CODEN: JASMAN

The Journal of the Acoustical Society of America

ISSN: 0001-4966

Vol. 123, No. 5, Pt. 1 of 2 May 2008

ACOUSTICAL NEWS-USA 2443

USA Meeting Calendar 2449

ACOUSTICAL NEWS-STANDARDS 2454

Standards Meeting Calendar 2454

BOOK REVIEWS 2459

REVIEWS OF ACOUSTICAL PATENTS 2461

LETTERS TO THE EDITOR

Influence of vehicle color on loudness judgments (L) — Daniel Menzel, Hugo Fastl, Ralf Graf, Jürgen Hellbrück — 2477

On the conservation of momentum for a sound pulse reflecting from a pressure-release boundary (L) — A. G. Voronovich — 2480

The high-frequency dispersion coefficient for the Rayleigh velocity in a vertically inhomogeneous anisotropic half-space (L) — A. L. Shuvalov — 2484

NONLINEAR ACOUSTICS [25]

Cubic nonlinearity in shear wave beams with different polarizations — Mark S. Wochner, Mark F. Hamilton, Yurii A. Ilinskii, Evgenia A. Zabolotskaya — 2488

Effect of an entrained air bubble on the acoustics of an ink channel — Roger Jeurissen, Jos de Jong, Hans Reinten, Marc van den Berg, Herman Wijshoff, Michel Versluis, Detlef Lohse — 2496

AEROACOUSTICS, ATMOSPHERIC SOUND [28]

Collective bubble oscillations as a component of surf infrasound — Joseph Park, Milton Garcés, David Fee, Geno Pawlak — 2506

Multilevel fast multipole algorithm for acoustic wave scattering by truncated ground with trenches — Mei Song Tong, Weng Cho Chew, Michael J. White — 2513

High-Reynolds-number turbulent-boundary-layer wall pressure fluctuations with skin-friction reduction by air injection — Eric S. Winkel, Brian R. Elbing, Steven L. Ceccio, Marc Perlin, David R. Dowling — 2522

UNDERWATER SOUND [30]

Boundary perturbation methods for high-frequency acoustic scattering: Shallow periodic gratings — David P. Nicholls, Fernando Reitich — 2531

Experimental validation and applications of a modified gap stiffness model for granular marine sediments — Masao Kimura — 2542

(Continued)

CONTENTS—*Continued from preceding page*

Fitting data, but poor predictions: Reverberation prediction uncertainty when seabed parameters are derived from reverberation measurements — Charles W. Holland — 2553

Optimization of transmitting beam patterns of a conformal transducer array — Zhengyao He, Yuanliang Ma — 2563

ULTRASONICS, QUANTUM ACOUSTICS, AND PHYSICAL EFFECTS OF SOUND [35]

Influence of spatial correlation function on attenuation of ultrasonic waves in two-phase materials — Dalie Liu, Joseph A. Turner — 2570

Theory and analysis of frequency-domain photoacoustic tomography — Natalie Baddour — 2577

TRANSDUCTION [38]

Pipe wall damage detection by electromagnetic acoustic transducer generated guided waves in absence of defect signals — Milos Vasiljevic, Tribikram Kundu, Wolfgang Grill, Evgeny Twerdowski — 2591

STRUCTURAL ACOUSTICS AND VIBRATION [40]

Comparison of spheroidal and eigenfunction-expansion trial functions for a membrane in an infinite baffle — Tim Mellow, Leo Kärkkäinen — 2598

NOISE: ITS EFFECTS AND CONTROL [50]

Calculations of modes in circumferentially nonuniform lined ducts — WenPing Bi — 2603

ARCHITECTURAL ACOUSTICS [55]

On the steering of sound energy through a supercritical plate by a near-field transducer array — Brian E. Anderson, W. Jack Hughes, Stephen A. Hambric — 2613

ACOUSTIC SIGNAL PROCESSING [60]

Statistically motivated design of input signals for modern ultrasonic array systems — Fredrik Lingvall, Tomas Olofsson — 2620

Sparsity constrained deconvolution approaches for acoustic source mapping — Tarik Yardibi, Jian Li, Petre Stoica, Louis N. Cattafesta, III — 2631

Model-based detection of synthetic bat echolocation calls using an energy threshold detector for initialization — Mark D. Skowronski, M. Brock Fenton — 2643

PHYSIOLOGICAL ACOUSTICS [64]

Stimulus-frequency otoacoustic emission: Measurements in humans and simulations with an active cochlear model — Yong-Sun Choi, Soo-Young Lee, Kourosh Parham, Stephen T. Neely, Duck O. Kim — 2651

PSYCHOLOGICAL ACOUSTICS [66]

Pitch strength decreases as F0 and harmonic resolution increase in complex tones composed exclusively of high harmonics — D. Timothy Ives, Roy D. Patterson — 2670

Speech detection in spatial and nonspatial speech maskers — Uma Balakrishnan, Richard L. Freyman — 2680

Relative weights for frequency glide detection using narrowband noise — Jinyu Qian, Virginia M. Richards — 2692

Perception and cortical neural coding of harmonic fusion in ferrets — Sridhar Kalluri, Didier A. Depireux, Shihab A. Shamma — 2701

(Continued)

CONTENTS—*Continued from preceding page*

SPEECH PRODUCTION [70]

Spatio-temporal quantification of vocal fold vibrations using high-speed videoendoscopy and a biomechanical model	Raphael Schwarz, Michael Döllinger, Tobias Wurzbacher, Ulrich Eysholdt, Jörg Lohscheller	2717
Nonlinear source–filter coupling in phonation: Theory	Ingo R. Titze	2733
Amplitude variations in coarticulated vowels	Ewa Jacewicz, Robert Allen Fox	2750
Focus, prosodic context, and phonological feature specification: Patterns of variation in fricative production	Noah Silbert, Kenneth de Jong	2769
What marks the beat of speech?	Greg Kochanski, Christina Orphanidou	2780

SPEECH PERCEPTION [71]

Differential contribution of envelope fluctuations across frequency to consonant identification in quiet	Frédéric Apoux, Sid P. Bacon	2792
A method to identify noise-robust perceptual features: Application for consonant /t/	Marion S. Régnier, Jont B. Allen	2801
Acoustic cues to tonal contrasts in Mandarin: Implications for cochlear implants	Yu-Ching Kuo, Stuart Rosen, Andrew Faulkner	2815
Compensation for coarticulation, /u/-fronting, and sound change in standard southern British: An acoustic and perceptual study	Jonathan Harrington, Felicitas Kleber, Ulrich Reubold	2825
Effect of spectral normalization on different talker speech recognition by cochlear implant users	Chuping Liu, John Galvin, III, Qian-Jie Fu, Shrikanth S. Narayanan	2836
Information transfer analysis: A first look at estimation bias	Elad Sagi, Mario A. Svirsky	2848
Intra- versus intermodal integration in young and older adults	Brent P. Spehar, Nancy Tye-Murray, Mitchell S. Sommers	2858

BIOACOUSTICS [80]

Suppression of shocked-bubble expansion due to tissue confinement with application to shock-wave lithotripsy	Jonathan B. Freund	2867
Mathematics of pulsed vocalizations with application to killer whale biphonation	Judith C. Brown	2875
Broadband backscatter from individual Hawaiian mesopelagic boundary community animals with implications for spinner dolphin foraging	Whitlow W. L. Au, Kelly J. Benoit-Bird	2884
The structure of vocal sounds produced with the mouth closed or with the mouth open in treefrogs	Marcos Gridi-Papp	2895
Human listeners attend to size information in domestic dog growls	Anna M. Taylor, David Reby, Karen McComb	2903
Carrier-dependent temporal processing in an auditory interneuron	Patrick Sabourin, Heather Gottlieb, Gerald S. Pollack	2910
The frequency response of rat vibrissae to sound	Lisa F. Shatz, Craig W. Christensen	2918
Frequency and level dependent masking of the multiple auditory steady-state response in the bottlenose dolphin (*Tursiops truncatus*)	Brian K. Branstetter, James J. Finneran, Dorian S. Houser	2928
Effect of combined source (*F*0) and filter (formant) variation on red deer hind responses to male roars	Benjamin D. Charlton, David Reby, Karen McComb	2936
Shape-based ultrasound tomography using a Born model with application to high intensity focused ultrasound therapy	Başak Ülker Karbeyaz, Eric L. Miller, Robin O. Cleveland	2944

(Continued)

CONTENTS—*Continued from preceding page*

JASA EXPRESS LETTERS

Contribution of onset/offset information of modulation to amplitude modulation depth discrimination	Derek R. Edwards, Jungmee Lee, Jennifer Andrews, Aileen Wong	EL111
Flexural wave dispersion in orthotropic plates with heavy fluid loading	Elizabeth Magliula, J. Gregory McDaniel	EL116

CUMULATIVE AUTHOR INDEX 2963

Contribution of onset/offset information of modulation to amplitude modulation depth discrimination[a)]

Derek R. Edwards, Jungmee Lee, Jennifer Andrews, and Aileen Wong
Department of Speech, Language, and Hearing Sciences, University of Arizona, 1131 E. 2nd Street, Tucson, Arizona 85721-0071
derek09@email.arizona.edu, jmlee6@email.arizona.edu, andrewsj@email.arizona.edu, annw16@email.arizona.edu

Abstract: A previous study by [J. Lee, G. Long, and C. Jeung, J. Acoust. Soc. Am. **119**, S3332 (2006)] found that information at the onset or offset of modulation could be utilized for improved amplitude modulation (AM) depth discrimination in a continuous carrier condition (carrier presented 250 ms earlier and later than the modulator). In this study, the relative contribution of information at the onset or offset of the modulation was examined with an onset-fringe carrier condition (carrier begins 250 ms earlier than the modulator) and an offset-fringe condition (carrier ends 250 ms later than the modulator). The results suggest that modulation information at the onset might be utilized more than at the offset.

© 2008 Acoustical Society of America
PACS numbers: 43.66.Mk, 43.66.Fe [Q-JF]
Date Received: November 27, 2007 **Date Accepted:** February 7, 2008

1. Introduction

Lee and Bacon (1997) studied the duration effect on amplitude modulation (AM) depth discrimination with a gated sinusoidal carrier condition (modulation begins and ends with the carrier). AM depth discrimination was found to be influenced by the number of modulation cycles. There was a critical duration of four cycles of modulation in which a dramatic threshold improvement (more than factor of 2) was observed when the stimulus duration increased from a shorter duration to this critical duration; only a slight or no improvement of threshold was observed when the stimulus duration exceeded this critical duration for modulation rates of 10, 20, 40, and 80 Hz. Lee and Bacon (1997) compared AM detection data (Sheft and Yost, 1990) with their AM depth discrimination data and found that AM detection lacks the critical duration effect observed in AM depth discrimination. In contrast, AM detection thresholds were found to decrease gradually with increasing duration from 25 to 400 ms. It should be noted, however, that Sheft and Yost (1990) used the noise carrier whose total duration was 51.2 ms longer (due to 25.6 ms rise/fall time) than modulation duration, while Lee and Bacon (1997) used a gated sinusoidal carrier. This difference between stimuli led to the study of Lee *et al.* (2006) in which both AM detection and AM depth discrimination were measured with the same stimulus conditions.

Lee *et al.* (2006) measured AM detection and AM depth discrimination with gated and continuous noise carrier conditions as a function of the number of modulation cycles. In the continuous noise carrier condition, the carrier was presented 250 ms earlier and 250 ms later than the modulator. A difference in thresholds between gated and continuous carrier conditions was observed for lower modulation rates of 10, 20, 40, and 80 Hz at less than four modulation cycles.

The critical duration of four cycles of modulation was observed for both AM detection and AM depth discrimination (for both standard depths of 0.1 and 0.4) in the gated carrier

[a)]A portion of this study was presented at the American Auditory Society meeting, 2007.

condition for lower modulation rates (10, 20, 40, and 80 Hz). For these lower modulation rates, there was a significant improvement in **both** AM detection and AM depth discrimination thresholds in the continuous carrier condition at fewer than four cycles of modulation. Thresholds were similar for both gated and continuous carrier conditions for modulation cycles greater than four. These results suggest that a difference in stimulus gating may have caused the absence of a critical duration effect in AM detection observed from the comparison of data from Sheft and Yost (1990) and Lee and Bacon (1997). For the gated carrier condition, shaping the onset/offset of stimuli with rise/fall times might reduce modulation information at the onset/offset, which might result in a dramatic change in threshold for a smaller number of modulation cycles. Therefore, the presence of a critical duration effect appears to be the result of gating differences.

In the continuous carrier condition used in Lee *et al.* (2006), the carrier was presented before and after the modulator. Therefore, it is impossible to determine from their data whether it was the modulation information at onset or offset of the modulator that was being used in the AM detection/discrimination task. The goal of the present study was to determine whether the onset or offset of modulation information is responsible for the observed improvement in AM depth discrimination at fewer than four cycles of modulation for lower modulation rates (10, 20, 40 and 80 Hz) in the continuous carrier condition. Four carrier conditions were compared: Gated (carrier gated on and off with the modulator), Onset/offset-fringe (carrier gated on 250 ms before modulator onset and gated off 250 ms after modulator offset), Offset-fringe (carrier gated on with the modulator and gated off 250 ms after modulator offset), and Onset-fringe (carrier gated on 250 ms before modulator onset and gated off with the modulator). For the purposes of this study, the continuous carrier condition of Lee *et al.* (2006) will be referred to as the onset/offset-fringe condition to make a clear distinction from the continuous carrier condition of Sheft and Yost (1990), where the wideband noise carrier was continuously on.

If it is the onset information of the modulator that contributes to the improved AM depth discrimination at fewer than four cycles of modulation, then the expected findings are: (1) the thresholds of the onset-fringe carrier condition will be lower than those of the offset-fringe carrier condition; (2) the thresholds of the onset-fringe and onset/offset-fringe carrier conditions will be similar or the same; (3) the thresholds of the gated carrier and offset-fringe carrier conditions will be similar or the same.

2. Methods

2.1 Subjects

Three normal hearing subjects participated in this study. Their ages ranged from 21 to 41. The subjects were paid for their participation.

2.2 Stimuli

Sinusoidally amplitude modulated noise was used as the stimulus throughout this experiment. The carrier was broadband noise low-pass filtered at 10,000 Hz.

Equation (1) defines the stimuli where A is the amplitude, m is the standard modulation depth, Δm is the change in the modulation depth, f_m is the modulation rate, and θ is the phase of modulation.

$$s(t) = A\{1 + [(m + \Delta m)\cos(2\pi f_m t + \theta)]\}X[\text{noise}], \quad (1)$$

Modulation frequencies of 10, 20, 40, or 80 Hz with a standard modulation depth of 0.1 were used. The phase of modulation was randomly chosen between trials. The onset and offset of all stimuli were shaped by a cosine-squared function resulting in a rise/fall time of 5 ms. The number of cycles for each modulation frequency was as follows: 2, 4, or 8 for 10 Hz; 2, 4, 8, or 16 for 20 Hz; 2, 4, 8, 16, or 32 for 40 Hz; 2, 4, 8, 16, 32, or 64 for 80 Hz. The overall level for each interval was randomized between 65 and 71 dB sound pressure level to ensure that depth discrimination was not based on a change in overall level due to modulation. The Tucker-Davis Technologies (TDT) system 3 was used to generate the stimuli with a 20 kHz sampling rate. Experiments were controlled by SykoFizX software. Four carrier conditions

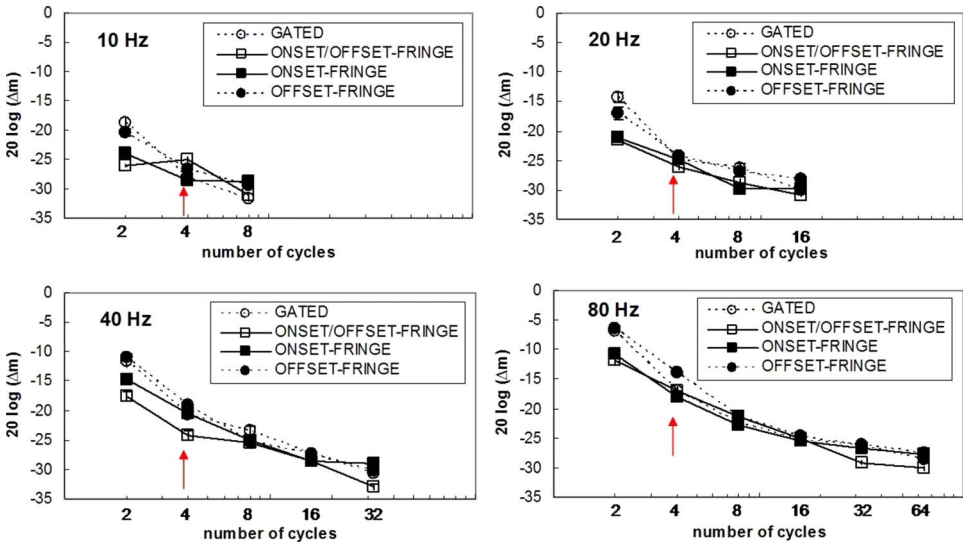


Fig. 1. (Color online) AM depth discrimination thresholds with gated (open circle), onset/offset-fringe carrier (open square), onset-fringe (closed square), and offset-fringe (closed circle) conditions were plotted as a function of the number of modulation cycles for $fm = 10$, 20, 40, and 80 Hz. These are the mean thresholds for three subjects. The standard errors are plotted and the size of symbols are smaller than the size of symbols.

were compared: Gated (carrier gated on and off with the modulator), onset/offset-fringe (carrier gated on 250 ms before modulator onset and gated off 250 ms after modulator offset), offset-fringe (carrier gated on with the modulator and gated off 250 ms after modulator offset), and onset-fringe (carrier gated on 250 ms before modulator onset and gated off with the modulator).

2.3 Procedure

AM depth discrimination thresholds were determined by a two alternative forced choice paradigm. The psychophysical task was to determine which interval contained the amplitude modulated sound with greater depth of modulation. The "standard" stimulus had a modulation depth of 0.1, and the "signal" stimulus had a modulation depth of $0.1+\Delta m$. The Δm was varied using a 3-down 1-up adaptive procedure (79.4% correct). The step size for the modulation depth change was 2 dB and was reduced to 1 dB after three reversals, and the trials were continued until obtaining seven reversals. The threshold for each run was an average of the final four reversals in the run. For each condition, three threshold estimations were averaged for the final threshold calculation if the standard deviation of the three threshold estimations was smaller than 3 dB. Additional threshold estimations were performed if the standard deviation was equal to or larger than 3 dB until the standard deviation was smaller than 3 dB, but the maximum number of threshold estimations did not exceed five.

Subjects were seated in a sound treated booth and listened to the stimuli through Sennheiser HD 250 linear II earphones. All stimuli were monaurally presented. Subject's responses were obtained with a push button response box with two buttons corresponding to two intervals. Practice trials were given before every run began and lasted until the subjects indicated that they understood the task. Correct answer visual feedback was provided after each response.

3. Results

All data in the figures are the mean of three subjects with standard error. In many cases, the standard error bars are smaller than the symbols. Figure 1 shows AM depth discrimination thresholds as a function of the number of modulation cycles for gated (open circles), onset/offset-fringe carrier (open square), onset-fringe (closed square), and offset-fringe (closed circle) conditions. Each panel represents different modulation rates. For a given modulation

rate, a two-way repeated analysis of variance (carrier type *x* number of cycles) indicated the main effect of carrier type is dependent on the number of modulation cycles since there is a significant interaction between the carrier type and the number of cycles ($p < 0.01$) for all modulation rates. Additional multiple comparison analysis (Holm–Sidak method) indicated that thresholds of gated and onset/offset-fringe conditions were not significantly different for four or greater number of cycles for all modulation rates except at 40 Hz for four modulation cycles, but the onset/offset-fringe condition thresholds were significantly better than those of the gated condition for two modulation cycles for all modulation rates ($p < 0.05$). Thresholds tend to increase as the number of modulation cycles decreases ($p < 0.025$) for all modulation rates. This finding is consistent with the results of Lee *et al.* (2006).

Comparison analysis of onset-fringe and offset-fringe conditions indicated that thresholds were not significantly different for four or greater number of cycles for all modulation rates except at 80 Hz for four modulation cycles, but the onset-fringe condition thresholds were significantly better than those of the offset-fringe condition for two modulation cycles for all modulation rates ($p < 0.05$).

Thresholds of offset-fringe and gated conditions were not significantly different for all modulation cycles for all modulation rates except at 20 Hz for two modulation cycles and at 80 Hz for four modulation cycles. Also, thresholds of onset-fringe and onset/offset-fringe conditions were not significantly different for all modulation cycles for all modulation rates except at 40 Hz for two and four modulation cycles.

Overall, at two modulation cycles, thresholds were better for conditions in which modulation information at the onset was well preserved (onset-fringe and onset/offset-fringe carrier) than for conditions in which modulation information at onset was distorted by the gating function (gated carrier and offset-fringe carrier). This supports our hypothesis that the modulation information at onset may contribute to better AM depth discrimination.

4. Discussion

For AM depth discrimination, conditions that included an unmodulated carrier prior to the modulator (onset-fringe and onset/offset-fringe carrier) had lower thresholds at two modulation cycles, resulting in gradual threshold improvement with increasing number of modulation cycles, than other conditions without an unmodulated carrier prior to the modulator (offset-fringe and gated carrier), resulting in an abrupt threshold improvement with increasing modulation cycles from two to four. Similar findings have been reported in studies with AM sounds (Sheft and Yost, 1990; Viemeister, 1979) and with recognition of syllables (Ainsworth and Meyer, 1994)

Sheft and Yost (1990) found that AM detection thresholds were reduced by the addition of 500 ms of carrier prior to the onset of modulation (fringe condition), which is similar to our onset-fringe condition. Their continuous condition (wideband noise carrier continuously on) produced lower thresholds than both gated and fringe conditions. This is different from the data reported here, which showed no significant difference between onset-fringe and onset/offset-fringe carrier conditions. Note, however, that their continuous carrier condition differs from our onset/offset-fringe condition. Our onset/offset-fringe had only 250 ms of noise present before and after the modulation, while their continuous carrier condition had a non-stop continuous carrier throughout the trials.

Viemeister (1979) measured AM detection for a gated and a continuous carrier condition (wideband noise carrier that was continuously on). Thresholds were found to be lower for the continuous carrier condition than for the gated carrier condition at low modulation rates (64 Hz and lower), while thresholds were similar across the two carrier conditions at higher modulation rates. The threshold difference between gated and continuous carrier conditions was larger for shorter stimulus durations. Viemeister speculated that improved thresholds for the continuous carrier condition at lower modulation rates may be due to a slow (100–200 ms) adaptation process occurring in the gated carrier condition. Short-term adaptation might reduce sensitivity to the modulation if the initial neural response to the onset of the stimulus is larger

relative to the change in neural response produced by the sinusoidal modulation. This reduced sensitivity effect is larger near carrier onset and will be more apparent for shorter durations; the first cycles of low frequency modulation would be masked.

Ainsworth and Meyer (1994) showed improved recognition of plosive syllables for a condition where noise was presented continuously (subjects were exposed to the noise at least 1 min before the task started), but this improved recognition was not present for a condition where noise was gated with syllables. They suggested that this may be the result of cochlear nerve fiber adaptation to the noise. Adaptation results in an increased dynamic range (increased saturation threshold) of the nerve fiber and could be the cause of improved recognition of syllables in continuous noise conditions (similar to our onset-fringe and onset/offset-fringe carrier conditions).

Therefore, it is possible that the improved AM depth discrimination at the shorter durations (usually corresponding to modulation cycles less than four) for the onset-fringe and onset/offset-fringe carrier condition in our study might be due to auditory nerve fibers' adaptation to the preceding noise. Another possible explanation is that unmodulated noise presented prior to the modulation could help preserve modulation information at the onset since the onset of modulation portion would not be shaped by the rise/fall time.

Acknowledgments

This work was supported by NIDCD Grant No. R03 DC06605. We would like to express our great appreciation to Dr. Andrew Lotto and Dr. Dianne Van Tasell for their valuable comments on this manuscript. Also we appreciate three anonymous reviewers for their helpful comments to improve this manuscript.

References and Links

Ainsworth, W. A., and Meyer, G. F. (**1994**). "Recognition of plosive syllables in noise: Comparison of an auditory model with human performance," J. Acoust. Soc. Am. **96**, 687–694.

Lee, J., and Bacon, S. (**1997**). "Amplitude modulation depth discrimination of a sinusoidal carrier: Effect of stimulus duration," J. Acoust. Soc. Am. **101**, 3688–3693.

Lee, J., Long, G., and Jeung, C. (**2006**). "Temporal integration functions of AM detection and AM depth discrimination," J. Acoust. Soc. Am. **119**, 3332.

Sheft, S., and Yost, W. A. (**1990**). "Temporal integration in amplitude modulation detection," J. Acoust. Soc. Am. **88**, 796–805.

Viemeister, N. F. (**1979**). "Temporal modulation transfer functions based upon modulation thresholds," J. Acoust. Soc. Am. **66**, 1364–1380.

Flexural wave dispersion in orthotropic plates with heavy fluid loading

Elizabeth Magliula
Naval Undersea Warfare Center, Division Newport, Newport, Rhode Island 02842 and
Department of Aerospace and Mechanical Engineering, Boston University, 110 Cummington Street, Boston, Massachusetts 02215
magliulaea@npt.nuwc.navy.mil

J. Gregory McDaniel
Department of Aerospace and Mechanical Engineering, Boston University, 110 Cummington Street, Boston, Massachusetts 02215
jgm@bu.edu

Abstract: Orthotropic plates support flexural waves with wavenumbers that depend on their angle of propagation. The present work investigates the effect of fluid loading on this angular dependence, and finds that the effect is relatively small for typical composite plate materials in contact with water. This finding results from an analytical model of the fluid-loaded plate, in which the plate is modeled by classical laminated plate theory and the fluid is modeled as an ideal acoustic fluid. The resulting dispersion relation is a tenth-order polynomial in the flexural wavenumber. Direct numerical solution, as well as analysis at frequencies below coincidence, reveals that the angular dependence of wavenumber is magnified but not significantly distorted by the addition of fluid loading.

© 2008 Acoustical Society of America
PACS numbers: 43.40.Dx, 43.20.Hq [AN]
Date Received: October 30, 2007 **Date Accepted:** February 7, 2008

1. Introduction

The bending rigidity of a composite plate may easily vary by an order of magnitude in its principal directions, even for classical composite materials. When the plate is *in vacuo*, this naturally causes substantial variations in the flexural wavenumber as the direction of wave propagation varies. The present work is concerned with the effects of fluid loading on these variations. Understanding this effect is expected to provide insights into the structural acoustics of finite orthotropic plates (Anderson and Bratos-Anderson, 2005), curved orthotropic structures (Ghinet and Atalla, 2005), and musical instrument models that involve thin orthotropic structures (Derveaux *et al.*, 2003).

Previous work by Fay (1948) on the propagation of flexural waves in fluid-loaded isotropic plates provides a foundation for the present work. Fay found that the dispersion relation for flexural waves involves a tenth-order polynomial in wavenumber. Further analysis at frequencies below coincidence revealed the existence of an unattenuated flexural wave that propagates with a subsonic sound speed. Fahy (1989) provided a simplified dispersion relationship below coincidence in which the effective mass of the fluid-loaded plate is a sum of the plate mass and the mass of a fluid whose volume is determined by the flexural wavenumber.

The present work derives the dispersion relation for a fluid-loaded orthotropic plate, following the derivation for the isotropic plate given by Fahy wherever possible. Next, a convenient method is presented for numerically computing the coefficients of the resulting tenth-order polynomial. The method involves the convolution of various polynomial coefficients, which avoids extensive algebraic manipulation. At frequencies below coincidence, a simplified dispersion relationship is found that is similar to that provided by Fahy. Examples involving classic composite materials indicate that the plate mass competes with the fluid mass for parameters of practical interest.

 © 2008 Acoustical Society of America

2. Dispersion relation

We begin by considering the equation of motion for an infinite orthotropic plate in contact with an acoustic fluid on one side (Leissa, 1969),

$$D_x\frac{\partial^4 w}{\partial x^4}+2D_{xy}\frac{\partial^4 w}{\partial x^2\,\partial y^2}+D_y\frac{\partial^4 w}{\partial y^4}+\rho_s h\frac{\partial^2 w}{\partial t^2}=f, \tag{1}$$

where w is the normal displacement and the coordinates x and y lie in the plane of the plate. This equation assumes that the plate thickness, h, is small relative to a flexural wavelength. The variables D_x and D_y represent the flexural stiffness of the plate in the x and y directions, respectively, and D_{xy} represents the "bending-torsional stiffness" of the plate (Anderson and Bratos-Anderson, 2005). Note that some authors, such as Timoshenko and Woinowsky-Krieger (1959), define the variable D_{xy} differently.

Derivation of the dispersion relation for the fluid-loaded orthotropic plate will follow a similar derivation by Fahy for isotropic plates, in which wave impedances for the plate and fluid act in mechanical parallel. Substitution of traveling wave representations for displacement and applied traction, $w=\Re\{W\exp[i(\omega t-k_x x-k_y y)]\}$ and $f=\Re\{F\exp[i(\omega t-k_x x-k_y y)]\}$, into Eq. (1) yields the wave impedance of the plate

$$Z_p=\frac{F}{i\omega W}=\frac{D_x k_x^4+2D_{xy}k_x^2k_y^2+D_y k_y^4-\rho_s h\omega^2}{i\omega}. \tag{2}$$

Similarly, substitution of a pressure field of the form $p=\Re\{P\exp[i(\omega t-k_x x-k_y y-k_z z)]\}$ into Euler's equation yields the acoustic wave impedance of the fluid,

$$Z_{fl}=\frac{P}{i\omega W}=\frac{\rho_0\omega}{k_z}, \tag{3}$$

and the acoustic wave equation provides a relationship between the wavenumbers,

$$k_0^2=k_x^2+k_y^2+k_z^2. \tag{4}$$

Finally, the dispersion relations are obtained by adding the impedances that are in mechanical parallel in the absence of excitation, $Z_p+Z_{fl}=0$, or

$$(k_0^2-k_x^2-k_y^2)(D_x k_x^4+2D_{xy}k_y^2k_x^2+D_y k_y^4-\rho_s h\omega^2)^2-(i\rho_0\omega^2)^2=0. \tag{5}$$

This polynomial is fifth order in k_x^2 when k_y^2 is specified. Only one of the roots represents a traveling flexural wave that is unattenuated when damping is not present. This wave is the sole focus for the remainder of this paper. For discussions of the other four roots, in the context of isotropic plates, the reader is referred to the paper by Fay.

In numerical simulations, it is convenient to numerically compute the coefficients of this polynomial by convolving vectors of coefficients whenever two polynomials are multiplied. This allows Eq. (5) to be written as $p(k_x^2)=0$, where $p(k_x^2)$ is a fifth-order polynomial in k_x^2. Its vector of coefficients, $\mathbf{p}$, is given by

$$\mathbf{p}=\mathbf{p}_1*\mathbf{p}_2*\mathbf{p}_2+\mathbf{p}_3, \tag{6}$$

where $*$ denotes a convolution defined by

$$(\mathbf{p}*\mathbf{q})_k=\sum_j \mathbf{p}_j\mathbf{q}_{k+1-j}. \tag{7}$$

The vectors are obtained by inspection of Eq. (5),

$$\mathbf{p}_1=\begin{bmatrix}-1 & (k_0^2-k_y^2)\end{bmatrix}. \tag{8}$$

$$\mathbf{p}_2=\begin{bmatrix}D_x & 2D_{xy}k_y^2 & (D_y k_y^4-\rho_s h\omega^2)\end{bmatrix}. \tag{9}$$

$$\mathbf{p}_3 = \begin{bmatrix} 0 & 0 & 0 & 0 & 0 & -(i\rho_0\omega^2)^2 \end{bmatrix}. \tag{10}$$

In this way, the coefficients $\mathbf{p}_1 - \mathbf{p}_3$ are computed from the above equations and the polynomial coefficients are computed from Eq. (6). This avoids extensive algebraic manipulations to analytically solve for the coefficients of the polynomial.

3. Low frequency approximation

In this section, we investigate flexural wave dispersion at low frequencies, where the inertia of the fluid dominates its compressibility. For simplicity in the derivation, let a coordinate x' be defined in the propagation direction of a flexural wave in an orthotropic plate. Since the displacement is independent of all other orthogonal coordinates, the equation of motion of the plate with fluid loading on one side assumes the form

$$D_{x'} \frac{\partial^4 w}{\partial (x')^4} + \rho_s h \frac{\partial^2 w}{\partial t^2} = f, \tag{11}$$

where $D_{x'}$ is algebraically related to D_x, D_y, and D_{xy}, as well as the angle between x and x'. Details of this relationship are given by Leissa (1969) [see Eq. (9.25) and following text].

Assuming a traveling wave of the form

$$w = \Re\{W \exp[i(\omega t - k_{x'} x')]\}, \tag{12}$$

and following the derivation in the previous section results in the dispersion

$$(k_0^2 - k_{x'}^2)(k_{x'}^4 D_{x'} - \rho_s h \omega^2)^2 - (i\rho_0 \omega^2)^2 = 0. \tag{13}$$

Introducing the low-frequency approximation

$$k_0 \ll k_{x'} \tag{14}$$

simplifies the dispersion relation in Eq. (13) to

$$D_{x'} k_{x'}^4 - \omega^2 h \left(\rho_s + \frac{\rho_0}{k_{x'} h} \right) = 0, \tag{15}$$

which has the same form as the corresponding result for the isotropic plate given in Fahy.

As in the case of the isotropic plate, the fluid loading represents an added mass that is inversely proportional to the fluid-loaded wavenumber. Larger flexural wavelengths will be increased by smaller amounts. For this reason, fluid loading is expected to make flexural waves less directive in orthotropic plates. The overall magnitude of this effect will depend on the relative values of ρ_s and $\rho_0/(k_{x'} h)$. Noting that classical plate theory is generally valid when $k_{x'} h < 1$ leads to the expectation that the fluid mass will often dominate the plate mass at low frequencies, as noted by Fahy.

Table 1. Material properties of graphite-epoxy, taken from Yuan and Hsieh (1998).

E_x	138 GPa
E_y	8.9 GPa
E_z	8.9 GPa
G_{xy}	5.176 GPa
G_{xz}	5.176 GPa
G_{yz}	2.89 GPa
ν_{xy}	0.3
ν_{xz}	0.3
ν_{yz}	0.54
ρ	1600 kg/m^3

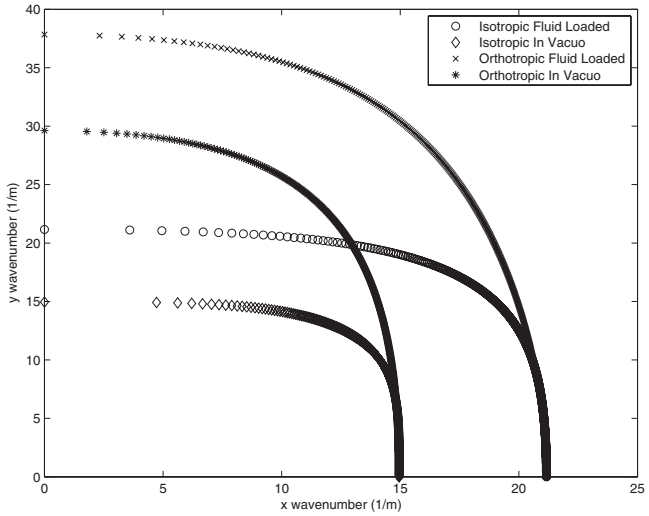


Fig. 1. Dispersion of flexural waves in a graphite-epoxy plate of thickness $h=0.01$ m, at 1 kHz.

4. Numerical results

The effects of fluid loading were numerically investigated for a plate constructed of graphite-epoxy with thickness $h=0.01$ m. Material properties are given in Table 1. Note that this material is at least an order of magnitude stiffer in the x direction than in the other directions. The fluid was taken as water with a sound speed $c_0=1500$ m/s and density $\rho_0=1$ kg/m^3. The wave number k_x corresponding to the propagating flexural wave was numerically computed from Eq. (5) for chosen values of k_y.

Results for a graphite-epoxy plate at frequencies of 1 kHz and 10 kHz are shown in Figs. 1 and 2. For comparison, results for the *in vacuo* case are plotted, as well as results for a similar isotropic plate whose properties are assumed to be those of the orthotropic plate in the x direction. These figures indicate a general magnification of the orthotropic wavenumbers due to

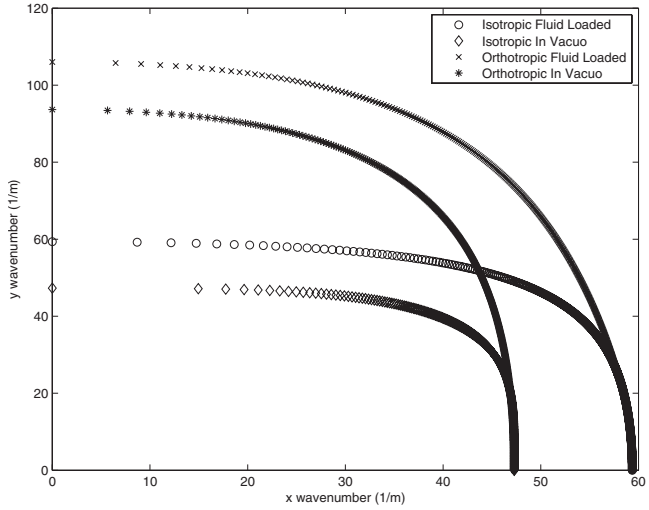


Fig. 2. Dispersion of flexural waves in a graphite-epoxy plate of thickness $h=0.01$ m, at 10 kHz.

Table 2. Percent increase in flexural wavenumber due to the addition of fluid loading to a composite plate.

	Case	% Increase in k_x	% Increase in k_y
1 kHz	Isotropic	41.54	41.54
	Orthotropic	41.54	27.73
10 kHz	Isotropic	25.56	25.56
	Orthotropic	25.56	13.19

fluid loading, however the variation with propagation angle is not significantly distorted when compared to the isotropic plate. This finding was more closely investigated in Table 2, which contains the percent increase in the flexural wavenumber due to fluid loading. This table supports the general conclusion that, for the cases studied, fluid loading does not distort the angular dependence of the flexural wave.

5. Summary

An analysis of the propagating flexural wave in a fluid-loaded orthotropic plate has been developed in order to better understand the effects of fluid loading. A method for numerically computing the coefficients of the resulting polynomial allows for direct calculation of the polynomial coefficients and hence the wavenumber. This work is expected to be important in numerically computing dispersion relations for more complicated geometries, such as cylindrical shells, where analytical derivation of the dispersion relation is difficult or impossible. When a single propagation angle is considered, this work shows that the equation of motion has the same form as that of an isotropic plate. This result reveals the underlying physics of flulid loading, particularly in the low-frequency regime where the fluid is primarily inertial and is likely to compete with the plate inertia.

Acknowledgments

The authors would like to acknowledge funding by ONR under Grant No. N000l4-05-1-0102 and NUWCNPT under the NUWCNPT In-House Laboratory Independent Research (I.L.I.R.) Program.

References and links

Anderson, J. S., and Bratos-Anderson, M. (**2005**). "Radiation efficiency of rectangular orthotropic plates," Acta. Acust. Acust. **91**, 61–76.
Derveaux, G., Chaigne, A., Joly, P., and Bécache, E. (**2003**). "Time-domain simulation of a guitar: Model and method," J. Acoust. Soc. Am. **114**(6), 3368–3383.
Fahy, F. (**1989**). *Sound and Structural Vibration*, 1st ed. (Academic, New York).
Fay, R. D. (**1948**). "Interactions between a plate and a sound field," J. Acoust. Soc. Am. **20**(5), 620–625.
Ghinet, S., and Atalla, N. (**2005**). "The transmission loss of curved laminates and sandwich composite panels," J. Acoust. Soc. Am. **118**(2), 774–790.
Leissa, A. W. *Vibration of Plates* (**1969**). (Acoustical Society of America, Melville).
Timoshenko, S., and Woinosky-Krieger, W. (**1959**). *Theory of Plates and Shells* (McGraw–Hill, New York).
Yuan, F. G., and Hsieh, C. C. (**1998**). "Three-dimensional wave propagation in composite cylindrical shells," Compos. Struct. **42**(2), 153–167.

ACOUSTICAL NEWS—USA

Elaine Moran
Acoustical Society of America, Suite 1NO1, 2 Huntington Quadrangle, Melville, NY 11747–4502

***Editor's Note**: Readers of this journal are encouraged to submit news items on awards, appointments, and other activities about themselves or their colleagues. Deadline dates for news and notices are 2 months prior to publication.*

New Fellows of the Acoustical Society of America



Susanna B. Blackwell—For contributions to the understanding of the effects of sound on marine mammals.



Vera Khokhlova—For contributions to theoretical nonlinear acoustics.

Reviewers of Manuscripts, 2007

Each year the Journal endeavors to publish a list of all the persons who reviewed manuscripts during the preceding year. Such a list is a compendium of names supplied by the Associate Editors. Because our peer review system depends strongly on the continuing anonymity of the reviewers, the Journal publishes these names in alphabetical order without identification of the associate editors who provided the names and without identification of the papers they reviewed. The primary reason for the publication of the list is to express the Journal's gratitude to its reviewers. Reviewing a paper is often a very time consuming and demanding task, and the anonymity requirement yields no professional recognition to those who generously provide their time to help the Associate Editors decide which papers should be published and to give constructive criticisms to the authors. The Journal is justifiably proud of this list, which includes a goodly proportion of all the researchers and eminent authorities in acoustics and related fields. In a compendium of this length, omissions and errors are inevitable. If anyone notices such, please send the corrections and missing names via e-mail or regular mail to either Elaine Moran (asa@aip.org) or Allan Pierce (adp@bu.edu).

Abascal, Ramon
Abawi, Ahmad T.
Abbas, Paul J.
Abdala, Carolina
Abel, Sharon M.
Abom, Mats
Abraham, Douglas A.
Adachi, Seiji
Adams, Norman
Adank, Patti
Agrawal, O.
Agus, Trevor R.
Ahnert, Wolfgang
Ahroon, William
Ainslie, Michael A.
Ajdler, Thibaut
Akay, Adnan
Akeroyd, Michael A.
Alain, Claude
Alberts, W. C. K., II
Aldridge, David F.
Aleshin, Vladislav
Alexander, Francis
Alexander, Joshua M.
Algazi, V. Ralph
Alghamdi, Mansour M.
Alipour, Fariborz
Allard, Jean-François F.
Allen, John S.
Allen, Jont B.
Alsius, Agnès
Altes, Richard A.
Amitay, Sygal
Ammi, Azzdine Y.
Anastasio, Mark A.
Anderson, John S.
Anderson, Sven E.
Ando, Yoichi
André-Obrecht, Régine
Andruski, Jean E.
Anemuller, Jorn
Anfosso-Ledee, Fabienne
Angster, Judit
Aoyama, Katsura
Arbisi-Kelm, Timothy
Arehart, Kathryn H.
Arieh, Yoav
Arnold, Walter
Aroyan, James
Arvelo, Juan I.
Ashmead, Daniel H.
Askenfelt, Anders G.
Assmann, Peter F.
Atalla, Noureddine
Atchley, Anthony A.
Atkins, Philip R.
Attenborough, Keith
Au, Whitlow W.
Auer, Edward T.
Austin, Steve
Avan, Paul A.
Averkiou, Michalakis A.
Baayen, R. Harald
Babisch, Wolfgang
Bacon, Sid P.
Bader, Rolf
Badiey, Mohsen
Badin, Pierre
Baer, Thomas
Baer, Tom
Baggeroer, Arthur B.
Bai, Mingsian R.
Bailey, Michael R.
Bailey, Peter J.
Bailliet, Hélène
Balaban, Evan S.
Balakrishnan, Uma
Barbone, Paul E.
Barlow, Claire
Barney, Anna
Barrera-Figueroa, Salvador
Barron, Michael
Barry, Johanna G.
Bartram, James F.
Baskent, Deniz
Bass, Andrew H.
Bass, Henry E.
Bauer, Jay J.
Beauchamp, James W.
Beaujean, Pierre-Philippe J.
Bech, Soren
Bécot, François-Xavier
Beddor, Patrice S.
Beedholm, Kristian
Benjamin, Kim C.
Bennert, T.
Benoit-Bird, Kelly J.
Bent, Tessa C.
Benyahia, Lazhar
Beranek, Leo L.
Berchok, Catherine L.
Berengier, Michel
Berg, Bruce G.
Berkhoff, Arthur
Bernstein, Joshua G.
Bernstein, Leslie R.
Bernstein, Lynne E.
Berry, David A.
Berryman, James G.
Berthommier, Frederic
Best, Virginia
Betlehem, Terence
Bharitkar, Sunil G.
Bian, Lin
Bickley, Corine A.
Bierer, Julie A.
Bigelow, Timothy A.
Bilbao, Stefan

 0001-4966/2008/123(5)/2443/11/$23.00 © 2008 Acoustical Society of America

Bilsen, Frans A.
Bisgaard, Nikolai
Bishop, Garner C.
Bjor, Ole-Herman
Blacklock, Oliver S.
Blackwell, Susanna B.
Blamey, Peter J.
Blanc-Benon, Philippe
Boe, Louis-Jean
Boersma, Paul
Boex, Colette
Bostrom, Anders
Bowles, Ann E.
Braasch, Jonas
Brachmanski, Stefan
Bradley, Charles
Bradley, John S.
Bradlow, Ann R.
Brambilla, Giovanni
Brand, Thomas
Branstetter, Brian K.
Braun, Christopher B.
Breazeale, Mack A.
Bregman, Al
Bresin, Roberto
Bressmann, Tim
Brink, Mark
Broad, David J.
Bronkhorst, Adelbert W.
Brooks, Bennett M.
Brooks, Thomas
Brown, Carolyn J.
Brown, Charles H.
Brown, Michael G.
Brown, Steve
Bruce, Ian C.
Bruce, Schneider
Bruecker, Christoph
Brungart, Douglas S.
Brungart, Timothy A.
Bucaro, Joseph A.
Buck, John R.
Buckingham, Michael J.
Buder, Eugene H.
Buell, Thomas N.
Buick, Jim
Buksnowitz, Christoph
Bull, Joseph
Bunnell, H. Timothy
Bunton, Kate E.
Burkhard, Mahlon D.
Burnett, David S.
Burnett, Theresa A.
Burroughs, Courtney B.
Busch-Vishniac, Ilene J.
Buss, Emily
Cabell, Randolph H.
Cable, Peter G.
Caiti, Andrea
Calamia, Paul T.
Calandruccio, Lauren
Calvo, David C.
Campanella, Angelo J.
Capus, Chris G.
Carcaterra, Antonio
Carey, William M.
Carlile, Simon
Carlyon, Robert P.
Carrell, Thomas D.
Carstensen, Edwin L.
Carter, G. Clifford
Castagnede, Bernard R.
Castaings, Michel
Castres, Fabrice O.
Catheline, Stefan
Cathignol, Dominique
Cawley, Peter
Cazzolato, Ben S.
Cebrian, Juli
Chadwick, Richard
Chaigne, Antoine J.
Chambers, David H.
Chambers, James P.
Chambers, Kyle
Chan, Roger W.
Chandiramani, Khushi L.
Chandler-Wilde, Simon
Chapman, Chris
Chapman, David M.
Chapman, John
Chapman, N. R.
Charrier, Isabelle
Chatterjee, Monita
Chebli, Hamid
Chen, Chi-Fang
Chen, Hongbin
Chen, Ming
Chen, Shigao
Chen, Sin-Horng
Chen, Yang
Cheney, Margaret
Cheng, Arthur C.
Chertoff, Mark
Chetouani, Mohammed
Chimenti, Dale E.
Ching, Teresa Y.
Chittivenkata, Krishnamurthy
Cho, Taehong
Choi, Jee Woong
Cholewiak, Roger
Chotiros, Nicholas P.
Chris, Plack
Christensen, Douglas
Chunchuzov, Igor
Church, Charles C.
Cienkowski, Kathleen M.
Cipolla, Jeffrey L.
Claesson, Ingvar
Clark, Bill
Clark, Cathy Ann
Clark, Christopher
Clark, William
Clarkson, Marsha G.
Cleary, Miranda
Clement, Gregory T.
Cleveland, Robin O.
Coady, Jeffry A.
Cobbold, Richard S.
Cobo, Pedro
Colburn, H. Steven S.
Cole, Ronald
Collet, Bernard
Collet, Manuel
Collins, Leslie M.
Collis, Jon M.
Colosi, John A.
Conant, David A.
Cone-Wesson, Barbara K.
Connine, Cynthia
Conoir, Jean-Marc
Cooke, Martin
Cornuelle, Bruce D.
Corsaro, Robert D.
Coulouvrat, François
Coussios, Constantin C.
Covey, Ellen
Cowan, Robert S. C.
Cox, Trevor J.
Craster, Richard
Creel, Sarah C.
Cudina, Mirko
Culling, John F.
Culver, Richard L.
Cunefare, Kenneth A.
Curcio, Daniella
Cusack, Rhodri
Cutler, Anne
Dacol, Dalcio K.
Dahl, Peter H.
Dai, Huanping
Daigle, Gilles A.
Dalecki, Diane
D'Alessandro, Christophe R.
Dalmont, Jean-Pierre
Dana, Murphy R.
Dancer, Armand L.
Dang, Jianwu
D'Antonio, Peter
Darwin, Christopher J.
Dasgupta, Nilanjan
Dasika, Vasant K.
Dau, Torsten
Davenny, Ben C.
David, Eddins
Davidson, Lisa
Davies, William J.
Davis, Rickie R.
Davy, John L.
Dayton, Paul A.
De Boer, Egbert
De Bruijn, Alex
De Cheveigné, Alain
Declercq, Nico F.
Defrance, Jerome
Degertekin, Levent
Dehnhardt, Guido
De Hoop, Adrianus T.
De Jong, Kenneth J.
Dejong, Richard
DelBalzo, Donald R.
Delgutte, Bertrand
Dellwo, Volker
DeLong, Caroline M.
Demany, Laurent
Demitriadis, Emilios
De Moustier, Christian P.
Deng, Cheri X.
Denisov, Gennady G.
Dent, Micheal L.
Depollier, Claude
De Rosa, Sergio
De Rosny, Julien
Desharnais, Francine
Destrade, Michel
Devasia, Santosh
Devillers, Laurence Y.
De Vries, Diemer
Dhar, Sumit
Di Scalea, Francesco L.
Dickey, Joe W.
Diehl, Randy L.
Dijksman, Frits
Dilley, Laura C.
Dittberner, Andrew B.
Divenyi, Pierre L.
Dizon, Roberto M.
Djikstra, Semme
Dobie, Robert
Dobrucki, Andrzej B.
Doellinger, Michael
Donaldson, Gail S.
Doo, Sejin
Dorman, Michael F.
Dos Santos, Serge
Dosso, Stan E.
Doty, Michael
Dougherty, Robert
Dowling, David R.
Dragonette, Louis R.
Drake, Robert M.
Drennan, Ward R.
Dreschler, Wouter A.
Drioli, Carlo
Drullman, Rob
D'Spain, Gerald L.
Dubus, Bertrand B.
Duda, Richard O.
Duda, Timothy F.
Dunlop, Rebecca A.
Dupere, Iain D.
Durlach, Nathaniel I.
Dusan, Sorin
Dushaw, Brian D.
Dutoit, Thierry
Dvorkin, Jack
Dye, Raymond H.
Dzieciuch, Matthew A.
Dzikowicz, Benjamin R.
Ebenezer, D. D.
Eddington, Donald K.
Eddins, David A.
Edds-Walton, Peggy
Edelmann, Geoffrey F.
Edmonds, Barrie A.
Edwards, Brent W.
Einhorn, Rebecca T.
Eisler, Thomas J.
Eisner, Frank
Ejsmont, Jerzy A.
Elberling, Claus
Eldredge, Jeff D.
Elhilali, Mounya
Elliott, Stephen J.
Ellison, William T.
Engwall, Olov
Epstein, Michael J.
Erath, Byron D.
Erbe, Christine
Ergun, Arif S.
Ericson, Mark A.
Ermann, Michael G.
Erpelding, Todd
Escudero, Paola
Espinoza-Varas, Blas
Espy-Wilson, Carol Y.
Evans, Bronwen G.
Evans, Richard B.
Everbach, Erich C.
Eversman, Walter
Ewert, Stephan D.
Faber, Alice
Fahey, Paul F.
Fahnline, John B.
Fais, Laurel
Falcone, Mauro
Fantini, Deborah A.
Farabee, Theodore M.
Farassat, Feri
Farina, Angelo
Farmer, David M.
Fastl, Hugo
Faulkner, Andrew
Fawcett, John A.
Fay, Richard R.
Feeney, M. Patrick
Feijoo, Gonzalo R.

Fellah, Zine el Abiddine
Fenton, Brock
Ferguson, Sarah H.
Festen, Joost M.
Fialkowski, Laurie T.
Fidell, Sanford
Fiebig, Andre
Fields, James M.
Filipanits, Frank
Fine, Michael L.
Finette, Steven I.
Finneran, James J.
Fishman, Yonatan I.
Fitch, Holly
Fitch, W. Tecumseh T.
Fitzpatrick, John A.
Flege, James E.
Fletcher, Neville H.
Fligor, Brian
Florentine, Mary
Folegot, Thomas
Foote, Kenneth G.
Ford, G.
Ford, John
Forrest, Karen
Forsythe, Stephen E.
Fox, Paul
Fox, Robert A.
Fox, Warren L.
Francis, Alexander L.
Francis, David T.
Franco, Francesco
Frank, Austin F.
Frank, Scott D.
Frankel, Adam S.
Frankel, Steven H.
Frankenthal, Shimshon
Franzoni, Linda P.
Frazer, L. Neil N.
Freeberg, Todd M.
Freed, Daniel J.
Freitag, Lee
Freyman, Richard L.
Friberg, Anders K.
Frijns, J.H.M
Frisk, George V.
Fritz, Claudia
Fromm, David M.
Fu, Qian-Jie
Fu, Tricia
Fu, Yibin
Fulop, Sean A.
Funnell, W. Robert J.
Furst, Miriam
Gabard, Gwenael
Gaeta, Rick
Galbrun, Laurent
Galland, M.A.
Gallun, Frederick J.
Galvin, John J.
Gan, Rong
Gannot, Sharon
Garcia-Lecumberri, Maria-Luisa L.
Gardonio, Paolo
Garrelick, Joel M.
Garrett, Steven L.
Gaskell, Gareth
Gaubitch, Nikolay D.
Gaumond, Charles F.
Gaunaurd, Guillermo C.
Gauthier, Philippe-Aubert
Gautier, Francois
Geers, Thomas L.
Gendron, Paul
Genuit, Klaus
George, Erwin L.J.
Gerratt, Bruce R.
Gerrits, Ellen
Gerstoft, Peter
Ghanem, Roger G.
Ghose, Kaushik
Ghosh Roy, Dilip N.
Gifford, Rene H.
Giguere, Christian
Gilbert, Kenneth E.
Gillespie, Douglas M.
Gillis, Keith A.
Ginsberg, Jerry H.
Giordano, Bruno L.
Givoli, Dan
Glasberg, Brian R.
Glegg, Stewart A.
Glorieux, Christ
Gockel, Hedwig E.
Goddard, Robert P.
Godin, Oleg A.
Goffman, Lisa
Goldinger, Stephen
Goldsworthy, Ray L.
Gomes, Joao P.
Gómez Vilda, Pedro
Gong, Xiu-Fen X.
Goodale, Melvyn
Goodman, Shawn S.
Goody, Michael
Gordon, Matthew K.
Gordon-Salant, Sandra
Gorga, Michael P.
Goto, Masahide
Gottfried, Terry L.
Goussev, Vitalyi
Gow, David W.
Grace, Sheryl M.
Gracewski, Sheryl M.
Gramtorp, Johan
Grantham, D. W.
Green, Dale
Green, Tim
Greene, Charles R., Jr.
Greenleaf, James F.
Gregory, Michelle L.
Griffiths, Timothy D.
Grinnell, Alan
Guastavino, Catherine
Guddati, Murthy N.
Guillon, Laurent
Guillot, Francois M.
Guinan, John J.
Guion, Susan G.
Gumerov, Nail A. A.
Gummer, Anthony W.
Guski, Rainer
Gutschalk, Alexander
Guyader, Jean-Luis
Haberman, Robert C.
Häb-Umbach, Reinhold
Hagiwara, Robert
Hahn, Mariah S.
Hahn, Thomas R.
Hald, Joergen
Hall, Deborah
Hall, Joseph W.
Hall, Neal A.
Hallé, Pierre A.
Halling, Dan C.
Hamdi, Mohamed-Ali
Hamilton, Mark F.
Hancock, Ken
Hanes, Peter
Hannon, Erin E.
Hansen, Colin H.
Hansen, John H.
Harkrider, Ashley W.
Harland, Edward J.
Harma, Aki S.
Harnsberger, James D.
Harris, Gerald R.
Harrison, Christopher H.
Harrison, Robert V.
Hartmann, William M.
Hartung, Klaus
Hasegawa-Johnson, Mark A.
Hawkins, Sarah
Hawley, Monica L.
Hayek, Sabih I.
Hayes-Harb, Rachel L.
Hazan, Valerie
Healy, Eric W.
Heaney, Kevin D.
Hedberg, Claes M.
Hedrick, Mark S.
Heffner, Henry E.
Heffner, Rickye
Hefner, Brian T.
Heil, Peter
Heimann, Dietrich
Heinz, Michael G.
Helfer, Karen S.
Heller, Laurie M.
Henderson, Paul D.
Henning, G. Bruce
Henyey, Frank S.
Hermand, Jean-Pierre
Hermansky, Hynek
Hermes, Dik J.
Hershey, John R.
Hertrich, Ingo
Herzel, Hanspeter
Herzing, Denise
Hess, Ursula
Hickey, Craig J.
Hickling, Robert
Hildebrand, John A.
Hinders, Mark K.
Hirata, Yukari
Hirose, Keikichi
Hirose, Sohichi
Hirshberg, Avraham
Hiryu, Shizuko
Hixon, Tom
Hodge, Megan M.
Hodgkiss, William S.
Hodgson, Murray R.
Hofmann, Heath
Hohmann, Volker
Holford, Richard
Holliday, Dale V.
Hollien, Harry
Holt, Lori L.
Holt, Marla M.
Holt, R. G.
Holzfuss, Joachim
Honda, Kiyoshi
Honing, Henkjan
Hoole, Philip A.
Hoover, K. Anthony
Hopgood, James R.
Hopkins, Kathryn
Horacek, Jaromir
Horne, John K.
Hornsby, Benjamin W.
Horoshenkov, Kirill V.
Horowitz, Seth S.
Hosokawa, Atsushi
Hosten, Bernard
Houde, John F.
Houle, Phil
House, Jill
Houser, Dorian S.
Houtgast, Tammo
Houtsma, Adrianus J.
Howe, Michael S.
Hu, Zhiwei
Huang, Jui-Ting
Huang, Lixi
Huber, Jessica E.
Hunter, Eric J.
Huntley Bahr, Ruth A.
Hursky, Paul
Hussain, Zahir M.
Hutchins, David A.
Hwang, Yun-Fan
Hynynen, Kullervo H.
Ian, Bruce
Ibsen, Stuart D.
Ih, Jeong-Guon
Ihlefeld, Antje
Ilinskii, Yurii A.
Ing, Ros Kiri
Insana, Michael F.
Isakov, Victor
Isakson, Marcia J.
Ishizuka, Kentaro
Iskarous, Khalil
Ito, Masashi
Iyer, Nandini
Jackett, David
Jackson, Darrell R.
Jackson, Philip J. B.
Jacobs, Laurence J.
Jacobsen, Finn
Jaeger, Stephen M.
James, Christopher J.
James, Howard
Jang, Seung-Ho
Janssen, Thomas
Jansson, Erik V.
Jarzynski, Jacek
Jech, Josef M.
Jedrzejczak, Wieslaw W.
Jensen, Finn B.
Jensen, Jakob
Jeon, Jin Yong
Jessen, Michael
Jesteadt, Walt
Jesus, Luis M.
Jesus, Sergio M.
Jiang, Qing
Jin, Craig
Jing, M.
Jing, Yun
Joe, Wolfe
John, Rosowski
Johnson, Blake W.
Johnson, Joel
Johnson, Michael T.
Johnson, Paul A.
Johnstone, Patti M.
Jones, Benjamin
Jones, Gary L.
Jones, Michael
Jonson, Michael
Jordan, Pedro M.
Joris, Philip
Jumars, Peter
Jurvelin, Jukka

Kaduchak, Gregory
Kain, Alexander
Kalluri, Rahda
Kanai, Hiroshi
Kang, Jian
Kargl, Steven G.
Karlsson, Inger
Kastelein, Ronald A.
Kates, James M.
Katz, Brian F.
Katz, J Lawrence
Kaufman, Jonathan
Kawahara, Hideki
Kazys, Rymantas
Keefe, Douglas H.
Keiffer, Richard S.
Keith, Stephen
Keith, William
Kemp, David
Keolian, Robert M.
Keppens, Veerle M.
Kergomard, Jean
Ketterling, Jeffrey A.
Khelif, Abdelkrim
Khokhlova, Vera A.
Khosla, Sid
Kidd, Gary R.
Kidd, Gerald
Kiefte, Michael
Kihlman, Tor S. D.
Kilfoyle, Daniel
Kim, Jaehwan
Kim, Jin O.
Kim, Kilsoo S.
Kim, Sang-Myeong
Kim, Yang-Hann
Kim, Yong Tae
Kimura, Masao
Kingston, John
Kirby, Raymond
Kirchhoff, Katrin
Kirkeby, Ole
Kistler, Doris J.
Kitamura, Tatsuya
Klaeboe, Ronny
Klapuri, Anssi
Kleiner, Mendel
Klemuk, Sarah A.
Klippel, Wolfgang
Klos, Jacob
Kloser, Rudy
Kluender, Keith R.
Klump, Georg M.
Knobles, David P.
Kob, Malte
Koehnke, Janet D.
Koenig, Laura L.
Kohler, Klaus J.
Kohlrausch, Armin
Koike, Takuji
Kolaini, Ali R.
Kolios, Michael C.
Kollmeier, Birger
Kong, Ying-Yee
Konrad-Martin, Dawn
Koopman, Gary
Kopco, Norbert
Korman, Murray S.
Korneliussen, Rolf J.
Kostek, Bozena
Krahe, Detlef
Krane, Michael H.
Krause, Jean C.
Krebes, Ed
Kreider, Wayne
Kripfgans, Oliver D.
Kristensen, Ryan
Kristiansen, Ulf R.
Kroeger, Bernd J.
Krolik, Jeffrey L.
Kroos, Christian
Krumbholz, Katrin
Krutyansky, Leonid M.
Kubin, Gernot
Kull, Robert C.
Kundu, Tribikram
Kuperman, William A.
Kushwaha, Manvir S.
Kuttruff, K. Heinrich
Kuznetsova, Iren E.
Kwon, Bom Jun
Kwon, Oh-Wook
Laback, Bernhard
Lacefield, James C.
Lachs, Lorin
Ladd, Robert
Ladich, Friedrich
Lafarge, Denis
Lafon, Cyril
Lam, Yiu W.
Lammers, Marc O.
Lane, Harlan
Langemann, Ulrike
Langley, Robin S.
Lanza di Scalea, Francesco
Larose, Eric
Larry, Humes
Larson, Gregg D.
Lasaygues, Philippe
Lasky, Robert E.
Lauchle, Gerald C.
Laugier, Pascal
Laukkanen, Anne-Maria
Lauriks, Walter
Laville, Frederic
Lawrie, Jane B.
Lawson, Gareth
Le Prell, Colleen
Lebourges-Dhaussy, Anne
Leclaire, Philippe
Lee, Haksue
Lee, Moohyung
Lee, Soo-Young
Lee, Sungbok
Lee, Tan
Lee, Young S.
Lehman, Sean K.
Leibold, Lori J.
Leighton, Timothy G.
Lentz, Jennifer J.
Leon, Fernand
LePage, Kevin D.
Lercher, Peter
Lesniewski, Peter J.
Leurer, Klaus C.
Levitin, Daniel
Levitt, Harry
Levy, Erika
Lewy, Serge
Leybaert, Jacqueline
Lhemery, Alain
Li, Kai Ming M.
Li, Weichang
Li, Wen L.
Lieberman, Philip
Lim, Raymond
Lingevitch, Joseph F.
Lipkens, Bart
Lister, Jennifer J.
Litvak, Leonid M.
Liu, Qing H.
Liu, Sheng
Lloyd, Christopher W.
Lobkis, Oleg I.
Locasto, Paul
Loeppert, Peter
Lofqvist, Anders
Loizou, Philipos C.
Lokki, Tapio
Lombard, Anthony
Long, Christopher J.
Lopez-Poveda, Enrique A.
Lorenzi, Christian
Loret, Benjamin L.
Lotto, Andrew J.
Loughlin, Patrick
Louisnard, Olivier
Lowe, Michael J.
Lu, Ching-Ta
Lu, Tom
Lu, Zhiqu
Lubman, David
Lucero, Jorge C.
Lugli, Marco
Lukashkin, Andrei N.
Luo, Li-Shi
Lütkenhöner, Bernd
Lutman, Mark E.
Lynch, James F.
Lyon, Richard H.
Lyzenga, Johannes
Mace, Brian R.
Mackersie, Carol L.
MacLeod, Andrea A.
Macmillan, Neil
Macpherson, Ewan A.
Madigosky, Walter M.
Madsen, Ernie L.
Madsen, Peter T.
Maekawa, Kikuo
Mainardi, Francesco
Majdak, Piotr
Makraki, George
Maltsev, Nick E.
Mamou, Jonathan
Mandelis, Andreas
Maniwa, Kazumi
Mann, David A.
Manoussaki, Daphne
Marchiano, Régis
Marengo, Edwin A.
Marklein, Rene
Marmottant, Philippe
Marshall, Bill
Marshall, Lynne
Marston, Philip L.
Martin, Brett
Martin, Glen K.
Martin, Paul
Martin, Steve W.
Martinez, Rudolph
Maruska, Karen
Maruvada, Subha
Maschke, Christian
Mason, Christine R.
Masserey, Bernard
Mast, T. Douglas
Masters, William M.
Mathevon, Nicolas
Matsukawa, Mami
Matsuo, Ikuo
Mattys, Sven L.
Matula, Thomas J.
Mauermann, Manfred
Maurel, Agnes
Maynard, Julian D.
Mayo, Catherine
Maze, Gerard
McAleavery, Steven
McAlpine, David
McCauley, Rob
McCowan, Brenda
McCoy, John J.
McDaniel, James G.
McDonald, Bryant E.
McFadden, Dennis
McGough, Robert J.
McGowan, Richard
McGuire, Grant L.
McKay, Colette M.
McLaughlin, Stephen
McLean, James S.
McRoberts, Gerald
Means, Steven L.
Meddis, Ray
Mehler, Jacques
Mellinger, David K.
Mercado, Eduardo
Meyer, Juergen
Miao, Jianmin
Michaels, Jennifer E.
Michalopoulou, Zoi-Heleni
Micheyl, Christophe
Mielke, Jeff
Migliori, Albert
Mignerey, Peter C.
Mignolet, Marc
Miksis-Olds, Jennifer L.
Miles, Ronald N.
Miller, Douglas L.
Miller, Eric L.
Miller, James G.
Miller, James H.
Miller, Lee A.
Mills, David M.
Milner, Ben P.
Minonzio, Jean-Gabriel
Mironov, Mikhail A.
Mitson, Ron
Mitterer, Holger
Miyashita, Toyokatsu
Miyoshi, Masato
Mobley, Joel
Mody, Maria B.
Moffett, Mark B.
Mohl, Bertel
Moilanen, Petro
Mokhtari, Parham
Mom, Thierry
Monahan, Edward C.
Mongeau, Luc G.
Monson, Brian
Montequin, Doug
Moonen, Marc
Mooney, T. Aran
Moore, Brian C.
Moore, Sue E.
Moorhouse, Andy T.
Mooshammer, Christine R.
Moreau, Stephane
Moretti, David J.
Morfey, Christopher L.
Morlet, Thierry
Morozov, Andrey K.
Morrison, Geoffrey S.
Morrissey, Ron

Morse, Scot F.
Moss, Cynthia F.
Moss, Heather
Mossbridge, Julia A.
Mottley, Jack G.
Mould, John
Mountain, David C.
Mozhaev, Vladimir
Muehleisen, Ralph T.
Mueller, Rolf
Muesch, Hannes
Muir, Thomas G.
Muller, Rolf
Mungiole, Michael
Munjal, M. L.
Munro, Murray J.
Munson, Benjamin R.
Murphy, Walter
Murphy, William J.
Murray, Todd W.
Murugesan, Venkatesan
Mutlu, Erhan
Nachtigall, Paul E.
Nagy, Peter B.
Nakatani, Tomohiro
Narayanan, Shrikanth S.
Nearey, Terrance M.
Neel, Amy T.
Neely, Stephen T.
Neff, Donna L.
Nehorai, Arye
Neild, Adrian
Nelken, Israel
Nelson, Doug
Nelson, Paul C.
Nelson, Peggy B.
Nemeth, Erwin
Nero, Redwood W.
Neubauer, Juergen
Newhall, Bruce K.
Newman, Rochelle S.
Ni, Kai
Nielsen, Peter L.
Nielsen, Traci
Niemiec, Jan M.
Niezrecki, Christopher
Nightingale, K.R. R.
Nilsson, Mats E.
Niquette, Patricia A.
Nishi, Kanae
Nissen, Shawn L.
Nittrouer, Susan N.
Noad, Michael
Nobile, Matthew A.
Noble, John M.
Noble, William
Nocke, Christian
Nolan, Francis
Nolte, Loren W.
Nordholm, Sven E.
Nordstrom, Karl I.
Norris, Andrew N.
Norris, David E.
Norris, Thomas F.
Nosal, Eva-Marie
Nowack, Robert L.
Nwokah, Eva
Nyborg, Wesley L.
Nygaard, Lynne C.
Oberfeld, Daniel
Obleser, Jonas
O'Brien Jr., William D.
Obrist, Martin
Odom, Robert I.
O'Donnell, Matthew
Oelze, Michael L.
Oertel, Donata
Ohde, Ralph N.
Ohl, Claus-Dieter
Ollivier, Sébastien
Olson, Elizabeth S.
Ona, Egil
Oppenheim, Irving J.
Orr, Rosemary
Orris, Gregory J.
Osler, John C.
Ostrovsky, Lev A.
Oswald, Julie N.
Outing, Donald A.
Ouyang, Huajiang
Owren, Michael J.
Oxenham, Andrew J.
Ozdamar, Ozcan
Pabon, Peter
Pack, Adam A.
Pagneux, Vincent
Paje, Santiago E.
Pan, Jie
Panetta, Paul D.
Panneton, Raymond E.
Papanicolaou, George C.
Paradiso, Joseph
Parks, Susan E.
Parsons, Jessica E.
Parthasarathi, Anand
Pascal, Laugier
Pastore, Richard E.
Patterson, Roy D.
Payton, Karen L.
Peat, Keith S.
Pecorari, Claudio V.
Pedersen, Michael
Pedersen, Peder C.
Peelle, Jonathan E.
Pelekasis, Nikos A.
Pelling, Andrew E.
Pelorson, Xavier
Peltier, Leonard J.
Peng, Shu-Chen
Penttinen, Henri
Perelomova, Anna
Persson Waye, Kerstin
Petersson, Björn A.
Pfingst, Bryan E.
Phatak, Sandeep A.
Photiadis, Douglas
Picaut, Judicaël
Pichora-Fuller, Margaret K.
Picton, Terence W.
Pierce, Allan D.
Pierucci, Mauro
Piquette, Jean C.
Piscoya, Rafael
Pishchalnikov, Yuri A.
Pitermann, Michel
Pitton, James
Piwakowski, Bogdan
Plack, Christopher J.
Plesniak, Michael
Plotkin, Kenneth J.
Poese, Matthew E.
Poissant, Sarah F.
Polack, Jean-Dominique
Pols, Louis C.
Pompei, F. Joseph
Poncelet, Olivier
Popelka, Gerald R.
Popov, Vladimir V.
Popovics, John S.
Popper, Arthur N.
Port, Robert F.
Porter, Michael B.
Posey, Joe W.
Post, John T.
Potty, Gopu R.
Prada, Claire
Prasanna, S.R.M.
Pratap, Rudra
Preisig, James C.
Pressnitzer, Daniel
Preumont, Andre
Prieve, Beth A.
Proctor, Michael
Prosperetti, Andrea
Protopapas, Athanassios
Purcell, David W.
Puria, Sunil
Pyrak-Nolte, Laura
Qian-Jie, Fu
Qin, Michael K.
Qin, Shengping
Quatieri, Thomas F.
Rabbitt, Richard
Radcliffe, Clark
Rafaely, Boaz
Raimbault, Manon
Rajagopal, Prabhu
Rajan, Subrahaniam D.
Rajapan, Dhilsha
Rakerd, Brad S.
Rakowski, Andrzej
Ramsay, Gordon J.
Rank, Erhard
Rankin, Shannon
Rao, Preeti
Raphael, Lawrence J.
Rasmussen, Arne N.
Rasmussen, Karsten B.
Ratilal, Purnima
Rayess, Nassif E.
Raymond, Scott
Reed, Charlotte M.
Reichmuth, Colleen
Reide, Tobias
Remez, Robert E.
Ren, Tianying
Repp, Bruno H.
Reuter, Karen
Reynolds, Mary
Richard, McGowan
Richards, Virginia M.
Richardson, Michael D.
Richie, Carolyn
Richter, Claus-Peter
Ricketts, Todd A.
Ridgway, Sam H.
Riede, Tobias
Rindel, Jens H.
Riquimaroux, Hiroshi
Robert, Jean-luc
Roger, Michel
Rogers, Catherine L.
Rogers, Peter H.
Rokhlin, Stanislav I.
Ronacher, Bernhard
Rose, Douglas
Rose, Joseph L.
Rosen, Stuart
Rosenblum, Lawrence D.
Rosner, Burton S.
Rosowski, John J.
Rossing, Thomas D.
Rouse, Jerry W.
Rouseff, Daniel
Roux, Philippe
Roy, Kenneth P.
Royer, Daniel
Royston, Thomas J.
Rubin, Gordon
Rudenko, Oleg V.
Ruggles, Dorea R.
Rumerman, Melvyn L.
Russell, Ian J.
Ruzzene, Massimo
Ryan, James G.
Ryden, Nils
Rypina, Irina I.
Sabatier, James M.
Saberi, Kourosh
Sabra, Karim G.
Sadegh, Nader
Sadhal, Satwindar
Saijyou, Kenji
Sakagami, Kimihiro
Sammelmann, Gary
Samuel, Arthur
Samuels, Stephen E.
Sanchez-Sesma, Francisco J.
Sanders, Lisa D.
Sangani, Ashok
Saoji, Aniket
Sapoval, Bernard
Sapozhnikov, Oleg A.
Sarkar, Kausik
Sarkissian, Angie
Sarradj, Ennes
Sarvazyan, Armen
Sato, Hiroshi
Savin, Eric M.
Sawada, Kouichi
Sawusch, James R.
Scalerandi, Marco
Scarborough, Rebecca
Scavone, Gary P.
Schairer, Kim S.
Scharf, Bertram
Scheifele, Peter M.
Scherer, Ronald C.
Scheuren, Joachim
Schirmacher, Rolf
Schlauch, Robert S.
Schmidlin, Dean J.
Schmidt, Henrik
Schmiedt, Richard A.
Schmitt, Denis P.
Schneider, Bruce A.
Schoentgen, Jean B.
Scholik-Schlomer, Amy
Schomer, Paul D.
Scott, Nigel
Scott, Sophie K.
Sebastián Gallés, Núria
Seeber, Bernhard U.
Sehgal, Chandra M.
Seiner, Jack
Seixas, Noah S.
Sek, Aleksander P.
Selamet, Ahmet
Selouani, Sid-Ahmed
Sen, Kamal
Sereno, Joan A.
Serniclaes, Willy
Sessarego, Jean-Pierre
Sethares, William A.
Seybert, Andrew F.
Shackleton, Trevor M.

Shamma, Shihab A.
Shannon, Robert V.
Sharp, David B.
Shaw, Adam
Sheft, Stanley
Shera, Christopher A.
Sherman, Charles H.
Shield, Bridget M.
Shih, Chilin
Shimizu, Yasushi
Shinn-Cunningham, Barbara G.
Shirron, Joseph J.
Shorter, Philip J.
Shrivastav, Mini N.
Shrivastav, Rahul
Shub, Daniel E.
Shung, K K.
Shuvalov, Alexander
Siderius, Martin
Siegel, Jonathan H.
Siegmann, William L.
Silva, David J.
Simmons, Andrea M.
Simmons, James A.
Simonetti, Francesco
Simons, Dick
Simpson, Adrian
Simpson, Brian D.
Sinex, Donal G.
Singh, Leher
Sinnott, Joan
Sisneros, Joseph A.
Skowronski, Mark D.
Skulina, David J.
Slabbekoorn, Hans
Slaton, William V.
Slifka, Janet L.
Smeulders, David
Smiljanic, Rajka
Smit, A.
Smith, John
Smith, John R.
Smith, Julius O.
Smith, Kevin B.
Smith, Zachary M.
Smotherman, Michael S.
Smurzynski, Jacek
Snellen, Mirjam
Snowdon, Charles
So Finegold, Michiko
Soize, Christian
Solna, Knut
Solodov, Igor
Song, Hee-Chun
Southall, Brandon L.
Souza, Pamela E.
Spicer, James B.
Spiesberger, John L.
Spoor, Philip S.
Spriet, Ann
Sprofera, Joseph D.
Stafford, Kathleen M.
Stallen, Pieter J.
Stanton, Timothy K.
Stecker, G. Christopher
Steele, Charles R.
Steinschneider, Mitchell
Stellmack, Mark A.
Stimpert, Alison
Stinson, Michael R.
Stojanovic, Milica
Strange, Winifred
Strasberg, Murray
Strickland, Elizabeth A.
Stride, Eleanor
Studebaker, Gerald A.
Stulov, Anatoli
Sturm, Frédéric
Stylianou, Yannis
Su, Zuhre
Sullivan, Edmund J.
Summerfield, Arthur Q.
Summers, Jason E.
Summers, Van
Sundberg, Johan E.
Supin, Alexander Y.
Surlykke, Annemarie
Surprenant, Aimee M.
Sussman, Joan E.
Sutherland, Louis C.
Suthers, Roderick A.
Sutin, Alexander
Svec, Jan G.
Svensson, Peter
Swearingen, Michelle E.
Swift, Gregory W.
Syrdal, Ann K.
Tabain, Marija
Tadeu, Antonio
Taherzadeh, Shahram
Takahashi, Daiji
Takeda, M.W.
Talmadge, Carrick L.
Tan, Chee Wee
Tang, Dajun
Tao, Chao
Taraldsen, Gunnar
Tarnow, Viggo
Taroudakis, Michael
Tartter, Vivien C.
Tasko, Stephen M.
Ten Bosch, Louis
TenCate, James A.
Ternström, Sten
Tesei, Alessandra
Teutsch, Heinz
Tewary, Vinod
Thomas, Jean-Hugh
Thomas, Jean-Louis
Thomenius, Kai Erik
Thompson, Michael W.
Thompson, Stephen C.
Thomsen, Frank
Thomson, Scott L.
Thornely-Taylor, Rupert M.
Thorsos, Eric I.
Tian, Jing
Tian, Yi
Tijani, Moulay E.
Timmerman, Nancy S.
Tindle, Christopher T.
Tinianov, Brandon
Titze, Ingo R.
Tjaden, Kris
Tobin, Jim
Tokuda, Isao
Tollefsen, Dag
Tollin, Daniel J.
Tolstoy, Alexandra I.
Toole, Floyd E.
Torres-Carrasquillo, Pedro A.
Tougaard, Jakob
Toyoda, Masahiro
Traunmuller, Hartmut
Treeby, Bradley E.
Tremblay, Kelly L.
Trevorrow, Mark V.
Treyssede, Fabien
Tsai, Chen-Gia
Tsao, Ying-Chiao
Tun, Pat
Turgut, Altan
Turner, Christopher W.
Turner, Joseph A.
Tyagi, Manav
Ueda, Mitsuhiro
Ulker Karbeyaz, Basak
Umesh, S.
Umnova, Olga
Uppanda, Ajith K.
Uther, Maria
Vagle, Svein
Valdivia, Nicolas P.
Valeau, Vincent
Valiere, Jean-Christophe
Valimaki, Vesa
Valin, Jean-Marc
Vallabha, Gautam K.
Valle, Christine
Van Alphen, Petra M.
Van de Par, Steven
Van Den Abeele, Koen
Van den Berg, Frits
Van der Heijden, Marcel
Van der Werf, Erik
Van Hoesel, Richard J.
Van Netten, Sietse M.
Van Parijs, Sofie M.
Van Renterghem, Timothy
Van Tasell, Dianne J.
Van Walree, Paul A.
Van Wassenhove, Virginie
VanBuren, Arnie L.
Vannoni, Elisabetta
Varghese, Tomy
Vaseghi, Saeed
Vatikiotis-Bateson, Eric A.
Vavrycuk, Vaclav
Vecherin, Sergey N.
Vercammen, Martijn
Verhey, Jesko L.
Versfeld, Niek J.
Versluis, Michel
Veuillet, Evelyn
Vieira, Jose
Vieira, Maurilio
Virovlyansky, Anatoly L.
Vitevitch, Michael S.
Vogt, Michael
Vorländer, Michael
Voronovich, Alexander G.
Vos, Johan
Voss, Susan E.
Vykhodtseva, Natalia L.
Waag, Robert C.
Wade, Travis
Wage, Kathleen E.
Wagner, Randall P.
Wagstaff, Ronald A.
Walhberg, Magnus K.
Walker, Shane C.
Wallace, Kirk D.
Wang, Chao
Wang, DeLiang
Wang, Ding
Wang, Emily Q.
Wang, Hsin-Min
Wang, Lijuan
Wang, Lily M.
Wang, Meng
Wang, Xiaoqin
Warner, Natasha L.
Warnock, Alf
Warren, Daniel M.
Warren, Joseph D.
Warren, Richard M.
Washburn, Karl B.
Wassink, Alicia B.
Waterhouse, Richard V.
Waters, Kendall R.
Watkins, Anthony J.
Wayland, Ratree
Wear, Keith A.
Weaver, Richard L.
Weber, Andrea
Weenink, David
Weisman, Ronald
Weismer, Gary G.
Weiss, Dan
Werner, Lynne A.
Westbury, John R.
Westwood, Evan K.
Whalen, Doug H.
Whitmal, Nathaniel A.
Wickesberg, Robert E.
Widen, Judy
Wiegrebe, Lutz
Wightman, Fred L.
Wilcox, Paul D.
Williams, Amber L.
Williams, Earl G.
Williams, Kevin L.
Wilmut, Mike J.
Wilson, Chris
Wilson, D. Keith
Wilson, Preston S.
Winfield, Ian
Winker, Douglas F.
Winkler, Istvan
Withnell, Robert H.
Wittstock, Volker
Wochner, Mark S.
Wojtczak, Magdalena
Wolfe, Joe
Woodhouse, Jim
Woods, William S.
Worcester, Peter F.
Wouters, Jan
Wright, Andrew B.
Wright, Beverly A.
Wright, William M.
Wu, Junru
Wu, Junru
Wu, Sean F.
Wu, Ting-Wen
Wurm, Lee
Wysocki, Lidia E.
Xiang, Ning
Xu, Min
Xu, Zhen
Yang, Tsih C.
Yang, Wen
Yano, Takeru
Yantis, Steven
Yonak, Serdar
Yoon, Suk Wang
Yost, William A.
Yost, William T.
Young, Eric D.
Yuan, Hanfeng
Yuen, Michelle M.
Yurk, Harald
Zabolotskaya, Evgenia A.
Zagrai, Andrei N.
Zahorian, Stephen A.
Zahorik, Pavel

Zaitsev, Vladimir
Zampolli, Mario
Zeegers, Jos
Zeitler, Berndt
Zemp, Roger J.
Zeng, Fan-Gang
Zhang, Honghu
Zhang, Shu-yi
Zhang, Victor Y.
Zhang, Zhaoyan
Zhao, Yunxin
Zhong, Pei
Ziemann, Astrid
Zimmer, Walter
Zinin, Pavel
Zorikov, Tengiz
Zotkin, Dmitry N.
Zuckewar, Allan
Zumberge, Mark
Zurek, Patrick
Zurk, Lisa M.

USA Meetings Calendar

Listed below is a summary of meetings related to acoustics to be held in the U.S. in the near future. The month/year notation refers to the issue in which a complete meeting announcement appeared.

2008

29 June–4 July	Joint Meeting of the Acoustical Society of America, European Acoustics Association and the Acoustical Society of France, Paris, France [Acoustical Society of America, Suite 1NO1, 2 Huntington Quadrangle, Melville, NY 11747-4502; Tel.: 516-576-2360; Fax: 516-576-2377; E-mail: asa@aip.org; WWW: http://asa.aip.org].
28 July–1 Aug	9th International Congress on Noise as a Public Health Problem (Quintennial meeting of ICBEN, the International Commission on Biological Effects of Noise). Foxwoods Resort, Mashantucket, CT [Jerry V. Tobias, ICBEN 9, Post Office Box 1609, Groton CT 06340-1609, Tel. 860-572-0680; Web: www.icben.org. E-mail: icben2008@att.net]
10–14 Nov	156th Meeting of the Acoustical Society of America, Miami, FL [Acoustical Society of America, Suite 1NO1, 2 Huntington Quadrangle, Melville, NY 11747-4502; Tel.: 516-576-2360; Fax: 516-576-2377; E-mail: asa@aip.org; WWW: http://asa.aip.org].

2009

18–22 May	157th Meeting of the Acoustical Society of America, Portland, OR [Acoustical Society of America, Suite 1NO1, 2 Huntington Quadrangle, Melville, NY 11747-4502; Tel.: 516-576-2360; Fax: 516-576-2377; E-mail: asa@aip.org; WWW: http://asa.aip.org].

Cumulative Indexes to the Journal of the Acoustical Society of America

Ordering information: Orders must be paid by check or money order in U.S. funds drawn on a U.S. bank or by Mastercard, Visa, or American Express credit cards. Send orders to Circulation and Fulfillment Division, American Institute of Physics, Suite 1NO1, 2 Huntington Quadrangle, Melville, NY 11747-4502; Tel.: 516-576-2270. Non-U.S. orders add $11 per index. Some indexes are out of print as noted below.

Volumes 1–10, 1929–1938: JASA, and Contemporary Literature, 1937–1939. Classified by subject and indexed by author. Pp. 131. Price: ASA members $5; Nonmembers $10.
Volumes 11–20, 1939–1948: JASA, Contemporary Literature and Patents. Classified by subject and indexed by author and inventor. Pp. 395. Out of Print.
Volumes 21–30, 1949–1958: JASA, Contemporary Literature and Patents. Classified by subject and indexed by author and inventor. Pp. 952. Price: ASA members $20; Nonmembers $75.
Volumes 31–35, 1959–1963: JASA, Contemporary Literature and Patents. Classified by subject and indexed by author and inventor. Pp. 1140. Price: ASA members $20; Nonmembers $90.
Volumes 36–44, 1964–1968: JASA and Patents. Classified by subject and indexed by author and inventor. Pp. 485. Out of Print.
Volumes 36–44, 1964–1968: Contemporary Literature. Classified by subject and indexed by author. Pp. 1060. Out of Print.
Volumes 45–54, 1969–1973: JASA and Patents. Classified by subject and indexed by author and inventor. Pp. 540. Price: $20 (paperbound); ASA members $25 (clothbound); Nonmembers $60 (clothbound).
Volumes 55–64, 1974–1978: JASA and Patents. Classified by subject and indexed by author and inventor. Pp. 816. Price: $20 (paperbound); ASA members $25 (clothbound); Nonmembers $60 (clothbound).
Volumes 65–74, 1979–1983: JASA and Patents. Classified by subject and indexed by author and inventor. Pp. 624. Price: ASA members $25 (paperbound); Nonmembers $75 (clothbound).
Volumes 75–84, 1984–1988: JASA and Patents. Classified by subject and indexed by author and inventor. Pp. 625. Price: ASA members $30 (paperbound); Nonmembers $80 (clothbound).
Volumes 85–94, 1989–1993: JASA and Patents. Classified by subject and indexed by author and inventor. Pp. 736. Price: ASA members $30 (paperbound); Nonmembers $80 (clothbound).
Volumes 95–104, 1994–1998: JASA and Patents. Classified by subject and indexed by author and inventor. Pp. 632, Price: ASA members $40 (paperbound); Nonmembers $90 (clothbound).
Volumes 105–114, 1999–2003: JASA and Patents. Classified by subject and indexed by author and inventor. Pp. 616, Price: ASA members $50; Nonmembers $90 (paperbound).

Revision List

New Associates

Abraham, Douglas, CausaSci LLC, PO Box 5892, Arlington, VA 22205
Aranchuk, Vyacheslav, NCPA, 1 Coliseum Dr., University, MS 38677
Arvanitis, Costas, Oxford Univ., Engineering Science, 43 Banbury Rd., Oxford, OX2 6PE, United Kingdom
Bahoura, Mohammed, Universite du Quebec Rimouski, Genie, 300, allee des Ursulines Rimouski, QC G5L 3A1, Canada
Barker, Gail, 1331 N. 78th St., Seattle, WA 98103
Beers, David, Progeny Systems Corp. 94-212 Hopoe Pl., Waipahu, HI 96797
Bell, Damien, Epsilon Associates, Inc., Noise, 3 Clock Tower Pl., Ste. 250, Maynard, MA 01754
Bernstein, Norman, 9 D Senate Rd., Milford, MA 01757
Bombien, Lasse, Institute of Phonetics Schellingstrasse 3 D-80779 Munich, Germany
Botchev, Vladimir, 20 Spindlewick Dr., Nashua, NH 03062
Branstetter, Brian, US Navy Marine Mammal Prog., Space and Naval Warfare System, Code 71510, 53560 Hull St., San Diego, CA 92152
Brown, Patrick, 203 Woodlawn Dr., Oxford, MA 38655
Capriotti, John, 2140 Kuhio Ave. #1602, Honolulu, HI 96815-2310,
Chavanu, Christopher, Electronic Contracting Company, Sales Engineer, 6501 N. 70th St., Lincoln, NE 68507
Chen, Yih-Yuh, National Taiwan Univ., Physics, No. 1, Sec. 4, Roosevelt Rd., Taipei 106, Taiwan
Cheng, Anping, GN Resound, Research & Development, 2601 Patriot Blvd., Glenview, IL 60026
Cheng, Jeffrey, Dept. Otology & Laryngology, EPL, Massachusetts Eye & Ear Infirmary, Harvard Medical School, 243 Charles St., Boston, MA 02114
Cooper, Russell, Jaffe Holden Acoustics, Inc. 114A Washington St., Norwalk, CT 06854
Czerski, Helen, 330 Kolmar St., La Jolla, CA 92037
Dajani, Hilmi, Univ. of Ottawa, SITE, 161 Louis Pasteur Ottawa, ON K1N 6N5, Canada
Decker, Jeremy, Charles M. Salter Associates, 130 Sutter St., 5th Fl., San Francisco, CA 94104
DeLaney, David, U.S. Army CERL, P. O. Box 9005, Champaign, IL 61826
Ellingson, Roger, 8515 SW Barnes Rd., Portland, OR 97225
Fan, Yan, 4590 Mercurio St., San Diego, CA 91230
Fandrich, Delwin, Fandrich Piano Company, Inc. 620 South Tower Ave., Centralia, WA 98531
Gao, Huidong, Innerspec Technologies, Inc., Research and Development, 4004 Murray Pl., Lynchburg, VA 24501
Giegold, Carl, Threshold Acoustics LLC, 53 W. Jackson Blvd., Ste. 1734, Chicago, IL 60604

Gerlovin, Mark, Revolabs, 63 Great Rd., Maynard, MA 01754
Ghorbanian, Kaveh, Sharif Univ. of Technolog, Aerospace Engineering, Azadi Ave., Tehran, Iran
Grant, Kevin, 1304 Constitution Dr., Slidell, LA 70458
Greenham, Edward, Noise, GDS Planning Consultants, 1160 Camp Ave., Mount Dora, FL 32757
Haldipur, Pranaam, Georgia Tech, ECE, 3230 Post woods Dr. #A, Atlanta, GA 30339
Haynes, Jared, 147 Church Hill Downs Ct, Madison, AL 35758
Henrick, Robert, 6687 Luster Dr., Highland, MD 20777
Hernandez, Daniel, 3366 North Torrey Pines Ct., Ste. 310, La Jolla, CA 92037
Hesse, Robert, Department of Defense, Army, AMSRD-AAR-AEP-A, 407 Buffington Rd., Picatinny Arsenal, NJ 07806-5000
Hingson, Dickson, 275 S. River Run #3, Flagstaff, AZ 86001
Hobbs, Christopher, Wyle Laboratories, Test, Engineering, & Research, 241 18th St. South, Ste. 701, Arlington, VA 22202
Hyeong, Kim, PCR, Environmental & Architectural Acoustics, One Venture, Ste. 150, Irvine, CA 92618
Iida, Kazuhiro, Chiba Institute of Technology 2-17-1 Tsudanuma Narashino, Chiba, 275-0016, Japan
Ikelheimer, Bruce, Blue Ridge Research and Consul, 13 1/2 W. Walnut St., Asheville, NC 28801
Iman, Larry, Architectone, Galeria 168 Kav. A9, Jl. Sersan Bajuri, Bandung 40559, Indonesia
Jaeger, Marion, Keferloherstr. 111, Munchen 80807 Germany
Jantzen, Mcneel, Western Washington Univ., Psychology, 516 High St., Bellingham, WA 98225
Jurevicius, Darren, Bassett Acoustics, Level 6, 100 Pirie St., Adelaide SA 5000 Australia
Kaufman, Greg, Pacific Whale Foundation, 300 Maalaea Rd., Ste. 211 Wailuku, HI 96793
Kawakami, Hiroshi, Nihon Univ., College of Art, 2-42-1 Asahigaoka, Nerima, Tokyo, 176-8525, Japan
Keene, James, Keene Building Products, 5910 Landerbrook Dr., Ste. 210, Mayfield Hts., OH 44124
Kim, Jeong-Woo, Foamex International Inc., R&D, 1500 East 2nd St., Eddystone, PA 19022
Kinsey, Kaolin, J & A Enterprises, Inc.,16 Broadway, Salem, MA 01970
Knorr, Aaron, Victory Industrial Products, Engineering, 4160 Half Acre Rd., Batavia, OH 45103
Korhonen, Petri, 633 S. Plymouth Ct. #301, Chicago, IL 60605
Kubota, Mikio, Seijo Univ. 6-1-20 Seijo, Setagaya-ku, Tokyo,157-8511, Japan
Kusi, Jim, 84 Amherst Dr., New Rochelle, NY 10804
Laprie, Yves, INRIA Lorraine Bbtiment C, 615 rue du jardin botanique, 54600, illers-Lhs-Nancy, France
Lee, Jae, 1 Aberdeen Way Ste. #211 Cambridge, MA 02138
Lefkowitz, Kimberly, CSTI Acoustics, 15835 Park Ten Pl., Ste. 105, Houston, TX 77084
Lopez, Jose J., Trafalgar 52-5-2C, Valencia 46023 Spain
Mueller, Reinhard, Justus-Liebig-Universitdt, AG-Hvrforschung, Aulweg 123 35392 Giessen, Germany
Maclean, Allan, Genentech, Inc., Corporate Security, Mail Stop #4, 1 DNA Way, South San Francisco, CA 94080
Marston, Brian, Unit 31,12 Meadow Crescent, Meadowbank, NSW 2114 Australia
Martinez, Loic, Universiti de Cergy, ECIME, Mail Gay Lussac 95031 Neuville Sur Oise, France
Matthew, Ian, 5089 Old Brock Rd., Claremont, ON L1Y 1B3, Canada
Mccaul, Stephen, Treyarch/Activision, 3420 Ocean Park #1000, Santa Monica, CA 90405
Merthayasa, I Gde Nyoman, Institute of Techn. Bandung, Engineering Physics, Jl. Ganesha No. 10 Bandung 40132, Indonesia
Mitchell, Stuart, 18712 23rd Ave. NE, Lake Forest Park, WA 98155
Marlot, Matija, FRI, Univ. of Ljubljana, Trzaska 25, Ljubljana 1000 Slovenia
Moulin, Annie, UMR CNRS 5020, Exploration fonctionnelle ORL, Pavillon U, Hopital E. Herriot, 69437 Lyon, France
Nava, Sue, 2590 Summer Brook St., Melbourne, FL 32940
Ng, Gim Pei, 1-9-11, Tingkat Paya Terubong 3, 11060 Air Itam, Pg, Malaysia., 11060 Air Itam/Penang, Malaysia
Ng, Gerald, 10 Oliver Rd., #1 Watertown, MA 02472
Novak, Colin, 1518 Bruce Ave., Windsor, ON N8X 1X9, Canada
Nyberg, Ross, Ross Nyberg Design LLC, 25210 SE 133rd St., Issaquah, WA 98027
Oppenheimer, Charles, Hewlett-Packard, Environmental Design Lab., 18110 SE 34th St., Vancouver, WA 98683
Orphanidou, Christina, 89 St. Marys Rd., Oxford, OX4 1QD, United Kingdom
Palmer, William, 146 Pinecrest Rd., Durham, NC 27705-5813
Plummer, Thomas, McQ Inc., Engineering, 1551 Forbes St., Fredericksburg, VA 22405
Pye, Christopher, Maya HTT Ltd., 4999 St. Catherine W., Ste. 400, Montreal, QC H3Z 1T3, Canada
Raiti, Peter, P.O. Box 428, Fort Washington, PA 19034-0428
Remillard, John, 1633 Smith Pl., Fort Collins, CO 80525
Roberts, Trefor, 32A Miranda Rd., London, N19 3RB, United Kingdom
Sanders, Lisa, Univ. of Massachusetts-Amherst, Dept. of Psychology, Tobin Hall, Amherst, MA 01003
Schlundt, Carolyn, 7174 Via Mariposa Norte, Bonsall, CA 92003
Schmitt, Jeff, 2512 Star Grass Cir., Austin, TX 78745
Seeger, Steffen, C-v-Ossietzky-Str 191, Chemnitz, Germany
Seo, Jongbum, Yonsei Univ., Biomedical Engineering, 108 Baekgun, Maeji, Hungup Wonju, 220710, Korea
Shackelford, Ronald, 908 Ash Court, Snohomish, WA 98290
Singleton, Herbert, 114 Sunnybrook Rd., Springfield, MA 01119
Stewart, Thomas, Marine Acoustics, Inc., 809 Aquidneck Ave., Middletown, RI 02842
Stride, Eleanor, University College London, Dept. Mechanical Engineering, Torrington Pl., London WC1E 7JE United Kingdom
Summers, Jason, 1222 4th St., SW, Washington, DC 20024
Sumner, Meghan, 1451 Kensington Dr., Fremont, CA 94539
Takahashi,Yoshinori, 6-8-18 Nakamachi, Nishi-Tokyo-shi, Tokyo, 202-0013, Japan
Tschiegg, Richard, Johns Hopkins Univ., Applied Physics Lab, National Security Technology Dept.,11100 Johns Hopkins Rd., Laurel, MD 20723
Testus, E. W., 873 Taughannock Blvd., Ithaca, NY 19850
Ulrich, Timothy, 3016 Orange St., Los Alamos, NM 87544
van der Veeke, Antonius, Mic-cell Co., Ltd., Business Development, Big One Complex 221/1-3 Moo 8, Poochaosamingprai Rd., Samrongklan, Prapr. Samutprakarn 10130 Thailand
Wolfram, Eric, Scott R. Riedel & Associates, Acoustics, 819 N Cass St., Milwaukee, WI 53202-3908
Wunderlich, Jens, Innomar Technologie GMBH, Schutower Ringstr. 4, Rostock D-18069, Germany
Xu, Zhen, Biomedical Engineering Dept., Univ. of Michigan, 2200 Bonisteel Blvd., Rm.1107
Gerstacker, Ann Arbor, MI 48109
Van Zanten, Bert, Dept. ENT/Audiology, University Medical Ctr., Heidelberglaam 100, Utrecht 3584 CX, The Netherlands
Yang, Yixin, Northwestern Polytechnical Univ., Insitute of Acoustic Engineering, PO Box 19, No.127 Youyixi Rd., Xian Shaanxi 71002, People's Republic of China
Ziegiebel, Molly, J & A Enterprises, Inc.,16 Broadway, Salem, MA 01970
Zoontjens, Luke, 14 Charlbury Rd., Medindie Gardens, SA 5081, Australia
Zwiebel, Richard, K2 Audio, LLC 4900 Pearl East Cir., Ste. 201E, Boulder, CO 80301

New Students

Allen, Ashley, 2902 Pearl St., Austin, TX 78705
Anderson, Shaun, Georgia Tech, Woodruff School of M.E., Graduate Box 1000, Atlanta, GA 30332-0405
Avgouleas, Kyriakos, 700 Huron Ave., Apt. 8H, Cambridge, MA 02138
Azizov, Ilgar, Univ. of Houston, Geoscience, 1910 Westmead Dr, #3512, Houston, TX 77077
Baumann, Simone, Scripps Inst. of Oceanography, MPL, 9500 Gilman Dr. #0205, La Jolla, CA 92093
Beck, Matthew, 536 Charles Court, Glendale Heights, IL 60139
Bernays, Michel, 4627 Edouard Montpetit, Montreal, QC H3W 1P6, Canada

Bidelman, Gavin, Purdue Univ., Speech, Language, and Hearing, 307 Montifiore, #217, Lafayette, IN 47905
Bissinger, Brett, 1621 Hawthorne Dr., State College, PA 16801
Block, Nicholas, 230 Littleton St., West Lafayette, IN 47906
Bridgewater, Benjamin, 826 Reba Pl., Evanston, IL 60202
Briley, Paul, MRC Institute of Hearing Research, University Park, Nottingham, NG7 2RD, United Kingdom
Brough, Samantha, Ikon Science, Fl. 2 Causeway House, The Causeway, Teddington, TW11 0JR, United Kingdom
Buzinski, Nicholas, 683 Prentis, 2D, Detroit, MI 48201
Cain, Jericho, 1802 Jackson Ave. West, Apt. 43, Oxford, MS 38655
Carpenter, Russell, Binghamton Univ., Binghamton Univ., BU Box 06778, Binghamton, NY 13902
Cheng, Chierh, University College London, Phonetics and Linguistics, Gower St., London,
WC1E 6BT, United Kingdom
Cheng, Min-Yu, 7625 N Eastlake Ter., Apt. 406, Chicago, IL 60626
Cho, Sang, 262 S. Corl St., Apt #3A, State College, PA 16801
Chuang, Yu-Ying, No.7, Ln. 3, Guanguang St., Banqiao City, 22070, Taiwan
Clark, Nick, Medical Research Council, Institute of Hearing Research, Nottingham Univ., University Park, Nottingham, NG7 2RD, United Kingdom
Clinard, Christopher, 31500 33rd Pl. SW, #Q-103, Federal Way, WA 98023
Cline, Douglas, 234 Oakville Rd., Beaver Falls, PA 15010
Crass, Kimberlee, Univ. of South Carolina, COMD, 210 Castlebury Dr., Columbia, SC 29229
Cristia, Alejandrina, Purdue Univ., Linguistics, 500 Oval Dr., West Lafayette, IN 47907
Devergie, Aymeric, CNRS, UMR 5020-Sensory Neuroscience/Behavior/Cognition, 50 avenue Tony, Garnier, Lyon Cedex 07 69366, France
Ding, Ran, P.O. Box44#, Pukou Campus of NJU, 210089 Nanjing, PRC
Dolder, Craig, 47 Fairfield St., Springfield, MA 01108
Duroux, Adelaide, 3200 Lenox Rd., Apt A307, Atlanta, GA 30324
Eickmeier, Justin, 101B Melbourne Ave., Indialantic, FL 32903
Elmgren, Mitchell, 157 Hathorn Hall, 620 S. Third St., River Falls, WI 54022
Evans, Neal, 2243 US 52 West, West Lafayette, IN 47906
Ferjan, Naja, 3927 B Miramar St., La Jolla, CA 92037
Ferrari, Riccardo, Via Hermada 13/3, 34151 Trieste, Italy
Gagnon, David, 7201 Hart Ln. Apt. 1087, Austin, TX 78731
Giglio Mark, 72 Rockvale Rd., Tewksbury, MA 01876
Gilbert, Keith, 123 State Rd., 2nd Fl., North Dartmouth, MA 02747
Gorman, Christopher, 1498 Waukon Cir., Casselberry, FL 32707
Gouedard, Pierre, LGIT - Maison des Geosciences, BP53, 38041 Grenoble Cedex 9, France
Goyette, Jennifer, 724 Doty, Green Bay, WI 54301
Greene, Chad, 2320 Gracy Farms Ln., Apt. 1431, Austin, TX 78758
Grenvall, Carl, Vstra Vallg. 35b, 22361 Lund, Sweden
Groener, David, 44 Bulkley Ave. North, Westport, CT 06880
Hall, James, 1616 Piedmont Ave., Apt. I-19, Atlanta, GA 30324
Hao, Yen-Chen, 2451 E. 10th St. (Apt. 1016), Bloomington, IN 47408
Harpin, Daniel, 71 Old Coach Highway, Hamden, CT 06518
Heer, Kyle, 412 S. Delaware Ave., # 1237, Tulsa, OK 74104
Hildebrand, Matt, 2303 Standish St., St. Paul, MN 55108
Ho, Sharon, 18753 Grace Court, Artesia, CA 90701
Holzinger, Tobias, Technische Universitdt Munchen, Thermodynamik, Boltzmannstr 15, 85748 Garching B. Munchen, Germany
Hool, Amy, 5049 N. Damen Ave., Apt. 1E, Chicago, IL 60625
Hopkins, Kathryn, Univ. of Cambridge, Experimental Psychology, Downing St., Cambridge, CB2 3EB, United Kingdom
Hornikx, Maarten, Chalmers Univ. of Tech., Applied Acoustics, Sven Hultinsgatan 8a, 41296 Gothenburg, Sweden
Inoue, Kenji, 4-18-15, Tanabe, Higashi-sumiyoshiku, Osaka, 546-0031, Japan
Islas, Alan, Univ. of Birmingham, Elect, Elect and Comp. Eng., Edgbaston, Birmingham, B15 2TT, United Kingdom
Jacobs, Aaron, 2116 Oak St., Apt. D, Santa Monica, CA 90405
Jelfs, Sam, 118 Admiral House, 38-42 Newport Rd., Cardiff, CF240DP, United Kingdom
Jones, Gary, Univ. of Wisconsin-Madison, Waisman Ctr., 1500 Highland Ave., Madison, WI 53705
Kaltenberg, Amanda, Oregon State Univ., College of Ocean & Atm. Sci., 104 COAS Admin. Bldg., Corvallils, OR 97331
Korakas, Alexios, LMFA - Centre Acoustique, Ecole Centrale de Lyon, 36, Avenue Guy de Collongue, 69134 Ecully Cedex, France
Kraemer, Jochen, Hilgenbacher Hoehe 15, 66265 Heusweiler, Germany
Krezanoski, Joseph, 2254 Clapton Way, Folsom, CA 95630
Krishnamurthy, Rohan, 544 Sunrise Cir., Kalamazoo, MI 49009
Kyriakou, Zoe, Biomedical Engineering, Engineering, Wolfson College, Linton Rd., Oxford, OX2 6UD, United Kingdom
Lanier, Stephanie, 133 Auriel Cir., Maumelle, AR 72113
Le Roux, Jonathan, Univ. of Tokyo, Information Physics & Computing, Sagayama/Ono Lab, 7-3-1, Hongo, Bunkyo-ku, Tokyo, 113-8656, Japan
Leblanc, Elisabeth, 180 2e rue ouest #3, Rimouski, QC G5L 4X7, Canada
Lee, Seung Hun, Rutgers Univ., Linguistics, 18 Seminary Pl., New Brunswick, NJ 08901
Leiby, Stephen, Purdue Univ., 500 N Martin Jischke Dr., West Lafayette, IN 47906
Levinson, Samantha, 6689 El Colegio Rd., Apartment #46, Isla Vista, CA 93117
Li, Zhiye, 2324 Short St., New Orleans, LA 70118
Li, Ming, Acoustics Research Centre, School of Architecture, The Univ. of Auckland, Private Bag, 92109, Auckland, New Zealand
Li, Qiang, Univ. of Rhode Island, Graduate School of Oceanography, 215 S Ferry Rd., Narragansett, RI 02882
Lindau, Alexander, Technical Univ. of Berlin, Audio Communication, Einsteinufer 17, 10587 Berlin, Germany
Liu, Shuangqin, Tufts Univ., Mechanical Engineering, 308 Boston Ave. #6, Medford, MA 02155
Lopez-Rivas, Rebeca, UNAM, FISICA, Circuito exterior s/n, Ciudad Universitaria, 04510 Mexico, D.F. FDM, Mexico
Marcus, Logan, 1802 Jackson Ave. West #167, Oxford, MS 38655
Marston, Timothy, Penn State, Acoustics, 425 Waupelani Dr., Apt. 306, State College, PA 16801
McCord, Cameron, 203 Riva Ridge, Wylie, TX 75098
McIver, Jordan, 1745 W. Latoka Dr., SW, Alexandria, MN 56308
Menzel, Daniel, TU Munich, AG Technische Akustik, MMK, Arcisstr. 21, 80333 Munich, Germany
Miranda Jofre, Luis, 403 King St., Newtown, Sydney, 2042, Australia
Mollica, Shannon, 286 Hollywood Ave., Bronx, NY 10465
Moreau, Danielle, The Univ. of Adelaide, School of Mech. Eng., North Terrace, Adelaide, STH 5005, Australia
Mulsow, Jason, UC Santa Cruz Long Marine Lab, Dept. of Ocean Sciences, 100 Shaffer Rd., Santa Cruz, CA 95060
Murray, Patrick, Boston Univ., Aerospace and Mechanical Eng, 110 Cummington St., Boston, MA 02215
Najafiyazdi, Alireza, No. 7035, Champagneur Ave., Apt 8., Montreal, QC H3N 2J6, Canada
Nakahashi, Laiyo, 203 West 108th St. #17, New York, NY 10025
Nelson, Misty, 121 33rd Ave. N, St. Petersburg, FL 33704
Okcu, Selen, 1631 Bridge Mill Dr., Apt. E, Marietta, GA 30067
Onan, Bridget, 1345 Washington St., River Falls, WI 54022
Osuna, Brenda, PO Box 5148, Frazier Park, CA 93222
Paglialonga, Alessia, CNR Ist. di Ing Biomedica, Dip Bioingegneria, Politecnico di Milano, piazza Leonardo da Vinci 32, 20133 Milan, Italy
Preece-Pinet, Melanie, University College London, Phonetics and Linguistics, 4, Stephenson Way, London, NW1 2HE, United Kingdom
Ran, Ding, Electronic Engineering Dept., Nanjing Univ., P.O. Box 44#, Pukuo Campus, Nanjing, People's Republic of China
Rao, Gayatri, Univ. of Texas - Austin, Dept. of Psychology, 1 University Station A8000, Austin, TX 78712-0187
Reisdorff, Jennifer, 1727 N. 58th St. Omaha, NE 6810
Rifai, Bassel, Oxford Univ., Institute for Biomedical Engin, 43 Banbury Rd., Oxford, OX2 6PE, United Kingdom
Rizzo Sierra, Carlos, BCN-NeuroImaging Ctr., Biomedical Engineering, Antonius deusinglaan 2,1 floor, 9700 AD, 9700 AD Groningen, The Netherlands
Roth, Ethan, UCSD/SIO, Marine Physical Lab., MC 0205, 9500 Gilman Dr., La Jolla, CA 92093
Schweizer, Miho, 29684 Meadow Ln., Coarsegold, CA 93614
Sedgman, Tom, Ground Floor Flat, 120 Raddlebarn Rd., Selly Oak, Birmingham, B29 6HQ, United Kingdom

Shim, Allison, 3941 Myra Ave., Los Alamitos, CA 90720
Shull, Thomas, P.O. Box 230131, Boston, MA 02123
Siciliano, Catherine, University College London, Phonetics and Linguistics, Wolfson House, 4 Stephenson Way, London, NW1 2HE, United Kingdom
Simon, Malene, Greenland Inst. Nat. Res., Birds and Mammals, P.O. Box 570, Kivioq 2, 3900 Nuuk, Greenland
Smith, Holly, 198 Etta St., Hot Springs, AR 71901
Sondkar, Pravin, 2921 Scioto Ln., Apt # 1206, Cincinnati, OH 45219
Speyer, Gavriel, 4747 30th Ave. NE, Apt D127, Seattle, WA 98105
Stamper, Sarah, Brown Univ., Psychology, 89 Waterman St., Box 1853, Providence, RI 02912
Stein, Joseph, 3321 16th St., South, Wisconsin Rapids, WI 54494
Stephey, Laurie, Rollins College, Physics, 1000 Holt Ave., Box 2366, Winter Park, FL 32789
Stetson, Kathleen, 1535 Bouton Rd., Troy, NY 12180
Stiefenhofer, Georg, Schiebenkamp 56, 26135 Oldenburg, Germany
Styler, William, 9025 Reed Hall, Boulder, CO 80310
Tavakoli Nia, Hadi, MIT, 550 Memorial Dr., Apt. # 18E3, Cambridge, MA 02139
Testa, Michael, Tempo Productions, 31 Tempo Dr, Danville, NH 03819
Tilsen, Sam, 1203 Dwinelle Hall, Berkeley, CA 94720
Torres-Jimenez, Jose, JTDA, 7979 NW 21st, SJO 967, Doral, FL 33122
Tremblay, Sara, 99 Maple Ave. Apt. 2R, Bristol, CT 06010
Turkocagi, Cemil, Merdivenkoy Yolu Birler Apt, 41/30 Goztepe Kadikoy, Istanbul, Turkey
Vadavalli,Venkata Phani Kirani, 737 Rue King George, Sherbrooke Quebec J1H 2G8 Canada
Vasquez Velez, Daniel, Flat 7, Faraday House, 26 Hornsey Ln., London, N6 5LX, United Kingdom
Vitela, Antonia, Univ. of Arizona, Speech, Language, Hearing Sci, P.O. Box 210071, 1131 E. 2nd St., Tucson, AZ 85721
Voelk, Florian, AG Technische Akustik, MMK, TU Muenchen, Arcisstrasse 21, 80333 Muenchen, Germany
Waters, Paul, 405 Suzzane, Pflugerville, TX 78660
Whyte, Stuart, 15 Glenway, Bognor Regis, PO22 8BU, United Kingdom
Wladichuk, Jennifer, Univ. of Bath, Mechanical Engineering, Claverton Down, Bath, BA2 7AY, United Kingdom
Woodson, Neil, 914 W. 26th St., Apt. #303, Austin, TX 78705
Wowk, Roman, PO Box 66479, Albuquerque, NM 87193
Wylie, Jennifer, 305 Galen Dr., Apt. 321, Key Biscayne, FL 33149
Xia, Jing, Boston Univ., Cognitive and Neural Systems, 677 Beacon St., Boston, MA 02215
Yousefzadeh, Behrooz, 7th Apt No.3, Bastan St.,, Firouzbakhsh St., Aghdasieh, 1957733411 Tehran, Iran
Yu, Kristine, UCLA, Linguistics, 3125 Campbell Hall, Los Angeles, CA 90095
Zietlow, Daniel, 1000 Holt Ave., Box 2667, Winter Park, FL 32789
Zoubek, Jeremy, 251 Lillian Pl., Bartlett, IL 60103

New Electronic Associates

Cardwell, Nina, Sandhills Community College, Education, 980 South Hardin St., Southern Pines, NC 28387

Cole, Jerry, SeaLandAire Technologies, Inc., 1510 Springport Rd., Ste. C, Jackson, MI 49202

Cusick, Suzanne, 171 Young Rd., Augusta, ME 04330

Deshpande, Chinmay, Flowserve Corp., Applied Technology, 2300 E. Vernon Ave., Vernon, CA 90058

Drebitt, Daniel, 5275 Keith Rd., West Vancouver, BC V7W 2M9, Canada

Esposito, Christina, Macalester College, Linguistics, 1600 Grand Ave., St. Paul, MN 55105

Fillon, Thomas, Research & Development, Sensitive Object, 696 Rue Yves Kertien, Boulogne-Billancourt 92100, France

Hohmann, Volker, Universitdt Oldenburg, Medizinische Physik, Postfach 26111 Oldenburg, Germany

Ikeda, Masahiro, Yamaha, CAST, CAG, 203 Matsunokishima Iwata, Shizuoka, 438-0192, Japan

Irwin, Julia, Haskins Laboratories, 300 George St., New Haven, CT 06511

Kulick, Roy, 529 Cochise, Ct., Cincinnati, OH 45215

Nielsen, Paul, Nielsen-Kellerman Co., 21 Creek Cir., Boothwyn, PA 19061

Penvenne, John, Penscil, Inc., PO Box 6249, Los Osos, CA 93412

Ramirez, Adriana Citlali, WesternGeco, Imaging Research, 10001 Richmond Ave., Houston, TX 77042

Ridgway, Stephen, 10, Offerton Rd., Hazel Grove, Stockport, SK7 4NJ, United Kingdom

Rohweder, Reimer, Deutsches Hvrgerdte Institut, Bessemerstr. 3 23627 Libeck, Germany

Roland, Andrew, Tech Environmental, 1601 Trapelo Rd., Waltham, MA 02451

Schevin, Olivier, Research & Development, Sensitive Object, 696 Rue Yves Kermen Boulogne-Billancourt 92100, France

Somit, Scott, 3750 Riviera Dr., #3, San Diego, CA 92109

Webster, Robert, Univ. of Tennessee, Computational Engineering, 701 East ML King Blvd., Chattanooga, TN 37403

Withgott, Margaret, 12348 Melody Ln., Los Altos Hills, CA 94022

Yilmaz, Hayriye, 45 Stirling Close, Streatham Vale, London, SW16 5HH, United Kingdom

Zanetti, Diego, Univ. of Brescia, Otorhinolaryngology, Piazzale Spedali Civili, 1 25100, Brescia, Italy

New Corresponding Electronic Associates

Dai, Wei, TIPC of CAS, Tech. Inst. of Phys & Chem, Zhong Guan Cun Bei Yi Tiao 2, Hai Dian, 100080 Beijing, PRC
Domitrovic, Hrvoje, Faculty of EE & Computing, Dept. of Electroacoustics, Unska 3,10000, Zagreb, Croatia
Li, Xiaodong, Institute of Acoustics, Communication Acoustics Lab, No. 21, Bei Si Huan Xi Lu, 100080 Beijing, PRC
Sepulveda, Alexander, Universidad Nacional, DEEEC, Km 6 via al Magdalena, Campus La Nubia, Manizales 57, Colombia
Wilkinson, Richardt, Cape Peninsula Univ. of Technology, PO Box 4578, Tyger Valley, 7536, Rep S. Africa

Members Elected Fellows

D. B. Bottledorn, D. M. Byrd, B. R. Glasberg, L. E. Humes, V. A. Khokhlova, A. P. Nash, J. C. Osler, R. M. Stern, B. H. Story

Associates Elected Fellows

M. A. Akeroyd, S. B. Blackwell, C. D. Micheyl

Associates Elected Members

R. M. Brenneman, L. J. Frizzell-Makowski, D. Lord, P. Moquin, R. O Rasmussen, D. J. Schmidlin, N. B. Sevener, Y. Tsurugaya, D. C. Waddington

Student Elected Member

M. Hisagi

Member to Electronic Associate

J. D. Van der Toorn

Member to Student

N. H. Philipp

Associates to Students

A. DiAngelo, B. E. Markham

Students to Associates

G. Acosta, J. A. Ballard, R. J. Barton, C. J. Beers, C. Bergevin, A. Blanc, A. Camacho, R. Campos-Astrorikiza, H. C. Chan, N. A. Chang, F. M. Del Solar Dorrego, B. Dunkin, L. E. Falco, C. H. Farney, R. A Felty, C. A. Garner, M. R. Haberman, S. R. Helgadottir, N. Hodoshima, E. M. Hoglund, W. B. Howard, A. B. John, E. Johnson, A. L. Joyce, N. Kawai, S. A. Klemuk, J. A. Konefall, M. Kuster, W. E. Kreider, J. Krivokapic, A. K. C.

Lee, K. Li, F. Liu, P. R. Messum, A. P. Michaud, N. Ogasawara, N. R. Owen, S. Phatak, C. A. Preissner, I. I. Rypina, Y. Samuel, B. M. Shafer, A. J. Stulgin, H. Sumoro, S. C. Sullivan, B. V. Tucker, I. A. Udovydchenkov, M. W. Urban, M. Vandam, M. Wirtzfeld, M. Yoshida, C. M. Zettler

Students to Electronic Associates

L. Calendruccio, A. N. Miller

Electronic Associates to Associates

F. Asdrubali, A. R. Bontomase, T. M. Lorenzen, G. Petculescu, C. M. Wu

Associates to Electronic Associates

R. C. Chapman, H. A. Gaberson, B. K. Mukherjee,

Electronic Associate to Corresponding Electronic Associate

H. Yoon

Student to Corresponding Electronic Associate

K. Jambrosic

Reinstated

J. H. Wyatt - Associate

Resigned

T. G. Birdsall, H. P. W. Gottlieb, S. Ohtsuki, - Fellows
A. Z. Davidsen, S. E. Dunn, J. K. Hall, E. Keller, M. B. Meikle, T. Tsumura, H. G. Urban - Members
K. W. Beach, A. P. Carito, K. D'Souza, T. Ferreira, M. C. Kelly, K. M. Powell, W. A. Russell,
H. K. Schutte, W. R. Short M. Sifakis, J. H. So, D. W. Sutton, T. Takahag, - Associates
B. R. M. Faehndrich, B. V. Hough, C. Mahaffey, M. H. Roe, A. I. Tlumak - Students
L. Krige - Corresponding Electronic Associate

Deceased

S. F. Clifford, J. F. Curtis, S. M. Flatte, R. Johnson, M. J. Kodaras, W. Kroll - Fellows
C. Barker, J. K. Cullen, J. Frarey - Members
O. E. Rodgers - Associate

Fellows	896
Members	2120
Associates	2637
Electronic Associates	648
Students	967
	7268

ACOUSTICAL STANDARDS NEWS

Susan B. Blaeser, Standards Manager
ASA Standards Secretariat, Acoustical Society of America, 35 Pinelawn Rd., Suite 114E, Melville, NY 11747 [Tel.: (631) 390-0215; Fax: (631) 390-0217; e-mail: asastds@aip.org]

George S.K. Wong
Acoustical Standards, Institute for National Measurement Standards, National Research Council, Ottawa, Ontario K1A 0R6, Canada [Tel.: (613) 993-6159; Fax: (613) 990-8765; e-mail: george.wong@nrc.ca]

American National Standards (ANSI Standards) developed by Accredited Standards Committees S1, S2, S3, and S12 in the areas of acoustics, mechanical vibration and shock, bioacoustics, and noise, respectively, are published by the Acoustical Society of America (ASA). In addition to these standards, ASA publishes Catalogs of Acoustical Standards, both National and International. To receive copies of the latest Standards Catalogs, please, contact Susan B. Blaeser.
Comments are welcomed on all material in Acoustical Standards News.
This Acoustical Standards News section in JASA, as well as the National and International Catalogs of Acoustical Standards, and other information on the Standards Program of the Acoustical Society of America, are available via the ASA home page: http://asa.aip.org.

Accredited Standards Committees S1, Acoustics; S2, Mechanical Vibration and Shock; S3, Bioacoustics; S3/SC 1, Animal Bioacoustics; and S12, Noise will meet in conjunction with the 156th meeting of the Acoustical Society of America in Miami, FL, during the week of **10 November 2008**. The U.S. TAGs to ISO/TC 43, ISO/TC 43/SC 1, ISO/TC 108 and its subcommittees, and IEC/TC 29 will also meet during the Standards Plenary meeting. Specific meeting dates and times will be announced soon.

Note that there will be NO standards committee meetings in Paris in June 2008.

Standards Meetings Calendar—International

8–12 September 2008 - Oslo, Norway
• ISO/TC 108/SC 4, Human exposure to mechanical vibration and shock

3–7 November 2008 - St. Louis, MO, USA
• ISO/TC 108, Mechanical vibration, shock and condition monitoring

• ISO/TC 108/SC 3, Use and calibration of vibration and shock measuring instruments

• ISO/TC 108/SC 6, Vibration and shock generating systems

Standards News From The United States

(Partially derived from *ANSI Standards Action,* with appreciation)

American National Standards - Call for Comment on Proposals Listed

This section solicits comments on proposed new American National Standards and on proposals to revise, reaffirm, or withdraw existing standards. The dates listed in parentheses are for information only.

ASA (ASC S1) (Acoustical Society of America)

REAFFIRMATIONS

BSR/ASA S1.14-1998 (R200x), Recommendations for Specifying and Testing the Susceptibility of Acoustical Instruments to Radiated Radio-Frequency Electromagnetic Fields (reaffirmation and redesignation of ANSI S1.14-1998 (R2003))

Provides recommendations for specifying and testing the susceptibility of acoustical instruments to radiated radio-frequency electromagnetic fields. It does not contain recommendations regarding the susceptibility of an instrument to conducted electromagnetic fields, or recommendations to limit the emission of electromagnetic fields from instruments. It covers two ranges of radio frequencies for the carrier signal: 25 MHz to 500 MHz, and an extended range from 25 MHz to 1 GHz. (March 10, 2008)

ASA (ASC S12) (Acoustical Society of America)

REAFFIRMATIONS

BSR/ASA S12.8-1998 (R200x), Methods for Determining the Insertion Loss of Outdoor Noise Barriers (reaffirmation and redesignation of ANSI S12.8-1998 (R2003))

Adopts insertion loss - the difference between acoustical levels before and after a noise-barrier installation - as the basis for evaluating the acoustical effectiveness of an outdoor noise barrier. Methods are provided to determine the insertion loss of outdoor noise barriers at selected receiver locations and under conditions of interest. It covers insertion loss determination, by measurement or by the combination of measurement and prediction, for outdoor noise barriers of all types. (April 7, 2008)

BSR/ASA S12.9-Part 2-1992 (R200x), Quantities and Procedures for Description and Measurement of Environmental Sound - Part 2: Measurement of Long-Term, Wide-Area Sound (reaffirmation and redesignation of ANSI S12.9-Part 2-1992 (R2003))

Describes recommended procedures for measurement of long-term, time-average environmental sound outdoors at one or more locations in a community for environmental assessment or planning for compatible land uses and for other purposes such as noise prediction validation and regulation. Its purpose is to provide for a commonality for measurement of outdoor environmental sound as it may affect people in and around dwellings. (April 7, 2008)

BSR/ASA S12.9-Part 3-1993 (R200x), Quantities and Procedures for Description and Measurement of Environmental Sound - Part 3, Short-Term Measurements with an Observer Present (reaffirmation and redesignation of ANSI S12.9-Part 3-1993 (R2003))

Describes recommended procedures for measurement of short-term, time-average environmental sound outdoors at one or more locations in a community for environmental assessment or planning for compatible land uses and for other purposes such as demonstrating compliance with a regulation. These measurements are distinguished by the requirement to have an observer present. Methods are given to correct the measured levels for the influence of background sound. (April 7, 2008)

 0001-4966/2008/123(5)/2454/4/$23.00 © 2008 Acoustical Society of America

REVISIONS

BSR S12.9/Part 6-200x, Quantities and Procedures for Description and Measurement of Environmental Sound - Part 6: Methods for Estimation of Awakenings Associated with Noise Events Heard in Homes (revision of ANSI S12.9-Part 6-2000 (R2005))

Defines noise levels that are associated with sleep disturbance in home settings in which people are familiar with the neighborhood noise environment. Sleep "disturbance" is restricted to behaviorally confirmed awakening, as demonstrated by pressing a button upon awakening. Noise levels are quantified as indoor sound exposure levels of events occurring less than 5 minutes prior to the awakening. The Standard further assumes a population of normal hearing individuals with no sleep disorders. (February 25, 2008)

BSR/ASA S12.2-200x, Criteria for Evaluating Room Noise (revision and redesignation of ANSI S12.2-1995 (R1999))

Provides three primary methods for evaluating room noise: a survey method that employs the A-weighted sound level; an engineering method that employs expanded noise criteria (NC) curves; and a method for evaluating low frequency fluctuating noise using room noise criterion (RNC) curves. (March 31, 2008)

HI (Hydraulic Institute)

REVISIONS

BSR/HI 9.6.4-200x, Rotodynamic Pumps for Vibration Measurements and Allowable Values (revision of ANSI/HI 9.6.4-2000)

Applies to the evaluation of vibration on rotodynamic pump applications absorbing more than 2 kw (3 hp) and of the types as indicated within the standard. This standard pertains to evaluation of vibration when the vibration measurements are made on nonrotating parts (hearing housing vibration). The general evaluation criteria are included for acceptance tests in field environments or at the manufacturer's test facility, as appropriate and as defined in the standard. (March 17, 2008)

CALL FOR MEMBERS

AHAM (Association of Home Appliance Manufacturers)

BSR/AHAM AC-2-2006 (R200x), Method for Sound Testing of Portable Household Electric Room Air Cleaners (reaffirmation of ANSI/AHAM AC-2-2006)

ARI (Air-Conditioning and Refrigeration Institute)

BSR/ARI 575-200x, Method of Measuring Machinery Sound Within an Equipment Space (new standard)

ASA (ASC S12) (Acoustical Society of America)

BSR/ASA S12.10/Part 2-200x, Declared Noise Emission Values of Information Technology and Telecommunications Equipment (new standard)

HI (Hydraulic Institute)

BSR/HI 9.1-9.5-200x, Pump - General Guidelines for Types, Definitions, Application, Sound Measurement and Decontamination (revision of ANSI/HI 9.1-9.5-2000)

BSR/HI 9.6.4-200x, Rotodynamic Pumps for Vibration Measurements and Allowable Values (revision of ANSI/HI 9.6.4-2000)

Project Initiation Notification System (PINS)

ANSI Procedures require notification of ANSI by ANSI-accredited standards developers (ASD) of the initiation and scope of activities expected to result in new or revised American National Standards (ANS). Early notification of activity intended to reaffirm or withdraw an ANS is optional. The mechanism by which such notification is given is referred to as the PINS process. For additional information, see clause 2.4 of the ANSI Essential Requirements: Due Process Requirements for American National Standards. Following is a list of proposed actions and new ANS that have been received recently from ASDs.

AHAM (Association of Home Appliance Manufacturers)

BSR/AHAM AC-2-2006 (R200x), Method for Sound Testing of Portable Household Electric Room Air Cleaners (reaffirmation of ANSI/AHAM AC-2-2006)

Establishes a method to determine the sound rating of portable household electric room air cleaners. The sound rating is comprised of a set of sound levels that include: (1) Overall A-weighted sound power level (Lwa) and (2) Loudness level in SONES. Established in the standard are definitions, tests, calculations, ratings, and minimum data requirements for published ratings and conformance conditions. Project Need: To reaffirm the existing standard. Stakeholders: Manufacturers, consumer groups, general interest.

ARI (Air-Conditioning and Refrigeration Institute)

BSR/ARI 575-200x, Method of Measuring Machinery Sound Within an Equipment Space (new standard)

Applies to water chilling systems, pumps and similar operating machines and parts thereof, which, for reasons of size or operating characteristics, are more practically evaluated in situ. Project Need: To establish a uniform method of measuring and recording the Sound Pressure Level of machinery installed in a mechanical equipment space. Stakeholders: Manufacturers, engineers, installers, contractors and users.

BSR/ARI 1140-200x, Sound Quality Evaluation Procedures for Air-Conditioning and Refrigeration Equipment (new standard)

This standard applies to factory-made, residential and commercial air conditioning as well as transport refrigeration equipment. Project Need: To establish sound quality evaluation procedures for air conditioning and refrigeration equipment and to provide definitions; test requirements; sound quality evaluation procedures; minimum data requirements for Published Ratings; and conformance conditions. Stakeholders: Manufacturers, engineers, installers, contractors and users.

ASA (ASC S12) (Acoustical Society of America)

BSR/ASA S12.10/Part 2-200x, Declared Noise Emission Values of Information Technology and Telecommunications Equipment (new standard)

Defines how to calculate and disclose two noise emission specification values: the declared A-weighted sound power level [LWAd] and the declared A-weighted sound pressure level [LpAm (a mean value)] at the operator or bystander positions. The declared sound power level enables 3rd party verification of the specifications, and permits consistent comparison of IT equipment by consumers, purchasing agencies, etc. Project Need: To create an American National Standard to govern noise emission declaration for IT products. Stakeholders: Information technology and telecommunications equipment manufacturers and purchasers.

HI (Hydraulic Institute)

BSR/HI 9.1-9.5-200x, Pump - General Guidelines for Types, Definitions, Application, Sound Measurement and Decontamination (revision of ANSI/HI 9.1-9.5-2000)

Applies to all industrial/commercial pumps including rotodynamic, rotary, and reciprocating types. It includes types, definitions, design and application, airborne sound measurement and decontamination. Project Need: To improve and update the existing ANSI/HI standard with latest content. Stakeholders: Pump manufacturers, specifiers, purchasers, and pump users.

Final actions on American National Standards

The standards actions listed below have been approved by the ANSI Board of Standards Review (BSR) or by an ANSI-Audited Designator, as applicable.

ASME (American Society of Mechanical Engineers)

REAFFIRMATIONS

ANSI/ASME Y32.18-1972 (R2008), Symbols for Mechanical and Acoustical Elements as Used in Schematic Diagrams (reaffirmation of ANSI/ASME Y32.18-1972 (R2003))

ASTM (ASTM International)

New Standards

ANSI/ASTM F1334-2008, Test Method for Determining A-Weighted Sound Power Level of Vacuum Cleaners (new standard)

ATIS (Alliance for Telecommunications Industry Solutions)

REAFFIRMATIONS

ANSI T1.518-1998 (R2008), Objective Measurement of Telephone Band Speech Quality Using Measuring Normalizing Blocks (MNBs) (reaffirmation of ANSI T1.518-1998 (R2003))

SCTE (Society of Cable Telecommunications Engineers)

New Standards

ANSI/SCTE 24-23-2007, BV32 Speech Codec Specification for Voice over IP Applications in Cable Telephony (new standard)

STANDARDS NEWS FROM ABROAD

(Partially derived from *ANSI Standards Action*, with appreciation)

Newly Published ISO and IEC Standards

Listed here are new and revised standards recently approved and promulgated by ISO - the International Organization for Standardization – and IEC – the International Electrotechnical Commission.

ISO Standards

PERFORMANCE OF HOUSEHOLD ELECTRICAL APPLIANCES (TC 59)

IEC 60704-2-13 Amd.1 Ed. 1.0 b:2008, Amendment 1 - Household and similar electrical appliances - Test code for the determination of airborne acoustical noise - Part 2-13: Particular requirements for range hoods

ENVIRONMENTAL CONDITIONS, CLASSIFICATION AND METHODS OF TEST (TC 104)

IEC 60068-2-27 Ed. 4.0 b:2008, Environmental testing - Part 2-27: Tests - Test Ea and guidance: Shock

MECHANICAL VIBRATION AND SHOCK (TC 108)

ISO 18434-1:2008, Condition monitoring and diagnostics of machines - Thermography - Part 1: General procedures

ISO 18436-3:2008, Condition monitoring and diagnostics of machines - Requirements for qualification and assessment of personnel - Part 3: Requirements for training bodies and the training process

ISO 21289:2008, Mechanical vibration and shock – Parameters to be specified for the acquisition of vibration data

IEC Standards

IEC 61196-1-325 Ed. 1.0 b:2008, Coaxial communication cables – Part 1-325: Mechanical test methods - Aeolian vibration

ISO and IEC Draft International Standards

ISO

ACOUSTICS (TC 43)

ISO/DIS 13474, Acoustics - Framework for calculating a distribution of sound exposure levels of impulsive sound events for purposes of environmental noise assessment

MECHANICAL VIBRATION AND SHOCK (TC 108)

ISO 13091-1/DAmd1, Mechanical vibration - Vibrotactile perception thresholds for the assessment of nerve dysfunction - Part 1: Methods of measurement at the fingertips - Amendment 1

ISO/DIS 22266-1, Mechanical vibration - Torsional vibration of rotating machinery - Part 1: Land-based steam and gas turbine generator sets in excess of 50 MW

SMALL CRAFT (TC 188)

ISO/DIS 14509-3, Small craft - Airborne sound emitted by powered recreational craft - Part 3: Sound assessment using calculation and measurement procedures

IEC

61F/737/FDIS, IEC 60745-2-12-A1 Ed 2.0: Hand-held motor-operated electric tools - Safety - Part 2-12: Particular requirements for concrete vibrators

104/448/FDIS, IEC 60068-2-27 Ed. 4.0: Environmental testing – Part 2-27: Tests - Test Ea and guidance: Shock

104/456/FDIS, IEC 60068-2-64 Ed. 2.0: Environmental testing – Part 2-64: Tests - Test Fh: Vibration, broadband random and guidance

Information Concerning:

Proposed Foreign Government Regulations

Call For Comment

U.S. manufacturers, exporters, regulatory agencies and standards developing organizations may be interested in proposed foreign technical regulations issued by Member countries of the World Trade Organization (WTO). In accordance with the WTO Agreement on Technical Barriers to Trade (TBT Agreement), Members are required to report proposed technical regulations that may significantly affect trade to the WTO Secretariat in Geneva, Switzerland. In turn, the Secretariat disseminates the information to all WTO Members. The purpose of this requirement is to provide global trading partners with an opportunity to review and comment on the regulations before they become final.

The National Center for Standards and Certification Information (NCSCI) at the National Institute of Standards and Technology (NIST) distributes these proposed foreign technical regulations to U.S. stakeholders via an online service, Notify U.S. Notify U.S. is an e-mail and Web service that allows interested U.S. parties to register, obtain notifications, and read full texts of regulations from countries and for industry sectors of interest to them. To register for Notify U.S., please go to Internet URL: http://www.nist.gov/notifyus/ and click on "Subscribe."

NCSCI is the WTO TBT Inquiry Point for the U.S. and receives all notifications and full texts of regulations to disseminate to U.S. Industry. For further information, please contact: NCSCI, NIST 100 Bureau Drive, Gaithersburg, MD 20899-2160; Telephone: (301) 975-4040; Fax: (301) 926-1559; E-mail: ncsci@nist.gov or notifyus@nist.gov.

International Organization for Standardization (ISO)

Call for International (ISO) Secretariat ISO/TC 86/SC 7 – Testing and Rating of Commercial Refrigerated Display Cabinets

ANSI has been advised The Air Conditioning and Refrigeration Institute (ARI) wishes to serve as delegated ANSI Secretariat for the above ISO subcommittee that was relinquished by the British Standards Institute (BSI). This SC is covered by the scope of the main Technical Committee (ISO/TC 86), having the following scope: Standardization in the fields of refrigeration and air conditioning, including terminology, mechanical safety, methods of testing and rating equipment, measurement of sound levels, refrigerant and refrigeration lubricant chemistry, with consideration given to environmental protection. The scope includes factory-assembled air conditioners (cooling), heat pumps, dehumidifiers, refrigerants, and refrigerant reclaiming and recycling equipment as well as other devices, components and equipment such as humidifiers, ventilation equipment, and automatic controls used in air conditioning and refrigeration systems that are not covered by other ISO technical committees. Anyone wishing to comment on the delegation of the International Secretariat to ARI please contact Henrietta Scully, ANSI, via e-mail, hscully@ansi.org.

BOOK REVIEWS

P. L. Marston
Physics Department, Washington State University, Pullman, Washington 99164

These reviews of books and other forms of information express the opinions of the individual reviewers and are not necessarily endorsed by the Editorial Board of this Journal.

Fundamentals of Voice Quality Engineering in Wireless Networks

Avi Perry

Cambridge University Press, 2006, 377 pp. Price: $90.00 (hardcover), ISBN: 0-521-85595-0

This book provides an excellent, practical, overview over the complete field of voice quality problems as encountered in wireless networks. Perry uses down to earth, sometimes nontechnical, descriptions to go over every aspect of voice quality, which sometimes leads to wordiness for those who are technically skilled in the field. However, it makes the book accessible for the larger field of nonexperts who want to gain insight into this topic, which has an ever-increasing impact on our daily telecommunication. The first two words of the title "Fundamentals Of" may be a little misleading because the fundamentals of voice quality itself are not worked out properly. Maybe the next issue of the book can take this criticism into account. The first part of the book, called "Voice-quality foundations," does not fulfill its promise, it should start with an ideal voice link as defined by the ITU (1 m air path) and then define the different aspects of conversational quality, listening quality (how do I perceive the other?), talking quality (how do I perceive my own voice?), and interaction quality (can we interrupt each other and what happens when we both talk?). Also the coding should be treated more fundamentally, Perry fails to make a distinction between redundancy and irrelevancy. Furthermore some ITU-T recommendations are not well treated (P.800, P.563, P.835, G.107, G.114).

The second part of the book, "Applications," gives an excellent overview of problems related to echo and noise problems and provides insights that go well beyond wireless networks. In fact most of the text can be applied to Voice over IP (VoIP) where the basic problems are more or less the same as in the wireless world, i.e., a longer end-to-end delay and consequently a need for more advanced (acoustic) echo canceling. Clear descriptions of both electric and acoustic echo problems are given in different network configurations. The impact of noise, noise reduction schemes, and level control are dealt with from a practical point of view and provide many useful discussion points that are very relevant in the operation of wireless networks. A minor point is that the reader may get a too optimistic view of the performance of noise suppressors/echo cancelers after reading part two.

The third part of the book deals with "Wireless architectures," where the voice quality topics are worked out and different architectures are discussed. It is well written with clear explanations of the relations between the architecture and voice quality problems for both mobile to fixed and mobile to mobile calls. An extra chapter devoted to the impact of radio parameters like RxQual, BLER, handover problems may be a good idea for the next issue.

Part four, "A network operator's guide for selecting, appraising and testing a voice-quality systems," provides many detailed tests for assessing voice-quality systems with a focus on the ITU-T recommendations G.160, G.167, and G.168 regarding objective testing. Also PESQ and other objective speech quality measurement systems are discussed and a warning is given not to rely on objective measurements too much. A nice list of different subjective tests that have to be carried out in the assessment of echo cancelers in order to have insight into their performance in "live" networks is given. Very useful are the subjective tests that relate to double talk conditions where especially the noise contrast and noise switching distortions are causing severe degradations in modern mobile and VoIP networks. This list should be used by anyone that is involved in designing and testing cancelers and by operators who want to have an idea of what their customers are experiencing.

Finally the remainder of the book provides a useful trouble-shooting overview where one can start with a voice-quality-related complaint and find a possible set of underlying technical problems and work toward a solution from that.

So overall Perry has succeeded to provide an excellent practical overview that is a good starting point for anyone in the field who needs a global picture on voice quality problems in wireless networks.

JOHN BEERENDS
TNO Information and Communication Technology
Delft, The Netherlands
john.beerends@tno.nl

 0001-4966/2008/123(5)/2459/1/$23.00 © 2008 Acoustical Society of America

REVIEWS OF ACOUSTICAL PATENTS

Sean A. Fulop
Dept. of Linguistics, California State University Fresno
5245 N. Backer Ave., Fresno, California 93740

Lloyd Rice
11222 Flatiron Drive, Lafayette, Colorado 80026

The purpose of these acoustical patent reviews is to provide enough information for a Journal reader to decide whether to seek more information from the patent itself. Any opinions expressed here are those of reviewers as individuals and are not legal opinions. Printed copies of United States Patents may be ordered at $3.00 each from the Commissioner of Patents and Trademarks, Washington, DC 20231. Patents are available via the internet at http://www.uspto.gov.

Reviewers for this issue:

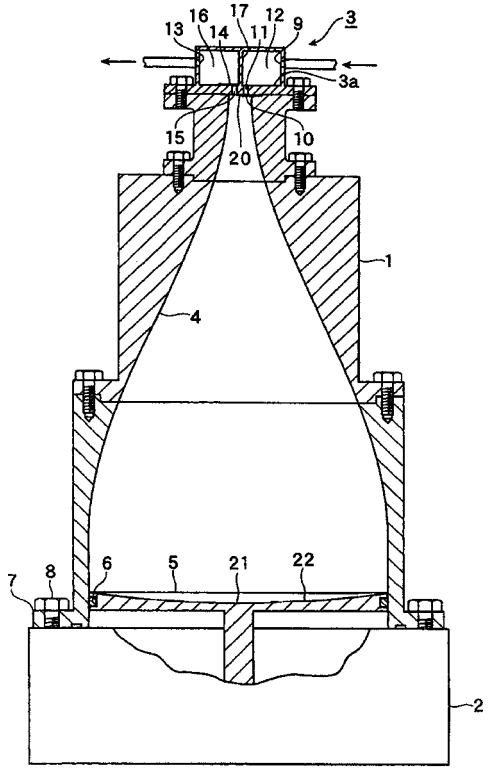
GEORGE L. AUGSPURGER, *Perception, Incorporated, Box 39536, Los Angeles, California 90039*
ANGELO CAMPANELLA, *3201 Ridgewood Drive, Hilliard, Ohio 43026-2453*
GEOFFREY EDELMANN, *Naval Research Laboratory, Code 7145, 4555 Overlook Ave. SW, Washington, DC 20375*
JEROME A. HELFFRICH, *Southwest Research Institute, San Antonio, Texas 78228*
DAVID PREVES, *Starkey Laboratories, 6600 Washington Ave. S., Eden Prairie, Minnesota 55344*
CARL J. ROSENBERG, *Acentech Incorporated, 33 Moulton Street, Cambridge, Massachusetts 02138*
NEIL A. SHAW, *Menlo Scientific Acoustics, Inc., Post Office Box 1610, Topanga, California 90290*
ERIC E. UNGAR, *Acentech, Incorporated, 33 Moulton Street, Cambridge, Massachusetts 02138*
ROBERT C. WAAG, *Department of Electrical and Computer Engineering, University of Rochester, Rochester, New York 14627*

7,299,894

43.20.Ks ACOUSTIC FLUID MACHINE

Masaaki Kawahashi *et al.*, assignors to *Anest Iwata Corporation*
27 November 2007 (Class 181/262); filed 2 July 2004

This gas pump is a close cousin to a hydraulic ram. Piston **5** is driven by actuator assembly **2** at a rate that coincides with the resonance frequency



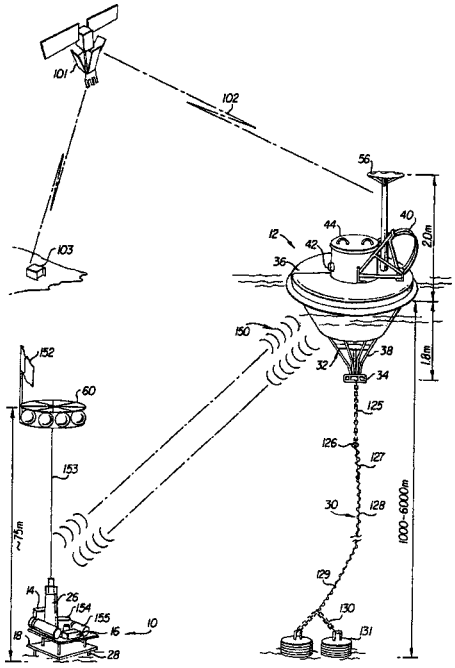
of chamber **4**. Inlet and outlet check valves maintain an efficient, unidirectional gas flow.—GLA

7,289,907

43.30.Ma SYSTEM FOR REPORTING HIGH RESOLUTION OCEAN PRESSURES IN NEAR REAL TIME FOR THE PURPOSE OF TSUNAMI MONITORING

Christian Meinig *et al.*, assignors to *The United States of America as Represented by the Secretary of Commerce*
30 October 2007 (Class 702/2); filed 20 May 2005

Tsunami early warning systems are terribly important; however, this disappointing submission merely claims that connecting the tsunameter (via



acoustic modem) to a buoy and the buoy (via RF) to a satellite is a non-obvious idea.—GFE

 0001-4966/2008/123(5)/2461/15/$23.00 © 2008 Acoustical Society of America

7,295,492

43.30.Vh METHOD AND APPARATUS FOR CORRELATION SONAR

Anthony L. Scoca, assignors to *Lockheed Martin Corporation*
13 November 2007 (Class 367/89); filed 6 January 2006

Incredibly, the authors assert that it is non-obvious that using extra receivers might just improve target velocity estimation.—GFE

7,289,389

43.30.Wi RESOLVING DIRECTIONAL INFORMATION IN SONAR ARRAYS

Rory Niland, *assignor to Sonartech Atlas Pty Limited*
30 October 2007 (Class 367/103); filed in Australia 4 September 2003

A formulaic recipe of using beamforming, the MUSIC algorithm, and expectation-maximization to improve the resolution of directional information, in that order, has been seized upon.—GFE

7,286,442

43.30.Yj METHOD AND APPARATUS FOR SEISMIC DATA ACQUISITION

Clifford H. Ray *et al.*, assignors to *Fairfield Industries, Incorporated*
23 October 2007 (Class 367/15); filed 25 October 2005

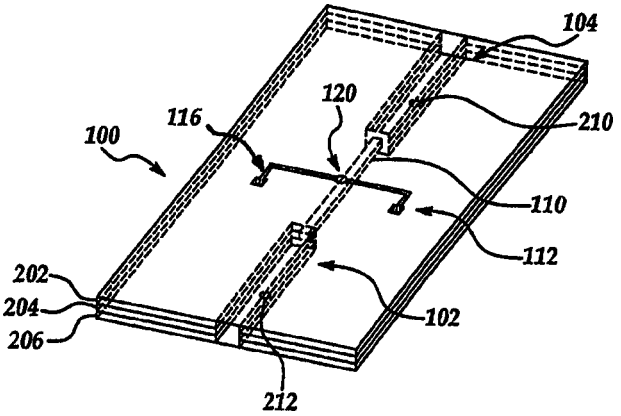
The involved details of one specific underwater seismic array are described.—GFE

7,304,732

43.35.Ud MICROELECTROMECHANICAL RESONANT PHOTOACOUSTIC CELL

Ronald G. Polcawich and Paul Pellegrino, assignors to *United States of America as represented by the Secretary of the Army*
4 December 2007 (Class 356/246); filed 19 November 2003

The authors describe a very simple MEMS cell constructed to allow a laser beam to pass through in one direction and contain a piezoelectric film microphone on another face. It is claimed that this planar geometry increases sensitivity to the photoacoustic interaction of light with the gas contained within. The cell as drawn is open to the air, so that the cavity inside is being used as an open-open resonant tube. The authors describe this arrangement as beneficial for trace gas monitoring of the atmosphere (as in waste gas monitoring, chemical warfare agent detection, etc.) It is claimed that the use of a MEMS cell allows for higher modulation frequencies and consequently higher detection sensitivities than in larger cavities. This seems counterintuitive, since the sensitivity of such microphones is rather poor, and the Q of any such small cavities must be low due to disadvantageous surface to volume area ratios. It would seem that the authors never actually built and tried such a device.—JAH

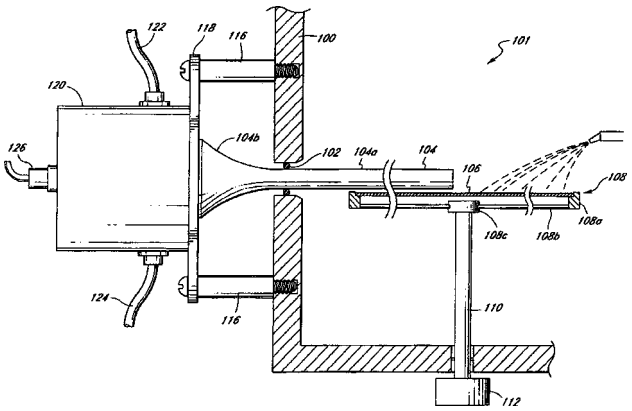


7,268,469

43.35.Zc TRANSDUCER ASSEMBLY FOR MEGASONIC PROCESSING OF AN ARTICLE AND APPARATUS UTILIZING THE SAME

Mario E. Bran, assignor to *Akrion Technologies, Incorporated*
11 September 2007 (Class 310/328); filed 15 March 2006

An ultrasonic cleaner **101** for semiconductor wafers is claimed comprising rod **104**–**104a** vibrating in its longitudinal mode at a megasonic (unspecified) frequency and in close proximity to wafer **106** on turntable



108–**108c**. Cleaning medium is sprayed onto the surface of rotating wafer **106**, moving cleaning droplets to and under the vibrating rod to be dispersed to clean surface **106**. Sprayed media may be various liquids and gases as well as dry ice snow.—AJC

7,289,038

43.38.Ar UNDERWATER SOUND RADIATION APPARATUS

Takayuki Watanabe and Shinji Kishinaga, assignors to *Yamaha Corporation*
30 October 2007 (Class 340/850); filed in Japan 13 July 2001

Anything can be patented these days; including the well-known idea of coupling a transducer to a wall or hull to increase the effective size of the radiation surface.—GFE

7,289,388

43.60.Cg ESTIMATION OF BACKGROUND NOISE AND ITS EFFECT ON SONAR RANGE ESTIMATION

Nathan Intrator *et al.*, assignors to *Brown University*
30 October 2007 (Class 367/100); filed 8 June 2004

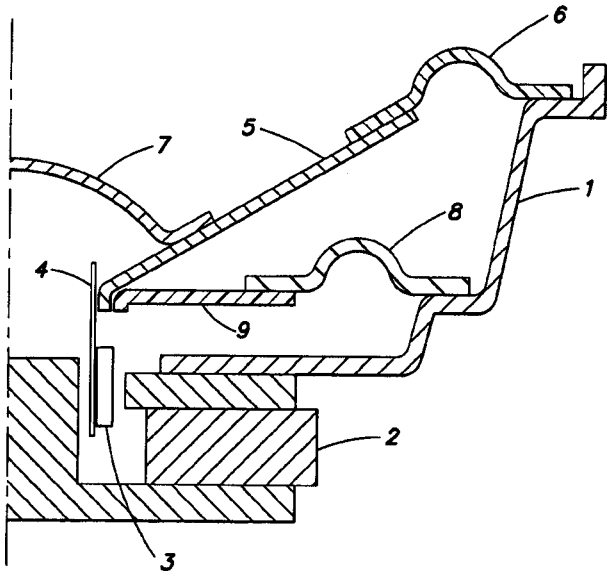
The straight-from-the-textbook method of measuring signal-to-noise ratio in different frequency bands via cross correlation is sadly nabbed.—GFE

7,292,707

43.38.Dv LOUDSPEAKER

Leonard Kreitmeier and Jürgen Ringlstetter, assignors to *Harman Becker Automotive Systems GmbH*
6 November 2007 (Class 381/398); filed in Germany 25 April 2001

For both cone type and flat panel loudspeakers with an electrodynamic drive, a "second bead" **8** is used instead of a conventional spider centering



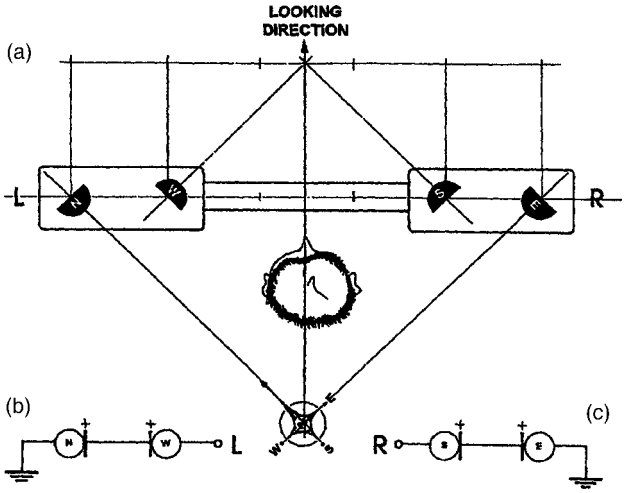
device. Multiple centering "beads" can be used.—NAS

7,263,034

43.38.Hz RESONATOR DEVICE AND CIRCUITS FOR 3-D DETECTION/RECEIVING SONIC WAVES, EVEN OF A VERY LOW AMPLITUDE/ FREQUENCY, SUITABLE FOR USE IN CYBERNETICS

Daniele Ramenzoni, Fidenza, Italy
28 August 2007 (Class 367/188); filed in Italy 18 March 2002

In rambling text, the author claims a transducer array for listening purposes operating at any frequency over a very wide range ("diapason") whose composite beam can be steered. Left transducers **N**–**W** (2.1 –10.8 cm apart) and right transducers **S**–**E** (also 2.1–10.8 cm apart) are arranged on line **L**–**R** spaced by 44 cm or less when operated in air. The pairs are connected in opposition as indicated in Figs. 1(b) and 1(c). Beam



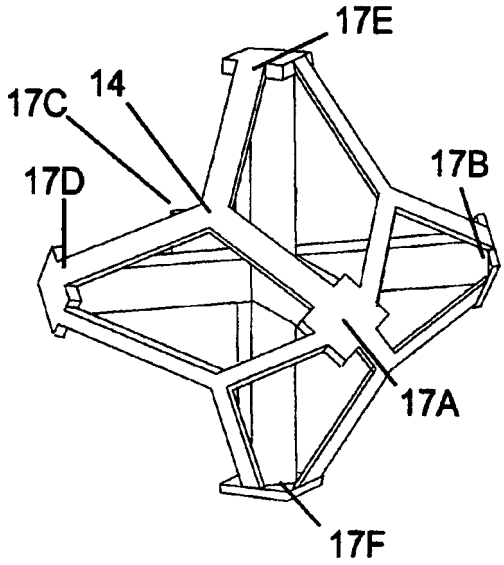
steering is provided by a variable resistor connected across **N** and one across **E**, while a fixed capacitor is connected across **W** and another across **S**. The resultant signals can be heard with earphones. Controlled directivity (beam steering) is claimed. It is also claimed that this transducer arrangement can be used to create and steer ultrasonic beams for therapeutic purposes in air and in liquid media in which case the spacings are increased (for water) by a factor of 4.395.—AJC

7,292,503

43.38.Hz MULTI PISTON ELECTRO-MECHANICAL TRANSDUCTION APPARATUS

Alexander L. Butler and John L. Butler, assignors to *Image Acoustics, Incorporated*
6 November 2007 (Class 367/163); filed 3 May 2004

Lever arm assembly **14** with piezoelectric drivers located below the square junctions **17** is surrounded by a spherical cover. This provides a



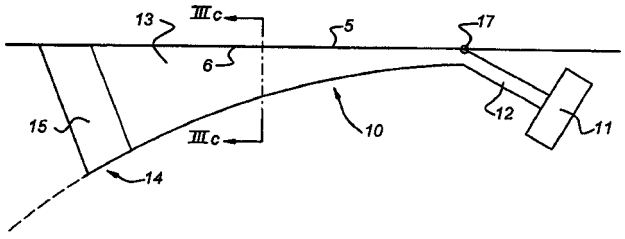
compact transducer that can find use in underwater applications. The patent also describes circular and cylindrical implementations using similar arrangements.—NAS

7,268,467

43.38.Ja ACOUSTIC TRANSDUCER

Gerard Hendrik Josephus De Vries, assignor to *Duran Audio B.V.*
11 September 2007 (Class 310/328); filed in Netherlands 14 February 2002

A high intelligibility loudspeaker assembly **10** for vehicle tunnels and multi-story parking lots is claimed. To avoid back-surface reflected waves that cause beam scalloping and delayed echoes, the speaker driver **11**–**12** is placed at the backing surface **5**. A surface **14** is added that parallels back surface **5** before widening to exit aperture **13**. In this way, the wave reflected



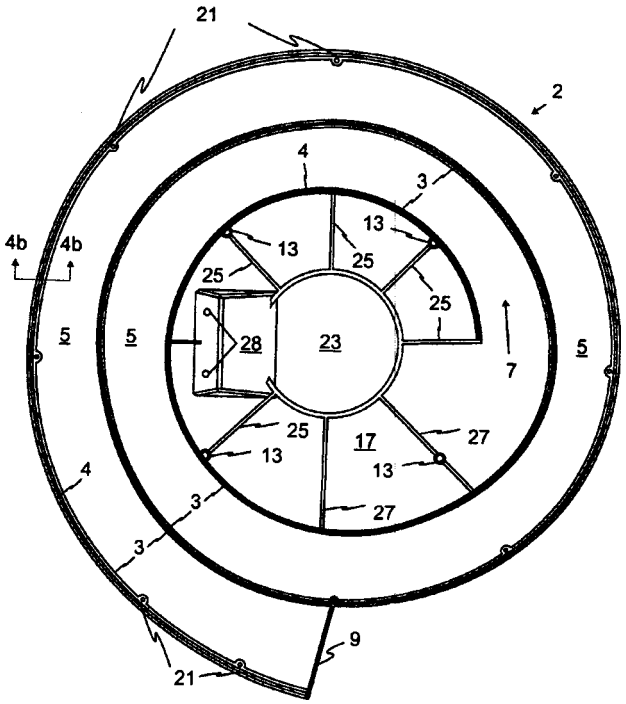
from the back surface **5** is not delayed in time. Both the direct and reflected waves **15** emerge in phase. The angular extent parallel to back surface **5** can be narrow, viz. 30 degrees as for a tunnel, or it can be a full 360 degrees, as for the ceiling of a multi-story parking lot.—AJC

7,284,638

43.38.Ja LOUDSPEAKER LOW PROFILE QUARTER WAVELENGTH TRANSMISSION LINE AND ENCLOSURE AND METHOD

Joseph Y. Sahyoun, Redwood City, California
23 October 2007 (Class 181/156); filed 8 May 2006

This reviewer thought that a transmission line design is used to completely absorb the rear wave from a driver in an enclosure. Here it is not and so appears to be more like a reflex or ported enclosure. Among the benefits



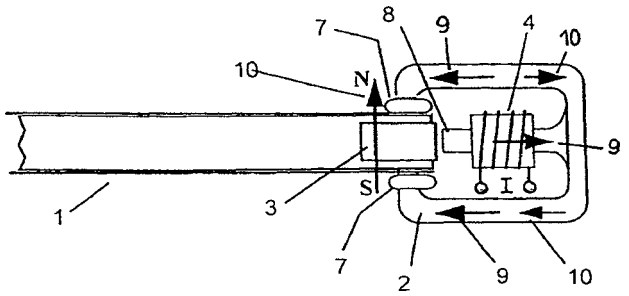
claimed for the design are reduced resistance to air flow (specifically exhale vs. inhale) as well as lower turbulence in the port, er, line. The design is also the enclosure.—NAS

7,302,077

43.38.Ja ELECTROMAGNETIC DRIVER FOR A PLANAR DIAPHRAGM LOUDSPEAKER

Wolfgang Bachmann *et al.*, assignors to *Harman/Becker Automotive Systems GmbH*
27 November 2007 (Class 381/412); filed in Germany 23 November 2000

The patent is a continuation of U.S. Patent No. 7,158,651 which described a kind of see-saw electromagnetic driver for a planar loudspeaker. In this variant, magnet **3** is embedded in an edge of planar diaphragm **1**. Flux generated by voice coil **4** flows through clamp-shaped armature **9**, causing



the magnet and the plate to vibrate. The patent argues that the push-pull arrangement causes the difference in forces to be proportional to the coil current.—GLA

7,292,423

43.38.Ja ACOUSTIC/UNDERWATER SIGNALING DEVICE

Andres Etchenique, Miami, Florida
6 November 2007 (Class 361/134); filed 6 June 2005

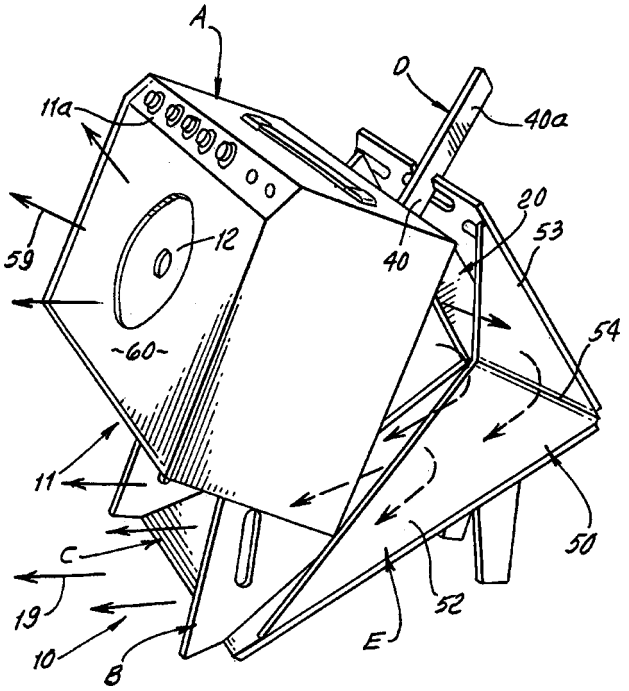
An underwater emergency siren is proposed. It is mechanical in nature and intended to be hand powered.—GFE

7,296,653

43.38.Ja SOUND CONTROL APPARATUS

Harold N. Smith, Jr. and Harold N. Smith III, both of Spring, Texas
20 November 2007 (Class 181/155); filed 7 January 2005

This patent describes a collapsible stand for an open-back musical instrument loudspeaker. When in use, sound from the rear is chaneled



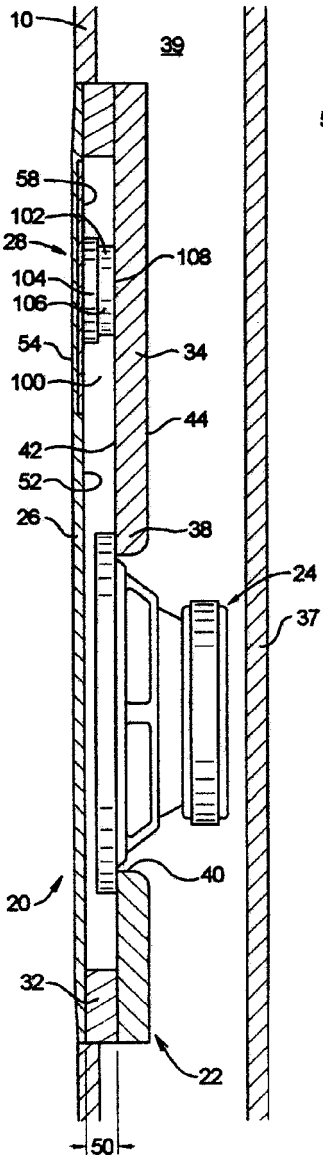
through a scoop-shaped reflector assembly, "…whereby control of ultimate sound effect is realized."—GLA

7,292,702

43.38.Ja IN-WALL SPEAKER SYSTEM METHOD AND APPARATUS

Paul N. Hagman, assignor to *Dimensional Communications, Incorporated*
6 November 2007 (Class 381/345); filed 28 April 2004

Radiating panel **26** has a high frequency area **58** that can be different in both thickness and laminations from low frequency "reciprocating" area **56**. Low frequency driver **26** is spaced a bit from panel **26** by frame **32**,



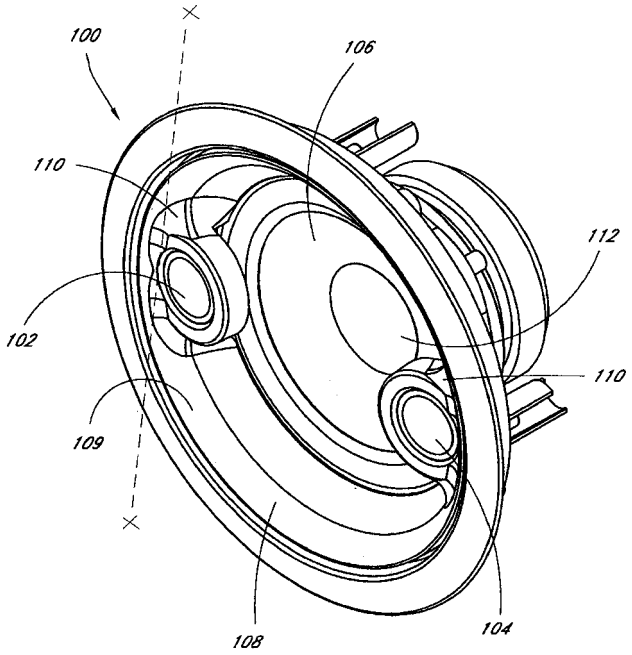
forming a chamber of sorts with back panel **34**, while high frequency drivers **102** are in contact with area **58**. Drivers **102** are NXT or similar drivers. A crossover network is also described.—NAS

7,302,061

43.38.Ja DUAL-TWEETER LOUDSPEAKER

Dean M. Rivera, assignor to *KSC Industries Incorporated*
27 November 2007 (Class 381/1); filed 12 December 2002

A non-coaxial two-way loudspeaker incorporates two tweeters **102**, **104** spaced as far apart as possible. When used as one speaker of a stereo



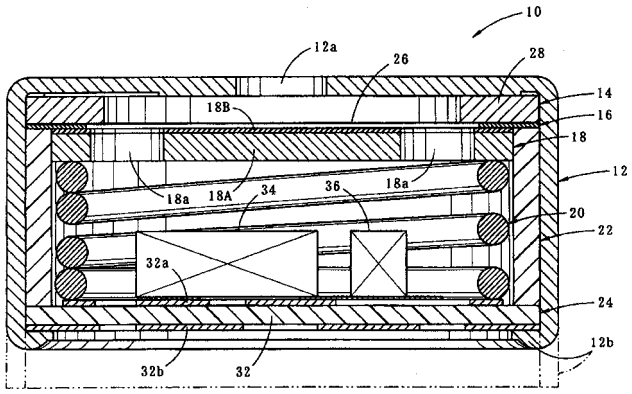
pair this geometry is said to provide improved imaging. Alternatively, the assembly can serve as a unitized stereo ceiling speaker in which the tweeters reproduce high frequencies from left and right channels, respectively. This is a continuation of earlier U.S. Design Patent No. 476,313.—GLA

7,287,327

43.38.Kb ELECTRET CAPACITOR MICROPHONE AND METHOD FOR PRODUCING THE SAME

Motoaki Ito and Kentaro Yonehara, assignors to *Star Micronics Company, Limited*
30 October 2007 (Class 29/886); filed in Japan 28 December 2001

Diaphragm material **26** is stretched under tension and bonded to ring **28** and assembled as shown into electret microphone assembly **10**. If the diaphragm tension is too high, the stiffness may be higher than desired and sensitivity suffers. The patent describes a process of first heating the ring/diaphragm, before assembly, for some time at certain temperatures (below



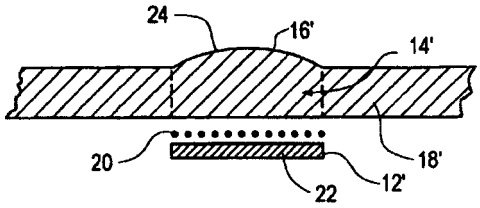
the melting point but above the second transition point of the thermoplastic material), sort of like annealing, and heated maybe more than once, to reduce the stiffness to a point where sensitivity is increased, but above the point where the diaphragm can "crinkle." This annealing-like process is widely used in the manufacture of tweeter diaphragms.—NAS

7,265,746

43.38.Rh ACOUSTIC WAVE TOUCH DETECTION CIRCUIT AND METHOD

Terence J. Knowles *et al.*, assignors to *Illinois Tool Works Incorporated*
4 September 2007 (Class 345/173); filed 4 June 2003

A touch sensor (switch) is claimed where raised portion **16** resonates at a vibrating frequency unique to its thickness **14** and mass. Transducer **12** may be an electromagnetic acoustic transducer (EMAT) comprising magnet



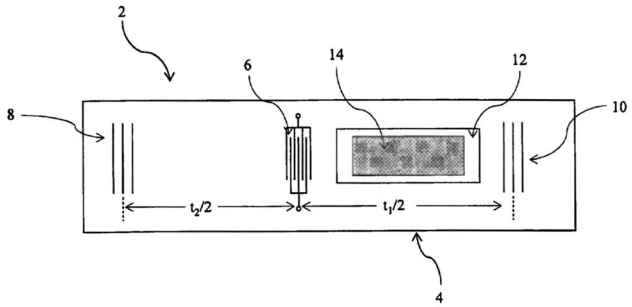
22 and winding **20**. A finger touching raised surface **24** will damp the resonant amplitude of the acoustic wave in resonator volume **14**, subsequently detected as evidence of the touch, and may be used for signal and command purposes.–AJC

7,268,662

43.38.Rh PASSIVE SAW-BASED HYDROGEN SENSOR AND SYSTEM

Jacqueline H. Hines and Leland P. Solie, assignors to *Applied Sensor Research & Development Corporation*
11 September 2007 (Class 338/34); filed 19 January 2006

A hydrogen gas concentration sensor **2** is claimed where palladium film **14** is arranged as a nano-cluster layer on siloxane monolayer **12**. Atmospheric hydrogen will absorb into palladium **14**, increasing its electrical conductivity which in turn slows down a surface acoustical wave (SAW) launched from fingers **12**. A SAW launched from **12** will be further delayed



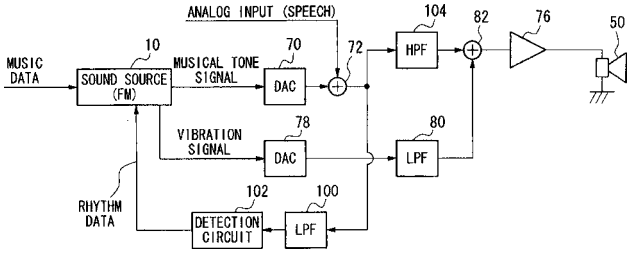
as it travels to and from reflector **10**, while a SAW from **6** to reflector **8** will not be further delayed. This sensor detects hydrogen in the atmosphere in concentrations from 25 ppm to 2% with a response time of a millisecond, is reversible and is operable at room temperatures.—AJC

7,301,094

43.38.Si DEVICE FOR DRIVING VIBRATION SOURCE

Masao Noro *et al.*, assignors to *Yamaha Corporation*
27 November 2007 (Class 84/645); filed in Japan 22 October 1999

Yamaha engineers have discovered a ghastly flaw in the evolution of the cellular telephone. Some current models can be set to notify the user of an incoming call using both sound (a custom ring melody) and vibration simultaneously. The problem is that the vibration and the music are not



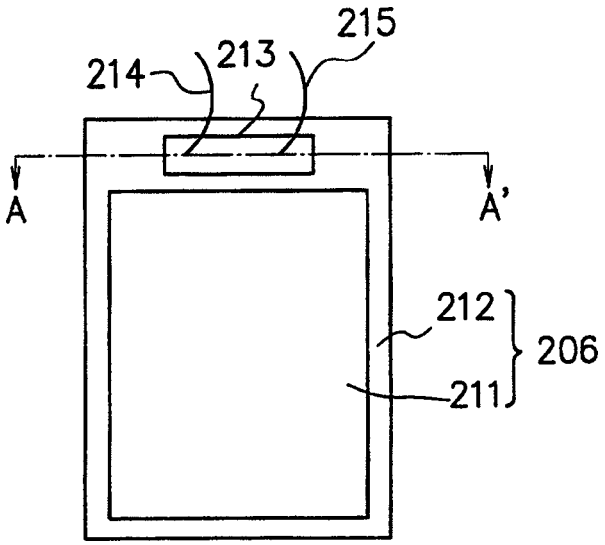
correlated, giving the user, "... a feeling of wrongness." How can this unacceptable oversight be corrected with minimal additional circuitry? The patent discloses a possible solution.—GLA

7,305,248

43.38.Si ELECTRONIC DEVICE

Ukyo Mori, assignor to *NEC Corporation*
4 December 2007 (Class 455/550.1); filed in Japan 28 November 2000

A transparent cover over the display panel of this cellular telephone also serves as a planar loudspeaker. This is hardly a new idea, and the patent



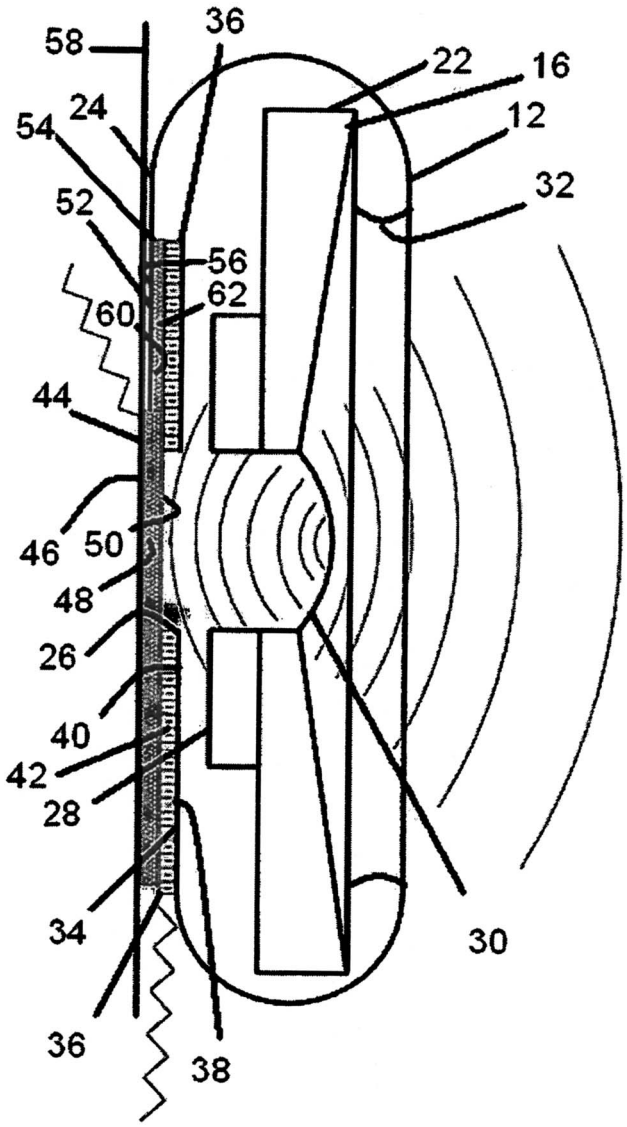
claims are restricted to a particular implementation involving a transparent section, a colored section, a planar voice coil, a resilient member, and two magnets.—GLA

7,308,108

43.38.Si HELMET-MOUNTED INTERCOMMUNICATIONS AND ENTERTAINMENT SYSTEM

William E. Davis, *Xenia*, **Ohio**
11 December 2007 (Class 381/376); filed 11 April 2005

Some motorcycle helmets include a microphone and headphone for two-way communication while riding. Instead of a conventional headphone, the inventor proposes enclosing a small loudspeaker in a padded fabric pouch that can be easily removed and reinstalled. This arrangement is said to optimize sonic performance, "…while eliminating the need for venting



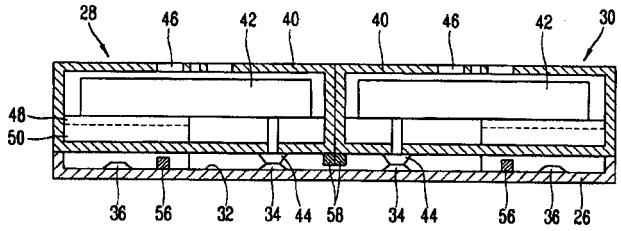
tubes or other cumbersome methods of properly porting a speaker for acoustic performance."—GLA

7,299,078

43.38.Vk MOBILE TERMINAL

Byung Jin Ahn, assignor to *LG Electronics Incorporated*
20 November 2007 (Class 455/575.4); filed 3 May 2004

Trying to reproduce surround sound from a cellular telephone may be a hopeless quest but inventors are nonetheless doing their best. In this example, left and right speakers are mounted on little extension sliders to



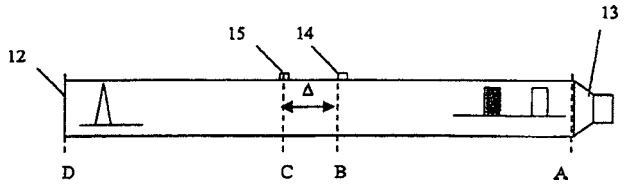
increase the distance between them. This is not a new idea, but apparently it has not previously been applied to cell phones.—GLA

7,266,992

43.40.Le REMOTE PIPELINE ACOUSTIC INSPECTION

Mohammad N Shamout *et al.*, assignors to *The Victoria University of Manchester*
11 September 2007 (Class 73/40.5A); filed in United Kingdom 30 November 2001

A pipe network inspection system is claimed where a sound pulse is introduced at **13-A** into one end of the pipe network while receiving transducers, **14**, **15**, etc., are inserted at various remote **B**–**C**, etc. locations along the pipe or pipe network. Received sound pulses and pulse echoes are analyzed by comparing them with a time-shifted reference pulse. Echo pulses



can arise from pipe transitions, by blockages by leaks and by pipe terminations **12-D**. The author claims a signal time shift and subtraction process to identify leaks and blockages.—AJC

7,289,391

43.40.Le NARROWBAND PHASE DIFFERENCE MEASUREMENT TECHNIQUE FOR SONAR APPLICATIONS

Byron W. Tietjen and Thaddeus J. Kurpiewski, assignors to *Lockheed Martin Corporation*
30 October 2007 (Class 367/125); filed 12 November 2004

In the this-will-never-work-in-real-life category, the authors plan to measure the phase difference between acoustic pulses at different frequencies in order to estimate the impedance (and thereby composition) of ocean bottom clutter.—GFE

7,296,654

43.40.Tm TUNABLE STACKED PLATE VIBRATION ISOLATOR

Morris S. Berman, assignor to *United States of America as Represented by the Secretary of the Army*
20 November 2007 (Class 181/207); filed 29 September 2004

This isolator, intended for the protection of electrical systems of projectiles and the like, consists of a stack of circular metal plates that are held together by a clamping arrangement. Damping results from friction between the plates and depends on their surface finish; the damping action may be adjusted by adjustment of the clamping force.—EEU

7,296,786

43.40.Tm COMPOSITE BUSHING HAVING DUAL DAMPING CAPABILITY

Erich Hees, assignor to *Honda Motor Company, Limited*
20 November 2007 (Class 267/293); filed 23 November 2004

This bushing in essence consists of an outer metal tube in the middle of which there is located a small metal tube, with a resilient connection between the two tubes. In a bushing according to this patent the resilient connection is provided by wedges of different resilient materials, so that the assembly has different stiffnesses in different radial directions.—EEU

7,299,698

43.40.Tm VIBRATION TEST MODULE HAVING CONTROLLABLE VIBRATION ATTRIBUTES

Gregg K. Hobbs, Westminster, Colorado
27 November 2007 (Class 73/649); filed 10 February 2005

The module to which this patent refers is a frame that is to be mounted on a shaker and that supports a test object. The support frame is provided with an array of spring-supported masses whose springs can be adjusted to change the natural frequencies of the spring-mass systems. Adjustment of the resonances of these systems permits one to shape the spectra of the vibrations to which the test article is exposed.—EEU

7,303,184

43.40.Tm ISOLATOR MOUNT FOR SHOCK AND VIBRATION MITIGATION

Bruce Bower and Gareth Knowles, both of Williamsport, Pennsylvania
4 December 2007 (Class 267/136); filed 12 September 2006

Equipment mounts, intended for shipboard use, consist of brackets made of a series of layers. In a typical mount the outer layers are relatively thick and of a material that can withstand repeated deflection. Sandwiched between these outer layers and bonded to these are thin layers capable of dissipating energy; these layers may consist of rare earth elements or alloys, ferromagnetic shape alloys, magnetic shape memory alloys, or super-elastic alloys.—EEU

7,306,082

43.40.Tm PASSIVE DAMPING OF VIBRATIONS IN A SUPPORT STRUCTURE

Ka Shing Kenny Kwan *et al.*, assignors to *ASM Technology Singapore PTE Limited*
11 December 2007 (Class 188/378); filed 8 April 2003

A component, such as one that supports devices that are rapidly repositioned in a microelectronics manufacturing machine, is subject to considerable accelerations. Damping of such components is desirable in order to suppress vibrations that may interfere with manufacturing accuracy. Damping of a device-supporting component is achieved according to this patent by introducing cylindrical cavities in the component and filling these at least partially with a composite material, such as butyl rubber loaded with carbon particles.—EEU

7,299,120

43.40.Vn METHOD FOR REDUCING JUDDERING VIBRATIONS

Boris Serebrennikov, assignor to *LuK Lamellen und Kupplungsbau Beteiligungs KG*
20 November 2007 (Class 701/67); filed in Germany 12 September 2002

This patent pertains to vibrations in the drive train of motor vehicles. As stated in the patent document, "juddering vibrations are…in particular vibrations of the transmission input against the vehicle." The system described here detects such vibrations and automatically adjusts an electronic clutch to suppress these.—EEU

7,299,141

43.40.Vn SYSTEM AND METHOD FOR CONTROLLING VIBRATION

Raymond Chin, assignor to *Hewlett-Packard Development Company, L.P.*
20 November 2007 (Class 702/56); filed 5 December 2002

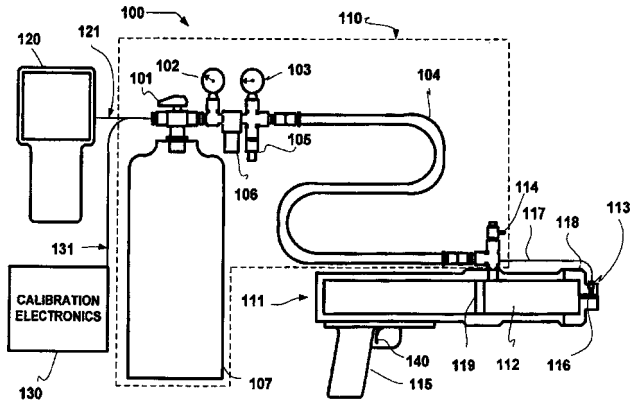
The vibrations of a drive cage that houses a number of data transfer devices are monitored and compared to a known standard. If the standard is exceeded, the data transfer rate of one or more of these devices is reduced and/or some of the devices are turned off in order to reduce the vibrations produced by these devices.—EEU

7,266,986

43.40.Yq PORTABLE SYSTEM FOR MEASURING DYNAMIC PRESSURE IN SITU AND METHOD OF EMPLOYMENT THEREFOR

Fred D. Shirley *et al.*, assignors to *The United States of America as represented by the Secretary of the Army*
11 September 2007 (Class 73/1.57); filed 18 November 2004

A backpack portable blast sensor dynamic calibrator is claimed where a controlled volume of pressurized gas is delivered to the input port of that sensor. Gases such as helium (fastest rise time), nitrogen or air are used. Pressure gauge **102** shows supply tank pressure and gauge **103** shows applied pressure, typically under 150 psi. The operator presses nozzle **116** to



the blast sensor input port, then pulls trigger **140** to release the gas charge **112** by moving **119** rearward to remove a poppet valve plunger (not shown) from blocking gas flow into nozzle **116**. Reference transducer **113** sends a pressure signal **117**–**121** for display and for archiving via **131** to microprocessor **130**.—AJC

7,308,368

43.40.Yq METHOD AND APPARATUS FOR VIBRATION DETECTION, METHOD AND APPARATUS FOR VIBRATION ANALYSIS, LITHOGRAPHIC APPARATUS, DEVICE MANUFACTURING METHOD, AND COMPUTER PROGRAM

Haico Victor Kok *et al.*, assignors to *ASML Netherlands B.V.*
11 December 2007 (Class 702/56); filed 15 September 2004

A lithographic apparatus is a machine that applies a desired pattern onto a target portion of a substrate. The pattern typically is provided by

radiation that passes through a patterning structure or by a beam that is made to scan along the substrate. Vibrations that may disturb the image produced by such a process are detected by projecting a test image onto the substrate and measuring its temporal intensity variations.—EEU

7,294,218

43.50.Fe COMPOSITE MATERIAL WITH IMPROVED STRUCTURAL, ACOUSTIC AND THERMAL PROPERTIES

Enamul Haque *et al.*, assignors to *Owens Corning Intellectual Capital, LLC*
13 November 2007 (Class 156/148); filed 18 November 2004

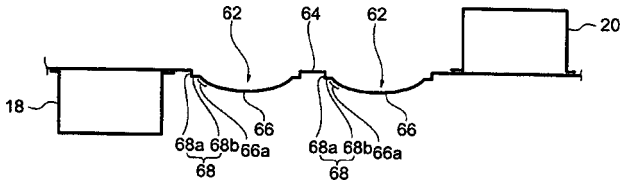
A method to produce multilayer acoustic and thermal insulation is put forth.—GFE

7,270,366

43.50.Gf AUTOMOTIVE FLOOR PANEL STRUCTURE

Takanobu Kamura *et al.*, assignors to *Mazda Motor Corporation*
18 September 2007 (Class 296/193.07); filed in Japan 11 November 2003

Reduction of noise emitted by vehicle floor panel **62**–**68** is claimed. Offending sound results from vibrations transferred from the car body **18**–**20** to floor panel **62**–**68**. Vibration arising from a 160 Hz suspension resonance and a 250 Hz tire cavity resonance that transmit to the floor panel can cause those panels to radiate sound into the vehicle cabin. Such sound radiation is reduced by forming the panel surface into at least two adjacent



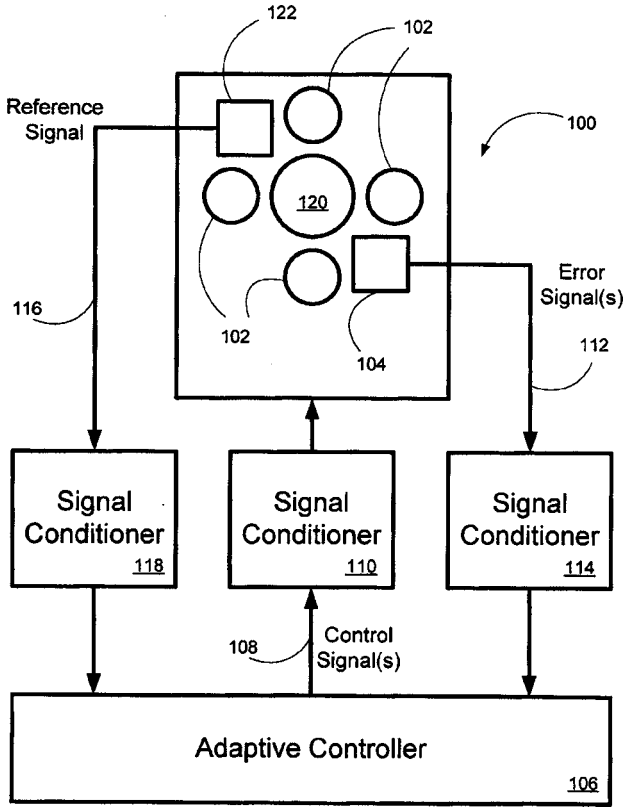
segments **62**, having predetermined stiffnesses. Bends of convex shape **62** and circular platform **66**, **68**-**a**-**b** stiffen both panel segments so as to not have a 1×1 resonance around 160 Hz, while also having a 1×2 resonance at 250 Hz. The 1×1 panel mode acts as a non-resonant stiff mass at 160 Hz, while the 1×2 panel mode has plus and minus phases which will cancel the sound radiated to a remote distance from that panel.—AJC

7,272,234

43.50.Ki MULTI-CHANNEL ACTIVE CONTROL SYSTEM AND METHOD FOR THE REDUCTION OF TONAL NOISE FROM AN AXIAL FAN

Scott D. Sommerfeldt and Kent L. Gee, assignors to *Brigham Young University*
18 September 2007 (Class 381/71.11); filed 4 April 2003

Reduction of tonal noise emission from small fans, etc. is claimed where error microphone **104** is placed in the near field of sound from noise source **120**. Loudspeakers **102** are placed as close as possible to, and in the near field of, source **120**. A blade passage sensor **122** provides a synchronizing signal for feed-forward control. Signal conditioning **106**–**118** provides separate and phased drives for each speaker **102** to implement noise



cancellation. Noise reduction of 19 dBA is reported for a fan fundamental of 370 Hz plus harmonics up to 1480 Hz.—AJC

7,296,977

43.55.Ti DAMPING MATERIAL, DAMPING ARRANGEMENT AND METHOD FOR DESIGNING A DAMPING ARRANGEMENT

Laurent Bonnet, assignor to *General Electric Company*
20 November 2007 (Class 416/230); filed in the European Patent Office 17 November 2004

This laminate for damping vibrations is comprised of a soft viscoelastic layer (elastomer based) and a stiff constrained layer (steel or aluminum, for example). It is attached in stripes oriented in an orthogonal grid to a vibrating element like a wind turbine.—CJR

7,297,407

43.55.Ti GLASS LAMINATES FOR REDUCTION OF SOUND TRANSMISSION

Jerrel C. Anderson, assignor to *E. I. du Pont de Nemours and Company*
20 November 2007 (Class 428/441); filed 19 September 2005

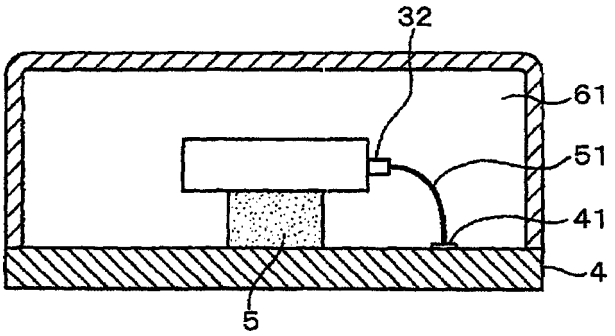
This patent describes a sound damping laminate that has at least three separate polymer layers. The laminate provides improved sound damping and transmission loss performance in glazing to be used in buildings or vehicles.—CJR

7,304,413

43.58.Hp PIEZOOSCILLATOR

Kenji Kasahara, assignor to *Nihon Dempa Kogyo Company, Limited*
4 December 2007 (Class 310/326); filed in Japan 10 August 2005

Referring to the figure, the author describes the temperature controlled crystal oscillator that he devised, which is isolated inside a case that can be temperature controlled. In addition, the crystal is mounted on a "buffer material" such as silicone gel or "…rubber, sponge, fiber, form material,



spring or the like can be used other than the previously-described gel." OK, so this person has just described and patented 50-year-old technology that is present in every watch and digital trinket made since then. The existence of this patent is a perfect example of how broken the patent review system is.—JAH

7,299,678

43.58.Wc SENSOR APPARATUS

Eric Atherton, assignor to *Baker Hughes Incorporated*
27 November 2007 (Class 73/24.06); filed in United Kingdom 27 March 2000

This patent discloses the use of tuning forks and other vibrational resonators as frequency-domain transducers for physical properties of the environment, such as temperature, pressure, and magnetic field. The advantage of doing this, it is claimed, is that many transducers can be chained on a single-conductor cable and operated at different frequencies. The electronics can all be situated at the interrogating end of the single-conductor cable, and thereby the sensors can be allowed to operate at temperatures well above the limit for active electronics. Although the author is primarily describing applications of this type of sensor in a borehole deep underground, it appears that it would also be useful in undersea monitoring operations. There are no specifics given of the sensor construction (both vibrating wires and tuning forks are mentioned), so little can be said about the validity of the chaining concept except that it requires either low-impedance sensors in series or high-impedance sensors in parallel.—JAH

7,289,796

43.60.Dh MOBILE COMMUNICATIONS TERMINAL DEVICE AND METHOD FOR IDENTIFYING INCOMING CALL FOR USE WITH THE SAME

Kazuhiro Kudoh, assignor to *NEC Corporation*
30 October 2007 (Class 455/415); filed in Japan 6 July 2000

Somehow, the idea of customized ringtones was claimed again.—GFE

7,289,390

43.60.Fg ULTRASONIC TRANSMITTING/RECEIVING APPARATUS AND SCANNING SONAR EMPLOYING SAME

Yasushi Nishimori *et al.*, assignors to *Furuno Electric Company, Limited*
30 October 2007 (Class 367/103); filed 19 July 2004

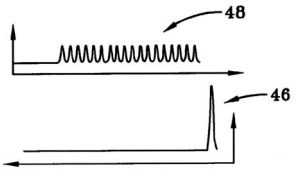
The well-known concept of multi-beam sonar at different frequencies is put forth again. Maybe that's what "employing same" means?—GFE

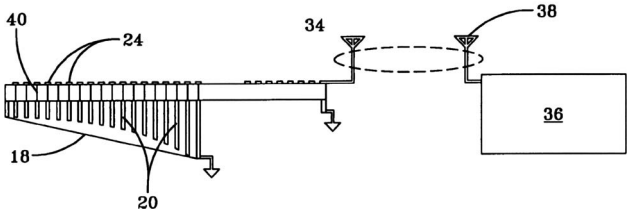
7,263,892

43.60.Qv PASSIVE TIRE PRESSURE SENSOR AND METHOD

Kent Bryant Pfeifer *et al.*, assignors to *The Goodyear Tire & Rubber Company*
4 September 2007 (Class 73/715); filed 23 January 2006

A transponding tire pressure gauge **34** is claimed. Sensor **18**–**34** receives a rf interrogation pulse **48** via antenna **34** whose energy is converted to a surface acoustic wave (SAW) in its substrate. This wave travels the length of that substrate and is reflected by any reflector **24** that is shorted by any contact **20** to cover **18**. The reflected SAW returns to the antenna with





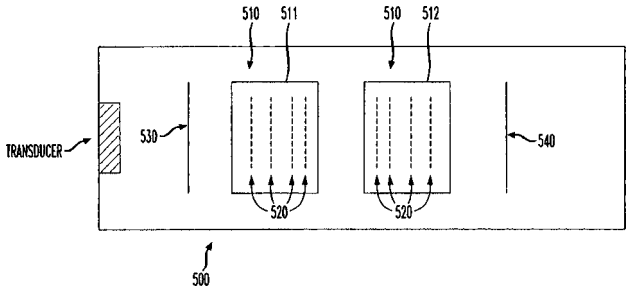
modulation **44**. Tire air pressure will depress cover **18** over a sealed cavity, to progressively touch contacts **20**. Delay time from the interrogation pulse to the reflected pulse **44** is progressively shortened by increased tire air pressures. Interrogation transceiver **38**–**36** and its processor convert this pulse time delay into a tire pressure alert signal to the driver.—AJC

7,264,149

43.60.Qv SAW IDENTIFICATION TAG DISCRIMINATION METHODS

Clinton S. Hartmann, Dallas, and John C. Bellamy, Coppell, both of Texas
4 September 2007 (Class 235/375); filed 15 September 2004

An error correcting radio frequency identification (RFID) tag is claimed for use in environments already rich in 2.8 GHz industrial, scientific and medical (ISM) signals, such as near a local area network (LAN) and microwave ovens. Surface acoustic wave (SAW) substrate **510** includes a transducer section, a start pulse reflector **530**, identical data encoder sections **511** and **512**, and a final reflector **540**. The subsequent pulse train received by an external interrogator (not shown) will contain two identical payload



pulse trains with an intervening pause. Improved discrimination is achieved for the desired RFID signal when in an environment rich in ISM radiation.—AJC

7,265,662

43.60.Qv APPARATUS AND METHOD FOR INSPECTING CONTAINERS

Paul Belanger, assignor to *Praxair Technology, Incorporated*
4 September 2007 (Class 340/521); filed 17 March 2005

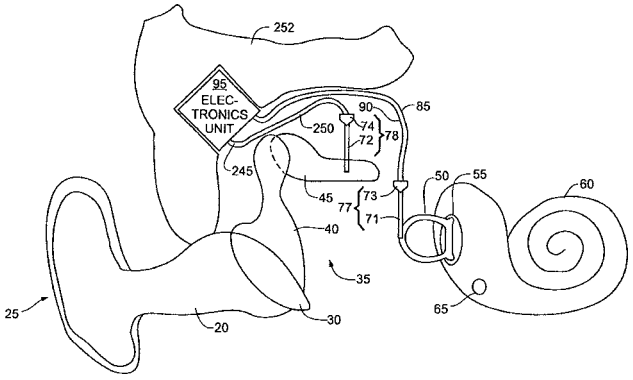
A system for inspecting empty pressurized gas storage cylinders prior to refilling is claimed using optical (video camera), sound and odor sensors. A microphone in the vicinity of the cylinder receives sound resulting from an impact by the operator or automatic impact device. The subsequent ring sound frequencies and other parameters are processed via a fast Fourier transform (FFT) or wavelet. These results are compared with database values to determine whether that cylinder is acceptable for refill.—AJC

7,297,101

43.66.Ts METHOD AND APPARATUS FOR MINIMALLY INVASIVE PLACEMENT OF SENSING AND DRIVER ASSEMBLIES TO IMPROVE HEARING LOSS

Johann J. Neisz *et al.*, assignors to *Envoy Medical Corporation*
20 November 2007 (Class 600/25); filed 17 January 2006

An implantable hearing system is mounted in the middle ear without performing mastoid surgery. By cutting a portion of the tympanic membrane, a trans-canal approach is used to mount the sensing/driver assembly



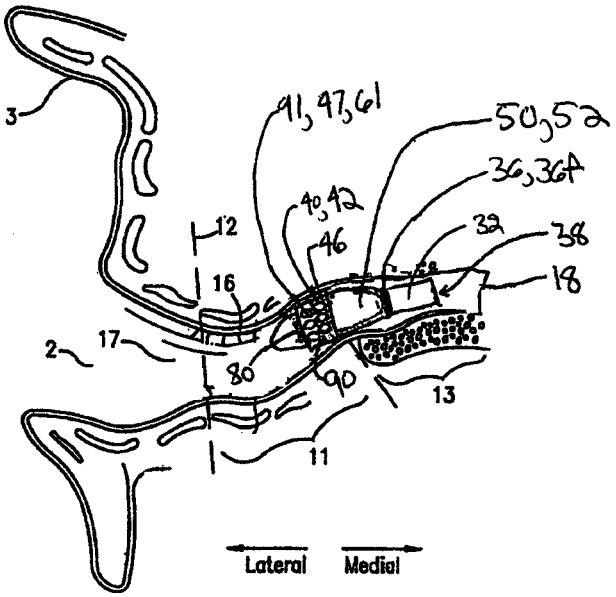
and secure it to a bone within the middle ear space. Leads from the electronics are coupled to the sensing/driver assembly through the skin near the ear canal.—DAP

7,298,857

43.66.Ts EXTENDED WEAR CANAL DEVICE WITH COMMON MICROPHONE-BATTERY AIR CAVITY

Adnan Shennib *et al.*, assignors to *Insound Medical, Incorporated*
20 November 2007 (Class 381/324); filed 7 February 2005

A deeply-fitting hearing device consists of a receiver assembly designed for location in the bony portion of the ear canal, a battery assembly hooked to the receiver assembly, and a microphone assembly that is attached to the battery assembly and oriented to prevent ingress of ear canal debris.



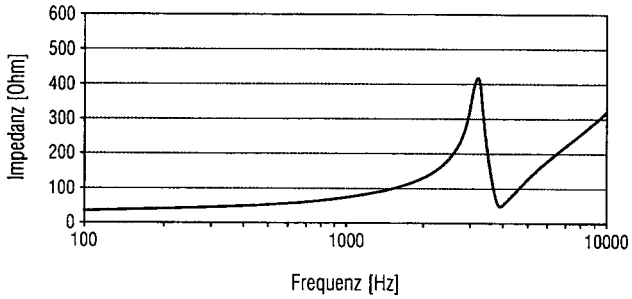
The microphone and battery assemblies are coupled to an air cavity, which may provide an air reservoir. A sealing retainer around the microphone or receiver assemblies helps to prevent acoustic feedback.—DAP

7,302,069

43.66.Ts HEARING AID AND METHOD FOR ADJUSTING A HEARING AID

Torsten Niederdränk and Christian Weistenhöfer, assignors to *Siemens Audiologische Technik GmbH*
27 November 2007 (Class 381/312); filed in Germany 18 September 2003

The acoustic impedance of a hearing aid wearer's ear canal is determined by measuring the electrical input impedance of the hearing aid receiver. The mechanical resonance frequency of the receiver is determined



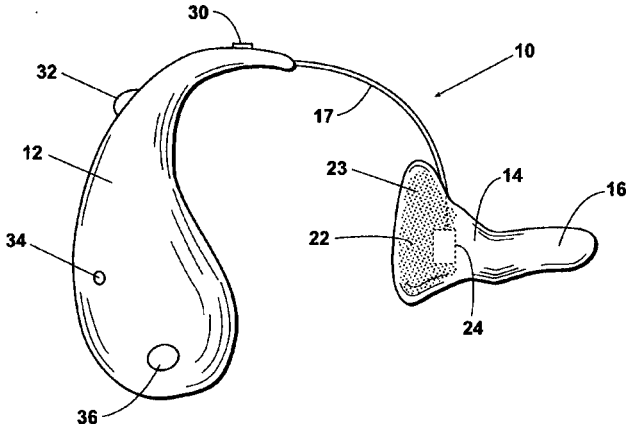
from the electrical input impedance versus frequency and is shifted to adjust the hearing aid frequency response in the wearer's ear.—DAP

7,302,071

43.66.Ts BONE CONDUCTION HEARING ASSISTANCE DEVICE

Daniel R. Schumaier, Elizabethton, Tennessee
27 November 2007 (Class 381/326); filed 15 September 2004

A two-part device has a bone vibrator packaged in an in-the-ear module. Vibrations are transferred from the portion of the in-the-ear module



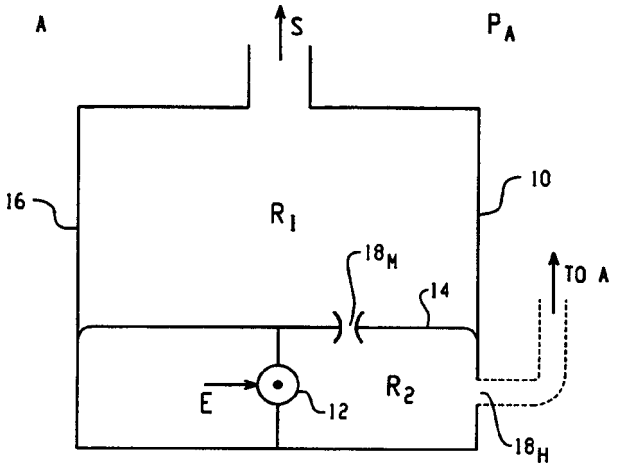
inserted into the ear canal to the cochlea via the adjacent mastoid bone. A behind-the-ear module houses the microphone, battery and electronics.—DAP

7,305,098

43.66.Ts HEARING DEVICE

Andi Vonlanthen and Hilmar Meier, assignors to *Phonak AG*
4 December 2007 (Class 381/312); filed 24 May 2002

The output transducer of a hearing device communicates with ambient air for pressure equalization. A membrane separates two spaces, each having



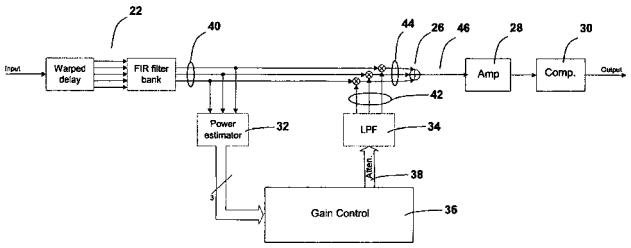
a passage with a low pass characteristic that blocks audible signals and passes lower frequency signals.—DAP

7,305,100

43.66.Ts DYNAMIC COMPRESSION IN A HEARING AID

Brian Dam Pedersen, assignor to *GN ReSound A/S*
4 December 2007 (Class 381/320); filed in Denmark 14 February 2003

Very basic and general methodology is outlined for a low power consumption multichannel digital compressor in a hearing aid. Linear phase



filters are utilized to obtain a low time delay for signals processed by the compressor.—DAP

7,308,107

43.66.Ts METHOD FOR ACTIVATING A HEARING DEVICE

Stefan Daniel Menzl and Ivo Hasler, assignors to *Phonak AG*
11 December 2007 (Class 381/312); filed 6 April 2004

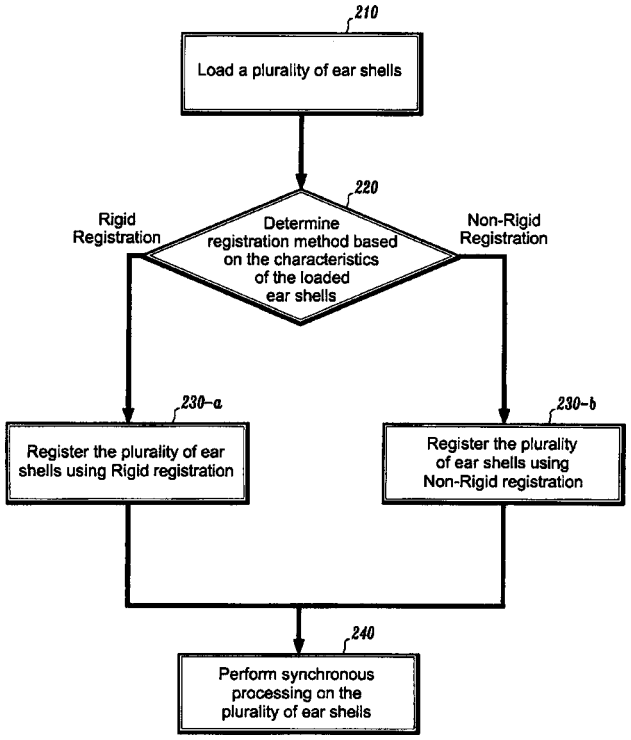
The occurrence of acoustic feedback oscillation is determined to confirm that the hearing device is working. Thereafter, the device is put into a reduced gain mode to prevent acoustic feedback oscillation occurrence while the device is placed on or into the wearer's ear. Mode switching may be manual or automatic via timeouts which may utilize changes in the feedback transfer function.—DAP

7,308,328

43.66.Ts SYNCHRONIZED PROCESSING OF EAR SHELLS FOR HEARING AIDS

Tong Fang *et al.*, assignors to *Siemens Medical Solutions USA, Incorporated*
11 December 2007 (Class 700/98); filed 11 May 2004

To speed up a first processing operation in the rapid prototyping manufacture of two shells in a custom binaural hearing aid, fitting for the two ears is synchronized if the shapes of the first and second ear shells are within a



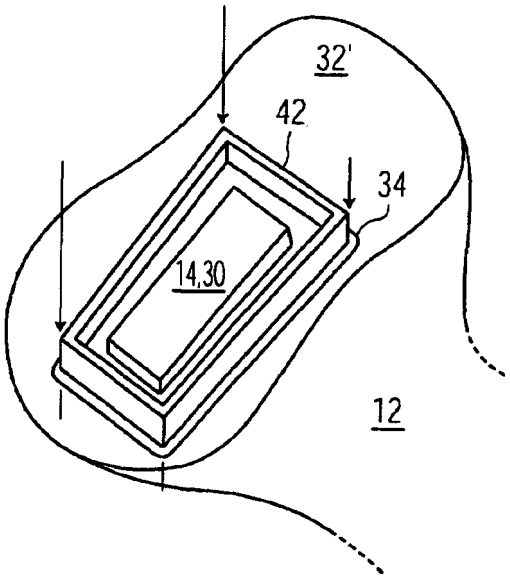
predetermined threshold. The images of the resulting ear shells are sent to a display device after the first processing operation.—DAP

7,305,101

43.66.Ts INSTRUMENT WITH AN INTERFACE FRAME AND A PROCESS FOR PRODUCTION THEREOF

George Doudoukjian, assignor to *Siemens Hearing Instruments, Incorporated*
4 December 2007 (Class 381/322); filed 15 January 2003

A modular approach for a custom hearing aid manufactured by rapid prototyping includes a faceplate integrated with the shell. The faceplate has a rectangular opening for a pivoting battery drawer cover and an electronic



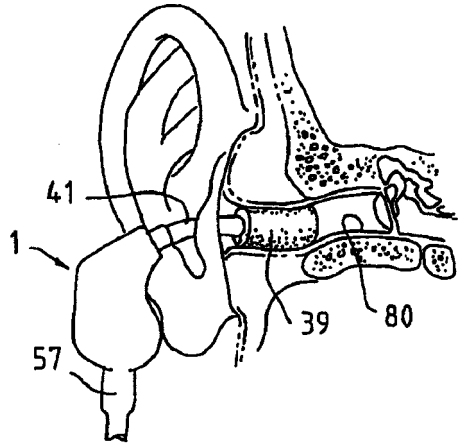
assembly that mounts precisely and securely onto an interior frame which has several rails.—DAP

7,298,858

43.66.Yw INSERT EARPHONE ASSEMBLY FOR AUDIOMETRIC TESTING AND METHOD FOR MAKING SAME

Donald L. Wilson and Steven J. Iseberg, assignors to *Etymotic Research, Incorporated*
20 November 2007 (Class 381/328); filed 23 September 2005

A sealed acoustic path is produced into an ear canal by the combination of a receiver attached to a tube nipple that is fastened to a flexible ear



tip. When an audio signal source drives the receiver, the output of the assembly at 6 kHz and/or 8 kHz is approximately the same as that of a TDH-39 headphone.—DAP

7,302,640

43.70.Fq LANGUAGE INPUT ARCHITECTURE FOR CONVERTING ONE TEXT FORM TO ANOTHER TEXT FORM WITH TOLERANCE TO SPELLING, TYPOGRAPHICAL, AND CONVERSION ERRORS

Kai-Fu Lee *et al.*, assignors to *Microsoft Corporation*
27 November 2007 (Class 715/533); filed 21 October 2004

This patent relates to acoustics if you think about the sounds of letters while you type. It turns out that if you're typing in Chinese, you have little choice. One of the two standard written languages has thousands of characters and although it has been done, it is rather impractical to build keyboards to type using those characters. This patent describes a system which lets you type those phonetic sounds and then makes a valiant effort to convert the phonetics into the desired Chinese words. There is extensive error correction built in, both at the phonetics level and at the final word level, along with a learning module that gets to know the kinds of errors that you most frequently make while typing.—DLR

7,299,172

43.72.Gy SYSTEMS AND METHODS FOR SOUND COMPRESSION

Jerome D. Wong, assignor to *J.W. Associates*
20 November 2007 (Class 704/212); filed 7 October 2004

To increase encoding resolution without increasing the number of encoding bits, an adaptive differential pulse code modulation (ADPCM) encoding scheme is skewed with an asymmetry based on the predicted sign of the ADPCM delta value and the predicted frequency of the audio signal.—DAP

7,302,393

43.72.Ne SENSOR BASED APPROACH RECOGNIZER SELECTION, ADAPTATION AND COMBINATION

Volker Fischer and Siegfried Kunzmann, assignors to *International Business Machines Corporation*
27 November 2007 (Class 704/254); filed in the European Patent Office 20 December 2002

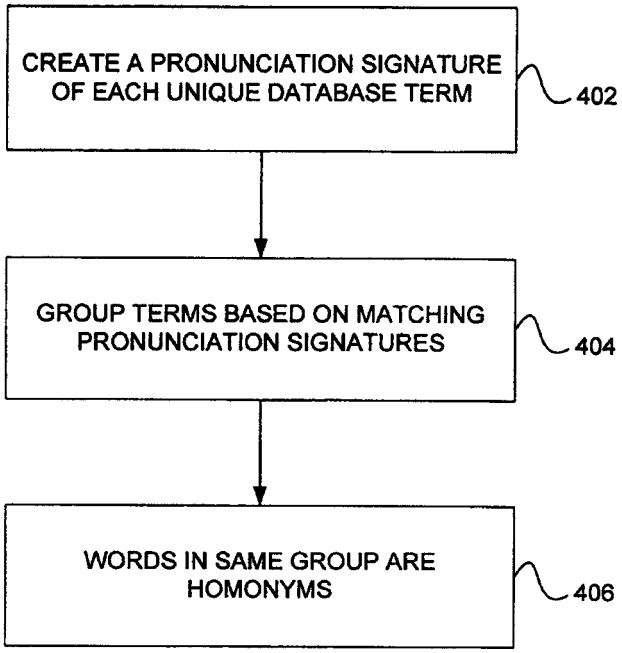
To improve recognition accuracy in noisy environments, the best one or best combination of available speech recognizers are selected from those available. The selection is based on the evaluation of collected data by a program-controlled arbiter that includes a decision engine, software and physical sensor like a microphone, camera or noise generating device.—DAP

7,299,181

43.72.Ne HOMONYM PROCESSING IN THE CONTEXT OF VOICE-ACTIVATED COMMAND SYSTEMS

Yun-Cheng Ju *et al.*, assignors to *Microsoft Corporation*
20 November 2007 (Class 704/257); filed 30 June 2004

Methodology is suggested to handle terms that are pronounced the same but are spelled differently for voice dialing or voice message applications. Terms within a database that are pronounced the same but spelled



differently are identified with a speech recognition or application dictionary and placed into distinct pronunciation classes. A grammar is constructed of a single spelling of a name to represent a set of terms having homonym characteristics.—DAP

7,297,115

43.80.Vj IMMERSIBLE ULTRASOUND PROBE AND CABLE

Kenneth N. Bates *et al.*, assignors to *Black Toe Medical III, Incorporated*
20 November 2007 (Class 600/437); filed 26 November 2003

This ultrasound probe and cable include connector housings that are sealed to prevent the entry of moisture and that allow the probe and cable to be sterilized.—RCW

7,297,117

43.80.Vj METHOD FOR OPTIMIZATION OF TRANSMIT AND RECEIVE ULTRASOUND PULSES, PARTICULARLY FOR ULTRASONIC IMAGING

Andrea Trucco and Simone Curletto, assignors to *Esaote, S.p.A.*
20 November 2007 (Class 600/443); filed in Italy 22 May 2003

The difference between an ideal beam pattern and an actual beam pattern is used to define an energy function. The energy function is minimized by adjusting beam parameters. The parameters that correspond to the minimum are used to determine pulses for excitation of elements in a transducer array.—RCW

7,297,118

43.80.Vj ULTRASOUND METHOD AND APPARATUS FOR MULTI-LINE ACQUISITION

Kjell Kristoffersen, assignor to *GE Medical Systems Global Technology Company*
20 November 2007 (Class 600/447); filed 21 November 2003

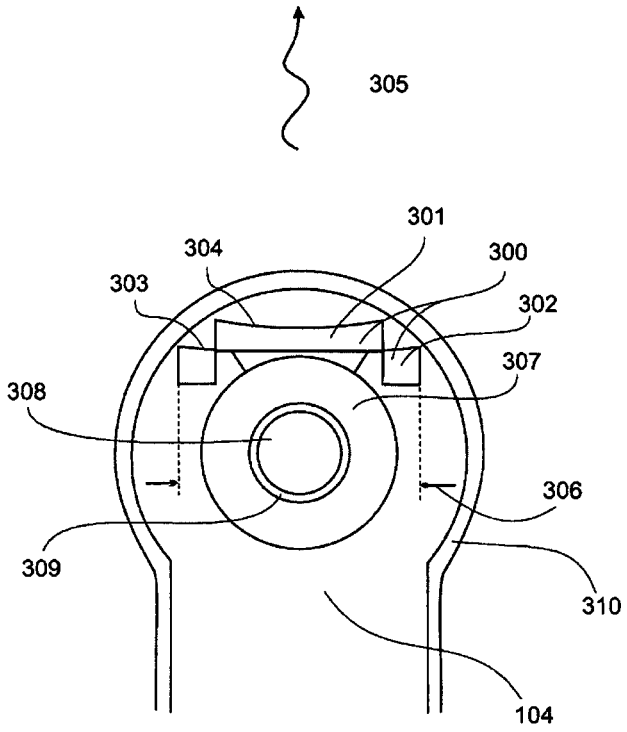
Echo signals are acquired and decimated by alternately removing at least two consecutive samples in a sample sequence and passing at least two consecutive samples in the sequence to reduce the bandwidth of the signals by one-half to three-quarters of the original bandwidth.—RCW

7,300,403

43.80.Vj WIDE APERTURE ARRAY DESIGN WITH CONSTRAINED OUTER PROBE DIMENSION

Bjørn A. J. Angelsen, Trondheim, Norway *et al.*
27 November 2007 (Class 600/447); filed 20 July 2004

The radiating surface of an array is divided into regions and the outer regions are physically displaced inward from the radiating surface that is



more central in the array to form a larger aperture than would otherwise be possible given the constraints of the probe outer dimensions.—RCW

7,302,850

43.80.Vj ULTRASONIC DIAGNOSTIC APPARATUS AND IMAGE PROCESSING APPARATUS

Naohisa Kamiyama, assignor to *Kabushiki Kaisha Toshiba*
4 December 2007 (Class 73/606); filed in Japan 28 April 2003

This apparatus switches between high acoustic pressure and low acoustic pressure transmissions. Echos from the low pressure transmissions are used to form real-time images. A still image obtained before switching to high pressure transmissions is displayed during the interval of the high pressure transmissions. With this operational sequence, an injected contrast agent is imaged using the low pressure transmissions and destroyed by the high pressure transmissions so re-entry of the contrast into the imaged region can be visualized.—RCW

7,303,530

43.80.Vj TRANSDUCER ARRAYS WITH AN INTEGRATED SENSOR AND METHODS OF USE

Stephen R. Barnes and Mirsaid Bolorforosh, assignors to *Siemens Medical Solutions USA, Incorporate***d**

4 December 2007 (Class 600/459); filed 22 May 2003

Sensors such as those for temperature, pressure, or audio are integrated with an array of ultrasound transducer elements to image and to monitor patient characteristics simultaneously.—RCW

7,306,561

43.80.Vj SYSTEMS AND METHODS FOR AUTOMATIC TIME-GAIN COMPENSATION !N AN ULTRASOUND IMAGING SYSTEM

Shashidhar Sathyanarayana, assignor to *Scimed Life Systems, Incorporated*

11 December 2007 (Class 600/443); filed 2 September 2004

A number of time-gain compensation functions are obtained, each from a separate set of echo signals, and the compensation functions are applied automatically without user intervention.—RCW

LETTERS TO THE EDITOR

This Letters section is for publishing (a) brief acoustical research or applied acoustical reports, (b) comments on articles or letters previously published in this Journal, and (c) a reply by the article author to criticism by the Letter author in (b). Extensive reports should be submitted as articles, not in a letter series. Letters are peer-reviewed on the same basis as articles, but usually require less review time before acceptance. Letters cannot exceed four printed pages (approximately 3000–4000 words) including figures, tables, references, and a required abstract of about 100 words.

Influence of vehicle color on loudness judgments (L)

Daniel Menzel[a] and Hugo Fastl
Arbeitsgruppe Technische Akustik, MMK, Technische Universität München, München, Germany

Ralf Graf and Jürgen Hellbrück
Arbeits-, Umwelt- und Gesundheitspsychologie, Katholische Universität Eichstätt-Ingolstadt, Eichstätt, Germany

(Received 18 October 2007; revised 7 February 2008; accepted 11 February 2008)

This experiment investigates the effect of images of differently colored sports cars on the loudness of a simultaneously perceived car sound. Still images of a sports car, colored in red, light green, blue, and dark green, were displayed to subjects during a magnitude estimation task. The sound of an accelerating sports car was used as a stimulus. Statistical analysis suggests that the color of the visual stimulus may have a small influence on loudness judgments. The observed loudness differences are generally equivalent to a change in sound level of about 1 dB, with maximum individual differences of up to 3 dB. © *2008 Acoustical Society of America.*
[DOI: 10.1121/1.2890747]

PACS number(s): 43.66.Lj, 43.66.Cb [BCM] Pages: 2477–2479

I. INTRODUCTION

Loudness plays an important role in sound-quality engineering and sound design. While loudness perception depends primarily on physical properties of the sound field, loudness judgments may also be influenced by nonacoustical factors (Blauert and Jekosch, 1997). For example, Namba *et al.* (1997) examined interior vehicle sounds and found that subjects tended to avoid extreme categorical ratings of loudness when a video of the scenery surrounding the driving car was presented. Thus loud sounds were rated softer, while soft sounds were rated louder. Dynamic visual information was also found to affect semantic differential ratings in a study reported by Suzuki *et al.* (2000). Different environmental sounds had to be rated with and without corresponding video sequences. The "volume" factor, which included adjectives such as powerful, loud, and noisy, had smaller loadings when there was additional visual stimulation. The influence of apparent size on the loudness of trucks was studied by Höger and Greifenstein (1988). In an eleven-point categorical scaling task, the sound accompanied by the video sequence of a small truck frequently was judged as being softer than the same sound combined with the video of a big truck.

Patsouras *et al.* (2002) and Rader *et al.* (2004) reported that the color of passenger trains may influence magnitude estimates of loudness. Still images which were electronically edited to show a bright red train caused subjects to give higher ratings when asked for the loudness of the sound of a passing train, while light-green trains elicited lower loudness judgments compared to purely auditory presentation. A summary of these and other studies concerning influences of visual stimulation on loudness estimation is given in Fastl (2004).

These phenomena of audio-visual interactions may also be of interest in the field of automotive design, especially regarding the typical bright red color of premium sports cars. It is expected that red cars cause an overestimation of loudness compared to cars of other colors.

II. EXPERIMENT

A. Stimuli

The picture of a British sports car (Aston Martin V8) was chosen as visual stimulus. Its dark-green (DG) color was digitally modified, so that in addition to the original color the images of a red (R), blue (B), and light-green (G) vehicle were available for the experiment (see Fig. 1). The images were shown on a 19 in. CRT computer monitor, with a viewing distance of 0.7 m. The monitor was positioned outside a soundproof booth and was visible through a window. The subjects were seated inside the booth and were instructed to keep their eyes focused on the image throughout the experiment.

The sound of an accelerating sports car with a duration of 4 s was used as auditory stimulus. It was presented diotically through calibrated electrodynamic headphones (Beyer

[a]Electronic mail: menzel@tum.de

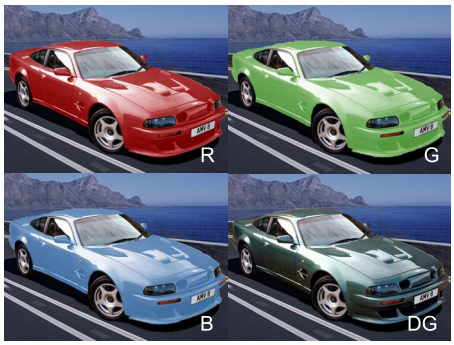


FIG. 1. (Color online) The four images used as visual stimuli. The original color of the car, a dark green, is depicted on the lower right-hand side.

DT 48), using a free field equalizer as described by Fastl and Zwicker (2007). To minimize memory effects during loudness judgments four different sound levels were chosen [L_{AFmax}=90,86,82, and 78 dB(A)].

B. Listeners

Sixteen subjects (four female, twelve male), aged 22 to 62 years (median 26 years), participated in the experiment. All had normal hearing, as verified by pure-tone audiometric measurements.

C. Procedure

Each subject participated in two sessions. Written instructions (in German) were given which informed the subjects that they were about to rate the perceived loudness of sounds accompanying the images of sports cars. They were told to do so by giving arbitrary positive numbers that correspond to perceived loudness ratios. In each session, all possible combinations of auditory and visual stimuli were presented four times in random order. At the beginning, a short training sequence was inserted consisting of four randomly chosen stimulus combinations. The subjects then judged the loudness of the sounds via free magnitude estimation, entering their answers on a computer keyboard. This resulted in 64 loudness ratings per subject per session.

D. Results

The data for each subject were normalized relative to the median of the ratings given for the dark-green image at 90 dB(A). The median rating of each stimulus combination across the four repetitions was then calculated and used in the following analysis.

Figure 2 shows a summary of the results. The median and interquartile ranges of each stimulus pair over all subjects are depicted. Regarding the median values, it seems that in most cases the sounds associated with images of red or dark-green vehicles were rated louder than those combined with light-green or blue ones.

To test the significance of these findings, a three-way repeated measures analysis of variance with session (1 and 2), level [90, 86, 82, and 78 dB(A)], and color (R, G, B, and DG) as within-subject factors was performed, which showed a significant interaction between session and color

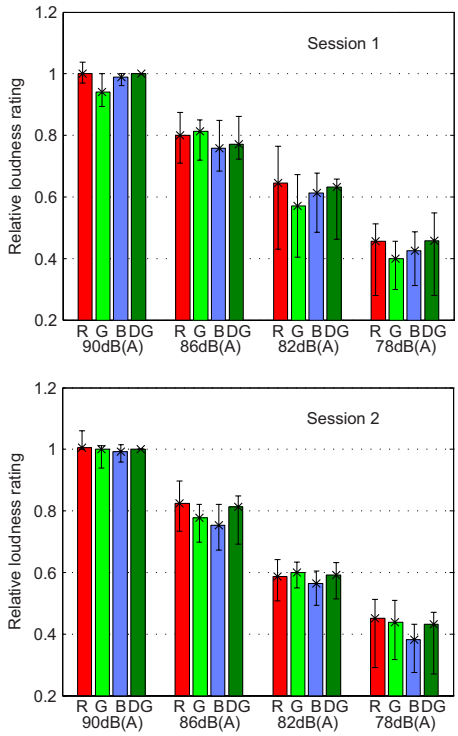


FIG. 2. (Color online) Median relative loudness ratings with interquartile ranges, grouped by level and normalized relative to the stimulus pair 90 dB(A)/DG.

[$F(3,45)=2.82$, $p<0.05$]. Therefore, the two sessions were analyzed separately using a two-way repeated measures analysis of variance with level [90, 86, 82, and 78 dB(A)] and color (R, G, B, and DG) as within-subject factors. Apart from the expected highly significant main effect of level [Session 1: $F(3,45)=222.24$, $p<0.0001$; Session 2: $F(3,45)=204.34$, $p<0.0001$], a significant main effect of color [Session 1: $F(3,45)=3.71$, $p<0.05$; Session 2: $F(3,45)=3.33$, $p<0.05$] was found, indicating that subjects were influenced in their loudness judgment by the color of the visual stimuli. No significant interaction (sound level by color) was found in either session ($p>0.05$).

To further investigate the influence of the visual conditions, a post-hoc comparison was performed using Scheffé's procedure. As can be seen in Table I, significant differences only occurred in Session 1 between the stimuli R and G ($p<0.05$) and in Session 2 between R and B ($p<0.05$). In both

TABLE I. Mean differences (D) between visual conditions. Critical differences (D_{crit}) were calculated according to Scheffé (α=0.05). Significant differences are marked with an asterisk.

	Session 1		Session 2	
	D	D_{crit}	D	D_{crit}
R-G	0.0359	0.0343*	0.0171	0.0331
R-B	0.0164	0.0343	0.0345	0.0331*
R-DG	0.0044	0.0343	0.0088	0.0331
G-B	−0.0195	0.0343	0.0174	0.0331
G-DG	−0.0316	0.0343	−0.0083	0.0331
B-DG	−0.0120	0.0343	−0.0257	0.0331

cases, sounds heard during the presentation of a red car produced higher loudness ratings. All other color combinations failed to reach statistical significance.

The mean difference between visual conditions R and G corresponds to a change in sound level of about 1 dB. Some subjects, however, seemed to be more strongly influenced by different colors and showed larger equivalent level differences of up to 3 dB.

III. CONCLUSIONS

In this experiment, small differences in magnitude estimates of loudness were found depending on visual stimulation by images of differently colored sports cars. These differences are equivalent to a change in sound level of about 1 dB, with maximum observed differences of 3 dB. Previous research concerning color influences on loudness was confirmed: Still images of red vehicles seem to elicit higher loudness ratings compared to light-green or blue vehicles. Similar tendencies were observed for dark green.

As light green and blue are rather untypical colors for sports cars, a tentative explanation could involve the degree to which the image displayed to the subjects gives the impression of a typical sports car. The general real life experience is that sports cars have certain visual and acoustical attributes, which separate them from "normal" cars. On the one hand, sports cars are usually built to reach high speeds, which requires for example a streamlined design and a powerful engine. On the other hand, certain colors like bright red are traditionally associated with premium sports cars. A visual stimulus that looks like a sports car (streamlined body structure, bright red color) thus could cause subjects to assume the vehicle possesses a powerful and therefore loud engine, which in turn could lead to higher loudness ratings. To test this hypothesis, other visual features of the vehicle apart from color could be modified to give the impression of more or less sportive cars. For example, race numbers on the door could suggest a professional racing car (with a corresponding powerful engine), and thus might influence loudness judgment even more. An additional questionnaire could give insight into introspection of the subjects, for example whether a particular vehicle during the experiment was identified as a sports car or not. A similar case of differences in loudness judgments caused by visual expectations was described by Aylor and Marks (1976).

There is evidence that the red/loud combination can raise physiological arousal and induce the perception of excitement (Wolfson and Case, 2000). Such a feeling of excitement may contribute to an overestimation of loudness.

ACKNOWLEDGMENTS

We wish to thank Mary Florentine and Brian Moore for most helpful comments on an earlier version of the paper.

Aylor, D. E., and Marks, L. E., (**1976**). "Perception of noise transmitted through barriers," J. Acoust. Soc. Am. **59**, 397–400.

Blauert, J., and Jekosch, U., (**1997**). "Sound-quality evaluation—A multi-layered problem," Acust. Acta Acust. **83**, 747–753.

Fastl, H., (**2004**). "Audio-visual interactions in loudness evaluation," in Proceedings of the 18th International Congress on Acoustics, Kyoto, Japan, pp. 1161–1166.

Fastl, H., and Zwicker, E., (**2007**). *Psychoacoustics. Facts and Models*, 3rd ed. (Springer, Berlin).

Höger, R., and Greifenstein, P., (**1988**). "Zum Einfluß der Größe von Lastkraftwagen auf deren wahrgenommene Lautheit (Influence of the size of trucks on their perceived loudness)," Z. Lärmbek. **35**, 128–131.

Namba, S., Kuwano, S., Kinoshita, A., and Hayakawa, Y., (**1997**). "Psychological evaluation of noise in passenger cars—The effect of visual monitoring and the measurement of habituation," J. Sound Vib. **205**, 427–433.

Patsouras, C., Filipou, T., and Fastl, H., (**2002**). "Influences of color on the loudness judgement," in Proceedings of the Forum Acusticum, Sevilla, PSY-05-002-IP (CD-ROM).

Rader, T., Morinaga, M., Matsui, T., Fastl, H., Kuwano, S., and Namba, S., (**2004**). "Cross-cultural effects in audio-visual interactions," in Transactions of the Technical Committee of Noise and Vibration of the Acoustical Society of Japan, Tokyo, Japan, N-2004-31.

Suzuki, Y., Abe, K., Ozawa, K., and Sone, T., (**2000**). "Factors for perceiving sound environments and the effects of visual and verbal information on these factors," in Contributions to Psychological Acoustics: Results of the Eighth Oldenburg Symposium on Psychological Acoustics, edited by A. Schick, M. Meis, and C. Reckhardt, Oldenburg, pp. 209–232.

Wolfson, S., and Case, G. (**2000**). "The effects of sound and colour on responses to a computer game," Interact. Comput. **13**, 183–192.

On the conservation of momentum for a sound pulse reflecting from a pressure-release boundary (L)

A. G. Voronovich[a)]
Physical Science Division, NOAA/Earth System Research Laboratory, 325 Broadway, Boulder, Colorado 80305

(Received 9 August 2007; revised 8 February 2008; accepted 8 February 2008)

When a "massless" one-dimensional sound pulse (mass of a sound pulse is defined as an integral of the perturbation of density over the pulse length) reflects from a pressure-release boundary, its momentum changes sign. This obviously violates momentum conservation. However, in contrast to the case of an unbounded medium, calculation of the momentum in a bounded region includes a second-order term as well. Apparently, the second-order correction to the linear solution ensures momentum conservation in this case. The purpose of this Letter is to find a concrete form of this second-order correction. It appears that, as a result of the nonlinear interaction of the pulse with a pressure-release boundary, the latter experiences second-order net shift. This leads to the generation of a massive second-order rarefaction pulse whose momentum is directed opposite to the direction of propagation of the pulse itself. Appearance of this pulse ensures total momentum conservation.
© *2008 Acoustical Society of America.*
[DOI: 10.1121/1.2890744]

PACS number(s): 43.25.Jh [OAS] Pages: 2480–2483

I. INTRODUCTION

Momentum of a wave motion in a one-dimensional (1D) case in an unbounded fluid is

$$P = \int_{-\infty}^{\infty} (\rho_0 + \rho)\varphi_x dx = \rho_0 \Delta\varphi + \int_{-\infty}^{\infty} \rho\varphi_x dx, \tag{1}$$

where ρ_0 and $\rho(x,t)$ are equilibrium density and its variation, respectively, $\varphi(x,t)$ is velocity potential, and $\Delta\varphi=\varphi(+\infty,t)-\varphi(-\infty,t)$ is total variation of the potential across the wave. If in the initial moment of time $\Delta\varphi=0$, then the jump of the potential will be equal to zero always, and to calculate momentum up to the lowest, (i.e., second) order value it is sufficient to substitute into the second term in Eq. (1) a linear solution. In the 1D case linear solution can be represented as a superposition of the right- and left-propagating pulses. At a later time when both pulses separate and do not overlap, one can easily find with the help of Eq. (11) that

$$P = \frac{E_+}{c_0} - \frac{E_-}{c_0}, \tag{2}$$

where E_+, E_- is an energy of the right- and left-propagating pulses, respectively. A similar situation takes place in the three-dimensional case as well.[1] Now let us assume that at $x=0$ there is a pressure-release boundary. After reflection from the boundary direction of the propagation and hence the momentum of the pulse changes without action of an external force. This obviously violates momentum conservation. However, now in Eq. (1) one has $\Delta\varphi=\varphi(\xi,t)$, where ξ is coordinate of the boundary, and momentum conservation can be ensured if after reflection due to nonlinear effects the reflected pulse acquires a second-order "tail" so that in Eq. (1) $\Delta\varphi\neq 0$. The purpose of this Letter is to find details of this process using second-order analysis.

Second-order solution of the 1D motion of an ideal compressible fluid was, of course, calculated for different purposes in numerous works. A review and detailed analysis of many situations related to this classical problem can be found, in particular, in relatively recent work.[2] However, the case of a pressure-release boundary was not considered there. The issue of momentum conservation for the sound pulse reflecting from a pressure-release boundary in the works known to the author has not been clarified yet.

In Sec. II we will present a solution of the problem in the form convenient for our analysis, and in Sec. III we will provide physical interpretation of the results.

II. CALCULATION

The equations of the adiabatic motion of an ideal fluid in 1D read:

$$\varphi_t + \tfrac{1}{2}\varphi_x^2 + w(\tilde{\rho}) - w(\rho_0) = 0, \tag{3}$$

$$\tilde{\rho}_t + (\tilde{\rho}\varphi_x)_x = 0, \tag{4}$$

where $\tilde{\rho}$ is a total density and $w(\tilde{\rho})$ is an enthalpy. We will consider a solution of these equations in a weakly nonlinear case up to the second-order terms only. In this case one can use for the enthalpy power expansion;

$$\frac{w(\tilde{\rho}) - w(\rho_0)}{c_0^2} = \frac{\tilde{\rho} - \rho_0}{\rho_0} + \alpha\left(\frac{\tilde{\rho} - \rho_0}{\rho_0}\right)^2 + \cdots, \tag{5}$$

where c_0 is an unperturbed sound speed and α is a constant coefficient determined by the equation of state. Since $dw = d\tilde{p}/\tilde{\rho}$ for the total pressure $\tilde{p}$ we obtain a similar expansion,

a)Electronic mail: alexander.voronovich@noaa.gov

$$\frac{\tilde{p}-p_0}{\rho_0 c_0^2}=\frac{\tilde{\rho}-\rho_0}{\rho_0}+\left(\alpha+\frac{1}{2}\right)\left(\frac{\tilde{\rho}-\rho_0}{\rho_0}\right)^2+\cdots, \tag{6}$$

where

$$\alpha=\frac{1}{2}\left(\frac{\rho_0 d^2\tilde{p}}{c_0^2 d\tilde{\rho}^2}-1\right)_{\rho=\rho_0}=\frac{1}{2}\left(\frac{\rho}{c^2}\frac{dc^2}{d\rho}-1\right)_{\rho=\rho_0}. \tag{7}$$

For the ideal gas with the equation of state $\tilde{p}/p_0=(\tilde{\rho}/\rho_0)^\gamma$ one finds $\alpha=\gamma/2-1$. Now we can rewrite Eqs. (3) and (4) to the accuracy of the second-order terms as follows:

$$\varphi_t+\frac{1}{2}\varphi_x^2+c_0^2\frac{\rho}{\rho_0}+\alpha c_0^2\left(\frac{\rho}{\rho_0}\right)^2=0, \tag{8}$$

$$\rho_t+\rho_0\varphi_{xx}+(\rho\varphi_x)_x=0, \tag{9}$$

where $\rho=\tilde{\rho}-\rho_0$. Differentiating Eq. (9) with respect to t and using Eq. (8) we obtain

$$\varphi_{tt}-c_0^2\varphi_{xx}=\frac{c_0^2}{\rho_0}(\rho\varphi_x)_x-\left(\frac{1}{2}\varphi_x^2+\frac{\alpha c_0^2}{\rho_0^2}\rho^2\right)_t. \tag{10}$$

In the linear approximation the right-hand side of Eq. (10) can be neglected. Let us consider the first-order solution in the form of a right-propagating pulse,

$$\varphi^{(1)}=f\left(t-\frac{x}{c_0}\right),\quad \rho^{(1)}=-\frac{\rho_0}{c_0^2}f'\left(t-\frac{x}{c_0}\right). \tag{11}$$

We will assume that function f is smooth and differs from zero at $0<t<T$ only. Let us calculate the second-order solution assuming the following initial conditions:

$$\varphi^{(2)}|_{t=0}=0,\quad \rho^{(2)}|_{t=0}=0. \tag{12}$$

It follows from Eqs. (8) and (12) that

$$\varphi_t^{(2)}|_{t=0}=-\frac{1}{c_0^2}\left(\frac{1}{2}+\alpha\right)\left[f'\left(-\frac{x}{c_0}\right)\right]^2. \tag{13}$$

Calculating the right-hand side of Eq. (10) in terms of the first-order values Eq. (11) we find:

$$\varphi_{tt}^{(2)}-c_0^2\varphi_{xx}^{(2)}=-\frac{1}{c_0^2}\left(\frac{3}{2}+\alpha\right)\frac{\partial}{\partial t}\left[f'\left(t-\frac{x}{c_0}\right)\right]^2. \tag{14}$$

One can easily check by inspection that the solution of Eqs. (12)–(14) is as follows:

$$\varphi^{(2)}=F(x,t)=-\frac{1}{2c_0^2}\left(\frac{3}{2}+\alpha\right)t\left[f'\left(t-\frac{x}{c_0}\right)\right]^2+\frac{1}{2c_0^2}\left(\frac{1}{4}-\frac{\alpha}{2}\right)\int_{-t-x/c_0}^{t-x/c_0}[f'(\tau)]^2 d\tau. \tag{15}$$

The original equations are invariant under substitution $x\to -x$; hence, one can replace in Eqs. (11) and (15) x by $-x$ and obtain a similar solution for the left-propagating pulse.

Let us now impose on our problem the pressure-release boundary condition $\tilde{p}|_{x=\xi(t)}=p_0$ or

$$\rho|_{x=\xi(t)}=0, \tag{16}$$

where $\xi(t)$ is the coordinate of the boundary which, apparently, satisfies

$$\xi_t=\varphi_x(\xi,t). \tag{17}$$

Now in the first approximation we have

$$\varphi^{(1)}=f\left(t-\frac{x}{c_0}\right)-f\left(t+\frac{x}{c_0}\right), \tag{18}$$

$$\rho^{(1)}=-\frac{\rho_0}{c_0^2}f'\left(t-\frac{x}{c_0}\right)+\frac{\rho_0}{c_0^2}f'\left(t+\frac{x}{c_0}\right), \tag{19}$$

$$\xi^{(1)}=-\frac{2}{c_0}f(t). \tag{20}$$

The solution Eqs. (18)–(20) represents a pulse which propagates from the region of negative x to the right and after reflection from the pressure-release boundary at $x=0$ changes its polarity.

Substituting into the right-hand side of Eq. (10) expressions (18) and (19) we obtain squares of the terms associated with the arguments $(t-x/c_0)$ and $(t+x/c_0)$ and a cross-product term. In Eq. (13) the cross-product term is absent, since the original pulse and its mirror image at $t=0$ do not overlap. According to this the second-order solution can now be represented as follows:

$$\varphi^{(2)}=F(x,t)+F(-x,t)-G(x,t)+Q\left(t+\frac{x}{c_0}\right), \tag{21}$$

where $F(x,t)$ is given by Eq. (15). Function G here is due to the cross-product term; it is a solution of

$$G_{tt}-c_0^2G_{xx}=\frac{1-2\alpha}{c_0^2}\frac{\partial}{\partial t}\left[f'\left(t-\frac{x}{c_0}\right)f'\left(t+\frac{x}{c_0}\right)\right], \tag{22}$$

satisfying the initial conditions $G=G_t=0$, $t=0$;

$$G(x,t)=\frac{1-2\alpha}{4c_0^2}\frac{\partial}{\partial t}\left[f\left(t-\frac{x}{c_0}\right)f\left(t+\frac{x}{c_0}\right)\right]. \tag{23}$$

Function G is even with respect to x and differs from zero only at $0<t<T$.

Apparently, Q in Eq. (21) is a solution of the homogeneous wave equation representing a second-order, left-propagating pulse. We will assume that Q turns to zero for negative arguments so that this term does not contribute to the initial condition (12) at $x<0$. The appearance of function Q is due to the necessity to satisfy boundary condition (17) at second order:

$$\rho^{(2)}|_{x=0}=-\rho_x^{(1)}|_{x=0}\xi^{(1)}=4\frac{\rho_0}{c_0^4}f''(t)f(t). \tag{24}$$

Calculating second-order terms in Eq. (8) at $x=0$ taking into account Eqs. (21) and (24) and integrating over time we find:

$$c_0^2Q(t)=\left(\frac{3}{2}+\alpha\right)t[f'(t)]^2-\left(\frac{7}{2}+\alpha\right)f(t)f'(t)+\left(\frac{7}{4}+\frac{\alpha}{2}\right)\int_0^t[f'(\tau)]^2 d\tau. \tag{25}$$

Now, let us evaluate total shift of the boundary in the second order [the first-order shift according to Eq. (20), equals, of course, zero]. From Eq. (17) we find:

$$\xi^{(2)}(\infty)=\int_0^\infty \varphi_x^{(2)}(0,t)dt+\int_0^\infty \varphi_{xx}^{(1)}(0,t)\xi^{(1)}(t)dt. \tag{26}$$

According to Eq. (18), $\varphi_{xx}^{(1)}(0,t)=0$. The sum of the first three terms in Eq. (21) is an even function of x, whence

$$\xi^{(2)}(\infty)=\int_0^\infty \varphi_x^{(2)}(0,t)dt=\int_0^\infty \frac{Q'(t)}{c_0}dt=\frac{Q(\infty)}{c_0}$$
$$=\frac{1}{c_0^3}\left(\frac{7}{4}+\frac{\alpha}{2}\right)\int_0^\infty [f'(\tau)]^2 d\tau \tag{27}$$

(actually integration here and in similar integrals to follow proceeds within the finite limits $0<\tau<T$). Thus, in the second order the boundary generally experiences positive shift (if $\alpha>-7/2$, what should normally be the case).

III. INTERPRETATION

Consider a linear pulse propagating to the right which shape is given by Eq. (11). Let us introduce a "mass" of the pulse,

$$M=\int_{-\infty}^\infty \rho dx=-\frac{\rho_0}{c_0^2}\int_{-\infty}^\infty f'\left(t-\frac{x}{c_0}\right)dx=\frac{\rho_0}{c_0}\Delta\varphi, \tag{28}$$

where

$$\Delta\varphi=\varphi(+\infty)-\varphi(-\infty) \tag{29}$$

is total change of the potential across the pulse. For the left-propagating pulse we will similarly find:

$$M=-\frac{\rho_0}{c_0}\Delta\varphi. \tag{30}$$

The total momentum of the right-propagating pulse is

$$P=\int_{-\infty}^\infty (\rho_0+\rho)\varphi_x dx=\rho_0\Delta\varphi+\frac{\rho_0}{c_0^2}\int_{-\infty}^\infty [f'(\tau)]^2 d\tau.$$

In the general case one thus obtains

$$P=\pm\left(Mc_0+\frac{\rho_0}{c_0^2}\int_{-\infty}^\infty [f'(\tau)]^2 d\tau\right), \tag{31}$$

where the plus or minus sign is related to the right- or left-propagating wave, respectively.

According to our assumption for the original pulse one has $\Delta\varphi=0$ and hence the mass of the original pulse is zero: $M=0$. At the initial moments of time: $0<t\ll T$, when one can assume that the reflected pulse did not appear yet, the second-order potential according to Eq. (15) is

$$\varphi^{(2)}=F(x,t)=-\frac{1}{2c_0^2}\left(\frac{3}{2}+\alpha\right)t\left[f'\left(t-\frac{x}{c_0}\right)\right]^2$$
$$+\frac{1}{2c_0^2}\left(\frac{1}{4}-\frac{\alpha}{2}\right)\int_{-t-x/c_0}^0 [f'(\tau)]^2 d\tau$$
$$+\frac{1}{2c_0^2}\left(\frac{1}{4}-\frac{\alpha}{2}\right)\int_0^{t-x/c_0} [f'(\tau)]^2 d\tau. \tag{32}$$

The first term here is due to the intrinsic nonlinearity of the process of propagation and describes steepening of the wave profile. The initial conditions given by Eq. (12) are chosen such that the wave motion at the initial moments of time corresponds to the right-propagating linear solution up to the second-order terms. One obtains proper solution by adding to the first term in Eq. (32) two second-order pulses which have the same mass

$$M_0=-\frac{\rho_0}{2c_0^3}\left(\frac{1}{4}-\frac{\alpha}{2}\right)\int_0^\infty [f'(\tau)]^2 d\tau, \tag{33}$$

but propagate in the opposite directions. These two massive pulses compensate the extra sources of mass, but do not introduce extra momentum. In other words, the two auxiliary pulses in Eq. (32) ensure required distribution of the initial second-order pressure and velocity fields at $t=0$. Since amplitude of these pulses is of second order already, one does not need to take into account for them nonlinear effects, and these pulses propagate to the second-order accuracy without changing shape.

Now let us consider how the solution looks at $x<0$ for sufficiently large moments of time $t>T$, when the process of interaction of the pulse with the boundary is completed. Equation (21), taking into account Eq. (25), gives

$$\varphi^{(2)}=\frac{1}{c_0^2}\left(\frac{3}{2}+\alpha\right)\left(\frac{t}{2}+\frac{x}{c_0}\right)\left[f'\left(t+\frac{x}{c_0}\right)\right]^2$$
$$-\frac{1}{c_0^2}\left(\frac{7}{2}+\alpha\right)f'\left(t+\frac{x}{c_0}\right)f\left(t+\frac{x}{c_0}\right)+\frac{1}{2c_0^2}\left(\frac{1}{4}\right.$$
$$\left.-\frac{\alpha}{2}\right)\int_{-t-x/c_0}^0 [f'(\tau)]^2 d\tau-\frac{1}{2c_0^2}\left(\frac{1}{4}-\frac{\alpha}{2}\right)$$
$$\times\int_0^{t+x/c_0} [f'(\tau)]^2 d\tau+\frac{2}{c_0^2}\int_0^{t+x/c_0} [f'(\tau)]^2 d\tau \tag{34}$$

(strictly speaking the solution for $\varphi^{(2)}$ at $t>T$ also includes a constant term which is of no consequence for the motion picture and was dropped). The first two terms in Eq. (34) represent the process of the steepening of the wave profile due to the nonlinearity of the process of pulse propagation. The third term in Eq. (34) represents the same left-propagating pulse as in Eq. (32); this pulse does not interact with the boundary and remains unchanged. The fourth term in Eq. (34) corresponds to the right-propagating pulse in Eq. (32) which was reflected from the pressure-release boundary and for this reason changed its polarity and hence sign of the mass. Since direction of propagation of this pulse has also changed, its momentum did not change, and total momentum of the two auxiliary pulses remains zero as it was at the initial moment. However, in Eq. (34) there is an additional left-propagating pulse corresponding to the last term in this equation. This pulse has a negative mass

$$M_*=-2\frac{\rho_0}{c_0^3}\int_0^\infty [f'(\tau)]^2 dt. \tag{35}$$

Note that the mass does not depend of the equation of state related to coefficient α in Eq. (5). In the case of rigid boundary which does not move the nonlinear effects lead to the

appearance of the radiation pressure.[2] In the case of the pressure-release boundary which cannot support the excess of pressure, the nonlinearity results in the second-order net shift of the boundary. However, total mass should be conserved, and shift of the boundary results in the appearance of the rarefaction pulse. From Eqs. (18) and (20) it is easy to see that after a right-propagating pulse of mass M_0 reflects from a pressure-release boundary, the boundary experiences in the linear approximation a net shift $\xi(\infty)=2M_0/\rho_0$. Similarly, a second-order, left-propagating pulse with mass M_* will produce a second-order shift—M_*/ρ_0. It is easy to see that the sum of these two shifts does correspond to the total shift given by Eq. (27),

$$\rho_0\xi^{(2)}(\infty)=2M_0-M_*. \tag{36}$$

According to Eq. (31) momentum of the left-propagating pulse with mass M_* is

$$P_*=-M_*c_0=2\frac{\rho_0}{c_0^2}\int_0^\infty [f'(\tau)]^2d\tau \tag{37}$$

[the second term in Eq. (31) is in this case of fourth order and has to be neglected]. The pulse propagates to the left, however its momentum is directed to the right since $M_*<0$. Together with the negative momentum of the reflected original pulse, momentum P_* ensures overall momentum conservation in the case of a pressure-release boundary:

$$\frac{\rho_0}{c_0^2}\int_0^\infty [f'(\tau)]^2d\tau=-\frac{\rho_0}{c_0^2}\int_0^\infty [f'(\tau)]^2d\tau+P_*. \tag{38}$$

The shape of this pulse is given by the last term in Eq. (34). If we assume that the initial pulse is narrow band with some envelope having final support, then the second-order pulse under consideration can be considered as a superposition of a high-frequency pulse with double carrier frequency and zero mass and a low-frequency massive pulse with the local amplitude of the velocity proportional to the square of the amplitude of the velocity in the original pulse. In the absence of dispersion (the case considered here) the low- and high-frequency pulses will be always superimposed. However, in the presence of a weak dispersion these two pulses will eventually separate.

It is interesting to compare the cases of a pressure-release and a rigid boundary which corresponds to the boundary condition $\varphi_x(0,t)=0$. In the latter case the second terms in the first-order solution given by Eqs. (18) and (19) change signs and it becomes $\xi^{(1)}=0$. Correspondingly, the second-order solution for the potential is given in this case by Eq. (21) with the sign of the third term (G) changed and the last term (Q) absent. Apparently, the boundary condition is satisfied in this case since $\varphi^{(2)}$ is an even function of x. Solution at small t, of course, coincides with Eq. (32), and at $t>T$ solution given by Eq. (34) as simple calculation shows has to be modified as follows. The first two terms in Eq. (34) are replaced by

$$-\frac{1}{2c_0^2}\left(\frac{3}{2}+\alpha\right)t\left[f'\left(t+\frac{x}{c_0}\right)\right]^2, \tag{39}$$

the fouth term changes sign (since corresponding pulse reflects now from rigid boundary), and the last term disappears. The total change of the momentum now becomes

$$\Delta P=\frac{\rho_0}{c_0^2}\int_0^\infty [f'(\tau)]^2d\tau-\left(-\frac{\rho_0}{c_0^2}\int_0^\infty [f'(\tau)]^2d\tau-2M_0c_0\right)$$
$$=\frac{\rho_0}{c_0^2}\left(\frac{7}{4}+\frac{\alpha}{2}\right)\int_0^\infty [f'(\tau)]^2d\tau. \tag{40}$$

The momentum change depends now on the equation of state. Using Eq. (6) one can check that

$$\Delta P=\int_0^\infty (\tilde{p}-p_0)_{x=0}dt, \tag{41}$$

as it should be according to Newton's second law.[2] It is interesting to note that the total momentum change in the case of the pulse reflected from the rigid boundary and the total shift of the pressure-release boundary according to Eqs. (40) and (27) are related as follows:

$$\Delta P=\rho_0c_0\xi^{(2)}. \tag{42}$$

A possible interpretation of this observation was suggested during the reviewing process. If one assumes that the radiation pressure on the right-hand side of Eq. (41) appearing in the case of a rigid boundary can be converted into the second-order velocity of the boundary in a pressure-release case through the medium impedance ρ_0c_0 according to the standard relation:

$$(\tilde{p}-p_0)_{x=0}=\rho_0c_0\dot{\xi}, \tag{43}$$

then Eq. (42) immediately follows from Eq. (41).

IV. CONCLUSION

When a sound pulse is reflected from a pressure-release boundary, the boundary experiences a second-order shift. This results in the appearance of a second-order massive rarefaction pulse whose momentum, which is also of the second order, is directed opposite to the direction of its propagation. Momentum of this pulse ensures overall momentum conservation. Its energy, however, is a fourth-order value; thus presence of this pulse does not violate energy conservation.

Thus, interaction of the massless sound pulses with the boundaries which are allowed to move can result in the appearance of the second-order massive pulses, and total variation of the potential across the wave will become nonzero: the situation which cannot arise as a result of nonlinear interactions in the unbounded fluid.

[1]L. D. Landay and E. M. Lifshitz, *Course of Theoretical Physics*, 2nd ed. (Elsevier, Amsterdam, 2004), Vol. 6, Sec. 65.
[2]G. G. Denisov, "The problem of wave momentum, radiation pressure and other quantities in the case of plane motion of an ideal gas," J. Appl. Math. Mech. **63**, 375–386 (1999).

The high-frequency dispersion coefficient for the Rayleigh velocity in a vertically inhomogeneous anisotropic half-space (L)

A. L. Shuvalov[a)]
Laboratoire de Mécanique Physique, Université Bordeaux 1, UMR CNRS 5469, F-33405 Talence Cedex, France

(Received 22 October 2007; revised 14 January 2008; accepted 8 February 2008)

For an arbitrary anisotropic half-space with continuous vertical variation of material properties, an explicit closed-form expression for the coefficient B of high-frequency dispersion of the Rayleigh velocity $v_R(\omega)\approx v_R^{(0)}(1+B/\omega)$ is derived. The result involves two matrices, one consisting of the surface-traction derivatives in velocity and the other of its Wentzel–Kramers–Brillouin coefficients, which are contracted with an amplitude vector of the Rayleigh wave in the reference homogeneous half-space. The "ingredients" are routinely defined through the fundamental elasticity matrix and its first derivative, both taken at $v=v_R^{(0)}$ and referred to the surface.
© *2008 Acoustical Society of America.* [DOI: 10.1121/1.2890743]

PACS number(s): 43.35.Cg [RLW] Pages: 2484–2487

I. INTRODUCTION

Inspecting the effect of surface curvature or continuous material inhomogeneity on the high-frequency Rayleigh wave is among the basic probing means in seismology. Theoretical analysis of this problem is commonly based on the well-established methods of the Wentzel–Kramers–Brillouin (WKB) expansion and ray theory.[1–4] A powerful though arduous technique has been developed for deriving the amplitude of Rayleigh wave in a three-dimensional inhomogeneous half-space with an arbitrary shape of the boundary.[5,6] A simpler case of a planar boundary and one-dimensional (1D) vertical inhomogeneity is often encountered in nondestructive testing of solids with a pronounced near-surface variation of material properties into the depth. In this case, the high-frequency dispersion of the velocity of Rayleigh wave is to the leading order inversely proportional to frequency, which is notably slower than an exponential falloff of the Rayleigh-velocity dispersion in materials with a buried continuous inhomogeneity or with a piecewise homogeneous (multilayered) structure. This feature may therefore be used for detecting and investigating a continuous inhomogeneity developing under the surface, see Refs. 7–9 and the bibliographies therein.

A simple model describing the case of 1D vertical inhomogeneity is as follows. Given is a half-space $y\geqslant 0$ with real nondispersive density $\rho(y)$ and elasticity coefficients $c_{ijkl}(y)$, which depend only on y and have nonzero first derivative in y at the traction-free planar surface $y=0$. Appealing to the Berry phase simplified for the case of 1D inhomogeneity in hand (Refs. 5 and 6), or directly using the WKB expansion of surface traction in powers of inverse frequency ω (Ref. 10) readily shows that the leading-order dispersion of the Rayleigh velocity at high ω is of the form

$$v_R(\omega)\approx v_R^{(0)}\left(1+\frac{B}{\omega}\right), \tag{1}$$

where B is real, $v_R^{(0)}$ is the Rayleigh velocity in a "reference" homogeneous half-space with constant ρ and c_{ijkl} equal to the surface values $\rho(0)$ and $c_{ijkl}(0)$ in the actual inhomogeneous material. The dependence (1) describes either a continuous high-frequency extent of the lowest curve of the dispersion spectrum if the half-space has no bulk-wave channels slower than $v_R^{(0)}$, or a sequence of exponentially close segments of successive branches if otherwise.[10] The high-frequency dispersion coefficient B for isotropic materials has been derived in Ref. 10, and the result may be written as follows:

$$B=v_R^{(0)}\frac{b_1}{b_2}:\quad b_1=(q_L+q_T)\left[\frac{4(\rho c_T^2)'}{\rho v_R^{(0)2}}-\frac{\rho'}{\rho}\right]+\frac{(1-q_T^2)q_L}{2-q_T^2}\frac{c_T'}{c_T}+\frac{(1-q_L^2)q_T}{2-q_L^2}\frac{c_L'}{c_L}-\frac{2(1+q_T^2)}{q_L+q_T}\times\left[\frac{(\rho c_T^2)'}{\rho c_T^2}\left(1+\frac{(1+q_T^2)(3+q_T^2)}{2(1-q_T^2)}\right)-\frac{\rho'}{\rho}\right],$$

$$b_2=2(1-q_T^2)\left(\frac{q_L}{q_T}+\frac{q_T}{q_L}\frac{c_T^2}{c_L^2}-1-q_T^2\right), \tag{2}$$

where $q_{L,T}=\sqrt{1-v^2/c_{L,T}^2}$, $c_L^2=c_{11}/\rho$, $c_T^2=c_{44}/\rho$, and the prime denotes a derivative with respect to y at $y=0$. Equation (2) has been used in Ref. 7 (with a notation $v_R^{(\infty)}$ in place of $v_R^{(0)}$) for comparing the leading-order asymptotics (1) with an exact dispersion curve computed numerically for a given profile of vertical inhomogeneity. A good accuracy of approximation has been observed in a rather broad high-frequency range.

An explicit form (2) of the coefficient B given in Ref. 10 for isotropic materials is fairly lengthy, and explicit expressions of Ref. 5 for an anisotropic body are further unwieldy

a)Electronic mail: a.shuvalov@lmp.u-bordeaux1.fr

 0001-4966/2008/123(5)/2484/4/$23.00 © 2008 Acoustical Society of America

even when these are reduced to the case of 1D inhomogeneity. The motivation of this letter is to present a closed-form solution for the high-frequency dispersion of Rayleigh velocity in a vertically inhomogeneous half-space of unrestricted anisotropy. The result amounts to a ratio of Hermitian forms of two 3×3 matrices of surface traction perturbations in v and ω^{-1} contracted with a vector of partial amplitudes of the Rayleigh wave in the "reference" homogeneous half-space.

II. BACKGROUND

The wave-propagation problem for a vertically inhomogeneous half-space $y\geqslant0$ maintaining zero traction $\sigma_{iy}=0$ at the surface $y=0$ with a normal $\mathbf{n}$ is considered in the transform domain $(\mathbf{k}_\parallel,y,\omega)$, where $\mathbf{k}_\parallel=k\mathbf{m}$ is orthogonal $\mathbf{n}$. The factor $e^{i(k\mathbf{m}\cdot\mathbf{r}-\omega t)}$ is suppressed hereafter. The governing equation of motion may be written as the first-order ordinary differential system of six equations

$$\left[\mathbf{Q}(y)-\frac{d}{dy}\right]\boldsymbol{\eta}(y)=\mathbf{0}, \tag{3}$$

where the state vector $\boldsymbol{\eta}(y)$ is a column of scalar multiples of displacement and traction vectors. An optional explicit form of the 6×6 matrix of system coefficients $\mathbf{Q}(y)$ can always be arranged so that

$$[\mathbf{TQ}(y)]^T=\mathbf{TQ}(y), \tag{4a}$$

$$\mathbf{Q}(y)=-\mathbf{Q}^*(y), \tag{4b}$$

where the superscript T and the asterisk mean transpose and complex conjugated, and $\mathbf{T}$ is a matrix with zero diagonal and identity off-diagonal 3×3 blocks. The system matrix $\mathbf{Q}(y)$ is composed of material coefficients $\rho(y)$, $c_{ijkl}(y)$ and also involves any two of dispersion parameters ω, k and $v=\omega/k$ (see Sec. III). At the same time, the eigenvectors $\boldsymbol{\xi}_\alpha(y)$ and eigenvalues $q_\alpha(y)$ of $\mathbf{Q}(y)$ are nondispersive in the sense that it is always possible to define $\boldsymbol{\xi}_\alpha(y)$ and $q_\alpha(y)$ for any fixed y as a function of v and as ω or k times function of v, respectively. For example, bearing in mind Eq. (4b), the eigenvalues of $\mathbf{Q}(y)$ can be introduced as $ikp_\alpha(y,v)$. Let $\hat{v}(y)$ be the threshold velocity, below which all $p_\alpha(y,v)$ at a given y are complex.

Denote the eigenspectrum of, specifically, $\mathbf{Q}(0)$ at the surface $y=0$ as follows:

$$[\mathbf{Q}(0)-ikp_\alpha\mathbf{I}]\boldsymbol{\xi}_\alpha=\mathbf{0},\quad \boldsymbol{\xi}_\alpha=(\mathbf{u}_\alpha\,\mathbf{f}_\alpha)^T,\quad \alpha=1,\ldots,6, \tag{5}$$

with p_α and $\boldsymbol{\xi}_\alpha$ understood as taken at $y=0$. Hence $\mathbf{u}_\alpha e^{ikp_\alpha y}$ and $\mathbf{f}_\alpha e^{ikp_\alpha y}$ are scalar multiples of displacements and tractions of partial modes in the reference homogeneous half-space [the one with constant $\rho=\rho(0)$ and $c_{ijkl}=c_{ijkl}(0)$]. Adopting the normalization $\boldsymbol{\xi}_\alpha\cdot\mathbf{T}\boldsymbol{\xi}_\alpha=1$ ensures that $\boldsymbol{\xi}_\alpha=\boldsymbol{\xi}_\alpha(v)$. Introduce the 6×6 matrix $\boldsymbol{\Xi}=\boldsymbol{\Xi}(v)$ whose columns are $\boldsymbol{\xi}_\alpha$. Note the identity

$$\boldsymbol{\Xi}^T\mathbf{T}=\boldsymbol{\Xi}^{-1}, \tag{6}$$

following from Eq. (4a) and incorporating the above-presented normalization. Assume hereafter that $v<\hat{v}(0)$, whence $p_\alpha(v)$ are complex and therefore complex conjugated. Let $\mathrm{Im}\,p_a(v)>0$ for $a=1,2,3$. Hence

$$\boldsymbol{\Xi}(v)=\begin{pmatrix}\hat{\mathbf{u}}(v) & \hat{\mathbf{u}}^*(v)\\ \hat{\mathbf{f}}(v) & \hat{\mathbf{f}}^*(v)\end{pmatrix}, \tag{7}$$

where the 3×3 matrices $\hat{\mathbf{u}}=\|u_{ia}\|$ and $\hat{\mathbf{f}}=\|f_{ia}\|$ involve displacements and tractions of the three partial modes $a=1,2,3$ decreasing into the depth of the reference homogeneous half-space. Denote the Rayleigh velocity in this homogeneous half-space by $v_R^{(0)}$ [see Eq. (1)] and introduce the abbreviated notations

$$\mathbf{u}_{0a}=\mathbf{u}_a(v_R^{(0)}),\quad \hat{\mathbf{u}}_0=\hat{\mathbf{u}}(v_R^{(0)}),\quad \mathbf{f}_{0a}=\mathbf{f}_a(v_R^{(0)}),$$

$$\hat{\mathbf{f}}_0=\hat{\mathbf{f}}(v_R^{(0)}). \tag{8}$$

The boundary condition $\sigma_{iy}=0$ at the surface $y=0$ implies that

$$\hat{\mathbf{f}}_0\mathbf{C}_0=0\Rightarrow\det\hat{\mathbf{f}}_0=0, \tag{9}$$

where $\mathbf{C}_0=(C_{01},C_{02},C_{03})^T$ is a vector of amplitudes of partial modes defined up to a constant scalar A. Denote the Rayleigh-wave displacement at $y=0$ in the reference homogeneous half-space by $\mathbf{u}_{0R}=\hat{\mathbf{u}}_0\mathbf{C}_0(=\Sigma_{a=1}^3C_{0a}\mathbf{u}_{0a})$. By virtue of Eqs. (6) and (9),

$$\mathbf{u}_{0R}^T\hat{\mathbf{f}}_0^*=\mathbf{0}, \tag{10a}$$

$$\hat{\mathbf{f}}_0^T\mathbf{u}_{0R}=\mathbf{C}_0. \tag{10b}$$

Hence $\mathbf{u}_{0R}=A(\mathbf{f}_{0a}^*\times\mathbf{f}_{0b}^*)$ and

$$\mathbf{C}_0=A([\mathbf{f}_{0a}^*\mathbf{f}_{0b}^*\mathbf{f}_{01}],[\mathbf{f}_{0a}^*\mathbf{f}_{0b}^*\mathbf{f}_{02}],[\mathbf{f}_{0a}^*\mathbf{f}_{0b}^*\mathbf{f}_{03}])^T, \tag{11a}$$

$$\mathbf{C}_0\cdot\mathbf{C}_0=0, \tag{11b}$$

where $[\cdot]$ is a mixed product and $a\neq b$ are any two of three modal numbers 1,2,3, unless the sagittal plane spanned by the vectors $\mathbf{m}$ and $\mathbf{n}$ is a symmetry plane. If it is, so that the Rayleigh wave is polarized in the sagittal plane $(\mathbf{m},\mathbf{n})$ and consists in the reference homogeneous half-space of two partial modes, say $a=1,2$, then $\mathbf{f}_{01}\|\mathbf{f}_{02}$, $\mathbf{u}_{0R}=A(\mathbf{f}_{01}^*\times\mathbf{f}_{03}^*)$, and, by Eq. (11b), $\mathbf{C}_0=A(1,\pm i)^T$, where $\pm$ is associated with an optional sign of a normalization constant supplied for each eigenvector in Eq. (5) by the condition $\boldsymbol{\xi}_\alpha\cdot\mathbf{T}\boldsymbol{\xi}_\alpha=1$.

Fundamentals of the surface-wave theory for homogeneous anisotropic solids are encompassed and referenced in Refs. 11 and 12. Details of the outlined state-vector formalism in vertically inhomogeneous materials may be found in Ref. 13.

III. THE COEFFICIENT OF HIGH-FREQUENCY DISPERSION

Let us proceed from specifying the high-frequency assumption. It is supposed to enable the WKB expansion and its truncation at the first-order term, also to free the consideration from possible turning points, and to allow a half-space model which discards a lower boundary. Denote by δ_1 and δ_2 typical values of, respectively, the first and second derivatives in y of $\rho(y)/\rho(0)$ and $c_{ijkl}(y)/c_{ijkl}(0)$ taken at $y=0$. Let $[0,y_c]$ be the depth range, within which there is no turning points and no abrupt boundaries with a jump of ma-

terial properties. The former implies that $v_R^{(0)} < \hat{v}(y)$ and hence that the eigenvalues $ikp(y,v)$ of $\mathbf{Q}(y)$ satisfy $\mathrm{Im}\, p_a(y, v_R^{(0)}) > 0$ $(a=1,2,3)$ for $y \leq y_c$. In these terms, we assume in the following that

$$\exp\left(-2\frac{\omega}{v_R^{(0)}}\int_0^{y_c} \mathrm{Im}\, p_a(y, v_R^{(0)})dy\right) \ll v_R^{(0)}\frac{\delta_1}{\omega} \ll v_R^{(0)2} \times \frac{\delta_2}{\omega^2} \ll 1. \tag{12}$$

Neglecting small exponential terms due to Eq. (12), the dispersion equation for the Rayleigh velocity in an inhomogeneous material at high frequency is

$$\det \hat{\mathbf{F}}(v,\omega) = 0, \tag{13}$$

where the columns of the 3×3 matrix $\hat{\mathbf{F}}(v,\omega)$ are the WKB expansions of "traction parts" of three partial solutions $\boldsymbol{\eta}_a(y)$ of Eq. (3) taken at $y=0$ and assuredly decreasing into the depth for $y \leqslant y_c$.

Seeking the solution of Eq. (13) in the form (1), we insert

$$\hat{\mathbf{F}}(v,\omega) = \hat{\mathbf{f}}(v) + \hat{\delta\mathbf{f}}(v_R^{(0)},\omega), \quad \hat{\mathbf{f}}(v) = \hat{\mathbf{f}}_0 + (d\hat{\mathbf{f}}/dv)_{v_R^{(0)}}\Delta v,$$

$$\hat{\delta\mathbf{f}}(v_R^{(0)},\omega) = \frac{1}{i\omega}(\hat{\mathbf{f}}_0\tilde{\mathbf{W}} + \hat{\mathbf{f}}_0^*\hat{\mathbf{W}}),$$

$$(d\hat{\mathbf{f}}/dv)_{v_R^{(0)}} = \frac{i}{v_R^{(0)}}(\hat{\mathbf{f}}_0\tilde{\mathbf{S}} + \hat{\mathbf{f}}_0^*\hat{\mathbf{S}}), \tag{14}$$

where the first-order WKB correction is introduced in its common form keeping i in $\hat{\delta\mathbf{f}} \sim (i\omega)^{-1}$, and the constant factor in the definition of $d\hat{\mathbf{f}}/dv$ is adjusted for convenience. Linearizing Eq. (13) in small $\Delta v = v - v_R^{(0)}$ and ω^{-1} leads us to the (approximate) equality

$$\frac{\Delta v}{v_R^{(0)}}\,\mathrm{trace}(\hat{\bar{\mathbf{f}}}_0\hat{\mathbf{f}}_0^*\hat{\mathbf{S}}) = \frac{1}{\omega}\,\mathrm{trace}(\hat{\bar{\mathbf{f}}}_0\hat{\mathbf{f}}_0^*\hat{\mathbf{W}}), \tag{15}$$

where $\hat{\mathbf{S}}$ and $\hat{\mathbf{W}}$ are Hermitian: $\hat{\mathbf{S}}=\hat{\mathbf{S}}^+$ and $\hat{\mathbf{W}}=\hat{\mathbf{W}}^+$ (see the following).

Next we note that the adjugate matrix $\hat{\bar{\mathbf{f}}}_0$ corresponds to $\hat{\mathbf{f}}_0$ with $\det \hat{\mathbf{f}}_0 = 0$ [see Eq. (9)], so that $\hat{\bar{\mathbf{f}}}_0\hat{\mathbf{f}}_0 = \hat{\mathbf{f}}_0\hat{\bar{\mathbf{f}}}_0 = \mathbf{I}\det\hat{\mathbf{f}}_0 = 0$ and therefore $\hat{\bar{\mathbf{f}}}_0$ is a dyadic product $\otimes$ of two vectors. The left vector is equal (up to an arbitrary factor A) to $\mathbf{C}_0$ according to the first half of Eq. (9), while the right vector is equal to $\mathbf{u}_R^*$ according to Eq. (10a). Hence, with reference to Eq. (10b),

$$\hat{\bar{\mathbf{f}}}_0\hat{\mathbf{f}}_0^* = (\mathbf{C}_0 \otimes \mathbf{u}_{0R}^*)\hat{\mathbf{f}}_0^* = \mathbf{C}_0(\mathbf{u}_{0R}^{*T}\hat{\mathbf{f}}_0^*) = \mathbf{C}_0\mathbf{C}_0^{*T}. \tag{16}$$

Plugging Eq. (16) into Eq. (15) yields Eq. (1) with the sought dispersion coefficient B in the form

$$B = \frac{\mathbf{C}_0^* \cdot \hat{\mathbf{W}}\mathbf{C}_0}{\mathbf{C}_0^* \cdot \hat{\mathbf{S}}\mathbf{C}_0} = \frac{\sum_{a=1}^3 W_{aa}|C_a|^2 + 2\,\mathrm{Re}\sum_{a,b=1;a>b}^3 W_{ab}C_a^*C_b}{\sum_{a=1}^3 S_{aa}|C_a|^2 + 2\,\mathrm{Re}\sum_{a,b=1;a>b}^3 S_{ab}C_a^*C_b}. \tag{17}$$

If the sagittal plane $(\mathbf{m},\mathbf{n})$ is a symmetry plane, then Eq. (17), with $a,b=1,2$ corresponding to the in-plane polarized modes, reduces to

$$B = \frac{W_{11} + W_{22} \mp 2\,\mathrm{Im}\, W_{12}}{S_{11} + S_{22} \mp 2\,\mathrm{Im}\, S_{12}}, \tag{18}$$

where the optional sign is inverse to that in $\mathbf{C}_0 \| (1, \pm i)^T$ [see the comment following Eq. (11)].

Let us now define an explicit form of the matrix $\hat{\mathbf{S}}$ of traction derivatives in v and the matrix $\hat{\mathbf{W}}$ of WKB coefficients, which are introduced in Eq. (14) and which appear in the resulting expressions (17) and (18). To do so, we need to specify an optional definition of the system matrix $\mathbf{Q}(y)$ of Eq. (3). The two most convenient and broadly used definitions, which enable a factorization of $\mathbf{Q}(y)$ with respect to one of the dispersion parameters, are the Stroh formulation $\mathbf{Q}(y,k,v) = ik\mathbf{N}_S(y,v)$ and the Thomson–Haskell formulation $\mathbf{Q}(y,\omega,v) = i\omega\mathbf{N}_{TH}(y,v)$, where

$$\mathbf{N}_S = \begin{pmatrix} \mathbf{N}_1 & \mathbf{N}_2 \\ \mathbf{N}_3 - \rho v^2\mathbf{I}_{(3)} & \mathbf{N}_1^{\mathrm{T}} \end{pmatrix},$$

$$\mathbf{N}_{TH} = \begin{pmatrix} s\mathbf{N}_1 & -\mathbf{N}_2 \\ -v^{-2}\mathbf{N}_3 + \rho\mathbf{I}_{(3)} & s\mathbf{N}_1^T \end{pmatrix},$$

$$\mathbf{N}_1 = -(nn)^{-1}(nm), \quad \mathbf{N}_2 = -(nn)^{-1},$$

$$\mathbf{N}_3 = (mm) - (mn)(nn)^{-1}(nm), \tag{19}$$

with $(ab) \equiv a_i c_{ijkl} b_l$ for $\mathbf{a},\mathbf{b}=\mathbf{m}$ or $\mathbf{n}$ (see Refs. 11–13 for the details). The matrix $\mathbf{N}$ is often called the fundamental elasticity matrix. Note that $\mathbf{N}_S \neq v\mathbf{N}_{TH}$, i.e., its two above formulations imply different (up to scalar factors) definitions of the state vector $\boldsymbol{\eta}$ in Eq. (3) and of the eigenvector $\boldsymbol{\xi}$ in Eq. (5). The eigenvalue problem (5) for the fundamental elasticity matrix taken at $v = v_R^{(0)}$ may be specialized correspondingly as

$$\left[\mathbf{N}_S(0, v_R^{(0)}) - p_{0\alpha}\mathbf{I}\right]\boldsymbol{\xi}_{0\alpha}^{(S)} = \mathbf{0}$$

or

$$\left[\mathbf{N}_{TH}(0, v_R^{(0)}) - \frac{p_{0\alpha}}{v_R^{(0)}}\mathbf{I}\right]\boldsymbol{\xi}_{0\alpha}^{(TH)} = \mathbf{0}, \tag{20}$$

where the both sets of eigenvectors $\boldsymbol{\xi}_{0\alpha} = (\mathbf{u}_{0\alpha}\,\mathbf{f}_{0\alpha})^T$ are normalized by the same condition $\boldsymbol{\xi}_{0\alpha} \cdot \mathbf{T}\boldsymbol{\xi}_{0\alpha} (= 2\mathbf{u}_{0\alpha} \cdot \mathbf{f}_{0\alpha}) = 1$, which renders the physical dimensions $1/\rho^{1/2}v$ and $\rho^{1/2}v$ to $\mathbf{u}_{0\alpha}^{(S)}$ and $\mathbf{f}_{0\alpha}^{(S)}$, and $1/(\rho v)^{1/2}$ and $(\rho v)^{1/2}$ to $\mathbf{u}_{0\alpha}^{(TH)}$ and $\mathbf{f}_{0\alpha}^{(TH)}$. In these terms, the components of matrices $\hat{\mathbf{S}}$ and $\hat{\mathbf{W}}$ are as follows:

$$S_{ab} = 2i\rho(0)v_R^{(0)2}\frac{\mathbf{u}_{0a}^{(S)*}\cdot\mathbf{u}_{0b}^{(S)}}{p_{0a}^{*}-p_{0b}} = 2i\rho(0)v_R^{(0)}\frac{\mathbf{u}_{0a}^{(TH)*}\cdot\mathbf{u}_{0b}^{(TH)}}{p_{0a}^{*}-p_{0b}}$$

$$= S_{ba}^{*},$$

$$W_{ab} = -v_R^{(0)}\frac{\boldsymbol{\xi}_{0a}^{(S)*}\cdot\mathbf{T}\left[\frac{d}{dy}\mathbf{N}_S(y,v_R^{(0)})\right]_{y=0}\boldsymbol{\xi}_{0b}^{(S)}}{(p_{0a}^{*}-p_{0b})^2} =$$

$$-\frac{\boldsymbol{\xi}_{0a}^{(TH)*}\cdot\mathbf{T}\left[\frac{d}{dy}\mathbf{N}_{TH}(y,v_R^{(0)})\right]_{y=0}\boldsymbol{\xi}_{0b}^{(TH)}}{(p_{0a}^{*}-p_{0b})^2} = W_{ba}^{*}, \quad (21)$$

where $a,b=1,2,3$ ($\mathrm{Im}\, p_{0a}>0$), and S_{ab} are physically dimensionless while W_{ab} are of dimension of frequency as they ought to be.

IV. SUMMARY

The high-frequency dispersion coefficient B in Eq. (1) is given by Eq. (17) or (18) as a ratio of Hermitian forms of the matrix $\hat{\mathbf{S}}$ of surface traction derivatives in v and of the matrix $\hat{\mathbf{W}}$ of the WKB coefficients incorporating the impact of inhomogeneity of material properties $\rho(y)$, $c_{ijkl}(y)$ via their first-order derivative taken with respect to y at the surface $y=0$. In the case of general anisotropy [Eq. (17)], these matrices are contracted with the vector $\mathbf{C}_0$ of partial amplitudes of the Rayleigh wave in the reference homogeneous half-space with constant $\rho=\rho(0)$ and $c_{ijkl}=c_{ijkl}(0)$. This result makes an evident physical sense linking the modal structure of the "zero-order" Rayleigh wave to the dispersive effect of inhomogeneity. The values of $\hat{\mathbf{S}}$, $\hat{\mathbf{W}}$, and $\mathbf{C}_0$ are defined by Eqs. (21) and (11) through the solutions p_{0a}, ξ_{0a} of the eigenvalue problem (20) for the fundamental elasticity matrix (19) taken at $v=v_R^{(0)}$ and $y=0$, and through its first derivative also taken at $y=0$.

ACKNOWLEDGMENTS

The author is grateful to A. P. Kiselev for a useful discussion, and to the anonymous reviewer for helpful comments.

[1] I. A. Viktorov, *Rayieigh and Lamb Waves: Physical Theory and Applications* (Plenum, New York, 1967).

[2] B. L. N. Kennett, *Seismic Wave Propagation in Stratified Media* (Cambridge University Press, Cambridge, 1983).

[3] C. H. Chapman and J. A. Orcutt, "The computation of body wave synthetic seismograms in laterally homogeneous media," Rev. Geophys. **23**, 105–163 (1985).

[4] L. M. Brekhovskikh and O. A. Godin, *Acoustics of Layered Media* (Springer, Berlin, 1992).

[5] V. M. Babich and N. Ya. Kirpichnikova, "A new approach to the problem of the Rayleigh wave propagation along the boundary of a non-homogeneous elastic body," Wave Motion **40**, 209–223 (2004).

[6] V. M. Babich and A. P. Kiselev, "'Nongeometrical' phenomena in propagation of elastic surface waves," in *Surface Waves in Anisotropic and Laminated Bodies and Defects Detection*, NATO Science Series II, Vol. **163**, edited by R. V. Goldstein and G. A. Maugin (Kluwer Academic, Dordrecht, 2004), pp. 119–131.

[7] C. Baron, A. L. Shuvalov, and O. Poncelet, "Impact of localized inhomogeneity on the surface-wave velocity and bulk-wave reflection in solids," Ultrasonics **46**, 1–12 (2007).

[8] V. Aleshin, V. Gusev, and V. Tournat, "Acoustic modes propagating along the free surface of granular media," J. Acoust. Soc. Am. **121**, 2600–2611 (2007).

[9] J. Goossens, P. Leclaire, X. Xu, C. Glorieux, L. Martinez, A. Sola, C. Siligardi, V. Cannillo, T. Van der Donck, and J.-P. Celis, "Surface acoustic wave depth profiling of a functionally graded material," J. Appl. Phys. **102**, 053508 (2007).

[10] A. G. Alenitsyn, "Rayleigh waves in a nonhomogeneous elastic half-space," J. Appl. Math. Mech. **27**, 816–822 (1963).

[11] T. C. T. Ting, *Anisotropic Elasticity* (Oxford University Press, Oxford, 1996).

[12] D. M. Barnett, "Bulk, surface, and interfacial waves in anisotropic linear elastic solids," Int. J. Solids Struct. **37**, 45–54 (2000).

[13] A. L. Shuvalov, O. Poncelet, and M. Deschamps, "General formalism for plane guided waves in transversely inhomogeneous anisotropic plates," Wave Motion **40**, 413–426 (2004).

Cubic nonlinearity in shear wave beams with different polarizations

Mark S. Wochner, Mark F. Hamilton,[a] Yurii A. Ilinskii, and Evgenia A. Zabolotskaya
Applied Research Laboratories, The University of Texas at Austin, Austin, Texas 78713-8029

(Received 29 August 2007; revised 6 February 2008; accepted 7 February 2008)

A coupled pair of nonlinear parabolic equations is derived for the two components of the particle motion perpendicular to the axis of a shear wave beam in an isotropic elastic medium. The equations account for both quadratic and cubic nonlinearity. The present paper investigates, analytically and numerically, effects of cubic nonlinearity in shear wave beams for several polarizations: linear, elliptical, circular, and azimuthal. Comparisons are made with effects of quadratic nonlinearity in compressional wave beams. © *2008 Acoustical Society of America.* [DOI: 10.1121/1.2890739]

PACS number(s): 43.25.Dc [OAS] Pages: 2488–2495

I. INTRODUCTION

The distinguishing feature of nonlinearity in shear waves is that it is primarily cubic rather than quadratic. A derivation of the nonlinear parabolic wave equation for shear wave beams in isotropic solids appeared in 1986.[1] Explicit expressions in terms of elastic moduli were presented for the coefficients of both the quadratic and cubic terms. The equation was solved by perturbation to demonstrate that while wavefront curvature introduces quadratic nonlinearity, it does not permit second harmonic generation directly by the fundamental. Rather, it was shown that the second harmonic is produced by interaction of the fundamental with the third harmonic generated by cubic nonlinearity.

A number of papers followed on wave propagation with cubic nonlinearity in nondispersive media. The 1987 paper by Lee-Bapty and Crighton[2] on plane waves develops a weak shock theory describing the discontinuities that form at both positive and negative gradients in the waveform. In the 1990s began a series of papers by Rudenko and co-workers on diffraction, self-focusing, and other effects in beams with cubic nonlinearity. For discussion of this body of work the reader is referred to two papers by Rudenko and Sapozhnikov[3,4] and the papers cited therein. The forms of the model equations used in these previous investigations restrict their application to nonlinear shear waves with linear polarization. A main purpose of the present investigation is to consider other types of polarization.

Our interest in nonlinear shear waves was motivated by experiments reported by Catheline *et al.*[5] that demonstrate clearly the harmonic generation and shock formation manifested by plane nonlinear shear waves propagating in soft tissue phantoms. The propagation speed of shear waves in soft tissue is extremely low, on the order of a few meters per second, making it relatively easy to generate disturbances with large acoustic Mach numbers. Catheline *et al.* reported a peak acoustic Mach number of 0.38, which is well in excess of acoustic Mach numbers ordinarily encountered with compressional waves. The close agreement they showed between measured waveforms containing shocks and numerical simulations based on a generalized Burgers equation confirmed that the nonlinearity was predominantly cubic.

The same group also reported measurements of elastic constants for soft tissue phantoms.[6] The enormous differences in the values of these constants for a given medium motivated development of a new expansion of the strain energy density in which the effects of shear deformation, which are associated with the small elastic constants, are separated from the effects of compressibility, which are associated with the large constants. The result is a much simplified expression for the strain energy density in nonlinear shear waves.[7] This new expansion was used to derive evolution equations for plane nonlinear shear waves in soft tissue-like media.[8]

In the present paper, the plane wave model[8] is extended to account for diffraction in nonlinear shear wave beams in arbitrary isotropic elastic media. Both components of the particle motion perpendicular to the beam axis are included to account for different polarizations of the beam, and not exclusively the linear polarization that is usually considered. A coupled pair of nonlinear parabolic wave equations is obtained that includes both quadratic and cubic nonlinearity. The present paper investigates, analytically and numerically, the effects of cubic nonlinearity in shear wave beams. Investigation of the quadratic nonlinearity is the subject of a future paper.

Selected results in the present paper have appeared previously in a conference proceedings.[9]

II. BASIC EQUATIONS

The general equation of motion in an elastic medium is[10]

$$\rho \frac{\partial^2 u_i}{\partial t^2} = \frac{\partial \sigma_{ik}}{\partial x_k}, \tag{1}$$

where ρ is the density of the material in its undeformed state, u_i are components of the particle displacement vector, and σ_{ik} is the stress tensor defined by

[a]Electronic mail: hamilton@mail.utexas.edu

 0001-4966/2008/123(5)/2488/8/$23.00 © 2008 Acoustical Society of America

$$\sigma_{ik} = \frac{\partial \mathcal{E}}{\partial(\partial u_i/\partial x_k)}. \tag{2}$$

The strain energy density $\mathcal{E}$ for an isotropic elastic medium may be expanded as follows:[1,7,10]

$$\mathcal{E} = \mu I_2 + \left(\tfrac{1}{2}K - \tfrac{1}{3}\mu\right)I_1^2 + \tfrac{1}{3}AI_3 + BI_1I_2 + \tfrac{1}{3}CI_1^3 + EI_1I_3 + FI_1^2I_2 + GI_2^2 + HI_1^4, \tag{3}$$

where the invariants

$$I_1 = \mathrm{tr}\,\mathbf{u} = u_{ii}, \quad I_2 = \mathrm{tr}\,\mathbf{u}^2 = u_{ik}u_{ki}, \quad I_3 = \mathrm{tr}\,\mathbf{u}^3 = u_{ik}u_{kl}u_{li}, \tag{4}$$

are defined in terms of the Lagrangian strain tensor

$$u_{ik} = \frac{1}{2}\left(\frac{\partial u_i}{\partial x_k} + \frac{\partial u_k}{\partial x_i} + \frac{\partial u_l}{\partial x_i}\frac{\partial u_l}{\partial x_k}\right). \tag{5}$$

Here μ and K are the shear and bulk moduli, respectively; A, B, and C are the third-order elastic constants of Landau and Lifshitz;[10] E, F, G, and H are the fourth-order elastic constants introduced by Zabolotskaya[1] (but without the coefficient D in Zabolotskaya's expansion which, as explained elsewhere,[7] is not required).

To develop equations that describe the propagation of shear waves, the first step is to express the right-hand side of Eq. (1) explicitly in terms of particle displacement, retaining all terms through cubic order. The quadratic terms are given by Gol'dberg.[11] The expression for the cubic terms is rather long and therefore not presented here.

Next, we consider a shear wave beam that propagates in the x_3 direction and introduce the retarded time $\tau = t - x_3/c$, where $c = (\mu/\rho)^{1/2}$ is the small-signal wave speed. As usual, a reduced wave equation is sought by introducing a slow scale corresponding to the moving coordinate system. The following ordering scheme is employed, in which ϵ characterizes the amplitude of the particle displacement transverse to the beam axis:

$$u_1 = \epsilon U_1(\tilde{x}_1, \tilde{x}_2, \tilde{x}_3, \tau), \quad u_2 = \epsilon U_2(\tilde{x}_1, \tilde{x}_2, \tilde{x}_3, \tau), \quad u_3 = \epsilon^2 U_3(\tilde{x}_1, \tilde{x}_2, \tilde{x}_3, \tau), \tag{6}$$

where $\tilde{x}_1 = \epsilon x_1, \tilde{x}_2 = \epsilon x_2$, and $\tilde{x}_3 = \epsilon^2 x_3$ are the slow-scale coordinates.

After substitution in Eq. (1) one obtains at leading (cubic) order in ϵ, for $i=1$,

$$\begin{aligned}\frac{2\mu}{c}\frac{\partial^2 U_1}{\partial \tilde{x}_3\,\partial\tau} &= \mu\left(\frac{\partial^2 U_1}{\partial \tilde{x}_1^2} + \frac{\partial^2 U_1}{\partial \tilde{x}_2^2}\right) + \left(K + \frac{\mu}{3}\right)\frac{\partial S}{\partial \tilde{x}_1} \\ &+ \frac{1}{c^2}\left(\mu + \frac{A}{4}\right)\left(\frac{\partial^2 U_m}{\partial\tau^2}\frac{\partial U_m}{\partial \tilde{x}_1} - \frac{1}{c}\frac{\partial^2 U_3}{\partial\tau^2}\frac{\partial U_1}{\partial\tau} + \frac{\partial^2 U_m}{\partial\tau^2}\frac{\partial U_1}{\partial \tilde{x}_m} - \frac{2}{c}\frac{\partial^2 U_1}{\partial\tau^2}\frac{\partial U_3}{\partial\tau} + 2\frac{\partial^2 U_1}{\partial \tilde{x}_m\,\partial\tau}\frac{\partial U_m}{\partial\tau}\right) \\ &+ \frac{1}{c^2}\left(K + \frac{\mu}{3} + \frac{A}{4} + B\right)\left(\frac{\partial^2 U_m}{\partial \tilde{x}_1\,\partial\tau}\frac{\partial U_m}{\partial\tau} + \frac{\partial S}{\partial\tau}\frac{\partial U_1}{\partial\tau}\right) + \frac{1}{c^2}\left(K - \frac{2\mu}{3} + B\right)S\frac{\partial^2 U_1}{\partial\tau^2} \\ &+ \frac{1}{c^4}\left(\frac{2\mu}{3} + \frac{K}{2} + \frac{A}{2} + B + G\right) \times \frac{\partial}{\partial\tau}\left\{\frac{\partial U_1}{\partial\tau}\left[\left(\frac{\partial U_1}{\partial\tau}\right)^2 + \left(\frac{\partial U_2}{\partial\tau}\right)^2\right]\right\},\end{aligned} \tag{7}$$

where $m=1,2$ is a summation index over components in the plane perpendicular to the x_3 axis, and

$$S = \frac{\partial U_1}{\partial \tilde{x}_1} + \frac{\partial U_2}{\partial \tilde{x}_2} - \frac{1}{c}\frac{\partial U_3}{\partial\tau}. \tag{8}$$

At leading order one also obtains for the divergence $\boldsymbol{\nabla}\cdot\mathbf{u} = \partial u_l/\partial x_l = \epsilon^2 S$. The result for $i=2$ is obtained by reversing the subscripts 1 and 2 in Eq. (7). For $i=3$, the leading order is quadratic in ϵ and one obtains

$$S = -\frac{1}{2c^2}\left(K + \frac{\mu}{3}\right)^{-1}\left(K + \frac{4\mu}{3} + \frac{A}{2} + B\right) \times \left[\left(\frac{\partial U_1}{\partial\tau}\right)^2 + \left(\frac{\partial U_2}{\partial\tau}\right)^2\right]. \tag{9}$$

Substitution of Eq. (9) in Eq. (7) and in the corresponding equation for U_2 yields, after reinstating the original coordinates and particle displacements, and using (x,y,z) in place of (x_1,x_2,x_3),

$$\frac{\partial^2 u_x}{\partial z\,\partial\tau} = \frac{c}{2}\nabla_\perp^2 u_x + \frac{1}{2c}\left(1 + \frac{A}{4\mu}\right)Q_{xy} + \frac{\beta}{3c^3}\frac{\partial}{\partial\tau}\left\{\frac{\partial u_x}{\partial\tau}\left[\left(\frac{\partial u_x}{\partial\tau}\right)^2 + \left(\frac{\partial u_y}{\partial\tau}\right)^2\right]\right\}, \tag{10}$$

$$\frac{\partial^2 u_y}{\partial z\,\partial\tau} = \frac{c}{2}\nabla_\perp^2 u_y + \frac{1}{2c}\left(1 + \frac{A}{4\mu}\right)Q_{yx} + \frac{\beta}{3c^3}\frac{\partial}{\partial\tau}\left\{\frac{\partial u_y}{\partial\tau}\left[\left(\frac{\partial u_x}{\partial\tau}\right)^2 + \left(\frac{\partial u_y}{\partial\tau}\right)^2\right]\right\}, \tag{11}$$

where $\nabla_\perp^2 = \partial^2/\partial x^2 + \partial^2/\partial y^2$ is the Laplacian in the plane perpendicular to the beam axis, all quadratic terms are contained in

$$Q_{xy} = \frac{\partial^2 u_y}{\partial\tau^2}\frac{\partial u_y}{\partial x} + \frac{\partial^2 u_y}{\partial\tau^2}\frac{\partial u_x}{\partial y} + 2\frac{\partial^2 u_x}{\partial y\,\partial\tau}\frac{\partial u_y}{\partial\tau} - \frac{\partial^2 u_y}{\partial y\,\partial\tau}\frac{\partial u_x}{\partial\tau} - 2\frac{\partial^2 u_x}{\partial\tau^2}\frac{\partial u_y}{\partial y} - \frac{\partial^2 u_y}{\partial x\,\partial\tau}\frac{\partial u_y}{\partial\tau}, \tag{12}$$

and the coefficient of nonlinearity for the cubic terms is

$$\beta = \frac{3}{4\mu}\left(K + \tfrac{4}{3}\mu + A + 2B + 2G\right) - \frac{3}{4\mu}\frac{\left(K + \frac{4}{3}\mu + \frac{1}{2}A + B\right)^2}{K + \frac{1}{3}\mu}. \tag{13}$$

Equations (10) and (11) differ only by the reversal of x and y.

In the absence of the second term in Eq. (13), Eqs. (10) and (11) agree with Eq. (14) of Zabolotskaya.[1] The second

term in Eq. (13) is associated with cubic nonlinearity arising from quadratic nonlinearity due to the fact that the right-hand side of Eq. (8), by virtue of Eq. (9), is quadratic at leading order when expressed in terms of only transverse particle displacements. The absence of this contribution to the cubic nonlinearity in Eq. (14) of Ref. 1 was noted by Enflo *et al.*[12] but their expression corresponding to the second term in Eq. (13) differs from ours.

The origin of the second term in Eq. (13) is not connected with diffraction and can be understood from Gol'dberg's[11] Eqs. (6) and (7) for plane waves. Gol'dberg defines a quadratic nonlinearity coefficient $\gamma=K+\frac{4}{3}\mu+\frac{1}{2}A+B$, the square of which appears in Eq. (13). The longitudinal wave generated by the quadratic nonlinearity of a shear wave is proportional to γ, and the shear wave generated by interaction of the longitudinal wave with the original shear wave introduces another factor of γ, resulting in the coefficient γ^2 associated with this third-order process. The corresponding term derived by Enflo *et al.*[12] contains only one factor of γ.

For soft elastic media characterized by $\mu \ll K$, the second term in Eq. (13) is negligible relative to the first. This can be shown by making use of the following relations between the elastic constants for such media:[7,13] $A=O(\mu)$, $B=-K+O(\mu)$, and $G=\frac{1}{2}K+O(\mu)$. Substitution in Eq. (13) reveals that the first term is $O(1)$ and second term is $O(\mu/K)$. For soft tissue, with μ/K of order 10^{-5} and possibly smaller, the second term in Eq. (13) is insignificant. In this case, the elastic energy density can be expressed in a reduced form that depends on only three elastic constants,[7]

$$\mathcal{E}=\mu I_2+\tfrac{1}{3}AI_3+DI_2^2, \tag{14}$$

rather than the nine in Eq. (3), and all three constants are of the same order. This reduced equation for the energy density leads to[8]

$$\beta=\frac{3}{2}\left(1+\frac{\frac{1}{2}A+D}{\mu}\right) \tag{15}$$

in place of Eq. (13).

Enflo *et al.*[12] present a result similar to Eq. (10) for a shear wave beam that is linearly polarized in the x direction, but without the quadratic terms, and without the corresponding equation for u_y. While Q_{xy} and Q_{yx} vanish for plane waves, they do not for beams. For a source that is linearly polarized in the x direction, u_y and therefore Q_{xy} are in fact zero in the source plane. However, in Eq. (11) the first and last terms in Q_{yx} depend only on u_x, giving rise to a nonzero value of u_y due to quadratic nonlinearity. Simply stated, quadratic nonlinearity prevents the existence of a pure linearly polarized shear wave beam.

Cubic nonlinearity can be more pronounced than quadratic nonlinearity due to the quasiplanar nature of wavefronts in directional sound beams. In the present paper we consider only the effects of cubic nonlinearity.

In the absence of quadratic nonlinearity, one may introduce the particle velocities $v_x=\partial u_x/\partial\tau$ and $v_y=\partial u_y/\partial\tau$ in Eqs. (10) and (11) to obtain, following integration with respect to τ, the coupled equations

$$\frac{\partial v_x}{\partial z}=\frac{\beta}{3c^3}\frac{\partial}{\partial\tau}[v_x(v_x^2+v_y^2)]+\frac{\eta}{2\rho c^3}\frac{\partial^2 v_x}{\partial\tau^2}+\frac{c}{2}\int_{-\infty}^{\tau}(\nabla_\perp^2 v_x)d\tau', \tag{16}$$

$$\frac{\partial v_y}{\partial z}=\frac{\beta}{3c^3}\frac{\partial}{\partial\tau}[v_y(v_x^2+v_y^2)]+\frac{\eta}{2\rho c^3}\frac{\partial^2 v_y}{\partial\tau^2}+\frac{c}{2}\int_{-\infty}^{\tau}(\nabla_\perp^2 v_y)d\tau', \tag{17}$$

where the terms accounting for the shear viscosity η are introduced as for plane waves.[8] Without the diffraction and absorption terms, Eqs. (16) and (17) are the same as Eqs. (53) and (54) in Ref. 8. When the source functions are axisymmetric and can be expressed as $v_{x0}(r,t)$ and $v_{y0}(r,t)$, where $r=(x^2+y^2)^{1/2}$, it is evident that the radiated sound beam is axisymmetric, in which case $\nabla_\perp^2=\partial^2/\partial r^2+r^{-1}(\partial/\partial r)$.

Comparisons will be made with nonlinear compressional wave beams, which are described by the KZK equation for the particle velocity component in the z direction:

$$\frac{\partial v_z}{\partial z}=\frac{\beta_l}{c_l^2}v_z\frac{\partial v_z}{\partial\tau}+\frac{\delta}{2c_l^3}\frac{\partial^2 v_z}{\partial\tau^2}+\frac{c_l}{2}\int_{-\infty}^{\tau}(\nabla_\perp^2 v_z)d\tau'. \tag{18}$$

The subscript l is used to identify parameters that are specific to compressional waves. Here, $\tau=t-z/c_l$ is the retarded time, $c_l=[(K+\frac{4}{3}\mu)/\rho]^{1/2}$ the small-signal compressional wave speed, δ is a diffusivity that accounts for sound absorption due to both shear and bulk viscosity, and also heat condition, and

$$\beta_l=-\frac{3}{2}-\frac{A+3B+C}{K+\frac{4}{3}\mu} \tag{19}$$

is the coefficient of nonlinearity. The coefficient of nonlinearity for a liquid is $\beta_l=1+B_l/2A_l$, where B_l/A_l is the parameter of nonlinearity for liquids that is obtained from the equation of state relating the pressure and density.

III. LINEAR POLARIZATION

For beams that are linearly polarized along the x axis, $v_y=0$ and Eq. (16) reduces to

$$\frac{\partial v_x}{\partial z}=\frac{\beta}{c^3}v_x^2\frac{\partial v_x}{\partial\tau}+\frac{\eta}{2\rho c^3}\frac{\partial^2 v_x}{\partial\tau^2}+\frac{c}{2}\int_{-\infty}^{\tau}(\nabla_\perp^2 v_x)d\tau'. \tag{20}$$

Without the diffraction term, Eq. (20) reduces to Eq. (37) in Ref. 8. Equation (20) is formally equivalent to Eq. (18) for compressional wave beams apart from the cubic rather than quadratic nonlinearity. The linearized forms of the two equations thus possess the same Green's function, which may be used to compare the corresponding solutions for harmonic generation.

We begin by assuming a source condition with time dependence $e^{i\omega t}$ and write $v_x=v_{x1}+v_{x3}$, where $|v_{x3}|\ll|v_{x1}|$ and

$$v_{xn}(r,z,\tau) = \mathrm{Re}[w_{xn}(r,z)e^{in\omega\tau}]$$
$$= \tfrac{1}{2}w_{xn}(r,z)e^{in\omega\tau} + \text{c.c.}, \quad n = 1,3. \tag{21}$$

The integral solutions of Eq. (20) for the first and third harmonic are thus (see, e.g., Ref. 14, Chap. 8)

$$w_{x1}(r,z) = 2\pi\int_0^\infty w_{x1}(r',0)g_1(r,z|r',0)r'dr', \tag{22}$$

$$w_{x3}(r,z) = \frac{i\pi\beta k}{2c^2}\int_0^z\int_0^\infty w_{x1}^3(r',z')g_3(r,z|r',z')r'dr'dz', \tag{23}$$

where $k=\omega/c$ and the Green's function is

$$g_n(r,z|r',z') = \frac{ink}{2\pi(z-z')}J_0\left(\frac{nkrr'}{z-z'}\right)$$
$$\times\exp\left[-n^2\alpha(z-z') - \frac{ink(r^2+r'^2)}{2(z-z')}\right], \tag{24}$$

and where $\alpha=\eta\omega^2/2\rho c^3$ is the absorption coefficient at the source frequency. For a source with Guassian amplitude shading described by $w_{x1}(r,0)=v_0\exp(-r^2/a^2)$ the integrals yield

$$w_{x1}(r,z) = \frac{v_0}{1-iz/z_0}\exp\left(-\alpha z - \frac{r^2/a^2}{1-iz/z_0}\right), \tag{25}$$

$$w_{x3}(r,z) = \frac{\beta v_0^3 k z_0}{4c^2(1-iz/z_0)^2}\exp\left(-9\alpha z - \frac{3r^2/a^2}{1-iz/z_0}\right.$$
$$\left.-i6\alpha z_0\right)\{E_2[-i6\alpha z_0(1-iz/z_0)]$$
$$-(1-iz/z_0)E_2[-i6\alpha z_0]\}, \tag{26}$$

where $z_0=ka^2/2$ is the Rayleigh distance, and $E_2(\xi)$ is the exponential integral defined by $E_m(\xi)=\int_1^\infty e^{-\xi t}t^{-m}dt$ with $m=2$. Equation (25) is the same as the solution for a compressional wave.

To facilitate comparison of Eq. (26) with the corresponding solution for second-harmonic generation in a compressional wave beam[14] we set $\alpha=0$ to obtain[1]

$$w_{x3}(r,z) = \frac{i\beta v_0^3 kz}{4c^2(1-iz/z_0)^2}\exp\left(-\frac{3r^2/a^2}{1-iz/z_0}\right). \tag{27}$$

The amplitude along the axis of the beam in the near field ($z\ll z_0$) increases in proportion to z, just like the second harmonic in a compressional wave. In the far field ($z\gg z_0$), however, Eq. (27) describes a z^{-1} decay rate, as for a spherical wave in the linear approximation. In contrast, the second harmonic in a compressional wave decays as $z^{-1}\ln z$ in the far field,[14] which is slower than spherical spreading due to the unending transfer of energy from the fundamental in a lossless medium. When absorption is negligible, all harmonics in the shear wave beam decay as z^{-1} in the far field, whereas all harmonics in the compressional wave beam decay more slowly than z^{-1}.

The decay rate of nonlinear shear waves in the far field can be explained by replacing the absorption and diffraction terms in Eq. (20) with a term that accounts only for spherical spreading:

$$\frac{\partial v_x}{\partial z} + \frac{v_x}{z} = \frac{\beta}{c^3}v_x^2\frac{\partial v_x}{\partial\tau}. \tag{28}$$

Given a waveform $v_x=f(\tau)$ prescribed at some distance $z=z_0$ in the spherical wave field, the implicit solution describing evolution of the waveform prior to shock formation may be written in the form

$$v_x(z,\tau) = \frac{z_0}{z}v(z,\tau), \quad \text{where} \quad v = f\left[\tau + \frac{\beta}{c^3}v^2 z_0\left(1-\frac{z_0}{z}\right)\right]. \tag{29}$$

At distances $z\gg z_0$ the waveform ceases to depend on z, which is to say that no further nonlinear distortion of the waveform takes place. The particle velocity waveform $v_x(z,\tau)$ thus ultimately decays as z^{-1} without further change in shape. This phenomenon is referred to as waveform freezing. Spherical spreading does not cause waveform freezing in compressional waves.

When absorption is taken into account the behavior of nonlinearly generated harmonics in the far field is quite different. The asymptotic forms of Eqs. (25) and (26) are

$$w_{x1}(\theta,z) \sim iv_0z_0\frac{e^{-\alpha z}}{z}D(\theta)\exp\left(-\tfrac{1}{2}ikz\tan^2\theta\right), \tag{30}$$

$$w_{x3}(\theta,z) \sim \frac{\beta v_0^3 k z_0^3}{24\alpha c^2}\frac{e^{-3\alpha z}}{z^3}D^3(\theta)\exp\left(-\tfrac{3}{2}ikz\tan^2\theta\right), \tag{31}$$

where

$$D(\theta) = \exp\left[-\tfrac{1}{4}(ka\tan\theta)^2\right] \tag{32}$$

is the directivity function for a Gaussian beam in the linear approximation, and θ is the angle with respect to the beam axis, defined by $\tan\theta=r/z$. The third harmonic is seen to be proportional to the cube of the fundamental.

Because of the quadratic dependence of the absorption coefficient on frequency, all higher harmonics in a linearly polarized beam follow the trend $w_{xn}(\theta,z)\propto w_{x1}^n(\theta,z)$ in the far field.[14] This absorption law also permits far-field solutions to be used in combination with geometrical acoustics to obtain asymptotic solutions for harmonics when an analytic solution for the primary wave radiated by a particular source may be available only in the far field. Such is the case for radiation by a circular disk of radius a, the source condition for which is $w_{x1}(r,0)=v_0H(a-r)$, where H is the Heaviside unit step function. The far-field solutions for the fundamental and third harmonic in this case are given again by Eqs. (30) and (31), respectively, but with

$$D(\theta) = \frac{2J_1(ka\tan\theta)}{ka\tan\theta}. \tag{33}$$

IV. ELLIPTICAL POLARIZATION

For elliptical polarization, the x and y components of the particle velocity are in phase quadrature, and one may write the source condition in the form

$$v_x(r,0,t) = v_0\,\mathrm{Re}[f(r)e^{i\omega t}], \quad v_y(r,0,t) = sv_0\,\mathrm{Im}[f(r)e^{i\omega t}], \tag{34}$$

where s varies from zero for linear polarization along the x axis to unity for circular polarization. For a Gaussian amplitude shaded source with $f(r)=\exp(-r^2/a^2)$ one obtains, in place of Eq. (27),

$$w_{x3}(r,z) = \frac{i(1-s^2)\beta v_0^3 kz}{4c^2(1-iz/z_0)^2}\exp\left(-\frac{3r^2/a^2}{1-iz/z_0}\right), \tag{35}$$

$$w_{y3}(r,z) = \frac{s(1-s^2)\beta v_0^3 kz}{4c^2(1-iz/z_0)^2}\exp\left(-\frac{3r^2/a^2}{1-iz/z_0}\right), \tag{36}$$

with $v_{x3}(r,z,\tau)=\mathrm{Re}[w_{x3}(r,z)e^{i3\omega\tau}]$ and $v_{y3}(r,z,\tau)=\mathrm{Im}[w_{y3}(r,z)e^{i3\omega\tau}]$. The two components differ only by the factor $-is$, as do the corresponding components at the source frequency. This same ratio is not maintained for the third and higher harmonics when higher-order nonlinear interactions are taken into account. Numerical solutions reveal that the main differences arise in the relative phases of the harmonics in the frequency spectra of v_x and v_y. For weak or moderate nonlinearity, the relative amplitudes remain nearly the same.

Note that the third harmonic vanishes for circular polarization, $s=1$, which is the case considered next.

V. CIRCULAR POLARIZATION

Given the absence of third-harmonic generation for circular polarization, we seek a monofrequency solution in the form

$$v_x(r,z,\tau) = \mathrm{Re}[w(r,z)e^{i\omega\tau}], \quad v_y(r,z,\tau) = \mathrm{Im}[w(r,z)e^{i\omega\tau}]. \tag{37}$$

Since

$$v_x^2(r,z,\tau) + v_y^2(r,z,\tau) = |w(r,z)|^2, \tag{38}$$

the quantity $v_x^2+v_y^2$ is independent of time and may be removed from under the time derivatives in Eqs. (16) and (17). For a circularly polarized plane wave in a lossless medium, where $w=\mathrm{const}\equiv v_0$, the wave propagates as a small signal and the only effect of nonlinearity is to change the propagation speed from c to $(1+\beta v_0^2/3c^2)c$.[8] The amplitude w is not constant in a diffracting beam, and in particular it varies across the beam. Different parts of the beam thus propagate at different phase speeds according to the square of the local acoustic Mach number and the sign of the nonlinearity coefficient. Self-defocusing occurs for $\beta>0$ because the beam propagates faster along its axis than off axis. Conversely, self-focusing occurs for $\beta<0$.

The evolution equation for w is obtained by substituting Eq. (37) into either Eq. (16) or Eq. (17) to obtain

$$i\left(\frac{\partial w}{\partial z}+\alpha w\right) - \frac{1}{2k}\nabla_\perp^2 w + \frac{\beta k}{3c^2}|w|^2 w = 0, \tag{39}$$

which is a damped nonlinear Schrödinger equation. In the absence of damping it is the classical model equation for self-focusing of linearly polarized optical beams, and it has also been analyzed in connection with circularly polarized optical beams.[15] For a circularly polarized shear wave beam that is radiated by a Gaussian source into a lossless medium, wavefront curvature due to self-action in the near field becomes comparable with wavefront curvature due to diffraction for v_0/c of order $|\beta|^{-1/2}(ka)^{-1}$.

The main point to be made is that cubic nonlinearity in circularly polarized shear wave beams produces no harmonic generation and therefore no waveform distortion. Its only effect is to cause self-focusing or self-defocusing depending on the sign of β.

VI. AZIMUTHAL POLARIZATION

Azimuthal polarization, which produces a torsional wave beam, results from a source that exhibits only rotational motion about the z axis. For simplicity the source is assumed to be axisymmetric, such that in the cylindrical coordinates (r,ϕ,z) one obtains for the components of the particle velocity vector in the plane perpendicular to the z axis $v_r=0$ and $v_\phi=v_\phi(r,z,\tau)$. Then $v_x=-v_\phi\sin\phi$, $v_y=v_\phi\cos\phi$, $v_x^2+v_y^2=v_\phi^2$, and both Eqs. (16) and (17) yield

$$\frac{\partial v_\phi}{\partial z} = \frac{\beta}{c^3}v_\phi^2\frac{\partial v_\phi}{\partial\tau} + \frac{\eta}{2\rho c^3}\frac{\partial^2 v_\phi}{\partial\tau^2} + \frac{c}{2}\int_{-\infty}^{\tau}\left(\frac{\partial^2 v_\phi}{\partial r^2}+\frac{1}{r}\frac{\partial v_\phi}{\partial r}-\frac{v_\phi}{r^2}\right)d\tau'. \tag{40}$$

Equation (40) differs from Eq. (20) for linear polarization only by the addition of the term $-r^{-2}$ to the transverse Laplacian $\nabla_\perp^2=\partial^2/\partial r^2+r^{-1}(\partial/\partial r)$. Torsional waves are often more conveniently expressed in terms of the angular velocity in the medium, $\Omega=\partial\phi/\partial\tau$, for which $v_\phi=r\Omega$ and Eq. (40) becomes

$$\frac{\partial\Omega}{\partial z} = r^2\frac{\beta}{c^3}\Omega^2\frac{\partial\Omega}{\partial\tau} + \frac{\eta}{2\rho c^3}\frac{\partial^2\Omega}{\partial\tau^2} + \frac{c}{2}\int_{-\infty}^{\tau}\left(\frac{\partial^2\Omega}{\partial r^2}+\frac{3}{r}\frac{\partial\Omega}{\partial r}\right)d\tau'. \tag{41}$$

From Eq. (41) it is evident that nonlinearity vanishes along the axis of the beam.

We again consider third-harmonic generation, here with $v_\phi=v_{\phi1}+v_{\phi3}$ and

$$v_{\phi n}(r,z,\tau) = \mathrm{Re}[w_{\phi n}(r,z)e^{in\omega\tau}], \quad n=1,3. \tag{42}$$

The integral solutions of Eq. (40) for the fundamental and third harmonic are given by Eqs. (22) and (23) with the subscript x replaced everywhere by ϕ, and with

$$g_n(r,z|r',z') = -\frac{nk}{2\pi(z-z')}J_1\left(\frac{nkrr'}{z-z'}\right) \times \exp\left[-n^2\alpha(z-z') - \frac{ink(r^2+r'^2)}{2(z-z')}\right]. \tag{43}$$

Equation (43) differs from Eq. (24) by a multiplicative factor i and by J_1 in place of J_0. The corresponding Green's function for Eq. (41) is obtained by multiplying the right-hand side of Eq. (43) by r'/r.

The source condition is expressed in the form

$$\Omega(r,0,t) = \Omega_0 \,\mathrm{Re}[f(r)e^{i\omega t}], \tag{44}$$

such that $w_{\phi 1}(r,0)=\Omega_0 r f(r)$. We first take $f(r)=\exp(-r^2/a^2)$ and obtain for the angular velocity at the source frequency

$$W_1(r,z) = \frac{\Omega_0}{(1-iz/z_0)^2}\exp\left(-\alpha z - \frac{r^2/a^2}{1-iz/z_0}\right), \tag{45}$$

with $\Omega_n(r,z,\tau)=\mathrm{Re}[W_n(r,z)e^{in\omega\tau}]$. In the far field the decay rate associated with spherical spreading is z^{-2} rather than z^{-1}. This is a consequence of the dipole-like nature of the source, and therefore the entire field, because $v_{x,y}(r,\phi,z,\tau)=-v_{x,y}(r,\phi+\pi,z,\tau)$. For any pair of points that are symmetric with respect to the z axis, the particle velocity vectors in the (x,y) plane are equal in magnitude and opposite in direction.

The integral for the third harmonic does not appear to admit a closed-form solution for a Gaussian beam. However, as discussed at the end of Sec. III, an analytic solution for the primary wave in the far field is sufficient to determine the corresponding asymptotic solution for the third harmonic. We thus consider radiation from a circular disk of radius a, for which $f(r)=H(a-r)$ in Eq. (44). The solutions for the fundamental and third harmonic in the far field are found to be

$$W_1(\theta,z) \sim -\frac{1}{2}\Omega_0 z_0^2 \frac{e^{-\alpha z}}{z^2} D(\theta)\exp\left(-\tfrac{1}{2}ikz\tan^2\theta\right), \tag{46}$$

$$W_3(\theta,z) \sim -\frac{i\beta\Omega_0^3 z_0^5}{384\alpha c^2}\frac{e^{-3\alpha z}}{z^4}(ka\tan\theta)^2 D^3(\theta) \times \exp\left(-\tfrac{3}{2}ikz\tan^2\theta\right), \tag{47}$$

where the directivity function for the primary wave,

$$D(\theta) = \frac{8J_2(ka\tan\theta)}{(ka\tan\theta)^2}, \tag{48}$$

is normalized to be unity on axis.

Like the linear solution for a Gaussian torsional beam, Eq. (46) exhibits a $z^{-2}e^{-\alpha z}$ decay rate. Unlike the linear solution for a Gaussian beam, the directivity function is different from that for a linearly polarized beam radiated by a source with the same amplitude distribution [compare Eqs. (25) and (45), and then Eqs. (33) and (48)]. Due to the factor $(ka\tan\theta)^2$ multiplying $D^3(\theta)$, the third harmonic vanishes along the axis of the beam in the far field. The maximum amplitude of the third harmonic in the far field is located at the angle θ_0 where $ka\tan\theta_0=1.92$, for which $(ka\tan\theta_0)^2D^3(\theta_0)=1.41$.

Equations (31) and (47) may now be used to compare the maximum amplitudes in a linearly polarized beam and an azimuthally polarized beam. To relate the source amplitudes, the kinetic energies associated with translation and rotation of the disk are matched to obtain $\Omega_0=2^{1/2}v_0/a$, for which the far-field formulas yield $|w_{\phi 3}(\theta_0,z)/w_{x3}(0,z)|\sim 0.12$. In terms of harmonic generation, azimuthal polarization is thus significantly less efficient than linear polarization.

VII. SOLUTION ALGORITHMS

Numerical results are presented in Sec. VIII for shear wave beams radiated in the z direction by a circular disk of radius a. The source condition for elliptically polarized beams, including linearly and circularly polarized beams, is

$$v_x(r,0,t) = v_0 H(a-r)\cos\omega t, \qquad v_y(r,0,t) = sv_0 H(a-r)\sin\omega t. \tag{49}$$

Diffraction is characterized by the Rayleigh distance $z_0=ka^2/2$, nonlinearity by the plane wave shock formation distance $z_{\mathrm{sh}}=c^2/\beta k v_0^2$, and absorption by the length $z_{\mathrm{abs}}=1/\alpha$. In terms of these length scales, the two dimensionless parameters used to characterize solutions of Eqs. (16) and (17) are $A=z_0/z_{\mathrm{abs}}$ for absorption and $N=z_0/z_{\mathrm{sh}}$ for nonlinearity. For plane waves, the Gol'dberg number $\Gamma=Z_{\mathrm{abs}}/z_{\mathrm{sh}}$ is used.

The source condition for azimuthally polarized beams is

$$\Omega(r,0,t) = \Omega_0 H(a-r)\cos\omega t. \tag{50}$$

Since in this case the peak particle velocity in the source plane is $a\Omega_0$, the characteristic shock formation distance is taken to be $z_{\mathrm{sh}}=c^3/\beta\omega a^2\Omega_0^2$. The parameters N and A are otherwise defined as for elliptically polarized beams.

Comparisons are made with solutions of Eq. (18) for compressional wave beams, the source condition for which is

$$v_z(r,0,t) = v_{z0}H(a-r)\cos\omega t. \tag{51}$$

The parameters N, A, and Γ are defined as for shear waves, except with the shock formation distance given instead by $z_{\mathrm{sh}}=c_l/\beta k_l v_{z0}$, where $k_l=\omega/c_l$, because the nonlinearity is quadratic.

For linear polarization, Eq. (20) is solved using the time domain algorithm in Ref. 16 after a minor change is made in the nonlinearity subroutine to account for the cubic nonlinearity. Equation (41) is solved for azimuthal polarization, again with the algorithm in Ref. 16 but without the coordinate transformation. Also, in addition to the change in the nonlinearity subroutine, a minor change is required in the diffraction subroutine. For elliptical polarization, Eqs. (16) and (17) must be solved simultaneously. No implicit analytical solution was discovered for the nonlinearity time step, and a weighted essentially nonoscillatory scheme[17] was used in place of the time base transformation in Ref. 16.

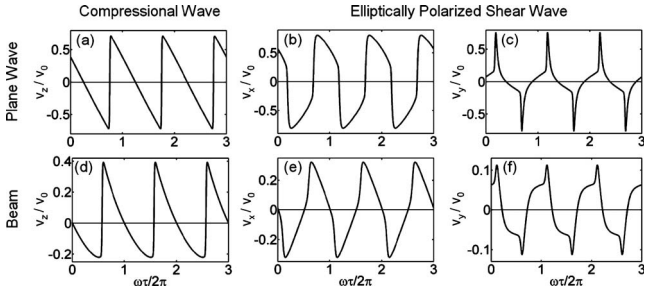


FIG. 1. Axial time waveforms in a compressional wave (first column, v_z) and an elliptically polarized shear wave with $s=0.25$ (second and third columns, v_x and v_y, respectively), both without diffraction [first row, (a)–(c)] and with diffraction [second row, (d)–(f)]. The distance for the plane waves is $z=3z_{sh}$ with $\Gamma=100$, and for the beams it is $z=3z_0$ with $N=1$ and $A=0.01$.

VIII. NUMERICAL RESULTS

Axial time waveforms are presented in Fig. 1 for a compressional wave (first column, v_z) and for an elliptically polarized shear wave with $s=0.25$ (second and third columns, v_x and v_y, respectively), both without diffraction [first row, Figs. 1(a)–1(c)] and with diffraction [second row, Figs. 1(d)–1(f)]. The distance for the plane waves is $z=3z_{sh}$ with $\Gamma=100$, and for the beams it is $z=3z_0$ with $N=1$ and $A=0.01$. The plane compressional waveform (a) has the classical sawtooth shape associated with quadratic nonlinearity. A distinctive feature of shear waves is that there are two shocks per period. In the y component, spikes appear at the locations where shocks appear in the x component. Effects of beam diffraction are illustrated in the lower row. Note that the waveform asymmetry in the compressional wave beam is absent from the shear wave beam. This is because the cubic nonlinearity generates only odd harmonics in the nonlinear shear wave, and any waveform that can be expressed as a Fourier series of odd harmonics is necessarily symmetric, regardless of the relative harmonic phase shifts introduced by diffraction. However, if the initial waveform contains even harmonics, diffraction will introduce some degree of waveform asymmetry in a nonlinear shear wave beam. Waveforms calculated for linear polarization are much the same as those shown in Figs. 1(b) and 1(e).

While unrelated to diffraction, the formation of secondary shocks was observed in simulations of elliptically polarized shear waves at high amplitude. Shown in Fig. 2 are waveforms at the three distances (a) $z=3z_{sh}$, (b) $10z_{sh}$, and (c) $15z_{sh}$ for an elliptically polarized plane wave with $s=0.25$ and $\Gamma=500$. In each frame, the velocity component v_x is on the top, v_y on the bottom. Note the small spikes that appear in v_x at $3z_{sh}$ (a). Their locations coincide with the large spikes in v_y. By $10z_{sh}$ (b) the spikes have evolved into small step shocks that have advanced in the waveform (to earlier retarded times, from right to left in the figure). By $15z_{sh}$ (c) the secondary shocks have disappeared. For sufficiently large Γ these secondary shocks may reappear.

Presented in Fig. 3 are harmonic beam patterns at $z=5z_0$ with $N=0.2$ and $A=0.01$ for (a) a compressional wave beam, and for the (b) x and (c) y components in an elliptically polarized shear wave beam with $s=0.25$. The beam

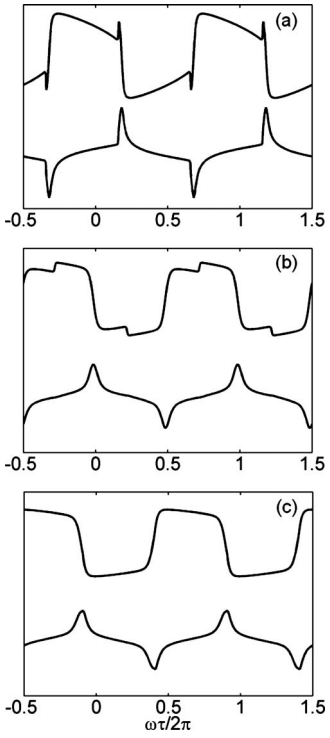


FIG. 2. Waveforms in an elliptically polarized plane wave with $s=0.25$ and $\Gamma=500$ at (a) $z=3z_{sh}$, (b) $10z_{sh}$, and (c) $15z_{sh}$. In each frame, the velocity component v_x is on the top, v_y on the bottom.

patterns for the even harmonics in the compressional wave are deemphasized by use of a lighter line weighting to facilitate comparison of the odd harmonics with those of the shear wave. As with compressional waves, the number of sidelobes in the nth harmonic beam pattern for the shear wave is n times the number in the beam pattern at the source frequency. This is not predicted by Eq. (31) for the third harmonic in the shear wave. The directivity function $D^3(\theta)$ indicates a beam pattern having the same number of sidelobes as at the source frequency, not three times as many. These additional sidelobes, also observed in the beam patterns for the compressional wave, are near-field effects that become less pronounced as either distance or absorption is increased.[14] For weak absorption, the far field for the nonlinearly generated harmonics is not reached until distances far beyond the Rayleigh distance z_0.

Results for an azimuthally polarized beam are presented in Fig. 4 for $N=3$ and $A=0.01$. Figure 4(a) shows harmonic beam patterns at $z=z_0$ for the source frequency and its third

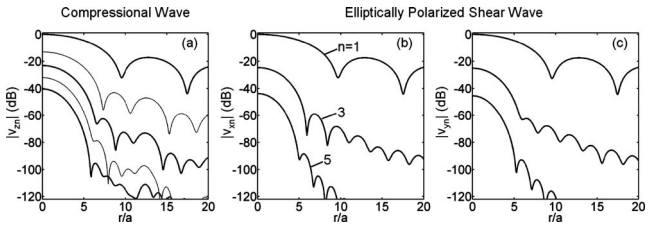


FIG. 3. Harmonic beam patterns at $z=5z_0$ with $N=0.2$ and $A=0.01$ for (a) a compressional wave beam, and for the (b) x and (c) y components in an elliptically polarized shear wave beam with $s=0.25$.

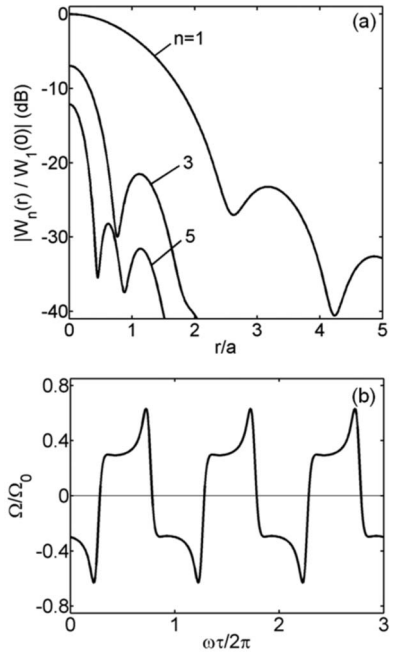


FIG. 4. (a) Harmonic beam patterns and (b) axial time waveform at $z=z_0$ in an azimuthally polarized beam with $N=3$ and $A=0.01$.

and fifth harmonics. Note that the levels of the third and fifth harmonics on the beam axis are maxima, not minima. The discrepancy with Eq. (47), which predicts zero for the amplitude of the third harmonic along the beam axis, is because the wave is not yet in the far field. Even though the nonlinear term in Eq. (41) is zero everywhere along the beam axis, harmonics generated nonlinearly off axis in the near field diffract into the axial region. Figure 4(b) shows the axial waveform at $z=z_0$. Like the waveforms in Figs. 1(e) and 1(f) for the elliptically polarized beam, the waveform in the azimuthally polarized beam is also symmetric.

IX. CONCLUSION

Effects of cubic nonlinearity in shear wave beams were analyzed for linear, elliptical, circular, and azimuthal polarizations, and comparisons were made with effects of quadratic nonlinearity in compressional wave beams. The coupled nonlinear evolution equations that were derived also include quadratic nonlinearity due to diffraction. Effects of quadratic nonlinearity, and the generation of longitudinal components in shear wave beams, are under investigation and will be reported in the future.

ACKNOWLEDGMENTS

This work was supported by NIH Grant No. R03-EB004336, and by the IR&D Program at Applied Research Laboratories.

[1]E. A. Zabolotskaya, "Sound beams in a nonlinear isotropic solid," Sov. Phys. Acoust. **32**, 296–299 (1986).
[2]I. P. Lee-Bapty and D. G. Crighton, "Nonlinear wave motion governed by the modified Burgers equation," Philos. Trans. R. Soc. London, Ser. A **323**, 173–209 (1987).
[3]O. V. Rudenko and O. A. Sapozhnikov, "Wave beams in cubically nonlinear nondispersive media," J. Exp. Theor. Phys. **79**, 220–229 (1994).
[4]O. V. Rudenko and O. A. Sapozhnikov, "Self-action effects for wave beams containing shock fronts," Phys. Usp. **47**, 907–922 (2004).
[5]S. Catheline, J.-L. Gennisson, M. Tanter, and M. Fink, "Observation of shock transverse waves in elastic media," Phys. Rev. Lett. **91**, 164301 (2003).
[6]S. Catheline, J.-L. Gennisson, and M. Fink, "Measurement of elastic nonlinearity of soft solid with transient elastography," J. Acoust. Soc. Am. **114**, 3087–3091 (2003).
[7]M. F. Hamilton, Yu. A. Ilinskii, and E. A. Zabolotskaya, "Separation of compressibility and shear deformation in the elastic energy density," J. Acoust. Soc. Am. **116**, 41–44 (2004).
[8]E. A. Zabolotskaya, M. F. Hamilton, Yu. A. Ilinskii, and G. D. Meegan, "Modeling of nonlinear shear waves in soft solids," J. Acoust. Soc. Am. **116**, 2807–2813 (2004).
[9]M. S. Wochner, M. F. Hamilton, Yu. A. Ilinskii, and E. A. Zabolotskaya, "Nonlinear shear wave beams in soft tissue-like media," *Proceedings of the 19th International Congress on Acoustics*, Madrid, Spain, 2–7 September 2007, Paper No. NLA-03-003-IP.
[10]L. D. Landau and E. M. Lifshitz, *Theory of Elasticity*, 3rd ed. (Pergamon, New York, 1986).
[11]Z. A. Gol'dberg, "Interaction of plane longitudinal and transverse elastic waves," Sov. Phys. Acoust. **6**, 306–310 (1961).
[12]B. O. Enfio, C. M. Hedberg, and O. V. Rudenko, "Wave motion in a medium with a cubic nonlinearity," *Proceedings of the Fourth Polyakov Readings*, St. Petersburg, Russia, 7–10 February 2006, pp. 65–74.
[13]S. Kostek, B. K. Sinha, and A. N. Norris, "Third-order elastic constants for an inviscid fluid," J. Acoust. Soc. Am. **94**, 3014–3017 (1993).
[14]*Nonlinear Acoustics*, edited by M. F. Hamilton and D. T. Blackstock (Academic, New York, 1998).
[15]G. Fibich and B. Ilan, "Self-focusing of circularly polarized beams," Phys. Rev. E **67**, 036622 (2003).
[16]Y.-S. Lee and M. F. Hamilton, "Time-domain modeling of pulsed finite-amplitude sound beams," J. Acoust. Soc. Am. **97**, 906–917 (1995).
[17]C.-W. Shu, "Essentially non-oscillatory and weighted essentially non-oscillatory schemes for hyperbolic conservation laws," in *Advanced Numerical Approximation of Nonlinear Hyperbolic Equations*, Lecture Notes in Mathematics Vol. 1697, edited by A. Quarteroni (Springer, Berlin, 1998), pp. 325–432.

Effect of an entrained air bubble on the acoustics of an ink channel

Roger Jeurissen and Jos de Jong
Physics of Fluids Group, Faculty of Science and Technology and Burgers Center of Fluid Dynamics, University of Twente, P.O. Box 217, 7500 AE Enschede, The Netherlands

Hans Reinten, Marc van den Berg, and Herman Wijshoff
Océ Technologies B.V., P.O. Box 101, 5900 MA Venlo, The Netherlands

Michel Versluis and Detlef Lohse
Physics of Fluids Group, Faculty of Science and Technology and Burgers Center of Fluid Dynamics, MESA+ Institute for Nanotechnology and Institute of Mechanics, Processes and Control-Twente (IMPACT), University of Twente, P.O. Box 217, 7500 AE Enschede, The Netherlands

(Received 15 August 2007; revised 18 December 2007; accepted 26 December 2007)

Piezo-driven inkjet systems are very sensitive to air entrapment. The entrapped air bubbles grow by rectified diffusion in the ink channel and finally result in nozzle failure. Experimental results on the dynamics of fully grown air bubbles are presented. It is found that the bubble counteracts the pressure buildup necessary for the droplet formation. The channel acoustics and the air bubble dynamics are modeled. For good agreement with the experimental data it is crucial to include the confined geometry into the model: The air bubble acts back on the acoustic field in the channel and thus on its own dynamics. This two-way coupling limits further bubble growth and thus determines the saturation size of the bubble. © *2008 Acoustical Society of America.* [DOI: 10.1121/1.2835624]

PACS number(s): 43.25.Yw, 43.20.Mv, 43.35.Ty [CCC] Pages: 2496–2505

I. INTRODUCTION

Drop-on-demand inkjet printing[1] has been and will be applied to many industrial applications,[2] which range from printing color filters for flat panel displays[3] to DNA microarrays.[4] Still, the most common application is the printing of text and graphics on paper. A small volume of ink is deposited on the paper in a very controlled way. The stability of the printing process is crucial, especially because the productivity and accuracy standards are continuously raised. The principle of a piezo printhead is a piezo element, which deforms an ink channel, thereby building up pressure at the nozzle.[5] One of the biggest challenges in piezo-acoustic printing is the entrapment of air bubbles.[6–8] They disturb the pressure buildup at the nozzle and lead to nozzle failure. Therefore, the monitoring of the printing process while printing is crucial.

Air entrapment at the nozzle can be detected by using the actuating piezo as a sensor.[8] An entrapped bubble has to be removed as quickly as possible to continue the printing process. However, waiting for the dissolution of the bubble is very time consuming and decreases the productivity of the printhead. Therefore, it is desirable to actively get rid of the air bubble. To accomplish this, first the bubble dynamics have to be understood. This article focuses on the dynamics of fully grown air bubbles where the jetting of droplets has completely broken down. The entrapped air bubble oscillates in the acoustic field. During bubble compression, gas is pressed out of the bubble, while during expansion dissolved gas enters into the bubble. For a large enough driving pressure the second effect dominates and a net growth of the air bubble results (rectified diffusion, see Refs. 9 and 10). Finally, the bubble reaches a dynamic equilibrium size.

The presence of an equilibrium radius signals the saturation: The bubble has become relatively large, thereby influencing the acoustic waves in the printhead, hence limiting its own oscillations and growth. During actuation, the bubble will then just remain in the ink channel oscillating around its equilibrium radius. By employing a glass connection channel and high speed imaging, the air bubble can be visualized and its dynamics can be resolved.

The dynamics of a bubble in a tube differ from the dynamics of a bubble in an infinite volume of liquid.[11,12] Due to the finite size of the ambient liquid, the natural frequency of oscillation usually decreases when the bubble becomes larger with respect to the pipe.[13,14,22] Qin *et al.*[15] showed that in some cases, the opposite occurs, indicating that the surrounding system and its behavior are relevant for the dynamics of the bubble. When the bubble touches the walls during expansion, the bubble can become nonspherical.[16,17] Cui *et al.*[18] found that for a bubble between two parallel plates, the acoustic field generated by the bubble is essential for the evolution of the bubble. For the saturated bubbles in an inkjet printhead, we find the two-way coupling effect, i.e., the backreaction of the bubble on the acoustic field, to be crucial, whereas for small bubbles this effect can be neglected.[19] To model the two-way coupling, the one-dimensional disk bubble model of Ref. 19 is extended to a fully coupled model. Moreover, the bubble itself is now modelled with a linearized Rayleigh–Plesset equation. We find that with such an extended model the experimental data can be described very well. The two-way coupling effect is found to be crucial. The pressure at the nozzle and the transfer function of

 0001-4966/2008/123(5)/2496/10/$23.00 © 2008 Acoustical Society of America

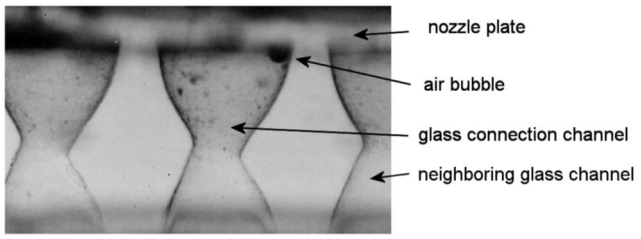


FIG. 1. The entrapped air bubble is trapped in the glass connection channel. When actuating, the fully grown air bubble will just remain oscillating in the channel. Note the position of the air bubble: due to the Bjerknes forces it is pushed against the glass walls. (The bubble is larger than its resonance size.) To the left and right of the channel with the bubble, the neighboring channels can be seen.

the velocity in the nozzle over the actuator voltage are changed significantly by the entrained air bubble.

The article is organized as follows: First, in Sec. II the details of the experimental setup are discussed. Next, in Sec. III, the experimental air bubble dynamics are presented. Section IV is devoted to the bubble model. For readability, some technical details of the model are separated in an appendix. The comparison between the experiments and the model is given in Sec. V. The paper ends with the conclusions and an outlook, Sec. VI.

II. EXPERIMENTAL SETUP

The setup consists of a side-shooter printhead,[19] developed by Océ Technologies. In this printhead, a 5 mm long rectangular ink channel is deformed by a piezo element, thereby generating acoustic waves in the channel. The waves result in a pressure and velocity field near the nozzle. To visualize the dynamics of the entrained air bubble, a glass connection channel was interposed between the ink channel and a glass nozzle plate, similar to Ref. 19. This channel has a length of 400 μm and an hourglass shape. The waist diameter is 80 μm and the maximum diameter 250 μm at the inlet and outlet. On top of the connection channel a glass nozzle plate is glued. The conical nozzles have a diameter of 30 μm at the exit and 50 μm at the inlet. The pulse applied to the printhead is trapezoidal lasting 8 μs (2 μs rise time, 4 μs plateau, and 2 μs fall time), with a repetition rate of 20 kHz.

After the bubble has been entrained, it is allowed to grow to its diffusive equilibrium. The droplet formation process has now ceased completely. The entrained air bubble is visualized by a Shimadzu HPV-1 high-speed camera (maximum frame rate of 1 Mfps) and a bright Olympus light source. The Shimadzu HPV-1 is capable of recording 100 frames and has an exposure time as short as 250 ns. A single frame showing the entrapped air bubble in the glass channel is depicted in Fig. 1. In this article we restrict ourselves to fully developed bubbles, so that the bubbles start every acoustic cycle with the same radius.

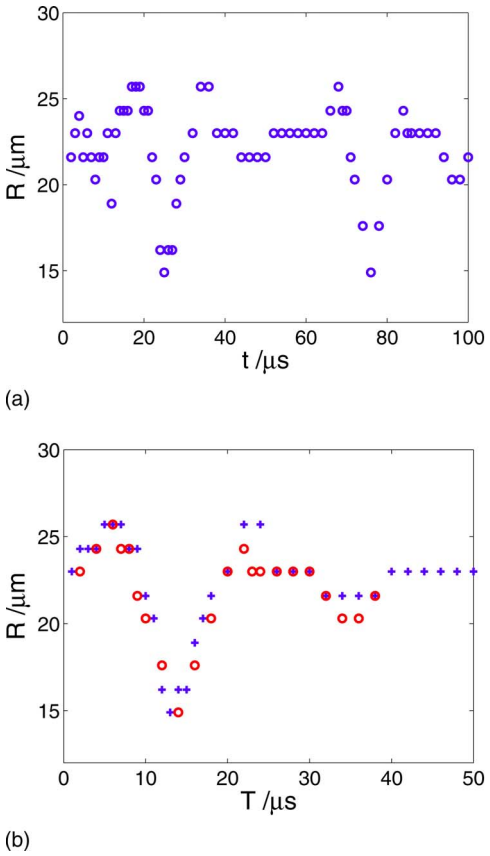


FIG. 2. (Color online) (a) Radius $R(t)$ of the entrained bubble actuated with 190 V as a function of time. The actuation frequency is 20 kHz. (b) To show the reproducibility of the bubble oscillations, the radius is plotted modulo its periodicity $T=1/f=50$ μs. The different cycles are denoted by different symbols.

III. EXPERIMENTAL RESULTS: BUBBLE OSCILLATIONS

For a driving voltage of 190 V, the radius of the bubble is plotted in Fig. 2(a). The equilibrium value was found to be $R_0=23$ μm, the minimum radius was 15 μm and the maximum radius was 26 μm. Two successive acoustic cycles (50 μs each) were captured by the camera with a frame rate of 1 Mfps. Plotting these acoustic cycles modulo the period $T=1/f=50$ μs shows the reproducibility of the oscillation, thereby confirming the assumption of a bubble in dynamical equilibrium, Fig. 2(b). The error in the data is caused by the assumed sphericity of the air bubble and by the limited resolution of the images. The error is estimated to be 2 μm in radius. Note that the expansion of the bubble is smaller than the compression. As we will see in the next section, this is due to the finite size of the ink channel. When reducing the actuating voltage to 120 V, we see a decrease in the saturation size of the air bubble, from $R_0=23$ μm to $R_0=18$ μm, see Fig. 3. The minimum bubble radius is now found to be13 μm, and its maximum is 22 μm.

Note the position of the air bubble: it is pushed against the nozzle plate. We attribute this to the flow field generated by the bubble oscillations. This flow field pulls the bubble toward the walls. This effect is called the secondary Bjerknes force.[20] Inspection of the obtained images reveals the bubble

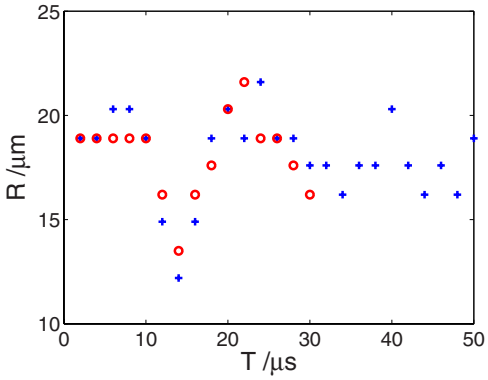


FIG. 3. (Color online) Radius $R(t)$ of the entrained bubble actuated with 120 V as a function of time. The actuation frequency is 20 kHz. Two acoustic cycles are displayed.

shape. When walls are nearby, the bubble oscillates nonspherically. After a large expansion, the shape of the bubble is nearly a quarter of a sphere that is bounded by the nozzle plate and the channel wall. When the bubble is compressed, it becomes nearly spherical. At lower actuation amplitudes, the bubble oscillations are more spherical. This is expected to be caused by a decrease in secondary Bjerknes force. By reducing the actuation voltage, the amplitude of the acoustic field is reduced, and so are the bubble oscillations. Therefore, when the bubble oscillations are decreasing, so is the secondary Bjerknes force that pulls the bubble toward the wall, resulting a less deformed bubble and a reduction of the error introduced by the assumed sphericity of the bubble.

The fast Fourier transform (FFT) is calculated to extract the frequencies present in the oscillations of the bubble, and is depicted in Fig. 4. To obtain a smooth spectrum, the bubble radius fluctuation $\Delta R(t)$ is padded with trailing zeros before calculating the FFT. At both the driving voltage of 120 V where $R_0=18$ μm, and at a driving voltage of 190 V

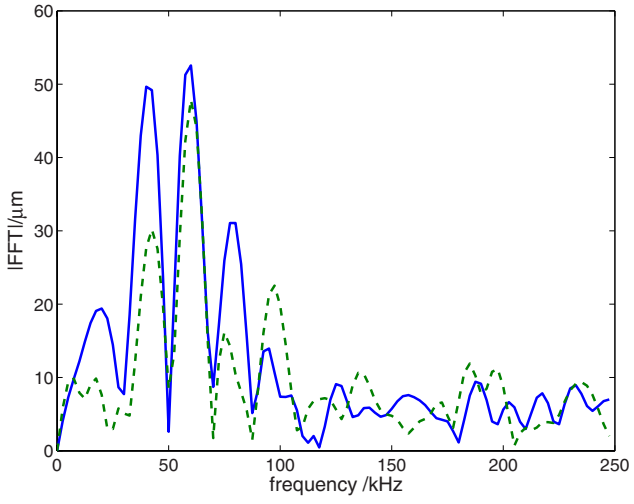


FIG. 4. (Color online) FFT of $\Delta R(t)$ for a driving voltage of 190 V, where the saturated ambient bubble radius is $R_0=23$ μm (solid), and for 120 V, where the saturated ambient bubble radius is $R_0=18$ μm (dashed): The largest maximum remains nearly unchanged at 60 kHz, whereas the second largest maximum at 40 kHz is larger at 190 V.

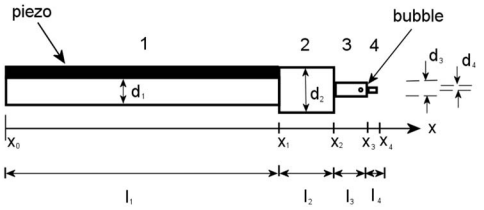


FIG. 5. A schematic overview of the ink channel. It is divided into four sections. Section I is the channel where the piezo is located. Section II is the standard connection channel. Section III is a representation of the glass connection channel, and section IV is the nozzle. The interfaces between the sections are positioned at, respectively, x_1, x_2, and x_3. The (undisturbed) diameters d_j for the four sections $j=1,2,3$, and 4 are $d_1=195$ μm, $d_2=250$ μm, $d_3=80$ μm, and $d_4=30$ μm, respectively.

where $R_0=23$ μm, the main frequency of the bubble oscillations is found to be 60 kHz.

IV. BUBBLE MODEL

A. Simplified geometry

To model the bubble oscillations in the ink channel, a one-dimensional model is used. The cylindrical channel is divided into four sections, see Fig. 5. Section 1 is the actuation channel, where the piezo is located. Section 2 is the standard connection channel. Section 3 is a model of the glass connection channel which we have included for visualization and section 4 is the nozzle. The interface between the sections is positioned at, respectively, x_1, x_2, and x_3. The channel acoustics, bubble dynamics, and nozzle flow are modeled. The bubble is located in the connection channel, and similar to the experiments it experiences the pressure at x_3 between the glass connection channel and the nozzle. The effect of the bubble on the channel acoustics is included in this model.

The channel acoustics is first treated section by section. Then the channel sections are coupled through the matching of interface conditions. The channel deformations are only represented by the cross-sectional variations.

B. Channel acoustics

The channel is actively deformed when applying a voltage to section 1, and passively by the pressure inside the channel. The channel cross-sectional area $A_j(x,t)$ of section j can be written as

$$A_j(x,t) = A_{0,j} + a_{a,j}(t) + a_{p,j}(x,t). \quad (1)$$

Here x is the spatial coordinate in the channel direction, $A_{0,j}$ is the undisturbed, equilibrium, cross-sectional area, $a_{a,j}(t)$ is the variation of cross-sectional area due to the actuator voltage V_j (obviously being nonzero only for section 1), and $a_{p,j}(x,t)$ is the passive deformation of the channel in response to the pressure, $P_j(x,t)$, inside the channel. Note that $a_{a,j}(t)$ is constant over a channel section. For frequencies below the Nyquist frequency $f_n=500$ kHz of the measurements, the wavelength $\lambda > 2.5$ mm is much larger than the channel radius $d_j < 250$ μm, so the radial component of the pressure gradient and velocity become negligible with

TABLE I. Parameters of the channel sections.

j	Section	α_j (V^{-1})	β_j ($m^2\,N^{-1}$)	d_j (μm)	$c_{\mathrm{eff,j}}$ ($m\,s^{-1}$)	l_j (μm)
1	Actuation channel	-3.43×10^{-6}	8.36×10^{-10}	195	803	5000
2	Connection channel	0	0	250	1250	1000
3	Glass connection	0	0	80	1250	149
4	Nozzle	0	0	30	1250	42

respect to the axial components. Linearize the channel deformations:

$$a_{a,j}(t) = \alpha_j V_j(t) A_{0,j}$$

$$a_{p,j}(x,t) = \beta_j P_j(x,t) A_{0,j} \tag{2}$$

with

$$\alpha_j = \frac{1}{A}\left(\frac{\partial A}{\partial V}\right)_P$$

$$\beta_j = \frac{1}{A}\left(\frac{\partial A}{\partial P}\right)_V \tag{3}$$

α_j, β_j, $A_{0,j}$, and $V_j(t)$, for $j=1,2,3,4$, are assumed to be constant over a channel section, α_j and β_j are calculated with a plane-strain calculation in the commercial solid mechanics model ANSYS by Océ Technologies B.V. Each channel section is characterized by the magnitude of these quantities, and the length l_j of the channel section. In Table I we have summarized the parameters characterizing the sections.

The wave equation for a deforming channel can be derived from the Navier–Stokes equation by a control volume analysis in the low reduced frequency approximation[21] where $R_c \ll \lambda$. Insert the linearized channel deformations, Eq. (2), into the wave equation for a deforming channel:

$$\partial_t^2 P_j = c_{\mathrm{eff},j}^2 \partial_x^2 P_j - \alpha_j \rho c_{\mathrm{eff},j}^2 \partial_t^2 V_j - c_{\mathrm{eff},j}^2 \frac{\mu}{A_{0,j}} \partial_x \oint_{\partial A_j} \partial_n u \, ds \tag{4}$$

where u is the axial velocity field, $\mu=0.01\ \mathrm{N\,m^{-2}\,s}$ is the viscosity, $\rho=1090\ \mathrm{kg\,m^{-3}}$ is the density of the ink, and $c_{\mathrm{eff},j}$ the effective phase velocity, which is given by

$$c_{\mathrm{eff},j} = \sqrt{\frac{c^2}{1+\beta_j c^2 \rho}} \tag{5}$$

where $c=1250\ \mathrm{m\,s^{-1}}$ is the velocity of sound in the ink. Equation (4) is linear, and can be solved in the frequency domain, so that in each channel section the pressure is given by

$$P_j(x,t) = p_{1,j} e^{i(\omega t - k_{1,j} x)} + p_{2,j} e^{i(\omega t - k_{2,j} x)} - \alpha_j c_{\mathrm{eff},j}^2 \rho v_j \tag{6}$$

where $p_{1,j}$ and $p_{2,j}$ are the amplitudes of the waves propagating in the negative and positive x direction, respectively. The driving voltage is $V_j = v_j e^{i\omega t}$, where v_j is the amplitude and ω is the angular frequency. Note again that only section I experiences direct driving, $v_1 \neq 0$, whereas sections II, III, and IV have $v_j=0$. The angular frequency ω ranges from $-2\pi\times10^7$ to $2\pi\times10^7\ \mathrm{rad\,s^{-1}}$. It is not to be confused with the drop-on-demand driving frequency $f_{\mathrm{DoD}}=5$ kHz, which is chosen such that the acoustic field is completely damped at the end of the acoustic cycle, $k_{1,j}$ and $k_{2,j}$ are the wave numbers of the waves propagating in the negative and positive x direction, respectively. Inserting the velocity profile of a cylindrical pipe given by Womersley[23] and dropping the $e^{i\omega t}$ term leads to

$$k_{n,j} = (-1)^n \frac{\omega}{c_{\mathrm{eff},j}} \left(1 + \frac{2\sqrt{i} J_1(\mathrm{Wo}_j i^{3/2})}{\mathrm{Wo}_j J_0(\mathrm{Wo}_j i^{3/2})}\right)^{-1/2} \quad (n \in \{1,2\}) \tag{7}$$

where $\mathrm{Wo}_j = 0.5 d_j \sqrt{\omega\rho\mu^{-1}}$ is the Womersley number. The functions J_0 and J_1 are the ordinary Bessel functions of the first kind, of zeroth and first order, respectively. With Eq. (7) substituted into Eq. (6) one finally obtains a general expression for the pressure $P_j(x,t)$ in section j.

The glass connection channel ($j=3$) and the nozzle ($j=4$) are not cylindrical but have a more complicated shape. However, both sections can be modeled by an equivalent cylindrical section, as shown in Appendices A and B. For the glass connection channel an equivalent diameter of $d_3=80\ \mu$m and an equivalent length of $l_3=148\ \mu$m are found. The conical nozzle is described by a cylinder of equivalent diameter $d_4=30\ \mu$m and equivalent length of $l_4=42\ \mu$m. Over most of their length, the radii of the real nozzle and glass connection channel are larger then the radii of the equivalent cylindrical sections. The equivalent lengths are chosen to keep the acoustic admittance constant. As the acoustic admittance is proportional to the ratio of the cross sectional area over the length of the cylinder, see the forthcoming Eq. (A8) the real lengths are also larger then the equivalent lengths.

The flow rate through the cylindrical nozzle is a function of the pressure drop over the nozzle in the frequency domain. The expression given by Womersley[23] for the amplitude of the volume flow rate q_j in a cylinder (the nozzle) is

$$q_j = p_j \frac{\pi d_j^2 i}{4 l_j \omega \rho} \left(1 - \frac{2 J_1(\mathrm{Wo}_j i^{3/2})}{i^{3/2} \mathrm{Wo}_j J_0(\mathrm{Wo}_j i^{3/2})}\right). \tag{8}$$

C. Matching the channel sections

We now have to match the pressure fields $P_j(x,t)$ for the different sections j. The boundary conditions at the ends of each section are continuity of pressure and flow. The pressure should be continuous at the matching positions x_1, x_2, x_3 (Fig. 5),

$$P_j(x_j) = P_{j+1}(x_j), \quad j = 1,2,3. \tag{9}$$

Moreover, continuity requires that the volume flow rate should also be continuous:

$$A_j u_j(x_j) = A_{j+1} u_{j+1}(x_j), \quad j = 1,2. \tag{10}$$

Here $u_j(x)$ is the velocity averaged over the cross section, $A_j(x_j)$. The effect of the bubble is included in the volume flow rate balance between section 3 and 4 where the bubble sits by explicitly considering the flux Q_b into the bubble,

$$A_3 u_3(x_3) = A_4 u_4(x_3) + Q_b \tag{11}$$

These boundary conditions together with equations (6) and (7) (the equation for the propagation of acoustic waves) provide a complete description of the channel acoustics.

D. Bubble volume oscillations

The behavior of spherical bubbles in large volumes is described by the Rayleigh–Plesset (RP) equation (see, e.g., Brennen[20])

$$R\ddot{R} + \frac{3}{2}\dot{R}^2 = \frac{1}{\rho}\left[\left(P_0 + \frac{2\sigma}{R_0} - P_v\right)\left(\frac{R_0}{R}\right)^{3\gamma} + P_v - \frac{2\sigma}{R} - \frac{4\mu\dot{R}}{R} - P_\infty(t)\right]. \tag{12}$$

Here $R(t)$ is the bubble radius, $\rho = 1090\ \mathrm{kg\ m^{-3}}$ is the ink density, σ is the surface tension, $\alpha = 0.028\ \mathrm{N\ m^{-1}}$, R_0 is the bubble radius at ambient pressure $P_0 = 101\,325\ \mathrm{N\ m^{-2}}$, $P_v = 2400\ \mathrm{N\ m^{-2}}$ is the vapor pressure, $\mu = 0.01\ \mathrm{N\ m^{-2}\ s}$ is the viscosity, and γ is the polytropic index. The bubble is assumed to oscillate isothermally, i.e., $\gamma = 1$. $P(t)$ is the pressure fluctuation caused by the actuator so that far from the bubble the pressure is

$$P_\infty(t) = P_3(x_3) = P_0 + P(t) + \Delta P(t). \tag{13}$$

Here $\Delta P(t)$ is the pressure disturbance caused by the bubble. This term can be neglected for bubbles in an infinite volume of liquid. In a channel however, this term is significant. It reflects the coupling between the channel acoustics and the bubble volume oscillations. The pressure $P_\infty(t)$ is the pressure at locations so far from the bubble, that the pressure due to the inertia of the radial flow field is negligible with respect to the imposed pressure fluctuations.

For small fluctuations of the driving pressure $P(t) \ll P_0$ and bubble radius $\Delta R(t) \ll R_0$ the RP equation, Eq. (12), can be linearized. The response of the bubble can be transformed to the frequency domain,

$$R(t) = \sum_{k=-\infty}^{\infty} r(\omega_k) e^{i\omega_k t}, \tag{14}$$

where $r(\omega)$ is the amplitude of the radius at frequency ω. Similarly,

$$P_\infty(t) = P_3(x_3) = \sum_{k=-\infty}^{\infty} p_3(\omega_k) e^{i\omega_k t}, \tag{15}$$

where $p_3(\omega)$ is the amplitude of the pressure at frequency ω at the position x_3. In the notation we suppress the explicit dependence on ω_k for compactness of formulation. Upon linearization, RP equation (12) becomes

$$-\omega^2 r = \frac{1}{R_0\rho}\left(-r\left(P_0 + \frac{2\sigma}{R_0} - P_v\right)\left(\frac{3\gamma}{R_0}\right) + r\frac{2\sigma}{R_0^2} - \frac{4\mu i\omega r}{R_0} - p_3\right). \tag{16}$$

The volume change of the bubble and thus the ink flow toward the position of the bubble center is:

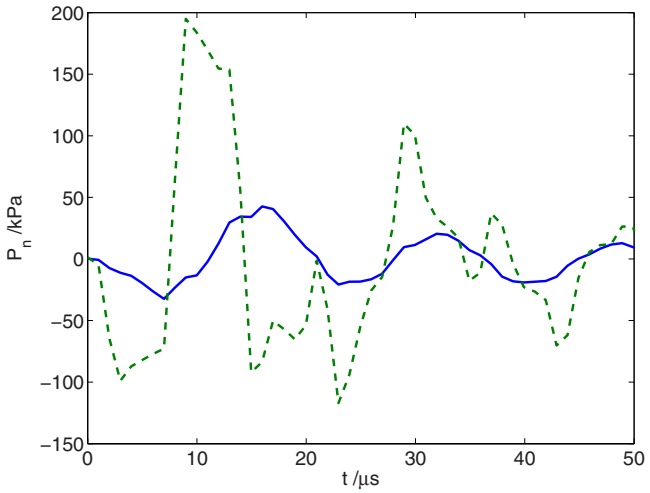


FIG. 6. (Color online) Pressure at the entrance of the nozzle $P_3(x_3)$ with (solid), and without (dashed) an entrained bubble of $R_0 = 23\ \mu\mathrm{m}$, as calculated by the model for a 2–4–2 pulse (2 μs rise time, 4 μs plateau, and 2 μs fall time), applied at 80 V. The pressure peak that starts at 10 μs would normally cause the formation of a droplet. With an entrained air bubble, this peak is reduced by a factor of four. The pressure reduction due to the bubble is strong enough to prevent the droplet formation.

$$Q_b(t) = -\frac{d}{dt}\left(\frac{4}{3}\pi R(t)^3\right) = \sum_{k=-\infty}^{\infty} q_b(\omega_k) e^{i\omega_k t}, \tag{17}$$

where $q_b(\omega)$ is the amplitude of the volume flow rate into bubble at frequency ω. Combining Eqs. (16) and (17) yields an expression for the amplitude of the volume flow rate:

$$q_b = -4\pi i p_3 R_0^2 \omega\left(R_0\rho\omega^2 - \left(P_0 + \frac{2\sigma}{R_0} - P_v\right)\left(\frac{3\gamma}{R_0}\right) + \frac{2\sigma}{R_0^2} - \frac{4\mu i\omega}{R_0}\right)^{-1}. \tag{18}$$

When inertia, vapor pressure, viscosity, and surface tension are neglected, Eq. (18) reduces to the expression for the disk bubble in de Jong *et al.*[19] This shows that the dynamics obtained for the disk bubble in Ref. 19 can be alternatively derived from the RP equation.

E. Model results

The model described in this section was developed to test the hypothesis that the two-way coupling between the bubble dynamics and channel acoustics is essential. The modification of the pressure fluctuation at the entrance of the nozzle by the bubble is significant, as shown in Fig. 6 for a bubble of $R_0 = 23\ \mu\mathrm{m}$, driven at 80 V.

The pressure fluctuations are reduced by a factor of 4 when a bubble is present. It is this pressure reduction which causes the nozzle to stop jetting droplets. Not only the pressure amplitude is reduced, also the higher frequencies in the signal are damped. This becomes evident when looking at the transfer function of the actuator voltage to the velocity in the nozzle, as shown in Fig. 7.

The velocity in the nozzle is reduced and the resonance peaks at 50 and 110 kHz are shifted to 20 and 60 kHz, respectively. Moreover, the higher frequencies are completely

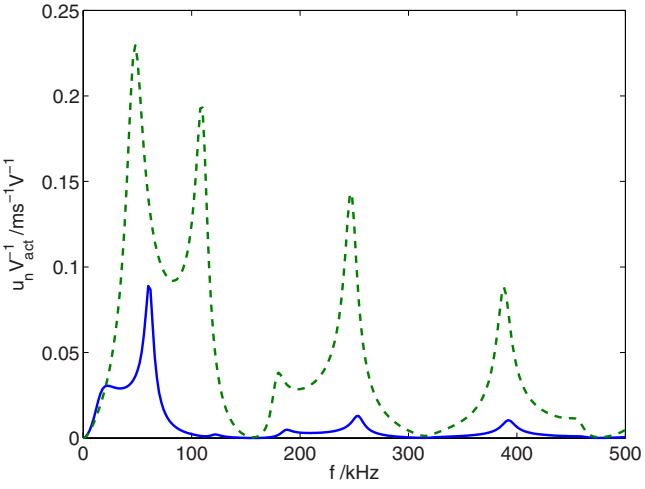


FIG. 7. (Color online) Transfer function amplitude of velocity in the nozzle over actuator voltage, with (solid) and without (dashed) an entrained bubble with a radius $R_0=23$ μm. Note the large reduction of the velocity, in particular at higher frequencies. The individual peaks are shifted as a result of the modification of the reflection at the nozzle. The bubble has a significant influence on the channel acoustics.

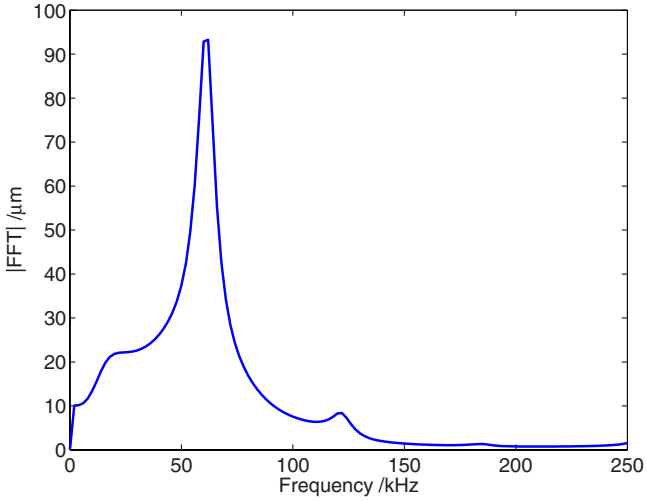


FIG. 9. (Color online) FFT calculated from the bubble oscillations for the case of Fig. 8 with two-way coupling. The main frequency is $f=60$ kHz. For this bubble radius, $R_0=23$ μm, the bubble reflects the acoustic waves in the ink channel. Therefore, the closed end (the nozzle) is replaced by an open end (the bubble).

damped by the air bubble. The zeros in the transfer function are not shifted as they are caused by the properties of section 1. The zeros occur at frequencies $f=nc_{\text{eff},1}l_1^{-1}$, where n is an integer.

The change in pressure fluctuation that the bubble experiences is accompanied by a change in bubble radius oscillation, as shown in Fig. 8. Here the bubble radius is shown, calculated with the described model, and calculated when neglecting the two-way coupling. Through the channel acoustics, the bubble loses energy, thus reducing the amplitude of the volume oscillations. When this effect is neglected, the bubble is driven beyond the linear regime, and the linearization is not justified. The bubble oscillations without two-way coupling were thus calculated with the full [nonlinear] RP equation, Eq. (12), driven by the pressure that would occur in the absence of a bubble, see Fig. 6. As seen in Fig. 8, the effect of the two-way coupling appears to be significant, and cannot be neglected.

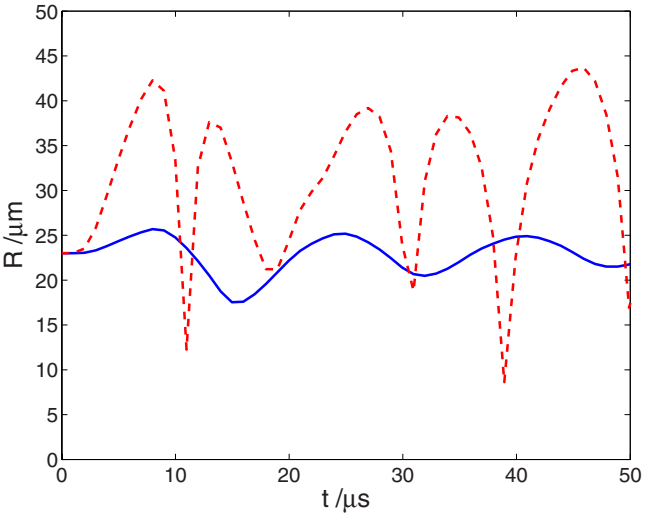


FIG. 8. (Color online) Bubble radius, neglecting the two-way coupling between bubble volume fluctuation and pressure (dashed), and with this two-way coupling taken into account (solid). The case with two-way coupling is calculated with the linearized analysis as described in the text for a trapezoidal 2–4–2 pulse and a driving of 80 V. The case where two-way coupling is neglected is calculated with the nonlinear Rayleigh–Plesset equation because in this case the bubble is driven beyond the linear regime. This is most evident in the violent collapse near $t=10$ μs, where the bubble is compressed within 3 μs from 48 to 10 μm.

The FFT is calculated from the oscillations of the $R_0=23$ μm, bubble and displayed in Fig. 9. The main frequency is 60 kHz. The same frequency is also found for the bubble of $R_0=18$ μm. This frequency does not depend on the bubble radius once it has reached a certain size. The reason for this is that once the bubble is large enough, it fully reflects the acoustic waves, acting like an open end of section 3 of the channel and decoupling it from the nozzle (section 4).

Air bubbles can be detected by monitoring the electric current through the piezo in the time domain, as it reacts to pressure fluctuations. This detection method has been described by de Jong *et al.*[8] The proposed model predicts the changes in this signal due to the entrained air bubble, as shown in Fig. 10, for the system considered by de Jong *et al.*[8] This printhead has an 8 mm actuation channel and a 50 μm trumpet shaped nozzle. A 5–6–3 (5 μs rise time, 6 μs plateau, and 3 μs fall time) trapezoidal pulse is employed, at a voltage of 44 V. The bubble is placed at the nozzle entrance, and has a radius of $R_0=23$ μm.

In the first part the piezo is deformed by the pulse. After $t=15$ μs, the piezo reacts to the pressure fluctuations in the ink channel. As our interest is focused on the acoustical signal from the piezo, the scale on the vertical axis is chosen such that the pressure change in the ink channel and its modification due to the bubble are resolved. The air bubble causes the signal to have a higher amplitude, a faster oscillation, and less high frequency fluctuation.

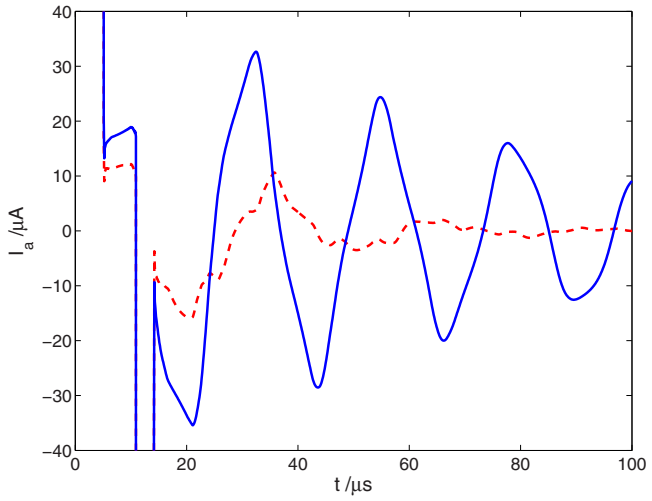


FIG. 10. (Color online) Piezo current with (solid) and without (dashed) an entrained air bubble of 23 μm radius. The printhead has an 8 mm actuation channel, a 50 μm trumpet shaped nozzle and is driven at 44 V with a 5–6–3 (5 μs rise time, 6 μs plateau, and 3 μs fall time) trapezoidal pulse. The signal is divided into two parts: first ($0<t<15$ μs), the piezo is deformed by a 44 V voltage, in the second part ($15<t<100$ μs), the piezo is only deformed by the pressure changes in the ink channel. Without a bubble, the piezo current is small after $t=50$ μs. The bubble however reflects the acoustic waves traveling toward the nozzle. As most damping is caused by the nozzle, the acoustic waves remain in the ink channel for a relatively long time.

V. COMPARISON BETWEEN MODEL AND EXPERIMENT

To compare the experimental data with the bubble model, the experimentally obtained equilibrium radius of the bubble is used in the model. A quantitative comparison can be seen in Fig. 11 for the 120 and the 190 V driving. As mentioned before, only the amplitude of the acoustic pressure for a driving of 190 V is adjusted to the pressure in the experiments so that for a bubble of $R_0=23$ μm the amplitude of the bubble oscillations fits to the experiment: The driving of 190 V in the experiments is found to be a driving of 80 V in the model. The difference in driving is assumed to be caused by the properties of the piezo, in particular the value of α_1. Upon adjusting this absolute size, a good agreement of the shape of the signal can be seen, showing the importance of the confined geometry in our printhead channel. In particular, the relatively small expansion of the bubble compared to its large compression is well captured. After about $t=30$ μs, the model slightly deviates from the experimental data. This is assumed to be due to the absence of thermal damping in the model, which is known to be relevant for bubbles of this size,[20] in particular in closed systems.[24]

The frequency spectrum (fast Fourier transform) is compared in Fig. 12. The bubble radius is $R_0=23$ μm in the experiments and in the model. The main frequency component found in the experiments is 60 kHz, as in the model.

VI. CONCLUSIONS AND OUTLOOK

When an air bubble is entrapped in the ink channel, it grows by rectified diffusion up to some saturation size. The oscillations of this bubble of saturated size are measured and

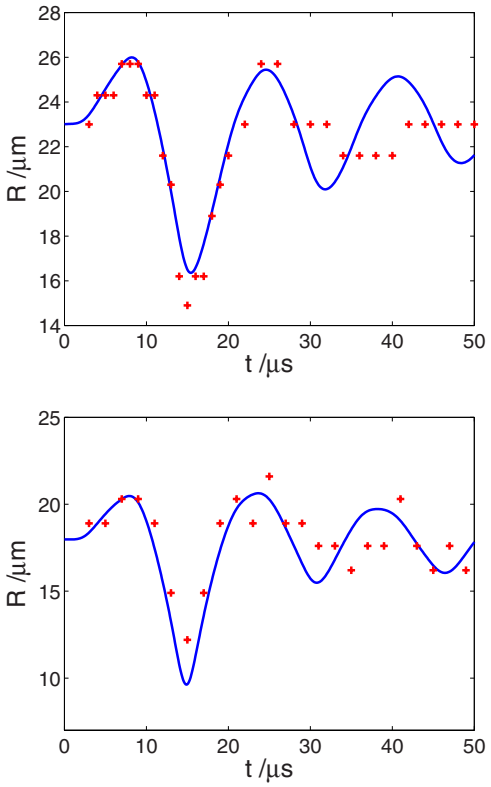


FIG. 11. (Color online) Comparison of the experimental bubble oscillations (crosses) with the numerical model (solid line). The air bubble of $R_0=23$ μm (top) and $R_0=18$ μm (bottom) is driven at 190 V (top) and at 120 V (bottom). The model driven at 80 V (top) and 51 V (bottom) captures the details of the initial expansion and the compression of the bubble. After $t=30$ μs, the model deviates from the bubble oscillations.

modeled. Due to the confined space the bubble acts back on the acoustic waves. This two-way coupling between the bubble and the channel acoustics results in the equilibrium size of the bubble. By employing a glass window the oscillations are measured with high speed imaging. The channel acoustics and bubble dynamics are modeled with a one-

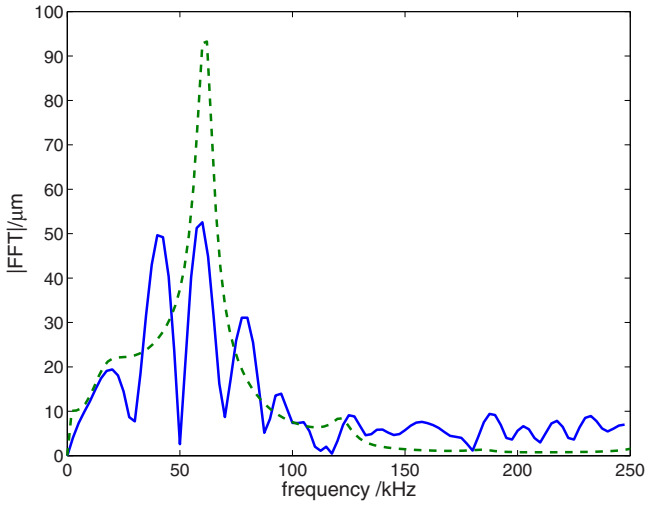


FIG. 12. (Color online) Fast Fourier transform (FFT) of the bubble oscillations in the experiments (dashed) and for the model (solid), for a bubble size of $R=23$ μm radius. The main frequency component at $f=60$ kHz agrees reasonably well.

dimensional model. This model incorporates coupling between the bubble and the ink channel. The bubble itself is modeled with a linearized Rayleigh-Plesset equation. It turns out that the confined geometry and therefore the two-way coupling is crucial. The result is a simple model that can be employed to study air bubble behavior and predict the effect of an entrapped air bubble on the acoustic field in the channel. In this way, air bubbles can be studied for different channel properties, $A_{0,j}$, l_j, α_j, β_j, and acoustic driving protocols.

ACKNOWLEDGMENTS

The authors thank Andrea Prosperetti for very helpful discussions. They thank the staff of Océ Technologies B.V. for support. This work is part of the research programme of the "Stichting voor Fundamenteel Onderzoek der Materie (FOM)" and "Stichting Technologie en Wetenschap (STW)," both of which are financially supported by the "Nederlandse Organisatie voor Wetenschappelijk Onderzoek (NWO)" and by Océ Technologies B.V.

APPENDIX A: NOZZLE REPRESENTATION

1. Conical nozzle representation

This appendix deals with the representation of the conical nozzle used in the experiments through the cylindrical nozzle that is employed in the model. A sketch of experimental nozzle and its cylindrical representation is shown in Fig. 13.

Two nozzle properties are important: the viscous friction on the walls, and the acoustic properties. The experimental nozzle can be described as a cylinder with an equivalent diameter and length. The equivalent diameter of the model nozzle, $d_4=2R_4$, is chosen equal to the minimum experimental nozzle diameter 30 μm in order to match the viscous friction in the nozzle. Now the correct equivalent length, l_4, has to be determined based on the acoustic properties.

The volume flow rate of ink through the nozzle, Q_n, is defined as

$$\int_{A_n} u_n dA = Q_n = \sum_{k=-\infty}^{\infty} q_n(\omega_k) e^{i\omega_k t}, \tag{A1}$$

where q_n is the amplitude of the volume flow rate through the nozzle.

The pressure can be obtained by integrating the linearized momentum equation over the axial coordinate

$$\partial_t u_j = \frac{-1}{\rho} \partial_x P_j \Rightarrow P_n(x) = P_n(x_3) + \int_{x_3}^{x} i\rho\omega \frac{q_n}{A_n(x)} dx. \tag{A2}$$

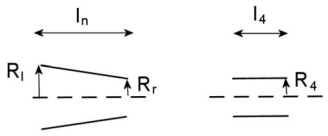


FIG. 13. (Left) Experimental nozzle, $R_l=25$ μm, $R_r=15$ μm, and $l_n=70$ μm. (Right) Cylindrical nozzle representation employed in the model, $R_4=15$ μm, and $l_4=42$ μm.

Transforming P_n to the frequency domain gives

$$P_n = \sum_{k=-\infty}^{\infty} p_n(\omega_k) e^{i\omega_k t}. \tag{A3}$$

After solving for the admittance (the volume flow divided by the pressure see, e.g., Refs. 25 and 26) and imposing zero pressure at the meniscus one gets

$$\frac{q_n}{p_n} = \frac{-1}{i\rho\omega \int_0^{l_n} \frac{1}{A_n(x)} dx}. \tag{A4}$$

Equation (A4) is a general solution depending on the geometry of the nozzle. This equation will now be evaluated for different nozzles and the glass connection channel.

The nozzle radius of the experimental conical nozzle is described by

$$R_n(x) = R_l\left(1 - \frac{x}{l_4}\right) + R_r \frac{x}{l_n}, \tag{A5}$$

where R_l is the entrance radius (25 μm), and R_r is the exit nozzle radius (15 μm). The length of the experimental nozzle is $l_n=70$ μm. Inserting Eq. (A5) into Eq. (A4) results in

$$\begin{aligned} \frac{q_n}{p_n} &= \frac{-\pi}{i\rho\omega \int_0^{l_n} \frac{1}{\left(R_l\left(1 - \frac{x}{l_n}\right) + R_r \frac{x}{l_n}\right)^2} dx} \\ &= \frac{-\pi R_l^2}{i\rho\omega l_n \int_0^1 \frac{1}{\left(1 + \left(\frac{R_r}{R_l} - 1\right)x\right)^2} dx}. \end{aligned} \tag{A6}$$

By evaluating the integral, the admittance of the experimental conical nozzle is obtained as

$$\frac{q_n}{p_n} = \frac{-\pi R_l R_r}{i\rho\omega l_n}. \tag{A7}$$

For the cylindrical nozzle of section 4, the admittance is

$$\frac{q_4}{p_n} = \frac{-\pi (R_4)^2}{i\rho\omega l_4}. \tag{A8}$$

If we now match the admittance of the experimental nozzle and the modeled cylinder, we can calculate the equivalent length l_4 of the nozzle based on the minimum radius, $1/2d_4=R_4=R_r=15$ μm:

$$\frac{q_4}{p_n} = \frac{-\pi (R_4)^2}{i\rho\omega l_4} = \frac{-\pi R_l R_r}{i\rho\omega l_n}. \tag{A9}$$

The equivalent length for the cylindrical nozzle is found to be:

$$l_4 = \frac{R_4^2}{R_l R_r} l_n = 42 \ \mu\text{m}. \tag{A10}$$

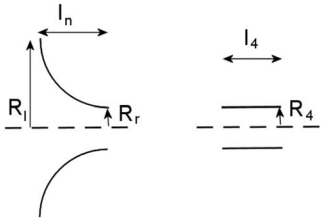


FIG. 14. (Left) Experimental nozzle, R_l=65 μm, R_r=15 μm, and l_n =50 μm. (Right) Cylindrical nozzle representation employed in the model, R_4=15 μm, and l_4=46 μm.

2. Trumpet shaped nozzle representation

The nozzle considered for the calculation of the electric current through the piezo in Fig. 10 is a trumpet shaped nickel nozzle. A sketch of the experimental nozzle and the nickel nozzle is depicted in Fig. 14.

We describe the radius of the trumpet-shape nozzle of Fig. 14 by

$$R_n(x) = R_l - l_n\sqrt{1-\left(1-\frac{x}{l_n}\right)^2}. \tag{A11}$$

The trumpet shaped nozzle is specified by two parameters: the nozzle length l_n=50 μm and the ratio $\lambda = R_l/l_n$ where R_l=65 μm is the entrance radius. The smallest radius is $R_n(l_n)=R_r=R_l-l_n=1/2d_4$=15 μm, and this is the radius at the meniscus. The radius is plotted as a function of x in Fig. 15.

Insert this nozzle shape into Eq. (A4) to obtain the admittance of the trumpet shaped nozzle:

$$\frac{q_n}{p_n} = \frac{-\pi l_n}{i\rho\omega}\frac{2(-1+\lambda^2)^{3/2}}{\pi + 2\arctan\left(\frac{1}{\sqrt{-1+\lambda^2}}\right) + 2\sqrt{-1+\lambda^2}}. \tag{A12}$$

This admittance is equal to the admittance of a cylindrical nozzle whose radius is equal to R_r and whose length is

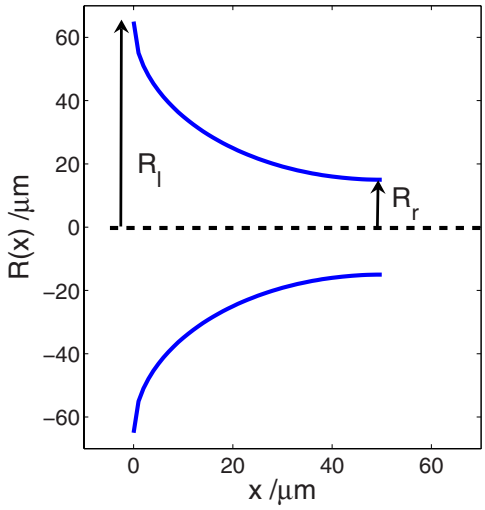


FIG. 15. (Color online) Approximation of the experimental nozzle radius.

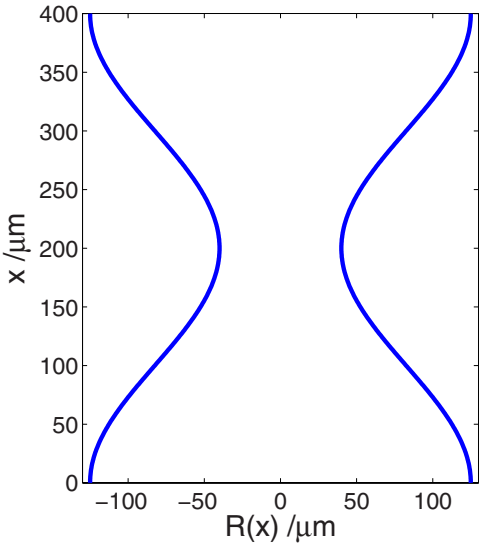


FIG. 16. (Color online) Approximation of the hour glass shape of Fig. 1.

$$l_4 = R_l\frac{1}{1+\sqrt{F}} \tag{A13}$$

with F equal to the second fraction on the right-hand side of Eq. (A12).

Therefore, the equivalent cylinder has a diameter of d_4 =30 μm and a length of l_4=46 μm.

APPENDIX B: GLASS CONNECTION CHANNEL REPRESENTATION

The method used to obtain equivalent cylindrical nozzles is also applied to the glass connection channel. The shape of the connection channel is approximately:

$$R_c(x) = R_{\max} - (R_{\max} - R_{\min})\left(\sin\frac{\pi x}{l_g}\right)^2, \tag{B1}$$

where l_g is the length of the glass connection channel, $R_{\max}$ is the maximum channel radius, and $R_{\min}$ is the minimum channel radius. The approximated shape of Eq. (B1) is plotted in Fig. 16.

Insert the channel cross-sectional area based on this radius into Eq. (A4) to obtain:

$$\frac{q_g}{p_g} = \frac{-\pi R_{\max}^2}{i\omega\rho l_g}\frac{2(1-\kappa)^{3/2}}{2-\kappa}, \tag{B2}$$

where p_g is the amplitude of the pressure drop over the glass connection channel, q_g is the amplitude of the volume flow rate through the glass connection channel, and

$$\kappa = \frac{R_{\max}-R_{\min}}{R_{\max}} = \frac{125\times10^{-6}-40\times10^{-6}}{125\times10^{-6}} = 0.68. \tag{B3}$$

The equivalent cylindrical connection channel with diameter d_3=80 μm has a length of l_3=149 μm. The admittance of the glass connection channel and the conical nozzle can be compared to obtain an estimate of the relative influence of the connection channel. The conical nozzle is approximated by a cylindrical nozzle of d_4=15 μm, and equivalent length of l_4=42 μm. The maximum glass channel

radius is $R_{max}=125\ \mu m$ and the channel length is $l_g=400\ \mu m$. The pressure drop ratio is $p_g/p_n=0.5$. The pressure drop over the connection channel is significant, with respect to the pressure drop over the nozzle.

[1]H. P. Le, "Progress and trends in ink-jet printing technology," J. Imaging Sci. Technol. **42**, 49–62 (1998).
[2]C. Williams, "Ink-jet printers go beyond paper," Phys. World **19**, 24–29 (2006).
[3]H. S. Koo, M. Chen, and P. C. Pan, "LCD-based color filter films fabricated by a pigment-based photo resist inks and printing technology," Thin Solid Films **515**, 896–901 (2006).
[4]O. A. Basaran, "Small-scale free surface flows with breakup: Drop formation and emerging applications," AIChE J. **48**, 1842–1848 (2002).
[5]J. F. Dijksman, "Hydrodynamics of small tubular pumps," J. Fluid Mech. **139**, 173–191 (1984).
[6]J. D. Brock, I. M. Cohen, I. P. Ivanov, H. P. Le, and J. Roy, "Oscillations of an air bubble in an ink jet," J. Imaging Technol. **10**, 127–129 (1984).
[7]N. P. Hine, "Deaeration system for a high-performance drop-on-demand ink jet," J. Imaging Technol. **17**, 223–227 (1991).
[8]J. de Jong, H. Reinten, M. van den Berg, H. Wijshoff, M. Versluis, G. de Bruin, and D. Lohse, "Air entrapment in piezo-driven inkjet printheads," J. Acoust. Soc. Am. **120**, 1257–1265 (2006).
[9]M. M. Fyrillas and A. J. Szeri, "Dissolution or growth of soluble spherical oscillating bubbles," J. Fluid Mech. **289**, 259–314 (1995).
[10]S. Hilgenfeldt, D. Lohse, and M. P. Brenner, "Phase diagrams for sonoluminescing bubbles," Phys. Fluids **8**, 2808–2826 (1996).
[11]C. Caskey, D. Kruse, P. Dayton, T. Kitano, and K. Ferrara, "Microbubble oscillation in tubes with diameters of 12, 25, and 195 microns," Appl. Phys. Lett. **88**, 033902 (2006).
[12]P. Zhong, Y. Zhou, and S. Zhu, "Dynamics of bubble oscillation in constrained media and mechanisms of vessel rupture in SWL," Ultrasound Med. Biol. **27**, 119–134 (2001).
[13]E. Sassaroli and K. Hynynen, "Resonance frequency of microbubbles in small blood vessels: a numerical study," Phys. Med. Biol. **50**, 5293–5305 (2005).
[14]S. Qin and K. Ferrara, "The natural frequency of nonlinear oscillation of ultrasound contrast agents in microvessels," Ultrasound Med. Biol. **33**, 1140–1148 (2007).
[15]S. Qin, Y. Hu, and Q. Jiang, "Oscillatory interaction between bubbles and confining microvessels and its implications on clinical vascular injuries of shock-wave lithotripsy," IEEE Trans. Ultrason. Ferroelectr. Freq. Control **53**, 1322–1329 (2006).
[16]E. Ory, H. Yuan, A. Prosperetti, S. Popinet, and S. Zaleski, "Growth and collapse of a vapor bubble in a narrow tube," Phys. Fluids **12**, 1268–1277 (2000).
[17]H. Yuan, H. Oguz, and A. Prosperetti, "Growth and collapse of a vapor bubble in a small tube," Int. J. Heat Mass Transfer **42** 3643–3657 (1999).
[18]J. Cui, M. Hamilton, P. Wilson, and E. Zabolotskaya, "Bubble pulsations between parallel plates," J. Acoust. Soc. Am. **119**, 2067–2072 (2006).
[19]J. de Jong, R. Jeurissen, H. Borel, M. van den Berg, H. Wijshoff, H. Reinten, M. Versluis, A. Prosperetti, and D. Lohse, "Entrapped air bubbles in piezo-driven inkjet printing: Their effect on the droplet velocity," Phys. Fluids **18**, 121511 (2006).
[20]C. E. Brennen, *Cavitation and Bubble Dynamics* (Oxford University Press, Oxford, 1995).
[21]H. Tijdeman, "On the propagation of sound waves in cylindrical tubes," J. Sound Vib. **39**, 1–33 (1975).
[22]H. N. Oğuz and A. Prosperetti, "The natural frequency of oscillation of gas bubbles in tubes," J. Acoust. Soc. Am. **103**, 3301–3308 (1998).
[23]J. R. Womersley, "Method for the calculation of velocity, rate of flow and viscous drag in arteries when the pressure gradient is known," J. Physiol. (London) **127**, 553–563 (1955).
[24]X. M. Chen and A. Prosperetti, "Thermal processes in the oscillations of gas bubbles in tubes," J. Acoust. Soc. Am. **104**, 1389–1398 (1998).
[25]J. Billingham and A. C. King, *Wave Motion* (Cambridge University Press, Cambridge, 2000).
[26]J. Lighthill, *Waves in Fluids* (Cambridge University Press, Cambridge, 1978).

Collective bubble oscillations as a component of surf infrasound

Joseph Park,[a] Milton Garcés, and David Fee
University of Hawaii, Infrasound Laboratory, 73-4460 Queen Kaahumanu Hwy #119, Kailua-Kona, Hawaii 96740, USA

Geno Pawlak
University of Hawaii at Manoa, Department of Ocean and Resources Engineering, 2540 Dole Street, Holmes Hall 404, Honolulu, Hawaii 96822, USA

(Received 14 June 2007; revised 13 November 2007; accepted 31 January 2008)

Plunging surf is a known generator of infrasound, though the mechanisms have not been clearly identified. A model based on collective bubble oscillations created by demise of the initially entrained air pocket is examined. Computed spectra are compared to infrasound data from the island of Kauai during periods of medium, large, and extreme surf. Model results suggest that bubble oscillations generated by plunging waves are plausible generators of infrasound, and that dynamic bubble plume evolution on a temporal scale comparable to the breaking wave period may contribute to the broad spectral lobe of dominant infrasonic energy observed in measured data. Application of an inverse model has potential to characterize breaking wave size distributions, energy, and temporal changes in seafloor morphology based on remotely sensed infrasound.
© *2008 Acoustical Society of America.* [DOI: 10.1121/1.2885743]

PACS number(s): 43.28.Dm, 43.30.Bp, 43.30.Pc [WMC] Pages: 2506–2512

I. INTRODUCTION

Oceanic ambient noise arises from a diverse set of geophysical, biological, and mechanical sources. This paper focuses on characterization of infrasound (1–20 Hz) produced from ocean waves breaking on coastlines-surf. Wave breaking processes are important contributors to the acoustic ambient field. Above roughly 500 Hz breathing-mode oscillation of individual air bubbles entrained by breaking waves constitute an important underwater sound source,[1] while at frequencies below 500 Hz it has been shown that collective bubble oscillations are significant generators of acoustic power.[2–6] In the infrasonic band known contributors include turbulence, machinery, and wave-wave interactions.[7,8] Analysis of oceanic infrasound by Nichols (1986) led to speculation that breaking waves could be capable sources,[9] followed by McCreery and Duennebier (1993) who postulated that hydroacoustic energy in the 0.5–10 Hz band might be attributed to coastal wave breaking.[10] It has been shown that near surface infrasonic sources can couple with insignificant power loss into the atmosphere,[11] and several studies have verified surf as a persistent and significant source of atmospheric infrasound.[12–15]

The type of breaking wave exerts a large influence on the generation of low frequency sound. Wave tank observations by Loewen and Melville revealed that plunging waves generate low frequency ($f>20$ Hz) energy correlated with breaking, while spilling waves do not.[5] Likewise, measurement of individual coastal breaking waves by Garcés *et al.* found that plunging waves were effective infrasonic sources ($f<20$ Hz), whereas spilling breakers were not.[16] Plunging waves are characterized by an overturning jet (or wall) of water which plunges forward of the wave and completely encloses a pocket of air (the tube, or barrel), while spilling breakers collapse into a bore of foam. Therefore, one can speculate that the unique water jet impact and enclosed vortex generation of plunging waves are candidate mechanisms for infrasound generation.

Even though specific generation mechanisms for surf infrasound have not been clearly identified, the foregoing observations suggest several likely sources: hydraulic impact of the plunging wave jet,[17] oscillations of the plunging wave jet-splash cycle,[18] impulse pressure "bounce back" from hydraulic impacts on elastic bodies (cliffs, reefs, seafloor),[19] multiple coherent vortex structure generation under the wave,[20] breathing-mode oscillation of the initially enclosed air volume,[5] and the collective oscillation of the collapsing bubble plume,[16,21]

Regarding the collective oscillation mechanism as a low frequency source, Carey speculated "If the spatial distribution of bubbles is related to the vorticity distribution, then the noise due to collective oscillations should have frequencies determined by the size of the vorticities".[22] The primary aim of this paper is to investigate the collective bubble oscillation mechanism as a potential generator of infrasound from plunging surf with sufficient energy and spatial scales. A model is developed in which bubble plume distributions are estimated from breaking wave spectra. Plume oscillations and temporal evolution lead to an estimate of acoustic radiation frequency as a function of breaking wave frequency, which is transformed into a relative acoustic amplitude spectrum. Model results are compared to field data and some inferences regarding bubble plume evolutions are presented.

[a]Author to whom correspondence should be addressed. Electronic mail: jpark@isla.hawaii.edu

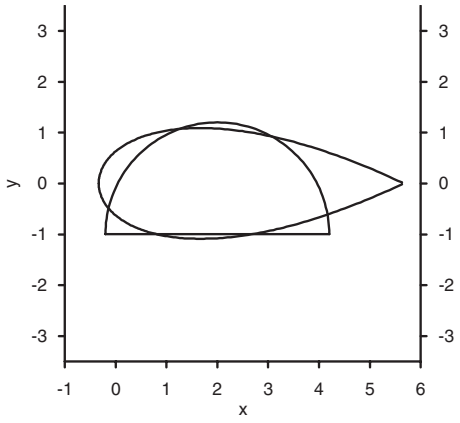


FIG. 1. Longuet-Higgins cubic vortex function compared to a semicylindrical cross section.

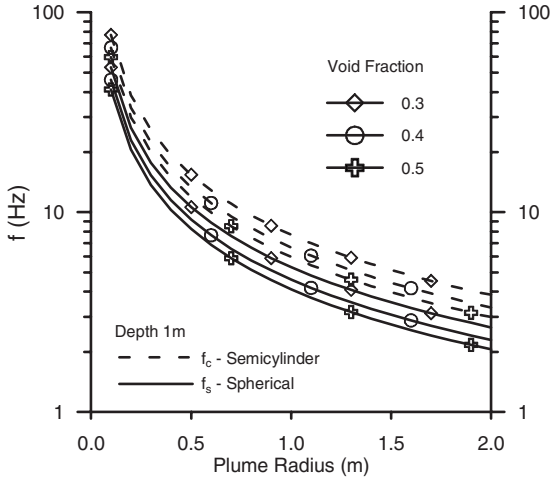


FIG. 2. Lowest eigenfrequency of collective bubble oscillation.

II. LOW FREQUENCY SOUND GENERATION FROM BUBBLE OSCILLATIONS

Wave breaking results in subsurface air entrainment which leads to both individual[5] as well as collective bubble oscillations,[2,4] each capable of generating low frequency acoustic radiation. According to Loewen and Melville, the low frequency sound produced by plunging waves contains two components.[5] The first is detected at the time of breaking and is attributed to "volumetric pulsation of the cylinder of pure air (100% void fraction) entrapped by the plunging wave crest." The second, which initiates some fraction of a wave period, later occurs when "the cylinder of pure air breaks up to form a bubble plume." It was noted by Loewen and Melville that the second component is a "slightly lower frequency signal" than the first.

Field observation and experiments indicate that the cross section of initial air entrainment by plunging waves is typically asymmetric.[5,23,24] Longuet-Higgins expressed the cross-section of the initial air volume in terms of a parametric cubic function with a shape resembling a teardrop (see Fig. 1).[23] Experimental work by Loewen and Melville found it convenient to model the bubble plume as a semicylindrical horizontal tube parallel to the crest of the wave.[5] As a comparison, Fig. 1 plots the Longuet-Higgins vortex function along with a semicylindrical cross section that has a radius the same dimension as the maximum vortex height.

Based on wave tank experiments Loewen and Melville fitted an empirical expression for the lowest eigenfrequency (see Fig. 2) of the semicylindrical horizontal bubble plume[5]

$$f_c \approx \frac{1}{2.5R_B}\sqrt{\frac{P_o}{\beta\rho}}, \tag{1}$$

where the range of approximation encompassed a plume radius R_B less than 1 m, and air volume fraction β less than 0.1. P_o denotes the ambient pressure and ρ the density of water. This expression is similar to that of the lowest eigenfrequency of a spherical cloud of radius R reported by Carey in Ref. 4

$$f_s = \frac{1}{2\pi R}\sqrt{\frac{3\gamma P_o}{\beta\rho}}, \tag{2}$$

where γ is the adiabatic ratio of specific heat. Comparison of Eqs. (1) and (2) reveals that $f_c \approx 1.45 f_s$, indicating that the asymmetric plume has a higher fundamental resonance than the spherical plume.

Using β values in the range measured by Deane,[24] $\gamma = 1$ (isothermal conditions, bubble surface tension is neglected), $P_o = 111{,}145$ Pa (depth 1 m) and $\rho = 1000$ kg/m^3, results of Eqs. (1) and (2) are shown in Fig. 2. These results indicate that for plunging breakers which produce approximately semicylindrical bubble clouds with characteristic radii larger than about 1/2 m, infrasonic generation from collective bubble oscillation is plausible.

III. ACOUSTIC MODEL

The model relies on a breaking wave spectrum to estimate the distribution of bubble plume sizes, which is transformed into an acoustic radiation spectrum. Considering only the entrained air oscillations, the model can be represented with a series of functional transformations applied to the deepwater wave spectrum.

Model input consists of a deepwater ocean wave spectrum $S(\omega)$ (Fig. 3), which can be constructed from wave

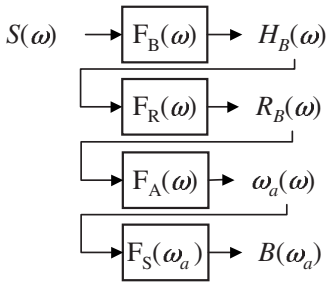


FIG. 3. Schematic of the acoustic transformation model: ω is the deepwater ocean wave frequency, ω_a the acoustic radiation frequency, S the deepwater wave spectrum, H_B the breaking wave height spectrum, R_B the bubble cloud characteristic length distribution and B the amplitude spectrum of acoustic radiation.

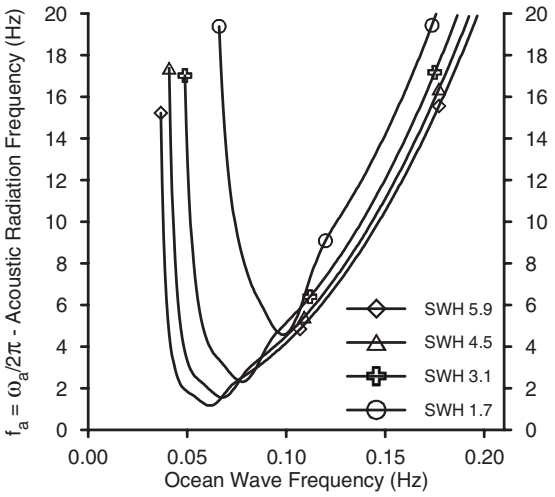


FIG. 4. Radiation frequencies of collective bubble oscillation from Eq. (6) versus the deepwater wave frequency for spectra with SWH of 1.7, 3.1, 4.5 and 5.9 m.

growth models applied to atmospheric weather conditions, or applied directly from observed ocean data buoys. The nonlinear transformation $F_B(\omega)$ produces a breaking wave height spectrum $H_B(\omega)$, which will depend on local bathymetry. $F_B(\omega)$ can be obtained from a breaker height index derived from empirical data,[25] or from a hydrodynamic wave model.[26] The breaking wave spectrum is then converted to a spectrum of bubble cloud characteristic lengths, $R_B(\omega)$, by the function $F_R(\omega)$ which can be modeled from data relating bubble cloud distributions to breaking wave height[27] and temporal evolution of plume dynamics.[6] The bubble cloud dimension is transformed into spectrum of acoustic radiation frequencies, $\omega_a(\omega)$ (see Fig. 4), based on the nonlinear transformation $F_A(\omega)$ which accounts for the radiation characteristics of the bubble plume.[5] Note that the deepwater wave frequency is denoted by ω, while the acoustic radiation frequency is denoted ω_a. Finally, the nonlinear distribution of radiation frequencies is summed and scaled across the acoustic frequency spectrum to estimate the acoustic radiation spectrum $B(\omega_a)$. Figure 3 is a schematic diagram of the model.

A. Breaking wave height spectrum

In the current model we employ the JONSWAP spectrum[28] as the deepwater wave generator, although other suitable distributions can be used. Median values of JONSWAP spectrum parameters were used (peak enhancement factor $\gamma=3.3$, peak width factor $\sigma=0.08$.) Model input consists of wind speed and fetch, from which the deepwater wave spectrum $S(\omega)$ is computed.

The function $F_B(\omega)$ transforms the deepwater wave spectrum into a breaking wave spectrum: $H_B(\omega)=F_B(S(\omega))$. One way to quantify the transition from deepwater-to-breaking wave height is with the breaker height index $h_B=H_B/H_o$ where H_B is the breaking wave height and H_o the deepwater wave height.[25] The breaker height index depends on beach slope and the incident wave steepness H_o/L_o, where L_o is the wavelength, and can be described with a power law of the form

$$h_B = c(H_o/L_o)^{-d} \tag{3}$$

with parameters $c=0.5784$, $d=0.23925$ for a beach slope of 1/10, and $c=0.5403$, $d=0.21618$ for a beach slope of 1/50.

Given a deepwater wave spectrum and slope of the beach where breaking will occur, a breaker height spectrum can be estimated by multiplying the deepwater spectrum with the corresponding breaker height index at each frequency.

$$H_B(\omega) = h_B(\omega) \cdot S(\omega) \tag{4}$$

With an estimate of the breaking wave spectrum at hand, the next step is to relate the breaking wave distribution to bubble cloud dimensions.

B. Bubble plume distribution

Application of Eq. (1) to estimate the acoustic spectrum of collective bubble radiation requires specification of the bubble plume radius, R_B, for each wave of the spectrum. Based on similarity between the Longuet-Higgins vortex function and a semicylinder of comparable scale (Fig. 1), the model assumes that the vortex height H_v, can be used as an approximation to the semicylindrical radius of Eq. (1). We therefore seek a variable, C_H, which scales the breaking wave height into an equivalent vortex height as shown in Eq. (5).

$$R_B(\omega) = H_v(\omega) = C_H \cdot H_B(\omega). \tag{5}$$

Mead and Black quantified ratios of vortex to breaking height at 26 surf locations,[27] from which we compute a mean value of $C_H=0.37$. The model estimate of initially entrained vortex height is therefore specified as: $H_v(\omega)=0.37 \cdot H_B(\omega)$.

C. Bubble radiation

The model assumes that the fundamental frequency f_c specified in Eq. (1) scales to plume dimensions larger than $R_B \approx 1$ m. This assumption is based on the scale invariance observed between Eqs. (1) and (2) in Fig. 2 as R exceeds 1 m. A spectrum of acoustic radiation frequencies associated with each incident breaking wave frequency can then be computed by combination of Eqs. (1) and (5):

$$\omega_a(\omega) = \frac{2\pi}{2.5H_v(\omega)}\sqrt{\frac{P_o}{\beta\rho}}. \tag{6}$$

Equation (6) does not quantify the spectral amplitude of radiation, rather, it defines a mapping between an incident breaking wave frequency and an estimate of the frequency of radiation of the collapsing vortex. Estimates of relative spectral amplitude are addressed in the next section.

To examine the evolution of bubble radiation with changes in wave group energy, Fig. 4 plots radiation frequencies of Eq. (6) for ocean wave spectra with deepwater significant wave heights of 1.7, 3.1, 4.5 and 5.9 m. As ocean wave group energy increases, with a corresponding increase in dominant wavelength and height, the acoustic radiation

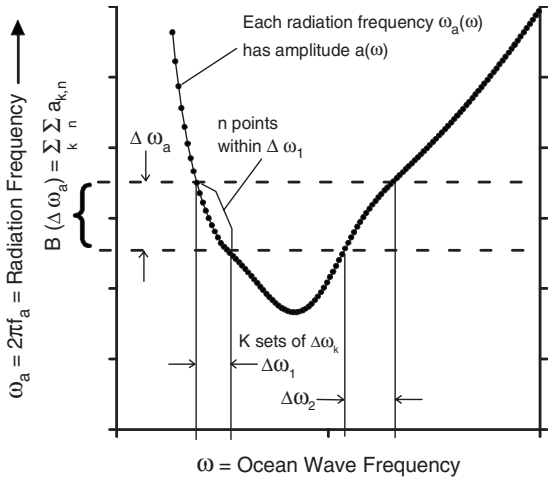


FIG. 5. Schematic of multiple contributions to bubble spectrum ω_a from ocean waves of different frequencies ω.

frequencies deepen into lower values. Thus we expect acoustic radiation spectra to exhibit stronger low frequency energy as incident ocean wave energy increases. One can also observe that the acoustic radiation broadens, covering a wider range of incident wave frequencies. This suggests that as incident wave energy increases, the acoustic radiation spectrum should also broaden around its main energy lobe.

D. Spectral amplitude estimates

The acoustic radiation frequencies of the model are computed from Eq. (6), we seek to transform this spectrum of radiation frequencies (such as shown in Fig. 4 where $\omega_a = 2\pi f_a$) into a spectrum of acoustic radiation amplitude, $B(\omega_a)$. The task is to identify the amplitude coefficient, B, associated with each acoustic radiation frequency ω_a.

It is clear from the nonlinear nature of $\omega_a(\omega)$ in Fig. 4 that bubble oscillations induced from multiple ocean wave frequencies can contribute to a single value of ω_a, and therefore B. This reflects the fact that for a given wave spectra, there can exist two frequencies with the same wave height. To account for these multiple sources, denote the acoustic radiation amplitude coefficient from each of k contributing ocean wave frequency as $a_k(\omega)$. In relation to Fig. 4 there are two contributing ocean waves at most values of ω_a, so that values of k are 1 and 2.

From an engineering perspective, there are a finite number of points in the spectra ω_a and B, and we denote the analysis binwidth of each component of B as $\Delta\omega_a$. Within each $\Delta\omega_a$ we designate the number of points for each of the k components as n. With an assumption of superposition, the discrete value of B within each analysis binwidth is given by

$$B(\Delta\omega_a) = \sum_k \sum_n a_{k,n}. \tag{7}$$

Figure 5 depicts the application of Eq. (7) to a representative radiation frequency spectrum $\omega_a(\omega)$.

Failure of superposition would arise from destructive interference between multiple, independent sources radiating at ω_a. However, the ocean wave periods and temporal persistence of the bubble plumes are an order of magnitude greater than the periods of ω_a. Given detector integration windows which are significantly greater than the wave period, it can be assumed that phase components are uniformly distributed and the amplitudes will be additive.

It is likely that a is a multiparametric function not just dependent on ω, but also a function of wave energy, site-specific wave breaking parameters such as beach slope, and other factors. Ideally, an estimate of the amplitude could be made from a low frequency acoustic model which considers both the bubble oscillation mechanics and the source-receiver transfer functions. For example, in the ocean layer the low frequency bubble oscillation models of Oguz[29] or Means[30] might assess the integrated behavior of the bubble plumes, while an additional aeroacoustic transfer function would be needed to model the atmospheric propagation to the infrasonic sensors. However, application of such models is beyond the scope of the present effort, and, it is useful to assess to what extent a simple first-order model can provide a robust and efficient estimator of breaking wave energy from remotely monitored infrasound. Here we make the assumption that $a(\omega)$ decays according to a simple $1/f$ scaling

$$a_n = A_n / f_{a_n}, \tag{8}$$

where A is a coefficient which can be used to describe the amplitude factors derived from higher order models such as those by Oguz[29] and Means,[30] and which can account for corrections due to the density of points summed in $\Delta\omega_a$. The discrete magnitude coefficients of B are then specified by

$$B(\Delta\omega_a) = \sum_k \sum_n A_{k,n} / f_{a_{k,n}}. \tag{9}$$

In the current model, $A \equiv 1$, and consequently this model is incapable of predicting absolute spectrum levels, it is limited to characterization of cutoff frequencies and spectral shape.

E. Bubble plume evolution

Bubble plumes from breaking ocean waves are known to persist for time scales on the order of seconds to tens of seconds. Given the dynamic environment in which the plumes are formed, and the unbalanced nature of the forces, plumes can evolve significantly within relatively short time scales (fractions of wave period). Two of the primary changes are a decrease in plume entrained air fraction, β, and an increase in plume cross-sectional area. Other important features include the horizontal and vertical velocities of the plume.

Lamarre and Melville[6] quantified plume dynamics in wavetank measurements and reported statistical moments of plume evolution. The mean void fraction as a function of time exhibited a nearly linear decrease for approximately one-half wave period after breaking. Based on their results, we have applied the following relationship to model the void fraction evolution:

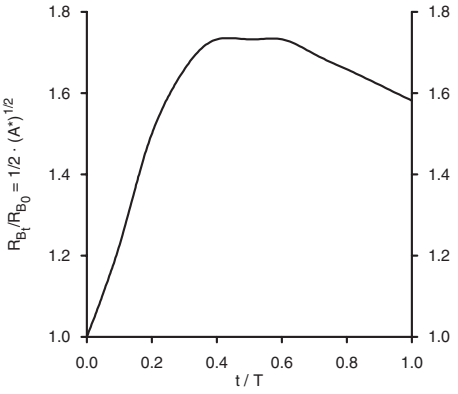


FIG. 6. Approximate evolution of plume cross-sectional area.

$$\beta(t) = \beta(0) - \frac{0.56t}{T};\ t \leqslant \frac{T}{2}, \tag{10}$$

where T is the wave period and $\beta(0)$ the initial air void fraction.

The bubble plume cross-sectional area normalized by the initial volume per unit width $(A*)$ was also reported as a function of time. It exhibited a nearly linear increase for the first several tenths of wave period after breaking, then tended to flatten out, and eventually decrease after times comparable to a wave period. There was considerable scatter in the data for times greater than about 0.2 T.

Equation (5) defines the initial bubble plume radius $R_B(\omega,t=0)$ as a function of breaking wave height. To model the evolution of plume radius, R_B is modulated with the relative radius length scale $\sqrt{A*}/2$

$$R_B(\omega,t) = \frac{\sqrt{A*(t)}}{2} R_B(\omega,t=0). \tag{11}$$

Values of $R_B(\omega,t)$ are then applied in Eq. (6) as the vortex height H_v to model time-varying plume growth. Figure 6 plots the evolution of the relative plume radius $\sqrt{A*}/2$, where values of $A*$ were taken from Ref. 6.

IV. KAUAI DATA

Figure 7 plots atmospheric infrasound recorded at a nearshore inland location on the island of Kauai during periods of moderate, high and extreme surf over the period March 4–March 10, 2005.[12] The spectra are parameterized in terms of significant wave height (SWH) measured from seafloor mounted pressure sensors offshore the surf zone. As the SWH increases there is a general increase in sound level, a shift to lower frequencies of the dominant energy, and a broadening of the dominant energy lobe. These observations are consistent with expectations of spectral evolution suggested by the computed radiation frequency spectra of Fig. 4.

Signal processing of the raw infrasound data collected at Kauai used an integration window of $\tau=3600$ s to estimate the spectral levels presented in Fig. 7. Since the model is based on transformation of radiation frequencies derived from a complete breaking wave distribution, model predictions are relevant only if the data window has sufficient length to sample a significant proportion of wavenumbers

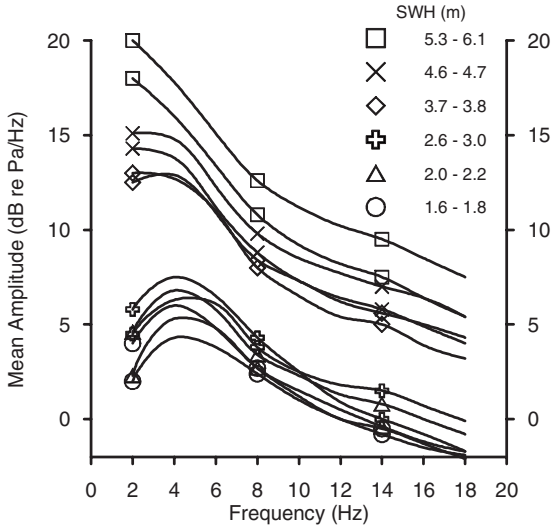


FIG. 7. Atmospheric infrasound from waves breaking at Polihale, Kauai.

represented in the breaking wave distribution. Most of the energy in the ocean wave spectra are contained in the 0.05–0.1 Hz bands, with dominant frequencies in the range 0.06–0.09 Hz corresponding to periods of 11–17 s. The long integration windows of the Kauai data allow for over 150 events with a period of 20 s, and therefore are deemed appropriate for model comparison.

V. MODEL RESULTS

This section presents comparisons of model results with measured data. Parameters used in model runs are as follows:

1. Slope of the breaking wave seafloor $m=0.06$.
2. Initial plume void fraction $\beta_0=0.35$, consistent with measured values by Deane.[24]
3. Initial vortex breaking height ratio $C_H=0.37$, from Sec. III B, Eq. (5).
4. Radiation spectrum (f_a) amplitude analysis binwidth $\Delta\omega_a=0.5$ Hz.

In default mode the model assumes that bubble plumes are static, there is a single bubble distribution that is summed in Eq. (9) to estimate the spectral shape. The model is capable of including contributions from additional bubble distributions according the evolution Eqs. (10) and (11). With this dynamic plume option, the void fraction values are decreased according to Eq. (10), and the plume effective radius is increased according to Eq. (11). Contributions for additional plumes in Eq. (9) are evaluated at fractional wave periods $t/T=0.1,0.2,0.3,0.4,0.5$.

Figure 8 plots results of Eq. (9) corresponding to deep-water significant wave heights of 1.8, 2.1, 2.4, 2.8, 3.7 and 4.6 m. Since the model computes only relative spectral levels, a bias term has been added to each computed spectrum to match the 10 Hz value of observed data.

Concerning the medium to large scale surf (SWH 1.8–2.4 m) represented in Fig. 8, characterization of the dominant infrasonic frequency is reasonable. This indicates that the presumed bubble oscillation mechanism is a candi-

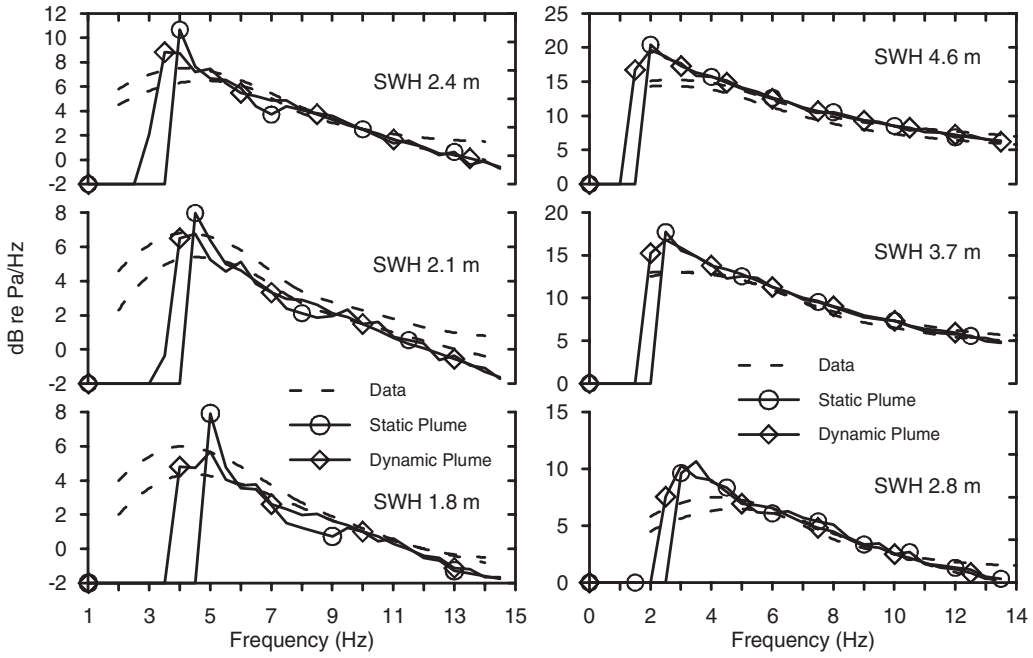


FIG. 8. Modeled infrasound spectra for ocean wave spectra with SWH of 1.8, 2.1, 2.4, 2.8, 3.7, 4.6 m compared to Kauai data.

date mechanism for generation of surf infrasound. It is also observed that the dynamic plume approximation has a broader main lobe, and lower cutoff frequency than the static plume, which is consistent with a larger sample of plume distributions that grow in size as the plume evolves. This result suggests that dynamic plume evolution is a significant factor contributing to the broad spectral lobes of dominant energy observed in field data.

Model results for the large and extreme surf conditions (SWH $>$ 2.5 m) estimate spectral shapes similar to the data, again with a slightly broader, lower frequency main energy lobe with the dynamic plume approximation. Prominence of the main energy lobe diverging from the spectral shape of the observed data may indicate that at these large spatial scales and energies the collective bubble oscillation mechanism is not a dominant contributor to infrasound generation. In this regime, the impact mechanisms may play a larger role.

VI. DISCUSSION

It has been recognized that remotely sensed infrasound has potential to provide "useful insight into coastal processes and permit an assessment of wave energy distribution in the littoral zone".[31] Indeed, Aucan *et al.* demonstrated that the bandpassed time series envelope of atmospheric infrasound generated by plunging surf can be used to estimate the dominant breaking wave period.[32] As an extension, we propose that based on an infrasound model such as that described above, an inverse model could be used to estimate a breaking wave height spectrum $H_B(\omega)$ from a measured infrasound spectrum $B(\omega_a)$.

Not only can an estimate of $H_B(\omega)$ be obtained, but one should also be able to estimate the bubble plume size distribution $R_B(\omega)$. Lamarre and Melville[33] found that dissipation of breaking ocean wave energy by air entrainment against buoyancy can account for up to 50% of the dissipated energy. Therefore, with an estimate of the initial wave energy spectrum and the entrained air volumes, the wave energy dissipated in breaking might be estimated. The residual could provide an estimate of the wave energy available for runup on the shore.

Another potential assessment of littoral dynamics is long term monitoring of surf zone bathymetric changes. Since bathymetry is a key variable in determination of the breaking wave spectrum, it is conceivable that parametric model fits to long term infrasonic monitoring could characterize seafloor morphology over times cales of days to months.

VII. CONCLUSION

A simple, functional transformation model of infrasound generated by collective bubble oscillations from collapsing air pockets entrained by plunging surf has been developed. The model is limited to estimation of relative spectral shape and cutoff frequencies since the amplitude coefficients of radiating spectral components are not quantified. Application of low frequency models which characterize the amplitude distributions, and source-receiver transfer functions[29,30] have potential to remove this limitation. Nonetheless, the model captures the observed characteristics of surf infrasound which include migration of dominant infrasonic energy to lower frequencies as ocean wave energy increases, and a broadening of the infrasonic energy distribution across the main lobe.

The model matches dominant infrasound frequencies and spectral shape reasonably well for medium to large scale surf, which may indicate that collective bubble oscillations are effective generators of surf infrasound. Further, it is suggested that dynamic plume evolution between breaking events is crucial to produce the observed broad spectral lobe around the dominant frequency of infrasonic energy. At the large and extreme scales of wave breaking, for example

when breaking wave heights exceed roughly 5 m, the model overestimates the relative amplitude of the lowest frequency components of the infrasound. This may indicate that at these larger spatial scales and energies the collective bubble oscillation mechanism is less important. In this regime hydrodynamic sources such as jet impact, vortex generation, impulse pressure bounce back, impact reverberations, as well as the massive bores of foam which persist shoreward of the plunging surf zone are potential contributors.

Estimation of acoustic radiation spectra from deepwater ocean wave spectra (forward model) constitutes a nonlinear transformation. Inversion of this model, for example with a neural network or other nonlinear state estimator, has potential to characterize surf-zone hydraulic and geomorphic dynamics based on remote infrasound sensing. In particular, it is suggested that the breaking wave height distribution, wave energy dissipation, wave energy runup potential, and long term bathymetric dynamics could be assessed.

ACKNOWLEDGMENT

The authors thank Dr. Robert M. Kennedy for his thoughtful review of the manuscript and suggestions which served to improve the paper.

[1]W. K. Melville, "The role of surface-wave breaking in air-sea interaction," Annu. Rev. Fluid Mech. **28**, 279–321 (1996).
[2]A. Prosperetti, "Bubble-related ambient noise in the ocean," J. Acoust. Soc. Am. **78**(S1), S2 (1985).
[3]A. Prosperetti, "Bubble-related ambient noise in the ocean," J. Acoust. Soc. Am. **84**(3), 1042–1054 (1988).
[4]W. Carey, "Low frequency noise from breaking waves," *Natural Physical Sources of Underwater Sound: Sea Surface Sound (2)*, edited by B. R. Kerman. (Kluwer Academic, Dordrecht, 1993).
[5]M. R. Loewen and W. K. Melville, "An experimental investigation of the collective oscillations of bubble plumes entrained by breaking waves," J. Acoust. Soc. Am. **95**(3), 1329–1343 (1994).
[6]E. Lamarre and W. K. Melville, "Void fraction measurements and sound-speed fields in bubble plumes generated by breaking waves," J. Acoust. Soc. Am. **95**(3), 1317–1328 (1994).
[7]S. C. Webb, "Broadband seismology and noise under the ocean," Rev. Geophys. **36**(1), 105–142 (1998).
[8]A. C. Kibblewhite and K. C. Evans, "Wave-wave interactions, microseisms, and infrasonic ambient noise in the ocean," J. Acoust. Soc. Am. **78**(3), 981–994 (1985).
[9]R. H. Nichols, "Infrasonic ocean noise sources: Wind versus waves," J. Acoust. Soc. Am. **82**(4), 1395–1402 (1987).
[10]C. S. McCreery and F. K. Duennebier, "Correlation of deep ocean noise (0.4–30 Hz) with wind, and the Holu Spectrum—A worldwide constant," J. Acoust. Soc. Am. **93**(5), 2639–2648 (1993).
[11]O. A. Godin, "Anomalous transparency of water-air interface for low-frequency sound," Phys. Rev. Lett. **97**, 164301 (2006).
[12]M. Garcés *et al.*, "Infrasound from large surf," Geophys. Res. Lett. **33**, L05611 (2006).
[13]S. J. Arrowsmith and M. A. H. Hedlin, "Observations of infrasound from surf in southern California," Geophys. Res. Lett. **32**, L09810 (2005).
[14]A. Le Pichon, V. Maurer, D. Raymond, and O. Hyvernaud, "Infrasound from ocean swells observed in Tahiti," Geophys. Res. Lett. **31**, L19304 (2004).
[15]M. Garcés, C. Hetzer, M. Merrifield, M. Willis, and J. Aucan, "Observations of surf infrasound in Hawaii," Geophys. Res. Lett. **30**, 2264 (2003).
[16]M. Garcés, D. Fee, S. McNamara, J. Aucan, and M. Merifield, "The deep sound of one wave plunging," J. Acoust. Soc. Am. **120**(5), 3032 (2006).
[17]D. H. Peregrine, "Breaking waves on beaches," Annu. Rev. Fluid Mech. **15**, 149–178 (1983).
[18]J. A. Battjes, "Surf-zone dynamics," Annu. Rev. Fluid Mech. **20**, 257–291 (1988).
[19]D. H. Peregrine, "Water-wave impact on walls," Annu. Rev. Fluid Mech. **35**, 23–43 (2003).
[20]Y. Watanabe, H. Saeki, and R. J. Hosking, "Three dimensional vortex structures under breaking waves," J. Fluid Mech. **545**, 291–328 (2005).
[21]D. Fee *et al.*, "Advances in surf infrasound monitoring," *2006 Infrasound Technology Workshop, Geophysical Institute, University of Alaska, Fairbanks*, September 25–28 (2006).
[22]W. Carey, "Low-to mid-frequency oceanic noise," *Natural Physical Processes Associated with Sea Surface Sound*, edited by T. G. Leighton, (University of Southampton, Southampton, 1997).
[23]M. S. Longuet-Higgins, "Parametric solutions for breaking waves," J. Fluid Mech. **121**, 403–424 (1982).
[24]G. B. Deane, "Sound generation and air entrainment by breaking waves in the surf zone," J. Acoust. Soc. Am. **102**(5), 2671–2689 (1997).
[25]U. S. Army Coastal Engineering Research Center, *Shore Protection Manual, Volume 1* (U. S. Government Printing Office, Washington D.C., 1977).
[26]N. Booij, R. C. Ris, and L. H. Holthuijsen, "A third-generation wave model for coastal regions, Part I, Model description and validation," J. Geophys. Res., [Oceans] **104**, 7649–7666 (1999).
[27]S. Mead and K. Black, "Predicting the breaker intensity of surfing waves," J. Coastal Res. Special Issue No. 29, 51–56 (2001).
[28]K. Hasselmann, W. Sell, D. B. Ross, and P. Müller, "A parametric wave prediction model," J. Phys. Oceanogr. **6**, 200–228 (1976).
[29]H. N. Oguz, "A theoretical study of low-frequency oceanic ambient noise," J. Acoust. Soc. Am. **95**(4), 1895–1912 (1994).
[30]S. L. Means, "Low-frequency sound generation from breaking surf," Acta Radiol. **5**(2), 13–18 (2004).
[31]M. Garcés, D. Fee, P. Caron, C. Hetzer, J. Aucan, M. Merrifield, R. Gibson, and J. Bhattacharyya, "Multiparameter studies of surf infrasound," J. Acoust. Soc. Am. **117**(4), 2452 (2005).
[32]J. Aucan, D. Fee, and M. Garcés, "Infrasonic estimation of surf period," Geophys. Res. Lett. **33**, L05612 (2006).
[33]E. Lamarre and W. K. Melville, "Air entrainment and dissipation in breaking waves," Nature (London) **351**, 469–472 (1991).

Multilevel fast multipole algorithm for acoustic wave scattering by truncated ground with trenches

Mei Song Tong[a] and Weng Cho Chew[b]
Department of Electrical and Computer Engineering, University of Illinois at Urbana-Champaign, Urbana, Illinois 61801

Michael J. White
Engineering Research and Development Center/Construction Engineering Research Laboratory, U.S. Army Corps of Engineers, P.O. Box 9005, Champaign, Illinois 61826

(Received 30 October 2007; revised 11 February 2008; accepted 24 February 2008)

The multilevel fast multipole algorithm (MLFMA) is extended to solve for acoustic wave scattering by very large objects with three-dimensional arbitrary shapes. Although the fast multipole method as the prototype of MLFMA was introduced to acoustics early, it has not been used to study acoustic problems with millions of unknowns. In this work, the MLFMA is applied to analyze the acoustic behavior for very large truncated ground with many trenches in order to investigate the approach for mitigating gun blast noise at proving grounds. The implementation of the MLFMA is based on the Nyström method to create matrix equations for the acoustic boundary integral equation. As the Nyström method has a simpler mechanism in the generation of far-interaction terms, which MLFMA acts on, the resulting scheme is more efficient than those based on the method of moments and the boundary element method (BEM). For near-interaction terms, the singular or near-singular integrals are evaluated using a robust technique, which differs from that in BEM. Due to the enhanced efficiency, the MLFMA can rapidly solve acoustic wave scattering problems with more than two million unknowns on workstations without involving parallel algorithms. Numerical examples are used to demonstrate the performance of the MLFMA with report of consumed CPU time and memory usage. © *2008 Acoustical Society of America.* [DOI: 10.1121/1.2897048]

PACS number(s): 43.28.Js, 43.20.Fn, 43.50.Pn [DSB] Pages: 2513–2521

I. INTRODUCTION

Fast multipole method (FMM) was introduced by Rokhlin to rapidly calculate Coulombic potentials for a large-scale particle system.[1] Later on, it was generalized by Greengard[2] to seek fast numerical solutions for two-dimensional and three-dimensional (3D) Laplace equations in particle simulations. This method was mainly applied to particle simulations in astrophysics and molecular dynamics at the beginning.[3,4] Later, it was extended to acoustic wave problem that follows from Helmholtz equation.[5] In electromagnetics (EM), it received intensive studies, and was extended to a multilevel scheme, known as multilevel fast multipole algorithm (MLFMA), in 1994.[6–8] The most distinctive feature of the method is the rapid evaluation of the matrix-vector multiply useful in an iterative method for solving a matrix equation. Also, the matrix elements are never explicitly stored except for those near-interaction entries, leading to a matrix-free scheme, where the memory requirement is dramatically reduced. In the iterative methods, the speed bottleneck is the matrix-vector multiply, which requires $\mathcal{O}(N^2)$ costs, where N is the number of unknowns in the matrix equation.

MLFMA wisely decomposes each element of the matrix, which represents the far interaction between a source point and a field point, into radiation pattern, translator, and receiving pattern. The matrix-vector multiply is then performed in three stages within a multilevel tree structure. The decomposition of a matrix element, which is the matrix representation of the Green's function, is based on the addition theorem.[9] The radiation pattern, translator, and receiving pattern can be constructed in advance and stored with much less memory. Due to the use of the multilevel tree structure, the diagonalization of the translation operator, and the interpolation or anterpolation for wave expansions at different levels, MLFMA can reduce the original $\mathcal{O}(N^2)$ complexity, both in CPU time and in memory usage, to a $\mathcal{O}(N \log N)$ complexity. This is a significant difference in computational costs when N is very large.

MLFMA has been widely used in solving EM integral equations.[10] With the help of supercomputers, the very large problems with 10–30 million unknowns have been solved.[11–14] Although FMM dealt with acoustic wave problems very early,[5] the development of the method in acoustics has been relatively slow,[15–19] compared with that in EM. Recently, there is a growing interest in the acoustic applications of MLFMA.[20–25] In Refs. 20 and 21, the authors considered scattering by multiple spheres based on the spherical harmonic expansion for the scattered fields. As semianalytical formulas instead of boundary integral equation (BIE) are used, the generation of matrix elements is simple. The scheme is not suitable for solving the scattering by arbitrarily shaped objects, although it has been demonstrated to solve

[a]Electronic mail: meisongt@uiuc.edu
[b]Currently on leave from UIUC to serve at The University of Hong Kong.

problems involving up to 10^4 spheres (about one million unknowns). In fact, the scheme is different from the BIE-based MLFMA, which we developed in this work. In Refs. 22–25, however, MLFMA together with BIE is applied to solve for acoustic scattering by 3D arbitrarily shaped scatterers, but the implementation is based on BEM.

We modify MLFMA for solving acoustic wave scattering by very large objects with 3D arbitrary shapes. In the studies for mitigating gun blast noise at proving grounds, we design a trench structure in the ground to block the propagation of sound wave. The simulation for acoustic wave scattering by such a structure requires solving a very large matrix equation resulting from acoustic BIE. MLFMA is then used to accelerate the solution process and fast solutions for problems with millions of unknowns can be obtained on workstations without involving parallel algorithms. Unlike the work in Refs. 21–25, our MLFMA is based on the Nyström method to form matrix elements. This is also different from the MLFMA implementation in EM, which is mainly based on the method of moments (MOM) with Rao-Wilton-Glisson (RWG) basis[26] to create matrix entries.

The Nyström method is an efficient numerical tool in solving integral equations.[27] Initially, this method was designed for solving integral equations with regular kernels. In recent years, it has been used to solve for the integral equations derived from Helmholtz equations for wave radiation and propagation problems.[28–31] Such integral equations include singular integral kernels related to the Green's function and special treatments are needed for self and near interaction terms. The Nyström method uses a collocation or point-matching process and wisely selects the quadrature points of a quadrature rule as the source points and observation points to transform an integral equation into a matrix equation. The matrix elements for far interactions are simply the direct evaluation of integrands. Due to its elegance, the Nyström method is simpler than MOM and BEM in incorporating MLFMA—this is also the first time that Nyström method is used with our version of MLFMA. However, the Nyström method usually has a lower accuracy than MOM for the same discretization of geometry with the same density of unknowns and the number of unknowns will dramatically increase if improving the accuracy by using a higher-order quadrature rule. For the near interaction terms of matrix in the MLFMA implementation, the original Nyström method is recalled and we derive very simple and efficient formulas for the singular or near-singular integrations of the acoustic BIE kernel. This technique is different from the regularization of singularity in BEM. Numerical examples from the simulation for mitigating gun blast noise show that the proposed MLFMA has a robust performance in solving for the acoustic wave scattering by very large and complex structures. A typical problem with one million unknowns can be solved within two days on a Dell Precision 690 machine using 5 GB memory. This machine has two dual-core 3.0 GHz CPU with 16 GB RAM, but we only employ one of CPU's as the series algorithm is utilized. All calculations in this work are realized on it.

II. IMPLEMENTATION OF MLFMA FOR ACOUSTIC BIE

MLFMA is described in the Appendix which factorizes Green's function, and hence, the matrix element that describes the interaction between a source point and a field point. In this section, we will describe the use of MLFMA for expediting the solution of the acoustic BIE.

A. Acoustic BIE

For EM wave scattering, the governing equation is a vector integral equation with the vector current as the unknown function, and MOM with RWG basis may be the appropriate method incorporating MLFMA. In contrast, acoustic wave scattering is represented by a scalar BIE,[32] i.e.

$$p^i(\mathbf{r}) + \int_S \left[\frac{\partial g(\mathbf{r},\mathbf{r}')}{\partial n'} p(\mathbf{r}') - g(\mathbf{r},\mathbf{r}') \frac{\partial p(\mathbf{r}')}{\partial n'} \right] dS' = \frac{1}{2} p(\mathbf{r}), \quad \mathbf{r} \in S, \tag{1}$$

where p is the pressure field, $g(\mathbf{r},\mathbf{r}')=e^{ikR}/(4\pi R)$ is the 3D Green's function, which is the same as that in EM, and $\hat{n}'$ is the outward unit normal vector on the surface S of a scatterer. The superscript i on p denotes the incident wave and $R=|\mathbf{r}-\mathbf{r}'|$ represents the distance between a field point (or observation point) $\mathbf{r}$ and a source point $\mathbf{r}'$. If we incorporate the impedance boundary condition[33]

$$\frac{\partial p(\mathbf{r}')}{\partial n'} - \eta p(\mathbf{r}') = 0, \tag{2}$$

where $\eta=i\omega\rho/z_s$ and z_s is the surface impedance, the previous BIE becomes

$$\frac{1}{2} p(\mathbf{r}) - \int_S G_0(\mathbf{r},\mathbf{r}') p(\mathbf{r}') dS' = p^i(\mathbf{r}), \quad \mathbf{r} \in S, \tag{3}$$

where $G_0=(\hat{n}'\cdot\nabla'-\eta)g(\mathbf{r},\mathbf{r}')$. Note that the previous BIE may have the possible internal resonance problem which refers to the nonuniqueness of the solution when the frequency of incident wave coincides with the resonance frequency of a cavity with the same shape as that of the scatter.[34] This problem can only be removed completely by using different BIEs, such as the combined Helmholtz integral equation formulation[35] or the Burton and Miller formulation.[36] We do not meet the internal resonance problem even using the BIE (1) in the solution because our iteration process converges normally. If the resonant frequency is approached or touched, the system matrix will be near-singular or singular and the iteration, which is very sensitive to the conditioning of the matrix, will tend to be divergent.

B. Radiation and receiving patterns

Due to the scalar property of the previous acoustic BIE, BEM, or the Nyström method may be more appropriate than MOM to combine with MLFMA in order to accelerate the solution. If the Nyström method with a one-point quadrature rule is used (the higher-order quadrature rules can be used,

but the number of unknowns will dramatically increases), the corresponding terms in the matrix equation in Eq. (A1) will be

$$A_{ji} = -\int_{\Delta S_i} dS' G_0(\mathbf{r}_j, \mathbf{r}'),$$

$$b_j = p^i(\mathbf{r}_j) \tag{4}$$

and a_i is the unknown pressure field at the centroid of the ith triangle patch ΔS_i. We do not include the identity or constant term (1/2) of the BIE in A_{ji} here because it belongs to the near terms (diagonal terms) and the matrix element here only represents the far interaction between a field point and a source point, which MLFMA works on. Using Eq. (A2) for the factorization of the Green's function, the integral kernel can be written as

$$G_0(\mathbf{r}_j - \mathbf{r}_i) = \frac{1}{4\pi}\int d^2\hat{k}(-\hat{n}' \cdot i\mathbf{k} - \eta) e^{i\mathbf{k}\cdot(\mathbf{r}_{jm} - \mathbf{r}_{im'})} \cdot \alpha_{mm'}(\mathbf{k}, \mathbf{r}_{mm'}). \tag{5}$$

With the previous kernel, the radiation and receiving patterns are

$$V_{sm'i}(\hat{k}) = \int_{\Delta S_i} dS' e^{-i\mathbf{k}\cdot(\mathbf{r}' - \mathbf{r}_{m'})}(-\hat{n}' \cdot i\mathbf{k} - \eta), \quad \mathbf{r}' \in \Delta S_i,$$

$$V_{fmj}(\hat{k}) = \frac{1}{4\pi} e^{i\mathbf{k}\cdot\mathbf{r}_{jm}} \tag{6}$$

and the translator is the same as Eq. (A3). We will implement Eq. (A2) based on Eq. (6) for far interactions and the solution process will be accelerated dramatically. The far interaction or well-separated interaction is defined as the interaction between a field point $\mathbf{r}_j$ and a source point $\mathbf{r}_i$ whose separation is at least one box at the same level.[10]

The previous integral over $\hat{k}$ is evaluated by the Gaussian quadrature rule with $Q=2L^2$ points, where L is the truncated number of the summation series in the translator in Eq. (A3). The use of the quadrature rule results in

$$A_{ji} = -\sum_{q=1}^{Q} V_{fjm}(\hat{k}_q) \cdot \alpha_{mm'}(\mathbf{k}_q, \mathbf{r}_{mm'}) \cdot V_{sm'i}(\hat{k}_q) = \mathbf{V}_{jm} \cdot \bar{\alpha}_{mm'} \cdot \mathbf{V}_{m'i}, \tag{7}$$

where

$$\mathbf{V}_{jm} = [w_1 V_{fjm}(\hat{k}_1), w_2 V_{fjm}(\hat{k}_2), \ldots, w_Q V_{fjm}(\hat{k}_Q)],$$

$$\bar{\alpha}_{mm'} = \mathrm{diag}\{\alpha_{mm'}(\mathbf{k}_1, \mathbf{r}_{mm'}), \alpha_{mm'}(\mathbf{k}_2, \mathbf{r}_{mm'}), \ldots, \alpha_{mm'}(\mathbf{k}_Q, \mathbf{r}_{mm'})\},$$

$$\mathbf{V}_{m'i} = [V_{sm'i}(\hat{k}_1), V_{sm'i}(\hat{k}_2), \ldots, V_{sm'i}(\hat{k}_Q)]^T, \tag{8}$$

and $w_1, w_2, \ldots, w_Q$ are the weights of the quadrature rule. We will store the previous vectors and matrix with an efficient manner in the preprocessing stage and they are used in each matrix-vector multiply in the iterative process.

C. Nyström method

In solving the boundary integral equation, we need to transform it into an algebraic matrix equation first. If the integral kernel is regular, the Nyström method directly replaces the numerical integration over a small patch with a summation under an appropriate quadrature rule, i.e.,

$$\int_{\Delta S} f(\mathbf{r}, \mathbf{r}') u(\mathbf{r}') dS' = \sum_{j=1}^{P} w_j f(\mathbf{r}, \mathbf{r}'_j) u(\mathbf{r}'_j), \tag{9}$$

where ΔS is the small patch, $f(\mathbf{r}, \mathbf{r}')$ is the integral kernel, $u(\mathbf{r}')$ is the unknown function, P is the number of quadrature points and w_j is the weights of the quadrature rule. The small patch usually represents a flat triangle in the discretization of the geometry and the quadrature rule has different choices.[37] This direct replacement will result in a very simple process to generate matrix elements when a collocation procedure is performed on the field point $\mathbf{r}$. The process is just the direct evaluation of the integrand multiplied by the weights at quadrature points and the unknown coefficients are chosen as the values of unknown function at quadrature points.

However, in wave physics, the integral kernel is related to Green's function which is not regular in the self and near interactions and a special treatment or local correction is needed.[28–30] We develop a very simple and efficient local correction scheme for EM[31,38] that can also be used for acoustic problems. We will implement the scheme to generate those self and near interaction terms in MLFMA.

D. Near terms

The near terms in MLFMA are calculated by the original numerical methods on which the solution of BIE is based without MLFMA acceleration. One usually employs MOM with RWG basis in EM and utilizes BEM in acoustics. Here we use the Nyström method to generate the near terms. The near terms include the self-interaction terms in which the source point and field point reside in the same triangle patch, and the near-interaction terms in which the source point and field point are located at different but nearby triangle patches. The acoustic BIE includes two kernels which are the Green's function itself and its gradient. The integral related to the Green's function itself has a week singularity which can be easily handled[38,39] and we will not deal with it here. The integral with the gradient of the Green's function has a $1/R^2$ singularity on which the special care should be taken. In a Cartesian coordinate system, the gradient of the Green's function becomes

$$\nabla g(\mathbf{r}, \mathbf{r}') = g_x\hat{x} + g_y\hat{y} + g_z\hat{z} = c_0(x - x')\hat{x} + c_0(y - y')\hat{y} + c_0(z - z')\hat{z}, \tag{10}$$

where

$$c_0 = \frac{(ikR - 1)}{4\pi R^3} e^{ikR}. \tag{11}$$

In Eq. (10), (x, y, z) and (x', y', z') are the coordinates of the field point and the source point on a triangle patch. If we create a local coordinate system on the source triangle patch plane whose origin is the projection of the field point on the

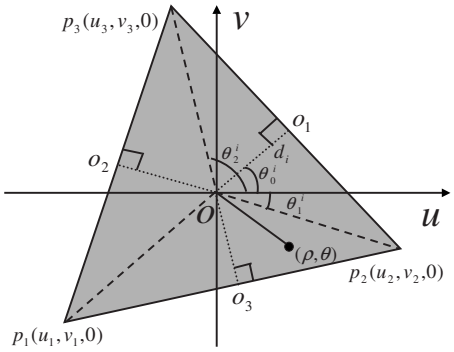


FIG. 1. Local coordinate system on a triangle patch plane.

plane, as shown in Fig. 1, then the three components of the gradient can be written as

$$g_u = c_0(-u); \quad g_v = c_0(-v); \quad g_w = c_0 w_0, \tag{12}$$

where $R=\sqrt{u^2+v^2+w_0^2}$. The source point is located at $(u,v,0)$ on the triangle patch and the field point is located at $(0,0,w_0)$ in the local coordinate system now. If we expand the exponential term in the Green's function into a series form

$$e^{ikR} = \sum_{m=0}^{\infty} \frac{(ik)^m}{m!} R^m \approx \sum_{m=0}^{M} \frac{(ik)^m}{m!} R^m, \tag{13}$$

which converges very rapidly (M is small) for near and self interaction terms as R is small, then the most singular integrals included in those three components of gradient will be

$$I_1 = \int_{\Delta S} \frac{u}{R^3} dS; \quad I_2 = \int_{\Delta S} \frac{v}{R^3} dS; \quad I_3 = \int_{\Delta S} \frac{w_0}{R^3} dS. \tag{14}$$

Other integrals are either regular or with a weak singular kernel of $1/R$ which are easily handled. By referring to Fig. 1, which includes a polar coordinate system (ρ,θ) for a source point on the triangle patch and $R=\sqrt{\rho^2+w_0^2}$, the first integral above can be written as

$$\begin{aligned} I_1 &= \int_{\Delta S} \frac{u}{R^3} dS = \sum_{i=1}^{3} \int_{\theta_1^i}^{\theta_2^i} d\theta \cos\theta \int_0^{d_\theta^i} \frac{\rho^2 d\rho}{(\rho^2+w_0^2)^{3/2}} \\ &= \sum_{i=1}^{3} \left[\int_{\theta_{10}^i}^{\theta_{20}^i} d\phi \frac{-d_i \cos(\phi+\theta_0^i)}{\sqrt{d_i^2 + w_0^2 \cos^2\phi}} + \int_{\theta_{10}^i}^{\theta_{20}^i} d\phi \cos(\phi \right. \\ &\quad + \theta_0^i) \ln(d_i + \sqrt{d_i^2 + w_0^2 \cos^2\phi}) - \int_{\theta_{10}^i}^{\theta_{20}^i} d\phi \cos(\phi \\ &\quad \left. + \theta_0^i) \ln(\cos\phi) \right] = \sum_{i=1}^{3} (I_{1a}^i + I_{1b}^i + I_{1c}^i), \end{aligned} \tag{15}$$

where $d_\theta^i = d_i/\cos(\theta-\theta_0^i)$, $\theta_{10}^i = \theta_1^i - \theta_0^i$, $\theta_{20}^i = \theta_2^i - \theta_0^i$. The first and third integrals above can be found analytically,[40] i.e.

$$\begin{aligned} I_{1a}^i &= -\frac{d_i}{w_0} \{\cos\theta_0^i [\arcsin(s_0 a_2^i) - \arcsin(s_0 a_1^i)] \\ &\quad + \sin\theta_0^i [\ln(w_0 b_2^i + \sqrt{d_i^2 + (w_0 b_2^i)^2}) \\ &\quad - \ln(w_0 b_1^i + \sqrt{d_i^2 + (w_0 b_1^i)^2})]\}, \end{aligned}$$

$$\begin{aligned} I_{1c}^i &= t_0[(1+a_2^i)\ln(1+a_2^i) - (1+a_1^i)\ln(1+a_1^i) \\ &\quad - (1-a_2^i)\ln(1-a_2^i) + (1-a_1^i)\ln(1-a_1^i) - 2(a_2^i \\ &\quad - a_1^i)] + \sin\theta_0^i [b_2^i \ln(b_2^i) - b_1^i \ln(b_1^i) - b_2^i + b_1^i], \end{aligned} \tag{16}$$

where $t_0=0.5\cos\theta_0^i$, $s_0=w_0/\sqrt{d_i^2+w_0^2}$, $a_1^i=\sin\theta_{10}^i$, $a_2^i=\sin\theta_{20}^i$, $b_1^i=\cos\theta_{10}^i$, and $b_2^i=\cos\theta_{20}^i$. The second integral I_{1b}^i is never singular no matter how the field point is close to the triangle patch, so it can be integrated numerically. We can use a similar way to handle I_2. For I_3, it is easy to show that

$$\begin{aligned} I_3 &= \int_{\Delta S} \frac{w_0}{R^3} dS = w_0 \sum_{i=1}^{3} \int_{\theta_1^i}^{\theta_2^i} d\theta \int_0^{d_\theta^i} \frac{\rho d\rho}{(\rho^2+w_0^2)^{3/2}} \\ &= t_1 \sum_{i=1}^{3} [\theta_2^i - \theta_1^i - \arcsin(s_0 a_2^i) + \arcsin(s_0 a_1^i)], \end{aligned} \tag{17}$$

where $t_1=\text{sign}(w_0)$. When the field point is inside the triangle patch, we can take a limit of $w_0 \to 0$ to obtain

$$I_1 = \sum_{i=1}^{3} [(\sin\theta_2^i - \sin\theta_1^i)\ln(d_i) - I_A \cos\theta_0^i + I_B \sin\theta_0^i],$$

$$I_2 = \sum_{i=1}^{3} [(\cos\theta_1^i - \cos\theta_2^i)\ln(d_i) - I_B \cos\theta_0^i - I_A \sin\theta_0^i],$$

$$I_3 = 0, \tag{18}$$

where

$$\begin{aligned} I_A &= 0.5\{(1+a_2^i)[\ln(1+a_2^i) - 1] - (1+a_1^i)[\ln(1+a_1^i) \\ &\quad - 1] - (1-a_2^i)[\ln(1-a_2^i) - 1] + (1-a_1^i)[\ln(1-a_1^i) \\ &\quad - 1]\}, \end{aligned}$$

$$I_B = b_2^i[1 - \ln(b_2^i)] - b_1^i[1 - \ln(b_1^i)]. \tag{19}$$

The formulas in Eq. (18) may not be necessary as the dot product of the unit normal vector with the gradient of the Green's function on a self-patch will vanish. We present these formulas for completeness, and also they may be useful for underwater acoustics in which a different BIE is employed.

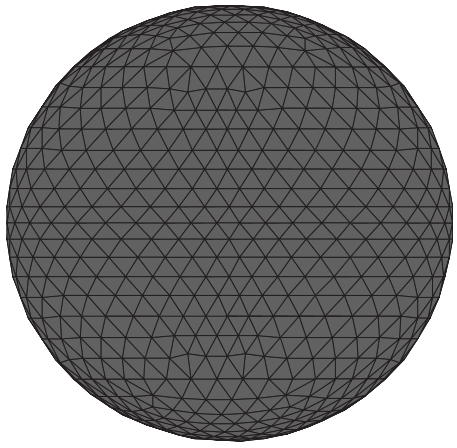


FIG. 2. A meshed sphere surface.

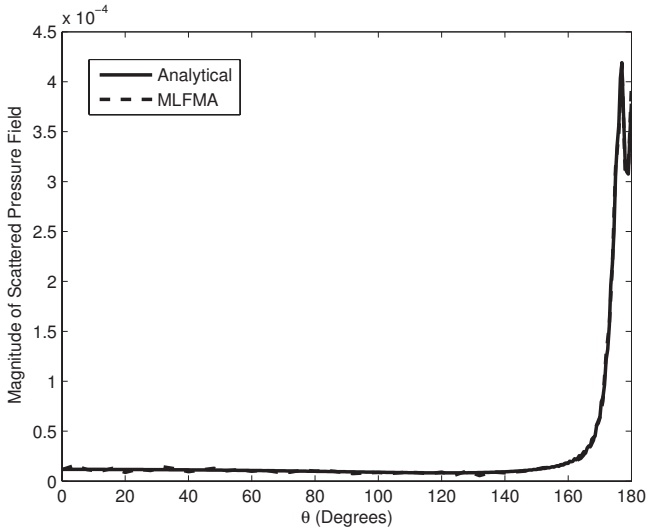


FIG. 3. Magnitude of scattered pressure field at the $r=50a$ principal cut, $a=20\lambda$ and $\eta=10-10i$.

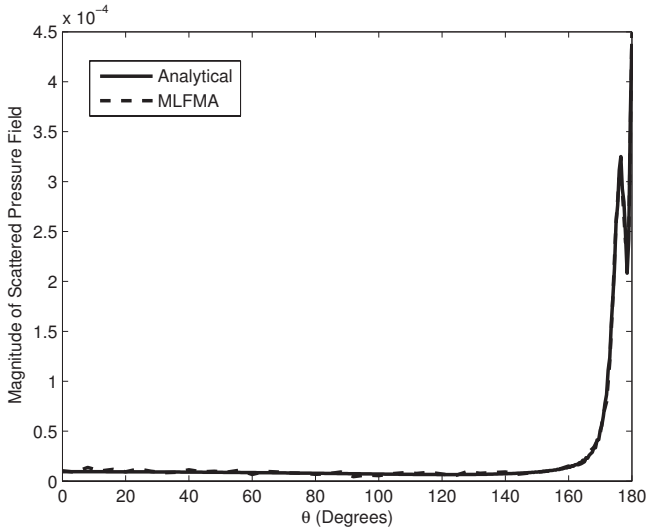


FIG. 5. Magnitude of scattered pressure field at the $r=50a$ principal cut, $a=25\lambda$ and $\eta=10-10i$.

III. NUMERICAL RESULTS

We use the developed MLFMA with the generalized minimal residual method as the iterative solver to solve for the acoustic wave scattering by very large scatterers. We first consider the scattering by a sphere so that the solutions can be verified by comparing with the corresponding analytical solutions. The sphere has a large radius $a=20\lambda$, 25λ, and 30λ, respectively, where λ is the wavelength in free space, and is meshed with flat triangle patches as illustrated in Fig. 2. The surface status of the sphere is characterized by the value of η and the incident wave is generated by a normalized point source located at $(0,0,10a)$ with a frequency $f=1700$ Hz. The propagation medium is the air with a standard acoustic velocity $c=340$ m/s.

Figures 3–6 show the scattered pressure fields along the principal cut ($\phi=0°$ and $\theta=0° \sim 180°$) at the $r=50a$ surface. Figure 7 is a zoom-in plot for the details between $\theta=160°$ and 180° for the $a=30\lambda$ case. We can see that the solutions are very close to the corresponding analytical solutions. Table I summarizes the CPU time T (s) and memory usage M (GB) for solving these large problems, where N is the number of unknowns. It is seen from the table that solving a one million unknown problem only consumes about 16 h when the stopping error of the iteration is set up 10^{-5}.

After validating the code, we apply it to solve for the acoustic wave scattering by large trench structures which are needed in the design for mitigating gun blast noise. Figures 8 illustrates a meshed trench structure embedded in a circularly truncated ground (top view) and 9 defines the geometrical sizes for each trench. We assume that the ground and trench surfaces are rigid, so $\eta=0$ here. The trenches are concentrically shaped and the entire structure is a body of revolution (BOR), but we treat it as a full 3D geometry and the solutions are compared with those obtained from BOR formulas

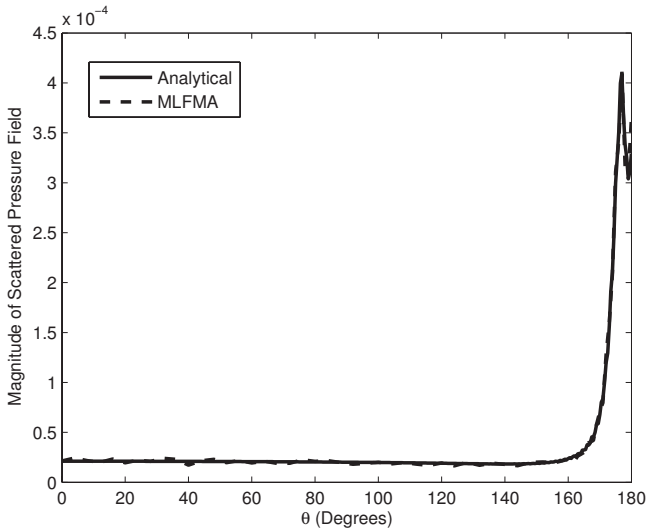


FIG. 4. Magnitude of scattered pressure field at the $r=50a$ principal cut, $a=20\lambda$ and $\eta=10$.

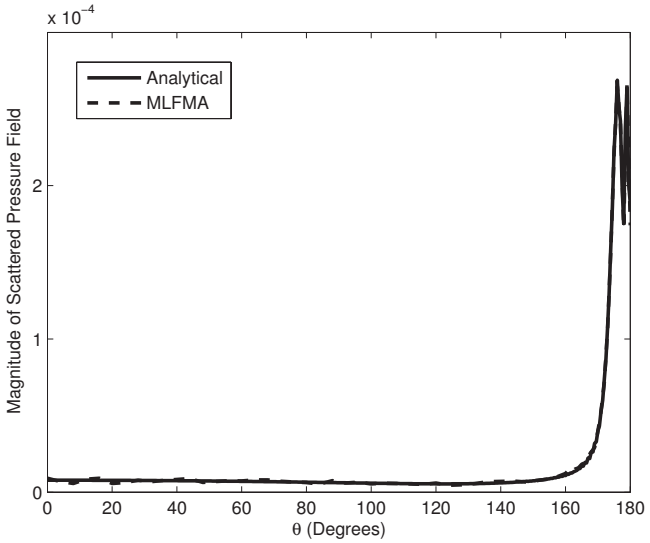


FIG. 6. Magnitude of scattered pressure field at the $r=50a$ principal cut, $a=30\lambda$ and $\eta=10-10i$.

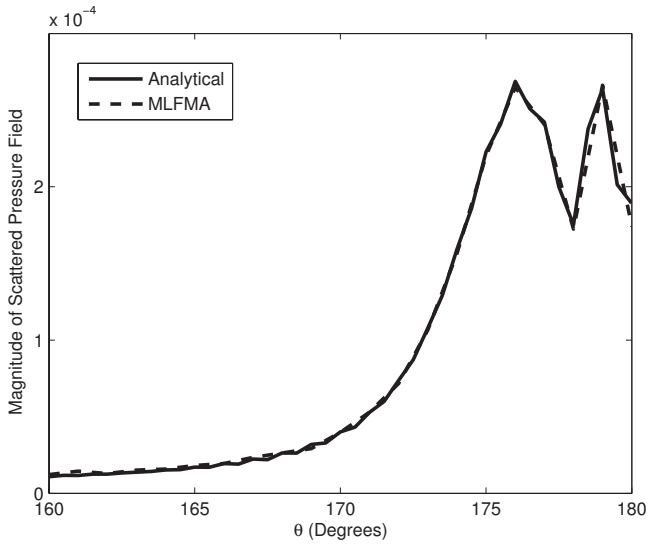


FIG. 7. Zoom-in plot for the magnitude of scattered pressure field at the $r=50a$ principal cut, $a=30\lambda$ and $\eta=10-10i$.

we developed previously. This can make sure the correctness of the solutions when lacking analytical solutions to compare with. In the calculations, we choose the frequency of the incident wave generated by a point source as $f=20$ Hz, which is close to the central frequency of a large-caliber gun blast noise, and the wave velocity as $c=350$ m/s.[41] The point source is located at a location above the ground center with a height of $h=0.1\lambda$. The truncated radius of the ground is chosen as $r_g=20\lambda$, which is large enough for the previous specific point source.[42] The trench geometry has a width of $w=0.1\lambda$, a periodicity of $t=0.2\lambda$ and a depth of $d=0.25\lambda$. The distance between the ground center and the inner wall of the first trench is $r_0=0.2\lambda$.

Figures 10–13 depict the radiation patterns (RP) or excess attenuations (EA) for the trench structures when the number of concentric trenches is $K=1$, 5, 10, and 50, respectively. RP or EA is defined as[43]

$$\mathrm{RP}=\mathrm{EA}=20\log_{10}\left|\frac{p(\mathbf{r})}{p_0(\mathbf{r})}\right|\mathrm{dB}, \tag{20}$$

where p is the total pressure field (with scatterer) and p_0 is the free-space pressure field (without scatterer) at an observation point $\mathbf{r}$. The observation points are located at the principal cut defined by $\theta=0°-90°$ and $\phi=0°$ and 180° on the sphere surface of $|\mathbf{r}|=2000$ m. It can be seen that the solutions based on MLFMA are close to those obtained from BOR formulas and also the propagation of acoustic wave is suppressed along the ground surface as the number of trenches increases. Figure 14 presents the comparison of radiation patterns when the larger truncated sizes of ground

TABLE I. CPU time and memory usage for scattering by a large sphere.

a	20	20	25	30
η	10-10i	10	10-10i	10-10i
N	1 046 528	1 046 528	1 635 840	2 556 800
T	54 267	58 728	107 037	145887
M	4.8	4.8	9.2	13.0

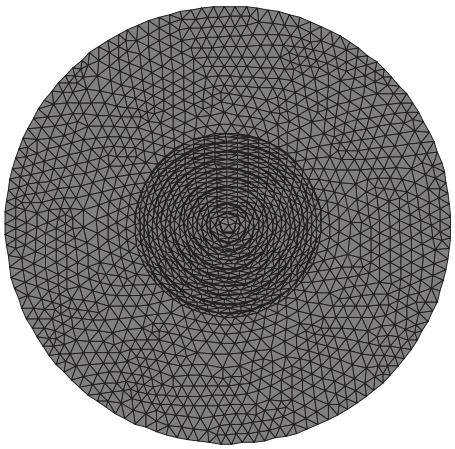


FIG. 8. A meshed trench structure embedded in a truncated ground (top view).

$r_g=30\lambda$ and 40λ with 50 trenches are chosen and it is clear that $r_g=20\lambda$ is large enough. Table II gives the CPU times and memory usage for running these cases, where K is the number of trenches. For the cases with more than 2 million unknowns in the two tables, we believe that they are the largest cases in acoustics that numerical solvers have solved without resorting to parallel algorithms and supercomputers. It should be noted that the commercial software IDEAS we employed to generate meshes in this work usually cannot generate more than one million triangular meshes. If more than one million triangular meshes are needed for a geometry, we have to generate coarse meshes using IDEAS first, and then refine these meshes by dividing a triangle into three smaller triangles. The three smaller triangles are formed by connecting three vertices with the centroid of the larger triangle. As such a refinement is based on the coarse IDEAS meshes, the small difference between three curves in Fig. 14 may be caused by the disagreement of geometrical approximation of the coarse IDEAS meshes between three cases.

IV. CONCLUSION

MLFMA is extended to solve for acoustic wave scattering by very large objects with 3D arbitrary geometries. In the implementation, We first use the Nyström method to generate

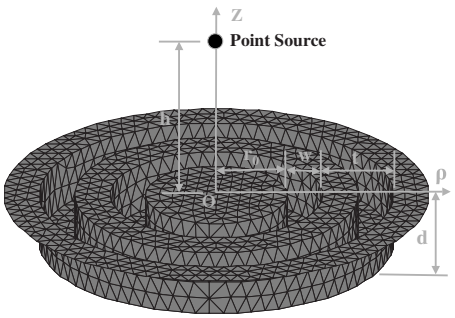


FIG. 9. Geometrical parameters of the trench structure, in which r_0 is the distance between the ground center and the inner wall of the first trench, w and d are the width and depth of each trench, respectively, and t is the periodicity of trenches. The ground width between two neighboring trenches is $t-w$.

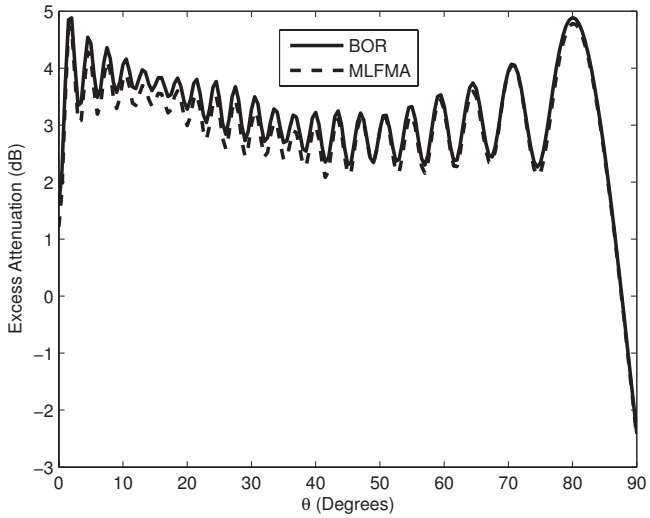


FIG. 10. Radiation pattern for the truncated ground with 1 trench.

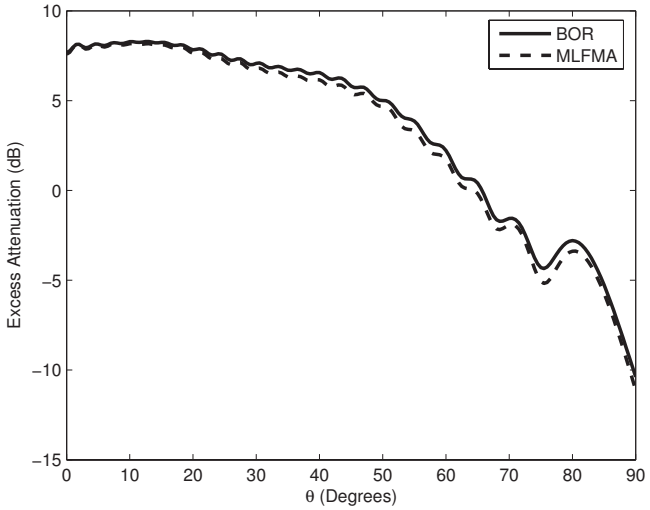


FIG. 12. Radiation pattern for the truncated ground with 10 trenches.

matrix equations. Due to the elegance of the Nyström method, i.e., the direct evaluation of integrands for far-interaction terms, the resulting radiation patterns and receiving patterns are more efficient compared with those in the BEM based fast multipole algorithm, which has been implemented in acoustics. Also, we develop a simple and efficient evaluation technique for those singular or near-singular integrals appearing in near terms. The technique is different from the singularity regularization used in BEM. The numerical examples from the simulations for mitigating gun blast noise have demonstrated the robustness of the proposed MLFMA. The fast solution for the problems with more than 2 million unknowns can be obtained on a workstation without involving parallel algorithms.

ACKNOWLEDGMENTS

This work was supported by CERL, U.S. Army under Grant No. W9132T-06-2-0006.

APPENDIX: MLFMA

The description of MLFMA can be found in details in many publications, such as Ref. 10. To facilitate the description of the proposed MLFMA in acoustics, we present a brief introduction for the algorithm here. In the iterative solution of matrix equation, the bottleneck is the matrix-vector multiply which requires $\mathcal{O}(N^2)$ operations in each iteration. MLFMA changes the computing strategy of the matrix-vector product for far-interaction terms by using the addition theorem for the Green's function and an inverted tree structure in the calculation. The inverted tree structure is illustrated in Fig. 15 and we have three stages, i.e., aggregation, translation, and disaggregation for calculating the far interaction between the grouped source points and field points. The aggregation process represented by β^t (vector) is to calculate the radiation pattern of the outgoing field from the source points. The translation process is characterized by $\bar{\alpha}$ (matrix) and is used to convert the outgoing waves to incoming waves. The disaggregation process denoted by β (vector) is to calculate the receiving pattern of the incoming field for

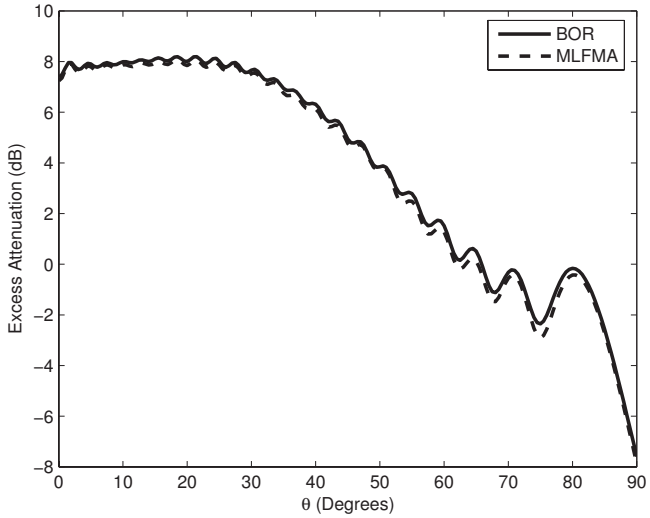


FIG. 11. Radiation pattern for the truncated ground with 5 trenches.

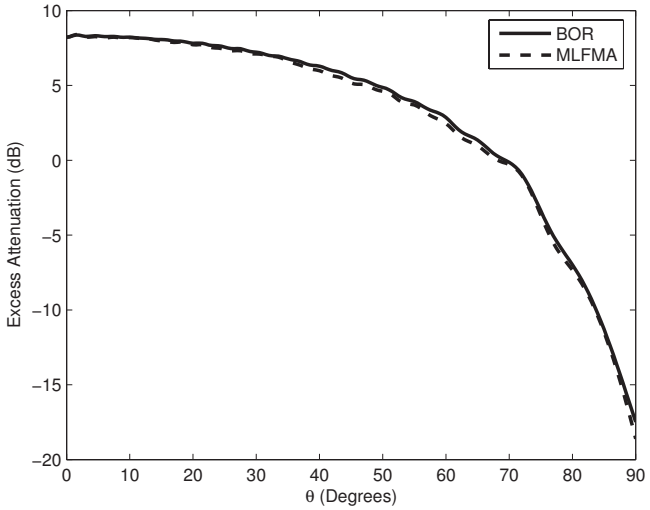


FIG. 13. Radiation pattern for the truncated ground with 50 trenches.

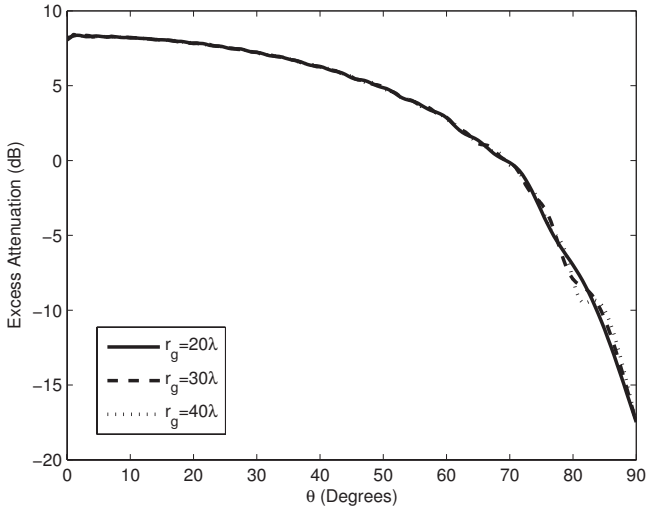


FIG. 14. Comparison of radiation patterns for different truncated sizes of ground with 50 trenches.

desired field points. In the multi-level version, the above is augmented by interpolation and anterpolation between levels.[6,7]

Consider a typical matrix equation

$$\sum_{i=1}^{N} A_{ji} a_i = b_j, \quad j = 1, \ldots, N, \tag{A1}$$

where N is the total number of unknowns after discretizing an integral equation, b_j is the known excitation in a wave equation, a_i is the unknown coefficient to be solved, and A_{ji} is the matrix element. In wave physics, the matrix element A_{ji} is related to the scalar Green's function which can be expanded as[15]

$$\frac{e^{ikr_{ji}}}{r_{ji}} = \int d^2\hat{k} e^{i\mathbf{k}\cdot(\mathbf{r}_{jm}-\mathbf{r}_{im'})} \alpha_{mm'}(\mathbf{k}, \mathbf{r}_{mm'}), \tag{A2}$$

where

$$\alpha_{mm'}(\mathbf{k}, \mathbf{r}_{mm'}) = \frac{ik}{4\pi} \sum_{l=0}^{L} i^l (2l+1) h_l^{(1)}(kr_{mm'}) P_l(\hat{r}_{mm'} \cdot \hat{k}) \tag{A3}$$

is the translator. Here, we have chosen $\mathbf{r}_m$ and $\mathbf{r}_{m'}$ as the centers of the mth and m'th groups in which the field point $\mathbf{r}_j$ and source point $\mathbf{r}_i$ reside, respectively. Also, $\mathbf{r}_{jm}$ denotes the distance vector from the field point to its group center, $\mathbf{r}_{im'}$ denotes the distance vector from the source point to its group center, and $\mathbf{r}_{mm'}$ denotes the distance vector from the field group center to source group center. Usually the integral kernels in wave integral equations will include the gradient operation on the scalar Green's function. The expansion for integral kernels can be obtained by simply replacing the gradient ∇ in space domain with multiplication of $i\mathbf{k}$ in the $\hat{k}$-domain in Eq. (A2). Thus the matrix element in Eq. (A1) can be written as

$$A_{ji} = \int d^2\hat{k} V_{fmj}(\hat{k}) \cdot \alpha_{mm'}(\mathbf{k}, \mathbf{r}_{mm'}) V_{sm'i}(\hat{k}), \tag{A4}$$

where

$$V_{fmj}(\hat{k}) = e^{i\mathbf{k}\cdot\mathbf{r}_{jm}},$$

$$V_{sm'i}(\hat{k}) = \int_{\Delta S_i} dS' e^{-i\mathbf{k}\cdot\mathbf{r}_{im'}} f(\hat{k}), \tag{A5}$$

are the receiving pattern and radiation pattern, respectively. Note that we do not include a basis function in the radiation pattern and a testing function in the receiving pattern as we do in MOM. In the previous, $f(\hat{k})$ denotes the $\hat{k}$-domain representation for the operation acting on the scalar Green's function in the integral kernels.

For the multilevel implementation, the outgoing wave expansions in the radiation pattern are calculated at the finest level and then the expansions for higher levels are obtained by interpolation. Similarly, the anterpolation or transpose interpolation is used to get the incoming wave expansion at a lower level from that at its parent level in the receiving pattern. The interpolation or anterpolation is recognized as one of the key techniques for reducing costs in MLFMA.

TABLE II. CPU time and memory usage for scattering by truncated ground with trenches.

r_g	20	20	20	20	30	40
K	1	5	10	50	50	50
N	801 116	804 718	822 476	991 943	1 736 988	2 441 136
T	63 202	66 547	71 281	108 259	167 642	248 357
M	3.6	3.6	3.9	4.7	9.5	12.0

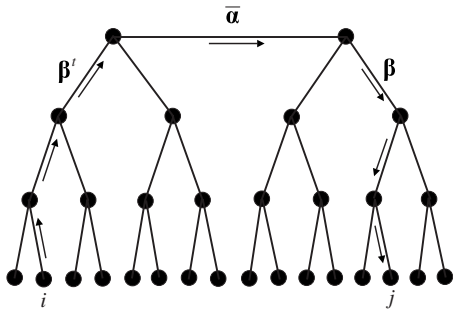


FIG. 15. Inverted tree structure in the calculation of matrix-vector multiply for far-interaction terms.

[1] V. Rokhlin, "Rapid solution of integral equations of classical potential theory," J. Comput. Phys. **60**, 187–207 (1985).
[2] L. Greengard, *The Rapid Evaluation of Potential Fields in Particle Systems* (MIT Press, Cambridge, 1987).
[3] L. Greengard and V. Rokhlin, "A fast algorithm for particle simulations," J. Comput. Phys. **73**, 325–348 (1987).
[4] J. Carrier, L. Greengard, and V. Rokhlin, "A fast adaptive multipole algorithm for particle simulations," SIAM J. Sci. Comput. (USA) **9**, 669–686 (1988).
[5] V. Rokhlin, "Rapid solution of integral equations of scattering theory in two dimensions," J. Comput. Phys. **86**, 414–439 (1990).
[6] C. C. Lu and W. C. Chew, "A multilevel algorithm for solving a boundary integral equation of wave scattering," Microwave Opt. Technol. Lett. **7**, 466–470 (1994).
[7] J. M. Song and W. C. Chew, "Multilevel fast-multipole algorithm for solving combined field integral equations of electromagnetic scattering," Microwave Opt. Technol. Lett. **10**, 14–19 (1995).

[8]B. Dembart and E. Yip, "A 3d fast multipole method for electromagnetics with multiple levels," Proc. 11th Ann. Rev. Prog. Appl. Comput. Electromagn. **1**, 621–628 (1995).
[9]W. C. Chew, *Waves and Fields in Inhomogeneous Media* (Van Nostrand Reinhold, New York, 1990).
[10]W. C. Chew, J. M. Jin, E. Michielssen, and E. J. M. Song, *Fast and Efficient Algorithms in Computational Electromagnetics* (Artech House, Boston, 2001).
[11]J. M. Song and W. C. Chew, "Large scale computations using fisc," IEEE Antennas Propagat. Int. Symp. **4**, 1856–1859 (2000).
[12]S. Velamparambil, W. C. Chew, and J. M. Song, "10 million unknowns: Is it that big?," IEEE Antennas Propag. Mag. **45**, 43–58 (2003).
[13]M. L. Hastriter, "A study of MLFMA for large scale scattering problems," Ph.D. dissertation, ECE Dept. Univ. Illinois, Urbana, 2003.
[14]L. Gurel and O. Ergul, "Fast and accurate solutions of extremely large integral-equation problems discretized with tens of millions of unknowns," Electron. Lett. **43**, 499–500 (2007).
[15]R. Coifman, V. Rokhlin, and S. Wandzura, "The fast multipole method for the wave equation: a pedestrian prescription," IEEE Antennas Propag. Mag. **35**, 7–12 (1993).
[16]V. Rokhlin, "Diagonal forms of translation operators for the helmholtz equation in three dimensions," Appl. Comput. Harmon. Anal. **1**, 82–93 (1993).
[17]M. A. Epton and B. Dembart, "Multipole translation theory for the three-dimensional laplace and helmholtz equations," SIAM J. Sci. Comput. (USA) **16**, 865–897 (1995).
[18]M. F. Gyure and M. A. Stalzer, "A prescription for the multilevel helmholtz fmm," IEEE Comput. Sci. Eng. **5**, 39–47 (1998).
[19]S. Koc and W. C. Chew, "Calculation of acoustical scattering from a cluster of scatterers," J. Acoust. Soc. Am. **103**, 721–734 (1998).
[20]N. A. Gumerov and R. Duraiswami, *Fast Multipole Methods for the Helmholtz Equation in Three Dimensions* (Elsevier, Oxford, UK, 2004).
[21]N. A. Gumerov and R. Duraiswami, "Computation of scattering from clusters of spheres using the fast multipole method," J. Acoust. Soc. Am. **117**, 1744–1761 (2005).
[22]T. Sakuma and Y. Yasuda, "Fast multipole boundary element method for large-scale steady-state sound field analysis. part i: Setup and validation," Acta. Acust. Acust. **88**, 513–525 (2002).
[23]Y. Yasuda and T. Sakuma, "Fast multipole boundary element method for large-scale steady-state sound field analysis. part ii: Examination of numerical items," Acta. Acust. Acust. **89**, 28–38 (2003).
[24]Y. Yasuda and T. Sakuma, "An effective setting of hierarchical cell structure for the fast multipole boundary element method," J. Comput. Acoust. **13**, 47–70 (2005).
[25]Y. Yasuda and T. Sakuma, "A technique for plane-symmetric sound field analysis in the fast multipole boundary element method," J. Comput. Acoust. **13**, 71–85 (2005).
[26]S. M. Rao, D. R. Wilton, and A. W. Glisson, "Electromagnetic scattering by surfaces of arbitrary shape," IEEE Trans. Antennas Propag. **30**, 409–418 (1982).
[27]J. S. Kot, "Solution of thin-wire integral equations by nyström methods," Microwave Opt. Technol. Lett. **3**, 393–396 (1990).
[28]L. S. Canino, J. J. Ottusch, M. A. Stalzer, J. L. Visher, and S. Wandzura, "Numerical solution of the helmholtz equation in 2d and 3d using a high-order nyström discretization," J. Comput. Phys. **146**, 627–663 (1998).
[29]S. D. Gedney, "On deriving a locally corrected nyström scheme from a quadrature sampled moment method," IEEE Trans. Antennas Propag. **51**, 2402–2412 (2003).
[30]S. D. Gedney, "Application of the high-order nyström scheme to the integral equation solution of electromagnetic interaction problems," 2000 IEEE Int. Symp. Electromag. Compat. **1**, 289–294 (2000).
[31]M. S. Tong and W. C. Chew, "A higher-order nyström scheme for electromagnetic scattering by arbitrarily shaped surfaces," IEEE Antennas Wireless Propag. Lett. **4**, 277–280 (2005).
[32]Y. W. Lam, "A boundary integral formulation for the prediction of acoustic scattering from periodic structures," J. Acoust. Soc. Am. **105**, 762–769 (1998).
[33]P. Ylä-Oijala and S. Järvenpää, "Iterative solution of high-order boundary element method for acoustic impedance boundary value problems," J. Sound Vib. **291**, 824–843 (2006).
[34]B. Chandrasekhar and S. M. Rao, "Elimination of internal resonance problem associated with acoustic scattering by three-dimensional rigid body," J. Acoust. Soc. Am. **115**, 2731–2737 (2004).
[35]H. A. Schenck, "Improved integral formulation for acoustic radiation problems," J. Acoust. Soc. Am. **44**, 41–58 (1968).
[36]A. J. Burton and G. F. Miller, "The application of integral equation methods to the numerical solution of some exterior boundary value problems," Proc. R. Soc. London, Ser. A **323**, 201–210 (1971).
[37]A. H. Stroud, *Approximate Calculation of Multiple Integrals* (Prentice–Hall, Englewood Cliffs, 1971).
[38]M. S. Tong and W. C. Chew, "Super-hyper singularity treatment for solving 3d electrical field integration equations," Microwave Opt. Technol. Lett. **49**, 1383–1388 (2007).
[39]M. G. Duffy, "Quadrature over a pyramid or cube of integrands with a singularity at a vertex," SIAM (Soc. Ind. Appl. Math.) J. Numer. Anal. **19**, 1260–1262 (1982).
[40]H. B. Dwight, *Tables of Integrals and Other Mathematical Data* (4th Ed., Macmillan, New York, 1961).
[41]G. W. J. Swenson, E. R. Sandeen, L. L. Pater, and H. C. Zhuang, "The potential for mitigation of gun blast noise through sheltering of the source," USACERL Technical Report No. N-92/09, 1992, pp. 1–26.
[42]M. S. Tong, W. C. Chew, and M. J. White, "Surface impedance design with ground corrugation for mitigation of large-caliber gun blast noise," CCEML Technical Report No. 4-07, 2007.
[43]D. Duhamel, "Efficient calculation of the three-dimensional sound pressure field around a noise barrier," J. Sound Vib. **197**, 547–571 (1996).

High-Reynolds-number turbulent-boundary-layer wall pressure fluctuations with skin-friction reduction by air injection

Eric S. Winkel, Brian R. Elbing, and Steven L. Ceccio
Department of Mechanical Engineering, University of Michigan, Ann Arbor, Michigan 48109

Marc Perlin
Department of Naval Architecture and Marine Engineering, University of Michigan, Ann Arbor, Michigan 48109

David R. Dowling[a)]
Department of Mechanical Engineering, University of Michigan, Ann Arbor, Michigan 48109

(Received 2 August 2007; revised 29 February 2008; accepted 29 February 2008)

The hydrodynamic pressure fluctuations that occur on the solid surface beneath a turbulent boundary layer are a common source of flow noise. This paper reports multipoint surface pressure fluctuation measurements in water beneath a high-Reynolds-number turbulent boundary layer with wall injection of air to reduce skin-friction drag. The experiments were conducted in the U.S. Navy's Large Cavitation Channel on a 12.9-m-long, 3.05-m-wide hydrodynamically smooth flat plate at freestream speeds up to 20 m/s and downstream-distance-based Reynolds numbers exceeding 200×10^6. Air was injected from one of two spanwise slots through flush-mounted porous stainless steel frits ($\sim$40 μm mean pore diameter) at volume flow rates from 17.8 to 142.5 l/s per meter span. The two injectors were located 1.32 and 9.78 m from the model's leading edge and spanned the center 87% of the test model. Surface pressure measurements were made with 16 flush-mounted transducers in an "L-shaped" array located 10.7 m from the plate's leading edge. When compared to no-injection conditions, the observed wall-pressure variance was reduced by as much as 87% with air injection. In addition, air injection altered the inferred convection speed of pressure fluctuation sources and the streamwise coherence of pressure fluctuations.
© *2008 Acoustical Society of America.* [DOI: 10.1121/1.2902169]

PACS number(s): 43.28.Ra, 43.50.Ed [GCL] Pages: 2522–2530

I. INTRODUCTION

[1]Pressure fluctuations produced on solid surfaces by turbulent flow are an important engineering concern as they are known to be a source of unwanted vibration, interior and exterior noise, and even structural fatigue—in extreme cases—in transportation systems. Thus, understanding and quantifying hydrodynamic pressure fluctuations is of interest for engineering design of watercraft. In addition, since wall-pressure fluctuations are directly related to the structure of boundary layer turbulence, changes in these fluctuations may yield insight into boundary-layer skin-friction drag-reduction mechanism(s). Thus, quantifying the modifications to wall-pressure fluctuations in a gas-laden liquid turbulent boundary layer (TBL) is a potentially important step prior to implementation of gas injection as a skin-friction drag-reduction technique for liquid flow over a solid surface.

Wall-pressure fluctuations beneath a TBL have been extensively studied and are well documented for single-phase gas or liquid flows. Reviews of single-phase wall-pressure-fluctuation research can be found in Bull (1996) and Keith *et al.* (1992). Likewise, skin-friction drag reduction by gas injection, herein termed bubble drag reduction (BDR), has been the focus of a number of experimental investigations; a review of BDR research can be found in Merkle and Deutsch (1992). However, scarcely any literature exists for wall-pressure fluctuations in liquid TBL flows with skin-friction drag reduction by gas injection, though two studies of an alternative skin-friction reduction technique (Brungart *et al.*, 2000; Barker, 1973) report pressure fluctuations beneath a polymer modified TBL. Brungart *et al.* simultaneously measured wall-pressure fluctuations and skin-friction reduction beneath the TBL on an axisymmetric body, 89 mm in diameter and 632 mm in length, in a polyethylene oxide (PEO) ocean at flow speeds up to 10.7 m/s. Spectral levels were reduced in proportion to the observed level of skin-friction drag reduction. Likewise, with the addition of dilute PEO solutions, Barker observed reductions in wall-pressure fluctuations as well as in the radiated noise from the TBL of a rotational flow apparatus. In contrast, no wall-pressure-fluctuation data have yet been reported for bubble-laden TBL flows even though local skin-friction drag reductions exceeding 80% have been experimentally observed for BDR.

While the mechanism(s) of BDR is (are) not yet fully understood, the phenomenon is associated with the modification of turbulent fluctuations and a reduced momentum exchange in the near-wall region (Merkle and Deutsch, 1992). Lumley (1977) reported that the presence of bubbles acts to increase the local viscosity in the buffer region of the TBL, resulting in a thickening of the viscous sublayer and a reduction in the near-wall velocity gradient. While measur-

[a)]Electronic mail: drd@umich.edu

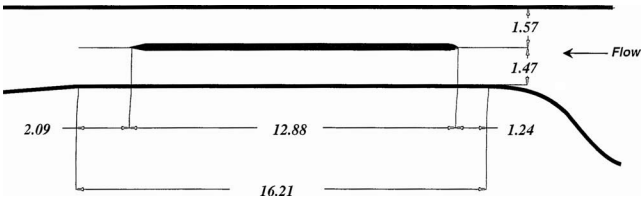


FIG. 1. Elevation side view of the test section geometry with the test model mounted slightly below the test section centerline. Dimensions are in meters.

ing shear stress indirectly with hot-film anemometry during BDR, Pal *et al.* (1989) observed suppressions in skin friction fluctuation levels, as well as reduction in the mean skin friction. Based on these prior findings, it is not surprising that similar suppressions of wall-pressure fluctuations were found in the study reported here.

This paper presents the results of a large scale BDR experiment designed to examine skin-friction drag reduction at large scales and high-Reynolds numbers on a hydrodynamically smooth surface when air was injected through the surface at one of two locations downstream of the surface's leading edge. A variety of data were gathered, but only skin-friction drag reduction and dynamic wall-pressure measurements are discussed herein. Wall-pressure fluctuations were observed with an array of dynamic pressure sensors flush mounted on the test model surface. Modifications to the spectral levels, and hence root-mean-square (rms) levels, convection velocities, and streamwise coherence of the wall pressure are reported for various levels of skin-friction drag reduction for a variety of freestream liquid speeds and gas injection rates. The remainder of this paper is divided into three sections that describe the experimental methods used in collecting and reducing the measurements, the results and their relationship to the no-injection or base line flow, and the conclusions drawn from this investigation.

II. EXPERIMENTAL METHODS

The experiments were conducted at the U.S. Navy's William B. Morgan Large Cavitation Channel (LCC), the world's largest low-turbulence (<0.5% free stream turbulence) recirculating water tunnel. The dimensions of the LCC test section are 16 m (length) and 3.05×3.05 m^2 (width and height). Details of the LCC test facility can be found in Etter *et al.* (2005).

The test model was a 12.9-m-long, 3.05-m-wide, and 18-cm-thick rigid flat plate. It spanned the entire width of the LCC test section and produced 6% blockage. The leading edge of the model was a 4:1 ellipse and the trailing edge was a 15° full-angle truncated wedge. A distributed roughness trip consisting of 120 μm particles embedded in epoxy was added near the leading edge. The trip spanned the entire test model and started 2.5 cm from the leading edge and extended 25.4 cm downstream. The model was positioned slightly below the vertical centerline of the LCC test section with the working surface facing downward, as shown in Fig. 1. The working surface was polished 304 stainless steel yielding a rms surface roughness, $k < 0.4$ μm, sufficiently small to be considered hydrodynamically smooth, even at the highest water-flow test speed, ~20 m/s. Figure 2 shows the location of the air injectors, skin-friction drag balances, and the dynamic-pressure transducer array. The downstream coordinate x has its origin ($x=0$) at the leading edge of the model.

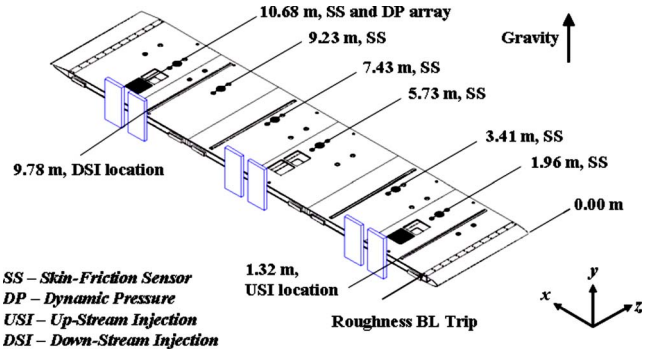


FIG. 2. (Color online) Schematic of the test model's working surface with the two air injectors and instrumental suite layout. Air injectors were located 1.32 and 9.78 m from the model leading edge and the six skin-friction drag balances span the model length. The dynamic pressure sensor array was located 10.68 m from the model leading edge and the velocity profile measurements were made at that location using a laser-Doppler velocimetry system.

Three test speeds, 6.6, 13.2, and 19.9 m/s, were investigated. These speeds were measured in the freestream with a laser-Doppler velocimetry system at the streamwise location of the dynamic pressure array. Boundary layer growth caused a slight favorable pressure gradient and freestream acceleration (<2.5%) along the length of the model. This flow acceleration, in terms of a dimensionless acceleration parameter K, is less than 10^{-9} for all freestream test speeds, where

$$K = \frac{\nu}{U_\infty^2}\frac{dU_\infty}{dx}, \tag{1}$$

where U_∞ is the freestream flow speed and ν is the kinematic viscosity of the fluid. Patel (1965) reported that the classical TBL log law remains unaltered for $K < 1.6 \times 10^{-6}$; therefore, the results presented herein are presumed to approach that of a zero-pressure-gradient TBL.

A. Skin-friction drag balances

Average skin-friction measurements were made at six streamwise locations using floating-plate-type force balances. Skin-friction drag reduction, calculated from measurements made at the same streamwise location as the transducer array using the furthest downstream balance ($x = 10.68$ m), is reported with the dynamic pressure measurements. Table I provides the base line (no-injection) skin-friction shear stresses, τ_w, local Reynolds numbers, and other TBL parameters measured with a laser-Doppler velocimetry system at the streamwise location of the dynamic pressure array. The force balances were designed at the Applied Research Laboratory of Pennsylvania State University. The floating elements of the force balances were polished stainless steel disks 15.2 cm in diameter and 0.79 cm thick, and each element was attached to a beryllium copper load cell instrumented with a full wheat-stone bridge of semiconductor strain gauges (model ESU-025-500, MSI Sensors®). The

TABLE I. Local base line (no-injection) Reynolds numbers, shear stress, and turbulent-boundary-layer parameters at the streamwise location of the dynamic pressure sensor array.

Parameter description	Symbol	Values		
Local freestream speed	U_∞	6.6 m/s	13.2 m/s	19.9 m/s
Downstream distance Reynolds number	Re_x ($\times 10^{-6}$)	69	139	209
Momentum thickness Reynolds number	Re_Θ ($\times 10^{-3}$)	66	126	186
Single-phase flow wall shear stress	τ_w (Pa)	37	136	292
Shear velocity$=(\tau_w/\rho)^{1/2}$	u_τ (m/s)	0.193	0.369	0.541
99% boundary layer thickness	δ_{99} (mm)	108	102	101
Boundary layer displacement thickness	δ (mm)	12.8	11.9	11.6
Boundary layer momentum thickness	θ (mm)	10.0	9.5	9.3

load cell and floating element were mounted in a stainless steel housing, which contained an eight-point leveling system to position the floating-plate flush with the housing. The gap between the floating element and the surrounding housing was measured to be 60 ± 20 μm. The balances were calibrated with a suction cup affixed to the floating element, a tensioning cable, and a precision load cell mounted on a translation stage.

B. Dynamic pressure sensors

Wall-pressure fluctuations were measured with 16 flush-mounted dynamic pressure sensors (model 138M101, PCB Piezotronics®) with a nominal sensitivity of 50 mV/psi, a low frequency cutoff of 1.6 Hz, and a resonant frequency greater than 300 kHz (leading to a rise time of less than 2 μs). The sensors had circular sensing surfaces with a diameter $d=5.6$ mm. The nominal factory-specified sensor calibration was used in the data processing. The sensors were connected to a multichannel excitation and signal-conditioning amplifier (model series 481, PCB Piezotronics®), and their signals were amplified with a gain of 150 and low-pass filtered at 4765 Hz. Each amplified and filtered signal was digitized at 10 kHz for a period of 20 s. The dynamic pressure sensors were flush mounted in a single "L-shaped" array located 10.7 m from the test model's leading edge (9.4 m from the upstream air injector and 0.9 m from the downstream air injector). The sensors were logarithmically spaced in each direction with the array spanning 27 cm in the streamwise direction and 40 cm in the cross-stream direction, as shown in Fig. 3.

C. Air injection

For the BDR experiments, air was injected through one of two spanwise air injectors located at $x=1.32$ m and $x=9.78$ m, designated upstream injection (USI) and downstream injection (DSI), respectively. Filtered air was delivered to the active injector through a symmetrical delivery manifold that fed 40 evenly spaced ports on the back of the injector housing. The air-flow rate was regulated with five mass flow meters (Sierra Instruments, model 840N3-0-0V1-S1-MP) each supplying eight of the 40 injector ports. Three layers of perforated brass plates with 0.5 mm diameter holes and 33% open area served to create a pressure drop in the injector that evenly distributed the air across the injector span. A cross-sectional schematic of the air injectors is shown in Fig. 4. They consisted of a contracting slot inclined at a mean angle of 25° with respect to the model surface, a full-angle contraction of 10°, and a final layer of sintered stainless steel with mean pore diameter of 40 μm (Mott Corporation®). The air injectors spanned the center 2.65 m

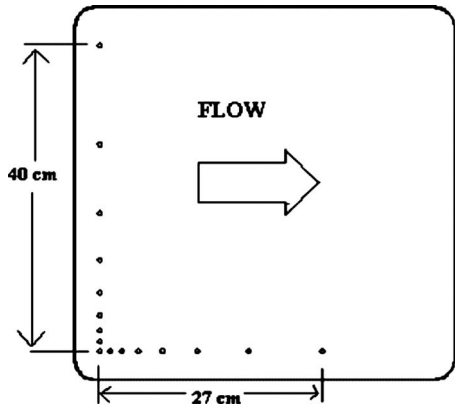


FIG. 3. Layout of the dynamic pressure sensor array located 10.7 m from the leading edge of the test model with the circles corresponding to locations of the dynamic pressure sensors. The array spanned 40 cm in the cross-stream direction and 27 cm in the spanwise direction.

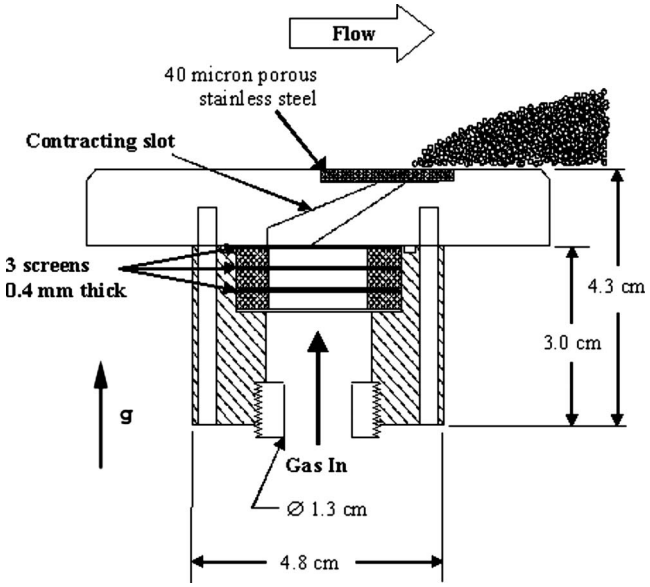


FIG. 4. Cross-sectional schematic of the air injectors that spanned the center 2.65 m of the test model. The air inlet consisted of 40–1.27 cm ID ports along the injector span, which supplied a manifold that spanned the entire injector length.

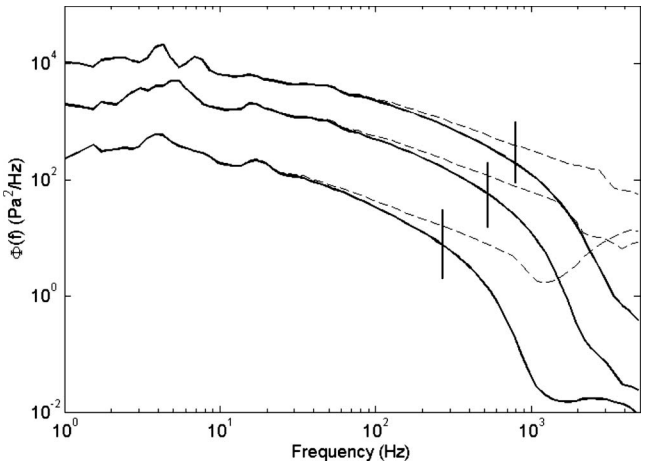


FIG. 5. Dimensional pressure spectra for single-phase flow at the three test speeds. The solid lines are the measured spectra and the dashed lines are the spectra after correction for sensor-size attenuation (Corcos, 1963). The vertical lines represent f_c, given in Table II, above which sensor size limitations become significant.

(87%) of the test model surface. *In situ* visual observations of bubble clouds, near and far from the injector, suggested that the air injection scheme had sufficient spanwise uniformity for these tests. Average-flux-based void fractions within the bubbly TBL were in the 1%–20% range with bubbles distributed in size between 200 and 700 μm (see Sanders *et al.*, 2006).

D. Test procedures

Air was injected at four nominal flow rates: 100, 200, 400, and 800 SCFM (standard cubic feet per minute) ranging from 17.8 to 142.5 l/s per meter of injector span. Dynamic pressure data acquisition was initiated once the skin-friction drag balances showed that force levels had reached steady state. At the lower air injection rates, the LCC test section static pressure could be maintained near the desired 138 kPa (absolute) so the true volumetric-flow rates were ~38% less than the specified volumetric-flow rates (given in SCFM above). However, at the highest injection rate (800 SCFM), a steady rise in test section pressure occurred during the injection process to a maximum of 240 kPa. Ignoring surface tension effects, this static pressure rise would cause bubble volume and void fraction to decrease by ~40% and bubble diameters to decrease by ~17%. Further details of the BDR experiment are reported in Sanders *et al.* (2006).

III. RESULTS

A. Base line spectra

The base line pressure spectra are shown in Fig. 5 (solid lines) in dimensional form for the three test speeds. The spectra presented are the average of the 16 sensors used in the experiment. Sensor-to-sensor differences in the base line flow pressure variance were less than 50%. When sensitivity differences between sensors are taken into account, variance differences are reduced to ~30%. Small unintended surface-flushness differences between sensors are the likely cause of the remaining variance differences. Unfortunately, further investigation of the observed variance differences became impossible once the experiment was disassembled. Thus, the experimental uncertainty of any single spectral measurement reported here is $\pm 10\log_{10}(1.3) \approx \pm 1$ dB. Wherever possible, results were averaged across sensors to further reduce this uncertainty, and, for clarity, the spectra were smoothed using a 1/20th decade top hat filter. The pressure spectra, $\Phi(\omega)$, presented herein are of the single-sided form.

TABLE II. Sensor size limitations and attenuation frequencies.

Freestream flow speed	6.6 m/s	13.2 m/s	19.9 m/s
Wall unit, l^+ (μm)	5.16	2.70	1.84
Sensor size, $d^+=d/l^+$	1100	2100	3000
Attenuation frequency, f_c	270 Hz	530 Hz	800 Hz

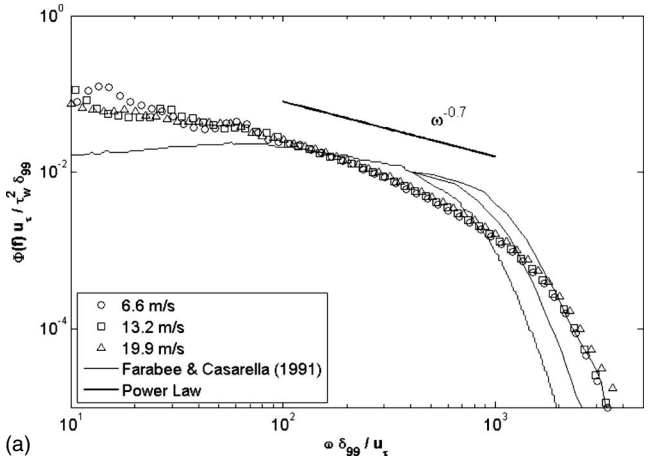
$$P_{\text{rms}}^2 = \int_0^\infty \Phi(\omega)d\omega, \tag{2}$$

$$\Phi(\omega) = \frac{1}{2\pi}\Phi(f), \tag{3}$$

where P_{rms}^2 is the pressure variance, and $\omega=2\pi f$ is the temporal frequency.

Unfortunately, the pressure spectra contain three types of noise: background tunnel noise, model vibration noise, and electrical noise. The first is most prevalent at low frequencies (below 10 Hz or so). Unfortunately, it was not separately quantified for these experiments. However, it does not dominate the measurements below 10 Hz because air injection was observed to alter pressure spectra in this frequency range. Model vibration noise covered much of the same frequency range as the pressure spectra but its spectral level was determined to be two or three orders of magnitude lower based on the separate test-surface acceleration measurements and the manufacturer-specified acceleration sensitivity for the pressure transducers. Similarly, broadband electrical noise levels were typically four or more decades below pressure spectrum levels. This is illustrated in Fig. 5 where the electrical noise spectral level is apparent as the nearly flat portion of the 6.6 m/s spectrum at frequencies above 1 kHz. In the results presented here, no noise reduction schemes have been implemented.

In addition, the pressure spectra are limited by the size of the transducer's sensing surface (d=diameter) relative to the inner TBL length scale, $l^+=\nu\sqrt{\rho/\tau_w}$, where ρ is the fluid density, which results in a suppression of the high-frequency fluctuations levels. The $d^+=d/l^+$ values of the sensors are presented in Table II for the three nominal flow speeds. Also listed in Table II is an estimated roll-off frequency, f_c, where the spectrum is attenuated by 50% due to the size of the sensor. Above this frequency, signal attenuation rapidly increases with frequency. According to prior work by Corcos (1963), this roll-off frequency occurs at $2\pi f_c d/U_c \sim 2.0$, where U_c is the convection velocity, which is approximately 70% of the freestream velocity, U_∞. The dashed lines in Fig. 5 show the spectra that have been corrected for sensor size



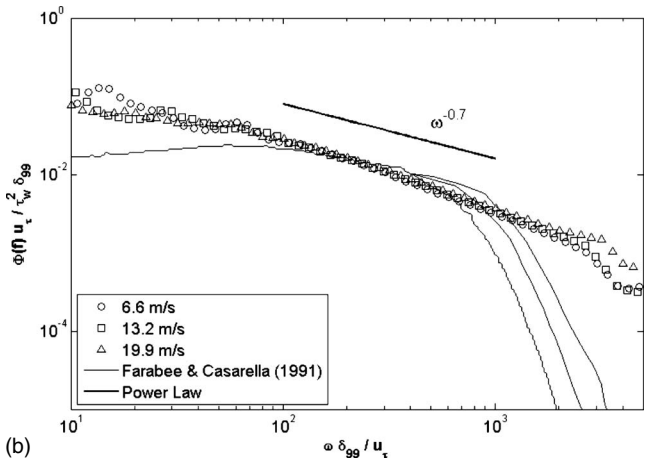


FIG. 6. Base line (single-phase) spectra scaled with outer flow variables for the three test speeds, (a) uncorrected for sensor size attenuation and (b) corrected for sensor size attenuation (Corcos 1963). Thin solid curves correspond to results obtained by Farabee and Casarella (1991), and the bold solid line has a slope of −0.7, as suggested by Goody (2004).

attenuation following the technique employed by Corcos. The short vertical lines mark f_c for each spectrum in this figure.

B. Base line TBL flow scaling

Work done by Farabee and Casarella (1991) identifies three frequency ranges for pressure fluctuation scaling: (1) a low frequency range, $\omega\delta^*/U_\infty \leqslant 0.03$; (2) a high frequency range, $\omega\nu/u_\tau^2 \geqslant 0.3$; and (3) a midfrequency range, $0.05 < \omega\delta^*/U_\infty < 10$, where δ^* is the boundary layer displacement thickness and $u_\tau = \sqrt{\tau_w/\rho}$ is the shear velocity. In this experiment, the low frequency range is possibly corrupted by background tunnel noise, and the high frequency range is largely lost because of finite-sensor-size attenuation. Therefore, the appropriate scaling range for the present data is the midfrequency range. Keith *et al.* (1992) and Brungart *et al.* (2000) have shown good collapse of data with mixed variable scaling: $\omega\delta^*/U_\infty$ and $\Phi U_\infty/\tau_w^2\delta^*$. Here, the data are scaled with outer variables and compared to the results of Farabee and Casarella (1991) in Fig. 6(a) without sensor size correction and in Fig. 6(b) with this correction. Table I provides the scaling parameters. The pressure spectra from these

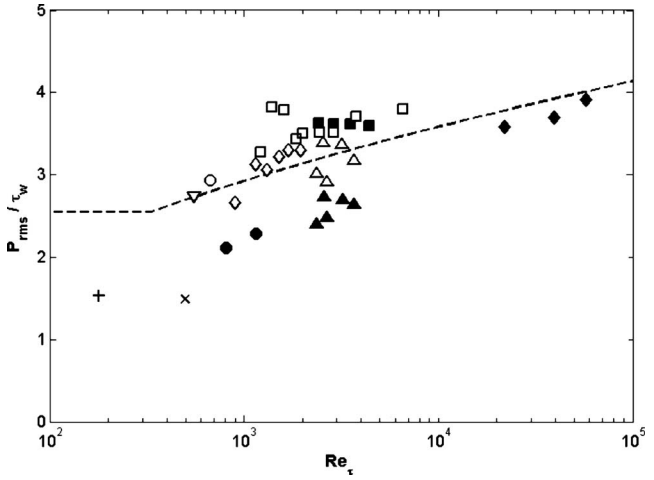


FIG. 7. Base line scaled rms pressure fluctuations for the current experiment, plotted as solid diamonds, along with other investigations compiled by Farabee and Casarella (1991). The dashed line corresponds to a scaling law purposed by Farabee and Cassarella.

two experiments collapse well from $10^2 < \omega\delta_{99}/u_\tau < 10^3$ when the current results are corrected for sensor-size attenuation. This is the spectral region where the most important changes occur when air is injected into the boundary layer. The lack of collapse outside this zone is a likely result of sensor-size limitations, imperfections in the sensor size corrections, and the higher Reynolds numbers of the present experiments compared to that of Farabee and Casarella. Note also that because the ratio of sensor size to boundary layer thickness (d/δ_{99}) is comparable between the current experiments (0.05) and those of Farabee and Casarella (0.03), the spectra from the two experiments in Fig. 6(a) are not as different as might be anticipated. More recently, Goody (2004) proposed a spectral scaling that includes the effects of Reynolds number. It suggests that pressure spectra should follow $\omega^{-0.7}$ in the midfrequency range (i.e., the bandwidth of interest in this study). Given the approximation inherent in the sensor-size correction, an $\omega^{-0.7}$ power law is close to that shown by the current corrected spectra [see Fig. 6(b)].

Scaling of the rms pressure fluctuation, P_{rms}, from different experiments has proven to be challenging due to the low frequency facility-specific noise contamination, high frequency attenuation due to the sensor size, and the dependence of wall-pressure fluctuations on Reynolds number. Results compiled in Farabee and Casarella (1991) illustrate this problem. For the current experiments, P_{rms} has been obtained by numerically integrating the pressure spectra corrected for sensor attenuation from 1 Hz, the lower frequency limit shown in Fig. 5, to the frequency where the sensor-size-induced attenuation is 99%. The potentially noisy frequency range from 1 to 10 Hz contributes only about 10% of the pressure variances. Figure 7 shows P_{rms}/τ_w from the investigations compiled by Farabee and Casarella along with the results from the current experiment plotted versus $\text{Re}_\tau = u_\tau\delta_{99}/\nu$. Also shown is the empirical scaling law proposed by Farabee and Casarella. Although the current results fall slightly below the proposed scaling law, they do confirm an overall trend of increasing P_{rms} with increasing Reynolds number.

For the present purposes, the results shown in Figs. 6 and 7 serve to validate the base line flow results via comparisons to prior higher-resolution, lower-Reynolds-number experiments. Thus, the effects of BDR on wall-pressure fluctuations are presented in the remainder of this manuscript by direct comparisons of BDR and single-phase flow results without the potential distractions associated with dimensionless scaling and sensor-size corrections. Given the importance of τ_w in the scaling of wall-pressure fluctuations and the large variations in τ_w that occur in BDR flows, presentation and comparisons of unscaled and uncorrected spectra are appropriate here for quantifying bubbly flow induced changes in wall-pressure fluctuations.

C. Spectral modifications during BDR

BDR wall-pressure spectra are compared to the base line spectra in Fig. 8. For reference, the skin-friction drag reduction (%DR at $x=10.68$ m), given by Eq. (4), is provided in the legends, where τ_w' is the BDR skin friction and τ_w is the base line skin friction.

$$\%\mathrm{DR} = \left(1 - \frac{\tau_w'}{\tau_w}\right) \times 100. \tag{4}$$

In the BDR spectra, an increase is observed in both the low ($f<10$ Hz) and the high ($f>1000$ Hz) frequency ranges. The low frequency spectral increase may be a result of the intermittency of an air film over the test model surface, which only occurs at the highest levels of skin-friction drag reduction, typically found at high air injection rates and lower freestream velocities. The high frequency spectral increase is likely associated with either (i) acoustic noise generated during the air injection process or (ii) the pressure fluctuations from small bubbles passing over the plate surface. Unfortunately, air injection measurements without flow in the LCC test section were not performed to readily discriminate between these two possibilities, and the complicated spatial filtering necessary to separate acoustic and convective noise sources for $f>1000$ Hz was not attempted.

Compared to the base line measurements, wall-pressure spectra in BDR flows were suppressed over a frequency range of at least a decade, and this range of reduction shifted upward in frequency with increasing freestream velocity. In general, the magnitude of this spectral suppression increases with increasing levels of skin-friction drag reduction, which agrees with the findings of Brungart *et al.* (2000) for polymer-based skin-friction drag reduction. In contrast, Brungart *et al.* observed reductions in spectral levels over the entire measured frequency range. However, this spectral suppression difference may be a result of differences in background noise in the two experiments. The injection of air in the current experiments audibly increased the background noise outside the water tunnel; presuming this was true inside the tunnel as well, air injection noise is likely the cause of the increase in BDR spectral levels at frequencies above 1 or 2 kHz seen in Fig. 8. There was no active injection system in the investigation of Brungart *et al.* (2000); thus, the suppression of pressure fluctuations in both types of skin-friction-drag-reduced flows may have common elements.

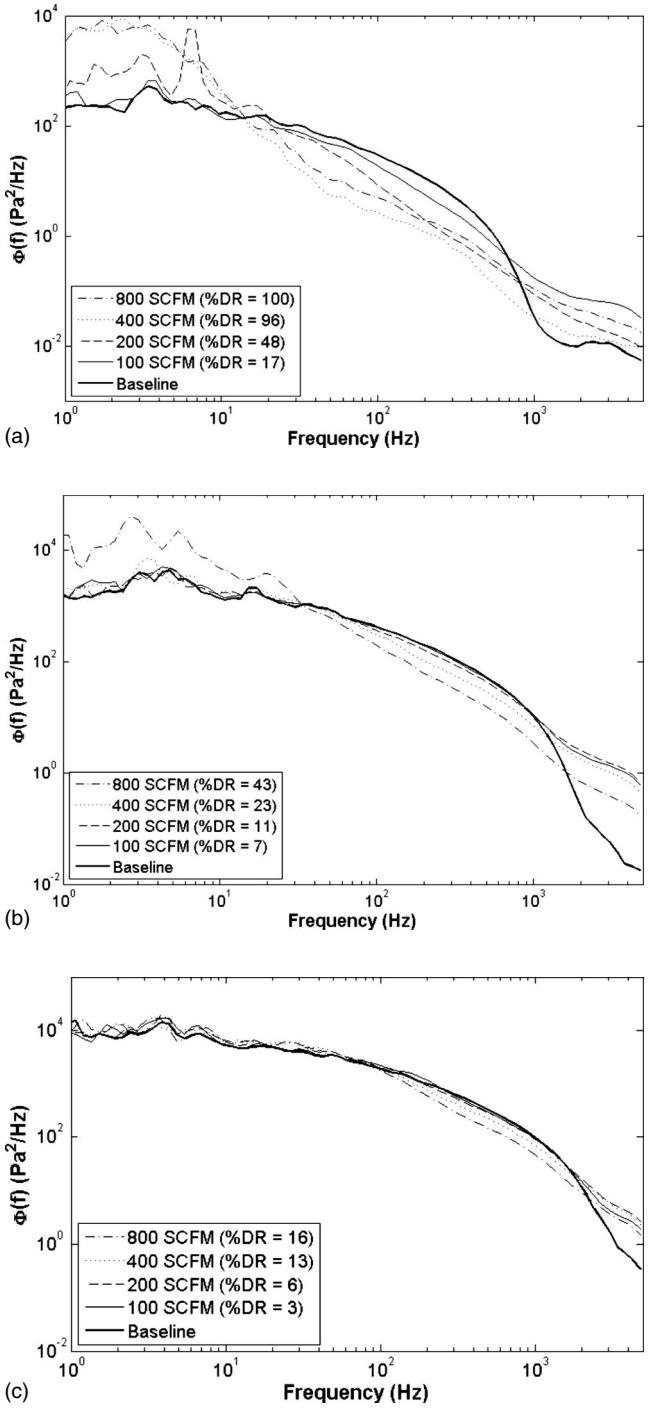


FIG. 8. Bubble modified pressure spectra for all air injection rates tested at (a) 6.6 m/s USI (b) 13.2 m/s DSI and (c) 19.9 m/s DSI. Also shown in the legend are the corresponding %DR measured by the skin-friction-drag balances at the same downstream location ($x=10.68$ m).

D. Reduction in mean-square pressure fluctuations

The ratio of pressure variance with bubbles, ${P'_{\mathrm{rms}}}^2$ to that of the baseline flow, P_{rms}^2 is plotted versus the reduction in skin friction, τ_w'/τ_w, in Fig. 9 for all the BDR measurements. The ${P'_{\mathrm{rms}}}^2$ values were computed by integrating the spectra over the frequency range where the spectral reductions occurred. This approach nearly eliminates the influence of high and low frequency noises in the BDR results, but it may also bias the results by under-reporting the ${P'_{\mathrm{rms}}}^2$ values. Also

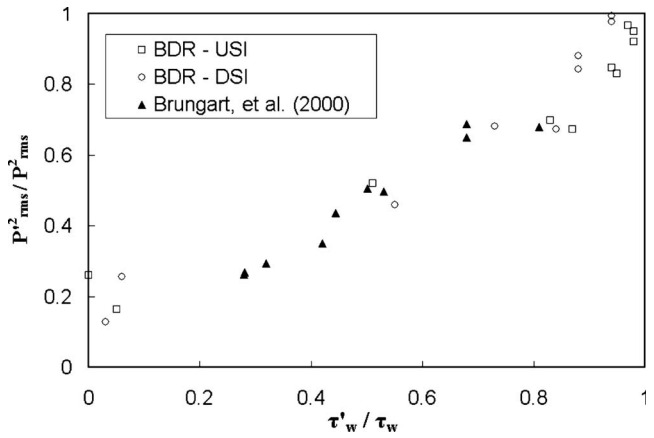


FIG. 9. Comparison of mean-square pressure fluctuations and skin-friction reductions during BDR. Also shown for comparison are data obtained from Brungart *et al.* (2000) where polymer was used to reduce the skin-friction drag.

shown in Fig. 9 are the results of the polymer skin-friction drag-reduction experiments of Brungart *et al.* (2000). The two data sets agree well with a simple linear trend with some additional scatter in the present data.

E. Convection velocity

The apparent convection velocity, U_c, of pressure fluctuations can be determined from the cross spectrum, Φ_{12}, of a streamwise sensor pair, as defined in Eq. (5), where ζ is the spacing between sensors and $\theta(\omega,\zeta)$ is the cross-spectrum phase defined in Eq. (6).

$$U_c(\omega,\zeta) = -\frac{\omega\zeta}{\theta(\omega,\zeta)}, \tag{5}$$

$$\theta(\omega,\zeta) = \tan^{-1}\left(\frac{\mathrm{Im}(\Phi_{12})}{\mathrm{Re}(\Phi_{12})}\right). \tag{6}$$

Figure 10 shows U_c/U_∞ for BDR at 13.2 and 19.9 m/s. The lower frequencies show an increase whereas the higher frequencies show a decrease in U_c relative to the base line results. The magnitude of these effects increases with increasing air injection rate and the corresponding skin-friction drag reduction achieved. The decrease in convection velocity at high frequencies indicates that the near-wall pressure fluctuations are moving slower with air injection and that the near-wall velocity gradient is decreased relative to the base line. The hydrodynamic BDR results reported in Sanders *et al.* (2006) put near-wall bubble velocities at 0.50–0.65 of U_∞; the present results at frequencies above about 300 Hz agree with this finding.

F. Streamwise coherence

A streamwise array of sensors can be used to measure the coherence of the pressure fluctuations as they are convected downstream. The coherence, $\Gamma(\omega,\zeta)$, given in Eq. (7), is a measure of the evolution and/or decay of the pressure fluctuations at frequency ω over a distance ζ. Here, Φ_{12} is the cross spectrum between a streamwise sensor pair, and Φ_{11}, Φ_{22} are the autospectra of each sensor.

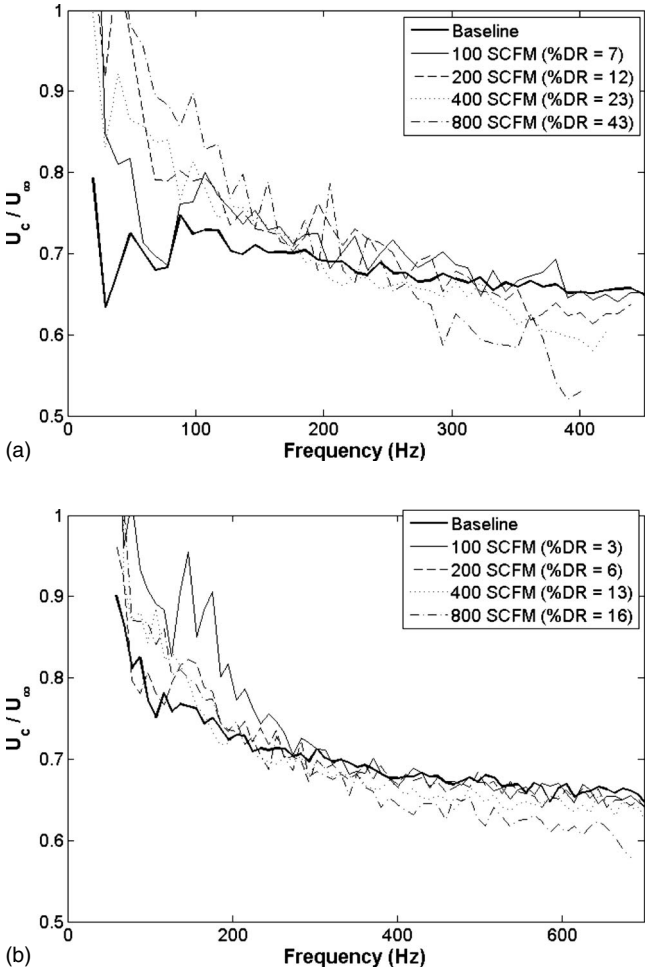


FIG. 10. Bubble modified convection velocity scaled using the freestream velocity for all air injection rates at (a) 13.2 m/s DSI and (b) 19.9 m/s DSI. The bold solid lines correspond to the base line (single-phase) convection velocity results.

$$\Gamma(\omega,\zeta) = \frac{|\Phi_{12}(\omega,\zeta)|}{\sqrt{\Phi_{11}\Phi_{22}}}. \tag{7}$$

The normalization shown in Eq. (7) prevents Γ from being significantly impacted by sensor size limitations. An empirical model for the decay of Γ, proposed by Corcos (1963),

$$\Gamma(\omega,\zeta) = \exp\left(-C_1\left|\frac{\omega\zeta}{U_c}\right|\right), \tag{8}$$

is based on a nondimensional spacing, $\omega\zeta/U_c$, and an empirical decay constant, C_1. The existing literature reports values of C_1 ranging from 0.10 to 0.19. Brooks and Hodgson (1981) reported a slight Reynolds number dependence for C_1, with C_1 decreasing with increasing Reynolds number. This agrees with the base line results from the present experiment, where $0.10 < C_1 < 0.12$ with the highest and lowest C_1 values corresponding to 6.6 and 19.9 m/s, respectively.

The base line coherence from two test speeds, 6.6 and 19.9 m/s, are given in Fig. 11 as a function of nondimensional spacing, $\omega\zeta/U_c$, with the corresponding empirical decay functions. Five sensor pair spacings, ranging from 2.0 to 9.1 cm, are shown. The data follow the exponential decay function reasonably well with the exception of the lowest

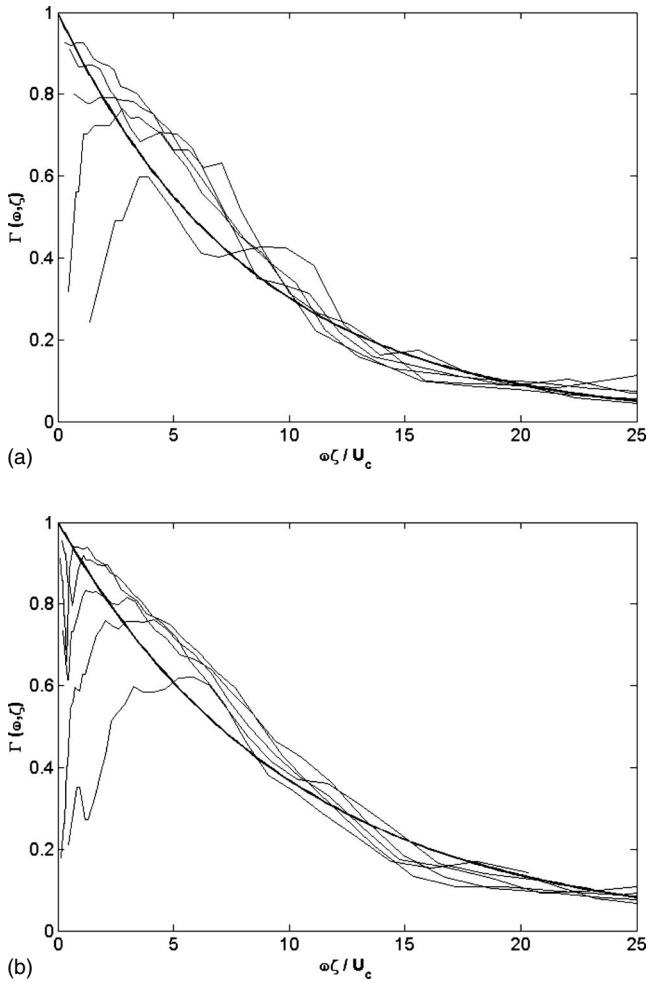


FIG. 11. Base line (single-phase) coherence and empirical decay model for five sensor pairings at two test speeds: (a) 6.6 m/s with C_1=0.12 and (b) 19.9 m/s with C_1=0.10.

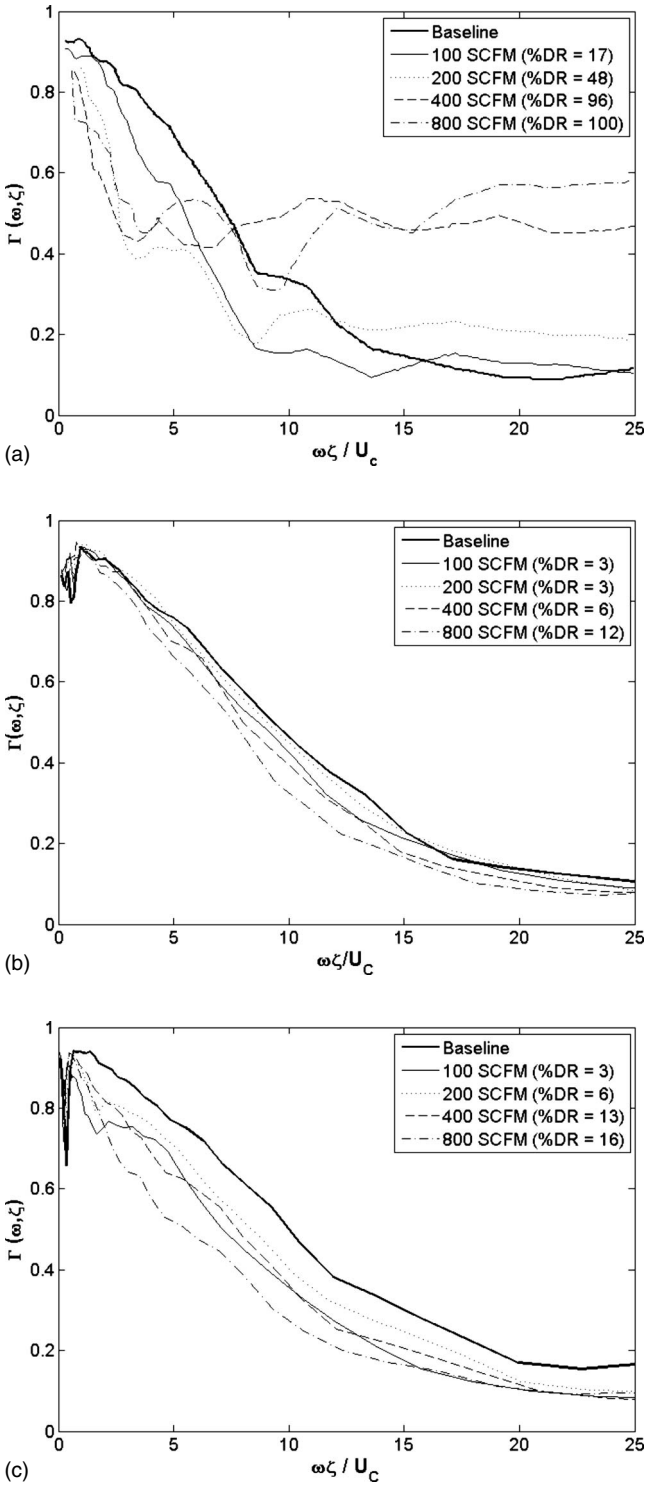


FIG. 12. Bubble modified streamwise coherence for a single sensor pair spacing (ζ=2.00 cm) and all air injection rates at (a) 6.6 m/s USI, (b) 13.2 m/s USI, and (c) 19.9 m/s DSI.

frequencies, where Γ peaks and then decreases or behaves erratically as $\omega\zeta/U_c$ approaches zero. This effect is a result of a breakdown of the similarity scaling embodied by $\omega\zeta/U_c$ for any finite sensor spacing as frequency approaches zero. This breakdown has been observed in other experiments (see Farabee and Casarella, 1991). To smooth the coherence results, the convection velocity, U_c, used to scale the coherence measurements in Figs. 11–13 was determined from a simple analytic form, $U_c/U_\infty = A\ \ln(B \cdot f)$, that was least-squares fit to the data for each flow condition shown in Fig. 10. Here, A and B are the fit constants and f is the frequency in hertz. In addition, the coherence spectra were postprocessed with a 1/20th decade top hat bandpass filter.

The coherence of surface pressure fluctuations during BDR is plotted in Fig. 12 for the three test speeds and all air injection rates. For clarity, results for only a single sensor pair spacing, ζ=2.00 cm, are shown in this figure. Relative to the base line, the coherence is typically suppressed over the entire frequency range shown and this suppression increases with increasing air injection rate. This observation implies that bubbles decrease the longevity of pressure sources within the boundary layer. The two exceptions to this observation are at the highest injection rates (400 and 800 SCFM) at 6.6 m/s, where a full or partial air film formed over the test surface. Here, the low frequency coherence is reduced, but the coherence at higher frequencies is elevated relative to the base line and it remains nearly constant at approximately 0.50. The reason for these changes is the different flow morphology. When a full or partial air layer forms, multiple irregularly shaped flat air pockets, with a thickness of ~1 cm and minimum horizontal dimension of δ(~10 cm) or greater, form and move downstream while

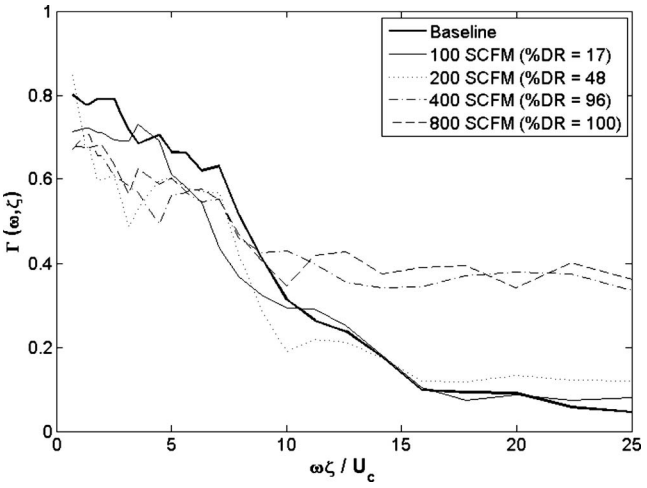


FIG. 13. Bubble modified streamwise coherence at 6.6 m/s with a single sensor pair spacing (ζ=4.6 cm) and all air injection rates.

slowly changing shape. As the air-flow rate increases, these air pockets merge and eventually form a complete air film. Thus, the enhanced high-frequency coherence in the 400 and 800 SCFM results in Fig. 12(a) can likely be attributed to passage of air-pocket edges over the pressure sensors. The decreased low frequency coherence is probably due to the air pockets altering or destroying large-scale base line TBL structures.

As a check of the similarity scaling of frequency and sensor spacing, BDR results from 6.6 m/s are provided in Fig. 13 for a sensor spacing of ζ=4.6 cm. A comparison of Figs. 12(a) and 13 shows that the differences are comparable (or nearly so) to differences in the single-phase coherence results at difference sensor spacings (see Fig. 11). Thus, the similarity variable $\omega\zeta/U_c$ appears to be equally valid in both single-phase and BDR TBL flows, even when a full or partial air layer forms. Hence, both turbulence- and bubble-originated pressure fluctuation sources move and evolve downstream in a similar manner.

IV. CONCLUSIONS

The data presented here show how the injection of air from the wall beneath a TBL modifies the spectra, coherence, and convection velocity of wall-pressure fluctuations. From this investigation, the following conclusions can be drawn. (1) rms pressure fluctuations without air injection have a Reynolds number dependence that is in good agreement with the scaling law proposed by Farabee and Casarella (1991). (2) With the injection of air, wall-pressure spectra are suppressed in the midfrequency range, approximately from $20 < \omega\delta/u_\tau < 2000$, where δ and u_τ are drawn from the equivalent single-phase base line boundary layer. However, air injection leads to increases in spectral levels above and below this range, likely caused by bubbles or pockets of air passing over the model surface and/or acoustic noise from the air injection process. In dimensional terms, the frequency range of this suppression shifts to slightly higher frequencies with increasing freestream velocity. The magnitude of this suppression increases monotonically with increasing skin-friction drag reduction. (3) Mean-square pressure fluctuations in BDR flows are reduced nearly in proportion to the reduction in skin friction, both relative to that measured in single-phase flow. (4) The convection velocity of pressure fluctuations above $\omega\delta/u_\tau \sim 50$ decreases with air injection, indicating that the pressure source terms for these frequencies are in a slower moving region of the flow. This convection velocity decrease becomes more apparent with increasing air injection rate. (5) The streamwise coherence of pressure fluctuations decreases during BDR, except when there is sufficient air to create an air layer between the liquid flow and the plate surface. (6) Comparisons of the base line coherence and the BDR coherence suggest that the usual frequency-distance similarity variable is equally valid when bubbles are present and when bubbles are absent.

ACKNOWLEDGMENTS

The authors are grateful for the support of the Defense Advanced Research Projects Agency under HR0011-04-1-000l (University of Michigan), Dr. Lisa Porter, Program Manager.

Barker, S. J. (**1973**). "Radiated noise from turbulent boundary layers in dilute polymer solutions," Phys. Fluids **16**, 1387–1394.
Brooks, T. F., and Hodgson, T. H. (**1981**). "Trailing edge noise prediction from measured surface pressures," J. Sound Vib. **78**, 69–117.
Brungart, T. A., Holmberg, W. J., Fontaine, A. A., Deutsch, S., and Petrie, H. L. (**2000**). "The scaling of wall pressure fluctuations in polymer modified turbulent boundary layer flow," J. Acoust. Soc. Am. **108**, 71–74.
Bull, M. K. (**1996**). "Wall-pressure fluctuations beneath turbulent boundary layers: some reflections on forty years of research," J. Sound Vib. **190**, 299–315.
Corcos, G. M. (**1963**). "Resolution of pressure in turbulence," J. Acoust. Soc. Am. **35**, 192–199.
Etter, R. J., Cutbirth, J. M., Ceccio, S. L., Dowling, D. R., and Perlin, M. (**2005**). "High Reynolds number experimentation in the U.S. Navy's William B. Morgan Large Cavitation Channel," Meas. Sci. Technol. **16**, 1701–1709.
Farabee, T. M., and Casarella, M. J. (**1991**). "Spectral features of wall pressure fluctuations beneath turbulent boundary layers," Phys. Fluids A **A3**, 2410–2420.
Goody, M. (**2004**). "A comparison of turbulent boundary layer wall-pressure spectra," AIAA J. **42**, 1788–1784.
Keith, W. L., Hurdis, D. A., and Abraham, B. M. (**1992**). "A comparison of turbulent boundary layer wall-pressure spectra," J. Fluids Eng. **114**, 338–347.
Lumley, J. L. (**1977**). "Drag reduction in two phase and polymer flows," Phys. Fluids **20**, S64–S70.
Merkle, C., and Deutsch, S. (**1992**). "Microbubble drag reduction in liquid turbulent boundary layers," Appl. Mech. Rev. **45**, 103–127.
Pal, S., Deutsch, S., and Merkle, C. L. (**1989**). "A comparison of shear stress fluctuation statistics between microbubble modified and polymer modified turbulent flow," Phys. Fluids A **1**, 1360–1362.
Patel, V. C. (**1965**). "Calibration of the Preston tube and limitations on its use in pressure gradients," J. Fluid Mech. **23**, 185–208.
Sanders, W. C., Winkel, E. S., Dowling, D. R., Perlin, M., and Ceccio, S. L. (**2006**). "Bubble friction drag reduction in a high-Reynolds-number flat-plate turbulent boundary layer," J. Fluid Mech. **552**, 353–380.

Boundary perturbation methods for high-frequency acoustic scattering: Shallow periodic gratings

David P. Nicholls[a)]
Department of Mathematics, Statistics, and Computer Science, University of Illinois at Chicago, Chicago, Illinois 60607

Fernando Reitich[b)]
School of Mathematics, University of Minnesota, Minneapolis, Minnesota 55455

(Received 29 June 2007; revised 4 February 2008; accepted 24 February 2008)

Despite significant recent advances in numerical methodologies for simulating rough-surface acoustic scattering, their applicability has been constrained by the limitations of state-of-the-art computational resources. This has been particularly true in high-frequency applications where the sheer size of the full-wave simulations render them impractical, and engineering processes must therefore rely on asymptotic models [e.g., Kirchhoff approximation (KA)]. However, the demands for high precision can make the latter inappropriate, thus efficient, error-controllable methodologies must be devised. This paper presents a computational strategy that combines the virtues of rigorous solvers (error control) with those of high-frequency asymptotic models (frequency-independent computational costs). These methods are based on *high-order* "boundary perturbations," which display high precision and unparalleled efficiency. This is accomplished by incorporating asymptotic phase information to effect a significant decrease in computational effort, simultaneously retaining the full-wave nature of the approach. The developments of this contribution are constrained to configurations that preclude multiple scattering; it is further explained how the schemes can be made applicable to general scattering scenarios, though implementation details are left for future work. Even for single-scattering configurations, the approach presented here gives significant gains in accuracy when compared to asymptotic theories (e.g., KA) with modest additional computational cost. © *2008 Acoustical Society of America.* [DOI: 10.1121/1.2897104]

PACS number(s): 43.30.Hw, 43.20.Fn, 43.20.Bi, 43.20.El [DSB] Pages: 2531–2541

I. INTRODUCTION

The significant advances in high-performance algorithms and hardware that have been attained over the last three decades have had a substantial impact on the classical engineering and design paradigm of repeated physical experimentation, interpretation, and modification in the most varied applications. Those relating to wave dynamics (e.g., acoustic, electromagnetic, elastic), such as in remote sensing,[1] nondestructive testing,[2] or imaging,[3] for instance, have increasingly relied on *numerical* simulations to accelerate assessment and/or prototyping projects. The success of such strategies has, in turn, provided further impetus to continue to migrate towards virtual experimentation and it has thus enhanced the need for evermore efficient and accurate simulators. These needs are, however, challenged by the increasing complexity of the processes to be numerically represented, which continuously test the limits of state-of-the-art computational methodologies and platforms. In the context of wave propagation these complexities can arise from that of the geometrical arrangement, from the intrinsic oscillations of the field quantities, or from both. Current simulation capabilities allow for the treatment of complicated geometries with a high degree of detail and accuracy. It is thus the requirement to resolve field quantities on the scale of the wavelength of oscillation that typically limits the applicability of advanced simulation schemes, and that consistently results in the need to abandon these in favor of approximate (high-frequency) asymptotic theories.

In this paper we introduce a family of numerical algorithms that are designed to overcome these limitations, simultaneously avoiding the inaccuracies that arise (at finite frequencies) from asymptotic solutions, such as those based on the classical Kirchhoff approximation[4] (KA) or on its corrected versions.[5–8] The schemes we present are based on *high-order* "boundary perturbations" (see, e.g., Refs. 9–16, and references cited therein) and can therefore be made to approximate the exact solution of full-wave scattering models to within any prescribed accuracy. As in classical implementations of these methods, the procedures we introduce here display a high degree of precision (owing to their spectral nature), and efficiency [stemming from the use of accelerated evaluations, e.g., based on fast-Fourier transforms (FFTs)]. In contrast with the classical approach, however, these characteristics are attained here, simultaneously avoiding the need to discretize the fields on the scale of the wavelength.

The basic observation that allows for such discretizations, and the consequent reduction in computational cost, relates to the possibility of predetermining the manner in

a)Electronic mail: nicholls@math.uic.edu
b)Electronic mail: reitich@math.umn.edu

which field quantities oscillate. More precisely, asymptotic high-frequency theories (e.g., geometrical acoustics) can be used *a priori* to predict the *phase* of the fields and, thus, to reduce the number of unknowns through its extraction, leaving only a slowly oscillatory modulation to be found. In the simplest case of impenetrable scatterers and wherein waves do not undergo multiple reflections, for instance, this phase takes on a particularly uncomplicated form, given by that of the incoming radiation on the surface of the obstacles and by the classical law of reflection away from these. This idea of phase extraction has been extensively used in the design of low-order analytical scattering theories (see, e.g., Refs. 5, 8, and 17–20) and, more recently, in the solution of integral equation formulations.[21–25] Here, in contrast, we explain how this can be incorporated into classical boundary perturbation algorithms to allow for efficient solutions of arbitrary accuracy.

Unlike low-order theories, the schemes we present here produce solutions that actually converge to that of the full-wave model. In fact, this characteristic also contrasts our approach with the high-order solutions of Refs. 21–23, which can be shown to be only asymptotic. Our methodology is perhaps most closely related to the work in Refs. 24 and 25, which introduces a *rigorous* approach to the numerical solution of high-frequency scattering problems based on the idea of phase extraction. This latter work is concerned with bounded scatterers for which an integral equation solver is designed to produce solutions with any prescribed accuracy in frequency-independent computational times. To this end, and in addition to the extraction of the phase, the work introduces suitable numerical mechanisms for a high-order treatment of the resulting singular and high-frequency integration problems, as well as of shadowing transitions[24] and multiple scattering effects.[25] Although a similar approach, based on integral equations, is certainly viable for the case we consider here of infinite (periodic) rough surfaces, the alternative perturbative procedures we advocate display some distinct advantages. In particular, for instance, these latter methodologies obviate the need to deal with the complications brought about by the corresponding Green's function (related to cost of its evaluation[26]), which are exacerbated at high frequencies, or with those related to the evaluation of oscillatory integrals.[25]

Although the derivations that follow apply to every boundary perturbation approach, for the sake of definiteness we shall detail these for two particularly popular schemes, namely the "field expansions" (FE) method of Bruno and Reitich[9–11] (a high-order, analytically continued version of the classical Rayleigh–Rice theory[27,28]); and the "operator expansion" (OE) method of Milder and co-worker[29–33] [based on perturbative expansions of the Dirichlet–Neumann Operator (DNO)]. In this initial contribution we constrain our developments to configurations that preclude multiple scattering, and are thus readily comparable with classical high-frequency approximations (e.g., KA). Extensions to cases wherein the effects of multiple scattering are significant can be attained through an iterative procedure that successively accounts for secondary reflections.[25] The numerical implementation of this procedure, however, is significantly more complicated (as it does, for instance, require the development of an accurate geometrical acoustics solver) and it is thus left for future work.

With these considerations, the rest of the paper is organized as follows: First, and for the sake of completeness, in Sec. II we recall the governing equations of rough surface scattering. Then, in Sec. III, we introduce the high-frequency versions of the OE and FE approaches that incorporate (single scattering) phase information to greatly reduce the number of degrees of freedom that are necessary to approximate the solution to any given accuracy. In Sec. IV we display results of numerical simulations which substantiate these claims and which show, in particular, that the approach can deliver significantly improved results when compared to classical asymptotic theories (e.g., KA) at a very modest additional computational cost. Finally, our conclusions follow in Sec. V.

II. GOVERNING EQUATIONS

The problem we consider is the scattering of time-harmonic acoustic waves from an impenetrable infinite surface which, for simplicity, is "sound soft" (our methods are easily modified to deal with other boundary conditions). We will consider the general three-dimensional case with crossed periodic gratings having shape represented by $y=g(x_1,x_2)$ where $g(x_1+d_1,x_2+d_2)=g(x_1,x_2)$ for periods d_1 and d_2.

If an incident plane wave,

$$v_i(x_1,x_2,y) = e^{i(\alpha x_1+\beta x_2-\gamma y)},$$

isonifies the surface, then this problem is governed by the Helmholtz equation with quasiperiodic lateral boundary conditions and a pressure release boundary condition at the scatterer, i.e.,

$$\Delta v + k^2 v = 0, \quad y > g(x_1,x_2), \tag{1a}$$

$$v(x_1,x_2,g(x_1,x_2)) = -v_i(x_1,x_2,g(x_1,x_2)) =: \xi(x_1,x_2), \tag{1b}$$

$$v(x_1+d_1,x_2+d_2,y) = e^{i(\alpha d_1+\beta d_2)} v(x_1,x_2,y), \tag{1c}$$

where v is the scattered field, ξ will denote the boundary data, and $k^2=\alpha^2+\beta^3+\gamma^2$. To specify a unique solution of Eq. (1) we need a boundary condition at infinity; this is given by an upward propagating condition,[34] which states that all scattered waves are "outgoing." It can be shown[15,16] that this can be explicitly enforced in the near-field with a "transparent boundary condition" at a hyperplane $y=a>\max|g|$. More precisely, Eq. (1) is equivalent to

$$\Delta v + k^2 v = 0, \quad g(x_1,x_2) < y < a, \tag{2a}$$

$$v(x_1,x_2,g(x_1,x_2)) = \xi(x_1,x_2), \tag{2b}$$

$$\partial_y v(x_1,x_2,a) - T[v(x_1,x_2,a)] = 0, \tag{2c}$$

$$v(x_1+d_1,x_2+d_2,y) = e^{i(\alpha d_1+\beta d_2)} v(x_1,x_2,y), \tag{2d}$$

where

$$T[\psi] := \sum_{p_1=-\infty}^{\infty} \sum_{p_2=-\infty}^{\infty} (i\gamma_{p_1,p_2}) \hat{\psi}_{p_1,p_2} e^{i(\alpha_{p_1} x_1 + \beta_{p_2} x_2)},$$

and

$$\alpha_{p_1} = \alpha + (2\pi/d_1)p_1, \quad \beta_{p_2} = \beta + (2\pi/d_2)p_2,$$

$$\gamma_{p_1,p_2} = \sqrt{k^2 - \alpha_{p_1}^2 - \beta_{p_2}^2}, \tag{3}$$

and $\mathrm{Im}\{\gamma_{p_1,p_2}\} \geq 0$. In this formula we have used the (generalized) Fourier series representation for quasiperiodic functions:

$$\psi(x_1,x_2) = \sum_{p_1=-\infty}^{\infty} \sum_{p_2=-\infty}^{\infty} \hat{\psi}_{p_1,p_2} e^{i(\alpha_{p_1} x_1 + \beta_{p_2} x_2)}. \tag{4}$$

Once computed, we can use the scattered field v to realize any of several near- and far-field quantities of interest. In the present context we will consider the normal derivative of the field at the surface of the scatterer:

$$\nu(x_1,x_2) := [\nabla v \cdot N_g]_{y=g},$$

where $N_g = (\partial_{x_1} g, \partial_{x_2} g, -1)^T$ is an exterior normal to the physical domain of the problem. As the "input" to our problem is the Dirichlet data ξ and the "output" is the Neumann information ν, this map is oftentimes called the DNO,[15,16] or Dirichlet-to-Neumann map.[35,36] We will denote this DNO by

$$G(g)[\xi] := [\nabla v \cdot N_g]_{y=g}$$
$$= [-\partial_y v + (\partial_{x_1} g)\partial_{x_1} v + (\partial_{x_2} g)\partial_{x_2} v]_{y=g}. \tag{5}$$

We note that knowledge of the DNO is exactly equivalent to that of the full solution to the scattering problem (2), as the field at any point can be readily recovered from this and the boundary pressure via Green's identities.

III. BOUNDARY PERTURBATION METHODS

The power and simplicity of boundary perturbation (BP) methods are based upon viewing the complicated problem domain as a perturbation of a much simpler one where the solution is trivial to compute. In the present context we view the shape of the grating, g, as a perturbation of a flat configuration, $g = \varepsilon f$ where, at the outset, ε will be small. Based upon this identification, one makes expansions of the form, e.g.,

$$v(x_1,x_2,y,\varepsilon) = \sum_{n=0}^{\infty} v_n(x_1,x_2,y)\varepsilon^n,$$

$$G(\varepsilon f)[\xi] = \sum_{n=0}^{\infty} G_n(f)[\xi]\varepsilon^n, \tag{6}$$

which can subsequently be shown to be *strongly convergent* under quite general conditions.[16,37] Additionally, these solutions can typically be continued analytically[16,38] so that, in fact, ε can be chosen quite large (provided that it remains real). In a numerical implementation this fact can be used to advantage if a suitable analytic continuation technique, such as Padé approximation,[39] is utilized. As we shall see, this combination of ideas leads to algorithms with quite remarkable properties of reliability, cost-effectiveness, and high-order accuracy.

A. Field expansions

The derivation of the FE method (originally named the "Method of Variation of Boundaries"[9–11]) begins with the expansion of the field, v:

$$v = v(x_1,x_2,y,\varepsilon) = \sum_{n=0}^{\infty} v_n(x_1,x_2,y)\varepsilon^n.$$

Upon insertion into Eq. (2) and evaluation at matching powers of ε, we realize the following system of equations to be solved:

$$\Delta v_n + k^2 v_n = 0, \quad 0 < y < a, \tag{7a}$$

$$v_n(x_1,x_2,0) = P_n(x_1,x_2), \tag{7b}$$

$$\partial_y v_n(x_1,x_2,a) - T[v_n(x_1,x_2,a)] = 0, \tag{7c}$$

$$v_n(x_1+d_1,x_2+d_2,y) = e^{i(\alpha d_1 + \beta d_2)} v_n(x_1,x_2,y), \tag{7d}$$

where

$$P_n(x_1,x_2) = \delta_{n,0}\xi(x_1,x_2) - \sum_{l=0}^{n-1} F_{n-l}(x_1,x_2)\partial_y^{n-l} v_l(x_1,x_2,0),$$

and

$$F_l(x_1,x_2) := \frac{f(x_1,x_2)^l}{l!}.$$

We recall that solutions v_n of Eqs. (7a), (7c), and (7d) can be written as

$$v_n(x_1,x_2,y) = \sum_{p_1=-\infty}^{\infty} \sum_{p_2=-\infty}^{\infty} d_{p_1,p_2} e^{i(\alpha_{p_1} x_1 + \beta_{p_2} x_2 + \gamma_{p_1,p_2} y)}, \tag{8}$$

c.f. Eq. (3). Given that ξ can be expressed as

$$\xi(x_1,x_2) = \sum_{p_1=-\infty}^{\infty} \sum_{p_2=-\infty}^{\infty} \hat{\xi}_{p_1,p_2} e^{i(\alpha_{p_1} x_1 + \beta_{p_2} x_2)},$$

c.f. Eq. (4), Eq. (7b) delivers a recursion formula for the $d_{p_1,p_2,n}$:

$$d_{p_1,p_2,n} = \delta_{n,0}\hat{\xi}_{p_1,p_2} - \sum_{l=0}^{n-1} \sum_{q_1=-\infty}^{\infty} \sum_{q_2=-\infty}^{\infty} F_{n-l,p_1-q_1,p_2-q_2} (i\gamma_{q_1,q_2})^{n-l} d_{q_1,q_2,l}, \tag{9}$$

where the coefficients F_{l,p_1,p_2} are defined by

$$F_l(x_1,x_2) =: \sum_{p_1=-\infty}^{\infty} \sum_{p_2=-\infty}^{\infty} F_{l,p_1,p_2} e^{i((2\pi/d_1)p_1 x_1 + (2\pi/d_2)p_2 x_2)}.$$

To compute the DNO, Eq. (5), we note that

$$\sum_{n=0}^{\infty} G_n(f)[\xi]\varepsilon^n = G(\varepsilon f)[\xi]$$

$$= [-\partial_y v + (\varepsilon\partial_{x_1} f)\partial_{x_1} v + (\varepsilon\partial_{x_2} f)\partial_{x_2} v]_{y=\varepsilon f}$$

$$= \sum_{n=0}^{\infty} \varepsilon^n \sum_{p_1=-\infty}^{\infty} \sum_{p_2=-\infty}^{\infty} (-i\gamma_{p_1,p_2} + (\varepsilon\partial_{x_1} f) i\alpha_{p_1} + (\varepsilon\partial_{x_2} f) i\beta_{p_2}) \times d_{p_1,p_2,n} e^{i(\alpha_{p_1} x_1 + \beta_{p_2} x_2 + \gamma_{p_1,p_2}\varepsilon f)}.$$

From this we deduce that

$$G_n(f) = \sum_{p_1=-\infty}^{\infty} \sum_{p_2=-\infty}^{\infty} \left(-\sum_{l=0}^{n} F_{n-l} (i\gamma_{p_1,p_2})^{n-l+1} d_{p_1,p_2,l} + \sum_{l=0}^{n-1} F_{n-l-1}((\partial_{x_1} f)(i\alpha_{p_1}) + (\partial_{x_2} f)(i\beta_{p_2})) \times (i\gamma_{p_1,p_2})^{n-l-1} d_{p_1,p_2,l} \right) e^{i(\alpha_{p_1} x_1 + \beta_{p_2} x_2)}. \tag{10}$$

B. High frequency field expansions

As we shall see in Sec. IV A, the FE method we have just described is not particularly well suited for high-frequency simulations. If the Fourier–Taylor coefficients $d_{p_1,p_2,n}$ from Eq. (9) are truncated after $N_{x_1} \times N_{x_2}$ Fourier modes and N Taylor terms, then the FE method has quite modest time $[\mathcal{O}(N_{x_1} \log(N_{x_1}) N_{x_2} \log(N_{x_2}) N)]$ and memory $[\mathcal{O}(N_{x_1} N_{x_2} N)]$ requirements. However, *all* features of the scattered field must be resolved to realize an accurate solution and, for this, the number of Fourier terms $N_{x_1} \times N_{x_2}$ *must* scale like $k \times k$.

However, the technique of phase extraction[5,8,19,21,22] gives us insight into how one can create a FE method which is specially designed for high-frequency calculations. In the present context, and in the absence of multiple scattering, it can be shown (see, e.g., Refs. 24 and 40) that

$$v(x_1,x_2) = e^{i(\alpha x_1 + \beta x_2 - \gamma g(x_1,x_2))} \mu(x_1,x_2), \tag{11}$$

where μ is a "slowly varying" envelope whose variations *do not* accentuate with increasing frequency. Note that this implies, in particular, that a uniformly accurate representation of μ can be attained with a number of degrees of freedom that is independent of the wave number k. Motivated by this realization we factor the *field*

$$v(x_1,x_2,y) = e^{i(\alpha x_1 + \beta x_2 - \gamma y)} w(x,y)$$

and substitute this into Eq. (2), which delivers

$$\Delta w + 2i(\alpha,\beta,-\gamma)\cdot\nabla w = 0, \quad g(x) < y < a, \tag{12a}$$

$$w(x_1,x_2,g(x_1,x_2)) = -1, \tag{12b}$$

$$w(x_1+d_1,x_2+d_2,y) = w(x_1,x_2,y). \tag{12c}$$

For the condition at the artificial boundary $y=a$, c.f. Eq. (2c), we begin with the calculation:

$$v(x_1,x_2,a) = e^{i(\alpha x_1+\beta x_2)} e^{-ia\gamma} w(x_1,x_2,a)$$

$$= e^{-ia\gamma} e^{i(\alpha x_1+\beta x_2)} \sum_{p_1=-\infty}^{\infty} \sum_{p_2=-\infty}^{\infty} \tilde{d}_{p_1,p_2} \times e^{i((2\pi/d_1)p_1 x_1 + (2\pi/d_2)p_2 x_2)}$$

$$= e^{-ia\gamma} \sum_{p_1=-\infty}^{\infty} \sum_{p_2=-\infty}^{\infty} \tilde{d}_{p_1,p_2} e^{i(\alpha_{p_1} x_1 + \beta_{p_2} x_2)},$$

where

$$\tilde{d}_{p_1,p_2} := \frac{1}{d_1 d_2} \int_0^{d_1} \int_0^{d_2} w(x_1,x_2,a) \times e^{-i((2\pi/d_1)p_1 x_1 + (2\pi/d_2)p_2 x_2)} dx_1 dx_2$$

is the (p_1,p_2)th Fourier coefficient of $w(x_1,x_2,a)$. Now, applying the operator T:

$$T[v(x_1,x_2,a)] = e^{-ia\gamma} T\left[\sum_{p_1=-\infty}^{\infty} \sum_{p_2=-\infty}^{\infty} \tilde{d}_{p_1,p_2} e^{i(\alpha_{p_1} x_1 + \beta_{p_2} x_2)} \right]$$

$$= e^{-ia\gamma} \sum_{p_1=-\infty}^{\infty} \sum_{p_2=-\infty}^{\infty} (i\gamma_{p_1,p_2}) \tilde{d}_{p_1,p_2} \times e^{i(\alpha_{p_1} x_1 + \beta_{p_2} x_2)}$$

$$= e^{i(\alpha x_1+\beta x_2)} e^{-ia\gamma} \sum_{p_1=-\infty}^{\infty} \sum_{p_2=-\infty}^{\infty} (i\gamma_{p_1,p_2}) \tilde{d}_{p_1,p_2} \times e^{i((2\pi/d_1)p_1 x_1 + (2\pi/d_2)p_2 x_2)}.$$

Finally, Eq. (2c) gives

$$0 = \partial_y v(x_1,x_2,a) - T[v(x_1,x_2,a)]$$

$$= \left(\partial_y w(x_1,x_2,a) - \sum_{p_1=-\infty}^{\infty} \sum_{p_2=-\infty}^{\infty} (i\gamma_{p_1,p_2} + i\gamma) \tilde{d}_{p_1,p_2} \times e^{i((2\pi/d_1)p_1 x_1 + (2\pi/d_2)p_2 x_2)} \right) e^{i(\alpha x_1+\beta x_2)} e^{-ia\gamma},$$

and we realize

$$\partial_y w(x_1,x_2,a) - T_0[w(x_1,x_2,a)] = 0, \tag{13}$$

where, for a *periodic* function $\zeta(x_1,x_2)$,

$$T_0[\zeta(x_1,x_2)] := \sum_{p_1=-\infty}^{\infty} \sum_{p_2=-\infty}^{\infty} (i\gamma_{p_1,p_2} + i\gamma) \times \hat{\zeta}_{p_1,p_2} e^{i((2\pi/d_1)p_1 x_1 + (2\pi/d_2)p_2 x_2)}. \tag{14}$$

Again, it can be shown that the (factored) field w can be expanded in a convergent Taylor series

$$w = w(x_1,x_2,y,\varepsilon) = \sum_{n=0}^{\infty} w_n(x_1,x_2,y)\varepsilon^n.$$

These w_n must satisfy

$$\Delta w_n + 2i(\alpha,\beta,-\gamma)\cdot\nabla w_n = 0, \quad 0 < y < a, \tag{15a}$$

$$w_n(x_1,x_2,0) = Q_n(x_1,x_2), \tag{15b}$$

$$\partial_y w_n(x_1,x_2,a) - T_0[w_n(x_1,x_2,a)] = 0, \tag{15c}$$

$$w_n(x_1+d_1,x_2+d_2,y) = w_n(x_1,x_2,y), \tag{15d}$$

where

$$Q_n(x_1,x_2) = -\delta_{n,0} - \sum_{l=0}^{n-1} F_{n-l}(x_1,x_2)\partial_y^{n-l} w_l(x_1,x_2,0).$$

Solutions of Eqs. (15a), (15c), and (15d) are given by

$$w_n(x_1,x_2,y) = \sum_{p_1=-\infty}^{\infty}\sum_{p_2=-\infty}^{\infty} b_{p_1,p_2,n} e^{(i\gamma_{p_1,p_2}+i\gamma)y} \times e^{i((2\pi/d_1)p_1x_1+(2\pi/d_2)p_2x_2)},$$

so that Eq. (15b) gives

$$b_{p_1,p_2,n} = -\delta_{n,0}\delta_{p_1,0}\delta_{p_2,0} - \sum_{l=0}^{n-1}\sum_{q_1=-\infty}^{\infty}\sum_{q_2=-\infty}^{\infty} F_{n-l,p_1-q_1,p_2-q_2} \times (i\gamma_{q_1,q_2}+i\gamma)^{n-l} b_{q_1,q_2,l}, \tag{16}$$

c.f. Eq. (9).

To compute the DNO we recall our factorization, Eq. (11), of the "fast" surface velocity ν as the product of an oscillatory term and a "slow" surface velocity μ. In terms of the slow field, w, we can write

$$\begin{aligned}\mu(x_1,x_2) &= e^{i(-\alpha x_1-\beta x_2+\gamma g(x_1,x_2))}\nu(x_1,x_2) = e^{i(-\alpha x_1-\beta x_2+\gamma g(x_1,x_2))}[-\partial_y v + (\partial_{x_1} g)\partial_{x_1} v + (\partial_{x_2} g)\partial_{x_2} v]_{y=g} = e^{i(-\alpha x_1-\beta x_2+\gamma g(x_1,x_2))}\\ &\times[(i\gamma)e^{i(\alpha x_1+\beta x_2-\gamma y)}w - e^{i(\alpha x_1+\beta x_2-\gamma y)}\partial_y w + (\partial_{x_1} g)(i\alpha)e^{i(\alpha x_1+\beta x_2-\gamma y)}w + (\partial_{x_2} g)(i\beta)e^{i(\alpha x_1+\beta x_2-\gamma y)}w\\ &+ (\partial_{x_1} g)e^{i(\alpha x_1+\beta x_2-\gamma y)}\partial_{x_1} w + (\partial_{x_2} g)e^{i(\alpha x_1+\beta x_2-\gamma y)}\partial_{x_2} w]_{y=g} = [(i\gamma)w - \partial_y w + (\partial_{x_1} g)(i\alpha)w + (\partial_{x_2} g)(i\beta)w + (\partial_{x_1} g)\partial_{x_1} w\\ &+ (\partial_{x_2} g)\partial_{x_2} w]_{y=g}.\end{aligned}$$

Now, if the w depends analytically upon ε then so will

$$\tilde{G}(\varepsilon f)[\psi(x_1,x_2)] := e^{i(-\alpha x_1-\beta x_2+\gamma\varepsilon f(x_1,x_2))} \times G(\varepsilon f)[e^{i(\alpha x_1+\beta x_2-\gamma\varepsilon f(x_1,x_2))}\psi(x_1,x_2)], \tag{17}$$

where $\psi\equiv -1$ corresponds to plane-wave scattering, i.e., $\tilde{G}(\varepsilon f)[-1]=\mu(x)$. Thus

$$\begin{aligned}\sum_{n=0}^{\infty}\tilde{G}_n(f)\varepsilon^n &= \tilde{G}(\varepsilon f)[-1]\\ &= [(i\gamma)w - \partial_y w + ((\varepsilon\partial_{x_1} f)(i\alpha) + (\varepsilon\partial_{x_2} f)\\ &\times(i\beta))w + (\varepsilon\partial_{x_1} f)\partial_{x_1} w + (\varepsilon\partial_{x_2} f)\partial_{x_2} w]_{y=g}\\ &= \sum_{n=0}^{\infty}\varepsilon^n\sum_{p_1=-\infty}^{\infty}\sum_{p_2=-\infty}^{\infty}[i\gamma - (i\gamma_{p_1,p_2}+i\gamma)\\ &+ (\varepsilon\partial_{x_1} f)i\alpha + (\varepsilon\partial_{x_2} f)i\beta + (\varepsilon\partial_{x_1} f)i(2\pi/d_1)p_1\\ &+ (\varepsilon\partial_{x_2} f)i(2\pi/d_2)p_2]\\ &\times b_{p_1,p_2,n} e^{i((2\pi/d_1)p_1x_1+(2\pi/d_2)p_2x_2+(\gamma+\gamma_{p_1,p_2})\varepsilon f)}.\end{aligned}$$

From this we have

$$\begin{aligned}\tilde{G}_n(f) = \sum_{p_1=-\infty}^{\infty}\sum_{p_2=-\infty}^{\infty}\Bigg(&\sum_{l=0}^{n} F_{n-l}(i\gamma)(i\gamma_{p_1,p_2}+i\gamma)^{n-l} b_{p_1,p_2,l}\\ &- \sum_{l=0}^{n} F_{n-l}(i\gamma_{p_1,p_2}+i\gamma)^{n-l+1} b_{p_1,p_2,l}\\ &+ \sum_{l=0}^{n-1} F_{n-l-1}[(\partial_{x_1} f)(i\alpha) + (\partial_{x_2} f)(i\beta)](i\gamma_{p_1,p_2}\\ &+ i\gamma)^{n-l-1} b_{p_1,p_2,l} + \sum_{l=0}^{n-1} F_{n-l-1}[(\partial_x f)i((2\pi/d_1)p_1)\\ &+ (\partial_{x_2} f)i(2\pi/d_2)p_2](i\gamma_{p_1,p_2}+i\gamma)^{n-l-1} b_{p_1,p_2,l}\Bigg).\end{aligned} \tag{18}$$

To reconstruct the DNO we simply multiply each of the $\tilde{G}_n$ by the factor $\exp(i(\alpha x_1+\beta x_2-\gamma g(x_1,x_2)))$.

C. Operator expansions

The OE method of Milder and co-worker[29–33] is a somewhat different approach than the FE algorithm as it endeavors to compute, given Dirichlet data, *only* the normal derivative (the DNO). Of course, as we mentioned, if the full field is desired then an appropriate integral can be used to recover this. To specify this OE algorithm we begin with the observation that the function

$$u_p(x,y) = e^{i(\alpha_{p_1}x_1+\beta_{p_2}x_2+\gamma_{p_1,p_2}y)}$$

satisfies Eqs. (2a), (2c), and (2d). Recalling the definition of the DNO, Eq. (5), and, again, setting $g(x_1,x_2)=\varepsilon f(x_1,x_2)$, we observe that

$$\begin{aligned} &G(\varepsilon f)[e^{i(\alpha_{p_1}x_1+\beta_{p_2}x_2+\gamma_{p_2,p_2}\varepsilon f(x_1,x_2))}] \\ &\quad = (-i\gamma_{p_1,p_2}+\varepsilon(\partial_{x_1}f)(i\alpha_{p_1})+\varepsilon(\partial_{x_2}f) \\ &\qquad \times(i\beta_{p_2}))e^{i(\alpha_{p_1}x_1+\beta_{p_2}x_2+\gamma_{p_1,p_2}\varepsilon f(x_1,x_2))}. \end{aligned} \tag{19}$$

Our goal is to, once again, take advantage of the analyticity properties of the DNO to find the Neumann data. This requires a formula for the nth term in the expansion of the DNO, G_n, c.f. Eq. (6), as applied to a generic quasiperiodic function $\xi(x_1,x_2)$. Making use of the representation

$$\xi(x_1,x_2) = \sum_{p_1=-\infty}^{\infty}\sum_{p_2=-\infty}^{\infty}\hat{\xi}_{p_1,p_2}e^{i(\alpha_{p_1}x_1+\beta_{p_2}x_2)}, \tag{20}$$

c.f. Eq. (4), it suffices to find a formula for G_n applied to a single harmonic $\exp(i(\alpha_{p_1}x_1+\beta_{p_2}x_2))$. For this we use Eq. (19):

$$\begin{aligned} &\left(\sum_{n=0}^{\infty}\varepsilon^n G_n(f)\right)\left[e^{i(\alpha_{p_1}x_1+\beta_{p_2}x_2)}\sum_{n=0}^{\infty}F_n(i\gamma_{p_1,p_2})^n\varepsilon^n\right] \\ &\quad = (-i\gamma_{p_1,p_2}+\varepsilon(\partial_{x_1}f)(i\alpha_{p_1})+\varepsilon(\partial_{x_2}f) \\ &\qquad \times(i\beta_{p_2}))e^{i(\alpha_{p_1}x_1+\beta_{p_2}x_2)}\sum_{n=0}^{\infty}F_n(i\gamma_{p_1,p_2})^n\varepsilon^n, \end{aligned}$$

where, again, $F_l := f^l/l!$. At order ε^0 we find

$$G_0[e^{i(\alpha_{p_1}x_1+\beta_{p_2}x_2)}] = -i\gamma_{p_1,p_2}e^{i(\alpha_{p_1}x_1+\beta_{p_2}x_2)},$$

which, using Eq. (20), gives

$$\begin{aligned} G_0[\xi] &= -i\gamma_D\xi \\ &:= \sum_{p_1=-\infty}^{\infty}\sum_{p_2=-\infty}^{\infty}(-i\gamma_{p_1,p_2})\hat{\xi}_{p_1,p_2}e^{i(\alpha_{p_1}x_1+\beta_{p_2}x_2)}, \end{aligned}$$

and defines the order-one Fourier multiplier G_0. At order ε^n, $n\geq 1$, we have

$$\begin{aligned} &G_n(f)[e^{i(\alpha_{p_1}x_1+\beta_{p_2}x_2)}] \\ &\quad = -F_n(i\gamma_{p_1,p_2})^{n+1}e^{i(\alpha_{p_1}x_1+\beta_{p_2}x_2)}+[(\partial_{x_1}f)F_{n-1}(i\alpha_{p_1}) \\ &\quad + (\partial_{x_2}f)F_{n-1}(i\beta_{p_2})](i\gamma_{p_1,p_2})^{n-1}e^{i(\alpha_{p_1}x_1+\beta_{p_2}x_2)} \\ &\quad - \sum_{l=0}^{n-1}G_l(f)[F_{n-l}(i\gamma_{p_1,p_2})^{n-l}e^{i(\alpha_{p_1}x_1+\beta_{p_2}x_2)}]. \end{aligned}$$

We can simplify the first two terms

$$\begin{aligned} R_n &:= -F_n(i\gamma_{p_1,p_2})^{n+1}e^{i(\alpha_{p_1}x_1+\beta_{p_2}x_2)}+(\partial_{x_1}f)F_{n-1}(i\alpha_{p_1}) \\ &\quad \times(i\gamma_{p_1,p_2})^{n-1}e^{i(\alpha_{p_1}x_1+\beta_{p_2}x_2)}+(\partial_{x_2}f)F_{n-1}(i\beta_{p_2}) \\ &\quad \times(i\gamma_{p_1,p_2})^{n-1}e^{i(\alpha_{p_1}x_1+\beta_{p_2}x_2)} \\ &= \{-F_n(i\gamma_{p_1,p_2})^2+(\partial_{x_1}f)F_{n-1}(i\alpha_{p_1}) \\ &\quad +(\partial_{x_2}f)F_{n-1}(i\beta_{p_2})\}(i\gamma_{p_1,p_2})^{n-1}e^{i(\alpha_{p_1}x_1+\beta_{p_2}x_2)} \end{aligned}$$

with the observation that, as $\alpha_{p_1}^2+\beta_{p_2}^2+\gamma_{p_1,p_2}^2=k^2$, we have

$$\begin{aligned} R_n &= \{F_nk^2+F_n(i\alpha_{p_1})^2+F_n(i\beta_{p_2})^2+(\partial_{x_1}f)F_{n-1}(i\alpha_{p_1}) \\ &\quad +(\partial_{x_2}f)F_{n-1}(i\beta_{p_2})\}(i\gamma_{p_1,p_2})^{n-1}e^{i(\alpha_{p_1}x_1+\beta_{p_2}x_2)}. \end{aligned}$$

Rewriting this using differential operators and the product rule we realize

$$\begin{aligned} R_n &= \{F_nk^2+F_n\partial_{x_1}^2+F_n\partial_{x_2}^2+(\partial_{x_1}f)F_{n-1}\partial_{x_1} \\ &\quad +(\partial_{x_2}f)F_{n-1}\partial_{x_2}\}(i\gamma_D)^{n-1}e^{i(\alpha_{p_1}x_1+\beta_{p_2}x_2)} \\ &= \{F_nk^2+\partial_{x_1}F_n\partial_{x_1}+\partial_{x_2}F_n\partial_{x_2}\}(i\gamma_D)^{n-1}e^{i(\alpha_{p_1}x_1+\beta_{p_2}x_2)}, \end{aligned}$$

resulting in

$$\begin{aligned} G_n(f)[\xi] &= k^2F_n(i\gamma_D)^{n-1}\xi+\partial_{x_1}F_n\partial_{x_1}(i\gamma_D)^{n-1}\xi \\ &\quad +\partial_{x_2}F_n\partial_{x_2}(i\gamma_D)^{n-1}\xi-\sum_{l=0}^{n-1}G_l(f)[F_{n-l}(i\gamma_D)^{n-l}\xi], \end{aligned} \tag{21}$$

where we have again used Eq. (20).

D. High frequency operator expansions

In a manner similar to that outlined in Sec. III B we can design a high-frequency OE method by making use of factorization (11). For this "high frequency operator expansions" (HFOE) method we wish to work directly with the DNO, however, now it should be scaled by the incident radiation so that it is slowly varying. Again, our goal is to find a formula for the nth term in the expansion acting on an *arbitrary* function. However, our surface function is the *periodic*, factored (slowly varying) incident radiation

$$\psi(x_1,x_2) := e^{i(-\alpha x_1-\beta x_2+\gamma g(x_1,x_2))}\xi(x_1,x_2) = -1.$$

Of course, this has a trivial Fourier series

$$\psi(x_1,x_2) = \hat{\psi}_{0,0}e^{i(0x_1+0x_2)} = (-1)e^{i(0x_1+0x_2)},$$

but we find it convenient to find the action of the nth term in the expansion of the reduced DNO applied to a general Fourier mode $\exp(i((2\pi/d_1)p_1x_1+(2\pi/d_2)p_2x_2))$.

As before, c.f. Eq. (17), we claim that $\tilde{G}(\varepsilon f)$ depends analytically upon ε, so that

$$\tilde{G}(\varepsilon f) = \sum_{n=0}^{\infty}\tilde{G}_n(f)\varepsilon^n.$$

To derive an explicit recurrence for the operators $\tilde{G}_n(f)$, we set

$$\psi(x_1,x_2) = e^{i((2\pi/d_1)p_1x_1+(2\pi/d_2)p_2x_2+\gamma g(x_1,x_2)+\gamma_{p_1,p_2}g(x_1,x_2))}. \tag{22}$$

Using this and the definition, Eq. (17), we find

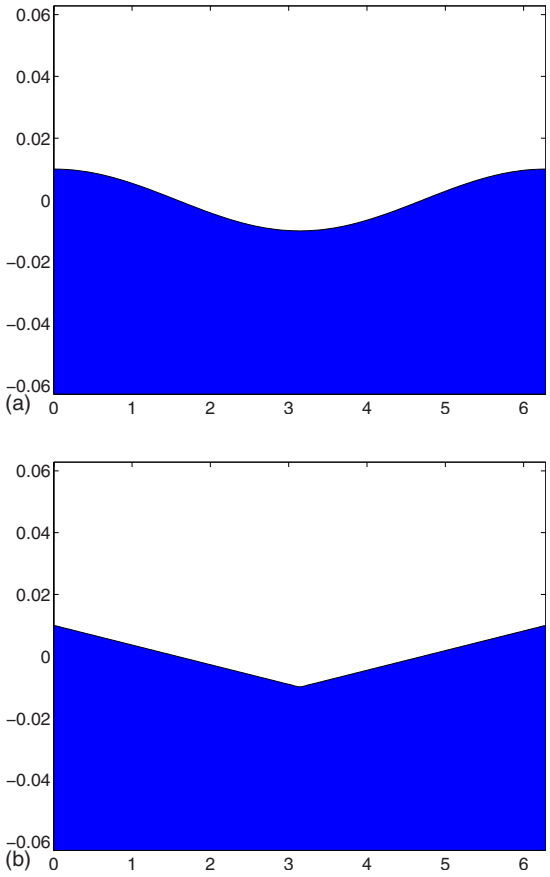


FIG. 1. (Color online) Plots of the two-dimensional profiles $f_s(x)=\cos(x)$, Eq. (24a), and $f_{L,40}$, Eq. (25).

$$\tilde{G}(g)[\psi] = e^{i(-\alpha x_1-\beta x_2+\gamma g(x_1,x_2))} \times G(g)[e^{i(\alpha_{p_1}x_1+\beta_{p_2}x_2+\gamma_{p_1,p_2}g(x_1,x_2))}] = e^{i(-\alpha x_1-\beta x_2+\gamma g(x_1,x_2))}[-\partial_y v(x_1,x_2,y) + (\partial_{x_1}g)\partial_{x_1}v(x_1,x_2,y) + (\partial_{x_2}g)\partial_{x_2}v(x_1,x_2,y)]_{y=g},$$

as the Dirichlet data, Eq. (22), we provide to G gives rise to the exact solution:

$$v(x_1,x_2,y) = e^{i(\alpha_{p_1}x_1+\beta_{p_2}x_2+\gamma_{p_1,p_2}y)}.$$

Continuing,

$$\tilde{G}(\varepsilon f)[\psi] = e^{i(-\alpha x_1-\beta x_2+\gamma\varepsilon f(x_1,x_2))}(-i\gamma_{p_1,p_2} + (\varepsilon\partial_{x_1}f)(i\alpha_{p_1}) + (\varepsilon\partial_{x_2}f)(i\beta_{p_2}))e^{i(\alpha_{p_1}x_1+\beta_{p_2}x_2+\gamma_{p_1,p_2}\varepsilon f(x_1,x_2))} = (-i\gamma_{p_1,p_2} + (\varepsilon\partial_{x_1}f)(i\alpha_{p_1}) + (\varepsilon\partial_{x_2}f)(i\beta_{p_2})) \times e^{i(2\pi/d_1)p_1x_1+i(2\pi/d_2)p_2x_2+(i\gamma_{p_1,p_2}+i\gamma)\varepsilon f(x_1,x_2)},$$

c.f. Eq. (19). Expanding as we did in the previous section:

$$\left(\sum_{n=0}^{\infty}\varepsilon^n\tilde{G}_n(f)\right)\left[e^{i((2\pi/d_1)p_1x_1+(2\pi/d_2)p_2x_2)}\sum_{n=0}^{\infty}F_n(i\gamma_{p_1,p_2} + i\gamma)^n\varepsilon^n\right] = (-i\gamma_{p_1,p_2} + \varepsilon(\partial_{x_1}f)(i\alpha_{p_1}) + (\varepsilon\partial_{x_2}f) \times i\beta_{p_2}))e^{i((2\pi/d_1)p_1x_1+(2\pi/d_2)p_2x_2)} \times\sum_{n=0}^{\infty}F_n(i\gamma_{p_1,p_2}+i\gamma)^n\varepsilon^n,$$

we find that, at order zero,

$$\tilde{G}_0[\psi] = -(i\gamma_D)\psi,$$

and at order $n\geq 1$,

$$\tilde{G}_n[\psi] = -F_n(i\gamma_D)(i\gamma_D+i\gamma)^n\psi + (\partial_{x_1}f)F_{n-1}(i\alpha_D)(i\gamma_D+i\gamma)^{n-1} \times\psi + (\partial_{x_2}f)F_{n-1}(i\beta_D)(i\gamma_D+i\gamma)^{n-1}\psi - \sum_{l=0}^{n-1}\tilde{G}_l[F_{n-l}(i\gamma_D+i\gamma)^{n-l}\psi]. \quad (23)$$

TABLE I. Relative error in FE, OE, HFFE, and HFOE algorithms (all with $N_x=16$) vs perturbation order N for the cosine profile, Eq. (24a), as compared to a highly resolved TFE simulation ($N_x=1024$, $N_y=64$, $N=28$); frequency is $(\alpha=1,\gamma=1)$.

N	FE	HFFE	OE	HFOE
0	9.91×10^{-3}	1.57×10^{-2}	9.91×10^{-3}	1.57×10^{-2}
2	1.37×10^{-6}	8.8×10^{-7}	1.37×10^{-6}	8.8×10^{-7}
4	3.53×10^{-10}	3.66×10^{-10}	3.53×10^{-10}	3.66×10^{-10}
6	3.53×10^{-10}	3.53×10^{-10}	3.53×10^{-10}	3.53×10^{-10}
8	3.53×10^{-10}	3.53×10^{-10}	3.53×10^{-10}	3.53×10^{-10}

IV. NUMERICAL TESTS

In this section we illustrate the superior accuracy one can realize with our new algorithms with cost *independent* of the frequency. We begin with a series of numerical tests in two dimensions, Sec. IV A, where we consider gratings which are invariant in one direction and the incident field is aligned precisely so that this invariant direction can be ignored. This configuration can be simulated with the algorithms outlined earlier by simply setting $\beta=0$, setting $d=d_1$, $x=x_1$, etc. In Sec. IV B we consider the full three-dimensional problem and show that our general conclusions are unchanged.

A. Two-dimensional tests

To test the usefulness of the two new algorithms, high-frequency field expansion (HFFE) and high frequency operator expansion (HFOE), outlined previously we will use them

TABLE II. Relative error in FE, OE, HFFE, and HFOE algorithms (all with $N_x=16$) vs perturbation order N for the cosine profile, Eq. (24a), as compared to a highly resolved TFE simulation ($N_x=1024$, $N_y=64$, $N=28$); frequency is $(\alpha=10,\gamma=10)$.

N	FE	HFFE	OE	HFOE
0	2×10^{0}	1.01×10^{-2}	2×10^{0}	1.01×10^{-2}
2	2×10^{0}	6.31×10^{-7}	2×10^{0}	6.31×10^{-7}
4	2×10^{0}	1.99×10^{-8}	2×10^{0}	1.99×10^{-8}
6	2×10^{0}	1.07×10^{-10}	2×10^{0}	1.07×10^{-10}
8	2×10^{0}	3.62×10^{-11}	2×10^{0}	3.62×10^{-11}

TABLE III. Relative error in FE, OE, HFFE, and HFOE algorithms (all with $N_x=16$) vs perturbation order N for the cosine profile, Eq. (24a), as compared to a highly resolved TFE simulation ($N_x=1024$, $N_y=64$, $N=28$); frequency is ($\alpha=100, \gamma=100$).

N	FE	HFFE	OE	HFOE
0	2×10^{0}	9.9×10^{-3}	2×10^{0}	9.9×10^{-3}
2	2×10^{0}	2.33×10^{-8}	2×10^{0}	2.33×10^{-8}
4	2×10^{0}	5.97×10^{-12}	2×10^{0}	5.97×10^{-12}
6	2×10^{0}	5.97×10^{-12}	2×10^{0}	5.97×10^{-12}
8	2×10^{0}	5.97×10^{-12}	2×10^{0}	5.97×10^{-12}

to compute the induced normal surface velocity for two scatterers with very different smoothness. For simplicity we assume the period to be $d=2\pi$, and we consider the following profiles:[15,16] A sinusoid

$$f_s(x)=\cos(x), \tag{24a}$$

and a nondifferentiable ("Lipschitz") function

$$f_L(x)=\begin{cases}-(2/\pi)x+1, & 0\le x\le \pi\\ (2/\pi)x-3, & \pi\le x\le 2\pi.\end{cases} \tag{24b}$$

For our simulations we point out that f_L admits an infinite Fourier series expansions:[15]

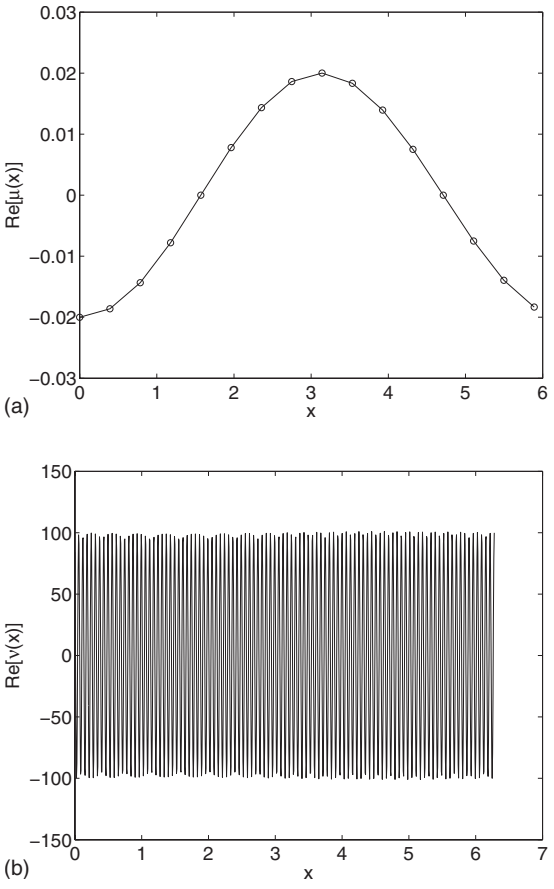


FIG. 2. Plots of the real parts of the slow surface velocity, $\mu(x)$, and fast surface velocity, $v(x)$. These plots are for profile (24a) and ($\alpha=100$, $\gamma=100$).

TABLE IV. Relative error in FE, OE, HFFE, and HFOE algorithms (all with $N_x=16$, $N=8$) vs perturbation size ε, for the cosine profile, Eq. (24a), as compared to a TFE simulation ($N_x=1024$, $N_y=64$, $N=28$); frequency is ($\alpha=100, \gamma=100$).

ε	FE	HFFE	OE	HFOE
0.02	2.01×10^{0}	2.9×10^{-12}	2.01×10^{0}	3.07×10^{-12}
0.03	2.06×10^{0}	4.01×10^{-12}	2.06×10^{0}	6.05×10^{-12}
0.04	2.22×10^{0}	5.63×10^{-12}	2.17×10^{0}	4.01×10^{-11}
0.05	2.33×10^{0}	9.8×10^{-12}	2.25×10^{0}	1.9×10^{-10}
0.06	2.34×10^{0}	2.09×10^{-11}	2.25×10^{0}	7.36×10^{-10}
0.07	2.21×10^{0}	5.72×10^{-11}	2.16×10^{0}	2.33×10^{-9}
0.08	2.53×10^{0}	7.73×10^{-10}	2.16×10^{0}	5.21×10^{-9}
0.09	2.23×10^{0}	2.21×10^{-9}	2.13×10^{0}	8.2×10^{-9}
0.1	2.13×10^{0}	1.83×10^{-9}	2.11×10^{0}	1.14×10^{-8}

$$f_L(x)=\sum_{r=1}^{\infty}\frac{8}{\pi^2(2r-1)^2}\cos((2r-1)x),$$

which, in our numerical simulations, we will truncate after P terms:

$$f_{L,P}(x)=\sum_{r=1}^{P/2}\frac{8}{\pi^2(2r-1)^2}\cos((2r-1)x); \tag{25}$$

please see Fig. 1 for depictions of, Eqs. (24a) and (25) ($P=40$).

Of course, for a generic profile there is no exact closed-form solution to the problem of plane-wave scattering by a grating so we resort to an alternative method to produce an "exact solution" with which we can compare. For this purpose we use the reliable, high-order "transformed field expansion" (TFE) method[16,41] for very large and/or very rough scatterers. For all of the two-dimensional simulations we present, a highly resolved reference solution was produced using this TFE algorithm with $N_x=1024$ (horizontal) Fourier modes, $N_y=64$ (vertical) Chebyshev coefficients, and $N=28$ Taylor orders; see Ref. 16 for a complete description of this method and these numerical parameters. These reference solutions can be shown to attain relative accuracies of the order of 10^{-10} which certainly suffice for our demonstration purposes. In this context then this becomes the smallest realizable "error," though the actual solutions we compute can be significantly more accurate when compared to the actual exact solution.

TABLE V. Relative error in HFFE and HFOE algorithms summed via Taylor and Padé algorithms (all with $N_x=32$) vs perturbation order N for the cosine profile, Eq. (24a), as compared to a highly resolved TFE simulation ($N_x=1024$, $N_y=64$, $N=28$); frequency is ($\alpha=100, \gamma=100$).

N	HFFE (Taylor)	HFFE (Padé)	HFOE (Taylor)	HFOE (Padé)
0	9.09×10^{-2}	9.09×10^{-2}	9.09×10^{-2}	9.09×10^{-2}
2	2.38×10^{-5}	2.38×10^{-5}	2.38×10^{-5}	2.38×10^{-5}
4	3.12×10^{-7}	2.85×10^{-8}	3.13×10^{-7}	2.85×10^{-8}
6	4.46×10^{-9}	2.1×10^{-9}	2.17×10^{-8}	4.86×10^{-8}
8	1.25×10^{-8}	4.22×10^{-9}	1.09×10^{-5}	4.88×10^{-8}
10	5.88×10^{-7}	2.16×10^{-9}	6.47×10^{-3}	3.26×10^{-8}
12	4.17×10^{-5}	1.54×10^{-8}	2.33×10^{0}	2.89×10^{-8}

TABLE VI. Relative error in FE, OE, HFFE, and HFOE algorithms (all with $N_x=256$) vs perturbation order N for the Lipschitz profile, Eq. (25), as compared to a highly resolved TFE simulation ($N_x=1024$, $N_y=64$, $N=28$); frequency is $(\alpha=1,\gamma=1)$.

N	FE	HFFE	OE	HFOE
0	2.02×10^{-2}	3.6×10^{-2}	2.02×10^{-2}	3.6×10^{-2}
2	9.59×10^{-6}	1.32×10^{-6}	9.59×10^{-6}	1.32×10^{-6}
4	3.5×10^{-10}	3.55×10^{-10}	3.55×10^{-10}	3.55×10^{-10}
6	3.46×10^{-10}	3.46×10^{-10}	3.64×10^{-10}	3.46×10^{-10}
8	3.46×10^{-10}	3.46×10^{-10}	3.75×10^{-10}	3.46×10^{-10}
10	3.46×10^{-10}	3.46×10^{-10}	3.72×10^{-10}	3.46×10^{-10}
12	3.46×10^{-10}	3.46×10^{-10}	3.72×10^{-10}	3.46×10^{-10}

TABLE VIII. Relative error in FE, OE, HFFE, and HFOE algorithms (all with $N_x=256$) vs perturbation order N for the Lipschitz profile, Eq. (25), as compared to a highly resolved TFE simulation ($N_x=1024$, $N_y=64$, $N=28$); frequency is $(\alpha=100,\gamma=100)$.

N	FE	HFFE	OE	HFOE
0	2.02×10^{-3}	8.08×10^{-3}	2.02×10^{-3}	8.08×10^{-3}
2	1.2×10^{-3}	9.01×10^{-6}	1.2×10^{-3}	9.01×10^{-6}
4	1.2×10^{-3}	1.73×10^{-5}	1.2×10^{-3}	1.73×10^{-5}
6	1.2×10^{-3}	2.78×10^{-7}	1.2×10^{-3}	2.78×10^{-7}
8	1.2×10^{-3}	3.57×10^{-9}	1.2×10^{-3}	3.57×10^{-9}
10	1.2×10^{-3}	3.21×10^{-10}	1.2×10^{-3}	3.22×10^{-10}
12	1.2×10^{-3}	2.71×10^{-10}	1.2×10^{-3}	2.72×10^{-10}

In Tables I–III we display results of FE, HFFE, OE, and HFOE simulations of plane-wave scattering from the sinusoidal profile, Eq. (24a), with $\varepsilon=0.01$ (to exclude the possibility of multiple reflections) for $(\alpha,\gamma)=(1,1)$, $(10,10)$, and (100,100), respectively. To exemplify the capabilities of our new methods, in all of these simulations we fix the number of Fourier modes at $N_x=16$ and study our solutions as the Taylor order is varied among $N=0$, 2, 4, 6, and 8. In this, and all future simulations, we have summed these Taylor series using Padé approximation[39] although, as the order N is quite small, the accuracy gains were typically modest.

In Table I we see that all four algorithms realize the optimal errors with respect to the TFE solution (of the order of 10^{10}) by perturbation order $N=6$ which is to be expected as this solution for $(\alpha,\gamma)=(1,1)$ is not very oscillatory. However, for this discretization, the FE and OE algorithms produce inaccurate results for $(\alpha,\gamma)=(10,10)$ and (100,100). Of course, this is not surprising as these algorithms attempt to resolve quite oscillatory functions with only $|r|<N_x/2=8$ modes. By contrast, as our new HFFE/HFOE methods simulate the *slowly* varying envelope μ, we notice *uniformly* excellent convergence behavior for all choices of (α,γ) where accuracies of 10^{-9} or 10^{-10} are always achieved with $N=8$ perturbation orders. For this final frequency we also display a plot of the slow, $\mu(x)$, and fast, $\nu(x)$, surface velocities in Fig. 2. From this we can clearly see how our new approach delivers such superior accuracy as the slowly changing function $\mu(x)$ can easily be represented with $N_x=16$ which is obviously insufficient for the highly oscillatory $\nu(x)$.

In Table IV we display results of FE, HFFE, OE, and HFOE simulations of plane-wave scattering from the sinusoidal profile, Eq. (24a), with various values of ε, $N_x=16$, $N=8$, and $(\alpha,\gamma)=(100,100)$. The results in this table exemplify the broad range of applicability of our scheme within the setting of single scattering configurations. To determine the limits of our new approach, a simple geometrical acoustics calculation is needed to determine the first appearance of multiple reflection for the given incidence and grating shape. For instance, in the present case of the sinusoidal profile, Eq. (24a), and incident radiation $\alpha=\gamma$ we have determined that multiple reflections occur once $\varepsilon\approx0.36$. By contrast, for the same profile but *normal* incidence, $\alpha=0$, we found that secondary reflections occur at $\varepsilon\approx0.82$.

TABLE VII. Relative error in FE, OE, HFFE, and HFOE algorithms (all with $N_x=256$) vs perturbation order N for the Lipschitz profile, Eq. (25), as compared to a highly resolved TFE simulation ($N_x=1024$, $N_y=64$, $N=28$); frequency is $(\alpha=10,\gamma=10)$.

N	FE	HFFE	OE	HFOE
0	1.06×10^{-2}	1.79×10^{-2}	1.06×10^{-2}	1.79×10^{-2}
2	1.31×10^{-4}	8.97×10^{-6}	1.31×10^{-4}	8.97×10^{-6}
4	1.82×10^{-10}	2.96×10^{-8}	1.85×10^{-10}	2.96×10^{-8}
6	4.04×10^{-11}	4.54×10^{-11}	6.06×10^{-11}	4.54×10^{-11}
8	4.04×10^{-11}	4.17×10^{-11}	7.3×10^{-11}	4.17×10^{-11}
10	4.05×10^{-11}	4.1×10^{-11}	6.97×10^{-11}	4.1×10^{-11}
12	4.05×10^{-11}	4.1×10^{-11}	6.99×10^{-11}	4.1×10^{-11}

In Table V we display results which illustrate the stabilizing effect which Padé summation can have on our algorithm. We again consider scattering from the cosine profile with incident radiation of frequency $(\alpha,\gamma)=(100,100)$, but now focus on the largest value of ε presented thusfar ($\varepsilon=0.1$) and compare, for values of the Taylor order $N=0,\ldots,12$ (for a slightly larger $N_x=32$ to avoid aliasing), the convergence of our high-frequency methods (HFFE and HFOE) with both Taylor and Padé summation. We see that through six orders all four calculations produce roughly the same precision, however, beyond eight orders the results from Taylor summation begin to deteriorate. This is particularly true for the HFOE algorithm, and highlights the advantageous properties of Padé summation even within the disk of convergence of these Taylor series.

We now present calculations for the Lipschitz profile, Eq. (25), (with $\varepsilon=0.01$) which features Fourier series which decay very slowly (as r increases). Due to this extremely slow decay we found it necessary to choose $N_x=256$ before our high-frequency algorithms gave uniformly good results. For this reason, the unmodified algorithms (FE and OE) were quite competitive up to $(\alpha,\gamma)=(10,10)$ (see Tables VI and VII). However, once the frequency reached (α,γ)

TABLE IX. Relative error in Kirchhoff Approximation for cosine, Eq. (24a) and Lipschitz profiles, Eq. (25), as compared to a highly resolved TFE simulation ($N_x=1024$, $N_y=64$, $N=28$).

Profile	$(\alpha,\gamma)=(1,1)$	$(\alpha,\gamma)=(10,10)$	$(\alpha,\gamma)=(100,100)$
Cosine	0.019 767 2	0.002 010 72	0.000 198 089
Lipschitz	0.040 357 3	0.021 093 1	0.003 682 25

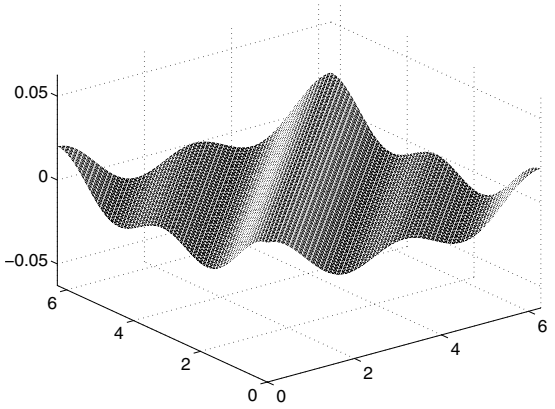


FIG. 3. Plot of the three-dimensional profile $f_r^{(3)}(x_1,x_2)$, Eq. (26).

$=(100,100)$ our specially designed algorithms were clearly superior, see Table VIII. Again, the range of applicability of our algorithm is determined by the onset of multiple scattering events which, we have calculated, to set in at $\varepsilon \approx 0.42$ for $\alpha=\gamma$ and $\varepsilon \approx 0.91$ for normal incidence, $\alpha=0$.

Finally, we make a comparison of our new methods to the KA for these configurations. The results are summarized in Table IX and show that, while the KA does give improved results as the frequency is increased, it never approaches the accuracy of our new HFFE/HFOE algorithms.

B. Three-dimensional test

We now present a set of illustrative numerical simulations to show that the HFFE and HFOE algorithms again deliver highly accurate solutions with very few degrees of freedom even in the three-dimensional case of scattering by a crossed grating. For this set of experiments we consider the three-dimensional smooth profile:

$$f_r^{(3)}(x_1,x_2) = \cos(x_1 - x_2) + \cos(2x_1 - 2x_2), \tag{26}$$

which is 2π periodic in both the x_1 and x_2 directions, and choose $\varepsilon=0.01$ to avoid multiple reflections (see Fig. 3). Again, we will use all four algorithms to compute the normal derivative of the field at the surface of the scatterer and compare this with a highly resolved TFE simulation, again accurate to around 10^{-10} ($N_{x_1}=128$, $N_{x_2}=128$, $N_y=64$, $N=28$). We display results of these simulations with $N_{x_1}=32$, $N_{x_2}=32$, and Taylor orders $N=0$, 2, 4, 6, and 8 in Tables X–XII for $(\alpha,\beta,\gamma)=(1,1,1)$, $(10,10,10)$, and $(100,100,100)$, respectively.

TABLE X. Relative error in FE, OE, HFFE, and HFOE algorithms (all with $N_{x_1}=32$ and $N_{x_2}=32$) vs perturbation order N for the three dimensional smooth profile, Eq. (26), as compared to a highly resolved TFE simulation ($N_{x_1}=128$, $N_{x_2}=128$, $N_y=64$, $N=28$); frequency is $(\alpha=1,\beta=1,\gamma=1)$.

N	FE	HFFE	OE	HFOE
0	3.25×10^{-2}	5.25×10^{-2}	3.25×10^{-2}	5.25×10^{-2}
2	3.78×10^{-5}	3.77×10^{-5}	3.78×10^{-5}	3.77×10^{-5}
4	2.79×10^{-9}	2.1×10^{-8}	2.79×10^{-9}	2.1×10^{-8}
6	1.62×10^{-10}	1.62×10^{-10}	1.62×10^{-10}	1.62×10^{-10}
8	1.61×10^{-10}	1.61×10^{-10}	1.61×10^{-10}	1.61×10^{-10}

TABLE XI. Relative error in FE, OE, HFFE, and HFOE algorithms (all with $N_{x_1}=32$ and $N_{x_2}=32$) vs perturbation order N for the three dimensional smooth profile, Eq. (26), as compared to a highly resolved TFE simulation ($N_{x_1}=128$, $N_{x_2}=128$, $N_y=64$, $N=28$); frequency is $(\alpha=10,\beta=10,\gamma=10)$.

N	FE	HFFE	OE	HFOE
0	5.34×10^{-3}	2.99×10^{-2}	5.34×10^{-3}	2.99×10^{-2}
2	7.39×10^{-4}	3.89×10^{-4}	7.39×10^{-4}	3.89×10^{-4}
4	5.3×10^{-5}	7.03×10^{-6}	5.3×10^{-5}	7.03×10^{-6}
6	5.3×10^{-5}	1.79×10^{-8}	5.3×10^{-5}	1.79×10^{-8}
8	5.3×10^{-5}	5.56×10^{-11}	5.3×10^{-5}	5.56×10^{-11}

For a relatively small frequency, $(\alpha,\beta,\gamma)=(1,1,1)$, all four algorithms work very well, c.f. Table X. However, at the more moderate frequency $(\alpha,\beta,\gamma)=(10,10,10)$ the standard FE/OE methods become disadvantaged and can only resolve the normal derivative of the field to 10^{-5}, see Table XI. Finally, once we reach the relatively high frequency $(\alpha,\beta,\gamma)=(100,100,100)$ the FE/OE approaches produce inaccurate results while the HFFE and HFOE methods produce solutions which are accurate to 10^{-10}.

To close, we note, for sake of comparison, that the KA delivers solutions with errors 0.065 260 7, 0.010 607 6, 0.000 975 237 for $(\alpha,\beta,\gamma)=(1,1,1)$, $(10,10,10)$, and $(100,100,100)$, respectively. Again, these errors are decreasing as the frequency is increased, but the KA solution cannot compete with the ones that HFFE/HFOE produce.

V. CONCLUSIONS

In this paper we have shown how asymptotic phase information can be incorporated into high-order boundary perturbation methods to produce numerical algorithms for acoustic scattering, which are error controllable with frequency-independent computational cost. A detailed specification has been given for two particularly popular boundary perturbation schemes, the "field expansions" method, based on perturbative expansions of the pressure, and the "operator expansion" method which works with expansions of the relevant Dirichlet–Neumann operator. Of particular note, these new methods *never* produce significantly worse results than the original FE/OE recursions, regardless of the frequency. Therefore it appears that these high-frequency schemes are to be recommended for *all* configurations where FE and OE are applicable. Also, provided that we have properly resolved the profile, there is *always* a smallest frequency for which these

TABLE XII. Relative error in FE, OE, HFFE, and HFOE algorithms (all with $N_{x_1}=32$ and $N_{x_2}=32$) vs perturbation order N for the three dimensional smooth profile, Eq. (26), as compared to a highly resolved TFE simulation ($N_{x_1}=128$, $N_{x_2}=128$, $N_y=64$, $N=28$); frequency is $(\alpha=100,\beta=100,\gamma=100)$.

N	FE	HFFE	OE	HFOE
0	1.21×10^{0}	2.66×10^{-2}	1.21×10^{0}	2.66×10^{-2}
2	1.21×10^{0}	1.29×10^{-6}	1.21×10^{0}	1.29×10^{-6}
4	1.21×10^{0}	4.33×10^{-10}	1.21×10^{0}	4.33×10^{-10}
6	1.21×10^{0}	1.43×10^{-10}	1.21×10^{0}	1.48×10^{-10}
8	1.21×10^{0}	1.43×10^{-10}	1.21×10^{0}	1.51×10^{-10}

new methods are significantly more accurate than the standard FE/OE algorithms. Further, for frequencies larger than this critical value the FE/OE recursions become unreliable, whereas our new procedures produce consistently accurate results. In this first contribution we have restricted our descriptions and numerical results to geometries which do not generate multiple reflections. However, we have discussed how these single-reflection methods can be rendered applicable to multiple scattering configurations, though we leave the specification and implementation to future work.

DISCLAIMER

Effort sponsored by the Air Force Office of Scientific Research, Air Force Materials Command, USAF, under Grant No. FA9550-05-1-0019. The U.S. Government is authorized to reproduce and distribute reprints for governmental purposes notwithstanding any copyright notation thereon. The views and conclusions contained herein are those of the authors and should not be interpreted as necessarily representing the official policies or endorsements, either expressed or implied, of the Air Force Office of Scientific Research or the U.S. Government.

ACKNOWLEDGMENTS

The first author (D.P.N.) gratefully acknowledges support from the NSF through Grant No. DMS-0537511. The second author (F.R.) gratefully acknowledges support from AFOSR through Contract No. FA9550-05-1-0019 and from NSF through Grant No. DMS-0311763.

[1]L. Tsang, J. A. Kong, and R. T. Shin, *Theory of Microwave Remote Sensing* (Wiley, New York, 1985).
[2]P. J. Shull, *Nondestructive Evaluation: Theory, Techniques, and Applications* (Marcel Dekker, New York, 2002).
[3]F. Natterer and F. Wübbeling, "Mathematical methods in image reconstruction," *SIAM Monographs on Mathematical Modeling and Computation* (Society for Industrial and Applied Mathematics, Philadelphia, PA, 2001).
[4]J. Ogilvy, *Theory of Wave Scattering from Random Rough Surfaces* (Institute of Physics Publishing, Bristol, UK, 1991).
[5]P. Lynch, "Curvature corrections to rough-surface scattering at high frequencies," J. Acoust. Soc. Am. **47**, 804–815 (1970).
[6]E. Liszka and J. McCoy, "Scattering at a rough boundary-extensions of the Kirchhoff approximation," J. Acoust. Soc. Am. **71**, 1093–1100 (1982).
[7]H. Chaloupka and H. Meckelburg, "Improved high-frequency current approximation for curved conducting surfaces," Arch. Elektrotech. (Berlin) **39**, 245–250 (1985).
[8]E. Rodriguez, "Beyond the Kirchhoff approximation," Radio Sci. **24**, 681–693 (1989).
[9]O. P. Bruno and F. Reitich, "Numerical solution of diffraction problems: A method of variation of boundaries," J. Opt. Soc. Am. A **10**, 1168–1175 (1993).
[10]O. P. Bruno and F. Reitich, "Numerical solution of diffraction problems: A method of variation of boundaries. II. Finitely conducting gratings, Padé approximants, and singularities," J. Opt. Soc. Am. A **10**, 2307–2316 (1993).
[11]O. P. Bruno and F. Reitich, "Numerical solution of diffraction problems: A method of variation of boundaries. III. Doubly periodic gratings," J. Opt. Soc. Am. A **10**, 2551–2562 (1993).
[12]O. P. Bruno and F. Reitich, "Calculation of electromagnetic scattering via boundary variations and analytic continuation," Appl. Comput. Electromagn. Soc. J. **11**, 17–31 (1996).
[13]O. P. Bruno and F. Reitich, "Boundary-variation solutions for bounded-obstacle scattering problems in three dimensions," J. Acoust. Soc. Am. **104**, 2579–2583 (1998).
[14]O. P. Bruno and F. Reitich, "High-order boundary perturbation methods," *Mathematical Modeling in Optical Science*, Frontiers in Applied Mathematics Series, Vol. **22** (SIAM, Philadelphia, PA, 2001), pp. 71–109.
[15]D. P. Nicholls and F. Reitich, "Shape deformations in rough surface scattering: Cancellations, conditioning, and convergence," J. Opt. Soc. Am. A **21**, 590–605 (2004).
[16]D. P. Nicholls and F. Reitich, "Shape deformations in rough surface scattering: Improved algorithms," J. Opt. Soc. Am. A **21**, 606–621 (2004).
[17]J. Cullen, "Surface currents induced on short-wavelength radiation," Phys. Rev. **109**, 1863–1867 (1958).
[18]V. Fock, *Electromagnetic Diffraction and Propagation Problems*, International Series of Monographs on Electromagnetic Waves Vol. **1** (Pergamon, Oxford, 1965).
[19]A. G. Voronovich, *Wave Scattering from Rough Surfaces*, 2nd ed. (Springer, Berlin, 1999).
[20]M. Charnotskii and V. Tatarskii, "Tilt-invariant theory of rough surface scattering," Waves Random Complex Media **5**, 361–380 (1995).
[21]O. Bruno, A. Sei, and M. Caponi, "High-order high-frequency solutions of rough surface scattering problems," Radio Sci. **37**, 1–13 (2002).
[22]F. Reitich and C. Turc, "High-order solutions of three-dimensional rough-surface scattering problems at high frequencies. I. The scalar case," Waves Random Complex Media **15**, 1–16 (2005).
[23]F. Reitich and C. Turc, "High-order solutions of three-dimensional rough-surface scattering problems at high-frequencies. II. The vector electromagnetic case," Waves Random Complex Media **15**, 323–337 (2005).
[24]O. P. Bruno, C. A. Geuzaine, J. A. Munro, and F. Reitich, "Prescribed error tolerances within fixed computational times for scattering problems of arbitrarily high frequency: The convex case," Philos. Trans. R. Soc. London, Ser. A **362**, 629–645 (2004).
[25]O. Bruno, C. Geuzaine, and F. Reitich, "A new high-order high-frequency integral equation method for the solution of scattering problems. ii: Multiple-scattering configurations," *Proceedings of the 20th Annual Review of Progress in Applied Computational Electromagnetics*, ACES, Syracuse, NY, April 2004.
[26]C. Linton, "The Green's function for the two-dimensional Helmholtz equation in periodic domains," J. Eng. Math. **33**, 377–402 (1998).
[27]L. Rayleigh, "On the dynamical theory of gratings," Proc. R. Soc. London, Ser. A **79**, 399–416 (1907).
[28]S. O. Rice, "Reflection of electromagnetic waves from slightly rough surfaces," Commun. Pure Appl. Math. **4**, 351–378 (1951).
[29]D. M. Milder, "An improved formalism for rough-surface scattering of acoustic and electromagnetic waves," Proc. SPIE **1558**, 213–221 (1991).
[30]D. M. Milder, "An improved formalism for wave scattering from rough surfaces," J. Acoust. Soc. Am. **89**, 529–541 (1991).
[31]D. M. Milder and H. T. Sharp, "Efficient computation of rough surface scattering," in *Mathematical and Numerical Aspects of Wave Propagation Phenomena*, Strasbourg, 1991 (SIAM, Philadelphia, PA, 1991), pp. 314–322.
[32]D. M. Milder and H. T. Sharp, "An improved formalism for rough surface scattering. ii: Numerical trials in three dimensions," J. Acoust. Soc. Am. **91**, 2620–2626 (1992).
[33]D. M. Milder, "Role of the admittance operator in rough-surface scattering," J. Acoust. Soc. Am. **100**, 759–768 (1996).
[34]S. N. Chandler-Wilde and B. Zhang, "Electromagnetic scattering by an inhomogeneous conducting or dielectric layer on a perfectly conducting plate," Proc. R. Soc. London, Ser. A **454**, 519–542 (1998).
[35]J. B. Keller and D. Givoli, "Exact nonreflecting boundary conditions," J. Comput. Phys. **82**, 172–192 (1989).
[36]F. Ihlenburg, *Finite Element Analysis of Acoustic Scattering* (Springer, New York, 1998).
[37]O. P. Bruno and F. Reitich, "Solution of a boundary value problem for the Helmholtz equation via variation of the boundary into the complex domain," Proc. R. Soc. Edinburgh, Sect. A: Math. **122**, 317–340 (1992).
[38]D. P. Nicholls and F. Reitich, "Analytic continuation of Dirichlet-Neumann operators," Numer. Math. **94**, 107–146 (2003).
[39]G. A. Baker, Jr. and P. Graves-Morris, *Padé Approximants*, 2nd ed. (Cambridge University Press, Cambridge, 1996).
[40]R. B. Melrose and M. E. Taylor, "Near peak scattering and the corrected Kirchhoff approximation for a convex obstacle," Adv. Math. **55**, 242–315 (1985).
[41]D. P. Nicholls and F. Reitich, "A new approach to analyticity of Dirichlet-Neumann operators," Proc. R. Soc. Edinburgh, Sect. A: Math. **131**, 1411–1433 (2001).

Experimental validation and applications of a modified gap stiffness model for granular marine sediments

Masao Kimura[a)]
School of Marine Science and Technology, Tokai University, 3-20-1 Orido, Shimizu-ku, Shizuoka, Shizuoka 424-8610, Japan

(Received 4 June 2007; revised 25 February 2008; accepted 3 March 2008)

The author has proposed a modified gap stiffness model, which is incorporated into the Biot model; the resultant model is called the BIMGS model. By using this model, it is theoretically demonstrated that the frame bulk modulus is dependent on frequency [M. Kimura, "Frame bulk modulus of porous granular marine sediments," J. Acoust. Soc. Am. **120**, 699–710 (2006)]. In this study, the modified gap stiffness model is reinvestigated and approximated expressions are derived for low- and high-frequency ranges. In particular, experimental validation of the BIMGS model is carried out. First, for glass beads and beach sands, the modified gap stiffness at a high frequency is experimentally obtained as a function of the grain size. Second, by using the measured values of the longitudinal wave velocities in the glass beads with two types of alcohol-water-mixed liquids, it is validated that the frame bulk modulus is a linear function of the fluid bulk modulus and that the frame bulk modulus is dependent on frequency, which can be derived from the BIMGS model. Finally, for applying the BIMGS model, it is shown that the reported velocity dispersion and the frequency dependence of attenuation, which cannot be explained by using the Biot-Stoll model with a constant frame bulk modulus, can be explained.
© *2008 Acoustical Society of America.* [DOI: 10.1121/1.2902179]

PACS number(s): 43.30.Ma [RR] Pages: 2542–2552

I. INTRODUCTION

Velocity dispersion in marine sediments is one of the important subjects that remains unresolved in the field of sediment acoustics.[1,2] The reported velocity dispersion is greater than the dispersion calculated by using the Biot-Stoll model with a constant frame bulk modulus.[1,3,4] Among the 13 physical parameters that are required by the Biot-Stoll model,[5–10] the value of the frame bulk modulus is one of the most difficult to estimate.[11] The author has proposed the BIMGS model (a modified gap stiffness model incorporated into the Biot model),[12] which is an improved version of Chotiros and Isakson's model.[13] In this model, the frame bulk modulus is the summation of the frequency-independent Hertz-Mindlin term and the frequency-dependent modified gap stiffness term, whose relaxation frequency is a function of the bulk modulus, viscosity of the fluid, and aspect ratio. That is, the frame bulk modulus in the BIMGS model is predicted to begin from a low-frequency asymptotic value and increase toward a high-frequency asymptotic value. Thus, the BIMGS model has been theoretically proposed. However, experimental validation of the model has not been carried out.

In this study, the BIMGS model is reinvestigated and approximated expressions are derived for the modified gap stiffness at low- and high-frequency ranges. In particular, the BIMGS model is experimentally validated. First, the modified gap stiffness at a frequency considerably higher than the relaxation frequency of it is experimentally obtained as a function of the grain size by using the measured results of the longitudinal wave velocities in the glass beads with 4 different kinds of grain sizes and 85 kinds of beach sands. In the BIMGS model, the frame bulk modulus at a high frequency is a linear function of the fluid bulk modulus, and the frame bulk modulus is dependent on frequency. The longitudinal wave velocities are measured in glass beads with two types of alcohol-water-mixed liquids with different viscosities and with different weight concentrations. Two types of alcohols—ethanol and methanol—with almost the same bulk moduli and with different ratios of the bulk modulus to the viscosity were used. By using these data sets, the BIMGS model was experimentally validated. Finally, for an application of the BIMGS model, it is shown that the reported velocity dispersion and the frequency dependence of the attenuation, which cannot be explained by using the Biot-Stoll model with a constant frame bulk modulus, can be explained by using this model.

In Sec. II, the BIMGS model will be reinvestigated and the expressions for the modified gap stiffness for low- and high-frequency ranges will be derived. In Sec. III, the modified gap stiffness at a high frequency will be experimentally obtained as a function of the grain size for glass beads and beach sands. Moreover, it will be experimentally validated that the frame bulk modulus is a linear function of the fluid bulk modulus and the frame bulk modulus is dependent on frequency. In Sec. IV, by using the BIMGS model, it will be shown that the reported velocity dispersion and the frequency dependence of attenuation can be explained. Finally, the paper will be concluded in Sec. V.

[a)]Present address: Poro-Acoustics Laboratory, 1115–11 Miyakami, Shimizu-ku, Shizuoka, Shizuoka 424–0911, Japan; Electronic mail: mk45@nifty.com

 0001-4966/2008/123(5)/2542/11/$23.00 © 2008 Acoustical Society of America

II. THE BIMGS MODEL

The BIMGS model has been developed by the author.[12] This model describes the acoustic relaxation due to the local fluid flow[14–16] in the gap between the grains. A porous grain contact has an effective normal stiffness. The effective normal stiffness k_n is the sum of the elastic stiffness of the solid-to-solid contact (contact stiffness) k_c and the effective stiffness of the contact gap (modified gap stiffness) k_g; this can be expressed as follows:

$$k_n = k_c + k_g. \tag{1}$$

The modified gap stiffness k_g is expressed as

$$k_g = \frac{\pi a^2 K_f}{h_0}\left(1 - \frac{1}{\frac{\kappa a}{2}\frac{J_0(\kappa a)}{J_1(\kappa a)}}\right), \tag{2}$$

where a denotes the contact radius, h_0 is the initial value of the gap separation distance, K_f is the fluid bulk modulus, and J_0 and J_1 are the Bessel functions of the first kind of the zeroth and first orders, respectively. κa is defined as follows:

$$\kappa a = \sqrt{-j2\pi\frac{f}{f_r}}, \tag{3}$$

where f_r is the relaxation frequency of the modified gap stiffness that is dependent on the bulk modulus K_f, viscosity η of the pore fluid, and the aspect ratio $\alpha(=h_0/a)$ as follows:[17]

$$f_r = \frac{1}{12}\frac{K_f}{\eta}\alpha^2. \tag{4}$$

The normalized modified gap stiffness k_{gn} is expressed as

$$k_{gn} = \frac{k_g}{k_{g\infty}} = 1 - \frac{1}{\frac{\kappa a}{2}\frac{J_0(\kappa a)}{J_1(\kappa a)}}\left(k_{g\infty} = \frac{\pi a^2 K_f}{h_0}\right). \tag{5}$$

The frequency characteristics of the normalized modified gap stiffness k_{gn} were investigated for low- and high-frequency ranges. At low frequencies $(f<2f_r)$, the normalized modified gap stiffness k_{gn} given in Eq. (5) can be approximated to the Maxwell model as follows:

$$k_{gn} = \frac{0.76}{1 - j\frac{f_r}{f}} \quad (f < 2f_r). \tag{6}$$

At high frequencies $(f>2f_r)$, the subsequent approximated expression

$$k_{gn} = 1 - \frac{0.925}{\left(\frac{\sqrt{\pi\frac{f}{f_r}}}{2} + \frac{1}{8}\right) + j\left(\frac{\sqrt{\pi\frac{f}{f_r}}}{2} - \frac{1}{8}\right)} \quad (f > 2f_r) \tag{7}$$

can be obtained by using the approximated expressions for the Bessel functions of the first kind of the zeroth and first orders[18] and fitting the coefficients of these equations for obtaining a better agreement between the approximated and exact values. A spring and dashpot model can be written for the modified gap stiffness k_g in each frequency range in Fig. 1. From this figure, it is observed that the Maxwell model can be applied for $f<2f_r$, that is, the loss factor is purely resistive. The factor of 0.76 in Eq. (6) appears in the BIMGS model for $f<2f_r$, under conditions in which the modified gap stiffness is normalized by that at an infinite frequency. However, the Maxwell model cannot be applied for $f>2f_r$. For $f>2f_r$, the frequency-dependent dashpot is replaced in parallel to the frequency-dependent spring k_η and dashpot η_g', that is, the loss factor is not purely resistive. The viscosity decreases and the elasticity increases with the frequency. At an infinite frequency, there is only the spring $k_{g\infty}(=\pi a^2 K_f/h_0)$, which means that the fluid has no time to flow in and out and the only compliant part of the gap is the bulk modulus of the fluid in the gap. The calculated results obtained by using the approximated equations [Eqs. (6) and (7)] are shown in Fig. 2. From this figure, it is observed that the calculated results obtained by using the approximated and exact equations are almost the same. The modified gap

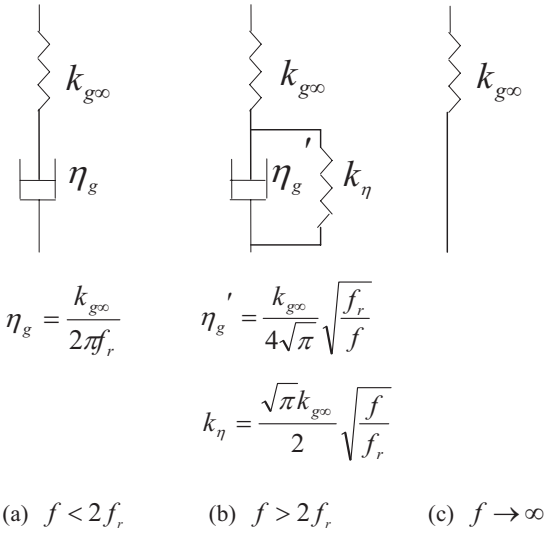


FIG. 1. Spring and dashpot models for the modified gap stiffness in each frequency. (a) Maxwell model for $f<2f_r$, (b) in series of the constant spring $k_{g\infty}$ and in parallel of the frequency dependent spring k_η and dashpot η_g' for $f>2f_r$, and (c) only the constant spring $k_{g\infty}$ for $f\to\infty$.

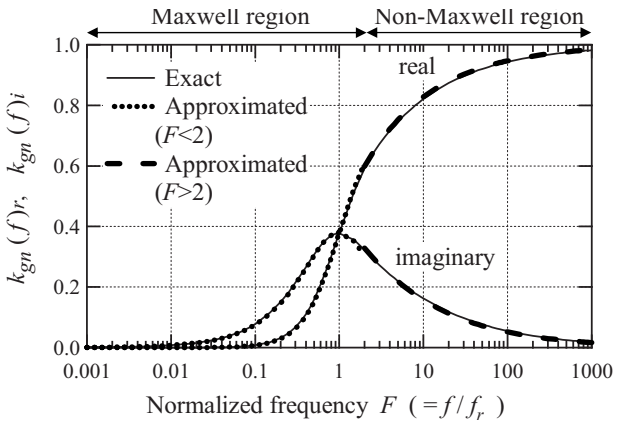


FIG. 2. Frequency dependence of the real and imaginary parts of the normalized exact and an approximated modified gap stiffness.

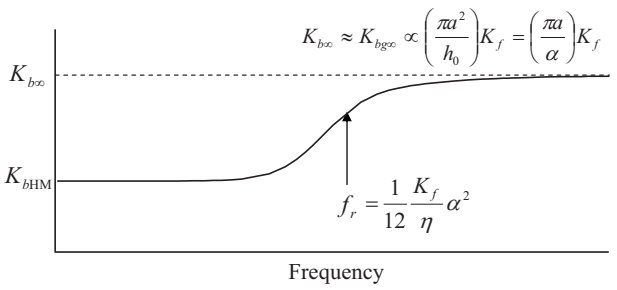


FIG. 3. Conceptual diagram of the frequency characteristics of the frame bulk modulus.

stiffness model is similar to the Maxwell model at a low frequency, except for the difference between the coefficients. However, the gap stiffness model is considerably different from the Maxwell model at high frequencies ($f > 2f_r$). In the Biot model with grain contact squirt flow and shear drag (BICSQS) model[13] in which the Maxwell model was used for the frame bulk modulus, there are no explicit physical parameters for the frame bulk modulus. On the contrary, there are some explicit physical parameters such as the bulk modulus, viscosity of the fluid, contact radius, and gap separation distance (or aspect ratio) for determining the frame bulk modulus in the BIMGS model.

The frame bulk modulus K_b is determined by the contact stiffness $k_c(\propto r)$ and gap stiffness k_g by using the following equation:[12]

$$K_b = \frac{C_n(1-\beta)}{12\pi r}(k_c + k_g) = \sqrt[3]{\frac{C_n^2(1-\beta)^2\mu_r^2}{18\pi^2(1-\sigma_r)^2}P} + \frac{C_n(1-\beta)}{12\pi r}k_g = K_{b\mathrm{HM}} + K_{bg}(f) = K_{b\mathrm{HM}} + (K_{b\infty} - K_{b\mathrm{HM}})k_{gn}, \tag{8}$$

where β denotes the porosity, C_n is the coordination number, r is the grain radius, μ_r is the shear modulus of the grain, σ_r is Poisson's ratio of the grain, and P is the hydrostatic confining pressure. Here, $K_{b\mathrm{HM}}$ is the frequency-independent term (Hertz-Mindlin term) and $K_{bg}(f)$ is the frequency-dependent term (gap stiffness term). A conceptual diagram of the frequency characteristics for the frame bulk modulus is shown in Fig. 3. In this figure, it is observed that the frame bulk modulus is predicted to begin from a low-frequency asymptotic value, $K_{b\mathrm{HM}}$, and increase toward a high-frequency asymptotic value, $K_{b\infty}$. The transition occurs over a frequency range that is approximately centered around the relaxation frequency.

III. VALIDATION OF THE BIMGS MODEL

A. Grain-size dependence of the modified gap stiffness of water-saturated glass beads and beach sands at a high frequency

The modified gap stiffness at a frequency considerably higher than the relaxation frequency of it cannot be theoretically determined as a function of the grain size. This relationship is experimentally studied by using the measured results of the longitudinal wave velocities in the glass beads with 4 different kinds of grain sizes and 85 kinds of beach sands at a high frequency by the author.[12]

The frame bulk modulus at a frequency considerably higher than the relaxation frequency of the modified gap stiffness can be approximated to

$$K_{b\infty} \approx K_{bg\infty} = \frac{C_n(1-\beta)}{12\pi r}k_{g\infty} = \frac{C_n(1-\beta)}{12\pi r}\frac{\pi a^2 K_f}{h_0}, \tag{9}$$

because the modified gap stiffness term at a high frequency $K_{bg\infty}(f)$ (the order of 10^9 Pa) is considerably higher than the Hertz-Mindlin term $K_{b\mathrm{HM}}$ (the order of 10^7 Pa). Therefore, the gap stiffness at a high frequency is expressed as follows:

$$k_{g\infty} = \frac{12\pi r}{C_n(1-\beta)}K_{bg\infty}. \tag{10}$$

The author measured the longitudinal wave velocities in 4 kinds of water-saturated glass beads with different grain sizes and 85 kinds of beach sands at the frequency of 500 kHz.[12] The grain size for a lowest ϕ is 0.78 mm and the wavelength at 500 kHz is approximately 4.0 mm. The ratio of the grain size to the wavelength at 500 kHz is about 1–5. Therefore, the grain sizes of most glass beads and sands are much smaller as compared to the wavelength at 500 kHz. The frame bulk modulus at a high frequency can be inverted by using the Biot model and the values of the longitudinal wave velocity and other Biot parameters, except the frame bulk modulus.[12] Subsequently, the modified gap stiffness at a high frequency is derived from the values of the frame bulk modulus at a high frequency $K_{bg\infty}$, grain radius r, porosity β, and coordination number C_n, which is expressed as[19,20]

$$C_n = 24.00\exp[-2.547\beta] - 0.3731. \tag{11}$$

The modified gap stiffness at a high frequency as a function of the grain size is shown in Fig. 4. Figures 4(a) and 4(b) show 4 kinds of water-saturated glass beads and 85 kinds of water-saturated beach sands, respectively. These figures show the strong grain-size dependence of the modified gap stiffness. The empirical equations of the modified gap stiffness at a high frequency as a function of the grain size are obtained as follows:

$$\log k_{g\infty} = 6.87 - 0.457\phi \rightarrow k_{g\infty} = (7.41 \times 10^6)d_m^{\,1.52} \quad \text{(for water-saturated glass beads)} \tag{12}$$

and

$$\log k_{g\infty} = 7.03 - 0.520\phi \rightarrow k_{g\infty} = (1.07 \times 10^7)d_m^{\,1.73} \quad \text{(for water-saturated beach sands, } N = 85\text{)}. \tag{13}$$

The difference between the results for the glass beads and sands shown in Fig. 4 and that between the empirical relationships in Eqs. (12) and (13) appears to exist due to the difference in the grain-size distribution of the sand and the shape of sand grains. From Eqs. (12) and (13), the following equations are obtained:

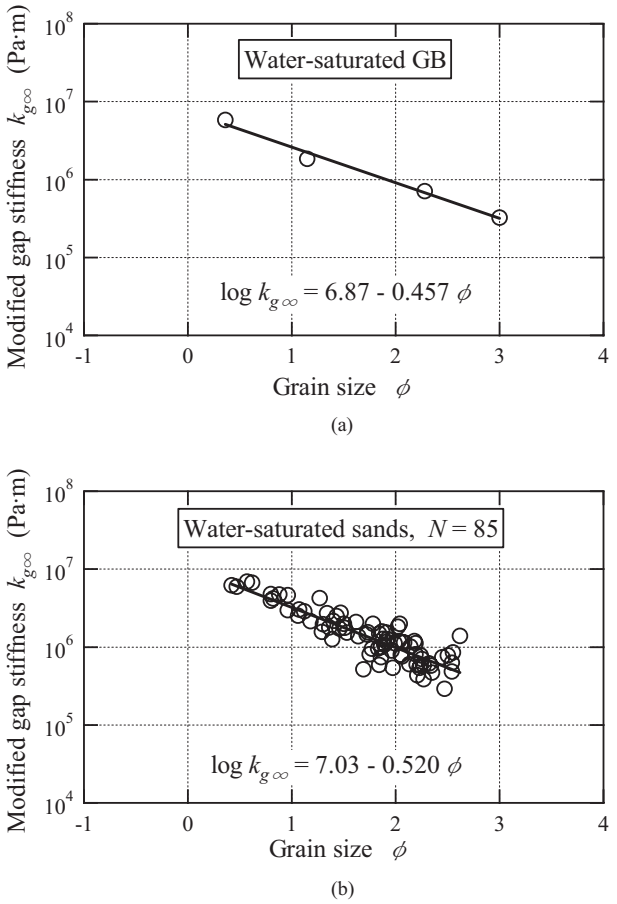


FIG. 4. Modified gap stiffness at a high frequency $k_{g\infty}$ as a function of the grain size ϕ for (a) water-saturated glass beads with 4 kinds of the grain sizes and (b) 85 kinds of water-saturated beach sands derived by the author's data.

$$\frac{a^2}{h_0} = \frac{a}{\alpha} \propto d_m^{1.52} \quad \text{(for water-saturated glass beads)} \quad (14)$$

and

$$\frac{a^2}{h_0} = \frac{a}{\alpha} \propto d_m^{1.73} \quad \text{(for water-saturated beach sands, } N = 85\text{)}. \quad (15)$$

Equations (14) and (15) indicate that the ratio of the gap radius to the aspect ratio exhibits grain-size dependence. In the future, it is necessary to investigate the grain-size dependence of the contact radius and the aspect ratio, separately.

Finally, the following equation can be obtained by using Eqs. (9), (12), and (13):

$$K_{bg\infty} \propto d_m^{0.52} \quad \text{(for water-saturated glass beads)} \quad (16)$$

and

$$K_{bg\infty} \propto d_m^{0.73} \quad \text{(for water-saturated beach sands, } N = 85\text{)}. \quad (17)$$

Thus, the frame bulk moduli of water-saturated glass beads as well as beach sands at a high frequency are expected to increase with the grain size.

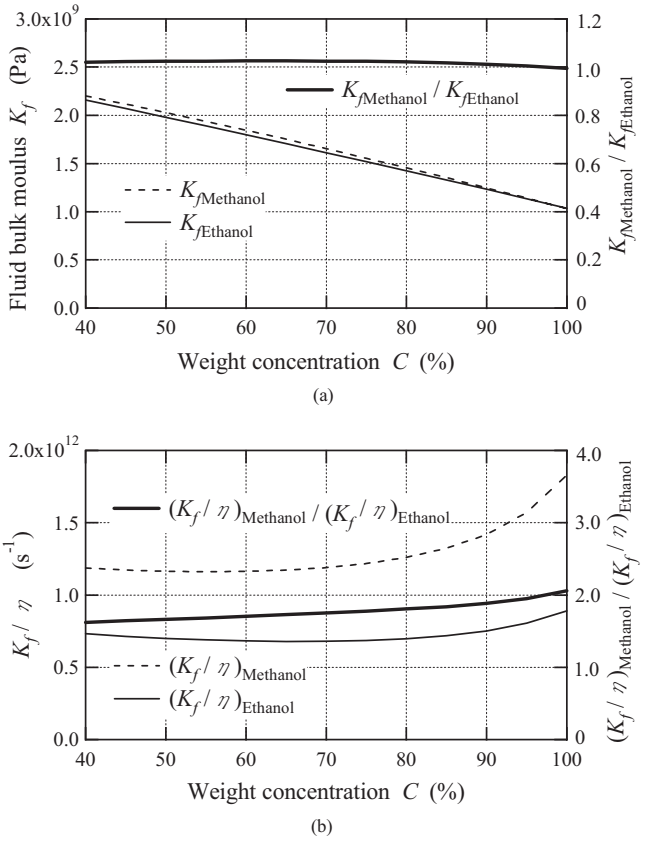


FIG. 5. (a) Fluid bulk modulus and (b) the ratio of the fluid bulk modulus to the viscosity of the mixed liquid as functions of the weight concentration of methanol and ethanol.

B. Fluid bulk modulus and frequency dependence of the frame bulk modulus

In the BIMGS model, the maximum value of the frame modulus is dependent on the contact radius a, gap separation distance h_0, and fluid bulk modulus K_f. Further, the relaxation frequency is dependent on the bulk modulus and viscosity η of the pore fluid and the aspect ratio α. Thus, the maximum value of the frame bulk modulus is a linear function of the fluid bulk modulus under the condition of the constant value of a^2/h_0, and the frequency characteristics of the frame bulk modulus are dependent on the relaxation frequency. Measurements of the frequency dependence of the frame bulk modulus using pore fluids with different bulk moduli and viscosities are necessary in order to confirm the validity of the BIMGS model. In this study, the glass beads saturated with two types of alcohols, ethanol- and methanol-water-mixed liquids, possessing a grain size of 0.192 mm were used for the measurements. The fluid bulk modulus and the viscosity of the alcohol-water-mixed liquid are dependent on the weight concentration of the alcohol. A liquid mixture of ethanol and water or methanol and water with a weight concentration ranging from approximately 50% to 100% was used for the pore fluids. The fluid bulk modulus and the ratio of the fluid bulk modulus to the viscosity of the mixed liquid as a function of the weight concentration are shown in Fig. 5. From this figure, it is observed that the relationships between the fluid bulk modulus and the weight concentration for methanol and ethanol are almost identical. However, the re-

lationships between the ratio of the fluid bulk modulus to the viscosity and the weight concentration for both the cases are considerably different. Therefore, it is expected that the maximum values of the frame bulk modulus are almost the same for both the mixed liquids; however, the relaxation frequencies are different in both the cases.

The author measured the longitudinal wave velocity in the glass beads saturated with the alcohol-water-mixed liquid by the time-of-flight method, which was also used in the previous measurements.[12] In the 500 kHz measurements, piezoelectric transducers with a resonance frequency of 500 kHz and a diameter of 2.54 cm were used for transmitting and receiving signals. A five-cycle sine wave pulse with a frequency of 500 kHz was used as the transmitting wave form. For the measurements, the depth was set to 30 mm in order to obtain the same stress condition. The external stress was hydrostatic.

The propagation distance was 40.2 mm. The longitudinal wave velocity is obtained by using the following equation:

$$c_l = c_w = \frac{1}{1 - \frac{\Delta t c_w}{d}} \rightarrow c_l = c_w \frac{1}{1 - \frac{\Delta t c_w}{d}} \tag{18}$$

where c_w(=1483 m/s) is the velocity in water at a temperature of 20 °C, d is the propagation distance, and $\Delta t = t_w - t_l$ (t_l, t_w=28.75 μs: propagation time in the sample and water at a temperature of 20 °C, respectively). For the measurements in the liquid-saturated samples, the removal of air in the sample is important. The alcohol-water-mixed liquid, which was degassed by vacuum deaeration for an hour, was poured into the vessels, and then the glass beads were carefully poured into the liquid little by little. The sample was deaerated again in the vacuum chamber for an hour. The measurements were conducted at a temperature of 20 °C in a constant temperature bath. The experimental vessel in which a sample was placed was vibrated by a vibrator for densely packing the sample. In the 50 kHz measurements, piezoelectric transducers with a resonance frequency of 50 kHz and a diameter of 3.8 cm were used for transmitting and receiving signals. A single-cycle sine wave pulse with a frequency of 50 kHz was used as the transmitting wave form. The depth for the measurement was again set as 30 mm and the external stress was hydrostatic. The propagation distance was 40.5 mm. The longitudinal wave velocity is obtained by using Eq. (18). In this case, the propagation time in water at a temperature of 20 °C, t_w, was 29.02 μs. The method used for deaeration was similar to that in the case of the 500 kHz measurements. The measurements were conducted at a temperature of 20 °C in a constant temperature bath. The experimental vessel in which a sample was placed was vibrated by a vibrator for densely packing the sample.

The measured results of the longitudinal wave velocity in the glass beads saturated with the alcohol-water-mixed liquid by the author are shown in Fig. 6. The frequencies for the measurements were 500 and 50 kHz. From Fig. 6, it is observed that the velocities at the frequency of 500 kHz are greater than those at 50 kHz for both the samples of glass

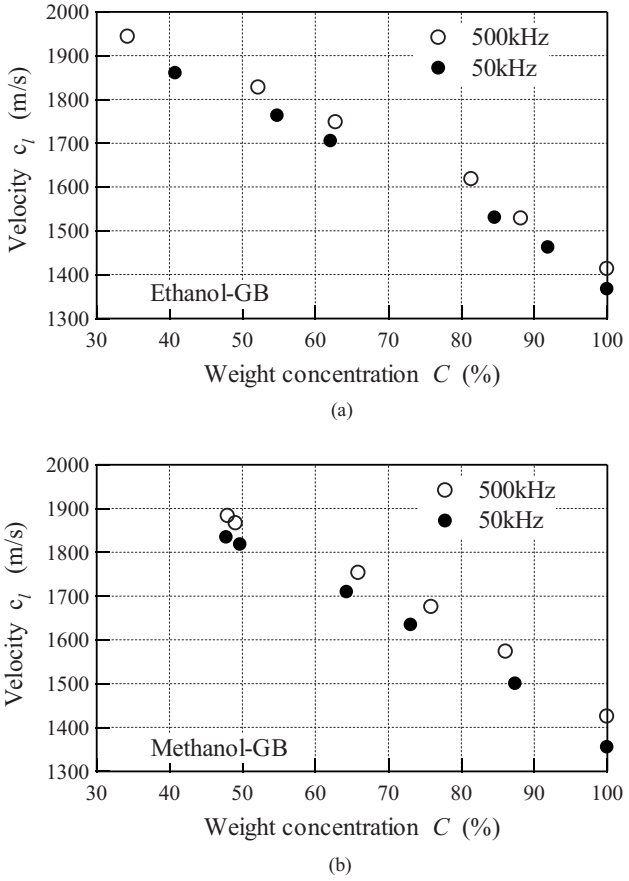


FIG. 6. Measured results of the longitudinal wave velocity in glass beads (GB) saturated with (a) ethanol- and (b) methanol-water-mixed liquids at the frequencies of 500 and 50 kHz by the author.

beads saturated with the alcohol-water-mixed liquid, and the velocities increase with a decrease in the weight concentrations for all the cases. The frame bulk modulus at a high frequency can be inverted by using the Biot model and the values of the longitudinal wave velocity and other Biot parameters, except the frame bulk modulus.[12] The inverted frame bulk modulus at 500 kHz as a function of the fluid bulk modulus by using the author's data is shown in Fig. 7. From this figure, it is observed that the frame bulk modulus is a linear function of the fluid bulk modulus for both the samples of glass beads saturated with the alcohol-water-mixed liquid. According to the BIMGS model, the maximum value of the frame bulk modulus is approximated, as shown in the following equation:

$$K_{bg\infty} \propto \frac{\pi a^2}{h_0} K_f. \tag{19}$$

The value of a^2/h_0 is considered to be a constant because the frame structure of the glass beads saturated with the alcohol-water-mixed liquid is considered to be the same for all the cases. Therefore, the results shown in Fig. 7 (K_b=0.748K_f for ethanol glass beads (GB) and K_b=0.781K_f for methanol GB) are consistent with those of the BIMGS model. The inverted frame bulk modulus at 50 kHz together with that at 500 kHz as a function of the fluid bulk modulus by using the author's data is shown in Fig. 8. In this figure, it is observed that the frame bulk modulus for ethanol GB at the frequency

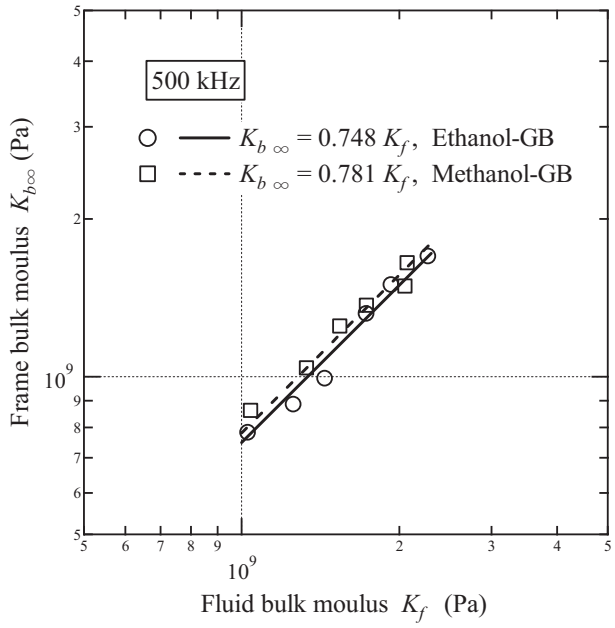


FIG. 7. Inverted frame bulk moduli at the frequency of 500 kHz as a function of the fluid bulk modulus for the glass beads with the ethanol- and methanol-water-mixed liquids by using the author's data.

of 50 kHz is larger than that for methanol GB. This is due to the difference in the ratios of the fluid bulk modulus to the viscosity. This ratio of ethanol is smaller than that of methanol. Therefore, the relaxation frequency for ethanol GB is lower than that for methanol GB. The frequency dependence of the frame bulk modulus for alcohol saturated glass beads with weight concentrations of 60%, 75%, and 90% inverted by using the author's data is shown in Fig. 9. In this figure, the circles and squares indicate the inverted values of the frame bulk modulus for both the samples of glass beads saturated with the alcohol-water-mixed liquid at 500 and 50 kHz,

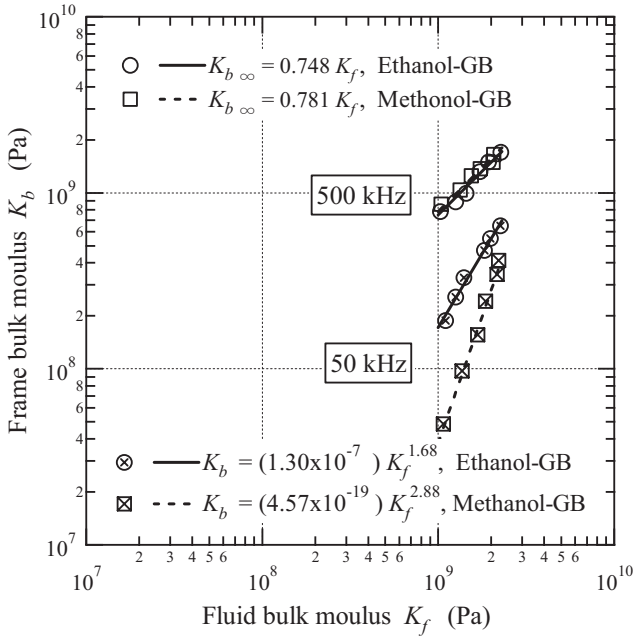


FIG. 8. Inverted frame bulk modulus at the frequencies of 500 and 50 kHz as a function of the fluid bulk modulus for the glass beads with the ethanol- and methanol-water-mixed liquids by using the author's data.

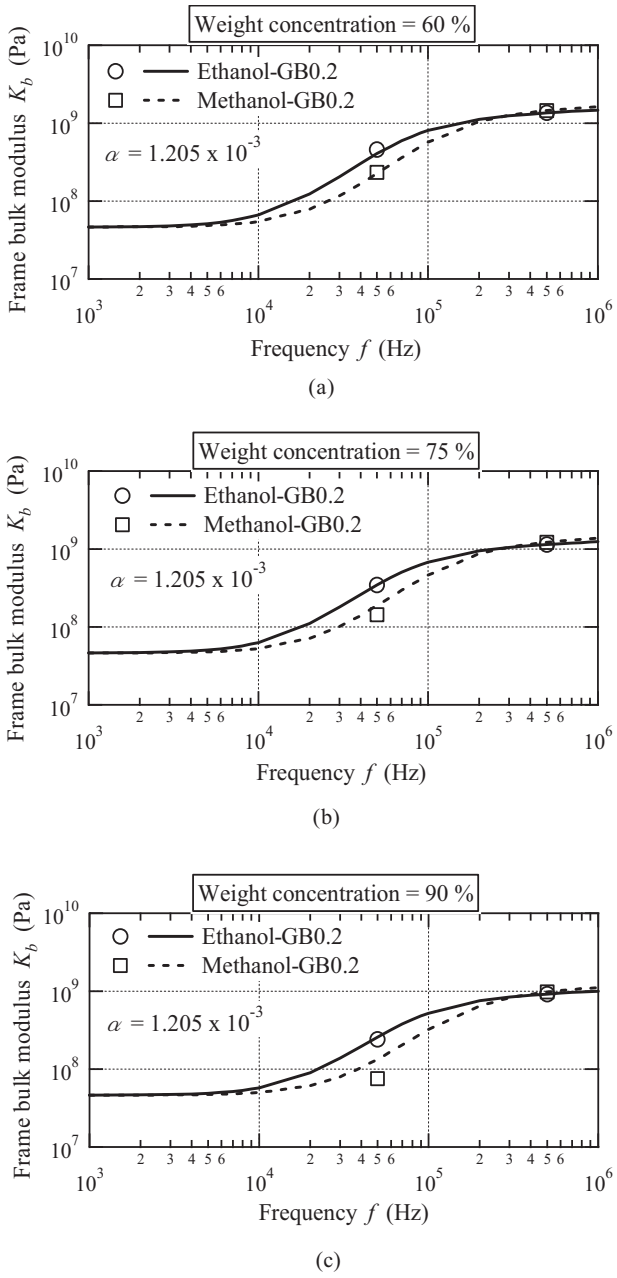


FIG. 9. Frequency dependence of the frame bulk modulus for the ethanol- and the methanol-saturated glass beads with the weight concentrations of 60%, 75%, and 90%. The circles and squares indicate the inverted values of the frame bulk modulus for the glass beads saturated with alcohol-water-mixed liquids at 500 and 50 kHz, respectively, by using the author's data. The solid and broken lines indicate the curves calculated for the glass beads saturated with ethanol- and methanol-water-mixed liquids for the aspect ratio α value of 1.205×10^{-3}, respectively.

respectively. The solid and broken lines indicate the calculated curves for the glass beads saturated with the ethanol- and methanol-water-mixed liquids with an aspect ratio α value of 1.205×10^{-3}, respectively. This value of the aspect ratio was selected by fitting the inverted values of the frame bulk modulus to the calculated values for the glass beads saturated with the ethanol-water-mixed liquid with a weight concentration of 75% at the frequencies of 500 and 50 kHz. The values of the parameters used in the calculation are shown in Table I. In Fig. 9, it is shown that the frame bulk modulus is constant at a low frequency, gradually increases

TABLE I. Values of parameters used for the calculation of the frame bulk modulus for glass beads saturated with alcohol-water-mixed liquid.

Grain	Diameter	d (mm)	0.192
	Density	ρ_r (kg/m^3)	2498
	Bulk modulus	K_r (Pa)	3.6×10^{10}
Pore fluid	Density	ρ_f (kg/m^3)	Measured
	Bulk modulus	K_f (Pa)	Inverted from the measured velocity
	Viscosity	η (Pa s)	Literature data
Frame	Porosity	β	0.362
	Permeability	k (m^2)	$k=\frac{d^2}{36k_0}\frac{\beta^3}{(1-\beta)^2}$ $(k_0=5)$[a]
	Pore size	a (m)	$a=\left(\frac{d}{3}\frac{\beta}{1-\beta}\right)$[a]
	Structure factor	α_t	1.25
	Shear modulus	μ (Pa)	μ (inverted using the measured c_s=59 m/s)
	Longitudinal logarithmic decrement	δ_l	0.15
	Shear logarithmic decrement	δ_s	0.15

[a]Reference 21.

at an intermediate frequency, and again becomes constant at a high frequency, as shown in Fig. 3. The inverted values of the frame bulk moduli are almost consistent with the calculated values. The frame bulk modulus of ethanol GB at 50 kHz is larger than that of methanol GB. This is because the relaxation frequency of ethanol GB is lower than that of methanol GB due to the difference in the values of K_f/η, as shown in Fig. 5.

IV. APPLICATIONS OF THE BIMGS MODEL

A. Velocity dispersion in air-saturated glass beads

First of all, the air-saturated case was investigated. The measured results of the frequency dependence of the longitudinal wave velocity in air-saturated glass beads with a grain size of 1.84 mm, which were obtained by Nomura *et al.*,[22] are shown in Fig. 10. A large velocity dispersion is observed in this figure. This dispersion cannot be explained by using a classical contact theory such as the Hertz-Mindlin model because there is no dispersion in the case of the Hertz-Mindlin model, as observed in Fig. 10. On the contrary, good agreement between the measured and calculated results can be achieved by using the BIMGS model. The values of the parameters used in the calculation are shown in Table II. This result implies that the elasticity of the air in the gap between the grains plays an important role in the determination of the frame bulk modulus, even in the case of air-saturated glass beads. In the author's previous study, the large grain-size dependence of the longitudinal wave velocity in air-saturated glass beads was obtained.[12] The velocity significantly increases with the grain size. First of all, it was assumed that this increase is due to the effect of some residual moisture at the grain contacts. Then, the velocity in the glass beads was measured after drying to remove the moisture. However, the results obtained were the same as those obtained before drying. Next, the velocity measurements were carried out in a vacuum chamber. The velocity decreases with the removal of air. The grain-size dependence in the vacuum-saturated case is relatively small (Fig. 8 in Ref. 12). From the above results, it is considered that the large velocity dispersion in Fig. 10 occurs due to the effect on the elasticity of air in the gap between the grains in the BIMGS model.

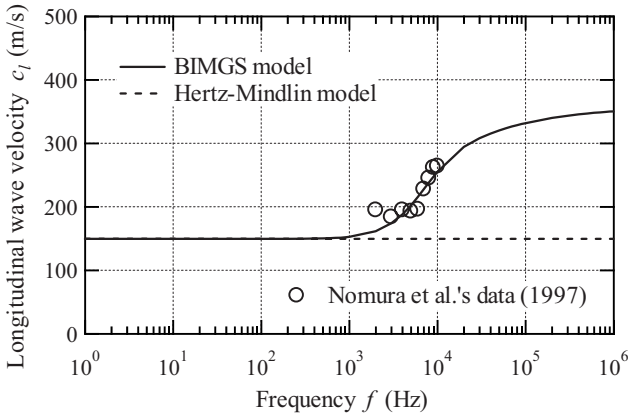


FIG. 10. Longitudinal wave velocity as a function of frequency for air-saturated glass beads with a diameter of 1.84 mm. The open circles indicate the data by Nomura *et al.* (Ref. 22), the broken line indicates the calculated result using the Hertz-Mindlin model, and the solid line indicates the calculated results using the BIMGS model for $K_{bHM}=2.70\times10^7$ Pa, $K_{bg\infty}=1.64\times10^8$ Pa, and $\alpha=3.76\times10^{-3}$.

TABLE II. Values of parameters used for the calculation of the longitudinal wave velocity for air-saturated glass beads.

Grain	Density	ρ_r (kg/m^3)	2492
Pore fluid	Density	ρ_f (kg/m^3)	1.21
	Bulk modulus	K_f (Pa)	1.43×10^5
	Viscosity	η (Pa s)	1.80×10^{-5}
Frame	Porosity	β	0.382
	Shear modulus	μ (Pa)	5.54×10^6
Hertz-Mindlin	Hertz-Mindlin bulk modulus	K_{bHM} (Pa)	2.70×10^7
BIMGS	Maximum of K_{bg} (f)	$K_{bg\infty}$	1.64×10^8
	Aspect ratio	α	3.76×10^{-3}

B. Velocity dispersion in water-saturated marine sediments

1. Turgut and Yamamoto's data

We investigate some velocity dispersion data that have been reported.[2,23,24] We begin by investigating Turgut and Yamamoto's data.[23] In their data, it is observed that there is a large dispersion at frequencies ranging from 1 to 27 kHz, as shown in Fig. 11. It is not possible to explain the dispersion data by using the Biot-Stoll model with a constant frame bulk modulus. If the calculated value of the velocity is adjusted to the measured value at a lower frequency by using a frame bulk modulus of 2.40×10^7 Pa, the measured and calculated values are found to be considerably different at a higher frequency, as shown in Fig. 11. On the contrary, if the calculated value of the velocity is adjusted to the measured value at a higher frequency by using a frame bulk modulus of 7.00×10^8 Pa, both the values are found to be considerably different at a lower frequency. Subsequently, the BIMGS model is applied for analyzing the dispersion data. The values of the parameters used for calculating the longitudinal wave velocity are shown in Table III. In Fig. 11, the calculated results obtained by using the BIMGS model are almost consistent with the measured results. Further, the frequency dependence of the attenuation is shown in Fig. 12. It includes Turgut and Yamamoto's data[23] and the calculated results. In this figure, it is observed that the calculated results obtained by using the BIMGS model are relatively consistent with the measured results.

2. SAX99 and SAX04 data

The SAX99 data obtained by Williams *et al.* provide excellent velocity dispersion and attenuation information.[2] Several researchers have measured velocity dispersion over a frequency range of 125 Hz–400 kHz and attenuation over a frequency range of 2.6–400 kHz for sand sediments. Almost all the physical parameters for the Biot-Stoll model could be obtained by *in situ* and laboratory measurements. The SAX99 dispersion data are shown in Fig. 13.[2] In this figure, a large dispersion is observed at frequencies ranging from 125 Hz to 400 kHz. At frequencies ranging from 1.7 to 400 kHz, the calculated results obtained by using the Biot-Stoll model with a constant frame bulk modulus is consistent with the measured results. However, an agreement between the calculated and measured results could not be obtained at low frequencies such as 125 and 400 Hz, which are indicated by the circles. The measured velocity is considerably low as compared to the calculated velocity obtained by using the Biot-Stoll model with a constant frame bulk modulus. Next, we attempted to adjust the fluid bulk modulus to match the measured results to the calculated results at a low frequency.[13] In this case, a good agreement could not

TABLE III. Values of parameters used for the calculation of the longitudinal wave velocity and attenuation for Turgut and Yamamoto's data.

			Constant K_b	BIMGS
Grain	Diameter	d (mm)	0.25	
	Density	ρ_r (kg/m^3)	2650	
	Bulk modulus	K_r (Pa)	3.6×10^{10}	
Pore fluid	Density	ρ_f (kg/m^3)	1000	
	Bulk modulus	K_f (Pa)	2.25×10^9	
	Viscosity	η (Pa s)	1.00×10^{-3}	
Frame	Porosity	β	0.44	
	Permeability	k (m^2)	1.75×10^{-11}	
	Pore size	a (m)	2.80×10^{-5}	
	Structure factor	α_t	1.25	
	Hertz-Mindlin bulk modulus	$K_{b\mathrm{HM}}$ (Pa)	7.00×10^8 2.40×10^7	2.40×10^7
	Shear modulus	μ (Pa)	2.40×10^7	
	Longitudinal logarithmic decrement	δ_l	0.15	
	Shear logarithmic decrement	δ_s	0.15	
BIMGS	Maximum of $K_{bg}(f)$	$K_{bg\infty}$	···	1.71×10^9
	Aspect ratio	α	···	2.50×10^{-4}

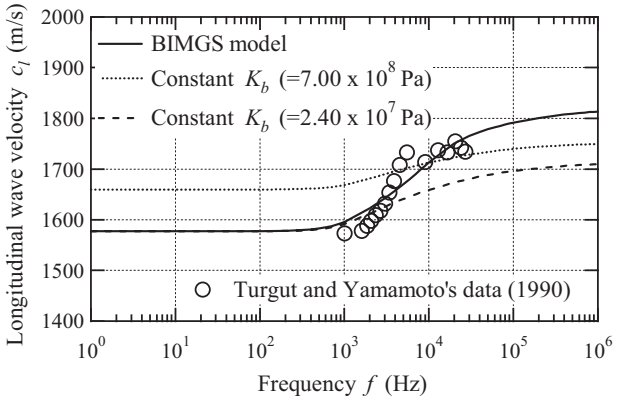


FIG. 11. Longitudinal wave velocity as a function of frequency for water-saturated marine sediments. The open circles indicate Turgut and Yamamoto's data (Ref. 23), the dotted and the broken lines indicate the calculated result using the Biot-Stoll model with a constant frame bulk modulus such as $K_b=7.00\times10^8$ and 2.40×10^7 Pa, respectively, and the solid line indicates the calculated results using the BIMGS model for $K_{b\mathrm{HM}}=2.40\times10^7$ Pa, $K_{bg\infty}=1.71\times10^9$ Pa, and $\alpha=2.50\times10^{-4}$.

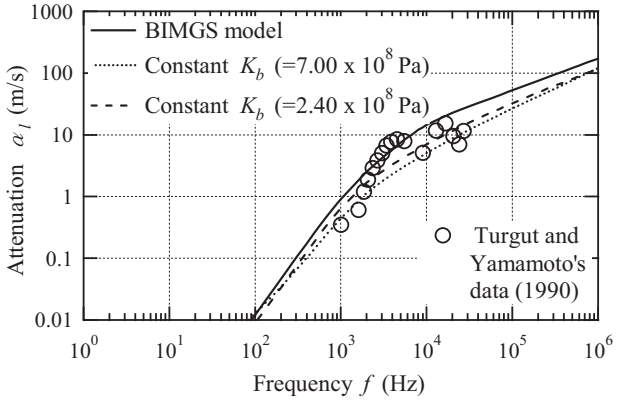


FIG. 12. Attenuation as a function of frequency for water-saturated marine sediments. The open circles indicate Turgut and Yamamoto's data (Ref. 23), the dotted and the broken lines indicate the calculated results using the Biot-Stoll model with a constant frame bulk modulus such as $K_b=7.00\times10^8$ and 2.40×10^7 Pa, respectively, and the solid line indicates the calculated results using the BIMGS model for $K_{b\mathrm{HM}}=2.40\times10^7$ Pa, $K_{bg\infty}=1.71\times10^9$ Pa, and $\alpha=2.50\times10^{-4}$.

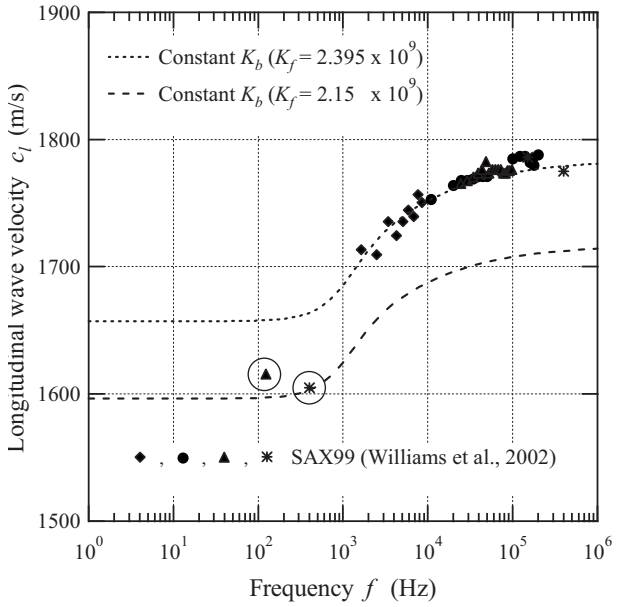


FIG. 13. Longitudinal wave velocity as a function of frequency for water-saturated marine sediments. Symbols indicate SAX99 data (Ref. 2) and the dotted and the broken lines indicate the calculated results using the Biot-Stoll model with constant frame moduli such as $K_f=2.395\times10^9$ and 2.15×10^9 Pa, respectively.

be obtained at a high frequency. Moreover, another SAX04 dispersion data set obtained by Hines *et al.*[24] is shown in Fig. 14 in conjunction with the SAX99 dispersion data set.[2] Further, a large dispersion occurs in the frequency range from 600 Hz to 20 kHz. We attempted to apply the BIMGS model to these dispersion data. Excellent agreement was achieved

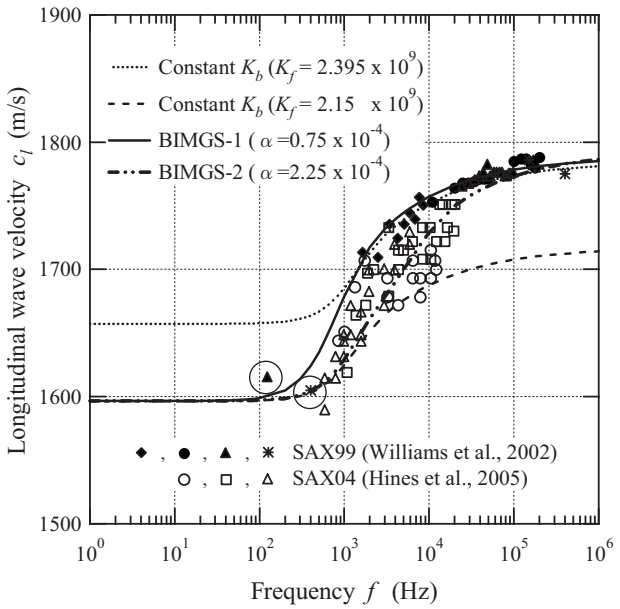


FIG. 14. Longitudinal wave velocity as a function of frequency for water-saturated marine sediments. Symbols indicate SAX99 (Ref. 2) and SAX04 data (Ref. 24). The dotted and the broken lines indicate the calculated result using the Biot-Stoll model with constant frame bulk moduli such as $K_f=2.395\times10^9$ and 2.15×10^9 Pa, respectively. The solid line indicates the calculated results using the BIMGS model for $K_{b\mathrm{HM}}=4.61\times10^7$ Pa, $K_{bg\infty}=1.24\times10^9$ Pa, and $\alpha=0.75\times10^{-4}$. The dashed and double-dotted lines indicate the calculated results using the BIMGS model for $K_{b\mathrm{HM}}=4.61\times10^7$ Pa, $K_{bg\infty}=1.31\times10^9$ Pa, and $\alpha=2.25\times10^{-4}$.

TABLE IV. Values of parameters used for the calculation of the longitudinal wave velocity and attenuation for SAX99 and SAX04 data.

			Constant K_b	BIMGS
Grain	Density	ρ_r (kg/m^3)	2690	
	Bulk modulus	K_r (Pa)	3.2×10^{10}	
Pore fluid	Density	ρ_f (kg/m^3)	1023	
	Bulk modulus	K_f (Pa)	2.395×10^9 / 2.15×10^9	2.15×10^9
	Viscosity	η (Pa s)	1.05×10^{-3}	
Frame	Porosity	β	0.385 / 0.37	0.37
	Permeability	k (m^2)	2.5×10^{-11}	
	Pore size	a (m)	2.85×10^{-5}	
	Structure factor	α_t	1.35	
	HM bulk modulus	$K_{b\mathrm{HM}}$ (Pa)	4.36×10^7	4.61×10^7
	Shear modulus	μ (Pa)	2.92×10^7	
	Longitudinal logarithmic decrement	δ_l	0.15	
	Shear logarithmic decrement	δ_s	0.15	
BIMGS	Maximum of K_{bg} (f)	$K_{bg\infty}$	...	1.24×10^9 / 1.31×10^9
	Aspect ratio	α	...	0.75×10^{-4} / 2.25×10^{-4}

between the measured SAX99 data and the calculated results with an aspect ratio of 0.75×10^{-4}. Further, the calculated result with an aspect ratio of 2.25×10^{-4} agrees relatively well with the SAX04 dispersion data. Several researches measured velocity and attenuation by some different methods; however, the data were obtained at a common location. Then, the author used the values of the Biot parameters for the SAX99 data, which were similar to the parameters used by Williams.[2] The environmental characteristics of the SAX04 data were assumed to be slightly different from those of the SAX99. However, the Biot parameters for the SAX04 data could not be obtained. Therefore, the author used the same values of the parameters for the SAX04 data as those used for the SAX99 data. Further, in order to match the data, two kinds of aspect ratios were used for the calculations for the SAX99 and SAX04 data. The values of the parameters used for calculating the longitudinal wave velocity are shown in Table IV. The measured attenuation as a function of the frequency[2] is shown in Fig. 15. The results calculated by using the BIMGS model ($\alpha=0.75\times10^{-4}$) almost agree with the measured results at frequencies ranging from 20 to 50 kHz. At frequencies below 10 kHz, the calculated values are larger than the measured values, which are similar to the values calculated for the Biot-Stoll model with a constant frame bulk modulus. On the other hand, at frequencies above 100 kHz, the values calculated by using the BIMGS model ($\alpha=2.25\times10^{-4}$) relatively agree with the measured values. Further investigations are required to understand the frequency dependence of the attenuation.

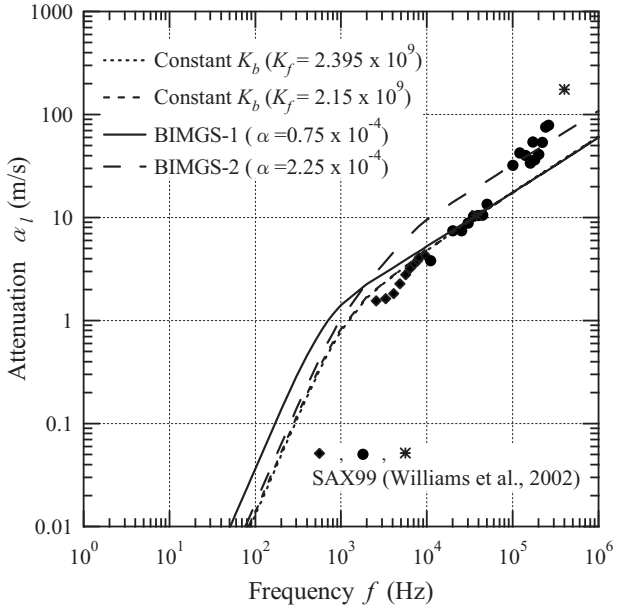


FIG. 15. Attenuation as a function of frequency for water-saturated marine sediments. Symbols indicate SAX99 data (Ref. 2) and the dotted and the broken lines indicate the calculated result using the Biot-Stoll model with constant frame bulk moduli such as $K_f=2.395\times10^9$ and 2.15×10^9 Pa, respectively. The solid line indicates the calculated results using the BIMGS model for $K_{b\mathrm{HM}}=4.61\times10^7$ Pa, $K_{bg\infty}=1.24\times10^9$ Pa, and $\alpha=0.75\times10^{-4}$. The dashed and double-dotted lines indicate the calculated results using the BIMGS model for $K_{b\mathrm{HM}}=4.61\times10^7$ Pa, $K_{bg\infty}=1.31\times10^9$ Pa, and $\alpha=2.25\times10^{-4}$.

V. CONCLUSIONS

In this study, the BIMGS model was reinvestigated and approximated expressions were derived for the modified gap stiffness at low- and high-frequency ranges. In particular, the BIMGS model was experimentally validated. First, the modified gap stiffness at a frequency considerably higher than the relaxation frequency of it was experimentally obtained as a function of the grain size by using the measured results of the longitudinal wave velocities in the glass beads with 4 different kinds of grain sizes and 85 kinds of beach sands. From the measured results, the gap stiffness at a high frequency was derived as a function of the grain size, that is, $k_{g\infty}=(7.41\times10^6)d_m^{1.52}$ for water-saturated glass beads and $k_{g\infty}=(1.07\times10^7)d_m^{1.73}$ for water-saturated beach sands. Moreover, it was validated that the modified gap stiffness at a high frequency is a linear function of the fluid bulk modulus and that the frame bulk modulus is dependent on frequency. Further, it was shown that the frame bulk modulus of ethanol-GB at 50 kHz was larger than that of methanol GB. This was because the relaxation frequency of ethanol GB was larger than that of methanol GB due to the difference in the values of K_f/η. Finally, for an application of the BIMGS model, it was shown that the reported velocity dispersion and the frequency dependence of the attenuation data, which were obtained from Turgut and Yamamoto's data and the SAX99 and SA04 data, could be explained.

ACKNOWLEDGMENTS

The author wishes to express his appreciation to Dr. Nicholas P. Chotiros of the Applied Research Laboratories, the University of Texas at Austin, for his valuable suggestions. The author is grateful to Professor Nicholas G. Pace and Dr. John C. Osler for presenting a proceedings and some papers to us. The author also thanks Ms. Nodoka Jinbo, who was a student in the School of Marine Science and Technology, Tokai University, during the year 2005, for her assistance in conducting the experiments.

APPENDIX

There are typographical errors in Eqs.(23) and (26) in Ref. 12. The corrected equations are as follows.

The normalized gap stiffness k_{gn} is expressed as follows:

$$k_{gn}=1-\frac{1}{\frac{\kappa a}{2}\frac{J_0(\kappa a)}{J_1(\kappa a)}}, \tag{23}$$

$$k_{gMn}=\frac{1}{1-j\frac{f_{rM}}{f}}. \tag{26}$$

[1]R. D. Stoll, "Velocity dispersion in water-saturated granular sediment," J. Acoust. Soc. Am. **111**, 785–793 (2002).
[2]K. L. Williams, D. R. Jackson, E. I. Thorsos, D. Tang, and S. G. Schock, "Comparison of sound speed and attenuation measured in a sandy sediment to predictions based on the Biot theory of porous media," IEEE J. Ocean. Eng. **27**, 413–428 (2002).
[3]M. Kimura, "Velocity dispersion in granular marine sediment," J. Acoust. Soc. Am. **111**, 2330 (2002).
[4]M. Kimura, "Velocity dispersion in water-saturated granular marine sediment," J. Acoust. Soc. Am. **120**, 3097 (2006).
[5]M. A. Biot, "Theory of elastic waves in a fluid-saturated porous solid. 1. Low frequency range," J. Acoust. Soc. Am. **28**, 168–178 (1956).
[6]M. A. Biot, "Theory of elastic waves in a fluid-saturated porous solid. 2. Higher frequency range," J. Acoust. Soc. Am. **28**, 179–191 (1956).
[7]M. A. Biot, "Mechanics of deformation and acoustic propagation in porous dissipative media," J. Appl. Phys. **33**, 1482–1498 (1962).
[8]M. A. Biot, "Generalized theory of acoustic propagation in porous dissipative media," J. Acoust. Soc. Am. **34**, 1254–1264 (1962).
[9]R. D. Stoll and G. M. Bryan, "Wave attenuation in saturated sediments," J. Acoust. Soc. Am. **47**, 1440–1447 (1970).
[10]R. D. Stoll, *Sediment Acoustics* (Springer-Verlag, Berlin, 1989).
[11]C. J. Hickey and J. M. Sabatier, "Choosing Biot parameters for modeling water-saturated sand," J. Acoust. Soc. Am. **102**, 1480–1484 (1997).
[12]M. Kimura, "Frame bulk modulus of porous granular marine sediments," J. Acoust. Soc. Am. **120**, 699–710 (2006).
[13]N. P. Chotiros and M. Isakson, "A broadband model of sandy ocean sediments: Biot-Stoll with contact squirt flow and shear drag," J. Acoust. Soc. Am. **116**, 2011–2022 (2004).
[14]W. F. MurphyIII, K. W. Winkler, and R. L. Kleinberg, "Acoustic relaxation in sedimentary rocks: Dependence on grain contacts and fluid saturation," Geophysics **51**, 757–766 (1986).
[15]J. Dvorkin and A. Nur, "Dynamic poroelasticity: A unified model with the squirt and the Biot mechanisms," Geophysics **58**, 524–533 (1993).
[16]J. Dvorkin, R. Nolen-Hoeksema, and A. Nur, "Squirt-flow mechanism: Macroscopic description," Geophysics **59**, 428–438 (1994).
[17]G. A. Gist, "Fluid effects on velocity and attenuation in sandstones," J. Acoust. Soc. Am. **96**, 1158–1173 (1994).
[18]*Handbook of Mathematical Functions*, edited by M. Abramowitz and I. A. Stegun (Dover, New York, 1970).
[19]G. Mavko, T. Mukerji, and J. Dvorkin, *The Rock Physics Handbook: Tools for Seismic Analysis in Porous Media* (Cambridge University Press, Cambridge, 1998).
[20]M. A. Zimmer, M. Prasad, G. Mavko, and A. Nur, "Seismic velocities of unconsolidated sands: Part 1—Pressure trends from 0.1 to 20 MPa," Geophysics **72**, E1–E13 (2007).
[21]J. M. Hovem and G. D. Ingram, "Viscous attenuation of sound in saturated

sand," J. Acoust. Soc. Am. **66**, 1807–1812 (1979).
[22]H. Nomura, T. Kamakura, and Y. Kumamoto, "Propagation characteristics of sound in granular material" (in Japanese), Proceedings of the Spring Meeting of the Acoustical Society of Japan (1997), pp. 1049–1050.
[23]A. Turgut and T. Yamamoto, "Measurements of acoustic wave velocities and attenuation in marine sediments," J. Acoust. Soc. Am. **87**, 2376–2383 (1990).
[24]P. C. Hines, J. C. Osler, J. Scrutton, and A. P. Lyons, "Time-of-flight measurements of acoustic wave speed in sandy sediments from 0.6–20 kHz," in *Boundary Influences in High Frequency, Shallow Water Acoustics*, edited by N. G. Pace and P. Blondel (University of Bath, Bath, 2005), pp. 49–56.

Fitting data, but poor predictions: Reverberation prediction uncertainty when seabed parameters are derived from reverberation measurements

Charles W. Holland[a)]
Applied Research Laboratory, The Pennsylvania State University, State College, Pennsylvania 16804

(Received 10 December 2007; revised 19 February 2008; accepted 20 February 2008)

For many decades, researchers have been developing inverse techniques for estimating seabed parameters from reverberation data, notably scattering strength. Generally, the angular dependence of the scattering kernel is unknown and is either solved for or assumed fixed. In either case, agreement is typically quite good between the measured reverberation and that modeled (by fitting scattering parameters). However, what are the resulting uncertainties in a reverberation prediction if the ocean or geometry changes? The main results of the paper are that (1) these prediction uncertainties are surprisingly large, of order 10 dB at 10 km and thus (2) traditional/current methods for reverberation inversion should be augmented, mitigating the large prediction uncertainties by an additional measurement. Several options for additional measurements are discussed.
© *2008 Acoustical Society of America.* [DOI: 10.1121/1.2897037]

PACS number(s): 43.30.Pc, 43.30.Gv, 43.30.Ma, 43.30.Vh [RCG] Pages: 2553–2562

I. INTRODUCTION

Predicting acoustic reverberation in a shallow water waveguide is an important problem for facilitating operation of active sonar. One of the quantities of interest is the predicted time decay of the received signal, sometimes called diffuse reverberation. Contributions to diffuse reverberation can originate from the sea surface, the ocean volume (i.e., bubbles or biologics), or the seabed (interface and/or subbottom structure). In shallow water regions, it is often the seabed that controls the reverberation decay and in this paper we focus on the seabed contributions to diffuse reverberation at low to midfrequencies (nominally 500–5000 Hz).

In order to predict diffuse reverberation in situations where the seabed contributions dominate, the seabed scattering kernel and the reflection coefficient (or equivalently the geoacoustic parameters) must be known. In an area without prior measurements, these are generally poorly known, thus predictions of diffuse reverberation in forward areas are expected to be quite poor. Ostensibly, one way to improve this state of affairs is to conduct long-range reverberation measurements in areas of interest and invert for the reflection coefficient and scattering kernel. Such measurements can be performed in a survey mode, or alternatively by using the very sonar system for which one wishes to make a prediction (this latter method is sometimes called "through the sensor" or "rapid environmental assessment"). Due to the considerable potential of such methods, a significant amount of work has been done on the inverse problem, i.e., to estimate the scattering kernel and/or reflection coefficient from reverberation data (e.g., Refs. 1–10, not intended to be exhaustive).

The objective of this paper is not to explore another inverse method, but rather to quantify the uncertainties in reverberation prediction that remain after a survey measurement (beyond this point we make no distinction between survey methods and rapid environmental assessment or through the sensor methods, since the uncertainties discussed here arise from all these methods). One of the reasons it is useful to study uncertainty is because it can help identify particular parameters that tend to drive the uncertainty; measurement assets can then be focused on those particular parameters. The total uncertainty of the reverberation prediction depends upon a variety of factors, including the uncertainty in the seabed parameters and how well the ocean environment (sound speed profiles, air–sea roughness, biologics, bubbles, etc.) is known during the survey measurement. However, here we ignore the latter uncertainties and ask "what are the prediction uncertainties if the ocean (above the seabed) is perfectly known?"[11]

After a brief review of the theory of reverberation in a waveguide (Sec. II), a simple example is provided to illuminate the issues associated with the large prediction uncertainties. Section III then explores more realistic examples of how uncertainties in the scattering kernel lead to reverberation prediction uncertainties. These uncertainties are examined under various environmental conditions in order to both determine the environmental dependencies and provide insight into ways of mitigating those uncertainties. Sediment reflection coefficient uncertainties (addressed in Sec. IV) are shown to have a smaller impact on the total uncertainty than scattering kernel uncertainty. The principal findings are discussed and summarized in the final section.

II. THEORY

In a range-independent waveguide with an arbitrary sound speed profile, the incoherent monostatic reverberation can be written (e.g., Refs. 12 and 13)

[a)]Electronic mail: holland-cw@psu.edu

$$I = I_0 \frac{4\gamma c\tau}{r\ 2} \int_0^{\theta_c} \int_0^{\theta_c} R(\theta_H)^{2r/r_c(\theta)} \frac{\cos\theta}{r_c(\theta)\sin\theta_H} M(\theta_H, \phi_H)$$

$$\times R(\phi_H)^{2r/r_c(\phi)} \frac{\cos\phi}{r_c(\phi)\sin\phi_H} d\theta d\phi, \quad (1)$$

where I_0 is the source intensity; r is range; r_c is cycle distance; γ is the horizontal beamwidth of the source or receiver; c is the sound speed; τ is pulse length; θ_c is the critical angle; R is the magnitude of the seabed plane wave pressure reflection coefficient; H is water depth; and M is the seabed scattering kernel which depends upon source and receiver vertical angles, θ and ϕ. The subscript H indicates angles at depth H, i.e., at the water–seabed interface.

The main assumptions are that: there are many modes, i.e., $kH \sin\theta_c/\pi \gg 1$, where k is the wave number; the receiver is many water depths from the source, i.e., $r/H \gg 1$; the single scatter approximation is valid, i.e., that there is only reflection at each forward bounce and only one scatter back to the receiver; and geometric dispersion can be ignored (typically has a small effect, less than about 1 dB). Lloyd mirror effects (i.e., when source/receiver are close to the boundaries) are ignored and source receiver are assumed to be omnidirectional. Finally, we impose certain assumptions about the environment: that the sea surface is a flat pressure release boundary; the water column is lossless; and that the scattering arises only from the seabed and is independent of azimuth. The environmental assumptions, the omnidirectionality for source/receiver, and proximity to the boundary (e.g., Ref. 14) could be easily removed, but are not limiting for this study.

Although R and M in Eq. (1) are completely general, it is helpful for the goals of the study to treat them simply, in a way that can be readily parametrized. With this in mind, consider a sediment half-space with a reflection coefficient calculated from nominal geoacoustic properties (see Table I) and an empirical scattering kernel,

$$M(\theta, \phi) = \mu \sin^m(\theta) \sin^m(\phi) \quad (2)$$

with a scattering strength parameter μ and an angular dependence parameter m (reciprocity requires the incoming and outgoing angle dependence to be identical). We could easily consider more complicated models, i.e., with layers and scattering arising from the subbottom volume and/or various layer roughnesses, but this level of detail may obscure the main points of the paper without changing the conclusions. What is important here is that the R and M are reasonably realistic,[15] even if simple. We also state up front that since we do not expect Eq. (2) to be representative of all possible scattering kernels, our estimates of reverberation uncertainties will not necessarily represent upper bounds.

TABLE I. Geoacoustic model for the case where geoacoustic properties (or equivalently the seabed reflection coefficient) are known *a priori* (see Figs. 1–5).

Sound speed (m/s)	Attenuation (dB/m/kHz)	Density (g/cm^3)
1600	0.5	1.8

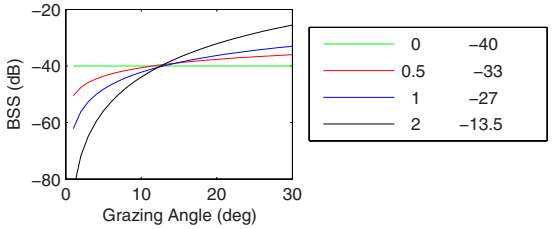


FIG. 1. (Color online) Various scattering kernels used in the study [the backscattering strength $\mathrm{BSS} = 10\log M(\theta, \theta)$]. The parameters m and $10\log\mu$ [see Eq. (2)] are given in the first and second columns of the legend, respectively.

In addition to simple scattering kernels, we also consider simple, i.e., linear, sound speed profiles (SSP) in the water column.

III. UNCERTAINTIES ASSOCIATED WITH THE SCATTERING KERNEL

We assume in this section that the ocean environment including the seabed reflection coefficient (or equivalently the geoacoustic properties) is perfectly known, except for the scattering kernel. Thus, the only uncertainties are due to the unknown seabed scattering kernel. An unbiased monostatic reverberation "survey" measurement is made and those data are employed to estimate the seabed parameters μ and m, Eqs. (1) and (2). Our intent is to determine the impact of the environmental uncertainties associated with estimating those parameters on the prediction of reverberation at future times (i.e., different sound speed profile and/or geometry).

The fundamental issues that lead to uncertainties are that (1) there is a limited angular range over which the scattering kernel can be observed and (2) there are many possible scattering kernels that can fit the observations (e.g., Ref. 16). For sake of argument, consider a situation where the reverberation is only sensitive to a single angle, say at 13°. In this case, any one of the scattering kernels in Fig. 1 could be used to accurately model the reverberation data (all the scattering kernels have the same value at 13°). Imagine for example that the true scattering kernel had a dependence of $m=0.5$, but that the model used to fit the data assumed $m=2$. Now consider the same seafloor region, but the sound speed profile and/or the source/receiver depths have changed so that the reverberation is only sensitive to scattering at 7°. The reverberation (using the scattering strength parameters derived from the measurements) would underpredict the true reverberation by 8 dB (the difference in scattering strengths between the two models at 7°).

This is a simplistic example. Generally, reverberation probes a distribution of angles (an exception would be a single propagating mode). The shape of the angular distribution is a function of the reflection coefficient, the SSP, the source–receiver depths and range. In the following, the bias errors associated with the unknown scattering kernel are examined using Eq. (1) for more realistic situations than the above-noted example. The cycle distance is obtained by ray theory, and the integral is evaluated numerically using Simpson's rule. The integrand, in general, is very well behaved, i.e., smoothly varying. Some care though is required in prop-

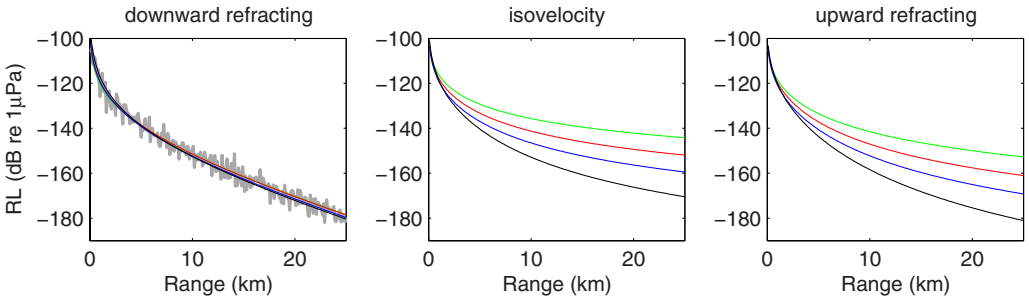


FIG. 2. (Color online) Reverberation predictions ($RL=10\log I$) for various sound speed profiles. The leftmost plot shows synthetic survey reverberation "data" (gray line) along with fits to the data using four scattering kernels shown in Fig. 1. The center and right-hand plots show reverberation predictions using the same scattering kernels under different sound speed profiles. The sound speed gradients from left to right are −0.3, 0, and 0.2. In the simulation the water depth is 100 m, sediment properties are given in Table I, and source/receiver depths are 10 m.

erly sampling the integrand for upward refracting cases at angles near the onset when the ray first interacts with the seabed.[17]

In Secs. III A and III B we consider bias errors if the sound speed profile during the survey measurement is (a) downward refracting and (b) isovelocity.

A. Bias errors in reverberation prediction: Downward refracting in survey

Consider a reverberation survey measurement conducted with a downward refracting profile with a gradient of $-0.3\ \mathrm{s}^{-1}$. Water depth is 100 m and the seabed properties are given in Table I. "Measured" (synthetic) data are shown in the gray line of Fig. 2(a) which were generated using $m=0.5$ summed with a zero-mean Gaussian distribution with a standard deviation of 3 dB. The synthetic data here and in the following sections are not frequency specific, but could apply to any frequency in the band of interest. A common method is to fit the data assuming a particular scattering kernel. Here we fit the data [Fig. 2(a)] using the four (out of an infinite number of possible) scattering kernels shown in Fig. 1. Note that all of the scattering kernels (see Table II) fit the data approximately equally well.

We can understand the reason why the ostensibly disparate scattering kernels fit the data by considering the angular distribution of the scattered intensity [i.e., the integrand of Eq. (1)]. The angular distribution depends somewhat on range,[18] but is approximately a truncated Gaussian with the main contributions around 13° [see Fig. 3(a)]. Since the scattering kernels all have similar levels near this angle (Fig. 1), the reverberation is also nearly the same [Fig. 2(a)] and in the absence of other information, it would be impossible to distinguish which (if any) of the models was the "correct" one. This is a specific example of the fundamental issue discussed previously, i.e., there is often a limited range of angles probed in reverberation measurements and thus many scattering kernels can be made to fit the data.

TABLE II. Scattering kernel possibilities for the case where geoacoustic properties (or equivalently the seabed reflection coefficient) are known *a priori*, but the scattering kernel is unknown (see Figs. 1–5).

m	$10\log(\mu)$
0	−40
0.5	−33
1	−27
2	−13.5

If the ocean and the source–receiver geometry were constant for all time, obviously each one of the four seabed parameter solutions would predict the reverberation equally well and there would be no need to inquire which one was correct. In reality (at least for database considerations), it is important to make predictions under changing ocean (SSPs) and geometries. At first blush one might be tempted to calculate the uncertainty associated with the reverberation prediction, simply by using the uncertainty associated with the estimate of μ. The uncertainty associated with any one of the scattering kernels would be a few decibels, and thus, one might conclude the total estimated prediction uncertainty would be a few decibels (the scattering strength parameter is a simple multiplier to the intensity). However, this method of predicting uncertainty severely underestimates the true uncertainties. The predicted uncertainties must take into account a wide variety of possible parametrizations, e.g., scattering kernels. This is done in the following paragraphs, showing how the predicted uncertainties evolve under changing ocean profiles and changing geometries.

1. Bias errors due to changing sound speed profile

Figure 2(b) shows reverberation predictions if the sound speed profile changed to isovelocity. The difference in the various curves is a measure of the prediction uncertainty associated with the uncertainty of the scattering kernels chosen. Recalling that the correct underlying scattering dependency was $m=0.5$; if it were erroneously assumed $m=1$ (Lambert's law) the resulting prediction would be 7 dB too low at 20 km. If one assumed $m=2$ or $m=0$, the resulting predictions at 20 km would be 16 dB too low or 7 dB too high, respectively. Figure 2(c) shows the bias errors if the SSP changes from downward to upward refracting where the results are similar (i.e., large bias errors) to the isovelocity case. The key point is that even with a reverberation measurement, the bottom properties that were extracted from it might only be useful when the SSP was similar to that of the original measurement, unless there was supplemental information about the nature of the scattering kernel.

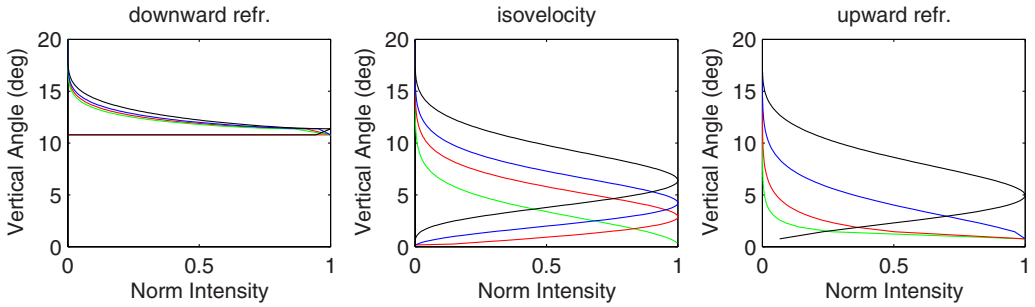


FIG. 3. (Color online) Vertical angle distributions for the reverberation of Fig. 2 at 10 km, normalized to the maximum value.

2. Bias errors due to changing source–receiver depths

Bias errors are also expected for changes in source–receiver depths (since the angular distribution on the seabed is a function of source–receiver depth). For example, the impact of changes in the source–receiver depths (monostatic) on the reverberation is shown in Fig. 4. The total spread in biases at 20 km at 90 m depth is about 12 dB. More complicated and larger errors due to changes in sound speed profile and source–receiver depths are possible. We wish first, though, to show the order of magnitude effects that might occur for separate environment and geometry changes.

It is of interest to quantify the bias error bounds as a function of sound speed gradient and source–receiver depth (see Fig. 5). Bias error bounds are defined here as the difference in reverberation from $m=0$ and $m=2$ at 10 km. The range of 10 km is somewhat arbitrary while the bounds of m are based on observations, theory, and current practice. At the upper end, $m=2$ is predicted at low angles by perturbation theory;[19] and is also observed in data at higher angles (e.g., Ref. 20, Fig. 25, Site 3, 10°–20° at 1200 Hz, 1800 Hz, where $m\sim 1.8$). For the lower bound, $m=0$ was chosen because theory predicts that the scattering can be approximately independent of angle over limited angle regions (e.g., see Fig. 4 of Ref. 21); it is also observed in data in some angular regimes (e.g., Ref. 20, Fig. 25, Site 2, below 1800 Hz) and $m=0$ is used in some reverberation inversion approaches (e.g., Refs. 1, 5, and 8).

Examining first the black line of Fig. 5(a) (same sediment parameters of Fig. 2), note that as the SSP changes from that applicable during the observation (in this case downward refracting), the errors rapidly increase to peak at isovelocity and then are roughly constant. We can understand this behavior by appealing to Figs. 3 and 1. As the sound speed gradient increases (away from that in the survey measurement, $-0.3\ \mathrm{s}^{-1}$), the dominant angles at the seabed decrease, and the difference in the respective scattering kernels increase (see Fig. 1). For the isovelocity profile, the angles are in the neighborhood of zero degrees grazing. For increasing gradients (i.e., upward refracting), the angles change but not substantially—hence the relatively constant bias errors.

How do the errors depend on the reflection coefficient (or geoacoustic properties)? The gray line of Fig. 5 shows the bias errors where sediment attenuation is reduced by a factor of 5. The bias errors as a function of changing SSP [Fig. 5(a)] are smaller for the less lossy seabed, though the overall shape of the two curves are similar. The smaller bias errors are due to the fact that with smaller reflection losses, the angular distribution at the bottom is broader and pushed toward higher angles (see Fig. 6). Both of these effects when considered in view of the scattering kernels (Fig. 1) tend to reduce the total error. In other words, the scattering kernels integrated over the angular distribution of Fig. 6 have less disparity than the scattering kernels integrated over the narrower angular distribution of Fig. 3. Increasing/decreasing the sediment sound speed has a similar effect, i.e., decreasing/increasing bias errors, but maintaining the overall shape of the curve.

The sensitivity of bias errors to source-receiver depth is shown in Fig. 5(b). Note that errors monotonically increase with distance away from the survey measurement geometry. Also note that the sensitivity is the same for both geoacoustic models. This is because the angular distribution is not very sensitive to differences in the geoacoustic models. The sensitivity of the bias errors to source–receiver depth is greatest for the downward refracting environment [see Fig. 5(c)].

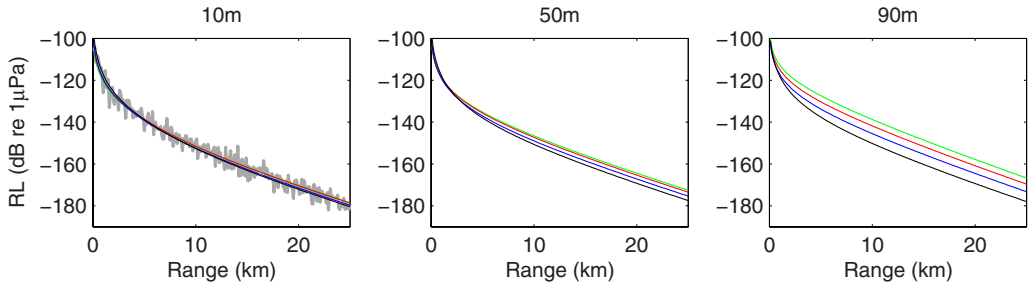


FIG. 4. (Color online) Reverberation for the four scattering kernels shown in Fig. 1 for various source–receiver depths; sound speed gradient is $-0.3\ \mathrm{s}^{-1}$.

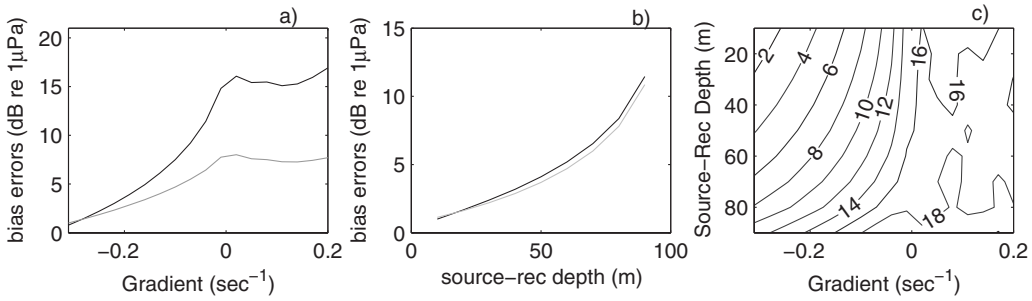


FIG. 5. Sensitivity of bias error bounds at 10 km range to: (a) sound speed gradient; (b) source–receiver depth; and (c) gradient and source–receiver depth (contours are bias errors in decibels). The black lines are errors where geoacoustic properties are given in Table I line; the gray lines are for an environment with a lower sediment attenuation (0.1 dB/m/kHz). Error bounds increase monotonically with range.

B. Bias errors in reverberation prediction: Isovelocity in survey

What happens if the survey measurement is conducted in isovelocity rather than in downward refracting conditions? "Measured" (synthetic) data from isovelocity conditions are shown in the gray line of Fig. 7 along with four scattering kernels that fit the data.

One salient point is that for isovelocity conditions there is a greater difference in the decay rates of the reverberation for the four scattering kernels than for downward refracting case [compare Fig. 7(a) with Fig. 2(a)]. Thus, if reverberation was measured over the entire 25 km as shown in Fig. 7, it would clearly be possible to eliminate several of the scattering kernels just based on the different decay rates. Imagine for the moment, however, because of high ambient noise and/or limited dynamic range, that reverberation could only be measured over ranges of 5–9 km. Over this limited range, all of the scattering kernels fit the data roughly equally well. In this case, the bias error bounds are very similar to those shown in Fig. 5(a) (with a shift in the curves so that the bias error of 0 is at isovelocity). If reverberation data were obtained over the entire range, and one could narrow the range of possible scattering kernel to say $0.5 \leqslant m \leqslant 1$, the error bounds at 10 km would be reduced from ~12 to ~4 dB. For the isovelocity case, the bias errors are zero with respect to changing source–receiver geometry since the incoherent field is independent of depth (except within a few wavelengths of the boundaries).

What happens if the survey measurement is conducted in upward refracting conditions? The results for the upward refracting case are similar to the isovelocity case, with the main difference being that the reverberation decay is even more distinct for the four scattering kernels. Thus, for a given set of reverberation versus range observations, and a perfectly known ocean with a smooth surface, the upward refracting case provides the greatest opportunity to minimize bias errors from the unknown scattering kernel. Also, the sensitivity of the bias errors to source–receiver depth is smaller than the downward refracting case.

In summary, the unknown scattering kernel can lead to substantial uncertainties in predicting reverberation for changing ocean conditions and/or changing source–receiver geometries. Bias errors as large as 10–18 dB were shown for simple, but not unrealistic cases.

IV. UNCERTAINTIES ASSOCIATED WITH THE REFLECTION COEFFICIENT

We now consider the case where the seabed scattering kernel is known, but the geoacoustic properties (or R) are unknown. Before examining specific cases, we point out that the range of reflection coefficients below the critical angle (supporting waveguide propagation) is much smaller than the range of scattering strengths at low angles. Thus, one might expect that the impact of an unknown reflection coefficient would tend to be less severe than the impact of an unknown scattering kernel. While we shall see that this is indeed the case, we note that while differences in R tend to be modest, those differences do get raised to the power $2r/r_c$ [see Eq. (1), where r/r_c is the number of bounces to the scattering patch] and so in principle might be significant.

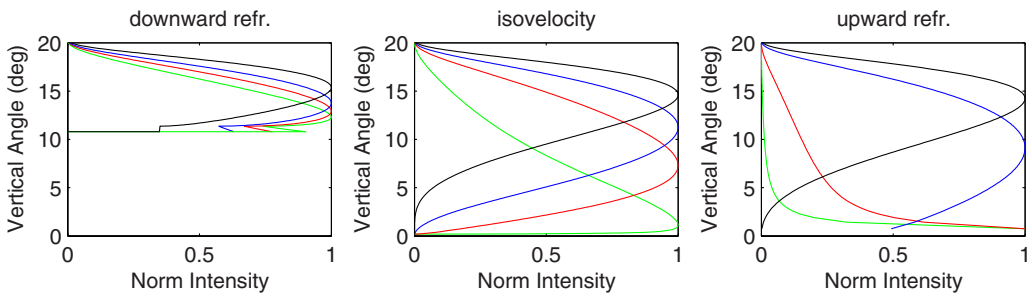


FIG. 6. (Color online) Normalized vertical angle distribution for the reverberation with attenuation of 0.1 dB/m/kHz. Note that the distributions include higher angles than in Fig. 3 due to less loss per bounce.

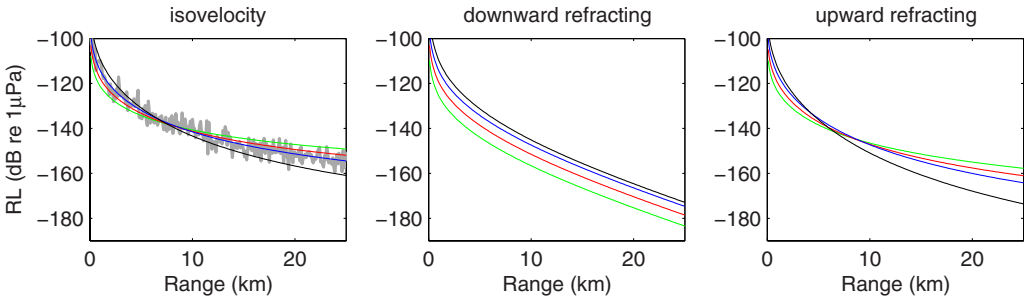


FIG. 7. (Color online) Reverberation predictions for various sound speed profiles. The leftmost plot shows synthetic survey reverberation data (gray line) along with fits to the data using four scattering kernels shown in Fig. 1. The center and right-hand plots show reverberation predictions using the same scattering kernels under different sound speed profiles. The sound speed gradients from left to right are 0, −0.3, and 0.2. In the simulation the water depth is 100 m, sediment properties are given in Table I, and source/receiver depths are 10 m.

A. Bias errors due to changed sound speed profile: Downward refracting in survey

In order to gain some insight, we examine a few specific cases. Three different reflection coefficients (corresponding to three geoacoustic models, see Table III) are shown in Fig. 8 that have similar levels at 13°. In our downward refracting environment with a gradient of $-0.3\ s^{-1}$, we expect [from Fig. 3(a)] that since the reverberation is dominated by angles near 13°, that the reverberation for all three reflection coefficients would be similar. The results of Fig. 9(a) show that indeed this is the case. Let us consider, as before, that any one of these curves could be a fit to a survey measurement. We are now interested in the uncertainties that occur if we make a prediction for a different SSP. The results of Figs. 9(b) and 9(c) indicate that the reverberation levels are similar for the three reflection coefficients under other SSPs; in other words, the uncertainty associated with the unknown reflection coefficient is rather small, on the order of a few decibels and nearly independent of range.

Why does uncertainty in the reflection coefficient (Fig. 9) lead to so much less uncertainty in reverberation than uncertainty in the scattering kernel (Fig. 2)? The answer is straightforward, inasmuch as the angles at the seabed for isovelocity and upward refracting sound speed profiles are all lower than that for the survey measurement (Fig. 3) and from Fig. 8 it is observed that the reflection coefficients are similar below 13°. Another way to say this is that the long-range reverberation in the mode stripping regime is not very sensitive to the individual geoacoustic properties, it is only sensitive to the slope of the reflection coefficient with angle (e.g., Refs. 2 and 22). Thus, there are an infinite number of reflection coefficients (or geoacoustic models) that could be used to fit the observations.

TABLE III. Three sediment half-space possibilities for the case when the scattering kernel is known *a priori* but the geoacoustic properties (or reflection coefficient) are unknown (see Figs. 8 and 9).

Sound speed (m/s)	Attenuation (dB/m/kHz)	Density (g/cm^3)
1600	0.5	1.8
1547	0.14	1.5
1670	1.0	2.0

It should be noted that the small uncertainties shown here do not necessarily represent the full range of possible uncertainties. For example, in fitting the data here we have assumed the "correct" parametrization, i.e., a half-space. If one were to assume, for example, that there was a sediment layer or layers, then the range of uncertainties associated with changing SSPs does indeed increase. However, some limited modeling (not shown) indicates modest and not dramatic increases in uncertainty, and much smaller uncertainties than seen for the scattering kernel in Sec. III.

The effect of changing geometry is similar to that of changing SSP, that is, the uncertainties are modest (a few decibels). The results here were calculated for a specific scattering kernel ($m=0.5$ and $10\log\mu=-33$ dB), however, the conclusions here are not sensitive to the particular scattering kernel chosen.

B. Bias errors due to changed sound speed profile: Isovelocity in survey

Since the reflection coefficients tend to be similar at low angles when fit to data, it does not matter very much whether the survey measurement is performed in downward refracting, isovelocity, or upward refracting conditions. All lead to similar (and modest) uncertainties.

However, we do comment that in the case where there is only a limited observation in range of the reverberation, the uncertainties could be significant. For example, consider a survey measurement of reverberation (isovelocity conditions) where because of noise and/or limited dynamic range, only ranges of 9–13 km could be observed. In this case, any

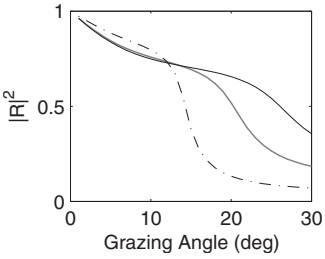


FIG. 8. Plane wave intensity reflection coefficients with similar levels at 13°. The geoacoustic models are in Table III [row 1 (gray line), row 2 (dash-dot), and row 3 (black)].

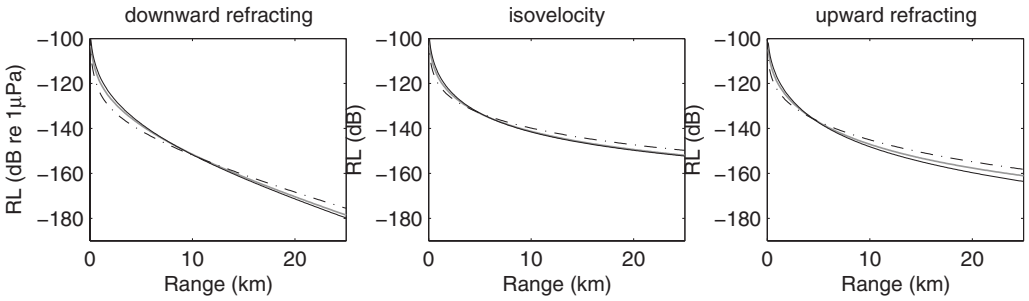


FIG. 9. Reverberation predictions for various sound speed profiles. The leftmost plot shows reverberation with the three reflection coefficients shown in Fig. 8 (with same line styles). The center and right-hand plots show reverberation predictions under different sound speed profiles. The sound speed gradients from left to right are −0.3, 0, and 0.2. In the simulation the water depth is 100 m, the sediment properties are provided in Table III, and source/receiver depths are 10 m.

one of the reflection coefficient curves of Fig. 10(d) could be made to fit the observations of Fig. 10(b). If predictions were made then under, say, downward refracting conditions [Fig. 10(a)], the errors at 10 km are about 6 dB.

C. Uncertainties associated with the reflection coefficient and the scattering kernel

In Sec. III, we showed that there was some advantage to conducting the survey measurement in an upward refracting or near isovelocity sound speed profiles when only the scattering kernel is unknown. Downward refracting gave the largest errors. It is of interest to determine whether this is true when both the scattering kernel and the reflection coefficient are unknown.

Fig. 11(a) shows fits to reverberation "data" for an upward refracting case in which both the scattering kernel and the reflection coefficient are unknown. The geoacoustic properties and scattering kernels are given in Table V. All of the sediment models fit the data reasonably well. If the SSP changes to downward refracting ($-0.3\ s^{-1}$), the predictions are shown in Fig. 11(b) where a very large spread in values (~60 dB at 10 km) is apparent. Thus, it is clear that if both the scattering kernel and reflection coefficient are unknown, there is no advantage to a particular SSP for the survey measurement.

Without attempting a complete treatment of prediction uncertainties in the case where both the scattering kernel and reflection coefficient are unknown, it suffices it to say that the error bounds can be quite large, many tens of decibels.

V. DISCUSSION AND CONCLUSIONS

A. Predicted uncertainties are large

The first and perhaps most important conclusion is that even in instances where a reverberation measurement is conducted, reverberation prediction uncertainties can be large when the sound speed profile changes or the source–receiver depths are different from that in the measurement. Uncertainties in reverberation prediction may be up to 18 dB at 10 km even when a measurement exists and everything is perfectly known about the ocean except the scattering kernel (which is obtained by fitting the data). Lossy bottoms (which have the

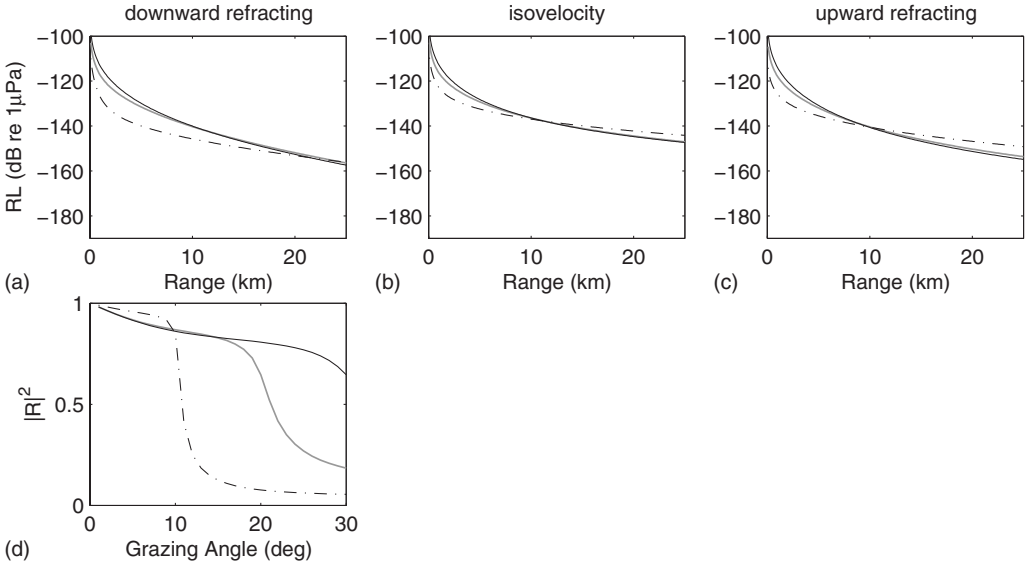


FIG. 10. (a)–(c) Reverberation predictions under various sound speed profiles and (d) reflection coefficients. The geoacoustic models for the reflection coefficients are given in Table IV.

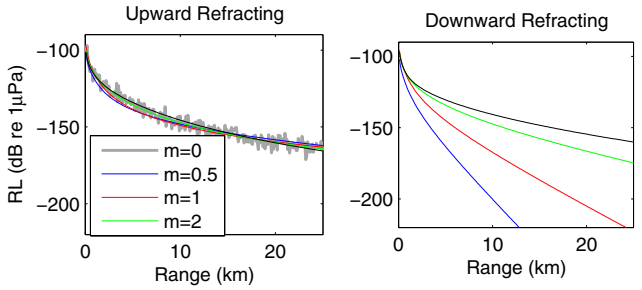


FIG. 11. (Color online) Example of no *a priori* knowledge of the scattering kernel or the reflection coefficient. "Synthetic" data (gray line) is compared with four scattering kernels (m=0, 0.5, 1, and 2) and variable reflection coefficients (see Table V) under upward refracting conditions in the left-hand plot. The right-hand plot shows predictions for the same four models if the sound speed profile changed to downward refracting ($-0.3\ s^{-1}$).

largest target echo-to-reverberation levels[22]) will generally have the largest bias errors from an unknown scattering kernel.

In realistic cases, the uncertainties are likely to be larger than predicted here since uncertainties, in the SSP, sea surface conditions, source/receiver calibrations, and seabed geoacoustic properties are not included in the order 10 dB uncertainties mentioned earlier. As an example, it was shown that uncertainties from lack of knowledge of both the scattering kernel and seabed geoacoustic properties can be very large (60 dB at 10 km). Thus our uncertainty bounds may underestimate the true uncertainties. It is the purpose here, however, to show order of magnitude uncertainties.

While we have used empirical models to quantify the order of magnitude bias errors that can occur, these same bias errors also occur for physics-based models when the underlying scattering kernel is unknown. Recalling the underlying cause that leads to the large uncertainties (a limited angular window to sample the scattering kernel), it does not matter whether the inverse approach assumes a fixed scattering kernel (e.g., Refs. 1, 3, 5, 6, and 8) or a variable scattering law including physics-based models (e.g., Refs. 2, 4, 7, 9, and 10). All of these approaches suffer from uncertainties in extrapolating from the angular window of observation to another angular window, which might be governed by a completely different scattering mechanism (see, e.g., Ref. 23, where low angles are controlled by volume scattering and intermediate angles by subbottom interface scattering).

B. Mitigating uncertainties

Reverberation prediction uncertainties of order 10 dB may be so large for some applications that the prediction is rendered of little value. Here we explore various ways to reduce the uncertainty. Given that the fundamental problem is a limited sampling of the scattering kernel in a reverberation measurement, the general idea in mitigation is to expand the angular sampling window (at the seabed). Various methods for accomplishing this are given in the following.

TABLE IV. Three sediment half-space possibilities for the case when the scattering kernel is known *a priori* but the geoacoustic properties (or reflection coefficient) are unknown (see Fig. 10).

Sound speed (m/s)	Attenuation (dB/m/kHz)	Density (g/cm^3)
1600	0.25	1.8
1525	0.02	1.5
1750	0.8	2.0

TABLE V. Geoacoustic models and scattering kernels for the case in which both the scattering kernel and the geoacoustic properties are unknown (Fig. 11).

Sound speed (m/s)	Attenuation (dB/m/kHz)	Density (g/cm^3)	m	$10\log(\mu)$
1530	0.9	1.8	0	−32
1600	1.5	1.8	0.5	−25
1600	0.5	1.8	1	−22
1600	0.25	1.8	2	−12

1. Mitigation of uncertainties by exploiting the sound speed profile

One possibility is to conduct the experiment during upward refracting or near isovelocity SSP. In the case of known seabed reflection coefficient, measuring reverberation over as large as possible range extent in an upward refracting profile offers the best chance for determining the correct scattering kernel from the data themselves. Strongly downward refracting profiles tend to lead to the largest bias errors (most difficult to distinguish various scattering kernels from the data themselves), with decreasing bias errors from decreasing sound speed gradients. Two caveats should be mentioned. First, in upward refracting cases, there is much greater likelihood for scattering from the sea surface, so it may actually become more difficult to determine the relative contributions of sea surface and seabed contributions. Second, if both the scattering kernel and the reflection coefficient are unknown, the bias errors might still be large (uncertainties of 60 dB at 10 km exist in the above–presented example) for the upward refracting or isovelocity case. Also note that, for some applications, waiting for a different SSP may be impractical.

2. Mitigation of uncertainties by multiple diverse reverberation measurements

Multiple reverberation measurements under diverse conditions permit the angular dependence of the scattering kernel (and also R) to be probed more widely. For example, reverberation in diverse SSPs or using diverse source–receiver depths in a single profile could reduce these uncertainties (also noted in Ref. 10). Generally, the greater disparity between the SSP or source–receiver depths for each measurement, the greater reduction in uncertainties will ensue (effectively probing the scattering over wider angular regions). However, it should be noted that in isovelocity (or near isovelocity) conditions, exploiting different source–receiver depths will not reduce the uncertainties, since in this case the reverberation is independent of source–receiver depth. Note again that in some cases, waiting for a diverse SSP may be impractical.

Another possibility is to exploit source–receiver vertical directionality[9] to probe the scattering kernel. That is, by ju-

dicious choice of directionality, one might be able to control the angles at the seabed and hence probe a wider angular window of the scattering kernel. If the directionality resides solely in the receiver, it might be possible to accomplish this with a single measurement.

3. Mitigation of uncertainties by measurement of the scattering kernel

Given that the prediction uncertainties tend to be dominated by scattering strength uncertainties (as opposed to reflection coefficient uncertainties), it suggests that measurement resources should be invested most heavily in measuring the scattering kernel directly. Perhaps the most obvious approach is to use the reverberation at short times when the reverberation is dominated by direct paths to the seabed (e.g., Ref. 24). However, the challenges include difficulty in isolating low angle scattering contributions (for which significant source–receiver directionality is required), the requirement to know geometry and source/receiver beampatterns accurately, and a large dynamic range (or adjustable gains). This is not to say that using a system designed for long-range reverberation cannot be used to measure short range scattering, it is only to say that considerable care is required.

Alternatively, the scattering kernel can be measured at low angles using techniques specifically designed for direct path (e.g., Refs. 20 and 25) measurements. Fortunately, uncertainties in vertically bistatic angular dependence have a minor impact on the uncertainties of the predicted reverberation,[26] therefore a measurement of backscatter is sufficient. The backscattering must be measured, however, over the range of angles that contribute to reverberation. For example, in shallow water this means angles below the critical angle.

There is evidence that scattering strength may be relatively constant over large areas in some environments (e.g., Ref. 27). Therefore, a promising strategy in a survey sense would be to use directional reverberation to determine provinces (i.e., areas where the scattering kernel appears to be reasonably constant in space) and then conduct a few direct path backscattering measurements to reduce reverberation prediction uncertainties.

C. Uncertainty estimation

In addition to the need for making an additional measurement to reduce or mitigate the large uncertainties, it would be useful for reverberation inversion approaches to report the estimated reverberation prediction uncertainties. A simple way might be similar to Fig. 5(c), where the range of sound speed profiles could be tailored to the particular area.

A straightforward, but potentially incorrect approach to estimating the uncertainties would be to simply propagate the uncertainties of the fitted seabed parameters. This would only be correct if the inverse problem is parametrized sufficiently broadly, including all possibilities for the seabed properties (for which the forward predictions are sensitive). For example, it is clear that the angular dependence of the scattering kernel has a large impact on prediction uncertainties. In the (not uncommon) case of assuming a fixed angular dependence in the inverse problem, the prediction of reverberation uncertainty must include a wide parametrization, allowing for other angular dependencies.

VI. SUMMARY

Reverberation measurements, either in a survey or through the sensor operation can be a powerful tool for reducing uncertainties in performance prediction for active systems. However, we have shown here that for current inversion methods where reverberation (and sometimes propagation) is inverted for seabed parameters, the remnant uncertainties even after the measurement can be quite large, of order 10 dB at 10 km, increasing with increasing range. These uncertainties are due to uncertainty in the scattering kernel, which generally cannot be obtained uniquely from long-range reverberation. Prediction uncertainties from the reflection coefficient (when the scattering kernel was known) were shown to be much smaller. However, in practice, when there are uncertainties in both the scattering kernel and the geoacoustic properties, the uncertainties can be much greater, several tens of decibels. Since the errors tend to depend most heavily on the (generally unknown) angular dependence of the scattering kernel, several methods were briefly explored for reducing the uncertainties. These methods allow a wider angular sampling of the scattering kernel than a single reverberation measurement.

In summary, the main points of the paper are as follows:

(1) Reverberation prediction uncertainties can be large, order 10 dB, even in the presence of high quality reverberation measurements at the same location, and ostensibly small uncertainties of the fitted seabed parameters.
   (a) Prediction uncertainties tend to be largest when there is a limited time/range window over which the observations are made.
   (b) However, increase of the range window does not necessarily guarantee a reduction in the prediction uncertainties (a case in point is for a downward refracting environment, see Fig. 2)

(2) Current methods for reverberation inversion should be modified, mitigating the large prediction uncertainties by at least one of the following:
   (a) Making independent measurements of the scattering kernel (backscattering strength is sufficient) from the critical angle to as low an angle as practical;
   (b) Conducting the reverberation measurements in isovelocity or upward refracting environments (or multiple sound speed profiles), if the angular dependence of the reflection coefficient is well known, and the scattering at the sea surface is negligible compared to the bottom scattering;
   (c) Conducting the reverberation measurements using multiple source/receiver depths, if the sound speed profile is not isovelocity or nearly isovelocity.

(3) Results for reverberation inversion should be accompanied by estimates of reverberation prediction uncertainty.

ACKNOWLEDGMENT

The author gratefully acknowledges the support of the Office of Naval Research Ocean Acoustics Program (Code OA321).

[1]R. J. Urick, "Reverberation-derived scattering strength of the shallow sea bed," J. Acoust. Soc. Am. **48**, 392–397 (1970).
[2]J. Zhuo, G. Dinghua, S. Erchang, and L. Ensheng, "Long range reverberation and bottom scattering strength in shallow water," Chin. J. Acoust. **1**, 54–63 (1982).
[3]D. D. Ellis and P. Gerstoft, "Using inversion techniques to extract bottom scattering strengths and sound speeds from shallow water reverberation data," Third European Conference on Underwater Acoustics, edited by J. S. Papadakis, Heraklion, Crete, 1996, pp. 557–562.
[4]G. A. Scanlon, R. H. Bourke, and J. H. Wilson, "Estimation of bottom scattering strength from measured and modeled mid-frequency sonar reverberation levels," IEEE J. Ocean. Eng. **21**, 440–450 (1996).
[5]P. G. Cable, K. D. Frech, J. C. O'Connor, and J. M. Steele, "Reverberation-derived shallow-water bottom scattering strength," IEEE J. Ocean. Eng. **22**, 534–540 (1997).
[6]M. Sundvik, E. Rabe, and M. Vaccaro, "Mapping seabed acoustic reflection and scattering coefficients using tactical sonar systems," *MTS/IEEE Oceans 99 Proceedings*, Seattle, WA, Sept. 13–16, 1999, Vol. 2, pp. 1070–1075.
[7]J. R. Preston, D. D. Ellis, and R. C. Gauss, "Geoacoustic parameter extraction using reverberation data from the 2000 Boundary Characterization Experiment on the Malta Plateau," IEEE J. Ocean. Eng. **30**, 709–732 (2005).
[8]P. G. Cable, T. W. Yudichak, Y. Dorfman, D. P. Knobles, R. Zhang, Z. Peng, F. Li, and Z. Li, "On shallow water bottom reverberation frequency dependence," IEEE J. Ocean. Eng. **31**, 145–155 (2006).
[9]C. H. Harrison and P. L. Nielsen, "Separability of seabed reflection and scattering properties in reverberation inversion," J. Acoust. Soc. Am. **121**, 108–119 (2007).
[10]M. A. Ainslie, "Observable parameters from multipath reverberation," J. Acoust. Soc. Am. **121**, 3363–3376 (2007).
[11]The latter uncertainties are not ignored because they are never important, rather we ignore them because we want to examine one specific aspect of the uncertainty budget.
[12]J. X. Zhou, "The analytical method of angular power spectrum, range and depth structure of echo-reverberation ratio in shallow water sound field," J. Med. Lab Technol. **5**, 86–99 (1980).
[13]X. Lurton, "The range averaged intensity model: A tool for underwater acoustic field analysis," IEEE J. Ocean. Eng. **17**, 138–149 (1992).
[14]K. V. Mackenzie, "Long-range shallow water reverberation," J. Acoust. Soc. Am. **34**, 62–66 (1962).
[15]As just one example, direct path scattering measurements confirmed by reverberation measurements indicate $m=0.5$ in one environment in the Straits of Sicily (Ref. 26). This angular dependence also conforms very closely to volume scattering from a slow sediment.
[16]C. W. Holland, "On errors in estimating bottom scattering strength from acoustic reverberation," J. Acoust. Soc. Am. **118**, 2787–2790 (2005).
[17]Note that the model predictions compare very closely with a normal mode reverberation model for various gradients.
[18]Note that the angular distribution is a function of both incident and scattered angles. For clarity, it is presented here at a single reference angle which is the mean of the incident and scattered angles. Also note that the shape of the angular dependence also depends weakly on frequency (here shown in the high frequency ray approximation) and will be smoothed and spread near the truncation at lower frequencies.
[19]E. T. Kuo, "Wave scattering and transmission at irregular surfaces," J. Acoust. Soc. Am. **36**, 2135–2142 (1964).
[20]C. W. Holland, R. Hollett, and L. Troiano, "A measurement technique for bottom scattering in shallow water," J. Acoust. Soc. Am. **108**, 997–1011 (2000).
[21]L. Guillon and X. Lurton, "Backscattering from buried sediment layers: The equivalent input backscattering model," J. Acoust. Soc. Am. **109**, 122–132 (2001).
[22]C. H. Harrison, "Closed-form expressions for ocean reverberation and signal excess with mode stripping and Lambert's law," J. Acoust. Soc. Am. **114**, 2744–2756 (2003).
[23]C. W. Holland and P. Neumann, "Sub-bottom scattering: A modeling approach," J. Acoust. Soc. Am. **104**, 1363–1373 (1998).
[24]W. E. Brown and M. L. Bartlett, "Mid-frequency through the sensor scattering measurements: A new approach," IEEE J. Ocean. Eng. **30**, 733–747 (2005).
[25]P. C. Hines, J. C. Osler, and D. J. MacDougald, "Acoustic backscatter measurements from littoral seabeds at shallow grazing angles at 4 and 8 kHz," J. Acoust. Soc. Am. **117**, 3504–3516 (2005).
[26]C. W. Holland, "A constrained comparison of ocean waveguide reverberation theory and observations," J. Acoust. Soc. Am. **120**, 1922–1931 (2006).
[27]C. W. Holland, "Mapping seabed variability: Rapid surveying of coastal regions," J. Acoust. Soc. Am. **119**, 1373–1387 (2006).

Optimization of transmitting beam patterns of a conformal transducer array

Zhengyao He[a] and Yuanliang Ma
Institute of Acoustic Engineering, Northwestern Polytechnical University, Xi'an, 710072, China

(Received 11 September 2007; revised 14 January 2008; accepted 22 February 2008)

A method is presented to calculate the driving-voltage weighting vector of a conformal array of underwater acoustic transmitting transducers to obtain a low-sidelobe beam pattern based on the measured receiving array manifold. The relationship among three quantities is given, which are, respectively, the radiated acoustic field, the measured receiving array manifold matrix and the driving-voltage weighting vector of the transducer array. Then, the driving-voltage weighting vector of the array is calculated using the optimization method to obtain a low-sidelobe transmitting beam pattern. At the frequency of 12.5 kHz, the receiving array manifold matrix of a 27-element conformal array is measured in an anechoic water tank. The driving-voltage weighting vector of the array is calculated using the proposed method. In addition, the computer simulation and experiments are carried out. The results agree well and show that the proposed method can obtain a low-sidelobe transmitting beam pattern and at the same time provide the largest amplitude of pressure in the axial direction when the maximum amplitude of the driving voltages of the array elements keeps unchanged. © *2008 Acoustical Society of America.* [DOI: 10.1121/1.2897046]

PACS number(s): 43.30.Yj, 43.60.Fg, 43.20.Rz [WMC] Pages: 2563–2569

I. INTRODUCTION

A low-sidelobe transmitting beam pattern and large radiated pressure amplitude of the mainlobe is always expected in an underwater acoustic transmitting transducer array of active sonar and autonomous underwater vehicle (AUV).[1] In the research of the radiated acoustic field of compact transducer arrays, the mutual interactions among elements must be considered.[2–4] In the conformal array of our research, the volume of the array is small with compact elements, and it is needed to transmit broadband signal. Consequently, the interactions among elements in the conformal array are definitely significant.[5] On the other side, the radiated acoustic field of the array may be greatly influenced by the baffle with a certain impedance boundary condition.[6] Diffraction is caused by the baffle when the conformal array transmits and receives acoustic signals. Thus, the diffraction constant is necessary to be considered when the transmitting beam pattern of the conformal array is controlled.

There is some preliminary research about the influence of the baffle and mutual interactions among elements on the performance of the transducer array. Carson[7] utilized the equivalent circuit principle to select appropriate tuning capacitors to control the vibration velocity of the transducer array. Audoly[8] adopted the improved Helmholtz boundary integral equation method[9] to calculate the acoustic radiation and mutual interactions of the 8-element and 32-element planar array set in the finite baffle. But, the above-mentioned research only analyzed how the baffle and mutual interactions greatly influenced the transmitting performance of the transducer array, yet they did not propose such methods that could reduce the influence in order to control the transmitting beam pattern and obtain a high transmitting source level. He and Ma[10] utilized the boundary element model to calculate the radiated acoustic field of the transducer array, and adopted optimization method to control the transmitting beam pattern of the array. However, a relatively big error existed when this theoretical calculation method was used practically. The experimental results were not very satisfactory when the transducer number in the array increases.

When the received signals of the conformal array of our research are processed by beam forming, the measured receiving array manifold of the array, which is composed of the receiving response of each element in the array including both amplitude and phase responses,[11] can be used to optimize the beam pattern of received signals. In the investigation of the conformal array, the acoustic reciprocity principle may be used. The basic concept of the acoustic reciprocity principle was given by Foldy and Primakoff[12] and Bobber[13] in detail. When the transducer array transmits acoustic signals, the array may be influenced by the baffle, the mutual interactions among elements, etc. When it receives acoustic signals, the array may also be influenced by these factors. Therefore, an idea emerges that the measured receiving array manifold may be used to calculate the driving-voltage weighting vector of the conformal array. Thus, comparing with the results using the theoretical model,[10] the error may decrease and the performance may increase.

In this paper, a new method is proposed to calculate the driving-voltage weighting vector of the conformal array based on the measured receiving array manifold in order to obtain a low-sidelobe transmitting beam pattern and good transmitting performance. Further, an experiment has been conducted to demonstrate the correctness and validity of the proposed method in an anechoic water tank.

[a]Electronic mail: hezhengyao@163.com

II. TRANSMITTING AND RECEIVING DIFFRACTION CONSTANTS OF TRANSDUCER

The concept of the transmitting and receiving diffraction constants[12] is given in the following. Assume that the surface vibration velocity of the transducer is uniform. Place a transducer with a volume velocity U in a free field, producing a pressure p in the far field at a distance d. Place a simple source with a volume velocity U_s at the point with the distance d, producing an average blocked pressure $\bar{p}_b$ on the transducer and a free-field pressure p_f at the transducer location. Then, the receiving diffraction constant of the transducer is

$$D = \frac{\bar{p}_b}{p_f}. \tag{1}$$

From the acoustic reciprocity theorem, it leads to

$$\frac{p}{U} = D\left(\frac{\omega\rho}{4\pi d}\right), \tag{2}$$

where ω is the sound wave angular frequency and ρ is the density of the medium.

Substitute a simple source for the transducer with the same volume velocity U, then the pressure at the point with the distance d is

$$p_0 = \left(\frac{\omega\rho}{4\pi d}\right)U. \tag{3}$$

From Eqs. (2) and (3), we can get

$$\frac{p}{p_0} = D. \tag{4}$$

The transmitting diffraction constant of the transducer is calculated by Eq. (4), which is the ratio of the pressure produced by a transducer at a remote point in a free field to the pressure produced at the same point when a simple source with the same volume velocity is substituted for the transducer. It is numerically equal to the receiving diffraction constant of the transducer. The transmitting diffraction constant D of the transducer can be calculated by the boundary element model. The transmitting and receiving diffraction constants include not only amplitude but also phase. Let the initial phase of the vibration velocity of the transducer when transmitting signals be zero and that of the simple source when receiving signals be zero. Then, according to the acoustic reciprocity principle, the phases of the transmitting and receiving diffraction constants are the same.

III. TRANSMITTING AND RECEIVING EQUIVALENT CIRCUITS OF TRANSDUCER

The transmitting and receiving equivalent circuits of the transducer are introduced in this section, which is preparation for the transmitting beam pattern optimization of the transducer array in the next section. Suppose that the transducers in the array are all piston transducers. The transmitting equivalent circuit of one transducer is shown in Fig. 1. C_0 is the static capacitance. n is the electromechanical transfer ratio, Z_m is the mechanical impedance, and Z_s is the radiation impedance. These parameters may be obtained by different models or by experiments.[14,15] E is the prescribed voltage on the transducer, I, I_0, and I_d are the electric currents in different branches, F is the mechanical force, and v is the vibration velocity of the transducer.

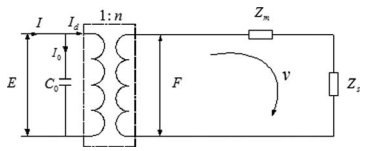


FIG. 1. Transmitting equivalent circuit of the transducer.

In the array composed of L identical transducers, the mechanical impedance of the transducers are all assumed to be Z_{m0}. Then, the mutual impedance matrix of the array can be written as

$$\mathbf{Z} = \begin{bmatrix} Z_{m0}+z_{11} & z_{12} & \cdots & z_{1L} \\ z_{21} & Z_{m0}+z_{22} & \cdots & z_{2L} \\ \vdots & \vdots & \vdots & \vdots \\ z_{L1} & z_{L2} & \cdots & Z_{m0}+z_{LL} \end{bmatrix}, \tag{5}$$

where z_{ii} is the self-radiation impedance of the ith transducer and z_{ij} is the mutual radiation impedance between the ith and jth transducer. Then, the driving voltage and the vibration velocity of the array satisfy the following relationship:

$$\mathbf{V} = n\mathbf{Z}^{-1}\mathbf{E}, \tag{6}$$

where n is the electromechanical transfer ratio of the transducers, $\mathbf{Z}$ is the mutual impedance matrix of the array, $\mathbf{E}$ is the column vector of the driving voltage, and $\mathbf{V}$ is the column vector of the vibration velocity of the array.

The receiving equivalent circuit of the transducer is shown in Fig. 2. F represents the mechanical force, which is exerted on the surface of the transducer by the free-field pressure p_f, D is the receiving diffraction constant, S is the surface area, Z_s is the radiation impedance, Z_m is the mechanical impedance, and Z_e is the electrical impedance when the vibration velocity is zero. According to the acoustic reciprocity principle, the mechanical impedance and radiation impedance of the transducer when receiving signals are the same as those when transmitting signals. n_r is the electromechanical transfer ratio when receiving signals, and v is the vibration velocity caused by the incident sound wave. The previous satisfies the following relationship:

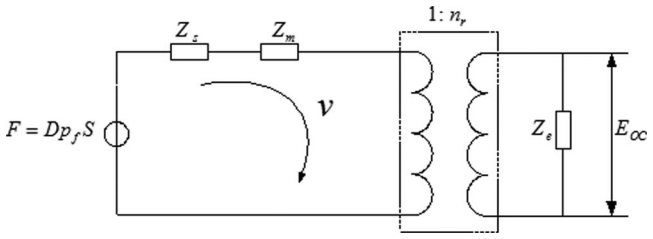


FIG. 2. Receiving equivalent circuit of the transducer.

$$F = Dp_f S = (Z_s + Z_m)v. \tag{7}$$

When the transducer receives signals, the open-circuit output voltage is

$$E_{OC} = n_r v, \tag{8}$$

where n_r is the electromechanical transfer ratio of the transducer when receiving signals and v is the vibration velocity of the transducer.

In the transducer array, the mutual impedance matrix when receiving signals is the same as that of transmitting, which is also $\mathbf{Z}$. Then, the mechanical force vector on the array exerted by the incident sound wave and the resultant vibration velocity vector of the array satisfy

$$\mathbf{F} = \mathbf{ZV}. \tag{9}$$

Using the transmitting and receiving equivalent circuits of the transducer and array introduced earlier, the relationship of the following quantities can be derived, which are, respectively, the driving voltage, diffraction constants, element mutual interactions, vibration velocity, and the receiving open-circuit voltage, and then the transmitting beam pattern of the transducer array can be optimized in the next section.

IV. TRANSMITTING BEAM PATTERN OPTIMIZATION PRINCIPLE OF THE TRANSDUCER ARRAY

Now, the transmitting beam pattern optimization principle of the transducer array is derived as follows. From Eqs. (3) and (4), the radiated acoustic pressure and vibration velocity of the transducer satisfy

$$p = Dp_0 = \frac{\omega \rho S}{4\pi d} Dv, \tag{10}$$

where S is the radiation surface area of the transducer, d is the distance between the far-field point and the equivalent acoustic center of the radiation area on the transducer, and D is the transmitting diffraction constant, including both amplitude and phase.

Suppose that the transducer array is composed of L transducers, the radiated acoustic pressure of the array is to be calculated. We uniformly divide the circle at a certain distance from the center of the array in the radiated acoustic field into M field points. The lines connecting these field points and the array center denote M directions of the radiated acoustic field. Assume that the transmitting diffraction constant of the jth transducer of the array in the ith direction is D_{ij}. Then, the transmitting diffraction constants of L transducers in M directions can form the constant matrix $\mathbf{D}$, which is

$$\mathbf{D} = \begin{bmatrix} D_{11} & D_{12} & \cdots & D_{1L} \\ D_{21} & D_{22} & \cdots & D_{2L} \\ \vdots & \vdots & \vdots & \vdots \\ D_{M1} & D_{M2} & \cdots & D_{ML} \end{bmatrix}. \tag{11}$$

From Eq. (6) and Eqs. (10) and (11), we can obtain the radiated acoustic pressure of the transducer array

$$\mathbf{P}_Q = \frac{n\omega\rho S}{4\pi d} \mathbf{DZ}^{-1}\mathbf{E}, \tag{12}$$

where $\mathbf{P}_Q$ denotes the vector constituted by the sound pressure in the M directions on the circle in the radiated far-field of the array.

When the transducer array receives acoustic signals, according to the acoustic reciprocity principle, the matrix of the receiving diffraction constant is the same as that of the transmitting diffraction constant, which is also determined by Eq. (11). Assume that the incident pressure p_f of each element in each direction is the same, and the surface area S of each transducer is also the same. From Eqs. (7)–(9) and Eq. (11), when the transducer array receives signals, the open-circuit output voltage is

$$\mathbf{E}_{OC} = n_r p_f S \cdot \mathbf{Z}^{-1}\mathbf{D}^T, \tag{13}$$

where $\mathbf{E}_{OC}$ is a $L \times M$ matrix, denoting the response to the far-field plane wave of L elements in M directions of the transducer array when receiving acoustic signals, including amplitude and phase responses, that is, $\mathbf{E}_{OC}$ is the receiving array manifold matrix of the transducer array, which can be obtained by experimental measurements. Because the mutual impedance matrix $\mathbf{Z}$ of the array is a symmetrical matrix, we can get

$$(\mathbf{Z}^{-1})^T = (\mathbf{Z}^T)^{-1} = \mathbf{Z}^{-1}. \tag{14}$$

Transposing the matrices on the two sides of Eq. (13) and substituting Eq. (14) into it, we get

$$(\mathbf{E}_{OC})^T = n_r p_f S \cdot \mathbf{DZ}^{-1}. \tag{15}$$

From Eq. (15), we obtain:

$$\mathbf{DZ}^{-1} = \frac{1}{n_r p_f S}(\mathbf{E}_{OC})^T. \tag{16}$$

Substituting Eq. (16) into Eq. (12) gives:

$$\mathbf{P}_Q = \frac{\omega\rho n}{4\pi d n_r p_f}(\mathbf{E}_{OC})^T\mathbf{E}. \tag{17}$$

Equation (17) relates the radiated acoustic field of the array with the measured receiving array manifold and the driving-voltage vector. Where $\mathbf{P}_Q$ is a $M \times 1$ vector, $(\mathbf{E}_{OC})^T$ is a $M \times L$ matrix, $\mathbf{E}$ is a $L \times 1$ vector, L denotes L elements of the array, and M denotes M directions on the circle in the radiated far field of the array. When the receiving array manifold matrix $\mathbf{E}_{OC}$ of the array is obtained by experimental measurements, the driving-voltage weighting vector of the array can be calculated by the optimization method to control the transmitting beam pattern of the array.

It is necessary to carry out the beam control for the transducer array in order to obtain a low-sidelobe transmitting beam pattern. Because the maximum amplitude of the driving voltages of the transducers in the array is limited, the result of the beam control may reduce the pressure amplitude in the axial direction of the array. For the purpose of making the transmitting source level of the array as high as possible, it needs to provide the largest pressure amplitude in the axial direction when the maximum amplitude of the driving voltages of the array elements keeps unchanged. That is, we

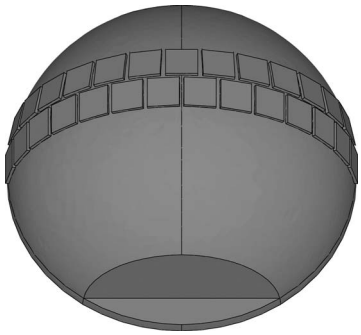


FIG. 3. Structure diagram of the conformal array which consists of 27 piston transducers and a hemispherical baffle.

make the maximum modulus of the driving-voltage weighting vector be minimum, simultaneously producing the same amplitude of pressure in the axial direction of the array and at the same time imposing constraints on the sidelobes of the transmitting beam pattern. Because what is to be calculated is the normalized vector, the coefficient $\omega\rho n/4\pi dn_r p_f$ in Eq. (17) can be left out of the calculation. It leads to the following optimization problem:

$$\begin{aligned} &\min_{\mathbf{W}_E} \mu \\ &\text{subject to} \quad \mathbf{E}_{\mathrm{OC}}(\theta_0)^T \mathbf{W}_E = 1 \\ &\qquad\qquad |\mathbf{W}_E(j)| \le \mu, \quad j = 1,2,\ldots,L \\ &\qquad\qquad |\mathbf{E}_{\mathrm{OC}}(\theta_s)^T \mathbf{W}_E| \le \delta_s, \quad \forall\, \theta_s \in \Theta_{\mathrm{SL}}, \end{aligned} \tag{18}$$

where $\mathbf{W}_E$ is the driving-voltage weighting vector of the array, μ is a nonnegative real variable, L is the transducer number of the array, θ_0 is the mainlobe direction, θ_s is the sidelobe direction, Θ_{SL} is the sidelobe regions which includes a number of directions, and δ_s controls the sidelobe level of the transmitting beam pattern. $\mathbf{E}_{\mathrm{OC}}(\theta_0)$ and $\mathbf{E}_{\mathrm{OC}}(\theta_s)$ are, respectively, the receiving array manifold vectors in θ_0 and θ_s directions, which can all be obtained by experimental measurements.

The optimization problem (18) can be solved by means of the optimization algorithm of the second-order cone programming.[16,17] Then, the required driving-voltage weighting vector $\mathbf{W}_E$ of the array is calculated. The practical driving voltage exerted on the transducers in the array is obtained by normalizing the calculated weighting vector, that is, the weighting vector is divided by the maximum modulus of the vector, and then multiplied by a voltage factor which must be less than the maximum voltage that can be exerted on the transducers of the array.

V. SIMULATION COMPUTATION

The structure diagram of the conformal array is shown in Fig. 3. This conformal array consists of 27 piston transducers. It is set in two arc lines of a hemispherical baffle. The cover board is on the underside of the baffle. The surface of the hemispherical baffle is made of rubber, the two sides of the baffle are of organic glass, and the cover board is of aluminum. The 27-element array is divided into two rows. The first row is in the middle. The left and right side of two rows are symmetrical. The first row consists of 14 transducers from a1 to a14. The second row consists of 13 transducers from b1 to b13. The distance between two adjacent transducers of the first row is 0.0452 m, and that of the second row is 0.0453 m. The angle between the planes of the first and second rows passing the hemispherical center is 12°. The radius of the hemispherical baffle is $r=0.216$ m. The radiation surface of each piston transducer is rectangular with the length $a=0.04$ m and width $b=0.04$ m. The sound frequency is $f=12.5$ kHz, speed underwater is $c=1500$ m/s and wavelength is $\lambda=0.12$ m. An experiment has been carried out to measure the receiving array manifold matrix of the conformal array in the anechoic water tank. The response of each element to the plane-wave acoustic signals, including amplitude and phase responses, is measured in the range of ±135° from the main axial direction of the array with the interval 3°, in this way, the receiving array manifold matrix of the conformal array is obtained. Then, two methods are used to calculate the driving-voltage weighting vector of the array. One is the conventional beam-forming method in which the weighting vector is calculated by phase compensation according to the geometrical positions of the elements using the plane-wave model.[18] The other is the proposed method in this paper, which uses Eq. (18) to calculate the weighting vector of the array. Figures 4–7 are, respectively, the radiated sound pressure amplitude and directivity of the 27-element conformal array calculated by simulation when the beam scan angles are 0° and 84°. The solid line represents the weighting vector calculated by the proposed method with the sidelobe level constrained to −20 dB. The dotted line represents the weighting vector calculated by the conventional beam-forming method with the plane-wave model. Then, the radiated acoustic pressure of the array is calculated by Eq. (17). The ordinates of Figs. 4 and 6 represent the radiated acoustic pressure amplitude of the array divided by the axial maximum pressure amplitude when the weighting vector is obtained by the conventional beam-forming method and the

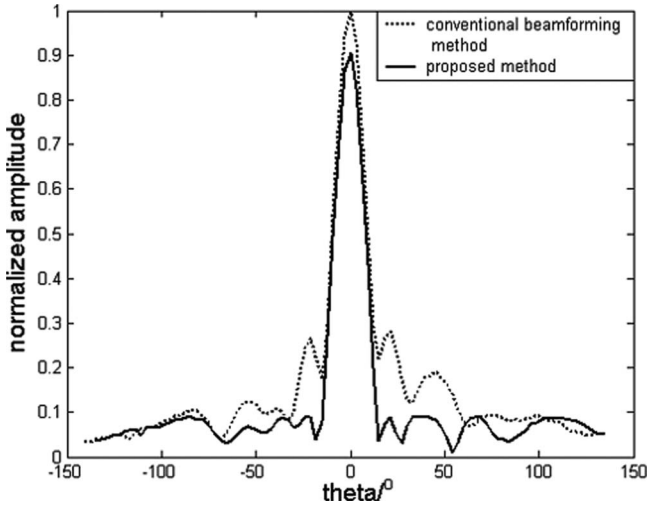


FIG. 4. Radiated sound pressure amplitude of the 27-element conformal array calculated by simulation of two weighting methods when the beam scan angle is 0°, where the pressure amplitude is divided by the axial maximum pressure amplitude when the weighting vector is obtained by the conventional beam-forming method. Revealed is the difference of the maximum amplitude in the axial direction of two weighting methods.

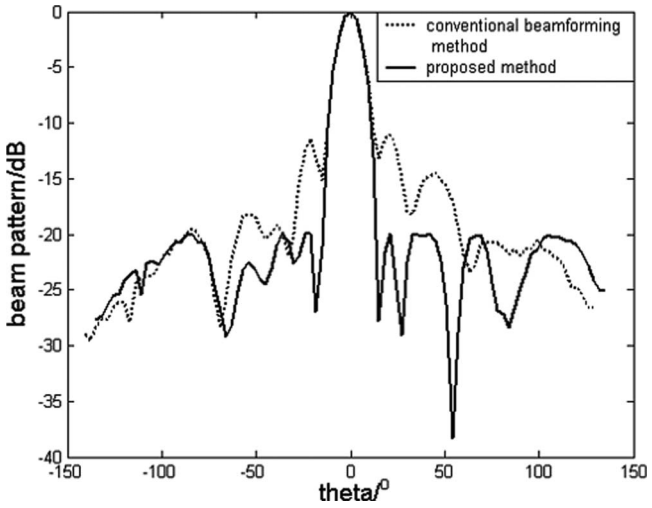


FIG. 5. Radiated sound pressure directivity of the 27-element conformal array calculated by simulation when the beam scan angle is 0°, in which the maximum value is normalized to 0 dB.

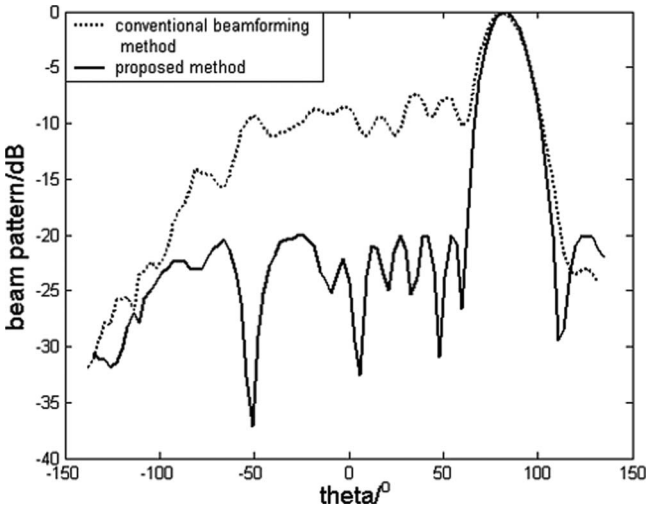


FIG. 7. Radiated sound pressure directivity of the conformal array calculated by simulation when the beam scan angle is 84°, in which the maximum value is normalized to 0 dB.

beam scan angle is 0°. Figures 4–7 show that the proposed method can control the sidelobes of the transmitting beam pattern of the conformal array and can obtain a low-sidelobe level. When the beam scan angles are 0° and 84°, using the proposed method, the highest sidelobe levels of the beam patterns of simulation are both −20 dB, whereas using the conventional beam-forming method, the highest sidelobe levels are, respectively, −11 and −7.3 dB. On the other hand, because the proposed method imposes constraints on the sidelobe level of the beam pattern, the maximum pressure amplitude of the mainlobe may reduce comparing with that of the conventional beam-forming method. However, the proposed approach can provide the largest pressure amplitude in the axial direction of the array when the maximum amplitude of the driving voltages of the array elements remains the same, simultaneously satisfying the sidelobe constraints. Corresponding to Figs. 4 and 6, using the proposed method, comparing with the conventional beam-forming method, the maximum pressure amplitude does not reduce much, with the reduction amounts of 0.87 and 0.3 dB, respectively. Because of the acoustic diffraction caused by the baffle and the element radiation directivity of each transducer in the array, the axial maximum pressure amplitude of the array, when the beam scan angle is in the side direction, may be lower compared to that in the main direction. The attainable beam scan angle of the conformal array of our research is broad, thus, the axial maximum pressure amplitude, when the beam scan angle is in the side direction 84°, does not reduce much compared with that in the main direction 0°, and the reduction amount is 3.2 dB. The simulation results show that the proposed approach can obtain a low-sidelobe transmitting beam pattern, and provide the largest pressure amplitude in the axial direction of the array when the maximum amplitude of the driving voltages of the array elements keeps unchanged.

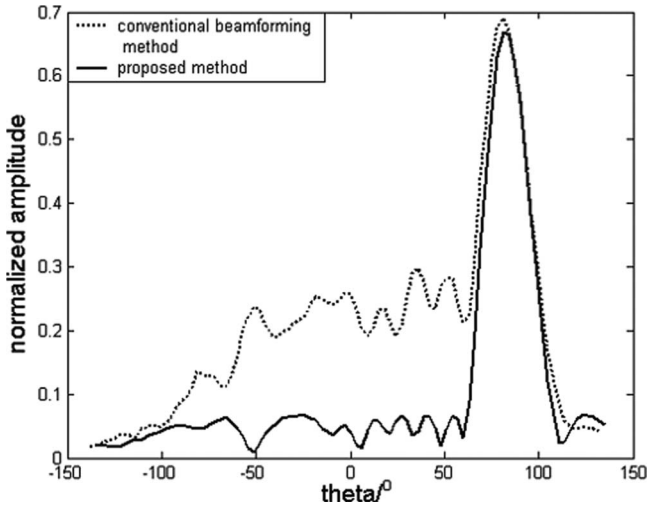


FIG. 6. Radiated sound pressure amplitude of the conformal array calculated by simulation when the beam scan angle is 84°. Pressure amplitude is divided by the axial maximum pressure amplitude when the weighting vector is obtained by the conventional beam-forming method and the beam scan angle is 0°. Revealed is the difference of the maximum amplitude in the axial direction of two weighting methods and two beam scan angles.

VI. EXPERIMENTAL RESULTS

An experiment has been conducted to measure the radiated acoustic pressure directivity of the conformal array in an anechoic water tank. The working frequency is $f=12.5$ kHz. The maximum driving voltage exerted on the transducers is 4 V, i.e., the normalized driving-voltage weighting vector calculated by Eq. (18) is multiplied by the voltage factor 4 V. Figures 8–11 are, respectively, the measured radiated sound pressure amplitude and directivity of the 27-element conformal array when the beam scan angles are 0° and 84°. The meanings represented by the solid and dotted lines in Figs. 8–11 are the same as those in Figs. 4–7. The ordinates of Figs. 8 and 10 represent the measured radiated acoustic pressure amplitude of the array divided by the axial maximum pressure amplitude when the weighting vector is calculated by the conventional beam-forming method and the beam scan angle is 0°. From Figs. 8–11, it is shown that the

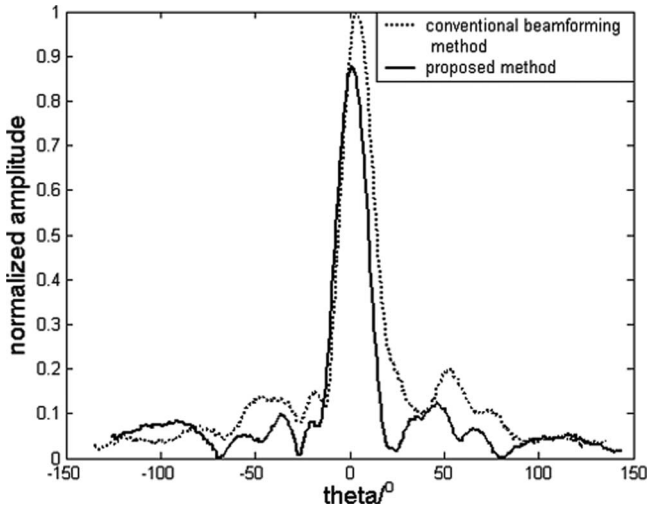


FIG. 8. Measured radiated sound pressure amplitude of the 27-element conformal array of two weighting methods when the beam scan angle is 0°. The pressure amplitude is divided by the axial maximum pressure amplitude when the weighting vector is obtained by the conventional beam-forming method. Revealed is the difference of the measured maximum amplitude in the axial direction of two weighting methods.

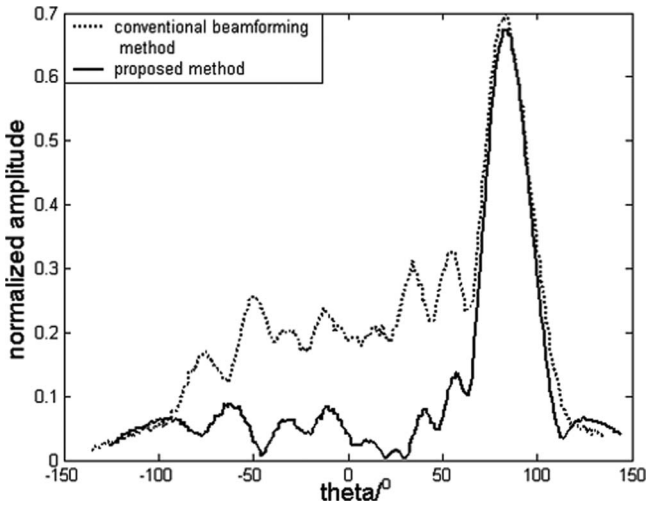


FIG. 10. Measured radiated sound pressure amplitude of the conformal array when the beam scan angle is 84°. Pressure amplitude is divided by the axial maximum pressure amplitude when the weighting vector is obtained by the conventional beam-forming method and the beam scan angle is 0°. Revealed is the difference of the measured maximum amplitude in the axial direction of two weighting methods and two beam scan angles.

measured results are consistent with the simulation results in Sec. V. Obviously, the proposed method can obtain a low-sidelobe transmitting beam pattern. Using the proposed method, the highest sidelobe levels of the measured beam patterns are, respectively, −17.1 and −13.9 dB when the beam scan angles are 0° and 84°. Although using the conventional beam-forming method, the highest sidelobe levels of the measured beam patterns are −13.9 and −6.6 dB, respectively. It is shown that the highest sidelobe levels are greatly reduced using the proposed method, compared to the conventional beam-forming method. There are some differences between the experimental and simulation results due to the measurement errors. On the other hand, similar to the simulation results, because the proposed method imposes constraints on the sidelobe level of the beam pattern, the maximum pressure amplitude of the mainlobe may be reduced compared to that of the conventional beam-forming method. The proposed method can provide the largest pressure amplitude in the axial direction of the array when the maximum amplitude of the driving voltages of the array elements are kept unchanged, and at the same time satisfying the sidelobe constraints. Corresponding to Figs. 8 and 10, by use of the proposed method contrasting with the conventional beam-forming method, the maximum pressure amplitude does not reduce much, with reduction amounts of 1.13 and 0.29 dB, respectively. From the experimental results, it is also shown that the attainable beam scan angle of the conformal array is broad, and the axial maximum pressure amplitude, when the beam scan angle is in the side direction 84°, does not reduce much compared to that in the main

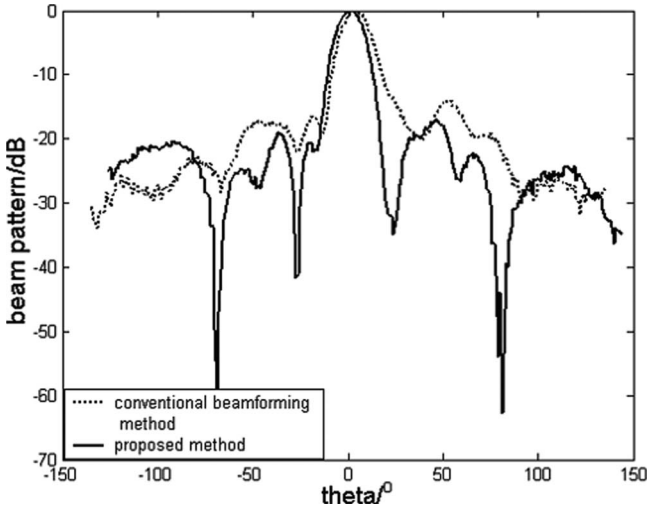


FIG. 9. Measured radiated sound pressure directivity of the 27-element conformal array when the beam scan angle is 0°, in which the maximum value is normalized to 0 dB.

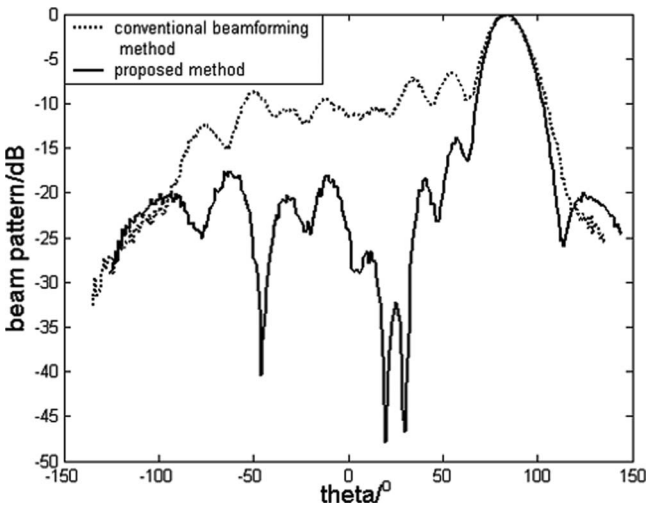


FIG. 11. The measured radiated sound pressure directivity of the conformal array when the beam scan angle is 84°, in which the maximum value is normalized to 0 dB.

direction 0°, with the reduction amount of 3.12 dB. It can be seen that the experimental results are greatly consistent with the simulation results, which verifies that the proposed method is valid and practical.

VII. CONCLUSIONS

In this paper, a new method is proposed to calculate the driving-voltage weighting vector of the conformal array based on the measured receiving array manifold in order to control the sidelobe of the transmitting beam pattern. According to the acoustic reciprocity principle, the relationship between the transmitting and receiving diffraction constants is given. The relationship among three quantities is presented, which are, respectively, the radiated acoustic field, the measured receiving array manifold, and the driving-voltage weighting vector of the transducer array. At last, the driving-voltage weighting vector of the array is calculated using the optimization method. The simulation results show that the proposed method can be adopted to calculate the driving-voltage weighting vector of the conformal array to obtain a low-sidelobe transmitting beam pattern and provide the largest pressure amplitude in the axial direction of the array when the maximum amplitude of the driving voltages of the array elements remains unchanged. An experiment has been carried out to measure the radiation directivity of the conformal array in the anechoic water tank and its results demonstrate that our method is valid and practical. There are still some differences between the experimental and simulation results due to measurement errors. The performance of the proposed method may be more perfect when the experimental measurements are more accurate.

ACKNOWLEDGMENTS

This work was supported by the National Natural Science Foundation of China under Grant No. 10734030.

[1] B. S. Liu and J. Y. Lei, *The Principle of Underwater Acoustics* (Harbin Shipbuilding Engineering Institute Press, Harbin, 1993), pp. 6–56 (in Chinese).
[2] J.-N. Decarpigny, "The design of low-frequency underwater acoustic projectors: Present status and future trends," IEEE J. Ocean. Eng. **16**, 107–122 (1991).
[3] G. H. Du, Z. M. Zhu, and X. F. Gong, *Fundamentals of Acoustics* (Nanjing University Press, Nanjing, 2001), pp. 308–382 (in Chinese).
[4] J. Lee and I. Seo, "Radiation power estimation for sonar transducer arrays considering acoustic interaction," Sens. Actuators, A **A90**, 1–6 (2001).
[5] Z. Y. He and Y. L. Ma, "Sound field calculation of underwater acoustic projecting transducer array of arbitrary shape," Appl. Acoust. **25**, 69–75 (2006) (in Chinese).
[6] LMS International, *SYSNOISE Rev 5.2 Manual* (LMS Company Leuven, 1995), pp. 1–300.
[7] D. L. Carson, "Diagnosis and cure of erratic velocity distribution in sonar projector arrays," J. Acoust. Soc. Am. **34**, 1191–1195 (1962).
[8] C. Audoly, "Some aspects of acoustic interactions in sonar transducer arrays," J. Acoust. Soc. Am. **89**, 1428–1433 (1991).
[9] H. A. Schenck, "Improved integral formulation for acoustic radiation problems," J. Acoust. Soc. Am. **44**, 41–58 (1968).
[10] Z. Y. He and Y. L. Ma, "Calculation of baffle effect and mutual interaction between elements for an underwater acoustic conformal array with application to the optimization of projecting beampattern," Chin. Sci. Bull. **52**, 2584–2591 (2007).
[11] R. Wu, Y. Ma, and R. D. James, "Array pattern synthesis and robust beamforming for a complex sonar system," IEE Proc., Radar Sonar Navig. **144**, 370–376 (1997).
[12] L. L. Foldy and H. Primakoff, "A general theory of passive linear electroacoustic transducer and the electroacoustic reciprocity theorem. I," J. Acoust. Soc. Am. **17**, 109–120 (1945).
[13] R. J. Bobber, "Diffraction constant of transducers," J. Acoust. Soc. Am. **37**, 591–595 (1965).
[14] W. S. Baidike and L. S. Fang, *Underwater Acoustic System Analysis* (Ocean Press, Beijing, 1992), pp. 39–58 (in Chinese).
[15] L. E. Kinsler, *Fundamentals of Acoustics* (Wiley, New York, 2000), pp. 390–406.
[16] J. F. Sturm, "Using SeDuMi 102, a MATLAB toolbox for optimization over symmetric cones," Optim. Methods Software **11–12**, 625–653 (1999).
[17] S. Yan, C. Hou, X. Ma, and Y. Ma, "Convex optimization based time-domain broadband beamforming with sidelobe control," J. Acoust. Soc. Am. **121**, 46–49 (2007).
[18] W. H. Kummer, "Basic array theory," Proc. IEEE **80**, 127–139 (1992).

Influence of spatial correlation function on attenuation of ultrasonic waves in two-phase materials

Dalie Liu and Joseph A. Turner[a)]
Department of Engineering Mechanics, University of Nebraska-Lincoln, W317.4 Nebraska Hall, Lincoln, Nebraska 68588, USA

(Received 28 June 2007; revised 15 January 2008; accepted 15 February 2008)

Successful processing of materials by powder sintering relies on the creation of strong interparticle bonds. During certain critical stages of the sintering process, the medium may be modeled as two phases consisting of the particles and a surrounding matrix. Ultrasonic methods have been proposed as a potential tool for monitoring such sintering processes. Thus, an understanding of the propagation and scattering of elastic waves in two-phase solids is of fundamental importance to these monitoring techniques. In this article, expressions for the ultrasonic attenuations are developed based on the spatial statistics of the density and Lamé parameters of the material constituents under assumptions of statistical homogeneity and statistical isotropy. The formulation is based on the solution of the elastodynamic Dyson equation within the limits of the first-order smoothing approximation. Since the geometric two-point correlation function plays a central role in the model, numerical models are developed using Voronoi polycrystals surrounded by a matrix of different material properties. The spatial statistics of the medium are extracted from these models. The results presented suggest new ultrasonic techniques may be developed to extract multiple correlation lengths for such two-phase microstructures. © *2008 Acoustical Society of America.*
[DOI: 10.1121/1.2896757]

PACS number(s): 43.35.Cg, 43.20.Bi, 43.20.Gp [PEB] Pages: 2570–2576

I. INTRODUCTION

Sintered metals and ceramics are very important in modern manufacturing. Many construction and engineering materials are produced by sintering of different crystal powders in mechanical engineering, energetics, metal-working industries, instrument making and electronics. An increased understanding of the sintering process would lead to intelligent process control, greater reliability of the production process, and improved quality of the end products. Therefore, continuous real-time monitoring of the microstructure evolution is necessary. More importantly, such monitoring techniques will provide valuable information for modeling sintering processes. Most current monitoring techniques are not *in situ* techniques. Ultrasonic and eddy current techniques have great potential for direct measurements during processing. However, eddy current techniques are limited to information predominantly about the material near the specimen surface.[1] Ultrasonic methods can provide information about the interior microstructure due to the penetration of ultrasonic waves and are capable of inspecting the sintering process at high temperatures.[2,3] However, the main difficulty with such ultrasonic techniques is the theoretical framework necessary to make the measurements quantitative.

The propagation and scattering of elastic waves through random medium has received considerable attention.[4,5] The basic premise of these analyses is to treat the material properties as random variables and use statistical methods to analyze the wave propagation. Most of those statistical theories require information about the spatial statistics of the microstructure to predict the macroscopic properties of heterogeneous materials. The model of Stanke and Kino[6] clearly established that the two-point correlation function is important for the attenuation within the second-order perturbation theory. Furthermore, the exponential correlation function used by Stanke and Kino for statistically isotropic, polycrystalline media is widely adopted in many works due to its simplicity.[7–11] The validity of this geometric autocorrelation function in polycrystalline media was examined by Man *et al.*[12] They found that the exponential formula fails to represent the correlation function for the grain boundary structure of a commercial aluminum alloy and that an alternative function is necessary. Such information will provide valuable insight for modeling the microstructure of complex materials during sintering processes.

In this article, the propagation and scattering of ultrasound in partially sintered materials is examined using a two-phase model consisting of the polycrystals and a surrounding matrix. The theory based on a stochastic, elastic wave model presented by Turner and Anugonda[10] is extended to study the attenuation of elastic waves in two-phase materials. The medium is assumed to be statistically homogeneous and statistically isotropic. The spatial statistics of the microstructure, also known as geometric correlation functions, are numerically evaluated and investigated. The attenuation of longitudinal and transverse elastic wave is presented in terms of the statistics of the density and Lamé parameters of the materials. The influence of correlation functions on the resulting attenuations is discussed.

[a)]Author to whom correspondence should be addressed. Electronic mail: jaturner@unl.edu.

 0001-4966/2008/123(5)/2570/7/$23.00 © 2008 Acoustical Society of America

II. STATISTICS OF MATERIAL PROPERTIES

The derivations for scattering attenuation rely on information regarding the statistics of the microstructure. Explicit expressions for the attenuation of longitudinal and transverse elastic waves used in this article are based upon the general description discussed by Turner and Anugonda.[10] In that work, the solution for the wave vector in the heterogeneous medium is based on the Dyson equation derived for the elastodynamic case. The Dyson equation was solved within the limits of the first-order smoothing approximation[13] for which the dimensionless combination of material fluctuation, bare wave number and correlation length must be smaller than unity. For more details, the reader may wish to refer to previous work using this approach.[9,10,14]

The spatial statistics of material properties are presented in this section. The material density, ρ, and Lamé parameters, λ and μ, are assumed to vary spatially and to have the form

$$\rho(\mathbf{x}) = \bar{\rho}[1 + \delta\rho(\mathbf{x})],$$

$$\lambda(\mathbf{x}) = \bar{\lambda}[1 + \delta\lambda(\mathbf{x})],$$

$$\mu(\mathbf{x}) = \bar{\mu}[1 + \delta\mu(\mathbf{x})], \tag{1}$$

where the over-bar terms are the average quantities and terms with δ represent a dimensionless measure of the spatial fluctuations about the average. It is assumed that the fluctuations are small and that the material properties are locally isotropic. The second-order statistics of the fluctuations are also required. The covariance of the density is given by

$$R_{\rho\rho}(\mathbf{x}-\mathbf{y}) = \langle \delta\rho(\mathbf{x})\delta\rho(\mathbf{y})\rangle. \tag{2}$$

The assumptions of statistical homogeneity and statistical isotropy imply that the correlation functions depend only on the distance, r, between the two positions. Thus

$$R_{\rho\rho}(\mathbf{x}-\mathbf{y}) = R_{\rho\rho}(|\mathbf{x}-\mathbf{y}|) = R_{\rho\rho}(r). \tag{3}$$

Autocorrelations of Lamé parameters, $R_{\lambda\lambda}$ and $R_{\mu\mu}$, as well as the cross correlation between different parameters $R_{\rho\lambda}$, $R_{\rho\mu}$, and $R_{\lambda\mu}$ can be defined in a similar manner.

For a material consisting of two uniform phases, a general and convenient description of the spatial variation is supplied by introducing the characteristic function[15]

$$\chi_1(\mathbf{x}) = \begin{cases} 1, & \text{if } x \in \Omega_1, \\ 0, & \text{otherwise}, \end{cases} \tag{4}$$

of the region Ω_1 occupied by phase "1." The complement Ω_2 is occupied by phase "2," and obviously, its characteristic function is $\chi_2(\mathbf{x}) = 1 - \chi_1(\mathbf{x})$. Starting from the definition of Eq. (3)

$$R_{\rho\rho}(r) = \frac{\langle(\rho(\mathbf{x}) - \bar{\rho})(\rho(\mathbf{y}) - \bar{\rho})\rangle}{\bar{\rho}^2}. \tag{5}$$

The density may then be described in terms of the characteristic functions

$$\rho(\mathbf{x}) = \rho_1\chi_1(\mathbf{x}) + \rho_2\chi_2(\mathbf{x}) \tag{6}$$

and

$$\bar{\rho} = \rho_1\langle\chi_1(\mathbf{x})\rangle + \rho_2\langle\chi_2(\mathbf{x})\rangle, \tag{7}$$

where ρ_1 and ρ_2 are the densities of phase "1" (grains) and "2" (matrix). After substitution into Eq. (5), we have

$$R_{\rho\rho}(r) = \frac{(\rho_1 - \rho_2)^2[\langle\chi_1(\mathbf{x})\chi_1(\mathbf{y})\rangle - \eta_1^2]}{\bar{\rho}^2}, \tag{8}$$

where $\eta_1 = \langle\chi_1(\mathbf{x})\rangle$ is the volume fraction of phase "1." The two-point correlation function $S_1 = \langle\chi_1(\mathbf{x})\chi_1(\mathbf{y})\rangle$ is noted as the probability that $\mathbf{x}$ and $\mathbf{y}$ are both in phase "1." As a result, the covariance reduces to the two-point moment[16] $M_2 = \langle\chi_1(\mathbf{x})\chi_1(\mathbf{y})\rangle - \eta_1^2$. For any statistically homogeneous medium, this two-point correlation moment, M_2, should be positive-definite such that its Fourier transform must be positive.[16,17] Similar derivations apply to the covariance of Lame parameters, $R_{\lambda\lambda}$ and $R_{\mu\mu}$, as well as the cross correlations between different parameters, $R_{\rho\lambda}$, $R_{\rho\mu}$, and $R_{\lambda\mu}$.

The spatial Fourier transform of the covariance is given by

$$\tilde{R}(\mathbf{p}) = \frac{1}{(2\pi)^3}\int d^3r R(\mathbf{r})e^{i\mathbf{p}\cdot\mathbf{r}}, \tag{9}$$

where $\mathbf{p}$ is the wave vector.

The general expressions of scattering attenuations from Turner and Anugonda[10] may then be simplified for the case of two-phase materials using the two-point correlation function. In the next section, the two-point correlation function is estimated from numerical simulations. The attenuations are then derived in terms of the two-point correlation function.

III. CORRELATION FUNCTION

The numerical models of the two-phase materials are constructed using Voronoi polycrystals surrounded by a matrix. This type of model allows the matrix structure to have different properties from the grain structure as dictated by typical sintering problems. Voronoi polycrystals are widely used in numerical analysis of many engineering problems. These models have been shown to model closely polycrystalline metals, ceramics and microstructures of many materials.[18–20] In Fig. 1, a Voronoi polycrystal diagram is created using a Voronoi tessellation,[21] demonstrating the two-phase geometry. A normal distribution of Voronoi nuclei is used such that the scattering theories assume uniform grain size, which is the average diameter D of the grains. The thickness of the matrix d is also assumed uniform. Various combinations of grain size and thickness of interface can be created as needed. Thus, the microstructural and statistical information of the medium may be obtained from such models.

Once such a model is created, the two-point correlation function can be measured in five steps: (i) Choose two random points $\mathbf{x}$ and $\mathbf{y}$ separated by a distance r repeatedly throughout the model; (ii) judge whether the points are inside grains or matrix; (iii) calculate $\delta\rho(\mathbf{x})$, $\delta\rho(\mathbf{y})$ for each point, and then calculate the covariance $\langle\delta\rho(\mathbf{x})\delta\rho(\mathbf{y})\rangle$ using the

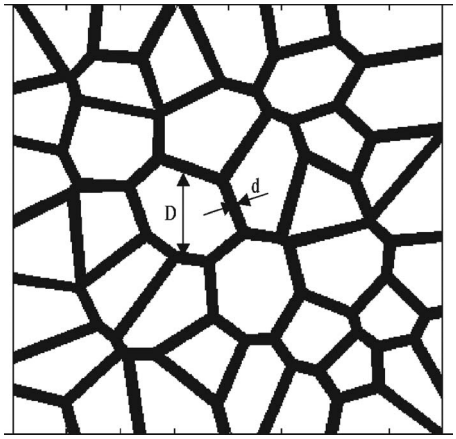


FIG. 1. Two-phase model using Voronoi polycrystals, with the grain diameter (size) D and the thickness of the matrix d.

definition of the ensemble average; (iv) average the covariance from different realizations of numerical models (here 100 realizations proved sufficient to obtain converged correlation behavior); (v) deduce the two-point correlation function $S_1=\langle\chi_1(\mathbf{x})\chi_1(\mathbf{y})\rangle$ using Eq. (8). Example correlation statistics of density from 100 realizations for a model of size 2.5 mm by 2.5 mm by 2.5 mm, grain size 0.8 mm, interface thickness 0.1 mm, are shown in Fig. 2. Note the step size Δr used was 0.006 mm for this result.

Although the two-point correlation function can be acquired directly from numerical simulations, the use of an analytical form is more helpful in evaluation of attenuation. The proper mathematical forms of these functions can allow us to investigate the details of the microstructure and therefore obtain the attenuation of ultrasound in the materials of interest. The use of appropriate forms of the two-point correlation functions has been investigated by Torquato and Stell,[22–26] Corson,[27,28] and Cule and Torquato,[29] to name a few. The exponential formula of the correlation function in Stanke and Kino's macroscopically isotropic model has been widely adopted in the studies of ultrasound attenuation in polycrystalline solids. They chose the following spatial autocorrelation function[6]

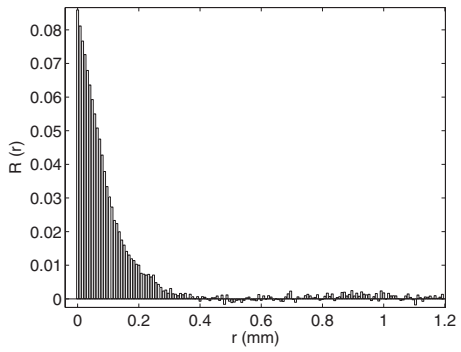


FIG. 2. Histogram of covariance from 100 realizations for a model of size 2.5 mm by 2.5 mm by 2.5 mm, grain size 0.8 mm, interface thickness 0.1 mm.

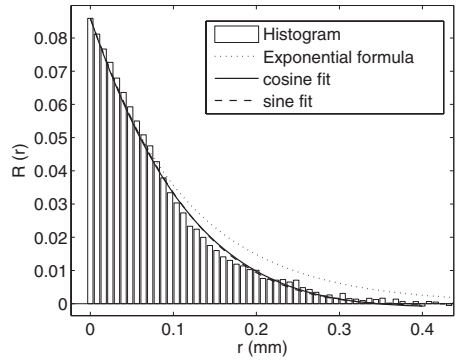


FIG. 3. Least squares fits to the measured data with the exponential formula and other models of correlation functions.

$$W(r) = e^{-r/L}, \tag{10}$$

which corresponds to the normalized two-point moment $\langle\chi_1(\mathbf{x})\chi_1(\mathbf{y})\rangle-\eta_1^2$ in our case. However, as shown in Fig. 3, this exponential formula is not valid to represent the numerical histogram data measured in the two-phase model. As mentioned above, this formula also failed for the geometric autocorrelation function in the grain boundary structure of a commercial aluminum alloy.[12] Therefore, finding a suitable formula for the two-phase medium is necessary. For a statistically homogeneous, isotropic microstructure, Cule and Torquato,[29] Yeong and Torquato,[30] proposed the following two-point correlation functions, respectively:

$$S_1(r) = \eta_1^2 + \eta_1\eta_2 e^{-br}\frac{\sin(qr)}{qr} \tag{11}$$

and

$$S_1(r) = \eta_1^2 + \eta_1\eta_2 e^{-b'r}\cos(cr), \tag{12}$$

where b, q, and b', c are characteristic spatial scale parameters, and $\eta_2=1-\eta_1$ is the volume fraction of phase "2." A least squares fit to the measured data using these two correlation functions in Fig. 3 shows that both of them are suitable to represent the two-point correlation function of this two-phase model. Note that only the positive part before oscillation is considered for curve fitting due to the short-range order observed. Therefore, the correlation function for the two-phase model is given by

$$S(r) = \begin{cases} \eta_1^2 + \eta_1\eta_2 e^{\frac{-br\sin(qr)}{qr}} \text{ or } \eta_1^2 + \eta_1\eta_2 e^{-b'r}\cos(cr), & 0 \le r \le r_0, \\ 0, & r > r_0, \end{cases} \tag{13}$$

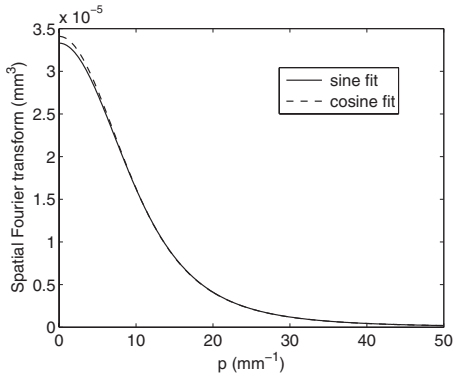


FIG. 4. Comparison of spatial Fourier transforms for the two correlation functions.

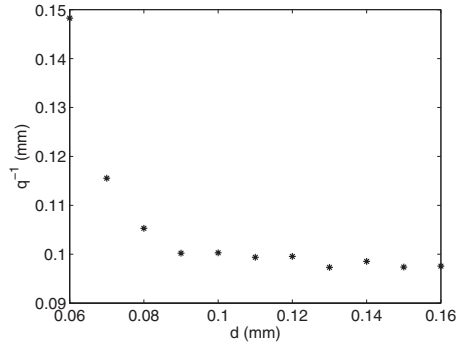


FIG. 6. Characteristic parameter q^{-1} vs. d for one combination of $D+d$ =0.83 mm.

where $r_0=\pi/q$ or $\pi/2c$ for models (11) and (12), respectively. The spatial Fourier transforms of the covariance obtained by curve fitting the histogram for both models are shown in Fig. 4. We found the difference between the two models is very small such that the attenuation results do not vary substantially. It is also found that the characteristic parameters in both models behave very similarly. Therefore, we conclude that both models provide good descriptions of the measured correlation functions. Here, only model (11) is used in the attenuation calculations that follow.

A least squares fit to the histogram of the measured two-point correlation function provides the two parameters b, q for the model given by Eq. (11). Note that there are also two independent parameters, grain size D and interface thickness d, for the two-phase geometry. Next the relationship between b, q and D, d is studied. Given a 2.5 mm by 2.5 mm by 2.5 mm cube, if we have the specified numbers of grains, the sum of $D+d$ is constant even when we change the thickness of the interface d. Figure 5 shows how b changes with the thickness d for the cube geometry with 80 grains, where $D+d=0.83$. The characteristic length scale b^{-1} appears to vary linearly with d. From Fig. 6, it seems q is a function of $(D+d)$ because it does not change significantly with d. Models with different numbers of grains are also created so that different values of $D+d$ are examined. A similar relationship between b^{-1} and d is observed in Fig. 7 for different combinations of $D+d$. However, from Fig. 8 the physical meaning of q is not clearly related with the geometric parameters, and is still under investigation. We also found out that these two models of correlation functions do not fit well to the histogram when the ratio of d/D is very small. Figure 9 shows the least squares fit to the histogram for the case of $d=0.03$, $D=0.80$. It is also seen that the exponential formula does not fit the data well. After investigation, it is believed that the ratio d/D needs to be larger than about 0.06 to apply the correlation function of Eq. (11).

The spatial Fourier transform of the two-point moment was then evaluated using numerical integration as

$$\tilde{S}(\mathbf{p}) = \frac{1}{(2\pi)^3}\int_0^{r_0}\int_0^{\pi}\int_0^{2\pi}\left(\eta_1\eta_2 e^{-br}\frac{\sin(qr)}{qr}\right) \times e^{-ipr\cos\theta}\sin\theta r^2 dr d\theta d\phi. \quad (14)$$

Expressions of attenuation for longitudinal and shear waves can then easily be obtained. In the next section, example numerical results and discussion are presented.

IV. EXAMPLE ATTENUATION RESULTS

Example results are presented for this two-phase model with known D and d. It is first assumed that the material properties are uncorrelated such that the cross correlations are zero ($R_{\rho\mu}=R_{\rho\lambda}=R_{\lambda\mu}=0$). In this case, the general expressions of scattering attenuations are given by[10]

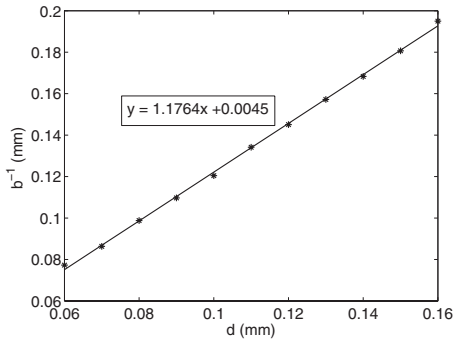


FIG. 5. Characteristic parameter b as a function of d for a 2.5 mm by 2.5 mm by 2.5 mm cubic model with 80 grains.

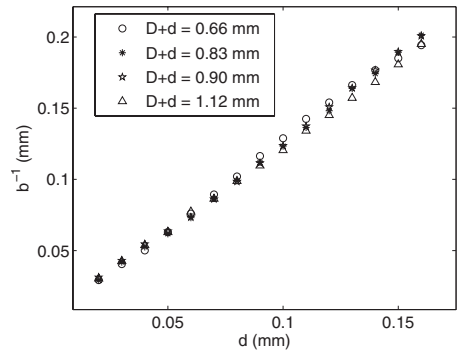


FIG. 7. Characteristic parameter b as a function of d for different combinations of $D+d$.

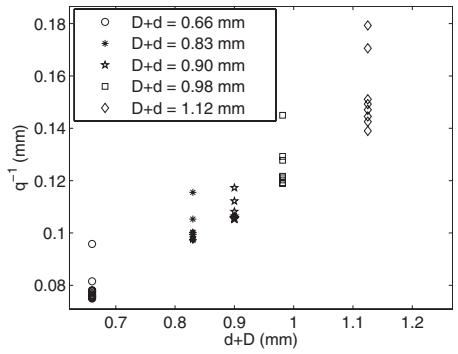


FIG. 8. Characteristic parameter q^{-1} in terms of $D+d$ for different combinations of $D+d$.

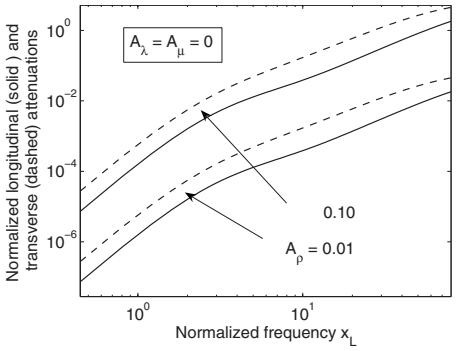


FIG. 10. Normalized longitudinal and transverse attenuations as a function of dimensionless frequency, $x_L=\omega D/c_L$, for density fluctuations only.

$$\alpha_{LL}=\frac{\pi^2\omega^4}{2c_L^4}\int_{-1}^{+1}\left\{\chi^2\tilde{R}_{\rho\rho}^{LL}(\chi)+\frac{(c_L^2-2c_T^2)^2}{c_L^4}\tilde{R}_{\lambda\lambda}^{LL}(\chi)+\frac{4c_T^4}{c_L^4}\chi^4\tilde{R}_{\mu\mu}^{LL}(\chi)\right\}d\chi, \tag{15}$$

$$\alpha_{LT}=\frac{\pi^2\omega^4}{2c_Lc_T^3}\int_{-1}^{+1}(1-\chi^2)\left\{\chi^2\tilde{R}_{\rho\rho}^{LT}(\chi)+\frac{(c_L^2-2c_T^2)^2}{c_L^4}\tilde{R}_{\lambda\lambda}^{LL}(\chi)+\frac{4c_T^2}{c_L^2}\chi^2\tilde{R}_{\mu\mu}^{LT}(\chi)\right\}d\chi,$$

$$\alpha_{TL}=\frac{1}{2}\left(\frac{c_T}{c_L}\right)^2\alpha_{LT},$$

$$\alpha_{TT}=\frac{\pi^2\omega^4}{4c_T^4}\int_{-1}^{+1}\{(\chi^2+1)\tilde{R}_{\rho\rho}^{TT}(\chi)+(1-3\chi^2+4\chi^4)\tilde{R}_{\mu\mu}^{TT}(\chi)\}d\chi,$$

where ω is the angular frequency. The $\tilde{R}$ terms are defined by

$$\tilde{R}^{ij}=\tilde{R}\left(\left|\frac{\omega}{c_i}\hat{\mathbf{p}}-\frac{\omega}{c_j}\hat{\mathbf{s}}\right|\right), \tag{16}$$

where i and j refer to the wave types, L or T (longitudinal or transverse). Here, $\hat{\mathbf{p}}$ defines the propagation direction and $\hat{\mathbf{s}}$ defines the scattered direction, with $\chi=\hat{\mathbf{p}}\cdot\hat{\mathbf{s}}=\cos\Phi$, where Φ is the angle between these directions. The correlation functions depend only on this angle due to the assumption of statistical isotropy. The final expressions for the total attenuations are given by[14]

$$\alpha_L=\alpha_{LL}+\alpha_{LT}, \tag{17}$$

$$\alpha_T=\alpha_{TL}+\alpha_{TT}. \tag{18}$$

For the two-phase material, since the material properties are assumed uncorrelated, from Eq. (8) the covariance can be written

$$R_{\tau\tau}(r)=A_\tau^2[S(r)-\eta_1^2], \tag{19}$$

where the subscript τ refers to the material parameters ρ, λ and μ. The contrast of the properties for the two phases is given by $A_\tau=(\tau_1-\tau_2)/\bar{\tau}$.

For the specific case shown here, the grain size and thickness of the matrix are chosen as $D=0.80$ mm and $d=0.10$ mm. The volume fraction of the grains is $\eta_1=0.684$. The parameters in the two-point correlation model are $b=8.09\ \text{mm}^{-1}$ and $q=8.90\ \text{mm}^{-1}$. The ratio of wave speed used here is $c_T/c_L=1/2$.

Numerical results of the attenuations are now presented. Figure 10 shows the normalized longitudinal $\alpha_L D$ and transverse attenuations $\alpha_T D$ as a function of dimensionless frequency, $x_L=\omega D/c_L$, for density fluctuations only ($A_\lambda=A_\mu=0$). The attenuations increase with the fourth power of frequency in the low frequency limit as expected. After a transition region, the attenuations scale with the square of frequency. The longitudinal attenuation is always smaller than the transverse attenuation as shown. It can be seen that the contrasts or fluctuations of material properties affect the ratio of the attenuations. Figure 11 shows the normalized longitudinal and transverse attenuations as a function of dimensionless frequency, x_L, for modulus fluctuations only ($A_\rho=0$). Similar results are seen as those in Fig. 10. From Eq. (15), attenuations of all material property fluctuations are just the sum of each component from these figures. Moreover, the contribution of density fluctuations to the attenuation weighs much more than modulus fluctuations for the same level of contrasts. All these results are in qualitative agreement with those of previous work.[10]

Finally, the influence of correlation functions is examined. Figure 12 is a plot of normalized longitudinal attenuations for $A_\rho=0.1$, $A_\lambda=A_\mu=0$ using the exponential formula

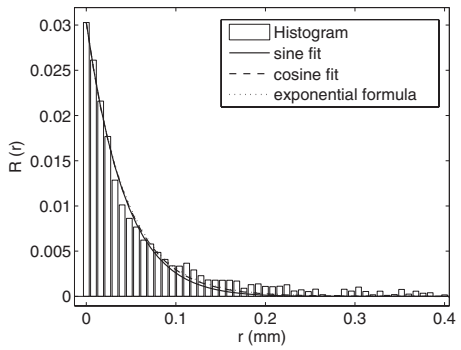


FIG. 9. Fitting of the correlation function for the model with a small ratio of d/D ($d=0.03, D=0.80$).

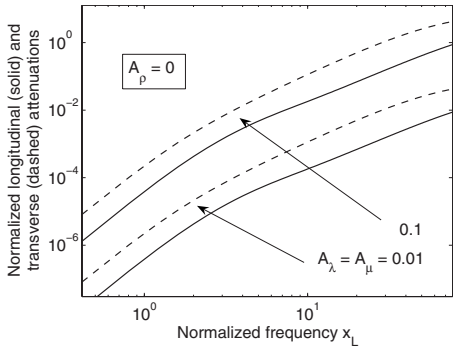


FIG. 11. Normalized longitudinal and transverse attenuations as a function of dimensionless frequency, x_L, for modulus fluctuations only.

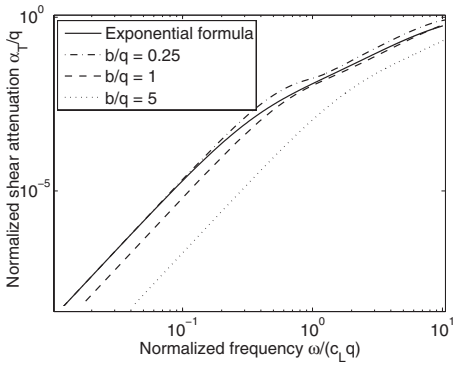


FIG. 13. Comparison of normalized transverse attenuations for $A_\rho=0.1$, $A_\lambda=A_\mu=0$ using exponential formula and Cule's correlation function.

and Cule and Torquato's model, respectively. Attenuations change with the ratio of b/q for this multiple parameter correlation model. When b/q is about 0.25, the attenuations of two models appear to have overlap in the low frequency range. However, as the frequency increases, the attenuations differ with each other. The results show that the multiple correlation lengths may not be detected at low frequencies. In this specific case, when the dimensionless frequency x_L is smaller than about 0.2, only one correlation length may be extracted. The most likely frequency range to extract both b and q is about $0.3<x_L<4$ as observed in this figure. Figure 13 is a plot of normalized transverse attenuations for different correlation functions. Similar results can be observed. The importance of extracting the correlation function from ultrasonic measurements has not been discussed before. All previous attenuation models use correlation functions with a single correlation length. The attenuation results presented here suggest that new ultrasonic techniques for characterization of multiple correlation parameters may be possible. The frequency to be used to extract the multiple correlation parameters may be determined based on the theoretical models developed here. In addition to the analysis presented here, numerical models for attenuation will also be necessary and will be investigated in subsequent work.

V. SUMMARY

The propagation of elastic waves in a statistical homogeneous and statistical isotropic two-phase solid has been investigated. The theory was derived for the case of both density and Lamé parameters which varied spatially. A numerical method to determine directly the geometric spatial correlation function of the microstructure has been presented. The exponential formula used previously was not applicable for the two-phase model compared with the numerical data. However, the models of two-point correlation functions given by Eqs. (11) and (12) would provide a suitable setting for the two-phase microstructure. The characteristic parameters in these models were also examined. Using those two-point correlation functions, the final expressions of attenuation were given in terms of the spatial statistics of density and Lamé constants. As mentioned, the fluctuations must be small and the volume fraction of each phase must not be so high $(d/D>0.06)$ for the validity of the correlation function model. Influence of the correlation functions on attenuations was observed. The results show that extracting the multiple correlation lengths may only be feasible in a specific frequency range. The general formulation here can be directly related to sintered metals, concrete, and polycrystals with decorated grain boundaries for which previous models had difficulty explaining the experimental results.[31,32] These results should be very useful for nondestructive testing and materials characterization research despite the simplicity of the assumptions made.

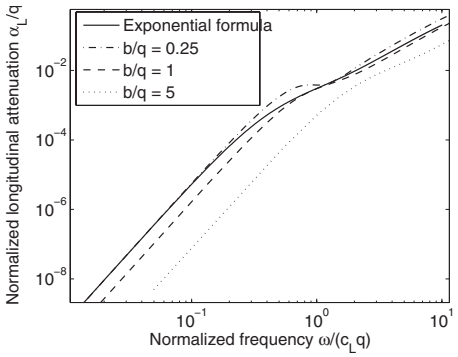


FIG. 12. Comparison of normalized longitudinal attenuations for $A_\rho=0.1$, $A_\lambda=A_\mu=0$ using exponential formula and Cule's correlation function.

ACKNOWLEDGMENT

The financial support of the U.S. Department of Energy (Grant No. DE-FG02-01ER45890) is gratefully acknowledged by the authors.

[1]M. J. Johnson and J. R. Bowler, "Pulsed eddy-current measurements for the characterization of thin layers and surface treatments," *Review of Progress in Quantitative Nondestructive Evaluation*, edited by D. O. Thompson and D. E. Chimenti (Plenum, New York, 1997), Vol. **17A**, pp. 251–257.

[2]N. Kulkarni, B. Moudgil, and M. Bhardwaj, "Ultrasonic characterization of green and sintered ceramics: I, time domain," Am. Ceram. Soc. Bull. **73**(7), 83–85 (1994).

[3]J. C. Foley and D. K. Rehbein, "In-situ nondestructive evaluation methods for characterizing sintering of aluminum powder metallurgy compacts," P/M Science and Technology Briefs **2**(1), 10–13 (2000).

[4]G. C. Papanicolaou, L. V. Ryzhik, and J. B. Keller, "Stability of the P-to-S energy ratio in the diffusive regime," Bull. Seismol. Soc. Am. **86**(4), 1107–1115 (1996).

[5]L. V. Ryzhik, G. C. Papanicolaou, and J. B. Keller, "Transport equations

for elastic and other waves in random media," Wave Motion **24**, 327–370 (1996).
[6]F. E. Stanke and G. S. Kino, "A unified theory for elastic wave propagation in polycrystalline materials," J. Acoust. Soc. Am. **75**, 665–681 (1984).
[7]F. E. Stanke, "Spatial autocorrelation functions for calculations of effective propagation constants in polycrystalline materials," J. Acoust. Soc. Am. **80**, 1479–1485 (1986).
[8]S. Ahmed and R. B. Thompson, "Propagation of elastic waves in equiaxed stainless-steel polycrystals with aligned [001] axes," J. Acoust. Soc. Am. **99**(4), 2086–2096 (1996).
[9]J. A. Turner, "Elastic wave propagation and scattering in heterogeneous, anisotropic media: Textured polycrystalline materials," J. Acoust. Soc. Am. **106**, 541–552 (1999).
[10]J. A. Turner and P. Anugonda, "Scattering of elastic waves in heterogeneous media with local isotropy," J. Acoust. Soc. Am. **109**, 1787–1795 (2001).
[11]L. Yang and J. A. Turner, "Scattering of elastic waves in damaged media," J. Acoust. Soc. Am. **113**, 2992–3000 (2003).
[12]C. Man, R. Paroni, Y. Xiang, and E. A. Kenik, "On the geometric autocorrelation function of polycrystalline materials," J. Comput. Appl. Math. **190**, 200–210 (2006).
[13]U. Frisch, "Wave propagation in random media," *Probabilistic Methods in Applied Mathematics*, edited by A. T. Barucha-Reid (Academic, New York, 1968), Vol. 1, pp. 75–198.
[14]R. L. Weaver, "Diffusion of ultrasound in polycrystasls," J. Mech. Phys. Solids **38**, 55–86 (1990).
[15]K. Z. Markov and J. R. Willis, "On the two-point correlation function for dispersions of nonoverlapping spheres," Math. Models Meth. Appl. Sci. **8**(2), 359–377 (1998).
[16]K. Z. Markov, "On the correlation functions of two-phase random media and related problems," Proc. R. Soc. London, Ser. A **455**, 1049–1066 (1999).
[17]E. Vanmarcke, *Random Fields, Analysis and Synthesis* (MIT Press, Cambridge, MA, 1983).
[18]S. Ghosh, Z. Nowak, and K. Lee, "Tessellation-based computational methods for the characterization and analysis of heterogeneous microstructures," Compos. Sci. Technol. **57**(9), 1187–1210 (1997).
[19]P. D. Zavattieri, P. V. Raghuram, and H. D. Espinosa, "A computational model of ceramic microstructures subjected to multi-axial dynamic loading," J. Mech. Phys. Solids **49**(1), 27–68 (2001).
[20]W. Brostow and V. M. Castano, "Voronoi polyhedra as a tool for dealing with spatial structures of amorphous solids and liquids and dense gases," J. Mater. Educ. **21**, 297 (1999).
[21]S. Kumar, S. K. Kurtz, J. R. Banavar, and M. G. Sharma, "Properties of a three-dimensional Poisson-Voronoi tesselation: A Monte Carlo study," J. Stat. Phys. **67**(3/4), 523–551 (1992).
[22]S. Torquato and G. Stell, "Microstructure of two-phase random media. I. The N-point probability function," J. Chem. Phys. **77**(4), 2071–2077 (1982).
[23]S. Torquato and G. Stell, "Microstructure of two-phase random media. II. The Mayer–Montroll and Kirkwood–Salsburg Hierarchies," J. Chem. Phys. **78**(6), 3262–3272 (1983).
[24]S. Torquato and G. Stell, "Microstructure of two-phase random media. III. The N-point matrix probability functions for fully penetrable spheres," J. Chem. Phys. **79**, 1505–1510 (1983).
[25]S. Torquato and G. Stell, "Microstructure of two-phase random media. IV. Expected surface area of a dispersion of penetrable spheres and its characteristics function," J. Chem. Phys. **80**(2), 878–880 (1984).
[26]S. Torquato and G. Stell, "Microstructure of two-phase random media. V. The N-point matrix probability functions for impenetrable spheres," J. Chem. Phys. **82**, 980–987 (1985).
[27]P. B. Corson, "Correlation functions for predicting properties of heterogeneous materials. I. Experimental measurement of spatial correlation functions in multiphase solids," J. Appl. Phys. **45**(7), 3159–3164 (1976).
[28]P. B. Corson, "Correlation functions for predicting properties of heterogeneous materials. II. Empirical construction of spatial correlation functions for two-phase solids," J. Appl. Phys. **45**(7), 3165–3170 (1976).
[29]D. Cule and S. Torquato, "Generating random media from limited microstructural information via stochastic optimization," J. Appl. Phys. **86**(6), 3428–3437 (1976).
[30]C. L. Y. Yeong and S. Torquato, "Reconstructing random media," Phys. Rev. E **57**(1), 495–506 (1998).
[31]X.-G. Zhang, W. A. Simpson, Jr., and J. M. Vitek, "Ultrasonic attenuation due to grain boundary scattering in copper and copper-Aluminum," J. Acoust. Soc. Am. **116**(1), 109–116 (2004).
[32]J. Mittleman, K. Y. Han, and R. B. Thompson, "Ultrasonic examination of Ti-6-4 and Ni-trided Ti-6-4 Materials," *Review of Progress in Quantitative NDE*, edited by D. O. Thompson and D. E. Chimenti (Plenum, New York, 1995), Vol. 14, pp. 1457–1464.

Theory and analysis of frequency-domain photoacoustic tomography

Natalie Baddour[a)]
Department of Mechanical Engineering, University of Ottawa, 161 Louis Pasteur, Ottawa Ontario, Canada K1N 6N5

(Received 8 August 2007; revised 2 January 2008; accepted 24 February 2008)

A new frequency-domain approach to photoacoustic tomography has recently been proposed, promising to overcome some of the shortcomings associated with the pulsed photoacoustic approach. This approach offers many of the benefits of pulsed photoacoustics but requires a different set of equations for modeling of the forward and inverse problems due to the longer time scales involved in the optical input signal. The theory of photoacoustic tomography with an optical input that is not necessarily a short pulse is considered in this paper. The full optical, thermal, and acoustic governing equations are derived. A transfer function approach is taken for the solution and analysis of this problem. The results and implications are compared with those of pulsed photoacoustics and traditional ultrasonic diffraction tomography. A Fourier diffraction theorem is also presented, which could be used as a basis for the development of tomographic imaging algorithms.
© *2008 Acoustical Society of America.* [DOI: 10.1121/1.2897132]

PACS number(s): 43.35.Ud, 43.20.Bi, 43.60.Pt [LLT] Pages: 2577–2590

I. INTRODUCTION

In recent years, noninvasive laser-based diagnostic and imaging techniques have been proposed and developed. Photoacoustic signal generation is a new technique, which has demonstrated great potential for visualization of the internal structures and function of soft tissue. It has particularly shown great potential for small animal imaging.[1,2] With this technique, a short-pulsed laser source is used to irradiate the sample. The energy absorbed produces a small temperature rise, which induces a pressure inside the sample through thermal expansion. This pressure acts as an acoustic source and generates further acoustic waves, which can be detected by ultrasound transducers positioned outside the sample. As there is a large difference in optical absorption between blood and surrounding tissue, the ultrasound wave induced by the laser irradiation carries information about the optical absorption property of the tissue. This approach is thus suitable for the imaging of the microvascular system or for tissue characterization.

This imaging technique has contrast similar to that of pure optical imaging and spatial resolution similar to that of pure ultrasonic imaging. It therefore combines the advantages of two imaging modalities in a single modality. The issue of the strong scattering of light in media such as biological tissue is overcome and the ability of acoustic waves to travel long distances without significant distortion or attenuation is also exploited. Photoacoustic detection has shown concrete promise of imaging in turbid media at depths greater than the full thickness of skin.[3,4]

The potential for high contrast is the most potent advantage of the technique. The large variation in the optical absorption and scattering properties of different tissue constituents can be exploited. Sources of naturally occurring absorption contrast include chromophores—features that selectively absorb light at certain wavelengths—such as blood vessels, tumors, hemoglobin (and its various oxygenated states), melanin, beta-carotene, and lipids. Of all of these, hemoglobin is perhaps the most significant. It offers strong optical contrast at optical wavelengths giving the technique the potential to image blood vessels for directly assessing arterial disease or mapping the vasculature. It can also be exploited to detect abnormal tissue morphologies such as cancerous lesions and vascular lesions that are accompanied by changes in the surrounding vasculature and tissue oxygenation status.[5,6] For three-dimensional (3D) imaging, the achievable resolution depends not only on the experimental approach but also on the choice of image reconstruction algorithm.[7–14] Careful design and verification of tomographic algorithms are required to ensure stable, rapid, and artifact-free imaging. A good review of photoacoustic imaging is given in Ref. 12.

The general field of photoacoustic tomography has so far been based entirely on pulsed laser excitation and time-of-flight measurements of acoustic transients to determine the position and optical properties of subsurface chromophores.[4,7,8,15–17] The field has recently experienced rapid development due to promising results for subsurface measurements and imaging of turbid media.[2,18]

A novel Fourier-domain photothermoacoustic (FD-PTA) imaging methodology has recently emerged.[5,19] For FD-PTA, the acoustic wave is generated by periodic modulation of a laser. In general, frequency-domain approaches in place of time-domain approaches have been shown to yield higher signal-to-noise ratios in other imaging modalities.[20] In this paper, the term photothermoacoustic imaging will be used to denote photoacoustic imaging where a short pulse is not necessarily used. This may imply a frequency-domain approach with narrow-band lock-in amplifiers or a time-domain approach where the pulse used is not necessarily short enough

[a)]Electronic mail: nbaddour@uottawa.ca

to fulfil the assumptions upon which photoacoustic imaging is based. Thus, the data can be acquired either as a steady-state complex intensity with measurable amplitude and phase or as time-varying intensities as the response to an input pulse. With the restriction of a short pulse removed, there is a greater degree of flexibility in the choice of input optical excitation. With this higher degree of flexibility and control available over the distribution in space and time of the illuminating sources, the potential to design an optimal acquisition system in a realistic fashion presents itself. Such a design must be based on a proper theoretical analysis. This paper aims to consider the theoretical development of the necessary background upon which to base the tomography algorithms and/or experiment design.

The layout of the paper is as follows: in Sec. II, the governing equations are derived. Sections III–V present sign conventions, geometry, and some background mathematics. Sections VI and VII present the solution to the presented problem, based on the use of the first Born approximation. Section VIII includes necessary mathematical simplifications, whereas Sec. IX considers the Green function theorem for a general illumination function. Section X presents an analysis of the implications of the mathematical results. Sections XI–XIII present the Fourier diffraction theorem for this problem, both for a generalized illumination function and for a planar illumination function and consider the implications of this theorem on the achievable resolution of this approach to imaging. Section XIV concludes the paper.

II. GOVERNING EQUATIONS

Governing equations for the coupled photothermoacoustic problem are presented here and are culled from,[5,21,22] where the photonic, thermal, or acoustic phenemena are separately discussed. The equations presented here are assembled to represent a complete model consisting of the full coupled photonic, thermal, and acoustic phenomena and are presented in infinite space in order to allow a diffraction tomographic approach. The first equation is the equation for the diffuse photon density waves (DPDW) that describes the propagation of photons in turbid media. The second equation uses the DPDW wave as a source term to the heat equation and describes the thermal expansion of the turbid media. Finally, the thermal term is used as an inhomogeneous source term to the acoustic wave equation where the variable of interest is the acoustic displacement potential.

A. Light propagation in scattering media

The gold standard for describing light propagation in turbid media is the radiative transport equation. The radiative transport equation governs light propagation in random media such as clouds, fog, and biological tissues. It takes into account scattering and absorption due to inhomogeneities in the propagating medium. Understanding the optical response due to inhomogeneities inside a uniform absorbing and scattering medium is important for imaging purposes. A commonly used approximation to the transport theory is the diffusion approximation, which describes time and frequency dependent photon diffusion. This approximation is particularly appealing due to its inherent mathematical tractability. This approximation is valid in the regime of multiple scattering such that the wavelength of light is much smaller than the thickness of the medium.[6] In this approximation, the multiply scattered light intensity is described by the diffusion equation. The equation for the DPDW, which describes the photon density $\rho_d(\mathbf{r},t)$ in the solid due to incident energy intensity $S(\mathbf{r},t)$ (optical source function) is given in the time domain by

$$D\nabla^2\rho_d(\mathbf{r},t) - \frac{1}{c}\frac{\partial}{\partial t}\rho_d(\mathbf{r},t) - \mu_a\rho_d(\mathbf{r},t) = -S(\mathbf{r},t). \tag{1}$$

In the preceding equation, μ_a is the optical absorption coefficient (m^{-1}), c is the speed of light in the turbid medium (m/s), and D is the optical diffusion coefficient (m). The optical diffusion coefficient is defined as

$$D = \frac{1}{3(\mu_a + \mu_s')}, \tag{2}$$

where μ_s' is the reduced scattering coefficient (m^{-1}). The reduced scattering coefficient μ_s' is related to the scattering coefficient μ_s such that $\mu_s' = (1-g)\mu_s$ where g is the mean cosine of the scattering function $p(\theta)$ of the photon over all spatial directions described by the solid angle Ω. It can be considered to be an assymetry parameter for anisotropic multiple scattering and can be defined as

$$g = \frac{\int_{4\pi} p(\theta)\cos\,\theta\, d\Omega}{\int_{4\pi} p(\theta) d\Omega}. \tag{3}$$

Note that $-1 \leq g \leq 1$. Isotropic scattering is given by $g=0$. Net backward scattering implies negative values of g while net forward scattering implies positive values of g. Clearly the reduced scattering coefficient μ_s' becomes equal to the scattering coefficient μ_s only in the case of isotropic scattering when $g=0$.

The diffusion approximation to the radiative transport equation, as given in Eq. (1) is valid when the absorption coefficient μ_a is much smaller than the reduced scattering coefficient μ_s', or $\mu_a \ll \mu_s'$.[23] It should be noted that even when this condition is satisfied, the diffusion approximation breaks down when the point-scatterer source is near the boundaries of the turbid medium and in general may not be applicable near the surface of a turbid medium.[6] This topic is addressed in Ref. 6, where it is found that for a turbid medium such as skin, the near-surface ballistic "skin layer" is on the order of 7–50 μm thick. A concise review of the literature on this subject is also included in that reference. It is noted that for the work considered here, an infinite domain is used and thus boundary layer effects are not considered.

Taking the Fourier transform of the DPDW equation, we obtain the Helmholtz pseudowave equation in the frequency domain:

$$\nabla^2\Psi_d(\mathbf{r},\omega) + k_p^2\Psi_d(\mathbf{r},\omega) = -\frac{S(\mathbf{r},\omega)}{D}, \tag{4}$$

where $k_p^2 = -\mu_a/D - i\omega/cD$ and $\Psi_d(\mathbf{r},\omega) = F\{\rho_d(\mathbf{r},t); t\rightarrow\omega\}$ is the Fourier transform of $\rho_d(\mathbf{r},t)$.

B. Thermal propagation equation

The equation describing the temperature rise in the material that follows as a result of the generation of the photonic diffuse density wave is given by the heat equation:

$$\nabla^2 T(\mathbf{r},t) - \frac{1}{\alpha}\frac{\partial}{\partial t}T(\mathbf{r},t) = -\frac{\mu_a}{\kappa_s}\rho_d(\mathbf{r},t). \tag{5}$$

In the frequency domain, this equation becomes another Helmholtz pseudowave equation given by

$$\nabla^2 T(\mathbf{r},\omega) + k_t^2 T(\mathbf{r},\omega) = -\mu_a \frac{\Psi(\mathbf{r},\omega)}{\kappa_s}, \tag{6}$$

where $k_t^2 = -i\omega/\alpha$ and $\Psi = \Psi_d + \Psi_c$. In the previous equation, $\Psi = \Psi_d + \Psi_c$ is the total DPDW wave and is the sum of the diffuse and coherent photon density waves. The variable α is the thermal diffusivity of the material and κ_s is the thermal conductivity of the material.

C. Acoustic propagation equation

Finally, the acoustic displacement potential is described by the wave equation, leading to the Helmholtz equation in the frequency domain. The wave equation can be dealt with by introducing a displacement potential $\phi_s(\mathbf{r},t)$, which is related to the displacement vector by[24]

$$u(\mathbf{r},t) = \nabla \phi_s(\mathbf{r},t). \tag{7}$$

Only longitudinal waves are assumed to propagate and as a result $\nabla \times u(\mathbf{r},t) = 0$ and the displacement potential satisfies the wave equation

$$\nabla^2 \phi_s(\mathbf{r},t) - \frac{1}{c_s^2}\frac{\partial^2}{\partial t^2}\phi_s(\mathbf{r},\omega) = \frac{\kappa_s \beta_s}{\rho_s c_s^2} T(\mathbf{r},t). \tag{8}$$

Taking the Fourier transform of this equation leads to a Helmholtz equation in the frequency domain with the thermal term acting as a source term, yielding

$$\nabla^2 \phi_s(\mathbf{r},\omega) + k_s^2 \phi_s(\mathbf{r},\omega) = \frac{\kappa_s \beta_s}{\rho_s c_s^2} T(\mathbf{r},\omega), \tag{9}$$

where $k_s^2 = \omega^2/c_s^2$. The thermoelastic pressure in the solid is then obtained from the displacement potential by $P(\mathbf{r},t) = -\rho_s(\partial^2/\partial t^2)\phi_s(\mathbf{r},t)$, which in the frequency domain becomes $P(\mathbf{r},\omega) = \rho_s \omega^2 \phi_s(\mathbf{r},\omega)$. Here c_s is the speed of sound in the medium, ρ_s is the material density, and β_s is the coefficient of thermal expansion of the material. Although the partial differential equation describing the variations of pressure is not an additional equation as the same information is contained in the equation for the displacement potential, it is nevertheless instructive to examine the equation for pressure:

$$\nabla^2 P(\mathbf{r},t) - \frac{1}{c_s^2}\frac{\partial^2}{\partial t^2}P(\mathbf{r},t) = -\frac{\kappa_s \beta_s}{c_s^2}\frac{\partial^2}{\partial t^2}T(\mathbf{r},t). \tag{10}$$

It can immediately be seen that the acoustic pressure is governed by the second time derivative ("acceleration") of the temperature dependence. It is noted that acoustic inhomogeneities and acoustic absorption are not modeled in this formulation.

In the preceding equations k refers to the wave number and the subscript indicates which phenomena (photonic, thermal or acoustic) the wave number is referring to. Specifically, k_p refers to the wave number for the DPDW (photonic) equation, k_t refers to the thermal wave number, and k_s refers to the acoustic wave number. It should be noted that only the acoustic wave number is real, with the thermal and photonic wave numbers being complex quantities, hence the use of the term "pseudowave" equation to describe the resulting Helmholtz equation in order not to avoid confusion with the proper Helmholtz equation with, the real wave number.

In this paper, our main interest lies in reconstructing the inhomogeneous distributions of optical absorption. Further, it is assumed in this formulation that the only inhomogeneities present are in the optical absorption coefficient.

III. NOTATION AND SIGN CONVENTIONS

From the preceding section, it can be seen that the photonic, thermal, and acoustic wave numbers are defined by the squares of their quantities and arise as a result of taking the Fourier transform of the corresponding equation. In particular,

$$k_p^2 = -\frac{\mu_a}{D} - \frac{i\omega}{cD}, \quad k_t^2 = -\frac{i\omega}{\alpha}, \quad k_s^2 = \frac{\omega^2}{c_s^2} \tag{11}$$

In the rest of the paper, we will have great use of the wave numbers themselves, namely, k_p, k_s, and k_t, which are the square roots of the equations in Eq. (11). Each k will be written as the sum of a real and an imaginary part, so that $k_p = k_{pr} + ik_{pi}$ with k_{pr} denoting the real part of k_p and k_{pi} denoting the imaginary part of k_p. Similar notations will apply to the other k's. As there are two square roots in the previous equations, we will use the convention that a particular (photonic, thermal, acoustic) k is the square root of the corresponding k^2 such that the *imaginary* part of k is positive. Hence k_p is the square root of k_p^2 such that $k_{pi} > 0$ and so forth. This convention will be important in derivations in order to ensure boundedness of solutions.

It is noted that the variable ω is the Fourier frequency variable corresponding to time. The (temporal) Fourier transform is defined in the conventional way as

$$\hat{F}(\omega) = \int_{-\infty}^{\infty} f(t) e^{-i\omega t} dt, \tag{12}$$

with the inverse transform defined by

$$f(t) = \frac{1}{2\pi}\int_{-\infty}^{\infty} \hat{F}(\omega) e^{i\omega t} d\omega. \tag{13}$$

The two-dimensional (2D) and 3D spatial Fourier transform of functions will be required and is defined as

$$\hat{F}_{3D}(\omega_x,\omega_y,\omega_z) = \int_{-\infty}^{\infty}\int_{-\infty}^{\infty}\int_{-\infty}^{\infty} f(x,y,z) \times e^{-i\omega_x x} e^{-i\omega_y y} e^{-i\omega_z z} dx\, dy\, dz. \tag{14}$$

In this case $(\omega_x, \omega_y, \omega_z)$ are the spatial frequency variables in

the Fourier domain. We will also require use of a variable of the form

$$\gamma^2 = \omega_x^2 + \omega_y^2 - k^2. \tag{15}$$

We will adopt the convention that the subscript on γ indicates the subscript of the corresponding k. That is, we define $\gamma_p^2 = \omega_x^2 + \omega_y^2 - k_p^2$, $\gamma_t^2 = \omega_x^2 + \omega_y^2 - k_t^2$, and $\gamma_s^2 = \omega_x^2 + \omega_y^2 - k_s^2$. Similarly, the use of γ will be more frequent than γ^2 and thus a convention is required to indicate which square root is being used. We will write $\gamma = \gamma_r + i\gamma_i$ where this is defined as the square root of γ^2 such that $\gamma_r \geq 0$. Similar to the convention for k_s the subscripts for γ get carried over to real and imaginary parts so that, e.g., $\gamma_s = \gamma_{sr} + i\gamma_{si}$ can be written.

IV. GEOMETRY

As for standard acoustic diffraction tomography theory, we assume a background medium infinite in extent and an inhomogeneity structure of finite extent. The previously given equations for the scattered field are valid for all points outside the inhomogeneity and for arbitrary source–detector configurations. The assumption of an infinite domain is the simplest case for physical insight and can later be modified for different geometries. As it is also the assumption typically made for standard acoustic diffraction tomography, as well as for diffuse photonic wave tomography, this assumption will allow for straightforward comparisons.

We further specialize our formulation to the case where the acoustic wave is measured by a plane of detectors so that the acoustic wave is measured in the $z = z_d$ plane. We are thus interested in the Fourier transform of the wave measured in the $z = z_d$ plane.

V. FIRST BORN APPROXIMATION

For tomographic imaging purposes, our main interest lies in reconstructing the inhomogeneous distributions of optical absorption. We therefore consider the Helmholtz equation for the photon density wave:

$$(\nabla^2 + k_p^2(\vec{r}))\Psi_d(\vec{r},\omega) = 0. \tag{16}$$

We now write

$$k_p^2(\vec{r}) = k_{p_0}^2 n^2(\vec{r}), \quad n^2(\vec{r}) = \frac{\mu_{a_0}}{\mu_a(\vec{r})}, \tag{17}$$

where $k_{p_0}^2 = -\mu_{a_0}/D - i\omega/cD$ and μ_{a_0} is the optical absorption coefficient of the assumed homogeneous medium surrounding the object region Q and $n(\vec{r})$ is a measure of the variation of the values of the optical absorption coefficient in the object from that of the surrounding homogeneous (reference) region. In this development, it is assumed that the only inhomogeneities are in the optical absorption coefficient. It is also assumed that the object has finite size. This leads to

$$(\nabla^2 + k_{p_0}^2)\Psi_d(\vec{r},\omega) = -\frac{1}{D} o_a(\vec{r})\Psi_d(\vec{r},\omega), \tag{18}$$

where the object function is given by

$$o_a(\vec{r}) = \begin{cases} k_{p_0}^2(n^2(\vec{r}) - 1), & \vec{r} \in Q \\ 0, & \vec{r} \notin Q. \end{cases} \tag{19}$$

It is noted that the preceding exactly follows the development of the diffraction tomography problem with the wave equation, with the exception of the complex nature of the photonic wave vector. The effect of the inhomogeneities of the object region appears as a source term on the right-hand side of the Helmholtz equation (18), with $o_a(\vec{r})$ being the object function representing the inhomogeneities of the scattering object region Q. The object function is zero outside the object region and its nonzero value within the object region represents the ratio of optical absorption coefficients.

The DPDW field $\Psi_d(\vec{r},\omega)$ shall be considered to be the sum of two components, $\Psi_{d0}(\vec{r},\omega)$ and $\Psi_{ds}(\vec{r},\omega)$, namely,

$$\Psi_d(\vec{r},\omega) = \Psi_{d0}(\vec{r},\omega) + \Psi_{ds}(\vec{r},\omega). \tag{20}$$

The component $\Psi_{d0}(\vec{r})$ is known as the incident field (or equivalently the illumination function) and is the field present without any inhomogeneities. It is given by the solution to

$$(\nabla^2 + k_{p_0}^2(\vec{r}))\Psi_{d0}(\vec{r},\omega) = 0. \tag{21}$$

The component $\Psi_{ds}(\vec{r},\omega)$, known as the secondary field, will be that part of the total field that can be attributed solely to the inhomogeneities. Note that this term is often referred to as the scattered field, however, the term "secondary" will be used here to avoid confusion with the true scattered field in the optical sense. The secondary component of the field will necessarily have to satisfy

$$(\nabla^2 + k_{p_0}^2)\Psi_{ds}(\vec{r},\omega) = -\frac{1}{D} o_a(\vec{r})\Psi_d(\vec{r},\omega). \tag{22}$$

It should be noted that $\Psi_d(\vec{r},\omega)$ in the right-hand side of Eq. (22) is unknown. However, for small enough inhomogeneities, $\Psi_d(\vec{r},\omega)$ can be replaced with its free-space value $\Psi_{d0}(\vec{r},\omega)$, which itself can be found from Eq. (21). Replacing $\Psi_d(\vec{r},\omega)$ with $\Psi_{d0}(\vec{r},\omega)$ on the right-hand side of Eq. (21) is known as the first Born approximation. Hence, under the first Born approximation, the secondary component of the DPDW field must satisfy

$$(\nabla^2 + k_{p_0}^2)\Psi_{dB}(\vec{r},\omega) = -\frac{1}{D} o_a(\vec{r})\Psi_{d0}(\vec{r},\omega), \tag{23}$$

where $\Psi_{dB}(\vec{r},\omega)$ is used to denote the first Born approximation to the secondary DPDW field. Thus, $\Psi_d(\vec{r},\omega) = \Psi_{d0}(\vec{r},\omega) + \Psi_{dB}(\vec{r},\omega)$, with $\Psi_{d0}(\vec{r},\omega)$ and $\Psi_{dB}(\vec{r},\omega)$ given by Eqs. (21) and (23), respectively. In the rest of what follows, we will use k_p to denote k_{p_0} for ease of notation, as no explicit reference to k_{p_0} is needed once the first Born approximation has been made.

VI. SOLUTION TO THE FORWARD PROBLEM

The complete problem formulation starts with Eq. (21) for the illumination function (which is a DPDW) along with Eq. (23), the Born solution to the inhomogeneous DPDW problem. The solution to this is subsequently used as source

terms in Eq. (6), the solution of which is then further used in Eq. (9). Hence the full problem consists of Eq. (21) along with Eqs. (6), (9), and (23).

To begin, a general illumination function is considered. That is, the sequentially coupled equations, Eqs. (6), (9), and (23), are solved without (yet) specifying a form for the illumination function. Next, we proceed by taking the spatial Fourier transform of both sides of the equations, however only with respect to the x and y variables leaving the z variable untransformed. This gives

$$\frac{d^2}{dz^2}\Psi_{dB}(\omega_x,\omega_y,z) - \gamma_p^2\Psi_{dB}(\omega_x,\omega_y,z,\omega) = -\frac{1}{D}O_a(\omega_x,\omega_y,z)\Psi_{d0}(\omega_x,\omega_y,z,\omega), \tag{24}$$

where $\gamma_p^2=\omega_x^2+\omega_y^2-k_p^2$. Denote $O_a\Psi_{d0}(\omega_x,\omega_y,z) := O_a(\omega_x,\omega_y,z)\Psi_{d0}(\omega_x,\omega_y,z,\omega)$ for brevity. Similarly, the thermal and acoustic equations become

$$\frac{d^2}{dz^2}T(\omega_x,\omega_y,z,\omega) - \gamma_t^2 T(\omega_x,\omega_y,z,\omega) = -\frac{\mu_a}{\kappa_s}\Psi_{dB}(\omega_x,\omega_y,z,\omega), \tag{25}$$

$$\frac{d^2}{dz^2}\phi_s(\omega_x,\omega_y,z,\omega) - \gamma_s^2\phi_s(\omega_x,\omega_y,z,\omega) = -\frac{\kappa_s\beta_s}{\rho_s c_s^2}T(\omega_x,\omega_y,z,\omega), \tag{26}$$

where $\gamma_t^2=\omega_x^2+\omega_y^2-k_t^2$ and $\gamma_s^2=\omega_x^2+\omega_y^2-k_s^2$. Note that Eqs. (24)–(26) can be solved using the one-dimensional (1D) Green function with the appropriate γ as the wave vector. Hence,

$$\Psi_{dB}(\omega_x,\omega_y,z,\omega) = \int_{-\infty}^{\infty}\frac{1}{2\gamma_p}e^{-\gamma_p|z-z_p|}\times\left\{\frac{1}{D}O_a\Psi_{d0}(\omega_x,\omega_y,z_p,\omega)\right\}dz_p. \tag{27}$$

The same Green function is also used to solve thermal equation (25) to give

$$T(\omega_x,\omega_y,z,\omega) = \int_{-\infty}^{\infty}\frac{1}{2\gamma_t}e^{-\gamma_t|z-z_t|}\frac{\mu_a}{\kappa_s}\Psi_{dB}(\omega_x,\omega_y,z_t,\omega)dz_t. \tag{28}$$

Using the expression in Eq. (27), this can be simplified to

$$T(\omega_x,\omega_y,z,\omega) = \frac{\mu_a}{4\kappa_s D\gamma_t\gamma_p}\int_{-\infty}^{\infty}\int_{-\infty}^{\infty}e^{-\gamma_t|z-z_t|}e^{-\gamma_p|z_t-z_p|}O_a\times\Psi_{d0}(\omega_x,\omega_y,z_p,\omega)dz_p dz_t. \tag{29}$$

Finally, the 1D Green expansion can also be used to solve acoustic equation (26) to give

$$\phi_s(\omega_x,\omega_y,z,\omega) = \int_{-\infty}^{\infty}\frac{1}{2\gamma_s}e^{-\gamma_s|z-z_s|}\frac{\kappa_s\beta_s}{\rho_s c_s^2}T(\omega_x,\omega_y,z_s,\omega)dz_s. \tag{30}$$

The expression for T from Eq. (29) is substituted into Eq. (30) and the order of integration is switched, yielding

$$\phi_s(\omega_x,\omega_y,z,\omega) = \frac{-\mu_a\beta_s}{8\gamma_p\gamma_t\gamma_s D\rho_s c_s^2}\int_{-\infty}^{\infty}\int_{-\infty}^{\infty}\int_{-\infty}^{\infty}e^{-\gamma_p|z_t-z_p|}\times e^{-\gamma_t|z_s-z_t|}e^{-\gamma_s|z-z_s|}O_a\Psi_{d0}(\omega_x,\omega_y,z_p,\omega)dz_s\,dz_t\,dz_p. \tag{31}$$

Recalling that the pressure is given by $P(\vec{r},\omega)=\omega^2\rho_s\phi_s(\vec{r},\omega)$, the Fourier transform of the pressure detected in a plane is obtained

$$\begin{aligned}P(\omega_x,\omega_y,z,\omega) &= \frac{-\mu_a\beta_s k_s^2}{D}\int_{-\infty}^{\infty}\int_{-\infty}^{\infty}\int_{-\infty}^{\infty}\frac{e^{-\gamma_p|z_t-z_p|}}{2\gamma_p}\times\frac{e^{-\gamma_t|z_s-z_t|}}{2\gamma_t}\frac{e^{-\gamma_s|z-z_s|}}{2\gamma_s}\\ &\quad\times O_a\Psi_{d0}(\omega_x,\omega_y,z_p,\omega)dz_s\,dz_t\,dz_p\\ &= \frac{-\mu_a\beta_s k_s^2}{D}\int_{-\infty}^{\infty}\int_{-\infty}^{\infty}\int_{-\infty}^{\infty}\times g_p(z_t-z_p;\gamma_p)g_t(z_s-z_t;\gamma_t)g_s(z-z_s;\gamma_s)O_a\Psi_{d0}(\omega_x,\omega_y,z_p,\omega)dz_s\,dz_t\,dz_p.\end{aligned} \tag{32}$$

In the integrand, the photonic, thermal and acoustic Green functions have been identified and labeled with the appropriate subscript, in keeping with the conventions of this paper. That is, for $i=p$, t, and s representing photonic, thermal and acoustic phenomena:

$$g_i(z;\gamma_i) = \frac{e^{-\gamma_i|z|}}{2\gamma_i}. \tag{33}$$

Equation (32) provides a good interpretation of the physics of the problem. In the Born approximation, the product of the object function and illumination function $O_a(x,y,z)\Psi_{d0}(x,y,z,t)$ can be considered as the input, with the only time dependence being in the incident diffuse photon density wave function. Let us refer to this product of object and illumination functions as the heterogeneity function. The system acts on this heterogeneity function input through the three Green functions. The system can be considered to be acting on the input with the photonic, followed by thermal, followed by acoustic Green function with the total system Green function being a product of the three. Essentially, we have

$$\begin{aligned}P(\omega_x,\omega_y,z,\omega) &= \frac{-\mu_a\beta_s k_s^2}{D}\int_{-\infty}^{\infty}\int_{-\infty}^{\infty}\int_{-\infty}^{\infty}\times g_{pts}(z,z_p,z_t,z_s;\gamma_p,\gamma_t,\gamma_s)O_a\\ &\quad\times\Psi_{d0}(\omega_x,\omega_y,z_p,\omega)dz_s\,dz_t\,dz_p,\end{aligned} \tag{34}$$

where $g_{pts}(z,z_p,z_t,z_s;\gamma_p,\gamma_t,\gamma_s)=g_p(z_t-z_p;\gamma_p)g_t(z_s-z_t;\gamma_t)\times g_s(z-z_s;\gamma_s)$.

This is a convenient way of thinking of the effect of the system as any simplifications or alternative modeling assumptions can be directly reflected in the individual Green functions and it is known that the total system Green function, given by g_{pts}, will be a product of the three individual ones and thus any changes can be analyzed directly. Note that the total system Green function, g_{pts}, is a four-dimensional (4D) function of (z,z_p,z_t,z_s) and when integrated can be considered to be the sequential convolution of the Green functions for the three subsystems. The integrations are performed over z_p, z_t, and z_s to ultimately yield a function of z. The γ's are considered to be parameters in the Green function(s). Simplifying this expression for the total system Green function will now be considered.

VII. SIMPLIFYING THE INTEGRALS

The expression for the pressure as given in Eq. (32) can be simplified. Using Lemma 1 (derived in the Appendix), the following results are important.

Result 1

$$\int_{-\infty}^{\infty}\frac{e^{-\gamma_t|z_s-z_t|}}{2\gamma_t}\frac{e^{-\gamma_s|z-z_s|}}{2\gamma_s}dz_s = \int_{-\infty}^{\infty}g_t(z_s-z_t;\gamma_t)g_s(z-z_s;\gamma_s)dz_s = \frac{g_s(z-z_t;\gamma_s)}{(k_s^2-k_t^2)} + \frac{g_t(z-z_t;\gamma_t)}{(k_t^2-k_s^2)}. \tag{35}$$

Proof: This result follows directly from the application of Lemma 1, which is given in the Appendix.

Result 2

$$\int_{-\infty}^{\infty}\int_{-\infty}^{\infty}\frac{e^{-\gamma_p|z_t-z_p|}}{2\gamma_p}\frac{e^{-\gamma_t|z_s-z_t|}}{2\gamma_t}\frac{e^{-\gamma_s|z-z_s|}}{2\gamma_s}dz_s\,dz_t = \int_{-\infty}^{\infty}\int_{-\infty}^{\infty}g_p(z_t-z_p;\gamma_p)g_t(z_s-z_t;\gamma_t)g_s(z-z_s;\gamma_s)dz_s\,dz_t = \frac{g_s(z-z_p;\gamma_s)}{(k_s^2-k_t^2)(k_s^2-k_p^2)} + \frac{g_t(z-z_p;\gamma_t)}{(k_t^2-k_s^2)(k_t^2-k_p^2)} + \frac{g_p(z-z_p;\gamma_p)}{(k_p^2-k_s^2)(k_p^2-k_t^2)} \tag{36}$$

Proof: We write

$$\int_{-\infty}^{\infty}\int_{-\infty}^{\infty}g_p(z_t-z_p;\gamma_p)g_t(z_s-z_t;\gamma_t)g_s(z-z_s;\gamma_s)dz_s\,dz_t = \int_{-\infty}^{\infty}g_p(z_t-z_p;\gamma_p)\left[\int_{-\infty}^{\infty}g_t(z_s-z_t;\gamma_t)g_s(z-z_s;\gamma_s)dz_s\right]dz_t \tag{37}$$

and then invoke Result 1.

VIII. GREEN FUNCTION THEOREM FOR A GENERAL ILLUMINATION FUNCTION

Results 1 and 2 can be used to simplify Eq. (32) to give

$$P(\omega_x,\omega_y,z,\omega) = \frac{-\mu_a\beta_s k_s^2}{D}\int_{-\infty}^{\infty}O_a\Psi_{d0}(\omega_x,\omega_y,z_p,\omega)\times\left[\frac{g_s(z-z_p;\gamma_s)}{(k_s^2-k_t^2)(k_s^2-k_p^2)} + \frac{g_t(z-z_p;\gamma_t)}{(k_t^2-k_s^2)(k_t^2-k_p^2)} + \frac{g_p(z-z_p;\gamma_p)}{(k_p^2-k_s^2)(k_p^2-k_t^2)}\right]dz_p. \tag{38}$$

Let us further define the following variables:

$$A_s := \frac{\mu_a^2k_s^2}{(k_s^2-k_t^2)(k_s^2-k_p^2)}, \tag{39}$$

$$A_t := \frac{\mu_a^2k_s^2}{(k_t^2-k_s^2)(k_t^2-k_p^2)}, \tag{40}$$

$$A_p := \frac{\mu_a^2k_s^2}{(k_p^2-k_s^2)(k_p^2-k_t^2)}. \tag{41}$$

With these new variables, Eq. (38) can be written as

$$P(\omega_x,\omega_y,z,\omega) = \frac{-\beta_s}{D\mu_a}\int_{-\infty}^{\infty}O_a\Psi_{d0}(\omega_x,\omega_y,z_p,\omega)g_{pts}\times(z-z_p;\gamma_s,\gamma_p,\gamma_t)dz_p, \tag{42}$$

where $g_{pts}(z;\gamma_s,\gamma_p,\gamma_t)=A_pg_p(z;\gamma_p)+A_tg_t(z;\gamma_t)+A_sg_s(z;\gamma_s)$

It can be seen that this is now a one dimensional (1D) problem with the pressure being given by a convolution of the heterogeneity function with the system Green function. Further, it is also clear that the system Green function, which was formerly 4D and a *product* of the subsystem Green functions, is now 1D and a *sum* of the subsystem Green functions.

A. Interpretation as a convolution

Equation (42) can be interpreted as a convolution where it can be written as

$$P(\omega_x,\omega_y,z,\omega) = \frac{-\beta_s}{D\mu_a}[O_a\Psi_{d0}(\omega_x,\omega_y,z,\omega)] * g_{pts}\times(z;\gamma_s,\gamma_p,\gamma_t)(z). \tag{43}$$

Taking the Fourier transform with respect to z of both sides turns products into convolutions and convolutions into products, leading to

$$P(\omega_x,\omega_y,\omega_z,\omega) = \frac{-\beta_s}{D\mu_a}O_a * \Psi_{d0}(\omega_x,\omega_y,\omega_z,\omega)\cdot G_{pts}\times(\omega_x,\omega_y,\omega_z,\omega), \tag{44}$$

where, $G_{pts}(\omega_x,\omega_y,\omega_z,\omega)=A_pG_p(\omega_x,\omega_y,\omega_z,\omega)+A_t\times G_t(\omega_x,\omega_y,\omega_z,\omega)+A_sG_s(\omega_x,\omega_y,\omega_z,\omega)$

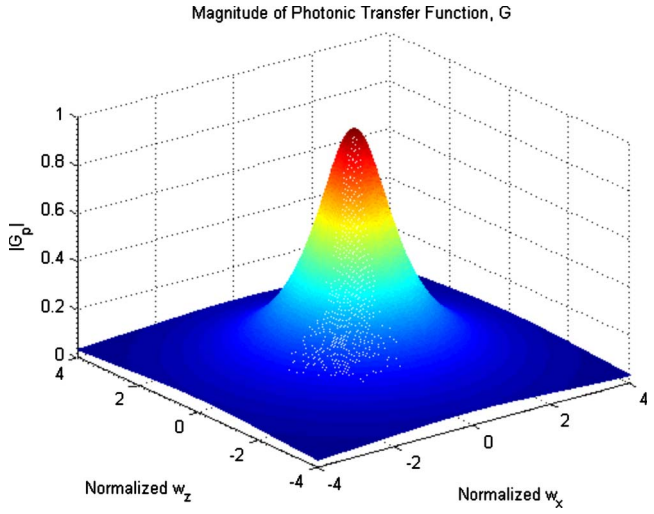


FIG. 1. (Color online) Photonic transfer function.

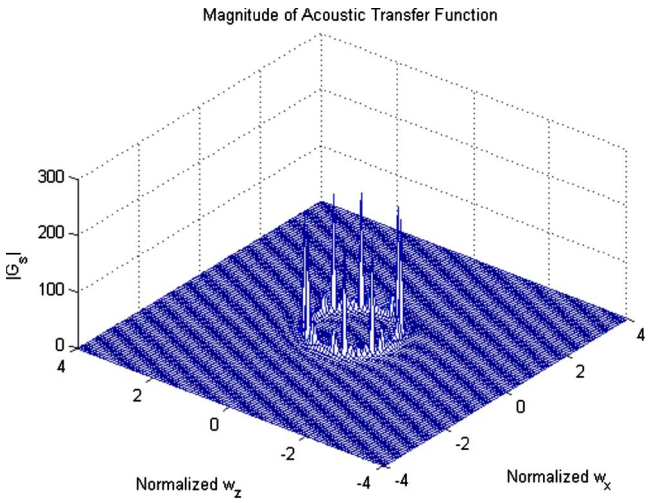


FIG. 3. (Color online) Acoustic transfer function.

The capital G is used to denote the full Fourier transform of each corresponding g function, for each of the photonic, thermal, and acoustic Green function. The form of each of these transfer functions is given by

$$G(\omega_x,\omega_y,\omega_z,\omega) = \mathbb{F}\left(\frac{e^{-\gamma_\omega|z|}}{2\gamma_\omega}\right) = \frac{2\gamma_\omega}{2\gamma_\omega}\frac{1}{\gamma_\omega^2+\omega_z^2} = \frac{1}{\omega_x^2+\omega_y^2+\omega_z^2-k^2}, \tag{45}$$

which is precisely the three-dimensional (3D) wave equation transfer function. In this form, it is easier to visualize the physical implications of the photonic, thermal, and acoustic transfer functions separately, as the combined transfer function is a sum of the three subsystem transfer functions. The magnitude of each transfer function is shown in Figs. 1–3, respectively. The transfer functions are 4D hypersurfaces in frequency space but have been plotted in Figs. 1–3 with $\omega_y = 0$ for clarity. In Figs. 1–3 each wave number in the denominator of the transfer function of the form of Eq. (45) has been normalized so that $|k| = 1$. Thus, the spatial frequencies displayed in the plots are normalized frequencies rather than true frequencies. To obtain the true frequency, each spatial frequency would have to be multiplied by the $|k|^2$ corresponding to that particular transfer function. The thermal transfer function dies off much more quickly in spatial frequency space than the photonic transfer function as the decay of both is primarily controlled by the exponent in the decaying exponential function. As the thermal wave number is smaller, the corresponding gamma exponent is larger for the thermal transfer function and thus the thermal transfer function goes to zero far more quickly than the photonic transfer function. As both the photonic and thermal wave numbers are complex, the corresponding transfer function reaches its maximum at $\omega_x = \omega_y = \omega_z = 0$ and then goes to zero for increasing spatial frequencies. Thus, the photonic and thermal transfer functions can be considered to be low-pass filters. However, the situation for the acoustic transfer function is not the same. The acoustic wave number is real, thus its transfer function, as given by Eq. (45) reaches a maximum when the denominator is zero. This would occur for $\omega_x^2 + \omega_y^2 + \omega_z^2 = k_s^2$. As illustrated in Fig. 3, in two dimensions this would be $\omega_x^2 + \omega_z^2 = k_s^2$, a circle in 2D spatial frequency space (and a sphere in 3D space). The variation in the heights of the spikes in Fig. 3 is an artifact of the discretization the Fourier space and not an inherent property of the transfer function. The acoustic transfer function can be considered to be a band-pass filter, with frequencies satisfying $\omega_x^2 + \omega_y^2 + \omega_z^2 = k_s^2$ passed on for detection.

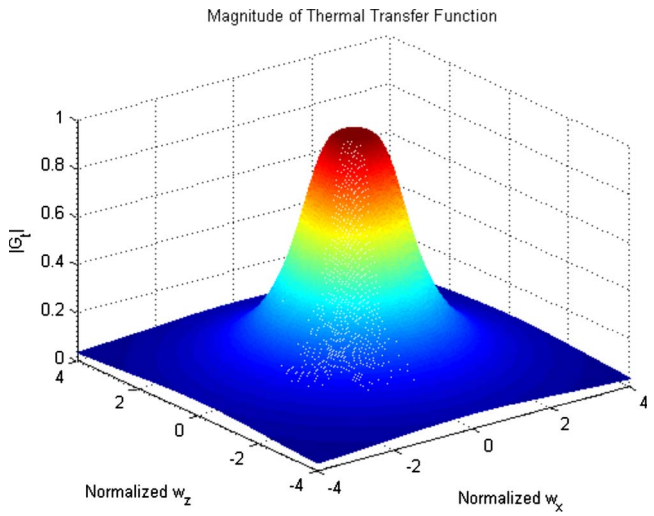


FIG. 2. (Color online) Thermal transfer function.

B. Block diagram and comparison with ultrasonic imaging

From Eq. (44), it can be seen that the detected pressure in Fourier frequency space (spatial and temporal) can be considered as a sequence of operations on the object (inhomogeneity) function. The object function is first convolved with the illumination function. This resulting function (termed the heterogeneity) function is then multiplied by the system transfer function. For the photothermoacoustics problem, this

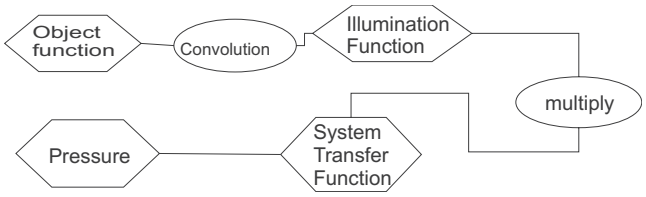


FIG. 4. Schematic of PTA process in the spatial and temporal frequency domain.

system transfer function is actually a sum of the three subsystem transfer functions. This process yields the pressure everywhere. This is shown schematically in Fig. 4. Clearly, the act of detecting the pressure on some surface is yet another transfer function, which acts on the resulting pressure function.

Viewing the photothermoacoustic process in the block diagram of Fig. 4 allows immediate comparison with the usual ultrasonic imaging modality. For traditional ultrasonic imaging, the inhomogeneity being imaged (i.e., the object function) represents inhomogeneities in the speed of sound in the object. In comparison, with PTA imaging, it is the inhomogeneities in the absorption coefficient of the tissue that are being imaged. The large variation in the optical absorption of different tissue constituents is thus expoited as these are the high-contrast inhomogeneities that are being imaged. For ultrasonic imaging, the illumination function is typically a plane-wave acoustic wave. This plane wave is a delta function in the spatial frequency domain and its convolution with the object function yields a shift of the object function in spatial Fourier space. In PTA imaging, the illumination function is a DPDW. Finally, the system transfer function for ultrasonic imaging is the acoustic transfer function alone, similar to the acoustic subsystem transfer function derived here. For PTA imaging, the system transfer function consists of the sum of the acoustic, photonic, and thermal transfer functions with the effect of each to be discussed shortly.

C. Comparison with pulsed photoacoustic imaging

In pulsed photoacoustic tomography, the pulse duration is so short that the thermal conduction time is greater than the thermoacoustic transit time and the effect of thermal conduction can be ignored.[25] The equation describing the resulting thermoacoustic pressure wave propagation is given by[12–14,25,26]

$$\nabla^2 p(\vec{r},t) - \frac{1}{c_s^2}\frac{\partial^2}{\partial t^2}p(\vec{r},t) = -\frac{\beta_s c_s}{C_p}\frac{\partial}{\partial t}H(\vec{r},t), \tag{46}$$

where C_p is the specific heat, H is the heating function defined as the thermal energy deposited by the energy source per time and volume, β_s is the coefficient of thermal volume expansion, and c_s is the speed of sound. The heating function can be written as the product of a spatial absorption function and a temporal illumination function of the rf source,

$$H(\vec{r},t) = I_0 o_a(\vec{r})\,\eta(t), \tag{47}$$

where I_0 is a scaling factor proportional to the incident radiation intensity and $o_a(\vec{r})$ describes the absorption properties of the medium—essentially the inhomogeneity whose image is sought. The function $\eta(t)$ describes the shape of the irradiating pulse and is a nonnegative function whose integration over time equals the pulse energy. Taking the Fourier transform with respect to time and the 3D Fourier transform with respect to space of Eq. (46) yields

$$P(\omega_x,\omega_y,\omega_z,\omega) = \frac{\beta I_0 i\omega}{C_p}\eta(\omega) \times O_a(\omega_x,\omega_y,\omega_z)G_s(\omega_x,\omega_y,\omega_z,\omega), \tag{48}$$

where

$$G_s(\omega_x,\omega_y,\omega_z,\omega) = \frac{1}{\omega_x^2+\omega_y^2+\omega_z^2-k_s^2} \tag{49}$$

is the acoustic transfer function. This can be directly compared with Eq. (43) for the full photo-thermo-acoustic problem. We see that there are several differences. First, the transfer functions are not the same. The pulsed photoacoustic problem yields the purely acoustic transfer function whereas the full photothermoacoustic problem has a transfer function, which is a sum of the acoustic, thermal, and photonic transfer functions. Second, for the pulsed photoacoustic problem, the system transfer function is directly multiplied with the object function. However, for the photothermoacoustic problem, the object function is first convolved with the illumination function before being multiplied by the system transfer function. As the choice of illumination function is somewhat under the control of the designer, it should be expected that the photothermoacoustic approach might yield greater ability to "probe" the object function and thus better imaging results.

IX. DIMENSIONAL ANALYSIS

The relative importance of acoustic, thermal, and photonic effects will be governed by three separate characteristic frequencies. To analyze the effects of acoustic, thermal, and photonic effects, let us define these characteristic frequencies as

$$\omega_s := \mu_a c_s =: \frac{1}{\tau_s}, \quad \omega_t := \mu_a^2\alpha =: \frac{1}{\tau_t}, \quad \omega_p := \mu_a c =: \frac{1}{\tau_p}. \tag{50}$$

The subscripts have been used along with this paper's convention of s,t, and p referring to acoustic, thermal, and photonic phenomena, respectively. Each characteristic frequency also defines a characteristic time, with this time defined as the inverse of the corresponding characteristic frequency. The time τ_s is the transit time of sound through the depth of light penetration. This is the time taken for stress to traverse the heated region. For frequencies $\omega > \omega_s$, or equivalently for times $t < \tau_s$, this condition is known as stress confinement.[12] For frequencies $\omega > \omega_t$, then heat conduction is considered to be negligible[25] as the thermal diffusion length is shorter than

the heating zone. Thus the time τ_t can be interpreted as a characteristic time scale for the heat dissipation of the absorbed photonic energy by thermal conduction.[12] It is a measure of the relative sizes of the depth of penetration of the diffuse photon density wave (heating zone) and the thermal diffusion length. This condition has been referred to as thermal confinement.[12] It follows that τ_s, τ_t, and τ_p can be interpreted as the times taken for acoustic, thermal, and photonic waves to traverse the depth of light penetration (the heating zone). Thermal and stress confinements are usually discussed in terms of time scales rather than frequencies. Generally, $\omega_p > \omega_s > \omega_t$.

In keeping with the work of Gusev and Karabutov,[25] we also define

$$\omega_\alpha = \frac{c_s^2}{\alpha} = \frac{\omega_s^2}{\omega_t}. \tag{51}$$

Gusev and Karabutov note that (Ref. 25, p. 16) the wave vector of the acoustic wave is much smaller than the wave vector of the thermal wave across the entire frequency range. This implies

$$\frac{\omega}{c_s} \ll \sqrt{\frac{\omega}{\alpha}} \rightarrow \frac{\omega\alpha}{c_s^2} \ll 1 \rightarrow \omega \ll \frac{\omega_s^2}{\omega_t} = \omega_\alpha. \tag{52}$$

This is simply the statement that the acoustic wavelength is much longer than the thermal wavelength, expressed in terms of input frequency and characteristic frequencies. It follows immediately from this statement that

$$\frac{k_s^2}{k_t^2} = \frac{\omega\alpha i}{c_s^2} = \frac{\omega\omega_t}{\omega_s^2} i \ll 1i, \tag{53}$$

where $i = \sqrt{-1}$, so that the magnitude of the ratio of the squared acoustic to thermal wave number is very small. Similarly,

$$\frac{k_p^2}{k_t^2} = -\frac{\mu_a \alpha i}{D\omega} + \frac{\alpha}{cD} = \frac{1}{\mu_a D}\left[\frac{\omega_t}{\omega_p} - \frac{\omega_t}{\omega} i\right] \approx \frac{-1}{\mu_a D}\frac{\omega_t}{\omega} i, \tag{54}$$

and can thus be considered as a measure of the degree of thermal confinement. If the input frequency $\omega \gg \omega_t$, then the magnitude of the ratios of the squared photonic to thermal wave number is very small (thermal confinement). Finally, we can also write

$$\frac{k_p^2}{k_s^2} = -\frac{\mu_a c_s^2}{D\omega^2} - \frac{i c_s^2}{cD\omega} = \frac{-\omega_s^2}{\omega^2}\left[1 + \frac{\omega}{\omega_p} i\right]\frac{1}{\mu_a D}. \tag{55}$$

This last ratio of squared wave numbers can be considered as a measure of the degree of stress confinement and in general cannot be considered to be a small quantity. In summary, we have that thermal confinement implies that k_p^2/k_t^2 is a small quantity and that stress confinement implies that k_p^2/k_s^2 is a small quantity. It is noted that both conditions can be expressed in terms of ratios of the appropriate wave numbers with thermal confinement involving the ratio of the photonic to thermal wave numbers and stress confinement involving the ratio of photonic to acoustic wave number.

Some typical examples of parameters are now given. From Ref. 12, it can be obtained that the absorption coefficients of the electric field in fat (low water content) and muscle (high water content) are about 0.1 and 0.9 cm^{-1}, respectively, at 3 GHz and about 0.03 and 0.25 cm^{-1}, respectively, at 300 MHz. Typical thermal diffusivity for most soft tissues is 1.4×10^{-3} cm^2/s. The speed of sound is 1.5 $\text{mm}/\mu\text{s}$. Telenkov *et al.* gives the thermal diffusivity of soft tissue as 0.11 mm^2/s.[27] Background optical properties are given as $\mu_a = 0.02$ cm^{-1} and $\mu_s' = 8.0$ cm^{-1}.[28] The speed of light in tissue, c, is on the order of 2×10^8 m/s.[29] Given these typical parameters, then $\omega_p = 2 \times 10^8$ s^{-1}, $\omega_s = 3 \times 10^3$ s^{-1}, and $\omega_t = 5.6 \times 10^{-7}$ s^{-1}. Given these numbers, it is easy to see that, in general, $\omega \gg \omega_t$ will be easily achieved whereas it is not necessarily true that $\omega > \omega_s$. Thus, in general, it follows that the magnitude of the ratio of the photonic and thermal wave numbers is very small and that the magnitude of the ratio of the acoustic and thermal wave number is also small. However, the ratio of photonic to acoustic wave number will depend on the frequency of the illumination function.

Based on the preceding analysis, the values of A_s, A_t, and A_p can be simplified. Using $\mu_a^2/k_s^2 = \omega_s^2/\omega^2$ and $\mu_a^2/k_t^2 = i\omega_t/\omega$, along with Eqs. (53) and (54), these can be rewritten as

$$A_t := \frac{-\omega_t^2/\omega_s^2}{(1 - k_s^2/k_t^2)(1 - k_p^2/k_t^2)} \approx -\frac{\omega_t^2}{\omega_s^2} \ll 1, \tag{56}$$

$$A_s := \frac{\omega_t i/\omega}{(k_s^2/k_t^2 - 1)(1 - k_p^2/k_s^2)} \approx -\frac{\omega_t i}{\omega}\frac{1}{(1 - k_p^2/k_s^2)}, \tag{57}$$

$$A_p := \frac{\omega_t i/\omega}{(k_p^2/k_s^2 - 1)(k_p^2/k_t^2 - 1)} \approx -\frac{\omega_t i}{\omega}\frac{1}{(k_p^2/k_s^2 - 1)} = -A_s. \tag{58}$$

Thus, the system Green function can now be written as

$$\begin{aligned} g_{pts}(z;\gamma_s,\gamma_p,\gamma_t) &= A_p g_p(z;\gamma_p) + A_t g_t(z;\gamma_t) + A_s g_s(z;\gamma_s) \\ &\approx A_s[g_s(z;\gamma_s) - g_p(z;\gamma_p)], \end{aligned} \tag{59}$$

and it follows that the thermal subsystem Green function has very little effect on the final output.

Stress confinement: As previously discussed, under the condition of stress confinement, k_p^2/k_s^2 becomes a small quantity. It then further follows that under stress confinement A_p and A_s simplify to

$$A_s = -\frac{\omega_t i}{\omega} = -A_p. \tag{60}$$

As previously discussed, A_t is considered small for most frequencies. The system Green function still has the same form as given by Eq. (59).

Near field and far field regions: It can be seen from Eq. (59) that the system Green function is a sum of photonic and acoustic Green functions. Recall that these functions are given by by the form,

$$g(z) = \frac{e^{-\gamma_\omega |z|}}{2\gamma_\omega}, \tag{61}$$

where γ_ω takes on the appropriate form for photonic and acoustic wave numbers and is an "effective" wave number. For acoustic waves, γ_ω is purely real for values of $k_s^2 < \omega_x^2 + \omega_y^2$ and thus decays exponentially. The Green function will approach zero for values of $|z|$ greater than about $5/\gamma_{\omega r}$—recalling that it is the real component of γ_ω that causes the decay in the Green function. As γ_s acts as an effective wave number, the inverse of γ_s behaves as an effective wavelength. For $k_s^2 > \omega_x^2 + \omega_y^2$, then γ_s is purely imaginary and thus does not decay. This is the "low-pass" version of the Green function as essentially only these lower spatial frequencies are propagated and the others are attenuated. More specifically, the acoustic Green function is really a band-pass function as spatial frequencies such that $\gamma_s = 0$, that is $\omega_x^2 + \omega_y^2 = k_s^2$, are the ones that are most highly selected, causing the denominator of the Green function to go to zero. The corresponding γ_ω for the DPDW is always complex and thus always has a decaying component. Hence, "far enough" away from a given inhomogeneity, only the acoustic contribution will remain as the photonic contribution to the system, as given in Eq. (59), will have completely decayed. As increasing spatial frequencies only serve to enhance the possible decay of the exponential term, the largest allowable z (before the Green function decays to zero) occurs at $\omega_x = \omega_y = 0$. It is the real part of k_p that dictates the rate of decay of the Green function. Recall that

$$k_p^2 = -\frac{\mu_a}{D} - \frac{i\omega}{cD}. \tag{62}$$

As the speed of light, c, is large, then for all but the highest of frequencies we can approximately write $k_p^2 = -\mu_a/D$ and thus $k_p = i\sqrt{\mu_a/D}$. For the typical values previously mentioned, $\sqrt{\mu_a/D} \approx 70\ \mathrm{m}^{-1}$ and it follows that the decay constant is roughly about 1.4 cm. If the detector is roughly within this order of magnitude or closer to the inhomogeneity then both the acoustic and photonic contributions to the final pressure should be considered. However, for distances about 4 to 5 times this far, then the photonic contribution becomes negligible and only the acoustic Green function plays a role. This distinction is of importance and should have an effect on any inversion algorithms employed.

X. GENERALIZED FOURIER DIFFRACTION THEOREM FOR GENERAL ILLUMINATION FUNCTION

Given the exponential functional form of the subsystem Green functions, Eq. (42) can be interpreted in terms of the Fourier transform. For a general Green function of the form $g(z - z_p) = e^{-\gamma_\omega |z - z_p|}/(2\gamma_\omega)$, we can write for any function h of space and temporal frequency:

$$\begin{aligned}
\int_{-\infty}^{\infty} h(\omega_x, \omega_y, z_p, \omega) \frac{e^{-\gamma_\omega |z - z_p|}}{2\gamma_\omega} dz_p &= \int_{-\infty}^{\infty} h(\omega_x, \omega_y, z_p, \omega) \frac{e^{-[\gamma_{\omega r} + i\gamma_{\omega i}]|z - z_p|}}{2\gamma_\omega} dz_p \\
&= \begin{cases} \dfrac{e^{-[\gamma_{\omega r} + i\gamma_{\omega i}]z}}{2\gamma_\omega} \displaystyle\int_{-\infty}^{\infty} h(\omega_x, \omega_y, z_p, \omega) e^{\gamma_{\omega r} z_p} e^{i\gamma_{\omega i} z_p} dz_p, & z > z_p \\ \dfrac{e^{[\gamma_{\omega r} + i\gamma_{\omega i}]z}}{2\gamma_\omega} \displaystyle\int_{-\infty}^{\infty} h(\omega_x, \omega_y, z_p, \omega) e^{-\gamma_{\omega r} z_p} e^{-i\gamma_{\omega i} z_p} dz_p, & z < z_p \end{cases} \\
&= \begin{cases} \dfrac{e^{-[\gamma_{\omega r} + i\gamma_{\omega i}]z}}{2\gamma_\omega} F_{3D}\{h(\vec{r}, \omega) e^{\gamma_{\omega r} z}\}\big|_{\omega_z = -\gamma_{\omega i}}, & z > z_p \quad \text{(transmission)} \\ \dfrac{e^{[\gamma_{\omega r} + i\gamma_{\omega i}]z}}{2\gamma_\omega} F_{3D}\{h(\vec{r}, \omega) e^{-\gamma_{\omega r} z}\}\big|_{\omega_z = \gamma_{\omega i}}, & z < z_p \quad \text{(reflection)}. \end{cases}
\end{aligned} \tag{63}$$

Here, F_{3D} denotes the 3D Fourier transform and it can be observed that each subsystem Green function has the effect of returning the 3D Fourier transform of the product of the heterogeneity function and a (decaying) exponential, evaluated on $\omega_z = \pm \gamma_{\omega i}$, weighted by appropriate factors. The positive sign is chosen for measurements in reflection and the negative sign for measurements in transmission. The weighting factor $e^{\pm[\gamma_{\omega r} + i\gamma_{\omega i}]z}/2\gamma_\omega$ is a constant for a fixed receiver plane and its form is very much reminiscent of the form of each subsystem Green function. In fact, as without loss of generality the inhomogeneity can be taken to be located at the origin, then the previous equation can be more compactly written as

$$\begin{aligned}
&\int_{-\infty}^{\infty} h(\omega_x, \omega_y, z_p, \omega) \frac{e^{-\gamma_\omega |z - z_p|}}{2\gamma_\omega} dz_p \\
&\quad = g_\omega(z) F_{3D}\{h(\vec{r}, \omega) e^{\gamma_{\omega r} |z|}\}\big|_{\omega_z = -\gamma_{\omega i}\, \mathrm{sgn}(z)},
\end{aligned} \tag{64}$$

where $g_\omega(z)$ is the appropriate (thermal, photonic or acoustic) Green function. Positive z's are chosen for transmission measurements and negative z's are chosen for reflection measurements. With respect to the convergence of the integrals in Eq. (63), it should be noted that the object function has finite

support, otherwise the basic premise of the Born approximation is no longer valid. With finite support, the integrals will converge, despite the presence of the exponential terms in the integrand.

Result: Applying the result of Eq. (63) on Eq. (42), we obtain the generalized Fourier diffraction theorem for the coupled PTA problem:

$$P(\omega_x,\omega_y,z,\omega)=\frac{-\beta_s}{D\mu_a}\int_{-\infty}^{\infty}O_a\Psi_{d0}(\omega_x,\omega_y,z_p,\omega)g_{pts}(z-z_p;\gamma_s,\gamma_p,\gamma_t)dz_p=\frac{-\beta_s}{D\mu_a}\sum_{\omega=p,t,s}A_\omega g_\omega(z)F_{3D}\times\{O_a\Psi_{d0}(\omega_x,\omega_y,z,\omega)e^{\gamma_{\omega r}|z|}\}\big|_{\omega_z=-\gamma_{\omega i}\,\mathrm{sgn}(z)}. \tag{65}$$

This Fourier diffraction theorem tells us that the spatial 2D Fourier transform of the measured response on a plane is proportional to the *sum* of three 3D Fourier transforms of the heterogeneity function (weighted with an exponential), evaluated at $\omega_z=\pm\gamma_{\omega i}$. The positive z is chosen for measurements in reflection and the negative z is chosen for measurements in transmission. The three separate 3D Fourier transforms are due to each of photonic, thermal, and acoustic generalized wave number, γ_ω. The γ has been defined as the square root of γ^2 such that the real part is positive, so that the exponential functions in front of the 3D Fourier transform are always well behaved at infinity.

XI. FOURIER DIFFRACTION THEOREM FOR PLANE-WAVE ILLUMINATION FUNCTION

We now specialize the Fourier diffraction theorem as derived earlier to the case of plane-wave illumination. Specifically, it is assumed that

$$\Psi_{d0}(\omega_x,\omega_y,z,\omega)=\Psi_{d0}(z,\omega)=e^{ik_p|z|}. \tag{66}$$

For plane-wave illumination, Eq. (65) becomes

$$P(\omega_x,\omega_y,z,\omega)=\frac{-\beta_s}{D\mu_a}\int_{-\infty}^{\infty}O_a(\omega_x,\omega_y,z)e^{ik_p|z|}g_{pts}(z-z_p;\gamma_s,\gamma_p,\gamma_t)dz_p=\frac{-\beta_s}{D\mu_a}\sum_{\omega=p,t,s}A_\omega g_\omega(z)F_{3D}\times\{o_a(\vec{r})e^{(\gamma_{\omega r}-k_{pi})|z|}\}\big|_{\omega_z=(-k_{pr}-\gamma_{\omega i})\mathrm{sgn}(z)}. \tag{67}$$

As $\gamma_{p/t/s}^2=\omega_x^2+\omega_y^2-k_{p/t/s}^2$, then the terms $g_\omega(z)$ in Eq. (67) always have a positive decaying component with the exception of $\gamma_s=\sqrt{\omega_x^2+\omega_y^2-k_s^2}$ when $\omega_x^2+\omega_y^2<k_s^2$. Hence for "large enough" z, the acoustic terms for which $\omega_x^2+\omega_y^2<k_s^2$ are propagated and the other terms are attenuated, effectively a low-pass filter. In this case, $\gamma_{si}=\sqrt{k_s^2-\omega_x^2-\omega_y^2}$, and the Fourier region of the 3D transform of $o_a(\vec{r})e^{(\gamma_{\omega r}-k_{pi})|z|}$ that is detected is where $\omega_z=\pm(k_{pr}+\gamma_{si})$ or $(\omega_z\pm k_{pr})^2=\gamma_{si}^2=k_s^2-\omega_x^2-\omega_y^2$, implying $(\omega_z\pm k_{pr})^2+\omega_x^2+\omega_y^2=k_s^2$. This last expression is for a sphere in 3D spatial frequency space, centered at $(0,0,\pm k_{pr})$ and of radius k_s and is the photothermoacoustic equivalent of the Fourier diffraction theorem as used in traditional ultrasonic detection.

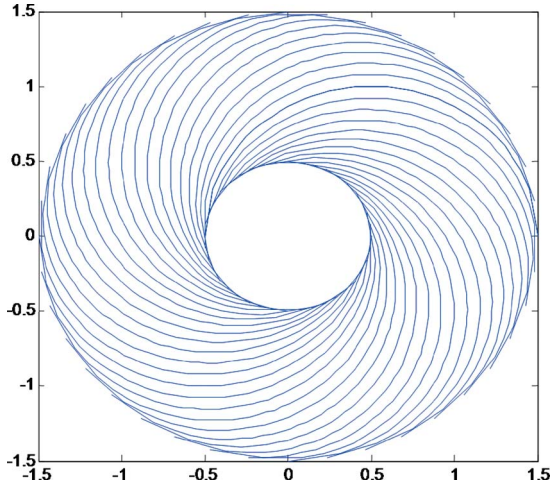


FIG. 5. (Color online) Rotated semicircle of radius 1, center at 0.5.

XII. FOURIER PLANE COVERAGE

As mentioned in the previous section, it can be seen that in the case of plane-wave illumination, the Fourier region is a hemisphere (depending on whether the detection is in transmission or reflection) centered at $(0,0,\pm k_{pr})$ and of radius k_s. It should be clear that the resolution with which the object can be imaged depends on how much of its Fourier transform can be measured. The Fourier plane coverage—the portion of the full 3D Fourier transform of the objection function that is obtained via measurement—is thus a good indicator of what it is theoretically possible to image. Further, as similar Fourier plane coverage results can be obtained or derived for both traditional ultrasonic imaging and pulsed photoacoustic imaging, different imaging modalities can be compared by comparing their Fourier plane coverage.

In particular, let us compare the Fourier plane coverage for the case of fixed frequency and multiple views. In other words, we compare the coverage of the object function if measurements are made at a specific frequency but the transmission/detection is made at various angles, eventually obtaining full 360° coverage of the subject.

For graphical simplicity, circles in the 2D Fourier plane rather than spheres in the 3D Fourier plane can be considered. For the ultrasonic case, this analysis is performed in Ref. 30. It can be observed that for the frequency domain photoacoustic modality, at fixed frequency and multiple views, the Fourier plane coverage is controlled by the location of the center of the circle, k_{pr} and the radius of the circle, k_s. By normalizing with k_s, the relevant quantities become the location of the center of the circle and the circle itself (of radius 1). As the view angle is changed, new information is obtained at a different location in the Fourier plane. The Fourier plane coverage for fixed frequency and multiple views is shown in Figs. 5–9. Various circle centers are shown. For Fig. 5, we see the Fourier coverage for a circle at center 0.5 and radius 1. It does not matter if the center is at (0,0.5) or (0.5, 0), etc. as these theoretical measurements are

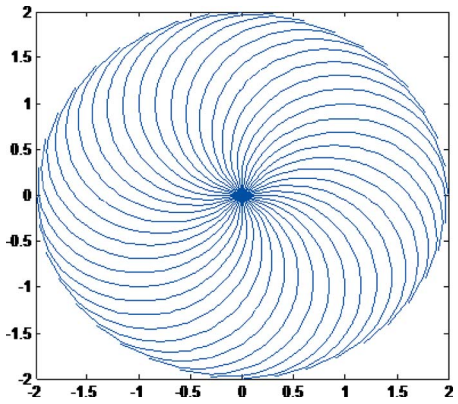


FIG. 6. (Color online) Rotated semicircle, radius 1, center at 1.

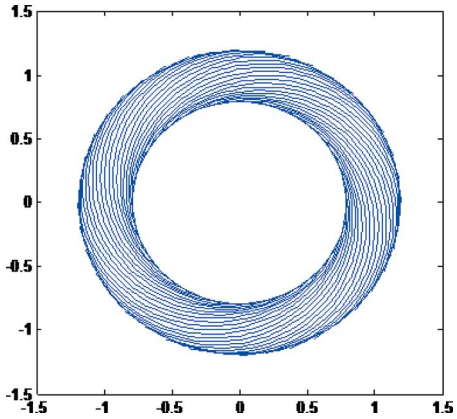


FIG. 8. (Color online) Rotated semicircle, radius 1, center at 0.2.

made through a full 360° rotation about the object. We see that this is essentially a band-pass filter for the object function as only information in an annulus type region of the Fourier plane is obtained. Figure 6 shows the Fourier coverage for a circle at center 1 and radius 1. This case corresponds to the ultrasonic case.[30] This case is a low-pass filter, in comparison with the band-pass filter of the previous case. The difference between the ultrasonic case and the photothermoacoustic case is that in the ultrasonic case, both the center of the circle and radius of the circle are controlled by k_s, whereas in the photothermoacoustic case, the center of the circle is controlled by k_{pr}, whereas the radius of the circle is controlled by k_s—two separate, although related, quantities. Figure 7 shows the case for a circle of radius 1, centered at 0. It can be shown that this corresponds to the pulsed photoacoustic case. In a way, this is an unreasonable comparison as in the case of pulse excitation more than one frequency would be present and thus it could be argued that the single-frequency-multiple-view scenario is unrealistic. However, for the sake of analysis we proceed with this case, in particular as this would also apply when k_{pr} is close to zero. We see that in this case, the band-pass filter narrows and essentially passes only those frequencies that are on the fixed circle. The Fourier coverage is minimal and in fact, no new information is gained by making measurements at various views. To gain more information about the rest of the Fourier plane, measurements would have to be made at additional frequencies, thus changing the radius of the circle. In Fig. 8, the case with center at 0.2 (a small center compared to radius) is demonstrated and it can be seen that this corresponds to a narrow band-pass filter. Clearly, the case where the center is at or close to zero is the limiting band-pass case. In Fig. 9, the case where the center is at 4, and thus greater than the radius of the circle (which is 1) is shown. This is again another band-pass case, although the location of the information on the Fourier plane is different. It can be seen from Fig. 9 that as the center of the circle starts to move away from the origin, additional measurements (more views) need to be made in order to "fill in" the information in the Fourier plane disk. In constrast, for the very narrow band-pass filters such those of Figs. 7 and 8, fewer views (measurements) need to be taken before all possible information at that frequency has been obtained. Hence, the higher k_{pr}, the more views need to be taken to fill in the Fourier disk and vice versa.

All of these simulations where done for the case of 40 views to achieve a full 360° rotation about the object. The smaller the center of the circle, as controlled by k_{pr}, the narrower the annulus of the band-pass filters. For small k_{pr}, less and less information is gained by making measurements at multiple views and the same frequency. In the limit of $k_{pr}=0$, additional views yield no new information, and measurements at different frequencies *must* be obtained in order to gain more information about the 3D Fourier transform of

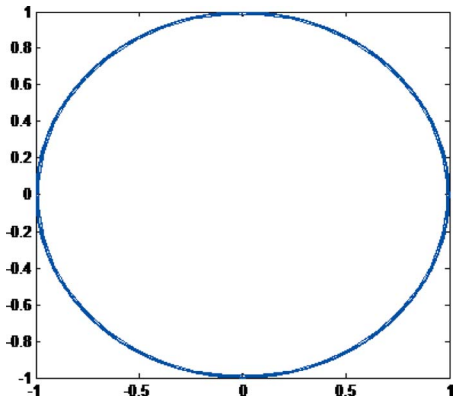


FIG. 7. (Color online) Rotated semicircles, radius 1, center at 0.

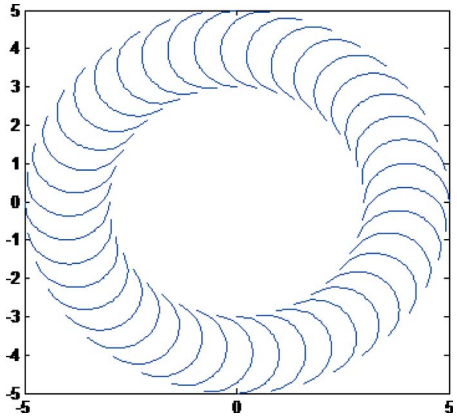


FIG. 9. (Color online) Rotated semicircle, radius 1, center at 4.

the object. The case where center and radius of the circle are equal corresponds to the traditional ultrasonic case and roughly speaking achieves best coverage of the Fourier plane *at a fixed frequency.* This case becomes a low-pass filter case in comparison with the band-pass filter of all the other cases. The power behind the photothermoacoustic modality is that the center and radius of the circle control the band-pass nature of the detection modality and these quantities are controlled by separate but related quantities, k_{pr} and k_s. Proper experiment design would be a matter of controlling the choice of frequencies and views in order to obtain coverage of the 3D Fourier transform of the object that is adequate for the intended application.

XIII. CONCLUSIONS

In conclusion, the governing equations for photoacoustic imaging were derived where a short input pulse is not assumed. The full coupled problem with diffuse photon density waves, thermal and acoustic waves was presented. It was shown that the forward problem could be interpreted as a convolution between the system transfer function and the heterogeneity function where the heterogeneity function is defined as the product of the object and illumination functions. Although truly a product of the three subsystem transfer function, the total system transfer function was eventually shown to be a sum of the three subsystem transfer function. Analysis of relative sizes of each showed that in general the thermal Green function can be neglected, whereas the photonic one may be negligible under certain circumstances. Finally, the preceding results led to a Fourier diffraction theorem for PTA imaging where the observed resulting pressure measured on a plane is shown to be a spherical slice of the 3D Fourier transforms of the object function. Fourier plane coverage was considered. It is expected that these findings will be useful in the design of experiments to ensure proper Fourier plane coverage and also as the basis of reconstruction algorithms for PTA imaging. Future work will extend these results to more general geometries and consider incorporating additional effects into the model.

APPENDIX

Define the following function:

$$f(z,z_t;\gamma_t,\gamma_s) := \int_{-\infty}^{\infty} e^{-\gamma_t|z_s-z_t|}e^{-\gamma_s|z-z_s|}dz_s. \tag{A1}$$

Note that z_s is a (dummy) integration variable and that (γ_t,γ_s) are parameters. We have used γ_t,γ_s in Eq. (A1) and we shall make use of their specific definition in what follows.

Lemma 1:

$$f(z,z_t;\gamma_t,\gamma_s) := \int_{-\infty}^{\infty} e^{-\gamma_t|z_s-z_t|}e^{-\gamma_s|z-z_s|}dz_s = \frac{2\gamma_t e^{-\gamma_s|z-z_t|}}{k_s^2-k_t^2} - \frac{2\gamma_s e^{-\gamma_t|z-z_t|}}{k_s^2-k_t^2}. \tag{A2}$$

Proof: As f is essentially a function of z and z_t, two possible cases need to be considered to evaluate the integral. In the first possible case, $z<z_t$, whereas in the second possible case, $z>z_t$. In the first case, if $z<z_t$, then f as given in Eq. (A1) can be written as

$$f(z,z_t;\gamma_t,\gamma_s) = \int_{-\infty}^{z} e^{-\gamma_t(z_t-z_s)}e^{-\gamma_s(z-z_s)}dz_s + \int_{z}^{z_t} e^{-\gamma_t(z_t-z_s)} \times e^{-\gamma_s(z_s-z)}dz_s + \int_{z_t}^{\infty} e^{-\gamma_t(z_s-z_t)}e^{-\gamma_s(z_s-z)}dz_s. \tag{A3}$$

This sum of integrals can be easily evaluated to give

$$f(z,z_t;\gamma_t,\gamma_s) = \frac{e^{-\gamma_t(z_t-z)}+e^{-\gamma_s(z_t-z)}}{\gamma_t+\gamma_s} + \frac{e^{-\gamma_s(z_t-z)}-e^{-\gamma_t(z_t-z)}}{\gamma_t-\gamma_s}. \tag{A4}$$

In the second case, if $z>z_t$, then f as given in Eq. (A1) can be written as

$$f(z,z_t;\gamma_t,\gamma_s) = \int_{-\infty}^{z_t} e^{-\gamma_t(z_t-z_s)}e^{-\gamma_s(z-z_s)}dz_s + \int_{z_t}^{z} e^{-\gamma_t(z_s-z_t)} \times e^{-\gamma_s(z-z_s)}dz_s + \int_{z}^{\infty} e^{-\gamma_t(z_s-z_t)}e^{-\gamma_s(z_s-z)}dz_s. \tag{A5}$$

This sum of integrals can similarly be easily evaluated to give

$$f(z,z_t;\gamma_t,\gamma_s) = \frac{e^{-\gamma_t(z-z_t)}+e^{-\gamma_s(z-z_t)}}{\gamma_t+\gamma_s} + \frac{e^{-\gamma_s(z-z_t)}-e^{-\gamma_t(z-z_t)}}{\gamma_t-\gamma_s}. \tag{A6}$$

Clearly, the preceding two cases can be summarized by use of the absolute value notation so that

$$\begin{aligned} f(z,z_t;\gamma_t,\gamma_s) &= \frac{e^{-\gamma_t|z-z_t|}+e^{-\gamma_s|z-z_t|}}{\gamma_t+\gamma_s} + \frac{e^{-\gamma_s|z-z_t|}-e^{-\gamma_t|z-z_t|}}{\gamma_t-\gamma_s} \\ &= \frac{2\gamma_t e^{-\gamma_s|z-z_t|}}{\gamma_t^2-\gamma_s^2} - \frac{2\gamma_s e^{-\gamma_t|z-z_t|}}{\gamma_t^2-\gamma_s^2} \\ &= \frac{2\gamma_t e^{-\gamma_s|z-z_t|}}{k_s^2-k_t^2} - \frac{2\gamma_s e^{-\gamma_t|z-z_t|}}{k_s^2-k_t^2}, \end{aligned} \tag{A7}$$

where we have made use of the definitions of γ so that $\gamma_t^2-\gamma_s^2=k_s^2-k_t^2$. The proof is complete.

[1] X. Wang, Y. Pang, G. Ku, G. Stoica, and L. V. Wang, "Three-dimensional laser-induced photoacoustic tomography of mouse brain with the skin and skull intact," Opt. Lett. **28**, 1739–1741 (2003).

[2] X. Wang, Y. Pang, G. Ku, X. Xie, G. Stoica, and L. V. Wang, "Noninvasive laser-induced photoacoustic tomography for structural and functional in vivo imaging of the brain," Nat. Biotechnol. **21**, 803–806 (2003).

[3] V. G. Andreev, A. A. Karabutov, S. V. Solomatin, E. V. Savateeva, V. Aleynikov, Y. V. Zhulina, R. D. Fleming, and A. A. Oraevsky, "Optoacoustic tomography of breast cancer with arc-array-transducer," Proc. SPIE **3916**, 36–47 (2000).

[4] A. P. Gibson, J. C. Hebden, and S. R. Arridge, "Recent advances in diffuse optical imaging," Phys. Med. Biol. **50**, 519-561 (2005).

[5] Y. Fan, A. Mandelis, G. Spirou, and I. A. Vitkin, "Development of a laser photothermoacoustic frequency-swept system for subsurface imaging: Theory and experiment," J. Acoust. Soc. Am. **116**, 3523–3533 (2004).

[6] A. Mandelis and C. Feng, "Frequency-domain theory of laser infrared

photothermal radiometric detection of thermal waves generated by diffuse-photon-density wave fields in turbid media," Phys. Rev. E **65**, 021909(2002).
[7]C. G. A. Hoelen and F. F. M. De Mul, "Image reconstruction for photoacoustic scanning of tissue structures," Appl. Opt. **39**, 5872–5883 (2000).
[8]A. A. Karabutov, N. B. Podymova, and V. S. Letokhov, "Time-resolved laser optoacoustic tomography of inhomogeneous media," Appl. Phys. B: Lasers Opt. **63**, 545–563 (1997).
[9]A. A. Karabutov, E. V. Savateeva, and A. A. Oraevsky, "Imaging of layered structures in biological tissues with opto-acoustic front surface transducer," Proc. SPIE **3601**, 284–295 (1999).
[10]K. P. Köstli and P. C. Beard, "Two-dimensional photoacoustic imaging by use of Fourier-transform image reconstruction and a detector with an anisotropic response," Appl. Opt. **42**, 1899–1908 (2003).
[11]K. P. Köstli, M. Frenz, H. Bebie, and H. P. Weber, "Temporal backward projection of optoacoustic pressure transients using Fourier transform methods," Phys. Med. Biol. **46**, 1863–1872 (2001).
[12]M. Xu and L. V. Wang, "Photoacoustic imaging in biomedicine," Rev. Sci. Instrum. **77**, 041101 (2006).
[13]M. Xu, Y. Xu, and L. V. Wang, "Time-domain reconstruction algorithms and numerical simulations for thermoacoustic tomography in various geometries," IEEE Trans. Biomed. Eng. **50**, 1086–1099 (2003).
[14]Y. Xu, D. Feng, and L. V. Wang, "Exact frequency-domain reconstruction for thermoacoustic tomography - I: Planar geometry," IEEE Trans. Med. Imaging **21**, 823–828 (2002).
[15]P. C. Beard and T. N. Mills, "Optical detection system for biomedical photoacoustic imaging," Proc. SPIE **3916**, 100–109 (2000).
[16]R. A. Kruger, W. L. Kiser, Jr., D. R. Reinecke, and G. A. Kruger, "Thermoacoustic computed tomography using a conventional linear transducer array," Med. Phys. **30**, 856–860 (2003).
[17]R. A. Kruger, P. Liu, Y. R. Fang, and C. R. Appledorn, "Photoacoustic ultrasound (PAUS)—Reconstruction tomography," Med. Phys. **22**, 1605–1609 (1995).
[18]A. A. Oraevsky, A. A. Karabutov, S. V. Solomatin, E. V. Savateeva, V. G. Andreev, Z. Gatalica, H. Singh, and R. D. Fleming, "Laser optoacoustic imaging of breast cancer in vivo," Proc. SPIE **4256**, 6–15 (2001).
[19]K. Maslov and L. V. Wang, "Continuous-wave photoacoustic microscopy," in *Progress in Biomedical Optics and Imaging, Proceedings of SPIE*, San Jose, CA, 2007.
[20]J. F. De Boer, B. Cense, B. H. Park, M. C. Pierce, G. J. Tearney, and B. E. Bouma, "Improved signal-to-noise ratio in spectral-domain compared with time-domain optical coherence tomography," Opt. Lett. **28**, 2067–2069 (2003).
[21]Y. Fan, A. Mandelis, G. Spirou, I. A. Vitkin, and W. Whelan, "Three-dimensional photothermoacoustic depth-profilometric imaging by use of a linear frequency sweep lock-in heterodyne method," Proc. SPIE **5320**, 113–127 (2004).
[22]Y. Fan, A. Mandelis, G. Spirou, I. A. Vitkin, and W. M. Whelan, "Laser photothermoacoustic heterodyned lock-in depth profilometry in turbid tissue phantoms," Phys. Rev. E **72**, 051908 (2005).
[23]S. R. Arridge, "Optical tomography in medical imaging," Inverse Probl. **15**, R41–R93 (1999).
[24]A. Mandelis, N. Baddour, Y. Cai, and R. G. Walmsley, "Laser-induced photothermoacoustic pressure-wave pulses in a polystyrene well and water system used for photomechanical drug delivery," J. Opt. Soc. Am. B **22**, 1024–1036 (2005).
[25]W. E. Gusev and A. A. A. A. Karabutov, *Laser Optoacoustics* (American Institute of Physics, New York, 1993).
[26]A. Tam, "Applications of photoacoustic sensing techniques," Rev. Mod. Phys. **58**, 381–431 (1986).
[27]S. A. Telenkov, G. Vargas, J. S. Nelson, and T. E. Milner, "Coherent thermal wave imaging of subsurface chromophores in biological materials," Phys. Med. Biol. **47**, 657–671 (2002).
[28]X. Li, D. N. Pattanayak, T. Durduran, J. P. Culver, B. Chance, and A. G. Yodh, "Near-field diffraction tomography with diffuse photon density waves," Phys. Rev. E **61**, 4295–4309 (2000).
[29]C. L. Matson, "A diffraction tomographic model of the forward problem using diffuse photon density waves," Opt. Express **1**, 6–11 (1997).
[30]M. Slaney and A. Kak, *Principles of Computerized Tomographic Imaging* (SIAM Philadelphia, 1988).

Pipe wall damage detection by electromagnetic acoustic transducer generated guided waves in absence of defect signals

Milos Vasiljevic[a] and Tribikram Kundu
Department of Civil Engineering and Engineering Mechanics, University of Arizona, Tucson, Arizona 85721

Wolfgang Grill and Evgeny Twerdowski
Institute of Experimental Physics II, University of Leipzig, Linnéstrasse 5, D-04103 Leipzig, Germany

(Received 29 November 2007; revised 27 February 2008; accepted 5 March 2008)

Most investigators emphasize the importance of detecting the reflected signal from the defect to determine if the pipe wall has any damage and to predict the damage location. However, often the small signal from the defect is hidden behind the other arriving wave modes and signal noise. To overcome the difficulties associated with the identification of the small defect signal in the time history plots, in this paper the time history is analyzed well after the arrival of the first defect signal, and after different wave modes have propagated multiple times through the pipe. It is shown that the defective pipe can be clearly identified by analyzing these late arriving diffuse ultrasonic signals. Multiple reflections and scattering of the propagating wave modes by the defect and pipe ends do not hamper the defect detection capability; on the contrary, it apparently stabilizes the signal and makes it easier to distinguish the defective pipe from the defect-free pipe. This paper also highlights difficulties associated with the interpretation of the recorded time histories due to mode conversion by the defect. The design of electro-magnetic acoustic transducers used to generate and receive the guided waves in the pipe is briefly described in the paper.
© *2008 Acoustical Society of America.* [DOI: 10.1121/1.2902188]

PACS number(s): 43.38.Dv, 43.35.Zc, 43.58.Vb, 43.35.Cg [TDM] Pages: 2591–2597

I. INTRODUCTION

Many catastrophic failures of gas and liquid transmission pipelines all over the world warrant more developments on reliable pipe inspection technology. A number of research papers have been published on various nondestructive evaluation techniques for early forecasting of the degradation process and for detecting existence of the mechanical defects in long pipelines. Cylindrical guided waves are useful for such defect detection and are becoming popular for pipe inspection.

Gazis[1,2] first analytically solved the harmonic wave propagation problem in an infinitely long elastic hollow cylinder. Greenspon[3,4] studied dispersion curves and displacement fields for an elastic cylindrical shell. Zemanek[5] presented numerical analyses of the frequency equation in an elastic cylinder. Some investigators[6,7] used guided wave modes for detecting wall thinning defects in cylindrical pipes. Cawley and co-workers[8–10] successfully used cylindrical guided waves for detecting crack and corrosion in pipes. Rose and co-workers[11,12] designed a special probe which can be used both as a transmitter and a receiver during the pipe inspection. Guo and Kundu[13,14] designed a new transducer holder mechanism for pipe inspection using cylindrical guided waves. Using those transducer holders, Na *et al.*[15–18] generated cylindrical guided waves in underwater pipes, concrete filled pipes, and steel bars embedded in concrete.

In most studies related to the pipe wall damage detection using guided waves investigators launched guided waves on the pipe and then let it propagate a long distance along the pipe before the wave is detected and analyzed. Received signal strengths are generally found to be different for defect-free and defective pipes. Thus comparing the received signal from a defect-free pipe one can conclude if the inspected pipe is defective. However, it will be shown in this paper that analysis and interpretation of the received signal from the defective pipe and detection of the small reflected signal from the defect are often not a trivial task. Difficulties associated with this interpretation and the technique to identify a defective pipe, even when the signal reflected from the defect is missed, are discussed below. In our experiment the guided wave is launched and recorded by electro-magnetic acoustic transducers (EMATs). One advantage of EMAT is that it does not need to be in direct contact with the pipe. Therefore, the pipe surface does not need to be very smooth and no coupling fluid between the transducer and the pipe is needed for launching the guided waves. It should be noted here that the ultrasonic piezoelectric transducers although preferred by many investigators, have a major shortcoming—they require either coupling fluids between the transducer and the pipe or a smooth pipe surface for the direct contact condition in the absence of any coupling medium.

II. EXPERIMENTAL INVESTIGATION

A. EMAT design

The electromagnetic field simulation program, "MAXWELL 2D" was used to model the optimal magnetic configu-

[a]Author to whom correspondence should be addressed. Electronic mail: milosv@email.arizona.edu

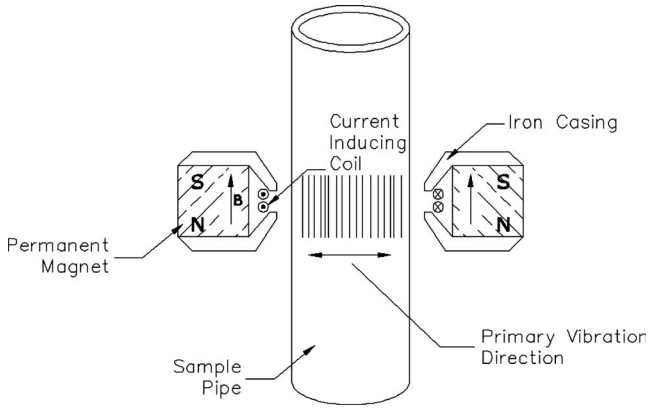


FIG. 1. Relative orientation of the electromagnetic acoustic transducer and the pipe. Note that the diagram shows the cross section of the EMAT which goes around the pipe.

ration for the EMAT. This finite element based program was used to create a two-dimensional model of the spatial distribution of the magnetic flux. The model of the EMAT is drawn on a two-dimensional plane which is intended for axisymmetric models. A typical drawing plane of the designed EMAT can be seen in Fig. 1, where the cross section is rotated about the axis of symmetry (z axis) in order to calculate the distribution of the magnetic induction.

Two shapes were considered for the EMAT design. The shape shown in Fig. 1 is the final shape used in the experiments. Note that this shape is different from the conventional EMAT design which uses only flat circular ferromagnetic disks. The conical shape of the disks of the EMAT shown in Fig. 1 increases the magnetic induction in the location of the coil. Computed results from the two designs are shown in Fig. 2. The simulation is based on the neodymium-iron-born (NdFeB) magnets with the outer and inner diameters equal to 60 and 20 mm, respectively, and the magnetization direction is along the positive Z axis. The magnetic induction distribution and the magnetic flux lines of the final design are shown in Figs. 3 and 4, respectively. Figure 5 shows the details of the EMAT assembly.

B. Specimens

Two different steel pipes—one is defect free and the second one is defective (dented)—are inspected. The two

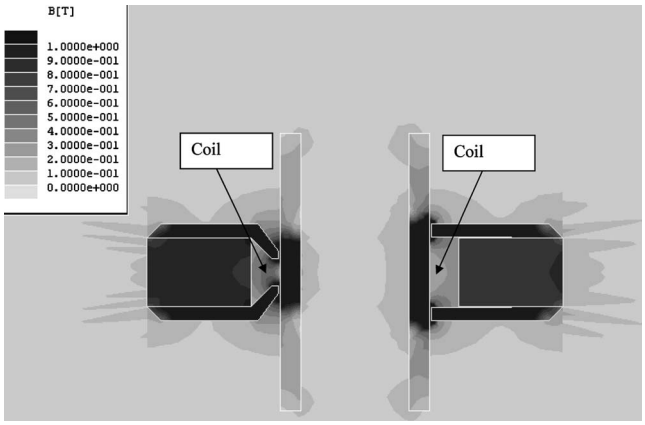


FIG. 2. Comparison of two designs of EMAT.

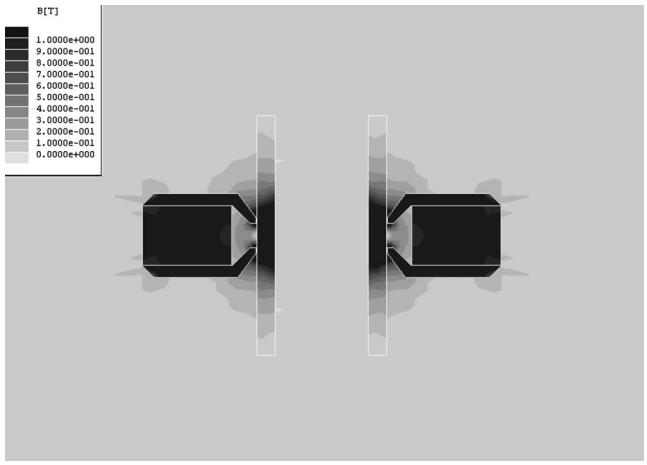


FIG. 3. Magnetic field distribution of the final EMAT design.

pipes have the same cross section; the outer and inner diameters of the pipes are 21.4 and 16.4 mm, respectively. The defect is fabricated by forming a dent (1 mm deep and 0.5 mm wide) along the circumference of a 6000-mm-long pipe. A dent is a localized depression or deformation in the pipe's cylindrical geometry resulting from an applied force.[17] Figure 6 shows the two pipes used in the experiment. These two pipes are denoted as (a) defect free and (b) defective pipes.

C. Experiment

Electromagnetic acoustic transducers (EMATs) were designed for exciting longitudinal wave modes in the pipe (see Fig. 1) as well as to receive the ultrasonic waves. EMATs were mounted on brass holders that helped to position the EMATs perpendicular to the pipe axis with a spacing of approximately 1 mm between the pipe wall and the EMAT. This position was fine tuned by small plastic screws in the brass holders (which were also the only points of contact between the entire EMAT system and the pipe). Figure 5 shows the details of the EMAT assembly. Digital oscilloscope TiePie Handyscope HS3 was used to generate chirp signals of varying frequencies controlled through the LABVIEW program written for this particular application. The signal generated by the transmitting EMAT propagated through the pipe and was received by the receiving EMAT. It was

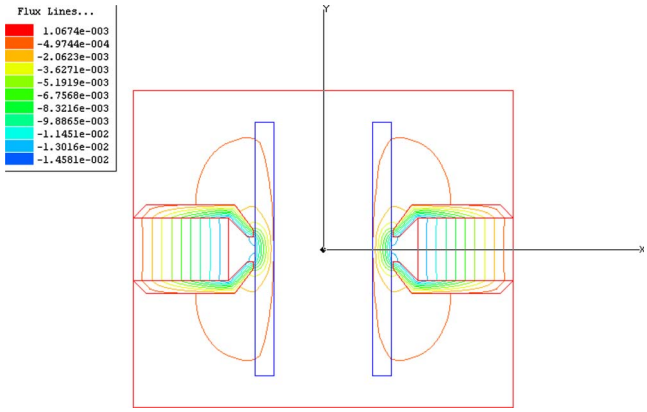


FIG. 4. (Color online) Flux line distribution of the final EMAT design.

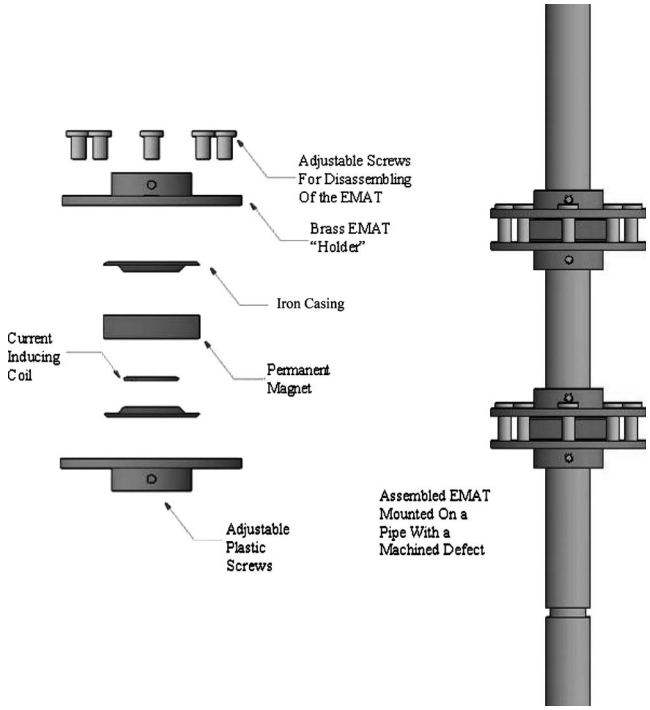


FIG. 5. Detailed diagram of the EMAT assembly.

then amplified by the Princeton Applied Research 113 Low Noise Preamplifier, digitized by the same Handyscope HS3 unit that was used to generate the signal, and displayed on the computer in the same LABVIEW program as a function of time, as well as a function of frequency. The signal strength for both time history and frequency spectrum was displayed in volts. The variation of the time versus signal strength is called time history or transient curve, and the variation of the signal amplitude versus frequency is called the spectral plots or the $V(f)$ curve. During the raw data collection, every time step was averaged by the program for at least 1024 times before being recorded to give a consistent value. Then it was analyzed in the new LABVIEW program created for the data analysis.

Figure 7 shows the experimental setup. The defect in the pipe is a total circumferential dent. EMAT to EMAT distance (dimension "b" in Fig. 7) is 2550 mm, EMAT to defect distance (dimension "d" in Fig. 7) is 250 mm, and the distance between the defect and the end of the pipe (dimension "c" in Fig. 7) is 1460 mm. A chirp signal with a frequency range of 100–150 kHz is sent to the transmitting EMAT. PAR 113 preamplifier has built-in low-pass and high-pass filters. The preamplifier amplifies signals in the frequency range

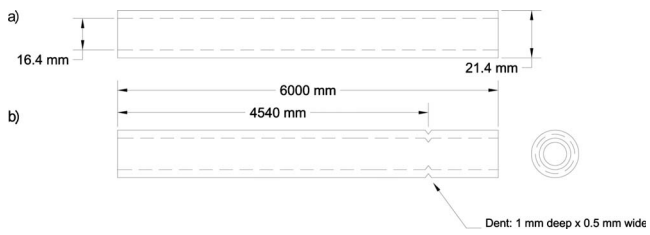


FIG. 6. Steel pipe specimens—(a) defect-free and (b) defective or dented pipe. Both pipes have the same inner and outer radii and length.

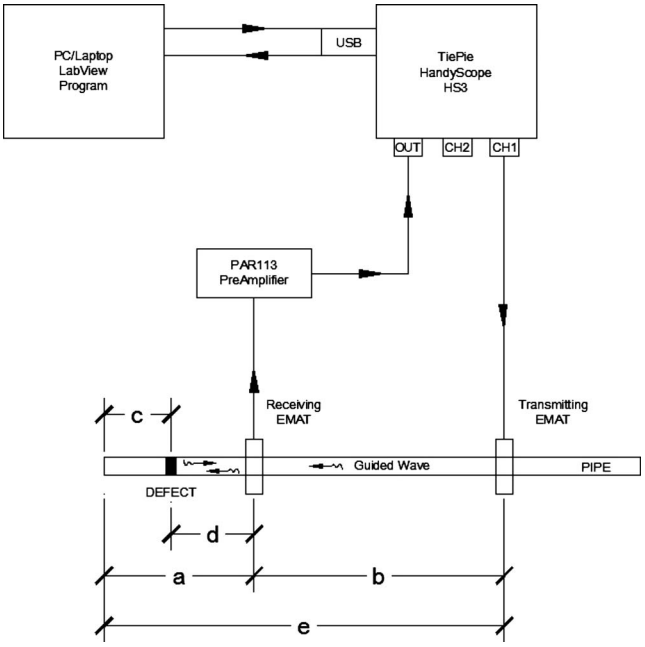


FIG. 7. Schematic of the experimental setup. Dimensions a, b, c, d and e are given in the text.

1–300 kHz. It magnifies the signal from the receiving EMAT ten thousand times. Excitation signal as well as the preamplifier setting stays the same for all experiments. Figure 8 shows the recorded time histories for the pipe with and without the defect. The first prominent peak is due to the radio frequency cross talk between the output and the input channels. Regions (1), (2), (3) and (4) marked in Fig. 8 are separately analyzed in the following section. Figures 9 through 12 show the $V(f)$ curves for Regions (1) through (4), respectively. The $V(f)$ curve for the entire recorded signal is plotted in Fig. 13.

III. ANALYSIS OF THE EXPERIMENTAL RESULTS

Time histories for defective and defect-free pipes shown in Fig. 8 clearly show significant differences. Therefore, the fabricated EMAT system used in this experiment is sensitive to the pipe wall defect. However, the time histories look very

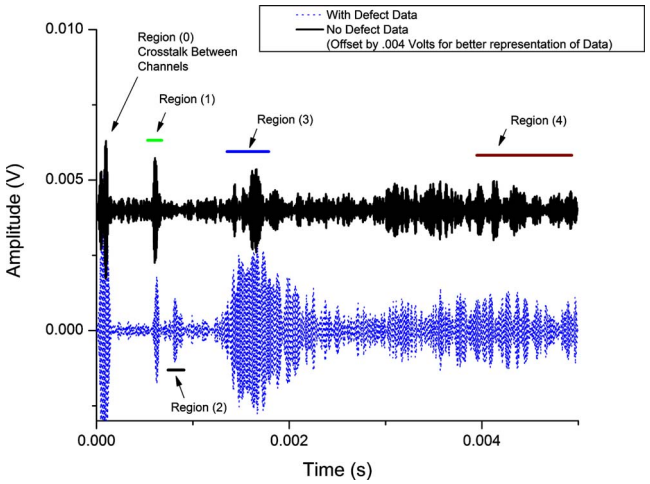


FIG. 8. (Color online) Recorded time histories for the defect-free and defective pipes.

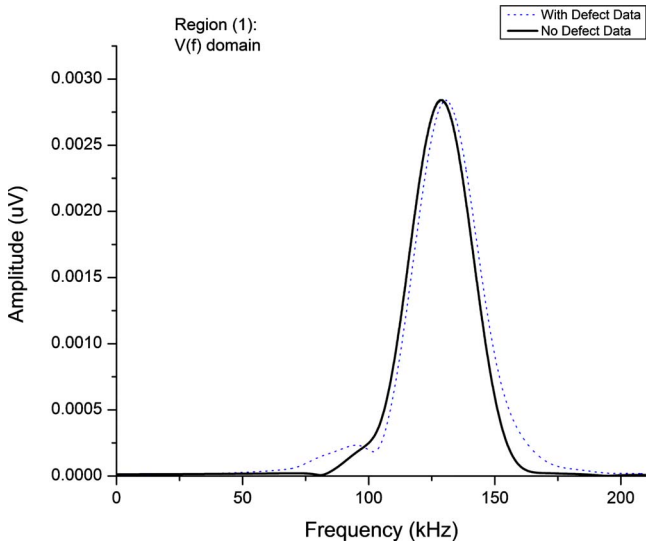


FIG. 9. (Color online) Spectral plots of Region 1 of the time histories shown in Fig. 8.

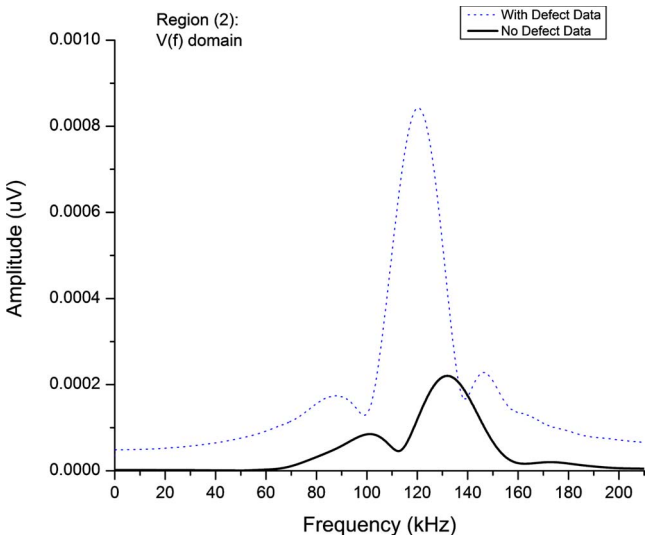


FIG. 10. (Color online) Spectral plots of Region 2 of the time histories shown in Fig. 8.

cumbersome and are not easy to interpret. The simple conclusion that can be drawn from these complicated plots is that the two time histories are significantly different. The first major peak [seen in Region (1)] in Fig. 8 appears at the same time in both time history plots. Spectral plots (see Fig. 9) of Region (1) show small differences between the defect-free and defective pipe signals. Therefore, this part of the signal must have been recorded before the wave encounters the defect and hence is not affected by the defect.

One clear distinction between these two time histories is that a relatively strong peak is observed in Region 2 for the defective pipe. Therefore, this peak must be the contribution of the defect. One can also observe a relatively strong packet of waves in the defective pipe signal in Region 3. To understand which peak corresponds to which guided wave mode, dispersion curves for the pipe are generated. Phase velocity and group velocity dispersion curves for $L(0,1)$ and $L(0,2)$ modes are shown in Fig. 14. Since the fabricated EMAT generates only the longitudinal wave modes in the frequency range 100–150 kHz, only $L(0,1)$ and $L(0,2)$ modes appear in the desired frequency range for the steel pipe considered here (P-wave speed=5.96 km/s, S-wave speed=3.26 km/s, density=7.932 gm/cm^3, outer diameter=21.4 mm and inner diameter=15.4 mm).

The group velocity of a propagating wave can be experimentally measured from the following equation

$$c_g(f) = \frac{s}{t}, \tag{1}$$

where group velocity c_g is a function of frequency f; s is the distance traveled by the wave and t is the time taken by the wave to travel the distance, s. Region 1 in Fig. 8 is where the first peak is observed. This peak corresponds to the wave traveling directly from the transmitting EMAT to the receiving EMAT. The time taken by this signal to travel a distance of 2550 mm is 0.524 ms (the distance between the cross talk region and Region 1 in Fig. 8) which gives the group velocity of 2.55/0.524=4.9 km/s. From Fig. 9, the dominant frequency at which this wave packet is propagating is found to be 130 kHz. Plotting these two values on the group velocity dispersion curves of Fig. 14, one can identify this wave mode as the $L(0,2)$ mode. Since $L(0,2)$ mode has higher velocity than $L(0,1)$ mode it arrives at the receiving EMAT first.

The peak in Region 2 of Fig. 8 appears only for the defective pipe. One can then conclude that this is the reflected signal from the defect. Since the distance between the receiving EMAT and the defect is 250 mm and the group velocity of $L(0,2)$ mode is 4.9 m/ms, the distance between the peaks of Regions 1 and 2 for the defective pipe should be 0.5/4.9 ms=0.102 ms if the wave travels twice the distance between the receiving EMAT and the defect as the L(0,2) mode. However, the measured time difference between these two peaks is found to be 0.189 ms in Fig. 8. This discrepancy can be explained in the following manner. If the wave travels from the EMAT to the defect as the $L(0,2)$ mode but returns to the EMAT as the slower $L(0,1)$ mode after being reflected by the defect, then the distance between the two peaks of Regions 1 and 2 should be greater than 0.102 ms. If the reflection by the defect causes mode conversion, then only such $L(0,2)$ to $L(0,1)$ mode conversion is possible.

The distance between the receiving EMAT and the defect is 250 mm. From Fig. 14 the group Velocity of $L(0,2)$ mode at 130 kHz is found to be 4.9 m/ms. Figure 10 shows that the peak value of the $V(f)$ curve for the defective pipe is between 110 and 120 kHz. At this frequency $L(0,1)$ mode has a group velocity of 1.8 m/ms. Therefore the total time taken by the wave to travel from the EMAT to the defect and back is

$$\frac{0.25}{4.9} + \frac{0.25}{1.8} = 0.051 + 0.138 = 0.189 \text{ ms}. \tag{2}$$

In Fig. 8, the time measured between Regions 1 and 2 is also found to be 0.189 ms. Therefore, it proves that the defect causes mode conversion. This problem can be reversed to calculate the distance of the defect from the EMAT, thus one

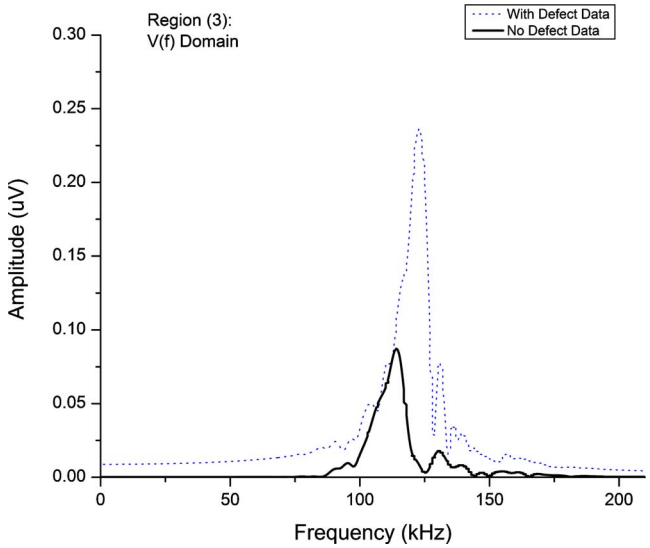


FIG. 11. (Color online) Spectral plots of Region 3 of the time histories shown in Fig. 8.

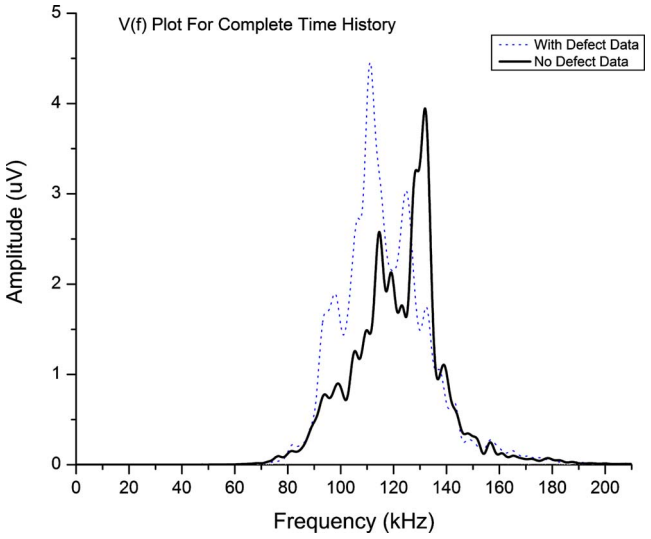


FIG. 13. (Color online) Spectral plots for the complete time histories of Fig. 8.

can predict the exact location of the defect in a pipe from the time of arrival of the reflected signal from the defect and knowing the modes of wave propagation between the receiving EMAT and the defect.

In the time history plots after Region 2, signals become quite complicated for defective and defect-free pipes after 1.4 ms time because $L(0,1)$ and $L(0,2)$ modes propagating directly from the transmitter to the receiver and those reflected from the pipe ends and the defect start overlapping. The recorded time history for the defective pipe appears to be more cumbersome because the defect causes mode conversion as well as reflection, transmission, and scattering of the ultrasonic energy. To investigate if any useful information can be extracted from the recorded signal beyond Region 2, frequency spectra of Regions 3, 4 and that of the complete and plotted in Figs. 11, 12, and 13, respectively.

Figure 11 shows that the spectral plot for the defective pipe is much greater than that for the defect-free pipe. The frequency corresponding to the highest peak is near 120 kHz for the defective pipe in both Figs. 10 and 11. Also, the peaks are higher for the defective pipe in both figures. However, the frequency corresponding to the highest peak for the defect-free pipe is close to 130 kHz in Fig. 10 and it is close to 115 kHz in Fig. 11. Clearly, the elastic waves generated by the defect have a strong influence on the time history signals in both Regions 2 and 3. Note that both have peaks near the same frequency (~120 kHz) and show much higher amplitude compared to that for the defect-free pipe. Therefore, even if someone misses the defect signal in Region 2 it is possible to identify the defective pipe from the spectral plots of Region 3.

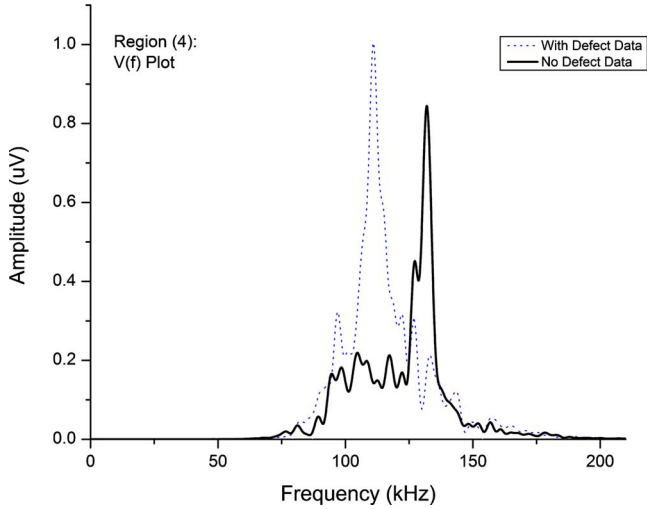


FIG. 12. (Color online) Spectral plots of Region 4 of the time histories shown in Fig. 8.

Next it is investigated if any consistent difference between the signals obtained from the defective and the defect-free pipes can be observed in the spectral plots from the time histories recorded well beyond the first arrivals of the reflected wave from the defect. With this goal in mind the $V(f)$ curves of Region 4 of Fig. 8 are plotted in Fig. 12. In Region 4, $L(0,1)$ and $L(0,2)$ modes and possibly some other modes generated by the defect strike the receiving EMAT multiple times after being reflected, transmitted, and scattered by the defect and the pipe boundaries multiple times. Therefore, in this region it is impossible to separately identify the contributions of different modes. However, the spectral plot shows a clear distinction between the defect-free and the defective pipe. The peak for the defective pipe is at 110 kHz while that for the defect-free pipe is at 130 kHz. The peak value for the defective pipe is also found to be slightly higher than that for the defective pipe. These two observations of Fig. 12 qualitatively agree with that in Fig. 10. Note that in Fig. 10 also a stronger peak at a lower frequency is observed for the defective pipe.

To investigate if this observation holds good if the spectral plots of the entire recorded time histories are compared, Fig. 13 is generated by taking the Fourier transform of the two time histories presented in Fig. 8. Note that although Figs. 12 and 13 are different, as one should expect, the strongest peak positions in both figures are observed at 110 kHz for the defective pipe and at 130 kHz for the defect-free

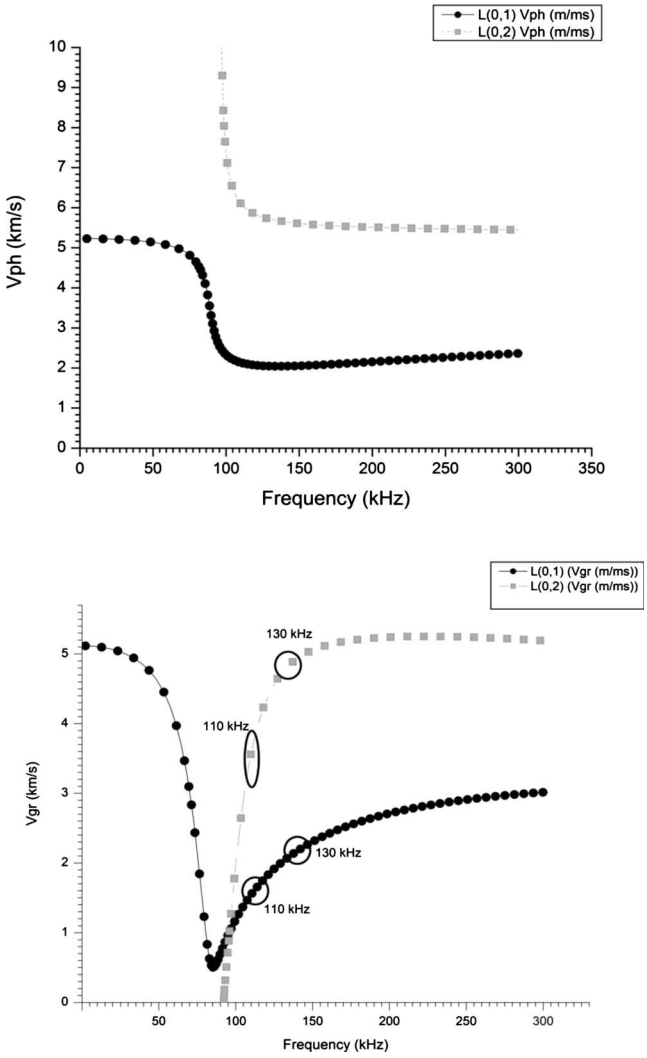


FIG. 14. Phase velocity (top) and group velocity (bottom) dispersion curves for the steel pipe.

pipe. The peak value for the defective pipe is stronger than that for the defect-free pipe in both figures. This is an important observation because it means that one can identify the defective pipe comparing the spectral plots of the complete time history (or that of the tail end, Region 4 of Fig. 8) without the need of pinpointing the exact position of the signal from the defect (Region 2 of Fig. 8) that may be hidden behind the noise level or other arriving modes for a different position of the defect or the receiving EMAT.

Justification of the frequency shift from 130 kHz for the defect-free pipe to 110 kHz for the defective pipe in Figs. 12 and 13 is given in the following. The mode conversion caused by the defect may explain this frequency shift. From the dispersion curves in Fig. 14, one can see that at frequencies greater than 100 kHz both $L(0,1)$ and $L(0,2)$ modes can exist in the pipe and that they have different phase and group velocities. Near 110 kHz, the curve for $L(0,2)$ mode has a steep slope that causes high dispersion. Therefore, the $L(0,2)$ mode traveling through the pipe near 110 kHz frequency is dispersed more than the $L(0,1)$ mode whose steep slope (high dispersion) is observed below 100 kHz. Therefore, if the defect generates $L(0,1)$ mode due to mode conversion then this mode can propagate multiple times through the pipe at 110 kHz without being significantly dispersed while the $L(0,2)$ mode at the same frequency decays sooner due to dispersion.

Identifying defective specimens by analyzing the reverberating tail end of the ultrasonic signal, also known as the diffuse ultrasonic signal,[19] has been attempted earlier. Michaels and Michaels[20] applied time domain differencing, spectrogram differencing, and local temporal coherence to diffuse ultrasonic waves in plates to identify defective plates in presence of temperature and environmental changes (wet and dry surface conditions). They found that time domain differencing and spectral analysis are generally ineffective in discriminating damage from environmental effects while local temporal coherence can successfully discriminate structural damage from both temperature change and modest change in the surface condition. Effect of the temperature and environmental change on the pipe damage detection capability using diffuse waves is currently under investigation. To the best of our knowledge this is the first attempt of using diffuse waves for pipe wall damage detection.

IV. CONCLUDING REMARKS

Longitudinal modes $L(0,1)$ and $L(0,2)$ of cylindrical guided waves have been generated and detected in a metal pipe by newly designed EMATs. Pipe dent could be easily detected by the EMAT.

In most guided wave based experiments one common question arises—what is the effect of reflection at the pipe ends on the defect detection capability? Often it is recommended that reflected waves from the pipe ends should be avoided as much as possible by truncating the signal right after the first arrival. However, in doing so slower modes are truncated. Also, often the small signal from the defect is hidden behind the other arriving modes and signal noise. To overcome the difficulties associated with identifying the small signal from the defect and truncating the signal right after the defect signal but before the arrival of the reflected signal from the pipe end, in this paper the signal is analyzed both before and well after different wave modes have propagated multiple times through the pipe. It is found that the defective pipe can be clearly identified by analyzing the signal well beyond the first arrival of the signal from the defect. Multiple reflections and scattering of the propagating wave modes by the pipe ends and the defects do not make the defect detection more difficult, on the contrary it apparently stabilizes the signal and consistent spectral plots clearly distinguish the defective pipe from the defect-free pipe. However, to predict the exact location of the defect the signal from the defect must be identified in the time history plots.

ACKNOWLEDGMENT

This research was financially supported from a research grant from the National Science Foundation CMS/CMMI program—Contract No. CMS-9901221, CMMI-0530991 Program Director—Dr. Shih-Chi Liu. The results and conclusions presented here are those of the writers and do not represent the views of the National Science Foundation.

[1]D. Z. Gazis, "Three dimensional investigation of propagation of waves in hollow circular cylinders. I. Analytical foundation," J. Acoust. Soc. Am. **31**, 568–573 (1959).
[2]D. Z. Gazis, "Three dimensional investigation of propagation of waves in hollow circular cylinders. II. Numerical results," J. Acoust. Soc. Am. **31**, 573–578 (1959).
[3]J. E. Greenspon, "Axially symmetric vibrations of a thick cylindrical shell comparison of the exact theory with approximate theories," J. Acoust. Soc. Am. **32**, 1017–1025 (1960).
[4]J. E. Greenspon, "Vibration of a thick walled cylindrical shell comparison of the exact theory with approximate theories," J. Acoust. Soc. Am. **32**, 571–578 (1960).
[5]J. ZemanekJr., "An experimental and theoretical investigation of elastic wave propagation in a cylinder," J. Acoust. Soc. Am. **51**, 205–225 (1972).
[6]M. G. Silk and K. F. Bainton, "The propagation in metal tubing of ultrasonic wave modes equivalent to lamb waves," Ultrasonics **71**, 11–19 (1979).
[7]M. Brook, T. D. K. Ngoc, and J. Eder, "Ultrasonic inspection of stem generator tubing by chemical guided waves," *Review of Progress in QNDE*, edited by D. O. Thomson and D. E. Chimenti (Plenum, New York, 1990), Vol. **9**, pp. 243–249.
[8]M. J. S. Lowe, D. N. Alleyne, and P. Cawley, "Defect detection in pipes using guided waves," Ultrasonics **36**, 147–154 (1998).
[9]M. J. S. Lowe, D. N. Alleyne, and P. Cawley, "Mode conversion of a guided wave by a part-circumferential notch in a pipe,"Trans. ASME, J. Appl. Mech. **65**, 649–656 (1998).
[10]A. Demma, P. Cawley, M. Lowe, A. G. Roosenbrand, and B. Pavlakovic, "The reflection of guided waves from notches in pipes: A guide for interpreting corrosion measurements," NDT & E Int. **37**, 167–180 (2004).
[11]J. L. Rose, J. J. Ditri, A. Pilarski, K. Rajana, and F. Carr, "A guided wave inspection technique for nuclear steam generator tubing," NDT & E Int. **27**, 307–310 (1994).
[12]J. L. Rose, K. M. Rajana, and F. T. Carr, "Ultrasonic guided wave inspection concepts for steam generator tubing," Mater. Eval. **52**, 134–139 (1994).
[13]D. Guo and T. Kundu, "A new sensor for pipe inspection by Lamb waves," Mater. Eval. **58**, 991–994 (2000).
[14]D. Guo and T. Kundu, "A new transducer holder mechanism for pipe inspection," J. Acoust. Soc. Am. **110**, 305–309 (2001).
[15]W. B. Na, T. Kundu, and M. R. Ehsani, "Ultrasonic guided waves for steel bar-concrete interface inspection," Mater. Eval. **60**, 437–444 (2002).
[16]W. B. Na, T. Kundu, and M. R. Ehsani, "Lamb waves for detecting delamination between steel bars and concrete," Comput. Aided Civ. Infrastruct. Eng. **18**, 57–62 (2003).
[17]W. B. Na and T. Kundu, "Underwater pipe inspection using guided waves," ASME J. Pressure Vessel Technol. **124**, 196–200 (2002).
[18]W. B. Na and T. Kundu, "EMAT-based inspection of concrete filled steel pipes for internal voids and inclusions," ASME J. Pressure Vessel Technol. **124**, 265–272 (2002).
[19]R. Weaver, "Laboratory studies of diffuse waves in plates," J. Acoust. Soc. Am. **79**, 919–923 (1986).
[20]J. E. Michaels and T. E. Michaels, "Detection of structural damage from the local temporal coherence of diffuse ultrasonic signals," IEEE Trans. Ultrason. Ferroelectr. Freq. Control **52**, 1769–1782 (2005).

Comparison of spheroidal and eigenfunction-expansion trial functions for a membrane in an infinite baffle

Tim Mellow[a)]
Nokia UK Ltd., Nokia House, Summit Avenue, Farnborough, Hants GU14 0NG, United Kingdom

Leo Kärkkäinen
Nokia Research Center, 00180, Helsinki, Finland

(Received 28 October 2007; revised 31 January 2008; accepted 15 February 2008)

The on-axis far-field pressure response of a circular membrane in an infinite baffle when driven by a uniformly distributed electrostatic force is calculated using two different trial functions for the surface velocity distribution. The first is an expansion based upon a solution to the free space wave equation in oblate spheroidal coordinates, which has already been derived in a previous paper [J. Acoust. Soc. Am. **120**(5), 2460–2477 (2006)], and the second is a membrane eigenfunction expansion (or Bessel series), which is rigorously derived in this letter. Although the latter can be used as a basis for calculating a number of different radiation characteristics such as the radiation impedance or directivity, etc., only the on-axis far-field sound pressure is considered here. The results are compared and discussed. © *2008 Acoustical Society of America.*
[DOI: 10.1121/1.2896756]

PACS number(s): 43.38.Ja, 43.20.Rz, 43.20.Tb, 43.40.Dx [TDM] Pages: 2598–2602

I. INTRODUCTION

In a previous paper,[1] the sound field of a circular membrane in an infinite baffle was calculated using a trial function for the surface velocity distribution based upon a solution to the free space wave equation in oblate spheroidal coordinates. No convergence problems were encountered because the chosen trial function has an inherent zero at the rim which matches the clamped rim boundary condition of the membrane. In a more recent paper,[2] the sound field of a shallow spherical shell was calculated, which differed from the membrane in that the surface velocity was non-zero at the rim. Initially, the authors tried using the spheroidal trial function, but encountered convergence problems because a very large number of terms were needed in the expansion in order to maintain the true non-zero velocity close to the rim where it is forced to zero by the trial function. Hence, an eigenfunction expansion based upon the solution to the wave equation of the shell itself was used instead. In this letter, this eigenfunction expansion method is retrospectively applied to the membrane and compared with the original spheroidal trial function. The authors originally obtained this result in order to verify the eigenfunction method before applying it to the shell. However, there are some differences in the derivations for the membrane and shell due to differences in their boundary conditions, as will be pointed out.

In Sec. II, both trial functions are presented in the form of summations with unknown coefficients. In Secs. III and IV, solutions to the free space and membrane wave equations respectively are given. In Sec. V, the solutions are then coupled and solved simultaneously in Sec. VI for the unknown trial function coefficients. Finally, in Sec. VII, expressions for the far-field sound pressure response are derived.

Electrostatic loudspeakers often have damping in the form of narrow sound holes in the electrodes which provide viscous losses in order to flatten what would otherwise be a highly modal response. The pressure response is calculated here without damping in order to obtain a response with strong modal features. This makes it easier to see whether the two calculation methods actually give the same results. Also, the lack of damping demonstrates more clearly the effect of coupling to the acoustic radiation load: Due to the radiation mass being considerably greater than the membrane mass, the modes are shifted downwards at low frequencies and the radiation resistance has a damping effect at high frequencies.

II. TRIAL FUNCTION

In the case of the membrane,[1] the following spheroidal trial function was used for the velocity distribution:

$$\tilde{u}_0(w_0) = \sum_{m=0}^{\infty} \tilde{A}_m \left(1 - \frac{w_0^2}{a^2}\right)^{m+(1/2)}, \tag{1}$$

where $\tilde{A}_m$ are the expansion coefficients (which have to be calculated), w_0 is the radial ordinate, and a is the radius of the membrane, as shown in Fig. 1. In the case of the shell,[2] an eigenfunction expansion was used instead, in order to guarantee convergence. A similar eigenfunction expansion can also be used as a trial function for a membrane as follows:

[a)]Author to whom correspondence should be addressed. Electronic mail: tim.mellow@nokia.com.

 0001-4966/2008/123(5)/2598/5/$23.00 © 2008 Acoustical Society of America

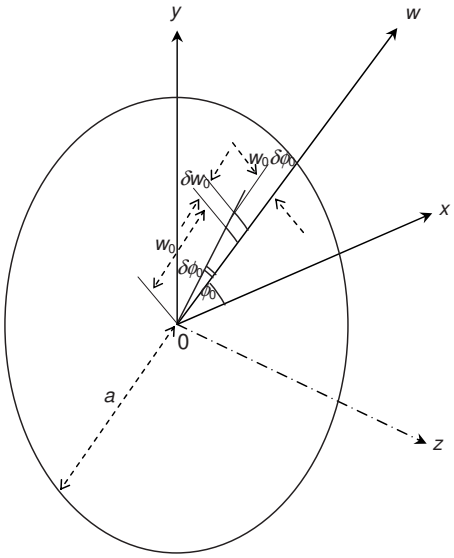


FIG. 1. Geometry of the membrane.

$$\tilde{u}_0(w_0) = \sum_{m=1}^{\infty} \tilde{A}_m J_0(\alpha_m w_0/a), \tag{2}$$

where α_m is the mth zero of $J_0(\alpha_m)$. However, this differs from the eigenfunction expansion for a shell in that a shell has bending stiffness which gives rise to a $I_0(\alpha_m w_0/a)$ term where I_0 is the Bessel function of the second kind. The shell also has a piston term which is proportional to the dome height. The uniform driving force is not expected to excite any axial modes, so only the 0th order Bessel function is included. Both of these trial functions satisfy the boundary condition of zero velocity at the rim of the membrane. The first is a solution to the wave equation for the surrounding medium to which the membrane is coupled and the second is a solution to the homogeneous wave equation for membrane itself. Only the latter is applied in this letter. In some ways, this method is slightly more direct because a set of simultaneous equations for the expansion coefficients is generated by simply equating the coefficients of $J_0(\alpha_n w/a)$ in the coupled equation. In the previous spheroidal derivation,[1] Eq. (1) was expanded as a Bessel series at one stage in order to generate the simultaneous equations. Both of these methods are fairly direct, though, and avoid the need for collocation or least squares minimization, which in turn leads to smaller errors and greater detail at high frequencies. Errors come mainly from the truncation of the expansion limits, as will be discussed.

III. SOLUTION TO THE FREE SPACE WAVE EQUATION

Using the King integral and doubling the amplitude due to the presence of the baffle, the pressure distribution is defined by

$$\tilde{p}(w,z) = 2\int_0^{2\pi}\int_0^a g(w,z|w_0,z_0) \times \frac{\partial}{\partial z_0}\tilde{p}(w_0,z_0)|_{z_0=0+} w_0 dw_0 d\phi_0, \tag{3}$$

where the Green's function is defined, in axisymmetric cylindrical coordinates, by

$$g(w,z|w_0,z_0) = \frac{i}{4\pi}\int_0^{\infty} J_0(\mu w)J_0(\mu w_0)\frac{\mu}{\sigma}e^{-i\sigma|z-z_0|}d\mu \tag{4}$$

and $\sigma=\sqrt{k^2-\mu^2}$, where k is the wave number given by $k=\omega/c=2\pi/\lambda$ and

$$\frac{\partial}{\partial z}\tilde{p}(w,z)|_{z=0\pm} = -ik\rho c\tilde{u}_0(w), \quad 0 \le w \le a, \tag{5}$$

where ρ is the density of air or any surrounding acoustic medium and c is the speed of sound in that medium. Inserting Eqs. (4) and (5) in Eq. (3) and integrating over the surface of the membrane while setting $z_0=0$ yields the sound pressure field as follows:

$$\tilde{p}(w,z) = ka\rho c\sum_{m=1}^{\infty}\tilde{A}_m\alpha_m J_1(\alpha_m) \times \int_0^{\infty}\frac{J_0(a\mu)J_0(\mu w)e^{-i\sigma z}}{(\alpha_m^2 - a^2\mu^2)\sigma}a\mu d\mu, \tag{6}$$

where the following identity[3] has been used:

$$\int_0^a J_0(\mu w_0)J_0(\alpha_m w_0/a)w_0 dw_0 = \frac{a^2}{\alpha_m^2 - a^2\mu^2}(\alpha_m J_0(a\mu)J_1(\alpha_m) - a\mu J_0(\alpha_m)J_1(a\mu)) \tag{7}$$

and taking into account that $J_0(\alpha_m)=0$. Let the power series coefficients $\tilde{A}_m$ be related to normalized dimensionless coefficients τ_m by

$$\tilde{A}_m = \tau_m\tilde{p}_I/(2\rho c), \tag{8}$$

where $\tilde{p}_I$ is the uniformly distributed driving pressure. Setting $z=0$ in Eq. (6) provides the surface pressure as follows:

$$\tilde{p}_+(w_0) = ka^2\frac{\tilde{p}_I}{2}\sum_{m=1}^{\infty}\tau_m\alpha_m J_1(\alpha_m)\int_0^{\infty}\frac{J_0(a\mu)J_0(\mu w_0)}{(\alpha_m^2 - a^2\mu^2)\sigma}\mu d\mu. \tag{9}$$

IV. SOLUTION TO THE MEMBRANE WAVE EQUATION

The solution[1] to the membrane wave equation $T(\nabla^2 - k_D^2)\tilde{\eta}(w) = \tilde{p}_+(w) - \tilde{p}_-(w) - \tilde{p}_I$, subject to the boundary conditions $\tilde{\eta}(a)=0$ and $\tilde{p}_+(w) = -\tilde{p}_-(w)$, is given by

$$\tilde{\eta}(w) = \frac{1}{T}\int_0^{2\pi}\int_0^a (2\tilde{p}_+(w_0) - \tilde{p}_I)G(w|w_0)w_0 dw_0 d\phi_0, \tag{10}$$

where $\nabla^2 = \partial^2/(\partial w^2) + w^{-1}\partial/(\partial w)$, $\tilde{\eta}(w)$ is the membrane deflection, T is the tension and k_D is the wave number of the membrane defined by $k_D=\omega\sqrt{\rho_D h/T}$, where ρ_D is the density

of the membrane and h is its thickness. The Green's function[4] for the membrane can be written suppressing the axial term in ϕ and ϕ_0 as follows:

$$G(w|w_0) = \frac{1}{\pi}\sum_{n=1}^{\infty} \frac{J_0(\alpha_n w/a)J_0(\alpha_n w_0/a)}{J_1^2(\alpha_n)(\alpha_n^2 - k_D^2 a^2)}, \quad 0 \le w \le a. \tag{11}$$

V. FORMULATION OF THE COUPLED PROBLEM

Substituting Eqs. (9) and (11) in Eq. (10) and equating the deflection with that given in Eq. (2) (where $\tilde{\eta}(w) = -i\tilde{u}_0(w)/kc$) leads to the following coupled equation (after integrating over the surface):

$$\frac{1}{\alpha_n J_1(\alpha_n)} = -i\tau_n \frac{\alpha_n^2 - k_D'^2 a^2}{4ka^2\rho c^2} T + ka\sum_{m=1}^{\infty} \tau_m \int_0^{\infty} \frac{\alpha_m \alpha_n J_0^2(a\mu) a\mu}{(\alpha_m^2 - a^2\mu^2)(\alpha_n^2 - a^2\mu^2)\sigma} d\mu, \tag{12}$$

which is obtained by equating the coefficients of $J_0(\alpha_n w/a)$ and again using the identity of Eq. (7) together with[5] $\int_0^a J_0(\alpha_n w_0/a) w_0 dw_0 = a^2 J_1(\alpha_n)/\alpha_n$.

VI. CALCULATION OF THE POWER SERIES COEFFICIENTS

A. Final set of simultaneous equations

From Eq. (12), the following set of M simultaneous equations in τ_m can be written

$$\sum_{m=1}^{M} {}_m\Psi_n(k_D' a, ka)\tau_m = 1, \quad n = 1,2,\ldots,M, \tag{13}$$

where ${}_m\Psi_n$ is an element of the mth column an nth row of the $M \times M$ matrix given by

$${}_m\Psi_n(k_D' a, ka) = \alpha_n J_1(\alpha_m)\left(-\frac{ika(\alpha_n^2 - k_D'^2 a^2)}{2\alpha^2(ka)}\delta_{mn} + \alpha_m \alpha_n I(k,m,n)\right), \tag{14}$$

where δ_{mn} is the Kronecker delta function and the infinite series limit has been truncated to order M. The dimensionless parameter α is the fluid-loading factor given by $\alpha(ka) = kac\sqrt{2a\rho/T}$. The integral $I(k,m,n)$ is defined by $I(k,m,n) = I_F(k,m,n) + iI_I(k,m,n)$, where

$$I_F(k,m,n) = ka\int_0^k \frac{J_0^2(a\mu)a\mu}{(\alpha_m^2 - a^2\mu^2)(\alpha_n^2 - a^2\mu^2)\sqrt{k^2 - \mu^2}} d\mu, \tag{15}$$

$$I_I(k,m,n) = -ka\int_k^{\infty} \frac{J_0^2(a\mu)a\mu}{(\alpha_m^2 - a^2\mu^2)(\alpha_n^2 - a^2\mu^2)\sqrt{\mu^2 - k^2}} d\mu. \tag{16}$$

It can be seen that the numerators and denominators of these integrals are simultaneously zero when $\alpha_m = a\mu$ or $\alpha_n = a\mu$, so these are indeterminate points. Using Taylor's series, it can be shown that the functions are actually continuous. Hence, the integrals can be solved numerically so long as these indeterminate points are avoided. Also, the weak singularity at $\mu = k$ can be removed by means of suitable substitutions, as shown in the following sections. However, the integrands are strongly oscillatory and the integral I_I has an infinite limit. Therefore, it is more efficient to solve these integrals analytically to yield fast converging expansions.

B. Solution of the finite integral

After substituting $\mu = k\sqrt{1-t^2}$, Eq. (15) for the finite integral becomes

$$I_F(k,m,n) = \int_0^1 \frac{k^2 a^2 J_0^2(ka\sqrt{1-t^2})}{(\alpha_m^2 - k^2a^2(1-t^2))(\alpha_n^2 - k^2a^2(1-t^2))} dt. \tag{17}$$

The Bessel functions can then be expanded using the following Lommel expansion:[6]

$$J_0(ka\sqrt{1-t^2}) = \sum_{p=0}^{\infty} \frac{J_p(ka)}{p!}\left(\frac{ka}{2}\right)^p t^{2p}, \tag{18}$$

so that the expanded integral can be written

$$I_F(k,m,n) = k^2a^2 \sum_{p=0}^{\infty}\sum_{q=0}^{\infty} \frac{J_p(ka)J_q(ka)}{p!\,q!}\left(\frac{ka}{2}\right)^{p+q} \times \int_0^1 \frac{t^{2p+2q}}{(\alpha_m^2 - k^2a^2(1-t^2))(\alpha_n^2 - k^2a^2(1-t^2))} dt. \tag{19}$$

After solving the integral,[3] and truncating the infinite expansion limits to P and Q, the final expression can be written

$$I_F(k,m,n)|_{m\neq n} = k^2a^2 \sum_{p=0}^{P}\sum_{q=0}^{Q} \frac{J_p(ka)J_q(ka)}{p!\,q!\,(2p+2q+1)(\alpha_m^2 - \alpha_n^2)} \times \left(\frac{ka}{2}\right)^{p+q} \left\{ \frac{1}{k^2a^2 - \alpha_m^2} {}_2F_1\left(1, u-1; u; \frac{k^2a^2}{k^2a^2 - \alpha_m^2}\right) - \frac{1}{k^2a^2 - \alpha_n^2} {}_2F_1\left(1, u-1; u; \frac{k^2a^2}{k^2a^2 - \alpha_n^2}\right)\right\}, \tag{20}$$

where $u = p+q+3/2$ and which is valid for $m \neq n$. It can be seen that if $m=n$, then $\alpha_m^2 - \alpha_n^2 = 0$, which leads to a singular expression. In the case of the shell, this problem did not arise due to the presence of damping resistance in the boundary conditions, which gave rise to complex eigenvalues so that the difference between the squares of two complex conjugate eigenvalues was non-zero. Here, for $m=n$ the following alternative expression has to be used:

$$I_F(k,m)|_{m=n} = k^2a^2 \sum_{p=0}^{P}\sum_{q=0}^{Q} \frac{J_p(ka)J_q(ka)}{p!\,q!\,(2p+2q+1)(k^2a^2 - \alpha_m^2)^2} \times \left(\frac{ka}{2}\right)^{p+q} {}_2F_1\left(2, u-1; u; \frac{k^2a^2}{k^2a^2 - \alpha_m^2}\right). \tag{21}$$

C. Solution of the infinite integral

After substituting $\mu = k\sqrt{t^2+1}$, Eq. (16) for the finite integral becomes

$$I_I(k,m,n) = -\int_0^\infty \frac{k^2a^2J_0^2(ka\sqrt{t^2+1})}{(\alpha_m^2 - k^2a^2(t^2+1))(\alpha_n^2 - k^2a^2(t^2+1))}dt. \tag{22}$$

The Bessel functions can then be expanded using Gegenbauer's summation theorem[5] as follows:

$$J_0(ka\sqrt{t^2+1}) = 2\sum_{p=0}^{\infty} \frac{(-1)^p}{1+\delta_{p0}} J_{2p}(ka)J_{2p}(kat), \tag{23}$$

so that the expanded integral can be written

$$I_I(k,m,n) = -4k^2a^2 \sum_{p=0}^{\infty}\sum_{q=0}^{\infty} \frac{(-1)^{p+q}J_{2p}(ka)J_{2q}(ka)}{(1+\delta_{p0})(1+\delta_{q0})} \times \int_0^\infty \frac{J_{2p}(kat)J_{2q}(kat)}{(\alpha_m^2 - k^2a^2(t^2+1))(\alpha_n^2 - k^2a^2(t^2+1))}dt. \tag{24}$$

After solving the integral,[3] and truncating the infinite expansion limits to P and Q, the final expression can be written

$$I_I(k,m,n)|_{m\neq n} = -\frac{ka}{\pi}\sum_{p=0}^{P}\sum_{q=0}^{Q} \frac{J_{2p}(ka)J_{2q}(ka)}{(1+\delta_{p0})(1+\delta_{q0})(v-2)_2(u-2)_2(\alpha_m^2-\alpha_n^2)} \times \left\{ {}_3F_4\left(1,1,\frac{3}{2};3-u,u,3-v,v;k^2a^2-\alpha_m^2\right) - {}_3F_4\left(1,1,\frac{3}{2};3-u,u,3-v,v;k^2a^2-\alpha_n^2\right)\right\}, \tag{25}$$

where $u=p+q+3/2$, $v=p-q+3/2$ and which is valid for $m\neq n$. Again, in order to avoid singularities, for $m=n$ the following alternative expression is provided:

$$I_I(k,m)|_{m=n} = \frac{3ka}{2\pi}\sum_{p=0}^{P}\sum_{q=0}^{Q} \frac{J_{2p}(ka)J_{2q}(ka)}{(1+\delta_{p0})(1+\delta_{q0})(u-3)_4(v-3)_4} \times {}_3F_4\left(2,2,\frac{5}{2};4-u,u+1,4-v,v+1;k^2a^2-\alpha_m^2\right). \tag{26}$$

It should be noted that in the case of the shell,[2] the solution to the infinite integral also contained Bessel functions of the second kind, in addition to the hypergeometric functions, due to the eigenvalues being complex. Here they are real, so those Bessel functions would not be valid and have been removed in order to obtain the correct result.

VII. FAR FIELD PRESSURE RESPONSE

The far field pressure is derived by inserting the following far-field Green's function in spherical-cylindrical coordinates

$$g(r,\theta,\phi|w_0,\phi_0,z_0) = \frac{1}{4\pi r}e^{-ik(r-w_0\sin\theta\cos(\phi-\phi_0)-z_0\cos\theta)} \tag{27}$$

in Eq. (3) and integrating over the surface of the membrane to obtain

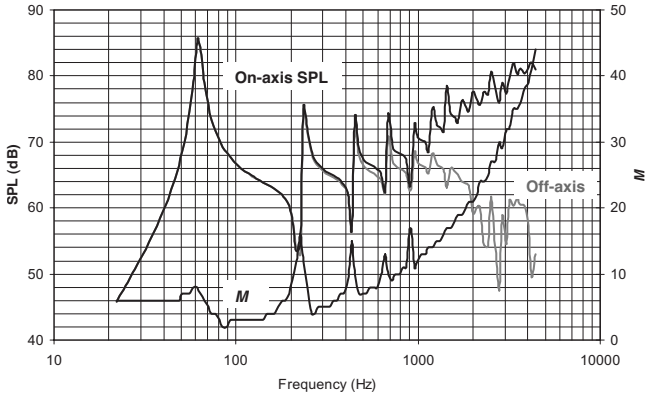


FIG. 2. On-axis and 45° off-axis pressure responses and summation limit M using the spheroidal trial function of Eq. (1), where $a=125$ mm, $h=12$ μm, $T=100$ N/m, $\rho_D=1667$ kg/m^3, $p_I=1$ Pa, and $r=1$ m.

$$\tilde{p}(r,\theta) = -\frac{ia}{4r}\tilde{p}_I e^{-ikr}D(\theta), \tag{28}$$

where r is the distance from the origin to the observation point and θ is the angle subtended to the axis of symmetry. The directivity function $D(\theta)$ is given by

$$D(\theta) = 2ka\sum_{m=1}^{M} \frac{\alpha_m J_1(\alpha_m)J_0(ka\sin\theta)}{\alpha_m^2 - (ka\sin\theta)^2}\tau_m. \tag{29}$$

For $\theta=0$ (i.e., on axis), this simplifies to

$$D(0) = 2ka\sum_{m=1}^{M} \frac{J_1(\alpha_m)}{\alpha_m}\tau_m. \tag{30}$$

The on-axis pressure response without damping is shown in Fig. 3 where the sound pressure level (SPL) is given by: $SPL=20\log_{10}|\tilde{p}(r,0)/(20\times10^{-6})|$. Figure 2 shows the response calculated using the surface-velocity trial function given in Eq. (1) and the far-field expression given in the previous paper.[1] The summation limit M is shown for each of the 114 points plotted. The summation limit was determined using a convergence criterion of 0.002 dB maximum difference between the SPL computed with M and $(M+1)$ terms. The remaining summation limits P and Q were set to $P=Q=2M$.

VIII. DISCUSSION OF THE RESULTS

The on-axis pressure responses shown in Figs. 2 and 3 are fairly typical of clamped membranes and plates in general. At the eigenfrequencies the membrane's displacement becomes very large. When most of the membrane's surface is moving in the same direction, large peaks are produced. Also, there are frequencies at which the displacement is still large, but different regions of the membrane are moving in opposite directions so as to cancel each other out: Instead of radiating sound, air is just moved back and forth between the areas of the surface that are moving in opposite phase. An excellent illustration of this has been provided by Streng.[7] The damping effect of the increasingly resistive radiation impedance at high frequencies is fairly evident. The direct nature of calculation method shows considerable detail in this region, enabled by the elimination of collocation or least

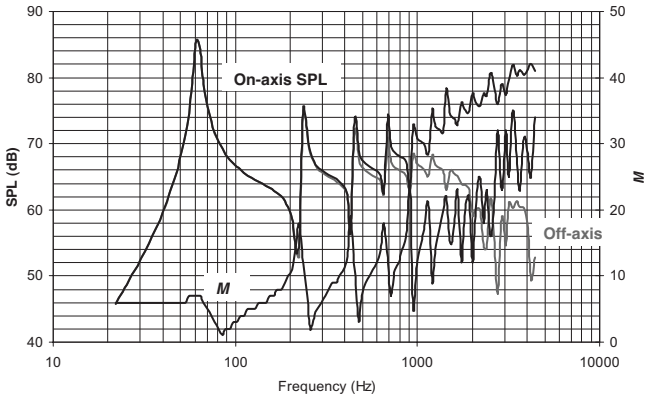


FIG. 3. On-axis and 45° off-axis pressure responses and summation limit M using the eigenfunction-expansion trial function of Eq. (2) with same parameters as Fig. 2.

squares methods. The actual differences between the pressures in Figs. 2 and 3 are fairly small. On axis, the maximum difference is 0.03 dB, rising to 0.1 dB at 45° off axis. As expected, the off axis response rolls off early due to high-frequency beaming, but still shows significant modal variations.

Also shown in these figures are the numbers of terms in the summations required to meet the convergence criterion of less than 0.002 dB difference in SPL when one extra term is added to the summation. Not surprisingly, it can be seen that generally more terms are required at higher frequencies due to the increasing complexity in the displaced membrane shape. Also, more terms are required at the eigenfrequencies because the driving force and acoustic pressure are distributed in such a way that excites not just that particular eigenfrequency, but a complex mixture of higher order modes too. Interestingly, fewer terms are required in the case of the eigenfunction method in between the eigenfrequencies, so here it must provide a more natural fit to the displaced shape. However, at the eigenfrequencies, the summation limit tends to be slightly greater than with the spheroidal method.

Regarding the speed of the calculations, this would of course vary considerably depending on whether a compiled or non-compiled program is used, numerical algorithms, type of hardware and other factors too. Suffice to say that the spheroidal method was found to be about ten times faster. This is mainly due to the fact that the hyperbolic functions in Eqs. (21) and (26) are functions of both p and q in the double summations, whereas in the case of the spheroidal method[1] the hypergeometric function is a function of q only.

IX. CONCLUSIONS

An alternative method has been presented for calculating the radiation characteristics of a membrane using a trial function based upon an eigenfunction expansion. This method, like the previous one which used a spheroidal trial function, does not require numerical integration.

Since the two methods give SPL values within 0.03 dB of each other on axis, it is not possible to state that one is necessarily more accurate than the other, but the fact that the two results are so consistent means that neither is likely to be wildly inaccurate.

The simpler formulas provided by the spheroidal series make it easier to derive expressions for other radiation characteristics such as the near field pressure and radiation impedance. Unfortunately, it appears to be restricted to cases where the surface velocity/deflection is either zero[1] or infinity[8] at the rim, such as circular membranes,[1] sound holes,[8] and clamped or simply supported plates and shells. Otherwise, for a finite rim velocity, the eigenfunction expansion has to be used. Examples of the latter are circular plates or shells[2] with non-zero rim velocity as in dynamic loudspeakers, earpieces and microphones, where the contribution of the surround is ignored (but its stiffness can still be included in the boundary conditions[2]). The rim velocity boundary condition affects the modal structure which, in turn, affects the computed sound pressure. Although the eigenfunction method is slower and therefore less attractive for the current problem, it has been verified and can therefore be applied with confidence to other uses where the spheroidal method is unsuitable.

[1]T. J. Mellow and L. M. Kärkkäinen, "On the sound field of a circular membrane in free space and an infinite baffle," J. Acoust. Soc. Am. **120**(5), 2460–2477 (2006).
[2]T. J. Mellow and L. M. Kärkkäinen, "On the sound field of a shallow spherical shell in an infinite baffle," J. Acoust. Soc. Am. **121**(6), 3527–3541 (2007).
[3]S. Wolfram, *The Mathematica Book*, 5th ed. (Wolfram Media, Champaign, IL, 2003).
[4]P. M. Morse and K. U. Ingard, *Theoretical Acoustics* (McGraw–Hill, New York, 1968), pp. 320, 365, 389, 390.
[5]I. S. Gradshteyn and I. M. Ryzhik, *Table of Integrals, Series, and Products*, 6th ed., edited by A. Jeffrey (Academic, New York, 2000), pp. 668, Eq. (6.561.5), pp. 930, Eq. (8.532.1), p. 980, Eqs. (8.930.1)–(8.930.7).
[6]G. N. Watson, *A Treatise on the Theory of Bessel Functions*, 2nd ed. (Cambridge University Press, London, 1944), p. 141, Sec. 5.22, Eq. (5).
[7]J. H. Streng, "Calculation of the surface pressure on a vibrating circular stretched membrane in free space," J. Acoust. Soc. Am. **82**(2), 679–686 (1987).
[8]T. J. Mellow, "On the sound field of a resilient disk in an infinite baffle," J. Acoust. Soc. Am. **120**(1), 90–101 (2006).

Calculations of modes in circumferentially nonuniform lined ducts

WenPing Bi[a)]
Laboratoire d'Acoustique de l'Université du Maine, UMR CNRS 6613, Faculté des sciences, 72085 Le Mans, France

(Received 28 June 2007; revised 15 January 2008; accepted 24 February 2008)

This paper proposes a computationally efficient method of determining eigenfunctions and eigenvalues of acoustic modes propagating in circular lined ducts with zero or uniform flow. Linings with circumferentially nonuniform impedance, as found in nacelle acoustics, are the focus. The method of solution adapts in two important respects—the presence of flow and the imposition of impedance boundary conditions—the series expansion method first proposed by Pagneux *et al.* [J. Acoust. Soc. Am. **110**, 1307–1314 (2001)] to calculate the eigenvalues of Lamb modes. The inclusion of flow, and a corresponding different method of solution leading to an improved convergence of eigenvalues ($O(N^{-5})$, N is the truncation of radial basis of expansion), is the important new feature as compared to the previous adaptation by Bi *et al.* [J. Acoust. Soc. Am. **122**, 280–291 (2007)]. As a result, it becomes possible to safely determine and in a simple manner the eigenvalues and eigenfunctions of circumferentially nonuniform lined ducts in the presence of uniform flow, up to relatively high frequencies (e.g., $30<kR<80$). All required eigenvalues are calculated at a time and no initial values guesses are needed. Results are presented and the method is discussed. © *2008 Acoustical Society of America.* [DOI: 10.1121/1.2897105]

PACS number(s): 43.50.Gf, 43.20.Mv, 43.20.Fn, 43.20.Hq [LLT] Pages: 2603–2612

I. INTRODUCTION

Determining the modal solutions is a very useful step in developing an understanding of sound propagation and attenuation in lined ducts with or without flow. The imaginary part of the axial wave number determines the rate of attenuation. The maximum attenuation is found for an impedance leading to the coalescence of two or more modes.[1] However, the determination of all different modes is generally difficult. As quoted in Astley *et al.*,[2] "The evaluation of the eigenvectors even for ducts of separable geometry, is a nontrivial exercise, particularly when flow is present. Surface modes exist for particular ranges of wall impedance, and the development of robust methods which are able to resolve all of the modes all of the time is not a simple matter." When the lining impedance is circumferentially nonuniform, especially when it is piecewise constant or includes small rigid splices, and when the frequency is relatively high, say the dimensionless frequency $30<K<80$, which are typical cases of interest in the lined intakes of an aeroengine, the calculations of modes are still not well resolved.

Calculations of modes in lined ducts (with uniform mean flow given by Mach number Ma_0) mean solving the following Laplacian eigenvalue problem:

$$\Delta_\perp \phi_i = -\gamma_i^2 \phi_i, \tag{1}$$

with the wall boundary condition[3]

$$\frac{\partial \phi_i}{\partial r} = Y(\theta)\left(1 - \mathrm{Ma}_0 \frac{K_{z,i}}{K}\right)^2 \phi_i, \quad \text{at } r = 1, \tag{2}$$

where

$$\Delta_\perp = \frac{1}{r}\frac{\partial}{\partial r}\left(r\frac{\partial}{\partial r}\right) + \frac{1}{r^2}\frac{\partial^2}{\partial \theta^2}, \tag{3}$$

$K=2\pi fR/c$ refers to the dimensionless frequency, f is frequency, R is radius, c is sound velocity in air, γ_i and ϕ_i refer to the transverse wave numbers and eigenfunctions respectively, $\gamma_i^2=(K-\mathrm{Ma}_0K_{z,i})^2-K_{z,i}^2$, $K_{z,i}$ are the axial wave numbers, $Y(\theta)=-jK\beta(\theta)$, and $\beta(\theta)$ is the liner admittance which can vary arbitrarily around the duct wall.

The equations are simple, but not evident to solve without resorting to purely numerical techniques. When the admittance β is uniform along θ, the dispersion relation equation can be written explicitly. Root finding methods, e.g., Newton–Raphson iteration, are generally used to solve it, after supposing some initial roots. In general, initial roots are unknown. Thus, in practice one often attributes a factor to the admittance of the lining, which is then increased step by step, from zero value (rigid duct with known solutions) to unit value (lining duct), using the solution of the preceding step as the initial solution. Another method is to start the computation at low frequencies where the admittance generally tends to zero, and to track the solutions when the frequency is increased step by step. Eversman and Cook[4] changed the eigenvalue equation into a differential one which can be integrated by using the Runge–Kutta algorithm. Montetagaud *et al.*[5] used this method with a more precise step. Rienstra[6] identified the modes in ducts in two categories: The duct modes resulting from the finiteness of

[a)]Electronic mail: wenping.bi@univ-lemans.fr

the duct geometry, and the surface waves that exist only near the wall surface in a way essentially independent of the rest of the duct. He was interested in the high frequency regime, which corresponds to typical cases in the turbofan engine duct applications. He gave the areas in the complex impedance Z plane in which the surface waves exist. He proposed a routine in the complex Z plane from $Z=\infty$ to the sought value to trace the eigenvalue as a function of Z. He pointed out that when the sought Z value is in the areas where the surface waves will exist we have to make sure to pick up these eigenvalues.

Finite Element Method (FEM) or Galerkin method are also proposed to solve the eigenvalue problem. The first instances of FEM used to calculate flow duct modes were devised by Astley and Eversman[7,8] for circumferentially uniform lined ducts. Other examples for circumferentially nonuniform lined ducts can be found in Refs. 2, 9, and 10. The eigenfunctions are expanded in terms of a basis which is independent of the eigenvalues. The Helmholtz equation (1) with boundary condition (2) is projected over this basis and then diagonalized. Other methods, e.g., Refs. 11–16, used to solve the eigenvalue problem in lined ducts are reviewed in detail in Ref. 17.

Recently, a multimodal expansion method was developed by Pagneux and Maurel[18] to calculate the eigenvalue spectrum of Lamb waves. They expanded the eigenfunctions of Lamb waves over a complete set of orthogonal functions. Application of this expansion converts the eigenproblem of Laplace operator and boundary conditions to a generalized eigenvalue problem of a matrix. There is widely available software for solving this matrix eigenvalue problem. All the required eigenvalues are calculated at a time and no initial values guesses are needed.

We extend in the present paper Pagneux's method to the problem of the determination of modes with zero or uniform flow and for ducts lined with circumferentially nonuniform lining. This work is motivated by the applications in the lined intake of an aeroengine in which the dimensionless frequency K may be up to 80, hundreds of modes are needed to calculate, the lining impedance may be circumferentially nonuniform, particularly, it may be in segments, leading to mathematically discontinuous boundary conditions.

In order to valuably apply the method it is necessary to address, in a convenient manner, two problems posed by the nature of the boundary conditions, namely, their "impedance" nature and the presence in them of the squared axial wave number. The first problem was addressed in a previous paper.[17] Impedance boundary conditions are difficult to fulfill by using, as is usual, the complete and orthogonal set of rigid duct eigenfunctions, resulting in a "slow" convergence of the method. A simple way to circumvent this problem consists of subtracting to the field we want to determine, a part suitably chosen to carry the information of the impedance boundary. Thanks to this subtraction, the remaining field to be developed on the usual rigid duct modes now fulfill the hard-wall boundary conditions, leading to an improved convergence.

The second problem, the inclusion of uniform flow, is specifically addressed in the present paper. This inclusion imposes modifying in suitable manner the mathematical treatment, in such a way that the benefits of the improved convergence will not be lost in presence of flow.

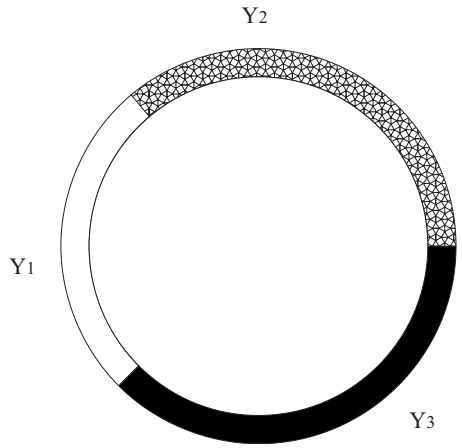


FIG. 1. A typical configuration of circumferentially nonuniform impedance boundary considered in this paper. Y_1, Y_2, and Y_3 are three segments of admittances.

The assumption of uniform flow, although being of course an important simplification, may provide useful insights on the main effects of flow. In practical applications the flow has a profile or may be more complicate. Including the shear flow in the present method, which will produce a continuous spectrum of hydrodynamic modes, is a very challenging work to be addressed in the future. At present time, precise numerical calculations of sound propagation in nonuniform lined ducts with true flow will take weeks or maybe more, even using huge computers. Those evaluations are only possible for some carefully chosen cases. The present method with the assumption of uniform flow may provide important information for those selections.

The paper is organized as follows. In Sec. II, the derivation of equations is presented for nonuniform boundary conditions. A validation of the method is presented in Sec. III. The convergence rates of eigenvalues and eigenfunctions are examined in Sec. IV. Then, in Sec V, some numerical examples are shown to illustrate the robustness of the method. In Sec. VI, we discuss two problem. In the first part, we show another important advantage of the method proposed in this paper. In the second part, we discuss a more general problem: The proper form of boundary conditions when the impedances are azimuthal discontinuous. Finally, conclusions are given in Sec. VII.

II. DERIVATION OF THE EQUATIONS

We consider a cylindrical lined duct of uniform cross section. The lining is assumed uniform along the duct axis z; at variance, any nonuniform lining pattern can be considered with respect to the azimuthal angle θ. A typical configuration is shown in Fig. 1. We wish to determine the possible modal solutions in this translational invariant lining duct in presence of a uniform flow. The sound propagation in air is assumed to be linear and lossless. Harmonic sound waves with a time factor $e^{j\omega t}$ are assumed.

The wanted eigenfunctions $\phi(r,\theta)$ may always be expanded in terms of the orthogonal and complete set of eigenfunctions $\Psi_{mn}=(1/\sqrt{\pi\Lambda_{mn}})(J_m(\alpha_{mn}r)/J_m(\alpha_{mn}))e^{-jm\theta}$ of the rigid duct, i.e.,

$$\phi(r,\theta)=\sum_{m=-\infty,n=0}^{\infty}\Phi_{mn}\Psi_{mn}(r,\theta), \tag{4}$$

where Λ_{mn} refer to the normalization coefficients, J_m is the m order bessel functions, α_{mn} is the solution of $\partial_r J_m(\alpha r)=0$ at $r=1$, m and n azimuthal and radial indices (the sum over index m will be suppressed in the case of circumferentially uniform impedance boundary condition). However, by definition these functions verify the boundary conditions $\partial_r\Psi_{mn}(r,\theta)|_{r=1}=0$. Thus, in order that ϕ may verify the wanted impedance boundary conditions (2), expansion (4) cannot be substituted directly in boundary condition (2) and derived term by term everywhere with respect to r. This means that the above expansion converges sufficiently slowly (with respect to index n) that the sum and derivative symbols do not commute. This suggests removing an arbitrary function $X(r,\theta)$, having nonzero derivative at $r=1$, before projecting as before over the Ψ_{mn}

$$\phi(r,\theta)-X(r,\theta)=\sum_{m=-\infty,n=0}^{\infty}\Phi_{mn}\Psi_{mn}(r,\theta). \tag{5}$$

This function will be chosen so as $\partial_r(\phi-X)|_{r=1}=0$, then ensuring that the expansion may be derived term by term, signature of an improved convergence [which will be of the type $O(n^{-4})$]. Then writing function $X(r,\theta)$ in the form (circumferentially nonuniform impedance boundary conditions)

$$X(r,\theta)=\sum_{m=-\infty}^{\infty}A_m\chi_m(r)e^{-jm\theta}, \tag{6}$$

with

$$\left.\frac{d\chi_m(r)}{dr}\right|_{r=1}=1, \tag{7}$$

it will be possible to arrange a choice of the A_m satisfying the condition $\partial_r(\phi-X)|_{r=1}=0$. In fact, as the left-hand side of Eq. (2) is determined by the $X(r,\theta)$ term only, this term need not appear in the right-hand side and our calculations will be simpler if we require additionally

$$\chi_m(r)|_{r=1}=0. \tag{8}$$

Notice that this is different from Ref. 17 where this condition is necessary.

A convenient choice for the $\chi_m(r)$ is then the following:

$$\chi_m(r)=B_m J_m(\beta_{m,0}r), \tag{9}$$

where $\beta_{m,0}$ is the first root of

$$J_m(\beta_m)=0, \tag{10}$$

and

$$B_m=\frac{-1}{\beta_{m,0}J_{m+1}(\beta_{m,0})}. \tag{11}$$

In Ref. 17, we consider a problem of propagation in the case of zero flow, we proceed by directly exploiting boundary condition (2). Substituting Eq. (5) in condition (2) and using conditions (7) and (8) and $\partial_r\Psi_{mn}(r,\theta)|_{r=1}=0$, yield the A_m in terms of the expansion coefficients Φ_{mn} [see Eqs. (17) and (27) in Ref. 17]. This leads to an expansion of eigenfunctions as [Eqs. (22) and (28) in Ref. 17]

$$\phi(r,\theta)=\mathbf{\Psi}^T\mathsf{M}\mathbf{\Phi}, \tag{12}$$

and a generalized eigenvalue problem of a matrix A_0 [Eqs. (24) and (30) in Ref. 17],

$$K_z^2\mathsf{M}\mathbf{\Phi}=\mathsf{A}_0\mathbf{\Phi}, \tag{13}$$

where matrices M and A_0 (A in Ref. 17) can be found in Ref. 17 by Eqs. (23), (25), (29), and (31). $\mathbf{\Phi}$ and $\mathbf{\Psi}$ are column vectors of dimension N_t, their elements are Φ_{mn} and Ψ_{mn}. $N_t=M\times N$, M and N are the truncations of indices m and n.

On the other hand, when the uniform flow is included, a multiplicative factor $(1-\mathrm{Ma}_0K_{z,i}/K)^2$ appears in the corresponding relations, showing that the A_m are now polynomial expressions of order two on the axial wave number $K_{z,i}$. Thus, if we were to proceed like in Ref. 17 [directly expressing the A_m from condition (2), substituting Eqs. (5) and (6) into Eq. (1) and projecting the latter over Ψ_{mn}] we would obtain a system of algebraic equations of order four with respect to $K_{z,i}$ (instead of order 2). This would require much computer memory to solve and the benefits of the introduction of the $X(r,\theta)$ term for an improved convergence would be lost.

Thus, in contrast to Ref. 17, we will not express A_m from the outset of the calculation. We instead follow the idea of Attanassoulis and Belibassakis[19] which keeps A_m as a set of unknown variables. Additional M equations are needed to calculate A_m, where M is the truncation number of index m. These will be the M equations obtained by projecting both sides of Eq. (1) over the (mutually orthogonal) $\chi_m(r)e^{-jm\theta}$. In the following, we consider the general case of uniform flow and nonuniform admittance $Y(\theta)$. The case of zero flow and/or uniform admittance are straightforward simplifications.

Let us project $\phi(r,\theta)$ over the basis Ψ_{mn} and the set of functions $\chi_m e^{-jm\theta}$. Following the matricial terminology, we yield

$$\int\phi(r,\theta)\mathbf{\Psi}^*dS=\mathbf{\Phi}+\mathbf{\Xi}\mathbf{A}, \tag{14}$$

$$\int\phi(r,\theta)\chi^*dS=\mathbf{\Xi}^T\mathbf{\Phi}+2\pi\mathbf{\Pi}\mathbf{A}, \tag{15}$$

where $\mathbf{\Xi}$ is a block diagonal matrix of dimension $N_t\times M$. In each block m of matrix $\mathbf{\Xi}$, it is a column vector of dimension N, its elements are $2\sqrt{\pi}/(\sqrt{\Lambda_{mn}}(\alpha_{mn}^2-\beta_{m,0}^2))$, with $n=1,2,\ldots,N$. Π is a diagonal matrix, $\|\chi_m\|^2=1/(2\beta_{m,0}^2)$ are in its main diagonal. $\mathbf{A}$ and χ are column vectors of dimension M, their elements are A_m and $\chi_m e^{-jm\theta}$. The superscript T and asterisk indicate the transpose and complex conjugate, respectively. The detailed derivation of Eqs. (14) and (15) are

shown in the Appendix. Equations (14) and (15) are combined to yield

$$\int \phi(r,\theta)\mathbf{\Psi}_{\mathbf{A}}^{*}dS = \mathsf{M}_1\mathbf{\Phi}_{\mathbf{A}}, \tag{16}$$

where

$$\mathbf{\Phi}_{\mathbf{A}} = \begin{bmatrix} \mathbf{\Phi} \\ \mathbf{A} \end{bmatrix}, \quad \mathbf{\Psi}_{\mathbf{A}} = \begin{bmatrix} \mathbf{\Psi} \\ \chi \end{bmatrix}, \tag{17}$$

M_1 is a $(N_t+M)\times(N_t+M)$ matrix, it is expressed as

$$\mathsf{M}_1 = \begin{bmatrix} \mathsf{I} & \Xi \\ \Xi^T & 2\pi\Pi \end{bmatrix}, \tag{18}$$

where I refers to identity matrix $(N_t\times N_t)$.

Using Eq. (16), we project Eq. (1), to yield (see the Appendix)

$$(\mathsf{A}_1K_{z,i}^2 + \mathsf{A}_2K_{z,i} + \mathsf{A}_3)\mathbf{\Phi}_{\mathbf{A}} = 0, \tag{19}$$

where matrix A_1, A_2, and A_3 are

$$\mathsf{A}_1 = \begin{bmatrix} \mathrm{Ma}_0^2\mathsf{I} + \dfrac{\mathrm{Ma}_0^2}{K^2}\mathsf{C} - \mathsf{I} & (\mathrm{Ma}_0^2-1)\Xi \\ (\mathrm{Ma}_0^2-1)\Xi^T & 2\pi(\mathrm{Ma}_0^2-1)\Pi \end{bmatrix},$$

$$\mathsf{A}_2 = 2K\mathrm{Ma}_0\begin{bmatrix} \mathsf{I} + \dfrac{1}{K^2}\mathsf{C} & \Xi \\ \Xi^T & 2\pi\Pi \end{bmatrix},$$

$$\mathsf{A}_3 = \begin{bmatrix} K^2\mathsf{I} - \mathsf{L}_1 + \mathsf{C} & (K^2\mathsf{I} - \mathsf{L}_1)\Xi \\ (K^2\mathsf{I}_2 - \mathsf{L}_2)\Xi^T - 2\sqrt{\pi}\Lambda & 2\pi K^2\Pi - \pi\mathsf{I}_2 \end{bmatrix}, \tag{20}$$

where matrices L_1 and L_2 are diagonal matrices, α_{mn}^2 and $\beta_{m,0}^2$ are in their main diagonal elements, respectively. Matrix Λ is a block diagonal matrix of dimension $M\times N_t$. Each block m of the matrix Λ is a row vector of dimension N, its elements are $1/\sqrt{\Lambda_{mn}}$, with $n=1,2,\ldots,N$. I_2 is an identity matrix of dimensions $M\times M$. Matrix C is

$$\mathsf{C} = \int_0^{2\pi} Y(\theta)\mathbf{\Psi}^*(1,\theta)\mathbf{\Psi}^T(1,\theta)d\theta. \tag{21}$$

Equation (19) is a nonlinear eigenvalue problem with respect to K_z of dimension $(N_t+M)\times(N_t+M)$, it can be recasted as a linear eigenvalue problem with respect to K_z of dimension $2(N_t+M)\times 2(N_t+M)$

$$K_z\mathsf{A}\mathbf{\Phi}_{\mathbf{B}} = \mathsf{B}\mathbf{\Phi}_{\mathbf{B}}, \tag{22}$$

where

$$\mathsf{A} = \begin{bmatrix} \mathsf{A}_1 & 0 \\ 0 & \mathsf{I} \end{bmatrix}, \quad \mathsf{B} = \begin{bmatrix} -\mathrm{j}\mathsf{A}_2 & \mathsf{A}_3 \\ -\mathsf{I} & 0 \end{bmatrix}, \quad \mathbf{\Phi}_{\mathbf{B}} = \begin{bmatrix} \mathbf{\Phi}_{\mathbf{C}} \\ \mathbf{\Phi}_{\mathbf{A}} \end{bmatrix}, \tag{23}$$

where $\mathbf{\Phi}_{\mathbf{C}}$ is a column vector which is dependent on $\mathbf{\Phi}_{\mathbf{A}}$.

Equation (22) is a generalized eigenvalue problem with generalized eigenvalue K_z and generalized eigenvectors $\mathbf{\Phi}_{\mathbf{B}}$, it can be easily solved by any packages of eigenvalue solver.

It is evident that in the zero flow case, the generalized eigenvalue problem Eq. (19) is

TABLE I. Eigenvalues calculated by method in this paper and FEM.

Mode order	method in this paper	FEM
(0,0)	$6.1154-0.2565j$	$6.1153-0.2565j$
(1,0)	$4.8555-0.4687j$	$4.8550-0.4690j$
(2,0)	$6.6284-1.1885j$	$6.6286-1.1884j$
(3,0)	$6.1375-1.3854j$	$6.1376-1.3853j$
(4,0)	$5.4127-1.6818j$	$5.4126-1.6817j$
(5,0)	$4.4252-2.1867j$	$4.4244-2.1868j$
(0,1)	$1.8901-1.2620j$	$1.8876-1.2647j$
(1,1)	$6.9038-1.0512j$	$6.9047-1.0522j$
(2,1)	$2.7758-0.9374j$	$2.7738-0.9386j$
(3,1)	$0.7916-3.5944j$	$0.7914-3.5982j$
(4,1)	$0.5219-5.8548j$	$0.5220-5.8594j$

$$K_z^2\mathsf{A}_1\mathbf{\Phi}_{\mathbf{A}} = \mathsf{A}_3\mathbf{\Phi}_{\mathbf{A}}, \quad \mathrm{Ma}_0 = 0. \tag{24}$$

It is noted that because the boundary condition is circumferentially nonuniform, rigid modes are coupled between azimuthal orders. The indices m and n of the above vectors and matrices are $-\infty < m < \infty$ and $0 \le n < \infty$.

III. VALIDATION OF THE METHOD

To validate the present method, we compare the results with those of FEM in partial differential equation (PDE) Toolbox of MATLAB. The PDE Toolbox defines a two-dimensional eigenvalue problem with local boundary conditions, and provides the solutions using a FEM. For simplicity, we chose to calculate the eigenvalues $K_{z,i}$ of circumferentially uniform lined ducts. The validation of circumferentially nonuniform lined ducts is straightforward. With dimensionless frequency $K=6.8$, lining impedance $Z/\rho c = 1.5-1.3132j$, the computed eigenvalues are shown in Table I.

It appears that the two results agree up to three significant digits for both real and imaginary parts.

IV. CONVERGENCE RATES

In this section, we numerically show the convergence rates of the method. The convergence rate of eigenfunctions means, in this paper, the coefficients $|\Phi_{mn}|$ of expansion (5) decrease as indices m and n increase. In the numerical analysis of convergence, the truncations of M and N, corresponding to the indices of m and n, respectively, are chosen as large as possible in order to obtain a stable comportment of $|\Phi_{mn}|$. The rate of radial convergence is $O(n^{-4})$ when m is fixed and the rate of circumferential convergence is $O(m^{-3})$ when n is fixed. They are same as in Ref. 17. More details for the convergence rates of eigenfunctions can be found in Ref. 17.

For the eigenvalues, the convergence rate means the relative errors $|K_z - K_{z,\mathrm{exa}}|/|K_{z,\mathrm{exa}}|$ versus the truncation $N(M)$ [not the indices $n(m)$]. It is shown in Figs. 2 and 3 for the azimuthally uniform and nonuniform boundary conditions, respectively, where the $K_{z,\mathrm{exa}}$ refers to the numerical exact values calculated by the root finding method.[11] As a result of the new treatment in this paper, the convergence rate of eigenvalues is improved and becomes $O(N^{-5})$ for azimuthal

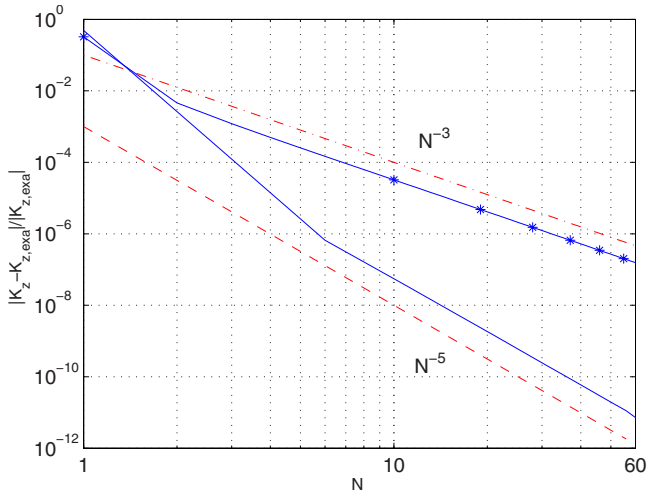


FIG. 2. (Color online) The relative errors of eigenvalues $|K_z-K_{z,\mathrm{exa}}|/|K_{z,\mathrm{exa}}|$ vs truncation N, azimuthally uniform boundary condition. $K=6.8$ and $Z/\rho c=1.5-1.3132j$. Solid line with star, method of Ref. 17 or solutions of Eq. (13), $K_{z,\mathrm{exa}}=4.855\,461\,748\,963\,631-0.468\,727\,712\,260\,302j$ no flow; solid line, method proposed in this paper or solutions of Eq. (22), $K_{z,\mathrm{exa}}=4.506\,069\,937\,543\,199-0.321\,062\,590\,157\,034j$, uniform flow, $\mathrm{Ma}_0=0.5$.

uniform boundary conditions. This is to be compared to the convergence rate of the treatment in Ref. 17 which is $O(N^{-3})$ and also shown in Fig. 2.

In absence of a direct mathematical substantiation of this difference, it may nevertheless be shown that the treatment in this paper will achieve a higher rate of convergence of eigenvalues than Ref. 17 does. For the sake of clarity, we assume uniform lining without flow. The eigenvalue equation obtained by the method proposed in Ref. 17 is in the form of Eq. (13). It can be rewritten as [see Eqs. (24) and (25) in Ref. 17]

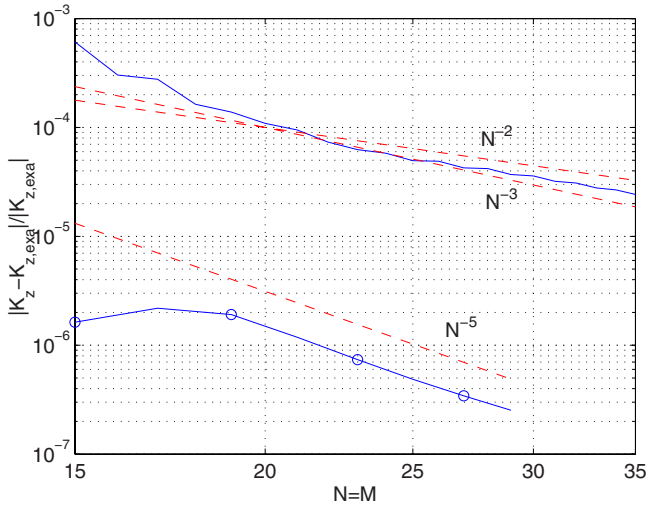


FIG. 3. (Color online) The relative errors of eigenvalues $|K_z-K_{z,\mathrm{exa}}|/|K_{z,\mathrm{exa}}|$ vs truncation $N=M$, azimuthally nonuniform boundary condition. $K=31.26$, two equal sized impedance $Z_1/\rho c=2-j$ and $Z_2/\rho c=2-0.5j$ distributed oppositely along the circumference of duct wall. Solid line, method of Ref. 17 or solutions of Eq. (13), $K_{z,\mathrm{exa}}=19.377\,398\,211\,660\,669-1.134\,878\,671\,886\,926j$, no flow; solid line with circle, method proposed in this paper or solutions of Eq. (22), $K_{z,\mathrm{exa}}=11.949\,004\,812\,788\,372-0.445\,168\,142\,112\,382j$, uniform flow, $\mathrm{Ma}_0=0.5$.

$$K_z^2\mathsf{M}\boldsymbol{\Phi}=(K^2\mathsf{I}-\mathsf{L}_1)\mathsf{M}\boldsymbol{\Phi}+\mathsf{C}\boldsymbol{\Phi}, \tag{25}$$

where C, as shown in Eq. (21), is a matrix of dimension $N\times N$, it depends only on m. The coefficient $\boldsymbol{\Phi}$ converges as $O(n^{-4})$, with m fixed as shown in Fig. 2 in Ref. 17. So the last term in the right-hand side converges as $O(n^{-4})$ with fixed m. But the other terms include $\mathsf{M}\boldsymbol{\Phi}$, the expansion coefficients of rigid mode basis $\boldsymbol{\Psi}$ as shown in Eq. (12). It converges as $O(n^{-2})$ with m fixed as shown in Eq. (42) in Ref. 17.

At variance, the eigenvalue equation proposed in this paper in zero flow case is shown in Eq. (24). It can be rewritten as

$$K_z^2\begin{bmatrix}\mathsf{I} & \boldsymbol{\Xi}\\ \boldsymbol{\Xi}^T & 2\pi\Pi\end{bmatrix}\begin{bmatrix}\boldsymbol{\Phi}\\ \mathbf{A}\end{bmatrix}=\begin{bmatrix}K^2\mathsf{I}-\mathsf{L}_1+\mathsf{C} & (K^2\mathsf{I}-\mathsf{L}_1)\boldsymbol{\Xi}\\ (K^2\mathsf{I}_2-\mathsf{L}_2)\boldsymbol{\Xi}^T-2\sqrt{\pi}\Lambda & 2\pi K^2\Pi-\pi\mathsf{I}_2\end{bmatrix}\begin{bmatrix}\boldsymbol{\Phi}\\ \mathbf{A}\end{bmatrix}. \tag{26}$$

In the case of uniform lining, as shown in the expansions of Eqs. (5) and (6), only one supplement term is needed to improve the convergence rate for a fixed azimuthal index m. The column vector $\mathbf{A}$ reduces to a scalar A_{m_0}. Matrices Π and I_2 also reduce to scalars; matrices I, C, and L_1 reduce to dimensions of $N\times N$; matrix $\boldsymbol{\Xi}$ reduces to a column vector of dimension $N\times 1$; matrix Λ reduces to a row vector of dimension $1\times N$. Details of the derivation are shown in the Appendix. In conclusion, in the case of uniform lining without flow, Eq. (26) is a system of $N+1$ equations. For the analysis of the properties of convergence, we can consider only the first N equations. It is rewritten as

$$K_z^2\mathsf{I}\boldsymbol{\Phi}=(K^2\mathsf{I}-\mathsf{L}_1)\boldsymbol{\Phi}+\mathsf{C}\boldsymbol{\Phi}+(K^2\mathsf{I}-\mathsf{L}_1-K_z^2)\boldsymbol{\Xi}A_{m_0}. \tag{27}$$

Consider first the last term in the right-hand side. The convergence behavior of this term depends only on $\boldsymbol{\Xi}$ and L_1 when n tends to infinity for fixed $m=m_0$. The elements of vector $\boldsymbol{\Xi}$ are (see Appendix, Eq. (A1))

$$\Xi_{m_0,n}=\frac{1}{\alpha_{m_0,n}^2-\beta_{m_0,0}^2}\frac{2\sqrt{\pi}}{\sqrt{\Lambda_{m0},n}}, \tag{28}$$

for fixed $m=m_0$ and behave like $1/\alpha_{m_0,n}^2$ in the limit $n\to\infty$ [see Ref. 17, Eq. (14)]. As we have indicated earlier, the elements of diagonal matrix L_1 are $\alpha_{m_0,n}^2$ on its main diagonal. So the term $(K^2\mathsf{I}-\mathsf{L}_1-K_z^2)\boldsymbol{\Xi}A_{m_0}$ tends to a constant c_0 when n tends to infinity for fixed m. Now Eq. (27) can be reduced as

$$K_z^2\mathsf{I}\boldsymbol{\Phi}=(K^2\mathsf{I}-\mathsf{L}_1)\boldsymbol{\Phi}+\mathsf{C}\boldsymbol{\Phi}+c_0,\quad n\to\infty. \tag{29}$$

The coefficient $\boldsymbol{\Phi}$ converges as $O(n^{-4})$, with m fixed, as shown in Fig. 2 of Ref. 17. Thus we should expect that Eq. (29) results in a faster rate of convergence of eigenvalues than Eq. (25) does.

For azimuthal discontinuous boundary conditions, the above convergence rates are approximately kept as shown in Fig. 3. The convergence rate is $O(N^{-5})$ with truncations $M=N$ for the treatment in this paper. The convergence rate of

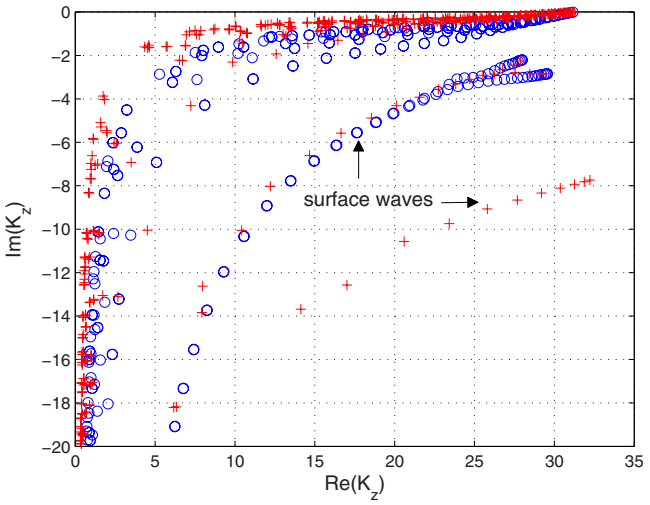


FIG. 4. (Color online) Axial wave numbers. $K=31.26$, ○: two equal sized impedance $Z_1/\rho c=2-j$ and $Z_2/\rho c=2-0.5j$ distributed oppositely along the circumference of duct wall; +: three equal sized impedance $Z_1/\rho c=2-j$, $Z_2/\rho c=2-0.5j$, and $Z_3/\rho c=1-j$ distributed uniformly along the circumference of duct wall, no flow, $N=20$, $M=35$.

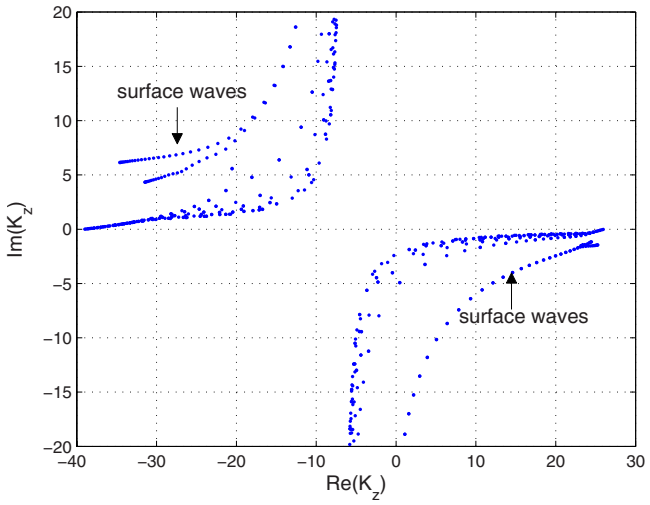


FIG. 5. (Color online) Axial wave numbers. $K=31.26$, two equal sized impedance $Z_1/\rho c=2-j$ and $Z_2/\rho c=2-0.5j$ distributed oppositely along the circumference of duct wall, uniform flow with Mach number $\mathrm{Ma}_0=0.2$, $N=25$, $M=35$.

the treatment in Ref. 17, i.e., Eq. (13), is between $O(N^{-2})$ and $O(N^{-3})$ with truncations $M=N$.

V. EXAMPLES

The present method with zero or uniform flow is especially adapted to calculate the modes in lined ducts with arbitrary nonuniform boundary conditions. In this section, we focus on the discontinuous boundary conditions which are the typical cases in the lined intakes of an aeroengine.

The first example, two and three equal sized impedance, is without flow. The dimensionless frequency is $K=31.26$. Two calculations are shown in Fig. 4, corresponding to Case 1 (symbol ○ in Fig. 4): two equal sized impedance $Z_1/\rho c=2-j$ and $Z_2/\rho c=2-0.5j$; and Case 2 (symbol + in Fig. 4): three equal sized impedance $Z_1/\rho c=2-j$, $Z_2/\rho c=2-0.5j$, and $Z_3/\rho c=1-j$. The surface waves, as indicated in Fig. 4, can be identified by the variations of eigenfunctions along r (not shown in the paper). It is well known that[6,20] when the impedance boundary condition is azimuthally uniform, there may exist two branches of surface waves propagating in opposite directions. When the lining impedance is azimuthally discontinuous, e.g., two segments of impedance as in the case 1, we find in Fig. 4, as we expect, that there exist four branches of surface waves (only the two branches having negative imaginary parts appear). One of the two branches shown in Fig. 4 corresponds to impedance $Z/\rho c=2-j$, but is modified by the presence of impedance $Z/\rho c=2-0.5j$; the other branch corresponds to impedance $Z/\rho c=2-0.5j$, but is modified by the presence of impedance $Z/\rho c=2-j$. As we expect, when the number of the lining segments increases to three as in the case 2, two other branches of surface waves appear (only one can be seen in Fig. 4) corresponding to the impedance $Z/\rho c=1-j$, which are of course modified by the presence of other impedance. It is worthy to note that when the impedance boundary condition is azimuthally uniform, distinct surface waves will appear for every azimuthal mode order m; but when the impedance boundary condition is nonuniform the different surface waves will be made of a complicate mixture of coupled components having different m values.

The second example (Fig. 5) is for a circumferentially nonuniform boundary condition with uniform flow. The nonuniform boundary is the same as Case 1 in the first example: two equal sized impedance $Z_1/\rho c=2-j$ and $Z_2/\rho c=2-0.5j$ distributed oppositely along the circumference of duct wall. The dimensionless frequency is $K=31.26$, the Mach number is $\mathrm{Ma}_0=0.2$. It is shown that the uniform flow makes the downstream split modes (with negative imaginary parts) to be closer and the upstream split modes (with positive imaginary parts) to be more separate.

Finally, we show in Fig. 6 the eigenfunctions modified by the presence of rigid splices, such as the ones generally found in the lined intakes of an aeroengine. The dimensionless frequency is $K=31.26$, the lining impedance is $Z/\rho c=2-j$. The centers of the two splices, with angle 0.3 rad, are at 0 and π.

VI. DISCUSSION

In this section, we first discuss another important advantage of the method proposed in this paper. We then turn to discuss a more general problem: Which form of the boundary conditions is more proper to use when the impedance boundary is circumferentially discontinuous?

The method proposed in this paper belongs to the general class of spectral or pseudospectral (collocation) methods but has one interesting feature we wish to stress. Those methods can calculate all needed eigenvalues one time without guessing the initial values. But as pointed out by Boyd,[21] in solving a linear eigenvalue problem by one conventional spectral method using $N+1$ terms in the truncated spectral series, the lowest $N/2$ eigenvalues are usually accurate to within a few percent while the larger $N/2$ eigenvalues differ from those of the differential equation by such large amounts

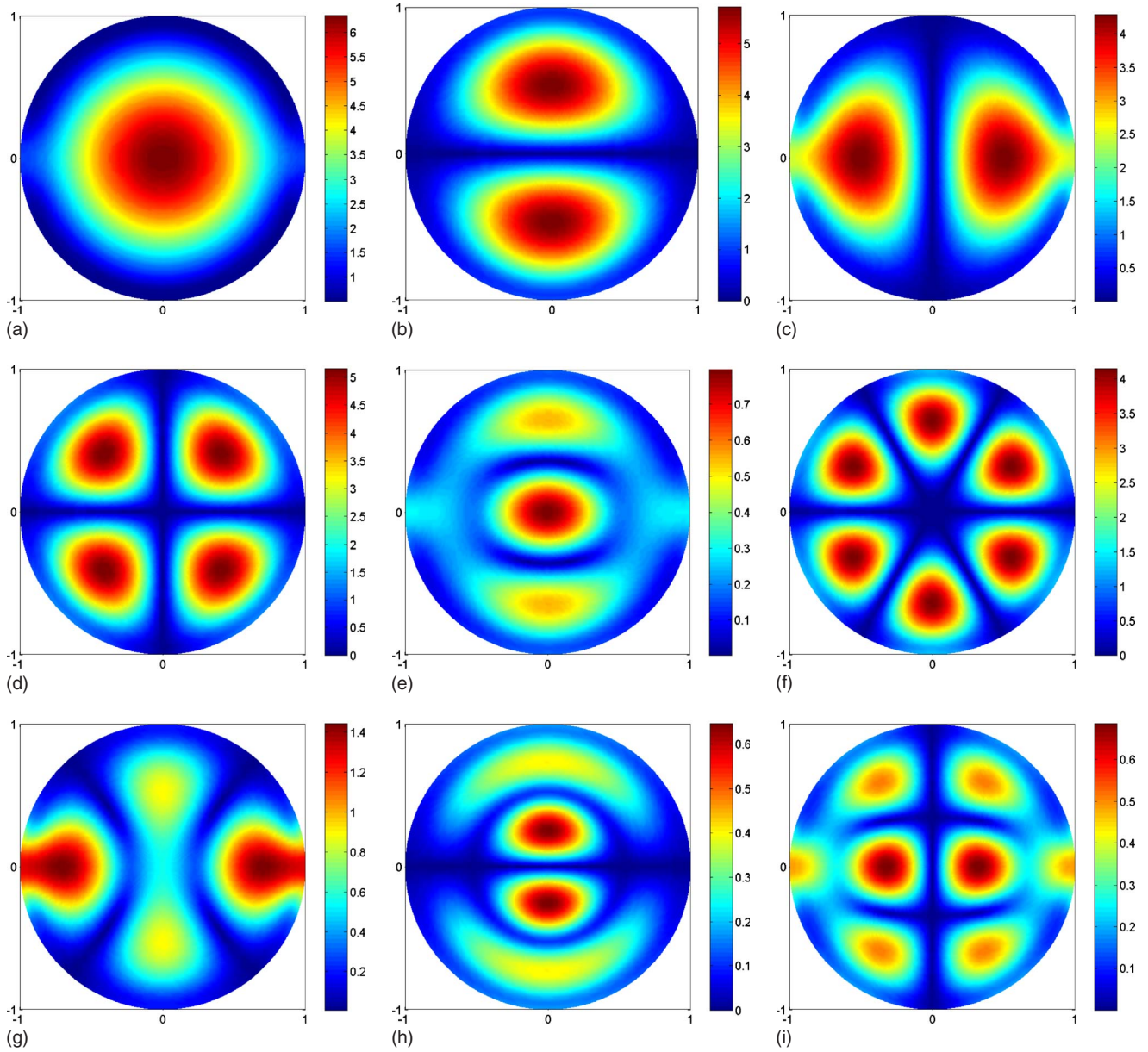


FIG. 6. (Color online) The first nine eigenfunctions (not normalized), according to the ascending order of the imaginary parts of the axial wave numbers, modified by the presence of rigid splices, (a), $K_{z,1}=31.16-0.01j$, (b), $K_{z,2}=31.01-0.03j$, (c), $K_{z,3}=31.02-0.05j$, (d), $K_{z,4}=30.81-0.06j$, (e), $K_{z,5}=30.75-0.07j$, (f), $K_{z,6}=30.56-0.09j$, (g), $K_{z,7}=30.85-0.09j$, (h), $K_{z,8}=30.40-0.11j$, and (i), $K_{z,9}=30.48-0.12j$. The dimensionless frequency is $K=31.26$, the lining impedance is $Z/\rho c=2-j$. The centers of the two splices, with angle 0.3 rad, are at 0 and π, no flow.

as to be useless. Boyd further proposed a strategy to verify the eigenvalues being well resolved. The strategy is to plot the logarithm of the reciprocal of the difference between corresponding eigenvalues as calculated at different truncation N, or named as the reciprocal eigenvalue drift ratios $1/(K_z(N_1)-K_z(N_2))$, where $K_z(N_1)$ and $K_z(N_2)$ refer to the nth eigenvalue calculated with different truncations N_1 and N_2, respectively. If the reciprocal eigenvalue drift ratios are very small for some eigenvalues, it means that those eigenvalues are not accurate. We plot the reciprocal eigenvalue drift ratios $1/(K_z(N_1)-K_z(N_2))$ in Fig. 7. It is an interesting feature of our method that all the 500 eigenvalues calculated using truncation $N_1=500$ are well resolved. This is explained by our addition of the $X(r,\theta)$ terms in Eq. (5), which are chosen so as to ensure that $\partial_r(\Sigma_{mn}\Phi_{mn}\Psi_{mn})|_{r=1}=0$, i.e., the basis Ψ_{mn} is used to represent a field verifying hard walled boundary conditions.

At the end of the paper, we hope to discuss a more general problem: When the impedance boundary is circumferentially discontinuous, which often occurs in the lined intake of an aeroengine where the lining impedance are in segments or with small rigid splices, which form of the boundary conditions is more proper to use to achieve a reasonable convergence rate? To answer this question, we do not restrict only the method proposed in the present paper. At variance, we use the root finding method, e.g., as in Refs. 11–14, to study this problem. In general, we may chose between the two forms (for simplicity, the case of without flow is considered only)

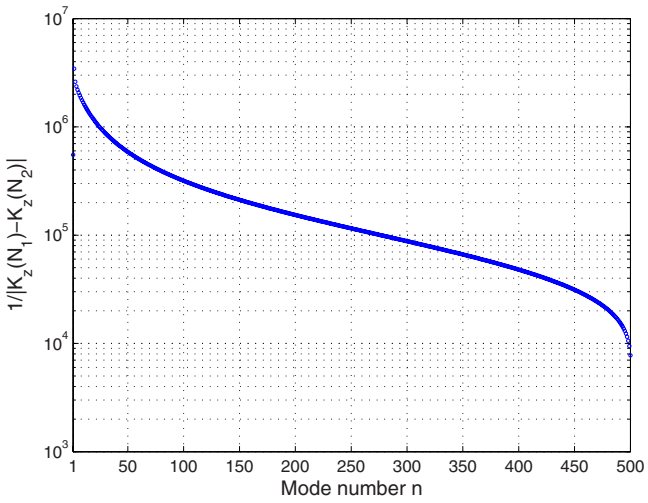


FIG. 7. (Color online) The reciprocal eigenvalue drift ratios $1/(K_z(N_1) - K_z(N_2))$ vs mode number n, $K_z(N_1)$ and $K_z(N_2)$ refers to the nth eigenvalue calculated with truncation $N_1=500$ and $N_2=1000$, respectively. $K=31.26$, circumferentially uniform impedance boundary condition, $Z/\rho c=2-j$, $m=26$.

$$\frac{\partial \phi_i}{\partial r} = Y(\theta)\phi_i, \quad r=1, \tag{30}$$

$$Z(\theta)\frac{\partial \phi_i}{\partial r} = \phi_i, \quad r=1. \tag{31}$$

Physically, the previous two forms are equivalent, but mathematically, they lead to significantly different convergence rates. This is shown in Fig. 8 by the relative error defined as $|(K_z - K_{z,\text{exa}})|/|K_{z,\text{exa}}|$ versus truncation M, where $K_{z,\text{exa}}$ refers to the numerically exact value. The eigenvalues K_z and $K_{z,\text{exa}}$ are calculated by a root finding method as Fuller's.[11] The convergence rate of form (30), in solid line with cross marks, is $O(M^{-3})$. It is considerably better than the convergence rate

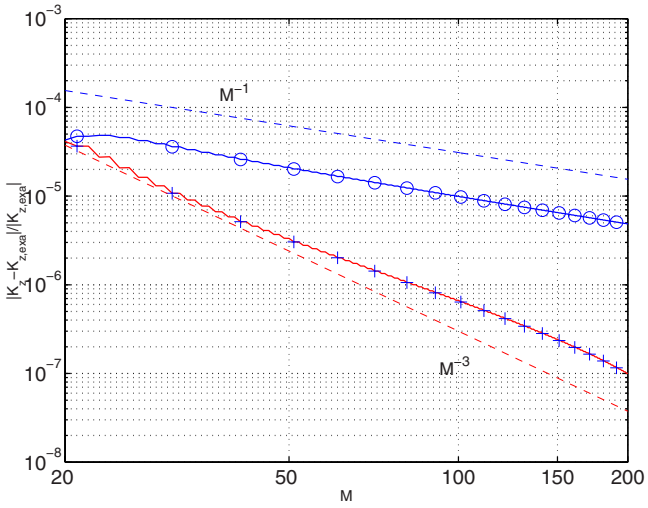


FIG. 8. (Color online) Convergence rates of different forms of boundary conditions by a root finding method as Fuller's (Ref. 11). Solid line with crosses corresponds to Eq. (30), solid line with circles corresponds to Eq. (31). The reference curves $O(M^{-1})$ and $O(M^{-3})$ are also plotted on the figure.

$O(M^{-1})$ of form (31) in solid line with circle marks. This result is a little puzzling. Elements for a clear understanding of it were given by Li[22]. He pointed out that in Eq. (31), the two functions $Z(\theta)$ and $\partial_r \phi_i(r,\theta)$ both have discontinuities, and their discontinuities are concurrent complementary (to assure $\phi_i(r,\theta)$ being continuous). In this case, the Fourier expansions of the left-hand side of Eq. (31) does not converge to the right-hand side which is continuous at those discontinuities.

The proper form of boundary condition (30) is used in this paper. The effects of circumferentially nonuniform impedance are expressed in the coupling matrix (21). It is obtained from the projection of $\nabla_\perp^2 \phi$ in the Appendix by using boundary condition (2). As we have shown earlier, the eigenvalues converge as $O(N^{-5})$ as the truncations $N=M$. This is because of the particular form we use of boundary condition (2) [reduced to condition (30) in the case of zero flow]. In fact, we are forced to set it in the given form.

VII. CONCLUSIONS

The series expansion method proposed in Ref. 18 to calculate Lamb modes has been extended to calculate the modes in nonuniformly lined ducts with zero and uniform flow, which is of important concern in nacelle acoustics applications. This results in a powerful method, capable to treat many demanding configurations (including nonuniform lining along the azimuthal direction, high-frequencies and presence of uniform flow) found in these applications.

The radial convergence rate of the eigenvalues is $O(N^{-5})$ for circumferentially uniform boundary conditions. For circumferentially discontinuous boundary conditions, the convergence rate of the eigenvalues is $O(N^{-5})$, when we chose equal truncations $N=M$ for the radial and azimuthal modes indices.

This method is an alternative to the usual root finding technique and FEM. It is easy to implement. For a given frequency, Mach number and lined impedance distribution, it is simple to evaluate the matrices A_1, A_2, and A_3 in Eq. (20), to put them in Eqs. (22) and (23), and then to use any eigenvalue solver package to obtain the eigenvalues and eigenfunctions. All modes are calculated at a time, with surface waves also well resolved.

Extension of the attractive features of the present method to account for nonuniform geometries and/or nonuniform flow would be worthwhile undertaking in view of providing a more generally applicable alternative to the FEM.

ACKNOWLEDGMENTS

The author is grateful to V. Pagneux for his invaluable advice. The author also wishes to thank D. Lafarge for his careful reading of the manuscript and greatly acknowledge Airbus for the financial support.

APPENDIX: PROJECTIONS OF Φ AND $\nabla_\perp^2\Phi$

In this appendix, we will show the derivation of the projections of ϕ and $\nabla_\perp^2\phi$ for a circumferentially nonuniform boundary condition. When the boundary condition is circumferentially uniform, the derivation in this appendix can be easily simplified. Using Eqs. (5), (9), and (11), the projection of ϕ over the basis $\mathbf{\Psi}^*$ for circumferentially nonuniform boundary condition is

$$\begin{aligned}\int \phi(r,\theta)\Psi_{mn}^* dS &= \int \left(\sum_{m'n'} \Phi_{m'n'}\Psi_{m'm'} + \sum_{m'} A_{m'}\chi_{m'}e^{-jm'\theta}\right)\Psi_{mn}^* dS \\ &= \Phi_{mn} + \frac{1}{\sqrt{\pi\Lambda_{mn}}}\frac{1}{J_m(\alpha_{mn})}\int_0^{2\pi}\sum_{m'} A_{m'}e^{-j(m'-m)\theta}d\theta\int_0^1 \chi_{m'}J_m(\alpha_{mn}r)rdr \\ &= \Phi_{mn} + \frac{1}{\sqrt{\pi\Lambda_{mn}}}\frac{1}{J_m(\alpha_{mn})}2\pi A_m B_m\int_0^1 J_m(\beta_{m,0}r)J_m(\alpha_{mn}r)rdr = \Phi_{mn} + \frac{1}{\alpha_{mn}^2-\beta_{m,0}^2}\frac{2\sqrt{\pi}}{\sqrt{\Lambda_{mn}}}A_m, \end{aligned} \tag{A1}$$

where we have used the relation[23]

$$\int_0^x tJ_\mu(at)J_\mu(bt)dt = \frac{x}{a^2-b^2}\left[J_\mu(ax)\frac{dJ_\mu(bx)}{dx} - J_\mu(bx)\frac{dJ_\mu(ax)}{dx}\right].$$

Following the matricial terminology, Eq. (A1) is written as

$$\int \phi(r,\theta)\mathbf{\Psi}^* dS = \mathbf{\Phi} + \Xi\mathbf{A}. \tag{A2}$$

For circumferentially nonuniform boundary conditions, Ξ is a block diagonal matrix of dimension $N_t\times M$, where N_t indicates $M\times N$, and M and N indicate the circumferential and radial mode truncation. In each block m of matrix Ξ, it is a column vector of dimension N, its elements are $2\sqrt{\pi}/(\sqrt{\Lambda_{mn}}(\alpha_{mn}^2-\beta_{m,0}^2))$, with $n=1,2,\ldots,N$. When the impedance boundary conditions are circumferentially uniform, Ξ reduces to column vector of dimension N for a fixed m_0. Its elements are $2\sqrt{\pi}/(\sqrt{\Lambda_{m_0n}}(\alpha_{m_0n}^2-\beta_{m_0,0}^2))$with $n=1,2,\ldots,N$. $\mathbf{A}$ is a column vector of dimension M. Its elements are A_m, each A_m corresponds to one circumferential index m. When the impedance boundary condition is circumferentially uniform, $\mathbf{A}$ reduces to scalar A_{m_0}, which means that only one term is needed to add in expansion (5). $\mathbf{\Phi}$ and $\mathbf{\Psi}$ are column vectors of dimension N_t, their elements are Φ_{mn} and Ψ_{mn}, respectively.

Similar to Eq. (A1), it is easy to obtain

$$\begin{aligned}&\int \phi(r,\theta)(\chi_m e^{-jm\theta})^* dS \\ &= \int \left(\sum_{m'n'} \Phi_{m'n'}\Psi_{m'n'} + \sum_{m'} A_{m'}\chi_{m'}e^{-jm'\theta}\right)(\chi_m e^{-jm\theta})^* dS \\ &= \sum_{n'} \Phi_{mn'}\frac{1}{\alpha_{mn'}^2-\beta_{m,0}^2}\frac{2\sqrt{\pi}}{\sqrt{\Lambda_{mn'}}} + 2\pi\|\chi_m\|^2 A_m, \end{aligned} \tag{A3}$$

where $\|\chi_m\|^2$ is

$$\|\chi_m\|^2 = \int_0^1 \chi_m^2 rdr = \frac{1}{2\beta_{m,0}^2}, \tag{A4}$$

where we have used Eqs. (9) and (11). Following the matrical terminology, Eq. (A3) is written as

$$\int \phi(r,\theta)\chi^* dS = \Xi^T\mathbf{\Phi} + 2\pi\Pi\mathbf{A}. \tag{A5}$$

Vector χ is a column vector of dimension M, its elements are $\chi_m\exp(-jm\theta)$. When the impedance boundary condition is curcumferentially uniform, χ reduces to be a scalar $\chi_{m_0}\exp(-jm_0\theta)$. Π is a diagonal matrix, $\|\chi_m\|^2$ are in its main diagonal. When the impedance boundary condition is curcumferentially uniform, it reduces to a scalar $\|\chi_{m_0}\|^2$.

Using Eqs. (14) [or Eq. (A2)] and (15) [or Eq. (A5)], we project $\nabla_\perp^2\phi$ to yield

$$\begin{aligned}\int \nabla_\perp^2\phi\mathbf{\Psi}^* dS &= \int \phi\nabla_\perp^2\mathbf{\Psi}^* dS + \oint\left(\mathbf{\Psi}^*\frac{\partial\phi}{\partial r} - \phi\frac{\partial\mathbf{\Psi}^*}{\partial r}\right)dC \\ &= \int \phi(-\mathsf{L}_1)\mathbf{\Psi}^* dS + \oint \mathbf{\Psi}^*(1,\theta) \\ &\quad\times Y(\theta)\left(1-\mathrm{Ma}_0\frac{K_{z,i}}{K}\right)^2\phi dC = -\mathsf{L}_1(\mathbf{\Phi}+\Xi\mathbf{A}) \\ &\quad + \left(1-\mathrm{Ma}_0\frac{K_{z,i}}{K}\right)^2\mathsf{C}\mathbf{\Phi}, \end{aligned} \tag{A6}$$

$$\begin{aligned}\int \nabla_\perp^2\phi\chi^* dS &= \int \phi\nabla_\perp^2\chi^* dS + \oint\left(\chi^*\frac{\partial\phi}{\partial r} - \phi\frac{\partial\chi^*}{\partial r}\right)dC \\ &= \int \phi(-\mathsf{L}_2)\chi^* dS - \oint \phi\frac{\partial\chi^*}{\partial r}dC \\ &= -\mathsf{L}_2(\Xi^T\mathbf{\Phi} + 2\pi\Pi\mathbf{A}) - 2\sqrt{\pi}\Lambda\mathbf{\Phi}, \end{aligned} \tag{A7}$$

where we have used Eqs. (9) and (11). Matrix L_1 is a diagonal matrix, $\alpha_{m,n}^2$ are in its main diagonal elements. Matrix C is

$$\mathsf{C} = \int_0^{2\pi} Y(\theta)\boldsymbol{\Psi}^*(1,\theta)\boldsymbol{\Psi}^T(1,\theta)d\theta. \quad \text{(A8)}$$

Matrix L_2 is a diagonal matrix, $\beta_{m,0}^2$ are in its main diagonal. Matrix Λ is a block diagonal matrix of dimension $M \times N_t$. In each block m of matrix Λ, it is a row vector of dimension N, its elements are $1/\sqrt{\Lambda_{mn}}$, with $n=1,2,\ldots,N$.

[1]B. J. Tester, "The optimization of modal sound attenuation in ducts in the absence of mean flow," J. Sound Vib. **27**, 477–513 (1973).
[2]R. J. Astley, V. Hii, and G. Gabard, "A computational mode matching approach for propagation in three-dimensional ducts with flow," AIAA Pap. **2006**, 2528 (2006).
[3]M. K. Myers, "On the acoustic boundary condition in the presence of flow," J. Sound Vib. **71**, 429–434 (1980).
[4]W. Eversman and E. L. Cook, "A method of weighted residuals for the investigation of sound transmission in non-uniform ducts without flow," J. Sound Vib. **38**, 105–123 (1975).
[5]F. Montetagaud, H. Batard, P. Lempereur, and C. Legros, "Modal conversion from untreated to treated cylindrical ducts," AIAA Pap. **1998**, 2309 (1998).
[6]S. W. Rienstra, "A classification of ducts modes based on surface waves," Wave Motion **37**, 119–135 (2003).
[7]R. J. Astley and W. Eversman, "A finite element formulation of the eigenvalue problem in lined ducts with flow," J. Sound Vib. **65**, 61–74 (1979).
[8]R. J. Astley and W. Eversman, "The finite element duct eigenvalue problem: An improved formulation with Hermitian elements and no flow condensation," J. Sound Vib. **69**, 13–25 (1980).
[9]M. C. M. Wright, "Hybrid analytical/numerical method for mode scattering in azimuthally nonuniform ducts," J. Sound Vib. **292**, 583–594 (2006).
[10]W. R. Watson, "Circumferentially segmented duct liners optimized for axisymmetric and standing wave sources," NASA-2075 (1982).
[11]C. R. Fuller, "Propagation and radiation of sound from flanged circular ducts with circumferentially varying wall admittances, I: semi-infinite ducts," J. Sound Vib. **93**, 321–340 (1984).
[12]C. R. Fuller, "Propagation and radiation of sound from flanged circular ducts with circumferentially varying wall admittances, II: Finite ducts with sources," J. Sound Vib. **93**, 341–351 (1984).
[13]L. M. B. C. Campos and J. M. G. S. Oliveira, "On the optimization of non-uniform acoustic liners on annular nozzles," J. Sound Vib. **275**, 557–576 (2004).
[14]L. M. B. C. Campos and J. M. G. S. Oliveira, "On the acoustic modes in a cylindrical duct with an arbitrary wall impedance distribution," J. Acoust. Soc. Am. **116**, 3336–3346 (2004).
[15]T. Elnady, H. Bodén, and R. Glav, "Application of the point matching method to model circumferentially segmented non-locally reacting liners," AIAA Pap. **2001**, 2202 (2001).
[16]M. C. M. Wright and A. McAlpine, "Calculation of modes in azimuthally nonuniform lined ducts with uniform flow," J. Sound Vib. **302**, 403–407 (2007).
[17]W. P. Bi, V. Pagneux, D. Lafarge, and Y. Aurégan, "An improved multimodal method for sound propagation in nonuniform lined duct," J. Acoust. Soc. Am. **122**, 280–291 (2007).
[18]V. Pagneux and A. Maurel, "Determination of Lamb mode eigenvalues," J. Acoust. Soc. Am. **110**, 1307–1314 (2001).
[19]G. A. Athanassoulis and K. A. Belibassakis, "A consistent coupled-mode theory for the propagation of small-amplitude water waves over variable bathymetry regions," J. Fluid Mech. **389**, 275–301 (1999).
[20]E. J. Brambley and N. Peake, "Classification of aeroacoustically relevant surface modes in cylindrical lined ducts," Wave Motion **43**, 301–310 (2006).
[21]J. P. Boyd, *Chebyshev and Fourier Spectral Methods*, (Springer, New York 1989).
[22]L. F. Li, "Use of Fourier series in the analysis of discontinuous periodic structures," J. Opt. Soc. Am. A **13**, 1870–1876 (1996).
[23]G. N. Watson, *A treatise on the Theory of Bessel Function* (Cambridge University Press, Cambridge, MA, 1952).

On the steering of sound energy through a supercritical plate by a near-field transducer array

Brian E. Anderson,[a] W. Jack Hughes, and Stephen A. Hambric
Applied Research Laboratory, The Pennsylvania State University, P.O. Box 30, State College, Pennsylvania 16804, USA

(Received 19 October 2007; revised 13 December 2007; accepted 7 February 2008)

The ability to direct sound energy through the flexural vibrations of a submerged plate at various angles of incidence using a near-field transducer array is investigated. An alumina bar is placed in front of a one-dimensional, eight-element transducer array, between the array and the water. Operating in a receive mode, data were taken as a function of angle of incidence and compared to data taken without the presence of the alumina bar. The array was also operated in transmit mode and results were compared to corresponding receive mode data, showing that reciprocity holds. Results show that in fact sound energy can be steered through a plate, and that the measurement method used provides a convenient method of measuring the angular dependence of transmission through a plate, including measurements at frequencies above the plate's critical frequency. Experimental results of sound transmission versus angle of incidence of finite sized plates agree qualitatively with theoretical results from an analysis of the transmission through an unbounded flexible partition. © *2008 Acoustical Society of America.* [DOI: 10.1121/1.2890738]

PACS number(s): 43.55.Rg, 43.38.Hz, 43.30.Yj, 43.20.Ye [DF] Pages: 2613–2619

I. INTRODUCTION

Arrays of transducer elements are often used to channel sound radiation into specific directivity patterns to image objects at specific angles. In some applications it is desirable to send sound through a plate or wall to allow imaging of objects on the other side, especially when it is not feasible to physically inspect the other side of the plate or wall. One potential application would be to place an array on the inner surface of the hull of a ship or submarine. There have been various studies on the effects of steering an array through acoustic windows, including modeling and testing,[1–7] but the main goal of those studies is to design an acoustically transparent barrier between the array electronics and the water. This paper investigates the steering of sound energy through a plate with an array mounted to the plate and proposes a method to measure the angular dependence of sound transmission through a plate.

The critical or coincidence frequency for sound transmission is the frequency at which the speed of sound in the acoustic fluid matches that of the speed of bending waves in a plate, resulting in nearly perfect transmission of sound at grazing incidence. As frequency is increased, the angle at which the coincidence effect occurs (high degree of sound transmission) shifts progressively away from grazing incidence and closer to normal incidence. The angular shifting of the coincidence effect occurs due to the dispersive nature of bending waves in plates. The theory of the coincidence effect and its frequency dependence is generally credited to Cremer.[8] Cremer's work in 1942 has influenced many other researchers in this field. Experimental verification of the coincidence effect was conducted in 1956 by Lamb,[9] and then also in 1957 by Eichler and Lambert.[10] Numerous studies have been conducted on the transmission of sound through partitions, but generally these studies are either done for subcritical plates or they measure the diffuse field transmission characteristics (an average over all angles of incidence, generally by using a reverberation chamber).

It was not until Davies and Gibbs' work in 1981 that a practical technique for measuring the angular dependence of sound transmission through a partition was proposed.[11] Davies and Gibbs used a method similar to that proposed by Louden[12] where an impulsive source sends sound through the partition under test at selected angles. The direct arrival of energy through a partition was compared to the direct arrival of energy received without the partition present, thus allowing the sound transmission to be characterized. They utilized various averaging schemes to improve upon their results. Unfortunately, their technique was contaminated by spherically incident wave fronts which excited bending waves in the partition which produced arrivals of energy shortly after the direct arrival (which was later termed the precursor phenomenon). Balilah and Gibbs further refined the technique proposed by Davies and Gibbs by making the technique more portable and by suggesting ways to reduce the effect of the precursor phenomenon.[13] Unfortunately these techniques require a large area of the material under test (partition) to avoid the arrival of the flanking transmission around the partition, thus smaller samples of material cannot be tested.

This paper proposes a technique in which a pulsed wave field is incident upon a plate which has an array of transducers mounted on the back side of the plate. The incident signal is emitted by a transmitter which is located in the far-field of the array. The measurement is repeated for many angles in the forward 180°. The signals detected by the array of transducers can be digitally steered in postprocessing to provide a

[a]Present address: Los Alamos National Laboratory, Geophysics Group, MS D443, Los Alamos, NM 87545. Electronic mail: bea@lanl.gov.

high degree of directivity in the direction of the incident wave energy. Thus the problem of incident spherical waves is avoided. The wave field detected from the same array without a plate is also measured. A comparison of the detected signals with and without the plate yields the transmission as a function of angle of incidence.

In this paper a comparison of theoretical analysis to experimental results is given for the angular dependence of sound transmission through a plate. The theoretical analysis utilizes an expression derived from unbounded/infinite plate theory (finite thickness). Experimental results were obtained with a finite sized plate. A more complete discussion of the theory, modeling, and experiments conducted in this study are given in the dissertation by Anderson.[14]

II. TRANSMISSION THROUGH UNBOUNDED FLEXIBLE PARTITIONS

This section will provide a brief presentation of the theory of sound transmission through an unbounded flexible partition vibrating in flexure (infinite-sized, thin-plate theory). A complete theoretical analysis of this theory is given by Fahy (Ref. 15, pp. 277–295). Theory for unbounded flexible partitions can also be used as an approximation for modeling the angular dependence of sound transmission for finite sized plates.

The specific acoustic impedance, $\tilde{z}_{SP}$, for an unbounded flexible plate partition is given by

$$\tilde{z}_{SP} = \frac{1}{\omega} D \eta \kappa^4 - j \frac{1}{\omega} (D\kappa^4 - m\omega^2), \tag{1}$$

where ω is the angular frequency, D is the bending stiffness of the plate, η is the damping loss factor in the plate, κ is the structural wave number in the plate, j is the imaginary number $\sqrt{-1}$, and m is the mass per unit area of the plate. The structural wave number in the plate depends on the wave speed of the type of wave excited. Two types of waves will be considered here, driven waves excited by an incident wave field, and bending waves which have dispersive wave speeds which increase as a function of $\sqrt{\omega}$ for low frequencies (at larger frequencies the bending wave speed asymptotically approaches the shear wave speed).

The general transmission coefficient, τ, for sound transmission through an unbounded flexible partition is given in Fahy's Eq. (5.36) (with some additional substitutions) as

$$\tau = \left| \frac{2\rho_2 c_2 \sec\theta_2}{\frac{1}{\omega} D \eta \kappa^4 - j \frac{1}{\omega} (D\kappa^4 - m\omega^2) + \rho_1 c_1 \sec\theta_1 + \rho_2 c_2 \sec\theta_2} \right|^2 \frac{\rho_1 c_1}{\rho_2 c_2} \left[\frac{1 - \left(\frac{c_2}{c_1} \sin\theta_1 \right)^2}{1 - \sin^2\theta_1} \right]^{1/2}, \tag{2}$$

where θ is an angle measured from normal incidence, ρ is the density, c is the acoustic speed of sound, and the subscripts 1 and 2 correspond to material properties of the incident and transmitted acoustic fluids (or the corresponding angle on either side of the partition). The term in the square brackets of Eq. (2) governs refraction of a wave from one fluid to the other, and if the fluid on both sides is the same then the refraction term and the impedance ratio term vanish and Eq. (2) becomes

$$\tau = \frac{(2\rho c \sec\theta)^2}{\left[2\rho c \sec\theta + \frac{1}{\omega} D \eta k^4 \sin^4\theta \right]^2 + \left[m\omega - \frac{1}{\omega} D k^4 \sin^4\theta \right]^2}, \tag{3}$$

where k is the acoustic wave number ($k \sin\theta = \kappa$). The second term in the denominator of Eq. (3) is governed by the damping in the plate, while the third and fourth terms are governed by the mass and stiffness in the plate, respectively. The standard equation for normal incidence mass law transmission results when Eq. (3) is evaluated at 0°, or when the bending stiffness term of Eq. (3) is very small compared to the mass term (η is generally much less than one).

The critical frequency, f_C, is defined as the frequency at which the acoustic sound speed in water equals the bending wave speed in the plate. The bending wave speed in a thin plate (thin plate theory ignores effects due to shear deformation and rotary inertia) is dispersive and increases with frequency,

$$c_B = \left(\omega^2 \frac{D}{m} \right)^{1/4}. \tag{4}$$

At the critical frequency transmission through a plate at grazing incidence is very high. Above the critical frequency, as the frequency is increased, the angle of high transmission (called the coincidence angle, θ_{CO}, which occurs when the imaginary part of the plate's impedance goes to zero) shifts toward normal incidence

$$\sin^2\theta_{CO} = \frac{c^2}{c_B^2} = \frac{c^2}{\omega} \sqrt{\frac{m}{D}}. \tag{5}$$

Thus, the coincidence angle is proportional to the arcsine of the inverse square root of frequency. The critical frequency may be solved for by evaluating Eq. (5) at grazing incidence ($\theta_{CO} = 90°$)

$$f_C = \frac{c^2}{2\pi}\left(\frac{m}{D}\right)^{1/2}. \tag{6}$$

The transmission coefficient at the coincidence angle is

$$\tau(\theta_{CO}) = \left(1 + \frac{\eta m\omega}{2\rho c}\sqrt{1 - \frac{c^2}{\omega}\sqrt{\frac{m}{D}}}\right)^{-2}. \tag{7}$$

A steered array of transmitting transducers effectively approximates a traveling wave in the plane of the array. The speed of this traveling wave must exceed the speed of sound in the fluid medium if the radiation is to be between grazing and normal incidence. This principle is called trace wave number matching (Ref. 15, pp. 175–177). In order to radiate sound at a given forward angle, θ_0, one must set up a traveling wave on a steered array such that

$$c_0 = \frac{c}{\sin\theta_0} = \frac{d}{\tau_0}, \tag{8}$$

where c_0 is the speed of the traveling wave, d is the center-to-center distance between consecutive transducers in the array, and τ_0 is the electronic time delay necessary to progressively implement across the array between consecutive transducers. Thus if one scans the surface of an array and measures the effective traveling wave sound speed, one can then determine at what angle the array is radiating.

III. EXPERIMENT SETUP

A. Array setup

Two different one-dimensional eight element arrays were mounted onto the polyurethane acoustic window of an array module. The transducers used are of a typical Tonpilz design with a nominal resonance frequency of 25 kHz. One array was placed directly on the acoustic window, while the other array was bonded onto an alumina bar with a 1.6-mm-thick layer of polyurethane between the array elements and the alumina bar. The alumina bar is a high purity 99.8% aluminum oxide ceramic (AmAlOx 68 alumina) and is 1.02 cm thick, 3.05 cm wide, and 24.4 cm in length. Plastic shims were placed between neighboring transducers to maintain a consistent spacing between all transducers. Figure 1(a) shows a photograph of a close up of the array bonded to the alumina bar. Figure 1(b) shows a photograph of the two arrays placed side by side on the window of the array module.

B. Scanning laser measurements

To confirm that the appropriate traveling flexural waves are generated in the plate driven by the array of transducers, a set of measurements was conducted using a PolyTec scanning laser vibrometer. The vibration of the plate induced by the array was imaged with the scanning laser. Reflective tape was placed on the acoustic window (assumed to be acoustically transparent) to provide high reflectivity of the laser signal and to provide an accurate measure of the plate vibration. A 7 by 43 point scan grid was used with a spacing of 6 mm between scan points. The measurements were conducted with the array module submerged in a small water tank with an optically transparent wall to allow the laser to scan the submerged surface while being physically located outside the water. Figure 2(b) shows a photograph of the scanning laser measurement setup. The array was operated in transmit mode at various frequencies and steer angles. Care was taken to eliminate the possibility of obstruction of the desired data from a reflected wave off the tank walls by applying an appropriate time window and transmit repetition rate.

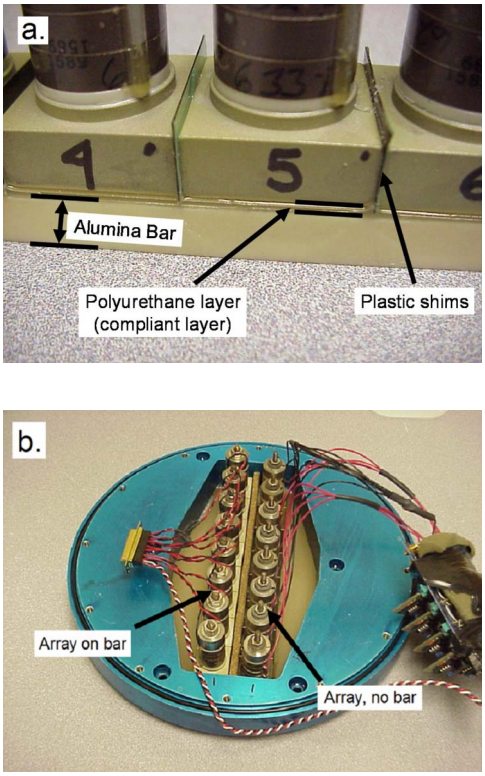


FIG. 1. (Color online) (a) Close up photograph of the alumina bar with an eight element line array mounted on it. (b) Photograph of the two eight element line arrays used in the water tank measurements.

C. Water tank measurements

The water tank facility at Penn State measures 5.3 $\times 5.5 \times 7.9$ m in size. The water tank is kept at a constant temperature and is lined with acoustical absorbing material. A calibrated transmitter or a calibrated receiver can be placed at one end of the tank to transmit/receive sound toward/from a transducer array under test at the other end of the tank. A computer controlled turntable can rotate the Array Under Test (AUT) with fractional degree increments. When the AUT is in a receive mode, up to 64 channels of complex data may be simultaneously acquired by a vector signal analyzer. The advantage of receive mode measurements is that in the postprocessing phase, the array can be arbitrarily steered to any angle by applying appropriate digital delays. In transmit mode each channel of the AUT must be amplified separately and set beforehand with fixed digital delays. Figure 2(a) shows a photograph of the array module just before being lowered into the water tank.

The array module was lowered into the water and connected up to the turntable. In one set of measurements the array mounted on the alumina bar was operated in a transmit

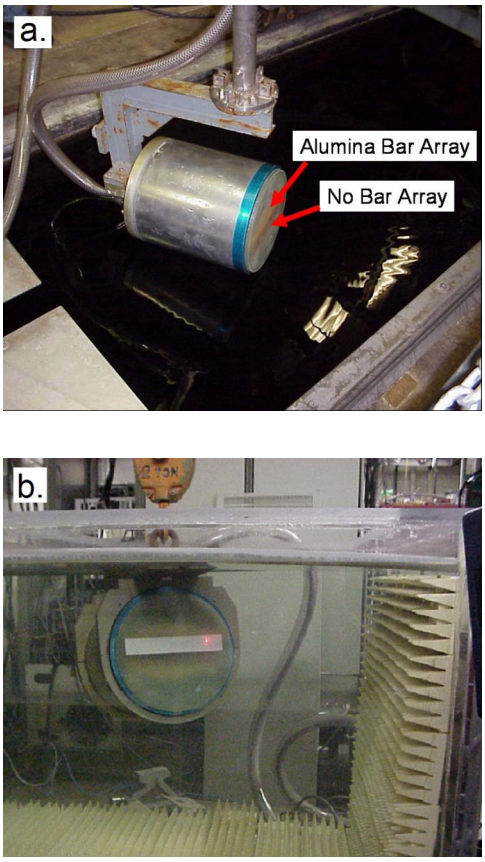


FIG. 2. (Color online) (a) Photograph of the array module before being lowered into the water tank. (b) Photograph of the array module in the small water tank while performing a scanning laser measurement.

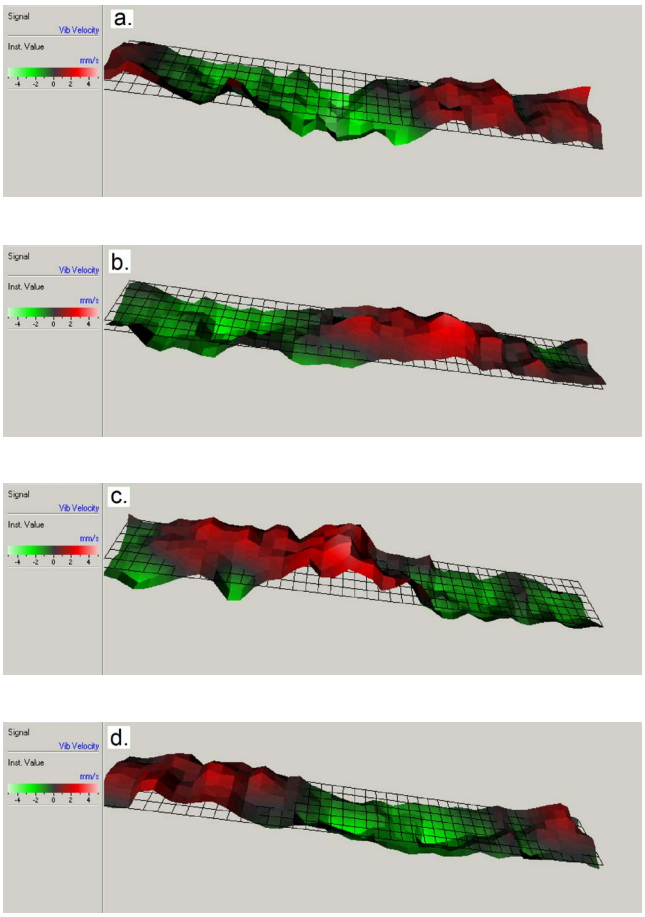


FIG. 3. (Color online) Velocity data from scanning laser data at 25 kHz and 15°. Each subplot represents progressive phase snapshots [(a) 0°, (b) 80°, (c) 180°, and (d) 280°] of the traveling wave progressing from right to left.

mode at various frequencies and also at various steer angles by applying appropriate digital delays. In another set of measurements the array mounted on the bar and the array without a bar were each operated in a receive mode at various frequencies while recording complex data on each receiver channel.

IV. RESULTS

A. Scanning laser measurements

The scanning laser results for a steer angle of 15° at a frequency of 25 kHz may be found in Fig. 3. The results are given at four different phase snapshots [(a) 0°, (b) 80°, (c) 180°, and (d) 280°] to illustrate the propagation of the traveling wave from right to left from Figs. 3(a)–3(d). According to Eq. (8), the speed of the steered array traveling wave, c_S, should approximately equal 1500 m/s/sin(15°)=5800 m/s. In Fig. 3(a), the peak on the right-hand side travels about 29 scan points (6 mm between points, therefore 174 mm) to its location in Fig. 3(d) in 280° of the phase cycle. That means that for a full 360° cycle, the wave travels 224 mm. The time duration, or period, of a cycle corresponds to the inverse of the frequency. Thus the duration of a period at 25 kHz is 40 μs. The traveling wave speed then is 224 mm/40 μs =5600 m/s. This value represents a fairly rough estimation, but it is within 3.5% of the 5800 m/s expected sound speed. Thus the scanning laser results show that the dominant traveling flexural wave on the radiating surface of the bar corresponds to the intended traveling wave setup by the transducer array.

B. Water tank measurements

Figure 4 displays sample plots comparing directivity patterns, normalized to their respective main lobe peak levels, from the transmit measurements and the receive measurements with the alumina bar array. The near perfect agreement of transmit and receive directivity patterns demonstrates that the array mounted on the alumina bar is a reciprocal system (Ref. 16, p. 378). The measurements of patterns from the array operated in a receive mode show that the data taken at large angles (approximately $>\pm 60°$) is corrupted by the noise floor of the system.

With array measurements in receive mode, the data may be processed to compute directivity patterns steered to any forward angular direction desired. Thus a 180° directivity pattern may be generated for each of the available 180° of steer angles. One convenient method of displaying these data is to create an amplitude map surface plot of receive angle versus steer angle, such that a vertical line (from −90° to +90°) at a fixed steer angle corresponds to the directivity pattern at that steer angle. Figure 5 displays sample surface plot maps of amplitude versus receive angle versus steer

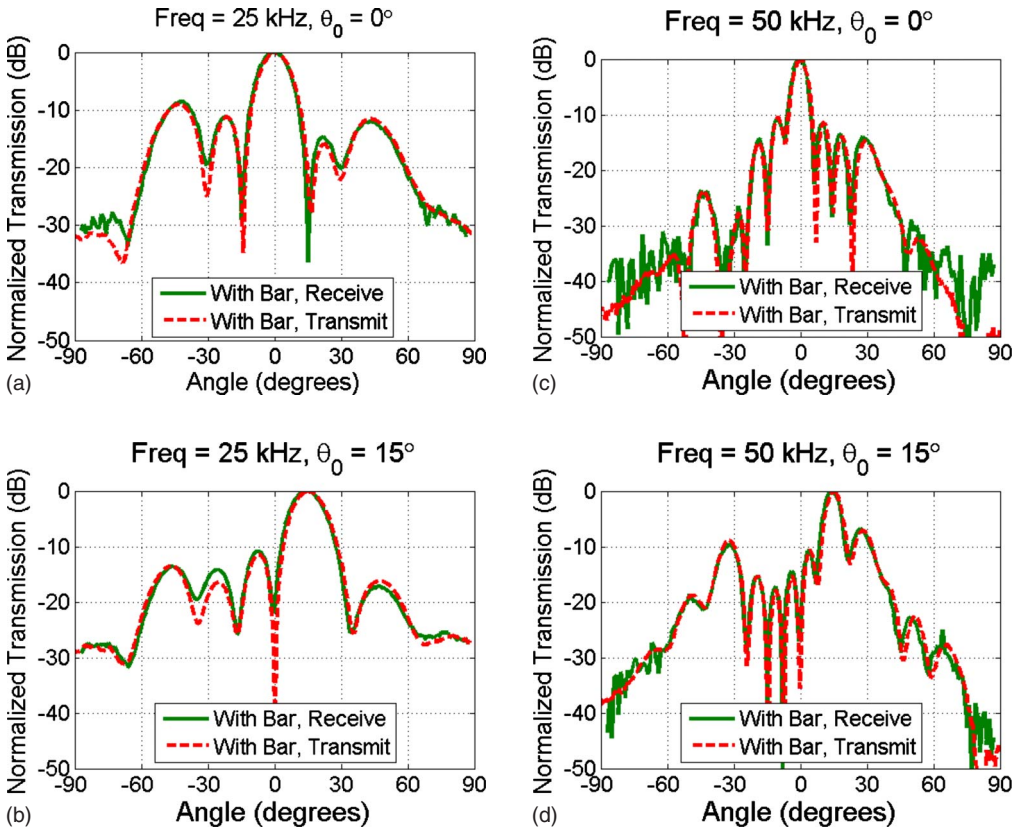


FIG. 4. (Color online) Directivity pattern plots of amplitude vs receive angle for the array mounted on the alumina bar operated in a transmit mode and in a receive mode at the frequencies and steer angles displayed in the titles of each subplot.

angle, with each vertical line of data normalized to its respective main lobe level, at 25 kHz (left subplots) and 50 kHz (right subplots) and for the array without the bar (upper subplots) and the array with the alumina bar (lower subplots). The dominant ridge in each subplot running from the lower left to the upper right corresponds to the main lobe at each steer angle. The presence of this ridge in the surface plots from the data taken from the array mounted on the bar demonstrates that the array can in fact steer sound energy through the alumina bar at the desired steer angle without refraction. Thus it is accurate to assume that the refraction term in square brackets in Eq. (2) may be discarded. Note that the width of the main lobe ridge in data taken from each of the two arrays is approximately the same, meaning that the presence of the alumina bar does not widen the main lobe. Thus the dispersive nature of bending waves in the bar does not alter the driven wave speed, since widening of a lobe would correspond to dispersion of wave speeds. The absence of refraction and dispersion, in the transmission of the driven wave through a plate, are important practical considerations when evaluating the feasibility of using an array to image objects behind a plate.

Note the horizontal ridges which occur in Figs. 5(b) and 5(d) located at receive angles of $\pm 45°$ and at $\pm 30°$, respectively. These horizontal ridges are located at the respective coincidence angles for each frequency [from Eq. (5), $\theta_{CO}(25\ \text{kHz}) = 45°$ and $\theta_{CO}(50\ \text{kHz}) = 30°$ for the alumina bar used]. The coincidence angle is the angle at which bending waves radiate most efficiently.

Another way to analyze the effect of the presence of the alumina bar is to compare the level of the main lobe at each steer angle from the data taken from each array configuration (with and without the alumina bar). The only difference between these two sets of steering data is due to the alumina bar, thus it provides a convenient method of measuring the sound transmission through the alumina bar as a function of angle. The theoretical expression for sound transmission through an undamped ($\eta = 0$) plate or bar given in Eq. (3) was evaluated at various frequencies using material property values which correspond to measured values for the alumina bar density ($\rho = 3956\ \text{kg/m}^3$), Young's modulus ($E = 391$ GPa), and bar thickness ($h = 1.02$ cm). [Thus the critical frequency for the alumina bar is $f_C = 12.0$ kHz, assuming the Poisson ratio specified by the manufacturer ($\sigma = 0.22$)].

Figure 6 shows a comparison of the theoretical and measured sound transmission through an alumina bar. Both plots are normalized to the normal incidence mass law sound transmission levels (measured plots were adjusted such that the small increase at normal incidence was ignored). The theoretical expressions were not evaluated at angles greater than $\pm 65°$ since the theoretical expression does not generally give accurate results at large angles, as noted by Fahy (Ref. 15, pp. 292–294). Also, measurements at large angles are corrupted by the measurement noise floor as noted in the reciprocity comparison discussion. Although the analytic approach is approximate (based on thin infinite plate theory), the simulated general behavior matches that observed in the

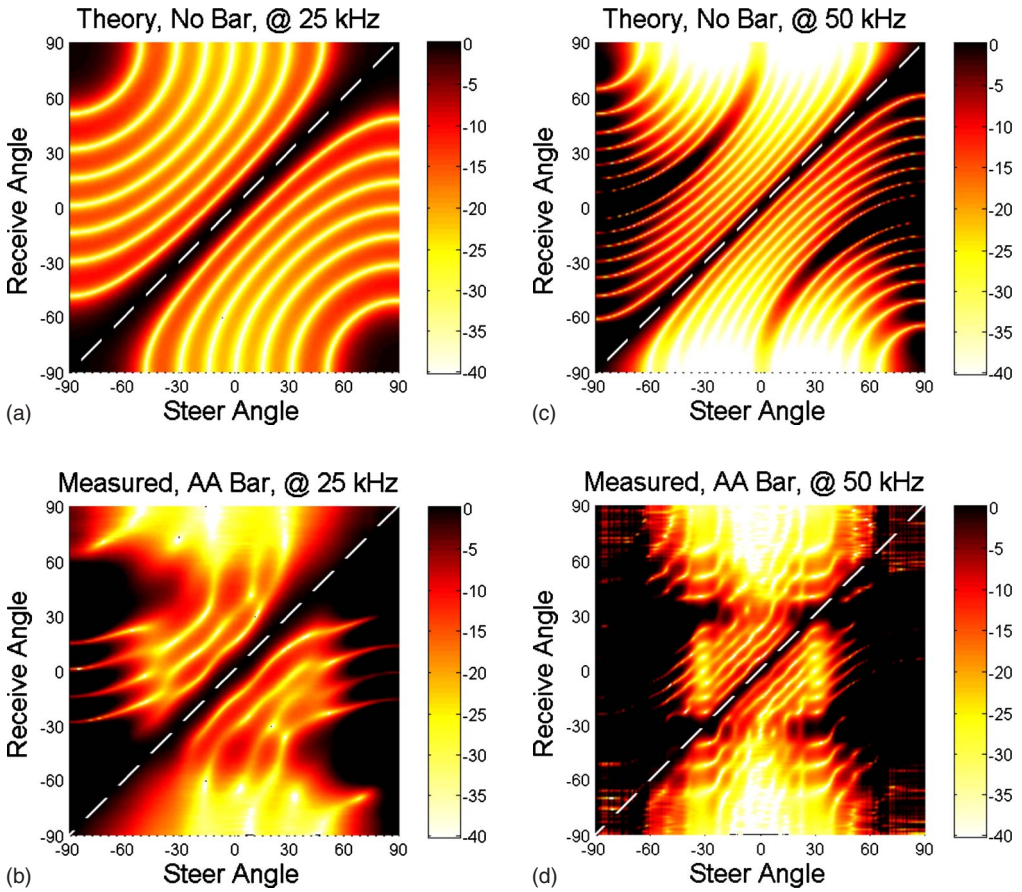


FIG. 5. (Color online) Surface plots of directivity amplitude vs steer angle and receive angle. The upper subplots are from data without the alumina bar, while the bottom subplots are from data with the alumina bar. The subplots on the left are for 25 kHz while the subplots on the right are for 50 kHz.

measurements. This means that the approximate analytic theory may be used for qualitative studies of other plate and array configurations. The discrepancies in levels at coincidence angles and at normal incidence are due to the approximate nature of the analytics used here (infinite, rather than finite plate; thin plate theory, rather than thick; approximate treatment of damping).

V. CONCLUSION

Results have shown that indeed a phased array of transducers can induce a traveling flexural wave on a rectangular bar which then radiates sound into the same direction as the phased array would radiate without a bar. Results also show that placing a bar in the near-field of the array allows measurement of transmission versus angle. The measured transmission versus angle for a finite sized plate does agree qualitatively with the theoretical transmission versus angle for an unbounded thin plate of the same thickness and material properties. It should be noted that the frequencies used in this study were above the plate's critical frequency. Below the critical frequency, one would not encounter the coincidence effects in the array's radiation pattern, since bending waves would not radiate efficiently even though they would be excited.

The ability to steer sound energy through a plate allows one to image objects on the other side of the plate when it is otherwise impossible to physically access that side of the plate. Sound transmission through a partition or plate is the highest at the coincidence angle, thus applications could be developed to exploit the ability to transmit and receive sound with a high degree of transmission at this angle. Conceivably, an array may be placed on the wall of a submarine hull or boat to image objects in the water.

A novel technique which allows measurement of the transmission coefficient as a function of angle has been presented in this paper. This technique is similar in nature to the techniques proposed by Louden,[12] Davies and Gibbs,[11] and Balilah and Gibbs[13] in that sound is sent through a plate at various angles, thus allowing measurement of the angular dependent transmission coefficient. However, the advantage of the proposed technique is that it exploits the high directivity of an array to avoid the flanking transmission and precursor waves encountered in the research done by Davies and Gibbs and Balilah and Gibbs which were due to using spherical wave sources. In addition, while the techniques proposed by the above-mentioned researchers essentially require relatively large partition samples, the proposed technique measures relatively small plate samples.

The results presented here were for one-dimensional measurements of the angular dependent transmission coefficient using a line array and a bar under test. The investigation has been extended to two dimensions by the authors, using a two-dimensional array of transducers.[14] The measurements yielded results consistent with the results found in

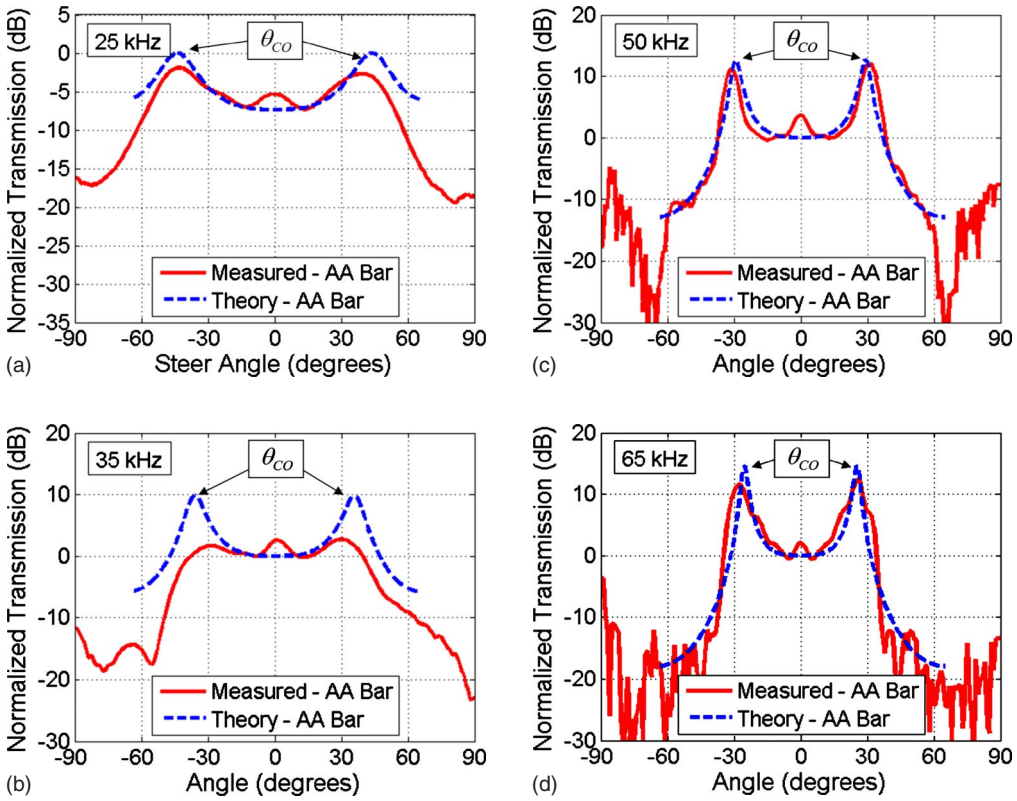


FIG. 6. (Color online) Plots of transmission through the alumina (AA) bar vs incidence angle for the frequencies indicated in the upper left of each subplot.

the material presented in this paper, and may be presented in a future paper. Finally, the analytic approach presented here (based on infinite thin plate theory) is approximate. Future analytic work in this area should focus on thick plate effects, and on finite dimensions, perhaps using numerical methods.

ACKNOWLEDGMENTS

This research was sponsored by the Office of Naval Research Code 333 Dr. David Drumheller. In addition to ONR support for B.A., support was also provided by a Penn State University Graduate Research Fellowship, a Penn State College of Engineering Fellowship, an Audio Engineering Society Educational Foundation Award, and Penn State Applied Research Laboratory Exploratory and Foundational Research Program funding. The assistance of Paul Bednarchik, Courtney Burroughs, Bob Dashem, Mark Geleskie, Greg Granville, Bill Thomas, Dave Van Tol, and Mark Wilson of the Penn State Applied Research Laboratory is recognized and appreciated. Facilities located in the Applied Research Laboratory of The Pennsylvania State University were used in this work. Electronic mail correspondence with Frank Fahy was also quite helpful in this work.

[1]J. S. Hickman, D. E. Risty, and E. S. Stewart, "Properties of sandwich-type structures as acoustic windows," J. Acoust. Soc. Am. **29**, 858–864 (1957).
[2]E. E. Mikeska and J. A. Behrens, "Evaluation of transducer window materials," J. Acoust. Soc. Am. **59**, 1294–1298 (1976).
[3]D. L. Folds and C. D. Loggins, "Transmission and reflection of ultrasonic waves in layered media," J. Acoust. Soc. Am. **62**, 1102–1109 (1977).
[4]C. M. Thompson, "Development of a structurally rigid, acoustically transparent plastic," J. Acoust. Soc. Am. **87**, 1138–1143 (1990).
[5]M. Kim and Y. F. Hwang, "An analysis of wave dispersion in coarsely laminated symmetric composite plates," J. Acoust. Soc. Am. **100**, 1981–1991 (1996).
[6]J. I. R. Blake, R. A. Shenoi, J. House, and T. Turton, "Strength modeling in stiffened FRP structures with viscoelastic inserts for ocean structures," Ocean Eng. **29**, 849–869 (2002).
[7]A. J. Hull, "Dynamic response of an insonified sonar window interacting with a Tonpilz transducer array," J. Acoust. Soc. Am. **122**, 794–803 (2007).
[8]L. Cremer, "Theorie der Schall damming dunner Wade bei Schragen Einfall," Akust. Z. **7**, 81–104 (1942).
[9]G. Lamb, Jr., "Transmission of a spherical wave through a thin elastic plate," J. Acoust. Soc. Am. **28**, 162 (1956).
[10]E. G. Eichler and R. F. Lambert, "Sound Transmission through thin plates at oblique incidence," J. Acoust. Soc. Am. **29**, 1253 (1957).
[11]J. C. Davies and B. M. Gibbs, "Oblique incidence measurement of transmission loss by an impulse method," J. Sound Vib. **74**, 381–393 (1981).
[12]M. M. Louden, "The single-pulse method for measuring the transmission characteristics of acoustic systems," Acustica **25**, 167–172 (1971).
[13]Y. A. Balilah and B. M. Gibbs, "The measurement of the transmission loss of single leaf walls and panels by an impulse method," J. Sound Vib. **123**, 229–245 (1988).
[14]B. E. Anderson, "Grating lobe reduction in transducer arrays through structural filtering of supercritical plates," Ph.D. thesis, The Pennsylvania State University, University Park, PA.
[15]F. Fahy and P. Gardonio, *Sound and Structural Vibration, Radiation, Transmission and Response*, 2nd Ed. (Academic Press, London, 2007).
[16]L. L. Beranek, *Acoustics* (McGraw-Hill, New York, 1954).

Statistically motivated design of input signals for modern ultrasonic array systems

Fredrik Lingvall[a)]
Department of Informatics, Group for Digital Signal Processing and Image Analysis, University of Oslo, P.O. Box 1080, Blindern, NO-0316 Oslo, Norway

Tomas Olofsson[b)]
Signals and Systems Group, Department of Engineering Sciences, Uppsala University, P.O. Box 528, SE-751 20 Uppsala, Sweden

(Received 5 April 2007; revised 8 January 2008; accepted 9 January 2008)

Modern array systems allow for excitation of separate elements using arbitrary wave forms. This is utilized in pulse compression and coded excitation techniques to improve the imaging performance. Such techniques are however somewhat inflexible since they use predefined excitation schemes. This paper presents a more flexible method for optimizing the input signals to an ultrasonic array in such a way that the scattering strengths at arbitrarily chosen control points in the insonified object can be estimated with as small an error as possible, measured with a mean squared error criteria. The statistically motivated method is based on a linear model of the array imaging system and the method takes into account both prior information regarding the scattering strengths and measurement errors. The input signals are found by using genetic optimization and are constrained to have finite duration and bounds on the maximum amplitudes. Different constellations of control points, and different signal-to-noise ratios, yield different excitation schemes. The design approach finds multiple selective focal laws when choosing relatively well separated control points and when the control points are closely spaced, the resulting excitations result in more diffuse fields. Because of the flexibility in choosing the control points, the design method will be useful when developing transmission schemes aiming at fast imaging of large image areas using few transmissions.
© *2008 Acoustical Society of America.* [DOI: 10.1121/1.2839139]

PACS number(s): 43.60.Fg, 43.60.Gk, 43.60.Uv, 43.60.Pt [EJS] Pages: 2620–2630

I. INTRODUCTION

Traditionally, acoustic array data have been processed by means of spatial filtering, or beamforming, to obtain an image of the scattering objects.[1–3] Beamforming using the classical time-domain delay-and-sum method is analogous to the operation of an acoustical lens and it can be performed efficiently using delay-line operations in real time or using postprocessing as in synthetic aperture systems.[4–7] Delay-and-sum beamforming, which is essentially based on a geometrical optics approach,[8] is computationally attractive due to its simplicity but it has several inherent drawbacks. One such drawback is that the resolution of traditional delay-and-sum beamforming methods is determined by the product of the transmitted and received beam patterns. These beam patterns are determined by the position-dependent point spread functions (PSFs) associated with the array system. These are determined by the aperture size, element size, and transmit pulse; hence resolution is directly related to the physical size of the array.[8] Classical beamforming can, therefore, not achieve higher resolution than the so-called diffraction limit.

Researches have developed various methods to improve resolution in ultrasonic array imaging using, for example, time-dependent (dynamic) receive focusing[9] or to select a transmit aperture so that the PSFs are as position invariant as possible over the region of interest (ROI).[10,11] Such approaches can, however, never circumvent the fundamental limitations of delay-and-sum methods.

Due to the inherent limitations of classical beamforming there has been an increasing interest in model-based array imaging methods. The idea with these methods is to set up a model for the imaging system that takes both electrical and acoustical (diffraction) effects into account[12,13] with the aim to compensate for both these effects. If this is successful then one can relax some of the restrictions normally imposed on array designs, that is, (i) undersampled arrays can be used since artifacts due to grating lobes can be compensated for, and (ii) long transmit sequences can be used which implies more transmitted acoustic energy, and as a consequence, the reconstructions become less noisy. Another potential benefit is that by using this methodology rather large areas can be reconstructed using a single, or at least very few transmissions, which is of interest in applications where a high frame rate is required.

The model-based methods can roughly be divided into two groups. In the first one the imaging problem is seen as an inverse problem where the goal is to remove effects of the so-called *propagation operator*. Since this type of problem is known to be "ill-posed," regularization is generally required in order to obtain numerically stable and noise resistant reconstructions.[14,15]

[a)]Electronic mail: fredrik.lingvall@ifi.uio.no
[b)]Electronic mail: tomas.olofsson@signal.uu.se

In the second group the imaging problem is seen as an inference problem[16,17] where the objective is to estimate the scattering strengths based on the information that is available. Such information is typically the PSFs associated with the array system (the propagation operator) and some assumptions regarding the scattering strengths.[18,19]

The main objective of this paper is the design of suitable transmit sequences to improve imaging performance. Input signal design for ultrasonic imaging has been studied extensively over the last two to three decades. Proposed approaches in ultrasonic imaging include, for example, coded-excitation methods and time-reversal-based methods.

Coded-excitation methods have become more popular in ultrasonic array imaging research in the last decade. In these methods a longer signal such as frequency modulated chirps or binary sequences, like Golay codes, are used instead of short pulses.[20–22] The temporal resolution is then restored on receive by pulse compression matched filtering. The benefit of these methods is an increased signal-to-noise ratio (SNR) in the beamformed images but they are still diffraction limited and the resolution is independent of the SNR (a high SNR will not improve resolution). The latter drawback can be alleviated by using spectral inversion[23] but these types of coded-excitation methods still have many of the deficiencies of conventional beamforming.

In time-reversal imaging, a pulse is first transmitted and after receiving the response, the acquired signals are reversed in time and then retransmitted.[24] The resulting field is then refocused to the strong scatterers even when the propagation medium is inhomogeneous. However, this approach has several drawbacks. First, a strong scatterer is needed to achieve focusing, and second, one may be interested in focusing at other points as well. Furthermore, the time-reversal operation is equivalent to the operation of a matched filter,[24] and although the matched filter approach is known to be robust[14,25] and has the property to optimize the SNR at the focal point, there are no restrictions on the estimation errors for points around the focal point resulting in a resolution similar to conventional array imaging.[14]

To alleviate these problems model-based inverse imaging can be included in the input signal design. A simple approach, suggested for transmit pulse design in nondestructive testing, is to use a weighted inverse of the double-path impulse response as an input signal for one-dimensional A-scan data.[26] In more advanced multidimensional imaging, a "stabilized" inverse of the propagation operator has been suggested for designing input signals so that a precise control over the intensity level at a predefined set of control points can be obtained.[14,27,28] This technique has also been used to improve the performance of coded-excitation methods.[29]

The input signal design approach taken in this paper is based on the second type of model-based imaging methods described earlier. Instead of specifying a desired response at some chosen control points, or specifying a coded excitation, the input signals are obtained by minimizing the *expected squared estimation error* for the optimal linear estimator[13,18,19] at a chosen set of control points.

The optimal linear estimator was chosen here since it allows for the estimation error to be expressed in a closed form which makes optimization of its performance feasible. Furthermore, the optimal linear estimator has the desirable properties to be able to compensate for both diffraction effects due to finite size of the array elements[30] as well as grating lobes or any other broad beam pattern.[13] The performance of the linear estimator is mostly determined by the SNR at the particular ROI. That is, if the signal energy at a region is sufficient then the optimal linear estimator can compensate for diffraction effects, arbitrary beam patterns, electrical characteristics of the transducer array, and very high resolution images can be obtained which are not diffraction limited.

Statistically motivated input signals have been used before in ultrasonic array imaging where temporal (one-dimensional) input signal optimization for the Wiener filter was considered.[31] It was shown that if an energy constraint was used, then the power spectrum of the input signal can be found leaving the phase of the signal arbitrary. It was also shown that genetic algorithms can be used to find binary input signals resulting in a low mean squared error (MSE) for the Wiener filter, which resulted in a superior range resolution, lower range sidelobes, and higher SNR compared to traditional pulse compression methods. However, the one-dimensional approach does not take into account the effects of the nonstationary PSFs, which is suboptimal since then not all of the diversity inherent in the array imaging problem is considered. In this paper a model is used that does take into account nonstationary PSFs and the constraints on the finite length input signals are only on the bounds of their maximum amplitude vales.

This paper is organized as follows: In Sec. II the linear model based on the impulse response method is introduced and in Sec. III the optimal linear estimator is presented. Section IV presents a performance criterion and suggests an optimization strategy. Some simulation examples are then shown in Sec. V, and finally in Sec. VI a discussion is given.

II. A DISCRETE LINEAR MODEL OF THE IMAGING SYSTEM

Here we will introduce the linear model, based on the impulse response concept,[32,33] that later will be used in the reconstruction algorithm (i.e., in the estimator presented in Sec. III). The objective is to model the double-path (pulse-echo) B-scan response given an array layout and a set of input signals, one separate input signal for each transmit element. To accomplish this we first describe the A-scan signal acquired at one receive element resulting from a scatterer at a single observation point, $\mathbf{r}=(x,y,z)$. This model is then extended to B-scan data for an arbitrary number of observation points.

Consider an array with K transmit elements and L receive elements and contributions from a scatterer at $\mathbf{r}$ with a scattering strength $o(\mathbf{r})$. The received A-scan signal from the lth receive element, $y_l(\mathbf{r},t)$ can be expressed as[19]

$$y_l(\mathbf{r},t) = \left(\sum_{k=0}^{K-1} h_k^{\text{f-SIR}}(\mathbf{r},t) * h_k^{\text{ef}}(t) * u_k(t) \right) \times o(\mathbf{r}) * h_l^{\text{b-SIR}}(\mathbf{r},t) * h_l^{\text{eb}}(t) + e_l(t), \quad (1)$$

where an asterisk (∗) denotes temporal convolution. The sum inside the parentheses in Eq. (1) represents the transmit process where $h_k^{\text{f-SIR}}(\mathbf{r},t)$ is the forward spatial impulse response (SIR) for the kth transmit element, $h_k^{\text{ef}}(t)$ is the forward electrical impulse response, and $u_k(t)$ is the kth input signal. The receive process is described by the backward SIR, $h_l^{\text{b-SIR}}(\mathbf{r},t)$, for the lth receive element and the corresponding backward electrical impulse response is denoted $h_l^{\text{eb}}(t)$. Finally, $e_l(t)$ represents the combination of measurement noise and any other model error for the lth receive element. The response for all observation points is obtained by superimposing the responses for all points in the ROI. For the discrete case, this summation can be written as a matrix-vector multiplication as follows:[19,30,34]

$$\mathbf{y} = \begin{bmatrix} \mathbf{y}_0 \\ \mathbf{y}_1 \\ \vdots \\ \mathbf{y}_{L-1} \end{bmatrix} = \mathbf{P}\mathbf{o} + \begin{bmatrix} \mathbf{e}_0 \\ \mathbf{e}_1 \\ \vdots \\ \mathbf{e}_{L-1} \end{bmatrix} = \mathbf{P}\mathbf{o} + \mathbf{e}. \quad (2)$$

The column vector $\mathbf{y}$ is the vectorized B-scan data and $\mathbf{o}$ is the vectorized image of scattering strengths; the L column vectors $\mathbf{y}_l$ in Eq. (2) represent the discrete-time A-scans for each receive element. The *propagation matrix*, $\mathbf{P}$, in Eq. (2) describes both the transmission and the reception process for an arbitrary excited array. Note that $\mathbf{P}$ is a function of the K arbitrary discrete input signals $\mathbf{u}_k$.

III. THE OPTIMAL LINEAR ESTIMATOR

The optimal linear estimator—also known as the linear minimum mean squared error estimator, the maximum *a posteriori* estimator under Gaussian assumptions, or the Wiener filter—is briefly introduced in this section. The estimator can be found by assuming a linear estimator, $\hat{\mathbf{o}} = \mathbf{K}_{\text{OPT}}\mathbf{y}$, and then minimize the mean squared error criteria given by[13,18]

$$\mathbf{K}_{\text{OPT}} = \arg\min_{\mathbf{K}} \mathrm{E}\{\|\mathbf{o} - \mathbf{K}\mathbf{y}\|^2\} = \mathbf{C}_o\mathbf{P}^T(\mathbf{P}\mathbf{C}_o\mathbf{P}^T + \mathbf{C}_e)^{-1}. \quad (3a)$$

where $\mathrm{E}\{\cdot\}$ is the expectation operator. The estimator (3a) can be rewritten in the equivalent form

$$\mathbf{K}_{\text{OPT}} = (\mathbf{P}^T\mathbf{C}_e^{-1}\mathbf{P} + \mathbf{C}_o^{-1})^{-1}\mathbf{P}^T\mathbf{C}_e^{-1}. \quad (3b)$$

The latter form (3b) can also be obtained by assuming a Gaussian distributed $\mathbf{o}$ and $\mathbf{e}$ and then choose the estimate $\hat{\mathbf{o}}$ where the *a posteriori* distribution has its maximum. Also, here we have assumed that $\mathbf{o}$ and $\mathbf{e}$ are mutually independent with covariance matrices $\mathbf{C}_o = E\{\mathbf{o}\mathbf{o}^T\}$ and $\mathbf{C}_e = E\{\mathbf{e}\mathbf{e}^T\}$, respectively.

Note that the performance of the estimator (3) is largely dependent on how the transmitted wave field is distributed in space. The most commonly used method to control the distribution of the wave field is by focusing, that is, a short pulse is transmitted on all array elements and appropriate delays are applied so that the field generated by the corresponding elements arrive at the focal point at the same time instant. The drawback of classical focusing is that only a small region will become insonified for each transmission. As mentioned earlier, modern array systems have the capability to transmit arbitrary wave forms and this feature can be utilized to design suitable input signals so the reconstruction performance for the estimator (3) is maximized. In order to accomplish this task we need a method to evaluate the performance, which is the topic of Sec. IV.

IV. THE PERFORMANCE CRITERION

In this section a performance measure and a criterion to optimize the performance is introduced. The performance measure is based on the reconstruction error, $\boldsymbol{\epsilon} = \hat{\mathbf{o}} - \mathbf{o}$, for the optimal linear estimator (3). First note that the covariance matrix for $\boldsymbol{\epsilon}$ can be expressed in a closed form which is given by[35]

$$\mathbf{C}_\epsilon = \mathbf{C}_o - \mathbf{C}_o\mathbf{P}^T(\mathbf{P}\mathbf{C}_o\mathbf{P}^T + \mathbf{C}_e)^{-1}\mathbf{P}\mathbf{C}_o = (\mathbf{C}_o^{-1} + \mathbf{P}^T\mathbf{C}_e^{-1}\mathbf{P})^{-1}. \quad (4)$$

Second, if we assume that there are no correlations between the scatterers and that the noise is white then $\mathbf{C}_o = \sigma_o^2\mathbf{I}$, $\mathbf{C}_e = \sigma_o^2\mathbf{I}$, and $\mathbf{C}_\epsilon$ reduces to

$$\mathbf{C}_\epsilon = \sigma_o^2\mathbf{I} - \sigma_o^2\mathbf{P}^T(\sigma_o^2\mathbf{P}\mathbf{P}^T + \sigma_e^2\mathbf{I})^{-1}\mathbf{P}\sigma_o^2 = (\mathbf{I}/\sigma_o^2 + \mathbf{P}^T\mathbf{P}/\sigma_e^2)^{-1}. \quad (5)$$

Since each diagonal element in $\mathbf{C}_\epsilon$ is the expected squared estimation error of the corresponding element in $\mathbf{o}$ (the expected error at the corresponding observation point) it can be used to evaluate and visualize performance. In particular, one can rearrange the diagonal elements of the $MN \times MN$ matrix $\mathbf{C}_\epsilon$ to form an $M \times N$ image, and then, one can directly see at which regions the error is small and where it is large.

To illustrate this technique we have simulated a 3.5 MHz, 16 element array with a pitch of 1 mm using the DREAM Toolbox.[36] The array was focused using traditional focusing at $z = 50$ mm. Two different SNRs were used, one high SNR and one low SNR, respectively, but the input signals were the same for both SNRs. The resulting error images are shown in Fig. 1 where a dark area indicates a region with low error and a white (bright) area indicates a region with a large error. The error image for the high SNR is shown in Fig. 1(a), and one can observe that the error is small in regions close to the center axis under the array, that is, in regions where the amplitude of the wave field is high. One can also observe that the region with a low error is considerably smaller for the low SNR error image, shown in Fig. 1(b), compared to the high SNR error image.

Note also that it is not required that the field is "focused" in the sense that it is closed to the focal point to obtain good reconstruction results since the expected error in Fig. 1(a) is small also at many points far from focal point. The error does, however, depend on the SNR and for low SNR, the error is only small for points close to the focal point.

From the example shown in Fig. 1 it is clear that if we want a small error over a larger region (from a single trans-

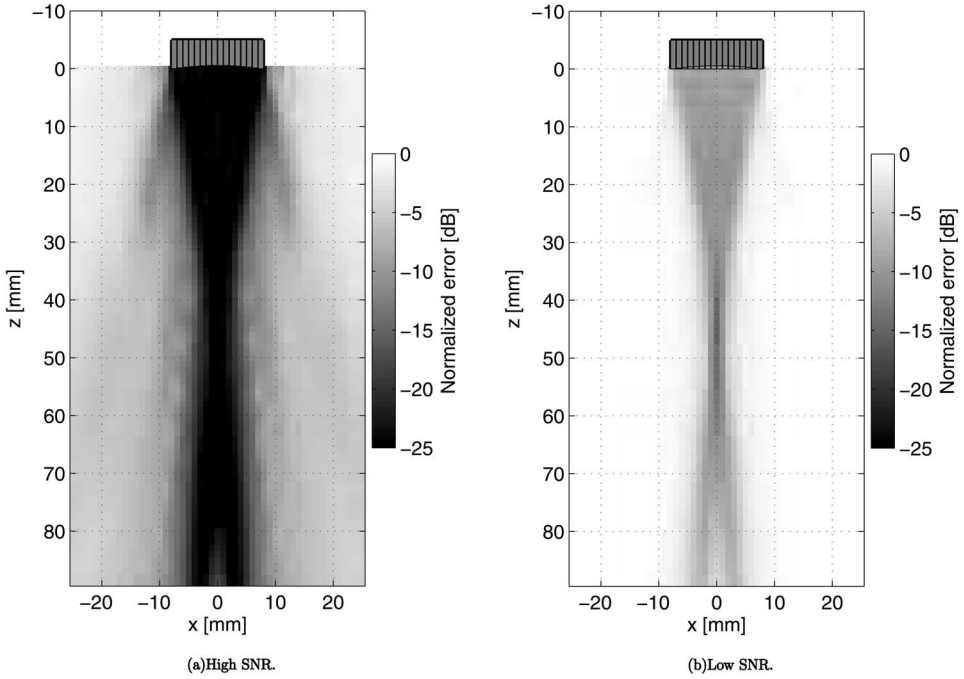


FIG. 1. Two examples of error images, normalized with respect to σ_o^2, for a 16 element array conventionally focused at $z=50$ mm. The error images are formed by rearranging the diagonal elements of the error matrix $\mathbf{C}_\epsilon$ [see Eq. (5)] for the optimal linear estimator (3) as an $M\times N$ image.

mission) then it is not sufficient to use traditional focusing and the objective here is then to minimize the error, for an arbitrarily chosen set of observation points, by means of finding suitable input signals for that task. To accomplish this first note that if the eigenvalues of the product $\mathbf{P}^T\mathbf{P}/\sigma_e^2$ are significantly larger than $1/\sigma_e^2$ then the expected error in Eq. (5) will become small. Moreover, since the elements in $\mathbf{P}$ are formed by convolutions with the input signals [cf., Eq. (1)], a small error can be achieved by simply increasing the amplitudes of the input signals. This will, however, force the input signals to infinity if there were no constraints on them.[31] For a practical system the input signals are limited and here we assume that we have an array system which have separate transmit and receive buffers for all channels; and these buffers have a limited size and the discrete representation of the signals limits the amplitudes to a predefined interval.

Let us denote the input signal's lengths L_u and let the amplitudes be restricted to the interval $(-u_{\max}\leqslant u_i\leqslant u_{\max})$. The criterion we have chosen to optimize is the MSE, $\Sigma_i E\{(\hat{o}_i-o_i)^2\}$, which is the sum over the diagonal elements (the trace) in $\mathbf{C}_\epsilon$

$$\hat{\mathbf{u}} = \arg\min_{\mathbf{u}} \mathrm{tr}\{\mathbf{C}_\epsilon\}$$
$$\text{subject to} \quad |u_i| \leqslant u_{\max}\forall_i, \tag{6}$$

where $\mathrm{tr}\{\cdot\}$ is the trace operator and $i=0,\ldots,L_u-1$. Note that the criterion (6) is nonlinear and we may have many local minima. Here we have used genetic optimization to find good input signal candidates.

It should be emphasized that this optimization approach to input signal design is very general in the sense that it is possible to find input signals for any array configuration provided the impulse responses for the model (2) can be obtained. Hence, both two- and three-dimensional imaging can be treated using, for example, one-dimensional linear arrays or two-dimensional arrays, which may or may not be undersampled.

In the remaining part of this paper a number of examples will be presented, from various setups, that show some properties and consequences of this input signal optimization approach.

V. SIMULATION EXAMPLES

Here we will present simulation examples for various single transducer and array imaging setups. The wave field simulations have been performed using the DREAM TOOLBOX,[36] which is a software package based on the *discrete representation* (DR) computational concept.[37]

A. The one-dimensional case: One transducer and a single observation point

Before we study the full multidimensional array case let us consider a single observation point and a single transducer operating in pulse-echo mode [see the illustration in Fig. 2(a)]. In such case the continuous-time model reduces to

$$\begin{aligned} y(t) &= h^{\text{f-SIR}}(t) * h^{\text{ef}}(t) * u(t)o \\ &\quad * h^{\text{b-SIR}}(t) * h^{\text{eb}}(t) + e(t) \\ &= h(t) * u(t)o + e(t), \end{aligned} \tag{7}$$

where $h(t)$ is the double-path impulse response for the single observation point where the dependence of $\mathbf{r}$ has been dropped in the notation here since we only have one observation point. In order to discretize Eq. (7) one can note that a discrete-time convolution of the signals $h(t)$ and $u(t)$, represented by the vectors $\mathbf{h}$ and $\mathbf{u}$, respectively, can be expressed as a matrix-vector multiplication of a Toeplitz matrix,[38] $\mathbf{H}$, consisting of delayed versions of $\mathbf{h}$ in its col-

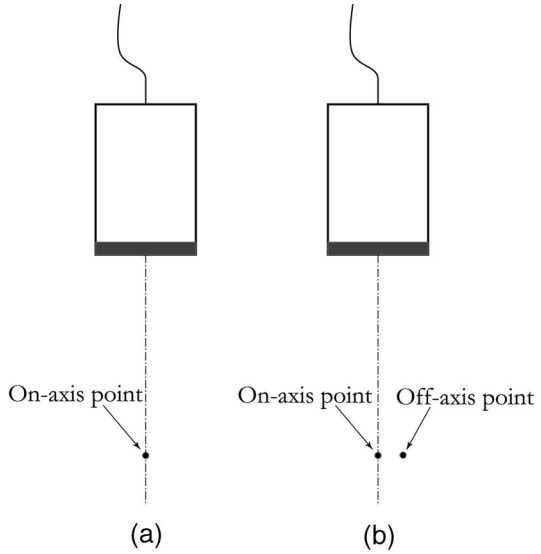


FIG. 2. Illustration of a single (circular) transducer with two configurations of observation points. (a) One on-axis observation point. (b) Two observation points, one located on-axis and one off-axis.

umns, and the vector $\mathbf{u}$. Hence, the discrete-time equivalent of Eq. (7) can be expressed as

$$\mathbf{y} = \mathbf{H}\mathbf{u}o + \mathbf{e}. \tag{8}$$

Thus, for this simple case the output signal only depends on the convolution of the input signal $\mathbf{u}$ and the impulse response $\mathbf{h}$ scaled with the (unknown) scattering amplitude o.

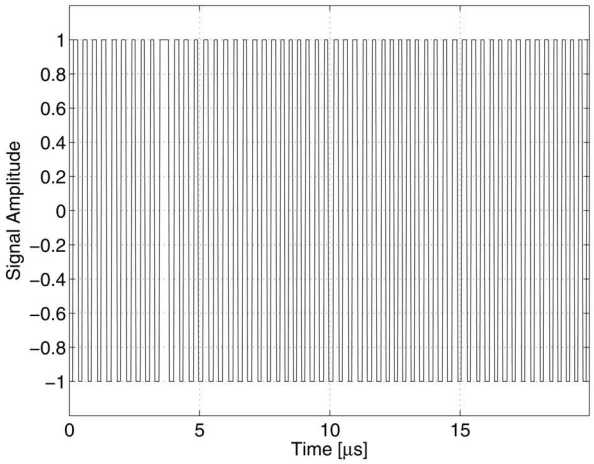
The expected error, found by using Eq. (8) in Eq. (5), then reduces to the scalar

$$\sigma_\epsilon^2 = (1/\sigma_o^2 + \mathbf{u}^T\mathbf{H}^T\mathbf{H}\mathbf{u}/\sigma_e^2)^{-1} = \frac{\sigma_e^2}{(\sigma_e^2/\sigma_o^2) + \mathbf{u}^T\mathbf{H}^T\mathbf{H}\mathbf{u}}. \tag{9}$$

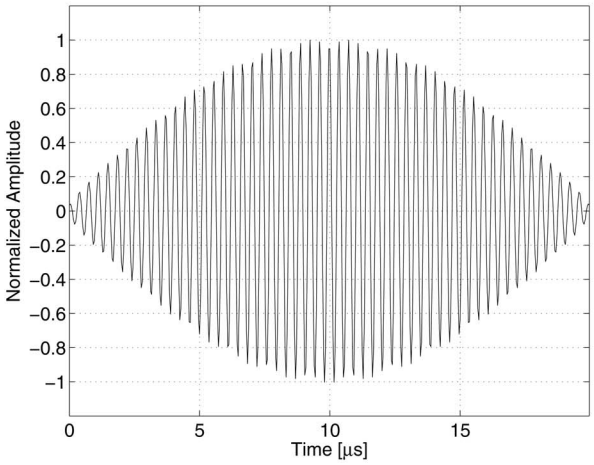
In this simple case we can immediately notice that it is sufficient to maximize the scalar $\mathbf{u}^T\mathbf{H}^T\mathbf{H}\mathbf{u}$ in order to minimize the error. That is, in this case the optimized input signals will not depend on the SNR.

An idea that may be tempting is to let $\mathbf{u}$ be the eigenvector corresponding to the largest eigenvalue of the matrix $\mathbf{H}^T\mathbf{H}$, since then, we will drive the system where it is most sensitive. This approach is, however, not optimal in the sense of the criterion (6); choosing the eigenvector as the input signal corresponds to a criterion where the restriction is on the energy, $\mathbf{u}^T\mathbf{u}$, of the input signals and not bounds of their max amplitudes. In order to use such eigenvectors as input signals they need to be scaled to fit within the amplitude bounds, which will result in a larger error compared to using signals specifically optimized to fit within these bounds.

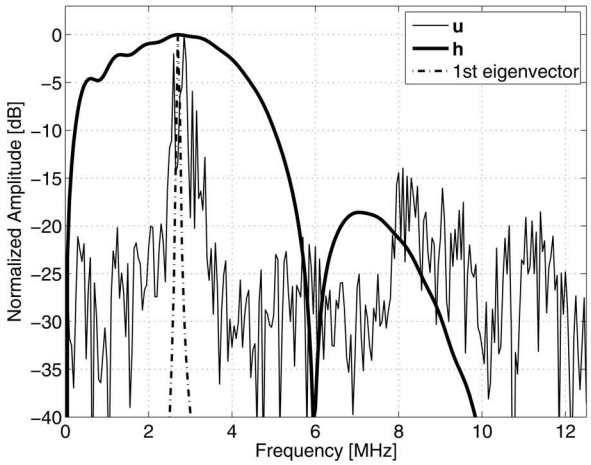
To illustrate this let us study a (broadband) 3.5 MHz circular transducer with a diameter of 10 mm and a single observation point at $(0,0,50)$ mm. An input vector with a length of L_u=500 samples was optimized for this scenario where the max amplitude, $u_{\max}$, was set to 1. The optimized input signal is shown in Fig. 3(a) and the eigenvector corresponding to the largest eigenvalue of $\mathbf{H}^T\mathbf{H}$ is shown in Fig. 3(b). Furthermore, in Fig. 3(c), the spectra for $\mathbf{u}$ (thin solid line), the eigenvector of $\mathbf{H}^T\mathbf{H}$ (dash-dotted), and the double-path impulse response, $\mathbf{h}$ (thick solid line) are also shown.



(a)Optimized input signal $\mathbf{u}$.



(b)Eigenvector corresponding to the largest eigenvalue, $\lambda_{\max}$, of $\mathbf{H}^T\mathbf{H}$.



(c)Thin line: amplitude spectrum of the input signal $\mathbf{u}$, thick line: amplitude spectrum of the impulse response $\mathbf{h}$, dash-dotted thick line: spectrum of the Eigenvector corresponding to the largest eigenvalue of $\mathbf{H}^T\mathbf{H}$.

FIG. 3. Simulation example of an optimized input signal for a 10 mm (in diameter), 3.5 MHz circular transducer and an observation point at $(0,0,50)$ mm.

By comparing the spectrum of the input signal to the spectrum of the double-path impulse response one can observe

that the peak of the input signal's spectrum coincides withthe peak of the impulse response's spectrum. Thus, the optimized input signal drives the system where it has the most sensitivity. This is also true for the eigenvector signal since its spectrum also peaks at the peak of the impulse response's spectrum. However, using the optimized signal will result in a smaller reconstruction error since the total energy in the optimized signal is always higher than for the eigenvector approach; for the example presented in Fig. 3 the error when using the eigenvector signal was 4.7 dB larger compared to using the optimized signal.

This is generally valid for all optimized signals presented in this paper. The optimal values of the input signals will always occur at corner points of the constraints in Eq. (6); that is, the value of the optimized signal will either be $-u_{\max}$ or $u_{\max}$. The discrete nature of the optimized signal is rather natural since the highest acoustic output will be attained when the input signal is maximal, e.g., since the system is linear a lowering of the input amplitude can never increase the total output energy. The form of the output signal is also attractive from a hardware design point-of-view since a binary output buffer can be used (e.g., $-u_{\max}$ can be represented with a "0" and $u_{\max}$ with a "1," and digital-to-analog converters are not needed).

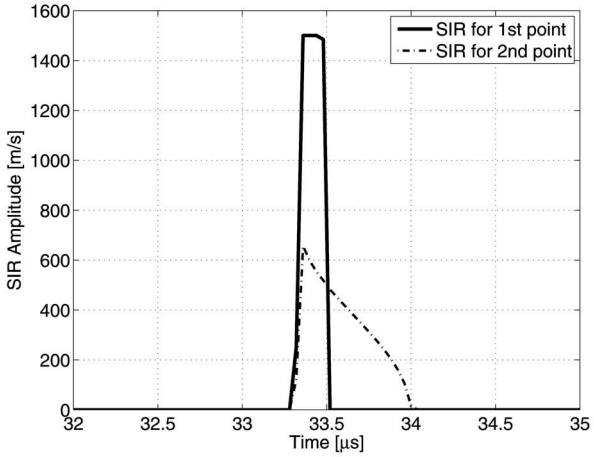
The optimized signal type, shown in Fig. 3, is known in the automatic control community as "bang-bang" signals. It has also been known from the 1960s in optimal experimental design that the bang-bang type of input signals are optimal in parameter estimation of linear dynamic systems when the constraints are of max/min type.[39,40]

B. One transducer and two observation points

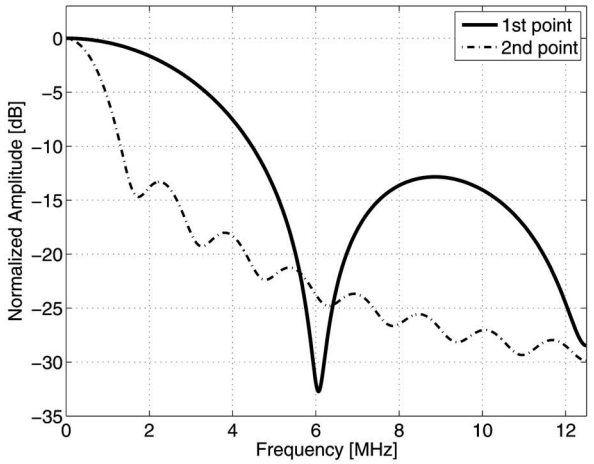
In the simple one-dimensional example presented in Sec. V A the optimized input signal did not depend on the SNR. This is, however, not true for more complex systems. To illustrate this let us consider two observation points and a single transducer [see the illustration in Fig. 2(b)]. Similar to the one-dimensional case, a discrete model can be obtained by expressing convolutions as matrix-vector multiplications. However, when we have two observation points the total A-scan response, $\mathbf{y}$, will now be a sum of two A-scan responses, one from each of the corresponding observation points. The total A-scan response can therefore be expressed as

$$\begin{aligned}\mathbf{y} &= \mathbf{H}_1\mathbf{u}o_1 + \mathbf{H}_2\mathbf{u}o_2 + \mathbf{e} \\ &= \mathbf{p}_1 o_1 + \mathbf{p}_2 o_2 + \mathbf{e} \\ &= (\mathbf{p}_1\mathbf{p}_2)\begin{pmatrix} o_1 \\ o_2 \end{pmatrix} + \mathbf{e}, \end{aligned} \tag{10}$$

where $\mathbf{H}_1$ and $\mathbf{H}_2$ are the Toeplitz matrices derived from the double-path impulse responses for the two observation points: 1 (on-axis) and, 2 (off-axis), $\mathbf{p}_1$ and $\mathbf{p}_2$ are the corresponding double-path (A-scan) responses (for unit area scatterers), and the two scalars o_1 and o_2 are the scattering strengths at observation point 1 and 2, respectively. The 2×2 error matrix, $\mathbf{C}_\epsilon$, for the linear estimator, based on Eq. (10), then becomes



(a) Spatial impulse responses (SIRs) for observation point 1 and 2.



(b) Normalized frequency responses of the SIRs for observation point 1 and 2.

FIG. 4. Spatial impulse responses and their corresponding frequency responses for a ∅10 mm circular transducer. Thick solid line: SIR corresponding to observation point 1 at (0,0,50) mm. Dash-dotted line: SIR corresponding to observation point 2 at (5,0,50) mm. (a) SIRs for observation points 1 and 2. (b) Normalized frequency responses of the SIRs for observation points 1 and 2.

$$\begin{aligned}\mathbf{C}_\epsilon &= \sigma_e^2 \begin{pmatrix} \mathbf{u}^T\mathbf{H}_1^T\mathbf{H}_1\mathbf{u} + \dfrac{\sigma_e^2}{\sigma_o^2} & \mathbf{u}^T\mathbf{H}_1^T\mathbf{H}_2\mathbf{u} \\ \mathbf{u}^T\mathbf{H}_2^T\mathbf{H}_1\mathbf{u} & \mathbf{u}^T\mathbf{H}_2^T\mathbf{H}_2\mathbf{u} + \dfrac{\sigma_e^2}{\sigma_o^2} \end{pmatrix}^{-1} \\ &= \sigma_e^2 \begin{pmatrix} \mathbf{p}_1^T\mathbf{p}_1 + \dfrac{\sigma_e^2}{\sigma_o^2} & \mathbf{p}_1^T\mathbf{p}_2 \\ \mathbf{p}_2^T\mathbf{p}_1 & \mathbf{p}_2^T\mathbf{p}_2 + \dfrac{\sigma_e^2}{\sigma_o^2} \end{pmatrix}^{-1}. \end{aligned} \tag{11}$$

Let us again consider a 10 mm circular transducer but now with two observation points at (0,0,50) mm and (5,0,50) mm, respectively. The corresponding SIRs and their frequency responses[33,41] are shown in Fig. 4. The SIR from the off-axis point (5,0,50) has a significantly lower cut-off frequency than the SIR for the on-axis point

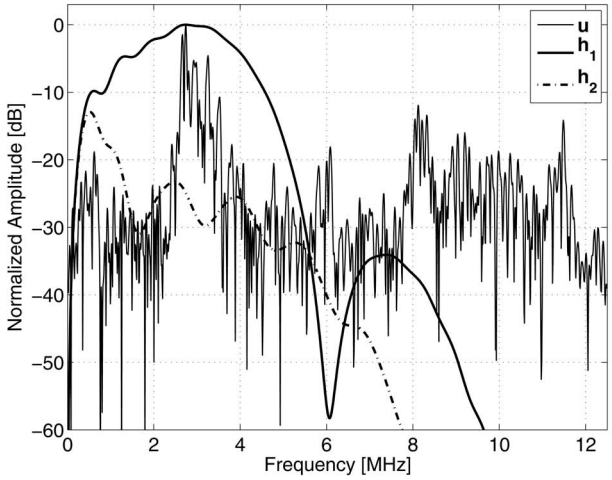
$(0,0,50)$, which corresponds to the fact that the beam width is frequency dependent. Thus, the transducer size effects, or the diffraction effects, result in a system that has a spatially varying frequency dependent sensitivity. In this particular example, the system is more sensitive at the on-axis point $(0,0,50)$ than at the off-axis point $(5,0,50)$.

Let us now study the elements $(\mathbf{C}_\epsilon)_{1,1}$ and $(\mathbf{C}_\epsilon)_{2,2}$ of the error matrix in Eq. (11). In order for the input signal to have a significant impact on the error, both the factors $\mathbf{p}_1^T\mathbf{p}_1$ and $\mathbf{p}_2^T\mathbf{p}_2$ cannot be much less in magnitude than σ_e^2/σ_o^2. If this would be the case then the acquired data basically do not give us any new information. If only one of the factors is small in comparison to σ_e^2/σ_o^2 then we will be "blind" at the corresponding observation point but not the other.

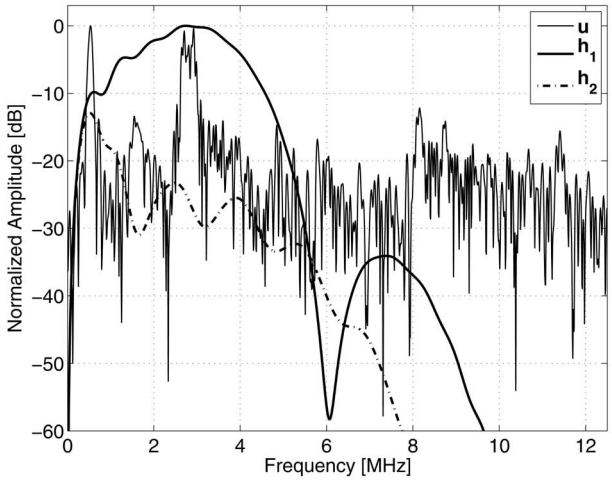
To illustrate the dependence of the SNR, simulations with three different SNRs are presented in Fig. 5. The thick solid lines indicate the double-path frequency responses corresponding to the on-axis point, $(0,0,50)$, the dash-dotted lines indicate the double-path frequency responses for the off-axis point, $(5,0,50)$, and the thin lines indicate the frequency responses for the optimized input signals.

In Fig. 5(a) the SNR was very low and only the error for the on-axis point could be affected by the input signal. This can be seen in the spectra in Fig. 5(a) where most of the input signal's energy is transmitted where the frequency response for the on-axis point has its peak. If the SNR is increased then also the off-axis point will contribute in the optimization and, as shown in Fig. 5(b), the spectra of the input signal now have significant contributions where the spectra for both the on-axis and off-axis points have their corresponding peaks. If we now increase the SNR even further, as shown in Fig. 5(c), then the input signal's spectra will be concentrated at the peak of the off-axis point's spectra. This phenomenon can be explained by the fact that the on-axis and off-axis spectra overlap and if the SNR is high enough then (1) it is possible to estimate scattering from both points using a signal with an "overlapping" spectra, and (2) the off-axis point will contribute most to the error so it makes sense to minimize that error contribution (the error contribution from the on-axis point is already small).

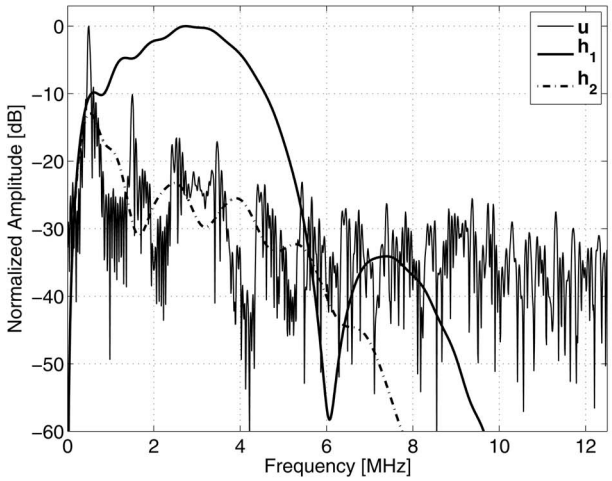
The conclusion from this example is that the distribution of the transmitted acoustic field will depend on the SNR and if the SNR is low then points close to the center axis under the transducer will be favored before points far from the center axis. Note that in the simple example presented here we could only control the error merely by sending the energy in suitable frequency bands. If we increase the number of transducers we have a greater possibility to improve the performance since then we have the possibility to adapt the beam pattern both in time and space which is the topic of the following.



(a)Low SNR ($\sigma_e^2 = 10^5$).



(b)Medium SNR ($\sigma_e^2 = 10^3$).

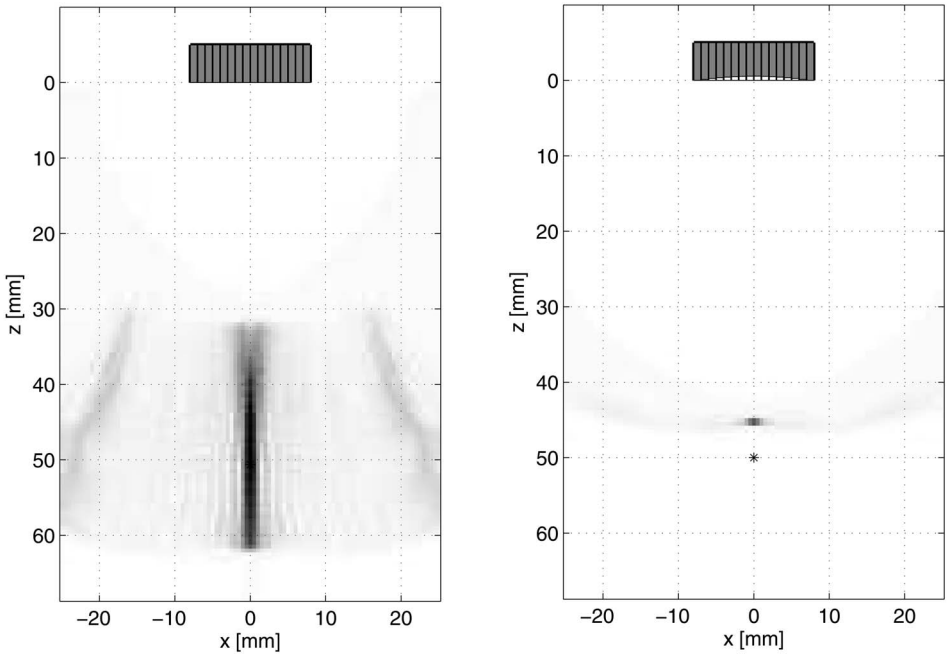


(c)High SNR ($\sigma_e^2 = 10^{-5}$).

FIG. 5. Simulation examples the frequency responses for optimized input signals for three different SNRs. The simulations were performed for a 10 mm (in diameter), 3.5 MHz circular transducer and two observation points at $(0,0,50)$ mm and $(5,0,50)$ mm, respectively. Thin solid line: Input signals. Thick solid line: Response for $\mathbf{h}_1$ corresponding to point $(0,0,50)$. Dash-dotted thick line: Response for $\mathbf{h}_2$ corresponding to point $(5,0,50)$.

C. Linear array examples

In this section we will present input signal design examples using a linear array. In the examples presented here the SNR can be considered as relatively high. A high SNR was chosen in order to show how the beam pattern can be adapted also for off-axis points; a very low SNR would oth-



(a)Wavefield snapshot at $t = 41.9\mu s$.

(b)Wavefield snapshot at $t = 31.1\mu s$ for a traditionally focused array.

FIG. 6. An example of a wave field resulting from using input signals optimized for a single control point. A 16 element array (with 0.9-mm-wide elements and a pitch of 1 mm) with 500-sample-long input signals optimized for a single point at (0,0,50.6) mm.

erwise, as was discussed in Sec. V B, force most of the energy to be transmitted directly under the aperture of the array.

Before we present the array examples it should be noted that our possibility to control the beam pattern and, therefore also the reconstruction error, depends very much on the experimental constraints. Longer input signals, higher amplitudes, and broadband transducers will give us more diversity and a higher degree of control of the acoustic field than using short signals, low signal amplitudes, and narrow band transducers.

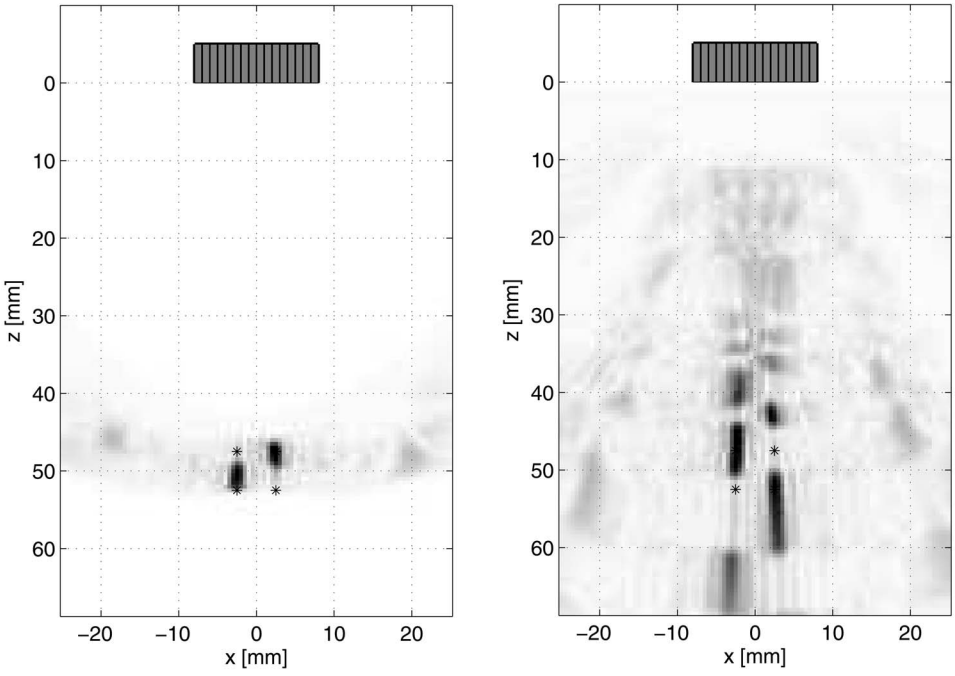
Also, let us define the set of observation points that we use in the optimization process as *control points* and reserve the name *observation points* for the points that are used in the reconstruction process. We make this distinction since one can optimize the input signals for one set of points and use a different set, typically more dense, in the actual reconstruction process.

Example 1 (The significance of input signal length). The input signal length has a direct effect on the reconstruction performance. With a longer signal one can transmit energy over a longer period of time, which results in a significantly lower estimation error compared to using very short pulses. To illustrate how input signal optimization, using a relatively long signal, influences the beam pattern a simulation for a 16 element array with 0.9 mm wide elements and a pitch of 1 mm is presented in Fig. 6. The array elements have center frequency of 3.5 MHz, corresponding to a wavelength of $\lambda \approx 0.4$ mm in water, and the length of the input signals, L_u was 500 samples (20 μs). Figure 6(a) shows a simulated wave field snapshot at $t=41.9$ μs and, for comparison, a snapshot at $t=33.5$ μs using traditional focusing is shown in Fig. 6(b). The optimization results in a transmitted wave field which has a time varying focus region and the single control point (0,0,50) is therefore insonified over a considerably longer time compared to using traditional focusing.

Example 2 (Time-space coding). Array imaging using long input signals offers a high degree of diversity and a possibility to control the wave field both in time and space. If the signals are long enough and the number of array elements is sufficient one can insonify very large ROIs. To illustrate how the time and space properties of the wave field are influenced by the optimization process let us consider the same array as used in Example 1 but now we have four control point instead of one. The control points were located at (−2.5,0,47.54), (2.5,0,47.5), (−2.5,0,52.5), and (−2.5, 0,52.5) mm, respectively. The simulation results are shown in Fig. 7, where the wave field resulting from optimization for four relatively closely spaced control points using two different signal lengths are displayed. Figure 7(a) shows a wave field snapshot for an input signal length of 100 samples and Fig. 7(b) shows the corresponding snapshot for a length of 1000 samples.

From Fig. 7(a) one can observe that the energy for control points at the same depth is, at each time instant, low for one control point and high for the other, which makes it easier for the estimator to discriminate from which direction the scattering originates. This phenomenon is seen in the wave fields from both signal lengths. The only difference is that the long signal allows for more of these "pulses" than the short signal resulting in a lower estimation error.

Example 3 (Distribution of energy). In order to reduce the number of transmissions it is desirable to be able to insonify large ROIs from a single transmission. Here this can be achieved by simply distributing the control points over a larger-than-normal area. The input signal optimization process will then try to find input signals, and the corresponding wave fields, so that all control points are sufficiently insoni-



(a)Input signal length $L_u = 100$ samples (snapshot at 35.6μs).

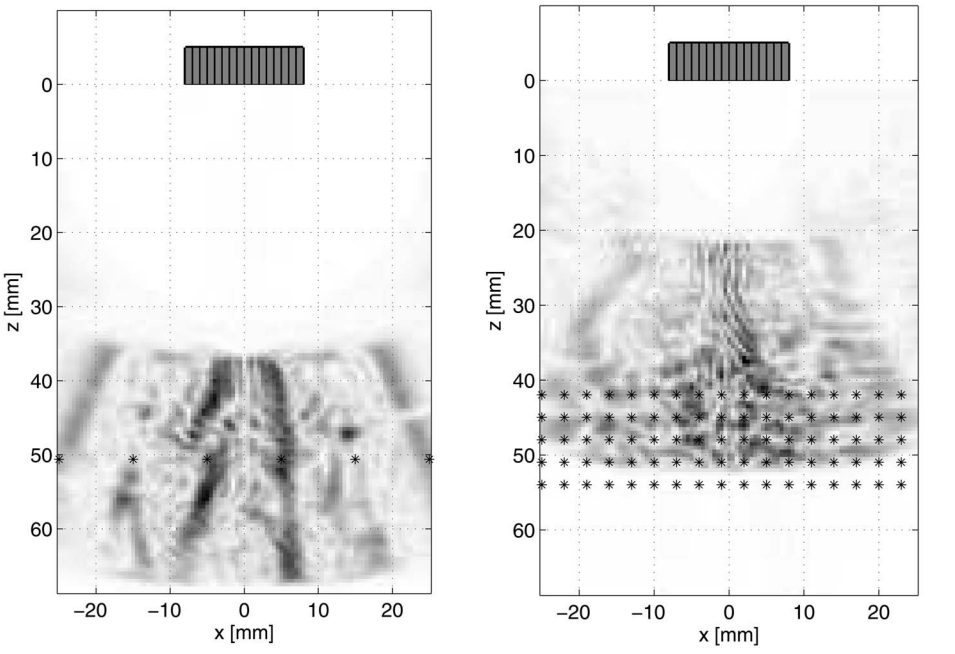
(b)Input signal length $L_u = 1000$ samples (snapshot at 47.9μs).

FIG. 7. Wave field snapshots for input signals optimized for four control points at: $(-2.5,0,47.5)$, $(x=2.5,0,47.5)$, $(-2.5,0,52.5)$, and $(-2.5,0,52.5)$ mm using the same array as in Fig. 6.

fied. It should, however, be noted that the error will most likely not be the same for all control points since, as mentioned in Sec. V B, the array system has a different sensitivity at different control points. The sensitivity is highest directly under the array aperture so a large aperture (with many elements) will perform better than a small one.

To illustrate how input signal optimization can generate laterally broad wave fields two examples are presented in Fig. 8 where the control points are distributed over a large region. Figure 8(a) shows an example with six horizontally located control points and one can observe that a multibeam field is obtained where most of the energy is concentrated around the control points. The example shown in Fig. 8(b) has a relatively large number of control points. Here, a more diffuse field is obtained insonifying the total region of control points.

The conclusion from the examples presented in this section is that the statistically motivated input signal design method proposed here is very flexible in the sense the input signals can be designed for any particular set of control points. The found signals will also result in the lowest possible estimation error for the optimal linear estimator (2) at



(a)Six control points horizontally aligned at $z = 50.6$ mm.

(b)85 control points uniformally located at $-25 < x < 25$, $42 < z < 52$ mm.

FIG. 8. Wave field snapshots at $t=45.5$ μs and $t=35.5$ μs, respectively, for $L_u=500$-sample-long optimized input signals.

the chosen control points for the array system at hand. Also, note that we have chosen to present the proposed method using a linear array and two-dimensional imaging only to facilitate the presentation, but the method can equally well be applied to two-dimensional arrays and/or three-dimensional imaging.

VI. DISCUSSION AND CONCLUSIONS

This paper treats the particular problem of input signal design for ultrasonic array imaging. This problem can be seen as a part of the general framework of optimal experimental design. Here the goal is to design the experiment in such a way that it is as informative as possible regarding the quantity that we want to study. In this case the quantity is the scattering strengths in some ROI and the objective is thus to design the experiment such that we get as much information as possible of the scattering using as much as possible of the capabilities of our measurement system.

When designing the experiment several decisions have to be made that will influence the outcome of the experiment. Typically the design of the experiment must account for several factors such as (from Goodwin[42]):

(1) "the goal of the experiment and the intended application of the results,"
(2) "the class of models to be used,"
(3) "the identification methods and the criterion of best fit,"
(4) "the extent of prior knowledge about the system," and
(5) "the constraints for the operation of the system, both to maintain safe operation and to ensure the system is not forced into an operation regime where the model becomes invalid."

Clearly our goal is to obtain the best image possible but we must first acknowledge the above-mentioned factors and specify the conditions and restrictions of our experiment. For example, if we acquire many signals over a long period of time we will improve the SNR in our estimates but then we cannot perform real-time imaging. Here we have focused on how to optimally design the experiment for so-called single-snapshot processing. If we would have time for more transmissions, mechanical scanning, etc., then the design may have been different.

Also, even though the model used here takes into account many of the properties not considered in traditional beamforming we have restricted the model to be linear. A more advanced model that, for example, has a quadratic term could also be considered. Such a model can better describe (first order) multiple scattering but it would also require a more complex estimator and therefore a more difficult design problem.

The choice of identification method and criterion used here is based on the capabilities of modern ultrasonic array systems and current research in high resolution imaging methods. Since many modern array systems have the capability to transmit arbitrary wave forms and high resolution algorithms can compensate for those wave forms[19] a less restrictive design than normally used can be allowed.

The constraints chosen here were only on the max/min amplitudes and the length of the input signals. These constraints were only due to the practical limitations of the hardware and we have aimed to make no further implicit or explicit restrictions that could degrade the performance. A typical example that results in reduced performance is aperture weighting, which is commonly used in sensor array processing; aperture weighting, or apodization, is a common technique in ultrasonic array imaging to suppress sidelobes. This is, however, clearly suboptimal since by apodizing the aperture less energy is transmitted and/or received, which essentially throws away valuable information.[43]

With these design decisions and restrictions in mind a method for input signal design in ultrasonic array imaging has been proposed in this paper. The method is capable of optimizing the input signals in such way that the scattering strengths at arbitrarily chosen control points can be estimated with as low an error as possible. The input signals, which take the form of binary bang-bang signals, are found by minimizing the expected error for the optimal linear estimator which is based on a linear model of the array system.

It is found that the optimized input signals depend on the SNR and to achieve good reconstruction results the acoustic field at a control point must be high enough relative to the noise. There is, however, no direct relation between the beamwidth of the field at that point since the used estimator has the capability to compensate for the beam patterns. Furthermore, the method automatically utilizes time–space coding possibilities inherent in ultrasonic array systems allowing multiple beams from a single transmission. This enables very fast imaging systems where the scattering amplitudes in large region of interests can be estimated using very few transmissions which is important in many applications such as in, for example, medical imaging where motion artifacts can be a problem if the frame rate is too low.[44]

ACKNOWLEDGMENT

We would like to acknowledge the Research Council of Norway (NFR) for funding of this work.

[1]O. T. von Ramm and S. W. Smith, "Beam steering with linear arrays," IEEE Trans. Biomed. Eng. **30**, 438–452 (1983).
[2]K. E. Thomenius, "Evaluation of ultrasound beamformers," in Proc.-IEEE Ultrason. Symp. **2**, 1915–1622 (1996).
[3]H. Krim and M. Viberg, "Two decades of array signal processing research," IEEE Signal Process. Mag. **22**, 67–94 (1996).
[4]J. A. Seydel, "Ultrasonic synthetic-aperture focusing techniques in NDT," *Research Techniques for Nondestructive Testing* (Academic, New York, 1982).
[5]S. R. Doctor, T. E. Hall, and L. D. Reid, "SAFT—The evolution of a signal processing technology for ultrasonic testing," NDT Int. **19**, 163–172 (1986).
[6]M. Karman and M. O'Donnell, "Synthetic aperture imaging for small scale systems," IEEE Trans. Ultrason. Ferroelectr. Freq. Control **42**, 429–442 (1995).
[7]J. A. Jensen, S. I. Nikolov, K. L. Gammelmark, and M. Pedersen, "Synthetic aperture ultrasound imaging," Ultrasonics **44**, 5–15 (2006).
[8]G. S. Kino, *Acoustic Waves: Devices, Imaging and Analog Signal Processing*, Prentice-Hall Signal Processing Series Vol. 6 (Prentice-Hall, Englewood Cliffs, NJ, 1987).
[9]T. L. Szabo, *Diagnostic Ultrasound Imaging: Inside Out* (Elsevier Academic, Amsterdam, 2004).
[10]J.-Y. Lu, "Bowtie limited diffraction beams for low-sidelobe and large

depth of field imaging," IEEE Trans. Ultrason. Ferroelectr. Freq. Control **42**, 1050–1063 (1995).
[11]Y. Zheng and S. Silverstein, "Novel transmit aperture for very large depth of focus in medical ultrasound B-scan," IEEE Trans. Ultrason. Ferroelectr. Freq. Control **53**, 1079–1087 (2006).
[12]R. J. Zemp, C. K. Abbey, and M. F. Insana, "Linear system models for ultrasound imaging: Application to signal statistics," IEEE Trans. Ultrason. Ferroelectr. Freq. Control **50**, 642–654 (2003).
[13]F. Lingvall, "A method of improving overall resolution in ultrasonic array imaging using spatio-temporal deconvolution," Ultrasonics **42**, 961–968 (2004).
[14]M. Tanter, J.-F. Aubry, J. Gerber, J.-L. Thomas, and M. Fink, "Optimal focusing by spatio-temporal inverse filter. I. Basic principles," J. Acoust. Soc. Am. **110**, 37–47 (2001).
[15]R. Lavarello, F. Kamalabadi, and W. D. O'Brien, "A regularized inverse approach to ultrasonic pulse-echo imaging," IEEE Trans. Med. Imaging **25**, 712–722 (2006).
[16]E. T. Jaynes, "Prior information and ambiguity in inverse problem," Inverse Probl. **14**, 151–166 (1984).
[17]E. T. Jaynes, *Probability Theory: The Logic of Science*, 1st ed. (Cambridge University Press, Cambridge, 2003).
[18]R. Stoughton and S. Strait, "Source imaging with minimum mean-squared error," J. Acoust. Soc. Am. **94**, 827–834 (1993).
[19]F. Lingvall and T. Olofsson, "On time-domain model based ultrasonic array imaging," IEEE Trans. Ultrason. Ferroelectr. Freq. Control **54**, 1623–1633 (2007).
[20]M. O'Donnell, "Coded excitation system for improving the penetration of real-time phased-array imaging system," IEEE Trans. Ultrason. Ferroelectr. Freq. Control **39**, 341–351 (1992).
[21]M. Pollakowski and H. Ermert, "Chirp signal matching and signal power optimization in pulse-echo mode ultrasonic nondestructive testing," IEEE Trans. Ultrason. Ferroelectr. Freq. Control **41**, 655–659 (1994).
[22]T. Misaridis and J. A. Jensen, "Use of modulated excitation signals in medical ultrasound. I. Basic concepts and expected benefits," IEEE Trans. Ultrason. Ferroelectr. Freq. Control **52**, 177–191 (2005).
[23]Y. Wang, K. Metzger, D. N. Stephens, G. Williams, S. Brownlie, and M. O'Donnell, "Coded excitation with spectrum inversion (CEXSI) for ultrasound array imaging," IEEE Trans. Ultrason. Ferroelectr. Freq. Control **50**, 805–823 (2003).
[24]C. Dorme and M. Fink, "Focusing in the transmit-receive mode through inhomogeneous media: The matched filter approach," J. Acoust. Soc. Am. **98**, 1155–1161 (1995).
[25]K.-S. Kim, J. Liu, and M. F. Insana, "Efficient array beam forming by spatial filtering for ultrasound B-mode imaging," J. Acoust. Soc. Am. **120**, 852–861 (2006).
[26]J. Schmolke, D. Hiller, H. Ermert, J. O. Schaefer, and G. Grabner, "Generation of optimal input signals for ultrasound pulse-echo system," Proc.-IEEE Ultrason. Symp. 929–934 (1982).
[27]E. S. Ebbini and C. A. Cain, "Multiple-focus ultrasound phased-array pattern synthesis: Optimal driving-signal distributions for hyperthermia," IEEE Trans. Ultrason. Ferroelectr. Freq. Control **36**, 540–548 (1989).
[28]K. Ranganathan and W. F. Walker, "A novel beamformer design method for medical ultrasound. I. Theory," IEEE Trans. Ultrason. Ferroelectr. Freq. Control **50**, 15–24 (2003).
[29]J. Shen and E. Ebbini, "A new coded-excitation ultrasonic imaging system I. Basic principles," IEEE Trans. Ultrason. Ferroelectr. Freq. Control **43**, 131–140 (1996).
[30]F. Lingvall, T. Olofsson, and T. Stepinski, "Synthetic aperture imaging using sources with finite aperture: Deconvolution of the spatial impulse response," J. Acoust. Soc. Am. **114**, 225–234 (2003).
[31]B. Haider, P. A. Levin, and K. Thomenious, "Pulse elongation and deconvolution filtering for medical ultrasonic imaging," IEEE Trans. Ultrason. Ferroelectr. Freq. Control **45**, 98–113 (1998).
[32]G. E. Tupholme, "Generation of acoustic pulses by baffled plane pistons," Mathematika **16**, 209–224 (1969).
[33]P. R. Stepanishen, "Transient radiation fom pistons in an infinite planar baffle," J. Acoust. Soc. Am. **49**, 1629–1638 (1971).
[34]T. Olofsson and E. Wennerström, "Sparse deconvolution of B-scan image," IEEE Trans. Ultrason. Ferroelectr. Freq. Control **54**, 1634–1641 (2007).
[35]S. M. Kay, *Fundamantals of Statistical Signal Processing: Estimation Theory* (Prentice Hall, Englewood Cliffs, NJ, 1993), Vol. 1.
[36]F. Lingvall and B. Piwakowski, "The DREAM Toolbox: An open source toolbox for MATLAB and OCTAVE for simulating acoustic fields radiated from common ultrasonic transducer types and arbitrarily complicated ultrasonic transducers arrays," 2007, available online at: http://www.signal.uu.se/Toolbox/dream/ (last viewed 7 January 2008).
[37]B. Piwakowski and K. Sbai, "A new approach to calculate the field radiated from arbitrarily structured transducer arrays," IEEE Trans. Ultrason. Ferroelectr. Freq. Control **46**, 422–440 (1999).
[38]R. A. Horn and C. R. Johnson, *Matrix Analysis* (Cambridge University Press, Cambridge, 1985).
[39]R. K. Mehra, "Optimal input signals for parameter estimation in dynamical systems—Survey and new results," IEEE Trans. Autom. Control **29**, 753–768 (1974).
[40]G. C. Goodwin and R. L. Payne, *Dynamical System Identification: Experiment Design and Data Analysis* (Academic, New York, 1977).
[41]J. C. Lockwood and J. G. Willette, "High-speed method for computing the exact solution for the pressure variations in the nearfield of a baffled piston," J. Acoust. Soc. Am. **53**, 735–741 (1973).
[42]G. C. Goodwin, "Identification: Experimental design," in *Encyclopedia of Systems and Control*, edited by M. Singh (Pergamon, New York 1987), pp. 2257–2264.
[43]E. T. Jaynes, "Detection of extra-solar-system planets," in *Maximum-Entropy and Bayesian Methods in Science and Engineering* (Kluwer, Dordrecht, 1988).
[44]G. E. Trahey and L. F. Nock, "Synthetic receive aperture imaging with phase correction for motion and for tissue inhomogeneities. II. Effects of and correction for motion," IEEE Trans. Ultrason. Ferroelectr. Freq. Control **39**, 496–501 (1992).

Sparsity constrained deconvolution approaches for acoustic source mapping

Tarik Yardibi and Jian Li[a)]
Department of Electrical and Computer Engineering, University of Florida, Gainesville, Florida, 32611

Petre Stoica
Department of Information Technology, Uppsala University, P.O. Box 337, SE-751 05 Uppsala, Sweden

Louis N. Cattafesta III
Department of Mechanical and Aerospace Engineering, University of Florida, Gainesville, Florida, 32611

(Received 2 November 2007; revised 11 February 2008; accepted 14 February 2008)

Using microphone arrays for estimating source locations and strengths has become common practice in aeroacoustic applications. The classical delay-and-sum approach suffers from low resolution and high sidelobes and the resulting beamforming maps are difficult to interpret. The deconvolution approach for the mapping of acoustic sources (DAMAS) deconvolution algorithm recovers the actual source levels from the contaminated delay-and-sum results by defining an inverse problem that can be represented as a linear system of equations. In this paper, the deconvolution problem is carried onto the sparse signal representation area and a sparsity constrained deconvolution approach (SC-DAMAS) is presented for solving the DAMAS inverse problem. A sparsity preserving covariance matrix fitting approach (CMF) is also presented to overcome the drawbacks of the DAMAS inverse problem. The proposed algorithms are convex optimization problems. Our simulations show that CMF and SC-DAMAS outperform DAMAS and as the noise in the measurements increases, CMF works better than both DAMAS and SC-DAMAS. It is observed that the proposed algorithms converge faster than DAMAS. A modification to SC-DAMAS is also provided which makes it significantly faster than DAMAS and CMF. For the correlated source case, the CMF-C algorithm is proposed and compared with DAMAS-C. Improvements in performance are obtained similar to the uncorrelated case.
© *2008 Acoustical Society of America.* [DOI: 10.1121/1.2896754]

PACS number(s): 43.60.Fg, 43.60.Jn, 43.60.Pt, 43.60.Mn [EJS] Pages: 2631–2642

I. INTRODUCTION

Microphone arrays have become an important element of aeroacoustic testing in recent years. These arrays can be electronically steered into desired regions in space to create an image of acoustic sources at a given frequency. This image consists of the sound pressure levels of each location in the region of interest.[1,2] Perhaps, the most commonly used beamforming algorithm in practice is the delay-and-sum beamformer,[1,3] which basically sums the delayed and weighted versions of each microphone signal so that the actual source signals are reinforced and the unwanted noise signals tend to cancel.

A well-known issue with the classical delay-and-sum approach is that the beamforming maps are usually contaminated by large sidelobes. Sidelobes can cause both the *smearing* and *leakage* of the sources.[4] Consider a scenario with two closely spaced sources so that the response of the array to the first source does not wither away before the response to the second source starts. This will result in the smoothing, or smearing, of the spectrum in the sense that the two peaks will be merged into a single broad peak. Looking from a different perspective, a strong source can yield power at other locations, where no source is present, through the convolution with the sidelobes. This latter form of degradation is called leakage. Therefore, it is usually difficult to identify the true source locations and strengths through the beamforming map obtained via the delay-and-sum method. Another problem with this method is that the beamwidth tends to increase with decreasing frequency.

Various other microphone array processing methods have been developed in order to mitigate the drawbacks of the delay-and-sum beamformer. Weighting schemes that maintain a constant beamwidth over a frequency range for the delay-and-sum beamformer have been discussed in the literature.[5,6] Also, several robust adaptive beamforming techniques have been proposed as alternatives to the delay-and-sum method.[7–9] The latter two of these techniques[8,9] are parametric approaches that require the number of sources to be known. Capon type beamformers cannot provide a sparse representation of the imaging scene and fail to work for coherent sources.[7]

In order to remedy the sidelobe problem of the delay-and-sum method, a postprocessing technique called the deconvolution approach for the mapping of acoustic sources (DAMAS) was developed.[10,11] This approach is considered a breakthrough in the area of aeroacoustic noise measurement

[a)]Author to whom correspondence should be addressed. Current address: Department of Electrical and Computer Engineering, P.O. Box 116130, University of Florida, Gainesville, FL 32611. Electronic mail: li@dsp.ufl.edu

and has been used widely in practice. DAMAS solves an inverse problem using the known steering vectors to decouple the actual source powers from the array characteristics based on the incoherence assumption of the noise sources. This inverse model can be written in a linear matrix equation form which, due to the structure of the matrices, cannot be solved easily. DAMAS uses an iterative scheme for solving this inverse problem. Many other algorithms related to DAMAS have been proposed in the literature.[12] LORE[13] is a deconvolution method that uses a two stage process to solve the inverse problem. In the first step a method similar to DAMAS is used to reduce the problem dimensions and in the second step an optimization scheme is used to solve the reduced inverse problem. DAMAS2 and DAMAS3[14] offer alternatives and extensions to DAMAS by using FFT and assuming that the point spread function is shift-invariant. DAMAS-C[15] extends DAMAS to the coherent sources case. Although requiring high computational resources, this approach is the first deconvolution algorithm considering correlated sources. DAMAS has also been applied to the three-dimensional source localization problem.[16]

In this paper, we introduce new approaches for solving the inverse problem for deconvolution via exploiting sparse signal representations. The sparse signal representation is extensively studied in many areas including statistics and signal processing for the recovery of signals consisting of only few nonzero elements with a known linear relation to the measured data. The sparse signal representation problem mainly aims to find the sparsest $\mathbf{x}$ such that $\mathbf{y}=\mathbf{A}\mathbf{x}$ is satisfied. Stated more formally, the objective is to minimize $\|\mathbf{x}\|_0$ such that $\mathbf{y}=\mathbf{A}\mathbf{x}$ where $\mathbf{A}$ is known and $\mathbf{y}$ is measured. The problem in its original form is a combinatorial problem and has an exponential complexity making it impractical.[17] Fortunately, when $\mathbf{x}$ is sufficiently sparse,[17] $\|\mathbf{x}\|_0$ can be replaced by $\|\mathbf{x}\|_1$ which leads to a convex optimization problem that can be solved much more easily using LASSO[18] or BP.[19] There are many works in the literature elaborating on this relaxation from the ℓ_0 norm to the ℓ_1 norm both in the noiseless and noisy case.[17,20–22] In a nutshell, when $\mathbf{x}$ contains a small number of nonzero elements with respect to its size, the solutions with the ℓ_0 and ℓ_1 norms coincide under some mild conditions. Alternatively, FOCUSS[23] can be used to iteratively solve the sparse problem. This method requires proper initialization of $\mathbf{x}$. Nevertheless, FOCUSS algorithms have been successfully applied to brain (EEG) signals and far field source localization problems. A Bayesian approach can also be used to estimate $\mathbf{x}$ using various prior probability distributions to enforce sparsity. Although these approaches do not require a user parameter,[24–26] they still need some kind of initialization. Note that LASSO can also be thought of as a Bayesian approach assuming a Gaussian likelihood for $\mathbf{y}$ and a Laplacian prior for $\mathbf{x}$ which is known to enforce sparsity. Another algorithm, the ℓ_1-SVD algorithm,[27] is proposed for estimating source locations in a manner similar to BP but for the multiple snapshot and complex case. The algorithm requires an initial estimate for the number of sources. Although this estimate does not have to be exact, a small error is required for good performance. Also, the algorithm has a user parameter whose selection is not trivial. Note that this method is designed to work with the time signals. In aeroacoustic applications, however, huge amounts of time data are collected and it is preferred to work with the covariance matrix since it requires much less storage space and is more convenient to deal with. Finally, Fuchs[28] also discusses methods for the recovery of source locations for the far-field linear array case by appending a noise basis vector to the steering matrix and using deconvolution together with sparsity. It is interesting to note that these approaches in the signal processing literature are similar to DAMAS. Fuchs also provides an extension to his method by using a uniform circular array and a sparse algorithm similar to BP.[29] In this method, the user parameter is selected to be a constant, which can introduce errors.

The remainder of this paper is organized as follows. In Sec. II we parametrize the aeroacoustic source localization problem. After reviewing DAMAS in Sec. III, we describe the sparsity constrained DAMAS algorithm (SC-DAMAS), which is an application of LASSO to the specific inverse problem of DAMAS, in Sec. IV. In contrast to selecting a constant,[29] the user parameter of the algorithm is selected by an adaptive and simple method which uses the eigenvalues of the sample covariance matrix. We also discuss a way to significantly speed up SC-DAMAS. Next in Sec. V, we propose another algorithm called the covariance matrix fitting (CMF) which also exploits sparsity for deconvolution but in a different way than the DAMAS formulation. Both of the algorithms are formulated as convex optimization problems and only use the sample covariance matrix. These algorithms are guaranteed to converge to the globally optimal solution and they take less computation time than DAMAS. The CMF algorithm is more robust to noise than both DAMAS and SC-DAMAS. In Sec. VI, we extend our analysis to deal with correlated sources. We propose CMF-C, which is an extension of CMF to the correlated signals case, and compare it with DAMAS-C. The performance of the algorithms is evaluated using synthetic data for various scenarios in Sec. VIII. The simulation results show that the proposed algorithms can be directly employed in aeroacoustic applications due to their simplicity and good performance. Finally, we conclude the paper in Sec. VIII.

II. PROBLEM FORMULATION

Consider the wave field generated by K near-field wideband sources located at $\mathbf{x}$ where $\mathbf{x}\triangleq[\mathbf{x}_1,\mathbf{x}_2,\ldots,\mathbf{x}_K]$ and $\mathbf{x}_k$ is the three-dimensional location of signal k, $k=1,\ldots,K$. At the pre-processing stage, the time data of each microphone is divided into I segments where each segment consists of L time samples. Each segment of data is then converted into L narrow frequency bins by the L-point discrete Fourier transform (or FFT). In this case, the $M\times 1$ array output vector of an M element microphone array in the presence of additive noise can be represented as,[4,30]

$$\mathbf{y}_i(\omega_l)=\mathbf{A}(\mathbf{x},\omega_l)\mathbf{s}_i(\omega_l)+\mathbf{e}_i(\omega_l),\quad i=1,\ldots,I, \tag{1}$$

for $l=1,\ldots,L$, where $\mathbf{A}$ is the $M\times K$ steering matrix defined as $\mathbf{A}(\mathbf{x},\omega_l)\triangleq[\mathbf{a}(\mathbf{x}_1,\omega_l),\mathbf{a}(\mathbf{x}_2,\omega_l),\ldots,\mathbf{a}(\mathbf{x}_K,\omega_l)]$ and the signal wave forms of the sources are given by

$\mathbf{s}_i(\omega_l) \triangleq [s_{i,1}(\omega_l), s_{i,2}(\omega_l), \ldots, s_{i,K}(\omega_l)]^T$, $i=1,\ldots,I$. The elements of $\mathbf{e}_i(\omega_l)$ and $\mathbf{s}_i(\omega_l)$ are assumed to be independent zero mean random variables for $i=1,\ldots,I$.

The steering vector for source k is

$$\mathbf{a}(\mathbf{x}_k,\omega_l) = \frac{1}{C(k,l)} \begin{bmatrix} \frac{1}{x_{1,k}} e^{-j\omega_l x_{1,k}/c_0} \\ \vdots \\ \frac{1}{x_{M,k}} e^{-j\omega_l x_{M,k}/c_0} \end{bmatrix} = \frac{\bar{\mathbf{a}}(\mathbf{x}_k,\omega_l)}{C(k,l)}, \tag{2}$$

where $x_{m,k}$ is the distance between the mth microphone and the kth source and $C(k,l)=\|\bar{\mathbf{a}}(\mathbf{x}_k,\omega_l)\|_2$, i.e., $C(k,l)$ is a constant used to normalize the columns of $\mathbf{A}(\mathbf{x}_k,\omega_l)$. Note that this does not restrict the following analysis in any way.

The sample covariance matrix, or the cross spectral matrix, for a given ω_l, $l=1,\ldots,L$, is calculated as

$$\hat{\mathbf{R}}(\omega_l) = \frac{1}{I}\sum_{i=1}^{I} \mathbf{y}_i(\omega_l)\mathbf{y}_i^H(\omega_l). \tag{3}$$

The problem is to estimate the power levels of the sources $\tilde{x}_k(\mathbf{x}_k,\omega_l)=(1/I)\Sigma_{i=1}^{I}|s_{i,k}(\omega_l)|^2$, for $l=1,\ldots,L$, $k=1,\ldots,K$, and their locations $\mathbf{x}$ from the observed data $\mathbf{y}_i(\omega_l)$, $l=1,\ldots,L$, $i=1,\ldots,I$.

The delay-and-sum beamformer output power at a given location $\mathbf{x}'$ and angular frequency ω_l, $l=1,\ldots,L$, is computed as

$$\tilde{y}(\mathbf{x}',\omega_l) = \frac{1}{M^2}\tilde{\mathbf{a}}^H(\mathbf{x}',\omega_l)\hat{\mathbf{R}}(\omega_l)\tilde{\mathbf{a}}(\mathbf{x}',\omega_l), \tag{4}$$

where,

$$\tilde{\mathbf{a}}(\mathbf{x}_k,\omega_l) = C(k,l)\begin{bmatrix} x_{1,k}e^{-j\omega_l x_{1,k}/c_0} \\ \vdots \\ x_{M,k}e^{-j\omega_l x_{M,k}/c_0} \end{bmatrix}. \tag{5}$$

In aeroacoustic noise measurement applications, the power levels are usually calculated separately for each frequency bin l, $l=1,\ldots,L$, and hence in the sequel ω_l will be dropped from the notation for simplicity.

III. REVIEW OF DAMAS

In this section, the inverse equation solved in DAMAS will be obtained from a slightly different perspective than the derivation in the original paper.[11] DAMAS uses the delay-and-sum beamformer results to obtain the deconvolved source strengths. Hence, substituting Eqs. (1) and (3) in Eq. (4) and dropping the $\mathbf{x}'$ term from $\tilde{\mathbf{a}}$, for notational simplicity, we obtain

$$\begin{aligned}\tilde{y} &= \frac{1}{M^2}\tilde{\mathbf{a}}^H\left[\mathbf{A}(\mathbf{x})\left(\frac{1}{I}\sum_{i=1}^{I}\mathbf{s}_i\mathbf{s}_i^H\right)\mathbf{A}^H(\mathbf{x}) + \sigma^2\mathbf{I}\right]\tilde{\mathbf{a}} \\ &= \frac{1}{M^2}\tilde{\mathbf{a}}^H\left[\frac{1}{I}\sum_{i=1}^{I}[\mathbf{a}(\mathbf{x}_1)s_{i,1} + \cdots + \mathbf{a}(\mathbf{x}_K)s_{i,K}][\mathbf{a}(\mathbf{x}_1)s_{i,1} \right. \\ &\quad \left. + \cdots + \mathbf{a}(\mathbf{x}_K)s_{i,K}]^H + \sigma^2\mathbf{I}\right]\tilde{\mathbf{a}}. \end{aligned} \tag{6}$$

The cross terms in Eq. (6) are assumed to be negligible which is a resonable assumption when $I \gg 1$. In DAMAS, this expression is approximated by also neglecting the noise term to obtain

$$\begin{aligned}\tilde{y}(\mathbf{x}') &= \frac{1}{M^2}\tilde{\mathbf{a}}^H(\mathbf{x}')\left[\sum_{k=1}^{K}\frac{1}{I}\sum_{i=1}^{I}|s_{i,k}|^2\mathbf{a}(\mathbf{x}_k)\mathbf{a}^H(\mathbf{x}_k)\right]\tilde{\mathbf{a}}(\mathbf{x}') \\ &= \sum_{k=1}^{K}\tilde{A}_k(\mathbf{x}')\tilde{x}(\mathbf{x}_k), \end{aligned} \tag{7}$$

where $\tilde{x}(\mathbf{x}_k) \triangleq (1/I)\Sigma_{i=1}^{I}|s_{i,k}|^2$ and

$$\tilde{A}_k(\mathbf{x}') = \frac{1}{M^2}|\tilde{\mathbf{a}}^H(\mathbf{x}')\mathbf{a}(\mathbf{x}_k)|^2, \quad k=1,\ldots,K. \tag{8}$$

Usually, the number of sources, K, is unknown and is replaced by N, which is the number of scanning points in the region. Also, $\mathbf{x}$ and $\mathbf{x}'$ are scanned over the same set of grid points for simplicity assuming that a certain minimum desired resolution is satisfied. If the power at each scanning point is stacked up to form a power vector $\tilde{\mathbf{y}}$, we arrive at

$$\begin{bmatrix} \tilde{y}(\mathbf{x}_1) \\ \tilde{y}(\mathbf{x}_2) \\ \vdots \\ \tilde{y}(\mathbf{x}_N) \end{bmatrix} = \begin{bmatrix} \tilde{A}_1(\mathbf{x}_1) & \tilde{A}_2(\mathbf{x}_1) & \cdots & \tilde{A}_N(\mathbf{x}_1) \\ \tilde{A}_1(\mathbf{x}_2) & \tilde{A}_2(\mathbf{x}_2) & \cdots & \tilde{A}_N(\mathbf{x}_2) \\ \vdots & \vdots & \ddots & \vdots \\ \tilde{A}_1(\mathbf{x}_N) & \tilde{A}_2(\mathbf{x}_N) & \cdots & \tilde{A}_N(\mathbf{x}_N) \end{bmatrix} \begin{bmatrix} \tilde{x}(\mathbf{x}_1) \\ \tilde{x}(\mathbf{x}_2) \\ \vdots \\ \tilde{x}(\mathbf{x}_N) \end{bmatrix}, \tag{9}$$

or $\tilde{\mathbf{y}}=\tilde{\mathbf{A}}\tilde{\mathbf{x}}$, each term of which can be expressed as

$$\tilde{y}_n = \tilde{A}_{n,1}\tilde{x}_1 + \tilde{A}_{n,2}\tilde{x}_2 + \cdots + \tilde{A}_{n,N}\tilde{x}_N, \tag{10}$$

where $n=1,\ldots,N$. The solution for $\tilde{\mathbf{x}}$ can be obtained by using the Gauss–Seidel method and noting that $\tilde{A}_{nn}=1$, from the definition of $\tilde{\mathbf{A}}$, as follows:

$$\tilde{x}_n^{(k)} = \max\left(0, \tilde{y}_n - \left[\sum_{j=1}^{n-1}\tilde{A}_{nj}\tilde{x}_j^{(k)} + \sum_{j=n+1}^{N}\tilde{A}_{nj}\tilde{x}_j^{(k-1)}\right]\right), \tag{11}$$

where k is the current iteration number limited above by a user defined maximum number of iterations, $\tilde{\mathbf{x}}^{(0)}=\mathbf{0}$ and the positivity of every element of $\tilde{\mathbf{x}}$ is enforced since $\tilde{\mathbf{x}}$ represents power.

The major drawbacks of this algorithm may be summarized as follows. First of all, neglecting the noise term in Eq. (7) introduces a modeling error since, in almost all practical cases, some kind of noise will contaminate the data. Second, the algorithm requires many iterations, on the order of thousands, to give reasonable results, which can become very time consuming depending on the resolution, i.e., the length of $\tilde{\mathbf{x}}$. Also, the delay-and-sum beamformer has to be implemented before using DAMAS which also means more processing time and effort. Finally, the Gauss–Seidel method is not guaranteed to converge unless $\tilde{\mathbf{A}}$ is diagonally dominant, i.e., for each row, the absolute value of the diagonal term is greater than the sum of absolute values of other terms which is usually not true.[12] Despite these drawbacks, the algorithm has been successfully employed in many practical applications.

Diagonal removal (DR). The first of the above-mentioned drawbacks can be overcome by the use of diagonal removal which eliminates the noise occurring in the diagonal of $\hat{\mathbf{R}}$ by removing the diagonal elements, i.e., making them zero.[2,10,11] In this case, the delay-and-sum output is calculated as

$$\tilde{y}^{\mathrm{DR}}(\mathbf{x}') = \frac{1}{M^2 - M}\tilde{\mathbf{a}}^H(\mathbf{x}')\tilde{\mathbf{R}}\tilde{\mathbf{a}}(\mathbf{x}'), \tag{12}$$

where $\tilde{\mathbf{R}}$ is obtained by removing the diagonal elements of $\hat{\mathbf{R}}$. Then, $\tilde{\mathbf{y}}^{\mathrm{DR}} = \tilde{\mathbf{A}}^{\mathrm{DR}}\tilde{\mathbf{x}}$, where

$$\tilde{A}_k^{\mathrm{DR}}(\mathbf{x}') = \frac{1}{M^2 - M}\tilde{\mathbf{a}}^H(\mathbf{x}')[\mathbf{a}(\mathbf{x}_k)\mathbf{a}^H(\mathbf{x}_k)]_{\mathrm{diag.}=0}\tilde{\mathbf{a}}^H(\mathbf{x}'), \tag{13}$$

for $k = 1, \ldots, K$.

In the rest of the paper, DAMAS is applied with diagonal removal in all cases. Otherwise, the performance becomes worse as σ^2 increases. Consequently, we will denote $\tilde{\mathbf{y}}^{\mathrm{DR}}$ and $\tilde{\mathbf{A}}^{\mathrm{DR}}$ as $\tilde{\mathbf{y}}$ and $\tilde{\mathbf{A}}$, respectively, in order to simplify the notation.

IV. SPARSITY CONSTRAINED DAMAS (SC-DAMAS)

A. Sparsity constrained formulation

Assume that a measured vector $\tilde{\mathbf{y}}$ exists which is known to satisfy the linear relation $\tilde{\mathbf{y}} = \tilde{\mathbf{A}}\tilde{\mathbf{x}}$ where $\tilde{\mathbf{A}}$ is known and $\tilde{\mathbf{x}}$ is an unknown quantity that is to be estimated, see Eq. (9). In its simplest form, sparse modeling can be stated as follows:

$$\text{minimize } \|\tilde{\mathbf{x}}\|_0 \text{ subject to } \tilde{\mathbf{y}} = \tilde{\mathbf{A}}\tilde{\mathbf{x}}. \tag{14}$$

Usually, this problem is a combinatorial problem which becomes intractable quickly as the dimension of $\tilde{\mathbf{x}}$ increases.[17] If the solution is sufficiently sparse, the ℓ_0 norm can be replaced with the ℓ_1 norm to make the problem convex.[17] The important point in Eq. (14) is that the matrix $\tilde{\mathbf{A}}$ is usually ill conditioned and not invertible. Otherwise, the solution could be obtained by taking the inverse, had $\tilde{\mathbf{A}}$ been a square matrix, or by the least-squares method otherwise.

Following the above-presented discussion, the problem in Eq. (9) is directly applicable in the sparse signal representation context by observing that $\tilde{\mathbf{x}}$ is sparse due to replacing K by N in Eq. (9) and noting that $N \gg K$. In other words, since $\tilde{\mathbf{A}}$ contains all the scanning points and only a small portion of the region is expected to possess strong sources, $\tilde{\mathbf{x}}$ will contain few nonzero elements with respect to its size. Thus, we can immediately think of applying a slightly modified version of LASSO[18] to this problem,

$$\begin{aligned} &\text{minimize} \quad \|\tilde{\mathbf{y}} - \tilde{\mathbf{A}}\tilde{\mathbf{x}}\|_2^2, \\ &\text{subject to} \quad \|\tilde{\mathbf{x}}\|_1 \leqslant \lambda, \quad \tilde{x}_n \geqslant 0, \quad n = 1, \ldots, N, \end{aligned} \tag{15}$$

where the modification is to enforce every element of $\tilde{\mathbf{x}}$ to be positive. Here, the user parameter λ is unknown and has to be empirically tuned or estimated from the observation vector $\tilde{\mathbf{y}}$ and $\tilde{\mathbf{A}}$. The following section describes a simple method for choosing the parameter λ automatically. Also, it is empirically observed that the method in Eq. (15) is not very sensitive to the selection of λ. In fact, if we let $\lambda \to \infty$, the formulation will reduce to a non-negative least-squares problem. However, using prior knowledge about the sparsity of $\tilde{\mathbf{x}}$ will improve the estimate in most cases. The problem in Eq. (15) is a quadratic convex optimization problem which can be solved efficiently via readily available interior point methods[31,32] to find the globally optimal solution for $\tilde{\mathbf{x}}$. *Self-Dual Minimization*[31] is an extensively used software package in the signal processing community for solving optimization problems over symmetric cones including linear, quadratic, second-order conic and semidefinite programs. The detailed discussion of advanced optimization methods is beyond the scope of this paper and the interested reader is referred to a text on convex optimization.[33]

B. Estimating the user parameter

In the formulation Eq. (15), λ constrains the ℓ_1 norm of $\tilde{\mathbf{x}}$, which represents the total power of the signals. Since this value is unknown, a way of determining λ has to be found for practicality. Let

$$\mathbf{R} = E\{\mathbf{y}_i\mathbf{y}_i^H\} = \mathbf{A}\mathbf{D}\mathbf{A}^H + \sigma^2\mathbf{I}, \tag{16}$$

where $\mathbf{D} = E\{\mathbf{s}_i\mathbf{s}_i^H\}$, which is a diagonal matrix for uncorrelated sources, is given by

$$\mathbf{D} = \begin{bmatrix} d_1 & 0 & \cdots & 0 \\ 0 & d_2 & \cdots & 0 \\ \vdots & \vdots & \ddots & \vdots \\ 0 & 0 & \cdots & d_K \end{bmatrix}, \tag{17}$$

where d_k, $k = 1, \ldots, K$ is the power of the kth source. The eigendecomposition of $\mathbf{A}\mathbf{D}\mathbf{A}^H$ can be written as $\mathbf{A}\mathbf{D}\mathbf{A}^H = \mathbf{U}\Lambda\mathbf{U}^H$, where the columns of the unitary matrix $\mathbf{U}$ denote the eigenvectors of $\mathbf{A}\mathbf{D}\mathbf{A}^H$ and the diagonal elements of the diagonal matrix Λ are the corresponding eigenvalues, denoted as $\lambda_1 \geqslant \lambda_2 \geqslant \cdots \geqslant \lambda_K \geqslant 0 = \cdots = 0$. Λ is an $M \times M$ matrix where $M \gg K$. Then, $\mathbf{R}$ can be written as

$$\mathbf{R} = \mathbf{U}(\Lambda + \sigma^2\mathbf{I})\mathbf{U}^H \triangleq \mathbf{U}\Gamma\mathbf{U}^H, \tag{18}$$

where the diagonal elements of the diagonal matrix Γ are $\gamma_1 \geqslant \gamma_2 \geqslant \cdots \geqslant \gamma_K \geqslant \sigma^2 = \cdots = \sigma^2$. Note that

$$\begin{aligned} \mathrm{Tr}(\Lambda) &= \mathrm{Tr}(\mathbf{U}\Lambda\mathbf{U}^H) = \mathrm{Tr}(\mathbf{A}\mathbf{D}\mathbf{A}^H) = \mathrm{Tr}(\mathbf{D}\mathbf{A}^H\mathbf{A}) = \mathrm{Tr}(\mathbf{D}) \\ &= \sum_{k=1}^{K} d_k, \end{aligned} \tag{19}$$

which is the total power of the sources. Here, we have used the fact that the columns in $\mathbf{A}$ have unit norm and $\mathbf{D}$ is diagonal.

In practice, we only have the estimated covariance matrix given in Eq. (3) instead of the true covariance matrix $\mathbf{R}$. Let $\hat{\mathbf{R}} = \hat{\mathbf{U}}\hat{\Gamma}\hat{\mathbf{U}}^H$ denote the eigendecomposition of $\hat{\mathbf{R}}$ with the eigenvalues of $\hat{\mathbf{R}}$, i.e., the diagonal elements of $\hat{\Gamma}$, arranged in nonincreasing order. Then, we can determine the user parameter λ in Eq. (15) as

$$\lambda = \mathrm{Tr}(\hat{\boldsymbol{\Gamma}} - \hat{\gamma}_M \mathbf{I}), \tag{20}$$

where $\hat{\gamma}_M$ is the smallest diagonal element of $\hat{\boldsymbol{\Gamma}}$. We refer to the approach of solving Eq. (15) using the λ determined in Eq. (20) as the sparsity constrained DAMAS (SC-DAMAS). We will show using numerical examples that SC-DAMAS is computationally more efficient than DAMAS. Note that, SC-DAMAS also uses the diagonal removal approach described for DAMAS.

C. A more efficient implementation of SC-DAMAS

The delay-and-sum estimate $\tilde{\mathbf{y}}$ usually contains redundant information due to its wide beamwidth. Therefore, it is not always necessary to beamform at all N locations in the region when using SC-DAMAS. Beamforming at fewer points reduces the size of $\tilde{\mathbf{y}}$ and increases the speed of SC-DAMAS. In this case, Eq. (9) becomes

$$\begin{bmatrix} \tilde{y}(\mathbf{x}_1) \\ \tilde{y}(\mathbf{x}_2) \\ \vdots \\ \tilde{y}(\mathbf{x}_{N_0}) \end{bmatrix} = \begin{bmatrix} \tilde{A}_1(\mathbf{x}_1) & \tilde{A}_2(\mathbf{x}_1) & \cdots & \tilde{A}_N(\mathbf{x}_1) \\ \tilde{A}_1(\mathbf{x}_2) & \tilde{A}_2(\mathbf{x}_2) & \cdots & \tilde{A}_N(\mathbf{x}_2) \\ \vdots & \vdots & \ddots & \vdots \\ \tilde{A}_1(\mathbf{x}_{N_0}) & \tilde{A}_2(\mathbf{x}_{N_0}) & \cdots & \tilde{A}_N(\mathbf{x}_{N_0}) \end{bmatrix} \begin{bmatrix} \tilde{x}(\mathbf{x}_1) \\ \tilde{x}(\mathbf{x}_2) \\ \vdots \\ \tilde{x}(\mathbf{x}_N) \end{bmatrix}, \tag{21}$$

where $N_0 < N$. Note that $\tilde{\mathbf{A}}$ has become a fat matrix, i.e., the number of its rows is smaller than the number of its columns. It will be shown in Sec. VII that this approach can save a significant amount of computation time without degrading the performance. A similar approach cannot be used with DAMAS since DAMAS requires N equations to solve for the N unknowns in $\tilde{\mathbf{x}}$. Formulating the same problem as a sparse problem alleviates the need for N equations.

V. COVARIANCE MATRIX FITTING

Instead of using the sample covariance matrix to obtain delay-and-sum estimates and then trying to deconvolve the results, we introduce a method for estimating source locations and strengths based directly on the sample covariance matrix in Eq. (3) and the steering vector in Eq. (2). Specifically, the covariance matrix fitting approach determines σ_0^2 and $\{d_n\}_{n=1}^N$ via

$$\begin{aligned} &\text{minimize}_{\{d_n\}_{n=1}^N, \sigma^2} \quad \|\hat{\mathbf{R}} - \mathbf{A}\mathbf{D}\mathbf{A}^H - \sigma^2 \mathbf{I}\|_F^2, \\ &\text{subject to} \quad d_n \geqslant 0, \quad n = 1, \ldots, N, \quad \sum_{n=1}^{N} d_n \leqslant \lambda, \\ &\qquad\qquad \sigma^2 \geqslant 0, \end{aligned} \tag{22}$$

which is a quadratic convex optimization problem where λ is defined in Eq. (20), d_n is the noise power level for grid n, $n = 1, \ldots, N$, and $\mathbf{D}$ is an $N \times N$ diagonal matrix with $\{d_n\}_{n=1}^N$ as its diagonals, see Eq. (17). Also recall that $\mathbf{A} = [\mathbf{a}(\mathbf{x}_1), \mathbf{a}(\mathbf{x}_2), \ldots, \mathbf{a}(\mathbf{x}_N)]$. The idea behind this method is quite intuitive in the sense that it basically tries to fit the unknown signal powers and the noise power to the model in Eq. (16) such that the solution is sparse. In contrast to deleting the diagonals of $\hat{\mathbf{R}}$, this method tries to extract the noise and use the signal components in the diagonal. Moreover, this formulation does not require the implementation of the delay-and-sum beamformer as an initial step and it converges quickly thanks to the convex formulation. Similar to SC-DAMAS, this algorithm also turns out to be quite insensitive to λ.

VI. CORRELATED SOURCES

DAMAS, SC-DAMAS, and CMF algorithms all assume that the noise sources are uncorrelated so that the cross terms in Eq. (6) can be neglected. However, if the sources are correlated, this assumption no longer holds and the algorithms have to be modified to deal with this case. After briefly reviewing DAMAS-C[15] for completeness, we will introduce the extension of the CMF approach to the correlated case.

A. DAMAS-C

DAMAS-C extends DAMAS to deal with correlated signals.[15] Similar to DAMAS, this algorithm uses Eq. (6) but without ignoring the cross terms. In this case, we end up with $N(N+1)/2$ unknowns and thus have to evaluate the delay-and-sum beamformer at more points. For this purpose, the cross-beamformer output is[15]

$$\acute{y}(\mathbf{x}', \mathbf{x}'') = \frac{1}{M^2} \tilde{\mathbf{a}}^H(\mathbf{x}') \hat{\mathbf{R}} \tilde{\mathbf{a}}(\mathbf{x}''), \tag{23}$$

which is similar to Eq. (4). Then, the inverse problem can be defined as in the following:

$$\begin{bmatrix} \acute{y}(\mathbf{x}_1, \mathbf{x}_1) \\ \acute{y}(\mathbf{x}_1, \mathbf{x}_2) \\ \vdots \\ \acute{y}(\mathbf{x}_1, \mathbf{x}_N) \\ \acute{y}(\mathbf{x}_2, \mathbf{x}_1) \\ \vdots \\ \acute{y}(\mathbf{x}_N, \mathbf{x}_N) \end{bmatrix} = \begin{bmatrix} \acute{A}_{1,1}(\mathbf{x}_1, \mathbf{x}_1) & \cdots & \acute{A}_{1,N}(\mathbf{x}_1, \mathbf{x}_1) & \cdots & \acute{A}_{N,N}(\mathbf{x}_1, \mathbf{x}_1) \\ \acute{A}_{1,1}(\mathbf{x}_1, \mathbf{x}_2) & \cdots & \acute{A}_{1,N}(\mathbf{x}_1, \mathbf{x}_2) & \cdots & \acute{A}_{N,N}(\mathbf{x}_1, \mathbf{x}_2) \\ \vdots & \ddots & \vdots & \ddots & \vdots \\ \vdots & \ddots & \vdots & \ddots & \vdots \\ \acute{A}_{1,1}(\mathbf{x}_N, \mathbf{x}_N) & \cdots & \acute{A}_{1,N}(\mathbf{x}_N, \mathbf{x}_N) & \cdots & \acute{A}_{N,N}(\mathbf{x}_N, \mathbf{x}_N) \end{bmatrix} \begin{bmatrix} \acute{x}(\mathbf{x}_1, \mathbf{x}_1) \\ \acute{x}(\mathbf{x}_1, \mathbf{x}_2) \\ \vdots \\ \acute{x}(\mathbf{x}_1, \mathbf{x}_N) \\ \acute{x}(\mathbf{x}_2, \mathbf{x}_1) \\ \vdots \\ \acute{x}(\mathbf{x}_N, \mathbf{x}_N) \end{bmatrix}, \tag{24}$$

or

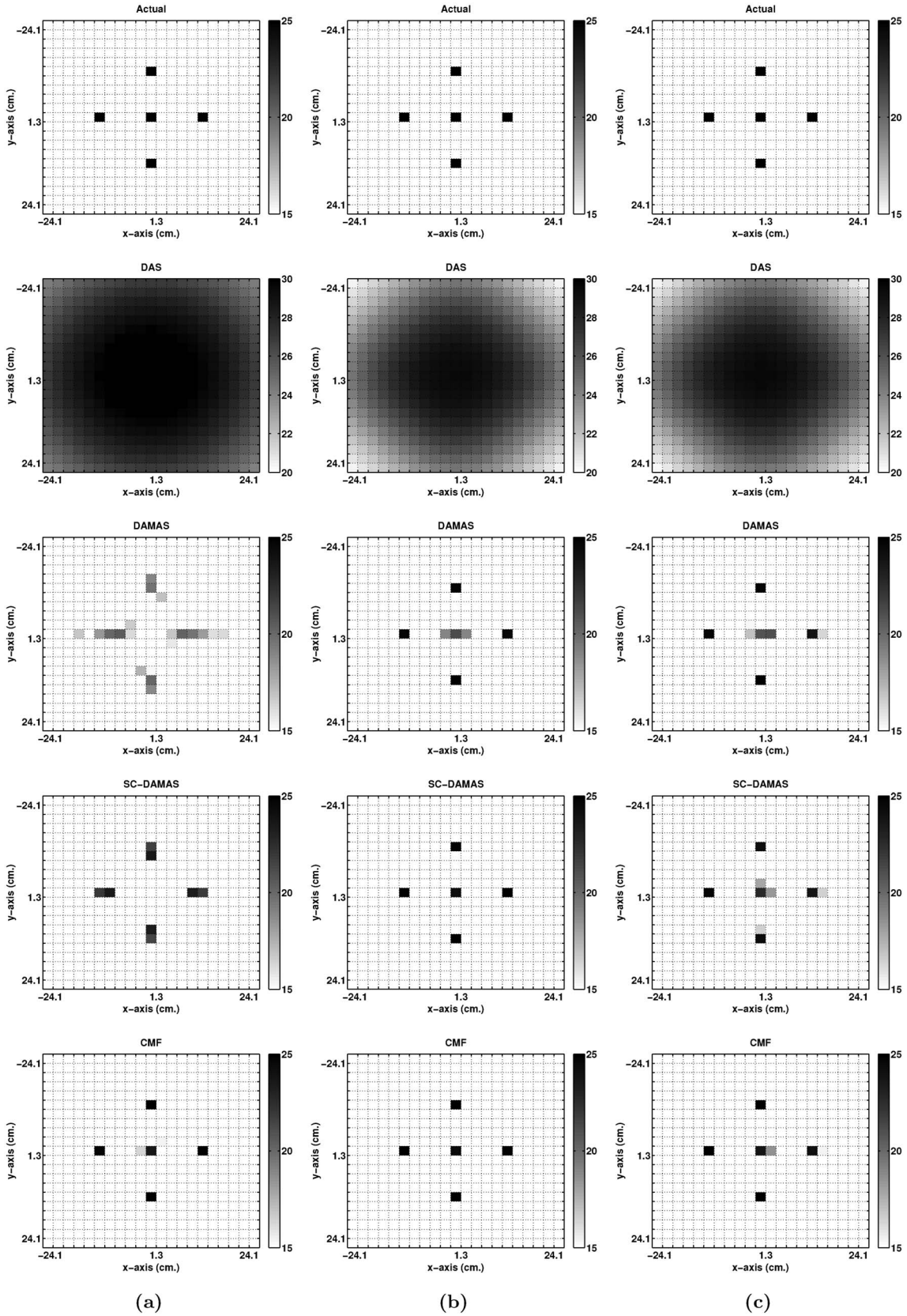
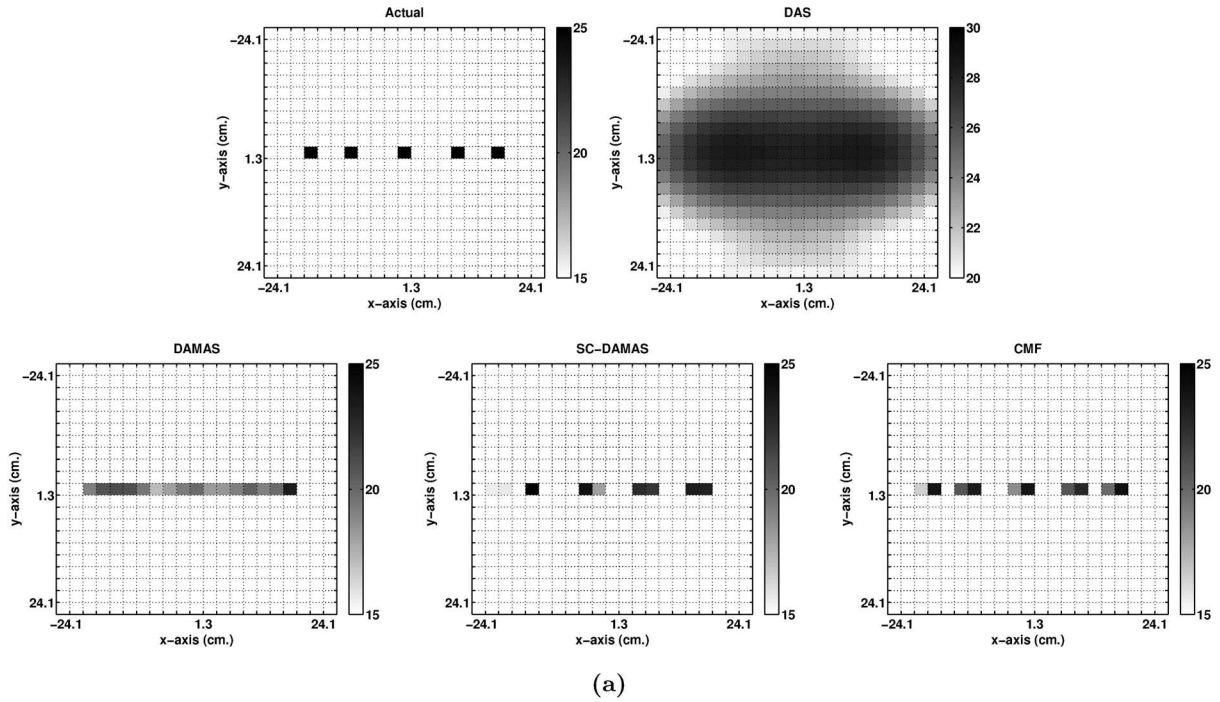


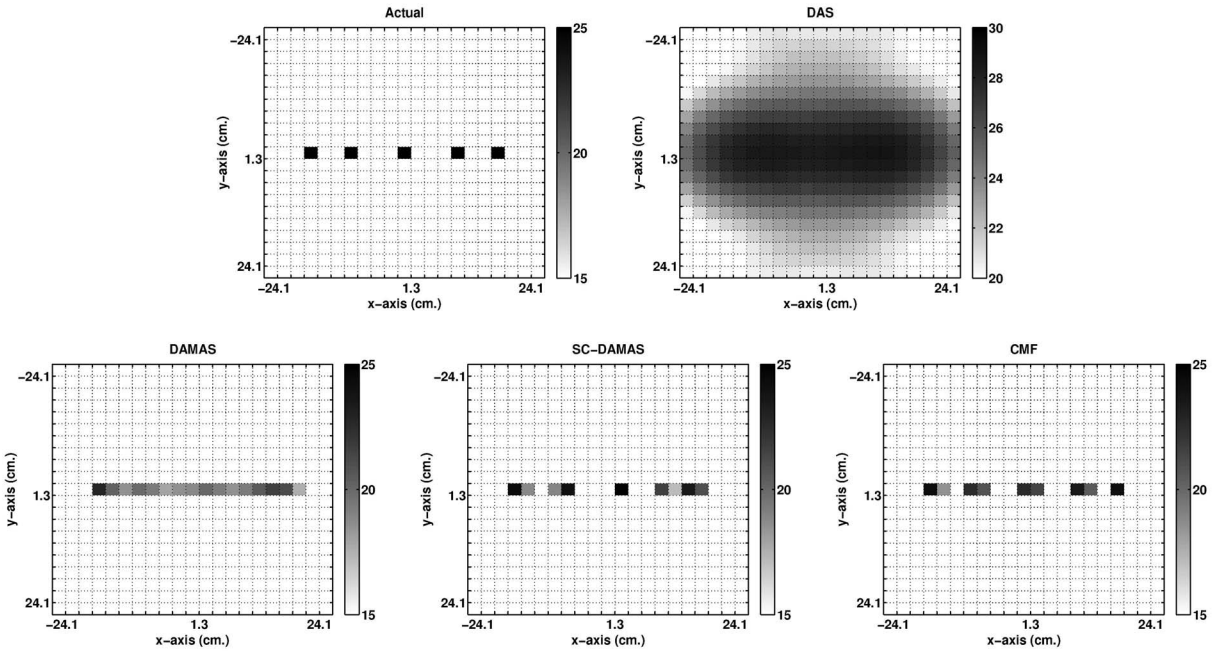
FIG. 1. The beamforming maps of the actual sources, DAS, DAMAS, SC-DAMAS, and CMF with three different settings as follows: $I=10\,000$, (a) $f=10$ kHz and $\sigma^2=0$, $f=15$ kHz: (b) $\sigma^2=0$, (c) $\sigma^2=100$. The 2D plots represent the beamforming area and the power levels are in decibels.

$$\acute{\mathbf{y}} = \acute{\mathbf{A}}\acute{\mathbf{x}}, \tag{25}$$

where $\acute{A}_{k,l}(\mathbf{x}',\mathbf{x}'')=(1/M^2)\tilde{\mathbf{a}}^H(\mathbf{x}')\mathbf{a}(\mathbf{x}_k)\mathbf{a}^H(\mathbf{x}_l)\tilde{\mathbf{a}}(\mathbf{x}'')$, $k,l=1,\ldots,K$. Although the derivation is straightforward, this equation is cumbersome. Note that the sizes of $\acute{\mathbf{y}}$, $\acute{\mathbf{A}}$, and $\acute{\mathbf{x}}$ are squares of the sizes of their uncorrelated counterparts $\tilde{\mathbf{y}}$, $\tilde{\mathbf{A}}$, and $\tilde{\mathbf{x}}$. This equation is solved for $\acute{\mathbf{x}}$ with a very similar



(a)



(b)

FIG. 2. The beamforming maps of the actual sources, DAS, DAMAS, SC-DAMAS, and CMF with two different settings as follows: $f=20$ kHz, $I=500$ and (a) $\sigma^2=0$, (b) $\sigma^2=5$. The 2D plots represent the beamforming area and the power levels are in decibels.

algorithm to DAMAS. Again, positivity is enforced as in Eq. (11). Yet, now there may be complex terms arising from the cross products and a suitable constraint has to be found for these terms too. The correlations are assumed to be in phase and real in DAMAS-C.[15] With this assumption, the positivity is enforced on every element of $\acute{\mathbf{x}}$, see Eq. (11), as the iterations proceed. As a final note, diagonal removal is also applied with DAMAS-C in our simulations.

B. CMF-C

The extension of CMF to the correlated case is as follows:

$$\text{minimize}_{\mathbf{D},\sigma^2} \quad \|\hat{\mathbf{R}} - \mathbf{A}\mathbf{D}\mathbf{A}^H - \sigma^2\mathbf{I}\|_F^2,$$

$$\text{subject to} \quad \mathbf{D} \geqslant 0, \quad \text{tr}(\mathbf{D}) \leqslant \lambda, \quad \sigma^2 \geqslant 0, \tag{26}$$

which looks simpler than the DAMAS-C formulation. Note that $\mathbf{D}$ is no longer a diagonal matrix and when the sources are uncorrelated, Eq. (26) reduces to the CMF formulation, Eq. (22). CMF-C is a semidefinite quadratic program and can also work with complex correlations between source signals in contrast to DAMAS-C. λ is determined as in Eq. (20).

Both CMF-C and DAMAS-C require extreme computation times as the number of grid points increases since the

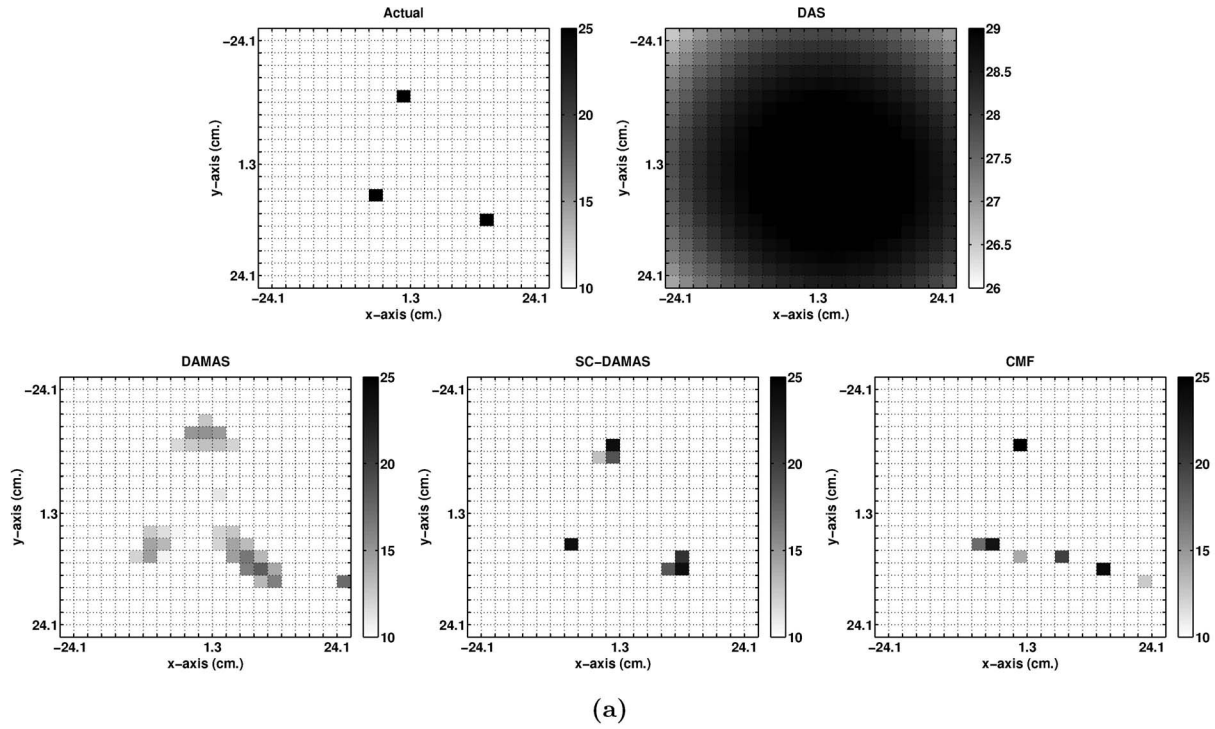


FIG. 3. The beamforming maps of the actual sources, DAS, DAMAS, SC-DAMAS, and CMF with two different settings as follows: $f=5$ kHz, $I=500$ and (a) $\sigma^2=0$, (b) $\sigma^2=4$. The 2D plots represent the beamforming area and the power levels are in decibels.

number of unknowns in both is approximately N^2. Nevertheless, a parallel implementation can make these algorithms usable in practice.[15] We will evaluate these algorithms only for a small grid size in Sec. VII. Note that a similar approach to SC-DAMAS can be used to solve the DAMAS-C problem given in Eq. (25) but this issue is not further explored here since our experience is that even in the uncorrelated case CMF usually results in better performance than SC-DAMAS. In results not shown here, it was observed that this is true in the correlated case, too.

VII. NUMERICAL EXAMPLES

In this section, we evaluate the performances of DAMAS, SC-DAMAS, and CMF for the SADA array.[1,34] SADA is a two-dimensional (2D) array consisting of 33 microphones and has a maximum diagonal aperture size of 19.71 cm. A microphone is located at the center and the others are arranged in four circles of eight microphones each where the diameter of each circle is twice the diameter of the circle it encloses. We assume that the SADA is at a distance

TABLE I. Characteristics of the acoustic imaging algorithms.

	DAS	DAMAS	SC-DAMAS	CMF
Resolution	Low	Medium	High	High
Sensitivity to noise	Low	Medium	Medium	Low
Computation Time	Low	High	Medium	Medium
Max. number of variables	High	Medium	Low	Low

of 1.52 m from the region of interest similar to the DAMAS paper.[10,11] The span for the x axes and y axes is from −25.4 to 25.4 cm and the resolution in both directions is 2.54 cm. We simulate the received signal at each microphone according to Eq. (1). The noise components $\mathbf{e}_i(\omega_l)$ in Eq. (1) are assumed to be uncorrelated with the source signals and distributed as circularly symmetric i.i.d. complex Gaussian random variables with mean zero and variance σ^2. The signal wave forms are also distributed as circularly symmetric i.i.d. complex Gaussian random variables with mean zero and a certain power level which is assumed to be 25 dB. This value is chosen without loss of generality since σ^2 will be varied throughout the experiments.

There are three parameters which affect the performances of the algorithms directly: number of snapshots I, noise variance σ^2, and frequency of interest $f=\omega/(2\pi)$. The incoherence assumption breaks down as the number of snapshots decreases since the cross terms in Eq. (6) are no longer negligible and also the additional noise term in Eq. (6) is no longer $\sigma^2\boldsymbol{I}$. Noise affects all the algorithms negatively as in all applications. Finally, the frequency determines the resolution of the algorithms since as the frequency increases, the difference in the steering vectors for nearby sources increases and hence it is easier for the algorithms to discriminate them. We will first evaluate DAMAS, SC-DAMAS, and CMF for uncorrelated sources and then evaluate DAMAS-C and CMF-C for correlated sources.

We start our simulations with a relatively easy scenario where the number of snapshots is large, $I=10\,000$, and $\sigma^2=0$ in which case the assumptions of the algorithms are almost correct. The resulting beamforming maps are shown in Figs. 1(a) and 1(b), where the horizontal axis and the vertical axis represent the 2D scanning plane and the power levels are represented in a gray color scale over a span of 10 dB. As expected, the delay-and-sum algorithm merges the peaks as if there were a single source. CMF works quite well and SC-DAMAS and DAMAS show good performance when the frequency is high. Next, the noise variance σ^2 is increased to 100. As shown in Fig. 1(c), CMF is more robust to noise than DAMAS and SC-DAMAS. Note that for all the examples in this section, DAMAS has been run for 10 000 iterations after which no significant improvement was observed.

TABLE III. Speeding up of SC-DAMAS for the example of Fig. 1(b). Timing values are in seconds.

N_0	441	196	121	81	36
Time	24.0	12.7	4.2	2.8	1.3

Next, we decrease the number of snapshots to 500 and increase the frequency to 20 kHz to resolve a more complicated source distribution. The results are shown in Fig. 2 for $\sigma^2=0$ and 5. The location estimates of SC-DAMAS for some of the sources are inaccurate and DAMAS is not able to discriminate the sources. CMF, however, is able to recover the sources reasonably well in both cases. If the frequency is decreased to $f=5$ kHz, DAMAS performance degrades significantly as also observed in other studies.[16] Figure 3 shows the imaging maps for $\sigma^2=0$ and 4 with $I=500$. DAMAS is not able to recover the source location for $f=5$ kHz even after 50 000 iterations. We again observe offsets in the location estimates of SC-DAMAS and when the noise is increased, the results become worse. This is due to the fact that SC-DAMAS is solving the same DAMAS inverse problem. In Fig. 3(a), the highest outlier for CMF is 5 dB below the actual signal levels and in Fig. 3(b), CMF provides the best performance. This performance gain can be attributed to the different formulation of CMF than DAMAS and SC-DAMAS. Recall that CMF does not rely on the delay-and-sum beamformer estimates and does not delete the diagonals. Note that the source distribtution considered for the last case is simpler than the other two since the frequency is low.

A qualitative assessment of the algorithms is given in Table I. The computational complexity of DAMAS was higher than that of SC-DAMAS and CMF in our simulations. Note that the public domain solver[31] we use for finding the optimal solutions to the SC-DAMAS and CMF problems works up to $N=1000$ grid points when the signals are complex valued. However, a commercial software designed for this purpose can go up to many more variables and hence the formulations are applicable to higher resolutions if desired. Table II shows the computation times of each algorithm for the examples considered in this section. We observe that SC-DAMAS is the fastest and CMF takes almost thrice the time of SC-DAMAS. DAMAS takes almost twice the time of CMF and eight times the time of SC-DAMAS. Furthermore, as mentioned in Sec. IV, the sparse formulation of SC-DAMAS allows us to reduce the size of $\tilde{\mathbf{y}}$ in Eq. (9) which provides more improvements in speed. In Table III, we noted the computation time of SC-DAMAS for different values of N_0 for the example considered in Fig. 1(b). The performance of SC-DAMAS undergoes only a minor degradation when

TABLE II. Computation times for DAMAS, SC-DAMAS, and CMF in seconds on personal computer, 2.0 GHz dual core processor, 2 Gbytes of RAM.

	Fig. 1(a)	Fig. 1(b)	Fig. 1(c)	Fig. 2(a)	Fig. 2(b)	Fig. 3(a)	Fig. 3(b)
DAMAS	160	165	161	160	160	180	162
SC-DAMAS	24	24	24	23	24	21	22
CMF	66	65	71	69	65	75	73

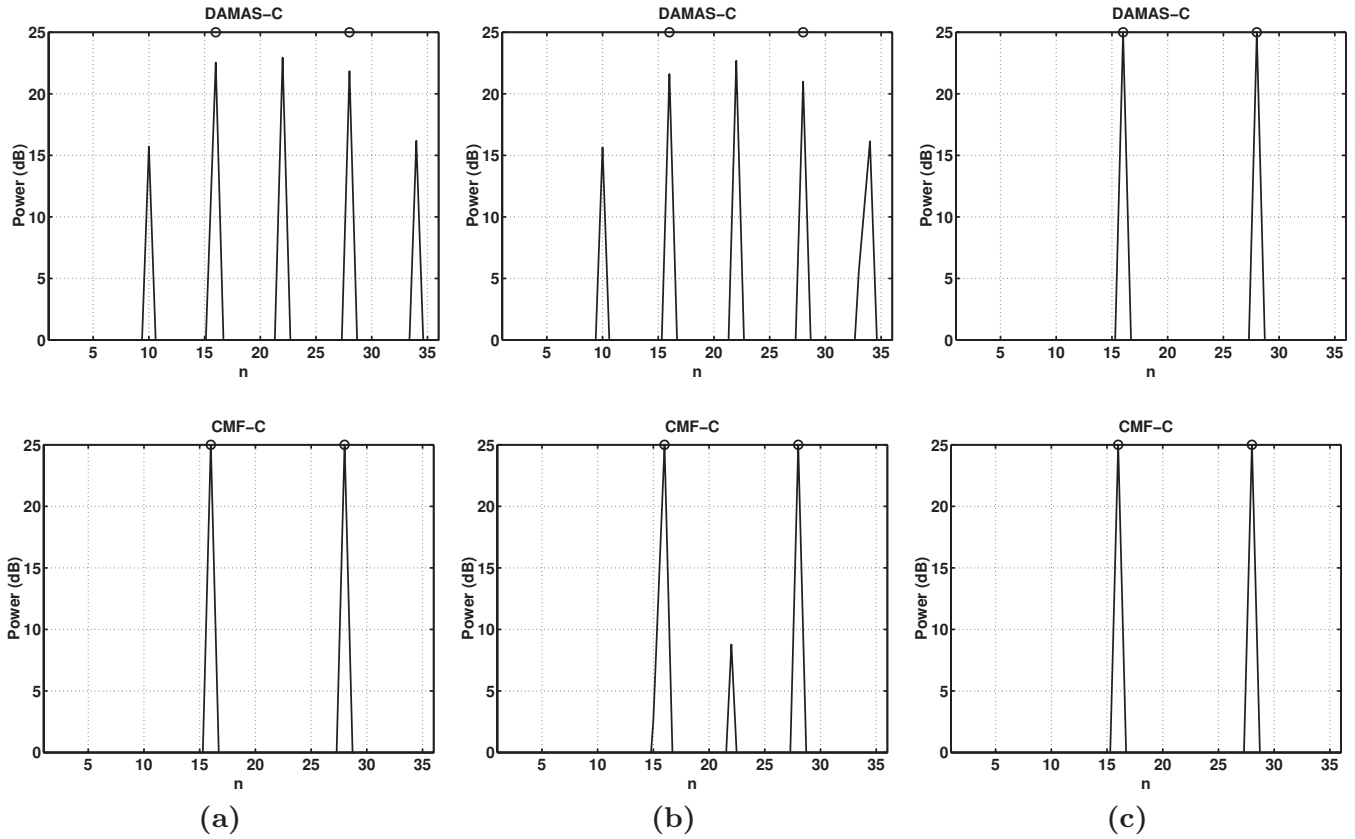


FIG. 4. The power estimates with DAMAS-C and CMF-C with three different settings as follows: $I=500$, (a) $f=10$ kHz and $\sigma^2=0$, (b) $f=10$ kHz and $\sigma^2=2$, (c) $f=20$ kHz and $\sigma^2=0$. DAMAS-C was run for 10 000 iterations. The y axis represents the power values in decibels and the x axis represents the index corresponding to the 2D grid point. The true source locations and powers are marked with circles.

$N_0 \geqslant 36$. Below that, the algorithm does not provide accurate results. The savings are huge and the problem can be solved in almost 1 s when $N_0=36$, which should be compared with 167 s for DAMAS and 62 s for CMF keeping in mind that CMF provides better results than SC-DAMAS and SC-DAMAS provides better results than DAMAS. In any case, SC-DAMAS offers a fast way of solving Eq. (9).

Finally, the performances of DAMAS-C and CMF-C are evaluated when there are two coherent acoustic signals in the scanning region. We assume a simple scenario which consists of 36 grid points between −12.7 and 12.7 cm with 5.08 cm increments in both x and y directions. Thus, the number of unknowns is 666 for each algorithm. The results are shown in Fig. 4. In these plots, rather than showing the 2D images, we plot the one-dimensional versions where the horizontal axis corresponds to the grid number n, where $n=1,\ldots,N$, and the vertical axis is the power levels in decibels since this way the power estimates are seen more clearly for this case. The actual noise locations and strengths are indicated with circles in the plots. We observe that DAMAS-C does not provide accurate estimates for the lower frequency scenario. But when the frequency increases, it can discriminate the sources. Note that results not shown here showed that DAMAS and CMF, which were designed for uncorrelated sources, cannot separate the two coherent sources, as expected. CMF-C can correctly identify the two sources even when $\sigma^2 \neq 0$ as shown in Fig. 4(b). The outlier occurring in this case is almost 16 dB below the correct estimates and is reasonable when compared to DAMAS performance. DAMAS-C and CMF-C take much more time than DAMAS and CMF due to the larger number of unknowns in the coherent case. As mentioned before, it is also possible to extend SC-DAMAS to the correlated case to achieve computational savings by sacrificing some accuracy as compared to CMF-C.

VIII. CONCLUSIONS

In this paper, a sparsity constrained deconvolution algorithm (SC-DAMAS) and a sparsity constrained covariance matrix fitting algorithm (CMF) were presented for the recovery of acoustic source locations and strengths. The former algorithm is an extension of DAMAS and tries to solve the same basic equation by exploiting sparsity. Similar to DAMAS, SC-DAMAS employs diagonal removal to mitigate the effects of noise, whereas the CMF algorithm eliminates noise without deleting the diagonals of the covariance matrix completely. Also, DAMAS and SC-DAMAS algorithms require the implementation of the delay-and-sum method and depend on the performance of this method. On the other hand, CMF is independent of the delay-and-sum algorithm. DAMAS, SC-DAMAS, and CMF were evaluated using synthetic data and the CMF approach showed the best performance both in terms of accuracy and robustness to noise. An alternative implementation of SC-DAMAS was provided which offers a very fast algorithm as compared to

DAMAS and CMF. Keeping in mind the better performance of SC-DAMAS than DAMAS, this could be a very practical deconvolution algorithm for aeroacoustic applications. DAMAS is observed to provide relatively worse performance as the frequency decreases. The number of snapshots affects all the algorithms significantly. Usually, large amounts of data are collected in aeroacoustic applications and the values used in the simulations are not far from being practical. An extension of CMF, CMF-C, was also proposed to deal with correlated sources and it was shown to provide better performance than DAMAS-C. The next step is to evaluate the algorithms on real data.

ACKNOWLEDGMENTS

This work was supported in part by NASA under Grant No. NNX07AO15A and the Swedish Science Council (VR).

LIST OF SYMBOLS

$\mathbf{a}(\mathbf{x}')$ = steering vector for location $\mathbf{x}'$
$\mathbf{A}(\mathbf{x}')$ = steering matrix
$\widetilde{\mathbf{A}}$ = matrix used in the inverse problem
$\widetilde{A}_{i,j}$ = (i,j)th element of $\widetilde{\mathbf{A}}$
BP = Basis pursuit
CMF = Covariance matrix fitting
CMF-C = extension of CMF to the correlated case
c_0 = sound propagation velocity in air, taken as 343 m/s
DAS = delay-and-sum beamformer
DAMAS = deconvolution approach for the mapping of acoustic sources
DAMAS-C = extension of DAMAS to the correlated case
DR = diagonal removal
$E\{.\}$ = expectation operation
$\mathbf{e}$ = noise
f = focusing frequency
FFT = fast Fourier transform
FOCUSS = focal underdetermined system solution
i.i.d. = independent identically distributed
I = number of snapshots
K = number of sources
L = number of frequency bins
LASSO = least absolute shrinkage and selection operator
LORE = localization and optimization of array results
M = number of microphones in the array
N = number of scanning points in the region
$\mathbf{R}$ = theoretical covariance matrix
$\hat{\mathbf{R}}$ = sample covariance matrix (cross spectral matrix)
SADA = small aperture directional array
SC-DAMAS = sparsity constrained DAMAS
SVD = singular Value Decomposition
$\mathbf{s}_k$ = signal wave form of source k
$\mathrm{Tr}(\cdot)$ = trace of the matrix argument
$\mathbf{x}_k$ = 3D location of source k
$\mathbf{x}$ = vector of all source locations
$\mathbf{x}', \mathbf{x}''$ = arbitrary 3D locations in space
$x_{m,k}$ = distance between the mth microphone and the kth source
$\widetilde{\mathbf{x}}$ = vector of $\{\widetilde{x}(\mathbf{x}_n)\}_{n=1}^{N}$
$\widetilde{x}_i$ = ith element of $\widetilde{\mathbf{x}}$
$\widetilde{x}(\mathbf{x}')$ = the actual source power level at $\mathbf{x}'$
$\mathbf{y}_i$ = measurement vector at snapshot i
λ = user parameter for SC-DAMAS and CMF
σ^2 = noise variance
ω = angular frequency
$\|\cdot\|_0$ = ℓ_0 norm: the number of nonzero elements
$\|\cdot\|_1$ = ℓ_1 norm: the absolute sum of the elements
$\|\cdot\|_2$ = ℓ_2 norm
$\|\cdot\|_{\mathrm{F}}$ = Frobenius norm
$(\cdot)^T$ = transpose of the argument
$(\cdot)^H$ = conjugate transpose of the argument
$(\cdot) \succcurlyeq 0$ = the matrix argument is positive semi-definite
$[\cdot]_{\mathrm{diag.}=0}$ = diagonal of the matrix argument is zero

[1]W. M. Humphreys, T. F. Brooks, W. W. Hunter, and K. R. Meadows, "Design and use of microphone directional arrays for aeroacoustic measurements," Fourth AIAA/CEAS Aeroacoustics Conference, Reno, NV, 1998, AIAA-98-0471.
[2]R. P. Dougherty, "Beamforming in acoustic testing," *Aeroacoustic Measurements*, edited by T. J. Mueller (Springer, New York, 2002), pp. 63–97.
[3]K. R. Meadows, T. F. Brooks, W. M. Humphreys, Jr., W. W. Hunter, and C. H. Gerhold, "Aeroacoustic measurements of a wing-flap configuration," Third AIAA/CEAS Aeroacoustics Conference, Atlanta, GA, 1997, AIAA Paper 97-1595.
[4]P. Stoica and R. L. Moses, *Spectral Analysis of Signals* (Prentice-Hall, Upper Saddle River, NJ, 2005).
[5]T. F. Brooks, M. A. Marcolini, and D. S. Pope, "A directional array approach for the measurement of rotor noise source distributions with controlled spatial resolution," J. Sound Vib. **112**, 192–197 (1987).
[6]J. Li, Y. Xie, P. Stoica, X. Zheng, and J. Ward, "Beampattern synthesis via a matrix approach for signal power estimation," IEEE Trans. Signal Process. **55**, 5643–5657 (2007).
[7]J. Li, P. Stoica, and Z. Wang, "On robust Capon beamforming and diagonal loading," IEEE Trans. Signal Process. **51**, 1702–1715 (2003).
[8]J. Li and P. Stoica, "Efficient mixed-spectrum estimation with applications to target feature extraction," IEEE Trans. Signal Process. **44**, 281–295 (1996).
[9]Z. Wang, J. Li, P. Stoica, T. Nishida, and M. Sheplak, "Wideband RELAX and wideband CLEAN for aeroacoustic imaging," J. Acoust. Soc. Am. **115**, 757–767 (2004).
[10]T. F. Brooks and W. M. Humphreys, "A deconvolution approach for the mapping of acoustic sources (DAMAS) determined from phased microphone arrays," J. Sound Vib. **294**, 856–879 (2006).
[11]T. F. Brooks and W. M. Humphreys, "A deconvolution approach for the mapping of acoustic sources (DAMAS) determined from phased microphone arrays," Tenth AIAA/CEAS Aeroacoustics Conference, Manchester, UK, 2004, AIAA-2004-2954.
[12]K. Ehrenfried and L. Koop, "A comparison of iterative deconvolution algorithms for the mapping of acoutic sources," 12th AIAA/CEAS Aeroacoustics Conference, Cambridge, MA, 2006, AIAA-2006-2711.
[13]P. A. Ravetta, R. A. Burdisso, and W. F. Ng, "Noise source localization and optimization of phased array results," 12th AIAA/CEAS Aeroacoustics Conference, Cambridge, MA, 2006, AIAA-2006-2713.
[14]R. Dougherty, "Extensions of DAMAS and benefits and limitations of deconvolution in beamforming," 11th AIAA/CEAS Aeroacoustics Conference, Monterey, CA, 2005, AIAA-2005-2961.
[15]T. F. Brooks and W. M. Humphreys, "Extension of damas phased array processing for spatial coherence determination (DAMAS-C)," 12th AIAA/CEAS Aeroacoustics Conference, Cambridge, MA, 2006, AIAA-2006-2654.
[16]T. F. Brooks and W. M. Humphreys, "Three-dimensional application of DAMAS methodology for aeroacoustic noise source definition," 11th AIAA/CEAS Aeroacoustics Conference, Monterey, CA, 2005, AIAA-2005-2960.
[17]D. L. Donoho and M. Elad, "Optimally sparse representation in general (nonorthogonal) dictionaries via ℓ^1 minimization," Proc. Natl. Acad. Sci.

U.S.A. **100**, 2197–2202 (2003).
[18]R. Tibshirani, "Regression shrinkage and selection via the lasso," J. R. Stat. Soc. Ser. B (Methodol.) **58**, 267–288 (1996).
[19]S. S. Chen, D. L. Donoho, and M. A. Saunders, "Atomic decomposition by basis pursuit," SIAM J. Sci. Comput. (USA) **20**, 33–61 (1998).
[20]J. A. Tropp, "Just relax: Convex programming methods for identifying sparse signals," IEEE Trans. Inf. Theory **51**, 1030–1051 (2006).
[21]J. J. Fuchs, "On sparse representations in arbitrary redundant bases," IEEE Trans. Inf. Theory **50**, 1341–1344 (2004).
[22]J. J. Fuchs, "Recovery of exact sparse representations in the presence of bounded noise," IEEE Trans. Inf. Theory **51**, 3601–3608 (2005).
[23]S. F. Cotter, B. D. Rao, E. Kjersti, and K. Kreutz-Delgado, "Sparse solutions to linear inverse problems with multiple measurement vectors," IEEE Trans. Signal Process. **53**, 2477–2488 (2005).
[24]D. P. Wipf and B. D. Rao, "Sparse Bayesian learning for basis selection," IEEE Trans. Signal Process. **52**, 2153–2164 (2004).
[25]M. A. T. Figueiredo, "Adaptive sparseness for supervised learning," IEEE Trans. Pattern Anal. Mach. Intell. **25**, 1150–1159 (2003).
[26]D. P. Wipf and B. D. Rao, "An empirical Bayesian strategy for solving the simultaneous sparse approximation problem," IEEE Trans. Signal Process. **55**, 3704–3716 (2007).
[27]D. M. Malioutov, M. Çetin, and A. S. Willsky, "A sparse signal reconstruction perspective for source localization with sensor arrays," IEEE Trans. Signal Process. **53**, 3010–3022 (2005).
[28]J. J. Fuchs, "Linear programming in spectral estimation. Application to array processing," in IEEE Proceedings of Acoustics, Speech, and Signal Processing, Atlanta, GA, 1996, pp. 3161–3164.
[29]J. J. Fuchs, "On the application of the global matched filter to DOA estimation with uniform circular arrays," IEEE Trans. Signal Process. **49**, 702–709 (2001).
[30]H. L. Van Trees, *Optimum Array Processing*, Detection, Estimation, and Modulation Theory Part IV (Wiley, New York, 2002).
[31]J. F. Sturm, "Using SeDuMi 1.02, a MATLAB toolbox for optimization over symmetric cones," Optim. Methods Software **11-12**, 625–653 (1999).
[32]J. Löfberg, "YALMIP: A toolbox for modeling and optimization in MATLAB," The 2004 IEEE International Symposium on Computer Aided Control Systems Design, Taipei, Taiwan, pp. 284–289.
[33]S. Boyd and L. Vandenberghe, *Convex Optimization* (Cambridge University Press, Cambridge, UK, 2004).
[34]T. F. Brooks and W. M. Humphreys, Jr., "Effect of directional array size on the measurement of airframe noise components," Fifth AIAA/CEAS Aeroacoustics Conference and Exhibit, Bellevue, WA, 1999, AIAA Paper 99-1958.

Model-based detection of synthetic bat echolocation calls using an energy threshold detector for initialization

Mark D. Skowronski[a] and M. Brock Fenton[b]
Department of Biology, University of Western Ontario, London, Ontario N6A 5B7, Canada

(Received 4 July 2007; revised 21 January 2008; accepted 14 February 2008)

Detection of echolocation calls is fundamental to quantitative analysis of bat acoustic signals. Automated methods of detection reduce the subjectivity of hand labeling of calls and speed up the detection process in an accurate and repeatable manner. A model-based detector was initialized using a baseline energy threshold detector, removing the need for hand labels to train the model, and shown to be superior to the baseline detector using synthetic calls in two experiments: (1) an artificial environment and (2) a field playback setting. Synthetic calls using a piecewise exponential frequency modulation function from five hypothetical species were employed to control the signal-to-noise ratio (SNR) in each experiment and to provide an absolute ground truth to judge detector performance. The model-based detector outperformed the baseline detector by 2.5 dB SNR in the artificial environment and 1.5 dB SNR in the field playback setting. Atmospheric absorption was measured for the synthetic calls, and 1.5 dB increased the effective detection radius by between 1 and 7 m depending on species. The results demonstrate that hand labels are not necessary for training detection models and that model-based detectors significantly increase the range of detection for a recording system. © *2008 Acoustical Society of America.* [DOI: 10.1121/1.2896752]

PACS number(s): 43.60.Uv, 43.80.Ev [MCH] Pages: 2643–2650

I. INTRODUCTION

Echolocation plays an important role in the lives of bats in the suborder Microchiroptera.[1,2] Bats use echolocation for orientation and prey detection. Echolocation calls also serve as part of bats' repertoire of social calls used to convey information among individual bats.[3,4] Biologists interested in surveying an area for bats often use acoustical methods to augment traditional capture-based research methods.[5,6] Acoustic monitoring can provide details about the species and relative abundances of bats in an area as well as an indication of where and when they forage. Acoustic sampling allows us to monitor bats that are difficult to catch and in situations that are difficult to cover with nets (e.g., over open water, in dense foliage, high above the ground).[7]

Historically, analysis of acoustical data from echolocating bats involved hand labeling the end points of calls by an expert using oscillograms, sonograms, and spectrograms to view data.[5,8,9] Values for global call features, such as duration, frequency of most energy, and bandwidth, were determined from various representations of the data either by hand or using automated algorithms. Recent advances in commercial acoustic recording equipment (e.g., Pettersson Elektronik AB, Uppsala, Sweden; Avisoft Bioacoustics, Berlin, Germany) allow observers to collect large amounts of call data, which poses practical problems for analysis by hand. First, hand labeling is a slow process: A minute of typical field recording data may take 60 min to rigorously detect all calls in the data, and field seasons may generate hundreds of hours of data to analyze. Second, hand labeling is subjective, and it can be difficult to obtain any absolute ground truth about the presence of calls in a recording. This means that the hand-labeling expert must decide which parts of the recorded data are calls and which parts are noise. Subjectivity is most pronounced for weak calls that may or may not be useful, based on the hand-labeling expert's opinion, because global call feature estimate error (e.g., for call duration, bandwidth, maximum frequency) is larger when less of the call is above the background noise level of the recording. Together, subjectivity and voluminous data challenge the repeatability of hand labeling.

Automated techniques have been used to address the issues of hand labeling bat calls. Conventional techniques for automated bat call detection use signal energy, either broadband or narrow band.[6,9] Skowronski and Harris (2006) showed that conventional automated bat call detection was inferior to model-based detection, inspired by the extensive research of acoustical analysis of human speech.[10] However, detection models require labeled data for training, and this can be generated in two ways: (1) hand labels or (2) another detector. The initializing detector can be any method that marks call end points.

The purpose of the current work was to investigate the effectiveness of initializing a model-based detector of bat calls with a conventional energy threshold detector. To provide an absolute ground truth of calls to detect, we used synthetic echolocation search-phase calls in the detection experiments. The merits and drawbacks of using synthetic calls are discussed in the following and then the results from two detection experiments: (1) an artificial noise environment and (2) an outdoor playback environment.

II. METHODS

Using synthetic calls in detection experiments allowed us to work with signals whose time and location were

[a]Electronic mail: mskowro2@uwo.ca
[b]Electronic mail: bfenton@uwo.ca

known, providing an absolute ground truth not available with real bat recordings. Subjective hand labeling is a limitation of conventional bat call detection experiments which has traditionally provided the ground truth for such experiments. Second, we had precise control over the signal-to-noise ratio (SNR) of each call in the artificial environment experiment, allowing us to vary the difficulty of the detection problem by varying the SNR. This advantage was sacrificed somewhat for the playback experiment to operate with more realistic noise and to better account for propagation effects (e.g., colored noise, echoes, atmospheric absorption). Third, we had practically an unlimited number of calls to use in our experiments, allowing us flexibility in our experiment design and scope. Call synthesis and the autodetection experiments were conducted using MATLAB 7.4 (The Mathworks, Natick, MA).

Using synthetic calls in detection experiments has limitations. The parametric functions that we used only approximate the frequency modulation curves (i.e., instantaneous frequencies) of real bat calls and cannot account for curves that are not monotonic or that have points of inflection (i.e., concavity sign change). The amplitude modulation of the synthetic calls that we used is simplistic and does not reflect, among other characteristics, the fact that real calls are emitted from moving bats and exhibit Doppler effects and intricate amplitude modulations due to interference. Furthermore, the synthetic calls do not contain harmonics or calls that overlap in time, and the calls used in the artificial environment experiment do not contain echoes, all of which are found in real echolocation recordings. Nevertheless, synthetic bat calls allowed us to perform rigorous detection experiments with an absolute ground truth and to compare the relative performance of various automated detector algorithms.

A. Synthetic calls

Synthetic bat calls consisting of a frequency-modulated sinusoid were constructed using a piecewise exponential curve. The exponential function was chosen as a basis for the synthetic calls based on the results from Parsons and Jones, who showed that the exponential curve was one of the most accurate functions of frequency modulation for species classification of bats.[11] The following is a normalized expression for the exponential frequency modulation (FM) curve, spanning unity time and frequency:

$$g(t) = \frac{e^{at} - 1}{e^{a} - 1}, \tag{1}$$

where $g(t)$ is normalized frequency over time $t \in [0,1]$ and $a \geqslant 0$ is the single model parameter that controls the curvature of the function. As $a \to 0$, the function becomes a linear curve, while the function approaches a right angle as a increases. The function is scaled such that $g(0)=0$ and $g(1)=1$.

To control the location of the point on the FM curve farthest from the diagonal line between the beginning and end of the curve, the *turning point*, we concatenated two exponential curves together (Fig. 1). The turning point has two degrees of freedom, $[t_0, g_0]$, and can be placed anywhere

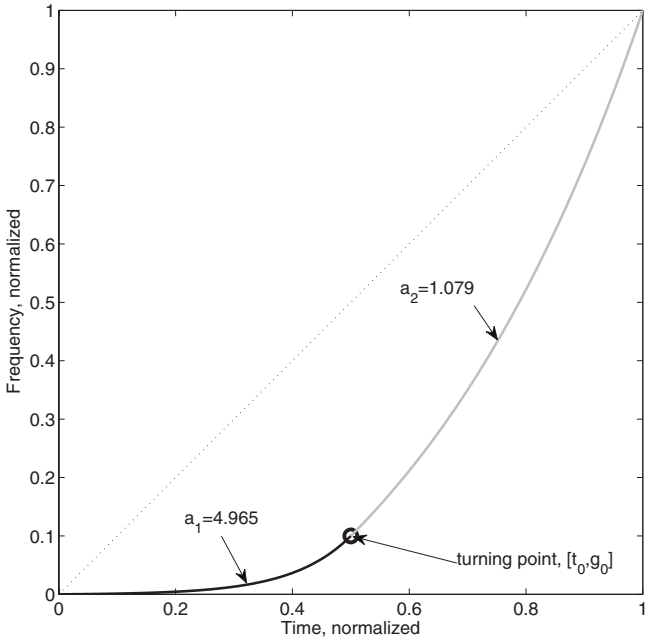


FIG. 1. Normalized piecewise exponential frequency modulation curve. The two exponential functions, shown with separate parameters a_1 and a_2 from Eq. (2), are joined at the turning point $[t_0, g_0]$. The diagonal line represents a linear modulation curve for comparison.

in the triangle space below the diagonal in Fig. 1 (since $a \geqslant 0$) to create a family of normalized monotonic curves. If the turning point is placed close to the diagonal, the FM curve is nearly linear, and long constant-frequency or steep frequency-modulated parts can be created by placing the turning point close to the horizontal or vertical legs of the lower triangle space, respectively.

The values for a for the two pieces of the FM curve are solved by the constraints that the pieces must pass through $[t_0, g_0]$ and have unity slope at $[t_0, g_0]$. Let $g_1(t)$ and $g_2(t)$ be the first and second pieces of the FM curve, respectively. Then

$$g_1(t) = g_0 \frac{e^{a_1 t/t_0} - 1}{e^{a_1} - 1}, \quad t \in [0, t_0],$$

$$g_2(t) = g_0 + (1 - g_0) \frac{e^{a_2 (t - t_0)/(1 - t_0)} - 1}{e^{a_2} - 1}, \quad t \in [t_0, 1], \tag{2}$$

where the extra shifting and scaling terms added to Eq. (1) ensure that $g_1(0)=0$, $g_1(t_0)=g_2(t_0)=g_0$, and $g_2(1)=1$. To solve for a_1 and a_2 in Eq. (2), the derivatives of g_1 and g_2 are equated to unity at $t=t_0$ which simplifies to

$$e^{a_1}(t_0 - g_0 a_1) - t_0 = 0,$$

$$(1 - t_0)(e^{a_2} - 1) - a_2(1 - g_0) = 0. \tag{3}$$

The expressions in Eq. (3) can be solved independently using empirical one-dimensional line search techniques (ignoring the trivial solutions $a_1=0$ and $a_2=0$).

The normalized frequency curve $g(t)$, the concatenation of $g_1(t)$ and $g_2(t)$, is upward-sweeping and concave up, which we refer to as call type I. Other types of calls can be constructed by flipping the time and/or frequency axes of

$g(t)$. A downward-sweeping and concave-up call is call type II with normalized frequency $\tilde{g}(t)=g(1-t)$. A type III call is downward sweeping and concave down with normalized frequency $\tilde{g}(t)=1-g(t)$, and a type IV call is upward sweeping and concave down with normalized frequency $\tilde{g}(t)=1-g(1-t)$.

To create a synthetic call, the process begins by selecting call parameters: starting frequency F_{start}, ending frequency F_{end}, duration T, turning point $[t_0, g_0]$, and sampling rate f_s. The starting and ending frequencies along with the turning point dictate the call type (I–IV, described earlier). To simplify the line searches used to solve Eq. (3), the turning point of the desired call type is translated to lie in the lower triangle space of a type I call shown in Fig. 1. For example, a downward-sweeping call with a turning point of [0.2, 0.1] (type II call) would be translated to [0.8, 0.1] before solving Eq. (3), while a downward-sweeping call with a turning point of [0.6, 0.7] (type III call) would be translated to [0.6, 0.3]. Once the parameters a_1 and a_2 are determined, the normalized FM curve of the desired call type $\tilde{g}(t)$ is shifted and scaled to fit between F_{start} and F_{end} for a call of duration T:

$$F(t) = F_{\min} + B\tilde{g}(t/T), \quad t \in [0,T], \tag{4}$$

where $F(t)$ is the instantaneous frequency of the synthetic call, $F_{\min}=\min(F_{\text{start}}, F_{\text{end}})$, and $B=|F_{\text{end}}-F_{\text{start}}|$ is the bandwidth of the call. The instantaneous frequency in Eq. (4) is integrated to form the instantaneous phase

$$\phi(t) = \int_0^t F(\tau)d\tau, \quad t \in [0,T], \tag{5}$$

which is used to form the synthetic call in the time domain

$$x(t) = A(t)\sin(2\pi\phi(t)), \quad t \in [0,T], \tag{6}$$

where $A(t)$ is an amplitude modulation function. For the current experiments, $A(t)$ was a Hamming window of length T. A discrete-time version of $x(t)$ is created using the desired sampling rate f_s.

B. Detection experiments

We performed two detection experiments using synthetic calls. The first was an artificial environment experiment in which the synthetic calls were embedded in additive white noise, while the second was a playback experiment in which the synthetic calls were broadcast in an outdoor environment using a high-frequency speaker and recorded using a microphone system.

In both experiments, we created calls from five hypothetical species. The parameters for each species were selected such that the calls had durations, bandwidths, and shapes typical of real species (compared with Vespertilionids[12] and neotropical species)[13] and that together the five species covered a wide range of frequency (Fig. 2; Table I). For each call, a set of parameters was selected from a uniform random distribution according to the value ranges listed in Table I.

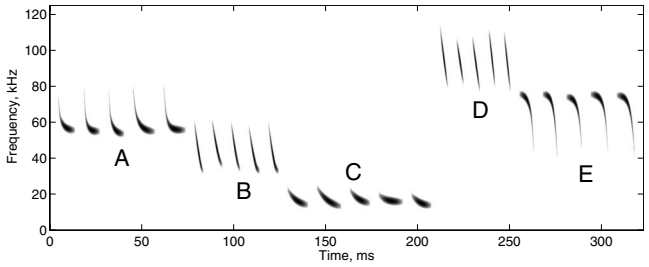


FIG. 2. Spectrogram of example calls for five hypothetical species, labeled A–E. See Table I for call parameters.

1. Artificial environment

In the first experiment, calls from each species were synthesized according to the parameter distributions listed in Table I and embedded in additive white Gaussian noise with zero mean and unity variance. To better mimic the analysis of real calls (e.g., the utility of spectral mean subtraction),[10,14] all calls were embedded into 16 bit files at a sampling rate of 250 kHz with 100 ms spacing between the beginning of adjacent calls. The files were uncompressed and encoded using pulse-code modulation. The SNR of each call was controlled by scaling the amplitude of the call to produce the desired signal power and SNR (i.e., noise power was constant for all calls). One file was created for each of the 12 SNRs tested (−13 to −3 dB in 1 dB increments and 0 dB), and each file contained 200 calls from each of the five species. A second file at 0 dB SNR with 200 calls from each species was created to train the model-based detector.

The primary advantage of using synthetic calls was that they provided an absolute ground truth for the detection experiments. While the calls of the five species used in the experiments were not designed to approximate calls from any real bat species, they contained the essence of real bat calls: frequency- and amplitude-modulated tones of relevant shape, bandwidth, and duration. Other characteristics typically found in real recordings of echolocating bats—echoes, harmonics, closely spaced or overlapping calls, feeding buzzes, insect noise, atmospheric absorption, source and microphone directionality—would add to the realism of the synthetic recording environment but were beyond the scope of the current study.

2. Playback recordings

In the second experiment, we created a file of synthetic calls for playback in an outdoor environment. The file was played through a ScanSpeak ultrasound speaker from Avisoft

TABLE I. Call parameters for five hypothetical species. Parameters selected from uniform distribution over listed range of values. See Fig. 2 for example call spectrograms.

Species	F_{start} (kHz)	F_{end} (kHz)	Duration (ms)	t_0	g_0
A	75–85	52.5–57.5	8–12	0.15–0.25	0.15–0.25
B	56–64	32.5–37.5	4–6	0.55–0.65	0.15–0.25
C	19.5–24.5	13.5–16.5	9–14	0.35–0.45	0.25–0.35
D	105–115	76.5–83.5	3–4	0.15–0.25	0.75–0.85
E	74–76	39–49	7–10	0.65–0.75	0.75–0.85

and recorded with an Avisoft UltraSoundGate 116 single-channel recorder using a CM16 condenser microphone capsule and CMPA preamplifier unit, both from Avisoft. The speaker and microphone were facing each other and aligned on axis (providing the flattest frequency response of both), and recordings were made in a flat grassy field. The speaker and microphone were spaced 4 m apart and mounted 1.76 m above the ground on tripods.

The file consisted of 200 calls of each of the five species embedded in additive white noise at SNRs from 11 to 50 dB in 1 dB increments (40 000 calls total). We used a range of embedded SNRs to accurately control the range of *recorded* SNRs of each species, which allowed us to compared the detectors in the same way as in the artificial environment experiment. The speaker and microphone gains were set well within their linear ranges such that calls with the highest embedded SNR were easily detected and calls with the lowest embedded SNR were not detectable better than random chance. The broadcast and recorded files were time-aligned using cross correlation.

3. Feature extraction and detectors

For both experiments, frame-based features were extracted from each file using 0.5 ms Blackman windows at 4000 frames/s (125 samples/frame at 250 kHz sampling rate and 50% overlap between adjacent frames). The spectrum of each frame was estimated using a 512-point zero-padded fast Fourier transform, and spectral mean subtraction was applied to each 2 s group of frames. The maximum energy of each frame, E (in dB), and the frequency of maximum energy, FME (in Hz), were determined. First-order temporal derivatives (Δ coefficients) of E and FME were estimated by linear regression using ± 3 frames around each frame, and second-order derivatives ($\Delta\Delta$ coefficients) were estimated by linear regression of the Δ coefficients.[10,15] The log-compressed mean-squared errors from the linear regression of E and FME were also included, called *smoothness* features. Peak energy and FME vary smoothly between frames of a call but coarsely between frames of background noise, making smoothness features useful for discriminating between calls and background noise. In summary, the following eight features were determined for each frame: E, FME, ΔE, ΔFME, $\Delta\Delta E$, $\Delta\Delta$FME, and smoothness of E and FME.

Three detectors were used in the experiments: (1) a baseline spectral peak detector, (2) a model-based detector trained with absolute ground truth endpoints, M_{abs}, and (3) a model-based detector trained with end points obtained from the baseline energy threshold detector, M_E. For the baseline detector, the variable E used by the model-based detector was compared to an energy threshold (described in the following). The model-based detectors used a Gaussian mixture model (GMM) to model both the frame-based call features and the background noise features,[10] and the output was the difference in log-likelihoods between the call and background GMMs. A threshold of 20 dB above the noise floor was used by the energy threshold detector to initialize M_E. Compared to M_{abs}, M_E should degrade in performance due to imperfect initial end point estimates provided by the baseline detector.

C. Detector evaluation

All detectors operated on a single measure for each analysis frame: peak energy E for the baseline detector, and log-likelihood difference for the model-based detectors. We evaluated the detectors by sweeping a detection threshold and generating a receiver operator characteristic (ROC) curve for each detector. For each detection threshold, all consecutive frames with a detector measure above the threshold were grouped together. The peak frame of each group was labeled a detected call peak. If the detected call peak was within 10 ms of the ground-truth end points of a call, a *hit* was recorded; otherwise, the detected call was recorded as a *false positive*. If no detected calls hit a ground-truth call, a *miss* was recorded for that call. The detection threshold controlled the tradeoff between hit rate (HR) and false positive rate (FPR):

$$\text{HR} = \frac{\text{hits}}{\text{hits} + \text{misses}},$$

$$\text{FPR} = \frac{\text{false positives}}{\text{hits} + \text{false positives}}, \tag{7}$$

where a higher detection threshold produced fewer false positives but more misses. Note that hits plus misses is the number of ground-truth calls and hits plus false positives is the number of detected calls. For the case of no detected calls (i.e., no hits and no false positives), FPR was set to 0 by convention.

A perfect detector has HR=1 and FPR=0. As a high detection threshold was lowered, fewer misses and more false positives were recorded, which produced a higher HR but higher FPR as well. Eventually, the detection threshold was so low that the HR and FPR were close to unity. Below this threshold level, HR and FPR decreased because separate calls merged into a single, large group and counted as a single detected call. When the threshold was below the minimum detector measure in a file, the entire file was detected as a single call. In the results to follow, we stopped decreasing the detection threshold when HR and FPR stopped increasing toward unity.

III. RESULTS AND DISCUSSION

A. Artificial environment

We embedded calls in files at SNRs of -13 to -3 dB, in 1 dB increments, and 0 dB. Figure 3 shows example spectrograms of a call from species A at various SNRs. All three detectors, the spectral peak baseline, M_{abs}, and M_E, were used to detect calls in each file. Figure 4 shows the ROC curves for the three detectors at -9 dB SNR. The model-based detectors outperformed the baseline detector, and M_E performed slightly better than the ground-truth-trained detector M_{abs} (Fig. 4). Results for all SNRs are shown in Fig. 5, which plots SNR versus the point on each ROC curve where HR=1−FPR (the cross-diagonal intersection in Fig. 4).

The results in Fig. 5 show that M_E outperformed the baseline detector by approximately 2.5 dB, meaning that M_E detected calls fainter by 2.5 dB compared to the baseline

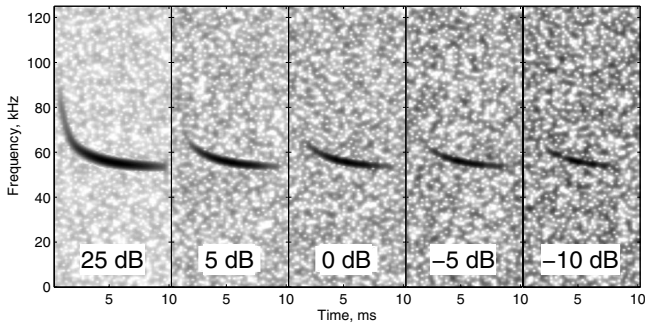


FIG. 3. Example noisy spectrograms. A synthetic call from species A was embedded in white noise at various SNRs, listed at the bottom of each pane. Less of the call is visible above the background noise for lower SNRs. All spectrograms were created using 250-point Blackman windows (1 ms) with 80% overlap, zero padded to 2048 points. The color map for each pane was scaled for maximum contrast.

detector for a given level of detector performance. In terms of "effective" detection range of a physical recording system, 2.5 dB translates into approximately 1.9 m increased detection radius of a recording system (1.32 dB/m atmospheric absorption at 40 kHz, 20 °C, and 50% relative humidity).[16] To better estimate the difference in effective detection range, we estimated the atmospheric absorption coefficient for calls from each species (described in the following).

The detector model M_E also slightly outperformed M_{abs}, even though M_{abs} was trained with absolute ground truth end points while M_E was trained using end points from the baseline detector which may be imperfect. Since M_{abs} and M_E were trained with calls at 0 dB SNR, the ends of each call were below the noise level because of the Hamming window amplitude modulation function $A(t)$ from Eq. (6) applied to

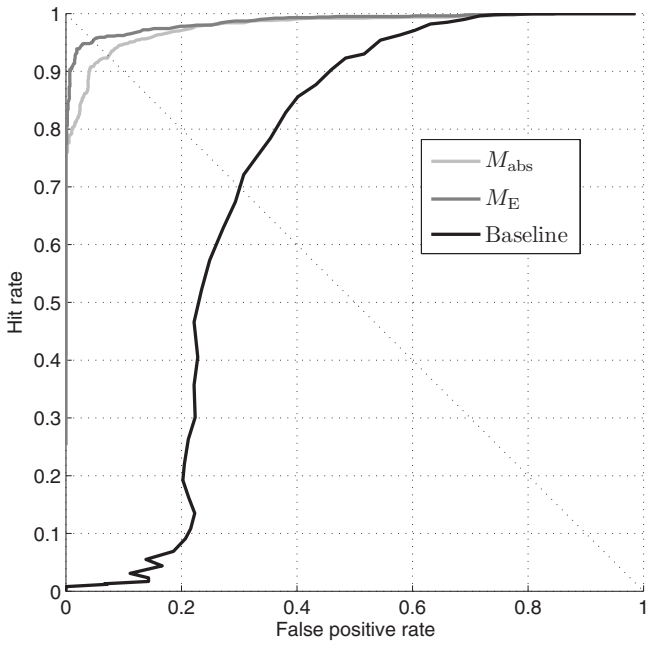


FIG. 4. Receiver operator characteristic curves for artificial environment detection experiment at −9 dB SNR. The cross diagonal line intersects each curve at the point where HR=1−FPR. The detectors are: ground-truth-trained model-based detector M_{abs}, the model-based detector initialized with the baseline detector M_E, and a spectral peak energy baseline detector.

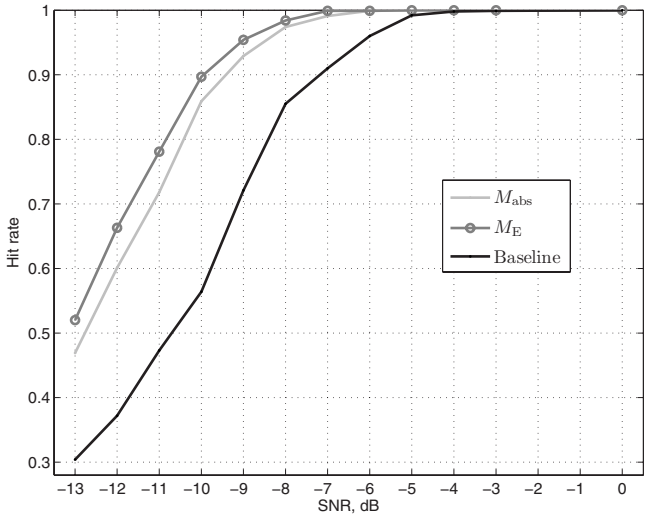


FIG. 5. HR vs SNR for artificial environment detection experiment. HR for each detector is for the point on each detector's ROC curve where HR=1−FPR.

each call. For M_E, the end points of each training call were set as two standard deviations above the noise peak distribution which effectively trimmed off the noise-corrupted ends of training calls. Since the training calls for M_{abs} contained some noisy frames, the call and background models for M_{abs} were more similar than those for M_E, resulting in less discriminability between the call and background models for M_{abs} and subsequently less detection power compared to M_E.

B. Playback recordings

Recordings were made outdoors in an open field at 31 °C and 52% relative humidity, measured using a Kestrel 4000 Pocket Weather Tracker (Nielsen-Kellerman Company, Boothwyn, PA). Since atmospheric absorption and off-axis misalignment between the speaker and microphone affected the recorded SNR of calls from each species differently, we analyzed the detectors for each species separately. Figure 6 shows embedded SNR versus HR where HR=1−FPR for species A through E. The plots in Fig. 6 are to the same scale, although the axis showing embedded SNR is shifted for each species depending on the propagation losses for each species' calls. For example, species D has the highest-frequency calls, which are most attenuated by the atmosphere, and required a higher embedded SNR to be detected at 4 m for a given level of detector performance compared to calls from the other species.

For all species except species D, the model-based detectors outperformed the baseline detector by 1–1.5 dB with little difference between the results for M_{abs} and M_E. The baseline and model-based detectors performed about the same for species D, whose calls were the highest in frequency and shortest in duration. The "jagged" look of the curves in Fig. 6 compared to similar curves from the artificial environment experiment in Fig. 5 is due to two sources: (1) the noise characteristics of the recordings made in the playback experiment and (2) the larger variance in recorded SNR due to atmospheric absorption and off-axis misalignment be-

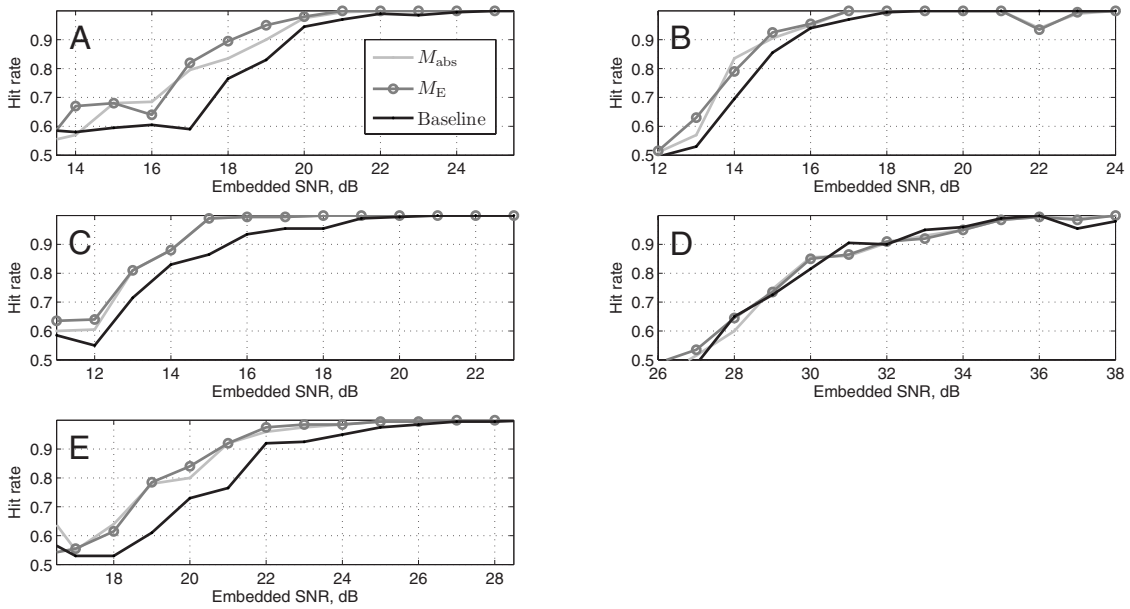


FIG. 6. HR vs embedded SNR for playback experiment. HR for each detector is for the point on each detector's ROC curve where HR = 1 − FPR. Species label, A–E, in upper left corner of each plot.

tween the speaker and microphone. The noise in the recorded files was not white and stationary like the noise in the artificial environment experiment and contained bursts of noise which increased FPR for the detectors.

To illustrate the relationship between SNR and effective detection radius, we estimated the atmospheric absorption coefficient for each species' calls. Using the same equipment and recording environment as the playback detection experiment, we played 200 calls from each species at 50 dB embedded SNR with a distance between the speaker and microphone of 1–12 m in 1 m increments. Recordings were made in an open field at 25 °C and 29% relative humidity. We extracted frame-based features from all recordings and found the spectral peak of each call using ground truth end points. To estimate the atmospheric absorption of each species' calls, we fit the spectral peak data to the following model:

$$\mathrm{E}(r) = -20\log_{10}(r) - \alpha r + \beta, \tag{8}$$

where $E(r)$, in decibels, is the spectral peak of a call at distance r, in meters, from the acoustic source. The log term accounts for spherical spreading loss, and α, in decibels per meter, is the atmospheric absorption coefficient. The term β is a gain term and accounts for the speaker and microphone gains. We used a least-squares curve fit function in MATLAB to find the model parameters in Eq. (8) for each species.

TABLE II. Curve fit parameters and coefficients of determination for models shown in Fig. 7.

Species	α (dB/m)	β (dB)	R^2
A	1.40	61.3	0.97
B	1.25	64.4	0.98
C	0.17	51.3	0.96
D	2.14	56.0	0.94
E	1.88	63.2	0.98

Figure 7 shows the mean ± standard deviation for each species at each distance along with the curve fit for each species, and Table II shows the curve fit parameters and coefficient of determination, R^2, for each model.

Table II shows that the atmospheric absorption term α ranged from 0.17 dB/m for the low-frequency species C to 2.14 dB/m for the high-frequency species D, and α for the other species fell in between in accordance with their frequency ranges. The term α for species D is probably underestimated since spectral peaks for $r \geq 10$ m were saturated by noise, as seen in Fig. 7. Comparing α in Table II to the SNR differences between the baseline and model-based detectors in Fig. 6, model-based detectors increased the effective detection range by the following: species A, 1.1 m; species B,

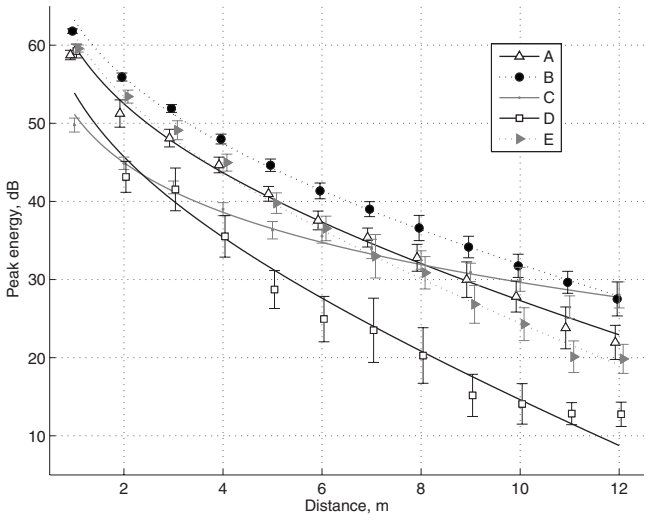


FIG. 7. Peak energy vs distance between speaker and microphone for each species in playback experiment. Symbols are mean ± standard deviation of 200 calls of each species, and lines are nonlinear regression expressions [Eq. (8)]. See Table II for model coefficients.

1.0 m; species C, 7 m; species D, 0 m; species E, 0.80 m. If a recording system has an effective detection range of 10 m using a spectral peak detector and an energy threshold that produces a hit rate of 0.75, then the same recording system would have an effective detection range of approximately 11 m for the majority of the species tested using a model-based detector with the same hit rate. Since detection volume is proportional to the cube of detection range (i.e., detection radius), this represents a 33% increase in effective detection volume.

Acoustic monitoring of bat activity has become a routine approach used by many bat biologists and others. Extending the volume of airspace sampled by acoustic monitoring has important repercussions, whether the monitoring is for an ecological and behavioral study, or associated with an assessment of bat activity tied to development such as a wind farm. Increasing the ability to detect and accurately assess the echolocation calls of bats is one part of the problem, the other is quickly and efficiently screening recordings to identify bat calls and extract information about them. Our model-based detection system both extends the volume of airspace sampled and makes it possible to quickly review and assess recordings of bat calls.

Real recordings of echolocating bats have several characteristics not included in the current experiments that greatly affect detector accuracy. For the baseline energy-based detector, *any* energy above the detection threshold produces a detected call, which tend to be false positives and can be quite numerous (e.g., recordings made near a pond full of croaking frogs). Such noises many times fall below the frequency range of interest and can be attenuated with appropriate filtering, but many insects produce acoustic noise in frequency bands that overlap with the frequency ranges of bat calls. Echoes also fall in the same frequency range as bat calls and can be detected as false positives with the baseline detector if they are intense enough. Echoes may last much longer than their original calls, potentially producing several false positives for each hit if the echo fluctuates above and below the detection threshold. This can be controlled by introducing a minimum time between detected calls, but such a solution tends to increase the number of misses because either calls from the same bat are closely spaced (e.g., feed buzz) or calls from separate bats with overlapping passes of calls are closely spaced or overlap in time.

Model-based detectors are less susceptible to real-world noise sources than the baseline detector because the model-based detector relies on more than just energy to determine if an analysis frame contains a bat call. However, other characteristics of real recordings of echolocating bats can hinder the performance of model-based detectors. The most significant is the so-called "test/train" mismatch phenomenon in the application of any statistical model. That is, the recorded (test) data are significantly different from the data used to train the models. The models could be trained on different species or with data recorded with different equipment (and associated equipment noise characteristics) or in environments with different acoustic noise characteristics (e.g., different insect populations). The training set may not contain any feeding buzzes or may not contain the full repertoire of search-phase calls of a species of interest (e.g., the high variability of calls from *Molossus* species)[17] or may contain calls with echoes of intensity different from that of test data. Closely spaced or overlapping calls would register as a single detected call as they would for the baseline detector. Therefore, the training data must be sufficiently broad for the model-based detectors to generalize well to novel recordings.

Characteristics of real calls not accounted for in the current experiments may also impact detector performance. Peak energy may jump between harmonics of a call (e.g., between the fundamental and second harmonics of calls from *Eptesicus fuscus*), causing a discontinuity in FME and erroneous slope and smoothness estimates. The model-based detectors may end a call at the discontinuity instead of the true end point, affecting global call feature measurements. Furthermore, calls may contain a notched amplitude modulation function that attenuates part of a call harmonic below the noise level at certain narrow frequency bands (e.g., calls from *Idionycteris phyllotis*),[18] which may produce multiple hits for the same call. A limitation of the model-based methods of detection is that likelihood is measured *locally* (within the neighborhood of a few frames), and global characteristics of calls are not utilized to make detection decisions. One method currently under study to address this limitation is the links detector which uses local and global call features to detect calls and call harmonics while rejecting echoes and noncall noises in a unified model-based framework.[19]

IV. CONCLUSIONS

We showed that a model-based bat call detector, trained with calls labeled by a baseline threshold energy detector, outperformed the baseline detector in terms of SNR of a call for a given level of detector performance. Skowronski and Harris (2006) showed that model-based detectors, trained with hand labels, were superior to energy-based detectors, and the current results extend those findings to show that models can be trained using labels from a simple detector instead of hand labels, resulting in a fully automated model-based detection algorithm.

We used synthetic echolocation calls, constructed with a piecewise exponential frequency modulation function, in the detection experiments to provide an absolute ground truth for call location and to accurately control the SNR of calls. We created random distributions of call parameters for five hypothetical species, which spanned a wide frequency range and were designed to approximate real echolocation calls. Using synthetic calls provided for us an unlimited number of labeled calls to use in our experiments, giving us flexibility in our experiment design and scope. In both experiments, a total of 65 000 synthetic calls were constructed. The piecewise exponential model can be extended to form more complex calls. For example, the "Z"-shaped calls of *Pteronotus davyi*[20] can be synthesized by concatenating a type III call with a type II call. The basic model in Eq. (1) can be extended to more than two pieces if extra constraints are included, or the model can be modified to included pure-tone

segments to better approximate the constant-frequency tails of calls from some species.

In the artificial environment experiment, the results in Fig. 5 show that, at a level of detector performance of 80% hit rate and 20% false positive rate, the baseline algorithm detected calls down to −8.4 dB SNR while the model-based detector M_E detected calls down to −11.9 dB SNR. Fainter calls by 2.5 dB were detected by the model-based detector, which translates into an increase in effective detection range of a physical acoustical recording system. The increase in performance of the model-based detector was due to the increase in information used by the model. Whereas the baseline detector only considered spectral peak energy, the model detector used spectral peak energy and spectral peak frequency as well as local shape information (i.e., slope, concavity, and smoothness).

The playback experiment was designed to repeat the artificial environment experiment using realistic noise sources and accounting for acoustic propagation effects. The results showed that model-based detection outperformed the baseline detector by 1–1.5 dB SNR, except for species D whose calls were equally detected by all algorithms. Our estimates for atmospheric absorption of calls from each species showed that 1–1.5 dB SNR difference translates into approximately 1 m increased effective detection range, except for the low-frequency species C whose calls could be detected 7 m farther away using the model-based detector. Adding 1 m of range to a recording system whose effective detection range is 10 m increases the effective detection volume by 33%. This result shows that calls can be detected in a significantly larger volume of space at a fixed level of detector performance (i.e., fixed hit rate) when using model-based detectors compared to the conventional energy threshold detector.

ACKNOWLEDGMENTS

The current work was funded by the International Fellowship Research Program from the National Science Foundation and the Natural Sciences and Engineering Research Council of Canada.

[1]D. R. Griffin, *Listening in the Dark: The Acoustic Orientation of Bats and Men* (Comstock, Ithaca, NY, 1958).

[2]*Echolocation in Bats and Dolphins*, edited by J. A. Thomas, C. F. Moss, and M. Vater (The University of Chicago Press, Chicago, IL, 2003).

[3]M. B. Fenton, *Communication in the Chiroptera* (Indiana University Press, Bloomington, IN, 1985).

[4]G. S. Wilkinson, "Social and vocal complexity in bats," in *Animal Social Complexity: Intelligence, Culture and Individualized Societies*, edited by F. B. M. de Waal and P. L. Tyack (Harvard University Press, Cambridge, MA, 2003), pp. 322–341.

[5]M. B. Fenton and G. P. Bell, "Recognition of species of insectivorous bats by their echolocation calls," J. Mammal. **62**, 233–243 (1981).

[6]M. K. Obrist, "Flexible bat echolocation: The influence of individual, habitat and conspecifics on sonar signal design," Behav. Ecol. Sociobiol. **36**, 207–219 (1995).

[7]W. L. Gannon, R. E. Sherwin, and S. Haymond, "On the importance of articulating assumptions when conducting acoustic studies of habitat use by bats," Wild. Soc. Bull. **31**, 45–61 (2003).

[8]M. J. O'Farrell, B. W. Miller, and W. L. Gannon, "Qualitative identification of free-flying bats using the Anabat detector," J. Mammal. **80**, 11–23 (1999).

[9]S. Parsons, A. M. Boonman, and M. K. Obrist, "Advantages and disadvantages of techniques for transforming and analyzing chiropteran echolocation calls," J. Mammal. **81**, 927–938 (2000).

[10]M. D. Skowronski and J. G. Harris, "Acoustic microchiroptera detection and classification using machine learning: Lessons learned from automatic speech recognition," J. Acoust. Soc. Am. **119**, 1817–1833 (2006).

[11]S. Parsons and G. Jones, "Acoustic identification of twelve species of echolocating bat by discriminant function analysis and artificial neural networks," J. Exp. Biol. **203**, 2641–2656 (2000).

[12]D. W. Thomas, G. P. Bell, and M. B. Fenton, "Variation in echolocation call frequencies recorded from North American Vespertilionid bats: A cautionary note," J. Mammal. **68**, 842–847 (1987).

[13]M. J. O'Farrell and B. W. Miller, "A new examination of echolocation calls of some neotropical bats (Emballonuridae and Mormoopidae)," J. Mammal. **78**, 954–963 (1997).

[14]B. S. Atal, "Effectiveness of linear prediction characteristics of the speech wave for automatic speaker identification and verification," J. Acoust. Soc. Am. **55**, 1304–1312 (1974).

[15]S. Furui, "Cepstral analysis technique for automatic speaker verification," IEEE Trans. Acoust., Speech, Signal Process. **29**, 254–272 (1981).

[16]International Organization for Standardization, *ISO 9613-1:1993: Acoustics—Attenuation of Sound during Propagation Outdoors—Part 1: Calculation of the Absorption of Sound by the Atmosphere* (ISO, Geneva, Switzerland, 1993).

[17]S. Biscardi, J. Orprecio, M. B. Fenton, A. Tsoar, and J. M. Ratcliffe, "Data, sample sizes and statistics affect the recognition of species of bats by their echolocation calls," Acta Chirop. **6**, 347–363 (2004).

[18]J. A. Simmons and M. J. O'Farrell, "Echolocation by the long-eared bat, plecotus phyllotis," J. Comp. Physiol. **122**, 201–214 (1977).

[19]M. D. Skowronski and M. B. Fenton, "Link-based feature extraction for model-based detection of echolocation calls," J. Acoust. Soc. Am. **122**, 2946 (2007).

[20]C. Ibanez, A. Guillen, J. Juste B, and J. L. Perez-Jorda, "Echolocation calls of Pteronotus davyi (Chiroptera: Mormoopidae) from Panama," J. Mammal. **80**, 924–928 (1999).

Stimulus-frequency otoacoustic emission: Measurements in humans and simulations with an active cochlear model

Yong-Sun Choi and Soo-Young Lee
Brain Science Research Center and Department of Bio and Brain Engineering, Korea Advanced Institute of Science and Technology, Daejeon 305-701, Republic of Korea

Kourosh Parham
Division of Otolaryngology, Department of Surgery, University of Connecticut Health Center, Farmington, Connecticut 06030, USA

Stephen T. Neely
Boys Town National Research Hospital, Omaha, Nebraska 68131, USA

Duck O. Kim[a)]
Department of Neuroscience, University of Connecticut Health Center, Farmington, Connecticut 06030, USA

(Received 17 September 2007; revised 3 March 2008; accepted 4 March 2008)

An efficient method for measuring stimulus-frequency otoacoustic emissions (SFOAEs) was developed incorporating (1) stimulus with swept frequency or level and (2) the digital heterodyne analysis. SFOAEs were measured for 550–1450 Hz and stimulus levels of 32–62 dB sound pressure level in eight normal human adults. The mean level, number of peaks, frequency spacing between peaks, phase change, and energy-weighted group delays of SFOAEs were determined. Salient features of the human SFOAEs were stimulated with an active cochlear model containing spatially low-pass filtered irregularity in the impedance. An objective fitting procedure yielded an optimal set of model parameters where, with decreasing stimulus level, the amount of cochlear amplification and the base amplitude of the irregularity increased while the spatial low-pass cutoff and the slope of the spatial low-pass filter decreased. The characteristics of the human cochlea were inferred with the model. In the model, an SFOAE consisted of a long-delay component originating from irregularity in a traveling-wave peak region and a short-delay component originating from irregularity in regions remote from the peak. The results of this study should be useful both for understanding cochlear function and for developing a clinical method of assessing cochlear status. © *2008 Acoustical Society of America.* [DOI: 10.1121/1.2902184]

PACS number(s): 43.64.Jb, 43.64.Bt, 43.64.Kc [BLM] Pages: 2651–2669

I. INTRODUCTION

Otoacoustic emissions (OAEs) are sounds generated by the inner ear (Kemp, 1978). As OAEs are related to movements of the cochlear partition, major goals of investigations of OAEs include: (1) to infer noninvasively basic characteristics of cochlear biomechanics of humans and animals in normal and pathological conditions (e.g., Kemp, 1978; Kim, 1980; Kim *et al.*, 1980; Zurek *et al.*, 1982; Kemp, 1986; Matthews and Molnar, 1986; Zwicker, 1986; Shera *et al.*, 2002; Goodman *et al.*, 2003; Siegel *et al.*, 2005) and (2) to assess the functional status of the cochlea noninvasively (e.g., Kemp *et al.*, 1990; Lonsbury-Martin and Martin, 1990; Probst *et al.*, 1991; Shera, 2004).

The present study is intended to contribute to these goals by: (1) introducing a new efficient method of measuring OAEs and providing human OAEs obtained with the method, and (2) interpreting experimentally observed OAEs in terms of an active cochlear model. Our study investigated stimulus-frequency OAEs (SFOAEs). A presumed advantage of SFOAE over distortion product OAEs (DPOAEs) is that the information conveyed by SFOAEs may be simpler than that by DPOAEs because SFOAEs involve only one frequency whereas DPOAEs involve multiple frequencies. Most likely, though, further studies of all types of OAEs will continue to be helpful in advancing our knowledge of cochlear biomechanics and in developments of methods for assessing the cochlear functional status.

In conventional methods of SFOAE measurement (e.g., Brass and Kemp, 1993; Shera and Guinan, 1999, 2003), the SFOAE is measured for one frequency at a time. It is thus necessary to make separate measurements at a large number of frequencies if one wishes to determine high-resolution fine structures of SFOAE level and phase versus frequency.

We have developed a new efficient method for measurement of SFOAEs whereby high-resolution fine structures of SFOAE versus frequency can be obtained more rapidly. The new method employs a stimulus where frequency is continuously swept and the response waveform is analyzed using the digital heterodyne analysis. Analogously, the present method can also obtain input-output functions of SFOAE where the

[a)]Author to whom correspondence should be addressed. Electronic mail: kim@neuron.uchc.edu.

stimulus level is continuously swept. The digital heterodyne analysis method was previously used for measurement of a time-dependent change (i.e., adaptation) of a DPOAE (Kim *et al.*, 2001) or an SFOAE (Guinan *et al.*, 2003) of a particular frequency. The latter studies involved using constant stimulus frequencies as opposed to time-varying stimulus frequencies used in the present study.

An important characteristic of SFOAEs is their fine structures in the frequency domain. Level of SFOAEs versus frequency exhibit a complex quasi-periodic pattern of peaks and troughs, while the phase of SFOAEs versus frequency also exhibits a complex pattern of many cycles of phase change indicating a frequency-dependent group delay (Kemp and Chum, 1980; Zweig and Shera, 1995; Shera and Guinan, 1999, 2003). The fine structures of SFOAEs have been interpreted to be a result of reflections of cochlear traveling waves arising from spatially distributed irregularities (or roughness) in cochlear-partition impedance (Shera and Zweig, 1991; Zweig and Shera, 1995; Talmadge *et al.*, 1998, 2000).

As an *in vivo* measurement of cochlear-partition motion is not feasible in humans, OAEs provide a useful basis for making indirect inferences for human cochlear mechanical responses. Along this line, one of the goals of the present study was to use features of human SFOAEs as a basis for specifying parameters of an active cochlear model and to make inferences about the human cochlear biomechanics. A cochlear model developed in the present study was able to reproduce salient features of the human SFOAE fine structures. Model parameters important for SFOAE simulation were the amount of cochlear amplification and the spatial-frequency contents of the partition-impedance irregularity. The correspondence between the human SFOAEs and the model results allowed us to infer characteristics of human cochlear-partition motion regarding the amount of amplification, sharpness of tuning and phase properties at various stimulus levels.

II. METHODS FOR MEASUREMENTS OF HUMAN SFOAES

The present SFOAE measurements were conducted at the University of Connecticut Health Center while Y.-S. Choi was visiting there.

A. Subjects

SFOAEs were obtained from eight ears of eight human subjects, five men and three women, aged 24–40 years. In a ninth (male, 32 years old) subject, SFOAE data were collected by the conventional method in addition to the current novel method for comparison. All of the subjects had normal hearing as documented by their audiometric thresholds being 20 dB hearing level (HL *re* American National Standards Institute S3.21, 1978) or better at octave frequencies in the range from 0.25 to 8 kHz. They also had normal patterns of tympanogram. For each subject, there were one or more recording sessions with each session typically taking 30–45 min. One session consisted of about 20 subsessions with each taking approximately 1.5 min. After groups of a few subsessions, the subjects had short breaks (~1 min each) to allow body movements for a comfortable posture, to relieve discomfort of the probe and ear mold (see below) being in the ear canal, and to remove any potential long-term adaptation.

During the recording sessions, the subjects remained awake sitting quietly on a chair in a double-walled acoustic chamber (Industrial Acoustics Co.). The present study was approved by the Institutional Review Board for Human Subjects of University of Connecticut Health Center.

B. Equipment

Stimuli were synthesized, stimulus presentation was controlled, and acoustic waveforms were recorded using a Windows-PC which contained a sound card (Card Deluxe, Digital Audio Labs) with 24 bit analog-to-digital and digital-to-analog converters operating at a sampling rate of 22 kHz. We used a program called SYSRES (Neely and Stevenson, 2002) to present the custom-synthesized stimulus and collect the acoustic waveforms.

The acoustic system included one microphone and two earphones (ER-10C, Etymotic Research) designed for ear-canal insertion. Individualized ear molds were made for the human subjects with silicon-based impression material. During the recording period, the ear mold was inserted into a subject's ear canal, and the tube of the ER-10C acoustic probe was inserted into the hole running through the ear mold. This arrangement, having a tight coupling between the acoustic probe and the ear canal, was intended to provide a higher signal-to-noise ratio and a more controlled positioning of the probe than a conventional arrangement where the probe was inserted in the ear canal with a foam tip.

C. Suppression method to extract SFOAEs

The measurement of SFOAEs requires separation of the recorded acoustic signal into the "stimulus" and emission components. The stimulus component represents both a signal generated by an earphone and passive acoustic properties of the earphone coupler and the passive acoustic input impedance looking into the ear canal. The emission component represents a signal generated by the ear. One method of such separation is based on the fact that an SFOAE is suppressed when a suppressor tone is added at a frequency near the probe tone (e.g., Kemp and Souter, 1988; Brass and Kemp, 1993; Shera and Guinan, 1999). In this method, the stimulus component is obtained from a condition where both a probe tone and a suppressor tone are applied as the stimulus. An SFOAE is then obtained by vector subtraction of the stimulus component from the signal containing both the stimulus and SFOAE. The present study used this method.

D. Frequency-sweeping method: Stimulus generation

The stimulus frequency was continuously swept from 500 to 1500 Hz in order to obtain high-resolution fine structures of SFOAEs. We applied a stimulus signal and recorded pressure response of the ear canal. At each measurement, the acoustic stimulus was repeated 32 times. As the duration of the stimulus was approximately 3 s, it took about 1.5 min for

TABLE I. Midway stimulus level in dB SPL and the range of levels obtained at the input attenuation level of −50 dB *re* maximum voltage into the earphone for each subject. The last column shows the corresponding information pooled for all subjects.

Subject ID No.	1	2	3	4	5	6	7	8	all
Mid-level (dB SPL)	49	39	39	37	42	40	37	39	42
Range (±dB)	2	3	7	4	3	8	4	3	10

a measurement covering 500–1500 Hz at one stimulus level. The stimulus had two channels delivered through two channels of the soundcard which were connected to two earphones of the ER-10C probe. One channel of the stimulus produced a probe tone whereas the other channel produced a suppressor tone. Each channel had two equal-length (32768 samples/(22000 samples/s=1.489 s) intervals. The two intervals of the probe channel were identical whereas the first interval of the suppressor channel was silence.

The probe and suppressor signals, $p(t)$ and $s(t)$, were:

$$p(t) = A_p \cdot \sin\left[2\pi \cdot \left\{500 \times \frac{f_{\text{sam}}}{31448} \times (t-0.03)^2 + 500 \times (t-0.03)\right\}\right], \quad (1)$$

$$s(t) = A_s \cdot \sin\left[2\pi \cdot \left\{500 \times \frac{f_{\text{sam}}}{31448} \times (t-0.03)^2 + 650 \times (t-0.03)\right\}\right]. \quad (2)$$

A_p and A_s represent amplitudes of the probe and suppressor tones, respectively, f_{sam} the sample rate in Hz. The unit of time, t, was seconds (s). The above equations included 0.03 s silent portions that were intended to avoid transients. The probe frequency was swept linearly from 500 to 1500 Hz. The suppressor frequency was also swept linearly such that it was 150 Hz above the probe frequency. For both $p(t)$ and $s(t)$, we used 30 ms rise/fall times with half Blackman windows. After subtracting the silent and rise/fall portions, the above signal waveform was stable for 1.37 s.

We converted the voltage amplitude of a stimulus tone to the earphone, A_p or A_s, relative to the maximum voltage as attenuation of the tone in dB. A constant attenuation corresponded to a variable sound pressure level (SPL) as a result of a frequency dependence of the earphone and the acoustic load impedance of the ear canal. In the present study, −50 dB attenuation, for example, corresponded to 37 ± 4 dB SPL (*re* 20 μPa) for 500–1500 Hz in one subject (No. 7). Further details on this topic are described in Sec. III A, Table I.

For each measurement, the probe stimulus was applied at a constant attenuation with the probe frequency swept from 500 to 1500 Hz. The attenuation level of the probe tone varied from −70 dB to −25 dB in 5 dB steps. In the present report, only the results with attenuation of −60 dB to −30 dB in 10 dB steps were systematically analyzed across all subjects. The suppressor level was 20–40 dB above that of the probe level; i.e., the suppressor level was −20, −15, −10, and −5 dB *re* max when the probe level was −60, −50, −40, and −30 dB *re* max, respectively. When the probe level was higher, we had to use smaller difference between the suppressor level and the probe level in order to keep the absolute level of the suppressor.

E. Digital heterodyne analysis of SFOAEs

We used the digital heterodyne method to determine SFOAE level and phase as a function of frequency which, in turn, are functions of time in the present study. The digital heterodyne method, a Fourier-transform application, was developed by Stephen T. Neely (Boys Town National Research Hospital, Omaha, NE, personal communication), and previously used to measure an OAE at a particular frequency as a function of time for a fixed stimulus (Kim *et al.*, 2001; Guinan *et al.*, 2003).

In the context of the present study, we took a discrete Fourier transform of the 1.43-s-long original response waveform sampled at 22 kHz. A band of positive frequencies (1000 spectral components) around an SFOAE analysis frequency was then selected in the frequency domain and shifted down ("heterodyned") such that the SFOAE frequency was set to be the zero frequency. Next, a Blackman low-pass filter was applied to the shifted spectrum.

The optimal bandwidth ("BW") of the heterodyne low-pass filter is proportional to square root of the frequency sweep rate. This is because opposing constraints on the BW are imposed in the frequency- and time-domain parts of the heterodyne analysis. An unduly wide BW of the low-pass filter will allow energy at a frequency remote from an analysis frequency to be included in the frequency-domain part of the heterodyne analysis whereas an unduly narrow BW of the filter (which has a long integration time), together with a frequency-swept stimulus, will allow energy at a frequency remote from the analysis frequency to be included in the time-domain part of the heterodyne analysis. We empirically found, for a Blackman low-pass filter used in this study, the optimal value of BW (defined as the bandwidth at a relative amplitude of 0.7):

$$\text{BW} = 0.345^*(\text{sr})^{0.5}, \quad (3)$$

where sr corresponded to sweep rate in Hz/s. [Note: the unit of $(\text{Hz/s})^{0.5}$ is Hz.] By substituting sr=699.3 Hz/s (1000 Hz/1.43 s) into Eq. (3), we obtained BW=9.1 Hz.

We then took an inverse discrete Fourier transform of the shifted and low-passed, yielding a complex-valued time-domain signal. The latter consisted of 1000 time points representing the magnitude and phase of the SFOAE of a particular analysis frequency as a function of time over 1.43 s with each time point representing 1.43 ms.

Originally, the heterodyne method was used to extract one specific frequency component as a function of time for a

fixed stimulus. A novel aspect of the present method is that a time dependence of the heterodyne analysis output is made to be equivalent to a frequency dependence by combining a frequency-swept stimulus with the heterodyne analysis.

To extract an SFOAE at a particular analysis frequency, the total 1.43 s recorded signal was first multiplied with a 227 ms Blackman window (spanning a frequency range of ± 79 Hz) centered at the point when the probe-tone frequency was equal to the analysis frequency to suppress the suppressor-tone signal; the suppressor frequency was 150 Hz higher than the probe frequency. The magnitude of the heterodyne-analysis output for a particular analysis frequency showed a peak near a time when the stimulus frequency was equal to the analysis frequency. A peak occurred slightly later (at a time to be called "$t_$peak") than the time when the stimulus frequency was equal to the analysis frequency ("$t_$stimulus"). The average delay between $t_$peak and $t_$stimulus among all of the present data was 3.1 ms. This delay represents a combination of a round-trip delay of the SFOAE signal and a delay of the measurement system.

Each original acoustic waveform was shifted by 3.1 ms to compensate for the delay described above. Then the heterodyne analysis was applied to the shifted waveform, and the magnitude, $m(f)$, and phase, $\theta(f)$, of an SFOAE for a particular analysis frequency, f, was determined by taking the magnitude and phase of the heterodyne-analysis output at the time when the stimulus frequency was equal to the analysis frequency. We converted the SFOAE magnitude, m in μPa, into an SFOAE level in dB SPL *re* 20 μPa by using

$$\text{SFOAE level} = 20 \cdot \log_{10}(m/20\ \mu\text{Pa}). \tag{4}$$

We repeated the above heterodyne analysis for a particular response waveform with a large number of analysis frequencies ranging from 550 to 1450 Hz in small steps. Because the analysis could be performed after the data were collected, the analysis time did not increase the recording time. The frequencies of 500–550 and 1450–1500 Hz were excluded to avoid transients. The minimum frequency separation where the contribution to an analysis frequency was less than 0.7 relative to the contribution by the analysis frequency itself was given by the bandwidth of the low-pass filter, ± 9.1 Hz. Thus, for the present SFOAE measure at each analysis frequency, the signal component at a frequency 9.1 Hz away from the analysis frequency had a relative contribution of 0.7. In describing our results, we chose to display the SFOAE measures versus frequency with a 5 Hz spacing rather than a 9.1 Hz spacing to improve visualization.

F. Noise floor computation

Noise floor was computed in separate steps from the normal SFOAE analysis. As stated above, the heterodyne output corresponds to the level and phase of a particular analysis frequency versus time; the full time range of measured waveform (0–1.43 s) in the present study was mapped to a probe-stimulus-frequency range of 500–1500 Hz. Such a heterodyne output typically exhibited high levels near the points where the probe frequency or suppressor frequency (150 Hz above the probe frequency) was equal to the analysis frequency. The level near the point of suppressor frequency was attenuated by applying a 227 ms Blackman window (spanning a frequency range of ± 79 Hz) centered at the probe frequency, as stated above. In a wide region of the full range of time/frequency in the heterodyne analysis output, neither the probe frequency nor the suppressor frequency was near the analysis frequency. In such a "remote region," consequently, the level of the heterodyne analysis output was quite low.

We defined a remote region to be a region spanning probe frequencies over a 400 Hz range. For this purpose, we treated the full probe frequency range of 550–1450 Hz as a circular range. For a particular analysis frequency, a probe frequency in the remote region was at least 150 Hz higher than, and at least 350 Hz lower than, the analysis frequency. For example, if the analysis frequency was 1000 Hz, the remote region consisted of two subregions of probe frequencies: (1) 550–650 Hz, and (2) 1150–1450 Hz.

For a particular analysis frequency, the 400-Hz-wide remote probe-frequency region consisted of 80 sample points separated by 5 Hz steps. For each of the 80 remote probe-frequency points, we multiplied the original response waveform with a 227 ms Blackman window centered at the "remote point" under consideration and then performed the heterodyne analysis yielding one remote level. We repeated the process 80 times for the 80 remote points and defined the average of the 80 remote levels to be the noise floor level for one analysis frequency under consideration. This process was repeated for each of all analysis frequencies.

G. Quantification of response features of SFOAE fine structures

SFOAEs exhibited fine structures, i.e., multiple peaks and troughs of level and many cycles of phase change over a frequency range of 550–1450 Hz. Based on such data in each subject, we quantified the following response features: (1) mean level (ML) of SFOAE in dB SPL; (2) number of peaks (NP); (3) frequency spacing (Δf) between SFOAE peaks in Hz; (4) number of cycles (NC) of SFOAE phase change; (5) energy-weighted group delay (EGD) in ms; and (6) standard deviation of EGD (σ_{EGD}) in ms.

Regarding NP, we required that an acceptable peak should be surrounded troughs each with a minimum 2 dB depth; the latter was measured between a relevant local minimum and the straight line connecting two neighboring peak candidates (local maxima). To determine energy-weighted group delays (EGDs), we first unwrapped SFOAE phase versus frequency where the neighboring phase values were constrained to be within one half cycle. The EGD was obtained by differentiating the unwrapped SFOAE phase, θ, with respect to frequency, f, with an energy weighting as follows:

$$\text{EGD}(f_c) = \frac{-\sum_{\text{f}} A^2(f) \cdot \frac{d\theta}{df}}{\sum_{\text{f}} A^2(f)}; \tag{5}$$

where, $A(f)$ and f_c represent the SFOAE amplitude at frequency f and the center of the processed frequency range,

respectively. The value of $d\theta/(df)$ was obtained by dividing the difference between the two neighboring phase values by the 5 Hz frequency difference. We used 25-Hz-wide ranges centered at various frequencies for information about how a narrowband EGD changes as a function of the center frequency, and a 900-Hz-wide range for information about the overall EGD processed for the whole 550–1450 Hz range. This definition of EGD was adapted from Goldstein *et al.* (1971) who indicated that EGD of a band-limited filter corresponds to the center of gravity of the impulse response of the filter. The advantage of EGD over the un-weighted group delay (GD) is that the former incorporates the fact that GD associated with a large amplitude is more meaningful than one associated with a small amplitude. We also determined normalized energy-weighted group delays (NEGDs) in units of cycles as follows:

$$\mathrm{NEGD}(f_c) = \mathrm{EGD} \times f_c. \tag{6}$$

The measure σ_{EGD} describes the variability of 25-Hz-wide EGDs over the 550–1450 Hz range in each subject.

H. Level-sweeping method

The level-sweeping method allowed us to measure the SFOAE input-output functions at specific frequencies. The frequency-swept data obtained at −40 dB *re* maximum were used to choose several peak and trough frequencies. Measurements were made at selected probe frequencies with swept stimulus levels. After the measurement, the probe (f_1) component was obtained using the heterodyne analysis method as above. The input-output functions of the SFOAE level and phase at a specific probe frequency were constructed by pairing the output level and phase with the corresponding input level.

At each measurement, the acoustic stimulus was repeated eight times. The duration of the stimulus was approximately 12 s hence each measurement required about 1.5 min. The stimulus had two channels with each having two intervals (as above). The probe frequency was fixed but level was varied, and the suppressor frequency was fixed at 150 Hz above the probe frequency and the level was varied. During the level sweep, the amplitudes of the waveforms were exponentially increased or decreased. These exponential changes of amplitudes over time correspond to linear sweeps of the stimulus levels in dB SPL versus time.

To construct the SFOAE input-output function, the heterodyne analysis was applied to extract the probe frequency component. Finally, the SFOAEs were extracted by taking the vector difference between the two intervals (as above). Generally, the probe level ranged from 10 to 70 dB SPL with the suppressor level ranging from 50 to 90 dB SPL; the suppressor level was 20–40 dB above the probe level. In cases where the maximum ear canal pressure of the suppressor channel was less than 90 dB SPL, the ranges of the probe and suppressor levels were adjusted. The present method of obtaining input-output functions with a continuously swept stimulus level is similar to that described by Neely *et al.* (2003).

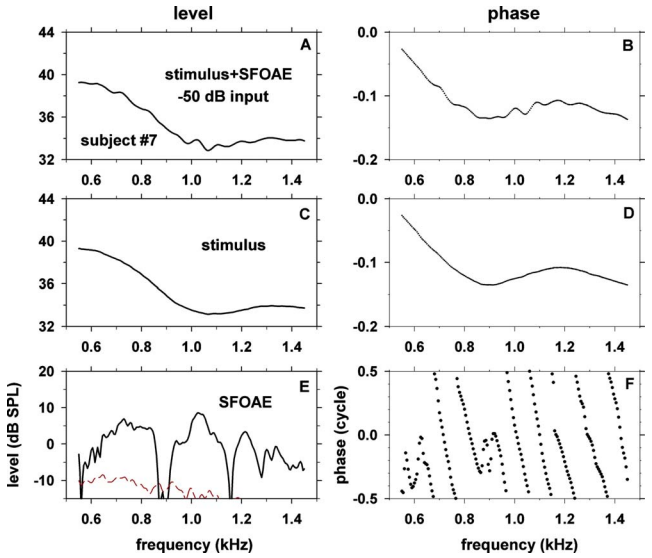


FIG. 1. (Color online) Procedure for obtaining SFOAE level and phase using frequency-swept stimuli illustrated with results obtained with a stimulus level of −50 dB *re* maximum voltage in one subject, No. 7. The left and right columns show signal level (in dB SPL) and phase (in cycles), respectively. In the top row (panels A and B), the signal (in the first interval) was a mixture of stimulus and SFOAE. In the second row (panels C and D), the signal (in the second interval) was stimulus with little SFOAE present as SFOAE was suppressed by the suppressor tone. The vector difference between the signals in the top two rows, shown in the third row (panels E and F), corresponds to SFOAE. Negative phase values were defined to be a phase lag. In panel E, dashed line represents noise floor.

III. RESULTS OF HUMAN SFOAES

A. Frequency-sweeping experiment

The procedure for obtaining SFOAE level and phase versus frequency is illustrated with an example obtained in one subject (No. 7) with a probe stimulus level of −50 dB *re* maximum voltage into the earphone (Fig. 1). As described in Methods, the stimulus consisted of two intervals where the first interval contained only the probe frequency component and the second interval contained both the probe and the suppressor frequency components. We obtained SFOAE level and phase versus frequency (Fig. 1, bottom row) by taking vector differences between the heterodyne outputs derived from the first interval (corresponding to SFOAEs plus probe stimuli, Fig. 1, top row) and those derived from the second interval (corresponding to probe stimuli, Fig. 1, middle row). The signals in the middle and bottom rows of Fig. 1 display a slowly varying pattern superimposed on a rapidly varying pattern. The slowly varying stimulus (middle row) represents the frequency-dependent properties of the stimulus-generating system and the input impedance looking into the ear. The dashed line in panel E shows the noise floor computed as described in Methods

The data of Fig. 1 are consistent with the concept that the stimulus+SFOAE fine structure has a frequency spacing the reciprocal of which corresponds to a round-trip delay (Zweig and Shera, 1995). The frequency spacing between peaks of the stimulus+SFOAE around 1 kHz [Fig. 1(A)] is 81 Hz. The reciprocal of 81 Hz is 12.3 ms. This value is close to the group delay of SFOAEs around 1 kHz, 11.1 ms [see below, Fig. 2(I)].

TABLE II. Comparison of SFOAEs obtained with the conventional analysis method against those obtained with the heterodyne analysis method. The two types of analysis methods were applied to a common set of data records obtained with conventional stimuli where the stimulus frequency was kept constant (at one of three values) over a 1.43 s stimulus period. The stimulus levels were 57, 54, and 52 dB SPL for 800, 1000, and 1100 Hz, respectively. Each entry is level (in dB SPL) and phase (in cycle) of SFOAE for a particular frequency. Results from one ear of Subject No. 9.

	800 Hz	1000 Hz	1100 Hz
Heterodyne	24.8 dB; 0.511 cyc.	23.6 dB; 0.480 cyc.	22.3 dB; 0.038 cyc.
Conventional	24.5 dB; 0.524 cyc.	23.3 dB; 0.482 cyc.	22.2 dB; 0.035 cyc.

As seen in panel C of Fig. 1, ear-canal sound pressure level varied as a function of frequency when the stimulus level was kept at a constant attenuation of voltage into the earphone. In this subject, −50 dB *re* maximum voltage corresponded to 37 ± 4 dB SPL *re* 20 μPa. The range of dB SPL values in various subjects at −50 dB *re* maximum voltage are described in Table I.

To verify that the current method generates results consistent with those of the conventional method (using a fixed-frequency stimulus), we analyzed a common dataset obtained with a constant stimulus frequency using two analysis methods: (1) a simple conventional Fourier transform, and (2) the heterodyne analysis. The results of one subject (No. 9) for three stimulus frequencies are summarized in Table II. The differences between the results obtained by the two analysis methods were within 0.3 dB in level and 0.013 cycle in phase. These data demonstrate that the results obtained with the current heterodyne analysis method are consistent with those obtained with the conventional method.

The results obtained with stimulus level from 27 to 57 dB SPL in subject No. 7 are shown in Fig. 2. The three columns represent SFOAE level, phase and 25-Hz-wide EGDs, respectively. The effective frequency resolution of the present data is 9.1 Hz as stated in Methods, and the data are plotted with 5 Hz steps. Prominent features of the data are: (1) SFOAE level versus frequency exhibits many quasi-periodic peaks and troughs; (2) when SFOAE phase is unwrapped, the phase versus frequency tends to be almost a straight line with a steep slope but there are conspicuous irregularities in the slope; (3) the 25-Hz-wide EGD varies irregularly as a function of frequency; and (4) all of the SFOAE fine-structure features change noticeably with stimulus level. The quasi-periodic peaks/troughs in SFOAE level versus frequency (Fig. 2, left column) should not be equated to quasi-periodic peaks/troughs seen in a mixture of SFOAE and stimulus [Fig. 1(A)]. An SFOAE itself (after removing the stimulus) still exhibits a quasi-periodicity. The mean level (ML) of SFOAE changed from −7.2 dB SPL at stimulus level of 27 dB SPL to 11.6 dB SPL at stimulus level of 57 dB SPL. The number of peaks (NP) of SFOAE in the 550–1450 Hz range decreased from 21 peaks at 27 dB SPL to six peaks at 57 dB SPL. The frequency spacing between peaks, Δf, increased from 42 to 121 Hz and the number of cycles of phase change (NC) decreased from 8.0 to 6.0 cycles over the same range of stimulus levels.

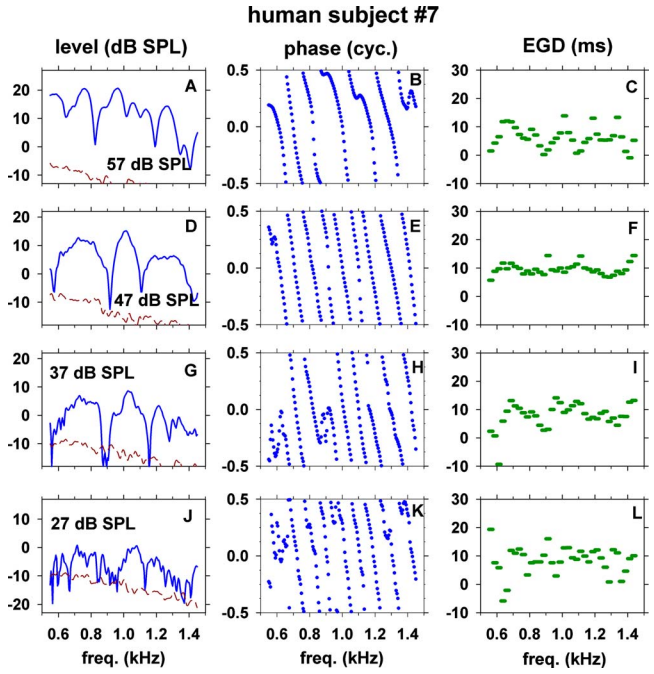


FIG. 2. (Color online) Level, phase, and 25-Hz-wide energy-weighted group delay (EGD) of SFOAE in one subject (No. 7) versus frequency at several stimulus levels (27–57 dB SPL). Dashed lines in the left panels show noise floor.

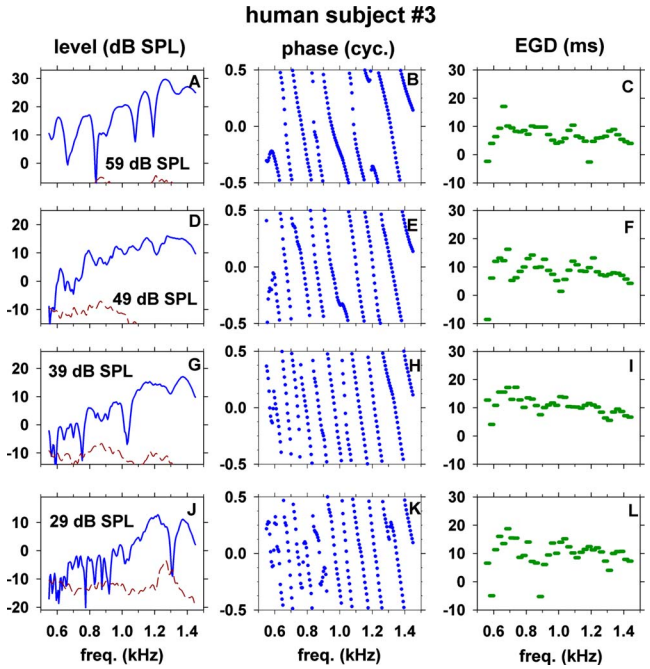


FIG. 3. (Color online) Level, phase, and 25-Hz-wide EGD of SFOAE in another subject (No. 3) versus frequency at several stimulus levels (29–59 dB SPL).

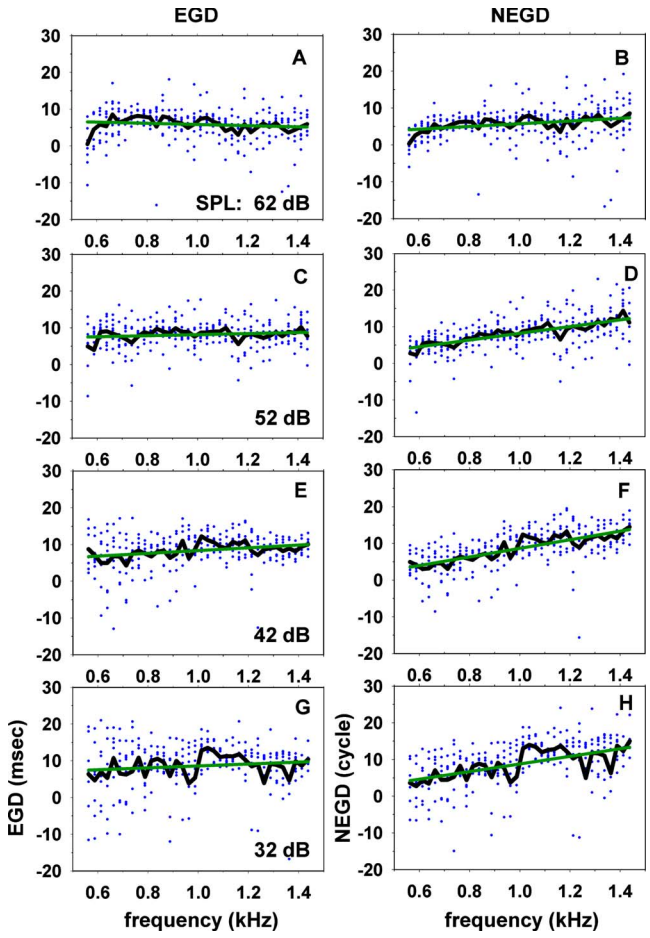


FIG. 4. (Color online) Energy-weighted group delays (EGDs) and normalized EGDs (NEGDs) of all subjects at several stimulus levels (32–62 dB SPL). Individual dots represent 25-Hz-wide EGDs or NEGDs of all subjects. At every 25 Hz band, individual EGDs or NEGDs were averaged and shown as a jagged line in each panel. A straight line is a linear regression line for the average values for various frequencies.

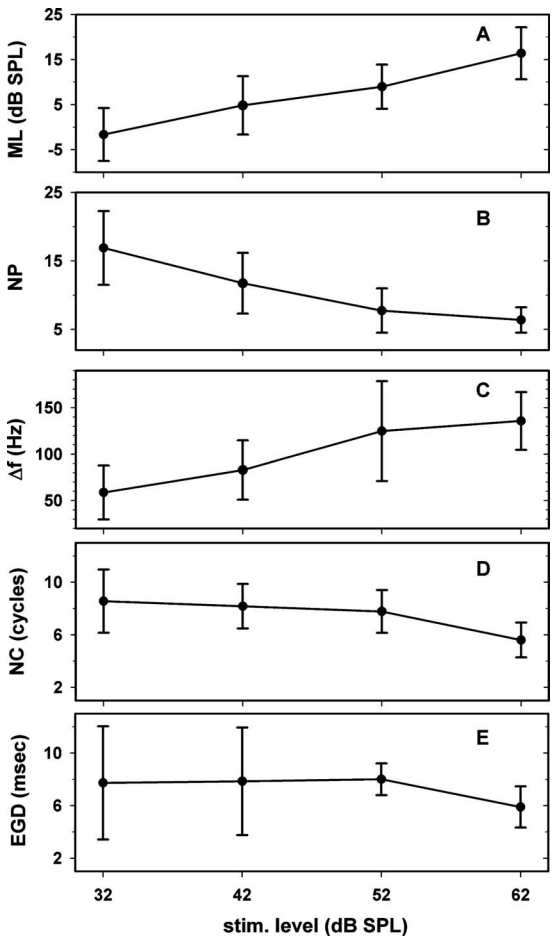


FIG. 5. Means ± standard deviations of five response features of SFOAEs among eight human subjects versus stimulus level: mean level (ML) of SFOAE, number of peaks (NP), frequency spacing (Δf), number of cycles of phase change (NC), and energy-weighted group delays (EGDs) in ms.

Results from another subject (No. 3) are shown in Fig. 3 for stimulus levels of 29–59 dB SPL to illustrate an intersubject variability. Although there are quantitative differences between the two subjects, the results from the two subjects are qualitatively similar; e.g., (1) there are many peaks/troughs of SFOAE level, (2) there are many cycles of phase change, (3) the 25-Hz-wide EGD varies irregularly as a function of frequency; and (4) NP, Δf, and NC change with stimulus level. ML changed from −0.5 dB SPL at stimulus level of 29 dB SPL to 17.5 dB SPL at stimulus level of 59 dB SPL. NP decreased from 16 to 7 peaks, Δf increased from 54 to 133 Hz and NC decreased from 9.2 to 6.6 cycles over the range of 29–59 dB SPL stimulus level.

Major troughs of SFOAE level tended to have concomitant rapid changes in phase slope and EGD. For example, there were major troughs at ~820, 1190, and 1410 Hz in Fig. 2(A) (57 dB SPL) and at ~910 and 1110 Hz in Fig. 2(D) (47 dB SPL). At such frequencies, the phase slopes abruptly changed [Figs. 2(B) and 2(E)] and the EGD values deviated from the neighboring values [Figs. 2(C) and 2(F)]. The phase slope became either steeper, shallower, or inverted with the EGD becoming longer, shorter, or negative. Analogous examples of concomitant microstructures of level, phase, and EGD of SFOAEs were also observed in another subject, e.g., troughs at ~1080 and 1200 Hz [Fig. 3(A)] were associated with rapid or irregular changes of phase slope [Fig. 3(B)] and EGD [Fig. 3(C)].

The 25-Hz-wide EGDs and normalized EGDs (NEGDs) of all eight subjects are plotted versus frequency as scattered dots in Fig. 4. The jagged and straight lines represent the average values and linear regression lines of the average values, respectively. There was a large variability in EGD and NEGD across subjects and across frequency. However, the linear regressions showed that EGDs tended to be almost constant and NEGDs tended to increase with increasing frequency across the 550–1450 Hz range. The value of EGD tended to decrease with increasing stimulus level. For example, EGD near 1 kHz tended to be ~9 ms at 32 dB SPL and ~6 ms at 62 dB SPL; the corresponding values of NEGD were 9 at 32 dB SPL and 6 at 62 dB SPL.

We determined ML, NP, Δf, NC and EGD for all subjects. Means and standard deviations of each of these measures across the subjects are shown at four stimulus levels in Fig. 5. For this figure, EGDs were calculated over the full 900-Hz-wide range NP, NC, and EGD decreased whereas ML and Δf increased with increasing stimulus level.

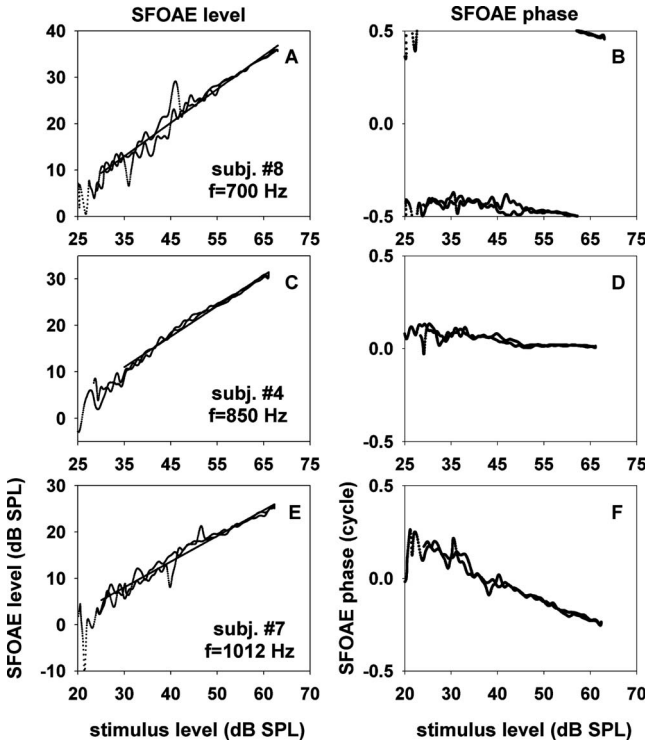


FIG. 6. SFOAE level and phase versus stimulus level for "peak stimulus frequencies." The latter were defined to be stimulus frequencies corresponding to peaks of SFOAE level versus frequency at 52 dB SPL. The three rows correspond to data from three different subjects; the subject identification numbers and the selected stimulus frequencies are shown in the insets. The input-output functions of SFOAE level were fitted with straight lines. The slopes of the fitting lines were 0.72, 0.66, and 0.55 dB/dB for panels A, C, and E, respectively.

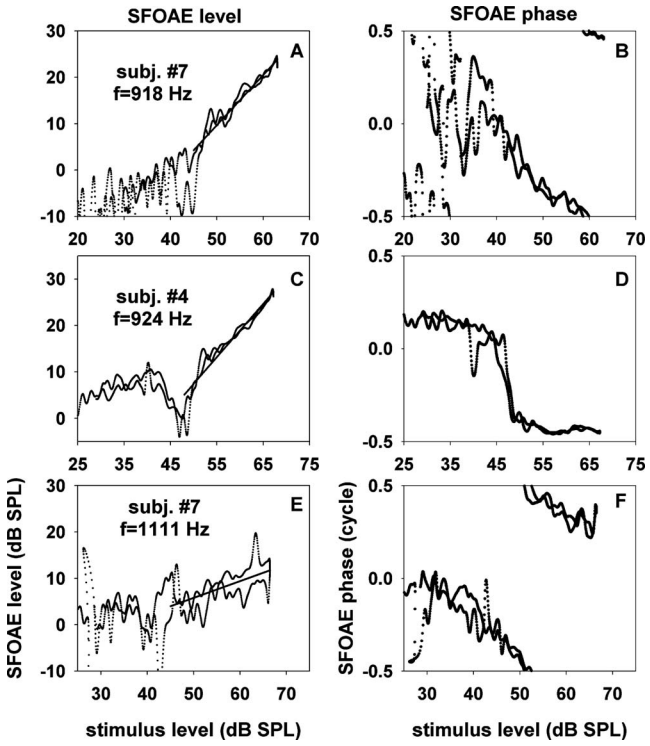


FIG. 7. SFOAE level and phase versus stimulus level for "trough stimulus frequencies." The latter were defined to be stimulus frequencies corresponding to troughs of SFOAE level versus frequency at 52 dB SPL. The three rows correspond to data from three different cases; the subject identification numbers and the selected stimulus frequencies are shown in the insets. The portions of the input-output functions of SFOAE level, where slopes could be ascertained, were fitted with straight lines. The slopes of the fitting lines were 1.08, 1.15, and 0.36 dB/dB for panels A, C, and E, respectively.

B. Level-sweeping experiment

We determined dependence of SFOAE level and phase upon stimulus level by using the stimulus level-sweeping method described in Sec. II H. For these measurements, we selected the probe frequency corresponding to a peak or a trough (in a graph like Figs. 2 and 3). Results obtained with a peak frequency in three subjects are shown in Fig. 6. The input-output functions in log-log plots were approximately straight lines. The data of Fig. 6 were fit with slopes ranging from 0.55 to 0.72 dB/dB. The phase of SFOAE remained nearly independent of stimulus level or became lagging as the stimulus level increased. The amount of phase change was small (<0.14 cycle) in two (panels B and D) of the three cases and larger (0.47 cycle) in the third case (panel F). Slope and phase change obtained with a peak frequency in each subject are described in Table III. The input-output slope ranged 0.52–0.72 whereas the amount of phase change ranged −0.13 to −0.47; a negative phase change corresponds to a phase lag.

Analogously, we determined dependence of SFOAE level and phase upon stimulus level for trough frequencies as shown in Fig. 7. These data illustrate that SFOAE versus stimulus level can be complex and variable if the probe frequency falls in a trough of SFOAE level versus frequency. The example of panel C is a clear illustration of a nonmonotonic input-output level function together with a rapid phase change of about a half cycle around the level notch. The present level-sweep method is particularly useful in characterizing such complex input-output functions because a high resolution of stimulus level is necessary to determine the nonmonotonic nature of emission level and a rapid phase change restricted to a small region of stimulus level.

In the left panels of Fig. 7, partial regions were selected where slopes could be measured. These slopes are summarized in Table IV. Two entries for a particular subject correspond to results obtained with two trough frequencies. The input-output slopes for trough frequencies ranged from 0.36 to 1.83. The range of slopes for trough frequencies was wider

TABLE III. Slopes of input-output functions of SFOAE level and changes of SFOAE phase with stimulus level at frequencies corresponding to SFOAE-level peaks.

Subject ID No.	2	3	4	5	7	8
Slope (dB/dB)	0.52	0.66	0.66	0.55	0.55	0.72
Δ phase (cycle)	−0.25	−0.26	−0.13	−0.47	−0.45	−0.14
Frequency (Hz)	820	961	850	1075	1012	700

TABLE IV. Slopes of input-output functions of SFOAE level at frequencies corresponding to SFOAE-level troughs in regions where slopes could be defined. Multiple entries within a subject represent multiple trough frequencies. There was no correlation between slope and frequency.

Subject ID No.	2	3	4	5	6	7	8
Slope (dB/dB)	0.50	0.37	0.87	0.61	0.48	0.36	0.75
Frequency (Hz)	1320	896	1121	1420	1200	1111	1450
Slope (dB/dB)	NA	1.83	1.53	0.75	0.75	1.08	0.78
Frequency (Hz)	NA	1014	1193	1295	1396	918	770

than that for peak frequencies. Measurements of phase changes in this case were omitted because the starting or ending points of the phases were not clear in most cases.

The facts that SFOAE level can change nonmonotonically with stimulus level and that the peak frequencies shift with stimulus level are illustrated with results from one subject in Fig. 8. It describes SFOAE level over a small range of frequencies (1000–1250 Hz) around a peak and the neighboring troughs for various stimulus levels. At 1160 Hz, SFOAE level was a nonmonotonic function of stimulus level similar to Fig. 7(C). The peak of SFOAE level was centered at 1140 Hz at stimulus level of 22 dB SPL but it gradually shifted toward lower frequencies with increasing stimulus level. The peak frequency decreased to 1065 Hz at 62 dB SPL.

IV. MODEL DEFINITION AND METHODS

A. Basic concept

The present model is intended to represent the human cochlea with a length of 35 mm. To simulate SFOAEs one needs to calculate the forward and backward waves in the cochlea by solving the wave equation. We adopted the one-dimensional transmission line model of the cochlea as described by Zweig *et al.* (1976). The nonuniform transmission line model incorporates a second-order differential equation for the wave propagation and reflection as

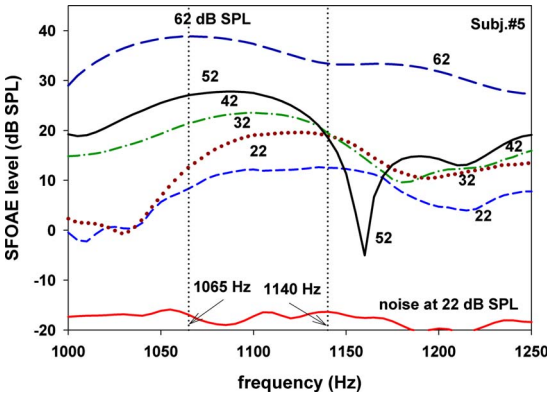


FIG. 8. (Color online) An example illustrating that a peak of SFOAE level shifted as a function of stimulus level. As the stimulus level increased, the position of the peak shifted to a lower frequency. The data also illustrate the fact that SFOAE level for a frequency near a trough (1160 Hz) can be a nonmonotonic function of stimulus level. The lowest curve shows noise floor at 22 dB SPL.

$$\frac{d^2P}{dx^2} - \frac{d\ln Z_s}{dx}\frac{dP}{dx} - Y_b Z_s P = 0, \tag{7}$$

where P is pressure difference between scalae, Z_s scala impedance per centimeter, Y_b cochlear-partition admittance per unit length, and x distance from the stapes. The cochlear-partition admittance and scala impedance were selected to maintain an approximate shift invariance. In other words, the excitation pattern shifts with frequency along the cochlea without much changing its shape. The model was made *active* by having Y_b include a region of negative damping (Neely and Kim, 1983, 1986, 2008).

$$Y_b(s) = \frac{7.186 \times 10^{-2} \exp(-1.51x)}{Z_b(s)}, \tag{8}$$

$$Z_b(s) = Z_1(s) + g \times \frac{1.666 \times Z_2(s) \cdot Z_3(s)}{Z_2(s) + Z_3(s)}, \tag{9}$$

where

$$Z_1 = sM_1 + R_1 + K_1/s, \tag{10}$$

$$Z_2 = sM_2 + R_2 + K_2/s, \tag{11}$$

$$Z_3 = R_3. \tag{12}$$

$$K_1 = 1.291 \times 10^8 \exp(-3.01x),$$
$$R_1 = 1.797 \times 10^2 \exp(-1.51x), \quad M_1 = 0.002. \tag{13}$$

$$K_2 = 6.455 \times 10^1 \exp(-3.01x),$$
$$R_2 = 3.595 \times 10^{-1} \exp(-1.51x), \quad M_2 = 6.0 \times 10^{-9}. \tag{14}$$

$$R_3 = -3.593 \times 10^{-1} \exp(-1.51x). \tag{15}$$

In these equations $s = i2\pi f$ is the Laplace-transform variable, while K, R and M represent the stiffness, damping and mass, respectively. Z_1 represents the cochlear-partition impedance when the cochlea is in a passive mode, and Z_2 and Z_3 create a frequency-dependent negative-damping region. Negative damping provided cochlear amplification and a proper shape of the cochlear excitation pattern (Neely and Kim, 1983, 1986, 2008). The parameter g in Eq. (9) determined the magnitude of negative damping and the amount of cochlear amplification. When g was zero, the cochlea was in a passive mode and exhibited no amplification. The model

was piecewise linear and represented the cochlear nonlinear behavior by increasing g (producing greater amplification) with decreasing stimulus level.

The scala impedance Z_s was chosen to have a decreasing cross-sectional area to compensate for the decreasing stiffness in the cochlear-partition impedance as

$$Z_s(s) = \rho s/A_s, \tag{16}$$

$$A_s = 3.592 \times 10^{-3} \exp(-1.51x). \tag{17}$$

In this equation, $\rho=1$ represents the fluid density. These parameter values were selected to keep the characteristic impedance of the transmission line $Z_c=\sqrt{Z_s/Y_b}$ as uniform as possible to minimize reflections.

The pressure difference P has both the forward (P_f) and backward (P_r) wave components, which may be decomposed as

$$P_f = \frac{1}{2}(P - P'/\beta), \tag{18}$$

$$P_r = \frac{1}{2}(P + P'/\beta). \tag{19}$$

where $P' \equiv dP/dx$ is the x derivative (or gradient) of P, and $\beta=\sqrt{Z_sY_b}$ is the propagation function. This decomposition formula was originally derived for a uniform transmission line (e.g., Durney and Johnson, 1969), and is exact only when the characteristic impedance is constant along the cochlea. We need to decompose the forward and backward waves only at the two ends of the cochlea, i.e., the stapes and helicotrema, for calculation of the reflectance (see below) and boundary conditions. The characteristic impedance is almost constant in these regions. Therefore, Eqs. (18) and (19) are applicable to the present model.

Cochlear reflectance, $\Re$, is defined as the ratio of the reverse-wave pressure to the forward-wave pressure wave at the stapes as

$$\Re = P_r/P_f. \tag{20}$$

If we assume that the effect of the middle ear is an amplitude scaling (see Sec. IV B below), then SFOAE can be modeled as the product of the cochlear reflectance, the round-trip middle ear gain, and the incident pressure at the eardrum (i.e., the stimulus) as

$$P_{\mathrm{SFOAE}} = \Re \cdot G_m \cdot P_S, \tag{21}$$

where P_{SFOAE}, G_m and P_S denote the pressure of SFOAE, round-trip middle ear gain, and the pressure of stimulus in the ear canal, respectively

We first solved the transmission line equation (7) numerically for pressure P along the length of the cochlea. The cochlear length $L=35$ mm was represented by $N=3501$ points (including both end points), and the differential equation was converted into difference equations by the finite-difference method. Since we are interested in the reflection coefficient only, the boundary condition at the stapes side was set as $P=1$. At the helicotrema there should be no backward wave, which results in $P=-P'/\beta$ as the helicotrema boundary condition. The resulting matrix equation was solved numerically for the pressure P, and the forward and backward pressures were calculated at the stapes.

B. Round-trip middle ear gain

Puria (2003) measured forward and reverse middle-ear pressure gain. These pressure gains varied slowly with frequency compared with SFOAE fine structures. In the current study, we are interested in the frequency range from 550 to 1450 Hz. In that range, the round-trip amplitude gain varied slowly between about −6 and −27 dB, and the phase changed between about 0.25 cycle and −0.4 cycle. From the data of Puria (2003), we determined that the average middle-ear round-trip amplitude gain over 500–1500 Hz was −17 dB. The phase part of the middle-ear round-trip function was negligible compared to the total phase change observed in SFOAE (i.e., NC). Therefore, we approximated the middle-ear round-trip function, G_m, with −17 dB and ignored the phase change.

C. Cochlear irregularity

Previous theoretical studies suggest that SFOAEs are generated by distributed irregularity in the cochlear-partition impedance (Zweig and Shera, 1995). It is not known which component of the impedance (i.e., stiffness, damping or mass) is most important for generation of SFOAE. Although we found that fine structures of the model cochlear reflectance could be generated with irregularity in only one of the three impedance components, irregularity in the overall impedance produced the widest range of model behavior. Therefore, we chose to apply irregularity to the overall impedance of the cochlear partition.

Irregularity in the cochlear-partition impedance was introduced by using:

$$\hat{Z}_1(x) = Z_1(x)[1 + I_r(x)], \tag{22}$$

$$I_r(x) = \alpha \cdot u_1(x)\exp[i \cdot 2\pi \cdot u_2(x)], \tag{23}$$

where $\hat{Z}_1(x)$, and $Z_1(x)$ are rough and smooth impedances, respectively, of the cochlear partition as functions of x. The relative irregularity, $I_r(x)$, is a complex quantity having a random magnitude between 0 and α ($\alpha<1$) and a random phase between 0 and 1 cycle; $u_1(x)$ and $u_2(x)$ are uniformly distributed random numbers ranging from 0 to 1. In the initial form of the model, the irregularities at different positions along the cochlea were independent of each other.

We modified the above concept of independently distributed irregularity along the cochlear distance by introducing a novel hypothesis that the spatial-frequency content of the distributed irregularity of the cochlear-partition impedance is low-pass filtered by the cochlear-amplifier mechanism and that both the amount of cochlear amplification and the spatial filter cutoff frequency change monotonically with stimulus level. Thus, $\hat{Z}_1$ was represented as:

$$\hat{Z}_1 = Z_1[1 + \hat{I}_r(x)], \tag{24}$$

$$\hat{I}_r(x) = F^{-1}[F\{I_r(x)\} \cdot L(f_s)], \tag{25}$$

$$L(f_s) = \left(1 + \left|\frac{f_s}{f_{s_0}}\right|^n\right)^{-1}, \tag{26}$$

where, $F\{\cdot\}$, $F^{-1}\{\cdot\}$, f_s, f_{s_0}, and n represent spatial Fourier transform, inverse spatial Fourier transform, spatial frequency, spatial low-pass filter cutoff frequency, and the order of the filter, respectively. The spatially filtered irregularity $\hat{I}_r(x)$ can be also expressed as

$$\hat{I}_r(x) = \alpha \cdot u_3(x)\exp[i \cdot 2\pi \cdot u_4(x)], \tag{27}$$

where $u_3(x)$ and $u_4(x)$ are random numbers which have low-pass filtered spatial profiles.

D. Fit-error function

To quantify the difference between human SFOAE data (target) and the model results, we defined a fit-error function as:

$$E_{\text{fit}}(52 \text{ dB SPL}) = 0.2 \times E_{\text{NP}} + 0.2 \times E_{\text{NC}} + 0.2 \times E_{\text{EGD}} + 0.2 \times E_{\sigma\text{EGD}} \tag{28}$$

$$E_{\text{fit}}(\text{other}) = 0.2 \times E_{\text{ML}} + 0.2 \times E_{\text{NP}} + 0.2 \times E_{\text{NC}} + 0.2 \times E_{\text{EGD}} + 0.2 \times E_{\sigma\text{EGD}} \tag{29}$$

$$E_X = 1 - \exp[-10 \times \{(V_X - T_X)/T_X\}^2] \tag{30}$$

$$E_{\text{ML}} = 1 - \exp[-0.01 \times (V_{\text{ML}} - T_{\text{ML}})^2], \tag{31}$$

where E_X is either E_{NP}, E_{NC}, E_{EGD} or $E_{\sigma\text{EGD}}$, and V_X is either V_{NP}, V_{NC}, V_{EGD} or $V_{\sigma\text{EGD}}$, which represent the model values of NP, NC, EGD and STD of 25-Hz-wide EGDs, respectively; T_X represents the corresponding target value, e.g., T_{NP} corresponds to the target NP. V_{ML} is the model value of ML and T_{ML} is the target ML. The target ML at stimulus levels other than 52 dB SPL was calculated from the model ML value at 52 dB SPL with a 0.58 dB/dB slope. The 0.58 dB/dB slope corresponds to the slope of the human SFOAE ML versus stimulus level. When the model reflectance was greater than 0 dB at any frequency, the model result was rejected (the fit-error function was assigned a value of infinity).

V. MODEL RESULTS

A. Frequency-distance map of the cochlea

The frequency-distance map of the model is compared with the Greenwood (1990) function of the human cochlear map (Fig. 9). The two maps are in close agreement except for a region near the apical end. This study is focused on the frequency range of 550–1450 Hz where the two maps were in agreement. This agreement supports the model as a representation of the human cochlea.

B. Model SFOAE fine structures

We adjusted model parameters attempting to reproduce mean values of response features (ML, NP, NC, EGD, and σ_{EGD}) of eight subjects in the frequency range 550–1450 Hz. The above measures, except for σ_{EGD}, were plotted in Fig. 5. We generated 11 versions of the impedance irregularity spatial profiles using 11 random seeds. We obtained the mean values of the model response features among the 11 random-seed cases for each of the four stimulus levels. The four model parameters (g, α, f_{s_0}, and n) were adjusted to find a best fit for the human SFOAE data for four stimulus levels as follows. Initially we adjusted g from 0.70 to 1.00 in steps of 0.05, α from 0.02 to 0.78 in steps of 0.04, f_{s_0} from 0.50 to 1.50 cycles/mm in steps of 0.1 cycles/mm, and n from 5 to 60 in steps of 5.

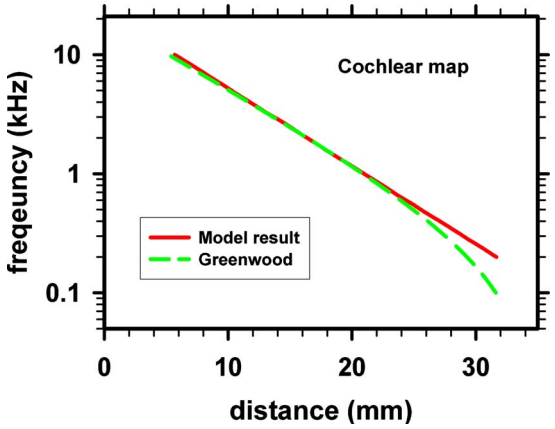


FIG. 9. (Color online) Cochlear frequency-distance map of the model (at 32 dB SPL) compared with the Greenwood (1990) function for the human cochlea.

During this adjustment, we first simulated the 52 dB SPL data. We treated the 52 dB data as the reference (or anchor) among the four stimulus levels. The fit-error function for 52 dB data, Eq. (28), included error components associated with four response features (NP, NC, EGD and σ_{EGD}) but excluded an error component associated with ML. We chose this approach because the model exhibited a difficulty of fitting all features including ML. Once we obtained the optimal model parameters for a best fit of the 52 dB data based on Eq. (28), we then attempted to simulate the optimal model behavior for other stimulus levels using all features including ML, i.e., using Eq. (29). This approach was intended to reproduce an optimal slope of SFOAE-level versus stimulus level. Accordingly, we derived target values of ML for 32, 42 and 62 dB SPL by combining the model ML at 52 dB and a slope of 0.58 dB/dB. The latter slope was obtained as the slope of a linear regression line fit for the human data of ML versus stimulus level [Fig. 5(A)].

During the search for optimal model parameters (g, α, f_{s_0}, and n), we imposed the constraint that each of the model parameters should vary monotonically and smoothly with stimulus level. A smooth change meant that the slope of each parameter versus stimulus level should also vary monotonically with stimulus level

We defined the total fit error to be the sum of four fit errors for the four stimulus levels. After finding the initial candidate optimal parameter set that minimized the total fit error based on the coarse steps of the parameter values, we performed a further search with fine steps of each parameter

TABLE V. Means ($\bar{m}$) and standard deviations (σ) of six response features of model SFOAE results obtained with 11 random seeds of the cochlear-partition irregularity under the condition of the optimal values of the model parameters. The response features were: mean level (ML) of SFOAE in dB SPL; number of peaks (NP); frequency spacing (Δf) between SFOAE peaks in Hz; number of cycles (NC) of SFOAE phase change; energy-weighted group delay (EGD) in ms; and standard deviation of EGD (σ_{EGD}) in ms.

Stimulus level (dB SPL)		Model result					
		ML	NP	Δf	NC	EGD	σ_{EGD}
32	$\bar{m}$	−13.9	15.0	56.6	7.2	9.0	6.8
	σ	1.5	1.2	4.3	2.3	2.7	1.8
42	$\bar{m}$	7.0	11.1	77.8	7.7	8.1	5.4
	σ	1.1	1.4	12.2	1.3	1.0	1.3
52	$\bar{m}$	1.5	7.1	111.7	7.1	7.9	3.8
	σ	1.6	1.0	24.8	0.8	1.5	0.7
62	$\bar{m}$	4.0	5.5	151.8	5.3	6.1	3.8
	σ	1.7	0.9	20.2	1.3	1.1	0.8

around the initial candidate optimal parameter values. The fine step size was 0.01 for g, 0.02 for α, 0.5 cycles/mm for f_{s_0}, and 1 for n. The set of model parameters that yielded the smallest average total fit error across the 11 random-seed cases representing the response features ML, NP, NC, EGD and σ_{EGD}, was chosen as *the optimal parameter set*. The model response features obtained with the optimal parameter set are summarized in Table V, and the optimal parameters of the model and the fit errors are shown in Table VI.

Figures 10 and 11 show simulated SFOAE level, phase, and 25-Hz-wide EGD versus frequency obtained with the optimal parameter set of the model and with two particular random seeds Nos. 6 and 1, respectively. The model exhibited SFOAE characteristics similar to those of the human SFOAEs shown in Figs. 2 and 3. Thus, the model successfully reproduced salient features of the human SFOAEs at stimulus levels of 32–62 dB SPL.

Analogous to the human SFOAEs, major troughs of SFOAE level of the model also tended to have concomitant rapid changes in phase slope and EGD values. For example, the SFOAE level in Fig. 10(G) exhibited major troughs at ~720 and 980 Hz. Around these frequencies, there were concomitant rapid changes in the phase slopes [Fig. 10(H)] and EGDs [Fig. 10(I)]. Analogous examples of troughs [Fig. 11(A)] and rapid changes of phase slopes [Fig. 11(B)] and EGDs [Fig. 11(C)] are also visible around 810 and 1210 Hz in results obtained with a different random seed.

The confidence intervals of model parameters were determined as follows. Within the confidence interval of a parameter, the fit error did not exceed twice the optimal fit error among the 11 random-seed cases. That is, the model generated sufficiently similar features of SFOAEs when the model parameters were within the confidence intervals. The confidence intervals are shown in Table VII. For example, for 52 dB SPL, optimal fit-error E_{fit} was 0.040 among 11 cases (Table VI). If we vary g in a range of 0.87–0.91 while fixing the other three parameters, then the fit error remained smaller than $2\times E_{\mathrm{fit}}$, i.e., 0.080. In some cases, fit-error values were

TABLE VI. Optimal values of the model parameters that produced minimal fit-errors (E_{fit}). E_{fit}, dimensionless, is defined in Eqs. (28) and (29). The model parameters were g (dimensionless amplification parameter), α (dimensionless scale factor for the cochlear-partition impedance irregularity), f_{s_0} (cutoff frequency, in cycles/mm, of a low-pass spatial-frequency filter acting on the irregularity), and n (dimensionless parameter for the slope of the low-pass spatial-frequency filter).

Stimulus level (dB SPL)	g	α	f_{s_0}	n	E_{fit}
32	0.93	0.42	0.85	9	0.13
42	0.91	0.22	1.20	13	0.073
52	0.88	0.10	1.40	24	0.040
62	0.73	0.08	1.40	50	0.053

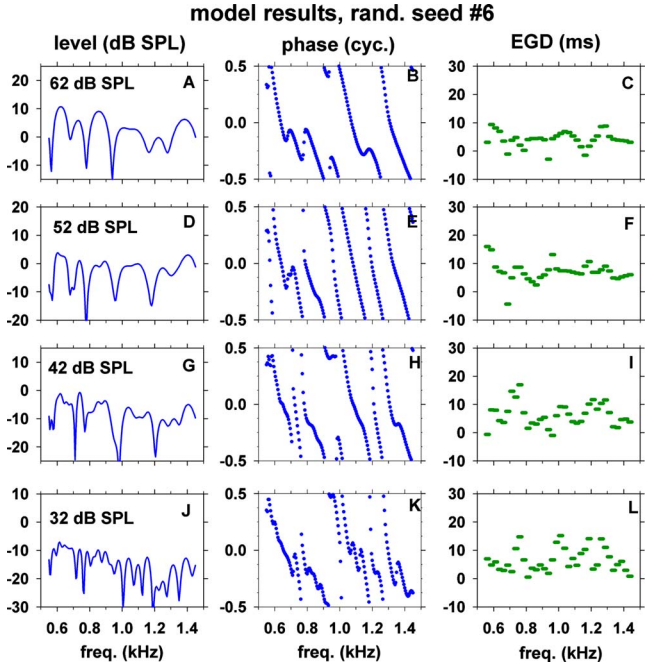


FIG. 10. (Color online) SFOAE fine structures of the model obtained with random seed No. 6 for the cochlear-partition impedance irregularity. The three columns correspond to the model SFOAE level, phase and energy-weighted group delay (EGD) versus frequency. The four rows correspond to four stimulus levels indicated in the insets. The model parameters were set to the optimal values described in Table VI.

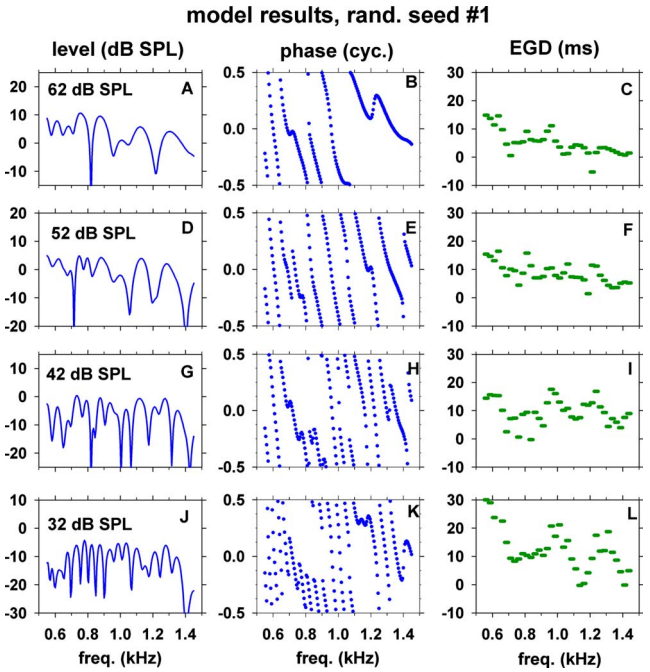


FIG. 11. (Color online) SFOAE fine structures of the model. All conditions of the model were the same as those of Fig. 10 except for the use of random seed No. 1 for the cochlear-partition impedance irregularity.

quite sensitive to the parameter change so that we introduced very small value ε which is smaller than 0.025 for f_{s_0} and 0.5 for n to represent the confidence interval. However, n value for 62 dB SPL in Table VII could be increased indefinitely because there was little effect on the low-pass filter when $n > 16$. Generally, the confidence intervals of the four model parameters shown in Table VII were narrow. That is, the model parameters for different stimulus levels were distinct with little overlaps. This indicates that the model parameters were well constrained by the human SFOAE features.

Changes of the model response features as results of changes in the model parameters are described in Table VIII using the 52 dB SPL stimulus condition as an example. Table VIII includes the optimal parameter set ($g=0.88$, $\alpha=0.10$, $f_{s_0}=1.40$ cycles/mm and $n=24$) together with other points of the parameter space corresponding to the extremes of the confidence interval of each parameter. Values of the model response features for the above conditions are shown. Within the confidence intervals, the relative magnitudes of changes in ML, NP, Δf, NC, EGD and $Q_{3\ \mathrm{dB}}$ were less than 2.2 dB, 8.5%, 9.7%, 8.5%, 11.4% and 4.2%, respectively Within the intervals, increases of g, α, or f_{s_0} led to increases of ML, NP, NC and EGD. A decrease of n led to a similar effect. Regarding $Q_{3\ \mathrm{dB}}$, only g among the four parameters affected $Q_{3\ \mathrm{dB}}$ such that an increase of g led to an increase of $Q_{3\ \mathrm{dB}}$.

C. Spatial profiles of irregularity

Spatial profiles of the amplitude (left column) and phase (right column) of the impedance irregularity under the condition of the optimal model parameters are described in Fig. 12. At 32 dB SPL, where the spatial low-pass cutoff frequency was the lowest, the spatial profile of amplitude and phase of the irregularity varied most slowly over cochlear distance among the four cases corresponding to four stimulus levels. With increasing stimulus level, the spatial low-pass cutoff gradually increased leading to increasingly more rapid changes of irregularity over distance.

D. Estimated human cochlear excitation patterns and transfer functions

Using the optimal model parameters described above, we determined cochlear excitation patterns and transfer functions of the model cochlear partition. The excitation patterns for 1 kHz stimulus frequency, corresponding to the ratio of cochlear-partition velocity to stapes velocity as a function of cochlear distance for a fixed frequency, are shown in Fig. 13, panels A and B. With decreasing stimulus level, the excitation pattern became sharper and the traveling-wave peak became higher moving slightly apically. The total phase lag of the excitation pattern was more than 15 cycles over the full cochlear distance. At the highest stimulus level, the phase-versus-distance slope became shallower.

The cochlear-partition transfer functions, corresponding to the ratio of cochlear-partition velocity to stapes velocity as a function of stimulus frequency for a fixed cochlear distance (i.e., the 1 kHz place), are shown in Fig. 13, panels C and D. The shapes of the partition responses versus distance (panel C) were quite similar to the partition responses versus stimulus frequency (panel A).

The sharpness of the partition transfer functions were quantified in terms of three types of quality factors and peak-to-shoulder ratio (PSR), also known as the tip-to-tail ratio.

TABLE VII. Confidence intervals of the model parameters g, α, f_{s_0}, and n. The confidence interval of each parameter was defined as one where the average fit error among the 11 random seed cases remained smaller than twice the optimal fit error. The confidence interval was determined by varying only one parameter at a time with the other parameters fixed at the optimal value (described in Table VI). The units of f_{s_0} are cycles/mm and the other three parameters are dimensionless. The symbol, ε, is intended to indicate a small quantity; it was less than the following values: 0.025 for f_{s_0}, and 0.5 for n.

	Stimulus level (dB SPL)			
Parameters	32	42	52	62
g	0.91–0.94	0.90–0.92	0.87–0.91	0.67–0.81
α	0.16–0.64	0.18–0.26	0.08–0.12	0.06–0.16
f_{s_0}	$(0.85-\varepsilon)$–$(0.85+\varepsilon)$	$(1.20-\varepsilon)$–$(1.20+\varepsilon)$	1.40–1.45	$(1.40-\varepsilon)$–$(1.40+\varepsilon)$
n	$(9-\varepsilon)$–$(9+\varepsilon)$	$(13\sim\varepsilon)$–$(13+\varepsilon)$	20–28	16–∞

TABLE VIII. Changes in model response features as results of changes in each model parameter at 52 dB SPL stimulus level. The range of each parameter was the confidence interval of the parameter described in Table VII. See the caption of Table VI for definitions of the model parameters.

		Model response features						
Parameter		ML (dB SPL)	NP	Δf (Hz)	NC (cyc.)	EGD (ms)	σ_{EGD} (ms)	$Q_{3\ dB}$
Optimal parameters		−1.5	7.1	111.7	7.1	7.9	3.8	7.1
g	0.87	−1.8	6.9	115.5	7.0	7.7	3.8	7.0
	0.91	−0.8	7.4	106.3	7.5	8.5	4.2	7.4
α	0.08	−3.5	6.5	122.5	7.0	7.7	3.7	7.1
	0.12	0.2	7.1	112.5	7.4	8.1	4.1	7.1
f_{s_0}	1.40	−1.5	7.1	111.7	7.1	7.9	3.8	7.1
	1.45	0.7	7.4	106.9	7.7	8.8	3.9	7.1
n	20	−1.0	7.3	108.6	7.2	8.2	4.1	7.1
	28	−1.7	6.6	117.9	6.9	7.8	3.9	7.1

Quality factors $Q_{3\ dB}$ and $Q_{10\ dB}$ correspond to the center frequency divided by the width of transfer function measured 3 and 10 dB below the peak, respectively. Q_{ERB} correspond to an analogous measure where the width of an equivalent rectangular bandwidth is used. For PSR, the shoulder corresponds to the part of the transfer function at a frequency below the peak where the curves of different stimulus levels converge. The values of these parameters for the model partition transfer functions are indicated in Table IX. $Q_{3\ dB}$ and Q_{ERB} ranged 5.5–8.0, $Q_{10\ dB}$ 3.2–4.3, and PSR 38–60 dB.

E. Decomposition of model SFOAE into long- and short-delay components

To determine the cochlear locations where SFOAEs are generated in the model, we examined the model behavior with the impedance irregularity confined either in a region around the traveling-wave peak or in regions remote from the peak. The traveling-wave peak region was associated with steeper phase-versus-distance slope [Figs. 13(B) and 14(B)]. In terms of wavelength (λ), i.e., the cochlear distance spanned by one cycle of phase change, the peak region has shorter λ than the remote regions [Fig. 14(C)]. We defined the peak region to be a cochlear region with $\lambda < 2.5$ mm, and the remote regions to be the remaining cochlear regions.

Besides the normal impedance irregularity distributed throughout the full cochlear length, we also prepared two other types of impedance irregularity profile: (1) irregularity restricted to the peak region with $\lambda < 2.5$ mm, and (2) irregularity restricted to the remote regions with $\lambda > 2.5$ mm.

The model SFOAEs obtained with three types of irregu-

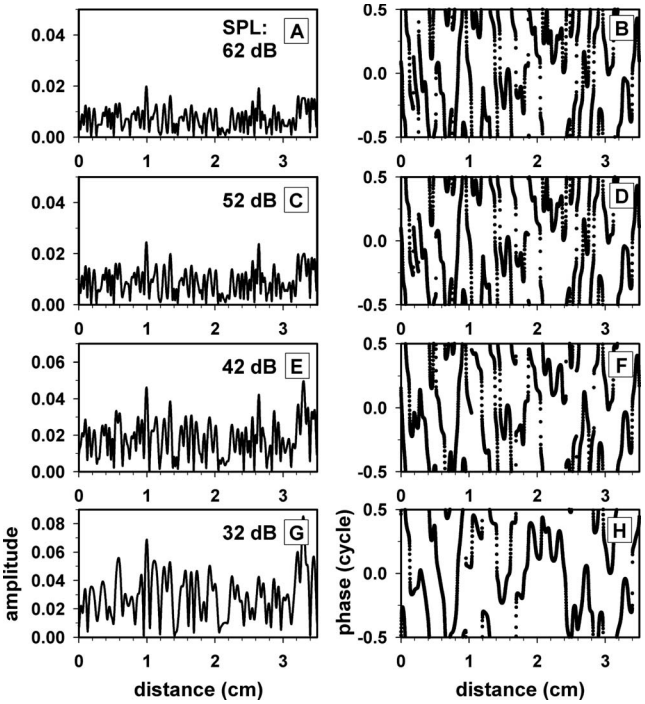


FIG. 12. Spatial profiles of amplitude (left column) and phase (right column) of the model cochlear-partition impedance irregularity. The four rows correspond to four stimulus levels. The model parameters were set to the optimal values described in Table VI.

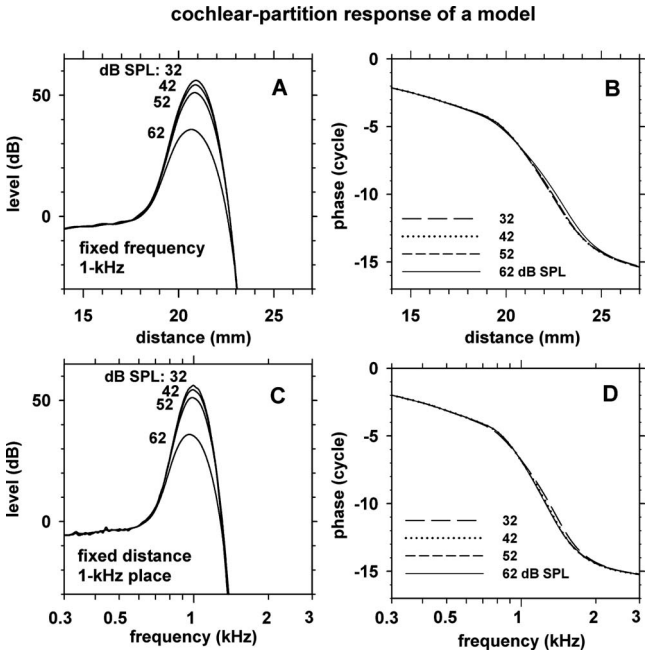


FIG. 13. Cochlear-partition response level and phase versus cochlear distance for 1 kHz stimulus frequency (panels A and B) and versus stimulus frequency for the 1 kHz cochlear place (panels C and D). Four curves in each panel correspond to four stimulus levels (32–62 dB SPL) indicated in the insets. The cochlear-partition response was relative to the stapes input. The model parameters were set to the optimal values described in Table VI.

TABLE IX. Response characteristics of the model cochlear-partition transfer functions at the 1 kHz place at stimulus levels of 32–62 dB SPL (described in Fig. 13). Means and standard deviations (STDs) were calculated for 11 random-seed cases. The results were obtained with the optimal model parameters described in Table VI. $Q_{3\ dB}$ and $Q_{10\ dB}$ are "quality factors" measured at 3 and 10 dB points relative to the peak; Q_{ERB} is a quality factor measured using the equivalent rectangular bandwidth (ERB). The quality factors are dimensionless. PSR stands for peak-to-shoulder ratio, also known as tip-to-tail ratio.

	Stimulus Level (dB SPL)							
	32		42		52		62	
	Mean	STD	Mean	STD	Mean	STD	Mean	STD
$Q_{3\ dB}$	8.0	0.53	7.6	0.30	7.1	0.19	5.8	0.07
Q_{ERB}	7.6	0.58	7.1	0.24	6.6	0.12	5.5	0.06
$Q_{10\ dB}$	4.3	0.24	4.1	0.12	3.9	0.05	3.2	0.02
PSR (dB)	60	1.6	57	0.8	54	0.3	38	0.2

larity profiles at 32 dB SPL are shown in Fig. 15. The three rows correspond to the three types of irregularity profiles: fully present (top), restricted to the peak region (middle), or to the remote regions (bottom). As the spatially restricted irregularity profiles were specifically associated with the 1 kHz traveling-wave peak, the model results of Fig. 15 are shown only for a narrow range of frequencies, 950–1050 Hz, around 1 kHz. The phase slope of the model SFOAE generated by the irregularity in the peak region [Fig. 15(D)] was steep with an EGD of 20.8 ms. The ratio of 20.8 ms to EGD of the 1 kHz place of the cochlea at 32 dB SPL (12.6 ms) is 1.7. This is slightly smaller than 2, expected from a situation where the signal propagates to the traveling-wave peak and back to the ear canal. In contrast, the phase slope of SFOAE generated by the remote regions [Fig. 15(F)] was shallow with an EGD of 4.1 ms, which is much shorter than the EGD of the 1 kHz cochlear place (12.6 ms.).

The results described in Fig. 15 demonstrate that, in the model, (1) the SFOAE consists of a long-delay component generated by irregularity in the traveling-wave peak region and a short-delay component generated by irregularity in the remote regions, (2) the levels of the long- and short-delay components are comparable to each other and they both change slowly with frequency, and (3) the rapidly changing fine structure of SFOAE of the model is a result of quasi-periodic vector cancellations between the long- and short-delay components.

VI. DISCUSSION

A. Main results

The main results of the present study are: (1) introduction of a novel method of efficiently measuring SFOAE level and phase as functions of frequency by a combined use of frequency-swept stimuli and the digital heterodyne analysis; (2) measurement of high-resolution data of SFOAE level, phase, and EGD versus frequency in normally hearing human adult subjects; (3) reproduction of salient features of the human SFOAEs in an active cochlear model; (4) inferences about characteristics of human cochlear-partition motion, and (5) demonstration that, in the model, an SFOAE consists of a long-delay component generated by irregularity in the traveling-wave peak region and a short-delay component generated by irregularity in cochlear regions remote from the peak.

B. Novelty and advantages of the present method of SFOAE measurement

The novelty of the present method lies in an unprecedented efficiency of measuring high-resolution SFOAEs by a combined use of *continuously* sweeping the stimulus frequency and the digital heterodyne analysis. The frequency resolution of the present method depends on the square root of the frequency sweep rate as stated in Methods, Eq. (3). Accordingly, a twofold higher frequency resolution can be

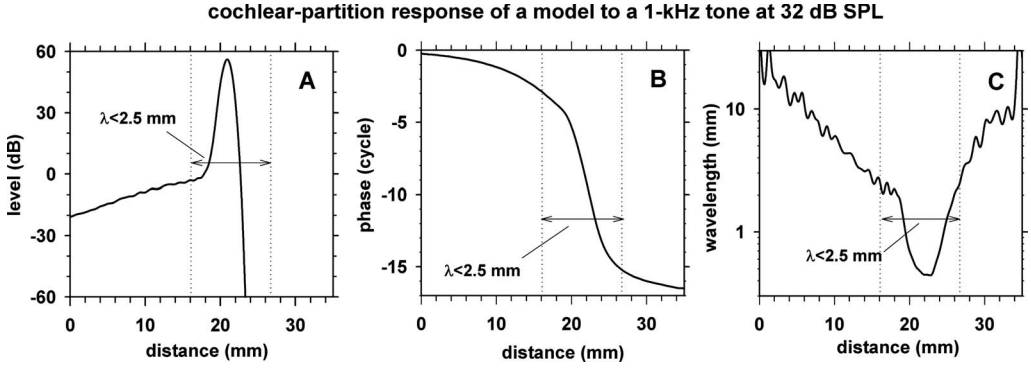


FIG. 14. Cochlear-partition response to a 1 kHz 32 dB SPL stimulus in terms of level (A), phase (B) and wavelength (C) as functions of cochlear distance. The cochlear-partition response was relative to the stapes input. The model parameters were set to the optimal values described in Table VI.

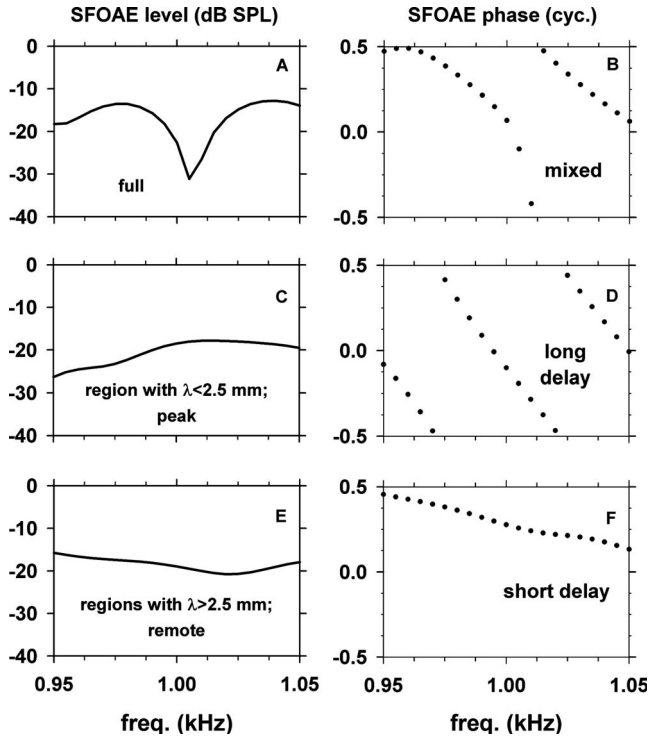


FIG. 15. Level and phase of the model SFOAE at 32 dB SPL versus frequency over a narrow range of frequencies (950–1050 Hz) obtained with three types of spatial profiles of the cochlear-partition impedance irregularity: fully present (*top*), restricted in a region around the traveling-wave peak with $\lambda < 2.5$ mm (*middle*) and in regions remote from the peak with $\lambda > 2.5$ mm (*bottom*).

achieved by decreasing the sweep rate four times. Equivalently, a fourfold faster sweep rate can be achieved if one is willing to decrease frequency resolution by a factor of 2.

In the conventional methods of SFOAE measurement (Shera and Guinan, 1999; Shera and Guinan, 2003; Goodman *et al.*, 2003; Schairer *et al.*, 2006), SFOAE fine structures are measured with many probe frequencies, one frequency at a time. Consequently, the conventional method has a greater overhead, i.e., rise and fall gating times and the times involved for saving the data on a storage device for each individual frequency rendering it inefficient.

An efficient recording method facilitates data collection with less variability and a higher signal-to-noise ratio for a given recording time. Data obtained over long recording times are more susceptible to artifacts arising from unavoidable random movements of the subjects making the data more variable.

C. Future applications of swept stimuli and heterodyne analysis

The present method can be used to obtain SFOAEs over a wider range of frequencies, e.g., 500–8000 Hz (Hill *et al.*, 2008). In such a study, an exponential frequency sweep is more desirable than a linear frequency sweep. A simple variation of the present method will allow one to measure DPOAEs as a continuous function of either primary frequencies (Long *et al.*, 2008) or primary levels. For example, one may sweep f_1, f_2 or f_2/f_1 over a period of time. The heterodyne analysis will then yield DPOAE level and phase (e.g., at $2f_1-f_2$) for various f_2, for example, by extracting DPOAE level and phase at various time points. A similar concept of measuring input-output functions of DPOAE level was introduced by Neely *et al.* (2003).

D. Why is SFOAE group delay far shorter than expected?

Prevailing concepts about SFOAEs are that: (1) SFOAEs are generated predominantly in a cochlear region around the traveling-wave peak, and (2) the SFOAE group delay at a frequency are approximately twice the group delay of the cochlear partition at the traveling-wave peak (Zweig and Shera, 1995). Siegel *et al.* (2005) observed that the group delays of SFOAEs in chinchillas were similar to (for frequencies >4 kHz), or shorter than (for frequencies <4 kHz) the group delays of the cochlear partition at the characteristic frequencies (the partition group delays were estimated from responses of cochlear nerve fibers in chinchillas). This observation is *inconsistent* with the prevailing concept indicated above. Siegel *et al.* highlighted this discrepancy as an important issue for the hearing-science field.

Shera *et al.* (2006) suggested that one approach to resolve the discrepancy between the Zweig–Shera model prediction and the Siegel *et al.* observation is to hypothesize that the total SFOAE is a mixture of a reflection-source emission component with a long delay and a nonlinear-distortion-source emission component with a short delay. (A similar suggestion was made by Goodman *et al.*, 2003) After Shera *et al.* separated ("un-mixed") the total SFOAE into short- and long-delay components, they found that the group delays of the long-delay component of SFOAE were closer to the predicted group delays. However, the group delays of the long-delay SFOAE component were still shorter than the predicted group delays for all frequencies with the differences being greater for frequencies <4 kHz. Furthermore, it remains unknown whether the short-delay component of SFOAE indeed represents a distortion-source emission or some other type of reflection-source emission.

The results of the present cochlear model (Fig. 15) provide a novel hypothesis that the short- and long-delay components of SFOAE are both reflection-source emissions but arise from different regions of the cochlea. In the model, the short-delay SFOAE component arises from irregularity located in cochlear regions remote from the traveling-wave peak whereas the long-delay component arises from irregularity in the peak region. Because the model is piecewise linear, there is no nonlinear-distortion-source emission in the model. Future experiments should verify the validity of this hypothesis.

E. Comparison with the coherent reflection model

The coherent reflection model of SFOAE [Zweig and Shera, 1995, Eq. (23), page 2023] states that reflected wavelets of a forward cochlear traveling wave combine in phase (i.e., creates coherent reflection) when $2^*\Delta x = \lambda$, or $\Delta x = \lambda/2$, where λ is the wavelength and Δx is distance between cochlear mechanical irregularities. An equivalent statement

is that reflected wavelets create coherent reflection when the spatial-frequency (f_s) content of the irregularity profile is large at $f_s=2/\lambda$.

In our model, λ at the peak of the traveling-wave envelope is ~0.5 mm for a 1 kHz sinusoidal stimulus at 32 dB SPL [Fig. 14(C)]. Thus, in order to produce coherent reflection at the traveling-wave peak, the spatial-frequency content of the irregularity profile has to be large at $f_s=2/\lambda=2/0.5=4$ cycles/mm.

A region of the cochlear model that includes the traveling-wave peak and nearby regions has shorter wavelengths [$\lambda=0.45-2.5$ mm, Fig. 14(C)] than the basal region further away from the peak [$\lambda=2.5-25$ mm, Fig. 14(C)]. In the peak region with $\lambda=0.45-2.5$ mm, generation of coherent reflection requires that the spatial-frequency content of the irregularity profile has to be large at $f_s=2/\lambda=0.8-4$ cycles/mm.

In contrast, the irregularity profiles in the model were filtered with a steep *low*-pass spatial-frequency filter with a cutoff frequency of 0.85 cycles/mm at 32 dB SPL; this parameter was obtained as a result of an objective fitting procedure. Therefore, the spatial-frequency content of the model irregularity profile was quite small at the 0.8–4 cycles/mm required for generation of coherent reflection in the short-λ peak region. Consequently, the SFOAE originating from the peak region of the model was much lower than expected from the coherent-reflection model which assumes that the spatial-frequency content of the irregularity profile is large at $f_s=2/\lambda$.

Because λ is much longer (2.5–25 mm) in the basal region, the spatial frequency for large irregularity required by coherent reflection is much lower ($f_s=2/\lambda=0.08-0.8$ cycles/mm) in the basal region than in the peak region. The low-pass spatial-frequency filter with a cutoff frequency of 0.85 cycles/mm preserves amplitudes of irregularity at the above required spatial frequencies. Therefore, the irregularity profile in the long-λ basal region of the model was in a more favorable condition for generation of coherent reflection than the irregularity profile in the short-λ peak region.

The above considerations provide an explanation of a surprising behavior of the present cochlear model. That is, in the model, the levels of the short- and long-delay SFOAE components originating from the remote and peak regions, respectively, are comparable to each other, thus creating rapidly changing peaks and troughs of SFOAE level versus frequency.

F. Comparison with previous studies

Changes in SFOAE fine structures with stimulus levels were reported by Goodman *et al.* (2003). Stimulus-level-dependent changes of frequency spacing, observed in the Goodman *et al.* study and the present study, represent a nonlinear behavior. This behavior was simulated by the present model with stimulus-level-dependent changes of the model parameters (g, α, f_{s_0}, and n).

Our observation of an increase of normalized group delay with frequency over 500–1500 Hz is consistent with previous studies (Shera and Guinan, 2003; Schairer *et al.*, 2006). The present observation of a decreasing group delay of SFOAE with increasing stimulus level (Figs. 4 and 5) is consistent with Schairer *et al.*, (2006). Mechanical responses of a basal part of the chinchilla cochlea also exhibited an analogous decrease of group delay with increasing stimulus level (Ruggero *et al.*, 1997).

G. Model assumptions

Although the model results successfully reproduced the six features of the human SFOAE fine structures (e.g., Fig. 5 and Table V), some differences between the model results and the human data were noticeable. One such example is the SFOAE phase versus frequency pattern. The human phase-frequency pattern (Figs. 2 and 3) tended to be more evenly spread out across the 550–1450 Hz range than the model counterpart (Figs. 10 and 11). It is not clear what changes in the model can improve in this regard.

There were other shortcomings of the model. We used a piecewise-linear frequency-domain model of the cochlea. Development of a nonlinear time-domain version of the model will be a desirable future goal. We used a one-dimensional cochlear model even though a cochlear model should ultimately be three dimensional. We believe, however, that important insights were gained by using a simplified one-dimensional model. Exploration of the parameter space of the model was facilitated by the simplified form of the model.

In addition, the boundary condition at the stapes did not include properties of the middle ear. A lossy-impedance boundary condition provided by the middle ear at the stapes should better represent reflection of the backward wave at the stapes (e.g., Shera and Zweig, 1991; Zweig and Shera, 1995; Talmadge *et al.*, 1998, 2000). Since the round-trip reflectance, i.e., the multiplication of reflectance from the cochlear-partition irregularities and the reflectance from the stapes, is small, the effects of multiple reflections may be small for the cases presented in this paper.

H. Is spatial profile of irregularity controlled by the cochlear amplifier?

In the model, the model parameters (g, α, f_{s_0}, and n), co-varied with stimulus level (Table VI). Specifically, as the stimulus level decreased, the model became more active (amplification increased), the base amplitude of the irregularity increased, and the spatial low-pass filter exhibited a lower cutoff and a steeper filter slope. These hypothesized relationships among the model parameters and stimulus level were found as a result of the objective fitting procedure searching for the optimal model parameters that best reproduced the human SFOAE fine structures at various stimulus levels.

A possible implication of the present hypothesis is that the spatial frequency content of the cochlear-partition impedance irregularity profile is controlled by the cochlear amplifier mechanism. When the model becomes more active at a lower stimulus level, the hypothesis implies that the active

mechanism exerts a more prominent longitudinal coupling of the organ of Corti whereby the partition impedance changes more slowly along the cochlear distance.

I. Inferences about the human cochlea

The present human SFOAE data together with an active cochlear model allowed us to make inferences about characteristics of the human cochlear-partition responses. The detailed and reliable measurements of SFOAE fine structures proved valuable in guiding the process of adjusting parameters of an active cochlear model. The optimal model parameters were well constrained by the six features of the SFOAE fine structures (Table V) with narrow confidence intervals (Tables VII and VIII). The present model suggests that: (1) the human cochlear-partition response at the 1 kHz place at 32 dB SPL has a sharp tuning ($Q_{3\ \mathrm{dB}}$ of 8.0) and a large amplification (peak-to-shoulder ratio of 60 dB), and (2) the tuning becomes broader and the amplification smaller as the stimulus level increased to 62 dB SPL.

Psychophysically observed Q_{ERB} of the human cochlear tuning at 1 kHz at a low stimulus level have been reported to be 7.5 (Glassberg and Moore, 1990), 12.7 (Shera *et al.*, 2002), and 11 (Oxenham and Shera, 2003). The present cochlear-model prediction of $Q_{\mathrm{ERB}}=7.6$ at 32 dB SPL is close to the value of Glassberg and Moore.

To compare the frequency-tuning characteristics of the present model with those of animal cochlear nerve fibers, we used the facts that the human 1 kHz cochlear place is located 60% from the stapes (Figs. 9 and 13) and that a 60% position corresponds to 2.8 kHz in cat (Liberman, 1982), 2 kHz in guinea pig (Wilson and Johnstone, 1975) and 1 kHz in chinchilla (Eldredge *et al.*, 1981). Because the tuning sharpness of a cochlear nerve fiber changes with the fiber's characteristic frequency (CF), it is appropriate to use a common relative cochlear position (60% from the stapes in this case) in a comparison of tuning sharpness across species. In cat, threshold tuning curves of cochlear nerve fibers with CF $=2.8$ kHz show an average $Q_{10\ \mathrm{dB}}=4.5$ (Liberman, 1990). In guinea pig, cochlear nerve fibers and medial olivocochlear nerve fibers with CF≈ 2 kHz show $Q_{10\ \mathrm{dB}}\approx 2.3\sim 4$ (Pickles, 1984; Brown *et al.*, 1998). In chinchilla, cochlear nerve fibers with CF≈ 1 kHz show $Q_{10\ \mathrm{dB}}\approx 1.7$ (Temchin *et al.*, 2005). Thus, the cochlear places at 60% from the stapes in these species exhibit a diverse range of $Q_{10\ \mathrm{dB}}$. The present human model prediction of $Q_{10\ \mathrm{dB}}=4.3$ at 32 dB SPL is similar to the $Q_{10\ \mathrm{dB}}$ value of cat (Liberman, 1990).

The present model predictions about the human cochlea are consistent with cochlear-partition responses of animals regarding the shapes of the amplitude and phase parts of the transfer function and stimulus-level-dependent changes in several response measures: (1) broadening of frequency tuning with increasing stimulus level, and (2) decrease of peak-to-shoulder ratio with increasing stimulus level (Rhode, 1971, 2007; Sellick *et al.*, 1982; Ruggero *et al.*, 1997 Robles and Ruggero, 2001; Ren *et al.*, 2006). Peak-to-shoulder ratio is related to the cochlear-amplifier gain. Cochlear amplifier gain, defined in various ways, has been observed in animals to be in a range of 40–80 dB (Ruggero *et al.*, 1997; Rhode, 2007). Peak-to-shoulder ratio of basal points of the chinchilla cochlear partition (CF$=5\sim 10$ kHz) were observed to be 33–50 dB at low stimulus levels (Ruggero *et al.*, 1997; Rhode, 2007). The present prediction of peak-to-shoulder ratio of the human cochlea, 60 dB at a stimulus level of 32 dB SPL, is slightly higher than those observed in the chinchilla cochlear partition.

ACKNOWLEDGMENTS

This study was supported in part by USA NIH-NIDCD Grant Nos. R01DC00360 (PI, D.O.K.) and R01DC08318 (PI, S.T.N.). The experiments were conducted while Y.-S.C. was visiting the University of Connecticut Health Center supported by Brain Korea 21 Project, the School of Information Technology, KAIST, in 2002–2003. Y.-S.C. and S.-Y.L. have been supported partly by the Brain Neuroinformatics Research Program sponsored by Korean MOST and MOCIE from 2001. We thank Dr. Gerhard Hill for assistance in making measurements using the conventional method, Dr. S. Puria for providing numerical middle-ear data, Dr. M. Ruggero and Dr. A. Temchin for providing numerical cochlear-partition data. We also thank Dr. J. Siegel, Dr. C. Shera, and Dr. M. Ruggero for helpful discussions on topics of this study.

American National Standards Institute (**1978**). Methods for Manual Pure-Tone Threshold Audiometry. ANSI S3.21-1978 (reaffirmed 1986).

Brass, D., and Kemp, D. T. (**1993**). "Suppression of stimulus frequency otoacoustic emissions," J. Acoust. Soc. Am. **93**, 920–939.

Brown, M. C., Kujawa, S. G., and Liberman, M. C. (**1998**). "Single Olivocochlear Neurons in the guinea pig. II. Response plasticity due to noise conditioning," J. Neurophysiol. **79**, 3088–3097.

Durney, C. H., and Johnson, C. C. (**1969**). *Introduction to Modern Electromagnetics* (McGraw–Hill, New York), pp. 365–368.

Eldredge, D. H., Miller, J. D., and Bohne, B. A. (**1981**). "A frequency-position map for the chinchilla cochlea," J. Acoust. Soc. Am. **69**, 1091–1095.

Glassberg, B. R., and Moore, B. C. J. (**1990**). "Derivation of auditory filter shapes from notched-noise data," Hear. Res. **47**, 103–138.

Goldstein, J. L., Baer, T., and Kiang, N. Y. S. (**1971**). "A theoretical treatment of latency, group delay and tuning. Characteristics for auditory nerve responses to clicks and tones," in *The Physiology of the Auditory System*, edited by M. B. Sachs (National Educational Consultants, Baltimore), pp. 133–141.

Goodman, S. S., Withnell, R. H., and Shera, C. A. (**2003**). "The origin of SFOAE microstructure in the guinea pig," Hear. Res. **183**, 7–17.

Greenwood, D. D. (**1990**). "A cochlear frequency-position function for several species—29 years later," J. Acoust. Soc. Am. **87**, 2592–2605.

Guinan, Jr., J. J., Backus, B. C., Lilaonitkul, W., and Aharonson, V. (**2003**). "Medial olivocochlear efferent reflex in humans: Otoacoustic emission (OAE) measurement issues and the advantages of stimulus frequency OAEs," J. Assoc. Res. Otolaryngol. **4**, 521–540.

Hill, G., Parham, K., Choi, Y.-S., and Kim, D. O. (**2008**). "Stimulus-frequency otoacoustic emissions in normally-hearing humans obtained with a frequency-sweeping method over 0.5 to 8 kHz," *Assoc. Res. Otolar. Meeting*, Abstr. No. 186.

Kemp, D. T. (**1978**). "Stimulated acoustic emissions from within the human auditory system," J. Acoust. Soc. Am. **64**, 1386–1391.

Kemp, D. T. (**1986**). "Otoacoustic emissions, traveling waves and cochlear mechanisms," Hear. Res. **22**, 95–104.

Kemp, D. T., and Chum, R. A. (**1980**). "Observations on the generator mechanism of stimulus frequency acoustic emissions—Two tone suppression," in *Physiological, Psychological, and Behavioral Studies in Hearing*, edited by G. van der Brink and F. A. Bilsen (Delft University Press, Delft, Netherlands), pp. 34–42.

Kemp, D. T., and Souter, M. (**1988**). "A new rapid component in the cochlear response to brief electrical efferent stimulation," Hear. Res. **34**,

49–62.
Kemp, D. T., Ryan, S., and Bray, P. (**1990**). "A guide to the effective use of otoacoustic emissions," Ear Hear. **11**, 93–105.
Kim, D. O. (**1980**). "Cochlear mechanics: Implications of electrophysiological and acoustical observations," Hear. Res. **2**, 297–317.
Kim, D. O., Molnar, C. E., and Matthews, J. W. (**1980**). "Cochlear mechanics: Nonlinear behavior in two-tone responses as reflected in cochlear-nerve-fiber responses and in ear-canal sound pressure," J. Acoust. Soc. Am. **67**, 1704–1721.
Kim, D. O., Dorn, P. A., Neely, S. T., and Gorga, M. P. (**2001**). "Adaptation of distortion product otoacoustic emission in humans," J. Assoc. Res. Otolaryngol. **2**, 31–40.
Liberman, M. C. (**1982**). "The cochlear frequency map for the cat: Labeling auditory-nerve fibers of known characteristic frequency," J. Acoust. Soc. Am. **72**, 1441–1449.
Liberman, M. C. (**1990**). "Effect of chronic cochlear de-efferentation of auditory-nerve response," Hear. Res. **49**, 209–224.
Long, G., Talmadge, C., Prieve, B., and Lahtinen, L. (**2008**). "Extraction of DPOAE generator and reflection components in the time domain in adults and infants," *Assoc. Res. Otolar. Meeting*, Abstr. No. 180.
Lonsbury-Martin, B. L., and Martin, G. K. (**1990**). "The clinical utility of distortion-product otoacoustic emissions," Ear Hear. **11**, 144–154.
Matthews, J. W., and Molnar, C. E. (**1986**). "Modeling intracochlear and ear canal distortion products $2f_1-f_2$," in *Peripheral Auditory Mechanisms*, edited by J. B. Allen, J. L. Hall, A. Hubbard, S. T. Neely, and A. Tubis (Springer-Verlag, New York), pp. 258–265.
Neely, S. T., and Kim, D. O. (**1983**). "An active cochlear model showing sharp tuning and high sensitivity," Hear. Res. **9**, 123–130.
Neely, S. T., and Kim, D. O. (**1986**). "A model for active elements in cochlear biomechanics," J. Acoust. Soc. Am. **79**, 1472–1480.
Neely, S. T., and Kim, D. O. (**2008**). "Cochlear models incorporating active processes," in *Active Processes and Otoacoustic Emissions in Hearing*, edited by G. A. Manley, R. R. Fay, and A. N. Popper (Springer, New York), Chap. 11, pp. 381–394.
Neely, S. T., Kim, D. O., and Gorga, M. P. (**2003**). "A novel method for making fast measurements of DPOAE as a continuous function of primary level," *Assoc. Res. Otolar. Meeting*, Abstr. No. 361.
Oxenham, A. J., and Shera, C. A. (**2003**). "Estimates of human cochlear tuning at low levels using forward and simultaneous masking," J. Assoc. Res. Otolaryngol. **4**, 541–554.
Pickles, J. O. (**1984**). "Frequency threshold curves and simultaneous masking functions in single fibers of the guinea pig auditory nerve," Hear. Res. **14**, 245–256.
Probst, R., Lonsbury-Martin, B. L., and Martin, G. K. (**1991**). "A review of otoacoustic emissions," J. Acoust. Soc. Am. **89**, 2027–2067.
Puria, S. (**2003**). "Measurements of human middle ear forward and reverse acoustics: Implications for otoacoustic emissions," J. Acoust. Soc. Am. **113**, 2773–2789.
Ren, T., He, W., Scott, M., and Nuttal, A. L. (**2006**). "Group delay of acoustic emissions in the ear," J. Neurophysiol. **96**, 2785–2791.
Rhode, W. S. (**1971**). "Observations of the vibration of the basilar membrane in squirrel monkeys using the Mössbauer technique," J. Acoust. Soc. Am. **49**, 1218–1231.
Rhode, W. S. (**2007**). "Basilar membrane mechanics in the 6–9 kHz region of sensitive chinchilla cochleae," J. Acoust. Soc. Am. **121**, 2792–2804.
Robles, L., and Ruggero, M. A. (**2001**). "Mechanics of the mammalian cochlea, Physiol. Rev. **81**, 1305–1352.
Ruggero, M. A., Rich, N. C., Recio, A., Narayan, S. S., and Robles, L. (**1997**). "Basilar-membrane responses to tones at the base of the chinchilla cochlea," J. Acoust. Soc. Am. **101**, 2151–2163.
Schairer, K. S., Ellison, J. C., Fitzpatrick, D., and Keefe, D. H. (**2006**). "Use of stimulus-frequency otoacoustic emission latency and level to investigate cochlear mechanics in human ears," J. Acoust. Soc. Am. **120**, 901–914.
Sellick, P. M., Patuzzi, R., and Johnstone, B. M. (**1982**). "Measurement of basilar membrane motion in the guinea pig using the Mössbauer technique," J. Acoust. Soc. Am. **72**, 131–141.
Shera, C. A. (**2004**). "Mechanisms of mammalian otoacoustic emission and their implications for the clinical utility of otoacoustic emissions," Ear Hear. **25**, 86–97.
Shera, C. A., and Guinan, J. J. (**1999**). "Evoked otoacoustic emissions arise by two fundamentally different mechanisms: A taxonomy for mammalian OAEs," J. Acoust. Soc. Am. **105**, 782–798.
Shera, C. A., and Guinan, J. J. (**2003**). "Stimulus-frequency-emission group delay: A test of coherent reflection filtering and a window on cochlear tuning," J. Acoust. Soc. Am. **113**, 2762–2772.
Shera, C. A., and Zweig, G. (**1991**). "Reflection of retrograde waves within the cochlea and at the stapes," J. Acoust. Soc. Am. **89**, 1290–1305.
Shera, C. A., Guinan, J. J., and Oxenham, A. J. (**2002**). "Revised estimates of human cochlear tuning from otoacoustic and behavioral measurements," Proc. Natl. Acad. Sci. U.S.A. **99**, 3318–3323.
Shera, C. A., Tubis, A., and Talmadge, C. L. (**2006**). "Delays of SFOAEs and cochlear vibrations support the theory of coherent reflection filtering," *Assoc. Res. Otolar. Meeting Abstr.*, Vol. **29**, revised poster No. 52.
Siegel, J. H., Cerka, A. J., Recio-Spinoso, A., Temchin, A. N., van Dijk, P., and Ruggero, M. A. (**2005**). "Delays of stimulus-frequency otoacoustic emissions and cochlear vibrations contradict the theory of coherent reflection filtering," J. Acoust. Soc. Am. **118**, 2434–2443.
Talmadge, C. L., Tubis, A., Long, G. R., and Piskorski, P. (**1998**). "Modeling otoacoustic emission and hearing threshold fine structure," J. Acoust. Soc. Am. **104**, 1517–1543.
Talmadge, C. L., Tubis, A., Long, G. R., and Tong, C. (**2000**). "Modeling the combined effects of basilar membrane nonlinearity and roughness on stimulus frequency otoacoustic emission fine structure," J. Acoust. Soc. Am. **108**, 2911–2932.
Temchin, A. N., Recio-Spinoso, A., van Dijk, P., and Ruggero, M. A. (**2005**). "Wiener kernels of chinchilla auditory-nerve fibers: Verification using responses to tones, clicks, and noise and comparision with basilar-membrane vibrations," J. Neurophysiol. **93**, 3635–3648.
Wilson, J. P., and Johnstone, J. R. (**1975**). "Basilar membrane and middle-ear vibration in guinea pig measured by capacitive probe," J. Acoust. Soc. Am. **57**, 705–723.
Zurek, P. M., Clark, W. W., and Kim, D. O. (**1982**). "The behavior of acoustic distortion products in the ear canals of chinchillas with normal or damaged ears," J. Acoust. Soc. Am. **72**, 774–780.
Zweig, G., Lipes, R., and Pierce, J. R. (**1976**). "The cochlear compromise," J. Acoust. Soc. Am. **59**, 975–982.
Zweig, G., and Shera, C. A. (**1995**). "The origin of periodicity in the spectrum of evoked otoacoustic emissions," J. Acoust. Soc. Am. **98**, 2018–2047.
Zwicker, E. (**1986**). "Otoacoustic emissions' in a nonlinear cochlear hardware model with feedback," J. Acoust. Soc. Am. **80**, 154–162.
Neely, S. T., and Stevenson, R. (**2002**). "SYSRES," Tech. Memo. 19, Boys Town National Research Hospital, Omaha, NE. (personal communication)

Pitch strength decreases as F0 and harmonic resolution increase in complex tones composed exclusively of high harmonics[a)]

D. Timothy Ives[b)] and Roy D. Patterson
Centre for the Neural Basis of Hearing, Department of Physiology, Development and Neuroscience, University of Cambridge, Downing Street, Cambridge, CB2 3EG, United Kingdom

(Received 15 January 2007; revised 4 February 2008; accepted 7 February 2008)

A melodic pitch experiment was performed to demonstrate the importance of time-interval resolution for pitch strength. The experiments show that notes with a low fundamental (75 Hz) and relatively few resolved harmonics support better performance than comparable notes with a higher fundamental (300 Hz) and more resolved harmonics. Two four note melodies were presented to listeners and one note in the second melody was changed by one or two semitones. Listeners were required to identify the note that changed. There were three orthogonal stimulus dimensions: F0 (75 and 300 Hz); lowest frequency component (3, 7, 11, or 15); and number of harmonics (4 or 8). Performance decreased as the frequency of the lowest component increased for both F0's, but performance was better for the *lower* F0. The spectral and temporal information in the stimuli were compared using a time-domain model of auditory perception. It is argued that the distribution of time intervals in the auditory nerve can explain the *decrease* in performance as F0, and spectral resolution *increase*. Excitation patterns based on the same time-interval information do not contain sufficient resolution to explain listener's performance on the melody task.
© *2008 Acoustical Society of America.* [DOI: 10.1121/1.2890737]

PACS number(s): 43.66.Ba, 43.66.Hg, 43.66.Lj [RAL] Pages: 2670–2679

I. INTRODUCTION

A series of experiments with filtered click trains and harmonic complexes has shown that pitch strength decreases as the lowest harmonic of a complex increases. The phenomenon has been demonstrated for the lowest harmonics using magnitude estimation (Fastl and Stoll, 1979; Fruhmann and Kluiber, 2005), and for higher harmonics using a variety of pitch discrimination tasks [e.g., Ritsma and Hoekstra, 1974; Cullen and Long, 1986; Houtsma and Smurzynski, 1990; see Krumbholz *et al.* (2000) for a review]. This paper reports an experiment that makes use of this phenomenon to demonstrate the importance of time-interval resolution for pitch strength. A harmonic complex with eight, adjacent components was used to measure performance on a melodic pitch task (Patterson *et al.*, 1983; Pressnitzer and Patterson, 2001), as a function of the frequency of the lowest harmonic in the complex. The important variable was the fundamental (F0) of the complex which was either low (75 Hz) or high (300 Hz), and the main empirical question was which fundamental supports better performance on the melodic pitch task?

In time-domain models of peripheral processing, the reduction in pitch strength with increasing harmonic number is associated with the loss of phase locking at high frequencies (e.g., Patterson *et al.*, 2000; Krumbholz *et al.*, 2000; Pressnitzer *et al.*, 2001). As a result, time-domain models predict that performance based on complexes limited to high harmonics will be worse for the *higher* fundamental (300 Hz); the higher harmonics occur above 3000 Hz for the 300 Hz fundamental, where the internal representation of the time interval information is smeared by the loss of phase locking.

In spectral models of pitch perception, the reduction in pitch strength with increasing harmonic number is associated with the loss of harmonic resolution at high harmonic numbers. This occurs because the frequency spacing between components of a harmonic complex is fixed, whereas the bandwidth of the auditory filter increases with filter center frequency. Thus, for all fundamentals, harmonic resolution (harmonic-spacing/center-frequency) decreases as harmonic number increases. It is also the case that the frequency resolution of the auditory filter improves somewhat with filter center frequency, where filter resolution is defined as the ratio of the center frequency (f_c) to the bandwidth (bw); it is referred to as the quality (Q) of the filter ($Q=f_c/\mathrm{bw}$). As a result, spectral models, which ignore the effects of phase locking, predict that performance will be worse for the *lower* fundamental with the lower value of Q.

The results of the experiment show that performance on the melodic pitch task is worse for the higher fundamental in support of the view that it is time-interval resolution rather than harmonic resolution that imposes the limit on pitch strength for these harmonic complexes.

[a)]Portions of this work were presented in "Why pitch strength decreases with increasing harmonic number in complex tones" at the 153rd Meeting of the Acoustical Society of America, Salt Lake City, 2007.
[b)]Electronic mail: dti20@cam.ac.uk

 0001-4966/2008/123(5)/2670/10/$23.00 © 2008 Acoustical Society of America

A. Spectral and temporal summaries of the pitch information in complex sounds

The logic of the experiment will be illustrated using a time-domain model of auditory processing, since such models make it possible to compare the spectral and temporal information that is assumed to exist in the auditory system at the level of the auditory nerve. There are a number of different time-domain models which are typically referred to by the representation of sound that they produce, for example, the "correlogram" (Slaney and Lyon, 1990), the "autocorrelogram" (Meddis and Hewitt, 1991), and the "auditory image" (Patterson *et al.*, 1992, 1995). The example is based on the auditory image model (AIM) and the specific implementation is that described in Bleeck *et al.* (2004). The first three stages of AIM are typical of most time-domain models of auditory processing. A bandpass filter simulates the operation of the outer and middle ears, and then an auditory filterbank simulates the spectral analysis performed in the cochlea by the basilar partition. The shape of the auditory filter is typically derived from simultaneous noise-masking experiments, rather than pitch experiments. In this case, it is the gammatone auditory filterbank of Patterson *et al.* (1995). The simulated membrane motion is converted into a simulation of the phase-locked, neural activity pattern (NAP) that flows from the cochlea in response to the sound; the simulated NAP represents the probability of neural firing, it is produced by compressing, half-wave rectifying and low-pass filtering the membrane motion, separately in each filter channel. The NAPs produced by AIM are very similar to those produced by correlogram and autocorrelogram models of pitch perception (e.g., Slaney and Lyon, 1990; Meddis and Hewitt, 1991; Yost *et al.*, 1996).

The NAPs produced in response to two complex sounds composed of harmonics 3–10 of a 300 Hz fundamental and a 75 Hz fundamental are shown in Figs. 1(a) and 1(b), respectively. The dimensions of the NAP are time (the abscissa) and auditory-filter center frequency on a quasilogarithmic axis (the ordinate). Figure 1 covers the frequency range from 50 to 12 000 Hz. The time range encompasses three periods of the corresponding fundamental; so for the 300 Hz F0 the range is 10 ms, and for the 75 Hz F0 the range is 40 ms. The vertical and horizontal side panels to the right and below each figure show the average of the activity in the NAP across one of the dimensions. The average over time is shown in the vertical (or spectral) profile; the average over frequency is shown in the horizontal (or temporal) profile. The spectral profiles are often referred to as excitation patterns (e.g., Glasberg and Moore, 1990), and they show that there are more resolved harmonics in the NAP of the sound with the higher F0 (300 Hz) [Fig. 1(a)] than for the lower F0 (75 Hz) [Fig. 1(b)]. This suggests that using the spectral profiles to predict pitch strength would lead to a higher value of pitch strength for the higher F0. The spectral summaries derived from other time-domain models and the spectral summaries used in spectral models of auditory processing would all lead to the same, qualitative, prediction. With regard to temporal information, the NAPs reveal faint ridges in the activity, which occur every 3.3 ms for the 300 Hz NAP and every 13.3 ms for the 75 Hz NAP. However, it is difficult to see the strength of the temporal regularity in the NAP because the propagation delay in the cochlea means that the temporal pattern in the lower channels is progressively shifted in time. Similarly, the temporal profiles provide only a poor representation of the temporal regularity in these sounds. This is a general limitation of time-frequency representations of the information in the auditory nerve.

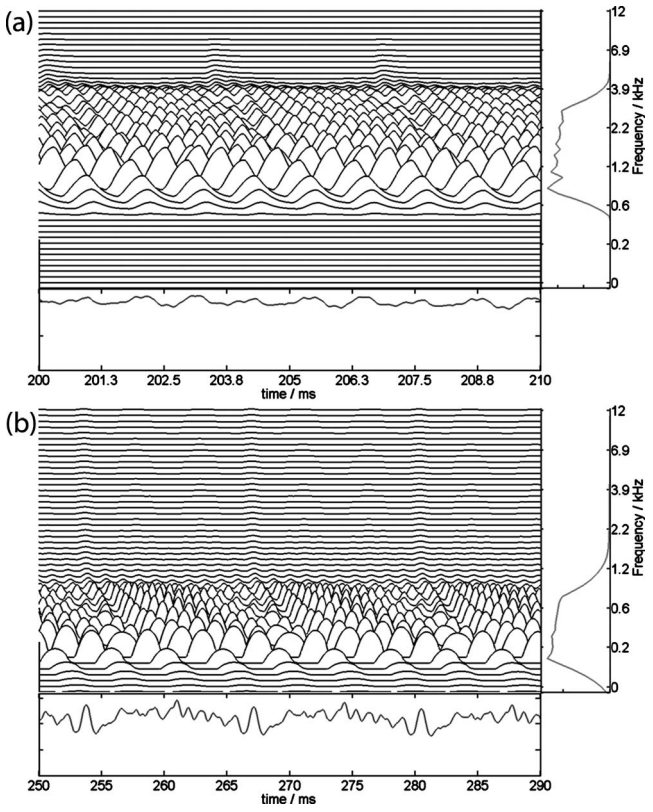


FIG. 1. Neural activity patterns (NAPs) for harmonic complex sounds composed of the third to tenth harmonics of (a) an F0 of 300 Hz, and (b) an F0 of 75 Hz. Side panels show the spectral profiles (vertical) and temporal profiles (horizontal) of the NAP.

The temporal information in the NAP concerning how the sound will be perceived is not coded by time, *per se*, but rather by the time intervals between the peaks of the membrane motion. For this reason, time-domain models include an extra stage, in which autocorrelation (e.g., Slaney and Lyon, 1990) or strobed temporal integration (Patterson *et al.*, 1992) is applied to the NAP to extract and stabilize the phase-locked, repeating neural patterns produced by periodic sounds. Broadly speaking, the time intervals between peaks within a channel are calculated and used to construct a form of time-interval histogram for that channel of the filterbank, and the complete array of time-interval histograms is the correlogram (Slaney and Lyon, 1990), or auditory image (Patterson *et al.*, 1992), of the sound. The histogram is dynamic and events emerge in, and decay from, the histogram with a half life on the order of 30 ms. It is argued that these representations provide a better description of what will be heard than the NAP. They have the stability of auditory perception (Patterson *et al.*, 1992) and they do not contain the between-channel phase information associated with the

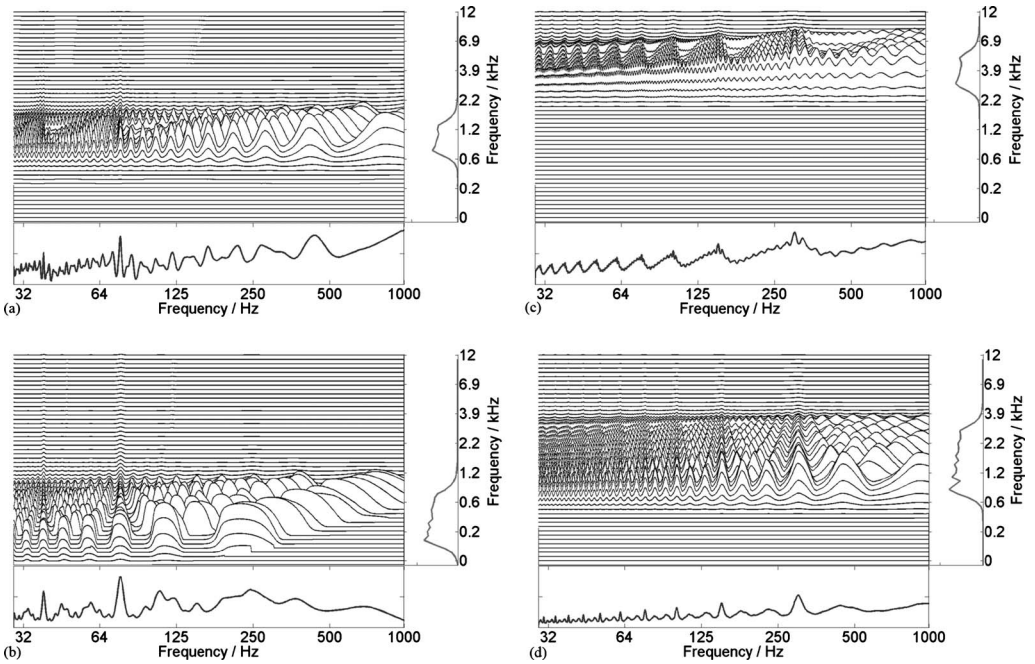


FIG. 2. Stabilized auditory images (SAI) of four harmonic complexes. All stimuli have eight consecutive harmonics; they differ in their fundamentals and lowest components. (a) F0=75 Hz, harmonics 11–18; (b) F0=75 Hz, harmonics 3–10; (c) F0=300 Hz, harmonics 11–18; (d) F0=300 Hz, harmonics 3–10. Side panels show the spectral profiles (vertical) and temporal profiles (horizontal) of the auditory images.

propagation delay which we do not hear (Patterson, 1987). However, all that matters in the current study is that they reveal the precision of the time-interval information in the auditory nerve and make it possible to produce a simple summary of the temporal information in the form of a temporal profile.

The auditory images of four harmonic complexes simulated by AIM are shown in Fig. 2. The stimuli all have eight consecutive harmonics but they differ in fundamental (F0) and/or lowest component (LC) as follows: (a) F0=75 Hz, LC=11; (b) F0=75 Hz, LC=3; (c) F0=300 Hz, LC=11; (d) F0=300 Hz, LC=3. The auditory images corresponding to the NAPs in Figs. 1(a) and 1(b) are shown in Figs. 2(d) and 2(b), respectively. In each channel of all four panels, there is a local maximum at the F0 of the stimulus, and together these peaks produce a vertical ridge in each panel that corresponds to the pitch that the listener hears. In the upper panels [Figs. 2(a) and 2(b)], where the lowest component is the 11th, and the auditory filters are wide relative to component density, the interaction of the components within a filter is clearly manifested by the asymmetric modulation of the pattern at the F0 rate. The corresponding correlograms of Slaney and Lyon (1990) and the autocorrelograms of Meddis and Hewitt (1991) would have a similar form in as much as there would be local peaks at F0 and prominent modulation for the stimuli where the lowest component is the 11th, but the pattern of activity within the period of the sound would be blurred and the envelope of the modulation would be more symmetric.

The vertical and horizontal side panels to the right and below each sub-figure show the average of the activity in the auditory image across one of the dimensions. The average over time interval is shown in the vertical, or spectral, profile; the average over frequency (or channels) is shown in the horizontal, or temporal, profile. The unit on the time-interval axis is the frequency equivalent of time interval, that is, time interval^{-1}. It is used to make the spectral and temporal profiles directly comparable. The spectral profile of the auditory image is very similar to that of the corresponding NAP. The temporal profile of the auditory image shows that the timing information in the neural pattern of these stimuli is very regular, and if the auditory system has access to this information it could be used to explain pitch perception. The advantage of time-domain models of auditory processing is that the spectral and temporal profiles are derived from a common simulation of the information in the auditory nerve, which facilitates comparison of the spectral and temporal pitch models based on such profiles. Moreover, the parameters of the filterbank are derived from separate, masking experiments, so the resulting models have the potential to explain pitch and masking within a unified framework.

In the spectral profile, when the lowest component is increased from three to eleven, the profile ceases to resolve individual components. This is shown by comparing the peaky spectral profile for the stimulus with a LC of 3 in Fig. 2(d), with the smoother profile for the stimulus with a LC of 11 in Fig. 2(c). The effect of increasing LC is similar for the lower F0 in the left column, but the harmonic resolution is reduced in both cases. In the temporal profile, when the lowest component is increased from three to eleven, the pronounced peak at 75 Hz in the left-hand column remains; compare Figs. 2(b) and 2(a). The 300 Hz peak in the temporal profile in the right-hand column becomes much less pronounced relative to the surrounding activity, [compare Figs. 2(d) and 2(c)] but there is still a small peak in Fig. 2(c).

As F0 is increased from 75 to 300 Hz, activity in the spectral profile shifts up along the frequency axis. For the stimuli with higher order components [Figs. 2(a) and 2(c)], there is little change in the resolution of the spectral profile when F0 is changed; the harmonic resolution remains poor. But for the stimuli with lower order components [Figs. 2(b) and 2(d)], the increase from a fundamental of 75 Hz to one of 300 Hz is accompanied by an increase in harmonic resolution, which is due to the increase in the Q of the filter with center frequency. As a result, a model based on spectral profiles would predict (a) that performance for stimuli with higher order components will be poor independent of F0, and (b) that performance for stimuli with lower order components will be better for the higher F0 (300 Hz).

As F0 is increased from 75 to 300 Hz, the peak in the temporal profile shifts to the right along the time-interval axis. For stimuli with lower order components [Figs. 2(b) and 2(d)], the ratio of the magnitude of the F0 peak to the magnitude of the neighboring trough is large, and a model based on temporal profiles would predict good performance in both conditions. For stimuli with higher order components [Figs. 2(a) and 2(c)], the peak to trough ratio is still reasonably large for the lower F0, but it is much reduced for the higher F0. So, a model based on temporal profiles would predict reasonable performance for the low F0 and poorer performance for the higher F0. Thus, there is a clear difference between the predictions of the two classes of model.

II. MAIN EXPERIMENT

The melody task is based on the procedure described previously by Patterson *et al.* (1983) and revived by Pressnitzer *et al.* (2001). Listeners were presented with two successive melodies. The second melody was a repetition of the first but had one of the notes changed by one diatonic interval up or down. The task for the listener was to identify which note had changed in the second melody. Melodies consisted of four notes from the diatonic major scale. The structure of the notes was such that only the residue pitch was consistent with the musical scale, and that sinusoidal pitch could not be used to make judgments. A melody task was used rather than a pitch discrimination task as it is a better measure of pitch strength.

A. Stimuli

The notes in the melodies were synthesized from a harmonic series whose lowest components were missing. The pitch of the note corresponded to the F0 of the harmonic series. The harmonics were attenuated by a low-pass filter with a slope of 6 dB/octave relative to the lowest component present in the complex. Performance on a melody task was measured as a function of three parameters: fundamental frequency (F0); average, lowest component number (ALC); and number of components (NC). There were two nominal F0's 75 and 300 Hz; the F0 was subject to a rove of half an octave. The ALC was 3, 7, 11, or 15. The NC was either 4 or 8. Stimuli were generated using MATLAB; they had a sampling rate of 48 kHz and 16 bit amplitude resolution. They were played using an Audigy-2 soundcard. The duration of each note was 500 ms, which included a 100 ms raised cosine onset and a 333 ms raised cosine offset. Stimuli were presented diotically using AKG K240DF Studio-Monitor headphones at a level of approximately 60 dB SPL. Difference tones in the region of F0 and its immediate harmonics (Pressnitzer and Patterson, 2001) were masked by bandpass filtered white noise; the frequency range was 20–160 Hz for the lower F0 and 50–400 Hz for the higher F0. The level of the noise was 50 dB SPL. Cubic difference tones just below the lowest harmonic were not masked as this would involve inserting a loud noise that would overlap in the spectrum with the stimulus. Cubic difference tones might increase pitch strength slightly in all conditions, but they would not be expected to contribute a distinctive cue to the melody that would affect performance differentially for a particular F0 or lowest harmonic number. The experiment was run in an IAC double-walled, sound-isolated booth.

B. Subjects

Three listeners participated in the first experiment; their ages ranged from 20 to 26 years. All listeners had normal hearing thresholds at 500 Hz, 1, 2, and 4 kHz. Listeners were not chosen on the basis of musical ability, but two of the listeners were trained musicians. All listeners were paid at an hourly rate. Listeners were trained on the melody task over a 2 h period, although they would be allowed to take frequent breaks so the actual training time was somewhat less than 2 h. The training program varied between listeners. Typically it involved starting with an easy condition having eight components, an ALC of three, and no roving of the lowest component. The difficulty of the task was then increased by including stimuli with fewer components (i.e., four), adding the rove, and finally presented stimuli with higher values of ALC. Three potential listeners were rejected after the training period because they were unable to learn the task sufficiently well within the allotted time.

C. Procedure

Listeners were presented with two consecutive four note melodies. The second melody had one of the notes changed, and listeners had to identify the interval with the changed note. The procedure is illustrated schematically in Fig. 3 as four bars of music: The two melodies are presented in the second and fourth bars; the tonic, which defines the scale for the trial, is presented twice before each of the melodies, as a pick up in the third and fourth beats of the first and third bars. After the presentation of the second melody, there was an indefinite response interval, which was terminated by the listener's response. Feedback was then given as to which note actually changed, then another trial begun. In the example shown in Fig. 3, it is the second note that has changed in the second melody as shown by the gray square.

The notes of the melodies were harmonic complexes without their lowest components. The melody was defined as the sequence of fundamentals (that is, the residue pitch) rather than the sequence of intervals associated with any of the component sinusoids. On each trial, the F0 of the tonic was randomly selected from a half-octave range, centered

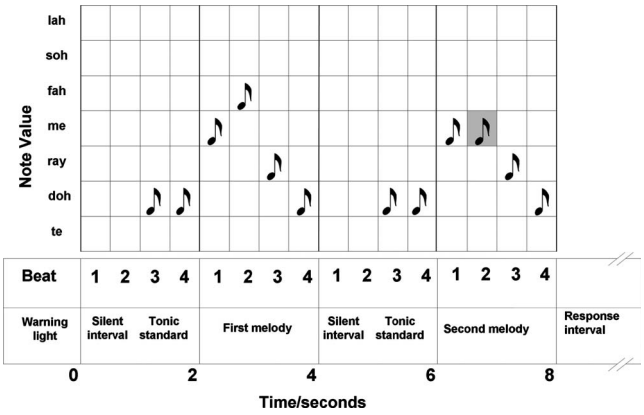


FIG. 3. Schematic of the procedure of the melody task, adapted from Patterson *et al.* (1983). One note changes by a single diatonic interval between the first and second presentations of the melody, and the listener has to identify the changed note, marked here by a grey square.

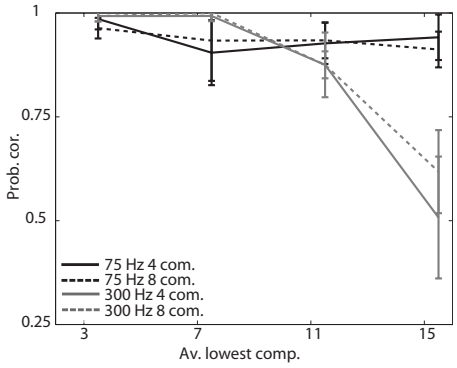


FIG. 4. Performance on the melody task with the 75 and 300 Hz fundamentals. The abscissa shows the average lowest component and the ordinate shows the probability of the listener correctly identifying the note which changed. Performance is plotted for each NC condition as a function of average lowest component. The black and grey lines show the results for the 75 and 300 Hz F0's, respectively. The solid and dashed lines show the results for the four- and eight-harmonic stimuli, respectively.

logarithmically on F0. The actual ranges were 63–89 and 252–357 Hz. The F0's of the other notes in the scale were calculated relative to the F0 of the tonic using the following frequency ratios: $2^{-1/12}$ (te); 1 (doh); $2^{2/12}$(ray); $2^{4/12}$(me); $2^{5/12}$(fah); $2^{7/12}$ (soh); and $2^{9/12}$(lah). Note that a ratio of $2^{1/12}$ produces an increase in frequency of one semitone on the equal temperament scale. The intervals are musical but, due to the randomizing of the F0, the notes of the melodies are only rarely the notes found on the A440 keyboard. The purpose of randomizing the F0 of the tonic was to force the listeners to use musical intervals rather than absolute frequencies to perform the task. The notes of the first melody of a trial were drawn randomly, with replacement, from the first five notes of the diatonic scale based on the randomly chosen tonic for that trial. The melody was repeated in the same key, and one of the notes was shifted up or down by a single diatonic interval. This shift can result in either a tone or a semitone change, since the size of a diatonic interval depends on its position in the scale.

The LC of each note in each melody was subjected to a restricted rove, the purpose of which was to preclude the use of the sinusoidal pitch of one of the components to perform the task. The degree of rove was one component, and so, the LC in each tone was either LC or LC+1. There were two further restrictions on the value of the LC: First, adjacent notes in a melody were precluded from having the same LC; second, each note had a different LC in the second melody from that which it had in the first melody. With these restrictions, it sufficed to alternate between the LC and the one above it using one of the patterns 1–0–1–0 or 0–1–0–1 for the first melody and the other pattern for the second melody.

The note-synthesis parameters were combined to produce 16 conditions ($2\times\mathrm{F0}, 2\times\mathrm{NC}, 4\times\mathrm{ALC}$). The order of these 16 conditions was randomized, and together they constituted one replication of the experiment. The listeners performed three or four replications in a 20 min block, with four or five blocks in a 2 h session. All listeners completed 45 or 46 replications.

D. Results of main experiment

The average results for the three listeners are shown in Fig. 4; the pattern of results was the same for all three listeners as shown by the analysis of variance (ANOVA) in Table I. The abscissa shows the ALC of the harmonic series; the ordinate shows the probability of the listener correctly identifying which of the notes changed in the second melody. Performance is plotted separately for the two NCs and the two F0's. The black and grey lines show the results for the 75 and 300 Hz F0's, respectively. The solid and dashed lines show the results for the four- and eight-harmonic stimuli, respectively. Figure 4 shows that, as ALC is increased, performance decreases, i.e., the probability of identifying which note changed in the second melody decreases in all conditions. However, the effect is much more marked for the 300 Hz F0, where performance decreases abruptly as ALC increases beyond 7. This is the most important result, as it differentiates the spectral and temporal models: Strictly spectral models would predict that there should be no reduction in listener performance when F0 is increased; indeed, performance should improve slightly with increasing F0 because the auditory filter becomes relatively narrower at higher center frequencies. Temporal models predict that there will be a decrease in performance with increasing F0 because of the progressive reduction in the phase locking of nerve fibers. The effect of increasing NC from four to eight had no consistent effect on listener performance.

An ANOVA was performed on the data; the results are presented in Table I, which confirms that the above-described effects are statistically significant at the $P<0.01$ level (bold type in Table I). There is a main effect of ALC, and one interaction, $\mathrm{F0}\times\mathrm{ALC}$. The interaction of F0 with ALC shows that ALC has a greater effect on performance for the higher F0.

III. ANCILLARY EXPERIMENTS

Prior to running the main experiment, two similar ancillary experiments were performed. They are presented briefly here inasmuch as they provide additional data concerning the

TABLE I. Results of an ANOVA of performance data (Dependent variable: SCORE). There is one significant ($P<0.01$) main effect and one significant interaction, both of which are shown in bold type; they are ALC, and F0×ALC.

Source	Type III sum of squares	df	Mean square	F	Sig.	Partial eta squared
F0	0.079	1	0.079	4.011	0.183	0.667
ALC	**0.412**	**3**	**0.137**	**18.477**	**0.002**	**0.902**
NC	0.002	1	0.002	3.728	0.193	0.651
SUB	0.012	2	0.006	0.273	0.782	0.186
F0*ALC	**0.347**	**3**	**0.116**	**27.632**	**0.001**	**0.933**
F0*NC	0.003	1	0.003	2.222	0.275	0.526
F0*SUB	0.039	2	0.020	3.834	0.080	0.545
ALC*NC	0.004	3	0.001	5.355	0.039	0.728
ALC*SUB	0.045	6	0.007	1.910	0.245	0.693
NC*SUB	0.001	2	0.001	0.443	0.717	0.421
F0*ALC*NC	0.012	3	0.004	7.181	0.021	0.782
F0*ALC*SUB	0.025	6	0.004	7.440	0.014	0.882
F0*NC*SUB	0.003	2	0.001	2.648	0.150	0.469
ALC*NC*SUB	0.002	6	0.000	0.480	0.803	0.324

effects observed in the main experiment, and they provide data on the effects of a larger component rove.

A. Method

The experimental task and the procedure were the same as those described for the main experiment in Sec. II. The design was slightly different. The F0 was 300 Hz in the first ancillary experiment and 75 Hz in the second. The ALC values were the same in the two ancillary experiments and the values were the same as in the main experiment, namely, 3, 7, 11, or 15. The number of components was 4 or 8, as in the main experiment; however, the ancillary experiments also included a condition with just two components. In the ancillary experiments, the lowest-component rove (LCR) was either one component (as in the main experiment) or three components. The LCR was subject to the same restrictions as to those in the main experiment. Specifically, for a rove of three, a random permutation of the four rove values was calculated for the first melody (e.g., 0–2–3–1) and recalculated for the second melody such that none of the notes in the second melody had the same lowest component as the corresponding note in the first melody (e.g., 1–0–2–3). Four listeners participated in each of the ancillary experiments, and three of the listeners were the same in the two experiments.

In the conditions where there were only two components in the sound, the pitch is ambiguous and the form of the ambiguity differs between musical and nonmusical listeners (Seither-Preisler *et al.*, 2007). The problem is that the sinusoidal pitches of the individual components are strong relative to the residue pitch produced by two components; this, in turn, makes it difficult for nonmusical listeners to focus on the residue pitch and not be distracted by the sinusoidal pitches. These problems reduced performance in the two-component conditions; the reduction was larger for the lower F0, and larger for the less musical listeners, but there was not enough data to quantify the interaction of F0 and listener. While it might be interesting to study how the pitch of the residue builds up with number of components, while the sinusoidal pitches of the individual components become less salient, that was not the purpose of these experiments. Consequently, the two-component condition was dropped from the design of the main experiment, and the two-component results from the ancillary experiments are omitted from further discussion.

B. Results

The remaining results of the two ancillary experiments are plotted together in Fig. 5; the pattern of results was the same for the four listeners in each of the experiments, so the figure shows performance averaged across listeners. The ab-

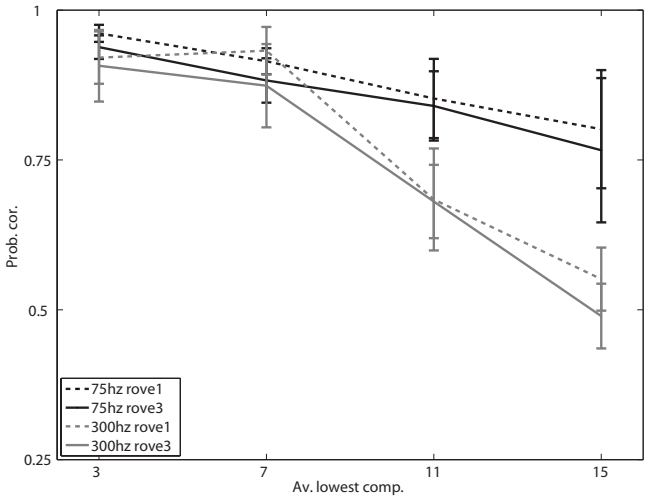


FIG. 5. Performance on the melody task in the ancillary experiments with the 75 Hz fundamental (black lines) and the 300 Hz fundamental (grey lines). The abscissa shows the average lowest component and the ordinate shows the probability of the listener correctly identifying the note which changed. Performance is plotted separately for the two rove conditions. The dashed and solid lines show the results for LCR values of one and three, respectively.

scissa shows the ALC of the harmonic series; the ordinate shows the probability of the listener correctly identifying which of the notes changed in the second melody, as before. Performance is plotted separately for the two LCRs and the two F0's. Performance was averaged over number of components (four and eight) because the variable did not affect performance; the same noneffect was later observed in the main experiment. The black and grey lines show the results for the 75 and 300 Hz F0's, respectively. The dashed and solid lines show the results for LCR values of one and three, respectively.

Consider first, the effect of roving the lowest component; compare the solid lines for a rove of one component with the dashed lines for the rove of three components. Although performance is slightly better for the rove of one, the pattern of results is the same, and the effect of rove magnitude is not significant. With this observation in mind, the results in Fig. 5 are seen to support the conclusions of the main experiment. The overall performance in the ancillary experiments is slightly lower overall, perhaps because two of the three listeners in the main experiment were trained musicians. However, the pattern of results is the same; whereas, performance decreases only slowly with increasing ALC when the F0 is 75 Hz, it decreases rapidly with ALC in the region above seven for an F0 of 300 Hz.

The comparison of performance for the two F0's must be made with some caution in this case, since three of the four listeners were common to the two ancillary experiments, and these three listeners performed the 300 Hz experiment before the 75 Hz experiment. However, there were more than 40 replications of all conditions for each listener in each ancillary experiment, *after* the initial training in the melody task, and an analysis showed that there was essentially no learning over the 40 replications in either experiment. It is also the case that the one listener who only participated in the 75 Hz experiment showed no learning over the course of the experiment, and had the same average level of performance as the other listeners in that experiment, indicating that training on the higher F0 was not required to produce good performance with the lower F0. Thus, it seems likely that the elevation of performance in the 75 Hz experiment for the higher ALC values is not simply due to learning, and probably represents the same effect as observed in the main experiment. Accordingly, in Sec. IV the data from the main and ancillary experiments are combined, so that the performance of the trained musicians is moderated by that of the rest of the listeners to provide the best estimate of what performance would be in the population.

IV. MODELING PITCH STRENGTH WITH DUAL PROFILES

The spectral and temporal profiles of the auditory image both describe aspects of the frequency information in a sound. They can be combined into a dual profile that facilitates comparison of the two kinds of frequency information by inverting the time-interval dimension of the temporal profile (Bleeck and Patterson, 2002). The dual profile for a typical stimulus in the current experiment is shown in Fig. 6. It had the following parameters: NC=4; ALC=3; and F0 =300 Hz. The temporal profile is the blue (darker gray) line with its maximum at 300 Hz; and the spectral profile is the red (lighter gray) line with its maximum at 900 Hz. The peak in the temporal profile at 300 Hz is the F0 of the harmonic series; the position of the peak is independent of the experimental parameters NC and ALC. Should the auditory system have a representation like the temporal profile, it would provide a consistent cue to the temporal pitch of these sounds. The spectral profile has four peaks at 900, 1200, 1500, and 1800 Hz. These peaks are at the four components of the signal, i.e., the third, fourth, fifth, and sixth harmonics of 300 Hz. The spectral profile shows that these four components are resolved, which means that a spectral model would be able to extract the F0 from the component spacing of this stimulus using a more central mechanism that computes subharmonics from a set of spectral peaks. As ALC increases, component resolution decreases and pitch strength decreases. In the following, we use the dual profile to assess the relative value of these spectral and temporal summaries of the sound as predictors of the data from the current experiment.

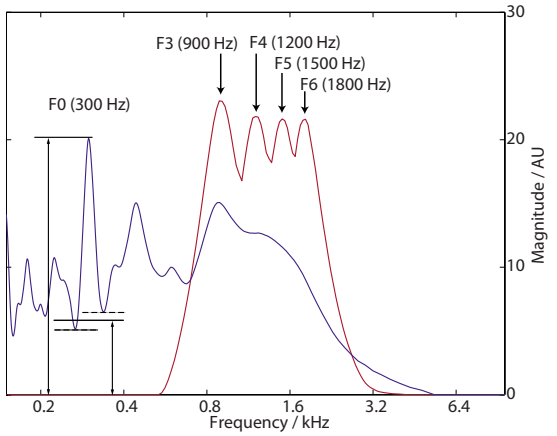


FIG. 6. (Color online) The dual profile for a stimulus with four resolved harmonics: NC=4, ALC=3, and F0=300 Hz. The temporal profile is the blue (dark) line and the spectral profile is the red (light gray) line. The F0 is represented in the temporal profile by the locating of the largest peak. In the spectral profile the F0 is represented by the spacing of the peaks.

A. The gammatone auditory filterbank

The dual profile shown in Fig. 6 was produced using a gammatone auditory filterbank (GT-AFB) (Patterson *et al.*, 1995) and the version of AIM described in Bleeck *et al.* (2004). The GT-AFB provides a linear simulation of the spectral analysis performed in the cochlea by the basilar partition. The dual profiles for all of the stimuli with F0's of 75 and 300 Hz are shown in Fig. 7. Figures 7(a)–7(h) show the profiles for an F0 of 75 Hz and Figs. 7(i)–7(p) show the profiles for an F0 of 300 Hz. Each row in Fig. 7 shows dual profiles with a constant NC; the value is eight for the top row, four for the middle row, eight for the second from bottom row, and four for the bottom row. Each column shows dual profiles for stimuli with a constant ALC, with values of three for the leftmost column, seven and eleven for the middle columns, and fifteen for the rightmost column. Thus, Fig. 7(a) is the dual profile for the stimulus with an F0 of

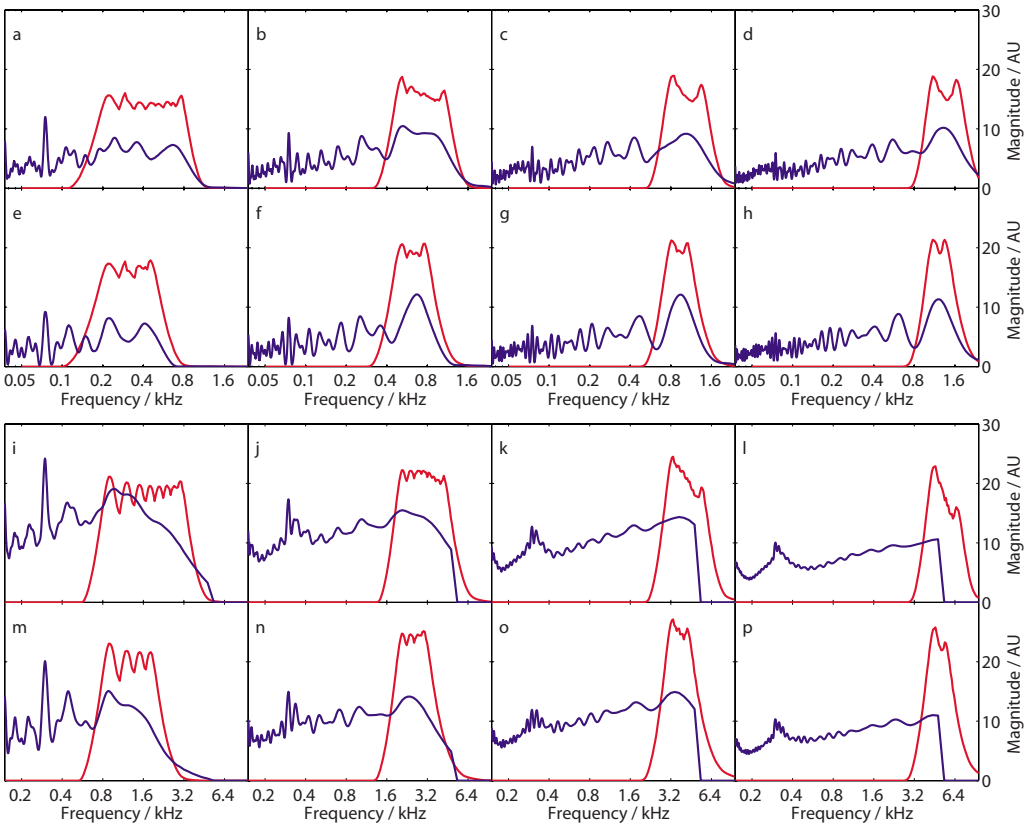


FIG. 7. (Color online) Dual profiles produced with the GT-AFB for stimuli with F0's of 75 and 300 Hz. Panels (a)–(h) Profiles for an F0 of 75 Hz. (i)–(p) Profiles for an F0 of 300 Hz. Each row shows dual profiles with a constant NC; the value is eight for the top row, four for the middle row, eight for the second from bottom row, and four for the bottom row. Each column shows dual profiles for stimuli with a constant ALC, with values of three for the leftmost column, seven and eleven for the middle columns, and fifteen for the rightmost column.

75 Hz, consisting of eight harmonics beginning from the third, and Fig. 7(p) is for an F0 of 300 Hz, consisting of four harmonics beginning from the fifteenth. Figure 7 shows that, generally, the spectral profiles do not contain many resolved harmonics for stimuli with lowest components above seven; this is shown in the three rightmost columns of Fig. 7.

The temporal profile always has a peak at the F0 of the harmonic series, 75 or 300 Hz, depending on the stimulus. The peak at F0 is not always the largest peak in the temporal profile; however, any other large peaks are spaced well away from the F0 in frequency. Sometimes the peaks are up to four octaves away, and as such, are far enough away not to interfere with the F0 peak. The peak used in the modeling was the largest peak within a two octave range centered on the fundamental. Thus, the temporal profile marks the F0 value by the location of a single peak and there is no need for a more central subharmonic generator. The height of the peak relative to the adjacent troughs can be used to estimate the strength of the pitch (Patterson *et al.*, 1996; Patterson *et al.*, 2000) and to explain the lower limit of pitch for complex harmonic sounds (Pressnitzer *et al.*, 2001). The pitch strength metric is illustrated in Fig. 6 by the faint lines; it is the height of the peak at F0, measured from the abscissa, minus the average of the trough values on either side of the peak, again measured from the abscissa. The effect of the loss of phase locking on this metric can be readily observed in the lower two rows of Fig. 7, where the F0 is 300 Hz and NC is either 8 or 4. As ALC increases from panel to panel across each row, the peak to trough ratio decreases progressively. The effect is much smaller in the upper rows where the energy of the stimulus is concentrated in the region below 2000 Hz, where phase locking is more precise.

There is a ceiling effect in the perceptual data at the lowest ALC values (3 and 7). Accordingly, the maximum value of the peak-to-trough ratio was limited to 7 in the modeling of pitch strength. This had the effect of limiting the model's estimate of pitch strength so that it did not rise further as ALC decreased from 7 to 3. The solid black and grey lines in Fig. 8 show the pitch strength estimates as a function of ALC for the 75 and 300-Hz F0's, respectively. The pitch strength values were averaged over the two NC conditions for each value of ALC. Figure 8 also shows the perceptual data for the listeners from both the main and the ancillary experiments averaged over NC for each F0. The perceptual data are presented separately for the two F0's with dashed black and grey lines for 75 and 300 Hz, respectively. Figure 8 shows that the model can explain the more rapid fall off in pitch strength with increasing ALC at the higher F0.

B. The dynamic, compressive gammachirp auditory filterbank

Unoki *et al.* (2006) have argued that the compressive GammaChirp auditory filter (cGC) of Irino and Patterson

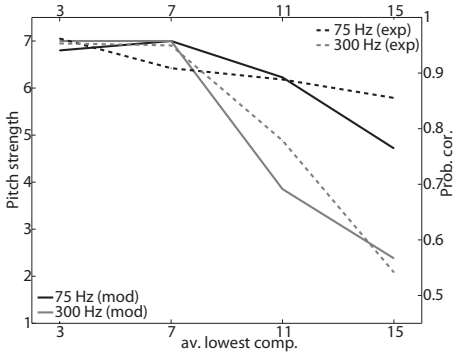


FIG. 8. Comparison of the experimental results with pitch-strength estimates from the dual profile model, based on a gammatone auditory filterbank, for an F0 of 75 Hz (black lines) and 300 Hz (grey lines). Dashed lines are the average experimental data plotted using the right ordinate (probability of correct identification as a function of average lowest component). Solid lines are the model values plotted using the left ordinate (pitch strength as a function of the average lowest component).

(2001) provides a better representation of cochlear filtering than the linear GT auditory filter in models of simultaneous masking. The magnitude characteristic of the cGC filter is asymmetric and level dependent with resolution similar to that described by Ruggero and Temchin (2005). At normal listening levels for speech and music, the bandwidth of the auditory filter is greater than the traditional ERB values reported by Glasberg and Moore (1990) as noted in Unoki *et al.* (2006). Moreover, Irino and Patterson (2006) have recently described a ***d****ynamic* version of the cGC filter with fast-acting compression which suggests that AIM can be extended to explain two-tone suppression and forward masking, as well as simultaneous noise masking. In an effort to increase the generality of the modeling, a version of AIM with the nonlinear dcGC filterbank was used to produce dual profiles for the stimuli in the experiment, to determine the pitch-strength values that would be derived from the temporal profiles of this more realistic time-domain model of auditory processing. The dual profiles produced with the dcGC filterbank were quite similar to those produced with the gammatone filterbank, primarily because the nonlinearities do not distort the time-interval patterns produced in the cochlea simulation as noted in Irino *et al.* (2007). The temporal profiles exhibited somewhat more pronounced peaks for the higher values of ALC, and the spectral profiles contained even less information, as would be expected with a broader auditory. But the differences were not large, and so the pattern of performance predicted for the melodic pitch task is quite similar for AIM with the dcGC filterbank. The results indicate that AIM with the dcGC filterbank would have the distinct advantage of being able to explain temporal pitch, masking, and suppression within one time-domain framework.

V. SUMMARY AND CONCLUSIONS

The decrease in pitch strength that occurs as the components of a harmonic complex are increased in frequency was used to demonstrate the importance of temporal fine structure in pitch perception. Performance on a melodic pitch task was shown to be better when the fundamental was lower (75 Hz) rather than higher (300 Hz), despite the fact that the internal representation of the harmonic complex has more resolved components when the fundamental is higher. A time-domain model of auditory processing (AIM) (Patterson *et al.*, 1995; Bleeck *et al.*, 2004) was used to simulate the neural activity produced by the stimuli in the auditory nerve and to compare the spectral and temporal information in the simulated neural activity in the form of the spectral and temporal profiles of the auditory image. Peaks in the time-interval profile can explain the *decrease* in performance as F0 *increases*. The corresponding spectral profiles show that spectral resolution increases when F0 increases, which suggests that spectral models based on excitation patterns would predict that performance on the melody task would improve as F0 increases, which is not the case.

The temporal profiles produced by the traditional version of AIM with the gammatone filterbank are similar to those produced by the most recent version of AIM, with a dynamic, compressive gammachirp filterbank. The latter model offers the prospect of being able to explain pitch, masking, and two-tone suppression within one time-domain framework.

ACKNOWLEDGMENTS

Research supported by the U.K. Medical Research Council (G0500221, G9900369). We would like to thank Steven Bailey, a project student, for his assistance in running the experiment, and his participation as a listener. The authors would also like to thank Alexis Hervais-Adelman for assistance with the ANOVA calculations.

Bleeck, S., Ives, T., and Patterson, R. D. (**2004**). "Aim-mat: The auditory image model in MATLAB," Acta Acust. **90**, 781–788.
Bleeck, S., and Patterson, R. D. (**2002**). "A comprehensive model of sinusoidal and residue pitch," poster presentation at Pitch: Neural Coding and Perception, Delmenhorst, Germany, 14–18 August.
Cullen, J. K. Jr., and Long, G. (**1986**). "Rate discrimination of high-pass filtered pulse trains," J. Acoust. Soc. Am. **79**, 114–119.
Fastl, H., and Stoll, G. (**1979**). "Scaling of pitch strength," Hear. Res. **1**, 293–301.
Fruhmann, M., and Kluiber, F. (**2005**). "On the pitch strength of harmonic complex tones," DAGA 05, Munchen, edited by H. Fastl and M. Fruhmann, DEGA, Berlin, Vol **II**, pp. 467–468.
Glasberg, B. R., and Moore, B. C. J. (**1990**). "Derivation of auditory filter shapes from notched-noise data," Hear. Res. **47**, 103–138.
Houtsma, A. J. M., and Smurzynski, J. (**1990**). "The central origin of the pitch of complex tones: Evidence from musical interval recognition," J. Acoust. Soc. Am. **87**, 304–310.
Irino, T., and Patterson, R. D. (**2001**). "A compressive gammachirp auditory filter for both physiological and psychophysical data," J. Acoust. Soc. Am. **109**, 2008–2022.
Irino, T., and Patterson, R. D. (**2006**). "A dynamic, compressive gammachirp auditory filterbank," IEEE Audio, Speech Lang. Proc. **14**, 2222–2232.
Irino, T., Walters, T. C., and Patterson, R. D. (**2007**). "A computational auditory model with a nonlinear cochlea and acoustic scale normalization," Proceedings of the 19th International Congress on Acoustics, Madrid.
Krumbholz, K., Patterson, R. D., and Pressnitzer, D. (**2000**). "The lower limit of pitch as determined by rate discrimination," J. Acoust. Soc. Am. **108**, 1170–1180.
Meddis, R., and Hewitt, M. J. (**1991**). "Virtual pitch and phase-sensitivity studied using a computer model of the auditory periphery. I. Pitch identification," J. Acoust. Soc. Am. **89**, 2866–2882.
Patterson, R. D. (**1987**). "A pulse ribbon model of monaural phase percep-

tion," J. Acoust. Soc. Am. **82**, 1560–1586.
Patterson, R. D., Allerhand, M., and Giguere, C. (**1995**). "Time-domain modeling of peripheral auditory processing: A modular architecture and a software platform," J. Acoust. Soc. Am. **98**, 1890–1894.
Patterson, R. D., Handel, S., Yost, W. A., and Datta, J. A. (**1996**). "The relative strength of the tone and noise components in iterated rippled noise," J. Acoust. Soc. Am. **100**, 3286–3294.
Patterson, R. D., Peters, R. W., and Milroy, R. (**1983**). "Threshold duration for melodic pitch," in *Hearing-Physiological Bases and Psychophysics*, edited by R. Klinke and R. Hartmann, Proceedings of the Sixth International Symposium on Hearing (Springer, Berlin), pp. 321–326.
Patterson, R. D., Robinson, K., Holdsworth, J., McKeown, D., Zhang, C., and Allerhand, M. (**1992**). "Complex sounds and auditory images," in *Auditory Physiology and Perception*, Proceedings of the Ninth International Symposium on Hearing, edited by Y. Cazals, L. Demany, and K. Horner (Pergamon, Oxford), pp. 429–446.
Patterson, R. D., Yost, W. A., Handel, S., and Datta, J. A. (**2000**). "The perceptual tone/noise ratio of merged iterated rippled noises," J. Acoust. Soc. Am. **107**, 1578–1588.
Pressnitzer, D., and Patterson, R. D. (**2001**). "Distortion products and the pitch of harmonic complex tones," in *Proceedings of the 12th International Symposium on Hearing, Physiological and Psychophysical Bases of Auditory Function*, edited by D. Breebaart, A. Houtsma, A. Kohlrausch, V. Prijs, and R. Schoonhoven (Shaker BV, Maastrict), pp. 97–104.
Pressnitzer, D., Patterson, R. D., and Krumbholz, K. (**2001**). "The lower limit of melodic pitch," J. Acoust. Soc. Am. **109**, 2074–2084.
Ritsma, R. J., and Hoekstra, A. (**1974**). "Frequency selectivity and the tonal residue," in *Facts and Models in Hearing*, edited by E. Zwicker and E. Terhardt (Springer, Berlin), pp. 156–163.
Ruggero, M. A., and Temchin, A. N. (**2005**). "Unexceptional sharpness of frequency tuning in the human cochlea," Proc. Natl. Acad. Sci. U.S.A. **102**, 18614–18619.
Seither-Preisler, A., Johnson, L., Krumbholz, K., Nobbe, A., Patterson, R. D., Seither, S., and Lütkenhöner, B. (**2007**). "Observation: Tone sequences with conflicting fundamental pitch and timbre changes are heard differently by musicians and non-musicians," J. Exp. Psychol. Hum. Percept. Perform. **33**, 743–751.
Slaney, M., and Lyon, R. F. (**1990**). "Visual representations of speech—A computer model based on correlation," J. Acoust. Soc. Am. **88**, S23.
Unoki, M., Irino, T., Glasberg, B. R., Moore, B. C. J., and Patterson, R. D. (**2006**). "Comparison of the roex and gammachirp filters as representations of the auditory filter," J. Acoust. Soc. Am. **120**, 1474–1492.
Yost, W. A., Patterson, R. D., and Sheft, S. (**1996**). "A time domain description for the pitch strength of iterated rippled noise," J. Acoust. Soc. Am. **99**, 1066–1078.

Speech detection in spatial and nonspatial speech maskers

Uma Balakrishnan[a] and Richard L. Freyman
Department of Communication Disorders, University of Massachusetts, 358 N. Pleasant Street, Amherst, Massachusetts 01003, USA

(Received 22 March 2007; revised 28 February 2008; accepted 3 March 2008)

The effect of perceived spatial differences on masking release was examined using a 4AFC speech detection paradigm. Targets were 20 words produced by a female talker. Maskers were recordings of continuous streams of nonsense sentences spoken by two female talkers and mixed into each of two channels (two talker, and the same masker time reversed). Two masker spatial conditions were employed: "RF" with a 4 ms time lead to the loudspeaker 60° horizontally to the right, and "FR" with the time lead to the front (0°) loudspeaker. The reference nonspatial "F" masker was presented from the front loudspeaker only. Target presentation was always from the front loudspeaker. In Experiment 1, target detection threshold for both natural and time-reversed spatial maskers was 17–20 dB lower than that for the nonspatial masker, suggesting that significant release from informational masking occurs with spatial speech maskers regardless of masker understandability. In Experiment 2, the effectiveness of the FR and RF maskers was evaluated as the right loudspeaker output was attenuated until the two-source maskers were indistinguishable from the F masker, as measured independently in a discrimination task. Results indicated that spatial release from masking can be observed with barely noticeable target-masker spatial differences.
© *2008 Acoustical Society of America.* [DOI: 10.1121/1.2902176]

PACS number(s): 43.66.Dc, 43.66.Pn, 43.66.Qp [RYL] Pages: 2680–2691

I. INTRODUCTION

The term informational masking has been used in a wide variety of contexts involving both speech and nonspeech signals. The use of this common terminology implies a common basis for this type of masking across speech and nonspeech stimuli. However, some key differences in methodology preclude the development of a global understanding of the concept of informational masking across both classes of signals. Not surprisingly, the majority of work with speech targets and maskers has involved *recognition* tasks (e.g., Carhart *et al.*, 1969; Freyman *et al.* 1999; Brungart, 2001; Arbogast *et al.*, 2005; Rakerd *et al.*, 2006). Some nonspeech studies have employed pattern identification or similar tasks (e.g., Watson *et al.*, 1976; Kidd *et al.*, 1995, 1998) and shown evidence of substantial informational masking. However, most of the work with nonspeech stimuli has involved *detection* experiments where the threshold of a tone is measured in the presence of a spectrally and/or temporally complex masker (e.g., Neff and Green, 1987; Wright and Saberi, 1999; Lutfi, 2003; Richards and Neff, 2004; Durlach *et al.*, 2005).

Only one study that we are aware of (Helfer and Freyman, 2005) examined detection of speech in conditions in which the focus was on informational masking. In that study, detection thresholds of topic-based sentences in the presence of masking sentences were obtained as part of an investigation of audiovisual speech perception. Sentence detection thresholds were obtained for both audiovisual and audio alone conditions for two spatial conditions. In the nonspatial condition the target sentence and the masker were presented from a single loudspeaker directly in front of the listener (the F-F condition). The spatial condition was the same except that an additional copy of the masker was presented 60° to the right and a 4 ms time advance was imposed on the right loudspeaker (the F-RF condition). In this condition, the masker was perceived to be well to the right of the target due to the precedence effect. Detection thresholds improved through the addition of visual cues or target-masker spatial separation only when the masker was speech (two talkers of the same sex as the target talker), not when it was noise. The fact that the F-RF condition produced no improvement for the noise masker was interpreted, as in previous recognition studies (e.g., Freyman *et al.*, 1999) to be evidence that this spatial configuration produced no release from energetic masking. Therefore, the observation of improvement in the F-RF condition with the speech masker was ascribed to release from informational masking. Monaural control experiments conducted by Freyman *et al.* (2001) had shown that, at least with recognition, such improvements were realized only with binaural listening, and presumed to result from perceived spatial differences between target and masker.

Because of the common use of detection for studying informational masking with nonspeech stimuli, its application to speech stimuli may offer improved opportunities to compare informational masking across speech and nonspeech signals. An additional important advantage of studying detection, relative to recognition, is that it would be expected to lower the signal-to-noise (S-N) ratio at which a threshold level of performance can be measured. The classic literature shows the speech detection threshold to be about 9 dB below the speech reception threshold (Thurlow *et al.*, 1948; Chaiklin, 1959). This difference could be useful when release from informational masking is measured in degraded

[a]Author to whom correspondence should be addressed. Electronic mail: umab@vermontel.net.

 0001-4966/2008/123(5)/2680/12/$23.00 © 2008 Acoustical Society of America

speech or in hearing-impaired populations. For example, Arbogast *et al.* (2005) showed that release from informational masking, and possibly informational masking itself, was reduced in a group of hearing-impaired subjects relative to normal-hearing listeners. However, the authors found that the base line nonspatial condition was so difficult for the hearing-impaired listeners that speech reception thresholds were often obtained at slightly positive S-N ratios. At positive S-N ratios, the target is louder than the masker, a condition that may not lend itself to informational masking. The vicinity of 0 dB S-N ratio may thus create a ceiling for informational masking, and the nonspatial threshold may have been truncated. Arbogast *et al.* (2005) suggested that because of this truncation it was not possible to determine conclusively whether informational masking differed between normal-hearing and hearing-impaired listeners. A speech detection paradigm could potentially avoid this issue because of the lower S-N ratios at which thresholds can be obtained.

The first experiment in the current paper employed a refined version of the detection paradigm used by Helfer and Freyman (2005) to study spatial release from informational masking. The sentence detection task used in that earlier study was most sensibly limited to single-interval trials because of the duration of the sentence stimuli. In the present study, we used words excised from the sentences and sought to determine whether a 4AFC paradigm could be employed successfully. The shortening of the stimuli from sentences to words also offered better control of stimulus variables and eliminated the potential use of semantic or syntactic connections between words available in sentence-level targets as cues, increasing the potential of making comparisons with nonspeech stimuli. Using this 4AFC paradigm, we investigated release from informational masking by creating target-masker spatial differences that do not produce unmasking with purely energetic maskers. These included the F-RF condition, described above, as well as an F-FR condition, which was identical to F-RF except that the front masker led the right masker by 4 ms. Both natural and time-reversed speech maskers were used.

In the course of Experiment 1 we (1) evaluated the extent to which a word detection paradigm lowered threshold S-N ratios, thereby mitigating the ceiling issues raised by Arbogast *et al.* (2005); (2) compared the amount of the informational masking that this detection paradigm produces relative to existing speech recognition data; (3) determined whether time-reversing the masker reduces spatial release from masking, a typical result in recognition studies; and (4) determined whether there is a difference in spatial release between the F-RF and F-FR conditions, where the former produces a large difference in perceived spatial location and the latter does not.

Experiment 2 explored in further detail the F-RF versus F-FR comparison and addressed the extent and type of spatial differences between target and masker that are essential for releasing informational masking. A classic study (Carhart *et al.*, 1969), as well as several recent studies (Freyman *et al.* 1999; Brungart *et al.*, 2005; Edmonds and Culling, 2005; and Rakerd *et al.*, 2006), have shown strong release from speech-on-speech masking even when spatial separation of target-masker images was not expected to create a clear separation in the centroid of target and masker auditory images. Freyman *et al.* (1999) found that spatial release from masking was almost as large for their F-FR condition as it was for the F-RF condition. The F-FR condition used the same loudspeaker configuration as the F-RF but with the time lead favoring the front loudspeaker. In this case the perceived horizontal location of target and masker was expected to be similar. Brungart *et al.* (2005) and Rakerd *et al.* (2006) explored the effect of masker delay over a wide range and found about the same masking release regardless of whether the time lead was imposed on the front or right loudspeaker. As the conditions where the masker time lead favors the front (target position) are not expected to create large horizontal shifts in the centroid of the masker image, their effectiveness may include or even be dominated by target-masker differences in other spatial properties, such as spatial width and shape. Blauert (1997) used the term "spaciousness" to describe this difference between two-source and single-source stimuli. Inasmuch as our two-loudspeaker spatial maskers simulate a source and a single reflection, the FR masker simulates only a reflection, whereas the RF masker simulates a reflection *and* also moves the masker source. It is not clear at this time whether the added spatial separation of masker source in the RF masker contributes to greater release from informational masking when the task is signal detection as opposed to recognition. In our second study we systematically attenuated the output of the right loudspeaker in both FR and RF spatial conditions and considered the difference in detection in these masking conditions in relation to their discriminability from the front only masker condition.

Finally, we investigated the effects of subject training on detection thresholds in the nonspatial (F-F) condition. This was motivated by the fact that in pilot listening, detection thresholds in the F-F condition showed considerable variability across runs and across listeners. Such variation was minimal in the spatial (F-RF and F-FR) conditions. Our purpose was to tease out any learning effects that might impact the overall amount of informational masking measured in the reference, nonspatial condition, so that we could make more accurate measurements of the release from informational masking provided by the spatial manipulations of the masker.

II. EXPERIMENT 1: RELEASE FROM MASKING IN DETECTION

A. Methods

1. Stimuli

Target stimuli were 20 consonant-vowel-consonant words excised from nonsense sentences recorded by a female talker. This was the same target talker used by Freyman *et al.* in previous studies (e.g., Freyman *et al.*, 1999). The 20 target words were chosen for clarity of production and ease of excision from the continuously produced sentence waveforms. Typically, the target word was the second "content" (meaning loaded) word of each utterance. In those instances where the second word in the sentence was not easy to extract from its surround, content words in other locations (first or third)

within the utterance were taken. The 20 target words were scaled to equate their root-mean-square (rms) amplitude and then padded with zeroes to match the duration of the longest word on the list (500 ms). The 20 words were concatenated to create a single file from which the experimental software randomly selected a single word and played it on each trial.

Two types of maskers were used: two-talker speech ("natural") and two-talker time-reversed speech ("reversed"). These were a 35 s duration mixture of the recording of two female talkers reciting nonsense sentences (see Freyman *et al.*, 2001). The choice of two-talker speech stream was determined by results shown by Freyman *et al.* (2004) that informational masking increased as number of talkers increased from one to two, and diminished thereafter as additional talkers were added. Other investigators have also shown that two to three-talker speech maskers are particularly effective in masking speech targets (Carhart *et al.*, 1975; Yost *et al.*, 1996; Brungart *et al.*, 2001; Hall *et al.*, 2002).

Each stereophonic masker was created by copying the two-talker masker signal into a second channel and imposing a 4 ms pad of zeroes at the beginning of one channel to delay it with respect to the other channel. Another 4 ms pad of zeroes was appended to the end of the second channel, to maintain equal duration of maskers in both channels. Both speech maskers were equated for rms as were the two channels of each masker. Two time-lead conditions were used for the natural masker: right-leading (RF) and front-leading (FR). Only the RF masker condition was used for the reversed speech masker. For comparison, a front-only (F) masker condition was created by turning off the right loudspeaker and playing the masker only from the loudspeaker that produced the target speech (the F-F condition). Thus for the front-only masker condition, the single-channel masker output was 3 dB less than that of the two-channel maskers. The target words always originated from the front loudspeaker. Therefore, for a given listening trial the target-masker configuration could be front-front (F-F), target front and masker right-front (F-RF) or target front and masker front-right (F-FR).

2. Apparatus

The experiments were conducted in an anechoic chamber measuring 4.9 m × 4.1 m × 3.12 m. The walls, floor, and ceiling are lined with 0.72 m foam wedges. Subjects were seated in the center of the room in front of a foam-covered semicircular arc on which two loudspeakers were positioned. The Front loudspeaker was at 0° horizontal azimuth; the Right loudspeaker was at 60° to the right. Both were 1.9 m from the approximate center of the subjects' head and were at ear height for the typical adult.

The target words were delivered via TDT System I instrumentation. The output of the 16 bit digital-to-analog converter (TDT DA1) running at 20 kHz was low-pass filtered at 8.5 kHz (TDT), attenuated (TDT PA3), and mixed with the masker before being delivered to a Crown D40 amplifier and a Realistic Minimus 7 loudspeaker. The masker was delivered from a second computer (Dell Dimension XPD 333) via audio software (Cool Edit Pro). The 35-s-long interference segment was played continuously in the loop mode over the duration of an adaptive track fed through PA4 attenuators (Tucker Davis System II). Calibration of target and maskers was by means of a 1 in. microphone (B&K 4145) fitted with a random incidence corrector and lowered to the position of the subjects' head with the subject absent. A sound level meter (B&K 2204) located outside the chamber measured the microphone output using the C-scale and Fast meter response. The target was calibrated to a sawtooth noise equated for average power to the target word stream. The maskers were calibrated for each channel using a speech-spectrum noise masker (Byrne *et al.*, 1994).

3. Subjects

Listeners were five young adult students. Four of the five subjects had hearing thresholds ≤20 dB hearing level (HL) in the tested frequency range 250–6000 Hz (ANSI S3.6, 1996). The fifth subject (coded as S1 in this paper) had hearing thresholds ≤20 dB HL in the frequency range 250–4000 Hz, and thresholds of 35 and 30 dB HL at 6000 Hz in the left and right ears, respectively, with recovery to within normal limits at 8000 Hz.

4. Procedures

For all conditions, masker level was fixed at 53 dBC in each masker channel while the target level was adapted. A four-alternative forced-choice (4AFC) paradigm with a 2-down 1-up stepping rule was employed to estimate the 70.7% criterion performance (Levitt, 1971). An individual adaptive track consisted of 10 reversals with the threshold computed as the arithmetic mean of the last six reversals. The initial step size for the adaptive track was 16 dB and the final, 2 dB. For all five subjects, data were collected for six listening conditions—two maskers (two-talker natural speech, two-talker reversed speech,) x three loudspeaker configurations (F-F, F-RF, F-FR). The masker was turned on prior to the initiation of each adaptive track and left running in loop play until the end of the track. Subjects responded using a button box with light-emitting diode (LED) lights that marked the four intervals, one of which contained the target. Feedback was provided via an LED, display that illuminated the target interval. For each condition, four adaptive tracks were obtained and threshold determined as the arithmetic mean of the four runs. All five subjects received the same order of listening conditions with two runs per condition before going on to the next. The sequence of presentation is shown in Table I.

At the beginning of the first listening session, subjects were verbally instructed, familiarized with the list of 20 target words (print and audio), and given practice runs in quiet and with the masker in F-F and F-RF loudspeaker conditions to familiarize them with the task. Listeners sat facing the front loudspeaker and were advised to not turn their heads; however, no head restraint was used. Subjects were given a brief break after the first six runs. A total of 12 runs completed the first listening session, with each subject returning for a second session to complete the second set of 12 adaptive tracks, again with a break after the first six runs of the

TABLE I. Order of presentation of listening conditions for Experiment 1. All subjects received the same sequence over two sessions. Maskers were two-talker speech natural and time reversed. Subjects received a final "Quiet" target track without any masker at the end of the second session.

Session 1	1, 2 Natural F-RF	3, 4 Natural F-F	5, 6 Natural F-FR	Break	7, 8 Reversed F-RF	9, 10 Reversed F-F	11, 12 Reversed F-FR	
Session 2	13, 14 Reversed F-FR	15, 16 Reversed F-F	17, 18 Reversed F-RF	Break	19, 20 Natural F-FR	21, 22 Natural F-F	23, 24 Natural F-RF	25 Quiet threshold

second session. Following the 12 adaptive tracks run with maskers, a "target only" track was run for each subject without the masker to ensure that target audibility in quiet was well below masker overall level. For all five subjects the quiet threshold was below 10 dBC.

B. Results

Figure 1 displays detection thresholds for the five subjects as well as the group mean for the two speech maskers. An additional set of four adaptive thresholds was obtained for S2 who showed high variability of F-F thresholds on the initial set (standard deviation of the mean=7.75). The second

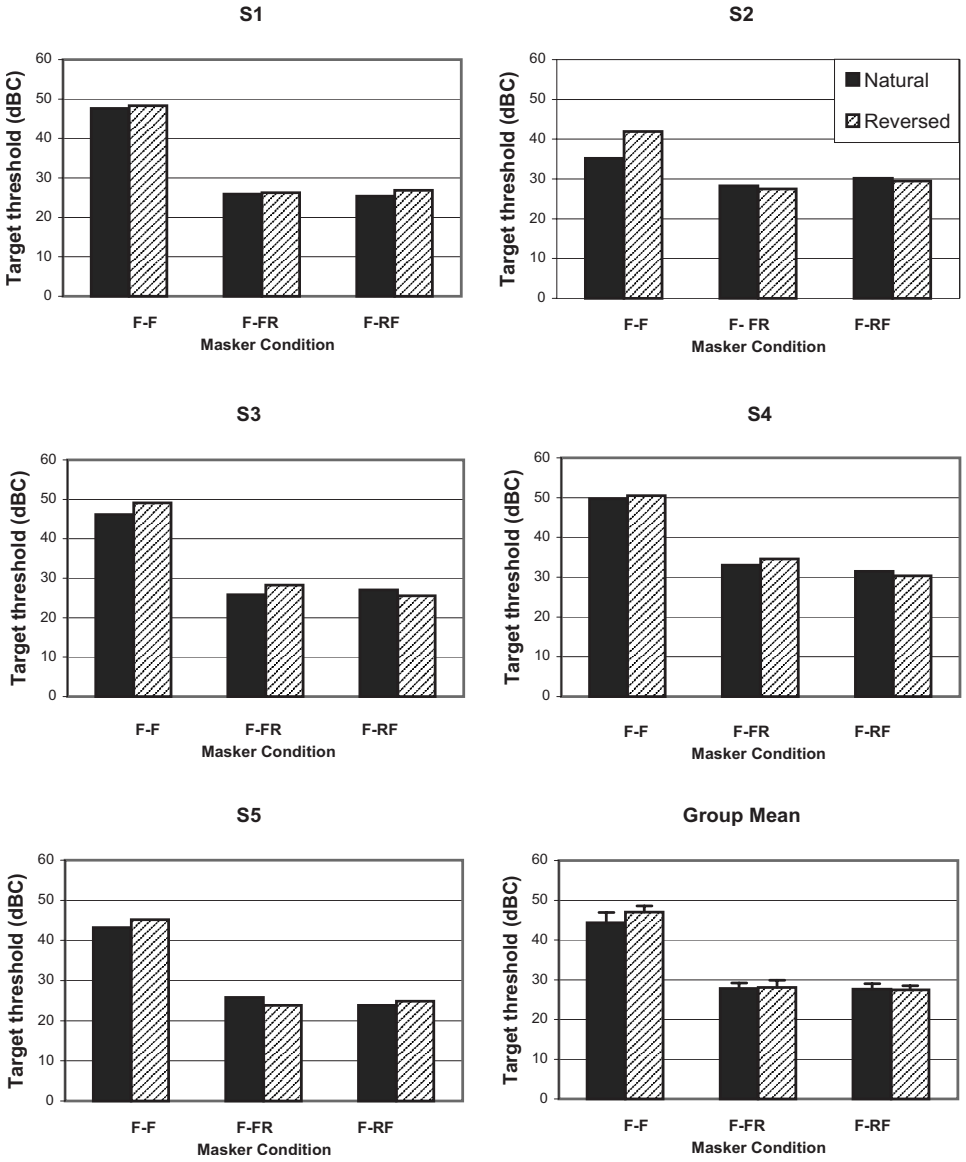


FIG. 1. Target thresholds for five subjects and group mean thresholds for the two-talker maskers in the F-F (nonspatial), F-FR (spatial, front-leading), and F-RF (spatial, right-leading) conditions. Solid bars represent the natural speech masker and the shaded bars represent the time-reversed speech masker. The group mean data (bottom left panel) also display one standard error of the mean.

set of four adaptive tracks also yielded a high standard deviation (6.37). Therefore, final threshold for the F-F condition for this subject was reported as the mean of all eight adaptive tracks.

As indicated earlier, masker output levels were fixed at 53 dBC for each loudspeaker. Threshold signal-to-noise (S-N) ratios are specified as the target level relative to 53 dBC. Across subjects target thresholds ranged from −2 dB S-N ratio for the nonspatial masker condition (S1) to nearly 30 dB below masker level for the RF spatial condition (S5). For individual subjects and the group, clear improvement in thresholds occurred for both spatial speech masker conditions (F-RF and F-FR) as compared to the F-F condition. Mean threshold improvement for the group (bottom right panel) in both spatial conditions relative to F-F was roughly 17 dB for the natural masker and 20 dB for the reversed masker. These values are substantially larger than those observed for nonsense sentence recognition using the same target talker and maskers (Freyman *et al.* 2001). It was also larger than the spatial advantages reported for detection by Helfer and Freyman (2005) for a different set of sentence stimuli using a single-interval task.

A noteworthy finding in the data displayed in Fig. 1 is the fact that both spatial speech masker conditions yielded substantial target threshold improvements, even though one (RF) was perceived well to the right of the target and the other (FR) was not. This is consistent with the findings reported in recognition studies (Freyman *et al.*, 1999; Brungart *et al.*, 2005; Rakerd *et al.*, 2006).

The improvement in the spatial conditions for the speech masker is interpreted here, as before, as indicating a release from informational masking. It is assumed that the high thresholds obtained in the F-F condition reflect approximately the same energetic masking as in the spatial conditions, with the difference of 17–20 dB reflecting informational masking. The fact that detection thresholds in the F-F condition were no better for the time-reversed speech than for the natural speech masker suggests that understandability of the masker is of virtually no importance in this detection experiment. If anything, the unintelligible time-reversed speech was a marginally more effective masker than the natural speech; the difference, however, was nonsignificant $t(4)=-1.962$; $p=0.121$. We suggest that this outcome is logical based on the brevity of the target signal used in this experiment (monosyllabic words) in conjunction with the nature of the detection task itself. That is, for our targets, the informational overlap between the target and masker occurs at the syllabic level, or, even more elementally, at the level of the phoneme. While natural and time-reversed speech streams are clearly differentiable from each other at the sentence level, they may be more similar to each other at the syllabic or phonemic level. For this reason, both types of speech maskers can be equally effective for the targets and the tasks we used. In contrast, when the same two maskers were used in a recognition experiment, the time-reversed masker was shown to be less effective than the natural masker in the F-F condition (Freyman *et al.*, 2001). Similar results have been reported for recognition by others (for example, Rhebergen *et al.*, 2005; Marrone *et al.*, 2007). These differences might suggest that the underlying psychometric functions created by time-reversed speech maskers might be steeper than those generated by natural speech, with the two functions converging at the lower end of the functions, near detection thresholds, and diverging at the higher end, where recognition performance is easier. In Freyman *et al.*, 2001 (Fig. 8, p. 2119) the backward and forward masker recognition performance functions for the F-F condition did converge at low S-N ratios (around −12 dB) while being divergent at high S-N ratios. However, because of the observed floor effects on performance, it is not possible to determine whether the convergence at low S-N ratios reflects an actual difference in the slopes of the two underlying functions.

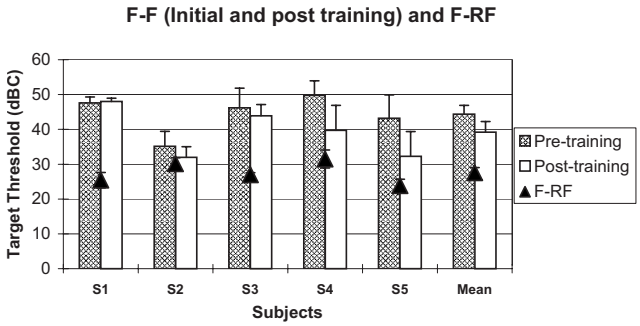


FIG. 2. Comparison of mean target thresholds for the initial four runs of Experiment 1 and the mean of the last four of ten training runs in the presence of the F-F (nonspatial) masker for five subjects and the group. Solid triangles are a replotting of the target thresholds obtained for the F-RF spatial masker condition for the natural speech masker shown in Fig. 1. Vertical bars show one standard deviation for individual subjects across the four pre- and post-training runs, and one standard error of the group mean data.

C. Learning effects in detection

In the F-F listening condition, four of the subjects showed higher variability in thresholds across the four adaptive tracks as compared to the F-RF condition. This raised the issue as to whether listeners could partially resolve the informational masking occurring in the F-F condition under some circumstances. To address this question, all five subjects were given ten successive adaptive tracks for the natural speech masker in the F-F condition. Results revealed variability across listeners, and while most listeners were able to improve performance on a given track, the gains did not carry over to successive tracks in a predictable or consistent manner.

Figure 2 treats the mean of the last four of the 10 runs as "post-training" and compares it to the mean of the initial four F-F runs of Experiment 1 for the five subjects and for the group. S1 shows no improvement, S2 and S3 show modest (less than 3 dB) gains, and S4 and S5 show large gains (about 10 dB). A paired-samples analysis of group mean data did not show a statistically significant difference between the pre- and post-training thresholds [$t(4)=2.316$; $p=.081$].

Also shown in Fig. 2 are the F-RF results for the natural speech masker reproduced from Fig. 1 (filled triangles). With the exception of S2, who did not show much spatial release from masking to begin with, subjects still showed substantial advantages in the F-RF condition even over the post-training

F-F results. Group mean differences between the F-F post-training and F-RF were statistically significant [$t(4)=3.182$; $p=.033$]. These results suggest that for most listeners, the release from masking provided by the spatial maskers was well beyond any improvement resulting from persistent listening and training. Inconsistent or limited responsiveness to extensive training has also been shown for nonspeech stimuli in informational masking tasks (for example, Neff and Callaghan, 1988; Neff and Dethlefs, 1995).

III. EXPERIMENT 2: REDUCING SPATIAL DIFFERENCES THROUGH RIGHT-CHANNEL ATTENUATION

In Experiment 1, listeners were able to benefit nearly equally from both the F-FR and F-RF spatial configurations, despite the fact that the spatial differences created are highly dissimilar. With the RF masker there is a substantial horizontal shift of the masker away from the target. As with any two-source sound, the RF masker is expected to have increased spaciousness relative to the F target, but the horizontal shift stands out as the most obvious difference. With the FR masker, the horizontal shift in position is expected to be fairly small and subjects may indeed use differences in spaciousness as a cue. Here, it may be worth noting an informal impression by the authors that listening to the F-FR condition does not require any special conscious or active effort to sort out how and where the target appears in relation to the masker. One listens for the target directly in front, and, at the relevant S-N ratios, the addition of the right loudspeaker causes it to stand out without any obvious increase in effort by the listener.

In the current experiment, target-masker spatial differences produced in the F-FR configuration were minimized by attenuating the right loudspeaker in graded steps. For comparison, we made the same right-loudspeaker attenuations for the RF masker, although in this case the time-intensity trade could create split or poorly defined spatial impressions. There were two parts to the experiment. In the first part, target words presented from the front loudspeaker were detected in the presence of the two-talker maskers as in Experiment 1, but now as a function of right-loudspeaker attenuation. In the second part, the spatial maskers were discriminated from the nonspatial (F) masker to determine the right-loudspeaker attenuation at which the addition of the right loudspeaker was undetectable. The goal of the combination of the two studies was to determine whether spatial release from masking could be observed with the front-right masker even when it was barely discriminable from the front masker.

A. Methods

Subjects were the same five listeners that completed Experiment 1. The speech target detection experiment used the same procedures as Experiment 1, except that the attenuation of the right loudspeaker in both the F-RF and F-FR conditions was increased from 0 dB (identical to the spatial conditions of Experiment 1) to 16 dB in 4 dB steps. Four adaptive tracks were obtained for each attenuation value. All subjects received the same stepwise order of presentation of conditions, starting with 0 dB and progressing to 16 dB of attenuation. One subject, (S3), received an additional attenuation step of 20 dB due to the fact that for this subject target threshold remained invariant as right loudspeaker attenuation was increased. The target words were the same as those used in Experiment 1 and the masker was the natural two-talker speech. Adaptive procedures and hardware setup were as described in Experiment 1.

For the discrimination task, 20 500 ms segments were randomly excised from a single channel version of the two-talker speech masker. Two kinds of average power relationships between segments were created. One set of 20 segments was allowed to retain the "natural" amplitude variation (N) (rms range=7.55 dB, standard deviation =1.93 dB), and in a second set the 20 segments were equated to each other for rms (Eq). The segments were converted into stereo waveforms by audio software (Cool Edit Pro), 20 ms linear rise/fall times were imposed, and 4 ms delays to one channel were added using zero padding as in Experiment 1. In each of the four intervals within a trial, an independent randomly selected segment was presented from among the 20 segments. In three of the intervals the stimulus was presented only from the front loudspeaker. The right loudspeaker was turned on during only one interval, to be detected by the listener, with feedback provided after each trial. Across trials, the right channel attenuation was adapted using the same tracking criteria and protocol employed in the other experiments described in this paper. Starting level for all stimuli was 40 dBC in both channels. Each subject received four adaptive tracks for each of four conditions in the following sequence: (1) FR-N–front-leading spatial masker with natural amplitude variation across segments; (2) RF-N–right-leading spatial masker with natural amplitude variation; (3) FR-Eq.–front-leading spatial masker rms equated; and (4) RF-Eq.–right-leading spatial masker rms equated. Subjects were the same five individuals who had participated in the previous experiments.

B. Results

The discrimination data are presented first (Fig. 3) so that they can be used to help interpret the target detection results later in Fig. 4. The abscissa marks the four spatial-amplitude combination conditions. The ordinate displays the relative level in the right loudspeaker required for discrimination from the front loudspeaker alone. Only small differences were noted between the results for the naturally roving level and the rms-equated stimuli. The purpose of the using the natural rove was to make the possible use of loudness cues available in the addition of the second loudspeaker less reliable. However, this appeared to have little effect. Because of the similarity across the "N" and "Eq." processing conditions, only the results for the natural rove will be discussed. There was a fairly wide variation across listeners, but the mean data show that the just-noticeable difference (jnd) for FR versus F alone occurred when the right loudspeaker was attenuated by 9 dB, whereas the jnd for the RF masker was obtained at a mean attenuation of approximately 16 dB.

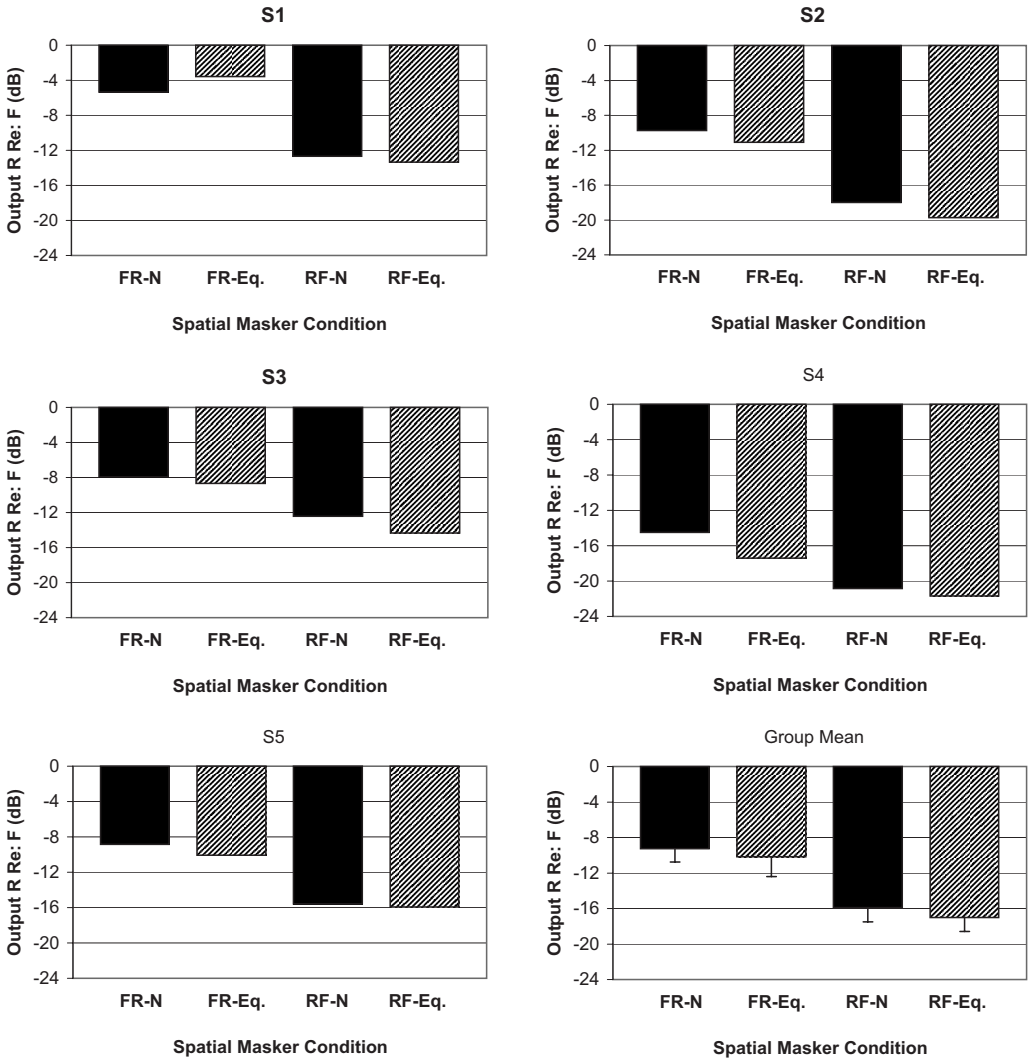


FIG. 3. Just-noticeable difference (jnd) in dB for discrimination of the spatial maskers from the nonspatial masker for five subjects and for the group. Jnd is expressed as right loudspeaker output relative to the fixed front loudspeaker output of 40 dBC. For each spatial masker, data are shown for the natural amplitude varying condition ("N") and the amplitude equated condition ("Eq."). Vertical bars for the group mean data display one standard error.

Paired samples *t*-test results showed that this was a statistically significant difference [$t(4)=10.6$; $p<0.001$]. The fact that the right loudspeaker output could be detected at a lower level for the RF masker may be attributable to a broadened or split spatial impression similar to that reported in lateralization studies in time-intensity trade conditions (Hafter and Jeffress, 1968; Hafter and Carrier, 1971). Rakerd and Hartmann (1985) suggested that the large variations in time-intensity trade data reported in the literature might be attributable to listeners expectations of the reliability and plausibility of conflicting directional cues.

Figure 4 displays target threshold for the two maskers as a function of right loudspeaker attenuation. Also shown for each subject is the F-F mean threshold for the last four of ten training runs (open square), which was assumed to be the value that the thresholds would approach as right loudspeaker output was attenuated and spatial release from informational masking was virtually eliminated. For all but S3, the functions for F-FR progressed from low thresholds averaging about 25 dB sound pressure level at 0 dB attenuation to higher thresholds approaching the F-F results at 16 dB attenuation. Thus, for the most part, 16 dB of attenuation effectively eliminated all effect of the right loudspeaker in producing release from masking. The progression varied among individual listeners. For example, S1's data show a large change between 12 and 16 dB while S4's data show the largest change with the first 4 dB of attenuation. For the other subject, S3, it appears that additional learning took place during the collection of the data such that performance actually improved as the experiment progressed and the attenuations increased. A 5 dB difference between F-FR with 0 dB attenuation (left-most data point) and the most attenuated condition occurred, but this was not nearly as large as the original F-FR versus F-F difference of 19 dB for that subject. The relationships between the F-RF and F-FR results are difficult to summarize on an individual subject basis, except to state that when there was a difference between the two thresholds the F-RF was usually lower. When thresholds were averaged across subjects (bottom-right panel), the RF masker provided a slightly but consistently greater release from masking relative to the FR masker for each right loudspeaker attenuation value (range of 0.55–2.93 dB). How-

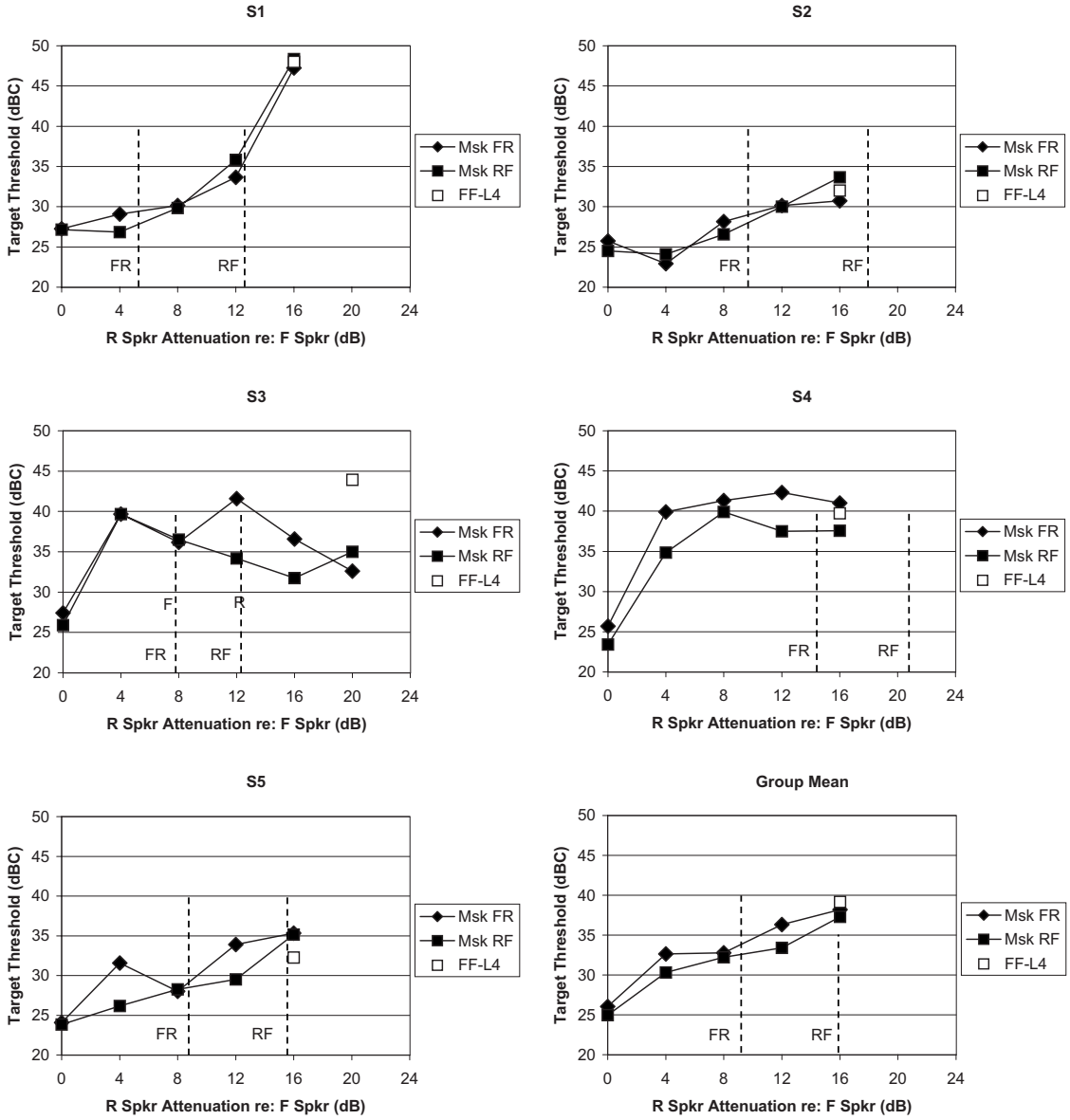


FIG. 4. Target thresholds for two spatial maskers for five subjects and for the group as a function of right loudspeaker attenuation. Dashed lines intersecting the abscissa replot the jnd values for each spatial masker from Fig. 3.

ever, analysis of variance results showed that these were not statistically significant [$F(4,1)=4.5$; $p=0.102$].

For comparison with the discrimination data, the natural-rove data from Fig. 3 are replotted in Fig. 4 as indicated by the dashed lines. These lines indicate the right loudspeaker attenuation values along the abscissa at which the spatial masker was just barely discriminable from the nonspatial. The comparison reveals the relationship between the threshold level of the right loudspeaker presentation and the effectiveness of the addition of the right loudspeaker in releasing masking for the front-only target words. Consider the group data first (bottom-right panel). The average just noticeable difference (jnd) for the F-FR configuration was approximately 9.3 dB of attenuation. Were the FR masker to be used with this right loudspeaker output level, the interpolated target detection threshold would be approximately 33.9 dBC (that is, the point at which the FR dashed line intersects the filled diamond trace depicting the FR threshold function). However, the nonspatial F-F threshold (unfilled square) was actually about 39.2 dBC. This means that 5.3 dB improvement in target detection for the FR masker took place at right loudspeaker attenuation values where the discrimination between FR and F was below 71% correct. In the case of one subject, S1, *most* of the improvement occurred at attenuations where FR and F configurations were less than one jnd apart. Thus, it must be concluded that spatial release from masking can occur with barely discriminable spatial differences between target and masker.

As had been shown in Fig. 3, detection of the signal from the right loudspeaker occurred at lower right loudspeaker output levels for the RF configuration than for FR (distance between the dashed lines along the abscissa). However, when the RF masker was used with the front-only target words, this RF-FR difference did not translate to correspondingly large or consistent changes in release from masking of the target words (difference between squares and

diamonds along the ordinate). This may have been because at low right-loudspeaker levels the RF masker likely produced split images, with one image remaining near the target and creating the same type of confusion caused by the front loudspeaker masking alone. If so, the lack of masking release would not be unlike what was observed by Brungart *et al.* (2005) and Rakerd *et al.* (2006). In those studies, masking release in the spatial maskers disappeared at long delays between the front and right loudspeakers where it was assumed that images were split.

IV. DISCUSSION

In these studies, a standard psychophysical multiple-interval forced-choice detection procedure using monosyllabic words revealed substantial evidence of spatial release from informational masking for speech stimuli. We believe that the general paradigm holds promise for helping to understand the commonalties and differences in what has been called informational masking for both speech and nonspeech stimuli.

In Experiment 1 we gathered basic information about informational masking and masking release using this word detection paradigm. We investigated (1) the S-N ratios at which base line performance could be obtained, (2) the size of the spatial release from informational masking that could be observed, (3) the dependence of informational masking on the understandability of the masker, and (4) the kinds of spatial differences that are required for spatial release from masking.

With regard to (1) above, the detection of words in the presence of two-talker masking was shown to produce thresholds of approximately −25 dB S-N ratio in spatial conditions, where informational masking was presumably minimal. By contrast, threshold *recognition* performance for sentence targets occurred around −10 dB S-N ratio in a recent study also using two-talker speech maskers (Freyman *et al.*, 2007). Others have found low threshold S-N ratios in recognition studies in spatial conditions using single-talker maskers (e.g., Hawley *et al.* 2004); however, less informational masking is expected than with two-talker maskers (e.g., Yost *et al.*, 1996; Freyman *et al.*, 2004). The advantage of the low threshold S-N ratio observed in the present study is that there is ample headroom to observe the effects of informational masking that may occur in nonspatial conditions without bumping into what might be a ceiling for informational masking at around 0 dB S-N ratio. The availability of this headroom could be useful for studying how a variety of stimulus manipulations affect informational masking, and could also make it easier to study informational masking in populations that have higher base line thresholds (see Arbogast *et al.*, 2005).

The second question concerned the size of the spatial release from masking that would be observed with these methods and stimuli. The answer was 17–20 dB for the natural and time-reversed speech maskers, respectively. All of the effect is presumed to be the result of release from informational masking. The basis for this assumption is that the spatial conditions used in this study have not been shown to produce masking release with purely energetic maskers (e.g., Freyman *et al.*, 1999; Brungart *et al.*, 2005; Rakerd *et al.*, 2006), even when using this very same detection paradigm (Freyman *et al.*, 2006). Under the further assumption that informational masking is approximately zero in the spatial conditions, a spatial release of 17–20 dB is indicative of informational masking of the same magnitude. This value is considerably larger than the approximately 5 dB of informational masking estimated with the same maskers for sentence-level target recognition (Helfer and Freyman, 2005; Freyman *et al.*, 2007). Helfer and Freyman (2005) also obtained detection thresholds for sentences against these maskers; the informational masking measured was about 6 dB, suggesting that the use of word level stimuli was a major contributing factor to the greater informational masking seen in the current experiment. A comparison of the word detection thresholds obtained in the current work with the sentence detection thresholds from Helfer and Freyman (2005) revealed that virtually all of the difference occurred in the nonspatial (F-F) condition (−17 dB S-N ratio in the earlier paper, and approximately −7 dB in the current study). This suggests that informational masking was greater for words than for sentences.

In restricting the task to word detection, our results more closely approximated the size of informational masking effects reported for brief nonspeech stimuli by other investigators. For instance, Kidd *et al.* (1998) obtained up to 15 dB of masking release at a spatial separation of 60° for pattern recognition in the presence of informational maskers. Using a detection paradigm, Oxenham *et al.* (2003) found on the average 10 and 25 dB of informational masking for a 1 kHz tone burst for musicians and nonmusicians, respectively. Oh and Lutfi (1999) estimated 11–12 dB informational masking for everyday sound maskers when they were easily recognized by subjects. It is also possible to observe large amounts of informational masking (on the order of 15 dB) in speech recognition studies (e.g., Arbogast *et al.*, 2005). However, these results have been reported for stimuli such as filtered coordinate response measure (CRM) sentences (Bolia *et al.*, 2000) and conditions specifically designed to maximize informational masking and minimize energetic masking.

The fact that spatial release is so large in our detection experiment may reflect a difference in the cues listeners are likely to use in the spatial and nonspatial conditions. In the two spatial conditions, F-RF and F-FR, the spatial image produced by the masker was different from that of the target, and the listener had only to detect the presence of any stimulus appearing to come from the front loudspeaker. By contrast, in the F-F condition both target and masking sounds appeared only from the front. In order to extract the target from the midst of an ongoing two-talker mixture of voices it was necessary to attend to other cues. At a minimum, subjects could have listened for the presence of the words with which they had been familiarized, abrupt amplitude changes, the voice characteristics of the target talker, or other linguistic features that separated the target speech from the masker speech. The threshold S-N ratios in the F-F condition (−7 dB average of natural and time-reversed maskers) suggest that none of these characteristics was easy to extract until the

target was within a few dB of the speech level of the individual talkers within the two-talker masking complex.

The third question considered in Experiment 1 was whether time reversing the masker would affect the amount of informational masking measured with this task. Results showed that masker time reversal produced no reduction in masking in either the spatial or nonspatial conditions. Indeed, a slight (though statistically insignificant) increase of about 2 dB was noted for the time-reversed speech masker. By contrast, sizable reduction of masking efficacy has been shown with masker time reversals for the recognition of short "everyday" sentences (Rhebergen *et al.*, 2005), nonsense sentences (Freyman *et al.*, 2001), and CRM stimuli (Marrone *et al.*, 2007). In recognition tasks, the absence of meaningful words in the masker could eliminate one of the main sources of confusion which, at least for CRM stimuli, is clearly supported by error patterns (Kidd *et al.*, 2005). By contrast, understandability could be less relevant in the detection paradigm used in this study, because any detectable portion of the target (such as a phoneme) can improve performance. The listener is able to use—and may even be dependent on—the phonological or linguistic information present in overlapping masker-target consonant and vowel segments rather than on word meaning and context cues. Thus, time reversing the speech masker does not reduce confusability between target and masker, because the confusion lies not at the word level but at the segmental level.

The absence of an effect of masker time reversal suggests that the speech-on-speech masking measured in the current study could be quite unlike the type of informational masking revealed when, for example, two or three CRM sentences compete with one another for attention (e.g., Ericson and McKinley, 1997; Arbogast *et al.*, 2002; Brungart and Simpson, 2002; Brungart *et al.*, 2005; Kidd *et al.*, 2005; Shinn-Cunningham *et al.*, 2005; Rakerd *et al.*, 2006). The difference may lead to the concern that a common terminology is being applied to different masking processes. However, although it would appear that in this study we measured the effect of a type of auditory confusion that is closer to what is seen in nonspeech informational masking, it would be premature to conclude that the speech-on-speech masking measured in this study had no linguistic basis. Even the time-reversed masker could be clearly recognized as speech. Listeners may have imposed the phonological and lexical rules of English to "extract" the target segment from the speech surround, in both natural and time-reversed speech maskers. It will likely require more work to identify the linguistic and nonlinguistic factors contributing to informational masking in this study.

A final question asked in Experiment 1 concerned the kinds of spatial differences between target and masker that are effective in releasing informational masking. The F-RF condition, where the masker from the right loudspeaker leads the presentation from the front loudspeaker, produces a dramatic target/masker spatial difference in which the masker is heard well to the right of the target. The F-FR condition, in which the front masker leads the right masker, still produces a noticeable spatial difference, but the change is more difficult to characterize. According to accounts from several papers (e.g., Shinn-Cunningham *et al.*, 1993; Litovsky and Macmillan, 1994; Chiang and Freyman, 1998) as well as classic texts on the spatial hearing (Blauert, 1997), the auditory image produced by a two-source masker such as the FR masker is expected to be less punctate than that of the single-source, front-only target, with the center of gravity shifted to the right by perhaps 5–10°. Despite the seemingly less obvious target-masker differences in the F-FR configuration, in *recognition* experiments release from masking relative to F-F was nearly the same for F-RF and F-FR configurations (Freyman *et al.*, 1999; Brungart *et al.*, 2005; Rakerd *et al.*, 2006). The current paper (Fig. 1) shows that this same result is obtained also for the word detection task. This suggests that small differences in spatial separation and/or spatial width cues are no less efficient in releasing informational masking than the dramatic spatial separation provided by the right-leading F-RF masker. The implication is that target-masker perceptual spatial differences other than spatial *separation* can be potent facilitators of release from masking.

In Experiment 2 we exploited the forced-choice word detection technique, and the large spatial release it produces, to explore further the subtlety of spatial difference required for masking release in the F-FR configuration. We titrated the more than 15 dB of difference in thresholds available between F and FR configurations by attenuating the output of the right loudspeaker in F-FR until the results were essentially no different than F-F. The functions were then related to the results of a second portion of the experiment, which determined the threshold of discrimination between F and FR maskers with systematic attenuation of the right loudspeaker in the FR condition. For comparison, all conditions were repeated with the RF masker, but still with attenuation of the right loudspeaker.

The 4AFC task with a two-down one-up stepping rule estimates a d' of 1.53 (Macmillan and Creelman, 1991). Using that threshold criterion, the mean just discriminable difference between FR and F alone occurred when the right loudspeaker was attenuated by 9 dB. With that same 9 dB of attenuation, an average of 5 dB of spatial release from masking still occurred in the F-FR configuration. Thus, it must be concluded that spatial release from masking can be observed with barely discernable target-masker spatial differences. This is consistent with other studies showing that small changes in masker-target spatial relationships can substantially affect target recognition (e.g., Brungart *et al.*, 2005; Gallun *et al.*, 2005).

There are also at least two observations in the literature where the opposite occurred, i.e., presumably large spatial differences between target and masker produced no release from masking (Brungart *et al.*, 2005; Rakerd *et al.*, 2006). In both of these cases release from masking disappeared when the delay in a two-source speech masker was increased from 32 to 64 ms. Presumably, the 64 ms delay produced split images for the masker, one near the front target and one near the lateral masker. Informational masking is attributed to the masker image located near the target. In the current Experiment 2, attenuations applied to the right loudspeaker were much more easily detected in the RF configuration than the FR configuration, but the release from masking created was

only marginally increased (Fig. 4) and did not reach statistical significance. It is possible that the severe attenuation applied to the leading (right) loudspeaker in the RF case produced a split image due to the time-intensity incompatibility and may have failed to produce increased release from masking for the same reasons presumed to occur in the Brungart *et al.* (2005) and Rakerd *et al.* (2006) studies. If this is indeed the explanation, then it is fascinating that listeners cannot use this additional synchronized separated image to inform them of the temporal characteristics of the masker in order better focus on the target. This kind of active study of the masker in order to learn what to ignore does not appear to be used or useful. Rather, barely discriminable differences between the spatial image produced by the target and the most similar image produced by the masker seem to facilitate improved attention on the target.

ACKNOWLEDGMENTS

The authors would like to thank Gail Brown, John Ackland Jones, Laurel Slongwhite, and Lauren Sullo for their assistance in data collection. We would also like to thank three anonymous reviewers and the associate editor for their thoughtful comments on earlier versions of this paper. This work was supported by a grant from the National Institute on Deafness and other Communicative Disorders (DC 01625).

ANSI (**1996**). ANSI S3.6-1996, "Specifications for audiometers" (American National Standards Institute, New York).

Arbogast, T. L., Mason, C. R., and Kidd Jr., G. (**2002**). "The effect of spatial separation on informational and energetic masking of speech," J. Acoust. Soc. Am. **112**, 2086–2098.

Arbogast, T. L., Mason, C. R., and Kidd Jr., G. (**2005**). "The effect of spatial separation on informational masking of speech in normal-hearing and hearing-impaired listeners," J. Acoust. Soc. Am. **117**, 2169–2180.

Blauert, J. (**1997**). *Spatial Hearing* (MIT, Cambridge, MA).

Bolia, R. S., Nelson, W. T., Ericson, M. A. and Simpson, B. D., (**2002**). "A speech corpus for multitalker communications research," J. Acoust. Soc. Am. **102**, 1065–1066.

Brungart, D. S., and Simpson, B. D. (**2001**). "Informational and energetic masking effects in the perception of two simultaneous talkers," J. Acoust. Soc. Am. **109**, 1101–1109.

Brungart, D. S., Simpson, B. D., Ericson, M. A., and Scott, K. R. (**2001**). "Informational and energetic masking effects in the perception of multiple simultaneous talkers," J. Acoust. Soc. Am. **110**, 2527–2538.

Brungart, D. S., and Simpson, B. D. (**2002**). "The effects of spatial separation in distance on the informational and energetic masking of a nearby speech signal," J. Acoust. Soc. Am. **112**, 664–676.

Brungart, D. S., Simpson, B. D., and Freyman, R. L. (**2005**). "Precedence-based speech segregation in a virtual auditory environment," J. Acoust. Soc. Am. **118**, 3241–3251.

Byrne, D., Dillon, H., Tran, K., Arlinger, S., Wilbraham, K., Cox, R., Hagerman, B., Hetu, R., Kei, J., Lui, C., Kiessling, J., Nasser Kotby, M., Nasser, N. H. A., El Kholy, W. A. H., Nakanishi, Y., Oyer, H., Powell, R., Stephens, D., Meridith, R., Sirimanna, T., Tavarkiladze, G., Frolenkovgi, G. I., Westerman, S., and Ludvigsen, C. (**1994**). "An international comparison of long-term average speech spectra," J. Acoust. Soc. Am. **96**, 2108–2120.

Carhart, R., Johnson, C., and Goodman, J. (**1975**). "Perceptual masking in mutliple sound backgrounds," J. Acoust. Soc. Am. **45**, 694–703.

Carhart, R., Tillman, T. W., and Greetis, E. S. (**1969**). "Perceptual masking of spondees by combinations of talkers," J. Acoust. Soc. Am. **58**, 694–703.

Chaiklin, J. B. (**1959**). "The relation among three selected auditory speech thresholds," J. Speech Hear. Res. **2**, 237–243.

Chiang, Y. C., and Freyman, R. L. (**1998**). "The influence of broadband noise on the precedence effect," J. Acoust. Soc. Am. **104**, 3039–3047.

Durlach, N. I., Mason, C. R., Gallun, F. J., Shinn-Cunningham, B. G., Colburn, H. S., and Kidd, G. (**2005**). "Informational masking for simultaneous nonspeech stimuli: Psychometric functions for fixed and randomly mixed maskers," J. Acoust. Soc. Am. **118**, 2482–2497.

Edmonds, B. A., and Culling, J. F. (**2005**). "The role of head-related time and level cues in the unmasking of speech in noise and competing speech," Acta. Acust. Acust. **91**, 546–553.

Ericson, M. A., and McKinley, R. L. (**1997**). "The intelligibility of multiple talkers separated spatially in noise," in *Binaural and Spatial Hearing in Real and Virtual Environments*, edited by R. H. Gilkey, and T. B. Anderson (Lawrence Erlbaum, Hillsdale, N. J.)

Freyman, R. L., Helfer, K. S., McCall, D. D., and Clifton, R. K. (**1999**). "The role of perceived spatial separation in the unmasking of speech," J. Acoust. Soc. Am. **106**, 3578–3588.

Freyman, R. L., Balakrishnan, U., and Helfer, K. S. (**2001**). "Spatial release from informational masking in speech recognition," J. Acoust. Soc. Am. **109**, 2112–2122.

Freyman, R. L., Balakrishnan, U., and Helfer, K. S. (**2004**). "Effect of number of masking talkers and auditory priming on informational masking and speech recognition," J. Acoust. Soc. Am. **115**, 2246–2256.

Freyman, R. L., Balakrishnan, U., and Helfer, K. S. (**2006**). "Exploration of spatial release from masking in a simulation of cochlear implant listening," paper presented at the *29th Mid-Winter Meeting of the Association for Research in Otolaryngology*, Baltimore, MD.

Freyman, R. L., Helfer, K. S., and Balakrishnan, U. (**2007**). "Variability and uncertainty in masking by competing speech," J. Acoust. Soc. Am. **121**, 1040–1046.

Gallun, F. J., Mason, C. R., and Kidd Jr., G. (**2005**). "Binaural release from informational masking in a speech recognition task," J. Acoust. Soc. Am. **118**, 1614–1625.

Hafter, E. R., and Jeffress, L. A. (**1968**). "Two-image lateralization of tones and clicks," J. Acoust. Soc. Am. **44**, 563–569.

Hafter, E. R., and Carrier, L. A. (**1972**). "Binaural interaction in low-frequency stimuli: the inability to trade time and intensity completely," J. Acoust. Soc. Am. **51**, 1852–1862.

Hall, J. W., Grose, J. H., Buss, E., and Dev, M. B. (**2002**). "Spondee recognition in a two-talker masker and a speech-shaped noise masker in adults and children," Ear Hear. **23**, 159–165.

Hawley, M. L., Litovsky, R. Y., and Culling, J. F. (**2004**). "The benefit of binaural hearing in a cocktail party: Effect of location and type of interferer," J. Acoust. Soc. Am. **115**, 833–843.

Helfer, K. S., and Freyman, R. L. (**2005**). "The role of visual speech cues in reducing energetic and informational masking," J. Acoust. Soc. Am. **117**, 842–849.

Kidd Jr., G., Arbogast, T. L., Mason, C. R., and Gallun, F. J. (**2005**). "The advantage of knowing where to listen," J. Acoust. Soc. Am. **118**, 3804–3815.

Kidd Jr., G., Mason, C. R., and Rohtla, T. L. (**1995**). "Binaural advantage for sound pattern identification," J. Acoust. Soc. Am. **98**, 1977–1986.

Kidd Jr., G., Mason, C. R., Rohtla, T. L., and Deliwala, P. S. (**1998**). "Release from masking due to spatial separation of sources in the identification of nonspeech auditory patterns," J. Acoust. Soc. Am. **104**, 422–431.

Levitt, H. (**1971**). "Transformed up-down methods in psychoacoustics," J. Acoust. Soc. Am. **49**, 467–477.

Litovsky, R. Y., and Macmillan, N. A. (**1994**). "Sound localization precision under conditions of the precedence effect: Effects of azimuth and standard stimuli," J. Acoust. Soc. Am. **96**, 752–758.

Lutfi, R. A., Kistler, D. J., Callahan, M. R., and Wightman, F. L. (**2003**). "Psychometric functions for informational masking," J. Acoust. Soc. Am. **114**, 3273–3282.

Macmillan, N. A., and Creelman, C. D. (**1991**). *Detection Theory: A User's Guide.*, (Cambridge U. P., Cambridge, England).

Marrone, N. L., Mason, C. R., and Kidd Jr., G. (**2007**) "Spatial release from speech-on-speech masking with symmetrically placed maskers," paper presented at the *30th Mid-winter Meeting of the Association for Research in Otolaryngology*, Denver, CO.

Neff, D. L., and Callaghan, B. P. (**1988**). "Effective properties of multicomponent simultaneous maskers under conditions of uncertainty maskers," J. Acoust. Soc. Am. **83**, 1833–1838.

Neff, D. L., and Dethlefs, T. M. (**1995**). "Individual differences in simultaneous masking with random frequency, multicomponent maskers," J. Acoust. Soc. Am. **98**, 125–134.

Neff, D. L., and Green, D. M. (**1987**). "Masking produced by spectral uncertainty with multicomponent maskers," Percept. Psychophys. **41**, 409–415.

Oh, E. L., and Lutfi, R. A. (**1999**). "Informational masking by everyday

sounds," J. Acoust. Soc. Am. **106**, 3521–3528.
Oxenham, A. J., Fligor, B. J., Mason, C. R., and Kidd Jr., G. (**2003**). "Informational masking and musical training," J. Acoust. Soc. Am. **114**, 1543–1549.
Rakerd, B., and Hartmann, W. M. (**1985**). "Localization of sound in rooms: The effects of a single reflecting surface," J. Acoust. Soc. Am. **78**, 524–533.
Rakerd, B., Aaronson, N. L., and Hartmann, W. M. (**2006**). "Release from speech-on-speech masking by adding a delayed masker at a different location," J. Acoust. Soc. Am. **119**, 1597–1605.
Rhebergen, K. S., Versfeld, N. J., and Dreschler, W. A. (**2005**). "Release from informational masking by time reversal of native and non-native interfering speech," J. Acoust. Soc. Am. **118**, 1274–1277.
Richards, V. M., and Neff, D. L. (**2004**). "Cueing effects for informational masking," J. Acoust. Soc. Am. **115**, 289–300.
Shinn-Cunningham, B. G., Zurek, P. M., and Durlach, N. I. (**1993**). "Adjustment and discrimination measurements of the precedence effect," J. Acoust. Soc. Am. **93**, 2923–2932.
Shinn-Cunningham, B. G., Ihlefeld, A., Satyavarta, and Larson, E. (**2005**). "Bottom-up and top-down influences on spatial unmasking," Acta. Acust. Acust. **91**, 967–979.
Thurlow, W. R., Silverman, S. R., Davis, H., and Walsh, T. E. (**1948**). "A statistical study of auditory tests in relation to the fenestration operation," Laryngoscope **58**, 43–66.
Watson, C. S., Kelly, W. J., and Wroton, H. W. (**1976**). "Factors in the discrimination of tonal patterns II: Selective attention and learning under various levels of stimulus uncertainty," J. Acoust. Soc. Am. **60**, 1176–1185.
Wright, B. A., and Saberi, K. (**1999**). "Strategies to detect auditory signals in small sets of random maskers," J. Acoust. Soc. Am. **105**, 1765–1775.
Yost, W. A., Dye, R. H., and Sheft, S. (**1996**). "A simulated cocktail party with up to three sound sources," Percept. Psychophys. **58**, 1026–1036.

Relative weights for frequency glide detection using narrowband noise[a)]

Jinyu Qian[b)] and Virginia M. Richards
Department of Psychology, 3401 Walnut Street, Suite 302C, University of Pennsylvania, Philadelphia, Pennsylvania 19104, USA

(Received 18 July 2006; revised 8 February 2008; accepted 18 February 2008)

Narrowband noise stimuli were used to derive relative weights for detecting frequency glides in a yes/no procedure. One stimulus set was restricted to the duration of the glide. For the second stimulus set, there were fringe noise bands preceding and following the glide. For both sets, the center frequency of the linear glide was either fixed at 1000 Hz or randomly chosen on each trial from the range of 800–1200 Hz. Relative weights as a function of time were derived using a linear model and the linear classification method [A. Ahumada, J. Vis., **2**, 121–131 (2002)]. Sensitivity was better for the fixed- than random-frequency conditions, and weight patterns from the random-frequency conditions were less reliable than those obtained from the fixed-frequency conditions. The magnitudes of the relative weights tended to be larger for the second half of the stimulus, suggesting that subjects paid more attention to the later than the earlier parts of stimuli. In the random-frequency conditions, the linear model failed to account for subjects' performance unless the stimuli were expressed in terms of relative changes in frequency rather than absolute frequency. © *2008 Acoustical Society of America.* [DOI: 10.1121/1.2897030]

PACS number(s): 43.66.Fe [RAL] Pages: 2692–2700

I. INTRODUCTION

Hartmann and Klein (1980) provided a signal-detection theoretical model to evaluate sensitivity to frequency modulation. As they point out, assuming the signal is known exactly, an ideal observer would cross correlate the stimulus with an internal template that is a copy of the signal to be detected. Noting that subjects can detect the modulation at signal levels smaller than those required in order to discriminate between forms of modulation (e.g., sinusoidal versus triangle frequency modulation), Hartmann and Klein suggested that the modulation form cannot be known exactly. Thus, they proposed that subjects sample the pitch of the stimulus, and difference the samples in order to detect the presence of modulation (see also Demany and Semal, 1989).

Here, the signal-detection theoretic approach noted by Hartmann and Klein is revisited with the goal of estimating the internal template for the detection of ascending frequency glides. The psychophysical estimate of the template is relative weights as a function of time, which will be referred to as the temporal weight pattern or TWP. The questions of interest include: What is the form of the TWP? And whether the TWPs can account for the human detection performance.

For the ideal observer model, the template for the detection of an ascending linear frequency glide is itself an ascending linear glide, with negative values for the first half and positive values for the second half of the template. In addition, the relative weights that form the template sum to zero. For each yes/no trial, a decision variable would be the inner product of the template and the stimulus vectors. A decision can be made by comparing the resulting decision variable to a criterion. Therefore, for the ideal observer, the decision variable for a constant-frequency tone (no-glide tone) would be zero and that for an ascending tonal glide would be positive valued. Additionally, the sum-to-zero template would lead to decision variables independent of the central frequency (the frequency at the temporal midpoint of the tonal glide) variation across presentations. Therefore, the ideal template predicts no effect of randomizing the central frequency of the glide stimuli.

Human listeners might likewise make their decisions based on a comparison between an internal template and the stimulus, noting that the template may not be ideal. In addition to the work of Hartmann and Klein (1980), two additional psychophysical results suggest possible deviations of the listeners' actual internal templates from the ideal template. First, several investigators (Madden and Fire, 1996; Moore and Sek, 1998; Sek and Moore, 1999) have reported that the threshold for detecting a change in the frequency extent of tonal linear glides is higher when the central frequencies of the stimuli are random across presentations compared to fixed. Second, Moore and Sek (1998) have shown that the effects of central frequency randomization on thresholds are not always as large as expected if subjects depended on the frequencies solely at the stimulus onset or solely at the stimulus offset.

When the central frequency is drawn at random, neither the beginning nor the ending portion of the stimulus alone indicates whether or not a glide is present. The difference between these two portions, however, is invariant with respect to central frequency randomization. In terms of tem-

[a)]Portions of this research were presented at the 151st meeting of the Acoustical Society of America [J. Acoust. Soc. Am.**119**, 3332 (2006)].
[b)]Author to whom correspondence should be addressed. Electronic mail: qianj@sas.upenn.edu.

 0001-4966/2008/123(5)/2692/9/$23.00 © 2008 Acoustical Society of America

plates, "listening" only at the beginning of the stimulus implies non-zero relative weights only at the stimulus onset. As a result, the decision variable would reflect only the initial frequency. For the strategy of "differencing" the beginning and the ending frequencies, similar to the ideal template, the relative weights at the stimulus onset and offset would be of equal magnitude, but opposite sign. On one hand, the available psychophysical data suggest a form of differencing the beginning and ending portions of the stimuli because the listeners' thresholds are superior to those expected if listeners were attending to, for example, just the initial frequency region of the stimuli (Moore and Sek, 1998). On the other hand, the differencing is not perfect; otherwise there would be no effect of frequency randomization at all. It is as though listeners fall between these two extremes, perhaps over weighting the initial or ending portions of the stimuli, but still differencing the frequencies of the initial and ending portions. Such a template would yield decision variables that are only somewhat influenced by central frequency randomization, consistent with the human literature.

Combining intuitions based on the ideal weight pattern and expectations based on psychophysical results, one might suggest the following expectation regarding the form of listeners' internal templates for detecting ascending frequency glides. The estimated internal templates should follow a negative-to-positive form, and the magnitudes of the initial negative and the ending positive regions should not be equal.

This prediction regarding subjects' internal templates suggests variations in the perceptual importance of different temporal segments of the glide stimuli. Since the beginning and ending frequencies are most informative for the detection of glides, they should be weighted heavily and the absolute values of the relative weights associated with these frequencies should be large. To emphasize the beginning and ending frequencies of glides, it is of interest to include conditions where two constant-frequency fringes were added at both ends of the glides to match the beginning and ending frequencies. The expected internal templates in these conditions should have large absolute values associated with the fringes.

In the current study, the internal templates for the detection of frequency glides were estimated when the central frequency of the stimuli were either fixed or randomly chosen across presentations. The stimuli were either frequency glides alone or glides with the beginning and the ending fringes depending on conditions.

The method used to estimate the template is based on Ahumada's (2002) "classification image" approach, where the template is the pattern of relative weights as a function of time. The advantage of Ahumada's approach for estimating relative weights, compared to other methods, is that the method can simply be applied to stimuli that vary continuously in time without requiring temporal "bins" (e.g., Berg and Green, 1990; Dai and Berg, 1992; Buus *et al.*, 1996; Turner *et al.*, 1998; Richards and Tang, 2006).

Ahumada's (2002) approach is, roughly, as follows. In a Yes/No procedure the subject indicates either "yes signal" or "no signal." Normally distributed random perturbations are added to the signal and no-signal stimuli. As an example, for a two-dimensional visual stimulus, the perturbations are added on a pixel-by-pixel case. After data collection, the stimuli are categorized conditioned on listeners' responses, yielding hit, false alarm, miss and correct rejection stimuli. Then, the perturbations for the trials that led to "yes" responses (hits and false alarms) are averaged (pixel-by-pixel) across trials, the perturbations for the trials that led to "no" responses (correct rejections and misses) are averaged across trials, and the latter image is subtracted from the former image. The resulting image provides an estimate of the subject's internal template, or a "classification image."

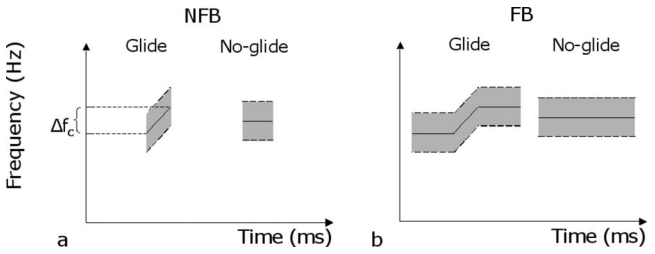


FIG. 1. Schematic spectrograms for the no-fringe-band (NFB, panel a) and fringe-band (FB, panel b) stimulus sets. The abscissa indicates time and the ordinate indicates frequency. Δf_c is the extent of the frequency glide. Solid lines show the carrier frequency of the narrowband of noise as a function of time and dashed lines delineate the 50 Hz noise bandwidth.

To apply this procedure to estimate the internal template for the detection of a frequency glide, perturbations in frequency as a function of time are required.[1] In the current experiment this was achieved by first applying a tonal frequency glide to a carrier tone and then multiplying the resultant glide by low-pass noise. The resulting narrow bands of noise have continuously changing frequencies. The difference, as a function of time, between the carrier frequency and the actual frequency of the narrow band of noise forms the perturbations in frequency as a function of time. Then, applying the method proposed by Ahumada (2002), the perturbations are used to estimate of the relative weights, which in turn provide a psychophysical estimate of the internal template.

II. METHODS

A. Stimuli and procedures

In a Yes/No paradigm, subjects indicated whether a 50-Hz-wide narrowband noise had a carrier with an ascending linear frequency glide (glide stimulus) or a constant-frequency carrier (no-glide stimulus). Two stimulus sets were tested, and both sets are shown in Fig. 1. The abscissa indicates time and the ordinate indicates frequency. The carrier frequency is shown using a solid line and the width of the narrow bands of noise are indicated using gray shading. The first stimulus set had a 120 ms duration, and the duration of the glide, when present, was also 120 ms. Figure 1(a) depicts these stimuli. For the second stimulus set, the glide-bearing 120 ms narrowband noise was preceded and followed by a 200 ms, 50 Hz band of noise [Fig. 1(b)]. The carrier frequencies of these "fringe bands" matched those of the initial and ending carriers of the glide-bearing portion of the band of noise. Thus, for a glide stimulus, the initial fringe band had a

carrier frequency lower than that of the ending fringe band, and for a no-glide stimulus, the initial and ending fringes had the same carriers. As a result, the listener could determine whether a glide was present using only the information in the fringe bands. This latter stimulus set will be referred to as the FB (fringe band) set, and the former stimulus set will be referred to as the NFB set (no fringe band). Note the NFB and FB stimulus sets parallel the "glide only" and "glide" conditions tested by Lyzenga *et al.* (2004), except that they used tonal glides.

The narrowband noise was generated digitally using the "quadrature multiplication" method (Bernstein and Trahiotis, 1992) in which two independent 25 Hz low-pass noises were multiplied by two tonal carriers, one in sine phase and the other in cosine phase, and the products summed to generate a 50-Hz-wide band of noise. For the NFB glide stimuli the 120 ms "sine" and "cosine" carriers varied linearly in frequency, whereas the no-glide stimuli had constant carrier frequencies. For the FB stimuli, stimulus generation was the same, except the carriers included two 200 ms constant carrier frequency fringes. All stimuli had 5 ms raised cosine rise/fall ramps at the stimulus onsets and offsets.

The central frequencies of the stimuli (the frequency at the temporal midpoint of the tonal carrier) were either fixed at 1000 Hz or randomly chosen from a uniform distribution ranging from 800 to 1200 Hz, yielding the *fixed-* or *random-frequency* conditions, respectively. In all, four conditions were tested: The 120 ms NFB stimuli with fixed (NFB-fixed) or random (NFB-random) central frequencies and the 520 ms FB stimuli with fixed (FB-fixed) or random (FB-random) central frequencies.

The extent of the tonal frequency glide, Δf_c, was the independent variable (see Fig. 1). The values of Δf_c ultimately tested were determined during two practice stages. In the first stage the threshold $\Delta f_c$was estimated using an adaptive tracking procedure in the FB-fixed condition (Levitt, 1971). This required approximately 1 h to complete. In the second stage, trials were blocked by condition and fixed Δf_c was used. The value of Δf_c was chosen with the goal of achieving performance of 75–80 percent correct. Depending on the subject and condition, this second practice stage required a total of 200–1300 trials.

Once the values of Δf_c were determined, data collection proceeded in blocks of 5 sets of 50 trials. Listeners rested between blocks. Listeners ran the FB conditions first. The FB-random and the FB-fixed conditions were intermixed such that blocks were tested using a random schedule. A total of five blocks for each condition were tested. Then the NFB conditions were tested using the same procedure. In all, a total of 1250 trials contributed to the final estimate of d' and to the formation of the TWPs.

Three young adults with normal hearing (<15 dB hearing level) served as subjects. The stimuli were presented diotically over Sennheiser HD410 SL headphones at an overall level of 57 dB sound pressure level with visual feedback following subjects' responses. Subjects were tested in a single-walled sound-attenuated booth in a quiet room. The stimuli were generated by TDT system II hardware controlled by MATLAB software.

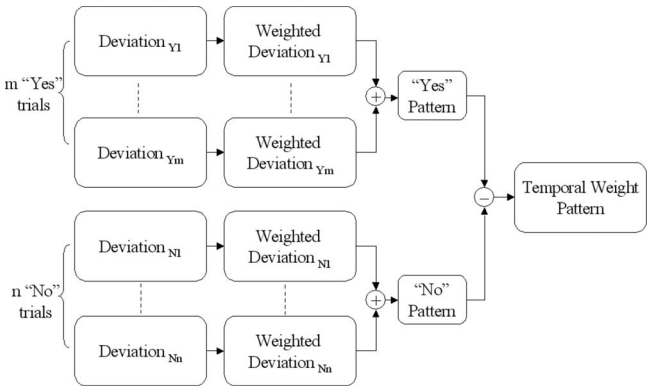


FIG. 2. The procedure for deriving the temporal weight pattern is shown.

B. Computational methods

1. Temporal weight pattern

Figure 2 shows the primary steps used to derive the TWPs. The columns show the computational steps and the rows emphasize that the procedure was applied to each stimulus tested, grouped by listeners' responses ("yes glide" and "no glide"). First, for each stimulus, the instantaneous frequency and envelope were estimated using a Hilbert transform. For stimulus, $x(t)$, with a Hilbert transform $H[x(t)]$, the envelope, $e(t)$, is given by: $e(t)=\sqrt{x(t)^2+H^2[x(t)]}$, and the instantaneous frequency, $f(t)$, is given by:

$$f(t)=\frac{1}{2\pi}\frac{\partial p(t)}{\partial t}, \tag{1}$$

where $p(t)=\tan^{-1}(H[x(t)]/x(t))$ (e.g., Green, 1998). Additionally, it is convenient to define the instantaneous carrier $f_c(t)$:

$$f_c(t)=f_0-\frac{\Delta f_c}{2}g(t), \tag{2}$$

where f_0 is the central frequency of the stimulus, Δf_c is the extent of the frequency glide when present. For the no-glide stimuli, $g(t)$ has a constant value of zero over time. For the glide stimuli in NFB conditions, $g(t)$ increases linearly from −1.0 to +1.0. For the glide stimuli in FB conditions, $g(t)$ has the constant value of −1.0 for the initial fringe, linearly increased values from −1.0 to +1.0 for the glide portion and the constant value of +1.0 for the latter fringe.

Next, the *deviation*, $\Delta f(t)$, of the instantaneous frequency from the instantaneous carrier was calculated as:

$$\Delta f(t)=f(t)-f_c(t). \tag{3}$$

The deviations are depicted in the leftmost column of Fig. 2.

In the third step, the deviations were weighted using a variant of the squared-envelope-weighted average of instantaneous frequency (SEWAIF) of Anantharaman *et al.* (1993; see also Dai, 1993), a model developed to predict pitch estimates for dynamically changing stimuli. In parallel with the SEWAIF model, the deviations of the instantaneous frequency from the carrier were weighted by the squared instantaneous envelope and then divided by the mean value of the squared instantaneous envelope, $\overline{e^2(t)}$:

$$\Delta f_w(t) = \frac{e(t)^2 \Delta f(t)}{\overline{e(t)^2}}, \quad (4)$$

The resulting *weighted deviations* are depicted in the second column of Fig. 2. The weighted deviations, $\Delta f_w(t)$, as a function of time formed the "perturbations" from the carrier frequency and allowed the estimation of the internal template or TWP using Ahumada's (2002) approach.

To form the TWP, i.e., relative weights as a function of time, the weighted deviations ($\Delta f_w(t)$) were categorized in accordance with subjects' responses (Ahumada, 2002). A "Yes" pattern was obtained by averaging the weighted deviations over all trials where the subject responded "Yes" the glide is present. Likewise, a "No" pattern was obtained by averaging the weighted deviations over the trials where the subject responded "No" glide. The ultimate TWP was subsequently formed by subtracting the "No" pattern from the "Yes" pattern, where the "Yes" and "No" patterns were weighted in proportion to the number of "Yes" and "No" responses[2] (final column of Fig. 2). Keep in mind that the estimated TWPs did not depend on the presence or absence of the glide because it was the deviations from the carrier frequency that were being averaged. However, the TWPs did depend on the responses, and therefore reflected subjects' decision processes.

This procedure for estimating the relative weights (Ahumada, 2002) assumes that the perturbations ($\Delta f_w(t)$ in this application) added to the stimulus (the carrier frequency) are normally distributed and statistically independent. The assumption of normal distribution was reasonably met,[3] but the assumption of independence was not. Evaluations of the autocorrelation functions of the $\Delta f_w(t)$ for several of the stimuli suggested consistent non-zero correlations for delays less than 40–50 ms. This represents a significant limitation in the current approach—changes in the estimated TWPs should be viewed with a conservative eye appreciating that there may be correlations in the TWPs that last 40 ms or so.

2. Model evaluation

The TWPs were evaluated from three perspectives. First, were the derived TWPs statistically discernable from zero? Second, was there sufficient information in the TWPs to account for subjects' performance? Third, were the magnitudes of relative weights corresponding to the initial and ending portions of the stimuli approximately the same? The procedures used to address these questions will be addressed in turn.

a. Bootstrap estimate: Are the TWPs statistically different from zero? A bootstrap procedure (Efron and Tibshirani, 1993) was used to evaluate whether the obtained TWPs were statistically different from those patterns based on random responses. For each subject and condition 1250 weighted deviations ($\Delta f_w(t)$) were drawn, with replacement, from the 1250 trials encountered by the subject. Responses of "Yes" and "No" were randomly assigned to each stimulus using proportions consistent with the "Yes" and "No" responses of the subject. Then a TWP was generated. This simulated TWP provided an estimated function for the null hypothesis that the subject-based TWPs contained no information concerning the internal template. The formation of a meaningful TWP requires that subjects' responses be systematically influenced by the perturbations, a relationship not present when responses were randomly assigned. The bootstrap simulation was repeated 100 times. Across the 100 repetitions, the average TWP were near zero. For each point in time, 96% confidence intervals about the average were estimated. The confidence intervals for all points were then averaged across time to form a single 96% confidence interval for each TWP. To the degree the psychophysically derived TWPs exceed the 96% confidence intervals, it would indicate that the obtained TWPs reflected properties of the subjects' responses (and so decision processes), not properties of the stimuli.

b. d' based on estimated TWPs. Values of d' based on TWPs (d'_{wgt}) were compared with the psychophysically obtained values of d' (d'_{obs}). The d'_{wgt} represents the best possible d'_{obs} subjects can reach if the derived TWPs were their exact internal templates on every trial, and there was no added "internal noise". Should the d'_{obs} exceed the d'_{wgt}, the linear model (specified below by Eq. 5) would fail to account for the psychophysical data. An opposite pattern would indicate that the TWPs contained enough information to account for subjects' performance. The approach used was similar to that used by Berg (1990).

The procedure used to estimate d'_{wgt} was as follows, and was repeated for each subject and condition. First, a decision variable β was computed for each trial. The decision variable was the inner product of the TWP (indicated as $W(t)$ below) and the weighted instantaneous frequency (i.e., $f_w(t) = \Delta f_w(t) + f_c(t)$) of the stimulus on that trial (trial i):

$$\beta_i = W(t) \bullet f_w(t)_i. \quad (5)$$

Equation (5) defines a linear detection model, in which the values of the decision variable β are a linear combination of the stimulus and the TWP. For a zero-mean TWP that resembled the form of the tonal carrier of the glide stimulus [see Fig. 1, solid lines] the βs for the glide stimuli would have a positive mean and the βs for the no-glide stimuli would have a zero mean.

Next, the βs were categorized depending on whether the stimulus was a glide or no-glide stimulus (β_g and β_{ng}, respectively). The distribution of the resulting βs was close to a normal distribution. Then, the two distributions of β_g and β_{ng} were fitted using a Gaussian distribution, $\hat{\beta}_g \sim N(\mu_g, \sigma_g^2)$ and $\hat{\beta}_{ng} \sim N(\mu_{ng}, \sigma_{ng}^2)$, where μ and σ^2 represent the mean and the variance of the estimated distributions. Finally, the d'_{wgt} was estimated as

$$\mathrm{d}'_{\mathrm{wgt}} = \frac{\mu_g - \mu_{ng}}{\sqrt{\frac{\sigma_g^2 + \sigma_{ng}^2}{2}}}. \quad (6)$$

A second model was also applied to the results of the random-frequency conditions. It was assumed that subjects formed representations of the frequency glides independent of the central frequency. For this model, the stimuli were translated to have the same central frequency, and the model was applied to the resulting stimuli. This model will be referred to as the *frequency-translation model*. The resulting values of d'_{wgt} will be indicated as $\tilde{d}'_{wgt}$ for this model. This model allows the determination of whether the predicted sensitivity improved when frequency randomization

TABLE I. For each subject and each condition, values of Δf_c (in Hz) and d' are listed.

		NFB			FB		
Conditions		S1	S2	S3	S1	S2	S3
Fixed frequency	Δf_c	46	44	42	16	18	20
	d'_{obs}	1.52	1.38	1.51	1.76	1.72	1.62
Random frequency	Δf_c	46	64	60	24	18	26
	d'_{obs}	1.60	1.42	1.72	1.76	1.49	1.52

was removed. The procedures used to estimate $\tilde{d}'_{wgt}$ were the same as those described above, except the central frequencies were translated to 1000 Hz prior to the formation of the decision variables, the β_is.

c. Comparisons of the magnitudes of the initial and ending portions of TWPs. As will be presented in the Results section, the TWPs derived from the current study were consistent with the expectations based on previous psychophysical results (Madden and Fire, 1996; Moore and Sek, 1998; Sek and Moore, 1999): The TWPs shared a negative-to-positive form, and unlike the ideal template, the magnitudes of the negative and positive weights tended to be different. That result led to two questions: (1) Whether subjects relied relatively more on the initial or the ending portion of the stimuli in order to make their detection decisions, and (2) was there a relation between the subjects' relative reliance on the initial/ending portion and their sensitivity? To address these questions, the ratio of the magnitudes of the relative weights from the ending *re*. initial portions of the TWPs was computed. If the ratio was approximately unity it would suggest equal weighting of the initial and ending portions of the stimuli. Additionally, consistent with the ideal template, should the TWP follow the negative-to-positive form, the initial negative and the latter positive portions would "cancel" the influence of the central frequency on decision variable β. This TWP would predict little or no effect of central frequency randomization. In contrast, a ratio either larger or smaller than unity would suggest subjects relied more on either the ending or initial portion of the stimuli, respectively. This result would predict a detrimental effect of central frequency randomization because the initial negative and the latter positive portions could not fully "cancel" the influence of the central frequency randomization.

These ratios of the magnitudes of the ending *re*. initial relative weights were estimated using different methods depending on the stimulus set. For the NFB conditions, the values were calculated by taking the ratio of the absolute values of the maximal (which occurred at toward the end of the TWP) *re*. the minimal (which occurred toward the initial part of the TWP) relative weights. For the FB conditions the relative weights from the initial and ending 200 ms fringe regions of the stimuli were separately averaged, and the ratio of the magnitudes of the averaged ending *re*. initial relative weights was computed.

To provide a statistical evaluation of the magnitude ratios, additional simulations were run. In each condition, the assumed TWP had the same form as the carrier frequency of the glide stimuli (see Fig. 1, solid lines), but the relative weight of the temporal middle of the TWP was zero. The stimuli from subject 2 (S2) were used for the simulation. First the 1250 stimuli were drawn, with replacement, from among the 1250 stimuli tested. Then, the inner product of the assumed TWP and $f_w(t)$ for each stimulus was obtained [Eq. (5)] and a zero-mean normal deviate was added to form the decision variable. The standard deviation of the zero-mean deviate was adjusted so as to approximate d'_{obs} for S2 in each condition. Simulated responses of "Yes" or "No" were assigned depending on whether the resulting decision variable was above or below the criterion, respectively. The criterion was the average decision variable across all trials. Once simulated responses were obtained, simulated TWPs were generated using the same methods as for the human subjects. This process was repeated 40 times, yielding 40 simulated TWPs for each of the four conditions. The ratio of the magnitudes of the ending and initial relative weights was calculated for each of the 40 replicate simulations. In each condition, the higher and lower boundaries of the 96% confidence interval of the ratios for the simulated TWPs were determined by adding or subtracting 2.054 times the standard deviations from the mean ratio across the 40 replicate indices.

III. RESULT AND DISCUSSION

A. Psychoacoustic results

Table I shows the frequency extents (Δf_c) used for each subject in each condition. The measured values of d'_{obs} are also listed. Given that the values were obtained from a Yes/No procedure, relative criteria (response bias) were also estimated (Macmillan and Creelman, 1991). The relative criteria were near zero, ranging from −0.1 to 0.2 across subjects and conditions, with S1 producing the largest relative criteria. For approximately equal values of d'_{obs}, Δf_cs were larger in the NFB than the FB conditions, and typically larger for random- than fixed-frequency conditions. These results were consistent with past work demonstrating the advantage of the fringe portions (e.g., Lyzenga *et al.*, 2004) and the disadvantages of frequency randomization (e.g., Madden and Fire, 1996; Moore and Sek, 1998; Sek and Moore, 1999), although in those studies the frequency extents at threshold were substantially smaller because the stimuli were tones rather than narrow bands of noises.

B. Estimated temporal weight patterns

The bold curves in Fig. 3 show the TWPs (relative weights as a function of time) for S1, whose results are as representative as any other subject. These results are shown separately to provide an example of the derived TWPs and the 96% confidence intervals associated with random responses. The left panels show the results for the NFB conditions and the right panels are for the FB conditions. Upper panels are for the fixed-frequency conditions and lower panels are for the random-frequency conditions. The shaded areas show the 96% of confidence intervals for TWPs derived

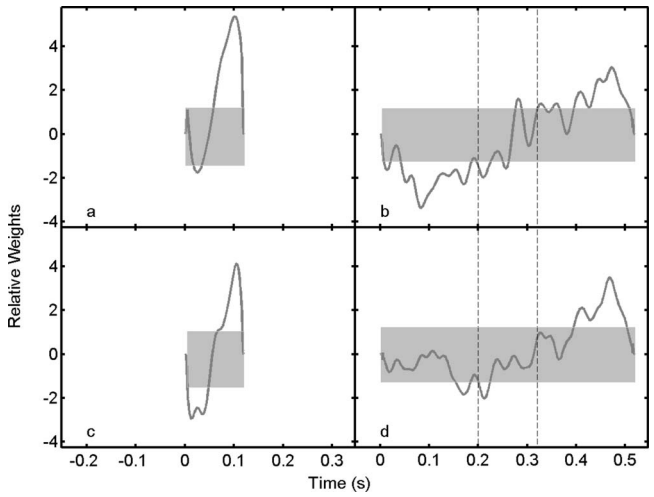


FIG. 3. Temporal weight patterns, i.e., relative weights as a function of time, derived from S1's responses for (a) NFB-fixed, (b) FB-fixed, (c) NFB-random and (d) FB-random conditions. The shaded areas specify the 96% confidence interval about the pattern derived from random responses. The vertical dashed lines in the right panels indicate the temporal regions associated with the glide-bearing portions of the stimuli.

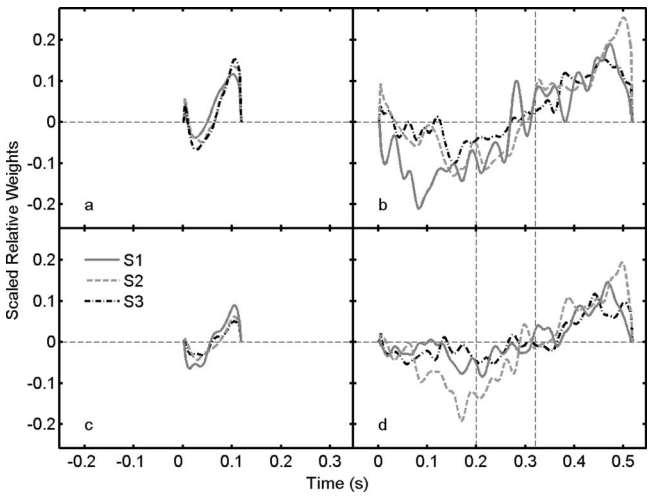


FIG. 4. Temporal weight patterns scaled by the inverse of Δf_c in (a) NFB-fixed, (b) FB-fixed, (c) NFB-random and (d) FB-random conditions. Data from different subjects (S1, S2, S3) are plotted using different line types. Weights of zero are specified by the horizontal dashed lines. The vertical dashed lines in the right panels indicate the temporal regions associated with the glide-bearing portions of the stimuli.

from unrelated to the presence/absence of the glide. The vertical dashed lines in the right panels indicate the temporal regions associated with the glide-bearing portions of the stimuli. The TWPs shifted from negative to positive values. This suggested that S1 contrasted the early and later frequencies rather than relying exclusively on just one or the other in making detection decisions. Moreover, there were substantial regions where the TWPs exceeded the confidence intervals, indicating that the obtained TWPs contained reliable information regarding S1's decision process. Note that the TWPs were constrained to start and end at zero.

The TWPs were scaled by the inverse of Δf_c in an effort to provide a direct comparison of the TWPs across conditions and subjects. For an ideal observer (assuming the linear model specified by Eq. (5) was correct and assuming the hypothetical observer maximized percent correct), such scaling would provide TWPs independent of Δf_c. In the current experiment the results were unlikely to be ideal, and so a slight error was assumed for this scaling procedure. Even so, this approach allowed a means of comparing the magnitudes of the relative weights across conditions and subjects.

Figure 4 shows subjects' individual TWPs scaled by the inverse of Δf_c for all conditions. The panels are arranged as in Fig. 3. The vertical dashed lines in the right panels indicate the temporal regions associated with the frequency glide. The results for different subjects are plotted using different line types. The results from Fig. 3, after scaling, are reproduced using the solid gray lines.

1. Comparisons of TWPs across conditions

Two common features were apparent in the obtained TWPs: (1) There was a clear negative-to-positive pattern in all TWPs, and (2) Most of the negative weights were in the first half of the TWPs and most of the positive weights were in the second half. Subjects' processing strategies were consistent with a linear model in which the first and second halves of the stimuli were differenced.

A third feature of the TWPs, not apparent in Fig. 4, was that for all but the FB-random conditions, the 96% confidence intervals were exceeded in both the beginning and ending portions of the TWPs. In the FB-random condition, the TWPs generally exceeded the confidence intervals only in the latter portion. This result might indicate a failure of the linear model in providing a reliable description of subjects' strategies in the FB-random condition, a possibility that will be considered more fully below (Sec. III B 2). Overall, however, the approach appears to have been successful in providing reliable and meaningful patterns of relative weights across time.

Across conditions, differences among TWPs were apparent. First consider the differences between the TWPs derived in the fixed- and random-frequency conditions. The magnitudes of the scaled weights were larger for the fixed than the random conditions. Moreover, the magnitudes of the weights were larger in the latter portion than the beginning portion of the TWPs. These greater magnitudes of the weights in the latter portion were clearer in the TWPs derived from the fixed- than random-frequency conditions. This suggested that, for the fixed-frequency conditions subjects relied more heavily on the ending frequency than the starting frequencies in decisions regarding the presence of a frequency glide. The relative magnitudes of the beginning and ending portions of the TWPs are considered more fully below (Sec. III B 3).

Next, consider the TWPs derived in the NFB and FB conditions. Restricting the comparison to just the glide portion of the TWPs, the extent of the scaled weights were roughly similar in the FB and NFB conditions, but the proportion of the TWP that fell outside the 96% confidence interval was much larger for the NFB condition (see Fig. 3 for an example). This suggests that subjects may have at-

TABLE II. Values of d'_{obs}, d'_{wgt}, and $\tilde{d}'_{wgt}$ are listed for each subject in fixed- and random-frequency conditions.

		NFB			FB		
Conditions/model		S1	S2	S3	S1	S2	S3
Fixed frequency	d'_{obs}	1.52	1.38	1.51	1.76	1.72	1.62
	d'_{wgt}	1.73	1.72	2.02	2.53	2.43	2.76
Random frequency	d'_{obs}	1.60	1.42	1.72	1.76	1.49	1.52
	d'_{wgt}	1.48	2.70	1.40	0.58	0.47	0.76
Random frequency - translated	$\tilde{d}'_{wgt}$	2.44	2.94	2.95	3.22	2.44	3.37

tended less to the glide portion in the FB conditions compared to the NFB conditions because there was additional information available in the fringe bands (Lyzenga *et al.*, 2004).

2. Comparison of d′ from observers and TWPs

The first four rows of Table II show the d'_{obs} and the d'_{wgt} for the four experimental conditions. The final row indicates the values of $\tilde{d}'_{wgt}$ for the frequency-translation model applied in the random conditions. The values of d'_{obs} are reproduced from Table I. For the NFB- and FB-fixed conditions, the values of d'_{wgt} were larger than the corresponding values of d'_{obs}, and this difference was magnified in the FB-fixed condition compared to the NFB-fixed condition. Because the TWP predicted better-than-obtained performance, the information in the TWPs was sufficient to describe subjects' performance in the fixed conditions.

Next, consider the random conditions. Except for S2 in the NFB-random condition, values of d'_{wgt} were smaller than the corresponding d'_{obs}. This indicated a failure of the linear model without frequency translation [i.e., Eq. (5)] because the model predicted lower-than-obtained values of d'. For the FB-random condition, the values of d'_{wgt} were even poorer. When Eq. (5) was altered to include frequency translation, the resulting predictions, $\tilde{d}'_{wgt}$, were much larger than the corresponding d'_{obs}. This result has two implications. First, the failure of the linear model in the random-frequency conditions does not reflect poorly estimated TWPs: $\tilde{d}'_{wgt}$ is much larger than d'_{obs} meaning that there was sufficient information in the TWPs to account for performance when frequency translation was applied. Second, there might be a psychophysical process corresponding to frequency translation but not captured by the linear detection model [in Eq. (5)], which allows the d'_{obs} to be higher than d'_{wgt}. By one potential process, the subject would form an internal representation of the stimulus distinct from the central frequency. This is simply the frequency translation model and predicts no effect of central frequency randomization, which is inconsistent with the data shown in Table I. If however, subjects failed to *completely* extract the stimuli away from the central frequencies, there would be on the one hand an effect of central frequency randomization, and on the other hand, a TWP that was successful in accounting for subjects' performance only after frequency translation.

3. Comparisons of the magnitudes of the initial and ending portions of TWPs

For TWPs in the fixed conditions, visual inspection suggested a tendency for the magnitudes of the weights to be smaller at the beginning than the end of the TWPs. This is consistent with the expectations of TWPs based on the previous psychophysical data (Madden and Fire, 1996; Moore and Sek, 1998; Sek and Moore, 1999): The unequal magnitudes of the initial negative and ending positive weights. Table III shows the ratio of the magnitudes of the ending *re.* initial portions of the TWPs. For the NFB conditions the ratio was based on the absolute values of the maximal and minimal weights and for the FB conditions the ratio was based on the absolute averaged values of the TWP associated with the ending *re*. initial fringe bands. The ratios in the first and second rows of Table III are from the fixed- and random-frequency conditions, respectively, and the columns are for the individual subjects in the NFB and FB conditions, respectively.

For the fixed-frequency conditions (first row) computer simulations indicated 96% confidence intervals surrounding unity of [0.58, 1.44] for the NFB-fixed condition and [0.75, 1.76] for the FB-fixed condition. In five of the six comparisons, the obtained ratios exceeded the 96% confidence intervals indicating that magnitudes of relative weights were larger at the ending than the initial portions of the TWPs. Subjects appeared to rely more heavily on the ending than the beginning portions of the stimuli in making their detection decisions. For the subjects with higher (lower) values of Δf_c the ratios were greater than (nearer) unity, although the comparisons are based on relatively few subjects and small differences.

For the random-frequency conditions (second row) computer simulations indicated the following 96% confidence intervals about a ratio of unity: [0.13, 1.74] for the NFB-random condition and [0.62, 1.55] for the FB-random condition. For the NFB condition, none of the ratios exceeded the

TABLE III. For each subject and each condition, the ratio of the magnitudes of the ending *re*. initial portions of the TWP are listed. Values in bold exceed the 96% confidence intervals about a ratio of unity.

	NFB			FB		
Conditions	S1	S2	S3	S1	S2	S3
Fixed frequency	**3.07**	**2.74**	**2.26**	0.82	**2.90**	**3.45**
Random frequency	1.40	1.43	1.59	**2.29**	1.09	**1.94**

96% confidence intervals and for the FB condition, the ratios for S1 and S3 exceeded the 96% confidence intervals. As in the fixed-frequency conditions, for the random-FB condition the two subjects with the larger ratios also had the poorer performance (greater values of Δf_c), but this reflects only three comparisons.

Subjects' reliance on the ending portion of the stimuli rather than the initial portion was stronger for the fixed- than random-frequency conditions. Potentially, in an effort to counteract the effect of central frequency randomization, subjects attempted to more equally rely on the initial and ending portions of the stimuli when the central frequency was random. However, to the degree subjects altered their strategies under the pressures of frequency randomization, they were not wholly successful. Such a strategy might, for example, introduce instability in their internal templates, which would potentially cause a failure of the linear model [outlined in Eq. (5)] to accurately estimate the TWPs in the random-frequency conditions.

C. Summary of computational results

The obtained TWPs were significantly different from the patterns associated with random responses for all three subjects in all four conditions, indicating that the patterns contained information regarding subjects' decision strategies. In the fixed-frequency conditions the TWPs indicated that subjects relied on both the starting and ending portions of the stimuli, although more so on the ending portion. In the random-frequency conditions, the stronger dependence on the ending portion was less apparent. Moreover, for the random-frequency conditions the linear detection model indicated by Eq. (5) failed to account for subjects' sensitivity. When frequency translation was applied to the stimuli, the model could at least account for subjects' sensitivity. Together, these results suggested that subjects altered their decision processes depending on whether the central frequency was randomized so as to more effectively difference the initial and ending portions of the stimuli.

IV. SUMMARY AND CONCLUSIONS

A linear classification model (Ahumada, 2002) was successfully used to derive relative weights as a function of time for the detection of an ascending frequency glide applied to 50-Hz-wide narrowband noise. Four conditions were tested, depending on whether the glide had onset and offset fringes or not (FB versus NFB) and depending on whether the central frequencies of the stimuli were fixed or random. Sensitivity to changes in frequency were superior in the FB relative to the NFB conditions, and for both the NFB and FB conditions sensitivity was superior for the fixed- than the random-frequency conditions. Although the current psychophysical data were obtained using narrow bands of noise, the pattern of results was consistent with previous results using tonal stimuli (Madden and Fire, 1996; Moore and Sek, 1998; Sek and Moore, 1999; Lyzenga *et al.*, 2004).

The pattern of relative weights as a function of time (TWPs), were derived for all four conditions. The estimated TWPs went from negative to positive, consistent with the ideal template. This negative-to-positive pattern also suggested that subjects did not rely on just the beginning or ending portion of the stimuli in detecting the glide. In most cases, the relative weights associated with the TWPs had larger magnitudes in the latter portion of the stimuli, especially for the fixed-frequency conditions. An analysis of d' based on the obtained TWPs indicated that the linear model could at least account for subjects' sensitivity in the fixed-frequency conditions. For the random-frequency conditions, although the estimated TWPs have the forms consistent with the expectations from the previous psychophysical results (Madden and Fire, 1996; Moore and Sek, 1998; Sek and Moore, 1999), the linear detection model [specified by Eq. (5)] nevertheless failed. An additional model representing the stimuli as changes in frequency (i.e., not actual frequencies) could account for subjects' sensitivity.

ACKNOWLEDGMENTS

This work was supported by Grant No. R01 DC002012 from the National Institutes of Health. We acknowledge the very helpful comments provided by two reviewers on earlier versions of this manuscript. Dr. Daniel Shub and Rong Huang also provided very helpful comments on earlier versions of the manuscript.

[1]Note that the frequency perturbations introduce variations in the decision variable, which results in more overlap between the two distributions of the decision variable for the glide and no-glide stimuli. This additional overlap due to the perturbations would make the glide more difficult to detect, and might cause the no-glide stimulus sound as though there is a glide.

[2]Ahumada (2002) derived a scaling procedure by which hit rates and false alarm rates are used to minimize the error in the weight patterns. Here, a somewhat less optimal scaling scheme, the proportion of "Yes" and "No" trials, is used. This approach ensures that the resulting weight patterns are in similar units (akin to deviations in Hz) across conditions.

[3]The distribution of the weighted deviations ($\Delta f_w(t)$) is roughly normal, with a mean near zero and a standard deviation of approximately 10. The kurtosis and skewness of the distribution are approximately the same as for a normal distribution.

Ahumada, Jr.A. J. (**2002**). "Classification image weights and internal noise level estimation," J. Vision **2**, 121–131.

Anantharaman, J. N., Krishnamurthy, A. K., and Feth, L. L. (**1993**). "Intensity-weighted average of instantaneous frequency as a model for frequency discrimination," J. Acoust. Soc. Am. **94**, 723–729.

Berg, B. G. (**1990**). "Observer efficiency and weights in a multiple observation task," J. Acoust. Soc. Am. **88**, 149–158.

Berg, B. G., and Green, D. M. (**1990**). "Spectral weights in profile listening," J. Acoust. Soc. Am. **88**, 758–766.

Bernstein, L. R., and Trahiotis, C. (**1992**). "Discrimination of interaural envelope correlation and its relation to binaural unmasking at high frequencies," J. Acoust. Soc. Am. **91**, 306–316.

Buus, S., Zhang, L., and Florentine, M. (**1996**). "Stimulus-driven, time-varying weights for comodulation masking release," J. Acoust. Soc. Am. **99**, 2288–2297.

Dai, H. (**1993**). "On the pitch of two-tone complexes," J. Acoust. Soc. Am. **94**, 730–734.

Dai, H., and Berg, B. G. (**1992**). "Spectral and temporal weights in spectral-shape discrimination," J. Acoust. Soc. Am. **92**, 1346–1355.

Demany, L., and Semal, C. (**1989**). "Detection thresholds for sinusoidal frequency modulation," J. Acoust. Soc. Am. **85**, 1295–1301.

Efron, B., and Tibshirani, R. J. (**1993**). *An Introduction to the Bootstrap* (Chapman and Hall/CRC, New York).

Green, D. M. (**1988**). *Profile Analysis: Auditory Intensity Discrimination* (Oxford U. P., New York).

Hartmann, W. M., and Klein, M. A. (**1980**). "Theory of frequency modula-

tion detection for low modulation frequencies," J. Acoust. Soc. Am. **67**, 935–946.
Levitt, H. (**1971**). "Transformed up-down methods in psychoacoustics," J. Acoust. Soc. Am. **49**, 167–177.
Lyzenga, J., Carlyon, R. P., and Moore, B. C. (**2004**). "The effects of real and illusory glides on pure-tone frequency discrimination," J. Acoust. Soc. Am. **116**, 491–501.
Macmillan, N. A., and Creelman, C. D. (**1991**). *Detection Theory: A User's Guide* (Cambridge U. P., Cambridge).
Madden, J. P., and Fire, K. M. (**1996**). "Detection and discrimination of gliding tones as a function of frequency transition and center frequency," J. Acoust. Soc. Am. **100**, 3754–3760.
Moore, B. C., and Sek, A. (**1998**). "Discrimination of frequency glides with superimposed random glides in level," J. Acoust. Soc. Am. **104**, 411–421.
Richards, V. M., and Tang, Z. (**2006**). "Estimates of effective frequency selectivity based on the detection of a tone added to complex maskers," J. Acoust. Soc. Am. **119**, 1574–1584.
Sek, A., and Moore, B. C. (**1999**). "Discrimination of frequency steps linked by glides of various durations," J. Acoust. Soc. Am. **106**, 351–359.
Turner, C. W., Kwon, B. J., Tanaka, C., Knapp, J., Hubbartt, J. L., and Doherty, K. A. (**1998**). "Frequency-weighting functions for broadband speech as estimated by a correlational method," J. Acoust. Soc. Am. **104**, 1580–1585.

Perception and cortical neural coding of harmonic fusion in ferrets

Sridhar Kalluri[a)]
Institute for Systems Research, University of Maryland, College Park, Maryland 20742, USA and Department of Anatomy and Neurobiology, University of Maryland, Baltimore, Maryland 21201, USA

Didier A. Depireux
Department of Anatomy and Neurobiology, University of Maryland, Baltimore, Maryland 21201, USA

Shihab A. Shamma
Institute for Systems Research, University of Maryland, College Park, Maryland 20742, USA

(Received 18 March 2007; revised 11 February 2008; accepted 3 March 2008)

This study examined the perception and cortical representation of harmonic complex tones, from the perspective of the spectral fusion evoked by such sounds. Experiment 1 tested whether ferrets spontaneously distinguish harmonic from inharmonic tones. In baseline sessions, ferrets detected a pure tone terminating a sequence of inharmonic tones. After they reached proficiency, a small fraction of the inharmonic tones were replaced with harmonic tones. Some of the animals confused the harmonic tones with the pure tones at twice the false-alarm rate. Experiment 2 sought correlates of harmonic fusion in single neurons of primary auditory cortex and anterior auditory field, by comparing responses to harmonic tones with those to inharmonic tones in the awake alert ferret. The effects of spectro-temporal filtering were accounted for by using the measured spectrotemporal receptive field to predict responses and by seeking correlates of fusion in the predictability of responses. Only 12% of units sampled distinguished harmonic tones from inharmonic tones, a small percentage that is consistent with the relatively weak ability of the ferrets to spontaneously discriminate harmonic tones from inharmonic tones in Experiment 1.
© *2008 Acoustical Society of America.* [DOI: 10.1121/1.2902178]

PACS number(s): 43.66.Hg, 43.66.Gf, 43.64.Qh [WPS] Pages: 2701–2716

I. INTRODUCTION

Two fundamentally important auditory perceptual phenomena, spectral fusion and virtual pitch, are intimately associated with sounds having harmonic spectra. The importance of harmonic sounds in auditory perception is such that auditory theory for at least 150 years has been driven in part by a quest for understanding the mechanisms underlying pitch perception (von Helmholtz, 1954). Despite intense investigation, many aspects of pitch perception have resisted explanation. One such problem is identifying its cortical neural correlates. More generally, not just pitch but the cortical encoding of harmonic sounds is not well understood, and forms the topic of this paper.

Listeners typically hear a harmonic complex tone as a coherent unitary entity with a clear pitch; this perceptual fusion due to harmonicity is used by the brain to organize complex acoustic environments into separate auditory objects (Bregman, 1990). An example of this brain function is the improvement obtained in the ability to distinguish two talkers when a fundamental frequency difference is imposed (Brokx and Nooteboom, 1980). This study focuses on fusion of tone components due to harmonic relationships, seeking correlates of this fusion in single cortical neurons. The highly salient pitch evoked by spectrally resolved harmonic complex tones, known as virtual pitch (when there can be no actual energy at the frequency of the perceived pitch), makes this study relevant for understanding cortical neural coding of pitch. We distinguish this pitch due to spectrally resolved harmonics from that due to spectrally unresolved harmonics, and use the term residue pitch to refer to the latter in this paper. The pitch due to spectrally resolved harmonics is the most important of the many distinct percepts that come under the rubric of pitch, because it underlies speakers' voices and speech prosody, as well as musical intervals and melody.

The percepts of virtual pitch and the spectral fusion of complex tones are closely related. There are a great many perceptual parallels, as in their similar insensitivity to the phases of low harmonics (Hartmann *et al.*, 1993; Houtsma and Smurzynski, 1990; Moore and Glasberg, 1985). Moreover, models for virtual pitch apply well to harmonic spectral fusion as well (Duifhuis *et al.*, 1982). For instance, in pattern recognition models, the pitch of a complex tone is equal to the fundamental frequency of the harmonic template that best fits the evoked neural activity arrayed along the tonotopic axis of the cochlea. In such models, template matching operates on the neural activity due to the resolved components of the complex tone (e.g., Goldstein, 1973; Srulovicz and Goldstein, 1983; Terhardt, 1974, 1979; Wightman, 1973). Such models predict well that the pitch of harmonic complex tones is not changed by the absence of the fundamental component: this is an important attribute for a model

[a)]Author to whom correspondence should be addressed. Current address: Starkey Hearing Research Center, 2150 Shattuck Ave., Suite 408, Berkeley, California 94704. Electronic mail: sridhar_kalluri@alum.mit.edu.

of pitch to possess (de Cheveigne, 2005). There is evidence that a template-matching operation also underlies the perceptual fusion of harmonically related components of a complex tone (Brunstrom and Roberts, 1998, 2000; Lin and Hartmann, 1998). However, the two processes are not entirely congruent, with virtual pitch depending on harmonic relations between components and perceptual fusion being due to spectral regularity (Roberts and Brunstrom, 1998, 2001, 2003). Nevertheless, the similarities of fusion and virtual pitch for harmonic stimuli suggest common mechanisms underlying the two and enable findings of one to be applied to the other. The study seeks to identify the neural basis for the special perceptual status of harmonicity; it approaches this issue from the perspective of the fusion or perceptual coherence of harmonic tones, and in the process it sheds light on the pitch evoked by such tones.

While spectral fusion and virtual pitch of complex tones are closely related, previous studies of the cortical coding of harmonic sounds have focused on the latter. One of the few studies that examined the role of human auditory cortex in harmonic fusion found support in measurements of event related potentials for the involvement of primary cortical areas (Dyson and Alain, 2004). Lesion studies show that the auditory cortex is needed for the perception of virtual pitch (Whitfield, 1980; Zatorre, 1988). Primary auditory cortex (AI) has failed, on the whole, to yield compelling correlates of virtual pitch. However, a study by Bendor and Wang (2005) in nonprimary auditory cortex of marmosets has yielded promising results that remain to be independently replicated and confirmed. See also further reservations discussed in McAlpine (2004).

In recordings from single neurons, Bendor and Wang (2005) found responses in rostral field tuned to the fundamental frequency of harmonic complex tones with and without the missing fundamental component. Such tuning to the fundamental frequency regardless of the physical presence of that component is suggestive of these neurons being tuned to pitch. Nevertheless, it is unclear if these neurons respond differently to harmonic tones than to inharmonic tones, as a pitch-selective or harmonicity-selective neuron might be expected to do.

Many studies of AI have examined pitch coding, and failed to yield harmonicity-selective neurons. Recordings from single units (Schwarz and Tomlinson, 1990) and multiple units (Fishman *et al.*, 1998) of monkey AI in response to missing-fundamental harmonic complex tones failed to show any rate tuning to the fundamental frequency. Multiunit activity and current-source-density patterns recorded in high-frequency areas of monkey AI directly encode the click rate of same- and alternating-polarity click trains in the temporal pattern of response (Steinschneider *et al.*, 1998); this click rate corresponds to the weak residue pitch. Consistent with observations from single-unit recordings (Schwarz and Tomlinson, 1990), resolved harmonics were represented as local maxima of activity determined by the tonotopic organization of the recording sites. However, the virtual pitch that would be derived from these local maxima was not encoded directly, in that neither the temporal pattern of response nor spatial distribution of activity reflected the fundamental frequency. Finally, several studies have reported mapping of the envelope periodicity of amplitude-modulated tones on an axis orthogonal to the tonotopic axis in AI of Mongolian gerbils (Schulze *et al.*, 2002; Schulze and Langner, 1997a, 1997b) and of humans (Langner *et al.*, 1997). These findings may indicate the presence of a map of virtual pitch, but three aspects of the experiments make the assertion inconclusive. First, the neurons forming the map of envelope periodicity were primarily sensitive to high-frequency energy (>5 kHz), a frequency region that does not evoke virtual pitch in human and cats (Heffner and Whitfield, 1976). Second, an extensive body of psychoacoustical literature shows that envelope periodicity, in general, is not predictive of the virtual pitch evoked by a stimulus (e.g., de Boer, 1956, 1976; Flanagan and Gutman, 1960). Third, rather than reflecting the virtual pitch due to the spectrally resolved components of the stimulus, the findings could instead be a mapping of the fundamental frequency (or modulation frequency for an amplitude-modulated tone) reintroduced by nonlinear distortion in the cochlea (McAlpine, 2002, 2004).

The lattermost of these reservations is also applicable to observations in monkey AI of similar responses to a pure tone and a missing-fundamental harmonic complex of the same pitch (Riquimaroux, 1995; Riquimaroux and Kosaki, 1995). Sensitivity to harmonic combinations of resolved components that would show tuning to the fundamental frequency of complex tones has been found in marmoset AI (Kadia and Wang, 2003) (also in bats, Suga *et al.*, 1983). Such neurons may underlie spectral fusion of harmonic complex tones. However, because these neurons preferred high frequencies and very high fundamental frequencies (typically greater than 4 kHz), the role of such neurons in the computation of virtual pitch and spectral fusion is unclear for sounds having predominantly low-frequency spectra such as speech, music, and many animal vocalizations.

In summary, previous studies of the cortical encoding of harmonic sounds have focused on correlates of virtual pitch. Several studies have yielded promising candidate neurons that encode pitch and may encode harmonic fusion, although these findings need to be further understood and replicated.

In this paper, we report experiments in domestic ferrets (*Mustela putorius*) aimed at understanding the cortical neural coding of harmonic sounds from the perspective of spectral fusion rather than virtual pitch. By comparing the neural representation of perceptually fused harmonic complex tones with that of perceptually unfused inharmonic complex tones in single AI and anterior auditory field (AAF) neurons, we expect to uncover neural computations specifically elicited by harmonic fusion in subcortical or primary cortical structures. The presence of such harmonicity-specific processing would have been missed by previous studies that employed harmonic sounds exclusively.

An assumption underlying the neurophysiology experiment is that ferrets automatically fuse components of harmonic complex tones, like humans do in typical listening conditions. Many animals can hear the pitch of the missing fundamental, including cats and monkeys (Heffner and Whitfield, 1976; Tomlinson and Schwartz, 1988), so it is not unreasonable to assume that ferrets might do the same. In order

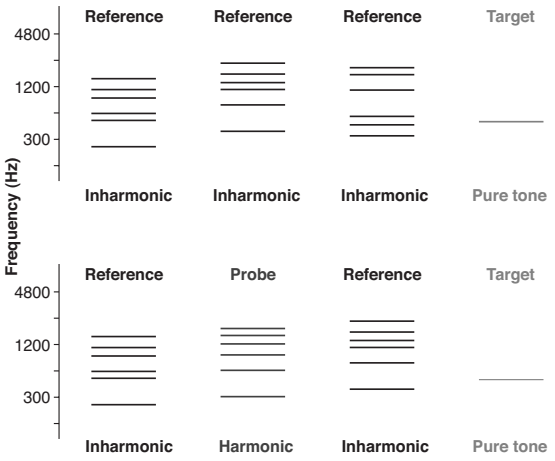


FIG. 1. Stimulus protocols for testing if ferrets automatically distinguish harmonic complex tones from inharmonic complex tones. (Top) In baseline sessions, ferrets were trained to detect pure-tone targets terminating a one-to-six-stimulus sequence of inharmonic complex tone reference sounds. Cues available for distinguishing the targets from the references were (i) differences in the quality of perceptual fusion and (ii) differences in timbre. (Bottom) In probe sessions conducted after ferrets attained proficiency in baseline sessions, a small fraction of the reference sounds were replaced by harmonic complex tone probe sounds. If harmonic complex tones were perceptually fused, then they might have been confused occasionally with the pure-tone targets, thereby indicating that ferrets can automatically distinguish harmonic tones from inharmonic tones.

to hear the pitch of the missing fundamental, the feline and primate subjects must have been able to estimate the fundamental from the components that were actually present in the stimuli. However, the animals did not necessarily fuse these components into a unitary entity.[1] The first experiment in this paper uses a conditioned avoidance behavioral-testing paradigm to study whether ferrets spontaneously fuse harmonic components of complex tones. Experiment 2 seeks neural correlates of harmonic fusion in ferret auditory cortex, specifically in areas AI and in AAF.

II. EXPERIMENT 1: PERCEPTION OF HARMONIC COMPLEX TONES

A. Rationale

In order to address whether ferrets can automatically fuse components of a harmonic complex, we asked if they can distinguish inharmonic complex tones from harmonic complex tones without receiving training on the distinction between the two classes of sounds. The experiment was performed in two stages comprising baseline sessions and probe sessions (Fig. 1). In baseline sessions, the ferrets were trained to detect pure-tone targets in a sequence of inharmonic complex tone reference sounds. By eliminating or making unreliable the differences in frequency range, level, and roughness, we left two cues available for reliably distinguishing targets from references: (i) differences in the degree of perceptual fusion, and (ii) differences in timbre.

When ferrets attained proficiency in these baseline sessions, probe sessions were conducted in which 10% of the reference sounds were replaced with harmonic complex tone probe sounds that were identical to the inharmonic complex tone references in every way except in the frequency relations between components. Because the timbre of the complex tones differs greatly from that of the pure tones, ferrets were expected, in most cases, to categorize the harmonic complex tones with the inharmonic complex tones based on similarity of timbre. This should be the case even if the ferrets heard the harmonic complex tones as fused. However, occasionally the putative fused nature of the harmonic complex tone might be confused with the unitary quality of the pure tone, prompting the ferret to respond to the harmonic probes as if it heard the pure-tone target. Therefore, detecting the probes at a rate greater than the false-alarm rate (i.e., the rate at which references were inadvertently detected as if they were targets) indicates that harmonic complex tones are heard differently than inharmonic complex tones. In contrast, failure to detect the probes in this experiment does not mean that the ferrets could not distinguish harmonic tones from inharmonic tones; they could simply have been using timbre exclusively to categorize the stimuli.

B. Methods

1. Behavioral testing

A conditioned-avoidance paradigm was used for testing how ferrets hear complex tones. The paradigm has been successfully used with many animals and it is described in detail by Heffner and Heffner (1995). We give a brief overview here.

A water-restricted ferret licked water from a continuously dripping spout while listening to reference sounds. At random intervals, an easily distinguishable target sound was presented followed by a light shock to the tongue delivered through the reward spout. Such pairings of stimulus and shock helped the ferret learn to break contact with the spout when it heard a target. The continuous water reward encouraged the ferret to maintain contact with the spout, providing a baseline behavior against which to measure responses. From the perspective of a ferret, the reference stimuli constituted safe trials because it could drink from the spout without getting shocked. On the other hand, target stimuli were warning trials, because they warned the ferret to break contact with the spout.

A computer registered successful withdrawal from the spout following a target as a *hit* and failure to withdraw as a *miss*. Because the animal occasionally withdrew in the absence of a target, a *false-alarm* rate was determined by registering how often it withdrew from the reward spout for reference trials. Both target and reference trials were ignored when the ferret did not contact the reward spout just before the trial; this was done in order to ensure that performance was evaluated only for trials on which the ferret attended to the stimuli. Figure 2 helps understand these measures by illustrating the presentation of trials and the timing of response intervals, while Table I shows which behaviors led to the different response categories.

During testing, two kinds of trial sequences were presented: (i) One to six reference trials followed by a target trial, and (ii) seven consecutive reference trials constituting a sham sequence. The number of reference trials in a given sequence was randomized such that the probability of the

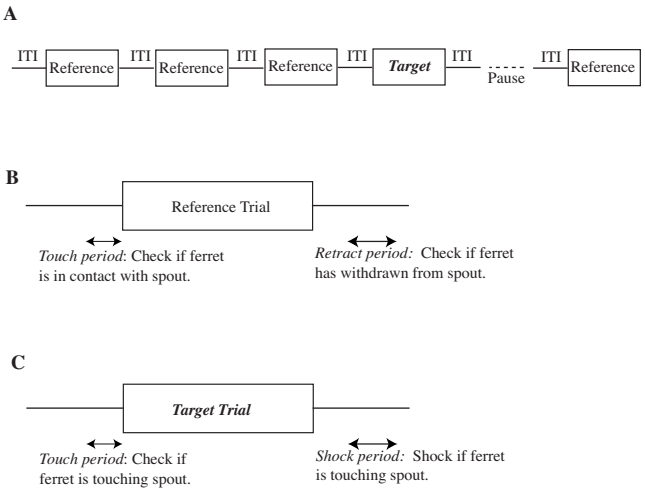


FIG. 2. (A) Schematic representation of a trial sequence, where the target sound was presented on trial 4. The presentation of trials was paused after a target trial until the ferret returned to the spout. (B) Schematic representation of a reference trial shows two time intervals, one before the stimulus onset and the second after stimulus offset. During the second interval, the ferret's contact with a reward spout determined the response class for the trial. If the ferret was not in contact with the spout during the first interval (the *touch* period), the response was classified as an "early" withdrawal and not counted toward overall performance on the experiment. If the ferret failed to contact the spout during the second interval (the *retract* period), the trial performance was scored as a "false alarm." (C) Schematic representation of a target trial shows the same two intervals of time. The first interval played the same role as on a reference trial. The second interval (the *shock* period) was a period when contact with the spout elicited a shock, and the trial performance was scored as a "miss." The *touch* period was 0.2 s while the *retract* and *shock* periods were 0.4 s in the experiment. The interval between the end of the stimulus and the start of the *retract* and *shock* periods was 0.2 s. Based on a figure from Heffner and Heffner (1995).

target sound occurring in trial position 2 through 7 was constant. This randomization was done so that the ferret could not preferentially respond on trials occurring at any given position. Sham sequences were interspersed between target sequences to discourage the ferrets from responding at regular intervals regardless of whether a target was presented. During probe sessions, probe trials were presented in exactly the same way as reference trials by replacing 10% of reference sounds by probe sounds; this percentage amounted, on average, to 40 probe sounds per session. Responses on the probe trials were scored in the same way as those on the reference trials. *Probe hits* and *probe misses* were equivalent to false alarms and safe responses respectively on reference trials.

TABLE I. Relationship between stimulus timing, ferret response, and performance measures.

Trial type	Spout contact (touch period)	Spout contact (retract/shock period)	Response class
Reference	Contact	No contact	Safe
Reference	Contact	Contact	False alarm
Reference	No contact	N/A	Early
Target	Contact	No contact	Hit
Target	Contact	Contact	Miss
Target	No contact	N/A	Early

2. Stimuli

For any given reference, target, or probe trial, stimuli were chosen randomly from a collection of inharmonic, pure-tone, and harmonic sounds that were synthesized and stored in memory just before placing a ferret in the testing cage. The stimuli were all 0.5 s long. Pure tones ranged in frequency from 150 to 4800 Hz. These frequencies were also the lower and upper bounds of the spectra of the complex tones, which had six components. To comply with these frequency limits, harmonic complex tones with components in random phase had fundamental frequencies between 150 and 800 Hz.

We constructed inharmonic complex tones by maintaining the same ratios or log spacings between consecutive components as in harmonic tones but reordering them to occur in different sequences than in harmonic tones. For example, a six-component harmonic tone had ratios between consecutive components of [2 3/2 4/3 5/4 6/5], and an exemplar inharmonic complex tone with lowest component at 200 Hz had components [200 267 320 480 960 1200] Hz corresponding to an ordering of the ratios of [4/3 6/5 3/2 2 5/4]. We constructed inharmonic complex tones in this manner so that these stimuli, if perceived as rough by ferrets, would have comparable roughness to the harmonic tones. The reasoning was that roughness is proportional to envelope fluctuations resulting from interactions between tone components within an auditory filter, and such interactions are comparable between harmonic complex tones and inharmonic complex tones constructed as above (Plomp and Levelt, 1965; Terhardt, 1974). The lowest component of the inharmonic complex tones was constrained between 150 and 800 Hz, so that any pitch cues from the edge of the spectrum were not reliably different from those generated by the spectral edge of the harmonic complex tones.

The levels of all stimuli were roved over a 6 dB range to prevent the use of intensity cues. Stimuli were played at a nominal level of 70 dB sound pressure level; this was the overall level of the complex tones, so individual components were lower in level. Levels were calibrated in an empty testing cage at the position occupied by the ferret's head with a sound level meter (Bruel and Kjaer). All stimulus parameters were restricted to narrower ranges during training sessions to help the ferrets learn the task.

3. Experimental apparatus

Behavior of the ferrets was tested in a custom-designed cage mounted inside a Sonex-foam lined and single-walled soundproof booth (Industrial Acoustics, Inc.). Sound was delivered through a speaker (Manger) mounted in the front of the cage at approximately the same height above the testing cage as the metal spout that delivered the water reward.

The testing cage had a metal floor so that the ferret formed a low-resistance electrical pathway between the spout and the floor when licking. The lowered resistance between floor and spout was used by a custom "touch" circuit to register when the ferret contacted the spout. Electromechanical relays switched between the touch circuit and a fence charger in order to deliver shocks to the ferret's

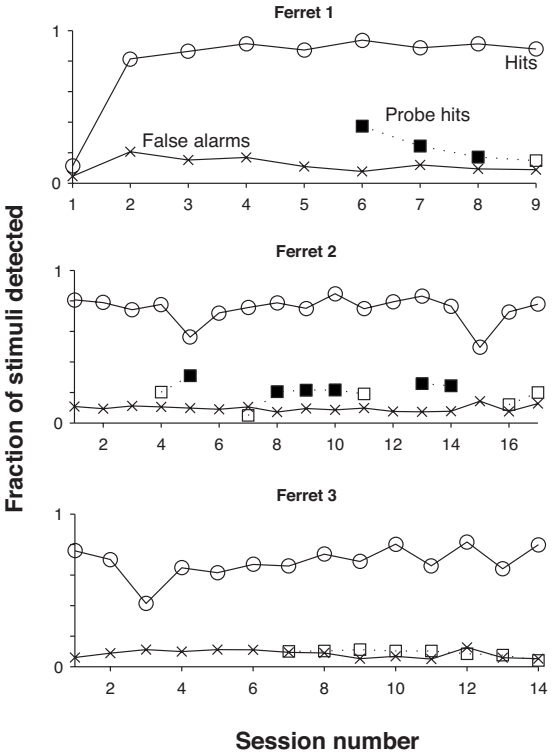


FIG. 3. Performance of three ferrets on baseline and probe sessions of experiment. Several training sessions occurred prior to the first session indicated on the abscissa of the figure for each of the ferrets. All three ferrets attained proficiency at the baseline task of distinguishing pure-tone targets from inharmonic complex tone references, as indicated by the hit rate exceeding 70% and the false-alarm rate not exceeding 20%. Two ferrets (top two panels) had probe hit rates that were significantly greater than the false-alarm rate during probe sessions (statistically significantly greater probe hit rates are indicated with a filled symbol), indicating that they sometimes heard harmonic complex tones as being different from inharmonic complex tones.

tongue. All procedures for behavioral testing of ferrets were approved by the institutional animal care and use committee (IACUC) of the University of Maryland, College Park.

C. Results: Ferrets can weakly distinguish harmonic tones from inharmonic tones during spontaneous behavior

Results from testing three female ferrets, in Fig. 3, indicate that ferrets automatically distinguish harmonic complex tones from inharmonic complex tones on about 20% of trials. The figure shows performance on consecutive sessions after a training period lasting 15–75 sessions had been completed. Hit rates greater than 70% and false-alarm rates less than 20% show that all three ferrets attained proficiency at the baseline task of distinguishing pure-tone targets from inharmonic complex tone references. Two ferrets (top two panels) out of three also detected harmonic complex tone probes at a significantly higher rate than the false-alarm rate, especially in the earliest probe sessions. For the sessions indicated with filled symbols for the probe hit rate, the null hypothesis of no difference between the probe hit rate and the false-alarm rate was rejected ($p < 0.05$) with a two-sided z test for independent proportions applied separately for each session and animal. The z test is a nonparametric test that is applicable when comparing two treatments (harmonic tones and inharmonic tones) and classifying measurements into two mutually exclusive types (hits and misses). Therefore, the ferrets, without receiving training on the distinction, occasionally heard harmonic complex tones to be different than inharmonic complex tones. Nevertheless, the considerable difference between the probe hit rate and the target hit rate indicates that harmonic tones were not treated equivalently to the pure tones.

D. Discussion

It is worth noting three points from the results. First, two ferrets heard harmonic complex tones to be different from inharmonic complex tones in about 15–20% of all trials. In these cases, they confused harmonic probes with pure-tone targets by responding to them as if they were pure tones, although the considerable difference between the hit rates for probes and targets suggests that these ferrets did not treat the two sound classes equivalently. A possible objection to the interpretation that probes and targets were confused, is that the ferrets simply heard the harmonic targets as a new kind of sound and responded (due to surprise) by withdrawing from the reward spout. This objection does not hold for two reasons. First, the parameters of the harmonic complex tones were matched in every way to those of the inharmonic complex tones. Thus, if harmonic probes were heard as a new category of sounds, it underscores the point that the ferrets could hear them to be different from inharmonic tones. Second, a novelty response should have declined rapidly as the ferret became accustomed to the harmonic probes. However, the elevated probe hit rate persisted for several sessions, especially in ferret 2.

Based on these results, we suggest that the ferrets sometimes distinguish harmonic tones from inharmonic tones on the basis of differences in perceived fusion. The results do not directly demonstrate that fusion was the relevant dimension for their judgments. However, we think it is a probable explanation because the harmonic and inharmonic complex tones were constructed to have no consistent differences in timbre or roughness. In analogy with human perception, we think perceptual fusion may be the logical dimension along which ferrets distinguish these two classes of sound. The results of the experiment also indicate that the ferrets occasionally distinguished harmonic tones from inharmonic tones automatically; it was automatic in the sense that they did not have to be taught the difference between these sound classes. In fact, the animals were not rewarded for making the distinction.

Second, the failure of ferret 3 to detect probes at a higher rate than the false-alarm rate does not necessarily indicate that it could not hear a difference between harmonic and inharmonic complex tones. Instead, the ferret may have learned to focus on the timbre cue in order to perform the baseline task. It may have continued to use the same cue during probe sessions and thus correctly categorized the harmonic probes to be similar to the inharmonic references along the perceptual dimension of timbre, while ignoring audible differences in fusion.

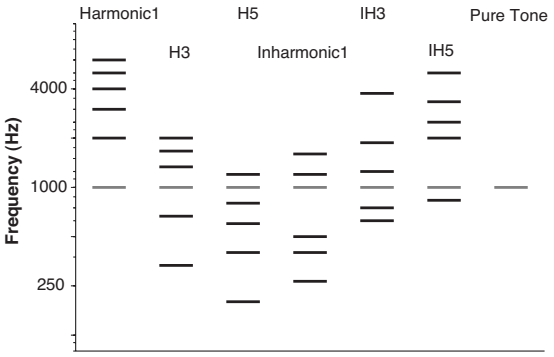


FIG. 4. Stimulus protocol for investigating cortical neural correlates of harmonicity in ferrets. Neural activity is recorded for a sequence of complex tones and a pure tone (*anchored tone sequence*), all of which share a component at the BF of the neuron under investigation. If cortical (or upstream) neurons treat harmonic sounds in a special manner, then the component at BF should elicit a qualitatively different response when presented in a harmonic context compared to an inharmonic context.

Finally, the probe hit rate for ferret 1 declined steadily after the first probe session. A probable reason is that the ferret, gradually learning that the harmonic probes were not associated with the shock, adjusted its judgments to use timbre exclusively rather than timbre in conjunction with fusion. Ferret 2, on the other hand, might not have adjusted its judgments simply because it more slowly learned that harmonic probes were not associated with the shock. Given more probe sessions, the ferret might have exhibited such a learning effect. Indeed, consistent with the notion that learning ability might underlie the difference between the declining probe hit rate for ferret 1 and the lack of such decline for ferret 2, the latter animal took almost five times more sessions than the former to attain proficiency at the baseline task.

In summary, two out of three ferrets discriminated harmonic tones from inharmonic tones. However, the low detection rate (15–20%) of harmonic tones was not comparable enough to that of pure tones to warrant a conclusion that these sound classes were perceptually equivalent to the animals.

III. EXPERIMENT 2: CORRELATES OF HARMONIC FUSION IN AUDITORY CORTICAL NEURONS

A. Rationale

To seek neural correlates of harmonic fusion, we recorded single-unit activity from primary auditory cortex (AI) and auditory anterior field (AAF) to a sequence of harmonic and inharmonic complex tones where all the sounds in the sequence shared a component at the best frequency (BF) of the unit under investigation (Fig. 4). The frequency of this shared component is known as the *anchor frequency* (AF) and the sequence is known as an *anchored tone sequence* in the rest of the paper. The anchor component was placed at the BF to ensure a robust response from the neuron for every complex tone. Any special cortical or upstream (subcortical) neural computation on harmonic sounds would be expected to result in a difference in the responses to the harmonic complex tones compared to those for inharmonic complex tones.

The effect of a harmonic context on the responses can be confused with the effects of spectro-temporal integration of stimulus spectrum by the spectro-temporal tuning of a cortical neuron (e.g., interaction of inhibitory sidebands with balance of spectrum above and below BF) (Depireux *et al.*, 2001; Kowalski *et al.*, 1996; Schreiner and Calhoun, 1994; Shamma *et al.*, 1995). To account for spectrotemporal filtering, we measured a neuron's spectro-temporal receptive field (STRF) and used it to predict the responses to the stimuli in the anchored tone sequences. An effect of harmonic context should then appear as a difference in the predictability of the responses to harmonic complex tones compared to those for inharmonic complex tones, because the predictions using the STRF account for the effect of the spectral context. The STRF is the best-fitting linear model for the transformation of the stimulus spectro-temporal envelope by a neuron. Because we measured STRFs using spectro-temporal envelopes imposed upon broadband noise (inharmonic) carriers, any effect of harmonic fusion is expected to manifest itself as a reduction in the predictability of responses to harmonic tones compared to that for inharmonic tones. A reduction is expected because the STRF, by definition, gives the best possible linear estimate of the response; any modification due to harmonicity must result in a degradation of this best estimate.

B. Methods

1. Experimental apparatus and methods

Experiments were performed at the University of Maryland, College Park and the University of Maryland, Baltimore. Animal preparation and neural-recording procedures were approved by the IACUCs of both institutions. Surgical procedures are described in detail in other publications (Dobbins *et al.*, 2007; Fritz *et al.*, 2003). We give a brief outline of the recording procedure here. During daily recording sessions lasting 3–6 h, ferrets were trained to lie motionless in a custom apparatus that restrained them. The auditory cortex was accessed through craniotomies of diameters in the range 0.5–6 mm. We took precautions to maintain sterility of the craniotomies at all times.

- In some experiments, the auditory cortex was accessed through a small hole of diameter less than 0.5 mm. Each hole was used for 5–7 days after which it was sealed with dental cement. The small size of the hole afforded stable recordings and lowered chances of infection. Closely spaced holes were made over auditory cortex, with particular focus on low-frequency areas for this study. Recordings were attributed to AI based on tonotopic organization and response properties (strong response to tones and relatively short response latency), but a few penetrations might have been from adjacent areas.
- In other experiments, we obtained recordings from both AAF and AI. In these experiments, the recordings were through relatively large craniotomies of diameter 5–6 mm. Larger craniotomies permitted us to identify recording locations as being from AI or AAF based on position relative to sulcal landmarks on the surface of the brain (Kowalski

et al., 1995). Such attribution of location would not have been possible with microcraniotomies because sulcal landmarks are not readily visible.

A variety of different methods were used for the recordings. These methods are described below, but they are not distinguished in the reporting of results because they did not lead to noticeably different findings. Most of the recordings were with single parylene-coated tungsten microelectrodes having impedance ranging from 2 to 7 MΩ at 1 kHz. Electrode penetrations were perpendicular to the surface of the cortex. We used a hydraulic microdrive under visual guidance via an operating microscope to position the electrodes. A few recordings were made with NeuroNexus Technologies silicon-substrate linear electrode arrays (four arrays, with each array having four electrodes in a straight line) or silicon-substrate tetrode arrays (four tetrode arrays, with each array having four closely spaced electrodes in a diamond-shaped configuration). Recordings yielded spikes from 1–3 neurons on a single electrode that were sorted offline with a combination of automatic spike-sorting algorithms (Lewicki, 1994; MClust-3.3, A. D. Redish *et al.*; KlustaKwik, K. Harris) and manual techniques. A spike class was included as a single unit for further analysis if less than 5% of interspike intervals were smaller than 1 ms, the putative absolute refractory period, and the spike waveform had a bipolar shape.

In some experiments, sounds were delivered with an Etymotic ER-2 earphone inserted into the entrance of the ear canal on the contralateral side of the cortex being investigated. All stimuli were generated by computer and fed through equalizers to the earphone. An Etymotic ER-7C probe-tube microphone was used to calibrate the sound system *in situ* for every recording session. An automatic calibration procedure gave flat frequency responses below 20 000 Hz. In other experiments, sounds were delivered by a speaker (Manger) placed 1 m straight above the head of the ferret. Stimuli were generated by a computer and sound levels were calibrated at the position of the ferret's head. Apart from a handful of cases, most of the recordings in these latter experiments were obtained without the sound system having been equalized to a flat frequency response, because the frequency response was flat even when not equalized.

2. Stimuli and analysis

a. Stimuli. After a cluster of single units was isolated using pure-tone and complex-tone search stimuli, its response area was measured with pure tones to get an estimate of the BF. The discharge rate was measured as a function of the level of pure tones at BF in order to estimate the threshold. Responses to a tone sequence anchored at the BF (as in Fig. 4) were measured at approximately 20 dB above BF-tone threshold. Finally, the neuron's spectro-temporal filtering characteristics were estimated at the same level as the anchored-tone sequence by measuring the STRF with temporally orthogonal-ripple-combination (TORC) stimuli (Klein *et al.*, 2000), which are described below.

b. Anchored tone sequences. Anchored-tone sequences consisted of six-component harmonic and inharmonic complex tones. Up to six different harmonic complex tones with components in random phase were part of the sequence, where each tone had a different component number at the anchor frequency. For most units, the first through sixth components were at the anchor frequency, but a few units had only the second through fifth or first through fifth components at the anchor frequency.

Inharmonic complex tones in the sequences were formed by reordering ratios between consecutive components of a harmonic complex tone, as in Experiment 1. The same sequences of ratios were used for almost all units.

In our later recording sessions, we imposed a slow sinusoidal amplitude modulation (4–20 Hz) with a modulation depth of 0.5 (peak to mean) upon the complex tones. All components were modulated coherently. We imposed this modulation to ensure that neurons responded vigorously throughout the complex tone, because cortical neurons are often unresponsive during the sustained portions of static stimuli (Clarey *et al.*, 1992; Shamma *et al.*, 1995) as was indeed the case for the majority of single units recorded during our early recording sessions. In contrast, most units responded vigorously to the amplitude-modulated complex tones. Sinusoidal amplitude modulation at slow rates may provide an additional grouping cue beyond that of harmonicity. However, this cue is in fact relatively weak compared to the unavoidable powerful (and quite similar) cue of the common rapid onset and offset of all (harmonic and inharmonic) tones. Since our goal is to compare the responses to the harmonic versus inharmonic complexes, then as they are treated the same, amplitude modulation should not confer any advantage to one complex over the other.

All components of the harmonic and inharmonic complex tones were presented at the same level.

c. Characterizing linear processing of spectro-temporal envelopes with STRFs. Underlying the measurement of a STRF is the observation (Kowalski *et al.*, 1996; Schreiner and Calhoun, 1994; Shamma *et al.*, 1995) that responses of many AI neurons have a large linear component with respect to the spectro-temporal envelope of sounds. The STRF (t,x), a two-dimensional function of time t and log frequency $x = \log(f/f_0)$, describes the linear component of the transformation between the spectro-temporal envelope of an acoustic stimulus and the neural response. This response component is given by

$$r(t) = \int \int \mathrm{STRF}(\tau,x) \cdot S(t-\tau,x) d\tau dx, \qquad (1)$$

where $r(t)$ is the instantaneous discharge rate of the neuron and $S(t,x)$ is the spectro-temporal envelope (or dynamic spectrum) of the stimulus; the equation describes a convolution in time and a correlation in log frequency. Intuitively, the neural response r at time t is the correlation of the STRF with the time-reversed dynamic spectrum of the stimulus S around that moment. This operation can be viewed as similar to a matched-filtering operation whereby the maximum response of the neuron occurs when the time-reversed dynamic spectrum most resembles the STRF.

The theory and practice of measuring STRFs with TORC stimuli are in Klein *et al.* (2000). A brief outline is given in the appendix. TORCs are composed of *moving*

ripples (Depireux *et al.*, 2001; Kowalski *et al.*, 1996), which are broadband sounds having sinusoidal temporal and spectral envelopes. Moving ripples are basis functions of the spectro-temporal domain, in that arbitrary spectro-temporal envelopes can be most efficiently expressed as combinations of these stimuli. The accumulated phase-locked responses to individual moving ripples give a spectro-temporal modulation transfer function (parameterized by ripple periodicity and ripple spectral density) whose two-dimensional inverse Fourier transform is the STRF. TORCs are special superpositions of moving ripples such that two components having different ripple spectral densities do not share the same ripple periodicity. This special combination of moving ripples enables rapid measurement of the STRF. We used random-phase tones densely spaced on a log-frequency axis as carriers (100 tones/octave, spanning 5–7 octaves) for the envelope of the TORC stimuli.

It is worth noting two properties of our STRF measurements.

1. Underlying our measurement of the STRF is an assumption that the neuronal system has reached a steady state (Schechter and Depireux, 2007). Consequently, the STRF quantifies changes of the discharge rate above and below a steady-state rate.
2. The mean of the STRFs is set to zero because the STRF is designed to predict response modulations, not the steady-state response. In order to predict the steady-state discharge rate, it is necessary to measure the terms of the STRF at a ripple periodicity of 0 Hz (i.e., static ripples). These responses cannot be measured by directly incorporating static ripples into TORC stimuli because responses to the static ripples are difficult to disambiguate from nonlinear responses to the moving ripples resulting from, for example, spiking rate saturation and positivity of spike rates. The 0 Hz ripple periodicity terms can be estimated separately using static ripples presented at a range of phases. We estimated such terms of the STRF for 13 units in some of the later recording sessions. However, because results from these units did not differ from other units, we do not distinguish them in the results.

d. Quantifying the effects of spectro-temporal filtering on responses to complex tones. In order to account for the effect of spectro-temporal filtering on responses of a unit to the anchored-tone sequence, we predicted the peri-stimulus time (PST) histogram of the response to each stimulus from the measured STRF. The lack of predictability of the PST histogram then served as a measure of the response to each stimulus that was not explainable by spectrotemporal filtering. Correlates of harmonic fusion were expected to show up as systematic differences in the predictabilities of the response for harmonic stimuli compared to those for inharmonic stimuli. In other words, the prediction of responses from the STRF accounts for the processing of slow spectrotemporal envelopes in the stimulus, a feature that has little to do with harmonic fusion and pitch. Any effects of harmonicity have to be in the remaining unpredicted portion of the response.

A discrete-time implementation of Eq. (1) was used to predict the response to each stimulus in the anchored tone sequence (visualized in Fig. 5). The predicted PST histogram ($p[n]$) for a stimulus was a function of the sum of two terms, one term due to spectrotemporal filtering ($p_{\text{strf}}[n]$) and a second term representing the steady-state discharge rate (p_{ss}). For a complex tone having L components, we used a two-step process to determine $p_{\text{strf}}[n]$, which is simply the convolution of the stimulus spectrogram with the STRF.

1. Convolve stimulus envelope $e[n]$ (flat in the early experiments that used unmodulated complex tones and sinusoidal in the later experiments that used modulated complex tones, both having 10 ms cosine-squared onset and offset ramps) with horizontal slices of the STRF at the frequencies x^i of the tone components, STRF $[n,x^i]$, to get the contributions of individual components to the overall prediction.

$$p^i_{\text{strf}}[n] = \frac{1}{N}(\text{STRF}[n,x^i] * e[n]), \tag{2}$$

where N is the length of $\text{STRF}^i[n]$ and $*$ indicates convolution in time.

2. Combine contributions of individual components to get the overall prediction from the STRF as the mean of the individual contributions.

$$p_{\text{strf}}[n] = \frac{1}{L}\sum_{i=1}^{L} p^i_{\text{strf}}[n]. \tag{3}$$

Finally, the predicted PST histogram was

$$p[n] = g(p_{\text{strf}}[n] + p_{\text{ss}}), \tag{4}$$

where $g(\cdot)$ indicates half-wave rectification representing the positivity of spike rates. Because the STRF does not predict the steady-state discharge rate (except in the handful of measurements where we measured responses to static ripples), we used the measured steady-state discharge rate r_{ss} instead of p_{ss}. In Fig. 5(E), shading is used to indicate one standard deviation above and below the mean prediction,[2] where the standard deviation is estimated by resampling the measured STRF using the bootstrap technique (Efron and Tibshirani, 1993; Klein *et al.*, 2006). Figures 5(C) and 5(D) show raster and PST histograms of the actual response of the cell to the same stimulus, demonstrating the relatively high quality of the prediction in this case.

We quantified the quality of the prediction with the cross-covariance between the response $r[n]$ and the prediction $p[n]$, defining it to be

$$\rho[m] = \frac{cov(r[n+m]\cdot p[n])}{\sigma_r \cdot \sigma_p}. \tag{5}$$

Because the covariance in the numerator is normalized by the standard deviations, $\rho[m]$ is insensitive to the magnitudes of $r[n]$ and $p[n]$ but it captures the similarity of the waveform shapes. We used $\rho = \max(\rho[m])$ to summarize the relationship of prediction and response independent of temporal misalignments between the waveforms; this quantity served

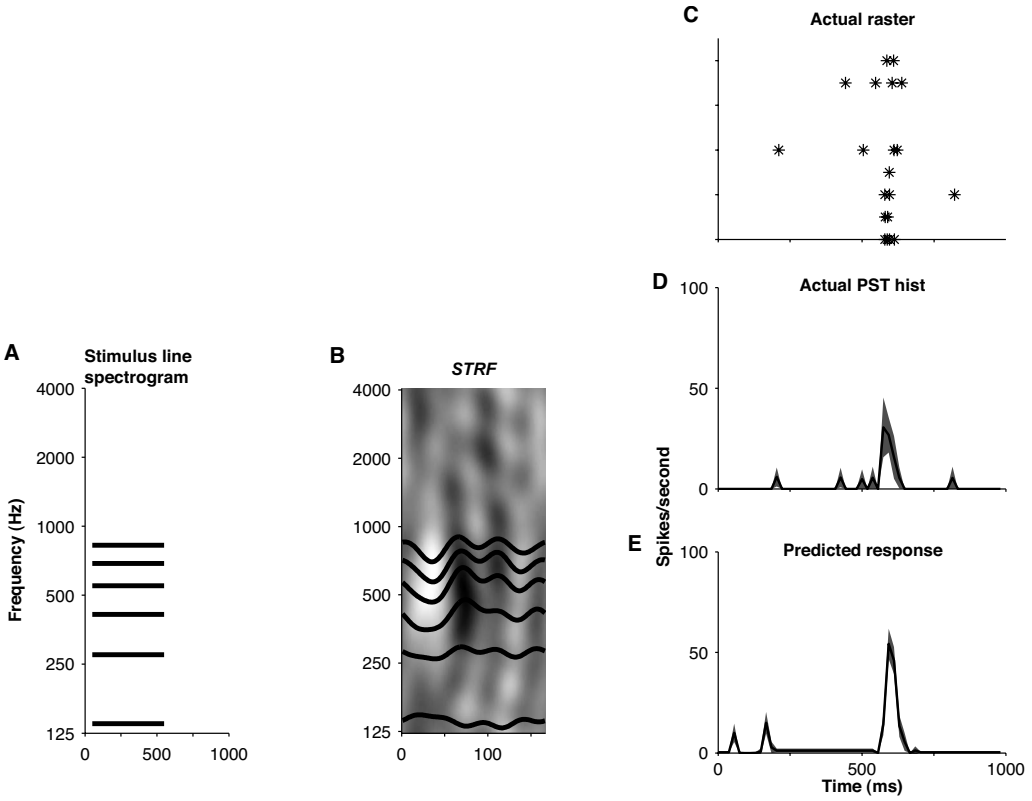


FIG. 5. Predicting responses to complex tones using STRFs. The predicted response (E) is the convolution of the spectrotemporal envelope of the stimulus (A, schematic spectrogram for complex tone having six components) with the STRF (B). More specifically, the operation can be seen as comprising two steps: (1) One-dimensional convolutions between the stimulus envelope (trapezoid-like with 10 ms cosine-squared onset and offset ramps) and horizontal slices of the STRF corresponding to the frequencies of each tone component; (2) Average of the results of the convolutions. These steps form part of an implementation of Eq. (4). Shown for comparison with the prediction are a raster plot (C) and a PST histogram (D) of the actual response of the neuron for ten stimulus presentations. Shading in D and E indicates one standard deviation above and below the mean prediction and the mean PST histogram, respectively, obtained with the bootstrap technique. The units of the STRF depicted in B are spikes/s/Pa. White pixels in the STRF indicate suppression, gray pixels indicate no change, and black pixels indicate elevation of discharge rate. Unit *d-46d*, *class 1*.

as a measure of the neuron's response after accounting for the effects of spectrotemporal filtering.

To quantify the extent to which a neuron distinguished a harmonic tone from each of the inharmonic stimuli, we used a measure analogous to the *d-prime* statistic from signal detection theory. We defined this measure to be the difference between the means of the distributions of ρ for each of the stimuli normalized by the geometric means of the standard deviations of the distributions, with the distributions having been generated by bootstrap replication.

$$d'_{\rho}(Hx,IHx) = \frac{\overline{\rho(Hx)} - \overline{\rho(IHx)}}{\sqrt{\sigma_{\rho(Hx)} \cdot \sigma_{\rho(IHx)}}}. \quad (6)$$

We did not compute this quantity when either stimulus of a *Hx*, *IHx* pair (denoting harmonic and inharmonic tones, respectively) did not evoke a change in discharge rate or a change in phase-locked response by visual inspection because predictability of the temporal pattern of discharge of a no response is not meaningful. Figure 7(B) gives an example of distributions of ρ generated by bootstrap resampling for a harmonic tone and several inharmonic tones. We take $d' = 1$ as the threshold at which the two distributions are significantly different (equivalent to 76% correct identification in a two-alternative forced-choice discrimination task) to determine if a neuron reliably distinguished a harmonic tone from all of the inharmonic stimuli. We revisit this example in the Results section below.

C. Results: A small fraction of cortical neurons distinguished harmonic complex tones from inharmonic complex tones

We selected data from 86 units in nine ferrets for this report, with many units rejected due to not having high enough signal-to-noise ratios. None of the nine ferrets were used in the behavioral study. The BFs of the units ranged from 210 to 13 600 Hz, with 11 having BF greater than 5000 Hz, 20 having BF greater than 3000 Hz, and 36 having BF greater than 1500 Hz. Of these units, 51 were from AI, 22 were from AAF, and 13 units were of uncertain location either in AI or AAF.

Figure 6 shows the responses of a single unit to unmodulated harmonic and inharmonic tones constituting the anchored tone sequences. Harmonic tones are labeled with the prefix "H" and the inharmonic tones are labeled with the prefix "IH;" the numerical suffix for the harmonic tones indicates the component at the AF (anchor frequency) while for inharmonic tones it is an arbitrary label not indicative of any status for the component at AF. The spectral context clearly influenced the responses of this unit to the different tones. For example, the harmonic tones labeled H3 and H4

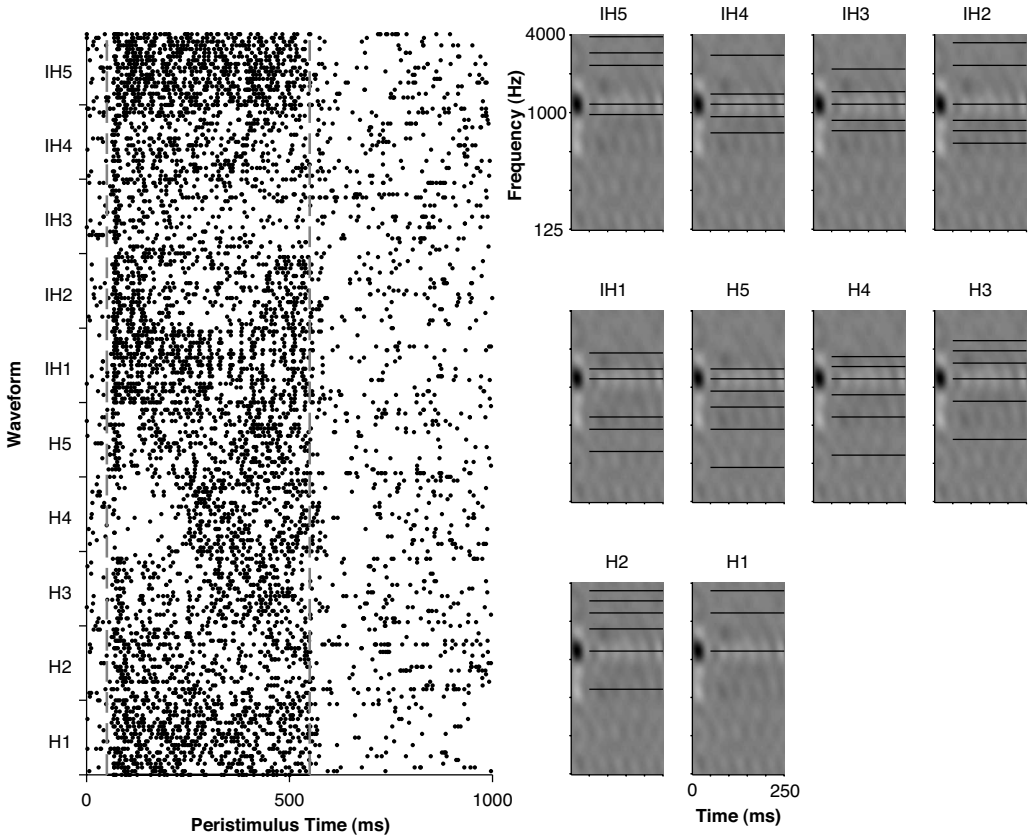


FIG. 6. Response of a unit to an anchored-tone sequence. Dot rasters (left) and schematic spectrograms of each tone in the anchored tone sequence overlayed on the STRF of the unit (right). Stimuli labeled as *Hx* (where *x* indicates the component number at *BF*) are harmonic tones. Those labeled as *IHx* are inharmonic tones, but in contrast to that for the harmonic tones, the numerical suffix is an arbitrary label not indicative of any status for the component at anchor frequency. Unit *d*-76*b*, *class 1*.

(third and fourth components at the AF, respectively) were inhibited for the first half of stimulus presentation, while none of the other stimuli elicited such a response. Similarly, the unit responded far more weakly to the inharmonic tones labeled IH3 and IH4 than to any of the other stimuli.

Interestingly for this unit, the response to stimulus IH1 shows temporal structure in the discharge pattern. This temporal structure reflects synchronization of discharges to envelope modulations resulting from interaction between tone components. Responses to all stimuli showed such synchronization to tone interactions up to 250 Hz. As a result of this 250 Hz upper limit, the temporal envelope for harmonic tones H1 through H4, where the fundamentals exceeded 250 Hz, was not reflected in the neural discharge patterns but the temporal envelope for H5 did produce synchronized discharges. The rate limit also makes such units unsuitable for encoding the virtual pitch of harmonic complex tones via synchronization to the envelope; instead, they are better suited for encoding residue pitch. A similar limit for synchronizing to the stimulus temporal envelope has been observed in previous studies of auditory cortex in awake animals (Bieser and Muller-Preuss, 1996; de Ribaupierre *et al.*, 1972; Elhilali *et al.*, 2004; Fishman *et al.*, 2000; Liang *et al.*, 2001; Steinschneider *et al.*, 1998). No other unit in our population exhibited such discharge patterns.

In order to account for the effect of spectrotemporal filtering in this unit, we used the STRF to predict PST histograms for the complex tones. Figure 7(A) shows actual PST histograms overlayed on predictions for the unit of Fig. 6. The response was better predicted for the inharmonic stimuli than for stimuli H3 and H4 because the STRF was unable to predict the late response to these harmonic stimuli. We summarized the linear predictability of the response using the maximum cross-covariance ρ (see Methods), between the response PST histogram and the predicted wave-form. Figure 7(B) shows distributions of ρ for stimulus H4 and for all the inharmonic stimuli. We quantified the extent to which this neuron distinguished H4 from each of the inharmonic stimuli using d'_ρ (see Methods). If we take $d'=1$ to be the threshold at which two distributions are significantly different, then this neuron reliably distinguished H4 from all of the inharmonic stimuli. Figure 7(C) summarizes d'_ρ for each of the harmonic stimuli compared to all of the inharmonic stimuli. The minimum d'_ρ for a given harmonic tone is a convenient measure of how well the neuron discriminated that harmonic tone from the inharmonic tone having the most similar response. This measure is greatest for H4 of all the harmonic tones, which means that this neuron was best at discriminating H4 from inharmonic tones.

Figure 8 shows an example of responses and predictions from a unit for amplitude-modulated complex-tone stimuli. Figure 8(A) shows period histograms of responses to a harmonic (H3) and an inharmonic tone[3] along with a single period of predictions for the same stimuli. Both the magnitudes and phases of the responses are predicted well by the STRF of this neuron. Figure 8(B) shows histograms of

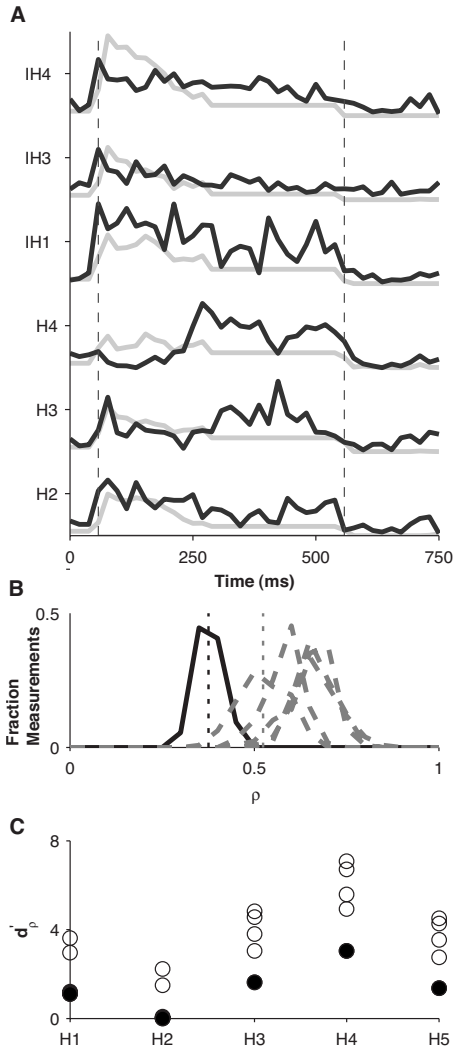


FIG. 7. Predictability of temporal patterns of discharge for unit of Fig. 6. (A) Actual (solid) PST histograms overlayed on predicted (dotted) PST histograms for some select stimuli in the anchored-tone sequence. Dashed vertical gray lines indicate stimulus onset and offset. Predictions are normalized by the maximum across stimuli of all prediction waveforms and actual PST histograms are normalized by the maximum across stimuli of all actual responses, because the magnitudes of the predictions are consistently greater than the magnitudes of the PST histograms. (B) Histograms of the correlation coefficient (ρ) between predicted and actual PST histograms for harmonic stimulus H4 (solid) and histograms of ρ for each of the inharmonic stimuli (dashed), where histograms are obtained from 128 bootstrap replicates of predicted and actual responses. Dotted vertical lines indicate means of the distributions of ρ for stimulus H4 and for the inharmonic stimulus whose response predictability was closest to that of H4. d'_ρ is the difference between such means normalized by the geometric mean of their standard deviations. (C) d'_ρ for each of the harmonic tones relative to each of the inharmonic tones. The minimum d'_ρ for a given harmonic number (solid circles) is a measure of how discriminable that particular harmonic tone is from the most similar inharmonic tone in terms of the predictability of the temporal discharge pattern.

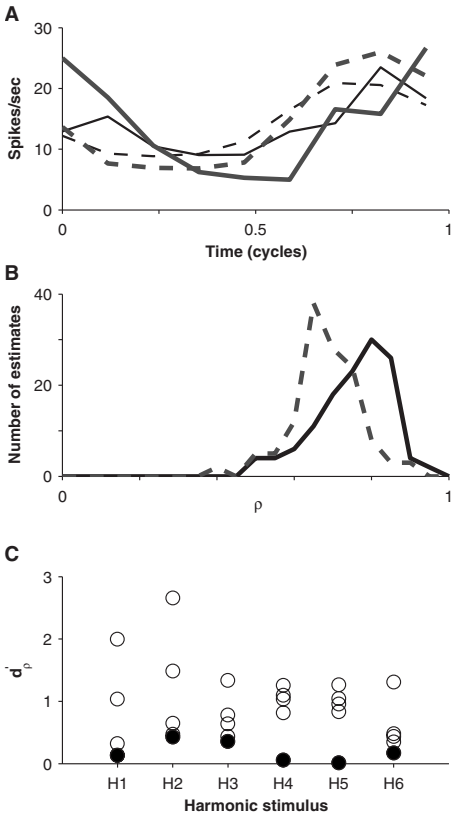


FIG. 8. Predictability of temporal patterns of discharge in a unit driven by amplitude-modulated complex tones. (A) A single period of predicted (dashed) and actual (solid) responses for harmonic tone H3 (thick gray) and an inharmonic tone (thin black). (B) Histograms of correlation coefficients between 128 bootstrap replicates of predicted and actual responses from panel (A). (C) d'_ρ for each of the harmonic tones relative to each of the inharmonic tones, with solid circles indicating the smallest d'_ρ for a given harmonic tone.

bootstrap-replicate ρ for stimulus H3 and the inharmonic tone of panel A. The distributions of ρ for these stimuli overlap a great deal, suggesting that the predictability of temporal discharge pattern does not readily distinguish H3 from the inharmonic tone. Figure 8(C) summarizes d'_ρ for each of the harmonic tones compared to all of the inharmonic tones. The minimum d'_ρ for each harmonic tone is less than 1, confirming the observation for stimulus H3 that this neuron was not effective at discriminating any of the harmonic tones from inharmonic tones.

Neurons were no more effective at discriminating harmonic tones from inharmonic tones when the stimuli were unmodulated compared to when they were amplitude modulated. Distributions of d'_ρ for responses to unmodulated tones overlapped greatly with those for responses to modulated tones. A large-sample normal approximation of the Wald–Wolfowitz runs test, a nonparameteric test for determining whether two samples are identically distributed, yielded a test statistic $z=1.42$. At this value of the test statistic, the null hypothesis of d'_ρ for modulated stimuli and d'_ρ for unmodulated stimuli being identically distributed cannot be rejected ($p>0.05$).

Most units in the population were ineffective at discriminating the harmonic tones from the inharmonic tones; that is, they were mostly like the unit of Fig. 8 rather than the unit of Fig. 7. Figure 9 summarizes for our entire population of neurons how well the predictability of the temporal pattern of discharge discriminated the harmonic tones from the inharmonic tones. Histograms of minimum d'_ρ in Fig. 9(A) show that values exceeding 1 were infrequently observed, indicating that few neurons discriminated any of the harmonic tones from inharmonic tones. Figure 9(B) gives an-

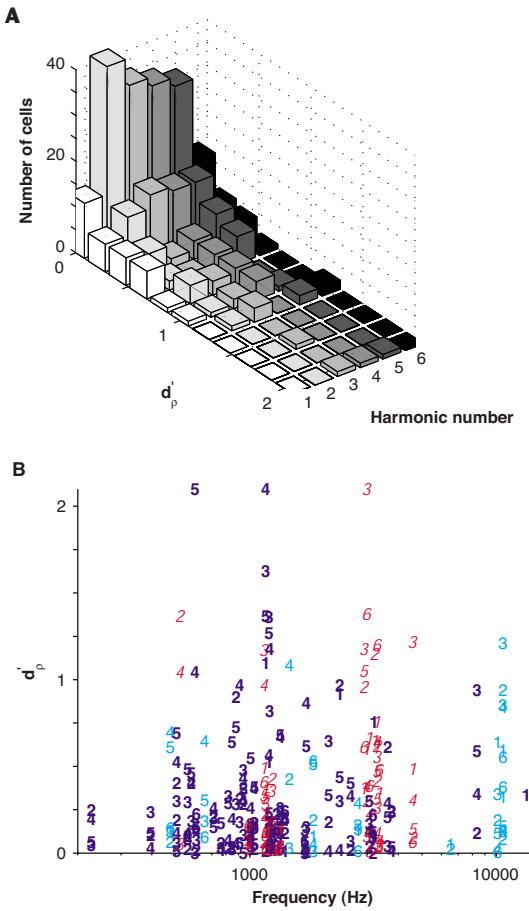


FIG. 9. (Color online) Summary of how distinguishable harmonic tones are from inharmonic tones across all recordings. (A) Histograms of the minimum d'_ρ for each harmonic tone across all recordings. (B) Minimum d'_ρ for each harmonic tone as a function of the best frequency for the recording. The recording location is indicated by font style (bold: AI, italic: AAF, plain: undetermined) and the identity of the harmonic tone is indicated by the numeric symbol.

other view of the same information. The figure shows the minimum d'_ρ for each harmonic tone as a function of the BF of the unit, while identifying the harmonic tone by digits corresponding to the number of the anchor component. The 13 units that had a minimum d'_ρ greater than 1 had BFs between 500 and 10 000 Hz (all but one unit having BFs less than 4400 Hz). Location of the units (indicated by the font style of the symbol) that discriminated harmonic tones from inharmonic tones could be either AI or AAF. In summary, these few discriminative units were not likely to occur in a particular cortical location nor biased to a particular range of BFs within the 500–4400 Hz range.

The maximum cross-covariance quantifies the similarity of the shapes of the predicted waveforms and the PST histograms. However, this measure fails to account for how the magnitude of the predicted waveform compares to the magnitude of the time-varying component of PST histograms, or any differences in latencies of the prediction and actual response. For modulated complex tones it fails to quantify synchronization of response to the amplitude modulation. Moreover, the steady-state discharge rate is not predicted by the STRF, but it must be affected by the interaction of the stimulus spectrum with the frequency tuning of the neuron. We accounted for these various other properties of response predictability in a manner similar to our examination of the maximum cross covariance (not shown). Our conclusions based on the maximum cross covariance were not significantly altered—between 10% and 15% of the units were capable of discriminating one of the harmonic tones from the inharmonic tones with these other measures.

D. Discussion

About 10%–15% of units in AI and AAF responded differently to harmonic tones than to inharmonic tones, so that they may be said to be sensitive to harmonicity. This relatively small fraction of harmonicity-encoding neurons may account for the weak ability of ferrets in Experiment 1 to discriminate harmonic tones from inharmonic tones.

The failure to find a robust neural discrimination of harmonic tones from inharmonic tones is consistent with the conclusion of previous studies that single AI neurons in naive animals for the most part are not concerned with the coding of harmonicity. On the other hand, the failure to find harmonicity coding in AAF neurons may be at odds with other studies. The correspondence of AAF in ferrets to cortical fields in other animals in uncertain (Bizley *et al.*, 2005). If AAF corresponds to the rostral field in primates, then our failure to find a significant percentage of neurons to be selective for harmonicity may be surprising given the promising observations of neurons tuned to the fundamental frequency of harmonic tones in marmosets (Bendor and Wang, 2005).

There are several possible reasons for the lack of congruence between the marmoset data and the ferret data. One possible reason is that AAF in ferrets may not correspond to rostral field in marmosets or that the marmoset data were mostly at very low frequencies (<0.8 kHz), while our data are at higher frequencies [mostly between 1 and 5 kHz—see Fig. 9(B)]. Another reason might be that the marmoset neurons were not harmonicity selective but instead were selective to waveform modulation rate. Future ferret studies having more recordings from the low-frequency region of AAF may yield data that are in line with the marmoset data. Moreover, there are some caveats to our conclusion that there are few harmonicity-sensitive neurons in AI and AAF of ferrets. First, our recordings were from multiple cortical layers and we had relatively few recordings per cortex. These characteristics may lead to a false conclusion that single AI and AAF neurons do not encode harmonicity if a population of harmonicity-selective neurons is concentrated in a specific subfield and layer of auditory cortex that we failed to sample. Second, different animals were used for the physiology and the behavior and it is possible that the physiology animals were incapable of spontaneously distinguishing harmonic tones from inharmonic tones. Finally, it is of course conceivable that our criteria for identifying harmonicity-sensitive cells are simply inadequate. Other formulations in the future may prove successful, such as distributed coding requiring comparison of spike timing across nearby neurons.

On the whole, our failure to find a robust encoding of harmonicity is not inconsistent with most previous studies

that have examined the encoding of harmonic sounds from the perspective of virtual pitch. Single-unit and multi-unit recordings have failed to reveal neurons selective to virtual pitch in AI (Fishman *et al.*, 1998; Schwarz and Tomlinson, 1990). Recent neuromagnetic and functional magnetic resonance imaging studies also support the conclusion that virtual pitch is not extracted in AI. Instead, investigations with regular-interval noise and filtered harmonic complex tones suggest that pitch is extracted at the anterolateral border of AI in humans (Krumbholz *et al.*, 2003; Patterson *et al.*, 2003; Penagos *et al.*, 2003; Warren *et al.*, 2003). Nevertheless, this conclusion about the role of the anterolateral border of AI has also recently come under doubt (Hall and Plack, 2006, 2007).

Several studies have investigated neural coding of harmonic fusion by seeking correlates of the perceptual popout of a mistuned component from an otherwise harmonic complex tone. Sinex *et al.* (2002, 2005) found that single inferior colliculus neurons in chinchilla could distinguish harmonic tones from mistuned-component harmonic tones based on distinctive temporal patterns of discharge. These temporal discharge patterns were understood as arising from envelope modulations due to interaction between adjacent tone components. This finding of a neural correlate for harmonicity in inferior colliculus is not inconsistent with our failure to find a robust correlate in auditory cortex, because the majority of cortical neurons do not encode first-order envelopes (modulations due to tone-tone interactions) but instead encode slower second-order envelopes (modulation of the first-order envelope) (Elhilali *et al.*, 2004).

The neural basis of the perceptual popout of a mistuned harmonic has also been investigated in human listeners with event-related brain potentials. These studies have found long latency (150–250 ms after stimulus onset) responses that are correlated with perceptual popout (Alain *et al.*, 2002; Hiraumi *et al.*, 2005; McDonald and Alain, 2005); such latencies imply an involvement of secondary auditory cortical areas. Involvement of primary auditory cortex is also suggested by small differences in middle latency responses between harmonic stimuli and mistuned-harmonic stimuli (Dyson and Alain, 2004). While these middle and long latency responses may reflect harmonicity processing, it is also possible that they indicate, more generally, the perception of concurrent auditory objects; this possibility may underlie our failure to find significant evidence for encoding of harmonicity.

In general, the present study differs in outlook from most previous single-unit and multi-unit neurophysiology studies of the cortical neural coding of harmonicity. Previous studies have sought correlates of harmonicity by focusing on two characteristics of the pitch percept: (1) virtual pitch is at the common fundamental of a sequence of harmonics, and (2) the pitch corresponds to that of a pure tone at the fundamental frequency. The former property is expected to endow the putative pitch neuron with inputs across a broad range of frequencies, while the latter property is expected to endow the neuron's tuning to pure tones to be at low frequencies below 1100 Hz (the range of virtual pitch in humans). These studies may be seen as employing a *pitch-equivalence method*.

The present study, employing a *fusion-based method*, exploits the fact that the brain uses harmonicity as a cue for grouping spectral components of a sound. It assumes that the fusion of harmonic components leaves an imprint on the neural representation of the individual components themselves; i.e., the brain maintains a pitch- or harmonicity-tagged representation of sound that is a by-product of the harmonic fusion process. Neurons that have an imprint of this harmonicity tagging would span a broad frequency range of best tuning up to 5000 Hz, the existence region for virtual pitch (Ritsma, 1962). This frequency range is greater than the expected frequency range of tuning for neurons whose selectivity to fundamental frequency corresponds to the pure-tone best frequency. The larger candidate pool of neurons in the fusion-based method compared to the pitch-equivalence method can be seen as an advantage when seeking correlates of harmonicity processing. On the other hand, a desirable feature of the latter method is that it can better reveal the actual neurons that combine harmonic components across frequency. A further advantage of the fusion-based method over the pitch-equivalence method is the potential for distortion products and combination tones to complicate interpretation of data in the latter method (McAlpine, 2004). Distortion and combination tones can regenerate missing components of missing-fundamental harmonic tones used in pitch-equivalence experiments; such nonlinearities are not a problem for the fusion-based method because it does not use missing-fundamental stimuli.

IV. GENERAL DISCUSSION

Our results show that ferrets can spontaneously distinguish harmonic tones from inharmonic tones, albeit weakly. We found relatively few neurons in AI and AAF that encoded harmonicity, which may explain the weak spontaneous behavior.

Perhaps one reason we did not find a large number of harmonicity-encoding neurons is that ferrets are not good at spontaneously distinguishing harmonic tones from inharmonic tones. Animals trained to discriminate harmonic tones from inharmonic tones may turn out to have significantly more harmonicity-encoding neurons. It is worth noting, however, that physiology studies that succeeded in finding candidate harmonicity-selective neurons were done on untrained animals (Bendor and Wang, 2005; Riquimaroux, 1995). Another possible explanation for finding few harmonicity-encoding neurons in AI and AAF is that such neurons exist aplenty, but elsewhere in the brain. If such is the case, then the relatively weak spontaneous behavior in Experiment 1 may be explainable if training is a necessary prerequisite for a strong behavioral response.

In conclusion, the neurons that confer a special perceptual status to harmonic sounds remain to be conclusively identified. Perhaps the puzzle of the cortical encoding of harmonicity will be unraveled by experiments having neural recordings coupled closely with functional brain imaging and behavioral measures in trained animals.

ACKNOWLEDGMENTS

S.K. was supported by T32 DC-00046 and F32 DC-05281, and D.A.D. was supported by RO1 DC-005937 from the National Institute of Deafness and Other Communication Disorders. The project was made possible by a grant from the Bresser Research Foundation to DAD. We also gratefully acknowledge funding from NIH R01 DC005779 and NIH Training grant No. DC00046-01 to S.A.S. We thank Shantanu Ray for expert programming and electronics assistance, Yadong Ji, Tamar Vardi, and Sarah Newman for help with training animals, as well as Heather Dobbins and Barak Shechter for assistance with physiological recordings. We are grateful to the three anonymous reviewers and the associate editor for helpful comments that greatly improved the manuscript.

APPENDIX: MEASURING THE STRF OF A NEURON WITH TORC STIMULI

The TORC stimulus is a particular combination of broadband stimuli known as *moving ripples*, whose spectrotemporal envelope is given by

$$S(t,x) = a_0 + a\cos[2\pi(\omega t + \Omega x) + \psi]. \quad \text{(A1)}$$

At each frequency location, the function describes a sinusoidal modulation of sound level at a rate of ω cycles/s around a mean a_0 and amplitude a; the relative phases of these modulations at different log frequency, $x=\log(f/f_0)$, produce a sinusoidal or rippled profile of density Ω cycles/octave. The rippled profile drifts across the spectral axis in time, hence leading to the name of moving ripples for these stimuli. Analogous to sinusoids for one-dimensional signals, moving ripples are basis functions of the spectrotemporal domain in that any arbitrary spectrotemporal profile can be constructed from a combination of them. And analogous to estimating the impulse response of a one-dimensional system using reverse correlation with white noise stimuli that have equal representation of all sinusoidal frequencies within the system bandwidth (de Boer and de Jongh, 1978), it is possible to estimate the STRF by reverse correlation with spectrotemporal white noise (STWN), which is a stimulus that has an equal representation of all moving ripples within the spectrotemporal bandwidth of the system[4] (Klein *et al.*, 2000, 2006).

However, because the STRF (x,t) transforms a two-dimensional input to a one-dimensional output, moving-ripple components of STWN that are spectrally orthogonal (different ripple densities, Ω, but same ripple periodicities, ω) can evoke overlapping response components that cannot be disambiguated; reverse correlation with such stimuli can result in inaccurate and noisy estimates of the STRF. The TORC stimulus overcomes this problem by ensuring that each moving ripple in the stimulus has a different absolute ripple periodicity $|\omega|$, so that each linear response component is uncorrelated with every ripple component of the stimulus except for the one evoking it. Therefore, when using reverse correlation with a TORC stimulus, response components of a given ripple periodicity contribute only to a single $[\omega,\Omega]$ component of the STRF.

[1]Spectral fusion of components and their contribution to virtual pitch are not entirely congruent in human listeners as well. For example, a component must be mistuned from a harmonic relation by 1.5%–2% in order to hear it apart from the remaining components, whereas it must be mistuned by 8% to stop contributing to the pitch of the complex (Ciocca and Darwin, 1993; Darwin and Ciocca, 1992; Moore *et al.*, 1986; Moore and Kitzes, 1985).

[2]The predictions are stochastic quantities because they are derived from STRFs that are estimated from spike train measurements having inherent variability.

[3]The period histogram accumulates the number of spikes occurring at a given phase of the modulation period of the amplitude-modulated complex tone. We accumulate all spikes occurring between 100 ms after stimulus onset and the end of the stimulus.

[4]For the cortical neurons investigated in this paper, ripple periodicities were less than 32 Hz and ripple densities were less than 1.4 cycles/octave.

Alain, C., Schuler, B. M., and McDonald, K. L. (**2002**). "Neural activity associated with distinguishing concurrent auditory objects," J. Acoust. Soc. Am. **111**, 990–995.

Bendor, D. A., and Wang, X. (**2005**). "The neuronal representation of pitch in primate auditory cortex," Nature (London) **435**, 341–346.

Bieser, A., and Muller-Preuss, P. (**1996**). "Auditory responsive cortex in the squirrel monkey: Neural responses to amplitude-modulated sounds," Exp. Brain Res. **108**, 273–284.

Bizley, J. K., Nodal, F. R., Nelken, I., and King, A. J. (**2005**). "Functional organization of ferret auditory cortex," Cereb. Cortex **15**, 1637–1653.

Bregman, A. S. (**1990**). *Auditory Scene Analysis* (MIT Press, Cambridge, MA).

Brokx, J., and Nooteboom, S. (**1980**). "Intonation and perceptual separation of simultaneous voices," J. Phonetics **10**, 23–36.

Brunstrom, J. M., and Roberts, B. (**1998**). "Profiling the perceptual suppression of partials in periodic complex tones: Further evidence for a harmonic template," J. Acoust. Soc. Am. **104**, 3511–3519.

Brunstrom, J. M., and Roberts, B. (**2000**). "Separate mechanisms govern the selection of spectral components for perceptual fusion and for the computation of global pitch," J. Acoust. Soc. Am. **107**, 1566–1577.

Ciocca, V., and Darwin, C. (**1993**). "Effects of onset asynchrony on pitch perception: Adaptation or grouping?," J. Acoust. Soc. Am. **93**, 2870–2878.

Clarey, J., Barone, P., and Imig, T. (**1992**). "Physiology of thalamus and cortex," in *The Mammalian Auditory Pathway: Neurophysiology*, edited by D. Webster, A. Popper, and R. Fay (Springer-Verlag, New York), pp. 232–334.

Darwin, C., and Ciocca, V. (**1992**). "Grouping in pitch perception: Effects of onset asynchrony and ear of presentation of a mistuned component," J. Acoust. Soc. Am. **91**, 3381–3390.

de Boer, E. (**1956**). "On the 'residue' in hearing," Ph.D. thesis, University of Amsterdam.

de Boer, E. (**1976**). "On the 'residue' and auditory pitch perception," in *Handbook of Sensory Physiology*, edited by W. Keidel and W. Neff (Springer, Verlag, Berlin), Vol. **3**, pp. 479–583.

de Boer, E., and de Jongh, H. R. (**1978**). "On cochlear encoding: Potentialities and limitations of the reverse-correlation technique," J. Acoust. Soc. Am. **63**, 115–135.

de Cheveigne, A. (**2005**). "Pitch perception models," in *Pitch: Neural Coding and Perception*, edited by C. J. Plack, A. J. Oxenham, R. R. Fay, and A. N. Popper, *Springer Handbook of Auditory Research* (Springer, New York).

de Ribaupierre, F., Goldstein, M. H., and Yeni-Komshian, G. (**1972**). "Cortical coding of repetitive acoustic pulses," Brain Res. **48**, 205–225.

Depireux, D. A., Simon, J. Z., Klein, D. J., and Shamma, S. A. (**2001**). "Spectro-temporal response field characterization with moving ripples in ferret primary auditory cortex," J. Neurophysiol. **85**, 1220–1234.

Dobbins, H. D., Marvit, P., Ji, Y., and Depireux, D. A. (**2007**). "Chronically recording with a multi-electrode array device in the auditory cortex of an awake ferret," J. Neurosci. Methods **161**, 101–111.

Duifhuis, H., Willems, L., and Sluyter, R. (**1982**). "Measurement of pitch in speech: An implementation of Goldstein's theory of pitch perception," J. Acoust. Soc. Am. **71**, 1568–1580.

Dyson, B., and Alain, C. (**2004**). "Representation of concurrent acoustic objects in primary auditory cortex," J. Acoust. Soc. Am. **115**, 280–288.

Efron, B., and Tibshirani, R. (**1993**). *An Introduction to the Bootstrap* (Chapman and Hall, New York).

Elhilali, M., Fritz, J., Klein, D., Simon, J., and Shamma, S. (**2004**). "Dy-

namics of precise spiking in primary auditory cortex," J. Neurosci. **24**, 1159–1172.
Fishman, Y., Reser, D. H., Arezzo, J. C., and Steinschneider, M. (**1998**). "Pitch versus spectral encoding of harmonic complex tones in primary auditory cortex of the awake monkey," Brain Res. **786**, 18–30.
Fishman, Y., Reser, D. H., Arezzo, J. C., and Steinschneider, M. (**2000**). "Complex tone processing in primary auditory cortex of the awake monkey. I. Neural ensemble correlates of roughness," J. Acoust. Soc. Am. **108**, 247–262.
Flanagan, J. L., and Gutman, N. (**1960**). "Pitch of periodic pulses without fundamental component," J. Acoust. Soc. Am. **32**, 1319–1328.
Fritz, J., Shamma, S., ElHilali, M., and Klein, D. (**2003**). "Rapid task-related plasticity of spectro-temporal receptive fields in primary auditory cortex," Nat. Neurosci. **6**, 1216–1223.
Goldstein, J. (**1973**). "An optimum processor theory for the central formation of the pitch of complex tones," J. Acoust. Soc. Am. **54**, 1496–1516.
Hall, D. A., and Plack, C. J. (**2006**). "Searching for a pitch center in human auditory cortex," in *Hearing — From Sensory Processing to Perception*, edited by B. Kollmeier (Springer Verlag, Berlin Heidelberg).
Hall, D. A., and Plack, C. J. (**2007**). "The human 'pitch center' responds differently to iterated noise and huggins pitch," NeuroReport **18**, 323-330.
Hartmann, W., McAdams, S., and Smith, B. (**1993**). "Hearing a mistuned harmonic in an otherwise periodic complex tone," J. Acoust. Soc. Am. **88**, 1712–1724.
Heffner, H., and Whitfield, I. (**1976**). "Perception of the missing fundamental by cats," J. Acoust. Soc. Am. **59**, 915–919.
Heffner, H. E., and Heffner, R. S. (**1995**). "Conditioned avoidance for animal psychoacoustics," in *Methods in Comparative Psychoacoustics*, edited by G. Klump (Birkhauser Verlag, Basel).
Hiraumi, H., Nagamine, T., Morita, T., Naito, Y., Fukuyama, H., and Ito, J. (**2005**). "Right hemispheric predominance in the segregation of mistuned partials," Eur. J. Neurosci. **22**, 1821–1824.
Houtsma, A., and Smurzynski, J. (**1990**). "Pitch identification and discrimination for complex tones with many harmonics," J. Acoust. Soc. Am. **87**, 304–310.
Kadia, S., and Wang, X. (**2003**). "Spectral integration in A1 of awake primates: Neurons with single- and multipeaked tuning characteristics," J. Neurophysiol. **89**, 1603–1622.
Klein, D. J., Depireux, D. A., Simon, J. Z., and Shamma, S. A. (**2000**). "Robust spectro-temporal reverse correlation for the auditory system: Optimizing stimulus design," J. Comput. Neurosci. **9**, 85–111.
Klein, D. J., Simon, J. Z., Depireux, D. A., and Shamma, S. A. (**2006**). "Stimulus-invariant processing and spectro-temporal reverse correlation in primary auditory cortex," J. Comput. Neurosci. **20**, 111–136.
Kowalski, N., Depireux, D., and Shamma, S. A. (**1996**). "Analysis of dynamic spectra in ferret primary auditory cortex. I. Characteristics of single unit responses to moving ripple spectra," J. Neurophysiol. **76**, 3503–3523.
Kowalski, N., Vernsel, H., and Shamma, S. A. (**1995**). "Comparison of responses in the anterior and primary auditory fields of the ferret cortex," J. Neurophysiol. **73**, 1513–1523.
Krumbholz, K., Patterson, R., Seither-Preisler, A., Lammertmann, C., and Lutkenhoner, B. (**2003**). "Neuromagnetic evidence for a pitch processing center in heschl's gyrus," Cereb. Cortex **13**, 765–772.
Langner, G., Sams, M., Heil, P., and Schulze, H. (**1997**). "Frequency and periodicity are represented in orthogonal maps in the human auditory cortex: Evidence from magnetoencephalography," J. Comp. Physiol., A **181**, 665–676.
Lewicki, M. (**1994**). "Bayesian modeling and classification of neural signals," Neural Comput. **6**, 1005–1030.
Liang, L., Lu, T., and Wang, X. (**2001**). "Neural representations of sinusoidal amplitude and frequency modulations in the primary auditory cortex of awake primates," J. Neurophysiol. **87**, 2237–2261.
Lin, J., and Hartmann, W. (**1998**). "The pitch of a mistuned harmonic: Evidence for a template model," J. Acoust. Soc. Am. **103**, 2608–2617.
McAlpine, D. (**2002**). "Are pitch neurones the result of difference tones on the basilar membrane?," Assoc. Res. Otolaryngol. Abstr. **25**, 154.
McAlpine, D. (**2004**). "Neural sensitivity to periodicity in the inferior colliculus: Evidence for the role of cochlear distortions," J. Neurophysiol. **92**, 1295–1311.
McDonald, K., and Alain, C. (**2005**). "Contribution of harmonicity and location to auditory object formation in free field: Evidence from event-related brain potentials," J. Acoust. Soc. Am. **118**, 1593–604.
Moore, B., and Glasberg, B. R. (**1985**). "Relative dominance of individual partials in determining the pitch of complex tones," J. Acoust. Soc. Am. **77**, 1853–1860.
Moore, B., Peters, R., and Galsberg, B. (**1986**). "Thresholds for hearing mistuned partials as separate tones in harmonic complexes," J. Acoust. Soc. Am. **80**, 479–483.
Moore, D., and Kitzes, L. (**1985**). "Projections from the cochlear nucleus to the inferior colluculus in normal and neonatally cochlea-ablated gerbils," J. Comp. Neurol. **240**, 180–195.
Patterson, R., Uppenkamp, S., Johnsrude, I., and Griffiths, T. (**2003**). "The processing of temporal pitch and melody information in auditory cortex," Neuron **36**, 767–776.
Penagos, H., Melcher, J. R., and Oxenham, A. J. (**2004**). "A neural representation of pitch salience in nonprimary human auditory cortex revealed with functional magnetic resonance imaging," J. Neurosci. **24**, 6810–6815.
Plomp, R., and Levelt, W. (**1965**). "Tonal consonance and critical bandwidth," J. Acoust. Soc. Am. **38**, 548–560.
Riquimaroux, H. (**1995**). "How to enjoy music by the brain not by the ears: Neuronal basis of pitch extraction," RIKEN Rev. **9**, 13–14.
Riquimaroux, H., and Kosaki, H. (**1995**). "Involvement of neurons in the primary auditory cortex in pitch extraction," Absr. Assoc. Res. Otolaryngol. **18**.
Ritsma, R. (**1962**). "Existence region of the tonal residue i," J. Acoust. Soc. Am. **34**, 1224–1229.
Roberts, B., and Brunstrom, J. M. (**1998**). "Perceptual segregation and pitch shifts of mistuned components in harmonic complexes and in regular inharmonic complexes," J. Acoust. Soc. Am. **104**, 2326–2338.
Roberts, B., and Brunstrom, J. M. (**2001**). "Perceptual fusion and fragmentation of complex tones made inharmonic by applying different degrees of frequency shift and spectral stretch," J. Acoust. Soc. Am. **110**, 2479–2490.
Roberts, B., and Brunstrom, J. M. (**2003**). "Spectral pattern, harmonic relations, and the perceptual grouping of low-numbered components," J. Acoust. Soc. Am. **114**, 2118–2134.
Schechter, B., and Depireux, D. A. (**2007**). "Stability of spectro-temporal tuning over several sessions in primary auditory cortex of the awake ferret," Neuroscience **148**, 806–14.
Schreiner, C. E. and Calhoun, B. M. (**1994**). "Spectral envelope coding in the cat primary auditory cortex: Properties of ripple transfer functions," Aud. Neurosci. **1**, 39–61.
Schulze, H., Hess, A., Ohl, F., and Scheich, H. (**2002**). "Superposition of horseshoe-like periodicity and linear tonotopic maps in auditory cortex of the Mongolian gerbil," Eur. J. Neurosci. **15**, 1077–1084.
Schulze, H., and Langner, G. (**1997a**). "Periodicity coding in the primary auditory cortex of the Mongolian gerbil (Meriones unguiculatus): Two different strategies for coding pitch and rhythm," J. Comp. Physiol., A **181**, 651–663.
Schulze, H. and Langner, G. (**1997b**). "Representation of periodicity pitch in the primary auditory cortex of the Mongolian gerbil," Acta Oto-Laryngol., Suppl. **532**, 89–95.
Schwarz, D. W., and Tomlinson, R. W. (**1990**). "Spectral response patterns of auditory cortex neurons to harmonic complex tones in alert monkey (macaca mulatta)," J. Neurophysiol. **64**, 282–298.
Shamma, S. A., Versnel, H., and Kowalski, N. (**1995**). "Ripple analysis in ferret primary auditory cortex. I. Response characteristics of single units to sinusoidally rippled spectra," Aud. Neurosci. **1**, 233–254.
Sinex, D., Henderson-Sabes, J., and Li, H. (**2002**). "Responses of inferior colliculus neurons to harmonic and mistuned complex tones," Hear. Res. **168**, 150–162.
Sinex, D., Li, H., and Velenovsky, D. (**2005**). "Prevalence of stereotypical responses to mistuned complex tones in the inferior colliculus," J. Neurophysiol. **94**, 3523–37.
Srulovicz, P., and Goldstein, J. (**1983**). "A central spectrum model: A synthesis of auditory-nerve timing and place cues in monaural communication of frequency spectrum," J. Acoust. Soc. Am. **73**, 1266–1276.
Steinschneider, M., Reser, D., Fishman, Y., Schroeder, C., and Arezzo, J. (**1998**). "Click train encoding in primary auditory cortex of the awake monkey: Evidence for two mechanisms subserving pitch perception," J. Acoust. Soc. Am. **104**, 2935–2955.
Suga, N., O'Neill, W., Kujirai, K., and Manabe, T. (**1983**). "Specificity of combination-sensitive neurons for processing of complex biosonar signals in auditory cortex of the mustached bat," J. Neurophysiol. **49**, 1573–1626.
Terhardt, E. (**1974**). "Pitch, consonance, and harmony," J. Acoust. Soc. Am. **55**, 1061–1069.
Terhardt, E. (**1979**). "Calculating virtual pitch," Hear. Res. **1**, 155–182.
Tomlinson, R. W. W., and Schwartz, D. W. F. (**1988**). "Perception of the

missing fundamental in nonhuman primates," J. Acoust. Soc. Am. **84**, 560–565.
von Helmholtz, H. (**1954**). *On the Sensations of Tone as a Physiological Basis for the Theory of Music* (Dover, New York).
Warren, J. D., Uppenkamp, S., Patterson, R. D., and Griffiths, T. D. (**2003**). "Separating pitch chroma and pitch height in the human brain," Proc. Natl. Acad. Sci. U.S.A. **100**, 10038–10042.
Whitfield, I. C. (**1980**). "Auditory cortex and the pitch of complex tones," J. Acoust. Soc. Am. **67**, 644–647.
Wightman, F. L. (**1973**). "The pattern-transformation model of pitch," J. Acoust. Soc. Am. **54**, 407–416.
Zatorre, R. (**1988**). "Pitch perception of complex tones and human temporal-lobe function," J. Acoust. Soc. Am. **84**, 566–572.

Spatio-temporal quantification of vocal fold vibrations using high-speed videoendoscopy and a biomechanical model

Raphael Schwarz[a)]
Department of Communication Sciences and Disorders, University of South Carolina, Columbia, South Carolina 29208

Michael Döllinger, Tobias Wurzbacher, Ulrich Eysholdt, and Jörg Lohscheller
Department of Phoniatrics and Pediatric Audiology, University Hospital Erlangen, Medical School, Erlangen, Germany 91054

(Received 20 December 2006; revised 25 February 2008; accepted 28 February 2008)

Pathologic changes within the organic constitution of vocal folds or a functional impairment of the larynx may result in disturbed or even irregular vocal fold vibrations. The consequences are perturbations of the acoustic speech signal which are perceived as a hoarse voice. By means of appropriate image processing techniques, the vocal fold dynamics are extracted from digital high-speed videos. This study addresses the approach to obtain a parametric description of the spatio-temporal characteristics of the vocal fold oscillations for the aim of classification. For this purpose a biomechanical vocal fold model is introduced. An automatic optimization procedure is developed for fitting the model dynamics to the observed vocal fold oscillations. Thus, the resulting parameter values represent a specific vibration pattern and serve as an objective quantification measure. Performance and reliability of the optimization procedure are validated with synthetically generated data sets. The high-speed videos of two normal voice subjects and six patients suffering from different voice disorders are processed. The resulting model parameters represent a rough approximation of physiological parameters along the entire vocal folds.
© *2008 Acoustical Society of America.* [DOI: 10.1121/1.2902167]

PACS number(s): 43.70.Aj, 43.70.Bk, 43.70.Dn, 43.72.Ar [AL] Pages: 2717–2732

I. INTRODUCTION

Supporting clinical diagnosis and classification of voice pathologies by means of objective measurements is an important issue in medical voice assessment. A widely used approach is the analysis of the acoustic speech signal.[1–3] However, voice signals provide only symptomatic information about the laryngeal dysfunction. Predications about the voice disorder itself are thus ambiguous.[4]

The reasons for perturbations of the acoustic speech signal are asymmetric or even irregular vocal fold vibrations which result from pathologic changes within the organic constitution of the vocal folds or an impairment of the laryngeal function.[5,6] For evaluating the direct effect of the laryngeal pathology, the observation of the vibrating vocal folds is an important method in clinical investigation of voice abnormalities.[7,8] Using state of the art digital high-speed imaging techniques, normal and pathologic vocal fold vibrations are observable during voice production with sufficient spatial and temporal resolution.[9,10] The analysis of high-speed recorded vocal fold vibrations has proven to be useful to study pathological and normal voice production.[9] The vocal folds are delineated by appropriate image processing algorithms.[11–14] For a quantitative analysis it is useful to derive a concise description of the vocal fold dynamics from the segmentation results.

One common approach is to compute the glottal area wave form, a plot of the area of the vocal fold opening, or glottal area, as a function of time.[15,16] Using the glottal area function, oscillation amplitude and frequency are commonly analyzed, as well as the ratio between open and closed duration of the glottis.[17] As a main shortcoming, this function does not distinguish between the influence of the left and the right vocal fold. Asymmetries concerning oscillation directions, velocities and amplitudes between the dynamics of the left and the right vocal fold are not evaluated. Local disturbances of the vibration pattern due to organic disorders are not incorporated sufficiently.

Further approaches for a quantitative analysis of segmented high-speed videos are deflection measurements of the vocal fold oscillations.[11,17] Here, the time-dependent distance of a specific point on the medial vocal fold edge to the longitudinal glottal axis is extracted (single-line kymography). In this way, the dynamic of each vocal fold is described by a one-dimensional trajectory. For a direct analysis of these trajectories, symmetry measures such as amplitude ratio or phase shift between left and right oscillation are introduced.[9,18] An alternative for evaluating the deflection measurements is a model-based approach.[6,19] The vocal fold dynamics can be reproduced with lumped-element models, such as the so-called two-mass model (2MM).[20] By means of automatic parameter optimization, the model oscillations are fitted to the bilateral motion curves.[19,21,22] The optimized model parameters enable an objective quantification of the vocal fold dynamics. The model-based method is advanta-

[a)]Author to whom correspondence should be addressed. Electronic mail: raphael.r.schwarz@googlemail.com

geous, as besides temporal oscillation properties like frequency, amplitude, and phase, also the specific wave forms of the oscillations are incorporated for the quantification. Additionally, the resulting model configurations facilitate further research into normal and pathologic human voice production by means of model simulations.[23] The model-based approach was successfully applied for an objective classification of vocal fold vibrations.[21,22]

Besides left-right asymmetries, alteration of wave forms also in longitudinal direction are observable as a consequence of voice disorders (e.g., due to organic impairments of the vocal folds). For analyzing such vibration patterns the deflection measurements by means of single-line kymography need to be extended. In Tigges *et al.*[24] and Neubauer *et al.*[10] the distances of the vocal fold edges from the longitudinal glottal axis are evaluated at multiple specific points (multi-line kymography). In this way a set of one-dimensional trajectories is obtained, describing the vocal fold vibrations at different points along each vocal fold. One method to analyze the trajectories is the evaluation of different symmetry measures.[25] In this way, amplitude differences and phase shifts between the left and the right vocal fold for the multiple longitudinal positions are evaluated. However, details concerning the time-varying shape of the vocal fold edges are not incorporated.

In this work a new model-based approach is proposed to enable an objective quantification of vocal fold vibration patterns that also takes longitudinal vibration modes into account. The so-called multi-mass model (MMM) based on Wong *et al.*,[26] a longitudinal extension of the 2MM as used in Schwarz *et al.*[21] and Wurzbacher *et al.*,[22] is introduced. Compared to other complex and high-dimensional models, ranging from multi-mass models with different surface modeling[27,28] to finite-element approaches,[29,30] the MMM allows to describe the pathologic vocal fold vibrations using only a limited parameter set.[26,31,32] This property enables a parameter optimization with suitable computing time. The MMM is combined with a new automatic optimization procedure based on a genetic algorithm. The performance of the model-based approach is validated with synthetic and clinical data sets. It is shown, that besides a spatio-temporal quantification, the proposed method allows to infer an estimation of physiological vocal fold parameters.

II. METHODS

A. Videoendoscopy and clinical data

High-speed videos are recorded during stationary sustained phonation of a vowel /a/ in a comfortable way (stationary phonation paradigm). The vocal fold vibrations are observed from a top-view position with a digital high-speed camera system (High-Speed Endocam, Wolf Corp., Knittlingen, Germany, temporal resolution 4000 frames/s, spatial resolution 256×256 pixels) which is coupled to a rigid endoscope, illuminated by a 250 W Xe light. Figure 1 shows the recording situation (left) and a single image from a high-speed video (right). From each high-speed video a sequence of $N=351$ frames (87.5 ms) is evaluated. The vocal fold edges are segmented, using the method after Lohscheller *et al.*[14] Within Fig. 1 (right) the segmented vocal fold edges are depicted as a dotted white line. The opening between the vocal folds is called glottis with opening area $a_v[n]$ for frame n. Posterior (pc) and anterior commissure (ac) mark the dorsal and ventral endings of the glottal axis. Within the short intervals of a high-speed sequence (less than 100 ms), changes of the vocal fold length are negligible due to the stationary phonation paradigm. Thus, the distance between the anterior and posterior commissure can be assumed to be constant during the evaluated sequence. In Fig. 1 (right), the points $\mathbf{g}_j$, with $j=1,\ldots,3$, are positioned at 25%, 50%, and 75% of the glottal axis length, starting from the posterior commissure. The dashed lines k_j are perpendicular to the glottal axis (intersection points $\mathbf{g}_j$). The intersection points $\mathbf{p}_j$ (right vocal fold) and $\mathbf{p}_{j+3}$ (left vocal fold), $j=1,\ldots,3$, of the vocal fold edges and the lines k_j are determined in each frame. For frame n, the distances $c_{v,j}[n]$ (right vocal fold) and $c_{v,j+3}[n]$ (left vocal fold) are calculated after

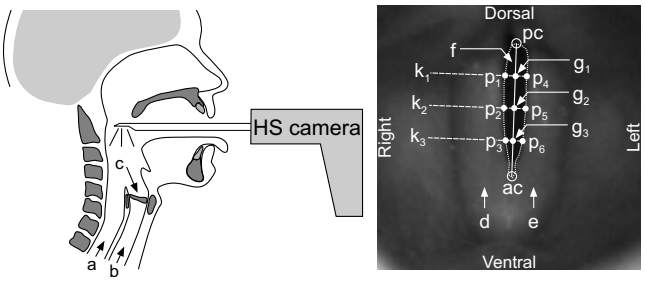


FIG. 1. Laryngeal high-speed videoendoscopy. Left: a rigid 90° endoscope connected to a digital high-speed camera is placed into the oropharynx (a–esophagus, b–trachea, c–vocal folds). Right: single image from a high-speed video (d,e–right and left vocal fold, f–glottis, ac–anterior commissure, pc–posterior commissure). The segmented vocal fold edges (dotted white line) and the glottal axis (solid white line from ac to pc) are shown.

$$c_{v,j}[n]=(-1)^{\kappa}\|\mathbf{p}_j-\mathbf{g}_j\|_2, \tag{1}$$

$$c_{v,j+3}[n]=(-1)^{\kappa+1}\|\mathbf{p}_{j+3}-\mathbf{g}_j\|_2, \tag{2}$$

with

$$\kappa=\begin{cases}1, & \text{mass crosses glottal axis}\\ 2, & \text{otherwise}\end{cases}. \tag{3}$$

In the sense of multi-line kymography, the vocal fold deflections are described by the *experimental curves* comprising the one-dimensional trajectories $c_{v,i}[n]$ and the glottal area function $a_v[n]$, with $i=1,\ldots,6$ and $n=1,\ldots,N$.

A reduced quality of the endoscopic images results in errors of the segmentation process. The applied image processing algorithm uses a threshold value to decide whether a certain pixel is part of the glottis or the vocal fold edges. If the transition between the glottis and the vocal folds is blurred within the high-speed data, the uncertainty of the edge segmentation increases. This uncertainty takes effect on the amplitudes of the extracted experimental curves. In this study, the typical deflection at medial position is about 10 pixels. The accuracy of the segmentation algorithm is about 1.5 pixel in lateral direction,[14] i.e., the relative segmentation error ϵ_s is about 15%. This error is mainly due to

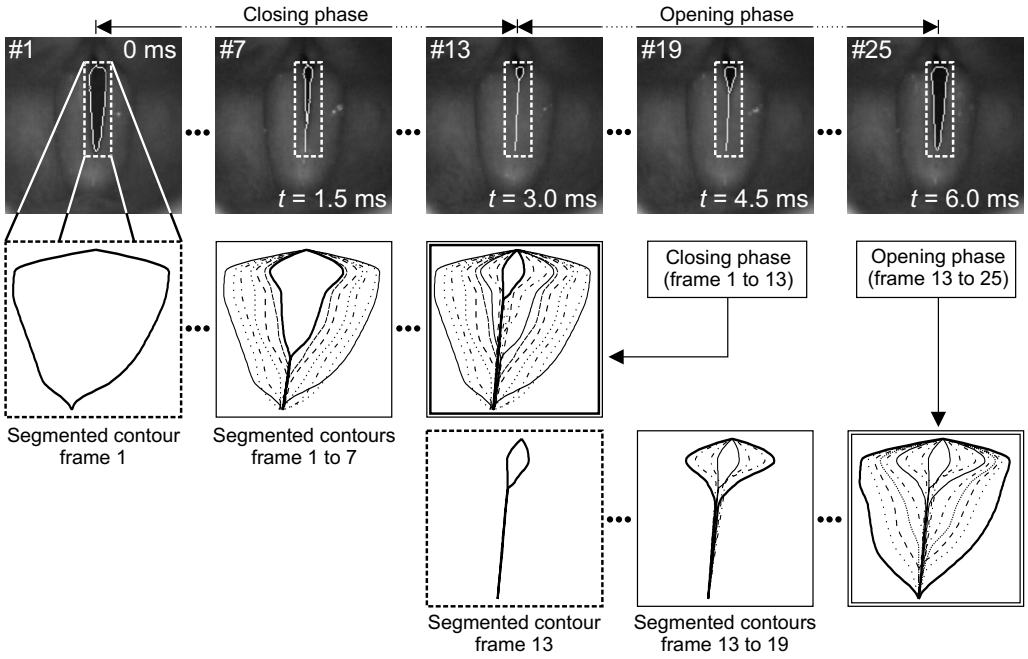


FIG. 2. Image sequence from a digital high-speed video. An oscillation cycle for normal vocal fold vibration is shown (first row). An alternative illustration of the vocal fold dynamics is depicted in the second (closing phase) and the third (opening phase) row.

the limited spatial resolution of the charge coupled device chip of the camera rather than from inaccurate segmentation of the glottal edges.

Figure 2 (first row) depicts an oscillation cycle in case of normal voice. The segmentation result is shown as a white line in each image. Here, the cycle starts with a maximum opening (frame 1). The glottal closing occurs with a longitudinal phase shift starting from the ventral part of the vocal folds (frame 7, after 1.5 ms). The minimum glottal area is achieved after 3 ms with a minor glottal closure insufficiency at the dorsal end (frame 13). After 6 ms the maximum opening is reached again (frame 25). The lower two rows show the construction of a compact illustration of the vocal fold dynamics. The first image of the second row represents the segmented contour of the first frame. The subsequent segmentation results are also drawn in the same figure (second image). In the third image (doubled border) the contours of the whole closing phase are depicted. For the opening phase, a second image is produced in the same way (third row). The resulting figure for the closing phase is shown in the third image of the third row. In the following, this compact illustration is used to represent the spatio-temporal characteristics of clinical data.

Within this study high-speed videos from two normal voice subjects (S1, S2) and six subjects (S3–S8) suffering from voice disorders are evaluated. Figures 3 and 4 give a survey of the corresponding vibration patterns. The left column shows a closing phase from each video. For subject S1, the sampling points of the trajectory $c_{v,2}$ (i.e., the dynamics of the right vocal fold at medial position) derived from the segmented contours are shown. For S1–S8 the intersection points $\mathbf{p}_2[n]$ of line k_2 and the right vocal fold edge are shown. The right column depicts the opening phase. It follows a brief description of the specific vibration characteristics:

- **S1**. Normal male voice. Left and right vocal fold oscillation are almost symmetric with respect to the glottal axis. Duration $\Delta t_c = 2.5$ ms of the closing phase is greater than the opening phase duration $\Delta t_o = 1.5$ ms. The glottal closure starts at the ventral end.
- **S2**. Normal female voice. Left and right vocal fold oscillation are almost symmetric. The closing phase is slightly longer ($\Delta t_c = 2.5$ ms) than the opening phase ($\Delta t_o = 2.0$ ms). The glottal closure starts at the ventral end. There is a glottal closure insufficiency at the dorsal end.
- **S3**. Functional dysphonia. The vibrational amplitude of the left vocal fold is reduced. The glottal closure is insufficient.
- **S4**. Unilateral paralysis (right sided). The glottal closure is insufficient and there is a phase shift between the left and right vocal fold oscillation. The left vocal fold reveals a longitudinal vibration mode.
- **S5**. Spasmodic dysphonia. The vocal fold oscillations are almost symmetric as for the normal voice subjects. However, spasms cause the vocal folds to slam together and stiffen. As a consequence Δt_c and Δt_o are decreased (1.0 and 0.75 ms, respectively) compared to the duration of the glottal closure (2.25 ms). The glottis is closed for more than half of the oscillation cycle.
- **S6**. Vocal fold scar (right sided). The right vocal fold shows a longitudinal vibration mode. The right oscillation amplitude is decreased compared to the left side. The du-

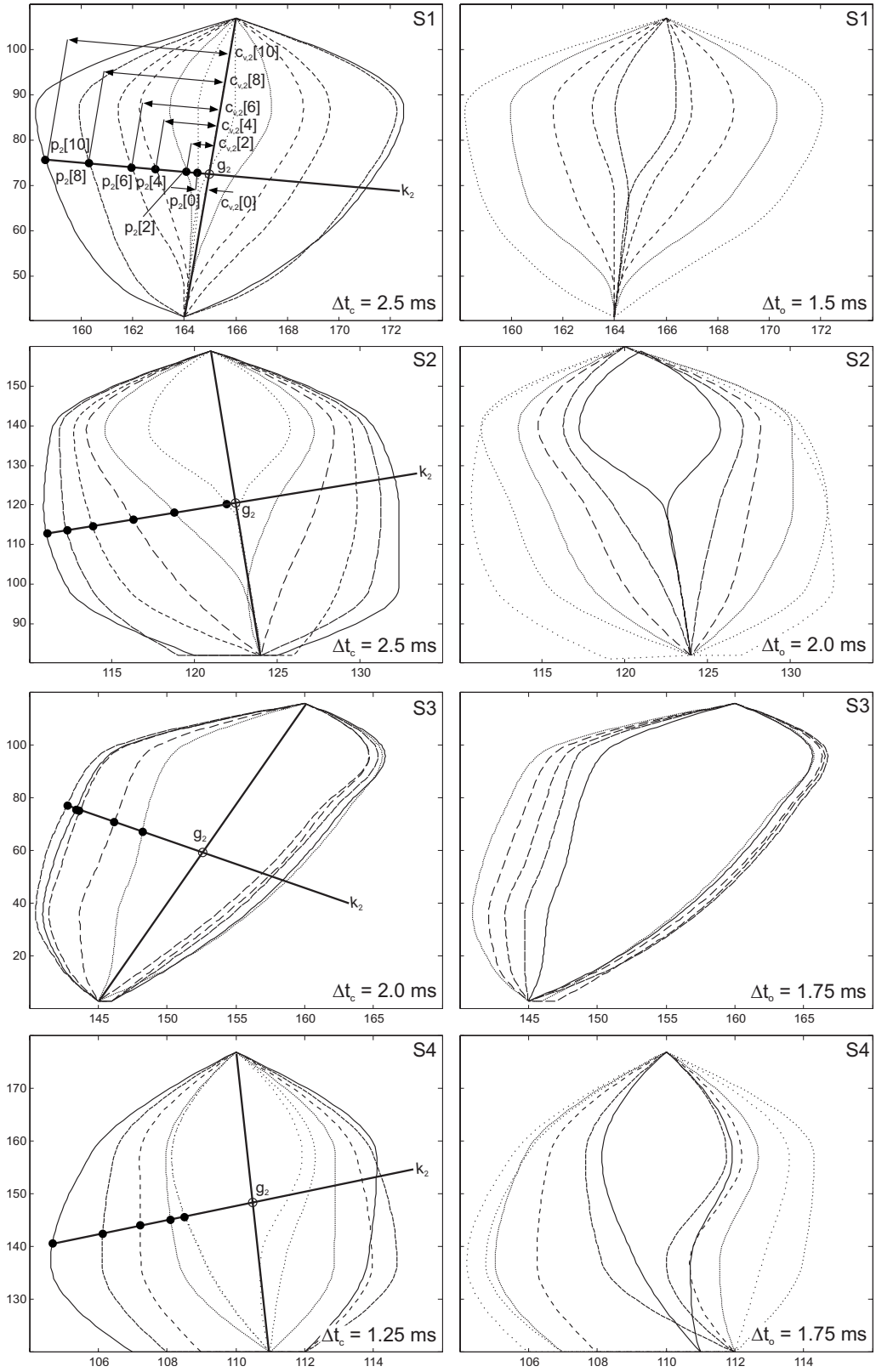


FIG. 3. Vocal fold vibration patterns for the subjects S1–S4. The left column shows the closing phase (duration Δt_c), the right column the opening phase (duration Δt_o). For subject S1, the sampling points of the experimental trajectory $c_{v,2}$ extracted during the closing phase from even-numbered frames are depicted.

ration of the glottal closure is short (0.5 ms) compared to the opening and closing phase (1.5 ms each).

- **S7**. Reinke's edema. The edema at the ventral end of the right vocal fold decreases the right oscillation amplitude. The glottal closure at the dorsal end is insufficient.
- **S8**. Nodules. The nodules are at medial position, symmetrical on both vocal folds. The glottal closure at the dorsal end is insufficient.

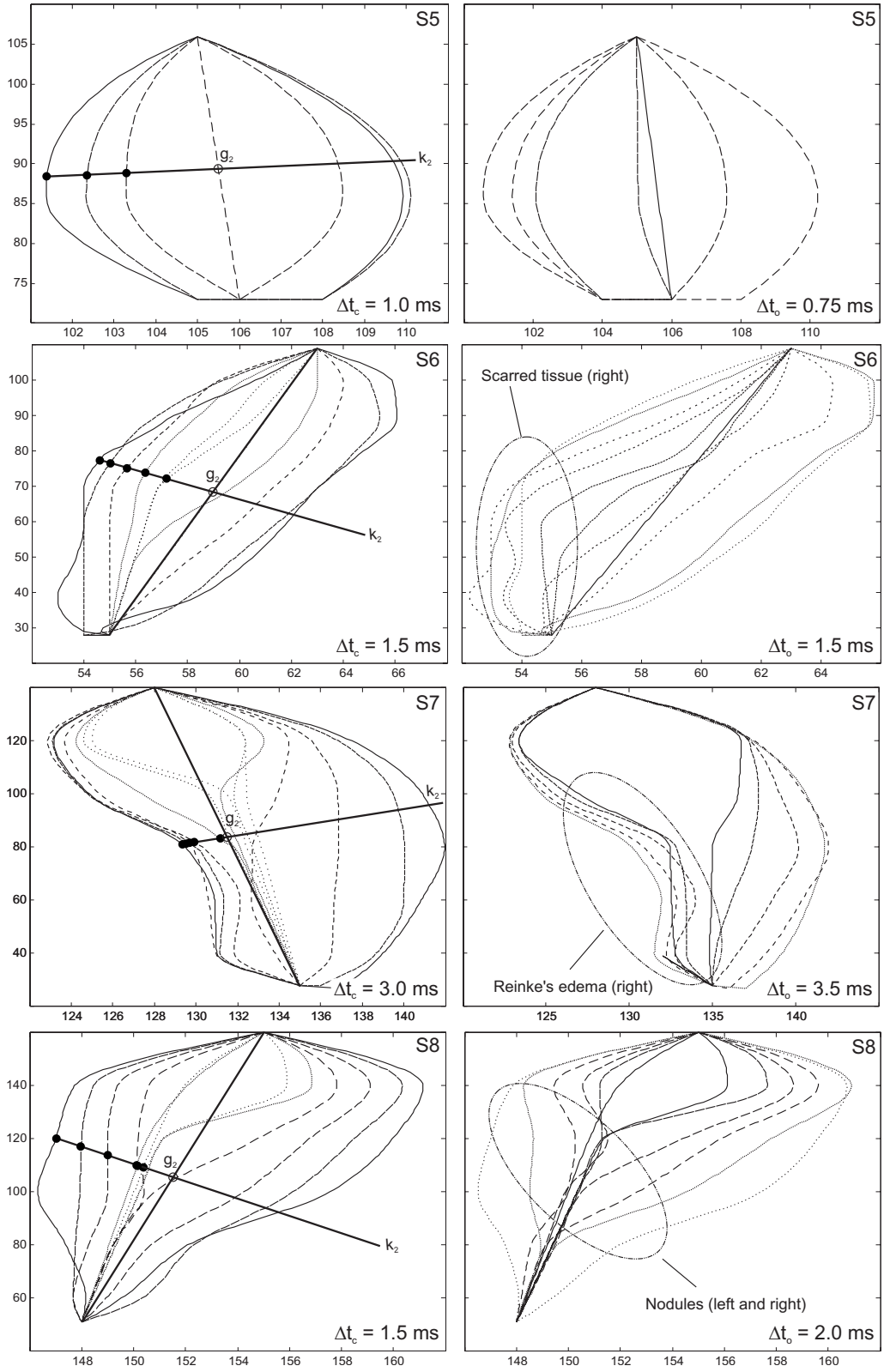


FIG. 4. Vocal fold vibration patterns for the subjects S5–S8. The left column shows the closing phase, the right column the opening phase.

B. Multi-mass model

For modeling the vocal fold dynamics a multi-mass model (MMM), similar to the model proposed in Wong *et al.*[26] (hereafter called the WO91 model), is used. Figure 5 shows a perspective view of the MMM. The coupled mass-spring oscillators numbered with $i=1,\ldots,6$ are the vibrating elements. In accordance to the view from the high-speed videos, the elements on the left ($i=1,\ldots,3$) model the dynamics of the right vocal fold, the elements on the right ($i=4,\ldots,6$) model the left vocal fold vibrations. Towards the posterior commissure, the vibrating elements are coupled to two fixed positions. These fixed positions correspond to the

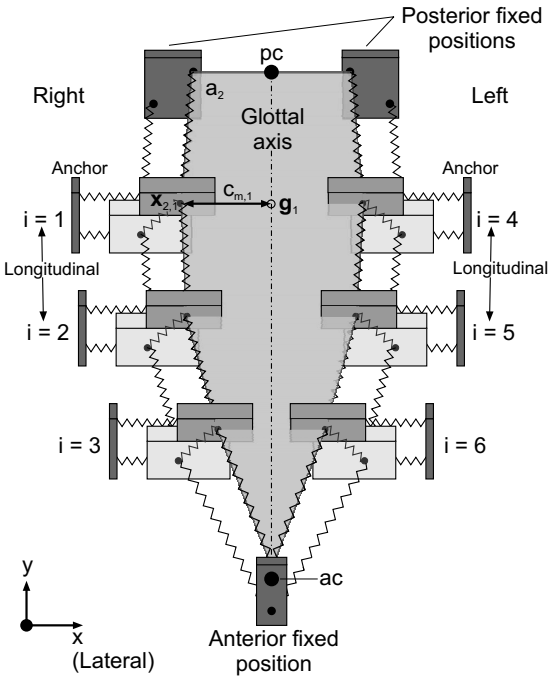


FIG. 5. Schematic representation of the multi-mass model of the vocal folds. The left model side represents the right vocal fold, the right side the left vocal fold. The minimum opening formed by the positions of the masses and fixed positions of both planes represents the glottal area (a_2). Posterior (pc) and anterior commissure (ac) define the glottal axis.

stiffened nonvibrating transition between the vocal cord and the arytenoid cartilage, the so-called vocal process.[33] At the ventral ending of the glottis the two model sides join together at a single fixed position (anterior commissure). In the following, the indices $s=1$ and $s=2$ denote the lower and the upper horizontal model plane. The vector $\mathbf{x}_{s,i}=(x_{s,i},y_{s,i})^T$, where $(\cdot)^T$ denotes the transposed vector, defines the position of the mass element $m_{s,i}$, with velocity $\dot{\mathbf{x}}_{s,i}$ and acceleration $\ddot{\mathbf{x}}_{s,i}$. Together with the fixed positions, the mass positions $\mathbf{x}_{s,i}$ define the model opening $a_s[n]$ of the horizontal plane s for the nth time step.

Compared to the WO91 model the following extensions are introduced for the MMM:

1. Besides different values of the anchor spring constances along each model side, variations of the longitudinal coupling stiffnesses are also considered.
2. The mass elements are allowed to move within the whole xy plane in longitudinal and lateral directions. This means a fully two-dimensional extension of the WO91 model.
3. The flow is calculated for the entire opening formed by the mass positions in each horizontal plane. Within the WO91 model, the glottal air flow is constricted to the sum of the parallel flows through each opposing pair of mass-spring oscillators.

The first extension is introduced to model alterations of the longitudinal stiffness within the vocal fold tissue, especially due to local tissue impairments. The applied image processing algorithm delivers a two-dimensional projection of the vocal fold movements. Following the second extension these

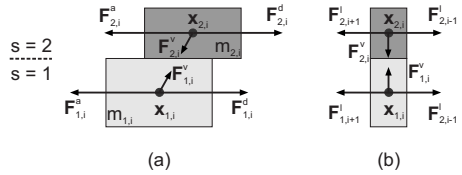


FIG. 6. Free body diagram of an oscillating element in lateral view (a) and frontal view (b).

movements can be reproduced by the MMM. The third extension of the WO91 model is necessary due to the second extension.

The equation of motion for a mass element $m_{s,i}$ is defined as

$$\mathbf{0}=m_{s,i}\ddot{\mathbf{x}}_{s,i}+\mathbf{F}^a_{s,i}+\mathbf{F}^v_{s,i}+\mathbf{F}^l_{s,i}+\mathbf{F}^c_{s,i}+\mathbf{F}^d_{s,i} \tag{4}$$

with the following forces:

$\mathbf{F}^a_{s,i}$ – force due to the anchor spring,

$\mathbf{F}^v_{s,i}$ – vertical coupling force,

$\mathbf{F}^l_{s,i}$ – longitudinal coupling force,

$\mathbf{F}^c_{s,i}$ – force due to collision with other masses or longitudinal coupling springs,

$\mathbf{F}^d_{s,i}$ – driving force generated by glottal flow.

Figure 6 shows a free body diagram of a single oscillator element with the acting forces. Compared with the WO91 model a more general definition of the forces is required according to the two-dimensional model extensions.

1. Anchor force

With stiffness $k^a_{s,i}$ and damping $r^a_{s,i}$ of the anchor spring as well as the rest position $\mathbf{x}^r_{s,i}$ of mass $m_{s,i}$ the anchor force $\mathbf{F}^a_{s,i}$ is defined as

$$\mathbf{F}^a_{s,i}:=k^a_{s,i}\|\mathbf{x}^r_{s,i}-\mathbf{x}_{s,i}\|_2\mathbf{u}^a_{s,i}+r^a_{s,i}(\mathbf{u}^a_{s,i})^T\dot{\mathbf{x}}_{s,i}\mathbf{u}^a_{s,i}. \tag{5}$$

For the definition of the unit vector $\mathbf{u}^a_{s,i}$, see Fig. 7.

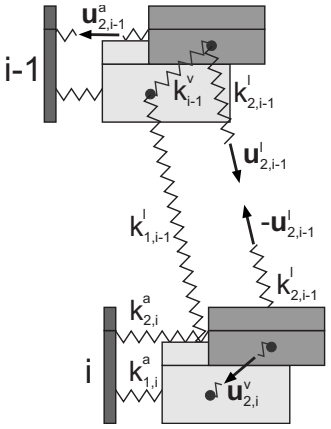


FIG. 7. Graphical definition of the unit vectors $\mathbf{u}^a_{s,i}$, $\mathbf{u}^l_{s,i}$, and $\mathbf{u}^v_{s,i}$ for the anchor force, longitudinal and vertical coupling.

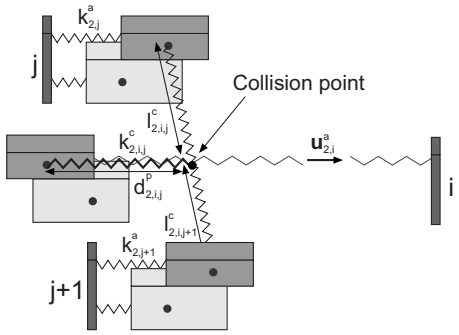


FIG. 8. Illustration of a single impact within the multi-mass model.

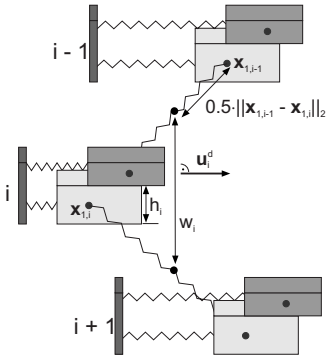


FIG. 9. Graphical definition of the unit vector $\mathbf{u}_{s,i}^{d}$ and the effective side length w_i for the driving force.

2. Vertical coupling force

The vertical coupling force $\mathbf{F}_{s,i}^{v}$ is calculated after

$$\mathbf{F}_{s,i}^{v} := k_i^{v}(\|\mathbf{x}_{s,i}^{r} - \mathbf{x}_{s^*,i}^{r}\|_2 - \|\mathbf{x}_{s,i} - \mathbf{x}_{s^*,i}\|_2)\mathbf{u}_{s,i}^{v} + r_i^{v}(\mathbf{u}_{s,i}^{v})^T(\dot{\mathbf{x}}_{s,i} - \dot{\mathbf{x}}_{s^*,i})\mathbf{u}_{s,i}^{v} \quad (6)$$

with the stiffness and damping coefficients k_i^{v} and r_i^{v} of the vertical coupling spring connecting masses $m_{1,i}$ and $m_{2,i}$. Index $s^*=1$ for $s=2$, otherwise $s^*=2$ is used. For the definition of the unit vector $\mathbf{u}_{s,i}^{v}$, see Fig. 7.

3. Longitudinal coupling force

The force $\mathbf{F}_{s,i}^{l}$ acting on mass $m_{s,i}$ due to the longitudinal coupling to $m_{s,i-1}$ and $m_{s,i+1}$ is defined as

$$\begin{aligned}\mathbf{F}_{s,i}^{l} := {} & k_{s,i-1}^{l}(\|\mathbf{x}_{s,i}^{r} - \mathbf{x}_{s,i-1}^{r}\|_2 - \|\mathbf{x}_{s,i} - \mathbf{x}_{s,i-1}\|_2)(-\mathbf{u}_{s,i-1}^{l}) \\ & + r_{s,i-1}^{l}(-\mathbf{u}_{s,i-1}^{l})^T(\dot{\mathbf{x}}_{s,i} - \dot{\mathbf{x}}_{s,i-1})(-\mathbf{u}_{s,i-1}^{l}) \\ & + k_{s,i}^{l}(\|\mathbf{x}_{s,i}^{r} - \mathbf{x}_{s,i+1}^{r}\|_2 - \|\mathbf{x}_{s,i} - \mathbf{x}_{s,i+1}\|_2)\mathbf{u}_{s,i}^{l} \\ & + r_{s,i}^{l}(\mathbf{u}_{s,i}^{l})^T(\dot{\mathbf{x}}_{s,i} - \dot{\mathbf{x}}_{s,i+1})\mathbf{u}_{s,i}^{l}, \end{aligned} \quad (7)$$

where $k_{s,i-1}^{l}$, $k_{s,i}^{l}$ and $r_{s,i-1}^{l}$, $r_{s,i}^{l}$ are the stiffness and damping coefficients of the longitudinal coupling springs, see Fig. 7.

4. Collision force

In case of collision an additional restoring force $\mathbf{F}_{s,i}^{c}$ acts on the mass $m_{s,i}$.[34] A collision is defined for $m_{s,i}$ if its anchor spring crosses the longitudinal coupling spring between two adjacent masses $m_{s,j}$ and $m_{s,j+1}$, as illustrated in Fig. 8. For the general case that $m_{s,i}$ causes more than one collision, the resulting collision force is given by

$$\mathbf{F}_{s,i}^{c} := \sum_{\forall j} k_{s,i,j}^{c} d_{s,i,j}^{p} \mathbf{u}_{s,i}^{a}, \quad (8)$$

with the stiffness of the restoring spring $k_{s,i,j}^{c}$ and the penetration depth $d_{s,i,j}^{p}$, defined as in Fig. 8. Derived from the 2MM[35] $k_{s,i,j}^{c}$ is calculated after

$$k_{s,i,j}^{c} := 3 \cdot \left(\frac{l_{s,i,j}^{c}}{l_{s,i,j}^{c} + l_{s,i,j+1}^{c}} k_{s,j}^{a} + \frac{l_{s,i,j+1}^{c}}{l_{s,i,j}^{c} + l_{s,i,j+1}^{c}} k_{s,j+1}^{a} \right), \quad (9)$$

where $l_{s,i,j}^{c}$ denotes the distance between the collision point and the position of the mass $m_{s,j}$, see Fig. 8.

5. Driving force

$\mathbf{F}_{s,i}^{d}$ is the driving force for the self-sustained MMM oscillation. It results from the pressure drop within the glottis. As the air flow is calculated for the entire model opening, the calculation of $\mathbf{F}_{s,i}^{d}$ differs from the definition in the WO91 model. The aerodynamic forces are described by the Bernoulli law and based on the following assumptions:[19,21–23,36,37]

- The subglottal pressure P^{sub} and the supraglottal pressure P^{supra} are constant with $P^{\text{supra}}=0$.[35]
- The interaction of the glottal flow with the subglottal and supraglottal vocal tract is neglected.[23,36]
- Pressure drop due to viscous losses within the glottis is neglected.[28]
- The Bernoulli force acts only below the narrowest part of the constriction and therefore only within the lower plane of the MMM.[19,38]

Following these assumptions the driving force is calculated as

$$\mathbf{F}_{s,i}^{d} = \begin{cases} P \cdot w_i \cdot h_i \cdot \mathbf{u}_i^{d}, & s=1 \\ \mathbf{0}, & s=2 \end{cases}, \quad (10)$$

with the height h_i of mass $m_{1,i}$ and the effective side length

$$w_i = \tfrac{1}{2} \cdot \|\mathbf{x}_{s,i+1} - \mathbf{x}_{s,i-1}\|_2. \quad (11)$$

The unit vector $\mathbf{u}_i^{d}$ indicates the direction of $\mathbf{F}_{s,i}^{d}$, see Fig. 9. The pressure P within the lower plane is calculated in accordance to Steinecke and Herzel[35] as

$$P = \begin{cases} P^{\text{sub}} \cdot \left(1 - \left(\dfrac{\min(a_1,a_2)}{a_1}\right)^2\right), & a_1 > 0 \\ 0, & a_1 \leqslant 0 \end{cases}. \quad (12)$$

The driving pressure P depends on the ratio of the areas a_s.

For the integration of the equations of motion a fourth-order Runge-Kutta algorithm is used. The step size is set to 0.25 ms. Due to the sampling frequency of the high-speed camera of 4000 frames/s no resampling is needed. The model runs with a computing time to real-time ratio of almost 1:1 (C# Pentium 4, 3 GHz).

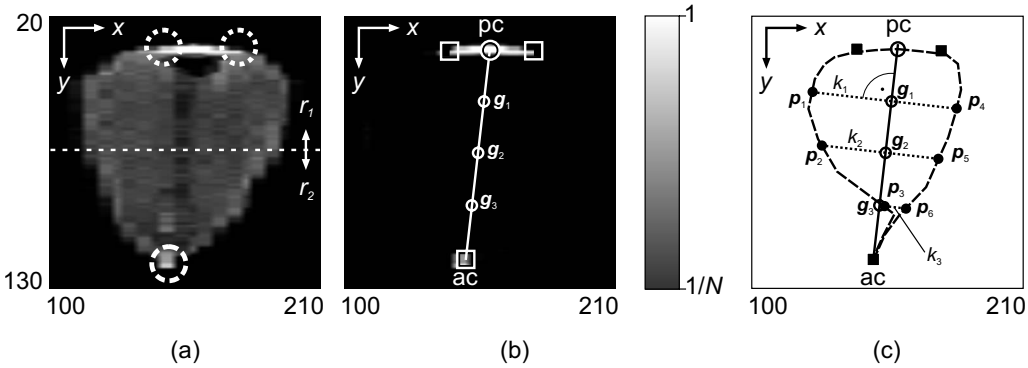


FIG. 10. (a) Representation of the histogram matrix H. The estimated positions of the anterior commissure (dashed circle) and the vocal processes (dotted circles) are shown. (b) Segmented regions at the anterior and the posterior commissure. The white squares represent the identified coordinates for the three fixed positions. The points $\mathbf{g}_j$ mark the dorsal, medial, and ventral position on the glottal axis. (c) The rest positions $\mathbf{p}_i$ for the oscillating elements are derived from the glottal contour with mean opening area (dashed line).

C. Automatic parameter optimization

The optimization procedure is constructed to simulate real vocal fold vibrations as exact as possible. For this aim, a model initialization, optimization parameters and an objective function consisting of two measures evaluating the fitting quality to the vocal fold vibrations are introduced in the following. The optimization parameters which result into the best fitting represent a quantitative description of the vocal fold vibrations patterns.

1. Model initialization

Precondition for the parameter optimization is a proper initialization of the MMM depending on the evaluated high-speed video. The applied image processing algorithm delivers the time-variant glottal contour but no information about the positions of the left and right vocal process which correspond to the two fixed positions near the posterior ending of the MMM. Also the anterior commissure where both vocal folds merge together is not determined. These fixed positions and subsequently the rest positions $\mathbf{x}_{s,i}^r$ for the masses are calculated with the following procedure: A histogram matrix $H(x,y)$ with 256×256 entries is derived from the segmentation results. The value of each entry $H(x,y)$ equals the number of time steps in which the corresponding pixel position (x,y) is part of the segmented glottal contour, normalized to the number of time steps N. For the pixel coordinates which are not passed by vocal fold edges the matrix entry is 0. Figure 10(a) depicts the matrix H for the high-speed video from a healthy voice subject (see Fig. 2). The black areas show the pixels which never belong to the segmented contour. The triangular-shaped region comprises the pixels contacted by the glottal edges during vocal fold oscillations. The boundary to the black area marks the maximum opening of the glottal area. The positions of the anterior commissure (dashed circle at the lower tip of the glottal area) as well as the left and right vocal process (dotted circles at the upper boundary of the glottal area) are represented by increased values within H. Thus, the characteristic positions can be identified by segmenting these parts of H which show maximum matrix entries. For this purpose, H is subdivided in the regions r_1 and r_2 as shown in Fig. 10(a). By definition the posterior commissure is located in r_1 while the anterior commissure can be found in r_2. Within each region a specific maximum $\eta_l=\max(H(x,y))$ with $(x,y)\in r_l$ and $l\in\{1,2\}$ occurs. Using threshold $\tau=\min(\eta_1,\eta_2)$, i.e., $H(x,y)=0$ if $H(x,y)<\tau$, the Matrix H can be segmented resulting in Fig. 10(b). Here, only matrix elements remain which are located near the posterior and anterior commissure. The pixel with minimum x within r_1 is used for the left posterior fixed position and the pixel with maximum x for the right one. The posterior commissure (pc) is on half way between these two points. The pixel with maximum y within r_2 defines the anterior commissure (ac). The three points $\mathbf{g}_j$ are defined as in Sec. II A. The frame n^* with the glottal area nearest to the mean opening is identified after

$$n^* = \underset{n}{\operatorname{argmin}} \left| a_u[n] - \frac{1}{N}\sum_{k=1}^{N} a_u[k] \right|. \tag{13}$$

Using the segmentation result of frame n^*, the contour points $\mathbf{p}_i$, $i=1,\ldots,6$, are determined, see Fig. 10(c). The initial rest positions of the upper plane are assigned with $\mathbf{x}_{2,i}^r-\mathbf{p}_i$ $(i=1,\ldots,6)$ and for the lower plane following

$$\mathbf{x}_{1,i}^r = \begin{cases} \begin{pmatrix} 0.95\cdot x_{2,i}^r \\ y_{2,i}^r \end{pmatrix}, & i=1,\ldots,3 \\ \begin{pmatrix} 1.05\cdot x_{2,i}^r \\ y_{2,i}^r \end{pmatrix}, & i=4,\ldots,6 \end{cases}. \tag{14}$$

2. Optimization parameters

Certain vibration patterns of the MMM can be simulated by means of modifying specific model parameters. According to model-based approaches[19,21,22] the variable model parameters are P^{sub}, $m_{s,i}$, $k_{s,i}$ and the rest positions $\mathbf{x}_{s,i}^r$. These variable model parameters are initialized by the standard parameter values as used in the WO91 model. A set of eight optimization parameters Q_p, $Q_1,\ldots,Q_6$, and Q_r is defined for modifying the standard values. By means of this set the actual model parameters $\hat{P}^{\text{sub}}$, $\hat{m}_{s,i}$, $\hat{k}_{s,i}$ and rest positions $\hat{\mathbf{x}}_{s,i}^r$ are derived from the initial values as follows:[19,21,22]

$$\hat{P}^{\text{sub}} = P^{\text{sub}}\cdot Q_p, \tag{15}$$

$$\hat{m}_{s,i} = m_{s,i}/Q_i, \tag{16}$$

$$\hat{k}_{s,i} = k_{s,i} \cdot Q_i, \tag{17}$$

$$\hat{\mathbf{x}}^r_{s,i} = \begin{pmatrix} g_{x,i} \mp Q_r \cdot |g_{x,i} - x^r_{s,i}| \\ y^r_{s,i} \end{pmatrix}, \quad \text{with } \mathbf{g}_i = \begin{pmatrix} g_{x,i} \\ g_{y,i} \end{pmatrix}. \tag{18}$$

In Eq. (18) the "−" sign is used for $i=1,\ldots,3$ and "+" for $i=4,\ldots,6$. The scaling of upper and lower springs and masses with Q_i couples four model parameters in one single optimization parameter for each oscillating element. The reciprocal coupling of spring stiffness and magnitude of mass was proposed and justified in former works.[19,31] In this way, the number of free optimization parameters is reduced, which assures a unique association between Q_i and the model dynamics.[39]

3. Objective function

For evaluating the adaptation quality achieved with the parameters $\hat{P}^{\text{sub}}$, $\hat{m}_{s,i}$ and $\hat{k}_{s,i}$, the consistency between the dynamics of the MMM and the vocal folds needs to be quantitatively described. For this aim first the model dynamics needs to be described in a way comparable with the vocal fold dynamics, i.e., *theoretical curves* have to be defined in accordance with the experimental curves. Second, criteria are defined for comparing the model dynamics with the vocal fold oscillations.

3.1 Definition of the theoretical curves

In this work the vocal fold dynamics is captured by means of the time-varying contours of the segmented glottis, see Fig. 2. These two-dimensional vibration patterns are presented in the model as time-variant polygons. The polygons are spanned by the anterior and posterior fixed positions and the mass positions $\mathbf{x}_i$ of the plane s with minimum opening, calculated after

$$\mathbf{x}_i[n] = \begin{cases} \mathbf{x}_{1,i}[n], & \text{for } a_1[n] < a_2[n] \\ \mathbf{x}_{2,i}[n], & \text{otherwise} \end{cases}. \tag{19}$$

From these polygons with opening area $a_m[n] = \min(a_1[n], a_2[n])$, one-dimensional model trajectories $c_{m,i}[n]$ with $i=1,\ldots,6$ and $n=1,\ldots,N$ are derived as described for the vocal folds, see Eqs. (1)–(3) and Fig. 1. Opening area a_m and trajectories $c_{m,i}$ define the theoretical curves.

3.2 Comparison between model dynamics and vocal fold dynamics

For quantifying the consistency between experimental and theoretical curves, two criteria are defined:

1. **Area consistency measure**. The energy Δa of the difference between the area functions of the MMM $a_m[n]$ and the vocal folds $a_v[n]$, $n=1,\ldots,N$, normalized to the energy of $a_v[n]$ is calculated after

$$\Delta a = \frac{\frac{1}{N}\Sigma_{n=1}^{N}(|a_m[n] - a_v[n]|)^2}{\frac{1}{N}\Sigma_{n=1}^{N}(|a_v[n]|)^2}. \tag{20}$$

2. **Trajectory consistency measure**. For each position i the trajectory $c_{m,i}$ is compared with the trajectory of the corresponding point at the vocal fold edge $c_{v,i}$ and the energy of the difference signal is calculated after

$$\Delta c_i = \frac{1}{N}\sum_{n=1}^{N}(|c_{m,i}[n] - c_{v,i}[n]|)^2,$$

$$\Delta c = \frac{\frac{1}{6}\Sigma_{j=1}^{6}\Delta c_j}{\frac{1}{6}\Sigma_{k=1}^{6}\frac{1}{N}\Sigma_{n=1}^{N}(|c_{v,k}[n]|)^2}, \tag{21}$$

with Δc normalized to the mean energy of the trajectories $c_{v,i}$.

For bounding the ranges of the two measures, the function $f(x)$ is introduced as

$$f(x) := \begin{cases} x, & 0 \leqslant x \leqslant 1 \\ 1, & x > 1 \end{cases}. \tag{22}$$

By means of $f(x)$ the values Δa and Δc are limited to values $\leqslant 1$. The two measures are combined to the objective function ϕ:

$$\phi := f(\Delta a) + f(\Delta c). \tag{23}$$

The smaller the value ϕ the better is the achieved fitting of the model oscillations to the vocal fold vibrations. In the following a method is introduced which uses the optimization parameters and the objective function ϕ for an automatic fitting of the model dynamics.

4. Optimization procedure

The objective function ϕ is a nonconvex function within the search space spanned by the introduced optimization parameters. Stochastic sampling methods as genetic algorithms (GA) are an appropriate technique solving optimization problems with such objective functions.[40,41] Therefore, the proposed procedure for the parameter optimization is based on a GA and in principle works as follows:[41]

1. Optimization parameters—the interface between GA and the variable model parameters—are combined in a group herein after referred to as *individual*. A set of M individuals forms the actual *population*.
2. Using the parameters of an individual, the variable model parameters are calculated from the standard values and a simulation is carried out with the modified MMM. This step is performed for each member of the population.
3. The match between the resulting model dynamics and the vocal fold vibrations is quantified with the objective function.
4. Using the parameter values of the individuals and their corresponding values of the objective function, the GA calculates the new population. This procedure is iterated from step 2 until a termination condition is fulfilled. The

fittest individual of the final population, i.e., the individual which results in the best adaptation, is the optimization result.

A general description of genetic algorithms can be found in Goldberg.[40] The termination of the optimization procedure can be obtained in two ways. Either a maximum number of iterations is passed through or all individuals of the actual population are located close to the fittest one. Due to the negligible diversity of the population the GA generates no more individuals with significantly differing values for the optimization parameters. Improvements for the fitness values no longer occur.

Applied in the described manner, the GA delivers no unique results, because of the extensive search space for the optimization parameters. Thus, the optimization procedure consists of three parts, the pre-, the coarse, and the fine optimization. For each part the steps 1–4 are passed through once. The aim of the first and the second part is a sufficient limitation of the search space and part 3 determines the final result of the optimization:

1. **Pre-optimization**. In this step, the theoretical area function a_m is fitted in frequency and amplitude to a_v. Longitudinal vibration properties are not evaluated in this part. Therefore, parameters $Q_{\text{left}}=Q_{1,\ldots,3}$ and $Q_{\text{right}}=Q_{4,\ldots,6}$ are used. All springs and masses representing one vocal fold are scaled with the same value following Eqs. (17) and (16). As initial search range [0.3,…,3] is used for each parameter. The parameter ranges are appropriate for simulating normal and pathologic vocal fold vibration patterns. Within the objective function it is sufficient to use only the measure Δa. The pre-optimization delivers the values Q_p^{pre}, $Q_{\text{left}}^{\text{pre}}$, $Q_{\text{right}}^{\text{pre}}$, and Q_r^{pre}.
2. **Coarse optimization**. The complete parameter set $Q_p, Q_1, \ldots, Q_6, Q_r$ is used. The search ranges for the eight parameters are derived from the pre-optimization results: $Q \in [Q^{\text{pre}}/1.2, \ldots, Q^{\text{pre}}/0.8]$. In consequence of the homogeneous scaling with Q_{left} and Q_{right} within the pre-optimization large deviations Δc_i occur, if the vocal fold dynamics demands a Q_i distinct from the other two values of the same model side. It is the aim of the coarse optimization to detect this situation as follows: For the left $(\alpha=l)$ and right $(\alpha=r)$ model side, the pair $(i,j)_\alpha$ with the least difference between the energies of the trajectory difference signals is identified after

$$(i,j)_\alpha = \underset{(i,j)}{\operatorname{argmin}} |\Delta c_i - \Delta c_j| \quad i,j \in \begin{cases} 1,\ldots,3, & \alpha = l \\ 4,\ldots,6, & \alpha = r \end{cases} \tag{24}$$

and the mean values $\Delta c_{\text{mean}}^{\alpha} = \frac{1}{2}(\Delta c_i + \Delta c_j)$ are calculated. The remaining difference energy Δc_k, $k \neq i,j$, for each side is assigned to $\Delta c_{\text{max}}^{\alpha} = \Delta c_k$. For $\Delta c_{\text{max}}^{\alpha} > 4 \cdot \Delta c_{\text{mean}}^{\alpha}$ the search range for the corresponding parameter Q_k is extended to [0.3,…,3]. The factor 4 avoids an unnecessary extension of the search space in case of small deviations. Due to the local search space extension, distinct values for Q_k compared to the remaining both vales (Q_i, Q_j) of a single model side are enabled. Within the objective function, Δa and Δc are evaluated.

3. **Fine optimization**. For this step, the optimization is coupled with a regularization. Besides the model dynamics, the mass and stiffness distributions along each model side are evaluated. For this aim, a further regularization condition is introduced in addition to the objective function ϕ.

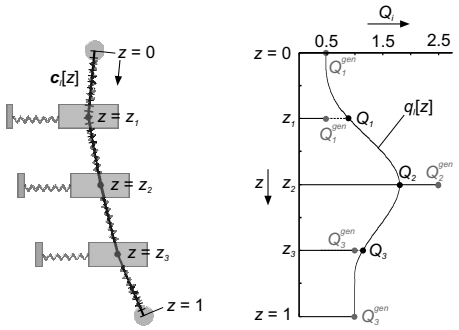


FIG. 11. Calculation of the longitudinal distribution $q_l[z]$ of the values Q_i $(i=1,\ldots,3)$ for the left model side.

For each model side (all masses are at rest position) contour lines $\mathbf{c}_\alpha[z]=(x[z],y[z])$ with the parametric domain $z \in [0,1]$ are determined as shown in Fig. 11. By means of approximation using cubic B splines, $q_\alpha[z]$ are derived from the sampling points $Q_j^{\text{gen}}(\alpha=l)$ and $Q_{j+3}^{\text{gen}}(\alpha=r)$, with $j=1,\ldots,3$. Thereby, Q_i^{gen} are the values for the optimization parameters delivered by the GA. Instead of using Q_i^{gen} for scaling the variable model parameters, the approximated values $Q_i=q_\alpha[z=z_i]$ are applied.

According to Eqs. (16) and (17) the function q_α approximates the mass and stiffness distributions along the model contour $\mathbf{c}_\alpha$. Following Hess *et al.*,[42] the mass and stiffness distributions along a vocal fold reveal a smooth course, i.e., a continuous behavior without excursive changes. To take this into consideration, the local smoothness s_i at position z_i is estimated as

$$s_i = \sum_{z=z_i-1}^{z_{i+1}} \left(\frac{q_\alpha[z-\Delta z] - 2q_\alpha[z] + q_\alpha[z+\Delta z]}{(\Delta z)^2} \right)^2, \tag{25}$$

the squared sum of the second order difference quotient with $\Delta z=0.01$. A mean value $\bar{s}$ of the s_i is calculated, whereby positions i with an extended search range during the coarse optimization are not considered:

$$\bar{s} = \frac{1}{\sum_{j=1}^{6} k_j} \sum_{i=1}^{6} k_i \cdot s_i,$$

with

$$k_i = \begin{cases} 0, & \Delta c_i = \Delta c_{\text{max}}^{\alpha} > 4 \cdot \Delta c_{\text{mean}}^{\alpha} \\ 1, & \text{else} \end{cases}. \tag{26}$$

For the regularization, a value $\bar{s}$ as low as possible, i.e., a function q_α as smooth as possible, is demanded. Extending the optimization procedure with the regularization, the final results $Q_p^*, Q_1^*, \ldots, Q_6^*$, and Q_r^* of the parameter optimization are calculated after

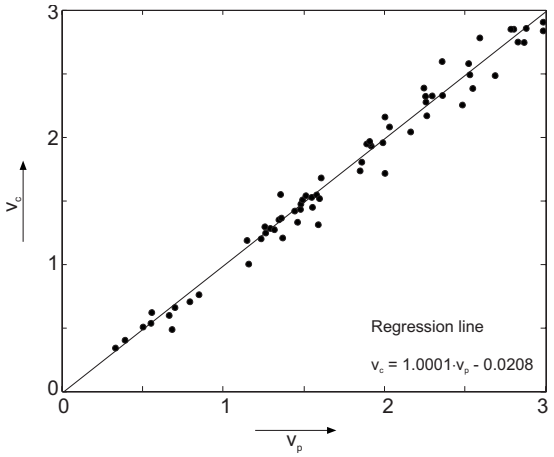


FIG. 12. Calculated parameter values v_c over the predefined parameter values v_p used for generating the synthetic vibration patterns.

$$\min_{Q_p,Q_1,\ldots,Q_6,Q_r}\left(\phi+\frac{\bar{s}}{\max_i(s_i)}\right). \tag{27}$$

The search spaces for the optimization parameters are derived from the results of the coarse optimization after $[Q^{\text{coarse}}/1.2,\ldots,Q^{\text{coarse}}/0.8]$.

5. Validation

Due to the nonconvex objective function ϕ with many local minima, it cannot be guaranteed to localize the global minimum. The different local minima of ϕ correspond to theoretical curves resulting from different values for the optimization parameters which fit more or less the experimental curves. In addition, the GA used for the optimization procedure is a stochastic approach and thus the calculated parameter values are not unique. Exact parameter values cannot be assured, as the results of the GA scatter within a certain interval. Therefore, the effects of the local minima of the objective function and the scattering of the optimization results has to be assessed. For this aim, the optimization procedure is applied to synthetic data sets. These data sets are generated by simulations with predefined model configurations. Eight model configurations are constructed, which simulate vibration patterns as observed for normal and pathologic voices as shown in Fig. 3 and 4. The time-variant contours formed by the modeled vocal fold edges are used as synthetic image processing results. For validation purposes, the parameter values resulting from the fitting of the MMM dynamics to the synthetic vibration patterns are compared with the predefined values. In this way, the reliability and performance of the optimization procedure is evaluated. Concerning the reproducibility of the optimization results, the parameter optimization is applied five times to each synthetic vibration pattern in addition to the first run. In this way, the scattering of the obtained parameter values and thus the reproducibility of the optimization results can be estimated.

TABLE I. Error between predefined and calculated parameter values averaged over all synthetic cases.

	Q_p	Q_1	Q_2	Q_3	Q_4	Q_5	Q_6	Q_r
Mean [%]	3.54	3.10	5.23	8.78	5.21	3.26	5.04	6.92

III. RESULTS

A. Validation of stability and reliability

In Fig. 12 the calculated parameter values v_c (comprising $Q_p^*,Q_1^*,\ldots,Q_6^*,Q_r^*$) resulting from the fitting to the eight synthetic vibration patterns are plotted over the predefined parameter values v_p. The correlation amounts 98%. The mean deviation of the predefined parameters from the values determined by the optimization are summarized in Table I. The error averaged over all eight parameters is 5.1%. The smallest error is achieved for parameter Q_1 with a mean error of 3.10%. The parameter Q_3 has the largest deviation with a mean error of 8.78%.

For the validation of the stability, the optimization procedure is applied additionally five times to each synthetic vibration pattern. The results are compared with the parameter values obtained in the first processing of the synthetic data. The variation of the resulting optimization parameters facilitates an appraisal of the stability of the proposed method. The mean deviation amounts to 5.5%, averaged across all parameters, see Table II. The smallest deviation is achieved for parameter Q_4 with a mean error of 3.36%. The greatest deviation reveals Q_1 with a mean error of 9.16%.

B. Application to real vocal fold oscillations

The automatic optimization procedure is applied to the eight digital high-speed videos of the subjects S1–S8. In Fig. 13 the vibration patterns of the optimized models are summarized. For each subject one entire closing phase is depicted. For comparison with the processed high-speed data, the corresponding vocal fold vibrations from Figs. 3 and 4 are also shown (gray lines). The frequency and amplitude of the vocal fold dynamics, as well as the time-varying shape of the glottis are reproduced by the MMM.

For giving a survey over the achieved fitting quality in all eight subjects, Table III summarizes the correlations between the area functions a_m and a_v (ρ_a) as well as the individual trajectories $c_{m,i}$ and $c_{v,i}$ (ρ_i). Concerning ρ_a a correlation of at least 0.89 is achieved with a mean value of 0.94. The correlation between the individual theoretical trajectories $c_{m,i}$ and the experimental trajectories $c_{v,i}$ amounts to (mean $\pm$ standard deviation (sd), averaged across all positions and subjects) 0.88 ± 0.09. The worst correlation is obtained at the position $i=3$ for S1 and at $i=5$ for S7, each with

TABLE II. Mean deviation of the optimization results from the predefined values after five additional applications of the optimization procedure to the same synthetic vibration patterns (averaged over all synthetic data sets).

	Q_p	Q_1	Q_2	Q_3	Q_4	Q_5	Q_6	Q_r
Mean [%]	3.80	9.16	4.69	3.46	3.36	8.64	7.10	3.87

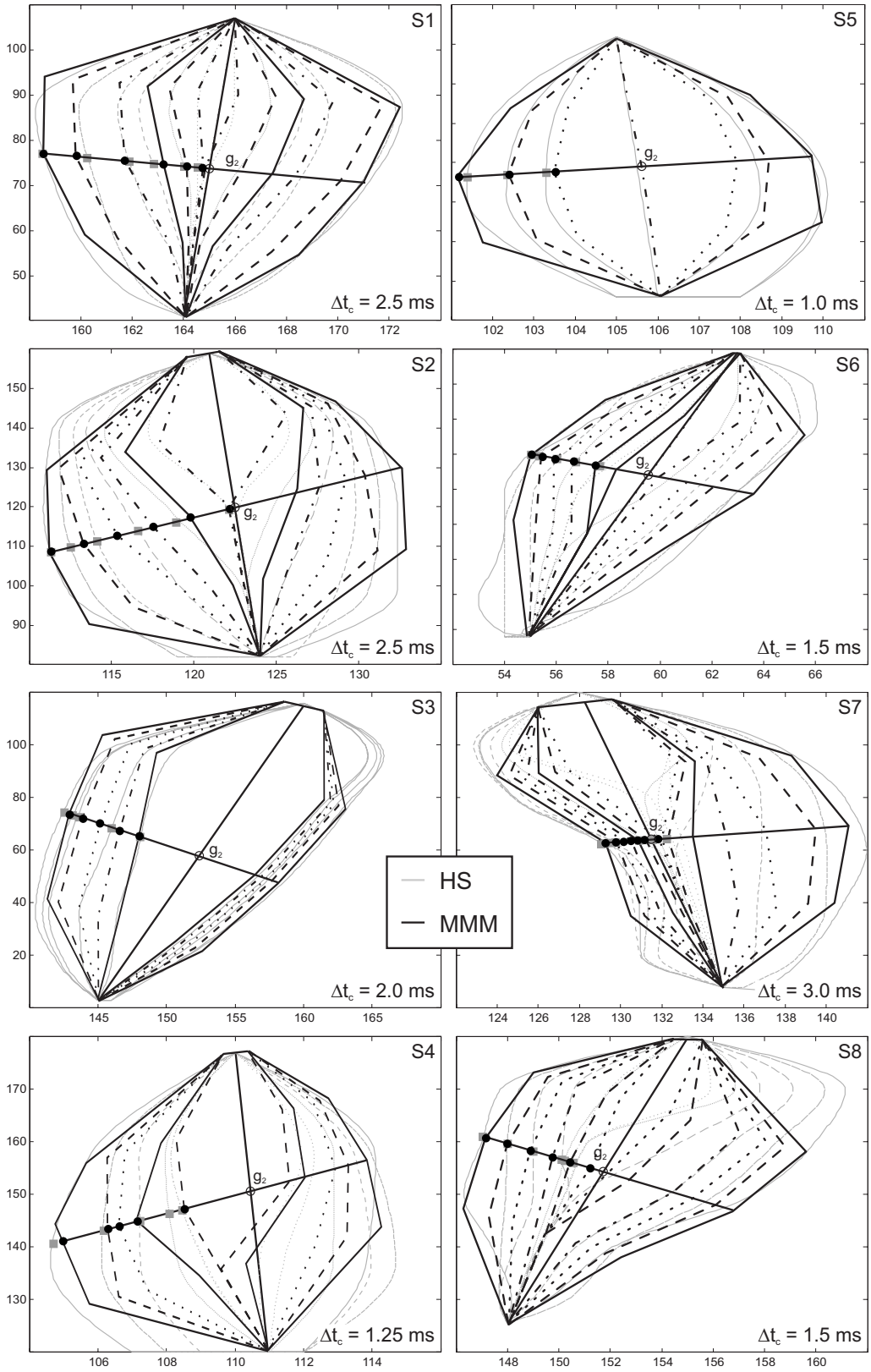


FIG. 13. Resulting vibration patterns for the optimized parameter values. For each subject the entire closing phase is presented (black lines). The evaluated vibrations extracted from the high-speed videos are also shown (gray lines).

0.63. In Table IV the relative errors ϵ_a and ϵ_i for the area functions and the individual trajectories are given. The experimental area functions are reproduced with a mean relative error of 7%. The experimental trajectories are reproduced with a mean relative error of 10.7%. The best result was achieved for subject S6 with $\epsilon_4 = 2.8\%$, the worst for S3 with $\epsilon_1 = 26.3\%$.

The parameter values resulting from the optimization

TABLE III. Correlation between the area functions a_m and a_v (ρ_a) as well as the trajectories $\mathbf{c}_{m,i}$ and $\mathbf{c}_{v,i}$ (ρi).

Subject	ρ_a	ρ_1	ρ_2	ρ_3	ρ_4	ρ_5	ρ_6
S1	0.94	0.91	0.88	0.63	0.73	0.85	0.89
S2	0.93	0.72	0.82	0.95	0.93	0.88	0.83
S3	0.99	0.76	0.98	0.91	0.97	0.89	0.83
S4	0.92	0.89	0.83	0.95	0.92	0.86	0.79
S5	0.95	0.92	0.97	0.99	0.95	0.82	0.88
S6	0.91	0.96	0.88	0.71	0.95	0.89	0.73
S7	0.89	0.85	0.71	0.72	0.88	0.63	0.82
S8	0.97	0.95	0.81	0.93	0.95	0.91	0.93
1st quartile	0.92			0.82			
median	0.94			0.88			
3rd quartile	0.96			0.93			

procedure are summarized in Table V and Fig. 14. Table V shows the values for the parameters Q_p and Q_r. Figure 14 shows the determined values for the optimization parameters Q_i (marked with small circles) and the interpolated distributions $q_\alpha[z]$, which represents an approximated distribution of mass and stiffness along left and right model side. In Fig. 14, q_l and q_r of each subject are graphically related to the morphology of the vibrating part of the vocal folds. Thereby, the normalized values $\hat{q}_\alpha[z]=q_\alpha[z]/\max_z(q_l[z],q_r[z])$ are plotted to facilitate a comparison between different subjects. In addition, μ_α indicates mean $\pm$ sd of $\hat{q}_\alpha$. For assessing the characteristics of the distributions q_α, Table VI summarizes the correlation ρ_q between q_r and q_l as well as mean and standard deviation of $\Delta q=|q_l-q_r|$ for each subject. For the normal voice subject S1 ρ_q is reduced to 0.12. Subject S6 shows a negative correlation with $\rho_q=-0.67$. For the normal voice subjects the mean for the difference Δq is 0.01 (S1) and 0.02 (S2), respectively. For the pathological subjects this value is at least three times increased to 0.06 for subject S6 (up to 0.27 in case of S3).

IV. DISCUSSION

The primary voice signal is generated by vocal fold vibrations and thus its temporal characteristics can also be found in the vocal fold dynamics. Therefore, the objective quantification of the vocal fold oscillations is an important precondition for supporting the clinical diagnosis of voice disorders. For quantification purpose, in this work a model-based method is proposed. Objective parameters representing the spatio-temporal properties of the vocal fold dynamics are identified by modeling vocal fold vibrations by means of the biomechanical MMM. The model is fitted to the vocal fold oscillations by modifying a set of model parameters. Appro-

TABLE IV. Relative errors (in [%]) between the area functions a_m and a_v (ϵ_a) as well as the trajectories $\mathbf{c}_{m,i}$ and $\mathbf{c}_{v,i}$ (ϵ_i).

Subject	ϵ_a	ϵ_1	ϵ_2	ϵ_3	ϵ_4	ϵ_5	ϵ_6
S1	5.8	14.3	8.6	10.0	14.3	8.6	10.0
S2	6.2	14.0	10.7	11.1	14.0	10.7	11.1
S3	7.1	26.3	15.4	17.1	20.0	16.7	16.7
S4	6.8	16.0	13.8	15.0	10.0	16.0	14.0
S5	4.2	2.5	4.0	4.4	7.8	3.8	9.1
S6	9.0	10.5	10.0	16.2	2.8	5.7	6.7
S7	10.5	6.0	10.0	13.3	12.8	5.5	8.7
S8	8.0	11.1	8.2	20.0	12.5	10.0	9.0
1st quartile	6.1			8.6			
median	7.0			10.7			
3rd quartile	8.3			14.3			

TABLE V. Results for the optimization parameters Q_p and Q_r.

Subject	Q_p^*	Q_r^*
S1	2.52	0.55
S2	2.87	0.70
S3	2.35	0.50
S4	2.25	0.38
S5	2.98	0.66
S6	1.90	0.55
S7	2.85	0.79
S8	2.35	0.32

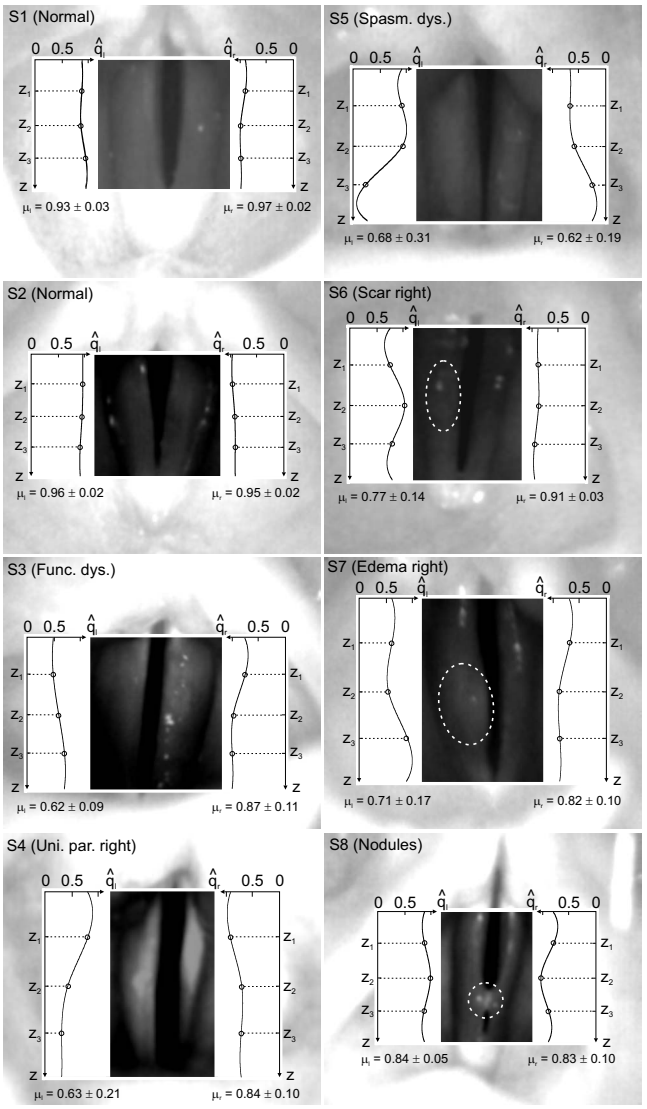


FIG. 14. Normalized distributions $\hat{q}_\alpha$ graphically related to the morphologies of the vocal folds. The values Q_1 to Q_3 and Q_4 to Q_6 along the left and right model side are marked with circles. The white dashed lines encircle tissue impairments on the vocal folds.

TABLE VI. Assessment of the distributions q_α. Left column: Correlation ρ_q between q_r and q_l. Right column: mean ± sd of the difference $\Delta q = |q_l - q_r|$.

Subject	ρ_q	mean ± sd of Δq
S1	0.12	0.02 ± 0.02
S2	0.85	0.01 ± 0.01
S3	0.91	0.27 ± 0.04
S4	0.96	0.21 ± 0.11
S5	0.98	0.13 ± 0.06
S6	−0.67	0.19 ± 0.12
S7	0.39	0.15 ± 0.12
S8	0.98	0.06 ± 0.02

priate values for the model parameters are determined with an automatic optimization procedure. In this way parameter values are identifiable which describe the time-varying two-dimensional contour of the vocal fold edges. In addition, the resulting parameter values serve for an approximation of physiological properties of the vocal fold as stiffness and mass distribution.

The applicability of our method was validated using eight synthetic model configurations, generated with predefined parameter values. The synthetic data sets were analyzed with the optimization procedure. A comparison of the calculated parameter values with the predefined values reveals a mean error of only 5.1% ± 3.8% (Table I) which represents a sufficient accuracy for the assessment of vocal fold vibrations extracted from high-speed videos. The resulting model deflection difference of less than 5%[22] is in the same range as the accuracy of the applied image processing for the vocal fold edge detection.[14]

The optimization procedure is based on a random-based search algorithm and thus the calculated parameter values are not unique with an immanent uncertainty. Thus, a certain resulting value cannot be guaranteed. To analyze the effect of the scattering, the procedure was applied six times to each synthetic data set. The mean deviation from the predefined values was 5.5% ± 4.3% (Table II). Following this, the uncertainty due to the scattering of the random-based optimization procedure is in the same range as the uncertainty of the segmentation algorithm with approximately 15% (see Sec. II A).

Besides a quantification of vocal fold dynamics, it is an additional motivation for the model-based approach to gain an estimation of physiological vocal fold properties. Primarily, these physiological parameters are stiffness and mass distribution along each vocal fold due to their influence on the vocal fold dynamics and the phonation process. To analyze the applicability of the optimization procedure and the interpretability of the obtained optimization results, clinical data of eight subjects are evaluated. The vibration patterns range from almost symmetric and regular oscillations for the normal voice subjects S1 and S2 to clearly asymmetric vibrations concerning the left and the right vocal fold (e.g., S3 and S4) and irregular shapes as for subject S6 and S7. Although the subjects show this high variability, the optimization procedure is capable of fitting the model dynamics to the vocal fold oscillations as indicated by the values in Tables III and IV. The mean relative error between the experimental and theoretical trajectories amounts to 10% which reflects the same accuracy as for the applied image processing algorithm. This result accounts for a sufficient accuracy of the model fitting.

For the aim of regularization within the fine optimization, distributions q_l and q_r are approximated using the values of the optimization parameters Q_j and $Q_{j+3}(j=1,\ldots,3)$ as sampling points. Following Eqs. (17) and (16) q_α describes the stiffness distribution and inverse mass distribution respectively along each model side. In Fig. 14 the normalized distributions $\hat{q}_\alpha$ derived from the final optimization result are related graphically to the morphology of the vocal folds. This allows a discussion of the optimized biomechanical model of the vocal folds with respect to the analyzed laryngeal configuration. The processed clinical data can be categorized in three groups: normal voice subjects, subjects with functional or paralytic voice disorders and voice disorders which result in local organic impairments on one or both vocal folds.

A. Normal voice subjects

For the normal voice subjects S1 and S2 the distributions q_α are almost symmetric for the left and the right side which results in mean difference between both sides of 1% (S1) and 2% (S2) of the maximum value of q_α. The standard deviation of only 3% and 2% of q_r and q_l for S1 and S2 reflects a low variability in longitudinal direction. Consequently, masses as well as stiffnesses vary only slightly along each model side with an obvious left/right symmetry. This result corresponds to the vocal fold constitution expected for normal voice subjects.

B. Functional and paralytic voice disorders

For the subjects with functional and paralytic voice disorders (S3, S4, S5) asymmetric model configurations are obtained. The mean difference between q_l and q_r is at least 0.13 (S5) which is about six times more than for the normal voice subjects. The correlation between q_l and q_r is at least 0.91 (S3). These high correlations result from almost identical courses in longitudinal direction for q_l and q_r.

The functional voice disorder of subject S3 results in a decreased stiffness and increased vibrating mass for the right side. The value for q_α increases towards the anterior commissure, but there is no distinct extremum for both sides. This is in accordance to the underlying functional voice disorder: a symmetric positioning and muscle activation is impeded, but there are no local changes of the tissue.[43]

In subject S4, the values of q_l, which models the right vocal fold, are reduced compared to the values of q_r (left vocal fold), especially towards the anterior commissure. Consequently, the stiffness for the side representing the paralyzed vocal fold is decreased compared to the unaffected side. This reflects the reduced muscle activation due to the unilateral paralysis. Towards the posterior commissure q_l and q_r increase symmetrically, thus the stiffness is increased. This result can be explained by reduced oscillation amplitudes of the vocal fold edges towards the dorsal endings.

In the case of spasmodic dysphonia (S5) spasms and involuntary muscle activations result in an asymmetric strain on the left and right vocal fold during phonation.[44] In accordance to this, the model configuration for subject S5 results in a decreased stiffness and increased vibrating mass for the left side.

C. Organic voice disorders

For the subjects S6, S7, and S8 with organic voice disorders, the distributions q_α reflect the local changes of the organic constitutions of the vocal folds. For S6 and S7 the standard deviation of Δq reaches the maximum compared to the other subjects due to the local effect of the tissue impairment. For both subjects the correlations between q_l and q_r are reduced compared to the normal voice subjects and the subjects with functional voice disorders. Along the scar on the right vocal fold (S6) the values for q_l are increased compared to the adjacent values. The localized stiffened scared tissue corresponds to an increased stiffness within the model. For the unaffected left vocal fold the behavior of q_r is comparable to the results of the normal voice subjects. The edema on the right vocal fold at ventral position for subject S7 corresponds to a maximum of q_l at this position. The symmetrical positioned nodules of subject S8 result in symmetrically increased values for q_α at medial position ($z=z_2$). Thus the standard deviation of the distribution q_α is increased compared to the normal voice subjects. However, as both vocal folds are effected symmetrically by tissue impairments, the symmetry between q_l and q_r is comparable to the normal voice subjects: The standard deviation of Δq is 0.02 as for S1 and the mean value is the minimum among the pathologic subjects.

The resulting model configurations reflect individual properties of the vocal fold vibrations and morphologic constitutions. The obtained distributions q_α are comprehensible by accounting physiological vocal fold properties as the longitudinal mass and stiffness distribution of the evaluated clinical cases: For the normal voice subjects a symmetric mass and stiffness distribution concerning left and right vocal fold with only a slight variance in longitudinal direction is approximated. The functional voice disorders result in an increased left to right asymmetry. For local tissue impairments in case of the organic voice disorders local changes of the stiffnesses and masses are obtained.

The proposed method enables a first approximation of physiological parameters along the entire vocal fold *in vivo*. This is an extension compared to other model-based approaches[21,22,45,46] or direct measurement techniques as proposed in Goodyer *et al.*,[47] where only global values for the vocal fold properties are derived *in vivo*. However, the relationship between the calculated parameters of the multi-mass model and the actual values of the corresponding vocal fold properties needs further investigation. In several works the measurement of biomechanical properties of the vocal folds using excised cadaver larynges were presented.[48–52] In Hess *et al.*[42] even local variations of the elasticity parallel and perpendicular to the vocal fold edge were measured *ex vivo*. Doellinger and Berry[32] comprises experiments with excised vocal folds and the high-speed imaging technique. Combining these methods with the proposed optimization procedure offers the possibility to investigate the relationship between the model parameters and the physiological vocal fold properties.

V. CONCLUSION

The observation of the vibrating vocal folds is essential for the clinical assessment of voice disorders. Videoendoscopic high-speed systems allow the recording of vocal fold vibrations during phonation. A comprehensive investigation of voice pathologies demands an objective and quantitative description of the observed vocal fold dynamics. In this work, a model-based approach is proposed, which allows to infer an approximation of the stiffness and mass distribution along the vocal folds. The validation with synthetic data sets shows the reliability and stability of the optimization procedure. In a study comprising a larger amount of clinical data sets with more different voice pathologies, the clinical significance of our proposed method has to be analyzed.

ACKNOWLEDGMENTS

This work was supported by the Collaborative Research Center 603 (Grant No. SFB 603, subproject B5), funded by the Deutsche Forschungsgemeinschaft (German Research Foundation, DFG).

[1] D. Huang, F. Kasuya, and S. Lin, "Measure of vocal function during changes in vocal effort level," J. Voice **9**, 429–438 (1995).
[2] S. Hadjitodorov and P. Mitev, "A computer system for acoustic analysis of pathological voices and laryngeal diseases screening," Med. Eng. Phys. **21**, 419–429 (2002).
[3] J. Godino-Llorente and P. Gomez-Vilda, "Automatic detection of voice impairments by means of short-term cepstral parameters and neural network based detectors," IEEE Trans. Biomed. Eng. **51**, 380–384 (2004).
[4] S. Niimi and M. Miyai, "Vocal fold vibration and voice quality," Folia Phoniatr Logop **52**, 32–38 (2000).
[5] N. Isshiki, M. Tanabe, K. Ishizaka, and D. Broad, "Clinical significance of asymmetrical vocal cord tension," Ann. Otol. Rhinol. Laryngol. **86**, 58–66 (1977).
[6] U. Eysholdt, F. Rosanowski, and U. Hoppe, "Vocal fold vibration irregularities caused by different types of laryngeal asymmetry," Eur. Arch. Otorhinolaryngol. **260**, 412–414 (2003).
[7] P. Kitzing, "Stroboscopy—a pertinent laryngological examination," J. Otolaryngol. **14**, 151–157 (1985).
[8] R. Sataloff, J. Spiegel, and M. Hawkshaw, "Strobovideolaryngoscopy: results and clinical value," Anal. Otorhinolaryngol. **100**, 725–727 (1991).
[9] U. Eysholdt, M. Tigges, T. Wittenberg, and U. Proschel, "Direct evaluation of high-speed recordings of vocal fold vibrations," Folia Phoniatr Logop **48**, 163–170 (1996).
[10] J. Neubauer, P. Mergell, U. Eysholdt, and H. Herzel, "Spatio-temporal analysis of irregular vocal fold oscillations: biphonation due to desynchronization of spatial modes," J. Acoust. Soc. Am. **110**, 3179–3192 (2001).
[11] T. Wittenberg, M. Moser, M. Tigges, and U. Eysholdt, "Recording, processing and analysis of digital highspeed sequences in glottography," Mach. Vision Appl. **8**, 399–404 (1995).
[12] S. Allin, J. Galeotti, G. Stetten, and S. Dailey, "Enhanced snake based segmentation of vocal folds," *IEEE International Symposium on Biomedical Imaging* (IEEE, Washington, DC, 2004), pp. 812–815.
[13] Y. Yan, X. Chen, and D. Bless, "Automatic tracing of vocal fold motion from high-speed digital images," IEEE Trans. Biomed. Eng. **53**, 1394–1400 (2006).
[14] J. Lohscheller, H. Toy, F. Rosanowski, U. Eysholdt, and M. Doellinger, "Clinically evaluated procedure for the reconstruction of vocal fold vibrations from endoscopic digital high-speed videos," Med. Image Anal. **4**, 400–413 (2007).

[15]J. Noordzij and P. Woo, "Glottal area waveform analysis of benign vocal fold lesions before and after surgery," Anal. Otorhinolaryngol. **109**, 441–446 (2000).
[16]Y. Yan, K. Ahmad, M. Kunduk, and D. Bless, "Analysis of vocal-fold vibrations from high-speed laryngeal images using a hilbert transform based methodology," J. Voice **19**, 161–175 (2005).
[17]Q. Qiu, H. Schutte, L. Gu, and Q. Yu, "An automatic method to quantify the vibration properties of human vocal folds via videokymography," Folia Phoniatr Logop **55**, 128–136 (2003).
[18]J. Svec and H. Schutte, "Videokymography: High-speed line scanning of vocal fold vibrations," J. Voice **10**, 201–205 (1996).
[19]M. Doellinger, U. Hoppe, F. Hettlich, J. Lohscheller, S. Schubert, and U. Eysholdt, "Vibration parameter extraction from endoscopic image series of the vocal folds," IEEE Trans. Biomed. Eng. **49**, 773–781 (2002).
[20]K. Ishizaka and J. L. Flanagan, "Synthesis of voiced sounds from a two-mass model of the vocal cords," Bell Syst. Tech. J. **51**, 1233–1268 (1972).
[21]R. Schwarz, U. Hoppe, M. Schuster, T. Wurzbacher, U. Eysholdt, and J. Lohscheller, "Classification of unilateral vocal fold paralysis by endoscopic digital high-speed recordings and inversion of a biomechanical model," IEEE Trans. Biomed. Eng. **53**, 1099–1108 (2006).
[22]T. Wurzbacher, R. Schwarz, M. Doellinger, U. Hoppe, U. Eysholdt, and J. Lohscheller, "Model-based classification of nonstationary vocal fold vibrations," J. Acoust. Soc. Am. **120**, 1012–1027 (2006).
[23]I. Titze and B. Story, "Rules for controlling low-dimensional vocal fold models with muscle activation," J. Acoust. Soc. Am. **112**, 1064–1076 (2002).
[24]M. Tigges, T. Wittenberg, P. Mergell, and U. Eysholdt, "Imaging of vocal fold vibration by digital multi-plane kymography," Comput. Med. Imaging Graph. **23**, 323–330 (1999).
[25]D. Kim, L. Kim, K. Kim, M. Sung, J. Roh, and M. Sung, "Videostroboky-mographic analysis of benign vocal fold lesions," Acta Oto-Laryngol. **123**, 1102–1109 (2003).
[26]D. Wong, M. Ito, N. Cox, and I. Titze, "Observation of perturbations in a lumped-element model of the vocal folds with application to some pathological cases," J. Acoust. Soc. Am. **89**, 383–394 (1991).
[27]X. Pelorson, A. Hirschberg, R. van Hassel, and A. Wijnands, "Theoretical and experimental study of quasisteady-flow separation within the glottis during phonation. Application to a modified two-mass model," J. Acoust. Soc. Am. **96**, 3416–3431 (1994).
[28]B. Story and I. Titze, "Voice simulation with a body-cover model of the vocal folds," J. Acoust. Soc. Am. **97**, 1249–1260 (1995).
[29]F. Alipour, D. Berry, and I. Titze, "A finite-element model of vocal fold vibration," J. Acoust. Soc. Am. **119**, 3003–3012 (2000).
[30]M. Rosa, J. Pereira, M. Grellet, and A. Alwan, "A contribution to simulating a three-dimensional larynx model using the finite element method," J. Acoust. Soc. Am. **114**, 2893–2905 (2003).
[31]P. Mergell, I. Titze, and H. Herzel, "Irregular vocal-fold vibration—high speed observation and modeling," J. Acoust. Soc. Am. **108**, 2996–3002 (2000).
[32]M. Doellinger and D. Berry, "Computation of the three-dimensional medial surface dynamics of the vocal folds," J. Biomech. **39**, 369–374 (2006).
[33]I. Titze, *Principles of Voice Production* (Prentice–Hill, Englewood Cliffs, NJ, 1994).
[34]H. Gunter, "A mechanical model of vocal fold collision with high spatial and temporal resolution," J. Acoust. Soc. Am. **37**, 1119–1124 (2004).
[35]I. Steinecke and H. Herzel, "Bifurcations in an asymmetric vocal fold model," J. Acoust. Soc. Am. **97**, 1571–1578 (1995).
[36]C. Driolo, "A flow waveform-matched low-dimensional glottal model based on physical knowledge," J. Acoust. Soc. Am. **117**, 3184–3195 (2005).
[37]M. de Vries, H. K. Schutte, A. E. P. Veldman, and G. Verkerke, "Glottal flow through a two-mass model: Comparison of Navier-Stokes solutions with simplified models," J. Acoust. Soc. Am. **111**, 1847–1853 (2002).
[38]N. Lous, G. Hofmans, R. Veldhuis, and A. Hirschberg, "A symmetrical two-mass vocal-fold model coupled to vocal tract and trachea, with application to prosthesis design," Acta Acust. **84**, 1135–1150 (1998).
[39]M. Doellinger, *Parameter Estimation of Vocal Fold Dynamics by Inversion of a Biomechanical Model* (Shaker Verlag, Aachen, Germany, 2002).
[40]D. Goldberg, *Genetic Algorithms in Search, Optimization, and Machine Learning* (Addison–Wesley, Reading, MA, 1989).
[41]C. Houck, J. Joines, and M. Kay, "A genetic algorithm for function optimization: A Matlab implementation," NCSU-IE, Technical Report No. 09-95 (1995).
[42]F. M. M. Hess, J. Kobler, S. Zeitels, and E. Goodyer, "Measurements of vocal fold elasticity using the linear skin rheometer," Folia Phoniatr Logop **58**, 207–216 (2006).
[43]R. Peppard, "Management of functional voice disorders in adolescents," Lang. Speech Hear. Serv. Sch. **27**, 257–270 (1996).
[44]E. Seifert and J. Kollbrunner, "Stress and distress in non-organic voice disorder," Swiss Med. Wkly. **135**, 387–397 (2005).
[45]C. Tao, Y. Zhang, and J. Jiang, "Extracting physiologically relevant parameters of vocal folds from high-speed video image series," IEEE Trans. Biomed. Eng. **54**, 794–801 (2007).
[46]T.-Y. Hsiao, C.-L. Wang, C.-N. Chen, F.-J. Hsieh, and Y.-W. Shau, "Elasticity of human vocal folds measured in vivo using color doppler imaging," Ultrasound Med. Biol. **28**, 1145–1152 (2002).
[47]E. Goodyer, F. Muller, B. Bramer, D. Chauhan, and M. Hess, "In vivo measurement of the elastic properties of the human vocal fold," Eur. Arch. Otorhinolaryngol. **263**, 455–462 (2006).
[48]A. Perlman and I. Titze, "Development of an in vitro technique for measuring elastic properties of vocal fold tissue," J. Speech Hear. Res. **31**, 288–298 (1988).
[49]R. Chan and I. Titze, "Viscoelastic shear properties of human vocal fold mucosa: Measurement methodology and empirical results," J. Acoust. Soc. Am. **106**, 2008–2021 (1999).
[50]R. Chan and I. Titze, "Viscoelastic shear properties of human vocal fold mucosa: Theoretical characterization based on constitutive modeling," J. Acoust. Soc. Am. **107**, 565–580 (2000).
[51]Y. Min, I. Titze, and F. Alipour-Haghighi, "Stress-strain response of the human vocal ligament," Ann. Otol. Rhinol. Laryngol. **104**, 563–569 (2005).
[52]E. Goodyer, S. Hemmerich, F. Muller, J. Kobler, and M. Hess, "The shear modulus of the human vocal fold, preliminary results from 20 larynxes," Eur. Arch. Otorhinolaryngol. **264**, 45–50 (2007).

Nonlinear source–filter coupling in phonation: Theory[a)]

Ingo R. Titze[b)]
Department of Speech Pathology and Audiology, The University of Iowa, Iowa City, Iowa 52242 and National Center for Voice and Speech, The Denver Center for the Performing Arts, Denver, Colorado 80204

(Received 2 August 2007; revised 10 December 2007; accepted 14 December 2007)

A theory of interaction between the source of sound in phonation and the vocal tract filter is developed. The degree of interaction is controlled by the cross-sectional area of the laryngeal vestibule (epilarynx tube), which raises the inertive reactance of the supraglottal vocal tract. Both subglottal and supraglottal reactances can enhance the driving pressures of the vocal folds and the glottal flow, thereby increasing the energy level at the source. The theory predicts that instabilities in vibration modes may occur when harmonics pass through formants during pitch or vowel changes. Unlike in most musical instruments (e.g., woodwinds and brasses), a stable harmonic source spectrum is not obtained by tuning harmonics to vocal tract resonances, but rather by placing harmonics into favorable reactance regions. This allows for positive reinforcement of the harmonics by supraglottal inertive reactance (and to a lesser degree by subglottal compliant reactance) without the risk of instability. The traditional linear source–filter theory is encumbered with possible inconsistencies in the glottal flow spectrum, which is shown to be influenced by interaction. In addition, the linear theory does not predict bifurcations in the dynamical behavior of vocal fold vibration due to acoustic loading by the vocal tract. © *2008 Acoustical Society of America.*
[DOI: 10.1121/1.2832337]

PACS number(s): 43.70.Bk, 43.75.Rs [BHS] Pages: 2733–2749

I. INTRODUCTION

The acoustic features of all vowel productions, and many consonant productions, have generally been described by a linear source–filter theory (Chiba and Kajiyama, 1958; Fant, 1960; Flanagan, 1972; Stevens, 1999). This linear theory is based on the assumption that the source of sound for vowels and voiced consonants (pulsatile airflow in the larynx) is independent of the filter, an acoustic resonator formed by airways known as the vocal tract. It is traditionally assumed that the source–filter combination can be characterized by mathematical convolution of source and filter functions in the time domain or by multiplication of Fourier-transformed source and filter functions in the frequency domain. Time domain convolution and frequency domain multiplication are linear mathematical operations that carry with them the superposition assumption; that is, the output of any combination of inputs is the linear combination of all the individual outputs. Stated another way, the output of any and all input frequencies can at most be an amplitude and phase changed version of these input frequencies. The filter cannot influence the source to produce new frequencies or change the overall energy level of the source. We will show here that this assumption is generally not valid, but under certain conditions is an appropriate simplification.

Many aspects of speech production have been successfully described by a linear source–filter theory. In particular, linear prediction of speech (Markel and Gray, 1976; Atal and Schroeder, 1978) has been the flagship of speech analysis, synthesis, and processing for over 30 years. But it has been recognized all along, however, that the linear theory is more applicable to male speech than female and child speech (e.g., Klatt and Klatt, 1990). As long as the dominant source frequencies lie well below the formant frequencies of the vocal tract, the source is influenced only in simple ways by the filter, mainly in terms of glottal flow pulse skewing and pulse ripple. This mild interaction occurs for most male adult speech, but greater interaction occurs for female and child speech, and even more for singing, where the fundamental frequency range spans more than two octaves and the lower partials of the source cross the formants. In these more intense interactions, bifurcations in the dynamics of vocal fold vibration can occur that may generate sudden F_0 jumps, subharmonic frequencies, or changes in the overall energy level at the source. The earliest computer simulations of source–filter coupling (Flanagan, 1968; Flanagan and Landgraf, 1968; Ishizaka and Flanagan, 1972) showed the interactivity clearly. The one-mass vocal fold model did not self-sustain oscillation without a vocal tract (a highly exaggerated coupling effect), and the two-mass model showed sudden frequency discontinuities when F_0 passed through the first formant frequency F_1. In human phonation, as our companion paper shows, the frequency discontinuities are clearly observable, but to a lesser extent than in these earlier models.

The purpose of this paper is to elucidate the underlying mechanisms of source–filter interaction, both with simple analytical models and with a highly sophisticated computational model. Specific questions of interest are: (1) what is the primary parameter that regulates the degree of interaction, (2) can new frequencies and greater output power be produced with increased interaction, (3) are there regions of

[a)]Readers are referred to [J. Acoust. Soc. Am.**123** (4), 1902–1915 (2008)] for a paper which reports on human subjects in this study.
[b)]Electronic mail: ingo-titze@uiowa.edu

harmonic stability and instability that can be exploited by a vocalist, (4) are sudden F_0 discontinuities (reported in a companion paper on human subjects) always triggered by F_0 interactions with F_1, the first formant frequency, or can higher harmonic-formant interactions contribute as well, and (5) how does the subglottal system contribute to nonlinear coupling differently from the supraglottal system?

It is hypothesized that humans (and perhaps many animals) have the ability to operate their source–filter system with either linear or nonlinear coupling. One way to express the degree of coupling is through the relative impedances of the source and filter. For linear source–filter coupling, the source impedance (transglottal pressure divided by glottal flow) is kept much higher than the input impedance to the vocal tract (vocal tract input pressure divided by the airflow into the vocal tract). This linear coupling is accomplished by adducting the vocal folds firmly and widening the epilarynx tube (a normally narrow region of the vocal tract above the vocal folds also known as the laryngeal vestibule). The glottal flow is then determined strictly by aerodynamics, while acoustic pressures above and below the glottis have little influence on either the transglottal pressure (which drives the glottal flow) or the intraglottal pressure (which drives the vocal folds). For nonlinear source–filter coupling, the glottal impedance is adjusted to be comparable to the vocal tract input impedance, making the glottal flow highly dependent on acoustic pressures in the vocal tracts (above and below the glottis). This is accomplished by setting specific adduction levels of the vocal folds that match a narrower epilarynx tube. Evidence of nonlinear coupling is the production of new frequencies in the form of distortion products, lowering of the oscillation threshold pressure (the Hopf bifurcation), production of subharmonics or modulation frequencies, sudden F_0 jumps, or chaotic vibrations, as either vowel or F_0 are changed (companion paper).

In many attempts to model the glottal airflow with explicit mathematical formulas (e.g., Rosenberg, 1971; Fant *et al.*, 1985; Fant and Lin, 1987), nonlinear source–filter coupling in the form of distortion products had already been introduced implicitly by making the glottal flow pulse shape different from the glottal area pulse shape. Usually, the peak of the flow pulse was delayed with respect to the area pulse shape. But such a delay (referred to as flow pulse skewing) cannot be justified if only quasisteady aerodynamic calculations are carried out (i.e., linear source–filter coupling). Rothenberg (1981) showed that the peak delay of the glottal flow pulse is a result of low-frequency source–filter interaction. Zhao *et al.* (2002) make a case for intraglottal pressure skewing for different glottal shapes based on an aerodynamic treatment that involves flow separation and vortex shedding, but the effect on glottal flow is likely to be small in comparison to the vocal tract loading effect, which has recently been further explored by this author (Titze, 2001; 2004a; b; 2006a). There is now strong evidence that glottal flow pulse skewing always involves the vocal tract, explicitly or implicitly. Constructing a glottal flow pulse shape without consideration of the vocal tract load can lead to inconsistencies in combining the source with the filter.

Source–filter interactions that involve changes in vocal fold vibration have been demonstrated by several investigators. Sudden changes in vocal fold vibration can be triggered by vocal tract length changes (Hatzikirou *et al.*, 2006), a good example of source–filter interaction. Further observations about source–filter coupling were reported by Švec *et al.* (1999) on human subjects and excised larynges, Mergell and Herzel (1997) on a female subject, Miller and Schutte (2005) on singers, Neumann *et al.* (2005) on male opera singers, Zhang et al. (2006a,b) on a physically constructed model, Zañartu *et al.*, (2007) with a computer simulation model, and Jiang and Tao (2007) with analytical mathematic methods. Some of these studies will be referred to in more detail later. In singing, vowel modifications (e.g., changing /u/ to /U/ or /i/ to /I/) are used routinely to strengthen a vowel on a certain pitch (Appelman, 1967; Coffin, 1987). Entire singing styles (operatic, musical theatre, yodeling) are based on the concept that certain vowels and voice qualities work best with certain pitches, a concept that would have no explanation if the source–filter system were linear. The entire voice register terminology is based on observed phenomena related to interaction within the source–filter building blocks, which includes the subglottal system (Titze, 2000; Chap. 10). Vocal pedagogues who invented terms like chest voice and head voice were not so naive to suggest that the source of sound moves from location to location, but rather that interactions with certain parts of the airway are stronger with certain source–filter adjustments and lead to special sensations along the airway. The role of the subglottal system for chest voice was implicated years ago by Van Den Berg (1957) and Vennard (1967). Chest voice production has both a glottal feature (a relatively long closed phase) and significant acoustic coupling to the trachea. For head voice, there appears to be more of an interaction with the supraglottal tract.

In an accompanying paper (Titze *et al.*, 2008), a primary objective is to differentiate purely source-generated bifurcations, including F_0 jumps, from vocal tract induced bifurcations. Three vocal exercises are designed in the accompanying paper to deliberately cross the fundamental frequency with the first formant frequency and to observe the resultant nonlinear effects in nine normal males and nine normal females. It is hypothesized that crossing F_0 with F_1 changes the acoustic load dramatically and that this crossing can destabilize vocal fold vibration. The main goal is to determine the proportion of irregularities that are due to nonlinear source–tract interactions. Expected manifestations of nonlinearity are sudden pitch jumps, subharmonic generation, or chaotic vocal fold vibration. Results indicate that the most frequent bifurcation is a sudden F_0 jump, as predicted by Fletcher (1993) for pressure-controlled valves in gas flows. The objective in this paper is to provide a theoretical framework for the bifurcation phenomena in vocal fold vibration with a nonlinear source–filter construct.

II. INTERACTION BASED ON VOCAL TRACT REACTANCE

Because the vocal tract is relatively short in comparison to a wavelength at typical speech fundamental frequencies

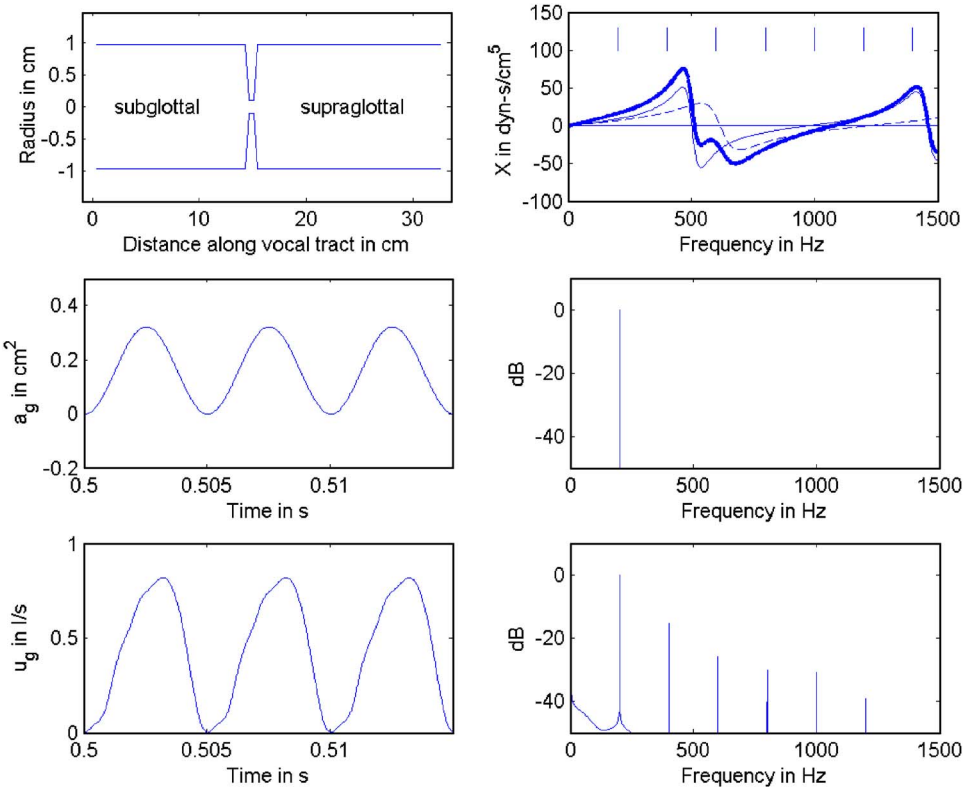


FIG. 1. (Color online) Harmonic frequency generation by source–filter interaction; (top left) vocal tract shape; (top right) reactance curves, thin solid line for supraglottal, dashed line for subglottal, and thick solid line for combined; (middle left) sinusoidal glottal area function; (middle right) spectrum of glottal area; (bottom left) glottal flow; (bottom right) spectrum of glottal flow.

(e.g., at F_0=200 Hz the vocal tract contains less than 1/8 of a wavelength), and because a speaker or singer wishes to convey all the phonetic variations of a spoken language, the length and shape of the vocal tract cannot be adjusted to resonate many of the source frequencies simultaneously. Thus, unlike in most musical instruments, for which the length and shape of the horn or bore is carefully designed to resonate the dominant source frequencies simultaneously, lining up source frequencies with vocal tract filter resonances is highly selective and rare in human phonation. Apparent "formant-harmonic tuning" occurs in high soprano singing (Sundberg, 1977; Joliveau *et al.*, 2004), but close inspection of the data reveals that F_0 is usually slightly less than the formant frequency F_1. In some cases, at very high F_0, oscillation occurs for $F_0 > F_1$. We will show that this is more likely for a falsetto-like vibration regime. Exact tuning of F_1 with a harmonic seems to occur only in so-called *overtone singing*, where a high frequency harmonic is reinforced by a formant that is tuned precisely to its frequency (Rachele, 1996).

For low-pitched speech or singing, the dominant source harmonics (typically F_0 through $3F_0$) are below the first resonance (formant) frequency F_1 of the vocal tract. For example, a bass or baritone speaking or singing a note G_2 (98 Hz) will reach the first formant of an /i/ or a /u/ vowel only with the third harmonic. For an /a/ vowel, source harmonics higher than the seventh are needed to reach the first formant. Because these higher harmonics often do not have a great influence on the nature of vocal fold vibration, their interaction with a formant is perceived as a vowel or voice quality characteristic, not a source change. But the flow pulse may nevertheless be influenced by higher harmonic source–filter interaction, as will be shown next.

A. Level 1 interaction: Flow pulse dependency on the subglottal and supraglottal vocal tract pressures

A first level of interaction is described in which vocal fold vibration is not significantly disturbed by oscillating pressures above or below the glottis, but glottal flow is. This level occurs in all speech and is therefore worthy of special consideration.

What is common about harmonics whose frequencies are less than F_1 is that they all experience positive (inertive) reactance from the vocal tract.[1] Figure 1 (top left) shows a uniform vocal tract (subglottal and supraglottal) separated by the glottis. The top right panel shows the reactance curves (subglottal as a dashed line, supraglottal as a thin solid line, and combined reactance as a thick solid line) up to 1500 Hz. The reactance curves were calculated with cascade transmission line matrices as originally outlined by Sondhi and Schroeter (1987) and further developed by Story *et al.* (2000). From 0 to 500 Hz, the supraglottal reactance is positive (inertive), whereas from 500 to 1000 Hz it is negative (compliant). The subglottal reactance stays inertive up to 600 Hz for this configuration.

Inertive reactance has been shown to skew the flow pulse (delay its peak relative to that of the glottal area), whether it is subglottal (X_1) or supraglottal (X_2). For a review of this flow pulse skewing, see Rothenberg (1981), Fant (1986), Fant and Lin (1987), or Titze (2006a). Note the delay in the peak of U_g in Fig. 1 (bottom left) in relation to a_g (middle left). Further discussion of these graphs will follow. For glottal flow calculation, the subglottal input impedance and the supraglottal input impedance add together algebraically (in complex form) to produce the effective load imped-

ance for the glottis. This can be shown by letting the input pressure to the vocal tract (epilarynx tube) be

$$P_e = Z_2 U_g, \tag{1}$$

where U_g is the complex (Fourier transformed) glottal flow and Z_2 is the complex supraglottal impedance. Similarly, the subglottal pressure is

$$P_s = Z_1(-U_g), \tag{2}$$

where Z_1 is the subglottal impedance. The transglottal pressure is then

$$P_s - P_e = -(Z_1 + Z_2)U_g = -(R_1 + R_2)U_g - i(X_1 + X_2)U_g, \tag{3}$$

where R_1 and R_2 are the subglottal and supraglottal resistances, $i = \sqrt{-1}$, and X_1 and X_2 are the corresponding reactances. Note that the combined reactance $X_1 + X_2$ shown in Fig. 1 (top right, thick line) is not necessarily symmetric about the horizontal axis because the subglottal and supraglottal peaks do not occur at identical frequencies.

For incompressible, quasisteady glottal flow, the transglottal pressure can also be expressed aerodynamically as

$$P_s - P_e = k_{t\frac{1}{2}} \rho u_g^2 / a_g^2, \tag{4}$$

where k_t is an empirically-determined transglottal pressure coefficient with an average value of about 1.1 (Scherer *et al.*, 1983; Alipour and Scherer, 2007; Fulcher *et al.*, 2006), ρ is the air density, u_g is the time-dependent flow, and a_g is the time-varying glottal area. Equation (4) is nonlinear in u_g and cannot easily be Fourier transformed, and since the resistances and reactances in Eq. (3) are in the frequency domain, Eqs. (3) and (4) cannot be equated. In previous work with a wave-reflection analog of the vocal tract (Titze, 1984), it was shown that the flow had the following closed-form solution:

$$u_g = \frac{a_g c}{k_t}\left\{-\left(\frac{a_g}{A^*}\right) \pm \left[\left(\frac{a_g}{A^*}\right)^2 + \frac{4k_t}{\rho c^2}(p_s^+ - p_e^-)\right]^{1/2}\right\}, \tag{5}$$

where c is the sound velocity, and A^* is an equivalent vocal tract area defined as

$$A^* = A_s A_e/(A_s + A_e), \tag{6}$$

with A_s and A_e being the subglottal and supraglottal (epilaryngeal) entry areas, respectively. Further, in the wave-reflection algorithm (Kelly and Lochbaum, 1962; Liljencrants, 1985; Story, 1995; Titze, 2006b) p_s^+ is the incident partial wave pressure arriving from the subglottis and p_e^- is the incident partial wave pressure arriving from the supraglottis. It should be noted that the wave-reflection analogs do not include the exact near-field pressures (Zhao *et al.*, 2002: Zhang *et al.*, 2002), but capture the most important fields for wave propagation in the vocal tract.

Equation (5) is critically important for understanding source–filter interaction because it defines explicitly a coupling parameter, a_g/A^*. Note that when a_g/A^* is small, the flow reduces to

$$u_g = a_g\left[\frac{4(p_s^+ - p_e^-)}{k_t \rho}\right]^{1/2}, \tag{7}$$

which becomes a direct proportion to the glottal area a_g. If a constant subglottal pressure were to be applied to produce the glottal flow, the incident partial pressure wave p_s^+ in the wave-reflection algorithm would be replaced by half of the lung pressure P_L with a +1 reflection coefficient, so that the subglottal pressure would then be $P_s = p_s^+ (1+r) = 2p_s^+ = P_L$ (Titze, 1984; Story, 1995). Furthermore, if the incident supraglottal pressure p_e^- were set to zero, then

$$u_g = a_g\left[\frac{2P_L}{k_t \rho}\right]^{1/2}, \tag{8}$$

which is the asymptotic condition for linear (noninteractive) source–filter coupling. For linear coupling, the relative phase delays between p_s^+ and p_e^- due to wave propagation are responsible for the nonproportionality between u_g and a_g.

The skewing of the flow pulse as a result of an overall inertive reactance produces new harmonic frequencies in the glottal airflow that are not part of the glottal area waveform. This result is not new (Rothenberg, 1981; Fant and Lin, 1987; Koizumi *et al.*, 1985), but most previous analyses have underestimated the amount of skewing because the exact geometry of the epilarynx tube was not known. The magnetic resonance images produced by Story (1995; 2005) have been the key data sets to validate strong source–filter interaction. The uniform tubes in Fig. 1 produce relatively weak interactions. In the middle panels, a sinusoidal a_g waveform is shown on the left and its corresponding single line spectrum is shown on the right. With this sinusoidal area (forced oscillation), glottal flow was produced (bottom left panel) with 0.8 kPa lung pressure in a voice simulator that could be switched between forced oscillation and flow-induced self-sustained oscillation. Equation (5) was combined with a 44 section uniform vocal tract with energy losses and the appropriate radiation impedance was used as previously described (Titze, 2006b). Note that the flow waveform is slightly skewed and has an entire spectrum of frequencies (bottom right). Wave propagation occurred in both subglottal and supraglottal tracts. The source–filter coupling is nonlinear because new frequencies (harmonic distortion frequencies) are created by the vocal tract.

The skewing of the flow pulse guarantees a dominant excitation near glottal closing and raises the energy in the harmonics (Fant, 1986). In the past it has been assumed that the harmonic spectrum of the source comes primarily from vocal fold collision. This may be true for many phonations, but this example shows that vocal fold collision is not essential to produce source harmonics. Nonlinear source–filter coupling can produce a spectrum of source frequencies, with a spectral slope of about −15 dB per octave in this case. Furthermore, the harmonic amplitudes are affected by the reactance curve. The short vertical lines in the top right panel above the reactance curves show the location of the harmonics in the bottom right figure. Note that harmonics 3 and 4 are in negative reactance territory and are depressed slightly in amplitude, relative to harmonics 2 and 5. The simplest explanation for this amplitude depression is that negative

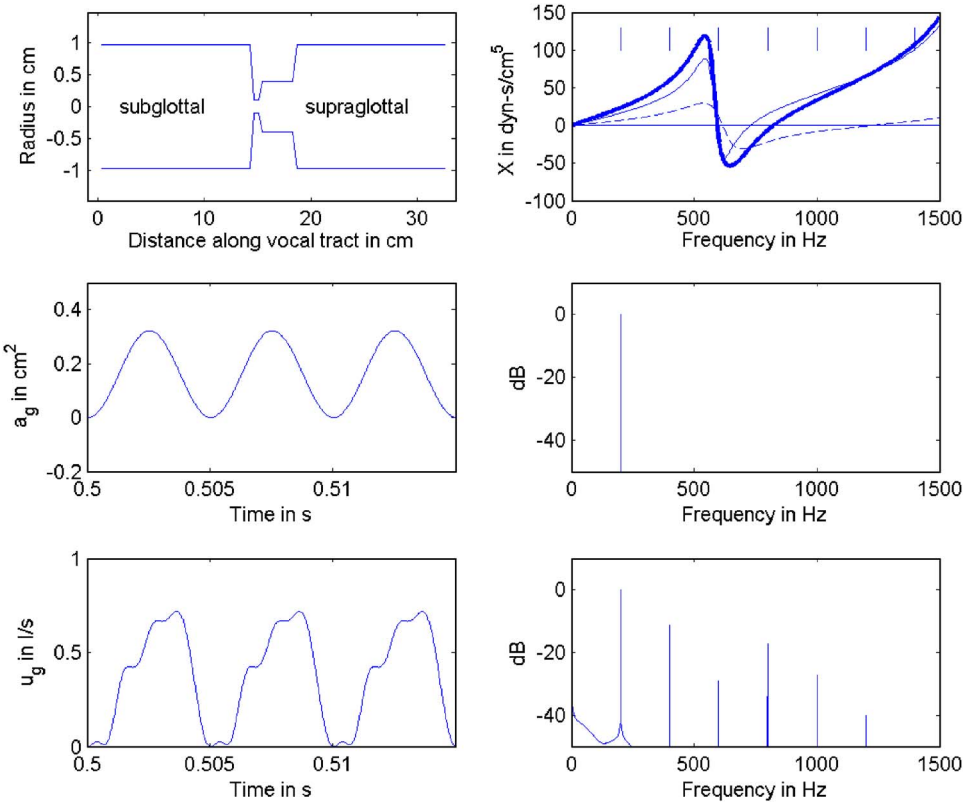


FIG. 2. (Color online) Harmonic frequency generation by source–filter generation with stronger coupling (A_e=0.5 cm^2); (top left) vocal tract shape; (top right) reactance curves, thin solid line for supraglottal, dashed line for subglottal, and thick solid line for combined; (middle left) sinusoidal glottal area function; (middle right) spectrum of glottal area; (bottom left) glottal flow; (bottom right) spectrum of glottal flow.

(compliant) reactance integrates the downstream flow and builds up an opposing pressure that reduces the flow at a given frequency. If negative reactance were present at all frequencies, the flow pulse would be skewed to the left because more flow would be accepted during glottal opening than glottal closing as the back pressure builds up. With frequency dependent reactance, selective components that would skew the pulse to the left are reduced in amplitude because, overall, the pulse is still skewed to the right. A more detailed discussion would require the consideration of all the phases of the components and how they are affected by variable reactance.

Figure 2 shows the same set of curves as in Fig. 1, but now the coupling between the source and the filter is increased to a more realistic value. By reducing the epilarynx tube cross-sectional area A_e from 3.0 cm^2 in Fig. 1 to 0.5 cm^2 in Fig. 2 (compare upper left graphs), the input impedance to the vocal tract has been increased. This input impedance is scaled by $\rho c/A_e$, the characteristic acoustic impedance of the first section of a tube, where ρ is the density of air and c is the sound velocity. The coupling parameter a_g/A^* in Eq. (5) was correspondingly increased from 0.1 to 0.35 because it contains A_e in the formula for A^* in Eq. (6). The mean glottal area a_g was held constant at 0.15 cm^2 and the subglottal area was held constant at 3.0 cm^2. Hence, the glottal source impedance remained the same. Note that the combined reactance curve (thick line, upper right in Fig. 2) now has a net upward shift toward positive (inertive) values. Specifically, over the entire 0–1500 Hz frequency range, negative (compliant) reactance occurs only between 600 and 800 Hz.

The harmonic frequencies produced in the flow wave form (bottom left panel of Fig. 2) reflect this increase in coupling strength. An apparent "closed phase" is seen, even though there was no glottal closure. As in Fig. 1, the area function a_g was sinusoidal and always remained above zero (no truncation). This brings into question that whole enterprise of inferring vocal fold vibration patterns from inverse-filtered glottal flow, especially in terms of an open phase and a closed phase. Rothenberg and Zahorian (1977) showed that inverse filtering to obtain the glottal area from mouth flow is fundamentally a nonlinear process. Linear prediction cannot accomplish this task.

Comparing the harmonic spectra (bottom right) across Figs. 1 and 2, we see that the strength of the harmonics is again related to the amount of inertive reactance present at the harmonic frequency. For the F_0 selected here (200 Hz), the third harmonic gained no strength with increased coupling because it still resides in negative (compliant) reactance territory, as in Fig. 1. The second and the fourth harmonics, however, both experience a slight amplitude increase due to higher reactance. In particular, the fourth harmonic, which was in negative territory, now experiences about zero reactance. This stronger fourth harmonic is responsible for the ripple seen in the flow waveform at the bottom left. (Only three ripple cycles are seen on the increasing flow; the fourth ripple cycle is hidden on the downward slope and on the flat portion near zero flow). The spectral slope is now only on the order of −10 dB per octave.

Because the source spectrum can be affected by vocal tract reactance, and because this reactance is frequency dependent, a spectrogram with an F_0 glide at constant vocal tract shape (identical to the shape shown in Fig. 2, top left) was investigated. This type of a pitch–glide spectrogram was

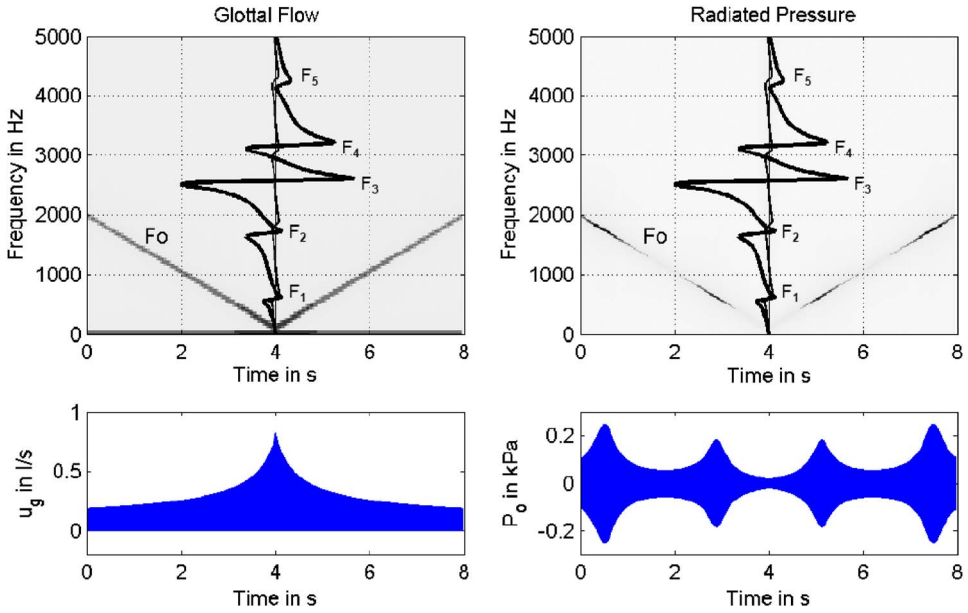


FIG. 3. (Color online) F_0 glide produced with a driven sinusoidal glottal area function with no source–filter interaction; (top left) spectrogram for glottal flow based on sinusoidal glottal area, with reactance curves overlaid vertically; (top right) spectrogram for radiated mouth pressure P_0; (bottom left) amplitude envelope of glottal flow; (bottom right) amplitude envelope of radiated mouth pressure.

analyzed for recordings of human subjects in the companion paper (Titze *et al.*, 2008). Figure 3 shows the noninteractive (linear) case as a control for later interactive cases. No interaction with tissue vibration was allowed because the vibration was still forced with a sinusoidal area rather than self-sustained. At the top left we see a spectrogram of the F_0 glide (straight sloping line), from 2000 to 100 Hz and back to 2000 Hz. The signal used in the spectrogram was the glottal flow u_g, a purely sinusoidal function derived from the sinusoidal area function a_g according to Eq. (8). The amplitude envelope of this sinusoidal flow is shown below the spectrogram on the left. Its peak at 4.0 s comes from the fact that the glottal area function (not shown) was programmed to vary inversely with the square root of frequency to approximate realistic amplitudes of vibration.

The spectrogram (top left panel) also shows the reactance curves of Fig. 2, now superimposed on the center of the spectrogram such that they are displayed vertically from 0 to 5000 Hz. Positive reactance is to the left and negative reactance is to the right of center. The reactance fluctuation in the third and fourth formant region (around 3000 Hz) is so large that the subglottal reactance is barely visible on the same scale. This large fluctuation is attributed to the epilarynx tube, which begins to establish its own characteristic quarter-wave resonance near the third formant at 2500–3000 Hz (Titze and Story, 1997).

Note again that no harmonic distortion frequencies are created by the vocal tract for this noninteractive F_0 glide, the control case. The single frequency component of the flow (F_0, sloping downward from 0.0 to 4.0 s and then upward from 4.0 to 8.0 s) is unaffected by the filter. What is affected by the filter is the oral radiated pressure P_o, shown on the right side of Fig. 3. As expected, P_o increases near 0.6 s when F_0 passes through F_2 and near 3.0 s when F_0 passes through F_1. These increases (and decreases on the other side of a formant) would be perfectly symmetric if the radiation at the mouth were independent of frequency. High frequencies radiate better than low frequencies, however, which produces a greater P_o at 2000 than at 100 Hz, even though the peak glottal flow was 0.2 vs 0.8 l/s at these extremes.

Figure 4 shows the flow-interactive case, with A_e remaining at 0.5 cm^2. Vocal fold vibration still remained forced (no interaction with tissue vibration). The confirming observation is that a series of extra harmonics ($2F_0$ through $4F_0$) is again created in u_g by vocal tract coupling. These harmonics are reinforced when there is positive reactance (positive reactance curve is left of the vertical center line) rather than at the center of the formants. This is especially noticeable in the second harmonic. [The dependence on reactance is also present in the fundamental, but the spectrogram gray scale was deliberately saturated for F_0 so that the higher harmonics could be seen.] At the formants, where the reactance changes suddenly from positive to slightly negative, the source harmonics are diminished in their amplitudes. This is further evidenced by the envelope of the flow wave form u_g, which is modulated by an uneven treatment of the harmonics by this reactance (note the valleys at 0.8 and 3.0 s in the bottom left panel). The peaks and valleys in the amplitude envelope are unmistakable evidence of nonlinear source–filter coupling because the glottal area and lung pressure were identical to the control case. As a result, the overall peak-to-valley ripple in the P_o waveform (bottom right) is less severe than in the linear case of Fig. 3. The dips in the u_g amplitude at the formants partially cancel the increase in energy transmission through the vocal tract at the formants (Rothenberg, 1987). Thus, the effect of nonlinear formant–harmonic coupling in the glottal flow (level 1 interaction) is to distribute the acoustic energy over the entire spectrum rather than to accentuate it at the center of a formant.

In summary, rather than attempting to resonate several source harmonics by tuning them to the tube resonances, as is done in many musical instrument designs, a vocalist may attempt to reinforce a cluster of several harmonics with favorable reactance. In most cases, as many harmonics as possible are placed on the lower frequency side of a formant (below the resonance frequency). For high-pitched singing,

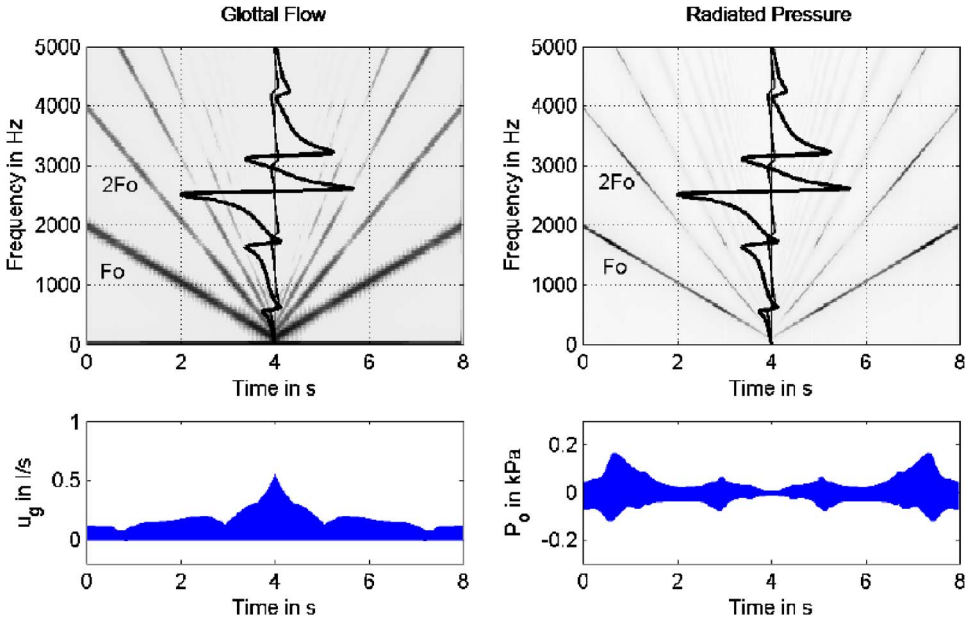


FIG. 4. (Color online) F_0 glide produced with a driven sinusoidal glottal area function with source–filter interaction (A_e=0.5 cm^2); (top left) spectrogram for glottal flow based on sinusoidal glottal area, with reactance curves overlaid vertically; (top right) spectrogram for radiated mouth pressure P_0; (bottom left) amplitude envelope of glottal flow; (bottom right) amplitude envelope of radiated mouth pressure.

this often requires a special vowel, so that at least F_0, $2F_0$, and $3F_0$ can all be reinforced over a reasonable pitch range. An example is shown in Fig. 5, where subglottal reactance is now shown by the thin line and supraglottal reactance by the thick line. Note the ranges of F_0, $2F_0$, and $3F_0$ below the reactance curves at the bottom of Fig. 5. Only the subglottal reactance is negative in the $2F_0$ range, but in the next discussion it will be shown that the combination of a compliant (negative) subglottal reactance and an inertive (positive) reactance provides ideal reinforcement of vocal fold vibration. So, the loss in level 1 interaction may in part be overcome by a gain in level 2 interaction. This example suggests that certain vowels will be favored over other vowels. The utility of this type of interaction is that source and filter frequencies do not need to match exactly, leaving some degree of freedom for articulation and vowel migration with the general goal of strengthening the dominant low-frequency harmonics.

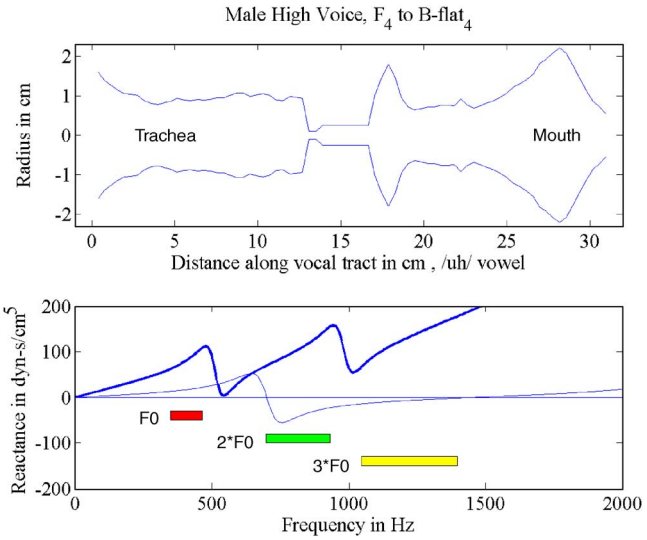


FIG. 5. (Color online) (Top) Vocal tract shape for the vowel /U/; (bottom) reactance curves, thick line supraglottal and thin line subglottal, and favorable ranges for F_0, $2F_0$, and $3F_0$ shown underneath.

B. Level 2 interaction: Mode of vibration dependency on vocal tract reactance

There is another level of interaction, identified as level 2, which involves a change of the vibration pattern of the vocal folds as a result of vocal tract changes. For this level of interaction, subglottal reactance and supraglottal reactance affect vocal fold vibration differently. While supraglottal reactance is generally most favorable when it remains inertive (positive), the subglottal reactance is sometimes more favorable if it is compliant (negative). The complicating factor is the geometry of the vocal folds, or shape of the glottis, in direct analogy to Fletcher's (1993) differentiation of inward, outward, and lateral striking valves that can self-sustain oscillation in a pipe. An added complexity, not discussed by Fletcher, is that vocal folds can propagate a surface wave in their tissue, which changes the shape of the valve dynamically. Based on this surface wave, a relation for the mean intraglottal driving pressure on the vocal fold surface was derived previously (Titze, 1988),

$$P_g = P_s\left(1 - \frac{a_2}{a_1}\right) + P_e\frac{a_2}{a_1}, \tag{9}$$

where P_g is the mean (entry to exit) intraglottal driving pressure, P_s is the subglottal pressure, P_e is the supraglottal (epilarynx tube) input pressure, a_1 is the glottal entry area (lower margin of the vibrating portion of the vocal folds), and a_2 is the glottal exit area (upper margin of the vibrating portion of the vocal folds). In deriving Eq. (9), the pressure profile in the glottis was assumed to follow the Bernoulli energy conservation law, the glottal area was assumed to vary linearly from bottom to top, the acoustic pressure P_e was assumed to be the only pressure recovery at glottal exit, and the transglottal pressure coefficient was set to 1.0 for simplicity. (For details of the full derivation, see Titze (1988), p. 1542.)

As a valve, the vocal folds are closest to the (+,+) case described by Fletcher (1993). In his notation, the valve is

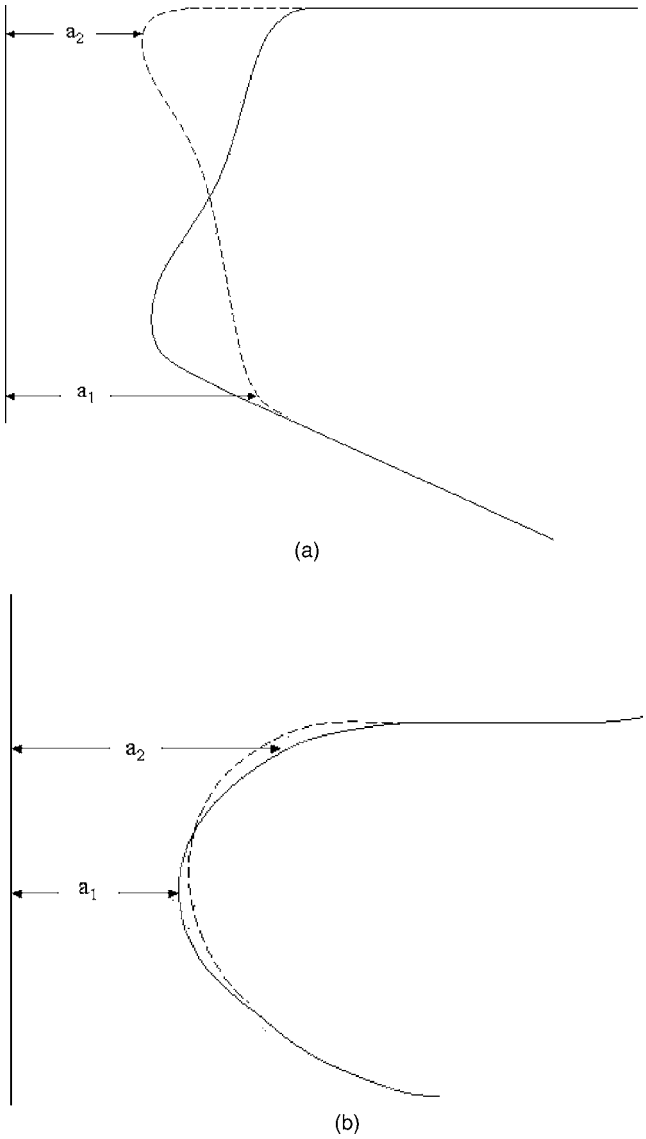


FIG. 6. Sketches of right vocal fold tissue displacement from the glottal midplane in coronal view of (a) modal register and (b) falsetto register. After Hirano, 1975.

(+,+) if tissue moves laterally with both increasing subglottal pressure (first +) and increasing supraglottal pressure (second +). But, as Eq. (9) indicates, intraglottal pressure is greater for a convergent glottis than for a divergent glottis. Tissue surface waves on the vocal folds (i.e., standing waves, or modes of vibration) can be excited by the airflow to produce self-sustained oscillation, even without vocal tract interaction (Titze, 1988). Note that, even if P_s is a constant and P_e is zero in Eq. (9), an alternating push–pull pressure can be created by an a_2/a_1 ratio that is less than 1.0 for lateral movement and greater than 1.0 for medial movement. Vocal tract interaction is therefore an important, but not a necessary, condition for self-sustained vocal fold oscillation.

Figure 6 shows a sketch of how the medial surface of the vocal folds may change during vibration, both in terms of the static and the time varying configuration. The sketch is patterned after Hirano (1975). Two different registers of phonation are identified. In the so-called modal register [Fig. 6(a)], vibration is observed over much of the thickness of the vocal folds, so that the entry area a_1, where vibration begins, is low in the glottis vertically. To the contrary, in the so-called falsetto register [Fig. 6(b)], vibration is confined mainly to the upper portion of the vocal folds, with a_1 being much higher in the glottis. (The point where vibration effectively begins vertically in the glottis has been called the mucosal upheaval point; Yumoto and Kadota, 1998). If we approximate the vibrating portion of the medial surface with a straight line, then the prephonatory shape is both convergent ($a_2<a_1$) and divergent ($a_2>a_1$) for the modal register but mainly divergent ($a_2>a_1$) for the falsetto register. Physiologically, the thyroarytenoid (TA) muscle controls this medial surface shape. When the TA muscle contracts, it thickens and bulges out the lower part of the vocal fold, thereby "squaring up" the glottis and producing modal register. When the TA muscle is relaxed, the bottom of the vocal fold retracts and only the top remains engaged in vibration. The medial surface is more rounded. The vocal ligament is used for adductory positioning and tensing of the vocal fold tissues.

It will now be shown how vocal tract pressures can assist or hinder vibration in these basic two registers. Neglecting vocal tract resistance and steady pressures for the first part of the discussion, basic acoustic theory would predict the vocal tract pressures to be

$$P_s = -I_1\frac{du}{dt} \quad \text{inertive subglottal tract} \tag{10}$$

$$= P_1 - \frac{1}{C_1}\int u\,dt \quad \text{compliant subglottal tract,} \tag{11}$$

$$P_e = +I_2\frac{du}{dt} \quad \text{inertive supraglottal tract} \tag{12}$$

$$= P_2 + \frac{1}{C_2}\int u\,dt \quad \text{compliant supraglottal tract,} \tag{13}$$

where P_1 and P_2 are constants of integration. With these relations, the intraglottal pressure of Eq. (9) has four possible forms:

$$P_g = -I_1\left(1-\frac{a_2}{a_1}\right)\frac{du}{dt} + I_2\frac{a_2}{a_1}\frac{du}{dt} \quad \text{inertive – inertive} \tag{14}$$

$$= P_1 - \frac{1}{C_1}\left(1-\frac{a_2}{a_1}\right)\int u\,dt + I_2\frac{a_2}{a_1}\frac{du}{dt} \quad \text{compliant – inertive,} \tag{15}$$

$$= -I_1\left(1-\frac{a_2}{a_1}\right)\frac{du}{dt} + P_2 + \frac{1}{C_2}\frac{a_2}{a_1}\int u\,dt \quad \text{inertive – compliant,} \tag{16}$$

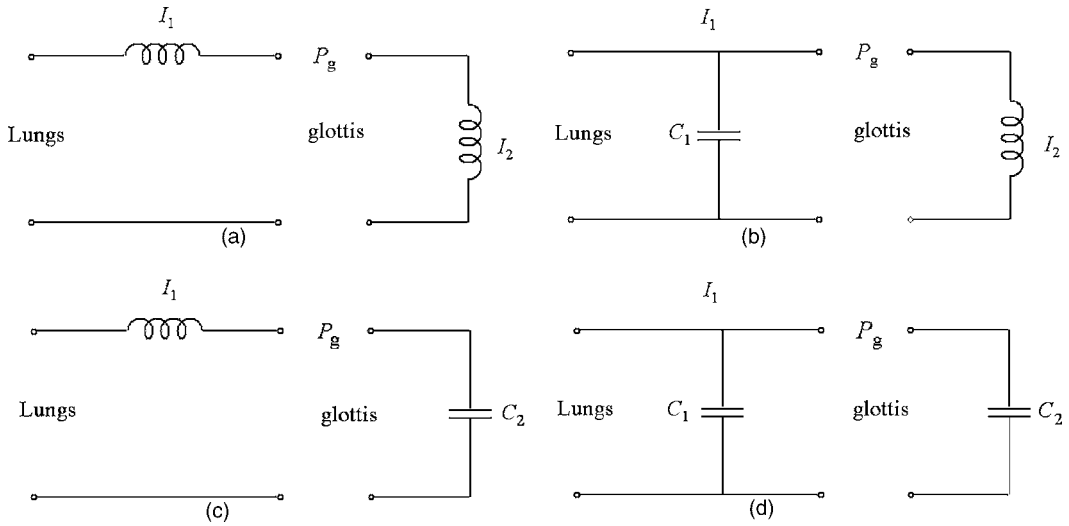


FIG. 7. Acoustic circuit diagrams for subglottal and supraglottal reactance, (a) inertive–inertive, (b) compliant–inertive, (c) inertive–compliant, and (d) compliant–compliant.

$$= P_1 - \frac{1}{C_2}\left(1 - \frac{a_2}{a_1}\right)\int udt + P_2 + \frac{1}{C_2}\frac{a_2}{a_1}\int udt \qquad \text{compliant – compliant.} \qquad (17)$$

These cases are basically the same as the four cases described by Fletcher (1993). An acoustic "circuit" representation of these relations is shown in Fig. 7. Inertance is represented by coils I_1 and I_2 and compliance is represented by parallel plates C_1 and C_2, following the symbolism of electric circuitry for inductance and capacitance, respectively. The driving pressure P_g from the above-presented mathematical expressions is also labeled in Fig. 7. For maximum reinforcement of vocal fold vibration, the driving pressure P_g should provide an alternating push–pull on the vocal fold tissue, a push when the glottis is opening and a pull when the glottis is closing. Thus, when du/dt is positive (flow is increasing during glottal opening), P_g should be positive; when du/dt is negative (flow is decreasing during glottal closing), P_g should be negative.

Consider first the *inertive – inertive* case [Eq. (14) and Fig. 7(a)]. Both coefficients in front of du/dt in Eq. (14) should be positive for the push–pull condition. The only way this can occur is if $a_2/a_1 > 1.0$ over most of the open portion of the glottal cycle, which means the glottis must be mainly divergent. Falsetto register may provide this configuration quite readily, referring to Fig. 6(b). It is known that the top of the vocal folds spread apart slightly in falsetto register. A net divergent glottis at the top created by this spread would appear to be beneficial to both terms in Eq. (14). For modal register, the divergent configuration occurs over a smaller fraction of the glottal cycle, prior to closure. But maximum pressures occur in this fraction of the cycle, yielding strong excitation in a pulse-like manner. Thus, subglottal inertance I_1 generally provides both a help and a hindrance to vocal fold vibration in modal register. On the other hand, supraglottal inertance I_2 always provides the favorable push–pull condition, for both registrations and both glottal configurations. The Flanagan and Landgraf (1968) and Ishizaka and Flanagan (1972) simulations had no subglottal tract. Hence, their vocal tract interaction effects were probably exaggerated. The Zhang *et al.* (2006a, b) investigations had only a subglottal tract, which could underestimate the overall interaction. The Zañartu *et al.* (2007) simulations included both a subglottal and a supraglottal tract. Given that their vocal fold model was composed of only a single mass, the results can be considered an excellent correction to the Flanagan and Landgraf (1968) model. In a later section, it will be shown that neglect of the subglottal reactance can be dramatic, even with greater degrees of freedom in tissue movement.

The *compliant–inertive* tract appears to be the most favorable for vocal fold vibration in modal register [Eq. (15) and Fig. 7(b)]. If the glottis is mostly convergent, with divergence occurring only over a small fraction of the cycle prior to closure, the integration of the flow in Eq. (15) produces a steady decrease in intraglottal pressure over the open portion of the glottal cycle (because $a_2 < a_1$). This gradual decrease in pressure (stronger during opening and weaker during closing) adds to the dominant push–pull produced by the inertive supraglottal tract, as described before. Tongue-tip trills (McGowan, 1992) have also been shown to be sustained by an upstream compliant reactance. The dominant compliance in tongue trills is a wall compliance (rather than an air compliance), but the effect is similar.

The *inertive – compliant* tract [Eq. (16) and Fig. 7(c)] is the least favorable for modal register. Supraglottal integration of the flow u raises the intraglottal pressure throughout the open portion of the cycle, creating a greater push during closing than during opening. This is contrary to the desired push–pull condition. In addition, when the glottis is convergent ($a_2/a_1 < 1.0$), the inertive subglottal tract further hinders oscillation, as discussed earlier. But some assistance is possible from subglottal inertance in falsetto register, if $a_2 > a_1$, also as discussed earlier.

Finally, a *compliant – compliant* tract [Eq. (17) and Fig. 7(d)] is also not favorable to modal register, but a little more

so than the inertive–compliant combination just discussed. For convergence, although the gradual pressure reduction from the first integration in Eq. (17) is favorable, the second integration is detrimental. The worst of all situations exists for divergence. The glottis is simply blown apart by a uniformly increasing intraglottal pressure. Thus a *compliant–compliant* vocal tract squelches phonation when the glottis diverges.

To determine how the above-noted driving pressures affect the frequency and amplitude of self-sustained oscillation, it is typical to develop an autonomous differential equation of motion for tissue displacement in terms of flow-dependent driving pressures. Fletcher's (1993) small amplitude analysis of autonomous vibration of simple pressure-controlled valves in gas flows is relevant to vocal fold vibrations, but the alternating convergent–divergent glottis created by surface waves on the tissues were not modeled. Hence, the analysis was basically for a one-mass model (or the x_{10} mode in the abbreviated mode nomenclature of Titze (2006b, Chap. 4). Adachi and Sato's (1996) treatment of two-dimensional lip vibration (transverse and longitudinal to the flow) captured a z_{10} mode in addition to the x_{10} mode, but also did not include the surface wave. Titze's earlier (1988) analysis did include the surface wave, but considered only downstream inertive reactance of the tract (the most typical for low F_0 speech). In Chan and Titze (2006) and in Titze (2006b, Chap. 7), upstream inertive reactance was also considered, but not compliant reactance. Thus, to date nobody has derived an autonomous differential equation that includes both inertive and compliant reactance, upstream and downstream, with the inclusion of a surface wave on the tissue.

Given that Fletcher's (1993) closed-form (analytical) solutions contain both subglottal and supraglottal reactance explicitly, his equations are utilized here to approximate frequency and amplitude changes for autonomous (self-sustained) oscillation. Equations (19) and (20), from Fletcher (1993) p. 2176, were solved with the following parameters (Fletcher's notation) that are relevant for human phonation: $\sigma_1=\sigma_2=+1$ (Fletcher's overpressure parameters that define the valve type); $W=1.0$ cm (vocal fold length); $m=0.05$ g (vocal fold mass in vibration); $S_1=S_2=S_3=0.5$ cm^2 (inferior, medial, superior surfaces of vocal folds, respectively); $x_0=0.03$ cm (neutral glottal half-width); $\bar{p}_2=10\,000$ dyn/cm^2 ≈ 1 kPa (mean subglottal pressure); $\theta=30°$=entry and exit angles into glottis; $k=(0.05)\,(2\pi F_0)$=tissue resonance bandwidth (157 Hz at $F_0=500$ Hz); X_1, X_2=subglottal and supraglottal reactances, respectively (variables).

Both X_1 and X_2 were varied according to the reactance curves of Fig. 2 (top right). They are redrawn for comparison at the top of Fig. 8. Recall that these reactances apply to a uniform 3.0 cm^2 subglottal tract and a uniform 3.0 cm^2 supraglottal tract that has a narrowed 0.5 cm^2 epilarynx tube.

Fletcher's analytical equations allow for direct specification of the natural frequency F_0 of the vocal fold oscillator in a no-load condition. This frequency was varied from 0 to 1500 Hz as a pitch glide to correspond to human ranges of F_0 and to predict the F_0 jumps observed in the data of the companion paper (Titze *et al.*, 2008). F was defined to be the

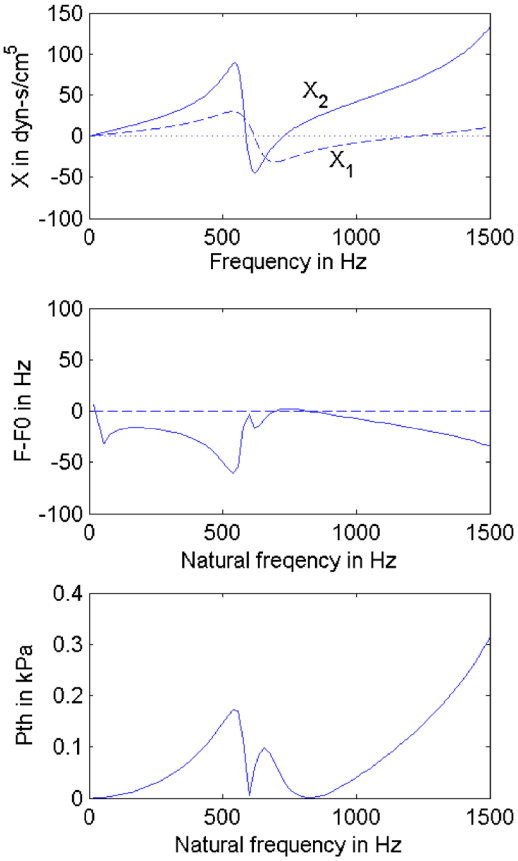


FIG. 8. (Color online) Fletcher's (1993) small oscillation analysis; (top) reactance curves; (middle) the difference between the oscillation frequency F and the no load frequency F_0; (bottom) oscillation threshold pressure P_{th}.

true oscillating frequency for any applied load. Figure 8 (middle graph) shows calculations for $F-F_0$, the difference in oscillation frequency from the no-interaction fundamental frequency. In the bottom graph we see the corresponding oscillation threshold pressure P_{th}.

Consider first some general trends. The oscillation frequency tends to be mostly below the no-interaction resonance frequency F_0. This is because inertive reactance dominates in airways that have a constricted region (the epilarynx tube in this case), creating effectively an increase in the mass of the oscillating system (tissue and air columns collectively). Note that there is a general inverse relation between $F-F_0$ and the supraglottal reactance X_2. The highest frequency is at 750 Hz, where $X_1=-30$ dyn s/cm^5 (compliant) and $X_2=0$. This frequency is slightly greater than F_0. The most notable drop in frequency (−50 Hz) occurs just above 500 Hz, where both X_1 and X_2 are highly positive. The small peak around 600 Hz is for $X_1=X_2=0$, the no-interaction condition for which $F=F_0$.

The threshold pressure P_{th} basically follows the sum of the reactance curves. Aside from a narrow dip near the tube resonances, where $X_1+X_2=0$, the lowest threshold pressure is found in the 750–1000 Hz region, where X_1 is negative (compliant) and X_2 is positive (inertive). Thus, as stated earlier, the *compliant – inertive* acoustic load is the most favorable to vocal fold oscillation. Titze and Sundberg (1992) have shown that every doubling of lung pressure above threshold raises the source intensity by about 6 dB. In addi-

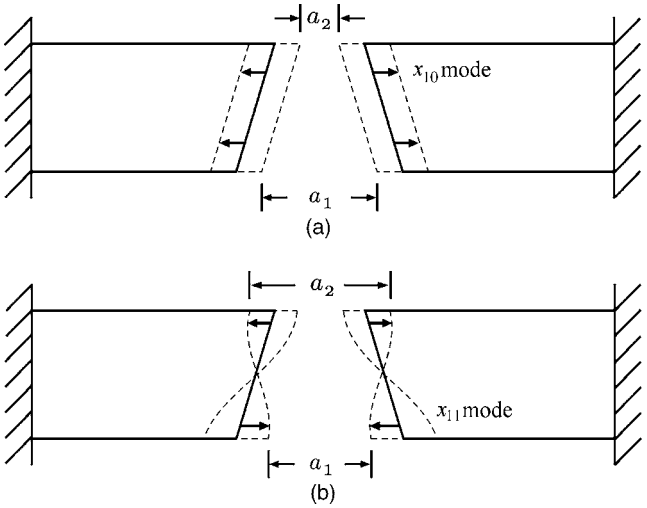


FIG. 9. Sketches of a convergent glottis with two vibrational modes, (a) the x_{10} mode and (b) the x_{11} mode.

tion, Alipour *et al.* (2001) showed that an approximate 6 dB increase in intensity was obtained in an excised larynx when a vocal tract was added by way of a physical tube that lowered the threshold pressure. Given that the threshold pressure in Fig. 8 varies from below 0.1 to above 0.3 kPa, and given that typical lung pressures for speech range between 0.5 and 1.0 kPa, it is possible that more than one doubling of P_{th} or 6–12dB in source intensity could be realized in the lower threshold regions with normal lung pressures. But a word of caution is in order. The Fletcher (1993) equations used for the Fig. 8 calculations did not contain vocal tract losses. Hence, the P_{th} fluctuations are probably overestimated. Nevertheless, significant changes in source energy are likely with only a few tenths of a kPa reduction in P_{th}.

In any vocal fold model other than the one-mass model, the a_2/a_1 ratio is variable throughout the glottal cycle. The amount of dynamic a_2/a_1 variation can be explained in terms of two dominant modes of vibration of vocal fold tissues (Fig. 9). For prephonatory (static) convergence, an x_{10} mode has no vertical variation in tissue displacement, as shown in Fig. 9(a). It produces less variation in the a_2/a_1 ratio than an x_{11} mode, which has a 180° phase difference between top and bottom displacement, as shown in Fig. 9(b). [For a complete description of tissue modes and their nomenclature, see Titze (2006b), Chap. 4]. The a_2/a_1 ratio for the x_{10} mode gradually increases and decreases over the open portion of the glottal cycle, but stays between 0.0 and 1.0. For the x_{11} mode, however, both convergence and divergence can be experienced over the cycle. Thus, the x_{11} mode is less dependent on vocal tract interaction than the x_{10} mode because the pushes and pulls from vocal tract pressures tend to cancel each other over the glottal cycle. This conclusion agrees with what Flanagan and Landgraf (1968) observed with a one-mass model, which only supports an x_{10} mode, and what Zhang *et al.* (2006a, b) observed on a physical model. It is also the reason why Zañartu *et al.* (2007) focused their recent analysis on the one-mass model. All models with a dominant x_{10} mode are highly affected by vocal tract reactance. In the two-mass model of Ishizaka and Flanagan (1972), the x_{11} mode was present and vocal tract interaction was reduced. Thus, the percentage of x_{11} mode excitation (relative to x_{10}) serves as a decoupler of vocal tract interaction, in direct opposition to the narrowing of the epilarynx tube. It offers a vocal tract-independence mechanism of self-sustained oscillation (Titze, 1988; Lucero and Koenig, 2007; Chan and Titze, 2006; Jiang and Tao, 2007). Speakers and singers who adjust their source and filter for linear coupling rely heavily on this mechanism of self-sustained oscillation.

III. SOURCE–FILTER INTERACTIONS WITH COMPUTER SIMULATIONS

Because of the many simplifications and limitations imposed by the low-dimensional vocal fold models and analytical treatments, it is important to balance the above-presented results with computer simulation models that are capable of handling all levels of interaction and many degrees of freedom in tissue movement.

A. Methods

An $L \times M \times N$ point-mass model of the vocal folds was used for simulation of flow-induced, self-sustained oscillation. The details of this model are beyond the scope of any single article, but are well documented in Titze (2006b, Chap. 4). L is the number of masses in the medio-lateral direction (7 in this simulation), M is the number of masses in the anterior–posterior direction (5 in this simulation), and N is the number of masses in the inferio–superior direction (5 in this simulation). Thus, the model had 175 point masses, each with two degrees of freedom (horizontal and vertical). Tissue properties were defined with a fiber-gel construct, where the fibers carried the nonlinear stress–strain characteristics of muscle, ligament, and mucosa, and the gel properties were defined with Young's moduli, shear moduli, and Poisson's ratios (Titze, 2006b; Chaps. 2–4). Aerodynamic pressures and glottal flow were calculated with a modified Bernoulli equation that included flow separation and jet formulation by rule (Titze, 2006b, Chap. 5). All vocal tract pressures were computed with the well-known wave-reflection analog (Liljencrants, 1985; Story *et al.*, 1996; Titze, 2006b, Chap. 6).

Based on the foregoing autonomous differential equation analyses, it was important to include both a subglottal and a supraglottal vocal tract to assess the individual and combined interaction effects. As in the previous section on level 1 interaction with forced oscillation, the subglottal system had 36 cylindrical sections, each 0.398 cm long, for a total length of 14.33 cm. The supraglottal system had 44 cylindrical sections, each of the same length, for a total of 17.51 cm. The first eight sections of the supraglottal tract again constituted the epilarynx tube, the diameter of which was kept uniform so that a single parameter (A_e) could be varied for coupling strength. The sampling frequency was 44.1 kHz. The medial surface of the vocal folds was nearly flat, with a slight convergence in the inferio–superior direction and a similar convergence (tapering) in the posterio–

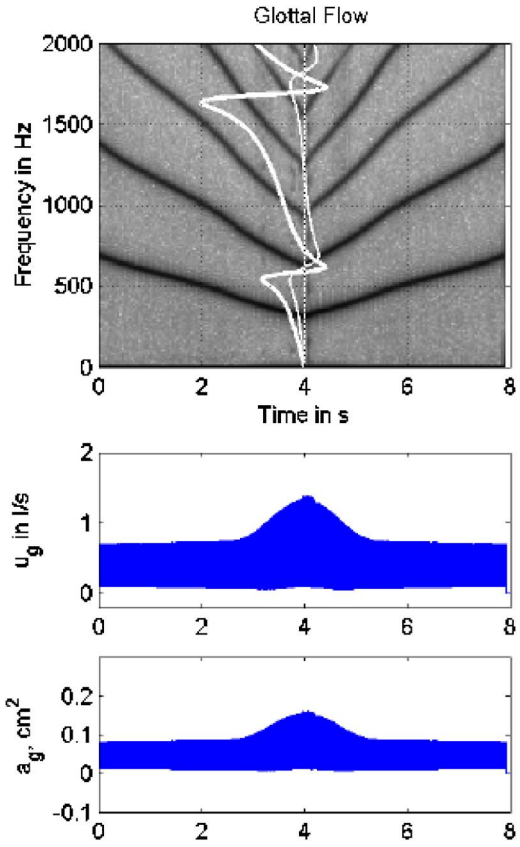


FIG. 10. (Color online) Simulation of downward and upward F_0 glide produced with a 175 point-mass self-oscillating biomechanical model of the vocal folds with no vocal tract interaction; (top) spectrogram, with reactance curves superimposed vertically, thick white line supraglottal and thin white line subglottal; (middle) glottal flow envelope; (bottom) glottal area envelope.

anterior direction. Dynamically, the shape of the glottis assumed a variety of mode configurations due to surface wave propagation.

Control parameters for this model were lung pressure P_L and simulated muscle activations of the intrinsic laryngeal muscles of the larynx: cricothyroid (CT), thyroarytenoid (TA), lateral cricoarytenoid (LCA), posterior cricoarytenoid (PCA), and interarytenoid (IA). These muscle activations (ranging from 0.0 for no activation to 1.0 for 100% activation) positioned the vocal folds (Titze, 2006b, Chap. 3; Titze and Hunter, 2007) and determined all of the tissue properties. Specific values will be given in the following sections.

B. Results

1. Simulation 1

A no-interaction case was first investigated as a control case. A high–low–high pitch glide was simulated under self-sustained oscillation, following the pattern produced earlier for level 1 interaction and produced by human subjects in the companion paper. Figure 10 shows a spectrogram for the glottal flow waveform, with both the subglottal reactance (thin white solid line) and the supraglottal reactance (thick white line) superimposed vertically. These reactances are the same as in previous figures (Figs. 2–4 and 8) for the uniform tubes with a 0.5 cm^2 epilarynx tube. The zero line for the reactance curves is set at time=4 s, and the scaling of the reactance magnitude can be obtained from Fig. 2. Underneath the spectrogram, the amplitude envelope for the glottal flow u_g is shown in the middle panel and the amplitude envelope for the glottal area a_g is shown in the bottom panel. The following parameters of the model were held constant in the simulations: P_L=1.5 kPa, LCA activity=31%, IA activity =30%, PCA activity=0.0%, vowel=uniform tube with narrowed epilarynx tube as in Fig. 2, with no nasal coupling. CT activity was varied from 90-0-90% and TA activity from 0-10-0%. Details of how these activities affect laryngeal posturing in a speech-like gesture can be found in Titze and Hunter (2007).

To simulate no vocal tract interaction, the pressures in the glottis were programmed as described previously in the forced oscillation case (level 1 interaction). Waves propagated through the vocal tract and were radiated from the mouth, but this propagation produced no load on the glottis because the incident pressures (traveling waves) were nullified by programming for glottal flow and pressure calculation. Only aerodynamic pressures and flows were retained. Note that this caused glottal flow and glottal area envelopes to be proportional, as in the forced oscillation case. The glottal area spectrogram (not shown) was identical to the glottal flow spectrogram, indicating that there was no interaction. Both spectrograms showed harmonics; however, these resulted from vocal fold collision in this case instead of flow pulse skewing. (It is difficult to obtain a perfectly sinusoidal area with no collision with self-sustained oscillation.) The broad peak in the center of the u_g and a_g envelopes was due to greater laxness of the tissue, which caused greater vibrational amplitude when F_0 was low. The fundamental frequency (F_0) in the glide ranged from 700 to 330 Hz. Note that F_0 passed through the positive peak of the reactance curve at about 1.0 s and again at about 7.0 s, but this had no effect on the flow or area waveforms, indicating linear source–filter coupling for this control case.

2. Simulation 2

For the next simulation, subglottal interaction alone was investigated. To uncouple the supraglottal tract, the supraglottal pressure was set to zero in the program for the purpose of glottal flow and intraglottal pressure calculation, but not for wave propagation. Figure 11 shows the result. Note first that the overall signal strength is a little less than for no interaction, judged by height of the a_g and u_g envelopes, and there is not an exact proportionality between the glottal area and glottal flow. More important, new frequencies have been created due to bifurcations in tissue movement, as seen in the spectrogram on top. At 0.8 s, a period-3 subharmonic occurs, which changes to a period-5 subharmonic at 1.6 s. The timing of the period-3 bifurcation agrees with F_0 being in the maximum negative reactance dip and the period-5 bifurcation occurs when $2F_0$ enters the negative reactance region. Much needs to be understood about the nature and onset of these subharmonic bifurcations, but this is a topic for subsequent research. Suffice it to say here that individual harmonics passing through rapidly changing reactance regions can destabilize the vibration regimes, as the foregoing analysis

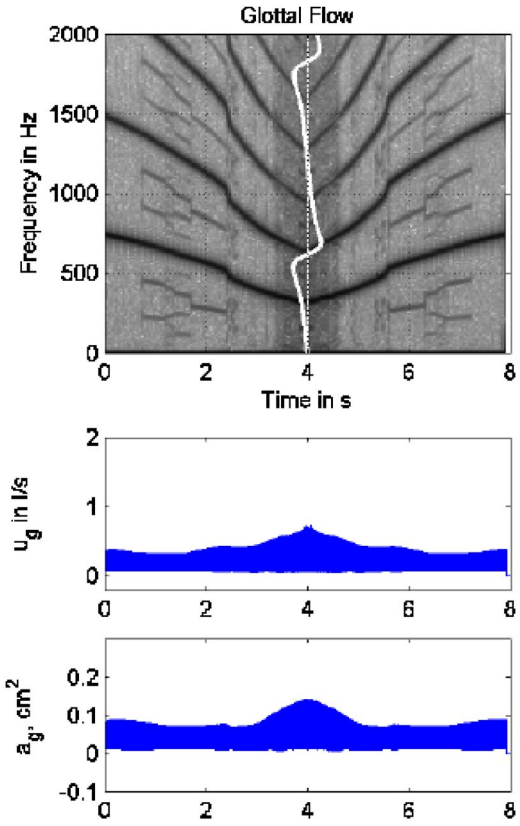


FIG. 11. (Color online) Simulation of downward and upward F_0 glide produced with a 175 point-mass self-oscillating biomechanical model of the vocal folds with subglottal interaction only; (top) spectrogram, with subglottal reactance superimposed vertically with white line; (middle) glottal flow envelope; (bottom) glottal area envelope.

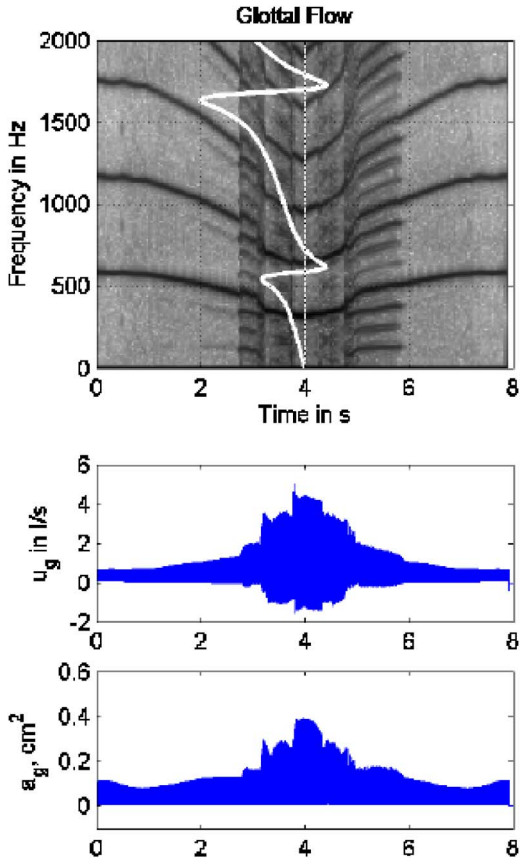


FIG. 12. (Color online) Simulation of downward and upward F_0 glide produced with a 175 point-mass self-oscillating biomechanical model of the vocal folds with supraglottal interaction only; (top) spectrogram, with supraglottal reactance superimposed vertically with white line; (middle) glottal flow envelope; (bottom) glottal area envelope.

demonstrated. Our quantitative interest here is in F_0 drops, because they are the most predictable instabilities and the most prevalent in our companion paper on human phonation.

An F_0 drop of about 50 Hz occurs at 2.4 s. This F_0 drop, predicted well by the foregoing small oscillation analysis with Fletcher's (1993) model (Fig. 8) and by Zhang *et al.* (2006a,b) on a physical laboratory model that had only subglottal interaction, was a "correction" from a higher F_0 that prevailed in the compliant reactance region. The starting F_0 was 750 Hz rather than the no-interaction F_0 of 700 Hz seen in Fig. 10. Compliance basically adds stiffness to the interactive vibrating system, thereby raising F_0, whereas inertance adds mass, thereby lowering F_0. An interesting observation is that the 50 Hz pitch jump occurred below the positive peak of the reactance curve. This may be related to the fact that the second harmonic $2F_0$ entered the compliant region at about 2.4 s, which could have delayed the jump by adding some stiffness to the system before inertive reactance took over. At 3.2 s in Fig. 11, some perturbed vibration occurred, as indicated by the darker (noisier) background. This aperiodic vibration is related to an impedance mismatch instability, i.e., the source impedance became lower, on average, than the vocal tract input impedance, and highly variable due to oscillation. The F_0 upglide showed a slight asymmetry in the duration of another brief noisy regime at 5.6 s, indicating a small hysteresis effect.

3. Simulation 3

The next simulation was for supraglottal interaction alone. Here subglottal pressure was set to the lung pressure, but supraglottal traveling waves were kept intact. Results are shown in Fig. 12. The waveform envelopes show that this case has the greatest overall signal energy. (The scale of u_g has been increased by a factor of 3 and the scale of a_g by a factor of 2 with respect to Figs. 10 and 11). A weak period-4 bifurcation occurred at 2.0 s, followed by a stronger one at 2.7 s. F_0 and $2F_0$ both went from higher to lower inertive reactance in this bifurcation region. With regard to fundamental frequency changes, note that F_0 started lower than in the noninteractive case, 570 Hz instead of 700 Hz. This "pulling down" of F_0 toward F_1, even when all muscle activities were the same as before, resulted from the inertive reactance of the vocal tract, which (as stated earlier) adds mass to the interactive oscillating system. A very small F_0 rise (10–20 Hz) is then seen at the beginning of the strong period-4 bifurcation, correlated with diminished reactance for both $2F_0$. This small rise, together with the subharmonic regime, delays the eventual larger drop in F_0 of about 100 Hz in positive reactance territory. Finally, the vocal fold vibrational amplitude became disproportionably large and slightly unstable in the 3.0–5.0 s region. A hysteresis effect was also seen in that the bifurcations were delayed on the upslope of the glide. Given that these bifurcations did not appear in the

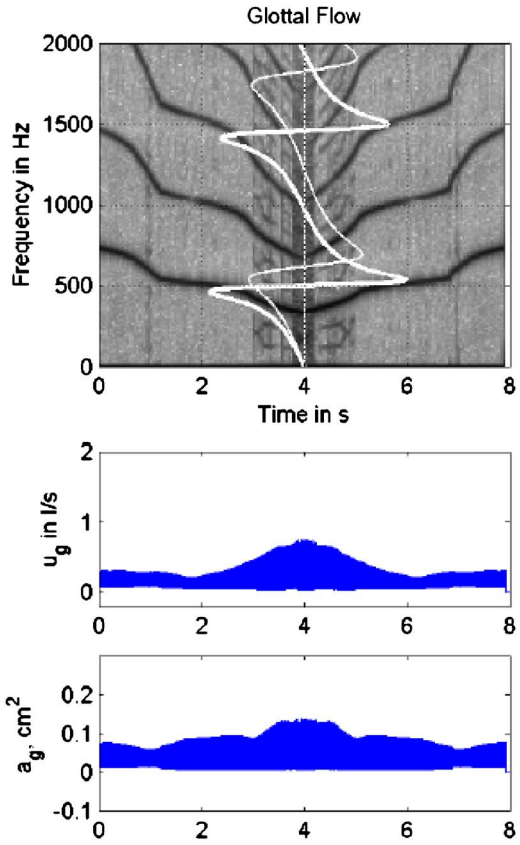


FIG. 13. (Color online) Simulation of downward and upward F_0 glide produced with a 175 point-mass self-oscillating biomechanical model of the vocal folds with both subglottal and supraglottal interaction, A_e=3.0 cm^2; (top) spectrogram, with subglottal reactance (thin white line) and supraglottal reactance (thick white line) superimposed; (middle) glottal flow envelope; (bottom) glottal area envelope.

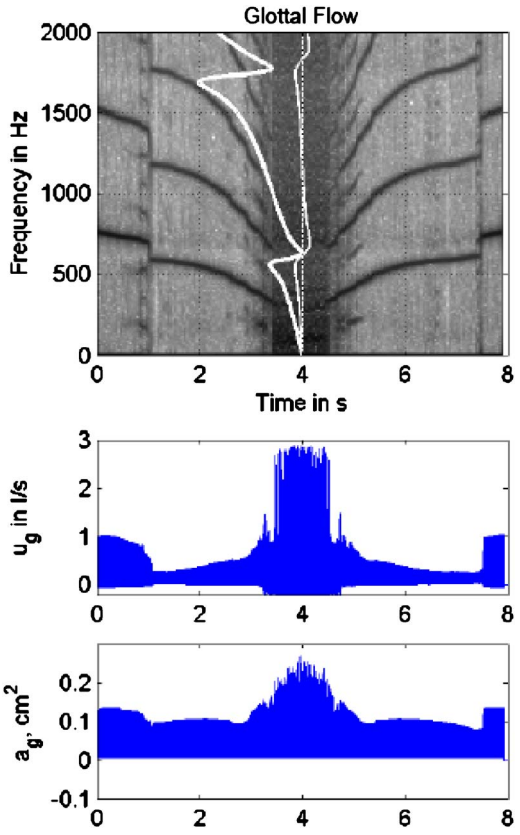


FIG. 14. (Color online) Simulation of downward and upward F_0 glide produced with a 175 point-mass self-oscillating biomechanical model of the vocal folds with both subglottal and supraglottal interaction, A_e=0.2 cm^2; (top) spectrogram, with subglottal reactance (thin white line) and supraglottal reactance (thick white line) superimposed; (middle) glottal flow envelope; (bottom) glottal area envelope.

noninteractive case (Fig. 10), we conclude that they are the result of supraglottal source–filter interaction.

4. Simulation 4

The next simulation was with combined subglottal and supraglottal interactions. Thus, it represented a realistic (nonrestricted) situation. The degree of supraglottal interaction was controlled by two separate values of the cross-sectional area of the epilarynx tube A_e. For the lowest degree of interaction (A_e=3.0 cm^2) the epilarynx tube diameter was equal to that of the uniform tube (recall Fig. 1, top left). Figure 13 shows the simulation results for this configuration. Both subglottal and supraglottal reactance curves are shown in white on the spectrogram, supraglottal being the thicker line. Again the scales are arbitrary, but the relative magnitudes between subglottal and supraglottal reactance are correct. There were two F_0 drops, one at about 0.8 s, where F_0 entered a region of rapidly changing overall F_1 reactance and $2F_0$ entered a region of positive supraglottal reactance, and another at drop about 3.0 s, where F_0 entered the region of positive supraglottal F_1 reactance. Also, $2F_0$ entered the *compliant–compliant* region at the second drop, and a period-3 bifurcation occurred when $2F_0$ entered this region, similar to what was seen in Fig. 12. Some evidence of chaotic vibration was seen near 4.0 s, where the lowest F_0 and the highest vibration amplitude occurred. The overall signal strength was slightly less than that of the noninteractive case (the scale for the signal envelopes was set back to that of Figs. 10 and 11).

5. Simulation 5

Figure 14 shows results for a severe case of epilaryngeal constriction (A_e=0.2 cm^2). The overall signal strength was much higher (scale on the glottal flow envelope was changed to 3.0 l/s), and stronger bifurcations occurred. A 100 Hz F_0 jump occurred at 1.0 s, which was preceded by a period-4 subharmonic, again as F_0 entered the rapidly changing reactance region. When $2F_0$ entered the minimum reactance regions, around 3.0 s, destabilization occurred in the vibration, as evidenced by further bifurcations. Strong hysteresis effects were also evident in that reverse bifurcations occurred at higher frequencies. Of particular significance is the fact that vibrational amplitude increased and decreased sharply (and irregularly) near the lowest F_0 (middle graph), while the flow amplitude reached a plateau (bottom graph). This plateau is attributed to the fact that the input impedance to the vocal tract became higher than the glottal impedance for A_e=0.2 cm^2, thus limiting the flow.

6. Changes in energy levels

Table I shows numerical results for a selected group of dynamical variables at all levels of interaction discussed earlier. (An intermediate case for A_e=0.5 cm^2 was added to

TABLE I. Output quantities for various degrees of interaction.

	Mean glottal area (cm^2)	Mean glottal flow (l/s)	Aerodynamic power (w)	Radiated power (w)	Efficiency (%)
No interaction	0.0381	0.3284	0.4825	0.0117	2.42
Subglottal only	0.0336	0.1835	0.2264	0.0033	1.44
Supraglottal only (A_e=0.5 cm^2)	0.0579	0.5014	0.7408	0.0523	7.07
Subglottal and supraglottal (A_e=3.0 cm^2)	0.0347	0.1717	0.2226	0.0014	0.62
Subglottal and supraglottal (A_e=0.5 cm^2)	0.0405	0.1860	0.2228	0.0035	1.59
Subglottal and supraglottal (A_e=0.2 cm^2)	0.0534	0.3200	0.2604	0.0143	5.49

show the progression with increased nonlinear coupling.) The output quantities for comparison are mean glottal area, mean glottal flow, aerodynamic power at the glottis, acoustic power radiated at the mouth, and glottal efficiency (the ratio of radiated power to aerodynamic power). The numbers represent time averages over the entire 8.0 s pitch glide. The "no interaction case" (top row) produced self-sustained oscillation by excitation of the x_{11} mode with aerodynamic pressures only. It serves as the control case. Consider first the "subglottal only" interaction case (row 2). In comparison to "no interaction," every dynamic quantity was reduced in magnitude. This is consistent with the expectation that subglottal inertance generally hinders vocal fold vibration, and such inertance was present over most of the F_0 glide. To the contrary, for the supraglottal only interaction case (row 3), every dynamic variable was increased, again consistent with previous predictions and discussions. Most variables increased by a factor of about 2 with supraglottal interaction only, but acoustic radiated power increased by a factor of more than 4. Glottal efficiency (the ratio of acoustic radiated power to glottal aerodynamic power) increased by a factor of about 3. Thus, supraglottal interaction alone would be a highly favored condition. Unfortunately, the trachea is always present in human phonation. Its effect cannot be removed, but perhaps altered for better reinforcement of vocal fold vibration by larynx lowering or raising.

With both subglottal and supraglottal interaction (rows 4–6), the results were dependent on the degree of interaction, which was controlled by the parameter A_e, the epilarynx tube area. For A_e=3.0 cm^2, the same as the area of the rest of the uniform tube, the radiated acoustic power was only 0.0014 W, nearly an order of magnitude less than for no interaction. This suggests that interaction is not necessarily an advantage. If the impedances are not well matched, more power can be absorbed internally in the system (Titze, 2002). Efficiency was only 0.62% compared to 2.43% for no interaction. Mean glottal flow was about half, as was the aerodynamic power. Mean glottal area remained about the same.

As the degree of interaction increased with a decrease in the epilarynx tube area A_e (rows 5 and 6), all dynamical variables increased. For the greatest interaction, A_e =0.2 cm^2, all quantities except aerodynamic power were greater than those for the "no interaction" case. This suggests a double advantage, getting more radiated power for less aerodynamic power used. Hence, the glottal efficiency had doubled, with the same lung pressure. Comparing mild interaction (A_e=3.0 cm^2) to strong interaction (A_e=0.2 cm^2), all variables increased categorically. The radiated acoustic power increased by a factor of 10, as did the glottal efficiency. We made no attempt to optimize the output variables by choosing the best value of A_e for the given glottal conditions, but we expect that such an optimization would yield an even higher efficiency.

IV. DISCUSSION AND CONCLUSIONS

Source–filter interaction has been divided into two levels. Level 1 is the interaction of glottal airflow with acoustic vocal tract pressures, even if vocal fold vibration is undisturbed. The interaction parameter is the mean glottal area divided by the effective (parallel combination) tube area of the subglottis and supraglottis. For constant adduction of the vocal folds and constant large tracheal diameters, the coupling parameter becomes the cross-sectional area of the epilarynx tube. Level 1 interaction produces harmonic distortion frequencies that contribute to the source spectrum. This interaction is present in all speech and singing, male and female. It has been described for nearly three decades, but generally underestimated in magnitude because details of the lower vocal tract were unknown. Level 1 interaction contributes to the spectral slope and the spectral ripple in the glottal sound source, even when the spectrum is purely harmonic and no bifurcations in vocal fold vibration occur. The supraglottal and subglottal impedances are additive for this interaction. If both impedances are inertive (positive), a maximum skewing of the flow pulse is achieved, which increases the maximum flow declination rate and thereby vocal intensity. Individual harmonics can be enhanced or suppressed by frequency-dependent reactances that change from positive to negative.

An interesting discovery was made in this investigation with regard to level 1 interaction. The entire spectrum of source frequencies can (theoretically) be produced without vocal fold collision. This finding could have an impact on voice therapy, particularly for vocal fold pathologies resulting from excessive tissue collision stress. With a sinusoidally varying glottal area and no vocal fold contact, a

−12 dB/octave spectral slope was shown here to be achievable with an epilarynx tube cross-sectional area of 0.5 cm^2.

Level 2 interaction is realized more in high F_0 productions for which the dominant harmonics $(F_0, 2F_0, 3F_0, \ldots)$ are near the formants. Frequency jumps and a variety of new source frequencies or instabilities can be produced, including subharmonics and non-random noise. The instabilities occur mostly when one of the dominant harmonics encounters sudden changes in reactance, destabilizing the modes of vibration of the tissue that are affected differently by reactance. The control parameter for these phenomena is the same as for level 1 interaction. Computer simulations with a high-dimensional model showed that vocal efficiency, the ratio of radiated acoustic power to aerodynamic power, can increase by an order of magnitude when the epilarynx tube area is narrowed from 3.0 to 0.2 cm^2, but this narrowing also produced greater instabilities when dominant harmonics were in unfavorable reactance regions (i.e., near formants).

A thick and pliable mucosal layer on the vocal folds can lead to self-sustained oscillation without much reliance on vocal tract reactance. A parameter for this is the strength of the x_{11} mode of vibration (characterized by large vertical phase differences) relative to the x_{10} mode. Some vocalists may have the choice to operate in either a nearly linear region, with maximum harmonic stability, or in a nonlinear region with greater output power and greater efficiency but at the expense of less harmonic stability.

In the companion paper (Titze *et al.*, 2008), the most frequently occurring instabilities in human subjects were F_0 jumps, in magnitude on the order of 30–40 Hz. But not all subjects exhibited these instabilities, suggesting that nonlinear interaction varies across subjects, and perhaps even within subjects for repeated vocalizations. The theoretical analyses here predicted the F_0 jumps, both with analytical treatments and with simulation. They are mostly triggered when F_0 passes through F_1, but occasionally when $2F_0$ passes through F_1, as both theory and measurement showed. Larger F_0 jumps tend to occur with greater coupling (i.e., a narrower epilarynx tube).

For the modal voice register, used largely in speech at relatively low F_0, the ideal vocal tract load for self-sustained oscillation would be subglottal compliance and supraglottal inertance. The x_{10} mode would get maximum reinforcement. Unfortunately, this combination does not exist at low F_0 in the human voice. Both reactances tend to be inertive because the trachea and the supraglottal tract are roughly of equal length. Although this *inertive–inertive* combination has been shown to be less favorable for self-sustained oscillation than the *compliant–inertive* combination, flow pulse skewing (level 1 interaction) benefits from dual inertive reactance. Hence the two effects are offsetting. The worst combination for self-sustained oscillation in the modal register is an inertive subglottal tract and a compliant supraglottal tract. This combination can occur in speech for low F_1 vowels such as /i/ and /u/. For example, if $F_0 = 300$ Hz, $F_1 = 250$ Hz, and $F_1^1 = 600$ Hz (first subglottal formant), then the *inertive–compliant* condition exists. If interaction is high (narrow epilarynx tube), the register can flip from modal to falsetto, which is more sustainable with this acoustic load. Females may have cultivated a mixed register for speech to avoid this instability, given that a 300 Hz fundamental frequency is well within their speaking range. The companion paper shows the females exhibit fewer instabilities on a pitch glide than males, even though the likelihood of $F_0 - F_1$ crossing is greater.

A great amount of future work is needed to determine the extent to which combinations of subglottal and supraglottal reactance can be exploited, especially in high-pitched speech, loud speech, and singing on a variety of vowels. In this paper, all discussions pertained to a neutral-shaped vocal tract. Detailed interaction effects need to be developed for all vowels and consonants. Finally, although humans do not have much control over tracheal diameters, tracheal lengths can be changed with larynx raising and lowering. Perhaps the subglottal entry configuration can also be changed for more compliance, and the soft wall construct of the trachea (the portion in contact with the esophagus) may be useful for introducing subglottal compliance.

ACKNOWLEDGMENT

Funding for this work was provided by the National Institute on Deafness and Other Communication Disorders, Grant No. 5 R01 DC004224 08.

[1]Reactance is the energy-storing part of impedance, in contrast to resistance, which is the energy-dissipating part. These two parts of impedance are written as a complex number (real and imaginary part), with reactance being the imaginary part of the impedance. Positive reactance is labeled inertive (because the acoustic flow lags behind the pressure in phase) and negative reactance is labeled compliant (because the acoustic flow leads the pressure in phase).

Adachi, S., and Sato, M. (**1996**). "Trumpet sound simulation using a two-dimensional lip vibration model," J. Acoust. Soc. Am. **99**, 1200–1209.

Alipour, F., Montequin, D., and Tayama, N. (**2001**). "Aerodynamic profiles of a hemilarynx with a vocal tract," Ann. Otol. Rhinol. Laryngol. **110**, 550–555.

Alipour, F., and Scherer, R. C. (**2007**). "On pressure-frequency relations in the excised larynx," J. Acoust. Soc. Am. **122**, 2296–2305.

Appelman, D. R. (**1967**). *The Science of Vocal Pedagogy: Theory and Application* (Indiana University Press, Bloomington, IN).

Atal, B. S., and Schroeder, M. R. (**1978**). "Linear prediction analysis of speech based on a pole-zero representation," J. Acoust. Soc. Am. **64**, 1310–1318.

Chan, R., and Titze, I. R. (**2006**). "Dependence of phonation threshold pressure on vocal tract acoustics and vocal fold tissue mechanics," J. Acoust. Soc. Am. **119**, 2351–2362.

Chiba, T., and Kajiyama, M. (**1958**). *The Vowel and Its Nature and Structure* (Tokyo-Kaisenikan, Tokyo).

Coffin, B. (**1987**). *Coffin's Sounds of Singing: Principles and Applications of Vocal Techniques with Chromatic Vowel Chart*, 2nd ed. (The Scarecrow Press, Metuchen, NJ).

Fant, G. (**1960**). *The Acoustic Theory of Speech Production* (Moulton, The Hague).

Fant, G. (**1986**). "Glottal flow: Models and interaction," J. Phonetics **14**, 393–399.

Fant, G., and Lin, Q. (**1987**). "Glottal voice source—Vocal tract acoustic interaction," Q. Prog. Status Rep. STL-QPSR **4**, 13–27.

Fant, G., Linjencrants, J., and Lin, Q. (**1985**). "A four-parameter model of glottal flow," STL Q. Prog. Status Rep. **4**, 1–13.

Flanagan, J. L. (**1968**). "Source-system interaction in the vocal tract," Ann. N.Y. Acad. Sci. **155**, 9–17.

Flanagan, J. L. (**1972**). *Speech Analysis, Synthesis, and Perception* (Springer, New York).

Flanagan, J., and Landgraf, L. L. (**1968**). "Self-oscillating source for vocal tract synthesizers," IEEE Trans. Audio. Electroacoust. **AU-16**, 57–64.

Fletcher, N. H. (**1993**). "Autonomous vibration of simple pressure-controlled valves in gas flows," J. Acoust. Soc. Am. **93**, 2172–2180.
Fulcher, L. P., Scherer, R. C., Zhai, G., and Zhu, Z. (**2006**). "Analytic representation of volume flow as a function of geometry and pressure in a static physical model of the glottis," J. Voice **20**, 489–512.
Hatzikirou, H., Fitch, W. T. S., and Herzel, H. (**2006**). "Voice instabilities due to source-tract interactions," Acta. Acust. Acust. **92**, 468–475.
Hirano, M. (**1975**). "Phonosurgery: Basic and clinical investigations," Otol. (Fukuoka) **21**, 239–440.
Ishizaka, K., and Flanagan, J. L. (**1972**). "Synthesis of voiced source sounds from a two-mass model of the vocal cords," Bell Syst. Tech. J. **51**, 1233–1268.
Jiang, J., and Tao, C. (**2007**). "The minimum glottal airflow to initiate vocal fold oscillation," J. Acoust. Soc. Am. **121**, 2873–2881.
Joliveau, E., Smith, J., and Wolfe, J. (**2004**). "Vocal tract resonances in singing: The soprano voice," J. Acoust. Soc. Am. **116**, 2234–2439.
Kelly, J. L., and Lochbaum, C. (**1962**). "Speech synthesis," *Proceedings of the Fourth International Congress on Acoustics*, Paper G42, pp. 1–4.
Klatt, D. H., and Klatt, L. C. (**1990**). "Analysis, synthesis, and perception of voice quality variations among female and male talkers," J. Acoust. Soc. Am. **87**, 820–857.
Koizumi, T., Taniguchi, S., and Hiromitsu, S. (**1985**). "Glottal source-vocal tract interaction," J. Acoust. Soc. Am. **78**, 1541–1547.
Liljencrants, J. (**1985**). "Speech synthesis with a reflection-type line analog," Doctoral dissertation, Department of Speech Communication and Music Acoustics, Royal Institute of Technology, Stockholm, Sweden.
Lucero, J. C., and Koenig, L. L. (**2007**). "On the relation between the phonation threshold lung pressure and the oscillation frequency of the vocal folds," J. Acoust. Soc. Am. **121**, 3280–3283.
Markel, J. D., and Gray, A. H. J. (**1976**). *Linear Prediction of Speech* (Springer, New York).
McGowan, R. S. (**1992**). "Tongue-tip trills and vocal-tract wall compliance," J. Acoust. Soc. Am. **91**, 2903–2910.
Mergell, P., and Herzel, H. (**1997**). "Modeling biphonation—The role of the vocal tract," Speech Commun. **22**, 141–154.
Miller, D. G., and Schutte, H. K. (**2005**). " 'Mixing' the registers: Glottal source or vocal tract?," Folia Phoniatr Logop **57**, 278–291.
Neumann, K., Schunda, P., Hoth, S., and Euler, H. A. (**2005**). "The interplay between glottis and vocal tract during male passaggio," Folia Phoniatr Logop **57**, 308–327.
Rachele, R. (**1996**). *Overtone Singing Study Guide*, 2nd ed. (Cryptic Voices Productions, Amsterdam, The Netherlands).
Rosenberg, A. (**1971**). "Effect of the glottal pulse shape on the quality of natural vowels," J. Acoust. Soc. Am. **49**, 583–590.
Rothenberg, M. (**1981**). "Acoustic interaction between the glottal source and the vocal tract," in *Vocal Fold Physiology*, edited by K. N. Stevens and M. Hinano (University of Tokyo Press, Tokyo), 305–328.
Rothenberg, M. (**1987**). "Cosi fan tutte and what it means or nonlinear source-tract acoustic interaction in the soprano voice and some implications for the definition of vocal efficiency," in *Laryngeal Function in Phonation and Respiration*, edited by T. Baer, C. Sasaki, K. S. Harris, . (College-Hill Press, Little, Brown and Company, Boston), pp. 254–269.
Rothenberg, M., and Zahorian, S. (**1977**). "Nonlinear inverse filtering technique for estimating the glottal-area waveform," J. Acoust. Soc. Am. **61**, 1063–1071.
Scherer, R. C., Titze, I. R., and Curtis, J. F. (**1983**). "Pressure-flow relationships in two models of the larynx having rectangular glottal shapes," J. Acoust. Soc. Am. **73**, 668–676.
Sondhi, M. M., and Schroeter, J. (**1987**). "A hybrid time-frequency domain articulatory speech synthesizer," IEEE Trans. Acoust., Speech, Signal Process. **35**, 955–967.
Stevens, K. (**1999**). "Current studies in linguistics," *Acoustic Phonetics* (MIT, Cambridge, MA).
Story, B., Laukkanen, A.-M., and Titze, I. R. (**2000**). "Acoustic impedance of an artificially lengthened and constricted vocal tract," J. Voice **14**, 455–469.
Story, B. H. (**1995**). "Speech simulation with an enhanced wave-reflection model of the vocal tract." Ph.D. dissertation, University of Iowa, Iowa City, IA.
Story, B. H. (**2005**). "Synergistic modes of vocal tract articulation for American English vowels," J. Acoust. Soc. Am. **118**, 3834–3859.
Story, B. H., Titze, I. R., and Hoffman, E. A. (**1996**). "Vocal tract area functions from magnetic resonance imaging," J. Acoust. Soc. Am. **100**, 537–554.
Sundberg, J. (**1977**). "The acoustics of the singing voice," Sci. Am. **236**, 82–91.
Svec, J. G., Schutte, H. K., and Miller, D. G. (**1999**). "On pitch jumps between chest and falsetto registers in voice: Data from living and excised human larynges," J. Acoust. Soc. Am. **106**, 1523–1531.
Titze, I. R. (**1984**). "Parameterization of the glottal area, glottal flow, and vocal fold contact area," J. Acoust. Soc. Am. **75**, 570–580.
Titze, I. R. (**1988**). "The physics of small-amplitude oscillation of the vocal folds," J. Acoust. Soc. Am. **83**, 1536–1552.
Titze, I. R. (**2000**). *Principles of Voice Production* (National Center for Voice and Speech, Denver, CO).
Titze, I. R. (**2001**). "Acoustic interpretation of resonant voice," J. Voice **15**, 519–528.
Titze, I. R. (**2002**). "Regulating glottal airflow in phonation: Application of the maximum power transfer theorem to a low dimensional phonation model," J. Acoust. Soc. Am. **111**, 367–376.
Titze, I. R. (**2004a**). "A theoretical study of F_0-F_1 interaction with application to resonant speaking and singing voice," J. Voice **18**, 292–298.
Titze, I. R. (**2004b**). "Theory of glottal airflow and source-filter interaction in speaking and singing," Acta. Acust. Acust. **90**, 641–648.
Titze, I. R. (**2006a**). "Theoretical analysis of maximum flow declination rate versus maximum area declination rate in phonation," J. Speech Lang. Hear. Res. **49**, 439–447.
Titze, I. R. (**2006b**). *The Myoelastic-Aerodynamic Theory of Phonation* (National Center for Voice and Speech, Denver, CO).
Titze, I. R., and Hunter, E. J. (**2007**). "A two-dimensional biomechanical model of vocal fold posturing," J. Acoust. Soc. Am. **121**, 2254–2260.
Titze, I. R., Riede, T., and Popolo, P. (**2008**). "Nonlinear source-filter coupling in phonation: Vocal exercises," J. Acoust. Soc. Am. **123**, 1902–1915.
Titze, I. R., and Story, B. H. (**1997**). "Acoustic interactions of the voice source with the lower vocal tract," J. Acoust. Soc. Am. **101**, 2234–2243.
Titze, I. R., and Sundberg, J. (**1992**). "Vocal intensity in speakers and singers," J. Acoust. Soc. Am. **91**, 2936–2946.
Van Den Berg, J. (**1957**). "Subglottal pressures and vibration of vocal folds," Folia Phoniatr. **9**, 65–71.
Vennard, W. (**1967**). *Singing: Mechanism and Technique* (Fisher, New York).
Yumoto, E., and Kadota, Y. (**1998**). "Pliability of the vocal fold mucosa in relation to the mucosal upheaval during phonation," Arch. Otolaryngol. Head Neck Surg. **124**, 897–902.
Zañartu, M., Mongeau, L., and Wodlicka, G. R. (**2007**). "Influence of acoustic loading on an effective single mass model of the vocal folds," J. Acoust. Soc. Am. **121**, 1119–1129.
Zhang, C., Zhao, W., Frankel, S. H., and Mongeau, L. (**2002**). "Computational aeroacoustics of phonation, 2. Effects of flow parameters and ventricular folds," J. Acoust. Soc. Am. **112**, 2147–2154.
Zhang, Z., Neubauer, J., and Berry, D. A. (**2006a**). "The influence of subglottal acoustics on laboratory models of phonation," J. Acoust. Soc. Am. **120**, 1558–1569.
Zhang, Z., Neubauer, J., and Berry, D. A. (**2006b**). "Aerodynamically and acoustically driven modes of vibration in a physical model of the vocal folds," J. Acoust. Soc. Am. **120**, 2841–2849.
Zhao, W., Zhang, C., Frankel, S. H., and Mongeau, L. (**2002**). "Computational aeroacoustics of phonation. 1. Computational methods and sound generation mechanisms," J. Acoust. Soc. Am. **112**, 2134–2146.

Amplitude variations in coarticulated vowels

Ewa Jacewicz[a] and Robert Allen Fox
Department of Speech and Hearing Science, The Ohio State University, Columbus, Ohio 43210-1002

(Received 19 February 2007; revised 13 February 2008; accepted 19 February 2008)

This paper seeks to characterize the nature, size, and range of acoustic amplitude variation in naturally produced coarticulated vowels in order to determine its potential contribution and relevance to vowel perception. The study is a partial replication and extension of the pioneering work by House and Fairbanks [J. Acoust. Soc. Am. **22**, 105–113 (1953)], who reported large variation in vowel amplitude as a function of consonantal context. Eight American English vowels spoken by men and women were recorded in ten symmetrical CVC consonantal contexts. Acoustic amplitude measures included overall rms amplitude, amplitude of the rms peak along with its relative location in the CVC-word, and the amplitudes of individual formants F1–F4 along with their frequencies. House and Fairbanks' amplitude results were not replicated: Neither the overall rms nor the rms peak varied appreciably as a function of consonantal context. However, consonantal context was shown to affect significantly and systematically the amplitudes of individual formants at the vowel nucleus. These effects persisted in the auditory representation of the vowel signal. Auditory spectra showed that the pattern of spectral amplitude variation as a function of contextual effects may still be encoded and represented at early stages of processing by the peripheral auditory system. © *2008 Acoustical Society of America.* [DOI: 10.1121/1.2897034]

PACS number(s): 43.70.Fq, 43.70.Bk [AL] Pages: 2750–2768

I. INTRODUCTION

This paper examines acoustic amplitude variation in naturally produced vowels as a function of vowel quality and its immediate consonantal context. Usually, formant frequencies are considered to be the primary factors determining vowel identity. However, although "secondary" acoustic cues such as duration, fundamental frequency (f_0), and amplitude have also been shown to contribute significantly to the phonetic identity of vowels, particularly little is known about the role of vowel amplitude. There is an extensive body of work supporting the linguistic use of vowel length distinctions and the perceptual importance of duration in vowel identification (e.g., Ainsworth, 1972, 1981; Mermelstein, 1978; Gottfried and Beddor, 1988; Whalen, 1989). The significance of f_0 to vowel quality has also been established (e.g., Nearey, 1989; Whalen and Levitt, 1995; Katz and Assmann, 2001). Yet, over the years, neither vowel amplitude nor the amplitudes of individual formants have been studied as systematically as have the other two secondary cues. Understandably, the literature on the subject, whether pertaining to vowel production or perception, is sparse.

Perhaps the best known set of studies exploring the role of formant amplitude comes from early speech perception research. Given the possibility of independent control over the formant amplitudes of static vowels using the parallel synthesis method, a number of experiments demonstrated that manipulations of the amplitudes of particular formants affected the perceived quality of the vowel (Lindqvist and Pauli, 1968; Carlson *et al.*, 1970; Ainsworth and Millar, 1972; Aaltonen, 1985; Schwartz and Escudier, 1987). If formant amplitudes indeed contribute to the perception of vowel quality, the question arises whether the auditory system is also sensitive to possible variations in formant amplitudes arising from coarticulation effects. However, before this question is addressed, we need to have a much better understanding of the nature, size, and range of such variation in naturally produced speech, especially in terms of the effect of immediate context. That is, given that naturally produced vowels are rarely static and dynamic cues such as formant transitions are coded primarily in the frequency domain, what is the nature and acceptable size of formant amplitude variation that may covary with dynamic frequency information? A better understanding of the nature and permissible range of such variation can help define more precisely the appropriate values in creating synthetic versions of vowels. In turn, by providing better controls, we may find that the contribution of formant amplitude to vowel perception may involve percepts other than phonetic quality, most likely vowel naturalness and timbre.

It needs to be pointed out that over the years, the primary interest in studying vowel amplitude was in determining its role in signaling linguistic prominence distinctions such as stress and accent (e.g., Fry, 1955; Lehiste and Peterson, 1959; Beckman, 1986; Sluijter and Van Heuven, 1996; Fant *et al.*, 2000a, b). However, this type of variation is fundamentally different in that it involves speaker-intended modification of vocal intensity. With regard to the basic amplitude variation, there is essentially one study which showed that vowel amplitude also varied as a function of its immediate consonantal context: House and Fairbanks (1953).

House and Fairbanks (1953) reported measurements of relative power for six American English vowels /i, e, æ, ɑ, o, u/ along with their duration and f_0. These vowels were produced in symmetrical stressed CVC syllables with twelve consonants /p, t, k, b, d, g, f, v, s, z, m, n/ differing in

[a]Electronic mail: jacewicz.1@osu.edu

 0001-4966/2008/123(5)/2750/19/$23.00 © 2008 Acoustical Society of America

voicing, manner, and place of articulation. Averaged across all consonantal contexts, the vowels fell in two groups: greater in relative power (/o, e, u/) and lesser in relative power (/i, æ, ɑ/). The differences within each group were not significant. A surprising result was that low vowels /æ, ɑ/ were the weakest in the entire set, contrary to what might have been expected given the greatest openness of both vowels. Another striking finding was that consonant voicing had a substantial effect on the vowel's amplitude: Vowels embedded in voiced consonants were more than twice as strong as vowels in the context of voiceless consonants. Considerable differences were also found as a function of consonant manner: Vowels in the context of fricatives were about 60% stronger than vowels in the context of stops. The effects of consonant place were small, showing that vowels in the contexts of velars were only slightly weaker that those in the contexts of either labials or alveolars.

These findings motivated the present study of the variation in formant amplitude in consonantal context. If specific contexts introduce such considerable changes to the overall vowel amplitude, we may expect these changes to be manifested also in the vowel spectrum. Furthermore, they may still be present at the vowel nucleus and not only at the vowel margins. There is a lack of empirical acoustic data which would relate the variability in the overall vowel amplitude as a function of consonantal context to the corresponding changes in amplitudes of particular formants. It is also unknown how the context affects formant amplitude of vowels differing in their articulation with respect to the tongue body position and degree of openness. We may only infer that context effects may be different for different vowel spectra, introducing local changes that might enhance a particular portion of the spectrum to which the perceptual system might be sensitive and may utilize it in processing and recognizing the vowel at the lexical level.

The contribution of formant amplitudes to the perception of vowel quality was recently examined in terms of manipulation of the global spectral tilt of synthetic vowels, based on the rules of formant amplitude in cascade filter model of the vocal tract (Ito *et al.*, 2001; Kiefte and Kluender, 2005). However, as demonstrated by Kiefte and Kluender (2005), spectral tilt seems to be more effective for steady-state vowels than for vowels with inherent spectral change. It becomes even more difficult to specify the synthesis values and to predict the perceptual efficacy of the global spectral tilt that may additionally vary as a function of the immediate phonetic context of the vowel.

In acoustic phonetic theory, it is generally accepted that the spectrum of a vowel is the spectrum of the glottal source filtered by the vocal tract and the vocal tract acts as a composite filter of several bandpass filters, one for each formant (e.g., Stevens, 1998; Titze, 2000). Although the vowel-specific spectral slope can be predicted from the complex interaction between glottal source and vocal tract filtering (e.g., Fant, 1956; Fant *et al.*, 1963; Fant and Lin, 1987), the size of the filter-related size variation in formant amplitude such as that found in vowels in context has not yet been integrated into the models. Yet, such spectral details may bolster speech production models, leading also to improved speech recognition schemes.

The present acoustic study is a partial replication and extension of House and Fairbanks (1953) to individual formants. The purpose of the replication is to verify the general patterns of amplitude variation in that study using current speech analysis tools. The investigation of the amplitude of individual formants, extending the original House and Fairbanks study, aims to relate the variability in the vowel spectrum to the changes in the overall vowel amplitude in consonantal context. The overall goal of this study is to characterize the nature, size, and range of acoustic amplitude variation in coarticulated vowels in order to determine its contribution and relevance to vowel perception.

II. METHODS

A. Speakers

Twenty speakers (ten men and ten women) of Midwestern American English with no known history of speech disorders participated in the present study—fourteen were born and raised in Ohio, four in Michigan, and two in Wisconsin. They were students aged 18–36 years enrolled in a variety of majors at The Ohio State University and were phonetically untrained.

B. Speech materials

Eight relatively monophthongal American English vowels were selected: /i, ɪ, ɛ, æ, ɑ, ɔ, ʊ, u/. Four of the vowels /i, æ, ɑ, u/ were among those studied by House and Fairbanks (HF), and four /ɪ, ɛ, ɔ, ʊ/ were new. Since the set in HF did not include short vowels, the vowels /ɪ, ʊ/ were added as the lax counterparts to the tense /i, u/ and the two diphthongal vowels /e, o/ were replaced by the relatively monophthongal vowels /ɛ, ɔ/. Consistent with HF, each vowel was embedded in a symmetrical C_1VC_1 context. The selected consonant set consisted of ten oral consonants /p, t, k, b, d, g, f, v, s, z/ as in HF. The two nasal consonants /m, n/ were not included in the present set. We decided to concentrate on oral vowels only because vowels in a symmetrical nasal context would have been produced with a significant degree of nasalization which would have introduced both nasal formants and nasal zeroes into the vowel spectra. In the present study, the CVCs were produced as monosyllables in a stressed position in a short phrase "It's a _____" [ɪtsə_____] and not as disyllables as in HF, in which each CVC was prefixed by unstressed [hə] (e.g., *hupeep*, *hudeed*, *hukeek*, etc.). This modification was introduced merely for practical reasons as the phonetically untrained subjects found it difficult to read a nonsense word with the above-mentioned prefix. However, in both HF and the present study the stressed target syllable was preceded by an unstressed schwa. The complete set of stimulus materials in the orthographic form presented to the speakers is listed in Table I. Each speaker recorded 240 utterances in a single session lasting approximately 1 h (8 vowels × 10 consonants × 3 repetitions). The data for /ɔ/ from three subjects and for /ɑ/ from three other subjects were subsequently discarded because it was determined during the

TABLE I. Orthographic representation of the recorded stimulus set.

Context	/i/ (heat)	/ɪ/ (hit)	/ɛ/ (bed)	/æ/ (bad)	/ɑ/ (lot)	/ɔ/ (law)	/ʊ/ (good)	/u/ (who)
[p]	peep	pip	pep	pap	pop	pawp	poup	poop
[t]	teet	tit	tet	tat	tot	tawt	tout	toot
[k]	keek	kik	kek	kak	kock	kawk	kouk	kook
[f]	feef	fif	fef	faf	fof	fawf	fouf	foof
[s]	sees	sis	ses	sas	sos	saws	sous	soos
[b]	beeb	bib	beb	bab	bob	bawb	boub	boob
[d]	deed	did	ded	dad	dodd	dawd	doud	dood
[g]	geeg	gig	geg	gag	gog	gawg	goug	goog
[v]	veev	viv	vev	vav	vov	vawv	vouv	voov
[z]	zeez	ziz	zez	zaz	zoz	zawz	zouz	zooz

analysis phase that these speakers had a complete merger of /ɔ/ and /ɑ/ (this was not true for the other speakers).

C. Procedure

Recordings were controlled by a program in MATLAB. The speaker was seated in a sound-attenuated IAC booth and was facing a LCD monitor placed outside the booth's window. A head-mounted Shure SM10A dynamic microphone was used, positioned at a distance of 2 in. from the speaker's lips. Speech samples were recorded and digitized at a 44.1 kHz sampling rate directly onto a hard disc drive. A model example word containing the vowel of interest was first displayed on the screen (e.g., "heat"). Next to the word, the stimulus sentence appeared (e.g, "It's a **beeb**"). The speaker read the sentence placing stress on the CVC word and producing the vowel quality as in the displayed word. To overcome any orthographic uncertainties, the presentation was blocked by vowel type. The order of consonantal contexts for each vowel type and the order of vowels themselves were randomized for each speaker. There was a short practice set completed before the start of each vowel category to assure that the speaker was comfortable with the spelling of the CVCs. After recording each sentence, the experimenter either accepted and saved the sentence or re-recorded it in the case of any mispronunciations. Speakers took short breaks upon request and the position of the microphone was monitored by the experimenter throughout the recording session to assure its constant distance from the speaker's lips.

D. Acoustic measurements

The set of measurements included overall rms amplitude, amplitude of the rms peak along with its location in the vowel, the amplitudes of individual formants F1–F4 along with their frequencies, vowel duration, and f_0. Prior to acoustic analysis, the tokens were digitally filtered and downsampled to 11.025 kHz. Measurements of both vowel duration and the duration of the whole CVC word served as input for subsequent automated measurements of rms peak location and the entire set of amplitude and frequency measurements. Standard measures of vowel duration were used (Peterson and Lehiste, 1960; Hillenbrand *et al.*, 1995). Vowel onsets and offsets were located by hand, primarily on the basis of a wave form display with segmentation decisions checked against a spectrogram. For vowels in the context of fricatives, vowel onset was measured from the cessation of noise in the periodic wave form following a frication offset and vowel offset was determined by the onset of noise in the wave form signaling the start of final frication. For vowels in the context of stops, vowel onset was measured from onset of periodicity (at a zero crossing) following the release burst. Vowel offset for voiceless stops was defined at the point at which the amplitude of the vowel dropped to near zero (which was also coincident with elimination of all periodicity in the wave form). The vowel offset for voiced stops was defined as that point when the amplitude dropped to near zero and any periodicity in the wave form contained no high frequency components (as expected for voicing produced during the stop closure). Because vowel amplitude was the primary focus, we eliminated those portions of the vowel near offset that were produced with creaky voice. This happened in about 20% of productions from three speakers who had a tendency to use irregular phonation at word offsets. All segmentation decisions were later checked and corrected (and then rechecked) by both experimenters using a MATLAB program that displayed the segmentation marks superimposed over a display of the CVC's wave form (in two different views—a view that included the entire CVC and an expanded view that concentrated on the vowel portion only).

Two measures of vowel amplitude were used in this study, the peak rms and the overall rms. The peak rms measure estimates the peak energy of the vowel, i.e., the highest amplitude of the vocalic portion or syllable nucleus. The overall rms (the quadratic mean) is a measure of vowel amplitude calculated from vowel onset to vowel offset. The choice of both measures instead of one was dictated by our desire to replicate the HF results choosing the amplitude values that would correspond most closely to the "maximum level for each syllable." HF measured the maximum level of each stressed syllable, defined as the point of maximum intensity reached during the production of the stressed vowel as indicated on an analog sound level meter and recorded graphically on paper. However, in reporting their result, HF used another measure called "relative power," which was a manipulation "to facilitate arithmetic treatment" (p. 110). Namely, each measurement for each subject was expressed in decibels above the lowest value for that subject and the difference N between the two values ($N_{\max} - N_{\min}$) was con-

verted to relative power for this subject which was equal to $\text{antilog}_{10} N/10$. Calculated in this way, each of these relative power values is a simple ratio value and there is no specific measure unit that can be assigned to them. In reporting their results as relative power, HF did not use any specific unit as they did in reporting their duration (in seconds) and f_0 (in Hz) measurements (see, for example, their Table 5). Their vowels were simply comparatively greater or smaller in relative power, which might be thought of as greater or smaller in magnitude, as all values were reported in relative power.

From the HF report, we do not know the exact decibel values for their "syllable maximum" measurements. Since our present focus was to relate the measures of overall vowel amplitude and the amplitude of individual formants, we measured both the peak rms and the overall rms amplitude to observe their relationship for individual vowels and consonantal contexts. The amplitudes of individual formants were then measured at the temporal location of the rms peak, which gives the best estimate of how spectral energy is distributed in the most "intense" region in the vowel. We expected higher decibel values for the peak rms measure as compared to the overall rms, but whether the effects of consonantal context would be the same for both measures could not be determined without empirical investigation. Based on how the analyses were done using the experimental apparatus available to HF, the overall rms measure may correspond more closely to HF measurements. Yet, examination of the overall rms measure alone would be problematic for the present focus which investigates changes to the amplitude spectrum in addition to the more "global" amplitude variation as a function of consonantal context. It was therefore decided to report the results for the overall rms in addition to the results for rms peak amplitude.

To find the location and size of the amplitude peak, the rms values of a series of overlapping 25 ms windows were calculated whose number varied with the duration of the vowel. The temporal location of the center of the 25 ms window with the highest rms value was defined as the location of the rms peak. The location of the rms peak was expressed as its relative position (with values ranging from 0 to 100%) with regard to the duration of the word.[1]

Formant frequency values and amplitudes of the first four formant peaks based on 14-pole LPC analysis were extracted automatically using a MATLAB program which determined the location of the rms peak. The program displayed these values along with the FFT and LPC spectrum and provided a wideband spectrogram of the entire vowel. No preemphasis was applied. In some cases, the formant frequency values obtained were compared to the formant peaks identified using smoothed FFT spectra and from the wideband spectrograms with formant tracks displayed (using the program TF32, Milenkovic, 2003). Errors in formant estimation in LPC analysis were then hand-corrected. The effects of consonantal context on formant amplitude were assessed by first examining the variation of A1, the strongest formant of each vowel. The decibel values for A1 (and for the higher formants A2, A3, and A4) were measured relative to the reference level of the speech analysis program (written in MATLAB), which is the lowest nonzero instantaneous amplitude that is coded by the A/D conversion. The differences between the amplitude of each higher formant and that of A1 were then analyzed. Because amplitude spectrum varies as a function of vowel category, the amplitude variation of the higher formants became more apparent when reported relative to A1. The (negative) decibel differences reflect the strength of the higher formant relative to A1. Smaller negative decibel difference values here denote a stronger higher formant. Conversely, greater negative decibel difference values imply its relative weakness.

The f_0 of the rms peak window was computed using cepstral analysis (Oppenheimer and Willsky, 1977) and hand-corrected when the method measured the frequency of a higher harmonic.

E. Statistical treatment of the amplitude results

In the HF study, the amplitude measures for each subject were expressed relative to the lowest value for that subject. A primary reason for this expression was to control for individual variation (in vocal characteristics, general amplitude levels, etc.). However, as HF note, the results of their analysis of variance (ANOVA) tests indicated that subject variation had not been "completely obliterated." The current study took the approach of using within-subject (also called repeated-measures) designs for all inferential statistical tests. The advantage of a within-subject design is that idiosyncratic variations among subjects (which is commonly found in phonetic experiments but is of no interest here) can be controlled for. In particular, in within-subject designs the differences among subjects are measured and separated from the error terms in the calculation of the test statistic (e.g., t and F values).

We used within-subject ANOVAs to assess the significance of amplitude variation. For each amplitude-related measure (i.e., location of rms peak, amplitude of rms peak, overall amplitude, and amplitudes of formants) an overall ANOVA was first completed with the within-subject factors vowel and consonantal context. Speaker gender was included as a between-subjects factor. To further explore significant consonant effects for each measure, separate repeated-measures ANOVAs were completed on individual vowels for the factors manner, voicing and place for the /b, p, d, t, v, f, z, s/ set, and for the factors place and voicing for the /b, p, d, t, g, k/ set. In each of these additional analyses, speaker gender was included as a between-subjects factor. For all reported significant main effects and interactions, the degrees of freedom for the F-tests were Greenhouse–Geisser adjusted when there were significant violations of sphericity. In addition to the significance values, a measure of the effect size—partial eta squared is reported (η^2, whose value can range from 0.0 to 1.0, should be considered a measure of the proportion of variance explained by a dependent variable when controlling for other factors). Post hoc analyses were completed using either additional ANOVAs on selected subsets of the data (with appropriate F tests) or Bonferroni-adjusted t-tests.

The results for vowel duration were assessed by within-subject ANOVAs and Bonferroni-adjusted t-tests. f_0 results

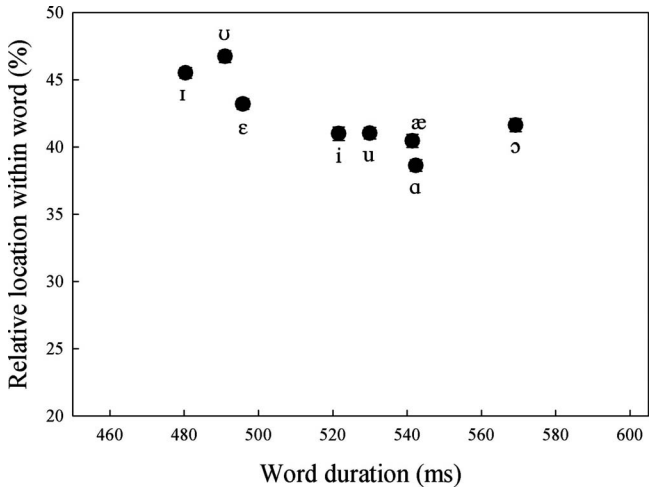


FIG. 1. Mean relative location of rms peak within a word as a function of each word's mean duration averaged across ten consonantal contexts.

were not assessed statistically because they are reported here merely to establish consistency with the HF data for all three secondary cues, including vowel amplitude, vowel duration, and f_0. At present, vowel duration and f_0 do not constitute a focus of the study.

III. RESULTS

A. Amplitude of rms peak and overall rms amplitude

The amplitude of rms peak was measured at its temporal location within the CVC word which varied for individual vowels. Despite the variation, the mean peak values for all vowels were still before vowel midpoint (Fig. 1). In general, the peaks of the short vowels /ɪ, ɛ, ʊ/ occurred later than the peaks of the remaining longer vowels.

The variation in the relative positions of rms peak within word as a function of consonantal context is summarized in Fig. 2. The peaks in the context of stops occurred later than in the context of fricatives and, statistically, the effect of manner was strong $[F(117)=306.16, p<0.001, \eta^2=0.947]$. The peaks were also significantly later in the context of

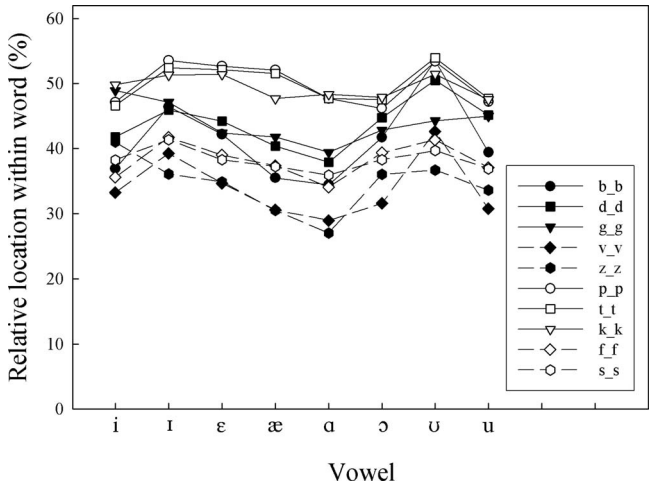


FIG. 2. Mean relative location of rms peak within a word shown for each vowel and for each individual consonantal context.

TABLE II. Mean vowel amplitude at rms peak and overall rms amplitude (in decibels) (s.d.) in consonantal contexts grouped by voicing, manner, and place of articulation. All vowels are pooled.

Grouped consonant environments	rms peak	Overall rms
Voicing		
Voiceless	−15.58 (3.89)	−18.26 (3.76)
Voiced	−15.45 (3.72)	−18.26 (3.62)
Manner of articulation		
Stop	−15.68 (3.79)	−18.28 (3.65)
Fricative	−15.27 (3.83)	−18.22 (3.74)
Place of articulation		
Labial	−15.01 (3.80)	−17.71 (3.69)
Alveolar	−15.79 (3.84)	−18.62 (3.72)
Velar	−15.97 (3.66)	−18.63 (3.50)

voiceless consonants than voiced $[F(1,17)=82.09, p<0.001, \eta^2=0.828]$. The effects of place were more variable and were mostly not significant.

Table II shows, following HF, means for amplitude of rms peak and overall rms amplitude grouped by consonant voicing, manner, and place across all vowels pooled. The mean amplitudes at rms peaks were consistently higher (2.74 dB) than the mean overall rms amplitudes. As is evident, however, neither amplitude values varied appreciably as a function of the consonantal features. This is in sharp contrast to HF results, particularly for voicing and manner.

Figure 3, drawn after HF, shows rms means for individual consonantal contexts (stops and fricatives) across all vowels pooled. Unlike the HF data, there is no sharp division

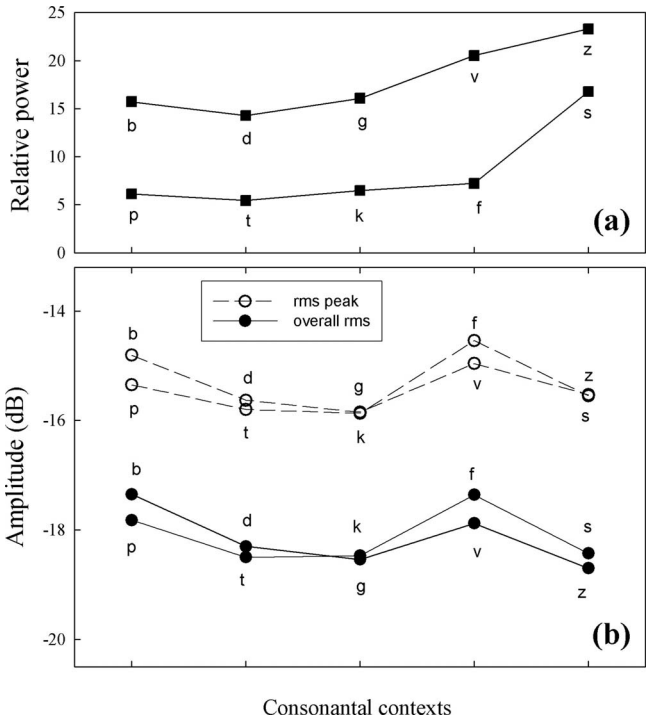


FIG. 3. Consonantal context effects on vowel amplitude pooled across all vowels. (a) Data from House and Fairbanks (1953) for their relative power measure (see the text). (b) Mean amplitudes (in decibels) of rms peak and overall rms in the present study.

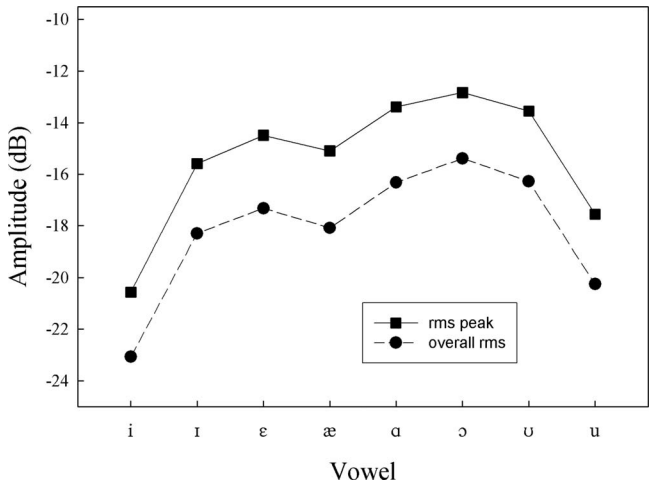


FIG. 4. Mean amplitudes of rms peak and overall rms for individual vowels averaged across all consonantal contexts.

between vowel amplitude in voiced and voiceless contexts. Although the general trends for all stops and the fricatives /v, f/ are consistent with HF, the results for the fricatives /z, s/ differ rather drastically. Unlike the HF results, the amplitudes of vowels in the environments of either /z/ or /s/ were not the greatest in the entire consonant set and did not differ appreciably from those in the context of alveolar stops. As shown in Table II, all amplitude values at rms peaks were about 3 dB higher than were overall rms amplitudes.

The amplitudes of individual vowels averaged across all consonantal contexts are shown in Fig. 4. Consistently with the trend already observed, amplitudes at rms peaks were about 3 dB higher than overall rms amplitudes. Back vowels had higher amplitude than front vowels. At rms peak, the overall mean for back vowels was −14.33 dB as opposed to −16.44 dB for front vowels. For overall rms, the mean values for back and front vowels were −17.06 and −19.19 dB, respectively. There was general regularity in the relationship between the degree of vowel openness and vowel amplitude: The two most closed vowels /i/ and /u/ had the lowest amplitudes while the most open back vowels /ɑ/ and /ɔ/ had the highest. However, the correspondence between greater openness of a vowel and its increased amplitude was less consistent for the remaining vowels. In particular, it was surprising that the amplitudes for both /ɪ/ and /ʊ/ were relatively high and comparable with those for /æ/ and /ɑ/, respectively. Paired two-tailed *t*-tests confirmed these observations, showing that there was no statistical difference in the amplitudes of the vowels /ɪ/ and /æ/ and the vowels /ʊ/ and /ɑ/. The difference was also not significant between /ʊ/ and /ɔ/. The differences for all remaining vowel pairs were significant for both rms peak and overall rms amplitude.

It may be recalled that the vowels /æ/ and /ɑ/ were drastically low in relative power in the HF study, approximating the relative power of the vowel /i/. Although various explanations for this unexpected outcome were offered, HF admitted that "a confident explanation of the atypical finding for

TABLE III. Summary of significant main effects from repeated measures ANOVAs for relative amplitude of rms peak and overall rms amplitude. Shown are partial eta squared values (η^2). (*) $p<0.050$, (**) $p<0.010$, (†) $p<0.001$; (---) not significant; fr=fricative, st=stop, vd=voiced, vl=voiceless, l=labial, alv=alveolar, vel=velar.

	/i/	/ɪ/	/ɛ/	/æ/	/ɑ/	/ɔ/	/ʊ/	/u/
rms peak								
/b, d, p, t, v, z, f, s/								
Manner	---	---	0.286* fr>st	0.452** fr>st	0.532** fr>st	---	---	---
Voicing	0.332** vd>vl	---	---	---	---	---	---	---
Place	0.414** l>alv	0.462** l>alv	0.503† l>alv	0.447** l>alv	0.438** l>alv	0.528** l>alv	0.311* l>alv	0.839† l>alv
/b, d, g, p, t, k/								
Voicing	0.337** vd>vl	---	---	---	---	---	---	---
Place	---	0.362† l>vel>alv	0.454† l>alv>vel	0.254** l>alv>vel	0.202* l>vel>alv	0.302** l>alv>vel	0.329** l>alv>vel	0.694† l>vel>alv
Overall rms								
/b, d, p, t, v, z, f, s/								
Manner	---	---	---	---	---	---	0.260* st>fr	0.201* st>fr
Voicing	---	---	---	---	---	0.375* vl>vd	---	---
Place	0.611† l>alv	0.699† l>alv	0.700† l>alv	0.565† l>alv	0.539** l>alv	0.689† l>alv	0.390** l>alv	0.850† l>alv
/b, d, g, p, t, k/								
Voicing	0.258* vl>vd	---	208* vd>vl	---	---	0.425** vl>vd	---	---
Place	---	0.512† l>alv>vel	0.610† l>alv>vel	0.388† l>alv>vel	---	0.353** l>alv>vel	0.407† l>alv>vel	0.730† l>vel>alv

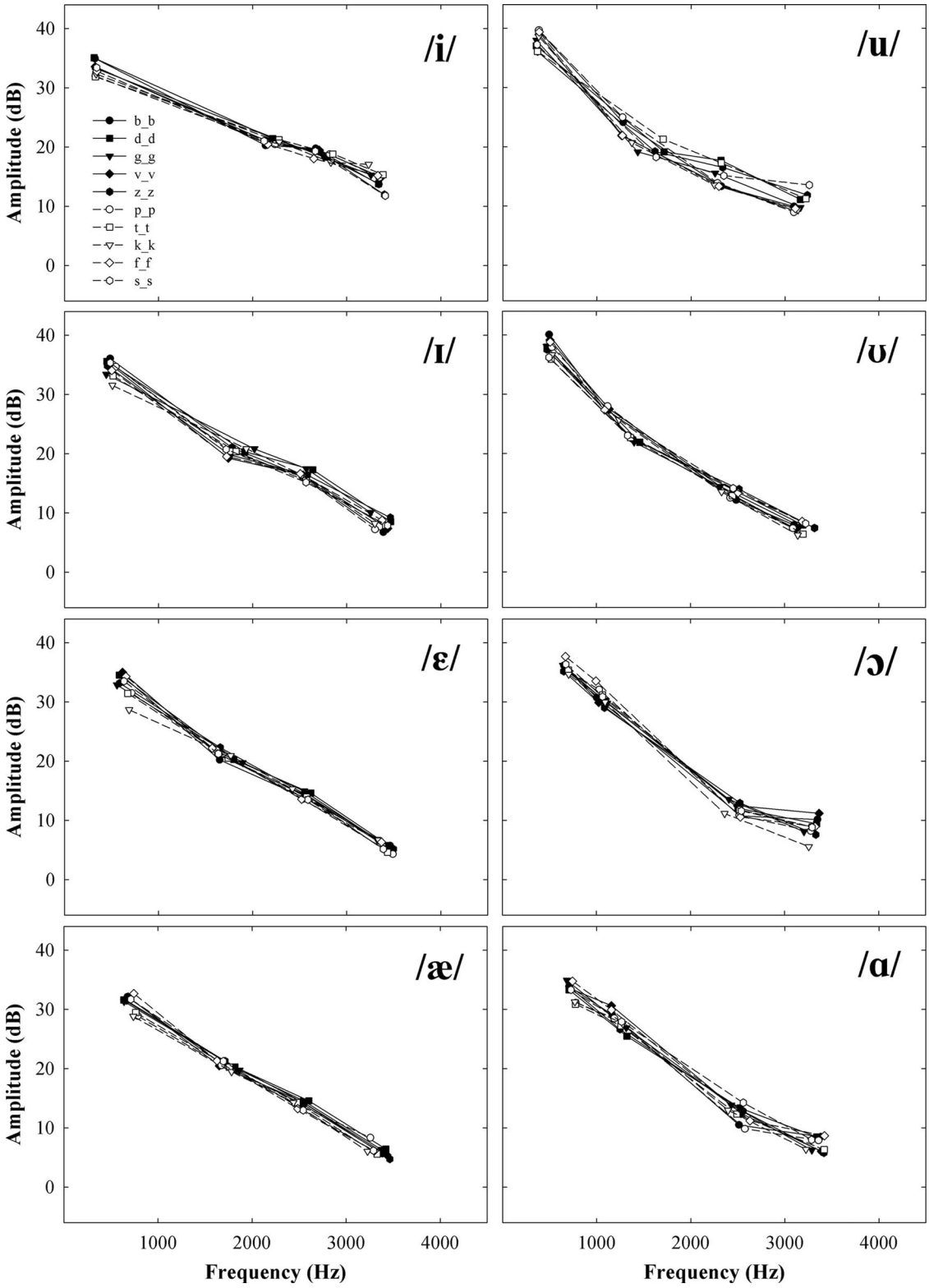


FIG. 5. Frequency and amplitude of formants 1–4 for individual vowels in ten consonantal contexts averaged for male speakers.

relative power cannot be advanced" (p. 112). The present results did not replicate this finding and did not provide any additional explanation for such atypically low amplitude values. However, in the current study, the amplitudes of these two vowels were not different from those for /ɪ/ and /ʊ/ within each front and back series, indicating that the greatest degree of opening may not automatically imply highest vowel amplitude.

Considering the consonantal context effects of voicing, manner, and place on amplitudes of individual vowels, the amplitude values did not differ greatly as a function of either voicing or manner. However, notable variation was found for consonant place: All vowels had higher amplitudes in the context of labials. The statistical assessments of the consonantal context effects are summarized in Table III. Table III lists the significant main effects only because significant in-

teractions were sparse and did not contribute greatly to the interpretation of the results. The main effect of voicing reached significance only for selected vowels (see Table III), and amplitude values were usually higher in the context of voiced stops. The main effect of manner was significant for the vowels /ɛ, æ, ɑ/ at rms peak. In each case, the peaks were higher in the context of fricatives. This tendency was consistent with HF results although decibel differences in the present data were much smaller, ranging from 0.5 to 0.7 dB, as compared to their relative power values. The effect of manner for the overall rms amplitude, however, produced greater amplitude in the context of stops. Overall, these results suggest that, generally, vowel amplitude does not change drastically as a function of either voicing or manner of articulation of the surrounding consonants.

To the contrary, the main effect of place was significant for all vowels except for /i/ for the stops-only analysis. Uniformly, the rms peaks were higher in the context of labial consonants as opposed to alveolar. The size of the place effects were greater too, with η^2 values ranging from 0.311 to 0.839. However, no consistent trend was found with respect to the alveolar and velar contexts (see Table III). The effects for the overall rms amplitude generally paralleled those at rms peak. The effect size of place was even stronger for the overall rms as evident from higher η^2 values listed in Table III. As a whole, the results for place do not match HF results, however, where vowels were greatest in relative power in the context of alveolars.

The main effect of gender was significant only for the vowel /i/ for both rms peak and overall rms, showing that male vowels had significantly higher amplitudes than female vowels. Given the relatively large degrees of freedom involved in the analyses, several interaction effects with gender as a factor were significant but had extremely low effect sizes ($\eta^2 < 0.10$), suggesting relatively unimportant (and, perhaps, even spurious) effects. They are not discussed here.

B. Relative amplitude of vowel formants

To get an overall picture of spectral variation for the present vowels in terms of both consonantal context and speaker gender, the mean frequency and amplitude values for the first four formants for each vowel in all ten consonantal contexts were plotted separately for males in Fig. 5 and for females in Fig. 6. As can be seen, consonantal context variously affected the amplitudes of individual formants and individual vowels. Frequency shifts are also detectable. Of particular note are the generally high F2 values for the vowel /u/ for both males and females which were additionally fronted in the context of alveolars. This is an outcome of regional variation in the vowel system of American English. The majority of the speakers for this study grew up in Ohio, where the variant of /u/ is significantly fronted. More acoustic evidence for the variation of F2 in the vowel /u/ as a function of speaker dialect can be found in Jacewicz *et al.* (2007a).

Figure 7 shows the mean differences between A2 and A1 (RelA2), A3 and A1 (RelA3), and A4 and A1 (RelA4) for each individual vowel and for each consonantal context. Because the first ANOVA showed that speaker gender was not significant for measure RelA2, RelA3, or RelA4, the display in Fig. 7 reflects amplitude values taken from Figs. 5 and 6 collapsed across speaker gender. As can be seen, mean RelA2 values remained rather steady for each front vowel (about −10 dB) whereas they were more variable for back vowels. In particular, they tended to increase with vowel openness, so that RelA2 for /u/ was about −18 dB and for /ɔ, ɑ/ was −5 dB. The variation as a function of consonantal context was quite extensive for most vowels although it was smaller for /u, ɑ/ and only minimal for /i, ɔ/.

Mean RelA3 values, although lower in general, tended to be higher for front vowels than for back (about −15 and −20 dB and lower, respectively). For back vowels, they were clearly the lowest for the vowel /ɔ/. The context-related variation was again evident for most vowels with the exception of /i, ɔ, ɑ/. The means for RelA4 again showed a sizeable variation as a function of consonantal context for some of the vowels.

The formant amplitude differences (RelA2, RelA3, and RelA4) were examined using separate ANOVAs which, for each vowel, assessed the effects of manner, voicing, and place separately for stops and fricatives sharing the same place of articulation (/b, d, p, t, v, z, f, s/) and for stops only differing in voicing and place (/b, d, g, p, t, k/) with gender as a between-subject factor. In the whole series of ANOVAs, the effect of speaker gender was significant only for the vowel /æ/ for RelA2 [$F(1,18)=6.65$, $p=0.019$, $\eta^2=0.270$] and RelA3 [$F(1,18)=7.76$, $p=0.012$, $\eta^2=0.301$] for the stops and fricatives analysis and for RelA2 [$F(1,18)=5.46$, $p=0.031$, $\eta^2=0.233$], RelA3 [$F(1,18)=8.97$, $p=0.008$, $\eta^2=0.333$], and RelA4 [$F(1,18)=4.77$, $p=0.042$, $\eta^2=0.210$] for the stops-only analysis, in each case indicating smaller decibel difference values for males. We therefore have chosen to exclude speaker gender as a factor for further consideration.

1. Variation of A1

In a separate analysis, we examined the variation of A1 as a function of consonantal context which is summarized in Fig. 8 for both male and female speakers.

The overall mean A1 values for male speakers were about 3 dB higher as compared to females (35 vs 32 dB). This relation was found in most vowels except for /i/ and /ʊ/ where the differences were greater (about 5 dB) and for /æ/, where mean male A1 was only 1 dB higher. As Fig. 8 shows, the variation as a function of consonantal context is particularly great for the vowels /ɪ, u/ for females and for /ɪ, ɛ/ for males.

We used separate ANOVAs with the within-subject factors manner, voicing, place, and gender as a between-subject factor to determine the significance of the A1 variations. A summary of significant effects is shown in Table IV.

The amplitude of A1, the strongest peak of a vowel, was affected by consonantal context to a relatively large extent. As can be seen, voicing had a significant effect on a number of vowels and was particularly strong for the short vowels /ɪ, ɛ, ʊ/. Unlike for the higher formants, all A1 peaks were higher in the context of voiced consonants and not voiceless. There were also significant effects of manner for three vow-

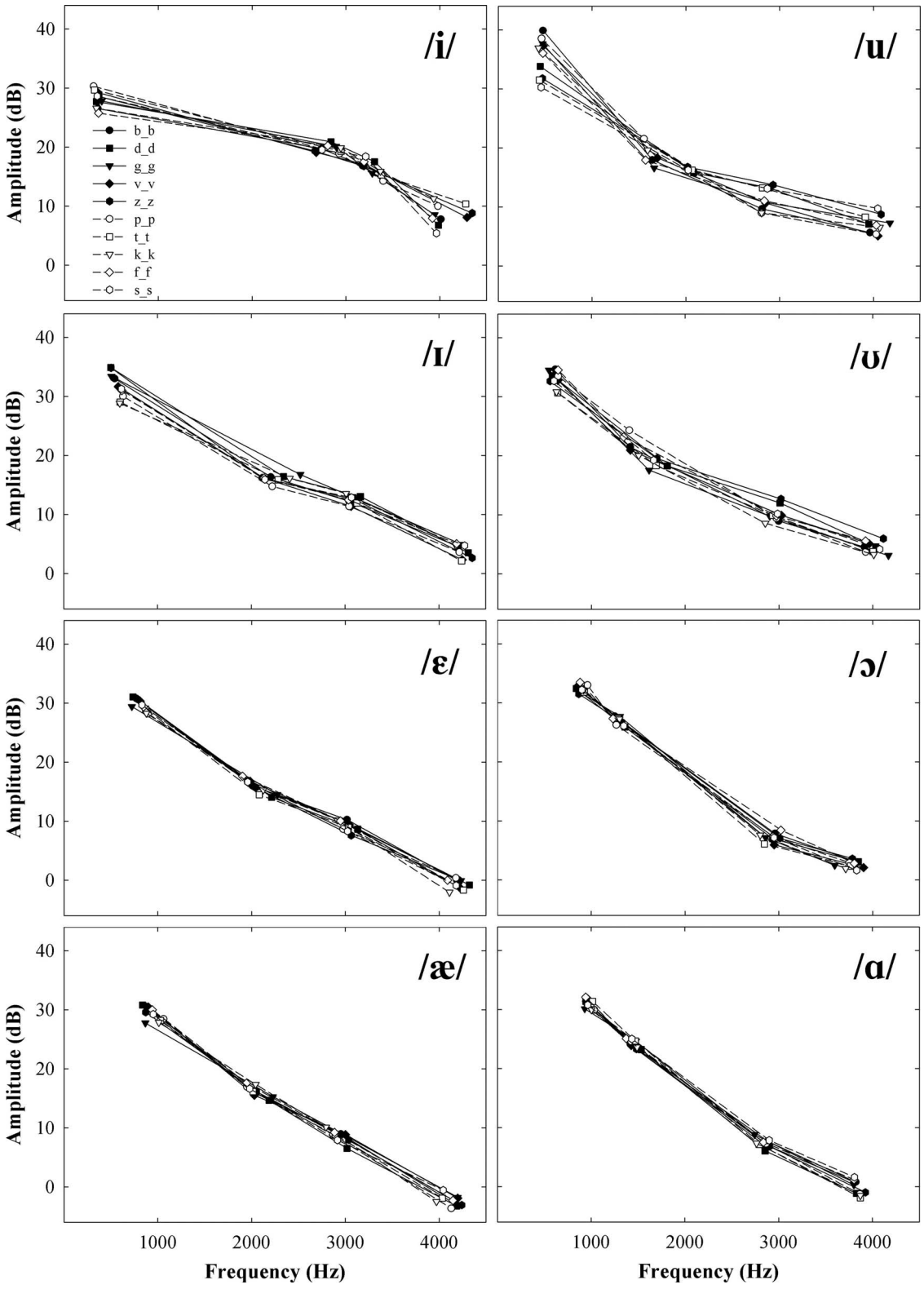


FIG. 6. Frequency and amplitude of formants 1–4 for individual vowels in ten consonantal contexts averaged for female speakers.

els /ɛ, æ, ɑ/, showing that A1 peaks were about 0.6–1.0 dB higher in the context of fricatives as opposed to stops. Place was significant for /ʊ, u/ for fricatives and stops, indicating that A1 in the context of labials was higher than in alveolars. For /u/, this effect was particularly strong (η^2=0.642) and A1 peaks were 4.4 dB higher. For the stops-only analysis, the results were variable. In general, the peaks in labial and alveolar contexts were higher as compared to velars. There were significant effects of gender for four vowels /i, ɛ, ɔ, ʊ/. In each case, A1 values for male speakers were higher than for female. One significant interaction deserves a mention here because it involved most of the vowels and showed a

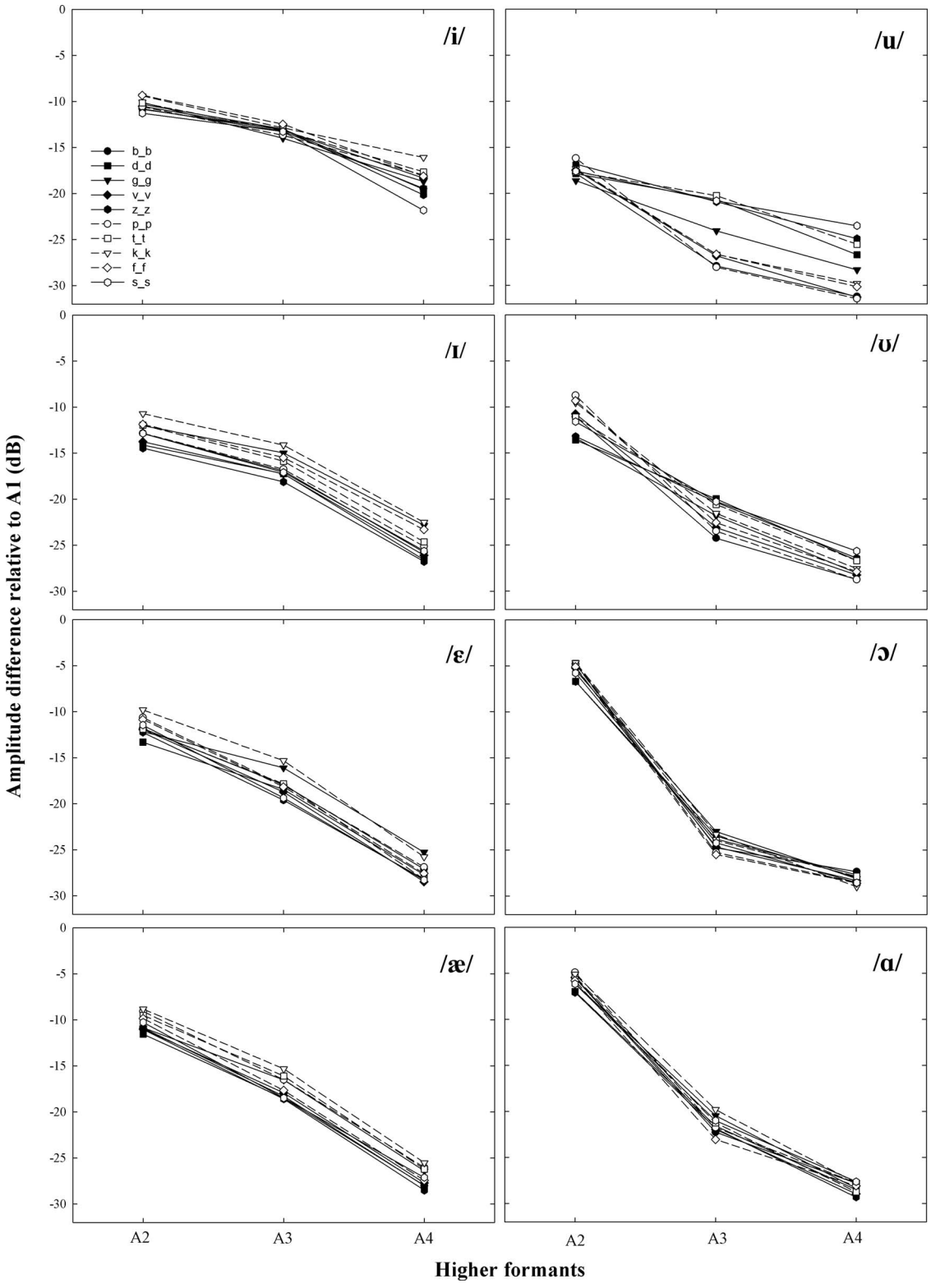


FIG. 7. Amplitude differences for each higher formant (A2, A3, A4) relative to A1 for individual vowels in ten consonantal contexts averaged across speaker gender.

consistent, relatively strong effect. The significant manner × voicing interaction arose from the fact that, for each affected vowel, the decibel difference between the higher A1 peak for voiced stops and the weaker A1 peak for voiceless stops was significantly greater (ranging from 2.18 to 2.88 dB) than the decibel difference between the A1 peaks for voiced and voiceless fricatives (ranging from −0.08 to 1.02 dB).

2. Results for RelA2, RelA3, and RelA4

Table V summarizes the statistical results for amplitude variations of the A2 and A3 relative to A1, i.e., RelA2 and RelA3. As can be seen, significant contextual effects were evident for all vowels except for /i/ and /ɔ/ for RelA2 and for /i, ɔ, ɑ/ for RelA3 analysis. In particular, the effect of voicing

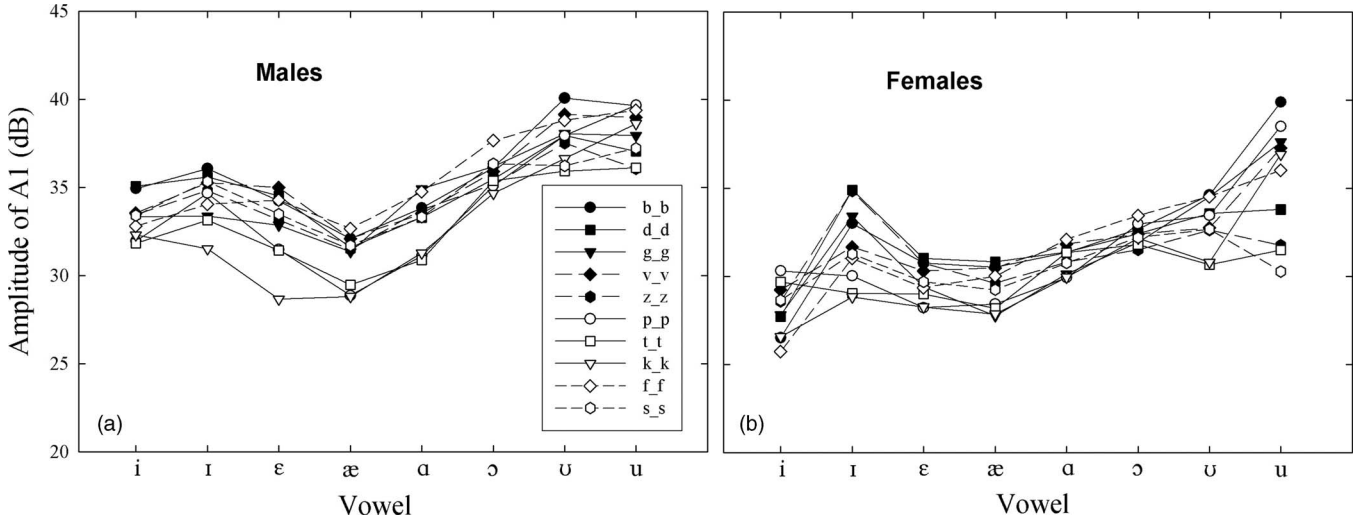


FIG. 8. Variation in the amplitude of the first formant (A1) for individual vowels in ten consonantal contexts averaged for male speakers (a) and for female speakers (b).

showed that the negative decibel differences were significantly smaller (about 2 to 3 dB) in the context of voiceless consonants as opposed to voiced, indicating that A2 was higher when surrounded by voiceless consonants. Consonant place introduced more variable results and affected primarily vowels in the context of stops. For front vowels, post-hoc analyses for stops revealed that decibel differences for both RelA2 and RelA3 were smallest in the context of velars, although this was not true for back vowels (compare Table V). The main effect of manner was not significant for any of the vowels. Significant interactions were sparse in the entire set and their small effects did not warrant a separate discussion.

While not necessarily related to consonantal context effects, visual inspection of Fig. 7 suggested that it was worthwhile to compare RelA3 values for front and back vowels. Across all contexts, these values tended to be smaller for front vowels than for back, indicating relatively stronger F3 peaks in front vowels. Results from a series of *t*-tests for RelA3 completed for all pairwise comparisons between vowels collapsed across all consonantal contexts confirmed these observations. There were no significant differences among the back vowels /u, ʊ, ɔ, ɑ/ except for /ɔ/ and /ɑ/ [$t(12) = -2.85$, $p = 0.015$]. For the front vowels, the differences among /ɪ, ɛ, æ/ were not significant. However, all pairwise comparisons with /i/ were significant, indicating that F3 for the vowel /i/ was significantly stronger than F3s for the remaining front vowels. No such consistency was found for all paired RelA2 and RelA4 comparisons, indicating that it is the relative amplitude of the third formant that most clearly marks the differences in spectral tilt between the front and back vowels.

TABLE IV. Summary of significant main effects and interactions from repeated measures ANOVAs for the amplitude of F1 (A1). Shown are partial eta squared values (η^2). (*) $p < 0.050$, (**) $p < 0.010$, (†) $p < 0.001$; (---) not significant; fr=fricative, st=stop, vd=voiced, vl=voiceless, l=labial, alv=alveolar, vel=velar, m=male, f=female.

	/i/	/ɪ/	/ɛ/	/æ/	/ɑ/	/ɔ/	/ʊ/	/u/
/b, d, p, t, v, z, f, s/								
Manner	---	---	0.206* fr>st	0.340** fr>st	0.241* fr>st	---	---	---
Voicing	---	0.441** vd>vl	0.546† vd>vl	0.326** vd>vl	---	---	0.246* vd>vl	---
Place	---	---	---	---	---	---	0.445** l>alv	0.642† l>alv
Manner × voicing	---	0.434**	0.227*	0.287*	---	0.301*	0.318*	---
Gender	0.312* m>f	---	0.364** m>f	---	---	0.361* m>f	0.371** m>f	---
/b, d, g, p, t, k/								
Voicing	---	0.544† vd>vl	0.432** vd>vl	0.357** vd>vl	0.418** vd>vl	---	0.506† vd>vl	---
Place	---	0.283** l>alv>vel	0.346† alv>l>vel	0.234** alv>l>vel	---	---	0.253** l>vel>alv	0.560† l>vel>alv
Gender	0.339** m>f	---	0.257* m>f	---	---	0.322* m>f	0.392** m>f	---

TABLE V. Summary of significant main effects from repeated measures ANOVAs for decibel difference A2-A1 (RelA2) and A3-A1 (RelA3). Shown are partial eta squared values (η^2). (*) $p<0.050$, (**) $p<0.010$, (†) $p<0.001$; (---) not significant; vd=voiced, vl=voiceless, l=labial, alv=alveolar, vel=velar.

	/i/	/ɪ/	/ɛ/	/æ/	/ɑ/	/ɔ/	/ʊ/	/u/
RelA2								
/b, d, p, t, v, z, f, s/								
Voicing	---	0.362** vl<vd	0.623† vl<vd	0.458** vl<vd	0.440** vl<vd	---	0.532† vl<vd	0.204* vl<vd
Place	---	---	0.252* l<alv	---	---	---	0.496** l<alv	---
/b, d, g, p, t, k/								
Voicing	---	0.433** vl<vd	0.632† vl<vd	0.667† vl<vd	0.427** vl<vd	---	0.575† vl<vd	0.339** vl<vd
Place	---	0.300** vel<alv<l	0.315** vel<l<alv	0.186* vel<l<alv	---	---	0.382† l<vel<alv	---
RelA3								
/b, d, p, t, v, z, f, s/								
Voicing	---	---	0.291* vl<vd	---	---	---	---	---
Place	---	---	---	---	---	---	0.466** alv<l	0.715† alv<l
/b, d, g, p, t, k/								
Voicing	---	0.253* vl<vd	0.289* vl<vd	0.287* vl<vd	---	---	0.233* vl<vd	---
Place	---	0.475† vel<alv<l	0.438† vel<l<alv	0.304** vel<l<alv	---	---	0.296** alv<vel<l	0.677† alv<vel<l

The context effects for RelA4 were comparatively smaller as shown in Table VI. The two high vowels /i, u/ were affected the most. Interestingly, place effects were different for each vowel. For /i/, the decibel difference was 1.3 dB smaller for the labial contexts as opposed to alveolar. The effect of place was particularly strong for the vowel /u/. For the stops and fricatives analysis, RelA4 was 7.5 dB higher in the context of alveolars as opposed to labials and the same tendency was also found for the stops-only analysis. Significant effects of place were also found for /ʊ/. For stops-only analyses, place was significant for /ɪ, ɛ, æ/ and the decibel differences were smallest in the context of velars, and for /u/, where the smallest decibel difference occurred in the context of alveolars. The effect of manner was significant for /u/ and /ɔ/, although showing opposite effects in that the decibel differences were smaller in the context of fricatives for /u/ (2.2 dB) and in the context of stops for /ɔ/ (1.4 dB). Voicing was significant for two vowels only, for /ɪ/ for fricatives and stops, and for /i/ for the stops-only analysis. In each case, the differences were about 2.5 dB smaller in the voiceless contexts as opposed to voiced.

Summarizing the results for formant amplitude, the consonantal context effects varied with vowel category and with a particular formant. For example, almost no significant effects were found for the vowel /ɔ/ across all three measures whereas numerous effects and interactions occurred for the short vowels /ɪ, ɛ, ʊ/. Similarly, there were no context effects for the vowel /i/ for RelA2 whereas they were abundant for

TABLE VI. Summary of significant main effects from repeated measures ANOVAs for decibel difference A4-A1 (RelA4). Shown are partial eta squared values (η^2). (*) $p<0.050$, (**) $p<0.010$, (†) $p<0.001$; (---) not significant; fr=fricaive, st=stop, vd=voiced, vl=voiceless, l=labial, alv=alveolar, vel=velar.

	/i/	/ɪ/	/ɛ/	/æ/	/ɑ/	/ɔ/	/ʊ/	/u/
/b, d, p, t, v, z, f, s/								
Manner	---	---	---	---	---	0.272* st<fr	---	0.288* fr<st
Voicing	---	0.261* vl<vd	---	---	---	---	---	---
Place	0.245* l<alv	---	---	---	---	---	0.235* alv<l	0.645† alv<l
/b, d, g, p, t, k/								
Voicing	0.216* vl<vd	---	---	---	---	---	---	---
Place	0.266** vel<alv<l	0.383† vel<l<alv	0.268** vel<l<alv	---	---	---	---	0.518† alv<vel<l

TABLE VII. Mean vowel durations (in milliseconds) (s.d.) in consonantal contexts grouped by voicing, manner, and place of articulation. All vowels are pooled. The data from House and Fairbanks (1953), shown as HF, are included for a comparison with the present results (JF).

Grouped consonant environments	JF females	JF males	HF males
Voicing			
Voiceless	200 (73)	172 (59)	174
Voiced	306 (68)	257 (67)	253
Manner of articulation			
Stop	235 (85)	200 (70)	203
Fricative	280 (85)	236 (80)	239
Place of articulation			
Labial	249 (85)	209 (73)	220
Alveolar	268 (91)	227 (80)	232
Velar	230 (82)	200 (71)	198

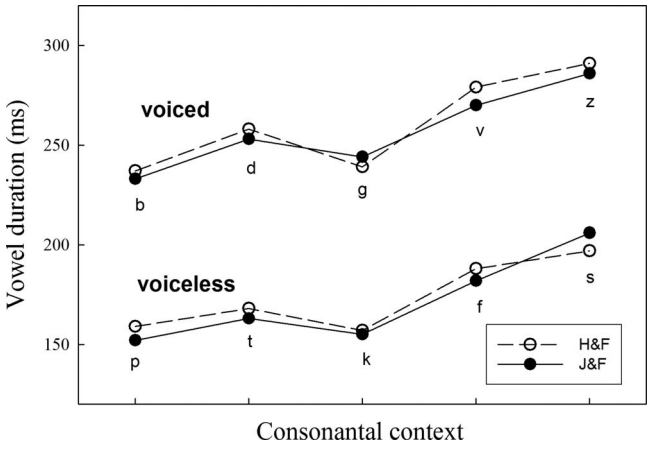


FIG. 9. Consonantal context effects on vowel duration pooled across all vowels. The present results, marked as JF, are compared with the data from House and Fairbanks (1953), marked as HF.

RelA4. Conversely, context affected RelA2 for /ɑ/ but not RelA3 or RelA4. Turning to the significant effects of consonantal features on formant amplitude variation, manner of articulation had almost no influence on amplitude changes except for a few interactions and main effects for RelA4. Both voicing and place affected formant amplitude variation to a much greater extent, as evident in a greater number of significant main effects. The effects of voicing were very consistent, showing uniformly that the formant peaks were higher in the voiceless contexts as opposed to voiced. Consonant voicing affected the greatest number of vowels and formants. The effects of place were more variable, although formant peaks tended to be higher in the context of labials as compared to alveolars. For stops only, the peaks were highest in the context of velars for front vowels whereas more variability was found in back vowels. Overall, there were more significant context-related main effects and interactions for front vowels (32) than for back (20).

C. Vowel duration

Although vowel duration was not of central interest to the study, this measure can be informative in light of the differences in amplitude results obtained between the HF study and the present report. Specifically, could differences in the articulation rates between the speakers in the two studies account for some of the discrepancies?

Table VII lists the duration values as a function of consonant environment grouped by voicing, manner, and place of articulation for all vowels pooled separately for males and females. With regard to the male data, the consistency with HF is remarkable given that only four vowels studied by HF were included in the present set.[2] The match is almost perfect despite the apparent differences in the way the material was recorded, i.e., as isolated disyllabic words in HF and as monosyllables in a short phrase in the present study. As might be expected, durations of female vowels were longer as compared to males (e.g., Adank *et al.*, 2007; Jacewicz *et al.*, 2007b).

Following HF, Fig. 9 displays mean durations for each individual consonantal context across all vowels pooled. Since the present focus was to compare the duration material with HF data,[3] only duration values from male speakers were included in Fig. 9. Again, the obtained pattern agrees remarkably with that found in HF. These results suggest that the articulation rates for the speakers in both the HF study and the present report were very similar.

As might be expected, the most robust duration differ-

TABLE VIII. Mean durations of individual vowels (in milliseconds) (s.d.) shown for voiced (Vd_Vd) and voiceless (Vl_Vl) environments and for all consonantal contexts pooled. Shown are also mean f_0 values (in hertz) (s.d.) for vowels for all consonantal contexts pooled.

Vowel	Duration Vd_Vd males	Duration Vl_Vl males	Duration Vd_Vd females	Duration Vl_Vl females	f_0 males	f_0 females
/ɪ/	204 (42)	125 (30)	250 (45)	142 (44)	138 (17)	217 (20)
/ʊ/	221 (43)	136 (35)	253 (42)	163 (47)	138 (16)	220 (23)
/ɛ/	225 (47)	153 (43)	277 (53)	172 (55)	131 (14)	213 (18)
/i/	257 (57)	173 (54)	305 (53)	205 (74)	145 (17)	237 (25)
/u/	267 (60)	166 (36)	309 (58)	209 (59)	144 (16)	235 (24)
/ɑ/	287 (70)	198 (56)	342 (58)	234 (68)	125 (14)	212 (19)
/ɔ/	300 (68)	211 (67)	374 (57)	246 (88)	129 (15)	207 (19)
/æ/	305 (66)	217 (62)	352 (63)	242 (69)	127 (15)	210 (18)

ences among the vowels came from the effects of consonant voicing. Table VIII lists durations of individual vowels (in ascending order) for male and female speakers, showing that vowels in the context of voiced consonants were longer than in the voiceless contexts. Also significantly longer vowels (18% longer) were produced by females [$F(1,10)=6.17$, $p=0.032$, $\eta^2=0.382$]. The main effect of consonant voicing was strong [$F(1,10)=134.7$, $p<0.001$, $\eta^2=0.931$] and the differences were very consistent within each gender group. On average, vowels in the context of voiced consonants produced by males were 36% longer than vowels in the voiceless contexts whereas the difference for female speakers was 37%. Comparing the present results with more recent published data, we found consistency with vowel duration material in Hillenbrand *et al.* (2001).

Considering the durations of individual vowels, the results for the voiced contexts were less variable than for the voiceless. In particular, paired two-tailed *t*-tests showed that there were no significant differences between /ɔ/ and /æ/ or between /æ/ and /ɑ/—the longest vowels or between the vowels /i/ and /u/—vowels of intermediate length. There were also no significant differences between /ɪ/ and /ʊ/ nor /ɛ/ and /ʊ/ —short vowels. All other differences were significant.

D. Variation in f_0

Although f_0 measure was also not of central interest to this study, the present f_0 values were compared with the results of HF for consistency. Following HF, f_0 values at the rms peak averaged across all vowels were plotted for each of the ten individual consonantal contexts (the plots are not included here). Although the present f_0 values for males were slightly higher than those in HF (on the order of 9%), the general trends were strikingly similar. Most important, f_0's of vowels in voiceless contexts were higher than those in voiced ones. As in HF, the difference in f_0 values as a function of voicing of the surrounding consonants tended to be greater for stops than for fricatives. These results match rather closely the f_0 material presented in HF. f_0 values for individual vowels averaged across all consonantal contexts and split by speaker gender are listed in Table VIII. The general tendency reflects the widely observed phenomenon that high vowels have higher intrinsic f_0 than low vowels (e.g., Whalen and Levitt, 1995).

IV. GENERAL DISCUSSION

The aim of this study was to characterize the nature, size, and range of acoustic amplitude variation in coarticulated vowels. Expecting large variation based on the findings in the House and Fairbanks (1953) study, we examined the changes to the amplitudes of the rms peak and the overall rms amplitude as a function of the consonantal features voicing, manner, and place. Contrary to the HF results, we found no systematic changes in vowel amplitude as a function of either consonant voicing or manner.

Both the present study and HF found significant effects of consonant place of articulation. However, although the small size of the amplitude variation was comparable, the directions of the effects for the place distinction differed. In particular, vowels in the context of alveolars were greater in relative power than labials in the HF data whereas the present results show the opposite: Both rms peak and overall rms amplitude were higher in the context of labials and not alveolars. In a similar fashion, vowels in the context of velars were lesser in relative power than in the context of alveolars in the HF study whereas no difference was found for these two contexts in the present study. On the whole, the present results show that consonantal context of a vowel does not introduce sizeable acoustic variation in vowel amplitude for either rms peak measure or overall rms amplitude.

A. Accounting for the discrepancy between the two sets of results

In attempting to explain the discrepancy between the central results of the HF study and the present results, we first considered the differences in the experimental protocol. Since the speech material in HF consisted of isolated words and the present stimuli were recorded in a short phrase, the possible differences in the articulation rate were a primary candidate for accounting for the discrepancy. As it turned out, the durations of vowels in the consonantal contexts in HF and in the present study were almost identical, indicating that the discrepancy was not due to a more formal or more casual speaking mode used in the recordings of the two sets of stimuli. We then turned to the equipment used in both studies and, although some slight incompatibilities might have been expected due to the analog and digital recordings, we considered each experimental setup to be adequate for the experimental purpose it served. The third possibility was in the way the acoustic measurements were made then and now. As will be shown in the following, the differences between the results of the two studies can probably be explained, at least to a great extent, by the different measurement techniques used.

Perhaps the greatest single discrepancy between the HF results and those presented here involves the voicing difference. In particular, HF's measurements indicated that vowels produced in the context of voiced consonants had twice the relative power of vowels produced in the context of voiceless consonants. One possible explanation for the difference lies in suggesting that the HF vowel measurements included some portion of the consonantal context, especially for voiceless consonants. In particular, we must assume that there was an integration window associated with their apparatus and associated measurement of intensity. If this window was large enough, then it might also have included a portion of the voiceless consonant context (syllable-initial, syllable-final, or both) since vowels produced in a voiceless context are significantly shorter than those in a voiced context. This account would explain many of the consonant context differences in relative power seen in HF (see their Fig. 3).

For example, we could expect that the voiced stops would show greater relative power than voiceless stops because the relative power measures for the vowels in a voiceless context would include portions of the voiceless stop itself. We would also expect vowels in the context of /s/ to

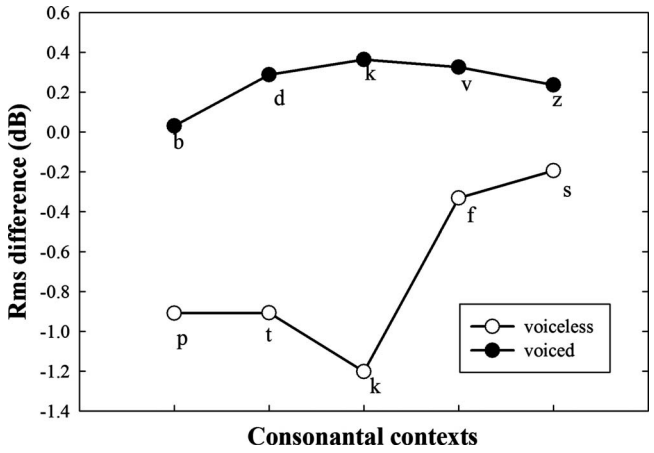


FIG. 10. Mean differences between overall rms (calculated from vowel onset to offset) and the rms from a 200 ms section of the utterance centered on the vowel across the ten consonantal contexts. Data are collapsed across two speakers and eight vowels.

show greater relative power than in the context of /f/ (since the relative power of the /s/ consonant, a portion of which is included in calculation of the vowel's power, is greater than that of the /f/). In turn, we would expect vowels in the context of /f/ to be slightly greater in relative power than when they occur in the context of /p, t, k/. This approach would thus also account for some of the differences between HF and the current study related to consonant manner. These patterns of consonantal feature differences were not found in the present study simply because our method only measured that portion of the speech signal that corresponded to the vowel.

As a test to determine whether this explanation is, in fact, plausible, the recordings from two speakers (one male, one female) were randomly selected and the rms of their vowels were analyzed in two separate ways. First, the rms of the target vowel, alone, was measured (this corresponded to the overall rms measure). Next, the rms of a 200-ms-long section of each utterance—centered on the midpoint of the target vowel—was measured. This 200 ms section of the utterance included portions of the initial and final consonants (which would lower the rms when the vowel was relatively short). Finally, the difference between the overall rms and the rms of the 200 ms section for each token was calculated. Shown in Fig. 10 are the mean rms differences collapsed across both speakers and all eight vowels. The pattern of the consonant context differences (between the voiced and voiceless contexts, and between the /p, t, k/ and /f, s/ context) shown in Fig. 10 bear a striking resemblance to HF (Fig. 3) suggesting the viability of this explanation for the obtained discrepancies.

B. Consonantal context effects on formant amplitude variation

Turning to the present results, we explored the possibility that significant context-related amplitude variations may affect specific spectral regions in a vowel (such as individual formants) rather than its overall energy. The changes in the amplitude of vowel formants were first examined by measuring amplitude of each higher formant relative to each vowel's strongest spectral peak, i.e., the amplitude of F1. This analysis revealed several systematic effects for each formant.

For F2, variation in A2 relative to A1 (RelA2) was significant for all vowels except for /i/ and /ɔ/. RelA2 was affected primarily by consonant voicing and place. For each vowel, the RelA2 values were uniformly smaller in the context of voiceless consonants as opposed to voiced, and they were variably affected by consonantal place. The variation ranged from 0.8 to 3.8 dB.

For F3, the RelA3 values did not vary greatly for the analysis involving labial and alveolar stops and fricatives. A large difference of 7.7 dB was found for the vowel /u/ as a function of place. However, more significant effects were found for the stops-only analysis. The RelA3 values were again smaller in the context of voiceless stops as opposed to voiced and the effects of place were variable. In general, the RelA3 variation was of the range 1.5–3.3 dB. The vowels /i, ɔ, ɑ/ remained unaffected by consonantal context. However, the place effects for the vowel /u/ were very strong. For this vowel, the decibel differences produced by context were large: 6.7 dB between alveolars and velars, and 8.7 dB between alveolars and labials. The consonant place effects for the vowel /u/ were thus the strongest in the entire set of vowels studied here. A3 peaks in the context of alveolars were higher than in the context of labials.

Finally, variation in the amplitude of F4, typically the weakest formant of a vowel, turned out significant for several vowels. Interestingly, the effects of place and voicing were significant for RelA4 for the vowel /i/ (1.3–2.6 dB) which otherwise was unaffected by contextual variation. The place effects for /u/ were again strong, reaching 7.5 dB difference for alveolars as opposed to labials for the contexts of stops and fricatives. For the stops-only analysis, A4 was 4.4 dB higher for alveolars as compared to velars and 7.3 dB higher in comparison with labials.

For the amplitude of F1 (A1), there was a significant effect of consonant voicing. A1 peaks had greater amplitude (ranging from 1.0 to 3.2 dB) in the voiced contexts than in the voiceless contexts. This was different from the patterns for the higher formants suggesting that A1 may be affected by other source characteristics. The results for place lead to the same conclusion. Although the amplitudes of higher formants were uniformly greater in the context of alveolars, A1 values were mostly greater in the context of labials. This was true for high vowels /u, ʊ, ɪ/ whose F1 frequency is low. For the vowels /ɛ, æ/ however, whose F1 frequencies are higher, A1 values were greater in the context of alveolars. This result was significant for the stops-only analysis. For the stop and fricatives analysis, the effect of place was not significant for these vowels.

C. Context-induced variation in relation to "basic rules of formant amplitude"

The observed amplitude variations as a function of consonantal context need to be situated within a well-established theoretical frame which lets us anticipate a substantial proportion of the effects found here. As Fant (1956) first noted,

formant frequencies and formant amplitudes are "intimately related" to the extent that two vowels differing in the frequency of F1 must also differ in the overall amplitude. This relation is carried over to the higher formants. Stevens 1998, (pp. 133–135) illustrates the three general rules of formant amplitude as stemming from the principles of linear resonances in series. All three rules are well represented in the present set of results, as shown in Figs. 4–6. In particular, the greater overall rms of back vowels as compared to front was due to the greater amplitude of F1 in back vowels. This can be accounted for by the first rule, which expresses the relation between the greater amplitude of F1 or higher frequency of F1 and the increased overall amplitude. Also, consistent with the first rule, the overall rms of the vowels increased as F1 rose in frequency. Although the overall rms of the vowels /æ, ɑ/ was slightly smaller than /ɛ, ɔ/ despite their higher F1 frequencies, this effect can be accounted for by the fact that the amplitude of F1 was on average about 2 dB greater for /ɛ, ɔ/ than for /æ, ɑ/.

A clear manifestation of the second rule, which states that increasing a particular formant frequency raises the amplitude of the spectrum at frequencies above that formant, can be found in front vowels. In the present set, the amplitude of F3 rose as a result of the increase in the frequency of F2 for the front series. This rule also explains the greater A3 for the vowel /u/ whose frequency of F2 rises in its variant spoken in Ohio. Finally, there is also an indication of the appearance of the third rule in the present set, which points to an increase in the amplitude spectrum in the vicinity of two or more formants coming close together. The increased amplitude of F2 in /ɔ, ɑ/ and of the F2–F3–F4 cluster in /i/ can be interpreted in light of the third rule.

The consonantal context effects on variation in formant amplitude observed in this study cannot be interpreted without reference to this pattern of expected changes to the amplitude spectrum. For example, consonant voicing did affect the amplitude of F1 but, apparently, the effect was not strong enough to influence the overall vowel amplitude and the first rule failed to apply. However, the context-induced variation in the frequency of a higher formant could in principle introduce changes to the amplitude spectrum at frequencies above that formant. The consonantal context effects on the vowel /u/ are the most illustrative example in the present set, where operation of the second and third rules cannot be excluded.

D. The role of formant amplitude variation in vowel perception

The size of variation in the amplitude of each higher formant observed here leads to the question of how relevant are these changes to the perception of vowel quality. In particular, one would not necessarily expect a vowel category change as a function of amplitude variation related to the place of articulation or voicing of consonants surrounding the vowel. In the typical speech perception paradigm involving isolated synthetic stimuli, the experiments demonstrated that adjustments made to formant amplitudes can change the perceived vowel quality (e.g., Miller, 1953; Lindqvist and Pauli, 1968; Carlson *et al.*, 1970; Ainsworth and Millar, 1972) and that a 8 dB change in the amplitude of A3 can be sufficient for the listener to perceive a different vowel category (Aaltonen, 1985). A much smaller difference limen was reported by Flanagan (1957) in a discrimination task, in which the 50%-crossover point for F2 of the vowel /æ/ was reached when the amplitude of this formant increased by 3 dB. Furthermore, listeners were shown to be equally sensitive to amplitude adjustments in F4 and in F2 for /ɪ/ and again, a 8 dB change caused a vowel category shift (Jacewicz, 2005).

These reports point to the potential role of variation in formant amplitudes in vowel perception. However, the variation ranging from 0.8 to 3.8 dB which was found in naturally produced vowels in this study is less likely to introduce a vowel quality change. After all, listeners do not depend on formant amplitude relations in making vowel quality distinctions to the extent that they rely on formant frequency pattern. Yet, the large 8.7 dB difference for the vowel /u/ produced by coarticulatory context as reported here has a great potential to affect the perception of vowel quality. In most cases, however, the sensitivity to formant amplitude variations may reflect listeners' experience with more subtle spectral changes which may contribute to the perceived vowel naturalness or timbre differences rather than vowel quality per se.

E. Consonantal context effects on amplitude spectrum at the auditory periphery

Before any expectations about the relevance of formant amplitude variation to vowel perception can be advanced, it is important to know whether such variation is still present in the auditory representation of the speech signal, at least at the auditory periphery. To estimate how the spectral amplitude variation may be encoded and represented at early stages of processing by the peripheral auditory system, we used the first level of the Perceptual Auditory Spectral Centroid model (Anantharaman, 1998) which simulates the peripheral processing through three psychoacoustically motivated stages corresponding to the middle-ear transduction, the filtering mechanism exhibited by basilar membrane, and hair cell activity transmitted in the auditory nerve which contributes to the sensation of loudness. Auditory spectra were calculated by passing the vowel spectra (as a positive time-frequency representation of the vowel signal) through the three stages of peripheral auditory processing: (1) equal-loudness preemphasis curve (provides a weighting along the frequency axis), (2) auditory filter bank (passes the output of the previous stage through 33 gammatone filters centered at each bin of the fft, center frequencies in ERBs), and (3) intensity-loudness compression (raises the output of the previous stage to the 0.3 power).

Figure 11 (bottom) shows the average auditory spectra of the vowel /ɪ/ in the contexts of labial, alveolar, and velar stops which were calculated from the productions of the present ten male speakers. For the same speakers, the corresponding measured mean frequencies of formants F1–F4 along with their amplitudes are included in the top panel. The formant peaks are situated within the four contiguous broad frequency bands B1–B4 [one band per octave, in kilohertz B1 (0–0.5), B2 (0.5–1.0), B3 (1.0–2.0), and B4 (2.0–

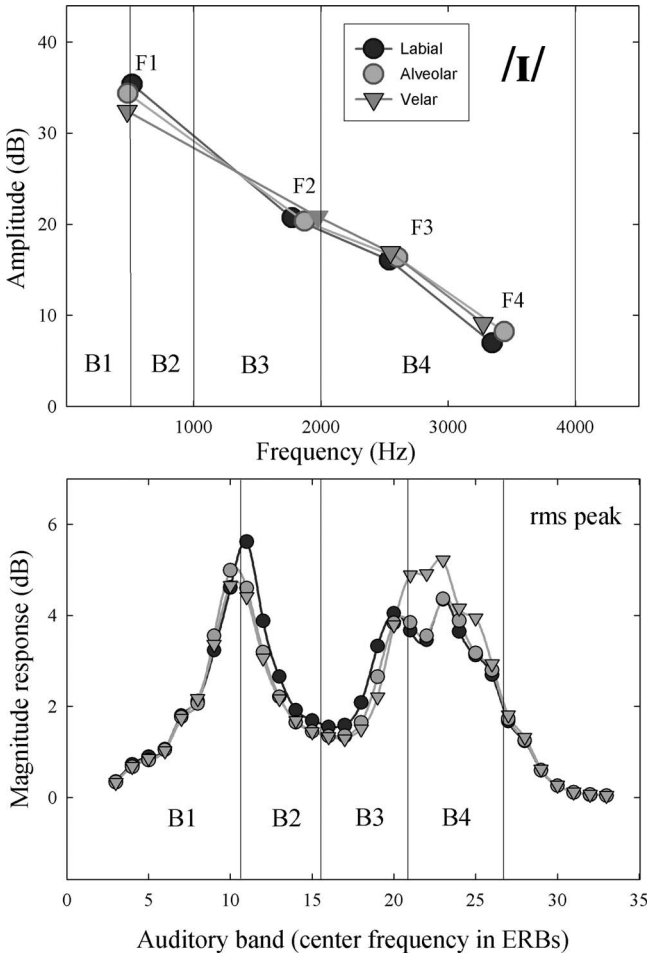


FIG. 11. Mean formant amplitude of the vowel /ɪ/ in the context of stops averaged across ten male speakers in this study (top) and the calculated auditory spectra based on the magnitude response of a gammatone filter bank (bottom).

4.0)]. These bands are also included in the auditory spectrum display to relate the two representations, i.e. acoustic (linear) and auditory (nonlinear), to one another. As evident, the acoustic amplitude variation is carried on through the early stages of auditory processing and the magnitude response in the auditory spectrum is remarkably consistent with the acoustic pattern. In particular, the specific significant consonantal context effects for the vowel /ɪ/ for the measures RelA2, RelA3, RelA4, and A1 summarized in Tables IV–VI can be clearly traced in the auditory spectrum. That is, the statistically strong place effects for RelA2, RelA3, RelA4 (see the results for the stops-only analysis for the vowel /ɪ/), indicating higher amplitude peaks in the context of velars are manifested in the auditory spectrum at the juncture of the bands B3 and B4 and throughout band B4. Clearly, the second peak in the auditory spectrum (which corresponds to the F2, F3, and F4 peaks) is highest in the context of velars. A close correspondence between the acoustic amplitude variations can also be found in the lower frequency region, representing F1 in the acoustic representation and the first peak in the auditory spectrum. The statistically strong effect of place for the A1 measure showing higher amplitude in the context of labials is also evident in the auditory spectrum.

The auditory spectra calculated from the measurements at rms peak show that two spectral regions—corresponding to the lower and higher parts of the measured acoustic spectrum—are emphasized. The question arises as to which spectral region contributes more to the overall vowel amplitude. In Table III, we observe that the significant effect of place for the vowel /ɪ/ for both the rms peak and the overall rms shows higher amplitude values in the context of labials. Relating this effect to the place effects within the spectral regions, we again find higher amplitude values in the context of labials for the lower spectral region (A1) but not for the higher (RelA2, RelA3, and RelA4), where the amplitude is greater in the context of velars. This may indicate that the lower spectral region dominates the vowel spectrum and the contribution of the higher region is comparatively smaller. However, despite the existing evidence (based upon psychophysical tuning) that in the region below 1000 Hz the ability to process spectral contrasts increases (e.g., Healy and Bacon, 2006), this interpretation needs to be tested in a series of further experiments.

At present, any generalization should be drawn with caution due to the large number of vowels and consonantal contexts used in this study. A more focused investigation should concentrate on selected vowels and contexts to gain more insight into the exact causes of differences in the size of amplitude variation found here. A detailed analysis deeply rooted in the acoustic theory of speech production is especially desirable in explaining some of the consonantal context effects on vowel amplitude variation. For example, spectral amplitude variations reflect a complex relation between the characteristics of the sound in the low-frequency region and acoustic attributes at frequencies above the first formant. These include the timing of acoustic events which depend on the length and the place of the consonantal constriction preceding the vowel. These events, such as rate of movement of F1 after the stop release and rate of movement of trajectories of higher formants following the release have an effect on amplitude spectrum (Stevens, 1998).

The significant effects of consonantal context on formant amplitude variations examined here were found at a time window relatively late in a vowel, i.e., at rms peak. This shows that significant variations do not occur only at vowel onsets and offsets (the vowel margins) whose formant frequencies are affected most by surrounding consonants but such effects can also be manifested at vowel nuclei. However, given the variable durations of the vowels and, understandably, variable locations of the rms peaks, it was not surprising to find different degrees of their susceptibility to the context effects. For example, the long vowels in the set such as /ɔ/ and /ɑ/ were relatively unaffected by contextual variation. This would indicate a greater temporal separation of their nuclei from syllable margins. However, this interpretation may not be true with respect to the vowel /æ/ which was the longest in the present set and exhibited more contextual effects than either /ɔ/ or /ɑ/. Also, the vowel /i/, being of intermediate length, was unaffected by contextual variation except for the variation in A4. These mixed results indicate that differences in vowel duration alone cannot entirely explain the varying degrees of context effects found at

vowel nucleus. Finally, there may also be a source variation in the vowel as a function of consonantal context—a study of contextual variations of the voice source can be found in Fant (1997). Fine-grained analyses of the voice source have shown that the influences on the vowel's mode of phonation depend on the manner of articulation of the consonant (Gobl and Ní Chasaide, 1999) and consonant voicing (Gobl and Ní Chasaide, 1993). The source variation in consonantal context may also have a profound effect on variation in the amplitudes of formants.

The type of variation in formant amplitude found in coarticulated vowels in the present study naturally co-occurs with speaker-intended changes to vocal intensity to convey emphasis, linguistic stress, emotions, or to communicate in noisy environments or over a longer distance. How listener deals with such complex interaction between several factors influencing vowel perception is a rich area for future research.

ACKNOWLEDGMENTS

This study was supported by the research Grant No. R03 DC005560 from the National Institute of Deafness and Other Communication Disorders, National Institutes of Health, to the first author. The authors would like to thank Chiung-Yun Chang for assistance at various stages of this research and Jeff Murray for editorial help. The comments and suggestions of the Associate Editor Anders Löfqvist and two anonymous reviewers on an earlier version of the paper are greatly appreciated.

[1]The location of the rms peak can be expressed in several ways. First, the peak rms position can be determined in terms of its absolute distance (in milliseconds) from vowel onset or CVC-word onset. Alternatively, the peak rms position can be expressed in terms of its relative position (with values ranging from 0 to 100%) with regard to the duration of the vowel or duration of the word. We experimented with each of these approaches to determine which measure best characterized the variation in the location of rms peak as a function of vowel category and consonantal context. Based on the statistical results, it became clear that the two relative positions (i.e., within the vowel and within the word) yielded the most comparable patterns. We therefore decided to present only the results for the most dependable measure.

[2]In the HF study, the voiced environments included the nasals /m, n/ which were absent in the present report. Also, in their Table 2, HF listed vowel durations separately for bilabial (/p, b, m/) and labiodental (/f, v/) consonants. In the present study, the HF's values for bilabials and labiodentals were averaged and listed in Table VII as labials. Also, postdental consonants in HF included /n/ which was absent in the present alveolar environments.

[3]HF data displayed in their Fig. 1 are taken from their Table 2.

Aaltonen, O. (**1985**). "The effects of relative amplitude levels of F2 and F3 on the categorization of synthetic vowels," J. Phonetics **13**, 1–9.

Adank, P., van Hout, R., and van de Velde, H. (**2007**). "An acoustic description of the vowels of northern and southern standard Dutch. II. Regional varieties," J. Acoust. Soc. Am. **121**, 1130–1141.

Ainsworth, W. A. (**1972**). "Duration as a cue in the recognition of synthetic vowels," J. Acoust. Soc. Am. **51**, 648–651.

Ainsworth, W. A. (**1981**). "Duration as a factor in the recognition of synthetic vowels," J. Phonetics **9**, 333–342.

Ainsworth, W. A., and Millar, J. (**1972**). "The effect of relative formant amplitude on the perceived identity of synthetic vowels," Lang Speech **15**, 328–341.

Anantharaman, J. N. (**1998**). "A Perceptual Auditory Spectral Centroid Model," Ph.D. dissertation, The Ohio State University, Columbus, OH.

Beckman, M. (**1986**). *Stress and Non-Stress Accent* (Foris, Dordrecht).

Carlson, R., Granström, B., and Fant, G. (**1970**). "Some studies concerning perception of isolated vowels," STL-QPSR 2-3/1970, pp. 19–35.

Fant, G. (**1956**). "On the predictability of formant levels and spectrum envelopes from formant frequencies," in *For Roman Jakobson: Essays on the Occasion of his Sixtieth Birthday*, edited by M. Halle, H. G. Lunt, H. McLean, and C. H. van Schooneveld (Mouton, The Hague), pp. 109–120.

Fant, G. (**1997**). "The voice source in connected speech," Speech Commun. **22**, 125–139.

Fant, G., Fintoft, K., Liljencrants, J., Lindblom, B., and Martony, J. (**1963**). "Formant-amplitude measurements," J. Acoust. Soc. Am. **35**, 1753–1761.

Fant, G., Kruckenberg, A., and Liljencrants, J. (**2000a**). "Acoustic-phonetic analysis of prominence in Swedish," in *Intonation: Analysis, Modeling and Technology*, edited by A. Botinis (Kluwer Academic, Dordrecht), pp. 55–86.

Fant, G., Kruckenberg, A., and Liljencrants, J. (**2000b**). "The source-filter frame of prominence," Phonetica **57**, 113–127.

Fant, G., and Lin, Q. (**1987**). "Glottal source–vocal tract acoustic interaction," STL-QPSR 1/1987, 13–27.

Flanagan, J. L. (**1957**). "Difference limen for formant amplitude," J. Speech Hear Disord. **22**, 205–212.

Fry, D. B. (**1955**). "Duration and intensity as physical correlates of linguistic stress," J. Acoust. Soc. Am. **27**, 765–768.

Gobl, C., and Ní Chasaide, A. (**1993**). "Contextual variation of the vowel voice source as a function of adjacent consonants," Lang Speech **36**, 303–330.

Gobl, C., and Ní Chasaide, A. (**1999**). "Techniques for analyzing the voice source," *Coarticulation: Theory, Data, and Techniques*, edited by W. J. Hardcastle and N. Hewlett (Cambridge University Press, Cambridge), pp. l00–321.

Gottfried, T. L., and Beddor, P. S. (**1988**). "Perception of temporal and spectral information in French vowels," Lang Speech **31**, 57–75.

Healy, E. W., and Bacon, S. P. (**2006**). "Measuring the critical band for speech," J. Acoust. Soc. Am. **119**, 1083–1091.

Hillenbrand, J. M., Clark, M. J., and Nearey, T. M. (**2001**). "Effects of consonantal environment on vowel formant patterns," J. Acoust. Soc. Am. **109**, 748–763.

Hillenbrand, J. M., Getty, L. A., Clark, M. J., and Wheeler, K. (**1995**). "Acoustic characteristics of American English vowels," J. Acoust. Soc. Am. **97**, 3099–3111.

House, A., and Fairbanks, G. (**1953**). "The influence of consonant environment upon the secondary acoustical characteristics of vowels," J. Acoust. Soc. Am. **22**, 105–113.

Ito, M., Tsuchida, J., and Yano, M. (**2001**). "On the effectiveness of whole spectral shape for vowel perception," J. Acoust. Soc. Am. **110**, 1141–1149.

Jacewicz, E. (**2005**). "Listener sensitivity to variations in the relative amplitude of vowel formants," ARLO **6**, 118–124.

Jacewicz, E., Fox, R. A., and Salmons, J. (**2007a**). "Vowel space areas across dialects and gender," in *Proceedings of the XVIth International Congress of Phonetic Sciences*, edited by J. Trouvain and W. J. Barry, Saarbrücken, Germany, pp. 1465–1468.

Jacewicz, E., Fox, R. A., and Salmons, J. (**2007b**). "Vowel duration in three American English dialects," Am. Speech **82**, 367–385.

Katz, W. F., and Assmann, P. F. (**2001**). "Identification of children's and adults' vowels: Intrinsic fundamental frequency, fundamental frequency dynamics, and presence of voicing," J. Phonetics **29**, 23–51.

Kiefte, M., and Kluender, K. R. (**2005**). "The relative importance of spectral tilt in monophthongs and diphthongs," J. Acoust. Soc. Am. **117**, 1395–1404.

Lehiste, I., and Peterson, G. E. (**1959**). "Vowel amplitude and phonemic stress in American English," J. Acoust. Soc. Am. **31**, 428–435.

Lindqvist, J., and Pauli, S. (**1968**). "The role of relative spectrum levels in vowel perception," STL-QPSR 2-3/1970, pp. 12–15.

Mermelstein, P. (**1978**). "On the relationship between vowel and consonant identification when cued by the same acoustic information," Percept. Psychophys. **23**, 331–336.

Milenkovic, P. (**2003**). TF32 software program. University of Wisconsin, Madison, WI.

Miller, R. L. (**1953**). "Auditory tests with synthetic vowels," J. Acoust. Soc. Am. **25**, 114–121.

Nearey, T. M. (**1989**). "Static, dynamic, and relational properties in vowel perception," J. Acoust. Soc. Am. **85**, 2088–2113.

Oppenheimer, A. V., and Willsky, A. S. (**1977**). *Signal and Systems* (Prentice Hall, New York).

Peterson, G. E., and Lehiste, I. (**1960**). "Duration of syllable nuclei in English," J. Acoust. Soc. Am. **32**, 693–703.
Schwartz, J., and Escudier, P. (**1987**). "Does the human auditory system include large scale spectral integration?" in *The Psychophysics of Speech Perception*, edited by M. Schouten (Nijhoff, Dordrecht), pp. 284–292.
Sluijter, A. M. C., and Van Heuven, V. J. (**1996**). "Spectral balance as an acoustic correlate of linguistic stress," J. Acoust. Soc. Am. **100**, 2471–2485.
Stevens, K. N. (**1998**). *Acoustic Phonetics* (MIT, Cambridge, MA).
Titze, I. R. (**2000**). *Principles of Voice Production* (National Center for Voice and Speech, Iowa City, IA).
Whalen, D. H. (**1989**). "Vowel and consonant judgments are not independent when cued by the same information," Percept. Psychophys. **46**, 284–292.
Whalen, D. H., and Levitt, A. G. (**1995**). "The universality of intrinsic F0 of vowels," J. Phonetics **23**, 349–366.

Focus, prosodic context, and phonological feature specification: Patterns of variation in fricative production

Noah Silbert[a] and Kenneth de Jong
Department of Linguistics and Department of Cognitive Science, Indiana University, Memorial Hall, Room 322, 1021 E. Third Street, Bloomington, Indiana 47405

(Received 12 March 2007; revised 6 February 2008; accepted 7 February 2008)

Because they consist, in large part, of random turbulent noise, fricatives present a challenge to attempts to specify the phonetic correlates of phonological features. Previous research has focused on temporal properties, acoustic power, and a variety of spectral properties of fricatives in a number of contexts [Jongman *et al.*, J. Acoust. Soc. Am. **108**, 1252–1263 (2000); Jesus and Shadle, J. Phonet. **30**, 437–467 (2002); Crystal and House, J. Acoust. Soc. Am. **83**, 1553–1573 (1988a)]. However, no systematic investigation of the effects of focus and prosodic context on fricative production has been carried out. Manipulation of explicit focus can serve to selectively exaggerate linguistically relevant properties of speech in much the same manner as stress [de Jong, J. Acoust. Soc. Am. **97**, 491–504 (1995); de Jong, J. Phonet. **32**, 493–516 (2004); de Jong and Zawaydeh, J. Phonet. **30**, 53–75 (2002)]. This experimental technique was exploited to investigate acoustic power along with temporal and spectral characteristics of American English fricatives in two prosodic contexts, to probe whether native speakers selectively attend to subsegmental features, and to consider variability in fricative production across speakers. While focus in general increased noise power and duration, speakers did not selectively enhance spectral features of the target fricatives.
© *2008 Acoustical Society of America.* [DOI: 10.1121/1.2890736]

PACS number(s): 43.70.Fq, 43.70.Jt [CHS] Pages: 2769–2779

I. INTRODUCTION

A. Stress, focus, strengthening, and reduction

Reduction is a pervasive property of motor behavior in speech. The extent of reduction of a speech action varies according to the context in which an utterance is produced, the position of the action within the utterance, the nature of surrounding actions, and the properties of the action itself. To create a framework in which to analyze this kind of variation, Lindblom (1990) formulated H&H Theory, in which speech production is constrained by the conflicting demands of motor economization and acoustic distinctiveness. Motor economization causes hypoarticulation, in which a production system "cuts corners," resulting in reduction effects (Lindblom *et al.*, 1971; Lindblom, 1963). However, according to the H&H framework, such effects are held in check by countervailing pressures to produce signs that are reliably recoverable by the hearer. Such shifts toward "output oriented" speech are called hyperarticulation. Various utterance contexts impose these opposing constraints to varying degrees, producing variation in the amount of reduction found in different contexts.

In concordaonce with the predictions of the H&H framework, the frequency of a lexical item seems to be correlated with weakening of output oriented constraints. High frequency words are shorter in overall duration than lower frequency items (Bell *et al.*, 2003), contain shorter consonantal segments in various positions (Umeda, 1977; Jurafsky *et al.*, 2001), and exhibit more extensive contextual assimilation (Ernestus *et al.*, 2006). However, such results need to be interpreted in light of other factors that also affect degree of reduction.

For example, the location of linguistic stress and focus affects degree of reduction. Linguistic stress is a conventional aspect of some languages that increases the prominence of certain syllables within a given word. Focus is the more general aspect of speech such that talkers mark particular items as centers of attention. de Jong (1995) used x-ray microbeam traces to investigate the effects of linguistic stress and focus on the articulation of a number of different vowels and consonants, arguing that stress functions as syllable-localized hyperarticulation (cf., Lindblom, 1990); phonological contrast effects are more apparent in stressed than unstressed syllables, and reduction is a general property of unstressed syllables. Although stress-induced hyperarticulation is generally taken to be localized to the syllable (at least in English), focus-induced hyperarticulation might apply to units larger than the syllable (Lindblom, 1990), and possibly those smaller than the syllable (van Heuven, 1994). The degree to which a segment is reduced also differs depending on the nature of the segment. For example, while both consonants and vowels tend to shorten, and vowels tend to exhibit centralized values of F2, coronal consonants are subject to exceptionally large amounts of reduction in poststress position (Umeda, 1977; de Jong, 1998).

The current study builds on previous work on the effects of linguistic stress and focus. The fact that stress accentuates local cues to linguistic contrasts was exploited in a pair of experiments probing cross-linguistic differences in vowel duration and consonant voicing (de Jong, 2004; de Jong and Zawaydeh, 2002). de Jong (2004) found stress and focus

[a]Electronic mail: nosilber@indiana.edu

both exaggerate durational differences between vowels and voicing-induced vowel duration differences, de Jong and Zawaydeh (2002) found similar effects on the duration difference between long and short vowels in Arabic, but no effect of voicing-induced durational differences.

These studies employed two types of focus, one in which talkers contrasted phonologically unrelated lexical items (lexical focus), and one in which talkers disambiguated particular segments (phonological focus). Lexical focus seems to operate primarily in locations picked out by linguistically specified stress, whereas phonological focus also serves to selectively enhance localized phonologically relevant features. de Jong (2004) also found a general effect on focus on vowel quality and less differentiation of vowel quality as a result of phonological focus; phonological focus effects on vowel quality were not significantly different than lexical focus effects.

The current paper extends this research program to an investigation of the effects of focus on place of articulation and voicing contrasts in American English fricatives. Less is known about the acoustic effects of focus and stress on consonants than on vowels, though several findings have been repeated in the literature. For example, stress and focus tend to create larger and more rapid transitions from a fricative into a following vowel (e.g., Tjaden, 1999). In addition, obstruents have greater duration in stressed position, though such increases in duration are smaller than those found in vowels (Crystal and House, 1988b).

No study to our knowledge has examined the effect of focus on the duration and quality of fricative productions, although the effects of low level prosodic context and stress on European Portuguese fricatives has been studied (Jesus and Shadle, 2002). Mooshammer *et al.*, (2006) similarly examined the effect of increased loudness on articulation of a variety of consonants, focusing on the relations of the jaw and tongue for different manners of articulation. While this study found sizable differences between loud and nonloud vowels, and some small positional differences for other consonants, they found very few differences between loud and nonloud sibilant fricatives, suggesting that the sibilant production exerts stringent requirements on jaw position, reducing variability in the loud and nonloud productions. It is also important to note that, while Jesus and Shadle (2002) found strong spectral tilt effects of increased airflow on sustained fricatives, they also showed that stress is not simply equivalent to increased effort.

In addition, there is evidence that levels of prosodic structure are distinguished by the "strength" of articulation of initial consonants in a number of languages; articulatory strengthening is similar to hyperarticulation, though it is not necessarily listener-oriented (Fougeron 2001; Keating *et al.* 2003). The current research examines strengthening and reduction patterns in the acoustics of fricatives in two (low level) prosodic contexts. While much research of this type has been applied to vowels and stop consonants, there is relatively little work on fricatives. In fact, aside from duration measures of sibilants in a variety of prosodic contexts (e.g., Klatt, 1974), duration and devoicing measures of European Portuguese fricatives in a variety of word positions and stress contexts (Jesus and Shadle, 2003a, b), and devoicing and spectral measures of sustained fricatives produced at various effort levels (Jesus and Shadle, 2002), the nature of prosodically induced acoustic variability in fricatives is relatively understudied.

B. Properties of fricatives

While vowels have been extensively examined, the physical properties of fricatives are less well understood. This may be due, in part, to the nature of fricatives. Because fricatives consist largely of turbulent noise, the wave form of a given fricative varies considerably from token to token. Because the characteristics of frication noise depend to an unknown degree on the unique shape of a given speaker's vocal tract, fricatives can also vary from speaker to speaker. Nonetheless, research indicates that fricatives do have a number of stable properties that vary consistently with phonological features. Broadly speaking, these may be categorized as temporal, spectral, and power properties.

1. Temporal properties

Although a number of factors may affect the duration of a given speech sound (see, e.g., Klatt, 1976) the effects of phonological feature specification and prosodic context are of interest here. The duration of the frication noise for voiceless fricatives at a given place of articulation is much greater than the duration of their voiced cognates (Crystal and House, 1988a, c; Klatt, 1976; Pirello *et al.*, 1997; Stevens, 1998; Stevens *et al.*, 1992). Stevens (1998) and Stevens *et al.* (1992) present a physiological explanation for this difference, arguing that the maintenance of voicing during the articulation of a fricative constriction results in later onset, earlier offset, and lower amplitude of frication noise. In addition, it is common to find that phonologically voiced fricatives undergo substantial devoicing (Haggard, 1978; Stevens *et al.* 1992). It is also possible that duration differences in fricatives may be "phonologized," or taken by speakers to be linguistically specified (as opposed to being a merely physiological byproduct of articulation).

Differences in place of articulation and prosodic context also correspond to duration differences, although place effects are typically much smaller than voicing effects. Voiceless coronal fricatives [s] and [ʃ] tend to be longer than voiceless interdentals [θ] and labiodentals [f] (Behrens and Blumstein, 1988; Jongman *et al.*, 2000), and phrase final segments tend to be lengthened (Klatt, 1976). Syllable affiliation (i.e., onset versus coda position) does not appear to correspond to reliable duration differences.

2. Spectral properties

Spectral properties of fricatives change with place of articulation, less so with voicing, across a number of languages (Hughes and Halle, 1956; Jassem, 1965; Jesus and Shadle, 2002; Jongman *et al.*, 2000; Stevens, 1998). Voicing seems to affect the spectra of fricatives primarily by reducing the amplitude of the noise (see, e.g., Jesus and Shadle, 2002; Stevens *et al.*, 1992). Differences in place of articulation can have drastic effects on the spectra of fricatives, largely be-

cause the noise source mechanism can change drastically with place: Labiodental and interdental frication noise is produced by airflow through a narrow constriction, whereas coronal frieation noise is produced both by this and the channeling of the air stream into the lower teeth (Shadle, 1990, 1991). In addition, the spectra of coronal fricatives are shaped by the resonant frequencies of the cavity anterior to the constriction (Stevens, 1998).

Because frication noise is highly variable, statistical techniques have proven to be especially useful in investigations of place of articulation differences in fricative spectra. For example, Jesus and Shadle (2002) fit two regression lines to the spectra of a number of European Portuguese fricatives. One regression line was fit to the spectra from the mean frequency of the highest amplitude peak up to 20 kHz, the other from 500 Hz to that mean frequency. Other work has exclusively employed so-called "spectral moments," in which the spectral representation of (a portion of) an obstruent is treated as a probability distribution. The first four (central) moments—the mean, variance, skewness, and kurtosis—are then taken as measures of the central tendency, variation, symmetry, and peakedness of the spectrum, respectively. Forrest *et al.* (1988) pioneered the use of spectral moments in a study of spectral differences in voiceless obstruents. Jongman *et al.* (2000) extended the use of these measures to a larger set of place of articulation distinctions in English fricatives, finding that interdental and labiodental fricatives tended to have lower spectral means and kurtosis than [s] and [z], higher spectral means and kurtosis than [ʃ] and [ʒ], higher spectral variance than either of the coron alpairs, and skewness higher than [s] and [z], but lower than [ʃ] and [ʒ]. Jesus and Shadle (2002) found similar, consistent changes in spectral shape across place of articulation in European Portuguese fricatives.

Although prosodic context has been studied with regard to articulatory measures (Fougeron, 2001; Keating *et al.*, 2003) as well as measures of duration and devoicing (Jesus and Shadle, 2003a; b), the spectral effects of prosodic context are unknown. Insofar as onset position is "stronger" than coda position, and insofar as strength corresponds to increased airflow, we should expect coda fricatives to exhibit a steeper spectral drop-off at higher frequencies (see Sec. I B 3). This will have predictable consequences for spectral measurements (see spectral measure hypotheses stated in Sec. II).

3. Power properties

As described earlier, the presence of voicing in a fricative tends to lower the overall amplitude of the frication noise. Noise amplitude can also be affected by place of articulation. For example, coronal fricatives have higher amplitude than labiodental or interdental fricatives (Jongman *et al.*, 2000). In addition, glottal excitation produces energy primarily at low frequencies (e.g., below 750 Hz). Finally, mechanical models of human vocal tracts show that increases in the volume velocity of air flowing through a constriction increase the power more at higher frequencies than at lower frequencies (Shadle, 1990, 1991).

4. Speaker-specific properties

Because many of the properties of fricatives are dependent on physiological features, the possibility of interspeaker variation must be allowed for. For example, the source spectrum for coronal fricatives depends in part on the shape and position of the lower teeth; the source spectrum for labiodental fricatives depends in part on the shape and size of the constriction between the lower lip and upper teeth; the resonant frequencies of a cavity vary with its size, which is itself variable. In addition, speaker gender has been shown to interact with, e.g., spectral peak location (Jongman *et al.*, 2000).

II. RESEARCH QUESTIONS AND HYPOTHESES

The present research seeks to probe the effects of focus on a subset of phonological contrasts in fricatives using a number of acoustic measures. Native speakers participated in an interactive fricative production experiment in which voicing and place of articulation distinctions in fricatives were explicitly disambiguated. Posed generally, the research questions to be investigated are as follows: What are the effects of focus on fricative production? How does prosodic context (i.e., syllable affiliation) modulate the effects of focus? Do native speakers selectively attend to subsegmental (i.e., contrastive) features in production? Answers to these questions were pursued by analyzing productions of singleton voiced and voiceless labiodental and coronal fricatives in onset and coda position in focus and neutral conditions.

Methods: *1. Corpus and materials.* The fricatives of interest were the labiodental [f] and [v], interdental [ɵ] and [ð], and coronal [s] and [z] in onset and coda positions in nonsense syllables. Every target syllable contained the same low vowel, [ɑ]. The exclusive use of "minimal pair" nonsense syllables was imposed to control for spectral and duration differences between English vowels, as well as potential confounds relating to differences in word frequency.

All fricative productions were elicited with orthographic representations. Both of the interdental fricatives were represented with the letters "th" accompanied by key words cuing the intended voicing specification. Because all but one participant exhibited considerable confusion with the interdental fricatives, trials involving these consonants were exempted from measurement and analysis.

Each recording was made with the first author present in a sound-attenuating booth. Target fricative productions were elicited in frame sentences in neutral, voicing disambiguation, and place disambiguation contexts. The neutral productions occurred in postfocus position, while the voicing and place disambiguation productions occurred in focus position. In each condition, a 3 by 5 in. card with a nonsense target syllable was displayed and the participants were instructed to read this nonsense syllable aloud. In the neutral (unfocused) condition, the experimenter then asked the participant "Did you say [target syllable]?" The participants were instructed to respond to this question with the frame sentence "No, Jeff/Jane said [target syllable]." The name in the response frame was fixed to match the gender of the participant.

In the voicing disambiguation and place disambiguation conditions, the experimenter asked "Did you say [disambiguation syllable]?" where [disambiguation syllable] indicates a syllable identical to the target syllable except for a difference in either voicing or place specification (i.e., the target syllable and the disambiguation syllable form a "minimal pair" contrastive in either voicing or place alone). The participants were instructed to respond to these questions with the frame sentence "No, I said [target syllable]." For example, for trials in which the target syllable was [fa], the voicing disambiguation question would be "Did you say [va]?," while the place disambiguation question would be "Did you say [sa]?" ln either case, the participant's response would be "No, I said [fa]."

For each talker, each target syllable was produced and recorded six times in each condition. Productions were blocked by repetition and partially blocked by focus condition. The disambiguation contexts, prosodic context, and target voicing and place specifications were randomized within blocks. Thus, for each repetition block, all of the neutral productions were elicited first, followed by all voicing and place disambiguation productions. The corpus consisted of six repetitions of four target fricatives produced in two prosodic contexts and three disambiguation conditions by four speakers. Thus, 576 tokens were measured and analyzed.

2. Participants. Four native speakers of Midwestern American English—two male and two female—were recorded in a single-walled sound attenuated booth using a head-mounted microphone. The participants' ages ranged from 18 to 21. At the time of recording, all participants were enrolled at a large Midwestern university. None reported any history of speech or hearing pathology, and all had limited, adult experience with at least one second language.

3. Recording. The microphone, a Shure SM10A (with frequency response from 50 to 15 000 Hz), was placed approximately 2 in. to the left and 2 in. below each participant's lips. Recordings were captured on digital audio tape (using a Panasonic SV3800) at a sampling rate of 44.1 kHz The participants' recordings were transferred to hard drive as wav files with a sampling frequency of 44.1 kHz and bit depth of 16 bits. These wav files were edited and subjected to acoustic analysis.

4. Measurement. Each target fricative alone and each full target syllable were manually extracted and saved as separate files using both wave form and spectrogram displays. All editing made use of two visual cues: high levels of energy in the frequency region above about 3 kHz relative to surrounding (vowel) regions in the spectrogram display, and the presence of noise (i.e., lack of periodicity) in the wave form display. The edited signals were preemphasized via a first-difference filter [as in Forrest *et al.* (1988) and Jongman *et al.* (2000)]. All measurements were taken automatically via a MATLAB script. Prior to measurement, all files were resampled to 30 000 Hz, fixing the highest frequency available for spectral analysis at 15 000 Hz. This value was chosen to match the upper bound of the frequency response of the microphone used to make the recordings.

Two temporal measurements were taken. Syllable duration was measured in milliseconds, and fricative duration was measured as a proportion of the syllable duration, in part to mitigate the effects of differences in speech rate across subjects (see Jongman *et al.*, 2000), in part to reduce as much as possible any correlation between the two temporal measures so as to increase the power of the multivariate statistical tests performed (Tabachnick and Fidell, 2001).

Four spectral measurements were taken. Twelve 17 ms (512 sample) sections were taken from each fricative. A full Hamming window was applied to each section, and a spectrum was calculated via fast fourier transform. All spectral moment measurements were taken from a single spectrum time-averaged across 12 individual spectra calculated from equally spaced windows. [See Jesus and Shadle (2002) for a discussion of time versus token averaging of fricative spectra.] Spectral moment measurements were restricted to frequencies above 750 Hz, as these were intended as descriptors of the noise component of the fricatives, and energy produced by glottal pulsing is located predominantly in the low frequency range. The energy below 750 Hz was used to measure the amount of glottal energy (see the following). The cutoff was chosen as 750 Hz based on visual inspection of the spectra analyzed here and on criteria used in other research (e.g., Jesus and Shadle (2002)).

The first four (central) spectral moments were calculated based on the formulas used in Forrest *et al.* (1988). Spectral moments were calculated using the portion above 750 Hz of a single spectrum (time) averaged across all 12 individual spectra taken from each fricative.

The noise power measurement for a given fricative was also taken from a single time-averaged spectrum and was also restricted to frequencies above 750 Hz. Glottal power measurements (i.e., power below 750 Hz) for each fricative were taken at three intervals, each based on a single spectrum averaged over four spectra. Thus, four 17 ms sections in the first third of a fricative were windowed, transformed, and averaged and the power below 750 Hz was calculated; the same was done for the middle third and final third of each fricative. All power measurements were decibel transformed with reference to a single bit.

5. Analysis. Each set of measures (two temporal measures, four spectral measures, and four power measures) was subjected to repeated measures multivariate analyses using the SPSS GLM algorithm. Plots and tables in Sec. III are based on a subset of the statistically significant results from the multivariate tests of between and within subject effects, as determined by the following hypotheses.

Temporal measures. Previous research leads us to expect the following hypotheses to hold. Regardless of prosodic context, phonologically voiceless fricatives will be longer than phonologically voiced fricatives, and coronal fricatives will be longer than labiodental fricatives. Phonologically voiced coda fricatives will be preceded by longer vowels than will phonologically voiceless coda fricatives. Phonological voicing in onset position will have no effect on vowel duration, so overall syllable duration will not vary across fricative voicing in coda position, but phonologically voiceless onset fricatives will appear in longer syllables than their voiced cognates.

If focus involves a general shift toward listener-oriented speech, syllables in focus position will have longer overall durations than will those in the nonfocus (neutral) position, as will individual fricatives. If focus involves adjustments in production specifically targeting contrastive dimensions, voicing disambiguation will selectively exaggerate duration differences due to phonological voicing. Although focus will generally increase fricative duration, phonologically voiceless fricatives will be lengthened more than phonologically voiced fricatives. Also, voiced-coda induced increases in vowel duration will be exaggerated by focus on voicing.

Note that, although the effect of voicing specification of coda obstruents on preceding vowel durations is quite large when found (see, e.g., Klatt, 1976, de Jong, 2004), it is not always found (see, e.g., Crystal and House, 1988a). Also, because all of the target syllables are in prepausal, phrase final position, coda fricatives will be longer than their onset counterparts (see, e.g., Klatt, 1976).

Spectral measures. Previous research leads us to expect that coronal fricatives will have higher spectral means, lower spectral standard deviations, higher spectral kurtosis, and lower spectral skewness than labiodental fricatives. More specifically, coronals will have negative spectral skewness, while labiodentals will have spectral skewness near zero. Phonologically voiced fricatives will have higher spectral standard deviations, lower (i.e., more negative) spectral skewness, and lower spectral kurtosis, regardless of prosodic context.

Although the effects of changes in cross-sectional area due to changes in place of articulation are well understood, relatively little is known about the acoustic effects of changes in cross-sectional area and shape of a fricative constriction within a given place of articulation (e.g., due to hyperarticulation). Because of this, all of the general focus hypotheses for spectral effects pertain to the effects of increase in volume velocity airflow. In order to state any such hypotheses, then, it is assumed that explicit focus will induce an increase in volume velocity airflow due to a general increase in articulatory effort. Because increased volume velocity airflow through a constriction with the same area increases the power more at higher frequencies than at low frequencies, fricatives in focus position will have higher spectral means than those in the neutral position, within each place of articulation and in any prosodic context. Coronal fricatives in focus position will have higher spectral standard deviation than those in the neutral position, while labiodental fricatives in focus position will have lower spectral standard deviation than those in the neutral position. Coronal fricatives in focus position will have lower (i.e., more negative) spectral skewness than those in the neutral position. Labiodental fricatives in focus conditions will also have lower (i.e., more negative) skewness and higher spectral kurtosis than those in the neutral position. If onsets are "stronger" than codas, and if articulatory strength is implemented, at least in part, through increased airflow, we expect the same general (focus) effects in onset but not in coda position.

If focus involves adjustments in production specifically targeting contrastive dimensions, place disambiguation will selectively exaggerate place differences as found in all four spectral moments. Insofar as voicing disambiguation increases the amount of glottal excitation, changes in the noise power will induce lower spectral mean, skewness, and kurtosis, higher spectral standard deviation for voiced fricatives.

Power measures. Based on previous research, we expect phonologically voiced fricatives to have more low-frequency power (near the co-syllabic vowel) than phonologically voiceless fricatives, regardless of prosodic context. Due to phrase and word edge effects, phonologically voiced coda fricatives will be devoiced more than their onset counterparts. Coronal fricatives will have higher noise power than labiodental fricatives. Phonologically voiced fricatives will have lower noise power than phonologically voiceless fricatives, although this effect may be modulated by the phrase edge effects discussed earlier.

If focus effects reflect a general increase in vocal output, fricatives in focus position will have higher noise power than those in the neutral position, regardless of place of articulation, voicing specification, and prosodic context. Phonologically voiced fricatives in focus position will have more low-frequency power (near the vowel in time) than those in the neutral position, regardless of place of articulation or prosodic context. Phonologically voiceless labial fricatives in focus position will have more low-frequency power (at all times) than those in the neutral position, whereas, due to zeros associated with the coronal place of articulation, phonologically voiceless coronal fricatives in focus position will have less low-frequency power than those in neutral position; we expect the same general pattern in onset and coda position. If focus effects are tuned to specific contrastive dimensions, voicing disambiguation will selectively increase the amount of low-frequency power in phonologically voiced fricatives.

III. RESULTS

A. Temporal measurements

Due to the large number of statistical tests carried out, a relatively conservative criterion ($\alpha=0.01$) was adopted. There were statistically significant main effects of voicing [$F(2,47)=120.15, p<0.001$], disambiguation condition [$F(2,96)=3.65, p=0.008$], prosodic context [$F(2,47)=106.92, p<0.001$], and speaker gender [$F(2,47)=12.90, p<0.001$]. Between-subject main described in detail in Table I. There were statistically significant interactions between voicing and prosodic context [$F(2,47)=6.35, p=0.004$] and between prosodic context and speaker gender [$F(2,47)=6.413, p=0.003$]. These interactions are illustrated in Fig. 1.

Phonologically voiced fricatives were shorter than phonologically voiceless fricatives, as shown by the main effect of voicing. However, there was no statistically significant main effect of place. The general focus prediction regarding temporal measures was confirmed, as shown by the main effect of disambiguation condition: In both focus conditions, overall syllable duration was increased by roughly the same amount. The disambiguation-specific predictions, however, were disconfirmed. Both focus conditions induced an approximately equal increase in consonant duration proportion.

TABLE I. Main effects, temporal DVs. Fricative duration is expressed as a proportion of syllable duration. Numbers indicate means (standard deviations).

Independent variable	Fricative duration		Syllable duration (ms)	
Voiced	0.302	(0.078)	409.876	(76.938)
Voiceless	0.426	(0.099)	428.843	(83.997)
Neutral	0.341	(0.104)	378.006	(75.899)
Voicing	0.376	(0.110)	440.605	(74.572)
Place	0.375	(0.108)	439.468	(76.595)
Onset	0.303	(0.072)	399.017	(84.437)
Coda	0.426	(0.104)	439.702	(72.079)
Female	0.341	(0.093)	400.373	(78.446)
Male	0.387	(0.118)	438.346	(79.236)

The main effect of prosodic condition was caused by the overall greater duration of coda fricatives. The voicing by prosodic context and prosodic context by gender interactions are depicted in Fig. 1. The gender main effect was caused by the male speakers' slightly longer syllables and fricatives. Both interactions are due to the male speakers' particularly long voiceless coda fricatives.

B. Spectral measurements

There were statistically significant main effects of voicing $[F(4,45)=7.41, p<0.001]$, place of articulation $[F(4,45)=363.49, p<0.001]$, prosodic context $[F(4,45)=11.26, p<0.001]$, speaker gender $[F(4,45)=25.34, p<0.001]$, and (within subjects) experimental block $[F(20,29)=3.40, p=0.001]$. Between-subject main effects are described in Table II. There were statistically significant interactions between voicing and place of articulation $[F(4,45)=6.54, p<0.001]$, place and speaker gender $[F(4,45)=38.90, p<0.001]$, place and prosodic context $[F(4,45)=5.29, p<0.001]$, voicing and prosodic context $[F(4,45)=4.08, p=0.007]$, experimental block and speaker gender $[F(20,29)=3.391, p=0.001]$, and between experimental block and place of articulation $[F(20,29)=2.837, p=0.005]$. Interactions involving only between-subjects effects are illustrated in Figs. 2–4.

TABLE II. Main effects, spectral DVs. M_s= spectral mean; s.d.$_s$= spectral standard deviation; S_s= spectral skewness; K_s= spectral kurtosis. Numbers indicate means (standard deviations). Spectral means and standard deviations are given in hertz. Spectral skewness and kurtosis are expressed in reference to spectral standard deviation (see formulas in Forrest *et al.*, 1988).

Independent variable	M_s		s.d.$_s$		S_s		K_s	
Voiceless	7049	(864)	2694	(505)	0.371	(0.372)	0.162	(0.758)
Voiced	6979	(885)	2820	(673)	0.369	(0.364)	0.143	(0.961)
Labiodental	6745	(707)	3302	(290)	0.337	(0.249)	−0.564	(0.317)
Coronal	7283	(942)	2212	(192)	0.403	(0.426)	0.870	(0.606)
Onset	7324	(851)	2770	(668)	0.284	(0.338)	0.123	(0.979)
Coda	6704	(785)	2744	(519)	0.456	(0.342)	0.182	(0.735)
Female	7274	(1012)	2689	(638)	0.237	(0.319)	0.301	(0.943)
Male	6754	(612)	2825	(548)	0.503	(0.330)	0.004	(0.752)

The main effect of place was as expected on three of the four of the spectral moments: coronal fricatives had higher spectral means, lower spectral standard deviations, and higher spectral kurtosis than did the labiodentals. The hypothesis concerning the effect of phonological voicing specification was only partially confirmed. While voicing does generally correspond to lower noise power in fricatives (see Sec. III C), this did not have the expected effect on the first, third, or fourth spectral moments. As can be seen in Fig. 2, phonologically voiced labiodental fricatives (diamond with solid variance axes) have higher spectral standard deviations (y axis) than do phonologically voiceless fricatives (star with solid variance axes), but no such effect was found for coronal fricatives (star and diamond with broken variance axes).

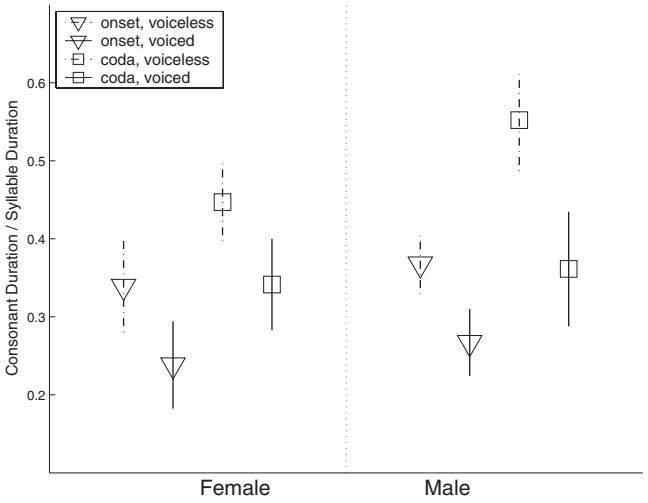


FIG. 1. Fricative duration (divided by syllable duration) as a function of fricative voicing, prosodic context, and speaker gender. Triangles indicate mean consonant duration for onset fricatives, squares for coda fricatives. Solid error bars indicate ±1 s.d. for voiced fricatives; broken error bars for voiceless fricatives. Values for female participants appear on the left, values for male participants on the right.

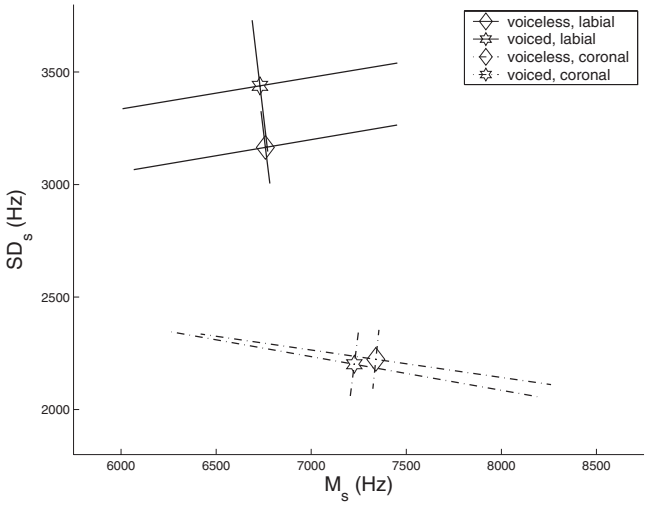


FIG. 2. The first and second spectral moments as a function of fricative voicing and place of articulation. The x axis indicates spectral mean values. The y axis indicates spectral standard deviation values. Diamonds indicate mean spectral moment values for voiceless fricatives, stars for voiced fricatives. Solid error bars indicate the major and minor axes of the variance ellipses for labial fricatives, broken error bars for coronal fricatives.

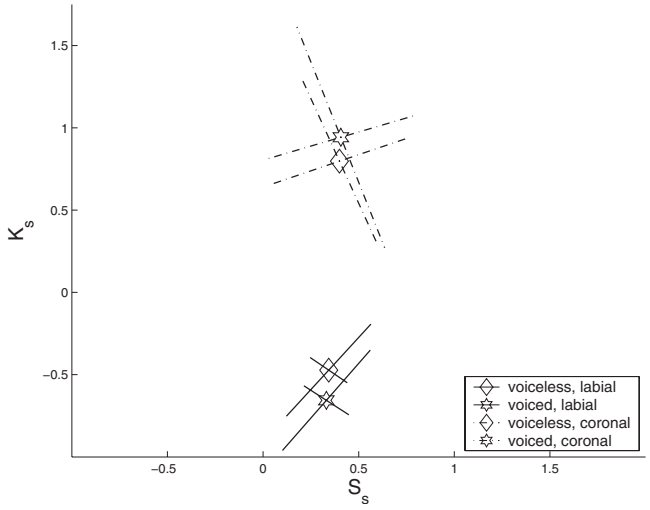


FIG. 3. The third and fourth spectral moments as a function of fricative voicing and place of articulation. The *x* axis indicates spectral skewness values. The *y* axis indicates spectral kurtosis values. Diamonds indicate mean spectral moment values for voiceless fricatives, stars for voiced fricatives. Solid error bars indicate the major and minor axes of the variance ellipses for labial fricatives, broken error bars for coronal fricatives.

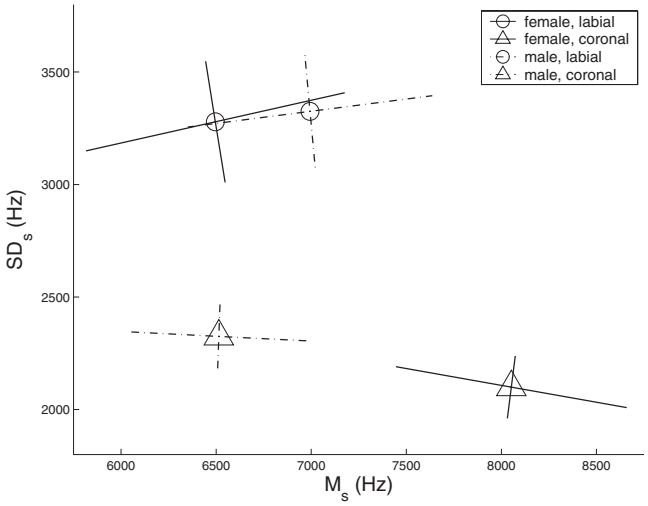


FIG. 5. The first and second spectral moments as a function of speaker gender and place of articulation. The *x* axis indicates spectral mean values. The *y* axis indicates spectral standard deviation values. Circles indicate mean values for labials, triangles for coronals. Solid error bars indicate the major and minor axes of the variance ellipse for female speakers, broken error bars for male speakers.

While the first and third moments were unaffected by phonological voicing, the difference in kurtosis between voiced labiodentals and coronals was larger than that between voiceless labiodentals and coronals (see Fig. 3). These two voicing-induced differences account for the place by voicing interaction.

All of the general focus and disambiguation-specific hypotheses were disproven, though the lack of statistical significance of the focus conditions was not due to a high degree of random variation in the fricatives, since there are a number of subtle prosodic and voicing differences that were statistically significant in the spectral measures. The main effect of prosodic context is due to higher spectral means in onset fricatives; the second, third, and fourth spectral moments are essentially identical across syllable position (see Table II). This main effect is due to an upward shift in spectral mean in voiceless onset fricatives and a larger difference in spectral standard deviation between labiodentals and coronals in onset position than in coda position. These differences are also responsible for the voicing by prosodic context interaction.

Place of articulation also interacts with prosodic context. The difference in spectral kurtosis between labiodentals and coronals is larger in onset position than in coda position, as depicted in Fig. 4.

Gender also affected the spectral measures. Both of the female speakers exhibited the expected patterns—coronal fricatives with high first and fourth but low second and third spectral moments, and labiodental fricatives with low first, third, and fourth spectral moments, and high spectral standard deviation. Both of the male speakers produced unexpectedly low first and fourth spectral moments and unexpectedly high second and third spectral moments in their coronal fricatives, although their labiodental fricatives conformed to expectations (see Figs. 5 and 6). All of the labiodental spectra are relatively flat across the four speakers, with small, idiosyncratic peaks in the spectra at various frequencies. The average coronal spectra, by contrast, all show energy concentrations in relatively narrow frequency bands. The lowest frequency of the concentrated energy is at approximately 5 kHz for the male speakers, and well above 6 kHz for the female speakers, consistent with a presumably shorter resonator for the female speakers. The difference between male and female speakers may also be due to idiosyncratic differences in (within category) place of articulation (e.g., differences in how far forward/back coronal fricatives are articulated). The different location of this peak relative to the center frequency of the spectral distribution explains the gender-based difference in skewness.

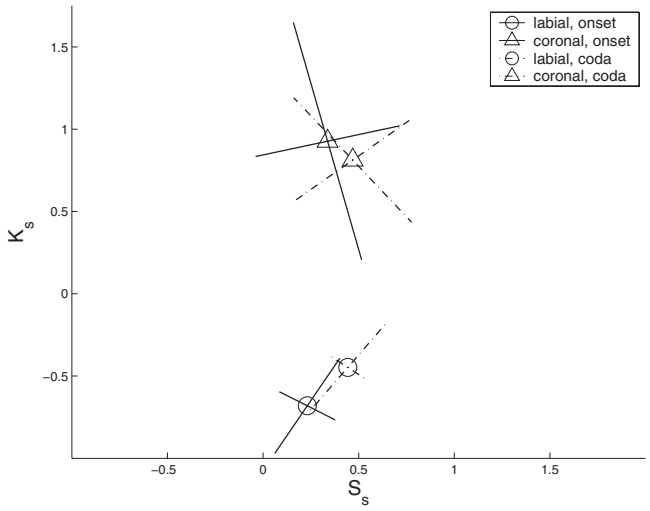


FIG. 4. The third and fourth spectral moments as a function of place of articulation and prosodic context. The *x* axis indicates spectral skewness values. The *y* axis indicates spectral kurtosis values. Triangles indicate mean spectral moment values for coronals, circles for labials. Solid error bars indicate the major and minor axes of the variance ellipses for onset fricatives, broken error bars for coda fricatives.

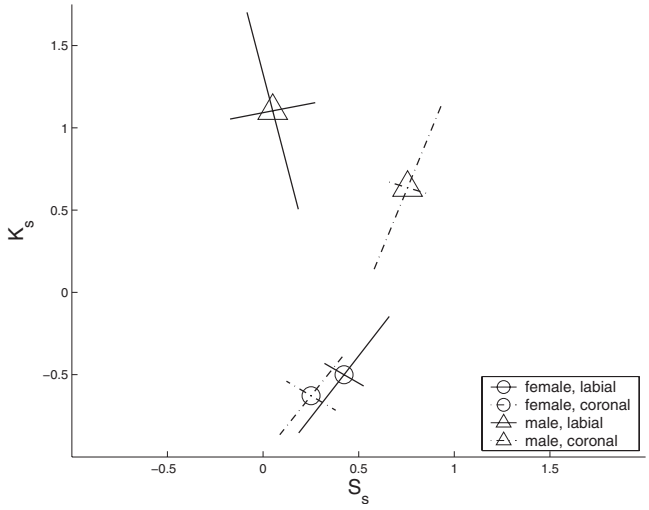


FIG. 6. The third and fourth spectral moments as a function of speaker gender and place of articulation. The *x* axis indicates spectral skewness values. The *y* axis indicates spectral kurtosis values. Circles indicate mean values for labials, triangles for coronals. Solid error bars indicate the major and minor axes of the variance ellipse for female speakers, broken error bars for male speakers.

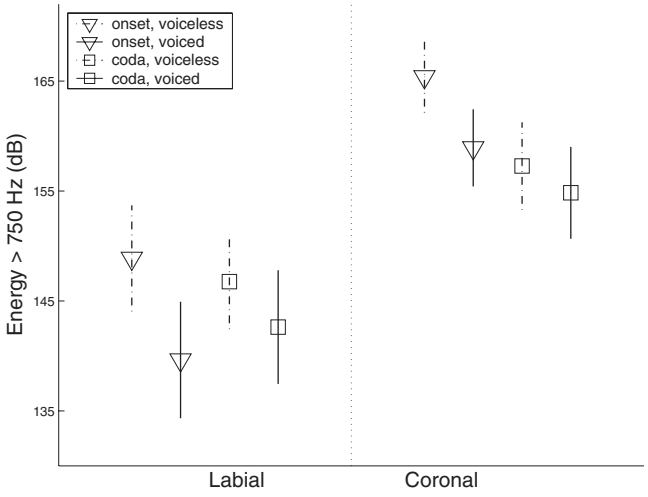


FIG. 7. Noise power (in dB re: 1 bit) as a function of voicing, prosodic context, and place of articulation. Triangles indicate mean noise power for onset fricatives, squares for coda fricatives. Solid error bars indicate ±/s.d. for voiced fricatives, broken error bars for voiceless fricatives. Noise power for labial fricatives is in the left panel, for coronals in the right.

Although these differences correspond with the gender of the speakers here, the small number of subjects in the present study and the apparent consistency across gender in other studies (e.g., Jongman *et al.*, 2000) limit the generality of the "gender" effect on spectral moments observed here. The "statistical" measures of the spectral properties of fricatives employed here cannot distinguish between plausible systematic (e.g., vocal tract size) and idiosyncratic (within-category place of articulation differences) causes for the observed gender difference.

The main effect of experimental block is due to an increase in spectral means, a decrease in spectral standard deviation and skewness, and general, nonmonotonic increase in spectral kurtosis over the course of the experiment. The experimental block by place interaction is due to nonmonotonic shifts in spectral means and skewness over the course of the experiment. All other spectral measurements remained more or less stable over the course of the six blocks.

C. Power measurements

There were statistically significant main effects of voicing $[F(4,45)=104.10, p<0.001]$, place of articulation $[F(4,45)=179.45, p<0.001]$, prosodic context $[F(4,45)=59.02, p<0.001]$, and experimental block $[F(20,29)=3.219, p=0.002]$. Between-subject main effects are described in detail in Table III. There were statistically significant interactions between voicing and prosodic context $[F(4,45)=18.039, p<0.001]$, place and prosodic context $[F(4,45)=29.03, p<0.001]$, voicing and speaker gender $[F(4,45)=8.03, p>0.001]$, and between experimental block and speaker $[F(20,29)=3.52, p=0.001]$. Interactions involving only between-subjects factors are illustrated in Figs. 7–9.

Phonologically voiceless fricatives have higher noise power than do phonologically voiced fricatives, as shown by the main effect of voicing on noise power in Table III. The main effect of place due to the higher noise power in coronals than labiodentals was also expected. Figure 7 illustrates the place by prosodic context and voicing by prosodic context interaction effects on noise power. The noise portion of the place by prosodic context interaction is due to the overall higher power for onset coronals relative to coda coronals, while labiodentals have roughly the same power across prosodic context (compare triangles to squares within each half of Fig. 7). The voicing by prosodic context interaction is due

TABLE III. Main effects, power DVs. Noise=power (dB) above 750 Hz. Voicing *N*=power (dB) below 750 Hz at *N*th third of the fricative. Numbers indicate means (standard deviations).

Independent variable	Noise	Voice 1	Voice 2	Voice 3
Voiceless	154.57 (8.46)	105.09 (4.75)	102.98 (4.93)	103.50 (5.58)
Voiced	149.00 (9.30)	114.58 (7.05)	108.92 (8.35)	109.36 (9.00)
Labiodental	144.47 (6.07)	110.21 (7.34)	106.70 (7.60)	106.69 (7.58)
Coronal	159.10 (5.41)	109.46 (7.95)	106.21 (7.78)	106.16 (8.84)
Onset	153.20 (10.71)	108.90 (8.56)	108.98 (8.45)	110.04 (8.60)
Coda	150.37 (7.40)	110.77 (6.51)	103.92 (5.83)	102.82 (5.43)
Neutral	150.30 (8.77)	108.64 (7.03)	105.28 (7.58)	105.87 (8.41)
Voicing	152.64 (9.51)	110.06 (8.23)	106.83 (7.66)	106.49 (7.61)
Place	152.42 (9.48)	110.80 (7.53)	107.24 (7.71)	106.91 (8.09)

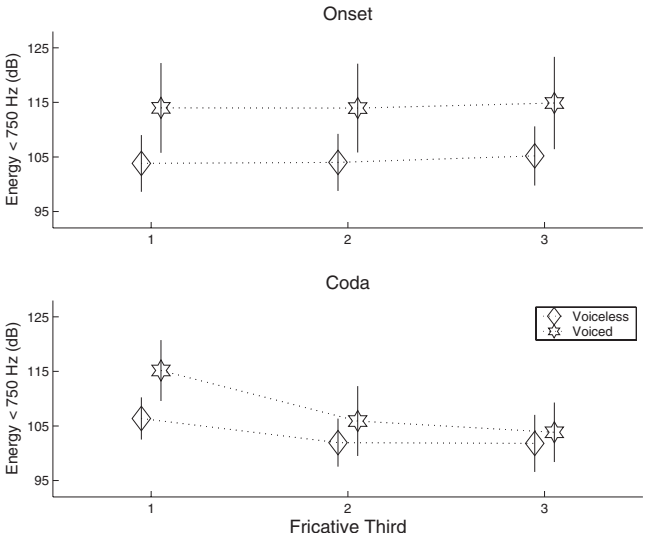


FIG. 8. Voicing power (in dB re: 1 bit) as a function of voicing, prosodic context, and fricative third. The *x* axis indicates "time," or the first, second, and middle third of the fricative. They *y* axis indicates power in decibels relative to one bit. Diamonds indicate mean voicing power for voiceless fricatives, stars for voiced fricatives. Solid error bars indicate ±1 s.d. The top panel indicates values for onset fricatives, the bottom panel for coda fricatives. The plots are staggered and nonvertical lines are plotted to ease comparison across voicing specification.

to the fact that, although the expected ordering is found between phonologically voiceless and voiced segments within each prosodic context, the difference between voiceless and voiced segments is larger in onset than in coda position (compare the difference between triangles with broken error bars and triangles with solid error bars to the difference between squares with broken error bars and squares with solid error bars in Fig. 7).

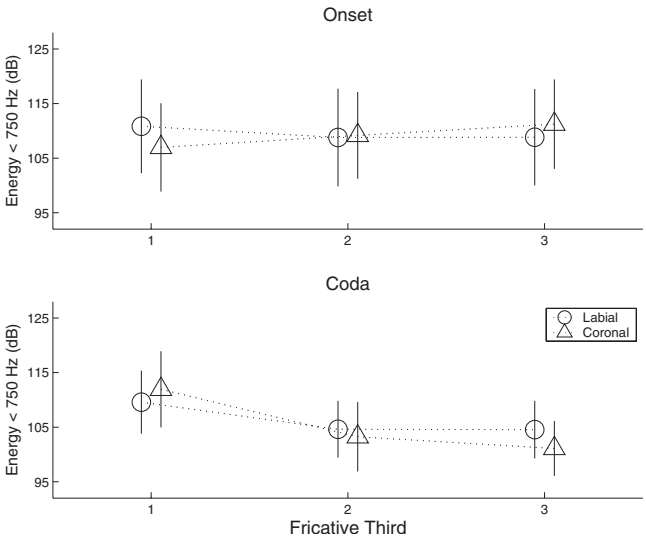


FIG. 9. Voicing power (in dB re: 1 bit) as a function of place of articulation, prosodic context, and fricative third. The *x* axis indicates time, or the first, second, and middle third of the fricative. The *y* axis indicates power in decibels relative to one bit. Circles indicate mean voicing power for labial fricatives, triangles for coronal fricatives. Solid error bars indicate ±1 s.d. The top panel indicates values for onset fricatives, the bottom panel for coda fricatives. The plots are staggered and nonvertical lines are plotted to ease comparison across voicing specification.

None of the general focus or disambiguation-specific power measure predictions were confirmed, though, as predicted, both of the focus conditions produced slightly higher noise and voicing power, as can be seen in Table 3.

Higher degree of voicing near the vowel should exhibit itself as a voicing by prosodic context interaction—onset fricatives should have higher power at the last measurement, whereas coda fricatives should have higher power at the first measurement. Figure 8 shows that, while phonologically voiced fricatives had higher low-frequency power than did phonologically voiceless fricatives, and while coda fricatives did indeed exhibit considerably more low-frequency power in the first third than at either of the other two thirds, onset fricatives had a more or less constant, perhaps slightly increasing level of low-frequency power.

The place by prosodic context interaction is also evident in the low frequency power measures. Figure 9 shows that voicing power in labiodentals decreased slightly over the three measurements (to a greater extent in coda than in onset position), whereas low frequency power increased for onset coronals and decreased for coda coronals.

The gender by voicing interaction is due to a much larger difference between phonologically voiced and phonologically voiceless fricatives in the first, and to a lesser degree the second, low-frequency power measurement in the productions of the male speakers than in productions of the female speakers. This is likely due, at least in part, to the fact that female speakers with higher fundamental frequencies would have fewer harmonics present below the 750 Hz cutoff employed.

IV. DISCUSSION AND CONCLUSION

Many previously documented differences between fricatives were observed here. The phonologically voiced fricatives were shorter than their voiceless counterparts. Coronal fricatives had higher spectral means, lower spectral standard deviations, higher spectral kurtosis, and had substantially more acoustic power than their labiodental counterparts. Phonological voicing increased the amount of low frequency power and reduced the acoustic power of frication noise, and had some, though not all, of the expected effects on the spectral moment measurements (e.g., voiced fricatives tended to have lower spectral means than their voiceless counterparts). The coda fricatives tended to be devoiced and lengthened.

Some expected properties of the fricatives were absent in the present data, however. Voiced coda fricatives were not preceded by longer vowels than their voiceless counterparts. For the male speakers, spectral skewness was higher for coronals than for labiodentals, and spectral means, while higher for coronals than for labiodentals, were much lower than expected. The duration of coronals was not statistically significantly different than the duration of labiodentals. Place of articulation also interacted with prosodic context with regard to the three low frequency power measurements—coronals had more low frequency power near the associated vowel (i.e., at the third time slice in onset position, at the first in coda position), whereas labiodentals in both prosodic contexts tended to decrease in low frequency power.

With regard to reduction effects, the general picture that is suggested by comparing onset and coda fricatives is that, as in vowels, fricative reduction is reflected, in part, in changes in acoustic power. However, unlike typical reduction effects, the coda fricatives in this corpus were longer than their onset counterparts, probably due to phrase-final lengthening. Interestingly, in coda position all spectral means are lower, while the spectral standard deviations take values intermediate between those of onset position. This suggests an acoustic characterization of reduction as consisting of a loss of higher frequency noise energy and the presence of relatively undifferentiated shaping effects.

The most obvious effect of focus was an increase in both fricative and syllable durations. Recall that fricative durations are expressed here as a proportion of syllable duration. The spectral mean increased slightly and spectral skewness decreased slightly in both focus conditions, and focus induced small increases in both noise and voicing power. All of these effects suggest that speakers were simply increasing articulatory effort. None of the disambiguation-specific predictions were borne out; both disambiguation conditions induced essentially the same general focus behavior.

The present results contrast with previous findings that focus induces hyperarticulation, which, in turn, selectively exaggerates linguistically important cues (de Jong, 2004; de Jong and Zawaydeh, 2002). A key difference between the present project and those reported in the above-mentioned papers is the nature of the segments under investigation, de Jong (2004) and de Jong and Zawaydeh (2002) studied the effects of focus (and stress) on vowel production, whereas this paper addresses fricatives. The differences in findings regarding the effects of focus between this and previous projects suggest that fricatives and vowels are subject to very different production pressures; vowels seem to be more malleable than fricatives. This finding is consistent with earlier articulatory research on prosodic position effects in which fricatives seem to be more resistant to changes in articulatory strength (Fougeron, 2001).

Although it is speculative to suggest a link, this idea is also consistent with work on word recognition wherein Dutch and Spanish native speakers were found to be more accurate and faster when required to change a vowel than when required to change a consonant, and more apt to change a vowel than a consonant when given a choice, in order to form real words from nonwords (Cutler *et al.*, 2000). Insofar as the present results reflect a difference in malleability between vowels and fricatives, we may conclude that the most one can hope for in cue-enhancing hyperarticulation in fricatives is increases in length and power. Longer and louder fricatives likely offer more and better opportunities to hear the relatively static phonetic cues for features like voicing and place of articulation.

However, one must be cautious in generalizing the current results to fricatives in general. The small set of fricatives examined here likely does not display the full range of variation in fricative production. For example, it is possible that the alveolar and palato-alveolar sibilants, which differ not just in lingual articulation but also secondary rounding, might exhibit focus-induced changes. If the lack of focus effects on fricative spectra depends on relatively stringent articulatory constraints on labial and lingual contact, it is still possible that the relatively free use of lip rounding might allow for focus variation. An obvious next step would be to extend the current approach to other segments and languages with different fricative inventories.

There are other possible reasons for the lack of focus effects here. Perhaps most obviously, while desirable for the control over extraneous factors (e.g., elimination of variables that were not of interest, such as word frequency), the use of nonwords as target syllables potentially reduces the communicative load of the carrier utterances. Because phonological contrasts function as cues to differences in meaning, by removing semantics from the picture (along with word frequency effects), the voicing and place contrasts' function was eliminated. Of course, it may also be the case that speakers are unable to attend selectively to subsegmental properties of speech sounds. The use of real words in a task in which a premium is placed on accurate communication of those words may better probe the speaker's ability and willingness to focus on the low-level characteristics that cue one contrast or another. Assuming that an appropriate set can be found, real words also offer the possibility of comparing current results with previous work, e.g., the effects of stress and focus in de Jong (2004) and the irregular differences in patterns of devoicing between real and nonwords in Jesus and Shadle (2002).

Finally, although an examination of within-subject variability is not the primary focus of the present research, it is noteworthy that statistically significant within-subjects main effects and interactions were found in the spectral measurements. Although some of these effects may be attributable to, e.g., changes in behavior over the course of the experiment, it seems that much of the variability across blocks is not due to task variables, but is a stable indicator of the different talkers. Of course, the existence of within-speaker and within-category variation is to be expected. However, given the differences in the variability of the spectral moments across place of articulation and speaker gender, a systematic investigation of this variation is called for, since such acoustic variation is a potentially important indicator of indexical differentiation in the face of linguistically specified aspects of the signal.

ACKNOWLEDGMENTS

This work was supported by the NSF Grant No. BCS-04406540. We would also like to thank Professor Diane Kewley-Port for her assistance in conducting this research, Dr. Christine Shadle for her comments and suggestions in her capacity as Associate Editor, and three anonymous reviewers for their helpful comments, all which have improved this work considerably.

Behrens, S. J., and Blumstein, S. E. (**1988**). "Acoustic characteristics of English voiceless fricatives: A descriptive analysis," J. Phonetics **16**, 295–298.

Bell, A., Jurafsky, D., Fosler-Lussier, E., Girand, C., Gregory, M., and Glidea, D. (**2003**). "Effects of disfluencies, predictability, and utterance position on word form variation in English conversation," J. Acoust. Soc. Am. **113**, 1101–1024.

Crystal, T. H., and House, A. S. (**1988a**). "Segmental durations in connected-speech signals: Current results," J. Acoust. Soc. Am. **83**, 1553–1573.
Crystal, T. H., and House, A. S. (**1988b**). "Segmental durations in connected-speech signals: Syllabic stress," J. Acoust. Soc. Am. **84**, 1574–1585.
Crystal, T. H., and House, A. S. (**1988c**). "A note on the durations of fricatives in American English," J. Acoust. Soc. Am. **84**, 1932–1935.
Cutler, A., Sebastián-Gallés, N., Soler-Vilageliu, O., and van Ooijen, B. (**2000**). "Constraints of vowels and consonants in lexical selection: Cross-linguistic comparisons," Mem. Cognit. **28**, 746–755.
de Jong, K. (**1995**). "The supraglottal articulation of prominence in English: Linguistic stress as localized hyperarticulation," J. Acoust. Soc. Am. **97**, 491–504.
de Jong, K. (**1998**). "Stress-related variation in the articulation of coda alveolar stops: Flapping revisited," J. Phonetics **26**, 283–310.
de Jong, K. (**2004**). "Stres, lexical focus, and segmental focus in English: Patterns of variation in vowel duration," J. Phonetics **32**, 493–516.
de Jong, K., and Zawaydeh, B. (**2002**). "Comparing stress, lexical focus, and segmental focus: Patterns of variation in Arabic vowel duration," J. Phonetics **30**, 53–75.
Ernestus, M., Lahey, M., Verhees, F., and Baayen, R. H. (**2006**). "Lexical frequency and voice assimilation," J. Acoust. Soc. Am. **120**, 1040–1051.
Forrest, K., Weismer, G., Milenkovic, P., and Dougall, R. N. (**1988**). "Statistical analysis of word-initial voiceless obstruents: Preliminary data," J. Acoust. Soc. Am. **84**, 115–123.
Fougeron, C. (**2001**). "Articulatory properties of initial segments in several prosodic constituents in French," J. Phonetics **29**, 109–135.
Haggard, M. (**1978**). "The devoicing of voiced fricatives," J. Phonetics **6**, 95–102.
Hughes, G. W., and Halle, M. (**1956**). "Spectral properties of fricatives consonants," J. Acoust. Soc. Am. **28** 303–310.
Jassem, W. (**1965**). "The formants of fricative consonants," Lang Speech **8**, 1–16.
Jesus, L. M. T., and Shadle, C. H. (**2002**). "A parametric study of the spectral characteristics of European Portuguese fricatives," J. Phonetics **30**, 437–464.
Jesus, L. M. T., and Shadle, C. H. (**2003a**). "Devoicing measures of European Portuguese fricatives," in *Computational Processing of the Portuguese Language*, edited by N. J. Mamede, J. Baptista, I. Trancoso, and M. das Graças Volpe Nunes (Springer, Berlin), pp. 1–8.
Jesus, L. M. T., and Shadle, C. H. (**2003b**). "Temporal and devoicing analysis of European Portuguese fricatives," in *Proceedings of the 15th International Congress of Phonetic Sciences*, Barcelona, Spain, pp. 779–782.
Jongman, A., Wayland, R., and Wong, S. (**2000**). "Acoustic characteristics of English fricatives," J. Acoust. Soc. Am. **108**, 1252–1263.
Jurafsky, D., Bell, A., Gregory, M., and Raymond, W. D. (**2001**). "Probablistic relations between words: Evidence from reduction in lexical production," in *Frequency and the Emergence of Linguistic Structure*, edited by J. L. Bybee and P. Hopper (Benjamins, Amsterdam), pp. 229–254.
Keating, P., Cho, T., Fougeron, C., and Hsu, C. (**2003**). "Domain-initial articulatory strengthening in four languages," in *Papers in Laboratory Phonology VI*, edited by R. Odgen, J. Local, and R. Temple (Cambridge University Press, Cambridge), pp. 145–163.
Klatt, D. H. (**1974**). "Duration of [s] in English words," J. Speech Hear. Res. **17**, 51–63.
Klatt, D. H. (**1976**). "Linguistic uses of segmental duration in English: Acoustic and perceptual evidence," J. Acoust. Soc. Am. **59**, 1208–1221.
Lindblom, B. E. F. (**1963**). "Spectrographic study of vowel reduction," J. Acoust. Soc. Am. **35**, 1773–1781.
Lindblom, B. E. F. (**1990**). "Explaining phonetic variation: A sketch of the H&H theory," in *Speech Production and Speech Modelling*, edited by W. J. Hardcastle and A. Marchal (Kluwer, Dordrecht), pp. 403–439.
Lindblom, B. E. F., Pauli, S., and Sundberg, J. (**1971**). "Modelling coarticulation in apical stops," in *Proceedings of the Speech Communication Seminar*, edited by G. Fant (Almqvist & Wiksell, Stockholm), Vol. **2**, pp. 87–94.
Mooshammer, C., Hoole, P., and Geumann, A. (**2006**). "Interarticulator cohesion within coronal consonant production," J. Acoust. Soc. Am. **120**, 1028–1039.
Pirello, K., Blumstein, S. E., and Kurowski, K. (**1997**). "The characteristics of voicing in syllable-initial fricatives in American English," J. Acoust. Soc. Am. **101**, 3754–3765.
Shadle, C. H. (**1990**). "Articulatory-acoustic relationships in fricative consonants," in *Speech Production and Speech Modelling*, edited by W. J. Hardcastle and A. Marchal (Kluwer, Dordrecht), pp. 187–209.
Shadle, C. H. (**1991**). "The effect of geometry on source mechanisms of fricative consonants," J. Phonetics **19**, 409–424.
Stevens, K. N. (**1998**). *Acoustic Phonetics* (MIT, Cambridge, MA).
Stevens, K. N., Blumstein, S. E., Glicksman, L., Burton, M., and Kurowski, K. (**1992**). "Acoustic and perceptual characteristics of voicing in fricatives and fricative clusters," J. Acoust. Soc. Am. **91**, 2979–3000.
Tabachnick, B. G., and Fidell, L. S. (**2001**). *Using Multivariate Statistics*. (Allyn & Bacon, Boston).
Tjaden, K. (**1999**). "Stress-induced variation in F2 trajectories as evidence for coproduction in CV syllables," Lang Speech **42**, 412–432.
Umeda, N. (**1977**). "Consonant duration in American English," J. Acoust. Soc. Am. **61**, 846–858.
van Heuven, V. J. (**1994**). "What is the smallest prosodic domain?," in *Phonological Structure and Phonetic Form: Papers in Laboratory Phonology III*, edited by P. A. Keating (Cambridge University Press, Cambridge), pp. 76–98.

What marks the beat of speech?

Greg Kochanski[a] and Christina Orphanidou
Phonetics Laboratory, University of Oxford, 41 Wellington Square, Oxford OX1 2JF, United Kingdom

(Received 4 December 2006; revised 7 February 2008; accepted 8 February 2008)

Which acoustic properties of the speech signal differ between rhythmically prominent syllables and non-prominent ones? A production experiment was conducted to identify these acoustic properties. Subjects read out repetitive text to a metronome, trying to match stressed syllables to its beat. The analysis searched for the function of the speech signal that best predicts the timing of the metronome ticks. The most important factor in this function is found to be the contrast in loudness between a syllable and its neighbors. The prominence of a syllable can be deduced from the specific loudness in an (approximately) 360 ms window centered on the syllable in question relative to an (approximately) 800-ms-wide symmetric window. © *2008 Acoustical Society of America.*
[DOI: 10.1121/1.2890742]

PACS number(s): 43.70.Fq, 43.70.Mn, 43.72.Ar, 43.75.Cd [PEI] Pages: 2780–2791

I. INTRODUCTION

Patterns of prominence define the rhythmicity of speech, which is an important characteristic of stress-timed languages, English among them. The purpose of this study is to find which acoustic properties of the speech signal mark rhythmic prominence. We investigate this with a new production-based experiment; it involves auditory perception only to the extent that subjects extract a beat from a metronome tick.

While a number of papers have studied acoustic correlates of prominence, human perception of speech has played a central part in most of them, with listeners being asked to identify prominent units in speech. The prototypical experiments are those of Fry (1955, 1958), who synthesized isolated disyllabic words and asked listeners to choose which syllable was stressed (≈ prominent). These papers are mostly of historic interest because the synthesis may not have been very realistic and the stimuli were very simple compared to natural speech.

Other workers (Beckman, 1986; Streefkerk *et al.*, 1999; Brenier *et al.*, 2005; Silipo and Greenberg, 2000; Kochanski *et al.*, 2005) have studied more realistic speech, some using actual conversations. These studies investigated the relative importance of a variety of acoustic factors to prominence. Streefkerk *et al.* (1999) tested several acoustic features such as duration, loudness, spectral slope of vowels, as well as median f_0 over a syllable, and the range of f_0 over a syllable. They concluded that all but the spectral slope had promise as predictors of prominence.

Brenier *et al.* (2005) tested 12 acoustic and lexical features and found that the maximum intensity was the most effective for emphasis detection, followed by duration and f_0. Silipo and Greenberg (2000) found that a combination of intensity and syllable duration was the best predictor of their "prosodic stress" (prominence by our definition). Kochanski *et al.* (2005) tested syllable prominence in seven dialects of British and Irish English and concluded that loudness and duration primarily marked prominence in speech, with f_0 relatively unimportant. The experimental consensus is that louder and longer syllables tend to be heard as prominent.

Most of these papers suffer from a common problem: The task used to define prominence is highly artificial and unnatural. Prominence was evaluated by a variant of the following experimental procedure:

(1) Display the speech wave form and f_0 trace on a computer monitor.
(2) Allow the subject (typically a linguist) to listen to the utterance or parts thereof many times.
(3) Have the subject find and mark prominent syllables on the computer screen.

Participants in a conversation normally do not see a graphical representation of their speech, and they hear each utterance only once. Further, they do not consciously classify each syllable as prominent or not,[1] nor is a mouse click the normal behavioral response to speech. Consequently, it is important to see if one would get similar results with a different task.

In our experiment, we employ a more natural approach by giving subjects a production rather than a perception task. The classic production experiment is that of Lieberman (1960), who built a machine classifier to study acoustic properties of prominence. He made perceptual judgments unimportant by selecting sentences that had unambiguous prominence patterns, at the cost of studying utterances that were presumably much more carefully articulated than normal speech. Fear *et al.* (1995) is a noteworthy modern representative of such experiments. Rhythmic speech, often spoken to a metronome, has been extensively studied in relation to stress in speech production and perception (Fowler, 1979; Cummins and Port, 1998; Lehiste, 1973). Boutsen *et al.* (2000) is a recent production experiment; they concluded that speakers use intensity to mark stress patterns, in agreement with the majority of perception-based experiments. Our experiment is most closely related to Cooper and Allen (1977), who collect very similar data, however we use a different analysis to look at the loudness contrasts in more

[a]Electronic mail: greg.kochanski@phon.ox.ac.uk.

 0001-4966/2008/123(5)/2780/12/$23.00 © 2008 Acoustical Society of America

detail. They focus on the differences between normal subjects and stutterers; we look at what aspects of the speech of normal speakers most accurately reflect the metronome rhythm.

We ask subjects to read text to a metronome, matching their reading to the beat. Before the experimental part of the task, there is a training part which is intended to accustom the subjects to treating metronome ticks as proxies for prominence. We then analyze the speech to find stable timing relationships between acoustic properties and the metronome ticks.

One important feature of our work is that we use naive native speakers, rather than linguists. This reduces the possibility that the prominence marks may be influenced by theoretical expectations. No conscious judgments of prominence are required and no visual cues are involved in this experiment. This experiment provides a different experimental view of prominence, with different biases and limitations from the classical technique.

One could argue that the task is not ideal in that the phrases must be spoken repetitively, which brings in the risk that repetitive speech is different from more natural speech. However, we have checked this possible problem in other, more recent work (Kochanski and Orphanidou, 2007). We found that spectral differences between repetitive speech and speech from a list of randomized phrases are not large, so one would expect other aspects of speech, like prominence, to be similarly unaffected.

Work has been published in the related field of music analysis, where algorithms have been designed to extract the beat and/or metrical pattern of music using metronomic stimulation. See Scheirer (1998), Klapuri *et al.* (2006), Todd and Brown (1996), Large and Palmer (2002), and references therein. The techniques differ from ours for various reasons, for instance, unlike speech, many musical sounds have sharp onsets (e.g., drums, pianos). Further, algorithms can exploit the fact that the beat of music is very nearly periodic; they can keep long-term correlations and use them to help predict the next beat. Conversely, our algorithm is designed to be applicable to normal speech, which is not very periodic. It therefore operates on a small window of time, with no explicit memory of previous prominences.

II. EXPERIMENTAL METHODS

The experiment involved several tasks and lasted for approximately 1 h; only some of the later tasks are analyzed. The earlier tasks were intended to train the subjects to put the metronome beat on metrically prominent syllables.[2]

A set of 53 short phrases (4–6 syllables) were central to the experiment (see Appendix B for a list). The phrases had four different metrical patterns: 12 of *SuSu*, 12 of *uSuS*, 13 of *SuuSuu*, and 16 of *SuuS*, where *S* denotes a stressed syllable and *u* unstressed.[3] The phrases were selected from Project Gutenberg (Hart *et al.*, 2006), based on patterns of stress predicted by UNISYN (Fitt and Isard, 1999; Fitt, 2002).[4] Phrases were selected for broad coverage of phonemes, minimal repetition of words, and a lack of obsolete and unusual vocabulary. They were reviewed to confirm that the UNISYN stress assignments led to a reasonable reading. All phrases have at least one polysyllabic word and they have an average of 1.4 monosyllabic words.

As a warm-up, subjects read out a poem (Nesbitt, 2001, "My Excuse") and then read it out again while tapping their finger to what they considered to be stressed syllables.

Next, a metronome was connected to an earphone, and subjects were asked to choose the two most comfortable rates at which they could read text with a strong metrical pattern. To pick a comfortable metronome rate, the metronome was started and the subject was asked to read the poem again. After a few lines, the subject was asked "faster, slower, or is that OK?" If necessary, the metronome was adjusted by one click (typically 4 beats per minute) and the process continued until the subject said "OK." They were then asked to pick a second rate, either four beats faster or slower than the first one. They then read the poem at both rates, matching their reading to the beats of the metronome.

In the next tasks, subjects read 48 short paragraphs from which the phrases had been extracted, then read a randomized list of 264 phrases, which included five repetitions each of the above-mentioned set of phrases.[5]

In the final set of tasks, subjects were presented with the above-mentioned set of phrases, from which four groups of 12 were randomly selected, with the groups balanced by metrical pattern. Subjects were asked to read out ten consecutive repetitions of each phrase. The repetitive task was intended to allow the subject to settle upon the easiest (perhaps the most natural) metrical pattern. The number of repetitions was intended to allow subjects to conveniently say them all in one breath. The first group of 12 was simply read out. For the second group, the subject was asked to read and simultaneously "Tap your finger to what you consider a stressed syllable."

We analyzed the data from the third and fourth groups of 12 phrases, which were read out to metronome ticks. One group was read at each of the two rates that the subjects chose earlier. Subjects were instructed to "Read, trying to follow the beat of the metronome." The metronome rates were 86 ± 7 beats per min (0.71 ± 0.06 s intervals between beats), and the mean length of ten repetitions of the phrase was 13.4 ± 2.4 s. (In this paper, means and standard deviations are given in the form $\mu \pm \sigma$, where σ is the standard deviation of the distribution, not the standard error of the mean.) There were 0.91 ± 0.15 metronome ticks per stressed syllable (assuming stress as predicted by UNISYN).

Participants were linguistically naive speakers of Standard Southern British English. All were either undergraduate or graduate students at Oxford University. Five females and four males were recruited by mailing list advertisements.

Each subject was recorded with an electret microphone positioned approximately 10 cm from his/her mouth, to the side of the breath stream. Recordings were taken in a acoustically insulated recording booth. The audio signals were sampled at 32 kHz with 16 bit resolution.

Metronome ticks were fed to the subjects through an "ear-bud" style earphone on the opposite side from the microphone that recorded their speech. It was adjusted to a comfortable loudness level for each subject. The metronome

ticks were recorded on one channel of a stereo recording and cannot be heard in the other channel which carries the microphone signal.

The start and end points of the speech were automatically determined by an algorithm that finds the borders of a loud interval, surrounded by quiet regions on both edges. It is a modified version of techniques used in Kochanski *et al.* (2005). All end points were manually checked at the same time we checked the tick marks. Fewer than 10% were adjusted. In total, approximately 3000 syllables (and tick positions) were examined.

III. ANALYSIS TECHNIQUES

In the analysis, we search for the function of the speech data that is best at predicting the metronome ticks. The function is expressed as a simple algorithm that has several adjustable parameters. It takes a wave form and yields a set of predictions; we compute the timing accuracy of the predictions and adjust the parameters to maximize that accuracy. We can then interpret the parameters to see how the subjects express rhythmical prominence.

A. The algorithm

The algorithm computes a signal from the speech wave form, convolves the signal with a kernel, and picks maxima of the result. Large maxima become predictions of metronome ticks. The signal we use is related to the perceived loudness of the speech, but we also try modifications that include information from the pitch of the speech, voicing, and the overall slope of the local speech spectrum.

It is motivated by perception experiments (Kochanski *et al.*, 2005) showing that prominent syllables are typically louder. The algorithm begins by computing a time series of the specific loudness, $L(t)$, from Kochanski *et al.* (2005),[6] derived originally from Stevens (1971). This specific loudness is then convolved with a kernel K to yield $x(t)$ as an intermediate result. We use[7]

$$x = K^*(Lg). \tag{1}$$

Other acoustic properties of the speech will be included via g, and will be described in more detail in Sec. III B. We will test different values for g, beginning with $g=1$, then functions of f_0, voicing periodicity, and spectral slope.

We chose a product form in Eq. (1) to express the fact that the other acoustic parameters become irrelevant as L approaches zero. For instance, if the signal is quiet enough relative to nearby regions, the pitch of the quiet region will be perceptually unimportant.

We chose a convolution kernel, K, which has a zero mean and is the difference between two Gaussians:

$$K(\tau) = e^{-(\tau - a\sigma)^2/2(b\sigma)^2} - be^{-\tau^2/2\sigma^2}, \tag{2}$$

where τ is the time delay, σ controls the overall width of the kernel, b (which is typically less than 1) is the relative width of the positive Gaussian, and a controls where the positive Gaussian sits. If $a=0$, K is symmetric in time and corresponds to the difference between a syllable and both of its neighbors; if $a \neq 0$, then the contrast with either the left or the right neighbor is more important. One can interpret σ as the width of the region that is used to normalize the local loudness information.

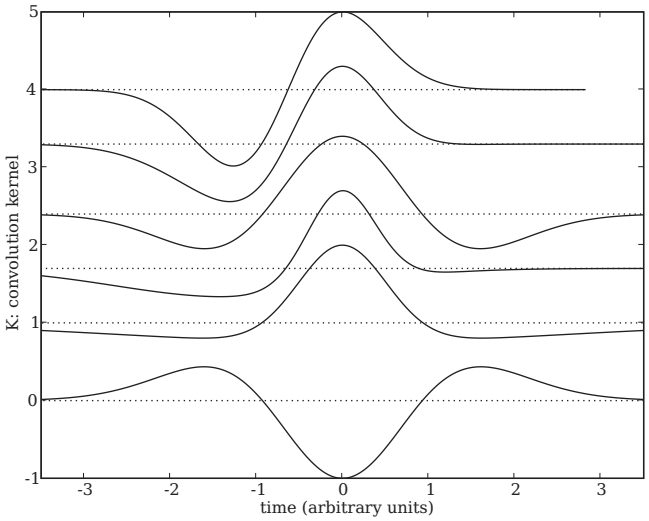


FIG. 1. Possible shapes for the convolution kernel, $K(\tau)$. More possible shapes can be obtained by reversing the time (delay) axis or the vertical axis.

Figure 1 shows the range of shapes that $K(\tau)$ can take. The top two would respond best to stepwise increases in Lg, the next down responds to the contrast of a syllable with the nearest syllable on each side. The next two show contrasts against broader regions than the nearest neighbor(s), and the lowest curve shows a kernel that responds to a local minimum in Lg.

In the next step, we consider regions where $x(t)$ is positive and take the time of the largest value in each region, $t_i^{\max}$. The final set of syllable times, T, is then computed by dropping any values of $t_i^{\max}$ where either $x(t_i^{\max}) < rx(t_{i-1}^{\max})$ or $x(t_i^{\max}) < rx(t_{i+1}^{\max})$. In other words, one drops t-values whose x is substantially smaller than their neighbors. The process is controlled by the adjustable parameter r: If $r \ll 1$ all the maxima are preserved, while if r is close to 1 only the largest few maxima in each utterance survive.

B. Acoustic properties beyond loudness

As there is some evidence that acoustic properties other than L contribute to prominence judgments, we investigated a set of alternatives for g in Eq. (1). They were as follows:

(1)

$$g_1 = 1. \tag{3}$$

The resulting timing estimates are based only on L.

(2)

$$g_2(t) = 1 + \eta V(t)\left(\frac{f_0(t)}{\langle f_0 \rangle} - 1\right), \tag{4}$$

where $f_0(t)$ is the speech fundamental frequency, as determined by the GET_F0 program from the ESPS package (Entropic Corp.). $V(t)$ is 1 or 0, indicating whether or not the speech is voiced (it also is produced by GET_F0), and $\langle f_0 \rangle$ is the average f_0 over the voiced parts of the utterance. Thus, if

$\eta > 0$, voiced sounds with relatively high f_0 are emphasized, while if $\eta < 0$, voiced sounds with relatively low f_0 would be treated as louder.

(3)

$$g_3(t) = 1 + \zeta V(t) \left| \frac{f_0(t)}{\langle f_0 \rangle} - 1 \right|, \tag{5}$$

with variables as noted earlier. Thus, if $\zeta > 0$, voiced sounds with either high or low f_0 are emphasized relative to those with f_0 near average. Conversely, if $\zeta < 0$, voiced sounds with near-average f_0 or unvoiced sounds would be treated as more important.

(4)

$$g_4(t) = 1 - \alpha A(t), \tag{6}$$

where $A(t)$ is the aperiodicity measure from Kochanski *et al.* (2005). [Related measures have been developed by de Krom (1993) and Boersma (1993).] Vowels have small aperiodicities (typically less than 0.5), while fricatives have aperiodicities near 1, so α controls how important fricatives (and other consonants) are in the expression of prominence.

(5)

$$g_5(t) = 1 - \gamma S(t), \tag{7}$$

where S is a measure of the average slope of the speech spectrum. It is related to the ratio of power below 1 kHz to the power above 1 kHz, and is described in detail in Appendix A. Related measures have been developed by Heldner (2001); Sluijter and van Heuven (1996), and references therein.

We define S so that its histogram is approximately centered around zero, and positive S corresponds to excess high-frequency power. Consequently, a positive γ would cause sounds with more high frequency power (like fricatives and harshly spoken vowels) to be treated as louder; on the other hand, sounds like /m/ and gently spoken vowels would be treated as emphasized if $\gamma < 0$.

(6)

$$g_6(t) = g_2(t) g_4(t) g_5(t). \tag{8}$$

We conduct an analysis where g is the product of Eqs. (4), (6), and (7). This allowed for prominence to be determined by an arbitrary combination of voicing irregularity, spectral slope, and f_0.

C. Optimizing the parameters

We based our analysis on the metaphor of coupled oscillators (Large and Kolen, 1994; Saltzman and Byrd, 2000; Port, 2003). Following that metaphor, we constructed a time series of phase for both the tick sequence and for the set of syllable times T produced by the algorithm. The phase is 0, 2π, 4π,… at successive ticks, linearly increasing in between. The metronome phase $\phi(t)$ is then a linear function of time, with a slope equal to 2π divided by the interval. A similar phase function, called $\psi(t)$, is defined from T; it increases by 2π for each element of T. It is defined between the first and last elements of T that fall within the speech.

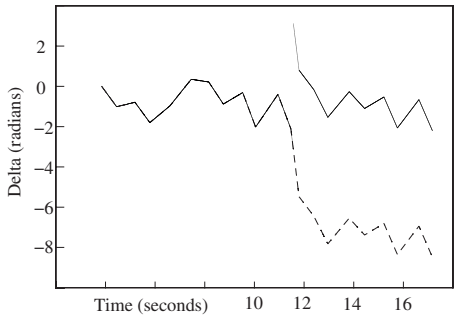


FIG. 2. The phase $\Delta(t)$ for a typical utterance plotted against time. The algorithm missed a prediction near $t = 10.8$ s, then behaved well for the rest of the utterance (dashed line). The solid line shows Δ, wrapped into the range from $-\pi$ to π to simulate the behavior of Eq. (10).

If the algorithm produced a periodic series of predictions in T, then $\psi(t)$ would also be a straight line. For a regular pattern with ticks and predictions coming at the same average rate, the slopes of ϕ and ψ will be equal, and the difference,

$$\Delta(t) = \phi(t) - \psi(t), \tag{9}$$

will be a constant. At each moment, Δ can be interpreted as a phase difference between the stream of ticks and the stream of predictions in T.

One could use the variance of $\Delta(t)$ as a measure of how well the two sequences are related, but it would be extremely sensitive to missed events. One missing or extra element in T would change Δ by 2π for the remainder of the utterance. Thus a single missed prediction could dramatically increase the variance, as can be seen from the dashed line of Fig. 2.

Instead, we compute[8]

$$I = \frac{1}{\mathbb{L}} \int \exp(i\Delta(t)) dt, \tag{10}$$

where the integral is taken over the part of the utterance where ψ and ϕ are both defined; $\mathbb{L}$ is the integral's length (in seconds).

If the times in T match the metronome ticks so that $\Delta(t)$ is constant, then the exponential will be a complex number of constant phase and unit magnitude, and the magnitude of I will be unity. This gives the largest possible magnitude for I; any mismatches will reduce it. So, $|I|$ tells how well the two sequences match, and the phase of I describes when the ticks occur relative to T.

Putting $\Delta(t)$ into an exponential makes the analysis relatively insensitive to dropping or adding one prediction. In either case, the argument to the exponential changes by 2π radians during the gap, but the value of the exponential swings around and returns to the value it had before the gap.[9] In such a case, $|I|$ would be reduced from 1 to about 0.9 for our conditions. The solid line in Fig. 2 shows the effect of the exponential, wrapping together values of Δ that differ by 2π.

We can interpret I in two related ways. Starting with $I = 1$ as implying perfect correlation, I is reduced whenever there is a missing or extra prediction. Alternatively, we note that when var(Δ) is much less than 1, $I \approx 1 - \text{var}(\Delta)$, so that a

decrease in I can be interpreted as an increase in the variance of Δ and thus as increased timing errors between the ticks and T.

Now we can compute I for an utterance, given the parameters that control the algorithm. Then, for a corpus, we can compute the average of the magnitude of I, i.e., $\langle|I|\rangle$. $\langle|I|\rangle$ is thus a function of the algorithm's parameters. It is an overall figure of merit for how well the algorithm's predictions match the ticks.

We then find the optimal parameters for the algorithm by evaluating $\langle|I|\rangle$ for 90 000 randomly chosen combinations of parameters and taking the one that produces the largest absolute value. This simple technique for finding the best parameters was chosen because I, and thus $\langle|I|\rangle$, is a discontinuous function of the algorithm's parameters. (More efficient optimization algorithms are not applicable, as they typically assume that the function to be optimized is continuous, and often that it has continuous first derivatives.)

By optimizing in this way, we are explicitly searching for acoustic properties that repeat with the same periodicity as the metronome ticks. The resulting parameters will be most representative of those utterances with one nominally stressed syllable per metronome tick.

D. Bootstrap resampling and confidence intervals

The above-presented technique is good for finding the parameters that give the best match to the data but it needs to be extended to find error bars and confidence intervals. For this purpose, we use a bootstrap resampling scheme (Davison and Hinkley, 1997). We compute 3400 artificial corpora, constructed by choosing utterances from the real corpus, sampling randomly with replacement. In each artificial corpus, most utterances appear once, but some do not appear at all and some appear several times. The same analysis procedure can then be repeated for each artificial corpus, leading to optimal parameters for each. In practice, we use a mathematically equivalent but faster technique. We compute the values of I for each combination of utterance and parameters, then the bootstrap resampling is implemented as a weighted average in the computation of $\langle|I|\rangle$. (Each weight is just equal to the number of times that datum was chosen.)

The resulting distribution of optimal parameters then approximates what one would get by replicating the entire experiment with new subjects drawn from the same pool. So, if one wishes to estimate the probability that some parameter p exceeds a threshold, X, one can simply count the fraction of artificial corpora where the optimal $p>X$. Thus, we use bootstrap resampling to generate confidence intervals for $|I|$ and the algorithm's parameters.

E. Timing data

We processed both the metronome and speech channels with the same algorithm (Sec. III A). Its use on the speech channel is a major focus of this paper; we used it to find the metronome ticks merely out of convenience. The metronome data are short bursts of oscillation amid silence, and almost any algorithm will be equally successful at finding the ticks.

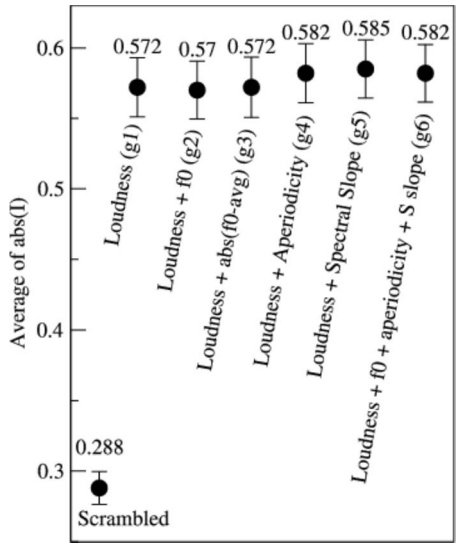


FIG. 3. Values if $|I|$, averaged over the corpus. The lower left measurement is the baseline, where acoustic data are shuffled with respect to ticks. Other conditions correspond to the six cases of Sec. III B, in order: running the analysis only on L ($g=g_1$), and L enhanced by other acoustical properties ($g=g_{2,\ldots,6}$).

For the metronome channel, rather than computing L (see Sec. III A), we used the rms power above 100 Hz in the metronome output, averaged over a 15 ms window. This signal was then used in Eq. (1) in place of L to yield an initial set of tick times. The algorithm's parameters were set by informal experiment to $g=1$, $a=0$, $\sigma=0.110$ s, $b\sigma=0.015$ s, and $r=0.5$. The result was inspected and no errors were found.

IV. RESULTS AND DISCUSSION

A. Relevant acoustic measures

We first confirm that the algorithm performs better when given acoustic data than it would without any data. This is the basic check that it can usefully predict anything. To do this, we first perform the analysis with $g=1$ and find $\langle|I|\rangle=0.572\pm0.02$. Then, we repeat the analysis, except we shuffle the data so that we use ticks from one utterance and acoustic data from another. Comparing, the shuffled results are substantially poorer than the actual analysis, with $\langle|I|\rangle$ only 0.290 ± 0.013. The difference between normal and shuffled analyses is statistically significant at $z>9$ or $P\ll10^{-5}$. Thus, based on L, metronome ticks can be predicted at much better than chance levels. All choices of g show similarly large and significant changes.

Next, we investigate which acoustic properties carry the most information, as shown by an improvement in the tick prediction. Can adding other information to L improve the tick prediction? To do this, we insert different choices of g from Sec. III B into Eq. (1) and see if $\langle|I|\rangle$ increases. The results are displayed in Fig. 3. Changing g to bring in other acoustic data gives little or no improvement over $g=1$.

Because the analysis with $g=g_6$ involves more parameters, it might be argued that we do not sample densely enough in the higher-dimensional parameter space to find the

maximum. While an exhaustive test is not practical, we did check for this possibility by recomputing the $g=g_6$ case with ten times as many samples (9×10^5 sets of parameters). This makes only a modest change: $\langle|I|\rangle$ increases by just 0.01. Since the change is small, it suggests that we have indeed sampled parameters close to the maximum even in the higher dimensional $g=g_6$ parameter space, and that little further increase would be expected even with more samples.

Figure 3 shows that L is an important correlate of the ticks, but it would not exclude the possibility that g is of comparable importance to L, if g and L marked the same locations. We can check that by looking at the distribution of α, γ, η, and ζ in suitable optimizations. If an acoustic measurement (e.g., f_0) were important, we would expect that the distributions of, e.g., η (which indicates changes in f_0—see Sec. III B) would be narrow. Assume, for instance, that ticks are marked by high f_0. In that case, we would expect a positive η so that the contributions of f_0 and L would reinforce each other. Running the algorithm with negative η would cause the contributions to cancel. L would then cancel the main effect of f_0 and vice versa, leaving only the fluctuations; one would not then expect the peaks of x to be correlated with either metronome ticks, L or f_0.

Similarly, if f_0 and L were anticorrelated, the same logic would apply and η would be negative. (If η were near zero, it would imply that the best tick predictions are done without the use of f_0, which contradicts the hypothesis that f_0 is important.) Either way, if f_0 were important, we would expect that η would have a reasonably narrow distribution, on one side or the other of zero. A broad distribution of η, roughly centered on zero, is thus evidence that the algorithm gets no useful information from f_0 via Eq. (4). The same logic applies to α, γ, and ζ.

For α, η, and ζ the distribution is broad and overlaps zero. The optimal values of η for the $g=g_2$ analysis is 0.0 ± 0.5. This provides additional evidence that f_0 does not usefully contribute to the prediction of metronome ticks (i.e., rhythmic prominence),[10] since the distribution includes $\eta=0$. The deviation of f_0 from the average ($g=g_3$) is also unimportant, with $\zeta=0.2\pm0.9$: subjects do not reliably mark prominent syllables by pushing f_0 away from the utterance mean. Likewise, the aperiodicity is not important; optimal $\alpha=-0.3\pm0.7$.

On the other hand, the spectral slope has some relationship to the ticks. The distribution of optimal values is $\gamma=0.6\pm0.3$, so that distribution overlaps zero only slightly: just 1% of the sets of optimal parameters are negative. So, syllables on the beat have some excess high frequency power. However, it is not a large effect; we estimate that $g_5(t)$ gives the same effect as a 20% change in L (roughly equivalent to a 5 dB change in acoustic power). (Perceptually, a 20% change in loudness is not large.) This is consistent with our result that $\langle|I|\rangle$ does not substantially increase when spectral slope information is added to L (Fig. 3). The small size of the effect is further confirmed by computing the correlation coefficient between $L(t)$ and $S(t)$, the spectral slope measure defined in Appendix A: It is just 0.03.

The straightforward interpretation of this is just that the specific loudnesses at frequencies over 1 kHz go up more, on the beat, than the specific loudnesses at lower frequencies. Such a shift in the spectral balance for vowels was measured by Glave and Rietveld (1975) and Gauffin and Sundberg (1989).

This weak correlation of a spectral slope measure with metronome ticks is in general agreement with the results of Kochanski *et al.* (2005), though the spectral slope computations differ. A comparison with Sluijter and van Heuven (1996) is not simple; they analyzed dependencies on focus (i.e., accent) and stress separately, while we effectively compare [+focus, +stress] with the neighboring syllables which are either [−focus] or [−stress]. Heldner (2001) showed that his measure, called "spectral emphasis," is a good predictor of accent. Our results do not support this (but are not inconsistent as his spectral emphasis measure is substantially different).

TABLE I. Parameters that yield the largest $\langle|I|\rangle$. The analysis operates on L only ($g=1$). The right column shows the distribution of values that were tested in the optimization procedure (90 000 samples), and the center column shows the distribution of optimal values that were found (3400 bootstrap corpora).

Parameter	Optimal value	Distribution of test evaluations: mean ± s.d.
σ	0.176 ± 0.028	Gaussian 0.19 ± 0.07
a	-0.01 ± 0.03	Gaussian 0 ± 0.4
b	0.83 ± 0.07	Uniform on [0.5,1]; thus 0.75 ± 0.16
r	0.04 ± 0.04	Uniform on [0,0.4]; thus 0.20 ± 0.12

B. How localized is prominence?

Since the primary acoustic marker of rhythmical prominence is L, we now focus on that case ($g=1$) and describe the remaining parameters. Three parameters (a,b,σ) define the shape of the convolution kernel K, and one (r) controls the rejection of small peaks. Table I shows optimal parameters. The rightmost column shows the distribution of parameters we sampled; in each case, the distribution of optimal parameters can be seen to be narrow and not too far off center, so our choice of sampling distribution is not seriously constraining the distribution of optimal parameters.

We also check that our analysis is not simply detecting the gap between repetitions. This is confirmed by noting that the median spacings between predictions in T (0.67 s for metronome for $g=1$) is substantially smaller than the median length of a repetition (1.30 s). Thus, we are not locked onto a single prediction per repetition; in fact, we are seeing close to one prediction per stress, or two predictions per repetition. Also, we note that the average integral over *uSuS* patterns is essentially the same as that for *SuSu* patterns (0.549 vs 0.558, not significantly different) while we might expect a substantial difference if predictions were tied to the beginning of each repetition but the metronome ticks followed the stresses.

The optimal values of r are small, so that the last step of the algorithm is almost moot; it rejects very few candidates.

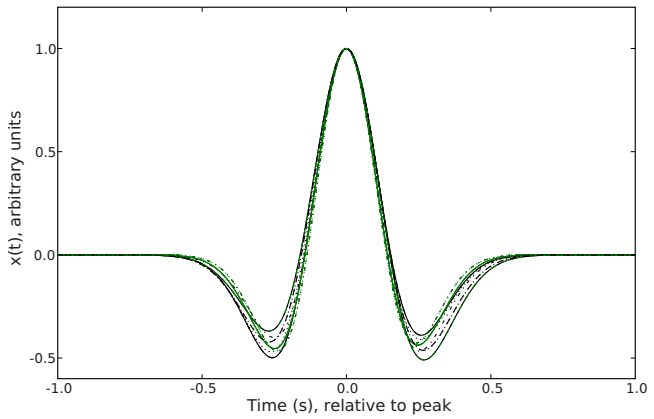


FIG. 4. (Color online) Convolution kernels, $K(\tau)$, that are optimal for bootstrap samples of the data. The maxima of the curves are aligned at $t=0$. (These kernels maximize $\langle|I|\rangle$, and have α, γ, and η zero, corresponding to $g=1$.)

The other three parameters are closely coupled, and can most easily be interpreted visually, by plotting $K(\tau)$. Figure 4 shows a set of convolution kernels that are computed from sets of (a,b,σ) which are optimal parameters for bootstrap corpora. The curves show examples of $K(\tau)$ that are consistent with the data, analyzed assuming $g=1$. Since the analysis procedure is invariant with respect to shifts of the peaks of x, we can align the peaks of K for clarity without changing $\langle|I|\rangle$. The shape of K is important because it tells us which contrasts are important for predicting a tick. In this case, the contrast is approximately symmetrical: the syllables preceding and following the metronome tick are equally quiet.

Figure 5 shows convolution kernels that are optimal for the $\langle|I|\rangle$, $g=g_6$ analysis. The analysis is entirely consistent with Fig. 4, but with somewhat larger scatter as we are fitting a more complex model to the data.

The widths and relative spacings of the peaks are remarkably consistent. Values for σ, which is related to the overall width of the kernel, are in Table I. The full-width at half-maximum (FWHM) for the highest peak in K is 0.184 ± 0.008 s, and the magnitude of the time interval between the most positive and most negative peaks is 0.31 ± 0.04 s for the $g=1$ analysis, so the entire window of relevant speech data spans approximately 800 ms. The numbers are similar for the $g=g_6$ analysis, 0.183 ± 0.01 for the FWHM and 0.26 ± 0.01 for the peak spacing.

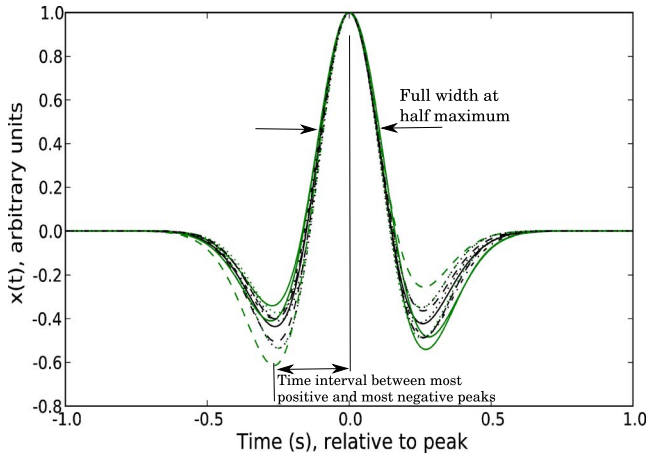


FIG. 5. (Color online) Optimal bootstrap samples of the convolution kernel, $K(\tau)$, for the $g=g_6$ analysis. The maxima of the curves are aligned at $t=0$. (These kernels maximize $\langle|I|\rangle$, and allow α, γ, and η to be nonzero.)

The positive peaks of the kernel are as wide or wider than a typical vowel, and about two-thirds of the mean syllable spacing, 0.27 s. The full extent of the kernel, given by $2\sigma\approx0.34$ s, is wider than the mean syllable spacing, and the time interval between the positive and negative peaks is just about equal to the mean syllable spacing. Ticks are thus correlated with the properties of a region larger than a single syllable. Our analysis is consistent with the hypothesis that ticks are related to a large loudness contrast between a syllable and its nearest neighbor(s).

This conclusion is consistent with findings by Kochanski *et al.* (2005), who show an (approximately) symmetric loudness pattern around syllables that were judged to be prominent. The loudness pattern observed there was somewhat narrower, as might be expected, given the faster speech in that study. There are some differences in detail, however. Kochanski *et al.* (2005) reported small but significant correlations of f_0 and A with prominence; but we see none here. The difference may be due to the different tasks (e.g., production versus perception).

An interesting feature of the these results is that the algorithm unifies loudness and duration changes into a single time series, $x(t)$. For vowel durations shorter than K's positive peak, an increase in duration has much the same effect as an increase in loudness; the convolution can be approximated as an integral of loudness over about 0.2 s. It can then be further approximated as the vowel's loudness times the vowel duration. Thus, peaks of $x(t)$ and consequently predictions in T will tend to occur on longer syllables, rather than shorter ones.

An analogous effect, but occurring in speech perception rather than production, can be found in the psychophysics literature. Munson (1947) showed that perceived loudness is a generally increasing function of duration, and Plomp and Bouman (1959) modeled the effect as a convolution of the specific loudness with a kernel. They obtained equivalent widths of their kernel near 0.25 s. This is sufficiently close to our results to support the idea that speech production should be matched to speech perception; the peak value of our $x(t)$ may simply be related to the perceived loudness of the syllable.

Our results are similar to those of Beckman (1986), who found strong correlations of prominence with a similar combination of amplitude and duration, and Silipo and Greenberg (1999, 2000), who had the best success at predicting prominence with a product of syllable-averaged amplitude and vowel duration. It also parallels (on the production side) at least one claim of Turk and Sawusch (1996)—viz. that duration and loudness are perceived together as a single percept.

This agreement with other work is perhaps remarkable, given the differences in experimental technique. Not least because the above-mentioned experiments involve percep-

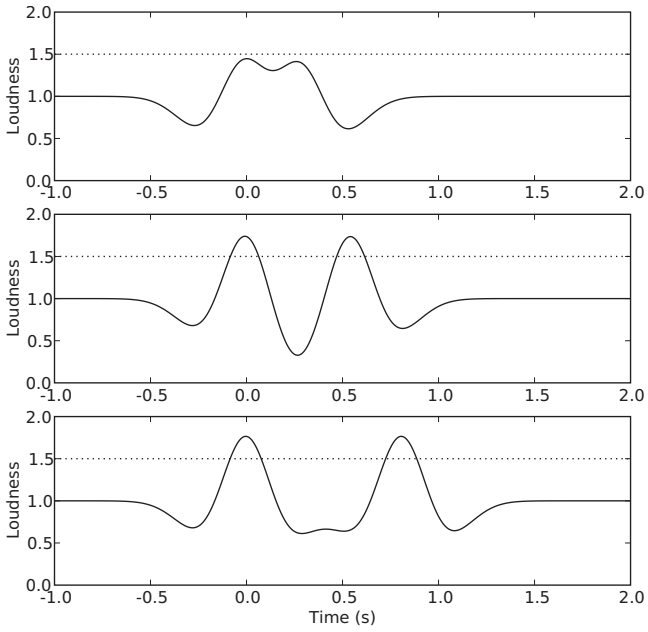


FIG. 6. Theoretical loudness contours based on this work for prominences that are (top) on adjacent syllables, (middle) separated by one, and (bottom) by two syllables. The dashed line is a loudness reference.

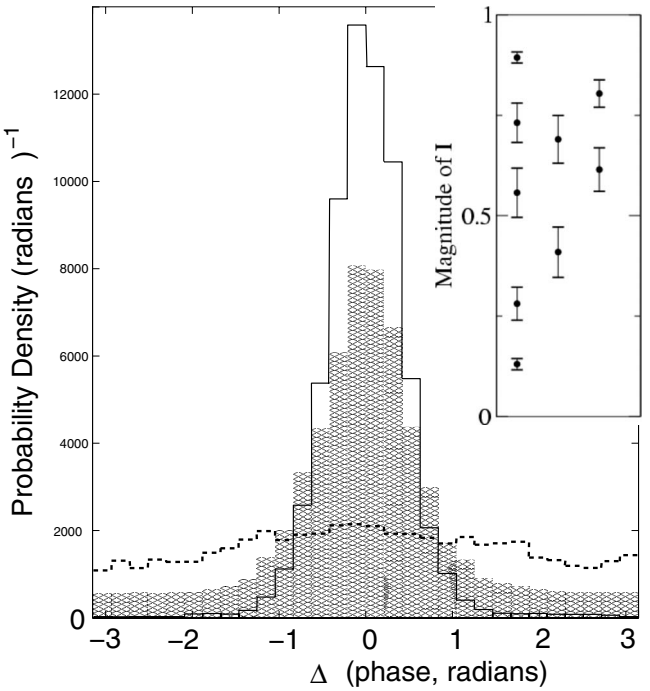


FIG. 7. Phase histograms (Δ, relative to the phase of I) for three different subjects. The subjects shown have (reading from top to bottom, in the center) the largest, median, and smallest value of $\langle|I|\rangle$. The sub-figure shows values of $\langle|I|\rangle$ for each subject, with 1 s.d. error bars on the average. (The horizontal axis in the subfigure has no meaning—it just separates subjects.)

tual judgments (e.g., which syllables are prominent), while our experiment is strictly a production experiment.

C. Alternating metrical patterns and implications for phonology

This result that prominence is expressed by a contrast between a syllable and its neighbors is interesting because it may provide a reductionist explanation of the alternating metrical patterns that are common in many languages.

Consider a loudness pattern like Fig. 4, and place it on a uniform background corresponding to the average loudness of speech. For the sake of argument, suppose that loudness patterns of different syllables add. Then, Fig. 6 shows the resulting loudness patterns for prominences that are separated by one, two, and three syllables.

One can see that the loudness patterns interfere with one another when the prominent syllables are adjacent, and the resulting loudness peaks are then not as dramatic as when the syllables are farther apart. If, hypothetically, the listener had a loudness threshold for the perception of prominence, the case of adjacent syllables would not be perceived as prominent.

To make the adjacent case appear prominent, the speaker would have to make those syllables unusually loud, and/or to push the syllables farther apart so that the loudness patterns would not interfere so strongly. We suggest that speakers may avoid this case because of the extra effort and complexity needed to ensure that a listener will perceive the correct prominences. Over time, this avoidance may become enshrined in phonological rules that reduce the number of adjacent stresses. If speakers avoid one-syllable feet because they are hard to produce clearly, the next simplest foot is two syllable and this potentially might help explain the cross language preference for an alternating metrical pattern.

D. Performance variation between subjects

Subjects differ substantially in terms of how consistently they follow the metronome. This performance variability is seen in Fig. 7, which shows the phase histograms for three speakers. Histograms for the other speakers are similar, displaying the same properties: Large $\langle|I|\rangle$ is correlated with a tall, narrow peak and a low background level, while small $\langle|I|\rangle$ implies a short broad peak sitting on a higher background.

From subject to subject, $\langle|I|\rangle$ varies from 0.13 to 0.90, while the uncertainty in each subject's mean due to intra-subject variation is just 0.05. This is a large range, as the possible range of $\langle|I|\rangle$ is just from 0 to 1.

Analysis of variance rejects the hypothesis that the subject means are equal with $P<10^{-6}$ $[F(9,214)=7.5]$. Some subjects are therefore speaking reliably along with the metronome, while the speech of some others has little consistent relationship to the ticks. By observation, the subjects with the lower values of $\langle|I|\rangle$ show a mixture of two problems: irregular pauses that lead to jumps in Δ, and speech that is simply not synchronized with the metronome rate, leading to a gradual drift in Δ.

For instance, if we select utterances that were spoken with approximately 1 tick per stressed syllable (i.e., 19–21 metronome ticks within the ten repetitions or 0.95–1.05 ticks per stressed syllable), we compute $\langle|I|\rangle=0.69\pm0.28$ for those utterances ($n=119$). This contrasts sharply with $\langle|I|\rangle=0.25\pm0.2$ for utterances which are apparently unsynchronized with the metronome, having 0.65–0.85 ticks per

stress ($n=44$). The three subjects who have the largest number of these unsynchronized utterances are also the three subjects with the smallest values of $\langle|I|\rangle$.

Because of the large range of subject performance, and because it can be automated, this task may be useful as a measure of the ability to process metrical patterns. One possible application is an evaluation tool for stuttering [e.g., Boutsen *et al.* (2000) and Cooper and Allen (1977) showed that stutterers had much larger timing variance in repetitive speech than normal subjects]. The wide range of intersubject performances that we have observed (cf. Fig. 7) parallels the results of Cooper and Allen (1977) for normal subjects, who found that some subjects had timing variances roughly ten times larger than others.

E. Analysis of high-performing subjects

Our analysis is designed on the assumption that metronome ticks are proxies for prominence. But, ticks are clearly not perfect proxies, especially for some subjects. This raises the possibility that our results are affected by utterances that are unsynchronized with the metronome or that have other synchronizations (e.g., two ticks per prominence).

The majority of the utterances were spoken with approximately a 1:1 ratio between metronome ticks and nominal stresses: 56% of the utterances contained 19–21 metronome ticks for their 20 nominally stressed syllables. A total of 18% were near other small-integer ratios that might suggest different patterns of synchronization: 5% contained 9–11 ticks (near a 1:2 ratio), 11% contained 14–16 (near a 2:3 ratio, but informal investigation shows that many of these utterances have no obvious synchronization), 1% contained 29–31 (3:2), and 1% contained 39–41 ticks (2:1). The ratios of the remaining 26% do not suggest synchronization between the speech and the metronome.

To check that possibility, we repeated our analysis on the subjects that gave us the five largest values of $\langle|I|\rangle$. These subjects generally produced utterances that are well synchronized, with one prominence per metronome tick, and thus are particularly well adapted to our analysis. By comparing the analysis on this subset to our main results (Sec. IV A), we can check that our results are robust.

As expected, the value of $\langle|I|\rangle$ for the shuffled analysis is statistically indistinguishable from the shuffled analysis for the full data set. Also, as expected, the values for the $g_{1,\ldots,6}$ analyses have increased: For the g_1 analysis, $\langle|I|\rangle$ has increased from 0.572 ± 0.02 to 0.739 ± 0.02. Even so, there are no differences among the various $\langle|I|\rangle$ values for the $g_{1,\ldots,6}$ analyses that are larger than the corresponding standard deviations. This supports our contention that the other acoustic properties are not very important.

Likewise, α, η, and ζ still have distributions that strongly overlap zero, providing further confirmation that f_0 does not play a role in the sense of Eqs. (4) and (5), and that $A(t)$ is likewise unimportant. The spectral slope remains weakly important, with just 4% of the optimal parameter sets having $\gamma<0$.

The shapes of K do not change substantially from those shown in Fig. 5; neither σ, a, b, nor r show changes larger than the error bars shown in Table I. This supports our use of the metronome tick as a proxy for rhythmic prominences.

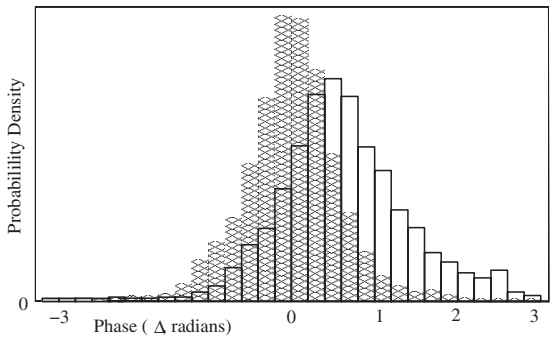


FIG. 8. Phase histogram (Δ) for a typical speaker (outline) and the histogram of Δ relative to the average phase of each utterance (filled). The peak of the dashed histogram shows the typical phase relationship between metronome ticks and the algorithm's predictions for that subject. The width of the histograms show timing inconsistencies between the subject's speech and the metronome.

F. Phase variation between utterances

The analysis so far only considers how stable the predictions (T) are, in relation to the ticks. Any uniform phase shift between the ticks and T will just change the phase of I but not its magnitude, so $|I|$ and $\langle|I|\rangle$ are insensitive to the average phase relation within an utterance. Our analysis essentially minimizes the variance of the difference between the predicted and actual tick positions. Thus, our analysis differs from that of Allen (1972), who assumes that the moment when the tick happens is the critical part of the syllable.

However, because the optimal K happens to be symmetrical and fairly compact, we can use it to identify the point in each phrase where $x(t)$ is maximal. The loudness contour in a region around this point gives the most consistent prediction of the metronome ticks. We computed this for $g=1$ and optimized parameters; peaks in $x(t)$ thus correspond fairly accurately to peaks in $L(t)$.

Figure 8 shows the histogram of Δ for all utterances produced by one subject. It also displays the histogram of Δ relative to the phase of I for the corresponding utterance. We display data from the subject who had the median value of $\langle|I|\rangle$. The histogram of relative phase is noticeably narrower and taller, as might be expected, indicating that different utterances have somewhat different alignments between the speech and the metronome.

For this subject, the peak of the Δ histogram (outline) is not at zero, indicating that the peak of $x(t)$ is not aligned with the metronome ticks, but that the metronome ticks occur somewhat before the peaks of $x(t)$. In other words, this subject speaks with the ticks early in the syllable, before the vowel's loudness peak. However, subjects differ in their average alignment.

Figure 9 shows a vector plot of the phases per utterance, for all subjects. The phases are distributed around zero, indicating that on average, subjects align the peaks of $x(t)$ [and thus $L(t)$] with the metronome ticks. If we wished to discuss a "pr(oduction)-center" in analogy to Allen's (1972) p(ercep-

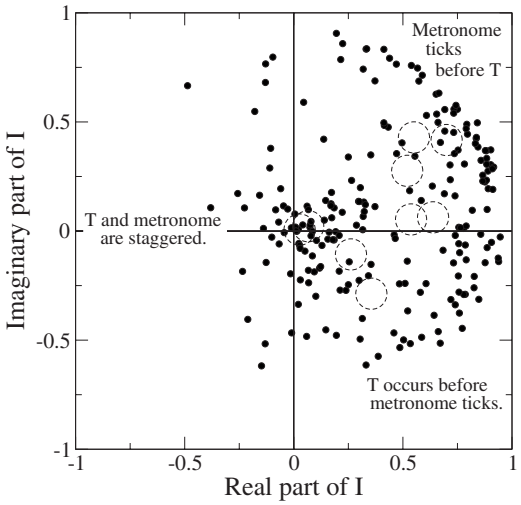


FIG. 9. The phase relationship between the metronome ticks and peaks of $x(t)$ (loudness, loosely speaking). Each utterance (i.e., ten repetitions of one text by one speaker) is represented by a dot at the (complex) value of I, with the real part on the horizontal axis and the imaginary part on the vertical axis. The distance from the origin is thus proportional to $|I|$ for that utterance. Dots near the origin represent utterances that did not have a consistent phase relationship between loudness and the metronome; dots on the unit circle would have a perfectly consistent phase relationship. The angle of the point, when viewed from the origin matches the phase of I, and dots just to the right of the origin come from utterances where the peak in $x(t)$ is aligned with the metronome ticks. Dashed circles represent the average of each subject's utterances.

tual) centers, the pr-center appears to be near the syllable's peak in L: the mean phase of the peak is $13 \pm 44°$ before the tick. The concept of pr-centers has been discussed by Morton, Marcus, and Frankish (1976), who have argued that P-centers are ambiguous and could possibly be exerting an influence on the production as well as the perception of words. However, there is substantial intersubject variation.[11] In Fig. 9, the dashed circles show averages of I for each subject. Apart from the two that are near zero and thus have no consistent phase relationship to the ticks, some subjects place the loudness peak before the tick, some almost on the tick, and some place it after the tick.

V. CONCLUSIONS

In English, the beat of repetitive speech is marked by an increase in the loudness relative to the immediate neighborhood. This neighborhood is approximately one syllable on either side of the beat, at the speech rates we studied.

The critical factor-appears to be the average loudness over an approximately 360 ms interval, so that as the vowel is shortened below 200–300 ms, the duration reduction will play the same role as a reduction in loudness. Other acoustical properties such as f_0 are not strongly correlated with the beat; one exception is that, on average, speakers produce somewhat more high frequency power on the beat than off.

We suggest that this preference for loudness contrasts as a marker of the beat may provide a partial explanation for the relative rarity of adjacent, prominent syllables. We note also that the width of the region over which prominence is expressed is well matched to human auditory perception, as might be expected.

We conducted a production experiment that had minimal involvement of speech perception, in contrast to much prior work on prominence. Despite that our results are in general agreement with prior experiments. Prominence seems a broadly useful idea, one that is shared both by linguists and naive speakers of English, and one that has a straightforward relationship to measureable acoustic quantities.

ACKNOWLEDGMENTS

We thank Burton Rosner for discussions and comments and 'Oiwi Parker Jones for comments. This research was funded by the UK's Economic and Social Research Council via Grant No. RES-000-23-1094.

APPENDIX A: DEFINITION OF SPECTRAL SLOPE MEASURE

The spectral slope measure we use is based on a comparison of specific loudnesses at high and low frequencies. The computation begins by filtering the speech into bands that are 1 Erb (see Moore and Glasberg, 1983) wide, on 1/2 Erb centers, between 50 and 6000 Hz. [We use the filterbank recommended by Baumgarte (2002).] Then, we half-wave rectify each filter output and take the cube root of the local intensity to approximate the nonlinear response of the ear. This yields a set of specific loudness measures, $\ell_k(t)$, where k indexes the frequency band. The center frequency of the kth band is $f(k)$ Hz.

Next, we low-pass filter these with a frequency-dependent time constant derived from Plomp and Bouman (1959) to yield $\tilde{\ell}_k(t)$. We approximate their time constants as

$$\tau(f) = 0.4 - 0.27\frac{\log(f/200)}{\log(10^4/200)}, \tag{A1}$$

where $\tau(f)$ is in seconds.

We sum the result into two broadband specific loudnesses,

$$L^H(t) = \sum_k \tilde{\ell}_k(t)$$

where

$$f(k) > 1000 \text{ Hz}, \tag{A2}$$

and

$$L^L(t) = \sum_k \tilde{\ell}_k(t)$$

where

$$f(k) < 1000 \text{ Hz}. \tag{A3}$$

Finally, we combine L^L and L^H into a spectral slope measure by computing

$$S(t) = \frac{cL^H(t) - L^L(t)}{\hat{s}}, \tag{A4}$$

where $c = 2.8$ is a constant chosen so that the average of $S(t)$ is approximately zero, and $\hat{s}$ (defined in the following) is a factor to normalize out the average loudness. This form for

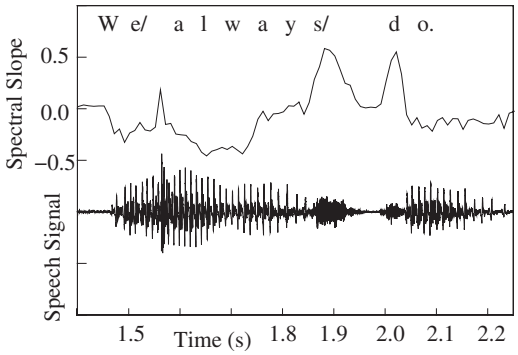


FIG. 10. Sample audio data along with the spectral slope, $S(t)$. This shows one repetition of "We always do."

$S(t)$ has the advantage that it is well-behaved in and near pauses, unlike measures based on intensity ratios of two frequency bands (Boersma, 1993; de Krom, 1993; Sluijter and van Heuven, 1996; Streefkerk *et al.*, 1999; Kochanski *et al.*, 2005). Also, it is well-behaved in regions of uncertain or no voicing, unlike the measure used by Heldner (2001).

We use

$$\hat{s} = c\frac{\Sigma_t s^2(t)}{\Sigma_t s(t)}, \tag{A5}$$

where $s(t)=cL^H(t)+L^L(t)$ and the sum over time is computed over the entire data file containing the utterance. (Typically, the data file contains about 20% silence, counting pauses between repetitions and a few hundred milliseconds at each end. We chose this form for $\hat{s}$ because it relatively insensitive to the amount of silence in the data file.) An example of $S(t)$ is shown in Fig. 10.

APPENDIX B: LIST OF PHRASES

Exactly so. Another time.
We always do. It surely is.
You never will. I understand.
Upon my word. She goes away.
They lie apart. The business here.
Indeed it had. I noticed that.
Nothing matters. Checker players.
William Roper. Scarlet Letter.
Goodness gracious! Lightning presses.
Worldly wisdom. Banking systems.
Phosphorescence. None whatever.
Good beginning. This is funny.
Testing the instruments. Philip was conquered
Love and integrity. Spare me your history.
Let us experiment. Notes on the editing.
Like you suggested. Here are the banners.
Not to my knowledge. Run for the cellar
Not that it mattered. Talking of wandering.
Wendy was scandalised. Going away.
Always ahead. Then I refuse.
Nothing at all. Open the door.
Maybe she had. Probably not.
Only a mouse. Say it again.
Billy was there. Under the desk.
Carrots and greens. Shirley declared.
That ruined me. Freddy Observed.
Tracy announced.

[1]As discussed in Kochanski (2006), it is not obvious to what extent people have accurate conscious access to the process of speech perception and understanding. For instance, several papers have raised the possibility (Dyde and Milner, 2002; Haffenden and Goodale, 1998; Aglioti *et al.*, 1995) that visual processing for perception is substantially different than processing for action. If so, reported perceptions could disagree on the actions we take in response to the same stimuli. If a similar effect occurs in speech, our reports of what we hear might not reflect our conversational behavior. Hickok and Poeppel (2000) argue for a similar distinction between tasks that require sublexical awareness and those that do not.

[2]Part of these data was intended for a similar finger-tapping experiment, but we dropped its analysis when we found that the finger-taps were too loud in the speech channel. However, the tapping parts of the experiment nicely serve the purpose of training the subjects to associate the beat with prominence.

[3]One male was accidentally given *uuSuuS* phrases instead of *SuuS*; these data were included in the analysis as we did not find any strong differences between metrical patterns. We do not include those phrases in the appendix because they were only used once.

[4]UNISYN is a software package for predicting pronunciation in a variety of English dialects. It is based on a lexicon and includes transformation rules.

[5]This part of the data was designed to check that the repetitive speech as not too different from a more typical laboratory experiment. See (Kochanski and Orphanidou, 2007) and the discussion in Sec. I.

[6]Note that calling $L(t)$ loudness as was done by Kochanski *et al.* (2005) is somewhat of a misnomer. $L(t)$ is closer to the sum of all the specific loudnesses at each moment, to use Zwicker's (1977) terminology. Munson (1947) and Plomp and Bouman (1959) showed that perceived loudness is an average of the specific loudness over approximately a 250 ms interval, while the Kochanski *et al.* (2005) measure averages only over a 25 ms (FWHM) window. Averaging $L(t)$ over a 250 ms window should approximate perceived loudness.

[7]The convolution $a*b$ is the integral $\int a(\tau)b(t-\tau)d\tau$. It can be thought of as taking a time-series b, and filtering it in a way specified by function a. If this were a perception experiment, this equation would correspond to Munson's (1947) sensation integral.

[8]Recall that $\exp(i\Delta)=\cos(\Delta)+i\sin(\Delta)$, so that it is periodic, not rapidly increasing as one would get by taking exp( ) of a real argument. If one plots the real and imaginary parts of $\exp(i\Delta)$, one finds that they trace out a unit circle, centered at zero.

[9]We rely on the fact that $\exp(i\Delta)=\exp(i(\Delta+2\pi))$ for any Δ.

[10]We recognize that f_0 *can* induce the perception of prominence, as shown by Gussenhoven *et al.* (1997); Rietveld and Gussenhoven (1985); Terken (1991). However, as shown in Kochanski *et al.* (2005), f_0 swings in speech are frequently not large enough to induce a prominence judgment. Consequently, f_0 is potentially important to prominence, but apparently not important in practice.

[11]Unfortunately a direct comparison to the p-center location is not practical in this experiment.

Aglioti, S., DeSouza, J. F., and Goodale, M. A. (**1995**). "Size-contrast illusions deceive the eye but not the hand," Curr. Biol. **5**, 579–685.
Allen, G. (**1972**). "The location of rhythmic stress beats in English: An experimental study I," Lang Speech **15**, 72–100.
Baumgarte, F. (**2002**). "Improved audio coding using a psychoacoustic model based on a cochlear filter bank," IEEE Trans. Speech Audio Process. **10**(7), 495–503.
Beckman, M. E. (**1986**). *Stress and Non-Stress Accent*, Netherlands Phonetic Archive Vol. **7** (Foris, Dordrecht).
Boersma, P. (**1993**). "Accurate short-term analysis of the fundamental frequency and the harmonics-to-noise ratio of a sampled sound," Proceedings of the Institute of Phonetic Sciences, University of Amsterdam, Vol. **17**, pp. 97–110, URL http://www.fon.hum.uva.nl/paul/papers/Proceedings_1993.pdf. Last viewed 3/14/2008.
Boutsen, F. R., Brutten, G. J., and Watts, C. R. (**2000**). "Timing and intensity variability in the metronomic speech of stuttering and nonstuttering speakers," J. Speech Lang. Hear. Res. **43**, 513–520.
Brenier, J. M., Cer, D., and Jurafsky, D. (**2005**). "The detection of emphatic words using acoustic and lexical words," in Proceedings of the Ninth European Conference on Speech Communication (EUROSPEECH-05),

International Speech Communications Association, Lisbon, Portugal, 4–8 September **2005**.
Cooper, M. H., and Allen, G. D. (**1977**). "Timing control accuracy in normal speakers and stutterers," J. Speech Hear. Res. **20**, 55–71.
Cummins, F., and Port, R. (**1998**). "Rhythmic constraints on stress timing in English," J. Phonetics **26**, 145–171.
Davison, A. C., and Hinkley, D. V. (**1997**). *Bootstrap Methods and their Application* (Cambridge University Press, Cambridge).
de Krom, G. (**1993**). "A cepstrum-based technique for determining a harmonics-to-noise ratio in speech signals," J. Speech Hear. Res. **36**, 254–266.
Dyde, R. T., and Milner, D. A. (**2002**). "Two illusions of perceived orientation: One fools all of the people some of the time; the other fools all of the people all of the time," Exp. Brain Res. **144**, 518–527.
Fear, B. D., Cutler, A., and Butterfield, S. (**1995**). "The strong/weak syllable distinction in English," J. Acoust. Soc. Am. **97**, 1893–1904.
Fitt, S. (**2002**). "Unisyn lexicon release," URL http://www.cstr.ed.ac.uk/projects/unisyn. Last viewed 3/14/08.
Fitt, S., and Isard, S. (**1999**). "Synthesis of regional English using a keyword lexicon," in Proceedings of Eurospeech 99, International Speech Communications Association, Vol. **2**, pp. 823–826, Budapest, Hungary, URL http://www.cstr.ed.ac.uk/downloads/publications/1999/Fitt_1999_a.ps. Last viewed 3/14/08.
Fowler, C. A. (**1979**). "'Perceptual centers' in speech production and perception," Percept. Psychophys. **25**, 375–388.
Fry, D. B. (**1955**). "Duration and intensity as physical correlates of linguistic stress," J. Acoust. Soc. Am. **27**, 765–768.
Fry, D. B. (**1958**). "Experiments in the perception of stress," Lang Speech **1**, 126–152.
Gauffin, J., and Sundberg, J. (**1989**). "Spectral correlates of glottal voice source waveform characteristics," J. Speech Hear. Res. **32**, 556–565.
Glave, R. D., and Rietveld, A. C. M. (**1975**). "Is the effort dependence of speech loudness explicable on the basis of acoustical cues?," J. Acoust. Soc. Am. **58**, 875–879.
Gussenhoven, C., Repp, B. H., Rietveld, A., Rump, H. H., and Terken, J. (**1997**). "The perceptual prominence of fundamental frequency peaks," J. Acoust. Soc. Am. **102**, 3009–3022.
Haffenden, A. M., and Goodale, M. A. (**1998**). "The effect of pictorial illusion on prehension and perception," J. Cogn Neurosci. **10**, 122–136.
Hart, M. S., Newby, G., Asscher, S., Choat, C., Bickers, J., Diogo, R. F., Price, D., Perathoner, M., Cook, M., Sly, A., Sutherland, J., Allen, T., Widger, D., Price, D., Viswanathan, S., Loewenstein, J., Lygarger, S., Haines, A., Marquardt, R., Franks, C., Smolenski, N., Stefanovic, S., Hutchinson, J., and volunteers who scanned the books used. (**2006**). "Project Gutenberg," URL www.gutenberg.org, project Gutenberg, (last viewed 3/26/2008).
Heldner, M. (**2001**). "Spectral emphasis as an additional source of information in accent detection," in Prosody in Speech Recognition and Understanding, Paper No. 10, 22–24 October, Molly Pitcher Inn, Red Bank, NJ.
Hickok, G., and Poeppel, D. (**2000**). "Towards a functional neuroanatomy of speech perception," Trends in Cognitive Sciences **4**(4), 131–138.
Klapuri, A. P., Eronen, A. J., and Astola, J. T. (**2006**). "Analysis of the meter of acoustical musical signals," IEEE Trans. Speech Audio Process. **14**, 342–355.
Kochanski, G. (**2006**). "Prosody beyond fundamental frequency," in *Methods in Empirical Prosody Research*, edited by S. Sudhoff, D. Lenertová, R. Meyer, S. Pappert, P. Augurzky, I. Mleinek, N. Richter, and J. Schließer, Language, Context and Cognition (de Gruyter, Berlin), pp. 82–122.
Kochanski, G., Grabe, E., Coleman, J., and Rosner, B. (**2005**). "Loudness predicts prominence: Fundamental frequency lends little," J. Acoust. Soc. Am. **118**, 1038–1054.
Kochanski, G., and Orphanidou, C. (**2007**). "Testing the ecological validity of repetitive speech," in Proceedings of the International Congress of Phonetic Sciences 2007, Saarbrucken, Germany, URL http://kochanski.org/gpk/papers/2007/icphs.pdf, URL viewed February 2008.
Large, E., and Kolen, J. F. (**1994**). "Resonance and the perception of musical meter," Connect. Sci. **6**(1), 177–208.
Large, E. W., and Palmer, C. (**2002**). "Perceiving temporal regularity in music," Cognit. Sci. Q. **26**, 1–37.
Lehiste, I. (**1973**). "Rhythmic units and syntactic units in production and perception," J. Acoust. Soc. Am. **54**, 1228–1234.
Lieberman, P. (**1960**). "Some acoustic correlates of word stress in American English," J. Acoust. Soc. Am. **32**, 451–454.
Moore, B. C. J., and Glasberg, B. R. (**1983**). "Suggested formulae for calculating auditory-filter bandwidths and excitation patterns," J. Acoust. Soc. Am. **74**, 750–753.
Morton, J., and Marcus, C. F., and Frankish, C. (**1976**). "Perceptual centers (p-centers)," Psychol. Rev. **83**, 405–408.
Munson, W. A. (**1947**). "The growth of auditory sensation," J. Acoust. Soc. Am. **19**, 734–735.
Nesbitt, K. (**2001**). *The Aliens Have Landed at Our School!* (Meadowbrook, Minnetonka, MN).
Plomp, R., and Bouman, M. A. (**1959**). "Relation between hearing threshold and duration for tone pulses," J. Acoust. Soc. Am. **31**, 749–758.
Port, R. F. (**2003**). "Meter and speech," J. Phonetics **31**, 599–611.
Rietveld, A. C. M., and Gussenhoven, C. (**1985**). "On the relation between pitch excursions and prominence," J. Phonetics **13**, 299–308.
Saltzman, E., and Byrd, D. (**2000**). "Task-dynamics of gestural timing: Phase windows and multifrequency rhythms," Hum. Mov. Sci. **19**, 499–526.
Scheirer, E. D. (**1998**). "Tempo and beat analysis of acoustic musical signals," J. Acoust. Soc. Am. **103**, 588–601.
Silipo, R., and Greenberg, S. (**1999**). "Automatic transcription of prosodic stress for spontaneous English discourse," in Proceedings of the XIVth International Congress of Phonetic Sciences (ICPhS99), edited by J. J. Olds, Y. Hasegawa, M. Ohala, and A. C. Bailey, The Regents of the University of California, San Francisco, CA, http://www.icsi.berkeley.edu/ftp/global/pub/speech/papers/icphs99–strss.pdf, pp. 2351–2354 (last viewed 3/26/2008).
Silipo, R., and Greenberg, S. (**2000**). "Prosodic stress revisited: Reassessing the role of fundamental frequency," in Proceedings of the NIST Speech Transcription Workshop, College Park, MD, http://silicon-speech.com/Media/PDF/2000_Silipo%26Greenberg_ProsodicStressRevisited.pdf (last viewed 3/26/2008).
Sluijter, A. M. C., and van Heuven, V. J. (**1996**). "Spectral balance as an acoustic correlate of linguistic stress," J. Acoust. Soc. Am. **100**, 2471–2485.
Stevens, S. S. (**1971**). "Perceived level of noise by Mark VII and decibels," J. Acoust. Soc. Am. **51**, 575–602.
Streefkerk, B. M., Pols, L. C. W., and ten Bosch, L. F. M. (**1999**). "Acoustical features used as predictors for prominence in read aloud Dutch sentences used in ANNs," in Proceedings of the Sixth European Conference on Speech Communication (EUROSPEECH-99), International Speech Communication Association, Budapest, Hungary, Vol. **1**, pp. 551–554.
Terken, J. (**1991**). "Fundamental frequency and perceived prominence of accented syllables," J. Acoust. Soc. Am. **89**, 1768–1776.
Todd, N. P. M., and Brown, G. J. (**1996**). "Visualization of rhythm, time and meter," Artif. Intell. Rev. **10**, 253–273.
Turk, A. E., and Sawusch, J. R. (**1996**). "The processing of duration and intensity cues to prominence," J. Acoust. Soc. Am. **99**, 3782–3790.
Zwicker, E. (**1977**). "Procedure for calculating loudness of temporally variable sounds," J. Acoust. Soc. Am. **62**, 675–682.

Differential contribution of envelope fluctuations across frequency to consonant identification in quiet

Frédéric Apoux[a] and Sid P. Bacon
Psychoacoustics Laboratory, Department of Speech and Hearing Science, Arizona State University, P.O. Box 870102, Tempe, Arizona 85287-0102

(Received 3 November 2006; revised 22 January 2008; accepted 25 February 2008)

Two experiments investigated the effects of critical bandwidth and frequency region on the use of temporal envelope cues for speech. In both experiments, spectral details were reduced using vocoder processing. In experiment 1, consonant identification scores were measured in a condition for which the cutoff frequency of the envelope extractor was half the critical bandwidth (HCB) of the auditory filters centered on each analysis band. Results showed that performance is similar to those obtained in conditions for which the envelope cutoff was set to 160 Hz or above. Experiment 2 evaluated the impact of setting the cutoff frequency of the envelope extractor to values of 4, 8, and 16 Hz or to HCB in one or two contiguous bands for an eight-band vocoder. The cutoff was set to 16 Hz for all the other bands. Overall, consonant identification was not affected by removing envelope fluctuations above 4 Hz in the low- and high-frequency bands. In contrast, speech intelligibility decreased as the cutoff frequency was decreased in the midfrequency region from 16 to 4 Hz. The behavioral results were fairly consistent with a physical analysis of the stimuli, suggesting that clearly measurable envelope fluctuations cannot be attenuated without affecting speech intelligibility. © *2008 Acoustical Society of America.* [DOI: 10.1121/1.2897916]

PACS number(s): 43.71.An, 43.71.Es, 43.66.Ba [KWG] Pages: 2792–2800

I. INTRODUCTION

For continuous speech in quiet, the dominant components of the modulation spectrum—the spectral representation of the temporal envelope—lie between 1 and 16 Hz with a peak around 4 Hz, reflecting the average syllable rate in speech (Arai and Greenberg, 1997; Greenberg, 1999). The speech modulation spectrum, however, also contains amplitude components above 16 Hz (Plomp, 1983; Houtgast and Steeneken, 1985). Consistent with the physical characteristics of the temporal structure of speech, a number of behavioral studies have demonstrated that speech intelligibility is only affected by reducing or removing modulation frequencies below a few tens of hertz, suggesting that higher envelope fluctuations do not contribute to overall intelligibility (Drullman *et al.*, 1994; Shannon *et al.*, 1995; Arai *et al.*, 1999; Xu *et al.*, 2005).

Although both physical and behavioral data suggest a limited role of high-frequency envelope fluctuations in speech intelligibility, listeners have been provided with envelope frequencies well beyond a few tens of hertz in many speech studies (Eisenberg *et al.*, 2000; Qin and Oxenham, 2003; Apoux and Bacon, 2004; Gonzales and Oliver, 2005). One motivation for this is related to the relative uncertainty about precisely which envelope frequencies are most important for speech. Another motivation is that some speech information (e.g., periodicity cues) has been associated with envelope fluctuations between 50 and 500 Hz (Rosen, 1992). In studies simulating hearing via a cochlear implant (CI), listeners are commonly provided fast envelope fluctuations (Dorman *et al.*, 1997, 1998; Friesen *et al.*, 2001; Faulkner *et al.*, 2003; Fu and Galvin, 2003; Baskent and Shannon, 2006). In this case, high-frequency cutoffs of the envelope filter (i.e., the low-pass filter used to extract the envelope) are used to conform to the cutoff frequencies commonly used in CI speech processors.

A. Factors affecting the bandwidth of the modulation spectrum

While it might seem reasonable to preserve high-frequency envelope fluctuations, it is unclear whether listeners can extract information from them. Even though humans are able to detect rates of amplitude modulation (AM) imposed on a broadband carrier as high as about 1000 Hz (Viemeister, 1979), filtering in the peripheral auditory system may limit the ability of the listeners to use high-frequency envelope cues in any given spectral region, as the maximum modulation frequency in a band-limited signal cannot exceed half the bandwidth of that band (see Lawson and Uhlenbeck, 1950). Modulation frequencies greater than half the bandwidth will be attenuated by the filter. Therefore, high-frequency AM should be available primarily from the high-frequency region of the speech spectrum. Similar limitations are also true for processing mimicking the resonant properties of the peripheral auditory system such as the analysis filters in CI and CI simulations (i.e., the filters used to decompose input signal spectra into a number of directly adjacent frequency bands for further processing). For example, Xu *et al.* (2005) examined the relative contribution of spectral and temporal cues for phoneme recognition by systematically varying the number of bands (1–16) and the cutoff frequency of the envelope low-pass filter (1–512 Hz) of a

[a]Author to whom correspondence should be addressed. Electronic mail: apoux@psycho.univ-paris5.fr

 0001-4966/2008/123(5)/2792/9/$23.00 © 2008 Acoustical Society of America

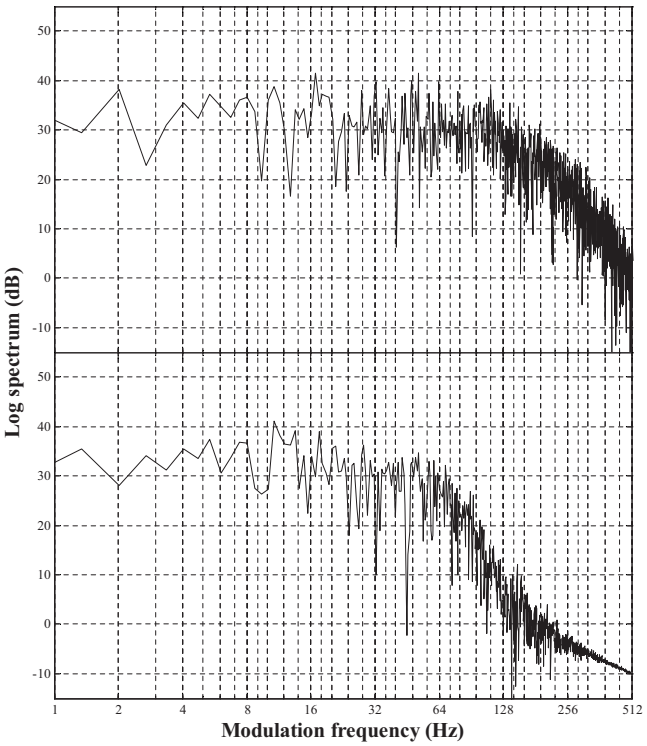


FIG. 1. Logarithm of the amplitude components of the modulation spectrum of a Gaussian noise, as computed at the output of a bandpass filter centered at 1000 Hz. The bandwidths of the bandpass filter were 1024 and 128 Hz for the upper and the lower panels, respectively. Prior to computation, the envelope of each band of noise was low pass filtered at 128 Hz.

noise-excited vocoder. According to their Table I, the bandwidth of the analysis filters ranged from 62 to 936 Hz in the 16-band condition. Therefore, it is clear that most, if not all, of the 16 unfiltered narrow-band envelopes could not exhibit fluctuations as high as 512 Hz. Moreover, if sidebands were introduced outside the passband of the analysis filter by AM, they would be significantly reduced by filtering after modulation (Eddins, 1993, 1999; Strickland and Viemeister, 1997). The effect of the bandwidth of the analysis filter is illustrated in Fig. 1. The two panels show the modulation spectrum of a Gaussian noise derived from the output of a bandpass filter centered at 1000 Hz. The bandwidth of the filter was 1024 Hz (upper panel) or 128 Hz (lower panel). The cutoff frequency of the envelope low-pass filter was 128 Hz in each condition. In the upper panel, it can be seen that only modulation frequencies above the cutoff of the envelope filter were attenuated. In contrast, modulation frequencies well below 128 Hz were attenuated when the bandwidth of the analysis filter was 128 Hz (lower panel). Only the modulation frequencies below half the bandwidth of the analysis filter (i.e., 64 Hz) were left intact.

B. Differential contribution of temporal envelope cues across frequency

From the above, it is apparent that the range of available envelope frequencies should differ across frequency because of the characteristics of the auditory filters and/or the analysis filters. Moreover, it is well established that the shape of the modulation spectrum of speech differs significantly across frequency. Greenberg *et al.* (1998) indicated that the high-frequency spectral region of speech contains a significantly greater amount of energy in the midfrequency modulation spectrum (10–25 Hz) than does the lower frequency spectral region. More recently, Crouzet and Ainsworth (2001) showed that temporal envelopes extracted from distant frequency regions are only partially correlated. Consistent with previous reports (Plomp, 1983; Houtgast and Steeneken, 1985), the results of Crouzet and Ainsworth indicate that for very low-frequency envelope modulations ($\leqslant$4 Hz) the correlation of envelope information between frequency bands is very high ($>$0.8). This high correlation reflects the syllabic rate in speech (i.e., syllables onsets and offsets are similar across the speech spectrum). For higher frequency envelope modulations ($>$8 Hz), the correlation remains significant only for adjacent spectral bands. Taken together, the fact that the shape of the modulation spectrum is not similar across spectral frequency and that narrow-band envelopes are only partially correlated across all spectral regions strongly suggest that temporal cues extracted from remote regions do not convey the same information.

Several behavioral studies with normal-hearing listeners reported data that are in good agreement with the above physical analysis. Grant *et al.* (1991) evaluated the benefits of the auditory presentation of envelope cues as a supplement to lip reading. Among the parameters assessed in this study, the authors investigated the effect of the frequency of the envelope low-pass filter and the effect of the center frequency of the analysis band. When the analysis band was located in the low-frequency region (500 Hz, 1 octave wide), some benefits to lip reading were observed for envelope cutoff frequencies up to 50 Hz. Benefits were observed up to 200 Hz when the analysis band was located in the high-frequency region (3150 Hz, 1 octave wide), suggesting a differential contribution of envelope cues across frequency. This result, however, may simply reflect the influence of auditory filters on the bandwidth of the modulation spectrum. More recently, Silipo *et al.* (1999) measured the intelligibility of one to four $\frac{1}{3}$-octave-wide bands of speech (sentences) presented simultaneously. The envelope of one or two of the bands was low pass filtered in a systematic fashion, allowing the authors to assess the importance of low-, mid-, and high-frequency modulations at different spectral regions. Their results indicated that (i) only modulation rates below 12 Hz play a significant role in the low spectral region and (ii) modulation rates between 10 and 25 Hz are of particular importance for encoding speech information in the spectral region above 1.5 kHz. Finally, Apoux and Bacon (2004) assessed the relative importance of temporal information in broad spectral regions for consonant identification. For the purpose of forcing listeners to use primarily temporal envelope cues, speech sounds were spectrally degraded using four noise-band vocoder processing. Frequency-weighting functions were determined using two methods. The first consisted of measuring the intelligibility of speech with a hole in the spectrum either in quiet or in noise. The second consisted of correlating performance with the randomly and independently varied signal-to-noise ratio within each band. Results demonstrated that all bands contributed equally to consonant

identification when presented in quiet. In noise, however, both methods indicated that listeners consistently placed relatively more weight on the highest frequency band.

The first experiment of the present study was designed to demonstrate the effect of auditory filter bandwidth on the transmission of high-frequency AM. As discussed above, modulation frequencies greater than half the critical bandwidth (see Zwicker *et al.*, 1957) are presumably attenuated. Therefore, it is inappropriate to discuss the effects of envelope cutoff frequency when the effective modulation bandwidth is, in fact, limited by the bandwidth of the auditory filters. To evaluate the effect of the auditory filter bandwidth on the transmission of high-frequency AM, a vocoder-like processor with the cutoff frequency of the envelope low-pass filter in each band proportional to the critical bandwidth of the auditory filter corresponding to that band was implemented. More specifically, envelope cutoffs were independently determined for each band so that, in theory, the desired modulation frequencies in a particular band could not be attenuated by the auditory filters (or the analysis filters). The results were compared with those obtained using a single high-frequency envelope cutoff for all bands. For completeness, low-frequency envelope cutoff frequencies were also tested.

The second experiment was designed to independently establish for different frequency regions which AM rates are critical for speech intelligibility. Previous studies evaluating the importance of low- and high-frequency amplitude fluctuations for speech intelligibility always filtered the temporal envelope in each speech band homogeneously across frequency (i.e., the same envelope cutoff frequency was used for each band). In one study, however, the authors investigated the critical AM for speech in three broad frequency regions independently (Christiansen and Greenberg, 2007). The three bands were centered at 750, 1500, and 3000 Hz and were presented either in isolation or combined with one or two other bands. The envelope cutoff frequency in each band was 3, 6, 12, or 24 Hz and was always the same across bands when two or more bands were simultaneously presented. From the data reported in their Table I, it seems that the effect of the envelope filter was similar across bands when presented in isolation. The authors, however, did not perform a statistical analysis of their percent correct data, making it difficult to determine whether or not the same range of AM was critical in each spectral region. In the second experiment of the present study, the envelope cutoff frequency in one band was systematically varied while keeping the envelope cutoff frequency for all the other bands fixed. Because it was anticipated that performance may not be affected by the manipulation of the envelope cutoff frequency in a single band, the cutoff frequency in two adjacent bands was also systematically and uniformly varied while keeping the envelope cutoff frequency for all the other bands fixed.

A potential complicating factor in the interpretation of the results may arise from recent studies suggesting that envelope filtering techniques might be inappropriate to estimate the range of the pertinent fluctuation rates in speech. Indeed, a series of theoretical and behavioral studies indicated that envelope filtering techniques might introduce artifacts when the speech fine structure is preserved (Ghitza, 2001; Atlas *et al.*, 2004). The exact reasons why envelope filtering techniques might be inappropriate are beyond the scope of the present study and, therefore, the reader is referred to a recent paper by Atlas *et al.* (2004) for further details. In short, it has been demonstrated that part of the original envelope information remains in the speech fine structure and that listeners are able to extract and use this information (Zeng *et al.*, 2004; Gilbert and Lorenzi, 2006). Accordingly, the possibility exists that listeners were, in fact, presented with rich envelope information in studies where the speech fine structure was preserved. Therefore, the speech fine structure was replaced by sinusoids in the present experiments. The use of spectrally degraded stimuli should also force listeners to primarily use temporal cues and, therefore, listeners likely should be more sensitive to modifications applied to the temporal structure of speech.

II. EXPERIMENT 1

A. Methods

1. Subjects

Six normal-hearing subjects participated—five females and one male [one of the authors, Apoux (S1), participated]. Their ages ranged from 20 to 32 years (average=23 years). Normal hearing was defined as having pure-tone air-conduction thresholds of 20 dB HL or better (ANSI, 1996) for octave frequencies from 250 to 8000 Hz. All participants, who, except for Apoux, were native American English speakers, had about 2 h of previous experience identifying spectrally degraded speech sounds and were paid an hourly wage for their participation.

2. Speech processing

The frequency range of speech stimuli was initially restricted to 0.1–5 kHz. The fine structure was replaced by sinusoidal carriers in the following manner. Each vowel-consonant-vowel (VCV) was first band passed in to N semi-logarithmic[1] frequency bands using 24th-order Butterworth filters (N=4, 8, 12, or 16). At the output of each analysis filter, the envelope was extracted by half-wave rectification and low-pass filtering at cf_m (eighth-order Butterworth). In all conditions but one, the envelope low-pass filter cutoff frequency was identical for each band (cf_m=4, 8, 16, 160, or 400 Hz). In the last condition, cf_m was independently computed for each band so that it was equal to half the critical bandwidth (HCB) of the auditory filter centered at the sinusoidal carrier frequency (Glasberg and Moore, 1990). The center frequency of each band and the corresponding envelope filter cutoff frequency in the HCB condition are given in Table I. The filtered envelopes were then used to modulate sinusoids with frequencies equal to the center frequencies of the bands. Each modulated sinusoid was passed through the same bandpass filter used in the original analysis band and the outputs of each band were finally combined. The overall level of each stimulus was normalized and calibrated to produce an average A-weighted output level of 70 dB.

TABLE I. Center frequencies of the analysis bands (in Hz). The envelope cutoff frequency—half the critical bandwidth—used for each band in the HCB condition is shown in italics.

Number of bands	Band															
	1	2	3	4	5	6	7	8	9	10	11	12	13	14	15	16
4	183	487	1 294	3 440												
	22	*38*	*82*	*198*												
8	132	214	350	570	930	1 517	2 473	4 033								
	19	*24*	*31*	*43*	*62*	*94*	*146*	*230*								
12	119	165	229	317	439	609	843	1 168	1 619	2 243	3 107	4 305				
	19	*21*	*24*	*29*	*36*	*45*	*58*	*75*	*99*	*133*	*180*	*244*				
16	114	145	186	237	303	387	494	630	805	1 028	1 313	1 676	2 141	2 734	3 491	4 458
	18	*20*	*22*	*25*	*28*	*33*	*39*	*46*	*56*	*68*	*83*	*103*	*128*	*160*	*201*	*253*

3. Speech material and procedure

The stimuli consisted of 16 consonants in /a/-consonant-/a/ environment recorded by four speakers (two for each gender) for a total of 64 VCV disyllables (Kwon and Turner, 2001). Each run or block presented the entire set of VCV stimuli and corresponded to a given combination between a band condition (4, 8, 12, or 16 bands) and an envelope cutoff condition (4, 8, 16, 160, 400 Hz or HCB). Therefore, each listener completed 24 blocks in which the 64 VCV stimuli were presented in random order. All conditions were presented in random order to avoid order effects. Stimulus presentation was computer controlled. Percent correct identification was measured using a single-interval, 16-alternative forced-choice procedure. The listeners were instructed to report the perceived consonant and responded using the computer mouse to select 1 of 16 buttons on the computer screen. Prior to data collection, each listener received 2 h of practice. No feedback was given during the practice or the experimental sessions. The listeners were tested individually in a double-walled, sound-attenuated booth. Stimuli were played to the listeners binaurally through Sennheiser HD 250 Linear II circumaural headphones.

B. Results and discussion

Figure 2 shows the percent correct identification score as a function of the number of bands averaged across listeners for each of the six envelope cutoff frequency conditions. The standard deviation across listeners was calculated for each condition, but for clarity these are not displayed. The standard deviation ranged from 6 to 21 percentage points (mean=13 percentage points). It generally increased with both increasing envelope cutoff and number of bands. Overall, the percent correct identification scores were slightly lower than in previous experiments. This apparent discrepancy, however, can be accounted for by differences in terms of the amount of practice. For example, Shannon *et al.* (1995) obtained about 90% correct but their subjects received between 8 and 10 h of practice. In studies with a similar amount of practice (e.g., 3 h in Xu *et al.*, 2005), the results were much more comparable. Other differences such as speech material and number of speakers may also account for these small discrepancies. Consistent with previous reports, consonant identification generally improved as a function of the number of bands. Intelligibility also improved as the envelope cutoff frequency increased. Beyond 160 Hz, however, performance seemed to reach an asymptote: scores in the 160- and 400-Hz conditions were within 5 percentage points of one another. Although it was systematically lower, performance in the HCB condition was very similar to that in the 160- and 400-Hz conditions. Overall, the envelope cutoff frequency exerted a more dominant effect on consonant identification than did the number of bands. A repeated measure analysis of variance (ANOVA) with factors of number of bands and envelope cutoff frequency revealed a significant effect for both factors ($p<0.001$). The interaction between the number of bands and the envelope cutoff frequency was also significant [$F(15,143)=2.21$, $p<0.05$]. *Post hoc* (Tukey) comparisons confirmed that increasing the envelope cutoff frequency from 4 to 8 Hz, from 8 to 16 Hz, and from 16 to 160 Hz significantly improved the performance of the listeners ($p<0.001$). Performance in the 400-Hz and HCB conditions did not differ significantly ($p=0.30$). The difference between the 4-band and the 8-band conditions was significant ($p<0.02$). The difference between the 8-band and the 12-band conditions was also significant ($p=0.04$), while

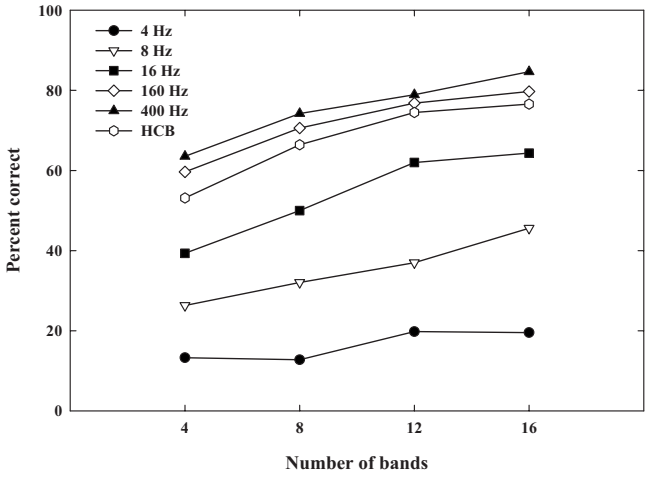


FIG. 2. Mean percent scores for consonant identification as a function of the number of bands. The parameter is the cutoff frequency of the envelope low-pass filter.

the difference between the 12-band and the 16-band conditions was not ($p=0.47$). This last result is fairly consistent with previous reports showing that asymptotic performance is usually achieved with eight bands for VCV stimuli presented in quiet (Dorman *et al.*, 1997).

Also consistent with previous research (van Tasell *et al.*, 1987; Shannon *et al.*, 1995), our results indicate that usable speech information is contained in fluctuation rates above 16 Hz. Indeed, providing modulation frequencies above 16 Hz markedly improved performance, irrespective of the number of bands that was available. Asymptotic performance was reached in the 160-Hz condition for all number of band conditions, suggesting that AM rates between 160 and 400 Hz do not play a significant role in speech intelligibility. Results in the HCB condition showed that consonant identification is not affected by eliminating AM rates greater than half the bandwidth of an auditory filter and, therefore, well below 160 Hz in some regions of the speech spectrum (see Table I).

Because performance did not improve when envelope fluctuations above HCB were provided to the listeners, it is reasonable to assume that, at least in quiet, the transmission of envelope fluctuations can be limited to those frequencies below half the bandwidth of the auditory filter in CI and CI simulations. The present results, however, do not provide much indication about the possible influence of those frequencies above half the bandwidth of the auditory filter when speech is presented against a background noise. Possibly, the intelligibility of speech presented in noise might even decrease when fluctuation rates above half the bandwidth of the auditory filter are provided. First, our results showed that fluctuation rates above half the bandwidth of the auditory filter do not convey any usable information in terms of intelligibility. Therefore, limiting the transmission of nonpertinent envelope fluctuations should help reduce the amount of noise in CI users *without affecting intelligibility*. Second, interference in the modulation domain has been demonstrated for speech in at least two studies (Kwon and Turner, 2001; Apoux and Bacon, 2008). Accordingly, fluctuation rates *above* half the bandwidth of the auditory filter pertaining to the noise background might interfere with fluctuation rates *below* half the bandwidth of the auditory filter pertaining to the target. Since the latter play a role in speech intelligibility, performance might be adversely affected by such interference. In view of the above, we suggest that the transmission of envelope fluctuations should be limited to those frequencies below half the bandwidth of the auditory filter in CI and CI simulations, particularly when background noise is present.

III. EXPERIMENT 2

A. Conditions

Twelve new subjects participated in the second experiment (11 females and 1 male). Their ages ranged from 20 to 40 years (average=25 years). All participants were native American English speakers and had pure-tone air-conduction thresholds of 20 dB HL or better for octave frequencies from 250 to 8000 Hz. Subjects were paid an hourly wage for their participation. The stimuli and processing were the same as for experiment 1 with the following exceptions.

(1) Speech stimuli were processed through an eight-band processor only. This condition was chosen (i) to allow a reasonable spectral resolution (i.e., a large number of bands) while limiting redundancy of information between bands and (ii) because results from experiment 1 indicated that consonant identification should be around 50% correct in this condition with the 16 Hz envelope cutoff and, therefore, base line scores should be sufficiently removed from ceiling and floor effects.
(2) In one condition (SING), the envelope cutoff frequency was set to 16 Hz for all but one band and the envelope in that single (test) band was low pass filtered at 4 Hz, 8 Hz, or HCB to quantify the range of modulation frequencies relevant for consonant identification in that particular band.
(3) In the other condition (CONT), the envelope cutoff frequency was set to 16 Hz for all but two contiguous bands (1 and 2, 2 and 3, 3 and 4, and so on) and the envelope in each of these two (test) bands was low pass filtered at 4 Hz, 8 Hz, or HCB.
(4) A baseline condition in which all narrow-band envelopes were filtered at 16 Hz was added. For comparison, a condition in which all eight narrow-band envelopes were filtered at half the critical bandwidth was also tested (HCB8).

The 12 listeners were divided into two groups. Each group first completed a series of seven blocks for practice. The first block corresponded to an unprocessed condition. The following six blocks corresponded to the conditions for which all bands were filtered at 16 Hz. We chose to train subjects in this particular condition because it was the reference condition. Then, the two speech band conditions were administrated separately. Six listeners completed the SING condition first and six completed the CONT condition first. The presentation order for the test band conditions was chosen randomly to avoid order effects. In addition, each listener completed three blocks in the 16-Hz condition and three blocks in the HCB8 condition. These 6 blocks were randomly dispersed among the 90 experimental blocks with the constraint to have at least one block for each condition in each part of the experiment.

B. Results and discussion

Figures 3 and 4 show the results for the SING and the CONT conditions, respectively. Each figure shows the performance averaged across the 12 listeners as a function of the test band(s) for each envelope cutoff condition. For reference, results for the baseline (all band at 16 Hz) and the HCB8 conditions are also reported. Note that individual performance in these two conditions corresponds to the average of 192 instead of 64 trials. The standard deviation across listeners was calculated for each condition, but for clarity these are not displayed. Overall, the standard deviation for a given condition was typically about 10 percentage points and did not vary systematically across conditions. Consistent

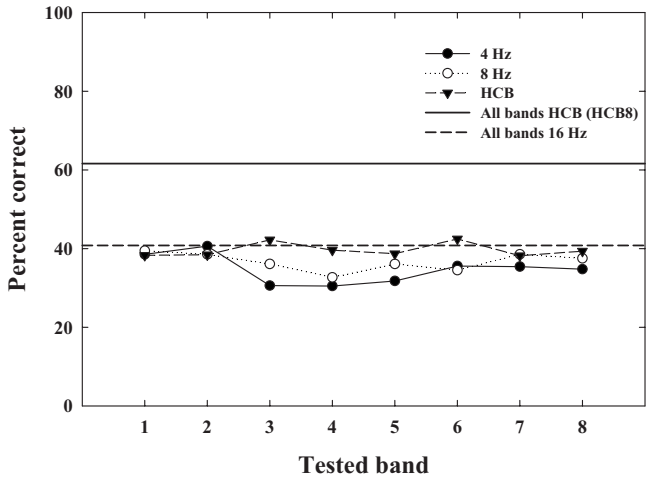


FIG. 3. Mean percent scores for consonant identification as a function of the band tested (SING condition). The parameter is the cutoff frequency of the envelope low-pass filter used for the tested band. Dashed and solid lines show the mean percent scores when the envelope filter for all bands was set to the same cutoff frequency, either 16 Hz or half the critical bandwidth (HCB8), respectively.

with our earlier finding, performance in the baseline condition was about 40% correct and increased up to about 60% correct in the HCB8 condition. First, consider the results for the SING condition (Fig. 3). Overall, the effects of test band frequency and envelope cutoff frequency were rather small. The latter had no influence on performance in the lower frequency region (test bands 1 and 2) for the most part. When the envelope cutoff was manipulated in test bands 3–8, some differences were observed. As a general rule, performance was only slightly reduced when the cutoff frequency was set to 4 or 8 Hz, while no effect was observed in the HCB condition. A repeated measures ANOVA with factors of test band frequency and envelope cutoff frequency showed a significant effect of test band frequency [$F(7,154)=2.84$, $p<0.020$] and envelope cutoff frequency [$F(2,154)=14.11$, $p<0.001$]. The interaction was also significant [$F(14,154)=2.47$, $p<0.005$]. *Post hoc* (Tukey) comparisons confirmed that the 4- and 8-Hz conditions did not differ significantly ($p=0.129$). However, performance in these two conditions was significantly lower than in the HCB condition ($p<0.001$ and $p<0.01$, respectively). *Post hoc* comparisons also revealed that scores for test bands 1 and 2 both differed significantly from performance for test band 4, indicating an effect of the frequency region ($p<0.03$ and $p<0.02$, respectively).

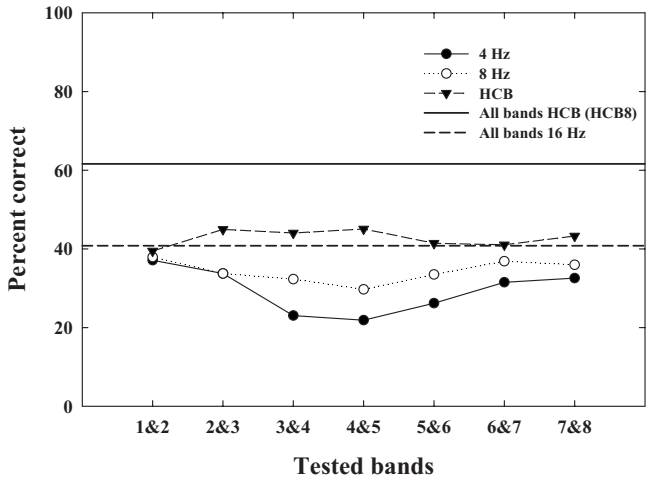


FIG. 4. Mean percent scores for consonant identification as a function of the bands tested (CONT condition). The parameter is the cutoff frequency of the envelope low-pass filter used for the tested bands. Dashed and solid lines show the mean percent scores when the envelope filter for all bands was set to the same cutoff frequency, either 16 Hz or half the critical bandwidth (HCB8), respectively.

By comparing Figs. 3 and 4, it is apparent that the same general pattern was observed in the CONT condition. However, the effects were noticeably amplified by the manipulation of two contiguous bands simultaneously. Again, no difference was observed between the three envelope cutoff conditions in the low-frequency region (test bands 1&2). In the other test band conditions, restricting envelope fluctuations to frequencies below 4 or 8 Hz typically deteriorated performance relative to the base line condition with the 4-Hz condition leading systematically to poorer scores. In this latter condition, percent correct may be reduced by as much as about 20 percentage points (test bands 3&4 and 4&5). In a few band conditions, consonant identification scores in the HCB condition increased relative to those in the baseline condition. However, the difference did not exceed 5 percentage points. A repeated measure ANOVA with factors of test band frequency and envelope cutoff frequency showed a significant effect of test band frequency [$F(6,132)=7.79$, $p<0.001$] and envelope cutoff [$F(2,132)=54.55$, $p<0.001$]. The interaction was also significant [$F(12,132)=5.06$, $p<0.001$]. *Post hoc* comparisons indicated that all three envelope cutoff conditions differed significantly from each other. They also indicated that consonant identification scores in the test band 4&5 condition differed from test band 1&2, 2&3, 6&7, and 7&8 conditions.

Increasing the cutoff of the envelope low-pass filter to half the critical band of an auditory filter in one band only (SING) did not lead to any substantial improvement in intelligibility. This finding may seem surprising at first given the 20 percentage points advantage observed when all eight narrow-band envelopes were filtered at half the critical bandwidth (compare solid and dashed lines in Fig. 3). One likely explanation is that envelope information in each band interacted in a way that was not simply additive. Such synergistic interactions have been reported previously for narrow bands of speech. For example, Warren *et al.* (1995) examined the intelligibility of $\frac{1}{20}$-octave-wide bands of speech presented either in isolation or in pairs. The authors found that two widely separated narrow bands of speech have intelligibility scores well above what would be predicted from the simple addition of their intelligibility scores when presented separately. The difference between the observed and the predicted performance, the synergistic effect, was about 17 percentage points in their study. To assess whether synergistic interactions also occurred in the CONT condition, the difference relative to the baseline condition in each test band condition was computed for both band conditions. A new condition, Sum Sing, was created in which the sum of differences ob-

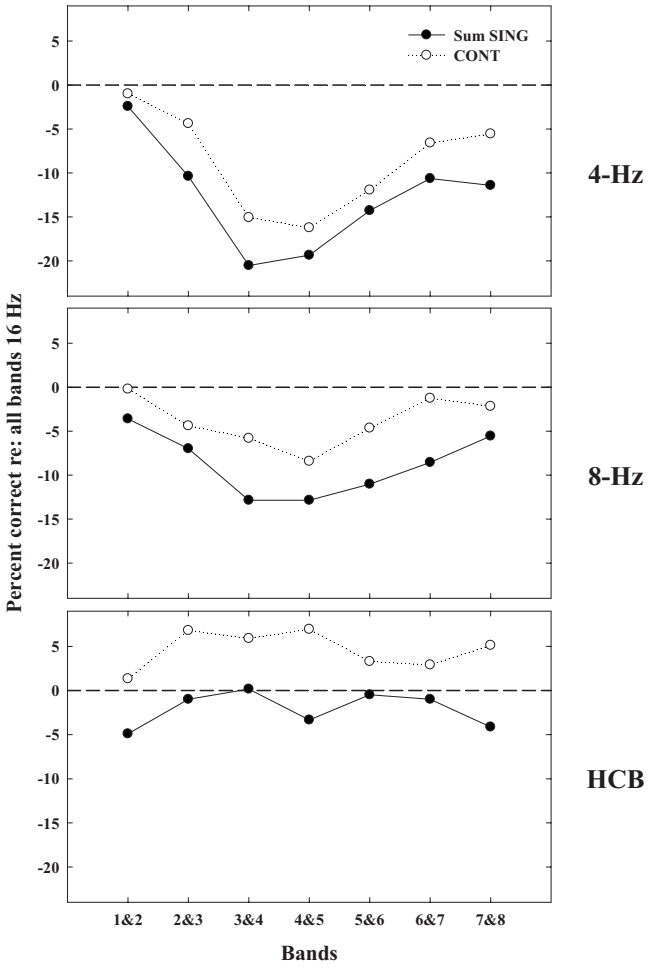


FIG. 5. The upper, middle, and lower panels show the percent correct relative to the base line condition (all bands at 16 Hz) in the 4 Hz, 8 Hz, and HCB conditions respectively, as a function of the tested bands. In each panel, the filled and unfilled circles show the results for the sum Sing and the CONT condition, respectively.

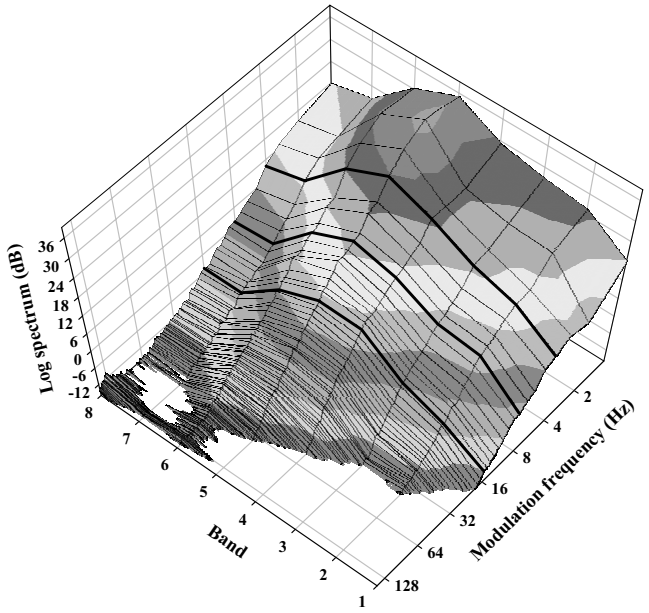


FIG. 6. Logarithm of the amplitude components of the modulation spectrum computed for all 64 VCVs used in the experiments as a function of the analysis band. The same eight bandpass filters used in the HCB condition were used for the analysis (i.e., the envelope low-pass filter cutoff frequency was equal to half the bandwidth of an auditory filter). Levels of gray indicate a 6 dB amplitude range. For clarity, lines on the modulation frequency axis corresponding to an envelope cutoff condition are in bold (4, 8, and 16 Hz).

tained for two bands was calculated for each pair of contiguous bands. For example, in the 1&2 band condition, the difference relative to the baseline condition computed for bands 1 and 2 was added together. This new condition allowed estimating the effect of manipulating two bands simultaneously (i.e., the synergistic effect). Figure 5 presents the results this way for the Sum Sing and the CONT conditions. The upper, middle, and lower panels show the results for the 4-Hz, 8-Hz, and HCB conditions, respectively. Positive values indicate an improvement over the baseline condition (cutoff frequency in all bands of 16 Hz). Statistical analyses were performed separately for each envelope cutoff frequency using repeated measures ANOVA with factors of test band frequency and "synergy" (i.e., Sum Sing versus CONT). The results indicated a significant effect of test band frequency for the 4- and 8-Hz conditions (all $p<0.001$), confirming a differential contribution of rate between 4 and 8 and between 8 and 16 Hz to consonant identification. In contrast, the effect of test band frequency was not significant for the HCB condition. All three analyses indicated no significant synergistic effect. In other words, the improvement observed with two contiguous bands (CONT) was not larger than the summed increase measured individually for each band (Sum Sing). The interaction between the two main factors was not significant in all three analyses. A likely explanation for the absence of synergistic interactions with two contiguous bands is that adjacent bands provide highly correlated information. Therefore, the 20 percentage points advantage observed when all eight narrow-band envelopes were filtered at half the critical bandwidth most likely reflects the synergistic interaction of distant bands. This assumption is consistent with the results of a recent study by Healy and Warren (2003). In this study, the authors measured the intelligibility of band pairs presented either contiguously or separated by 1, 2, 3, or 4 octaves. Their results showed an improvement in sentence intelligibility as band pairs were moved apart. Although a band separation of 3 and 4 octaves resulted in no improvement relative to the contiguous condition, a 20 percentage points improvement was observed for band separation of 1 and 2 octaves.

An interesting question that emerges is how the present results can be related to the amount of "temporal information" that was physically present in each band. The modulation spectrum associated with each band is illustrated in Fig. 6, as computed for all 64 VCV stimuli at the output of the analysis filters used in the HCB condition. For clarity, the modulation frequencies corresponding to envelope cutoff conditions used in experiment 2 are marked by a bold line (4, 8, and 16 Hz). As can be seen, the peak of the spectrum lies around 2 Hz in all bands and the energy decreases rapidly with increasing modulation frequency beyond this value. The frequency of the peak presumably reflects the average duration of the stimuli. At most modulation frequencies, the

amount of energy is greatest in band 5 (cf=930 Hz) and lowest in bands 1, 7, and 8. The four remaining bands have an intermediate amount of energy with bands 4 and 6 being in the upper end of this intermediate range and bands 2 and 3 in the lower end. This pattern is fairly consistent with the effects of the envelope filter's cutoff frequency on consonant identification in that behavioral data indicated a primary role of modulation frequencies between 4 and 16 Hz in the midfrequency region of the speech spectrum and a negligible contribution of these rates in the lower and upper frequency regions. Minor discrepancies may have resulted from at least two factors. First, it should be noted that a seven-point drop in percent correct can result from the deterioration of intelligibility for one VCV only. Therefore, the average identification scores may have been influenced by the results for a particular VCV or subset of VCVs and this effect might not be apparent when averaged behavioral and physical data are compared. Second, as discussed in the Introduction, the correlation of envelope information between adjacent bands is very high and, therefore, one can reasonably assume a certain degree of redundancy across bands. Accordingly, the loss of envelope information in a restricted frequency region may have been compensated by the presence of similar information in an adjacent band, reducing the observed effect. Comparisons across SING and CONT conditions provide at least some indirect support for this interpretation in that a larger effect of envelope cutoff was observed when the envelope cutoff was manipulated in two adjacent bands.

Results from experiment 2 suggest that the accuracy of methods developed for the prediction of speech intelligibility such as the speech transmission index (STI) (Steeneken and Houtgast, 1980) might be increased by measuring independently for different frequency regions which AM rates are critical for speech intelligibility. The STI is based on a weighted sum of modulation transfer functions, each of which specifies how modulation depth in seven octave-wide frequency bands is affected by interference or signal processing. This reduction in modulation depth of a test signal (Houtgast and Steeneken, 1985) or speech signal (Payton and Braida, 1999; Steeneken and Houtgast, 1999) has been shown to be highly correlated with intelligibility. Because STI calculation is based on the transmission of AM, one important parameter is the range of modulation frequencies considered. Based on the modulation spectra of octave-band filtered speech, modulation frequencies of 0.63–12.5 Hz in $\frac{1}{3}$-octave steps have been typically used. According to our data, however, the upper limit of the pertinent fluctuations rates for speech intelligibility varies across the speech spectrum. Although our results were obtained with VCVs, it is reasonable to assume that the same range of modulation frequencies should not be used for each of the seven-octave-wide bands. In some bands, only the modulation frequencies below a few hertz should be considered. Conversely, modulation frequencies well above 12.5 Hz should be considered in other bands.

IV. SUMMARY AND CONCLUSIONS

The goal of the present study was to determine which modulation frequencies contribute significantly to the identification of spectrally degraded speech in specific frequency regions. The results from experiment 1 suggest that envelope fluctuations above 16 Hz play a critical role in consonant identification. They also demonstrate that the preservation of modulation frequencies greater than half the bandwidth of an auditory filter has no significant effect on consonant identification in quiet. Taken together, these findings indicate that most of the temporal information necessary to preserve accurate consonant identification is conveyed by envelope fluctuations equal or lower than half the critical bandwidth of an auditory filter. Although not surprising, this result stands out against the use of a high envelope cutoff frequency as typically used in CI and CI simulations.

The second experiment indicates that the range of critical modulation frequencies for consonant identification depends on the region of the speech spectrum. Behavioral data showed a primary role of modulation frequencies between 4 and 16 Hz in the midfrequency region of the speech spectrum and a negligible contribution of these rates in the lower and upper frequency region of the speech spectrum. Accordingly, previous studies showing that the removal of modulation frequencies between 4 and 16 Hz significantly affects speech intelligibility (Drullman *et al.*, 1994; Arai *et al.*, 1999) only reflect the importance of these rates *in a specific region of the speech spectrum*. A comparison between the analysis of the speech stimuli used in the present experiment and the behavioral data obtained with these stimuli suggests that understanding spectrally reduced speech (eight-band vocoder) relies on most, if not all, the *available* envelope fluctuations in each band. In other words, envelope fluctuations present in narrow bands of speech *with enough power* cannot be attenuated without affecting intelligibility.

ACKNOWLEDGMENTS

This research was supported by a grant from the National Institute of Deafness and Other Communication Disorders (NIDCD Grant No. DC01376). We thank Ken Grant and two anonymous reviewers for their helpful comments on a previous version of the manuscript.

[1]The upper cutoff frequency f_n of the nth band was computed according to the equation

$$f_n = F_{\mathrm{lo}} \times 10^{\log_{10}(F_{\mathrm{up}}/F_{\mathrm{lo}})(1/N)n},$$

where F_{lo} and F_{up} are, respectively, the lower and upper limits of the filterbank in hertz (i.e., 100 and 5 000 Hz) and N is the total number of bands.

ANSI (**1996**). "Specifications for audiometers," ANSI Report No. S3.6-1996, American National Standards Institute, New York.

Apoux, F., and Bacon, S. P. (**2004**). "Relative importance of temporal information in various frequency regions for consonant identification in quiet and in noise," J. Acoust. Soc. Am. **116**, 1671–1680.

Apoux, F., and Bacon, S. P. (**2008**). "Selectivity of modulation interference for consonant identification in normal-hearing listeners," J. Acoust. Soc. Am. **123**, 1665–1672

Arai, T., and Greenberg, S. (**1997**). "The temporal properties of spoken Japanese are similar to those of English," Proceedings of the Eurospeech, Rhodes, Greece, pp. 1011–1014, September.

Arai, T., Pavel, M., Hermansky, H., and Avendano, C. (**1999**). "Syllable intelligibility for temporally filtered LPC cepstral trajectories," J. Acoust. Soc. Am. **105**, 2783–2791.

Atlas, L., Li, Q., and Thompson, J. (**2004**). "Homomorphic modulation spectra," Proceedings of the 29th International Conference on Acoustics, Speech, and Signal Processing, Montreal, Canada, pp. 761–764, May.
Baskent, D., and Shannon, R. V. (**2006**). "Frequency transposition around dead regions simulated with a noiseband vocoder," J. Acoust. Soc. Am. **119**, 1156–1163.
Christiansen, T. U., and Greenberg, S. (**2007**). "Distinguishing spectral and temporal properties of speech using and information-theoric approach," XVIth International Congress of Phonetic Sciences, Saarbrücken, Germany, December.
Crouzet, O., and Ainsworth, W. A. (**2001**). "On the various influences of envelope information on the perception of speech in adverse conditions: An analysis of between-channel envelope correlation," Workshop on Consistent and Reliable Cues for Sound Analysis, Aalborg, Denmark, September.
Dorman, M. F., Loizou, P. C., and Rainey, D. (**1997**). "Speech intelligibility as a function of the number of channels of stimulation for signal processors using sine-wave and noise-band outputs," J. Acoust. Soc. Am. **102**, 2403–2411.
Dorman, M. F., Loizou, P. C., Fitzke, J., and Tu, Z. (**1998**). "The recognition of sentences in noise by normal-hearing listeners using simulations of cochlear-implant signal processors with 6-20 channels," J. Acoust. Soc. Am. **104**, 3583–3585.
Drullman, R., Festen, J. M., and Plomp, R. (**1994**). "Effect of temporal envelope smearing on speech reception," J. Acoust. Soc. Am. **95**, 1053–1064.
Eddins, D. A. (**1993**). "Amplitude modulation detection of narrow-band noise: Effects of absolute bandwidth and frequency region," J. Acoust. Soc. Am. **93**, 470–479.
Eddins, D. A. (**1999**). "Amplitude-modulation detection at low- and high-audio frequencies," J. Acoust. Soc. Am. **105**, 829–837.
Eisenberg, L. S., Shannon, R. V., Martinez, A. S., Wygonski, J., and Boothroyd, A. (**2000**). "Speech recognition with reduced spectral cues as a function of age," J. Acoust. Soc. Am. **107**, 2704–2710.
Faulkner, A., Rosen, S., and Stanton, D. (**2003**). "Simulations of tonotopically mapped speech processors for cochlear implant electrodes varying in insertion depth," J. Acoust. Soc. Am. **113**, 1073–1080.
Friesen, L. M., Shannon, R. V., Baskent, D., and Wang, X. (**2001**). "Speech recognition in noise as a function of the number of spectral channels: Comparison of acoustic hearing and cochlear implants," J. Acoust. Soc. Am. **110**, 1150–1163.
Fu, Q. J., and Galvin, J. J. (**2003**). "The effects of short-term training for spectrally mismatched noise-band speech," J. Acoust. Soc. Am. **113**, 1065–1072.
Gilbert, G., and Lorenzi, C. (**2006**). "The ability of listeners to use recovered envelope cues from speech fine structure," J. Acoust. Soc. Am. **119**, 2438–2444.
Ghitza, O. (**2001**). "On the upper cutoff frequency of the auditory critical-band envelope detectors in the context of speech perception," J. Acoust. Soc. Am. **110**, 1628–1640.
Glasberg, B. R., and Moore, B. C. J. (**1990**). "Derivation of auditory filter shapes from notched-noise data," Hear. Res. **47**, 103–138.
Gonzales, J., and Oliver, J. C. (**2005**). "Gender and speaker identification as a function of the number of channels in spectrally reduced speech," J. Acoust. Soc. Am. **118**, 461–470.
Grant, K. W., Braida, L. D., and Renn, R. J. (**1991**). "Single band amplitude envelope cues as an aid to speechreading," Q. J. Exp. Psychol. A **43**, 621–645.
Greenberg, S., Arai, T., and Silipo, R. (**1998**). "Speech intelligibility derived from exceedingly sparse spectral information," International Conference on Spoken Language Processing, Sydney, Australia, pp. 74–77, December.
Greenberg, S. (**1999**). "Speaking in shorthand—A syllable-centric perspective for understanding pronunciation variation," Speech Commun. **29**, 159–176.
Healy, E. W., and Warren, R. M. (**2003**). "The role of contrasting temporal amplitude patterns in the perception of speech," J. Acoust. Soc. Am. **113**, 1676–1688.
Houtgast, T., and Steeneken, H. J. M. (**1985**). "A review of the MTF concept in room acoustics and its use for estimating speech intelligibility in auditoria," J. Acoust. Soc. Am. **77**, 1069–1077.
Kwon, B. J., and Turner, C. W. (**2001**). "Consonant identification under maskers with sinusoidal modulation: Masking release or modulation interference?," J. Acoust. Soc. Am. **110**, 1130–1140.
Lawson, J. L., and Uhlenbeck, G. E. (**1950**). *Threshold Signals*, Radiation Laboratory Series Vol. **24** (McGraw-Hill, New York).
Payton, K. L., and Braida, L. D. (**1999**). "A method to determine the Speech Transmission Index from speech waveforms," J. Acoust. Soc. Am. **106**, 3637–3648.
Plomp, R. (**1983**). "The role of modulation in hearing," in *Hearing—Physiological bases and psychophysics*, edited by R. Klinke and R. Hartmann (Springer-Verlag, New York).
Qin, M. K., and Oxenham, A. J. (**2003**). "Effects of simulated cochlear-implant processing on speech reception in fluctuating maskers," J. Acoust. Soc. Am. **114**, 446–454.
Rosen, S. (**1992**). "Temporal information in speech: Acoustic, Auditory and Linguistic aspects," Philos. Trans. R. Soc. London, Ser. B **336**, 367–373.
Silipo, R., Greenberg, S., and Arai, T. (**1999**). "Temporal constraints on speech intelligibility as deduced from exceedingly sparse spectral representation," Proceedings of the Eurospeech, Budapest, Hungary, pp. 2687–2690, September.
Shannon, R. V., Zeng, F. G., Kamath, V., Wygonski, J., and Ekelid, M. (**1995**). "Speech recognition with primarily temporal cues," Science **270**, 303–304.
Steeneken, H. J. M., and Houtgast, T. (**1980**). "A physical method for mearuring speech-transmission quality," J. Acoust. Soc. Am. **67**, 318–326.
Steeneken, H. J. M., and Houtgast, T. (**1999**). "A physical method for mearuring speech-transmission quality," J. Acoust. Soc. Am. **67**, 318–326.
Strickland, E. A., and Viemeister, N. F. (**1997**). "The effects of frequency region and bandwidth on the temporal modulation transfer function," J. Acoust. Soc. Am. **102**, 1799–1810.
van Tasell, D. J., Soli, S. D., Kirby, V. M., and Widen, G. P. (**1987**). "Speech waveform envelope cues for consonant recognition," J. Acoust. Soc. Am. **82**, 1152–1161.
Viemeister, N. F. (**1979**). "Temporal modulation transfer functions based upon modulation thresholds," J. Acoust. Soc. Am. **66**, 1364–1380.
Warren, R. M., Riener, K. R., Bashford, J. A., and Brubaker, B. S. (**1995**). "Spectral redundancy: Intelligibility of sentences heard through narrow spectral slits," Percept. Psychophys. **57**, 175–182.
Xu, L., Thompson, C. S., and Pfingst, B. E. (**2005**). "Relative contributions of spectral and temporal cues for phoneme recognition," J. Acoust. Soc. Am. **117**, 3255–3267.
Zeng, F.-G., Nie, K., Liu, S., Stickney, G., Del Rio, E., Kong, Y.-Y., and Chen, H. (**2004**). "On the dichotomy in auditory perception between temporal envelope and fine structure cues," J. Acoust. Soc. Am. **116**, 1351–1354.
Zwicker, E., Flottorp, G., and Stevens, S. S. (**1957**). "Critical band width in loudness summation," J. Acoust. Soc. Am. **29**, 548–557.

A method to identify noise-robust perceptual features: Application for consonant /t/

Marion S. Régnier and Jont B. Allen[a)]
ECE Department and The Beckman Institute for Advanced Science and Technology, University of Illinois at Urbana-Champaign, 405 North Mathews, Urbana, Illinois 61801, USA

(Received 11 August 2007; revised 24 February 2008; accepted 25 February 2008)

This study focuses on correlating speech *confusion patterns*, defined as consonant-vowel confusion as a function of the speech-to-noise ratio, and a model acoustic feature (AF) representation called the *AI gram*, defined as the *articulation index density* in the spectrotemporal domain. By collecting many responses from many talkers and listeners, the AF and psychophysical feature (*event*) is shown to be correlated via the AI-gram model and the confusion matrices at the utterance level, thereby explaining the listener confusion. Consonant /t/ is used as an example to identify its primary robust-to-noise feature, and a precise correlation of the acoustic information with the listeners' confusions is used to label the event. The main spectrotemporal cue defining the /t/ event is an across-frequency temporal coincidence, wherein frequency spread and robustness vary across utterances, while the event remains invariant. The cross-frequency timing event is shown to be the key perceptual feature for consonants in a vowel following context. Coincidences are found to form the basic element of the auditory object. Neural circuits used for coincidence in binaural processing for localization across ears are proposed to be used within one ear across channels. It is further concluded that the event is based on the audibility of the /t/ burst rather than on any superthreshold property. © *2008 Acoustical Society of America.* [DOI: 10.1121/1.2897915]

PACS number(s): 43.71.An, 43.71.Gv, 43.66.Ba [ADP] Pages: 2801–2814

I. INTRODUCTION

After 50 years of work, even a basic understanding of speech's robustness to masking noise remains a mystery. Having a theory of human speech recognition (HSR) is critical for the development of new hearing aids and cochlear implants, and for automatic (machine) speech recognition (ASR). Given the importance of such a theory, other than a hand full of papers, little attention has been paid to the basic relations between acoustic and perceptual speech features. To research this long-standing problem, we measured a large number of listeners' responses to individual consonant-vowel (CV) syllables in noise and then correlated the confusions with each utterances' acoustic cues. *Utterances* are defined as CV sounds spoken by a particular talker, whereas a *token* is an utterance specified by its signal-to-noise ratio. We can prove the existence of these perceptual cues, denoted here as *events*, by identifying the spectrotemporal features used by listeners to discriminate consonants in noise.

Our approach is to correlate tokens to listeners's responses. By assuming that human communication is an "information channel" in the Shannon (1948) sense, we use Shannon's receiver to model the robust detection of speech cues in noise. We specifically show that across-frequency onset timing plays a crucial role in speech perception (Heil, 2003).

One might reasonably wonder why we study CV phonology rather than meaningful sounds having context. Context effects are critical when decoding natural language. However, with very limited context, listeners are still able to discriminate nonsense CV speech sounds below −16 dB speech-to-noise ratio (SNR) (Allen, 2005a; Phatak and Allen, 2007). This is now clear from our analysis of confusion matrices (CMs) of CV sounds, measured by Miller and Nicely (1955) (denoted MN55), as emphasized by Allen (2005a, 2005b) and Phatak and Allen (2007). Noise robustness has been a major area of debate in both the HSR and ASR literature (Hermansky, 1998).

Other than in a handful of studies (Blumstein and Stevens, 1979; Delattre *et al.*, 1955; Repp *et al.*, 1978; Kewley-Port, 1983; Lisker, 1985; Stevens and Klatt, 1974; Klunder *et al.*, 1995) little is known about the specific spectrotemporal information present in each wave form that causes (or prevents) specific confusions. Much remains to be done. Only a few studies (Fletcher and Galt, 1950; Summerfield and Haggard, 1977; Dubno and Levitt, 1981; Dubno *et al.*, 1987; Kamm *et al.*, 1985; Hant and Alwan, 2003) have used masking noise on real speech signals to study the confusions via the confusion matrix method. To explore the effects of noise and its spectrum, the University of Illinois at Urbana-Champaign (UIUC) Human Speech Recognition Group at the Beckman Institute conducted two basic studies, denoted PA07 and PA05 (Lovitt and Allen, 2006) and analyzed by Phatak and Allen (2007). PA05 used the same CVs as MN55 presented in white noise but expanded the MN55 experiment by including more vowels, talkers, and listeners and by updating the testing methodology. The present paper extends the analysis of Phatak and Allen (2007) by correlating the audible speech information with the scores for individual utterances from these two experiments. Our goal is to identify and label the common robust-to-noise features in the spectrotemporal domain (Strope and Alwan, 1997).

[a)]Electronic mail: jontalle@uiuc.edu.

Previous studies [Cooper *et al.*, 1952; Delattre *et al.*, 1955; see Hawkins, 2003; Nguyen and Hawkin, 2003 for reviews] pioneered the analysis of spectrotemporal cues discriminating consonants. Their goal was to study the acoustic properties of consonants /p/, /t/, and /k/ in different vowel contexts. One of their main results is the empirical establishment of a physical to perceptual map, derived from the presentation of synthetic CVs to human listeners. These synthetic "speech sounds" consisted of a short noise burst (10 ms, 400 Hz bandwidth), representing the consonant, followed by artificial formant transitions composed of tones, simulating the vowel. They discovered that for each of these synthetic voiceless stops, the spectral position of the noise burst was vowel dependent. This *coarticulation* was mostly obvious for /p/ and /k/, with bursts above 3 kHz giving the percept of /t/ for all vowel contexts. A burst located at the second formant frequency or slightly above would create a percept of /k/, and that below would create /p/. Consonant /t/ could therefore be considered to have less coarticulation. No information was provided about the robustness of their synthetic speech samples to masking noise nor about the importance of the presumed features relative to other cues that are present in natural speech but missing in their synthetic speech samples.

The spectrotemporal location of events has been found to vary due to the natural variability of speech. Cooper *et al.* (1952) determined the most relevant parts of the speech based on perceptual criterion. We have done the same. However, unlike Cooper *et al.* (1952), our results depend on natural speech and variable amounts of masking noise (Miller and Nicely, 1955; Allen, 2005a; Phatak and Allen, 2007; Régnier and Allen, 2007a, 2007b).

In summary, by collecting many responses from many talkers and listeners, we were able to build a large database of CPs (Allen, 2005b; Phatak and Allen, 2007). We relate the perceptual and physical domains at the utterance level via our measurement of speech audibility, the articulation index (AI) model (Fletcher and Galt, 1950; French and Steinberg, 1947), and thereby explain listeners' confusions via the spectrotemporal acoustic perceptual features. Throughout this paper, we will take the example of consonant /t/ and show how we can reliably identify its primary robust-to-noise feature. In order to identify and label events, we precisely correlate the acoustic information with the listeners' confusions. We show that the main spectrotemporal cue defining the /t/ event is composed of across-frequency temporal coincidence (perceptual features), which is represented by correlated acoustic properties (acoustic features). These can vary on an utterance basis. Our observations support these coincidences as a basic element of the auditory object formation, the cross-frequency timing event being the main perceptual feature for consonants in a vowel context. It seems reasonable that similar neural circuits used for coincidence in binaural processing for localization across ears (Joris *et al.*, 1998) could be used within one ear across channels (Delgutte *et al.*, 1998).

II. THE ARTICULATION INDEX: AN AUDIBILITY MODEL

The *articulation* is defined as the score P_c(SNR) for nonsense sound. The *articulation index* is the foundation stone of speech perception, laid down by Fletcher and Galt (1950) and French and Steinberg (1947). The AI is a *sufficient statistics* of the articulation (Allen, 2005a). It follows that the score is a function of the AI, giving P_c(AI). The basic concept of the AI is to quantify maximum entropy (MaxEnt, also called nonsense speech) average phone scores. It is based on the SNR in critical bands, expressed in decibel sensation level, scaled by the dynamic range of speech (30 dB) (Allen, 1994, 2005a; Phatak and Allen, 2007).

Allen (2005a) showed that French and Steinberg's (1947) expression for the maximum entropy average phone score P_c(AI), corrected for chance, may be written as

$$P_c(\mathrm{AI}) = 1 - P_e = 1 - e_{\mathrm{chance}} e_{\mathrm{min}}^{\mathrm{AI}}, \tag{1}$$

where the recognition error e_{min} is the minimum error at AI=1, and the error $e_{\mathrm{chance}}=1-1/16=15/16$ at chance performance (AI=0) for the 16 consonant case (Kamm *et al.*, 1985).

The articulation index is the basis of many standards, and its long history and utility, as discussed in length in several papers and books (French and Stemberg, 1947; Allen, 1994; Fletcher, 1995; Allen, 1996, 2005a, 2000b). Phatak and Allen (2007) extended the AI formula following French and Steinberg (1947) to account for the peak-to-rms [root-mean-squared $x_{\mathrm{rms}}=\sqrt{\overline{(x-\bar{x})^2}}$] ratio for the speech r_k in each band as

$$\mathrm{AI}_k = \min\left(\tfrac{1}{3}\log_{10}(1 + r_k^2 \mathrm{SNR}_k^2), 1\right), \tag{2}$$

where AI_k is called the *specific AI*, and SNR_k is the SNR (i.e., the ratio of the rms of the speech to the rms of the noise) in the kth articulation band. The total AI is then the average over the specific AI:

$$\mathrm{AI} = \frac{1}{K}\sum_{k=1}^{K} \mathrm{AI}_k. \tag{3}$$

The parameter $K=20$ bands defines the number of articulation bands and is determined empirically to give an equal band contribution in score for consonant-vowel materials (French and Steinberg, 1947). Each of these 20 bands corresponds to 1 mm along the basilar membrane, from about 0.3 to 7.5 kHz (Fletcher and Galt, 1950).

We denote the AI density over time and place (frequency) as the *AI gram* and noted it as $\mathrm{AI}(t, X_k)$. This is a simple graphical extension of the AI, as defined by French and Steinberg (1947). This function of time and *place* (defined as the distance X along the basilar membrane) is computed from a cochlear model or cochlear filter bank, with bandwidths equal to human critical bands, followed by a simple model of the auditory nerve (Lobdell and Allen, 2006). Figure 1 shows the block diagram of how the AI gram is computed from a masked speech signal $s(t)$. As a practical matter, the noise spectrum $\sigma_n^2(f)$ is based on the noise in isolation, but if necessary, it may be estimated directly from the noisy speech but with some loss of accuracy. The AI gram includes a conversion of the basilar membrane vibration to a neural firing rate via an envelope detector representing the mean rate of the neural firing pattern across the cochlear output. The speech+noise signal is scaled by the long-

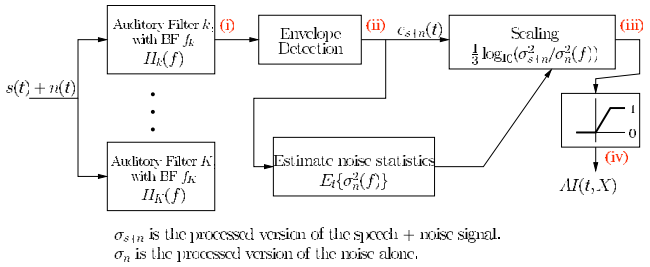


FIG. 1. (Color online) AI-gram block diagram. Derived from the work of French and Steinberg (1947) and Fletcher (1995), the output of the AI gram relates to the audibility of a sound. When a speech signal is visible in different degrees of black on the AI gram, it is above the masked threshold (i.e., audible). It follows that all noise and inaudible sounds having a SNR less than 0 dB appear in white due to the band normalization by the noise.

term average noise power $\sigma_n^2(f)$ so that the power SNR in each frequency band is $\mathrm{SNR}_k^2=\sigma_{s+n}^2/\sigma_n^2\approx 1+\sigma_s^2/\sigma_n^2$. The scaled value of SNR_k (in decibels) [as defined by Eq. (2)] yields the AI density $\mathrm{AI}(t,X)$. The audible speech modulations across frequency give a spectrotemporal representation in the form of the AI gram (Lobdell and Allen, 2006), as shown in Fig. 2.

The AI gram represents a simple *perceptual model*, and based on the pioneering work of French and Steinberg (1947) and Fletcher and Galt (1950), its output is assumed to be correlated with our psychophysical experiments. Different degrees of black on the AI gram are correlated with the audibility of the region of interest. Noise and inaudible speech sounds are represented by white (where the SNR is less than 0 dB), while audible speech is dark. The greater the $\mathrm{AI}(t,X)$, the darker the corresponding region.

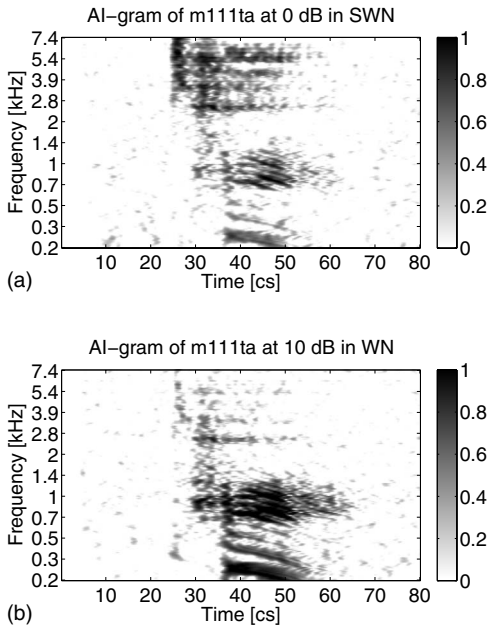


FIG. 2. AI gram of male speaker 111 speaking /tɑ/ in (a) SWN at 0 dB SNR and (b) WN at 10 dB SNR. The audible speech information is dark, the different levels representing the degrees of audibility. Since the two different noises have different spectra, the speech is masked differently. Speech-weighted noise masks low frequencies and high frequencies equally on average. One may clearly see the strong masking due to WN at high frequencies. The AI gram is an important tool used here to explain the differences in CPs observed in many studies to connect the physical and perceptual domains.

Figure 2 provides two AI grams of utterance /tɑ/ in (a) speech-weighted noise (SWN) and (b) white noise (WN). We shall demonstrate that this model of audibility is useful when explaining the decrease of recognition and for identifying the correlated masked events.

III. PILOT EXPERIMENTS

The purpose of this pilot study section is to draw out previously unpublished results from two major studies, called PA05 and PA07 here. PA05 is a modern version of the study of Miller and Nicely (1955). Results are unpublished. It uses 16 consonants and a single vowel with white noise. PA07 is an extension of MN55, with 64 CVs (16 consonants and 4 vowels), using speech-weighted noise (Phatak and Allen, 2007). Both experiments are further analyzed here in terms of confusion patterns (CPs) $P_{h|s}(\mathrm{SNR})$ (Allen, 2005b) and then correlated against AI grams. We have carried out this analysis on the consonant /t/ using an analysis tool denoted the *four-step method*. This novel detailed analysis will provide some useful insights that we believe to be new.

The next section describes the methods and results of these Miller-Nicely-type experiments, PA07 and PA05, run by members of the Human Speech Recognition Group in 2004 (Phatak and Allen, 2007).

A. PA07 and PA05

Experiment PA07 measured normal hearing listeners' responses to 64 CV sounds (16 C × 4 V, spoken by 18 talkers). PA05 included the subset of these CVs containing vowel /ɑ/, to match MN55's CVs.

B. Methods

For PA07, the masking noise was SWN having SNRs of $[Q,12,-2,-10,-16,-20,-22]$ (Q for quiet), and that for PA05 WN was used with SNRs of $[Q,12,6,0,-6,-12,-15,-18,-21]$. All conditions were randomized and presented only once to each of the approximately 20 listeners. The CV speech stimuli for all experiments described in this paper are taken from the Linguistic Data Consortium at the University of Pennsylvania (corpus LDC-2005S22) (Fousek, *et al.* 2004) database composed of a large number of CV, VC, CCV, and VVC utterances, spoken by 20 talkers having different language backgrounds. Talkers' labels start with a talker gender label (f, m), followed by the talker ID (a three-digit number) and the sound label (e.g., m115pa).

The experiments were implemented using MATLAB©. The presentation program was written by student Andrew Lovitt, run on a desktop PC with a Linux kernel 2.4 (Mandrake 9) located outside an acoustic booth (Acoustic Systems model number 27930). Only the keyboard, liquid crystal display monitor, headphones, and mouse were inside the booth. Subjects sitting in the booth are presented with the speech files via a 16 bit PC sound card (Soundblaster Live) and Sennheiser HD280 headphones. Subjects responded as to which CV they heard via a graphical interface.

1. SNR calculations

To set the rms level, the following procedure was used. The rms level for the speech and the noise was set to 1 by computing the rms level for each, and dividing each waveform by that number. Second, the SNR was converted to a decimal value using the formula $g=10^{\text{snr}/20}$, where SNR is the decibel value. Third, the speech and noise were added according to the formula $\text{fix}(S=s+g*n)$ where s,n are the vector speech and noise wave forms. Finally, the absolute peak was found and the vector signal S was converted to an integer wave form, in preparation for outputting to the codec. This transformation is $KS(t)/S_{\max}$ where $K=32\,767=2^{15}-1$ is the maximum positive integer supported by the codec corresponding to the maximum codec voltage.

The rms for the speech was based on either a Volume Unit (VU) calculation (Lobdell and Allen, 2007) or a true rms calculation depending on the data set in question (Phatak and Allen, 2007). The rms of the noise was based on a true rms calculation.

To prevent loud sounds, the maximum allowed rms pressure was limited to 80 dB sound pressure level (SPL) by a hardware attenuator box located between the sound card and the headphones. This limit was based on a 1 kHz long-duration pure tone. The earphone sensitivity calibration (in Pa/V) was based on a 1 kHz tone SPL level on a flat plate coupler using an Etymotic ER7C probe microphone. When frequently asked, the subjects never requested any further level adjustment.

Subjects were volunteers from the University of Illinois student and staff population who had normal hearing (self-reported) and were native English speakers. They were compensated for their participation. Further details on methods may be found in the references.

C. Confusion pattern analysis

CPs [a row of the CM versus SNR, $P_{h|s}(\text{SNR})$] corresponding to a specific CV "spoken" (s) versus "heard" (h) utterance provide the representation of the scores as a function of SNR. CPs may be made for individual utterances or averaged over all talkers/utterances of the same CV. In the following analysis, we shall look at CPs for specific utterances.

Examples of CP plots for an individual /tɑ/ utterance from PA05 and PA07 are shown in Fig. 3, averaging data for 14 listeners for PA07 and 24 for PA05. Many important observations are supported by these charts.

1. Utterance variability

As SNR is reduced (noise increased), the target consonant score starts to measurably decrease at the *saturation threshold*, denoted SNR_s. This *robustness threshold* is defined as the SNR at which the consonant had an error equal to chance performance (6.25%). For example, in Fig. 3, corresponding to utterance f105ta, SNR_s is located at −16 dB SNR for SWN [left panel (a)] and at 0 dB SNR in WN [right panel (b)]. Each utterance presents a different threshold depending on its physical properties. This dependence will be explored in detail in the next section, Sec. III D, and then discussed in Sec. III E.

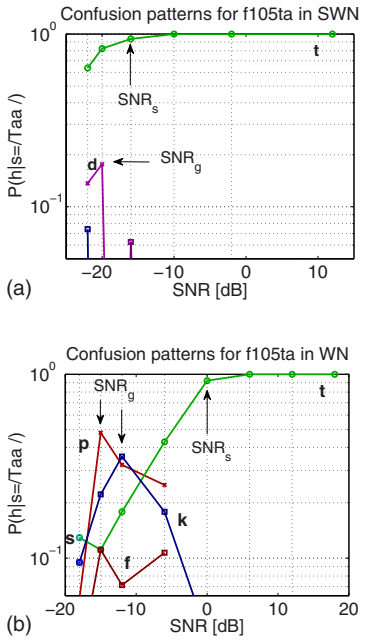


FIG. 3. (Color online) Confusion patterns for /tɑ/ spoken by female talker 105 in (a) SWN and (b) white noise. Note the significant robustness difference depending on the noise spectrum. In SWN, /t/ is correctly identified down to −16 dB SNR, whereas it starts to decrease at 0 dB in WN. SNR_s corresponds to the SNR at which the error starts to increase. The confusions are also more significant in WN, with the scores for /p/ and /k/ overcoming that of /t/ below −6 dB. We call this surprising observation morphing. The maximum confusion score is denoted SNR_g. The reasons for this robustness difference depend on the audibility of the /t/ event, which will be analyzed in the next section.

2. Spectral effects

It is clear from Fig. 3 that the noise spectrum (WN or SWN) strongly influences both SNR_s and the confusions occurring well below the saturation threshold. The *confusion group* of this /tɑ/ utterance in WN [Fig. 3(b)] is [/p/, /t/, /k/]. The SNR corresponding to the maximum in the confusion score is denoted SNR_g, and for this example is located close to (indicated with arrows) −18 dB SNR for /p/ and −15 dB for /k/, with respective scores of 50% and 35%. In SWN (a), /d/ is the only significant competitor (at a 20% level. $\text{SNR}_s=-16$ dB, $\text{SNR}_g=-20$ dB) due to its natural robustness to SWN. Summarizing then, the same utterance presents different robustness and confusion thresholds depending on the masking noise and the consonant spectral support. We shall further explore this in Sec. III D.

3. Morphing

As WN is mixed with utterance f105ta, /t/ *morphs* to /p/ or /k/, meaning that the probability of recognizing /t/ drops while that of /p/ and /k/ increases above that of /t/. At a SNR of −9 dB (WN), the /p/ and /k/ confusions overcome the target /t/ score. As shown in the CP plot of Fig. 3(b), the recognition of /p/ is maximum $[P_{/p/|/t/}(\text{SNR}_g=-16)=50\%]$, that of /k/ peaks at 35% at −12 dB, whereas the score for /t/ is about 10%. This morphing effect, while at first surprising,

is typical in our database for many consonant in white noise but much less common in SWN. The robustness of /t/ to SWN makes morphing rare in PA07 (SWN), as will be exampled later on, due the large difference in SNR spectral balance.

4. Priming

Listening experiments show that when the scores for consonants of a confusion group are similar, listeners can *prime* between these phones. Priming is defined as the ability to mentally select the consonant heard by making a conscious choice between several possibilities having neighboring scores. As a result of priming, given random presentations, a listener must randomly choose one of several priming consonants. The SNR range for which priming takes place is listener dependent; the CPs presented here are averaged across listeners and, therefore, are representative of an average priming range. At a given SNR, each listener has a bias toward one or the other sound, causing score differences. However, most listeners prime between /t/, /p/, and /k/ at around −10 dB SNR, whereas they typically have a bias for /p/ at −16 dB SNR and for /t/ above −5 dB. Based on our studies, we suspect that priming occurs when events, shared by consonants of a confusion group, are at the threshold of audibility, and when the distinguishing feature is at its masked threshold.

In summary, four major observations may be drawn from our analysis of many CPs of CVs similar to those of Fig. 3: (i) *robustness variability across utterances* as measured by SNR_s, (ii) *confusion group variability across noise spectra and utterances*, (iii) *morphing*, and (iv) *priming*. We conclude that each utterance presents different *saturation thresholds*, different *confusion groups, morphs* (or not), and may be subject to *priming* in some SNR range, depending on the masking noise spectrum and the consonant.

Our approach is to take advantage of this natural variability across tokens. As exampled in the above discussion, we will quantitatively relate the confusion patterns and robustness to the audible cues at a given SNR. Finding such relations enables us to identify events, namely, to label the acoustic features that map to "perceptual space."

Using the four-step method, described in the next section, we demonstrate that events are common across utterances of a particular consonant, whereas the *acoustic correlation* of the events, namely, the spectrotemporal and energetic properties, depends on the utterances, the noise spectrum, and the SNR. That is, while the acoustic features are highly variable, events are not. While in this report we only study /t/ and its confusions, we believe that /t/ is representative of other sounds in this regard.

5. Conclusion of confusion pattern analysis

We have used an AI-gram analysis on a large number of responses to many CV sounds in noise and related the scores to the audible speech features, with the end goal of finding events. These events represent the acoustic features that are robust to noise since they survive at very low SNRs (typically much less than 0 dB). Several features of the CPs have been defined, such as morphing, priming, and utterance variability in noise. The identification of a saturation threshold SNR_s (Fig. 3), located at the 93.75% point, is a quantitative measure of utterance robustness, and is a function of the noise spectrum. The natural utterance variability, quantified by this robustness threshold, causes utterances of the same phone category to behave differently with different types of noise.

The existence of morphing demonstrates that noise can mask an essential feature for the recognition of a sound, leading to consistent confusions among our subjects. However, such morphing is not ubiquitous, as it depends on the type and amount of masking noise. Different morphs are observed for different noise spectra. Morphing demonstrates that consonants are not uniquely characterized by independent features, but that they share *common cues* that appear to be weighted differently in perceptual space. This conclusion is supported by CP plots for /k/ and /p/ utterances, showing a well defined [/p/, /t/, /k/] confusion group structure in WN.

From the strong confusions, it seems clear that [/t/, /p/, /k/] share common perceptual features. A similar conclusion can (arguably) be derived from the results observed by Miller and Nicely (1955) (Allen, 2005b). The /t/ event is more easily masked by WN than by SWN, and the usual [/k/, /p/] confusion for /t/ in WN demonstrates that when the /t/ burst is masked, the remaining features are shared by all three voiceless stop consonants. As exampled in the next section, in Fig. 4(a), when the primary /t/ event is masked at high SNRs in SWN, we see strong [/p/, /t/, /k/] confusion groups. Our working hypothesis is that the common features shared by this group are masked by speech-weighted noise due to their localization in frequency, whereas the /t/ burst itself is usually robust in SWN.

We shall further show in Sec. III that this *common feature* hypothesis is also supported by temporal truncation experiments, similar to those of Furui (1986). It is shown that confusions take place when the acoustic features defining the primary /t/ event are inaudible due to noise or truncation, and that the remaining cues are part of what perceptually characterizes /t/'s competitors (/p/, /k/).

D. Four-step method to identify events

Our four-step method (steps 1–4) is an analysis that uses the perceptual models and correlates them with the CPs. This leads to the development of the *event gram*, derived from the AI gram, and uses human confusion responses to identify the relevant acoustic features. Here, we used the four-step method to draw conclusions about the /t/ event. There is some evidence that we may be able to explain other stop consonants using the four-step method. This will be studied in the near future. In Fig. 4(a), we identify and analyze the spectral support of the primary /t/ perceptual feature for two /tɛ/ utterances in SWN spoken by different talkers.

1. Step 1: CPs and robustness

Step 1 of our four-step analysis consists of the collection of confusion patterns described in the previous section, as in the bottom right panels of Figs. 4(a) and 4(b).

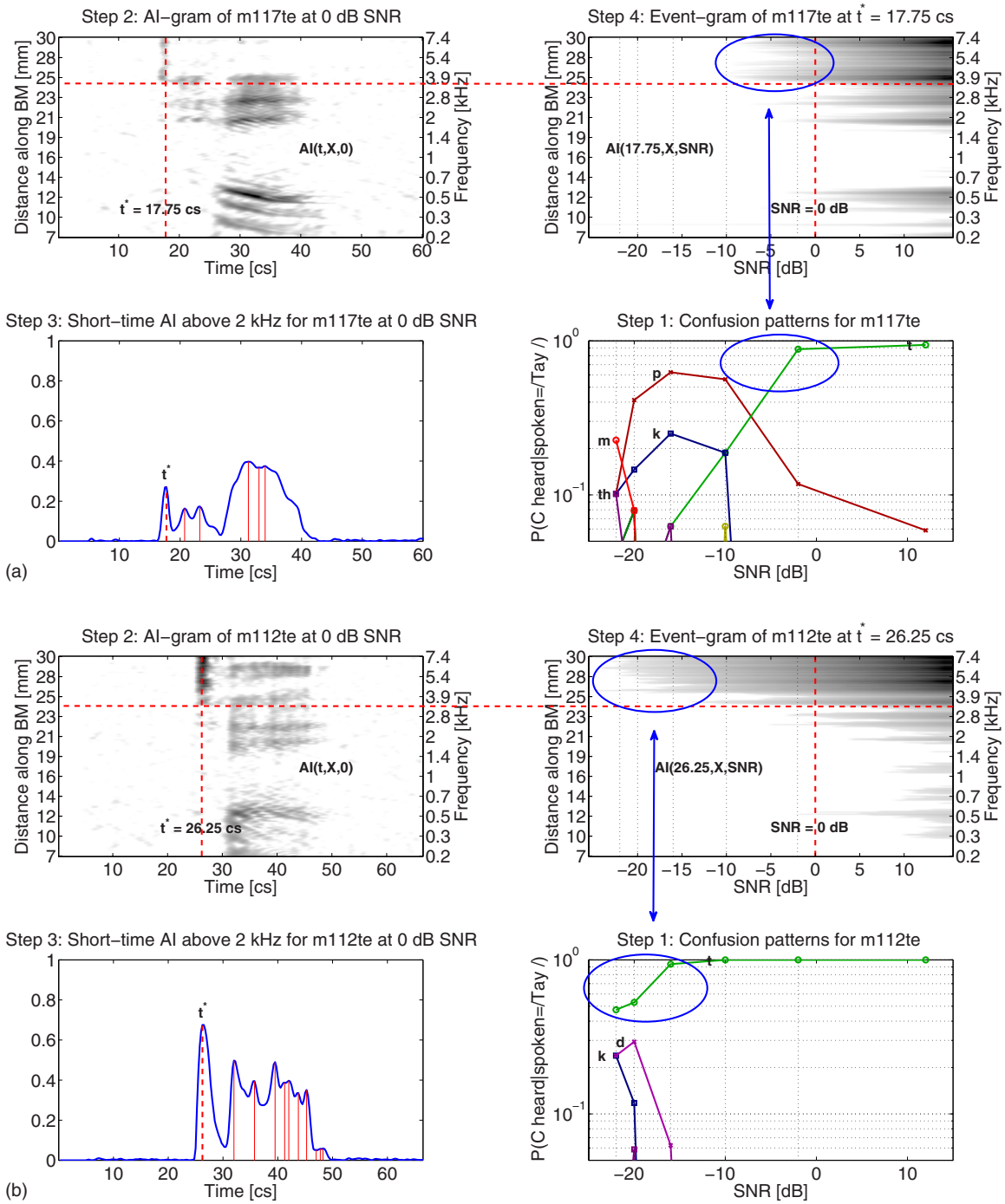


FIG. 4. (Color online) Comparison between a "weak" (top, m117te) and a "strong" (robust) (bottom, m112te) /tɛ/. The arrangement of the four panes is optimized for inner subfigure comparisons. Step 1 provides to the CPs (bottom right), step 2 to the AI gram at 0 dB SNR in SWN, step 3 to the mean AI above 2 kHz where the local maximum t^* in the burst is identified, leading to step 4, the event gram (vertical slice through AI grams at t^*). Note that for the same SWN masking noise, these utterances behave differently and present different competitors. Utterance m117te strongly morphs to /pɛ/. Many of these differences can be explained by the AI gram and more specifically by the event gram which quantifies the /t/-burst threshold, and therefore its robustness to noise. This threshold is precisely correlated with the human responses (encircled). This leads to the conclusion that this 2–8 kHz across-frequency onset transient is the primary /t/ event. (a) Analysis of sound /tɛ/ spoken by male talker 117 in SWN. This utterance is not robust to noise since the /t/ recognition starts to decrease at −2 dB SNR. Identifying t^*, time of the burst maximum at 0 dB SNR in the AI gram (top left), and its mean in the 2–8 kHz range (bottom left), leads to the event gram (top right). The vertical dashed line on the AI gram shows t^*. On the event gram, the dashed line shows the SNR at which the AI gram was displaced (similar to a vertical slice). In both cases, the horizontal dashed line marks the lower frequency limit of the burst (here 3.7 kHz) This representation of the audible phone /t/ burst information at time t^* is highly correlated with SNR_s and the CPs: when the burst information becomes inaudible (white on the AI gram), /t/ score decreases, as indicated by the ellipses. (b) Analysis of sound /tɛ/ spoken by male talker 112 in SWN. Unlike the case of m117te, this utterance is robust to SWN and identified down to −16 dB SNR. Again, the burst threshold defined by the event gram (top right) is related to SNR_s defined by the CP, accounting for the robustness of consonant /t/.

For male talker 117 speaking /tɛ/ [Fig. 4(a), bottom right panel], the saturation threshold is ≈−6 dB SNR (ellipsed), forming the /p/, /t/, /k/ confusion group. This weak /t/ morphs to /p/ [Fig. 4(a)]: the recognition of /p/ is maximum $[P_{/p/|/t/}(\mathrm{SNR}_g)=60\%]$ at a $\mathrm{SNR}_g=-16$ dB, where the score for /t/ is 6%. Morphing not only occurs in WN (Fig. 3

f105ta) but also in SWN for this weaker /tɛ/ sound (m117te). Confusion patterns and robustness vary dramatically across utterances of a given CV masked by the same noise: unlike for talker m117, /te/ spoken by talker m112 does not morph to /p/ or /k/, and its score is higher [Fig. 4(b), bottom right panel]. For this more robust utterance, /t/ was accurately identified down to $SNR_s = -16$ dB SNR (ellipsed) and was still well above chance performance (1/16) at −22 dB. Its main competitors /d/ and /k/ have 25%–30% scores and which only appear well below SNR_s.

It is clear that these two /tɛ/ sounds are dramatically different. Note that utterance differences are only seen with the addition of a masking noise. There is confusion pattern variability not only across noise spectra but also within a masking noise category (e.g., WN versus SWN). These two /tɛ/'s are an example of *utterance variability*, as shown by the analysis of step 1: two sounds are heard the same when it is quiet, but they are heard quite differently as the SNR is varied. The next section will detail the physical properties of consonant /t/ in order to relate spectrotemporal features to the score using our audibility model.

2. Steps 2 and 3: Utilization of a perceptual model

For talker 117, Fig. 4(a) (top left panel) shows the AI gram at 0 dB SNR. We observe that the high-frequency burst having a sharp energy onset, stretches from 2.8 to 7.4 kHz and runs in time from 16 to 18 cs (a duration of 20 ms). According to the CPs previously discussed [Fig. 4(a), bottom right panel], at 0 dB SNR consonant, /t/ is recognized 88% of the time. The burst for talker 112 has higher intensity and spreads from 3 kHz up, as shown by the AI gram for this utterance [Fig. 4(b), top left panel], which results in a 100% recognition at and above −10 dB SNR.

These observations lead us to step 3, the integration of the AI gram over frequency [bottom right panels of Figs. 4(a) and 4(b)]. One obtains a representation of the average audible speech information over a particular frequency range Δf as a function of time, denoted the short-time AI, AI(t) (Rhebergen *et al.*, 2006). Here, AI(t) is computed in the 2–8 kHz bands, corresponding to the limits of this high-frequency /t/ burst. In contrast, the traditional AI is the area under the entire frequency range. (In this case, if we integrated over all frequencies, there would be only a very small difference.) The first maximum, AI(t^*) [vertical dashed line on the top and bottom left panels of Figs. 4(a) and 4(b)] is an indicator of the audibility of the consonant /t/ burst. Since the frequency content is collapsed, t^* indicates the time of the relevant perceptual information for /t/.

3. Step 4: The event gram

The identification of t^* allows step 4 of our correlation analysis. The top right panels of Figs. 4(a) and 4(b) represent the event grams for the two utterances. The event gram, AI(t^*, X, SNR), is defined as a cochlear place (or frequency, via Greenwood's cochlear map) versus SNR slice at one instant of time. The event gram is the link between the CPs and the AI gram. The event gram represents the AI density as a function of SNR at a given time t^* (determined in step 3). If several AI grams computed at different SNRs were stacked, the event gram would be a vertical slice through this stack. In summary, the event grams displayed in the top right panels of Figs. 4(a) and 4(b), plotted at t^*, characterize the /t/ burst's threshold. A horizontal dashed line, from the bottom of the burst on the AI gram to the bottom of the burst on the event gram at SNR=0 dB, provides the visual link between the two plots.

The significant result visible on the event gram is that for these two utterances, the event gram is correlated with the average normal listener score, as seen in the ellipses linked by a double arrow. Indeed, for utterance 117te, the recognition of consonant /t/ starts to drop at −2 dB SNR, when the burst above 3 kHz is completely masked by the noise [top right panel of Fig. 4(a)]. On the event gram, below −2 dB SNR (circle), one can note that the energy of the burst at t^* decreases, and the burst becomes inaudible (white). A similar relation is seen for utterance 112, but since the energy of the burst is much higher, the /t/ recognition starts to fall at −15 dB SNR, at which point the energy above 3 kHz becomes sparse and decreases, as seen in the top right panel of Fig. 4(b) and highlighted by the circles.

There is an obvious correlation in this example between the variable /t/ confusions and the score for /t/ [step 1, bottom right panel of Figs. 4(a) and 4(b)], the strength of the /t/ burst in the AI gram (step 2, top left panels), and the short-time AI value (step 3, bottom left panels), all quantifying the event gram (step 4, top right panels). Because these panels are correlated with the human score, the burst constitutes our model of the perceptual cue (the event), upon which listeners rely to identify consonant /t/ in noise.

A systematic quantification of this correlation for a large number of consonants will be described in the next section, where we analyze the effect of the noise spectrum on the perceptual relevance of the /t/ burst in noise to account for the differences previously observed across noise spectra.

4. Effect of the noise samples

A classical question is the difference between internal and external noises in masking (Allen and Neely, 1997). Internal noise is due to the internal representation of the signal in a critical band while external noise is due to the uncertainty from the external noise added to the signal. Given this classical classification scheme, it was natural to wonder about the significance of the different ensemble noise samples on the variability of the event gram. Our experiment procedure was designed so that a new noise sample was used for each token presentation, so listeners never hear a signal (speech sound) mixed with the same masker (noise) even when presented at the same SNR.

To study this effect, we analyzed the variance using different noise samples having the same spectrum (the phase of the noise varied from trial to trial) and computed event grams for ten different noise samples. The resulting variance is shown in Fig. 5 for utterance f103ta in SWN. The result is that both regions of high and low SNRs show a small variance. Only where the SNR is near zero do the speech and noise interact, giving a finite variance. It makes sense that the only noticeable variance is seen near threshold. The

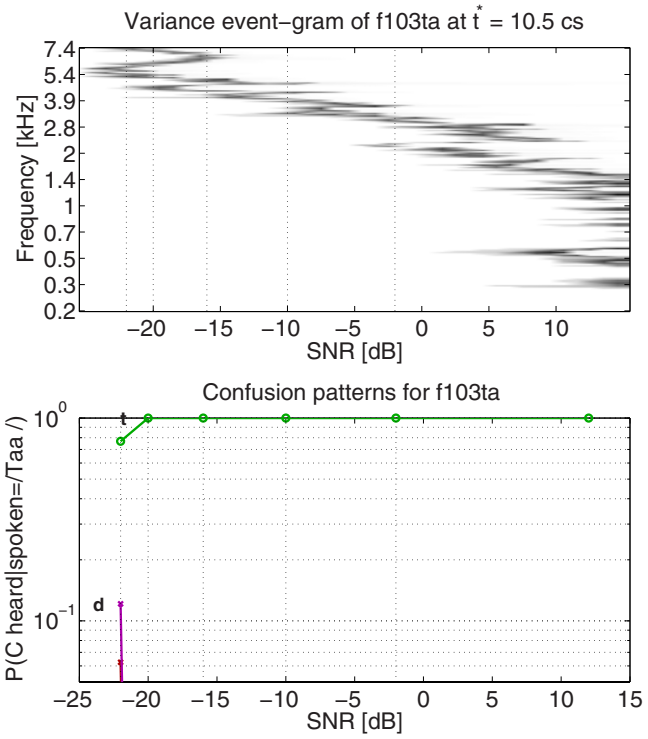


FIG. 5. (Color online) This variance event gram was computed by taking event grams of a /tɑ/ utterance for ten different noise samples in SWN (PA07). We can see that all the variance is located on the edges of the audible speech energy, where the noise and speech have similar level, located between regions of high audibility and regions of noise. However, the spread is thin, showing that the use of different noise samples will not significantly impact the perceptual scores.

thickness of the line is a measure of the trial variance. The small spread of the line indicates that using a new noise on every trial has little impact on the scores of our psychophysical experiment, and the correlation between noise and speech is unlikely to impact the features significantly, and to the extent it does, only over a small SNR range.

E. Discussion: Relating CPs and audibility for /t/

Using a four-step method analysis, we found that the discrimination of /t/ is due to its robustness, defined by a sharp onset burst from 2 to 8 kHz. Robustness, measured by SNR_s and CPs (confusion groups), are highly dependent on the specific utterance due to variations in this burst. Each instance of the /t/ burst typically presents different characteristics. As shown in Fig. 3, SNR_s changes with the noise type for a given sound. This correlation demonstrates that a consonant presents different perceptual thresholds. Additionally, in Fig. 4, we found that the /t/ event is invariant for two utterances and is masked at different SNRs and correlated with SNR_s.

As compared to SWN, WN provides more masking at high frequencies, accounting for the decrease of the /t/ at high SNR recognition. Once the burst starts being masked, at SNR_s, the /t/ score quickly drops below 100%. The acoustic representations in the physical domain of the perceptual features is highly variable (e.g., 16 dB in our example), while the perceptual features themselves (events) remain invariant.

We wish to more precisely quantify the /t/ event in the physical domain; however, improved characterization of the spectrotemporal location of the burst is needed to fully quantify its impact on robustness across utterances.

To further quantify the correlation between the audible speech information from the event gram and the perceptual information given by our listeners, we have correlated *event-gram thresholds*, denoted SNR_e, with the 90% score SNR, denoted SNR_{90}. Based on our regressions between SNR_e and the score, the 90% score point represents the /t/ feature with a smaller residual error over the wide range of conditions we studied. Thus, the onset drop in score appears to be more highly correlated with SNR_e than SNR_s. Here, we wish to identify the optimal set of parameters that will maximize the correlation between SNR_e and SNR_{90}). Our previous results, based on the four-step method, enable us to limit the search above 2 kHz, a frequency ranged *assumed* to be most relevant to /t/ recognition.

The parameters used here are an AI density threshold T and an adaptive bandwidth B. For given values of T,B, we determined the SNR range where there is continuous speech information in frequency above AI threshold T. To start the search for the optimum values of T and B, a set of values of SNR_e is determined for different pairs of parameters, within 5 Hz steps for the bandwidth and steps of 0.005 for the threshold. The value corresponding to the lowest mean square error for the correlation with SNR_{90} gives SNR_e. The procedure was followed independently for PA05 and PA07 and gave two slightly different optimized parameters, namely, $B=570$ Hz in SWN for $T=0.335$, and $B=450$ Hz for $T=0.125$ in WN.

Fourteen of the /ɑ/ utterances tested in PA07 were also in PA05; therefore, sound common to both experiments appears twice on the scatter plot. Scatter plots for PA05 (in WN) are at higher SNRs than those for PA07 (in SWN) due to the stronger masking of the /t/ burst in WN, leading to higher SNR_e and SNR_{90}.

The high correlation between SNR_{90} and the event-gram thresholds for the parameters used, represented by their proximity to the 45° line, proves that our AI-gram audibility model and the event gram are good predictors of the average normal listener score. The 120 Hz difference between optimal bandwidths for WN and SWN seems insignificant. The identification of an intermediate value for both noise spectra would be the basis of additional work. The difference in optimal AI thresholds T is likely due to the spectral emphasis of each noise (low frequencies in SWN and high frequencies in WN). The lower value obtained in WN could also be the result of other cues at lower frequencies, contributing to the score, when the burst is weak. More research will be needed to identify the optimal parameters and to precisely characterize the correlation between the scores and the event-gram model.

Figure 6(b) shows an event gram in SWN, for utterance f106ta, with the optimal bandwidth between the two horizontal dashed lines, leading to the identification of SNR_e. Below

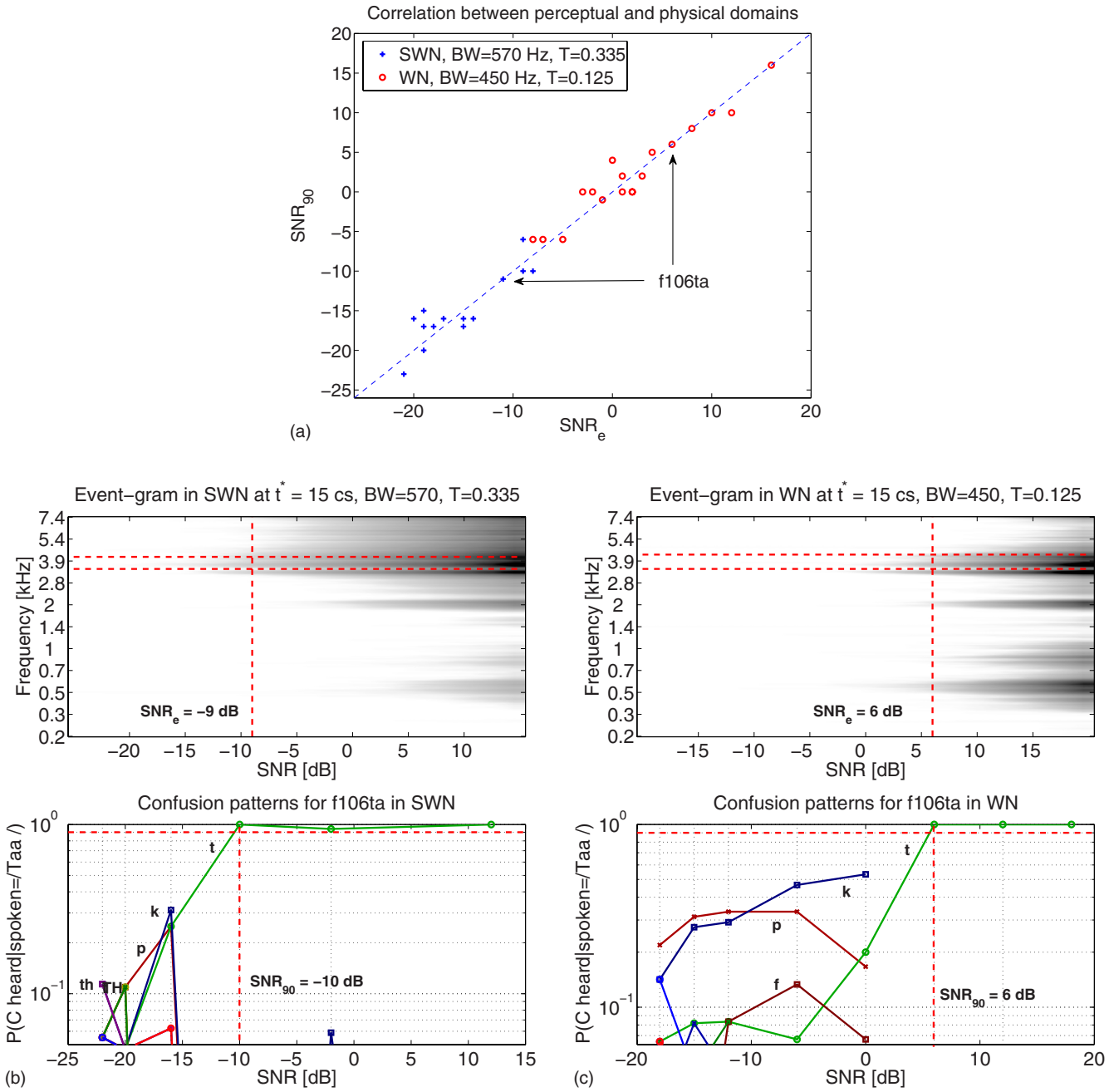


FIG. 6. (Color online) (a) Scatter plot of the event-gram thresholds SNR_e above 2 kHz, computed for the optimal burst bandwidth B having an AI density greater than the optimal threshold T compared to the SNR of 90% score. Utterances in SWN (+) are more robust than those in WN (○), accounting for the large spread in SNR. We can see that most utterances are close to the 45° line, showing the high correlation between the AI-gram audibility model (middle pane) and the event gram (right pane). The detection of the event-gram threshold SNR_e is shown on the event gram in SWN [top pane of (b)] and WN [top pane of (c)], between the two horizontal lines, for f106ta, and placed above their corresponding CPs. SNR_e is located at the lowest SNR where there is continuous energy above 2 kHz and spread in frequency with a width of B above AI threshold T. We can notice the effect of the noise spectrum on the event gram, accounting for the difference in robustness between WN and SWN.

are the CPs where $SNR_{90}=-10$ dB is shown by a vertical dashed line (thresholds are chosen in 1 dB steps, and the closest SNR integer value above 90% is chosen for SNR_{90}). Panel (c) shows the event gram and CPs for the same utterance in WN. The points corresponding to utterance f106ta are denoted by arrows.

Regardless of the noise type, we can see on the event grams the relation between the audibility of the 2–8 kHz range at t^* (in dark) and the correct recognition of /t/ even though the thresholds are much lower in SWN than in WN. More specifically, the strong masking of WN at high frequencies accounts for the early loss of the /t/ audibility as compared to SWN.

We conclude that the burst, as a high-frequency coinciding onset, is the main event accounting for the robustness of consonant /t/ independent of the noise spectrum. It presents different physical properties depending on the masker spectrum, but its audibility is strongly related to human responses in both cases. The event is therefore based on the audibility of the /t/ burst, not on any superthreshold property.

To further amplify the conclusions of the four-step method, we decided to run a psychophysical experiment where the /t/ burst would be truncated and study the resulting responses under lower noise conditions. We hypothesize that since the /t/ burst is the most robust-to-noise event, it is the strongest feature cuing the /t/ percept even at higher SNRs. A truncation experiment would therefore remove this crucial /t/ information.

IV. EXPERIMENT 2: TIME TRUNCATION

We next strengthen our conclusions drawn from Fig. 4 based on a confusion pattern and the event-gram analysis. Inspired by the work of Furui (1986), we truncated CV sounds in 5 ms steps and studied the resulting morphs. Our goal is to answer a fundamental research question raised by the four-step analysis of /t/: can the truncation of /t/ cause a morph to /p/, implying that the /t/ event is prefixed to consonant /p/, thereby showing that they share common features? Such a conclusion would be consistent with our observation that many /t/'s strongly morph to /p/ when the energy at high frequencies around t^* is masked by the noise.

A. Methods

Two SNR conditions, 0 and 12 dB SNRs, were used with SWN. The noise spectrum was identical to that used in PA07 (Phatak and Allen, 2007). In preliminary pilot studies, we identified the most common responses, and 22 were chosen that seem to accommodate our subjects. The final response task was then a forced choice among the 22 possible consonant CV responses or vowel only. A "vowel only" button was provided for those cases where no consonant could be identified. When queried, our subjects never expressed a need to add more response choices. Ten subjects participated in the final experiment.

1. Stimuli

The six tested CVs were /tɑ/, /pɑ/, /sɑ/, /zɑ/, /ʃɑ/, and /ʒɑ/ spoken by ten different talkers, for a total of 60 utterances. The times of the onset of each consonant and vowel were hand labeled. Onset truncations were generated automatically from these timing markers every 5 ms, including a "no truncation" condition and a "total" truncation condition, where only the vowel was played. One-half second of noise was prefixed to the CVs. The truncation was created by ramping the clean speech with half of a 10 ms Hamming window (5 ms ramp). The noise was added following the ramping. We only report the /t/ results here.

B. Results

The main conclusion of the /tɑ/ truncation experiment is the strong morph obtained for *all* of our stimuli when less than 30 ms of the /t/ burst are removed relative to the hand-labeled onset of the consonant. When presented with our truncated /tɑ/ sounds, listeners most commonly reported hearing /p/. Occasionally, /k/ or /h/ is reported, but when so, they have much lower average scores than /p/. In all cases, transitions took place within a 5–10 ms time frame. Specifically, the /t/ recognition abruptly dropped from above 90% at the onset of morphing to less than 10% within 5–10 ms.

Two main trends can be observed. Four out of ten utterances followed a hierarchical $/t/ \rightarrow /p/ \rightarrow /b/$ morphing pattern (group 1). In these cases, the consonant was first identified as /t/ for truncation times less than 30 ms; then /p/ is reported over a period spreading from 30 to 110 ms (one extreme case) and to finally reported as /b/.

The results (all four utterances) of group 1 are shown in Fig. 7. Note the significant variability in the crossover truncation times (the duration that the target and the morph scores overlap). This is due to both the natural variability in the /t/ burst duration and variation in the subject's responses. We have not analyzed the relative magnitudes of these two sources of variation. As a rule, the change in SNR from 12 to 0 dB had only a negligible impact on the scores (see Fig. 7).

The second trend (group 2) consisted of utterances that morph from $/t/ \rightarrow /p/$ but are also confused with /h/ and /k/. Five out of ten utterances (shown in Figs. 8 and 9) are in this group. The /h/ confusion is represented by the black dashed line and is stronger for the two top utterances, m102ta and m104ta [Figs. 8(a) and 8(b)]. A decrease in SNR from 12 to 0 dB caused a small increase in the /h/ score, almost bringing scores to chance performance (e.g., 50%) between those two consonants for the top two panels. This suggests a priming situation between these two sounds. The four lower panels show results for talkers m107 and m117, where a decrease in SNR causes a /k/ confusion which is as strong as the /h/ confusion but which differs from the 12 dB case, where competitor /k/ was not reported. The final example for the truncation of utterance f113ta (Fig. 9) shows a weak /h/ confusion to the /p/ morph, not significantly affected by a SNR change.

A noticeable difference of group 2 from group 1 is the absence of /b/ as a significant competitor. This discrepancy could simply be due to the limit of the truncation times. Utterances m104ta and m117ta [Figs. 8(b) and 8(d)] show weak /b/ confusions at the last truncation time tested. More test conditions would be needed to confirm this. Alternatively, since /p/ is a midstate between /t/ and /b/, we might simply study /pɑ/ truncations. In our /pɑ/ truncation data (not shown), not all /pɑ/s morph to /bɑ/; in most cases, no consonant is heard for the maximum truncation condition (i.e., only the vowel is reported). Therefore, if our $/t/ \rightarrow /p/$ results suggest that /p/ could be a precursor for /t/, we have not yet drawn this conclusion for $/p/ \rightarrow /b/$. More experiments will be required to resolve this apparent discrepancy. Of course, it is possible that the confusions with /h/ play a role in the loss of /b/ confusions.

In the figures, notice that for both groups 1 and 2, the onset time of the /t/ confusion depends on SNR. In most of the 0 dB case, the score for /t/ drops 5 ms earlier than for the 12 dB cases. This is likely due to masking of both sides of the burst energy, making them less audible and more difficult to be heard as an onset cue. When we study the AI grams for these cases, we see that the /t/-burst energy is weaker at t^*

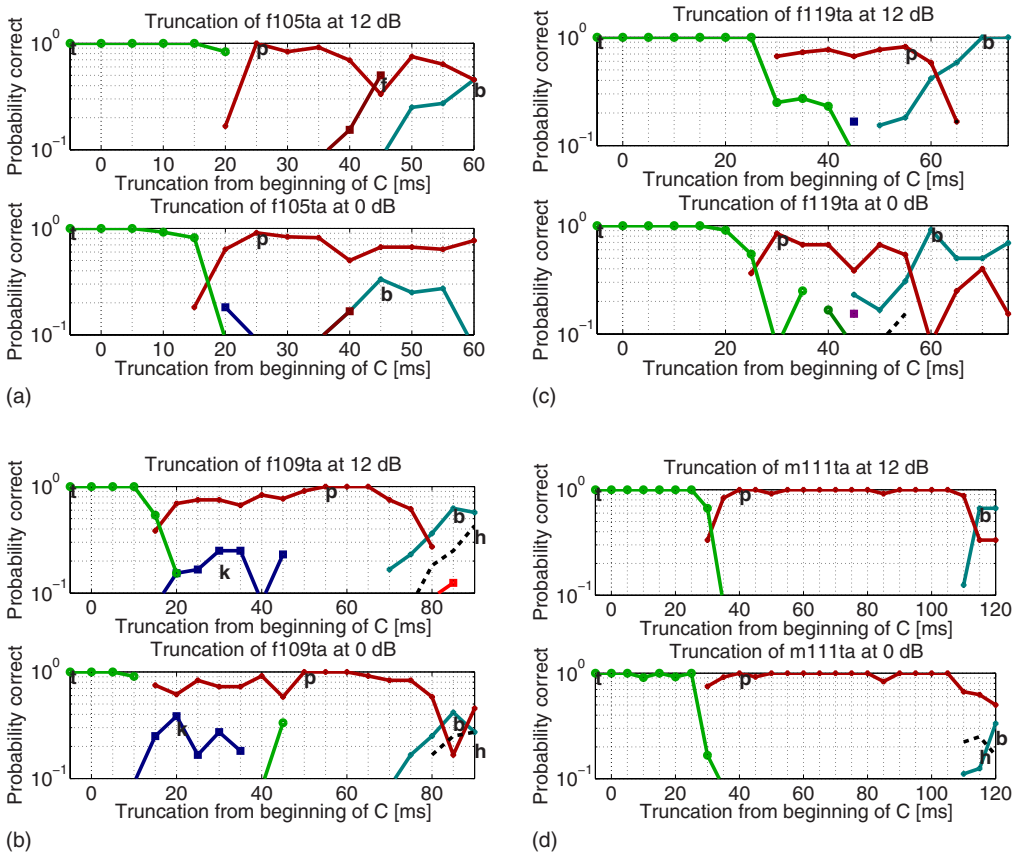


FIG. 7. (Color online) Group 1 utterances are defined as those which morph as /t/ → /p/ → /b/. For each panel, the top plot represents responses at 12 dB SNR and the lower those at 0 dB SNR. There is no significant SNR effect for these sounds. (a) Truncation of f105ta at 12 (top) and 0 dB SNRs (bottom). (b) Truncation of f109ta at 12 (top) and 0 dB SNRs (bottom). (c) Truncation of f119ta at 12 (top) and 0 dB SNRs (bottom). (d) Truncation of m111ta at 12 (top) and 0 dB SNRs (bottom).

(where the /t/ burst energy has its maximum). The best example of this somewhat subtle SNR effect is shown in Fig. 7(d).

As shown in Fig. 10, the pattern for the truncation of utterance m120ta was totally different from the other nine utterances included in the experiment. First, the score for /t/ did not decrease significantly after 30 ms of truncation. Second, /k/ confusions were present at 12 but not at 0 dB SNR, causing the /p/ score to reach 100% only at 0 dB. Third, the effect of SNR was pronounced. Figure 10 shows AI grams of this /tɑ/ at 12 (a) and 0 (b) dB SNRs. We can see that the burst is very strong for about 35 ms for both SNRs, which accounts for the high /t/ recognition in this range. For truncation times greater than 35 ms, /t/ is still identified with an average probability of 30%. This effect appears to be due to the level of high-frequency energy following the onset. As a result of the truncation, a coinciding onset of energy in the /t/-burst event frequency range is created, the duration of which is close to the natural /t/ burst.

For the 12 dB SNR case and for truncation times greater than 4 cs, this artificial /t/ burst appears to be weaker than the original strong onset burst. This explains the lower /t/ score compared to that in the untruncated version.

An unanticipated score inversion appears at 55 ms for the 0 dB SNR case. This /t/ peak is also weakly visible at 12 dB (left). We hypothesize that midfrequency energy, most likely around 0.7 kHz, is cuing /p/ at 12 dB but being masked at 0 dB SNR, enabling the /t/ recognition to rise. For the first 30 ms of truncation, this behavior is similar to that of the other utterances. The pattern observed for later truncation times is a demonstration of utterance variability, and can thus be explained without violating the /t/ burst event hypothesis. As shown by the truncation plots, when the /t/ burst is gone, beyond 80 ms, the /t/ score finally drops.

We conclude from the CV-truncation data that the *consonant duration* is an important timing cue used by listeners to distinguish /t/ from /p/. This duration depends on the natural duration of the /t/ burst. When only 5–10 ms more are truncated, the scores can drop dramatically. This demonstrates the high temporal sensitivity of the /t/ burst. As discussed earlier, we found in additional results (not shown) on truncated /pɑ/ that utterances are frequently confused with /bɑ/. This is consistent with the idea of a hierarchy of speech sounds, clearly present in our group 1 /tɑ/ examples. At the core of this hierarchy is /p/. By prefixing a short-duration burst, this can become /tɑ/ or /kɑ/. We have limited preliminary data that show that this works for several other vowels as well.

In summary, using our truncation procedure, we have independently verified that the high-frequency burst accounts for the noise-robust event corresponding to the discrimination between /t/ and /p/ even in moderate noisy conditions. Thus, we confirm that our approach of adding noise to iden-

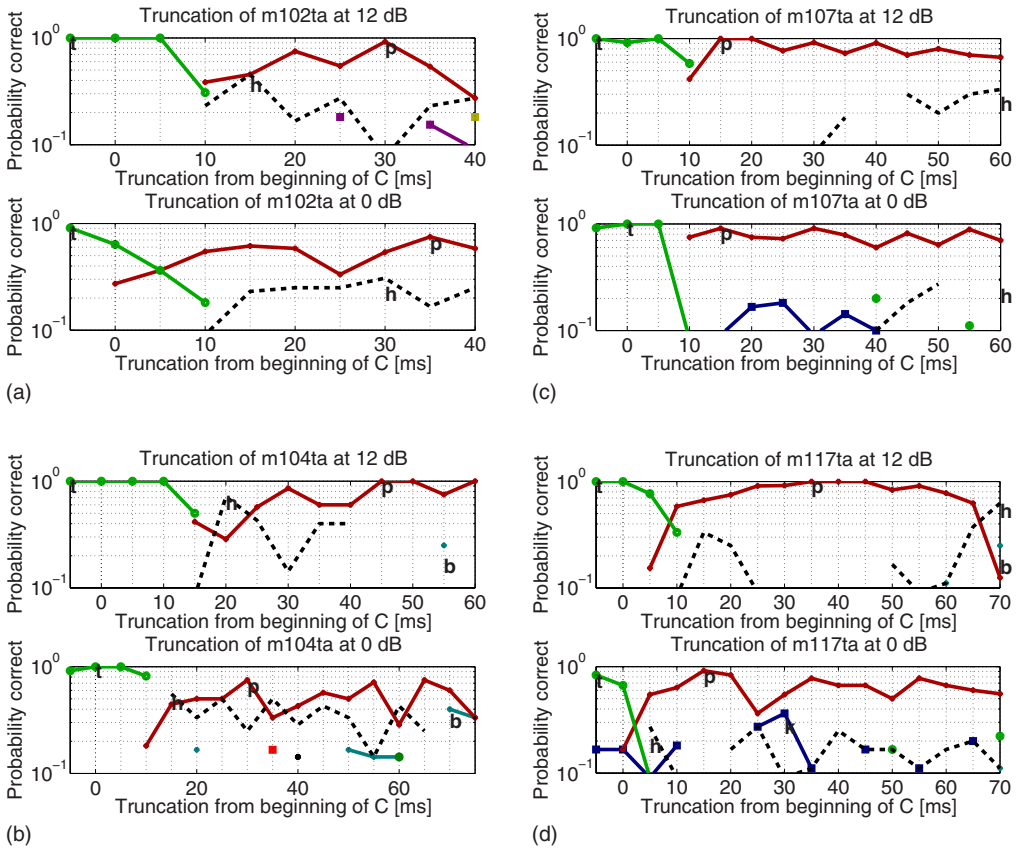


FIG. 8. (Color online) Utterances of group 2: Consonant /h/ strongly competes with /p/ (top), along with /k/ (bottom). For the top right and left panels: increasing the noise to 0 dB SNR causes an increase in the /h/ confusion in the /p/ morph range. For the two bottom utterances, decreasing the SNR causes a /k/ confusion that was nonexistent at 12 dB, equating the scores for competitors /k/ and /h/. (a) Truncation of m102ta at 12 (top) and 0 dB SNRs (bottom). (b) Truncation of m104ta at 12 (top) and 0 dB SNRs (bottom). (c) Truncation of m107ta at 12 (top) and 0 dB SNRs (bottom). (d) Truncation of m117ta at 12 (top) and 0 dB SNRs (bottom).

tify the most robust, and therefore crucial perceptual information, enables us to identify the primary feature responsible for the correct recognition of /t/.

C. Discussion

The results of our truncation experiment demonstrate that the /t/ recognition is masked after 30 ms for nine out of ten of our stimuli. This is in locked agreement with our analysis of the AI gram and event gram emphasized by our four-step analysis. We proved, therefore, that the leading edge of the /t/ burst from 2 to 8 kHz is used by our listeners to identify /t/ at all SNRs. We conclude that this burst is an across-frequency coincidence over a specific frequency range, and it plays the key role in the robust recognition of /t/.

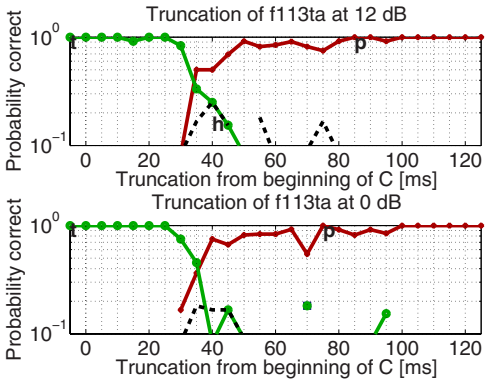


FIG. 9. (Color online) Truncation of f113ta at 12 (top) and 0 dB SNRs (bottom): Consonant /t/ morphs to /p/, which is slightly confused with /h/. There is no significant SNR effect.

Moreover, the /p/ morph that consistently occurs when the /t/ burst is truncated shows that consonants are not perceptual independent; thus, they share common cues. This hypothesis leads to the possible existence of "root" consonants. We presently view /p/ as a voiceless stop consonant root containing raw but crucial spectrotemporal information to which primary robust-to-noise cues can be added to form the various consonant of /p/'s confusion group. We have only demonstrated this here for the case of /t/. When CVs are mixed with masking noise morphing and priming are important empirical observations that are correlated with this conclusion.

Future work would need to verify that the /t/ recognition significantly drops when 30 ms of *only* the above 2 kHz burst region is removed. Such an experiment would further prove that it is an exclusively high-frequency /t/-burst event, making it not just sufficient but a necessary condition.

Dynamically modifying such timing events using signal processing techniques could lead to a new family of hearing

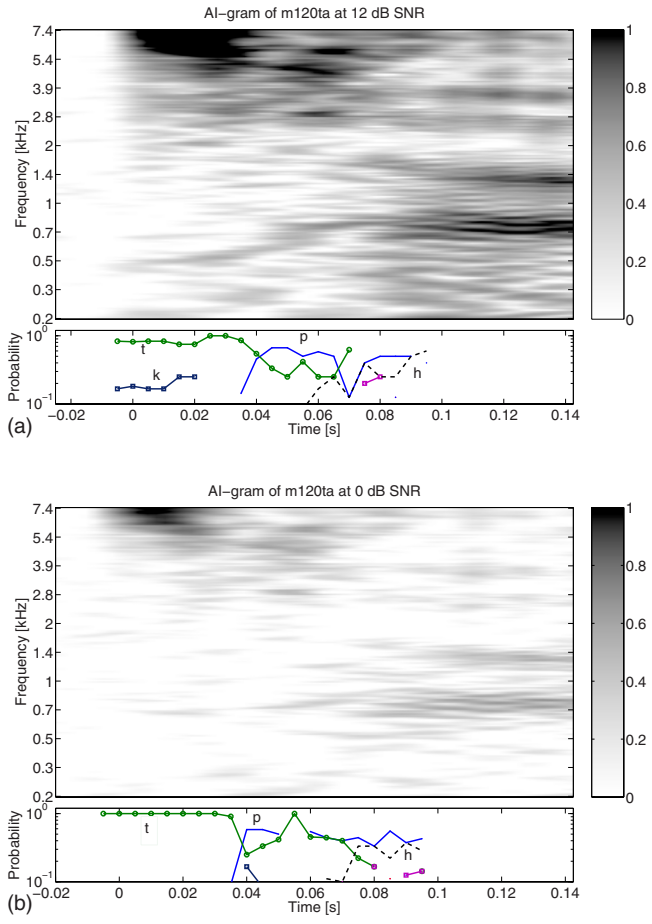


FIG. 10. (Color online) (a) 12 dB SNR zoomed AI gram. (b) 0 dB SNR zoomed AI gram. AI grams of m120ta, zoomed to a duration of 160 ms, in the consonant and transition regions at (a) 12 dB SNR and (b) 0 dB SNR. Below each AI gram are plotted the listener responses as a function of the truncation time, time synchronized. Uniquely for this utterance, the /t/ identification is still high after 30 ms of truncation, presumably because of the long-duration residual high-frequency (i.e., 2–8 kHz) energy. The target probability even overcomes the score for /p/ at 0 dB SNR at a truncation time of 55 ms, most likely because of a strong relative /p/ event present at 12 dB but weaker at 0 dB.

aids (Braida *et al.*, 1979), cochlear implants (Rabinowitz *et al.*, 1992; Shannon *et al.*, 1995), and robust automatic speech recognition (Hermansky, 1998).

Making automatic speech recognizers robust to noise, based on knowledge of human speech recognition, would be a tremendous breakthrough in an area where significant improvement is sorely needed (Lippmann, 1997; Dusan and Rabiner, 2005).

V. CONCLUSION

Our overall approach aims at directly relating our model of *speech audibility* in noise, the AI gram, a generalization of the AI, to the *confusion pattern discrimination measure* for consonant /t/. The AI gram represents an "input" measure, while the CPs are the "output" measure of the auditory speech processing system. Our approach is novel and represents a significant contribution toward solving the speech robustness problem as it has successfully led to the identification of the /t/ event as a synchronous 2–8 kHz temporal burst. This event is common across CVs identified with /t/ even if its physical properties widely vary across utterances. The strength of this acoustic feature leads to different degrees of robustness to noise. We have harnessed its natural variability to allow us to establish a correlation between the acoustic features and the scores. The correlation we observed between event-gram thresholds and 90% CP scores [Fig. 6(a)] confirms our hypothesis. This nearly perfect correlation between the /t/ burst strength and /t/ masked threshold scores has been demonstrated in a systematic manner across a large number of utterances.

Our results are consistent with the idea that the auditory brain is listening for onset transients. There is a small but significant literature on the importance of onset transients in both cortical research (Heil, 1997; Oertel, 2005; Heil, 2003; Shamma, 2003) and in the music perception research where timing onsets are known to carry important information about instrument identity.

Our onset-timing interpretation of speech cues resulted in a second experiment where we truncated the sounds from the onset and to the concept of a hierarchy of consonants forming the confusion group. It confirms our hypothesis that consonants forming a confusion group share common events. Finally, we have clearly shown that the /t/ burst is the primary feature for the identification of /t/ even in small amounts of noise. Primary events, along with a shared base of perceptual features, are used to discriminate consonants and characterize the consonant's degree of robustness to masking noise.

We have concluded that the event is therefore based on the audibility of the /t/ burst, not on any superthreshold property.

We believe that a hearing aid, tuned to such onset transients, could extract these cues and amplify them on a listener basis, resulting in significant improvement of speech identification in noisy environments for hearing impaired (HI) listeners.

ACKNOWLEDGMENTS

The authors wish to acknowledge the support of the Human Speech Recognition Group for the valuable comments and data collection. The authors would like to thank Etymotic Research and Starkey Laboratories for the financial support used to pay the subjects in the many experiments. Financial support was mostly provided by the ECE Department, UIUC. This work constitutes a portion of the first author's MS thesis.

Allen, J. B. (**1994**). "How do humans process and recognize speech?," IEEE Trans. Speech Audio Process. **2**, 567–577.
Allen, J. B. (**1996**). "Harvey Fletcher's role in the creation of communication acoustics," J. Acoust. Soc. Am. **99**, 1825–1839.
Allen, J. B. (**2005a**). *Articulation and Intelligibility* (Morgan and Claypool, LaPorte, CO).
Allen, J. B. (**2005b**). "Consonant recognition and the articulation index," J. Acoust. Soc. Am. **117**, 2212–2223.
Allen, J. B., and Neely, S. T. (**1997**). "Modeling the relation between the intensity JND and loudness for pure tones and wide-band noise," J. Acoust. Soc. Am. **102**, 3628–3646.
Blumstein, S. E., and Stevens, K. N. (**1979**). "Acoustic invariance in speech production: Evidence from measurements of the spectral characteristics of

stop consonants," J. Acoust. Soc. Am. **66**, 1001–1017.
Braida, L. D., Durlach, N. I., Lippmann, R. P., Hicks, B. L., Rabinowitz, W. M., and Reed, C. M. (**1979**). "Hearing aids: A review of past research on linear amplification, amplitude compression, and frequency lowering," American Speech and Hearing Association Monograph No. 19.
Cooper, F., Delattre, P., Liberman, A., Borst, J., and Gerstman, L. (**1952**). "Some experiments on the perception of synthetic speech sounds," J. Acoust. Soc. Am. **24**, 579–606.
Delattre, P., Liberman, A., and Cooper, F. (**1955**). "Acoustic loci and translational cues for consonants," J. Acoust. Soc. Am. **24**, 769–773 (Haskins work on painted speech).
Delgutte, B., Hammond, B., and Cariani, P. (**1998**). "Neural coding of the temporal envelope of speech: Relation to modulation transfer functions," in *Psychophysical and Physiological Advances in Hearing*, edited by A. Palmer, A. Reese, A. Summerfield, and R. Meddis (Whurr, London), pp. 596–603.
Dubno, J. R., Dirks, D., and Schaefer, A. (**1987**). "Effects of hearing loss on utilization of short-duration spectral cues in stop consonant recognition," J. Acoust. Soc. Am. **81**, 1940–1947.
Dubno, J. R., and Levitt, H. (**1981**). "Predicting consonant confusions from acoustic analysis," J. Acoust. Soc. Am. **69**, 249–261.
Dusan, S., and Rabiner, L. (**2005**). "Can automatic speech recognition learn more from human speech perception?," in *Trends in Speech Technology* Romanian Academy, pp. 21–36.
Fletcher, H. (**1995**). "Speech and hearing in communication," in *The ASA Edition of Speech and Hearing in Communication*, edited by J. B. Allen (Acoustical Society of America, New York).
Fletcher, H., and Galt, R. (**1950**). "Perception of speech and its relation to telephony," J. Acoust. Soc. Am. **22**, 89–151.
Fousek, P., Svojanovsky, P., Grezl, F., and Hermansky, H. (**2004**). "New nonsense syllables database — Analysis and preliminary ASR experiments," in Proceedings of the International Conference on Spoken Language Processing, (JEJU Island, Korea).
French, N. R., and Steinberg, J. C. (**1947**). "Factors governing the intelligibility of speech sounds," J. Acoust. Soc. Am. **19**, 90–119.
Furui, S. (**1986**). "On the role of spectral transition for speech perception," J. Acoust. Soc. Am. **80**, 1016–1025.
Hant, J., and Alwan, A. (**2003**). "A psychoacoustic-masking model to predict the perception of speech-like stimuli in noise," Speech Commun. **40**, 291–313.
Hawkins, S. (**2003**). "Roles and representations of systematic fine phonetic detail in speech understanding," J. Phonetics **31**, 373–405.
Heil, P. (**1997**). "Auditory cortical onset responses revisited. I. First-spike timing," J. Neurophysiol. **77**, 2616–2641.
Heil, P. (**2003**). "Coding of temporal onset envelope in the auditory system," Speech Commun. **41**, 123–134.
Hermansky, H. (**1998**). "Should recognizers have ears?," Speech Commun. **25**, 3–27.
Joris, P., Smith, P., and Yin, T. (**1998**). "Coincidence detection in the auditory system: 50 years after Jeffress," Neuron **21**, 1235–1238.
Kamm, C., Dirks, D., and Bell, T. (**1985**). "Speech recognition and the articulation index for normal and hearing-impaired listeners," J. Acoust. Soc. Am. **77**, 281–288.
Kewley-Port, D. (**1983**). "Time varying features as correlates of place of articulation in stop consonants," J. Acoust. Soc. Am. **73**, 322–335.
Klunder, K. R., Lotto, A. J., and Jenison, R. L. (**1995**). "Perception of voicing for syllable-initial stops at different intensities: Does synchrony capture signal voiceless stop consonants?," J. Acoust. Soc. Am. **97**, 2552–2567.
Lippmann, R. P. (**1997**). "Speech perception by humans and machines," Speech Commun. **22**, 1–15.
Lisker, L. (**1985**). "The pursuit of invariance in speech signals," J. Acoust. Soc. Am. **77**, 1199–1202.
Lobdell, B., and Allen, J. B. (**2006**). "An information theoretic tool for investigating speech perception," in Proceedings of Interspeech, p. 87.
Lobdell, B., and Allen, J. B. (**2007**). "Modeling and using the vu-meter (volume unit meter) with comparisons to root-mean-square speech levels," J. Acoust. Soc. Am. **121**, 279–285.
Lovitt, A., and Allen, J. (**2006**). "Using listener and talker variability to understand confusion patterns," in International Hearing Aid Research Conference.
Miller, G. A., and Nicely, P. E. (**1955**). "An analysis of perceptual confusions among some English consonants," J. Acoust. Soc. Am. **27**, 338–352.
Nguyen, N., and Hawkins, S. (**2003**). "Temporal integration in the perception of speech: Introduction," J. Phonetics **31**, 289–291 (overview of the special issue).
Oertel, D. (**2005**). "Importance of timing for understanding speech: Focus on Perceptual consequences of disrupted auditory nerve activity," J. Neurophysiol. **93**, 3044–3045 (editorial focus).
Phatak, S., and Allen, J. B. (**2007**). "Consonant and vowel confusions in speech-weighted noise," J. Acoust. Soc. Am. **121**, 2312–2326.
Rabinowitz, W., Eddington, D., Delhome, L., and Cuneo, P. (**1992**). "Relations among different measures of speech reception in subjects using a cochlear implant," J. Acoust. Soc. Am. **92**, 1869–1881.
Régnier, M., and Allen, J. B. (**2007a**). "Perceptual cues of some CV sounds studied in noise," *Abstracts* (AAS, Scottsdale).
Régnier, M., and Allen, J. B. (**2007b**). "The importance of across frequency timing coincidences in the perception of some English consonants in noise," *Abstracts* (ARO, Denver, CO).
Repp, B., Liberman, A., Eccardt, T., and Pesetsky, D. (**1978**). "Perceptual integration of acoustic cues for stop, fricative, and affricate manner," J. Exp. Psychol. **4**, 621–637.
Rhebergen, K., Versfeld, N., and Dreschler, A. (**2006**). "Extended speech intelligibility index for the prediction of the speech reception threshold in fluctuating noise," J. Acoust. Soc. Am. **120**, 3988–3997.
Shamma, S. (**2003**). "Physiological foundations of temporal integration in the perception of speech," J. Phonetics **31**, 495–501.
Shannon, C. E. (**1948**). "The mathematical theory of communication," Bell Syst. Tech. J. **27**, 379–423; 1948) Bell Syst. Tech. J. **27**, 623–656.
Shannon, R. V., Zeng, F. G., Kamath, V., Wygonski, J., and Ekelid, M. (**1995**). "Speech recognition with primarily temporal cues," Science **270**, 303–304.
Stevens, K., and Klatt, D. (**1974**). "Role of formant transitions in the voiced-voiceless distinstion for stops," J. Acoust. Soc. Am. **55**, 653–659.
Strope, B., and Alwan, A. (**1997**). "A model of dynamic auditory perception and its application to robust word recognition," IEEE Trans. Acoust., Speech, Signal Process. **5**, 451–464.
Summerfield, Q., and Haggard, M. (**1977**). "On the dissociation of spectral and temporal cues to the voicing distinction in the initial stop consonants," J. Acoust. Soc. Am. **62**, 51–61.

Acoustic cues to tonal contrasts in Mandarin: Implications for cochlear implants

Yu-Ching Kuo[a)]
Department of Special Education, Taipei Municipal University of Education, No. 1, Ai-Guo West Road, Taipei, 10042, Taiwan and Department of Phonetics and Linguistics, University College London, 4 Stephenson Way, London NW1 2HE, United Kingdom

Stuart Rosen and Andrew Faulkner
Department of Phonetics and Linguistics, University College London, 4 Stephenson Way, London NW1 2HE, United Kingdom

(Received 5 January 2007; revised 14 February 2008; accepted 14 February 2008)

The present study systematically manipulated three acoustic cues—fundamental frequency (f0), amplitude envelope, and duration—to investigate their contributions to tonal contrasts in Mandarin. Simplified stimuli with all possible combinations of these three cues were presented for identification to eight normal-hearing listeners, all native speakers of Mandarin from Taiwan. The f0 information was conveyed either by an f0-controlled sawtooth carrier or a modulated noise so as to compare the performance achievable by a clear indication of voice f0 and what is possible with purely temporal coding of f0. Tone recognition performance with explicit f0 was much better than that with any combination of other acoustic cues (consistently greater than 90% correct compared to 33%–65%; chance is 25%). In the absence of explicit f0, the temporal coding of f0 and amplitude envelope both contributed somewhat to tone recognition, while duration had only a marginal effect. Performance based on these secondary cues varied greatly across listeners. These results explain the relatively poor perception of tone in cochlear implant users, given that cochlear implants currently provide only weak cues to f0, so that users must rely upon the purely temporal (and secondary) features for the perception of tone. © *2008 Acoustical Society of America.*
[DOI: 10.1121/1.2896755]

PACS number(s): 43.71.Es, 43.70.Fq, 43.71.Ky [AJO] Pages: 2815–2824

I. INTRODUCTION

In Mandarin Chinese, four tones are one of the phonetic determinants of lexical meaning (e.g., Chao, 1948; 1968; Yip, 1980). These four tones are mainly distinguished by their variations in fundamental frequency (e.g., Howie, 1976; Lin, 1988). The four tonal patterns are often described in terms of the pitch range of the particular speaker. Tone 1, the level tone, starts within a speaker's high pitch range and maintains approximately the same pitch to the end of the syllable. Tone 2, the rising tone, starts in a middle pitch range, then shows a rise, which is sometimes preceded by a small dip. Tone 3, the falling–rising tone, also starts in a middle pitch range, falls gradually toward a low pitch and then rises. Tone 4, the falling tone, starts at a high pitch, and drops to a low one. A syllable with different tones represents different words. For example, the syllable *ba* expressed with tones 1, 2, 3, and 4 means "eight," "to pull," "to hold," and "father," respectively.

Although tone 3 is often referred to as a falling–rising pattern, it also appears in other forms (e.g., Chao, 1948; 1968; Shih, 1988; Chen, 2000). This variation is due to phonological processes that are described by the third tone sandhi rule. A falling–rising pattern appears in isolated words and in sentence-final position. However, in nonfinal positions, a low-falling pattern occurs. In addition, if a syllable with tone 3 is followed by another syllable with the same tone, the first syllable will be pronounced as tone 2, a rising tone. Therefore, tone 3 appears in three patterns: the falling–rising pattern, the low-falling pattern, and the rising pattern. Previous studies have shown that tone 3 was sometimes misidentified as the falling tone (tone 4) or the rising tone (tone 2) (Gårding *et al.*, 1986; Shen and Lin, 1991).

The usage of the falling–rising and the low–falling patterns also varies according to dialect and/or speaking style (Shih, 1988). Northern Chinese speakers use the falling–rising pattern in sentence-final position in all speech. By contrast, southern speakers use the low-falling pattern even in the final position in casual speech, and use the falling–rising pattern in emphatic speech and in yes–no questions. Dialect may also influence Mandarin tone. Fon and Chiang (2000) reported that Taiwan Mandarin showed a narrower tonal range, lower tonal heights, and more conservative tonal contours compared to Beijing Mandarin. This could be attributed to an influence from Taiwanese, which has a lower tonal register than Mandarin (Lin and Repp, 1989).

While the four tones are mainly distinguished by fundamental frequency, other acoustic characteristics such as overall intensity and duration tend to vary systematically with tone (Howie, 1976; Zee, 1978; Blicher *et al.*, 1990; Tseng, 1990; Whalen and Xu, 1992; Fu and Zeng, 2000). Tone 4 is often the most intense one and has the shortest duration,

[a)]Electronic mail: ykuo@tmue.edu.tw

while tone 3 is the least intense with the longest duration. However, different patterns of tone 3 differ in duration as well as in pitch contour. While the falling–rising pattern shows the longest duration among the four tones, the low-falling pattern has the shortest duration (Shih, 1988). Amplitude envelope has also been found to be highly correlated with f0 contour for tones 3 and 4 (Whalen and Xu, 1992; Fu and Zeng, 2000).

Several studies have investigated tone perception from purely temporal cues using various noise stimuli modulated by envelopes derived from natural speech stimuli. Three temporal envelope cues were defined by Fu and Zeng (2000): periodicity, amplitude contour, and duration. As in Rosen (1992), "periodicity" referred to fluctuations in the overall amplitude at a rate between 50 and 500 Hz, whereas "amplitude contour" referred to fluctuations at a rate between 2 and 50 Hz. Although percepts of pitch are strongest for truly periodic sounds, they can also be elicited by temporal fluctuations in amplitude-modulated noise (Burns and Viemeister, 1976). When the temporal envelope of speech is derived from rectified speech with an envelope-smoothing filter which includes the voice f0 range, listeners can perceive the quasiperiodic amplitude modulations imposed on a noise carrier as pitch changes. The temporal regularities in the modulated noise can be referred to as periodicity information (Rosen, 1992). However, when the cutoff frequency of an envelope-smoothing filter falls below the fundamental frequency range, the periodicity information is not included in the envelope signal.

Whalen and Xu (1992) used signal-correlated-noise (SCN) to investigate the extent to which tone recognition can be aided by amplitude contour and duration. Their results showed high recognition scores for tones 2–4, averaging 87.6%, but only 38.5% correct for tone 1. To further examine the contribution of amplitude contour, they used stimuli with controlled duration, and found that recognition scores were still well above chance in the absence of the duration cue (45%, 55.3%, 69.5%, and 92.3% for tones 1, 2, 3, and 4, respectively). However, SCN is equivalent to wide-band noise modulated with an envelope extracted using a smoothing filter with a very high cut-off frequency on full-wave rectified speech. Therefore, SCN stimuli contain not only amplitude contour and duration cues, but also the periodicity of the natural tokens on which they were based, albeit in weakened form. Green *et al.* (2002) showed listeners to have some ability to label glides in fundamental frequency at low frequency ranges in stimuli that were similar to, although not identical to, SCN. Thus, periodicity information, directly related to the change in fundamental frequency, was likely to influence subject performance as well (Rosen, 1992; Van Tasell *et al.*, 1987).

Fu *et al.*, 1998 investigated the importance of periodicity and amplitude envelope to tone recognition by using amplitude-modulated noise. In this study, duration was not examined and retained its natural variations. When no spectral information was available (1-band condition), recognition scores of up to 80% could be achieved in a condition that preserved amplitude envelope, periodicity, and duration information, while accuracy was about 67% in a condition preserving only amplitude envelope and duration information. Tones 3 and 4 were identified best, nearly twice as well as tone 1 and tone 2. In another study, Fu and Zeng (2000) used SCN to further explore the contribution of periodicity, amplitude contour, and duration to tone recognition. These three cues were manipulated in isolation, in pairs, and all together. Results showed that the highest score, nearly 70%, was achieved in the condition with all three cues. Around 55% correct recognition was shown in conditions that preserved either the amplitude contour or periodicity cues. A condition preserving only the duration cue had the lowest recognition score of about 35% correct. The duration cue was found to contribute to recognition of tone 3, and the amplitude cue contributed to the recognition of both tones 3 and 4. The periodicity cue contributed to recognition of all four tones.

In a recent study by Xu *et al.* (2002), amplitude envelope and periodicity were manipulated by varying the low-pass cutoff frequency of an envelope-smoothing filter from 1 to 512 Hz in 1 octave steps. Tone recognition improved slightly but consistently as cutoff frequency increased in the 1-channel condition in which there was no spectral information available. Consistent with the results of Fu *et al.* (1998), around 50% correct recognition was achieved with only amplitude envelope and duration cues (when the envelope cutoff frequency was as low as 1 or 2 Hz), while accuracy approached 65% when periodicity cues were also available (with an envelope cutoff frequency at 512 Hz). When the duration cue was removed, scores dropped significantly, with tones 3 and 4 affected the most (the decreases were by 12.5, 8.5, 19.5, and 19.7 percentage points for tones 1, 2, 3, and 4, respectively). These decreases in performance indicated that duration did show a significant effect on tone recognition mainly on tones 3 and 4.

To sum up, results from the above-mentioned studies confirm that tone recognition can be assisted by temporal envelope cues. Although the pitch from modulated noise is considerably less salient than the pitch of harmonic signals for which there are spectral cues to pitch, listeners can perceive the periodicity information in the modulated noise and use it to recognize tone (Burns and Viemeister, 1976). The amplitude and duration cues also play significant roles for tone recognition, and contribute to tones 3 and 4 the most. The studies showed an inconsistency of effects of duration. Duration contributed to the identification of both tones 3 and 4 in Xu *et al.* (2002), but only affected tone 3 in Fu and Zeng (2000). It appears that duration did not consistently contribute to tone 4 recognition in the latter study because tone 4 was not significantly different from tone 1 in duration. In Xu *et al.*, tone 4 was the shortest tone. Therefore, although duration can sometimes be used to aid tone recognition, it varies in natural tokens so it may not always be a reliable cue.

The aim of the current study was to investigate the extent to which tonal contrasts can be recognized with different acoustic cues. Although these three main cues to tonal contrasts in Mandarin (f0, amplitude envelope, and duration) have been investigated in several studies, only the study by Fu and Zeng (2000) systematically combined different cues to examine their contributions. Modulated noises were used

to carry all possible combinations of the three cues. However, the pitch information was conveyed by the temporal fluctuations in the speech envelope which is a far less salient cue than that which arises from true periodic sounds. Here, we introduce a sawtooth wave form created period by period to match the f0 of original speech, and used this to carry pitch information. The f0-controlled sawtooth wave form contains both spectral and temporal cues to pitch, and was expected to give a clearer indication of voice pitch than would be possible from the temporal envelope of noise alone. The same three cues in all combinations were conveyed both by sawtooth and noise carriers [the latter as in Fu and Zeng (2000), but with some modifications in signal processing]. With the same testing materials, the results of the present study allow the comparisons of the level of correct tone recognition with different combinations of acoustic cues.

Stimuli with explicit f0 information (f0 carried by sawtooth carriers) were expected to be recognized the best among all stimuli. For stimuli with the relatively weak temporal f0 information (f0 carried by temporal fluctuations of noise carriers), listeners were expected to be able to identify some tonal information, but their performance would not be as good as the performance when f0 was represented explicitly. It is well known that amplitude-modulated noise stimuli, with no regularity in fine structure, lead to weak pitch sensations. According to Lin's (1988) study, when explicit f0 is presented, amplitude envelope and duration are unlikely to contribute much to the recognition of tonal contrasts. However, when f0 information is absent or presented in a rather weak form, as in Whalen and Xu (1992) and Fu *et al.* (1998), amplitude envelope and/or duration could be of use. Even so, the effect of amplitude envelope and/or duration would be less significant.

II. METHODS

A. Speech stimuli

Four syllables (/i/, /ba/, /fu/ and /tɕʰi/) with each of four tones were used as stimuli. Four different syllable structures (vowel only, three point vowels with initial plosive, fricative, and affricative consonants) were included, so as to contain more variability and be more representative of the information in real life. All these syllables were Mandarin words with a high frequency of occurrence. Natural models for the stimuli were produced by two young adults, one male and one female, who were native speakers of Mandarin from Taiwan. All stimuli were randomized and produced in the carrier phrase "qǐ tiao chu-" ("Please choose—") to avoid inconsistency in pitch range. Six repetitions were produced for the four syllables with each of the four tones. The recording was conducted in an anechoic chamber with speech and laryngograph signals (*Lx*) recorded at the same time using a Sony DAT recorder at a 44.1 kHz sampling rate. The first two tokens sounded natural and contained no creaky voice, as judged by a native speaker of Mandarin (the first author), and so were selected as stimuli. There were a total of 64 speech stimuli (4 syllables X 4 tones X 2 tokens X 2 speakers).

TABLE I. Mean fundamental frequency (Hz), rms amplitude (dB re 1, where all amplitudes are within the range ±1), and duration for the four tones (standard deviations in parentheses).

		Fundamental frequency (Hz)				rms amplitude (dB re 1)	Duration (ms)
		Male		Female			
Tone 1	Average	158	(6)	257	(12)	−23.5 (3.5)	308.8 (38)
Tone 2	Initial	121	(16)	201	(11)	−27.7 (2.9)	347.7 (47)
	Final	143	(15)	222	(15)		
Tone 3	Initial	120	(13)	198	(15)	−30.7 (2.5)	323.7 (66)
	Turning point	91	(9)	113	(41)		
	Final	119	(9)	147	(37)		
Tone 4	Initial	171	(32)	264	(18)	−25.0 (3.0)	256.2 (72)
	Final	108	(14)	150	(42)		
Average						−26.7 (3.6)	309 (65)

B. Acoustic analysis of speech stimuli

Table I shows the f0 values of average pitch curves, mean rms amplitude, and duration for the four tones.

1. F0 contour

Figure 1 shows pitch contours for all speech tokens by the male and female speakers. Note that the pitch contours of tone 3 for the female appeared to be more variable. While the male speaker used the falling–rising pattern consistently, the female speaker used both falling–rising and low-falling patterns. Some of the pitch contours kept falling throughout while others rose slightly at the end.

2. Overall intensity

An analysis of variance (ANOVA) showed a significant difference of rms amplitude of the four tones [$F(3,60)=17.22$, $p<0.001$]. *Post-hoc* comparisons revealed that tone 3 was the least intense tone with significantly lower intensity than the other three tones. Tones 1 and 4 had no significant difference between their overall intensities, and both had significantly higher levels than tone 2.

3. Duration

Tone 2 had the longest duration, followed by tone 3, then tone 1, and finally tone 4. An ANOVA showed a significant effect of duration [$F(3,60)=7.3$, $p<0.001$]. *Post-hoc* comparisons revealed that tones 2 and 3 were significantly longer than tone 4.

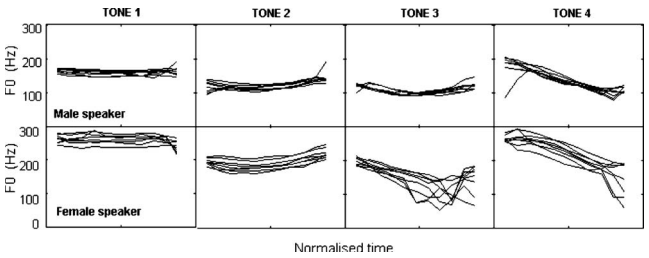


FIG. 1. F0 contours for speech stimuli from the two speakers (all the pitch contours were normalized using a linear time scaling to give the same duration).

TABLE II. Summary of stimuli used in the present study and the study of Fu and Zeng (2000). Cues *A*, *F*, and *D* represent amplitude contour, f0, and duration, respectively.

Cues		Carrier		
		Present study		Fu and Zeng 2000
		Sawtooth carrier	*Noise* carrier	*Noise* carrier
Natural duration	*AFD*	f0-controlled sawtooth carrier envelope extracted at 30 Hz	*AFDcis* Noise carrier × envelope extracted at 400 Hz *AFD* f0-controlled sinusoidal modulated noise × envelope extracted at 30 Hz	Noise carrier × envelope extracted at 500 Hz
	AD	Random-frequency sawtooth carrier envelop extracted at 30 Hz	Noise carrier × envelope extracted at 30 Hz	Noise carrier × envelope extracted at 50 Hz
	FD	f0-controlled sawtooth carrier	f0-controlled sinusoidal modulated noise	f0-controlled 100% amplitude modulated noise (no further detials provided)
Duration fixed at 309 ms	*AF*	Sawtooth carrier controlled by the 309 ms time-scaled f0 contour × time-scaled envelope extracted at 30 Hz	Time-scaled f0-controlled sinusoidal modulated noise × time-scaled envelope extracted at 30 Hz	Linear interpolation was applied to AFD-stimulito give a fixed duration at 400 ms (the range of f0 variation may change althoughthe same percentile of f0 change remains)
	A	309 ms random-frequency sawtooth carrier × time-scaled envelope extracted at 30 Hz	Noise carrier × time-scaled envelope extracted at 30 Hz	Linear interpolation was applied to *AD* stimuli togive a fixed duration at 400 ms (the range of f0 variation may change)
	F	Sawtooth carrier controlled by the 309 ms time-scaled f0 contour	Time-scaled f0-controlled sinusoidal modulatednoise	Linear interpolation was applied to *FD* stimuli(the range of f0 variation may change)
Duration cue only	*D*	Random-frequency sawtooth carrier with original duration	Noise carrier with original duration	Noise carrier with original duration

While tone 3 was often reported as the longest tone in many early studies (e.g., Howie, 1976; Tseng, 1990; Whalen and Xu, 1992; Fu and Zeng, 2000), tone 3 had a shorter duration than tone 2 in this study (348 and 324 ms for tones 2 and 3, respectively). The short tone 3 might be due to the female speaker using both falling–rising and low-falling patterns. As mentioned in Sec. I, the falling–rising tone 3 had the longest duration and the low-falling tone 3 had the shortest duration. Both our speakers were native Mandarin speakers from Taiwan, while most speakers in earlier studies were native speakers from Beijing. The short tone 3 might be a dialect difference between Beijing and Taiwan.

Another possible reason for the short tone 3 was the speech stimuli used in the current study. The speech stimuli in our study included vowels in four different phonetic contexts (vowels only and with different initial consonants), while stimuli in most of early studies used vowels only. The potential effects of the four phonetic contexts might result in the differences in duration relative to other studies. A short tone 3 can also be found in previous studies. For instance, Howie (1976) reported some of the recorded syllables had longer tone 2 than tone 3 (e.g., syllable /hu/ had 260 and 235 ms vowel duration for tones 2 and 3, respectively; syllable /yan/ had 190 and 180 ms vowel duration for tones 2 and 3, respectively).

C. Signal processing

All stimuli in this study were simplified from the originally recorded speech stimuli. Table II summarizes the method used to generate these stimuli, compared to Fu and Zeng's (2000) study. Each speech stimulus was used to produce 15 simplified stimuli with all possible combinations of f0 (*F*), amplitude envelope (*A*), and duration (*D*) in isolation, pairs, and all together, and carried by either sawtooth or noise carriers. Figure 2 shows some examples of the simplified stimuli.

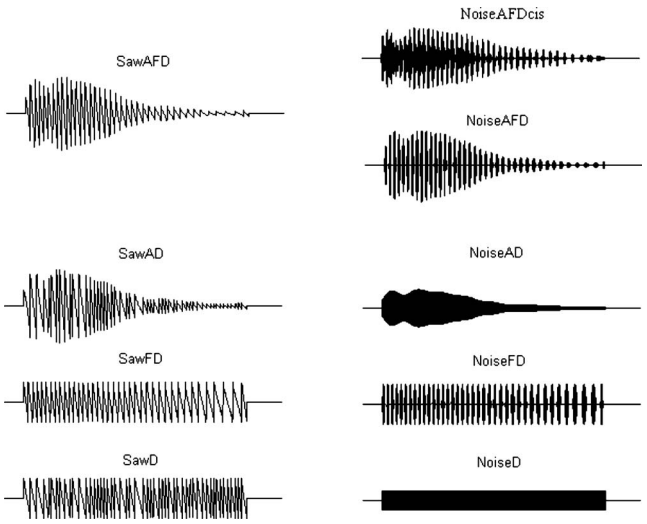


FIG. 2. Examples of some simplified stimuli (conditions *AFD*, *AD*, *FD*, and *D*, using both sawtooth and noise carriers and *NoiseAFDcis*) for the syllable /ba/ with tone 4 produced by the male speaker. Other simplified stimuli *AF*, *A*, and *F* are similar to *AFD*, *AD*, and *FD*, respectively, except with duration fixed at 309 m.

1. AFD (amplitude envelope, f0, and duration)

a. Sawtooth carrier The times between successive regular vocal fold closures (referred to as *Tx*) were measured from laryngograph signals, and used to generate a sawtooth wave form period by period. The f0-controlled sawtooth wave form preserved the f0 contour of the original speech with constant amplitude contour. The amplitude envelope was extracted by full-wave rectification, followed by forward and backward filtering with a 30 Hz cutoff frequency fourth-order elliptical low-pass filter. The f0-controlled sawtooth carrier was then multiplied by the amplitude envelope to generate the *SawAFD* stimulus.

b. Noise carrier In the present study, the signal processing used to generate the *AFD* stimulus by a noise carrier was different from that used in Fu and Zeng's study (2000). A sinusoidal wave form was generated from *Tx* values period by period, half-wave rectified, and then used to modulate a noise carrier. The *NoiseAFD* stimulus contained all three cues, but the temporal cue to pitch was expected to be rather weak. Another condition, which was almost the same as one used by Fu and Zeng (2000), except using a slightly different cutoff frequency (see Table II), was also generated. A noise carrier was multiplied by a speech envelope extracted by half-wave rectification and low-pass filtering with a 400 Hz cutoff frequency to generate the *NoiseAFDcis* stimulus ("cis" refers to "continuous interleaved sampling, CIS," one commonly used speech coding strategy in current cochlear implant systems). Since the range of voice pitch was included, the envelope with 400 Hz cutoff frequency would be expected to preserve some pitch information. The *NoiseAFD* stimulus, because of its clearer pattern of f0-related modulations, might contain slightly better pitch information than the *NoiseAFDcis* stimulus, although the difference should not be large (Green *et al.*, 2002). In any case, the use of an explicit modulator based on f0 allowed condition *NoiseAFD* to be comparable to condition *NoiseFD*, and also to make the f0 information contained in the noise conditions more comparable to that contained in the sawtooth carriers.

2. AD (amplitude envelope and duration)

a. Sawtooth carrier. A random-frequency sawtooth carrier was generated by taking *Tx* randomly from the *Tx* values of the 64 original speech signals across four tones and two speakers, with the same duration as the original speech. The random-frequency sawtooth carrier eliminated the f0 cue to tonal contrasts. A fixed frequency sawtooth carrier was not used because a constant f0 would sound like tone 1, the level tone. The random-frequency sawtooth carrier was then multiplied by the amplitude envelope to generate the *SawAD* stimulus.

b. Noise carrier. A noise carrier was multiplied by the amplitude envelope extracted at 30 Hz to generate the *NoiseAD* stimulus.

3. FD (f0 and duration)

a. Sawtooth carrier. The *SawFD* stimulus was the f0-controlled sawtooth carrier, which preserved the f0 contour and the duration of the original speech but no variation in amplitude.

b. Noise carrier. The *NoiseFD* stimulus was the f0-controlled sinusoidally modulated noise. This stimulus contained the temporal cue to pitch with constant amplitude envelope.

4. AF (amplitude envelope and f0)

a. Sawtooth carrier. A linear time scaling was applied to the f0 contour so as to give a constant duration of 309 ms (the average duration of the voiced parts of all original speech signals), thus eliminating the duration cue. To create a sawtooth wave form with the original f0 contour but a fixed duration at 309 ms, the following procedure was used. The fundamental periods measured from the larygograph signal were converted to a pitch contour first. Then, a linear time scaling was applied to the pitch contour to produce a new pitch contour with the same shape but duration fixed at 309 ms. The new pitch contour was converted back to a new set of *Tx* periods. The first *Tx* period was the same as that in the original speech. The second *Tx* period was determined by the f0 value in the time-scaled pitch contour at the end of this first period. Similarly, the third and subsequent *Tx* periods were determined from the f0 value of the time-scaled contour at the end of the immediately preceding period. The new sets of *Tx* values preserved the original pitch contours without changing the overall f0 range.

The amplitude envelopes extracted at 30 Hz were also scaled in time to give the 309 ms duration, and then multiplied against the sawtooth carriers controlled by time-scaled f0 contour. The *SawAF* stimulus preserved both the f0 and amplitude contours in the original speech but with duration fixed at 309 ms.

b. Noise carrier. A sinusoidal wave form was generated from the time-scaled *Tx* values and half-wave rectified, and then used to modulate a noise carrier. The time-scaled f0-controlled sinusoidal wave form was then multiplied by the time-scaled amplitude envelopes extracted at 30 Hz. The *NoiseAF* stimulus contained the same temporal pitch and amplitude information as in *NoiseAFD* stimulus but without the duration cue.

5. A (amplitude envelope only)

a. Sawtooth carrier. A random-frequency sawtooth carrier with duration fixed at 309 ms was multiplied by the time-scaled amplitude envelope extracted at 30 Hz, resulting

in the *SawA* stimulus.

b. Noise carrier. A noise carrier was multiplied by the time-scaled amplitude envelope extracted at 30 Hz, resulting in *NoiseA* stimulus.

6. F (f0 only)

a. Sawtooth carrier. The *SawF* stimulus was the constant amplitude sawtooth carrier generated from the time-scaled *Tx* values.

b. Noise carrier. The *NoiseF* stimulus was the time-scaled f0-controlled sinusoidal modulated noise. This stimulus contained the temporal cue to pitch with a constant amplitude envelope and a fixed duration.

7. D (duration only)

a. Sawtooth carrier. The *SawD* stimulus was a fixed-amplitude random-frequency sawtooth carrier with duration varied as in the original speech.

b. Noise carrier. The *NoiseD* stimulus was a noise carrier with the duration of the original speech.

D. Subjects

Eight normal hearing adults, three male and five female, participated in the experiment. All were native speakers of Mandarin from Taiwan, aged between 27 and 35.

E. Procedure

Stimuli were blocked by condition, so were presented in 15 blocks. A graphical user interface built in MATLAB was used for running the experiment. In each block, a learning session and a training session were given before a testing session started. Subjects were given sample stimuli for all 15 processing conditions in the learning session, and these stimuli were played randomly in the training session with feedback given. Subjects were allowed to spend as much time as desired in these two sessions. No stimuli used for familiarization were used in the testing session. In the testing session, the four corresponding Mandarin characters of the stimulus were shown first, and the stimulus was played. The Mandarin characters with the Chinese phonetic alphabet, the jùyīnfúhaù, were also shown on the screen. Four push buttons labeled with Tone 1 to Tone 4 were presented below the corresponding characters. Subjects made their identification response using a computer mouse to click one of the four buttons. Then the four corresponding characters of the next stimulus were shown, and the next stimulus was played. No feedback was given in the testing session.

Stimuli were presented through Sennheiser HD 414X headphones, with intensity varied randomly within a 3 dB range around the original level on each trial to reduce cues derived from the overall intensity of the stimuli. The 3 dB range was chosen as it approximated the standard deviation of the rms amplitude of the natural tokens. The order of the 15 processing conditions was randomized and counterbalanced across subjects. In each block, stimuli from male and female speakers were presented in a randomized order. The 15 blocks with 64 simplified stimuli in each resulted in a total of 960 stimuli.

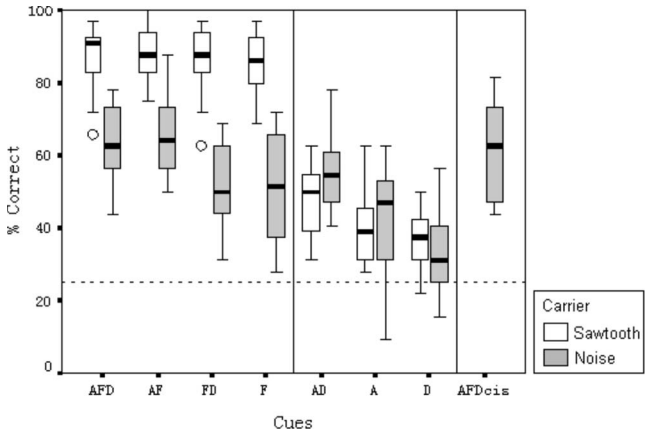


FIG. 3. Boxplots of percentage of correct tone recognition across conditions of different acoustic cues carried by sawtooth or noise carriers. The box represents the 25 to 75 percentile range of the data over subjects and speakers, and the bar within each box represents the median. The whiskers represent the range of data points, except for outliers which are shown as asterisks (more than 3 box lengths from the box edge) or open circles (more than 1.5 box lengths). The dashed line represents chance performance (25% correct).

III. RESULTS AND DISCUSSION

A. Contribution of f0, amplitude envelope, and duration

For stimuli in which f0 information is conveyed by sawtooth carriers (*SawAFD*, *SawAF*, *SawFD*, and *SawF*), a pitch percept can be evoked from both resolved lower harmonics and unresolved higher harmonics. For stimuli with f0 carried by noise carriers (*NoiseAFD*, *NoiseAF*, *NoiseFD*, *NoiseF*, and *NoiseAFDcis*), pitch can only be derived from regular fluctuations in the amplitude of the noise. Since pitch perception in the normal auditory system is mainly determined by resolved lower frequency harmonics (e.g., Moore and Peters, 1992; Ritsma, 1967), stimuli *SawAFD*, *SawAF*, *SawFD*, and *SawF* would be expected to give the most clear information about tonal contrasts. Figure 3 shows the percentage correct tone recognition for the various acoustic cues. Conditions with f0-controlled sawtooth carriers (*SawAFD*, *SawAF*, *SawFD*, and *SawF*) led to the highest levels of performance (around 90% correct), but conditions with other acoustic cues also allowed tone recognition to some extent (varying between 33% and 65%). Performance on all conditions was significantly above chance, except marginal effects for conditions with the duration cue only (36.3% and 33.6% for conditions *SawD* and *NoiseD*; a binomial distribution reveals that scores of 23 or more out of 64, or over 35.9%, are statistically different from chance performance, $p < 0.05$).

Conditions *NoiseAFDcis* and *NoiseAFD* would be expected to carry similar information for tonal contrasts, and an *a priori* comparison confirmed that there was no significant difference between performances on these two conditions. *A priori* comparisons were also carried out to examine the effect of periodicity, amplitude envelope, and duration, by using contrasts of conditions with and without one of these three cues (for instance, comparison of conditions *NoiseAFD/NoiseAF/NoiseFD* vs *NoiseAD/NoiseA/NoiseD* was used to examine the effect of periodicity; contrasts of

TABLE III. Results of Bonferroni post hoc comparisons for pairs of conditions with different acoustic cues. An asterisk indicates a significance level of 0.05.

	Sawtooth Carrier							Noise Carrier						
	AFD	AF	FD	F	AD	A	D	AFD	AF	FD	F	AD	A	D
AFD														
AF	-							-						
FD	-	-						-	*					
F	-	-	-					-	*	-				
AD	*	*	*	*				-	-	-	-			
A	*	*	*	*	-			-	-	-	-	-		
D	*	*	*	*	*	*		*	*	-	-	-	-	

NoiseAFD/AF/AD vs *NoiseFD/F/D*, and *NoiseAFD/FD/AD* vs *NoiseAF/F/A* were used for amplitude envelope and duration, respectively). These revealed that there were significant differences for the periodicity and amplitude envelope cues ($[F(1,7)=20.3,\ p<0.01]$ and $[F(1,7)=48.8,\ p<0.01]$, respectively), but not for the duration cue.

A repeated-measures ANOVA was performed for factors of cue, carrier, and speaker. This showed significant effects of carrier $[F(1,7)=131.3,\ p<0.001]$ and cue $[F(6,42)=51.3,\ p<0.001]$, and significant interactions of carrier by cue $[F(6,42)=27.3,\ p<0.001]$ and speaker by carrier $[F(1,7)=15.0,\ p<0.05]$. No other two-way or three-way interaction was significant.

The interaction of carrier by cue was almost certainly due to performance with the two carriers differing greatly only in those conditions in which f0 information was presented (*AFD*, *AF*, *FD*, and *F*). Bonferroni-corrected *post-hoc* comparisons, with an alpha of 0.05, were used to examine the effect of the two different carriers on each of seven conditions, revealing that this was indeed the case. All conditions involving f0 information (*AFD*, *AF*, *FD*, and *F*) were significantly different according to carrier, whereas conditions which had no f0 information (*AD*, *A*, and *D*) were statistically equal. This confirmed our expectation that a sawtooth carrier generated period by period from f0 provided better information for tone recognition than could possibly be conveyed by a modulated noise, with no significant difference for using a random-frequency sawtooth carrier and a noise carrier for conveying information about amplitude envelope and duration.

To examine the relative importance of the different acoustic cues to tonal contrasts, the effect of different combinations of cues on tone recognition was also compared, with sawtooth and noise carriers separately. Table III summarizes the results. For the sawtooth carrier, no significant difference was found between the four conditions with salient f0 (*SawAFD*, *SawAF*, *SawFD*, and *SawF*), and they were all significantly higher than the three conditions without f0 information. There was no significant difference between the two conditions with amplitude envelope cue presented (*SawAD* and *SawA*), and they were significantly higher than the condition with duration only (*SawD*). This indicated that information about f0 conveyed by a periodic sound contributed to tone recognition the most, and neither amplitude envelope nor duration affected tone recognition

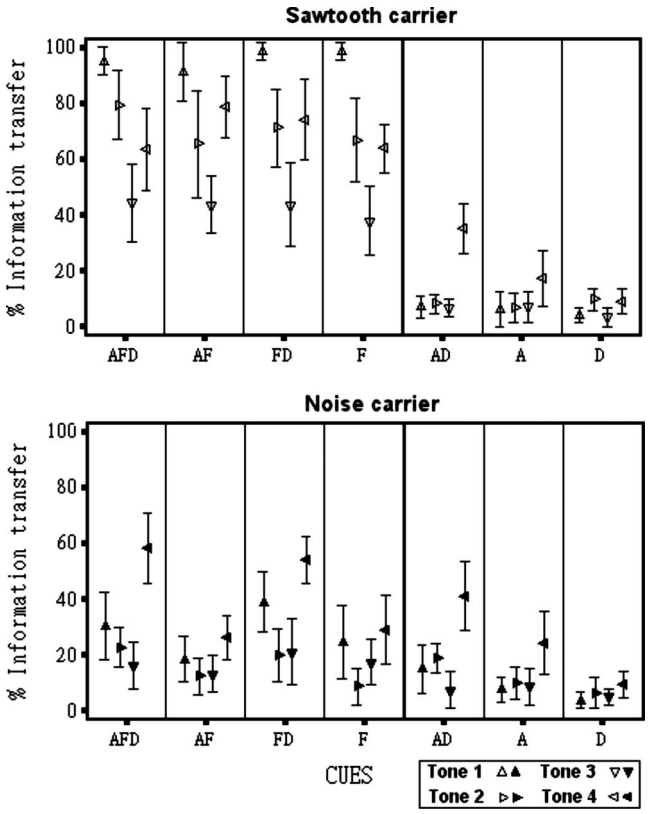


FIG. 4. Percentage of information transfer score of tone recognition for four tones across conditions with different combinations of three acoustic cues. Performance on conditions using the sawtooth carrier is displayed in the upper panel, and performance on conditions using the noise carrier is displayed in the lower panel. Error bars indicate the 95% confidence interval for the means averaging over 16 data points (8 subjects × 2 speakers).

performance while f0 was present. In the absence of salient f0, amplitude envelope appeared to contribute more to tone recognition than duration.

For noise carriers, only a few comparisons showed significant effects, even though several pairs of conditions had considerably different means (for instance, the mean score of *NoiseAFD* was more than 20% higher than that of *NoiseD*, yet, not significant). This was due to there being larger variations in some conditions than others, and the Bonferroni correction leads to relatively conservative tests.

B. Performance for the four tones

Previous studies have shown that the recognition for the four tones in Mandarin can vary with different acoustic cues available (e.g., Whalen and Xu, 1992; Fu *et al.*, 1998; Fu and Zeng, 2000). Here, performance for the four tones in conditions with different combinations of cues was further examined. To give an unbiased measure of identification performance for individual tones, information transfer scores were computed using the procedures of Miller and Nicely (1955) from tone confusion matrices (e.g., a 2 × 2 matrix classifying stimuli as tone 1 versus all other tones, and responses in the same way). The percentage of information transferred for the four tones across conditions is shown in Fig. 4.

A repeated-measures ANOVA was performed for factors of tone and condition, demonstrating a significant interac-

TABLE IV. (a) Response matrices (in percentage) for stimuli with the amplitude envelope cue only (results were summed over conditions *SawA* and *NoiseA*). (b) Cross correlations between amplitude contours and pitch contours for male and female speakers.

(a)		Response to male speaker				Response to female speaker			
	Stimulus	1	2	3	4	1	2	3	4
	Tone 1	31.3	43.0	16.5	9.4	35.9	28.9	16.4	18.8
	Tone 2	15.6	48.4	25.8	9.4	19.5	42.2	26.6	11.7
	Tone 3	7.8	44.5	38.3	9.4	17.2	19.5	25.8	37.5
	Tone 4	23.4	10.2	13.3	53.3	17.2	9.4	16.4	57.0
(b)	Amp	Male speaker F0				Female speaker F0			
		1	2	3	4	1	2	3	4
	Tone 1	0.38	−0.07	0.22	0.69	0.62	−0.01	0.69	0.72
	Tone 2	0.34	0.68	0.45	0.04	0.33	0.45	0.33	0.25
	Tone 3	0.43	0.40	0.78	0.51	0.43	−0.02	0.79	0.85
	Tone 4	0.41	−0.01	0.37	0.77	0.49	−0.19	0.88	0.89

tion $[F(39,273)=18.2,\ p<0.001]$, and significant main effects for condition $[F(13,91)=96.5,\ p<0.001]$ and tone $[F(3,21)=65.7,\ p<0.001]$. Bonferroni-corrected *post-hoc* comparisons were used to examine performance of the four tones on conditions with different combinations of cues. For conditions with explicit f0 included (*SawAFD*, *SawAF*, *SawFD*, and *SawF*), information transfer scores for the four tones showed similar patterns: Tone 1 was significantly higher than tones 2 and 4, and there was no significant difference between these two tones. All these three tones were significantly higher than tone 3. Tone 1 might be recognized best because it had a higher and more distinct frequency range compared to the other three tones. As for tone 3, the variation of its realization presumably was responsible for its relatively low scores. In the two conditions with the duration cue only (*SawD* and *NoiseD*), information transfer scores were all very low, with not much difference among the four tones. For the rest of conditions with little or no f0 presented, tone 4 was generally recognized well compared to the other three tones.

C. The use of amplitude envelope for tone recognition

Table IV(a) shows subject response for stimuli with the amplitude envelope cue only. The confusion matrices were summed over conditions *SawA* and *NoiseA* for male and female speakers separately. Percent correct for each of the four tones is shown along the diagonal of each table. Results from previous studies have shown that listeners were able to use the amplitude cue to label tones to some extent, though performance based on the amplitude envelope cue was often highly variable across tones and speakers. Whalen and Xu (1992) suggested that listeners either recognized the consistent correlation between pitch and amplitude contours or interpreted amplitude change as f0 change. The variation in performance might arise from the fact that a significant correlation between pitch and amplitude contours was only found for certain tones and speakers (Whalen and Xu, 1992; Fu and Zeng, 2000). To examine if subject responses could be explained by the similarity of pitch and amplitude contours, the correlations between pitch and amplitude contours were calculated and compared with the frequency of subject response for stimuli with the amplitude envelope cue only.

The similarity of the amplitude contour of one tone to the pitch contour of each of the four tones was examined by calculating a cross correlation. The average pitch and amplitude contours, averaged over eight normalized contours with the duration of 309 ms of the four tones for the male and female speaker, were used (see Fig. 5). To obtain approximately independent samples, points along a contour were sampled separated by an interval determined by calculating autocorrelation coefficients for pitch and amplitude contours of several sentences. Since a sample point and its neighbor become less related to each other when they are further apart,

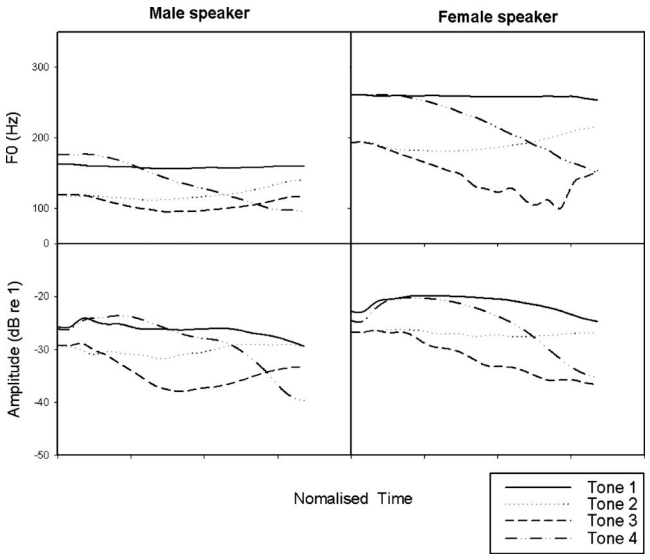


FIG. 5. Average pitch and amplitude contours for the four tones for the two speakers. Each line was averaged over eight speech tokens after a linear time scaling.

the autocorrelation coefficients were often not significant when the time lag was over 55 ms. Therefore, six samples for each of normalized amplitude and pitch contours were calculated by dividing one contour into six sections and taking the average value in each section. Correlations for the lags of −1, 0, and +1 were calculated, and the maximum value was selected. Table IV(b) shows the average correlation between the amplitude contour of one tone and the pitch contours of the four tones. The amplitude contour of a tone did not always correlate most highly with the pitch contour of that same tone. For instance, the amplitude contour of tone 1 for the male speaker was highly correlated to the pitch contour of tone 4 (r=0.69) rather than that of tone 1 (r =0.38). Also, for the female speaker, the amplitude contour of tone 3 was highly correlated with the pitch contours of both tone 3 and tone 4 (r=0.79 and 0.85, respectively), so as the amplitude contour of tone 4 to the pitch contours of tone 4 and tone 3 (r=0.89 and 0.88, respectively). This might be due to, as shown in Fig. 1, the female tone 3 sometimes appeared as low-falling pattern which could correlated well with tone 4, the falling tone.

To further investigate whether response frequencies to stimuli with only the amplitude envelope cue [Table IV(a)] could be explained by the similarity between pitch and amplitude contours [Table IV(b)], the relationship between subject responses and the correlation of pitch and amplitude was examined. Generally speaking, high response frequencies were associated with high correlation coefficients. Although a high correlation coefficient did not always lead to a high proportion of subject responses, a low correlation coefficient seldom did. This indicated that a certain relationship between identification responses and the correlation between amplitude and pitch contour exists.

IV. GENERAL DISCUSSION

While lexical tones are mainly distinguished by their f0 patterns, early studies often suggested that other acoustic cues such as amplitude and duration were of little importance for tone recognition. Recent studies have reported that these temporal cues have a more substantial contribution when f0 information is weak or completely absent. However, results from the present study clearly demonstrate that performance with any combination of these temporal cues was still much lower than with explicit f0 information. The results here might be used to indicate the extent to which information about tonal contrasts could possibly be obtained by current cochlear implant users with CIS-like speech processors, and what may possibly be achieved in future devices. While voice f0 is indubitably the most essential cue for recognizing tonal contrasts, it is not transmitted sufficiently well through current implants. The f0 information available in implant systems is very similar to that conveyed by temporal fluctuations of a noise carrier in the present study. Without the presence of explicit f0 information, this temporal pitch information could help tone recognition, as could amplitude envelope and duration. However, even with all available temporal cues, tone recognition performance was hardly above 70% correct. This is consistent with clinical results, which have reported that users of tonal languages often encounter great difficulty in tone recognition (e.g., Barry *et al.*, 2002; Peng *et al.*, 2004, Wei *et al.*, 2004).

While these temporal cues (temporal coding of f0, amplitude envelope, and duration) could aid in tone recognition to a certain extent and could be used by implant users, none of them is always reliable. Listeners often vary greatly in their ability to make use of these temporal cues, as shown in this study (see Fig. 3) and in previous research. For instance, in Green *et al.* (2002), glide labeling performance based on temporal envelope cues was limited and varied greatly across subjects. Also, the amplitude envelope and duration cues in Mandarin have been reported to be highly variable across speakers and different tones (Fu and Zeng, 2000). The performance in those conditions with noise carriers may represent what can be achieved when listeners are able to perceive one, two, or all of these three cues. The average performance across conditions varies greatly between 35% and 65%, and this low level is about what has been observed in many implant users. Furthermore, these temporal cues are likely to be even less salient in a real life situation of running speech in less-than-ideal acoustic environments.

V. SUMMARY

As would be expected, the explicit f0 cue contributed to tone recognition the most, irrespective of the presence of amplitude envelope and/or duration cues. In the absence of explicit f0, the temporal f0, amplitude envelope, and duration cues also contributed to tone recognition to different extents: the temporal coding of f0 and amplitude envelope both demonstrated substantial contributions to tone recognition, while duration had only a marginal effect. The differences in the utility of duration relative to other studies might be due to: (a) a dialect difference between Beijing and Taiwan and/or (2) the speech syllables used here including different phonetic contexts (vowels only and with different initial consonants). Performance based on these secondary cues varied greatly across subjects, indicating listener variability in perceiving these temporal cues. The contribution of the amplitude envelope cue to the identification of certain tones, especially for tone 4, might be explained by the relatively high correlation between their amplitude and pitch contours.

ACKNOWLEDGMENTS

Thanks go to the Chiang Ching-kuo Foundation for International Scholarly Exchange (Taiwan) for the Ph.D. dissertation fellowship to the first author (DF 020-U-02). We also thank Andrew Oxenham and two anonymous reviewers of the current manuscript and the anonymous reviewers of the early version of this paper, for their helpful comments.

Barry, J. G., Blamey, P. J., Martin, L. F. A., Lee, K. Y. S., Tang, T., Ming, Y. Y., and van Hasselt, C. A. (**2002**). "Tone discrimination in Cantonese-speaking children using a cochlear implant," Clin. Linguist. Phonetics **16**, 79–99.

Blicher, D. L., Diehl, R. L., and Cohen, L. B. (**1990**). "Effects of syllable duration on the perception of the Mandarin Tone2/Tone 3 distinction: Evidence of auditory enhancement," J. Phonetics **18**, 37–49.

Burns, E. M., and Viemeister, N. F. (**1976**). "Nonspectral pitch," J. Acoust. Soc. Am. **60**, 863–869.

Chao, Y. R. (**1948**). *Mandarin Primer: An Intensive Course in Spoken Chinese* (Harvard University Press, Cambridge, MA).
Chao, Y. R. (**1968**). *A Grammar of Spoken Chinese* (University of California Press, Berkeley, CA).
Chen, M. Y. (**2000**). *Tone Sandhi: Patterns Across Chinese Dialects* (Cambridge University Press, Cambridge).
Fon, J., and Chiang, W. Y. (**2000**). "What does Chao have to say about tones?—A case study of Taiwan Mandarin," Can. J. Phys. **27**, 13–37.
Fu, Q. J., and Zeng, F. G. (**2000**). "Identification of temporal envelope cues in Chinese tone recognition," J. Speech Lang. Hear. Res. **5**, 45–57.
Fu, Q. J., Zeng, F. G., Shannon, R. V., and Soli, S. D. (**1998**). "Importance of tonal envelope cues in Chinese speech recognition," J. Acoust. Soc. Am. **104**, 505–510.
Gårding, E., Kratochvil, P., Svantesson, J. O., and Zhang, J. (**1986**). "Tone 4 and Tone 3 discrimination in modern Standard Chinese," Lang. Speech**29**, 281–293.
Green, T., Faulkner, A., and Rosen, S. (**2002**). "Spectral and temporal cues to pitch in noise-excited vocoder simulations of continuous-interleaved-sampling cochlear implants," J. Acoust. Soc. Am. **112**, 2155–2164.
Howie, J. M. (**1976**). *Acoustic Studies of Mandarin Vowels and Tones* (Cambridge University Press, Cambridge).
Lin, H. B., and Repp, B. (**1989**). "Cues to the perception of Taiwanese tones," Lang Speech **32**, 25–44.
Lin, M.-C. (**1988**). "The acoustic characteristics and perceptual cues of tones in Standard Chinese," Chin. Yuwen **204**, 182–193.
Miller, G. A., and Nicely, P. E. (**1955**). "An analysis of perceptual confusions among some English consonants," J. Acoust. Soc. Am. **27**, 338–352.
Moore, B. C. J., and Peters, R. W. (**1992**). "Pitch discrimination and phase sensitivity in young and elderly subjects and its relationship to frequency selectivity," J. Acoust. Soc. Am. **91**, 2881–2893.
Peng, S. C., Tomblin, J. B., Cheung, H., Lin, Y. Y., and Wang, L. S. (**2004**). "Perception and production of Mandarin tones in prelingually deaf children with cochlear implants," Ear Hear. **25**, 251–264.
Ritsma, R. J. (**1967**). "Frequencies dominant in the perception of the pitch of complex sounds," J. Acoust. Soc. Am. **42**, 191–198.
Rosen, S. (**1992**). "Temporal information in speech: Acoustic, auditory and linguistics aspects," Philos. Trans. R. Soc. London, Ser. B **336**, 367–373.
Shen, X. S., and Lin, M. (**1991**). "A perceptual study of Mandarin Tones 2 and 3," Lang Speech **34**, 145–156.
Shih, C. L. (**1988**). "Tone and intonation in Mandarin," Working Pagers Cornell Phonetics Lab. **3**, 83–97.
Tseng, C. Y. (**1990**). *An Acoustic Phonetic Study on Tones in Mandarin Chinese* (The Institute of History and Philology Academia Sinica, Taipei).
Van Tasell, D. J., Soli, S. D., Kirby, V. M., and Widin, G. P. (**1987**). "Speech waveform envelope cues for consonant recognition," J. Acoust. Soc. Am. **82**, 1152–1161.
Wei, C. G., Cao, K., and Zeng, F. G. (**2004**). "Mandarin tone recognition in cochlear-implant subjects," Hear. Res. **197**, 87–95.
Whalen, D. H., and Xu, Y. (**1992**). "Information for Mandarin tones in the amplitude contour and in brief segments," Phonetica **49**, 25–47.
Xu, L., Tsai, Y., and Pfingst, B. E. (**2002**). "Spectral and temporal features of stimulation affecting tonal-speech perception: Implication for cochlear prostheses," J. Acoust. Soc. Am. **112**, 247–258.
Yip, M. (**1980**). "The tonal phonology of Chinese," Ph.D. dissertation, MIT; published (Garland, New York, **1990**).
Zee, E. (**1978**). "Duration and intensity as correlates of F0," J. Phonetics **6**, 213–220.

Compensation for coarticulation, /u/-fronting, and sound change in standard southern British: An acoustic and perceptual study

Jonathan Harrington,[a] Felicitas Kleber, and Ulrich Reubold
Institute of Phonetics and Speech Processing (IPS), University of Munich, Munich, Germany

(Received 17 September 2007; revised 10 February 2008; accepted 21 February 2008)

The aim of the study was to establish whether /u/-fronting, a sound change in progress in standard southern British, could be linked synchronically to the fronting effects of a preceding anterior consonant both in speech production and speech perception. For the production study, which consisted of acoustic analyses of isolated monosyllables produced by two different age groups, it was shown for younger speakers that /u/ was phonetically fronted and that the coarticulatory influence of consonants on /u/ was less than in older speakers. For the perception study, responses were elicited from the same subjects to two minimal word-pair continua that differed in the direction of the consonants' coarticulatory fronting effects on /u/. Consistent with their speech production, young listeners' /u/ category boundary was shifted toward /i/ and they compensated perceptually less for the fronting effects of the consonants on /u/ than older listeners. The findings support Ohala's model in which certain sound changes can be linked to the listener's failure to compensate for coarticulation. The results are also shown to be consistent with episodic models of speech perception in which phonological frequency effects bring about a realignment of the variants of a phonological category in speech production and perception. © *2008 Acoustical Society of America.*
[DOI: 10.1121/1.2897042]

PACS number(s): 43.71.Es, 43.71.An, 43.70.Mn [AJ] Pages: 2825–2835

I. INTRODUCTION

Many studies in recent years have shown that /u/ (lexical set GOOSE in Wells, 1982) of the standard accent of England, Received Pronunciation (RP) has become phonetically fronted. One of the earliest reports of this phenomenon was in Gimson (1966) and some 30 years later, Roach and Hartman (1997) described RP /u/-fronting as a radical shift that had taken place in the last 20–30 years. These and other similar auditory impressions (e.g., Wells, 1982, 1997) have been supported by various acoustic studies showing that the second formant frequency of /u/ both in RP and in standard southern British (SSB), a variety spoken by the majority of RP speakers, is raised for young compared with older speakers (e.g., Bauer, 1985; de Jong *et al.*, 2007; Hawkins and Midgley, 2005; Henton, 1983; McDougall and Nolan, 2007).

Diachronic /u/-fronting has also been found in longitudinal studies of Queen Elizabeth II (Harrington *et al.*, 2000a, b) who speaks a variety of the standard accent known as U-RP [see also Wells (1982, 1997) for the distinction between mainstream RP, or SSB, and U-RP and their relationship to Estuary English]. In these acoustic analyses of the Christmas broadcasts, /u/ was shown to have fronted between the 1950s and 1980s, but the Queen's 1980s /u/ was not as front as /u/ that was typical of SSB speakers of the 1980s. Harrington (2007) suggests that this sound change could be related to the prevalence with which RP /u/ follows consonants with a high F2 locus, both after alveolars in words like *noon*, *soon*, and after /j/, the latter context being somewhat more frequent in RP and SSB (and other related accents such as Australian and New Zealand English in which GOOSE is a high central vowel) because of the additional contexts with /coronal+j/ like *duty*, *news*, *tune* which are without /j/ in general American.

Thus, it is possible that the synchronic vowel fronting caused by consonant-on-vowel perseverative coarticulation in these contexts is related to diachronic /u/ -fronting in the last 50 years. Some evidence for this was provided in Harrington (2007), who showed that the distance between the F2 locus of the preceding consonant and the F2 target of /u/ had progressively diminished over a 50 year period in the Queen's Christmas broadcasts suggesting an increase in the influence of the preceding consonant on /u/ which, for various reasons that are also discussed in Harrington (2006), could not be explained away by a waning of the formality of speaking style leading to greater coarticulation and a shrinkage of the vowel space.

The above-provided explanation gives emphasis to speaker-hypoarticulation and speech production as a basis for diachronic change, but as argued by Ohala in a number of studies concerned with establishing a relationship between synchronic variability and diachronic change, there is also experimental evidence to show that the origin of sound changes is often as likely to be in the ear of the listener as in the mouth of the speaker (e.g., Ohala 1981, 1990, 1993, 2005; Ohala and Feder, 1994). For Ohala, the source of many hypoarticulation-induced sound changes—that is those that

[a]Author to whom correspondence should be addressed at Institut für Phonetik und Sprachverarbeitung, Ludwig-Maximilans Universität München, Schellingstraße 3, D 80799 München, Germany. Electronic mail: jmh@phonetik.uni-muenchen.de

can be related to contextual influences synchronically—is an unintentional error on the part of the listener that comes about because of a failure to compensate for the effects of coarticulation. Central to this idea is that listeners may incorrectly parse phonetic events from one phoneme that are temporally distributed and interwoven with those of another. For example, in a dissociation parsing error, two events in speech production that should be associated or parsed together are not (Ohala and Busà, 1995). Thus, as argued in Hombert *et al.* (1979), the development of phonological tone in certain daughter dialects of middle Chinese and some Southeast Asian languages can be attributed to listeners parsing the speaker's unintended f0 microperturbation not with the voicing status of the preceding consonant, but with tonal properties of the following vowel. The extension of Ohala's model to the analysis in the present study is that /u/-fronting may have come about because listeners fail to parse the fronting effect on /u/ either with a preceding palatal consonant or with a preceding coronal consonant that has a high F2 locus.

The evidence that listeners compensate for coarticulation at all has been demonstrated in various studies (see, e.g., Fujisaki and Kunisaki, 1976; Lindblom and Studdert-Kennedy, 1967; Mann and Repp, 1980 for some of the earliest of these) in which listeners are shown to categorize differently exactly the same acoustic token when it is embedded in two contexts that are known to exert different influences on its phonetic structure. Consider a hypothetical example which is entirely relevant to the present study from Lindblom *et al.* (1995), in which speakers are presumed to produce a back vowel as a fronted variant in an alveolar context because of consonant-on-vowel coarticulation: thus /tut/ which in the speaker's phonological plan is specified with a back vowel may be produced as [tʉt] with a central vowel due to the phonetic fronting effects of the flanking alveolars. However, assuming that listeners have an internalized knowledge of such rules of coarticulation, they can nevertheless recover the speaker's planned /tut/ by factoring out the proportion of /u/-fronting that they assume to be attributable to the alveolar context: that is they undo or compensate perceptually for coarticulation. However, if (for whatever reason) compensation for coarticulation should fail to apply, then the listener recovers not /tut/ but /tʉt/: that is, the listener assumes that a central /ʉ/ formed part of the speaker's phonological (rather than phonetic) speech production plan. A minisound change would then occur according to Ohala, if the listener turned speaker replaces /u/ with /ʉ/, especially if this is done in contexts like *move* in which a phonetically advanced /u/ has no coarticulatory *raison d'être*.

One of the main aims of the present study was to investigate whether there was any evidence for this relationship between the failure to compensate for coarticulation and /u/-fronting that has been taking place in SSB over the last 50 years. We reasoned that if young listeners are more likely to interpret a fronted production of /u/ as intended (i.e., as part of the speaker's phonological speech production plan), then they should show less evidence of compensation for the coarticulatory effects of fronting compared with older listeners from the same SSB-speaking community. A second and related aim was to assess whether, commensurate with the studies cited earlier showing /u/-fronting as a change in progress in SSB, the perceptual boundary along an /i-u/ continuum is shifted to the left for younger listeners—that is, whether young listeners are more likely to label a given token from an /i-u/ continuum as /u/ compared with older listeners from the same community.

In the present study, these perceptual effects were investigated by embedding /i-u/ continua in two sets of minimal pairs: *yeast-used* (*used*, past tense, as in "they used to study"), /jist-just/; and *sweep-swoop*, /swip-swup/.

Based on the foregoing discussion, we made the following predictions.

(1) The /i-u/ boundary should be left-shifted (greater proportion of /u/-responses) for younger listeners in both contexts. This is because, if young listeners' /u/ category boundary has fronted, then it is likely that they will interpret a greater number of stimuli with high F2 on an /i-u/ continuum as /u/.
(2) The /i-u/ boundary should be left-shifted for *yeast-used* compared with *sweep-swoop* for both young and old listeners, if a certain degree of variation in /u/ is interpreted as due to the different coarticulatory influences of the initial consonants. This follows entirely from the theory of, and experimental findings for, perceptual compensation for coarticulation (Beddor *et al.*, 2002; Beddor and Krakow, 1999; Fujisaki and Kunisaki, 1976; Kawasaki, 1986; Mann and Repp, 1980).
(3) The difference in the responses between these two sets of minimal pairs should be less for younger listeners. This is because, if young listeners compensate less for coarticulation—i.e., if they tend to ignore perceptually the influence of the consonant on /u/—then their responses to the same synthetic token whether embedded in a fronting or nonfronting context should be fairly similar, whereas they are predicted to diverge much more for older listeners, assuming that they compensate perceptually to a greater extent for the effects of coarticulation.

Another aim of this study was to relate these predictions from speech perception to speech production in two ways. First (and trivially), younger listeners should show evidence of a left-shifted category boundary in production, i.e., /u/ is expected to be phonetically fronted compared with that of an older group of speakers. Second, if perceptual compensation for coarticulation has weakened in younger listeners, then evidently the perceptual influence of the consonant on /u/ is reduced. We might then expect the coarticulatory influences of the consonant on /u/ also to be reduced in their speech production compared with that of older speakers. Thus we would expect diphones in which the consonant does (e.g., /ju/) and does not (e.g, /wu/) have a fronting effect on the vowel to be phonetically less divergent in the younger than in the older speakers.

In summary, then, there are five hypotheses to be tested, two in production and three in perception:

H1: /u/ is fronted in the production of young SSB speakers.

H2: The coarticulatory consonant-on-vowel influences in /Cu/ are less in younger SSB speakers.

H3: The /i-u/ perceptual boundary is left-shifted (greater proportion of /u/-responses) in younger listeners.

H4: Listeners (young and old) compensate perceptually for the expected coarticulatory influence of a consonant on /u/.

H5: Young listeners compensate less for the influence of a consonant on /u/ compared with older listeners.

II. SPEECH PRODUCTION

A. Method

1. Subjects

The subjects were recruited from the University of Cambridge and through the University College London and included 30 speakers of SSB. The subjects were recruited into a Young and an Old group. The Young group included 14 subjects (3 male, 11 female) aged between 18 and 20 and with an average age of 18.9 years; and the Old group 17 subjects (10 male, 7 female) over the age of 50 and with an average age of 69.2 years. Seven members of the Old group had been taken from the same subject pool as in Hawkins and Midgley (2005). Due to various scheduling difficulties, one subject from the Old group participated only in the production experiment (II) but not in the perception experiment (III); and four other subjects from the Old group participated only in the perception experiment (III) but not in the production experiment. Most of the subjects were tested and recorded in quiet rooms in the Phonetics Laboratory of the University of Cambridge, but some of the older subjects were tested and recorded in a quiet room at their homes. There were no apparent differences in the quality of the recorded speech signal and no differences in the subjects' performance related to the testing location. The equipment (for both the production and the perception experiment) was the same (Sennheiser stereo headset pc165 USB and a Toshiba Tecra notebook) for all recordings.

2. Materials, procedure, and parameters

Subjects produced a number of isolated monosyllabic words with different vowel nuclei to cover most of the RP vowel space. The words were displayed individually on a notebook computer screen in a quiet room and recordings were made with the "SpeechRecorder" software that is routinely used at the University of Munich for speech recording outside the laboratory (Draxler and Jänsch, 2004). A total of 540 words were produced in this way from a randomized list of 10 repetitions of 54 words. Any words that were mispronounced were excluded from the analysis.

The words that were analyzed in the present study included only a subset of these: /i/ (lexical set FLEECE), /u/ (lexical set GOOSE), and /ɑ/ (lexical set START) nuclei. The words with other types of nuclei, of which some will be analyzed in a future study, served mainly as filler and distractor items as far as the present study was concerned. The design of the words with /u/ and /i/ nuclei was shaped by five main criteria:

(1) The two sets of minimal word pairs used in the perception experiment *yeast*, *used*, *sweep*, *swoop* were included.
(2) There was a matched set of /Cu/ and /Cju/ words (e.g., *cooed* and *queued*)
(3) Words were included whose initial consonants had a minimal (*food*, *who'd*), a fronting (*soup*), and a backing (*cooed*) influence on /u/.
(4) There were matched minimal word-pairs between /Cid/ and /Cud/ (e.g. *keyed*, *cooed*)
(5) The final consonant was /d/ as far as possible.

A total of 4296 words were analyzed in this study including 2412 with /u/ nuclei, 1614 with /i/ nuclei, and 270 with /ɑ/ nuclei all taken from the word *hard*. The purpose of including /ɑ/, which in SSB is phonetically open, a monophthong (SSB is nonrhotic), and slightly fronter than cardinal vowel 5, was to provide a relative quantitative measure of /u/-fronting, as described in further detail in Sec. II A 2. The distribution of these 4296 words by age and gender is shown in Table I.

The words were digitized at 44.1 kHz and the first four formant frequencies were calculated using the EMU speech database analysis system (Cassidy and Harrington, 2001). The parameters for formant calculation were: LPC order of 10, a preemphasis of 0.95, and a 30 ms Blackman window with a frame shift of 5 ms. All of the data were segmented and labeled into phonetic segments.

The first two formant frequencies of all vowels in the words in Table I were checked manually both by inspecting the trajectories on the spectrogram and by identifying outliers from ellipse plots in the F1 × F2 formant plane. All the formant frequencies were converted to bark using the formula in Traunmüller (1990).

The quantitative analysis of /u/-fronting was carried out in a three-dimensional space formed from the first three coefficients of the discrete cosine transformation (DCT) applied separately to the Bark-scaled F2 trajectory between the onset and offset of each vowel. The DCT breaks down any trajectory into $\frac{1}{2}$ cycle cosine waves which, if summed, reconstruct the original signal [Watson and Harrington (1999); see also Nossair and Zahorian (1991) and Milner and Shao (2006) for the relationship between DCT and cepstral coefficients]. For an N-point F2-trajectory, $x(n)$, extending in time from $n=0$ to $N-1$ points, the mth DCT coefficient, C_m $(m=0,1,2)$ was calculated with

$$C_m = \frac{2k_m}{N}\sum_{n=0}^{N-1} x(n)\cos\left(\frac{(2n+1)m\pi}{2N}\right)$$

$$k_m = \frac{1}{\sqrt{2}},\ m=0, \quad k_m = 1,\ m \neq 0 \tag{1}$$

Thus the F2 trajectory between the acoustic onset and offset of each vowel was represented by a single point in a three-dimensional space whose axes were formed from the first three DCT coefficients or equivalently from the amplitudes of the cosine waves at frequencies $k=0$, 0.5, and 1 cycles. Since these first three DCT coefficients are proportional to

TABLE I. Number of tokens for each word analyzed in this experiment for young (Y), old (O), male (M), and female (F) speakers shown separately by vowel and with the left consonantal context shown in the left column.

		Y		O		
C(C)	Word	M	F	M	F	Σ
/u/						
j	**used**	30	109	70	60	269
fj	**feud**	29	109	70	58	266
hj	**hewed**	30	108	70	58	266
kj	**queued**	30	110	70	60	270
f	**food**	29	110	70	60	269
s	**soup**	30	110	70	60	270
k	**cooed**	30	110	69	55	264
h	**who'd**	30	110	70	60	270
sw	**swoop**	29	110	70	59	268
	Σ	267	986	629	530	2412
/i/						
j	**yeast**	30	109	70	60	269
f	**feed**	30	109	69	59	267
h	**heed**	30	110	70	60	270
k	**keyed**	30	110	70	60	270
s	**seep**	30	110	70	59	269
sw	**sweep**	30	109	70	60	269
	Σ	180	657	419	358	1614
/ɑ/						
h	**hard**	30	110	70	60	270

the trajectory's mean, linear slope, and curvature, respectively (Guzik and Harrington, 2007), this form of data reduction encodes a significant amount of dynamic information of the F2 trajectory's changing shape in time.

Using a methodology in Harrington (2006) and Guzik and Harrington (2007) we quantified the extent of /u/-fronting by calculating separately for each speaker the relative Euclidean distances of all the speaker's /u/ tokens to the same speaker's /ɑ/ (a back vowel) and /i/ (a front vowel) centroids in the three-dimensional DCT-space described earlier. This is illustrated in Fig. 1 in two dimensions, in which E_1 and E_2 are the Euclidean distances of a given /u/ token to the same speaker's /ɑ/ and /i/ centroids, respectively. The parameter d_u in the following:

$$d_u = \log(E_1/E_2) = \log(E_1) - \log(E_2), \quad (2)$$

is a quantification of the relative proximity of the /u/-token to these two centroids: When d_u is zero, then the token is equidistant between /i/ and /ɑ/; when it is positive, then it is closer to /i/ than to /ɑ/; and when it is negative, it is closer to /ɑ/ than to /i/. We calculated d_u over all /u/-tokens in this way separately for each speaker and using the speaker-specific /i/ and /u/ centroids as illustrated in Fig. 1 (but in a three-dimensional space). The hypothesis to be tested, then, is that if /u/ is phonetically fronted for younger speakers, then d_u should be smaller, reflecting its relatively closer Euclidean proximity to /i/ than to /ɑ/, compared with d_u for older speakers.

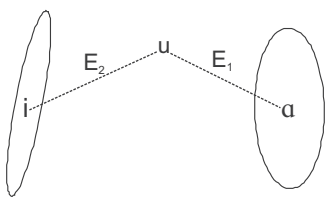


FIG. 1. E_1 and E_2 are the Euclidean distances in an arbitrary two-dimensional space from a single /u/ token to the same speaker's /ɑ/ and /i/ centroids, respectively.

Finally, for the purposes of comparing the influence of C-on-/u/ coarticulation with perceptual responses, we measured the Euclidean distances again separately for each speaker but this time between *used* and *swoop* in the same three-parameter DCT space described earlier. The more that the consonants exert a coarticulatory influence on /u/, then the further apart *used* and *swoop* should be in the parametrized F2 space. Where m_{sw} is the (speaker specific) mean (centroid) of *swoop* in the DCT space, we calculated the Euclidean distances from all tokens of *used* to the same speaker's m_{sw}; and where m_{ju} is the mean of *used* in the same DCT space, we calculated the Euclidean distances from all tokens of *swoop* to the same speaker's m_{ju}. If, for the reasons described in Sec. I, the coarticulatory influences of the initial consonant on /u/ are greater for the older speakers, then they should show greater values on this Euclidean metric (commensurate with a greater F2-trajectory divergence between *used* and *swoop*) compared with younger speakers.

B. Results

We begin by presenting some graphical analyses which were then quantified using the metrics described in Sec. II A 2.

Figure 2 shows the average position in the Bark-scaled F1 × F2 plane of formant values extracted at the temporal

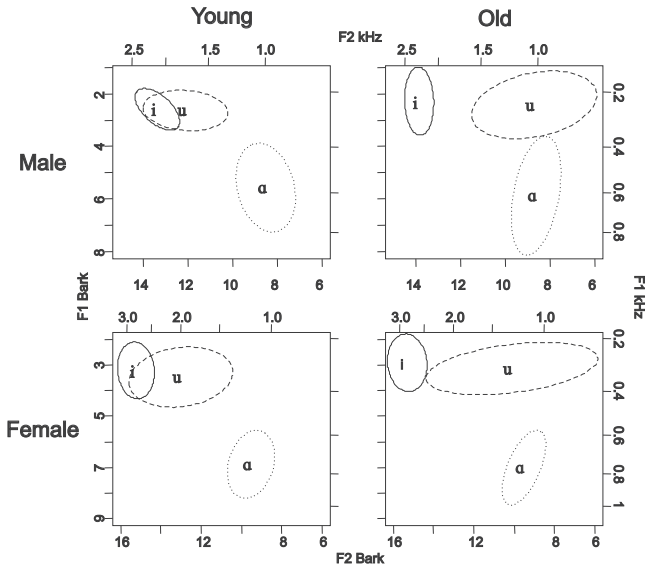


FIG. 2. 95% confidence ellipses for /iuɑ/ in a Bark-scaled formant plane shown separately for the age and gender groups in formant data extracted at the vowels' temporal midpoints.

midpoint of /i, u, ɑ/ separately for the gender and age groups. It is evident that F2 of /u/ is higher for young speakers, which is consistent with the various findings discussed in Sec. I that it is also phonetically fronter. The ellipses for /u/ are also somewhat larger for old speakers which would suggest that consonantal context had a more marked coarticulatory effect on /u/ than for young speakers.

Figure 3 shows linearly time-normalized trajectories for the second formant frequency over the extent of /ju/ in *used* and /wu/ in *swoop*, averaged separately for the four gender × age combinations. The formant trajectory shapes across gender (left and right panels) are fairly similar, but there are markedly different F2 patterns across the two age groups. In particular, three features characterize the old as opposed to the young group of speakers:

(1) F2 of *used* falls much more steeply and to a lower value (of roughly 1600 Hz in males and 1800 Hz in females) than in the young group for which F2 is more or less level (at around 2000 Hz for the male speakers and just over 2000 Hz for the female speakers).

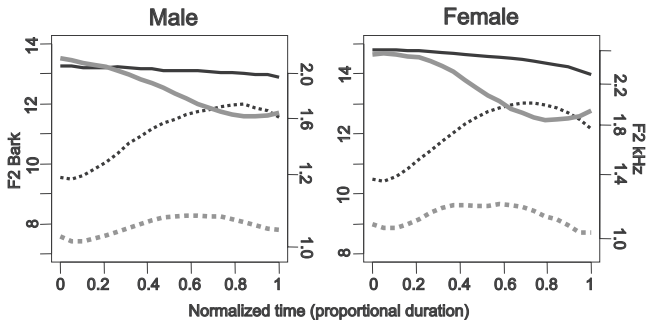


FIG. 3. Bark-scaled F2 trajectories between the onset and offset of /ju/ in *used* (solid) and /wu/ in *swoop* (dotted) that were linearly time-normalized and averaged across the young (black) and old (gray) groups shown separately for male (*left*) and female (*right*) speakers.

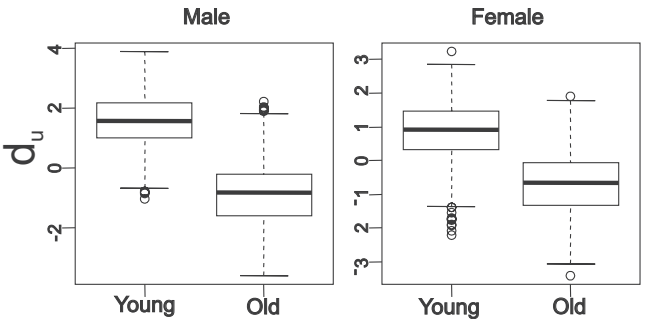


FIG. 4. Boxplots showing the median (thick horizontal bar), interquartile range and outliers (circles) on the parameter d_u, the log Euclidean distance ratio, across the young and old groups separately for male (*left*) and female (*right*) speakers.

(2) F2 of *swoop* rises but to a much lower frequency than for the young group.
(3) There is a considerably greater difference especially at F2 onset but also throughout the entire trajectories between *used* and *swoop* than for the young group. This suggests that the extent of C-on-V coarticulation is somewhat greater in the old group and for two reasons. First, because there is a more substantial deviation for the old group between the F2 onsets and by extension between the F2 loci of /w/ and /j/; and second because there is evidently a greater convergence in F2 toward a common vowel target across these two word contexts in the young group, as shown by the smaller separation between the *used* and *swoop* trajectories in both young male and female speakers.

We quantified the differences in the extent of /u/-fronting between the two age groups by calculating d_u, the log. Euclidean distance ratios in a three-dimensional DCT space, using the formula in Eq. (2) as described in Sec. II A 2. The results of these calculations are shown as boxplots for /u/ and /ju/ words in Fig. 4.

For both males and females, it is evident that the log Euclidean distance ratio, d_u, is greater for the younger speakers. Moreover, for the younger speakers, d_u is positive, which suggests that /u/ is closer to /i/ than to /ɑ/ on F2; by contrast, d_u is negative for the older speakers and so for them /u/ is closer on F2 to /ɑ/ than to /i/.

The results of a repeated measures analysis of variance (ANOVA) with dependent variable log Euclidean distance ratio, two between-subjects factors, Age (Young vs Old) and Gender, and a within-subjects factor for Word (9 levels corresponding to the 9 word types shown in Table I with a /u/ or /ju/ nucleus) showed a significant effect for Age [$F(1,13)=117.1$, $p<0.001$]. There was also an (unsurprising) significant effect for Word [$F(1,8)=167.7$, $p<0.001$], which simply means that F2 in the different words in Table I with /u/ or /ju/ nuclei were not all equally close to /i/ as to /ɑ/. There was no significant effect for Gender which may have come about because of the small number of male speakers in the young group.

The only interaction that was significant was Word × Age [$F(1,8)=10.1$, $p<0.001$]. This means that the extent of

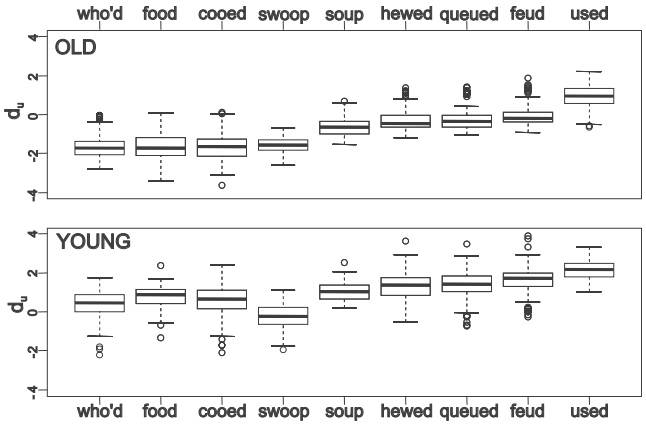


FIG. 5. Boxplots showing the median (thick horizontal bar), interquartile range, and outliers (circles) on the parameter d_u, the log Euclidean distance ratio, for the old (*above*) and young (*below*) groups separately for each word. The boxplots are rank ordered from lowest to highest median d_u in the old group in both cases.

/u/-fronting for the young relative to the old group was not the same in all words. Three findings emerged from a subsequent analysis of the word-specific distributions which are shown separately for the two age groups in Fig. 5. First, as also shown by *post-hoc* Tukey tests, there is a marked and significant ($p<0.001$) difference between the age groups for all words. As Fig. 5 shows, the median log Euclidean distance ratio is greater than zero for all words except *swoop* in the young speakers, which means they are all acoustically closer on (DCT and Bark-transformed) F2 to front /i/ than to back /ɑ/. There is exactly the opposite pattern in the older speakers for which the vowels of all words except *used* are closer to /ɑ/ (since median d_u is negative in these cases). Second, the relative positions and therefore rank order from lowest to highest d_u is very similar for both age groups: The main exception is *swoop* which has a roughly similar median value as the other back variants of /u/ in *cooed*, *who'd*, *food* for the older speakers, but which has a lower value in comparison with the three words in the younger speakers. The third finding falls out from the first two: The differences between the age groups were greatest in words with retracted /u/: that is, the difference between the age groups on the log Euclidean distance ratios was, as Fig. 5 shows, evidently greater for *cooed*, *who'd*, *food* than for *queued*, *hewed*, and *feud*.

We quantified these word-specific differences more precisely by measuring in the same Bark-transformed DCT space the Euclidean distances between the age groups separately for each word. More specifically, we calculated for *swoop* the Euclidean distances from all the young speakers' *swoop* tokens to the old group's *swoop* centroid; and the Euclidean distances from all the old speakers' *swoop* tokens to the young group's *swoop* centroid. The more these word-specific distributions of younger and older speakers overlap with each other, then the closer these distances should be to zero. We then carried out the same word-specific Euclidean measure for all word types separately. As Fig. 6 shows, the pattern of the resulting distribution on this measure is very similar to that obtained from the metric used for quantifying

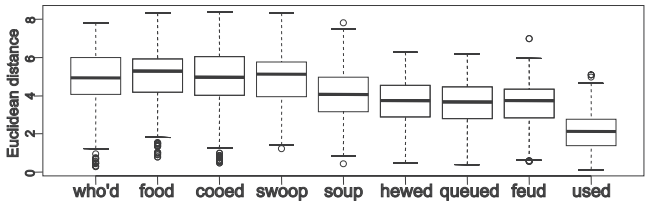


FIG. 6. Boxplots showing the median (thick horizontal bar), interquartile range and outliers (circles) on the inter-Euclidean distances (arbitrary units) between the young and old groups calculated in a Bark-scaled and DCT-transformed F2 space separately for each word. The words are arranged in the same order as in Fig. 5.

the relative position of the old speakers' vowels on a phonetic front–back dimension (Fig. 5). Thus, the greatest difference between the two age groups is for those vowels whose allophones are most retracted in the older speakers. This provides further evidence that the sound change involves a realignment in production of the phonetically back allophones of /u/ toward a phonetically front position (as a result of which, phonetically front variants of /u/ show the least displacement).

As far as the measures of coarticulation described in Sec. II A 2 are concerned, Fig. 7 shows the logarithm of the Euclidean distances from *used* tokens to the *swoop* centroid and from *swoop* tokens to the *used* centroid by age and gender: These distances are clearly greater for the old compared with the young group. A repeated measures ANOVA with dependent variable log Euclidean distances and two between-subjects factors, Age (Young vs Old) and Gender, and a within-subjects factor for Word (*used* and *swoop*) showed a significant effect for Age [$F(1,20)=36.5$, $p<0.001$] but no other significant effects.

III. SPEECH PERCEPTION

A. Method

For the perception experiment, HLsyn (High Level Parameter Speech Synthesis System, version 2.2) was used for creating the synthetic stimuli. With the exception of five subjects from the Old group, of which one participated only in the production experiment and of which four participated

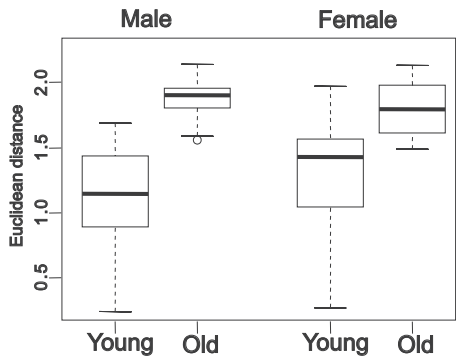


FIG. 7. Boxplots showing the median (thick horizontal bar), interquartile range and outliers (circles) on the logarithm of the inter-Euclidean distances (arbitrary units) calculated in a Bark-scaled and DCT-transformed F2 space between *used* and *sweep* shown separately for age and gender.

only in the perception experiment, listening responses were obtained from the same subjects who had participated in the production experiment (see Sec. II A 1 for further details).

We carried out various pretests with trained L1-English phoneticians to obtain naturalness judgments to a number of continua in the two word-contexts described more fully in the following, both in order to guarantee that our synthesized end points were intelligible as the intended words and to determine the perceptually most natural continuum as far as F2 changes were concerned.

We created two 13-step synthetic continua, one each between two sets of minimal-word pairs: *yeast-used* (/jist/-/just/ and henceforth /jVst/) and *sweep-swoop* (/swip/-/swup/ and henceforth /swVp/). These word pairs were chosen because the anterior /j_s/ context in the former is expected to have a phonetic fronting effect in speech production for which listeners might be expected to compensate perceptually relative to /sw_p/, as described in Sec. I.

The continua in both cases were created by varying F2 in the following ways. For the /jVst/ continuum, F2 was varied from 1278 Hz (stimulus 1 nearest /u/) to 2428 Hz (stimulus 13 nearest /i/) in equal 0.45 Bark-size steps. The following parameters were fixed for all stimuli in /jVst/: the F2-locus of the preceding /j/ at 2450 Hz; a transition phase of 90 ms in which F2 decreased linearly; a following steady-state vowel of 120 ms in duration; a level F1 and F3 from the periodic onset to the offset at 280 and 2700 Hz, respectively.

For /swVp/, F2 varied between 1014 Hz (stimulus 1) to 2320 Hz (stimulus 13) in 0.35 Bark steps. The /w/ locus was fixed at 600 Hz. There was a transition phase of 45 ms which was followed by a steady vowel of 140 ms with F1 and F3 fixed from the periodic onset to the offset at 280 and 2544 Hz, respectively. The reason why the two continua in /jVst/ and /swVp/ did not have the same formant end points was for reasons of perceived naturalness.

The 26 stimuli were randomized and individual synthetic word tokens were presented from both continua in one session 5 times (5 repetitions × 13 steps × 2 continua=130 randomized stimuli). For the perception experiment, subjects listened to each stimulus separately and carried out a forced-choice identification task in which they responded to each stimulus with one of *used*, *yeast*, *swoop*, or *sweep*.

Since, as described earlier, the two continua were synthesized with different end points, we had to map them onto the same F2-scale for the purposes of comparing the responses between them. The matching was done by aligning in frequency the responses to /jVst/ with those of /swVp/ at the closest F2 correspondences between the stimuli. For example, we compared responses to stimulus 4 from /swVp/ (F2=1260 Hz) with responses to stimulus 1 from /jVst/ with F2=1278 Hz because these were the two stimuli with the smallest F2 difference (Δ_{F2}=1278−1260=18 Hz) between them. As Table II shows, we had to exclude from the analysis responses to stimuli 1–3 from /swVp/ and to stimulus 13 from /jVst/ for which no closest F2 matches from the other continuum were available. We also had to collapse the responses to stimuli 4 and 5, and to 9 and 10 in /jVst/ for the same reason (see Table II for further details). The responses to the continua in Sec. III B are therefore presented for 10 stimuli based on the matched F2 values shown in the right column of Table II.

TABLE II. F2 values on the 13-point synthetic continuum for *sweep-swoop* (column 2), *yeast-used* (column 3), and the derived F2-aligned, 10-point continuum analyzed in this study (far right column).

Stimulus No.	/swVp/ F2 values (Hz)	/jVst/ F2 values (Hz)	Mean F2 value (Hz)
1	01. 1014		
2	02. 1092		
3	03. 1173		
4	04. 1260	01. 1278	1. 1269
5	05. 1351	02. 1350	2. 1351
6	06. 1447	03. 1426	3. 1437
7	07. 1549	04. 1505+05. 1588=1546.5	4. 1548
8	08. 1658	06. 1675	5. 1667
9	09. 1773	07. 1766	6. 1770
10	10. 1897	08. 1872	7. 1885
11	11. 2028	09. 1964+10. 2070=2017	8. 2023
12	12. 2169	11. 2183	9. 2176
13	13. 2320	12. 2302	10. 2311
		13. 2428	

Two types of analyses were carried out on the perceptual responses. First, the results were analyzed with a repeated measures ANOVA with the stimulus number from the synthetic continua as a repeated-measure dependent variable, and with Context (a within-subject factor with two levels, /jVst/ vs /swVp/) and Age (between-subject factor with two levels, Old and Young) as the independent variables. Second, we carried out another repeated measures ANOVA with the same independent variables but with the category boundary obtained separately for each listener (i.e., the F2 frequency for which responses with /i/ or /u/ were 50%) as the dependent variable (Fig. 8). The 50% category boundary was calculated using probit analysis following exactly the same procedure as in, e.g., Lotto *et al.* (1996).

B. Results

The results of the comparison of the entire continua showed significant effects for Age [$F(1,28)=6.163$; $p<0.05$], and for Context [$F(1,28)=34.3$, $p<0.001$], as well

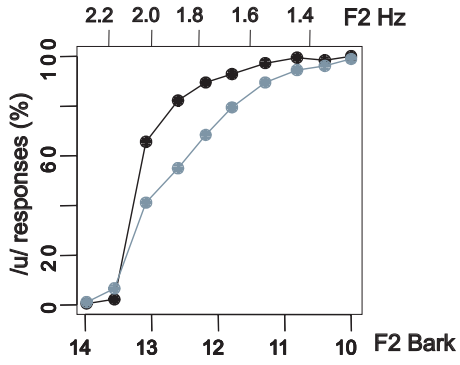


FIG. 8. (Color online) Percentage of /u/ responses as a function of decreasing F2 by young (*black*) and old (*gray*) listeners to synthetic continua pooled across *yeast-used* and *sweep-swoop*.

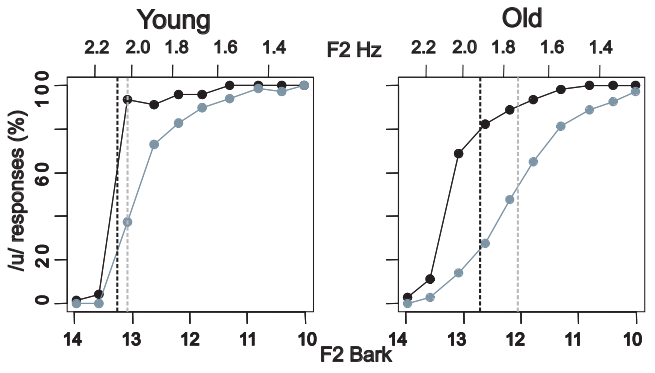


FIG. 9. (Color online) Percentage of /u/ responses as a function of decreasing F2 by young (*left panel*) and old (*right panel*) listeners to *used-yeast* (*black*) and *sweep-swoop* (*gray*). The vertical dotted lines show the mean category boundaries in *yeast-used* (*black*) and *sweep-swoop* (*gray*).

as a significant Context × Age interaction [$F(1,28)=4.3$, $p<0.05$]. The results of the comparison of the category boundaries, whose means for the four Age × Content conditions are superimposed on Fig. 9, were broadly consistent with those obtained from comparing the entire continua. There was a significant effect for Age [$F(1,28)=5.63$; $p<0.05$], for Context [$F(1,28)=39.7$, $p<0.001$], although a not quite significant Context × Age interaction [$F(1,28)=3.67$, $p=0.066$].

The effect across both sets of results for Age shows that, consistent with H3 (Sec. I), the /i-u/ boundary was left-shifted for the Young group: that is younger listeners were more likely to hear the same synthetic token as /u/ compared with older listeners, an effect which is clearly shown in Fig. 8. The effect across both sets of results for Context shows that the /i-u/ boundary was left-shifted in /jVst/: that is, listeners were more likely to hear the same synthetic token as /u/ in *yeast-used* compared with *sweep-swoop* (Fig. 9). This result is a replication of various experiments reviewed in Sec. I showing that listeners compensate perceptually for the effects of coarticulation.

The result of the Context × Age interaction which was significant in comparing the entire continua and not quite significant in comparing category boundaries, together with the data in Fig. 9 showing the responses separately to the two continua by age, is, in general, compatible with Hypothesis 5: Evidently, the young listeners did not compensate as much as the old listeners for coarticulation since the differences in their responses to *yeast-used* versus *sweep-swoop* were less than for older listeners. Thus, *post-hoc* Tukey tests showed that there were no significant differences between *yeast-used* versus *sweep-swoop* for the young listeners, neither in comparing the entire continua nor in comparing category boundaries; but that there were significant differences in older listeners' responses to *yeast-used* versus *sweep-swoop* both in comparing the entire continua ($p<0.001$) and in comparing category boundaries ($p<0.001$).

However, Fig. 9 also shows that the relatively diminished perceptual compensation for coarticulation in younger listeners came about because of differences in responses by the two age groups to /swVp/. More specifically, the results of *post-hoc* Tukey tests showed that there were no significant differences between the two age groups in their responses to /jVst/, either based on comparing the entire continua ($p=0.88$), or based on comparisons between the category boundaries ($p=0.86$). On the other hand, there were significant differences between the age groups in their responses to /swVp/, both in comparing continua ($p<0.01$) and in comparing category boundaries ($p<0.05$). This means that the main reason why there were overall different perceptual responses between the age groups (Fig. 8) was because the /i-u/ boundary on *sweep-swoop* was left-shifted in younger relative to that of the older listeners. We discuss the further implication of this result together with those from the acoustic analysis in Sec. IV.

IV. DISCUSSION

The hypothesis H4, that listeners compensate for the effects of coarticulation, is supported by the results from this experiment. Listeners attribute a certain proportion of vowel fronting on an /i-u/ continuum to the effects of consonantal context and factor this out: Accordingly, there is a greater probability that the same stimulus token will be perceived as /u/ in a fronting context such as /j_s/ than in a backing consonantal context such as /sw_p/. These findings are consistent with various studies showing perceptual compensation for coarticulation (Beddor *et al.*, 2002; Beddor and Krakow, 1999; Kawasaki, 1986; Fujisaki and Kunisaki, 1976; Mann and Repp, 1980), but also more generally with speech perception models (Fowler, 1984; Fowler and Smith, 1986; Ohala, 1993) in which listeners are sensitive to the nature and extent of coarticulatory overlap between segments.

The results of the production study showed unequivocally that younger speakers have a fronter realization of /u/ than older speakers (consistently with H1): this result lends support to other acoustic and auditory studies (Gimson, 1966; Hawkins and Midgley, 2005; Roach and Hartman, 1997) as well as to the longitudinal analysis in Harrington (2007) that /u/ in SSB has fronted in the last 40 years. The present investigation extends these analyses by showing that young listeners not only produce a fronter realization of /u/, but they also have a fronter category boundary in perceiving this vowel. Thus, H3, that young and old listeners respond differently to the same continuum that spans a sound-change in progress, was also supported by these data. In light of these data as well as other recent experimental studies on sound change in progress (e.g., Warren *et al.*, 2007), we have to abandon the notion that there is a uniform relationship between the phonological system and phonetic output for all members of the same speech community. Instead, phonological category boundaries are likely to be specific to different groups of speakers of the same speaking community and above all strongly related to the differences in their own speech production. The model that seems to be best able to account for these differences is an episodic or exemplar-based model of speech perception (Johnson, 1997; Pierrehumbert, 2002, 2003a, b, 2006). In this model, a phonological category is defined by a distribution in a perceptual space that depends on its remembered exemplars. Moreover, speech production involves the selection of one of the

exemplars—typically one that is most probable and nearest the center of the distribution (Pierrehumbert, 2001). Two features from this model are consistent with the results from the present study. First, that the phonological category boundaries can be (and are likely to be) different from one individual to the next, given that the remembered exemplars from which a phonological category is constructed will certainly be different across different individuals, even of the same speaking community. Second that, since in speech production an exemplar is selected from the phonological category that is built out of perceived and remembered exemplars, there is a close link between the category boundaries in speech perception and production: Thus our interpretation of these data within this model is that younger members of the community who place the category boundary closer to /i/ on /i-u/ in perception are also more likely to produce a more fronted /u/ than older members of the same community (because if the category boundary shifts toward /i/, then so does the center of gravity from which tokens are most likely to be selected in speech production).

The most important hypothesis in this paper, H5, was that if, following Ohala (1981, 1993), sound change comes about because listeners fail to undo perceptually the effects of consonant on vowel coarticulation, then the differences in the responses to the two continua should be a good deal less for younger listeners. Before we assess in detail the extent to which this hypothesis was substantiated, we will briefly recap the three main findings from the perception experiments. First, the results showed that, compatible with H5, there was a significantly greater difference in responses to the two continua by the older listeners. Evidently this shows that the older listeners' responses were influenced by consonantal context to a far greater degree than those of the younger listeners. Here there is, once again, compatibility with their speech production because the acoustic influence of consonantal context on the vowel was also greater (H2), as shown by the older speakers' greater divergence between *used* and *swoop* in a (bark and DCT-parametrized) F2 space. Second, the two age groups differed minimally and not significantly in their perceptual responses to *yeast-used*. And third, they differed extensively and significantly in their perceptual responses to *sweep-swoop*.

We now consider in further detail whether these three findings can be reconciled with Ohala's (1981, 1993) model in which a minisound change occurs as a result of a failure to compensate for coarticulation which is then carried over into speech production. Our starting point in this interpretation is the finding that young and old listeners have more or less the same responses to the *yeast-used* continuum. Here we would argue that although both age groups cut up the *yeast-used* continuum in a similar way, the difference is in the classification: Older listeners classify the distinction as /i-u/ as opposed to the younger listeners who classify it as /i-ʉ/. Thus, suppose there is a token midway between the synthesis end points which we denote as [ʉ]. Older listeners compensate for coarticulation and attribute a certain amount of fronting to the consonantal context and classify it perceptually as a back vowel /u/. Younger listeners compensate far less, or minimally, for the effects of consonantal context and classify it perceptually as a central vowel /ʉ/. So, in both cases, the *position* of the category boundary on the *yeast-used* continuum may be roughly the same (left-*shifted* in old speakers because they compensate for coarticulation, but *positioned* to the left and near /i/ in young listeners because /ʉ/, being a central vowel, is characterized in speech production by a mid-high F2) but the *classification* is different. Now consider the results for *sweep-swoop*. Here there is of course no reason to compensate for the fronting effects of coarticulation and so the category boundary for older listeners shifts to the right commensurate with their classification of the low end of the F2 continuum as a back /u/, resulting in a relatively greater proportion of /i/ responses and a marked and significant difference compared with their responses to *yeast-used*. Since younger listeners compensate minimally for coarticulation, their category boundary is not significantly different from their *yeast-used* but it is significantly to the left of the older listeners' *sweep-swoop* boundary (who divide the continuum into /i-u/). Thus all of the findings from the perception experiment and their relationship to those from the production experiment are consistent with the following two ideas. First, older listeners compensate perceptually for the coarticulatory fronting effects of a consonantal context in *yeast-used* but younger listeners do not (or compensate much less). Second, there is a difference of *phonological* category between the two groups: Older listeners make a contrast between /i/ and /u/ whereas for younger listeners of the same speaking community, the contrast is between /i/ and a central vowel /ʉ/. It is because the two age groups cut up the *sweep-swoop* continuum differently and because the young listeners show neither significant evidence of coarticulatory compensation in perception nor of a back vowel allophone in contexts like *swoop* in production that we wish to argue for a difference in phonological category: this is, of course, very different from suggesting that the two age groups have the same /i-u/ contrast and differ because the young speaker-listeners realize /u/ phonetically as [ʉ].

The stages that give rise to the sound change within Ohala's model might then be as follows. The divergence between front and back variants of /u/ 40–50 years ago was very large (and is still considerable in older speakers) necessitating compensation for coarticulation in the front consonantal context to bring about a perceptual realignment of front realizations of /u/ with retracted variants, thereby maintaining the phonetic integrity of the phonological category /u/. With the assumed waning of perceptual compensation for coarticulation, the integrity of the phonological category was preserved by shifting diachronically *in production* the back toward the front variants. This suggests that the extent of this shift was greatest in the phonetically most retracted variants and some evidence to support this has been presented in Figs. 5 and 6 in which, for example, the difference between young and older speakers' production of *food* or *who'd* was greater than for *feud* or *hewed*.

In the above-presented analysis, the failure to compensate perceptually for coarticulation is the trigger for the sound change in which /u/ changes to /ʉ/. However, the data from the present study might be just as compatible with an episodic model of perception and production in which the

frequency and probability with which /u/ occurs in a certain context is the trigger for sound change. An analysis of the CELEX database (Baayen *et al.*, 1997) in Harrington (2007) reported that just over 70% of SSB /u/ occur in words following a consonant with a high F2 locus, either after /j/ (*argue*, *cute*, *duty*, *few*) or after alveolars (*lose*, *noon*, *soon*). In an episodic model of speech perception, frequency of occurrence emerges as a direct consequence of remembered instances of words and it exerts an influence on speech perception by way of activation strength (Pierrehumbert, 2001). Essentially, more frequently occurring remembered exemplars have higher resting levels of activation and are therefore more likely to be selected than low frequency tokens in matching a remembered exemplar to an incoming speech signal in speech perception: This type of association between statistical frequency and activation strength can explain why in speech perception there is a bias toward perceiving more frequently occurring phonotactic consonant clusters, as shown by Hay *et al.* (2003). In speech production, an exemplar is, according to Pierrehumbert (2001), selected at random from a cloud of remembered tokens, but in such a way that the selection is weighted by the same frequency effects and activation strengths that bias speech perception. Since this model of speech production is probabilistic, then an exemplar may sometimes be selected from the exemplar cloud for /u/ that is not always quite appropriate for the consonantal context. Moreover, since fronted allophones of /u/ are statistically more frequent and therefore have a higher activation strength, the probability that the speaker inappropriately selects a front allophone of /u/ for a context like *swoop* is greater than the probability of inappropriately selecting a back allophone of /u/ for a fronting context like *yeast*. This greater probability of misselecting front allophones may be the mechanism by which the center of gravity of the entire /u/ cloud is incrementally shifted toward the front part of the vowel space [see Pierrehumbert (2001) for further details on the way in which this kind of bias and incremental shift can be introduced over time into speech production]. Thus the evidence that high frequency labels are advantaged perceptually because of their stronger perceptual representations (Pierrehumbert, 2003a) and that low frequency items are less robust than high frequency items (Hay *et al.*, 2003; Silverman, 2004) may then have been the trigger for back variants of /u/ to front. As the back variants were fronted, the center of gravity of the entire /u/ distribution would necessarily be fronted even further; and this may be the reason why there is some further minor phonetic advancement of vowels even in fronted /j/ contexts, as the difference between the age groups in the relative positions in production of words like *used* and *feud* shows (Fig. 5). With the progression of the sound change, listeners would need to compensate less for coarticulation in the front context because the divergence between the front and back variants of /u/ would be lessened as the sound change progressed (thus progressively reducing the need for perceptual realignment). So in this model, the waning of perceptual compensation for coarticulation would be an *effect*, not the *cause* or trigger for /u/-fronting.

In summary, we have found evidence that /u/-fronting is a sound change in progress in SSB both in production and perception. Since for the younger speaker-hearers, the phonological category is fronted relative to that of the older speaker-hearers, they produce phonetically fronted [ʉ] vowels and their category boundary is nearer /i/ than for older listeners. However, because older listeners compensate perceptually for the coarticulatory fronting influences of the consonant on a vowel, this age-group difference manifests itself perceptually only in contexts in which the consonant causes the vowel to be phonetically fronted. These coarticulatory-dependent perceptual differences between the age groups are commensurate with their speech production: The coarticulatory influences of the consonant in a fronting context are much more pronounced for the older speakers leading to consonant-dependent divergent vowel variants that are not in evidence for the young. Finally, the finding that there are perceptual differences between the age groups is consistent with Ohala's (1981, 1993) model in which a coarticulatory-dependent allophone may be phonologized (leading to sound change) if listeners give up on compensating perceptually for coarticulation in the same context. It may, however, also be compatible with an episodic model of speech perception and production in which phoneme frequency effects trigger a realignment in production between phonetically markedly divergent variants. Further research, possibly involving an analysis of a different hypo-articulation-induced sound change whose variants are less distinguished by statistical frequency effects, would be needed to resolve this issue further.

ACKNOWLEDGMENTS

The authors thank Ann-Kathrin Killguss for help with labeling, Sarah Hawkins of the Department of Linguistics, University of Cambridge, as well as Valerie Hazan and Moira Yip of the University College London for their help in recruiting subjects, and Allard Jongman and two reviewers for their comments. We are also very grateful to all the subjects at Cambridge and London for participating in this study. This research was supported by German Research Council Grant No. HA3512/3-3, "Sound change, lexical frequency, and variability: an experimental study of Southern British English, Received Pronunciation."

Baayen, R., Dijkstra, T., and Schreuder, R. (**1997**). The CELEX Lexical Database, Linguistic Data Consortium, University of Pennsylvania, Philadelphia (CD-ROM).

Bauer, L. (**1985**). "Tracing phonetic change in the received pronunciation of British English," J. Phonetics **13**, 61–81.

Beddor, P., Harnsberger, J., and Lindemann, S. (**2002**). "Language-specific patterns of vowel-to-vowel coarticulation: Acoustic structures and their perceptual correlates," J. Phonetics **30**, 591–627.

Beddor, P., and Krakow, R. (**1999**). "Perception of coarticulatory nasalization by speakers of English and Thai: Evidence for partial compensation," J. Acoust. Soc. Am. **106**, 2868–2887.

Cassidy, S., and Harrington, J. (**2001**). "Multi-level annotation in the Emu speech database management system," Speech Commun. **33**, 61–77.

de Jong, G., McDougall, K., Hudson, T., and Nolan, F. (**2007**). "The speaker discriminating power of sounds undergoing historical change: A formant-based study," *Proceedings of the 16th International Congress of Phonetic Sciences*, Saarbrücken, Germany, pp. 1813–1816.

Draxler, C., and Jänsch, K. (**2004**). "SpeechRecorder—A universal platform independent multichannel audio recording software," *Proceedings of the Fourth International Conference on Language Resources and Evaluation*, Lisbon, Portugal, pp. 559–562.

Fowler, C. A. (**1984**). "Segmentation of coarticulated speech in perception," Percept. Psychophys. **36**, 359–368.
Fowler, C. A., and Smith, M. R. (**1986**). "Speech perception as 'vector analysis:' An approach to the problems of segmentation and invariance," in *Invariance and Variability of Speech Processes*, edited by J. Perkell and D. Klatt (Erlbaum, Hillsdale, NJ), pp. 123–139.
Fujisaki, H., and Kunisaki, O. (**1976**). "Analysis, recognition and perception of voiceless fricative consonants in Japanese," Annual Bulletin RILP No. 10, 145–156.
Gimson, A. C. (**1966**). *An Introduction to the Pronunciation of English*, 1st ed. (Arnold, London).
Guzik, K., and Harrington, J. (**2007**). "The quantification of place of articulation assimilation in electropalatographic data using the similarity index (SI)," Advances in Speech–Language Pathology **9**, 109–119.
Harrington, J. (**2006**). "An acoustic analysis of 'happy-tensing' in the Queen's Christmas broadcasts," J. Phonetics **34**, 439–457.
Harrington, J. (**2007**). "Evidence for a relationship between synchronic variability and diachronic change in the Queen's annual Christmas broadcasts," in *Laboratory Phonology 9*, edited by J. Cole and J. Hualde (Mouton de Gruyter, Berlin), pp. 125–143.
Harrington, J., Palethorpe, S., and Watson, C. (**2000a**). "Does the Queen speak the Queen's English?" Nature (London) **408**, 927–928.
Harrington, J., Palethorpe, S., and Watson, C. (**2000b**). "Monophthongal vowel changes in Received Pronunciation: An acoustic analysis of the Queen's Christmas broadcasts," J. Int. Phonetic Assoc. **30**, 63–78.
Hawkins, S., and Midgley, J. (**2005**). "Formant frequencies of RP monophthongs in four age groups of speakers," J. Int. Phonetic Assoc. **35**, 183–199.
Hay, J., Pierrehumbert, J., and Beckman, M. (**2003**). "Speech perception, wellformedness and the statistics of the lexicon," in *Papers in Laboratory Phonology VI: Phonetic Interpretation*, edited by J. Local, R. Ogden, and R. Temple (Cambridge University Press, Cambridge), pp. 58–74.
Henton, C. (**1983**). "Changes in the vowels of received pronunciation," J. Phonetics **11**, 353–371.
Hombert, J.-M., Ohala, J. J., and Ewan, W. G. (**1979**). "Phonetic explanations for the development of tones," Language **55**, 37–58.
Johnson, K. (**1997**). "Speech perception without speaker normalization," in *Talker Variability in Speech Processing*, edited by K. Johnson and J. W. Mullennix (Academic, San Diego), pp. 145–166.
Kawasaki, H. (**1986**). "Phonetic explanation for phonological universals: The case of distinctive vowel nasalization," in *Experimental Phonology*, edited by J. J. Ohala and J. J. Jaeger (Academic, New York), pp. 81–103.
Lindblom, B., Guion, S., Hura, S., Moon, S.-J., and Willerman, R. (**1995**). "Is sound change adaptive?" Rivista Di Linguistica **7**, 5–37.
Lindblom, B., and Studdert-Kennedy, M. (**1967**). "On the role of formant transitions in vowel recognition," J. Acoust. Soc. Am. **42**, 830–843.
Lotto, A. J., Kluender, K. R., and Green, K. P. (**1996**). "Spectral discontinuities and the vowel length effect," Percept. Psychophys. **58**, 1005–1014.
Mann, V. A., and Repp, B. H. (**1980**). "Influence of vocalic context on perception of the [ʃ]-[s] distinction," Percept. Psychophys. **28**, 213–228.
McDougall, K., and Nolan, F. (**2007**). "Discrimination of speakers using the formant dynamics of /u:/ in British English," *Proceedings of the 16th International Congress of Phonetic Sciences*, Saarbrücken, Germany, pp. 1825–1828.
Milner, B., and Shao, X. (**2006**). "Clean speech reconstruction from MFCC vectors and fundamental frequency using an integrated front-end," Speech Commun. **48**, 697–715.
Nossair, Z. B., and Zahorian, S. A. (**1991**). "Dynamical spectral features as acoustic correlates for initial stop consonants," J. Acoust. Soc. Am. **89**, 2978–2991.
Ohala, J. J. (**1981**). "The listener as a source of sound change," in *Papers from the Parasession on Language and Behavior*, edited by C. S. Masek, R. A. Hendrick, and M. F. Miller (Chicago Linguistic Society, Chicago), pp. 178–203.
Ohala, J. J. (**1990**). "The phonetics and phonology of aspects of assimilation," in *Papers in Laboratory Phonology I: Between the Grammar and the Physics of Speech*, edited by J. Kingston and M. Beckman (Cambridge University Press, Cambridge), pp. 258–275.
Ohala, J. J. (**1993**). "The phonetics of sound change," in *Historical Linguistics: Problems and Perspectives*, edited by C. Jones (Longman, London), pp. 237–278.
Ohala, J. J. (**2005**). "Phonetic explanations for sound patterns. Implications for grammars of competence," in *A Figure of Speech. A Festschrift for John Laver*, edited by W. J. Hardcastle and J. M. Beck (Erlbaum, London), pp. 23–38.
Ohala, J. J., and Busà, M. G. (**1995**). "Nasal loss before voiceless fricatives: A perceptually-based sound change, " Rivista di Linguistica **7**, 125–144.
Ohala, J. J., and Feder, D. (**1994**). "Listeners' identification of speech sounds is influenced by adjacent 'restored' phonemes," Phonetica **51**, 111–118.
Pierrehumbert, J. (**2001**). "Exemplar dynamics: Word frequency, lenition, and contrast," in *Frequency Effects and the Emergence of Linguistic Structure*, edited by J. Bybee and P. Hopper (J Benjamins, Amsterdam), pp. 137–157.
Pierrehumbert, J. (**2002**). "Word-specific phonetics," in *Laboratory Phonology VII*, edited by C. Gussenhoven and N. Warner (Mouton de Gruyter, Berlin), pp. 101–140.
Pierrehumbert, J. (**2003a**). "Probabilistic phonology: Discrimination and robustness," in *Probabilistic Linguistics*, edited by R. Bod, J. Hay, and S. Jannedy (MIT Press, Cambridge), pp. 177–228.
Pierrehumbert, J. (**2003b**). "Phonetic diversity, statistical learning, and acquisition of phonology," Lang Speech **46**, 115–154.
Pierrehumbert, J. (**2006**). "The next toolkit," J. Phonetics **34**, 516–530.
Roach, P., and Hartman, J. (**1997**). *English Pronouncing Dictionary*, 15th ed. (Cambridge University Press, Cambridge).
Silverman, D. (**2004**). "The diachrony of labiality in Trique, and the functional relevance of gradience and variation," in *Papers in Laboratory Phonology 8*, edited by L. M. Goldstein, D. H. Whalen, and C. T. Best (Mouton de Gruyter, Berlin).
Traunmüller, H. (**1990**). "Analytical expressions for the tonotopic sensory scale," J. Acoust. Soc. Am. **88**, 97–100.
Warren, P., Hay, J., and Thomas, B. (**2007**). "The loci of sound change effects in recognition and perception," in *Laboratory Phonology 9*, edited by J. Cole and J. Hualde (Mouton de Gruyter, Berlin), pp. 87–112.
Watson, C. I., and Harrington, J. (**1999**). "Acoustic evidence for dynamic formant trajectories in Australian English Vowels," J. Acoust. Soc. Am. **106**, 458–468.
Wells, J. C. (**1982**). *Accents of English II: The British Isles* (Cambridge University Press, Cambridge).
Wells, J. C. (**1997**). "Whatever happened to Received Pronunciation?" in *II Jornadas de Estudios Ingleses*, edited by C. Medina and P. Soto (Universidad de Jaén, Spain), pp. 19–28.

Effect of spectral normalization on different talker speech recognition by cochlear implant users

Chuping Liu[a)]
Department of Electrical Engineering, University of Southern California, Los Angeles, California 90089

John Galvin III
Department of Auditory Implants and Perception, House Ear Institute, 2100 West Third Street, Los Angeles, California 90057

Qian-Jie Fu
Department of Biomedical Engineering, University of Southern California, Los Angeles, California 90089 and Department of Auditory Implants and Perception, House Ear Institute, 2100 West Third Street, Los Angeles, California 90057

Shrikanth S. Narayanan
Department of Electrical Engineering, University of Southern California, Los Angeles, California 90089

(Received 25 January 2007; revised 12 February 2008; accepted 23 February 2008)

In cochlear implants (CIs), different talkers often produce different levels of speech understanding because of the spectrally distorted speech patterns provided by the implant device. A spectral normalization approach was used to transform the spectral characteristics of one talker to those of another talker. In Experiment 1, speech recognition with two talkers was measured in CI users, with and without spectral normalization. Results showed that the spectral normalization algorithm had small but significant effect on performance. In Experiment 2, the effects of spectral normalization were measured in CI users and normal-hearing (NH) subjects; a pitch-stretching technique was used to simulate six talkers with different fundamental frequencies and vocal tract configurations. NH baseline performance was nearly perfect with these pitch-shift transformations. For CI subjects, while there was considerable intersubject variability in performance with the different pitch-shift transformations, spectral normalization significantly improved the intelligibility of these simulated talkers. The results from Experiments 1 and 2 demonstrate that spectral normalization toward more-intelligible talkers significantly improved CI users' speech understanding with less-intelligible talkers. The results suggest that spectral normalization using optimal reference patterns for individual CI patients may compensate for some of the acoustic variability across talkers.
© *2008 Acoustical Society of America.* [DOI: 10.1121/1.2897047]

PACS number(s): 43.71.Gv, 43.64.Me, 43.72.Fx, 43.66.Ts [ARB] Pages: 2836–2847

I. INTRODUCTION

Normal hearing (NH) listeners are able to understand speech from a variety of talkers, despite differences in acoustic characteristics (e.g., voice pitch, speaking rate, accent, etc.). NH listeners are thought to use some form of "speaker normalization" to process speech from multiple talkers, thereby preserving the perceptual constancy of the linguistic message (Pisoni, 1993). Speaker normalization may affect processes at an early segmental acoustic-phonetic level (Verbrugge *et al.*, 1976; Assmann *et al.*, 1982), and is associated with some central processing cost, as reflected in the reduced speech performance as the number of talkers is increased (Mullennix *et al.*, 1989; Sommers *et al.*, 1994).

Despite the operation of such speaker normalization processes, speech intelligibility varies considerably across different talkers. Different talkers have been shown to produce different levels of speech intelligibility in NH listeners (e.g., Hood and Poole, 1980; Cox *et al.*, 1987). For example, Cox *et al.* (1987) studied the intelligibility of speech materials produced from three male and three female talkers in different listening conditions in NH listeners. Results indicated significant differences in intelligibility across talkers, even in listening environments that allowed for full intelligibility of everyday conversations. These cross-talker effects have also been observed in cochlear implant (CI) users. For example, Green *et al.* (2007) recently studied the effects of cross-talker differences on speech intelligibility in CI users and NH listeners listening to acoustic CI simulations. In their study, two groups of talkers (high or low intelligibility talkers) were established according to mean word error rates, based on previous data collected with NH listeners; each group consisted of one male adult, one female adult, and one female child talker. Results showed differences in intelligibility between the two talker groups, for a variety of listening conditions; talker group differences were maintained even when overall speech performance was reduced in the more difficult listening conditions. In CIs, speech patterns are represented by a limited number of spectral and temporal cues. In addition, electrically evoked speech patterns may be further dis-

[a)]Electronic mail: chupingl@usc.edu

 0001-4966/2008/123(5)/2836/12/$23.00 © 2008 Acoustical Society of America

torted due to the spectral mismatch between the input acoustic frequency and electrode place of stimulation. Previous CI acoustic simulation studies with NH listeners have shown differences in speech understanding for different talkers (e.g., Dorman *et al.*, 1997a; Fu and Shannon, 1999). While talker variability may not have been the main research focus, these studies suggest that the degree of spectral distortion may significantly affect intelligibility with different talkers. Thus, compared with NH listeners whose spectral resolution may better support perceptual normalization across talkers, CI users' speech recognition may be more susceptible to acoustic differences across talkers.

Although widely studied, the relation between speech intelligibility and the acoustic-phonetic properties for different talkers remains unclear. For example, while Bradlow *et al.* (1996) found no correlation between speaking rate and intelligibility in NH listeners, Bond and Moore (1994) found that, compared with more-intelligible talkers, less-intelligible talkers produced words and vowels with shorter durations. Besides speaking rate, other acoustic-phonetic correlates of intelligibility across talkers have been studied, e.g., fundamental frequency (F0; Bradlow *et al.*, 1996), amplitude of stressed vowels (Bond and Moore, 1994), and long-term average spectrum and consonant-vowel intensity ratio (Hazan and Markham, 2004). Typically, no single acoustic feature was able to explain the intelligibility difference across talkers. Hazan and Markham (2004) suggested that highly intelligible speech may depend on combinations of different acoustic-phonetic characteristics.

Some researchers have tried to improve speech intelligibility by compensating for differences along one acoustic dimension. For example, Luo and Fu (2005) studied an acoustic rescaling algorithm to normalize the formant space across talkers; the algorithm was evaluated in NH subjects listening to acoustic CI simulations. In their study, mean third formant frequency (F3) values (across vowels) were calculated for each talker in the stimulus set. The ratio between the mean F3 value for each talker and the reference talker (the talker that produced the best vowel recognition for each subject) was used to adjust the analysis filter bank of an acoustic CI simulation to match an optimal reference pattern. Multitalker Chinese vowel recognition was tested in NH subjects listening to a four-channel acoustic CI simulation, with and without the acoustic rescaling algorithm. Results showed a small but significant improvement in subjects' overall multitalker vowel recognition with the acoustic rescaling algorithm. Note that in the Luo and Fu study (2005), the largest improvements in performance were not always for the least-intelligible talkers. Nejime and Moore (1998) examined the effects of reduced speaking rates for speech intelligibility in noise, using a simulation of cochlear hearing loss in NH subjects. Reducing the speaking rate did not significantly improve intelligibility in the context of the simulated hearing loss. This lack of effect may have been due to the relatively weak contribution of speaking rate to intelligibility, or to processing artifacts associated with the signal modification.

In the present study, rather than normalize speech in one acoustic dimension or by linearly rescaling the formant space, we used a spectral normalization method based on statistical modeling of acoustic features to compensate for complex and dynamic acoustic variability at the speech segment level. As described earlier, no single acoustic feature can fully account for intelligibility difference across talkers. As a statistical modeling does not depend on any single feature, this approach may be more beneficial. The term "spectral normalization" is used because: (a) the spectral envelope was used to analyze the acoustic variability and (b) the proposed algorithm was intended to normalize spectral characteristics across different talkers. Note that spectral normalization in this study refers to a signal processing procedure rather than a perceptual process (e.g., "speaker normalization," as in Pisoni, 1993). The proposed spectral normalization algorithm was used for "front-end" processing (before CI speech processing), and was evaluated in CI users and NH subjects. In Experiment 1, recognition of sentences produced by two different talkers (one male and one female) was measured in CI listeners, with and without spectral normalization conditions; sentence recognition was measured in quiet for each talker independently. In Experiment 2, sentence recognition was measured in CI and NH listeners, with and without spectral normalization, using pitch-stretched transformations to simulate different talkers, i.e., speech was systematically pitch-stretched to produce different F0 and vocal tract configurations while preserving temporal characteristics such as speaking rate, overall duration, and amplitude. Subjective quality ratings and stimulus discriminability data were also collected from NH listeners.

II. METHOD

A. Spectral normalization algorithm

In the present study, the spectral normalization algorithm was based on a continuous statistical model to compensate for acoustic differences between talkers. By using a continuous model, speech from a variety of talkers may be adjusted to match a listener's optimal speech patterns. Specifically, the algorithm used a Gaussian mixture model (GMM) to represent spectral characteristics of a "source" talker at the segmental level, and transformed the source talker's spectral characteristics to that of a "target" talker using a trained spectral conversion function.

A GMM represents the distribution of the observed parameters $\mathbf{x}$ by m mixture Gaussian components in the form of

$$p(\mathbf{x}) = \sum_{i=1}^{m} \alpha_i N(\mathbf{x}; \mu_i, \Sigma_i), \tag{1}$$

where α_i denotes the prior probability of component i ($\Sigma_{i=1}^{m} \alpha_i = 1$ and $\alpha_i \geq 0$) and $N(\mathbf{x}; \mu_i, \Sigma_i)$ denotes the normal distribution of the ith component with mean vector μ_i and covariance matrix Σ_i, in the form of

$$N(\mathbf{x}; \mu_i, \Sigma_i) = \frac{1}{(2\pi)^{p/2} \Sigma_i^{1/2}} \times \exp\left[-\frac{1}{2} (\mathbf{x} - \mu_i)^T \Sigma_i^{-1} (\mathbf{x} - \mu_i) \right], \tag{2}$$

where p is the number of vector dimensions. The parameters

of the model (α,μ,Σ) can be estimated using the well-known expectation maximization (EM) algorithm (Huang *et al.*, 2001).

After GMM modeling of the source talker's spectral distribution, the conversion function $F(x_t)$ is chosen such that the total conversion errors of n spectral vectors

$$\varepsilon = \sum_{t=1}^{n} (\mathbf{y}_t - F(\mathbf{x}_t))^2 \tag{3}$$

is minimized for training data, and where $\mathbf{x}_t$ is a spectral vector produced by the source talker and $\mathbf{y}_t$ is the time-aligned spectral vector produced by the target talker. Assuming that the source vector $\mathbf{x}_t$, follows a GMM model and that the source and target vectors are jointly Gaussian, the conversion function (Stylianou *et al.*, 1998; Kain and Macon, 1998; Mendel, 1995) is given in the form of

$$F(X_t) = \sum_{i=1}^{m} P(C_i|\mathbf{x}_t)[\mathbf{v}_i + \mathbf{T}_i\Sigma_i^{-1}(\mathbf{x}_t - \mu_i)], \tag{4}$$

where $P(C_i|\mathbf{x}_t)$ is the posterior probability of the ith Gaussian component given $\mathbf{x}_t$. $P(C_i|\mathbf{x}_t)$ is calculated by the application of Bayes theorem:

$$P(C_i|\mathbf{x}_t) = \frac{\alpha_i N(\mathbf{x}_t;\mu_i,\Sigma_i)}{\sum_{j=1}^{m} \alpha_j N(\mathbf{x}_t;\mu_j,\Sigma_j)}. \tag{5}$$

The unknown parameters $\mathbf{v}_i$ and $\mathbf{T}_i$ are computed by solving the following set of over-determined linear equations for all feature vector $t=(1,\ldots,n)$:

$$y_t = \sum_{i=1}^{m} P(C_i|\mathbf{x}_t)[\mathbf{v}_i + \mathbf{T}_i\Sigma_i^{-1}(\mathbf{x}_t - \mu_i)]. \tag{6}$$

Note that Eqs. (4) and (6) are identical on the right-hand side but are different on the left side [$F(\mathbf{x}_t)$ for Eq. (4), y_t for Eq. (6)]. Hence, the minimum mean square error (MMSE) solutions for $\mathbf{v}_i$ and $\mathbf{T}_i$ from Eq. (6) will guarantee that the total conversion error of Eq. (3) is minimized. Estimating parameters $\mathbf{v}_i$ and $\mathbf{T}_i$ from Eq. (6) determines the conversion function in Eq. (4). Given a certain source vector $\mathbf{x}_t$, the MMSE estimate of the target vector is equivalent to the right-hand side of Eq. (4).

B. Implementation of spectral normalization

Once the spectral conversion function had been estimated from training data, the spectral conversion was performed as depicted in Fig. 1.

In the above-mentioned system, a Mel-scaled line spectral frequency (LSF) feature (Huang *et al.*, 2001) was used to train the GMM, as it is perceptually based and has smooth interpolation characteristics (Kain and Macon, 1998). Specifically, the Mel-scaled LSF coefficients were obtained as follows. After frame-based speech analysis and linear predictive coding (LPC) coefficients extraction, the LPC spectrum was transformed to a Mel-warped spectrum (Huang *et al.*, 2001) according to the relationship $M(f)=1125\ln(1+f/700)$, where f is frequency in hertz and $M(f)$ is the corresponding Mel frequency in Mels. The warped spectrum

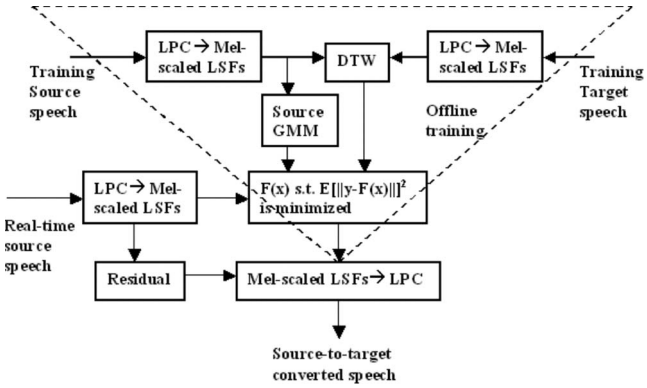


FIG. 1. Implementation framework of the GMM-based spectral normalization algorithm.

was then uniformly resampled using splined cubic phase interpolation to obtain the Mel-scaled LPC spectrum. A least-squares fit was used to transform the Mel-scaled LPC spectrum to Mel-scaled LPC coefficients, which were then transformed to Mel-scaled LSF coefficients.

To transform a given utterance, spectral feature vectors from the source talker's speech were extracted and transformed by the spectral conversion function that was trained using the GMM (as described in Sec. II A). The residual from the spectral extraction was then convolved with the modified spectral parameters to render the transformed speech signal. In the present study, there was no attempt to match the prosodic characteristics of source and target talkers. Hence, the source talker's average fundamental frequency (F0), speaking rate, and articulation rhythms were preserved after transformation.

To reduce computational load, a diagonal conversion was used [i.e., the $\mathbf{T}_i$ and Σ_i in Eq. (4) were in diagonal form]. This is a common practice in GMM training, as the correlation between distinct cepstral coefficients is very small (Stylianou *et al.*, 1998). The number of GMM components [i.e., m in Eq. (1)] was set to 64, as the contribution of additional GMM components to the acoustic distance between target and transformed speech is marginal beyond 64 components (Liu *et al.*, 2006).

C. Objective verification of the spectral normalization algorithm in cochlear implant simulations

Spectral conversion has been shown to effectively transform the spectral characteristics (e.g., formant position/bandwidth, spectral tilt, energy distribution, vocal tract length) of a source talker to that of a target talker without spectral degradation (Stylianou *et al.*, 1998; Kain and Macon, 1998; Liu *et al.*, 2006). For CI users, speech recognition performance is most strongly influenced by parameters that affect spectral resolution (e.g., the number of electrodes/channels). In general, speech recognition in quiet improves with increasing numbers of spectral channels (Fu, 1997; Dorman *et al.*, 1997b; Fishman *et al.*, 1997). To see the effect of spectral conversion on spectrally degraded speech (as is typi-

cally encountered by CI users), the proposed algorithm was evaluated using distance measurements with an acoustic CI simulation.

The acoustic CI simulation was implemented similarly to Shannon *et al.* (1995). The signal was first preemphasized with a filter coefficient of 0.95. The input frequency range (100–6000 Hz) was then bandpassed into 16, 8, 6, or 4 frequency analysis bands (24 dB/octave filter slope), distributed according to Greenwood's formula (Greenwood, 1990). The temporal envelope was then extracted from each frequency band by half-wave rectification and low-pass filtering (160 Hz envelope filter). The envelope of each band was then used to modulate a wideband noise, which was then spectrally limited by the same bandpass filter used for frequency analysis. Finally, the modulated carriers of each band were summed to render spectrally degraded speech. To measure the degree of spectral conversion for spectrally degraded speech, the acoustic distance between the transformed speech and the target speech was calculated as follows:

$$d^2_{\mathrm{MFCC}} = \frac{1}{N}\sum_{n=1}^{N}\sum_{k=1}^{p}[c^{n,k}_{\mathrm{converted}} - c^{n,k}_{\mathrm{target}}]^2, \quad (7)$$

where N is the total frame numbers in feature streams, $c^{n,k}$ is the kth component of the Mel-frequency cepstral coefficients (MFCC) vector in frame n, and p is the MFCC order (14, in the present case). Lower values of d^2 indicate greater spectral similarity between the transformed speech and the target speech. When the spectrum of the transformed speech perfectly aligns with that of the target speech, $d^2=0$.

The objective analysis was performed using IEEE sentences (IEEE, 1969), recorded with one male (M1) and one female (F1) talker. Spectral normalization from F1 to M1 was analyzed. The GMM training data set included 100 sentences randomly selected from the database; the testing data set included the entire database (720 sentences). The average acoustic distance between the source (F1) and target (M1) speech was calculated across the whole testing data set. The average acoustic distance for each condition was then converted to decibel units referenced to the acoustic distance between the unprocessed source and target speech (i.e., no acoustic CI simulation or spectral normalization). Figure 2 shows the mean acoustic distance (in decibels) between the source and target speech, as a function of the number of spectral channels. The acoustic distance decreased similarly with (dashed line) or without (solid line) spectral normalization as the number of spectral channels was reduced. The acoustic distance was significantly reduced (paired t-test: $p < 0.05$) with the spectral normalization algorithm; the mean reduction in acoustic distance was −2.73 dB, across all spectral resolution conditions. The objective analysis showed that spectral normalization was efficient in transforming the source speech in mimicking the target speech, regardless of the number of spectral channels.

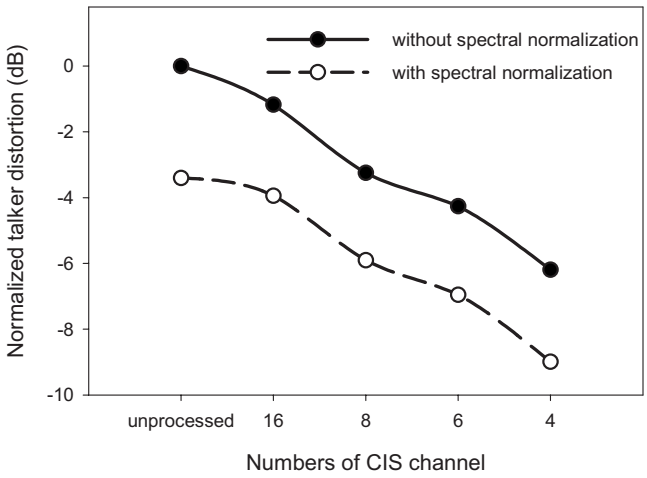


FIG. 2. Normalized talker distortion as a function of number of channels. Solid line: Without spectral normalization. Dashed line: With spectral normalization. Note that the talker distortion between talkers F1 and M1 (unprocessed speech) was used as the reference.

III. EXPERIMENT 1: EFFECT OF SPECTRAL NORMALIZATION ON SENTENCE RECOGNITION WITH TWO DIFFERENT TALKERS

A. Methods

1. Subjects

Nine postlingually deafened adult CI users (7 men, 2 women) participated in this experiment. Table I lists relevant demographics for the CI subjects. All subjects were native speakers of American English and had extensive experience in speech recognition experiments. All subjects provided informed consent and all were paid for their participation.

TABLE I. Subject demographics for the cochlear implant patients who participated in the present study.

Subject	Age	Gender	Etiology	Implant Type	Strategy	Duration of Implant use (years)
S1	67	M	Hereditary	Nucleus-22	SPEAK	14
S2	75	M	Noise induced	Nucleus-22	SPEAK	9
S3	72	F	Unknown	Nucleus-24	ACE	5
S4	54	M	Unknown	Nucleus-22	SPEAK	11
S5	62	F	Genetic	Nucleus-24	ACE	2
S6	55	M	Hereditary	Freedom	ACE	1
S7	52	M	Unknown	Clarion-CII	HiRes	6
S8	48	M	Trauma	Nucleus-22	SPEAK	13
S9	64	M	Trauma/unknown	Nucleus-22	SPEAK	15

2. Stimuli and speech processing

IEEE sentences (IEEE, 1969), recorded with one male (M1) and one female (F1) talker, were used in this experiment. The mean F0, across all sentences was 92 Hz for M1 and 185 Hz for F1. It is assumed that, in practice, spectral normalization is beneficial only when a less intelligible talker is transformed toward a more intelligible talker. Because it was unknown which talker might produce better recognition performance in individual CI subjects, the spectral transformation was performed between both talkers (i.e., M1 was transformed to F1, and F1 was transformed to M1). The GMM for the source talker was trained with 100 randomly selected sentences, resulting in over 60,000 Mel-scaled LSF feature vectors (25th order). The function to transform the source talker to the target talker was estimated according to Eq. (4). After training the conversion function, all sentences with each source talker were spectrally transformed toward the target talkers. Note that the training sentences were also transformed and included in the listening test to increase the available speech materials for the experiment. For descriptive purposes, when the source talker was M1 and the target talker was F1, the transformed speech was labeled M1-to-F1 (and vice versa). In Experiment 1, IEEE sentence recognition was tested for four talker conditions: M1 (unprocessed), F1 (unprocessed), M1-to-F1, and F1-to-M1.

3. Procedure

Subjects were tested using their clinically assigned speech processors and self-adjusted comfortable volume/sensitivity settings; once testing began, these settings were not changed. Subjects were tested while seated in a double-walled sound-treated booth (IAC). Stimuli were presented via a single loud speaker at 65 dBA. The sentences in the IEEE database were divided into 72 lists, with 10 sentences per list. For each run, a list was randomly chosen (without replacement) and the sentences from within the list were presented in random order. Subjects were asked to repeat what they heard; the experimenter tabulated all correctly identified words. Performance was calculated according to the ratio between correctly identified words and all words presented in the list; performance was typically averaged across four to five lists for each talker condition. To familiarize subjects with the different talkers and test procedures, a practice session with one randomly selected list (without replacement) was provided prior to the sentence recognition test in each condition. Note that the speech stimuli used in the practice session were not included in test stimulus set. The test order for the different talker conditions was randomized for each subject. No feedback was provided during the test.

B. Results and discussion

Figure 3 shows individual subjects' sentence recognition performance for the M1 and F1 unprocessed source talkers, as well as the mean performance across subjects. Subjects are ordered according to talker sensitivity. Note that throughout the paper, "talker sensitivity" refers to the magnitude of the difference in performance between the two talkers. Mean

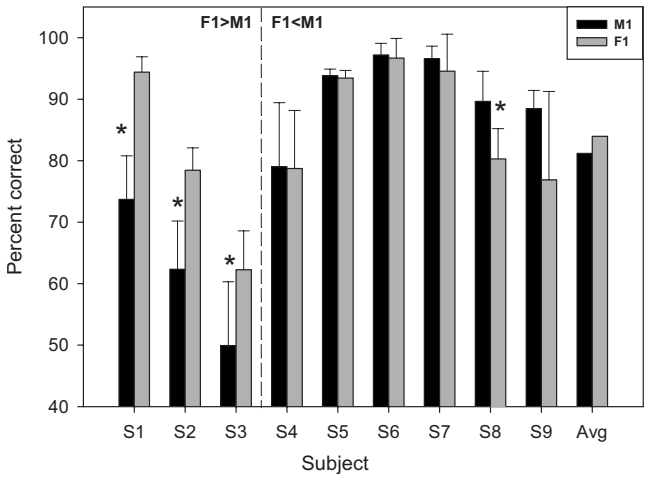


FIG. 3. Individual and mean sentence recognition performance for talkers M1 and F1. For subjects S1–S3, performance with F1 was better than that with M1; for subjects S4–S9, performance was better with M1 than with F1. The error bars show 1 s.d., and the asterisks show significantly different performance between the two talkers ($p<0.05$).

performance with talker F1 was 2.8 percentage points greater than that with M1; however, the difference was not significant [one-way repeated measures (RM) analysis of variance (ANOVA): $F(1,8)=0.560$, $p=0.476$]. For subjects S1–S3, performance was better with F1 than with M1; for subjects S4–S9, performance was better with M1 than with F1. The difference in performance between talkers was significant for subjects S1, S2, S3, and S8 (t-test: $p<0.05$; analysis performed within individual subjects using raw data from multiple sentence lists). There was intersubject variability in terms of talker sensitivity, ranging from 0.3 percentage points for subject S4 to 21 percentage points for subject S1.

Because the talker that produced better speech understanding differed among individual subjects, the most relevant comparison between unprocessed and spectrally transformed speech is in terms of the "Better" and "Worse" talker. Ideally, after spectral transformation, performance with the Worse talker would be equivalent to that with the Better talker (and vice versa). For convenience, the term "Worse-to-Better" refers to the transformation of the Worse toward the Better talker (and vice versa). Table II compares performance with unprocessed speech to that with spectrally normalized speech in terms of the Better and Worse talkers. Note that individual subject data were analyzed with t-tests, using raw performance data from multiple sentence lists; mean performance data (across subjects) were analyzed using mean data from each subject (across sentence lists). While the Better talker differed among individual subjects, the mean baseline performance difference between the Better and Worse talker was 8.1 percentage points; this difference was significant [one-way RM ANOVA: $F(1,8)=10.164$, $p=0.013$]. For the Better-to-Worse transformation, mean performance was significantly poorer than that with the Better talker [one-way RM ANOVA: $F(1,8)=5.558$, $p=0.046$]. The difference was significant for subjects S1, S2, and S4. There was no significant difference in mean performance between the Better-to-Worse transformation and the Worse talker

TABLE II. Performance difference between unprocessed source talkers (i.e., M1 vs F1), and between spectrally normalized and unprocessed talkers. Note that because the performance with talkers M1 and F1 differed among individual subjects, comparisons are made in terms of the "Better" and "Worse" talker. Bold numbers indicate significant differences in performance across different sentence lists ($p<0.05$).

			Performance difference (percentage points)				
			Better	Better-to-Worse		Worse-to-Better	
Subject	Better talker	Worse talker	vs Worse	vs Better	vs Worse	vs Better	vs Worse
S1	F1	M1	**20.7**	**−10.2**	**10.5**	**−15.5**	5.2
S2	F1	M1	**16.1**	**−11.6**	4.5	−7.8	8.3
S3	F1	M1	**12.4**	5.3	**17.7**	−10.6	1.7
S4	M1	F1	0.3	**−21.6**	**−21.3**	−0.5	−0.2
S5	M1	F1	0.4	−0.7	−0.3	1.7	2.1
S6	M1	F1	0.5	−0.2	0.3	0.8	1.3
S7	M1	F1	2.0	−3.2	−1.2	−0.4	1.6
S8	M1	F1	**9.4**	−4.9	4.4	−6.0	3.3
S9	M1	F1	11.6	−8.7	2.9	−6.8	4.8
Avg across all nine subjects			**8.1**	**−6.2**	2.0	**−5.0**	**3.1**
Avg across subjects S1, S2, S3 and S8			**14.7**	−5.4	9.3	**−10.0**	**4.6**

[one-way RM ANOVA: $F(1,8)=0.308$, $p=0.594$]; however, performance differed significantly for subjects S1, S3, and S4. For the Worse-to-Better transformation, mean performance remained significantly poorer than that with the Better talker [one-way RM ANOVA: $F(1,8)=6.624$, $p=0.033$]; the difference was significant only for subject S1. Interestingly, performance with the Worse-to-Better transformation was significantly better than that with the Worse talker [one-way RM ANOVA: $F(1,8)=12.967$, $p=0.007$], although the difference was not significant for any individual subject.

Figure 3 shows that only four out of the nine subjects exhibited significant differences in intelligibility between the F1 and M1 talkers. This may have been due to ceiling performance effects in some subjects (S5, S6, and S7). Further analysis was performed using only the subjects whose baseline performance was significantly affected by talker (S1, S2, S3, and S8). Results are shown in Table II alongside the analyses with all nine subjects. For the Better-to-Worse transformation, mean performance was 5.4 percentage points lower than that with the Better talker; however, this difference was not significant [one-way RM ANOVA: $F(1,3)=1.957$, $p=0.256$]. Mean performance for the Better-to-Worse transformation was 9.3 percentage points better than that with the Worse talker; however, this difference was not significant [one-way RM ANOVA: $F(1,3)=8.757$, $p=0.060$]. For the Worse-to-Better transformation, mean performance remained 10.0 percentage points poorer than that with the Better talker; this difference was significant [one-way RM ANOVA: $F(1,3)=23.383$, $p=0.017$]. Mean performance for the Worse-to-Better transformation was 4.6 percentage points better than that with the Worse talker [one-way RM ANOVA: $F(1,3)=10.672$, $p=0.047$], Thus, the subanalyses using subjects S1, S2, S3, and S8 showed similar performance patterns to those with the previous analyses using all nine subjects.

In general, the spectral normalization algorithm produced the intended results, i.e., performance improved when a Worse talker was transformed toward a Better talker and vice versa. For some subjects, performance with the transformed talkers did not always follow this general trend. For example, for subject S3, performance improved when the Better talker was transformed to the Worse talker. Conversely, performance slightly declined for subject S4 when the Worse talker was transformed to the Better talker. This adverse effect may have been because the spectral normalization could not completely compensate for all the acoustic/perceptual differences between the source and target talkers. Alternatively, the transformation may have resulted in "talkers" that were not included or sampled in the test materials.

Sensitivity to the spectral normalization algorithm also varied among subjects. For example, there was only a 2 percentage point difference in performance among the four conditions for subjects S5 and S6. For subject S4, performance with the Better-to-Worse transformation was 22 percentage points poorer than that with the Better talker; there was only ~1 percentage point difference in performance among the remaining three talker conditions. In general, the effect of spectral normalization was strongest for subjects whose performance differed substantially between M1 and F1 (i.e., subjects S1, S2, S3, S8, and S9). In terms of mean performance, note that the Better-to-Worse transformation resulted in a decrement of ~6 percentage points, while the Worse-to-Better transformation resulted in an improvement of ~3 percentage points. While this is a relatively small difference in terms of effect size, there are three possible explanations for this bidirectional imbalance. First, the mean performance deficit with the Better-to-Worse transformation may have been primarily due to the large drop in performance for subject S4. Second, artifacts associated with the spectral normalization algorithm (e.g., spectral discontinuities, unnaturalness) may have limited any improvements in performance with the Worse-to-Better transformation and may have contributed more strongly to "worsening" performance with the Better-to-Worse transformation. Third, ceiling effects may

have limited the degree of improvement with spectral normalization, but not the degree of deterioration in performance.

The results of Experiment 1 demonstrated that spectral normalization, using a GMM model trained with relatively few stimuli, significantly improved speech understanding with less-intelligible talkers, especially for CI users whose speech performance was sensitive to different talkers. The objective acoustic measures using the CI simulation showed that spectral normalization was efficient in transforming the source speech toward the target speech, regardless of the number of spectral channels. Although some CI subjects were more sensitive than others to talker differences and the subsequent spectral normalization, the perceptual measures showed relatively small effects, on average. The modest effects may have been due to the small number and/or quality of the test talkers (1 male and 1 female) who may not have elicited sufficient baseline talker sensitivity effects. Also, ceiling performance effects associated with sentence recognition may have limited the effects of spectral normalization.

IV. EXPERIMENT 2: EFFECT OF SPECTRAL NORMALIZATION ON SENTENCE RECOGNITION WITH SIMULATED TALKERS

In Experiment 1, the speech materials differed between the two talkers not only in terms of spectral cues, but also in terms of temporal cues, even for the same sentences. Previous studies have shown that speech intelligibility may be influenced by speaking rate (Kurdziel *et al.*, 1976; Miller and Volaitis, 1989; Gordon-Salant and Fitzgibbons, 1997). Cross-talker temporal variability such as voice-onset-time may also affect speech recognition (Allen *et al.*, 2003). Temporal cue effects have been observed in NH listeners (Miller and Volaitis, 1989), elderly listeners (Kurdziel *et al.*, 1976), HI listeners (Gordon-Salant and Fitzgibbons, 1997; Kirk *et al.*, 1997), and CI users (Liu *et al.*, 2004). In Experiment 1, the spectral normalization algorithm was intended to modify only the spectral information. However, it is possible that modified spectral information may interact with temporal information (which was not modified) and thereby affect speech understanding. It would be preferable to test the spectral normalization algorithm using different talker speech materials that have been normalized in terms of temporal information. It is very difficult to constrain temporal cues (i.e., speaking rate, total duration, emphasis, etc.) across different talkers with naturally produced speech materials. Therefore, in Experiment 2, the different talker conditions were simulated by adjusting the voice pitch and vocal tract characteristics of a reference talker (F1).

A. Methods

1. Subjects

The same 9 CI subjects from Experiment 1 also participated in Experiment 2. Four NH subjects (2 men, 2 women) also participated in Experiment 2, and served as a control group. All NH subjects had sensitivity thresholds better than 15 dB hearing level for audiometric test frequencies from 250 to 8000 Hz; all were native speakers of American English. Informed consent from each subject was obtained for the study.

2. Stimuli and speech processing

In Experiment 2, talker differences were simulated by systematically altering the acoustic characteristics of a reference talker (F1), while preserving speaking rate (i.e., duration of utterances) and prosodic characteristics, in the form of relative changes in F0. The IEEE sentences produced by talker F1 from Experiment 1 were used as the reference. To simulate different talkers, sentences were altered by using the "pitch-stretch" processing feature in COOL EDIT PRO (Version 2.0; Syntrillium Software). The pitch-stretching algorithm changed the fundamental frequency of the original speech and hence the spectral envelope, mimicking different vocal tract configurations. Each sentence produced by talker F1 was processed using six different pitch-stretch ratios: 0.6, 0.8, 1.0, 1.2, 1.4, and 1.6. Higher ratios resulted in lower-pitched speech, and smaller ratios resulted in higher-pitched speech; when the ratio was equal to 1.0, there was no pitch shift (i.e., the original speech tokens from talker F1). For example, the average F0 for talker F1 across all sentences was 185.10 Hz; when pitch-stretched by a ratio of 1.6, the average F0 was 116.96 Hz (i.e., 185.10/1.6=115.69 Hz), simulating a male voice. Note that because the reference talker F1 was female, the minimum ratio was 0.6 in this experiment, as lesser values produced overly high F0 values. Thus, ratios of 0.6, 0.8, and 1.0 were intended to simulate female talkers, while ratios of 1.2, 1.4, and 1.6 were intended to simulate male talkers. Note that as the pitch-stretching ratio deviated from 1.0, speech increasingly sounded less natural. For reference purposes, the transformations associated with the different pitch-stretching ratios are labeled T0.6, T0.8, T1.0 (unprocessed speech by talker F1), T1.2, T1.4, and T1.6.

After generating the different pitch-shift transformations, the spectral normalization algorithm was applied, with T1.0 as the target talker. The same 100 sentences used in Experiment 1 were used to train the GMM model, while the entire database (720 sentences) was used for testing. Spectral normalization was performed exactly as in Experiment 1. The stimuli in Experiment 2 included 11 sets of talkers: one source talker (T1.0), five pitch-shift transformations (T0.6, T0.8, T1.2, T1.4, and T1.6), and five spectral transformations (T0.6-to-T1.0, T0.8-to-T1.0, T1.2-to-T1.0, T1.4-to-T1.0, and T1.6-to-T1.0). For the spectral transformations, T0.6-to-T1.0 and T0.8-to-T1.0 represented female-to-female transformations, while T1.2-to-T1.0, T1.4-to-T1.0, and T1.6-to-T1.0 represented male-to-female transformations.

Table III shows the pitch and formant analysis for the pitch-shifted and spectrally transformed speech. Table III shows that voice pitch was well-scaled by the pitch-stretching operation, and was maintained by spectral transformation. While formant frequencies were not maintained or scaled by the pitch-stretching algorithm (relative to the source speech T1.0), spectral normalization largely restored formant frequencies to those of the source speech. The mean difference of all formant frequencies between the target

TABLE III. Pitch and formant analysis for the pitch-shift and spectral transformations in Experiment 2. The target F0 for the pitch-shift transformations was scaled according to the pitch-stretching ratio used for processing; the target F0 for the spectral transformation refers to the measured F0 values after pitch-stretching. The F0s and formant frequencies were measured with software WAVESURFER 1.8.5. The F0s were averaged across all IEEE sentences. The formant frequencies were estimated for the vowel /IY/ from the sentence "Glue the sheet to the dark blue background." Note that reference talker T1.0 (in bold) was F1 from Experiment 1.

Transformation	Condition	Target F0	Measured F0	Measured F1	Measured F2	Measured F3
Pitch-shift	T0.6	185/0.6 = 308	298	326	582	4040
	T0.8	185/0.8=231	228	422	2051	3046
	T1.0	**185/1.0=185**	**185**	**344**	**2440**	**2859**
	T1.2	185/1.2=154	155	290	2062	2405
	T1.4	185/1.4=132	133	248	1816	2232
	T1.6	185/1.6=116	117	214	1610	2267
Spectral	T0.6-to-T1.0	298	300	291	2497	2996
	T0.8-to-T1.0	228	230	290	2408	2871
	T1.2-to-T1.0	155	157	279	2366	2750
	T1.4-to-T1.0	133	135	274	2151	2744
	T1.6-to-T1.0	117	118	278	1750	2498

speech (i.e., T1.0) and the spectral transformation was only 118 Hz, with a standard deviation of 199 Hz.

Figure 4 shows example wave forms for the sentence "Glue the sheet to the dark blue background," produced by source talker T1.0 and two pitch-shift transformations (T0.6, T1.6); note that the duration and modulation depth is nearly identical across the wave forms. The top panel of Fig. 5 shows the spectral envelope for a speech segment within the vowel /IY/ from the word "sheet;" note the relative stretch in the spectral envelope for the two pitch-shift transformations. The bottom panel of Fig. 5 shows the spectral envelope for the same speech segment, as produced by two spectral trans-

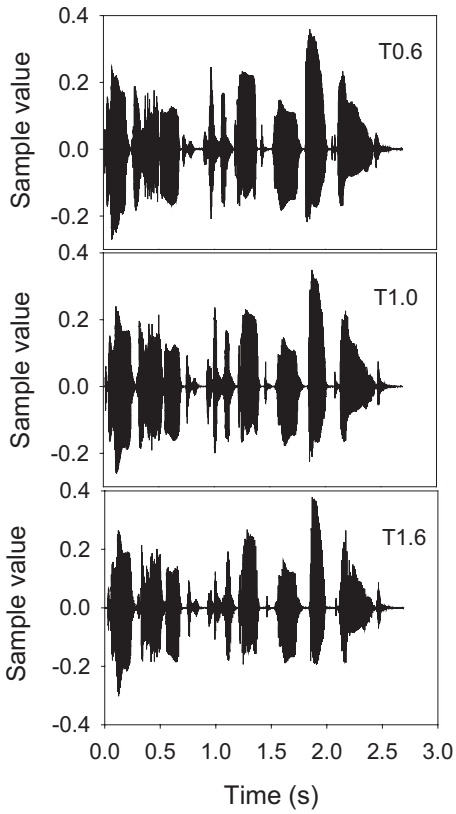


FIG. 4. Wave forms for the sentence "Glue the sheet to the dark blue background." Top panel: Pitch-shift transformation T0.6 (upward pitch shift). Middle panel: Reference talker T1.0 (unprocessed speech from talker F1). Bottom panel: Pitch-shift transformation T1.6 (downward pitch shift).

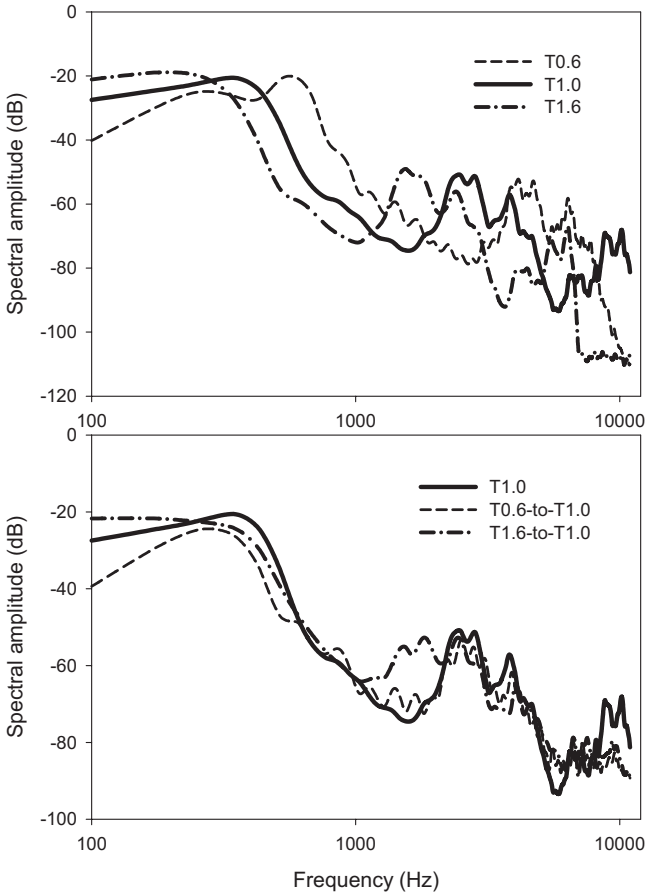


FIG. 5. Spectral envelopes for different processing conditions in Experiment 2. Top panel: Spectral envelopes for reference talker T1.0 and pitch-shift transformations T0.6 and T1.6. Bottom panel: Spectral envelopes for T1.0 and spectral transformations T0.6-to-T1.0 and T1.6-to-T1.0.

formations (T0.6-to-T1.0, T1.6-to-T1.0) and reference talker T1.0; note that the spectral envelopes are quite similar for the two spectral transformations and T1.0.

3. Procedure

For all talker conditions, IEEE sentence recognition was measured using the same procedures described in Experiment 1. After the speech recognition test, subjective quality ratings were obtained from the same NH subjects. Subjects were asked "How would you rate the overall speech quality on a scale from 1 to 10, with larger values indicating better overall speech quality?" Subjective ratings were anchored to T1.0, which was given the highest rating (10, on a 10-point scale). For each pitch-shift and spectral transformation, speech quality ratings were averaged across subjects. In addition to sentence recognition, discriminability among the pitch-shift transformations was also measured in NH subjects to verify whether the pitch-stretching algorithm produced different "talker identities." During the discriminability test, subjects were presented with a sentence produced by T1.0 and a different sentence produced by one of the pitch-shift transformations. NH subjects were asked whether the sentences were produced by the same or different talkers. Each of the five pitch-shift transformations was compared to talker T1.0 six times. The presentation order of the processed and unprocessed sentences was randomized, and the test sentences were randomly selected (without replacement) from the test materials.

B. Results and discussion

In terms of stimulus discriminability, for three out of the four NH subjects, all of the pitch-shift transformations sounded like different talkers, relative to the reference talker T1.0 (i.e., 100% discrimination across all six trials). For the remaining NH subject, pitch-shift transformations T1.2, T1.4, and T1.6 were easily discriminated from talker T1.0 (100% discrimination across all six trials); however, T0.8 and T0.6 were judged to be the same as T1.0 in four out of six trials. Thus, the pitch-shift transformations were judged, for the most part, to represent different talker identities.

Figure 6 shows the overall speech quality ratings for the 4 NH subjects, with and without spectral normalization, as a function of pitch-shift transformation. A two-way RM ANOVA showed that overall speech quality ratings were significantly affected by pitch-shift [$F(5,15)=15.352$, $p<0.001$]. While spectral normalization also seemed to affect quality ratings, the effect failed to reach significance [$F(1,15)=9.517$, $p=0.054$]. Except for pitch-shift transformation T1.2, all the pitch-shift and spectral transformations produced significantly lower ratings, relative to reference talker T1.0 (t-test: $p<0.05$). Quality ratings were generally lower after spectral transformation; the decrements were only significant for T1.2-to-T1.0 (t-test: $p<0.05$). This suggests that pitch shifting may have introduced one set of artifacts, and the spectral normalization (intended to compensate only for spectral differences) may have introduced a second set of artifacts. Artifacts associated with spectral normalization may have added to the pitch-shift artifacts, further reducing the speech quality ratings.

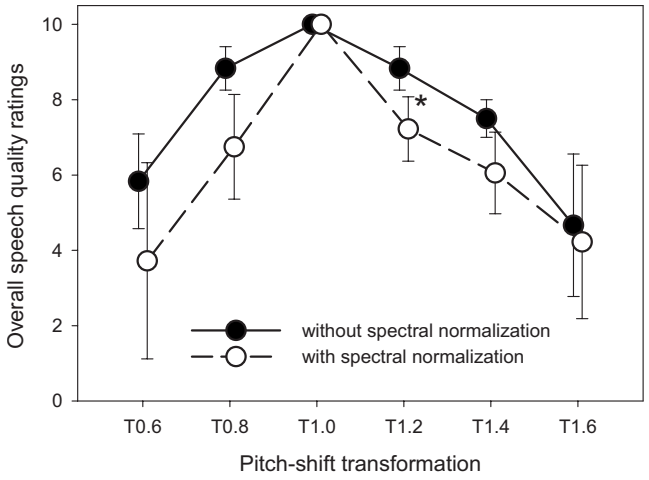


FIG. 6. NH subjects' overall speech quality ratings for the pitch-shift transformations, with (open symbols) and without (closed symbols) spectral normalization. The error bars show 1 s.d., and the asterisks indicate significantly different ratings with spectral normalization ($p<0.05$). Note that source talker T1.0 (unprocessed speech from talker F1) was used to anchor the subjective quality ratings.

Figure 7 shows sentence recognition performance for CI and NH listeners (circle and diamond symbols, respectively), with and without spectral normalization (open and closed symbols, respectively), as a function of pitch-shift transformation. For NH subjects, sentence recognition remained nearly perfect for all conditions, except for T0.6-to-T1.0 (94% correct, significantly lower than performance with T0.6). CI subjects were very sensitive to the different pitch-shift and spectral transformations. Mean peak performance was 84% correct with T1.0. Performance with the pitch-shift transformations sharply declined as the shift ratios became more extreme. With T0.6, mean performance was only 20% correct, and with T1.6, mean performance was only 31%

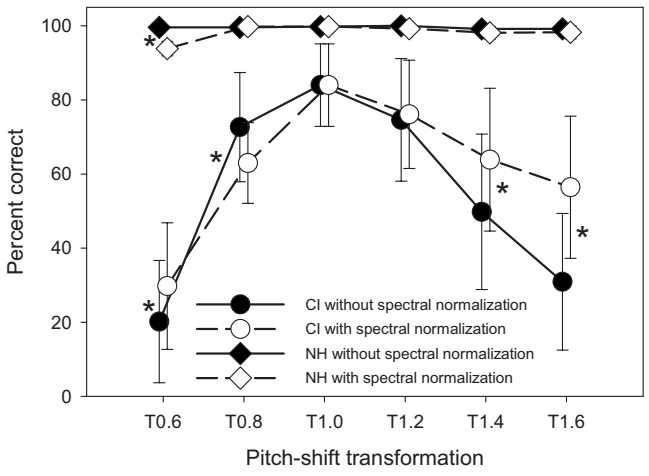


FIG. 7. Sentence recognition performance for NH and CI subjects, with (open symbols) and without (closed symbols) spectral transformation, as a function of pitch-shift transformations. The error bars show 1 s.d., and the asterisks indicate significantly different performance after spectral transformation ($p<0.05$).

correct. Performance with spectral normalization also declined for the more extreme pitch-shift transformations, but the decline was less steep than without spectral normalization. A two-way repeated measures ANOVA showed that performance was significantly affected by pitch-shift [$F(5,40)=124.014$, $p<0.0001$] and spectral normalization [$F(1,40)=64.770$, $p<0.001$]. There was a significant interaction between the pitch-shift and spectral transformations [$F(5,40)=21.557$, $p<0.001$]. Post-hoc Bonferroni t-tests showed that performance with T1.0 was significantly better than that with T0.6, T0.8, T1.4, and T1.6, before or after spectral normalization ($p<0.05$). Post-hoc Bonferroni t-tests also showed that spectral normalization significantly improved performance for T0.6, T1.4, and T1.6 ($p<0.001$). In contrast, performance with T1.2 was not significantly different from that with T1.0, with ($p=0.271$) or without spectral normalization ($p=0.078$). Performance with T0.8 significantly declined after spectral normalization ($p=0.012$).The failure of spectral normalization to significantly improve performance with T0.8 and T1.2 may have been due to the relatively small differences in baseline performance between T0.8, T1.0, and T1.2, before normalization. The potential benefits of spectral normalization may not have been large enough to overcome processing artifacts associated with the speech modification and synthesis.

The results suggest that, despite potential signal processing artifacts, spectral normalization may benefit CI users. It is important to note that, as suggested from Fig. 6, the artifacts associated with spectral normalization may have added to the artifacts associated with the pitch-shift algorithm. Note that the spectral normalization was intended to modify the spectral envelope toward that of the reference talker, not to reduce the artifacts associated with the pitch-shift processing. Ultimately, spectral normalization significantly improved CI users' speech understanding with the pitch-shift transformations. This implies that CI listeners may not have been sensitive to these processing artifacts (due to the reduced spectral resolution), or that CI listeners were able to ignore these artifacts and receive the benefits of spectral normalization.

Given the probable artifacts associated with pitch-shift and spectral normalization, it is possible that some learning may have occurred during testing. Note that the test order was randomized within and across subjects for the measurements with pitch-shift and spectral transformations. A two-way ANOVA was conducted for each individual subject (with the pitch-shift ratio and test session as factors), for both the baseline and spectral normalization conditions. While there were significant effects for the pitch-shift ratio (both with and without spectral normalization), there were no significant effects for test session, for any subject in any condition ($p>0.05$). Note also that the effects of spectral normalization were measured acutely. It is possible that long-term experience or explicit training might have influenced baseline performance and/or further enhanced the benefit of spectral normalization.

GENERAL DISCUSSION

The results of the present study demonstrate that the proposed spectral normalization algorithm can significantly improve CI users' speech understanding with less-intelligible talkers. In Experiment 1, spectral normalization provided the greatest benefit to CI subjects who exhibited the greatest talker sensitivity. In Experiment 2, a pitch-shift algorithm was used to simulate different talkers while keeping temporal cues (e.g., speaking rate, overall sentence duration, temporal modulation depth) constant. While pitch-shifting and subsequent spectral normalization produced some undesirable processing artifacts, CI users' speech recognition improved with the spectral normalization algorithm. Taken together, the results suggest that this spectral normalization approach may benefit CI users' understanding of speech produced by less-intelligible talkers. However, some considerations should be kept in mind when interpreting these results, and in designing an effective spectral normalization algorithm for real-time speech processing.

In Experiment 1, only four of the nine CI subjects exhibited significant better performance with one of the two test talkers (S1, S2, and S3 with talker F1; S8 with talker M1). The best-performing subjects exhibited no significant difference in performance with talkers F1 or M1. It is possible that a greater number of source talkers would have elicited stronger talker sensitivity effects in all subjects, albeit with different talkers for each subject. It is also possible that interfering noise may have elicited more talker sensitivity across subjects. Note that both F1 and M1 produced the IEEE stimuli in the manner of "clear" speech, i.e., relatively slow speaking rate, well articulated, etc. Thus, the normalization algorithm largely addressed spectral envelope differences between talkers, which might have to be more extreme to produce talker sensitivity effects. Temporal differences between talkers (e.g., speaking rate, overall duration, emphasis, etc.) may produce equal if not greater talker sensitivity effects. An effective speaker normalization algorithm may also need to compensate for temporal differences between talkers, as well as spectral differences.

Experiment 2 was designed to factor out possible contributions of varying temporal information and to expand the range of talker characteristics presented in Experiment 1. While the pitch-shift algorithm may not have been the ideal method to create different talker characteristics, it is difficult to control temporal variations among different talkers. One would have to record a very large database to include the range of spectral and temporal characteristics encountered in everyday listening experience. Alternatively, judicious amounts of duration adjustments (via cut and splicing or duplication of speech segments) might offer some experimental control, albeit with another set of possible signal processing artifacts. In Experiment 2, the pitch-shift transformations significantly reduced performance relative to the reference source talker F1. The results were in agreement with those from Experiment 1, in that spectral normalization generally improved speech understanding with less-intelligible talkers. However, it should be noted that the pitch-shift algorithm simulated only some of the acoustic characteristics that may differ between real talkers. Also, NH subjects' overall speech quality ratings suggest that the spectral normalization algorithm may introduce undesirable artifacts when talker differences are sufficiently extreme. While CI listeners generally

TABLE IV. r^2 significance values for linear regressions performed between the unprocessed talkers from Experiment 1 (M1 and F1) and the pitch-shift transformations from Experiment 2 (T0.6, T0.8, T1.2, T1.4, T1.6).

	Pitch-shift transformation (Exp. 2)				
Talker (Exp. 1)	T0.6	T0.8	T1.2	T1.4	T1.6
M1	r^2=0.409	r^2=0.532	r^2=0.718	r^2=0.521	r^2=0.635
	p=0.064	**p=0.026**	**p=0.004**	**p=0.028**	**p=0.010**
F1	r^2=0.393	r^2=0.725	r^2=0.688	r^2=0.470	r^2=0.358
	p=0.071	**p=0.004**	**p=0.006**	**p=0.041**	p=0.089

benefited from spectral normalization in Experiment 2, it is unclear whether the proposed spectral normalization algorithm would sufficiently compensate for differences between real talkers. Further testing with a more diverse group of real source talkers is needed to verify the feasibility of the proposed technique.

Individual CI subjects' talker sensitivity may have also contributed to the pattern of results in Experiments 1 and 2. For example, it might be expected that subjects who performed better with talker F1 in Experiment 1 would also perform better with the upwardly shifted transformations T0.6 and T0.8 in Experiment 2, as these pitch shifts were smaller relative to F1 than to M1. It might also be expected that these same subjects would benefit more greatly from the spectral transformations T1.2-to-T1.0, T1.4-to-T1.0 and T1.8-to-T1.0. Data were compared between experiments to see whether individual subjects' performance in Experiment 1 was reflected in Experiment 2. In the first analysis, subjects were divided into two groups: Group 1 (S1, S2, and S3; better performance with F1) and Group 2 (S4–S9; better performance with M1). A two-way ANOVA, with subject group (Group 1 or 2) and pitch-shift transformation (T0.6 or T0.8) showed no significant effect for subject group [$F(1,7)$ =0.0584, p=0.816]; post-hoc Bonferroni t-tests showed no significant effect for subject group, for either T0.6 (p =0.987) or T0.8 (p=0.643). One issue with this analysis is that for five out of the six subjects in Group 2, there was no significant difference in performance between M1 and F1. Individual subject performance with talker M1 or F1 in Experiment 1 was also compared to that with the pitch-shift transformations in Experiment 2. Table IV shows the r^2 and significance values for the linear regression analysis across different subjects. Subject performance with the F1 talker in Experiment 1 was fairly well correlated with performance for T0.8 and T1.2 from Experiment 2 (both were relatively close to the original F1 talker). Similarly, subject performance with the M1 talker in Experiment 1 was fairly well correlated with performance with T1.6 from Experiment 2 (the most "male" of the pitch-shift transformations). However, one issue with this analysis is that the better performers in Experiment 1 performed equally well with the M1 and F1 source talkers. Thus, it is difficult to separate talker sensitivity from overall performance with this regression analysis. In the present study, it is difficult to know how talker sensitivity for the top-performing subjects may have been limited by performance ceiling effects. Again, sufficiently different talkers or difficult listening conditions might allow talker sensitivity effects to emerge in even good CI users. It may be true that better CI performers may be less sensitive to talker differences, and therefore may benefit less from spectral normalization. For these CI users, the acoustic input may be better matched to the electrode locations in the cochlea, or other patient-related factors may contribute to the better overall performance.

While the results from these two experiments are promising, special care is needed when designing a real-time normalization algorithm that will be robust to ambient noise, interfering speech, and the wide variety of talker characteristic found in everyday listening environments. A standard set of talkers and listening conditions might help to quickly identify a reference talker (or maybe even several reference talkers) that could be used in the algorithm. Ideally, the algorithm would be continuously updated as new talkers and listening conditions are introduced. Finally, CI patients would likely experience a period of adaptation to such a normalization algorithm (and any adverse processing artifacts). In the present study, the effects of spectral normalization were acutely measured, which may have underestimated the benefits after long-term experience.

V. CONCLUSIONS

The present study showed substantial differences in cross-talker intelligibility in CI users' speech recognition. A spectral normalization algorithm was used to compensate for acoustic differences between the less-intelligible and more-intelligible speech patterns from different talkers. In Experiment 1, spectral normalization was shown to significantly improve overall CI speech performance; however, some CI users were more sensitive than others to talker differences and the subsequent spectral normalization. In Experiment 2, the spectral normalization algorithm was applied to simulated talkers, in which the fundamental frequency and vocal tract characteristics were modified while preserving temporal information such as speaking rate. Compared to NH listeners, CI users' speech understanding was more sensitive to the pitch-shift transformations and subsequent spectral normalization. The results suggest that spectral normalization, as a front end to CI speech processing, may help CI users maintain perceptual constancy when presented with multiple and/or less-intelligible talkers.

ACKNOWLEDGMENTS

We are grateful to all subjects for their participation in these experiments. We thank three anonymous reviewers for their insightful comments and recommendations. Research was supported in part by NIH (No. DC-004993).

Allen, J. S., Miller, J. L., and DeSteno, D. (**2003**). "Individual talker differences in voice-onset-time," J. Acoust. Soc. Am. **113**, 544–552.

Assmann, P. F., Nearey, T. M., and Hogan, J. T. (**1982**). "Vowel identification: Orthographic, perceptual, and acoustic aspects," J. Acoust. Soc. Am. **71**, 975–989.

Bond, Z. S., and Moore, T. J. (**1994**). "A note on the acoustic-phonetic characteristics of inadvertently clear speech," Speech Commun. **14**, 325–337.

Bradlow, A. R., Torretta, G. M., and Pisoni, D. B. (**1996**). "Intelligibility of

normal speech 1. Global and fine-grained acoustic-phonetic talker characteristics," Speech Commun. **20**, 255–272.
Cox, R. M., Alexander, G. C., and Gilmore, C. (**1987**). "Intelligibility of average talkers in typical listening environments," J. Acoust. Soc. Am. **81**, 1598–1608.
Dorman, M. F., Loizou, P. C., and Rainey, D. (**1997a**). "Stimulating the effect of cochlear implant electrode insertion depth on speech understanding," J. Acoust. Soc. Am. **102**, 2993–2996.
Dorman, M. F., Loizou, P. C., and Rainey, D. (**1997b**). "Speech intelligibility as a function of the number of channels of stimulation for signal processors using sine-wave and noise-band outputs," J. Acoust. Soc. Am. **102**, 2403–2411.
Fu, Q. -J. (**1997**). "Speech perception in acoustic and electric hearing," Ph.D. dissertation, University of Southern California, Los Angeles, CA..
Fu, Q. -J., and Shannon, R. V. (**1999**). "Recognition of spectrally degraded and frequency shifted vowels in acoustic and electric hearing," J. Acoust. Soc. Am. **105**, 1889–1900.
Fishman, K., Shannon, R. V., and Slattery, W. H. (**1997**). "Speech recognition as a function of the number of electrodes used in the SPEAK cochlear implant speech processor," Hear. Res. **40**, 1201–1215.
Gordon-Salant, S., and Fitzgibbons, P. J. (**1997**). "Selected cognitive factors and speech recognition performance among young and elderly listeners," J. Speech Lang. Hear. Res. **40**, 423–431.
Green, T., Katiri, S., Faulkner, A., and Rosen, S. (**2007**). "Talker intelligibility differences in cochlear implant listeners," J. Acoust. Soc. Am. **121**, EL223–EL229.
Greenwood, D. D. (**1990**). "A cochlear frequency-position function for several species—29 years later," J. Acoust. Soc. Am. **87**, 2592–2605.
Hazan, V., and Markham, D. (**2004**). "Acoustic-phonetic correlates of talker intelligibility for adults and children," J. Acoust. Soc. Am. **116**, 3108–3118.
Hood, J. D., and Poole, J. P. (**1980**). "Influence of the speaker and other factors affecting speech intelligibility," Audiology **19**, 434–455.
Huang, X. -D., Acero, A., and Hon, H.-W. (**2001**). *Spoken Language Processing—A Guide to Theory, Algorithm, and System Development*, (Prentice Hall, Englewood Cliffs, NJ).
IEEE (**1969**). *IEEE Recommended Practice for Speech Quality Measurements* (IEEE, New York).
Kain, A., and Macon, M. W. (**1998**). "Spectral voice conversion for text-to-speech synthesis," IEEE, ICASSP, **1**, 285–288.
Kirk, K. I., Pisoni, D. B., and Miyamoto, R. C. (**1997**). "Effects of stimulus variability on speech perception in listeners with hearing impairment," J. Speech Lang. Hear. Res. **40**, 1395–1405.
Kurdziel, S., Noffsinger, D., and Olsen, W. (**1976**). "Performance by cortical lesion patients on 40 and 60% time-compressed materials," J. Am. Aud Soc. **2**, 3–7.
Liu, C., Fu, Q. -J., and Narayanan, S. S. (**2006**). "Smooth GMM based multi-talker spectral conversion for spectrally degraded speech," IEEE ICASSP **5**, 141-144.
Liu, S., Rio, E. D., Bradlow, A. R., and Zeng, F.-G. (**2004**). "Clear speech perception in acoustic and electric hearing," J. Acoust. Soc. Am. **116**, 2374–2383.
Luo, X., and Fu, Q. -J. (**2005**). "Speaker normalization for Chinese vowel recognition in cochlear implants," IEEE Trans. Biomed. Eng. **52**, 1358–1361.
Mendel, J. M. (**1995**). *Lessons on Estimation Theory for Signal Processing, Communications and Control* (Prentice Hall, Englewood Cliffs, NJ).
Miller, J. L., and Volaitis, L. E. (**1989**). "Effect of speaking rate on the perceptual structure of a phonetic category," Percept. Psychophys. **46**, 505–512.
Mullennix, J. W., Pisoni, D. B., and Martin, C. S. (**1989**). "Some effects of talker variability on spoken word recognition," J. Acoust. Soc. Am. **85**, 365–378.
Nejime, Y., and Moore, B. C. (**1998**). "Evaluation of the effect of speech-rate slowing on speech intelligibility in noise using a simulation of cochlear hearing loss," J. Acoust. Soc. Am. **103**, 572–576.
Pisoni, D. B. (**1993**). "Long term memory in speech perception: Some new findings on talker variability, speaking rate, and perceptual learning," Speech Commun. **13**, 109–125.
Shannon, R. V., Zeng, F. -G., Kamath, V., Wygonski, J., and Ekelid, M. (**1995**). "Speech recognition with primarily temporal cues," Science **270**, 303–304.
Sommers, M. S., Nygaard, L. C., and Pisoni, D. B. (**1994**). "Stimulus variability and spoken word recognition. I. Effects of variability in speaking rate and overall amplitude," J. Acoust. Soc. Am. **96**, 1314–1324.
Stylianou, Y., Cappe, O., and Moulines, E. (**1998**). "Continuous probabilistic transform for voice conversion," IEEE Trans. Speech Audio Process. **6**, 131–142.
Verbrugge, R. R., Strange, W., Shankweiler, D. P., and Edman, T. R. (**1976**). "What information enables a listener to map a talker's vowel space?," J. Acoust. Soc. Am. **60**, 198–212.

Information transfer analysis: A first look at estimation bias

Elad Sagi and Mario A. Svirsky[a)]
Department of Otolaryngology, New York University School of Medicine, 550 First Avenue, NBV-5E5, New York, New York 10016, USA

(Received 2 August 2007; revised 8 January 2008; accepted 25 February 2008)

Information transfer analysis [G. A. Miller and P. E. Nicely, J. Acoust. Soc. Am. **27**, 338–352 (1955)] is a tool used to measure the extent to which speech features are transmitted to a listener, e.g., duration or formant frequencies for vowels; voicing, place and manner of articulation for consonants. An information transfer of 100% occurs when no confusions arise between phonemes belonging to different feature categories, e.g., between voiced and voiceless consonants. Conversely, an information transfer of 0% occurs when performance is purely random. As asserted by Miller and Nicely, the maximum-likelihood estimate for information transfer is biased to overestimate its true value when the number of stimulus presentations is small. This small-sample bias is examined here for three cases: a model of random performance with pseudorandom data, a data set drawn from Miller and Nicely, and reported data from three studies of speech perception by hearing impaired listeners. The amount of overestimation can be substantial, depending on the number of samples, the size of the confusion matrix analyzed, as well as the manner in which data are partitioned therein.
© *2008 Acoustical Society of America.*
[DOI: 10.1121/1.2897914]

PACS number(s): 43.71.Gv, 43.66.Ts, 43.71.Es [MSS] Pages: 2848–2857

I. INTRODUCTION

Information transfer (IT) analysis, introduced by Miller and Nicely (1955), is an application of Shannon's (1948) information measure to data obtained from a speech identification task. The data are typically categorized into distinctive features (e.g., voicing, nasality, affrication, manner and place of articulation, etc.) and then organized into a confusion matrix. An IT score is obtained from this matrix by calculating the number of bits received by the listener and dividing this result by the number of bits available in the stimuli. When the listener has received all the bits available in the stimuli, e.g., when no errors appear in the feature confusion matrix, an IT score of 100% is obtained. When the listener's responses are independent of the stimuli, e.g., in a case of random guessing, the listener receives no bits of information producing an IT score of 0%. With IT analysis, one can construct a picture of how each speech feature contributes to the intelligibility of the phonemes as a whole. That is, when phonemes are viewed as a bundle of several distinctive features (Stevens, 2002), IT analysis tells us what fraction of the original information has been transmitted for each feature independently.

The IT metric is particularly advantageous over the percent correct score in cases where a listener's responses are independent of the stimuli presented. For example, purely chance performance can yield different percent correct, depending on how speech stimuli are organized into features. If out of 16 consonants, say, 9 are voiced and 7 are voiceless, then purely chance performance produces an average percent correct score of 51%. If out of 16 consonants, say, 2 are nasal and 14 are non-nasal, then purely chance performance produces an average percent correct score of 78%. Even more anomalous is when a listener's responses are biased even though the responses are independent of the stimuli presented. In the case of nasality, for example, if the listener always identified each consonant as non-nasal, the 2×2 matrix for this feature will yield a percent correct score of 87.5%. Conversely, if the listener always identified each consonant as nasal, the percent correct score in the 2×2 feature matrix for nasality becomes 12.5%. In all these cases, input and output are independent and the IT metric for these features yields a score of 0%, regardless of the type of feature or whether the listener's responses are biased.

IT analysis is pertinent beyond the speech, language, and hearing sciences, having been applied to areas such as rehabilitation, acoustics, communication engineering, computer science, psychology, and neuroscience. The ISI Web of Science indicates more than 800 papers that have cited Miller and Nicely (1955). In IT analysis, the percent information transfer is obtained by applying a maximum-likelihood estimate (MLE) of the transmitted information to a confusion matrix. In a parenthetical note of their 1955 study, Miller and Nicely state, "like most maximum likelihood estimates, this estimate will be biased to overestimate [IT] for small samples." They also state that in their study the bias can be safely ignored as each confusion matrix contained a total of 4000 entries, obtained by pooling data across subjects. Surprisingly few of the articles that cite Miller and Nicely (1955) mention this bias, or, to our knowledge, have provided a quantitative description of the overestimation, or a guideline as to the number of confusion matrix entries required to overcome the bias.

Previous efforts in other related fields have been made to describe the bias in information estimates (e.g., Miller, 1955; Rogers and Green, 1955; Carlton, 1969; Houtsma, 1983; Rabinowitz *et al.*, 1987; Wong and Norwich, 1997; Sagi and Norwich, 2002). However, to provide an accurate bias cor-

[a)]Electronic mail: Mario.Svirsky@nyumc.org.

rection for data sets with small numbers of samples, these methods require at least some model of how data will be distributed across confusion matrix elements. Such models are available for the more simple sensory stimuli such as pure tones varying in pitch or intensity. For speech stimuli, predicting how data will distribute across confusion matrix elements is a far more complicated affair.

The goal of this study is to examine the potential effect of the bias in information estimates on IT analysis, and to establish a rough guideline for avoiding this bias. First to be discussed is the case of IT overestimation bias that occurs in a situation of purely random performance, where IT should be 0%. Second, some data from Miller and Nicely (1955) will be used to demonstrate how the bias in IT estimates could arise in actual data obtained from a standard speech perception identification task. Finally, possible examples of overestimation bias in IT estimates reported in the literature shall be discussed.

II. METHODS

IT is defined as the ratio of transmitted information, I_t, to input entropy, H_x (Miller and Nicely, 1955), and is commonly expressed as a percent. The true probabilities that comprise the input entropy (denominator) are typically known *a priori*. Conversely, the probabilities that comprise the transmitted information (numerator) must be estimated from the contents of a confusion matrix. The MLE for the probability of a given event is obtained by dividing the number of times this event was observed by the number of times all events were observed. If N is the total number of observations of all events, n_x is the number of times input x was presented, n_y is the number of times output y was observed, and n_{xy} is the number of times x and y were observed together, then the MLE of the information transfer, $\hat{\mathrm{IT}}$ (the caret on top of $\hat{\mathrm{IT}}$ means "estimate"), is defined as

$$\hat{\mathrm{IT}} = \frac{\hat{I}_t}{H_x} = \frac{-\sum_x \frac{n_x}{N}\log\frac{n_x}{N} - \sum_y \frac{n_y}{N}\log\frac{n_y}{N} + \sum_x\sum_y \frac{n_{xy}}{N}\log\frac{n_{xy}}{N}}{-\sum_x p_x \log p_x}, \quad (1)$$

where p_x in the denominator is the true probability that the input x occurred. There are other ways to express the numerator in Eq. (1), but this form describes the MLE of the transmitted information as a summation of the input entropy plus the output entropy less the joint entropy. In a confusion matrix, N is equal to the total number of times all stimuli were presented, n_x is the sum of row x, n_y is the sum of column y, and n_{xy} is in the main body of the matrix at the intersection of row x and column y.

It is important to differentiate between information transfer as obtained from true probabilities and the estimation of information transfer from an experimental confusion matrix. The former will be depicted symbolically as IT, and the latter as $\hat{\mathrm{IT}}$. By definition, an estimator converges to its true value after a large enough number of samples. That is, $\hat{\mathrm{IT}}=\mathrm{IT}$ when N is large. However, to be considered an unbiased estimator, this result would have to be true *on average* for any value of N. That is, one calculates the estimate for a given number of samples N, repeats this process many times, and then computes the average of these estimates. If this average estimate equals IT for any value of N, then the estimator is considered unbiased. It will be shown that the average estimate of $\hat{\mathrm{IT}}$ is larger than IT when N is small, i.e. that $\hat{\mathrm{IT}}$ is a biased estimator, and that in some cases this bias can be large.

As a first step in demonstrating the bias in $\hat{\mathrm{IT}}$ we consider a situation where the true information transfer is equal to zero, i.e., IT=0%. This will occur whenever input and output are independent, for example when listeners guess their responses at random. Chance performance can be modeled by assuming that responses are drawn from a uniform distribution, i.e., when responses are equally likely given any stimulus. Three cases were considered. In the first case, the relationship between $\hat{\mathrm{IT}}$ and IT (i.e., the relationship between sample estimates and true values of IT) was examined as a function of two variables: the number of samples, N, and the size of the confusion matrix m (i.e., m rows and m columns). In the second case, the relationship between $\hat{\mathrm{IT}}$ and IT from the first case was reexamined as a function of the number of samples per matrix category, i.e., N/m. In the third case the relationship between $\hat{\mathrm{IT}}$ and IT was examined as a function of N for matrices of equal size, but obtained using different partitions of a larger matrix.

For the first case, $\hat{\mathrm{IT}}$ was applied to nine confusion matrices ranging in size from 2×2 to 10×10 as each matrix was progressively filled with data. Data samples were obtained with a MATLAB subroutine instructed to generate two numbers for each sample, one "input" and one "output." The input indicates the row and the output indicates the column of the confusion matrix to be updated by this sample. Both numbers are sampled pseudorandomly from a uniform distribution, but with one important difference. In many experiments, in addition to being presented in random order, stimuli are also presented the same number of times. This sampling constraint was employed strictly so that each input was repeated the same number of times every number of samples equal to the size of the confusion matrix. That is, for the 10×10 matrix, each input was represented exactly once every $N=10$ samples, whereas for the 5×5 matrix, each input was represented exactly once every $N=5$ samples, etc. In contrast to sampling of input, the uniform sampling of output was left otherwise unconstrained. $\hat{\mathrm{IT}}$ was calculated every cycle of samples for which all input were repeated until the number of samples reached closest to $N=1000$. This process was repeated 10 000 times so as to calculate the average $\hat{\mathrm{IT}}$ as a function of N. This average was then compared with the true value for IT, which is 0% for each confusion matrix in this case.

For the second case, the values of average $\hat{\mathrm{IT}}$ obtained in the first case were analyzed as a function of the number of

	p	t	k	f	Θ	s	ʃ	b	d	g	v	ð	z	ʒ	m	n	Total
p	**51**	53	65	22	19	6	11	2	0	2	3	3	1	5	8	5	256
t	64	**57**	74	20	24	22	14	2	3	1	1	2	1	1	5	1	292
k	50	42	**62**	22	18	16	11	4	1	1	1	2	0	0	4	2	236
f	31	22	28	**85**	34	15	11	3	5	0	8	8	3	0	3	0	256
Θ	26	22	25	63	**45**	27	12	6	9	3	11	9	3	2	7	2	272
s	16	15	16	33	24	**53**	48	3	5	6	3	1	6	2	0	1	232
ʃ	23	32	20	14	27	25	**115**	1	4	5	3	0	6	3	4	2	284
b	4	2	2	18	7	7	1	**60**	18	18	44	25	14	6	20	10	256
d	3	0	1	4	7	4	11	18	**48**	35	16	24	26	14	9	12	232
g	3	1	1	1	4	5	7	20	38	**29**	16	29	29	38	10	9	240
v	0	1	1	12	5	4	5	37	20	23	**71**	16	14	4	14	9	236
ð	0	1	4	17	2	3	2	53	31	25	50	**33**	23	5	13	6	268
z	6	1	2	2	6	14	8	23	29	27	24	19	**40**	26	3	6	236
ʒ	3	2	2	1	0	6	7	7	30	23	9	7	39	**77**	5	14	232
m	0	1	0	0	1	1	0	11	3	6	8	11	0	1	**109**	60	212
n	1	0	0	1	0	1	0	2	2	6	7	1	1	9	84	**145**	260
Total	281	252	303	315	223	209	263	252	246	210	275	190	206	193	298	284	4000

	Voiceless	Voiced	Total
Voiceless	**1630**	198	1828
Voiced	216	**1956**	2172
Total	1846	2154	4000

FIG. 1. 16-consonant confusion matrix (top) from Miller and Nicely (1955) partitioned along gray lines into a 2×2 voicing feature matrix (bottom). In both matrices, correct responses are emphasized in bold.

samples per matrix category, from 1 to 100 samples per category. In the case of the 10×10 matrix, 100 samples per category are obtained after $N=1000$ samples. For the 2×2 matrix, 100 samples per category are obtained after $N=200$ samples, and so on.

For the third case, five 2×2 matrices were constructed from a 10×10 matrix as the latter matrix was filled with data using the strict sampling constraint described above. Each 2×2 matrix was constructed by using a different partition of the 10×10 matrix. For example, an equal partition of the 10×10 matrix would result in a 2×2 matrix with each category consisting of five categories from the original 10×10 matrix. Let us represent this partition as (5, 5). The other four 2×2 matrices were constructed using the following partitions: (4, 6), (3, 7), (2, 8), and (1, 9). $I\hat{T}$ was calculated from each 2×2 matrix every $N=10$ samples until $N=1000$. This process was repeated 10 000 times to obtain an average $I\hat{T}$ as a function of N.

The next example we used to demonstrate the overestimation bias employed data from Miller and Nicely (1955). Samples were drawn from the 16×16 consonant confusion matrix in Fig. 1 (Table II in Miller and Nicely, 1955). Normal hearing listeners were required to identify which of 16 consonants was heard in a stimulus that contained one of the consonants followed by the vowel /a/. For this confusion matrix, stimuli were presented in the presence of background noise with a fairly low signal-to-noise ratio of −12 dB. From this matrix, one can produce 4000 input–output pairs. For example, consider the cell at the intersection of the first row and third column of the consonant confusion matrix. One observes that the number of times the consonant /p/ was confused with consonant /k/ is 65. Hence, there are 65 input–output pairs for the input /p/ and the output /k/. From the list of 4000 pairs, 1600 were selected at random and updated into a 16×16 consonant confusion matrix. The random selection of input–output pairs was constrained so that each input was represented exactly once every 16 samples. To achieve this, all responses to each input were randomly permuted, and then the first 100 responses for each input were entered into the matrix 16 at a time, once for each input. $I\hat{T}$ was calculated from the matrix as each set of 16 samples were entered to obtain a measure of $I\hat{T}$ as a function of N, for $N=16,32,48,\ldots,1600$. This was repeated 10 000 times using a different random permutation of the original data to obtain a measure of the average $I\hat{T}$ at each number of samples. The standard deviation about the mean was also calculated.

TABLE I. Miller and Nicely (1955) classification of feature categories for 16 consonants. Voicing: 0=voiceless and 1=voiced; nasality: 0=non-nasal and 1=nasal; affrication: 0=nonaffricate and 1=affricate; and place of articulation: 0=front, 1=middle, and 2=back.

	Features			
Consonant	Voicing	Nasality	Affrication	Place
p	0	0	0	0
t	0	0	0	1
k	0	0	0	2
f	0	0	1	0
Θ	0	0	1	1
s	0	0	1	1
ʃ	0	0	1	2
b	1	0	0	0
d	1	0	0	1
g	1	0	0	2
v	1	0	1	0
ð	1	0	1	1
z	1	0	1	1
ʒ	1	0	1	2
m	1	1	0	0
n	1	1	0	1

This procedure for obtaining the curve of average $I\hat{T}$ from the consonant confusion matrix in Fig. 1 was repeated for the following four features: voicing, nasality, affrication, and place of articulation. At the bottom of Fig. 1 is an illustration of how a 2×2 voicing matrix is constructed from the consonant matrix. The gray lines represent the partition of the consonant matrix into feature categories of voiced and voiceless consonants. The classification of consonants into feature categories for each of the four features is summarized in Table I, taken from Miller and Nicely (1955). For a given input–output consonant pair sampled from Figure 1, Table I was used to reclassify the pair as an input and output for the appropriate feature confusion matrix. For example, the consonant pair /p/ and /k/ mentioned previously would yield a feature input–output pair of (0, 0) for voicing and (0, 2) for place. That is, both consonants are voiceless (i.e., 0), but /p/ is produced with a constriction at the front of the oral cavity (i.e., 0) whereas /k/ is produced with a constriction at the back of the oral cavity (i.e., 2). As with the 16×16 consonant matrix, the average $I\hat{T}$ was calculated from each feature matrix at $N=16,32,\ldots,1600$. For each feature, the *a priori* probabilities for the denominator of Eq. (1) were calculated from Table I. For example, one can see from Table I that the

a priori probabilities for nasal and non-nasal consonants are 2/16 and 14/16, respectively. To compare with the 16×16 consonant matrix, the standard deviation about the mean $\hat{IT}$ was calculated for the voicing feature. For each of the above five cases, the consonant matrix in Fig. 1 as well as the four features in Table I, the values of average $\hat{IT}$ as a function of the number of samples N are compared with the true values for IT, approximated by the value of $\hat{IT}$ at $N=4000$.

As an example of how bias in IT estimates appears in the IT literature, data sets from three studies with cochlear implant (CI) listeners are analyzed; Donaldson and Kreft (2006), van Wieringen and Wouters (1999), and Tye-Murray and Tyler (1989). In each case, the average $\hat{IT}$ was reported for different speech features. In these investigations, the average was obtained by first calculating $\hat{IT}$ from each listener's confusion matrix, and then averaging across the group of listeners tested. Also reported in these studies was a confusion matrix containing data pooled from all listeners as well as a table depicting the classification of consonants into feature categories. We calculated $\hat{IT}$ for each feature by applying their feature classification table to the pooled matrix, and compared the result with the average $\hat{IT}$ reported in the respective papers. The difference between these two measures is that the former was calculated from a large number of samples, i.e., a confusion matrix with data pooled across listeners, whereas the latter consists of measurements obtained with far fewer samples, i.e., confusion matrices with data from individual listeners. If no small-sample bias existed in IT estimation, the two measures should be close. As IT estimates tend to overestimate the true value for smaller samples, we expect that the average $\hat{IT}$ values reported would be larger than the $\hat{IT}$ obtained from the pooled matrix.

In Donaldson and Kreft (2006), $\hat{IT}$ averaged from 20 CI users was reported for the consonant features voicing, manner and place of articulation. Stimuli were 19 consonants in initial and medial position for three vowel contexts, produced by male and female talkers. Only the average $\hat{IT}$ data reported for the initial consonants in three vowel contexts from female talkers was examined here. Each averaged estimate was obtained from matrices consisting of $N=285$ samples per listener. Also reported for each testing condition was a confusion matrix with data pooled across listeners. Each of these matrices contained $N=5700$ samples. We conducted IT analysis on the pooled matrices for the stimulus conditions examined here, for the features voicing, manner, and place of articulation using the feature table reported in Donaldson and Kreft (2006). The pooled $\hat{IT}$ were compared with the reported averaged $\hat{IT}$.

In van Wieringen and Wouters (1999), IT estimates were reported for vowel and consonant features for 24 CI users partitioned into three groups of better, intermediate, and poor performers with 8 listeners in each group. The vowel features analyzed were duration, first (F1) and second (F2) formant frequencies. The consonant features analyzed were voicing, burst, amplitude envelope, place, affrication, manner, and nasality. Two sets of IT estimates were reported for each group, an average score and a pooled score. The pooled confusion matrices for each group were also reported. We compiled three sets of IT estimates from the data of van Wieringen and Wouters (1999) for all speech features analyzed. The first set is the average of the 24 individual $\hat{IT}$ values obtained by averaging the averaged estimates reported for the three performance groups. The matrices from which these estimates were obtained consist of $N=120$ samples per matrix for vowels and $N=192$ samples per matrix for consonants. The second set of estimates are the pooled $\hat{IT}$ per group, averaged over the three performance groups. The matrices for these estimates contained $N=960$ samples per matrix for vowels and $N=1536$ samples per matrix for consonants. The second set of estimates is depicted as "Pool8" to indicate that each estimate represents the pooling of data from 8 listeners, pooled for each group, but averaged for the three groups. The third set of estimates is $\hat{IT}$ obtained by pooling all data into one matrix of $N=2880$ for vowels and $N=4608$ for consonants. These estimates were obtained by combining the pooled matrices for the three performance groups into one matrix. The third estimate is depicted as "Pool24." We compared the three sets of IT estimates, i.e., averaged, Pool8 and Pool24, to examine how much overestimation, if any, occurs as one moves from the Pool24 estimate to the averaged estimate.

In Tye-Murray and Tyler (1989) IT estimates were reported for users of several CI devices for the consonant features voicing, place, nasality, duration, frication and envelope. We examined their IT estimates reported for 7 Nucleus users and 10 Symbion users. The number of samples in the matrices from which IT estimates were obtained for each listener ranged from $N=280$ to $N=630$ samples per Nucleus user and $N=280$ to $N=350$ samples per Symbion user. We averaged the reported estimates for each feature across users for each device group. Also reported was the pooled confusion matrix for each device group, consisting of $N=2940$ samples for the Nucleus group and $N=3430$ samples for the Symbion group. We performed IT analysis on the pooled matrices to obtain $\hat{IT}$ estimates for each feature and for each device group. The averaged and pooled $\hat{IT}$ estimates obtained were compared to test for overestimation bias.

III. RESULTS

In a system where input and output are sampled independently from a uniform distribution, it is known from the outset that information transfer is zero, i.e., IT=0%. In Fig. 2 are values of the average estimate of information transfer as a function of the number of samples for confusion matrices ranging in size from 2×2 to 10×10 filled with uniformly distributed pseudorandom data. Two observations are worth noting. First, average $\hat{IT}$ overestimates IT when the number of samples N is small, and approaches IT=0% as N becomes large. Hence, although $\hat{IT}$ is an estimator for IT, it is a biased estimator. Second, the size of the overestimation depends on both the number of samples N and the size of the matrix.

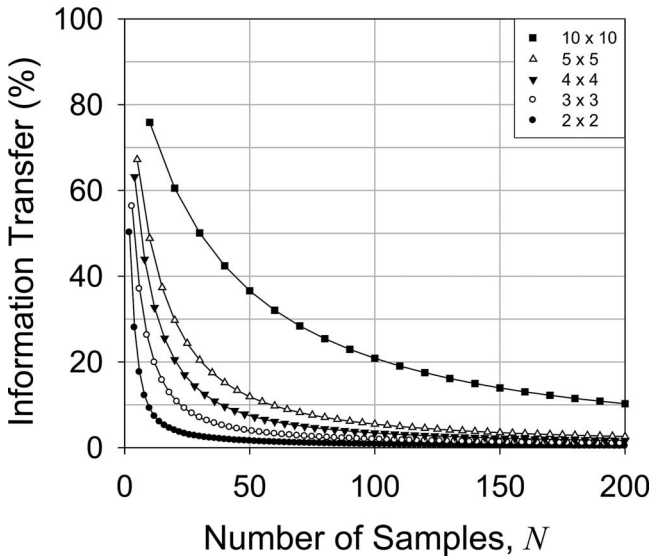


FIG. 2. Average information transfer estimate as a function of the number of samples for matrices filled with uniformly distributed pseudorandom data. Average was obtained from 10 000 iterations. Size of matrices ranges from 2×2 to 10×10. In each case, the true value for IT is 0%.

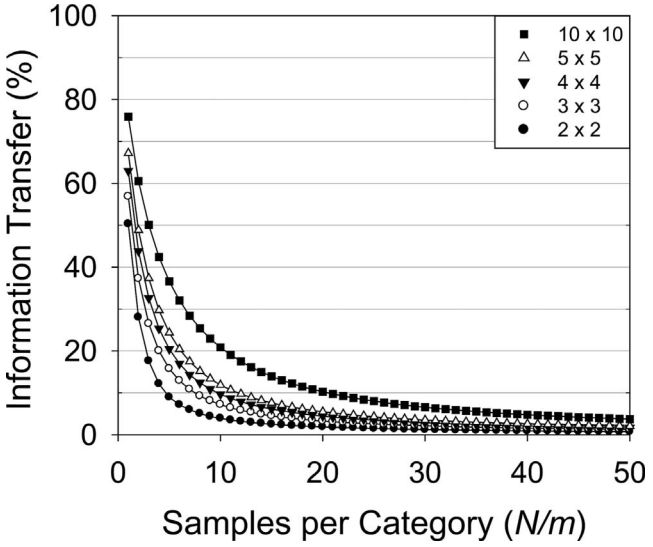


FIG. 3. Average information transfer estimate as a function of the number of samples per matrix category (N/m) for $m\times m$ matrices of size $m=2,\ldots,10$ filled with uniformly distributed pseudorandom data.

Larger matrices will tend to produce a larger overestimation and require more samples before $\hat{IT}$ estimates will asymptote to their true value.

The sampling constraint we employed allowed us to examine the bias in another manner, as a function of the number of samples per matrix category. If an $m\times m$ matrix is filled with N samples so that each of the m possible inputs are presented the same number of times every cycle of m samples, then the number of samples per matrix category every m samples is N/m. Could the overestimation bias be the same when examined on a per category basis, irrespective of matrix size? In Fig. 3, it is clear that this is not the case. For the same number of samples per matrix category, larger matrices will still tend to produce a larger overestimation. The data depicted in Fig. 3 are also summarized in Table II, for matrix sizes ranging from 2×2 to 10×10 using up to 100 samples per matrix category. The overestimation in the 2×2 matrix is nearly negligible, less than 2%, after as few as 20 samples per category ($N=40$ samples). In contrast, the overestimation in the 10×10 matrix becomes less than 2% after as many as 100 samples per matrix category ($N=1000$ samples). Clearly, using too many feature categories relative to the number of samples collected could give rise to problematic estimates.

One must keep in mind that the matrices in Table II were generated so that each category has the same number of samples per matrix category. Very often in IT analysis, feature matrices are produced by partitioning a larger matrix into feature categories where the numbers of samples per feature category are not equal. The effect of unequal samples per category on the overestimation bias is depicted in Fig. 4, where five 2×2 matrices were constructed using different partitions of a 10×10 matrix as the latter was filled with uniformly distributed data using the strict sampling constraint. For purposes of comparison, the bias due to a 3×3 matrix with a uniform partition is also plotted in Fig. 4 in gray (i.e., the same 3×3 data plotted in Fig. 2). The different 2×2 partitions are represented as (5, 5), (4, 6), (3, 7), (2, 8), and (1, 9), where (1, 9) means that the first category of the 10×10 matrix became the first category in the 2×2 matrix and the other 9 categories of the 10×10 matrix were combined to produce the second category in the 2×2 matrix. From Fig. 4, it is evident that a 2×2 matrix constructed from a less uniform partition of the 10×10 matrix tends to pro-

TABLE II. Average estimated information transfer as a function of samples per matrix category (N/m) for $m\times m$ matrices of size $m=2,\ldots,10$. Matrices filled with data sampled from a uniform distribution using the strict sampling constraint described in the text. The true value for information transfer should be 0%.

$\hat{IT}$ (%)	Matrix size ($m\times m$)								
N/m	2×2	3×3	4×4	5×5	6×6	7×7	8×8	9×9	10×10
10	4.0	7.0	9.6	11.9	14.1	15.9	17.7	19.3	20.8
20	1.9	3.2	4.4	5.5	6.5	7.5	8.4	9.4	10.2
30	1.2	2.1	2.8	3.5	4.2	4.8	5.4	6.0	6.5
40	0.9	1.6	2.1	2.6	3.1	3.5	3.9	4.4	4.8
50	0.7	1.2	1.6	2.0	2.4	2.8	3.1	3.4	3.7
100	0.4	0.6	0.8	1.0	1.2	1.3	1.5	1.7	1.8

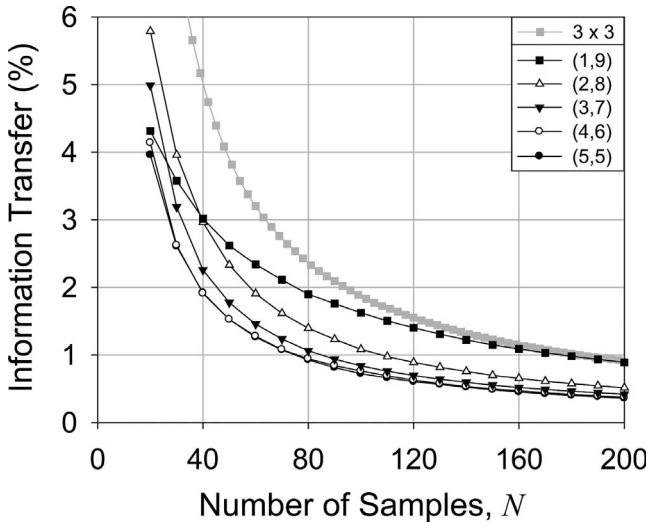


FIG. 4. Average information transfer as a function of the number of samples for five 2×2 matrices obtained from different partitions of a larger 10×10 matrix filled with pseudorandom data. For comparison, the bias due to a 3×3 matrix with a uniform partition filled with pseudorandom data is plotted in gray.

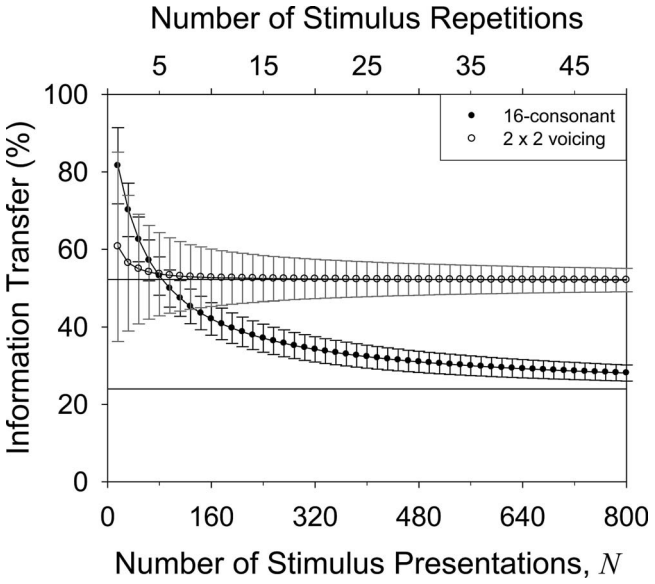


FIG. 5. Average information transfer estimate as a function of the number of samples for the 16-consonant matrix (filled circles) and 2×2 voicing matrix (empty circles) depicted in Fig. 1. Averages were obtained from 10 000 iterations of randomly selecting samples from the consonant matrix using the strict sampling constraint. Black and gray error bars depict 2 standard deviations above and below the average for the 16-consonant and 2×2 matrices respectively. Horizontal lines depict approximate true value for *IT*.

duce greater overestimation than a more uniform partition. That is, a less uniform partition will tend to require more samples than a more uniform partition before the bias becomes negligible. Indeed, after $N=200$ samples, the bias in the 2×2 matrix with the (1, 9) partition becomes very nearly equal to the bias in the 3×3 matrix with a uniform partition. Hence, a very extreme non-uniform partition in a smaller matrix can increase the bias, as if it came from a larger matrix size.

To understand the difference between the curves in Fig. 4, it is useful to refer to Table II. For example, in Fig. 4, the average $\hat{IT}$ for the (1, 9) 2×2 matrix at $N=100$ samples is 1.6%. In this matrix, the first input category consists of 10 samples whereas the second input category consists of 90 samples. In Table II, 10 samples per category for a 2×2 matrix will result in an average $\hat{IT}$ of 4% whereas 90 samples per category will result in an average $\hat{IT}$ of 0.4%. The average $\hat{IT}$ in the (1, 9) 2×2 matrix with 10 samples in one category and 90 samples in the other category falls in between these two extremes, and is largely determined by the input category with fewer samples per category.

Turning now to the data of Miller and Nicely (1955), the average $\hat{IT}$ for the 16-consonant confusion matrix and 2×2 voicing matrix in Fig. 1 are plotted in Fig. 5 as a function of the number of samples (filled and empty circles respectively). When applying $\hat{IT}$ to the 16×16 consonant matrix, each consonant is treated as a separate feature category. Although this is not the most common way of conducting IT analysis, it is presented here as a contrast to the 2×2 voicing matrix. Because each consonant stimulus was selected once every 16 samples, the average $\hat{IT}$ are also plotted as a function of the number of stimulus repetitions (abscissa on top), i.e., the number of times all stimuli were repeated. Each value of average $\hat{IT}$ includes an error bar (black for the 16-consonant matrix and gray for the voicing feature matrix) that represents ±2 standard deviations about the mean. The horizontal lines represent the value of $\hat{IT}$ after 4000 samples in each case (24% for the 16-consonant matrix and 52% for the 2×2 voicing matrix). Although a small amount of bias may still exist after 4000 samples it is negligible at this point and the horizontal lines can be considered close enough to the actual asymptote, i.e., the true value of IT for each matrix. In both matrices, the average $\hat{IT}$ is not equal to its true value for all numbers of samples (or stimulus repetitions) showing again that $\hat{IT}$ is a biased estimator. Although in both matrices, the average $\hat{IT}$ overestimates its true value for small numbers of samples, the bias is clearly different between the two cases. The average $\hat{IT}$ for the voicing feature matrix approaches to within 1% of its true value after only 7 stimulus repetitions (112 samples), whereas even after 50 stimulus repetitions not only does the average $\hat{IT}$ for the 16-consonant matrix overestimate its true value by 4%, but the true value remains lower than 2 standard deviations below the mean $\hat{IT}$. Of course, the average $\hat{IT}$ for the 16-consonant matrix will eventually approach the "true value" depicted in Fig. 5 as the latter was estimated from the same matrix filled with $N=4000$ samples.

Another difference in $\hat{IT}$ values between the two matrices is that the 2×2 voicing feature matrix produces a larger standard deviation about the mean $\hat{IT}$ than the 16-consonant matrix. Hence, for the voicing matrix, even though the average $\hat{IT}$ reaches to within 1% of its true value after 7 stimulus repetitions, the amount of variability about this mean is ±9%. At the same number of stimulus repetitions the amount of variability about the mean $\hat{IT}$ for the 16-consonant matrix is ±5%, though this mean overestimates the true

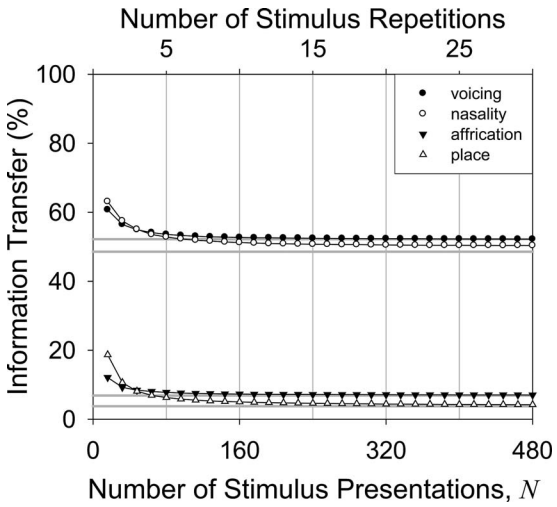


FIG. 6. Average information transfer estimate as a function of the number of samples for the features voicing, nasality, affrication, and place of articulation. For each curve, average was obtained from 10 000 iterations of randomly selecting samples from the 16-consonant matrix depicted in Fig. 1 using the strict sampling constraint, and categorizing samples into features according to Table I. For each feature, horizontal gray lines depict approximate true value for *IT*.

value by 23%. The error bars for both matrices demonstrate that in addition to being a biased estimator $\hat{IT}$ will also yield estimates that can vary considerably above and below the expected value, and that this variability will diminish as one uses a greater number of samples. This variability, due to the type of sampling error one encounters with any statistical estimator, is not explored further here.

In Fig. 6 are plots of average $\hat{IT}$ for the features voicing, nasality, affrication, and place using the data of Miller and Nicely (1955). The data are plotted both as a function of the number of samples *N* (abscissa on bottom) as well as the number of stimulus repetitions (abscissa on top), where each stimulus repetition occurs every 16 samples. The average $\hat{IT}$ for the voicing feature is the same as in Fig. 5. The horizontal gray lines represent, approximately, the true value of IT for each feature. To reach within 1% of the true value, the average $\hat{IT}$ required 7 stimulus repetitions (112 samples) for the voicing feature, 5 stimulus repetitions (80 samples) for the affrication feature, and 13 stimulus repetitions (208 samples) for the place feature. For nasality, even after 50 stimulus repetitions (800 samples) the average $\hat{IT}$ failed to reach within 1% of its true value, though it did reach 3% of this value after 9 stimulus repetitions (144 samples).

TABLE IV. Information transfer estimates for vowel features in 24 cochlear implant users from van Wieringen and Wouters (1999). Next to each feature in parentheses is the number of feature categories. Avg: average estimate per user, $N=120$ samples per matrix; Pool8: estimate obtained by averaging the pooled estimate between better, intermediate, and poorer performers (8 listeners per group with $N=960$ samples per matrix); and Pool24: estimate obtained by pooling data from all 24 listeners into one matrix with $N=2880$ samples. Without the small-sample bias, numbers in a given row should be similar.

	Vowels		
$\hat{IT}$ (%)	Avg	Pool8	Pool24
Duration (2)	34	28	23
F1 (3)	28	24	19
F2 (3)	31	24	19

In Tables III–VI are examples of averaged and pooled IT estimates taken from three representative studies. The pooled estimate is obtained from one aggregate confusion matrix that includes the trial-by-trial data of all test subjects. Conversely, with the averaged estimate, each test subject's confusion matrix is considered separately. As the number of samples in the aggregate matrix is much larger than the number of samples in each subject's confusion matrix, we would expect that the pooled estimate would provide a less biased estimate of the true value for the average IT among all the subjects, whereas the averaged estimate of this true value would incur a larger overestimation. The number of samples per matrix for the pooled and averaged IT estimates and the number of feature categories per feature are specified in Tables III–VI. In Table III are averaged and pooled IT estimates for three consonant features from the data of Donaldson and Kreft (2006). In each case the average $\hat{IT}$ is larger than the pooled $\hat{IT}$, but not by a large amount. The overestimation ranged from 2% to 6% with the largest overestimation coming from the manner feature with 4 categories. In Tables IV and V are averaged, Pool8 and Pool24 IT estimates from data reported in van Wieringen and Wouters (1999) for vowel (Table IV) and consonant (Table V) features. In Tables IV and V there is a consistent drop in $\hat{IT}$ between the average estimates and those pooled for 8 listeners, and between those pooled for 8 listeners and those pooled for 24 listeners. Overall, the average $\hat{IT}$ overestimates the pooled $\hat{IT}$ for 24 listeners by 9%–12% for the vowel features in Table IV, and by 6%–9% for the consonant features in Table V. In Table VI are averaged and pooled IT

TABLE III. Information transfer estimates for consonant features in 20 cochlear implant users from Donaldson and Kreft (2006). Next to each feature in parentheses is the number of feature categories. Avg: average estimate per user, $N=285$ samples per matrix; Pool: estimate obtained from data pooled in one matrix with $N=5700$ samples; and diff=Avg-Pool. Without the small-sample bias, diff should be close to zero.

	/Ca/			/Ci/			/Cu/		
$\hat{IT}$ (%)	Avg	Pool	diff	Avg	Pool	diff	Avg	Pool	diff
Voicing (2)	59	56	3	63	60	3	67	65	2
Place (3)	35	33	2	23	21	2	27	25	2
Manner (4)	60	54	6	59	54	5	56	52	4

TABLE V. Information transfer estimates for consonant features in 24 cochlear implant users from van Wieringen and Wouters (1999). Next to each feature in parentheses is the number of feature categories. Avg: average estimate per user, $N=192$ samples per matrix; Pool8: estimate obtained by averaging the pooled estimate between better, intermediate, and poorer performers (8 listeners per group with $N=1536$ samples per matrix); and Pool24: estimate obtained by pooling data from all 24 listeners into one matrix with $N=4608$ samples. Without the small-sample bias, numbers in a given row should be similar.

	Consonants		
$\hat{IT}$(%)	Avg	Pool8	Pool24
Voicing (2)	41	35	33
Burst (2)	57	53	51
Amp Env (2)	63	59	56
Nasal (2)	43	41	37
Affrication (2)	52	46	43
Manner (3)	58	53	49
Place (4)	15	10	8

estimates from data reported in Tye-Murray and Tyler (1989) for six consonant features for users of the Nucleus and Symbion CI devices. The difference between the average and pooled estimates, i.e., average minus pooled, ranges between −2% and 9% with the largest overestimation occurring for the place and envelope features which comprise 4 feature categories; the other features consist of 2 feature categories. Differences in how phonemes were partitioned among the various features did not appear to play a large role in the amounts of bias reported in Tables III–VI.

IV. DISCUSSION

Miller and Nicely (1955) stated that the MLE for the information transfer will be biased to overestimate its true value for small samples. This study clarifies their assertion. Three approaches were followed to examine the small-sample bias in information transfer estimates. The first approach was to examine a case in which the bias is very clear and easy to interpret, where input and output are independent and drawn from a uniform distribution and the true value for the information transfer is 0%. The second approach was to reconstruct the bias in the original data set of Miller and Nicely (1955) by sampling data from one of the confusion matrices reported therein and calculating the amount of overestimation as a function of the number of samples for different speech features. Information transfer analysis was born out of this classic study and though the authors mentioned the small sample bias parenthetically, no indications or guidelines were presented about the magnitude of the bias or how to overcome it other than a statement to the effect that the bias is very small after a very large number of samples on the order of $N=4000$. Hence, the Miller and Nicely data set was included here to provide an explicit description of the bias referred to in their study. The third approach was to ascertain whether the problem of overestimation bias is relevant in a practical sense by examining the tendency of overestimation bias in information transfer estimates reported in three contemporary studies representative of how IT analysis is commonly used. Each of these approaches provides insight into the magnitude of the overestimation and a rough picture on the requirements to reasonably overcome this bias.

The case where input–output pairs are independent and drawn from a uniform distribution is a model of chance performance and demonstrates how the overestimation bias depends on the number of samples relative to the size of the confusion matrix, as well as how these samples are partitioned among the input categories of the matrix. In Fig. 2, the peak overestimation ranges from 50% to 76% depending on whether the confusion matrix was from 2×2 to 10×10. As for the number of samples before $\hat{IT}$ drops below 2%, 40 samples were sufficient for the 2×2 case, whereas 1000 samples were required for the 10×10 case. Hence, larger matrices will tend to produce a larger overestimation and require more samples to reach the true information transfer. Figure 3 and Table II show how the effect of matrix size persists when the bias is examined as a function of the number of samples per matrix category. For example, at 10 samples per category, the bias ranges from 4% to 21% depending on whether the confusion matrix was 2×2 to 10×10. Figure 4 shows the effect on the bias when the number of samples per category is unequal among the matrix input categories. This occurs when a matrix is constructed from a non-uniform partition of a larger matrix. In such a case, the bias will be dominated by the input category with fewest samples and require more samples to be overcome relative to a matrix constructed from a uniform partition of a larger

TABLE VI. Information transfer estimates for consonant features in 7 Nucleus and 10 Symbion cochlear implant users from Tye-Murray and Tyler (1989). Next to each feature in parentheses is the number of feature categories. Avg: average estimate per user, about $N=420$ and $N=343$ samples per matrix for Nucleus and Symbion users, respectively; Pool: estimate obtained from pooled data in one matrix with $N=2940$ and $N=3430$ samples for Nucleus and Symbion users, respectively; and diff: Avg-Pool. Without the small-sample bias, diff should be close to zero.

	Nucleus			Symbion		
$\hat{IT}$ (%)	Avg	Pool	diff	Avg	Pool	diff
Voicing (2)	22	22	0	49	43	6
Nasality (2)	24	23	1	56	51	5
Frication (2)	17	19	−2	34	36	−2
Duration (2)	14	12	2	33	31	2
Place (4)	18	13	5	20	11	9
Envelope (4)	29	24	5	54	46	8

matrix. These model systems demonstrate how chance performance could yield a nonzero information transfer estimate depending on the number of samples, the size of the confusion matrix, and how samples are partitioned amongst the input categories of the matrix.

These three effects on the overestimation bias are also demonstrated in the curves of average $\hat{IT}$ in Figs. 5 and 6, resampled from Miller and Nicely (1955). In Fig. 5, the bias in information transfer estimates for a 16-consonant matrix is contrasted with the bias when the consonants are partitioned into a 2×2 voicing matrix. Whereas the bias is fairly large for the 16×16 matrix and requires over 50 stimulus repetitions for the average information transfer to reach within 3% of its true value, the average bias in the 2×2 voicing matrix falls below 3% after just 3 stimulus repetitions, though considerable variability about the mean does exist ($\pm15\%$). That is, although the average $\hat{IT}$ in a small feature matrix can converge to its true value after relatively few stimulus repetitions, one should not expect the same from a single estimate of IT as considerable variability can remain even after a much larger number of stimulus repetitions. As depicted in Fig. 6, similar results for the average $\hat{IT}$ were obtained for the other feature matrices. After a relatively small number of stimulus repetitions, the overestimation in the average information transfer became quite small. Even nasality, for which the bias persisted the most relative to the other features, reached within 3% of its true value using less than 10 stimulus repetitions (160 samples). This many stimulus repetitions is well within the number typically obtained in the speech and hearing fields and may be sufficient to overcome the bias when dealing with a small number of feature categories on the order of 2 or 3.

Some differences do exist amongst the curves of average $\hat{IT}$ in Fig. 6. The order of features from least to greatest in terms of the number of stimulus repetitions required before the average $\hat{IT}$ approached its true value was affrication, voicing, place, and then nasality. As one can observe in Table I, the affrication and voicing features result in 2×2 matrices with partitions (8, 8) and (7, 9), respectively. The small matrix size accompanied by a fairly uniform partition of consonant stimuli results in a small bias that converges to its true value after relatively few stimulus repetitions. The place feature results in a relatively larger matrix (3×3) and hence requires more stimulus repetitions to converge to its true value. Finally, although the nasality feature results in a small matrix (2×2), its partition is highly skewed (14, 2) and so its bias is predominantly determined by the nasal category which accrues samples only twice every 16 samples. Hence, the effects of numbers of samples, matrix size, and how the samples are distributed among the feature categories combine to provide an account for the differences in small sample bias among the features in Fig. 6.

The three CI studies that were examined in this study, whose results are analyzed in Tables III–VI, were chosen specifically because they published sufficient data to illustrate two different ways of calculating information transfer from a population of CI users. Each method can result in different amounts of overestimation bias. First, one can calculate the information transfer from each user's confusion matrix and average the results. Second, one can pool data from all subjects into one aggregate confusion matrix and then calculate the information transfer. In general, the information transfer estimate obtained by averaging individual IT estimates from individual subject matrices will incur a larger overestimation than the information transfer estimate obtained from the pooled matrix. The averaging approach utilizes confusion matrices with a relatively smaller number of samples per matrix, whereas the pooled approach utilizes a confusion matrix with a relatively large number of samples. In addition to the number of samples, the amount of overestimation also depends on the size of the feature matrices analyzed.

In Table III and Table VI, one observes how the difference between averaged and pooled information transfer can be relatively small (3% or less) for feature matrices of 2×2 or 3×3 when the number of samples per matrix in the averaged estimate is larger than $N=250$. However, this difference becomes more substantial once the size of the feature matrix analyzed becomes 4×4. In Tables IV and V, the individual matrices contained less than 200 samples resulting in a larger discrepancy between the averaged and pooled information transfer, even for features with 2 or 3 categories. For these matrices, an intermediate category between averaged and pooled results was included, showing a steady decrease in information transfer estimates between the averaged matrices and the pooled matrix, as the number of samples per matrix for each category was increased.

Some overestimation remained between features in the intermediate Pool8 category and features in the Pool24 category in Tables IV and V, between 2% and 5%, even though the pooled matrices for the intermediate category consisted of about 1000 samples. Some overestimation also remained between the average and pooled estimates in Table VI for the voicing and nasality features among Symbion patients, 5% and 6% respectively, even though the averaged estimates involved 2×2 feature matrices with more than 250 samples per matrix. These results may be attributed to the variability in information transfer estimates in addition to the bias, as depicted by the confidence intervals for the curves in Fig. 5. Indeed, the curves of Fig. 6 would suggest that the bias is nearly overcome after 200 samples for features with 2 or 3 categories. However, these curves were obtained from an average of 10 000 iterations. Hence, one should not presume that a number of samples on the order of $N=250$ will guarantee an information transfer estimate equal to its true value for small matrices since sometimes $N=1000$ might not be enough due to the randomness involved.

Both the averaged and pooled approaches to obtaining IT estimates have a disadvantage and an advantage. With the averaged approach, one is likely to obtain a result that overestimates the true value, whereas the pooled approach will likely yield an unbiased result. However, the averaged approach also yields confidence intervals with which one can conduct statistical analyses to test for differences between experimental groups. The pooled approach only yields one

estimate for each condition, obviating any statistical comparisons between groups. So which approach should one follow?

If one is not interested in the absolute value of the information transfer for a given feature, but rather in relative differences between groups, then the averaged approach is a viable option and statistical differences thus obtained are valid. However, using a small number of samples per matrix will increase the inherent variability of IT estimates, in addition to inter-individual differences within the group, and thus make it more difficult to demonstrate significant differences between groups. Furthermore, if one decides to implement the averaged approach it is important to ensure that each confusion matrix, both between and within experimental groups, contains the same number of samples. Although the amount of bias in a group of IT estimates may differ within the group even when the number of samples obtained for each matrix within the group are the same, there is less chance of confounding the bias in the average IT for the group than if the number of samples per matrix is not fixed. Also, caution is required when comparing IT estimates between features with different numbers of feature categories or with very different partitions of the same phoneme matrix, because the bias becomes more prevalent as the number of feature categories increases and when the feature categories consist of very nonuniform partitions of phoneme stimuli.

If one is interested in the absolute value of the information transfer for the group, then one needs to ensure that the matrices to be analyzed have a sufficient number of samples. This can be achieved by pooling several matrices, or by ensuring that each individual matrix has an adequate number of samples. An example of when the absolute value of the information transfer is required is in sequential information transfer analysis (Wang and Bilger, 1973), where larger IT estimates determine the order for which features are sequentially partialed out of the confusion matrix. The effect of the small-sample bias on sequential IT analysis has not been explored here, and is yet to be determined.

V. CONCLUDING REMARKS

Until more sophisticated techniques are developed to correct for small-sample bias in IT estimates, it is important to keep the bias in mind when planning one's experimental paradigm. For example, based on the results of this study, we would suggest obtaining at least 250 samples per subject when examining information transfer for features with 2 or 3 categories. For features with 4 or 5 categories, we would suggest obtaining at least 500 samples. This number of samples should yield an average IT estimate that is within 3% of its true value. However, this suggestion is more of a rough guideline than a hard rule, because the actual sample estimate may be higher or lower than the average. To assess the amount of overestimation bias, it may be useful to report the pooled IT estimate in addition to the average IT estimate for each group, and compare the two results.

ACKNOWLEDGMENTS

This research was supported by Grant No. R01-DC003937 from the National Institute on Deafness and Other Communication Disorders (NIH).

Carlton, A. G. (**1969**). "On the bias of information estimates," Psychol. Bull. **71**, 108–109.

Donaldson, G. S., and Kreft, H. A. (**2006**). "Effects of vowel context on the recognition of initial and medial consonants by cochlear implant users," Ear Hear. **27**, 658–677.

Houtsma, A. J. M. (**1983**). "Estimation of mutual information from limited experimental data," J. Acoust. Soc. Am. **74**, 1626–1629.

Miller, G. A. (**1955**). "Note on the bias of information estimates," in *Information Theory in Psychology; Problems and Methods*, edited by H. Quastler (The Free Press, Glencoe, IL), pp. 95–100.

Miller, G. A., and Nicely, P. E. (**1955**). "An analysis of perceptual confusions among some english consonants," J. Acoust. Soc. Am. **27**, 338–352.

Rabinowitz, W. M., Houtsma, A. J. M., Durlach, N. I., and Delhorne, L. A. (**1987**). "Multidimensional tactile displays: identification of vibratory intensity, frequency, and contactor area," J. Acoust. Soc. Am. **82**, 1243–1252.

Rogers, M. S., and Green, B. F. (**1955**). "The moments of sample information when the alternatives are equally likely," in *Information Theory in Psychology; Problems and Methods*, edited by H. Quastler (The Free Press, Glencoe, IL) pp. 101–108.

Sagi, E., and Norwich, K. H. (**2002**). "Weighing the anchor in categorization of sound level," Can. Acoust. **30**, 15–24.

Shannon, C. E., (**1948**). "A mathematical theory of communication," AT & T Tech. J. **27**, 623–656.

Stevens, K. N. (**2002**). "Toward a model for lexical access based on acoustic landmarks and distinctive features," J. Acoust. Soc. Am. **111**, 1872–1891.

Tye-Murray, N., and Tyler, R. S. (**1989**). "Auditory consonant and word recognition skills of cochlear implant users," Ear Hear. **10**, pp. 292–298.

van Wieringen, A., and Wouters, J. (**1999**). "Natural vowel and consonant recognition by Laura cochlear implantees," Ear Hear. **20**, 89–103.

Wang, M. D., and Bilger, R. C. (**1973**). "Consonant confusions in noise: a study of perceptual features," J. Acoust. Soc. Am. **54**, 1248–1266.

Wong, W., and Norwich, K. H. (**1997**). "Simulation of human sensory performance," BioSystems **43**, 189–197.

Intra- versus intermodal integration in young and older adults

Brent P. Spehar[a] and Nancy Tye-Murray
Department of Otolaryngology, Washington University School of Medicine, St. Louis, Missouri 63110

Mitchell S. Sommers
Department of Psychology, Washington University, St. Louis, Missouri 63130

(Received 6 February 2007; revised 11 February 2008; accepted 12 February 2008)

The ability to integrate information across sensory channels is critical for both within- and between-modality speech processing. The present study evaluated the hypothesis that inter- and intramodal integration abilities are related, in young and older adults. Further, the investigation asked if intramodal integration (auditory+auditory), and intermodal integration (auditory+visual) resist changes as a function of either aging or the presence of hearing loss. Three groups of adults (young with normal hearing, older with normal hearing, and older with hearing loss) were asked to identify words in sentence context. Intramodal integration ability was assessed by presenting disjoint passbands of speech (550–750 and 1650–2250 Hz) to either ear. Integration was indexed by factoring monotic from dichotic scores to control for potential hearing- or age-related influences on absolute performance. Intermodal integration ability was assessed by presenting the auditory and visual signals. Integration was indexed by a measure based on probabilistic models of auditory-visual integration, termed integration enhancement. Results suggested that both types of integration ability are largely resistant to changes with age and hearing loss. In addition, intra- and intermodal integration were shown to be not correlated. As measured here, these findings suggest that there is not a common mechanism that accounts for both inter- and intramodal integration performance. © *2008 Acoustical Society of America.* [DOI: 10.1121/1.2890748]

PACS number(s): 43.71.Ky, 43.71.Lz, 43.71.Rt, 43.71.Gv [DOS] Pages: 2858–2866

I. INTRODUCTION

The ability to combine sensory information, both intra- and intermodally, is essential for efficient interaction with the environment. For example, *intramodal integration* across critical bands is a prerequisite for accurate perception of the broadband speech signal. Integration across ears, which is another type of intramodal integration, enhances sound localization and provides about a 3-dB boost for binaural as compared to monaural speech perception (Humes, 1994). Finally, *intermodal integration*, like the integration of the visual and auditory signals during face-to-face conversations, can provide large improvements in speech perception compared to listening or viewing alone (Sommers *et al.*, 2005a; Sumby and Pollack, 1954). The current study was designed to determine whether there is overlap in the processes mediating these intra- and intermodal integration abilities and to determine whether and how some integrative abilities are affected by age and hearing loss.

For the current investigation, intramodal integration was defined as the process of combining two or more channels of speech information within the same modality (i.e., auditory +auditory information). It was assessed using spectral fusion tasks (Cutting, 1976), in which disjoint bands of spectral information are presented to participants monotically (all information presented to one ear) or dichotically (different information presented to each ear).[1] Intermodal integration was defined as the process of combining speech information across modalities (auditory+visual information). Audiovisual integration was used as the index of intermodal integration ability.

Two similarities have been observed between intra- and intermodal integration (Cutting, 1976; McGurk and MacDonald, 1976). The first similarity entails the combination of two different speech segments into a single percept. In a task that required intramodal integration, Cutting (1976) simultaneously presented two different speech signals, /ba/ and /ga/, to opposite ears (dichotic presentation). Individuals perceived a third, nonpresented, phonetic segment (/da/) about 68% of the time (termed *psychoacoustic fusion*). In a task that required intermodal integration, McGurk and MacDonald (1976) presented two different phonemes simultaneously to participants with normal hearing, one as a visual signal and the other as an auditory signal. An auditory presentation of /ba/ coupled with a visual presentation of /ga/ often led to the percept of /da/ or /θa/, occurring around 70% of the time (the *McGurk effect*). Spectral fusion and the McGurk effect are both instances in which the fused perception of two stimuli (auditory stimuli in the case of spectral fusion and auditory and visual stimuli in the case of the McGurk effect) leads to a percept that corresponds to neither of the individual elements.

A second similarity between intra- and intermodal integration is that both can provide superadditive (sometimes called synergetic) benefit. In the case of spectral fusion, Ronan *et al.* (2004) compared participants' perception of widely separated bands of filtered speech presented simultaneously to the participants' perception of the individual bands. Identification for the two bands exceeded what would have been

[a]Electronic mail: speharb@ent.wustl.edu

 0001-4966/2008/123(5)/2858/9/$23.00 © 2008 Acoustical Society of America

predicted from simply multiplying the error probabilities from the scores for each band alone. Also, presentations of single narrow bands (1/3 octave or less) of speech usually result in floor performance for word- and sentence-level speech perception, whereas the simultaneous presentation of the same narrow bands can result in superadditive performance as high as 90% words correct with sentences (Warren *et al.*, 1995; Spehar *et al.*, 2001).

In the case of audiovisual speech perception, Walden *et al.* (1993) compared the performance obtained in an audiovisual (AV) condition with performance obtained in visual-only (V) and auditory-only (A) conditions in older adults with hearing loss. Visual-only and auditory-only scores were 16.7% and 42.7% key words correct in sentence context, respectively. In the AV condition, scores were better than additive, averaging 92.0% (see also Grant *et al.*, 1998; Sommers *et al.*, 2005a).

The existence of these two similarities suggest that an ability to integrate intramodally may be related to the ability to integrate intermodally. That is, similarities may exist because a common process mediates both forms of integration. However, to date, no investigation has specifically addressed whether the two abilities are correlated. One goal of the present investigation was to relate intra- and intermodal integration performance.

A third similarity between the two types of integration ability might also exist, and if so, its existence would provide additional support for the present interpretation. It may be that aging and hearing loss affect both inter- and intramodal integration in like ways because they both affect a common process. Although some research has considered the effects of aging and hearing loss on integration, no investigation has specifically examined whether either aging or hearing loss affects intermodal integration similarly.

Recent findings concerning aging and intermodal integration indicate that the ability to merge the auditory and visual signal is relatively stable across the adult lifespan (Massaro, 1987; Cienekowski and Carney, 2002; 2004; Sommers *et al.*, 2005a). For example, Cienkowsi and Carney (2002) demonstrated that older and younger adults were equally susceptible to the McGurk effect (McGurk and MacDonald, 1976). The investigators suggested that aging does not degrade one's ability to integrate auditory and visual information. Likewise, Sommers *et al.* (2005a) reached a similar conclusion, finding that older adults (over 65 years) demonstrated similar auditory enhancement (the benefit of adding auditory speech information to a visual-only speech recognition task) as young adults (18–26 years).

Whether or not aging affects intramodal integration remains unclear. One concern in measuring age-related changes in a spectral fusion task is that the findings may be confounded by presbycusic hearing loss and the resultant reduction of audibility of the two bands. For example, Palva and Jokinen (1975) studied spectral fusion ability across the life-span (5–85 years) in 289 healthy persons. Word-level stimuli were presented in both monotic and dichotic conditions without a carrier phrase. Filter settings included a low passband from 480 to 720 Hz and a high passband from 1800 to 2400 Hz. Results indicated a peak in performance scores (>80% words correct) at the ages of 15–35 years for both monotic and dichotic conditions. A gradual decline in scores was seen from the ages of 35 to 85 years, with scores averaging around 40% words correct in the 85-years old group. Since Pavla and Jokinen did not control for hearing loss, it is not possible to determine if age-related reductions in performance were due to a reduced ability to perceive the filtered speech signal or to a decline in the ability to integrate the two channels of spectral information, or some combination of the two.

Franklin (1975) assessed the effects of hearing loss on monotic and dichotic spectral fusion for consonant perception in a group of young adults with moderate to severe sensorineural hearing loss. Scores were based on the perception of consonants presented in real words. Stimuli were presented at or near threshold levels. Filter settings included a low passband from 240 to 480 Hz and a high passband from 1020 to 2040 Hz. The participants scored better in the dichotic relative to the monotic condition. This finding was opposite to that found in an earlier study with participants with normal hearing. This latter group performed better in the monotic condition relative to the dichotic condition (Franklin, 1969). Taken together, these two studies indicate listeners with normal and impaired hearing may differ in their monotic versus dichotic spectral fusion ability.

Results from Pavla and Jokinen (1975) and Franklin (1975) indicated possible age or hearing-related differences in spectral fusion ability. However, results were not analyzed for intramodal integration ability. Specifically, it is not possible to determine if observed reductions in dichotic performance were due to a reduced ability to perceive the filtered speech signal or a decline in the ability to integrate the two channels. To assess intramodal integration ability, the current investigation used monotic performance as a covariate when comparing dichotic performance across groups. Any decline seen in dichotic performance, after accounting for monotic ability, was considered to be an index of less than perfect intramodal integration ability.

In summary, some similarities have been found between results for audiovisual integration and results for spectral fusion. Both have been shown to be superadditive and both have shown the phenomenon of eliciting the perception of a third unique phoneme when conflicting information is merged from two channels of speech. The working hypothesis was that a common process underlies the integration of multiple channels of speech information, whether the input is received intermodally or intramodally. Moreover, it was predicted that age and hearing impairment would have comparable effects on intramodal integration. To address these questions, the current investigation included three groups of participants: young adults with normal hearing, older adults with normal hearing, and older adults with hearing loss. Comparisons between the two groups with normal hearing assessed the effects of age, independent of hearing loss. Comparisons between the two older groups assessed the effects of hearing loss.

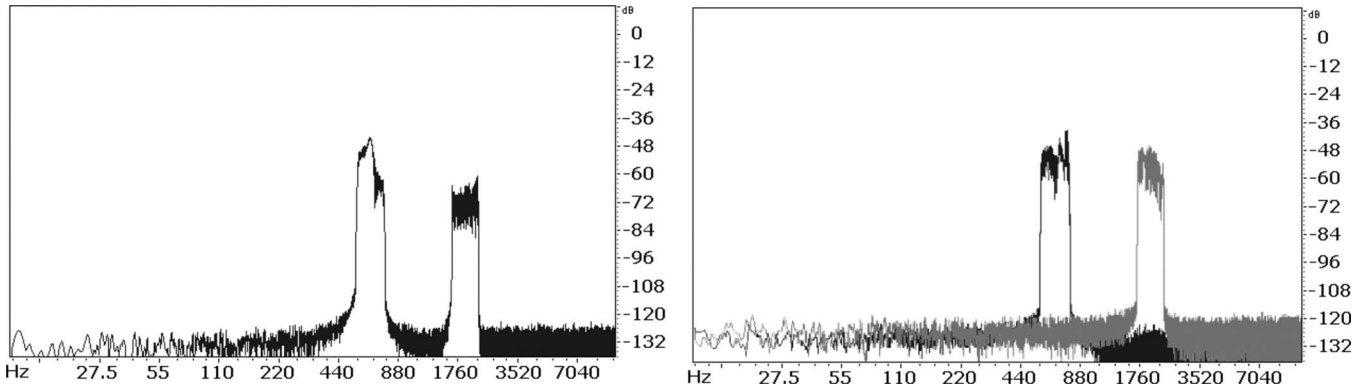


FIG. 1. Example of spectra from single band and combined band stimuli. Left and right panels are the monotic and dichotic conditions, respectively. *Y* axis represents distance from peak clipping in a 16-bit digital clip (i.e., 0 dB is the maximum value before clipping occurs).

II. METHODS

A. Participants

Thirty-nine young adults (YNH) and 63 older adults [39 with normal hearing (ONH) and 24 with hearing impairment (OHI)] were tested. All participants were tested as part of a larger study investigating AV integration in young and older adults (See Tye-Murray *et al.*, 2007). Only those participants who received the spectral fusion conditions as presented here were included. Older adults (22 men and 41 women, mean age=73.0 years, s.d.=5.1, Min=65.4, Max=85.3) and young adults (17 men and 22 women, mean age=21.3 years, s.d. =2.0, Min=18.1, Max=26.4) were community-dwelling individuals who were recruited from the participant pool maintained by the Aging and Development program at Washington University. All participants were paid $10 per hour or assigned class credit for participating in the study.

Participants were screened to include only those with pure-tone-averages (PTA; average of pure tone threshold values at 500, 1000, and 2000 Hz) at or below 55 dB HL in each ear. Average PTA for the young participants was 4.9 dB HL (s.d.=2.1, Min=−5.8, Max=16.7). Among the older adults, participants were grouped by hearing status. Thirty-nine were considered normally hearing with PTAs at or below 25 dB HL (mean=15.1, s.d.=6.3, Min=5, Max=25) and the remaining 24 had some degree of mild to moderate hearing loss (mean=42.9, s.d.=6.1, Min=32.5, Max=55.8) (Roeser *et al.*, 2000). The differences in sample size for the older groups are the result of the strict criteria for relatively flat responses across the audiometric test frequencies. Volunteers with interoctave slopes greater than 15 dB at frequencies between 500 and 4000 Hz were screened out. No age difference between the ONH and the OHI groupings was found [$t(61)=0.331$, $p=0.742$]. All participants were also screened to include those with visual acuity equal to or better than 20/40 using the standard Snellen eye chart and contrast sensitivity better than 1.8 as assessed with the Pelli-Robison Contrast Sensitivity Chart (Pelli *et al.*, 1998). Participants taking medications that might affect the CNS were excluded.

B. Stimulus preparation and testing procedures

1. Intramodal integration stimuli

Intramodal integration ability in young and older adults was assessed using both monotic and dichotic presentations of bandpass filtered sentences. The stimuli were digital quality productions in.wav (PCM) file format of the CUNY Sentences (Boothroyd *et al.*, 1988) obtained by request from Dr. Boothroyd. The CUNY sentences consist of 72 lists of 12 sentences. Each list is consistent with respect to the topic of the sentences and the type of sentences included. For example, each list contains one sentence each about a common topic, such as family, weather, holidays, money, and each list contains an equal number of statements, imperatives and interrogatives. Lists 7–9 were used for the dichotic condition and lists 10–12 were used for the monotic condition. Each condition consisted of 36 sentences, with a total of approximately 336 content words. Scoring was based on correct identification of these content words. The same female talker spoke all sentences.

The original stimulus files were in mono, 16-bit format with a sample rate of 22050 samples/s. Filtering was accomplished using COOL EDIT, a PC-based wave-form-editing software package. Filtering was performed using Blackman-windowing with a 4096 sample fast Fourier transform (FFT) size. Separate filtering of the original files preserved both low-frequency (LB) and high-frequency (HB) passband information (LB, 550–750 Hz; HB, 1650–2250 Hz). These filter settings yielded approximately 0.5 octave bandwidths for the LB and HB bands. Cutoff frequencies for the two passbands were selected so that the remaining passband was in frequency regions where potential effects from sloping high frequency hearing loss would be minimal. Filter parameters were chosen based on results of pilot testing with young adults which indicated that these filter parameters were adequate to avoid ceiling effects in the monotic condition and floor effects in the dichotic condition (Spehar *et al.*, 2001). After filtering, all sentences were equated for amplitude to the same rms level using IL-16, another PC-based wave-form editing package. No peak clipping was detected before or after filtering. The monotic and dichotic stimuli were produced by combining the filtered files for each sentence into stereo files with the appropriate information in each left or right channel. Figure 1 shows a schematic representation of the frequency spectra and band configuration for each condition. Light grey indicates the spectral information presented to one ear, where dark grey is what was pre-

sented to the other (i.e., only the dichotic condition presented information to both ears at the same time).

2. Intramodal integration testing procedure

Participants were asked to sit in a double-walled sound-treated booth and listen to the prepared sentences under headphones (Sennheiser HD 265 Linear) presented at 50 dB SPL for the YNH and ONH groups and 70 dB for the OHI participants. The relatively low presentation level was necessary to lessen the "sharp" sensation commonly experienced with narrowly filtered speech stimuli. Participants consistently reported the stimuli to be audible but difficult to understand. Calibration was accomplished using an inline Ballantine rms meter and checked before testing each participant. Condition order (monotic or dichotic first) was counterbalanced across participants so that approximately half of all participants received the monotic condition first, while the other half received the dichotic condition first. Halfway through each condition the presentation to each headphone was switched. For example, the dichotic condition began by presenting the LB to the left ear and the HB to the right. After the first 18 sentences in that condition, the presented filter band was switched to the other ear. In the monotic condition, the first 18 sentences were presented to the left ear and the last 18 to the right ear. To familiarize participants with the test stimuli, practice was provided before testing began. During practice, three unfiltered sentences were presented to familiarize the participant with the speaker's voice followed by blocked presentations of six sentences from each condition, monotic first. Practice items were not scored. It was confirmed that all participants were able to hear the stimuli at a comfortable level before proceeding.

Filtered practice items were taken from list 13 of the CUNY sentences. The experimenter listened to the responses of the participant via intercom and selected all correctly identified key words from a touch-screen. Key words were considered correct only if the participant identified all phonemes correctly (e.g., saying "cars" for "car" was considered incorrect). Presentation of the next trial did not occur until the experimenter finished entering the response from the previous trial. Sentence testing took approximately 30 min to complete. Experiment flow and scoring was conducted on a Windows-based PC equipped with a SoundBlaster Pro sound card via software programmed with LABVIEW specifically for audio presentation of digital wave forms. Participants were asked to repeat the sentences that were heard and encouraged to repeat "any or all words" that they could identify and encouraged to guess when not sure. Scoring was based on the percent of all content words correctly identified.

3. Intermodal integration stimuli

Audiovisual sentence stimuli were digitized from Laserdisc recordings of the Iowa Sentences Test (see Tyler *et al.*, 1986, for additional details). The output of the Laserdisc player (Laservision LD-V8000) was connected into a commercially available PCI interface card for digitization (Matrox RT2000). Video capture parameters were 24-bit, 720 $\times$480 in NTSC-standard 4:3 aspect ratio and 29.97 frames/s to best match the original analog version.

The Iowa Sentence Test includes 100 sentences, spoken by 20 adult talkers, speaking five sentences, with Midwest American dialects (10 female, 10 male). For our purposes, the test was divided into five lists of 20 sentences each. Each list included one sentence spoken by each of the talkers and each list included approximately the same number of words. Thus, within a list, participants saw and heard a new talker on every trial. Two of the lists were used for practice and establishing a babble level while the remaining three were used for testing. Each condition (A, V, and AV) was presented using one list. An approximately equal number of participants viewed each list in each condition. For example, in the A condition, one-third of the participants received list A, while one-third received list B, and the remaining received list C, likewise for the V and AV conditions.

4. Intermodal integration testing procedures

Participants were tested while sitting in a sound-treated room. All stimuli were presented via a PC (Dell 420) equipped with a Matrox (Millennium G400 Flex) three-dimensional video card. A dual screen video configuration was used so that stimuli could be presented to participants in the test booth while the experimenter scored responses and monitored testing progress. Experiment flow, headphones, and scoring were identical to that of the spectral fusion testing. Signal levels for the A and AV stimuli were approximately 60 dB SPL for the YNH and ONH groups and 80 dB SPL for the OHI participants. Stimuli were presented along with six-talker babble (the V also included background babble for consistency across the conditions). The background babble was adjusted for each individual during a pretesting phase using a modified speech-reception-threshold procedure (ASHA, 1988). Background noise prevented ceiling effects in the AV condition and helped equate participants' performance in the A condition. The goal in the audiovisual speech testing battery was to equate performance across the groups to between 40% and 50% key words correct in the A condition and to use this same babble level in the other two conditions (AV and V). Signal-to-noise ratios averaged −7.5 dB (s.d.=1.8) for the YNH group, −6.0 dB (s.d.=0.9) for the ONH group, and −1.0 dB (s.d.=2.7) for the OHI group.

Similar to the intramodal integration testing, trials were blocked by presentation condition (A, V, and AV) and condition order was counterbalanced. Because data were collected as part of a larger battery (see Sommers *et al.*, 2005a, b for details), presentation for the A, V, and AV conditions occurred on three separate days of a three-day test protocol. Practice for the AV sentence testing consisted of five sentences in clear (i.e., no babble) auditory-only speech presented before the testing to establish the appropriate babble level. Stimuli were taken from the two remaining lists of the

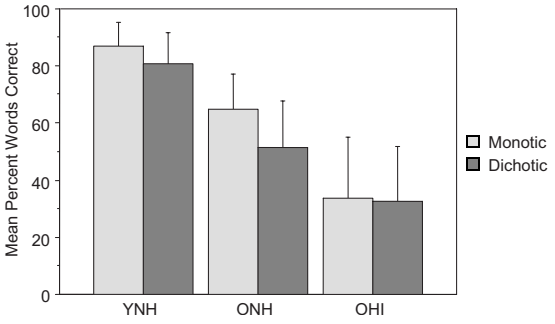


FIG. 2. Mean percent content words correct for three groups, split by condition. Error bars indicate standard deviation.

Iowa Sentences Test. Scores on the practice items were required to be 100% before further testing could begin.

III. RESULTS AND ANALYSES

Results from the study are described in three sections. The first two present the results of testing with the two types of integration (intramodal and intermodal). In the last section, the results of the analyses correlating intra- and intermodal integration are described.

A. Spectral fusion and intramodal integration

1. Absolute differences in spectral fusion

Figure 2 shows the mean percent content words correct for the monotic and dichotic spectral fusion testing as a function of group. To investigate differences in absolute performance levels in the monotic and dichotic conditions, arcsine transformed scores were analyzed using a mixed-design analysis of varience (ANOVA) with age group (older and young) as a between-subjects variable, and condition (monotic and dichotic) as a repeated measures variable (Studebaker, 1985; Sokal and Rohlf, 1995). Results indicated overall differences between the groups [$F(2,99)=110.0$, $p<0.001$], with older adults performing significantly poorer than the young adults. Significant differences were also observed between the two conditions, with performance better in the monotic than in the dichotic presentation format $F(1,99)=43.35$, $p<0.001$). There was an interaction between group and condition $F(2,99)=8.79$, $p<0.001$. Bonferroni/Dunn corrected post-hoc testing indicated that the interaction was due to the OHI group's lack of significant difference between the monotic versus dichotic conditions [monotic=33.8% (s.d.=21.26) and dichotic=32.5% (s.d.=19.23)], whereas the other two groups did show significant differences between the two conditions [ONH, monotic=65.0% (s.d.=12.0) and dichotic=51.4% (s.d.=16.5) ($p<0.001$); YNH, monotic=87.1% (s.d.=8.0) and dichotic=80.7% (s.d.=11.0) ($p<0.001$)].

2. Intramodal integration and age

To investigate the effects of age and hearing impairment on intramodal integration ability, scores were analyzed using hierarchical regression analysis. Figure 3 shows the scatter plot of monotic and dichotic scores for all participants. Scores for the two conditions were highly correlated for all

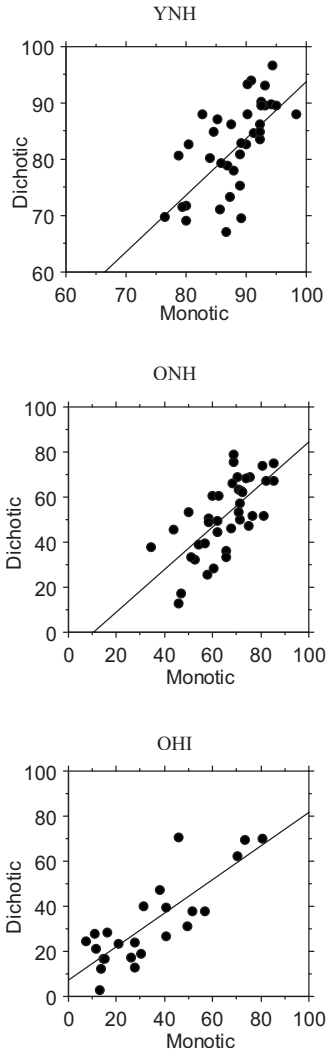


FIG. 3. Scatter plots of monotic vs dichotic performance for the three groups (top panel, young normal hearing adults (YNH), $r=0.82$; middle panel, older adults with normal hearing (ONH), $r=0.69$; bottom panel, older adults with hearing impairment (OHI), $r=0.74$; overall $r=0.89$). Please note the different axes scales for the YNH panel.

three groups (OHI, $r=0.82$, ONH, $r=0.69$, YNH, $r=0.74$, overall $r=0.89$; all p values <0.001). To measure integration, it was necessary to control for the variability already captured by the monotic performance. Thus, a hierarchical stepwise regression was performed in which scores from the monotic condition were entered into the model as step 1. A residual score near the regression line would produce a value close to zero, indicating that the dichotic performance for this individual was similar to that of his or her monotic performance. A residual score below the regression line would suggest relatively poor integration in the dichotic condition while a residual score above the line would suggest relatively good integration.

The variability in the dichotic condition, not accounted for by the monotic condition, reflected intramodal integration ability. It was analyzed for an effect of age group (entered as a coded variable, Older=1, Young=0) and PTA (average PTA across both ears entered as a single continuous variable). The analysis, using arcsine transformed data, indicated that a small proportion of variance in the dichotic scores

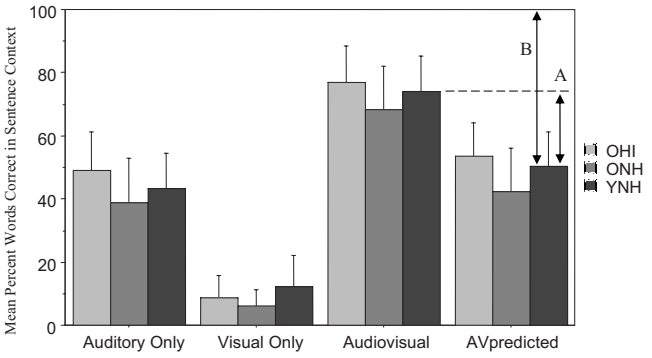


FIG. 4. Mean percent content words correct in the A, V, and AV testing the three groups. Error bars indicate standard deviation. Lines labeled A and B are aids in the conceptualization of the auditory enhancement measure for the young adults. Line A is the amount of performance beyond the AV predicted score that was actually obtained. Line B represents the amount that could have been improved, and is used for normalizing scores to determine the amount benefit afforded by having an integration process or mechanism.

could be attributed to age group [2.3% (F change (1,99) =12.86, beta=−10.99, p=0.001] beyond the large proportion of variance already accounted for by the monotic condition [79.2%, F(1,100)=380.91, $p<0.001$]. The average PTA measure did not account for enough independent variability in the dichotic scores to be included in the model (partial correlation=0.091, beta=0.105).

B. Audiovisual testing

1. Group differences in audiovisual testing

Scores from the AV testing as a function of group are presented in Fig. 4. Figure 4 also includes the results of a multiplicative error formula (AV predicted) and a schematic representation of the derived integration enhancement measure to be discussed in the following. Auditory-only scores averaged 43.4% words correct (s.d.=11.2) for the YNH group, 38.7% (s.d.=14.2) for the ONH group, and 48.9% (s.d.=12.2) for the OHI group (see also Tye-Murray *et al.*, 2007). Although we attempted to equate A performance across groups, results of a one-way ANOVA with three groups (YNH, ONH, OHI) indicated a group effect for the A scores [F (2,99)=4.914, $p<0.01$]. Bonferroni/Dunn corrected post-hoc analysis indicated that the group differences were driven by the OHI and ONH comparison ($p<0.01$), with the OHI group performing better than the other two groups. All other post-hoc comparisons for the A scores were not significant. The use of individually determined signal-to-babble ratios, however, was effective in keeping AV scores away from ceiling performance [YNH=73.9% words correct (s.d.=11.4); ONH=68.3% (s.d.=13.7); OHI=76.8% (s.d. =11.8)]. Results of a one-way ANOVA for the AV scores indicated an overall group difference in AV performance [F(2,99)=3.977, p=0.02.] Post-hoc analysis indicated that group differences were due to the ONH versus OHI comparison ($p<0.01$), with none of the remaining individual comparisons reaching significance. A one-way ANOVA on the V scores revealed an overall group difference [F(2,99)=6.019, $p<0.01$]. The post-hoc analysis indicated that differences were primarily due to the YNH versus ONH comparison ($p<0.01$). The analysis of the V condition should be interpreted with caution owing to the possibility of floor effects [YNH=12.2% words correct (s.d.=10.1); ONH=6.1% (s.d. =5.2); OHI=8.6% (s.d.=7.3)].

2. Intermodal integration

To quantify audiovisual integration ability without the confounding factors of unimodal performance, a measure termed *integration enhancement* (IEnh) was computed (Sommers *et al.*, 2005b; Tye-Murray, *et al.*, 2007). IEnh represents the proportion of obtained AV performance beyond that predicted by a probabilistic model of integration (arrow A, Fig. 4), normalized for the proportion of (p) possible improvement in AV scores (arrow B). Predicted AV performance is shown by

$$(p)\text{AV predicted} = 1 - ((1 - (p)A)(1 - (p)V)). \quad (1)$$

In this model, errors in the AV condition only occur following errors in both unimodal conditions (Fletcher, 1953; Massaro, 1987; Ronan *et al.*, 2004). The measure has been used in previous investigations of both intra- and intermodal integration (Blamey *et al.*, 1989; Grant and Braida, 1991; Ronan *et al.*, 2004) to predict performance in multichannel conditions from performance in single-channel conditions. In general, individuals outperform predicted performance and this difference between predicted and obtained scores has been attributed to integration ability (Grant, 2002). Thus, IEnh is calculated according to

$$\text{IEnh} = ((p)\text{AV}_{\text{observed}} - (p)\text{AV}_{\text{predicted}})/(1 - (p)\text{AV}_{\text{predicted}}). \quad (2)$$

Consistent with previous studies using probabilistic models (cf. Blamey *et al.*, 1989), predicted performance for all three groups' AV performance was lower than obtained AV scores (see Fig. 4). IEnh for the YNH (0.463 s.d.=0.22), ONH (0.452, s.d.=0.19), and OHI (0.492, s.d.=0.25) groups were compared using one-way ANOVA. Results indicated that integration ability for sentence-level material was not significantly different between the groups [F(2,99)=−0.261, p=0.771.].

C. Intra- versus intermodal integration

The relationship between intra- and intermodal integration ability was determined by semipartial (sr) correlation analysis. IEnh served as the measure of intermodal integration. As mentioned earlier, the intelligibility of single narrow bands of speech is very small (Warren *et al.*, 1995; Spehar *et al.*, 2001). The application of the IEnh formula to predict intramodal integration in a manner similar to intermodal integration would have required the use of floor-level scores as predictors of integration performance. Therefore, the measure of intramodal integration was the residuals obtained in the hierarchical regression analysis (i.e., the variability in dichotic performance not associated with monotic scores). Figure 5 shows the scatter plot for the residual dichotic val-

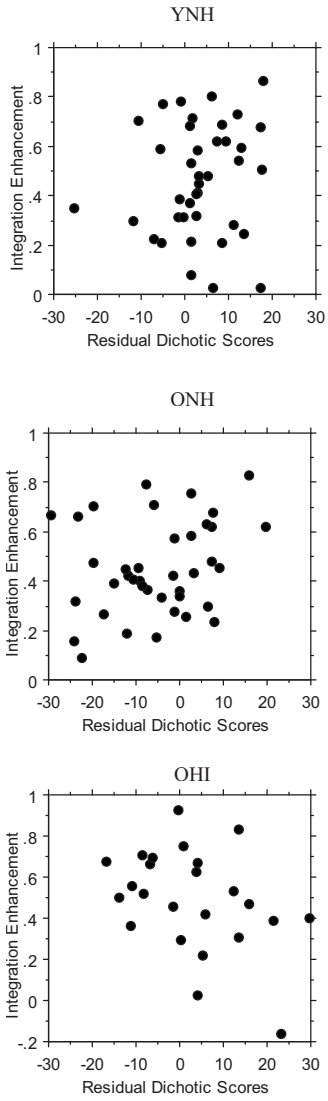


FIG. 5. Scatter plots comparing residual dichotic (arcsine transformed) values and integration enhancement [top panel, young normal hearing adults (YNH), sr=0.12, p=0.460; middle panel, older adults with normal hearing (ONH), sr=0.26, p=0.118; bottom panel, older adults with hearing impairment (OHI), sr=−0.38, p=0.065, Fisher's r to Z].

ues versus the IEnh calculation. The overall semipartial correlation between intra- and intermodal integration was not significant (sr=0.03, p=0.760). Comparisons within groups also indicated that the two types of integration were not correlated (YNH, sr=0.12, p=0.460; ONH sr=0.26, p=0.118; OHI, sr=−0.38, p=0.065).

IV. DISCUSSION

The current study had two goals. One goal was to determine whether aging and hearing loss affect intra- and intermodal integration similarly. A second goal was to determine whether the ability to integrate information intramodally correlates with the ability to integrate information intermodally.

The intramodal integration abilities of young and older adults with varying degrees of hearing acuity were compared using a spectral fusion task. Results indicated a possible age-related decline in intramodal integration ability. However, this effect was small, accounting for only 2.3% of the variance in dichotic performance. Therefore, in general, older and younger adults appear similarly able to combine disjoint bands of speech presented dichotically.

Similar to the current findings, the results of Murphy *et al.* (2006) suggested a resistance to age-related change in the ability to identify multiple tones presented diotically. Murphy *et al.* asked older and young participants to separate and identify multiple channels of information presented simultaneously, whereas the current investigation assessed their ability to merge two disjoint channels of spectral information. Results from the two studies, however, are similar in that the older listener appeared equally able to process the separate channels of spectral information to that of their younger counterparts.

The finding that age-related differences in integration abilities were relatively small is counter to the general findings of large age differences in many aspects of speech perception (cf. CHABA, 1988). For example, age-related hearing loss has been found to diminish the peripheral encoding of the speech signal (van Rooij *et al.*, 1989; Humes *et al.*, 1994). Beyond the effects of absolute sensitivity changes, reduced central auditory function has also been shown to affect speech perception in older adults through changes in the processing of the encoded auditory speech stimuli (Wilson and Jaffe, 1996). Further, cognitive deficits associated with aging have also been shown to influence speech perception ability (Pichora-Fuller *et al.*, 1995; Wingfield, 1996; Gordon-Salant and Fitgzibbons, 1997). The current results showing no age-related change in dichotic spectral fusion, therefore, add to a relatively small list of centrally mediated auditory abilities that remain largely unchanged with age. On the other hand, the current findings are similar to other results demonstrating that the integration of auditory and visual speech information (Massaro, 1987; Cienkowski and Carney, 2002; 2004; Sommers *et al.*, 2005a) is largely preserved across the lifespan. Thus, one picture that may be beginning to emerge is one in which a select set of speech perception processes are unaffected by aging. Both, intra- and intermodal integration, appear to be among this relatively rare set of age-resistant abilities.

To assess whether intra- and intermodal integration are correlated, audiovisual integration was measured and compared to intramodal integration ability. Audiovisual integration ability was indexed by a measure derived by Tye-Murray *et al.* (2007) termed integration enhancement. Results suggested that the two types of integration do not share a common mechanism and may be of separate ability. The lack of correlation could be a consequence of the two measures engaging independent process within the two domains. However, the absence of correlations between intra- and intermodal integration are consistent with those of Grant *et al.* (2004) who found that, for temporal processing among young adults with normal hearing, the two types of integration (called cross-modal and cross-spectral integration) were not mediated by similar mechanisms. Grant *et al.* measured differences in detecting a temporal asynchrony using stimuli presented either in a single (auditory) modality or two (auditory-visual) modalities. Young participants were asked to determine if the presented stimulus seemed "out of synch"

when presented at various temporal asynchronies. Results indicated that a relatively large time difference between the auditory+visual channels (approximate range, −50 to 220 ms) could go undetected when compared to that of the differences between the filtered auditory+auditory stimuli (average range, −17 to 23 ms). Based on these findings, the authors suggested that, at least for temporal processing, the two types of integration are not mediated by similar mechanisms because of the large differences in the thresholds for detecting asynchrony. In the current investigation we assessed individuals' actual perceptual ability while fusing disjoint frequency bands of speech information and integrating auditory and visual information. Taken together, results from Grant *et al.* and the current investigation both support a model of sensory integration that includes distinct or separate processes for the integration of audiovisual information and the fusion of spectral information within the hearing system.

A. Group differences in monotic and dichotic spectral fusion

Unlike the YNH and ONH groups, the OHI group did not show a decline from monotic to dichotic performance. These results resemble those reported by Franklin (1969; 1975), who reported that participants with hearing impairment performed better in a dichotic task relative to a monotic task, whereas participants with normal hearing performed worse in the dichotic task. In the current study, 41.6% of the OHI participants also performed better in the dichotic task, whereas only 15.4% of the ONH and 20.5% of the YNH participants did.

The differential results for the three groups on the two spectral fusion tasks may provide an avenue for future investigation. Franklin (1975) suggested that low-frequency masking occurs when the two bands are presented to the same ear (monotic). Franklin's suggestion was supported by subsequent investigations on the effects of hearing loss on the upward spread of masking within speech signals (Florentine *et al.*, 1980; Klein *et al.* 1990; Richie *et al.*, 2003). Those with hearing impairment were found to be more susceptible to monaural low-frequency masking. Further, Hannley and Dorman (1983) found that the degree masking of the upper vowel formants by the first formant was more pronounced depending on the etiology of the hearing impairment. Older participants with noise-induced hearing impairment showed a larger amount of upward formant masking.

Taken together with results for low frequency masking among persons with hearing impairment, the findings for no difference between the monotic and dichotic conditions in the OHI group may be the result of some of the OHI participant's increased susceptibility to the upward spread of masking in the monotic condition. This would result in lower monotic than dichotic scores relative to the two normally hearing groups. Specifically, the differential results seen for the OHI group may be the result of poorer monotic performance, due to the upward spread of masking, creating relative dichotic performance that is better than what is seen in the NH groups. Our present results suggest that further research is needed to determine if some older hearing-impaired persons or some types of sensorineural hearing losses might gain from signal processing strategies that include dichotic spectral fusion as a way to overcome the increased susceptibility to the upward spread of masking seen in a monaural speech signal.

B. Clinical implications

The practice of aural rehabilitation could benefit from a clinically feasible index of audiovisual integration such as the integration enhancement measure used here. Current practices of aural rehabilitation focus on assessing and improving communication ability among persons with hearing impairment. For the evaluation of baseline performance and progress throughout aural rehabilitation, the testing of lipreading ability and the audibility of speech through a hearing device (e.g., cochlear implant, hearing aid, or other assistive device) are important parts of a rehabilitation plan. However, without determining the ability to combine the two sources of sensory information, an equally important piece of information may be left unknown and untapped as a potential source for improving communication ability. The inclusion of integration ability to the assessment battery not only provides a valuable tool for counseling the patient, but also another measure by which to track improvement. For future research, it will be helpful to the practice of aural rehabilitation to be able to determine if integration ability can be improved. This could be accomplished through multisensory training designed to force patients to integrate information from the two modalities and counseling for awareness to the potential benefits of using all information available in face-to-face communication.

The use of narrow bands of filtered speech is found in the application of multi-channel hearing aids and cochlear implants (Loizou *et al.*, 2003; Lunner *et al.*, 1993). The finding that dichotic spectral integration remains relatively intact among older adults with and without hearing loss is encouraging to developing signal processing strategies for the binaural use of sensory aids. [2]

ACKNOWLEDGMENTS

This research was supported by a grant from the National Institute of Aging (NIA Grant No. AG018029). We thank the anonymous reviewers for their helpful comments on a previous version of the manuscript.

[1]The measure of intramodal integration used in the present study (comparison of monotic and dichotic spectral fusion) is one index of within-modality integration. Other measures, such as monotic spectral fusion (sometimes called critical-band integration) could also be considered examples of intramodal integration. The decision to use a comparison of monotic and dichotic presentations as a measure of within-modality integration in the present study was based on two factors. First, measuring critical band integration requires testing single bands (i.e., low-frequency only and high-frequency only) and pilot testing indicated that bandwidths for the single bands that did not produce floor level performance when tested alone yielded ceiling level performance in the combined band condition. Second, critical band integration measures the integration within the auditory periphery, whereas the dichotic fusion task used in the present study is more centrally mediated. As the goal was to compare within- and between-modality integration, the dichotic task was selected as it is more analogous to the centrally mediated between-modality AV integration task.

[2]The two measures of integration compared in the current study were derived from two different methods, both attempting to index the ability to merge independent channels of information. The use of different measures was necessary to avoid the improper use of the IEnh formula. As mentioned earlier, the intelligibility of single narrow bands of speech is very small (Warren *et al.*, 1995; Spehar *et al.*, 2001). The application of the IEnh formula to predict intramodal integration in a manner similar to intermodal integration would have required the use of floor-level scores as predictors of integration performance.

ASHA (**1988**). *Guidelines for Determining Threshold Level for Speech* (Am. Speech Lang. Hearing Assn., Rockville), pp. 85–89.

Blamey, P., Alcantara, J., Whitford, L., and Clark, G. (**1989**). "Speech perception using combinations of auditory, visual, and tactile information," J. Rehabil. Res. Dev. **26**, 15–24.

Boothroyd, A., Hnath-Chisolm, T., Hanin, L., and Kishon-Rabin, L. (**1988**). "Voice fundamental frequency as an auditory supplement to the speechreading of sentences," Ear Hear. **9**, 306–312.

Cienkowski, K., and Carney, A. (**2002**). "Auditory-visual speech perception and aging," Ear Hear. **23**, 439–449.

Cienkowski, K., and Carney, A. (**2004**). "The integration of auditory-visual information for speech in older adults," J. Speech Lang. Pathol. Audiol. **28**(4), 166–172.

Committee for Hearing, Bioacoustics and Biomechanics (CHABA). (**1988**). "Speech understanding and aging," J. Acoust. Soc. Am. **83**, 859–895.

Cutting, J. E. (**1976**). "Auditory and linguistic processes in speech perception: Inferences from six fusions in dichotic listening," Psychol. Rev. **83**, 114–140.

Fletcher, H. M. (**1953**), *Speech and Hearing in Communication* (Van Nostrand, New York).

Florentine, M., Buus, S., Scharf, B., and Zwicker, E. (**1980**). Frequency selectivity in normally-hearing and hearing-impaired observers, J. Speech Hear. Res. **23**, 646–669.

Franklin, B. (**1969**). "The effect on consonant discrimination of combining a low-frequency passband in one ear and a high-frequency passband in the other ear," JETP Lett. **9**, 365–378.

Franklin, B. (**1975**). "The effect of combining low- and high-frequency passbands on consonant recognition in the hearing impaired," J. Speech Hear. Res. **18**, 719–727.

Gordon-Salant, S., and Fitzgibbons, P. J. (**1997**). "Selected cognitive factors and speech recognition performance among young and elderly listeners," J. Speech Lang. Hear. Res. **40**, 423–431.

Grant, K. (**2002**). "Measures of auditory-visual integration for speech understanding: A theoretical approach," J. Acoust. Soc. Am. **112**, 30–33.

Grant, K., and Braida, L. (**1991**). "Evaluating the articulation index for auditory-visual input," J. Acoust. Soc. Am. **89**, 2952–2960.

Grant, K., van Wassenhoven, V., and Poeppel, D. (**2004**). "Detection of auditory (cross-spectral) and auditory-visual (cross-modal) synchrony," Speech Commun. **44**, 43–53.

Grant, K. W., Walden, B. E., and Seitz, P. F. (**1998**). "Auditory-visual speech recognition by hearing-impaired subjects: Consonant recognition, sentence recognition, and auditory-visual integration," J. Acoust. Soc. Am. **103**, 2677–2690.

Hannley, M., and Dorman, M. F. (**1983**) "Susceptibility to intraspeech spread of masking in listeners with sensorineural hearing loss," J. Acoust. Soc. Am. **74**, 40–51.

Humes, L. E. (**1994**) "Psychoacoustic considerations in clinical audiology," *Handbook of Clinical Audiology*, 4th ed., edited by J. Katz (Williams and Wilkins, Baltimore).

Humes, L. E., Watson, B. U., Christensen, L. A., Cokely, C. G., Halling, D. C., and Lee, L. (**1994**). "Factors associated with individual differences in clinical measures of speech recognition among the elderly," J. Speech Hear. Res. **37**, 465–474.

Klein, A. J., Mills, J. H., and Adkins, W. Y. (**1990**). "Upward spread of masking, hearing loss, and speech recognition in young and elderly listeners," J. Acoust. Soc. Am. **87**, 1266–1271.

Loizou, P. C., Mani, A., and Dorman, M. F. (**2003**). "Dichotic speech recognition in noise using reduced spectral cues," J. Acoust. Soc. Am. **114**, 475–483.

Lunner, T., Arlinger, S., and Hellgren, J. (**1993**). "8-channel digital filter bank for hearing aid use: Preliminary results in monaural, diotic and dichotic modes," J. Acoust. Soc. Am. **38**, 75–81.

Massaro, D. W. (**1987**) *Speech Perception by Ear and Eye: A Paradigm for Psychological Inquiry*, (Erlbaum, Hillsdale, NJ).

McGurk, H., and MacDonald, J. (**1976**). "Hearing lips and seeing voices," Nature (London) **264**, 746–748.

Murphy, D. R., Schneider, B. A., Speranza, F., and Moragalia, G. (**2006**). "A comparison of higher order auditory processes in younger and older adults," Psychol. Aging **21**, 763–773.

Palva, A., and Jokinen, K. (**1975**). "The role of the binaural test in filtered speech audiometry," Acta Oto-Laryngol. **79**, 310–314.

Pelli, D., Robson, J., and Wilkins, A. (**1998**). "The design of a new letter chart for measuring contrast sensitivity," Clin. Vision Sci. **2**, 187–199.

Pichora-Fuller, K. M., Schneider, B. A., and Daneman, M. (**1995**). "How young adults listen to and remember speech in noise," J. Acoust. Soc. Am. **97**, 593–608.

Richie, C., Kewely-Port, D., and Coughlin, M. (**2003**). "Discrimination of vowels by young, hearing impaired adults," J. Acoust. Soc. Am. **114**, 2923–2933.

Roeser, R., Buckley, K., and Stickney, G. (**2000**). "Pute tone tests," *Audiology: Diagnosis*, edited by R. Roser, M. Valente, and H. Hosford-Dunn (Thieme, New York), pp. 227–252.

Ronan, D., Dix, A. K., Shah, P., and Braida, L. D. (**2004**). "Integration across frequency bands for consonant identification," J. Acoust. Soc. Am. **116**, 1749–1762.

Sokal, R. R., and Rohlf, F. J. (**1995**). *Biometry: The Principals and Practice of Statistics in Biological Research* (Freeman, New York).

Sommers, M. S., Spehar, B., and Tye-Murray, N. (**2005b**). "The effects of signal-to-noise ratio on auditory-visual integration: Integration and encoding are not independent," J. Acoust. Soc. Am. **117**, 2574.

Sommers, M. S., Tye-Murray, N., and Spehar, B. (**2005a**). "Auditory-visual speech perception and auditory-visual enhancement in normal-hearing younger and older adults," Ear Hear. **26**, 263–275.

Spehar, B. P., Tye-Murray, N., and Sommers, M. S. (**2001**) "Auditory integration of bandpass filtered sentences," J. Acoust. Soc. Am. **109**, 2439.

Studebaker, G. A. (**1985**). "A rationalized arcsine transform," J. Speech Hear. Res. **28**, 455–462.

Sumby, W. H., and Pollack, I. (**1954**). "Visual contribution to speech intelligibility in noise," J. Acoust. Soc. Am. **26**, 212–215.

Tye-Murray, N., Sommers, M. S., and Spehar, B. P. (**2007**). "Audiovisual integration and lipreading abilities of older adults with normal and impaired hearing," Ear Hear. **28**, 656–668.

Tyler, R. D., Preece, J., and Tye-Murray, N. (**1986**). *The Iowa Laser Videodisk Tests* (University of Iowa Hospitals, Iowa City, IA).

Walden, B. E., Busacco, D. A., and Montgomery, A. A. (**1993**). "Benefit from visual cues in auditory-visual speech recognition by middle-aged and elderly persons," J. Speech Hear. Res. **36**, 431–436.

Warren, R. M., Riener, K. R., Bashford, J. A., Jr., and Brubaker, B. S. (**1995**). "Spectral redundancy: Intelligibility of sentences heard through narrow spectral slits," Percept. Psychophys. **57**, 175–182.

Wilson, R. H., and Jaffe, M. S. (**1996**). "Interactions of age, ear, and stimulus complexity on dichotic digit recognition," J. Am. Acad. Audiol **7**, 358–369.

Wingfield, A. (**1996**). "Cognitive factors in auditory performance: Context, speed of processing, and constraints of memory," J. Am. Acad. Audiol **7**, 175–182.

van Rooij, J. C. G. M., Plomp, R., and Orlebeke, J. F. (**1989**). "Auditive and cognitive factors in speech perception by elderly listeners. I. Development of test battery," J. Acoust. Soc. Am. **86**, 1294–1309.

Suppression of shocked-bubble expansion due to tissue confinement with application to shock-wave lithotripsy

Jonathan B. Freund[a)]
Mechanical Science and Engineering and Aerospace Engineering, University of Illinois at Urbana-Champaign, 1206 West Green Street MC-244, Urbana, Illinois 61801, USA

(Received 12 October 2007; revised 29 February 2008; accepted 29 February 2008)

Estimates are made of the effect of tissue confinement on the response of small bubbles subjected to lithotriptor shock pressures. To do this the Rayleigh–Plesset equation, which governs the dynamics of spherical bubbles, is generalized to treat a bubble in a liquid region (blood), which is in turn encased within an elastic membrane (like a vessel's basement membrane), beyond which a Voigt viscoelastic material models the exterior tissue. Material properties are estimated from a range of measurements available for kidneys and similar soft tissues. Special attention is given to the constitutive modeling of the basement membranes because of their expected importance due to their proximity to the bubble and their toughness. It is found that the highest expected values for the elasticity of the membrane and surrounding tissue are insufficient to suppress bubble growth. The reduced confinement of a cylindrical vessel should not alter this conclusion. Tissue viscosities taken from ultrasound measurements suppress bubble growth somewhat, though not to a degree expected to resist injury. However, the higher reported viscosities measured by other means, which are arguably more relevant to the deformations caused by growing bubbles, do indeed significantly suppress bubble expansion. © *2008 Acoustical Society of America.* [DOI: 10.1121/1.2902171]

PACS number(s): 43.80.Gx, 43.35.Wa, 43.40.Ng [ROC] Pages: 2867–2874

I. INTRODUCTION

There is strong evidence that inertial cavitation causes much of the injury to renal tissue that can accompany the treatment of kidney stones with shock-wave lithotripsy (e.g., Bailey *et al.*[1]). However, the detailed mechanisms of how a growing and collapsing cavitation bubble interacts with the tissue to cause injury are not understood. It is curious, for example, that ~1000 shocks are required before significant injuries are observed.[2] (A typical treatment delivers ~2000 shocks.) It can be speculated that this delay might be due to the scarcity of cavitation nuclei, and that some other mechanism such as shear[3,4] initiates injury. Artificially adding cavitation nuclei has been shown to increase injury,[5] but it remains unclear what happens under normal physiological conditions. In this paper, we develop and parametrize a simple model to assess whether or not the confinement afforded by the renal structures where injury is observed might play a role in suppressing cavitation. The main question we ask with the model is what tissue mechanical properties are needed to suppress damaging bubble expansion: is the tissue expected to be weak or strong as far as an expanding cavitation bubble is concerned? Mechanical properties from several types of experiments on kidneys and other soft tissues are considered.

The possibility that expanding bubbles rupture renal blood vessels was analyzed in some detail by Zhong *et al.*[6,7] They showed that confinement, either by tissue[6] or in blood vessel phantoms,[7] reduces time to bubble collapse and therefore presumably also the size and potential for injury of the expanding cavitation bubbles. However, the phantom vessels they used were significantly larger than most of the blood vessels in kidney tissue, especially in the medulla toward the papilla tip where damage is first observed,[8] and their elasticity relative to that expected for renal vessels and tubules was not characterized. Nevertheless, the experiments clearly showed that only a few shocks were necessary to rupture them via expanding cavitation bubbles. Zhong *et al.*[7] used arguments based on the energetics of expanding bubbles at the critical radius—the radius at which they would encounter the inner vessel wall—to suggest that smaller vessels would be even more susceptible to this mechanism. This approach assumes that the elastic confinement of the vessel is not coupled to the dynamics of the bubble. We account for this in this paper. The opposite extreme would be to study bubble dynamics with completely rigid confinement, such as recently done by Cui *et al.*,[9] who studied the dynamics of spherical bubbles between parallel rigid walls. In this case, of course, it is not possible to tell if actual tissue would be strained to the point of tearing.

The Rayleigh–Plesset equation and related spherical bubble models have been extended to treat bubbles in viscoelastic material[10–12] or bubbles in liquids surrounded by viscoelastic material.[13] These show, as expected, that sufficient elastic resistance suppresses bubble growth and subsequent dynamics. We generalize this approach to a configuration that accounts for more microscopic features of kidney tissue: the bubble is in a liquid bounded by an elastic membrane beyond which is viscoelastic tissue. We do this for a simple geometry, our main objective being to couple viscoelastic properties, as estimated from experimental measurements of kidney and similar tissues, with bubble dynamics. As seen in Fig. 1, the basic geometry is indeed crude. It is a spherical gas bubble in a concentric liquid-filled spheri-

a)Electronic mail: jbfreund@uiuc.edu.

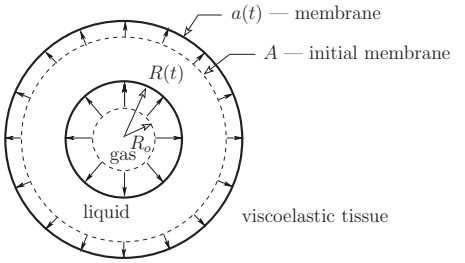


FIG. 1. Model geometry schematic. A bubble radius $r(t)$ [initially $r(0)=R_0$] is positioned at the center of an elastic membrane radius $a(t)$ [initially $a(0)=A$]. The elastic membrane is surrounded by a Voigt viscoelastic material that models tissue.

cal elastic membrane, the tissue beyond which is viscoelastic. The membrane dynamics are coupled with the bubble, liquid, and viscoelastic region dynamics in Sec. II for a model lithotriptor shock pressure history (Sec. II B). Constitutive models and estimates of properties are developed in Sec. III.

Clearly this model was selected for its geometric simplicity and is only a crude model of the geometry of the blood vessels in the kidney, which are approximately cylindrical. However, if spherical confinement is estimated to be unsuccessful in restricting the expansion of the bubble, it is not expected that the weaker confinement afforded by a cylindrical vessel would be more significant. In this sense, we are establishing an upper bound on confinement. If the bubble does not "feel" the confinement in this artificial sphere case, it is even less likely to do so in a cylindrical geometry, where flow along the cylindrical tubule or vessel would facilitate release of the pressure. We shall see in Sec. IV that this is indeed the case for upper estimates on the confinement afforded by elasticity. Further justification of this perspective is provided in the appendix via estimates of the time scales for pressure release by flow along the vessel in both inertia- and viscosity-dominated limits. Both mechanisms are estimated to be too slow to fundamentally change the confinement. The detailed simulations of Ye and Bull[14] show how deformations of an arteriole wall in an embolotherapy application significantly reduce the pressure environment of a confined bubble relative to a rigid wall.[15] This also supports our neglect of flow along the vessel as a pressure release mechanism in making our estimates.

II. BUBBLE DYNAMICS

A. Generalization of the Rayleigh–Plesset equation

Adding the effect of the concentric membrane and exterior viscoelastic material shown in Fig. 1 to the Rayleigh–Plesset equation is straightforward, constituting only a minor change to its derivation. As usual, we neglect any dynamics of the gas phase in the bubble. Under the conditions of interest in shock-wave lithotripsy, the inertia and viscosity of the gas will be negligible relative to that of the liquid except perhaps at collapse, which is not considered in detail in this study. Spherical symmetry and our assumption of an incompressible medium dictate that the radial velocity has the form

$$u(r,t)=\frac{F(t)}{r^2}, \tag{1}$$

where r is the radial coordinate. At the bubble surface $[r=R(t)]$, the fluid velocity must match the bubble surface velocity $[u(R,t)=R]$, which gives $F(t)=R^2\dot{R}$, where the overset dot indicates a time derivative. The appropriate incompressible-medium momentum equation in spherical coordinates is[16]

$$\rho\left(\frac{\partial u}{\partial t}+u\frac{\partial u}{\partial r}\right)=-\frac{\partial p}{\partial r}+\frac{\partial \tau_{rr}}{\partial r}+\frac{3\tau_{rr}}{r}, \tag{2}$$

where p is the pressure, ρ is the density, and τ_{rr} is the radial-normal deviatoric stress. As assumed recently by Yang and Church[12] for a bubble directly in a viscoelastic material, we employ a Voigt model for the viscoelasticity,

$$\tau_{rr}=2(G\gamma+\mu_t\dot{\gamma}). \tag{3}$$

Here, G is the shear modulus of the medium, which for an incompressible medium is one-third the Young's modulus, and μ_t is its viscosity. The simple combination of elastic and viscous effects in the Voigt model is appropriate given the level of detail available in experimental measurements of tissue properties. In Eq. (3), γ is the strain and $\dot{\gamma}$ is the rate of strain,

$$\dot{\gamma}=\frac{\partial u}{\partial r}. \tag{4}$$

Applying Eq. (1) to Eq. (4) gives

$$\dot{\gamma}=-\frac{2R^2\dot{R}}{r^3}, \tag{5}$$

and the corresponding strain from the reference condition (for which $R=R_0$) is thus

$$\gamma=-\frac{2}{3r^3}(R^3-R_0^3). \tag{6}$$

The standard next step in the derivation of the Rayleigh–Plesset equation is an integration of Eq. (2) from $r-R(t)$ to $r\to\infty$,

$$\rho\int_R^\infty\left(\frac{\dot{F}}{r^2}-\frac{2F^2}{r^5}\right)dr=\int_R^\infty\left(-\frac{\partial p}{\partial r}+\frac{\partial \tau_{rr}}{\partial r}+\frac{3\tau_{rr}}{r}\right)dr, \tag{7}$$

where Eq. (1) has been used and ρ has been assumed constant (1000 kg/m^3) for $r>R$. The membrane at $r=a$ is assumed to have negligible thickness and therefore no mass. It is also assumed to exert a singular stress upon the fluid directed normal to its surface. Because this stress is singular, and because the material properties discontinuously change at the membrane, it is appropriate to split the integration operator on the right-hand side of Eq. (7) as

$$\int_R^\infty \Rightarrow \int_R^{a^-}+\int_{a^+}^\infty, \tag{8}$$

which upon integration yields

$$\rho\left(\frac{\dot{F}}{R}-\frac{1}{2}\frac{F^2}{R^4}\right)=p_R-p_{a^-}+p_{a^+}-p_\infty(t)+\tau_{rr}^{a^-}-\tau_{rr}^{a^+}-\tau_{rr}^{R}+\tau_{rr}^{\infty}+\int_R^{a-}\frac{3\tau_{rr}}{r}dr+\int_{a^+}^{\infty}\frac{3\tau_{rr}}{r}dr. \quad (9)$$

A force balance at the bubble surface $r=R$ yields

$$p_B=p_R+\frac{4\mu}{R}\dot{R}+\frac{2\sigma}{R}, \quad (10)$$

which is the usual expression relating bubble internal pressure p_B to the liquid pressure on the bubble surface p_R via the viscous and surface tension stresses. We neglect any vapor or gas exchange between the bubble and liquid so the bubble pressure is assumed to depend only on its volume according the usual polytropic relation

$$p_B=p_{B_0}\left(\frac{R_0}{R}\right)^{3\gamma}, \quad (11)$$

with $p_{B_0}=2\sigma/R_0+p_0$ being the equilibrium bubble pressure when $R=R_0$. The bubble volume change is fast, so we assume that it is effectively adiabatic before collapse and accordingly set $\gamma=1.4$. A force balance at $r=a$, corresponding to the usual one at $r=R$ quoted in Eq. (10), yields

$$-p_{a^-}+\tau_{rr}^{a^-}+\frac{2T(\lambda)}{a}=-p_{a^+}+\tau_{rr}^{a^+}, \quad (12)$$

where $T(\lambda)$ is the elastic tension in the membrane with stretch λ. The remaining integrals in Eq. (9) can be easily evaluated given Eqs. (5) and (6). Doing this, taking $\tau_{rr}^{\infty}=0$, applying Eqs. (10) and (12), neglecting elasticity of the liquid, and invoking $F=R^2\dot{R}$, yields

$$R\ddot{R}+\frac{3}{2}\dot{R}^2=\frac{1}{\rho}\left[p_B-p_\infty(t)-\frac{2\sigma}{R}-4\mu\frac{\dot{R}}{R}-\frac{2T(\lambda)}{a}-\frac{4}{3}\frac{G}{a^3}(R^3-R_0^3)-4(\mu_t-\mu)\frac{R^2\dot{R}}{a^3}\right]. \quad (13)$$

The final three terms of this expression are extensions to the standard Rayleigh–Plesset equation. In order of appearance in Eq. (13), they are the effects of the membrane tension, the elasticity beyond the membrane, and the viscosity jump across the membrane. We consider ranges of $T(\lambda)$, G, and μ_t for kidney tissue in Sec. (3).

So long as there is no significant liquid compressibility in the neighborhood of and beyond the membrane, which would be the case in our application, a similar modification can be made to compressible forms of the bubble dynamics equations, as done for a bubble in a weakly compressible viscoelastic medium by Yang and Church.[12] This, however, is not necessary here since we do not study collapse and rebound, the only cases where compressibility is expected to play a substantive role.

The membrane tension T in Eq. (13) is a function of stretch $\lambda=a/A$ [see Eq. (22)] and other terms in Eq. (13) depend on radius a, which changes according to the local velocity [Eq. (1)] as

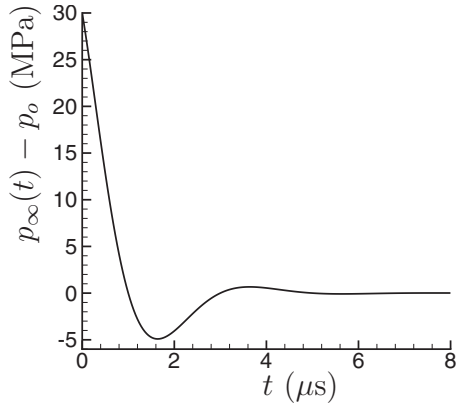


FIG. 2. Assumed lithotriptor shock profile: maximum of 30 MPa, minimum of −4.9 MPa.

$$\dot{a}=u[r=a(t),t]=\frac{R^2\dot{R}}{a^2}. \quad (14)$$

Equations (13) and (14) are solved with a stiff equation solver [LSODE (Ref. 17)] with initial conditions

$$R(0)=R_0, \quad \dot{R}(0)=0, \quad a(0)=A. \quad (15)$$

Results are relatively insensitive to R_0; we take $R_0=1$ μm for all cases. The initial membrane radius is taken to be $A=5$ μm, as appropriate for a small vessel.

B. Lithotriptor shock profile

The pressure field in a kidney of a shock from any particular lithotriptor is not precisely known and probably varies considerably depending on the various parameters of the configuration. It is thought to have a peak positive pressure, which abruptly rises to tens of megapascals, that is followed for about 2 μs by a negative pressure of $\lesssim$10 MPa. We assume a profile

$$p_\infty(t)=p_0+p_A e^{-t/\tau}\cos\left(\frac{\pi t}{2\tau}\right), \quad (16)$$

where $p_A=30$ MPa, $p_0=0.101$ MPa ($\approx$1 atm), and $\tau=1$ μs. This profile is plotted in Fig. 2. It resembles measured lithotriptor pressure histories.[18] The conclusions of this paper are independent of the details of the assumed shock profile.

III. MATERIAL PROPERTIES ESTIMATES

We assume that the bubble nuclei are in small blood vessels, and so we set viscosity $\mu=0.005$ Pa s, which is typical for microcirculation hematocrit values and high rates of strain.[19] Blood's surface tension under normal conditions is approximately $\sigma=0.06$ N/m.[20,21] The blood vessels in the kidney have a collagenous basement membrane with interstitial cells, extracellular material, and other vessels beyond that.[22] Mechanical properties of these materials are estimated in the following subsections.

A. Membrane constitutive model

Given the regular, tubular structure of kidney tissue (e.g., Jamison and Kriz[22]), we expect the membrane encasing

a bubble to have by far the largest influence on the bubble for two reasons. The first is simply proximity: the velocity and deformation fields of the bubble will decay as $1/r^2$ so the closest material will have dominant elastic influence. The second reason is that thin-walled shell-membrane structures are significantly more resistant to expansion from the inside than crushing from the outside, which causes them to buckle. Beyond the vessel we consider containing the bubble nucleus, which resists expansion, the nearby vessels in the kidney will be crushed and are therefore expected to be more fluidlike than elastic. There is cellular and extracellular matrix materials between the basement membranes, but it is thought[23,24] that basement membranes are the most important structural components of small vessels. We shall see in Sec. IV that even the highest estimate we can justify for the overall tissue elasticity is insufficient to significantly suppress cavitation.

The simplest way to proceed for modeling the elastic behavior of the membranes is simply by choosing Young's modulus, but like many biological materials the elasticity of basement membranes is significantly nonlinear. Welling *et al.*[24] reported that the effective modulus is $Y \approx 2-5$ MPa for small deformations, but $Y \approx 20$ MPa for large deformations. Since we need to track the entire range of deformations in our model, a more complete description is warranted.

Our constitutive model is constructed to reproduce the pressure-diameter data for the inflation of a renal tubule.[24] We start from well-known continuum mechanics results for membrane elasticity (e.g., Humphrey[25]) that relates the stress tensor $\mathbf{t}$ to a strain energy function W,

$$ht_{\alpha\beta} = \frac{2H}{J_{2D}} F_{\alpha\Sigma} F_{\beta\Delta} \frac{\partial W}{\partial C_{\Sigma\Delta}}, \tag{17}$$

where H is the initial predeformation thickness of the membrane of current thickness h so $F_{33}=\lambda_3=h/H$, $\mathbf{C}$ is the right Cauchy–Green tensor $\mathbf{C}=\mathbf{F}^T\cdot\mathbf{F}$, and $\mathbf{F}$ is the deformation gradient tensor. For a thin membrane the form of $\mathbf{F}$ is

$$\mathbf{F} = \begin{bmatrix} F_{11} & F_{12} & 0 \\ F_{21} & F_{22} & 0 \\ 0 & 0 & F_{33} \end{bmatrix}. \tag{18}$$

In principal coordinates, it is diagonal with the principal stretches on its diagonal: $\mathbf{F}=\mathrm{diag}[\lambda_1,\lambda_2,\lambda_3]$. In Eq. (17), the subscripted indexes α, β, Σ, and Δ each take values of only 1 or 2 reflecting the two-dimensional character of the membrane. J_{2D} in Eq. (17) is the determinant of the two-dimensional deformation gradient: $J_{2D}=F_{11}F_{22}-F_{12}F_{21}$.

We assume a simple strain energy function

$$W = W_0 e^{\alpha(I_C-3)}, \tag{19}$$

where $I_C=C_{11}+C_{22}+C_{33}$ is the first invariant of the Cauchy–Green tensor. In terms of principal stretches, it is $I_C=\lambda_1^2+\lambda_2^2+\lambda_3^2$. More general formulas than Eq. (19) might improve the apparent fit to the data, but pursuing this is unnecessary for our objectives and also probably unwarranted given that the data available for fitting are limited. The experiments were not designed with the intent to develop constitutive models, and so are missing some of the details (e.g., the stretch along the tubule) that would be needed to refine the constitutive model with confidence.

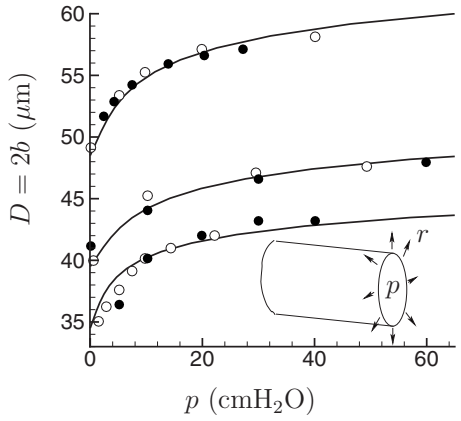


FIG. 3. Pressure-diameter relation for a renal tubule. The symbols show the data of Welling *et al.* (Ref. 24) for rabbit renal tubules. The (—) are from the effective stress of Eq. (21) with $\alpha=12$, $W_0=5000$ N/m^2, and $H=0.1$, 0.25, and 0.25 μm for the three sets of data shown. (The H were selected from the range reported (Ref. 24) to provide the best fit for constant B and α.)

For the inflation of the approximately cylindrical membrane of Welling *et al.*,[24] we assume that $\lambda_1=1$ and take $\lambda_2=\lambda=b/B$, where b and B are the radius and initial zero-stress radius, respectively. The axial boundary conditions are unclear from the experimental setup so the $\lambda_1=1$ assumption seems best for making our estimates. With this assumption, Eq. (17) using Eq. (19) yields azimuthal principal tension,

$$T_2 \equiv ht_{22} = \frac{2W_0\alpha H}{\lambda}\left(1-\frac{1}{\lambda^4}\right)e^{\alpha(\lambda^2+1/\lambda^2-2)}, \tag{20}$$

with corresponding pressure

$$p = \frac{T_2}{r} = \frac{T_2}{\lambda R}. \tag{21}$$

The fitted pressure-diameter curves are shown in Fig. 3 along with the experimental data.

For the spherical membrane inflation we consider in the current model, $\lambda_1=\lambda_2=\lambda=a/A$. where a is the radius and A is the initial radius of the sphere. In this case, both principal tensions are

$$T = 2W_0\alpha H\left(1-\frac{1}{\lambda^6}\right)e^{\alpha(2\lambda^2+1/\lambda^4-3)}, \tag{22}$$

with corresponding pressure

$$p_m = \frac{2T}{a}. \tag{23}$$

This pressure appears in Eq. (13). The membranes are observed to rupture for $\lambda \gtrsim 1.22$,[24] so we set $p_m=0$ when this occurs.

B. Bulk viscoelasticity

There are other components to renal tissue aside from basement membranes that we need to consider. We focus the present discussion on the inner medulla where injury is typically first observed.[8] The membranes of various capillary vessels and vasa recta, collecting ducts, and thin limbs of the

loops of Henle are lined with endothelial cells on their insides and surrounded by extracellular material with relatively low collagen content[26] and interstitial cells that bridge between them. As previously discussed,[3] none of these are expected to have any significant elasticity. Reported values of linear elastic moduli for cells are ~1 kPa, well less than that of basement membranes of 1–20 MPa.[24] Yang and Church[12] showed that elastic moduli of ~1 MPa for the entire material surrounding a bubble would suppress bubble growth for 1 MPa peak-to-peak, 1 MHz ultrasound. In the inner medulla, only the basement membranes are expected to have >1 MPa stiffness and they account for less than 1% of the volume of the overall tissue. Supporting this, Welling *et al.*[24] found no difference in the elasticity of renal tubule elasticity before and after the epithelial cells were chemically removed. However, with this type of reasoning, we would expect only $G \approx 1$ kPa for $r > a(t)$, but the tissue structure is complex and there are other measurements to consider.

Aside from the renal tubules, there are no detailed measurements of the microstructural material properties of renal tissue. So we must estimate the effective elastic response of the material surrounding the basement membrane based on bulk tissue measurements. Even for these studies, though, the deformations are either significantly slower than the ~10 μs expected for bubble expansion or deduced from ultrasound frequency shear wave dynamics, whose amplitude is small and whose deformation character is expected to be significantly different than that of an expanding bubble. Nevertheless, the available measurements allow us to establish bounds for making our estimates. Given the uncertainty of the data, we craft the discussion around linear elasticity moduli for our estimation purposes. The deformations are, of course, large, which would need to be more formally treated if data were available for crafting more precise models.

Basic stress-elongation data of Melvin *et al.*[27] suggest whole live organ linear elasticity with modulus $E \lesssim 2$ MPa. Measurements of sections of cortex tissue show this same stiffness, but only after 20%–30% strains are applied.[28] Before this level of deformation, the apparent modulus of elasticity appears to be <100 kPa.[29] This is consistent with the 20 Hz small strain (<2%) measurements of cortex tissue of Nasseri *et al.*,[29] which show $Y \approx 10$ kPa. Extrapolation of their data to the ~100 kHz expected for bubble growth still suggests $Y \lesssim 100$ kPa. Ultrasound measurements of other soft tissues also support these relatively low moduli. Experimental limitations of Firzzell *et al.*[30] set an upper bound of $Y < 1$ MPa for liver. Madsen *et al.*[31] fitted similar ultrasound data with a Voigt viscoelasticity model to suggest $Y \approx 10$ kPa. All these values will be considered in parametrizing the model in Sec. IV.

We also need estimates of the expected tissue viscosity for $r > a(t)$. Though only ultrasound measurements[30–32] reach the deformation rates expected in the neighborhood of a growing cavitation bubble, they are thought to yield relatively low values because the viscosity arises from dissipation at the macromolecular rather than cellular scale due to the short wavelength of the sound.[30] Ultrasound measurements at 1 MHz suggest a viscosity for liver of 0.15 Pa s,[32] which is about a factor of 10 higher than the viscosity predicted by fitting a Voigt model through 2–14 MHz ultrasound measurements for liver[31] or a Voigt-like model for 6–20 MHz ultrasound measurements for kidney.[33] It is possible that the longer sound wavelength at 1 MHz causes more cell-scale deformations leading to higher viscosity. The deformation caused by bubble expansion will be larger than cell scale, and so we expect the ultrasound measurements to provide a lower bound on viscosity, with significantly more viscous resistance possible. Mechanical testing of kidneys and most soft tissues at 20 Hz suggest much higher viscosities: Nasseri *et al.*[29] reported ~100 Pa s for sections of kidney cortex. Extrapolation with their power law fit to 100 kHz suggests 0.15 Pa s.

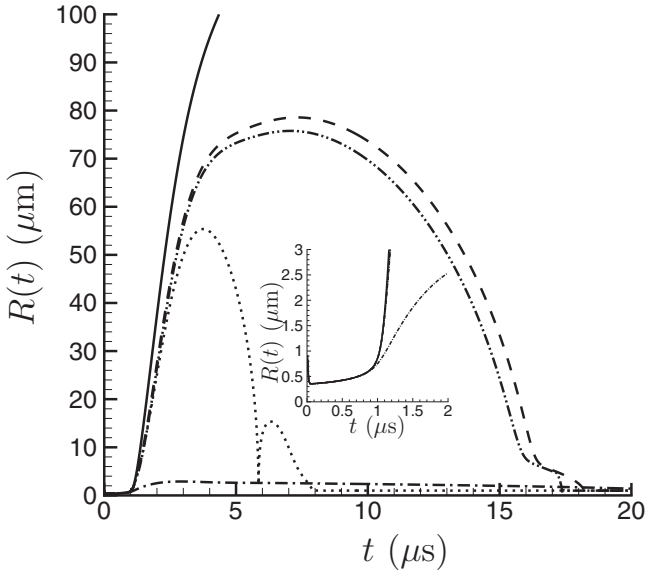


FIG. 4. Bubble radius evolution: (—) $Y=0$, $f_t=0$, $\mu_t=0$; (- - - -) $Y=10$ kPa, $f_t=1$, $\mu_t=0.15$ Pa s; (–··–) $Y=10$ kPa, $f_t=100$, $\mu_t=0.15$ Pa s; (·····) $Y=1$ MPa, $f_t=1$, $\mu_t=0.15$ Pa s; (–·–) $Y=10$ kPa, $f_t=1$, $\mu_t=15.0$ Pa s.

IV. MODEL PREDICTIONS

We consider five cases, the results of all of which are shown in Fig. 4. The first is a baseline unconfined Rayleigh–Plesset solution, which corresponds to $A \to \infty$. This is shown as the solid line in the figure. As expected, the bubble grows to be well over $R=100$ μm radius in this case. For cases with a membrane ($A=5$ μm) and elastic tissue beyond, the eventual size of the bubble and membrane cannot be regarded as quantitatively relevant unless it is substantially suppressed in its growth. If it grows large, it will exceed the yielding or tearing thresholds of the materials, which would be even more challenging to make reliable estimates for. Thus, our main conclusions will be concerning whether or not the bubble grows large and not its eventual size *per se*.

For the second case, we consider the least confining constitutive properties from the discussions in Sec. III. We thus take the membrane dynamics as modeled in Sec. III A, Young's modulus in $r > a$ to be $Y=10$ kPa as suggested for relatively small deformation[29] and by ultrasound,[31] and the tissue viscosity of 0.15 Pa s as suggested from ultrasound[32] and extrapolation from low frequencies.[29] This confinement

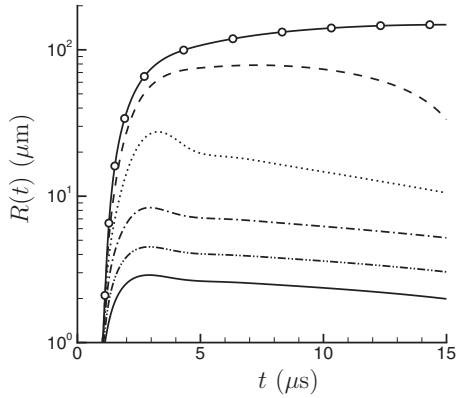


FIG. 5. Bubble radius evolution for (−∘−) $Y=0$, $f_t=0$, $\mu_t=0$, and $Y=10$ kPa, $f_t=1$, with viscosities (- - - -) $\mu_t=0.15$ Pa s, (·····) $\mu_t=0.47$ Pa s, (−·−) $\mu_t=1.5$ Pa s, (−··−) $\mu_t=4.7$ Pa s, and (——) $\mu_t=15$ Pa s.

does suppress the bubble growth somewhat, though it still grows to a radius of nearly $R\approx 80$ μm, far exceeding any expectations of the yield strain for the membrane and surrounding tissue.

For the final three cases, we in turn increase membrane elasticity $T(\lambda)$, G, and μ_t by factors of 100. This brings their properties into the high end of the ranges estimated in Sec. III. Though it is expected to be the stiffest component of the tissue, increasing the stiffness of the basement membrane model by a factor $f_T=100$ (i.e., $T'=f_T T$) does little to additionally constrain the bubble. As seen in the figure, it only reduces the maximum radius by only a few micrometers. More surprisingly, increasing the elastic modulus of the exterior material by a factor of 100 to 1 MPa, bringing it into the range expected for the largest deformations at the slowest rates,[29] still does not suppress bubble growth. The maximum radius is still more than 50 μm as seen in the figure, and the material would be expected to yield well before this point. This level of exterior elasticity was sufficient to suppress bubble growth in the ultrasound experiments and simulations of Caskey *et al.*,[34] which have weaker forcing, but it is not clear that such a high level of elasticity is justified, at least not for the whole range of deformation. Tissue viscosity was also neglected in that study. Here, we find that tissue viscosity is actually the most effective restriction of bubble growth. Increasing μ_t to 15 Pa s, which is well within the range measured for tissues by methods other than by ultrasound, significantly suppresses the growth. For this tissue viscosity, the membrane would not be expected to rupture. Plots for several viscosities are shown in Fig. 5.

The differences in the behavior of the different cases come from the expansion and do not significantly involve the bubble collapse, as can be seen from the inset in Fig. 4. When the bubble is small, changes in its size have little effect on the membrane and the viscoelastic tissue beyond because of the R^2/a^2 relation in displacements and velocities. For fixed bubble size, larger membranes (larger A) would also be significantly less confining for the same reason.

V. CONCLUSIONS AND ADDITIONAL DISCUSSION

The first principal conclusion of these model simulations is clear: the measured elasticity of a renal basement membrane is of itself far too weak to significantly alter the growth of a cavitation bubble confined within it, at least for a lithotriptor pressure pulse with $P_-\approx 5$ MPa. A spherical confinement model was employed for analytical simplicity, but the effect of the membrane elasticity on the bubble is so small that it does not seem possible that a cylindrical membrane would offer any significant confinement either. We show that the elasticity of the tissue beyond the membrane would also need to exceed all reported measurements for kidney tissue in order to avoid large, presumably tearing strains. Given these predictions for elastic confinement, we are left to address what suppresses cavitation and injury in shock-wave lithotripsy, at least for the first 1000 or so shocks. A possible explanations is that there are insufficient cavitation nuclei in the tissue so other mechanisms such a shear[3,4] are needed to initiate injury. We cannot make an assessment of the normal density of cavitation nuclei here, but our estimates indicate that any confining effects on bubble dynamics are more likely to come via viscosity than elasticity. The largest reported elastic moduli for kidney tissue at any deformation rates do not substantially suppress bubble growth in our model. The largest viscosities, however, easily do, and even the smallest values reported, those that come from ultrasound measurements, have a significant suppressing effect on the maximum size reached by a bubble. The second principal conclusion is, therefore, that any tissue confinement of lithotriptor-shocked bubbles will most likely derive from tissue viscosity. It is well known that sufficient viscosity will suppress any motion, as has been specifically discussed for lithotriptor driven bubbles by Church;[35] our estimates suggest that tissues might have sufficient viscosity to suppress bubbles in small vessels. We can go on to speculate that it might be a slow reduction of tissue viscosity that eventually facilitates the more widespread injuries observed after ~1000 shocks are delivered. Pooling of blood in lesions, whatever their cause, is potentially a route to reduced viscous confinement. Similarly, examination of kidney tissue injured by shock-wave lithotripsy shows that the entire microstructure is disrupted,[36] which will also tend to reduce its viscosity and thereby perhaps also facilitate bubble growth and spreading cavitation damage.

ACKNOWLEDGMENTS

The author is grateful for fruitful discussions with M. Bailey about shock-wave lithotripsy and bubble confinement in tissue. This work was partially supported by NIH Grant No. PO1-DK043881.

APPENDIX: AXIAL PRESSURE RELEASE ESTIMATES IN ELASTIC CYLINDERS

This appendix serves as supplemental justification of the relevance of the spherical confinement for the more realistic, but more analytically challenging, case of cylindrical confinement. The strongest argument in this regard, however, remains the fact that the bubble is not substantively confined

by the spherical membrane, which is in a sense maximally confining. If the spherical membrane does not suppress expansion, we cannot expect a more realistic cylindrical membrane to either.

We make estimates in two limits of how quickly flow along the vessel would release confinement in the neighborhood of the bubble. In one limit, the pressure is countered by inertia along the tubule and in the other the pressure is countered by viscous forces in the tubule. For making some of our estimates, it will be simpler to revert to a linear elasticity model. In this case we take $T=T_y(\lambda-1)$ and use $T_y=0.16$ N/m as in a previous effort.[3]

1. Inertia mediated pressure release

Elastic fluid filled cylindrical membranes are known to support waves, the pulse wave in the arterial system being the most celebrated, and the speed of this wave governs the rate of pressure release along the vessel. For small amplitudes, the speed of such waves is[37]

$$c=\sqrt{\frac{T}{2\rho r_0}}, \tag{A1}$$

where T is the elastic tension modulus and r_0 is the undeformed radius of the tubule. For $T=0.16$ N/m and $r_0=5$ μm, this wave speed is 4 m/s so it takes 2.5 μs to travel the distance of the tubule's diameter $(2r_0)$. This is comparable to the time scale of the bubble growth to the point at which it would stretch the membrane to the breaking point, so we do not expect an inertia based mechanism of this sort to play a dominant role in releasing the excess membrane induced pressure in the neighborhood of the bubble. This analysis neglects the mass of any attached surrounding tissue, but this would serve only to slow the wave speed. However, for inertia to be the dominant mechanism, the Reynolds number of the system should be large. The velocity depends on the bubble dynamics, but is slower than the wave speed, which we therefore use to establish an upper bound on the Reynolds number: $\mathrm{Re}=\rho c r_0/\mu=4$. This is too low to expect a purely inertial behavior, so we also make an estimate in the viscous limit.

2. Viscosity mediated pressure release

In this case, a similar set of quasi-one-dimensional assumptions to those used[37] in is establishing the elastic tube wave speed is used in the viscous limit. To this end, the flow is assumed to be one dimensional and to have the well-known Poiseuille parabolic velocity profile for which the volumetric flow rate q is related to the pressure drop Δp along a tubule segment length ℓ by

$$q=\frac{\pi r^4 \Delta p}{8\mu\ell}. \tag{A2}$$

In the limit of an infinitesimal tube segment length $\ell\to dx$,

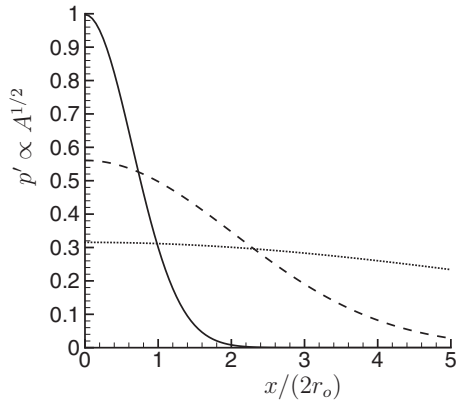


FIG. 6. Estimated pressure distribution for a viscous mediated pressure release along a flexible cylindrical membrane (see text) at times of (—-) 1 μs, (- - - -) 10 μs, and (·····) 100 μs.

$$q=-\frac{\pi r^4}{8\mu}\frac{\partial p}{\partial x}. \tag{A3}$$

This is a consequence of conservation of momentum. A differential form of conservation of mass, again assuming one-dimensional flow with volume flux q, is

$$\frac{\partial A}{\partial t}+\frac{\partial q}{\partial x}=0, \tag{A4}$$

where A is the fluid-filled area of the tube. Assuming linear elasticity, as appropriate for our estimates which are made in the small deformation limit, the internal pressure in Eq. (A3) is related to the tube radius by

$$p-p_0=\frac{\tau}{r}=T\left(\frac{1}{r_0}-\frac{1}{r}\right). \tag{A5}$$

Substituting this into Eq. (A3) and the result into Eq. (A4) yields a differential equation for the tube's area

$$\frac{\partial A}{\partial t}-\frac{\partial}{\partial x}\left(\alpha A^{1/2}\frac{\partial A}{\partial x}\right)=0, \tag{A6}$$

where

$$\alpha=\frac{T}{16\pi^{1/2}\mu}. \tag{A7}$$

Small perturbations A' to initial undeformed area A_0 evolve according to

$$\frac{\partial A'}{\partial t}-\beta\frac{\partial^2 A'}{\partial x^2}=0, \tag{A8}$$

where $\beta=A_0^{1/2}\alpha$. Plotting $p'\propto\sqrt{A'}$ for the fundamental solution of this equation [initial condition $A'(x,t=0)=\delta(x)$] in Fig. 6 with $T=0.16$ N/m shows that the pressure should also slowly spread relative to the bubble growth by this viscous mechanism.

[1]M. R. Bailey, L. A. Crum, A. P. Evan, J. A. McAteer, J. C. Williams, Jr., O. A. Sapozhnikov, R. O. Cleveland, and T. Colonius, "Cavitation in shock wave lithotripsy," in *The Fifth International Symposium on Cavitation*, Osaka, Japan, November 2003, Paper No. Cav03 OS-2-1-006.
[2]A. P. Evan, L. R. Willis, J. E. Lingeman, and J. A. McAteer, "Renal trauma and the risk of long-term complications in shock wave lithotripsy,"

Nephron **78**, 1–8 (1998).
[3]J. B. Freund, T. Colonius, and A. P. Evan, "A cumulative shear mechanism for tissue damage initiation in shock-wave lithotripsy," Ultrasound Med. Biol. **33**, 1495–1503 (2007).
[4]M. Lokhandwalla, J. A. McAteer, J. C. Williams, Jr., and B. Sturtevant, "Mechanical haemolysis in shock wave lithotripsy (SWL): II. *In vitro* cell lysis due to shear," Phys. Med. Biol. **46**, 1245–1264 (2001).
[5]D. Dalecki, C. H. Raeman, S. Z. Child, D. P. Penney, R. Mayer, and E. L. Carstensen, "The influence of contrast agents on hemorrhage produced by lithotripter fields," Ultrasound Med. Biol. **23**, 1435–1439 (1997).
[6]P. Zhong, I. Cioanta, S. Zhu, F. H. Cocks, and G. M. Perminger, "Effects of tissue constraint on shock wave-induced bubble expansion *in vivo*," J. Acoust. Soc. Am. **104**, 3126–3129 (1998).
[7]P. Zhong, Y. Zhou, and S. Zhu, "Dynamics of bubble oscillations in constrained media and mechanisms of vessel rupture in SWL," Ultrasound Med. Biol. **27**, 119–134 (2001).
[8]P. M. Blomgren, B. A. Connors, J. E. Lingeman, L. R. Willis, and A. P. Evan, "Quantitation of shock wave lithotripsy-induced lesion in small and large pig kidneys," Anat. Rec. **249**, 341–348 (1997).
[9]J. Cui, M. F. Hamilton, P. S. Wilson, and E. A. Zabolotskaya, "Bubble pulsations between parallel plates," J. Acoust. Soc. Am. **119**, 2067–2072 (2006).
[10]J. S. Allen and R. A. Roy, "Dynamics of gas bubbles in viscoelastic fluids. II. Nonlinear viscoelasticity," J. Acoust. Soc. Am. **108**, 1640–1650 (2000).
[11]S. Y. Emelianov, M. F. Hamilton, Y. A. Ilinskii, and E. A. Zabolotskaya, "Nonlinear dynamics of a gas bubble in an incompressible elastic medium," J. Acoust. Soc. Am. **115**, 581–588 (2004).
[12]X. Yang and C. C. Church, "A model for the dynamics of gas bubbles in soft tissue," J. Acoust. Soc. Am. **118**, 3595–3606 (2005).
[13]C. C. Church and X. Yang, "A theoretical study of gas bubble dynamics in tissue," in *Proceedings of the 17th International Symposium on Nonlinear Acoustics*, edited by A. A. Atchley, V. W. Sparrow, and R. M. Keolian (American Institute of Physics, Melville, 2006), pp. 217–224.
[14]T. Ye and J. L. Bull, "Microbubble expansions in a flexible tube," J. Biomed. Eng. **128**, 554–563 (2006).
[15]T. Ye and J. L. Bull, "Direct numerical simulations of micro-bubble expansion in gas embolotherapy," J. Biomed. Eng. **126**, 746–759 (2004).
[16]A. Prosperetti, "A generalization of the Rayleigh–Plesset equation of bubble dynamics," Phys. Fluids **25**, 409–410 (1982).
[17]A. Hindmarsh, "LSODE. Ordinary differential equation system solver," Lawrence Livermore National Laboratory, Technical Report No. ESTSC–000216CY0MP00, 1983.
[18]R. O. Cleveland, M. R. Bailey, N. Fineberg, B. Hartenbaum, M. Lokhandwalla, G. A. McAteer, and B. Sturtevant, "Design and characterization of a research electrohydraulic lithotripter patterned after the Dornier HM3," Rev. Sci. Instrum. **71**, 2514–2525 (2000).
[19]R. L. Whitmore, *Rheology of the Circulation* (Pergamon, Oxford, 1968).
[20]E. Hrncir and J. Rosina, "Surface tension of blood," Physiol. Res. **46**, 319–321 (1997).
[21]J. Rosina, E. Kvasnak, D. Suta, H. Kolarova, J. Malek, and L. Krajci, "Temperature dependence of blood surface tension," Physiol. Res. **56** (Supplement 1), S93–S98 (2007).
[22]R. L. Jamison and W. Kriz, *Urinary concentrating mechanism: structure and function* (Oxford University Press, New York, 1982).
[23]J. B. West, K. Tsukimoto, O. Mathieu-Costello, and R. Prediletto, "Stress failure in pulmonary capillaries," J. Appl. Physiol. **40**, 1731–1742 (1991).
[24]L. W. Welling, M. T. Zupka, and D. J. Welling, "Mechanical properties of basement-membrane," News Physiol. Sci. **10**, 30–35 (1995).
[25]J. D. Humphrey, *Cardiovascular Solid Mechanics: Cells, Tissues, and Organs* (Springer, New York, 2002).
[26]L. Osvaldo and H. Latta, "Interstitial cells and the renal medulla," J. Ultrastruct. Res. **15**, 589–613 (1966).
[27]J. W. Melvin, R. L. Stalnaker, and V. L. Roberts, "Impact injury mechanisms in abdominal organs," Proceedings of the 17th Stapp Car Crash Conference, SAE Trans. 730968, 115–126 (1973).
[28]M. Farshad, M. Barbezat, P. Flüeler, F. Schmidlin, P. Graber, and P. Niederer, "Material characterization of the pig kidney in relation with the biomechanical analysis of renal trauma," J. Biomech. **32**, 417–425 (1999).
[29]S. Nasseri, L. E. Bilston, and N. Phan-Thien, "Viscoelastic properties of pig kidney in shear, experimental results and modelling," Rheol. Acta **41**, 180–192 (2002).
[30]L. A. Frizzell, E. L. Carstensen, and J. F. Dyro, "Shear properties of mammalian tissues at low megahertz frequencies," J. Acoust. Soc. Am. **60**, 1409–1411 (1977).
[31]E. L. Madsen, H. J. Sathoff, and J. A. Zagzebski, "Ultrasonic shear wave properties of soft tissues and tissue like materials," J. Acoust. Soc. Am. **74**, 1346–1355 (1983).
[32]S. Girnyk, A. Barannik, E. Barannik, V. Tovstiak, A. Marusenko, and V. Volokhov, "The estimation of elasticity and viscosity of soft tissues in vitro using the data of remote acoustic palpation," Ultrasound Med. Biol. **32**, 211–219 (2006).
[33]X. Yang and C. C. Church, "A simple viscoelastic model for soft tissues in the frequency range 6-20 MHz," IEEE Trans. Ultrason. Ferroelectr. Freq. Control **53**, 1404–1411 (2006).
[34]C. F. Caskey, S. M. Stieger, S. Qin, P. A. Dayton, and K. W. Ferrara, "Direct observations of ultrasound microbubble contrast agent interaction with the microvessel wall," J. Acoust. Soc. Am. **122**, 1191–1200 (2007).
[35]C. C. Church, "A theoretical study of cavitation generated by an extracorporeal shock wave lithotripter," J. Acoust. Soc. Am. **86**, 215–227 (1989).
[36]Y. Shao, B. A. Connors, A. P. Evan, L. R. Willis, D. A. Lifshitz, and J. E. Lingeman, "Morphological changes induced in the pig kidney by extracorporeal shock wave lithotripsy," Anat. Rec. **275A**, 979–989 (2003).
[37]J. Lighthill, *Mathematical Biofluiddynamics* (Society for Industrial and Applied Mathematics, Philadelphia, 1989).

Mathematics of pulsed vocalizations with application to killer whale biphonation

Judith C. Brown[a)]
Physics Department, Wellesley College, Wellesley, Massachusetts 02481 and
Media Lab, Massachusetts Institute of Technology, Cambridge, Massachusetts 02139

(Received 19 August 2007; revised 18 January 2008; accepted 8 February 2008)

Formulas for the spectra of pulsed vocalizations for both the continuous and discrete cases are rigorously derived from basic formulas for Fourier analysis, a topic discussed qualitatively in Watkins' classic paper on "the harmonic interval" ["The harmonic interval: Fact or artifact in spectral analysis of pulse trains," in Marine Bioacoustics 2, edited by W. N. Tavogla (Pergamon, New York, 1967), pp. 15–43]. These formulas are summarized in a table for easy reference, along with most of the corresponding graphs. The case of a "pulse tone" is shown to involve multiplication of two temporal wave forms, corresponding to convolution in the frequency domain. This operation is discussed in detail and shown to be equivalent to a simpler approach using a trigonometric formula giving sum and difference frequencies. The presence of a dc component in the temporal wave form, which implies physically that there is a net positive pressure at the source, is discussed, and examples of the corresponding spectra are calculated and shown graphically. These have application to biphonation (two source signals) observed for some killer whale calls and implications for a source mechanism. A MATLAB program for synthesis of a similar signal is discussed and made available online. © *2008 Acoustical Society of America.*
[DOI: 10.1121/1.2890745]

PACS number(s): 43.80.Ka [WWA] Pages: 2875–2883

I. INTRODUCTION

Marine mammals, such as killer whales, produce a wide range of vocalizations, among which pulsed calls have the most interesting and complex spectra. In general the mathematical properties of these calls have been discussed qualitatively (Watkins, 1967), and the initial goal of this paper is to derive general formulas for the spectra of some common shapes of pulsed wave forms showing rigorously, for example, the reason for missing spectral lines.

The mathematics of pulsed calls can give important information on call production. An example is given for a killer whale sound with a treatment of biphonation or simultaneous sound production by two independent sources. For many of these calls the signal from one source is modulated by the signal from the other source in a nonlinear interaction (Tyson, 2006; Tyson *et al.*, 2007). In this case involving multiplication in the time domain, the spectrum is obtained from the convolution of the individual spectra in the frequency domain; it is shown that these results can also be understood with a simple trigonometic formula giving amplitude information as well as frequency shifts. It is interesting to compare to human speech production where the source is filtered by vocal cavities giving rise to convolution in the time domain and multiplication in the frequency domain.

Finally results are given from a MATLAB (made available on the internet) program which can simulate two independent sources with one signal modulating the other. The spectrum of the simulation is compared to that of a recorded killer whale sound, and the implication of the dc components (net positive pressure) for a source mechanism is discussed.

II. BACKGROUND

A. Watkins

In 1967 Watkins published a seminal article on what he called the "harmonic interval." This included a treatment of the spectra of pulse trains with varying ratios R of period (of the pulse train) to width of the pulses comprising the pulse train. He called the fundamental frequency of the pulse train the pulse repetition rate. He then considered the case where this pulse train is multiplied by a sinusoid of higher frequency called the pulse tone (shifting the original spectrum up by this higher frequency) and discussed the spectra resulting from varying R and making the point that the repetition rate of the pulse train can be obtained from the spacing between spectral lines. He also discussed the symmetry of the temporal wave form and how this leads to missing lines (Fourier components) in the spectrum.

We will derive Watkins' results to give explicit formulas for Fourier analysis of continuous time wave forms and of the discrete Fourier transform for a digitized time wave form for cases of interest. As an aside we make a comparison to the identical problem in the spatial domain of diffraction by a variable number of slits. Our terminology will follow that of the more recent literature (Miller and Bain, 2000, and references therein) referring to Watkins' pulse train (or "burst pulse train") as the low frequency component (LFC) and to his pulse tone as the high frequency component (HFC). In the case of his pulse tone with sidebands, the spectrum is an example of convolution of the LFC and HFC spectra in the

[a)]Electronic mail: brown@media.mit.edu

frequency domain and hence arises from the multiplication of the LFC and HFC in the time domain. Or equivalently, the LFC is amplitude modulating the HFC, which implies a nonlinear interaction between the two sources.

B. Two-voiced and biphonic calls

In Watkins' work on marine mammals sounds he treats the simultaneous production of two signals. There are a number of examples of this phenomenon both in the animal world and in that of musical instruments. Bird calls (Suthers, 1990, 2006) with two signals are classified as two-voiced when there are two independent sources and biphonic when a single source emits two signals. Some musical instruments produce what are called multiphonics. For example, a brass player can play one note and sing another with the sum of these two producing a third frequency. With the flute and clarinet, the fingering can be changed to enhance a higher harmonic and make its amplitude comparable to that of the fundamental. Similarly with Tuvan throat singing, the shape of the vocal cavities are changed to selectively amplify a higher harmonic of the sound wave being produced and resulting in the perception of two voices.

Biphonation by a group of Northern resident killer whales has been included in a discussion of nonlinear sources (Tyson, 2006; Tyson *et al.*, 2007). Although it is probable that there are two sources for these sounds, no distinction in terminology has been made in the marine mammal literature between two voiced and biphonic sound production. Calculations on this same group of sounds are found in Brown and Miller (2006, Brown *et al.* (2006, 2007), Tyson (2006), Tyson *et al.* (2007), and Miller *et al.* (2007).

III. CALCULATIONS

Results of the following calculations are summarized in the upper section of Table I for the continuous time cases and in the lower section for the discrete calculations. Note the period P of the pulse train is the reciprocal of its frequency and is also referred to as the pulse separation in the case of a finite pulse train.

A. Continuous time

1. Fourier series: Pulse train of infinite length and finite width W

The case of a pulse train with period P and pulse width W is graphed in Fig. 1.

From Fourier series analysis for a periodic function of time $f(t)$ with period T, the kth Fourier coefficient a_k is

$$a_k = \frac{1}{T}\int_{-T/2}^{T/2} f(t)\exp(-jk2\pi t/T)dt. \quad (1)$$

With parameters W and P from Fig. 1 and using the fact that the function is zero outside the interval $(-W/2, W/2)$

$$a_k = \frac{1}{P}\int_{-W/2}^{W/2} f(t)\exp(-jk2\pi t/P)dt = \frac{1}{k\pi}\sin(k\pi W/P). \quad (2)$$

TABLE I. Summary of results. The upper part gives formulas for the spectra of continuous temporal wave forms with the lower part for the sampled wave forms. Note the symbol M for the number of pulses in the window is written as $m_{\max}$ in the corresponding figures.

CONTINUOUS with PERIOD P (in seconds)

Physical example	Length	Width of pulse	Magnitude formula in frequency domain	Figure
Diffraction grating	Infinite	W	$\frac{1}{k\pi}\sin(k\pi W/P)$	1 and 2
Diffraction grating	Infinite	δ	$\frac{1}{P}\Sigma_{k=-\infty}^{+\infty}\delta\left(\omega - k\frac{2\pi}{P}\right)$	
M slits	MP	δ	$\frac{\sin(\omega MP/2)}{\sin(\omega P/2)}$	3
M slits	MP	W	$\frac{\sin(\omega MP/2)}{\sin(\omega P/2)}\frac{\sin(\omega W/2)}{\omega/2}$	4

DISCRETE with PERIOD P (in samples)

Length	Number of Pulse	Width of Pulse	Magnitude formula in Frequency domain	Figure
N	1	W	$\frac{\sin(\pi kW/N)}{\sin(\pi k/N)}$	
N	M	1	$\frac{\sin(\pi kMP/N)}{\sin(\pi kP/N)}$	5
N	M	W	$\frac{\sin(\pi kMP/N)}{\sin(\pi kP/N)}\frac{\sin(\pi kW/N)}{\sin(\pi k/N)}$	6 and 7

In the frequency domain this is the amplitude of the kth Fourier component and has radial frequency $k2\pi/P$, with frequency separation $2\pi/P$ (Watkins' "harmonic interval") of the components. The coefficients are plotted against k, the harmonic number, in the lower half of Fig. 1 for the case

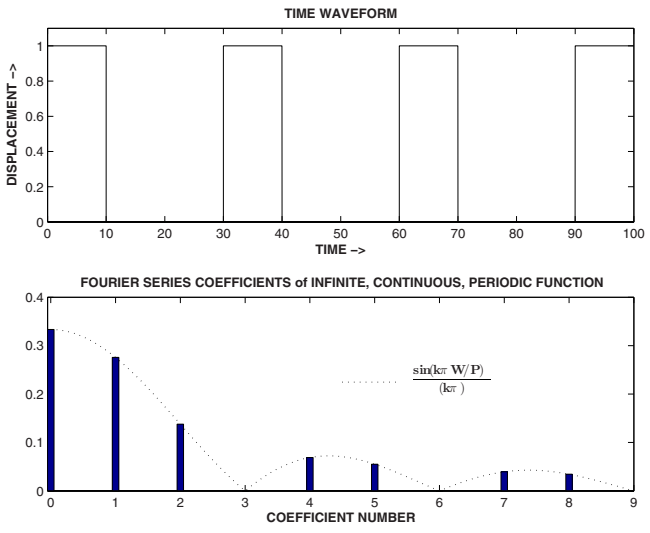


FIG. 1. (Color online) Temporal wave form (upper panel) and magnitude Fourier series coefficients (lower panel) of a pulse train with pulse width $W=10$ and pulse period $P=30$. Here $P/W=3$ and every third coefficient is missing. The dotted curve is the Fourier transform of a single pulse of width W and determines the amplitudes of the coefficients.

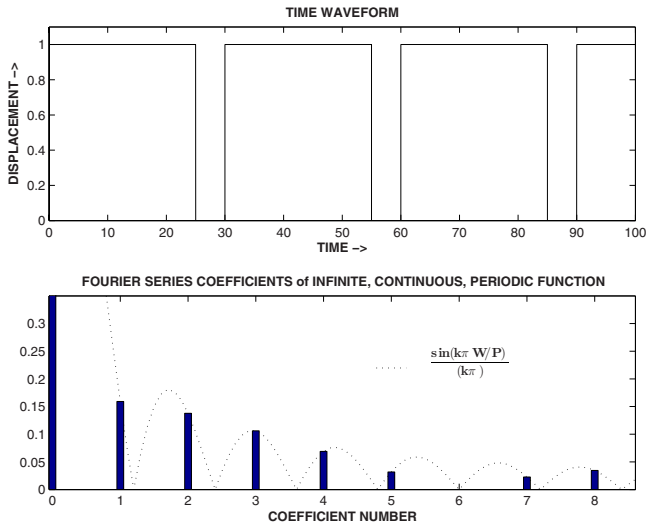


FIG. 2. (Color online) Temporal wave form (upper panel) and magnitude Fourier series coefficients (lower panel) of a pulse train with pulse width $W=25$ and pulse period $P=30$. Here $P/W=6$ to 5 and every sixth coefficient is missing. Note that the coefficients do not drop off as rapidly as in Fig. 1.

$P/W=3$, which shows clearly that every third Fourier coefficient is missing. Or in general for an arbitrary ratio P/W any coefficient which is a multiple of P/W will be missing. This is a simple, yet rigorous way to see Watkins' statements about missing spectral components. This case is equivalent in the spatial domain to a diffraction grating with slit width b and slit separation d (Brown, 1971).

Another case which has not been treated explicitly but is more widely applicable to pulsed animal vocalizations is that of the pulse width W greater than half the period P or P/W less than 2. The same formula applies for this case but the condition for missing Fourier components becomes

$$k\pi W/P = q\pi$$

with k and q integers or

$$kW/P = q.$$

This condition will be met for any k which is an integral multiple of P. The lowest value of k for which this can occur is $k=P$. This case is graphed in Fig. 2 for the case of $P=k=6$ and $W=5$. This can be interpreted (as seen in this graph) as the positions of integral k "beating" with the zeros of the amplitude function. The result is that there are fewer missing components and the radial frequency separation is $2\pi/P$ for most of the components. Physically, if the individual harmonics corresponding to each k value are graphed against time and compared to the time wave form, the missing components are those having maxima (or minima) at the beginning and end of the pulse, i.e., the transition from 0 to 1 or 1 to 0.

2. Fourier series: Pulse train of infinite length and negligible width

As the pulse width approaches zero, the ratio of P/W becomes very large with the central lobe (dotted curve in Fig. 1 spreading to ∞, and qualitatively one expects that the Fourier series coefficients will have equal amplitude with radial frequency separation $2\pi/P$).

More formally, the periodic function to be analyzed is an impulse train and can be written as a sum of delta functions,

$$f(t) = \sum_{m=-\infty}^{+\infty} \delta(t - mP)$$

giving

$$a_k = \frac{1}{P}\int_{-P/2}^{P/2} \delta(t)\exp(-jk2\pi t/P)dt = 1/P, \tag{3}$$

which is constant, independent of k as predicted, and has the same separation of components as in the previous case. Stated otherwise the transform of an impulse train of periodicity P in the time domain is an impulse train in the frequency domain with radial frequency separation $2\pi/P$, and equal to $1/P\Sigma_{k=-\infty}^{+\infty}\delta(\omega-k2\pi/P)$.

3. Fourier transform: Impulse train of finite length

Changing from an infinite impulse train to a finite one, the Fourier series gives rise to the Fourier transform given by

$$g(\omega) = \int_{-\infty}^{\infty} f(t)\exp(-j\omega t)dt. \tag{4}$$

Considering a finite impulse train with period P and M pulses

$$f(t) = \sum_{m=0}^{M-1} \delta(t - mP).$$

Substituting in Eq. (4),

$$g(\omega) = \int_{-\infty}^{\infty} \sum_{m=0}^{M-1} \delta(t - mP)\exp(-j\omega t)dt = 1 + \exp(-j\omega P) + \cdots + \exp(-j(M-1)\omega P) = \sum_{m=0}^{M-1} \exp(-jm\omega P). \tag{5}$$

This is a geometric series with sum:

$$g(\omega) = \frac{1 - \exp(-j\omega MP)}{1 - \exp(-j\omega P)} = \frac{\sin(\omega MP/2)}{\sin(\omega P/2)}\exp(j\omega P/2 - j\omega MP/2), \tag{6}$$

where the phase factor can be dropped in a consideration of spectral magnitudes. An example for the case of $M=5$ is found in Fig. 3.

4. Fourier transform: Pulse train of finite length and pulse width W

The Fourier transform can be obtained by considering a time wave with M pulses of width W and integrating in Eq. (4) directly. This case is treated in texts on physical optics for M slits with finite width b in the spatial domain. See, for

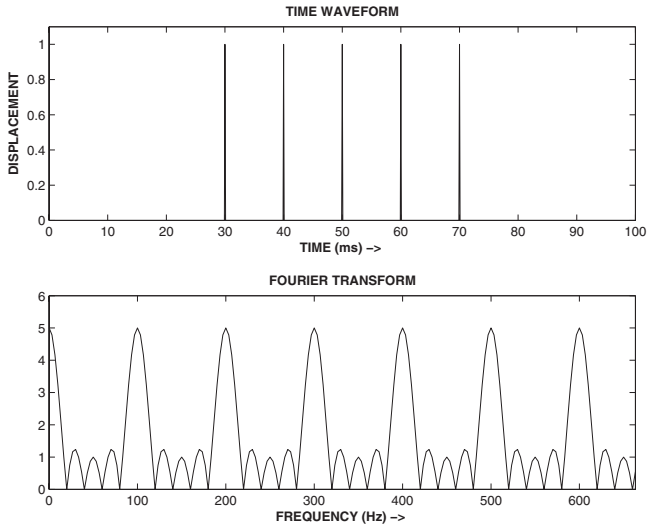


FIG. 3. Temporal wave form (upper panel) and magnitude Fourier transform (lower panel) of a finite impulse train. Here there are five impulse functions with separation $P=10$.

example, Jenkins and White (1976). It is simpler and will provide a useful tool for later sections to use the convolution theorem (Oppenheim *et al.*, 1983) which states that, if two functions are convolved in the time domain, their Fourier transform is the product of their individual transforms (and conversely from frequency domain to time domain).

The time wave form describing the pulse train is the convolution of the finite impulse train from the previous section and a single pulse of width W. The convolution is identical to a cross correlation except that one function is time reversed. The result is the temporal wave form for the example of five pulses of width W equal to 3.33 ms shown in Fig. 4.

To obtain the Fourier transform, we need the transforms from Eq. (6) and the transform of a single pulse of width W.

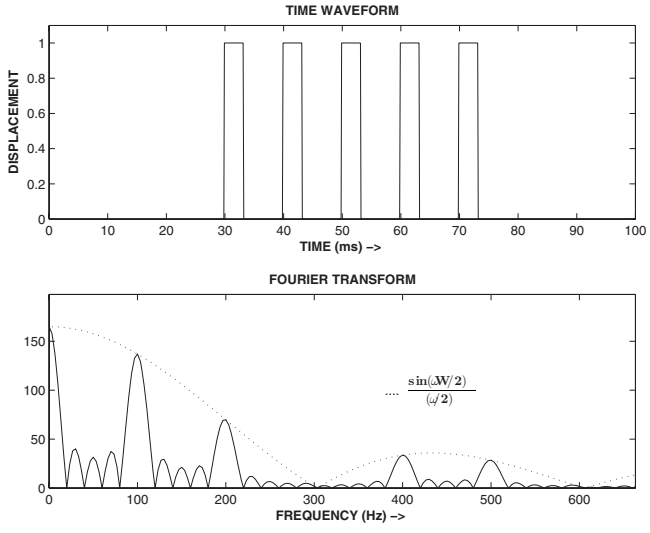


FIG. 4. Temporal wave form (upper panel) and magnitude Fourier transform (lower panel) of a finite pulse train with five pulses having pulse separation 10 and pulse width 3.33 such that $P/W=3$ as in Fig. 1. Here there are secondary maxima between the principal maxima, but as in Fig. 1 every third principal maximum is missing.

The latter can be obtained using Eq. (4) to evaluate an integral identical to that of Eq. (2) with the result:

$$g(\omega)_{\text{pulse}} = \frac{\sin(\omega W/2)}{\omega/2}. \tag{7}$$

This is the dotted function plotted in the lower half of Fig. 4 (scaled to match the maximum of the solid curve).

Using the convolution theorem to obtain the transform we multiply the transforms from Eqs. (6) and (7) to obtain

$$|g(\omega)| = \frac{\sin(\omega MP/2)}{\sin(\omega P/2)} \frac{\sin(\omega W/2)}{\omega/2}. \tag{8}$$

This is the function plotted with a solid line in the lower half of Fig. 4. Clearly it is the product of the transform of a single pulse of width W with that of the five impulses plotted in Fig. 3. In the spatial domain this formula describes diffraction by M slits with width b corresponding to W.

B. Discrete time: Discrete Fourier transform implemented with fast Fourier transform

The previous calculations for the continuous time cases are interesting and instructive; and they form a basis for the derivation and understanding of the formulas describing implementation of the discrete Fourier transform (DFT) as a fast Fourier transform (FFT) on a sampled wave form.

Traditional notation is followed in considering a window of N samples of a function $x[n]$. For comparison with Section A above, the pulse trains will have period P and width W, but now in units of samples. If desired these quantities can be converted to seconds by dividing by the sample rate, which is 100 in the examples.

For any window of N samples of the function $x[n]$, the inverse of its DFT will be replicated with periodicity N (whatever the shape or periodicity of $x[n]$), and the DFT, $X[k]$, has periodicity in the frequency domain equal to the sample rate. Since the magnitudes of $X[k]$ and $X[-k]$ are equal, there are $N/2$ unique magnitudes of the Fourier components. Note that a rectangular window is assumed in the following examples to make them tractable algebraically. Most software packages include the option of multiplying by a windowing function; this effect can be obtained by a convolution in the frequency domain of the Fourier transform of the window function with the formulas which are derived in the following (Harris, 1978).

1. Discrete Fourier transform: Single pulse of width W

Consider first a single pulse of width W samples. The general expression for the discrete Fourier transform is (Oppenheim and Schafer, 1975)

$$X[k] = \sum_{n=0}^{N-1} x[n]\exp(-j2\pi kn/N). \tag{9}$$

Here $x[n]=1$ for $0 \leqslant n \leqslant W-1$ and 0 over the remaining interval, and $X[k]$ is the kth Fourier component with angular frequency $2\pi k/N$ in units of radians/sample. Substituting for $x[n]$,

$$X[k] = \sum_{n=0}^{W-1} \exp(-j2\pi kn/N).$$

This is a geometric series identical to that evaluated following Eq. (5) and gives

$$|X[k]| = \frac{\sin(\pi kW/N)}{\sin(\pi k/N)} \tag{10}$$

for $k=0$ to $N/2-1$ magnitudes. Its shape can be seen as the dotted curve at the top of Fig. 6. It is interesting to compare this formula to Eq. (2). Here the window length N appears instead of P the period of the pulse train; and in the denominator a sin function appears replacing the argument alone. Both functions in Eq. (10) show that there is an overall periodicity in N due to sampling.

2. Discrete Fourier transform: Impulse train

Consider a windowed region $x_N[n]$ of the function $x[n]$ containing M impulses with spacing P. With the restriction that the first impulse occurs at the origin, M is the quotient of N/P rounded down to an integer, i.e., the number of complete periods in the window. Then

$$x_N[n] = \sum_{m=0}^{M-1} \delta(n - mP).$$

Substituting in Eq. (9)

$$X[k] = \sum_{n=0}^{N-1} \sum_{m=0}^{M-1} \delta(n - mP)\exp(-j2\pi kn/N). \tag{11}$$

This double sum can be evaluated as described leading to Eq. (6) with $2\pi k/N$ replacing ω. The result is

$$|X[k]| = \frac{\sin(\pi kMP/N)}{\sin(\pi kP/N)}. \tag{12}$$

Equation (12) is plotted at the top of Fig. 5 with points corresponding to integral k indicated. The middle graph is the sampled impulse train (chosen so that the impulse falls on a sampled point), and the bottom graph is the FFT of this impulse train with integral k points taken from the formula to demonstrate its accuracy as well as showing exactly how the calculated DFT samples compare to the function. Note that M in Eq. (12) corresponds to $m_{\max}$ in the formula in the figure.

3. Discrete Fourier transform: General case—pulse train with M pulses of width W and period P

This is the sampled analog of M pulses of width W treated previously. As discussed the input pulse train is the convolution of the function representing M impulses and that for a single pulse of width W. As before, the transform is the product of their transforms, and the results from sub sections 1 and 2 above give

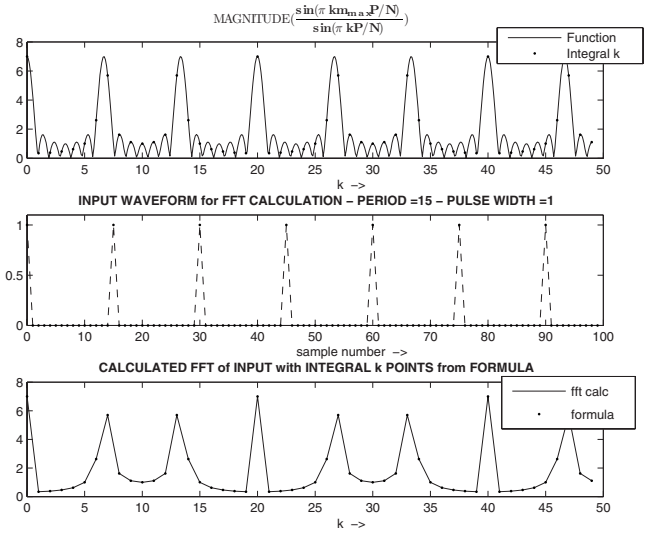


FIG. 5. Upper panel: Calculated magnitude function for the DFT of a sampled impulse train with period 15 samples. The points corresponding to integral k are indicated with a dot. Middle panel: Input wave form for the calculation, chosen so that samples occur at the maxima. Samples are indicated with a dot and connected with dashes. Lower panel: Actual calculation of FFT on samples in the middle panel. The points correspond to the samples for integral k indicated for the function in the top panel.

$$|X[k]| = \frac{\sin(\pi kMP/N)}{\sin(\pi kP/N)} \frac{\sin(\pi kW/N)}{\sin(\pi k/N)}. \tag{13}$$

Examples for ratios of pulse period to pulse width of 3 to 1 and 5 to 4 are plotted in Figs. 6 and 7. These can be compared to the continuous cases of Figs. 1 and 2.

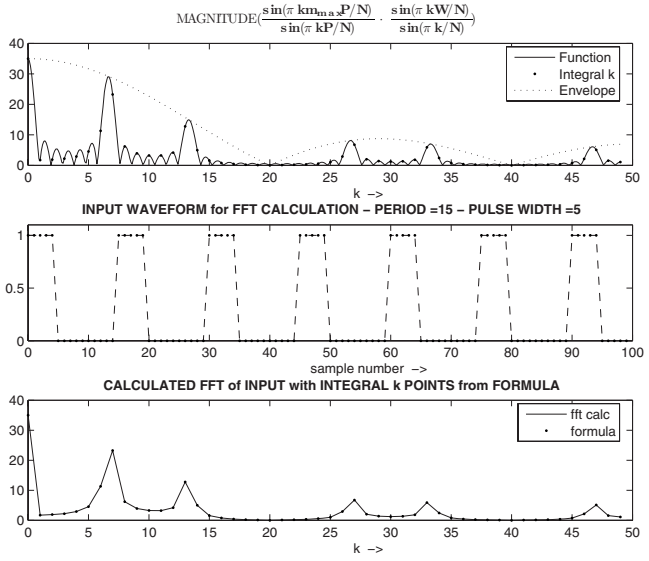


FIG. 6. Upper panel: Magnitude function for the DFT of a sampled pulse train with period 15 samples and pulse width 5 samples. The points corresponding to integral k are indicated with a dot. Middle panel: Input wave form for the calculation. Samples are indicated with a dot and connected with dashes. Lower panel: Actual calculation of FFT on the samples from the input wave form. The points correspond to the samples for integral k indicated for the function in the top figure.

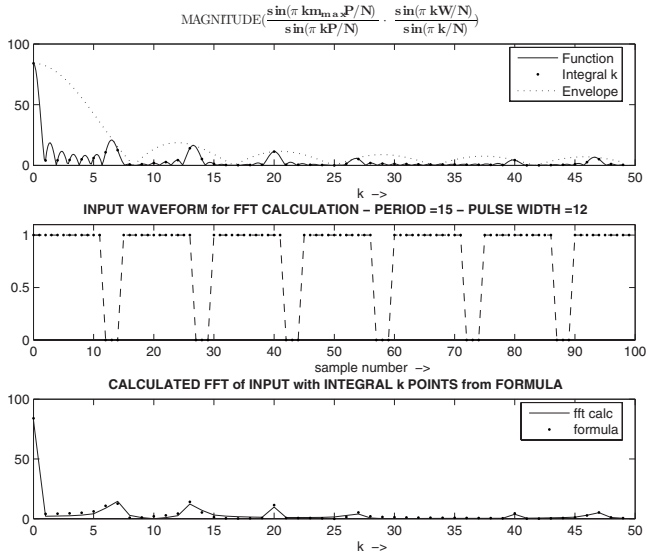


FIG. 7. Upper panel: Magnitude function for the DFT of a sampled pulse train with period 15 samples and pulse width 12 samples. The points corresponding to integral k are indicated with a dot. Middle panel: Input wave form for the calculation. Samples are indicated with a dot and connected with dashes. Lower panel: Actual calculation of FFT on the samples from the input wave form. The points correspond to the samples for integral k indicated for the function in the top figure.

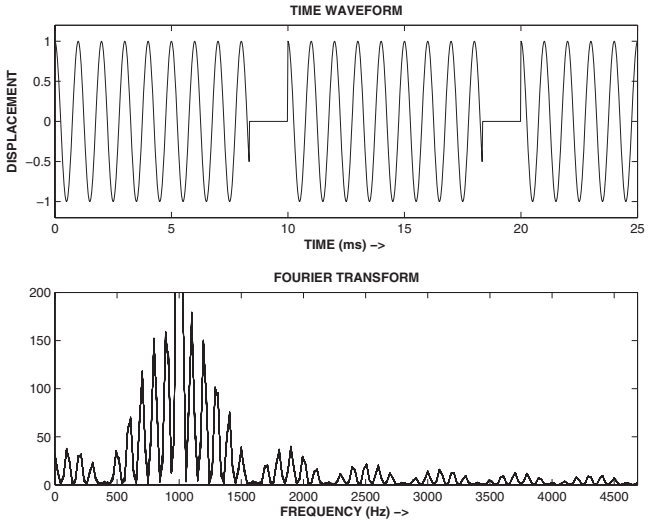


FIG. 8. Upper panel: Wave form of a sinusoid of frequency 1000 Hz multiplied by a pulse train of frequency 100 Hz having a ratio of pulse period to pulse width of 6 to 5. Lower panel: Fourier transform of the above wave form showing that the spectrum of the pulse train is shifted up in frequency by 1000 Hz.

C. Product of two signals

It is of interest to compare to the case of the sum of two signals having, for example, frequencies of ω_L and ω_H. Taking the transform is a linear operation, and the spectrum consists of two lines at these frequencies, i.e., the superposition of their individual transforms. Far more interesting effects occur for the nonlinear case of a product.

1. Convolution in the frequency domain

We can now consider Watkins' case of a pulse train spectrum shifted by the presence of a pulse tone, which corresponds to the multiplication of two signals. As pulse train we take the example from Fig. 2 with ratio of pulse period to pulse width of 6 to 5, and for clarity multiply it by a single sinusoid of higher frequency. The result is found in Fig. 8 where the sinusoid has frequency 1000 Hz and the pulse train has frequency 100 Hz. The effect in the frequency domain of this multiplication in the time domain is to shift the center of the spectrum of the pulse train from dc to 1000 Hz.

This is an example of multiplication in the time domain giving rise to convolution in the frequency domain. When we convolve the spectrum of the pulse train with the spectrum of the sinusoid (a single peak at 1000 Hz), each of the peaks of the original spectrum is shifted up in frequency by 1000 Hz. This can also be "derived" from the trigonometric identity:

$$\cos(\omega_L t)\cos(\omega_H t) = 1/2[\sin((\omega_L + \omega_H)t) + \sin((\omega_H - \omega_L)t)]. \quad (14)$$

Each component ω_L of the pulse train will appear as its sum and difference with ω_H, the higher frequency. Or in other words ω_H acts as the new baseline, and since ω_L represents any of the components of the pulse train, the entire spectrum with positive and negative frequency components is shifted upwards by ω_H.

Since the spacing of the components relative to each other is preserved, this gives rise to Watkins' statement that the pulse repetition rate can be obtained from the separation between harmonic bands.

2. Importance of the dc component

The displacement in Fig. 2 is positive with respect to a zero baseline and thus has a positive average. With this duty cycle it is a fairly high number. This is reflected in the frequency domain by the center component at 1000 Hz in Fig. 8 which goes off scale. Note that the unshifted spectrum of this pulse train would look like that of Fig. 2 (also having an offscale dc component).

Figure 9 shows the effect of a dc component on the spectrum of two sinusoids (chosen for simplicity), which are multiplied. The upper and middle parts of Fig. 9 show the LFC and HFC with a dc component turned on and off and its appearance and disappearance in the spectrum. The spectrum is plotted against time to show this more clearly. At the bottom of Fig. 9 is found the product of these two functions with and without a dc component.

To examine the lower part of Fig. 9 quantitatively, Eq. (14) can be modified to include a dc component A_{0L} and A_{0H} for each of the individual components (now with amplitudes A_{ω_L} and A_{ω_H}) to give

$$(A_{oL} + A_{\omega_L}\cos(\omega_L t))(A_{oH} + A_{\omega_H}\cos(\omega_H t)) = A_{oL}A_{oH} + A_{oH}A_{\omega_L}\cos(\omega_L t) + A_{oL}A_{\omega_H}\cos(\omega_H t) + (1/2)A_{\omega_L}A_{\omega_H}[\sin((\omega_L + \omega_H)t) + \sin((\omega_H - \omega_L)t)]. \quad (15)$$

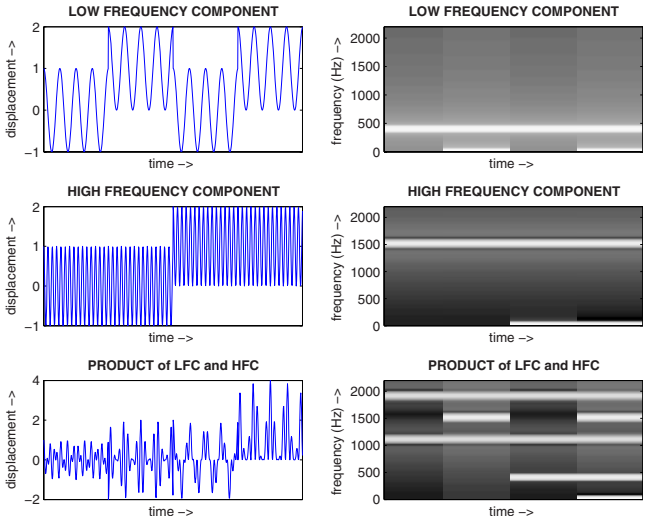


FIG. 9. (Color online) Upper panel: Wave form (left) and spectrum (right) of a low frequency sinusoid with and without a dc component. Middle panel: Wave form and spectrum of a higher frequency sinusoid with and without a dc component. Lower panel: Wave form and spectrum of the product of the wave forms in the upper and middle panels.

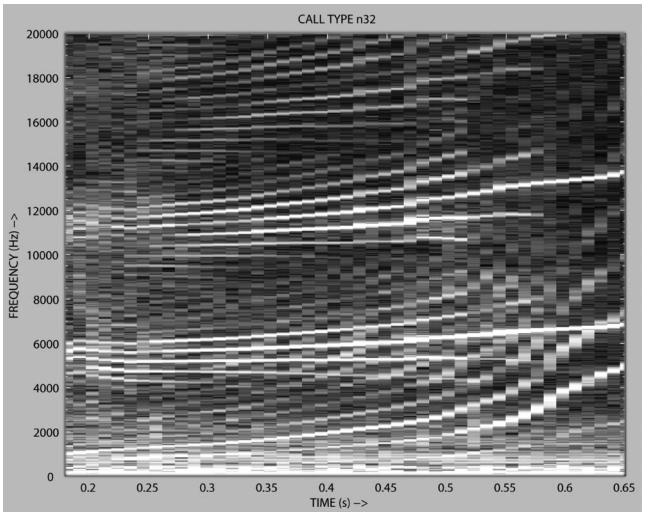


FIG. 10. Example of a Northern resident killer whale call of type n32 with a rising low frequency component having a number of harmonics and a high frequency component (HFC) with fundamental starting around 5800 Hz and rising slowly. The HFC also has a second and third harmonic visible.

From Fig. 9, it is clear that to have a component at the center frequency ω_H of the shifted spectrum, there must be a dc component present for the LFC. This corresponds to the third term on the right in Eq. (15). And to see the unshifted spectrum of the LFC in Fig. 9, there must be a dc component for the HFC; this corresponds to the second term on the right. The strength of the sum and difference terms is independent of the presence of dc terms and is equal to the product of their individual amplitudes, shown in the last two terms. They should appear symmetrically around the center frequency (i.e., the frequency of the HFC).

The presence of a dc component is physically meaningful as it implies a net positive pressure at the source. A biological example of this effect in sound production for an anuran (frogs and toads) is discussed in Bradbury and Vehrencamp (1998). An example for a killer whale having a dc component for both the LFC and the HFC follows in Sec. IV. The discussion presented above can then apply, by extension, to any two spectral lines from the more complex sounds originating from two real sources.

IV. BIPHONATION EXAMPLES

A. Killer whale

An example of a Northern resident killer whale called type n32 (cataloged by Ford, 1987) is found in Fig. 10. This is one of a set of calls recorded off Vancouver Island, Canada in 1998 and 1999 using a beamforming array (Miller and Tyack, 1998; Miller *et al.*, 2007). Digital recordings were made with Tascom recorder with a 48 kHz sampling rate and 16 bit samples.

This is an excellent example of a call where the HFC has a fundamental and two upper harmonics (and probably more that go off scale). Here the spectrum of the LFC can be seen with respect to dc and then shifted up by the frequency of each line in the spectrum of the HFC. Note the negative frequency components of the LFC appear as mirrored by each HFC harmonic. The LFC has a number of harmonics, which can be seen most clearly after 0.5 s where the fundamental frequency is rising and its harmonics 3, 4, and 5 intersect the fundamental of the HFC.

This is an excellent example of the relevance of the previous discussion of the dc components since the unshifted spectrum of the LFC is present and indicates a dc component for the HFC. Also the center line of the LFC is seen at the frequency of each of the harmonics of the HFC, indicating a dc component for the LFC. This is somewhat counterintuitive but follows from Eq. (15). If the unshifted LFC spectrum is present, it means there is a dc component for the HFC; and if the spectral lines of the HFC are present (rather than just seeing the LFC mirrored about a central position), it means that there is a dc component of the LFC.

B. Synthetic signal

As a test of the analysis of the call of Fig. 10, a MATLAB program[1] was written to synthesize a similar sound. A model of the low frequency call consists of a pulse train similar to that of Fig. 2 with fundamental frequency varying from 450 to 900 Hz. This was filtered to drop off at around 3000 Hz for less overlap with components due to the HFC. The shape of this LFC is shown with the dotted line of Fig. 11 on the left.

The HFC consists of a fundamental varying from 5800 to 6500 Hz with second and third harmonics each having amplitudes reduced by a factor of 10. Two periods of the product of the LFC and HFC are shown in the time wave at the left of Fig. 11. The spectrum is given on the right side of Fig. 11 and is the convolution of the individual (not shown but easily inferred) LFC and HFC spectra as predicted.

The Fourier transform as a function of frequency is shown in Fig. 12 and shows amplitudes which can be inferred from Eq. (15). For example, each of the sum and difference lines has the same amplitude. This is not rigor-

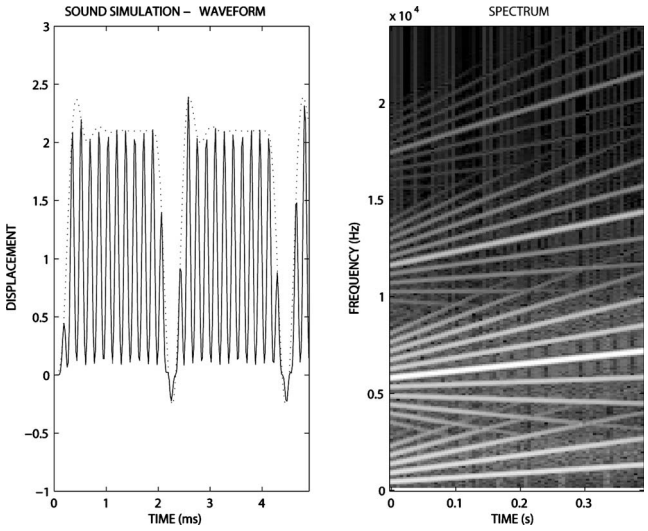


FIG. 11. Simulation of the wave form (left) and spectrum (right) of the killer whale call of Fig. 10. The wave form is the product of an HFC with fundamental varying from 5800 to 6500 Hz and a LFC (dotted) with ratio of period to pulse width of 6 to 5. The LFC is filtered to drop off at around 3000 Hz for less overlap, and this gives rise to the distortion of the square pulse.

ously true for the killer whale sound of Fig. 10 and thus implies some formant structure in the killer whale production anatomy amplifying spectral regions selectively.

V. DISCUSSION

The mathematics of pulsed calls can give important information on call production. For calls such as the example given for the killer whale, the fact that there is a convolution in the frequency domain implies that there are two sources and that they are interacting nonlinearly. This means that they are multiplied, and the LFC is amplitude modulating the HFC. The presence of dc components for each source implies a net positive pressure for each source.

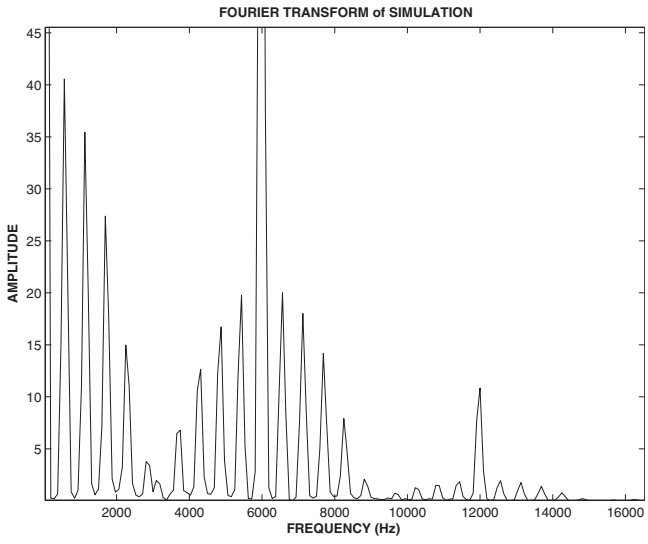


FIG. 12. Magnitude of the Fourier transform for the simulation in Fig. 11 at time 0.05 s plotted against frequency.

These observations support a source mechanism for odontocetes proposed by Cranford and others (Cranford *et al.*, 1996; Cranford, 2000; 2006) in a series of papers over the past decades. Two sets of phonic lips (also called monkey lips dorsal bursae complexes or MLDB) are set in vibration by two independent sources of air under pressure in the nasal passages implying a net positive pressure as discussed earlier. The vibrations are independent despite the experimental observation that the pressure in the two nasal passages does not differ (Cranford, 2006) for the case of the bottlenose dolphin. These vibrations may be coupled through the dorsal bursae to the melon which acts as an acoustic lens and impendence match to the ocean water.

As postulated the two sources would produce independent vibrations, and the spectrum would be that of the sum of those due to the individual vibrations. This is in fact observed for many killer whale calls (Hodgins-Davis, 2004). Others (see Fig. 1 in Miller *et al.*, 2007) show a nonlinear coupling, though in general it is less strong than that of Fig. 10. Qualitatively the MLDB complexes are located near each other and the motion of one could easily affect the vibration of the other leading to the observed nonlinearity (Fletcher, private communication, 2007). It would be very interesting to see a theoretical treatment of this effect.

ACKNOWLEDGMENTS

I would like to thank Patrick Miller for the killer whale sound in Fig. 10 as well as Neville Fletcher and Ted Cranford for some interesting "electronic" discussions on a source mechanism.

[1]MATLAB code can be obtained from http://www.media.mit.edu/~brown

Bradbury, J. W., and Vehrencamp, S. L. (**1998**). *Principles of Animal Communication* (Sinauer Associates, Sunderland, MA).
Brown, J. C. (**1971**). "Spatial filtering and fourier analysis," Am. J. Phys. **39**, 797–801.
Brown, J. C., Hodgins-Davis, A., and Miller, P. J. O. (**2006**). "Classification of vocalizations of killer whales using dynamic time warping," J. Acoust. Soc. Am. **119**, EL34–EL40.
Brown, J. C., and Miller, P. J. O. (**2006**). "Classifying killer whale vocalization using time warping," Acoustics Today **16**, 45–47.
Brown, J. C., and Miller, P. J. O. (**2007**). "Automatic classification of killer whale vocalizations using dynamic time warping," J. Acoust. Soc. Am. **122**, 1201–1207.
Cranford, T. (**2006**). "Odontocete nasalizations: Morphology, physiology, and evolution of sonar signal generation in toothed whales," J. Acoust. Soc. Am. **120**, 3189–3190.
Cranford, T. W. (**2000**). "In search of impulse sound sources in Odontocetes," in *Hearing by Whales and Dolphins*, edited by W. W. L. Au, A. N. Popper, and R. R. Fay (Springer, New York), pp. 109–155.
Cranford, T. W., Amundin, M. E., and Norris, K. S. (**1996**). "Functional morphology and homology in the odontocete nasal complex: Implications for sound generation," J. Morphol. **228**, 223–285.
Ford, J. K. B. (**1987**). "A catalogue of underwater calls produced by killer whales (Orcinus orca) in British Columbia," Can. Data Rep. Fish. Aq. Sci. No. 633.
Harris, F. J. (**1978**). "On the use of windows for harmonic analysis with the discrete Fourier transform," Proc. IEEE **66**, 51–83.
Hodgins-Davis, A. (**2004**). "An analysis of the vocal repertoire of the captive killer whale population at marineland of Antibes, France," thesis, Wellesley College, Wellesley, MA.
Jenkins, F. A., and White, H. E. (**1976**). *Fundamentals of Optics*, 4th ed. (McGraw-Hill, New York).
Miller, P. J. O., and Bain, D. E. (**2000**). "Within-pod variation in the sound

production of a pod of killer whales, Orcinus orca," Anim. Behav. **60**, 617–628.
Miller, P. J. O., Samarra, F. I. P., and Perthuison, A. (**2007**). "Caller sex and orientation influence spectra of 'two-voice' stereotyped calls produced by free-ranging killer whales," J. Acoust. Soc. Am. **121**, 3932–3937.
Miller, P. J. O., and Tyack, P. L. (**1998**). "A small towed beamforming array to identify vocalizing resident killer whales (Orcinus orca) concurrent with focal behavioral observations," Deep-Sea Res., Part II **45**, 1389–1405.
Oppenheim, A. V., and Schafer, R. W. (**1975**). *Digital Signal Processing* (Prentice-Hall, Englewood Cliffs, NJ).
Oppenheim, A. V., Wilsky, A. S., and Young, I. T. (**1983**). *Signals and Systems* (Prentice-Hall, Englewood Cliffs, NJ).
Suthers, R. A. (**1990**). "Contributions to birdsong from the left and right sides of the intact syrinx," Nature (London) **347**, 473–477.
Suthers, R. A., Beckers, J. G. L., and Nelson, B. S. (**2006**). "Vocal mechanisms for avian communication," in *Behavior and Neurodynamics for Auditory Communication*, edited by J. Kanwal and G. Ehret (Cambridge University Press, Cambridge), pp. 3–35.
Tyson, R. B. (**2006**). "The presence and potential functions of nonlinear phenomena in cetacean vocalizations," thesis, Florida State University, Tallahassee, FL.
Tyson, R. B., Nowacek, D. P., and Miller, P. J. O. (**2007**). "Nonlinear phenomena in the vocalizations of North Atlantic right whales (Eubalaena glacialis) and killer whales (Orcinus orca)," J. Acoust. Soc. Am. **122**, 1365–1373.
Watkins, W. A. (**1967**). "The harmonic interval: Fact or artifact in spectral analysis of pulse trains," in *Marine Bioacoustics 2*, edited by W. N. Tavogla (Pergamon, New York), pp. 15–43.

Broadband backscatter from individual Hawaiian mesopelagic boundary community animals with implications for spinner dolphin foraging

Whitlow W. L. Au[a)]
Marine Mammal Research Program, Hawaii Institute of Marine Biology, P.O. Box 1106, Kailua, Hawaii 96734, USA

Kelly J. Benoit-Bird
College of Atmospheric and Oceanic Sciences, 104 COAS Administration Building, Oregon State University, Corvallis, Oregon 97331, USA

(Received 19 November 2007; revised 4 March 2008; accepted 5 March 2008)

Broadband simulated dolphin echolocation signals were used to measure the *ex situ* backscatter properties of mesopelagic boundary community (MBC) in order to gain a better understanding of the echolocation process of spinner dolphins foraging on the MBC. Subjects were captured by trawling with a 2-m-opening Isaacs-Kidd Midwater Trawl. Backscatter measurements were conducted on the ship in a 2000 L seawater tank with the transducer placed on the bottom pointed upwards. Backscatter measurements were obtained in both the dorsal and lateral aspects for seven myctophids and only in the dorsal aspect for 16 more myctophids, six shrimps, and three squids. The echoes from the myctophids and shrimps usually had two highlights, one from the surface of the animal nearest the transducer and a second probably from the signal propagating through body of the subject and reflecting off the opposite surface of the animal. The squid echoes consisted mainly of a single highlight but sometimes had a low amplitude secondary highlight. The backscatter results were used to estimate the echolocation detection range for spinner dolphins foraging on the mesopelagic boundary community. The results were also compared with multi-frequency volume backscatter of the mesopelagic boundary community sound scattering layer. © *2008 Acoustical Society of America.* [DOI: 10.1121/1.2902187]

PACS number(s): 43.80.Ka, 43.30.Sf, 43.30.Ft, 43.20.Fn [JAS] Pages: 2884–2894

I. INTRODUCTION

The mesopelagic boundary community (MBC) found in waters over the slopes of the Hawaiian Islands is a midwater sound-scattering layer. This distinct land-associated community is made up of micronektonic fish, mainly from the myctophid family, shrimp and squid (Reid *et al.*, 1991). The MBC undergoes a diel migration with a vertical component towards the surface and a horizontal migration towards shore after dusk and then a reverse migration to deeper waters after midnight (Benoit-Bird and Au, 2004). The Hawaiian spinner dolphin (*Stenella longirostris*) is one of the high trophic level predators that forage on the micronekton of the MBC (Norris and Dohl, 1980; Benoit-Bird and Au, 2003c; Benoit-Bird, 2004). The spatial and temporal dynamics and behavior of the MBC affect the foraging behavior of spinner dolphins (Benoit-Bird and Au, 2003a) and consequently has been studied extensively by Benoit-Bird using a 200 kHz echosounder (e.g., Benoit-Bird *et al.*, 2001, Benoit-Bird and Au 2003a, 2003b, 2004). The target strength of a number of individual restrained MBC organisms was also measured by Benoit-Bird and Au (2001) using a 200 kHz echosounder. In order to gain insight into role of echolocation by spinner dolphins while foraging, it is important to examine reflections from these micronekton using broadband simulated dolphin echolocation signals. One of the questions of interest is the strength of the echoes that foraging dolphins may receive. Another question involves the determination of cues in the echoes that may allow dolphins to discriminate between fish, shrimp and squid. Madsen *et al.* (2007) have recently measured the backscatter properties of Loligo pealeii using odontocete-like echolocation signal, however their subjects were about five times larger than the MBC species.

Since the earlier studies using a single 200 kHz echosounder, more recent work has involved the multi-frequency Simrad EK-60 system operating at 38 kHz, 70 kHz, 120 kHz, and 200 kHz to study the MBC in Hawaii (Benoit-Bird and Au, 2006; Benoit-Bird, 2006). With the use of multi-frequency echosounders, it becomes important to understand the frequency dependency of the acoustic backscatter process for individual micronekton in order to understand the volume backscattering process of a complex environment with many different types of acoustically reflective entities. It is also important to gain a better understanding of the backscatter process from ship-based surveys with multi-frequency echosounder as we continue to study the interaction of dolphins and small whales with the mesopelagic boundary community.

One of the goals of this study was to determine the broadband target strength of MBC micronekton based on the total energy in the incident and backscattered signals and

[a)]Author to whom correspondence should be addressed. Electronic mail: wau@hawaii.edu

 0001-4966/2008/123(5)/2884/11/$23.00 © 2008 Acoustical Society of America

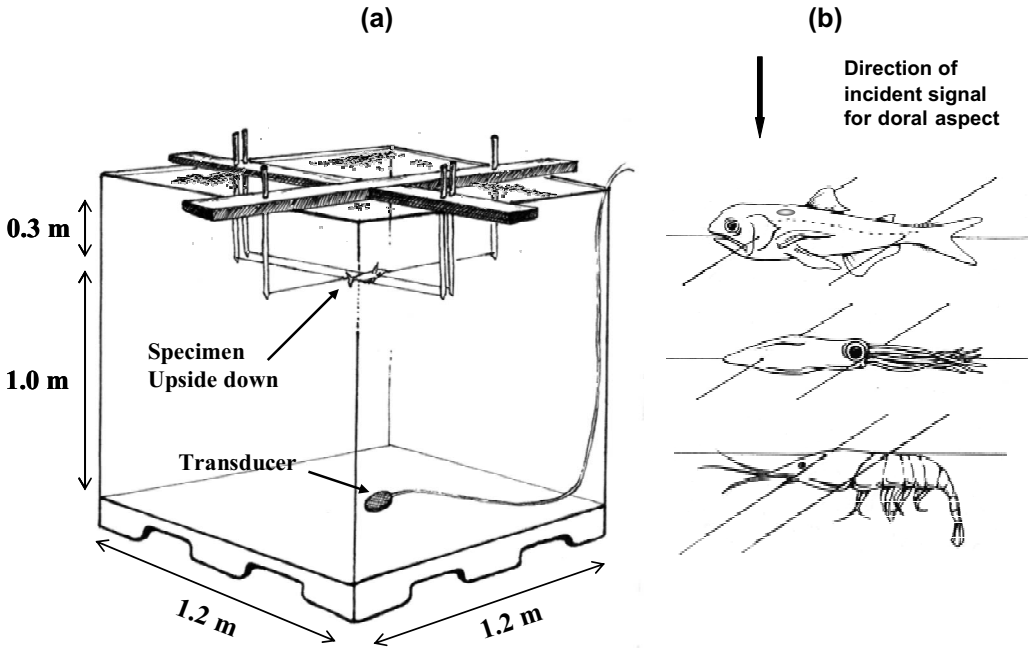


FIG. 1. (a) Schematic of the plastic holding tank in which the backscatter measurements were made. A broadband transducer was mounted on the bottom of the tank pointing upwards and the subjects were attached to monofilament lines and a special support assembly. (b) Pictures of the three classes of micronecton that were measured acoustically.

relate the results to spinner dolphin foraging on the MBC. The second goal was to measure the target strength of individual micronekton using a broadband simulated dolphin echolocation signal to determine the frequency dependency of the target strength. Simulated dolphin echolocation signals have been used extensively since 1980 (Au and Snyder, 1980) for different types of targets used in dolphin echolocation experiments (Au, 1993) and by Au and Benoit-Bird (2003) to measure the spectral structure of backscatter from lutjanid snappers.

The previous study of Benoit-Bird and Au (2001) indicated that the swimbladders of the myctophids used in our study were empty or wax invested. The specimens used in this study were a subset of the earlier study. The shrimps and squids did not contain any gas pockets. Chu and Stanton (1998) found that acoustic reflections from decapod shrimp occurred at the front water-animal interface and a secondary reflection occurred at the back animal-water interface. Therefore, it is expected our backscatter results will also have reflections from the front surface of the animals and from the signal propagating through the animals and reflecting off the back surface and any skeletal structures and also the possibility of the signals propagating along a circumferential path along the skin surface. These multiple echo components or highlights will contribute to deep local minima in the echo spectrum affecting the frequency dependency of the echoes, as was shown by Chu *et al.*, 1992 and Stanton *et al.*, 1996 for decapod shrimp.

II. APPROACH

A. Backscatter measurements

The broadband acoustic backscatter measurements were carried out in conjunction with measurements performed by Benoit-Bird and Au (2001) and much of the details regarding animal collection and preparation can be found in that reference. Micronekton were collected using a 2 m opening Isaccs-Kidd Midwater Trawl during a cruise in July, 2000 aboard the NOAA ship R/V Townsend Cromwell. The trawl was towed obliquely for 20–30 min, reaching a maximum depth of 200 m. Live animals were transferred into an aerated seawater container on deck to await acoustic measurements. Within one-half hour of initial retrieval, a single individual was transferred into a container filled with 1 l of water and tranquilized with bubbling CO_2 using an Alka-Seltzer tablet, introduced 1/4 quarter at a time until the animal was subdued. Air bubbles were removed from the surface of the animal and the monofilament tethers using streaming seawater. Measurements were first performed using a 200 kHz system (Benoit-Bird and Au, 2001). These were followed by the broadband measurements using a broadband transducer that simply flipped in place resting on the 200 kHz transducer. The animals were held 0.3 m from the surface of the water, 1 m above the transducers [Fig. 1(a)]. The subjects were mounted with monofilament lines [Fig. 1(b)] and tied to a wooden frame which rested on the top of a 2000 l freestanding shipboard tank filled with seawater.

A custom-made transducer consisting of a 6.35 cm circular disk of 1–3 composite piezoelectric that had a thickness of 6.35 mm (Material Systems Inc.) was used to project a dolphin-like echolocation signal and receive the corresponding echoes. The transmission and receiving characteristics of the transducer was known from previous calibration using tone bursts and comparasion with a standard hydrophone. The transducer in a transmit-receive mode using dolphin-like clicks was also calibrated for amplitude using an indirect procedure incorporating a 0.79-cm-diam solid steel sphere

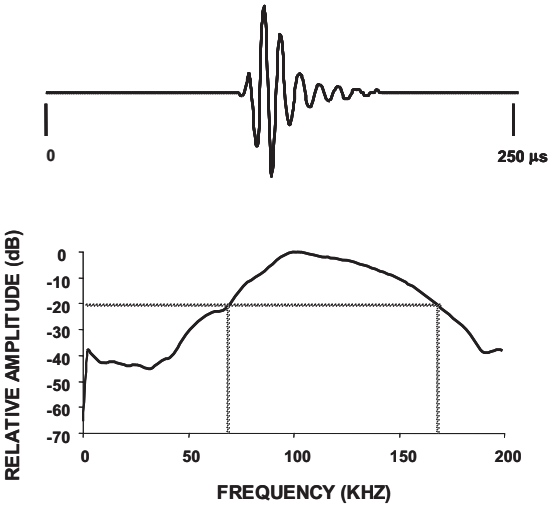


FIG. 2. The waveform and frequency spectrum of the simulated dolphin echolocation signals used in the backscatter measurements.

and a 38.1-mm-diam tungsten carbide reference sphere in a test tank as prescribed by Foote *et al.* (1987). The results from both spheres were consistent (after accounting for differences in diameters) as they should be but the process was done as a check. The incident signal waveform was measured in the same test tank by reflecting the projected signal off an acoustic mirror consisting of a 30.5×30.5-cm-square aluminum plate that was 6.35 mm thick and covered with a close-cell neoprene sheet. The diameter of the closed cells was not known. The plate was suspended by lines tied to a 61.0-cm-long aluminum channel that was attached at its center to a rotor. The plate was rotated so that the incident signal was perpendicular to its surface. This technique has been used for many years (see Au and Snyder, 1980) and the authenticity of the reflected waveform has been verified by using a small B&K 8103 hydrophone to first record the incident signal and later the reflection from the plate, with the same face of the hydrophone directed towards the signal to minimize any hydrophone effects. The incident signal was generated with a Qua-Tech WA-10 board housed in a transportable "lunch-box" personal computer using a 1 MHz sampling rate and fed to a Hafler Transnova amplifier and a step-up transformer which drove the transducer. The waveform and frequency spectrum of the incident signal are shown in Fig. 2. The −20 dB points occurred at 70 and 170 kHz. Echoes were received via a custom-built T/R switch and gated amplifier unit before being digitized.

Twenty echoes were obtained from the dorsal aspect of all animals examined and also the lateral aspect for selected subjects. The echoes were digitized at a sampling rate of 1 MHz with a Rapid System R1200 data acquisition system and 512 points per echo were stored on the hard drive of the computer. Before conducting measurements with animals, echoes with only the frame present were collected in order to ensure that unwanted reverberation would not interfere with the collection of echoes from the subjects.

B. Data analysis

The peripheral auditory system of dolphins can be modeled as an energy detector that integrates the energy in the acoustic signal (Johnson, 1968; Au *et al.*, 1988). Therefore, target strength most appropriate to a dolphin should be calculated in terms of energy in the broadband incident and reflected signals. Target strength based on energy can be defined as

$$TS_E = 10\,\mathrm{Log}\left(\frac{\int_0^{T_e} s_e^{\,2}(t)dt}{\int_0^{T_i} s_i^{\,2}(t)dt}\right) = 10\,\mathrm{Log}\left(\frac{\int_0^{F_e}|S_e(f)|^2 df}{\int_0^{F_i}|S_i(f)|^2 df}\right), \tag{1}$$

where $s_e(t)$ and $s_i(t)$ are the pressure waveforms of the echo referenced to 1 m from the target and the incident signal at the target, respectively, $S_e(f)$ and $S_i(f)$ are the Fourier transform of the echo and incident waveforms, respectively, T_e and T_i are the durations of the echo and incident signal, respectively, F_e and F_i are the maximum frequencies in the spectrum of the echo and incident signals, respectively, so that $S_e(f)$ and $S_i(f) \cong 0$ for $f > F_i$ and F_e, respectively. The expressions inside the right most logarithm of Eq. (1) are the energy flux density of the echo, $E_e(f)$, and the incident signal, $E_i(f)$, in the frequency domain. The frequency dependent target strength of a target can be simply written as

$$TS(f) = 10\,\mathrm{Log}\left(\frac{|E_e(f)|}{|E_i(f)|}\right). \tag{2}$$

In order to examine the waveform in the time domain and examine the time differences between highlights, the envelope of the cross correlation function was calculated using the equation

$$c(t) = env[\Im^{-1}(S_e(f)S_i(f))], \tag{3}$$

where $\Im^{-1}$ is the inverse Fourier transform and the product $S_e(f)S_i(f)$ is the cross-correlation function between the echo and incident waveforms. The envelope was determined using the Hilbert transform procedure (Rihaczek, 1969).

A convenient approach to analyzing multi-highlight echoes is to consider the Fourier transform of such signals. We can express a two-highlight echo and its Fourier transform by the equation

$$\Im[s_e(t) + as_e(t-\tau)] = |S_e(f)|\sqrt{1 + a^2 + 2a\cos(2\pi f\tau)}, \tag{4}$$

where $\Im$ denotes the Fourier transform of the variables in the bracket, $S_e(f)$ is the Fourier transform of $s_e(t)$, "a" is the reflection coefficient of the secondary reflecting element, and τ is the time delay between the primary and secondary reflection. Equation (4) will have local minima at frequencies where the argument of the cos is equal to odd multiples of π, so that

$$f_{l\,\min} = \frac{2n+1}{2\tau}, \tag{5}$$

where $n = 0, 1, 2\ldots$. The frequency spacing (Δf) between two consecutive local minima will be $1/\tau$. In a special case of two secondary highlights, both having the same amplitude, $f_{l\,\min}$ will be the same as in Eq. (2) but τ will be the sum of the two time delays. If the two secondary highlights are not of the same amplitude, a simple analytical solution cannot be found, however, the spectrum of the echo will still follow the basic form as indicated by Eq. (4) with a rippled pattern and

TABLE I. Summary of Mesopelagic boundary animals measured with a simulated dolphin echolocation signal.

Family	Species	Numbers	Size range (cm)	Mean size (cm)
Fishes				
	Myctophidae			
	Benthosema fibulatum	12	2.9–7.9	5.3
	Diaphus adenomus	4	3.7–6.3	5.3
	Diaphus chrysorhynchus	2	3.8–5.4	5.0
	Diaphus trachops	2	3.3–3.9	3.6
	Myctophum brachygnathos	3	5.2–8.2	7.0
Shrimps				
	Grathophausidae			
	Grathophausia lonispina	2	4.5–7.4	6.0
	Pasiphacidae			
	Pasiphaea truncata	1	6.8	6.8
	Sergestidae			
	Sergia fulgens	3	7.1–8.3	7.6
Squids				
	Endoploteuthidae			
	Abralia trigonura	2	2.2–4.2	3.2
	Cranchiidac			
	Liocranchia reinhardti	1	3.6	3.6

local minima at $f_{l\,\min}$. A 512 point fast Fourier transform (FFT) was used to compute all spectra.

III. RESULTS

A. Myctophids

Broadband echoes were collected from 23 myctophids, six shrimps and three squids from the dorsal aspect [the direction of the sound source with respect to the subjects in the dorsal aspect is shown in Fig. 1(b)]. A summary of the microneckton for which broadband echoes were collected is shown in Table I. Echoes were also collected from seven myctophids in the lateral aspect [the direction of the signal was perpendicular to the plane of the page shown in Fig. 1(b)]. These lateral aspect echoes were collected from four *Benthosema fibulatum*, two *Diaphus* sp., and one *Myctophum brachygnathos*. For both the dorsal and longitudinal aspects, the subjects were oriented so that the incident signal was nearly perpendicular to the longitudinal axis of the subjects.

The average echo waveform for each species was obtained for the 20 echoes obtained per subject. The average echo waveform was calculated by aligning the peaks of the envelope of each echo. The average spectrum was obtained by averaging the absolute value of the Fourier transform of each echo expressed in dB. The averaged echo waveform, the cross-correlation function between the incident and echo waveforms, and the envelope of the correlation function, and the echo spectrum for a *Benthosema fibulatum*, *Diaphus adenomus*, and *Myctophum brachygnathos* in the dorsal and lateral aspect are shown in Fig. 3. The standard deviation of the spectrum was calculated for the 20 echoes collected per species. In some cases the envelop of the cross-correlation function can be useful in showing the presence and time of occurrence of echo highlights. Interference between the echo from the front surface (surface closest to the transducer) and secondary echoes from other structures including the back surface of the animal can be seen in the echo waveforms. From a dolphin perspective, the backscatter of myctophids in the lateral aspect would apply to a situation in which the dolphin and the prey are at the same depth. The target strength based on energy for all the mythophid measured in the lateral aspect varied from a high of -51.7 ± 0.2 dB to a low of -59.5 ± 0.8 dB.

Interference between the echo from the front surface (surface closest to the transducer) and secondary echoes from other structures including the back surface of the animals can be seen in the echo waveforms and sometimes in the envelope of the cross-correlation function for the dorsal aspect of the three species represented in Fig. 3. Although the presence of multi-pulse interference effects is more obvious in the echo waveform than in the cross-correlation function, the envelope of the cross-correlation function is useful in obtaining the time separation between multiple echo components. The structures of the echoes for the dorsal and lateral aspects were not very different from one another. This is because the multi-highlights were caused by the same structures but from different aspects, although the thickness of the fish was narrower in the lateral aspect than in the dorsal aspect. The echoes from the *Myctophum brachygnathos* in the lateral aspect had more structure than those of the other two myctophids in Fig. 3 and were slightly longer in duration than its corresponding dorsal reflection. This may have been caused by the longitudinal axis of the fish being slightly off the normal to the direction of the incident signal so that the secondary echoes had slightly longer propagation paths. Unfortunately, we cannot specify the specific parts of the fish anatomy that contributed to specific secondary reflections because the resolution capability of the incident signal was not fine enough.

Target strength calculation based on Eq. (2) was limited to frequencies above 70 kHz. Below 70 kHz, the spectral amplitude of the incident signal dropped below the −20 dB

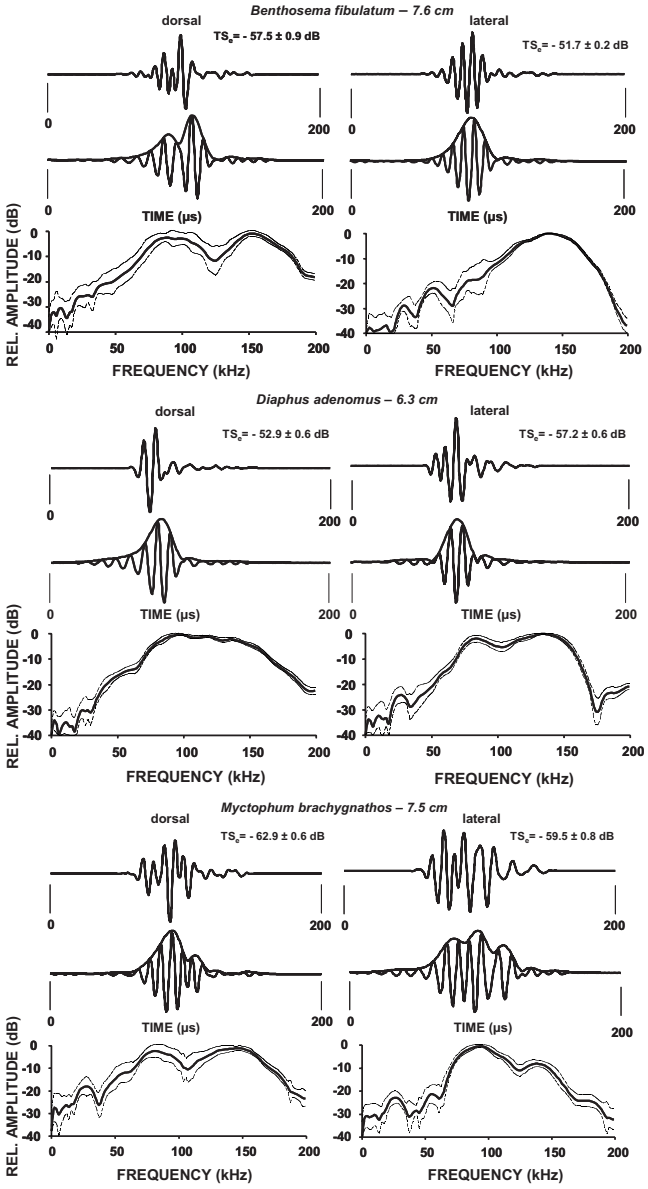


FIG. 3. The averaged echo waveform, the cross-correlation function between the averaged incident signal, and averaged echo waveform, the envelop of the correlation function and the averaged echo spectrum along with its standard deviation over the 20 pings for each orientation are shown for a *Benthosema fibulatum*, *Diaphus adenomus*, *Myctophum brachygnathos* in the dorsal and lateral aspects.

point and the target strengths fluctuated considerably with frequency within a ping and between pings. This type of behavior was probably caused by having a progressively smaller value in the denominator of an equation and by quantization errors inherent in the 12 bit digitization process. The fluctuation problem did not exist for frequencies above 170 kHz, however, target strength results above 170 kHz were denoted by a dashed curve to suggest that the results may not be as reliable as those between 70 and 170 kHz. The averaged target strengths as a function of frequency for the same subjects shown in Fig. 3 are shown in Fig. 4 for both the dorsal and lateral aspects. The thick solid curve is the averaged target strength and the thin curves represent the ± one standard deviation values over the 20 echoes collected per subject. The presence of a weak cosine ripple structure in both the echo and the target strength spectra was most obvious for the *Diaphus adenomus* in the lateral aspect, having two distinct local minima, and for the *Myctophum brachygnathos* in both aspects. Less developed cosine ripple structure can also be seen in the spectra for the *Myctophum brachygnathos* in both aspects and for the *Diaphus adenomus* in the dorsal aspect. The target strength spectra from all of the subjects shown in Fig. 4 had relatively deep local minima between −70 and −80 dB except for *Diaphus adenomus* in the dorsal aspect. Unfortunately, the bandwidth of the incident signal was not wide enough so that more than one ripple could be seen except for *Diaphus adenomus* in the lateral aspect. Nevertheless, the presence of the local minima and ripples are clear indicators of the presence of multiple highlight components in the waveform of the echoes.

The presence of multiple reflective components in an echo will also tend to increase the length of the echo compared with the incident signal. The greater the number of reflective components in the echo, the longer the echo will be. The larger the sum of all the echo delay will also make the frequency spacing between local minimas shorter. The echo from the lateral aspect of both the *Diaphus adenomus* and *Myctophum brachygnathos* are longer in duration than for the dorsal aspect. The sum of the highlight delays was large enough to make the frequency spacing between two consecutive local minima small enough so that both minima could be seen in the target strength spectra.

The frequency at which the local minima occurred in the target strength as a function of length is shown in Fig. 5 for the 18 *Benthosema fibulatum* that were insonified in the dorsal aspect. The data fell into two distinct groups: (1) length smaller than 5.75 cm and minima frequencies less than 107 kHz, and (2) length greater than 7.25 cm and minima frequencies clustered about 60 kHz. The linear regression line has a negative correlation between the frequency of the local minima and fish length (R^2=0.772). Unfortunately, we did not capture any specimen with lengths between the two clusters. Within both clusters, there is hardly any trends of $f_{l\,\mathrm{min}}$ with frequency, probably because the length differences were small. It is only when all the data are considered together that a negative correlation with minima frequency was found. Nevertheless, the regression line suggests a general tend of decreasing local minima frequency with length and since height should increase with length, longer delays between multiple echo components and lower local minima frequencies should occur. However, the possibility exists that the decrease in $f_{l\,\mathrm{min}}$ may not be best represented by a linear regression curve. The length variable was used because we unfortunately did not measure the height or thickness of the subjects. However, we were able to obtain ten *Benthosema fibulatum*, preserved in formaldehyde and measured the length, height, and thickness of the samples. The height measurements are shown as a function of length in Fig. 6. The longest *Benthosema* was 4.3 cm and the linear regression line fitting the data had a R^2 value of 0.88. Therefore, the height of myctophids with length smaller than 4.3 cm was directly proportional to height.

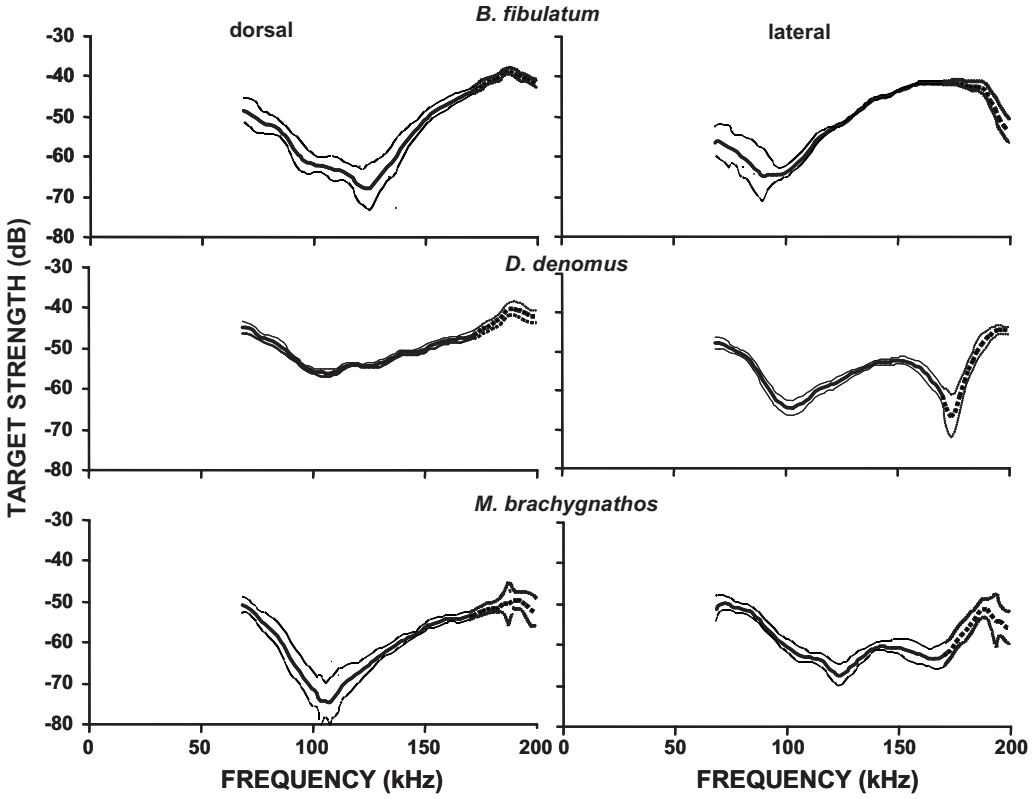


FIG. 4. The mean and standard deviation of the target strength spectra taken over 20 pings for the subjects of Fig. 3 in both the dorsal and lateral aspects.

B. Shrimps and squids

The averaged echo waveform, the cross-correlation function between the averaged incident signal and averaged echo waveform, the envelope of the correlation function and the averaged echo spectrum for three shrimps, *Sergia fulgen*, *P. truncata*, and *Gnathophausia longispina*, are depicted in Fig. 7 and for two squids, *Liocranchia reinhardti* and *Abralia trigonura* in Fig. 8. All echoes from the shrimp and squid were collected with the animals in the dorsal aspect. The effects of multipath interference can be seen in the waveform and the cross-correlation function of both echoes by an abrupt change in the shape of the curves consisting of a sharp drop off in the amplitude when compared with the incident signal. The echo waveforms are less complex in shape than those of the myctophids, with fewer echo components. As with the other micronekton, the effects of multipath interference can be seen in the waveform and the cross-correlation function of both echoes.

The target strength spectra for the three shrimps and two squids are shown in Fig. 9. The effect of multi-path interference is clearly seen by the presence of a local minima in the frequency spectra. Both spectra suggest that a rippled pattern would be present if the frequency range of the incident signal extended beyond 200 kHz. The target strength spectra for the squids had the largest variations throughout the entire frequency range (68–200 kHz) on a ping to ping basis, suggesting that the echo formation process was more sensitive to slight changes in aspect angle caused by the movement of the ship than for the other micronekton.

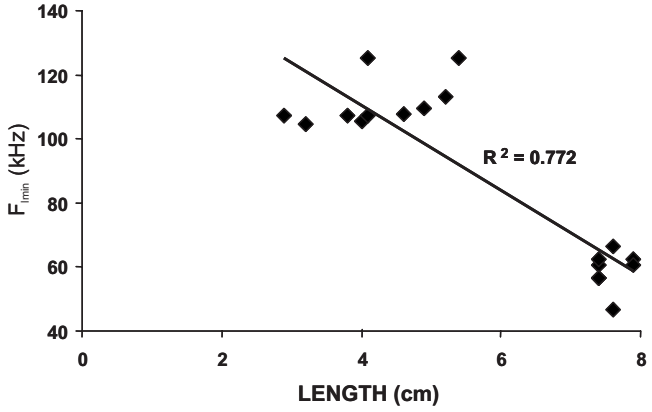


FIG. 5. The local minima frequency (associated with $n=0$) in the target strength and echo spectra plotted as a function of length echoes from the dorsal aspect for all the *Benthosema fibulatum*. The averaged echo waveforms and spectra were taken over the 20 echoes recorded per orientation for each animal.

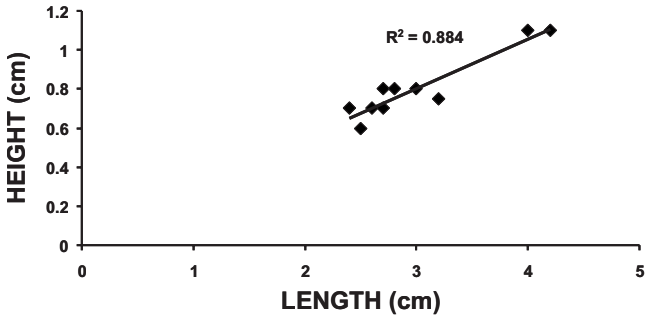


FIG. 6. Results of height versus length for *Benthosema fibulatum* preserved in formaldehyde.

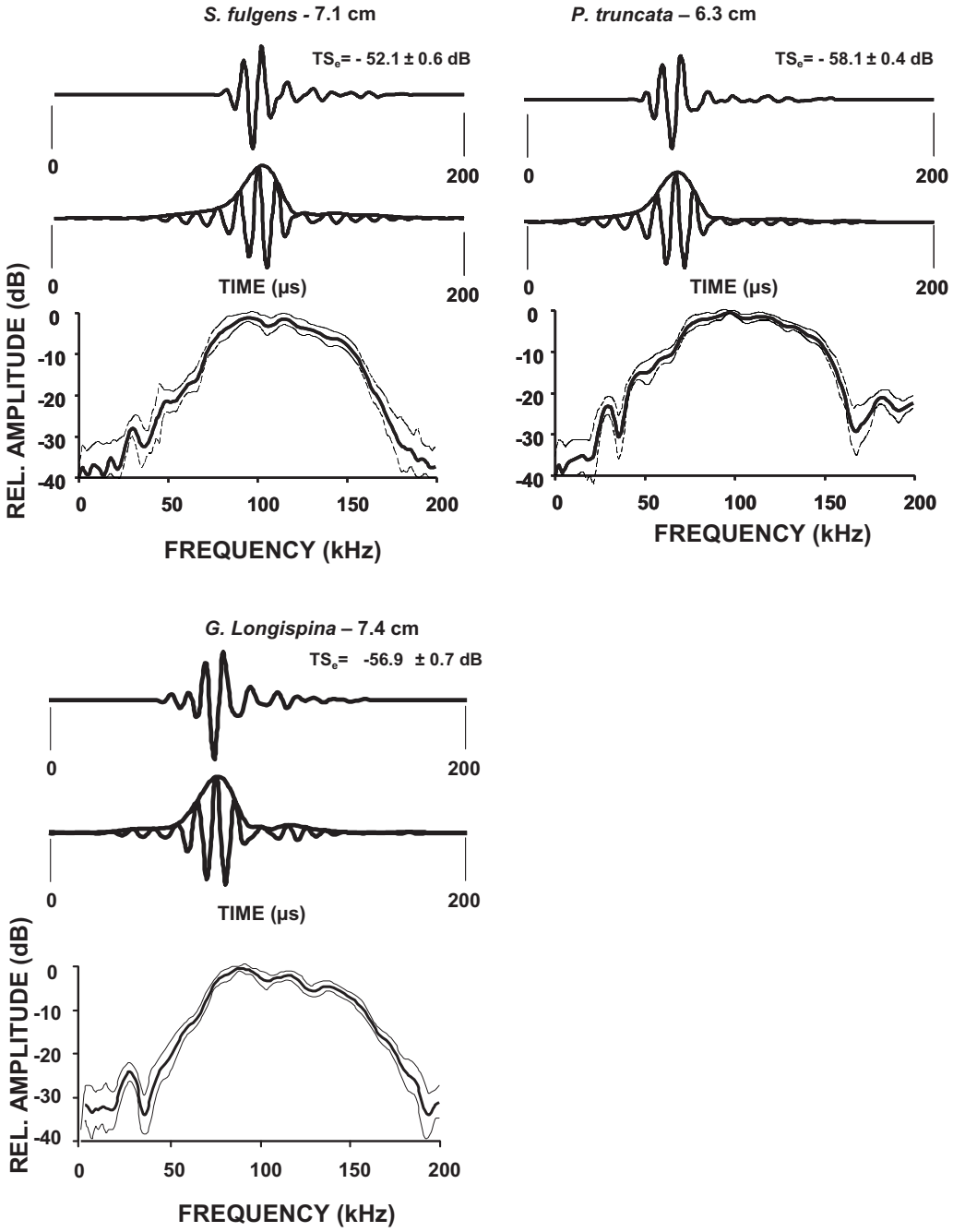


FIG. 7. The echo waveform, cross-correlation function, the envelope of the cross-correlation function, and the echo spectra for three species of shrimps, *Sergia fulgens* and *Pasiphaea truncate* and *Gnathophausia longispina*. The length of the specimen is denoted below the species name. The averaged echo waveforms and spectra were taken over the 20 echoes recorded per orientation for each animal.

IV. DISCUSSION AND CONCLUSIONS

The spectra of all of the target strength results were dominated by the presence of minima and associated ripple-like variations in the echo and target strength spectra. The results are relatively consistent with the broadband acoustic backscatter work of Chu *et al.* (1992), Stanton *et al.* (1996), and Chu and Stanton (1998). Their studies involved zooplankton from several groups including decapod shrimps, euphausiids, hard shelled gastopods, and gas bearing siphonosphores. Because of the small size of the organisms, higher frequency modulated signals from 400 to 800 kHz were used. The broadband dolphin-like signal used in this study had a usable band between 70 and 200 kHz, slightly larger than the octave band used by Chu and Stanton (1998). The shrimp-like krill, euphasusiid and decapod shrimp are similar to the shrimp species used in this study. We could not find any references of broadband acoustic studies with myctophids, the main subject of our study.

We can gain a general appreciation of the role of echolocation by spinner dolphins while foraging on the MBC by relating results obtained here with our knowledge of the echolocation signals used by spinner dolphins and the echolocation detection capability of bottlenose dolphin in waters inhabited by snapping shrimp. The echolocation signals emitted by spinner dolphins (Schotten *et al.*, 2003) are relatively similar in spectra and source energy flux density to

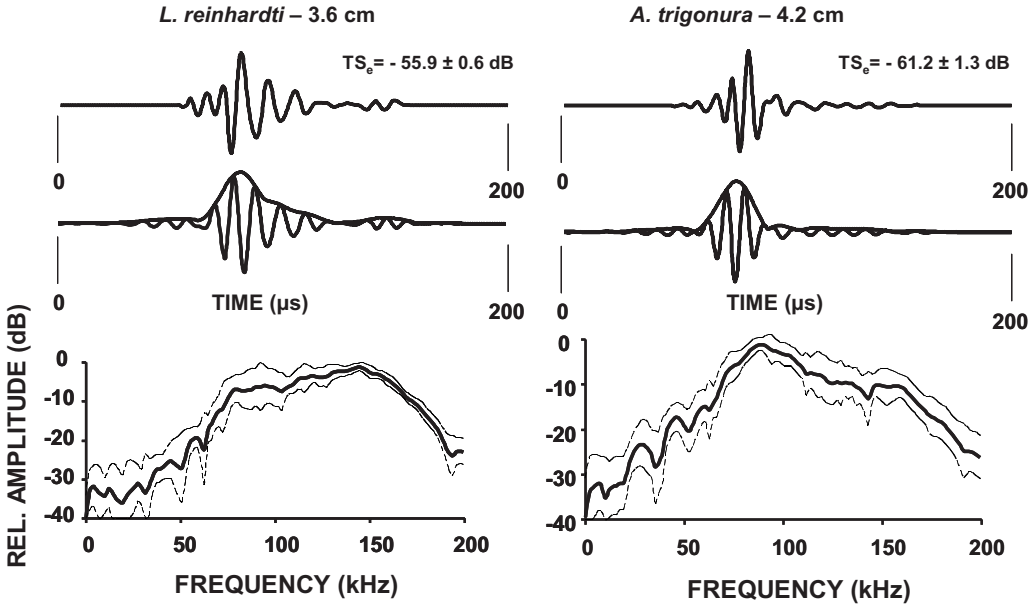


FIG. 8. The echo waveform, cross-correlation function, the envelope of the cross-correlation function and the target strength for two species of squid, *Liocranchia reinhardti* and *Abralia trigonura*. The length of the specimen is denoted below the species name. The averaged echo waveforms and spectra were taken over the 20 echoes recorded per orientation for each animal.

those used by bottlenose dolphins (Au, 1993). The target strength based on energy (−51.7 to −59.5 dB) of myctophids in the lateral aspects can be used to estimate the echolocation detection ranges of spinner dolphins swimming at about the same depth as a single fish. The target detection threshold of a bottlenose dolphin for a 2.54-cm-diam solid stainless steel sphere with a target strength of −41.0 dB was 73 m in waters inhabited by snapping shrimp (Au, 1993). The inshore waters around the Hawaiian Islands where spinner dolphins forage are also inhabited by snapping shrimp (Lammers *et al.*, 2008). If we assume that the snapping shrimp noise levels are about the same as for the waters of Kaneohe Bay, Oahu, Hawaii, where the bottle experiment was conducted and that the echolocation detection capability of bottlenose and spinner dolphins are roughly equivalent, then we can estimate range at which myctophids may be detected. Following the approach of Au *et al.* (2007) the echo energy flux density in dB that a dolphin will receive can be expressed by the equation

$$\mathrm{EE} = \mathrm{SE} - 2\mathrm{TL} + \mathrm{TS}, \tag{6}$$

where SE is the source energy flux density, TL is the one way transmission loss and TS is the target strength based on energy. If we assume that the source energy flux density and received echo energy flux density are the same for the bottlenose and spinner dolphins, we will have the following equation to satisfy:

$$-2\mathrm{TL}_\mathrm{B} + \mathrm{TS}_\mathrm{B} = -2\mathrm{TL}_\mathrm{S} + \mathrm{TS}_\mathrm{S}, \tag{7}$$

where the subscript B and S refer to the bottlenose and spinner dolphins, respectively. Assuming spherical spreading, we have

$$40\,\mathrm{Log}(r_\mathrm{S}) + 2\alpha r_\mathrm{S} = 40\log(r_\mathrm{B}) + 2\alpha r_\mathrm{B} + \mathrm{TS}_\mathrm{S} - \mathrm{TS}_\mathrm{B}, \tag{8}$$

where r_B=73 m, TS_B=−41 dB, TS_S=−52 to −60 dB, and the absorption loss at 120 kHz is approximately 0.044 dB/m. Inserting the values appropriate to the bottlenose and spinner dolphin situations, the detection range of MBC organisms can be estimated. However Eq. (8) belongs to a class of transedental equation that does not have a closed-form solution so it must be solved numerically. Inserting the appropriate values into Eq. (8), we obtained a maximum detection range for a single myctophid to be between 30 and 45 m. The MBC contains patches that can be quite dense over spatial scales of tens of meters (Benoit-Bird and Au, 2003c) with the orientation of the swimming myctophids dynamically varying with respect to a dolphin so that the use of a broadside target strength values should be appropriate. The detection range of an ensemble within the two-way beam of echolocating dolphins will increase over that of a single mycthophid if their echoes are within the short integration time of the dolphin (264 μs, Au, 1993) or about 40 cm. Given the animal densities reported from field studies (2001, 2006), micronekton in these layers can be spaced 1 every 8.5 cm. With the averaged sized individual being about 7 cm, the resulting spacing between animals in the scattering layer would be less than 2 cm, well within the integration time of the dolphin. Only at densities below about 10 animals/m3 would an animal of this size be detected individually by the dolphin. If for example four additional myctophids at the normal aspect are within the beam, the target strength will increase by 6 dB and the maximum detection range would increase to about 57 m. This rough calculation suggests that spinner dolphins may be able to detect patches in the MBC at sufficient range to influence their foraging behavior.

The detection of patches in the MBC will probably depend on the presence of myctophids rather than either squids or shrimps. Benoit-Bird and Au (2001) had slightly more squid and shrimp speciments and obtained results that clearly showed the target strength of myctophids at 200 kHz was

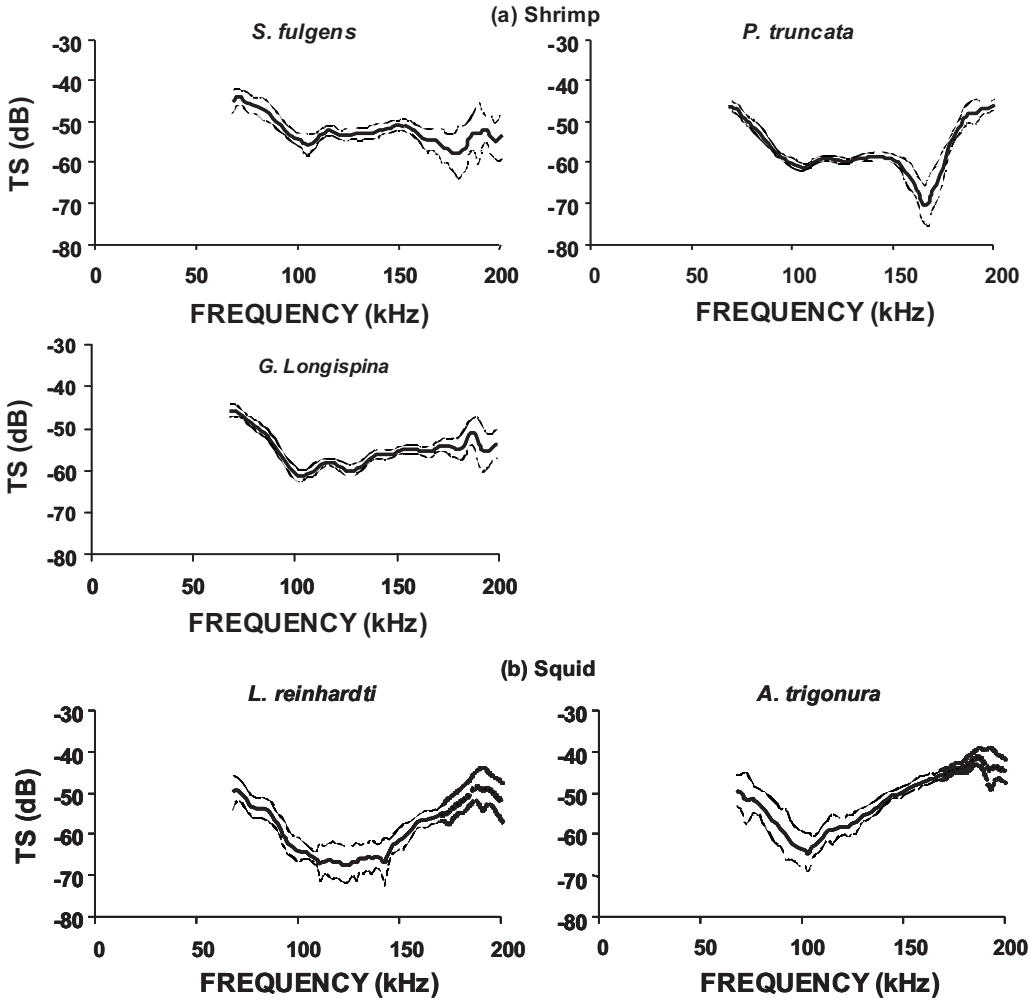


FIG. 9. The target strength spectra calculated from the dorsal aspect echoes for the shrimp species of Fig. 7 and the squid species of Fig. 8.

about 5 dB higher than squid and about 15 dB higher than shrimp of equivalent length. The three squids captured in this study were relatively small (2.2, 3.6, and 4.4 cm length) with the target strengths between −56 and −61 dB. The five shrimps were larger than the squids with lengths between 4.5 and 8.3 cm and target strength between −52 and −58 dB.

In order to consider whether or not an echolocating spinner dolphin can discriminate between myctophids, squids, and shrimps based on their echoes, the two-way 3 dB beamwidth of about 10° for the bottlenose dolphin (Au, 1992) must be taken into account. If we assume that the spinner dolphin would have approximately the same two-way beamwidth, then in most situations, a spinner dolphin echolocating on the MBC would have more than one micronekton within its beam. The example provided by Benoit-Bird and Au (2003c) of broadband backscatter from the MBC obtained with a planar transducer having a two-way beamwidth of 8° showed a series of echoes highlights within a 200 μs window, making it difficult to separate echoes from different organisms. Madsen *et al.* (2005) suggest that beaked whales can discriminate prey type in a relatively dense prey field. However, the prey field of the beaked whale is not nearly as dense as the MBC. The example in Madsen *et al.* (2005) shows a single echo from a prey in a 5 m range space. The example provided by Benoit-Bird and Au (2003a) had eight echoes, one following immediately after another in less than a meter range space. This would make discrimination of different species highly unlikely. Besides, the echo spectra for the different micronekton examined were complex and without any specific features useful for species identification. A species may be recognized from information on its swimming behavior collected over several echolocation transmissions, however, this process will be complicated by the presence of several micronekton within the beam. Furthermore, dolphin echolocation signals are Doppler tolerant so that negligible Doppler information can be obtained from a single echo (Au, 1993).

Although all animal groups in our study, myctophid, shrimp and squid, exhibited relatively similar patterns of variation with frequency, the presence of a skeletal structure in the mytophid made the backscatter process slightly more complicated than for shrimp and squid. In all three groups of animals, the presence of the minima were directly associated with the presence of multi echo components, the first being a reflection of the incident acoustic signal at the front surface, the surface nearest to the transducer, and the second being a reflection of the signal that penetrated into the body of the organisms and then reflected either off the skeletal structure or the back surface of the specimen. The minima in the spectra are not as deep as would be suggested by Eq. (4). In Eq.

(4), the assumption of perfect reflection off flat surfaces that are perpendicular to the direction of the incident signal was made. In our case, the reflective surfaces were not flat but curved. Furthermore, the front surface of the mycthophids in the dorsal aspect had a slight concave shape while the back surface had a convex shape. Therefore, the secondary highlights may have been correlated with the primary highlight off the front surface. The correlation was probably far from perfect, however, affecting the spectral interference between the highlights.

The frequency of the first local minima between 60 and 200 kHz had a strong negative correlation with the length of *Benthosema fibulatum*. This characteristic is consistent with the notion that the height is directly proportional to the length of the fish, at least for fish smaller than 6 cm. As the height of the fish increase, the delay time between echo components should increase, causing the frequency of the local minima to decrease as our data showed in Fig. 5.

Recent measurements at 38, 70, 120, and 200 kHz of the volume backscatter of the mesopelagic boundary community by Benoit-Bird (2006) in the waters of Oahu, Hawaii indicated that the volume scattering decreased with frequency whereas our target strength results exhibited a local minima between 100 and 150 kHz. The frequency dependency of individual micronektons of the MBC may not be directly related to volume scattering from an ensemble of the same organisms suggesting that the volume scattering process is very complex and not well understood. It should also be noted that Benoit-Bird (2008) did not use the same pulse length at the four frequencies so that the same volume of water was not examined. The 70, 120, and 200 kHz versions of the Simrad EK-60 have conical beams of approximately the same width so that the volume of water examined at any depth will be a truncated cone with its height being determined by the pulse length (Urick, 1983). The pulse lengths were 256 μs at 38 kHz, 128 μs at 70 and 64 μs at 120 and 200 kHz making the height of the examined region four times greater at 38 kHz and two times greater at 70 kHz than at 120 and 200 kHz. The effects of examining different volumes are not known.

Backscatter from a mesopelagic layer can be rather complex if the density of organism is high and a number of organisms are within the beam of the echosounder. In such a case, there will be a large amount of constructive and destructive interference, making the backscatter process so complicated that any analogy with a simple frequency response from individual organisms seems irrelevant. To illustrate this, we created a simulated echo using the dorsal aspect echo from the *B. fibulatum* in Fig. 3 by adding seven versions of the echo but with arbitrary delays between each echo and obtained the echo waveform shown in Fig. 10. Below the waveform are the echo and target strength spectra. There are obvious differences in the spectra shown in Fig. 10 and Fig. 3. The results of our simulation suggest that the spectral integrity of echoes from individual animals will not be preserved when echoes contain backscatter from several identical animals.

It is important to understand the relationship between backscatter measured by an echo-sounder and that which an echolocating spinner dolphin receives. Clearly, the backscatter process from either an echosounder or dolphin perspective is very complicated and deserves more attention. The complexity of the backscatter process results from the high density of mixed species and inhomogenity that seems inherent in the mesopelagic layer. Zooplankton may contribute to some of the volume backscatter obtained by an echosounder since the micronekton of the mesopelagic boundary migrate horizontally over 2 km towards shore to forage on zooplankton at night. It stands to reason that zooplanton density should be several orders of magnitude higher than the density of micronekton, otherwise the long horizontal migration would not result in sufficient energetic gain. The contribution of a large zooplankton population on the volume backscatter cannot be overlooked.

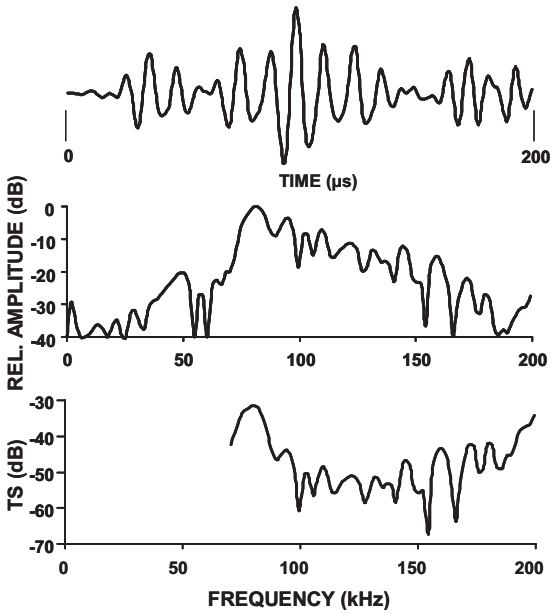


FIG. 10. Waveform for a simulated *Benthosema fibulatum* echo consisting of seven versions of the dorsal aspect echo waveform shown in Fig. 3, summed together with an arbitrary delay for each replica. The echo and target strength spectra are shown below the echo waveform.

ACKNOWLEDGMENTS

The authors would like to express their appreciation to the officers and crew of the NOAA ship Townsend Cromwell. We also thank Robert Humprey, cruise chief scientist for providing ship time and support and to Bruce Monday for assistance in fish species identification, both from the Pacific Islands Science Center of the National Marine Fisheries Service in Honolulu. Curt Fiedler assisted in identification of the shrimp species and Christopher Bird assisted in constructing the mounting frame; both are from the Hawaii Institute of Marine Biology. We would express our thanks to Dr. Jeffrey Drazen of the Oceanography Department, University of Hawaii, for allowing us to use his laboratory to measure the morphometrics of his *Bentoshema fibulatum* collection. Finally, we thank Dr. Julie Oswald of the Hawaii Institute of Marine Biology for her helpful comments.

This work was supported in part by Office of Naval Research Grant No. N00014-98-1-068, Dr. Robert Gisiner,

Program Manager. This work was also funded by a grant from the National Oceanic and Atmospheric Administration, Project No. R/FM-7, which is sponsored by the University of Hawaii Sea Grant College Program, SOEST, under Institutional Grant No. NA86RG0041 from NOAA Office of Sea Grant, Department of Commerce. The views expressed herein are those of the authors and do not necessarily reflect the views of NOAA or any of its subagencies. UNIHISEAGRANT-JC-02-17. This is HIMB contribution 1306.

Au, W. W. L. (**1993**). *The Sonar of Dolphins* (Springer-Verlag, New York).

Au, W. W. L. (**1992**). "Application of the reverberation-limited form of the sonar equation to dolphin echolocation," J. Acoust. Soc. Am. **92**, 1822–1826.

Au, W. W. L., and Snyder, K. J. (**1980**). "Long-range target detection in open waters by an echolocating atlantic bottlenose dolphin (*Tursiops truncatus*)," J. Acoust. Soc. Am. **68**, 1077–1084.

Au, W. W. L., Moore, P. W. B., and Pawloski, D. A. (**1988**). "Detection of complex echoes in noise by an echolocating dolphin," J. Acoust. Soc. Am. **83**, 662–668.

Au, W. W. L., and Benoit-Bird, K. (**2003**). "Acoustic backscattering by Hawaiian Lutjanid snappers II: Broadband temporal and spectral structure," J. Acoust. Soc. Am. **114**, 2767–2774.

Au, W. W. L., Benoit-Bird, K. J., and Kastelein, R. A. (**2007**). "Modeling the detection range of fish by echolocating bottlenose dolphins and harbor porpoises," J. Acoust. Soc. Am. **121**, 3954–3962.

Benoit-Bird, K. J., and Au, W. W. L. (**2001**). "Target strength measurements of hawaiian mesoplegic boundary community animals," J. Acoust. Soc. Am. **110**, 812–819.

Benoit-Bird, K. J., Au, W. W. L., Brainard, R. E., Lammers, M. O. (**2001**). "Diel horizontal migration of the Hawaiian mesopelagic boundary community observed acoustically," Mar. Ecol.: Prog. Ser. **217**, 1–14.

Benoit-Bird, K. J., Au, W. W. L., Brainard, R. E., and Lammers, M. O. (**2001**). "Diel horizontal migration of the Hawaiian mesopelagic boundary community observed acoustically," Mar. Ecol.: Prog. Ser. **217**, 1–14.

Benoit-Bird, K. J., and Au, W. W. L. (**2003a**). "Prey dynamics affect foraging by a pelagic predator (*Stenella longirostris*) over a range of spatial and temporal scales," Behav. Ecol. Sociobiol. **53**, 364–373.

Benoit-Bird, K. J., and Au, W. W. L. (**2003b**). "Spatial dynamics of the Hawaiian mesopelagic boundary community," ICES J. Mar. Sci. **60**, 899–913.

Benoit-Bird, K., and Au, W. W. L. (**2003c**). "Target strength and density structure of Hawaiian mesopelagic boundary community patches," J. Acoust. Soc. Am. **114**, 1888–1897.

Benoit-Bird, K. J., and Au, W. W. L. (**2004**). "Fine-scale diel migration dynamics of an island-associated sound-scattering layer," Deep-Sea Res., Part I **59**, 707–719.

Benoit-Bird, K. J. (**2004**). "Prey value and energy needs: Foraging predictions for wild spinner dolphins," Mar. Biol. (Berlin) **145**, 435–444.

Benoit-Bird, K. J., and Au, W. W. L. (**2006**). "Extreme diel horizontal migrations by a tropical nearshore resident micronekton community," Mar. Ecol.: Prog. Ser. **319**, 1–14.

Benoit-Bird, K. J. (**2006**). "Effects of scattering layer composition, animal size, and numerical density on the frequency response of volume backscatter," J. Acoust. Soc. Am. **120**, 3001.

Chu, D., Stanton, T. K., and Wiebe, P. H. (**1992**). "Frequency dependence of sound backscattering from live individual zoolplankton," ICES J. Mar. Sci. **49**, 97–106.

Chu, D., and Stanton, T. K. (**1998**). "Application of pulse compression techniques to broadband acoustic scattering by live individual zoolplankton," J. Acoust. Soc. Am. **104**, 39–55.

Foote, K. G., Vestnes, G., Maclennan, D. N., and Simmonds, E. J. (**1987**). "Calibration of acoustic instruments for fish density information: A practical guide," in *International Council for the Exploration of the Sea Cooperative Research Report No.* 144.

Johnson, C. S. (**1968**). "Relation between absolute threshold and duration of tone pulse in the Bottlenosed propoise," J. Acoust. Soc. Am. **43**, 757–763.

Lammers, M. O., Brainard, R. E., Au, W. W. L., Mooney, T. A., and Wong, K. (**2008**). "An ecological acoustic recorder (EAR) for long-term monitoring of biological and anthropogenic sounds on coral reefs and in nearby waters," J. Acoust. Soc. Am. **123**, 1720–1728.

Madsen, P. T., Wilson, M., Johnson, M., Hanlon, R. T., Bocconcelli, A., Aguilar de Soto, N., and Tyack, P. L. (**2007**). "Clicking for calamari: Toothed whales can echolocate squid Loligo pealeii," Aquat. Biol. **1**, 141–150.

Madsen, P. T., Johnson, M., Aguilar de Soto, N., Ximmer, W. M., and Tyack, P. (**2005**). "Biosonar performance of foraging beaked whales (*Mesoplodon densirostris*)," J. Exp. Biol. **208**, 181–194.

Norris, K. S., and Dohl, T. P. (**1980**). "Behavior of the Hawaiian spinner dolphin, *Stenella longirostris*," Fish. Bull. **77**, 821–849.

Reid, S. B., Hirota, J., Young, R. E., and Hallacher, L. E. (**1991**). "Mesopelagic-boundary community in Hawaii: Micronekton at the interface between neritic and oceanic ecosystems," Mar. Biol. (Berlin) **109**, 427–440.

Rihaczek, A. W. (**1969**). *Principles of High-Resolution Radar* (McGraw–Hill, New York).

Stanton, T. K., Chu, D., and Wiebe, P. H. (**1996**). "Acoustic scattering characteristics of several zooplankton group," ICES J. Mar. Sci. **53**, 289–295.

Schotten, M., Au, W. W. L., Lammers, M. O., and Aubauer, R. (**2003**). "Echolocation recordings and localizations of wild spinner dolphins (*Stenella longirostris*) and pantropical spotted dolphins (*Stenella attenuata*) using a four hydrophone array," in *Echolocation in bats and dolphins*, edited by J. Thomas, C. Moss, and M. Vater (University of Chicago Press, Chicago), pp. 393–409.

Urick, R. J. (**1983**). *Principles of Underwater Sound*, McGraw–Hill, New York.

The structure of vocal sounds produced with the mouth closed or with the mouth open in treefrogs

Marcos Gridi-Papp[a)]
Section of Integrative Biology C0930, University of Texas, 78712 Austin, Texas, USA

(Received 1 July 2007; revised 14 February 2008; accepted 17 February 2008)

Frogs and toads mostly call with their mouths shut, unlike many other vertebrates. Sound is generated when air crosses the larynx, but there is no direct airflow to the external environment and radiation occurs at the skin. This study directly compares the acoustic output obtained from euthanized frogs with the mouth open against the output obtained with the mouth closed during activation of the larynx by airflow. With the mouth closed, the vocal sac was inflated and the acoustic energy was concentrated in the same harmonics as in the advertisement call, whereas with the mouth open, energy was spread in a wide range of harmonics. The acoustic output at the dominant frequency was more intense with the mouth closed than with the mouth open. More sound was radiated through the vocal sac and head than through the rest of the body. The spectral differences between open and closed mouth treatments matched the differences observed between natural advertisement calls, produced with the mouth closed, and distress calls, produced with the mouth open. By calling with the mouth closed, treefrogs can potentially produce advertisement calls with the energy concentrated in a narrower frequency range than with the mouth open.
© *2008 Acoustical Society of America.* [DOI: 10.1121/1.2897001]

PACS number(s): 43.80.Ka, 43.64.Tk [JAS] Pages: 2895–2902

I. INTRODUCTION

Many species of frogs can produce strikingly intense advertisement calls and, unlike most terrestrial vertebrates, they do so with their mouth and nares closed (Gerhardt, 1975; Passmore, 1981; Gans and Pyles, 1983). Air flows from the lungs through the larynx into the mouth and vocal sac, and it is returned to the lungs after each call (Martin and Gans, 1972; Dudley and Rand, 1991; Walkowiak 2006). The vocal sac has been assumed to enhance the intensity of the calls (McAlister, 1959).

Resonance can produce amplitude gain and it is common in vocalizing animals (Bradbury and Vehrencamp, 1988; Fletcher, 1992; Hoese *et al.*, 2000). Tests for resonance of the air inside the vocal sac of frogs, however, did not detect any cavity resonance. These tests included puncturing the vocal sacs of toads (Martin, 1972; Capranica and Moffat, 1983), and recording frogs calling in an atmosphere with nitrogen replaced by helium (Capranica and Moffat, 1983; Rand and Dudley, 1993).

Instead of resonance of the air inside the sac, Purgue (1995, 1997) investigated acoustic resonance of the tissues of the animal. He injected sound tones at various frequencies into the carcass of euthanized frogs and used a capacitance probe to measure the magnitude of the sound transfer function at several points of the body. The tissues transferred frequencies unequally, and many areas were tuned to the frequencies present in the natural calls. The vocal sacs of *Pseudacris triseriata*, *Hyla regilla* and *Hyla gratiosa* were tuned to the frequency that is emphasized in natural advertisement calls. While in *P. triseriata* the vocal sac transferred sound to the environment without amplitude loss or gain at the dominant frequency, the vocal sacs of *Hyla regilla* and *Hyla gratiosa* produced a gain of about 15 dB in relation to the sound perceived by the microphone with the frog tissues removed from the setup.

The reasons why frogs call mostly with their mouths closed are not fully understood and several hypotheses remain untested (Rand and Dudley, 1993; Purgue, 1995). Determining how the calling apparatus would behave with the mouth open or closed can indicate if sound spectral composition or intensity might play a role in the maintenance of this behavior. In this study, I employed the technique of laryngeal activation by airflow (Paulsen, 1965; Martin, 1971; Suthers *et al.*, 2006) to obtain artificial calls from euthanized frogs by passive vibration of the vocal folds. The temporal structure of the natural call is lost with this method, as the anuran larynx has four pairs of muscles that contract at different moments during phonation (Trewavas, 1933; Martin and Gans, 1972). The spectral structure of the artificial calls, however, approximates that of the natural calls (Martin, 1971; Suthers *et al.*, 2006), allowing for a meaningful comparison between the mouth open or closed. In addition, I used a sound attenuator to investigate the relative contribution of body parts to the radiated call.

II. MATERIALS AND METHODS

Seven calling male *Hyla versicolor* (LeConte 1825) and four *Pseudacris streckeri* (Wright and Wright 1933) were collected in the Lexington Wildlife Management Area in Lexington, OK, and seven *Hyla cinerea* (Schneider 1799) at Brackenridge Field Laboratory in Austin, TX, in May 2002.

[a)]Electronic mail: mgpapp@ucla.edu. Present address: Department of Physiological Science, University of California, 621 Charles E. Young Dr. South, 90095-1606 Los Angeles, California.

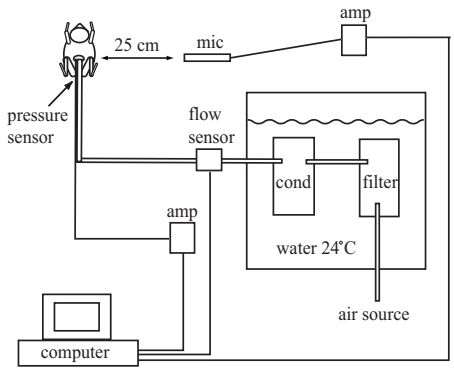


FIG. 1. Artificial laryngeal activation of frogs. Moist air is passed through the lungs of the euthanized frog and activates the vocal membranes in the larynx to produce sound. Pulmonary air pressure, airflow and sound are recorded. Abbreviations: mic=microphone, amp=amplifier, cond =condenser.

A. Laryngeal activation

The animals were euthanized with external application of benzocaine gel at 5% and immediately prepared for experimentation (see Fig. 1). The tip of one lung was cannulated through an abdominal incision and the connection was sealed with cyanoacrylate adhesive. A pressure sensor (Millar SPR-524, Houston, TX) was inserted in the cannula to monitor pulmonary pressure. The abdominal muscles and skin at the incision were also glued to the cannula, sealing the body cavity. The air fed into the larynx was saturated with humidity at 24 °C, to prevent dehydration of the vocal folds. Pressure was controlled by the experimenter by blowing into the end of the tubing. The air then passed through a filter, a condenser and a thermal mass airflow sensor (Cole-Parmer EW-32707-16, Vernon Hills, IL; range $0-10\pm1.5\%$ L/min) before reaching the frog. An electret microphone (RadioShack 33-3003) was placed at 25 cm from the preparation, perpendicular to the longitudinal axis of the animal.

The microphone-recorder setup was calibrated within the experimental chamber in reference to a sound pressure level meter (GenRad 1982, IET Labs, Westbury, NY; Fig. 2). After each experiment, the preparation was inspected for air leaks and anatomical damage. The calibration and linearity of the pressure sensor were verified by immersion of its tip in a graduated water column at nine known depths for which theoretical values of pressure could be calculated. The response of the airflow sensor was factory calibrated and was verified by comparison with a fan-based airflow sensor at various levels of constant flow.

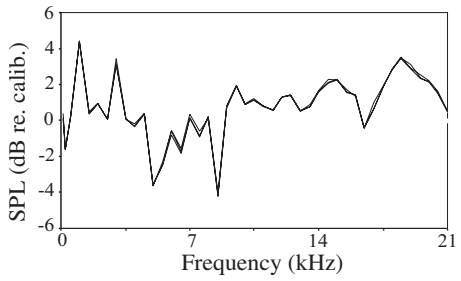


FIG. 2. Spectral response of the microphone. Ordinate presents the amplitude level of the signal recorded by the experimental microphone in relation to the amplitude registered by the sound pressure level meter. The loudspeaker output was calibrated *in situ* with a sequence of sinusoidal tones ranging from 500 Hz to 21 kHz at 500 Hz intervals, having a precision sound pressure level meter as reference.

A human-based air source was used as opposed to a mechanical one, for providing adequate pressure range, pressure feedback shutoff to prevent over inflation, and air saturated with humidity. A mechanical-electronical system is under development to replace the current air source in future experiments, providing more precise control of the input and faster pressure feedback.

A wide range of sound frequencies and amplitudes was produced at each experiment by varying pulmonary pressure up to 5 kPa. The preparation was installed in a custom made anechoic container to attenuate any echo or external noise. The container measured $0.76\times0.76\times1.1$ m, with its exterior composed of plywood with a thickness of 12 mm, followed by 54 mm of high-density foam, another layer of 8 mm of plywood and two more layers of 54 mm high-density foam. Pure tones played and recorded within the container produced sinusoid waveforms with smooth amplitude envelope and less then 1.5% variation in amplitude among cycles at frequencies within 250 Hz to 20 kHz.

1. Experimental treatments

At least ten artificially generated calls were recorded from each treatment and individual. The three treatments were: open mouth, closed mouth and cut vocal sac. In the first treatment, the euthanized animal was positioned on its back without being fixed to the foam substrate and the mouth was held open at 45° by contact with an entomological pin fixed to the substrate. Removal of the pin did not alter the sound unless the mouth closed completely. The vocal sac did not inflate in this treatment. In the closed mouth treatment, the jaws and nares were sealed with cyanoacrylate glue and a cannula was protruded through the nares into the oral cavity. A tygon tube of 60 cm in length was attached to this cannula to remotely allow or prevent the deflation of the vocal sac after each artificial call. The cut vocal sac treatment followed the closed mouth treatment. A ventral incision was produced on the vocal sac, perpendicular to the longitudinal axis of the animal, to allow the air to escape and therefore prevent inflation.

Two additional treatments consisted of repetitions of the closed mouth treatment with placement of an acoustic attenuator over the head and vocal sac only, or over the rest of the body. The goal was to access the relative contribution of the two regions of the body to the radiation of sound in these animals. The attenuator consisted of a styrofoam box with $135\times115\times110$ mm in external dimensions and 22 mm in thickness with an arch carved at one side to adjust to the animal's body shape. Its transfer spectrum was uneven but produced adequate attenuation within the range of interest (Fig. 3).

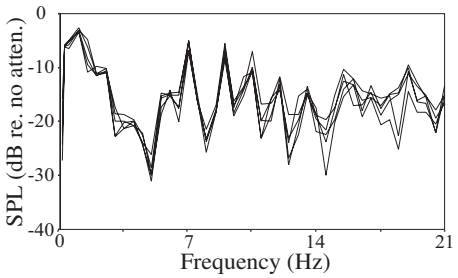


FIG. 3. Spectral profile of the attenuator. Ordinate presents the amplitude level with attenuator, in relation to without. A loudspeaker was placed in the position normally occupied by the frog in the experimental chamber. A sequence of sinusoidal tones ranging from 500 Hz to 21 kHz at 500 Hz intervals was played and recorded having the loudspeaker covered or not by the attenuator.

B. Data analysis

Sounds were produced at various laryngeal pressures and airflows to explore the range of the vocal apparatus. The fundamental frequency and intensity of such calls are correlated with each other and with air pressure and airflow (Martin, 1971; Gridi-Papp, unpublished). A direct comparison of the structure of calls produced with the mouth open with those produced with the mouth closed would be weakened by the variation in fundamental frequency of the calls. To avoid such constraint, calls were compared having fundamental frequency as a covariate and spectral patterns were analyzed in relation to harmonic number, instead of absolute frequency.

Fundamental frequency, root mean square amplitude of the sound above 90% of its peak amplitude, and relative amplitude of the first 20 harmonics were determined for each artificial call using SoundRuler (soundruler.sourceforge.net, version 0.937b). I assumed that all of the energy of each call was contained in its first 20 harmonics. That allowed for mathematical subtraction of the effect of the attenuator on each call, harmonic by harmonic. By placing the attenuator over the head and vocal sac only, the output contained the sum of the attenuated sound radiated by the head and vocal sac, and the full sound radiated by the rest of the body. Subtracting this sound from the average full sound without attenuator revealed the sound that was retained by the attenuator. Multiplication of the sound retained at the attenuator by the inverse of the attenuator's spectral profile reconstructed the original signal produced by the head and vocal sac only. The same procedure was repeated for the body. Sound multiplication by the attenuator's spectral profile was performed one harmonic at a time, interpolating its frequency in the spectral profile to find the appropriate correction factor and multiplying it by the harmonic's amplitude. Attenuated sounds were subtracted from the average non-attenuated sound harmonic by harmonic. As non-attenuated sounds varied in fundamental frequency, average spectral profiles were built at intervals of 50 Hz fundamental frequency and the fundamental frequency of each sound to be subtracted was interpolated between the closest average profiles to determine the harmonic amplitudes to be subtracted.

Pearson correlation was used to examine relations between continuous variables in laryngeal activation. Sound amplitude with the mouth open was compared to amplitude with the mouth closed or the vocal sac cut through analysis of variance with Bonferroni corrected post-hoc multiple comparisons. Radiation by the head or the body were compared using t-tests. All test were two tailed.

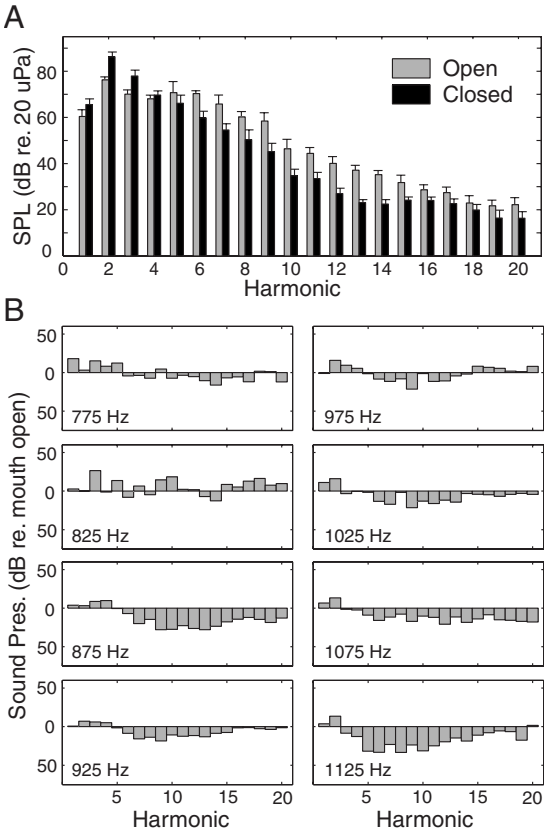


FIG. 4. Harmonic structure of artificial calls in *Hyla versicolor*. A. Pooled call spectral structure, showing how the amplitude in calls produced with the mouth open or closed is distributed in the first 20 harmonics. Error bar =standard error of the mean. B. Spectral structure of the amplitude level with the mouth closed, in relation to the mouth open. Calls grouped by fundamental frequency at intervals of 50 Hz.

III. RESULTS

A. Hyla versicolor

Artificial calls produced with the mouth open differed from calls produced with the mouth closed, by concentrating the acoustic energy at the lower harmonics [Fig. 4(A)]. This pattern was held over most of the fundamental frequency range over which the larynx was excited [Fig. 4(B)]. While these animals produce reduced frequency modulation in their natural calls, a wide range of fundamental frequencies was produced by varying the air pressure applied to the lungs to make sound (Martin, 1971). Fundamental frequency was positively correlated with amplitude with the mouth open ($r^2=0.58$, $N=105$, $P<0.001$) and with the mouth closed ($r^2=0.63$, $N=152$, $P<0.001$).

As expected, artificial calls lacked the temporal properties of natural calls, but they matched the fundamental frequency of natural calls (Fig. 5). Calls produced with the mouth closed were more similar to natural calls in harmonic structure than calls produced with the mouth closed.

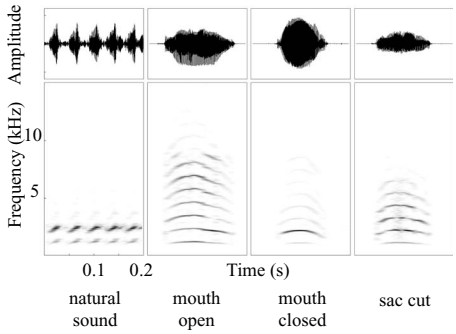


FIG. 5. Oscillogram and spectrogram of natural and artificial calls generated in three treatments of laryngeal activation in *Hyla versicolor*. The amplitude axis is not comparable among plots.

Call energy was concentrated in the second harmonic, when the mouth closed, as in the natural call. With the mouth open, the energy was more distributed among higher harmonics. Calls produced with the mouth closed were more intense than calls produced with the mouth open (mean difference = 0.12 Pa, $P<0.001$ Fig. 6). The amplitude of the dominant frequency was also higher with the mouth closed than with the mouth open (mean difference = 0.21 Pa, $P<0.001$). The smaller amplitude obtained with the mouth open could be due to displacement of the calling apparatus, related to the opening of the mandible. This hypothesis was tested and rejected by cutting the vocal sac in preparations with the mouth closed. Those cut preparations produced sounds with reduced energy in the second harmonic (mean difference = 0.20 Pa, $P<0.001$). They also exhibited energy more widely spread in higher harmonics, as the preparations with the mouth open (Fig. 5).

When the head and vocal sac were attenuated, a larger loss in call amplitude occurred than when the body was attenuated (mean difference = 0.23 Pa, $t=10.8$, $N=94, 94$, $P<0.001$).

B. Pseudacris streckeri

Artificial calls produced with the mouth open or closed were even more divergent in this species than in *Hyla versicolor* (Fig. 7). Mouth closure concentrated the acoustic energy of the call at the low frequencies, especially at the second harmonic. As in *Hyla versicolor*, the natural harmonic structure was best matched by artificial calls produced with the mouth of the frog closed (Fig. 8).

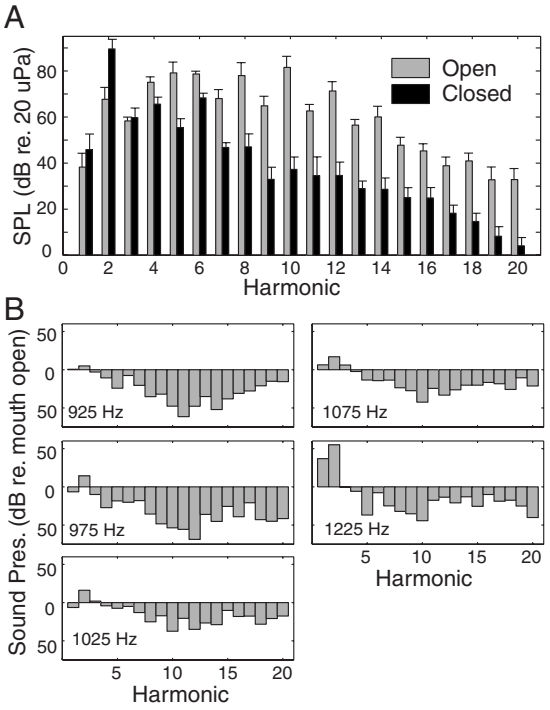


FIG. 7. Harmonic structure of artificial calls in *Pseudacris streckeri*. A. Pooled call spectral structure, showing how the amplitude in calls produced with the mouth open or closed is distributed in the first 20 harmonics. Error bar=standard error of the mean. B. Spectral structure of the amplitude level with the mouth closed, in relation to the mouth open. Calls grouped by fundamental frequency at intervals of 50 Hz.

Call amplitude was not significantly higher with the mouth closed than with the mouth open (mean difference = 0.24 Pa, $t=1.6$, $P=0.124$, Fig. 9), except when only the dominant harmonic was compared (mean difference = 0.91 Pa, $t=9.1$, $P<0.001$). The peak at the dominant frequency of the natural call was radiated at higher amplitude by the head and vocal sac than by the body (mean difference = 0.27 Pa, $t=2.4$, $N=37, 57$, $P=0.018$). The dominant fre-

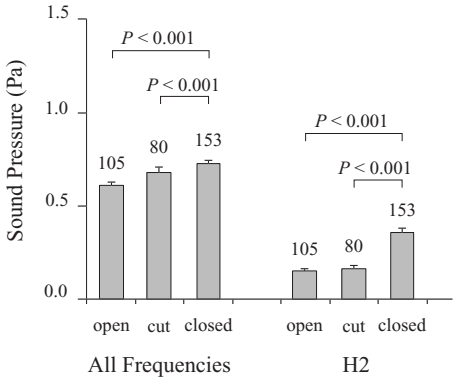


FIG. 6. Sound pressure of artificial calls in *Hyla versicolor*. "Open" refers to calls obtained with the mouth open, "closed" refers to the mouth closed with the vocal sac inflating, and "cut" refers to the mouth closed and the sac cut. Error bar = standard error of the mean.

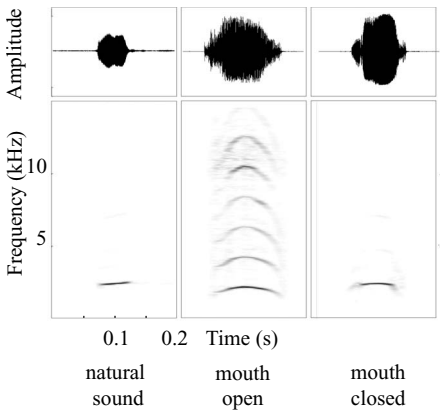


FIG. 8. Oscillogram and spectrogram of natural and artificial calls generated in two treatments of laryngeal activation in *Pseudacris streckeri*. The amplitude axis is not comparable among plots.

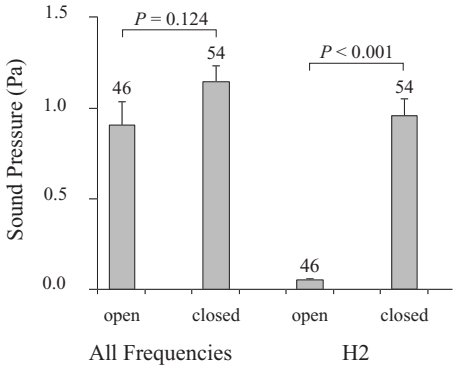


FIG. 9. Sound pressure of artificial calls in *Pseudacris streckeri*. "Open" refers to calls obtained with the mouth open and "closed" refers to the mouth closed with the vocal sac inflating. Error bar = standard error of the mean.

quency of the natural advertisement calls of ten individuals from the population where these animals were collected was the second harmonic near 2.2 kHz (the first harmonic is too weak to be seen in Fig. 8).

C. Hyla cinerea

The artificial calls of the green treefrogs also exhibited concentration of energy at low frequencies when the mouth was closed, producing reduction of amplitude at high harmonics and an increase in amplitude at low harmonics (Fig. 10). These frogs, however, produced a harmonic structure that matched every third frequency band of the natural calls (Fig. 11). The intermediate frequencies could not be recreated with artificial activation, indicating that some muscular contraction might be necessary to achieve the full natural acoustic structure. Natural calls of *H. cinerea* in the population studied have the call energy concentrated on two frequency peaks near 850 and 2500 Hz. In the artificial calls, the dominant frequency was the third harmonic in trials with the mouth closed (Fig. 11). The frequency corresponds to the high band of dominant frequency in the natural call. When the mouth was open, the dominant frequency was the second harmonic. When the vocal sac was cut in a preparation with the mouth closed, the dominant frequency switched from the third harmonic to the second harmonic. The vocal sac, or the integrity of the closed system, seems to be necessary for tuning the call energy to the high frequency peak of the advertisement call.

The amplitude of the calls of *H. cinerea* was not altered significantly by opening the mouth (mean difference = 0.02 Pa, $P > 0.937$, Fig. 12). The dominant frequency had higher amplitude when the mouth was closed (mean difference = 0.10 Pa, $P < 0.001$). The head and vocal sac radiated more energy than the body (mean difference = 0.25 Pa, $t = 7.5$, $N = 49, 64$, $P < 0.001$).

IV. DISCUSSION

In all three species, artificial calls produced with the mouth closed had the acoustic energy concentrated in a narrower band of the spectrum, and presented more energy at the dominant harmonic than calls produced with the mouth

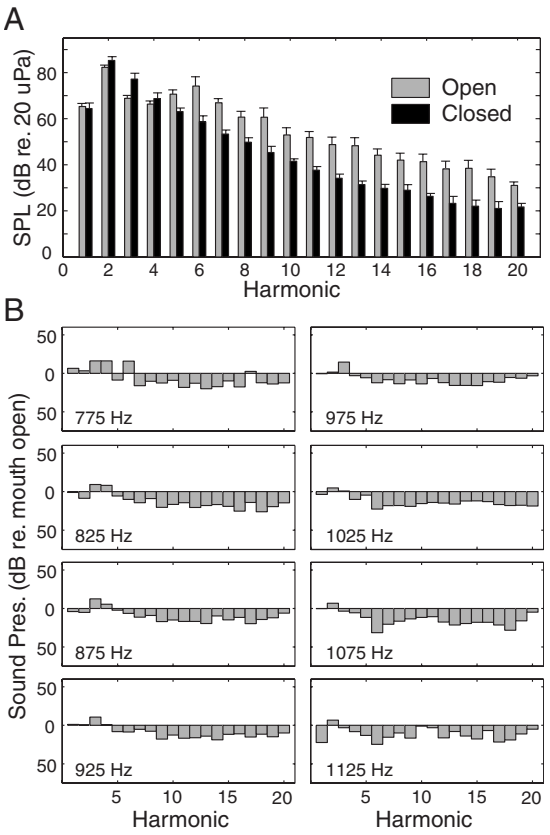


FIG. 10. Harmonic structure of artificial calls in *Hyla cinerea*. A. Pooled call spectral structure, showing how the amplitude in calls produced with the mouth open or closed is distributed in the first 20 harmonics. Error bar =standard error of the mean. B. Spectral structure of the amplitude level with the mouth closed, in relation to the mouth open. Calls grouped by fundamental frequency at intervals of 50 Hz.

open. In one of the three species, total call amplitude was higher when the mouth was closed. Artificial calls closely matched the fundamental frequency and harmonic structure of natural calls when the mouth was closed only. Opening the mouth or cutting the vocal sac open did not alter the fundamental frequency of the call, but dispersed the acoustic energy toward high frequency harmonics.

The results show that the passive calling apparatuses of the anurans in this study can produce sounds with a narrower frequency range and higher intensity when the mouth is closed than when the mouth is open.

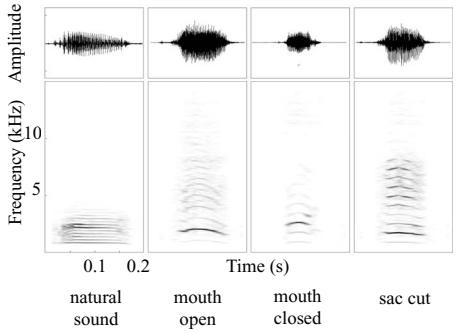


FIG. 11. Oscillogram and spectrogram of natural and artificial calls generated in three treatments of laryngeal activation in *Hyla cinerea*. The amplitude axis is not comparable among plots.

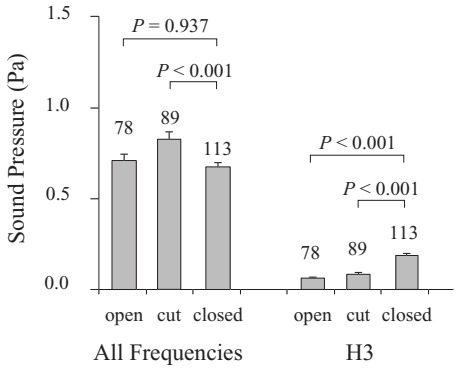


FIG. 12. Sound pressure of artificial calls in *Hyla cinerea*. "Open" refers to calls obtained with the mouth open, "closed" refers to the mouth closed with the vocal sac inflating, and "cut" refers to the mouth closed and the sac cut. Error bar = standard error of the mean.

A. Bandwidth

The narrowing in bandwidth with the mouth closed could be explained by alteration of the vibration patterns of the vocal folds, due to the increased impedance downstream from the larynx when the mouth is closed. Such effect should become more pronounced as the call progresses, because the buccal air pressure increases. It should generate a pattern of gradual change in distribution of energy among harmonics along the call. The increase in pressure in the mouth is exponential. The connection between the vocal sac and the mouth in these frogs stayed wide open during inflation. Buccal air pressure exhibits a markedly exponential relation with volume in all the three species, with very little increase in pressure during the first half of the inflation (ln(pressure)= −2.82+1.21∗ volume in *H. versicolor*, ln(pressure)=−2.97 +4.37∗ volume in *P. streckeri* and ln(pressure)=−2.90 +1.91∗ volume in *H. cinerea*, pressure in kPa and volume in ml, ln=natural logarithm; Gridi-Papp, in preparation). Most of the differences between open and closed mouth should have been evident in the second half of the calls, but the distribution of energy among harmonics within the duration of the artificial calls was rather constant (Figs. 5, 8, and 11).

Filtering by the frog's tissues when the mouth is closed seems to provide a more likely explanation for the narrowing of call bandwidth. This would be in agreement with the observations by Purgue (1995) that the transfer functions of the tissues that mostly radiate the energy of the calls match the acoustic structure of the calls. The vocal folds would produce a long series of harmonics, and the filtering properties of the radiating structures would determine the harmonic structure of the call in the environment.

B. Intensity

The increased intensity at the dominant harmonic when the mouth was closed is unlikely to be due to resonance in the buccal cavity. Previous studies on several species of frogs of different families failed to detect cavity resonance (Martin, 1972; Capranica and Moffat, 1983; Rand and Dudley, 1993). The concept is also unlikely because the volume of the cavity in the studied species exhibits extensive and constant change during the call.

The observed intensity peaks could be caused by resonance of the vocal sac tissues. This would corroborate the findings by Purgue (1995) when he connected an artificial sound source to euthanized frogs. The vocal sac of *Pseudacris regilla* and *Hyla gratiosa* showed increased resonance at the frequency that is emphasized in the call. The smaller intensity gain observed in this study at the dominant frequency of the natural call in *H. versicolor* and *H. cinerea* might be due to real differences in the calling apparatuses, or to methodological limitations. Purgue (1995) also found variation in vocal sac resonance among hylids. The vocal sac of *P. triseriata* produced no gain at the frequency that it transferred best, whereas *P. regilla* and *P. gratiosa* produced about 15 dB gain in relation to the artificial source in free field. The gain in amplitude could also be partly attributed to the increase in radiation surface of the vocal sac during its inflation. Such effect would be counteracted by the increase in buccal pressure at the end of the call, causing the middle of the call to exhibit the peak amplitude.

All the musculature was passive in the present experiments. Tension in the buccal musculature or the body wall might be required for proper resonance of the tissues.

C. Natural versus artificial calls

Two out of three species in this study produced artificial calls that matched the fundamental frequency and the harmonic structure of the natural calls. *Hyla cinerea* did not produce, passively, the same harmonic structure that it produces actively. The method of passive laryngeal activation by airflow is very simplistic and relies on a simple laryngeal structure that does not require muscular contraction for the onset of sound. This method seems to work well for some groups of frogs, like *Rana* (Paulsen, 1965) and *Bufo* (Martin, 1971) but not for others like the genus *Physalaemus* (Gridi-Papp, unpublished data). This study shows that even within the same genus (*Hyla*), there is relevant variation in the mechanism of sound production. Most frogs have four pairs of laryngeal muscles (Trewavas, 1933) and their function is currently not well understood, giving margin for many possible explanations for laryngeal control in animals like *H. cinerea* (Martin and Gans, 1972; Schmidt, 1973; Schneider, 1988).

D. Head and vocal sac versus body as radiators

In this study, the head and vocal sac radiated more sound than the body. Purgue (1995) found that in hylids the vocal sacs were responsible for a large amount of the total radiated sound. In male bullfrogs (*Rana catesbeiana*), the tympanic membranes are the major sound radiators in the head (Purgue, 1997), but in the treefrogs studied, the ears are relatively smaller than those of male bullfrogs.

The abdominal concretion formed by cannulation, in this study, reduced the ventral area of the trunk by up to 8% in the smallest specimens. Such reduction in radiation surface does not explain the results. Conducting the experiments with the ventral side of the animal up should not have been a relevant issue either, as the body of these frogs weighs a few grams only, and calling air pressure overcomes the effect of

gravity on the tissues. Proper inflation of the lungs could be verified visually in these treefrogs, as the shape of the trunk is mostly defined by the amount and position of the air in the lungs. The ventral side of the treefrog is probably more important as a radiator than the dorsal side, for not being surrounded by skeleton, besides the externum, and it was therefore left unimpeded.

The reduced radiation by the body might result from it being positioned upstream from the larynx and experiencing considerable airflow during phonation (Martin, 1971). The trunk also has a thicker tissue structure than the vocal sac, with the lungs being involved by two layers of strong oblique muscles that generate pressure for sound production and covered by a thick skin. Finally, the oblique muscles were fully relaxed in this study while they contract during live calling, possibly altering the radiation patterns of the trunk.

E. Biological relevance

The reduced frequency range obtained in this study for calls produced with the mouth closed matches the evidence observed in nature. While most anurans produce advertisement calls with the mouth and nares closed, distress calls are generally produced with the mouth wide open (Sazima, 1975; Hödl and Gollmann, 1986; Martins and Haddad, 1988; Kanamadi *et al.*, 1993; Souza and Haddad, 2003). Descriptions of distress calls are available for frog species of several families and most of these calls exhibit a wide range of harmonics that are not observed in the advertisement calls. The lack of data on intensity and laryngeal airflow in distress calls prevents further corroboration of the laboratory findings.

If advertisement calls produced with the mouth closed exhibit narrow bandwidth and increased intensity at the dominant frequency, they should stand out of the background noise better then if they were produced with the mouth open. Such gain in acoustic conspicuousness might be selectively advantageous for increasing the male's active space and improving its energetic efficiency at advertising (Prestwich *et al.*, 1989; Wells, 2001). Female acoustic preferences can also benefit males that produce intense and species-specific calls and facilitate distinction from heterospecifics (Gerhardt, 1981; Duellman and Pyles, 1993; Rand *et al.*, 1992; Pfennig, 1998; Gerhardt and Huber, 2002; Chek *et al.*, 2003).

In contrast with communication among conspecifics, the fact of being directed towards other species might explain why distress calls in frogs are generally produced with the mouth open (Sazima, 1975; Hödl and Gollmann, 1986; Martins and Haddad, 1988; Kanamadi *et al.*, 1993; Souza and Haddad, 2003). Such distress calls have the energy widely distributed across harmonics and have been suggested to have the role of startling the predator or attracting a secondary predator that might disturb the attack. A wide frequency spectrum could be beneficial for facilitating perception by a variety of potential predators with different hearing sensitivity ranges. As an alternative, distress calls could be produced with the mouth open to enhance duration or intensity. These calls are produced a single or a few times in a predation event. A single call produced with the mouth open permits exhalation of the whole pulmonary volume without limitation by the vocal sac, potentially resulting in a call with increased duration or same duration but increased airflow and intensity. Alarm calls are also produced infrequently and are supposed to alert conspecifics about the presence of a danger (Evans *et al.*, 1993). If anuran alarm calls are also produced with the mouth open, that will favor the sound intensity hypothesis over the spectrum width hypothesis, but the data currently available are too limited.

While producing advertisement calls with the mouth closed may result in an advantageous acoustic structure, other physiological, mechanical and behavioral factors could influence the maintenance of the behavior of shutting the mouth to call. By dispensing the buccal pump, calling with the mouth closed might be more energetically efficient (Bucher *et al.*, 1982; Dudley and Rand, 1991; Purgue, 1995; Jaramillo *et al.*, 1997), allow for faster lung reinflation and high call rates (Pauly *et al.*, 2006), add a visual component to the advertisement signal through the movement of the vocal sac (Narins *et al.*, 2003; Rosenthal *et al.*, 2004), and avoid desiccation by recirculating the same air after each call. A satisfactory explanation for the behavior of calling with the mouth closed will require the evaluation of each of the factors above while integrating aspects of mechanism, behavior and history.

ACKNOWLEDGMENTS

I am thankful to M. J. Ryan, C. Gans, D. Cannatella, D. Hillis, R. Dudley, and W. Wilczynski for advice and logistic support for the study; B. Borrell, E. Chen, A. Fowler, M. L. Garrison, C. O. Gridi-Papp, K. Heubel, E. M. Lemmon, E. S. Miller for field and lab assistance; Lexington Wildlife Management Area and Brackenridge Field Laboratories for logistic support; and CAPES – Brazil and NSF through Grant No. 99–81631 to D. C. Cannatella at the University of Texas for financial support. This study was conducted under Texas Parks and Wildlife permits SPR-0600-105 and the Animal Utilization Protocol number 01021501 of the Animal Resource Center of the University of Texas.

Bradbury, J. W., and Vehrencamp, S. (**1988**). *Principles of Animal Communication* (Sinauer Associates, Sunderland, Massachusetts).

Bucher, T. L., Ryan, M. J., and Bartholomew, G. A. (**1982**). "Oxygen consumption during resting, calling and nest building in the frog *Physalaemus pustulosus*," Physiol. Zool. **55**, 10–22.

Capranica, R. R., and Moffat, A. J. M. (**1983**). "Neurobehavioral correlates of sound communication in anurans," in *Advances in Vertebrate Neuroethology*, edited by J. P. Ewert, R. R. Capranica, and D. J. Ingle (Plenum, London) pp. 701–730.

Chek, A. A., Bogart, J. P., and Lougheed, S. C. (**2003**). "Mating signal partitioning in multi-species assemblages: A null model test using frogs," Ecol. Lett. **6**, 235–247.

Dudley, R., and Rand, A. S. (**1991**). "Sound production and vocal sac inflation in the túngara frog, *Physalaemus pustulosus* (Leptodactylidae)," Copeia **1991**, 460–470.

Duellman, W. E., and Pyles, R. A. (**1983**). "Acoustic resource partitioning in anuran communities," Copeia **1983**, 639–649.

Evans, C. S., Evans, L., and Marler, P. (**1993**). "On the meaning of alarm calls: Functional reference in an avian vocal system," Anim. Behav. **46**, 23–38.

Fletcher, N. H. (**1992**). *Acoustic Systems in Biology* (Oxford University Press, Oxford.).

Gans, C., and Pyles, R. (**1983**). "Narial closure in toads; which muscles?," Respir. Physiol. **53**, 215–223.
Gerhardt, H. C. (**1975**). "Sound pressure levels and radiation patterns of the vocalizations of some North American frogs and toads," J. Comp. Physiol. [A] **102**, 1–12.
Gerhardt, H. C. (**1981**). "Mating call recognition in the green treefrog (*Hyla cinerea*): Importance of two frequency bands as a function of sound pressure," J. Comp. Physiol. [A] **144**, 9–16.
Gerhardt, H. C., and Huber, F. (**2002**). *Acoustic Communication in Insects and Anurans* (University of Chicago Press, Chicago).
Hödl, W., and Gollmann, G. (**1986**). "Distress call of neotropical frogs," Amphib.-Reptil. **7**, 11–21.
Hoese, W. J., Podos, J., Boetticher, N. C., and Nowicki, S. (**2000**). "Vocal tract function in birdsong production: Experimental manipulation of beak movements," J. Exp. Biol. **203**, 1845–1855.
Jaramillo, C., Rand, A. S., Ibáñez, R., and Dudley, R. (**1997**). "Elastic structures in the vocalization apparatus of the túngara frog *Physalaemus pustulosus* (Leptodactylidae)," J. Morphol. **233**, 287–295.
Kanamadi, R. D., Schneider, H., Hiremath, C. R., and Jirankali, C. S. (**1993**). "Vocalization of the tree frog *Polypedates maculatus* (Rhacophoridae)," J. Biosci. **18**, 239–245.
Martin, W. F. (**1971**). "Mechanics of sound production in toads of the genus *Bufo*: passive elements," J. Exp. Zool. **176**, 273–294.
Martin, W. F. (**1972**). "Evolution of vocalization in the genus bufo," in *Evolution in the Genus Bufo*, edited by W. F. Blair (The University of Texas Press, Austin), pp. 279–309.
Martin, W. F., and Gans, C. (**1972**). "Muscular control of the vocal tract during release signaling in the toad *Bufo valliceps*," J. Morphol. **137**, 1–27.
Martins, M., and Haddad, C. F. B. (**1988**). "Vocalizations and reproductive behaviour in the smith frog, *Hyla faber* Wied Amphibia; Hylidae)," Amphib.-Reptil. **9**, 49–60.
McAlister, W. H. (**1959**). "The vocal structures and method of call production in the genus *Scaphiopus*," Tex. J. Sci. **2**, 60–77.
Narins, P. M., Hödl, W., and Grabul, D. S. (**2003**). "Bimodal signal requisite for agonistic behavior in a dart-poison frog, *Epipedobates femoralis*," Proc. Natl. Acad. Sci. U.S.A. **100**, 577–580.
Passmore, N. I. (**1981**). "Sound levels of mating calls of some African frogs," Herpetologica **37**, 166–171.
Paulsen, K. (**1965**). "Beitraege zur Anatomie und Physiologie des Froschkehlkopfes, mit besonderer Berucksichtigung der Stimmbildung" ("Contributions to the anatomy and physiology of the frog larynx, with special consideration of vocalization"), Z. Wiss. Zool. **172**, 1–16.
Pauly, G. B., Bernal, X. E., Rand, A. S., and Ryan, M. J. (**2006**). "The role of the vocal sac in increasing call rate in *Physalaemus pustulosus*," Physiol. Biochem. Zool. **79**, 708–719.
Pfennig, K. S. (**1998**). "The evolution of mate choice and the potential for conflict between species and mate-quality recognition," Proc. R. Soc. London, Ser. B **265**, 1743–1748.
Prestwich, K. N., Brugger, K. E., and Topping, M. (**1989**). "Energy and communication in three species of hylid frogs: Power input, power output, and efficiency," J. Exp. Biol. **144**, 53–80.
Purgue, A. P. (**1995**). "The sound broadcasting system of the bullfrog (*Rana catesbeiana*)," Ph.D. thesis, University of Utah.
Purgue, A. P. (**1997**). "Tympanic sound radiation in the bullfrog *Rana catesbeiana*," J. Comp. Physiol. [A] **181**, 438–445.
Rand, A. S., and Dudley, R. (**1993**). "Frogs in helium: The anuran vocal sac is not a cavity resonator," Physiol. Zool. **66**, 793–806.
Rand, A. S., Ryan, M. J., and Wilczynski, W. (**1992**). "Signal redundancy and receiver permissiveness in acoustic mate recognition by the túngara frog *Physalaemus pustulosus*," Am. Zool. **32**, 81–90.
Rosenthal, G. G., Rand, A. S., and Ryan, M. J. (**2004**). "The vocal sac as a visual cue in anuran communication: An experimental analysis using video playback," Anim. Behav. **68**, 55–58.
Sazima, I. (**1975**). "Distress call in newly metamorphosed smith frog, *Hyla faber Wied*," Herpetologica **31**, 471–472.
Schmidt, R. S. (**1973**). "Vocal cord mechanisms of release calling in the northern leopard frog," Copeia **1973**, 624–627.
Schneider, H. (**1988**). "Peripheral and central mechanisms of vocalization," in *The Evolution of the Amphibian Auditory System*, edited by B. Fritzsch, M. Ryan, W. Wilczynski, T. Hetherington, and W. Walkowiak (Wiley, New York), pp. 537–558.
Souza, M. B., and Haddad, C. F. B. (**2003**). "Redescription and reevaluation of the generic status of *Leptodactylus dantasi* (Amphibia, Anura, Leptodactylidae) and description of its unusual advertisement call," J. Herpetol. **37**, 490–497.
Suthers, R. A., Narins, P. M., Lin, W. Y., Schnitzler, H. U., Denzinger, A., Xu, C.-H., and Feng, A. (**2006**). "Voices of the dead: Complex nonlinear vocal signals from the larynx of an ultrasonic frog," J. Exp. Biol. **209**, 4984–4993.
Trewavas, E. (**1933**). "The hyoid and the larynx of the Anura," Philos. Trans. R. Soc. London, Ser. B **222**, 401–527.
Walkowiak, W. (**2006**). "Call production and neural basis of vocalization," in *Springer Handbook of Auditory Research Vol. (22) Hearing and Sound Communication in Amphibians*, edited by Peter Narins, Albert Feng, Arthur Popper, and Richard, R. Fay (Springer-Verlag, New York).
Wells, K. D. (**2001**). "The energetics of calling in frogs," in *Anuran Communication*, edited by M. J. Ryan (Smithsonian Institution Press, Washington).

Human listeners attend to size information in domestic dog growls

Anna M. Taylor,[a] David Reby, and Karen McComb
Department of Psychology, University of Sussex, Falmer, BN1 9QH United Kingdom

(Received 21 September 2007; revised 29 January 2008; accepted 17 February 2008)

The acoustic features of vocalizations have the potential to transmit information about the size of callers. Most acoustic studies have focused on intraspecific perceptual abilities, but here, the ability of humans to use growls to assess the size of adult domestic dogs was tested. In a first experiment, the formants of growls were shifted to create playback stimuli with different formant dispersions (Δf), simulating different vocal tract lengths within the natural range of variation. Mean fundamental frequency ($F0$) was left unchanged and treated as a covariate. In a second experiment, $F0$ was resynthesized and Δf was left unchanged. In both experiments Δf and $F0$ influenced how participants rated the size of stimuli. Lower formant and fundamental frequencies were rated as belonging to larger dogs. Crucially, when $F0$ was manipulated and Δf was natural, ratings were strongly correlated with the actual weight of the dogs, while when Δf was varied and $F0$ was natural, ratings were not related to the actual weight. Taken together, this suggests that participants relied more heavily on Δf, in accordance with the fact that formants are better predictors of body size than $F0$. © *2008 Acoustical Society of America.* [DOI: 10.1121/1.2896962]

PACS number(s): 43.80.Ka, 43.80.Lb, 43.71.Bp [JAS] Pages: 2903–2909

I. INTRODUCTION

Although originally developed for human speech, the source-filter model of sound production has now been applied to the study of vocal communication in many animal species (see Fitch, 2000 and Munhall and Byrne, 2007, for overviews). The source-filter model presumes that there are two independent mechanisms involved in vocal production. The source signal is first produced when air expelled from the lungs passes through the vocal folds in the larynx and sends them into periodic vibration at a rate known as the fundamental frequency ($F0$). The signal then passes through the vocal tract, which, acting as a narrowband filter, enhances those frequencies associated with the resonances of the vocal tract while attenuating all others (Titze, 1994; also see Fitch, 2000). The amplification of the resonant frequencies causes broad energy bands in the spectrum, which are known as formants (Fant, 1960). $F0$ is thus determined by the length, mass, and tension of the vocal folds, while the values and spacing of formants are determined by the length of the vocal tract, leading to a negative correlation between formant dispersion (hereafter referred to as Δf) and vocal tract length in many mammals (see Fitch, 1997).

Formants and fundamental frequency are thus independent components in the vocal spectrum. This is important for human speech, which as a multidimensional form of communication can convey meanings as well as indexical information such as age, sex, individual identity, or geographical origin (see Rendall *et al.*, 2005). It is also significant for other mammal vocalizations that may need to communicate identity, affective state, or physical characteristics (e.g., Fitch and Hauser, 2002; Seyfarth and Cheney, 2003a; 2003b; Vannoni and McElligot, 2006; Munhall and Byrne, 2007). Fundamental frequency, for example, has previously been linked to identity and emotional content in domestic dog barks (Yin, 2002; Yin and McCowan, 2004), while Δf has been linked to caller size because of its dependence on the vocal tract (Riede and Fitch, 1999). Indeed, anatomical constraints on the length of the vocal tract impose acoustic limits on formant dispersion, making formants an honest cue to size in many mammals (Fitch and Hauser, 2002; Reby and McComb, 2003a). In other words, larger animals produce lower and more closely spaced formants, whereas smaller animals produce higher, more widely spaced formants (macaques: Fitch, 1997; dogs: Riede and Fitch, 1999; red deer: Reby and McComb, 2003a; elephant seals: Sanvito *et al.*, 2007). Although there is some evidence for a correlation between vocal tract length and body size in humans (see Fitch and Giedd, 1999), the great flexibility of the human vocal tract generally means that Δf is a poor predictor of size in adult humans (e.g., González, 2004; Feinberg *et al.*, 2005; Rendall *et al.*, 2005).

Unlike the vocal tract, the vocal folds can develop independently of skeletal influences. As a result, correlations between $F0$ (which is a direct product of vocal fold length) and body size are generally weak or nonexistent in both humans and nonhuman mammals (Kunzel, 1989; McComb, 1991; Reby and McComb, 2003b; Rendall *et al.*, 2005). It should be noted, however, that when comparing individuals across age and sex, the vocal folds become a more reliable cue to body size. In those circumstances, associations between $F0$ and body size may be observed (Fischer *et al.*, 2002; Pfefferle and Fischer, 2006).

Many studies have now shown that animals naturally attend to formants in conspecific vocalizations (Sommers *et al.*, 1992; Fitch and Fritz, 2006; Charlton *et al.*, 2006) and that they are able to respond to size-related acoustic cues in a

[a]Author to whom correspondence should be addressed. Electronic mail: a.m.taylor@sussex.ac.uk

functionally significant way (Reby and McComb, 2003a; 2003b; Reby *et al.*, 2005; Charlton *et al.*, 2007). Furthermore, Ghazanfar *et al.* (2007) showed that rhesus monkeys were able to use formant cues to make accurate assessments of caller body size and age in conspecific vocalizations. Humans also attend to formants and formant-related parameters (e.g., Smith *et al.*, 2005); however, due to the greater flexibility of the human vocal tract, it is often difficult to assess the body size of adult humans using only formants (e.g., Collins, 2000; González, 2004; Feinberg *et al.*, 2005). It is also unclear whether listeners can assess size differences from Δf in the vocalizations of species other than their own. The domestic dog is an interesting candidate to investigate interspecific vocal communication, as its primary social companion is human rather than conspecific. Because of this distinct evolutionary background, most humans are likely to be exposed to dog vocalizations in their everyday life, and to thus have some degree of familiarity with these vocalizations.

To date there has been no attempt to investigate the intra- or interspecific perception of size information in dog vocalizations, despite it being a unique species in terms of the morphological variability found between breeds. No other has such a huge range of shapes and sizes (from under 2 kg to over 100 kg; see Sutter *et al.*, 2007). Although in a previous study we found little evidence of context information encoded in the acoustic features of growls (growls recorded in a playful and in an aggressive context were compared; unpublished data), size information is likely to be present (see Riede and Fitch, 1999). The harsh broadband nature of growls makes them an ideal vocalization to investigate the role of formants in the transmission of size-related information by domestic dogs.

For an interspecific approach it is important to understand how humans normally perceive formants and how we interpret size information in speech. Several studies have demonstrated that humans are actually surprisingly bad at judging speaker size, mainly because we appear to base our assessment on acoustic features that are only weakly correlated with size in adult humans (Collins, 2000; González, 2004; Feinberg *et al.*, 2005; Bruckert *et al.*, 2006). Collins (2000) showed that women incorrectly associated lower frequency parameters with masculine traits such as larger size and body hair. Similarly, Feinberg *et al.* (2005) found that manipulations of Δf and $F0$ influenced the perceived attractiveness of male voices, with lower frequencies being rated as more attractive and belonging to larger men. Formant dispersion is thus perceptually salient to humans and ratings of size appear to be relatively consistent across different trials and individuals (Feinberg *et al.*, 2005; Bruckert *et al.*, 2006); however, they do not correspond to reality due to the poor relationship between formant and fundamental frequencies and body side in adult humans.

In a study of interspecific size perception solely based on a vocalization, we first investigate the relationship between formant dispersion and fundamental frequency in dog growls and caller body size. The predicted relationship between Δf and body size has previously been confirmed by Riede and Fitch (1999); however, the relationship between fundamental frequency and body size has not yet been examined in domestic dogs. Previous research on other species (Fitch, 1997; Fischer *et al.*, 2002; Pfefferle and Fischer, 2006) suggests that this relationship will be very weak or even nonexistent. We then test the ability of humans to assess size information in dog growls with two psychoacoustic experiments that investigate on which acoustic parameters human listeners rely to attribute size to adult domestic dogs. In the first playback experiment, the formant dispersion of growls is modified but the fundamental frequency is left unchanged, whereas in the second playback experiment, fundamental frequency is modified and formant dispersion is left unchanged—this enables us to examine the independent effects of each of these acoustic features on size assessment. For the reasons previously discussed, it is expected that participants will assess the size of dogs using the same strategy as they use to assess human speaker size, relying on both formant dispersion and fundamental frequency.

II. METHODS

A. Dogs and recordings

The growls used in this study were recorded from 30 privately owned domestic dogs of 22 different breeds. The ages of the dogs ranged from 1 to 13 years; there were 13 females and 17 males, and all dogs except two (both Dobermanns) were neutered or sterilized. The dogs were recruited when their owners responded to a local advertisement and were recorded on their home territory in the presence of their owners between October 2005 and August 2006. The recordings were all made in the same context: Upon arrival at the house, the experimenter (A.M.T.) approached the dog while staring it in the eyes to elicit a defensive growling response (similar to the method used by Riede and Fitch, 1999). A Sennheiser MKH 416 directional microphone connected to a Marantz PMD670 digital audio recorder was used, with the microphone typically held at around one meter from the dog's head (although this varied a little as the dogs sometimes moved around). Recording levels were manually adjusted to avoid audio clipping. Finally, the dogs were weighed using PS250 veterinary floor scales.

B. Acoustic analyses

All audio manipulations and analyses were done with Praat acoustical analysis software, version 4.4.32 [by Boersma and Weenink (1996)]. The first high quality growl (defined as clearly audible with a well-defined beginning and ending and no background noise) from each dog was extracted in mono AIFF format with a 16 bit resolution and 44.1 kHz sampling rate. A Praat macro script, using the robust autocorrelation method described by Boersma (1993), was used to extract mean $F0$ from the whole duration of the signal, using a time step of 100 ms. The frequency range for the analysis was selected as 50–180 Hz. Two dogs in the present study were found to have a mean $F0$ outside the predicted range—both were Jack Russel terriers. Their mean $F0$ was thus separately extracted. Following Owren and Bernacki (1998), a second script relying on Linear Predictive Coding was used to measure formant frequencies in each

TABLE I. Biological and acoustic information collected for each dog.

Dog	Sex	Age (years)	Weight (kg)	Mean fundamental frequency (Hz)	Formant dispersion (Hz)
German shepherd	F	6	35.4	95	927
American cocker	M	3	12	148	1290
Basset hound	F	5	34.6	98	861
Cairn terrier	F	3.5	6.8	120	1285
Collie 1	M	3	18	117	944
Collie 2	F	2.5	12.5	130	1274
Dobermann 1	F	8	33	172	844
Dobermann 2	M	5	32	130	875
English cocker	F	2	5.8	127	1316
Flat-coated retriever	F	1	35	111	859
Jack Russell 1	F	6	4.2	204	1393
Jack Russell 2	M	7	6.8	193	1443
Jack Russell 3	M	2	8.5	114	1225
King Charles spaniel	M	4	8.3	189	1293
Labrador	M	10.5	26.5	124	1108
Lurcher 1	M	13	13.9	111	1143
Lurcher 2	M	2	17.6	134	993
Miniature dachshund	M	1	5	98	1433
Miniature schnauzer	F	2	6.6	185	1205
Old English sheepdog	M	12	35	110	948
Patterdale terrier	M	13	16	107	1186
Rhodesian ridgeback	M	6.5	25.1	178	871
Rottweiler	M	4	35.2	88	1143
Shi Tzu	M	8	7	119	1237
Springer spaniel 1	M	8	26.1	115	1153
Springer spaniel 2	F	1.5	20	149	1318
Staffordshire bullterrier 1	F	2	16.9	110	1435
Staffordshire bullterrier 2	F	6	17.7	138	1045
Staffordshire bullterrier 3	F	5	14	108	1291
Standard schnauzer	M	11	22.6	154	1049

growl. Where possible, five formants were measured; however, the number of formants varied from three to six. This is in line with previous observations in formant variations between different breeds of dogs (Riede and Fitch, 1999). Formant locations were also visually verified using a broadband spectrogram. Formant dispersion (Δf) was then computed using the linear regression method described in Reby and McComb (2003b). For each dog, there was thus a record of weight, mean $F0$, and Δf (see Table I for qualitative data).

C. Resynthesis

1. First playback experiment

Acoustic resyntheses were performed using pitch-synchronous overlap and add (PSOLA) based algorithms as coded into the "change gender" function in Praat. PSOLA algorithms enable signals to preserve their overall shape as target features are allometrically manipulated without affecting other acoustic parameters (see Goncharoff and Gries, 1998).

The durations of the stimuli were standardized to 2.8 s. Stimuli were never lengthened or shortened by more than 10% of their original duration to preserve the quality of the call. In addition, 1 s of silence was inserted before and after each stimulus. The use of PSOLA enables the manipulation of formants without changing $F0$, pitch envelope, amplitude contour, or temporal structure; so only the formant frequencies were resynthesized in the first experiment while the other parameters were left natural. Resynthesized growls with formant dispersions of 844 (simulating a vocal tract length of 20.7 cm), 995 (17.6 cm), 1146 (15.3 cm), 1294 (13.5 cm), and 1443 Hz (12.1 cm) were created; 844 and 1443 Hz were the smallest and largest Δf observed in our natural population—the resynthesized stimuli thus represented a wide range within the natural variation of dog growls. Figure 1 shows spectrograms of one of the resynthesized stimuli, in which the dark energy bands of the formants are clearly visible. It is notable that formants in dog growls sometimes show dynamic modulation as seen in Fig. 1, and the occurrence and function of these still require further investigation. The resynthesis failed for ten growls, which were removed from the study. In total there were thus 100 resynthesized stimuli, originating from 20 individuals. Finally, all stimuli were double checked to make sure that no other acoustic parameters had been altered and their amplitudes were normalized to 75 dB (± 5 dB).

2. Second playback experiment

PSOLA was also applied to change the mean $F0$ of the growls without altering the formants or any other acoustic parameters. The way PSOLA affects $F0$ is by applying a

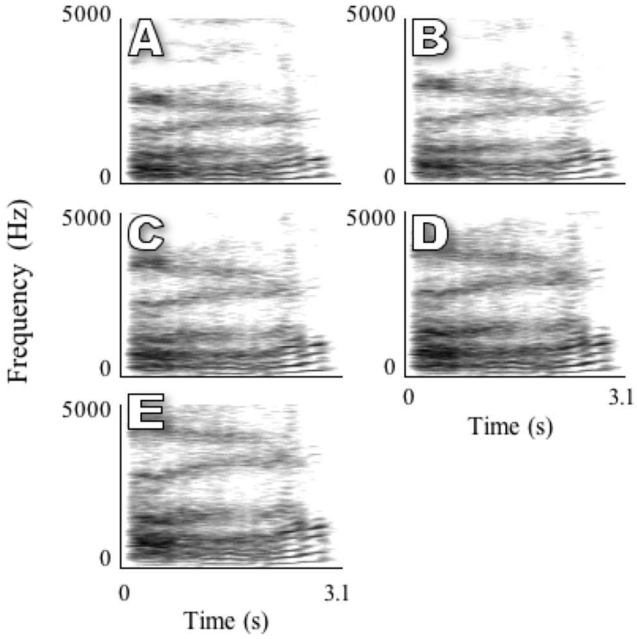


FIG. 1. Spectrograms (FFT window size=512 pts, window length=0.15 s) of the resynthesized stimuli created from the natural growl of a male Jack Russell terrier. The formant dispersions of the resynthesized stimuli are (A) 844, (B) 995, (C) 1146, (D) 1296, and (E) 1443 Hz. Note how the formants are shifted in comparison to the original signal, while all other acoustic parameters, including fundamental frequency, remain unchanged.

multiplicative transformation and thus controlling for relative frequency modulation in the signal (see Goncharoff and Gries, 1998). This preserves the natural shape of the signal. Each growl was resynthesized five times to give mean fundamental frequencies for our playback stimuli of 90, 119, 148, 177, and 200 Hz. The lowest and highest observed *F*0 in our sample were 90 and 200 Hz, respectively, so all the resynthesized stimuli were within the natural variation of dog growls. The resynthesis failed for 13 growls, which were removed from the study. In total there were thus 80 resynthesized stimuli originating from 17 individuals.

D. Playback protocol

1. First playback experiment

Thirty undergraduate students of the University of Sussex participated in the first playback experiment (25 females and five males; mean age=23 years). An MFC Praat experiment script running on an eMac (Apple Mac OS X, 1.4 GHz PowerPC G4) was used to run the playback. Participants were individually tested in the same lab. Testing was standardized by the use of the same location and equipment for all participants. They listened to each of the 100 stimuli in a randomized order through Koss Porta-pro headphones (frequency response: 15–25 000 Hz), and were then asked to rate each stimulus after the question "What is the size of this dog?" by clicking on a Likert scale from 1 (very small) to 7 (very big). The script automatically recorded the participant number, stimulus number, order of presentation, and size rating in a table file. Participants were then asked to state their previous dog experience from 1 (no experience) to 5 (regular contact with dogs). These data were transferred into an Excel file including the fundamental frequency of each stimulus (which varied between, but not within, dogs).

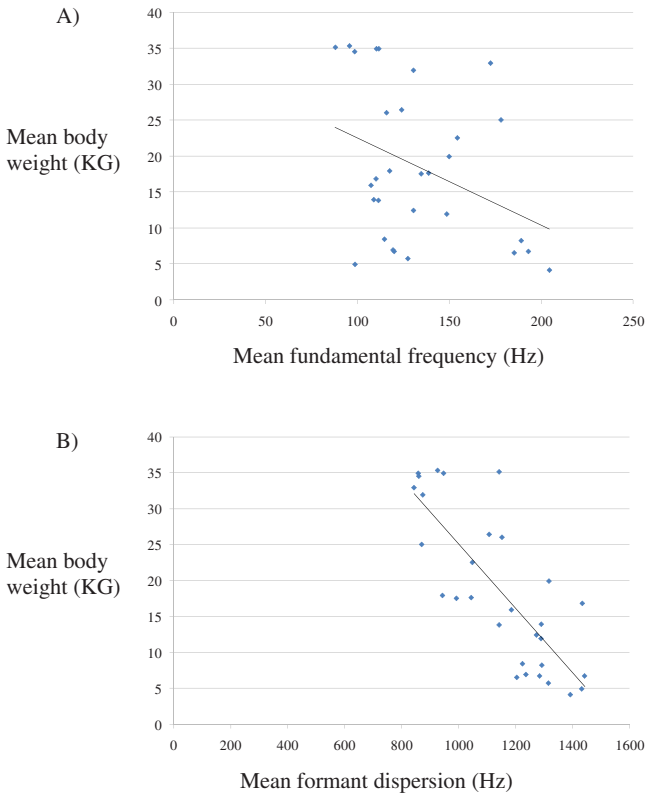


FIG. 2. (Color online) Single regression plots showing the relationship between the body weight of the dogs as a function of the two acoustic variables under study: mean (A) fundamental frequency and (B) formant dispersion.

2. Second playback experiment

An identical protocol was used for the second playback experiment using a different group of 22 participants (19 females and three males; mean age=21). In this second experiment, participants listened to the playback stimuli within which only the fundamental frequency was resynthesized.

III. RESULTS

A. Acoustic analyses

Table I shows qualitative information about the 30 dogs that were recorded for this study, as well as the mean *F*0 and Δf measured in their growls. As we were interested in finding out to what extent these acoustic measures were predictive of caller weight, a multiple regression model was built entering Δf and mean *F*0 as predictors. The model found that, together, Δf and *F*0 accounted for $R^2_{(adj)}=66.3\%$ of the variation in weight ($F_{(2,27)}=29.48$, $p<0.001$). This was a stronger fit than a single regression model based solely on formant dispersion ($R^2_{(adj)}=62.3\%$, $F_{(1,28)}=48.84$, $p<0.001$) or on *F*0 ($R^2_{(adj)}=9\%$, $F_{(1,28)}=32.24$, $p=0.05$), demonstrating that when studying a species with a large morphological range, fundamental frequency can be weakly and negatively associated with body size. Plots of the single regressions are shown in Fig. 2 with body weight shown as a function of

acoustic parameters.

B. First playback experiment: Effect of formant dispersion on size ratings

A linear mixed model using a scaled identity covariance structure was used to analyze the data. The order of stimulus presentation and subject identity were entered as random factors in the model, Δf as a fixed factor and $F0$ and previous dog experience as covariates. The model was run with a maximum likelihood estimation and identified a significant main effect of Δf ($F_{(4,2300)}=56.28$, $p<0.001$) on size ratings. Ratings were also influenced by mean $F0$ ($F_{(1,2300)}=1027.07$, $p<0.001$) and previous dog experience ($F_{(4,2300)}=32.24$, $p<0.001$). These results indicate that recordings resynthesized to simulate a longer vocal tract (closely spaced formants) were rated as belonging to larger dogs and recordings resynthesized to simulate a shorter vocal tract (more widely spaced formants) were rated as belonging to smaller dogs. Examination of the residuals showed a homogeneous distribution, confirming a good fit of the linear mixed model (see Venables and Ripley, 2002). There was no significant interaction effect between manipulated Δf and natural $F0$ on size ratings ($p=0.107$).

C. Second playback experiment: Effect of fundamental frequency resynthesis on size ratings

Using the same statistical protocol as above, we found significant effects of resynthesized mean $F0$ ($F_{(4,3740)}=73.25$, $p<0.001$) on size ratings. Ratings were also influenced by natural Δf ($F_{(1,3740)}=49.11$, $p<0.001$) and previous experience ($F_{(1,3740)}=4.04$, $p=0.044$). Again, there was no significant interaction effect between natural Δf and manipulated $F0$ on size ratings ($p=0.120$). These results are in accord with the findings of the first playback experiment and confirm that humans rely on both formant dispersion and $F0$ to judge the size of dogs. Reliance on these cues appears to be influenced by previous dog experience, and indeed participants with a higher level of experience appear to show more reliance on Δf than participants with a lower levels of experience (see Sec. D).

D. Accuracy of the ratings

An investigation of the association between the mean size rating given to each dog (across all stimuli) and the actual weight of subjects revealed no correlation between these factors in the first playback, where Δf was resynthesized but $F0$ was natural ($r=0.35$, $p=0.13$). In the second playback, however, where $F0$ was resynthesized but formants were natural, there was a significant correlation between ratings and actual weight ($r=0.72$, $p=0.001$). This result held true within every level of experience, as shown in Table II. Interestingly, the strongest correlation between ratings and weight was found within the highest level of experience ($r=0.73$, $p=0.001$), suggesting that greater previous experience of dogs increases the ability to correctly assess their size. This result indicates that although both Δf and $F0$ were used to assess the size of callers, participants relied more strongly on Δf and were thus not misled by manipulation of $F0$ in the second playback experiment.

TABLE II. Correlation coefficients between *participant size ratings* and *actual dog weight* within each level of previous dog experience.

Level of experience	First experiment		Second experiment	
	r	p	r	p
1[a]	…	…	…	…
2	0.29	0.22	0.67**	0.003
3	0.44*	0.05	0.64**	0.005
4	0.43	0.06	0.65**	0.004
5	0.38	0.10	0.73**	0.001

[a]No statistics were computed for this level of experience, as only one participant chose this option.

IV. DISCUSSION

The acoustic analyses confirmed that formant dispersion in domestic dog growls is strongly predictive of caller weight, and thus growls have the potential to provide an honest cue to body size. This is in line with previous analyses in domestic dogs (Riede and Fitch, 1999) and other mammals (e.g., Fitch, 1997, Reby and McComb, 2003a). In addition, there was a weak, but significant, association between fundamental frequency and caller weight. Although correlations between $F0$ and body size have typically been found to be unreliable in adult mammals within a given species (McComb, 1991; Fitch, 1997; Fitch and Hauser 2002; Reby and McComb, 2003a), there is evidence that $F0$ can be indicative of body size in certain circumstances, for example when considered across age and/or gender (Pfefferle and Fischer, 2006). The great morphological variability between different dog breeds is likely to have led to broad variation in the length and mass of the vocal folds, and as such it is not surprising that there should be a link between $F0$ and caller weight in our mixed-breed sample.

Both Δf and $F0$ thus have the potential to convey body size in dogs, and in fact the results of our playback experiments showed that both these parameters had a significant effect on size ratings by participants. Stimuli resynthesized to simulate dogs with a longer vocal tract (closely spaced formants) were rated as larger than stimuli resynthesized to simulate dogs with a shorter vocal tract (widely spaced formants). Likewise, stimuli resynthesized to have a lower $F0$ were rated as larger than stimuli resynthesized to have a higher $F0$. The use of both Δf and $F0$ to make size assessments is not surprising, for it is already known that humans rely on both to judge speaker size within their own species. Because neither Δf nor $F0$ are reliably indicative of body size in adult humans (Kunzel, 1989; van Dommelen, 1993; van Dommelen and Moxness, 1995), this means that speaker size assessments are generally inaccurate (Collins, 2000; González, 2004; Feinberg *et al.*, 2005).

Two plausible theories have been proposed for why human size assessments are so imprecise. First, the $F0$ of human speech is determined by the amount of testosterone present during puberty, at which point the larynx descends

into its mature position and vocal fold length is established (Titze, 1994); this means that *F*0 is to some extent linked to age (mature versus immature). In addition, because of differences in male and female puberty, *F*0 is also a sexually dimorphic trait in humans. The *F*0 of adult males is thus approximately half that of adult females (Huber *et al.*, 1999). Developmental changes in *F*0 (within call types) have also been observed in some nonhuman animals such as red deer, where subadult stags have a higher *F*0 than adult stags (Fitch and Reby, 2001; Reby and McComb, 2003b). The perceived association between *F*0 and body size may thus stem from an overgeneralization of the existing association across age and sex (see Collins, 2000, and Feinberg *et al.*, 2005 for comprehensive discussions). Another possible reason for the inaccuracy of human size assessment could stem from our evolutionary history. *F*0 may have originally been a salient cue to maturity with formant cues providing additional information about the size of the mature male. Attendance to both *F*0 and Δf would thus have provided an evolutionary advantage before the development of the flexible vocal tract seen in modern humans (Collins, 2000). The overgeneralization and evolutionary advantage hypotheses are not mutually exclusive and may both have contributed to how humans assess speaker size, although further research into size perception mechanisms in humans will be necessary to determine which theory carries more weight.

We found no interaction effect of Δf and *F*0 on the ratings (in our playback protocol each set of participants was exposed to either resynthesized formants with natural *F*0 or resynthesized *F*0 with natural formants; a future study could investigate how formant dispersion and *F*0 affect size perception when both variables are resynthesized). Similarly, when assessing female mate preference based on red deer stag roars, researchers found no interaction effect when Δf and *F*0 were simultaneously varied (Charlton *et al.*, 2008). Red deer hinds, however, unlike humans, do not appear to use *F*0 for size estimation (Charlton *et al.*, 2006; 2007, McComb, 1991).

From our results, it is clear that participants used the same strategy to rate dog size as they use to rate the size of human speakers. Since both Δf and *F*0 are to some degree related to size across different breeds of dogs, it follows that reliance on both cues is justified when assessing the size of dogs. Formant dispersion was found to provide the strongest cue to size, as supported by the finding that size ratings from the second playback experiment were correlated with the actual weight of subjects. In this experiment, *F*0 was resynthesized but Δf was left unchanged, so it seems that participants were able to extract accurate size cues from the natural Δf without being misled by the resynthesized *F*0. In contrast the ratings of the first playback experiment (resynthesized Δf but unchanged *F*0) were not correlated with actual weights.

Overall, this shows that human listeners are able to accurately assess the size of domestic dogs, based on vocal signals alone. It also raises the question as to what (if any) significance human listeners attribute to *F*0. While there do not appear to be any acoustic differences between play growls and aggressive growls, it is possible that humans might perceive vocalizations with a lower *F*0 as more aggressive, in the same way that they perceived human speech with a lower *F*0 as more masculine in Collins' (2000) experiments. In addition, an effect of previous dog experience was found in both playback experiments—from this we propose that dog owners become more accurate at judging size as exposure to dogs teaches them not to over-rely on *F*0. Indeed, in the second experiment, the size ratings of the participants with the most previous dog experience were also the closest to reality, indicating that those participants were most confident about basing their ratings on the natural Δf and were less confused by the resynthesized pitch (see Table II).

This is the first evidence of interspecific size assessment based on vocal signals alone and suggests that fundamental acoustic principles that are common to mammals are relied on to make size assessments. This could have important evolutionary implications in terms of antipredator and/or prey selection strategies, as it would mean that signaling relationships are not confined to one species, and thus, as in the case of dogs and humans, interspecific size assessments based on acoustic signals alone can provide important information for listeners. Our findings also suggest, however, that humans with little experience of dogs may to some extent be vulnerable to manipulation by dog growls. Within a certain anatomical range, smaller dogs may be able to partly exaggerate their perceived size (or aggressiveness) by means of a lower *F*0. Capitalization on a propensity to over-relate *F*0 to body size becomes possible if smaller dogs are able to produce vocalizations with a lower *F*0 than would normally be expected for their size. Furthermore, it is also worth considering that a certain amount of vocal plasticity is anatomically possible in domestic dogs, who may be able to lengthen their vocal tracts by lowering the larynx to a small degree (see Fitch, 2000 for cine-radiographic evidence of vocal plasticity in several mammal species including the domestic dog). It is, however, not currently known whether dogs are able to use this potential to manipulate the acoustic features of their vocalizations.

In summary, human listeners used both Δf and mean *F*0 to assess the size of domestic dogs. As both of these acoustic parameters are reliably linked to caller weight, it follows that humans are able to accurately assess size in dogs by listening to their growls. Δf provided the more salient cue for size assessment; this was reflected by the fact that when *F*0 but not Δf was resynthesized, participants were still able to use the natural Δf to rate size and were not fooled by the resynthesized *F*0. Furthermore, experience played a role in both playbacks, and we suggest that the most plausible explanation for this is that dog owners learn by exposure not to over-rely on *F*0. People with a high level of previous dog experience might thus learn to more strongly focus on Δf than people who are less familiar with dogs (who may thus be more likely to over-rely on *F*0). Although learning may to some extent influence size assessment, this study nevertheless showed that humans were able to accurately rate the size of another species based solely on a vocal signal. Future research will reveal whether this ability exists in other interspecific signaling relationships or whether it is linked to the close evolutionary history between humans and dogs.

ACKNOWLEDGMENTS

Many thanks go to the many dog owners who offered access to their companions for recordings and observation and to the students of the University of Sussex who participated in the psychoacoustic experiments. Thanks also to Ben Charlton for comments on an earlier manuscript of this paper. Funding for this research was provided by a B.B.S.R.C. studentship to the primary investigator (A.M.T.).

Boersma, P. (**1993**). "Accurate short-term analysis of the fundamental frequency and the harmonics-to-noise ratio in a sampled sound," Proc. Inst. Phonetic Sci. Univ. Amsterdam **17**, 97–110.

Boersma, P., and Weenink, D. (**1996**). "Praat: A system for doing phonetics by computer (version 4.4.32)," Computer software, downloaded from http://www.praat.org/.

Bruckert, L., Liénard, J.-S., Lacroix, A., Kreutzer, M., and Leboucher, G. (**2006**). "Women use voice parameters to assess men's characteristics," Proc. R. Soc. London, Ser. B **273**, 83–89.

Charlton, B., Reby, D., and McComb, K. (**2006**). "Female perception of size-related formant shifts in red deer," Anim. Behav. **74**, 707–714.

Charlton, B., Reby, D., and McComb, K. (**2007**). "Female red deer prefer the roars of larger males," Cell. Mol. Biol. Lett. **3**, 382–385.

Charlton, B., Reby, D., and McComb, K. (**2008**). "Effect of combined source (F0) and filter (formant) variation on red deer hind responses to male roars," J. Acoust. Soc. Am. **123**, XXX.

Collins, S. A. (**2000**). "Men's voices and woman's choices," Anim. Behav. **60**, 773–780.

Fant, G. (**1960**). *Acoustic Theory of Speech Production* (Mouton, The Hague, The Netherlands).

Feinberg, D. R., Jones, B. C., Little, A. C., Burt, D. M., and Perrett, D. I. (**2005**). "Manipulations of fundamental and formant frequencies influence the attractiveness of human male voices," Anim. Behav. **69**, 561–568.

Fischer, J., Hammerschmidt, K., Cheney, D. L., and Seyfarth, R. M. (**2002**). "Acoustic features of male baboon loud calls: Influences of context, age and individuality," J. Acoust. Soc. Am. **111**, 1465–1474.

Fitch, W. T. (**1997**). "Vocal tract length and formant frequency dispersion correlate with body size in rhesus macaques," J. Acoust. Soc. Am. **102**, 1213–1222.

Fitch, W. T. (**2000**). "The phonetic potential of nonhuman vocal tracts: Comparative cineradiographic observations of vocalizing animals," Phonetica **57**, 205–218.

Fitch, W. T., and Fritz, J. B. (**2006**). "Rhesus macaques spontaneously perceive formants in conspecific vocalizations," J. Acoust. Soc. Am. **120**, 2132–2141.

Fitch, W. T., and Giedd, J. (**1999**). "Morphology and development of the human vocal tract: A study using magnetic resonance imaging," J. Acoust. Soc. Am. **106**, 1511–1522.

Fitch, W. T., and Hauser, M. D. (**2002**). "Unpacking 'honesty:' vertebrate vocal production and the evolution of acoustic signals," in *Acoustic Communication*, edited by A. M. Simmons, R. R. Fay, and A. N. Popper (Springer-Verlag, New York), pp. 65–137.

Fitch, W. T., and Reby, D. (**2001**). "The descended larynx is not uniquely human," Proc. R. Soc. London, Ser. B **268**, 1669–1675.

Ghazanfar, A. A., Turesson, H. K., Maier, J. X., van Dinther, R., Patterson, R. D., and Logothetis, N. H. (**2007**). "Vocal tract resonances as indexical cues in the rhesus monkeys," Curr. Biol. **17**, 425–430.

Goncharoff, V., and Gries, P. (**1998**). "An algorithm for accurately marking pitch pulses in speech signals," *Proceedings of the International Conference on Signal and Image Processing 1998*. Retrieved from http://ieeexplore.ieee.org/iel5/9711/30650/01415093.pdf on 08/27/2007.

González, J. (**2004**). "Formant frequencies and body size of speaker: A weak relationship in adult humans," J. Phonetics **32**, 277–287.

Huber, J. E., Stathopoulos, E. T., Curione, G. M., Ash, T. A., and Johnson, K. (**1999**). "Formants of children, women and man: The effects of vocal intensity variation," J. Acoust. Soc. Am. **106**, 1532–1542.

Kunzel, H. (**1989**). "How well does average fundamental frequency correlate with speaker height and weight?," Phonetica **46**, 117–125.

McComb, K. E. (**1991**). "Female choice for high roaring rates in red deer, *Cervus elaphus*," Anim. Behav. **41**, 79–88.

Munhall, K. G., and Byrne, S. K. (**2007**). "Animal communication: Big talkers and small talk," Curr. Biol. **17**, 247–249.

Owren, M. J., and Bernacki, R. H. (**1998**) "Applying Linear Predictive Coding (LPC) to frequency-spectrum analysis of animal acoustic signals," in *Animal Acoustic Communication*, edited by S. L. Hopp, M. J. Owren, and C. S. Evans, pp. 299–346.

Pfefferle, D., and Fischer, J. (**2006**). "Sounds and size: Identification of acoustic variables that reflect body size in hamadryas baboons, *Papio hamadryas*," Anim. Behav. **72**, 43–51.

Reby, D., and McComb, K. (**2003a**). "Anatomical constraints generate honesty: Acoustic cues to age and weight in the roars of red deer stags," Anim. Behav. **65**, 519–530.

Reby, D., and McComb, K. (**2003b**). "Vocal communication and reproduction in deer," Adv. Stud. Behav. **33**, 231–264.

Reby, D., McComb, K., Cargnelutti, B., Darwin, C., Fitch, W. T., and Clutton-Brock, T. (**2005**). "Red deer stags use formants as assessment cues during intrasexual agonistic interactions," Proc. R. Soc. London, Ser. B **272**, 941–947.

Rendall, D., Kollias, S., and Ney, C., and Lloyd, P. (**2005**). "Pitch (F0) and formant profiles of human vowels and vowel-like baboon grunts: The role of vocalizer body size and voice-acoustic allometry," J. Acoust. Soc. Am. **117**, 944–955.

Riede, T., and Fitch, T. (**1999**). "Vocal tract length and acoustics of vocalization in the domestic dog (Canis familiaris)," J. Exp. Biol. **202**, 2859–2867.

Sanvito, S., Galimberti, F., and Miller, E. H. (**2007**). "Vocal signalling of male southern elephant seals is honest but imprecise," Anim. Behav. **73**, 287–299.

Seyfarth, R. M., and Cheney, D. L. (**2003a**). "Meaning and emotion in animal vocalizations," Ann. N.Y. Acad. Sci. **1000**, 32–55.

Seyfarth, R. M., and Cheney, D. L. (**2003b**). "Signalers and receivers in animal communication," Annu. Rev. Psychol. **54**, 145–173.

Smith, D. R. R., Patterson, R. D., Turner, R., Kawahara, H., and Irino, T. (**2005**). "The processing and perception of size information in speech sounds," J. Acoust. Soc. Am. **117**, 305–318.

Sommers, M. S., Moody, D. B., Prosen, C. A., and Stebbins, W. C. (**1992**). "Formant frequency discrimination by Japanese macaques (*Macaca fuscata*)," J. Acoust. Soc. Am. **91**, 3499–3510.

Sutter, N. B., Bustamante, C. D., Chase, K., Gray, M. M., Zhao, K., Zhu, L., Padhukasahasram, B., Karlins, E., Davis, S., Jones, P. G., Quignon, P., Johnson, G. S., Parker, H. G., Fretwell, N., Mosher, D. S., Lawler, D. F., Satyaraj, E., Nordborg, M., Lark, K. G., Wayne, R. K., and Ostrander, E. A. (**2007**). "A single IGF1 allele is a major determinant of small size in dogs," Science **316**, 112–115.

Titze, I. R. (**1994**). *Principles of Vocal Production* (Prentice–Hall, Englewood Cliffs, N.J.).

van Dommelen, W. A. (**1993**). "Speaker height and weight identification: Reevaluation of some old data," J. Phonetics **21**, 337–341.

van Dommelen, W. A., and Moxness, B. H. (**1995**). "Acoustic parameters in speaker height and weight identification: Sex-specific behaviour," Lang Speech **38**, 267–287.

Vannoni, E., and McElligot, A. G. (**2006**). "Individual acoustic variation in fallow deer (*Dama dama*), Common and harsh groans: A source-filter theory perspective," Ethology **113**, 223–234.

Venables, W. N., and Ripley, B. D. (**2002**). *Modern Applied Statistics with S*, 2nd ed. (Springer-Verlag, New York).

Yin, S. (**2002**). "A new perspective on barking in dogs (*Canis familiaris*)," J. Comp., Psych. **116**, 189–193.

Yin, S., and McCowan, B. (**2004**). "Barking in domestic dogs: Context specificity and individual identification," Anim. Behav. **68**, 343–355.

Carrier-dependent temporal processing in an auditory interneuron

Patrick Sabourin, Heather Gottlieb, and Gerald S. Pollack[a)]
Department of Biology, McGill University, Montréal, Québec, Canada H3A1B1

(Received 6 September 2007; revised 24 January 2008; accepted 17 February 2008)

Signal processing in the auditory interneuron Omega Neuron 1 (ON1) of the cricket *Teleogryllus oceanicus* was compared at high- and low-carrier frequencies in three different experimental paradigms. First, integration time, which corresponds to the time it takes for a neuron to reach threshold when stimulated at the minimum effective intensity, was found to be significantly shorter at high-carrier frequency than at low-carrier frequency. Second, phase locking to sinusoidally amplitude modulated signals was more efficient at high frequency, especially at high modulation rates and low modulation depths. Finally, we examined the efficiency with which ON1 detects gaps in a constant tone. As reflected by the decrease in firing rate in the vicinity of the gap, ON1 is better at detecting gaps at low-carrier frequency. Following a gap, firing rate increases beyond the pre-gap level. This "rebound" phenomenon is similar for low- and high-carrier frequencies.
© *2008 Acoustical Society of America.* [DOI: 10.1121/1.2897025]

PACS number(s): 43.80.Lb [JAS] Pages: 2910–2917

I. INTRODUCTION

A hallmark of auditory systems is the ability to encode temporal features of acoustic stimuli. Such features carry behaviorally relevant information to the signal recipients, including, for a number of animals, the species and/or individual identity of the signaler (e.g., Gerhardt and Huber, 2002) and, for humans, the information content of speech (Shannon *et al.*, 1995). Among the methods used to characterize auditory temporal processing are measurements of integration time (an indicator of the time over which input can be accumulated), of the detection of gaps in an ongoing stimulus (presumed to reflect the rate at which excitatory input dissipates) and of phase locking to periodic stimuli (which will be affected by both of the temporal characteristics described above). In this paper we apply these methods to study temporal processing in the auditory system of crickets.

At least two classes of acoustic signals are behaviorally important for crickets: Intraspecific signals (songs) which serve to attract mates, to elicit copulation, and to repel rivals; and echolocation sounds emitted by insectivorous bats. Conspecific songs of *Teleogryllus oceanicus* are emitted with carrier frequency around 4.5 kHz, and consist of brief pulses repeated at stereotypic intervals (from 6.8 to 22.8 Hz for calling songs, Walker and Cade, 2003). Echolocating bats that prey on flying insects emit trains of ultrasonic (up to 100 kHz) pulses at highly variable rates, ranging from a few Hz during target search up to 200 Hz during pursuit (Griffin *et al.*, 1960).

Many neurons in the first stages of auditory processing are specialized for processing a specific type of sound. For instance, an auditory receptor's threshold is minimal at either low (around 4.5 kHz), mid (around 10 kHz), or ultrasonic frequency (above 18 kHz; Imaizumi and Pollack, 1999). As another example, Ascending Neuron 2 (AN2), a neuron involved in the bat avoidance response, is most sensitive to high-frequency sounds (Moiseff and Hoy, 1983).

Other neurons, such as the Omega Neuron 1 (ON1), are implicated in both types of sound processing and thus face the problem of having to process sounds with highly variable temporal structures. In ON1, this problem is overcome through distinct temporal filtering characteristics for low- and high-carrier frequencies. Marsat and Pollack (2004) showed that the information content of ON1 response to stimuli with randomly varying amplitude is adapted to the specific temporal characteristics of signals with different carrier frequencies. For stimuli with low, cricket-like carrier frequency, ON1 exhibits low-pass temporal filtering, which closely corresponds to the narrow range of temporal features of cricket songs, whereas for stimuli with high carrier frequency (which characterizes bat sounds), ON1 is more wideband, corresponding to the broad range of temporal components of bat echolocation sounds.

In the present paper, we extend the work of Marsat and Pollack (2004) by examining whether carrier frequency affects integration time of ON1, its ability to detect gaps, and its ability to phase lock to a periodic stimulus.

II. MATERIALS AND METHODS

A. Electrophysiology

Teleogryllus oceanicus were reared in the laboratory. Virgin females were used for experiments 10–20 days after the final molt. They were anesthetized by chilling and mounted on a support ventral side uppermost. The prothoracic ganglion was exposed by ventral dissection, supported on a metal platform, and bathed in physiological saline (Strausfeld *et al.*, 1983). The cricket's front legs (which bear the ears) were held flexed against the pronotum in a position similar to that assumed during flight.

[a)]Author to whom correspondence should be addressed. Electronic mail: gerald.pollack@mcgill.ca

 0001-4966/2008/123(5)/2910/8/$23.00 © 2008 Acoustical Society of America

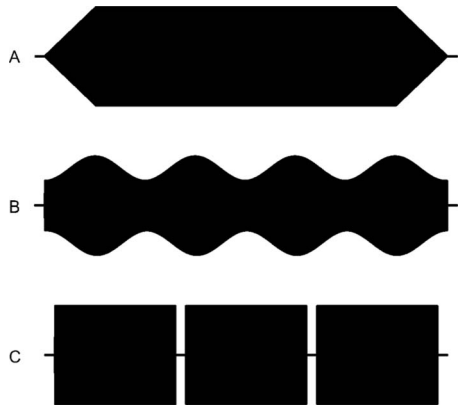


FIG. 1. Auditory stimuli presented in each of the three experiments. (A) Pulse used in the energy integration experiment. (B) SAM tone used in phase-locking experiment. (C) Gapped tone used in the gap detection experiment.

ON1 was extracellularly recorded from its soma-contralateral processes in the prothoracic ganglion, using blunt glass microelectrodes filled with 1 M NaCl or KCL (resistance, 5–10 MΩ). ON1 can be identified in this recording configuration by its preference for electrode-contralateral stimuli, as well as its greater sensitivity, but longer latency, to 4.5 kHz stimuli compared with ultrasound stimuli (Faulkes and Pollack, 2000).

B. Stimuli

Stimuli were generated via a National Instruments (Austin, TX) analog-to-digital/digital-to-analog board with 12 bits of resolution, at a sampling rate of 100 kHz. Sound was broadcast from a loudspeaker situated to the cricket's left or right, perpendicular to the longitudinal axis. Sound level was adjusted with a programmable attenuator (Mike Walsh Electronics) and calibrated using Bruël and Kjaer (Naerum, Denmark) instruments (4135 microphone; 2610 sound-level meter).

Three types of stimuli were presented in three different experiments: Pulses, sinusoidally amplitude modulated (SAMs) and constant tones interrupted by gaps (see Fig. 1).

1. Sound pulses

Pulses had a carrier frequency of either 5 or 30 kHz and duration ranging from 1 to 200 ms, including 0.2 ms rise and fall ramps and a constant-amplitude plateau [see Fig. 1(A)]. Note that 5 kHz was used as the low carrier frequency (instead of 4.5 kHz, which is the conspecific carrier frequency) to ensure that each pulse began and ended with the carrier sine at phase 0 (i.e., there was an integer number of carrier cycles within a pulse), thus preventing discontinuities.

2. SAM stimuli

SAMs were produced by modulating a constant tone with a sinusoidal envelope as shown in Fig. 1(B). The amplitude modulation (AM) rate was defined as the frequency of the modulating sine (10, 25, 50, 100, or 150 Hz) and the modulation depth (MD) as 100% minus the amplitude ratio (in percentage) between a trough and a peak of the signal (0, 2, 4, 6, 10, or 20%). SAMs were generated with a carrier frequency of 4.5 or 30 kHz at 15 dB above threshold for a total of 52 different signals (0 MD is actually a constant tone).

3. Interrupted tones

Gaps (segments of zero signal amplitude) with duration 0, 1, 2, 5, 10, or 20 ms were inserted within a constant tone (5 or 30 kHz) every 0.5 s [see Fig. 1(C)]. Each signal lasted 20 s (i.e., includes 38 gaps) and was played at 10, 20, or 30 dB above auditory threshold (for a total of 36 different stimuli).

C. Analysis

1. Integration time

The analysis is based on an energy integration paradigm as described by Plomp and Bouman (1959). The neuron under study is considered to be a leaky integrator that accumulates energy until it reaches firing threshold. Using this model, it is possible to estimate the "integration time"—the time it takes to reach threshold—at a given intensity by evaluating τ in the following formula:

$$Th_{\text{rel to }\infty} = -10\log(1 - e^{-t/\tau}), \tag{1}$$

where $Th_{\text{rel to }\infty}$ is the threshold of a neuron relative to its auditory threshold when stimulated with a pulse of infinite duration, t is the duration of the pulse and τ is the integration time. For very long pulses ($t \gg \tau$), the relative threshold settles at 0 dB whereas it approaches infinity for infinitely short pulses (that is infinite energy is needed to reach threshold). In practice, Th_{∞} was defined as the minimum auditory threshold measured during an experiment, which occurred at relatively long pulse durations (mean: 89.8 ± 43.6 ms for low frequency, 63.8 ± 47.6 ms for high frequency).

The parameter τ was found for each neuron by fitting the relative threshold data to Eq. (1) using a nonlinear least squares method (MATLAB curve-fitting toolbox).

2. Phase locking to SAM stimuli

Responses to SAMs were evaluated using standard vector strength analysis (Goldberg and Brown, 1969). The first three seconds of the response were discarded to avoid the confounding effects of adaptation, and the synchronization coefficient was calculated from the following formula:

$$r = \frac{\sqrt{(\Sigma_1^n \cos\theta_i)^2 + (\Sigma_1^n \sin\theta_i)^2}}{n}, \tag{2}$$

where θ_i is the phase of the ith spike (spike timing was determined with 0.5 ms resolution) with respect to the stimulus envelope and n is the total number of spikes. One-tailed significance of the synchronization coefficient was assessed using Rayleigh's Z statistic (Batschelet, 1981) computed from the following formula:

$$\text{Rayleigh's } Z = nr^2, \tag{3}$$

where n and r are defined as in Eq. (2). Significance level was set at $p=0.001$ ($Z>6.9$ for $n=\infty$, which would be the

most conservative criterion) to limit type I errors.

3. Gap detection

Responses to gap stimuli were analyzed by inspecting firing rate around the gap. First, spike trains were converted to firing rate by setting the value at each time point as the inverse of the interspike interval from the previous to the next spike. The firing rate at the point where a spike occurs was set as the average of the previous and the next firing-rate values. The firing-rate signal was then low-pass filtered (cutoff frequency=1 kHz) to remove high-frequency noise. Although filtering slightly affected the magnitude of gap-induced decreases in firing rate this was offset by the benefits of noise filtering. The firing rates from 100 ms before onset to 100 ms after offset of each gap were then averaged over all gaps. The maximum and minimum mean firing rates from the onset of the gap to 100 ms after the end of the gap were recorded and the baseline (average firing rate for 100 ms preceding the onset of gap) subtracted to yield the maximum increase and decrease in firing rate around gaps. This procedure necessarily results in nonzero baselines (i.e., the maximum value of a data set minus the mean will always give a positive value). To correct for this, a bootstrapping method was used. A new spike train was constructed by shuffling the order of interspike intervals of the original response, thus obliterating any changes in firing rate that are time locked to the gaps. The maximum increase and decrease in firing rate was then computed as described above. This procedure was repeated 1000 times in order to obtain a distribution of values. The maximum increase and decrease in firing rate measured for the actual response were then corrected by subtracting the mean of the corresponding distribution for shuffled spike trains. Equations (4) and (5) below summarize the calculation

$$\Delta fr_{\text{increase}} = (fr_{\max} - fr_{\text{mean}}) - mean(fr_{\text{maxdist}} - fr_{\text{meandist}}), \tag{4}$$

$$\Delta fr_{\text{decrease}} = (fr_{\min} - fr_{\text{mean}}) - mean(fr_{\text{mindist}} - fr_{\text{meandist}}), \tag{5}$$

where $fr_{\max}$ and $fr_{\min}$ are the maximum and minimum firing rates obtained from the original spike train, fr_{maxdist} and fr_{mindist} are the distributions of maximum and minimum firing rates obtained from the shuffled spike trains, and fr_{mean} and fr_{meandist} are the average firing rates over the 100 ms preceding the gaps.

To determine whether a neuron had detected the gaps, the ranks of $(fr_{\max}-fr_{\text{mean}})$ or $(fr_{\min}-fr_{\text{mean}})$ in their respective distributions (derived from the shuffled spike trains) were converted to p values by dividing by 1000. The value of $p=0.001$ was set as the threshold for significant detection (i.e., none of the 1000 randomly generated values exceeded the original value).

Data analysis, including statistical tests, was done using MATLAB (Rel. 2006a, The Mathworks) and R for Windows (www.r-project.org).

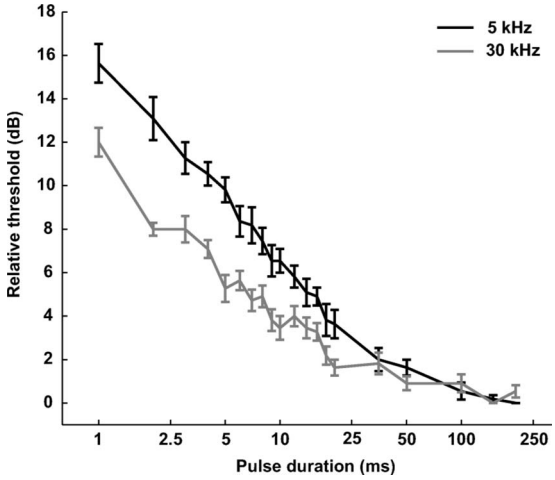


FIG. 2. Auditory threshold in dB as a function of pulse duration. Threshold is relative to the lowest threshold measured. Black curve: 5 kHz carrier frequency; gray: 30 kHz ($N=11$). Two-way ANOVA is significant for both pulse-duration and carrier-frequency effects ($p<0.001$).

III. RESULTS

A. Integration time

Minimum thresholds were 43.8 ± 9.0 dB sound pressure level (SPL) for 5 kHz and 58.2 ± 4.1 for 30 kHz stimuli. Relative thresholds were significantly higher at low frequency for most pulse durations (see Fig. 2; two-way analysis of variance (ANOVA), carrier-frequency effect, $p<0.001$). For stimuli with 5 kHz carrier frequency, the slope of the relationship between pulse duration and threshold was −2.82 dB per doubling of duration (calculated for durations ⩽20 ms), which is quite close to the expected value of −3 dB for the energy-integration model of Plomp and Bouman (1959). The slope was lower (−2.13) for 30 kHz stimuli, resulting in a significant interaction between pulse duration and carrier frequency (ANOVA, $p<0.001$).

Relative threshold curves of each neuron were fit to Eq. (1) with a standard error on τ of less than 2.2 ms in all cases [Fig. 3(A)]. The integration time (as defined by the value of τ) was significantly lower for high-frequency (18.6 ms) than for low-frequency stimuli [42.0 ms, Fig. 3(B); paired t-test,

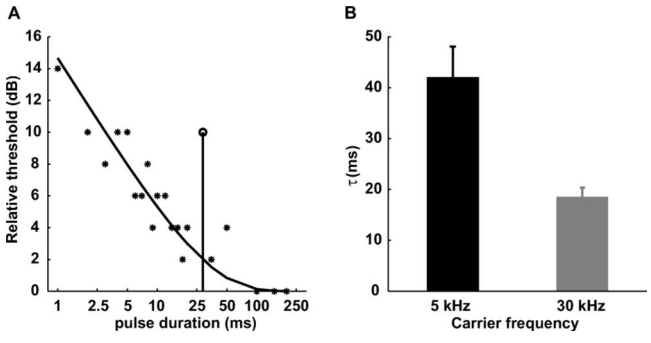


FIG. 3. Integration times. (A) Relative threshold as a function of pulse duration for an example neuron stimulated with low-carrier frequency pulses. The line illustrates the best fit to the equation $Th_{\text{rel to}\infty}=-10\log(1-e^{-t/\tau})$; τ of best fit is indicated by the vertical line. (B) Mean integration time (τ) was longer at 5 kHz than at 30 kHz ($N=11$; $p=0.002$, paired t-test). Error bars show standard errors.

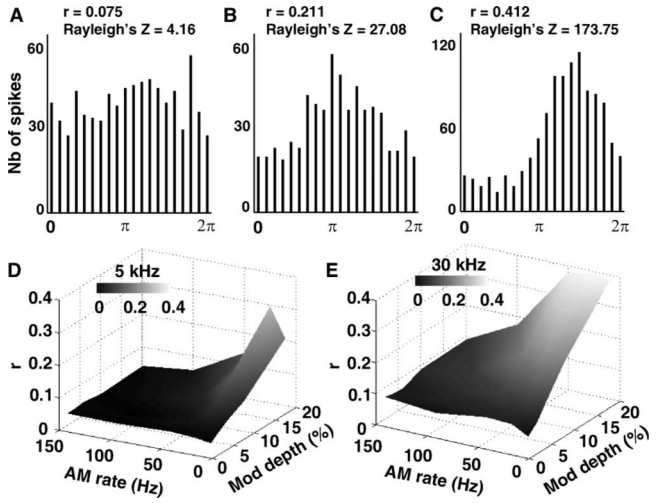


FIG. 4. (A)–(C) Examples of phase histograms constructed from neural responses to SAM stimuli: (A) Cf=30 kHz, AM=10 Hz and MD=2%, r =0.075 (Rayleigh's Z=4.16, $p>0.001$). This response is not considered phase locked to the stimulus. (B) Cf=30 kHz, AM=100 Hz and MD =10%; r=0.211 (Rayleigh's Z=27.08, $p<0.001$). (C) Cf=30 kHz, AM =25 Hz and MD=10%; r=0.412 (Rayleigh's Z=173.75, $p<0.001$). Both (B) and (C) show significant phase locking. (D)–(E) Mean synchronization coefficients as a function of modulation depth and AM frequency at (D) 4.5 kHz and (E) 30 kHz (N=13).

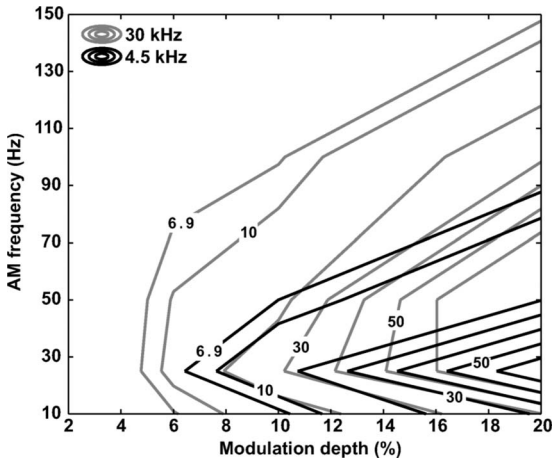


FIG. 5. Superimposed contour plots of Rayleigh's Z values for low- and high-carrier frequencies. Gray contours are for 30 kHz stimuli, black are for 4.5 kHz. Contours for Z=6.9 (threshold for significant detection), 10, 20, 30, 40, 50, and 60 are shown. The graph shows that ON1 is more wideband when stimulated with high-carrier frequency (N=13).

p=0.002]. Integration time across all neurons was more variable for low-frequency (s.d., 20.1 ms) than for high-frequency stimuli (5.9 ms; Bartlett's test for homogeneity of variance, $p<0.001$).

B. Phase locking to SAM stimuli

ON1 showed better phase locking to the stimulus envelope at high than at low-carrier frequency. Figures 4(A)–4(C) illustrate various phase histograms along with their corresponding synchronization coefficient values, where 4(A) shows no phase locking at all, 4(B) shows moderate phase locking, and 4(C) shows strong phase locking. Synchronization coefficients were generally higher at high-carrier frequency, particularly at higher AM rates and lower modulation depths [Figs. 4(D) and 4(E); ANOVA, $p<0.001$; see also Fig. 5]. The contour plot in Fig. 5 illustrates, in two dimensions, Rayleigh's Z for all combinations of AM frequency and modulation depth. This clearly shows that the passband (i.e., the area delimited by each line) is much larger for high-carrier frequency than for low-carrier frequency. The left-most contour, which shows Z=6.9, represents the limit for significance ($p<0.001$).

C. Gap detection

Figure 6 illustrates the responses of a typical neuron. Upon occurrence of a sufficiently long gap, firing rate decreases. When the sound resumes, firing increases beyond the pregap mean level [Figs. 6(A) and 6(B)]. As a result of the method that we used to calculate firing rate (inverse of interspike interval; see Sec. II), the minimum firing rate (i.e., within the gap) is determined by the duration of the pause in firing that is caused by the gap. Generally, this pause lasted longer for low-carrier stimuli [compare Figs. 6(A) and 6(B)].

The effect of gaps on firing rate is clear from comparison of the mean perigap firing rate (solid lines) with firing rates computed from shuffled spike trains (dotted lines). The longer (20 ms) gaps resulted in clear changes in firing rate [Figs. 6(A) and 6(B)], whereas 1 ms gaps were not detected by this neuron [Figs. 6(C) and 6(D)].

The drop in firing rate following onset of a gap was

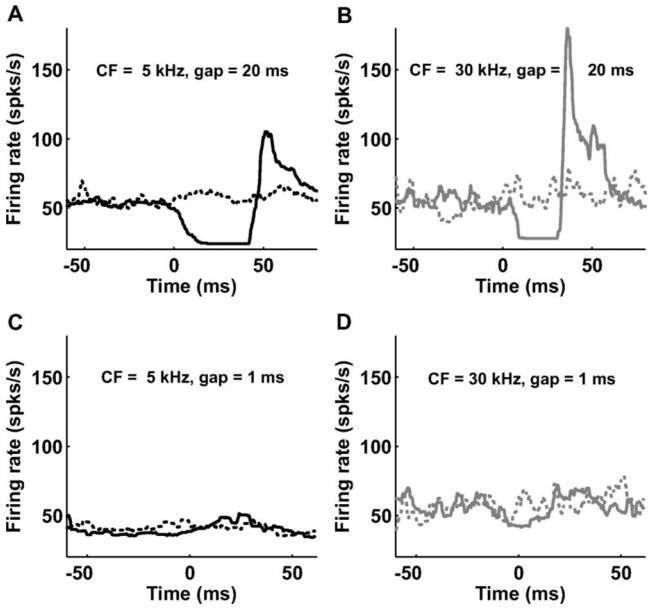


FIG. 6. Firing rate averaged over all gaps within a stimulus, illustrating the results observed in $\Delta fr_{decrease}$ (Fig. 7) and $\Delta fr_{increase}$ (see Fig. 8) at 20 dB above threshold. Data are from a single representative experiment. Gaps begin at time 0. Solid line shows average rate of original spike train and dotted line shows the average firing rate of a shuffled spike train (see Sec. II). (A) $\Delta fr_{decrease}$=−22.7 spks/s and $\Delta fr_{increase}$=39.4 spks/s. CF=5 kHz and gap width=20 ms. (B) $\Delta fr_{decrease}$=−14.5 spks/s and $\Delta fr_{increase}$ =99.8 spks/s. CF=30 kHz and gap width=20 ms. Notice that $\Delta fr_{decrease}$ is smaller and that $\Delta fr_{increase}$ is larger than at 5 kHz. (C) $\Delta fr_{decrease}$= −0.1 spks/s and $\Delta fr_{increase}$=2.7 spks/s. CF=5 kHz and gap width=1 ms. (D) $\Delta fr_{decrease}$=−0.1 spks/s and $\Delta fr_{increase}$=−6.0 spks/s. CF=30 kHz and gap width=1 ms.

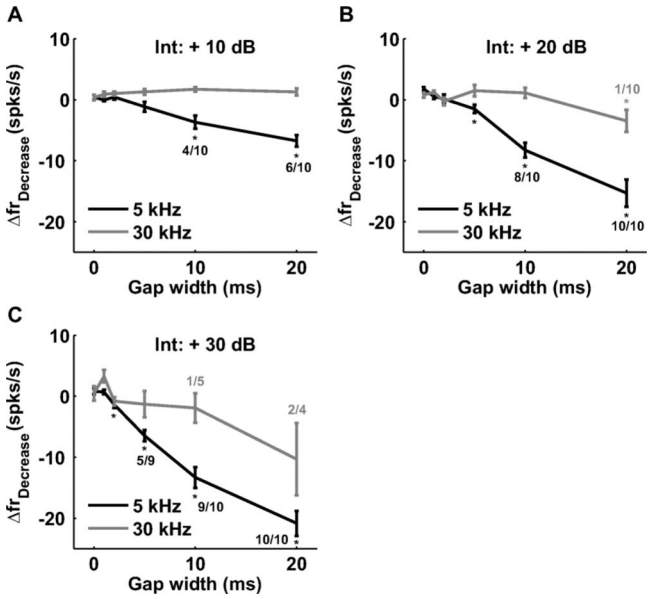


FIG. 7. Decrease from average firing rate as a function of gap width at (A) +10 dB, (B) +20 dB and (C) +30 dB (the + sign indicates that the intensities are relative to threshold). Black: 5 kHz stimuli; gray: 30 kHz. Error bars show standard error. Decrease in firing rate is significantly different between low and high frequency; gap width and intensity were significant factors as well (three-way ANOVA, all $p<0.001$). The proportion of neurons that detected the gaps (a neuron was "successful" when none of the values obtained from the shuffled spike trains exceeded the value obtained from the original spike train) is indicated when it is non-zero. A star next to the error bar further indicates that the mean $\Delta fr_{\text{decrease}}$ is significantly different from zero (t-test, $p<0.05$). At any given gap width that was successfully detected, more neurons were able to detect the gaps at low-carrier frequency than at high-carrier frequency. $N=9$ to 11 for all data points, except for 30 kHz at 30 dB above threshold where $N=3-5$; threshold for 30 kHz stimuli is relatively high (58.2 ± 4.1 dB SPL), and 30 dB above threshold often exceeded the 90 dB SPL upper limit of our stimulation system.

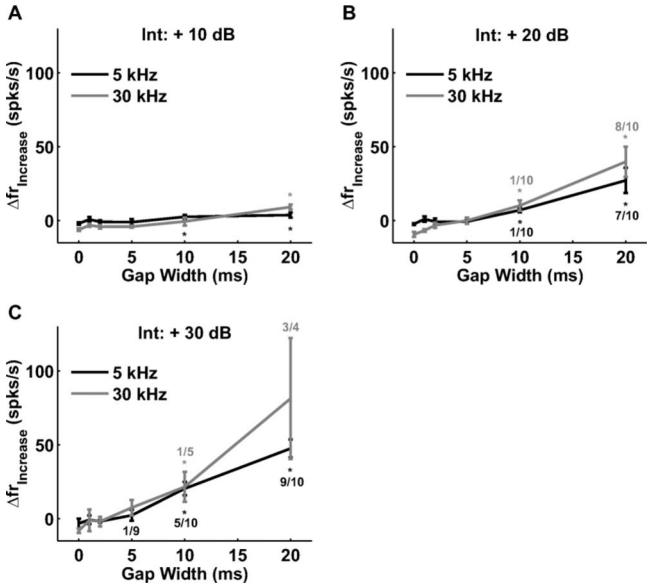


FIG. 8. Increase from average firing rate as a function of gap width at (A) +10 dB, (B) +20 dB and (C) +30 dB (the + sign indicates that the intensities are relative to threshold). Black: 5 kHz carrier; gray: 30 kHz. Error bars show standard error. Effects of gap width and intensity were significant (ANOVA, $p<0.001$), but there was no effect of carrier frequency (ANOVA, $p>0.05$). The proportion of neurons that detected the gaps (a neuron is "successful" when none of the values obtained from the shuffled spike trains exceeded the value obtained from the original spike train) is indicated when it is non-zero. A star next to the error bar further indicates that the mean $\Delta fr_{\text{increase}}$ is significantly different from zero (t-test, $p<0.05$). A similar proportion of neurons was able to detect the gap at each frequency for most gap widths (excluding 30 dB above threshold, where N is too small to establish precise proportion for 30 kHz. N is as in Fig. 7).

generally greater at low-carrier frequency, and increased for higher sound levels and larger gap widths (Fig. 7; three-way ANOVA, all $p<0.001$). For 5 kHz stimuli, a significant decrease in firing rate could be detected at the population level for gaps as brief as 2 ms [Fig. 7(C)], although gap detection was not significant for any single neuron. For 30 kHz stimuli, consistent (i.e., population-level) gap detection occurred only for the longest gap tested (20 ms), at 20 dB above threshold [Fig. 7(B)], although statistical power was limited at 30 dB above threshold. The difference between the two carrier frequencies was significant for gaps of at least 5 ms (Fig. 7; post-hoc t-tests, $p<0.05$ for all gaps $>=5$ ms). In addition, the percentage of neurons able to detect the gap was systematically higher at low-carrier frequency (see Fig. 7).

The post-gap rebound increases with gap width and sound level (Fig. 8, ANOVA: $p<0.001$ for both effects). However, unlike the decrease in firing rate, the postgap increase is similar for low- and high-carrier frequencies (ANOVA, $p>0.05$). No neuron at either low or high-carrier frequency had a significant rebound at 10 dB above threshold. At 20 dB above threshold, the number of neurons with significant rebounds was similar for both carrier frequencies (as for Fig. 7, sample size is limited at 30 dB).

The changes in firing rate that we report above depend not only on the effects of gaps, but also on mean firing rate, and this in turn depends on carrier frequency (and, of course, intensity—but not gap width: ANOVA: intensity and carrier effects, $p<0.001$; gap-width effect, $p>0.9$). Mean firing rate is higher for low-carrier stimuli. To examine the effect of mean firing rate on gap detection, we plot gap-related changes in firing rate as a function of mean rate in Fig. 9. For 20 ms gaps [Figs. 9(A) and 9(B)], carrier-specific differences in the effects of gaps remain evident even when mean firing rate is taken into account. That is, the responses to gaps differ between carriers, for 20 ms gaps, even when firing rates are similar. This is confirmed by the difference in the slopes of the regression lines for low- and high-carrier frequencies [$p<0.001$ in Fig. 9(A), <0.002 in Fig. 9(B), t-test]. Moreover, a difference in post-gap rebound is revealed, with larger rebounds at a given firing rate for ultrasound stimuli. For decrease in firing rate, mean rate has a more pronounced effect (steeper slope) for low-carrier than for high-carrier stimuli, whereas the opposite is true for the post-gap rebound. For 5 ms gaps [Figs. 9(C) and 9(D)], slopes do not differ for low- and high-carrier stimuli [$p>0.2$ in Fig. 9(C), >0.5 in Fig. 9(D)].

IV. DISCUSSION

The results presented above confirm and extend the earlier demonstration, by Marsat and Pollack (2004), that the temporal processing properties of ON1 differ for stimuli with

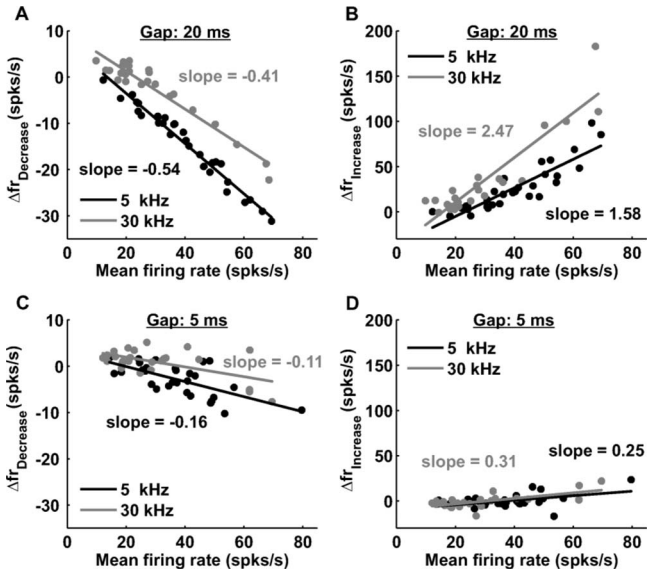


FIG. 9. Correlation between mean firing rate in the 100 ms before gap onset and gap-induced changes in firing rate. Graphs include data points for all stimulus intensities. Black: 5 kHz stimuli; gray: 30 kHz. (A) $\Delta fr_{\text{decrease}}$ vs mean firing rate for 20 ms gaps. Correlation coefficient is $r=-0.962$ for 5 kHz and $r=-0.984$ for 30 kHz (all $p<0.001$). (B) $\Delta fr_{\text{increase}}$ vs mean firing rate for 20 ms gaps. Correlation coefficient is $r=0.893$ for 5 kHz and $r=0.919$ for 30 kHz (all $p<0.001$). (C) $\Delta fr_{\text{decrease}}$ vs mean firing rate for 5 ms gaps. Correlation coefficient is $r=-0.681$ for 5 kHz and $r=-0.587$ for 30 kHz (all $p<0.001$). (D) $\Delta fr_{\text{increase}}$ vs mean firing rate for 5 ms gaps. Correlation coefficient is $r=0.673$ for 5 kHz and $r=0.467$ for 30 kHz (all $p<0.05$). Mean firing rates are strongly correlated with $\Delta fr_{\text{decrease}}$ and $\Delta fr_{\text{increase}}$, but the correlations weaken as the gap width decreases.

cricket-like and bat-like carrier frequencies. As assessed by integration time and by synchronization to periodic modulations in amplitude, ON1 is "faster" (i.e., shorter integration time, phase locking to higher AM rates) for ultrasound stimuli. By contrast, brief gaps in an ongoing stimulus are more reliably detected for low-carrier stimuli, at least as assessed by the gap-induced decrease in firing rate.

These differences might arise, in principle, at any stage along the auditory processing chain, including the mechanics of the tympanum and/or of the linkage to receptor neurons, the electrophysiological properties (e.g., membrane time constant) of the receptor neurons, and the properties of synaptic connections between receptors and ON1. Tympanal mechanics can be ruled out, as the time constants of the tympana of several insects are on the order of 200 μs or less (Schiolten *et al.* 1981; Larsen, 1981; Gollisch and Herz, 2005), at least an order of magnitude smaller than the time scales of the present measurements. Estimates of membrane time constants for auditory receptor neurons (of locusts) range from <1 ms (Gollisch and Herz, 2005) to 5–10 ms (Hill, 1983). The former is again too short to account for our results, but the latter value corresponds reasonably well to our measurements of gap detection and of phase locking (a time constant of 5–10 ms would predict an upper limit for phase locking of 100–200 Hz, which ON1 approaches, at least for 30 kHz stimuli with large modulation depths; Fig. 5, cf. Marsat and Pollack, 2004). However, although separate groups of receptors are tuned to low and high frequencies (Imaizumi and Pollack, 1999) there are as yet no data indicating whether their membrane time constants differ. The two groups of receptors do differ in other respects, including numerosity, slope of intensity-response function, and probable synaptic weighting (Imaizumi and Pollack 1999, 2001; Pollack and Faulkes, 1998; Pollack, 1994). We discuss below how these differences might contribute to the temporal-processing characteristics of ON1.

A. Integration time

The integration time of ON1 was much shorter (by a factor of 2) at high- than at low-carrier frequency. This is consistent with published data on the shorter latency of ON1 at high-carrier frequency compared to low-carrier frequency (Pollack 1994). Interestingly, integration time in an identified interneuron of a katydid was also found to be about half as long for high-frequency (40 kHz; integration time 6 ms) compared to low-frequency (15 kHz, 15 ms) stimuli (Faure and Hoy, 2000). Examples where integration time is generally shorter at higher frequency also exist in vertebrates, notably in frogs (Dunia and Narins, 1989), cats (Costalupes, 1983), rhesus monkeys (Clack, 1966), and humans (Plomp and Bouman, 1959; Watson and Gengel, 1969).

For 5 kHz stimuli, the relationship between duration and integration time rather closely matched the expectation (−3 dB per doubling of duration) for an intensity-integration model. For 30 kHz, however, the slope was less steep. This resembles previous findings for katydids, where the slopes for low- (15 kHz) and high- (40 kHz) stimuli were −2.7 and −2.0 dB per doubling of duration, respectively (Faure and Hoy, 2000). For crickets, the discrepancy between theoretical and measured values for 30 kHz stimuli may reflect nonlinearities of ultrasound processing. Marsat and Pollack (2004) measured both linear and nonlinear contributions to information coding by ON1, and found that nonlinearity was much more pronounced in responses to ultrasound.

We do not yet know where, within the auditory processing chain, the carrier-related difference in integration time arises. This might already be present at the level of auditory afferents, as is the case, e.g., in frogs (Dunia and Narins, 1989). Another (nonexclusive) possibility is that the difference results from the characteristics of the synaptic connections between auditory afferents and ON1. Previous experiments strongly suggested that unitary excitatory postsynaptic potentials (EPSPs) evoked in ON1 by high-frequency receptors are large compared to those evoked by low-frequency stimuli (Pollack, 1994; Faulkes and Pollack, 2001). This suggests that at low frequency, membrane potential in ON1 may be brought to threshold by summation of a large number of small EPSPs, whereas only a few well-timed large EPSPs from high-frequency receptors would be required to reach threshold.

B. Phase locking to SAM stimuli

Marsat and Pollack (2004) showed that, for SAM stimuli with 100% modulation depth, ON1 is better able to phase lock to the envelope of high-carrier than of low-carrier stimuli. We extended these results by varying modulation depths down to very low levels. Strong synchronization oc-

curred even for modulation depth of only 5%, which is comparable to the minimum modulation depth detectable by humans (Rodenburg, 1977). We confirmed that ON1 is more "wideband," with respect to both AM rate and modulation depth, for high-carrier frequency stimuli (see Fig. 5). Faure and Hoy (2000) found that katydid T-cells synchronized better to trapezoidally amplitude-modulated stimuli at high- than at low-carrier frequency. However, their measure of synchronization emphasized the probability of responding to varying AM rates, rather than the precise timing of responses.

As for integration time, the carrier-dependent difference might already be occurring at the receptor level. However, in a related insect, locust, phase-locking characteristics of low- and high-frequency receptor neurons are similar (Prinz and Ronacher, 2002). Another hypothesis is that the better phase locking at high AM rates for ultrasound carrier might be attributed to unitary EPSP size and membrane potential dynamics. Slow buildup of EPSPs for low-carrier stimuli may be unable to follow fast AM rates. In addition, several observations suggest that responses of receptors and of ON1 to ultrasound stimuli are more sensitive to changes in stimulus amplitude than those to low-carrier frequencies, i.e., intensity-response functions are steeper (Pollack, 1994; Imaizumi and Pollack, 2001; Marsat and Pollack, 2004). Thus, small amplitude modulations would induce a larger change in firing rate at high carrier frequency, and this might contribute to improved phase locking.

C. Gap detection

Introduction of a gap in an ongoing tone had two effects on the response of ON1: An early decrease in firing rate, followed by a postgap increase (cf. Zhang *et al.*, 1990; Kuwada and Batra, 1999). Either or both of these effects might be informative for downstream neurons. The minimum detectable gap duration, 2–5 ms, is comparable to that of human subjects (Buus and Florentine, 1985), but longer than that achieved by another insect (Ronacher and Stumpner, 1988). The decrease in firing rate is more pronounced at low-carrier frequency, whereas the post-gap increase does not significantly differ between the two carrier frequencies. The decrease in firing rate reflects not only the absence of excitatory input, but also the latency of the postgap response upon resumption of input. As discussed above, response latency of ON1 is longer for low-frequency than for ultrasound stimuli, possibly because of the increased requirement for postsynaptic summation. The same effect may explain the longer pause in firing induced by gaps. The postgap increase in firing rate may have several causes. One of these is almost certainly recovery from adaptation. ON1 experiences profound adaptation when stimulated with a long-lasting tone, with firing rate decreasing by as much as 96.4%. For the neuron showing the strongest adaptation, firing rate in response to a 30 kHz tone presented at 20 dB above threshold decreases from a maximum of 526.1 Hz immediately after tone onset, to 19.2 Hz a few seconds later. The pause in excitatory input caused by a gap presumably affords an opportunity for at least partial recovery. It is also interesting to note that adaptation was slightly stronger at high carrier frequency (means: $94.4 \pm 1.0\%$ for high carrier frequency versus $89.6 \pm 3.1\%$ for low carrier frequency; t-test, $p < 0.001$). A second cause might be an intrinsic tendency of ON1 to fire at a high rate following rapid increases in amplitude of ultrasound stimuli (bursting; Marsat and Pollack, 2007). We further consider this below.

There was a strong correlation between mean firing rate before gaps and the gap-induced changes in firing rate (see Fig. 9). The correlation between the gap-induced decrease in firing rate and mean rate was to be expected, since the higher the mean firing rate preceding a gap, the larger the potential decrease after the gap. Unexpectedly, however, firing rate has a more pronounced effect on responses to low-carrier than to high-carrier stimuli. The probable explanation for this is apparent in Fig. 6. The pause in firing during a gap is typically longer in duration for low-carrier stimuli [compare Figs. 6(A) and 6(B)], resulting in an additional decrease in firing rate beyond that for high-carrier stimuli. This additional constant time period in the gap-induced interspike interval carries increasing weight in the calculation of $\Delta fr_{\text{decrease}}$ as mean firing rate increases (i.e., as the average interspike interval decreases), resulting in a steeper slope for the relationship between these values. There was also a positive relationship between mean firing rate and $\Delta fr_{\text{increase}}$ for both low- and high-carrier frequencies at 20 ms gaps [respectively, $r = 0.893$ and $r = 0.919$, $p < 0.001$; see Fig. 9(B)]. In this case, the relationship may stem in part from the fact that we pooled all stimulus intensities in the analysis, so that stimuli evoking higher mean firing rates were on average more intense. Earlier work showed, both for receptors (Givois and Pollack, 2000) and for another identified interneuron (Samson and Pollack, 2002), that adaptation is more pronounced for more intense stimuli. Thus, to the extent that the postgap rebound represents recovery from adaptation, it might be expected to be greater for higher mean rates. The rebound would also be expected to increase with longer-lasting gaps, which presumably would allow more time for recovery. Nevertheless, the magnitude of the rebound is larger, for similar mean rates, for high-carrier stimuli. This may reflect a tendency of ON1 to fire at high rates in response to rapid amplitude increases in ultrasound stimuli. For example, in our data set, maximum firing rates at the onsets of constant tones at 20 dB above threshold were 536.1 ± 106.9 spikes/s for 30 kHz compared to 299.6 ± 84.2 for 5 kHz. This characteristic of the response of ON1 serves to match the structure of its spike train to that of a synaptic partner, AN2. Brief periods of high-rate firing of AN2 (bursts) reliably signal large and rapid increases in amplitude of an ultrasound stimulus, such as those that occur in bat echolocation sounds. ON1 is a source of contralateral inhibition of AN2 and, like AN2, it also produces bursts for rapid increases in ultrasound amplitude. This matching of the spike-train structure between the two neurons increases the effectiveness of contralateral inhibition, resulting in better representation of the location of the stimulus (Marsat and Pollack, 2007).

V. CONCLUSION

The above results are based on the study of the temporal dynamics of events (spikes) with respect to the amplitude dynamics of a given stimulus. The causes of differential signal processing in ON1, however, must be sought in its membrane potential dynamics. Some clues are already available—for instance, the EPSPs evoked in ON1 by low- and high- frequency afferents are suspected to be quite different in size (Faulkes and Pollack 2001), but further investigation (both theoretical and experimental) is required (and is under way) to determine the precise intracellular dynamics at the root of the differences in the spike-train temporal structure.

ACKNOWLEDGMENTS

This research was supported by the Natural Sciences and Engineering Research Council of Canada and the Fonds québécois de la recherche sur la nature et les technologies.

Batschelet, E. (**1981**). *Circular Statistics in Biology* (Academic, London).

Buus, S., and Florentine, M. (**1985**). "Gap detection in normal and impaired listeners: The effect of level and frequency," In: *Time Resolution in Auditory Systems*, edited by A. Michelsen (Springer-Verlag, Berlin), pp. 159–179.

Clack, T. D. (**1966**). "Effect of signal duration on the auditory sensitivity of humans and monkeys (*Macaca mulatta*)," J. Acoust. Soc. Am. **40**, 1140–1146.

Costalupes, J. A. (**1983**). "Temporal integration of pure tones in the cat," Hear. Res. **9**, 42–54.

Dunia, R., and Narins, P. M. (**1989**). "Temporal integration in an anuran auditory nerve," Hear. Res. **39**, 287–298.

Faulkes, Z., and Pollack, G. S. (**2000**). "Effects of inhibitory timing on contrast enhancement in auditory circuits in crickets (*Teleogryllus oceanicus*)," J. Neurophysiol. **84**, 1247–1255.

Faulkes, Z., and Pollack, G. S. (**2001**). "Mechanisms of frequency-specific responses of omega neuron 1 in crickets (*Teleogryllus oceanicus*): A polysynaptic pathway for song?," J. Exp. Biol. **204**, 1295–1305.

Faure, P. A., and Hoy, R. R. (**2000**). "Neuroethology of the katydid T-cell. I. Tuning and responses to pure tones," J. Exp. Biol. **203**, 3225–3242.

Gerhardt, H. C., and Huber, F. (**2002**). *Acoustic Communication in Insects and Anurans* (University of Chicago, Chicago).

Givois, V., and Pollack, G. S. (**2000**). "Habituation of auditory receptor neurons: Implications for sound localization," J. Exp. Biol. **203**, 2529–2537.

Goldberg, J. M., and Brown, P. B. (**1969**). "Functional organization of the dog superior olivary nucleus: An anatomical and electrophysiological study," J. Neurophysiol. **31**, 639–656.

Gollisch, T., and Herz, A. V. M. (**2005**). "Disentangling sub-millisecond processes within an auditory transduction chain," PLoS Biol. **3**, 144–154.

Griffin, D. R., Webster, F. A., and Michael, C. R. (**1960**). "The echolocation of flying insects by bats," Anim. Behav. **8**, 141–154.

Hill, K. G. (**1983**). "The physiology of locust auditory receptors. II. Membrane potentials associated with the response of the receptor cell," J. Comp. Physiol. **152**, 483–493.

Imaizumi, K., and Pollack, G. S. (**1999**). "Neural coding of sound frequency by cricket auditory receptors," J. Neurosci. **19**, 1508–1516.

Imaizumi, K., and Pollack, G. S. (**2001**). "Neural representation of sound intensity by functionally different auditory receptors in crickets," J. Acoust. Soc. Am. **109**, 1247–1260.

Kuwada, S., and Batra, R. (**1999**). "Coding of sound envelopes by inhibitory rebound in neurons of the superior olivary complex in the unanesthetized rabbit," J. Neurosci. **19**, 2273–2287.

Larsen, O. N. (**1981**). "Mechanical time resolution in some insect ears. II. Impulse sound transmission in acoustic tracheal tubes," J. Comp. Physiol. [A] **143**, 297–304.

Marsat, G., and Pollack, G. S. (**2004**). "Differential temporal coding of rhythmically diverse acoustic signals by a single interneuron," J. Neurophysiol. **92**, 939–948.

Marsat, G., and Pollack, G. S. (**2007**). "Efficient inhibition of bursts by bursts in the auditory system of crickets," J. Comp. Physiol., A **193**, 625–633.

Moiseff, A., and Hoy, R. R. (**1983**). "Sensitivity to ultrasound in an identified auditory interneuron in the cricket: a possible link to phonotactic behavior," J. Comp. Physiol. **152**, 155–167.

Plomp, R., and Bouman, M. A. (**1959**). "Relation between hearing threshold and duration for tone pulses," J. Acoust. Soc. Am. **31**, 749–758.

Pollack, G. S. (**1994**). "Synaptic inputs to the omega neuron of the cricket *Teleogryllus oceanicus*: Differences in EPSP waveforms evoked by low and high sound frequencies," J. Comp. Physiol., A **174**, 83–89.

Pollack, G. S., and Faulkes, Z. (**1998**). "Representation of behaviourally relevant sound frequencies by auditory receptors in the cricket Teleogryllus oceanicus," J. Exp. Biol. **201**, 155–163.

Prinz, P., and Ronacher, B. (**2002**). "Temporal modulation transfer functions in auditory receptor fibers of the locust (*Locusta migratoria L.*)," J. Comp. Physiol., A **188**, 577–587.

Rodenberg, M. (**1977**). "Investigation of temporal effects with amplitude modulated signals," In: *Psychophysics and Physiology of Hearing*, edited by E. F. Evans and J. P. Wilson (Academic, London), pp. 429–437.

Ronacher, B., and Stumpner, A. (**1988**). "Filtering of behavioral relevant temporal parameters of a grasshopper's song by an auditory interneurone," J. Comp. Physiol., A **163**, 517–523.

Samson, A.-H., and Pollack, G. S. (**2002**). "Encoding of sound localization cues by an auditory interneuron: Effects of stimulus temporal pattern," J. Neurophysiol. **88**, 2322–2338.

Schiolten, P., Larsen, O. N., and Michelsen, A. (**1981**). "Mechanical time resolution in some insect ears. I. Impulse responses and time constants," J. Comp. Physiol. [A] **143**, 289–295.

Shannon, R. V., Zeng, F.-G., Kamath, V., Wygonski, J., and Ekelid, M. (**1995**). "Speech recognition with primarily temporal cues," Science **270**, 303–304.

Strausfeld, N. J., Seyan, H. S., Wholers, D., and Bacon, J. P. (**1983**). "Lucifer yellow histology," In: *Functional Neuroanatomy*, edited by N. J. Strausfeld (Springer-Verlag, Berlin), pp. 132–155.

Walker, S. E., and Cade, W. H. (**2003**). "The effects of temperature and age on calling song in a field cricket with a complex calling song, *Teleogryllus oceanicus* (Orthoptera: Gryllidae)," Can. J. Zool. **81**, 1414–1420.

Watson, C. S., and Gengel, R. W. (**1969**). "Signal duration and signal frequency in relation to auditory sensitivity," J. Acoust. Soc. Am. **46**, 989–997.

Zhang, W., Salvi, R. J., and Saunders, S. S. (**1990**). "Neural correlates of gap detection in auditory nerve fibers of the chinchilla," Hear. Res. **46**, 181–200.

The frequency response of rat vibrissae to sound

Lisa F. Shatz[a)]
Electrical and Computer Engineering Department, Suffolk University, 41 Temple St. Boston, Massachusetts 02114 and Boston University Hearing Research Center, 44 Cummington St., Boston, Massachusetts 02215, USA

Craig W. Christensen
Electrical and Computer Engineering Department, Suffolk University, 41 Temple St. Boston, Massachusetts 02114, USA

(Received 3 August 2007; revised 4 March 2008; accepted 4 March 2008)

The motion of isolated rat vibrissae due to low frequency sound has been modeled and measured with good agreement (within a factor of 2) between the data and the model's predictions. As had been done in previous studies on the response of rat vibrissae to tactile stimulation [Hartmann, M. J., Johnson, N. J., Towal, R. B., and Assad, C., J. Neurosci **23**, 6510–6519 (2003) and Neimark, M. A., Andermann, A. L., Hopfield, J. J., and Moore, C. I., J. Neurosci **23**, 6449–6509 (2003)] the vibrissae were modeled as thin conical beams. The force of the vibrating air on a vibrissa was modeled using the exact solution for a vibrating infinite cylinder in linear fluid. A finite element method was used to model the motion of a single vibrissa fixed at its base, using the aforementioned fluid force. Values for Young's modulus and vibrissa mass density were taken from a previous study [Neimark *et al.* (above)]. The model had no freely fitted parameters. Motion of isolated vibrissae was measured using a video camera with microscope. The sound stimulation was created using a stereo speaker connected to a signal generator. The tuning was found to be sharp, with quality factors that varied between 3 and 7, much sharper than the motion of cricket cercal hairs or in vitro inner ear hair bundles. © *2008 Acoustical Society of America.* [DOI: 10.1121/1.2902181]

PACS number(s): 43.80.Lb, 43.20.Ks, 43.40.Cw, 43.20.Tb [JAS] Pages: 2918–2927

I. INTRODUCTION

Sensor hairs are found in hearing organs, lateral line organs of fish and amphibians, and in spiders, crickets and cockroaches; and these hairs are used to detect sound-induced or mechanically induced motion of the fluid surrounding the hairs. The sensor hair system in crickets and spiders has been shown to be far superior to most man-made devices (such as microphones and anemometers); only laser anemometers are known to have comparable sensitivity (Kamper and Kleindeist, 1990). Sensor hairs are also found in vestibular organs to detect fluid motion caused by head movements in order to maintain postural equilibrium.

Vibrissae or whiskers are also types of sensor hairs, and for certain organisms, these play a vital role in detecting disturbances in their surrounding fluid, which could be air or water. Pinnipeds like seals use their vibrissae to track water waves as small as a micron in amplitude left in the wake of their prey (Dehnhardt *et al.*, 2001). Manatees have vibrissae over their whole bodies, analogous to a lateral line system, with which they detect changes in water motion caused by mechanical or sound stimuli (Reep *et al.*, 2002).

Significant progress has been made to understanding the mechanics of sensor hairs in the inner ear (Freeman and Weiss, 1990a; Freeman and Weiss, 1990b; Freeman and Weiss, 1990c; Freeman and Weiss, 1990d; Shatz, 2000; Aranyosi, 2002; Shatz, 2004), as well as in the mechanics of the sensor hairs found in crickets, spiders and cockroaches (Shimozawa, 1984; Barth *et al.*, 1993; Humphrey *et al.*, 1993; Shimozawa *et al.*, 1998a; Shimozawa *et al.*, 1998b). These sensor hairs have been shown to be frequency selective; each sensor hair has been shown to have a frequency or range of frequencies to which it responds best. Shorter hairs have been shown to respond best to higher frequencies while longer hairs respond best to lower frequencies.

Vibrissae have also been shown to be frequency selective in their response to tactile stimulation, and a preliminary effort has been made to model the mechanics of rat vibrissae (Hartmann *et al.*, 2003; Neimark *et al.*, 2003). A thin elastic beam model has been used to predict a rat vibrissa's resonant frequencies, but it could not predict the actual motion of the vibrissae and it has not been used to study the response of the vibrissae to sound.

This study looks at how rat vibrissae respond to sound. Measurements were taken of the motion of isolated rat vibrissae, fixed at their bases, in response to sound at several frequencies emanating from a stereo speaker. A finite element model, which uses the exact solution for the fluid force of a cylinder in linear vibrating fluid to model the fluid forces on a vibrissa, is used. The model predicts the motion of vibrissae well.

This work has applications for designing sound sensors, for understanding the neural responses of vibrissa sensing, and will serve as a preliminary study to understanding the vibrissae of aquatic mammals.

[a)]Author to whom correspondence should be addressed. Electronic mail: lshatz@suffolk.edu

 0001-4966/2008/123(5)/2918/10/$23.00 © 2008 Acoustical Society of America

II. THE EXPERIMENT

Vibrissae are plucked from rats that had already been sacrificed, preserved, and vacuum packed. The vibrissae are stimulated by the motion of the surrounding fluid (air) that is driven by the sound coming from the speaker[1] (Fig. 1). The motion of the air next to the vibrissa could not easily be measured and an estimate of the air displacement next to the vibrissa is derived from a measurement of the speaker displacement and an estimate of the attenuation of the air displacement from its peak value next to the speaker. The estimate of the attenuation was found, using a velocity microphone,[2] to be about a factor of 2. This attenuation was observed by viewing the output of the microphone on an oscilloscope when it was adjacent to the speaker, and when it was in the vicinity of the vibrissa location.[3] Errors in this approximation come from the fact that the speaker is concave[4] and so the distance of the sound source to the vibrissa is not uniform; the vibrissa are curved which also results in the distance to the sound source varying by several millimeters[5] with position along the vibrissa; the microphone is 5.2 cm in diameter and so its output does not reflect the fluid displacement at any particular point along a vibrissa; and the distance to the speaker varies with the to and fro oscillation of the vibrissae.

As controls, the motion of thin gold-plated tungsten and copper wires was also observed. The advantages of using these wires are that their characteristics (mass density, Young's modulus) have been well established[6] and that their shape is cylindrical with widths that are set by industrial standards. In contrast, the characteristics of vibrissae have been measured in only two studies (Hartmann *et al.*, 2003; Neimark *et al.*, 2003) and the results for the Young's modulus and mass density vary. Moreover, the shape of the vibrissae is that of a truncated cone and the measurement of the base and tip widths adds additional uncertainties.

Measuring the vibrissae and speaker displacements was done by viewing a movie of the vibrissa and speaker oscillation [Figs. 1(B) and 1(C)]. The movie was taken at a frame rate of 27.97 frames per second with two images per frame. The camera was not synchronized to the speaker, but the speaker motion and the vibrissa motion were recorded simultaneously.[7] The fundamental frequency and, occasionally, the first harmonic (when it was noticeable) were found by manually sweeping through frequencies and observing the output through the video microscope. The responses at those resonant frequencies were then used for measurements. The other frequencies used were frequencies at multiples of 10 or 4 Hz intervals from the resonant frequencies.[8] For instance, for an observed fundamental frequency of 54 Hz,[9] the output was measured at 44, 54, 64, and 74 Hz. The lowest and highest frequencies used were those frequencies for which a response was measurable.

The maximum displacements were found by viewing the movie, frame by frame, using the software *Measurement in Motion*™. The maximum displacements were found by inspecting several complete cycles of the motion[10] and were recorded for each input frequency. The ratio of the maximum tip displacements to the maximum air velocity[11] was plotted as a function of input frequency, and was compared to the same curve generated by a finite element model.

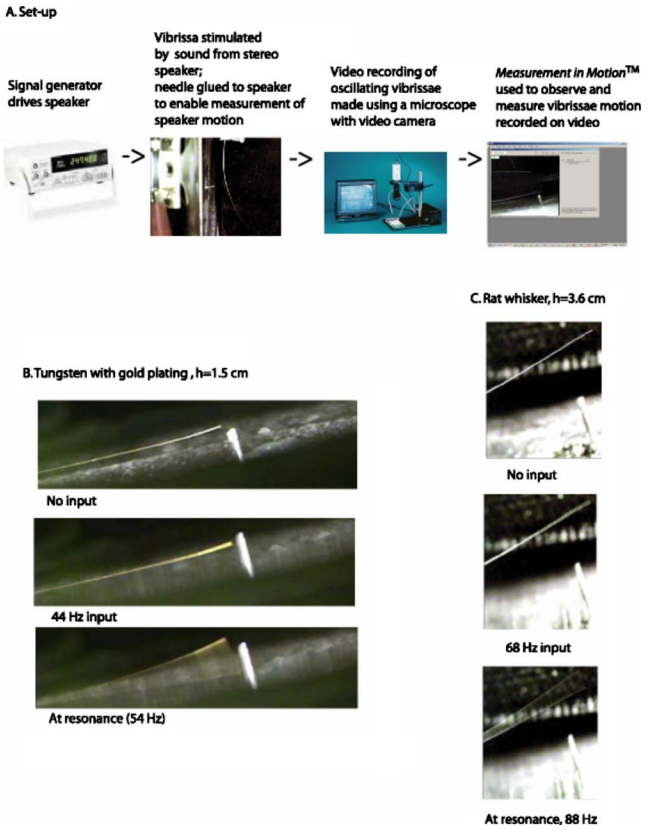


FIG. 1. (Color online) (A) Vibrissae bend back and forth in response to air motion driven by the speaker. Wires were also used but are not shown. Air displacement measured to be about a factor of 2 less than speaker displacement. (B) Motion of tungsten with gold plating, h=1.5 cm (1.2 cm of 1.5 cm length is shown). Note that off resonance, the bending is mainly at the tip. (C) Motion of rat whisker, h=3.6 cm (0.95 cm of 3.6 cm length is shown).

To obtain information about the phase of the whisker motion, the motion of the whisker and the speaker were observed at frequencies for which the strobe effect of the camera allowed the viewing of complete cycles of motion, i.e., frequencies close to multiples of 60 Hz.

III. THE MODEL

A. Equations of motion

As had been done previously (Hartmann *et al.*, 2003; Neimark *et al.*, 2003), the vibrissae are modeled as thin elastic beams shaped as truncated cones. The vibrissae are fixed at their bases, and are surrounded by linear, incompressible fluid.[12] Equation (1) describes the displacement of the vibrissa in response to the force of the surrounding fluid:

$$\frac{\partial^2}{\partial x^2}\left(\mathrm{EI(x)}\frac{\partial^2 y(x,t)}{\partial x^2}\right) - \mathrm{F_{fluid}} = -\rho\frac{\partial^2 y(x,t)}{\partial \mathrm{t}^2}\mathrm{A}(x), \qquad (1)$$

where $y(x,t)$ (m) represents displacements of the vibrissa as a function of x, the distance from the base; E (Pa) represents the vibrissa's Young's modulus; $I(x)$ (m^4) represents the second moment of area; $\rho(\mathrm{kg/m}^3)$ represents the vibrissa's mass density; $A(x)$ (m^2), the cross-sectional area of the vibrissa;

and F_{fluid} (N/m) represents the force due to translational oscillations of the surrounding air. The first term on the left of Eq. (1) represents stiffness forces that resist the bending due to the driving external forces represented by the second term on the left. The term on the right represents the vibrissa's inertia that resists acceleration. For sinusoidal motion $y(x,t)$ can be represented as $y(x,t)=y(x)e^{-j\omega t}$ where ω represents the radian frequency of oscillation. Equation (1) can then be represented as

$$\frac{\partial^2}{\partial x^2}\left(\mathrm{EI(x)}\frac{\partial^2 y(x)}{\partial x^2}\right) - \mathrm{F_{fluid}} = \rho\omega^2 A(x)y(x). \tag{2}$$

Since the cross section of the vibrissa varies slowly over its length, we will approximate the derivatives of $I(x)$ as zero and represent Eq. (2) as

$$\mathrm{EI}(x)\left(\frac{\partial^4 y(x)}{\partial x^4}\right) - \mathrm{F_{fluid}} = \rho\omega^2 A(x)y(x). \tag{3}$$

In order to solve Eq. (3), a finite element method (FEM) is used. To model the fluid force, the exact solution for the force on an infinite oscillating cylinder in linear fluid is used.

B. Model for fluid force

Equations (4) and (5) describe the motion of moving linear fluid[13] surrounding the vibrissa:

$$\rho_{\text{air}}\frac{\partial \mathbf{u}(\mathbf{r},t)}{\partial t} = -\nabla P(\mathbf{r},t) + \mu\nabla^2\mathbf{u}(\mathbf{r},t) \tag{4}$$

$$\nabla\cdot\mathbf{u}(\mathbf{r},t) = 0, \tag{5}$$

where ρ_{air} represents the mass density of air; $\boldsymbol{u}(\boldsymbol{r},t)$ represents the air's velocity as a function of position $\boldsymbol{r}$ and time t; $P(\boldsymbol{r},t)$ represents the air's pressure; and μ represents the air's viscosity. Equation (4) describes conservation of momentum, with the two terms on the right representing forces due to fluid pressure and fluid viscosity. Equation (5) describes conservation of mass for an incompressible fluid. Note that although sound is a wave, its wave properties are negligible in stimulating the vibrissa motion, since, at the frequencies and sound amplitudes of interest, the sound's wavelength is much, much greater than the size of the vibrissa, its motion, and any of the fluid displacements.[14] Equations (4) and (5) have been solved exactly for an infinite cylinder surrounded by linear, oscillating fluid (Batchelor, 1967) and approximately for very thin prolate hemispheroids whose shape is similar to that of a truncated cone, using a singularity method (Shatz, 2005). These solutions can be used as approximate solutions for the effects of oscillating fluid on the vibrissa.

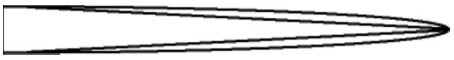


FIG. 2. A comparison of the shape of a hemispheroid with that of a truncated cone. The force on a hemispheroid was computed using a singularity method. The force on the truncated cone was computed by dividing the cone into n elements, computing for force on each element using the exact solution for the force/length of an infinite cylinder whose radius is equal to the mean radius of the element, and then summing the results.

The results for the fluid force on a prolate hemispheroid calculated using a singularity method, and the fluid force on a truncated cone (Fig. 2), calculated using the exact solution for an infinite cylinder, are shown in Table I. Each structure has a height to base radius ratio of 1000, which is roughly the shape of a vibrissa. The force on the truncated cone was computed by dividing the cone into n elements, computing for force on each element using the exact solution for the force/length of an infinite cylinder,[15] and then summing the results. It is clear that the forces are about the same, and, since the computation is much faster using an exact solution than a numerical one, and since a hemispheroidal shape is not the same as a truncated cone, the results for the cylinder were used to represent the fluid force on the vibrissa.

C. Finite element method

Equation (3) was solved using the FEM derived from a minimum energy formulation. The vibrissa is divided into n elements,[16] and a cubic displacement function is used to solve for the displacements and rotations ($y(x)$ and $dy(x)/dx$, respectively) of each element. Since the vibrissa is fixed at its base, $y(x)$ and $dy(x)/dx$ are set to zero in the first element at the bottom (Fig. 3).

IV. RESULTS

A. Tuning curves features

The results of the experiment and the model (Figs. 4 and 5) show that the vibrissae have resonant frequencies, i.e., frequencies for which the motion is maximum. We can understand the shape of the tuning curves by first discussing the tuning curve in the vicinity of the first resonant frequency,

TABLE I. A comparison of the force on a vibrissa using two different methods.

Vibrissa length (cm)	Frequency (Hz)	Force on hemispheroid (magnitude) (μN)	Force on truncated cone (magnitude) (μN)	% Difference between force magnitudes	Force on hemispheroid [phase (deg)]	Force on truncated cone [phase (deg)]	Phase difference
4	225	1.5	1.7	−10	−33	−19	−14
3	100	2.3	2.5	−10	−33	−19	−14
4	55	3	2.2	+29	−33	−17	−16
2	55	1.5	1.3	+11	−15	−14	−1
3	15	2.2	2.0	+11	−15	−15	0
4	15	2.9	2.6	+11	−15	−14	−1

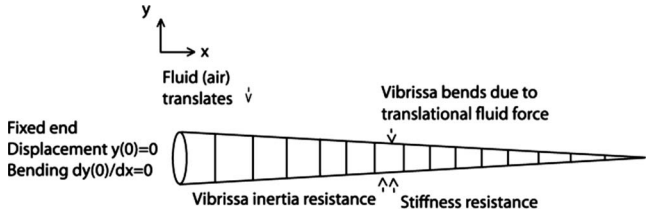


FIG. 3. In the FEM the vibrissa is divided into n elements, and a minimum energy equation, derived from Eq. (3) is solved for each element.

also known as the fundamental frequency. For frequencies lower than the fundamental, the term that represents the stiffness forces is larger than the inertia term, $(\mathrm{EI}(x)\,\partial^4 y(x)/\partial x^4) \gg \rho\omega^2 A(x) y(x)$, and Eq. (3) can be written as

$$\mathrm{EI}(x)\left(\frac{\partial^4 y(x)}{\partial x^4}\right) = \mathrm{F}_{\mathrm{fluid}}. \tag{6}$$

Therefore, the frequency dependence of the displacement $y(x)$ is determined by F_{fluid}. For frequencies above the fundamental frequency, the inertia term is much larger than the stiffness term $(\mathrm{EI}(x)\,\partial^4 y(x)/\partial x^4) \ll \rho\omega^2 A(x) y(x)$, and we can represent the displacement of the whisker as

$$-\frac{\mathrm{F}_{\mathrm{fluid}}}{\rho\omega^2 A(x)} = y(x). \tag{7}$$

The $1/\omega^2$ dependency for $y(x)$ can be seen in the steeper slopes of the tuning curves for frequencies beyond the fundamental frequency than for frequencies below it. For resonant frequencies greater than the fundamental frequency, the aforementioned description about the behavior of the tuning curves below the resonant frequency and above it are still valid. The magnitude of the stiffness term becomes large and dominates as kinetic energy is converted to elastic potential energy for frequencies below a resonant frequency. As the magnitude of the stiffness term becomes less significant, a resonant frequency is approached and inertial forces dominate at frequencies above a resonant frequency. For each resonant frequency, there is a 180° phase shift in the motion

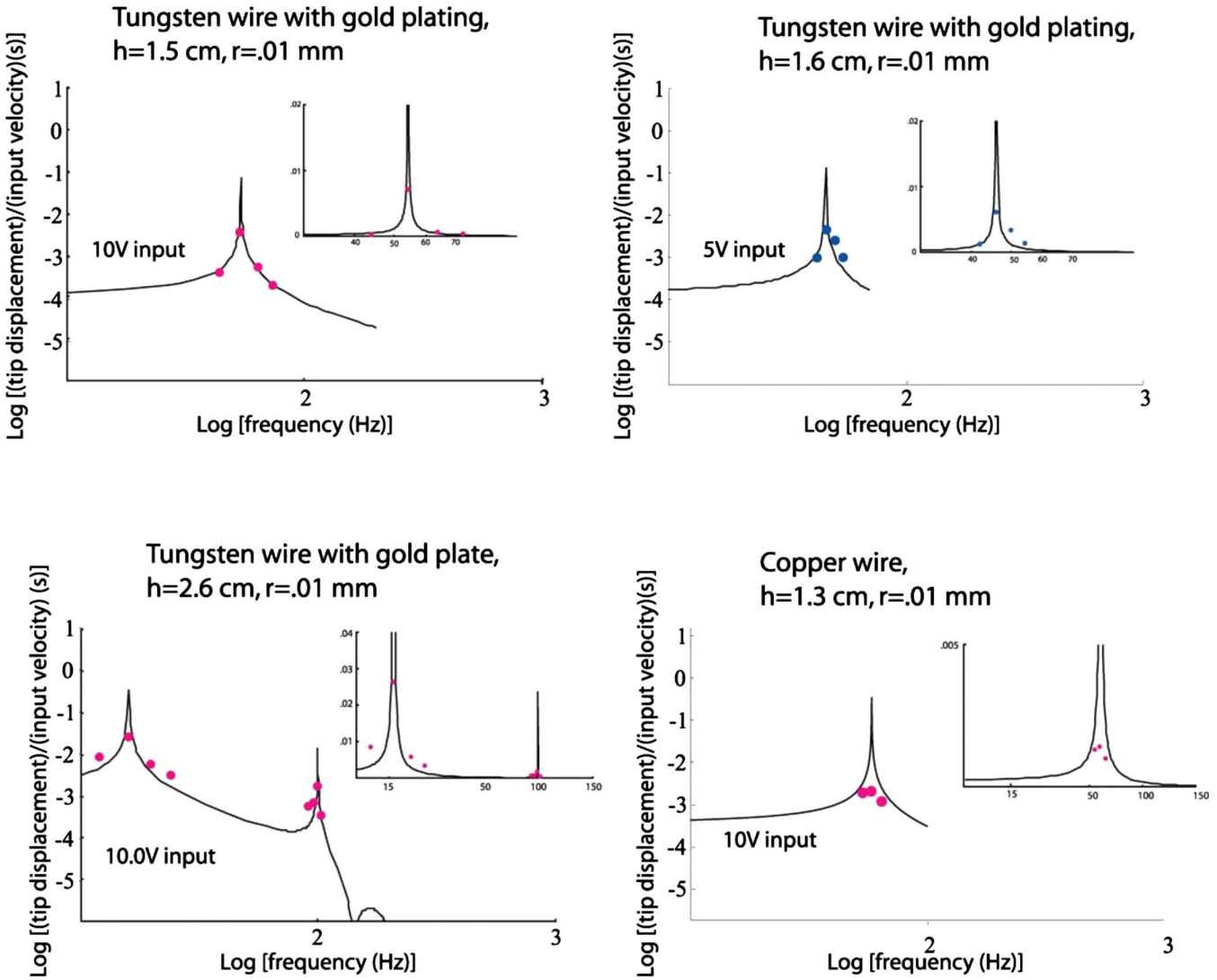


FIG. 4. (Color online) A comparison of the measurements and the FEM's predictions (solid lines) for a very thin tungsten wire with gold plating and for a very thin copper wire. A factor of 2 was used to account for attenuation of the sound in the air. For 5 V input to the speaker, speaker amplitudes of displacement ranged from 0.25 mm for a 10 Hz signal to 0.6 mm for a 100 Hz signal. For the 10 V input, the speaker amplitudes of displacement were 2–3 times as large as for the 5 V input. The ratio of tip displacement to input displacement (not shown) varied between 1.7 and 2.6. Log-linear plots shown in insets.

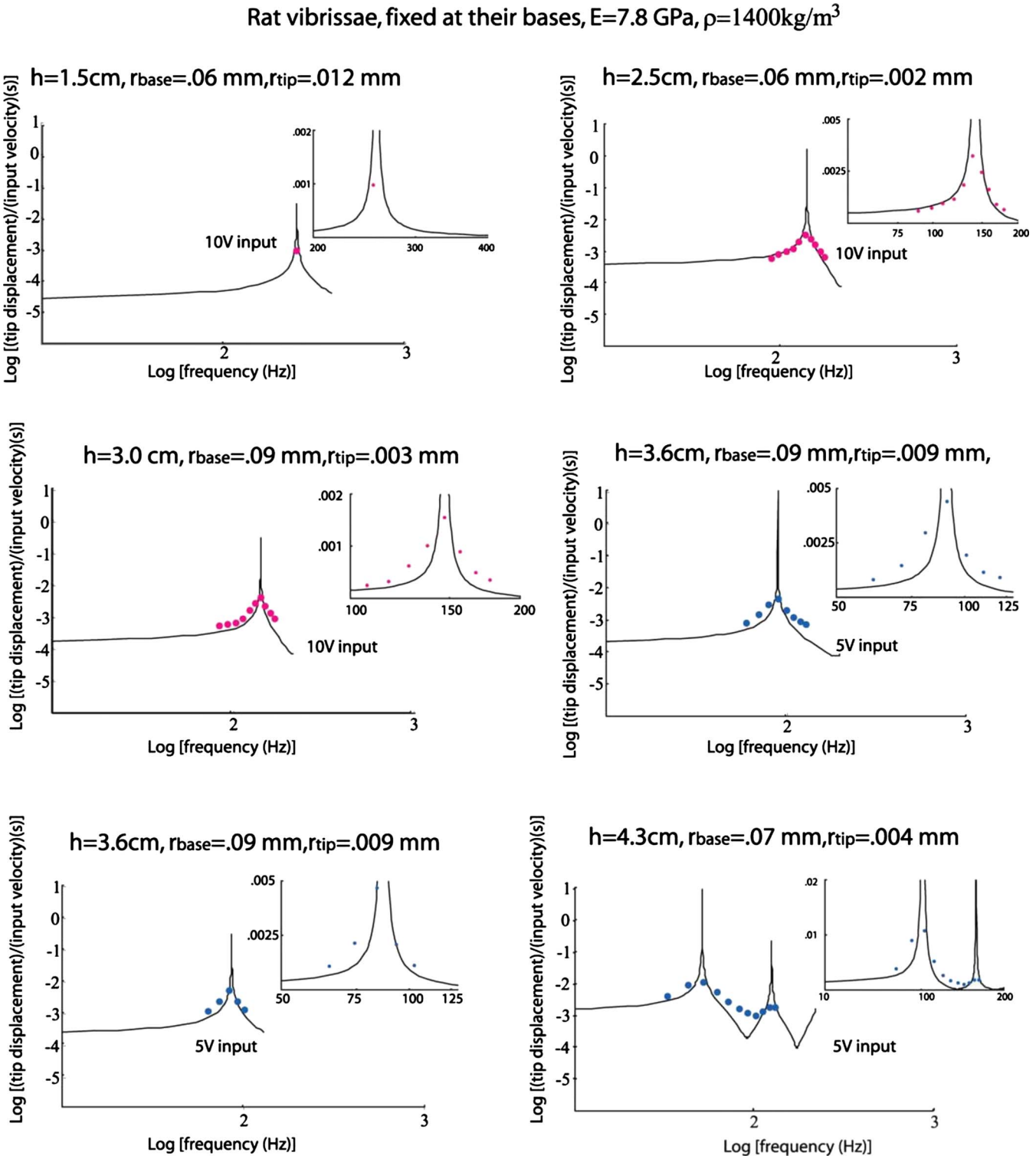


FIG. 5. (Color online) A comparison of the measurements and the FEM's predictions (solid lines) for vibrissae. For 5 V input, speaker amplitudes of displacement ranged from 0.25 mm for a 10 Hz signal to 0.6 mm for a 100 Hz signal, and then decreased to 0.35 mm for a 130 Hz signal. For frequencies above 100 Hz, 10 V signals had speaker amplitudes of displacement that were 1–2 times larger than those for 5 V signals. The ratio of tip displacement to input displacement (not shown) varied between 0.7–1.8. Log-linear plots shown in insets; r_{base} and r_{tip} are the base and tip radii of a vibrissa and were obtained from micrometer measurements.

between frequencies below that resonant frequency and frequencies above it.

B. Measurement and model comparisons for metals and vibrissae

A comparison of the results of the measurements and the FEM model for tungsten and copper wires, stimulated by sound, is shown in Fig. 4 and those for vibrissae are shown in Fig. 5. Motion of the wires and vibrissae could only be measured near the resonant frequencies; it was too small to be seen for frequencies that were too far away. Although there are no free parameters in the model, the measured length of the wires and vibrissae was determined to have an

TABLE II. A comparison of the measured lengths and those used in the model.

Type of whisker	Measured length (cm)	Length used in model (cm)
Tungsten with gold plate	1.50	1.52
Tungsten with gold plate	1.60	1.56
Tungsten with gold plate	2.50	2.65
Copper	1.30	1.32
Rat whisker	1.60	1.52
Rat whisker	2.55	2.46
Rat whisker	2.95	2.96
Rat whisker	3.65	3.55
Rat whisker	3.70	3.62
Rat whisker	4.30	4.31

error of ~1 mm due to bending and in determining where the glue ends. This was the dominant error, so the model parameter for length was chosen to be the best fit to the data; it was almost always within ~1 mm of the measured length (see Table II).[17]

Note that in all cases the model's tuning at the best frequency is sharper than the actual measurements. This is because the model does not account for air resistance due to the vibrissa's bending back and forth, which, for small displacements, is mainly near the tip. As in any resonant system, resistance serves to decrease the sharpness of tuning. This air resistance is modeled in the discussion section.

C. The phase

As was previously mentioned, since the source was not synchronized to the camera, the phase of the motion could not be observed except at frequencies that are nearly integer multiples of the rates of the interlaced scans (59.94 Hz), where full cycles of the oscillation could be seen.[18] Unfortunately, at frequencies near integer multiples of 60 Hz, effects of the electronic equipment which operate at 60 Hz may interfere with the results. Nonetheless, some corroboration of our model could be obtained. The measurements of the phase of the vibrissa oscillation with respect to the speaker oscillation are shown in Fig. 6. The phase measurements were obtained by computing the smallest difference in frame numbers between a maximum of the whisker displacement and a maximum in the speaker displacement, dividing that difference by the number of frames for a complete cycle,[19] and then multiplying the result by 360°. The fundamental frequency of the 2-cm-long vibrissa was 110 Hz, and a 180° phase addition between 61 and 181 Hz is seen in both the model and data. The 4-cm-long vibrissa has two resonant frequencies evident, one at 63 Hz and one at 169 Hz,[20] and the phase shifts of the data agreed with those predicted by the model.

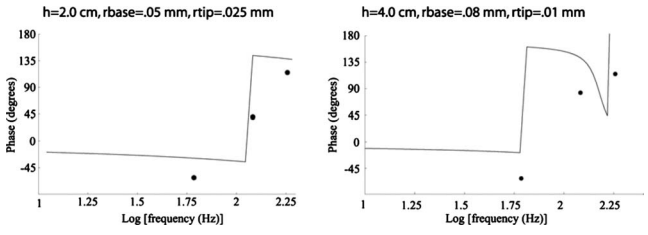


FIG. 6. The phase of the vibrissa oscillation with respect to the speaker oscillation for a 2-cm-long vibrissa (left) and a 4-cm-long vibrissa (right) at 61, 121, and 181 Hz. The solid curve indicates the model's predictions. For the shorter vibrissa, the 180° phase shift due to resonance can clearly be seen since there is only one resonant frequency in this frequency range.

The measurements indicated a 180° phase shift as predicted by the model but had lower phase shifts than the model, by ~40°. Perhaps these lower phase shifts result from the effects of the electronic equipment. Also, due to only having three data points, the effect of drag could not be discerned.

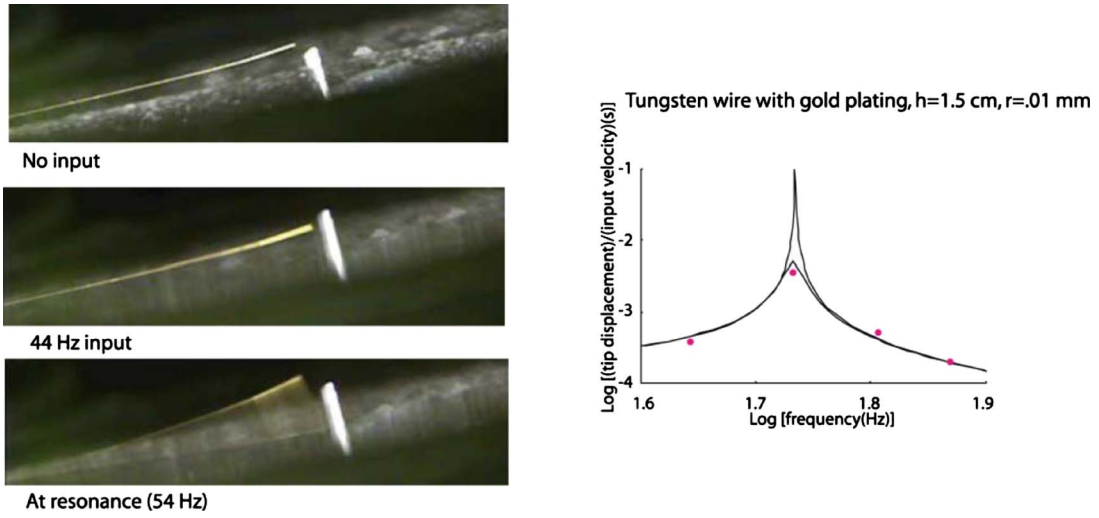
V. DISCUSSION

A. Effect of air resistance (drag) on the motion

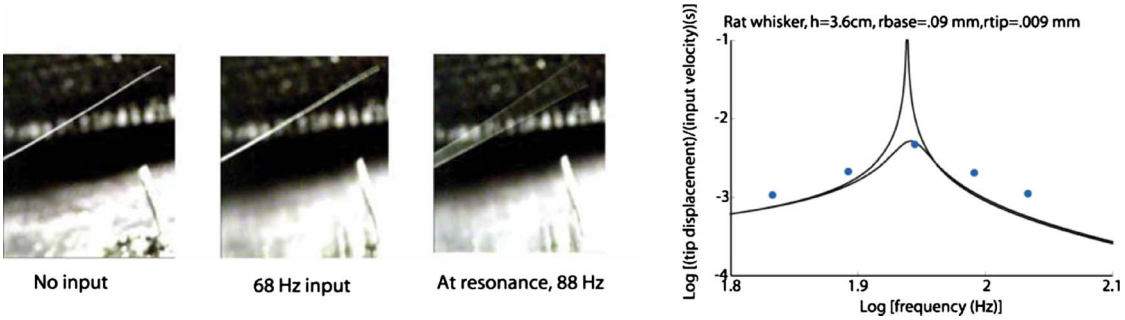
A drag term is introduced to model the effect of air resistance or drag on the motion of the vibrissa. This drag term differs from the driving fluid force. The driving fluid force is caused by the speaker motion and exists throughout the length of the vibrissa. The drag term is proportional to the vibrissa displacement $y(x)$ and therefore only exists where the vibrissa bends. A drag term was introduced into Eq. (3) giving Eq. (8):

$$\mathrm{EI}(x)\left(\frac{\partial^4 y(x)}{\partial x^4}\right) - i\omega Z(x)y(x) - \mathrm{F}_{\mathrm{fluid}} = \rho\omega^2 A(x)y(x). \quad (8)$$

The solution for an oscillating cylinder is also used to approximate the drag term, and was added to the finite element model. Figure 7 illustrates the model's predictions for the effect of air resistance. Also shown is the motion with no drag present. It is clear the drag mainly affects the motion at resonance, which makes sense because at this frequency, the vibrissa bends the most. Table III compares the response at resonance for the measurements, the model with no drag, and the model with drag. It is clear from Table III and Fig. 7 that the drag accounts for most of the discrepancies between the model's predictions and the measurements at the resonant frequencies. Accounting for the drag, most of the data (55 out of 64 data points) differ from the model's predictions by a factor of 2 or less.



A. Tungsten with gold plating



B. Rat whisker

FIG. 7. (Color online) The model's predictions for the effect of drag on a tuning curve. These results are obtained for the wire and whisker shown [also shown in Figs. 1(B) and 1(C)].

B. Comparison to other sensor hairs

It is interesting to compare tuning curves of rat vibrissae to those of other sensor hairs. Figure 8 illustrates the tuning curves for an inner ear hair bundle of an alligator lizard (in vitro[21]), a cercal hair of a cricket, and a rat vibrissa. All of these sensor hairs are surrounded by fluid, although the fluid of the inner ear hair bundle is mostly water as opposed to air for the other two sensor hairs. Also, the sensor hairs of the inner ear come in bundles that move as a single unit so their widths are effectively larger, and they are much shorter than the cercal hair or vibrissae, so their shape is considerably less prolate than the tall and thin cercal hairs and vibrissae. The main difference between the vibrissae and the other two types of sensor hairs is that vibrissae are elastic, and for small displacements, the bend is close to their tips, whereas the other sensor hairs are rigid and only bend at their bases. Moreover, because they are elastic, vibrissae display higher harmonics where the other sensor hairs do not. Another difference is that vibrissae are about one order of magnitude longer than cercal hairs and three orders of magnitude longer than inner ear hair bundles.

What is noticeable in Fig. 8 is that the tuning of a vibrissa is sharper than that of the cercal hair and the inner ear hair bundle. The quality factor Q is a measure of the selectivity of a system, and can be defined as

$$Q = \frac{f_{\text{res}}}{f_h - f_l}, \tag{9}$$

where f_{res} is the resonant frequency and f_h and f_l are the frequencies at which the amplitude is half of its value at resonance. For the inner ear hair bundle and cercal hair, $Q \approx 1$. For vibrissae and the thin metal wires, $3 \leq Q \leq 7$. This larger quality factor is likely due to the smaller effect of fluid resistance on the vibrissa, which only bends near its tip than for the other two types of sensor hairs, which bend at their bases, and are affected by fluid resistance throughout their lengths.

VI. CONCLUSION

The response of vibrissae and thin metal wires to sound has been both measured and modeled with good agreement between the model and the data. A finite element model was used to represent the mechanics with a linear fluid model used to represent the force of the air on the vibrissae and wires. The elastic vibrissae and wires were found to have

TABLE III. A comparison of the results (*tip displacement/input velocity*) at resonance: Measurements, model with no drag, model with drag. Note that the response of model with no drag at the exact resonant frequency is actually infinite. The response shown in the table is at the resonant frequency rounded to the nearest 0.1 Hz.

Whisker type	Length (cm)	Measured response at the resonant frequency (s)	Model response at resonant frequency, no drag (s)	Model response at resonant frequency, with drag (s)
Tungsten and gold plating	1.5	0.0035	0.102	0.0044
Tungsten and gold plating	1.6	0.003	1.2	0.0052
Tungsten and gold plating (two resonant frequencies measured)	2.6	0.026	0.88	0.015
		0.0017	0.056	0.001
Copper	1.3	0.0014	0.32	0.004
Rat whisker	1.5	0.00098	2.2	0.0017
Rat whisker	2.5	0.0032	0.72	0.0029
Rat whisker	3.0	0.0039	0.30	0.0033
Rat whisker	3.55	0.0047	1.1	0.0049
Rat whisker	3.62	0.0047	0.38	0.0050
Rat whisker (two resonant frequencies measured)	4.3	0.011	0.89	0.0074
		0.0018	0.61	0.0011

larger quality factors $3 \leq Q \leq 7$ than the rigid cricket cercal hairs and inner ear hair bundles, likely because fluid drag has less of an effect on bodies that can bend close to their tips than on rigid bodies that can bend only at their bases.

These findings may be of use in the development of artificial vibrissae, and in the understanding of vibrissae functioning.

ACKNOWLEDGMENTS

The authors would like to thank Christopher Moore, Jason Ritt, and Mark Andermann of MIT's Brain and Cognitive Science Department; Sandy Mulcahy, Angela Buffone, and Carl Merrill of Suffolk University's Biology Department; Bill Walcott and Patrick O'Hanlan of SU 's Media Services; Pat Hogan of SU's Environmental Engineering Department; Tom Vales of SU's Electrical and Computer Engineering Department and Michael Shatz.

APPENDIX

The Navier–Stokes equation,

$$\rho_{\text{air}} \frac{\partial \mathbf{u}(\mathbf{r},t)}{\partial \mathrm{t}} + \rho_{\text{air}}(\mathbf{u}(\mathbf{r},t)\cdot\nabla)\mathbf{u}(\mathbf{r},t) = -\nabla P(\mathbf{r},t) + \mu\nabla^2\mathbf{u}(\mathbf{r},t), \tag{A1}$$

represents conservation of momentum in a fluid. If the magnitude of the linear inertial term of Eq. (A1) $\rho_{\text{air}}\partial\mathbf{u}(\mathbf{r},t)/\partial t$ is much greater than the convective nonlinear term, $|\rho_{\text{air}}\partial\mathbf{u}(\mathbf{r},t)/\partial \mathrm{t}| \gg |\rho_{\text{air}}(\mathbf{u}(\mathbf{r},t)\cdot\nabla)\mathbf{u}(\mathbf{r},t)|$, the fluid can be considered linear. Let $\mathbf{u}(\mathbf{r},t)=U_f e^{\mathrm{j}\omega t}$. The magnitude of the linear inertial term can be approximated as $\omega\rho_{\text{air}}U_f$ and the compressive nonlinear term can be approximated as $\rho_{\text{air}}U_f^2/d$, where d represents the smallest distance over which the velocity changes significantly (Freeman and Weiss, 1986). Let us approximate d by the boundary layer thickness $d \approx \sqrt{2\mu/(\rho_{\text{air}}\omega)}$. The ratio of the nonlinear term to the linear term can be represented as

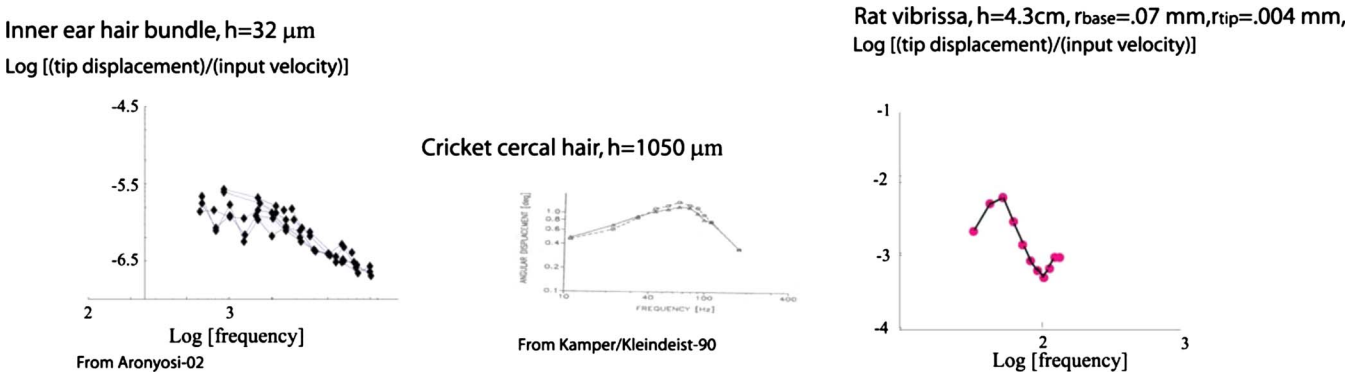


FIG. 8. (Color online) A comparison of the tuning curve measurements for an inner ear alligator lizard hair bundle (right), a cercal cricket hair (middle) and rat vibrissa (left). Each curve has the same scale.

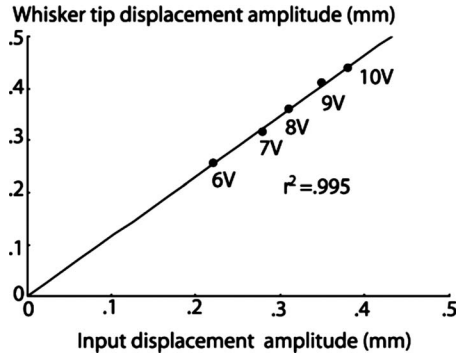


FIG. 9. A test of the linearity assumption. Whisker displacement is shown as a function of the input displacement (half of the speaker displacement). Linearity is clearly demonstrated. For whisker h=5.3 cm, r_{base}=0.14 mm, r_{tip}=0.08 mm, at resonance, f=43 Hz.

$$R_{nl} = \frac{U_f}{\omega d} = \frac{X_f}{d} = X_f \sqrt{\frac{\rho_{air}\omega}{2\mu}},$$

where X_f is the air displacement. With the physiological relevant parameters, $\rho_{air}=1.2\ kg/m^3$, $\mu=1.7\cdot10^{-5}\ kg/(m\ s)$, and with the sound amplitude of $X_f=0.0004$ m (corresponding to a 10 V input to the speaker, with a factor of 2 attenuation at the body), at the lowest frequency f=30 Hz makes $R_{nl}=1$. At higher frequencies X_f decreases and R_{nl} remains roughly equal to 1 throughout the frequency range.

This result would indicate that using a linear approximation would result in some errors; however, the linearity of the fluid was tested by observing the tip displacement as a function of input displacements (Fig. 9). Linearity was clearly observed with a correlation coefficient value of 0.995.

[1]Radioshack™ Model FE-103, 9.2 cm in diameter.
[2]ShinyBox™ Ribbon Microphone, Model 46 MX.
[3]The vibrissae are within ~20 mm from the innermost point of the speaker.
[4]Radius of curvature of the speaker is 14 mm.
[5]The lengths of vibrissa used in this study fall in the range of 15–43 mm.
[6]Tungsten with gold plating has a mass density of 19300 kg/m^3 (Hodgeman, C. D., Ed. (1962). Handbook of Chemistry and Physics. Cleveland, The Chemical Rubber Publishing Company.) and has a Young's modulus, measured with an Instron 8845 Microtester™ at the MIT NanoMechanical Technology Laboratory, of 312 GPA. Copper has a mass density of 8920 kg/m^3 (Winter, M. (1993–2007). WebElementsTM, the periodic table on the WWW, The University of Sheffield and WebElements Ltd., UK. ⟨http://www.webelements.com/webelements/scholar/elements/copper/physical.html⟩) and a Young's modulus of 116 GPA (De Keulenaer, H. (2007), European Copper Institute. Leonardo Energy, European Copper Institute, ⟨http://www.leonardo-energy.org/drupal/node/1032⟩).
[7]A needle was glued to the speaker to facilitate the measurements of its displacements.
[8]For some of the metal wires, the data were taken at 4 Hz intervals.
[9]This is the resonant frequency of the tungsten with gold plating wire with a length of 1.5 cm [Fig. 1(B)].
[10]Note that the cycle of the motion of the vibrissa in the movie is not the same as its period of oscillation due to the effects of the frame rate with interlacing. The differences in maximum displacements between the cycles were not measurable.
[11]Air velocity is $2\pi f$ times the maximum air displacement.
[12]The validity of the linear approximation for the fluid will be discussed in the Appendix.
[13]The validity of assuming the fluid is linear will be discussed on the Appendix.
[14]For the frequencies used in this study: 10 Hz$<f<$340 Hz, λ, the wavelength of sound varies between: 34 m>λ>1 m. Since these wavelengths are much greater than the vibrissa and wire displacements, which are on the order of 0.1 mm, the wave properties of the sound have an insignificant effect.
[15]The width of the cylinder is taken to be the mean width of the element.
[16]n=19 for all the model simulations described in this paper.
[17]One measurement, that for a tungsten with gold plate wire with h=2.5 cm had a model length that was 1.5 mm more than its measurement. See Table II for a list of the measured lengths and those used in the model.
[18]The shutter speed of the camera also needed to be increased to observe two images per frame.
[19]For 61 Hz, the number of frames per cycle was 28–29; for 121 Hz it was 26–27; for 181 Hz it was 25–26.
[20]This is the models' predicted first harmonic frequency. The measured first harmonic was difficult to measure but appeared to be at a somewhat lower frequency, between 131 and 161 Hz.
[21]An inner ear hair bundle in vivo is much more sharply tuned due to active mechanisms in the inner ear (Manley, G. A., Kirk, D. L., Koppl, C., and Yates, G. K. (2001)). "In vivo evidence for a cochlear amplifier in the hair-cell bundle of lizards," Proc. Natl. Acad. Sci. U.S.A. **98**, 2826–2831.

Aranyosi, A. J. (**2002**). "Measuring sound-induced motions of the alligator lizard cochlea," Massachusetts Institute of Technology, Ph.D. thesis.
Barth, F., Wastl, U., Humphrey, J., and Devarakaonda, R. (**1993**). "Dynamics of arthropod filiform hairs. II Mechanical properties of spider trichobothria (Cupiennius salei Keys.)," Philos. Trans. R. Soc. London, Ser. B **340**, 445–461.
Batchelor, G. K. (**1967**). *An Introduction to Fluid Dynamics*, (Cambridge University Press, London).
Dehnhardt, G., Mauck, B., Hanke, W., and Bleckmann, H. (**2001**). "Hydrodynamic trail-following in harbor seals (phoca vitulina)," Science **293**, 102–104.
De Keulenaer, H. (**2007**). European Copper Institute. Leonardo Energy, European Copper Institute. ⟨http://www.leonardo-energy.org/drupal/node/1032⟩(last accessed April 1, 2008).
Freeman, D. M., and Weiss, T. F. (**1986**). "On the role of fluid inertia and viscosity in stereociliary tuft motion: Analysis of isolated bodies of regular geometry," in *Peripheral Auditory Mechanisms*, edited by J. B. Allen, J. L. Hall, S. T. Neely, and A. Tubis (Springer Verlag, New York), 147–154.
Freeman, D. M., and Weiss, T. F. (**1990a**). "Superposition of hydrodynamic forces on a hair bundle," Hear. Res. **48**, 1–16.
Freeman, D. M., and Weiss, T. F. (**1990b**). "Hydrodynamic forces on hair bundles at high frequencies," Hear. Res. **48**, 31–36.
Freeman, D. M., and Weiss, T. F. (**1990c**). "Hydrodynamic forces on hair bundles at low frequencies," Hear. Res. **48**, 17–30.
Freeman, D. M., and Weiss, T. F. (**1990d**). "Hydrodynamic analysis of a two-dimensional model for micro-mechanical resonance of free-standing hair bundles," Hear. Res. **48**, 37–68.
Hartmann, M. J., Johnson, N. J., Towal, R. B., and Assad, C. (**2003**). "Mechanical characteristics of rat vibrissae: Resonant frequencies and damping in isolated whiskers and in the awake behaving animal," J. Neurosci. **23**, 6510–6519.
Hodgeman, C. D., Ed. (**1962**). *Handbook of Chemistry and Physics* (Chemical Rubber, Cleveland).
Humphrey, J., Devarakaonda, R., Iglesias, I., and Barth, F. (**1993**). "Dynamics of arthropod filiform hairs. I. Mathematical modeling of the hair and air motions," Philos. Trans. R. Soc. London, Ser. B **340**, 424–443.
Kamper, G., and Kleindeist, H. (**1990**). "Oscillation of cricket sensory hairs in a low frequency sound field," J. Comp. Physiol., A **167**, 193–200.
Manley, G. A., Kirk, D. L., Koppl, C., and Yates, G. K. (**2001**). "In vivo evidence for a cochlear amplifier in the hair-cell bundle of lizards," Proc. Natl. Acad. Sci. U.S.A. **98**, 2826–2831.
Neimark, M. A., Andermann, A. L., Hopfield, J. J., and Moore, C. I. (**2003**). "Vibrissa resonance as a transduction mechanism for tactile encoding," J. Neurosci. **23**, 6449–6509.
Reep, R. L., Marshall, C. D., and Stoll, M. L. (**2002**). "Tactile hairs on the post-cranial body in Florida manatees: A mammalian lateral line?," Brain Behav. Evol. **59**, 141–154.
Shatz, L. (**2000**). "The effect of hair bundle shape on hair bundle hydrodynamics of inner ear hair cells at low and high frequencies," Hear. Res. **141**, 39–50.
Shatz, L. (**2004**). "The effect of hair bundle shape on hair bundle hydrodynamics of non-mammalian inner ear hair cells for the full frequency range," Hear. Res. **195**, 41–53.
Shatz, L. (**2005**). "Slender body method for slender prolate spheroids and hemispheroids on planes in linearized oscillatory flow," Phys. Fluids **17**,

113603–113603.
Shimozawa, T. (**1984**). "The aerodynamics and sensory physiology of range fractionation in the cercal filiform sensilla in the cricket gryllus bimaculatue," J. Comp. Physiol., A **155**, 495–505.
Shimozawa, T., Kumagai, T., and Baba, Y. (**1998a**). "Structural scaling and functional design of the cercal wind-receptor hairs of cricket," J. Comp. Physiol., A **183**, 171–186.
Shimozawa, T., Kumagai, T., and Baba, Y. (**1998b**). "The shape of wind-receptor hairs of cricket and cockroach," J. Comp. Physiol., A **183**, 187–192.
Winter, M. (**1993-2007**). WebElements, The periodic table on the WWW, The University of Sheffield and WebElements Ltd., UK. ⟨http://www.webelements.com/webelements/scholar/elements/copper/physical.html⟩ (last viewed 4/10/2008).

Frequency and level dependent masking of the multiple auditory steady-state response in the bottlenose dolphin (*Tursiops truncatus*)

Brian K. Branstetter[a] and James J. Finneran
U.S. Navy Marine Mammal Program, Space and Naval Warfare Systems Center, San Diego, Code 71510, 53560 Hull Street, San Diego, California 92152

Dorian S. Houser
Biomimetica, 7951 Shantung Drive, Santee, California 92071

(Received 8 August 2007; revised 11 February 2008; accepted 14 February 2008)

The potential for interactions between steady-state evoked responses to simultaneous auditory stimuli was investigated in two bottlenose dolphins (*Tursiops truncatus*). Three experiments were conducted using either a probe stimulus (probe condition) or a probe in the presence of a masker (probe-plus-masker condition). In the first experiment, the probe and masker were sinusoidal amplitude-modulated (SAM) tones. Probe and masker frequencies and masker level were manipulated to provide variable masking conditions. Probe frequencies were 31.7, 63.5, 100.8, and 127.0 kHz. The second experiment was identical to the first except only the 63.5 kHz probe was used and maskers were pure tones. For the third experiment, thresholds were measured for the probe and probe-plus-masker conditions using two techniques, one based on the lowest detectable response and the other based on a regression analysis. Results demonstrated localized masking effects where lower frequency maskers suppressed higher frequency probes and higher amplitude maskers produced a greater masking effect. The pattern of pure tone masking was nearly identical to SAM tone masking. The two threshold estimates were similar in low masking conditions, but in high masking conditions the lowest detectable response tended to overestimate thresholds while the regression-based analysis tended to underestimate thresholds.
© *2008 Acoustical Society of America.* [DOI: 10.1121/1.2896753]

PACS number(s): 43.80.Lb, 43.64.Ri, 43.66.Dc, 43.66.Gf [WWA] Pages: 2928–2935

I. INTRODUCTION

The emergent use of the multiple auditory steady-state response (ASSR) has proven to be a useful and efficient method for odontocete audiometric assessment (Finneran and Houser, 2007; Finneran *et al.*, 2007a; d). When multiple sinusoidal amplitude-modulated (SAM) tones, each with a unique carrier and modulation frequency, are simultaneously presented, the ASSR to each carrier frequency occurs at the corresponding modulation frequency, allowing hearing to be simultaneously tested at multiple frequencies (Lins and Picton, 1995; John *et al.*, 1998). This method has been used to test up to nine simultaneous frequencies in dolphins (Finneran *et al.*, 2008), significantly reducing the time required for estimating a complete audiogram.

Although the multiple ASSR technique offers significant time advantages, interactions between the SAM tones have the potential to attenuate aspects of the evoked response, thus, confounding threshold measurements. In humans, significant interactions between SAM tones occur when stimuli are separated by a half octave or less (John *et al.*, 1998). Higher-amplitude SAM tones have a greater masking effect than low-amplitude SAM tones; however, when up to four SAM tones are each separated by one octave, no significant interactions are observed in human subjects (John *et al.*, 1998). Popov *et al.* (1997; 1998) demonstrated that the ASSR for a bottlenose dolphin could be suppressed when a flanking pure tone was added to a SAM tone. Suppression was most salient with higher amplitude flanking pure tones that were similar in frequency (within 1/6 of an octave) to the SAM tone probe. Similar interactions occur for psychophysical measurements of two-tone masking (Johnson, 1971). Dolphin listeners exhibit a pattern of masking where lower-frequency pure tones tend to mask higher-frequency pure tones, a result consistent with human listeners in an analog task (Wegel and Lane, 1924). Excitation patterns on the differentially responsive basilar membrane have been implicated in this asymmetrical pattern known as the upward spread of masking.

The effects of tone interactions on the resulting threshold estimates may also be affected by the specific threshold estimation procedure. Two common methods for estimating thresholds for single SAM tones are: (1) a threshold based on the lowest-detectable response (LDR) (Finneran *et al.*, 2007b) and (2) a regression-based analysis (REG) (Popov and Supin, 1985; Nachtigall *et al.*, 2005). In the application of the LDR, thresholds are defined as the lowest stimulus level producing a statistically determined detectable response, the average stimulus level associated with the lowest detection and the next highest nondetection, or by averaging the stimulus levels corresponding to a set number of reversals (a change from response detection to nondetection, or

[a]Electronic mail: branstet@hawaii.edu

 0001-4966/2008/123(5)/2928/8/$23.00 © 2008 Acoustical Society of America

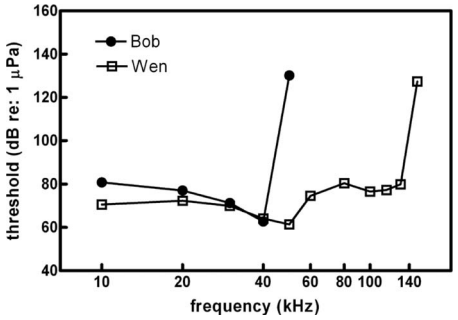


FIG. 1. Previously measured AEP audiograms for BOB and WEN using single SAM tone stimuli. WEN had normal hearing to 130 kHz and BOB had high frequency hearing loss with normal hearing to 40 kHz.

vice versa). For the REG method, a linear regression is first performed on the ASSR input–output (I/O) function (the relationship between stimulus level and ASSR amplitude). Thresholds are then calculated by interpolating/extrapolating the regression line to determine the stimulus level producing some predefined ASSR amplitude, often 0 V, i.e., the stimulus amplitude that would produce a 0 V ASSR is arbitrarily chosen as the threshold. Conditions that produce masking during the multiple ASSR procedure have the potential to attenuate the evoked response, thus biasing thresholds using either procedure. For example, masking may inflate thresholds calculated by the LDR by reducing the ability to detect responses at lower stimulus levels. REG based thresholds, on the other hand, may be affected if the I/O function is altered by interactions between multiple tones.

The main goals of the present study were to (1) identify the conditions (the relative amplitude and frequency spacing between tones) that would produce significant interaction when using the multiple ASSR procedure, (2) to determine the extent that commonly used threshold estimation procedures (LDR and REG) would be biased as a result of probe–masker interactions, and (3) to provide general guidelines in choosing methodology and stimuli configuration when employing the multiple ASSR procedure during audiometric testing.

II. SUBJECTS

The subjects were two male bottlenose dolphins (WEN, 24 years; BOB, 29 years) with extensive experience in electrophysiological audiometry. Prior testing revealed normal hearing sensitivity up to 130 kHz for WEN and high frequency hearing loss for BOB with normal hearing up to 40 kHz (Fig. 1). Of three experiments performed, WEN participated in all three experiments and BOB only participated in experiment I. The subjects were housed in 9×9 to 9×18 m netted enclosures (pens) located in San Diego Bay CA. The study followed a protocol approved by the Institutional Animal Care and Use Committee of the Biosciences Division, Space and Naval Warfare Systems Center, San Diego, and all applicable U.S. Department of Defense guidelines for the care of laboratory animals.

TABLE I. Stimuli parameters for experiment I.

Probe			Masker	
Carrier frequency (kHz)	Modulation rate (kHz)	Sound pressure level (dB re 1 μPa)	Carrier frequency (kHz)	Modulation rate (kHz)
31.7	1.0	100	15.9, 20.0, 25.2, 40.0, 50.4, 63.5	1.1
63.5	1.0	105	31.7, 40.0, 50.4, 80.0, 100.8, 127.0	1.1
100.8	1.0	114	50.4, 63.5, 80.0, 127, 160	1.1
127.0	1.0	113	50.4, 63.5, 80.0, 100.8, 160.0	1.1

III. EXPERIMENT I: TWO SAM-TONE MASKING

The goal of experiment I was to determine the relationship between the relative amplitude and frequency separation of two SAM tones and the resulting ASSR amplitudes. We predicted similar results to that of John *et al.* (1998), where only high amplitude maskers with frequencies within one octave would contribute to the masking of the probe stimulus. Furthermore, we predicted a masking pattern consistent with an upward spread of masking.

A. Methods

Two stimulus conditions were used: a probe alone stimulus (baseline) and a probe-plus-masker stimulus. Each probe consisted of a SAM tone with a 100% amplitude-modulation depth and modulation rate of 1.0 kHz. A modulation rate of 1.0 kHz was chosen because the bottlenose dolphin's modulation rate transfer function displays good sensitivity around 1.0 kHz (Dolphin *et al.*, 1995; Supin and Popov, 1995; Finneran *et al.*, 2007c). Four probe carrier frequencies were used: 31.7, 63.5, 100.8, or 127.0 kHz. WEN was tested at each probe frequency, while BOB, because of high frequency hearing loss, was only tested at 31.7 kHz. Each probe was presented at a sensation level (SL) of 30 dB (i.e., 30 dB above previously measured ASSR thresholds). For each probe-plus-masker condition, a single masker was simultaneously presented with the probe. Each masker consisted of a SAM tone with a 100% depth and a rate of 1.1 kHz. The carrier frequency of the masker in each probe-plus-masker condition is presented in Table I. In humans, significant interactions occurred when the probe and masker carrier frequencies were separated by less than an octave (John *et al.*, 1998). We therefore chose the frequency separation between the carrier and the masker to be spaced by 1/3 octave steps with the assumption that a measurable interaction would occur for at least several of the probe-plus-masker conditions. This frequency separation also roughly reflects the frequency selectivity of mammalian peripheral auditory filters (Fletcher, 1940; Johnson, 1968; Patterson, 1976) allowing us to assess if interactions are related to this mechanism. Each masker was presented at seven different amplitudes, covering the range of ±30 dB relative to the

probe amplitude in 10 dB steps. Both masker and probe stimuli were 32 ms in duration with 1 ms cosine onset–offset envelopes.

Stimulus generation and evoked potential recording was performed using the Evoked Response Study Tool [EVREST, Finneran (2008)]. Each SAM tone instantaneous voltage, $v(t)$, was created by multiplying a pure tone carrier by a sinusoidal modulator:

$$v(t) = \frac{A}{2}[1 - \cos(2\pi ft)]\sin(2\pi Ft), \quad (1)$$

where A is the tone amplitude, t is time, F is the carrier frequency, and f is the modulation frequency. The resulting signal possessed a frequency spectrum containing a center frequency at F with flanking tones located at $F \pm f$. The probe and masker were summed prior to digital-to-analog conversion using a 2 MHz update rate and 16 bit resolution (National Instruments PCI-6251). Stimuli were bandpass filtered (200 Hz to 150 kHz, Krohn-Hite 3C series module), attenuated if necessary, and presented via a "jawphone" transducer (a piezoelectric sound projector embedded in a silicon rubber suction cup) that was attached to the left pan region of the dolphin lower jaw [for details see Finneran and Houser (2006)]. In-air auditory evoked potential (AEP) thresholds using a similar jaw phone have been strongly correlated to underwater behavioral thresholds in dolphins (Finneran and Houser, 2006), thus validating this technique.

During experimental sessions, each dolphin was cued by a trainer to "beach" himself, and remained on a padded mat within a floating wooden hut adjacent to the pens. The inside of the hut was lined with sound attenuating foam and provided enough room for the dolphin, a trainer, a researcher operating a portable computer, and an assistant. Between each measurement sequence (approximately 5–10 min), dolphins were rewarded with fish for remaining still and their skin was kept moist with a water hose. At the end of the session the dolphin was reinforced for sliding back into the pens. Each session lasted approximately 30–45 min.

AEPs were recorded for each condition using three suction cups embedded with 10 mm gold cup surface electrodes. The noninverting electrode (+) was positioned behind the blow hole and slightly contralateral to the receiving jaw phone. The inverting electrode (−) was placed near the contralateral meatus relative to the jawphone. A common electrode was placed on the back of the dolphin anterior to the dorsal fin. Conductive gel was applied to each electrode before placement. Electrode signals were amplified and filtered ($\times 10^5$, 300–3000 Hz, Grass ICP511), then digitized (PCI-6251) at a 10 kHz sampling rate. Recordings were made over 40 ms epochs synchronized with the start of each stimulus. Stimuli were presented at a rate of approximately 25/s. Frequency analysis was performed on a 30 ms rectangular window centered on the ASSR. Coherent averaging was performed in the frequency domain using a total of 500 epochs for each measurement. AEP peak voltages exceeding 12 μV were considered artifacts and excluded from averaging. The amplitude of the spectral peak at 1.0 kHz (corresponding to the probe stimulus) was compared between the probe-alone and probe-plus-masker conditions to assess the level of masking. AEPs were recorded first for the probe-alone condition followed by the probe-plus-masker condition for each masker frequency. The presentation of masker frequency was randomized while masker levels were presented in an ascending order. The procedure was repeated for each probe frequency.

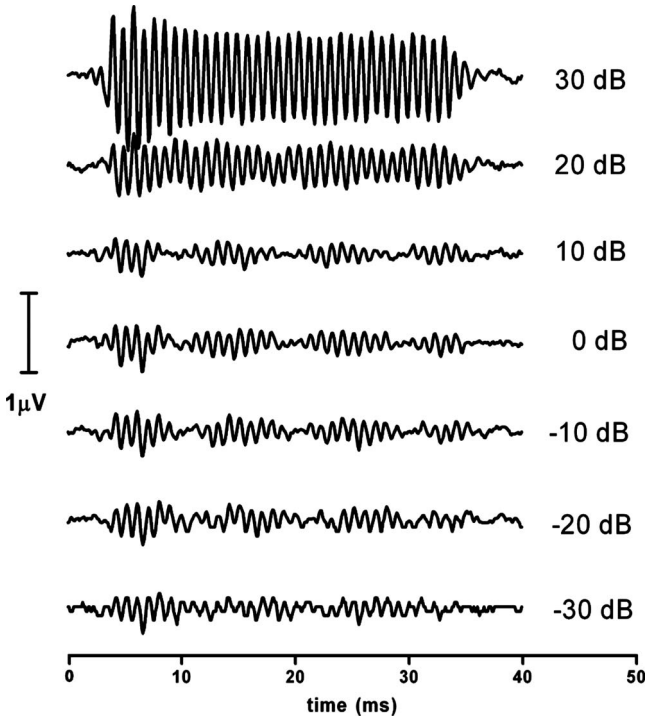


FIG. 2. ASSR waveforms from WEN in response to a stimulus consisting of a SAM probe at 31.7 kHz and a SAM masker at 25.2 kHz. The level of the probe was at a constant 30 dB SL and the level of the masker varied ±30 dB relative to the level of the probe, indicated by the numbers to the right of each trace.

B. Results

A total of three experimental sessions were conducted resulting in three replicated AEP measurements for each condition for each subject. Figure 2 displays a series of AEP waveforms recorded from WEN in response to a 31.7 kHz SAM probe and a 25.2 kHz SAM masker. Figure 3 displays the frequency spectra from the waveforms in Fig. 2. The peaks at 1.0 and 1.1 kHz represent the amplitude of the ASSR to the probe and masker AM rates, respectively. As the level of the masker increased, the response to the probe was suppressed until it was no longer visible.

Figures 4 and 5 display the probe ASSR relative amplitude as a function of the relative masker frequency and level for WEN and BOB, respectively. The vertical dashed line indicates the frequency of the probe stimulus. The frequency scale has been converted to an octave scale (re: probe frequency) to better facilitate comparisons between conditions. The relative probe response amplitude was calculated by dividing the probe ASSR amplitude for the probe-plus-masker condition by the probe ASSR amplitude for the probe alone (baseline) condition from the same test session. Lower rela-

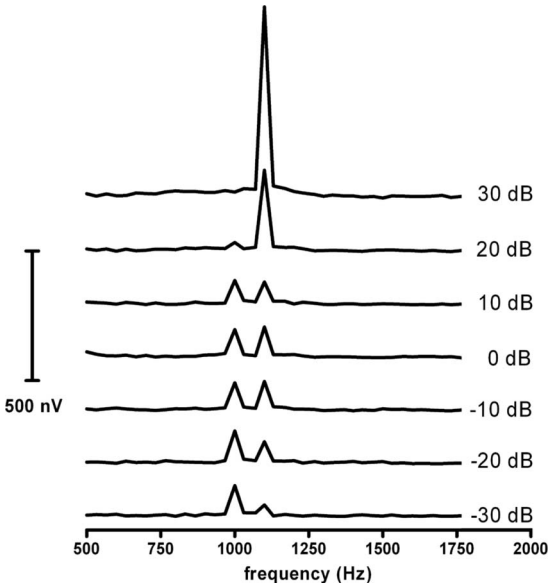


FIG. 3. Frequency spectra from the waveforms in Fig. 2. The numbers to the right of each trace indicate the masker level relative to the probe level, which was 30 dB SL. The peaks at 1.0 and 1.1 kHz represent the ASSR amplitude response to the probe and masker modulation rates, respectively. As the level of the masker increased, the spectral peak corresponding to the probe increased, while the spectral peak corresponding to the masker decreased until it was no longer visible.

tive amplitudes indicate greater masking of the probe ASSR. A value of 1 indicates no interaction. Each data point represents the mean of three measurements.

For each probe frequency, the main effects (masker frequency and amplitude) and the interaction between the main effects were evaluated with a repeated measures, two-way analysis of variance (ANOVA). For all probe frequencies, the amplitude of the masker had a significant effect ($p<0.01$) as did the frequency of the masker ($p<0.05$), for both dolphins. A significant interaction between masker amplitude and masker frequency occurred for the 31.7 kHz probe ($p=0.005$), and the 63.5 kHz probe ($p<0.001$) for WEN. No significant interactions occurred for BOB. Several data points suggest the interaction between the probe and masker may have had a subtle additive effect (values greater than 1). The largest example occurred for BOB, for the masker frequency of 15.9 kHz (one octave below the 31.7 kHz probe frequency) at the highest masker amplitude decibel. However, this apparent large response was not significantly different from the corresponding probe alone condition (two-tailed t-test, $p=0.11$). Inconsistencies inherent to the AEP procedure (e.g., electrode and jaw phone placement) likely accounted for much of the variability for values near the normalized amplitude of 1. On average, amplitude, frequency, and interaction accounted for 25.9%, 10.4%, and 14.1% of the total variance, respectively, for WEN. High amplitude maskers less than an octave below the probe produced the greatest amount of masking.

IV. EXPERIMENT II. SAM TONE VERSUS PURE TONE MASKING

This experiment was created to compare masking levels between SAM and pure-tones since Popov *et al.* (1998) demonstrated that a pure-tone could mask a SAM tone with a similar carrier in dolphins. The comparison between SAM and pure tone masker permits the relative importance of amplitude modulation to masking to be ascertained.

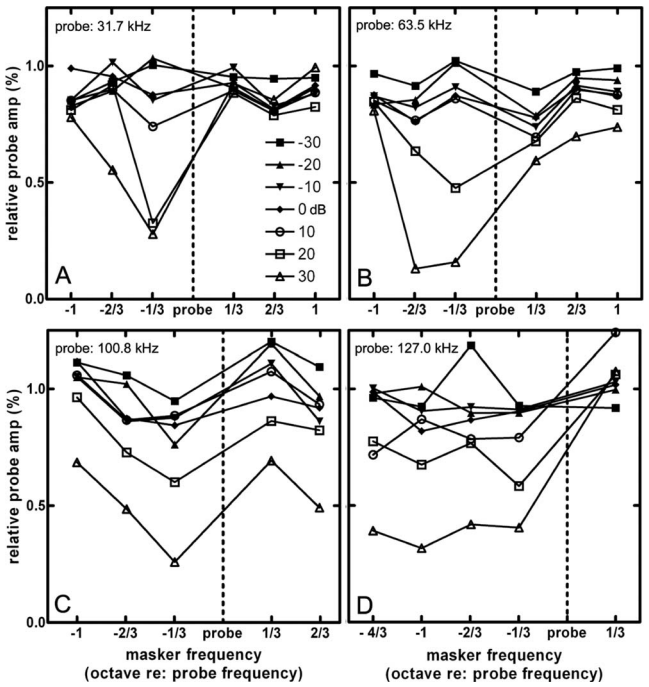


FIG. 4. Probe ASSR amplitudes as a function of masker frequency (in octaves relative to the probe frequency) and masker level (for WEN only). The vertical dotted line indicates the frequency of the probe stimulus. (A), (B), (C), and (D) correspond to probe frequencies of 31.7, 63.5, 100.8, and 127.0 kHz, respectively. The amplitude of the probe ASSR in the masker-plus-probe condition was normalized to the level of the probe in the baseline probe-alone condition. Lower values indicate greater masking and a value of 1 indicates no interaction. Each data point represents the mean of three measurements. Error bars were excluded for clarity, however, the average standard deviation around these data points was 0.15.

A. Methods

The stimuli and recording procedures in this experiment were identical to those of the 63.5 kHz probe condition in

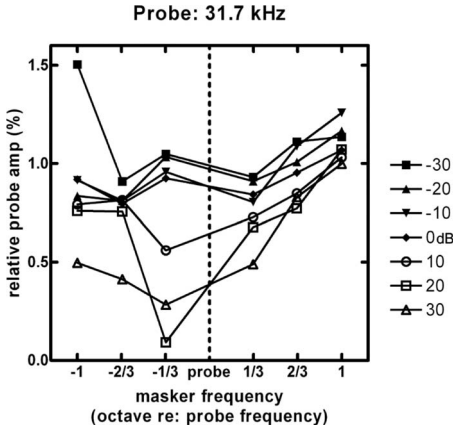


FIG. 5. Probe ASSR levels as a function of masker frequency and masker level (for BOB). Each data point represents the average of three measurements. Error bars were excluded for clarity.

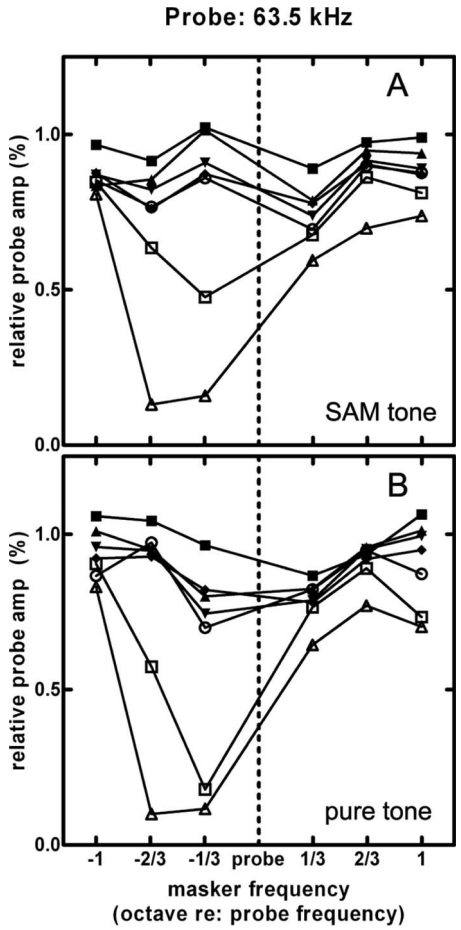


FIG. 6. Probe ASSR levels for both SAM tone maskers (A) and pure tone maskers (B) at 63.5 kHz (data from WEN, experiments I and II).

experiment I, except the maskers were pure tones instead of SAM tones. The subject for this experiment was WEN.

B. Results

The AEP measurements obtained for WEN in each pure tone masking condition were compared against corresponding SAM tone conditions in experiment I. Figure 6 displays the 63.5 kHz probe with both SAM and pure-tone maskers. The pattern of SAM and pure tone masking are very similar, with no significant difference (multifactorial, repeated measures ANOVA: $p=0.52$) between the main effect of masker type (SAM versus pure tone). This suggests that the frequency and amplitude component of the stimuli, rather than the amplitude modulation, are the key factors affecting masking.

V. EXPERIMENT III: THRESHOLD ESTIMATION PROCEDURE

We compared two commonly used threshold estimation procedures (LDR and REG) to test their susceptibility to threshold estimation biases during conditions likely to produce masking.

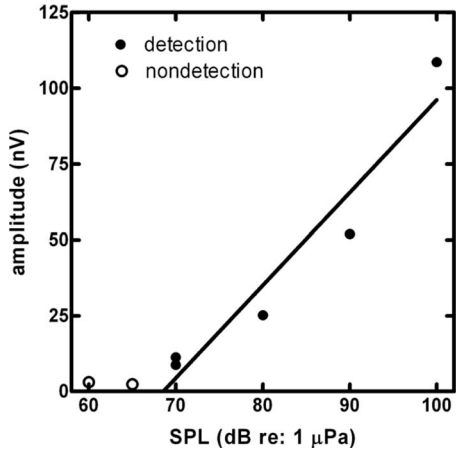


FIG. 7. ASSR amplitude as a function of probe SPL. Thresholds were computed for both LDR and REG using the same data set. Closed circles represent detections and open circles represent nondetections. A line was fit to the descending detections only for REG. [Note: There are two points for 70 dB, one before the reversal (descending staircase) and one after the reversal (ascending staircase) and the *x*-axis intercept is used as the threshold estimation. LDR thresholds are computed by averaging the highest nondetection and the lowest detection.]

A. Methods

Stimuli were presented using an adaptive up/down staircase procedure (Finneran and Houser, 2006). After each stimulus presentation, the magnitude-squared coherence (MSC) was calculated for the probe ASSR (using a total of 500 epochs with 20 subaverages, 25 epochs per subaverage) and compared to critical values for the MSC, based on $\alpha=0.01$ (Dobie and Wilson, 1989, 1996; Finneran *et al.*, 2007b). If the MSC exceeded the critical value, the evoked response due to the probe (i.e., at the probe modulation rate) was considered to be detected. After each detection, the stimulus SPL was decreased by 10 dB until the response was no longer detected. After the first nondetection, the SPL was increased by 5 dB until a response was detected. LDR thresholds were calculated by averaging the SPL corresponding to the lowest detection and the highest nondetection (Finneran *et al.*, 2007b). For REG based thresholds, a regression line was fit to a subset of this data, using only the detections that occurred before the first nondetection (see Fig. 7). The SPL where the regression line crossed an amplitude value of zero was used as the arbitrary threshold level. Thus, LDR and REG thresholds were estimated from the same data set.

Thresholds were estimated for three experimental conditions: (1) probe alone, (2) equal probe plus masker (EPM), and (3) unequal probe plus masker (UPM). In the probe alone condition the stimulus consisted of a SAM tone with a carrier frequency of 31.7 kHz and a modulation rate of 1.0 kHz. Thresholds for each condition were estimated four times in a random order and then averaged. The initial SPL was 100 dB re 1 μPa. This condition represents a commonly used procedure of estimating the threshold at a single frequency (Nachtigall *et al.*, 2005; Finneran and Houser, 2006). The EPM stimulus consisted of the probe stimulus (31.7 kHz SAM tone described earlier) and a masker at

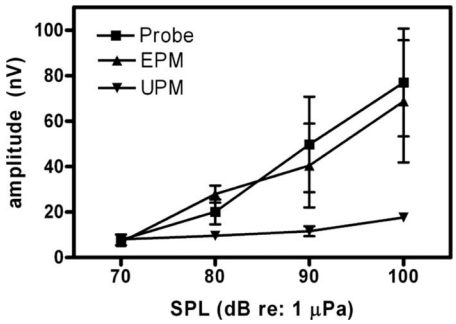


FIG. 8. ASSR (nV) as a function of SPL (error bars represent the standard deviation). Probe is the probe alone condition, EPM is equal probe plus masker (masker and probe have the same SPL), and UPM is unequal probe plus masker condition (masker is 30 dB greater than probe). Only detections during the initial descending staircase are included.

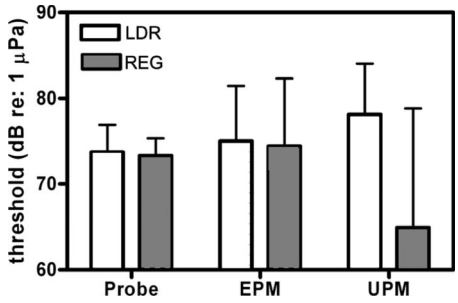


FIG. 9. Threshold estimates using LDR and REG techniques for probe alone (probe), probe+masker with equal SPL (EPM), and probe+masker with unequal SPL (UPM). Error bars represent the standard deviation.

25.2 kHz (1/3 octave below the probe) with a modulation rate of 1.1 kHz. Both the masker and probe had initial levels of 100 dB re 1 μPa. The decibel level of both the masker and the probe were adjusted by the adaptive staircase procedure described earlier. This condition was chosen because: (1) the frequency separation produced considerable masking in experiment I, and (2) starting the adaptive staircase with each component at equal amplitude is an acceptable procedure when an animal's thresholds are unknown. In the UPM condition, the stimuli were identical to the EPM condition; however, the initial SPLs of the probe and masker were 100 and 130 dB re 1 μPa, respectively, representing a condition where significant masking effects would be more likely. Again, the decibel level of both the masker and the probe were adjusted by the adaptive staircase procedure described earlier. Stimulus durations, rise and fall times, and AEP recording parameters were identical to experiment I. The subject for this experiment was WEN.

B. Results

Figure 8 displays the mean ASSR amplitude (spectral peak at 1.0 kHz) as a function of SPL for the three conditions of probe alone, EPM, and UPM. Only detections during the initial descending staircase are included because, after the first miss, the EVREST software independently varied the probe and masker levels. As a result, after the first nondetection of either the probe or masker, the amplitude relationship between the probe and the masker was variable and unpredictable. A clear masking effect is visible in the UPM condition, whereas the probe alone and EPM functions are nearly identical (Fig. 8). Masking was greater at the larger amplitudes and became progressively less as stimulus levels approached threshold. Figure 9 illustrates threshold estimates for each of the experimental conditions. A two-way ANOVA (threshold estimation procedure versus stimulus types) resulted in no significant main effects or interactions (threshold estimation procedure, $p=0.14$; stimulus type, $p=0.70$; interaction, $p=0.18$). Threshold levels for the probe and EPM conditions were similar regardless of the threshold estimation procedure employed (Fig. 9). However, in the UPM condition where a large masking effect was expected, the average threshold for the LDR was the highest (78 dB re 1 μPa) while the average threshold for the REG condition was the lowest (65 dB re 1 μPa). While neither of these two thresholds were significantly different from their corresponding probe alone conditions (one-tailed t-test, $p>0.05$), a significant difference did exist between the thresholds estimated with the two procedures (LDR and REG) within the UPM condition (one-tailed t-test, $p=0.047$). In addition, the REG procedure within the UPN condition produced a mean threshold estimate with a relatively large standard deviation (s.d.=13.89).

VI. DISCUSSION

A. Masker amplitude and frequency separation

The interaction between two SAM tones can be generally characterized by a localized masking effect, where lower frequency tones mask higher frequency tones, and a direct relationship exists between the degree of masking and the amplitude of the masker. SPL contributes to a greater masking effect than frequency.

The effect of amplitude on masking (i.e., suppression of the ASSR) has been modeled by a nonlinear compressive rectifier (John *et al.*, 1998). The unidirectional response of basilar membrane hair cells become increasingly saturated with increased stimulus levels. When a masking tone is added to a probe of similar frequency, the hair cell response of the probe will be suppressed because it is responding to summated energy from both the probe and masker. Although a compressive rectifier may account for amplitude suppression, basilar membrane mechanics likely account for the pattern of masking asymmetry in the frequency domain.

The basilar membrane is differentially sensitive, with lower frequency (longer wavelength) sounds producing greater relative displacement toward the apical end (von Bekesy, 1960). Lower-frequency tones have a relatively broader basilar membrane excitation pattern with a much steeper decay on the apical end (von Bekesy, 1960; Sellick *et al.*, 1982). As sound level increases, the excitation pattern broadens with a greater shift toward the base (Ren, 2002) resulting in an increased upward spread of masking.

Although several studies (Wegel and Lane, 1924; Johnson, 1971; Ruggero *et al.*, 1992) have demonstrated the same upward spread of masking (low frequencies mask high frequencies) as the current study, opposite results were obtained by John *et al.* (1998) and Dolphin and Mountain

(1993) where high frequencies suppressed lower frequencies. Although various mechanisms have been suggested to account for the reverse in asymmetry, a definitive explanation has yet to be offered.

The pattern of masking in the current study is much wider and more asymmetrical than peripheral-filter bandwidths measured from critical bands (Au and Moore, 1990), critical ratios (Johnson, 1968), and notched noise (Lemonds *et al.*, 1997; Finneran *et al.*, 2002). All of these studies adjusted the level of the probe while the masker level remained constant. In notched-noise masking tasks where the level of the probe is held constant and the level of the masker varied, filter shapes derived from human listeners closely resembled asymmetrical basilar membrane displacement (Rosen *et al.*, 1998). In experiment I from the current study, the level of the probe was also held constant and the level of the masker was varied, producing masking patterns similar to Rosen *et al.* (1998). Low-amplitude maskers are only effective within a narrower bandwidth while high-amplitude maskers produce a much wider and asymmetrical pattern of masking. The current data suggest the shape of dolphin auditory filters are level dependent and thus the filters are nonlinear. The level-dependent effects of masking on human auditory filter shapes has been well defined (Rosen *et al.*, 1998; Irino and Patterson, 2001), but has yet to be thoroughly investigated with an odontocete.

The SL of the stimuli may also have contributed to the broad asymmetry found with the higher frequency probes. The masking of the 100.8 and 127 kHz probes appears more broadband than that of the 31.7 and 63.5 kHz probes. Although all probe frequencies were presented at 30 dB SL, the higher frequency probes had higher absolute decibel levels (re 1 μPa) due to their corresponding higher audiogram thresholds. This resulted not only in higher probe levels but also higher masker levels. The resulting asymmetrical and broader masking patterns for higher probe frequencies may be due, in part, to increased SLs for their corresponding low frequency maskers. Similar masking trends were found for a two-tone masking study (Wegel and Lane, 1924) where an 80 dB SL masker had a much broader masking effect than a 44 dB SL masker of the same frequency. With two-tone masking, and apparently with two-SAM tone masking, higher amplitude maskers have an overall greater masking effect that extends across a wider range of frequencies.

B. SAM tone versus pure tone masking

Within the conditions tested, pure-tone maskers appear to have the same effect as SAM-tone maskers. This suggests that the amplitude and frequency content, rather than AM, is the salient feature related to masking. This result is consistent with findings from John *et al.* (1998) where no masking effects related to AM rate were found. Similar masking patterns have been demonstrated between pure-tone masking (Wegal and Lane, 1924; Johnson, 1971; current study), narrow-band-noise masking (Egan and Hake, 1950), and SAM-tone masking (current study) when similar experimental procedures are used. Similarity between the masking patterns for these studies suggests the same masking mechanism(s) may have been active.

C. Threshold estimation procedure

When no masking or small amounts of masking occur, thresholds estimated using a REG-based analysis or a LDR procedure yielded similar values. However, when large amounts of masking occur (such as in the UPM condition), differences between the LDR and REG threshold estimates became significant. Because regression-based thresholds rely on fitting data points across a range of SPL values, if ASSR amplitudes are masked (as in the UPM condition in Fig. 8), the resulting linear fit will have a lower slope. For example, the slope for the EPM and UPM conditions were 2.04 and 0.30, respectively. This resulted in a lower mean threshold (Fig. 9) and a larger variance for the UPM condition. The variance will increase because, with lower slope values, small changes in I/O data points can cause a large difference in estimated thresholds. For steeper I/O slopes, minor differences do not alter the x intercept to such a degree.

In the LDR procedure, thresholds were overestimated. One method that could reduce threshold biases due to masking using the LDR procedure is to only calculate thresholds when all SAM components have simultaneously reached threshold level (i.e., multiple reversals). If all stimuli components are at threshold levels, minimal masking will occur. Another potential option would be to use an ascending staircase so levels would never get high enough to produce salient masking.

D. Audiometry

Conducting a quick and accurate audiometric test on a marine mammal has advantages in several situations including opportunistic strandings and measuring the transient effects of temporary threshold shift (TTS) growth and recovery. Because the dolphin auditory system can track multiple SAM rates simultaneously (Dolphin, 1996; Finneran and Houser, 2007), the simultaneous presentation of multiple SAM tones could be used to estimate an entire audiogram in less time than the repetitive use of single SAM tones for estimating individual frequency thresholds (Finneran *et al.*, 2007a, d). This approach may also be used to assess the presence/absence of TTS at multiple frequencies simultaneously (Finneran *et al.*, 2007d), a process which is both desirable and necessary given current concerns over the potential impact of anthropogenic sound on marine mammals. In TTS studies where the fatiguing stimuli are broadband (i.e., broadband noise or a short duration impulse), the multiple ASSR could allow the simultaneous tracking of growth and recovery functions over a wide range of frequencies. In both situations, the multiple ASSR technique could limit the amount of potentially aversive exposures required.

VII. CONCLUSIONS

Because of variability inherent to the AEP procedure, statistical significance of the masking effect may have been diluted. Therefore, these results should be considered a conservative measurement of masking between a probe and masker stimulus. With caution in mind, the following conclusions can be drawn:

(1) Masking is localized, where lower frequency maskers (both SAM and pure tone) suppressed higher frequency probes and higher amplitude maskers produced a greater masking effect.
(2) Interactions are likely to occur for stimuli within a 2/3 octave bandwidth when the masker is 20–30 dB above the probe level.
(3) Simple basilar membrane mechanics in conjunction with a nonlinear rectifier appear to provide a reasonable explanation to the masking in the current study and similar studies (Johnson, 1971; Wegel and Lane, 1924) using a diverse set of stimuli (pure tone, SAM, narrow-band noise), i.e., lower frequency maskers are more effective than higher frequency maskers at masking a given stimulus.
(4) When estimating thresholds using multiple ASSRs, LDR and REG threshold estimates were similar in low masking conditions, but in high masking conditions the LDR tended to overestimate thresholds while the REG tended to underestimate thresholds.

ACKNOWLEDGMENTS

We would like to thank Randall Dear and Carolyn Schlundt for their help in data collection. We would like to thank Liz Testa, Laura Lewis, John Orr, and Linda Green for animal training. We also thank Colleen Reichmuth, Jason Mulsow, and an anonymous reviewer for their helpful and extremely thorough comments of an earlier manuscript draft. Financial support was provided by the Office of Naval Research and a fellowship awarded to the first author by the National Research Council.

Au, W. W. L., and Moore, P. W. B. (**1990**). "Critical ratio and critical bandwidth for the Atlantic bottlenose dolphin," J. Acoust. Soc. Am. **88**, 1635–1638.
Dobie, R. A., and Wilson, M. J. (**1989**). "Analysis of auditory evoked potentials by magnitude-squared coherence," Ear Hear. **10**, 2–13.
Dobie, R. A., and Wilson, M. J. (**1996**). "A comparison of *t*-test, *F* test, and coherence methods of detecting steady-state auditory-evoked potentials, distortion-product otoacoustic emissions, or other sinusoids," J. Acoust. Soc. Am. **100**, 2236–2246.
Dolphin, W. F. (**1996**). "Auditory evoked responses to amplitude modulated stimuli consisting of multiple envelope components," J. Comp. Physiol., A **179**, 113–121.
Dolphin, W. F., Au, W. W., Nachtigall, P. E., and Pawloski, J. (**1995**). "Modulation rate transfer functions to low-frequency carriers in three species of cetaceans," J. Comp. Physiol., A **177**, 235–245.
Dolphin, W. F., and Mountain, D. C. (**1993**). "The envelope following response (EFR) in the Mongolian gerbil to sinusoidally amplitude-modulated signals in the presence of simultaneously gated pure tones," J. Acoust. Soc. Am. **94**, 3215–3226.
Egan, J. P., and Hake, H. W. (**1950**). "On the masking pattern of a simple auditory stimulus," J. Acoust. Soc. Am. **22**, 622–630.
Finneran, J. J. (**2008**). *Evoked Response Study Tool (EVREST) User's Guide* (SSC San Diego, San Diego).
Finneran, J. J., and Houser, D. S. (**2006**). "Comparison of in-air evoked potential and underwater behavioral hearing thresholds in four bottlenose dolphins (*Tursiops truncatus*)," J. Acoust. Soc. Am. **119**, 3181–3192.
Finneran, J. J., and Houser, D. S. (**2007**). "Bottlenose dolphin (*Tursiops truncatus*) steady-state evoked responses to multiple simultaneous sinusoidal amplitude modulated tones," J. Acoust. Soc. Am. **121**, 1775–1782.
Finneran, J. J., Houser, D. S., Blasko, D., Hicks, C., Hudson, J., and Osborn, M. (**2008**). "Estimating bottlenose dolphin (*Tursiops truncatus*) hearing thresholds from single and multiple simultaneous auditory evoked potentials," J. Acoust. Soc. Am. **123**, 542–551.
Finneran, J. J., Houser, D. S., Blasko, D., Hicks, C., Hudson, J., Osborn, M., and Walsh, K. M. (**2007a**). "Hearing screening in bottlenose dolphins using single and multiple auditory evoked potentials," J. Acoust. Soc. Am. **121**, 3093–3094(A).
Finneran, J. J., Houser, D. S., and Schlundt, C. E. (**2007b**). "Objective detection of bottlenose dolphin (*Tursiops truncatus*) steady-state auditory evoked potentials in response to AM/FM tones," Aquat. Mamm. **33**, 43–54.
Finneran, J. J., London, H. R., and Houser, D. S. (**2007c**). "Modulation rate transfer functions in bottlenose dolphins (*Tursiops truncatus*) with normal hearing and high-frequency hearing loss," J. Comp. Physiol., A **193**, 835–843.
Finneran, J. J., Schlundt, C. E., Branstetter, B., and Dear, R. L. (**2007d**). "Assessing temporary threshold shift in a bottlenose dolphin (*Tursiops truncatus*) using multiple simultaneous auditory evoked potentials," J. Acoust. Soc. Am. **122**, 1249–1264.
Finneran, J. J., Schlundt, C. E., Carder, D. A., and Ridgway, S. H. (**2002**). "Auditory filter shapes for the bottlenose dolphin (*Tursiops truncatus*) and the white whale (*Delphinapterus leucas*) derived with notched noise," J. Acoust. Soc. Am. **112**, 322–328.
Fletcher, H. (**1940**). "Auditory patterns," Rev. Mod. Phys. **12**, 47–65.
Irino, T., and Patterson, R. D. (**2001**). "A compressive gammachirp auditory filter for both physiological and psychophysical data," J. Acoust. Soc. Am. **109**, 2008–2022.
John, M. S., Lins, O. G., Boucher, B. L., and Picton, T. W. (**1998**). "Multiple auditory steady-state responses (MASTER): Stimulus and recording parameters," Audiology **37**, 59–82.
Johnson, C. S. (**1968**). "Masked tonal thresholds in the bottlenosed porpoise," J. Acoust. Soc. Am. **44**, 965–967.
Johnson, C. S. (**1971**). "Auditory masking of one pure tone by another in the bottlenosed porpoise," J. Acoust. Soc. Am. **49**, 1317–1318.
Lemonds, D. W., Au, W. W. L., Nachtigall, P. E., Vlanchos, S., and Roitblat, H. L. (**1997**). "Auditory frequency selectivity and masked hearing capabilities in an Atlantic bottlenose dolphin (A)," J. Acoust. Soc. Am. **102**, 3102.
Lins, O. G., and Picton, T. W. (**1995**). "Auditory steady-state responses to multiple simultaneous stimuli," Electroencephalogr. Clin. Neurophysiol. **96**, 420–432.
Nachtigall, P. E., Yuen, M. M. L., Mooney, T. A., and Taylor, K. A. (**2005**). "Hearing measurements from a stranded infant Risso's dolphin, *Grampus griseus*," J. Exp. Biol. **208**, 4181–4188.
Patterson, R. D. (**1976**). "Auditory filter shapes derived with noise stimuli," J. Acoust. Soc. Am. **59**, 640–654.
Popov, V. V., and Supin, A. Y. (**1985**). "Determining hearing characteristics in dolphins using evoked potentials of brain stem," Dokl. Akad. Nauk SSSR **283**, 496–499.
Popov, V. V., Supin, A. Y., and Klishin, V. O. (**1997**). "Paradoxical lateral suppression in the dolphin's auditory system: Weak sounds suppress response to strong sounds," Neurosci. Lett. **234**, 51–54.
Popov, V. V., Supin, A. Y., and Klishin, V. O. (**1998**). "Lateral suppression of rhythmic evoked responses in the dolphin's auditory system," Hear. Res. **126**, 126–134.
Ren, T. (**2002**). "Longitudnal pattern of basilar membrane vibration in the sensitive cochlea," Proc. Natl. Acad. Sci. U.S.A. **99**, 1–6.
Rosen, S., Baker, R. J., and Darling, A. (**1998**). "Auditory filter nonlinearity at 2 kHz in normal hearing listeners," J. Acoust. Soc. Am. **103**, 2539–2550.
Ruggero, M. A., Robles, L., and Rich, N. C. (**1992**). "Two-tone suppression in the basilar membrane of the cochlea: Mechanical basis of auditory-nerve rate suppression," J. Neurophysiol. **68**, 1087–1099.
Sellick, P. M., Patuzzi, R., and Johnstone, B. M. (**1982**). "Measurement of basilar membrane motion in the guinea pig using the Mössbauer technique," J. Acoust. Soc. Am. **72**, 131–141.
Supin, A. Y., and Popov, V. V. (**1995**). "Envelope-following response and modulation transfer function in the dolphin's auditory system," Hear. Res. **92**, 38–46.
von Bekesy, G. (**1960**). *Experiments in Hearing* (McGraw-Hill, New York).
Wegel, R. L., and Lane, C. E. (**1924**). "The auditory masking of one pure tone by another and its probable relation to the dynamics of the inner ear," Phys. Rev. **23**, 266–285.

Effect of combined source (*F*0) and filter (formant) variation on red deer hind responses to male roars

Benjamin D. Charlton,[a] David Reby, and Karen McComb
Department of Psychology, School of Life Sciences, University of Sussex, BN1 9QH, United Kingdom

(Received 14 June 2007; revised 7 February 2008; accepted 17 February 2008)

Studying female response to variation in single acoustic components has provided important insights into how sexual selection operates on male acoustic signals. However, since vocal signals are typically composed of independent components, it is important to account for possible interactions between the studied parameter and other relevant acoustic features of vocal signals. Here, two key components of the male red deer roar, the fundamental frequency and the formant frequencies (an acoustic cue to body size), are independently manipulated in order to examine female response to calls characterized by different combinations of these acoustic components. The results revealed that red deer hinds showed greater overall attention and had lower response latencies to playbacks of roars where lower formants simulated larger males. Furthermore, female response to male roars simulating different size callers was unaffected by the fundamental frequency of the male roar when it was varied within the natural range. Finally, the fundamental frequency of the male roar had no significant separate effect on any of the female behavioral response categories. Taken together these findings indicate that directional intersexual selection pressures have contributed to the evolution of the highly mobile and descended larynx of red deer stags and suggest that the fundamental frequency of the male roar does not affect female perception of size-related formant information. © *2008 Acoustical Society of America.* [DOI: 10.1121/1.2896758]

PACS number(s): 43.80.Lb, 43.80.Ka [AL] Pages: 2936–2943

I. INTRODUCTION

Male courtship signals are often subject to sexual selection through female mating preferences (Searcy and Andersson, 1986; Ryan, 1998; Kokko *et al.*, 2003). However, in order to appreciate how intersexual selection is generated it is necessary to understand how females perceive and react to signal variation. Since acoustic signals can be easily separated from other aspects of the male phenotype, they are ideally suited for studying female responses to variation in their properties (Gerhardt, 1991; Searcy, 1992). Indeed, many studies have shown how female preferences are affected by variation in single acoustic parameters (Andersson, 1994). However, as acoustic signals are typically composed of several components, possible interactions between them can mean that female responses to variation in single acoustic parameters may not predict how females respond to variation in different combinations of acoustic components (Ryan and Rand, 2003; Olvido and Wagner, 2004; Scheuber *et al.*, 2004).

The generalization of the source-filter theory of voice production (Fant, 1960) to nonhuman mammals allows specific acoustic features of mammal calls to be linked to their production mechanisms. Furthermore, by doing so, predictions about which acoustic features of mammal calls have the potential to provide receivers with reliable information on the caller's phenotype can be made. The source-filter theory states that mammal vocalizations result from a source signal, generated by vibrations of the vocal folds in the larynx, which is then filtered by the cavities of the vocal tract. The source signal determines the pitch, i.e., the fundamental frequency (*F*0), of the vocalization. When this signal passes through the vocal tract, which acts as a tube of air with natural resonances, some frequencies are selectively amplified: These frequencies are termed "formants." Because source and filter components are independently produced, either or both have the potential to provide receivers with important information on the caller's genetic quality and/or current physical condition.

The source-filter theory has been successfully applied to the study of mammal vocal communication, including male red deer roaring (Fitch and Reby, 2001; Reby and McComb, 2003a; Reby *et al.*, 2005; Vannoni and McElligott, 2007). In particular, a number of studies have confirmed that formants provide accurate information to receivers on the caller's body size (Fitch, 1997; Riede and Fitch, 1999; Reby and McComb, 2003a; Harris *et al.*, 2006; Sanvito *et al.*, 2007), due to a close relationship between the formant spacing, the caller's vocal tract length (VTL), and overall body size (Fitch, 2000). This reliable information on body size may also allow receivers to gauge the caller's maturity (Reby and McComb, 2003a), and even, in size dimorphic species, the caller's sex (Rendall *et al.*, 2004).

Both red and fallow deer males have a descended and highly mobile larynx that enables them to increase their VTL during vocalizations (Fitch and Reby, 2001; McElligott *et al.*, 2006), thereby lowering their formant frequencies independently of *F*0. While size exaggeration as previously suggested as a possible mechanism for the evolution of this anatomical innovation (Fitch and Reby, 2001), the maximum extension of the vocal tract, achieved in most roars by red

[a]Author to whom correspondence should be addressed. Electronic mail: b.d.charlton@sussex.ac.uk.

 0001-4966/2008/123(5)/2936/8/$23.00 © 2008 Acoustical Society of America

deer stags, is morphologically constrained by the sternum and hence minimum formant values are honest indicators of body size (Fitch and Reby, 2001; Reby and McComb, 2003a). Moreover, playback experiments using resynthesized roar stimuli have shown that both male and female red deer do actually attend to formants in the roars of simulated rivals (Reby *et al.*, 2005) and potential mates, respectively (Charlton *et al.*, 2007a, 2007b). Accordingly, we would only expect display characteristics that provide an honest advertisement of body size to be maintained by selection in these contexts (Grafen, 1990).

In contrast, mean fundamental frequency ($F0$) is not correlated with aspects of male quality in red deer (Reby and McComb, 2003a) and has proven to be a poor predictor of body size within mammal species (Masataka, 1994; Rendall *et al.*, 2005; but see Pfefferle and Fischer, 2006). In addition, red deer hinds show no preferences when presented with the choice between roars with low and high fundamental frequencies (McComb, 1991). Notwithstanding this, there are theoretical reasons for suspecting that $F0$ may contribute to the perception of the formant frequencies in the male roar and consequently affect the attractiveness of the signal to females. When roars are delivered with a low fundamental frequency the density of harmonics sampling the formant envelope is increased, which may be expected to increase the salience of the formant structure (Ryalls and Lieberman, 1982) and hence, affect the differential response of red deer hinds to size-related variation in formant spacing.

In the current study, we used resynthesis techniques to create roar stimuli in which we independently manipulated the formant frequencies and $F0$, while leaving all other acoustic parameters (e.g., duration, amplitude, other timbral cues, etc.) unchanged. We then used these stimuli in playback experiments to examine the behavioral response of red deer hinds to male roars characterized by different combinations of these acoustic components. This allowed us to separately determine female responses to formant variation but also test whether the value of $F0$ affects female response to size-related formant variation.

II. MATERIALS AND METHODS

A. Experimental site and animals

The playback experiments were conducted at Invermay Agricultural Centre and Tony Pearse's Deer Farm in Mosgiel, New Zealand, during March and April 2006. A total of 96 adult red deer hinds from 20 different groups, all identified by numbered collars and ear tags, were used as subjects in the playback experiments. As our experiments were conducted early in the breeding season some of the hinds already had a resident stag placed (as a sire) in their enclosure. To minimize habituation, individuals within the same groups were presented with playbacks on separate days.

B. Selection of roars for resynthesis

To create the playback stimuli we selected two roaring bouts from each of four mature stags (aged 5–8 years). These roaring bouts, each comprising two roars, had been previously recorded at Redon Experimental Deer Farm, France, using a Telinga pro-III-S/(DAT) microphone and a DAT Sony TCD-D7 recorder (amplitude resolution: 16 bits, sampling rate: 48 kHz). This ensured that the current hinds were unfamiliar with these males that, ranging in weight from 210 to 230 kg, were representative of farmed stags. The original DAT recordings were transferred onto an Apple Macintosh G3 computer via a Digidesign Audiomedia III soundcard, saved in AIFF format as separate Sound-Edit 16 Version 2 sound files (16 bits amplitude resolution, 48 kHz sampling rate) and normalized to 100% peak amplitude.

C. Acoustic analyses

In order to determine the appropriate readjustment factors by which to resynthesize the roar stimuli, we initially measured the formant and fundamental frequency ($F0$) values for each roar using the Praat 4.2.06 DSP package (Boersma and Weenink, 2005).

1. Formant frequency and spacing estimation

The frequency values of the first eight formants ($F1, F2, \ldots, F8$) were extracted using Linear Predictive Coding via the "LPC: To Formants (Burg)" command in Praat. The analysis parameters were time step, 0.05 s; window analysis, 0.1 s; maximum formant values, 1700–1900 Hz; maximum number of formants, eight; pre-emphasis, 6000 Hz. The male roar is characterized by an initial drop in formant frequencies, which then plateau at minimum values before they rise again at the end of the roar. This is due to the mobile larynx of red deer stags that enables them to lengthen their vocal tract during vocalizations (Fitch and Reby, 2001), which in turn lowers the formant values and decreases the overall spacing of the formants across the roar (see Fig. 1). Therefore, in order to standardize formant measurement, the Praat output for each entire roar was examined and ten readings (at a time step of 0.05 s), from an area where the formants reach their minimum values, were selected and the values for each formant frequency averaged. These average minimum formant frequencies were used to estimate the minimum formant spacing achieved during each roar by finding the best fit for the equation

$$F_i = \frac{2i-1}{2}\Delta F. \quad (1)$$

This equation describes the relationship between individual formant frequencies (i=formant number 1, 2, 3,…) and the average overall formant spacing (ΔF) in a vocal tract approximated as a straight uniform tube closed at one end (the glottis) and open at the other end (the mouth) (Titze, 1994). Finally the estimated apparent VTL, was directly deduced from formant spacing by using the equation

$$VTL = \frac{c}{2\Delta F}, \quad (2)$$

where c=the approximate speed of sound in a mammal vocal tract (350 m/s) (Titze, 1994). Full details of this procedure are available in another paper (Reby and McComb, 2003a).

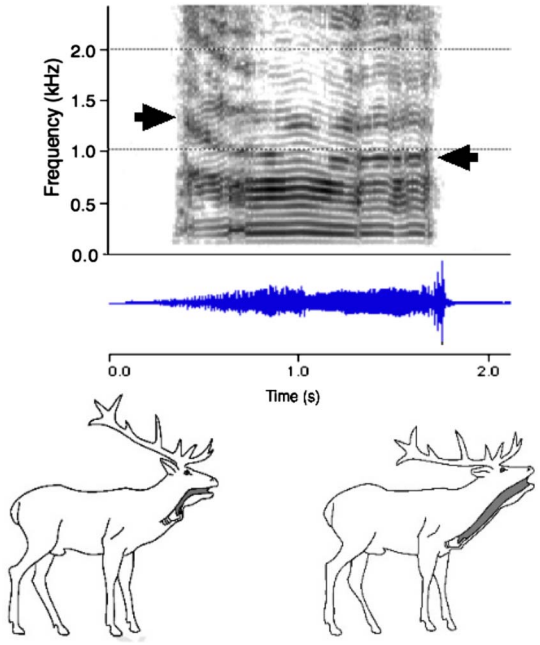


FIG. 1. (Color online) The mobile larynx of red deer stags allows them to lengthen their vocal tracts during vocalizations. The formants, visualized as darkened energy bands, plateaux at the midpoint of the spectrogram when the larynx is fully descended. Hence, the minimum formant frequency values produced at this time provide honest information about body size. The arrow indicates the position of a formant (illustrations of roaring stags taken from Fitch and Reby, 2001).

2. Fundamental frequency estimation

The mean fundamental frequency ($F0$) values for each roar were extracted using a forward cross-correlation [to pitch (cc) command] algorithm in Praat. The time step in the analysis was 0.05 s and the specified range for the lower and upper limits of the expected range of $F0$ were 30 and 250 Hz, respectively. A five point average smoothing filter removed any rapid variations in the $F0$ contour before the mean value for $F0$ across the entire roar was determined using the "get mean" command in Praat.

D. Resynthesis of roar stimuli

Previous data from a population of adult Scottish red deer males showed a variation of ~5% around the mean for the largest and smallest adult apparent VTLs measured (Reby and McComb, 2003a). Therefore, in order to realistically simulate natural variation in male VTL between the largest and smallest adults representative of a population, we used values shifted ±5% from the measured mean of our stag exemplars of 81.5 cm: Creating adult size variants with apparent VTLs of 85.7 and 77.5 cm, respectively. To simulate male callers with VTLs outside of the natural adult range, the formants of the roar stimuli were shifted ±20% to represent abnormally large and small adult males with VTLs of 101.7 and 67.8 cm, respectively (see Fig. 2). This was done to test the hind's responses to supernormal stimuli and to determine whether any innate directional preferences existed for males with abnormally long vocal tracts.

We conducted three levels of pitch manipulation for each of the four size variant conditions, corresponding to adult red deer males roaring at low (70 Hz), medium (100 Hz), and high (130 Hz) fundamental frequencies (see Fig. 2). Previous data taken from a population of 22 adult Scottish stags (in which the minimum, mean, and maximum

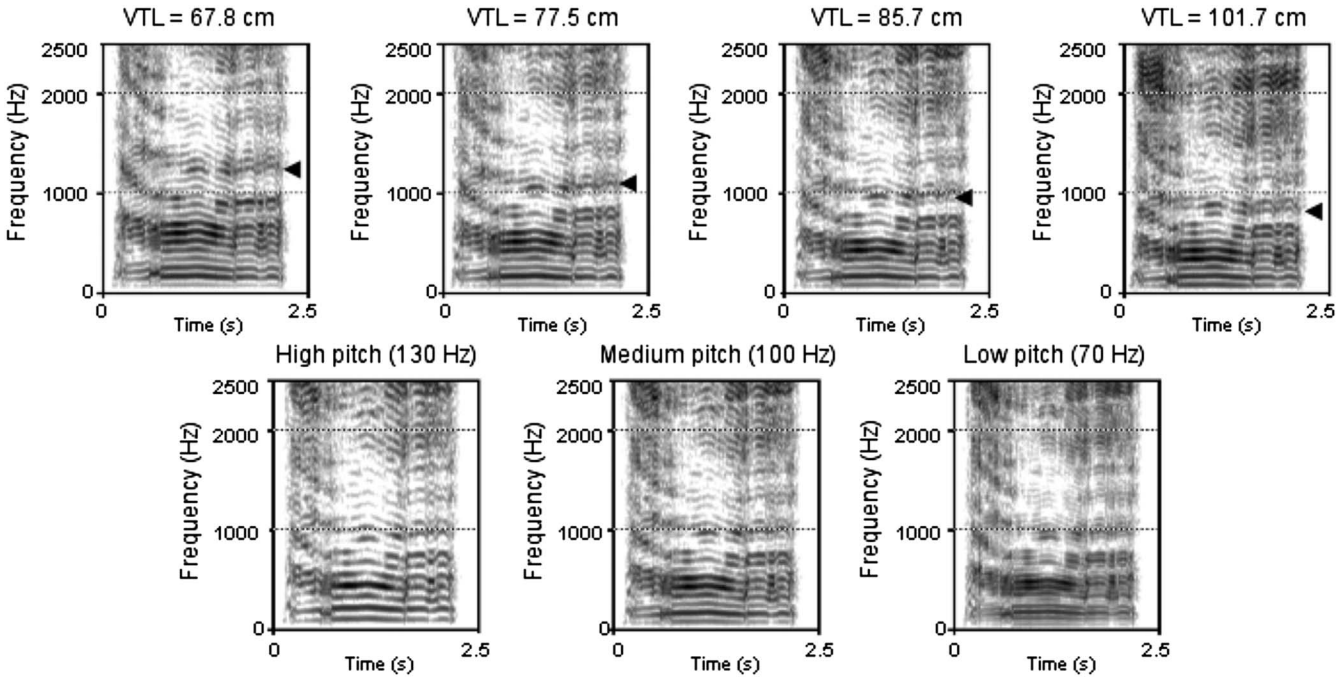


FIG. 2. Resynthesized roar stimuli used in playback experiments. The upper section of the diagram shows spectrograms of a roar from one of the stag exemplars resynthesized to correspond to males with vocal tract lengths of 67.8, 77.5, 85.7, and 101.7 cm. The arrow indicates the position of an individual formant, which decreases in frequency as apparent vocal tract length increases from very small adult to very large adult (full details in text). The lower section shows the VTL=85.7 cm roar after the three pitch manipulations: high (130 Hz), medium (100 Hz), and low (70 Hz). Note that the harmonic spacing decreases as you go from the high (130 Hz) to the low (70 Hz) pitch condition.

measured mean fundamental frequency values were 65.7, 111.7, and 168.3 Hz, respectively) indicate that these pitch variants fall within the natural range for adult male red deer (Reby and McComb, 2003a). The resynthesis factors for these mean fundamental frequency values were simply deduced by dividing the intended value by the original measured value for each roar.

A Praat script (originally written by C. J. Darwin) was used to batch process roar stimuli for the modification of formants and fundamental frequency ($F0$). Formant modification was achieved using a Pitch-Synchronous Overlap and Add (PSOLA) based algorithm that alters the apparent vocal-tract lengths of the roar stimuli by shifting the formant frequencies by a factor ($k1$), while leaving all other acoustic parameters unchanged. This program works by initially multiplying $F0$ by $k1$ and duration by $1/k1$ using PSOLA, before resampling at the original sampling frequency multiplied by $k1$ and finally playing the samples at the original sampling frequency. The fundamental frequency ($F0$) was adjusted at the same time by adding an additional line to this script, further raising or lowering the "pitch tier" (a Praat vector of $F0$ estimates) by the appropriate factor ($k2$).

E. Playback sequences

A total of 48 different playback sequences were created from the four stag exemplars and the 12 different combinations of size and pitch variation (four different adult size variants each with three levels of pitch manipulation, see Fig. 2). The playback sequences ranged between 9.6 and 10.6 s and consisted of two two-roar roaring bouts from the same stag exemplar separated by 0.5 s. In order to standardize the roaring rate for each stag exemplar, the roars within each bout were separated by 1 s of silence. This ensured that each of the four roars within a sequence was equally spaced across exemplars.

F. Playback experiments

Individual hinds with their head down grazing and at the periphery of a group were targeted for the playbacks. In this way we aimed to provide a standardized context for the playbacks and also to ensure that in each case the hind's attention was not already directed toward the speaker position. The 48 different playback sequences (see above) were played back to 96 different hinds, making a total of 96 playback experiments. The playback sequences were presented to the hinds using an Anchor Audio Liberty 6000HIC speaker at sound pressure levels (SPLs) of 105 dB peak SPL at 1 m from the source (determined using a Radio Shack Sound Level Meter, set for C-weighted fast response). The loudspeaker was connected by a coaxial cable to an Apple Powerbook G4 with an external imic soundcard (Griffin technology) and a Sony digital camera (model DCR/TRV19E) used to capture behavioral responses on videotape for 2 min after each playback presentation.

G. Behavioral analysis

The videotapes were analyzed frame by frame (frame $=0.04$ s) using Gamebreaker 5.1 digital video analysis system for Mac OS 10. In order to quantify the strength of the hind's response to each playback condition, the duration of the first look given by the hind while stationary toward the speaker position and the total time that each hind spent stationary with their head up looking around during the 2 min period after each playback presentation were measured. Looking was defined as having begun the frame before that in which the hind raised her head to look around or, in the case of the first look duration, turned her head to face the speaker, having previously faced away. This behavior ended the frame before that in which the head began to move back down to a grazing position or in which the hind ceased to be stationary. The time between the onset of the playback and the first behavioral response (latency to first response) and the number of looks given during the 2 min period after each playback presentation were also quantified.

H. Statistical analysis

Log (10) transformations were used to normalize the data distribution for parametric statistics. Additionally, in order to normalize the data distribution for latency to first response without removal of data, subjects responding more than 10 s after playback onset were given maximum values of 10. A principal components analysis was made using first look duration, total look duration, and number of looks to reduce these highly correlated variables to one "looking response component" explaining 70% of the variance (subjects with greater first look duration, total look duration, and number of looks had the highest scores).

Separate univariate analyses of covariance (ANCOVA) were computed for looking response component and latency to respond to compare the response of hinds to both the size and pitch variant conditions, in which the presence or not of a resident stag was the single covariate (a resident stag was present for 66 out of 96 playback experiments). A preliminary analysis indicated that the presence of a resident stag was negatively correlated to total look duration ($F1,96=4.473, P=0.037$) and bordering on significance for number of looks given ($F1,96=3.885, P=0.052$). Pair-wise comparisons were also used to compare the behavioral responses to the different size and pitch variant conditions. Finally, Levene's tests were used to determine whether the variance of hind response to size-related formant information was reduced by lower fundamental frequencies, as might be expected if lower fundamental frequencies significantly improved the ability of hinds to perceive the formant structure in the male roar. Alpha levels were set at 0.05 and two-tailed probability values quoted.

III. RESULTS

A. Looking response component

The univariate ANCOVA revealed that the looking response component was significantly affected by the size variant condition [$F(3,96)=6.694, p<0.001$] but not the pitch variant played back [$F(2,96)=0.863, p=0.426$] [see Figs. 3(a) and 3(b)]. Moreover, no interaction between the size and pitch variant played back was detected [$F(6,96)=0.423, P=0.862$], indicating that the pitch of the male roar had no

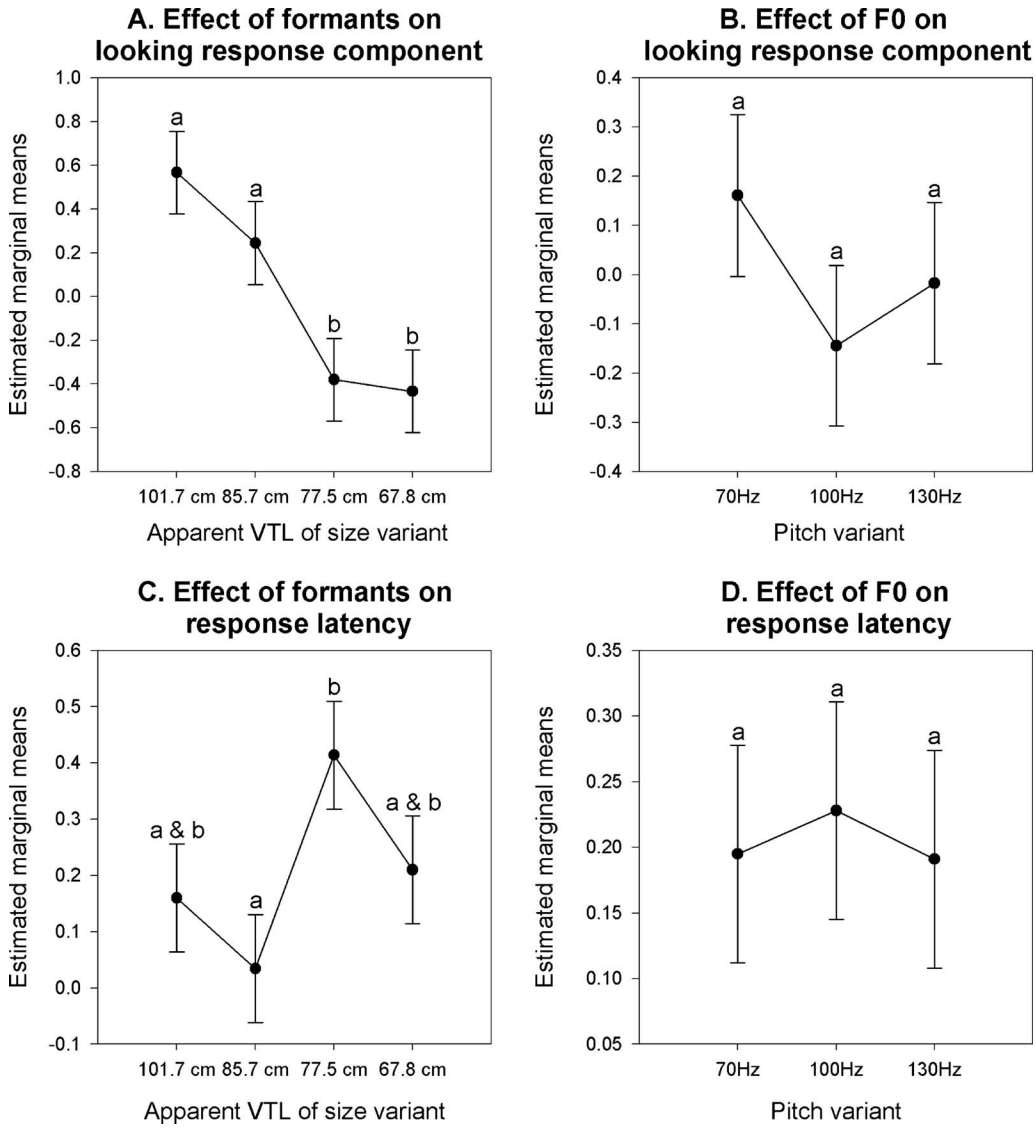


FIG. 3. Female [(A), (B)] looking responses and [(C), (D)] latency to respond to resynthesized male roars simulating the different size and pitch variants. Estimated marginal means ±S.E are taken from pair-wise comparisons; those sharing the same letter are not significantly different.

effect on the looking response of hinds to the different size variants. The pair-wise comparisons showed that looking response was significantly greater for hinds presented with male roars simulating abnormally large adults (VTL =101.7 cm) than those simulating both small (VTL =77.5 cm) (p=0.001) and abnormally small adult size variants (VTL=67.8 cm) ($p<0.001$). In addition, looking response was significantly greater when hinds were presented with male roars simulating a large adult (VTL=85.7 cm) than those simulating both small (VTL=77.5 cm) (p =0.022) and abnormally small adults (VTL=67.8 cm) (p =0.013). Last, no significant differences were detected in looking response between the small and abnormally small fadult (p=0.842) or between the large and abnormally large adult size variants (p=0.228). In addition, no differences in the variance of hind response to the pitch variants [Levene's test: $F(2,93)=0.895$, $p=0.412$] or the different combinations of size and pitch variant were detected [Levene's test: $F(11,84)=1.181$, $p=0.312$].

B. Latency to respond

The univariate ANCOVA revealed that latency to respond was significantly affected by the size variant [$F(3,96)=2.726$, $p=0.049$] but not the pitch variants played back [$F(2,96)=0.061$, $p=0.941$] [see Figs. 3(c) and 3(d)]. Moreover, no interaction between the size and pitch variant played back was detected [$F(6,96)=0.471$, $p=0.828$], indicating that the pitch of the male roar had no effect on the response latency of hinds to the different size variants. The pair-wise comparisons showed that latency to respond was lower for playbacks simulating abnormally large adults (VTL=101.7 cm) than those simulating small adult size variants (VTL=77.5 cm) (bordering on significance: p =0.064). Additionally, hinds responded significantly faster to male roars simulating large adults (VTL=85.7 cm) than those simulating small adult size variants (VTL=77.5 cm) (p=0.006). Lastly, no significant differences for latency to respond were detected between the abnormally large versus

large ($p=0.356$), abnormally large versus abnormally small ($p=0.713$), large versus abnormally small ($p=0.199$), and small versus abnormally small ($p=0.136$) size variant conditions. In addition, no differences in the variance of hind response to the pitch variants [Levene's test: $F(2,93)=0.207$, $p=0.814$] or the 12 different combinations of size and pitch variant were detected [Levene's test: $F(11,84)=0.308$, $p=0.982$], indicating the fundamental frequency did not significantly affect the variability of hind response.

IV. DISCUSSION

There are three main results from this study. The first is that red deer hinds showed greater overall attention, judged on the number and duration of looks, and had lower response latencies to playbacks simulating adult males with VTLs (and hence body sizes) greater than the natural population mean. The second is that the value of the fundamental frequency in the playback stimuli had no effect on the response of the hinds. The final result is that there was no interaction between the value of the fundamental frequency and the value of the formant spacing affecting the observed response of the hinds; suggesting that the value of the fundamental frequency in roars does not affect how receivers perceive size-related variation in formant frequency spacing.

A. Formants and female response

We know from previous work that red deer hinds move preferentially toward male roars in which the formants indicate larger callers when they are in peak oestrus (Charlton *et al.*, 2007b). Our findings here suggest that males producing roars with lower formant values, indicative of longer vocal tracts and larger bodies, would also elicit greater attention from peri-oestrous females during the breeding season. Accordingly, roars with lower formants may serve as an initial attractor for females just prior to oestrus, making them more likely to join the harems of larger males. Such a preference would be adaptive for females because they would then be better positioned to mate with larger males when they came into oestrus and hence, gain the indirect genetic benefits of larger more competitive offspring. It also seems likely that by joining the harems of larger males during the breeding season, discriminating females could get direct fitness benefits such as increased protection from male harassment (Clutton-Brock *et al.*, 1982; Reale *et al.*, 1996).

Interestingly, although female response increased most steeply across the natural range of male size variants, our results showed that hinds gave their greatest responses to roars simulating abnormally large males with VTLs outside of the normal population range. This is consistent with previous work demonstrating that, when given a relative choice between roars simulating large and small male callers, oestrous red deer hinds moved preferentially toward the larger size variant (Charlton *et al.*, 2007b). Moreover, these findings lend support to the hypothesis that directional intersexual selection pressures have contributed to the evolution of the mobile larynx of red deer stags and other cervids (Fitch and Reby, 2001; McElligott *et al.*, 2006), enabling them to lengthen their vocal tract and lower their formants during vocalizations. Future studies would be needed to determine whether this female sensory bias was pre-existing (Ryan *et al.*, 1990) or evolved to select for roars with the very lowest formant values, in order to maximize the chances of mating with the largest available male (Enquist and Arak, 1998).

B. Fundamental frequency and female response

The fundamental frequency manipulation had no significant separate effect on any of the female response parameters. This is consistent with another study in which red deer hinds showed no preference when presented with the choice between roars with high and low fundamental frequencies (McComb, 1991). Nevertheless, male roars with the lowest fundamental frequencies of 70 Hz appeared to induce the greatest average response from hinds across formant frequency variants (although this was not statistically significant), particularly when large and small adult size variants within the normal range were played back. Indeed, although no known correlations between mean fundamental frequency and aspects of male quality have previously been detected in red deer, the fundamental frequency (mean and max) is significantly higher in the roars of subadult than adult stags (Reby and McComb, 2003a) and therefore has the potential to act as an additional cue to the maturity of the caller alongside the formants.

In addition, studies on humans suggest that speakers with lower *F*0's have higher testosterone levels (Evans *et al.*, 2006) and female listeners rate male speakers with lower pitched voices as more attractive (Feinberg *et al.*, 2005). Interestingly, human females find male speakers with low formants and fundamental frequency particularly attractive when they are ovulating (Feinberg *et al.*, 2006). Accordingly, although we found no evidence of female preferences based on fundamental frequency in the current study, future work on oestrous red deer hinds may show that this acoustic component is relevant in a mate choice context, possibly as a cue to the caller's maturity or hormonal quality.

C. The effect of fundamental frequency on female perception of size-related formant variation

Our analysis revealed no interactions between the size and pitch variants played back for any of the response categories, indicating that the overall response pattern observed across the size variant conditions was similar for all the pitch variations (70, 100, and 130 Hz). This suggests that the ability of females to perceive size-related formant information in the roars of stags is unaffected by the fundamental frequency of the call when it is varied within the natural range.

Given that denser spectral sampling provided by lower fundamental frequencies improves human perception of formants (Ryalls and Lieberman, 1982), we may have predicted that lower fundamental frequencies would increase the salience of the formant structure, in turn increasing the magnitude of the differential responses to the size variants and/or lowering the variance of the hinds' response. The fact that neither of these were observed suggests that lower fundamental frequencies do not significantly enhance the percep-

tion of the formant structure within the male roar nor alter the behavioral response of red deer hinds to the signal. One possible reason for this result is that the mean fundamental frequency values that we used (70–130 Hz) were lower than the minimum formant frequency spacing of our four size variant conditions (ranging from 172 to 258 Hz), therefore providing a sufficiently dense spectral source for revealing the vocal tract resonances. Accordingly, as the perception of size-related formant information by red deer hinds does not appear to be affected when the spectral envelope is sampled at a lower rate than that known to significantly impair human vowel discrimination (Ryalls and Lieberman, 1982), we suggest that using formants to estimate a caller's size is less likely to rely on the precise judgment of individual formants (as it is for vowel perception) than an estimate of overall formant spacing.

Further studies comparing the effect of a wider range of fundamental frequencies on the perception of size-related formant information in red deer are warranted. As the peak fundamental frequency of male roars in this species can exceed 200 Hz (Reby and McComb, 2003a), it would be particularly interesting to see the effect of mean fundamental frequency values that are comparable to or even exceed the formant frequency spacing. It may be that the fundamental frequency only begins to affect the perception of size-related formant information when the harmonic spacing is wide enough to be comparable with the formant spacing. It is also important to note that the fundamental frequency of red deer roars is often strongly modulated (Reby and McComb, 2003b), and that this could theoretically provide additional information for receivers about the spectral envelope for a range of values around each harmonic. Accordingly, modulation of the fundamental frequency could be expected to improve formant perception, particularly at high fundamental frequencies when the spectral envelope is sampled more sparsely.

In conclusion, the use of multicomponent signals for female mate choice in animals has received recent theoretical (Johnstone, 1995; Candolin, 2003) and empirical attention (Patricelli *et al.*, 2003; Scheuber *et al.*, 2004; Poole and Murphy, 2007). In this study we examined the combined effect of variation in two separate components of a male mammals sexual call on female response. Our results reinforce the idea that formants, being a long-term indicator of male body size and hence genetic quality, are important to red deer hinds as acoustic cues for mate assessment during the breeding season. Moreover, as the fundamental frequency does not appear to influence the perception of the formant structure in the male red deer roar, we suggest that the extremely low-pitched male rutting calls of Corsican (*Cervus elaphus corsicanus*) and fallow deer (*Dama dama*) (Reby and McComb, 2003b) are unlikely to represent an adaptation to facilitate the transmission of size-related formant information.

However, fundamental frequency variation may be functionally significant to oestrous red deer and other female mammals during their time of peak conception. Fundamental frequency is often highly modulated within the roars of red deer stags and both the range and mean values are variable between and within individuals (Reby and McComb, 2003a). In addition, minimum *F*0 is positively correlated to reproductive success in red deer (Reby and McComb, 2003a). In fact, because higher fundamental frequencies require greater stiffness and tension of the vocal folds, and probably higher subglottal pressures to produce, the fundamental frequency may dynamically reflect a callers' short-term condition (Gerhardt, 1991) of direct importance to receptive females. We suggest that future work should adopt the same resynthesis techniques and playback approach to present male sexual calls with different combinations of fundamental frequency and formants not only to oestrous red deer hinds but also to other female mammals, to explore these possibilities.

ACKNOWLEDGMENTS

Many thanks go to the staff at Invermay Agricultural Research station and Agresearch in New Zealand for allowing Ben Charlton to conduct his research there. Special thanks go to Geoff Asher without whom the project could not have been a success and Tony Pearse for free access to his deer farm. Funding for the research was provided by a B.B.S.R.C. studentship to B.C. and a Nuffield Grant to D.R.

Andersson, M. (**1994**). *Sexual Selection* (Princetown, University Press, Princetown,).

Boersma, P., and Weenink, D. (**2005**), *Praat: Doing phonetics by computer (Version 4.3.22)* [Computer program]. Retrieved from http://www.praat.org/ (last viewed online March 2007).

Candolin, U. (**2003**). "The use of multiple cues in mate choice," Biol. Rev. Cambridge Philos. Soc. **78**, 575–595.

Charlton, B. D., Reby, D., and McComb, K. (**2007a**). "Female perception of size-related formant shifts in red deer, Cervus elaphus," Anim. Behav. **74**, 707–714.

Charlton, B. D., Reby, D., and McComb, K. (**2007b**). "Female red deer prefer the roars of larger males," Cell. Mol. Biol. Lett. **3**, 382–385.

Clutton-Brock, T. H., Albon, S., and Guinness, F. E. (**1982**), *Red Deer: Behavior and Ecology of Two Sexes* (University of Chicago Press, Chicago).

Enquist, M., and Arak, A. (**1998**). "Neural representation and the evolution of signal form," in *Cognitive Ecology*, edited by R. Dukas (Chicago University Press, Chicago), pp. 12–87.

Evans, S., Neave, N., and Wakelin, D. (**2006**). "Relationships between vocal characteristics and body size and shape in human males: An evolutionary explanation for a deep male voice," Biol. Psychol. **72**, 160–163.

Fant, G. (**1960**). *Acoustic Theory of Speech Production* (Mouton, The Hague, The Netherland).

Feinberg, D. R., Jones, B. C., Law-Smith, M. J., Moore, F. R., DeBruine, L. M., Cornwell, R. E., Hillier, S. G., and Perrett, D. I. (**2006**). "Menstrual cycle, trait estrogen level, and masculinity preferences in the human voice," Horm. Behav. **49**, 215–222.

Feinberg, D. R., Jones, B. C., Little, A. C., Burt, D. M., and Perrett, D. I. (**2005**). "Manipulations of fundamental and formant frequencies influence the attractiveness of human male voices," Anim. Behav. **69**, 561–568.

Fitch, W. T. (**1997**). "Vocal tract length and formant frequency dispersion correlate with body size in rhesus macaques," J. Acoust. Soc. Am. **102**, 1213–1222.

Fitch, W. T. (**2000**). "Skull dimensions in relation to body size in nonhuman mammals: The causal bases for acoustic allometry," Zoology **103**, 40–58.

Fitch, W. T., and Reby, D. (**2001**). "The descended larynx is not uniquely human," Proc. R. Soc. London, Ser. B **268**, 1669–1675.

Gerhardt, H. C. (**1991**). "Female mate choice in treefrogs—Static and dynamic acoustic criteria," Anim. Behav. **42**, 615–635.

Grafen, A. (**1990**). "Biological signals as handicaps," J. Theor. Biol. **144**, 517–546.

Harris, T. R., Fitch, W. T., Goldstein, L. M., and Fashing, P. J. (**2006**). "Black and white colobus monkey (Colobus guereza) roars as a source of both honest and exaggerated information about body mass," Ethology **112**, 911–920.

Johnstone, R. A. (**1995**). "Honest advertisement of multiple qualities using

multiple signals," J. Theor. Biol. **177**, 87–94.
Kokko, H., Brooks, R., Jennions, M. D., and Morley, J. (**2003**). "The evolution of mate choice and mating biases," Proc. R. Soc. London, Ser. B **270**, 653–664.
Masataka, N. (**1994**). "Lack of correlation between body-size and frequency of vocalizations in young female japanese macaques (Macaca fuscata)," Folia Primatol. **63**, 115–118.
McComb, K. E. (**1991**). "Female choice for high roaring rates in red deer, *Cervus elaphus*," Anim. Behav. **41**, 79–88.
McElligott, A. G., Birrer, M., and Vannoni, E. (**2006**). "Retraction of the mobile descended larynx during groaning enables fallow bucks (Dama dama) to lower their formant frequencies," J. Zool. **270**, 340–345.
Olvido, A. E., and Wagner, W. E. (**2004**). "Signal components, acoustic preference functions and sexual selection in a cricket," Biol. J. Linn. Soc. **83**, 461–472.
Patricelli, G. L., Uy, J. A. C., and Borgia, G. (**2003**). "Multiple male traits interact: Attractive bower decorations facilitate attractive behavioral displays in satin bowerbirds," Proc. R. Soc. London, Ser. B **270**, 2389–2395.
Pfefferle, D., and Fischer, J. (**2006**). "Sounds and size: Identification of acoustic variables that reflect body size in hamadryas baboons, Papio hamadryas," Anim. Behav. **72**, 43–51.
Poole, K. G., and Murphy, C. G. (**2007**). "Preferences of female barking treefrogs, Hyla gratiosa, for larger males: Univariate and composite tests," Anim. Behav. **73**, 513–524.
Reale, D., Bousses, P., and Chapuis, J. L. (**1996**). "Female-biased mortality induced by male sexual harassment in a feral sheep population," Can. J. Zool. **74**, 1812–1818.
Reby, D., and McComb, K. (**2003a**). "Anatomical constraints generate honesty: Acoustic cues to age and weight in the roars of red deer stags," Anim. Behav. **65**, 519–530.
Reby, D., and McComb, K. (**2003b**). "Vocal communication and reproduction in deer," Adv. Stud. Behav. **33**, 231–264.
Reby, D., McComb, K., Cargnelutti, B., Darwin, C., Fitch, W. T., and Clutton-Brock, T. H. (**2005**). "Red deer stags use formants as assessment cues during intrasexual agonistic interactions," Proc. R. Soc. London, Ser. B **272**, 941–947.
Rendall, D., Kollias, S., and Ney, C. (**2005**). "Pitch (*F*0) and formant profiles of human vowels and vowel-like baboon grunts: The role of vocalizer body size and voice-acoustic allometry," J. Acoust. Soc. Am. **117**, 944–955.
Rendall, D., Owren, M. J., Weerts, E., and Hienz, R. D. (**2004**). "Sex differences in the acoustic structure of vowel-like grunt vocalizations in baboons and their perceptual discrimination by baboon listeners," J. Acoust. Soc. Am. **115**, 411–421.
Riede, T., and Fitch, W. T. (**1999**). "Vocal tract length and acoustics of vocalization in the domestic dog (Canis familiaris)," J. Exp. Biol. **202**, 2859–2867.
Ryalls, J. H., and Lieberman, P. (**1982**). "Fundamental-frequency and vowel perception," J. Acoust. Soc. Am. **72**, 1631–1634.
Ryan, M. J. (**1998**). "Sexual selection, receiver biases, and the evolution of sex differences," Science **281**, 1999–2003.
Ryan, M. J., Fox, J. H., Wilczynski, W., and Rand, A. S. (**1990**). "Sexual selection for sensory exploitation in the frog Physalaemus-pustulosus," Nature (London) **343**, 66–67.
Ryan, M. J., and Rand, A. S. (**2003**). "Sexual selection in female perceptual space: How female tungara frogs perceive and respond to complex population variation in acoustic mating signals," Evolution (Lawrence, Kans.) **57**, 2608–2618.
Sanvito, S., Galimberti, F., and Miller, E. H. (**2007**). "Vocal signalling in male southern elephant seals is honest but imprecise," Anim. Behav. **73**, 287–299.
Scheuber, H., Jacot, A., and Brinkhof, M. W. G. (**2004**). "Female preference for multiple condition-dependent components of a sexually selected signal," Proc. R. Soc. London, Ser. B **271**, 2453–2457.
Searcy, W. A. (**1992**). "Song repertoire and mate choice in birds," Am. Zool. **32**, 71–80.
Searcy, W. A., and Andersson, M. (**1986**). "Sexual selection and the evolution of song," Annu. Rev. Ecol. Syst. **17**, 507–533.
Titze, I. R. (**1994**) "Principles of Voice Production" (Prentice–Hall, Englewood Cliffs, NJ).
Vannoni, E., and McElligott, A. G. (**2007**). "Individual acoustic variation in fallow deer (Dama dama) common and harsh groans: A source-filter theory perspective," Ethology **113**, 223–234.

Shape-based ultrasound tomography using a Born model with application to high intensity focused ultrasound therapy

Başak Ülker Karbeyaz[a)]
Analogic Corporation, Peabody, Massachusetts 01960, USA

Eric L. Miller[b)]
Department of Electrical and Computer Engineering, Tufts University, Medford, Massachusetts 02215, USA

Robin O. Cleveland[c)]
Department of Aerospace and Mechanical Engineering, Boston University, Boston, Massachusetts 02115, USA

(Received 30 June 2007; revised 20 February 2008; accepted 21 February 2008)

A shaped-based ultrasound tomography method is proposed to reconstruct ellipsoidal objects using a linearized scattering model. The method is motivated by the desire to detect the presence of lesions created by high intensity focused ultrasound (HIFU) in applications of cancer therapy. The computational size and limited view nature of the relevant three-dimensional inverse problem renders impractical the use of traditional pixel-based reconstruction methods. However, by employing a shape-based parametrization it is only necessary to estimate a small number of unknowns describing the geometry of the lesion, in this paper assumed to be ellipsoidal. The details of the shape-based nonlinear inversion method are provided. Results obtained from a commercial ultrasound scanner and a tissue phantom containing a HIFU-like lesion demonstrate the feasibility of the approach where a 20 mm×5 mm×6 mm ellipsoidal inclusion was detected with an accuracy of around 5%. © *2008 Acoustical Society of America.* [DOI: 10.1121/1.2897045]

PACS number(s): 43.80.Sh, 43.20.Fn, 43.20.Rz, 43.20.Bi [TDM] Pages: 2944–2956

I. INTRODUCTION

Motivated by the need to develop noninvasive methods for monitoring high intensity focused ultrasound (HIFU) treatment of cancer, we consider the problem of localizing and characterizing the structure of a penetrable ellipsoidal scatterer embedded into a lossy homogeneous medium given backscatter ultrasound data. We propose an inversion method based on a Born forward model that can be potentially used to characterize HIFU lesions based on changes in sound speed and attenuation from rf data collected using a standard ultrasound array.

Over the past 15 years, there has been a significant interest in the development and clinical evaluation of HIFU for therapeutic applications, in particular the treatment of cancer.[1–10] HIFU uses focused ultrasound to raise the temperature of the target tissue to above 60 °C in 2 to 3 s, creating a lesion of order a few millimeters in size.[11,12] For example ter Haar *et al.*[13] reported that a 1.7 MHz transducer, which had a focal pressure of 6 MPa, created ellipsoidal-shaped lesions in beef liver that were about 20 mm long (in the direction of the HIFU beam) and 4 mm in diameter. Two major advantages of HIFU compared to the other tumor ablation techniques, e.g., radiation or cryogenic therapy, is that it uses nonionizing radiation and can generate tissue necrosis at depth with minimal impact on the surrounding tissues. One of the challenges required to make HIFU a practically useful tool for clinical application is the need for guidance of the HIFU treatment. As this treatment method is noninvasive it is necessary that an imaging method be available to guide the treatment and ensure full necrosis of the region of interest.

The current state of the art to monitor the HIFU lesions is magnetic resonance imaging (MRI), which can monitor time-dependent temperature elevation.[14–16] Despite the success of MRI as a tool for monitoring HIFU, it is a relatively expensive option and requires the development and use of specialized MRI-compatible HIFU hardware. Also patients with metal or electrical implants (e.g., pacemakers) are excluded from MRI. These issues motivate the use of diagnostic ultrasound for HIFU monitoring and guidance.

Ultrasound is sensitive to the acoustic properties of the tissue, specifically, the sound speed, acoustic absorption, and density. It is potentially suitable for HIFU guidance as it has been reported that HIFU treatments affect both the sound speed and the attenuation values of the tissue while forming lesions.[17–22] The change in sound speed is less than 20 m/s (about 1%) and peaks at temperatures between 50 and 70 °C and then decreases with further increase in the temperature. In most cases the change is reported to be reversible. The attenuation coefficient significantly increases within the values ranging from 80% to 700% and the change is irreversible.[23]

These effects have been employed previously in ultrasound-based monitoring of HIFU. For example Simon *et al.*[24] and Pernot *et al.*[25] were able to estimate the changes in the temperature from the sound speed measurements. However, because of the reversible nature of the sound

a)Electronic mail: bkarbeyaz@analogic.com.
b)Electronic mail: elmiller@ece.tufts.edu.
c)Electronic mail: robinc@bu.edu.

 0001-4966/2008/123(5)/2944/13/$23.00 © 2008 Acoustical Society of America

speed, the lesion will not be visible using this method once the tissue cools. The change in the attenuation is irreversible, hence an imaging approach based on capturing the changes in the attenuation should be more robust. The attenuation in the necrosed tissue is much higher than that of the surrounding healthy tissue, hence, the tissue behind the HIFU lesion would appear slightly darker in standard B-scan images. Processing the B-scan data, Baker and Bamber,[26] Annad and Kaczkowski,[27] and Zhong *et al.*[28] detected the changes in the ultrasound images behind the lesion.

Traditional medical ultrasound scanners employ beamforming to generate two-dimensional images. These techniques have enjoyed a great deal of success both because of their inherent computational efficiency as well as the quality of the imagery they provide. Less common is the use of tomographic approaches for processing ultrasound data. In cases where an ultrasound system can fully encircle a region of interest then it is possible to employ tomographic approaches as a diagnostic tool[29,30] or to detect HIFU lesions.[31] However, in the body the breast is perhaps the only organ that provides this access and most applications of HIFU therapy yield imaging problems for which only backscatter data, as are typically acquired by commercial ultrasonic transducers, will be available. As such, one would not expect image-formation type methods to yield the same high resolution results as in Ref. 29–31. Moreover, the fast backprojection computational methods of Refs. 29 and 30 are no longer applicable so that one must employ a discretized physical model for the interaction of ultrasound with tissue leading to some rather formidable computational challenges.

In this paper, we develop and validate a shape-based inversion designed for limited view, ultrasound tomographic applications such as HIFU lesion characterization. In the development of the inverse problem we invoked the following assumptions:

(1) The shape of the object is taken to be ellipsoidal.
(2) A Born-type model is assumed for describing the scattering processes.
(3) The medium in which the object is embedded is taken to be homogeneous and lossy.

Each of these assumptions has been made more as a matter of convenience to allow us to concentrate on the primary objectives of the paper, which is the formulation of a shape-based tomography problem and the validation of this idea using experimentally acquired data from an off-the-shelf transducer. We address the relevance and impact of these assumptions in the following paragraphs and discuss how they can be lifted in Sec. VI.

In terms of shape-based modeling, we note that there has been considerable work in the past decade on the use of such models as the basis for inverse processing. For example, the reconstructions of ellipsoids have been considered using low frequency acoustic and electromagnetic data.[32–36] However these methods do not address to penetrable scatterers, assume low-frequency plane wave excitation, and rely on the fact that the scattering amplitude is known. Our own efforts consider the use of ellipsoids as models for problems in diffuse optical tomography,[37] another diffusive imaging-type application, where an ellipsoidal model was employed to describe perturbations in optical absorption properties for a breast imaging application. The work in this paper build most closely on that of Ref. 38 in that here we also consider the estimation of the parameters modeling the shape of an ellipsoid. Here, though, we generalize the problem to the case where there are multiple physical properties that are of interest (sound velocity, absorption, and density) each of which can, in theory, be associated with its own ellipsoid. We also consider specifically the high frequency, ultrasound problem rather than the diffusive applications cited earlier.

The use of a Born model in this paper and the assumption of spatial homogeneity are both closely related. They are driven by the size of the problem we were addressing. As will be discussed in Sec. III, the computational size of the relevant three-dimensional (3D) ultrasound problem renders impractical the straightforward use of a full wave field model. Given that our objective was to provide initial validation of the inversion scheme we are proposing as well as the success in processing experimental data, as demonstrated in Sec. V C, we have elected to delay to the future the substantial investment in effort that would be required to develop a fully nonlinear inversion scheme.

II. FORWARD MODEL

A. Derivation of the scattered field

The propagation of time harmonic ultrasound through an inhomogeneous, lossy medium can be described by the following frequency domain wave equation:[39]

$$\nabla^2 p(r,\omega) - \nabla \ln \rho(r) \nabla p(r,\omega) + k^2(r,\omega) p(r,\omega) = q(r,\omega), \tag{1}$$

where r is a point in three space, ω is the angular frequency, $p(r,\omega)$ is the pressure at r and ω, $\rho(r)$ is the density, $k(r,\omega)$ is the wave number, and $q(r,\omega)$ is the source that creates the acoustic disturbance in the medium. In dispersive attenuating media, $k(r,\omega)$ has the form: $k(r,\omega)=\omega/c(r,\omega)-j\alpha(r,\omega)$ where $c(r,\omega)$ is the dispersive speed of sound and $\alpha(r,\omega)$ is the frequency-dependent attenuation coefficient.

In most tissue, dispersion is weak and the attenuation follows a power law. The sound speed can then be expressed as $c(r,\omega)=c_b+c_p(r)$, where c_b is the background sound speed and $c_p(r)$ the spatially dependent perturbation. Similarly, $\alpha(r,\omega)=\alpha_b(\omega)+\alpha_p(r,\omega)$ where $\alpha_b(\omega)=\alpha_{bo}\left(\frac{\omega}{\omega_o}\right)^n$ is the background attenuation (typically $1<n<1.5$ for soft tissue) and $\alpha_p(r,\omega)=\alpha_{po}(r)(\omega/\omega_o)^n$ the perturbation. The square of the wave number can then be expressed as

$$k^2(r,\omega) \approx \frac{\omega^2}{c_b^2} - j\frac{2\omega\alpha_b(\omega)}{c_b} - c_p(r)\left[\frac{2\omega^2}{c_b^3}\right] - \alpha_p(r,\omega) \times \left[j\frac{2\omega}{c_b}\right]. \tag{2}$$

This can be decomposed into a background term

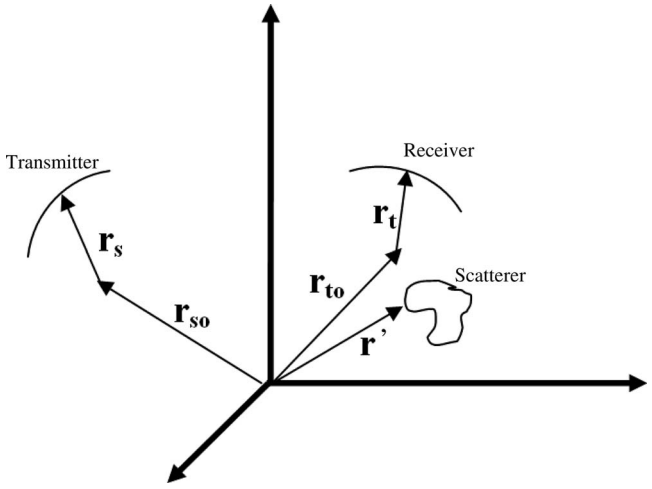


FIG. 1. Transmitter, receiver, and the scatterer location vectors.

$$k_b^2(\omega) = \frac{\omega^2}{c_b^2} - j\frac{2\omega\alpha_b(\omega)}{c_b} \tag{3a}$$

and a perturbation term

$$k_s^2(r,\omega) = c_p(r)\left[-\frac{2\omega^2}{c_b^3}\right] + \alpha_p(r,\omega)\left[-j\frac{2\omega}{c_b}\right], \tag{3b}$$

which is a *linear* function of scattering parameters.

We invoke the Born approximation to determine the scattered field in terms of the perturbation to the background properties:[40]

$$p_s(r,\omega) = \int_{V'} G(r,r',\omega)k_s^2(r',\omega)p_b(r',\omega)d^3r' - \int_{V'} G(r,r',\omega)\,\nabla\,\sigma_p(r')\,\nabla\,p_b(r',\omega)d^3r', \tag{4a}$$

where $\sigma=\ln(\rho(r))=\sigma_b+\sigma_p(r)$. After some algebraic manipulations the scattered field is given by[41]

$$p_s(r,\omega) = \int_{V'} \{G(r,r',\omega)k_s^2(r',\omega)p_b(r',\omega) + \sigma_p(r')\,\nabla\,p_b(r',\omega)\,\nabla\,G(r,r',\omega)\}d^3r', \tag{4b}$$

where $p_s(r,\omega)$ is the scattered field (i.e., the Fourier transform of the ultrasonic echoes), $p_b(r',\omega)$ is the background field; that is, the ultrasound field in the medium in the absence of the scatterer, $G(r,r',\omega)$ is the 3D free space lossy Green's function and V' is the boundary of the scattering volume.

B. Derivation of the measured pulse echo signal

Having presented the major equations, we now calculate the received signal, measured echo data, for a bistatic pulse-echo configuration.[42] The configuration for the transmitter, receiver, and the scatterer locations is given in Fig. 1. The scatterer is identified by $\mathbf{r}'$ and the origin of the transmitter and receiver coordinates are denoted by $\mathbf{r}_{so}$ and $\mathbf{r}_{to}$, respectively. The vectors that are traversing the surface of the transmitter and receiver transducers are given by $\mathbf{r}_s$ and $\mathbf{r}_t$, respectively.

For this bistatic pulse-echo system the scattered field is given by

$$p_s(\mathbf{r}_{to}+\mathbf{r}_t,\omega) = \int_{V'} G(\mathbf{r}_{to}+\mathbf{r}_t,\mathbf{r}',\omega) \times (k_s^2(\mathbf{r}',\omega)p_b(\mathbf{r}',\mathbf{r}_{so},\omega) - \nabla\sigma_p(\mathbf{r}')\cdot\nabla p_b(\mathbf{r}',\mathbf{r}_{so},\omega))d^3\mathbf{r}, \tag{5}$$

where the background signal can be obtained from

$$p_b(\mathbf{r}',\mathbf{r}_{so},\omega) = V_i(\omega)e_T(\omega)\int_S \frac{e^{-jk|\mathbf{r}'-(\mathbf{r}_s+\mathbf{r}_{so})|}}{4\pi|\mathbf{r}'-(\mathbf{r}_s+\mathbf{r}_{so})|}d^2\mathbf{r}_s. \tag{6}$$

$V_i(\omega)$ is the Fourier transform of the uniform excitation voltage and $e_T(\omega)$ is the Fourier transform of the transmit electromechanical response of the transducer. The integral in Eq. (6) is the spatial transfer function and it relates the transducer geometry to the acoustic field.[43–45] By means of this function, we can write

$$p_b(\mathbf{r}',\mathbf{r}_{so},\omega) = V_i(\omega)e_T(\omega)H(\mathbf{r}',\mathbf{r}_{so},\omega). \tag{7}$$

The received signal is the product of the scattered pressure field integrated over the receiver transducer surface and the electromechanical impulse response of the receiver, $e_R(\omega)$,

$$v_o(\mathbf{r}_{to},\omega) = e_R(\omega)\int_S p_s(\mathbf{r}_{to}+\mathbf{r}_t,\omega)d^2\mathbf{r}_t. \tag{8}$$

Using this definition and integrating Eq. (5) with respect to r_t, one readily obtains

$$v_o(\mathbf{r}_{to},\omega) = e_{pe}(\omega)\int_{V'} H(\mathbf{r}_{to},\mathbf{r}',\omega)(k_s^2(\mathbf{r}',\omega)H(\mathbf{r}',\mathbf{r}_{so},\omega) - \nabla\sigma_p(\mathbf{r}')\cdot\nabla H(\mathbf{r}',\mathbf{r}_{so},\omega))d^3\mathbf{r}', \tag{9}$$

where $e_{pe}(\omega)=V_i(\omega)e_T(\omega)e_R(\omega)$. Finally using Green's theorem:

$$v_o(\mathbf{r}_{to},\omega) = e_{pe}(\omega)\int_{V'} k_s^2(\mathbf{r}',\omega)H(\mathbf{r}_{to},\mathbf{r}',\omega)H(\mathbf{r}',\mathbf{r}_{so},\omega)d^3\mathbf{r}' + e_{pe}(\omega)\int_{V'} \sigma_p(\mathbf{r}')\,\nabla\,H(\mathbf{r}_{to},\mathbf{r}',\omega)\cdot\nabla H(\mathbf{r}',\mathbf{r}_{so},\omega)d^3\mathbf{r}'. \tag{10}$$

The primary characteristic of Eq. (10) is that it provides a linear relation between the measured backscatter data, $v_o(\mathbf{r}_{to},\omega)$, and the medium parameters k_s^2 and σ_p.

III. INVERSION METHOD

The forward model for a medium with weak scatterers is obtained by substituting Eq. (3b) in Eq. (10) in which case

$$v_o(\mathbf{r}_{to},\omega) = \int_{V'} K_1(r,r',\omega)c_p(r')d^3r' + \int_{V'} K_2(r,r',\omega)\alpha_p(r')d^3r' + \int_{V'} K_3(r,r',\omega)\sigma_p(r')d^3r', \quad (11)$$

where K_i, $i=1,2,3$ depend only on the background properties. To represent the forward model for point sources, Eq. (4b) will be used to obtain K_i.

For the imaging system of interest in this work, it is assumed that multiple transmitters and receivers are used to obtain the measurements. For the case of N_T transmitters and N_R receivers with N_S frequency samples, the measured data $\mathbf{y}$ can be written as a column vector of size $N_T \times N_S \times N_R$. Discretizing Eq. (11) at any position r', the received echo voltage can be written in a matrix-vector model of the form:

$$\mathbf{y} = [\mathbf{K}_1\mathbf{K}_2\mathbf{K}_3][\mathbf{f}_1^T\mathbf{f}_2^T\mathbf{f}_3^T]^T + \mathbf{n} = \mathbf{K}\mathbf{f} + \mathbf{n}, \quad (12)$$

where $\mathbf{K}$ is the matrix representation of the integral; $\mathbf{f}_1$ is the column vector containing the voxel values of sound speed perturbation, c_p; $\mathbf{f}_2$ is the column vector containing the voxel values of attenuation perturbation, α_p; $\mathbf{f}_3$ is the column vector containing the voxel values of density perturbation, σ_p; and $\mathbf{n}$ is the additive sensor noise.

The ultimate goal is to estimate the unknown medium parameters $\mathbf{f}_1$, $\mathbf{f}_2$, and $\mathbf{f}_3$, from measured backscatter data. One approach to this problem would be to use linear inversion methods, and try to reconstruct voxelated images of the sound speed, density, and absorption. The nominal wavelength for imaging in tissue is about 0.3 mm at 5 MHz and the physical size of the region to be imaged could be on order of 30 mm on a side. An accurate discretization of the problem, with a step of a tenth of a wavelength (0.03 mm), could require up to a billion voxels. The linear inversion problem is ill-posed for this case due to the large number of voxels defining each of the three unknown vectors $\mathbf{f}_1$, $\mathbf{f}_2$, $\mathbf{f}_3$.

Our approach to the problem is based on the specification of the parameters describing the shape of the perturbations. We assume the shape of the perturbations is known, ellipsoids, but the locations, sizes, and orientations are unknown. Specifically, perturbations in Eq. (11), c_p, α_p, and σ_p, are represented by ellipsoidal shapes.

Therefore, to completely characterize the perturbation in one variable, we only need the location of the center, the lengths of the three axes of the ellipsoid, three angles that orient the ellipsoid in space, and contrast of the perturbation. Thus rather than having to invert for up to a billion voxels we have only $3\times10=30$ quantities to estimate from the measured data. In the case when c_p, α_p, and σ_p share the same geometry the number of unknowns reduces to 12. The inverse problem cast in this manner is therefore much better posed than the fully voxelated image.

A. Ellipsoid modeling

An ellipsoid can be defined mathematically with four elements:

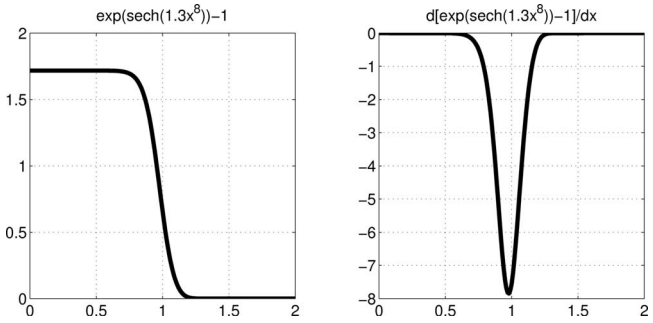


FIG. 2. The function $S(x)=\exp(\mathrm{sech}(1.3x^8))-1$ and its derivative.

(1) A length three vector, c, denoting the center of the ellipsoid, (x_o,y_o,z_o).
(2) A diagonal matrix $D=\mathrm{Diag}(d)$ whose diagonal entries are inverses of the semiaxes lengths, (l_1,l_2,l_3).
(3) An orthonormal matrix U defining the ellipse in 3D using three Euler angles, $(\theta_1,\theta_2,\theta_3)$.
(4) A constant M, defining the contrast of the object.

A point $r'=[x',y',z']^T$ is determined to be on or in the ellipsoid if

$$\|DU^T(r'-c)\|_2^2 \leqslant 1. \quad (13)$$

Hence, the ellipsoidal perturbations can be defined as

$$\gamma(r') = MS(1-\|DU^T(r'-c)\|_2^2) = \begin{cases} M & r' \in \text{ellipsoid} \\ 0 & \text{otherwise} \end{cases}. \quad (14)$$

For an infinitely sharp interface $S(x)$ could be a step function. However, the step function model of the ellipsoid gives a discontinuity at the boundary of the ellipsoid. For purposes of inversion, where we wish to use gradient descent type methods to estimate the parameters of interest, we employ a smooth, analytical approximation to the step function as is common in many geometric-type processing methods.[46] It is more computationally efficient to have an analytical representation of the Jacobian which motivates choosing a differentiable expression that maps the parameters describing the shape to any point r' in the region of interest. Here the step function is approximated with a hyperbolic secant, see Fig. 2, and define the perturbations as

$$\gamma(r') = \exp(\tilde{M}\ \mathrm{sech}(1.3\|DU^T(r'-c)\|_2^{16})) - 1. \quad (15)$$

The coefficient 1.3 is chosen so that without the scaling from the exponential function, the boundary value of the shape is set to 0.5 (the mean value of the change in the boundary).

If a point r_1 is within the ellipsoid, $\|DU^T(r_1-c)\|_2^2$ is less than 1 and the value of $\gamma(r_1)$ approaches a constant value $[\exp(\tilde{M})-1]$. On the other hand, if r_1 is not within the ellipsoid, the value of Eq. (13) is larger than 1 and $\gamma(r_1)$ approaches 0. Around the boundary, the function provides a transition from 1 to 0. Therefore the expression approximates a step function, and classifies the points in the region of interest.

Our use of the hyperbolic secant function was motivated not by a desire to represent the transition from lesion to

healthy tissue, but rather as a mathematical convenience for use with the optimization method we use. With respect to the boundary in the tissue, there are data that indicate that the transition from necrosed to healthy tissue is very sharp—on the order of tens of cells.[47,48] Relative to the ultrasonic wavelength the exact nature of the discontinuity is not resolvable and therefore could be represented by any number of functions. For the inversion, it was necessary to have differentiable functions and for that purpose we chose the sech function. We tested other functions to represent the sharp boundary, including arctan and arctanh, and found that the sech function provided marginally better results over the full range of experiments considered in the paper.

B. Inverse problem

The parameters that will be used to characterize the ellipsoids of the three acoustic properties will be

$$\beta_i = [x_{oi}, y_{oi}, z_{oi}, l_{1i}, l_{2i}, l_{3i}, \theta_{1i}, \theta_{2i}, \theta_{3i}, M_i],$$

where the subscripts $i=c,a,d$ will be used to represent the perturbations in sound speed, attenuation, and density, respectively. The representation of the perturbations given in Eq. (15a), $\gamma(r')$, will be replaced by $\gamma_i(r',\beta_i)$ to account for the parameters of each individual ellipsoid, where

$$\gamma_i(r',\beta_i) = \exp(\tilde{M}_i \operatorname{sech}(1.3\|D_i U_i^T (r' - c_i)\|_2^{16})) - 1. \quad (16)$$

The problem to be solved given data $\mathbf{y}$, is the nonlinear least squares problem:

$$\min_{\beta_c,\beta_a,\beta_d} \|\mathbf{y} - \mathbf{K}\mathbf{f}(\beta)\|_2^2 \quad (17a)$$

$$\beta = \begin{bmatrix} \beta_c \\ \beta_a \\ \beta_d \end{bmatrix} \quad (17b)$$

In this work the minimization problem in Eq. (17a) was solved using the Gauss–Newton method.[49] For this purpose, an initial guess is provided for the ellipsoid parameters (β^0). Subsequent guesses (β^k) for the parameter vectors are then produced by the recurrence relation:

$$\beta^{k+1} = \beta^k + \alpha^k t^k, \quad (18)$$

where α^k is the sense optimal and t^k is the search direction obtained from the solution of

$$(J^T J)t^k = -J^T \|\mathbf{y} - \mathbf{K}\mathbf{f}(\beta^k)\|_2, \quad (19)$$

where J is the Jacobian. The computation of the Jacobian matrix is given in the Appendix. The search algorithm iterates until a termination tolerance is satisfied which is described in Sec. V.

IV. APPLICATION TO HIFU LESIONS

The equations presented in Sec. II A can be used to express the measured backscatter data from a lesion embedded in a weakly scattering medium as follows. The use of the Born approximation requires that the incident field is negligibly impacted by the presence of the lesion. In the case of HIFU lesions, the change in sound speed due to heating is less than 1%, which is within the Born approximation. The attenuation coefficient increase by 80%–700% appears large but the constraint on the attenuation is defined as the smallness of α_p/k_b. The nominal attenuation in human tissue is 35.6 Np/m at 3.5 MHz. For the sound speed of 1551 m/s and 700% perturbation in attenuation, the ratio of α_p/k_b is 1.7% also within the Born approximation. Although our model accounts for changes in the density of tissue, the link between density and HIFU lesions has not yet been established. However, the density perturbations are included here for the completeness of the model. We were not able to identify measurements of density change in response to HIFU and therefore in this work the change in the density was limited to 1% to validate the Born model.

The applicability of the inversion method described in Sec. III to HIFU lesions is based on the fact that in HIFU there is substantial prior information about the target. The approximate size, location, and orientation of the lesion can be determined from the parameters of the HIFU source. In this work we will assume that the lesions are ellipsoidal in shape which is a reasonable model for purely thermal lesions.

We note that, after several excitations, the heated area may well lose its initial simple, ellipsoidal shape. Also, the morphology of the necrosed region may depend upon how the tissue is ablated, i.e., how the beam is scanned across the region of interest, and at what repetition rate. Depending upon these, the shape of the necrosed area may be quite arbitrary. However, the paradigm we introduce in this work can be extended to other shapes and this is addressed in the discussion.

V. INVERSION EXAMPLES AND RESULTS

In this section, the 3D shape-based inversion results for ellipsoidal Born scatterers are presented. In Sec. V A, the transducers are assumed to be point sources where the scattered field is represented by Eq. (4b) and in Sec. V B, a Monte Carlo analysis is done to determine the robustness of the inversion. In Sec. V C the proposed method is validated with measured ultrasound backscatter data from an ellipsoidal target that mimics a HIFU lesion. In this case the scattered field is represented by Eq. (10). In both cases the model given by Eq. (16) is used for the lesion structure and the contrast of the ellipsoidal-shaped perturbations in sound speed, attenuation, and density are estimated.

A. Numerical simulations and results

Here we present the numerical simulations that were used to validate the inversion idea on a problem of manageable size while the laboratory experiments presented in Sec. V C were dictated by the underlying, motivating application as well as the fact that the 3.5 MHz transducer is what is readily available in practice. In what follows we will employ a Monte Carlo approach to determine the behavior of the inversion and therefore to reduce the computational complexity for the numerical simulations, frequency values lower than those employed in the medical imaging applications were used, and the overall size of the problem was

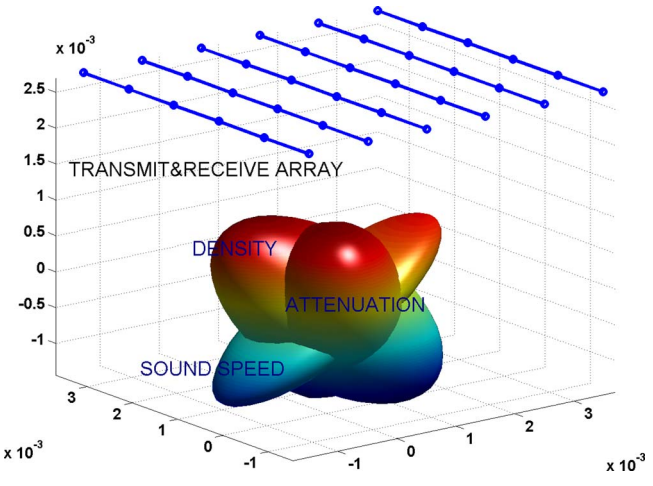


FIG. 3. (Color online) Setup for the numerical simulation showing three noncongruent perturbations. The connected dots show the six locations of the six element array that was used to detect the lesions.

reduced to 5 mm×5 mm×5 mm. Exploring ideas such as our ability to recover one ellipsoid per physical quantity could not be done easily at higher frequencies due to the long computational time associated with the size of the matrices for the high frequency case.

To demonstrate the flexibility of the shape-based approach three numerical simulation experiments were performed. Two cases were presented where three different ellipsoids were assumed for three different acoustic parameters and another case in which the spatial changes in the acoustic properties were represented by three overlapping ellipsoids (i.e., single ellipsoid). In practice, and indeed in the laboratory experiments, we assume a single ellipsoid in which the spatial changes in acoustic properties were enclosed within a single ellipsoid.

The numerical simulation conditions are given in Fig. 3. A linear array of six point sources are scanned across the anomaly at six different measurement points. At each measurement point, a single transmitter insonifies the medium where the echo data are calculated for each element of the array. Six frequencies equally spaced between 300 and 425 kHz were used in the simulations. Gaussian noise was added to the data to set the signal to noise ratio to 25 dB. The background properties were chosen to match those of a tissue mimicking phantom that we have employed previously:[41] $c_b=1551$ m/s, $\rho_b=1045$ kg/m^3, $\alpha_b=3.6$ Np/m $(\omega/\omega_o)^{1.2}$ where $\omega_o=2\pi 350$ kHz. The values of the contrasts for a realistic problem were chosen as explained in the following. The total number of voxels in the region of interest was 4096 ($16\times16\times16$). The discretization step in terms of the smallest wavelength was one-tenth of a wavelength.

The bounds for the contrasts, M_i, were chosen as follows:

(1) 0 m/s$<M_c<$20 m/s.
(2) 0 Np/m$<M_a<$20 Np/m.
(3) 0 kg/m$^3<\sigma_p<$10 kg/m^3, hence $0<M_d<9.5\times10^{-3}$.

The inversion method described in Sec. III B was implemented in MATLAB where the "lsqnonlin" function with Gauss–Newton option was used. The geometric parameters and the contrasts of the ellipsoids, β_i were scaled to the same order (between 1 and 2) prior to the optimization routine to maximize the performance. The bounds for the geometric parameters are given in Table I. The lower limits for the lengths of the semiaxes were set to a small number (0.5 μm) to prevent the solution producing zero volume ellipses.

TABLE I. Lower and upper limits for the geometric parameters of the ellipsoid.

	Lower limit	Upper limit
x_o	−2.5 mm	2.5 mm
y_o	−2.5 mm	2.5 mm
z_o	−2.5 mm	2.5 mm
l_1	0.5 μm	2.5 mm
l_2	0.5 μm	2.5 mm
l_3	0.5 μm	2.5 mm
θ_1	0	2π
θ_2	0	π
θ_3	0	2π

The lower and the upper bounds for the "lsqnonlin" function were set to 1 and 2, respectively, to ensure that the boundary of the ellipsoid was in the region of interest and the contrasts were within the above-defined limits. The termination tolerance on the function value, $\mathbf{y}-\mathbf{Kf}(\beta^k)$, was 10^{-5}.

In Figs. 4–6 the true and estimated ellipsoid distributions are displayed. For comparison purposes, the true shapes are plotted with lines on the estimated ellipsoids. Two measures are introduced to describe the error between the real and simulated ellipsoids. The estimation error in contrast is defined as

$$E_c\,\% = 100\left|\frac{M_i-\bar{M}_i}{M_i}\right|, \tag{20}$$

where M_i and $\bar{M}_i$ represent the actual and estimated contrasts, respectively. The volumetric estimation error is defined as

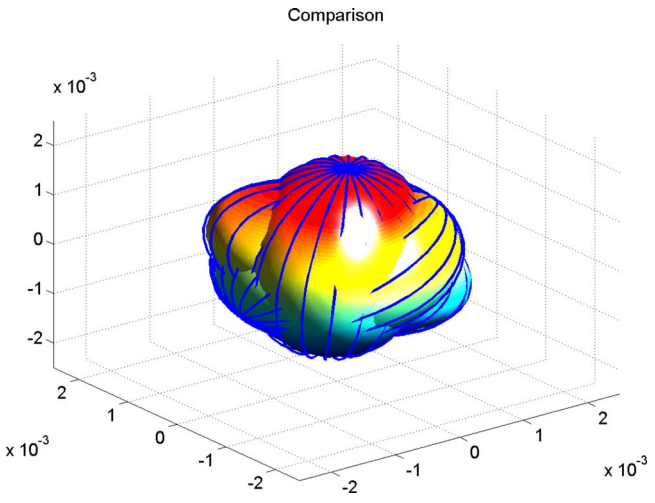


FIG. 4. (Color online) Case 1: Inversion for similarly sized and shaped ellipsoids.

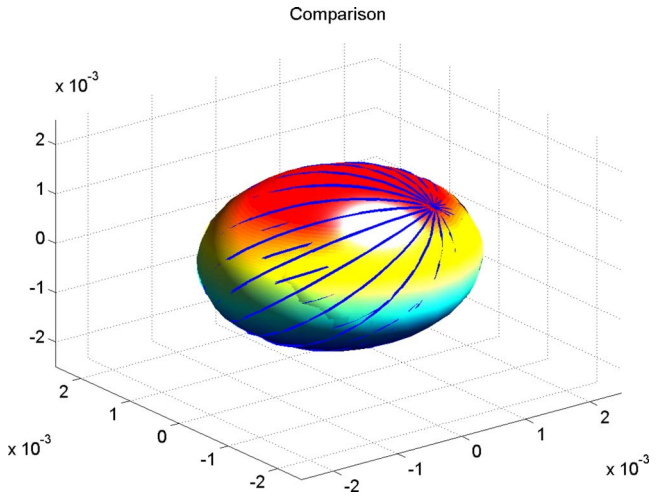


FIG. 5. (Color online) Case 2: Inversion for concentric and overlapping ellipsoids.

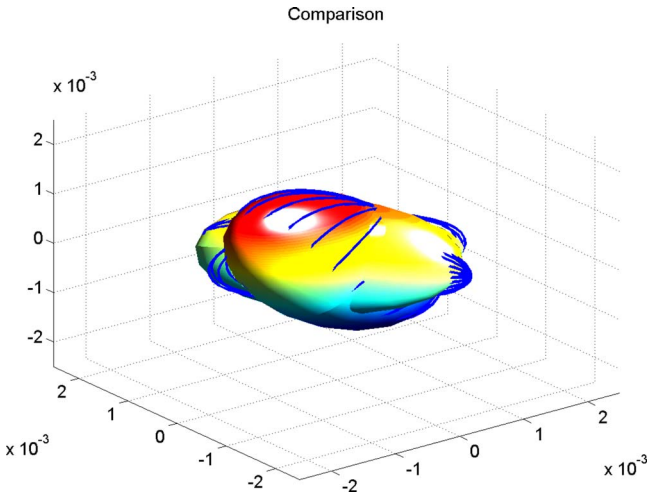


FIG. 6. (Color online) Case 3: Inversion for significantly different ellipsoids.

$$E_v\,\% = 100\left(1 - \frac{\text{Volume}(E_a \cap E_e)}{\text{Volume}(E_a \cup E_e)}\right), \tag{21}$$

where E_a and E_e represent the actual and estimated ellipsoids, respectively. For comparison purposes, the real, initial, and estimated contrast values for all the simulations are given in Table II with the error values.

Figure 4 shows a case where the inclusion consists of similarly sized and shaped ellipsoids with different orientations. Given little prior information about the shape and the contrasts it was possible to recover the geometry and the contrasts quite accurately, with all errors less than 4%. The number of required iterations was 99, which took 14 min on a 1 GHz Linux workstation.

Figure 5 shows the HIFU lesion type anomaly where the inclusion consists of three concentric, overlapping ellipsoids. This represents the case of HIFU lesion where the changes of the acoustic properties are confined into a single region of space rather than individual ellipsoids. Although it appears that a single ellipsoid anomaly has been detected, the algorithm classified three distinct ellipsoids. Although the initial estimates for the contrasts were considerably different than the real values, a very good estimate was obtained for the contrasts and the geometries. The method proposed here to define the contrast of the object as a nonlinear parameter of the problem, greatly improved the contrast detection. The number of required iterations was 98, which took 14 min on a 1 GHz Linux workstation.

In the third case, Fig. 6, the scenario consisted of three significantly different ellipsoids. Although this does not model what we expect to observe in a HIFU application it demonstrates the utility of the approach to a wider class of problems. The localization of the perturbations was successful although the differences were larger than for the other two cases. Our observations revealed that the rotation angles are the most difficult parameters to estimate for this type of shape-based inversion problem. The number of required iterations was 299, which took 24 min on a 1 GHz Linux workstation. The same experiment was repeated with signal-to-noise ratio of 40 dB and a better localization was obtained for the anomaly where the errors were less than 5%.

B. Monte Carlo analysis

A statistical error analysis was done to assess more thoroughly the performance of the inversion method presented in this study. For this purpose, Monte Carlo simulations were performed in which 140 estimation problems were considered. For each realization, a randomly oriented ellipsoid was selected so that it had up to 15% deviation in contrast, volume, and orientation from an *a priori* ellipsoid. Gaussian

TABLE II. Contrast and error values for the sound speed, attenuation, and density.

		Real	Initial	Estimate	E_c %	E_v %
Case 1	Speed (m/s)	3.58	20.00	3.71	3.59	3.00
	Density (kg/m^3)	4.99	10.00	4.87	2.32	2.05
	Attenuation (Np/m)	3.58	20.00	3.63	1.20	2.69
Case 2	Speed (m/s)	7.42	20.00	7.50	0.95	3.19
	Density (kg/m^3)	9.01	10.00	8.93	0.87	5.73
	Attenuation (Np/m)	7.42	20.00	8.16	9.88	2.26
Case 3	Speed (m/s)	13.57	20.00	10.52	22.01	32.94
	Density (kg/m^3)	10.00	10.00	10.00	0	1.41
	Attenuation (Np/m)	12.30	19.00	5.92	51.01	1.89

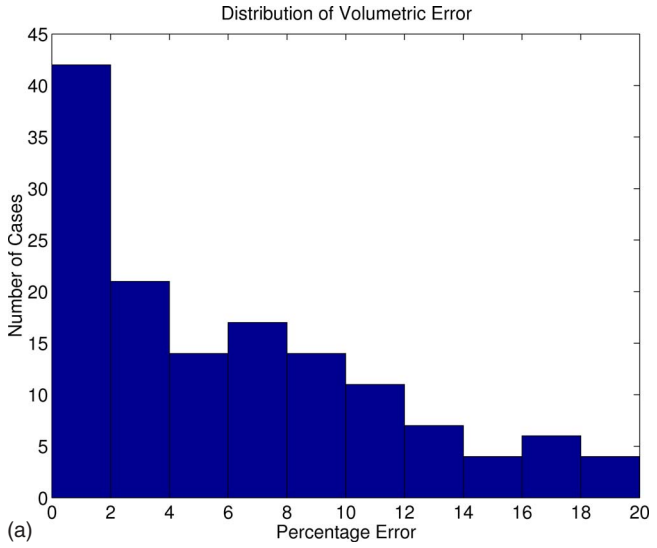


FIG. 7. (Color online) Distribution of volumetric (a) and contrast (b) errors. The total number of reconstructions was 140.

noise was added to the data to set the signal to noise ratio to 25 dB. The error distributions in volume and contrast are given in Fig. 7.

The algorithm was successful in localizing the ellipsoidal shapes but the performance was slightly poorer for contrast estimation. In 75% of the cases the localization error was less than or equal to 10%. For the problem of determining HIFU lesion position, the localization is more important than the contrast errors. On the other hand, the contrast estimation provides a means to construct a "safety zone" by which one can be assured that the tissue has in fact been necrosed. For all the cases where the error was high, the rotation parameters were significantly different (22%) than the actual values. This is consistent with the previous observation that the rotation parameters are the most difficult parameters to estimate.

The results showed that the method given in this study was generally successful in estimating the randomly oriented ellipsoids.

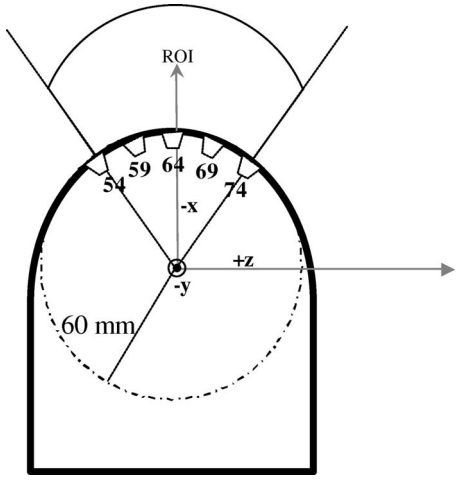


FIG. 8. Schematic of the locations of the transducers on the transducer array.

C. Laboratory experiment and results

A laboratory experiment with a clinical ultrasound transducer was performed to validate the inversion method developed in this paper. The probe (Model 8665, BK Medical, Wilmington, MA) was a curvilinear array with a 60 mm radius of curvature convex surface upon which 128 elements (13 mm high $\times$ 0.5 mm wide) were placed with a pitch of 0.525 mm. Each element had a center frequency of 3.5 MHz and in the elevation plane was focused to 70 mm. Each element could be individually controlled using a real time ultrasound scanner (AN2300, Analogic Corporation, Peabody MA) with a MATLAB interface.

For this experiment five elements, Nos. 54, 59, 64, 69, and 74, were employed to take the measurements. The angle between each element used in this study was 0.0438 rad. The schematic showing the location of the cylindrically concave transducers on the linear array is given in Fig. 8.

The array transducer and the phantom were placed in a water tank (35 cm $\times$ 53 cm $\times$ 35 cm) that was filled with deionized, degassed water at approximately 21 °C. Each cylindrically concave element was operated in transmit mode individually and the unbeamformed echo data from other elements in the array were recorded and stored for post processing.

The laboratory experiment settings are given in Fig. 9. The origin of the region of interest (ROI) was defined as the geometric focus of the 64th element. The linear array was scanned across the ellipsoid anomaly at five different measurement locations. At each measurement location, a single element insonified the medium and the backscattered signal was measured by all five elements of the array. This was repeated using all elements of the array as a transmitter. The array was scanned across the anomaly between $y=-6$ mm to $y=6$ mm with 3 mm step size.

An ellipsoidal shaped phantom (20 mm $\times$ 5 mm $\times$ 6 mm) was carved from an agar tissue mimicking phantom which had the nominal acoustic properties of $c_p = 1551$ m/s, $\rho_p = 1045$ kg/m^3, and $\alpha_p = 10.17$ Np/m/MHz. The ellipsoid was immersed into a polyacrylamide hydrogel

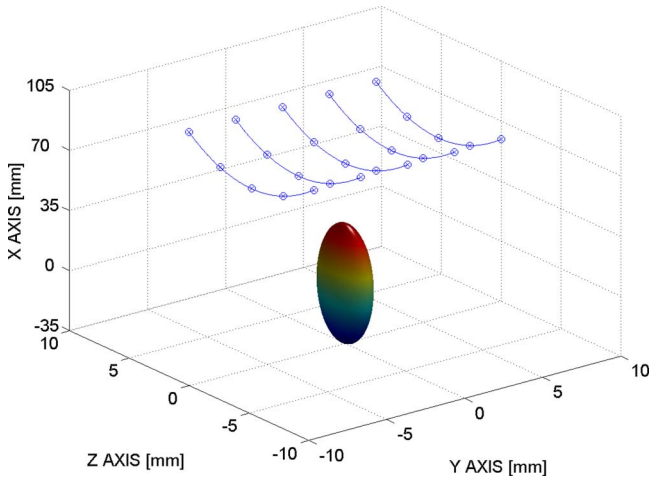


FIG. 9. (Color online) Setup for the laboratory experiment showing agar perturbation. The connected dots show the five elements of the linear array that was used to detect the lesion. The array was scanned across the ellipsoid anomaly at five different measurement locations.

with 7% Bovine Serum Albumin (BSA) protein concentration in a cylindrical container. The acoustic properties of the background phantom were: $c_b=1540$ m/s, $\rho_b=1045$ kg/m^3, and $\alpha_b=1.5$ Np/m/MHz.[50] The polyacrylamide hydrogel was used because it was optically transparent (allowing visualizing of the ellipsoidal anomaly), had the same density as the agar phantom, and had differences in sound speed and attenuation that were representative of a HIFU lesion. That resulted in an experiment environment of which there was a single ellipsoidal anomaly and altered sound speed and attenuation values compared to the background. A photograph of the BSA phantom showing the ellipse is given in Fig. 10. The inversion algorithm involves solving the same minimization problem as in Sec. V A, Eq. (17a). The only difference is that the transducer elements cannot be modeled as point sources. Therefore, the method described in Ref. 51 was used to compute the spatial transfer function of the cylindrical elements and incorporated into computing K_1,K_2, and K_3 in Eq. (11). The inversion was carried out at five frequency values equally sampled between 2.5 and 3 MHz.

D. Results

The inversion was carried out using the following bounds on for the contrasts: $0 \text{ m/s} < M_c < 20 \text{ m/s}$ and



FIG. 10. (Color online) Optical image of phantom showing the ellipsoid—the dark region at the center of the image.

TABLE III. Lower and upper limits for the geometric parameters of the ellipsoid.

	Lower limit	Upper limit	Real value
x_o	−3.70 mm	0.3 mm	−1.70 mm
y_o	0 mm	4 mm	2.00 mm
z_o	−4.00 mm	3.20 mm	−2.80 mm
l_1	1.48 mm	8.30 mm	1.60 mm
l_2	0.50 mm	16.10 mm	2.60 mm
l_3	9.86 mm	12.40 mm	9.90 mm
θ_1	0.37	0.50	0.43
θ_2	0.24	0.30	0.27
θ_3	0.43	0.55	0.49

$0 \text{ Np/m} < M_a < 440 \text{ Np/m}$. Since there was no density perturbation with respect to background, M_d was set to 0. In HIFU problems, the location and orientation of the lesion can be initially estimated from the geometry of the HIFU transducer. Therefore, for this problem, it was assumed that the location and the orientation of the ellipsoid were roughly known but the lengths and contrasts were given larger bounds. The bounds for the geometric parameters used in the inversion are given in Table III.

In Fig. 11 the true ellipsoid, initial guess provided to the estimation method and the final result are displayed. For comparison purposes, the estimated ellipsoid is plotted with lines on the actual ellipsoid in Fig. 12. The number of iterations required was 116 and the total computation time was about 26 min. We were able to recover the geometry information with 5.7% volumetric estimation error. The maximum error in x, y, and z was determined to be 4.6%. The quantitative acoustic parameters of the ellipsoid is also of interest here. The initial contrast values provided to the optimization routine and the expected values are given in Table IV. Although the initial values were considerably different than the real values, we were able to determine the attenuation perturbation to within 5%. The sound speed estimate was not so accurate, with an error of 16%, however we note that the contrast in the sound speed was very small (5 m/s in 1550 m/s) and as was mentioned in Sec. I this may not be a robust parameter to determine a lesion once the lesion has cooled.

VI. CONCLUSIONS

The use of wave-based inversion methods for medical ultrasound imaging is not common. Primarily, the size of the region of interest and the limited view nature associated with most data acquisition scenarios make the traditional inversion methods, which yield complete images, impractical. However, in the case of lesions formed during HIFU the goal is to characterize objects for where there is significant prior information about the size, location, and orientation of lesions as well as their acoustic contrasts in attenuation and sound speed. Motivated by this application a shape-based method was developed for determining the acoustic properties and the spatial structure of an ellipsoidal scatterer in the Born approximation. The application of this method to HIFU-like lesions was demonstrated. This preliminary work

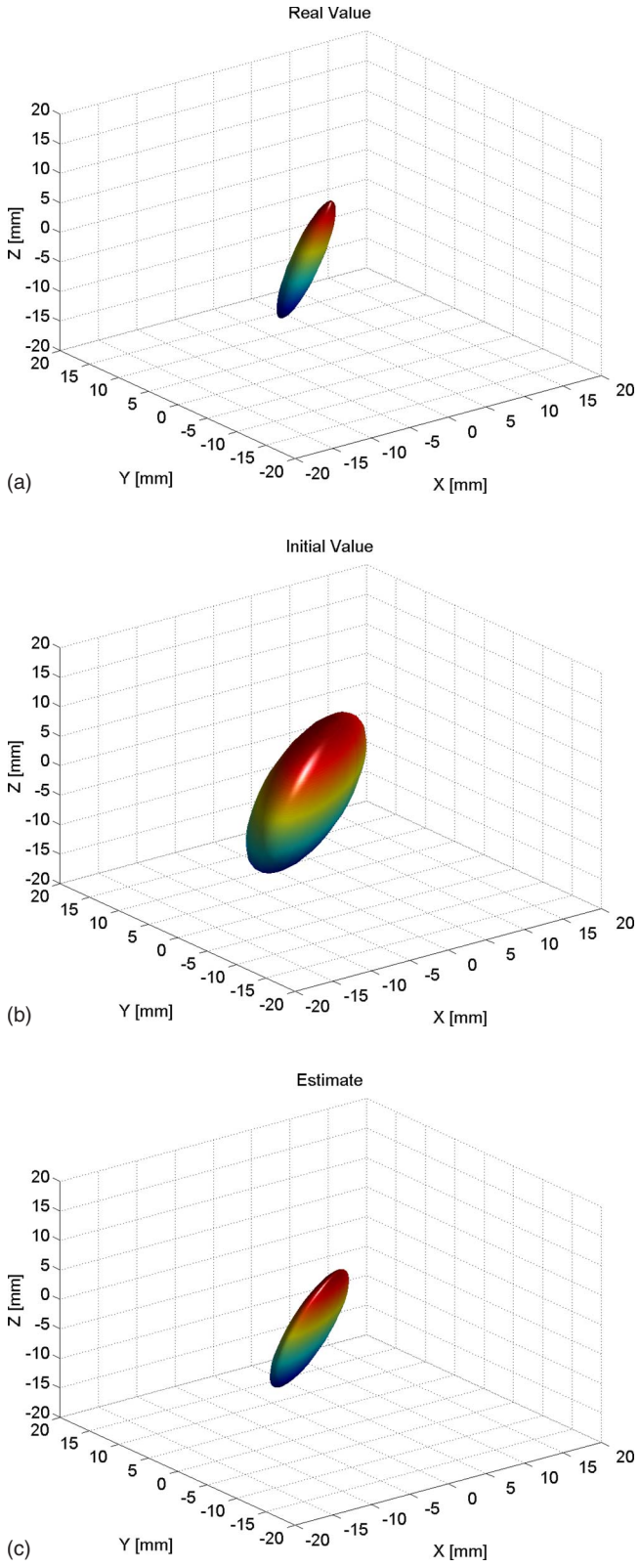


FIG. 11. (Color online) Inversion result of the experiment. The true ellipsoid (a), initial guess provided to the estimation method (b), and the final result (c) are shown.

indicates that a linearized physics-based model, coupled with a shape-based inversion routine, might provide a feasible method to monitor the progress of image guided therapy. We exploited the fact that the treatment results in an ellipsoidal-

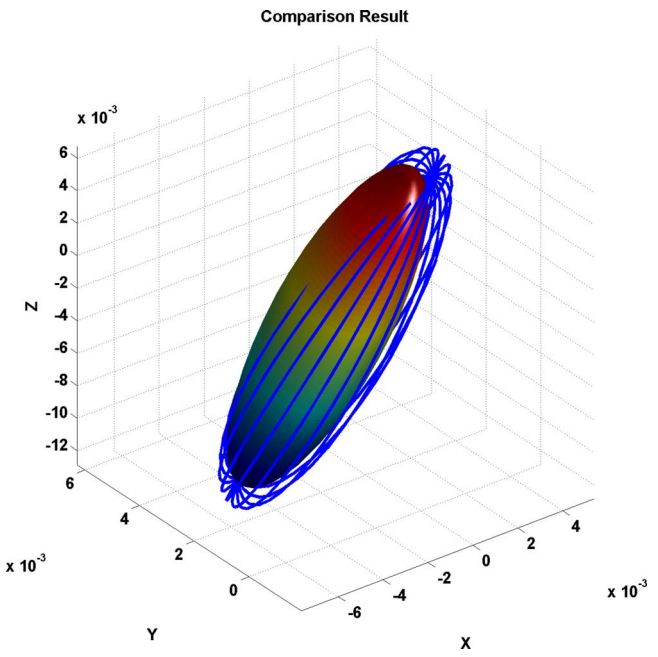


FIG. 12. (Color online) Comparison of actual and estimated ellipsoids. The estimated ellipsoid is plotted with lines on the actual ellipsoid.

shaped region and proposed a differentiable function to describe the boundary and the contrast of the ellipsoid.

Numerical simulations were used to illustrate the potential of the shape-based inversion and to show the robustness by means of a Monte Carlo approach. The Monte Carlo simulations showed that the algorithm was able to determine most of the parameters of an ellipsoid to within 10%, with the exception of the orientation angles which were found to be the hardest to accurately predict. A laboratory experiment was also considered using a clinical curvilinear array transducer. A roughly ellipsoidal HIFU lesion-like phantom was used which had perturbation in sound speed and attenuation only. We were able to reconstruct the geometry of the ellipsoid and the contrasts accurately. The results were obtained with 116 iterations using a MATLAB implementation in 26 min on a 667 MHz workstation. In practice one would need faster inversion, less than 1 min and ideally on the order of 1 s, to guide the therapy. We note that MATLAB is not an ideal computational platform to perform real-time operations. It is the experience of the authors that converting MATLAB code to a fully compiled code, using, e.g., C or FORTRAN, results in a speed up of two to three orders of magnitude. Therefore we anticipate that practical computation times will be achievable with sufficient engineering effort.

In this work we employ the Gauss–Newton method, a local optimization routine, for solving the parameter estimation problem. This method is highly sensitive to prior infor-

TABLE IV. Contrast and error values for the sound speed and attenuation.

	Real	Initial	Estimate	Err_c %	Err_v %
Sound (m/s)	5	20	5.80	16.2	5.7
Attenuation (Np/m)	48.7	440	46.3	4.9	5.7

mation particular with respect to the initial position of the ellipsoid and was motivated by the fact that for HIFU such data are readily available. With regards to the contrast parameters other experiments (not reported here) indicate that high accuracy terms of prior information are not necessary to obtain useful final results. If this technique should be applied to a case where there is no *a priori* information available, either a brute force method or global minimization technique (genetic algorithm, particle swarm, etc.) should be used to find the best initial parameters for the Gauss–Newton method as in Ref. 52.

As discussed in Sec. I, the approach we have presented is based on a number of assumptions concerning the shape of the scatterer, the nature of the medium in which it is embedded, and the physical model used in the processing. In terms of the shape assumption, the experiments in this paper indicate that accurate results can be obtained even for objects that are not perfect ellipsoids, which was indeed the case for the phantom considered in Sec. V C. Current work on this project[53] confirms these findings on a broader range of phantom experiments. Moving forward in making our approach more suitable for addressing the clinical form of the HIFU problem, there are many possible generalization of the ellipsoidal model which provide for the modeling of more complex shapes without the need to solve a large-scale inverse problem. We point specifically to the use of spherical harmonic expansions as the basis for modeling individual scatterers as described for example in Refs. 54–56 as well as level set methods such as those developed by Miller's group[57,58] and others[59–61] for which the number of objects need not be specified *a priori*.

The method that is developed in this work is valid for homogeneous, lossy, power-law attenuating medium in which a Born scattering model is employed in the processing. Certainly, to make this approach of practical use, it will be necessary to move beyond the assumption of spatial homogeneity. Here, we must account both for fine-scale tissue inhomogeneities that give rise to typical speckle patterns in ultrasound imagery as well as large scale structures including aberrating layers, organs, etc. Our recent work[53] indicates a strong degree of resilience of the shape-based method for problems in which the only source of heterogeneity is the small-scale structures.

In the case of large-scale structures, many options can be explored. There are a number of approaches that have been employed to address abberation in B-mode ultrasound that could be a starting point for an inhomogeneous background model, see, e.g., Refs. 62–64. Alternatively, one could consider the use of distorted wave Born methods[65–67] for constructing linearized models about heterogeneous media. Such an approach would allow us to easily capture large scale inhomogeneities such as the presence of organs, layers of fat, etc. Initial ideas for jointly estimating the contrast parameters when the shape of the inhomogeneities is known as well as the perturbation itself have been considered in Ref. 68. Determining the gross structure of these regions may require the acquisition and processing of, e.g., CT or MRI data prior to HIFU treatment. A major issue to be considered here is whether the lesions themselves are "small" perturbations against this inhomogeneous medium. For the homogeneous problem here, the results of our work in Sec. V C indicate that for isolated lesions, the Born model is adequate. It remains to be seem whether this holds as HIFU therapy continues and produces lesions of increasing complexity. Should that not be the case then a fully nonlinear inversion routine may be needed. Here the work of Ref. 31 where an efficient contrast-source method was employed may be of use. Such techniques are well known for pixel-based image formation methods and adapting the idea for shape-based schemes would require some effort.

ACKNOWLEDGMENTS

This work was supported in part by CenSSIS (The Bernard M. Gordon Center for Subsurface Sensing and Imaging Systems), under the Engineering Research Centers Program of the National Science Foundation (Award No. EEC-9986821) the NIH under Grant No.,R21 CA123253–01 and the National Science Foundation under Grant 0208548. The authors are grateful for technical assistance provided by Dr. Emmanuel Bossy and Ersel Karbeyaz.

APPENDIX: JACOBIAN CALCULATION

The Jacobian matrix associated with Eq. (12) is

$$\frac{\partial y}{\partial \mu} = -[\mathbf{K}_1\mathbf{K}_2\mathbf{K}_3]\begin{bmatrix}\frac{\partial \mathbf{f}_1}{\partial \mu}\\ \frac{\partial \mathbf{f}_2}{\partial \mu}\\ \frac{\partial \mathbf{f}_3}{\partial \mu}\end{bmatrix}, \tag{A1}$$

where μ is the unknown geometric parameter of the ellipsoid and each $\mathbf{f}_i$ a column vector containing the voxel values of the perturbations. To obtain the Jacobian matrix, the derivatives of Eq. (16) with respect to the unknown ellipsoid parameters are required.

Using the chain rule:

$$\frac{\partial \gamma_i(r',\beta_i)}{\partial \mu} = -10.4\tilde{M}_i \operatorname{sech}(1.3x^8)\tanh(1.3x^8)x^7 \times \exp(\tilde{M}_i \operatorname{sech}(1.3x^8))\frac{\partial x}{\partial \mu}, \tag{A2a}$$

$$\frac{\partial \gamma_i(r',\beta_i)}{\partial M_i} = \operatorname{sech}(1.3x^8)\exp(\tilde{M}_i \operatorname{sech}(1.3x^8)), \tag{A2b}$$

where $x=\|D_iU_i^T(r-c_i)\|_2^2$. Using matrix algebra x can be written as

$$x = (r'-c_i)^T U_i D_i^T D_i U_i^T (r'-c_i).$$

The derivatives of x with respect to the various ellipsoid parameters can be expressed as

$$\frac{\partial x}{\partial x_{oi}, y_{oi}, z_{oi}} = 2\frac{\partial (r'-c_i)^T}{\partial x_{oi}, y_{oi}, z_{oi}} U_i D_i^T D_i U_i^T (r'-c_i), \tag{A3a}$$

where

$$\frac{\partial(r'-c_i)}{\partial x_{oi}}=\begin{bmatrix}-1\\0\\0\end{bmatrix}\frac{\partial(r'-c_i)}{\partial y_{oi}}=\begin{bmatrix}0\\-1\\0\end{bmatrix}\frac{\partial(r'-c_i)}{\partial z_{oi}}=\begin{bmatrix}0\\0\\-1\end{bmatrix}, \tag{A3b}$$

$$\frac{\partial x}{\partial l_{1i},l_{2i},l_{3i}}=2(r'-c_i)^T U_i D_i^T \frac{\partial D_i}{\partial l_{1i},l_{2i},l_{3i}} U_i^T (r'-c_i), \tag{A4a}$$

where

$$\frac{\partial D_i}{\partial l_{1i}}=\begin{bmatrix}-1/l_{1i}^2 & 0 & 0\\ 0 & 0 & 0\\ 0 & 0 & 0\end{bmatrix},$$

$$\frac{\partial D_i}{\partial l_{2i}}=\begin{bmatrix}0 & 0 & 0\\ 0 & -1/l_{2i}^2 & 0\\ 0 & 0 & 0\end{bmatrix},$$

$$\frac{\partial D_i}{\partial l_{3i}}=\begin{bmatrix}0 & 0 & 0\\ 0 & 0 & 0\\ 0 & 0 & -1/l_{3i}^2\end{bmatrix} \tag{A4b}$$

and

$$\frac{\partial x}{\partial \theta_{1i},\theta_{2i},\theta_{3i}}=2(r'-c_i)^T \frac{\partial U_i}{\partial \theta_{1i},\theta_{2i},\theta_{3i}} D_i^T D_i U_i^T (r'-c_i), \tag{A5a}$$

where

$$\frac{\partial U_i}{\partial \theta_{1i}}=\begin{bmatrix}-\sin(\theta_{1i}) & \cos(\theta_{1i}) & 0\\ -\cos(\theta_{1i}) & -\sin(\theta_{1i}) & 0\\ 0 & 0 & 0\end{bmatrix} U_{2i} U_{3i}, \tag{A5b}$$

$$\frac{\partial U_i}{\partial \theta_{2i}}=U_{1i}\begin{bmatrix}-\sin(\theta_{2i}) & 0 & \cos(\theta_{2i})\\ 0 & 0 & 0\\ -\cos(\theta_{2i}) & 0 & -\sin(\theta_{2i})\end{bmatrix} U_{3i}, \tag{A5c}$$

$$\frac{\partial U_i}{\partial \theta_{3i}}=U_{1i} U_{2i}\begin{bmatrix}-\sin(\theta_{3i}) & \cos(\theta_{3i}) & 0\\ -\cos(\theta_{3i}) & -\sin(\theta_{3i}) & 0\\ 0 & 0 & 0\end{bmatrix}. \tag{A5d}$$

[1]L. Poissonnier, A. Gelet, J. Chapelon, R. Bouvier, O. Rouviere, C. Pangaud, D. Lyonnet, and J. Dubernard, "Results of transrectal focused ultrasound for the treatment of localized prostate cancer (120 patients with PSA <or+10 ng/ml)," Prog. Urol. **13**, 60–72 (2003).

[2]T. A. Gardner, M. O. Koch, A. Shalhav, R. Bihrle, R. S. Foster, C. Steidle, I. Grunberger, A. S. M. Resnick, J. Cochran, V. Rao, and N. T. Sanghvi, "Minimally invasive treatment of benign prostatic hyperplasia with high intensity focused ultrasound using the Sonablate™ system: An updated report of phase III clinical studies conducted in the USA," Proc. SPIE **4609**, 107–114 (2002).

[3]N. T. Sanghvi, J. Syrus, R. S. Foster, R. Bihrle, R. Casey, and T. Uchida, "Noninvasive surgery of prostate tissue by high intensity focused ultrasound: An updated report," Proc. SPIE **3907**, 194–200 (2000).

[4]S. Madersbacher, C. Kratzik, and M. Marberger, "Prostatic tissue ablation by transrectal high intensity focused ultrasound: Histological impact and clinical application," Ultrason. Sonochem. **4**, 175–179 (1997).

[5]K. Nakamura, S. Baba, S. Saito, M. Tachibana, and M. Murai, "High-intensity focused ultrasound energy for benign prostatic hyperplasia: Clinical response at 6 months to treatment using sonablate 200," J. Endourol **11**, 197–201 (1997).

[6]E. D. Mulligan, T. H. Lynch, D. Mulvin, D. Greene, J. M. Smith, and J. M. Fitzpatrick, "High-intensity focused ultrasound in the treatment of benign prostatic hyperplasia," Br. J. Urol. **79**, 177–180 (1997).

[7]C. Chaussy, S. Thuroff, F. Lacoste, and A. Gelet, "HIFU and prostate cancer: The European experience," in *Proceedings of the Second International Symposium on Therapeutic Ultrasound*, July 29–Aug. 1; Seattle, WA (2002).

[8]J. Kennedy, G. T. Haar, and D. Cranstron, "High intensity focused ultrasound: Surgery of the future?," Br. J. Radiol. **76**, 590–599 (2003).

[9]F. Wu, W. Chen, J. Bai, Z. Zou, Z. Wang, H. Zhu, and Z. Wang, "Pathological changes in human malignant carcinoma treated with high-intensity focused ultrasound," Ultrasound Med. Biol. **27**, 1099–1106 (2001).

[10]F. Wu, Z. Wang, W. Chen, W. Wang, Y. Gui, M. Zhang, G. Zheng, Y. Zhou, G. Xu, M. Li, C. Zhang, H. Ye, and R. Feng, "Extracorporeal high intensity focused ultrasound ablation in the treatment of 1038 patients with solid carcinomas in China: An overview," Ultrason. Sonochem. **11**, 149–154 (2004).

[11]G. T. Clement, "Perspectives in clinical uses of high-intensity focused ultrasound," Ultrasonics **42**, 1087–1093 (2004).

[12]Z. Wang, J. Bai, F. Li, Y. Du, S. Wen, K. Hu, G. Xu, P. Ma, N. Yin, W. Chen, F. Wu, and R. Feng, "Study of a 'biological focal region' of high-intensity focused ultrasound," Ultrasound Med. Biol. **29**, 749–754 (2003).

[13]G. ter Haar, D. Sinnett, and I. Rivens, "High intensity focused ultrasound—A surgical technique for the treatment of discrete liver tumors," Phys. Med. Biol. **34**, 1743–1750 (1989).

[14]H. Cline, K. Hynynen, C. Hardy, R. Watkins, F. Schenck, and F. Jolesz, "MR temperature mapping of focused ultrasound surgery," Magn. Reson. Med. **31**, 628–636 (1994).

[15]N. McDannold, L. King, F. Jolesz, and K. Hynynen, "Usefulness of MR imaging-derived thermometry and dosimetry in determining the threshold for tissue damage induced by thermal surgery in rabbits," Radiology **216**, 517–523 (2000).

[16]K. Hynynen, O. Pomeroy, D. Smith, P. Huber, N. McDannold, J. Kettenbach, J. Baum, S. Singer, and F. Jolesz, "MR imaging-guided focused ultrasound surgery of fibroadenomas in the breast: A feasibility study," Radiology **219**, 176–185 (2001).

[17]J. C. Bamber and C. R. Hill, "Ultrasonic attenuation and propagation speed in mammalian tissues as a function of temperature," Ultrasound Med. Biol. **5**, 149–157 (1979).

[18]N. L. Bush, I. Rivens, G. R. ter Haar, and J. C. Bamber, "Acoustic properties of lesions generated with an ultrasound therapy system," Ultrasound Med. Biol. **19**, 789–801 (1993).

[19]C. A. Damianou, N. T. Sanghvi, F. J. Fry, and R. Maass-Moreno, "Dependence of ultrasonic attenuation and absorption in dog soft tissues on temperature and thermal dose," J. Acoust. Soc. Am. **102**, 628–634 (1997).

[20]S. H. Bloch, M. R. Bailey, L. Crum, P. Kaczkowski, G. Keilman, and P. Mourad, "Measurements of sound speed in excised tissue over temperature expected under high-intensity focused ultrasound conditions," J. Acoust. Soc. Am., **103**(5), pp. 2868 (1998).

[21]A. E. Worthington and M. D. Sherar, "Changes in ultrasound properties of porcine kidney tissue during heating," Ultrasound Med. Biol. **27**, 673–682 (2001).

[22]U. Techavipoo, T. Varghese, Q. Chen, T. A. Stiles, J. A. Zagzebski, and G. R. Frank, "Temperature dependence of ultrasonic propagation speed and attenuation in excised canine liver tissue measured using transmitted and reflected pulses," J. Acoust. Soc. Am. **116**, 2859–2865 (2004).

[23]P. D. Tyréus and C. Diederich, "Two-dimensional acoustic attenuation mapping of high-temperature interstitial ultrasound lesions," Phys. Med. Biol. **49**, 533–546 (2004).

[24]C. Simon, P. VanBaren, and E. S. Ebbini, "Two-dimensional temperature estimation using diagnostic ultrasound," IEEE Trans. Ultrason. Ferroelectr. Freq. Control **45**, 1088–1099 (1998).

[25]M. Pernot, M. Tanter, J. Bercoff, K. Waters, and M. Fink, "Temperature estimation using ultrasonic spatial compound imaging," IEEE Trans. Ultrason. Ferroelectr. Freq. Control **51**, 606–615 (2004).

[26]L. A. S. Baker and J. C. Bamber, "Effect of dynamic receive focusing on reflex transmission imaging (RTI)," Proc.-IEEE Ultrason. Symp. **2**, 1581–1584 (2002)

[27]A. Anand and P. J. Kaczkowski, "Monitoring formation of high intensity focused ultrasound (HIFU) induced lesions using backscattered ultrasound," ARLO **5**, 88–94 (2004).

[28]H. Zhong, M. Xi Wan, Y.-F. Jiang, and S. Pin Wang, "Monitoring imaging

of lesions induced by high intensity focused ultrasound based on differential ultrasonic attenuation and integrated backscatter estimation," Ultrasound Med. Biol. **33**, 82–94 (2007).
[29]N. Duric, P. Littrup, A. Babkin, D. Chambers, S. Azevedo, A. Kalinin, R. Pevzner, M. Tokarev, E. Holsapple, O. Rama, and R. Duncan, "Development of ultrasound tomography for breast imaging: Technical assessment," Med. Phys. **32**, 1375–1386 (2005).
[30]R. G. Pratt, L. Huang, N. Duric, and P. Littrup, "Sound-speed and attenuation imaging of breast tissue using waveform tomography of transmission ultrasound data," Proc. SPIE **6510**, 65104S (2007).
[31]K. W. A. van Dongen and W. M. D. Wright, "A full vectorial contrast source inversion scheme for three-dimensional acoustic imaging of both compressibility and density profiles," J. Acoust. Soc. Am. **121**, 1538–1549 (2007).
[32]G. Dassios, "The inverse scattering problem for the soft ellipsoid," J. Math. Phys. **28**, 2858–2862 (1987).
[33]R. J. Lucas, "An inverse problem in low-frequency scattering by a rigid ellipsoid," J. Acoust. Soc. Am. **95**, 2330–2333 (1994).
[34]R. J. Lucas, "The inverse problem for scattering by an ellipsoidal boss," J. Acoust. Soc. Am. **97**, 2645–2650 (1995).
[35]G. Dassios and R. J. Lucas, "An inverse problem in low-frequency scattering by an ellipsoidally embossed surface," Wave Motion **20**, 33–39 (1994).
[36]T. S. Angell and R. E. Kleinman, "Polarizability tensors in low-frequency inverse scattering," Radio Sci. **22**, 1120–1126 (1987).
[37]M. E. Kilmer, E. L. Miller, A. Barbaro, and D. Boas, "Three-dimensional shape-based imaging of absorption perturbation for diffuse optical tomography," Appl. Opt. **42**, 3129–3144 (2003).
[38]M. Kilmer, E. L. Miller, A. Barbaro, and D. A. Boas, "3d shape-based imaging for diffuse optical tomography," Appl. Opt. **42**, 3129–3144 (2003).
[39]P. M. Morse and K. U. Ingard, *Theoretical Acoustics* (Princeton University Press, Princeton, NJ, 1986).
[40]B. U. Karbeyaz, E. L. Miller, R. O. Cleveland, and R. A. Roy, "Adaptive linearized modeling and inversion for 3d tissue characterization," J. Acoust. Soc. Am. **114**, 2379–2380 (2003).
[41]B. U. Karbeyaz, "Modeling and shape based inversion for frequency domain ultrasonic monitoring of cancer treatment," Ph.D. thesis, Northeastern University, Boston, MA, 2005.
[42]J. A. Jensen, "A model for the propagation and scattering of ultrasound in tissue," J. Acoust. Soc. Am. **89**, 182–190 (1991).
[43]M. Arditi, F. Foster, and J. Hunt, "Transient fields of concave annular arrays," Ultrason. Imaging **3**, 37–61 (1981).
[44]E. Madsen, M. Insana, and J. A. Zagzebski, "Method of data reduction for accurate determination of acoustic backscatter coefficients," J. Acoust. Soc. Am. **76**, 913–923 (1984).
[45]T. L. Szabo, B. U. Karbeyaz, R. O. Cleveland, and E. L. Miller, "Determining the pulse-echo electromechanical characteristic of a transducer using flat plates and point targets," J. Acoust. Soc. Am. **116**, 90–96 (2004).
[46]S. J. Osher and R. P. Fedkiw, *Level Set Methods and Dynamic Implicit Surfaces* (Springer, New York, 2002).
[47]G. Ter Haar, "Acoustic surgery," Phys. Today **54**, 29–34 (2001).
[48]W. F. , W.-Z. Chen, J. Bai, J.-Z. Zou, Z.-L. Wang, H. Zhu, and Z.-B. Wang, "Pathological changes in human malignant carcinoma treated with high-intensity focused ultrasound," Ultrasound Med. Biol. **27**, 1099–1106 (2001).
[49]P. E. Gill, W. Murray, and M. H. Wright, *Practical optimization* (Academic, New York, 1981).
[50]C. Lafon, P. J. Kaczkowski, S. Vaezy, M. Noble, and O. A. Sapozhnikov, "Development and characterization of an innovative synthetic tissue-mimicking material for high intensity focused ultrasound (HIFU) exposures," Proc.-IEEE Ultrason. Symp. **2**, 1295–1298 (2001).
[51]B. U. Karbeyaz, E. L. Miller, and R. O. Cleveland, "Semi-analytical computation of the acoustic field of a segment of a cylindrically concave transducer in lossless and attenuating media," J. Acoust. Soc. Am. **121**, 1226–1237 (2007).
[52]J. Stalnaker and E. Miller, "Particle swarm optimization as an inversion tool for a nonlinear uxo model," IEEE International Geoscience and Remote Sensing Symposium, IGARSS 23-28 July 2007, 432–435.
[53]B. Durning, R. O. Cleveland, and E. L. Miller, "Parametric study of a shape based inversion for detecting high-intensity focused ultrasound lesions," J. Acoust. Soc. Am. **121**, 3082 (2007).
[54]G. Boverman and E. L. Miller, "Estimation-theoretic algorithms and bounds for three-dimensional polar shape-based imaging in diffuse optical tomography," *Proceedings of the 2006 IEEE International Symposium on Biomedical Imaging: From Nano to Macro*, Arlington, VA, April 6–9, 1132–1135 (2006).
[55]G. Boverman, Q. Fang, E. Miller, D. H. Brooks, R. H. Moore, D. B. Kopans, and D. A. Boas, "Estimation and statistical bounds for three-dimensional polar shapes in diffuse optical tomography," IEEE Trans. Med. Imaging (in press).
[56]A. Zacharopoulos, S. Arridge, O. Dorn, V. Kolehmainen, and J. Sikora, "3d shape reconstruction in optical tomography using spherical harmonics and bem," J. Electromagn. Waves Appl. **20**, 1827–1836 (2006).
[57]O. Dorn, E. Miller, and C. Rappaport, "A shape reconstruction method for electromagnetic tomography using adjoint elds and level sets," Inverse Probl. **16**, 1119–1156 (2000).
[58]M. K. Ben Hadj Miled, and E. L. Miller, "A projection-based level-set approach to enhance conductivity anomaly reconstruction in electrical resistance tomography," Inverse Probl. **23**, 2375–2400 (2007).
[59]M. Soleimani, O. Dorn, and W. R. B. Lionheart, "A narrow-band level set method applied to eit in brain for cryosurgery monitoring," IEEE Trans. Biomed. Eng. **53**, 2257–2264 (2006).
[60]M. Soleimani, W. R. B. Lionheart, and O. Dorn, "Level set reconstruction of conductivity and permittivity from boundary electrical measurements using experimental data," Inverse Probl. **14**, 193–210 (2006).
[61]O. Dorn and D. Lesselier, "Level set methods for inverse scattering," Inverse Probl. **22**, R67–R131 (2006).
[62]D.-L. Liu and R. C. Waag, "Correction of ultrasonic wavefront distortion using back-propagation and a reference waveform method for time-shift compensation," J. Acoust. Soc. Am. **96**, 649–660 (1994).
[63]S.-E. Masoy, T. Varslot, and B. Angelsen, "Iteration of transmit-beam aberration correction in medical ultrasound imaging," J. Acoust. Soc. Am. **117**, 450–461 (2005).
[64]N. M. Ivancevich, J. J. Dahl, G. E. Trahey, and S. W. Smith, "Phase-aberration correction with a 3-d ultrasound scanner: Feasibility study," IEEE Trans. Ultrason. Ferroelectr. Freq. Control **53**, 1432–1439 (2006).
[65]Y. Fei and A. J. Devaney, "Inverse scattering for real-valued scattering potentials," Inverse Probl. **21**, L7–L12 (2005).
[66]M. L. Dennison and A. J. Devaney, "Inverse scattering in inhomogeneous background media: II. Multi-frequency case and svd formulation," Inverse Probl. **20**, 1307–1324 (2004).
[67]A. J. Devaney and M. Dennison, "Inverse scattering in inhomogeneous background media," Inverse Probl. **19**, 855–870 (2003).
[68]G. Boverman, E. L. Miller, A. Li, Q. Zhang, T. Chaves, D. H. Brooks, and D. A. Boas, "Quantitative spectroscopic diffuse optical tomography of the breast guided by imperfect a priori structural information," Phys. Med. Biol. **50**, 3941–3956 (2005).

Session 1aID

Opening Ceremony

The Opening Ceremony will include a special welcome from the Vice-President of Ile de France Regional Council, addresses by National sponsors, and addresses by the Presidents of the Acoustical Society of America, the European Acoustics Association, and the French Acoustical Society. Musical interludes will be given and two plenary lectures will be presented.

Plenary Lectures

Introduced by George Frisk, Florida Atlantic University, USA

10:30

1aID1. How sound from human activities affects marine mammals. Peter Tyack (Woods Hole Oceanographic Institution, Applied Ocean Physics & Engineering Dept., Woods Hole, MA 02543, USA, ptyack@whoi.edu)

Effects of sound on marine mammals have traditionally been defined either as injury or disruption of behavior. The earliest concern about behavioral disruption was that elevated noise could reduce the range of communication by masking faint signals. Few studies have documented this effect, but recent work emphasizes mechanisms animals use to compensate for elevated noise. Many studies have documented changes in behavior as a function of exposure, but it has proven difficult to relate these to effects on the welfare of individual animals or on the status of populations. Promising approaches to interpreting effects include avoidance of habitat, energetics of foraging, and applying models of anti-predator behavior to human disturbance. During the 1990s acoustic criteria for injury were designated based upon temporary hearing loss. Accumulating evidence of atypical mass strandings of beaked whales coincident with naval sonar exercises suggest that injury or death may result from behavioral responses of some species at lower exposure levels in some settings. A tagged beaked whale showed similar but weaker responses to experimental playback of a mid-frequency sonar sound compared to calls of killer whales, suggesting that anti-predator response may harm animals after exposure to levels of sound very unlikely to cause injury directly.

Introduced by Luigi Maffei, Second University of Naples, Italy

11:10

1aID2. New Trends in Aeroacoustics: From acoustic analogies to direct numerical simulations. Daniel Juvé (Ecole centrale de Lyon, 36 avenue Guy de Collongue, 69134 Ecully cedex, France, daniel.juve@ec-lyon.fr)

Modern aeroacoustics started in the early 1950's when Lighthill developed his famous acoustic analogy in an attempt to understand, and reduce, the terrifying noise generated by jet aircrafts. For nearly 50 years the subject of aerodynamic sound was dominated by approaches based upon this analogy or variants of it. Recently, the availability of powerful computing facilities combined with the development of numerical algorithms specially designed to simulate sound propagation over large distances has paved the way for ″a second golden age of aeroacoustics″ (to quote Lighthill himself). In this talk we will first give an overview of this evolution from acoustic analogies to computational aeroacoustics (CAA). Typical illustrations of the CAA approach will then be presented and applications for transportation systems will be discussed.

Session 1pAAa

Architectural Acoustics and Noise: Acoustics of Open-Plan Spaces I

Kenneth P. Roy, Cochair
Armstrong Building Products, 2500 Columbia Ave, Lancaster, PA 17603, USA

Valtteri O. Hongisto, Cochair
Finnish Institute of Occupational Health, Lemminkäisenkatu 14-18 B, Turku, 20520, Finland

Stephen Sinclair, Cochair
Centre for Interdisciplinary Research in Music Media & Technology, Schulich School of Music, McGill Univ., Montreal H3A IE3, QC, Canada

Invited Papers

1:00

1pAAa1. Spatial decay, behaviour and space planning models European and International standards on open office acoustics. Pierre Chigot (Saint Gobain Ecophon SA, box 30030, 60 291 Rantigny, France, pierre.chigot@saint-gobain.com)

Recent standardisation work on open plan offices acoustics is characterized by a shift in the way room acoustics is handled. Spatial decay (expressed through rate of spatial decay per doubling of distance, DL2) is preferred to temporal decay (expressed through reverberation time, RT). The complexity of open plan office acoustic design results from the fundamental contradiction of communication and concentration. DL2 reflects better the challenges of sound control in such rooms, which is basically sound propagation control. Beyond, this contradiction, specific space analysis models and tools can help to visualize the acoustic interactions between workstations, teams and departments accommodated in the same room. These models are now ready to be included in standardization work. International technical standard for field measurements of DL2 integrates new descriptive models for open plan office acoustics, taking into account geometric proportions, presence of screens and furniture as well as group behaviour and speech characteristics, such as increased energy contents at low frequencies, voice levels, raised hearing sensitivity at high frequencies. Also, normative guidelines from Netherlands and France integrating this approach will be presented.

1:20

1pAAa2. Acoustics and sustainable design in exposed structures. Kenneth P. Roy (Armstrong Building Products, 2500 Columbia Ave, Lancaster, PA 17603, USA, kproy@armstrong.com), Anita L. Snader (Armstrong World Industries, 2500 Columbia Ave, R&D Bldg. 5, Lancaster, PA 17604, USA, alsnader@armstrong.com)

Two very important emerging architectural trends in the USA are to 1) 'open up' the space design as exposed structures, and 2) incorporate sustainable design into building interiors. We as acoustic designers would like to know the consequences of both on acoustics performance and occupant satisfaction and work performance. The first concern is addressed in a study by CISCA evaluating the effects of ceiling plenum vs. exposed structures in both office and retail spaces. And the second issue of compatibility of sustainable design objectives with acoustic performance is addressed by a pertinent field survey by the Center for the Built Environment (CBE at Univ. of CA, Berkeley) on occupant satisfaction and performance. The issue of the availability and use of 'green' acoustic building materials that not only meet sustainability and energy goals, but also serve to ensure that our buildings actually work for their intended purposes will be addressed. Finally, the increased awareness of the acoustic impact of 'green' design on occupant satisfaction is being seen in the evolution of LEED and other 'green' rating systems.

1:40

1pAAa3. Differences in perception of noise and privacy in different office types. Christina Bodin Danielsson (The Royal Institute of Technology, KTH, Roslagsgatan 37, 113 54 Stockholm, Sweden, c.danielsson@comhem.se)

Differences between office types with regard to their architectural and functional features may have an impact on the employees' disturbance by noise and perception of privacy. These aspects may in its turn have an impact on employees' satisfaction and psychological responses to the office environment. In a study 469 employees in 26 different companies have rated their satisfaction with the office environment in seven different office-types: cell-office, shared room office, small open plan office, medium open plan office, large open plan office, flex-office and combi-office. This paper discusses the results concerning the employees' perception of noise and privacy and put the results in relation to the two different aspects of privacy, visual and acoustic privacy, and the role of personal control. In the statistical analysis adjustments for potential confounders as age, gender, job rank and line of business were done, which are known to have an influence on perception and satisfaction. Substantial differences between employees in different office-types were found. The fact that there were such differences between different types of offices that mean sharing of workspace and work facilities was a surprise. Architectural and functional features of the offices are discussed as the main exploratory factors for these results.

Contributed Paper

2:00

1pAAa4. Effect of sound masking on workers in an open office. Annu Haapakangas (Finnish Institute of Occupational Health, Lemminkäisenkatu 14-18 B, 20520 Turku, Finland, annu.haapakangas@ttl.fi), Valtteri O. Hongisto (Finnish Institute of Occupational Health, Lemminkäisenkatu 14-18 B, 20520 Turku, Finland, valtteri.hongisto@ttl.fi)

Appropriate masking sound is necessary for reaching acceptable speech privacy in open offices. However, the electronic masking systems have not become very popular although the importance of masking is emphasized in design guidelines worldwide. One reason may be that very few scientific field experiments have been published in this area. The aim of this pilot study was to investigate the effects of artificial masking sound on workers in a small department of 15 workers. Measurements and questionnaires were conducted before and after launching the system. Masking sound 44 dBA was produced using centralized pink noise generator and ceiling loudspeakers. The spectrum reminded ventilation noise. Initial background noise level was 36 dBA. Acoustic measurements showed that masking sound reduced the radius of distraction rD from 15 m to 7 m, i.e. acoustic privacy improved significantly. The questionnaire revealed several positive changes attributable to masking. Distraction caused by speech and other varying office sounds was reduced. Noise-related stress was reduced. Evaluations of acoustic environment, speech privacy and self-rated work efficiency were improved. The results showed no adverse effects of masking on workers.

Invited Papers

2:20

1pAAa5. Speech Privacy Options for the Open Ceiling Office Environment. Dana S. Hougland (Shen Milsom Wilke, Inc., 1822 Blake Street, Suite 2A, Denver, CO 80202, USA, dhougland@smwinc.com)

The popularity of the open ceiling and loft office environment continues to grow. The design and effectiveness of sound masking systems in an open office environment are well established for traditional office spaces with acoustically absorptive ceilings systems. Aesthetic preferences for open ceilings with minimal ceiling treatment popular in the creative reuse of older buildings and more minimalist industrial spaces limit the sound masking options available to achieve an acceptable level of speech privacy in an open office environment. Traditional sound masking systems are often subjectively viewed as harsh, unpleasant or visually inappropriate. Several options for alternative designs are evaluated as to the evenness of coverage, effectiveness in achieving an appropriate level of speech privacy, aesthetic integration into the environment and subjective impression of the occupants.

2:40

1pAAa6. Effective sound masking for speech privacy in open plan offices. Joel Lewitz (Rosen Goldberg Der & Lewitz, Inc., 1100 Larkspur Landing Circle, Suite 354, Larkspur, CA 94939, USA, jlewitz@RGDLacoustics.com)

For over 30 years acousticians have studied, measured and evaluated open plan offices to improve speech privacy and freedom from distraction. This paper addresses the relative importance of the many factors affecting speech privacy in open plan offices. Adjusting the background noise level at the receiver has proven to be a very powerful and relatively inexpensive method to optimize the acoustical environment in open plan offices. However, sound masking systems are not always properly tuned to achieve the maximum benefit. In this paper, the importance of the shape, smoothness and level of the masking sound spectrum are discussed and demonstrated with case studies. Recent legislation in the U.S., such as the Healthcare Insurance Portability and Accountability Act of 1996, also known as HIPAA, has broadened speech privacy concerns from open plan to closed plan. Sound masking is an attractive option for both configurations. Differences in sound masking design and tuning between open plan and closed plan are explored in this paper.

3:00

1pAAa7. Room acoustical measures for open plan spaces. Erling Nilsson (Saint-Gobain Ecophon AB, Box 500, SE-260 61 Hyllinge, Sweden, erling.nilsson@ecophon.se), Björn Hellström (ÅF-Ingemansson AB, Box 47321, SE-100 74 Stockholm, Sweden, Bjorn.Hellstrom@afconsult.com), Björn Berthelsen (Saint-Gobain Ecophon AB, Box 500, SE-260 61 Hyllinge, Sweden, bjorn .berthelsen@ecophon.se)

In an ongoing Nordic cooperation project the acoustical conditions in open-plan spaces are investigated. Of special interest is to find suitable acoustical parameters that reveal the acoustical conditions in these spaces and also are of importance for the subjective perceived acoustics. Measurements have so far been carried out in five open plan offices accompanied with an inquiry gathering the subjective judgments by the staff. A program for the acoustical measurements was designed specifying how to perform the measurements, which type of parameters to measure and how to report the results. The acoustical parameters included in the measurements are Reverberation time T20, Early Decay Time (EDT), Deutlichkeit (D50), Speech transmission index (STI), Speech intelligibility index (SII), Privacy Index (PI), Rate of spatial decay of sound pressure levels per distance doubling (DL2), Excess of sound pressure level with respect to a reference curve (DLf), background noise levels in occupied and unoccupied offices. The behavior of these parameters will be discussed and suitable parameters for evaluation of open plan spaces will be suggested.

3:20-3:40 Break

3:40

1pAAa8. Characterization of acoustics in open offices - four case studies. Jukka S. Keränen (Finnish Institute of Occupational Health, Lemminkäisenkatu 14-18 B, 20520 Turku, Finland, jukka.keranen@ttl.fi), Petra Virjonen (Finnish Institute of Occupational Health, Lemminkäisenkatu 14-18 B, 20520 Turku, Finland, petra.virjonen@gmail.com), Valtteri O. Hongisto (Finnish Institute of Occupational Health, Lemminkäisenkatu 14-18 B, 20520 Turku, Finland, valtteri.hongisto@ttl.fi)

Acoustic design in open offices aims to reduction of distractions and improvement of speech privacy. Room acoustical design includes high room absorption, high and absorptive screens and appropriate masking sound level. The aim of this study is to show, how these individual design components can affect on room acoustics, using modern room acoustical descriptors. Individual acoustical remedies were studied in four case studies independently. The implemented room acoustical changes were increased ceiling absorption,

sound-absorptive screens, curtains between workers and increased masking sound level. Radius of distraction, r_D, spatial decay rate of speech, DL_2, and speech level at 4 m from speaker, $L_{p,S,4m}$, were determined before and after the room acoustical change. These three simple and robust single-number parameters are recommended to characterize the acoustic conditions of open offices because they react logically to room acoustical changes.

Contributed Papers

4:00

1pAAa9. Possibilities for acoustic improvement of the far field in open-plan offices. Catrin Humer (TGM Federal Institute of Technology, Wexstrasse 19-23, 1200 Vienna, Austria, catrin.humer@tgm.ac.at), Herbert Muellner (TGM Federal Institute of Technology, Wexstrasse 19-23, 1200 Vienna, Austria, herbert.muellner@tgm.ac.at)

An increase in open-plan offices has occurred recently. This makes it necessary to examine and, if necessary, to improve the acoustic conditions in the planning phase. With acoustic simulations it is possible to verify the acoustic quality of offices without much increase in money and time. In order to get the needed absorption area of the room to reduce the reverberation time and the sound level, open-plan offices are usually partitioned with screens. To improve the acoustics in the close range, special conditions, which mainly concern the height, have to be met. Also the absorption and the height of the ceiling have a strong influence on the acoustic quality of the neighbouring workstations. In the far field additional planning bases apply - particularly to raise the horizontal absorption and to get the optimal screening effect. This report highlights the possibilities of the acoustic improvements in the far field in open-plan offices and shows examples of simulated and improved options.

4:20

1pAAa10. Modeling the sound field of open spaces using a diffusion equation model. Yun Jing (Rensselaer Polytechnic Institute, Greene Building, School of Architecture, 110 8th Street, Troy, NY 12180, USA, jingy@rpi.edu), Ning Xiang (Rensselaer Polytechnic Institute, Greene Building, School of Architecture, 110 8th Street, Troy, NY 12180, USA, xiangn@rpi.edu)

Steady-state and transient sound field modeling of open spaces, such as urban squares, courtyard-type traditional Chinese theaters, is discussed in this paper. It is well known that the application of the statistical room-acoustic theory is strongly limited in this case, because of the high non-uniformity of the absorption coefficient. In this study, a diffusion equation along with a recently proposed modified boundary condition [Y. Jing and N. Xiang, J. Acoust. Soc. Am., 123, 2008, 145-153] is used to predict the acoustic characteristics of open spaces, in terms of both sound pressure level distributions and reverberation times. Three different types of open spaces are presented, including urban squares, quasi-cubic open rooms, and urban streets. This paper will compare the simulation results with the experimental results conducted in all these three cases (scale model), to verify the validity and efficiency of the diffusion equation model.

MONDAY AFTERNOON, 30 JUNE 2008 ROOM 252B, 1:00 TO 7:20 P.M.

Session 1pAAb

Architectural Acoustics: Acoustics of Concert Halls I

Takayuki Hidaka, Cochair
Takenaka R&D Institute, 1-5-1, Otsuka, Inzai, Chiba, 270-1395, Japan

Daniel E. Commins, Cochair
Commins Acoustics Workshop, 15 rue Laurence Savart, Paris, 75020, France

Invited Papers

1:00

1pAAb1. From backward integration to number-theoretic diffusors. Manfred Schroeder (University of Goettingen, Rieswartenweg 8, 37077 Goettingen, Germany, mrs17@aol.com)

As a student of physics at Göttingen I was interested in the statistics of electromagnetic resonances in metallic cavities when Erwin Meyer offered me a scholarship in concert-hall acoustics. So we compromised and my thesis eventually appeared under the double heading ″The statistical parameters of the frequency responses of large enclosures. Experiments with electromagnetic waves″.-After moving to Bell Laboratories in New Jersey, I continued to explore, with Heiner Kuttruft, frequency responses in concert halls by digital simulation, confirming my earlier theory that, above a critical frequency, these responses are just ″noise″ in the frequency domain. Later I dabbled in anti-feedback circuits and explored, with Ben Logan, artificial reverberation that spawned a minor industry-now dubbed sound scapes (first realized by John Chowning) and virtual reality. Then came the work (with Gerhard Sessler, Jim West, Bishnu Atal and Carol Bird) on Philharmonic Hall in New York, which lead to a new method of measuring reverberation time (″backward″ integration) and new surface structures, based on number theory, for better sound diffusion. (The idea came to me during a talk by André Weil on ″Gauss Sums″ during the celebration of the 200th anniversary of Gauss' birth.)

1:20

1pAAb2. Echo suppression effect and coloration of periodic-type diffusers. Masahiro Toyoda (Pioneering Research Unit, B104, Kyoto University Katsura, Nishikyo-ku, 615-8530 Kyoto, Japan, masahiro.toyoda@kupru.iae.kyoto-u.ac.jp), Tomohiro Furukawa (Kajima Corporation, Akasaka 6-5-30, Minato-ku, 107-8502 Tokyo, Japan, furuktom@kajima.com), Daiji Takahashi (Pioneering Research Unit, B104, Kyoto University Katsura, Nishikyo-ku, 615-8530 Kyoto, Japan, tkhs@archi.kyoto-u.ac.jp)

Walls and ceilings are often designed to suppress undesirable echoes. For that purpose, walls and ceilings are given absorptive surfaces which absorb sound energy or uneven surfaces which provide wave diffusion. While it is not difficult to predict the degree of echo suppression effects in the case of absorptive surfaces, it is generally difficult to do that in the case of uneven surfaces. In addition, if the surfaces have periodicity, unintended effects called coloration can distort tonal characteristics of the sound field. Thus, many acoustic designers would hesitate to employ this kind of periodic-type diffusers. However, there are some cases where it is necessary to suppress echoes without any energy loss. Periodic-type diffusers have the advantages of easy estimation of diffusion properties, simple method of design, and ready availability. In this study, a subjective experiment with simulated stimuli was carried out to clarify the echo suppression effect of the periodic-type diffusers from the viewpoint of reflected energy level. Although coloration interfered in subjective judgments in some cases of the experiment, it is shown that the periodic-type diffusers have echo suppression effect if coloration does not occur. This study is also devoted to discussion about the cause of the coloration.

1:40

1pAAb3. Experimental analysis of the acoustical behaviour of Musikverein in concert and ballet configurations. Angelo Farina (University of Parma, Via delle Scienze 181/A, Industrial Engineering Dept., 43100 Parma, Italy, farina@unipr.it), Daniel E. Commins (Commins Acoustics Workshop, 15 rue Laurence Savart, 75020 Paris, France, d.commins@comminsacoustics.com), Nicola Prodi (Engineering Dept. - Univ. of Ferrara, Via Saragat, 1, 44100 Ferrara, Italy, nicola.prodi@unife.it)

Musikverein is among the best concert halls in the world. But the hall is also employed for open-to-the-public ballets. All seats in main stalls are removed, and packed under the wooden floor thanks to a large opening. Detailed acoustical measurements have been performed, with the aim of evaluating the different acoustical behavior with and without the seats. Furthermore, it was attempted to assess the contribution of the air volume under the floor, as a possible ″resonant chamber″, with volume and absorption significantly different when it is filled with packed seats. The results did show that the main acoustical parameters vary significantly between the ″concert″ setup and the ″public ballet″ setup, which is more reverberant, with lesser clarity and more envelopment. Regarding the hypothesis that the volume under the floor has some effect on the acoustical behaviour of the room, the experimental results excluded that this is possible. Furthermore, measurements with accelerometers and pressure/velocity probes did not reveal any difference between the behaviour of the ″openable″ part of the floor and the surrounding ″fixed″ floor. So it was concluded that the large difference in acoustical behaviour is simply caused by the removal of the seats, and by changes in fittings of the stage.

2:00

1pAAb4. Acoustical considerations in the design for 'La Philharmonie de Paris'. Harold Marshall (Marshall Day Acoustics LTD, P O Box 5811, Wellesley St., 1000 Auckland, New Zealand, harold.marshall@marshallday.co.nz), Joanne O. Valentine (Marshall Day Acoustics LTD, P O Box 5811, Wellesley St., 1000 Auckland, New Zealand, joanne.valentine@marshallday.co.nz), Thomas Scelo (Marshall Day Acoustics LTD, P O Box 5811, Wellesley St., 1000 Auckland, New Zealand, thomas.scelo@marshallday.co.nz)

The 2006 competition instructions for ″La Philharmonie de Paris″ included a detailed acoustical specification and the general requirement that the design should be a ″new typology″. The early and late sound fields respectively should be controlled independently. This paper gives an account of the acoustical aspect of the winning design, its relationship to the architecture at the competition phase, and the methodology for developing the design in subsequent phases. The new typology developed here is called the ″bicameral adaptable concert hall″. There are partial precedents for the concepts advanced and these will be identified. Reference is also made to a related paper (at this conference) which discusses the issue of coupling between the acoustical spaces.

2:20

1pAAb5. Acoustical design of Shenzhen Concert Hall, Shenzhen China. Keiji Oguchi (Nagata Acoustics Inc., 2130 Sawtelle Blvd., Suite 307A, Los Angeles, CA 90025, USA, oguchi@nagata.co.jp), Yasuhisa Toyota (Nagata Acoustics Inc., 2130 Sawtelle Blvd., Suite 307A, Los Angeles, CA 90025, USA, toyota@nagata.co.jp)

The Shenzhen Concert Hall complex opened in Shenzhen, China on October 12, 2007. The complex contains the Symphony Hall with 1,800 audience seats, the Theater Studio with 400 - 580 seats and some rooms for rehearsing. The Symphony Hall has a vineyard configuration with a steep audience block arrangement, called ″canyon terrace″. At the widest point of the audience seating, the room spans 45m, is 60m long and has a ceiling height of 25 m. The polycarbonate ensemble reflector panels are suspended at the height of approx.15m above the stage. The acoustical design and characteristics of the Concert Hall are reported.

2:40

1pAAb6. A comparison between shoebox and non-shoebox halls based on objective measurements in actual halls. Takayuki Hidaka (Takenaka R&D Institute, 1-5-1, Otsuka, 270-1395 Inzai, Chiba, Japan, hidaka.takayuki@takenaka.co.jp), Leo L. Beranek (975 Memorial Drive, Suite 804, Cambridge, MA 02138, USA, beranekleo@ieee.org), Noriko Nishihara (Takenaka R&D Institute, 1-5-1, Otsuka, 270-1395 Inzai, Chiba, Japan, nishihara.noriko@takenaka.co.jp)

In recent papers, the sound absorption by chairs and audiences were determined for shoebox (SB) and non-shoebox (NSB) types of concert halls (Beranek, JASA 120, 1399 (2006); Hidaka, Proc. ICA2007). The purpose of this paper is to examine objective differences in the sound fields in these two hall types. This investigation follows reports of music goers that the average subjective sound quality

in NSB and SB halls differs appreciably and that there are greater subjective differences in sound quality from one seating location to another in NSB halls. Special attention is given to the temporal and amplitude structure in the early part (before 80 msec) of the impulse responses measured at various seat positions in six well-known halls (three SB and three NSB). To the extent the data permit, the usual objective parameters are also analyzed, both averaged and at various seat locations, in a total of 12 halls: reverberation time, early decay time, C80 (3-band), interaural cross-correlation coefficient (3-band middle frequency early before 80 ms), initial-time-delay-gap, bass ratio, and strength factors at low- and mid-frequencies. The differences found are discussed with reference to the subjective reports.

3:00

1pAAb7. Changing seating arrangements of the orchestras - a challenge for the concert hall design. Jürgen Meyer (Bergiusstr. 2a, D-38116 Braunschweig, Germany, juergen.meyer-bs@t-online.de)

For the future of concert hall design, two aspects will play an increasing role: the search for new shapes created by the architects and changing seating arrangements preferred by the conductors. Whereas in the last decades, acoustic consultants could assume that e.g. celli and double basses were positioned on the right side of the stage, they will to have consider now that more and more conductors - particularly those of high international reputation - go back to the classic seating arrangement (celli in the center, 2nd violins on the right side. Among others, this distinct tendency leads to the following questions: Which are the tonal (acoustic) advantages of the German seating arrangement and by which roomacoustical means can they been supported? In which directions - seen from the player - exist important reflection areas for timbre, clarity and spaciousness? How should risers on the stage be designed for improving the listeners' sound impression and supporting the musicians' mutual hearing? Do celli and basses need podium areas capable of vibrating? Furthermore, where are critical areas and delay times for generating echos or erroneous localization of French horns or other winds? These questions shall be discussed from physical and psychoacoustic aspects.

3:20

1pAAb8. Acoustical analysis of a variable roof configuration concert hall: The São Paulo Hall. Roberto A. Tenenbaum (Instituto Politecnico, Universidade do Estado do Rio de Janeiro, Rua Alberto Rangel, S/N, 28630-050 Nova Friburgo, Brazil, tenenbaum@iprj.uerj.br), Lenine V. Oliveira (Universidade Federal do Rio de Janeiro, Av. Marechal Trompowsky S/N, 21970-000 Rio de Janeiro, Brazil, leninevas@ig.com.br), Swen Müller (Instituto Nacional de Metrologia e Controle da Qualidade, Av. N.S. das Graças, S/N, 21000-000 Xerem, Brazil, smuller@inmetro.gov.br)

The São Paulo Hall (SPH) is recognized by musicians and musical critics in general by its good acoustical quality. It has, as an important feature, variable acoustics due to its movable roof, which is employed by musicians to tune the room according to the musical style. This work addresses the acoustical quality of SPH and its dependence on the roof configuration. Impulse responses for one source, eight microphone and two dummy head positions, using the sweep-sine technique with pre-emphasis, were obtained for seven roof configurations. Some details of the measurement procedure to ensure good accuracy are discussed. The measurement results were then used to compute the main room acoustical quality parameters, for each octave band between 63 and 8000 Hz. The spatial average and deviation of these data are presented as a function of the frequency band. The influence of the roof configurations on the obtained acoustical parameters is also discussed. Furthermore, comparative plots among SSP at the chosen roof configurations and two famous and representative halls from the classical and romantic periods are reported and discussed. It is concluded that the movable roof is very effective in modifying the room acoustics and that the musician's choices are quite good.

3:40

1pAAb9. The acoustic design of the Elisabeth Murdoch Hall, Melbourne, Australia. Raf Orlowski (Arup Acoustics, St Giles Hall Pound Hill, CB3 0AE Cambridge, UK, Raf.Orlowski@arup.com)

The Elisabeth Murdoch Hall is a 1000 seat recital space which will be completed in the latter half of 2008. The overall geometry is based on a classical shoebox shape to provide acoustic excellence although the internal appearance is wholly contemporary. The walls and ceiling of the hall are clad in timber panelling which is stepped in and out and also modulated to provide diffusion at mid and low frequencies. In addition, the surface layer of the panels is grooved or cut away to form an abstract pattern which is both decorative and diffusing at high frequencies. A notable aspect of the hall is that it has no orchestral reflector. The important early reflections for good orchestral ensemble are provided by articulating and shaping the surfaces around the stage. Although the hall is primarily for recitals of classical music, provision is made for amplified music by introducing acoustic drapes.

4:00-4:20 Break

4:20

1pAAb10. Trends in preference, programming and design of concert halls for symphonic music. Anders C. Gade (Dept. of Acoustic Technology, Technical University of Denmark, Building 352, DK 2800 Lyngby, Denmark, acg@oersted.dtu.dk)

This paper discusses the evolution in taste regarding concert hall acoustics and how this can be reflected in the new halls being built today. The clients' and listener's preferences are not only based on listening in existing halls; but also on listening to reproduced music recorded with microphones close to the orchestra and with artificial reverberation added. The result may be a desire for higher clarity as well as a more full reverberation than what is found in most existing halls. Without being very specific in the brief regarding geometrical detailing - which is not desirable as it will limit architectural freedom and evolution - we can only specify a desire for acoustic conditions in this direction by setting targets for standardized objective room acoustic parameters. In this paper, measured ISO 3382 data are used to illustrate typical differences between ″live″ and recorded concert experiences, and it is seen how visionary hall designs over the last four decades tend to move the acoustics of halls in the same direction. Finally, it is suggested how target values for ISO 3382 parameters - in spite of their limitations - can be set up to drive the design in such a direction.

4:40

1pAAb11. Describing measurement uncertainties in room acoustics with the concept of GUM. Ingo Witew (Institute of Technical Acoustics, Templergraben 55, 52056 Aachen, Germany, Ingo.Witew@akustik.rwth-aachen.de), Renzo Vitale (Institute of Technical Acoustics, Templergraben 55, 52056 Aachen, Germany, renzo.vitale@akustik.rwth-aachen.de)

Considering the uncertainties in room acoustical measurements is a crucial step towards quality evaluation, comparability between different measurements methods and instrumentation. In the preceding discussion it was shown that the concepts specified in the ″Guide to the expression of Uncertainty in Measurements″ (GUM) can well be applied for room acoustical measurement tasks. In this initiatory step a detailed analytical formulation of a model function was avoided for reasons of simplicity and practicability. The waiving of complex modeling, however, requires comprehensive series of measurements to assess the measurement uncertainties. In this paper it is discussed how modeling can reduce such requirements. A special focus is placed on the influence of the directional radiation properties of sound sources.

5:00

1pAAb12. Simplified Room Acoustic Measurements. Tor Halmrast (Statsbygg, Biskop Gunnerus gt 6, pb 8106, Dep, NO-0032 Oslo, Norway, th@statsbygg.no), Anders Buen (Brekke & Strand akustikk as, Hovfaret 17, 0275 Oslo, Norway, Anders.Buen@bs-akustikk.no)

Standardised room acoustic measurements are needed for concert halls etc., but they imply heavy equipment. Thus, many interesting rooms are not measured. Most musicians (and even some acousticians) find that clapping and shouting in a room/hall might give an overview of the room acoustics. In the literature we even find that acoustic parameters are derived from scratchy recordings of music. Modern handheld high quality recording technology and possibilities of analysing sound files gives that one should investigate simpler (non standardised) measurements for simpler rooms/halls. This paper gives analysis of Impulse-Responses recorded from balloons, paper bags, clapping, compared with measurements taken with more academic measurement equipment.

Contributed Papers

5:20

1pAAb13. Acoustics of concert halls with organs in Russia: trends and problems. Pavel Kravchun (Moscow State University, Faculty of Physics, Department of Acoustics, Box 15, 125130 Moscow, Russian Federation, gedackt@mail.ru)

Over the past decades the organ music has become one of the most popular kinds of classical music in Russia. About 30 new organs were built in concert halls, and several old instruments were restored or rebuilt. Acoustical properties of 15 well-known Russian concert halls with organs (Moscow, St. Petersburg, Perm, Kazan, Astrakhan, etc.) are presented and considered in the paper. In many cases acoustics in the concert halls is not so good for the solo organ music. The reasons are discussed. Acoustics of the Russian concert halls with adjustable acoustics is considered (Moscow, Kazan). It was noted that the "optimum" reverberation time recommended by different acousticians for organ music had a tendency to be longer and longer in the 20th century. Values of the average sound absorption coefficient for organ front were estimated. Some problems in organ-building connected with the concert hall acoustics are discussed.

5:40

1pAAb14. Dexterity and Spirit: The Peter Kiewit Concert Hall at the Holland Performing Arts Center. Dawn Schuette (Threshold Acoustics, 53 W. Jackson Blvd, Suite 1734, Chicago, IL 60604, USA, dschuette @thresholdacoustics.com)

Bathed in natural light, the Peter Kiewit Concert Hall is the focal point of the architecturally innovative Holland Performing Arts Center. The space features cast plaster panels for acoustic diffusion, a tunable canopy over stage for acoustic support, and natural felt banners for reverberation and reflection control. The space transforms easily from an orchestral concert setting to an environment friendly to amplified sound, allowing orchestral music one night to seem as naturally suited to the room as amplified music the following evening. The world-class concert hall acoustics provided by this venue meld seamlessly with the amplified use as well resulting in a unique venue for the music community. This hall is an excellent starting point for a continued discussion about how to successfully incorporate variability in high quality acoustic venues. [Work completed while author was employed as a Principal Consultant at Kirkegaard Associates.]

6:00

1pAAb15. A new symphonic hall, Musikhuset Aarhus, Denmark. Carsten Lemvigh Fog (COWI A/S, Parallelvej 2, DK 2800 Kgs. Lyngby, Denmark, clf@cowi.dk), Richard M. Ballinger (COWI A/S, Odensevej 95, DK 5260 Odense S, Denmark, rmb@cowi.dk)

During the past 3 years Musikhuset Aarhus in Denmark has been enlarged by an area of approximately 17.000 m^2 to a new total area of approximately 34.000 m^2. The new part of the complex contains a symphonic concert hall for Aarhus Symphonic Orchestra with 1200 seats, a hall for rythmic contemporary music with 600 seats and a hall for classical music with 160 seats. The complex also houses the new premises for Aarhus Academy of Music. Important design considerations will be highlighted in the paper and the results of the preliminary and final computer modeling of room acoustics will be presented using examples of auralisation. In conclusion the room acoustic parameters (measured according to ISO 3382 standard) will be discussed, also in respect of the initial reaction from ochestral musicians.

6:20

1pAAb16. Qualitative Standard for Symphonic Concert Environment. Christopher Jaffe (167 East Rocks Road, Norwalk, CT 06851, USA, ADK117@GMAIL.COM)

All acousticians strive to obtain a symphonic concert environment that will be well received by musicians, professional music critics and the general public. Currently, this environment corresponds to the reflective energy measurements found in what might be designated as the rectangular European or American Concert Hall of the late nineteenth century, such as the Grosser Musikvereinssaal in Vienna and Symphony Hall in Boston Massachusetts. It is well known that these measurements can be correlated to subjective musical judgments and that halls incorporating these measurements have been universally designated as having excellent environments for symphonic concerts. But how did these specific reflections become an acoustical standard. This paper presents a theory of how the rectangular European and American style concert hall became an acoustical standard at the beginning of the twentieth century and poses the question as to whether this standard is still applicable in the twenty first century?

6:40

1pAAb17. Acoustical characterization of orchestra platforms. Maria Giovannini (Politecnico di Torino, Corso Duca degli Abruzzi, 24, 10129 Turin, Italy, maria.giovannini@polito.it), Arianna Astolfi (Politecnico di Torino, Department of Energetics, Corso Duca degli Abruzzi, 24, 10129 Turin, Italy, arianna.astolfi@polito.it), Giulio Barbato (Politecnico di Torino, Corso Duca degli Abruzzi, 24, 10129 Turin, Italy, giulio.barbato @polito.it)

In concert halls and other performance spaces it is important that acoustic conditions allow the musicians to hear each other and that there is a sufficient response from the room. Acoustical characterization of spaces for musicians, such as orchestra platforms, orchestra pits, and rehearsal rooms requires the measurements of the Early and Late Support, and other acoustical parameters described in the ISO/DC 3382-1 and in Literature. This work shows results from measurements carried out on five orchestra platforms, different in shape, size and materials of the boundary surfaces. Up to eight source positions were chosen in order to represent the main instrumental sections of the orchestra playing on the platform. Measurements were carried out without musicians, in conditions of empty stage and stage equipped as in concert configuration with stands, chairs, and risers. Some metrological problems connected with the reproducibility of results are considered as the directivity of the source and the small movements of the source and the microphone. The correlations between objective data show that the measured parameters are not always independent, but some groups of correlated measures, not completely separated, are found. The comparison of results allows to draw some connections with the main stage architectural features.

7:00

1pAAb18. On the Reverberation time of Gamelan Bali Concert Hall based on the Physio-Acoustic Responses. I Gde Nyoman Merthayasa (Institute of Technology Bandung, Dept. of Engineering Physics - ITB, Jln. Ganesha no. 10, 40132 Bandung, Indonesia, ignmerth@tf.itb .ac.id), Farida Idealistina Muchtadi (Institute of Technology Bandung, Dept. of Engineering Physics - ITB, Jln. Ganesha no. 10, 40132 Bandung, Indonesia, lies@tf.itb.ac.id)

Based on the fourth orthogonal acoustic factors of a concert hall design theory, it is possible to calculate the acoustical quality at any position in a proposed Gamelan Bali concert hall. And, it is well known that the value of preferred sound fields depends upon the characteristics of the sound source signal. Previous research has reported the most preferred value of the four orthogonal factors of Gamelan Bali sound fields based on the subjective response. It would be important to obtain the objective response, based on the physio-acoustics measurement using Electroechepalograph (EEG), when the subjects were excited by a certain variation of sound fields while other parameters were kept constant. In this research, the subjects were excited by a serial variation of the subsequent reverberation time of Gamelan Bali music. The brain activities were measured using EEG in the temporal areas. The result shows that the maximum power spectral of Alpha Waves of the subjects occurred when the reverberation time of Gamelan Bali were between 750 mS to 1750 mS.

MONDAY AFTERNOON, 30 JUNE 2008 ROOM 253, 1:00 TO 5:00 P.M.

Session 1pAAc

Architectural Acoustics and Psychological and Physiological Acoustics: Speech Segregation in Rooms I

Barbara Shinn-Cunningham, Cochair
Boston University Hearing Research Center, 677 Beacon Street, Boston, MA 02215, USA

Mathieu Lavandier, Cochair
Cardiff University, School of Psychology, Tower Building, Park Place, Cardiff, CF10 3AT, UK

Invited Papers

1:00

1pAAc1. Issues in the perception of multiple speech sources under reverberant listening conditions. Chris J. Darwin (University of Sussex, Psychology, School of Life Sciences, BN1 9QG Brighton, UK, cjd@sussex.ac.uk)

This paper will review the changes that room acoustics can make to the cues available for speech perception and those available for the localisation of sound sources, and give an overview of the perceptual mechanisms underlying the causes of the reduced intelligibility that reverberant room acoustics can make to the intelligibility of speech that is masked by additional sources of speech. Major factors that contribute to the interference of one source of speech by another are the obscuring of primary speech cues either by masking or by the failure of simultaneous grouping mechanisms, and the failure to track the sounds of an individual talker across time. The role of spatial localisation mechanisms to both these factors will be discussed.

1:20

1pAAc2. Room-acoustic factors in attentional tracking. Anthony J. Watkins (Reading University, Department of Psychology, RG6 6AL Reading, UK, syswatkn@rdg.ac.uk), Simon J. Makin (Reading University, Department of Psychology, RG6 6AL Reading, UK, S.J.Makin@reading.ac.uk), Andrew Raimond (Reading University, Department of Psychology, RG6 6AL Reading, UK, a.raimond@reading.ac.uk)

In a "busy" auditory environment listeners can selectively attend to one of several simultaneous messages by tracking one listener's voice characteristics. Here we ask how well other cues compete for attention with such characteristics, using variations in the spatial position of sound sources in a (virtual) seminar room. Listeners decided which of two simultaneous target words belonged in an attended "context" phrase when it was played with a simultaneous "distracter" context that had a different wording. Talker difference was

in competition with a position difference, so that the target-word chosen indicates which cue-type the listener was tracking. The main findings are that room-acoustic factors provide some tracking cues, whose salience increases with distance separation. This increase is more prominent in diotic conditions, indicating that these cues are largely monaural. The room-acoustic factors might therefore be the spectral- and temporal-envelope effects of reverberation on the timbre of speech. By contrast, the salience of cues associated with differences in sounds' bearings tends to decrease with distance, and these cues are more effective in dichotic conditions. In other conditions, where a distance and a bearing difference cooperate, they can completely override a talker difference at various distances.

1:40

1pAAc3. Effects of reverberation on spatial release from masking. Richard L. Freyman (Univ. of Massachusetts, Dept. of Communication Disorders, 358 N. Pleasant St., Amherst, MA 01003, USA, rlf@comdis.umass.edu), Patrick M. Zurek (Sensimetrics Corp, 48 Grove St., Somerville, MA 02144, USA, pat@sens.com)

When sounds that we want to listen to (targets) and interfering sounds (maskers) are separated spatially, several advantages are observed relative to the baseline condition in which target and masker come from the same location. This paper will discuss how and to what extent these advantages are disrupted by room reverberation, which reduces better-ear signal-to-noise ratios and interaural intensity differences, and obscures interaural time differences. Statistical analysis of room acoustics combined with a model of binaural release from masking can, with the articulation index, help quantify expected reductions in speech recognition benefits of target/masker spatial separation in reverberation. This paper will also discuss some advantages of target/masker spatial separation that appear to be well preserved in reverberant rooms. Specifically, reverberation does not eliminate the perceptual differences between target and masker that arise from their different physical locations. The advantages of perceived spatial differences are seen when target and masking sounds share similar characteristics and are confusable with one another. In such cases spatial differences appear to resolve the confusion. This paper will describe research indicating that barely discriminable spatial differences between target and masker are sufficient for spatial release from masking in these circumstances. [Work supported by NIH DC-01625]

2:00

1pAAc4. Some Temporal and Spatial Effects of Room Acoustics on Speech Privacy. John S. Bradley (National Research Council, 1200 Montreal Rd, Ottawa, ON K1A 0R6, Canada, john.bradley@nrc-cnrc.gc.ca), Marina Apfel (National Research Council, 1200 Montreal Rd, Ottawa, ON K1A 0R6, Canada, Marina.Apfel@gmx.de), Brad N. Gover (National Research Council, 1200 Montreal Rd, Ottawa, ON K1A 0R6, Canada, Brad.Gover@nrc-cnrc.gc.ca)

The speech privacy of meeting rooms relates to the possibility of eavesdroppers outside the room being able to understand speech from within the meeting room. Although the speech privacy of meeting rooms is usually assumed to relate to the level of the speech transmitted from the room relative to the ambient noise outside the room, the intelligibility of the transmitted speech is also influenced by room acoustics. However, the audibility of speech is only influenced by the levels of the transmitted speech and ambient noise. This paper reports on a series of speech intelligibility tests in which the components of the problem were systematically added. As expected, adding early reflections of speech from various directions increases intelligibility but later-arriving speech sounds decrease intelligibility. While a spatial separation of speech and noise sources in free field conditions increases speech intelligibility (spatial release from masking), in more realistic conditions, representing a diffuse ambient noise field, the effects are much smaller. Conditions are further complicated by the sever filtering of the speech on transmission through typical walls. The combined effects can be estimated and are significant. If ignored costly over-design of the sound isolation of the meeting room could occur.

2:20

1pAAc5. Binaural room acoustics - cross-correlation. William M. Hartmann (Michigan State University, Dept. of Physics and Astronomy, East Lansing, MI 48824, USA, hartmann@pa.msu.edu), Neil L. Aaronson (Michigan State University, Dept. of Physics and Astronomy, East Lansing, MI 48824, USA, AARONSON@PA.MSU.EDU)

The subject of ''Binaural room acoustics″ combines the disciplines of room acoustics with facts and models of human binaural physiology and psychology. It considers the linear effects of rooms on the inputs to the two ears of a listener, and it considers the nonlinear effects of binaural hearing processes on perceptually relevant acoustical characterizations of rooms. Linear effects of interest are binaural differences in amplitude and phase spectra, which are combined in the cross-correlation function (CCF). A psychophysically relevant CCF is computed over frequency bands approximately corresponding to auditory filters. Because the bands are narrow, the effects on the CCF of frequency-dependent interaural parameters, most importantly dispersion, can be modeled analytically. The roles of amplitude incoherence and dispersion can also be independently modelled. A systematic experimental approach begins with the dependence of the CCF on head related transfer functions (HRTF) as measured at different azimuths in a free field. Although there are notable individual differences, the effects of HRTFs appear to be almost entirely below detection threshold. An empirical relationship between the CCF for a waveform and for its envelope has been established numerically and in extensive room experiments. [Work supported by the NIDCD, grant DC00181.]

2:40

1pAAc6. Speech segregation in rooms: Importance of the interferer interaural coherence. Mathieu Lavandier (Cardiff University, School of Psychology, Tower Building, Park Place, CF10 3AT Cardiff, UK, lavandiermn@cardiff.ac.uk), John F. Culling (Cardiff University, School of Psychology, Tower Building, Park Place, CF10 3AT Cardiff, UK, CullingJ@cardiff.ac.uk)

When an interferer is present, reverberation degrades speech intelligibility not only by its direct effect on the target, but also by affecting the interferer [Lavandier & Culling, J. Acoust. Soc. Am., **122** (3), 2007]. This latter effect occurs at lower levels of reverberation than the former intrinsic degradation of the target, and can be explained by a binaural mechanism. We show here that the interaural coherence of the interferer is the principal parameter predicting the resulting loss of intelligibility. Speech reception thresholds were measured under headphones, using running speech targets and speech-shaped noise interferers. The stimuli were created by con-

sidering a listener and a spatially-separated target and interferer in virtual rooms. The reverberation was varied by modifying the absorption coefficient of every room surfaces simultaneously. Different absorption coefficients were used for target and interferer. With the target anechoic, the interferer was tested in several configurations, in rooms with different sizes and absorptions, at different distances and azimuths from the listener. Several computations of coherence were compared, in order to reveal the one allowing the best prediction of intelligibility.

3:00

1pAAc7. Effects of pitch and spatial separation on selective attention in anechoic and reverberant environments. Scott Bressler (Boston University Hearing Research Center, 677 Beacon Street, Boston, MA 02215, USA, SCBressler@verizon.net), Barbara Shinn-Cunningham (Boston University Hearing Research Center, 677 Beacon Street, Boston, MA 02215, USA, shinn@cns.bu.edu)

Subjects identified a random, spoken sequence of five monotonized digits (F_0 = 100 Hz) presented from 0° azimuth. A monotonized masking sentence (F_0 = 84, 89, 94, 100, 106, 112, or 119 Hz) was presented simultaneously from either 0° and $+90^\circ$ azimuth (chosen randomly on each trial). The same talker recorded both target and masker speech. KEMAR-derived transfer functions simulated either a reverberant or anechoic environment. In contrast to previous studies, in the anechoic condition, differences in pitch provided little benefit and differences in location gave improvements explainable by improvements in the target-to- masker ratio at the acoustically better ear. In reverberant conditions, differences in target and masker location improved performance more than differences in pitch; however, performance was best when there were differences in both location and pitch. Results suggest that when a target utterance is easy to segregate and select (such as in anechoic space when the target is a digit sequence embedded in a competing sentence), high-level attributes such as pitch and location do not improve the ability to selectively attend in a speech-on-speech task. However, in more challenging, reverberant conditions, location and pitch cues can aid segregation and/or selection.

3:20

1pAAc8. Effects of reverberation on perceptual segregation of competing voices by difference in fundamental frequency. Mickael Deroche (Cardiff University, School of Psychology, Tower Building, Park Place, CF10 3AT Cardiff, UK, derochem@cf.ac.uk), John F. Culling (Cardiff University, School of Psychology, Tower Building, Park Place, CF10 3AT Cardiff, UK, CullingJ@cardiff.ac.uk)

Three experiments investigated the effect of reverberation on listeners' ability to use the difference in fundamental frequency (F0) between a target and an interfering voice to perceptually separate them. Speech reception thresholds (SRTs) were measured for a monotonized or frequency-modulated male voice against one or two other monotonized or frequency-modulated male voices or against a speech-shaped, pulse train within a virtual room with controlled reverberation. The sources of targets and interferers were always co-located both straight ahead of the listener. In the two first experiments, the beneficial effect of a F0 difference was reduced in reverberation when the target and interferer's F0 were frequency-modulated at 5 Hz. Experiment 3 investigated this interaction between reverberation, a F0 difference and the target and/or interferer F0's modulation: the results highlighted the relevance of the interferer F0's modulation alone in the presence of reverberation. This finding is consistent with the idea that the effect of F0 difference is mediated by a harmonic-cancellation process. The cancellation of the interferer is disrupted by the reverberation only when the interferer's F0 is frequency-modulated, irrespective of the modulation of the target's F0. A frequency-overlap between the F0 of the target and the maskers does not seem a cause of worse impairment in intelligibility.

3:40-4:00 Break

4:00

1pAAc9. The effects of fluctuating interaural cues on the segregation of speech in rooms: Revisited. Douglas S. Brungart (AFRL, 2610 Seventh Street, WPAFB, OH 45433, USA, douglas.brungart@wpafb.af.mil), Nandini Iyer (AFRL, 2610 Seventh Street, WPAFB, OH 45433, USA, nandini.iyer@wpafb.af.mil)

Spatial separation is known to improve the segregation of talkers in anechoic environments, but spatial auditory cues can be severely degraded in reverberant rooms. One might expect the random disruptions in the interaural time and level differences (ILDs and ITDs) that occur in reverberant environments to eliminate many of the intelligibility benefits that normally occur for spatially separated speech. However, the precedence effect often leads to a robust perception of spatial location even in extremely echoic environments. This can result in an apparent separation between talkers that may facilitate selective attention to the location of the target speech even in a highly reverberant room. Also, random fluctuations in ITD and ILD may lead to differences in the apparent source widths of the target and masking sounds, which might serve as a segregation cue. In this talk, we examine the effects fluctuating interaural difference cues have on the segregation of target speech from competing speech or noise. These results, originally scheduled for presentation at the 152nd meeting, suggest that differences in apparent source width can be used to segregate competing speech signals even when the target and masking signals appear to originate from the same direction relative to the listener.

4:20

1pAAc10. A reverberation-robust automatic speech recognition system based on temporal masking. Guy J. Brown (University of Sheffield, Dept. of Computer Science, Regent Court, 211 Portobello Street, S1 4DP Sheffield, UK, g.brown@dcs.shef.ac.uk), Kalle J. Palomäki (Adaptive Informatics Research Centre, Helsinki University of Technology, P.O. Box 5400, 02015 Espoo, Finland, kalle .palomaki@tkk.fi)

Previously, we have proposed a reverberation-robust system for automatic speech recognition (ASR) based on a temporal masking principle. In the first pathway of this system, speech is analysed by a bank of auditory filters, in order to provide acoustic features for the recogniser. In the second pathway, a bandpass modulation filter (1.5 Hz - 8.2 Hz) detects regions of the envelope in each filter

channel that contain strong speech energy. Regions of the modulation filter output that exceed a threshold are labelled as reliable evidence for the speech in a time-frequency mask; regions that fall below the threshold are dominated by reverberation and labelled as unreliable. The acoustic features and time-frequency mask are then decoded by a "missing data" ASR system. Here we describe modifications of this system that bring it into closer agreement with purported mechanisms of human perceptual compensation for reverberation, as determined by psychophysical studies [Watkins & Makin, JASA 121, 257-266]. Specifically, we use a metric for identifying regions of reliable speech that gives greater emphasis to reverberation "tails," and is computed independently for each frequency band. The performance of the system is evaluated on a corpus of spoken digits convolved with recorded room impulse responses.

4:40

1pAAc11. Monaural segregation of reverberant speech. Zhaozhang Jin (Ohio State University, Department of Computer Science & Engineering, 2015 Neil Ave., Columbus, OH 43210, USA, jinzh@cse.ohio-state.edu), Deliang Wang (Ohio State University, Department of Computer Science & Engineering, 2015 Neil Ave., Columbus, OH 43210, USA, dwang@cse.ohio-state.edu)

A major source of signal degradation in realistic environments is room reverberation. Monaural speech segregation in reverberant environments is a particularly challenging problem. Although inverse filtering has been proposed to partially restore the harmonicity of reverberant speech before segregation, this approach is sensitive to different room configurations. In this study, we investigate monaural segregation of reverberant speech by employing a supervised learning approach to map from a set of pitch-based auditory features to a grouping cue, which encodes the posterior probability of a time-frequency unit being target dominant given observed features. We devise a novel objective function for the learning process, which relates to the goal of maximizing SNR directly. The models trained using this new objective function yield significantly better results for unit labeling. In our segregation system, a segmentation and grouping framework is utilized in order to capture segments reliably under reverberant conditions and organize them into streams. Systematic evaluations show that our approach produces very promising results.

MONDAY AFTERNOON, 30 JUNE 2008 ROOM 202/203, 4:40 TO 7:20 P.M.

Session 1pAAd

Architectural Acoustics and Musical Acoustics: Surround Sound Acoustics I

Anthony Hoover, Cochair
McKay Conant Hoover Inc., 5655 Lindero Canyon Rd, Suite 325, Westlake Village, CA 91362, USA

Alexander Case, Cochair
Fermata Audio & Acoustics, PO Box 1161, Portsmouth, NH 03802, USA

Etienne Corteel, Cochair
Sonic Emotion, Eichweg, 6, Oberglatt, CH-8154, Switzerland

Contributed Papers

4:40

1pAAd1. Virtual acoustic environments for music performance, rehearsal, and recording. Wieslaw Woszczyk (McGill University, Schulich School of Music, 555 Sherbrooke Street West, Montreal, QC H3A 1E3, Canada, wieslaw@music.mcgill.ca), Doyuen Ko (McGill University, Schulich School of Music, 555 Sherbrooke Street West, Montreal, QC H3A 1E3, Canada, doyuen.ko@mail.mcgill.ca), Tom Beghin (McGill University, Schulich School of Music, 555 Sherbrooke Street West, Montreal, QC H3A 1E3, Canada, tom.beghin@mcgill.ca), Martha De Francisco (McGill University, Schulich School of Music, 555 Sherbrooke Street West, Montreal, QC H3A 1E3, Canada, martha.defrancisco@mcgill.ca), Jeremy Tusz (McGill University, Schulich School of Music, 555 Sherbrooke Street West, Montreal, QC H3A 1E3, Canada, tusz@mac.com), Ryan Miller (McGill University, Schulich School of Music, 555 Sherbrooke Street West, Montreal, QC H3A 1E3, Canada, ryan.miller@mail.mcgill.ca)

A comprehensive 24-channel sound field rendering system was built at McGill University's CIRMMT Centre to immerse scholar/performer Tom Beghin in virtual concert spaces where Haydn composed and performed his keyboard sonatas, or expected them to be performed. The virtual rooms were reconstructed from detailed measurements made in Haydn's historical rooms in Europe using a high-resolution 24 bit/96 kHz impulse-response measuring system. In an acoustically treated laboratory, 24 custom loudspeaker arrays were arranged on a surface of a hemisphere surrounding the performer. Multiple fast DSP engines convolved live signals with 24 impulse responses allowing the performer to rehearse and record in each room with low-latency virtual acoustics. This paper describes the details of system design, the method of measurement, and discusses various aspects of recording and performing in virtual acoustic environments. The method has also been tested in a large room during public performance by having virtual-room responses and high-definition photo images projected from the stage. Surround sound recordings of Haydn's complete solo keyboard music made in several virtual rooms and matched to specific historical instruments will be released in a collection of 13 commercial SA-CD's by the end of 2008.

5:00

1pAAd2. Prediction of spatial perceptual attributes of reproduced sound across the listening area. Philip J. Jackson (University of Surrey, Centre for Vision, Speech and Signal Processing, GU2 7XH Guildford, UK, p.jackson@surrey.ac.uk), Martin Dewhirst (University of Surrey, Institute of Sound Recording, GU2 7XH Guildford, UK, m.dewhirst@surrey.ac.uk), Slawomir Zielinski (University of Surrey, Institute of Sound Recording, GU2 7XH Guildford, UK, s.zielinski@surrey.ac.uk), Francis J. Rumsey (University of Surrey, Institute of Sound Recording, GU2 7XH Guildford, UK, f.rumsey@surrey.ac.uk), Robert Conetta (University of Surrey, Institute of

Sound Recording, GU2 7XH Guildford, UK, r.conetta@surrey.ac.uk),David Meares (DJM Consultancy, Winthrift, Nuthurst, RH13 6RG Horsham, UK, meares_david@yahoo.co.uk), Søren Bech (Bang & Olufsen A/S, Peter Bangsvej 15, DK-7600 Struer, Denmark, sbe@bang-olufsen.dk)

Audio systems and recordings are optimized for listening at the "sweet spot," but how well do they work elsewhere? An acoustic-perceptual model has been developed that simulates sound reproduction in a variety of formats, including mono, two-channel stereo, five-channel surround and wave-field synthesis. A virtual listener placed anywhere in the listening area is used to extract binaural signals, and hence interaural cues to the spatial attributes of the soundfield. Using subjectively-validated models of spatial sound perception, we can predict the way that human listeners would perceive these attributes, such as the direction (azimuth) and width of a phantom source. Results will be presented across the listening area for different source signals, sound scenes and reproduction systems, illustrating their spatial fidelity in perceptual terms. Future work investigates the effects of typical reproduction degradations.

Invited Papers

5:20

1pAAd3. Measuring perceived spatial quality changes in surround sound reproduction. Francis J. Rumsey (University of Surrey, Institute of Sound Recording, GU2 7XH Guildford, UK, f.rumsey@surrey.ac.uk), Slawomir Zielinski (University of Surrey, Institute of Sound Recording, GU2 7XH Guildford, UK, s.zielinski@surrey.ac.uk), Philip J. Jackson (University of Surrey, Centre for Vision, Speech and Signal Processing, GU2 7XH Guildford, UK, p.jackson@surrey.ac.uk), Martin Dewhirst (University of Surrey, Institute of Sound Recording, GU2 7XH Guildford, UK, m.dewhirst@surrey.ac.uk), Robert Conetta (University of Surrey, Institute of Sound Recording, GU2 7XH Guildford, UK, r.conetta@surrey.ac.uk), Søren Bech (Bang & Olufsen A/S, Peter Bangsvej 15, DK-7600 Struer, Denmark, sbe@bang-olufsen.dk), David Meares (DJM Consultancy, Winthrift, Nuthurst, RH13 6RG Horsham, UK, meares_david@yahoo.co.uk)

The spatial quality of audio content delivery systems is becoming increasingly important as service providers attempt to deliver enhanced experiences of spatial immersion and naturalness in audio-visual applications. Examples are virtual reality, telepresence, home cinema, games and communications products. The QESTRAL project is developing an artificial listener that will compare the perceived quality of a spatial audio reproduction to a reference reproduction. The model is calibrated using data from listening tests, and utilises a range of metrics to predict the resulting spatial sound quality ratings. Potential application areas for the model are outlined, together with exemplary results obtained from some of its component parts.

5:40

1pAAd4. Dynamic sound image creation by un-directional sound beam reproduction toward an interior surface with a DSP controlled line array speaker for Surround Sound Composition. Yasushi Shimizu (Center for Advanced Sound Technologies, Yamaha, 203 Matsunokijima, 4380192 Iwata, Shizuoka, Japan, yasushi_shimizu@gmx.yamaha.com), Masato Hata (Yamaha, 203 Matsunokijima, 4380192 Iwata, Shizuoka, Japan, hata@beat.yamaha.co.jp), Atsuko Ito (Center for Advanced Sound Technologies, Yamaha, 203 Matsunokijima, 4380192 Iwata, Shizuoka, Japan, atsuko1_ito@gmx.yamaha.com), Akira Miki (Yamaha, 203 Matsunokijima, 4380192 Iwata, Shizuoka, Japan, akira_miki@gmx.yamaha.com), Masato Hatanaka (Hashimoto Bldg, 301, 4-1-25, Komazawa, Setagaya, 1540012 Tokyo, Japan, info@hatanakamasato.net)

Surround Sound Composition in an indoor space is frequently provided with spatial sounds, giving both a sound localization and surround sound effect. Systems have been installed in public spaces such as a museum and retail shops. However, technical improvements are required to provide a small sweet spot and to address architectural designs for speaker installation, because multiple speakers are required for surround sound effect. Recently, we have been applying DSP beam-forming technology with a line-array speaker to create a 3D sound image by scanning a focused sound beam onto an interior surface. The DSP array speaker is capable of providing static and dynamic control in beam steering and sound focusing. Therefore, dynamic spatial sound effect on the interior surface is possible, wherein un-directional sound reproduction is analogous to un-directional lighting. We present three case studies; 1) Virtual 3D Surround Sound in multi-media improvisation, 2) 3D Spatial Sound Synthesis in sound installation and 3) Sound Installation with a Dynamic Sound Beam Scanning.

6:00

1pAAd5. How does spatial auditory perception impact how we enjoy surround sound? Barbara Shinn-Cunningham (Boston University Hearing Research Center, 677 Beacon Street, Boston, MA 02215, USA, shinn@cns.bu.edu), K Anthony Hoover (McKay Conant Hoover, Inc., 5655 Lindero Canyon Road, Suite 325, Westlake Village, CA 91362, USA, thoover@mchinc.com)

Surround sound has become an essential element of enormously popular home entertainment systems, with consumers becoming increasingly eager to invest in high-quality audio systems. While even a cursory web search can uncover numerous criteria, standards, and blogs describing how to select and set up surround-audio equipment, architectural effects are typically ignored or, at best, treated naively. However, architectural acoustics profoundly affect the perceptual experience of a surround-sound listener. Similarly, sound engineers, producers, and artists agonize over every aspect of soundtrack design and production, including the spatial cues embedded in a surround-sound recording, but they have no control over the acoustic environments in which consumers experience their art. How do the acoustics of surround-listening spaces influence the perceptual experiences of the ordinary listener? Is accurate sound localization a proper, desirable, or achievable goal? Would more loudspeakers or higher fidelity improve the surround experience of a typical consumer? These issues will be discussed, taking into account basic psychophysical issues as well as disheartening truths about how ordinary consumers experience sound from their expensive home entertainment systems.

6:20

1pAAd6. Acoustics of a large immersive environment, The Allosphere. David Conant (McKay Conant Hoover, Inc., 5655 Lindero Canyon Road, Suite 325, Westlake Village, CA 91362, USA, dconant@mchinc.com), William Chu (McKay Conant Hoover, Inc., 5655 Lindero Canyon Road, Suite 325, Westlake Village, CA 91362, USA, wchu@mchinc.com), Thomas McNally (McKay Conant Hoover, Inc., 5655 Lindero Canyon Road, Suite 325, Westlake Village, CA 91362, USA, tmcnally@mchinc.com), K Anthony Hoover (McKay Conant Hoover, Inc., 5655 Lindero Canyon Road, Suite 325, Westlake Village, CA 91362, USA, thoover@mchinc.com), Stephen Pope (Center for Research in Electronic Art Technology, U. C. Santa Barbara, 220 Santa Anita Road, Santa Barbara, CA 93105, USA, Stephen@HeavenEverywhere.com)

The Allosphere is a new audio/visual immersion space for the California Nanosystems Institute at The University of California, Santa Barbara, used for both scientific and performing-arts studies. This three-story sphere with central-axis catwalk permits an unusually large experiential region. The huge perforated-metal visual-projection sphere, with its principle listening locations centered inside the sphere, introduces multiple considerations and compromises, especially since the ideal acoustical environment is anechoic. Video projection requires opaque light reflectivity of the concave projection surface, while audio solicits extreme sound transmissibility of the screen plus full-range sound absorptivity outside the sphere. The design requires high-fidelity spatialization of a large number of simulated sound sources over a large region near the core, and support of vector-based amplitude panning, Ambisonic playback, and wavefield synthesis. This paper discusses considerations that both conform to, and lie outside of, traditional acoustical analysis methodologies, and briefly reviews the electroacoustic systems design.

6:40

1pAAd7. Case study on assessing audibility by ″Perspicuity″ for sounds added to factory noise, using different types of speaker in directional performance. Yasushi Shimizu (Center for Advanced Sound Technologies, Yamaha, 203 Matsunokijima, 4380192 Iwata, Shizuoka, Japan, yasushi_shimizu@gmx.yamaha.com), Mai Fujiwara (Center for Advanced Sound Technologies, Yamaha, 203 Matsunokijima, 4380192 Iwata, Shizuoka, Japan, mai_fujiwara@gmx.yamaha.com), Atsuko Ito (Center for Advanced Sound Technologies, Yamaha, 203 Matsunokijima, 4380192 Iwata, Shizuoka, Japan, atsuko1_ito@gmx.yamaha.com)

Music and other sounds have been played to provide a pleasant sound environment for workers in a factory. In terms of ″Sound Perspicuity″ this case study was conducted to assess audibility of spatial sounds, which were adjusted in level without increasing total sound pressure level (SPL) at the workstation. Furthermore, the added sounds were not audible at other workstations. Three speaker systems, including line-array speaker (60 cm in length), were used for the case study. The ratio of added sound (Signal) to factory noise (Noise) was analyzed at every measuring point on a grid of 50 cm by 50 cm. Audibility listening tests were performed for the added sounds, such as natural-environment sounds and musical instrument tones, with Signal to Noise ratios analyzed from three types of speaker. As a result, a sound is recognized as ″Kiwadachi″ by a Japanese adjective word even when the factory noise has higher levels than the added sounds. Audibility test results for each added sound are discussed with different Signal to Noise ratios.

Contributed Paper

7:00

1pAAd8. Spatial Audio Reproduction Using Distributed Mode Loudspeakers. Joshua Atkins (Johns Hopkins University, 853 West 35th Street, Baltimore, MD 21211, USA, joshatkins@jhu.edu), James West (Johns Hopkins University, Department of Electrical Engineering, 3400 North Charles Street, Baltimore, MD 21218, USA, jimwest@jhu.edu)

For future telecommunication systems to become more pervasive in society they must have the ability to produce high quality surround sound audio for multiple listeners. Current 5.1 audio systems lack the capacity to handle large group telecommunications because of their limited optimal listening positions (″sweet spots″) and their preference for sound generated in front of the listeners. This is due in part to the non-optimal position of the loudspeakers and also to the fact that very directional speakers are commonly used. Recently, a new form of speaker has been developed called a distributed mode loudspeaker (DML). These speakers use bending waves in a panel to radiate sound. Consequently, they can be very good omnidirectional sources throughout nearly all of the human hearing range. Experiments using a higher order ambisonics (HOA) approach to sound field capture and generation will be presented to show how conventional electrodynamic speaker arrays compare to equivalent DML arrays for spatial sound reproduction. This work is funded by NSF Grant IIS-0534221.

Session 1pAAe

Architectural Acoustics and Noise: Low Frequency Absorption: Mechanisms, Measurement Methods, and Application I

Peter D'Antonio, Cochair
RPG Diffusor Systems, Inc., 651-C Commerce Drive, Upper Marlboro, MD 20774, USA

Christian Nocke, Cochair
Akustikbüro Oldenburg, Katharinenstr. 10, Oldenburg, 26121, Germany

Invited Papers

5:00

1pAAe1. Overview of low frequency control options in rooms. Peter D'Antonio (RPG Diffusor Systems, Inc., 651-C Commerce Drive, Upper Marlboro, MD 20774, USA, pdantonio@rpginc.com)

Low frequency control of modes and speaker boundary interference in rooms has been a persistent problem that affects the sound field in rooms. However, many innovative techniques have been developed to address these problems. This presentation will be an overview of approaches that address the optimization of room dimensions to provide the flattest room response and speaker/listener placement to minimize speaker-boundary interference; the mechanism and design of passive absorption devices based on Helmholtz resonators, diaphragmatic limp mass membranes, plate resonators and microperforated panels will be described and characterized; as well as electro-acoustic approaches, using equalization, active absorbers and the optimal placement of multiple in-phase subwoofers.

5:20

1pAAe2. Low frequency sound absorption measurements - limits and ideas. Christian Nocke (Akustikbüro Oldenburg, Katharinenstr. 10, 26121 Oldenburg, Germany, nocke@akustikbuero-oldenburg.de)

Many (standardised) measurement procedures for sound absorption rely on geometrical approximations or statistical approaches. They fail whenever the limit of geometrical acoustics is reached. Also many room acoustic modeling procedures assume geometrical spreading of sound and neglect the wave characteristics of sound waves. In this paper various approaches towards the measurement of sound absorption are briefly reviewed and discussed in the light of low frequency applications. Approaches towards analytic descriptions for sound fields in room at low frequencies from the early 1930s are reviewed. The approaches might be the basis for future developments on new procedures for measurement techniques. Finally measurement results on the deduction of sound absorption at low frequencies are presented.

5:40

1pAAe3. Enhancing bass absorbers using activated carbon. Fouad Bechwati (University of Salford, Acoustics Research Centre, Newton Building, M5 4WT Salford, UK, f.bechwati@pgr.salford.ac.uk), Trevor J. Cox (University of Salford, Acoustics Research Centre, Newton Building, M5 4WT Salford, UK, t.j.cox@salford.ac.uk), Olga Umnova (University of Salford, Acoustics Research Centre, Newton Building, M5 4WT Salford, UK, o.umnova@salford.ac.uk), Mark R. Avis (University of Salford, Acoustics Research Centre, Newton Building, M5 4WT Salford, UK, m.r.avis@salford.ac.uk)

Bass absorbers, either Helmholtz or membrane devices, are commonly used in small rooms to reduce the effects of standing wave modes. Previously, it has been shown that activated carbon can be used to change the compliance of loudspeaker enclosures. It has also been shown that activated carbon displays excess absorption at low frequencies. It has been suggested that the change in compliance and absorption is due to adsorption and desorption of air molecules on the surface of the carbon, caused by the compressions and rarefactions of sound waves. This paper investigates the extent of these effects to and their significance for resonant absorbers. The results show that activated carbon can lower the resonant frequency of a Helmholtz absorber, and also increases the quality factor of the resonance. The paper will discuss what the results mean in terms of the physical interaction between activated carbon and sound, as well as the practical application of the material to bass absorbers.

6:00

1pAAe4. An improved low frequency radiation model for finite sound reflectors. Jonathan Rathsam (Univ. of Nebraska - Lincoln, Architectural Eng. Program, 1110 S. 67th St., Omaha, NE 68182-0681, USA, jrathsam@mail.unomaha.edu), Lily M. Wang (University of Nebraska - Lincoln, 1110 S. 67th St., Omaha, NE 68182-0681, USA, LWang4@UNL.edu), Jens Holger Rindel (Odeon A/S, Scion DTU, Diplomvej Buildling 381, DK-2800 Lyngby, Denmark, jhr@odeon.dk), Claus Lynge Christensen (Odeon A/S, Scion DTU, Diplomvej Buildling 381, DK-2800 Lyngby, Denmark, clc@odeon.dk)

Geometric computer models for room acoustics, such as ODEON, predict sound fields most reliably at high frequencies. At low frequencies, algorithms must be modified to account for deviations from geometrical acoustics caused by wave phenomena. For finite reflectors, a common low frequency model is based on the Kirchhoff-Fresnel Diffraction Approximation, which predicts a uniform 6 dB

per octave slope below a reflector's geometrical limiting frequency. As discussed in this paper, highly accurate Boundary Element Method simulations, not subject to the Kirchhoff Approximation, suggest the use of an additional, lower limiting frequency and slope of 12 dB per octave to represent the reflector's response at the lowest frequencies. This second limiting frequency and 12 dB per octave slope, referred to as the dipole limiting frequency, are presented in a form suitable for insertion into a geometric computer model. [Work supported by the National Science Foundation.]

Contributed Papers

6:20

1pAAe5. Control of low-frequency sound to improve spatial uniformity in music production spaces. Ronald Eligator (Acoustic Dimensions, 145 Huguenot Street, New Rochelle, NY 10801, USA, religator @acousticdimensions.com)

Commercial music post-production spaces are often less than 300 ft^2 (28 m^2) and 2700 ft^3 (76.5 m^3), and it is not uncommon for them to be one-third to one-half this area. Even with careful room design, creating spatially-uniform sound fields, especially at low-frequencies, can be thwarted by the physical restraints imposed by the room's dimensions, boundary conditions and restraints imposed by other functional requirements and budget. This paper presents successful, and not so successful, approaches to managing these challenges through speaker selection, placement and mounting, as well as room shaping and finishes and furniture design. Results of design analysis, room acoustic testing, and listening tests are compared.

6:40

1pAAe6. The Perforated Panel Resonator with Flexible Tube Bundles and its Appliations. Yadong Lu (Institute of Acoustics, Chinese Academy of Sciences, P. O. Box 2712, 21 Beisihuanxilu St., 100080 Beijing, China, yadong@mail.ioa.ac.cn), Huide Tang (Tianjin Hearing-aid Factory, Chenglinzhuang Rd. No. 93, 300161 Tianjin, China, tanghuide@eyou.com), Qiang Wang (Jinyusun Ventilation and Air-conditioning Equipment Ltd., Golden-delta Development Region. Tongzhou Dist., 101112 Beijing, China, jinyushun2003@yahoo.com.cn), Jing Tian (Institute of Acoustics, Chinese Academy of Sciences, P. O. Box 2712, 21 Beisihuanxilu St., 100080 Beijing, China, tian@mail.ioa.ac.cn), Youli Qu (Beijing Electrical Designing Institute, 15 Guananmenxijie St., 100055 Beijing, China, thgink@tom.com), Bo Qiu (Institute of Acoustics, Chinese Academy of Sciences, P. O. Box 2712, 21 Beisihuanxilu St., 100080 Beijing, China, nkcubert@yahoo.com.cn)

The sound absorptive mechanism and properties of the perforated panel resonator with flexible tube bundles are presented. Based upon that, some practical applications of the sound absorbing structure are introduced as follows. First of all, the perforated panel resonator with flexible tube bundles is used in designing a highly sound absorptive chamber, which is used as an audio-video laboratory. The acoustical performances of the chamber are presented. Second, the perforated panel resonator with flexible tube bundles is used in highly efficient duct silencer. The total noise level of axial fan source is attenuated to background noise level. Not only middle and high frequency noise is reduced, but also low frequency noise is suppressed considerably. Third, the perforated panel resonator with flexible tube bundles is used in a small-type centrifugal fan's casing treatments. The cut-off region of the centrifugal fan's casing is also acoustically treated. After the acoustical treatments, total sound power level of the fan is reduced obviously. Fourth, the perforated panel resonator with flexible tube bundles is used in designing the exhaust ducts and sound absorptive channel walls for an electrical transformer substation. The noise emitted from the transformer substation is reduced to surrounding background noise level.

7:00

1pAAe7. Shape-optimization of several multi-modal resonators accounting for room/resonator acoustical coupling. Octávio Inácio (Musical Acoustics Laboratory - ESMAE-IPP, Rua da Alegria, 503, 4000-045 Porto, Portugal, OctavioInacio@esmae-ipp.pt), José Antunes (Applied Dynamics Laboratory, Instituto Tecnológico e Nuclear, Estrada Nacional 10, 2686-953 Sacavém, Portugal, jantunes@itn.pt)

Helmholtz resonators are often applied for the sound equalisation of control rooms, through adequate leveling of the low frequency acoustic modal room responses. In several recent papers we proposed to improve the efficiency of such devices by, instead of using basic Helmholtz resonators with uniform cross-section, develop shape optimized multi-modal resonators in order to cope with a larger number of intrusive room modes. We thus showed the feasibility of resonator shape-optimization, in order to obtain a target set of acoustic eigenvalues, within imposed physical and/or geometrical constraints. More recently, we developed an efficient substructure theoretical approach to compute the coupled acoustical modes of rooms fitted with several multi-mode resonators, later also including viscous boundary layer absorption effects at the room/resonator interfaces. In the present paper we extend a further step these results by applying the previously developed optimization techniques to the fully coupled room/resonator model. We thus obtain truly representative results for the optimized complex acoustical problem, which highlight the potential of the proposed corrective methodology.

Session 1pAB

Animal Bioacoustics, Noise, and ECUA: Anthropogenic Noise Effects on Animals I

Michael Stocker, Cochair
Ocean Conservation Research, P.O. Box 559, Lagunitas, CA 94938, USA

Jonathan Gordon, Cochair
Sea Mammal Research Unit, Gatty Marine Laboratory, University of St Andrews, St Andrews, KY16 8LB, UK

Contributed Papers

1:00

1pAB1. Automated classification of odontocetes in open ocean environments using a novel multiclass suport vector machine. Susan Jarvis (Worcester Polytechnic Institute, 100 Institute Rd, Worcester, MA 01609, USA, sjarvis@ece.wpi.edu), Nancy A. Dimarzio (Naval Undersea Warfare Center Division Newport, 1176 Howell Street, Bldg 1351, 2nd Floor, Newport, RI 02841, USA, dimarziona@npt.nuwc.navy.mil), Ronald P. Morrissey (Naval Undersea Warfare Center Division Newport, 1176 Howell Street, Bldg 1351, 2nd Floor, Newport, RI 02841, USA, morrisseyrp@npt.nuwc.navy.mil), Jessica Ward (NAVSEA, Newport Undersea Warfare Center, Newport, RI RI 02841, USA, wardja@npt.nuwc.navy.mil), David Moretti (NAVSEA, Newport Undersea Warfare Center, Newport, RI RI 02841, USA, MorettiDJ@npt.nuwc.navy.mil)

Mid-frequency active sonar has recently been implicated in several marine mammal stranding events in various geographic locations. This has caused increased interest in monitoring and mitigating the effects of anthropogenic noise on marine mammals. Some species can be more susceptible sonar than others. For example, beaked whales (particularly Mesoplodon densirostris) have been the predominant species involved in most of the strandings. Key to effective monitoring and mitigation is the ability to automatically detect and identify the animals present, especially the species of high interest like beaked whales. This paper presents a novel class-specific support vector machine (CS-SVM) methodology for automated, species-level classification of small odontocetes. A CS-SVM has been developed and trained to identify click vocalization from several species of odontocetes including Mesoplodon densirostris. The algorithm processes time series data in a fully automated fashion first detecting and then classifying click vocalizations. The current CS-SVM configuration correctly identifies clicks from M. densirostris over 95% of time. Further results from the application of this automated classifier to data recorded at the AUTEC and SCORE undersea range facilities will be presented.

1:20

1pAB2. Effect of vessels and swimmers on the behavior of spinner dolphins (Stenella longirostris) off the Big Island of Hawai'i. Carmen Bazúa Durán (UNAM, Facultad de Ciencias, Depto. Física, Lab Acústica, Circuito exterior s/n, Cd. Universitaria, 04510 Mexico, D.F., Mexico, bazua@servidor.unam.mx), Nina V. Luna Valiente (UAM-Xochimilco, División de Ciencias Biológicas y de la Salud, 04960 Mexico, D.F., Mexico, bazua@servidor.unam.mx)

Many cetaceans live in coastal waters that are accessible to humans. In Kealakekua Bay, Hawai'i human activities occur during morning hours, when spinner dolphins rest and socialize (feeding occurs at night). Five human activities (swimmers, kayaks, motorized-boats, and narrow- or broad-band engine noises) within 200 m of the dolphins were monitored to investigate their effect on dolphin behavior. Dolphin behavior was measured as aerial behavior (high, medium, low energy), acoustic behavior (whistles, burst-pulses, echoclick-trains), herd size, herd coordination (high, medium, low), and diving interval (DI$<$1 min, 1 min$<$DI$<$2 min, DI$>$2 min) in the presence or absence of each human activity. Interactions between human activities and dolphins occurred 71% of the time, having simultaneous presence of several human activities. When only one human activity was present, motorboats and broad-noise increased herd-coordination and number of aerial behaviors; motorboats and both engine-noises reduced number of acoustic behaviors; kayaks and narrow-noise increased herd-coordination, DI and some acoustic behaviors; swimmers reduced herd-coordination and increased number of acoustic behaviors. Therefore, all five human activities studied changed dolphin behavior and changed it differently. Spinner dolphins probably can distinguish efficiently between human activities and may be interrupting their rest cycle to warn each other, which could have effects on this species welfare.

Invited Papers

1:40

1pAB3. Effects of sound on the behavior of toothed whales. Peter Tyack (Woods Hole Oceanographic Institution, Applied Ocean Physics & Engineering Dept., Woods Hole, MA 02543, USA, ptyack@whoi.edu), Ian Boyd (Sea Mammal Research Unit, Gatty Marine Laboratory, University of St Andrews, KY16 8LB St Andrews, UK, ilb@st-andrews.ac.uk), Diane Claridge (Bahamas Marine Mammal Research Organisation, P.O. Box AB-20714, Abaco, 0 Marsh Harbour, Bahamas, bmms@oii.net), Christopher W. Clark (Cornell University Laboratory of Ornithology, Bioacoustics Research Program, 159 Sapsucker Woods Road, Ithaca, NY 14850, USA, cwc2@cornell.edu), David Moretti (NAVSEA, Newport Undersea Warfare Center, Newport, RI RI 02841, USA, MorettiDJ@npt.nuwc.navy.mil), Brandon Southall (National Marine Fisheries Service, 1315 East West Hwy, SSMC III #12539, Silver Spring, MD 20910-6233, USA, Brandon.Southall@noaa.gov)

We report initial results from a study on behavioral responses of beaked and other whales to sonar and other sounds. This research is designed to provide new science-based approaches for mitigating the risk of sonar to beaked and other whales. The study was conducted at the Atlantic Undersea Test and Evaluation Center (AUTEC) range near Andros Island in the Bahamas, where Blainville's beaked whales (Mesoplodon densirostris) can regularly be detected using passive acoustic monitoring of their echolocation clicks. Tags recorded sound at the whale and behavior of the whale. Data were collected from 10 tag deployments, 6 on Blainville's beaked whales and 4 on pilot whales. 109 hours of data were collected from tags, 74 hours from beaked whales and 34 hours from pilot whales.

Playbacks of mid-frequency sonar and killer whale calls were performed on 3 of the tagged whales, 1 beaked whale and 2 pilot whales. The tagged beaked whale responded to both sonar and killer whale sounds by premature cessation of clicking during foraging dives (RL = ~117 dB re 1 μPa for the killer whale sound, ~145 dB for the sonar), and an unusually slow and long ascent.

2:00

1pAB4. Acoustic flexibility in singing birds under noisy urban conditions. Hans Slabbekoorn (Leiden University, Kaiserstraat 63, 2311 GP Leiden, Netherlands, H.W.Slabbekoorn@Biology.LeidenUniv.NL)

Birds rely on song for defending a territory and attracting a mate. More and more breeding areas are affected by human activities and anthropogenic noise has become almost omnipresent. Consequently, song function in and around cities, and alongside highways, train tracks and airports, is increasingly hampered by noise interference. Several counter strategies in producing sounds, related to changes in loudness, pitch, and timing, can help out under these noisy urban conditions. Observational data have yielded several interesting patterns which show remarkable singing flexibility in different species that are typically common in cities. Here I present data for a new species, the chiffchaff (Phylloscopus collybita) showing spectral and temporal adaptation which reduces masking alongside a highway in the Netherlands. Furthermore, experimental field data reveal for the first time that this species is able to adjust immediately to exposure to highway noise via artificial playback in quiet territories. Acoustic flexibility may be key to efficient use of the 'left-over acoustic space' and may determine whether individual birds can maintain their territory and breed successfully. Variation in flexibility among species may explain which birds will remain widespread in our noisy world and which will be pushed back into 'silent' habitat pockets.

Contributed Papers

2:20

1pAB5. Comodulation masking release in the bottlenose dolphin (Tursiops truncatus). Brian K. Branstetter (US Navy Marine Mammal Program, Space and Naval Warfare Systems Center, 53560 Hull St., Code 71510, San Diego, CA 92152, USA, branstet@hawaii.edu), James J. Finneran (US Navy Marine Mammal Program, Space and Naval Warfare Systems Center, 53560 Hull St., Code 71510, San Diego, CA 92152, USA, james.finneran@navy.mil), Linda S. Green (Science Applications International Corporation, 4065 Hancock St., San Diego, CA 92110, USA, branstet@hawaii.edu), Erik E. Robinson (Science Applications International Corporation, 4065 Hancock St., San Diego, CA 92110, USA, branstet@hawaii.edu), Megan N. Tormey (Science Applications International Corporation, 4065 Hancock St., San Diego, CA 92110, USA, branstet@hawaii.edu), Randall L. Dear (Science Applications International Corporation, 4065 Hancock St., San Diego, CA 92110, USA, RANDALL.L.DEAR@saic.com)

The power spectrum model of masking, derived from critical band or critical ratio measurements is often cited and used to extrapolate the effects of masking noise on the signal detection abilities of marine mammals. However, the power spectrum model may not generalize well to environmental noise that is often coherently amplitude-modulated across frequency regions. The current study demonstrates a pattern of masking where temporally fluctuating comodulated noise produces lower masked thresholds (up to a 17 dB difference) compared to Gaussian noise of the same spectral density level. Noise possessing wide bandwidths, low temporal modulation rates, and across-frequency temporal envelope coherency resulted in lower masked thresholds, a phenomenon known as comodulation masking release. The results are consistent with a model where dolphins compare temporal envelope information across auditory filters to aid in signal detection. Furthermore, results suggest conventional models of masking derived from experiments using random Gaussian noise may not generalize well to environmental noise that dolphins actually encounter.

2:40

1pAB6. Investigating noise effects on the call amplitude of endangered Southern Resident killer whales (Orcinus orca). Marla Holt (NOAA Northwest Fisheries Science Center, Marine Mammal Program, 2725 Montlake Blvd East, Seattle, WA 98112, USA, Marla.Holt@noaa.gov), Val Veirs (Colorado College, Department of Physics, Colorado Springs, CO 80903, USA, vveirs@coloradocollege.edu), Scott Veirs (Beam Reach Marine Science and Sustainability School, 7044 17th Ave NE, Seattle, WA 98115, USA, scott@beamreach.org)

Anthropogenic sound exposure has been identified as a potential threat to endangered Southern Resident killer whales (SRKWs). Such exposure can mask important biological sounds including those used for social functions. Vocal animals might compensate for increased background noise by calling louder (the Lombard effect). In this study, amplitude compensation was investigated in SRKW communication calls recorded off of San Juan Island, WA, U.S.A. Data were obtained from two calibrated recording systems, a shore-based hydrophone array [V. Veirs, J. Acoust. Soc. Am., **116**, 2615 (2004)] and a boat-based vertical array. Calls were localized using time of arrival differences to estimate range and apparent source levels after background levels were subtracted from the signal. Call levels were calculated assuming spreading loss functions determined from sound propagation observations made in situ. Results demonstrated a positive relationship between call levels and background levels. Costs of such vocal flexibility are unknown, but may include changes in energetic demand and/or communicative functionality. Within the data ranges measured in this study, killer whales communicatively adjusted for fluctuating background noise levels. However, other sounds detected during passive listening (e.g. prey sounds) might be more susceptible to masking effects [Work supported by NOAA and Colorado College.]

Invited Papers

3:00

1pAB7. Effects of noise on hearing in odontocetes. James J. Finneran (US Navy Marine Mammal Program, Space and Naval Warfare Systems Center, 53560 Hull St., Code 71510, San Diego, CA 92152, USA, james.finneran@navy.mil), Carolyn E. Schlundt (EDO Professional Services, 3276 Rosecrans St., San Diego, CA 92110, USA, carolyn.melka@edocorp.com), Sam H. Ridgway (University of California, San Diego, Dept. of Pathology, School of Medicine, 9500 Gilman Drive, La Jolla, CA 92093, USA, ridgway@spawar.navy.mil)

Increased public concern and regulation of activities involving anthropogenic sound have resulted in a pressing need for specific information regarding safe limits for marine mammals exposed to underwater noise. Since many marine mammals have sensitive hearing and rely upon underwater sound for communicating, foraging, and navigating, the potential effects of noise on their hearing is of particular concern. One of the most familiar consequences of noise exposure is an increase in threshold that persists after the cessation of the noise, called a temporary thresholds shift (TTS) or permanent threshold shift (PTS). Although there are no PTS data for marine

mammals, there have been TTS measurements in a number of species, including bottlenose dolphins and belugas. These studies compare hearing thresholds before and after subjects are exposed to intense sounds. The results are analogous to data from terrestrial mammals, where TTS depends on the exposure frequency, sound pressure, duration, and temporal pattern. This talk reviews the major findings related to the growth of and recovery from TTS in bottlenose dolphins and belugas and discusses the application of these data to acoustic exposure guidelines.

3:20

1pAB8. Noise-induced permanent threshold shift in a harbor seal. David Kastak (UCSC Institute of Marine Sciences, Long Marine Lab - University of California, 100 Shaffer Road, Santa Cruz, CA 95060, USA, kastak@ucsc.edu), Jason Mulsow (UCSC Institute of Marine Sciences, Long Marine Lab - University of California, 100 Shaffer Road, Santa Cruz, CA 95060, USA, jmulsow@ucsc.edu), Asila Ghoul (UCSC Institute of Marine Sciences, Long Marine Lab - University of California, 100 Shaffer Road, Santa Cruz, CA 95060, USA, asila@ucsc.edu), Colleen Reichmuth (UCSC Institute of Marine Sciences, Long Marine Lab - University of California, 100 Shaffer Road, Santa Cruz, CA 95060, USA, coll@ucsc.edu)

Investigation of auditory temporary threshold shift (TTS) in marine mammals has provided a means of predicting the harmful effects of underwater anthropogenic noise. As complete recovery of hearing is requisite in these studies, they have been considered appropriate in light of subject availability and ethical considerations. In our psychophysical studies of TTS in pinnipeds, we have employed methods designed to safely titrate from sound levels of noise inducing no TTS to levels of significant but completely recoverable hearing loss. In the present study, these methods were used with a harbor seal (*Phoca vitulina*) exposed to an underwater 4.1 kHz pure tone fatiguing stimulus. Sound levels and durations were gradually increased to a maximum received sound pressure of 184 dB re 1 μPa with a duration of 60 s (SEL=202 dB re 1 $\mu Pa^2 s$). Upon the second exposure to this fatiguing stimulus, an initial threshold shift in excess of 50 dB was estimated at a test frequency of 5.8 kHz, a half-octave above the fatiguing tone. Recovery from this unexpectedly large shift occurred at a rate of -10 dB per log(min), with an apparently permanent threshold shift of 7 to 10 dB evident after more than two months following exposure.

3:40-4:00 Break

4:00

1pAB9. Anthropogenic sounds - Potential effects on fish. Arthur Popper (Dept. of Biology, University of Maryland, College Park, MD 20742, USA, apopper@umd.edu), Svein Løkkeborg (Fish Capture Division, Institute of Marine Research, P.O. Box 1870, Nordnes N-5817 Bergen, Norway, svein.loekkeborg@imr.no), Robert McCauley (Curtin University, Centre for Marine Science and Technology, GPO Box U 1987, 6845 Perth, Australia, r.mccauley@cmst.curtin.edu.au)

There is concern that human-generated sounds may have deleterious effects on fish. This paper will review some of what is currently known about these effects, and consider the questions that have to be answered before developing models to enable ″prediction″ of sound effects on particular fish species. A major restriction is that there are few peer-reviewed data on effects of anthropogenic sources on fish. Extrapolation from these results is further confounded since experiments differ in many ways, each of which may alter the resultant impact on fish. For example, studies vary in sounds types tested (e.g., pile driving vs. ship noise), signal parameters (intensity, number of repetitions), species used, fish age, etc. Moreover, a singularly important issue is that while many of the issues and impact mechanisms are potentially amenable to experimental lab study, the ultimate questions regarding the effects of sound on fish behavior need to field based and require long-term observations where behaviour of wild fish is not constrained. Only by observing fish in the wild will we ultimately understand if, and how, anthropogenic sounds impact fish both during exposure and, more importantly, for extended periods after the termination of the sound.

4:20

1pAB10. Characterizing the relative contributions of large vessels to total ocean noise fields: a case study using the Gerry E. Studds Stellwagen Bank National Marine Sanctuary. Leila T. Hatch (US NOAA, Stellwagen Bank National Marine Sanctuary, 175 Edward Foster Road, Scituate, MA 02066, USA, leila.hatch@noaa.gov), Christopher W. Clark (Cornell University Laboratory of Ornithology, Bioacoustics Research Program, 159 Sapsucker Woods Road, Ithaca, NY 14850, USA, cwc2@cornell.edu), Sofie Van Parijs (US NOAA, Northeast Fisheries Science Center, 166 Water Street, Woods Hole, MA 02543, USA, sofie.vanparijs@noaa.gov), Richard Merrick (US NOAA, Northeast Fisheries Science Center, 166 Water Street, Woods Hole, MA 02543, USA, richard.merrick@noaa.gov), Dimitri Ponirakis (Cornell University Laboratory of Ornithology, Bioacoustics Research Program, 159 Sapsucker Woods Road, Ithaca, NY 14850, USA, dwp22@cornell.edu), Kurt Schwehr (University of New Hampshire, Center for Coastal and Ocean Mapping Joint Hydrographic Center, 24 Colovos Road, Durham, NH 03824, USA, kurt@ccom.unh.edu), Michael A. Thompson (US NOAA, Stellwagen Bank National Marine Sanctuary, 175 Edward Foster Road, Scituate, MA 02066, USA, michael.a.thompson@noaa.gov), David Wiley (US NOAA, Stellwagen Bank National Marine Sanctuary, 175 Edward Foster Road, Scituate, MA 02066, USA, david.wiley@noaa.gov)

Understanding and mitigating the effects of underwater noise on marine species requires substantial information regarding acoustic contributions from shipping. In 2006, we used the U.S. Coast Guard's Automatic Identification System (AIS) to describe patterns of large commercial ship traffic within a U.S. National Marine Sanctuary. AIS data were combined with low-frequency acoustic data from an array of nine-ten autonomous recording units deployed throughout 2006. Analysis of received sound levels (10-1000 Hz, root-mean squared decibels re 1 μPascal ± standard error) averaged 119.5 ± 0.3 at high traffic locations. High traffic locations experienced double the acoustic power of less trafficked locations for the majority of the time period analyzed. Average source level estimates (71-141 Hz, root-mean squared decibels re 1 μPascal ± standard error) for individual vessels ranged from 158 ± 2 (research vessel) to 186 ± 2 (oil tanker). Tankers were estimated to contribute two times more acoustic power to the region annually than cargo ships, and over one

hundred times more than research vessels. Our results indicate that noise produced by large commercial traffic was at levels and within frequencies that warrant concern among managers regarding the ability of endangered whales to maintain acoustic contact within greater sanctuary waters.

Contributed Papers

4:40

1pAB11. Estimates of chronic SNR exposure levels of sperm whales (Physeter macrocephalus) to airguns in the Gulf of Mexico. Aaron Thode (Marine Physical Laboratory, Scripps Institution of Oceanography, 9500 Gilman Dr, MC 0238, La Jolla, CA 92093-0238, USA, athode@ucsd.edu), Martha Winsor (Hatfield Marine Science Center, Oregon State University, Newport, CA 97365, USA, martha.winsor@oregonstate.edu), Bruce Mate (Hatfield Marine Science Center, Oregon State University, Newport, CA 97365, USA, bruce.mate@oregonstate.edu), Matt Howard (Dept. of Oceanography, Texas A&M University, 3146 TAMU, College Station, TX 77843, USA, mkhoward@tamu.edu), Katherine Kim (HLS Research, Inc., 3366 N. Torrey Pines Ct., Ste. 310, La Jolla, CA 92037, USA, Katherine.Kim@HLSResearch.com), John Diebold (Lamont-Doherty Earth Observatory of Columbia University, 61 Route 9W, Palisades, NY 10964-8000, USA, johnd@ldeo.columbia.edu), Maya Tolstoy (Lamont-Doherty Earth Observatory of Columbia University, 61 Route 9W, Palisades, NY 10964-8000, USA, tolstoy@ldeo.columbia.edu)

A synthesis effort by the Sperm Whale Seismic Study (SWSS) has estimated chronic levels of low-level, long-term acoustic exposures of sperm whales in the Gulf of Mexico due to seismic airgun activity. Between 2002 and 2005, satellite-tags were attached to 53 whales of both sexes in the northern Gulf, with an average tag viability of 187 days. Data provided by the International Association of Geophysical Contractors (IAGC) permitted the range estimation of active seismic vessels to each whale location. The ray-tracing model BELLHOP was used to estimate received levels from each seismic vessel for every space-time data point at frequencies between 10 to 1000 Hz, using simulated source signatures from a 3590 in 3 seismic array. Winds speeds from numeric models at each space-time location were converted into ambient noise levels, and shipping noise levels were crudely estimated. The preliminary synthesis using a simple spherical spreading transmission loss model suggests that over 95% of the whale positions reported during times of airgun activity occurred in circumstances where the received airgun pulses had 0 dB signal-to-noise ratio (SNR) or greater compared to ambient levels, and between 25-60% of all locations have received SNRs of 20 dB or greater, depending on the SNR definition used. [Sponsored by US Minerals Management Service].

5:00

1pAB12. Underwater radiated noise due to the piling for the Q7 Offshore Wind Park. Christ A.f. De Jong (TNO Science and Industry, P.O. Box 155, 2600 AD Delft, Netherlands, christ.dejong@tno.nl), Michael A. Ainslie (TNO Defence, Security and Safety, Oude Waalsdorperweg 63, 2597 AK The Hague, Netherlands, michael.ainslie@tno.nl)

The Q7 is the second offshore wind farm in the Dutch sector of the North Sea and, at 23 km off the Dutch coast, the world's first to be located outside the 12-mile limit. To support the wind turbines, monopiles (54 metres long steel pipes with a diameter of 4 metres) are hammered into the seabed using a pile-driver. The underwater radiated noise during the impulsive hammering of 9 out of 61 monopiles was monitored. Although there is a wide concern about the impact of piling noise on the marine life in the area, there are no criteria for the maximum acceptable noise levels. A quantitative comparison of the results of various studies in which the underwater noise from pile driving has been measured and reported is difficult, due to the lack of standardization in the level definitions and data processing. The Q7 data have been analyzed in terms of a broadband sound exposure level, peak pressure and pulse duration and a 1/3-octave band frequency spectrum of the sound pressure at different hydrophone locations, for each hammer stroke that has been recorded. The results are discussed in relation to the stroke energy and the hydrophone distance and depth.

5:20

1pAB13. Monitoring the temporal and spatial characteristics of the noise radiated from marine piling. Paul A. Lepper (Loughborough University, Electronic & Electrical Engineering, LE11 3TU Leicestershire, UK, p.a.lepper@lboro.ac.uk), Stephen P. Robinson (National Physical Laboratory, Hampton Road, TW11 OLW Teddington, UK, Stephen.Robinson@npl.co.uk)

Noise is often an unintended by-product of offshore activities, and a significant source of impulsive underwater noise is marine piling, where a pile is driven into the sea-bed using a hydraulic hammer. This paper describes work undertaken to monitor the underwater radiated noise during offshore marine piling. The measurements made include full characterisation of the temporal variation of the resulting sound field, including frequency content of the pulses and the increasing amplitude typically observed during the soft start period. Results are also shown for the spatial variation of the field, including the effect on propagation of significant bathymetry changes (for example, due to the presence of a sand bank). The energy within each acoustic pulse is an appropriate measure of the sound field, having the advantage that it is relatively straightforward to add the contributions from each pulse in order to derive an overall sound exposure level (SEL) in a manner analogous to methods familiar from air acoustics. An example is then given of how the measured data and predictive modeling may be used to calculate an overall exposure for an animal in the vicinity, using various assumptions about the location and mobility of the animal.

5:40

1pAB14. Monitoring, measuring and describing ocean noise over ecologically viable scales with applications to impacts on large whales. Christopher W. Clark (Cornell University Laboratory of Ornithology, Bioacoustics Research Program, 159 Sapsucker Woods Road, Ithaca, NY 14850, USA, cwc2@cornell.edu), Chris Tremblay (Cornell University Laboratory of Ornithology, Bioacoustics Research Program, 159 Sapsucker Woods Road, Ithaca, NY 14850, USA, cjt35@cornell.edu), Melissa Fowler (Cornell University Laboratory of Ornithology, Bioacoustics Research Program, 159 Sapsucker Woods Road, Ithaca, NY 14850, USA, mcf3@cornell.edu), Christi Diamond (Cornell University Laboratory of Ornithology, Bioacoustics Research Program, 159 Sapsucker Woods Road, Ithaca, NY 14850, USA, cd254@cornell.edu), Dimitri Ponirakis (Cornell University Laboratory of Ornithology, Bioacoustics Research Program, 159 Sapsucker Woods Road, Ithaca, NY 14850, USA, dwp22@cornell.edu), Clara McCarthy (Cornell University Laboratory of Ornithology, Bioacoustics Research Program, 159 Sapsucker Woods Road, Ithaca, NY 14850, USA, cmm255@cornell.edu), Janelle Morano (Cornell University Laboratory of Ornithology, Bioacoustics Research Program, 159 Sapsucker Woods Road, Ithaca, NY 14850, USA, jlm394@cornell.edu), Charles Muirhead (Cornell University Laboratory of Ornithology, Bioacoustics Research Program, 159 Sapsucker Woods Road, Ithaca, NY 14850, USA, cam236@cornell.edu), Anita Murray (Cornell University Laboratory of Ornithology, Bioacoustics Research Program, 159 Sapsucker Woods Road, Ithaca, NY 14850, USA, am678@cornell.edu), Liz Rowland (Cornell University Laboratory of Ornithology, Bioacoustics Research Program, 159 Sapsucker Woods Road, Ithaca, NY 14850, USA, edr6@cornell.edu), Catherine Vannicola (Cornell University Laboratory of Ornithology, Bioacoustics Research Program, 159 Sapsucker Woods Road, Ithaca, NY 14850, USA, cmv44@cornell.edu), Ann Warde (Cornell University Laboratory of Ornithology, Bioacoustics Research Program, 159 Sapsucker Woods Road, Ithaca, NY 14850, USA, amw38@cornell.edu)

Large whales communicate primarily in the low ($<$1000 Hz) frequency bands; the same frequency range within which anthropogenic ocean noise has been increasing over the last half century at approximately 3-5 dB/decade. The working assumption and hypothesis hold that rising ambient noise levels negatively impact whales by interfering with communication, navigation and predator detection, and that over the long-term such effects

could reduce breeding success and population size. There is a lack of empirical data on the spatial-temporal dynamics of ambient noise by which to assess potential impacts. One year of continuous acoustic data from an ongoing distributed array of 19 continuous seafloor recorders covering a 1000 km^2 area in Massachusetts Bay, USA were analyzed for ambient noise statistics and the occurrences, locations and vocal behaviors of fin, humpback and right whales. Noise levels were greater than 120 dB rms re 1 μPa in the 10-1000 Hz band throughout the 1000 km^2 area for ⩾50% of the season when whales were present. If animals are relying on acoustic cues to coordinate feeding and social interactions, these high noise levels impose a significant loss of acoustic habitat during the whales' residency in the area.

6:00

1pAB15. Environmental Risk Management Capability: Advice on minimising the impact of sonar on marine mammals. Colin Schofield (BAE Systems Integrated System Technologies, Unit D1, Marabout Industrial Estate, DT1 1YA Dorchester, UK, colin.schofield @baesystems.com)

The Environmental Risk Management Capability - Sonar (ERMC(S)) has now been accepted into service by the UK Royal Navy. ERMC(S) is the first operational software package that provides a comprehensive risk assessment of the common concern of the potential impact of sonar usage on marine mammals. The algorithms include allowance for extended periods of use and advice on achievable mitigation options. Now that the system has achieved this significant milestone, this paper reviews the elements of the system that have made progress to this stage so successful: -The techniques and data used by the algorithms. -The inclusive development approach that allowed all the concerned stakeholders to be satisfied with the processes utilised. -The annual review cycle that will enable the tool to maintain its links with forefront research in this area. -The application of the system to non-military sound sources as the benchmark approach. This paper will show how ERMC(S) can be develop into a tool for both commercial and military sound sources using proving and established techniques.

6:20

1pAB16. Proposed Marine Mammal Noise Exposure Criteria: Current Data Base, Limitations, and Research Needs. Darlene R. Ketten (Woods Hole Oceanographic Institution, Applied Ocean Physics & Engineering Dept., Woods Hole, MA 02543, USA, dketten@whoi.edu), Ann E. Bowles (Hubbs-Sea World Research Institute, 2595 Ingraham Street, San Diego, CA 92109, USA, abowles@hswri.com), William T. Ellison (Marine Acoustics, Inc, 809 Aquidneck Ave, Middletown, RI 02842, USA, WEMAI@aol.com), James J. Finneran (US Navy Marine Mammal Program, Space and Naval Warfare Systems Center, 53560 Hull St., Code 71510, San Diego, CA 92152, USA, james.finneran@navy.mil), Roger L. Gentry (ProScience Consulting, LLC, P.O. Box 177, Dickerson, MD 20842-0177, USA, roger.gentry@comcast.net), Charles R. Greene (Greeneridge Sciences, Inc., 4512 Via Huerto, Santa Barbara, CA 93110, USA, cgreene@greeneridge.com), David Kastak (UCSC Institute of Marine Sciences, Long Marine Lab - University of California, 100 Shaffer Road, Santa Cruz, CA 95060, USA, kastak@ucsc.edu), James H. Miller(University of Rhode Island, Department of Ocean Engineering, Narragansett Bay Campus, Narragansett, RI 02882, USA, miller@egr.uri.edu), Paul E. Nachtigall (University of Hawaii, Hawaii Institute of Marine Biology, P.O. Box 1106, Kailua, HI 96734, USA, nachtiga@hawaii.edu), W J. Richardson (LGL Ltd., Environmental Research Associates, P.O. Box 280, 22 Fisher St, King City, AB L7B 1A6, Canada, wjr@lgl.com), Brandon Southall (National Marine Fisheries Service, 1315 East West Hwy, SSMC III #12539, Silver Spring, MD 20910-6233, USA, Brandon.Southall@noaa.gov), Jeanette A. Thomas (Western Illinois University Quad Cities, Department of Biological Sciences, 3561 60th St., Moline, IL 61265, USA, j-thomas@wiu.edu), Peter Tyack (Woods Hole Oceanographic Institution, Applied Ocean Physics & Engineering Dept., Woods Hole, MA 02543, USA, ptyack@whoi.edu)

This paper presents the findings of an inter-disciplinary expert panel based on comprehensive review of hearing and noise effects data for marine and land mammals. The principal motivation for the review was to assist formulation of data-based noise exposure criteria in light of rapidly evolving research advances in marine mammal hearing and underwater noise effects. Levels estimated to induce permanent hearing loss were determined for single exposure events for cetaceans (in water) and pinnipeds (in air and water) for each of 15 sound type/animal group combinations. These recommendations represent a current best estimate only and are modular, with modifiable key variables; e.g., source and exposure, to facilitate revision as data improve. In some cases, relatively explicit injury limits are proposed, e.g., 186 dB re: $1\mu Pa^2$-s (frequency-weighted sound exposure level) and 218 dB re: $1\mu Pa_{peak}$ (unweighted peak sound pressure level) for pinnipeds in water exposed to multiple sound pulses. In others, particularly for behavioural effects of multiple-pulse and non-pulse exposures, response severity and significance are quantitatively scored, but the data do not allow identification of specific broadly-applicable disturbance thresholds. These findings are a current best effort and include a discussion of limitations and recommended research needed to address data gaps.

6:40

1pAB17. A simple acoustical exposure metric based on biological thresholds and integrating a temporal characteristics exposure axis. Michael Stocker (Ocean Conservation Research, P.O. Box 559, Lagunitas, CA 94938, USA, mstocker@OCR.org), Tom Reuterdahl (505 LaVerne Ave, Mill Valley, CA 94941, USA, euler1@sbcglobal.net), Libbie Horn (975 Black Mountain Rd., Hillsborough, CA 94-1-, USA, libbie.horn@gmail.com), Gail Hurley (768 Lovell Ave., Mill Valley, CA 94941, USA, hurleyitaly@hotmail.com)

Anthropogenic noise is compromising habitat for marine mammals, fish and potentially other marine organisms. Determining acceptable exposure thresholds is confounded by the fact that marine animals have adapted to some exceedingly loud naturally occurring sounds, while exposure to certain anthropogenic noises at equivalent or lower amplitudes causes harm. It is clear that mitigation levels can not be established by signal amplitude alone and that other signal characteristics are significant factors in biological responses to noise exposure. This proposed metric continues ongoing work on a simple exposure metric based on broadband frequency and amplitude representation of a subject noise with the time domain represented in the Z axis.

Session 1pAOa

Acoustical Oceanography and ECUA: Acoustical Oceanography of Polar Environments I

Peter N. Mikhalevsky, Cochair
Science Applications International Corporation, 4001 N. Fairfax Dr. Suite 850, Arlington, VA 22203, USA

Hanne Sagen, Cochair
Nansen Environmental and Remote Sensing Center, Thormølensgt. 47, Bergen, 5006, Norway

Invited Papers

1:00

1pAOa1. Acoustic communication and navigation in the Arctic Ocean. Arthur B. Baggeroer (MIT, Department of Mathematics, 77 Massachusetts Avenue, Cambridge, MA 02139, USA, abb@boreas.mit.edu), Lee Freitag (Woods Hole Oceanographic Inst., 266 Woods Hole Road, MS 18, Woods Hole, MA 02543, USA, lfreitag@whoi.edu), James E. Priesig (Woods Hole Oceanographic Inst., 266 Woods Hole Road, MS 18, Woods Hole, MA 02543, USA, jreisig@whoi.edu), Daniel Nagle (Naval Undersea Systems Center, 1176 Howell Street, Newport, RI 02841, USA, nagledt@npt.nuwc.navy.mil)

Acoustic communication and navigation in the Arctic usually implies surface interaction because of the upward refracting profile. While open water leeds and polyna exist, sensors must also be deployed beneath the ice. Nominal roughness of several meters plus ubiquitous ice keels all lead to complicated multipath propagation typically of durations from 0.1 to 10 seconds. Pack ice drifts at scales of 0.1-0.2 nm/s leading to doppler shifts/spreads of 2 - 8 Hz at 10-20 kHz carriers. These lead to highly spread channels with lots of ISI. Wise signal and code designs coupled with equalizers are critical to successful performance of acomms system even at low rates. Navigation such as by long base line systems encounter the same multipath. Path detectors and trackers are easily confused in determining interactions with the underside of the ice cover. Often, first arrivals are weak and do not trigger detectors. This leads to ″lane″ skipping by tracking algorithms and sychonization errors for acomms. This implies clever ″track association″ algorithms to identify the arrival patterns and then transform them to locations which move with ice drift. This presentation outlines acoustic problems which communicaton and navigation systems must overcome using data take from several Arctic experiments.

1:20

1pAOa2. Propagation, scattering and reverberation in an ice-covered Arctic ocean. Henrik Schmidt (MIT, 77 Mass Ave, 5-204, Cambridge, MA 02139, USA, henrik@mit.edu), Kevin D. Lepage (Naval Research Laboratory, 4555 Overlook Ave SW, Washington, DC 20375, USA, kevin.lepage@nrl.navy.mil)

The Arctic Ocean is a unique acoustic environment due to the ice cover and the strongly upward refracting sound speed profile. A large amount of theoretical and experimental research has focused on the significance of the scattering of sound by the rough ice cover. In spite of this, a strong anomali persisted until the early 1990s in the propagation of low-frequency sound in particular, with prevailing rough-surface scattering theories incapable of explaining the frequency dependence of transmission loss observed experimentally. More recent modeling was cabable of reproducing the observed transmission losses by combining the effects of ice elasticity, rough interface scattering, and waveguide propagation [JASA, **96**:1783-1795,1994]. Thus, it was demonstrated that incoherent scattering into Lamb waves in the ice provided a significant loss mechanism. This mechanism itself did not explain the frequency dependence, but when incorporating the bilinear sound speed profile of the arctic ocean, it was found that the lower-order modes become disproportionately attenuated, explaining the high attenuation observed at low frequencies. The finding was later confirmed by succesfully modeling the modal losses observed in 1994 Trans-Arctic Propagation experiments, and the ability of the same model to accurately predict observed, long-range reverberation measurements [JASA, **111**:747-760,2001]. [Work supported by ONR.]

1:40

1pAOa3. Long-term variations of ice breaking noise in Antarctica. Alexander Gavrilov (Curtin University of Technology, Centre for Marine Sci & Tech, GPO Box U1987, 6845 Perth, WA, Australia, a.gavrilov@cmst.curtin.edu.au), Binghui Li (Curtin University of Technology, Centre for Marine Sci & Tech, GPO Box U1987, 6845 Perth, WA, Australia, binghui.li@postgrad.curtin.edu.au)

Numerous low frequency transient signals arriving from Antarctica have been detected in five-year sea noise recordings in 2002-2006 at the hydroacoustic listening station deployed off Cape Leeuwin in Western Australia as part of the International Monitoring System of the Comprehensive Nuclear-Test-Ban Treaty. The majority of these signals consist of a single arrival of mode 1 which dominates the higher modes and undergoes strong frequency dispersion due to long-range propagation in the polar ocean environment. These signals are believed to be emitted primarily by ice rifting and breaking events on the Antarctic shelf. Several regions along the Antarctic coast associated with certain glaciers and ice tongues were found to persistently be much more active in generating ice noise than other

parts of the Antarctic shelf. An analysis of long-term changes in the frequency of occurrence of ice events showed noticeable seasonal cycles, but did not reveal any significant interannual variations against the background of short-term fluctuations. Some of the ice events detected at the Cape Leeuwin station were also identified in sea noise recordings made on autonomous acoustic loggers deployed on the Antarctic shelf, which allowed us to investigate characteristics of the acoustic signals from ice events near their origins.

Contributed Papers

2:00

1pAOa4. Localization of Antarctic ice breaking events by frequency dispersion of the signals received at a single hydroacoustic station in the Indian Ocean. Binghui Li (Curtin University of Technology, Centre for Marine Sci & Tech, GPO Box U1987, 6845 Perth, WA, Australia, binghui.li@postgrad.curtin.edu.au), Alexander Gavrilov (Curtin University of Technology, Centre for Marine Sci & Tech, GPO Box U1987, 6845 Perth, WA, Australia, a.gavrilov@cmst.curtin.edu.au)

Transient acoustic signals from Antarctic ice cracking and breaking events, featuring significant frequency dispersion, were observed at the hydroacoustic stations deployed in the Indian Ocean as part of the International Monitoring System (IMS) of the Comprehensive Nuclear-Test-Ban Treaty. Based on a comparison with numerical predictions, the measured dispersion characteristics were used to estimate the range between ice events and the receiver. Combined with the bearing capability of the IMS stations, these estimates allow us to locate ice events from a single hydroacoustic station. An analysis of range estimation errors due to uncertainty of the measured time-frequency structure of signal arrivals and due to variations of the sound speed profiles was also conducted. The analysis showed that the location accuracy from a single hydroacoustic station for the typical ice events was of the same order, as that determined from an intersection of bearings from two remote stations, if the signal frequency bandwidth is as wide as at least 5 Hz and lies within 5 Hz to 35 Hz frequency range. This localization method was examined by analysing several ice events detected at both the Cape Leeuwin IMS station and a sea noise logger deployed off the Antarctic shelf.

2:20

1pAOa5. Year-round acoustic monitoring of large whales in polar environments: a comparison of Davis and Bransfield Straits. Kathleen Stafford (University of Washington Applied Physics Lab, 1013 40th St NE, Seattle, WA 98105, USA, stafford@apl.washington.edu), Malene J. Simon (University of Aarhus, Institute of Biology, C.F. Mollers Alle 1131, 8000 Aarhus C, Denmark, MaSi@natur.gl), Robert Dziak (Oregon State Univ. and NOAA, 2030 SE Marine Science Dr., Newport, OR 97365, USA, robert.p.dziak@noaa.gov), David K. Mellinger (Oregon State Univ. and NOAA, 2030 SE Marine Science Dr., Newport, OR 97365, USA, David .Mellinger@oregonstate.edu)

Both Davis Strait, in the Arctic between Canada and Greenland, and Bransfield Strait, in the Antarctic between the Antarctic Peninsula and the South Shetland Islands, are areas that experience extreme inter-seasonal differences in temperature, ice cover and productivity. The seasonally productive nature of both of these ice-influenced areas provides habitat for foraging large whales such as blue (Balaenoptera musculus) and fin (B. physalus) whales. In order to monitor and compare the seasonal occurrence of these species at high latitude regions at opposite ends of the globe, autonomous underwater hydrophone packages were deployed for one year in each Strait. Three instruments were deployed and recovered in Davis Strait from October 2006-07 and five in Bransfield Strait from November 2006-07. Blue and fin whales were recorded seasonally in both regions and exhibited the geographic acoustic distinctions between northern and southern hemisphere populations. Comparisons of the seasonal occurrence and the influence of ice cover on this occurrence will be compared and contrasted between north and south.

Invited Papers

2:40

1pAOa6. Acoustic navigation and communications for high latitude ocean research (ANCHOR). Craig M. Lee (Applied Physics Laboratory, University of Washington, 1013 NE 40th St, Seattle, WA 98105-6698, USA, craig@apl.washington.edu), Jason I. Gobat (Applied Physics Laboratory, University of Washington, 1013 NE 40th St, Seattle, WA 98105-6698, USA, jgobat@apl .washington.edu)

Recent community reports on autonomous and Lagrangian platforms and Arctic observing identify the development of under-ice navigation and telemetry technologies as one of the critical factors limiting the scope of autonomous (e.g. floats, AUVs and gliders) high-latitude measurement efforts. These platforms could provide persistent, high-resolution, basin-wide sampling in ice-covered regions and collect measurements near the critical ice-water interface. Motivated by the dramatic advances in temporal and spatial reach promised by autonomous sampling and by the need to coordinate nascent efforts to develop navigation and communication system components, an international group of acousticians, platform developers, high-latitude oceanographers and marine mammal researchers gathered in Seattle, U.S.A. from 27 February - 1 March for an NSF Office of Polar Programs sponsored Acoustic Navigation and Communication for High-latitude Ocean Research workshop. Workshop participants summarized the current state of knowledge concerning Arctic acoustics, navigation and communications, developed an overarching system specification to guide community-wide engineering efforts and established an active community and steering group to guide long-term efforts and ensure interoperability between elements developed by disparate teams. This presentation will summarize workshop findings and provide an update on recent developments stemming from the EU DAMOCLES and US NSF Arctic Observing Network programs.

3:00

1pAOa7. Sound fixing and ranging beneath sea-ice. Jean-Claude Gascard (University Pierre & Marie Curie, 4 place Jussieu, Locean tour 45-46, 5e, 75005 Paris, France, jga@locean-ipsl.upmc.fr)

Sound fixing and ranging techniques, the so-called SOFAR technique, is widely used in the field of oceanography for tracking neutrally buoyant floats underwater over large distances (several thousands of kilometres) and for long periods of time (several years). The range propagation depends largely on the existence or not of the SOFAR sound channel. Twenty years ago we investigated SOFAR acoustic propagation under sea-ice over large distances and at various frequencies from 80 Hz up to 1560 Hz. We discovered the range for acoustic propagation was much reduced (100 kms to 150 kms) no matter the frequency used. This was due to large scattering induced by under sea-ice topography since there is no way to avoid acoustic rays to bounce back to the surface towards sea-ice and create multiple reflections. More recently during the Tara Damocles transpolar drift across the Arctic Ocean, we reinvestigated the

SOFAR acoustic range propagation under sea-ice for longer periods of time in various conditions (summer and winter conditions). Our results confirmed those obtained 20 years ago and indicated a high sensitivity to the ambient conditions. We are presenting the results obtained during the late fall- early winter months of the Tara transpolar drift across the Arctic Ocean.

Contributed Papers

3:20

1pAOa8. The Fram Strait acoustic tomography system. Hanne Sagen (Nansen Environmental and Remote Sensing Center, Thormølensgt. 47, 5006 Bergen, Norway, hanne.sagen@nersc.no), Stein Sandven (Nansen Environmental and Remote Sensing Center, Thormølensgt. 47, 5006 Bergen, Norway, stein.sandven@nersc.no), Peter Worcester (MPL, Scripps Institution of Oceanography, University of California, San Diego, La Jolla, CA 92093-0238, USA, pworcester@ucsd.edu), Matthew Dzieciuch (MPL, Scripps Institution of Oceanography, University of California, San Diego, La Jolla, CA 92093-0238, USA, mad@ucsd.edu), Emmanuel Skarsoulis (FORTH/IACM, N. Plastira 100, Vasilika Voutes, GR-70013 Heraklion, Greece, eskars@iacm.forth.gr)

The deep and wide Fram Strait between Greenland and Spitzbergen is the main influx and efflux gate to the Arctic Basin. Although major resources are invested in measurements of current and temperature here (http://asof.npoar.no), the flux estimates still have significant deficiencies and errors. Our objective is to build, test, validate and use an innovated integrated observing and modeling system, including acoustic tomography, for improved monitoring of volume, heat and freshwater transports in the Fram Strait. As part of the DAMOCLES-IP, (=Developing Arctic Modeling and Observing Capabilities for Long-term Environmental Studies - Integrated Project) a first step acoustic tomography system is to be installed in the Fram Strait between East Greenland and West Spitzbergen in August 2008. The first step tomography system consists of one acoustic source near the Svalbard shelf and one receiver array in the middle of the Fram Strait. An extended acoustic system serving both tomography and glider navigation is planned implemented in 2009 within the recently funded project ″Acoustic technology for observing the interior of the Arctic Ocean″ (ACOBAR). We will present the specification of the tomography systems; our experimental plans, and plans for data analysis, including data assimilation.

3:40

1pAOa9. Ocean acoustic tomography: Travel-time inversion in the eastern Fram Strait. Emmanuel Skarsoulis (FORTH/IACM, N. Plastira 100, Vasilika Voutes, GR-70013 Heraklion, Greece, eskars@iacm.forth.gr), George Piperakis (FORTH/IACM, N. Plastira 100, Vasilika Voutes, GR-70013 Heraklion, Greece, piperak@iacm.forth.gr), Michael Kalogerakis (TEI Crete/FORTH/IACM, Vassilika Vouton, GR-711 10 Heraklion, Crete, Greece, mixalis@iacm.forth.gr), Hanne Sagen (Nansen Environmental and Remote Sensing Center, Thormølensgt. 47, 5006 Bergen, Norway, hanne.sagen@nersc.no)

The Fram Strait is the main passage through which the mass and heat exchange between the Atlantic and the Arctic Ocean takes place. In the framework of DAMOCLES project (EU/FP6) a tomography experiment is planned to be conducted at latitude of 78N50 between 1E and 7E. A near-real-time discrete inversion scheme has been developed relying on the matched-peak inversion approach seeking to maximize agreement between theoretical and observed peaks. The model relations between model parameters (temperature distributions) and travel times are implemented using a ray-tracing code accounting for the effects of range dependence. The parameter space is discretized and the corresponding model relations are stored in a database for later use - stored model relations greatly accelerate the inversion process. In the absence of real measurements the performance of the inversion scheme was tested using synthetic data relying on 3-year long time series of temperature data. The particular propagation conditions give rise to different inversion errors at different depths, with the minimum obtained at 250 m depth, in the core of the northward flowing Atlantic water. For the implementation of the tomographic analysis a software system called SMTAS has been developed running in a dedicated server connected to the internet.

MONDAY AFTERNOON, 30 JUNE 2008 ROOM 342A, 4:20 TO 7:20 P.M.

Session 1pAOb

Acoustical Oceanography and ECUA: Marine Ecosystem Acoustics I

Kenneth G. Foote, Cochair
Woods Hole Oceanographic Institution, Woods Hole, MA 02543, USA

Olav R. Godoe, Cochair
Institute of Marine Research, PO Box 1870, Bergen, 5817, Norway

Invited Papers

4:20

1pAOb1. Ecosystem acoustics: meeting management needs. Olav Rune Godoe (Institute of Marine Research, C. Sundtsgt 64, Nordnes, 5817 Bergen, Norway, olavrune@imr.no)

Marine ecosystems and their exploited resources are often monitored through quasi-synoptic scientific surveys that produce estimates of population characteristics at periodic intervals. Spatial and temporal variability is an integral part of ecosystem function but is often ignored in traditional assessment methodology due to the inability of conventional surveys to resolve and quantify such effects. This confounds estimates of the state of the ecosystem and its main populations and obscures understanding of its dynamics and function. The concept and approach of ecosystem acoustics, which are elaborated and illustrated in this presentation, exploit both active and passive acoustics over their full bandwidth from a range of platforms giving temporal and spatial resolution sufficient for assessing

the state of ecosystems including their main component organisms. Application of new platforms and sensors, as well as combinations of these, is enhancing the power of the approach. Ecosystem acoustics enables observations of marine life to be made on spatial and temporal scales relevant to understanding ecosystem function and assessment of system dynamics and state.

4:40

1pAOb2. Acoustical methods that provide an integrated view of the marine ecosystem. Anne Lebourges-Dhaussy (IRD, Technopole de la Pointe du Diable, BP 70, 29280 Plouzane, France, Anne.Lebourges.Dhaussy@ird.fr), Erwan Josse (IRD, Technopole de la Pointe du Diable, BP 70, 29280 Plouzane, France, Erwan.Josse@ird.fr)

The fish stock assessment are not anymore the sole purpose of the ″fisheries acoustics″ as it appears clearly that the fish belongs to a whole ecosystem, of which functioning mechanisms must be understood to better assess the fish populations' health state. The biotic factors, as prey availability, are of great importance and can be studied also by acoustic tools. The multifrequency systems (echosounders or profilers), increase the size range of the organisms that can be detected; new multibeam sonars provide a high resolution allowing studies close to boundaries. The results of the SIMFAMI European program are presented. It aimed at marine organism classification through multifrequency information, including fish/plankton separation and classification of meso/macroplankton. It provided new methods to classify and describe the various biotic components of the ecosystem from fish to plankton. A link between the use of these new methods and the former micro/mesoplankton classification tools as well as passive acoustic tools allows to reach the classification of a huge range of organisms and to study their interactions. Results of such experiences done on various upwelling ecosystems are shown. Additionally for complex fields, new multibeam sonars can advantageously help in the description of fish distributions.

5:00

1pAOb3. Three-dimensional structure of thin zooplankton layers is impacted by foraging fish. Kelly Benoit-Bird (Oregon State University, 104 COAS Admin Bldg, Corvallis, OR 97333, USA, kbenoit@coas.oregonstate.edu)

The role of predation by fish in the formation and persistence of zooplankton thin layers was assessed from three-dimensional observations using a multibeam sonar attached to a mechanical rotator. Zooplankton in Monterey Bay, CA, USA were found in intense layers with vertical scales of 0.5-2.5 m at night. These features comprised more than 90% of the zooplankton biomass and had volume scattering strengths of up to -35 dB. These thin zooplankton layers showed complex structure with significant though gradual undulations in their depth, thickness, and intensity. Fish spent significantly more time within zooplankton layers than was expected by chance, suggesting concentrated foraging activity. Sonar tracks of individual fish showed them diving through zooplankton layers. These dives were correlated with a decrease in the intensity of zooplankton scattering at the scale of tens of centimeters, resulting in the appearance of holes in the layer. Continued observation of layers revealed that these voids slowly filled in with zooplankton after the fish's departure. At the level of foraging observed, fish can have a significant effect on the distribution of zooplankton layers, however, the layers are resilient to apparent foraging by fish with reformation of the distinct layer often occurring post-predation.

5:20

1pAOb4. Acoustic assessment of trophic dominance in a marine ecosystem. Richard E. Thorne (Prince William Sound Science Center, P.O. Box 705, Cordova, AK 99574, USA, rthorne@pwssc.org), Gary L. Thomas (University of Miami, RSMAS, 4600 Rickenbacker Causeway, Miami, FL 33149, USA, gthomas@rsmas.miami.edu)

High-frequency acoustic surveys over the past 15 years show that the trophic structure in Prince William Sound (PWS), Alaska, functions as a wasp-waist ecosystem. Three dominant biomasses in PWS are: (1) Pacific herring (2) walleye pollock and (3) the large-bodied copepods (Neocalanus spps.) that dominate the spring zooplankton assemblage. The acoustic surveys and associated ecosystem observations suggest that the relative dominance of herring and pollock affects the composition of the apex predators. The near-shore and near-surface distribution of herring provides access by surface-oriented marine mammal and seabird predators, such as sea lions, seals, murres and cormorants, to a crucial winter-period food source. In contrast, the deep, off-shore distribution of the pollock favors large benthic predators, such as demersal sharks, halibut, and flounder. The acoustic surveys also demonstrated that the abundance of large-bodied copepods in PWS is critical to ecosystem productivity, including survival of juvenile pink salmon, and may affect the relative dominance of herring and pollock. An additional outcome of the long-term database on Pacific herring was the discovery of linkages between the 1989 Exxon Valdez oil spill and a subsequent collapse of the herring along with associated predators.

5:40

1pAOb5. Saguenay fjord entrance whale feeding ground: Acoustic study of sill dynamics and tidal aggregation of forage fish. Yvan Simard (Fisheries and Oceans Canada & ISMER-UQAR, 850 route de la Mer, P.O. Box 1000, Mont-Joli, QC G5H-3Z4, Canada, simardy@dfo-mpo.gc.ca), Nathalie Roy (Fisheries and Oceans Canada & ISMER-UQAR, 850 route de la Mer, P.O. Box 1000, Mont-Joli, QC G5H-3Z4, Canada, royn@dfo-mpo.gc.ca), François Saucier (Marine Sciences Institute, University of Québec, 310 Allée des Ursulines, P.O. Box. 3300, Rimouski, QC G5L-3A1, Canada, francois_saucier@uqar.qc.ca), Jacques Gagné (Fisheries and Oceans Canada, 850 route de la Mer, P.O. Box 1000, Mont-Joli, QC G5H-3Z4, Canada, gagneja@dfo-mpo.gc.ca), Samuel Giard (Fisheries and Oceans Canada, 850 route de la Mer, P.O. Box 1000, Mont-Joli, QC G5H-3Z4, Canada, giards@dfo-mpo.gc.ca)

The Saguenay fjord entrance in the St. Lawrence Estuary at Tadoussac is a world famous site where beluga and minke whales can be regularly observed from the coast. Strong tidal upwelling over the shallow sill of the fjord controls the exchanges with the St. Lawrence. In May 2005, an intensive oceanographic and acoustic survey was conducted to understand how the complex 3D hydrodynamics may contribute to concentrating whale preys. High time-space resolution acoustics (38 and 120 kHz split-beam), ADCP (acoustic Doppler current profilers), CTD profiles, plankton and micronekton sampling were used to track the 3D movements of water masses, zooplankton and forage fish. During flood, the dense cold waters that jump over the sill block the Saguenay outflow and subduct into the fjord with their fish and zooplankton content. This complex 3D circulation generates fronts and convergence zones where

biomass is concentrating until current reversal occurs during ebb. These concentrations are then advected and dispersed downstream over the sill with the Saguenay surface plume. This whale prey tidal concentrating process depends on the existence of sufficient forage fish densities in the mesoscale neighbourhood. It is likely at the basis of the persistent high frequentation of this area by whales.

6:00

1pAOb6. Multibeam sonar and echosounder to study schooling behaviour and predator-prey interactions of marine animals. Leif Nøttestad (Institute of Marine Research, Distribution and Trophic Interactions, P.O. Box 1870 Nordnes, N-5817 Bergen, Norway, leif.nottestad@imr.no)

In the past the technological developments and improved spatial and temporal resolution in hydro-acoustics, have made it possible to study schooling and aggregation behaviour of fish and predator-prey interactions in considerable detail. Hydro-acoustic methodology have thus revealed new and interesting scientific findings on animal behaviour and ecology previously difficult to observe and document from the marine environment. A fundamental challenge is still to be able to track individual fish within a school or animal aggregation at the same time as we observe the collective movements. The spatial resolution of hydro-acoustics is usually not sufficient enough to track individual fish within dense aggregations. Underlying mechanisms and motivations of individual animals swimming in aggregations are needed, in order to improve our understanding and predictability of collective behaviour. Improved post-processing programs for quantitative analysis of multi-beam sonar data are also needed. High-resolution underwater cameras, Crittercam-technology and individual tagging will offer complementary data sources to our understanding of detailed behaviour of marine animals. I will present synoptic ecological studies using multi-beam sonar and echosounder on schooling behaviour and predator-prey interactions including fish, seabirds and marine mammals.

6:20

1pAOb7. Acoustic characteristics of vertically migrating and non-migrating organisms observed in the North Pacific Ocean. Kouichi Sawada (Nat. Res. Inst. Fish. Engine., FRA, 7620-7 Hasaki, 314-0408 Kamisu, Japan, ksawada@fra.affrc.go.jp), Hiroki Yasuma (Hokkaido Univ., 3-1-1 Minato-machi, 041-8611 Hakodate, Japan, ANB52615@nifty.com), Taro Ichii (Nat. Res. Inst. Fish. Sci., FRA, 2-12-4 Fukuura, Kanazawa, 235-8648 Yokohama, Japan, ichii@fra.affrc.go.jp), Hideyuki Takahashi (Nat. Res. Inst. Fish. Engine., FRA, 7620-7 Hasaki, 314-0408 Kamisu, Japan, hideyuki@fra.affrc.go.jp), Koki Abe (Nat. Res. Inst. Fish. Engine., FRA, 7620-7 Hasaki, 314-0408 Kamisu, Japan, abec@fra.affrc.go.jp)

Acoustic characteristics of vertically migrating and non-migrating organisms in a day were investigated for species identification. In July 27-30, 2004, both organisms were observed using ship echosounders (38 kHz and 120 kHz) and a tethered acoustic-optical composite system (J-QUEST) from several hours before sunset to several hours after the sunrise, drifting a research vessel, Shunyo-maru, in the North Pacific Ocean. The J-QUEST is an instrumental package composed of an split-beam echosounder (70 kHz) and a stereo TV camera system. The J-QUEST depth was changed from 220 m to 25 m to observe vertical migration. Boreopacific gonate squids were observed by the stereo TV camera and they are considered to conduct diurnal vertical migration to feed migrating organisms. Average TS of the ascending layer and Boreopacific squid were measured in situ using the J-QUEST. Average area scattering strength (SA) values of the ascending layer, non-migrating layer, descending layer, aggregation of Boreo pacific squids, and that of Japanee anchovy were measured at 38 kHz and 120 kHz, There was a constant and different SA difference between the two frequencies at each layer except migrating layer. The ascending and the descending layer have almost the same SA differences. It indicates that the both layers composed of the same organisms.

6:40

1pAOb8. Acoustic GIS-based monitoring of Atlantic cod ecosystems in coastal Newfoundland. George A. Rose (Memorial Univ. of Newfoundland, Marine Inst., 155 Ridge Rd., St. John's, NL A1C5R3, Canada, grose@mi.mun.ca)

Several bays in Newfoundland hold the largest extent groups of overwintering and spawning Atlantic cod (Gadus morhua), and are spawning areas for capelin (Mallotus villosus), the most important forage species. These species co-exist in coastal ecosystems whose physical features and ecological sensitivities restrict monitoring using conventional fisheries methods. Active and passive acoustic methods, acoustic telemetry, oceanographic instrumentation and ROV video have been used to monitor overwintering and spawning distributions and abundance of cod, using mobile and fixed platforms. Cod behaviour is complex and features high mobility both horizontally and vertically, especially during migratory and spawning periods. Overwintering cod have school packing densities $>>1$ fish.m^{-3}. Spawning features increased mobility and vertical structures or ″columns″ of individual fish and sound production captured using stationary hydrophones. Acoustic returns from aquatic vegetation and bottom types have been used to map juvenile habitat. Acoustic telemetry has established the movement patterns of male and female fish during spawning and the homing characteristics of cod as the basis of their stock structure. The movements and spawning behaviour of capelin can also be monitored as can interactions between predators and prey. An experiment using real-time and 3D location telemetry in a comprehensive GIS system will be described.

7:00

1pAOb9. Using multifrequency acoustic scattering techniques to study mixed zooplankton populations. Andone Lavery (Woods Hole Oceanographic Institution, Applied Ocean Physics & Engineering Department, 98 Water Street, MS #11, Woods Hole, MA 02543, USA, alavery@whoi.edu), Peter Wiebe (Woods Hole Oceanographic Institution, Biology Department, 45 Water Street, MS #33, Woods Hole, MA 02543, USA, pwiebe@whoi.edu), Timothy K. Stanton (Woods Hole Oceanographic Institution, Applied Ocean Physics & Engineering Department, 98 Water Street, MS #11, Woods Hole, MA 02543, USA, tstanton@whoi.edu), Gareth Lawson (Stanford University, Hopkins Marine Station, 120 Oceanview Blvd, Pacific Grove, CA 93950, USA, glawson@stanford.edu), Mark Benfield (Louisiana State University, Department of Oceanography & Coastal Sciences, 2179 Energy, Coast & Environment Building, Baton Rouge, LA 70803, USA, mbenfie@lsu.edu), Nancy Copley (Woods Hole Oceanographic Institution, Biology Department, 45 Water Street, MS #33, Woods Hole, MA 02543, USA, ncopley@whoi.edu)

Zooplankton populations can be highly heterogeneous and variable on spatial scales of centimeters to kilometers and temporal scales of minutes to years. High-frequency acoustic scattering techniques allow a synoptic view of zooplankton distribution and abundance on these scales. However, there are well-known complications in the interpretation of acoustic scattering returns, often limiting the inference of quantitative parameters (such as size or abundance) to restricted locations and conditions. Multifrequency and broadband acoustic scattering techniques, combined with sophisticated instrument platforms that combine multiple sensors allowing acoustical, optical, and other environmental measurements, reduce the ambiguities typically associated to the interpretation of acoustic scattering at single frequencies and expand the conditions under which inference of quantitative biological parameters is possible. The focus of this talk is a decade-long study aimed at understanding the distribution and abundance of mixed zooplankton populations in the Gulf of Maine. Simultaneous multifrequency acoustic, optical, environmental, and net measurements were performed. Insights gained from this study are presented together with recent measurements involving broadband acoustic scattering from zooplankton in the presence of nonlinear internal solitary waves. These studies highlight the importance of an integrated approach to understanding heterogeneous zooplankton populations on relevant spatial and temporal scales.

MONDAY AFTERNOON, 30 JUNE 2008 ROOM 352B, 1:00 TO 5:20 P.M.

Session 1pBBa

Biomedical Ultrasound/Bioresponse to Vibration: High-Intensity Focused Ultrasound I

Lawrence A. Crum, Cochair
Center for Industrial and Medical Ultrasound, Applied Physics Lab., University of Washington, 1013 NE 40th St., Seattle, WA 98105, USA

Jean Yves Chapelon, Cochair
INSERM, U556, 151 Cours Albert Thomas, Lyon, 69003, France

Invited Papers

1:00

1pBBa1. The feasibility of local harmonic motion imaging for the guidance and control of focused ultrasound surgery. Kullervo Hynynen (University of Toronto, Sunnybrook Health Sciences Centre, Suite S6 65b, 2075 Bayview Ave, Toronto, ON M4N 3M5, Canada, khynynen@sri.utoronto.ca), Laura Curiel (University of Toronto, Sunnybrook Health Sciences Centre, Suite S6 65b, 2075 Bayview Ave, Toronto, ON M4N 3M5, Canada, lcuriel@sri.utoronto.ca), Rajiv Chopra (University of Toronto, Sunnybrook Health Sciences Centre, Suite S6 65b, 2075 Bayview Ave, Toronto, ON M4N 3M5, Canada, chopra@sri.utoronto.ca)

A local harmonic motion (LHM) can be generated within the tissues by the periodic induction of radiation force using a focused ultrasound (FUS) transducer. Tissue motion can then be tracked by collecting RF signals during the excitation using a separate transducer. Finally, displacement estimates can be obtained by cross-correlating the collected RF signals. The characteristics of the induced LHM depend on the local elastic properties of the tissues making it an attractive tool for imaging and therapy control applications. LHM measurements have been obtained in vivo on rabbit muscle and it was observed that the amplitude of the motion was significantly reduced after coagulation. LHM was successfully used to spatially detect the presence of the coagulation lesions within the tissues as a drop in LHM amplitude. It was also possible to detect the location of an implanted VX2 tumor when a spatial scan was performed as the LHM amplitude was lower inside the tumor because of an increased stiffness. Measurements of LHM during tissue heating using FUS reflected the changes in stiffness and revealed the apparition of coagulation showing the potential of these measurements as an alternative control for the FUS exposure. [Work supported by NIH GrantR33 CA102884 and CRC.]

1:20

1pBBa2. Clinical experiences with extracorporeal Ultrasound-guided high-intensity focused ultrasound treatment for cancer patients. Feng Wu (Chongqing Medical University, Institute of Ultrasound Engineering in Medicine & Clinical Centre for Tumour Therapy, 1 Medical College Road, 400016 Chongqing, China, mfengwu@yahoo.com)

Noninvasive, image-guided tumour thermal ablation with extracorporeal high-intensity focused ultrasound (HIFU) has received increasing interest in the treatment of patients with solid tumours. Since December 1997, an extracorporeal ultrasound-guided HIFU system (Mode-JC, Haifu Technology Co. Ltd., Chongqing, China) has been used to treat approximately 10,000 patients with solid tumours in China, including those of liver, breast, bone, kidney, pancreas, soft tissue, and uterus. The same device has been recently introduced into the UK, Italy, Japan, and South Korea, and so far, more than 1,000 patients have received HIFU treatment outside China. The purpose of this article is to introduce our clinical experiences using extracorporeal, ultrasound-guided HIFU ablation for solid tumours. Five-year follow-up data are observed in patients with primary liver cancer, breast cancer, and osteosarcoma. Among patients treated with HIFU, an extremely low major complication rate is observed. In conclusion, our clinical studies indicate that HIFU treatment is a safe, effective, and feasible modality in the treatment of cancer patients.

1:40

1pBBa3. Adaptive focusing for bone and motion artifacts corrections in High Intensity Focused Ultrasound Therapy. Mickael Tanter (Laboratoire Ondes et Acoustique, ESPCI, Université Paris 7, CNRS, 10 rue Vauquelin, 75005 Paris, France, michael.tanter@espci.fr), Mathieu Pernot (Laboratoire Ondes et Acoustique, ESPCI, Université Paris 7, CNRS, 10 rue Vauquelin, 75005 Paris, France, mathieu.pernot@espci.fr), Jean-François Aubry (Laboratoire Ondes et Acoustique, ESPCI, Université Paris 7, CNRS, 10 rue Vauquelin, 75005 Paris, France, jean-francois.aubry@espci.fr), Mathias Fink (Laboratoire Ondes et Acoustique, ESPCI, Université Paris 7, CNRS, 10 rue Vauquelin, 75005 Paris, France, mathias.fink@espci.fr)

Despite extensive and fast progress of HIFU clinical applications, many issues still need to be addressed. Distortions caused by defocusing obstacles, such as the skull or ribs, on the ultrasonic therapeutic beam are still being investigated. Multi-element transducer technology must be used in order to achieve such transcranial or transcostal adaptive focusing. Second, the problem of motion artifacts, a key component in the treatment of abdominal lesions, has been shown to significantly influence the efficacy and treatment time. Though many methods have been proposed for the detection of organ motion, little work has been done to develop a comprehensive solution including motion tracking and feedback correction in real time. This paper is a review of the work achieved by authors in transcranial HIFU, transcostal HIFU, and motion compensated HIFU. For these three issues, the optimal solution can be reached using the same technology of multi-element transducers devices able to work both in Transmit and Receive modes.

Contributed Papers

2:00

1pBBa4. Using a toroid transducer for thermal ablation by high-intensity-focused ultrasound increases the coagulated volume. David Melodelima (INSERM, U556, 151 Cours Albert Thomas, 69003 Lyon, France, melodelima@lyon.inserm.fr), William N'Djin (INSERM, U556, 151 Cours Albert Thomas, 69003 Lyon, France, ndjin@lyon.inserm.fr), Hubert Parmentier (INSERM, U556, 151 Cours Albert Thomas, 69003 Lyon, France, hubert.parmentier@chu-lyon.fr), Michel Rivoire (Institut de Chirurgie Experimentale - Centre Léon Berard, 28 rue Laennec, 69008 Lyon, France, rivoire@lyon.fnclcc.fr), Jean Yves Chapelon (INSERM, U556, 151 Cours Albert Thomas, 69003 Lyon, France, chapelon@lyon.inserm.fr)

Here, we report that a new design of High Intensity Focused Ultrasound transducer can significantly enlarge the coagulated volume over short periods of time, and that treatment in the liver can be guided in real-time using an integrated ultrasound imaging probe. Eight ultrasound emitters, divided into 256 elements, were created by sectioning a single toroid piezocomposite transducer. The focal zone was conical in shape and located 70 mm from the transducer; enabling the treatment of deep-seated tumors. A single thermal lesion was created when the eight emitters performed alternative and consecutive 5 s ultrasound exposures. This paper presents in vivo evidence that the coagulated volume obtained from a 40 s total exposure in the liver was 7.0 ± 2.5 cm^3 (min 1.5 - max 20.0 cm^3). All lesions were visible with high contrast on sonograms. The correlation between the diameter of lesions observed on sonograms and during gross examination was 92%. This method also allowed the user to easily enlarge the coagulated volume by juxtaposing single lesions. This approach may have a role in treating unresectable colorectal liver metastases and may also be used in conjunction with resection to extend its limits.

2:20

1pBBa5. Temperature measurements and determination of cavitation thresholds during High Intensity Focused Ultrasound (HIFU) Exposures in ex-vivo porcine muscle. Subha Maruvada (U.S. Food and Drug Administration, 10903 New Hampshire Ave., Silver Spring, MD 20993, USA, subha.maruvada@fda.hhs.gov), Yunbo Liu (U.S. Food and Drug Administration, 10903 New Hampshire Ave., Silver Spring, MD 20993, USA, yunbo.liu@fda.hhs.gov), Bruce A. Herman (U.S. Food and Drug Administration, 10903 New Hampshire Ave., Silver Spring, MD 20993, USA, bruce.herman@fda.hhs.gov), William F. Pritchard (U.S. Food and Drug Administration, 10903 New Hampshire Ave., Silver Spring, MD 20993, USA, william.pritchard@fda.hhs.gov), Gerald R. Harris (U.S. Food and Drug Administration, 10903 New Hampshire Ave., Silver Spring, MD 20993, USA, gerald.harris@fda.hhs.gov)

Cavitation in HIFU procedures can yield unpredictable results, particularly when the same location is targeted for more than several seconds. To study this effect, temperature rise was measured in fresh ex-vivo porcine tissue during HIFU exposures. Immediately following euthanasia, a section of back muscle (latissimus dorsi) was resected and a 50 μm diameter fine bare wire thermocouple was placed via needle through the tissue. 825 kHz HIFU was then applied to the tissue focused at the thermocouple junction. Thirty second HIFU exposures of increasing pressure from 1-7.5 MPa were applied and the temperature rise and decay during and after sonication were recorded. B-mode imaging was used to monitor any cavitation activity during sonication. If cavitation was noted during the sonication, the sonication was repeated at the same pressure level two more times at 20 minute intervals in order to characterize the repeatability given that cavitation has occurred. The cavitation threshold of porcine muscle was determined to be between 4 and 7 MPa. Temperature traces obtained at various pressure

levels demonstrated a wide range of heating profiles in fresh ex-vivo tissue due to both the occurrence of cavitation and viscous heating artifacts. (This research was supported by DARPA IAG # 224-05-6016).

2:40

1pBBa6. Therapeutic ultrasound induced cell death from a histological perspective. Andrew Brayman (Center for Industrial and Medical Ultrasound, Applied Physics Lab., University of Washington, 1013 NE 40th St., Seattle, WA 98105, USA, brayman@apl.washington.edu), Peter Kaczkowski (Center for Industrial and Medical Ultrasound, Applied Physics Lab., University of Washington, 1013 NE 40th St., Seattle, WA 98105, USA, peter@apl.washington.edu), Yak-Nam Wang (Applied Physics Laboratory, University of Washington, 1013 NE 40th Street, Seattle, WA 98105, USA, ynwang@apl.washington.edu), Marilee Andrew (Center for Industrial and Medical Ultrasound, Applied Physics Lab., University of Washington, 1013 NE 40th St., Seattle, WA 98105, USA, marilee@apl.washington.edu), Lawrence A. Crum (Center for Industrial and Medical Ultrasound, Applied Physics Lab., University of Washington, 1013 NE 40th St., Seattle, WA 98105, USA, lac@apl.washington.edu),Steven Kargl(Applied Physics Laboratory, University of Washington, 1013 NE 40th Street, Seattle, WA 98105, USA, kargl@troutmask.apl.washington.edu), Gavriel Speyer (Center for Industrial and Medical Ultrasound, Applied Physics Lab., University of Washington, 1013 NE 40th St., Seattle, WA 98105, USA, gavriel@u.washington .edu)

High-power, short-exposure time, High Intensity Focused Ultrasound (HIFU) treatment protocols are under development that offer the potential to increase procedure throughput and optimize individual therapies. Histological examination and optical image analysis of tissues following dynamic HIFU exposure in ex vivo bovine liver have revealed that cells undergo a fundamentally different form of cell death. The rapid temperature rise due to the HIFU exposure leaves the cells structurally intact but no longer viable, similar to the cell ″fixation″ induced by snap-freezing. These results suggest that careful choice of both staining technique and metric for determining cell death are important in quantifying type and morphology of cell ablation, and more broadly, safety and efficacy of treatment. This finding is similar to those obtained and under discussion in the laser and RF ablation communities. Specifically, the NADH staining technique is superior to H&E for assessing cell viability, and an alternative measure of cell death may be preferable to the binary thermal dose threshold currently the standard for HIFU treatment. [Work supported by NIH.]

Invited Papers

3:00

1pBBa7. Ultrasound interstitial applicators for thermal ablation in liver. Cyril Lafon (INSERM, U556, 151 Cours Albert Thomas, 69003 Lyon, France, lafon@lyon.inserm.fr), Rares Salomir (INSERM, U556, 151 Cours Albert Thomas, 69003 Lyon, France, salomir@lyon.inserm.fr), Guillaume Bouchoux (INSERM, U556, 151 Cours Albert Thomas, 69003 Lyon, France, bouchoux@lyon.inserm.fr), Alain Birer (INSERM, U556, 151 Cours Albert Thomas, 69003 Lyon, France, birer@lyon.inserm.fr), Neil Owen (INSERM, U556, 151 Cours Albert Thomas, 69003 Lyon, France, Neil.Owen@lyon.inserm.fr), Eric Delabrousse (INSERM, U556, 151 Cours Albert Thomas, 69003 Lyon, France, delabrousse@lyon.inserm.fr), François Mithieux (INSERM, U556, 151 Cours Albert Thomas, 69003 Lyon, France, mithieux@lyon.fnclcc.fr), Jean Yves Chapelon (INSERM, U556, 151 Cours Albert Thomas, 69003 Lyon, France, chapelon@lyon.inserm.fr)

Aggressive treatment of localized hepatic metastases, by surgery or other means, was proven to be a viable strategy for improving the prognoses of many patients. In that context, thermal ablation by high intensity ultrasound was proposed and used in clinics. However, for treating deep-seated tumors and in most cases, radiofrequency and cryotherapy probes are applied interstitially. Interstitial ultrasound applicators were proposed as an intermediate solution. The treatment can be focused, deeper than with other physical agents, and the transducer can eventually both treat and image tissues. In our experience, two approaches were investigated: percutaneous and intratissular, or endo vascular. The active element was a miniature flat transducer operating at a frequency of 5 MHz, for a satisfactory tradeoff between beam penetration and energy absorption. In vivo trials on a porcine model demonstrated that both procedures are minimally invasive and that large thermal lesions, up to 20 mm deep, can be obtained. Technological improvements such as the use of dual mode transducers (for imaging and therapy) or the performance under MRI guidance allowed monitoring the treatment in real-time.

3:20

1pBBa8. Histotripsy and the developing role of microbubbles in ultrasound therapy. Jeffrey B. Fowlkes (University of Michigan, Department of Radiology, Kresge III, R3320, Ann Arbor, MI 48109-0553, USA, fowlkes@umich.edu)

Microbubbles in therapeutic ultrasound has seen increasing interest in recent years. Once thought to be problematic, bubble production and interactions with ultrasound fields are yielding promising new methods and this presentation will review two areas of collaborative research at the University of Michigan investigating therapeutic applications utilizing microbubbles. Histotripsy uses short pulses of high intensity ultrasound produce cavitation in vivo and subdivide tissue at a subcellular level. The highly localized bubble activity homogenizes tissue to the point of reducing acoustic backscatter enabling lesion detection. Lesion margins are remarkably fine, even yielding fractional disruption of cells. The homogenized material is readily absorbed thus debulking tissue with little residual scar. At the other end of the acoustic intensity scale, microbubbles can be produced by triggering vaporization of superheated liquid droplets, termed acoustic droplet vaporization (ADV). ADV requires diagnostic levels of ultrasound to yield localized microbubbles production. The method is being investigated for direct occlusion therapy and perfusion control to augment other therapeutic methods including drug delivery among other potential applications. These methods highlight the growing field of microbubble-based therapies, which will expand with our increasing understanding of microbubbles and their interactions with surrounding environments. Supported in part by NIH EB00281, HL077629 and EB006476.

3:40-4:00 Break

4:00

1pBBa9. Localization and enhancement of cavitation and heating during HIFU exposure using microparticles of high surface roughness. Manish Arora (University of Oxford, Medical Engineering Unit, 43 Banbury Road, OX2 6PE Oxford, UK, manish.arora@eng.ox.ac.uk), Costas Arvanitis (University of Oxford, Medical Engineering Unit, 43 Banbury Road, OX2 6PE Oxford, UK, costas.arvanitis@eng.ox.ac.uk), Emma Cox (University of Oxford, Medical Engineering Unit, 43 Banbury Road, OX2 6PE Oxford, UK, eflcox@gmail.com), Constantin C. Coussios (University of Oxford, Medical Engineering Unit, 43 Banbury Road, OX2 6PE Oxford, UK, constantin.coussios@eng.ox.ac.uk)

The occurrence of cavitation during HIFU exposure is associated with higher heating rates than in the absence of bubble activity. However, the peak rarefaction pressures required to initiate cavitation in vivo are high (7-10 MPa), making it difficult to localize, sustain, and confine cavitation activity and its associated bioeffects. In this work, we explore the use of rough microparticles to promote and localize cavitation nucleation during HIFU exposures. Polystyrene microparticles of mean diameter ~2 μm are embedded in a polyacrylamide tissue mimicking phantom, which has a high cavitation threshold similar to tissue. The temperature rise during HIFU exposure is measured using an embedded needle thermocouple, whilst cavitation activity is simultaneously monitored using a passive cavitation detector (PCD). The presence of particles is shown to lower the cavitation threshold significantly and, above this threshold, to result in higher heating rates than in the absence of particles for the same focal intensity. Furthermore, it is found that particles make it possible to repeatedly initiate cavitation at the same location and lead to increased broadband noise emissions. Finally, a strong correlation is found between enhanced heating and the broadband emissions arising from inertial cavitation.

4:20

1pBBa10. Local heating by a bubble excited by high intensity focused ultrasound. Wayne Kreider (Center for Industrial and Medical Ultrasound, Applied Physics Lab., University of Washington, 1013 NE 40th St., Seattle, WA 98105, USA, wkreider@u.washington.edu), Michael S. Canney (Center for Industrial and Medical Ultrasound, Applied Physics Lab., University of Washington, 1013 NE 40th St., Seattle, WA 98105, USA, mcanney@u.washington.edu), Michael R. Bailey (Center for Industrial and Medical Ultrasound, Applied Physics Lab., University of Washington, 1013 NE 40th St., Seattle, WA 98105, USA, bailey@apl.washington.edu), Vera A. Khokhlova (Center for Industrial and Medical Ultrasound, Applied Physics Lab., University of Washington, 1013 NE 40th St., Seattle, WA 98105, USA, vera@acs366.phys.msu.ru), Lawrence A. Crum (Center for Industrial and Medical Ultrasound, Applied Physics Lab., University of Washington, 1013 NE 40th St., Seattle, WA 98105, USA, lac@apl.washington.edu)

A current topic of interest for high intensity focused ultrasound (HIFU) treatments involves the relative roles of bubbles and nonlinear acoustic propagation as heating mechanisms. At high amplitudes, nonlinear propagation leads to the generation of boiling bubbles within milliseconds; at lower amplitudes, cavitation bubbles can enhance heating through viscous dissipation, acoustic radiation, and heat conduction. In this context, understanding the physics attendant to HIFU bubbles requires consideration of gas-vapor bubble dynamics, including thermal effects in the nearby liquid. To this end, recent experimental observations with high-speed photography suggest that bubbles undergo a brief period of growth after application of HIFU has stopped. To explain this observation, a model is implemented that couples the thermodynamic state of a strongly driven bubble with thermal conditions in the surrounding liquid. From model simulations, liquid heating in the vicinity of a HIFU bubble is estimated. Calculations suggest that thermal conduction and viscous dissipation can lead to the evolution of a nontrivial thermal boundary layer. Development of a boundary layer that reaches superheated temperatures would explain the aforementioned experimental observation. As such, cavitation bubbles and boiling bubbles share important characteristics during HIFU. [Work supported by NIH DK43881 and NSBRI SMS00402.]

4:40

1pBBa11. Temperature and size-dependence of the vaporization threshold of phase-shift emulsions. Tyrone Porter (Boston University, 110 Cummington Street, Boston, MA 02215, USA, tmp@bu.edu), Peng Zhang (Boston University, 110 Cummington Street, Boston, MA 02215, USA, pzhang@bu.edu)

Acoustic cavitation has proven to be important for several therapeutic applications of ultrasound. However, acoustic cavitation is difficult to initiate and sustain in the absence of cavitation nuclei, particularly in tissue. Phase shift emulsions are ideal candidates for cavitation nuclei for in vivo applications. These emulsions, which consist of superheated liquid perfluorocarbon droplets enclosed by albumin shells, may be vaporized with acoustic pulses, a process known as acoustic droplet vaporization (ADV). In this study, we determined the ADV threshold at 2 MHz as a function of temperature and droplet size. Studies were conducted with micro- and nano-sized emulsions in a closed-flow system immersed in a temperature controlled water bath. The emulsions were injected into a flow system and exposed to high intensity focused ultrasound (HIFU; acoustic parameters: 2 MHz, 10 cycles, 100 Hz pulse repetition frequency). A portable diagnostic ultrasound scanner was used to monitor for vaporization. Upon vaporization, the peak rarefactional pressure of the acoustic pulse and the water bath temperature were recorded. It was determined that the vaporization threshold was independent of droplet size and inversely proportional to temperature. The utility of these emulsions in cancer therapy, particularly for bubble-enhanced heating during HIFU exposure, will be discussed.

5:00

1pBBa12. In vitro evaluation of an oscillating 5-element dual-mode transducer. Neil Owen (INSERM, U556, 151 Cours Albert Thomas, 69003 Lyon, France, Neil.Owen@lyon.inserm.fr), Guillaume Bouchoux (INSERM, U556, 151 Cours Albert Thomas, 69003 Lyon, France, bouchoux@lyon.inserm.fr), Alain Birer (INSERM, U556, 151 Cours Albert Thomas, 69003 Lyon, France, birer@lyon.inserm.fr), Rémi Berriet (Imasonic, Z.A. rue des Savourots, 70190 Voray sur l'Ognon, France, Remi.Berriet@imasonic.com), Jean Yves Chapelon (INSERM, U556, 151 Cours Albert Thomas, 69003 Lyon, France, chapelon@lyon.inserm.fr), Gérard Fleury (Imasonic, 15 rue Alain Savary, 25000 Besançon, France, Gerard.Fleury@imasonic.com), Cyril Lafon (INSERM, U556, 151 Cours Albert Thomas, 69003 Lyon, France, lafon@lyon.inserm.fr)

Miniature dual-mode transducers can be used for minimally invasive treatment of deep-seated tumors. While in contact with the tissue, the transducer guides and monitors localized necrosis. Here, an oscillating 5-element piezo-composite transducer was characterized, and then evaluated in vitro using porcine liver. Each element was 3.0 x 3.8 mm^2 with a geometric cylindrical focus of 14 mm. The transmit frequency was determined by the maximal electro-acoustic efficiency, 65%, which was found at 5.6 MHz. The transmit-receive impulse response was 400 ns long at -6 dB, and the -6 dB fractional bandwidth, centered at 5.6 MHz, was 30%. Axial and lateral resolution measured with a 0.1 mm diameter wire was 0.5 mm and 2.0 mm, respectively. For therapy, all elements radiated simultaneously, and for imaging, independently. Treatment was performed at increments of 20° to form a composite volume of necrosis. At each angle, ultrasound was applied for 60 s at a transducer surface intensity of 15 W/cm^2. Pulse-echo data were recorded while the transducer oscillated over a 180° sector to form images before and after treatment at each angle. Gross examination of lesion size agreed well with echogenic region size in the images. [Supported by ANR and Inserm Post-doctoral Fellowship.]

Session 1pBBb

Biomedical Ultrasound/Bioresponse to Vibration: Quantitative Ultrasound Methods for Diagnosis and Therapy I

Jonathan Mamou, Cochair
Riverside Research Institute, 156 William St., 9th Floor, New York, NY 10038, USA

Geneviève Berger, Cochair
Université Paris 6, Laboratoire d'Imagerie Paramétrique, 15 rue de l'Ecole de médecine, Paris, France

Invited Papers

1:00

1pBBb1. Techniques and modalities for high resolution imaging and assessment of skin with high-frequency ultrasound (20 to 100 MHz). Michael Vogt (Institute of High-Frequency Engineering, Ruhr-University Bochum, IC 6/133, 44780 Bochum, Germany, Michael.Vogt@rub.de), Helmut Ermert (Institute of High-Frequency Engineering, Ruhr-University Bochum, IC 6/133, 44780 Bochum, Germany, Helmut.Ermert@rub.de)

High-frequency ultrasound (HFUS) in the 20 MHz range is routinely used in dermatological diagnosis for morphological skin imaging in order to support the identification of suspicious skin lesions and to evaluate the success of therapies. In this presentation, technical developments for the utilization of higher ultrasound frequencies in the range up to 100 MHz are presented, which allow for high-resolution imaging and assessment of skin structures with an axial resolution down to 10 μm. Furthermore, a new HFUS system for the assessment of elastic skin properties and quantitative strain imaging with 20 MHz ultrasound is presented as a new imaging modality. Also, a reflection-tomography skin imaging concept was implemented with a 20 MHz ultrasound limited-angle spatial compound system, which allows for multi-directional analysis of backscattered and reflected ultrasound waves from different insonation angles. The proposed techniques and modalities have been evaluated by measurements on phantoms and in vivo. Results show that high-resolution qualitative and quantitative skin assessment methods have been successfully implemented. HFUS based strain imaging enables the non-invasive assessment of skin and lesion properties, and HFUS limited-angle spatial compounding allows for improved skin analysis compared to the conventional linear-scan imaging approach.

1:20

1pBBb2. Quantitative intravascular ultrasound elasticity imaging as an imaging biomarker in clinical trials. Ton Van Der Steen (Thorax centre ErasmusMC, Ee23.02, pobox 2040, 3000 CA Rotterdam, Netherlands, a.vandersteen@erasmusmc.nl), Johannes A. Schaar (Biomedical Engineering, Erasmus MC, P.O. Box 2040, 3000 CA Rotterdam, Netherlands, j.schaar@erasmusmc.nl), Frits Mastik (Biomedical Engineering, Erasmus MC, P.O. Box 2040, 3000 CA Rotterdam, Netherlands, f.mastik@erasmusmc.nl), Hector Garcia (Biomedical Engineering, Erasmus MC, P.O. Box 2040, 3000 CA Rotterdam, Netherlands, HGarcia@cardialysis.nl), Mike Danilouchkine (Biomedical Engineering, Erasmus MC, P.O. Box 2040, 3000 CA Rotterdam, Netherlands, m.danilouchkine@erasmusmc.nl), Radj Baldewsing (Biomedical Engineering, Erasmus MC, P.O. Box 2040, 3000 CA Rotterdam, Netherlands, radj.baldewsing@hewitt.com), Patrick W. Serruys (Biomedical Engineering, Erasmus MC, P.O. Box 2040, 3000 CA Rotterdam, Netherlands, p.w.j.c.Serruys@erasmusmc.nl)

The composition and morphology of an atherosclerotic lesion are currently considered more important determinants of acute coronary ischemic syndromes that the degree of stenosis. When a lesion is unstable, it can rupture and cause an acute thrombotic reaction. An unstable plaque can be characterized by a lipid core that is covered by a thin fibrous cap, which has been locally weakened by inflammatory cells. Intravascular Ultrasound Palpography is an intravascular ultrasound based technique that is capable to measure the local strain in coronaries and atherosclerotic plaque. This strain is induced by varying intraluminal pressure. This lecture will show principles of the technology and how this technology is used in clinical trials. Results from a trial with traditional lipid lowering treatment (IBIS1) and from a trial on the efficacy of a new medication (IBIS2) will be presented. Furthermore the potential of Intravascular Ultrasound Modulography will be discussed. This work is financially supported by the Dutch Technology Foundation, The Dutch Heart Foundation and a research grants from Volcano Corporation and Glaxo Smith Kline

1:40

1pBBb3. Recent progress of acoustic microscopy for medicine and biology. Yoshifumi Saijo (Tohoku University, 4-1 Seiryo-machi, Aoba-ku, 980-8575 Sendai, Japan, saijo@idac.tohoku.ac.jp), Kazuto Kobayashi (Honda Electronics Co. Ltd., 20 Oyamazuka, Oiwa-cho, 441-3193 Toyohashi, Japan, kazuto@honda-el.co.jp), Takahiro Iwamoto (Tohoku University, 4-1 Seiryomachi, Aoba-ku, 980-8575 Sendai, Japan, iwamoto@yoshizawa.ecei.tohoku.ac.jp), Nagaya Okada (Honda Electronics Co. Ltd., 20 Oyamazuka, Oiwa-cho, 441-3193 Toyohashi, Japan, nagaya@honda-el.co.jp), Akira Tanaka (Fukushima University, 1 Kanayagawa, 960-1296 Fukushima, Japan, a-tanaka@sss.fukushima-u.ac.jp), Naohiro Hozumi (Aichi Institute of Technology, 1247 Yachigusa, Yakusa-cho, 470-0392 Toyota, Japan, hozumi@aitech.ac.jp)

Dramatic shortening of the calculation time provided by the recent progress of the computer technology has made biomedical researchers possible to assess nonlinear acoustic phenomena in soft materials which had been assumed as acting linearly. Besides, the spread of Windows-based personal computer and peripheral devices enabled easier and cheaper configuration of the whole acoustic microscope system such as pulse generation, analogue/digital conversion, mechanical scanning and image processing. According to

these progresses, conventional acoustic microscopy with only C-mode imaging has widened its data acquisition mode to B-mode, C-mode, surface acoustic impedance mode, and three-dimensional (3D) imaging. The base of our acoustic microscope system was consisted of (1) PVDF transducer with the central frequency of 100 MHz, (2) ultrasonic pulser made of high speed semiconductor switching, (3) mechanical scanner using two linear servo motors, (4) high speed PCI card digitizer with the sampling frequency of 2 GHz, and (5) personal computer controlling the whole system. For skin imaging, 3D imaging of the fingerprint was reconstructed by consecutive B-mode imaging. Surface acoustic impedance imaging of the fingerprint can be obtained by just putting a finger on a thin plastic plate of the transducer. Conventional C-mode imaging of thinly sliced skin sample presented quantitative values of thickness, attenuation and sound speed of the tissue.

2:00

1pBBb4. Improved cancer detection and classification using multi-parameter quantitative ultrasound. Michael L. Oelze (University of Illinois at Urbana-Champaign, Beckman Institute, 405 N Mathews, Urbana, IL 61801, USA, oelze@uiuc.edu), William D. O'Brien, Jr. (University of Illinois at Urbana-Champaign, Beckman Institute, 405 N Mathews, Urbana, IL 61801, USA, wdo@uiuc.edu)

Quantitative ultrasound (QUS) has been used successfully to differentiate benign from malignant solid tumors in animal models of breast cancer. In these studies, QUS made use of estimates of average scatterer diameter (ASD) and average acoustic concentration (AAC) from the ultrasonic backscatter. However, initial attempts to classify different kinds of malignant tumors based on ASD and AAC estimates were not successful. New models for ultrasonic backscatter were created by considering the cytoskeletal structure of cells. In addition, the homodyned K distribution was used to model the amplitude of the envelope from regions-of-interest in the malignant tumors. The homodyned K distribution yielded two parameters: the S parameter, which quantified the randomness of scatterer spacings, and the β parameter, which quantified the amount of clustering of scatterers in the interrogated tissue. Statistically significant differences ($P < 0.05$) were observed between average S and β parameters from the malignant tumors. Furthermore, statistically significant differences ($P < 0.05$) were observed between ASD and AAC estimates from the malignant tumors using the new scattering models at ultrasonic frequencies above 16 MHz. The use of four parameters, as opposed to two, improved the ability to uniquely classify different kinds of malignant tumors. [Supported by NIH R01CA111289.]

2:20

1pBBb5. Modeling scattering from cells and biological structures. Michael C. Kolios (Ryerson University, Department of Physics, 350 Victoria Street, Toronto, ON M5B2K3, Canada, mkolios@ryerson.ca), Gregory J. Czarnota (Sunnybrook Health Sciences Centre, Department of Radiation Oncology and Imaging Research, 2075 Bayview Ave, T2-Wing, Toronto, AB M4N 3M5, Canada, Gregory.Czarnota@sunnybrook.ca)

The goal of ultrasonic tissue characterization is to extract information over and above the information conventionally displayed on imaging instruments which is typically the backscatter strength (B-mode image). The driving hypothesis of our work is that as the ultrasound wavelength approaches the size of a cell, the backscatter characteristics become more sensitive to the cells' physical attributes (size, structure, and composition) and changes in the cell structure due to therapeutic intervention. A better understanding of the interaction of acoustic waves with cells is required to interpret the backscatter data. An overview of our efforts to model scattering from individual cells, cell ensembles, and in-vivo cancer will be presented. Theoretical results will be presented comparing scattering from individual cells with experimental data from a variety of cells in suspension, cell ensembles with pellets (compact aggregates of cells) and in-vivo tumors. It will be shown that for the tumors we have studied there is a very good correlation of scattering characteristics between cell pellets and in-vivo tumors, indicating that in the tumors studied cell structure was the factor that dominated the scattering response. The goal of this work is to use quantitative ultrasound methods for diagnosis and monitoring the response to therapy.

2:40

1pBBb6. Estimation of heterogeneity of scatterer densities for diagnosis of liver fibrosis. Tadashi Yamaguchi (Research C. for Frontier Med. Eng., Chiba University, 1-33 Yayoicho, Inageku, 263-8522 Chiba, Japan, yamaguchi@faculty.chiba-u.jp), Hiroyuki Hachiya (Dept. of Mech. and Cntr. Eng., Tokyo Inst. of Tech., 2-12-1 Ookayama, Meguroku, 152-8550 Tokyo, Japan, hachiya@ctrl.titech.ac.jp)

In the quantitative diagnosis using ultrasound, existence of the high or low echo which was indistinguishable from speckle serves as an index of diagnosis. In this study, we tried to clarify the relation between the scattering condition in the tissue and the probability density function of echo amplitude. Parameters to estimate the scattering condition were derived by Q-Q probability plot at computer simulation models and the clinical data of liver fibrosis. In the simulation model of heterogeneous medium, the result of Q-Q plot became a curve and the curvature was dependent on the difference of the scatterer density of two intermingled media. In the clinical data of liver fibrosis, curvature was large when many fibers were contained. On the other hand, curvature was small when cysts or minute blood vessels were intermingled in the speckle and the whole distribution function was able to be approximated by k-distribution. Moreover, the crooked point of the Q-Q plot was changed depending on the scatterer density of a mixture part. These results show that the mixture rate and scatterer distributions of two different distribution functions can be recognized parametrically in the liver in which minute diseased tissue was intermingled.

3:00

1pBBb7. Noninvasive temperature estimation using diagnostic ultrasound: In vivo results. Dalong Liu (University of Minnesota, 200 Union St SE, Rm 4-174 EECS Bldg, Minneapolis, MN 55455, USA, liuxx293@umn.edu), Ajay Shrestha (University of Minnesota, 200 Union St SE, Rm 4-174 EECS Bldg, Minneapolis, MN 55455, USA, ajay@ece.umn.edu), Rachana Visaria (University of Minnesota, 200 Union St SE, Rm 4-174 EECS Bldg, Minneapolis, MN 55455, USA, visar001@umn.edu), John Bischof (University of Minnesota, 200 Union St SE, Rm 4-174 EECS Bldg, Minneapolis, MN 55455, USA, bischof@umn.edu), Emad S. Ebbini (University of Minnesota, 200 Union St SE, Rm 4-174 EECS Bldg, Minneapolis, MN 55455, USA, emad@umn.edu)

In this paper, we present temperature imaging data obtained before and after HIFU-induced lesions in implanted tumors in the hind limb of nude mice in vivo. The RF data was acquired using a 9 MHz 192-element linear probe on a diagnostic scanner at 90 frames per second. Approximately 2 s of frame data was collected before, during and after sub-therapeutic exposures of 0.2 s duration. The frame rates were sufficiently high to capture the effects of local tissue deformation due to breathing and pulsation near blood vessel. Using a physics-based spatial-temporal filtering of tissue displacement, we were able to produce accurate spatial-temporal maps of the temperature change with fine spatial and temporal resolution. These results are in good agreement with directly measured temperatures using fine temperature sensors near the HIFU focal spot. The results show that robust temperature estimation in the presence of tissue motion/deformation is feasible. Applications of this method in measuring the local thermal properties of tissue will be addressed. In particular, tissue absorption can be estimated and it appears to increase by a factor of 2 - 4 after lesion formation.

3:20

1pBBb8. Transient elastography: changing clinical practice in hepatology. Laurent Sandrin (Echosens, R&D department, 153 avenue d'Italie, 75013 Paris, France, laurent.sandrin@echosens.com), Sylvain Yon (Echosens, R&D department, 153 avenue d'Italie, 75013 Paris, France, sylvain.yon@echosens.com), Céline Fournier (Echosens, R&D department, 153 avenue d'Italie, 75013 Paris, France, celine.fournier@echosens.com), Veronique Miette (Echosens, R&D department, 153 avenue d'Italie, 75013 Paris, France, veronique.miette@echosens.com)

Transient elastography is one of several new approaches that have recently been proposed to manage liver diseases. This quantitative method is used in clinical practice to assess liver fibrosis noninvasively and rapidly. The technique consists in generating low-frequency elastic shear waves through the liver and measuring their velocity using ultrafast pulse-echo ultrasound acquisition. Liver stiffness is directly related to shear waves velocity. Nowadays more than 400 devices (Fibroscan®, Echosens, Paris, France) are being used worldwide in clinical practice. Studies reported a strong correlation between liver stiffness and the fibrosis stage obtained by liver biopsy in patients with chronic liver diseases: hepatitis B and/or C, HCV co-infection, HIV, alcoholism, etc. Stiffness measurements obtained using transient elastography are in good agreement with measurements performed using other elastography techniques (magnetic resonance elastography and radiation force). Main limitations of transient elastography are related to the morphology of the patients. Examinations may be difficult or impossible in overweighted to obese patients and in children. New probes have been developed for children and obese patients. Using these probes and dedicated measurement procedures the performance of transient elastography is significantly improved. The development of transient elastography currently focuses on heterogeneous stiffness measurement.

3:40-4:00 Break

Contributed Papers

4:00

1pBBb9. Transient elastography in heterogeneous tissues. Cécile Bastard (Echosens, R&D department, 153 avenue d'Italie, 75013 Paris, France, cecile.bastard@echosens.com), Jennifer Oudry (Echosens, R&D department, 153 avenue d'Italie, 75013 Paris, France, jennifer.oudry@echosens.com), Yassine Mofid (Echosens, R&D department, 153 avenue d'Italie, 75013 Paris, France, mofid@echosens.com), Laurent Sandrin (Echosens, R&D department, 153 avenue d'Italie, 75013 Paris, France, laurent.sandrin@echosens.com)

The Fibroscan® (Echosens, Paris, France) is a transient elastography based device used to quantify liver fibrosis by following the propagation of a low frequency shear wave and measuring the mean Young's modulus of the liver. This device has been successfully applied to homogeneous tissues such as liver in patients with chronic hepatitis C. Current developments in transient elastography are now headed toward the characterization of heterogeneous tissues. The estimation of the shear wave velocity can be achieved by solving the elastic wave equation taking into account either the 1D, the 2D, or the 3D components of the displacement spatial derivatives. The objective of this study is to characterize focal nodules in human liver and to quantify heterogeneous fibrosis. We present the methods used to estimate the local shear wave velocity and the results of experiments conducted on heterogeneous phantoms and in the liver in vivo.

4:20

1pBBb10. Improvements in liver diseases evaluation using transient elastography for obese patients. Magali Sasso (Echosens, R&D department, 153 avenue d'Italie, 75013 Paris, France, magali.sasso@echosens.com),Veronique Miette(Echosens, R&D department, 153 avenue d'Italie, 75013 Paris, France, veronique.miette@echosens.com), Laurent Sandrin (Echosens, R&D department, 153 avenue d'Italie, 75013 Paris, France, laurent.sandrin@echosens.com)

Transient elastography (Fibroscan®, Echosens, Paris, France) is a non invasive and rapid technique used to assess liver fibrosis by measuring liver stiffness. Clinical interest of liver stiffness measurement using Fibroscan® has been demonstrated for chronic liver diseases in adult patients. Clinically, the liver stiffness evaluation can be tricky in obese patients due to their large subcutaneous fat thickness. Obesity is a growing public health concern which requires dedicated liver evaluation procedures due to the patients' morphology and/or the specific diseases associated with obesity. Our study aims to show how Fibroscan® can adapt for liver diseases evaluation in obese patients. Clinical adaptations dedicated to over-weighted patients are shown: ultrasound guidance procedure, development of a dedicated probe for patients with a large subcutaneous fat thickness, development of new algorithms based on attenuation of both ultrasonic and shear waves. Performance is assessed and clinical interest of each adaptation is discussed in over-weighted, obese and morbid obese patients (body mass index greater than 25). These new procedures dedicated to obese patients improve liver diseases assessment using Fibroscan®.

4:40

1pBBb11. Towards the modeling of high-frequency ultrasound scattering from cells. Omar Falou (Ryerson University, Department of Physics, 350 Victoria Street, Toronto, ON M5B2K3, Canada, ofalou

@ryerson.ca),J. Carl Kumaradas(Ryerson University, Dept. of Physics, 350 Victoria Street, Toronto, ON M5B 2K3, Canada, ckumarad@ryerson.ca), Michael C. Kolios (Ryerson University, Department of Physics, 350 Victoria Street, Toronto, ON M5B2K3, Canada, mkolios@ryerson.ca)

High-frequency ultrasound is a novel method to detect cell death based on changes in cell morphology that cause alterations in the acoustic properties of cell ensembles in tissues. In previous work, our group has suggested that for cells with a nucleus to cell volume ratio of 0.33, the backscatter response from single cells was best modeled as a fluid sphere. However, for cells with a larger nucleus, neither the fluid nor the elastic sphere models showed a good agreement. We hypothesize that cells with a large nucleus ratio ($>$ 0.33) may be modeled as an elastic sphere surrounded by a fluid shell. In this work, the backscatter response from non-nucleated cells (Strongylocentrotus purpuratus oocytes) was measured Experimental RF lines were acquired using the VisualSonics VS40B ultrasound biomicroscope using 20 and 40 MHz transducers. A finite-element model of wave propagation was developed to solve high-frequency ultrasound scattering from spheres. A very good agreement was found suggesting that the cytoplasm of the oocytes is of fluid nature. Finally, a finite-element model treating the cells as having an elastic nucleus surrounded by a fluid shell is compared to experimental measurements. The implications of these findings on the prediction of ultrasound backscatter from cells are discussed.

5:00

1pBBb12. High-frequency quantitative ultrasound imaging methods for human lymph nodes characterization ex vivo. Jonathan Mamou (Riverside Research Institute, 156 William St., 9th Floor, New York, NY 10038, USA, mamou@rrinyc.org), Alain Coron (Université Paris 6, Laboratoire d'Imagerie Paramétrique, 15, rue de l'Ecole de Médecine, 75006 Paris, France, alain.coron@lip.bhdc.jussieu.fr), Masaki Hata (J. A. Burns School of Medicine, 405 N. Kuakini Street, Honolulu, HI 96817, USA, masakihata4999@yahoo.co.jp), Junji Machi (J. A. Burns School of Medicine, 405 N. Kuakini Street, Honolulu, HI 96817, USA, junji@hawaii.edu), Eugene Yanagihara (J. A. Burns School of Medicine, 405 N. Kuakini Street, Honolulu, HI 96817, USA, kplety@earthlink.net), Pascal Laugier (Université Paris 6, Laboratoire d'Imagerie Paramétrique, 15, rue de l'Ecole de Médecine, 75006 Paris, France, laugier@lip.bhdc.jussieu.fr), Ernest J. Feleppa (Riverside Research Institute, 156 William St., 9th Floor, New York, NY 10038, USA, feleppa @rrinyc.org)

High-frequency ($>$15 MHz, i.e., wavelength $<$100 μm) ultrasound has the potential to characterize biological tissues quantitatively at the microscopic level. In this study, quantitative ultrasound (QUS) methods were developed to evaluate freshly excised human lymph nodes from patients with possible metastatic cancer. The objectives were to improve detection of small but clinically significant lymph-node metastases that often are missed during routine histological evaluation. Three-dimensional (3D) ultrasound data acquisition was conducted on freshly excised nodes using a spherically-focused transducer with a center frequency of 21 MHz. Average scatterer sizes and acoustic concentrations were estimated using QUS methods with a Gaussian scattering model over a bandwidth extending from 11 to 27 MHz. Strategies were developed to recover lymph-node orientation and size after histological sectioning to allow for spatially matching QUS estimates to histology. The signal- and image-processing aspects of QUS estimation are presented and the preliminary results are shown that demonstrate our ability to acquire 3D ultrasound and histological data, to co-register them spatially, and to obtain scatterer-size and acoustic-concentration estimates for specific tissue types (cancer versus non-cancer) within the nodes. In future studies, these QUS estimates will be used to identify histologically difficult-to-detect micrometastases in lymph-nodes. [Supported by NIH R01CA100183.]

5:20

1pBBb13. Extraction of the multiple scattering contribution in weakly scattering media: Application to human soft tissues. Alexandre Aubry (Laboratoire Ondes et Acoustique, ESPCI, Université Paris 7, CNRS, 10 rue Vauquelin, 75005 Paris, France, alexandre.aubry@espci.fr), Arnaud Derode (Laboratoire Ondes et Acoustique, ESPCI, Université Paris 7, CNRS, 10 rue Vauquelin, 75005 Paris, France, arnaud.derode@ujf-grenoble.fr), Mickael Tanter (Laboratoire Ondes et Acoustique, ESPCI, Université Paris 7, CNRS, 10 rue Vauquelin, 75005 Paris, France, michael.tanter@espci.fr)

Waves scattered by a weakly scattering random medium contain a predominant single scattering contribution as well as a multiple scattering contribution which is usually neglected. But its investigation can be fruitful for characterization purposes because it provides measurements of statistical parameters such as the scattering mean free path. Our aim is to extract the multiple scattering contribution in a weakly scattering random medium. The experimental set up consists in an array of programmable transducers placed in front of the sample. The impulse responses between each couple of transducers are measured and form the interelement matrix. Our technique allows the extraction of multiple scattering signals by taking advantage of their randomness, contrary to single scattering contributions which are shown to exhibit a deterministic coherence along the antidiagonals of the array response matrix, whatever the distribution of scatterers. To illustrate the interest of this technique, we applied it to a synthetic medium (Agar gel) and to breast tissues. Surprisingly, the multiple scattering contribution is far from negligible in the breast around 4.3 MHz. The temporal evolution of its intensity can provide a new tool to complete information provided by standard echography; it also constitutes an experimental test of the Born approximation.

5:40

1pBBb14. Ultrasonic vibrometer for tissue characterization. James S. Martin (Georgia Institute of Technology, Mechanical Engineering, 771 Ferst Drive, Atlanta, GA 30332-0405, USA, james.martin@me.gatech.edu), Peter H. Rogers (Georgia Institute of Technology, Mechanical Engineering, 771 Ferst Drive, Atlanta, GA 30332-0405, USA, peter.rogers@me.gatech.edu), Michael D. Gray (Georgia Institute of Technology, Mechanical Engineering, 771 Ferst Drive, Atlanta, GA 30332-0405, USA, michael.gray@me.gatech.edu)

Ultrasonic vibrometers are well suited to a variety of tissue-characterization tasks because they exploit the lateral resolution and depth of field available with diagnostic ultrasound systems for measurements at lower frequencies. In the past, ultrasonic vibrometers have been used to measure the motion of surfaces with high impedance contrast to their surroundings (otoliths, swim bladders, and lung tissue). New ultrasonic vibrometry techniques have been developed and tested that permit calibrated real-time (amplitude and phase) transduction of sub-nanometer-amplitude vibrations at audio frequencies. These can be configured using either analog or digital demodulation for carrier signals up to 10 MHz. In the fully digital configuration, the vibrometer offers better displacement resolution than has been previously reported for analog systems. It also has the capability to simultaneously distinguish between the displacements of multiple discrete vibrating scatterers or regions within a continuum of scatterers by exploiting a multi-sine carrier signal. Individual vibrating targets are separated by pulse compression and windowing. This reduces the problem of carrier drop-out or speckle noise that occurs when multiple reflections destructively interfere at the receiver of a narrow-band signal. The technique should permit the vibrometer a depth resolution comparable a typical pulse-echo ultrasound system. [Work supported by ONR.]

6:00

1pBBb15. An acoustic technique for mapping and sizing particles following needle-free transdermal drug and vaccine delivery. Jamie Condliffe (University of Oxford, Medical Engineering Unit, 43 Banbury

Road, OX2 6PE Oxford, UK, jamie.condliffe@magd.ox.ac.uk),Heiko Schiffter (University of Oxford, Medical Engineering Unit, 43 Banbury Road, OX2 6PE Oxford, UK, heiko.schiffter@eng.ox.ac.uk), Constantin C. Coussios (University of Oxford, Medical Engineering Unit, 43 Banbury Road, OX2 6PE Oxford, UK, constantin.coussios@eng.ox.ac.uk)

Needle-free ballistic particle injection enables painless transdermal delivery of pharmaceuticals. To improve the efficacy of this technique, a non-invasive method of assessing particle penetration depth, distribution and changes in particle size following injection is required. Polydisperse distributions of polystyrene particles, mean diameter 25 μm, and insulin particles, mean diameter 44 μm, were injected into both tissue-mimicking phantoms and porcine skin, which they penetrate to a mean depth of 300 μm. Following injection, the surface of the targets was scanned using a 50 MHz focused ultrasound transducer driven in pulse-echo mode. The received waveforms were post-processed to estimate particle penetration depth and distribution in the plane perpendicular to injection. The targets were then sectioned and optical microscopy was used to validate the acoustic results. Furthermore, computational implementation of an exact solution for sound scattering by an elastic sphere allows prediction of the frequency response of the insonified particles. Direct comparison of the theoretical model with the frequency content of experimental data is shown to provide an accurate means of estimating particle size, and is being extended to correlating particle size with penetration depth. The acoustic technique shows great promise as a non-invasive means of mapping, sizing, and assessing stability of drug particles following needle-free injection.

6:20

1pBBb16. Noninvasive vascular ultrasound elastography of carotid arteries for stroke prevention. Guy Cloutier (Laboratory of Biorheology and Medical Ultrasonics, University of Montreal Hospital Research Center, 2099 Alexandre de Sève (room Y-1619), Montreal, QC H2L 2W5, Canada, guy.cloutier@umontreal.ca), Roch Maurice (Laboratory of Biorheology and Medical Ultrasonics, University of Montreal Hospital Research Center, 2099 Alexandre de Sève (room Y-1619), Montreal, QC H2L 2W5, Canada, maurice.roch.chum@ssss.gouv.qc.ca), Elizabeth Mercure (Laboratory of Biorheology and Medical Ultrasonics, University of Montreal Hospital Research Center, 2099 Alexandre de Sève (room Y-1619), Montreal, QC H2L 2W5, Canada, elizabeth.mercure@UMontreal.CA), Marie-France Giroux (Department of Radiology, University of Montreal Hospital, 1560 Sherbrooke Est, Montreal, QC H2L 4M1, Canada, m_fgiroux@videotron.ca), Gilles Soulez (Department of Radiology, University of Montreal Hospital, 1560 Sherbrooke Est, Montreal, QC H2L 4M1, Canada, gilles.soulez.chum@ssss.gouv.qc.ca)

Carotid plaque rupture leading to stroke involves alteration of arterial wall mechanical properties. This paper addresses reproducibility and potential clinical impact of non-invasive vascular elastography. Fifteen symptomatic and 15 asymptomatic patients with greater than 50% stenoses of their internal carotids, and 15 control subjects were scanned independently by two radiologists. Radio-frequency cine-loops were acquired on left and right common and proximal internal carotids. For control subjects, homogeneous strains with successive compression and dilatation of the vascular wall from systole to diastole and few shear patterns were observed. The axial strain did not differ between recording sites, sides and radiologists (ANOVA, $p > 0.19$). For patients, heterogeneous axial strain patterns with both compression and dilatation of tissues within plaques were noted along with shear concentrations at interfaces of tissue structures. Despite similar blood pressures, larger mean instantaneous axial strains were measured in symptomatic ($1.5 \pm 0.6\%$) versus asymptomatic ($1.2 \pm 0.5\%$) patients in systole for common carotids (t-test, $p < 0.02$). To conclude, reproducible results were obtained for control subjects and in patients, larger axial strains in common carotids may be associated with plaque rupture. This new imaging method may become a unique approach to characterize vulnerable plaques for stroke prevention.

6:40

1pBBb17. ANAIS: An ultrasound mammograph. Serge Mensah (Laboratory for Mechanics and Acoustics CNRS, 31 chemin Joseph Aiguier, 13009 Marseille, France, mensah@lma.cnrs-mrs.fr), Philippe Lasaygues (Laboratory for Mechanics and Acoustics CNRS, 31 chemin Joseph Aiguier, 13009 Marseille, France, lasaygues@lma.cnrs-mrs.fr), Eric Debieu (Laboratory for Mechanics and Acoustics CNRS, 31 chemin Joseph Aiguier, 13009 Marseille, France, debieu@lma.cnrs-mrs.fr), Emilie Franceschini (CNRS - LMA, 31 Chemin Joseph Aiguier, 13009 Marseille, France, franceschini@lma.cnrs-mrs.fr)

It is well established that ultrasonography is a cost-effective, patient-friendly imaging modality available for breast imaging. The main aim of this paper is concerned with a tomographic ultrasound mammograph allowing 3D-reconstruction of the uncompressed breast immersed in a water tank. The scanner, based on a 1024 semi-circular motorized antenna, provides more efficient way to view anatomical ductal structures of the breast. Quantitative volume parameter cartography is the unique means to make objective, reproducible, and operator-independent diagnoses (Computer Aided Diagnosis). The recovery of quantitative acoustical parameters requires solving a nonlinear inverse scattering problem from large amount of measurements. This is achieved using advanced computing resources; a front-end acquisition system based on $32*1024$ multiplexed channels and specific reconstruction procedures. The objective is not only to offer a multiparameter tissue characterization using reflection and transmission measurements but also to provide a systemic inspection of the ductal tree.

7:00

1pBBb18. A reflex transmission method for ultrasound thermometry. Caleb H. Farny (Harvard Medical School, Focused Ultrasound Lab - BWH Radiology, 221 Longwood Ave RM 521, Boston, MA 02115, USA, cfarny@bwh.harvard.edu), Gregory Clement (Harvard Medical School, Focused Ultrasound Lab - BWH Radiology, 221 Longwood Ave RM 521, Boston, MA 02115, USA, gclement@hms.harvard.edu)

It is of great interest to develop ultrasound-based thermal imaging for monitoring thermal ablation procedures and as a tissue characterization technique. A phase contrast analysis for temperature mapping has been investigated, based on the temperature dependence of sound speed of water and tissue. The method employs reflex transmission imaging principles, planar projection and tomographic reconstruction techniques, for interrogating a region featuring a temperature contrast. Through-transmission and pulse-echo configurations were both used to image phase contrasts caused from a change in sound speed, in experimental measurements and numerical simulations. Tissue phantoms were used as a medium in which to create a steady-state sound speed contrast, and a raster scan was performed to acquire the sound field with a hydrophone. Two scans were acquired, a reference sound field and a scan featuring a phase contrast which corresponded to a 7 - 10°C peak temperature rise. The through-transmission configuration employed a 0.2-mm diameter needle hydrophone, while the pulse-echo measurement employed a custom-built thin-wire hydrophone to acquire the sound field between the interrogation transducer and tissue phantom. The method successfully located the location and amplitude of the phase contrast, and future steps necessary for tracking dynamic temperature changes will be discussed.

Session 1pBBc

Biomedical Ultrasound/Bioresponse to Vibration and Engineering Acoustics: High-Intensity Focused Ultrasound Metrology and Standards I

Peter Kaczkowski, Cochair
Center for Industrial and Medical Ultrasound, Applied Physics Lab., University of Washington, 1013 NE 40th St., Seattle, WA 98105, USA

Gail Ter Haar, Cochair
Institute of Cancer Research, 15 Cotswold Road, Belmont, Sutton, Surrey, SM2 5NG, UK

Invited Papers

5:40

1pBBc1. On the need for basic theoretical, numerical, and experimental research in the development of useful standards for focused ultrasound therapy. Peter Kaczkowski (Center for Industrial and Medical Ultrasound, Applied Physics Lab., University of Washington, 1013 NE 40th St., Seattle, WA 98105, USA, peter@apl.washington.edu), Michael R. Bailey (Center for Industrial and Medical Ultrasound, Applied Physics Lab., University of Washington, 1013 NE 40th St., Seattle, WA 98105, USA, bailey@apl.washington.edu), Vera A. Khokhlova (Center for Industrial and Medical Ultrasound, Applied Physics Lab., University of Washington, 1013 NE 40th St., Seattle, WA 98105, USA, vera@acs366.phys.msu.ru), Oleg A. Sapozhnikov (Center for Industrial and Medical Ultrasound, Applied Physics Lab., University of Washington, 1013 NE 40th St., Seattle, WA 98105, USA, oleg@acs366.phys.msu.ru)

High intensity focused ultrasound (HIFU) is rapidly gaining widespread clinical use in China, and is undergoing regulatory evaluation in Europe and the US for many target diseases. There is rising concern within the HIFU community that no standards exist for measuring or reporting of HIFU fields, inhibiting broad clinical adoption of HIFU. This paper addresses current technical gaps for the development of such standards. High power and strong focusing combine to make accurate measurements of focal fields difficult. No simple way exists to extrapolate in-water field measurements directly to patients, and thus to calculate temperature rise and therapeutic dose in tissue. To arrive at a set of characteristic parameters for HIFU systems that are both clinically relevant and are practical to measure reliably, we believe several avenues of research are needed. Numerical models that include nonlinear acoustic propagation must be carefully validated with experiments, and both numerics and experimental methods must be standardized for broad dissemination. Mechanisms of enhanced tissue heating due to nonlinear effects must be experimentally quantified, and robust accurate models developed. These advances in understanding must be transitioned into practical recommendations for standard metrics and methodologies to facilitate industrial development and regulatory oversight.

6:00

1pBBc2. A method of HIFU field characterization in water and deration to tissue. Vera A. Khokhlova (Center for Industrial and Medical Ultrasound, Applied Physics Lab., University of Washington, 1013 NE 40th St., Seattle, WA 98105, USA, vera@acs366.phys.msu.ru), Michael S. Canney (Center for Industrial and Medical Ultrasound, Applied Physics Lab., University of Washington, 1013 NE 40th St., Seattle, WA 98105, USA, mcanney@u.washington.edu), Michael R. Bailey (Center for Industrial and Medical Ultrasound, Applied Physics Lab., University of Washington, 1013 NE 40th St., Seattle, WA 98105, USA, bailey@apl.washington.edu), Olga V. Bessonova (Center for Industrial and Medical Ultrasound, Applied Physics Lab., University of Washington, 1013 NE 40th St., Seattle, WA 98105, USA, olga@acs366.phys.msu.ru), Oleg A. Sapozhnikov (Center for Industrial and Medical Ultrasound, Applied Physics Lab., University of Washington, 1013 NE 40th St., Seattle, WA 98105, USA, oleg@acs366.phys.msu.ru), Lawrence A. Crum (Center for Industrial and Medical Ultrasound, Applied Physics Lab., University of Washington, 1013 NE 40th St., Seattle, WA 98105, USA, lac@apl.washington.edu)

Acoustic characterization of nonlinear HIFU fields is important for both the accurate prediction of ultrasound induced bioeffects and the development of regulatory standards for clinical HIFU devices. In this work a new characterization method is proposed and tested in water, tissue phantoms, and ex-vivo tissues. The method is based on the combined use of measurements and modeling. Experiments were performed with a 2 MHz transducer of 4.2 cm aperture and 4.5 cm focal length. Low amplitude measurements in water were used to establish boundary conditions for modeling based on the KZK-type equation. High amplitude focal waveforms then were simulated and measured with a fiber optic probe hydrophone in water, within tissue phantom, or adjacent to excised tissue. It was shown that at high amplitudes, the simulations of shock waveforms were more accurate than the measurements. The focal waveforms obtained in water were found to be in a good agreement with those produced in tissue with higher source pressure scaled to compensate for the linear attenuation on the way to focus. This result establishes a method to derate the focal HIFU pressures determined in water to tissue. [Work supported by NIH DK43881, NSBRI SMS00402 and RFBR.]

6:20

1pBBc3. Uncertainty of power and intensity measurement in focused fields. Adam Shaw (National Physical Laboratory, Hampton Road, Teddington, TW11 0LW Middlesex, UK, adam.shaw@npl.co.uk), Pierre Gelat (National Physical Laboratory, Hampton Road, Teddington, TW11 0LW Middlesex, UK, pierre.gelat@npl.co.uk)

Currently, the methodology employed to measure acoustic intensity and acoustic power relies on the plane wave assumption, resulting in a simple relation between acoustic power and the normal component of the radiation force vector, and acoustic intensity and pressure magnitude. For a range of ultrasonic transducers, and for positions in the field beyond the last axial maximum, this assumption is a valid one. Nevertheless, there is a range of situations where the plane wave assumption may introduce significant uncertainty in the measurement, such as in near field measurements and in fields resulting from highly focused devices. This investigation looks at the acoustic fields generated by axisymmetric rigidly vibrating curved pistons over a range of diameters and radii of curvature at megahertz frequencies. Finite element and boundary element methods are used to evaluate the acoustic pressure field and the components of the particle velocity vector at specified field positions. The time-averaged acoustic intensity vector, the acoustic power, as well as the normal component of the radiation force vector on a perfectly absorbing target may then be derived. Experimental results are will also be presented comparing theory with radiation force measurements and with the new and more accurate buoyancy change method.

6:40

1pBBc4. Towards a standardized approach for quantifying inertial cavitation activity. Jamie R. Collin (University of Oxford, Medical Engineering Unit, 43 Banbury Road, OX2 6PE Oxford, UK, jamie.collin@magd.ox.ac.uk), Ian Webb (University of Oxford, Medical Engineering Unit, 43 Banbury Road, OX2 6PE Oxford, UK, ian.webb@eng.ox.ac.uk), Ronald A. Roy (Boston University, Dept. of Aerosp. and Mech. Eng., 110 Cummington St., Boston, MA 02215, USA, ronroy@bu.edu), Constantin C. Coussios (University of Oxford, Medical Engineering Unit, 43 Banbury Road, OX2 6PE Oxford, UK, constantin.coussios@eng.ox.ac.uk)

Relative measures of the energy radiated as broadband noise emissions by inertially cavitating bubbles, such as the mean square voltage received using a passive cavitation detector (PCD), have been recently shown to be directly relatable to cavitation-mediated bioeffects. Even though numerous techniques exist to detect inertial cavitation qualitatively, there is presently a lack of a unified approach that makes it possible to quantify and compare levels of cavitation activity across different experimental setups and conditions. A technique has been developed that uses a calibrated sound source, a hydrophone, and a point spherical scatterer of known frequency response embedded in a tissue-mimicking material to achieve an absolute calibration of a PCD on receive. This makes it possible to relate the PCD signal during inertial cavitation activity to the acoustic power radiated as broadband noise in the proximity of the bubble cloud. The technique is validated against PCD measurements of single-bubble inertial cavitation activity in a tissue-mimicking material and compared to theoretical predictions using the Keller-Miksis model. Calibrated measurements of acoustic power radiated as broadband noise emissions could thus provide a quantitative measure of cavitation dose that can be directly related to resulting bioeffects, such as increased sonoporation or enhanced heating.

7:00

1pBBc5. Standardisation and metrology for High Intensity focused ultrasound: a clinical perspective. Gail Ter Haar (Institute of Cancer Research, 15 Cotswold Road, Belmont, Sutton, SM2 5NG Surrey, UK, gail.terhaar@icr.ac.uk)

The clinical application of HIFU is a young and rapidly expanding field, and it is essential that validated methods for measurement and testing are made available as soon as possible. These issues have not been addressed to date in any systematic fashion. There is, therefore, an urgent need to produce standard registration, testing equipment and methodology to allow users to characterize clinical HIFU systems for checking safety and reproducibility of a machine's output, comparing different devices or commissioning new systems. HIFU is delivered to the target volume via a number of routes. Extra-corporeal and trans-rectal probes are the most commonly used, although preliminary testing of intra-cavitary, catheter based devices is also underway19. These different devices present a wide range of different transducer geometries, f-numbers (~0.8-1.8), operating frequencies (~0.8 - 5 MHz), and focal peak intensities (~7.5 10^2 - 3 104 W cm^{-2}). Clinical HIFU systems are currently assessed on an ad hoc basis by individual clinical departments and manufacturers, using methods, many of which are unpublished. The main requirements from a clinical perspective are for the quantification of parameters which relate directly to individual HIFU treatments, allow reproducible treatments between different patients, and allow clinical trial data to be compared.

Session 1pEAa

Engineering Acoustics, Underwater Acoustics, Signal Processing in Acoustics, and ECUA: Sensor Technologies for Autonomous Acoustic Sensing Systems I

Henrik Schmidt, Cochair
MIT, 77 Massachusetts Ave, 5-204, Cambridge, MA 02139, USA

Andrea Caiti, Cochair
University of Genova, Via Opera Pia 13, 15614 Genova, Italy

Contributed Paper

1:00

1pEAa1. SLITA: A new slim towed array for AUV applications. Alain Maguer (NURC Nato Undersea Research Centre, Viale San Bartolomeo 400, 19026 La Spezia, Italy, maguer@nurc.nato.int), Rodney Dymond (NURC Nato Undersea Research Centre, Viale San Bartolomeo 400, 19026 La Spezia, Italy, dymond@nurc.nato.int), Marco Mazzi (NURC Nato Undersea Research Centre, Viale San Bartolomeo 400, 19026 La Spezia, Italy, mazzi@nurc.nato.int), Stefano Biagini (NURC Nato Undersea Research Centre, Viale San Bartolomeo 400, 19026 La Spezia, Italy, biagini@nurc.nato.int), Stefano Fioravanti (NURC Nato Undersea Research Centre, Viale San Bartolomeo 400, 19026 La Spezia, Italy, fioravanti@nurc.nato.int), Piero Guerrini (NURC Nato Undersea Research Centre, Viale San Bartolomeo 400, 19026 La Spezia, Italy, guerrini@nurc.nato.int)

The typical 70 mm diameter towed array was developed for blue-water detection at long range and low frequencies in the 1960s. Since then, there has been a need for towed arrays that are lighter and less expensive, especially since the maturing field of autonomous vehicles has expanded the potential of such arrays. The marriage of AUVs and lightweight towed arrays is a natural progression in the development of littoral autonomous sensing networks for applications such Anti-Submarine Warfare, marine mammals, or ambient noise measurements. In August 2007, NURC began to design and build a new thin diameter (31 mm) high-frequency (up to 20 kHz) nested towed array for ASW purposes. An engineering at-sea trial of the array towed by OEX AUV was performed beginning of November 2007. The flow noise level of the array while towed and the potential influence of the AUV self-noise on the acoustic array were also measured. This paper will first describe the array design, its acquisition system and its integration on the OEX AUV. Then, the results obtained from the data analysis are presented. It is shown that the SLITA array has performance that will make it easily fit requirements of the applications previously mentioned.

Invited Paper

1:20

1pEAa2. An autonomous moored ocean profiler. Benjamin Cray (Naval Undersea Warfare Center, Code 821, 1176 Howell Street, Newport, RI 02841-1708, USA, crayba@npt.nuwc.navy.mil)

An unconventional set of environmental and acoustic data, measured from an autonomous moored ocean profiler, is presented. The profiler is a programmable robotic underwater winch and data acquisition system that cycles vertically through the water column. The system profiles at pre-determined time intervals, surfaces to transmit data via RF links, and can be deployed for up to 180 days. Built by WETLabs Incorporated (Western Environmental Technology Laboratories) for the Naval Underwater Systems Center (NUWC), the system is outfitted with three environmental sensors and two acoustic vector sensors. The environmental sensors include; a Nortek Vector velocimeter which samples current components and characterizes surface wave velocities, a Seabird FastCAT Conductivity, Temperature, Depth (CTD) sensor; and a Wetlabs Fluorometer-Turbidity optical sensor that measures both chlorophyll-a and turbidity. The Wilcoxon acoustic vector sensors measure acoustic pressure and the three components of acoustic particle acceleration. Wilcoxon Research (a subsidiary of Meggitt Corporation) and Applied Physical Sciences (APS) have developed underwater acoustic vector sensors for many applications. The quality and sensitivity of these vector sensors has steadily improved. A review of early (pre-2002) vector sensor development efforts is discussed.

Contributed Papers

1:40

1pEAa3. Experimental validation of a chirp-based underwater acoustic communication method. Maria Palmese (DIBE - Dept. of Biophysical and Electronic Engineering - University of Genoa, Via Opera Pia 11a, 16145 Genova, Italy, palmese@dibe.unige.it), Giacomo Bertolotto (Fincantiere - Cantieri Navali Italiani S.p.A., Via Cipro 11, 16126 Genova, Italy, Giacomo.bertolotto@fincantieri.it), Alessandro Pescetto (Vulnerability & Signature Department, CETENA S.p.A., Via Ippolito d'Aste 5, 16121 Genova, Italy, alessandro.pescetto@cetena.it), Andrea Trucco (DIBE - Dept. of Biophysical and Electronic Engineering - University of Genoa, Via Opera Pia 11a, 16145 Genova, Italy, trucco@ieee.org)

A wireless underwater acoustic communication algorithm based on the combination of chirp modulation and direct-sequence spread-spectrum signaling is presented. In this paper, the processing chain design is proposed, discussed, and demonstrated using real data. The communication algorithm is made of a transmission block encoding the bits with adequate linear chirps multiplied by pseudo noise (PN) sequences, and a rake receiver that allows one to positively exploit the energy present in the most significant propagation paths. The use of chirp signals takes advantage of the low Doppler sensitivity in the matched filter operation whereas the choice of PN sequences allows one to reduce narrowband interference arising from other users and self-interference due to multipath propagation. Moreover a tracking

procedure that allows an adaptation to the instantaneous Doppler shift has been devised and tested. Some experiments have been carried out changing the distance and the speed between transmitter and receiver. Results show that the developed communication method is able to handle the multipath phenomenon and the Doppler effect, allowing one to achieve a bit error rate less than 10 (-3) for long ranges for bit rates of about 15 and 230 bit/s.

2:00

1pEAa4. Broadband transducers for underwater communications. David Brown (BTech Acoustics, LLC and Universtity of Massachusetts Dartmouth, ATMC, Electro-Acoustics Research Laboratory and ECE Dept., 151 Martine St, Fall River, MA 02723, USA, dbAcoustics@cox.net), Corey Bachand (BTech Acoustics, LLC and Universtity of Massachusetts Dartmouth, ATMC, Electro-Acoustics Research Laboratory and ECE Dept., 151 Martine St, Fall River, MA 02723, USA, corey.bachand@cox.net),Boris Aronov (BTech Acoustics, LLC and Universtity of Massachusetts Dartmouth, ATMC, Electro-Acoustics Research Laboratory and ECE Dept., 151 Martine St, Fall River, MA 02723, USA, baronov@comcast.net)

Properties of underwater acoustic cylindrical piezoelectric (PZT) transducers currently used for broadband underwater communications with unmanned underwater vehicles (UUV) and new transducers under development utilizing single crystal relaxor ferroelectrics (PMN-PT) with significantly higher material coupling coefficients and lower sound speed are presented. Characteristics including resonance frequency, coupling coefficient, transmit (TVR) and receive (OCVS) frequency response, maximum drive and achievable source levels, tuned and untuned power factor, and directivity factors are discussed. Results for experimental calibrations and field tests will be compared with detailed equivalent electrical circuit models of the transducer and transducer channel. Work supported in part by BTech Acoustics and Office of Naval Research.

Invited Papers

2:20

1pEAa5. High resolution angular measurements with single vector sensors and arrays. Joseph A. Clark (NSWCCD, Code 7340, 9500 MacArthur Blvd., West Bethesda, MD 20817-5000, USA, joseph.a.clark1@navy.mil), Dehua Huang (Naval Undersea Warfare Center, 1176 Howell St., Newport, RI 02841, USA, HuangD@Npt.NUWC.Navy.Mil)

The direction finding capability of acoustic sensors that directly measure acoustic particle velocity alone or in combination with pressure measurements (vector sensors) is well known. The angular resolution of the measurements can be improved by using arrays of vector sensors. It is also possible to improve angular resolution by additional processing of data from even a single vector sensor. This approach could be especially advantageous for sonar systems designed to operate from small platforms such as autonomous underwater vehicles. In this talk linear and non-linear methods for processing data from one or more vector sensors to achieve high angular resolution will be reviewed. Experimental investigations comparing the methods will be reported and factors found to limit the localization and detection performance of sonar systems employing the methods will be discussed.

2:40

1pEAa6. Hydroflown: MEMS-based Underwater Acoustical Particle Velocity Sensor. Tuncay Akal (SUASIS: Underwater Systems Technology Development, Tubitak-Marmara Research Center, Tech. D. Free Zone, Block A - L4, Gebze, 41470 Kocaeli, Turkey, tuakal@yahoo.com), Hans-Elias De Bree (Microflown Technologies Inc., PO BOX 300, 6900 AH Zevenaar, Netherlands, debree@microflown.com), Piero Guerrini (NURC Nato Undersea Research Centre, Viale San Bartolomeo 400, 19026 La Spezia, Italy, guerrini@nurc.nato.int), Alain Maguer (NURC Nato Undersea Research Centre, Viale San Bartolomeo 400, 19026 La Spezia, Italy, maguer@nurc.nato.int)

The increasing problems related to homeland security and harbour/infrastructure protection have increased the level of interest on vector sensors. Market surveys carried out during the last three years gave the conclusion that there is a need for a new generation, small size, and low-cost underwater sensors capable of measuring particle velocity in three dimensional plain within a broad frequency band (2 Hz - 50 kHz) and with high angular resolution. The small size MEMS-based sensors developed by Microflown Technologies BV Inc are the world's only commercially available transducers that are capable of measuring the particle velocity, instead of pressure, in air. The development of a new generation, innovative and low-cost underwater sensors and technologies based on that in-air nano technology is therefore considered. This technology has a great potential to become a revolutionary underwater acoustic sensor using nanotechnology, capable of finding many applications like sensors for Autonomous Underwater Vehicles, sensors for directional receivers for underwater acoustic systems, Floating autonomous systems, Sensors for seismic towed arrays for underwater oil and mineral prospecting and harbour and water-side infrastructure protection. This paper describes how Microflown technology can be adapted to underwater applications.

Contributed Papers

3:00

1pEAa7. Concurrent detection, classification and localization of seabed targets using virtual time reversal. Alexis J. Dumortier (MIT, 77 Mass Ave, 5-204, Cambridge, MA 02139, USA, adumorti@mit.edu), Henrik Schmidt (MIT, 77 Mass Ave, 5-204, Cambridge, MA 02139, USA, henrik@mit.edu), Karim G. Sabra (Georgia Institute of Technology, School of Mechanical Engineering, 771 Ferst Drive, NW, Atlanta, GA 30332-0405, USA, karim.sabra@me.gatech.edu)

During the last decade, the use of unmanned vehicles to detect seabed objects has been revolutionized by the rapid development of AUV technology. The reduced power budget imposed by autonomous operations limits the amount of processing allowable onboard and calls for simple and efficient detection algorithms. Time reversal techniques have proved to be a robust way of focusing sound on reflective objects in complex environments and only require minimal computation. The method proposed here uses a virtual time reversal mirror in monostatic configuration to localize the origin of the field scattered by objects located on the seafloor. The waveguide is insonified with a low frequency source (~kHz) mounted on the AUV and the resulting scattered field is sampled by a receiving array towed behind the vehicle. The recorded signals are then used to simulate the time reversed transmissions onboard, generating a map of reflectors present on the seabed. The rejection of clutter using singular value decomposition and the sensitivity of this method to environmental misknowledge are addressed along with the presentation of experimental results. [Work supported by ONR.]

3:20-3:40 Break

3:40

1pEAa8. Computational fluid dynamic analysis of optimized windscreens for UAV based acoustic arrays. Wayne E. Prather (Miltec Research & Technology, 9 Industrial Park Dr., Oxford, MS 38655, USA, wprather@mil-tec.com), David H. Bridges (Mississippi State University, Dept. of Aerospace Engineering, Mississippi State, MS 39762, USA, dbridges@AE.MsState.EDU), Tom Edwards (Raspet Flight Research Laboratory, 114 Airport Road, Starkville, MS 39759, USA, edwards@raspet.msstate.edu), David S. Thompson (Mississippi State University, Dept. of Aerospace Engineering, Mississippi State, MS 39762, USA, dst@simcenter.msstate.edu)

As part of an overall effort to place acoustic sensors on airborne platforms for surveillance applications, analysis studies were performed of acoustic probe windscreens that could minimize wind noise and be made relatively insensitive to small angle of attack and sideslip excursions. Through a collaborative effort between Miltec Research & Technology, Mississippi State University Department of Aerospace Engineering, Raspet Flight Research Laboratory, and the Engineering Research Center several probe designs were developed and analyzed using inviscid and viscous simulations with the objective of characterizing their flow fields and identifying potential modifications that could improve suitability for use as acoustic measurement probes. Several of the recommended probe shapes were fabricated and tested under real world conditions on an acoustically optimized 1/3 scale Schleicher ASH26 glider test bed.

4:00

1pEAa9. Acoustical methods for azimuth, range and heading estimation in underwater swarms. Uwe R. Zimmer (The Australian National University, 0200 Canberra, Australia, uwe.zimmer@ieee.org), Navinda Kottege (The Australian National University, 0200 Canberra, Australia, navinda.kottege@anu.edu.au)

Acoustical Methods for Azimuth, Range and Heading Estimation in Underwater Swarms Enhanced, embodied autonomy in small submersibles enables the design and deployment of practical swarms of autonomous underwater vehicles (AUVs). The swarming paradigm requires for each vehicle location awareness of at least its near neighbors. The Serafina AUV swarming project additionally requires a localisation system which could cope with the dynamic and fast changing vehicle configurations while being small, reliable, robust, and energy efficient and not dependent on pre-deployed acoustic beacons. The short-range acoustical relative localisation system proposed here, uses hyperbolic and spherical localization concepts and provides each vehicles with the azimuth, range and heading of its near neighbours. The implementation utilises an acoustically transmitted MLS signal which provides extremely high robustness against interference by stochastic and systematic disturbances which are typical for underwater environments. The azimuth is obtained via hyperbolic positioning with improved resolution and accuracy with respect to conventional methods. Range and heading estimation is achieved by two independent methods for increased robustness; one uses the implicit synchronisation provided by the underlying inter-vehicle communication scheduling system to measure the difference of TOAs of an acoustic and a long-wave radio signals; the second relies on TDOAs and a reverse hyperbolic localisation scheme.

Invited Paper

4:20

1pEAa10. Integrated sensing, modeling, and control in undersea sensor networks. Arjuna Balasuriya (MIT, 77 Mass Ave, 5-204, Cambridge, MA 02139, USA, arjunab@mit.edu), Henrik Schmidt (MIT, 77 Mass Ave, 5-204, Cambridge, MA 02139, USA, henrik@mit.edu), Michael B. Benjamin (MIT, 77 Mass Ave, 5-204, Cambridge, MA 02139, USA, mikerb@csail.mit.edu)

The way forward in adaptively sampling the vast ocean environment is by deploying a network of sensors with different capabilities. Due to the complex nature of the environment, covering such an area cannot be achieved by simply deploying underwater sensor nodes at predefined locations. The undersea network topology should dynamically adapt to the events and changes in the environment. However, the main challenge for undersea network autonomy is due to the limitations in underwater acoustic communication. In order to overcome such limitations, Nested Autonomy architecture is being developed and demonstrated in programs such as PLUSNet and Ocean Observatories. This paper looks into the implementation of such autonomy architecture in different sensor nodes with different capabilities. This is achieved by separating the ″low-level″ tasks of a sensor node with its ″high-level″ tasks. Low-level tasks will be sensor specific while the high-level tasks looks into the autonomy required for the adaptive sampling applications, which here refers to as the ″Backseat-driver paradigm″. The ″backseat″ carries the on-board intelligence required for the mission at hand. Behavior-based autonomy architecture which is used in the back-seat significantly improves the sensor performance by selecting the best behavior for the given state of the vehicle, mission at hand and the observations being made.

Contributed Paper

4:40

1pEAa11. Artificial characteristic landmarks for SLAM navigation. Yan Pailhas (Ocean Systems Laboratory, School of Eng. & Phys. Sciences, Heriot-Watt University, EH14 4AS Edinburgh, UK, Y.Pailhas@hw.ac.uk), Chris Capus (Ocean Systems Laboratory, School of Eng. & Phys. Sciences, Heriot-Watt University, EH14 4AS Edinburgh, UK, C.Capus@hw.ac.uk), Keith E. Brown (Ocean Systems Laboratory, School of Eng. & Phys. Sciences, Heriot-Watt University, EH14 4AS Edinburgh, UK, K.E.Brown@hw.ac.uk)

The use of autonomous underwater vehicles (AUVs) for a variety of purposes is set to increase in the future. A key issue in the navigation processing, especially for survey applications, is the lack of accuracy or cumulative error introduced by the various position sensors: accelerometer; DVL; compass. Algorithms such as SLAM (simultaneous localisation and mapping) rely on accurate landmark recognition in order to correct the vehicle position. This paper proposes a solution based on broadband sonar and artificial coded landmarks to improve the navigation. Through resolution of the wave equation for acoustic propagation in a multilayer concentric sphere, we will show that there is a great diversity in the echo spectrum with small changes in internal structure. This enables the design of a set of passive landmarks which can be identified unambiguously, since each has a characteristic signature or 'spectral code' when insonified with a broadband sonar.

Invited Paper

5:00

1pEAa12. Acoustic sensor systems on a flying wing underwater glider and two prop-driven autonomous underwater vehicles. Gerald D'Spain (Marine Physical Lab, Scripps Institution of Oceanography, 291 Rosecrans St., San Diego, CA 92106, USA, gld@mpl.ucsd.edu), Richard Zimmerman (Marine Physical Lab, Scripps Institution of Oceanography, 291 Rosecrans St., San Diego,

CA 92106, USA, richard@mpl.ucsd.edu),Scott A. Jenkins (Marine Physical Lab, Scripps Institution of Oceanography, 291 Rosecrans St., San Diego, CA 92106, USA, sjenkins@ucsd.edu), Dennis B. Rimington (Marine Physical Lab, Scripps Institution of Oceanography, 291 Rosecrans St., San Diego, CA 92106, USA, drimington@ucsd.edu), James C. Luby (Applied Physics Lab, Univ. of Washington, 1013 NE 40th St., Seattle, WA 98105, USA, jcl@apl.washington.edu), Peter Brodsky (Applied Physics Lab, Univ. of Washington, 1013 NE 40th St., Seattle, WA 98105, USA, brodsky@apl.washington.edu)

The Marine Physical Laboratory, Scripps Institution of Oceanography operates several underwater vehicles including an autonomous underwater glider based on a flying wing design and two prop-driven autonomous underwater vehicles (AUV) manufactured by Bluefin Robotics. The objective of this presentation is to describe the acoustic sensor systems on these platforms and provide sample results from the at-sea data. The glider, with a 6.1-m wing span, was developed jointly by the Marine Physical Lab and the Applied Physics Laboratory, University of Washington. It is designed to maximize the horizontal distance traveled between changes in buoyancy (i.e., maximize its ″finesse″) while quietly listening to sounds in the ocean. A 27-element hydrophone array with 5 kHz per channel bandwidth is located in the sonar dome all along the wing's leading edge. In addition, it has a four-component acoustic vector sensor in its nose. The two prop-driven AUVs have been equipped with hull-mounted hydrophone arrays with 10 kHz bandwidth for passive synthetic aperture studies, an acoustic vector sensor, and active acoustic imaging systems for ocean bottom/subbottom mapping. Results from the data processing illustrate the tight coupling between acoustic sensor systems, signal/array processing methods, and vehicle behavior. [Work supported by the Office of Naval Research.]

MONDAY AFTERNOON, 30 JUNE 2008 ROOM 353, 1:00 TO 4:00 P.M.

Session 1pEAb

Engineering Acoustics and Signal Processing in Acoustics: Microphone Array Signal Processing I

Gary Elko, Cochair
mh acoustics LLC, 25-A Summit Ave., Summit, NJ 07901, USA

Walter Kellermann, Cochair
Univ. of Erlangen-Nuremberg, 90158 Erlangen, Germany

Contributed Papers

1:00

1pEAb1. Spherical harmonic analysis applied to the reconstruction of the sound field radiated by a loudspeaker. Filippo M. Fazi (ISVR, University of Southampton, Highfield, SO171BJ Southampton, UK, ff1@isvr.soton.ac.uk), Vincent Brunel (ISVR, University of Southampton, Highfield, SO171BJ Southampton, UK, Vincent.Brunel@eurocopter.com), Philip A. Nelson (ISVR, University of Southampton, Highfield, SO171BJ Southampton, UK, P.A.Nelson@soton.ac.uk)

The three dimensional acoustic radiation patterns generated by different models of loudspeaker have been measured in an anechoic environment using an array of 40 omnidirectional microphones, arranged on a hemispherical surface. The acquired data have been numerically processed in order to obtain the complete three dimensional reconstruction of the analysed sound field. The theory of the applied method is based on the spherical harmonic decomposition of the sound field defined over the surface of a sphere containing the sound source and sampled at a finite number of positions. The reconstruction of the sound field in the region of the space inside and outside the measurement surface has been obtained by multiplying each coefficient of the spherical harmonic series by the corresponding spherical propagator, defined as the ratio of two spherical Hankel functions. The conditioning of the inverse problem related to the reconstruction of the sound field in the interior of the measurement surface has been analysed and put in relation to the behaviour of the spherical propagators of different orders.

1:20

1pEAb2. Surround sound echo cancellation in the spherical harmonic domain. Joshua Atkins (Johns Hopkins University, 853 West 35th Street, Baltimore, MD 21211, USA, joshatkins@jhu.edu), James West (Johns Hopkins University, Department of Electrical Engineering, 3400 North Charles Street, Baltimore, MD 21218, USA, jimwest@jhu.edu)

The problem of creating a multiuser hands-free immersive telecommunications environment poses many challenges for acoustic signal processing. The most pressing is the creation of a fast multichannel acoustic echo canceller (MCAEC) to eliminate acoustic feedback created in the speaker-microphone loop. Traditional multichannel adaptive algorithms for echo cancellation are not fast enough to work in systems with highly correlated multichannel signals like those found in the traditional telecommunications setup. This work presents analysis of a proposed acoustic echo cancellation system that operates in the spherical harmonic domain. Transforming the microphone and speaker signals into the spherical harmonic domain reduces both the number of channels and the correlation between channels for faster convergence of the adaptive MCAEC filters. This method also has the added benefit of being independent of the microphone and speaker array configuration, resulting in a hybrid mono/stereo/multichannel acoustic echo canceller. This work is funded by NSF Grant IIS-0534221.

1:40

1pEAb3. Improving the directivity of a Soundfield microphone using least-squares estimation. Craig Jin (University of Sydney, School of Electrical and Information Engineering, Bldg. J03, 2006 Sydney NSW, Australia, craig@ee.usyd.edu.au), Alan Kan (University of Sydney, School of Electrical and Information Engineering, Bldg. J03, 2006 Sydney NSW, Australia, alan@carlab.ee.usyd.edu.au), Andre Van Schaik (University of Sydney, School of Electrical and Information Engineering, Bldg. J03, 2006 Sydney NSW, Australia, andre@ee.usyd.edu.au)

Faller [1] has recently shown that highly directive microphone systems can be obtained using coincident microphones and appropriate signal processing to separate direct and ambient sound. We apply this approach to a Soundfield microphone in which coincident virtual first-order microphone patterns pointing in any direction are available. The variation with our ap-

proach is that we apply a specific gain pattern across a set of coincident cardiod or hypercardiod microphones to determine the pick-up direction. A least-squares estimate is made of the spectrum of the on-axis sound. We empirically investigate the performance of this directive microphone technique. [1] C. Faller, ″A highly directive 2-capsule based microphone system,″ in Proc. of 123rd Audio Engineering Convention, New York, U.S.A., October 5-8, 2007.

2:00

1pEAb4. A comparison of measured and theoretical performance of a co-centred rigid and open spherical microphone array. Craig Jin (University of Sydney, School of Electrical and Information Engineering, Bldg. J03, 2006 Sydney NSW, Australia, craig@ee.usyd.edu.au), Abhaya Parthy (University of Sydney, School of Electrical and Information Engineering, Bldg. J03, 2006 Sydney NSW, Australia, aparthy@it.usyd.edu.au), Andre Van Schaik (University of Sydney, School of Electrical and Information Engineering, Bldg. J03, 2006 Sydney NSW, Australia, andre@ee.usyd.edu.au)

We present a comparison of the measured and theoretical performance of a dual co-centred spherical microphone array that consists of an open spherical microphone array with a smaller, rigid spherical microphone array at its centre. The dual co-centred spherical microphone array has 64 microphones, with 32 microphones on the open spherical microphone array of radius 6.30 cm and 32 microphones on the rigid spherical microphone array of radius 1.63 cm. We have previously shown [1] that this even distribution of microphones, between the two spherical microphone arrays, provides a greater frequency range of operation for a third-order, 64-channel spherical microphone array compared to a single rigid 64-channel spherical array. The performance of the dual co-centred spherical microphone array is measured in an anechoic chamber using a speaker mounted on a robotic arm. A comparison is made between the theoretical and measured directivity pattern for various frequencies. [1] A. Parthy, C. Jin, and A. van Schaik ″Optimisation of Co-centred Rigid and Open Spherical Microphone Arrays,″ in Proc. of 120th Audio Engineering Convention, Paris, France, May 20-23, 2006.

2:20

1pEAb5. Towards 'not so spherical' microphone arrays. Nicolas Epain (France Telecom R&D, 2 avenue Pierre Marzin, 22300 Lannion, France, nicolas.epain@orange-ftgroup.com), Jérôme Daniel (France Telecom R&D, 2 avenue Pierre Marzin, 22300 Lannion, France, jerome.daniel @orange-ftgroup.com)

An increasing number of applications require that the sound field spatial properties are accurately described. Using arrays consisting of omnidirectional microphones distributed at the surface of a rigid sphere has been proven to be an efficient yet practical strategy to obtain such three dimensional sound field descriptions. However these sensor arrays are known to suffer from frequency limitations, mainly due to the sphere directivity properties. In this paper, it is proposed to optimize the shape of the object upon which the microphones are located, in order to make them more directive. Results of measurements and simulations show that such ″not so spherical″ shapes could help at widening the microphone array frequency range.

2:40

1pEAb6. Global synthesis of superdirective frequency-invariant beam patterns. Marco Crocco (DIBE - Dept. of Biophysical and Electronic Engineering - University of Genoa, Via Opera Pia 11a, 16145 Genova, Italy, crocco@dibe.unige.it), Stefania Repetto (DIBE - Dept. of Biophysical and Electronic Engineering - University of Genoa, Via Opera Pia 11a, 16145 Genova, Italy, stefania@dibe.unige.it), Andrea Trucco (DIBE - Dept. of Biophysical and Electronic Engineering - University of Genoa, Via Opera Pia 11a, 16145 Genova, Italy, trucco@ieee.org)

Frequency-invariant beam patterns are often required by systems using an array of sensors to process broadband signals. If the spatial aperture is shorter than the involved wavelengths, the use of a superdirective beam pattern is essential to attain an efficient system. In this context, robustness to array imperfections is a crucial feature. In the literature, only a few approaches have been proposed to design a robust, superdirective, frequency-invariant beamformer, based on a filter and sum architecture: in all of them, the frequency invariance is achieved imposing an a priori desired beam pattern. However the choice of a suitable desired beam pattern is not trivial and depends on the specific design case: an improper selection of the desired beam pattern can produce unsatisfactory performances. We propose a new method of global synthesis, computationally inexpensive, allowing to design a robust broadband beam pattern with an optimal trade-off between the frequency invariance and the directivity, without the need of imposing a priori a desired beam pattern. The results show that the synthesized beam patterns have a directivity, a frequency-invariance, and a robustness that are very similar to or better than those of the beam patterns obtained by the literature methods.

3:00

1pEAb7. The generation of binaural signals from a regularly sampled soundfield using a beamforming approach. Mark Poletti (Industrial Research Ltd., PO Box 31-310, 310 Lower Hutt, New Zealand, M.Poletti@irl.cri.nz), Peter Svensson (Norwegian Univ. of Science and Technology, O.S. Bragstads plass 2B, Dept. of Electronics and Telecommunications, NO-7491 Trondheim, Norway, svensson@iet.ntnu.no)

Auditorium designs can be evaluated prior to construction by numerical modeling of the design. Subjective assessment of the design requires auralization of the computed soundfield at a desired listener position and the binaural format is dominant for representation of the soundfield. For high accuracy the modeling is based on solving the wave equation numerically, which typically produces the sound pressure on a rectangular grid. Such a sampled soundfield is not straightforward to convert to a binaural format. This paper investigates binaural conversion from the sound pressure at a selected number of grid points using a least squares beamforming approach. Low-frequency axisymmetric emulations are derived assuming a solid sphere model of the head, and an open spherical array of 640 microphones is used to emulate ten measured HRTF data sets from the CIPIC database for half the audio bandwidth. The microphone positions might be displaced from the exact spherical surface to fit the mesh sample points. The spherical array can produce high-accuracy band-limited emulation of any human subject's measured HRTFs for a fixed listener position by using individual sets of beamforming impulse responses.

3:20

1pEAb8. New measurements of head-related transfer functions with an optimized ear-canal microphone. Christopher Haut (Oldenburg University, Institute for Physics, 26111 Oldenburg, Germany, christopher@aku.physik.uni-oldenburg.de), Jacqueline Rausch (Oldenburg University, Institute of Physics - Acoustics, Carl-von-Ossietzky Str. 9-11, 26111 Oldenburg, Germany, jacqueline@aku.physik.uni-oldenburg.de), Volker Mellert (Oldenburg University, Institute for Physics, 26111 Oldenburg, Germany, volker.mellert @uni-oldenburg.de)

Affecting the ear-canal impedance by inserting a microphone produces considerable changes in the directional characteristics of the ear with increasing frequency. Head-related transfer functions (HRTFs) are measured in the horizontal and median plane under systematic change of the ear-canal microphone more or less blocking the ear-canal entrance. A microphone arrangement is developed which minimizes the influence on the given impedance of the ear canal entrance. New measurements of HRTFs are reported and compared with well-known literature results. The ″undisturbed″ HRTFs serve as objective functions for a microphone array which substitutes the dummy head in head-related (stereophonic) recordings. The (complex) objective functions are modified for the microphone array according to the relevance in directional hearing.

3:40

1pEAb9. Study of a concert harp's radiation using acoustic imaging methods. Quentin Leclere (Laboratoire Vibrations Acoustique - INSA Lyon, 25 bis avenue Jean Capelle, Bâtiment Saint-Exupéry, F-69621 Villeurbanne cedex, France, quentin.leclere@insa-lyon.fr), Jean-Loic Le Carrou (Laboratoire d'Acoustique de l'Université du Maine, Avenue Olivier Messiaen, 72085 Le Mans, France, jean-loic.le_carrou@univ-lemans.fr), François Gautier (Laboratoire d'Acoustique de l'Université du Maine, Avenue Olivier Messiaen, 72085 Le Mans, France, francois.gautier@univ-lemans.fr)

Recent studies have been conducted to understand the low frequency radiation of a concert harp. Experiments have been carried out in a semi-anechoic room: the harp's soundboard is excited with a shaker and the pressure is measured at more than 600 positions on a nearly hemispherical surface at a distance of about 2 m from the instrument. Simple source models with a set of monopoles have been optimized to fit the measured acoustic radiation. These models are very satisfactory in the low frequency domain but cannot properly reproduce the measured field above 350 Hz. The aim of this paper is to present the application of acoustic imaging tools to this academic case: volumetric velocity and acoustic power maps in the harp plane are computed with an optimized beamforming and with a regularized inverse FRF method up to 1 kHz. The optimization of the beamforming is realized using a variable windowing factor, and the regularization of the inverse FRF method with a Tikhonov approach. The presented results permit the evaluation of the importance of the bass reflex effect in the harp, of the contribution of the first bending modes and of the contribution of the soundbox vibrations in the radiated sound field.

MONDAY AFTERNOON, 30 JUNE 2008 ROOM 353, 4:20 TO 7:40 P.M.

Session 1pEAc

Engineering Acoustics and Psychological and Physiological Acoustics: Hearing Aid Engineering I

Daniel M. Warren, Cochair
Knowles Electronics, 1151 Maplewood Dr, Itasca, IL 60143, USA

Stefan Launer, Cochair
Phonak AG, Laubisrütistr. 28, CH-8712 Stäfa, Switzerland

Invited Paper

4:20

1pEAc1. Model-based signal processing for hearing aids. Volker Hohmann (Carl von Ossietzky Universität Oldenburg, Ammerländer Heerstraße 114-118, 26111 Oldenburg, Germany, volker.hohmann@uni-oldenburg.de)

The aim of the work presented in this talk is to investigate potential applications of models of human auditory processing to signal processing in hearing aids. In particular, it is shown that auditory models may be used as objective indicators of the perceptual quality of single- and multichannel noise reduction strategies. Furthermore, a general framework for computational auditory scene analysis (CASA) is introduced and applied to the problem of estimating spatial direction and spectral envelope of super-imposed sound sources from a binaural input signal. Finally, implications of using nonlinear peripheral models for the design of compression systems in hearing aids are discussed. In particular, results from a multiband instantaneous compression scheme are presented, which is based on a novel nonlinear auditory filterbank controlled by the instantaneous frequency calculated in frequency sub-bands.

Contributed Paper

4:40

1pEAc2. The sound field in life-size replicas of human ear canals occluded by a hearing aid. Mike R. Stinson (Inst. for Microstructural Sciences, National Research Council of Canada, Bldg. M-36, Ottawa, ON K1A 0R6, Canada, mike.stinson@nrc-cnrc.gc.ca), Gilles A. Daigle (Inst. for Microstructural Sciences, National Research Council of Canada, Bldg. M-36, Ottawa, ON K1A 0R6, Canada, gilles.daigle@nrc-cnrc.gc.ca)

In addition to the longitudinal sound pressure distributions that form in the human ear canal, large transverse variations can arise in the vicinity of an occluding hearing aid. These effects are being studied, numerically and experimentally, making use of life-size ear canal replicas. Using digital representations of real ear canal geometries [Stinson and Lawton, J. Acoust. Soc. Am. 85, 2492-2503 (1989)], a polyjet fabrication process forms replicas with a spatial accuracy of better than 0.1 mm. A hearing aid test fixture, with vent, receiver, and an inner microphone, occludes the replica canal and provides the acoustical input. The sound field inside the canal is measured using a 0.2 mm o.d. probe microphone. In parallel, the interior sound field is calculated using a boundary element method, using the same ear canal geometry as the replicas and accounting for the acoustical boundary conditions presented by the eardrum and the hearing aid. In the current series of ear canal replicas, the eardrum is rigid. Measurements and calculations are in good agreement. Large transverse variations of sound pressure level, as much as 20 dB at 8 kHz, are observed across the inner face of the hearing aid, particularly near the receiver and vent ports.

Invited Papers

5:00

1pEAc3. Acoustics of open fittings. Matthias Blau (Institut für Hörtechik + Audiologie, FH OOW, Ofener Str. 16, D-26121 Oldenburg, Germany, matthias.blau@fh-oldenburg.de), Tobias Sankowsky (Institut für Hörtechik + Audiologie, FH OOW, Ofener Str. 16, D-26121 Oldenburg, Germany, tobias.sankowsky@fh-oldenburg.de), Alfred Stirnemann (Phonak AG, Laubisrütistr. 28, CH-8712 Stäfa, Switzerland, alfred.stirnemann@phonak.ch), Hannes Oberdanner (Phonak AG, Laubisrütistr. 28, CH-8712 Stäfa, Switzerland, hannes.oberdanner@phonak.ch), Nicola Schmitt (Phonak AG, Laubisrütistr. 28, CH-8712 Stäfa, Switzerland, nicola.schmitt@phonak.ch)

The use of so-called ″open fittings″ instead of individual ear shells has become very popular in hearing aid fitting, in particular because the open fittings avoid the occlusion effect, but also because they are more comfortable, easier to manufacture, and cosmetically preferred. On the other hand however, there are acoustical issues with open fittings, including the mixture of direct and amplified sound, a poor low-frequency performance, an increased risk of feedback and a supposedly less reproducible position of the sound delivering device (tubing or speaker) in the ear canal, which in turn may result in a greater variability of acoustic parameters such as RECD and REOG. The two latter issues are addressed here in a study with 20 subjects, for individual shell and a number of open fittings, comprising closed and open domes of different diameters with tubings as well as with ear canal receivers. It was observed that in comparison to individual shell fittings, the open fittings did not exhibit higher interindividual differences of RECD and REOG, but up to 15 dB (closed domes) to 25 dB (open domes) lower feedback thresholds.

5:20

1pEAc4. Estimation of maximum stable gain in a hearing aid. Ivo L. Merks (Starkey Laboratories, 6600 Washington Ave S, Eden Prairie, MN 55344, USA, ivo_merks@starkey.com), Karrie Recker (Starkey Laboratories, 6600 Washington Ave S, Eden Prairie, MN 55344, USA, karrie_recker@starkey.com), Harikrishna P. Natarajan (Starkey Laboratories, 6600 Washington Ave S, Eden Prairie, MN 55344, USA, harikrishna_natarajan@starkey.com), Lalin S. Theverapperuma (Starkey Laboratories, 6600 Washington Ave S, Eden Prairie, MN 55344, USA, lalin_theverapperuma@starkey.com)

Feedback cancellation (FBC) algorithms have become an important part of hearing aids, allowing the Maximum Stable Gain (MSG) to be increased by up to 25 dB beyond what is possible without an FBC. Although FBC algorithms have improved the usability of hearing aids, it is difficult to predict the MSG for a given individual with a particular hearing aid. Knowledge of this information would enable the audiologist to make more informed decisions regarding the appropriateness of a hearing aid/earmold, and it could be used to counsel the patient regarding feedback. A method of estimating the MSG of a hearing aid with and without an FBC will be presented. The method uses a finite impulse response filter to approximate the acoustic path. The filter coefficients are estimated during the initialization of the FBC. From these filter coefficients, the MSG for the hearing aid with and without FBC are calculated. This method has been implemented in the firmware and fitting software. Using a variety of device styles, microphone modes and feedback paths, it has been verified that the estimated MSG matches the actual MSG within 6 dB for 90% of hearing aids.

5:40

1pEAc5. ″Auditory scene analysis″ in hearing instruments. Matthias Froehlich (Siemens Medical Solutions SAT, 91058 Erlangen, Germany, Matthias.froehlich@siemens.com)

The term ″auditory scene analysis″ generally refers to a categorization of a given acoustic situation based on the acoustic signal only, where the results determine the subsequent processing of the acoustic signal within some auditory context. According to this definition, several approaches can be differentiated in the field of hearing instrument development. They differ in the computational complexity of the particular analysis methods applied, as well as in the subsequent action. Some of these approaches have been realized in commercially available hearing instruments, others lie still ahead. A simple example of the former category is noise reduction algorithms that address different classes of noises, examples of the latter are MPEG4-like virtual arrangements of media objects. In the presentation, different approaches will be discussed in terms of potential benefit and technical realization, as well as their limitations. For approaches already realized in commercially available hearing instruments, the expected benefit will be aligned with results from clinical studies.

Contributed Paper

6:00

1pEAc6. Prediction of perceived sound quality of hearing aids (algorithms) using perceptual models. Rainer Huber (Kompetenzzentrum HörTech, Marie-Curie-Str. 2, 26129 Oldenburg, Germany, Rainer.Huber@HoerTech.de)

This contribution presents an overview of basic approaches for predicting the perceived sound quality of hearing aids and hearing aid algorithms using auditory processing models for hearing impaired. Comparison-based concepts will be considered in particular. The main characteristic of these concepts is the comparison of internal representations (the outputs of the auditory models) of a test and a reference signal. While this approach is straight-forward and has proven to be successful for the prediction of sound quality of lossy speech and audio processing systems perceived by normal-hearing listeners, the requirement of a reference representing the optimal quality can pose a problem in the case of hearing aids and hearing-impaired listeners. The potential and limitations of comparison-based approaches will be illustrated by example results from different studies obtained with an extended version of the perceptual audio quality model PEMO-Q.

Invited Papers

6:20

1pEAc7. Real-world effectiveness of directional microphone hearing aids. Ruth Bentler (University of Iowa, 250 Hawkins Drive, Wendell Johnson Clinic, Iowa City, IA 52242, USA, ruth-bentler@uiowa.edu)

Single, dual, triple, and array microphone designs that are static, automatic and/or adaptive are now available in marketed hearing aids. The cost of designing and producing these more sophisticated systems is significant; yet, studies of user benefit are often equivocal, particular those involving self-report or field-obtained measures. In a series of studies we have attempted to characterize (model) the function of a number of these designs in simple and complex environments in an effort to explain the results obtain in both laboratory and field studies. Rather than directivity limitations, factors such as internal noise, loudness preference and visual cues have all been implicated in the limited user benefit, and will be discussed in this presentation.

6:40

1pEAc8. Whispering in your ear: a recent history of subminiature transducers. Daniel M. Warren (Knowles Electronics, 1151 Maplewood Dr, Itasca, IL 60143, USA, daniel.warren@knowles.com)

For 50 years, the history of hearing aid transducer development could be read in a simple photograph and timeline, where the size of the transducer was inversely correlated to the year it was developed. This size curve corresponds to hearing aid development over the same time period, progressing from body-worn aids in the 1940s to large behind-the-ear (BTE), smaller BTE's, in-the-ear (ITE), and successively deeper in- the-canal (ITC) devices through the 1990s. Although size still matters, in the last decade there has been less effort in reducing the size of hearing aids and more on increasing features, usability, and comfort. Development of hearing aid transducers has become similarly multidimensional. This paper charts the progress from the linear smaller-is-better design model to lower vibration, higher acoustic output, lower current draw, reduced radio frequency interference, wider bandwidth, and other multifaceted challenges of modern hearing aid transducer design.

Contributed Papers

7:00

1pEAc9. High sound quality and concha headphones: where are the limitations? Lola Blanchard (Bang&Olufsen ICEpower/DTU, Gl. Lundtoftevej 1b, st., 2800 Lyngby, Denmark, lob@bang-olufsen.dk)

Concha headphones (the small type of headphone that rests at the entrance of the ear canal) are the most popular type of headphones for everyday use. However, the sound quality produced by even ″high quality″ concha headphones is rather poor. This paper gives an overview of the different factors that affect the quality of this type of headphones, describes the measurement difficulties, and presents a model. The leakage between the headphone and the ear changes every time the headphone is inserted in the ear. This alters the perceived sound quality, especially at low frequencies, and makes measurements very difficult. Moreover, because of energy efficiency considerations, a typical transducer design is prone to nonlinear behaviour, and a high distortion rate can be measured for most concha headphones. The measured transducer parameters and leakage have been implemented in a model realised in Simulink. The simulation model, which makes it possible to study the influence of the various parameters including the uncontrolled leakage, is the first step towards developing a compensation technique.

7:20

1pEAc10. A two-stage binaural speech enhancement approach for hearing aids with preserving binaural benefits in noisy environments. Junfeng Li (Japan Advanced Institute of Science and Technology, 1-1, Asahidai, Nomi, 923-1292 Ishikawa, Japan, junfeng@jaist.ac.jp),Shuichi Sakamoto (R.I.E.C., Tohoku University, 2-1, Katahira, Aoba-ku, 980-8577 Sendai, Japan, saka@ais.riec.tohoku.ac.jp), Satoshi Hongo (Faculty of Design and Computer Applications, Miyagi National College of Technology, 48, Nodayama, Medeshima Shiote, 981-1239 Natori, Japan, hongo@miyagi-ct.ac.jp), Masato Akagi (Japan Advanced Institute of Science and Technology, 1-1, Asahidai, Nomi, 923-1292 Sendai, Japan, akagi@jaist.ac.jp), Yôiti Suzuki (R.I.E.C., Tohoku University, 2-1, Katahira, Aoba-ku, 980-8577 Sendai, Japan, yoh@ais.riec.tohoku.ac.jp)

Speech enhancement is one of the most crucial functions, if not the most, in hearing aids, as hearing impaired people have great difficulty in understanding speech in noisy environments. In this paper, we propose a two-stage binaural speech enhancement approach for hearing aids, which consists of interference estimation by pre-trained adaptive filters and speech enhancement using the Wiener filters. Main attention is then paid to the theoretical analysis of this system and the experimental comparisons with the traditional binaural speech enhancement approaches. The comparisons are conducted with the following two considerations: interference suppression performance and the ability in preserving binaural cues which give birth to listener's own "binaural gain." We finally give the general discussion on this proposed binaural speech enhancement algorithm from the viewpoints of theory, through implementation, to evaluation.

Session 1pEAd

Engineering Acoustics, Underwater Acoustics, and ECUA: Sonar Transducer Design and Modeling I

John B. Blottman, Chair
Naval Undersea Warfare Center, Division Newport, 1176 Howell Street, Newport, RI 02841-1708, USA

Invited Papers

5:40

1pEAd1. Advanced application-motivated design techniques for high performance piezocomposite underwater sonar transducers and arrays. Sandy Cochran (Institute for Medical Science and Technology, University of Dundee, Wilson House, 1 Wurzburg Loan, DD2 1FD Dundee, UK, s.cochran@dundee.ac.uk), Christine E. Demore (Institute for Medical Science and Technology, University of Dundee, Wilson House, 1 Wurzburg Loan, DD2 1FD Dundee, UK, c.demore@dundee.ac.uk), Pablo Marin (Piezo Composite Transducers Ltd, Aberdeen Science Park, Balgownie Drive, Bridge of Don, AB22 8GU Aberdeen, UK, pablo.marin@pct-ltd.co.uk), Richard Marsh (Tritech International Ltd, Peregrine Road, Westhill Business Park, Westhill, AB32 6LJ Aberdeen, UK, richard-marsh@tritech.co.uk), Keith Mayne (Piezo Composite Transducers Ltd, Aberdeen Science Park, Balgownie Drive, Bridge of Don, AB22 8GU Aberdeen, UK, keith.mayne@pct-ltd.co.uk), Graeme McRobbie (University of the West of Scotland, High Street, PA1 2BE Paisley, UK, graeme.mcrobbie@uws.ac.uk), Michelle Wallace (Doosan Babcock Energy, Porterfield Road, PA4 8DJ Renfrew, UK, mwallace@doosanbabcock.com), Mark P. Walsh (Piezo Composite Transducers Ltd, Aberdeen Science Park, Balgownie Drive, Bridge of Don, AB22 8GU Aberdeen, UK, mark.walsh@pct-ltd.co.uk), Richard Wright (Tritech International Ltd, Peregrine Road, Westhill Business Park, Westhill, AB32 6LJ Aberdeen, UK, dick-wright@tritech.co.uk)

Developments in areas as diverse as advanced piezoelectric materials and low cost digital electronics continue to offer new possibilities to the designer of high performance underwater sonar transducers and arrays. Many of these are likely to be realised with complex composite materials comprising a polymer matrix with rods of piezoelectric ceramic such as PZT 5H or crystal such as PMN-PT which require advanced design techniques. This paper first briefly reviews relevant capabilities of conventional equivalent circuit and wave equation transducer models, and the composite homogenisation technique of Smith and Auld. The increasing possibilities offered by finite element analysis (FEA) running on relatively low-cost computing hardware are also considered. Whichever design technique is adopted, accurate material properties are crucial and this is reported through reference to a range of piezoelectric and passive materials. The potential variation of such properties across the operating temperature range of underwater transducers is also considered, illustrated with experimental measurements. As understanding of high performance transducer structures grows, future possibilities also become evident, such as the 3-1 connectivity multilayer composite. The paper is therefore completed with an outline of these complex structures and a stochastic mathematical technique that can be used to optimise their designs automatically.

6:00

1pEAd2. Leveraged motion underwater sound piston transducers. John Butler (Image Acoustics, Inc., 97 Elm Street, Cohasset, MA 02025, USA, jbutler@imageacoustics.com), Alexander L. Butler (Image Acoustics, Inc., 97 Elm Street, Cohasset, MA 02025, USA, abutler@imageacoustics.com)

Flextensional transducers use leveraged shell motion to produce enhanced acoustic radiation from compact sources, which are often used in low frequency underwater sound applications. The most commonly used flextensional is the Class IV where an oval shell is driven along its major axis by a stack of piezoelectric ceramic elements. We present here a review of a new class of leveraged transducers in which the shell motion drives pistons attached to the shell at the location of maximum magnified motion. Because of the uniform motion of the pistons, greater source strength and radiation load is attained compared to the tapered motion of flextensional shells. The leveraged motion typically yields a motion magnification of approximately three and an impedance load magnification of approximately nine, resulting in reasonably low Q for a compact low frequency transducer. Various designs are presented and illustrated including one in which the piezoelectric drive simultaneously acts as a tail mass and one which operates in a high impedance velocity control mode under array conditions. Lumped models as well as FEA models and measured results are presented to illustrate the concept and performance of PZT and PMN-PT driven designs. [Work supported in part by ONR.]

6:20

1pEAd3. Electro-active polymer transduction for distributed netted sensing. Dennis F. Jones (Defence R&D Canada - Atlantic, P.O. Box 1012, Dartmouth, NS B2Y 3Z7, Canada, dennis.jones@drdc-rddc.gc.ca), John B. Blottman (Naval Undersea Warfare Center, Division Newport, 1176 Howell Street, Newport, RI 02841-1708, USA, blottmanjb@npt.nuwc.navy.mil), Roger T. Richards (Naval Undersea Warfare Center, Division Newport, 1176 Howell Street, Newport, RI 02841-1708, USA, richardsrt@npt.nuwc.navy.mil)

The Naval Undersea Warfare Center in Newport, RI is developing an electro-active polymer-based sensing node for use in a persistent distributed underwater surveillance system. Persistence demands extreme energy conservation measures. The node will resemble a jellyfish in form, complete with tentacles housing a volumetric array of light-weight piezoelectric polyvinylidene fluoride trifluoroethylene (PVDF-TrFE) copolymer cylindrical hydrophones designed for an ultra-low power acoustic receiver. Each cylinder has con-

ductive silver electrodes on the inside and outside surfaces, a length of 2.5 cm, an outside diameter of 11 mm, a 1 mm wall thickness, and a mass less than 2 g. Operating in the hydrostatic mode, the hydrophone sensitivity is typically -195 dB//1 V/μPa and is stable with both hydrostatic pressure (50 to 1000 psi) and temperature (-1 to 35°C). [Work supported by the Office of Naval Research.]

6:40

1pEAd4. Magnetostrictive compacted sonar transducer design. Stephen C. Butler (Naval Undersea Warfare Center, 1176 Howell St, Newport, RI 02841, USA, butlersc@npt.nuwc.navy.mil), Julie Slaughter (Etrema Products, Inc., 2500 N. Loop Drive, Ames, IA 50010, USA, julie.slaughter@etrema.com)

A compact modular high power magnetostrictive sound source that is capable of producing scanning Cardioid beams every 45 degrees in the horizontal plane and operates over one octave has been fabricated. The device consists of 8 transducer elements in the form of a ring that radiates acoustic energy radially outward. This design uses the operation principles of a peizoceramic transducer of similar design [J. L. Butler and A. L. Butler, J. Acoust. Soc. Am. **119**, 3409 (2006)], which operated in a higher frequency band. The sound source can be driven to form omni-directional, dipole, and quadrupole beam patterns. By combining the measured electrical drive and acoustic pressure amplitude and phase coefficients of these beam patterns a narrower type Cardioid beam pattern is generated. The transducer elements are of a tonpilz type vibrator consisting of magnetostrictive Terfenol-D drive rods sandwiched between radiating head mass and a tail mass that is common to all elements with tie bolts consolidating the parts together. The Terfenol-D rods are interlaced with rare earth magnets to provide the DC magnetic bias field for the AC drive field provided by a coil. FEA models using ATILA and COMSOL are used for structural and magnetic analysis predictions of the device. [Work supported by ONR.]

7:00

1pEAd5. Broadband tonpilz transducers based on single crystal relaxor ferroelectrics: Design and modeling. Richard J. Meyer (The Applied Research Laboratory/ The Pennsylvania State University, P.O. Box 30, State College, PA 16801, USA, rmeyer@psu.edu), Douglas C. Markley (The Applied Research Laboratory/ The Pennsylvania State University, P.O. Box 30, State College, PA 16801, USA, dcm13@psu.edu)

Very broad bandwidth transduction capability has been made possible by high coupling piezoelectric single crystal materials. Recent work has shown that PMN-PT based tonpilz elements with a single resonance have a device electromechanical coupling coefficient greater than 0.86 and can easily achieve more than two octaves of source level bandwidth. Implementing single crystal based tonpilz elements reduces array packaging volume and weight while maintaining source level. In addition, high coupling projectors reduce transmit system complexity when compared to traditional materials. This paper will describe approaches to creating broadband SONAR projectors using single crystal materials. Crystal anisotropy plays a key role in transducer design. This anisotropy requires final designs to be modeled in three dimensions. ATILA finite element code was used to capture all of the modes of vibration and performance predictions. Motor section geometries and material compositions will be compared. The model predictions will also be compared to measured data.

MONDAY AFTERNOON, 30 JUNE 2008 AMPHI MAILLOT, 1:00 TO 4:00 P.M.

Session 1pMUa

Musical Acoustics: Acoustic Measurements on Wind Instruments I

Noam Amir, Cochair
Tel Aviv University, Dept. of Communications Disorders, Sheba Medical Center, Tel Hashomer, 52621, Israel

David B. Sharp, Cochair
Acoustics Research Group, DDEM, MCT Faculty, Open University, Walton Hall, Milton Keynes, MK7 6AA, UK

Invited Papers

1:00

1pMUa1. A new impedance sensor for wind instruments. Jean-Pierre Dalmont (Laboratoire d'Acoustique de l'Université du Maine, Avenue Olivier Messiaen, 72085 Le Mans, France, Jean-Pierre.Dalmont@univ-lemans.fr), Jean Christophe Le Roux (CTTM, 20, rue Thales de Milet, 72000 Le Mans, France, jcleroux@cttm-lemans.com)

Our aim was to build a low cost but accurate portable impedance sensor. The adopted technique is the one using a source with a back cavity. A first elctret microphone on the front of the source measures the pressure at the input of the instrument weather a second one measures the pressure in the cavity, which is proportional to the volume flow supplied by the source. By choosing a sufficiently small sealed cavity and a small piezoelectric source the system do not exhibit any cut-off frequency in the measurement range. The calibration is then simplified and only few parameters are needed to model the three complex calibration functions. This calibration is performed with three nonresonant calibration loads. Moreover, it is shown that the geometry of the sensor being known, the measurement with a rigid wall is sufficient to calibrate the sensor. Results show that it is possible to achieve a measurement with an accuracy lower than 1dB in the range 50-4000 Hz.

1:20

1pMUa2. Input impedance measurements of conical acoustic systems using the two-microphone technique. Antoine Lefebvre (Schulich School of Music, McGill University, 555 Sherbrooke Street West, Montreal, QC H3A 1E3, Canada, antoine.lefebvre2@mail.mcgill.ca), Gary Scavone (Schulich School of Music, McGill University, 555 Sherbrooke Street West, Montreal, QC H3A 1E3, Canada, gary@music.mcgill.ca)

The two-microphone technique with a broadband excitation has been used for the measurement of various objects including straight conical waveguides and alto saxophones. An improved procedure has been developed whereby the noise excitation signal is pre-filtered by the inverse frequency response of the system under consideration. This approach helps reduce distortion and improves the SNR of the measurement. Results with and without pre-filtering are compared for different fingerings of an alto saxophone. The input impedance of a straight conical waveguide is compared with theory and discrepancies are analyzed. The input impedance of saxophones are evaluated with the transmission matrix approach and compared with measurements. A software environment for efficient comparison and analysis of measurement data with theoretical calculations is presented. We also propose a framework for sharing raw measurement data among researchers to allow comparison of results obtained with different apparatus on similar objects to better quantify their accuracy.

Contributed Paper

1:40

1pMUa3. Improved precision in acoustic impedance measurements by using calibration loads without resonances. Paul Dickens (University of New South Wales, Music Acoustics, School of Physics, NSW 2052 Sydney, Australia, PDickens@resmed.com.au), John Smith (University of New South Wales, Music Acoustics, School of Physics, NSW 2052 Sydney, Australia, john.smith@unsw.edu.au), Joe Wolfe (University of New South Wales, Music Acoustics, School of Physics, NSW 2052 Sydney, Australia, J.Wolfe@unsw.edu.au)

Although the input impedance of a one-dimensional waveguide is simply defined by the ratio of pressure to volume flow measured at its input, the deficiencies of available transducers require a more complicated approach for precise measurements. These can involve multiple transducers at points within an impedance head connected to the measured load. However, resonances and/or singularities during calibration and/or measurement often limit the precision of acoustic impedance spectra. This paper reviews and compares several established techniques, and describes a technique that incorporates three features that can considerably improve precision. The first feature involves minimising the problems due to resonances by calibrating the instrument using up to three different acoustic reference impedances that do not themselves exhibit resonances: an acoustically infinite waveguide, an acoustic open circuit and an acoustically infinite flange. The second feature involves using multiple pressure transducers to reduce the effects of measurement singularities. The third involves iteratively tailoring the spectrum of the stimulus signal to control the distribution of errors across the particular measured impedance spectrum. Examples are given of the performance of the technique on simple cylindrical waveguides and some wind instruments, including the saxophone and clarinet.

Invited Paper

2:00

1pMUa4. A practical way to measure intonation quality of woodwind instruments using standard equipment without custom made adapters. Wilfried Kausel (Inst. f. Wiener Klangstil, Univ. f. Music, Anton von Webernplatz 1, A-1030 Vienna, Austria, kausel@mdw.ac.at), Helmut Kuehnelt (Inst. f. Wiener Klangstil, Univ. f. Music, Anton von Webernplatz 1, A-1030 Vienna, Austria, Helmut.Kuehnelt@arsenal.ac.at)

Woodwinds are not much different from brass instruments in how intonation is determined by air column resonances. Nevertheless, it is easier to measure input impedance of brasses because the input cross-section at the mouthpiece rim is circular, plane and big enough to be easily coupled to standard measuring heads. In reed instruments the input cross-section is neither flat nor circular nor well defined. Flute instruments not even have any definable input cross-section as this is controlled by the player's lower lip. On top of that, flutes are played at an open end where some coupled impedance considerably influenced by the nearby environment like lips, mouth, and face of the player has to be taken into account. Existing approaches to measure input impedance of woodwind instruments usually require custom made adaptors optimised to yield nearly accurate intonation results for a specific instrument and playing range only. The proposed new approach is to separate instrument head or mouthpiece from the body and measure both parts from their cylindrical ends. During the measurement a natural playing condition can be simulated at the now available end. Both measurements can be assembled computationally yielding useful intonation results as will be demonstrated for flutes and saxophones.

Contributed Paper

2:20

1pMUa5. Measured and calculated sounding frequencies of pipes coupled with free reeds. James Cottingham (Coe College, 1220 First Avenue NE, Cedar Rapids, IA 52402, USA, jcotting@coe.edu), Eric A. Dieckman (Truman State Univ., Physics Dept., Kirksville, MO 63501, USA, ead603@truman.edu)

The Asian free-reed mouth organs incorporate approximately symmetric free reeds coupled to pipe resonators. Previous research has shown that the reeds in these instruments behave as "blown-open" reeds in which the playing frequency is above both the natural frequency of the reed and the first peak of the measured impedance curve. Measurements of the input impedance have been made for a variety of these instruments. Detailed calculations of input impedance have also been made using transmission matrices, taking into account the position of the reed along the pipe, tuning slots, finger holes, and nonuniform cross sections. These calculations are in good agreement with the measured impedances of the same instruments. If the reed is treated as a damped, driven harmonic oscillator, the sounding frequencies of these reed-pipes can be predicted using a phase relation between the reed vibration and the phase of the complex impedance. [Research supported by National Science Foundation REU Grant PHY-0649007.]

Invited Papers

2:40

1pMUa6. Calibration of apparatus for wave separation in wind instruments. Giovanni De Sanctis (Queen's University Belfast, University Road, BT7 1NN Belfast, UK, gdesanctis01@qub.ac.uk), Maarten Van Walstijn (Sonic Arts Research Centre, Queen's University Belfast, BT7 1NN Belfast, UK, m.vanwalstijn@qub.ac.uk)

Knowledge of the forward and backward traveling waves inside the bore of a wind instrument is a useful starting point for the estimation of its playing parameters. These are mainly parameters describing the mouthpiece embouchure and the states of the tone holes. Due to the highly nonlinear behaviour of the excitation mechanism, a precise estimation is needed. The separation method under investigation relies on a model inversion, starting from the pressure measured by three microphones. For this reason the estimation is very sensitive to the relative positions of the microphones, and the latter must therefore be known very precisely. A geometrical measurement would not be reliable because of construction tolerances, including uncertainties about the acoustic centers of the microphones; therefore the distances are gathered through audio measurements. A number of approaches to such a calibration of the measurement system have been investigated, using a purposely constructed apparatus which will also be described.

3:00

1pMUa7. Acoustic pulse reflectometry for the measurement of horn crooks. Jonathan Kemp (Edinburgh University, 4201 JCMB, Kings Buildings, Mayfield Road, EH9 3JZ Edinburgh, UK, jonathan@ph.ed.ac.uk), John Chick (Edinburgh University, 4201 JCMB, Kings Buildings, Mayfield Road, EH9 3JZ Edinburgh, UK, john.chick@ed.ac.uk), Murray Campbell (Edinburgh University, 4201 JCMB, Kings Buildings, Mayfield Road, EH9 3JZ Edinburgh, UK, dmc@ph.ed.ac.uk), Darren Hendrie (Edinburgh University, 4201 JCMB, Kings Buildings, Mayfield Road, EH9 3JZ Edinburgh, UK, darrenhendrie@hotmail.com)

The echo-based technique of acoustic pulse reflectometry can be used to measure tubular objects to determine the bore profile. In this paper, measurements of historic orchestral horn crooks are presented showing how the technique can help to determine the method of construction of historic crooks and can provide valuable information to manufacturers of reproduction period instruments. Comparison of the bore profile measured by pulse reflectometry and the known exit radius of the crook can be used to determine the presence of leaks. The technique is shown to be sensitive enough to find a leak in a horn crook that behaves reasonably under playing conditions and was not suspected of having a leak prior to testing.

Contributed Papers

3:20

1pMUa8. Industrial applications of acoustic pulse reflectometry. Noam Amir (Tel Aviv University, Dept. of Communications Disorders, Sheba Medical Center, 52621 Tel Hashomer, Israel, noama@post.tau.ac.il), Oded Barzelay (AcousticEye LTD., 4 Harechev st., 67771 Tel Aviv, Israel, oded@acousticeye.com), Tal Pechter (AcousticEye LTD., 4 Harechev st., 67771 Tel Aviv, Israel, tal@acousticeye.com)

Acoustic pulse reflectometry (APR) has been used extensively in the study of wind instruments, for measuring input impedance, bore reconstruction, and fault detection. Industrial applications have often been mentioned in the literature, though they have barely been exploited. Academic APR systems are extremely bulky, which limits their industrial use severely. Two requirements from such an industrial system are that the source tubes be as short as possible, and that they be able to measure long objects, often much longer than most musical instruments, e.g., condenser tubes which are at least 8 m long. This creates difficult calibration problems and difficulties in obtaining sufficient SNR levels, especially at low frequencies. In this paper we describe a system with the necessary adaptations for industrial use. We demonstrate the problems that are encountered, and introduce solutions which we have implemented. Modifications to the deconvolution phase improve low frequency SNR, which is further improved using nonlinear filtering. Adaptive filters are then used to discriminate between a faulty and intact system. When faults are detected, they are identified using several identification algorithms based on matched filtering and local inverse scattering.

3:40

1pMUa9. Influence of the bocal on the sound of the bassoon. Johannes Baumgart (Technische Universität Dresden, Institute for Aerospace Engineering, 01062 Dresden, Germany, johannes.baumgart@tu-dresden.de), Timo Grothe (Technische Universität Dresden, Institute for Aerospace Engineering, 01062 Dresden, Germany, timo.grothe@tu-dresden.de), Roger Grundmann (Technische Universität Dresden, Institute for Aerospace Engineering, 01062 Dresden, Germany, roger.grundmann@tu-dresden.de)

The bocal of a bassoon is characterized by geometrical parameters such as the bore, the outer contour and the wall-thickness as well as material parameters and the coating. Professional bassoonists select bocals extremely carefully and report influences on the playability and sound colour. In order to understand the underlying effects, several experiments were performed with bocals of the same bore bent in two different shapes and with two different materials. Images of a high-speed camera show a periodic motion of the bocal tip while the instrument is artificially blown. A modal analysis of the bocals was performed experimentally and numerically to investigate the dynamic behaviour of the structure. The first bending mode of the bocals is around 70 Hz. While the material properties shift the modal frequencies less than 2%, the shift due to the geometry is more than 10%. The experimental program included playing experiments with professional bassoonists. The setup was fixed and the players used the same reed. For each player, slight shifts in the sound spectra could be found due to the use of different bocals. The harmonic structure showed changes in the frequency bands where the bending modes differ.

Session 1pMUb

Musical Acoustics: Edge Tone and Flue Pipes I

Shigeru Yoshikawa, Cochair
Dept. of Acoustic Design, Kyushu University, Fukuoka 815-8540, Japan

Judit Angster, Cochair
Fraunhofer Institute for Building Physics, Nobelstrasse 12, Stuttgart, 70569, Germany

Invited Papers

4:20

1pMUb1. Influence of the geometrical parameters in flue instruments on the vorticity modulation near the separation points of the jet. François Blanc (Institut Jean Le Rond d'Alembert/LAM (UPMC/CNRS/Ministère Culture), 11, rue de Lourmel, 75015 Paris, France, blanc@lam.jussieu.fr), Pierre-Yves Lagrée (Institut Jean le Rond d'Alembert - FCIH team, 4 place Jussieu, 75006 Paris, France, pyl@ccr.jussieu.fr), Patricio De La Cuadra (Centro de Investigación en Tecnologias de Audio (CITA), Universidad Católica de Chile, Alameda 340, Oficina 13, Casilla 114-D Santiago, Chile, pcuadra@uc.cl), Benoit Fabre (Institut Jean Le Rond d'Alembert/LAM (UPMC/CNRS/Ministère Culture), 11, rue de Lourmel, 75015 Paris, France, fabreb@ccr.jussieu.fr)

In the making of the recorder, great care is given to the shape of the chamfers at the exit of the channel. Makers insist on the need of sharp chamfers, for a good tone quality. Recorders made with rounded chamfers present a noisy sound. On the other hand, in the flute, the channel is made by the lips of the musician, defining a rounder geometry. Previous work show that variations of the geometry of the exit of the channel has little influence on the velocity profile of the jet and on the position of the separation points. Thus, variations of the geometry are expected to affect mainly the interaction between the air jet and the acoustic field. The paper will present measurements together with direct Navier Stokes calculations for different geometrical configurations of a jet emerging in a transverse oscillating velocity field. We investigate the modulation of the vorticity of the jet shear layers by the acoustical field, in the vicinity of the separation points, in an attempt to develop a model that allows to predict the influence of the geometry.

4:40

1pMUb2. Mode transition of a flue organ pipe. Seiji Adachi (Fraunhofer Institute for Building Physics, Nobelstrasse 12, 70569 Stuttgart, Germany, seiji.adachi@ibp.fraunhofer.de), Judit Angster (Fraunhofer Institute for Building Physics, Nobelstrasse 12, 70569 Stuttgart, Germany, an@ibp.fhg.de), Andras Miklos (Fraunhofer Institute for Building Physics, Nobelstrasse 12, 70569 Stuttgart, Germany, an@ibp.fhg.de)

A flue organ pipe can be excited in various acoustic modes by changing the air pressure supplied to it. This research aims to reconstruct this behavior from the result of numerical flow simulation of a jet deflected by sound and from physical modeling simulation of the total sound production system. In the numerical flow simulation, motion of the jet in the pipe mouth was replicated: The jet emerges from a flue and travels in a space where the air oscillates laterally to the jet direction. As a result, the jet oscillates with the same frequency as the oscillation of the air i.e., sound. From the flow simulation, a model of the jet deflection was developed. This model was then used as a model of the sound source in the physical modeling simulation where not only the sound source but the resonance of the pipe is also modeled in a set of differential equations with delayed feedback. The mode transition observed in the physical modeling simulation was discussed by comparing with that experimentally observed.

5:00

1pMUb3. Frequency and phase characteristics of the edge tone. György Paál (Budapest University of Technology and Economics, P.O. Box 91, 1521 Budapest, Hungary, paal@hds.bme.hu), István Vaik (Budapest University of Technology and Economics, P.O. Box 91, 1521 Budapest, Hungary, vaik@hds.bme.hu)

Extensive experimental and computational work was performed to characterize the edge tone phenomenon. The dependence of the oscillating frequency on some of the main parameters of the configuration including the nozzle-wedge distance and the profile and the mean velocity of the jet was measured. The frequency was obtained from the FFT of a pressure sensor signal. The measured and computed frequencies are compared and show a very good agreement. For both the CFD simulations and the experiments the phase of the oscillation and the pressure at specified points on the wedge are correlated. For the experiments the phase of the flow oscillation is determined with the help of flow visualization pictures obtained by a high speed digital camera. From the CFD results spatial distribution of acoustical sources are also observed and correlated with pressure distribution on the wedge and with the phase of the oscillating flow. Some aspects of the initial transients are also presented.

5:20

1pMUb4. Influence of the edge tone (mouth tone) on the sound of flue organ pipes as a function of pipe scaling. Judit Angster (Fraunhofer Institute for Building Physics, Nobelstrasse 12, 70569 Stuttgart, Germany, an@ibp.fhg.de), Andras Miklos (Steinbeis Transfer Center Applied Acoustics, Landauer Str. 24, D-70499 Stuttgart, Germany, Andreas.Miklos@urz.uni-heidelberg.de)

The sound quality of an organ pipe is mainly influenced by the attack transients. This onset is first dominated by the edge tone, while later the pipe resonator will play a more important role. To understand the physics of a flue organ pipe, it is necessary to analyse the edge tone, the acoustic properties of the pipe resonator, the attack transient and the stationary sound of the pipe. Several pipe ranks have been investigated in the anechoic room of the Fraunhofer IBP: Nachthorn, Diapason, Gamba, Octave, Flute, Geigenprinzipal, Salizional. By the evaluation all physical effects contributing to the production of sound were taken into account. In the present paper about the physical effect of the edge tone on the production of the pipe sound will be reported.

5:40

1pMUb5. Development of an adjustable pipe-foot model of a labial organ pipe. Hubert Außerlechner (Fraunhofer Institute for Building Physics, Nobelstrasse 12, 70569 Stuttgart, Germany, hubert.ausserlechner@ibp.fraunhofer.de), Judit Angster (Fraunhofer Institute for Building Physics, Nobelstrasse 12, 70569 Stuttgart, Germany, an@ibp.fhg.de), Andras Miklos (Steinbeis Transfer Center Applied Acoustics, Landauer Str. 24, D-70499 Stuttgart, Germany, Andreas.Miklos@urz.uni-heidelberg.de)

In order to understand the physical processes involved in the build-up of the sound signal in a pipe (in our case a labial organ pipe) a pipe-foot model has been developed, with which the main important parameters, such as positions of the lower- and upper-labium, the wind pressure in the foot and the width of the flue can be adjusted. Moreover, different types of languids and pipe bodies (resonators) can be attached to the model. For the reason of corresponding to a real metal organ pipe these parts of the model are made of "organ metal." The reproducibility of measurements is provided by the micrometer screws applied for the adjustments. Flow and edge-tone measurements were carried out with the help of this model. A comparison with real organ pipes gives some indications for the range of the parameters. Because of the flexible adjustments and the large range of values of every parameter, it is possible to find different ranges with varying parameter settings for the occurrence of the edge-tone. The analysis of these measurement results shows the dependency of the edge-tone of the adjusted parameters.

MONDAY AFTERNOON, 30 JUNE 2008 AMPHI MAILLOT, 6:00 TO 7:20 P.M.

Session 1pMUc

Musical Acoustics and Psychological and Physiological Acoustics: Acoustics and Psychoacoustics of Pipe Organs

Jonas Braasch, Cochair
Rensselaer Polytechnic Institute, Greene Bldg., 110 8th St., Troy, NY 12180, USA

David M. Howard, Cochair
University of York, Department of Electronics, Heslington, York, YO10 5DD, UK

Invited Papers

6:00

1pMUc1. Voicing documentation of a pipe organ. Christophe D'Alessandro (LIMSI-CNRS, B.P. 133, 91403 Orsay, France, cda@limsi.fr)

The paper begins with a brief presentation on the Parisian organ landscape, and then focuses on sound documentation of the historical organ of Sainte Elisabeth (Suret 1853, 3 keyboards and pedal, 40 stops, about 2500 pipes). Calibrated recordings of all the notes have been performed inside and outside the organ case, using several microphone positions. The methodology proposed by Pollard (J. Acoust. Soc. Am. **106**(1), July 1999, 360-370) is extended and applied to sound analysis for all the notes of the instrument. The analogies between the proposed sound description (or "voicing quality," described in terms of sharpness, loudness, tristimulus coordinates, transient building, and spectral centre of gravity) and human voice quality description are discussed. Both voicing of individual pipes and voicing of the instrument are analysed. "Voicing of the instrument" means voicing variations of the pipes for different notes or registers of a same stop, for different stops of a same division, and for different divisions of the instrument. This methodology may be applied to documentation and characterisation of the "style" of the instrument in terms of its acoustic signature, provided additional information on recording conditions and room acoustics are available.

6:20

1pMUc2. Documenting the acoustics of the Silbermann pipe organ at the Catholic Cathedral in Dresden before and after the restoration of 2002. Christian Ahrens (Musikwissenschaftliches Institut, Ruhr-Universität Bochum, Universitätsstr. 150, 44780 Bochum, Germany, christian.ahrens@rub.de), Jonas Braasch (Rensselaer Polytechnic Institute, Greene Bldg., 110 8th St., Troy, NY 12180, USA, braasj@rpi.edu), Sebastian Schmidt (Institute of Communication Acoustics, Ruhr-Universität Bochum, IC 1/142, Universitätsstr. 150, 44780 Bochum, Germany, sebastian.schmidt@rub.de)

Gottfried Silbermann's pipe organ at the Catholic Cathedral of the Saxonian Court in Dresden was, with 47 stops, the largest instrument he had ever built. The instrument was evacuated during World War II and luckily survived intact, while the church itself was badly damaged. The instrument received a more romantic sound ideal after its resurrection in 1971. The biggest deviation from the original concept of Silbermann was the change from church pitch (A_4=415 Hz) to chamber pitch (A_4=440 Hz). In 2002, the instrument was renovated again with the goal to restore the instrument to the original design of 1755. The work was commissioned to two local organ builders, Kristian Wegscheider and Jehmlich Orgelbau, and the authors received the unique opportunity to measure the instrument before and after the restoration. During the measurements, the pipes of each stop were recorded in the near field in steps of a third. The acoustical comparison between each pipe before and after the restoration shows significant differences that match the informal observations of expert listeners. In general, the pipes received more energy in the higher partials and had a better attack response. Another interesting finding is the improvement of the pipes' formants after the restoration.

Contributed Papers

6:40

1pMUc3. The physical characteristics of mechanical pipe organs and how much they allow the organist to influence the initial transient. Jose Grossinho (R. Francisco da Silva Marques, n°5, 2°Dto, 2825-125 Caparica, Portugal, zefino@netcabo.pt)

It has been accepted by organists that one can change the timbre of the organ simply by varying the velocity of the key. Previous research (Nolle, 1941, 1992) shows clearly that there is a change in the initial transient of the sound with different pressure rise times (PRT) on the foot of the pipe. More recent research (Woolley, 2006) shows that in mechanical action organs there is no major difference in the velocity of the key when the organist thought there was. The velocity of opening of the pallet is one of the main aspects that influence the PRT. Calculations of the flexibility of mechanical parts from organs in Mafra, Portugal, were taken, as well as motion of the key, pressure on the pipe's foot and sound measurements on a model organ, using human touch on the key. Due to the pressure differences in the wind chest and the groove, it is difficult to control the pallet movement after it starts to open. The results show that there is a more efficient control of the velocity of opening of the pallet on more rigid actions, giving a better control to the organist over the timbre of the instrument.

7:00

1pMUc4. Very-low frequency range influence for free reed instruments physical modeling. Laurent P. Millot (IDEAT (University Paris 1), ENS Louis-Lumière, 7 allée du Promontoire, 93161 Noisy-le-grand, France, l.millot@ens-louis-lumiere.fr)

Measurements of the inner and outer over-pressure for a diatonic harmonica were performed during blown, drawn, and bend notes notably. Using an energy analysis based on a nonregular spectral decomposition of the energy with only 10 frequency subbands, the IDS analysis, we have compared the relative weights of each subbands for both inner and outer pressure signals. This comparison underlines the key role played by the very low frequency range (0-50 Hz) and justifies a physical modeling without any waves occurrences but taking into account only acoustical flows descriptions. Within the presentation the audience will listen these phenomena and will access an explanation of the details of the physical modeling which has been used and which permits to refind chromatical playing on a diatonic harmonica, including the vocal tract player. We will also propose some clues to include a pipe in the modeling in order to study instruments like the sheng or the harmonium for instance.

Session 1pNSa

Noise, Physical Acoustics, and EURONOISE: Aeroacoustics I

Philip J. Morris, Cochair
Penn State University, 233C Hammond Building, University Park, PA 16802, USA

Christophe Bailly, Cochair
Ecole Centrale de Lyon, 36, avenue Guy de Collongue, LMFA, Ecully, 69134, France

Invited Papers

1:00

1pNSa1. Jet noise from large-scale turbulent structures. Philip J. Morris (Penn State University, 233C Hammond Building, University Park, PA 16802, USA, pjm@psu.edu)

The generation sound by large-scale turbulent structures in jets, where the structures are convecting supersonically with respect to the ambient speed of sound, is well understood. The pressure pattern generated by the large-scale structures couples directly with the radiated sound field. An instability wave model for the development of the large-scale structures gives excellent predictions of both the near and far acoustic fields. However, when the structures are convecting subsonically, there is no general agreement as to how or even whether they generate any noise directly. Recent experimental evidence has shown a remarkable similarity between the jet noise spectra in the vicinity of the peak noise radiation direction for both subsonic and supersonic jets. This suggests that the large-scale structures do contribute directly to jet noise radiation at all jet operating conditions. In the present paper a model is developed for the noise generation mechanism. Using experimental measurements of the far field noise, the near field pressure pattern required to generate the noise can then be calculated. The question of whether this pattern is consistent with a reasonable physical model for the evolution of the large-scale turbulent structures is then discussed.

1:20

1pNSa2. Effect of jet temperature on jet noise: data and requirements for modeling. Krishnamurthy Viswanathan (The Boeing Company, M/S 67-ML, P.O. Box 3707, Seattle, WA 98124, USA, k.viswanathan@boeing.com)

The modifications to the jet spectra caused by the heating of the jet have been the subject of experimental and theoretical research since the early 1970s. Early experimental data produced ambiguous and contradictory trends, which complicated the modeling efforts. Disparate theories have been proposed; however, no fundamental explanation or theory exists to date. First of all, a comprehensive experimental program has been carried out to establish the effect of temperature on jet noise. Detailed analyses indicate that in addition to the jet velocity (Vj/a), the jet temperature ratio, either stagnation or static, is an independent controlling parameter. The spectral shape at the lower radiation angles (measured from the jet inlet) is universal and independent of the jet Mach number and temperature. In the aft directions, the spectral shape is controlled by the jet temperature ratio, regardless of the jet velocity. These recently established trends have not been incorporated in any existing theory. The modeling of the effects of jet temperature and the suitability of the proposed formulations in existing theories are examined; the need for fresh thinking and the requirements for a good model are highlighted.

Contributed Paper

1:40

1pNSa3. Correlations between the turbulent and the acoustic fields of a hot co-axial jet simulated by large-eddy simulation. Christophe Bogey (Ecole Centrale de Lyon, 36, avenue Guy de Collongue, LMFA, 69134 Ecully, France, christophe.bogey@ec-lyon.fr), Francois Coiffet (Ecole Centrale de Lyon, 36, avenue Guy de Collongue, LMFA, 69134 Ecully, France, francois.coiffet@ec-lyon.fr)

Correlations between the turbulent and the acoustic fields of a high-speed hot co-axial jet are calculated, in order to study noise generation mechanisms by a causality method. The jet flow was computed by a large-eddy simulation using specific aeroacoustic schemes. The simulation also provided directly the near-presure field, which was then extrapolated in the far field by solving the linear acoustic equations. The causality method is applied using flow quantities such as the velocity components, density, and temperature in the jet and the far field pressure, in the temporal as well as in the spectral domains. To exhibit and characterize the regions of noise generation, we are focusing on the correlation peaks, and in particular their location and corresponding frequencies. Moreover, there is an attempt to link the noise generation with the jet turbulence properties including intermittency and convection velocity. For instance, the turbulence at the end of the primary potential core was found to show high correlations with the far field pressure and significant intermittency, in a similar way as in single-stream jets.

Invited Papers

2:00

1pNSa4. Simulation of jets exhausting from chevron nozzles and their noise. Ali Uzun (Florida State University, School of Computational Science, 400 Dirac Science Library, Tallahassee, FL 32306, USA, uzun@scs.fsu.edu)

Environmental concerns and strict noise regulations around major airports have made jet noise a crucial problem in present day aeroacoustics research, as it is the jet engine exhaust that is responsible for much of the noise generation during aircraft takeoff. Chevron nozzles have drawn a lot of attention recently due to their noise reduction benefits. Chevrons typically reduce low frequency noise at aft angles while providing an increase in high frequency noise at broadside angles relative to the jet. The streamwise vorticity generated by the chevrons affects the jet shear layer mixing and thus is responsible for the decrease or increase in noise over certain frequency ranges. The ultimate goal in chevron design is to decrease low frequency noise as much as possible while preventing the increase in high frequency noise. In our research, we are performing high-fidelity numerical simulations of jets exhausting from chevron nozzles to gain a better understanding of chevron jet shear layer mixing. These simulations employ a large eddy simulation tool utilizing state-of-the-art numerical techniques. In this talk, representative results from our research will be presented and an assessment of our current prediction capability of chevron jet noise will be provided.

2:20

1pNSa5. Reduced-order models for jet noise. Ann P. Dowling (University of Cambridge, Department of Engineering, Trumpington Street, CB2 1PZ Cambridge, UK, apd1@cam.ac.uk), Mohammed Afsar (University of Cambridge, Department of Engineering, Trumpington Street, CB2 1PZ Cambridge, UK, ma357@cam.ac.uk), Sergey Karabasov (University of Cambridge, Whittle Laboratory, Department of Engineering, Madingley Road, CB3 0DY Cambridge, UK, sak36@eng.cam.ac.uk), Tom P. Hynes (University of Cambridge, Whittle Laboratory, Department of Engineering, Madingley Road, CB3 0DY Cambridge, UK, tph@eng.cam.ac.uk)

The research reported here leads to a simple prediction methodology based on a reduced-order model for jet noise. The approach is a hybrid one made up of three components. Each component uses modeling and numerical techniques optimised to suit a particular purpose. The propagation of noise to the far field is captured via a new method for solution of the adjoint linearised Euler equations, describing how sound emitted by the jet is modified by propagation through the time-averaged but spatially varying jet flowfield. The directivity of the quadrupole sources is more general than is usually assumed and their statistical properties are modeled based on a RANS solution for the jet: the cross-correlation of the turbulent quadrupoles is modelled as Gaussian with length and time parameters proportional to the local length and timescales from the RANS solution, The constants of proportionality are determined through comparison with correlations from LES and from experimental data. Hence the source model is determined entirely from near field data and the far-field sound is then predicted with no empirical constants. Comparison between this predicted noise and experimental data is very good, across a wide spectral range and even at angles close to the jet axis.

Contributed Paper

2:40

1pNSa6. Numerical study of the influence of temperature and microjets on the radiated noise for a subsonic jet. Maxime Huet (ONERA, BP 72-29 avenue de la Division Leclerc, 92322 Châtillon, France, Maxime.Huet@onera.fr), Gilles Rahier (ONERA, BP 72 - 29 avenue de la Division Leclerc, 92322 Châtillon, France, Gilles.Rahier@onera.fr), François Vuillot (ONERA, BP 72 - 29 avenue de la Division Leclerc, 92322 Châtillon, France, francois.vuillot@onera.fr)

Jet noise remains the principal nuisance source for an aircraft at take-off conditions. A previous work [1] showed that using micro-jets could be effective to modify the turbulence development and thus decrease the radiated pressure. This micro-jets effect is numerically studied for two jets. LES simulations of a cold (M = 0.9) and a hot (M = 0.636) jets, with and without micro-jets, are computed and the acoustic post-processing is performed using the Ffowcs-Williams and Hawkings surface formulation. The temperature effect on the noise is analyzed for the reference computations and, with micro-jets, the noise reduction is compared to measurements for a similar configuration [1]. Aerodynamic comparisons with experiments give a good comparison, excepted a too short potential core and overestimated turbulent kinetic energy. The noise decrease with the higher temperature and the modifications of the spectral densities are well captured by the simulations. The micro-jets provide a reduction up to more than 2 dB for the best angles. Turbulence modification is still under investigation and results will be presented. [1] Castelain, T., Béra, J., Sunyach, M., and Juvé, D., "Effect of microjets on a high-subsonic jet. Parametric study of far-field noise reduction," 12th AIAA/CEAS Aeroacoustics Conference (2006).

Invited Papers

3:00

1pNSa7. On the separation of hydrodynamic and acoustic waves in linear free-shear flows. Anurag Agarwal (Institute of Sound and Vibration Research, University of Southampton, Highfield, SO17 1BJ Southampton, UK, aa2@isvr.soton.ac.uk), Gwenael Gabard (Institute of Sound and Vibration Research, University of Southampton, Highfield, SO17 1BJ Southampton, UK, gabard@soton.ac.uk)

The governing equations for sound propagation through free-shear flows, like jets and mixing layers, are the linearized Euler equations. These equations support both hydrodynamic and acoustic waves. For an aeroacoustician wishing to study the refraction effects of a sound source by shear flows, it is important to distinguish the acoustic solution from the hydrodynamic waves. Agarwal et al. (AIAA J., Vol. 42, No. 1, 2004) presented a technique to achieve this in the frequency domain. In this talk, we present a time-domain technique to separate the hydrodynamic and acoustic waves. The idea is to implement a filter that filters out only the acoustic wave solution from the linearized Euler equations. Some sample solutions are presented for two-dimensional free-shear flows and comparisons are made against known analytical solution for parallel flows and from solution obtained by approximate methods, which have a limited range of applicability. The advantage for the present technique is that it is applicable to arbitrary frequencies and flow profiles.

3:20

1pNSa8. Turbulent flow noise around a zero-incidence airfoil. Olivier Marsden (Ecole Centrale de Lyon, 36, avenue Guy de Collongue, LMFA, 69134 Ecully, France, olivier.marsden@ec-lyon.fr), Christophe Bogey (Ecole Centrale de Lyon, 36, avenue Guy de Collongue, LMFA, 69134 Ecully, France, christophe.bogey@ec-lyon.fr), Christophe Bailly (Ecole Centrale de Lyon, 36, avenue Guy de Collongue, LMFA, 69134 Ecully, France, christophe.bailly@ec-lyon.fr)

A large eddy simulation (LES) of the flow around a NACA 0012 airfoil at zero incidence, at a chord-based Reynolds number of 500,000 and a Mach number of 0.22, is presented. The aim is to show that high-order numerical schemes can successfully be used to perform direct acoustic computations of compressible transitional flow on curvilinear grids. At a Reynolds number of 500,000, the boundary layers around the airfoil transition from an initially laminar state to a turbulent state before reaching the trailing edge. Results obtained in the LES show a well-placed transition zone, and turbulence levels in the boundary layers in agreement with analytical developments as well as experimental data. Furthermore, the radiated acoustic field is determined directly by the LES, without the use of an acoustic analogy. Third-octave acoustic spectra are compared to experimental data, with deviations of around 3 dB per band exhibited.

Contributed Paper

3:40

1pNSa9. Preliminary screening of flow behavior around airfoils using a microphone phased array. Marcel C. Remillieux (Virginia Tech, Mechanical Engineering, 153 Durham 0238, Blacksburg, VA 24061, USA, mremilli@vt.edu), Ricardo A. Burdisso (Virginia Tech, Mechanical Engineering, 153 Durham 0238, Blacksburg, VA 24061, USA, rburdiss@vt.edu), William J. Devenport (Virginia Tech, Aerospace and Ocean Engineering, 224E Randolph Hall, Blacksburg, VA 24061, USA, devenport@vt.edu)

Recently, as a part of research projects for the National Renewable Energy Laboratory (NREL) and Sandia National Laboratories, several full-scale, wind-turbine airfoils were tested at various speeds (high Reynolds numbers) and angles of attack in the Virginia Tech Stability Wind Tunnel. This unique facility is aerodynamically closed and acoustically open, which allows better aerodynamic performance than a free jet facility, while maintaining comparable acoustic performance. Flow measurements consisted of monitoring the surface pressure around the airfoils with a distribution of pressure taps on the airfoil surface. Acoustic measurements were carried out with a microphone phased array. The phased-array data was post-processed to generate acoustic maps of the noise generated by the airfoils exposed to the flow as well as their noise spectra. In addition to the tests, two-dimensional CFD computations of the flow field around the airfoils were carried out using a k-ϵ turbulent model. The acoustic maps clearly show the noise sources generated by potential turbulent flow around the airfoils. The very good correlation between the acoustic maps and the flow characteristics of the airfoils, both numerical and experimental, allows for phased-array measurements to be used as a tool for preliminary screening of the flow behavior around a given airfoil.

4:00-4:20 Break

Invited Paper

4:20

1pNSa10. Experimental analysis of the wall aerodynamics and acoustic radiation of the trailing edge of an airfoil in subsonic flow. Cyrille Bonamy (Laboratoire d'Etudes Aérodynamiques (LEA), Université de Poitiers - ENSMA - CNRS, Bâtiment K, 40 Avenue du Recteur Pineau, 86022 Poitiers, France, cyrille.bonamy@lea.univ-poitiers.fr), Yves Gervais (Laboratoire d'Etudes Aérodynamiques (LEA), Université de Poitiers - ENSMA - CNRS, Bâtiment K, 40 Avenue du Recteur Pineau, 86022 Poitiers, France, yves.gervais@lea.univ-poitiers.fr)

This experimental study treats of the trailing edge noise mechanisms, especially broadband noise, resulting from the hydrodynamic wave diffraction on the sharp edge of a foil in flow, with the aim of improving its modeling. A detailed review of the dynamic behaviour of the phenomenon characteristic aerodynamic quantities (wall pressure and velocity fluctuations) has been made on a Naca 0012 airfoil and particular statistical data analysis have been performed (POD, temporal and spectral visualizations, spatial filtering by transducer array). Some models from the literature related to the wall pressure statistics (Corcos, Chase) have been adjusted and validated, and finally used for the modeling of the noise from the trailing edge of the airfoil. To conclude, measurements of the radiated acoustic pressure have been made in an anechoic wind tunnel, showing as a result the validity and limits of the implemented aeroacoustic model. The approach proposed by Chase in terms of wall pressure statistic modeling appears to be able to correctly represent the influence of the problem main parameters (Reynolds number, airfoil incidence).

Contributed Papers

4:40

1pNSa11. A numerical insight into the effect of confinement on trailing edge noise. Thomas Le Garrec (Arts et Métiers Paris Tech - Sinumef Lab, 151 bd de l'Hopital, 75013 Paris, France, thomas.le-garrec@paris.ensam.fr), Xavier Gloerfelt (Arts et Métiers Paris Tech - Sinumef Lab, 151 bd de l'Hopital, 75013 Paris, France, xavier.gloerfelt@paris.ensam.fr), Christophe Corre (LEGI Lab, BP 53, 38041 Grenoble Cedex 9, France, christophe.corre@hmg.inpg.fr)

The flow and the acoustic field around a 3D NACA 0018 airfoil at Reynolds 160 000 with an angle of attack of 6° are investigated numerically by direct noise computation to make comparisons with the experimental results of Nakano et al. (Experiments in Fluids, 2005) and the numerical simulations of Kim et al. (Heat and Fluid Flow, 2006). The direct noise computation of the flow around a 3D airfoil reaches the limits of current computational capacities. Indeed the main difficulty of such simulations comes from the large disparities between the fine scales of turbulence and the large wavelengthes of acoustic radiation which impose severe constraints on the meshes. In order to limit the number of points and to reduce the calculation cost, a multisize-mesh multitime-step strategy is adopted. The main purpose of the paper is to study numerically the influence of the confinement due to the top and bottom surfaces of the wind tunnel used in the experiments of Nakano et al. on the flow around the airfoil. The numerical results for a con-

fined airfoil will be compared to the results obtained when the top and bottom walls are removed. So the noise can be directly linked to the vortices which develop in the wake of the airfoil.

5:00

1pNSa12. Coupled oscillations in the aeroacoustics of a Katana blade. Michel Roger (Ecole Centrale de Lyon, 36 Avenue Guy de Collongue, Centre Acoustique, 69134 Ecully, France, michel.roger@ec-lyon.fr)

The paper investigates experimentally the tonal characteristics of the aerodynamic sound of a Katana blade handled at high speed. Katana is the name of the Japanese sword used in martial arts. It is designed with a sharp cutting edge, a thick black-edge, and sometimes so-called blood-grooves. When handled through the air, the blade radiates sound at different frequencies. First a low-frequency, dominant sound is heard due to the von Karman vortex shedding in the wake of the blade. Second high-frequency tones are produced in the case of a Katana with grooves. The tones result from the self-sustained oscillations of the detached shear layers over the grooves which behave like cavities under a grazing flow. In the case of a Katana with no groove, other high-frequency tones are heard due to acoustic back-reaction on the Tollmien-Schlichting waves growing in the boundary layers. The variations of the acoustic signature with varying angle of attack and relative flow speed are analyzed in the paper, with emphasis on the coupling between the different mechanisms. The main trends are compared to simple self-sustained oscillation formulae. Finally the possible use of the sound as a criterion of inaccuracies in the handling of the Katana is discussed.

5:20

1pNSa13. Large-eddy simulation of roughness-generated boundary-layer noise. Meng Wang (University of Notre Dame, Departmernt of Aerospace and Mechanical Engineering, Notre Dame, MD 46556, USA, m.wang@nd.edu), Qin Yang (University of Notre Dame, Departmernt of Aerospace and Mechanical Engineering, Notre Dame, MD 46556, USA, qyang@nd.edu)

A computational study is carried out to predict rough-wall boundary layer noise and elucidate noise generation mechanisms. As a first step, the sound radiation from a single hemispherical roughness element in a turbulent boundary layer at Re_θ=7500 is investigated. The roughness height is 3.6% of the boundary layer thickness, or 95 wall units. The flow field is computed by large-eddy simulation. The velocity statistics show reasonable agreement with the experimental data measured at Virginia Tech. Acoustic calculations are performed based on the Curle-Powell integral solution to the Lighthill equation. The sound radiation is dominated by unsteady drag dipoles and their images in the wall, with the spanwise dipole of similar magnitude or stronger compared to the streamwise dipole. The viscous contribution to the drag dipole is negligible relative to the pressure contribution. Numerical experiments are performed to isolate the roles of vortex shedding and diffraction of convected hydrodynamic pressure by the roughness element; both are shown to be important noise source mechanisms. The effects of roughness height, upstream wake, and multiple roughness elements are discussed as well.

5:40

1pNSa14. The mechanisms of roughness noise. William J. Devenport (Virginia Tech, Aerospace and Ocean Engineering, 224E Randolph Hall, Blacksburg, VA 24061, USA, devenport@vt.edu), Stewart A. Glegg (Florida Atlantic University, Department of Ocean Engineering, Boca Raton, VA 33431, USA, glegg@oe.fau.edu), Nathan Alexander (Virginia Tech, Aerospace and Ocean Engineering, 224E Randolph Hall, Blacksburg, VA 24061, USA, alexande@vt.edu), Ben Smith (Virginia Tech, Aerospace and Ocean Engineering, 224E Randolph Hall, Blacksburg, VA 24061, USA, besmith5@vt.edu)

The interaction of turbulence and a rough surface results in the radiation of sound that is not produced in smooth wall flows. The mechanisms by which this sound is generated are not well understood. Scattering of the convected turbulent pressure field by the surface irregularities seems to be a probable source when the roughness size is small compared to the boundary layer. The bluff body mechanisms of vortex shedding and unsteady drag from the roughness elements appear more likely to be dominant sources when those elements are large compared to the boundary layer. Demonstrating the existence of these mechanisms, their range of dominance, the extent to which they are distinct and can be characterized in terms of flow parameters that can be realistically modeled (such as the surface pressure spectrum), are all pre-requisites to the development of a robust prediction method. New insight into these issues has been obtained through measurements made with using a purpose built roughness noise facility in combination with fundamental theoretical analysis of the problem. The measurements include roughness noise spectra, wall pressure spectra and aerodynamics for a large variety of rough surfaces. This work is supported by the Office of Naval Research.

Invited Paper

6:00

1pNSa15. Modeling and prediction of fan noise. Edmane Envia (NASA Glenn Research Center, Acoustics Branch, M.S. 54-3, 21000 Brookpark Road, Cleveland, OH 44135, USA, edmane.envia-1@nasa.gov)

Fan noise is a significant contributor to the total noise signature of a modern high bypass ratio aircraft engine and, with the advent of ultrahigh bypass ratio engines like the geared turbofan, it is likely to remain so in the future. As such, accurate modeling and prediction of the basic characteristics of fan noise are necessary ingredients in designing quieter aircraft engines in order to ensure compliance with ever more stringent aviation noise regulations. In this paper, results from a comprehensive study aimed at establishing the utility of current tools for modeling and predicting fan noise will be summarized. It should be emphasized that these tools exemplify present state of the practice and embody what is currently used at NASA and industry for predicting fan noise. The ability of these tools to model and predict fan noise is assessed against a set of benchmark fan noise databases obtained for a range of representative fan cycles and operating conditions. Detailed comparisons between the predicted and measured narrowband spectral and directivity characteristics of fan noise will be presented in the full paper. General conclusions regarding the utility of current tools and recommendations for future improvements will also be given.

6:20

1pNSa16. Contra-rotating fans noise prediction for jet engine performance optimization. Dax Au (ISAE, 10, av Edouard Belin, 31055 Toulouse, France, dax.au@isae.fr), Alexandre Leblanc (ISAE, 10, av Edouard Belin, 31055 Toulouse, France, alexandre.leblanc@isae.fr)

This work fits within the framework of the European research project VITAL, which is dedicated to the development of technologies aimed at reducing the environmental impact of jet engines. In this respect, a new concept of ducted contra-rotating fans is investigated. The present contribution to this project is to elaborate a noise prediction tool for performances optimization. On the basis of the helicoidal surface theory, Hanson previously developed a harmonic formulation for the propfan rotor/rotor interaction. This method is here extended in order to take into account the duct effects and the noise radiated by the rear struts. A computer program has been written to predict the pressure distribution in the near field and to estimate the noise spectra in the far field. The results are validated with computational fluid dynamics simulations and compared with available public data. Those predictions are then included in a global noise computation with the other engine acoustic sources (coaxial jet, combustor and so on), and a multidisciplinary optimizer is used for the engine noise minimization.

6:40

1pNSa17. Design of a low noise radial fan with computational aeroacoustics. Esra Sorgüven (Yeditepe University, Kayisdagi, 34755 Istanbul, Turkey, sorguven@yeditepe.edu.tr),Yilmaz Dogan(Arcelik A.S., Tuzla, 34950 Istanbul, Turkey, yilmaz.dogan@arcelik.com), Ergin Arslan (Arcelik A.S., Tuzla, 34950 Istanbul, Turkey, ergin.arslan@arcelik.com)

Aim of this study is to employ computational aeroacoustics methods in order to design a fan system. Design objectives of this study are to decrease the flow-induced noise, to provide the necessary flow rate and pressure increase. During the design, modern computational methods will be employed in addition to traditional turbomachinery design methods. The design procedure begins with a baseline fan system design, which is based on traditional semi-empirical correlations. Flow through this fan system is analyzed via computational fluid dynamics. Pressure fluctuations on rotating and stationary solid surfaces are determined to calculate sound sources of the system. The baseline design is improved by eliminating the areas where powerful sound sources occur. Flow analysis and sound prediction is repeated to improve fan system further. This step is repeated until the desired sound power level is achieved. This design procedure employs numerical analysis instead of experiments. Therefore it will be more effective and less time consuming than the experimental trial and error design procedures. The number of prototypes and necessary measurements are decreased dramatically.

Invited Paper

7:00

1pNSa18. Computational AeroAcoustics of Realistic Co-Axial Engines. Stephane Redonnet (ONERA (French Aerospace Center), CFD & Aeroacoustics Department, BP 72, 29 avenue de la division Leclerc, 92322 Chatillon Cedex, France, stephane.redonnet@onera.fr), Ciprian D. Mincu (ONERA (French Aerospace Center), CFD & Aeroacoustics Department, BP 72, 29 avenue de la division Leclerc, 92322 Chatillon Cedex, France, dmincu@onera.fr), Eric Manoha (ONERA (French Aerospace Center), CFD & Aeroacoustics Department, BP 72, 29 avenue de la division Leclerc, 92322 Chatillon Cedex, France, eric.manoha@onera.fr), Yann Druon (Airbus S.A.S, Department of Acoustic & Environment, 316 route de Bayonne, 31000 Toulouse, France, yann.druon@airbus.com), Bastien Caruelle (Airbus S.A.S, Department of Acoustic & Environment, 316 route de Bayonne, 31000 Toulouse, France, bastien.caruelle@airbus.com)

This study, that is relevant from the turbofan engines noise prediction/reduction, aims at CAA-computing the aft fan noise propagation/radiation of a realistic full-3D exhaust (with pylon and internal bifurcations), the latter being affected of (i) typical in-flight (take-off) thermodynamic conditions and of (ii) a representative fan noise modal content. As for previous studies conducted over baseline geometries, this CAA computation is conducted following the usual hybrid process, where a preliminary aerodynamic calculation provides a heterogeneous steady mean flow on which an acoustic calculation is then conducted A RANS computation is first performed, delivering the stationary jet mean flow characterizing the 3D exhaust in its typical 'take-off flight' ($M\infty = 0.25$). A CAA grid (22 blocks, 28 millions cells) is then derived from the CFD one, before the RANS steady jet mean-flow is interpolated on it. After what the CAA computation is computed, a fan noise mode (26, 1) being emitted at a reduced frequency of $kR = 30$ (1 BPF) in the upstream of the engine's secondary exhaust, and numerically propagated along and outside the latter. Finally, a Kirchhoff post-treatment provides the far-field radiation characterizing these engine geometry, modal content and thermodynamic conditions.

Session 1pNSb

Noise and EURONOISE: Action Planning and Global Solutions for Urban Noise I

Klaus Genuit, Cochair
HEAD acoustics GmbH, Ebertstrasse 30a, Herzogenrath, 52134, Germany

Itziar Aspuru Soloaga, Cochair
Labein-Tecnalia, C/Geldo-Parque Tecnologico de Bizkaia, Derio, 48160, Spain

Invited Papers

1:00

1pNSb1. Strategies for noise action plans. Paul De Vos (DHV BV, Postbus 1132, NL 3800 BC Amersfoort, Netherlands, paul.devos@dhv.com)

Following the requirements of the Environmental Noise Directive, Noise Action Plans should have been produced. The plans are supposed to build on two important pillars: the strategic noise maps and the consultation with the local residents. In some cases, the plan is considered as a mere statement of the long term policy of the authority under concern. In other cases, it is set up as an implementation plan with clear and measurable targets. Also the focus varies: only the highest noise levels could be attacked or the large numbers of exposed citizens, or even the overall annoyance. Target noise levels may lead to confusion both for local decision makers and citizens. Also, the preservation and possible creation of quiet areas can be envisaged. The use of an equal annoyance indicator helps to set the targets in the right perspective. Translation into different levels of quality of life is recommended. In terms of cost and benefits, the options for city councils are very limited. Due to a lack of European legislative power, cities tend to set their own rules, e.g. for road vehicles. Several initiatives to propose toolkits for action plans, comparable to the best practice guide for noise mapping, are welcomed but require harmonization and dissemination.

1:20

1pNSb2. From strategic noise maps to action plan: Perspective of Spanish main roads. Maria Dolores Jimenez (Dirección General de Carreteras del Ministerio de Fomento, Paseo de la Castellana 67, 28071 Madrid, Spain, mdjimenez@fomento.es), Jesus Rubio (Dirección General de Carreteras del Ministerio de Fomento, Paseo de la Castellana 67, 28071 Madrid, Spain, jjrubio@fomento.es), Fernando Segues (CEDEX Centro de Estudios de Técnicas Aplicadas, Alfonso XII, 3-5, 28014 Madrid, Spain, fsegues@cedex.es), Pilar Fernandez (Labein Tecnalia, Parque Tecnologico Bizkaia, 48160 Derio, Spain, pfernandez@labein.es)

The Direccion General de Carreteras of the Spanish Ministry of Transport is finishing the process of Strategic Noise Mapping of Spanish major roads (EGRA). The whole National road network that has been noise mapped for the first END has a length of 6.400 km round. The present paper contains - Some conclusions from the process of noise mapping; - A general view of the process of making decisions about Action Plans; - Definition of the first steps to decide the scope of Action Plans: design of a pilot study to establish the elements needed technical studies, coordination with other administration bodies and public involvement.

1:40

1pNSb3. Decision support system for Action Planning in the framework of the European Noise Directive. Jeroen Borst (TNO Science and Industry, Stieljesweg 1, 2628CK Delft, Netherlands, jeroen.borst@tno.nl), Walter J. Lohman (TNO, P.O. Box 49, NL-2600 AA Delft, Netherlands, walter.lohman@tno.nl), Arno R. Eisses (TNO, Stieltjesweg 1, P.O. Box 155, 2600 AD Delft, Netherlands, Arno.Eisses@tno.nl), Henk M. Miedema (TNO, P.O. Box 49, NL-2600 AA Delft, Netherlands, henk.miedema@tno.nl)

The European Noise Directive (END) requires assessment of noise exposures as well as the formulation of Action Plans for the reduction of the number of people harmfully affected by environmental noise. TNO is developing a decision support system for noise mitigating measures. The proof of concept of such a system for road noise is presented here. On the basis of a detailed noise map, for each road segment an indication is given for the amount of negative effect (e.g., number of people being highly annoyed) per meter it is causing. On the basis of the characteristics of the road segment, the system suggests possible noise mitigation measures. The effect of the measure chosen by the user, such as the application of silent road surface types or lowering speed limits, can be interactively explored with the system. It directly shows the updated detailed noise contour maps as well as indicators describing the impact after a measure has been applied though the interactive interface.

2:00

1pNSb4. Urban Noise Action Planning - an integrated approach towards noise abatement in the frame of urban development: Tools and recommendations developed within the SILENCE project. Melanie Kloth (Polis, rue du Trône 98, 1050 Brussels, Belgium, mkloth@polis-online.org)

Noise action planning following the European Directive on Environmental Noise is for many cities a new, additional task. It will probably be not very successful when considered as mere duty separated from other urban policy areas. Today, noise does not rank high on the local political agenda. Human and financial resources provided for noise abatement tend to be low. Furthermore, looking at concrete noise abatement measures it becomes clear that most effective measures also impact on other policy areas (air quality, mobility, etc.). Therefore it is advisable to link noise action planning closely with other urban plans like development plans, mobility plans, clean air programmes, etc. This requires a strong involvement of the relevant stakeholders as well as knowledge about the potential impact of noise abatement measures on other policy areas. To support local authorities in this complex task the SILENCE project developed a guidebook which comprises recommendations on organisational settings, on the involvement of stakeholders and the public, the action planning process as well as on a range of noise abatement measures. The description of these measures refers not only to their noise abatement potential but takes also into account their - positive or negative - impact on other policy areas.

2:20

1pNSb5. Noise Action Plan in the Ile-de-France region: a complex process. Fanny Mietlicki (Bruitparif, 25 rue Coquillière, 75001 Paris, France, fanny.mietlicki@bruitparif.fr)

The transposition of the European Noise Directive (END) into French law was achieved in April 2006. Noise maps have to be established before June 30, 2007 and action plans have to be set up before July 18, 2008 for agglomerations with more than 250,000 inhabitants and for major infrastructures. The State representatives at the departmental scale are in charge of the infrastructure maps, while the local authorities are in charge of the agglomeration maps. The Paris agglomeration which counts 11 million inhabitants is made of 396 towns. Since some of them are grouped into cooperation structures for noise issues, there are 238 entities in charge of the application of the END in the Paris agglomeration. To face this administrative complex situation, Bruitparif has developed a program to help local authorities in setting up the END. Different actions are lead: - providing information and technical assistance on how to establish noise maps and action plans, - conducting noise measurements in order to validate maps and to provide complementary information, - coordinating actions and initiatives, - consolidating the map of the Paris agglomeration from the local maps in order to estimate the noise exposure, - preparing guidelines for the action plans.

2:40

1pNSb6. Action planning procedures and realized action plans of municipalities and cities - results from the implementation of END. Markus Petz (ACCON GmbH, Ingenieurbüro für Schall- und Schwingungstechnik, Gewerbering 5, 86926 Greifenberg, Germany, markus.petz@accon.de)

For many federal states of Germany the Strategic Noise Maps were calculated and published in 2007. For some cities it will be shown, how a standard procedure for preparation of a noise action plan was defined together with responsible authorities from the municipality. The chosen procedure also considered the deadline for finalisation and the commencement of an action plan at July, 2008. Based on Strategic Noise Maps and hot spot analyses a catalogue of measures for noise reduction within a community was investigated and evaluated (cost/effectiveness). Together with representatives of traffic-, town- and environmental planning departures of the municipalities efficient measures were discussed and selected considering other local planning interests, financial possibilities and public acceptance. The draft action plan were published and public demurs have been weighted. In July, 2008 the action plans came into force.

Contributed Papers

3:00

1pNSb7. Action plans (PPBE) : experience of municipal noise fighting plans. Eric Gaucher (Acoustique & Conseil, 17-19 rue des Grandes Terres, 92508 Rueil-Malmaison, France, eg@acoustique-conseil.com)

The European Noise Directive (END) relating to the assessment and management of environmental noise requires the elaboration of action plans (Plans de Prévention du Bruit dans l'Environnement PPBE). However, these plans are limited to their concerned sources: trains, roads, planes and industrial plants. Municipal noise fighting plans (Plans Municipaux de Lutte contre le Bruit PMLB) taking equally into account any annoying sound situation, regardless of its nature, have been developed and implemented in around forty towns in France, with increasing success before the END was published. Acoustique & Conseil have already implemented thirty PLMBs. This experience has lead us to think that the strict application of PPBEs will in most cases not answer all the expectations of the concerned populations, in terms of solutions to their daily noise problems. It therefore seemed relevant for us to present a synthesis of the situations encountered during our works in order to enrich the approach of towns willing to enlarge their actions beyond those of the END. Now that it is time to elaborate the PPBE, it seems relevant and appropriate to implement PLMBs equally for the towns concerned.

3:20

1pNSb8. Urban and building acoustics management in the next decades: a matter of prevention, simplification and education. João G. Baring (Univ. of São Paulo - Facty. of Archt. and Urban., Rua Rafael Clark 85, 05526 - 010 São Paulo, Brazil, jbaring@uol.com.br)

In Brazil, in cities like São Paulo and Rio de Janeiro, noise pollution control has been carried out mainly in the form of repression. In the seventies and eighties, people joined together to fight against noisy government projects, and government fought noisy industries and commercial establishments. Since then, people have become aware of their rights, but have learned little about their own obligations on the matter. The author researched this process in order to find a better way for the future and concluded that prevention must be enforced through noise codes, standards must include easier survey methods, and low cost devices for noise control must be available. Most important, education must be improved in all levels, to make every citizen a partner of noise control at home, at work and elsewhere in the cities. This paper points out some ways of dealing with this process.

3:40

1pNSb9. NERS-analysis extended to include the existence of neighbouring quiet areas. Åsa Stenman (Acoustic Control AB, Tumstocksvägen 1, SE-187 66 Täby, Sweden, stenman@acoustic.se), Peter

Malm(Acoustic Control AB, Tumstocksvägen 1, SE-187 66 Täby, Sweden, peter.malm@acoustic.se), Magnus Lindqvist (Stockholm Environmental & Health Administation, Box 38024, SE-100 64 Stockholm, Sweden, magnus .lindqvist@miljo.stockholm.se)

One of the goals for the EC financed Integrated Project Quiet City Transport (QCITY), is to provide European city administrations with validated analysis tools and technical noise control solutions for the efficient production of noise action plans. A part of the QCITY project work is to produce complete noise maps and hot-spot analysis for a part of Stockholm. This paper will focus on the Noise Environmental Rating System (NERS), a tool for performing hot-spot analysis on noise maps, developed within the QCITY project. The input parameters that have been used in previous studies [Internoise-07_411, Å. Stenman, P.-Malm, 2007] are outdoor noise on all floors, number of inhabitants per building and the facade sound insulation index. Previous studies, such as the ″Stockholm score rating model (Trafikbuller och planering II, Stockholm, 2004) show a strong correlation between noise annoyance and the existence of quiet nearby areas. The NERS-analysis in this work has therefore been extended to include quiet areas.

4:00-4:20 Break

4:20

1pNSb10. NERS-analysis extended to include noise levels measured on city courtyards. Peter Malm (Acoustic Control AB, Tumstocksvägen 1, SE-187 66 Täby, Sweden, peter.malm@acoustic.se), Åsa Stenman (Acoustic Control AB, Tumstocksvägen 1, SE-187 66 Täby, Sweden, stenman@acoustic.se), Thomas Hammarlund (Environment Administration, Karl Johansgatan 23, SE-414 59 Göteborg, Sweden, thomas .hammarlund@miljo.goteborg.se)

One of the goals for the EC financed Integrated Project Quiet City Transport (QCITY), is to provide European city administrations with validated analysis tools and technical noise control solutions for the efficient production of noise action plans. A part of the QCITY project work is to produce complete noise maps and hot-spot analysis for the entire Gothenburg area. Earlier studies have shown that calculated noise levels from traffic at inner city courtyard are lower compared to actual measurements. Gothenburg city have performed over 700 measurements on city courtyards. The measurements are included in the NERS-analysis to show the influence of the actual courtyard noise levels. The study covers a smaller area in the central part of Gothenburg where the measurements have been made.

Invited Papers

4:40

1pNSb11. Auralisation and psychoacoustic evaluation of traffic noise scenarios. Sandro Guidati (HEAD acoustics GmbH, Ebertstrasse 30a, 52134 Herzogenrath, Germany, claudia.erens@head-acousitcs.de)

The evaluation of vehicle noise is mostly done using the A-weighted sound pressure level, e.g., the Lmax for pass-by noise or the Leq for community noise. Unfortunately, the dB(A)-value does not reflect the annoyance effect of vehicle noise correctly. During the first phase of the European Research Project QCity a metric for psychoacoustic evaluation of single pass-by events has been developed. In the next step this metric is adapted for the evaluation of complex traffic scenarios calculated by traffic flow simulations. Psychoacoustic evaluation requires time signals. Single values or third octave spectra are not sufficient to investigate all relevant effects (e.g., annoying time patterns, masking). The time signals are calculated combining advanced resynthesis with exterior noise simulation techniques. Hereby, it is possible to investigate the effect of e.g., low noise surfaces or various traffic control measures (traffic light vs. roundabout). Since a standard traffic scenario includes a very large number of single pass-by events special focus lies on fast processing techniques. This paper gives an overview of the developed algorithms and presents first results of the psychoacoustic evaluation of traffic scenarios.

5:00

1pNSb12. Lions Bay noise mitigation program. Duane E. Marriner (Wakefield Acoustics Ltd., 301-2250 Oak Bay Avenue, Victoria, BC V8R 1G5, Canada, duane@wakefieldacoustics.com)

The Ministry of Transportation (MoT) of the Province of B.C. noise abatement policy requires that environmental community noise impacts of highways projects involving new or substantially upgraded highways be assessed and mitigation implemented where warranted. This paper presents an extraordinary noise model developed to mitigate residential areas of the Village of Lions Bay on the rugged B.C. coastline from the Sea-to-Sky Highway connecting Vancouver, B.C. to Whistler, B.C. home of the Winter Olympic and Para-Olympic Games in 2010. The Cadna/A Version 3.9.15 software was used to develop a new 4 lane split grade alignment model incorporating two mini-interchanges. With the objective of achieving a 10 dBA noise reduction benefit, mitigation in the form of quiet pavement (OGA), traffic calming and 5 meter high absorptive sound walls or noise barriers were introduced into the model which included 150 mountain side residential receptors along the 2 km long corridor at elevations up to 35 meters above the project. Noise reduction benefits for dwellings were further analyzed to determine contributions during each stage of project development by creating a super user, modular, multi-layer noise model of Lions Bay. This work was carried out under the sponsorship of BCMoT.

5:20

1pNSb13. Tire/road noise reduction. Alexander Ossipov (Goodyear, Ave G. Smith, L-7750 Colmar - Berg, Luxembourg, alexander_ossipov@goodyear.com), Marc Engel (Goodyear, Ave G. Smith, L-7750 Colmar - Berg, Luxembourg, marc_engel @goodyear.com)

Traffic running on high speed roads is a considerable source of noise annoyance and is frequently a source of complaint by the general public. One of the components of this noise is generated by the interaction between motor vehicles tires and the road surface. The amplitude and frequency content of this noise is a function of many parameters, including the road surface texture, tire dimensions, tire materials, and construction and the tread pattern design. The paper provides detailed insight concerning the factors influencing exterior (environmental) and interior (vehicle) tire/road noise reduction and includes recommendations with regard to optimize tire design.

5:40

1pNSb14. Calculations of low height noise barriers efficiency by using Boundary Element Method and optimisation algorithms. Marine Baulac (CSTB, 24 rue Joseph Fourier, 38400 Saint-Martin-d'Hères, France, marine.baulac@cstb.fr), Arnaud Guillou (Institut National de Métrologie (LNE-INM/Cnam), 61 rue du Landy, 93210 La Plaine Saint Denis, France, guillou.arnaud@gmail.com), Jérôme Defrance (CSTB, 24 rue Joseph Fourier, 38400 Saint-Martin-d'Hères, France, jerome.defrance@cstb.fr), Philippe A. Jean (CSTB, 24 rue Joseph Fourier, 38400 Saint-Martin-d'Hères, France, philippe.jean@cstb.fr)

Nowadays, roads and railways are often quoted as the most annoying source of noise for the living environment. This problem of ground transportation noise is present in extra-urban environments as well as in town centres. Traditional noise barriers are in many cases not suited for acoustic protection in urban areas mainly because of their height. Previous studies have shown a significant efficiency of low height noise protections (kind of urban furniture) for the decreasing of noise levels in semi-opened areas such as city parks, places, and large avenues. However, the simulations of low height noise protections requires specific numerical codes since ray tracing methods are not suited for barriers lower than around 2 m. This paper proposes a way to implement an approach with allow to simulate low height noise protections in engineering calculation methods. This can be done by creating a database using a Boundary Element Method numerical code combined with optimisation algorithms. Work is still in progress since only 2D configurations are considered at the moment.

6:00

1pNSb15. Status of noise abatement measures for roads in Switzerland. Laurent Cosandey (Office Fédéral de l'Environnement, OFEV, 3003 Berne, Switzerland, laurent.cosandey@bafu.admin.ch), Kirk Ingold (Office Fédéral de l'Environnement, OFEV, 3003 Berne, Switzerland, kirk.ingold@bafu.admin.ch), Tommaso Meloni (Office Fédéral de l'Environnement, OFEV, 3003 Berne, Switzerland, tommaso.meloni@bafu.admin.ch), Nicole Luethi (Grolimund und Partner AG, Entfelderstr. 41, 5000 Aarau, Switzerland, Nicole.Luethi@gundp.ch), Hansueli Pestalozzi (Grolimund und Partner AG, Entfelderstr. 41, 5000 Aarau, Switzerland, hansueli.pestalozzi@gundp.ch)

In 2006, a comprehensive survey on the status of noise abatement measures for all roads was carried out in Switzerland for the first time. This survey recorded the costs of remedial work and noise protection measures completed to date (approx. CHF 1 billion) or still outstanding (approx. CHF 3 billion). An account is also given of the distribution among different types of measures, and of the protective effects on the public. As well as indicating the financial resources required for remediation of the Swiss road network on schedule, the survey highlights measures for controlling noise emissions at source which need to be implemented urgently.

6:20

1pNSb16. Influence of noise source representation on the estimation of specific descriptors close to traffic signals. Arnaud Can (LICIT, ENTPE/INRETS - Université de Lyon, rue Maurice Audin, 69518 Vaulx-en-Velin Cedex, France, can@entpe.fr), Ludovic Leclercq (LICIT, ENTPE/INRETS - Université de Lyon, rue Maurice Audin, 69518 Vaulx-en-Velin Cedex, France, leclercq@entpe.fr), Joel Lelong (INRETS, 25 av. F. Mitterrand, case 24, 69675 Bron, France, lelong@inrets.fr)

Considering traffic dynamics greatly improves noise estimation in urban area. This can be achieved by coupling a dynamic traffic model with both emission laws and sound propagation calculation. This paper focuses on the influence of noise source representations in the combination with the traffic model. Several representations are tested: point sources and homogeneous line sources of different sizes. We aim at evaluating how these representations correctly estimate classical descriptors (LAeq and statistical descriptors) and specific descriptors able to capture noise dynamics at a traffic signal scale. Three typical urban situations are studied: in front of, upstream and downstream a traffic signal. Noise source representation can be coarse for classical descriptors calculation if traffic dynamics is precisely described. On the contrary, noise source representation should be refined to precisely assess noise dynamics.

6:40

1pNSb17. Evaluation of Directive 2000/14/EC on outdoor machinery noise. Michael G. Dittrich (TNO Science and Industry, PO Box 155, 2600 AD Delft, Netherlands, michael.dittrich@tno.nl)

The European Directive 2000/14/EC sets a requirement for noise labeling for the sound power level of 57 types of outdoor equipment, and sound power limits for 22 of these. In the NOMEVAL project the Directive and its amendment 2005/88/EC were evaluated, resulting in recommendations for an update of the equipment list, the noise limits and the test codes. A European database of noise emission data was assessed, and environmental bodies and industry were consulted. The recommendations were also based on environmental, technical and economic impact assessments. A new environmental indicator was applied to rank the impact of the different equipment types. It was found that many types currently without noise limits have a higher impact than those with noise limits. Some new types of equipment have been identified including snowmobiles, mobile waste breakers and screens, motorised brooms, handheld cut-off saws, and power pruners. The technical impact assessment was based on current technology and trends and the feasibility of new or stricter limits. The economic impact assessment was based on estimated societal benefits versus the estimated additional cost to the consumer or purchaser. Finally, a number of instruments for further reduction of outdoor equipment noise were proposed.

7:00

1pNSb18. Some algebra and statistics on isolated noise events. Michel Maurin (INRETS-LTE, case 24, 69 675 Bron cedex, 69 500 Bron, France, maurin@inrets.fr)

Noise indices related to isolated emerging noise events are calculated on variable finite durations ΔT_{ev}, as opposed to instantaneous levels or indices on constant conventional periods ΔT (1 h, 24 h, ...). Here they are defined by TEL (transit exposure levels) or $Leq_{\Delta Tev}$ on every ΔT_{ev}. There are classical formulas to pass from many TEL_i to the Leq on a longer period including many events. When TEL_i are supposed equal to TEL one gets classicaly $Leq_{\Delta T}$ = TEL + 10 log n + K, (CNR, NEF for instance). In algebra, the approach develops some algebraic relations and conditions between total duration ΔT, the global part of all $\Delta T_{ev,i}$ and their number n, in a way that TEL is clearly emerging from noise level without the isolated events. It is a manner to find a general result like "events kill events," say that too many events render not emerging any new one. One finds the same with a statistical approach and other appropriate technics (quantiles for instance). And coming on with probabilistic tools, the Bêta distribution renders possible some characterisation of the graphical look of the time evolution of noise level during ΔT_{ev}. This work has partly been done with V. Catto of Lyon 1 University.

Session 1pNSc

Noise and EURONOISE: Noise Mapping Techniques and Uncertainties I

Richard Peppin, Cochair
Scantek, Inc., 7060 Oakland Mills Rd., Columbia, MD 20146, USA

Wolfgang Probst, Cochair
DataKustik GmbH, Gewerbering 5, Greifenberg, 86926, Germany

Contributed Paper

1:00

1pNSc1. Optimizing localization of noise monitoring stations for the purpose of inverse engineering applications. Malgorzata Reiter (Gdansk University of Technology, Multimedia Systems Department, 11/12 Gabriela Narutowicza Street, 80-952 Gdansk, Poland, reiter.m@sound.eti.pg.gda.pl), Jozef Kotus (Gdansk University of Technology, Multimedia Systems Department, 11/12 Gabriela Narutowicza Street, 80-952 Gdansk, Poland, joseph@sound.eti.pg.gda.pl), Andrzej Czyzewski (Gdansk University of Technology, Multimedia Systems Department, 11/12 Gabriela Narutowicza Street, 80-952 Gdansk, Poland, andcz@sound.eti.pg.gda.pl)

Long-term environmental monitoring of noise levels can be done using autonomous measurement stations. Because of the high cost of monitoring systems and management of these stations, it is essential to identify how many of measuring localization points are really required. In cases related to complex noise generation schemes, when there are various noise sources, the differences between calculations and measurements can be difficult to estimate. Therefore, it is vital to find some most appropriate locations for measurement stations which would ensure obtaining an adequate number of measurement results to be employed in the reverse engineering. These measurements can be then utilized to update dynamic noise maps. Furthermore, predictive noise models may be developed accordingly to certain local requirements. This could result in a better accuracy of dynamic noise maps. The paper focuses on defining the proper choice of the measurement points localizations. The experiments described include a comparison between real-life measurement results performed with the Multimedia Noise Monitoring System developed at the Multimedia Systems Department of the Gdansk University of Technology and the noise level prediction results. The optimization of the number and location of noise monitoring points with regard to the measurement accuracy is also discussed.

Invited Paper

1:20

1pNSc2. Acoustical design margins: Uncertainty in prediction and measurement of community noise. Robert Putnam (Siemens Power Generation, 4400 Alafaya Trail, Orlando, FL 32826, USA, bob.putnam@siemens.com), Roland Hetzel (Siemens Power Generation, Beethovenring 8a, 91090 Effeltrich, Germany, roland.hetzel@siemens.com)

Compliance with regulatory requirements for sound levels in communities adjacent to industrial or power generating facilities is typically a contractual commitment, with the potential for significant financial penalties in the event of noncompliance. Uncertainties at any stage of the design, specification or prediction of plant sound level may be accounted for as part of the overall plant acoustical design margins. There are also additional uncertainties in terms of compliance sound measurement surveys, that are commonly referred to as either "test tolerance," or "instrumentation tolerance and measurement uncertainty." From the viewpoint of the plant equipment supplier all of the uncertainties associated with equipment design and specification are simply additive to all of the uncertainties of compliance measurements, since they all contribute to, or affect the selection of, the overall plant acoustical design margin. The discussion will address the types of uncertainties in source sound power levels and measurement error, tolerances, and confidence limits of field sound surveys, highlighting some seldom-treated aspects of uncertainty. Measurement uncertainties and the applicable combinatorial rules will be treated.

Contributed Papers

1:40

1pNSc3. Possibilities of supporting municipal authorities in processes of acoustical environment management. Jan Ka Mierczak (Silesian University of Technology, Faculty of Organization and Management, ul. Roosevelta 26/28, 41-800 Zabrze, Poland, Jan.Kazmierczak@polsl.pl)

EU directives and state law acts oblige municipal authorities of European towns to create and exploit strategic acoustic maps. The further decisions of these authorities, considering both sustainable local development strategies and results of analysis of environmental effects (such as noise), ought to form suitable living conditions in the towns. The people, responsible for such decisions, ought to dispose suitable knowledge and skills. Author of this paper leaded in recent years the consortium of R&D units involved in the research project, focussed on preparing technology of creating acoustic maps of urban areas. The project resulted in the method of acoustic mapping, based on GIS technology. Apart of "purely acoustical" problems, the forming of competencies of these members of municipal staff, responsible on preparation and then exploitation of acoustic maps, has been mentioned as a problem of essential importance in this research. In result of discussions with potential users of strategic acoustic maps, the need was formulated to give municipal units some effective tools of supporting them by means of offering necessary knowledge and expertises in the field of management of acoustical environment in urban areas. The concept of network-based system focussed on such a target is presented in the paper.

2:00

1pNSc4. Evaluation models for the noise diminution due to the phonique barrier walls. Mariana Arghir (Technical University of Cluj-Napoca, Faculty of Machines Design; Department of Mechanics and Computer Programming, B-dul Muncii; Nr. 103-105, 400 641 Cluj-Napoca,

Romania, marianaarghir@yahoo.com),Dan Borza(National Institute of Applied Sciences of Rouen, INSA Rouen, LMR, Ave l'Universite, BP8 76800 Rouen, France, dan.borza@insa-rouen.fr), Florin Blaga (University of Oradea, Str. Universitatii nr.1, 400 641 Cluj-Napoca, Romania, florin_blaga2000@yahoo.com), Tiberiu Vesseleny (University of Oradea, Str. Universitatii nr.1, 400 641 Cluj-Napoca, Romania, vasitata@yahoo.com), Geamilia Solea (Technical University of Cluj-Napoca, Faculty of Machines Design; Department of Mechanics and Computer Programming, B-dul Muncii; Nr. 103-105, 400 641 Cluj-Napoca, Romania, marylandprod@gmail.com), Mariana Runcan (National Institute of Applied Sciences of Rouen, INSA Rouen, LMR, Ave l'Universite, BP8 76800 Rouen, France, mariruncan@yahoo.com)

The present paper contains our study regarding the diminution of the urban noise using the phonique barrier walls conformed to the EMPARA procedure, which is based on the simplified of the standard method for the measurements and computes of the surface traffic inside the urban agglomeration, as they are given in SRM2 laws (Netherlands standards). There are made the studies taking into account all the parameters that characterize the the noise and they are graphical representations having the "n-1" constant parameters and only one having the time variation law. In this way we are obtained the influence of each parameter in the diminution of the urban noise using the phonique barrier walls. In addition we realized a measurement for a real barrier wall inside the Oradea town. The comparison between them was enough good, that means our theoretical study is correct and characterizes the noise pollution and its diminution on the urban agglomeration. The measurement device was a CENTER 322 Sound Lever Meter. This study contains the two steps for the "noise map" asked for the Romania integration in the European Union, and was made by the researchers of the Oradea University under the direction of the Prof. Dr. Ing. Mariana ARGHIR from the Technical University of Cluj-Napoca.

2:20

1pNSc5. Environmental impact of noise from mobile outdoor equipment. Foort De Roo (TNO Science and Industry, Stieljesweg 1, 2628CK Delft, Netherlands, foort.deroo@tno.nl), Eddy Gerretsen (TNO Science and Industry, Stieljesweg 1, 2628CK Delft, Netherlands, eddy.gerretsen@tno.nl), Jeroen Borst (TNO Science and Industry, Stieljesweg 1, 2628CK Delft, Netherlands, jeroen.borst@tno.nl)

As part of an evaluation study of European Directive 2000/14/EC relating to the noise emission by equipment for use outdoors, an environmental impact assessment was required to investigate the need for new or tighter noise limits. In contrast to other environmental noise sources, the operating location of outdoor machines is not fixed. As conventional environmental noise mapping could not be used for this purpose, an environmental indicator was developed. This indicator takes the following factors into account: numbers of equipment in use in the EU, typical average sound power level, tonal/impulsive/intermittent sound content, annual duration of operation, day/night operation and typical areas of use. The numbers of people affected were assessed by means of a series of noise maps, resulting in distribution curves characteristic for different types of environment (urban, suburban, rural, and others). The newly developed environmental indicator is a relatively simple quantity taking all relevant factors into account including annoyance.

Invited Papers

2:40

1pNSc6. Procedures of large scale noise mapping - examples based on German projects. Markus Petz (ACCON GmbH, Ingenieurbüro für Schall- und Schwingungstechnik, Gewerbering 5, 86926 Greifenberg, Germany, markus.petz@accon.de)

Noise mapping projects for the German Federal States Baden-Wuerttemberg, Hesse, and Schleswig-Holstein and for the cities Munich, Frankfurt, and Wiesbaden are presented. These large projects have been performed using newest software technology like fully automated parallel computing applying the PCSP technique (Program Controlled Segmented Processing) and by using all CPU cores of the noise mapping computer cluster (multithreading). With the noise mapping for all main roads and railways in Austria the 64 Bit technology has been applied - this allows to handle even files of more than 10 GB without the need of manual intervention. The influence of these techniques on uncertainties is discussed using the strategy of DIN 45687 and it is shown that such complete 3D models are the optimal basis to develop noise reduction measures in the frame of Action Planning.

3:00

1pNSc7. Noise mapping for large urban areas - the city of Vienna. Werner Talasch (Magistrat der Stadt Wien - Magistratsabteilung 22, Dresdner Straße 45, A-1200 Wien, Austria, office@talasch.at)

The Environmental Noise Directive 2002/49/EG requires noise maps for the main noise sources railway, road and aircraft and as well for agglomerations. For agglomerations there are also industrial sites (restricted to IPPC plants) a relevant noise source. The noise maps for the agglomeration of Vienna includes the City of Vienna and 5 further municipalities. These are Brunn am Gebirge, Maria Entersdorf, Mödling, Perchtoldsdorf, and Wiener Neudorf. The area of the agglomeration is about 460 km^2. The most difficult part in the task of creating the noise maps was the 3D model of the agglomeration. Most of the relevant objects were available as 3D objects. Only some objects are only available as 2D objects and caused therefore a lot of work.

3:20-3:40 Break

3:40

1pNSc8. The United Kingdom noise mapping experience. Nick Hawkins (ACCON UK Limited, Unit B, Fronds Park, Frouds Lane, Aldermaston, RG7 4LH Reading, UK, nick.hawkins@accon-uk.com), Graham Parry (ACCON UK Limited, Unit B, Fronds Park, Frouds Lane, Aldermaston, RG7 4LH Reading, UK, graham.parry@accon-uk.com)

The paper describes the noise mapping of the Bristol and Bournemouth agglomerations for the United Kingdom Noise Mapping Initiative in compliance with the European Directive on Environmental Noise and the challenges of delivering both compliant noise mapping, noise mapping outputs and shape files, and the associated methodology reports. The paper examines the noise model utilised for the mapping, the various efficiencies built into the system to provide error checking, the external data acquisition and the effects that any uncertainties may have in strategic noise mapping. Additionally, the use of a GIS based toolkit for identifying and amending the location of noise barrier objects was utilised.

Contributed Paper

4:00

1pNSc9. A comparison between predicted and measured noise levels at the Rijeka - Zagreb motorway. Sanja Grubesa (Faculty of EE and Computing, Unska 3, Department of Electroacoustics, HR-10000 Zagreb, Croatia, sanja.grubesa@fer.hr), Marko Horvat (Faculty of EE and Computing, Unska 3, Department of Electroacoustics, HR-10000 Zagreb, Croatia, marko.horvat@fer.hr), Hrvoje Domitrovic (Faculty of EE and Computing, Unska 3, Department of Electroacoustics, HR-10000 Zagreb, Croatia, hrvoje.domitrovic@fer.hr)

The current calculations used for predicting the levels of road traffic noise can and usually do give results that can differ significantly from the results of measurements of noise levels performed in the field. In order to examine these discrepancies, levels of road traffic noise have been measured on two locations on the Rijeka - Zagreb Motorway. After that, the geographical layout of these locations has been prepared and then input into a computer simulation program with the goal of obtaining simulated road traffic noise levels. Following the assumption that these results will be different, the goal is to determine which of the simulation models used today will provide results that are in the best agreement with the results obtained from the actual field measurements, with the emphasis on this particular geographic region, namely, the Republic of Croatia.

Invited Paper

4:20

1pNSc10. City noise mapping without traffic data. Laurent Droin (Acouphen-Environnement, Campus de La Doua, 66 BD Niels Bohr, BP 52132, 69603 Villeurbanne, France, laurent.droin@acouphen-environnement.com), Pierre Odent (MVAConsultancy, 12-14 rue Jules Cesar, 75012 Paris, France, podent@mvaconsultancy.com)

The authers have a large experience on transport and noise planning and mapping with projects on many communities of different size in France. Within the time scale of a mapping project, it is very common to have a large variation of the accuracy in traffic data, especially for roads (largest source data base). In many cases, no traffic data is available on less exposed roads. This paper illustrates how variation of input data accuracy and lack of data were tackled in both large and small territories (population between 50 000 and 1 000 000) in order to provide maps with the required accuracy and information for political action and communication.

Contributed Papers

4:40

1pNSc11. Definition of traffic scennaries, application on a practise case of the criteria followed by the guide of good practises for elaboration of strategic traffic noise maps in urban routes. Igone García Pérez (Labein-Tecnalia, C/Geldo-Parque Tecnologico de Bizkaia, 48160 Derio, Spain, igarcia@labein.es), Itziar Aspuru Soloaga (Labein-Tecnalia, C/Geldo-Parque Tecnologico de Bizkaia, 48160 Derio, Spain, iaspuru@labein.es)

Configuration of noisy environment in towns mostly depends upon the characterization of traffic noise in urban routes. Frequently there is a lack of information when it is a question of having data from the whole urban area. To solve this lack of information the above-mentioned guide (WG-AEN 002.2006) proposes some suppositions for this characterization which can turn out to be very general in practical applications. Through the presentation of these criteria applied to a practical case it can be seen the tools necessary to adjust real traffic characterization to the elaboration of noise maps and definition of an Action Plan. The analyzed variables are: AVT, % of heavy vehicles, time distribution and speed considering, for this last factor, the lacks shown by the interim method and the applicable supposes based upon the state of the art.

5:00

1pNSc12. Urban noise mapping - an approach to the establishment of standard making procedure. Predrag Vukadin (Brodarski institut d.o.o., Avenija V.Holjevca 20, 10 020 Zagreb, Croatia, prevuk@hrbi.hr), Ivan Bublic (Brodarski institut d.o.o., Avenija V.Holjevca 20, 10 020 Zagreb, Croatia, ivan.bublic@hrbi.hr), Ivan Tudor (Brodarski institut d.o.o., Avenija V.Holjevca 20, 10 020 Zagreb, Croatia, ivan.tudor@hrbi.hr)

The Directive 2002/49 relating to the assessment and management of environmental noise and the Croatian legislative derived from it defines the basic rules to carry out strategic noise mapping. However, in real life situations, each mapping project implies a different approach, depending on various case related distinctions e.g. availability and quality of input data, extent of noise annoyance, the form and the volume of output data to be presented, etc. Based on the experience from various urban noise mapping projects, this work is an approach to defining key steps in urban noise map production and establishing standard step-by step procedure, and an attempt to define the procedure for each step. Examples for each step are given based on the case studies from our previous urban noise mapping projects.

Session 1pNSd

Noise and EURONOISE: Environmental Noise Mapping I

Kenneth Cunefare, Cochair
Woodruff School of Mechanical Engineering, The Georgia Inst. of Technol., Atlanta, GA 30332 USA

Gaetano Licitra, Cochair
ARPAT - Dept. Firenze, Via Porpora, 22, Firenze, 50144, Italy

Invited Papers

5:40

1pNSd1. Differences among European noise mapping methods. Stylianos Kephalopoulos (European Commission, via e. fermi, 1, 21020 Ispra, Italy, Stylianos.Kephalopoulos@jrc.it), Marco Paviotti (European Commission, via e. fermi, 1, 21020 Ispra, Italy, marco.paviotti@jrc.it)

This article will present the differences among noise maps of Lden and Lnight levels produced following the EU Interim methods and those produced following other national methods used in the EU MS. Lden and Lnight are the two indicators required by the European Environmental Noise Directive (2002/49/EC) defined at the position of 4 m height and 2 m away from the facade of a building. Four different comparisons will be presented for road, railway, industrial, and aircraft noise. This article will also focus on the methodology used to assess the equivalence among the national methods against the interim ones as well as the statistical approach used to consider uncertainties. Finally, the input values used, the parameters and the lay-outs of the four protocols corresponding to the four environmental noise sources (i.e., road traffic, railway, industrial, and aircraft noise) adopted for the equivalence exercise will be also presented.

6:00

1pNSd2. Challenges and opportunities for noise mapping in the United States. Kenneth Kaliski (Resource Systems Group (RSG), 55 Railroad Row, White River Junction, VT 05001, USA, kkaliski@rsginc.com)

Primarily through the impetus of European Union Directive 2002/49/EC, EU cities have been on the forefront of noise mapping and the community planning that results from it. The United States has no similar legislation at federal or state levels. As a result, noise mapping for towns and cities in the U.S., and indeed, awareness of noise issues by planners, appears to lag behind their European counterparts. However, metropolitan areas in the U.S. have invested a great deal in transportation modeling. As a result, the data foundation for noise mapping, that is, road and rail geometry and traffic volumes, is in place in many metropolitan areas. In addition, digital terrain elevation data, aerial photography, and GIS data are generally available on a state or national basis at no charge over the internet. The Chittenden County, Vermont noise map is one example of how publically available data can be used to create a useful community noise map over a large area. Other examples will be discussed.

6:20

1pNSd3. Presenting Noise Mapping Information to the Public. John F. Hinton (Birmingham City Council, Regulatory Services, 581 Tyburn Road, B24 9RF Birmingham, UK, bham.acoustics@dsl.pipex.com), Soren Rasmussen (Cowi-Odense, Odensevej 95, Postboks 444, Hjallese, DK-5260 Odense, Denmark, SRS@cowi.dk)

Directive 2002/49/EC of the European Parliament and of the Council of 25 June 2002 relating to the assessment and management of environmental noise requires Member States to undertake strategic noise mapping. It also refers to legislation regarding access to the information from strategic noise maps, since it requires "that the strategic noise maps ... are made available and disseminated to the public in accordance with relevant Community legislation ... and in conformity with Annex IV ... to this Directive." Under its terms of reference for 2007 the European Environment Agency's (EEA) Working Group on the Assessment of Exposure (WG-AEN) was asked to produce a Position Paper containing the Group's ideas and suggestions on good practice and associated strategies for presenting noise mapping information to the public at local and national levels. Many of these ideas and suggestion were developed from the outcomes of a workshop held in London in October, 2006. The final draft of the Position Paper was completed in December, 2007. This conference paper and associated verbal presentation will provide an overview of the contents of the Position Paper and report on developments since December, 2007.

6:40

1pNSd4. Limits and advantages of Good Practice Guide to Noise Mapping. Gaetano Licitra (ARPAT - Dept. Firenze, Via Porpora, 22, 50144 Firenze, Italy, g.licitra@arpat.toscana.it), Gianluca Memoli (Imperial College London, Department of Chemical Engineering, Exhibition road, SW7 2AZ London, UK, g.memoli@imperial.ac.uk)

The Pisa Noise Mapping Project has recently presented to the public what turned out to be the first noise map for road traffic in Italy, developed taking into account the Good Practice Guide version 2 (GPG2) of WG-AEN and the main results of the IMAGINE project. This paper will discuss the results of this noise map, relative to road traffic, in terms of Lden and Lnight and their uncertainties, obtained by comparing the calculated values with a set of noise measurements taken across the territory. The uncertainties so defined were compared with the ones predicted by GPG2 considering, in particular, two different ways to model the source. To do this, input traffic flow were assigned first by taking direct measurements and performing a road classification and then, at a second stage, using a static traffic model (the latter method should give less uncertainty, according to GPG2). The expected change in uncertainty will be discussed, together with advantages and disvantages of the two different choices. A comparison of exposed population with other EU realities will be also presented.

Contributed Paper

7:00

1pNSd5. A noise mapping study of a large metropolitan city with a heterogeneous traffic. Ramachandra Alur (Indian Institute of Technology, Acoustics Laboratory, Dept of Civil Engg, IIT- M, 600036 Chennai, India, ram_alur@yahoo.com), Kalaiselvi Ramasamy (Indian Institute of Technology, Acoustics Laboratory, Dept of Civil Engg, IIT- M, 600036 Chennai, India, kalai_archi@yahoo.com)

Traffic noise characteristics in some of the cities in a developing country like India are slightly varied by virtue of the fact that the composition of the traffic is heterogeneous accompanied by variance in road geometry and varying density of the buildings on the either side of the road. To study the feasibility of noise reduction in some of the areas a noise mapping study has been attempted along with field measurements of L10, L50, L90 and Leq. In the noise mapping parameters such as Ld, LN, Lden have been arrived at by taking into consideration the geometrical features of the roads and varying heights of the buildings. In this study noise mapping through computer simulation model (soundplan) is used by considering several noise sources and propagation of noise to the receiver point. This paper describes how the local characteristics of the city affect the propagation of noise and describes an integrated approach to control noise pollution in these areas. A three dimensional acoustical model has been developed for two locations of the city. Methodologies of noise control through noise contours around traffic are illustrated.

MONDAY AFTERNOON, 30 JUNE 2008 AMPHI HAVANE, 1:00 TO 7:40 P.M.

Session 1pPAa

Physical Acoustics: Acoustics of Porous Media I

Walter Lauriks, Cochair
Lab. ATF, Katholieke Universiteit Leuven, Celestijnenlaan 200D, Leuven, B-3001, Belgium

Keith Attenborough, Cochair
Open University, Department of Design, Development, Materials and Environment, Walton Hall, Milton Keynes, MK7 6AA, UK

Invited Papers

1:00

1pPAa1. Nonlinear acoustic acceleration waves in porous media flow. Pedro M. Jordan (U.S. Naval Research Lab., Code 7181, Stennis Space Center, MS 39529-5004, USA, pjordan@nrlssc.navy.mil)

Acoustic acceleration waves are defined as jumps in the first derivatives of the velocity, pressure, or density across a propagating singular surface (or wavefront). In this talk, the temporal evolution of the amplitude and the propagation speed of such waves are investigated in the context of finite-amplitude acoustic propagation in Darcy-type porous media. It is shown that there exists a critical value, $\alpha^*(>0)$, of the initial jump amplitude such that the acceleration wave magnitude either goes to zero, as $t \leftarrow \infty$, or blows up, in finite time, depending on whether the given initial jump amplitude is less than or greater than α^*. In addition, a connection to traveling wave solutions is noted and the linearized case is examined. Finally, the numerical solution of a (1D) nonlinear IBVP involving sinusoidal signaling in a fluid-saturated porous slab is used to illustrate the finite-time transition from acceleration wave to shock wave, which occurs when the initial jump amplitude is greater than α^*. [Supported by ONR/NRL funding (PE 061153N).]

1:20

1pPAa2. New equipment for the measurements of flow resistivity and porosity of open cell ceramic and metal foams. Benjamin Jados (Illinois Institute of Technology, Civil, Architectural and Environmental Engineering, 3201 S. Dearborn St., Room 228, Chicago, IL 60616, USA, jadoben@iit.edu), Ralph T. Muehleisen (Illinois Institute of Technology, Civil, Architectural and Environmental Engineering, 3201 S. Dearborn St., Room 228, Chicago, IL 60616, USA, muehleisen@iit.edu)

Two of the most important measurements in the acoustic analysis of porous media are the flow resistivity and porosity. To reduce the errors in the measurements of these parameters, new instruments have been developed, which incorporate recent technological advances. The new equipment helps to streamline the user experience and improve the confidence of the results. The current design includes the use of LabVIEW and COMSOL Multiphysics software, the use of thermal press-fit sample holders, and the use of low differential pressure transducers. The new instruments were used to study the flow resistivity and porosity of various pore sizes of open cell ceramic and metal foams. Data are presented with accompanying errors, as well as a discussion of the shortcomings and possible improvements of the measurement system.

1:40

1pPAa3. Semi-empirical time domain model of sound attenuation in porous materials. Olga Umnova (University of Salford, Acoustics Research Centre, Newton Building, M5 4WT Salford, UK, o.umnova@salford.ac.uk), Diego Turo (University of Salford, Acoustics Research Centre, Newton Building, M5 4WT Salford, UK, d.turo@pgr.salford.ac.uk)

A semi-empirical model for complex tortuosity function, which satisfies physically correct low and high frequency limits and allows analytical transformation into the time domain has been developed. It is based on the assumption, that a network of pores with two characteristic sizes can approximate the internal structure of the material, and thus requires the knowledge of two relaxation times. It is proven, however, that the model can predict sufficiently well the acoustical properties of rigid porous materials with various microstructures when is complete with the tortuosity as an additional parameter. It is shown that relaxation times can be easily related to the "equivalent fluid" model parameters. Numerical time domain calculations confirm that the contribution of both viscous and inertial effects on the evolution of acoustical pulses as they propagate through a porous material can be accounted for simultaneously within the framework of the model. It is shown that the extended version of the model, which accounts for the thermal effects can also be explicitely used for time-domain computations.

2:00

1pPAa4. Acoustical and micro-structural properties of recycled grains and fibres. Kirill V. Horoshenkov (University of Bradford, School of Engineering, Design and Technology, BD7 1DP Bradford, UK, k.horoshenkov@Bradford.ac.uk), Amir Khan (University of Bradford, School of Engineering, Design and Technology, BD7 1DP Bradford, UK, a.khan72@bradford.ac.uk), Hadj Benkreira (University of Bradford, School of Engineering, Design and Technology, BD7 1DP Bradford, UK, h.benkreira@bradford.ac.uk), Giulio Pispola (Umbra Group, Umbra Cuscinetti S.p.A., Zona Industriale, Localita Paciana, 06034 Foligno, Italy, gpispola@umbracus.com)

This paper presents a systematic study into the production, characterisation and modeling of the acoustic behaviour of highly heterogeneous, low density porous layers having a complex pore size distribution. A new cold extrusion production method was developed at the University of Bradford to process recycled polymeric fibres and grains so that accurate control of the pore size distribution and the porosity of the resultant porous product could be attained. In this way high values of the acoustic absorption coefficient could be obtained in a relatively thin porous layer throughout the design frequency range . Two approaches were used to model the acoustic performance of the manufactured porous media. The first approach requires the direct numerical integration of the Biot viscosity correction function which depends on the probability density function of the pore size. The other approach assumes a low permeability contrast between the two porous scales so that the acoustic properties could be estimated using the semi-phenomenological models of Johnson and Lafarge for the viscous and thermal dynamic permeabilities. Numerical results predicted by the two models were then compared with impedance tube experimental data showing good accuracy of the selected prediction methods.

2:20

1pPAa5. Deduction of porous material properties using a point source. Jean François Allard (Laboratoire d'Acoustique de l'Université du Maine, Avenue Olivier Messiaen, 72085 Le Mans, France, jean-francois.allard@univ-lemans.fr), Olivier Dazel (Laboratoire d'Acoustique de l'Université du Maine, Avenue Olivier Messiaen, 72085 Le Mans, France, olivier.dazel@univ-lemans.fr), Laurens Boeckx (Lab. ATF, Katholieke Universiteit Leuven, Celestijnenlaan 200D, B-3001 Leuven, Belgium, laurens.boeckx@fys.kuleuven.be), Nathalie Geebelen (Lab. ATF, Katholieke Universiteit Leuven, Celestijnenlaan 200D, B-3001 Leuven, Belgium, Nathalie.Geebelen@bwk.kuleuven.be), Walter Lauriks (Lab. ATF, Katholieke Universiteit Leuven, Celestijnenlaan 200D, B-3001 Leuven, Belgium, Walter.Lauriks@fys.kuleuven.be)

The acoustic field created by a point source above the plane boundary between two semi-infinite fluid layers has been previously studied by Brekhovskikh. A straightforward generalization can be performed by replacing the fluid under the source by the fluid equivalent to a rigid-framed porous medium. This leads to a method of evaluating, from pressure measurements, the surface impedance close to grazing incidence and the Brewster angle of total refraction of the porous medium. The model by Brekhovskikh can also be generalized when a thin porous layer is set under the point source. A pole of the reflection coefficient exists for an angle of incidence close to grazing incidence. This pole is related to an acoustic field similar to a surface wave above the layer. The measurement of this angle provides an evaluation of the surface impedance close to grazing incidence. The point source induces frame vibrations that can be predicted with the Biot theory. The rigidity coefficients of the frame at audible frequencies can be evaluated from measurements of the frame velocity with a laser velocimeter.

2:40

1pPAa6. Acoustic waves propagation along mechanically free surface of unconsolidated granular porous media. Xavier Jacob (LPEC/UMR 6087/CNRS/Université du Maine, Avenue Olivier Messiaen, 72085 Le Mans Cedex 09, France, xavier.jacob@univ-lemans.fr), Vladislav Aleshin (LPEC/UMR 6087/CNRS/Université du Maine, Avenue Olivier Messiaen, 72085 Le Mans Cedex 09, France, aleshinv@mail.ru), Vincent Tournat (LPEC/UMR 6087/CNRS/Université du Maine, Avenue Olivier Messiaen, 72085 Le Mans Cedex 09, France, vincent.tournat@univ-lemans.fr), Philippe Leclaire (Lab. de Recherche en Mécanique et Acoustique, I.S.A.T - Univ. de Bourgogne, 49, rue Mademoiselle Bourgeois, 58000 Nevers, France, philippe.leclaire@gmail.com), Walter Lauriks (Lab. ATF, Katholieke Universiteit Leuven, Celestijnenlaan 200D, B-3001 Leuven, Belgium, Walter.Lauriks@fys.kuleuven.be), Vitali Gusev (LPEC/UMR 6087/CNRS/Université du Maine, Avenue Olivier Messiaen, 72085 Le Mans Cedex 09, France, vitali.goussev@univ-lemans.fr)

Unconsolidated granular materials exhibit strong dependence of elastic properties on pressure due to high sensitivity of the inter-grain contacts to magnitude of loading. As a consequence the gravity field makes these granular assemblages highly elastically inhomogeneous particularly near mechanically free surface. Theoretical and experimental investigations conducted recently have demonstrated that multiple waveguide surface acoustic modes propagate along the free surface of the solid-state skeleton in the disordered air-saturated granular packings. These modes are localized near the surface. In ordered granular packing the acoustic waves can travel along the surface inside the horizontal channels, which are localized beneath the surface. The waves of different frequencies are travelling at different depths. The anisotropy of these inhomogeneous granular phononic crystals has an important influence of the existence of the waveguide modes. The experiments with acoustic waves traveling in the vicinity of a free surface provide fundamental information on the mechanical behaviour of unconsolidated granular media at very low pressures in the vicinity of the jamming transition. The perspectives of this research could be related to the analysis of the role which could be played in the considered phenomena by the acoustic waves predominantly travelling in these granular porous assemblages through the fluid-saturated pores.

3:00

1pPAa7. The Biot Type II wave in the fluid and matrix of soils. James M. Sabatier (University of Mississippi, NCPA, 1 Coliseum Drive, University, MS 38677, USA, sabatier@olemiss.edu), Chris McNeill (University of Mississippi, NCPA, 1 Coliseum Drive, University, MS 38677, USA, cmcneil1@olemiss.edu)

When an acoustic wave is incident on the surface of the porous ground energy is coupled into the soil matrix and fluid. To investigate the depth dependence of the Type I and II waves from the ground surface, the ground is modeled as a semi-infinite air-filled poroelastic medium. Using a modified form of Biot-Stoll theory the magnitude and phase of the matrix velocity and fluid pressure caused by the two possible dilatational waves are determined. Traditionally speaking the type I (fast) wave is the nondispersive wave traveling in the solid, and the type II (slow) wave is dispersive and travels primarily in the fluid (air). Previous experiments have shown the possibility that the type II wave travels in the solid near the surface and influences the measured matrix velocity and fluid pressure. Calculations have been done showing that near the surface of the ground the type II wave actually does have a large effect on the particle velocity of the matrix. After the first few centimeters the type II wave is completely attenuated and the type I wave is responsible for the displacement and pressure in the medium

3:20

1pPAa8. Anisotropy effects on the acoustical properties of porous materials. Olivier Dazel (Laboratoire d'Acoustique de l'Université du Maine, Avenue Olivier Messiaen, 72085 Le Mans, France, olivier.dazel@univ-lemans.fr), Jean François Allard (Laboratoire d'Acoustique de l'Université du Maine, Avenue Olivier Messiaen, 72085 Le Mans, France, jean-francois.allard@univ-lemans.fr), Laurens Boeckx (Lab. ATF, Katholieke Universiteit Leuven, Celestijnenlaan 200D, B-3001 Leuven, Belgium, laurens.boeckx@fys.kuleuven.be), Nathalie Geebelen (Lab. ATF, Katholieke Universiteit Leuven, Celestijnenlaan 200D, B-3001 Leuven, Belgium, Nathalie.Geebelen@bwk.kuleuven.be), Poonam Khurana (Lab. ATF, Katholieke Universiteit Leuven, Celestijnenlaan 200D, B-3001 Leuven, Belgium, Poonam.Khurana@fys.kuleuven.be), Walter Lauriks (Lab. ATF, Katholieke Universiteit Leuven, Celestijnenlaan 200D, B-3001 Leuven, Belgium, Walter.Lauriks@fys.kuleuven.be)

Porous materials are now widely used in noise control for their acoustic properties in sound absorption and transmission. These properties are function of the internal porous medium structure. Generally, most of the models assume that the porous medium is isotropic. Mineral wools (as well as some foams) clearly present an anisotropic structure. This communication is concerned with the adaptation of recent works on isotropic materials to the case of anisotropic porous materials. The general theory will be exposed for sound absorbing materials with anisotropic acoustical and mechanical parameters. The case of transverse isotropic materials (with fibers organized in planes running parallels one to each other) will then be detailed in particular in the case when the plane of fibers is not the same than the normal plane of the sample. The influence on the acoustical properties anisotropic porous materials will then be presented. Illustrations are then provided with measurements performed on wools and it will be shown that the rigidity coefficients of a sample can be evaluated at audible frequencies from measurements in particular from the speed of the Rayleigh wave in different directions.

3:40

1pPAa9. Low frequency implementation of the full Kramers-Kronig relationships for the description of dispersion and attenuation of acoustical waves in porous media. Bernard R. Castagnede (Laboratoire d'Acoustique de l'Université du Maine, Avenue Olivier Messiaen, 72085 Le Mans, France, bernard.castagnede@univ-lemans.fr), Denis Lafarge (Laboratoire d'Acoustique de l'Université du Maine, Avenue Olivier Messiaen, 72085 Le Mans, France, denis.lafarge@univ-lemans.fr), Claude Depollier (Laboratoire d'Acoustique de l'Université du Maine, Avenue Olivier Messiaen, 72085 Le Mans, France, claude.depollier@univ-lemans.fr), Naima Sebaa (Laboratoire d'Acoustique de l'Université du Maine, Avenue Olivier Messiaen, 72085 Le Mans, France, naima.sebaa@univ-lemans.fr), Michel Henry (Laboratoire d'Acoustique de l'Université du Maine, Avenue Olivier Messiaen, 72085 Le Mans, France, michel.henry@univ-lemans.fr)

It is well known that the causality principle which applies during the acoustic propagation of a wave packet inside any material should be described by the universal Kramers-Kronig (K-K) relationships, enabling to formally link dispersion to attenuation curves. The application of the K-K formalism to porous networks has been studied lately, but unfortunately, the metrology of dispersion features at very low frequency is intricate. The use of parametric arrays of nonlinear acoustics enables to get at the same time, some precise information on dispersion and absorption on various porous media, for instance in the frame of the "equivalent fluid" model. In the present work, we describe some very recent findings obtained along these ideas for a truly relevant application of the full KK formalism in various fibrous materials. We have checked numerical predictions of the absorption versus frequency computed from the dispersion curves with the K-K modeling, as well as confrontation of these numerical predictions with experimental data on absorption obtained with various set-ups, on different fibrous materials.

4:00-4:20 Break

4:20

1pPAa10. On the diffusion of sound energy in porous materials. Nicola Prodi (Engineering Dept. - Univ. of Ferrara, Via Saragat, 1, 44100 Ferrara, Italy, nicola.prodi@unife.it)

The sound intensity was used in the past to describe the surface properties of porous materials. Actually no extensive study used the same concepts to describe the properties of the energy flow inside the material. As known, the sound intensity has a twofold nature, that is an active part transferring the energy out of a point and a reactive one localizing the energy. These features are crucial in the development of the new model for the propagation of the energy inside porous materials developed in this work. In fact, by means of the intensimetric approach, it is shown that the one-dimensional transfer of sound energy can be fully described as a diffusion process. The role of the active and reactive sound intensities is outlined and specific parameters are defined to account for the material behaviour with respect to the transfer of the sound energy. Moreover the sinks of energy and the sources of reactivity in the material are derived and discussed.

4:40

1pPAa11. Optimal sound absorbing and manufacturable two-dimensional, hexagonal-like porous structure. Camille Perrot (Groupe d'Acoustique de l'Université de Sherbrooke, 2500, Boul. de l'Université, Département de génie mécanique, Sherbrooke, QC J1K-2R1, Canada, camille.perrot@usherbrooke.ca), Fabien Chevillotte (Groupe d'Acoustique de l'Université de Sherbrooke, 2500, Boul. de l'Université, Département de génie mécanique, Sherbrooke, QC J1K-2R1, Canada, fabien.chevillotte@usherbrooke.ca), Raymond Panneton (Groupe d'Acoustique de l'Université de Sherbrooke, 2500, Boul. de l'Université, Département de génie mécanique, Sherbrooke, QC J1K-2R1, Canada, raymond.panneton@usherbrooke.ca)

Results from a numerical study examining micro-macro relations linking local geometry parameters to sound absorption properties are presented. For an hexagonal structure of solid fibers, the porosity ϕ, the thermal characteristic length Λ', the static viscous permeability ko, the tortuosity α_∞, the viscous characteristic length Λ, and the sound absorption coefficient are computed. Numerical solutions of the steady Stokes and electrical equations are employed to provide ko, α_∞, and Λ. Hybrid estimates based on direct numerical evaluation of porosity ϕ, Λ', ko, α_∞, Λ and the analytical model derived by Johnson, Champoux, and Allard are used to relate varying (i) throat size, (ii) pore size, and (iii) fibers cross-section shapes to the sound absorption spectrum. The result of this paper tends to demonstrate the important effect of throat size in the sound absorption level, cell size in the sound absorption frequency selectivity, fibers cross-section shape in the porous material weight reduction. In a hexagonal porous structure with solid fibers, the sound absorption level will tend to be maximized with a 48 ± 10 μm throat size corresponding to an intermediate resistivity, a 13 ± 8 μm fiber radius associated with small pores, and convex triangular cross-section shape fibers allowing weight reduction.

5:00

1pPAa12. Analytical microstructural model for acoustical porous materials with single or double porosity. Emmanuel Gourdon (Université de Lyon, Ecole Nationale des Travaux Publics de l'Etat, CNRS, URA 1652, Département Génie Civil, 3, rue Maurice Audin, F-69120 Vaulx-en-Velin, France, emmanuel.gourdon@entpe.fr), Luc Jaouen (Matelys - Acoustique & Vibrations, 20/24 rue Robert Desnos, 69120 Vaulx-en-Velin, France, luc.jaouen@matelys.com)

An analytical model of sound propagation for porous materials with single or double scale of porosity is described. For each scale, pores and interconnections between them are modeled by a serie of two cylinders; a cylindrical periodical cell is thus considered. Scales are supposed to be separated, the porous medium is supposed to be periodic and to have a motionless skeleton. The geometrical parameters needed to quantify visco-thermal effects are directly related to the microstructure of the material. These parameters: lengths and radii of pores and interconnections can be extracted from image analysis for example. From additional conditions on cell morphology, independent parameters per porosity scale can be reduced to a number of three. Good comparisons between theoretical calculations of the sound absorption coefficient at normal incidence and impedance tube measurements are obtained for single and double porosity (meso-perforated) materials.

5:20

1pPAa13. Adsorption in activated carbon and its effects on the low frequency performance of hearing defenders. Fouad Bechwati (University of Salford, Acoustics Research Centre, Newton Building, M5 4WT Salford, UK, f.bechwati@pgr.salford.ac.uk), Trevor J. Cox (University of Salford, Acoustics Research Centre, Newton Building, M5 4WT Salford, UK, t.j.cox@salford.ac.uk), Mark R. Avis (University of Salford, Acoustics Research Centre, Newton Building, M5 4WT Salford, UK, m.r.avis@salford.ac.uk), Olga Umnova (University of Salford, Acoustics Research Centre, Newton Building, M5 4WT Salford, UK, o.umnova @salford.ac.uk)

Activated carbon displays interesting behaviours at low frequencies due to its large internal surface area and complex network of pores of various sizes and shapes. The material can produce larger than expected absorption and change the compliance of acoustic enclosures. This paper investigates the performance of hearing defenders which utilize activated carbon as the lining material of the cup. Compared to a standard foam liner, the introduction of activated carbon increases the insertion loss by up to 15 to 20 dB at frequencies between 31.5 and 250 Hz. The enhanced insertion loss is due to the increase in stiffness and apparent volume of the cup cavity as the activated carbon is introduced. This is probably due to the substantial change in local density as air molecules adsorb onto, and desorb from, the activated carbon pores during sound propagation. There is a change in entropy and energy loss from the sound wave during the adsorption/ desorption process due to the existence of a hysteresis loop. This additional absorption enhances performance.

5:40

1pPAa14. Ultrasonic behaviour of high pressure air filled porous media. Stephane Griffiths (LAUM, CNRS, Université du Maine, Av. O. Messiaen, 72085 Le Mans, France, stephane.griffiths@live.fr), Christophe Ayrault (LAUM, CNRS, Université du Maine, Av. O. Messiaen, 72085 Le Mans, France, christophe.ayrault@univ-lemans.fr)

This paper deals with the acoustic behaviour of porous media when the saturating fluid is high pressured. These observations are performed by ultrasonic transmission through a porous sample with variations of the static pressure of the saturating fluid. In order to characterize high damping materials, measurements are performed for high static pressure (up to 18 bars). It is shown that the behaviour of transmission coefficient and speed with pressure follow the Biot's theory. Moreover, measurements are strongly dependant on temperature, which is not visible in modelizations with Biot's model, although this parameter is taken into account in thermodynamical parameters. It is therefore assumed that mechanical characteristics vary with temperature and pressure. An estimation of mechanical parameters is then performed by minimization between the Biot's model and experimental data. First results, obtained in suitable cases for which measurements quality is good and minimization process converges correctly, show that mechanical parameters follow the evolution with frequency described by Pritz at low frequencies. Further researches are still necessary to determine dependance to temperature.

6:00

1pPAa15. Automatic characterisation of ground surfaces from in situ measurements. Guillaume Dutilleux (Lab. Régional des Ponts et Chaussées, 11, rue Jean Mentelin, BP 9, 67035 Strasbourg Cedex 2, France, Guillaume.Dutilleux@equipement.gouv.fr), David Ecotiere (Lab. Régional des Ponts et Chaussées, 11, rue Jean Mentelin, BP 9, 67035 Strasbourg Cedex 2, France, david.ecotiere@equipement.gouv.fr)

The study of long term acoustic performance of road pavements requires to access the evolution of the intrinsic parameters of these surfaces, such as resistivity or tortuosity. In long range sound propagation as well, it is well known that ground absorption is time varying. The understanding of this variation is an important issue. In both application cases, nondestructive measurement methods are required. The present contribution focuses on the 2-parameter model by Delany and Bazley for outdoor surfaces and the 4-parameter one by Hamet-Berengier for porous road pavements. It is shown that for both models the absorption coefficient spectrum obtained by an ISO 13472-1 compliant measurement contains enough data for the automatic identification. For the 2-parameter model the identification is based on a suitable cost function. The complexity of the function is low enough for a resolution by exhaustive search. It turns out that, for a large set of soft ground samples, the cost function is convex. Therefore the resolution can be done quite efficiently by classical gradient descent methods. Regarding the 4-parameter model, although the cost function is no longer convex, the resolution can be performed using a global optimization tool, like an evolutionary algorithm.

6:20

1pPAa16. A new setup for measuring the mechanical properties of porous materials. Nicolas Dauchez (Laboratoire d'Acoustique de l'Université du Maine, Avenue Olivier Messiaen, 72085 Le Mans, France, nicolas.dauchez@univ-lemans.fr), Olivier Doutres (Laboratoire d'Acoustique de l'Université du Maine, Avenue Olivier Messiaen, 72085 Le Mans, France, olivier.doutres.etu@univ-lemans.fr), Jean Michel Genevaux (Laboratoire d'Acoustique de l'Université du Maine, Avenue Olivier Messiaen, 72085 Le Mans, France, jean-michel.genevaux@univ-lemans.fr), Guy Lemarquand (Laboratoire d'Acoustique de l'Université du Maine, Avenue Olivier Messiaen, 72085 Le Mans, France, guy.lemarquand@univ-lemans.fr)

A new device for determining complex Young's modulus of porous materials in a extended frequency range is proposed. Classical methods are based on quasitatic or dynamic response of porous material. These methods generaly neglect the coupling between the surrounding fluid and the porous frame so that they are restricted to low frequency range ($<$100 Hz) or specific sample shape. Dynamic methods provide relevant information only at the resonance frequencies of the frame. The proposed method extends the quasistatic method towards high frequencies: 1. the porous sample is setup in a cavity in order to avoid the coupling with the external fluid, 2. a specific electrodynamic transducer has been developped to get the mechanical impedance of the sample from the measurement of the electrical impedance, 3. mechanical properties of the frame are derived by inverse method using Biot theory so that the frequency range is not restricted to the quasistatic domain. First results obtained with a prototype validate the method in comparison with two classical methods.

6:40

1pPAa17. Quasistatic evaluation of mechanical properties of poroelastic materials: static and dynamic strain dependence and in vacuum tests. Paolo Bonfiglio (Dipartimento di Ingegneria - University of Ferrara, Via Saragat 1, 44100 Ferrara, Italy, paolo.bonfiglio@unife.it), Francesco Pompoli (Dipartimento di Ingegneria - University of Ferrara, Via Saragat 1, 44100 Ferrara, Italy, francesco.pompoli@unife.it), Paresh Shravage (Dipartimento di Ingegneria - University of Ferrara, Via Saragat 1, 44100 Ferrara, Italy, paresh.shravage @unife.it)

A complete description of the vibro-acoustical behavior of a poroelastic material requires the knowledge of both geometrical quantities, related to the structure of the fluid-filled pores to account the sound propagation within them, and mechanical parameters (i.e. Young Modulus, Poisson's ratio, and loss factor) in order to model the wave propagation through the elastic structure constituting its skeleton. Because the nonlinear nature of poroelastic media, those mechanical properties are shown depending on static preload and dynamic strain applied to them. In the present work a well established quasi-static method, based on the measurement of mechanical impedance and the use of adequate polynomial relations, has been used to determine the dependence of the mechanical properties on the applied deformations. Furthermore, tests have been also carried out in a vacuum chamber in order to evaluate the real contribution of the filling fluid on the total vibro-acoustical response of the material.

7:00

1pPAa18. Sound absorbing properties of materials made of rubber crumbs. Francesco Asdrubali (Università degli studi di Perugia, Via G. Duranti 67, 06125 Perugia, Italy, fasdruba@unipg.it), Francesco D'Alessandro (Università degli studi di Perugia, Via G. Duranti 67, 06125 Perugia, Italy, dalessandro.unipg@ciriaf.it), Samuele Schiavoni (Università degli studi di Perugia, Via G. Duranti 67, 06125 Perugia, Italy, schiavo81 @libero.it)

Recycled tyre granules can be used for manufacturing acoustic insulating and absorbing materials, with applications in buildings and road barriers. Therefore, the production of these materials is a valid alternative to the disposal into landfill or incineration of used tyres. This paper presents the results of sound absorbing coefficient measurements of several samples manufactured at the Acoustics Laboratory of the University of Perugia. The sound absorbing panels were produced by mixing rubber crumbs and an adequate binder in a proper proportion and then by compacting the obtained mix. The methodology used to evaluate coefficient of absorption coefficient is indicated in ISO 10534-2 standard, thanks to an impedance tube. The influence on the absorption performance of granules size, binder concentration, thickness and compaction ratio of the samples was investigated and an optimization process was carried out, in order to produce a sample with satisfying acoustical performances.

7:20

1pPAa19. Measurement of acoustic and mechanical parameters of poroelastic materials by mean of active control and wave-based methods. Cedric Batifol (Centre Acoustique du LMFA, Ecole Centrale de Lyon, 36 avenue Guy de Collongue, 69134 Ecully cedex, France, cedric.batifol@ec-lyon.fr), Marie-Annick Galland (Centre Acoustique du LMFA, Ecole Centrale de Lyon, 36 avenue Guy de Collongue, 69134 Ecully

cedex, France, marie-annick.galland@ec-lyon.fr),Mohamed Ichchou(Centre Acoustique du LMFA, Ecole Centrale de Lyon, 36 avenue Guy de Collongue, 69134 Ecully cedex, France, mohamed.ichchou@ec-lyon.fr)

Poroelastic materials are used in sound barriers for sound insulation and absorption. At low frequencies, the medium is modeled using the Biot theory. This homogenised model needs to be feed by at least eight parameters using the Johnson-Allard approach. The presented characterisation method relies on two specific test facilities. First, acoustic parameters are obtained thanks to a modified Kundt tube. The porosity and resistivity are obtained by direct measurements of the surface impedance with hard wall and zero pressure boundary conditions on the rear face of the sample, respectively. This last boundary conditions is achieved thanks to active control procedure. Finally, the remaining acoustic parameters are obtained in a least mean square sense. Mechanical parameters are then measured on a second test bench. A beam made of the poroelastic sample is subjected to mechanical broadband forcing. The transverse displacement is measured along the beam thanks to a laser vibrometre. Dispersion curves are then obtained by calculating the Inhomogeneous Wave Correlation (IWC) ratio. The Young modulus and loss factor of the sample are estimated thanks to an optimisation procedure applied to the finite element model of the test. Results are compared to those obtained using more classical quasi-static methods.

MONDAY AFTERNOON, 30 JUNE 2008 ROOM 351, 1:00 TO 7:00 P.M.

Session 1pPAb

Physical Acoustics: Phononic Crystals I

Pierre Deymier, Cochair
University of Arizona, Materials Science and Engineering Department, Mines Bldg., P.O. Box 210012, Tucson, AZ 85721, USA

Jérôme Vasseur, Cochair
IEMN, UMR CNRS 8520, avenue Poincaré, BP 60069, Villeneuve d'Ascq, 59652, France

Contributed Papers

1:00

1pPAb1. Rubber/air acoustic band gap materials: Elastic and viscoelastic effects. Bassam Merheb (University of Arizona, Materials Science and Engineering Department, Mines Bldg., P.O. Box 210012, Tucson, AZ 85721, USA, bassam@merheb.net), Pierre Deymier (University of Arizona, Materials Science and Engineering Department, Mines Bldg., P.O. Box 210012, Tucson, AZ 85721, USA, deymier@u.arizona.edu), Manish Jain (3M Corporation, Corporate Research Materials Laboratory, Bldg. 201-3N-04, 3M Center, St. Paul, MN 55144-1000, USA, mjain@mmm.com), Marie Aloshyna-Lesuffleur (3M Corporation, Corporate Research Materials Laboratory, Bldg. 201-3N-04, 3M Center, St. Paul, MN 55144-1000, USA, mlesuffleur@mmm.com), Richard Greger (3M Corporation, Corporate Research Materials Laboratory, Bldg. 201-3N-04, 3M Center, St. Paul, MN 55144-1000, USA, rgreger@mmm.com), Sanat Mohanty (3M Corporation, Corporate Research Materials Laboratory, Bldg. 201-3N-04, 3M Center, St. Paul, MN 55144-1000, USA, smohanty@mmm.com), Ali Berker (3M Corporation, Corporate Research Materials Laboratory, Bldg. 201-3N-04, 3M Center, St. Paul, MN 55144-1000, USA, aberker@mmm.com)

Two-dimensional elastic and viscoelastic phononic crystals structures are investigated theoretically and experimentally. These are two-dimensional arrays of cylinders of air inclusions in a solid silicone rubber matrix as well as arrays of silicone rubber cylinders in an air matrix. In this study, viscoelasticity is modeled with a compressible general linear viscoelastic fluid model. Numerical calculations of transmission spectra and band structures are conducted by extending the finite difference time domain (FDTD) method to account for linear viscoelastic materials which exhibit time-dependent moduli. These systems demonstrate very wide band gaps in their transmission spectra that extend to frequencies in the audible range of the spectrum. Experimental and calculated transmission spectra for a rubber matrix/air inclusions phononic crystal show that the system behaves as a fluid/fluid composite with respect to the longitudinal polarization of acoustic waves due to the large contrast between the transverse and longitudinal speeds of sound. We also demonstrate that viscoelasticity can attenuate transmission over very wide ranges of frequency leaving only passing bands at very low frequency. These phononic crystals demonstrate the practical design of elastic or viscoelastic solid rubber/air acoustic band gap sound barrier with small dimensions.

1:20

1pPAb2. Development of a suitable PML for an harmonic study of a finite 1D phononic crystal. Maxime Bavencoffe (LOMC FRE-3102 CNRS, Groupe Ondes Acoustiques, University of Le Havre, Place Robert Schuman, BP 4006, 76610 Le Havre, France, maxime.bavencoffe@univ-lehavre.fr), Bruno Morvan (LOMC FRE-3102 CNRS, Groupe Ondes Acoustiques, University of Le Havre, Place Robert Schuman, BP 4006, 76610 Le Havre, France, bruno.morvan@univ-lehavre.fr), Anne-Christine Hladky (IEMN, UMR CNRS 8520, avenue Poincaré, BP 60069, 59652 Villeneuve d'Ascq, France, anne-christine.hladky@isen.fr), Olivier Bou Matar (IEMN, UMR CNRS 8520, avenue Poincaré, BP 60069, 59652 Villeneuve d'Ascq, France, olivier.boumatar@iemn.univ-lille1.fr), Jean-Louis Izbicki (LOMC FRE-3102 CNRS, Groupe Ondes Acoustiques, University of Le Havre, Place Robert Schuman, BP 4006, 76610 Le Havre, France, jean-louis.izbicki@univ-lehavre.fr)

This paper deals with the interaction of ultrasonic Lamb waves with a 1D phononic crystal. The studied structure is a finite plate with a periodic corrugated surface. Two types of forbidden bands arise in the Lamb wave dispersion curves. The first one is located at the limit of the first Brillouin zone, the second one exists at the crossing of dispersion curves of two different Lamb modes. These forbidden bands lead to conversion phenomena. In order to study accuratly the conversion phenomena in the band gaps, harmonic finite element analysis are performed. Perfect matching layers (PML) on both sides of the plate are then necessary to avoid stationnary waves. PML, adapted for Lamb modes involved at a given frequency, must be designed. By using these PML, the attenuation of Lamb waves propagating in the phononic crystal is clearly shown and is related to the existence of the forbidden band.

1:40

1pPAb3. Plate waves in phononic crystals slabs. Jiu-Jiu Chen (CNRS and Paris VI University, INSP - 140 rue de Lourmel, 75015 Paris, France, chen99nju@gmail.com), Bernard Bonello (CNRS and Paris VI University, INSP - 140 rue de Lourmel, 75015 Paris, France, bernard.bonello@insp.jussieu.fr)

We have computed the dispersion curves of plate waves propagating in periodic composite structures composed of isotropic tungsten cylinders

embedded in a isotropic silicon background. The phononic crystal has a square symmetry and the calculation is based on the plane wave expansion method. The direction of propagation is defined by the angle φ between ΓX in the reduced Brillouin zone and the wave vector k. If φ=0 {0} or φ=90 {0}, SH modes are simple hyperbolas and do not couple to the Lamb wave modes polarized in the sagittal plane. If is different from 0 {0} or 90 {0}, SH modes convert to Lamb wave modes and couple with the flexural and dilatational modes. The symmetric modes splitting in the band structures along this direction and all three components of the particle displacements demonstrate this phenomenon which is different from the pure isotropic plate case where SH waves decouple to Lamb waves whatever the propagating direction.

2:00

1pPAb4. Analysis of bandpass spectra of phononic defect-mode waveguides based on mode coupling between point defects. Toyokatsu Miyashita (Dept. Electronics & Informatics, Ryukoku University, Seta Oecho Yokotani 1-5, 520-2194 Otsu, Japan, miya@rins.ryukoku.ac.jp)

Pass bands of defect-mode waveguides fabricated in sonic/phononic crystals have desirable characteristics for their practical applications to acoustic bandpass filters. Their mechanism is considered to originate in mode-coupling characteristics of point defects, a chain of which composes a defect-mode waveguide. Especially, mode confinement in each point defect or their mode coupling is found to decide the flatness of the pass band. For example, with a relatively strong mode confinement, the transmission of the pass band swings between 0 and -16 dB with frequency, although the transmission outside the pass band remains still typically at -50 dB. On the contrary with a moderate mode confinement, the transmission remains fairly flat only with a swing of 2 dB. We have obtained these characteristics not only by an elastic FDTD method but also by acoustic experiments. These have been investigated theoretically and experimentally based on analyses of the mode coupling between point defects. Two sonic/phononic crystals are considered; one is composed of acrylic-resin cylinders in air, and the other steel cylinders in water.

2:20

1pPAb5. Design and characterization of stop-band filters using PZT layer on silicon substrate phononic crystals. Jérôme Vasseur (IEMN, UMR CNRS 8520, avenue Poincaré, BP 60069, 59652 Villeneuve d'Ascq, France, jerome.vasseur@univ-lille1.fr), Anne-Christine Hladky-Hennion (IEMN, UMR CNRS 8520, avenue Poincaré, BP 60069, 59652 Villeneuve d'Ascq, France, Anne-Christine.Hladky@isen.fr), Bertrand Dubus (IEMN, UMR CNRS 8520, avenue Poincaré, BP 60069, 59652 Villeneuve d'Ascq, France, Bertrand.Dubus@isen.fr), Bahram Djafari-Rouhani (IEMN, UMR CNRS 8520, avenue Poincaré, BP 60069, 59652 Villeneuve d'Ascq, France, Bahram.Djafari-Rouhani@univ-lille1.fr), Bruno Morvan (LOMC FRE-3102 CNRS, Groupe Ondes Acoustiques, University of Le Havre, Place Robert Schuman, BP 4006, 76610 Le Havre, France, bruno.morvan@univ-lehavre.fr)

Phononic crystals are periodic structures exhibiting absolute band gaps i.e. frequency bands in which the propagation of elastic waves is forbidden in all directions. Filtering is then a possible application of phononic crystals. Recently, the existence of absolute band gaps has also been theoretically demonstrated for guided elastic waves in a piezoelectric plate on a substrate [J. Vasseur et al, J. Appl. Phys, **101**, 114904 (2007)], which is a geometry of interest for possible co-integration on silicon chip. The 2D phononic crystal was constituted by a square arrangement of cylindrical holes in a PZT layer deposited on a silicon substrate. In this communication, the realization of a stop-band filter constituted by a periodically patterned PZT layer, polarized along thickness, on silicon substrate and interdigitated electrodes (IDE) for emission/reception of guided elastic waves, is investigated. The filter characteristics are theoretically evaluated by using finite element simulations: dispersion curves of patterned PZT layer are computed for various pattern geometries to obtain the absolute band gap. Complete structure is then modeled, with appropriate IDE to propagate a guided mode in the piezoelectric layer. Finally, filtering capability of the structure is evaluated. Work supported by STMicroelectronics (Nano2008 program of French ministry of industry).

2:40

1pPAb6. Acoustic response of a soniclike crystal within a rigid frame porous plate. Jean-Philippe Groby (DRE/L2S - UMR8506 CNRS/Supelec/Univ. Paris Sud 11, Département de Recherche en Electromagnétisme/Laboratoire des signaux et systèmes, 3 rue Joliot-Curie, 91192 Gif-sur-Yvette cedex, France, groby@lss.supelec.fr), Armand Wirgin (CNRS-Laboratoire de Mécanique et d'Acoustique, 31 Chemin Joseph Aiguier, 13402 Marseille, France, wirgin@lma.cnrs-mrs.fr), Erick Ogam (Laboratoire de Mécanique et d'Acoustique CNRS UPR-7051, 31, Chemin Joseph Aiguier, 13402 Marseille Cedex 20, France, ogam@lma.cnrs-mrs.fr), Laurent De Ryck (Lab. ATF, Katholieke Universiteit Leuven, Celestijnenlaan 200D, B-3001 Leuven, Belgium, Laurent.DeRyck@fys.kuleuven.be), Walter Lauriks (Lab. ATF, Katholieke Universiteit Leuven, Celestijnenlaan 200D, B-3001 Leuven, Belgium, Walter.Lauriks@fys.kuleuven.be), Claude Depollier (Laboratoire d'Acoustique de l'Université du Maine, Avenue Olivier Messiaen, 72085 Le Mans, France, claude.depollier@univ-lemans.fr)

The acoustic response (in particular, the transmission) of a periodic distribution of macroscopic inclusions within a rigid frame, porous plate (similar to a sonic crystal) is studied by the multipole method. Numerical results show that the addition of grating stacks leads to band gaps within the audible frequency range for a small number of stacks, this being associated with a large decrease of the transmission coefficient of the initial plate. The first band gap is of practical interest for noise suppression. The second band gap enables total acoustic absorption within a narrow frequency range due to the fact that a modified mode of the plate lies within this band gap.

3:00

1pPAb7. K-dependent polarization of sagittal acoustic waves in phononic crystals. Felipe Ramos-Mendieta (Universidad de Sonora, Rosales y Boulevard Luis Encinas, Colonia Centro, 83000 Hermosillo, Mexico, framos@cajeme.cifus.uson.mx), Betsabe Manzanares-Martinez (Division de Ciencias e Ingenieria, Unidad Sur Universidad de Sonora, Boulevard Lazaro Cardenas 100, 85390 Navojoa, Mexico, mbmm@cajeme.cifus.uson.mx)

By calculating the longitudinal and transverse strain energy averages we studied the polarization states of sagittal acoustic waves in one- and two-dimensional phononic crystals. Our theoretical results show the continuous variation of the field displacement components when the Bloch wave vector sweeps the Brillouin zone; thus, the vibrational modes of a same dispersion curve can have different polarization. First we present the polarization map of sagittal waves for an epoxy/Sn superlattice. Then we discuss the band polarization of an array of cylindrical holes in epoxy. As we shall see, the mixed modes can be either predominantly transverse of predominantly longitudinal. For calculations we have used an energy balance criterion.

3:20

1pPAb8. Proof of the existence of large complete band gaps in high frequency silicon phononic crystal plates. Saeed Mohammadi (Georgia Institute of Technology, 338083 Georgia Tech Station, Atlanta, GA 30332, USA, saeedm@gatech.edu), Ali Asghar Eftekhar (Georgia Institute of Technology, 338083 Georgia Tech Station, Atlanta, GA 30332, USA, eftekhar@ece.gatech.edu), Abdelkrim Khelif (Institut FEMTO-ST/CNRS, 32 avenue de l'Observatoire, 25044 Besançon cedex, France, abdelkrim.khelif@femto-st.fr), William D. Hunt (Georgia Institute of Technology, 338083 Georgia Tech Station, Atlanta, GA 30332, USA, bill.hunt@ee.gatech.edu), Ali Adibi (Georgia Institute of Technology, 338083 Georgia Tech Station, Atlanta, GA 30332, USA, adibi@ece.gatech.edu)

We show, for the first time, the evidence of the existence of large phononic band gaps (PBGs) in two-dimensional phononic crystal (PC) plates formed by etching a hexagonal (honeycomb) array of air holes through a free standing plate of silicon (Si). A CMOS compatible fabrication process is used on a Si on insulator (SOI) substrate to realize the PC devices. More than 30 dB attenuation is observed for eight periods of the hexagonal lattice PC at high frequency region, i.e. 133 MHz with a band gap to mid gap ratio of 25%. We show that the experimental results agree very well

with the theoretical predictions for the PBG. This result opens a new direction in the implementation of high frequency practical PC structures for a variety of applications especially wireless communication, and sensing.

3:40

1pPAb9. Acoustic defect mode in a finite 1-dimension lattice. Kanghyun Chu (Center for Noise and Vibration Control, Korea Advanced Institute of Science and Technology, 4114, Department of Mechanical Engineering, Guseong-dong, Yuseong-gu, 305-701 Daejon, Republic of Korea, kanghyunchu@kaist.ac.kr), Yang-Hann Kim (Center for Noise and Vibration Control, Korea Advanced Institute of Science and Technology, 4114, Department of Mechanical Engineering, Guseong-dong, Yuseong-gu, 305-701 Daejon, Republic of Korea, yanghannkim@kaist.ac.kr)

If there is a defect in a periodic lattice, then the defect modes are expected. The wave localization can be one of representative examples of defect modes applications. However, it is not likely possible to deal with an infinite-periods lattice in practice, and this implies that it is impossible to obtain a perfect wave localization. This motivates us to study a lattice with a finite period which allows the wave tunneling through it. Therefore, the behavior of the acoustic wave in a 1-dimension periodic lattice containing a defect with a finite period has been studied. For simplicity, we considered the lattice composed of two kinds of media with different characteristic impedance in the repeating order with finite periods and the defect with arbitrary size and characteristic impedance Finally, the limitation of wave localization in the real world application is discussed.

4:00-4:20 Break

4:20

1pPAb10. Review of phononic crystals, nonlinear processes, devices and prospects. Sergey Nikitov (Institute of Radioengineering and Electronics, Russian Academy of Sciences, 11, bldg. 7, Mokhovaya St., 125009 Moscow, Russian Federation, nikitov@cplire.ru), Yurii Gulyaev (Institute of Radioengineering and Electronics, Russian Academy of Sciences, 11, bldg. 7, Mokhovaya St., 125009 Moscow, Russian Federation, nikitov@cplire.ru), Valery Grigorevsky (Institute of Radioengineering and Electronics, Russian Academy of Sciences, 11, bldg. 7, Mokhovaya St., 125009 Moscow, Russian Federation, vig324@ms.ire.rssi.ru), Alexander Grigorevsky (Institute of Radioengineering and Electronics, Russian Academy of Sciences, 11, bldg. 7, Mokhovaya St., 125009 Moscow, Russian Federation, vig324@ms.ire.rssi.ru), Ivan Lisenkov (Institute of Radioengineering and Electronics, Russian Academy of Sciences, 11, bldg. 7, Mokhovaya St., 125009 Moscow, Russian Federation, lisenkov@cplire.ru), Roman Popov (Institute of Radioengineering and Electronics, Russian Academy of Sciences, 11, bldg. 7, Mokhovaya St., 125009 Moscow, Russian Federation, rspopov@gmail.com)

The review of current state of the art of bulk and surface linear and nonlinear acoustic wave propagation in phononic crystals (PhC) is given. First, theoretical analysis of bulk acoustic waves propagation in 2D phononic crystals composed of elastic medium with periodic systems of air holes with different symmetry is considered. The properties of hypersonic bulk and surface acoustic waves (Love, Lamb) in PhC are considered theoretically and expermentally. We studied bulk waves propagation in microstructured optical fiber preforms made of quartz. The study of simultaneous propagation of acoustic waves and light in structures being both photonic and phononic crystals was done. We study also properties of guided waves (Lamb modes) propagating in layered structures containing the magnetic films with two-dimensional periodic structures. In these structures we discovered a strong coupling between elastic and magnetic properties leading to effective waves transformation between magnetic and elastic systems. Such structures are so called magnonic-phononic crystals. The recommendations of use such unusual BAW and SAW properties in PhC for development of solid state devices are given. This work is supported by RFBR grant 08-02-00785.

4:40

1pPAb11. Omnidirectional phononic reflection and selective transmission in solid/fluid superlattices. El Houssaine El Boudouti (Faculté des Sciences, Département de Physique, Université Mohamed I, 60000 Oujda, Morocco, elboudouti@yahoo.fr),Youssef El Hassouani (Faculté des Sciences, Département de Physique, Université Mohamed I, 60000 Oujda, Morocco, hassouani@yahoo.fr), Hassan Aynaou (Faculté des Sciences, Département de Physique, Université Mohamed I, 60000 Oujda, Morocco, haynaou_2004@yahoo.fr), Bahram Djafari-Rouhani (IEMN, UMR CNRS 8520, avenue Poincaré, BP 60069, 59652 Villeneuve d'Ascq, France, Bahram.Djafari-Rouhani@univ-lille1.fr)

We present a theoretical analysis of the occurrence of omnidirectional reflection in one-dimensional phononic crystal. We discuss the conditions for a one-dimensional layered structure, made of alternating solid and fluid layers, to exhibit total reflection of acoustic incident waves in a given frequency range for all incident angles. In general, this property cannot be fulfilled with a simple finite superlattice if the incident wave is launched from an arbitrary fluid. Therefore, we propose two solutions to obtain such an omnidirectional band gap, namely: (i) cladding of the superlattice with a layer of high acoustic velocities that acts like a barrier for the propagation of phonons, or (ii) the association in tandem of two different superlattices in such a way that the superposition of their band structures exhibits an absolute acoustic band gap. We discuss the appropriate choices of the material and geometrical parameters to realize such structures. The behavior of the transmission coefficients is discussed in relation with the dispersion curves of the finite structure embedded between two fluids. By inserting a defect layer in the structure, we show that selective transmission may occur in the forbidden bands.

5:00

1pPAb12. Bubble phononic crystals. Alice Bretagne (Laboratoire Ondes et Acoustique, ESPCI, Université Paris 7, CNRS, 10 rue Vauquelin, 75005 Paris, France, alice.bretagne@espci.fr), Arnaud Tourin (Laboratoire Ondes et Acoustique, ESPCI, Université Paris 7, CNRS, 10 rue Vauquelin, 75005 Paris, France, arnaud.tourin@espci.fr), Patrick Tabeling (MMN ESPCI, 10 rue vauquelin, 75005 Paris, France, patrick.tabeling@espci.fr), Valentin Leroy (Laboratoire Ondes et Acoustique, ESPCI, Université Paris 7, CNRS, 10 rue Vauquelin, 75005 Paris, France, valeroy77@yahoo.fr), Nicolas Pannacci (MMN ESPCI, 10 rue vauquelin, 75005 Paris, France, nicolas.pannacci@espci.fr), Hervé Willaime (MMN ESPCI, 10 rue vauquelin, 75005 Paris, France, herve.willaime@espci.fr), Mathias Fink (Laboratoire Ondes et Acoustique, ESPCI, Université Paris 7, CNRS, 10 rue Vauquelin, 75005 Paris, France, mathias.fink@espci.fr)

Our aim is to investigate phononic crystals consisting of periodic arrangements of micron size gas bubbles. Such crystals are of great potential interest. Because of the high compressibility and high acoustic impedance contrasts between gas and water, a gas filled bubble in water is indeed a strong acoustic scatterer with a large value of its resonant wavelength compared with its size and a scattering cross section several orders of magnitude larger than its geometrical cross section. In that sense a microbubble can be viewed as the equivalent of an acoustic atom and even a small size sample made with such bubbles is expected to have a dramatic impact on acoustic propagation. Using microfluidics techniques we were able to produce perfectly monodisperse gas bubbles in a liquid. When these bubbles (radius=50 μm) are then injected into a liquid with surfactant, they are found to organize themselves to form an hexagonal close packed crystal. Its stability has still to be optimised before testing it successfully with acoustic waves. The calculation of the band structure of that crystal with the plane wave expansion (PWE) method confirms its interest for controlling propagation of MHz-ultrasounds: a 800-kHz wide band gap around 1.85 MHz is predicted.

5:20

1pPAb13. Floquet Lamb modes in periodic plates. Vincent Pagneux (Laboratoire d'Acoustique de l'Université du Maine, UMR CNRS 6613, AV. O. Messiaen, 72085 Le Mans, France, vincent.pagneux@univ-lemans.fr), Agnes Maurel (LOA/ESPCI, 10 rue Vauquelin, 75005 Paris, France, agnes.maurel@espci.fr)

An elastic waveguide with periodic perturbation of its thickness or of its elastic properties can support Floquet modes that are the extension of the classical Lamb modes. In this work, we obtain the spectra of the Floquet modes by using a new numerical coupled mode method which is based on a

pseudospectral discretization in the transverse direction and a Magnus exponential integration in the longitudinal direction. The Floquet mode spectra are analyzed and compared to the Lamb mode spectra for different configuration of the periodic perturbation of the plate. A particular emphasis is given to the existence of backward wave propagation and to the number of propagating modes as the frequency is increased.

5:40

1pPAb14. Acoustic transparency by switching of phononic band gaps. José Sanchez-Dehesa (Polytechnic University of Valencia, Cami de Vera s/n, 46022 Valencia, Spain, jsdehesa@upvnet.upv.es), Helios Sanchis-Alepez (Polytechnic University of Valencia, Cami de Vera s/n, 46022 Valencia, Spain, hesana@alumni.uv), Daniel Torrent (Politechnic University of Valencia, Wave Phenomena Group. Department of Electronic Engineering, C/Camino Vera s.n, ES-46022 Valencia, Spain, datorma1@upvnet.upv.es), Liang-Wu Cai (Kansas State University, Mechanical and Nuclear Engineering, Manhattan, KS 66506, USA, cai@ksu.edu)

Acoustic transparency is here studied in two-dimensional phononic crystals made of hexagonal arrangements of layered cylinders. These layered cylinders, which have their acoustical properties radially dependent, can be achieved by using the recently proposed acoustical metamaterials [D. Torrent and J. Sanchez-Dehesa, New J. Phys., **9**, 323 (2007)]. The transparency condition is here achieved by switching of the phononic band gaps, which is governed by the scattering form factor of the acoustic parameters (bulk modulus and sound speed). Various dependence have been studied. The feasibility of this proposal is demonstrated by multiple scattering simulations of the proposed metamaterials [Work supported by NSF of USA and MEC of Spain.]

6:00

1pPAb15. Three-dimensional phononic crystals made by brazing aluminum beads to form an opal structure. John H. Page (Dept. of Physics and Astronomy, Univ. of Manitoba, Winnipeg, MB R3T 2N2, Canada, jhpage@cc.umanitoba.ca), Hefei Hu (Dept. of Physics and Astronomy, Univ. of Manitoba, Winnipeg, MB R3T 2N2, Canada, hefeihu2@uiuc.edu), Yukihiro Tanaka (Division of Applied Physics, Graduate School of Engineering, Hokkaido University, 060 8628 Sapporo, Japan, yuki@eng.hokudai.ac.jp), Takuro Okada (Department of Applied Physics, Hokkaido University, 060-8628 Sapporo, Japan, broaden_my_outlook@yahoo.co.jp), Shin Tamura (Department of Applied Physics, Hokkaido University, 060-8628 Sapporo, Japan, s-tamura@eng.hokudai.ac.jp)

Most phononic crystals studied so far are constructed from periodically arranged objects (e.g., spheres or rods) immersed in a continuous solid or fluid medium. In this presentation, we investigate the properties of a different type of phononic crystal made by weakly brazing 4-mm-diameter aluminum beads in a face-centred cubic array, producing a large-scale opal. In this crystal, wave propagation proceeds through the network of coupled beads rather than through the surrounding medium (air in our case), and the main band gaps that we observe result from coupled resonances of the beads rather than from Bragg scattering. Using ultrasonic techniques, we measure the transmission coefficient and the dispersion relation along the ΓL direction, and show that the lowest-frequency gap occurs between about 500 and 600 kHz - a frequency range that is just below the lowest resonance of an isolated aluminum sphere. We have also measured the group velocity, which we find to be negative in the lowest frequency band gap. Further insight into the properties of these phononic crystals is obtained by performing finite difference time domain (FDTD) calculations, in which the coupling between spheres is taken into account by allowing the spheres to overlap.

6:20

1pPAb16. Band gaps in a phononic crystal constituted by cylindrical dots on a homogeneous plate. Bahram Djafari-Rouhani (IEMN, UMR CNRS 8520, avenue Poincaré, BP 60069, 59652 Villeneuve d'Ascq, France, Bahram.Djafari-Rouhani@univ-lille1.fr), Yan Pennec (IEMN, UMR CNRS 8520, avenue Poincaré, BP 60069, 59652 Villeneuve d'Ascq, France, yan.pennec@univ-lille1.fr), Hocine Larabi (IEMN, UMR CNRS 8520, avenue Poincaré, BP 60069, 59652 Villeneuve d'Ascq, France, hocine.larabi@wanadoo.fr), Jérôme Vasseur (IEMN, UMR CNRS 8520, avenue Poincaré, BP 60069, 59652 Villeneuve d'Ascq, France, jerome.vasseur@univ-lille1.fr), Anne-Christine Hladky (IEMN, UMR CNRS 8520, avenue Poincaré, BP 60069, 59652 Villeneuve d'Ascq, France, anne-christine.hladky@isen.fr)

Using the finite difference time domain (FDTD) and the finite element (FE) methods, we investigate theoretically the band structure of a phononic crystal constituted by a periodic array of cylindrical dots deposited on a thin homogeneous plate. We demonstrate that such a structure can exhibit a very low frequency absolute band gap as compared to the wavelength in the constituent materials. The occurrence of this gap requires an appropriate choice of the geometrical parameters and, in particular, of the thickness of the plate as compared to the period or to the height of the cylinders. However, the same behavior can be obtained for various combinations of the materials constituting the homogeneous plate and the dots. We study in detail the width of this band gap as a function of the geometrical and physical parameters of the structure. On the other hand, the structure can also exhibit one or more higher gaps whose numbers can be increased by increasing the height of the cylinders.

6:40

1pPAb17. Laser-generated surface acoustic waves in copper line arrays on silicon. Alexei A. Maznev (Department of Applied Physics, Hokkaido University, Kita 13 Nishi 8, Kita-ku, 060-8628 Sapporo, Japan, alexei.maznev@gmail.com)

Laser-generated acoustics waves are widely used to control the fabrication on metal interconnect structures in the semiconductor industry. On the other hand, acoustic properties of such structures, typically comprised of periodic arrays of metal lines embedded in a dielectric film on a silicon substrate, pose some interesting wave propagation problems. We will report measurements of surface acoustic waves (SAWs) performed using laser-induced transient grating technique on periodic arrays of micron-wide copper lines. As expected, SAW dispersion curves yield small band gaps at the Brillouin zone boundary. However, much larger band gaps are observed within the 1st Brillouin zone. We believe that these giant band gaps are formed due to avoided crossing of the 1st and 2nd order surface acoustic modes of the film/substrate structure when the 1st mode dispersion curve becomes folded due to periodicity. Another observed phenomenon is a spectacularly sharp increase in the acoustic attenuation occurring when the folded surface mode becomes coupled to a bulk wave.

Session 1pPAc

Physical Acoustics and Signal Processing in Acoustics: Acoustic Landmine Detection I

James M. Sabatier, Cochair
University of Mississippi, NCPA, 1 Coliseum Drive, University, MS 38677, USA

Keith Attenborough, Cochair
Open University, Department of Design, Development, Materials and Environment, Walton Hall, Milton Keynes, MK7 6AA, UK

Invited Papers

1:00

1pPAc1. Combined seismic, radar, and induction sensor for landmine detection. Waymond R. Scott (Georgia Institute of Technology, School of Electrical and Computer Engineering, 777 Atlantic Dr., Atlanta, GA 30332-0250, USA, waymond.scott@ece.gatech.edu), Kangwook Kim (Dept. Machatronics, GIST, 1 Oryong-dong, Buk-gu, 500-712 Gwangju, Republic of Korea, mkkim@gist.ac.kr), Gregg D. Larson (Georgia Institute of Technology, G. W. Woodruff School of Mechanical Engineering, 777 Atlantic Dr., Atlanta, GA 30332-0250, USA, gregg.larson@me.gatech.edu), Ali C. Gurbuz (Georgia Institute of Technology, School of Electrical and Computer Engineering, 777 Atlantic Dr., Atlanta, GA 30332-0250, USA, gtg173p@mail.gatech.edu), James H. McClellan (Georgia Institute of Technology, School of Electrical and Computer Engineering, 777 Atlantic Dr., Atlanta, GA 30332-0250, USA, jim.mcclellan@ece.gatech.edu)

An experimental system to collect co-located ground penetrating radar (GPR), electromagnetic induction (EMI), and seismic data was developed to investigate possibilities of using the sensors in a cooperative manner and to investigate the benefits of the fusion of the sensors. These sensors were chosen because they can sense a wide range of physical properties. The seismic sensor is sensitive to the differences between the mechanical properties of a landmine and the soil while the GPR is sensitive to the dielectric properties, and the EMI sensor is sensitive to the conductivity. In the experiments, a range of mines and clutter objects were buried at various depths in a sandbox. Multiple burial scenarios were investigated with a variety of antipersonnel and antitank mines and typical clutter objects. The GPR makes use of modified resistive-vee antennas. The EMI sensor collects broadband data so that the relaxation spectra of the buried targets can be used to aid discrimination. The system uses electrodynamic shakers to generate seismic waves, and a radar is used to measure the displacement of the surface caused by the seismic waves. The responses of each of these sensors to the buried targets will be shown. [Work supported by ARO.]

1:20

1pPAc2. Information-based sensor management for landmine detection using electromagnetic induction, ground-penetrating radar, and seismic sensors. Mark P. Kolba (Duke University, Department of Electrical and Computer Engineering, Box 90291, Durham, NC 27708, USA, mpk6@ee.duke.edu), Peter A. Torrione (Duke University, Department of Electrical and Computer Engineering, Box 90291, Durham, NC 27708, USA, pt@ee.duke.edu), Waymond R. Scott (Georgia Institute of Technology, School of Electrical and Computer Engineering, 777 Atlantic Dr., Atlanta, GA 30332-0250, USA, waymond.scott@ece.gatech.edu), Leslie M. Collins (Duke University, Department of Electrical and Computer Engineering, Box 90291, Durham, NC 27708, USA, lcollins@ee.duke.edu)

An information-based sensor management framework is presented that enables the automated tasking of a suite of sensors when detecting static targets. The sensor manager chooses the sensors to use and the grid-based locations to observe in order to maximize the expected information gain that will be obtained with each new sensor observation. Initially, sensor probabilities of detection and false alarm, Pd and Pf, are assumed to be known by the sensor manager. In a field setting, however, Pd and Pf cannot be known exactly, and so uncertainty modeling for Pd and Pf is also presented. The sensor manager is tested on real landmine data using electromagnetic induction (EMI), ground-penetrating radar (GPR), and seismic sensors. A matched subspace detector is used to process the EMI data, an adaptive pre-screening algorithm based on the least mean squares (LMS) adaptive filter is used to process the GPR data, and whitening followed by an energy detector is used to process the seismic data. The sensor manager is able to detect the landmines more quickly and more effectively than an unmanaged, blind-search approach. Using all three sensor modalities also results in superior detection performance to that achieved by only a single modality.

1:40

1pPAc3. Nonlinear seismo-acoustic landmine detection. Dimitri Donskoy (Stevens Institute of Technology, Dabvidson Lab., 711 Hudson Street, Hoboken, NJ 07030, USA, ddonskoy@stevens.edu)

The seismo-acoustic methods are among the most promising emerging techniques for the detection of landmines. Numerous field tests have demonstrated that buried landmines manifest themselves at the surface through resonance and nonlinear responses (or signatures) to acoustic/seismic excitation at the frequencies below 1000 Hz. The resonance signatures are primarily due to mine's housing structural resonances. The nonlinear signatures explained by high contact nonlinearity at the mine-soil interface. These phenomena are utilized for landmine detection demonstrating high provability of detection and low false alarms. The paper provides overview of theoretical and experimental investigations conducted by the author and his colleagues at Stevens Institute of Technology. Among major

accomplishments are discovery and explanation of mine's resonance behavior; soil/depth effect on buried mine's resonances; discovery and analysis of nonlinear acoustic interactions at the soil-mine interface; development of nonlinear quadratic and intermodulation detection algorithms based on dual-frequency excitation. Work supported by the U.S.Army NVESD, ARO and ONR.

2:00

1pPAc4. Hysteresis effects in nonlinear acoustic landmine detection. Murray S. Korman (Physics Dept., United States Naval Academy, Chauvenet Hall Room 295, 572 C Holloway Road, Annapolis, MD 21402, USA, korman@usna.edu)

In nonlinear acoustic landmine detection the vibration interaction of the top-plate of the buried plastic landmine with the adjacent soil is a subject of interest due to the strong nonlinear coupling. Using airborne sound excitation (in buried plastic anti-tank inert VS 1.6 and VS 2.2 landmine experiments) tuning curve behavior and generation of combination frequencies from two-tone tests were similar to the mesoscopic/nanoscale nonlinear elastic behavior observed in geomaterials like sandstone [J. Acoust. Soc. Am. **116**, 3354-3369 (2004)]. Tuning curve measurements near resonance for increased acoustic amplitude (exhibiting softening) can be explained if hysteresis effects (characteristic of mesoscopic nonlinearity) are considered. The backbone curve (peak amplitude vs. corresponding resonant frequency from a family of tuning curves) exhibits mostly linear behavior for "off target" soil surface vibration measurements of a soil layer resonating over a rigid boundary. Backbone curves for "on target" measurements exhibit significantly more bending and curvature when a soil layer resonates over the compliant top-plate of the landmine. An oscillator with hysteresis modeled by a distribution of parallel spring elements each with a different threshold slip condition seems to describe the "off target" behavior, while a single bilinear hysteresis element describes the "on target" results. [Support by USNA.]

2:20

1pPAc5. Accelerometer measurements of acoustic-to-seismic coupling above buried objects. Keith Attenborough (Open University, Department of Design, Development, Materials and Environment, Walton Hall, MK7 6AA Milton Keynes, UK, Keith .Attenborough@ioa.org.uk)

The surface velocity of sand inside a large PVC container, induced by the sound pressure from either a large loudspeaker radiating into an inverted cone and pipe or a B&K point source loudspeaker mounted with its axis vertical, has been measured using accelerometers. Results of white noise and stepped frequency excitation are presented. Without any buried object the mass loading of an accelerometer creates resonances in the spectral ratio of sand surface velocity to incident acoustic pressure i.e. the acoustic-to-seismic (A/S) admittance spectra. The A/S responses above a buried compliant object are larger and distinctive. The linear A/S admittance spectra in the presence of a buried electronic components box have been studied as a function of burial depth and sand state. The nonlinear responses above the buried box have been studied as a function of depth, sand state and amplitude. Predictions of a modified 1D lumped parameter model have been found to be consistent with the observed nonlinear responses. Also the modified model has been used to explain features of the A/S responses observed when using an accelerometer without any buried object [Work supported by DSTL, UK.]

2:40

1pPAc6. Acoustic-laser land mine detection: Operationally enabling technologies. Robert Haupt (MIT Lincoln Laboratory, 244 Wood St., Lexington, MA 02421, USA, haupt@LL.mit.edu)

Reliable and cost effective methods are critically needed to locate the vast number of land mines left behind from military conflicts. Many mine location systems being developed fall short of being operationally practical since they may detect only metal or a specific mine feature, have limited standoff ranges, or have slow search speeds. An approach that may overcome operational issues is the acoustic-laser method. Acoustic waves generated by a noncontact/standoff source and transmitted through air can couple to the ground and induce resonances from a large variety of mines. The vibration field above these mines can be measured remotely using laser Doppler vibrometry. In this paper, enabling technologies that can significantly increase search area speed, improve standoff range, and reduce size in an acoustic-laser system are discussed. We take a novel approach to excite mines by using a high powered parametric acoustic array source developed at MIT Lincoln Laboratory that transmits a highly directive sound beam from a safe distance. The avalanche photo diode (APD) array developed at MIT Lincoln Laboratory will also be discussed as the enabling technology of a proposed 4096 multipixel laser system that can sense a wide vibration field out in front of a moving vehicle.

3:00

1pPAc7. Fast acoustic landmine detection using multiple beam laser Doppler vibrometry. Vyacheslav Aranchuk (University of Mississippi, NCPA, 1 Coliseum Drive, University, MS 38677, USA, aranchuk@olemiss.edu), James M. Sabatier (University of Mississippi, NCPA, 1 Coliseum Drive, University, MS 38677, USA, sabatier@olemiss.edu), Richard D. Burgett (Planning Systems, Inc., NCPA, 1 Coliseum Drive, University, MS 38677, USA, rburgett@olemiss.edu)

An acoustic method of buried landmine detection consisting of excitation of the ground using airborne sound or seismic waves in the frequency range from about 50 Hz to 1000 Hz, and obtaining a velocity image of the ground surface with a laser Doppler vibrometer (LDV) has been developed and successfully tested in the laboratory and field experiments. The presence of a buried landmine can be detected by an abnormality in the velocity image. Initially, the scanning single-beam LDV created a velocity image of the ground through point-by-point measurements, which resulted in a long measurement time. To reduce this measurement time, a multiple beam LDV having 16 beams configured in a linear array was developed and successfully used in field experiments. To further reduce the time of measurement, a full-field LDV capable of making 256 vibration measurements in parallel on the target, configured as 16x16 square array of points equally separated in x- and y-directions has been recently developed. The system is capable of creating a two-dimensional vibrational velocity image of the ground surface in the time defined by the required frequency resolution. The parallel measurement makes the system a unique tool to measure transient vibrations.

3:20

1pPAc8. Mechanical resonances in the low-frequency vibration spectrum of a cylindrically symmetric, anti-tank landmine. William C. Alberts (U.S. Army Research Laboratory, 2800 Powder Mill Rd, Adelhi, MD 21044, USA, kirk.alberts@arl.army.mil), James M. Sabatier (University of Mississippi, NCPA, 1 Coliseum Drive, University, MS 38677, USA, sabatier@olemiss.edu), Roger Waxler (University of Mississippi, NCPA, 1 Coliseum Drive, University, MS 38677, USA, rwax @olemiss.edu)

Acoustic-based landmine detection methods have enjoyed success, in part, because of structural resonances in many landmines. The unburied VS 1.6, a member of a family of plastic, cylindrically symmetric anti-tank landmines, exhibits seven modes below 1.6 kHz and a large frequency shift of the first symmetric mode such that its frequency is greater than that of the first asymmetric mode, a phenomenon observed in timpani of reduced kettle volume [Christian et al., J. Acoust. Soc. Am., **76**(5), 1336-1345 (1984)]. An elastically supported, thin, elastic plate acceptably models the unperturbed modes of the pressure plate. Coupling of the acoustic analog of the first symmetric mode to the cavities beneath the plate shows those cavities to be the cause of the perturbation. Shallow burial in sand effectively removes the frequency shift of the first symmetric mode. Comparisons to burial simulation experiments in water will be made, thus allowing a qualitative explanation of the effect sand has on the first symmetric mode of the plate. [This work was sponsored by US Army Research, Development, and Engineering Command, Night Vision and Electronic Sensors Directorate under Contract DAAB15-02-C-0024.]

3:40

1pPAc9. Review of a model for the response of a buried landmine to an airborne acoustic signal. Doru Velea (QinetiQ North America, Technology Solutions Group, 12030 Sunrise Valley Dr., Suite 400, Reston, VA 20191, USA, dvelea@plansys.com), Roger Waxler (University of Mississippi, NCPA, 1 Coliseum Drive, University, MS 38677, USA, rwax@olemiss.edu), James M. Sabatier (University of Mississippi, NCPA, 1 Coliseum Drive, University, MS 38677, USA, sabatier@olemiss.edu)

Buried landmines can be found acoustically by insonifying the ground and detecting a contrast between the vibratory motion of the ground surface directly above the mine and a short distance away from the mine. Experiments have revealed a short-ranged spatial response and a frequency response that peaks around 100-200 Hz for anti-tank mines. The peak is believed to be a response to mechanical resonances of the mine itself. A model was developed to explain these experimental observations and to predict how the mine's resonance is influenced by the surrounding soil. In the model the soil was assumed to be an effective fluid while the mine was modeled as a right cylinder with a compliant top. The response of the top of the mine was modeled by an impedance condition. Predictions of the model are presented and compared with the phenomena observed in the field.

MONDAY AFTERNOON, 30 JUNE 2008 ROOM 352A, 4:00 TO 8:00 P.M.

Session 1pPAd

Physical Acoustics: Sonic, Ultrasonic, and Megasonic Cleaning I

Ralph T. Muehleisen, Cochair
Illinois Institute of Technology, Civil, Architectural and Environmental Engineering, 3201 S. Dearborn St., Room 228, Chicago, IL 60616, USA

Claus-Dieter Ohl, Cochair
University of Twente, P.O. Box 217, Department of Science and Technology, Enschede, 7500 AE, Netherlands

Invited Papers

4:00

1pPAd1. Global Trend of Precision Cleaning Technology and the Application in Hard Disk Drive Industry. Jun Zhang (Data Storage Institute, DSI bldg, 5 Eng Dr 1 (Off Kent Ridge Crescent, NUS), 117608 Singapore, Singapore, zhang_jun@dsi.a-star.edu.sg) , Yun Fook Liew (Data Storage Institute, DSI bldg, 5 Eng Dr 1 (Off Kent Ridge Crescent, NUS), 117608 Singapore, Singapore, zhang_jun@dsi.a-star.edu.sg)

As industry trends for hard disk drive and related electronic devices are moving toward high capacity and miniaturization. A big challenge is to find increasing the efficient ways to clean the parts which are regarded as the most stringent in cleanliness. The critical issues include the methodology for identifying the contaminants and how to choose a correct cleaning chemical and cleaning technology. Today's hard disk media, particularly the perpendicular recording media, is capable of storing up to 300GB per disk under which the distance between the recording head/disk have to be reduced to a few nanometers. It will bring more difficulties for increasing the reliability and disk capacities. On the other hand, all components within the hard disk drive are required to avoid submicron particulate contamination ($<0.1\mu m$). Megasonic and ultrasonic cleaning are the most effective and promising technologies to remove such contaminants. This presentation will discuss the technical trend and possible solution of precision cleaning and the strategy for selecting the cleaning chemicals and technologies to meet the cleanliness requirement through a case study.

4:20

1pPAd2. Accoustic cleaning in nanoelectronics. Paul Mertens (Imec, Kapeldreef 75, B-3001 Leuven, Belgium, paul.mertens@imec.be)

The fabrication of state-of-the-art electronic integrated circuits involves multiple cleaning steps in which residues of the order of ten or a few tens of nm need to be removed with very high efficiency. Historically cleaning was obtained by chemical undercutting (order of a few nm). The dimensions of nanoelectronic devices become so small that the amount of substrate etching involved in a cleaning step should be kept below 0.05 nm. Therefore other cleaning mechanism, involving a mechanical force, have to be considered such as acoustic agitation of the cleaning liquid or high-velocity aerosol bombardment. These forces, however, can damage fine structures already fabricated on the substrate, particularly the "up-features." This implies that a trade-off needs to be made between avoiding damage and obtaining an acceptable cleaning performance. This presentation includes typical hardware configurations and possible mechanisms for particle removal and use of megasonic agitation in nonaqueous liquid solutions.

4:40

1pPAd3. Cleaning of semiconductor substrates by controlled cavitation. Frank Holsteyns (SEZ AG, SEZ-Strasse 1, 9500 Villach, Austria, F.Holsteyns@at.sez.com), Alexander Lippert (SEZ AG, SEZ-Strasse 1, 9500 Villach, Austria, A.Lippert@at.sez.com), Florian Lechner (SEZ AG, SEZ-Strasse 1, 9500 Villach, Austria, F.Lechner@at.sez.com), Andrea Otto (Göttingen University, Friedrich-Hund-Platz 1, 37077 Göttingen, Germany, aotto@physik3.gwdg.de), Till Nowak (Göttingen University, Friedrich-Hund-Platz 1, 37077 Göttingen, Germany, tnowak@physik3.gwdg.de), Robert Mettin (Göttingen University, Drittes Physikalisches Institut, Friedrich-Hund-Platz 1, 37077 Göttingen, Germany, R.Mettin@physik3.gwdg.de), Alexander A. Doinikov (Belarus State University, 11 Bobruiskaya Street, 220030 Minsk, Belarus, doinikov@bsu.by), Harald Okorn-Schmidt (SEZ AG, SEZ-Strasse 1, 9500 Villach, Austria, H.Okorn-schmidt@at.sez.com)

The continuing downscaling of device geometries in the semiconductor industry is driving the requirements for both process and contamination control. Historically, the physical and the chemical processes required for contamination control were evolutionarily scaled with device geometry. However, today's tailored wet-chemical cleaning approaches must strive to meet stringent requirements to assure a minimal material loss and no damage to extremely fragile structures. While chemical solutions exist for the control of molecular-organic and metallic ion contamination, the physico-chemical solutions for the removal of nanosized particulate contamination to critical diameters below 20 nm are still undetermined. Therefore, the potential and the limitations of megasonic cleaning, which is mainly based on cavitation, are carefully balanced and a detailed understanding of the ongoing physical mechanisms is necessary to maintain a stable window of operation. The relevant active mechanisms present in such a cavitation driven cleaning process, will depend in great part on the characteristics of the applied sound field; that is to say on frequency, amplitude and uniformity and also on the properties of the cleaning liquid, i.e., the level of gasification, temperature, surface tension, and many others. Different techniques in conjunction with simulations and modeling are under development to improve the design of a novel cleaning tool that can address the challenges.

5:00

1pPAd4. Using megasonic agitation to extend chemical cleaning for nanotechnology device production. Cole Franklin (1241 East Dyer Road, Santa Ana, CA 92672, USA, colesfranklin@yahoo.com)

Aqueous and solvent chemicals are widely used in the semiconductor industry and as the technology nodes shrink device makers are working to extend these cleaning fluids to the next technology node. Internal data shows megasonic agitation can enhance polymer removal without complete dissolution for both aqueous and solvent chemicals. Data has shown solvents and semi-aqueous solutions show better selectivity with advanced material stacks over aqueous solution. It has been established that megasonic energy can enhance particle removal from semiconductor devices during cleaning processes. However, applied megasonic energy can also damage sensitive semiconductor devices during cleaning, especially in aqueous solutions. Aqueous fluids appear to promote much more damage for the same applied megasonic power than do most solvents. We show that some solvents have a higher threshold for cavitation than deionized water mixes. Since device manufacturers are working to extend their current cleaning chemicals to the 65 and 45 nm pilot production and research nodes, we studied several ways to accomplish this goal for aqueous or solvent chemicals. Described here we apply a methods to predict the damage of nanostructures by various liquids using signal analysis to better understand the mechanical that promotes improved control of cleaning without damage.

5:20

1pPAd5. On frequency scaling of ultrasonic cavitation and cleaning. Robert Mettin (Göttingen University, Drittes Physikalisches Institut, Friedrich-Hund-Platz 1, 37077 Göttingen, Germany, R.Mettin@physik3.gwdg.de)

In virtually all applications of acoustic cavitation, variations of the effects with sound frequency are observed. However, a simple comparison of analogical setups at different frequencies can be misleading, as other parameters, like wavelength or emitted transducer power, change jointly with the driving frequency. Indeed, the similarity of acoustically cavitating systems under scaling of frequency is not well defined yet, in particular because it is not clear what observable should stay the same. A possible way of characterization of "similar" systems could be the observation of similar cavitation bubble structures, "such as" for hydrodynamic flow patterns or hydrodynamic cavitation structures. This idea is debated on experimental and theoretical basis, and the consequences for cleaning applications in the higher frequency range are discussed.

5:40

1pPAd6. Surface cavitation on micro- and nanometer scales. Detlef Lohse (Physics of Fluids, University of Twente, P.O. Box 217, 7500 AE Enschede, Netherlands, d.lohse@utwente.nl), Nicolas Bremond (University of Twente, P.O. Box 217, Department of Science and Technology, 7500 AE Enschede, Netherlands, Nicolas.Bremond@espci.fr), Bram Borkent (University of Twente, P.O.

Box 217, Department of Science and Technology, 7500 AE Enschede, Netherlands, b.m.borkent@tnw.utwente.nl),Claus-Dieter Ohl (University of Twente, P.O. Box 217, Department of Science and Technology, 7500 AE Enschede, Netherlands, c.d.ohl@utwente.nl), Manish Arora (University of Twente, P.O. Box 217, Department of Science and Technology, 7500 AE Enschede, Netherlands, m.arora@tnw.utwente.nl), Julius Vancso (University of Twente, P.O. Box 217, Department of Science and Technology, 7500 AE Enschede, Netherlands, g.j.vancso@tnw.utwente.nl), Holger Schoenherr (University of Twente, P.O. Box 217, Department of Science and Technology, 7500 AE Enschede, Netherlands, h.schonherr@utwente.nl)

Heterogeneous bubble nucleation at surfaces has been notorious because of its irreproducibility. Here controlled multibubble surface cavitation is achieved by heterogenous nucleation of bubbles on a hydrophobic surface patterned with microcavities. The expansion of the nuclei in the microcavities is triggered by an impulsive lowering of the liquid pressure. The procedure allows to control and fix the bubble-distance within the bubble cluster. We observe a perfect quantitative reproducibility of the cavitation events where the inner bubbles in the two-dimensional cluster are shielded by the outer ones, reflected by their later expansion and their delayed collapse. Apart from the final bubble collapse phase (when jetting flows directed towards the cluster's center develop), the bubble dynamics can be quantitatively described by an extended Rayleigh-Plesset equation, taking pressure modification through the surrounding bubbles into account. When repeating the same experiments with flat polyamide and hydrophobized silicon surfaces populated with surface nanobubbles (as can be seen through atomic force microscopy), these nanobubbles do not act as nucleation sites for cavitation bubbles, in contrast to the expectation. This implies that surface nanobubbles are not just stable under ambient conditions but also under enormous reduction of the liquid pressure down to -6 MPa. We denote this feature as superstability.

6:00

1pPAd7. In-situ monitoring of megasonic cleaning. Aaldert G. Zijlstra (Physics of Fluids, University of Twente, P.O. Box 217, 7500 AE Enschede, Netherlands, a.g.zijlstra@tnw.utwente.nl), Tom Janssens (IMECvzw, Kapeldreef 75, 3001 Heverlee, Belgium, janssent@imec.be), Paul Mertens (Imec, Kapeldreef 75, B-3001 Leuven, Belgium, paul.mertens@imec.be), Michel Versluis (Physics of Fluids, University of Twente, P.O. Box 217, 7500 AE Enschede, Netherlands, m.versluis@utwente.nl)

Acoustic agitation is used in ultrasonic cleaning to induce a physical force to remove nanoparticles in semiconductor processing. The performance of cleaning tools is commonly quantified ex-situ by the particle removal efficiency η (i.e. the ratio of the remaining to the original particle concentration). The resulting η-wafer maps often reveal spatial nonuniformities related to tool design. The local study of the cleaning dynamics, quantified by the removal frequency ($f_R[s^{-1}]$) also indicates that the density of cleaning events over a wafer can be strongly non homogeneous. Because the sound frequencies used in industrial tools are in the MHz range, visualization of the cavitating bubbles (resonant size 3 μm) is highly challenging, both in time and in spatial resolution. Considering that the cleaning effect of a cavitating bubble is permanent a method is presented here to determine the acoustic cleaning event size ($A_{event}[\mu m^2]$) and the event flux ($\phi[\mu m^{-2}s^{-1}]$) through visualization techniques. The method consists of time-resolved imaging of the removal of a nanoparticle layer deposited on a transparent substrate. The microscopic cleaning activity can then be correlated to the actual removal frequencies f_R through the relation $f_R = \phi A_{event}$ to further clarify the cleaning mechanisms in industrial tools.

6:20

1pPAd8. Potential uses of ultrasound in the dairy ultrafiltration processes. Shobha Muthukumaran (School of Engineering and Information Technology, Deakin University, Pigdons Road, Waurn Ponds, Victoria, 3217 Geelong, Australia, shobha.muthukumaran@deakin.edu.au), Sandra Kentish (Department of Chemical and Biomolecular Engineering, The University of Melbourne, Parkville, Victoria, 3010 Melbourne, Australia, sandraek@unimelb.edu.au), Muthupandian Ashokkumar (Department of Chemical and Biomolecular Engineering, The University of Melbourne, Parkville, Victoria, 3010 Melbourne, Australia, masho@unimelb.edu.au), Geoff Stevens (Department of Chemical and Biomolecular Engineering, The University of Melbourne, Parkville, Victoria, 3010 Melbourne, Australia, gstevens@unimelb.edu.au)

There has been a growing interest in the industrial application of ultrasound, especially in the food industry. Power ultrasound can have a number of physical effects; it can increase turbulence through both the introduction of vibrational energy and through acoustic streaming, it can cause both particle dispersion and particle agglomeration and clean surfaces with a scouring action. Our work in this area has focused on the use of ultrasound to enhance membrane processing. Low frequency ultrasound has been used to facilitate cross flow ultrafiltration of dairy whey solutions for both during the ultrafiltration production cycle and the cleaning cycle. During the production cycle, the use of ultrasound reduces both pore blockage and the specific resistance of the fouling cake layer. This leads to higher flux rates and the potential for longer production cycles. During the cleaning cycle, ultrasound systematically increases cleaning efficiency, thus has the potential to reduce both total chemical consumption and system downtime. There was no deterioration in cleaning effectiveness or membrane condition, which implies that sonication, has not damaged the membrane itself. Similarly, there was no change in the chemical nature of soluble proteins following sonication.

6:40

1pPAd9. Ultrasonic cleaning of particle and natural organic matter fouled cross-flow membranes. Linda K. Weavers (The Ohio State University, 470 Hitchcock Hall, 2070 Neil Ave, Columbus, OH 43210, USA, weavers.1@osu.edu), Harold W. Walker (The Ohio State University, 470 Hitchcock Hall, 2070 Neil Ave, Columbus, OH 43210, USA, walker.455@osu.edu), Dong Chen (Lamar University, Department of Civil Engineering, Beaumont, TX 77710, USA, dchen@my.lamar.edu), Mikko O. Lamminen (The Ohio State University, 470 Hitchcock Hall, 2070 Neil Ave, Columbus, OH 43210, USA, m.o.lamminen@gmail.com)

Membrane filtration has arguably been the most significant development in the area of water purification in the past 50 years. It has enabled many processes to become more reliable and to achieve purities that have not been achieved previously. One of the drawbacks of membrane use is fouling. In this research the ultrasonic cleaning of particle-fouled membranes was investigated. Specifically, we have explored the mechanisms responsible for ultrasonic cleaning and how solution conditions, particle conditions, cake layer effects,

and ultrasonic conditions affect cleaning using scanning electron microscopy (SEM) and permeate flux measurements. We have investigated continual cleaning during membrane filtration in addition to cleaning after fouling. Results of this work will be discussed for cross-flow system configurations.

Contributed Papers

7:00

1pPAd10. Measurements and simulations on the wall shear stress from single cavitation bubbles. Rory Dijkink (University of Twente, Physics of Fluids, Building Meander, Postbus 217, 7500 AE Enschede, Netherlands, r.j.dijkink@tnw.utwente.nl), Evert Klaseboer (Institute of High Performance Computing, 1 Science Park Road, #01-01 The Capricorn, 117528 Singapore, Singapore, evert@ihpc.a-star.edu.sg), Boo Cheong Khoo (National University of Singapore, Dept of Mechanical Engineering, 10 Kent Ridge Crescent, 119260 Singapore, Singapore, mpekbc@nus.edu.sg), Claus-Dieter Ohl (University of Twente, P.O. Box 217, Department of Science and Technology, 7500 AE Enschede, Netherlands, c.d.ohl@utwente.nl)

Cavitation bubbles collapsing near a solid boundary manifest a jetting effect towards the closest rigid boundary. After impacting on the boundary the jet spreads out radially thereby shearing the surface. It is speculated that cavitation bubbles clean through the resulting shearing forces, e.g. they drag adherent contaminants through the radial spreading jet. Although the cleaning through bubbles is used in a wide set of technologies, for example for pre-cleaning surgical equipment, for bio-film removal in medical and drinking water applications, and in ultraclean processing of semiconductor wafers, very limited experimental studies on the wall shear stress exist. In an effort to shed light on the shear forces caused by no spherical oscillating cavitation bubbles close to boundaries we implement a constant temperature anemometer together with high-speed imaging to elucidate the fluid dynamics near the boundary. Additionally, we perform potential flow simulations with a boundary element method. The boundary layer is resolved with a convolution integral to the solution of Stokes' first problem. In general we find the generation of wall shear stress both in experiment and simulations during the growth and collapse of the bubble. Yet, very high shear stress is generated once the jet impacts and spreads on the boundary.

7:20

1pPAd11. Cinephotographic observations of particle removal from a surface by acoustic cavitation. Lawrence A. Crum (Center for Industrial and Medical Ultrasound, Applied Physics Lab., University of Washington, 1013 NE 40th St., Seattle, WA 98105, USA, lac@apl.washington.edu), Michael R. Bailey (Center for Industrial and Medical Ultrasound, Applied Physics Lab., University of Washington, 1013 NE 40th St., Seattle, WA 98105, USA, bailey@apl.washington.edu), Michael S. Canney (Center for Industrial and Medical Ultrasound, Applied Physics Lab., University of Washington, 1013 NE 40th St., Seattle, WA 98105, USA, mcanney@u.washington.edu), Hong Chen (Center for Industrial and Medical Ultrasound, Applied Physics Lab., University of Washington, 1013 NE 40th St., Seattle, WA 98105, USA, hopechen@u.washington.edu),Thomas Matula(Center for Industrial and Medical Ultrasound, Applied Physics Lab., University of Washington, 1013 NE 40th St., Seattle, WA 98105, USA, matula@apl.washington.edu), Christopher McInnes (Ultreo, Inc., 9461 Willows Road NE, Redmond, WA 98052, USA, chris@ultreo.com)

It is commonly believed that ultrasonic cleaners remove particles from a surface through acoustic cavitation, presumably in which a pulsating bubble interacts directly with the particle. We are unaware of any direct evidence of this interaction. Recently, however, we have used a high-speed movie camera to observe the removal of biofilm attached to a solid surface during exposure to a cavitation field. The biofilm consisted of Streptococcus mutans, a common oral bacterium, grown on a glass slide and observed under magnification to be both thinly coating the glass surface and clustered in larger colonies. The cavitation field was created by an Ultreo^{TM} toothbrush which combines both vibrating bristles and an ultrasound transducer with waveguide, operating at a frequency of 324 kHz. When the waveguide was immersed in water containing bubbles from an ultrasound contrast agent (Optison^{TM}), visual observations could be made with the naked eye of biofilm removal. With high-speed cinephotography, it was possible to observe bacteria removal by the direct interaction of a cavitation bubble (cloud) and the colony. These observations will be presented along with our interpretations of the data. [Work supported in part by Ultreo^{TM}, Inc.]

7:40

1pPAd12. Pressure fields and their effects in membrane cleaning applications. Fabian Reuter (Göttingen University, Drittes Physikalisches Institut, Friedrich-Hund-Platz 1, 37077 Göttingen, Germany, freuter@physik3.gwdg.de), Robert Mettin (Göttingen University, Drittes Physikalisches Institut, Friedrich-Hund-Platz 1, 37077 Göttingen, Germany, R.Mettin@physik3.gwdg.de), Werner Lauterborn (Göttingen University, Friedrich-Hund-Platz 1, 37077 Göttingen, Germany, W.Lauterborn @physik3.gwdg.de)

It is known that the use of ultrasonic cavitation can support the cleaning of filtration membranes. We study the final purification step in drinking water production by ultrafiltration through a submerged filter module. The module consists of parallel polymer membrane sheets. Its filtration efficiency is rapidly decreased by fouling. Here, the removal of membrane attached fouling layers by backflushing can successfully be enhanced using ultrasound without membrane damage. To better understand the cleaning mechanism and cavitation properties for further optimization of efficiency, the sound pressure field is measured and the bubble distribution is characterized. Different sound field arrangements are investigated with respect to cleaning performance, while membrane integrity is controlled by turbidity and particle monitoring of the permeate. Results show that a strong influence due to the geometrical configuration can be present, for instance due to impedance effects of the membrane layers.

Session 1pPAe

Physical Acoustics: Mathematical and Numerical Methods I

Andrew Piacsek, Cochair
Central Washington University, Department of Physics, 400 E. University Way, Ellensburg, WA 98926, USA

B. D. Zaitsev, Cochair
Institute of Radio Engineering and Electronics of RAS, Saratov Branch, Zelyonaya str., 38, 410019 Saratov, Russian Federation

Contributed Papers

7:00

1pPAe1. The peculiarities of energy characteristics of acoustic waves. Boris D. Zaitsev (Institute of Radio Engineering and Electronics of RAS, Saratov Branch, Zelyonaya str., 38, 410019 Saratov, Russian Federation, zai-boris@yandex.ru), Andrey A. Teplykh (Institute of Radio Engineering and Electronics of RAS, Saratov Branch, Zelyonaya str., 38, 410019 Saratov, Russian Federation, teplykhaa@mail.ru), Iren E. Kuznetsova (Institute of Radio Engineering and Electronics of RAS, Saratov Branch, Zelyonaya str., 38, 410019 Saratov, Russian Federation, kuziren@yandex.ru)

Acoustic waves propagating in piezocrystals transport kinetic and potential energies. Potential energy consists of mechanical, electrical, and mutual contributions. At that the change in potential energy of the voluentary unit of medium is identified with the work of mechanical stress for infinitesimal displacement. Versus method of integrating this equation there are two different expressions for density of potential energy. In case 1 (traditional approach) the density of energy is equal to the half-product of mechanical stress and strain. At that for any type of plane acoustic wave the instantaneous density of total energy in given point of medium depends on time and there is no mutual transformation of potential and kinetic energies. For this case there exists well-known traditional expression for power flow. In case 2 suggested by authors the density of potential energy is equal to half-product of mechanical stress gradient and displacement. At that the density of total energy does not depend on time. It means the mutual transformation of potential and kinetic energies according to motion equation. The new expression for power flow is derived for this case. The peculiarities of energy characteristics for piezoactive waves are discussed. The work is supported by RFBR grant N°08-08-00793.

7:20

1pPAe2. Audio acoustic modeling using full-wave methods. Timo Lahivaara (University of Kuopio, P.O. Box 1627, 70211 Kuopio, Finland, timo.lahivaara@uku.fi), Tomi Huttunen (University of Kuopio, P.O. Box 1627, 70211 Kuopio, Finland, tomi.huttunen@uku.fi),Simo-Pekka Simonaho (University of Kuopio, P.O.Box 1627, 70211 Kuopio, Finland, simo-pekka.simonaho@uku.fi)

The numerical simulation of wave propagation poses a significant challenge in scientific computation. Historically, several approaches are explored in order to get a stable method that can be efficiently used for approximating wave propagation without excessive numerical dissipation or dispersion. Unfortunately, the traditional approaches, such as the finite element and the finite difference, require many discretization points per wavelength to obtain reliable solutions. In this study, two alternative full-wave methods for reducing the computational complexity are consider. The methods are the time-domain discontinuous Galerkin method and the ultraweak variational formulation in the frequency domain. Using these techniques, the directivity and the frequency response of a loudspeaker are studied. Moreover, the simulated results are compared to experimental measurements.

7:40

1pPAe3. Propagation in a dispersive medium: a phase-space approach. Leon Cohen (City University of New York, Hunter-Phyiscs, 695 Park Ave., New York, NY 10021, USA, leon.cohen@hunter.cuny.edu)

We derive exact moments for pulse propagation in a dispersive medium. These moments are not only inherently interesting but clarify the validity of a recently proposed approximation scheme for wave propagation. The approximation method for pulse propagation is based on the Wigner position-wave/number representation and is very accurate, easy to apply, and moreover is physically illuminating. In particular one obtains the evolved approximate Wigner distribution from the initial Wigner distribution by a simple linear translation in phase space. Propagation with damping is also taken into account. We will show that the reason for the high accuracy of the approximation is that the important low order moments are exactly given by the approximation and that these low order moments preserve very well the basic shape of the pulse. Moreover, now that we understand why the approximation method works well, the approximation can be systematically improved. We give a number of specific examples of exactly calculable moments to illustrate the method and we compare exact and approximate moments. Research supported by the AFOSR.

Session 1pPPa

Psychological and Physiological Acoustics: Integrated Approaches to Auditory Scene Analysis I

Mounya Elhilali, Cochair
Johns Hopkins University, Dept of Electrical and Computer Engineering, Barton Hall 105, 3400 N. Charles Street, Baltimore, MD 21218, USA

Daniel Pressnitzer, Cochair
CNRS UMR 8158 ; Univ. Paris Descartes; Ecole Normale Supérieure, 29 rue d'Ulm, Paris, 75005, France

Invited Papers

1:00

1pPPa1. Sequential integration in the perception of tone sequences. Leon Van Noorden (Rassonstraat 39, B-1030 Brussels, Belgium, leonvannoorden@mac.com)

The seminal book of Albert Bregman on Auditory Scene Analysis had not yet appeared at the time of my dissertation research (1970-1975). One of the major difficulties that I had was to come at grips with the concept of a sequence of tones that form a 'gestalt' of tones 'belonging' together. This Sequential Integration, as coined by Bregman, has not received as much attention as the 'Differentiation' aspect. A number of experiments show that this sequential integration process is characterised by a resonance process with a broad peak near 2 Hz. This resonance process can explain several phenomena such as subjective rhyhmisation, the data on tapping along polyrhythms and the histogram of musical tempi. Confronting these findings with the measurements of the Temporal Cohence Boundary may indicate where pitch movement detectors may play a role. Recent publications have linked this resonance with a movement control process.

1:20

1pPPa2. On the binding of successive tones: Implicit versus explicit pitch comparisons. Laurent Demany (CNRS UMR 5227; Univ. Victor Segalen, 146 rue Léo Saignat, 33076 Bordeaux, France, laurent.demany@psyac.u-bordeaux2.fr), Daniel Pressnitzer (CNRS UMR 8158; Univ. Paris Descartes; Ecole Normale Supérieure, 29 rue d'Ulm, 75005 Paris, France, Daniel.Pressnitzer@ens.fr), Catherine Semal (CNRS UMR 5227; Univ. Victor Segalen, 146 rue Léo Saignat, 33076 Bordeaux, France, catherine.semal@u-bordeaux2.fr)

Listeners were presented with sound sequences in which one pure tone (T) was followed by a set (S) of five synchronous or asynchronous pure tones 550 cents apart. In a "present/absent" condition, T was either identical to a randomly selected component of S or halfway in frequency between two components, and listeners had to indicate if T was present in S or not. In an "up/down" condition, T was 100 cents below or above a randomly selected component of S, and listeners had to identify the direction of the frequency shift. When the components of S were asynchronous, the present/absent task was easier than the up/down task. When the components of S were synchronous, the opposite trend was observed. In case of asynchrony, the components of S could be heard out individually, so listeners presumably compared explicit (conscious) pitch percepts to make their judgments. In case of synchrony, the components of S were difficult to hear out individually; apparently, pitch comparisons were then made implicitly by "frequency-shift detectors" (Demany and Ramos, 2005) which, we argue, participate in auditory scene analysis. It seems that such detectors relate automatically consecutive tones, and are generally less efficient for comparisons between nonconsecutive tones.

1:40

1pPPa3. Concurrent sound segregation and peripheral frequency resolution. Christophe Micheyl (University of Minnesota, Department of Psychology, 75 E. River Road, Elliott Hall N218, Minneapolis, MN 55455, USA, cmicheyl@umn.edu), Michael V. Keebler (University of Minnesota, Department of Psychology, 75 E. River Road, Elliott Hall N218, Minneapolis, MN 55455, USA, keeb0002@umn.edu), Andrew J. Oxenham (University of Minnesota, Department of Psychology, 75 E. River Road, Elliott Hall N218, Minneapolis, MN 55455, USA, oxenham@umn.edu)

In everyday environments where multiple sound sources coexist, listeners often have to follow a harmonic source of interest (e.g., someone's voice) among other such sources (e.g., other talkers). Here, we review psychoacoustical findings suggesting that this form of auditory scene analysis is related to the degree of peripheral "resolvability" of harmonics in the auditory system. We present experimental results, which indicate a systematic relationship between harmonic resolvability and the ability of normal-hearing listeners to "track" (or discriminate) changes in the fundamental frequency (F0) of a target harmonic complex mixed with another (interferer). We show that poor harmonic resolvability is associated not only with poor performance, but also with an inability to take advantage of normally potent cues for concurrent sound segregation, including F0 differences, laterality differences, and onset-offset asynchronies. While it remains unclear whether this relationship is causal, these findings may have important implications for the design of artificial auditory-scene-analysis systems, and for our understanding of the listening difficulties experienced by hearing-impaired listeners in whom peripheral frequency resolution is reduced. [Work supported by NIDCD R01DC05216.]

2:00

1pPPa4. Temporal fine structure cues in auditory stream segregation of complex tones. Nicolas Grimault (Laboratoire Neurosciences Sensorielles, Comportement, Cognition, UMR 5020, Université Lyon 1 - CNRS, 50 av. Tony Garnier, 69366 Lyon Cedex 07, France, ngrimault@olfac.univ-lyon1.fr), Etienne Gaudrain (Laboratoire Neurosciences Sensorielles, Comportement, Cognition, UMR 5020, Université Lyon 1 - CNRS, 50 av. Tony Garnier, 69366 Lyon Cedex 07, France, egaudrain@gmail.com)

The ability to understand speech-in-speech is generally described to be related to the capacity to segregate one auditory stream among others sound sources. The channeling theory suggests that sequential stream segregation is basically sustained by frequency selectivity. However, it has been evidenced that sequences of stimuli that evoked the same excitation pattern can be streamed apart based on temporal cues only. Other results involving hearing impaired listeners with enlarged auditory filters hardly fit in with this theory. More recently, several reports in the literature and new attempts of modelization underline the potential interest of temporal fine structure cues for stream segregation. The current study is dedicated to test further the potential interest of temporal fine structure cues to stream apart sequences of unresolved complex tones with alternating fundamental frequencies. Several conditions of envelope saliency (positive and negative Schroeder phase complex tones) and several conditions of fine structure will be used in a streaming test leading to an objective measure related to segregation.

2:20

1pPPa5. Auditory streaming and coherence. Shihab Shamma (ECE Department, AV Williams Bldg., 2203, University of Maryland, College Park, MD 20742, USA, sas@eng.umd.edu), Mounya Elhilali (Johns Hopkins University, Dept. of Electrical and Computer Engineering, Barton Hall 105, 3400 N. Charles Street, Baltimore, MD 21218, USA, mounyaelhilali@gmail.com)

Auditory streaming is a phenomenon that manifests itself in the everyday ability of humans and animals to parse complex acoustic information arising from multiple sound sources into meaningful auditory "streams." For instance, the ability to follow a conversation at a noisy cocktail party or hear the violin in the orchestra both rely on the formation of auditory streams. While seemingly effortless, the neural mechanisms underlying auditory streaming remain a mystery. In this talk, we shall discuss physiological experiments that address the role of coherence in mediating this percept. The experiments contrast the perception and neural responses evoked by the classic two-tone stimuli when presented in alternating or synchronous modes. Briefly, while the percepts in these two conditions are very different, being much more "streamed" in the alternating case, physiological responses to the tones did not differ significantly enough to explain this change in percept. This result casts doubt on the simple spatial segregation hypothesis, and instead argues for a substantial role of coherence of stimuli across different channels in mediating streaming.

Contributed Paper

2:40

1pPPa6. Auditory temporal edge detection in human auditory cortex. Maria Chait (UCL Ear Institute, 332 Gray's Inn Road, WC1X 8EE London, UK, m.chait@ucl.ac.uk)

Auditory objects are detected if they differ acoustically from the ongoing background. In simple cases, the appearance or disappearance of an object involves a transition in power, or frequency content, of the ongoing sound. However, it is more realistic that the background and object possess substantial nonstationary statistics, and the task is then to detect a transition in the pattern of ongoing statistics. How does the system detect and process such transitions? We use magnetoencephalography (MEG) to measure early auditory cortical responses to transitions between constant tones, regularly alternating, and randomly alternating tone-pip sequences, where the dimension of change is either frequency, loudness, or spatial location. Such transitions embody key characteristics of natural auditory temporal edges. Our data demonstrate that the temporal dynamics and response polarity of the neural temporal-edge-detection processes depend in specific ways on the generalized nature of the edge (the context preceding and following the transition) and suggest that distinct neural substrates in core and noncore auditory cortex are recruited depending on the kind of computation (discovery of a violation of regularity, vs the detection of a new regularity) required to extract the edge from the ongoing fluctuating input entering a listener's ears.

Invited Papers

3:00

1pPPa7. Perception of simultaneous sentences with frequency-shifted voiced excitation. Brian Roberts (Aston University, Psychology, Life and Health Sciences, B4 7ET Birmingham, UK, b.roberts@aston.ac.uk), Stephen D. Holmes (Aston University, Psychology, Life and Health Sciences, B4 7ET Birmingham, UK, S.D.Holmes@aston.ac.uk), Chris J. Darwin (University of Sussex, Psychology, School of Life Sciences, BN1 9QG Brighton, UK, cjd@sussex.ac.uk)

Identification of key words in one of two simultaneous sentences is substantially improved when the sentences differ in fundamental frequency (F0). When the sentences are constructed to be almost continually voiced, identification can improve from 20% at 0 semitones difference to 80% at 8 semitones difference (J. Bird & C.J. Darwin 1998 in Psychophysical and Physiological Advances in Hearing, Ed A.R. Palmer et al., Whurr, London, pp. 263-269). We recorded the same monotone sentences as Bird and Darwin. These were first resynthesised using PSOLA to give a range of harmonic F0 differences (0, 1, 3, and 10 semitones) and then additionally resynthesised by LPC with the LPC residual frequency shifted by 25% of F0, to give excitation with inharmonic but regularly spaced components. Experiment 1 showed that frequency-shifted sentences gave the same large improvement with nominal F0 difference as did the harmonic sentences, although overall performance was about 10% poorer. Experiment 2 replicated the finding by Bird and Darwin that swapping the F0 difference across spectral regions only reduced the improvement in recognition for large F0 differences, and extended this finding to frequency-shifted voiced excitation. The results extend the range of perceptual phenomena originally attributed to harmonic processing.

3:20-3:40 Break

3:40

1pPPa8. Signal duration modulates age differences in neuromagnetic brain activity associated with concurrent sound segregation. Claude Alain (Rotman Research Institute, Baycrest Centre, 3560 Bathurst Street, Toronto, ON M6A 2E1, Canada, calain@rotman-baycrest.on.ca), Kelly McDonald (Rotman Research Institute, Baycrest Centre, 3560 Bathurst Street, Toronto, ON M6A 2E1, Canada, kmcdonald@rotman-baycrest.on.ca)

Listeners' ability to parse concurrent sounds is a prerequisite in solving the cocktail party problem. Here, we examine whether deficits in periodicity coding can account for older adults' difficulties in understanding speech in noise. In two experiments, we measured auditory evoked fields (AEFs) while young and older adults listened to complex sounds that either had all of their harmonics in tune or had the third harmonic mistuned by 4 or 16% of its original value. For each participant, the AEFs were modeled with a pair of dipoles in auditory cortex and the effects of age on the resulting source waveforms were examined. Older adults were less likely to report hearing the mistuned harmonic as a separate sound than young adults, but only for short duration signals (50 ms). This age difference was paralleled by reduced neuromagnetic activity indexing the processing of the mistuned harmonic. For longer duration signals (e.g., 200 ms), older adults show comparable amplitude, but a delay in latency. These findings show an age-related decline in concurrent sound perception based on harmonicity, which could partly be alleviated by increasing signal duration. The implications of these findings for speech perception in noise will be discussed.

Contributed Paper

4:00

1pPPa9. Influence of noise type, degree of comodulation and interaural phase difference on the combined monaural and binaural masking release. Bastian Epp (Universität Oldenburg, Medizinische Physik, Carl-von-Ossietzky Str. 9-11, 26111 Oldenburg, Germany, Bastian.Epp@uni-oldenburg.de), Jesko Verhey (Universität Oldenburg, Medizinische Physik, Carl-von-Ossietzky Str. 9-11, 26111 Oldenburg, Germany, jesko.verhey@uni-oldenburg.de)

Several masking experiments have shown that the auditory system is able to use coherent envelope fluctuations of the masker across frequency within one ear as well as differences in interaural disparity between signal and masker to enhance signal detection. The two effects associated with these abilities are comodulation masking release (CMR) and binaural masking level difference (BMLD). The aim of the present study was to investigate the combination of CMR and BMLD. Thresholds of a sinusoidal signal were measured in a flanking band paradigm, i.e., in the presence of several narrowband noise maskers, (i) for two noise types (Gaussian and multiplied noise), (ii) various degrees of comodulation, and (iii) various interaural phase differences (IPD) of the signal. Thresholds decreased as the signal IPD increased and decreased as the masker comodulation increased. For both noise types, the maximum CMR was about 10 dB and the maximum BMLD was about 14 dB. Thresholds where monaural and binaural cues were present showed an addition of the single effects, i.e., a maximum masking release of 24 dB. A simplified model of the auditory system assuming a serial alignment of the across-frequency and the binaural processing stages is able to reproduce the dataset.

Invited Papers

4:20

1pPPa10. Speech in noise and the medial olivo-cochlear efferent system. Raymond Meddis (University of Essex, Department of Psychology, Wivenhoe Park, CO7 9SW Colchester, UK, rmeddis@essex.ac.uk), Robert Ferry (University of Essex, Department of Psychology, Wivenhoe Park, CO7 9SW Colchester, UK, rferry@essex.ac.uk), Guy J. Brown (University of Sheffield, Dept. of Computer Science, Regent Court, 211 Portobello Street, S1 4DP Sheffield, UK, g.brown@dcs.shef.ac.uk)

A central question in auditory scene analysis is how we are able to follow speech against a background of interfering noise. The question is particularly acute for artificial speech recognition algorithms and the hearing impaired. The medial efferent system has been suggested as one contributor to our ability to hear speech in noise. We have recently added efferent suppression to our model of the auditory periphery and evaluated it against physiological observations at the level of the basilar membrane and auditory nerve. We have also replicated a study using compound action potentials where a tone in a noise background became more salient when the efferent system was artificially activated. Visual representations of the computed auditory nerve response to speech in noise show considerable improvement when the efferent system is activated. Tests using the auditory model as a front end to a connected-word recognition algorithm also showed improved performance in the presence of noise when efferent effects were included. The benefits of efferent suppression include reduced compression and extension of the dynamic range of individual auditory nerve fibers.

4:40

1pPPa11. Contributions of the brainstem and below to auditory scene analysis. Ian M. Winter (Centre for the Neural Basis of Hearing, The Physiological Laboratory, Downing Street, CB2 3EG Cambridge, UK, imw1001@cam.ac.uk)

We are increasingly aware of the cues the auditory system uses in the segregation and fusion of auditory objects, however, we have very little evidence for how, or where, these cues are extracted in the auditory pathway. Here I will show how the inner ear and cochlear nucleus contribute to three classical auditory scene analysis phenomena. In the first, grouping by common onset; adaptation, lateral suppression, and recovery from suppression all play a role. In the second phemonenon, a sequential streaming task, commonly referred to as ABA, the contributing low-level mechanisms are frequency tuning and neural adaptation. Finally, in the third phenomenon, comodulation masking release, which describes the seemingly paradoxical situation whereby the detection of a masked signal is improved by the addition of coherently modulated energy remote from the signal frequency, lateral suppression is an important mediator. Taken together these studies suggest that neurophysiological processes at, or before, the level of the cochlear nucleus make an important contribution to auditory scene analysis.

5:00

1pPPa12. The European starling as a model for understanding mechanisms underlying auditory scene analysis. Georg Klump (Oldenburg University, Zoophysiology & Behavior Group, IBU, Fak 5, Carl von Ossietzky Str. 9-11, 26129 Oldenburg, Germany, georg.klump@uni-oldenburg.de)

The European starling is a songbird that has evolved mechanisms for the analysis of acoustic scenes exhibiting a number of similarities with human perception. Segregation of signals and background noise from different sources is enhanced due to the processing of differences in modulation patterns as is evident in experiments on the comodulation detection difference and and comodulation masking release. Similarly to auditory streaming in human subjects, integration of sequential signals into streams occurs in the European starling and it is affected by spectral and temporal properties of the sounds. The presentation reviews results from psychophysical experiments and compares these to observed neural response patterns of auditory forebrain neurons in starlings.

5:20

1pPPa13. Identifying auditory events at a cocktail party: Principles of temporal integration and stream segregation. Elyse Sussman (Albert Einstein College of Medicine, Dept. of Neuroscience, 1410 Pelham Parkway S, Bronx, NY 10461, USA, esussman@aecom.yu.edu)

The question of how sequential sound elements are grouped into meaningful percepts has been within the focus of researchers for decades. This talk takes a new perspective by addressing how within-stream temporal integration occurs in the context of a cocktail party. In a noisy environment, the ability to identify specific events depends upon multiple processes: the overall segregation of sounds into streams as well as the within-stream integration of sequential sounds into meaningful units. This talk presents two studies that address the interaction of these two complex processes. Event-related potentials were used to determine effects of timing (Experiment 1) and of attention (Experiment 2) on the perception of within-stream sound events in multistream environments. Experiment 1 shows that within-stream temporal integration of sequential elements uses previously segregated streams as input. Experiment 2 shows that attention can override stimulus-driven processing biases to facilitate task demands. These results demonstrate different time courses for segregation of sounds into separate streams and for integration of sound elements into within-stream units. Thus, the findings suggest that different neural mechanisms interact in the perceptual organization of sequential sound elements.

Contributed Papers

5:40

1pPPa14. Object formation versus object selection. Barbara Shinn-Cunningham (Boston University Hearing Research Center, 677 Beacon Street, Boston, MA 02215, USA, shinn@cns.bu.edu)

Auditory scene analysis is intricately linked to our ability to understand one acoustic source amidst competing sources. However, studies of selective attention often fail to distinguish between the roles of object formation (estimating the spectro-temporal content of a particular auditory object) and object selection (determining which object will be the focus of attention) in performance. Part of the difficulty in trying to disentangle these effects is that they are intimately related. However, listeners in a selective attention task often report sound elements that are similar in a sound dimension they know is task irrelevant when trying to selectively attend to a different sound attribute (e.g., location, pitch, intensity, timbre). Such results suggest a model of selective attention in which the focus of attention is an auditory object that is formed through interactions between automatic grouping processes and top-down selection. A conceptual model of these interactions will be presented along with data in support of this framework. [Work supported by AFOSR and ONR.]

6:00

1pPPa15. Auditory scene analysis emerges from a distributed yet integrated network. Rhodri Cusack (MRC CBU, 15 Chaucer Road, Cambridge, CB2 7EF Cambridge, UK, rhodri.cusack@mrc-cbu.cam.ac.uk), Daniel Pressnitzer (CNRS UMR 8158; Univ. Paris Descartes ; Ecole Normale Supérieure, 29 rue d'Ulm, 75005 Paris, France, Daniel.Pressnitzer@ens.fr)

Three architectures that have been explicitly or implicitly proposed for auditory scene analysis were evaluated: (1) that some single module is responsible for scene analysis after feature extraction; (2) that scene structure is elaborated through feed-forward stages of auditory processing; and (3) that scene analysis is integrated yet distributed. It is argued that the available evidence points towards the third model. Against (1), scene analysis is influenced by features that are best represented across a broad range nodes in the auditory network, and transmitting this information to a single module would not be parsimonious. Furthermore, neurophysiology has shown a range of nodes reflect scene analysis, ranging from the cochlear nucleus, through auditory cortex to the parietal cortex. Against both (1) and (2) is the high degree of reciprocal interaction between the behavioural derivation of features and scene analysis, and the integration evident from the exclusivity of scene organisations. In contrast, model (3) naturally predicts these observations and is compatible with auditory anatomy, which is not "feed forward" or hublike. Finally, we highlight outstanding issues important to a fuller understanding of scene analysis, such as the neural code for perceptual groups and the mechanism for extraction of statistical regularities.

Invited Papers

6:20

1pPPa16. Perceptual dynamics of auditory streaming and its neural correlates. Makio Kashino (NTT Communication Science Laboratories, NTT Corporation, 3-1, Morinosato Wakamiya, 243-0198 Atsugi, Japan, kashino@avg.brl.ntt.co.jp), Hirohito M. Kondo (NTT Communication Science Laboratories, NTT Corporation, 3-1, Morinosato Wakamiya, 243-0198 Atsugi, Japan,hkondo@brl.ntt.co.jp), Minae Okada (ERATO Shimojo Implicit Brain Function Project, JST, 3-1, Morinosato Wakamiya, 243-0198 Atsugi, Japan, mokada@shimojo.jst.go.jp)

Prolonged listening to a repeated sequence consisting of low and high tones produces spontaneous transitions in the perceptual state between a single coherent stream and two segregated streams. The dissociation between constant physical stimulation and fluctuating perceptual experience in auditory streaming provides a compelling means for studying how auditory percepts are formed in the brain. First, we psychophysically examined the nature of such perceptual transitions in various frequency differences (Δf) between low and

high tones. After the initial buildup of streaming, perceptual transitions occurred frequently even at the Δfs that were previously thought to produce a stable percept, and the dominant perceptual state changed depending on Δf. Next, we explored brain activities correlated with the perceptual transitions using functional magnetic resonance imaging (fMRI). An event- related analysis revealed that the auditory cortex and thalamus were activated at the timing of perceptual transitions. The response onset of the activity in the auditory cortex was earlier than that in the thalamus for the transition from dominant to non-dominant percepts, and later for the transition from non-dominant to dominant percepts. These results imply that the interaction of the auditory cortex and thalamus plays a crucial role for perceptual transitions in auditory streaming.

6:40

1pPPa17. What can binocular rivalry tell us about auditory streaming? Susan Denham (University of Plymouth, Drake Circus, PL4 8AA Plymouth, UK, sdenham@plymouth.ac.uk), István Winkler (Department of General Psychology, Institute for Psychology, Hungarian Academy of Sciences, P.O. Box 398, 1394 Budapest, Hungary, iwinkler@cogpsyphy.hu), Kinga Gyimesi (Department of General Psychology, Institute for Psychology, Hungarian Academy of Sciences, P.O. Box 398, 1394 Budapest, Hungary, kgyimesi@cogpsyphy.hu), Gábor Stefanics (Department of General Psychology, Institute for Psychology, Hungarian Academy of Sciences, P.O. Box 398, 1394 Budapest, Hungary, gstefanics@cogpsyphy.hu)

Although sensory systems share the common goal of building accurate representations of the environment, differences in the physical nature of stimuli from different modalities seem to argue against similar processing strategies. Nevertheless, our experiments have revealed surprisingly deep parallels between the dynamics of perceptual organisation in auditory streaming and binocular rivalry. These parallels provide evidence for an interpretation of auditory streaming in terms of rivalry between competing temporal associations, which helps to explain the distribution of perceptual switching with respect to stimulus features, strong differences between first and steady-state phases in ongoing switching, the nonmonotonic dependence of switching rate on stimulus "strength," the range of relationships between phase duration and stimulus features, and the existence and distribution of "transition" phases during which subjects simultaneously experience what are usually thought to be mutually exclusive perceptual states.

7:00

1pPPa18. Multistability in audiovisual speech scene analysis: behavioral and neurophysiological data on multimodal verbal transformations. Jean-Luc Schwartz (ICP-GIPSA, INPG, 46 Av. Félix Viallet, 38031 Grenoble, France, schwartz@icp.inpg.fr), Anahita Basirat (ICP-GIPSA, INPG, 46 Av. Félix Viallet, 38031 Grenoble, France, basirat@icp.inpg.fr), Marc Sato (ICP-GIPSA, INPG, 46 Av. Félix Viallet, 38031 Grenoble, France, sato@icp.inpg.fr)

The multistable perception of speech refers to the perceptual changes experienced while listening to a speech form cycled in rapid and continuous repetition, the so-called Verbal Transformation Effect. Because distinct interpretations of the same repeated stimulus alternate spontaneously, this effect provides an invaluable tool to examine how speech percepts are formed in the listener's mind. In a series of behavioural studies, we demonstrated that (1) articulatory-based representations play a key part in the endogenously driven emergence of auditory speech percepts; (2) vision penetrates into the transformation process, intervening both in the stability of a given pattern, and in the temporal dynamics of perceptual switches. Furthermore, we determined the cortical circuit in charge for the emergence of a shift of percept associated to a given audio input. This circuit involves a cortical "dorsal route" for speech perception, linking temporal, parietal, and frontal regions. Current experiments involve further tests about the nature of both perceptuo-motor and audiovisual interactions in verbal transformations. Altogether, these results shed some new lights on the cognitive and neurobiological bases of speech perception, in which multimodal interactions between sensory and motor representations play a crucial role.

Session 1pPPb

Psychological and Physiological Acoustics: Cochlear Implants: Going Beyond the Envelope I

Bernhard U. Seeber, Cochair
MRC Institute of Hearing Research, Science Rd / University Park, Nottingham, NG7 2RD, UK

H. Steven Colburn, Cochair
Boston University, 44 Cummington St., Boston, MA 02215, USA

Contributed Paper

1:00

1pPPb1. A new approach to electric-acoustic stimulation. Christopher A. Brown (Arizona State University, Dept. of Speech & Hearing Science, P.O. Box 870102, Tempe, AZ 85287-0102, USA, c-b@asu.edu), Sid P. Bacon (Arizona State University, Dept. of Speech & Hearing Science, P.O. Box 870102, Tempe, AZ 85287-0102, USA, spb@asu.edu)

When low-frequency acoustic stimulation is combined with either real or simulated electric stimulation from a cochlear implant (electric-acoustic stimulation, or EAS), speech intelligibility in noise can improve dramatically. This improvement has been shown in simulation to be due in part to the presence of fundamental frequency (F0) and amplitude envelope information in the low-frequency region. The current experiment extends those findings to implant patients. Six patients who had residual low-frequency hearing in either their implanted or unimplanted ear participated. A target talker was combined with multitalker babble and presented to the implant. In the low-frequency region, patients heard either no stimulus, target speech, or a tone that was modulated in frequency to track the dynamic changes in F0, and in amplitude with the amplitude envelope of the low-pass target speech. Results showed that the tone provided, on average, about 58 percentage points of improvement over electric-only stimulation. Both the tone and target speech provided a statistically significant benefit over electric stimulation only ($p<0.0001$), and were statistically equivalent to each other ($p>0.05$). These results demonstrate that a tone that conveys F0 and amplitude envelope information can provide significant benefit in EAS.

Invited Papers

1:20

1pPPb2. Temporal pitch processing by cochlear implant users. Robert P. Carlyon (MRC CBU, 15 Chaucer Rd., CB2 7EF Cambridge, UK, bob.carlyon@mrc-cbu.cam.ac.uk), Ying-Yee Kong (Notheastern University, 106A Forsyth, Boston, MA Ma 02115, USA, yingyeekong@googlemail.com), Cathy Lynch (Addenbrooke's NHS Trust, Hills Rd, CB2 2QQ Cambridge, UK, catherine.lynch@addenbrookes.nhs.uk), John Deeks (MRC CBU, 15 Chaucer Rd., CB2 7EF Cambridge, UK, john.deeks@mrc-cbu.cam.ac.uk)

Modern cochlear implants (CIs) convey fundamental frequency (F0) information using a purely temporal code. However, temporal pitch processing - as measured by the discrimination of the changes in the rate of a pulse train applied to a single electrode - is often worse than in normal hearing (NH) at low pulse rates, and usually deteriorates dramatically at rates above about 300 pps. We will describe evidence that at low pulse rates, the value of the pitch perceived can be affected by refractory effects at the level of the auditory nerve (AN), and can also be influenced by small (< 0.5 dB) changes in stimulus level. In contrast, the deterioration in rate discrimination at high rates appears to be impervious to a wide range of manipulations that would be expected to strongly affect the representation of the stimulus at the level of the AN. One example of this is the finding that the variation in rate discrimination performance with baseline rate for single-pulse-per-period pulse trains correlates, across listeners, with discrimination of different rates of sinusoidal amplitude modulation imposed on a 5000-pps carrier. The implications of these findings for attempts to improve pitch coding in CIs will be discussed.

1:40

1pPPb3. Investigating the influence of pulse rate and duration on pitch perception in cochlear implants. Joshua S. Stohl (Duke University, Department of Electrical and Computer Engineering, Box 90291, Durham, NC 27708, USA, jss@ee.duke.edu), Chandra S. Throckmorton (Duke University, Department of Electrical and Computer Engineering, Box 90291, Durham, NC 27708, USA, cst@ee.duke.edu), Leslie M. Collins (Duke University, Department of Electrical and Computer Engineering, Box 90291, Durham, NC 27708, USA, lcollins@ee.duke.edu)

Multirate sound processing strategies may potentially provide improved speech recognition and music perception in cochlear implants (Nie et al., 2005; Throckmorton et al., 2006), although it may be necessary to tune these strategies using psychophysical data to provide maximum benefit to the user (Throckmorton et al., 2006). To investigate the need for tuning, cochlear implant users participated in several rate-based psychophysical experiments. Subjects performed single- and two-rate pitch ranking tasks to investigate the influence of pulse rate on the overall pitch structure. The introduction of a second rate resulted in frequent pitch reversals between closely spaced electrodes. In addition to the multi-rate pitch structure, the duration necessary to perceive a rate change must also be considered. Experiments were performed using ABA stimuli, where rate B was higher than rate A. Subjects completed an embedded rate discrimination task in which the duration of B was fixed and its rate varied adaptively for durations ranging from 20-200 ms. The rate of segment B was then fixed, and its duration varied adaptively. Results imply that embedded rate difference limens may be a function of duration, and that the minimum duration required for detecting a change in pulse rate is subject specific.

2:00

1pPPb4. Use of simultaneous stimulation to represent fine structure in cochlear implant processors. Leonid Litvak (Advanced Bionics, 12740 San Fernando Rd., Sylmar, CA 91342, USA, LeonidL@AdvancedBionics.Com), Aniket Saoji (Advanced Bionics, 12740 San Fernando Rd., Sylmar, CA 91342, USA, Aniket.Saoji@AdvancedBionics.Com), Anthony Spahr (Arizona State University, Lattie F. Coor Hall, Room 3462, Tempe, AZ 85287, USA, Tony.Spahr@Asu.Edu), Abhijit Kulkarni (Advanced Bionics, 12740 San Fernando Rd., Sylmar, CA 91342, USA, Abhijit.Kulkarni@AdvancedBionics.Com), Michael Marzalek (Advanced Bionics, 12740 San Fernando Rd., Sylmar, CA 91342, USA, mikemarz@sonic.net)

In cochlear implants, simultaneous stimulation of adjacent electrodes, can be used to shape the electric fields generated within the cochlea. For example, simultaneous in-phase stimulation of nearby electrodes can be used to create activation patterns which may have maxima at locations that are intermediate to the locations of the stimulated electrodes. Psychophysically, such "virtual channels" give rise to intermediate pitch sensations. Simultaneous out-of-phase stimulation of two flanking electrodes in addition to the center electrode can be used to presumably produce more focused activation at the cost of larger overall stimulation currents. Forward masking patterns indicate that for sufficiently large compensation currents, such "focused" stimulation can lead to a more spatially contained excitation. In some cases, current focusing also could lead to sensations that are more tonal relative to monopolar. This presentation will review recent results obtained in our laboratories with both "virtual channel" and "focused" configurations. We will also address how both techniques can be used to better represent the within-channel fine structure in a wearable sound processing strategy.

2:20

1pPPb5. Effect of channel interactions on sensitivity to binaural timing cues in electrical hearing. Gary Jones (University of Wisconsin, 1500 Highland Ave, Waisman Center, Madison, WI 53705, USA, gjones@waisman.wisc.edu), Ruth Litovsky (University of Wisconsin, 1500 Highland Ave, Waisman Center, Madison, WI 53705, USA, litovsky@waisman.wisc.edu), Richard Van Hoesel (CRC HEAR, 384-388 Albert St, VIC 3002 East Melbourne, Australia, rvanh@bionicear.org)

With bilateral cochlear implant (BICI) users it is possible to test sensitivity to interaural timing differences (ITDs) while bypassing peripheral auditory processing. Ongoing work in our lab suggests that at low pulse rates ITD JNDs in the tens of microseconds can be achieved by BICI users with postlingual onset of deafness at single pairs of electrodes at the base, middle or apex of the electrode array. The current project is concerned with channel interactions and, specifically, performance when there is activation of more than one electrode pair and when more than one ITD is presented to the auditory system simultaneously. We examined ITD sensitivity in BICI users with bilateral pairs of pitch-matched electrodes on which unmodulated pulse trains were presented at 100 pulses per second. A probe pulse train and an added pulse train were temporally interleaved. ITD JNDs for the probe train were measured while varying the added train's: a) frequency place, b) level, and c) ITD (matched to probe or fixed at 0 μs). Results suggest that stimulation of multiple electrodes can result in a range of interaction effects that can have either facilitatory or interfering effects on binaural sensitivity. Work supported by NIH-NIDCD (R01 DC003083-09, F31 DC009361).

2:40

1pPPb6. Binaural jitter improves sensitivity to interaural time differences in electric and acoustic hearing. Bernhard Laback (Austrian Academy of Science/Acoustics Research Institute, Wohllebengasse 12-14, 1040 Vienna, Austria, Bernhard.Laback@oeaw.ac.at), Piotr Majdak (Austrian Academy of Science/Acoustics Research Institute, Wohllebengasse 12-14, 1040 Vienna, Austria, piotr@majdak.com), Matthew J. Goupell (Austrian Academy of Science/Acoustics Research Institute, Wohllebengasse 12-14, 1040 Vienna, Austria, matt.goupell@gmail.com)

Cochlear implant (CI) listeners are often sensitive to fine structure ITD at low pulse rates, but their sensitivity declines at higher pulse rates which are required for speech coding. We hypothesized that this limitation is related to the binaural adaptation phenomenon [Hafter and Dye, J. Acoust. Soc. Am. **73** 644-651 (1983)], associated with periodic stimulation. With five CI listeners, we tested the effect of introducing binaurally-synchronized jitter (binaural jitter) in the stimulation timing, assuming that this reduces the periodicity in the neural response and thus avoids binaural adaptation. Pulse rates from 400 to 1515 pulses per second (pps) were tested. In addition, we performed a similar experiment with normal-hearing (NH) listeners using bandpass-filtered acoustic pulse trains and testing the pulse rates 600 and 1200 pps. The CI listeners showed large improvements in ITD sensitivity from binaural jitter at high pulse rates (800 - 1515 pps). The NH listeners also showed large improvements from binaural jitter. The results are consistent with the hypothesis that random temporal variation reactivates the adapted binaural auditory system. Thus, binaurally-jittered stimulation improves the access of bilateral CI listeners to ITD information. Partly supported by the Austrian Science Fund, FWF, project number P18401-B15.

3:00

1pPPb7. Parameters affecting the precedence-effect with cochlear implants. Bernhard U. Seeber (MRC Institute of Hearing Research, Science Rd., / University Park, NG7 2RD Nottingham, UK, seeber@ihr.mrc.ac.uk), Ervin R. Hafter (University of California, Department of Psychology, 3210 Tolman Hall, Berkeley, CA, CA 94720-1650, USA, hafter@berkeley.edu)

Monaural spectral and temporal cues as well as binaural cues provide the information to analyze the auditory scene. Subjects using bilateral cochlear implants (CIs) have limited access to those cues, particularly to interaural time differences (ITDs) and to spectral information. Nevertheless, many subjects can localize sounds in quiet based on the evaluation of interaural level differences (ILDs) but this might be impaired by the presence of reflections. We studied the precedence effect with patients wearing bilateral CIs and found that localization was abolished in most subjects when the echo was present, but some subjects showed dominance of the leading sound on localization. The reasons for the different outcomes were studied with simulations of CIs. Using a noise-band vocoder simulation, subjects could not fuse lead and lag into a single object and they localized both separately. With a sinusoidal vocoder, lead-lag fusion and the precedence effect could be obtained provided that frequencies of the carrier sinusoids were matched across ears. Interaural phase of the carrier played only a limited role. We conclude that precedence of ongoing sounds can solely be based on ILDs and envelope-ITDs and that proper place matching of CI-electrodes would help the analysis of concurrent sounds.

3:20-3:40 Break

3:40

1pPPb8. Neural cross-correlation metrics to quantify envelope and fine-structure coding in auditory-nerve responses. Michael Heinz (Purdue University, 500 Oval Drive, West Lafayette, IN 47907, USA, mheinz@purdue.edu), Jayaganesh Swaminathan (Purdue University, 500 Oval Drive, West Lafayette, IN 47907, USA, jswamy@purdue.edu)

Fundamental questions about the relative perceptual importance of envelope and fine structure are often addressed using specialized acoustic stimuli, such as temporal-fine-structure speech or auditory chimaeras. Interpretation of these perceptual studies assumes envelope and fine structure can be isolated at the output of the cochlea. Narrowband cochlear filtering constrains the ability to isolate fine structure from envelope; however, envelope recovery from fine structure has been difficult to evaluate physiologically. Separate neural cross-correlation coefficients (CCCs) for envelope and fine-structure were developed based on shuffled auto- and cross-correlograms. Neural CCCs have a wide dynamic range for both within-fiber, cross-stimulus and cross-fiber, within-stimulus correlations based on both model and recorded spike-train data from auditory-nerve fibers. Results provide physiological evidence consistent with perceptual findings that envelope recovery is reduced as the number of analysis bands increases, but is not completely eliminated for 8- and 16-band conditions. Neural CCCs were also used to evaluate across-fiber temporal coding, which has been implicated in the difficulties that hearing-impaired listeners have in understanding speech in complex acoustic backgrounds. Results demonstrate the potential of these neural CCC metrics to quantitatively evaluate a wide range of perceptually significant temporal coding issues relevant to normal and impaired hearing. Supported by NIH-NIDCD.

Contributed Paper

4:00

1pPPb9. Transmission of temporal fine structure by a penetrating auditory nerve implant. John C. Middlebrooks (University of Michican, KHRI, 1301 E. Ann St., Ann Arbor, MI 48109-5506, USA, jmidd@umich.edu), Russell L. Snyder (University of California, Epstein Laboratory, Room U-490, P.O. Box 0526, San Francisco, CA 94143 0526, USA, rsnyder@ohns.ucsf.edu)

We are quantifying the transmission of temporal fine structure from a penetrating auditory nerve electrode array to the inferior colliculus (IC) in anesthetized cats. We stimulate with biphasic electrical pulse trains and determine the maximum pulse rate eliciting phase-locked activity. Many IC neurons showed significant phase locking to rates as high as 600 pulses per second (pps) when the nerve was stimulated with the penetrating array, whereas phase locking reached only 300 pps when stimulated with a conventional intrascalar cochlear implant. Phase locking to rates $>$300 pps was found primarily among IC units with characteristic frequencies (CFs) $<$2 kHz. Such low frequency fibers are not stimulated selectively by conventional intrascalar cochlear implant. We selectively stimulated apical fibers by placing ball electrodes on the apical spiral lamina. Activation of these balls selectively stimulated low-CF IC neurons. These neurons phase locked to 600 pps. Based on these results, we conclude that transmission of temporal information from a penetrating intraneural electrode array is superior to that obtained with a conventional cochlear implant but only insofar as the intraneural electrodes provide more selective access to low-CF pathways. Supported by NIDCD NO1-DC-5-0005.

Invited Papers

4:20

1pPPb10. Why is sensitivity to interaural time differences (ITD) poorer than normal with bilateral cochlear implants? Neurophysiological considerations. Bertrand Delgutte (Massachusetts Eye & Ear Infirmary, Eaton-Peabody Lab., 243 Charles St., Boston, MA 02114, USA, Bertrand_Delgutte@meei.harvard.edu), Kenneth E. Hancock (Massachusetts Eye & Ear Infirmary, Eaton-Peabody Lab., 243 Charles St., Boston, MA 02114, USA, ken_hancock@MEEI.HARVARD.EDU)

Bilateral cochlear implantation improves sound localization and speech reception in noise. Yet ITD sensitivity is clearly poorer than normal with bilateral implants, even when the stimulation bypasses the processors (which discard the temporal fine structure of the stimulus). This poor behavioral ITD sensitivity is surprising from a physiological perspective because (1) electric stimulation produces precise temporal patterns of activity in the auditory nerve, and (2) most neurons in the inferior colliculus of acutely-deafened, bilaterally-implanted cats show precise tuning to ITD of pulse trains at the appropriate intensity (Smith and Delgutte, J. Neurosci. **27**:6740). We will present physiological and modeling results bearing upon two hypotheses for reconciling neural and psychophysical observations. One hypothesis is that plastic changes to the neural circuitry resulting from binaural deprivation may impair the binaural processing in long-term deafened animals (and humans), particularly if deafening occurs during the neonatal period. Alternatively, the abnormal spatio-temporal pattern of activity across the population of binaural neurons (due in part to limited dynamic range with electric stimulation) may impair the ability of the central decoding stages to extract the ITD information available in individual binaural neurons.

4:40

1pPPb11. Modeling responses of brainstem neurons to electrical stimuli. H Steven Colburn (44 Cummington St., Boston, MA 02215, USA, colburn@bu.edu), Yoojin Chung (44 Cummington St., Boston, MA 02215, USA, yjchung@bu.edu), Andrew Brughera (44 Cummington St., Boston, MA 02215, USA, brughera@bu.edu), Yi Zhou (Johns Hopkins University, Dept. of Biomedical Eng.; School of Medicine, Ross 424 Wang, Baltimore, MD 21205, USA, zhouyi@jhu.edu)

This talk describes modeling efforts to understand brainstem neural responses to electrical cochlear stimulation. Our approach is to combine brainstem models developed for acoustic stimulation with descriptions of auditory-nerve (AN) responses to electric stimulation. Predictions for the behavior of neurons at several levels of the brainstem are compared to available physiological data. Specifically, the AN model predicts differences in discharge probability, degree of phase-locking, and adaptation of discharge rate of the AN response to stimuli, inlcuding both electrical and acoustical cases. Predicted neural responses are generated for several brainstem

nuclei, including cell populations in the cochlear nucleus (CN), the superior olive (SOC) and the inferior colliculus (IC). Specific attention is given to two special topics: 1) responses to the simultaneous stimulation of multiple electrodes, and 2) the effects of amplitude modulation on the tuning of binaural neurons to interaural time delay (ITD). [Work supported by US National Institutes of Health grants DC04663, DC00100, and DC05775 (Delgutte, PI).]

Contributed Papers

5:00

1pPPb12. Higher sensitivity of human auditory nerve fibers to positive electrical currents. Olivier Macherey (MRC CBU, 15 Chaucer Rd., CB2 7EF Cambridge, UK, olivier.macherey@mrc-cbu.cam.ac.uk), Robert P. Carlyon (MRC CBU, 15 Chaucer Rd., CB2 7EF Cambridge, UK, bob.carlyon@mrc-cbu.cam.ac.uk), Astrid Van Wieringen (ExpORL, Dept. Neurosciences, K.U. Leuven, Herestraat 49 bus 721, O. & N2, B-3000 Leuven, Belgium, astrid.vanwieringen@med.kuleuven.be), John Deeks (MRC CBU, 15 Chaucer Rd., CB2 7EF Cambridge, UK, john.deeks@mrc-cbu.cam.ac.uk), Jan Wouters (ExpORL, Dept. Neurosciences, K.U. Leuven, Herestraat 49 bus 721, O. & N2, B-3000 Leuven, Belgium, jan.wouters@med.kuleuven.be)

Most contemporary cochlear implants (CIs) stimulate the auditory nerve with trains of amplitude-modulated, symmetric biphasic pulses. Although both polarities of a pulse can depolarize the nerve fibers and generate action potentials, it remains unknown which of the two (positive or negative) phases has the stronger effect. Animal experiments have shown that cathodic (negative) current flows are more effective than anodic (positive) ones in eliciting neural responses, and this finding has motivated the development of novel speech-processing algorithms. Here we show electrophysiologically and psychophysically that the human auditory system exhibits the opposite pattern, being more sensitive to anodic stimulation. We measured electrically evoked compound action potentials in CI listeners for phase-separated pulses, allowing us to tease out the responses to each of the two opposite-polarity phases. At an equal stimulus level, the anodic phase yielded the larger response. This finding was corroborated by a measure of psychophysical masking patterns and may relate to a particular orientation of the nerve fibers relative to the electrode or to a substantial degeneration/demyelination of the peripheral processes. Potential applications to improve CI speech-processing strategies are discussed.

5:20

1pPPb13. 3D-localization of virtual sound sources in normal-hearing and cochlear-implant listeners. Piotr Majdak (Austrian Academy of Science/Acoustics Research Institute, Wohllebengasse 12-14, 1040 Vienna, Austria, piotr@majdak.com), Bernhard Laback (Austrian Academy of Science/Acoustics Research Institute, Wohllebengasse 12-14, 1040 Vienna, Austria, Bernhard.Laback@oeaw.ac.at), Matthew J. Goupell (Austrian Academy of Science/Acoustics Research Institute, Wohllebengasse 12-14, 1040 Vienna, Austria, matt.goupell@gmail.com)

The ability to localize sound sources in 3D-space was tested in humans. Five normal-hearing (NH) subjects listened via headphones to noises filtered with subject-specific head-related transfer functions. Four bilateral cochlear implant (CI) subjects listened via their clinical speech processors to noises filtered with subject-specific behind-the-ear head-related transfer functions. A virtual structured environment was presented via head mounted display. Two conditions were used: a condition where the subjects were naive and had no response feedback and a learning condition where the subjects were trained by providing extensive feedback during the test. Response feedback was provided via the visual virtual environment. The results show that the CI listeners performed generally worse than NH listeners, both in the horizontal and vertical dimensions. Both subject groups were able to learn to better localize sound sources, which is supported by lower localization errors in the learning condition. However, in the learning condition, the CI listeners showed a front/back confusion rate comparable to naive NH listeners, which was two times higher than for the trained NH listeners. These results indicate the necessity of new CI processing strategies which include spectral localization cues. Funding by FWF (P18401-B15).

5:40

1pPPb14. Emergence of sound localization acuity in children who are fitted with bilateral cochlear implants. Ruth Litovsky (University of Wisconsin, 1500 Highland Ave, Waisman Center, Madison, WI 53705, USA, litovsky@waisman.wisc.edu), Tina Grieco-Calub (University of Wisconsin, 1500 Highland Ave, Waisman Center, Madison, WI 53705, USA, grieco@waisman.wisc.edu), Shelly Godar (University of Wisconsin, 1500 Highland Ave, Waisman Center, Madison, WI 53705, USA, godar @waisman.wisc.edu)

Sound localization was investigated in children who are born deaf and hear with either monaural or bilateral cochlear implants (CIs). Using a 2AFC discrimination task with stimuli to the right/left, in a sound proof booth, loudspeaker locations varied along the horizontal plane between +/-70 deg. Minimum audible angle (MAA) thresholds were estimated adaptively. In study 1, 4-14 year-old children who received two CIs in sequential procedures participated. They were first tested while functioning monaurally, then at 3- and 12-months following activation of bilateral hearing. Following bilateral activation, MAA thresholds were significantly lower, especially after 12 months. In study 2 children were 2.5 years old, with 6-20 months of bilateral experience. MAAs were typically better when children had $\geqslant$12 months of exposure to bilateral stimulation. Overall, these findings suggest that binaural hearing abilities can be established in an auditory system that is strictly stimulated with electrically pulsed signals, but that unlike a normal auditory system, here a year of exposure may be required before localization acuity is better under bilateral than monaural conditions. These findings are especially relevant to considerations of localization in absence of fine-structure, a cue that is discarded by the speech processors utilized in CIs.

Session 1pSAa

Structural Acoustics and Vibration and EURONOISE: Vibration and Radiation from Complex Structural Systems I

David Feit, Cochair
Applied Physical Sciences Corp., Ste. 300, 2 State St., New London, CT 06320, USA

Jean-Louis Guyader, Cochair
INSA de Lyon - LVA, Bâtiment St. Exupéry, 25 bis avenue Jean Capelle, Villeurbanne Cedex, F-69621, France

Invited Papers

1:00

1pSAa1. Development of a general SEA subsystem formulation using FE periodic structure theory. Vincent Cotoni (ESI Group, 12555 High Bluff Dr., Suite 250, San Diego, CA 92130, USA, vincent.cotoni@esi-group-na.com), Phil S. Shorter (ESI Group, 12555 High Bluff Dr., Suite 250, San Diego, CA 92130, USA, pjs@esi-group-na.com), Robin S. Langley (University of Cambridge, Trumpington Street, CB5 8HU Cambridge, UK, rsl21@hermes.cam.ac.uk)

Statistical Energy Analysis (SEA) represents a field of study in which statistical descriptions of a system are employed in order to simplify the analysis of complicated vibro-acoustic problems. In SEA, a vibro-acoustic system is represented by a collection of subsystems that can receive, store, dissipate and transmit vibro-acoustic energy. Traditionally, the SEA parameters for a given subsystem are formulated analytically based on consideration of wave propagation through the subsystem. While such analytical algorithms can be readily applied to the majority of systems encountered in practical problems, there are certain types of sections that are difficult to describe using existing analytical formulations. Examples include: isogrid in launch vehicle fairings, extruded aluminum sections in train floors and modern corrugated aircraft fuselage constructions. This paper describes the development of a generic SEA subsystem formulation based on the use of finite element (FE) periodic structure theory. A small unit cell of the section is created and computationally efficient algorithms are developed to calculate wave propagation through a large array of such cells. The resulting algorithms are used to calculate the SEA parameters for the section. The approach is described and a number of numerical validation examples are presented.

1:20

1pSAa2. Structure/cavity coupling using Statistical Energy Analysis: Coupling loss factors and energy maps into subsystems. Nicolas Totaro (INSA de Lyon - LVA, Bâtiment St. Exupéry, 25 bis avenue Jean Capelle, F-69621 Villeurbanne Cedex, France, nicolas.totaro@insa-lyon.fr), Jean-Louis Guyader (INSA de Lyon - LVA, Bâtiment St. Exupéry, 25 bis avenue Jean Capelle, F-69621 Villeurbanne Cedex, France, jean-louis.guyader@insa-lyon.fr)

Prediction of interior noise is one of the most concerning issues of vehicle industry. Statistical Energy Analysis theoretically allows to determine energy spread over a structure divided into subsystems when one subsystem is submitted to a rain-on-the-roof excitation. Subsystems can be either a part of the structure or a cavity. Recently, a method (SmEdA) based on modal bases of uncoupled subsystems have been derived. This method permits to compute CLF using standard FEM software. This method has been successfully applied on structure/structure coupling and is extended to estimation of CLF between a structure and a cavity in the present article. In addition, in the case of interior noise, SEA can only provide a global energy into the cavity on frequency bands. No information on energy repartition into the subsystem is given. In the present article, an extension of SmEdA method is proposed to quickly estimate energy repartition into subsystems (structure or cavity).

1:40

1pSAa3. Theory and application of pseudo-damping in structures. Adnan Akay (Carnegie Mellon University, Mechanical Engineering Department, Pittsburgh, PA 15213, USA, akay@cmu.edu), Antonio Carcaterra (Università di Roma, 'La Sapienza,' Dipartimento di Meccanica ed Aeronautica, Via Eudossiana, 18, 00184 Roma, Italy, a.carcaterra@dma.ing.uniroma1.it)

This presentation describes the underlying physics and theory of pseudo damping to reduce vibration of conservative structures. The theoretical approach is based on particular properties of harmonic functions that lead to construction of a complex system that exhibits nearly irreversible energy transfer. This approach also provides the ability to tailor energy absorption from a particular structure in the absence of damping. The authors will also discuss extension of the concept to continuous systems and its application to waveguides. The presentation will illustrate test results including application to reduce vibrations in a satellite. [Research carried out while AA served at NSF.]

2:00

1pSAa4. Localization and mesoscopics in structures and rooms I. Richard Weaver (Dept. of Physics, University of Illinois, Urbana, IL 61801, USA, r-weaver@uiuc.edu)

Diffuse field methods such as reverberation room acoustics and statistical energy analysis predict wave energy flow in complex structures. They are predicated on an incorrect assumption of incoherence. The consequent failures of otherwise successful theories are occasionally striking. The most noteworthy among these are related to Anderson - and other kinds of - localization. Residual coherence manifests also in time-reversal invariance and Green's function retrieval in field-field correlations. It is sometimes possible in special cases to make ad hoc corrections to the diffuse field theories. It would be preferable, however, to augment them with more a fundamental quantitative theory applicable to a wide variety of systems. This talk reviews mesoscopic phenomena such as weak Anderson localization, modal echoes, Anderson localization, Thouless localization, and Greens function retrieval. It sets out the phenomena and concepts behind the new theory to be presented in "Localization and Mesoscopics in Structures and Rooms II" at a later session.

2:20

1pSAa5. Spherical harmonic analysis of the field radiated by a source embedded in a two-layer coating of a spherical shell. Jerry H. Ginsberg (Georgia Insitute of Technology, G. W. Woodruff School of Mechanical Engineering, Atlanta, GA 30332-0405, USA, jerry.ginsberg@me.gatech.edu)

The acoustic field generated by a small source embedded in a viscoelastic layer encapsulating a spherical shell was modeled previously by treating each layer as a dissipative fluid [J. H. Ginsberg, JASA, **122**, 3067 (2007)]. Using spherical harmonic series for each layer was shown to lead to profoundly ill-conditioned equations because of the enormous differences of scale of the spherical Bessel functions having complex argument and high order. Mie series is not directly applicable because the present source is embedded in a layer. Scaling of the spherical Bessel functions and the alternatives of using Bessel and Neumann or two Hankel functions are examined for their efficacy in addressing ill-conditioning. The specfic system that is analyzed consists of a soft inner layer that coats the shell, covered by an outer layer that encapsulates the source. The impedance of the outer layer nominally matches the surrounding water, so reflection of the source from the soft inner layer might seem to have the effect of creating a dipole. However, depending on the wavelength in the inner layer, it might seem that the source "sees" the shell, in which case one would expect the behavior to be like a simple source whose strength is doubled.

Contributed Papers

2:40

1pSAa6. Periodic assembly of multicoupled beams: Wave propagation and natural modes. Guillaume Gosse (Laboratoire Vibrations Acoustique - INSA Lyon, 25 bis avenue Jean Capelle, Bâtiment Saint-Exupéry, F-69621 Villeurbanne cedex, France, guillaume.gosse@insa-lyon.fr), Charles Pezerat (Laboratoire Vibrations Acoustique - INSA Lyon, 25 bis avenue Jean Capelle, Bâtiment Saint-Exupéry, F-69621 Villeurbanne cedex, France, charles.pezerat@insa-lyon.fr), François Bessac (CETIAT, Domaine Scientifique de la Doua, 25 avenue des Arts, BP 2042, F-69603 Villeurbanne cedex, France, francois.bessac@cetiat.fr)

The present work is concerned with the vibrations of a discrete multicoupled periodic system. It lies within a larger study on the vibroacoustic behaviour of a heat exchanger. These structures are usually made of a succession of huge number of identical parallel fins (around 600 per meter) connected by tubes conveying the coolant fluid. By now their behaviour can not be calculated using FE model. As a first step, the periodicity principles are applied on a simpler structure, i.e.. an assembly of identical beams linked by several damped springs. The basic unit is symmetric and composed of one flexural beam with several springs on each side. Using the Floquet-Bloch's theorem and the works of Denys Mead (receptance matrix), it is possible to completely describe the whole structure behaviour (natural modes, response) only from the vibroacoustic knowledge of the basic unit. This has be done analytically and the results were confirmed by a (very time consuming) FE model calculation. The study of the basic unit can also give valuable information on the physical phenomena governing the transmission from one unit to the next, and then the propagation in the whole structure.

3:00

1pSAa7. The response of a complex dynamical system to a complex external forcing. John McCoy (Catholic University, 620 Michigan Ave, Washington, DC 20064, USA, mccoy@cua.edu)

The response of a dominant grounded spring/mass to which are attached a large number of significantly less massive sprung masses, when subject to an external forcing acting on the dominant mass, is revisited. Distinguishing the new study is a focus on the net force that the attached systems cause to act on the dominant mass and the derivation of a semi-analytic, time domain representation of the system operator that transforms the history of the external force acting on the adorned dominant spring/mass to the history of an effective force that acts on the unadorned dominant spring/mass. The mathematical framework provided by the concept of an ″effective force″ acting on the unadorned simple system gives additional insight to a commonly accepted concept of an ″effective dissipation″ modifying the unadorned simple system, when subject to simple external force histories; i.e., force histories with limited time extents or with limited bands of spectral content. Of greater practical interest is the mathematical framework allows investigation of external force histories that are not simple.

3:20

1pSAa8. General absorbing boundary for acoustic and elastic waves. Denis Duhamel (ENPC, UR Navier, 6 et 8 Avenue Blaise Pascal, Cité Descartes, Champs sur Marne, 77455 Marne la Vallée, France, duhamel@lami.enpc.fr)

In the finite element computation of unbounded acoustic problems, the domains must be of finite size and artificial absorbing conditions have to be introduced in order to avoid reflections at the truncated boundary. This communication proposes a new method in the frequency domain to generate efficient absorbing boundary conditions without the need to consider high order derivatives on the boundary. Moreover the approach is quite general and can consider media with mean flow or be applied to structural vibrations. It needs the knowledge of the dynamic stiffness matrix of only one element which can be obtained from any finite element software. The final result is an impedance condition linking the forces and displacements on the boundary which is determined numerically from a wave analysis of one element of the media. Using this impedance condition a finite element problem can be solved by standard methods. This is then applied to study some examples for 2D standard acoustic, acoustic problems with mean flow and vibrations of plates.

3:40

1pSA9. Dynamic response of an insonified sonar window. Andrew J. Hull (Naval Undersea Warfare Center, Code 8212, 1176 Howell St., Newport, RI 02841, USA, hullaj@npt.nuwc.navy.mil)

This talk derives and evaluates an analytical model of an insonified sonar window in contact with an array of Tonpilz transducers operating in

receive mode. The window is fully elastic so that all wave components are present in the analysis. The output of the model is a transfer function of a transducer element output voltage divided by input pressure versus arrival angle and frequency. This model is intended for analysis of sonar systems that are to be built or modified for broadband processing. The model is validated at low frequency with a comparison to a previously derived thin plate model. Once this is done, an example problem is studied so that the effects of higher order wave interaction with acoustic reception can be understood. It was found that these higher order waves cause multiple nulls in the region where the array detects acoustic energy and that their locations in the arrival angle-frequency plane can be determined. The effects of these nulls in the beam patterns of the array are demonstrated.

4:00-4:20 Break

4:20

1pSAa10. Circumferential admittance approach for vibro-acoustic prediction of a submerged cylindrical shell with rib aperiodicity and transversal bulkheads. Laurent Maxit (DGA (Defence Agency), CTSN/SDP/CMPF, B.P. 28, 83800 Toulon, France, laurent.maxit@dga.defense.gouv.fr)

The circumferential admittance approach is presented to predict the vibro-acoustic behaviour of an externally fluid loaded shell with aperiodic stiffeners and transversal bulkheads. It consists to consider the circumferential spectral displacements of the shell and to use a partitioning of the structure such that the fluid loaded shell constitutes one subsystem and the stiffeners/bulkheads constitute others subsystems. Each subsystem is characterised independently by the circumferential admittances. For the stiffeners/bulkheads, a standard FE code is used to calculate these admittances with a shell description. The admittances of the fluid load shell are estimated by a spectral approach. Developments are proposed in this paper to improve the numerical convergence of the spectral approach. The final assembly is obtained using the continuity relations. Excitations like mechanical forces, acoustic diffuse fields or plane waves can be easily taken into account. For submarine applications, this model permits to study the noise radiated by the pressure hull and to analyse the acoustic target strength of the shell with its internal frames. The whole submarine pressure hull can be described with the assumption that it is extended by a cylindrical rigid baffle. Numerical validations are presented and results at several kHz are shown for a submarine application.

4:40

1pSAa11. Enhanced coupled mechanical-acoustic field computations on nonmatching grids. Simon Triebenbacher (Univ. Erlangen-Nuremberg, Dept. of Sensor Technology, Paul-Gordan-Str. 3/5, 91052 Erlangen, Germany, simon.triebenbacher@lse.eei.uni-erlangen.de), Manfred Kaltenbacher (Univ. Erlangen-Nuremberg, Dept. of Sensor Technology, Paul-Gordan-Str. 3/5, 91052 Erlangen, Germany, manfred.kaltenbacher@lse.eei.uni-erlangen.de), Martin Meiler (Simetris GmbH, Am Weichselgarten 7, 91058 Erlangen, Germany, martin.meiler@simetris.de), Hermann Landes (Simetris GmbH, Am Weichselgarten 7, 91058 Erlangen, Germany, hermann.landes@simetris.de)

In this work we extend our research on nonmatching finite element grids, as used in the analysis of coupled mechanical-acoustic systems, from standard (bi-)linear grids to higher order Lagrangian grids. In practical applications, such as the simulation of thin membranes, the use of higher order finite elements is often advantageous to prevent locking effects. For the comparison of the radiated sound from a loudspeaker with measurements an acoustic propagation domain is required which is very large in relation to the size of the speaker. To keep the number of unknowns in this domain low the discretization should be chosen as coarse as possible without becoming susceptible to numerical dispersion. Due to the same reason it is also desirable to use a uniform discretization and to be able to adjust the approximation order. To gain more flexibility, we introduce a nonmatching interface between the subdomains and discretize them independently, both in space and approximation order. Our enhanced scheme applies the mortar finite element method to coupled mechanical-acoustic field problems. We demonstrate the applicability of our approach to practical applications. We analyze the system response of an electrodynamic loudspeaker and the sound radiation of an electric transformer.

5:00

1pSAa12. Comparison of numerical techniques for the vibro-acoustic behaviour of a flexible structure. Yvon Goth (CETIM, 52 av Felix Louat, BP 80067, F-60304 Senlis Cedex, France, yvon.goth@cetim.fr)

The tractors bonnets are large flexible parts that radiate noise under the excitation of the forces exerted on the contact points and the sound pressure fluctuations coming from the engine. The vibro-acoustic behaviour of such a bonnet, excited by local forces or a diffuse pressure field, has been computed using various techniques: - In the low frequency domain, the finite element method has been used to compute the structural behaviour, while the acoustic radiation has been computed by using the boundary element method and the finite element method with approximated boundary conditions to simulate the free field conditions. - In the high frequency domain, the computation has been made using the SEA method, with an approximation of the radiation coefficients. -In the medium frequency domain, both techniques have been used and compared. Software used where VA-One, from ESI, and Code-Aster, from EDF. The paper presents the numerical results obtained, associated to the computing time. Approximated methods can be largely faster than 'exact' ones (finite elements associated with boundary elements) and, for engineering use, represent a good compromise between quality and efficiency.

5:20

1pSAa13. Structure-borne modeling of a vehicle in the mid-frequency range using Virtual SEA: experimental validation. Denis Thenail (PSA Peugeot Citroën, Route de Gisy, 78943 Vélizy-Villacoublay Cedex, France, denis.thenail@mpsa.com), Julien Baratier (Faurecia AST, Center of Acoustic Technology, Dämmstoffwerk 100, 38524 Sassenburg, Germany, julien.baratier@faurecia.com), Arnaud Duval (Faurecia AST, Center of Acoustic Technology, Dämmstoffwerk 100, 38524 Sassenburg, Germany, arnaud.duval@faurecia.com), Gérard Borello (InterAC, 10 impasse Borde-Basse, ZA. La Violette, 31240 L'Union, France, gerard.borello@interac.fr), Laurent Gagliardini (PSA Peugeot Citroën, Route de Gisy, 78943 Vélizy-Villacoublay Cedex, France, laurent.gagliardini@mpsa.com)

Virtual SEA is a modeling process using FE computations to build an SEA model including equivalent masses, modal densities, and CLF, but excluding DLF since damping modeling in the mid-high frequency range is still an open issue. This technique, previously proposed by some of the authors, is applied to a production vehicle in the range 200-1000 Hz. The actual vehicle is simultaneously measured at a subset of the FE nodes. The automated sub-structuring provided by Virtual SEA (20 subsystems at 630Hz) is used to favorably position 64 sensors on the body. Next, an experimental SEA procedure is performed: a full transfer matrix is measured between more than 1000 excitation (hammer) locations and the sensors. In order to compensate for structural heterogeneity, input mobilities are measured at every point and used to normalize the transfer matrix As all measurement points are associated to FE nodes, computed input mobilities can be compared to measurements. Finally, the SEA model identification is carried out for both experimental and virtual SEA. As far as damping (DLF) can only be known experimentally, comparisons of the numerical and experimental approach only concern the orher SEA parameters (CLFs, modal densities ...) and transfer functions.

5:40

1pSAa14. Measurement of SEA damping loss factor for complex structures. Maxime Bolduc (Univ. de Sherbrooke, Mechanical Engineering Depart., 2500 Boulevard de l'Université, Sherbrooke, QC J1K 2R1, Canada, maxime.bolduc@usherbrooke.ca), Noureddine Atalla (Univ. de Sherbrooke, Mechanical Engineering Depart., 2500 Boulevard de l'Université, Sherbrooke, QC J1K 2R1, Canada, Nouredinne.Atalla@Usherbrooke.ca)

Statistical Energy Analysis has become extremely popular in the transportation industry. As a prediction tool, it offers appealing advantages such as its wide frequency range and short computational time, which conventional methods do not offer. Critical parameter in every SEA model, the

damping characteristics of the subsystems must be determined by way of experimentations. A variety of different techniques of measuring the damping loss factor were developed. These techniques can be divided into three main groups: (i) method based on the identification of modal damping by curve-fitting frequency response function, (ii) decay techniques based on-determination of the reverberation time and, (iii) steady-state techniques involving measurements of power input method much closely related to the definition of SEA since its starting point is the power balance. This work presents an experimental study of these techniques for various structures such as flat metallic panels, aircraft side walls (ribbed curved panels) and sandwich-composite panels in both low and high damping configurations (additions of damping materials, sound packages in both single wall and double wall configurations, mounting effects, ...). In particular, a critical discussion is made on the implementation, advantages and drawbacks of each method regarding its use in SEA modeling of complex structures.

6:00

1pSAa15. Transmission loss of a panel with tuned vibration absorbers. Carl Q. Howard (The University of Adelaide, School of Mechanical Engineering, North Terrace, 5005 Adelaide, Australia, carl.howard@adelaide.edu.au)

The transmission loss of a rectangular panel with numerous discrete tuned vibration absorbers is investigated both theoretically and experimentally. The 49 tuned vibration absorbers have a linear distribution of resonance frequencies and were arranged in grid pattern on the rectangular plate. The transmission loss of the plate was measured between two reverberation chambers and was compared with theoretical predictions. In addition, theoretical predictions and experimental measurements were conducted on a similar system where each vibration absorber was replaced with the equivalent mass of the absorber. The numerical computations were conducted on a distributed computing network comprising 200 desktop computers. The results indicate the improvement in sound transmission loss that can be achieved, greater than merely increasing the thickness of the panel (mass law), and also provides a data set for comparison with predictions involving the use of fuzzy-structure theory.

6:20

1pSAa16. A 'concatenation' study of wave energy transport among three coupled plates. Nick Wolff (Dept. of Mechanical Science and Engineering, University of Illinois, 1206 W Green St. MC 244, Urbana, IL 61801, USA, nlwolff@uiuc.edu), Richard Weaver (Dept. of Physics, University of Illinois, Urbana, IL 61801, USA, r-weaver@uiuc.edu)

We address the problem of constructing predictions for the diffuse transport and distribution of mean spectral acoustic energy density in an undamped complex linear structure, without appeal to SEA and by taking information gleaned from short time cost-effective, direct numerical simulations (DNS). A numerical model is constructed consisting of three finite plates coupled by sets of springs. Coupling is chosen to be sufficiently strong to avoid localization and sufficiently weak that the notion of substructures remains valid. Numerical simulations of transient responses to each of several sources are carried out; responses are recorded at each of several receivers. The resulting time-domain diffuse waveforms are analyzed for the work done at each source, and the transient spectral energy density at each receiver at times shortly after the action of the sources. This information is used in a 'concatenation' ansatz to predict the evolution and distribution of spectral energy density at these receivers at later times. The resulting prediction is compared favorably with the actual energy densities observed in the DNS at late times. It is described how the results also apply directly to the more conventional but closely related problem of damped systems and/or steady state input. Work supported by NSF CMS-0528096.

6:40

1pSAa17. Modification of an interface parameter between sub-system and vehicle: case of a fan system attached to the front end of a car. Saul Mapagha (CEVAA, Technopole du Madrillet, 2 Rue Joseph Fourier, 76800 Saint Etienne du Rouvray, France, s.mapagha@cevaa.com), Vincent Martin(Institut Jean Le Rond d'Alembert, UMR CNRS 7190, UPMC, 2 Place de la Gare de Ceinture, 78210 Saint-Cyr l'Ecole, France, vmartin@ccr.jussieu.fr)

The car industry, as well as many others, is constantly undergoing modifications to comply security and comfort regulations. Among the major causes for concern is the integration of sub-systems on vehicles. In fact, when a sub-system runs on a vehicle, it can lead to vibrations on the body of the car and thus acoustical radiations, causing trouble for the passengers, and also outside the vehicle. The frequency response functions (FRF)-based substructuring technique and impedances coupling methods are used to predict the forces entering the vehicle from those measured on a test bed. When a given constraint on the forces entering the vehicle is not satisfied, the car supplier may choose to modify the interface parameters between the substructures. In this paper an analytical approach to filter the entering forces by elastic suspension is proposed. An application is given by way of numerical experiments on a fan system attached to the front end of a car, both subsystems being identified through measurements.

7:00

1pSAa18. Sound radiation induced force vibration of submerged and fluid filled multilayered spherical shell. Sadeq Malakooti (Acoustics Research Laboratory, Dept. of Mechanical Engineering, Iran University of Science and Technology, Narmak, 16844 Tehran, Iran, s_malakooti@mecheng.iust.ac.ir), Seyyed M. Hasheminejad (Acoustics Research Laboratory, Dept. of Mechanical Engineering, Iran University of Science and Technology, Narmak, 16844 Tehran, Iran, hashemi@iust.ac.ir), Nader Mohammadi (Univ. of Tehran, School of Mechanical Engineering, 1439957131 Tehran, Iran, nmohamady@ut.ac.ir)

Nowadays sound radiation from spherical shells is attracted for aviation industry. In this paper, the general approach is presented for predicting a coupled fluid solid interaction problem. Therefore, a fully elasticity solution is applied in conjunction with laminated shell model for considering of the sound field over the shell. For each plies the elasticity coefficients are assumed to be constant. The main objectives of this work are investigating the influence of internal and external acoustic mediums and also radially inhomogeneity on acoustic performance of the spherical shell. Numerical results are presented for a three layered spherical shell. For each excitation frequency, sound pressure over zenith angle in polar coordinate is plotted. Also pressure levels against excitation frequency for resonance spectroscopy are investigated.

7:20

1pSAa19. Particular analysis of vibration energy transmission in connections of thin plates. Jacek Cieslik (AGH-UST University of Science and Technology, Al. Mickiewicza 30, 30-059 Krakow, Poland, cieslik@agh.edu.pl)

Analyses of energy balance in the mechanical systems are done by the quantitative and qualitative assessment. Qualitative assessment is possibly by the use of energy flow descriptors and observation of energy density distribution in the mechanical structure. The work presents the results of investigation of welded connections of rectangular steel plates. The aim of the analysis was the quantitative estimation of vibrational energy transmitted though the welded connection depending on the inclination angle of plates. The structural intensity was used as the parameter for the analysis. Method of structural intensity evaluation enabled the elaboration of intensity vector field. Unification of shape and size of finite elements made possible the summation of only the magnitude of intensity. Summation was performed in the plate's cross sections far from the places of excitation and the damping. The detailed information on vibration energy flow was achieved. The obtained results of calculation give the quantitative information on amount of energy transmitted, reflected and the damped in welded joints of plates. The analyzed case was intentional to show the utility of intensity method in diagnostics of joints in mechanical constructions. The calculation results were verified experimentally with application of thermograph measurements of stress and vibration velocity.

Session 1pSAb

Structural Acoustics and Vibration and EURONOISE: General Topics in Structural Acoustics and Vibration I

Wolfgang Kropp, Cochair
Chalmers University of Technology, Division of Applied Acoustics, Gothenburg, SE-41296, Sweden

Sean Wu, Cochair
Wayne State Univ., 5050 Anthony Wayne Dr., Detroit, MI 48202, USA

Contributed Papers

1:00

1pSAb1. Efficient computation of the radiated sound power of vibrating structures using a modal approach. Nicolas Roy (Top Modal, 5, rue de la ZA de Ribaute, 31130 Quint-Fonsegrives, France, nicolas.roy@topmodal.fr), Marc Lapi (DGA/DCE/CTSN, Site du Mourillon, BP 28, 83800 Toulon Armées, France, marc.lapi@dga.defense.gouv.fr)

The optimal design of structures in terms of noise control is of great interest in many fields such as automotive, aerospace, and naval. Since design strategies require simple design parameters, the sound power is often used to characterize the sound radiated from a structure. The CTSN in collaboration with TOP MODAL has recently developed a software tool to efficiently compute the radiated sound power of a vibrating structure using modes obtained by finite element analysis. The modal analysis has been enhanced to take into account the presence of fluid cavities and damping elements via the introduction of residual modes. The radiated sound power is computed from the volume velocities of the vibrating surface using a lumped parameter method requiring no explicit modeling of the acoustic medium. The modal contributions to the total sound power may also be calculated. The underlying methods are described including the improved coupled fluid-structure modal analysis and the computation of the radiated sound power. Next an overview of the tool's architecture is presented. Finally, several industrial applications are presented to illustrate the features and interest of the tool.

1:20

1pSAb2. High resolution modal analysis. Kerem Ege (Laboratoire de Mécanique des Solides, Ecole Polytechnique, 91128 Palaiseau Cedex, France, kerem.ege@lms.polytechnique.fr), Xavier Boutillon (Laboratoire de Mécanique des Solides, Ecole Polytechnique, 91128 Palaiseau Cedex, France, boutillon@lms.polytechnique.fr), Bertrand David (Télécom Paristech (ENST) / TSI - CNRS LTCI, 46, rue Barrault, 75634 Paris Cedex 13, France, bertrand.david@enst.fr)

The Fourier-transform-based traditional modal analysis techniques perform poorly when modal overlap η exceeds 30%, due to the $\Delta T.\Delta f$ limitation. In view of filling the gap between the low- and the high-frequency domains where modal analysis and statistical methods respectively apply, a technique based on the high resolution analysis algorithm ESPRIT (Roy & Kailath, IEEE Transactions on Acoustics Speech and Signal Processing, **37**(7), 984-995, 1989) has been developed. A pulselike force is repeatedly applied to the structure and the response is measured in a number of points. In each point, the impulse response of the structure is retrieved by deconvolving the pulselike force and filtering the response with the result. In a second step, the number of modes in the reconstructed impulse response is evaluated by the novel procedure ESTER (Badeau et al., IEEE Transactions on Signal Processing, **54**(2), 450-458, 2006) and various preconditioning techniques are applied. The ESPRIT algorithm finally extracts the modal frequencies, damping factors, and complex amplitudes at each point. Two applications are presented: the separation of twin modes of a square plate ($\eta = 200\%$) and the partial modal analysis of a $1620 \times 1000 \times 5$ mm aluminum plate up to a modal overlap $\eta = 70\%$.

1:40

1pSAb3. Vibration of a submarine hull under harmonic propeller-shaft excitation. Mauro Caresta (University of New South Wales, 2052 Sydney, Australia, maurorestaca@yahoo.it), Nicole J. Kessissoglou (University of New South Wales, 2052 Sydney, Australia, n.kessissoglou@unsw.edu.au)

A model to describe the dynamic response of submarine hull to a harmonic propeller shaft excitation is presented. The submarine is modeled as a ring stiffened cylindrical shell, with bulkheads and end caps. The stiffeners are introduced using a smeared approach. The bulkheads are modeled as circular plates with in plane and bending motion, and the end closures are modeled as truncated conical shells. External fluid loading is introduced to take into account the interaction of the structure with the acoustic medium. The propeller introduces a harmonic varying force in both the axial and transverse directions. The force is transmitted to the structure through the shaft that is connected to the end plate of the cylindrical hull and supported by the conical end cap. The axial component excites the axisymmetric modes of the structure. The transverse force component excites the hull through the conical shell and excites the higher circumferential modes. Since these modes are mainly flexure in nature, they can result in a high noise signature level. Results are presented in terms of FRFs calculated analytically and compare the axisymmetric vibration caused by the axial excitation and the asymmetric response due to the transverse component of the force.

2:00

1pSAb4. Application of guided flexural waves in immersed plates to aquatic propulsion of mono-hull marine vessels. Victor V. Krylov (Loughborough University, Department of Aeronautical and Automotive Engineering, Ashby Road, LE11 3TU Loughborough, UK, V.V.Krylov@lboro.ac.uk), Ewan Porteous (Loughborough University, Department of Aeronautical and Automotive Engineering, Ashby Road, LE11 3TU Loughborough, UK, wan2001@hotmail.com)

The present paper describes the results of the experimental investigation of a small-scale mono-hull model boat propelled by a localised flexural wave propagating along the plate of finite width forming the boat's keel. Forward propulsion of the boat was achieved through flexural wave propagation in the opposite direction, which is similar to the aquatic propulsion used in nature by stingrays. The model boat under consideration underwent a series of tests both in a Perspex water tank and in the experimental pool. In particular, the forward velocity of the boat has been measured for different frequencies and amplitudes of the flexural wave. The highest velocity achieved was 32 cm/s. The thrust and propulsive efficiency have been measured as well. The obtained value of the propulsive efficiency in the optimum regime was 51%. This indicates that efficiency of this type of aquatic propulsion is comparable to that of dolphins and sharks (around 75%) and to that of a traditional propeller (around 70%). In contrast to a propeller though, the wavelike aquatic propulsion has the following advantages: it does not generate underwater noise and it is safe for people and marine animals.

2:20

1pSAb5. The structural acoustic properties of stiffened shells. Yu Luan (DTU, Building 352, Oersted. DTU, 2800 Lyngby, Denmark, yl @oersted.dtu.dk)

Plates stiffened with ribs can be modeled as homogeneous isotropic or orthotropic plates, and modeling such an equivalent plate numerically with, say, the finite element method is, of course, far more economical in terms of computer resources than modelling the complete, stiffened plate. This is important when a number of stiffened plates are combined in a complicated structure composed of many plates. However, whereas the equivalent plate theory is well established there is no similar established theory for stiffened shells. This paper investigates the mechanical and structural acoustic properties of curved shells with stiffening ribs. Finite element simulations and experimental data will be compared and discussed.

2:40

1pSAb6. Multi-bay double panel system with heterogeneous blanket treatment: A comparison between theory and experiment. Kamal Idrisi (Virginia Tech, Mechanical Engineering, 143 Durham 0238, Blacksburg, VA 24061, USA, idrisi@vt.edu), Marty Johnson (Virginia Tech, Mechanical Engineering, 143 Durham 0238, Blacksburg, VA 24061, USA, martyj@vt.edu), Alessandro Toso (Virginia Tech, Mechanical Engineering, 143 Durham 0238, Blacksburg, VA 24061, USA, aletoso@vt.edu)

This study is part of an effort to improve the low frequency performance of acoustic blankets used to reduce the noise inside aircraft cabins. This is achieved by embedding small masses inside the poro-elastic layer such that they act like distributed mass spring damper systems. These mass-spring-damper systems can then be designed to reduce the sound transmission through the double panel system at low frequencies where traditional poro-elastic materials have little effect. A mathematical model of a multi-bay double panel system with frames, stringers, an acoustic cavity and porous-/mass layer was developed using impedance and mobility methods (IMM). The multi-bay double panel system includes four skin pockets with four HG blankets of different dimensions such that the interaction between the panels can be analyzed. The predicted responses of the source and receiver panel due to a point force are validated with experimental measurements. The results indicate that proper tuning of the mass insertions can improve the broadband noise reduction below 500 Hz with less than 10% added mass without losing the performance of the acoustic foam at high frequencies.

3:00

1pSAb7. Acoustic radiation from vibrating panels subject to high-frequency broadband excitation. Donald B. Bliss (Duke University, Mechanical Engineering and Materials Science, 148B Hudson Hall, Durham, NC 27708, USA, dbb@duke.edu), Linda P. Franzoni (Duke University, Mechanical Engineering and Materials Science, 148B Hudson Hall, Durham, NC 27708, USA, franzoni@duke.edu)

Radiation from a baffled panel subject to high-frequency broadband excitation is studied. If the panel flexural waves are subsonic, the radiation comes from edges. For supersonic waves the entire surface is important. Characterization of the radiation is surprisingly straightforward in the high-frequency broadband limit, with simple analytical expressions for directivity patterns. For subsonic waves, a series expansion of the surface velocity wave number transform, convergent in the radiating region, can be reinterpreted physically as singularity functions along the panel perimeter, namely the delta function and its derivatives. This interpretation leads to monopole, dipole, and higher-order edge radiators with relative strengths that depend on surface-wave Mach number. Both propagating and evanescent structural waves contribute to the radiation. A proper physical explanation of the radiation is provided both in physical space and transform space. The common interpretation of edge radiation in terms of uncancelled volumetric sources is not correct; the higher order edge singularities are very significant. For low structural damping, this approach leads to a very simple way to calculate the radiated field. The relationship between radiation and structural power flow is potentially useful in energy-intensity based prediction methods with application to vehicle interior noise. (Sponsor NSF)

3:20

1pSAb8. Active noise control at a moving location in a modally dense three-dimensional sound field using virtual sensing. Danielle J. Moreau (The University of Adelaide, School of Mechanical Engineering, North Terrace, 5005 Adelaide, Australia, danielle.moreau@adelaide.edu.au), Ben S. Cazzolato (The University of Adelaide, School of Mechanical Engineering, North Terrace, 5005 Adelaide, Australia, benjamin.cazzolato@adelaide.edu.au), Anthony C. Zander (The University of Adelaide, School of Mechanical Engineering, North Terrace, 5005 Adelaide, Australia, anthony.zander@adelaide.edu.au)

Local active noise control systems generate a zone of quiet at the physical error sensor using secondary sources to cancel the acoustic pressure at the sensor location. The resulting zone of quiet is generally limited in size and as such, placement of the physical error sensor at the location of desired attenuation is required, which is often inconvenient. Virtual acoustic sensors overcome this by projecting the zone of quiet away from the physical error sensor to a remote location. While virtual acoustic sensors have shown potential to improve the performance of local active noise control systems, it is, however, likely that the desired location of maximum attenuation is not spatially fixed. The work described here presents a virtual sensing method capable of tracking a desired location in a modally dense three-dimensional sound field. The developed algorithm has been experimentally verified in a three-dimensional enclosure and the experimental results are presented.

3:40

1pSAb9. Active modal control in rooms - practical approach. Pierre-Jean Rene (Acoustical Engineering & Research, Ch. de la Vuachère, 20D, 1012 Lausanne, Switzerland, pjrene@a-e-r.ch), Hervé Lissek (Ecole Polytechnique Fédérale de Lausanne, EPFL STI LEMA, Station 11, CH 1015 Lausanne, Switzerland, herve.lissek@epfl.ch)

Engineers dealing with noise reduction in habitations close to transportation traffic or industrial facilities encounter several problems to decrease noise level in rooms at low frequencies. Passive materials and current building construction knowledge enable to avoid noise transmission in habitations at medium and high frequencies and the regulations based on the dBA scale can often be respected. But these regulations do not take into account the real unpleasantness of noise for the inhabitants who are still disturbed by low frequency noise. Because of the modal behavior of rooms, air-borne and structure-borne noise generate high sound pressure level at the first modal frequencies, even with small amount of energy. The aim of this work is to decrease noise level in rooms at these specific and most annoying frequencies. Usual techniques of room acoustics and acoustic insulation reach their limits and cannot be improved due to cost and volume constraints. To reach our goal, active modal control seems to be the best way. The principle of the AMC is to decrease only the 2 or 3 first modal frequencies with a unique microphone-controller-loudspeaker system. Several results are presented for different excitations and room configurations. The controller setup has to be the more autonomous and flexible system as possible.

4:00-4:20 Break

4:20

1pSAb10. Resonant frequencies of a cantilevered timoshenko beam with an attached general point-connected vibratory system. Robert M. Koch (NUWC, 1176 Howell Street, Code 8232, Bldg. 1302, Newport, RI 02841-1708, USA, kochrm@npt.nuwc.navy.mil)

The literature is full of technical papers that have examined the free vibration of cantilevered Bernoulli-Euler beams with both rigidly and elastically-attached point masses at the free end. Additionally, much work has been published in the last ten years on cantilevered Timoshenko beams (which includes the effects of shear deformation and rotatory inertia) with a similar, yet more restricted, set of free end boundary conditions. Rossit and Laura published in the Journal of the Acoustical Society of America in 2001 a formulation for a Timoshenko beam with a simple single DOF spring-mass system attached to the free end. The present paper extends Rossit and Laura's mathematical formulation to account for a general, damped, multi-

DOF system point-connected to a cantilevered Timoshenko beam's free end. To demonstrate the formulation, mathematical relations and numerical results for a single DOF damped system and both damped/undamped 2DOF vibration absorbers are presented.

4:40

1pSAb11. Damage detection in composite laminates using coin-tap method. Sung Joon Kim (Korea Aerospace Research Institute, 45 Eoeun-Dong, Youseong-Gu, 305-333 Daejeon, Republic of Korea, yaelin@kari.re.kr)

The ″coin-tap″ test has the ability to indicate damage in a composite structural element due to a localized change of stiffness. The change in vibration signature may be detected by ear or more precisely by measurement of the dynamic contact force. It has been shown that the characteristics of radiated sound from a structure during a tap are changed by the presence of defect beneath the surface of the composite structure. For structurally radiated noise, the sound field is directly coupled to the structural motion. Therefore, impact response analysis should be computed. In this study, the radiated sound induced by impact is obtained by solving the Rayleigh integral equation. Experimental results for the delaminated composite structure are presented and correlations between analytical predictions and measured data are shown. It is shown that the sound based tap test is useful and practical diagnostic tool for detecting localized delamination in composite laminates

5:00

1pSAb12. Identification of noise sources by means of inverse finite element method using measured data. Matthias Weber (Helmut-Schmidt-Universität - Universität der Bundeswehr Hamburg, Holstenhofweg 85, 22043 Hamburg, Germany, mweber@hsuhh.de), Thomas Kletschkowski (Helmut-Schmidt-Universität - Universität der Bundeswehr Hamburg, Holstenhofweg 85, 22043 Hamburg, Germany, thomas.kletschkowski@hsuhh.de), Delf Sachau (Helmut-Schmidt-Universität - Universität der Bundeswehr Hamburg, Holstenhofweg 85, 22043 Hamburg, Germany, sachau@hsuhh.de)

Identification of noise sources in airplane cabins proves to be difficult particularly at low frequencies. A new approach reconstructs the spatial distribution of sound pressure and particle velocity based on the inverse finite element (FE) method. This procedure requires measurements in the cavity of the cabin. If all sound sources are located on the boundary of the cabin, the equation system resulting from a matching FE model can be resorted in such way that computation of the unknown boundary data is possible, even with distorted measurement data. The method is explained using a simplified 2D laboratory experiment consisting of a flat sound-hard bounded rectangle with a loudspeaker included in the boundary. A corresponding FE model with given boundary conditions is verified by mapping the sound pressure in the test bed. The inner part of the measurement data is used to compute the boundary values. Regularization methods are applied to find an optimal solution. To prepare a verification of this technique in real world conditions, the sound field in the cavity of an airplane mock-up (Airbus A340) exited by both an interior and exterior noise source is mapped with a custom-built microphone array. Taking advantage of the results of the 2D examination, the current status of this verification process is shown.

5:20

1pSAb13. Reconstruction of Rayleigh-Lamb dispersion spectrum based on noise obtained from an air-jet forcing. Eric Larose (LGIT - CNRS - Université Joseph Fourier, Maison des Géosciences, 1381 rue de la Piscine, BP 53, 38041 Grenoble, France, Eric.Larose@obs.ujf-grenoble.fr), Philippe Roux (LGIT - CNRS - Université Joseph Fourier, Maison des Géosciences, 1381 rue de la Piscine, BP 53, 38041 Grenoble, France, philippe.roux@obs.ujf-grenoble.fr), Michel Campillo (LGIT - CNRS - Université Joseph Fourier, Maison des Géosciences, 1381 rue de la Piscine, BP 53, 38041 Grenoble, France, Michel.Campillo@obs.ujf-grenoble.fr)

The time-domain cross-correlation of incoherent and random noise recorded by a series of passive sensors contains the impulse response of the medium between these sensors. By using noise generated by a can of compressed air sprayed on the surface of a plexiglass plate, we are able to reconstruct not only the time of flight but the whole waveforms between the sensors. From the reconstruction of the direct A_0 and S_0 waves, we derive the dispersion curves of the flexural waves, thus estimating the mechanical properties of the material without a conventional electromechanical source. The dense array of receivers employed here allow a precise frequency-wave number study of flexural waves, along with a thorough evaluation of the rate of convergence of the correlation with respect to the record length, the frequency, and the distance between the receivers. The reconstruction of the actual amplitude and attenuation of the impulse response is also addressed in this paper [Larose et al, J. Acoust. Soc. Am **122** (2007)].

5:40

1pSAb14. Interaction of a pair of complex dynamical systems under impact conditions. Joseph F. Vignola (Catholic University, 620 Michigan Ave., Washington, DC 20064, USA, vignola@cua.edu), John A. Judge (Catholic University, 620 Michigan Ave., Washington, DC 20064, USA, judge@cua.edu), John McCoy (Catholic University, 620 Michigan Ave., Washington, DC 20064, USA, mccoy@cua.edu)

An important class of complex dynamical systems has members that are comprised of a dominant simple system, made complex by attaching a large number of significantly less massive subsystems. The response of such systems to a simple forcing that acts on the dominant system has received considerable attention. A simple forcing is understood here to be represented by a time series that has very limited support when represented in either temporal or spectral space. Little attention has be paid to the response of such systems to a complex forcing, understood to be one represented by a time series that has extended support when represented in both temporal and spectral spaces. In the reported study, the interaction of two systems drawn from the described class, under impact conditions are investigated. Significantly, the action of each system on the other during the time interval of their contact is represented by an interaction force that is complex in the sense described. The investigation is accomplished via numerical simulation, physical experiments and analysis.

6:00

1pSAb15. Reduction of radiated sound from a continuum using low-damping vibration absorbers. Zenzo Yamaguchi (Kobe Steel, Ltd., 1-5-5, Takatsukadai, Nishi-ku, 651-2271 Kobe, Hyogo, Japan, zyamaguc@purdue.edu), Akio Sugimoto (Kobe Steel, Ltd., 1-5-5, Takatsukadai, Nishi-ku, 651-2271 Kobe, Hyogo, Japan, sugimoto.akio@kobelco.com), Yoshio Yano (Kobe Steel, Ltd., 1-5-5, Takatsukadai, Nishi-ku, 651-2271 Kobe, Hyogo, Japan, yano.yoshio@kobelco.com), J. Stuart Bolton (Ray W. Herrick Labs., School of Mech. Eng., Purdue University, 140 S. Martin Jischke Drive, West Lafayette, IN 47907-2031, USA, bolton@purdue.edu)

When reducing the sound radiated from a resonant structure, it is necessary to ensure that the driving frequency does not correspond to any of the system resonance frequencies. In addition, it may be desirable to use dynamic vibration absorbers to reduce the response at the driving frequency. In this paper, a low-damping vibration absorber is studied for solving noise radiation problems from a resonant, light-gauge structure driven by a force whose frequency and amplitude are constant and whose frequency does not match any of the system natural frequencies. When the driving frequency and the structure's natural frequency are different, the structure cannot be represented by as a SDOF system. Therefore, the conventional design method, based on equivalent mass, is inapplicable. In this paper, a design method based on the mobility of the structure is proposed. By means of the proposed method, the sound power radiated from a simply supported beam with an attached absorber is calculated and it leads to the following results: 1) When the absorber is installed at the driving point, it reduces the sound power as predicted; 2) An increase in radiated noise may occur when the absorber is not installed at the driving point.

6:20

1pSAb16. A fluid level sensor using A0 Lamb wave mode. Fouad Boubenider (University of Science and Technology Houari Boumediene (USTHB), Laboratoire de Physique des Matériaux BP32, El Alia 16111, DZ Alger, Algeria, fboubenider@yahoo.fr)

The aim of this study was to examine the feasibility of creating a fluid level sensor operating in A0 Lamb wave mode. The experimental sensor is composed of a plate of stainless steel 1.3 meters high, in which, an A0 Lamb wave mode is generated. The choices of the material, the plate thickness and the wave vibration mode are all important. We therefore plotted the phase and group velocity curves, and the transversal and longitudinal displacements versus the product frequency x thickness. These curves enabled us to visualize the best target point for the excitation energy on a suitably guided wave mode at an appropriate frequency; this point is referred to as the operating point. When the chosen wave mode is generated, the echo from the reflection at the guide-water interface is easily detected by the transmitter-receiver transducer and can be worked efficiently.

MONDAY AFTERNOON, 30 JUNE 2008 ROOM 240, 1:00 TO 4:00 P.M.

Session 1pSCa

Speech Communication: Speech Technology I

Deliang Wang, Chair
Ohio State University, Department of Computer Science & Engineering, 2015 Neil Ave., Columbus, OH 43210, USA

Contributed Papers

1:00

1pSCa1. Automatic testing of speech understanding. Tom Francart (ExpORL, Dept. Neurosciences, K.U. Leuven, Herestraat 49 bus 721, O. & N2, B-3000 Leuven, Belgium, tom.francart@med.kuleuven.be), Marc Moonen (ESAT/SISTA, K.U. Leuven, Kasteelpark Arenberg 10, B-3001 Leuven, Belgium, marc.moonen@esat.kuleuven.be), Jan Wouters (ExpORL, Dept. Neurosciences, K.U. Leuven, Herestraat 49 bus 721, O. & N2, B-3000 Leuven, Belgium, jan.wouters@med.kuleuven.be)

Speech reception tests are commonly administered by manually scoring the oral response of the test subject. This requires a test supervisor to be continuously present, which can be avoided by having the subject type the response on a computer keyboard and automatically scoring the response. However, spelling errors may then be counted as recognition errors, and hence influence the test results. We demonstrate an autocorrection approach based on two scoring algorithms to cope with spelling errors. The first algorithm deals with sentences and is based on word score. The second algorithm deals with single words and is based on phoneme score. Both algorithms are evaluated with a corpus of typed answers based on three different Dutch speech materials. The percentage of differences between the autocorrection algorithm and the manual correction was calculated, in addition to the mean difference in speech recognition threshold between automatic and manual scoring. The sentence correction algorithm performed at higher accuracy than commonly obtained with these speech materials. The word correction algorithm performed better than the human operator. Both algorithms can be used in practice and allow speech reception tests with open set speech materials over the internet.

1:20

1pSCa2. A comparison between two methods for speech transmission quality assessment with noise simulation at receiver's side. Marcel Wältermann (Deutsche Telekom Laboratories, Berlin Institute of Technology, Ernst-Reuter-Platz 7, 10587 Berlin, Germany, marcel.waeltermann@telekom.de), Nicolas Côté (France Télécom, 2 avenue Pierre Marzin, 22300 Lannion, France, nicolas.cote@orange-ftgroup.com), Alexander Raake (Deutsche Telekom Laboratories, Berlin Institute of Technology, Ernst-Reuter-Platz 7, 10587 Berlin, Germany, alexander.raake@telekom.de), Sebastian Möller (Deutsche Telekom Laboratories, Berlin Institute of Technology, Ernst-Reuter-Platz 7, 10587 Berlin, Germany, sebastian.moeller@telekom.de)

Two auditory experiments are presented that were designed in order to compare two different methods for the assessment of speech quality when noise at listener's side is present: (1) Headphone presentation with samples pre-recorded over a head and torso simulator, and (2) test participants located in a noisy environment, rendered by a 4.1 loudspeaker system. Real-world types of background noise were employed as well as a variety of user terminals. The correlation between corresponding overall quality scores amounts to $r = 0.9$. Hence, a headphone presentation can replace a loudspeaker noise simulation in principle, leading to the consequence that a simpler experimental set-up is sufficient for assessing the speech quality when noise is present at the receiver's side. However, there exist certain differences between both quality scores. For example, in most cases clean wideband (50-7000 Hz) and standard narrow-band (300-3400 Hz) speech are rated slightly lower if the samples are presented over a headphone and noise is simultaneously present. Since the separation between speech and noise is potentially easier when the noise is played back over loudspeakers, participants may mainly judge the speech rather than the overall quality, leading to higher scores for the clean channel conditions.

1:40

1pSCa3. Predicting speech quality under noise in wideband speech transmission. Juan-Pablo Ramirez (Deutsche Telekom Laboratories, Berlin Institute of Technology, Ernst-Reuter-Platz 7, 10587 Berlin, Germany, juan-pablo.ramirez@telekom.de), Alexander Raake (Deutsche Telekom Laboratories, Berlin Institute of Technology, Ernst-Reuter-Platz 7, 10587 Berlin, Germany, alexander.raake@telekom.de), Marcel Wältermann (Deutsche Telekom Laboratories, Berlin Institute of Technology, Ernst-Reuter-Platz 7, 10587 Berlin, Germany, marcel.waeltermann@telekom.de), Sebastian Möller (Deutsche Telekom Laboratories, Berlin Institute of Technology, Ernst-Reuter-Platz 7, 10587 Berlin, Germany, sebastian.moeller@telekom.de)

Prediction of users' opinion of speech quality in telecommunication is of a major issue in speech transmission planning. For this purpose, reliable models, such as the E-model (ITU-T Rec. G.107, 2005) were developed for narrow-band (NB) transmission. Meanwhile, telephony using the Internet Protocol (VoIP) has enabled an enlargement of the transmission band, introducing wideband (WB; 50-7000 Hz and beyond) to every day communication. The quality improvement thanks to the bandwidth extension was found to be 29%, as compared with NB [3]. Consequently, an updated planning model is required to assess quality in WB speech transmission. We performed two listening only tests to study the quality impairment due to signal attenuation, different noise types and level and various codecs. The tests showed that user's quality perception in case of WB was similar to NB for the noisy conditions. However, considerably higher judgments were given to WB than to NB for the low-noised conditions. With increasing noise level, the quality of NB and WB become more and

more alike, and quality differences between codecs decrease. Following the lines of thoughts of the E-model, we propose a model assessing the quality impairment in WB speech transmission resulting from noise and/or signal attenuation.

2:00

1pSCa4. Effect of degradations' distribution in a corpus test on auditory ratings. Nicolas Côté (France Télécom, 2 avenue Pierre Marzin, 22300 Lannion, France, nicolas.cote@orange-ftgroup.com), Virginie Durin (France Télécom, 2 avenue Pierre Marzin, 22300 Lannion, France, virginie.durin@orange-ftgroup.com)

Speech quality of telecommunications systems is usually evaluated thanks to auditory tests, which must be carried out in accordance with ITU-T Recommendations. In these tests, subjects are asked to assess the quality of speech sample by giving a score on a five-level scale. The averaging of subjects' scores yields the Mean Opinion Score (MOS) which represents the speech quality for a given condition. However, MOS values can be strongly influenced by many factors. In this paper, we focus on a specific bias: the distribution of the impairments in the stimuli set. In effect the rating of a narrow-band stimulus (300-3400 Hz) may have a lower quality score in a mixed-band set (mixed of narrow-band and wideband (50-7000 Hz) conditions) than in a purely narrow band set. This effect is detailed through results of auditory tests recently carried out. Consequently, the validity of MOS value is theoretically limited within a test which prevents MOS comparison between different tests. Finally, two solutions are proposed to avoid this effect: first, an improvement of auditory tests methodology and then, a new approach to assess speech quality, based on the subject's behaviour.

2:20

1pSCa5. Influence of informational content of background noise on speech quality evaluation for VoIP application. Adrien Leman (France Telecom, 2, Avenue Pierre Marzin, 22300 Lannion, France, adrien.leman@orange-ftgroup.com), Julien Faure (France Telecom, 2, Avenue Pierre Marzin, 22300 Lannion, France, julien.faure@orange-ftgroup.com), Etienne Parizet (Laboratoire Vibrations Acoustique, Insa Lyon, 25 bis, av. J. Capelle, 69621 Villeurbanne Cedex, France, etienne.parizet@insa-lyon.fr)

With the rise of mobile communication systems, the background noise in the speaker's environment and its interaction with VoIP network impairment affects speech quality perception. This effect should be taken into account in nonintrusive models in order to improve accuracy of end user perception measurement. The aim of this study is to determine the impact of information contained in background noise (background speech, environmental sources) on speech quality perception. A subjective test on the speech quality perception in real network conditions has been done comparing the effect of stationary background noise mainly due to transmission equipment (electrical humming or blowing noises) with the effect of nonstationary environmental noise (public place, traffic noise, background conversation). Interactions between these different background noise condition and realistic network impairments (coders and packets loss) were also studied. The speech quality was evaluated through the Mean Opinion Score determined from an Absolute Category Rating method.

2:40

1pSCa6. Speech perception in noise with binary gains. Deliang Wang (Ohio State University, Department of Computer Science and Engineering, 2015 Neil Ave., Columbus, OH 43210, USA, dwang@cse.ohio-state.edu), Ulrik Kjems (Oticon A/S, Kongebakken 9, DK-2765 Smørum, Denmark, uk@Oticon.dk), Michael S. Pedersen (Oticon A/S, Kongebakken 9, DK-2765 Smørum, Denmark, msp@Oticon.dk), Jesper B. Boldt (Oticon A/S, Kongebakken 9, DK-2765 Smørum, Denmark, jeb@Oticon.dk), Thomas Lunner (Oticon Research Centre Eriksholm, Kongevejen 243, DK-3070 Snekkersten, Denmark, TLU @Oticon.dk)

For a given mixture of speech and noise, an ideal binary time-frequency mask is constructed by whether SNR within individual time-frequency units exceeds a local SNR criterion (LC). With linear filters, co-reducing mixture SNR and LC does not alter the ideal binary mask. Taking this manipulation to the limit by setting both mixture SNR and LC to minus infinity produces an output that contains only noise with no target speech at all. This particular output corresponds to turning on or off the filtered noise according to a pattern prescribed by the ideal binary mask. Our study was designed to test on speech intelligibility of noise gated by the ideal binary mask obtained this way. It is observed that listeners achieve nearly perfect speech recognition from gated noise. Only sixteen filter channels and a frame rate of one hundred Hertz are sufficient for high intelligibility. The results show that, despite a dramatic reduction of speech information, a pattern of binary gains provides an adequate basis for speech perception in noise.

3:00

1pSCa7. Low-dimensional, auditory feature vectors that improve vocal-tract-length normalization in automatic speech recognition. Jessica J. Monaghan (Centre for the Neural Basis of Hearing, Department of Physiology, Development and Neuroscience, University of Cambridge, Downing Site, CB23EG Cambridge, UK, jjmm2@cam.ac.uk), Christian Feldbauer (Centre for the Neural Basis of Hearing, Department of Physiology, Development and Neuroscience, University of Cambridge, Downing Site, CB23EG Cambridge, UK, feldbauer@tugraz.at), Tom C. Walters (Centre for the Neural Basis of Hearing, Department of Physiology, Development and Neuroscience, University of Cambridge, Downing Site, CB23EG Cambridge, UK, tcw24@cam.ac.uk), Roy D. Patterson (Centre for the Neural Basis of Hearing, Department of Physiology, Development and Neuroscience, University of Cambridge, Downing Site, CB23EG Cambridge, UK, rdp1@cam.ac.uk)

Human speech recognition is robust to large changes in vocal tract length (VTL) but automatic speech recognition is not. In an effort to improve VTL normalization, an auditory model was used to derive formant-like features from syllables. The robustness supported by these auditory features was compared to the robustness provided by traditional MFCCs (Mel-Frequency Cepstral Coefficients), using a standard HMM recognizer (Hidden-Markov-Model). The speech database consisted of 180 syllables, each scaled with the vocoder STRAIGHT to have a wide range VTLs and glottal pulse rates. Training took place with syllables from a small, central range of scale values. When tested on the full range of scaled syllables, average performance for MFCC-based recognition was 73.5%, with performance falling close to 0% for syllables with extreme VTL values. The feature vectors constructed with the auditory model led to much better performance; the average for the full range of scaled syllables was 91%, and performance never fell below 65% even for extreme combinations of VTL and GPR. Moreover the auditory feature vectors contain just 12 features whereas the standard MFCC vectors contain 39 features. Research supported by the UK-MRC (G0500221) and EOARD (FA8655-05-1-3043).

3:20

1pSCa8. A Portable robot audition software system for multiple simultaneous speech signals. Hiroshi G. Okuno (Kyoto University, Graduate School of Informatics, Yoshida-Honmachi, Sakyo, 606-8501 Kyoto, Japan, okuno@i.kyoto-u.ac.jp), Shunichi Yamamoto (Kyoto University, Graduate School of Informatics, Yoshida-Honmachi, Sakyo, 606-8501 Kyoto, Japan, shunichi@kuis.kyoto-u.ac.jp), Kazuhiro Nakadai (Honda Research Institute Japan Co., Ltd., 8-1 Honcho, Wako, 351-0114 Saitama, Japan, nakadai@jp.honda-ri.com), Jean-Marc Valin (CSIRO ICT Center, Cnr Vimiera & Pembroke Rds, NSW 2122 Marsfield, Australia, jean-marc.valin@csiro.au), Tetsuya Ogata (Kyoto University, Graduate School of Informatics, Yoshida-Honmachi, Sakyo, 606-8501 Kyoto, Japan, ogata@kuis.kyoto-u.ac.jp), Kazunori Komatani (Kyoto University, Graduate School of Informatics, Yoshida-Honmachi, Sakyo, 606-8501 Kyoto, Japan, komatani@kuis.kyoto-u.ac.jp)

Since a robot is deployed in various kinds of environments, the robot audition system should work with minimum prior information on environments to localize, separate and recognize utterances by multiple simultaneous talkers. For example, it should not assume either the number of speakers, the location of speakers for sound source separation (SSS), or specially

tuned acoustic model for automatic speech recognition (ASR). We developed a portable robot audition that uses eight microphones installed on the surface of robot's body such as Honda ASIMO, and SIG-2 and Robovie-R2 at Kyoto University with different microphone configurations. The system integrates SSS and ASR by using the Missing-Feature Theory. For SSS, we use Geometric Source Separation (GSS) [Parra 2002] and multichannel post-filter [Cohen 2002] to separate each utterance. Since separated speech signals are distorted due to interfering talkers and sound source separation, multichannel post-filter enhanced speech signals. At this process, we create a missing feature mask that specifies which acoustic features are reliable in time-frequency domain. Multiband Julius [Nishimura 2004], a missing-feature-theory based ASR, uses this mask to avoid the influence of unreliable features in recognizing such distorted speech signals. The system demonstrated a waitress that accepts meal orders placed by three actual human talkers and a voice ″Rock-Scissors-Paper″ game referee that decides who wins the game.

3:40

1pSCa9. Ambiguity in the recognition of phonetic vowels when using a bone conduction microphone. Véronique Zimpfer (ISL, 5 rue du Général Cassagnou BP 70034, 68301 Saint Louis, France, veronique.zimpfer@isl.eu),Karl Buck(French German Institut of Saint Louis (ISL), 5 rue du Général Cassagnou, 68301 Saint-Louis, France, karl.buck@isl.eu)

When speaking, not only air conducted noise is generated, but also vibrations can be recorded at different places on the head using accelerometers. The bone conduction microphones are less sensitive to noise than regular acoustical microphones, they are usable in harsh environments and they are compatible with head equipment such as NBC protection devices. This paper reports the first results of a study designed to evaluate the differences in perception between speech recorded via a acoustic microphone and speech recorded using bone conduction. These differences may cause of a bad intelligibility of bone conduction communication, even if presented in an undisturbed environment. We study the recognition of ten French phonetic vowels recorded by a bone conduction microphone. A listening test is designed to show the confusions of phonetic vowels when listening to speech picked up by an air or bone conduction microphone. The tests show confusion between the vowels [i] [y] [u]. All of these have the frequency of their first formant in common. The sonograms are distinctly different when recorded with an aero-acoustic microphone, become almost identical if the bone conducted speech is analyzed. Moreover, the confusions of the phonetic vowels depend on the speaker.

MONDAY AFTERNOON, 30 JUNE 2008 ROOM 250B, 1:00 TO 4:00 P.M.

Session 1pSCb

Speech Communication: Measurement of Sociophonetic Variation in Speech

Ewa Jacewicz, Cochair
The Ohio State University, 110 Pressey Hall, 1070 Carmack Road, Columbus, OH 43210, USA

Jonathan Harrington, Cochair
Institute of Phonetics and Speech Processing, University of Munich, Munich, 80799, Germany

Invited Papers

1:00

1pSCb1. Inter- and intra-speaker variation: some methodological consequences for sociophonetic research. Gerard J. Docherty (Newcastle University, School of ECLS, KG VI Building, NE3 1YB Newcastle upon Tyne, UK, g.j.docherty@ncl.ac.uk), Paul Foulkes (University of York, Department of Language & Linguistic Science, Heslington, YO10 5DD York, UK, pf11@york.ac.uk)

In recent years there has been a rapidly growing awareness of the importance of sociophonetic variation for advancing models of speech production, perception and learning. Meanwhile within sociolinguistic research there has been an equally rapidly evolving recognition that full accounts of the social marking functions of speech communication require greater focus on the manner in which individuals deploy phonetic resources variably as a reflection of the fluid identities which they project across the diverse interactions which they participate in. The aim of this talk is to explore some of the methodological consequences of these developments. We explore the ways in which an approach to sociophonetic variation which rightly focuses on how it plays out in the performance of individual speakers can be reconciled with the development of models of speech production and perception which to date have typically been driven by what is found to be common across individual speakers/listeners and much less by those factors which differentiate them.

1:20

1pSCb2. Sociophonetic methods for studying substratal effects and new dialect formation. Erik R. Thomas (North Carolina State University, Department of English, Box 8105, Raleigh, NC 27695-8105, USA, ethomas@social.chass.ncsu.edu)

Studies of substratal effects in the formation of new language varieties have seldom combined both acoustic sophistication and the examination of a broad suite of pronunciation features. This study provides an example of how such work can be conducted. The study focuses on Pearsall, Texas, a community in southern Texas in which Mexican Americans have formed an established community for four generations and exhibit a shift from Spanish dominance to English dominance. A variety of segmental and prosodic variables are examined, both for different generations of Mexican Americans and for Anglo speakers of the contact dialect, and the variables are compared statistically. Results show that some Spanish interference features are discarded, while others take on a life of their own as markers of Mexican American identity.

1:40

1pSCb3. Modeling dialect-related variability in American English plosives. Thomas Purnell (University of Wisconsin, 1168 Van Hise, 1220 Linden Drive, Madison, WI 53706, USA, tcpurnell@wisc.edu)

Socially motivated variation in speech often lies in the differential use of phenomena described in identical or near-identical terms. This paper investigates the hypothesis that dialect differences may result from the relative distribution of an acoustic characteristic with respect to trading relations with other co-varying characteristics, or by variations in the characteristic within regions of linguistic stability. Plosive variation among European American and African American English speakers in the upper Midwest is examined. Speakers from both dialect groups may produce plosives instead of interdental fricatives in syllable initial position, and devoice or glottalize apical plosives in syllable final position. Additionally, speakers of both dialects have been observed to hypervoice voiced plosives word-initially. The current experiment explores the boundary characteristics of a trading relations model within the plosive system of both dialect groups. The specific question addressed by the paper is whether the range of plosive variation suggests a shared property of nonstandard dialects, or whether the relation among acoustic measures is dialect specific. Results are discussed in light of acoustic, perceptual and categorical stability.

2:00

1pSCb4. The acoustic and perceptual bases of diachronic /u:/-fronting in Standard Southern British. Jonathan Harrington (Institute of Phonetics and Speech Processing, University of Munich, 80799 Munich, Germany, jmh@phonetik.uni-muenchen.de), Felicitas Kleber (Institute of Phonetics and Speech Processing, University of Munich, 80799 Munich, Germany, kleber@phonetik.uni-muenchen.de), Ulrich Reubold (Institute of Phonetics and Speech Processing, University of Munich, 80799 Munich, Germany, reubold@phonetik.uni-muenchen.de)

In a recent experiment concerned with diachronic /u:/-fronting in Standard Southern British, it was shown both that the /u:/ category boundary was perceptually retracted for older compared with younger listeners of this variety, and that they compensated perceptually to a greater extent for the coarticulatory fronting effects of the preceding consonant on /u:/ in words like used. In the present study, these perceptual differences were related to the same speakers' productions of words containing a /u:/ nucleus in a fronting (e.g., 'used') and non-fronting (e.g., 'swoop') contexts. The relative acoustic distance of /u:/ between front and back vowels was measured in a three-dimensional space formed by applying the discrete-cosine-transformation to the entire F2-trajectory shape separately for each speaker. Compatibly with their perceptual responses, older listeners had a more retracted /u:/ on this measure and exhibited a greater coarticulatory influence of the preceding consonant. The mechanism of this sound change is considered both from the point of view of a shift in the perceptual compensation for coarticulation and recent developments in episodic models of speech perception

2:20

1pSCb5. Speech processing and dialect variation in the American Midwest. Cynthia G. Clopper (Ohio State University, 1712 Neil Ave, Oxley Hall 222, Columbus, OH 43210, USA, clopper.1@osu.edu)

The Midwestern United States is divided into two dialect regions: North and Midland. The Northern dialect is characterized by the clockwise rotation of the low and low-mid vowels in the acoustic-phonetic vowel space. The Midland dialect is characterized by back vowel fronting and the merger of the low back vowels. A series of experiments exploring the effects of dialect variation on spoken word recognition has revealed systematic linguistic processing costs associated with these dialect-based vowel system differences for Midwestern listeners. While word recognition performance in noise is equally accurate for both dialects, the patterns of errors that listeners produce reveal systematic confusions between phonologically different vowels that overlap in the acoustic-phonetic space across the two dialects. In addition, speeded lexical classification performance is highly accurate for both dialects, but performance is slower for Northern vowels than Midland vowels of the same phonological class. The results from these studies suggest that even in the absence of striking intelligibility differences between the two dialects, processing costs associated with the perception of dialect variation can be observed using traditional speech perception and spoken word recognition tasks.

2:40

1pSCb6. Analysis of total vowel space areas in three regional dialects of American English. Robert A. Fox (The Ohio State University, 110 Pressey Hall, 1070 Carmack Road, Columbus, OH 43210, USA, fox.2@osu.edu), Ewa Jacewicz (The Ohio State University, 110 Pressey Hall, 1070 Carmack Road, Columbus, OH 43210, USA, jacewicz.1@osu.edu)

The acoustic characteristics of vowel systems in different varieties of American English are greatly affected by regional variation. Given the significant positional differences of vowels within the acoustic space across regional dialects of English, one should expect that the size and extent of the vowel space is also affected by this type of variation. Traditionally, the size of the acoustic vowel space has been measured as the triangular area defined by the three corner vowels. An obvious weakness of this approach is that it underestimates the actual ″working space″ of vowel system in that the onsets and/or offsets of other vowels are often found outside this triangular area. This paper proposes a procedure to estimate the area of a complete vowel space, taking into account dynamic formant pattern of all vowels and diphthongs. Complete vowel space areas are calculated for individual speakers and compared across three distinct regional varieties (representing Inland North, Southern Appalachian, and a Midland variety). The comparison also examines possible changes to vowel space area as a function of speaker generation (younger and older adults).

3:00

1pSCb7. Regional variation in vowels and vowel systems: normalization and optimization. Roeland Van Hout (Department of Linguistics - Radboud University, Post Box 9103, 6500 HD Nijmegen, Netherlands, hout@let.ru.nl)

We made an acoustical description of regional variation patterns in the vowel system of Dutch spoken in the Netherlands and Flanders. The speech material consisted of read monosyllabic utterances in a neutral consonantal context, representing the vowels of

Dutch. A discriminant analysis applied on the raw measurements to classify each speaker into one of the eight regions involved (sociogeographic variation) gave a correct regional classification for 72.0% of the 160 speakers. When normalization procedures were applied, the percentages of proper classification increase to 82.5%. Several questions have to be answered though. Which normalization procedure is the best one and why, and how can we be sure that specific parts of sociophonetic variation are not distorted by the normalization procedure? We will present additional materials collected on the same set of speakers in reading aloud a strictly controlled list of words containing all Dutch vowels in different consonantal contexts. Another question is how to reduce the amount of information used in a normalization procedure. The z transformation (Lobanov) performs well, but is rather expensive in the amount of information needed. Can we minimize the information needed and yet uncover the patterns of sociophonetic variation?

3:20

1pSCb8. A new speaker-intrinsic vowel formant frequency normalization algorithm for sociophonetics. Anne Fabricius (Roskilde University, Department of Culture and Identity, Postboks 260, DK4000 Roskilde, Denmark, fabri@ruc.dk), Dominic Watt (University of York, Department of Language & Linguistic Science, Heslington, YO10 5DD York, UK, dw539@york.ac.uk)

This paper evaluates the strengths and weaknesses of a speaker-intrinsic vowel formant frequency normalization algorithm initially proposed in Watt and Fabricius (2002) and modeled by Thomas and Kendall (2007) for direct comparison with other normalization algorithms. We evaluate the merits of the new routine as a sociophonetic research tool relative to those of two well-known speaker-intrinsic methods documented in Lobanov (1971) and Nearey (1977) through comparisons of the values of two parameters: degree of overlap of vowel spaces and vowel space area ratios. Measurements of angles and Euclidean distances between pairs of points in the vowel space (a method presented in Fabricius 2007) also provide a comparative parameter revealing how different algorithms model the vowel space. The study uses two existing datasets: 1) a corpus of RP vowels compiled from Hawkins and Midgley (2005) and Moreiras (2006) and 2) previously unpublished data from Aberdeen, northeast Scotland.

3:40

1pSCb9. Stability and variation in the pronunciation of French: A corpus-based approach. Jacques Durand (Laboratoire Cognition, Langues, Langage, Ergonomie (CLLE), Université Toulouse - Le Mirail & CNRS, 5, Allées Antonio Machado, 31058 Toulouse, France, jacques.durand@univ-tlse2.fr), Noel Nguyen (LPL, Aix-Marseille Université & CNRS, 29, avenue Robert Schuman, 13100 Aix-en-Provence, France, Noel.Nguyen@lpl-aix.fr)

This contribution relates to the project ″La Phonologie du Français Contemporain″ (PFC), the largest and most ambitious survey of modern French ever conceived. The PFC project involves over thirty researchers from a variety of countries and aims at the recording, partial transcription and phonetic analysis of over 600 speakers from the francophone world. It aims at a broad coverage of varieties of contemporary French by selecting groups of speakers from approximately 60 different locations in the francophone world. So far around 600 speakers have already been recorded in various parts of the francophone world beside France, including Belgium, Burkina Fasso, Canada, Côte d'Ivoire, Louisianne, and Switzerland. The recordings involve formal and informal conversation, the reading aloud of a word-list and a passage. Current work conducted on the database ranges from auditory exploitation of the data to automatic speech recognition via classical experimental phonetics. We address theoretical and empirical issues related to liaison as well as vowel systems, and examine sociogeographical variation and changes in progress in these respects within French, using a variety of quantitative methods for the empirical assessment of phonological hypotheses.

Session 1pSCc

Speech Communication: General Topics in Speech Communication I (Poster Session)

Erika Levy, Cochair
Biobehavioral Sciences, Teachers College, Columbia University, New York, NY 10027, USA

Susanne Fuchs, Cochair
ZAS, Schuetzenstr. 18, 10117 Berlin, Germany

Patti Adank, Cochair
F.C. Donders Centre for Cognitive Neuroimaging, University College London, London WC1N 3AR, UK

All posters will be on display from 4:20 p.m. to 6:00 p.m. To allow contributors an opportunity to see other posters, contributors of odd-numbered papers will be at their posters from 4:20 p.m. to 5:10 p.m. and contributors of even-numbered papers will be at their posters from 5:10 p.m. to 6:00 p.m.

Contributed Papers

1pSCc1. Acoustic validation of the analysis of diadochokinesis in normal speech using the motor speech profile program. Yu-Tsai Wang (National Yang-Ming University, School of Dentistry, Rm. 411, No. 155, Sec. 2, Li-Nong St. Beitou District, 11221 Taipei, Taiwan, yutsaiwang@ym.edu.tw), Yuh-Mei Chung (Dept. of Physical Medicine and Rehabilitation, Taipei Veterans General Hospital, No. 201, Sec. 2, Shih-Pai Rd., 11217 Taipei, Taiwan, ymchung@vghtpe.gov.tw), Ray D. Kent (Waisman Center, Rm. 435, University of Wisconsin-Madison, 1500 Highland Avenue, Madison, WI 53705-2280, USA, kentray@waisman.wisc.edu), Hsiu-Jung Lu (National Yang-Ming University, School of Dentistry, Rm. 411, No. 155, Sec. 2, Li-Nong St. Beitou District, 11221 Taipei, Taiwan, hsiujung_lu@hotmail.com)

The purpose of this study is to evaluate the suitability, reliability, and concurrent validity of the analysis of diadochochinesis (DDK) in normal speech using a computer program, Diadochokinetic Rate Analysis (DRA) in the KayPENTAX Motor Speech Profile. Fifteen healthy participants were recorded at UW-Madison as they repeated various syllables as quickly and steadily as possible. The DDK samples were executed by the DRA protocol to generate immediate quantitative information at different thresholds and were also hand-measured. When the lowest peak intensity during consonant-vowel syllables is lower than the highest peak intensity during intersyllable pauses, the DRA output is incorrect and the DDK sample is defined as nonexecutable. Analyses were based on the percentage of nonexecutable DDK samples and the comparisons of the results between repeated analyses at different thresholds and between automatic and manual measuring methods. Results: (1) One-ninth of the DDK samples was nonexecutable; (2) when the protocol was executable, the reliability at different thresholds and validity between different measuring methods were both satisfactory; and (3) the temporal variation between different measuring methods were larger than the intensity variation. Implications of the findings will be discussed in terms of the application of the DRA to general clinical purposes.

1pSCc2. Analysing cockpit and laboratory recordings to determine fatigue levels in pilots' voices. Claude Legros (Université de Toulouse-Le Mirail, Laboratoire d'Acoustique LAUTM, 5, allées Antonio Machado, 31058 Toulouse Cedex 1, France, legros@univ-tlse2.fr), Robert Ruiz (Université Toulouse II, LARA, 5 allée Antonio Machado, 31058 Toulouse Cedex, France, robert.ruiz@univ-tlse2.fr), Philippe Plantin De Hugues(Ministère des Transports, Bureau Enquêtes Analyses, 200 rue de Paris, Bât 153, Aéroport du Bourget, 93352 Le Bourget Cedex, France, plantindehugues@bea-fr.org)

Analysis of pilots' voices was undertaken under controlled laboratory conditions, using aeronautical terminology, standard professional equipment, and a standardized recording environment. The aim of the experiment was to determine the way the acoustic characteristics of the voice are modified after a phase of sleep. The results, which are presented in this paper, show very significant variations in the dispersion parameters, like jitters, associated with the fundamental frequency. In an aircraft cockpit, the electro-acoustic and environmental conditions are not so good. Therefore, it is essential to improve and adapt voice analysis methods to achieve reliable results. Cockpit Voice Recorder recordings have poor acoustic characteristics due to microphone quality and the signal to noise ratio, in addition to the non-predetermined vocabulary range. This paper will outline the modifications made to the laboratory methodology and the comparative results obtained, to improve the analysis of CVR recordings. Comparisons of the test recordings meant that it was feasible to determine, via voice analysis, the state of drowsiness of a pilot and, made possible the study of CVR recordings from accidents using new analytical techniques.

1pSCc3. The temporal location of rms peak in coarticulated vowels. Ewa Jacewicz (The Ohio State University, 110 Pressey Hall, 1070 Carmack Road, Columbus, OH 43210, USA, jacewicz.1@osu.edu), Robert A. Fox (The Ohio State University, 110 Pressey Hall, 1070 Carmack Road, Columbus, OH 43210, USA, fox.2@osu.edu)

The acoustic energy peak of the vowel, here defined as the rms peak, occurs typically before the temporal vowel midpoint. This study examines whether and how the location of the rms peak varies as a function of consonantal context and vowel duration. Four measures of rms peak location were explored: its distance (in ms) from vowel onset and from CVC-word onset (absolute measures) and its relative position (ranging from 0 to 100%) within the vowel and within the CVC-word (relative measures). Analysis of eight American English vowels produced in ten consonantal contexts by twenty speakers shows that the two relative measures yielded the most comparable and consistent patterns. The relative location of rms peak varied significantly as a function of consonantal context. It occurred earlier (i.e., closer to vowel or word onset) in the context of fricatives (and not stops), voiced consonants (as opposed to voiceless), and labials (as opposed to

alveolars). The temporal location of rms peak was also closer to the vowel onset (or word onset) for long vowels as opposed to short. Explanation of these patterns will be provided.

1pSCc4. Analysis of short-time speech transmission index algorithms. Karen Payton (ECE Dept., UMass Dartmouth, 285 Old Westport Rd., Dartmouth, MA 02747, USA, kpayton@umassd.edu), Mona Shrestha (ECE Dept., UMass Dartmouth, 285 Old Westport Rd., Dartmouth, MA 02747, USA, g_mshrestha@umassd.edu)

Various methods have been shown to compute the Speech Transmission Index (STI) using speech as a probe stimulus (Goldsworthy & Greenberg, J. Acoust. Soc. Am., **116**, 3679-3689, 2004). Frequency-domain methods, while accurate at predicting the long-term STI, cannot predict short-term changes due to fluctuating backgrounds. Time-domain methods also work well on long speech segments and have the added potential to be used for short-time analysis. This study investigates the accuracy of two time-domain STI methods: envelope regression (ER) and normalized correlation (NC), as functions of window length, in various acoustically degraded environments with multiple talkers and speaking styles. Short-time STIs are compared with a short-time Theoretical STI, derived from octave-band signal-to-noise ratios and reverberation times. For windows as short as 0.3 s, the ER and NC Methods track the short-time Theoretical STI and both the Theoretical and ER Methods converge to the long-term result for windows greater than 4 s. Short-time STIs are also compared to intelligibility measurements on clear/conversational speech. Correlations between STI and intelligibility scores are high at the sentence and word levels and, consistent with the scores, short-time methods predict a higher average value of STI for clear than for conversational speech.

1pSCc5. An acoustic investigation into coarticulation and speech motor control: high vs. low frequency syllables. Frank Herrmann (University of Sheffield, Human Communication Sciences, 31 Claremont Crescent, S10 2TA Sheffield, UK, F.Herrmann@Sheffield.ac.uk), Sandra P. Whiteside (University of Sheffield, Human Communication Sciences, 31 Claremont Crescent, S10 2TA Sheffield, UK, s.whiteside@sheffield.ac.uk), Stuart Cunningham (University of Sheffield, Human Communication Sciences, 31 Claremont Crescent, S10 2TA Sheffield, UK, s.cunningham@sheffield.ac.uk)

Levelt & Wheeldon's concept of the mental syllabary (1994) suggests that articulatory routines for syllables are stored in the form of gestural scores in a library. Cholin et al. (2006) found a syllable frequency effect on naming latency of nonsense words and interpret this as supporting evidence for the existence of such a syllabary. This paper presents a data set from a project investigating speech motor learning and coarticulation. Acoustic-based coarticulation measures, such as F2 locus equations, are used to indirectly determine the degree of gestural overlap in articulatory movements. Greater degrees of coarticulation can be indicators of cohesive articulatory gestures and therefore, motor speech skill. It is hypothesised that high frequency syllables, as well trained articulatory gestures, should exhibit a greater degree of coarticulation, less variation, and shorter duration times than low frequency syllables. Fifteen native speakers of English listened to, and repeated 16 mono-syllabic stimuli which belonged to either of two categories: high and low frequency (CELEX). Acoustic measurements included the transitions of the first three formants (C-to-V coarticulation), transition times and syllable duration. Patterns of coarticulation were quantified using F2 locus equations and the absolute changes in formant frequency. The results are presented and discussed.

1pSCc6. Segmental and supra-segmental contributions to cross-language speech intelligibility. Melanie Preece-Pinet (University College London, Department of Phonetics and Linguistics, 4, Stephenson Way, NW1 2HE London, UK, m.pinet@ucl.ac.uk), Paul Iverson (University College London, Department of Phonetics and Linguistics, 4, Stephenson Way, NW1 2HE London, UK, p.iverson@ucl.ac.uk)

Non-native accents affect speech recognition in noise, and previous work has shown that intelligibility is modulated by listener-talker interaction; a matched linguistic background between the two seems to maximise intelligibility. The present study examined the contribution of segmental and supra-segmental cues, as well as how the degree of L2 experience affects non-native speech perception. A group of monolingual native English listeners and two groups of French native listeners with different amounts of L2 experience were presented with English sentences produced by native and non-native (French) speakers in noise. The stimuli were digitally processed to swap the pitch and segment durations between recordings of the same sentences produced by different speakers (e.g., imposing a French-accented prosody onto recordings made from English speakers). The results revealed that English listeners were more accurate at recognizing speech with English segments but were little affected by prosody; low proficiency French listeners were more accurate when the speech had both French-accented segments and prosody; and high proficiency French listeners varied in the cues that they used depending on the noise level. The use of segmental and supra-segmental cues thus appears to vary with language experience and listening context.

1pSCc7. A multidimensional acoustic analysis of vowels in two Polish dialects. Wieslawa Cholewa (UMR 7018, CNRS/Univ. Paris III, 19, rue des Bernardins, 75005 Paris, France, Wieslawa.Cholewa@univ-paris3.fr), Charalampos Karypidis (UMR 7018, CNRS/Univ. Paris III, 19, rue des Bernardins, 75005 Paris, France, ch_karypidis@yahoo.com)

In this paper, we attempt to examine the acoustic (oral) vowel spaces of two main Polish dialects: the Polish spoken in Cracow and that spoken in the wider region of Warsaw. A semi-spontaneous corpus consisting of four speakers (two male, two female) of each dialect was recorded with approximately 2000 vowel occurrences for each speaker. The segmentation was performed manually and was subsequently corrected with an intensity-based algorithm. The tokens were submitted to acoustic analyses, and two multidimensional representations were then prepared, one based on formants (accompanied with bandwidths and amplitudes) and the other on critical bands. Both representations included measurements for duration, F0, spectral center of gravity, skewness, and kurtosis. These values served as input for discriminant and principal component analysis which allowed us: (a) to compare the relative weight of each cue, (b) to isolate those parameters that allow a differentiation of the members of a vowel system (in a language such as Polish, F1 and F2 are traditionally the sole cues regarded as relevant), and (c) to detect any (dis)similarities between the two dialects in the three aforementioned aspects.

1pSCc8. Automatic data enhancement for language identification using voice generation. Aaron Lawson (RADC, Inc., 525 Brooks Road, Rome, NY 13441, USA, aaron.lawson.ctr@rl.af.mil), Matthew Linderman (Air Force Research Laboratory, 525 Brooks Road, Rome, NY 13441, USA, matthew.linderman@gmail.com), Michael Carlin (Air Force Research Laboratory, 525 Brooks Road, Rome, NY 13441, USA, Michael.Carlin@rl.af.mil), Allen Stauffer (RADC, Inc., 525 Brooks Road, Rome, NY 13441, USA, stauffar@clarkson.edu)

Approaches to LID require very large sets of training (often greater than six hours per language) for accurate results. This study looks at ways of automatically reducing the amount of training data required to train a LID model, while maintaining or increasing accuracy. Initial experiments found that speaker density, i.e., the number of speakers per time unit, had a very dramatic influence on the accuracy of models (absolute increase of 15%). In order to accomplish the goal of increasing the number of speakers available for LID training without having to collect additional audio, the STRAIGHT algorithm was used to synthesize ″novel″ speakers for use in training language models for a LID system. The mean pitch and vocal tract length of the speaker in each LID training file was scaled to generate four additional voices per original speaker to artifically augment the training data. The resulting models yielded an improvement of 10% over the baseline system (from 80% to 90%). This study shows that automatically generated speakers

have a great impact on the accuracy of LID models, in this case an initial training set of 15 minutes per language was augmented and performed comparably to a set trained with six hours.

1pSCc9. Channel mitigation approach for automatic language identification. Allen Stauffer (RADC, Inc., 525 Brooks Road, Rome, NY 13441, USA, stauffar@clarkson.edu), Aaron Lawson (RADC, Inc., 525 Brooks Road, Rome, NY 13441, USA, aaron.lawson.ctr@rl.af.mil)

A major obstacle to overcome in language identification (LID) performance is the impact of varying channel conditions. In house experiments show that LID performance drops between 10-12% across channels. The focus of this project is to mitigate the impact of channel conditions and artifacts on LID, and to provide an understanding of how channel robust models may be created by combining data from across corpora. Our approach involved creating composite cross-channel language models from multiple corpora that were tested with data from three corpora whose results were compared to results obtained from same-channel and pure cross-channel experiments. Our hypotheses were that 1) same-channel models would be the most accurate, 2) purely cross-channel models would be considerably less accurate, and 3) composite model accuracy would fall in between that of the same-channel and cross-channel models. Results were surprising: while pure cross-channel tests performed the worst, with an average of 11% loss in accuracy, composite models outperformed matched condition models in tests by 0.5% to 15% for all four combinations tested. These findings provide evidence that cross-channel augmentation does not just make for more robust LID models across channel conditions, but improves model robustness within channel conditions as well.

1pSCc10. Newborn pain cry analysis based on pitch frequency tracking. Delphine Bard (Lund University, Division of Engineering Acoustics, John Ericsson väg 1, 221 00 Lund, Sweden, delphine.bard@acoustics.lth.se), Per Runefors (Department of Paediatrics, Växjö Hospital, 351 85 Växjö, Sweden, per.runefors@vaxjo.mail.telia.com), Einar Arnbjörnsson (Department of Paediatric Surgery, University Hospital Lund, 221 00 Lund, Sweden, einar.arnbjornsson@telia.com)

The aim of the newborn pain cry analysis is to test the hypothesis that cry can be used as a tool to detect signs of nocioceptive pain. Previous studies applying signal processing techniques to analyze the sound of these cries have been done. The subject of this paper is to adapt and improve the original method with the help of new signal processing methods. The pitch frequency is extracted from the waveform of the recorded babies' cries using time domain methods. The fluctuations of this parameter are analyzed in terms of jitter. In particular, a sliding buffer approach is presented, as well as an improvement of the Average Mean Difference Function (AMDF). Comparison between original and news results has been done.

1pSCc11. Age effects of pitch-shifted auditory feedback on reflexive and volitional voice F0 control. Kyoko Nagao (Center for Pediatric Auditory and Speech Sciences, Nemours Biomedical Reserach, A.I. du Pont Hospital for Children, 1600 Rockland Road, Wilmington, DE 19803, USA, nagao@asel.udel.edu), Katie E. McCurdy (Indiana University, Dept. of Speech and Hearing Sciences, 200 S Jordan Avenue, Bloomington, IN 47405, USA, kemccurd@indiana.edu), Theresa A. Burnett (Indiana University, Dept. of Speech and Hearing Sciences, 200 S Jordan Avenue, Bloomington, IN 47405, USA, burnett@indiana.edu)

Research on voice fundamental frequency (F0) control suggests that when making a voluntary vocal response to a pitch change in voice auditory feedback, the pitch-shift reflex typically occurs before the volitional response is initiated. The current study examined the effects of aging on reflexive and volitional voice F0 responses to pitch-shifted auditory feedback. Thirty participants (age range 19 to 78 years) repeatedly sustained an /u/ vocalization at a steady pitch and loudness while listening to their voice fed backed over headphones. Once per vocalization, feedback pitch was randomly shifted upward or downward for 100 milliseconds and 20 or 100 cents. In the Sustain condition, participants attempted to ignore the pitch change in auditory feedback voice. In the Follow condition, participants immediately changed their pitch in the same direction as the auditory pitch shift they heard. Preliminary results from thirteen participants indicate that there appears to be no effect of aging on the first F0 responses for both magnitude and latency. Voluntary voice F0 changes were delayed in older participants compared to younger participants as expected due to age-related general slowing. Results broaden our understanding of typical reflexive and volitional voice control capabilities across the age span.

1pSCc12. Do Japanese speakers perceive nonexistent vowels in non-native consonant clusters? Seiya Funatsu (The Prefectural Univ. of Hiroshima, 1-1-71 Ujinahigashi Minami-ku, 734-8558 Hiroshima, Japan, funatsu@pu-hiroshima.ac.jp), Satoshi Imaizumi (The Prefectural Univ. of Hiroshima, 1-1 Gakuen-machi, 723-0053 Mihara, Japan, imaizumi@pu-hiroshima.ac.jp), Masako Fujimoto (The National Inst. for Japanese Language, 10-2 Midori-machi, 190-8561 Tachikawa, Japan, mfuji@viola.ocn.ne.jp), Akira Hashizume (Hiroshima Univ., 1-2-3 Kasumi Minami-ku, 734-8553 Hiroshima, Japan, wj8uc6@bma.biglobe.ne.jp), Kaoru Kurisu (Hiroshima Univ., 1-2-3 Kasumi Minami-ku, 734-8553 Hiroshima, Japan, kuka422@hiroshima-u.ac.jp)

Vowel epenthesis is a well known phenomenon that non-native speakers insert epenthetic vowels inside non-native consonant clusters. Vowel epenthesis is assumed as perceptual ″illusory vowels″ (Dupoux et al. 1999). We analyzed vowel epenthesis shown by native Japanese speakers during reading and repetition tasks for non-native consonant clusters, and analyzed their brain responses using magnetoencephalographic methods. Under the reading task, in which subjects read English words and nonsense words, native Japanese speakers (eight females) inserted vowel /o/ after /t/ and /d/ in consonant clusters, and vowel /u/ after other consonants. Under the repetition task, in which subjects repeated utterances of a native English speaker, native Japanese speakers did not produce epenthetic vowels with few exceptions. The length of exceptional epenthetic vowels found under the repetition task was shorter than those under the reading task. The magnetoencephalographic mismatch responses were elicited by epenthetic vowels, suggesting that the native Japanese detected epenthetic vowels as real segments. Based on these results, we conclude that vowel epenthesis by native Japanese speakers did not arise from ″illusory vowels″, but rather from the difficulty of articulating consonant clusters which are not found in Japanese and/or Japanese phonological rules.

1pSCc13. Fine-phonetic variation in a computational model of word recognition. Odette Scharenborg (Centre for Language and Speech Technology, Radboud University Nijmegen, Erasmusplein 1, 6525 HT Nijmegen, Netherlands, O.Scharenborg@let.ru.nl)

There is now considerable evidence from psycholinguistic and phonetic research that fine-phonetic variation in the speech signal modulates human speech processing (HSP), and helps the listener segment a speech signal into syllables and words [e.g., Salverda et al., Cognition **90**, 51-89 (2003)]. This kind of information also appears to help the human perceptual system distinguish short words (like 'ham') from the longer words in which they are embedded (like 'hamster'). Salverda et al. showed that the lexical interpretation of an embedded sequence is related to its duration; a longer sequence tends to be interpreted as a monosyllabic word more often than a shorter one. Until recently, no computational models of HSP existed that are able to model this fine-phonetic variation [Hawkins, J. of Phonetics **31**, 373-405 (2003)]. In this paper, we present Fine-Tracker, a novel computational model of human word recognition that it is able to capture and use this fine-grained acoustic-phonetic variation during speech recognition. Simulations using the recordings from the listener experiments by Salverda et al. show that Fine-Tracker is able to capture and use duration variation in the speech signal to distinguish short words from the longer words in which they are embedded. [Research supported by NWO.]

1pSCc14. Lombard speech: effects of task and noise type. Youyi Lu (Sheffield University, Computer Science Department, Regent Court, 211 Portobello St., S1 4DP Sheffield, UK, y.lu@dcs.shef.ac.uk), Martin

Cooke(Sheffield University, Computer Science Department, Regent Court, 211 Portobello St., S1 4DP Sheffield, UK, m.cooke@dcs.shef.ac.uk)

An analysis of the effect of noise on speech production requires material recorded while undertaking realistic tasks in the presence of realistic noise backgrounds. This study examined speech produced in a number of types of ″noise″ in tasks with and without a communication factor. In one task, individual speakers were asked to speak aloud while solving ″sudoku″ puzzles, while in another task pairs of speakers solved these puzzles cooperatively. In both cases the background was quiet or contained one of three types of noise: competing talker, babble-modulated noise and speech-shaped noise. Individual digit words ″one″ to ″nine″ and speech/nonspeech sections were manually segmented for acoustic analysis. Both tasks produced Lombard effects observed in previous studies: increases in duration, energy, F0 and spectral centre of gravity. Relative to the non-communicative task, the presence of a communication factor led to words with shorter duration, more overall energy and higher spectral centre of gravity. Speakers actively avoided overlapping with the competing speech masker, with a stronger effect in the communicative task. These results suggest that speakers can, to some extent, compensate for both energetic and informational masking at the ears of the interlocutor.

1pSCc15. Differences in the time-course of accent adaptation: a comparison of adaptation to foreign-accented and unfamiliar regionally-accented speech. Bronwen G. Evans (Department of Phonetics and Linguistics, University College London, 4 Stephenson Way, NW12HE London, UK, bronwen.evans@ucl.ac.uk), Patti Adank (F.C. Donders Centre for Cognitive Neuroimaging, Kapittelweg 29, 6525EN Nijmegen, Netherlands, patti.adank@fcdonders.ru.nl)

Recent work in speech perception has demonstrated that listeners are able to rapidly adapt to foreign- accented speech (Clarke and Garrett, 2004). However, it is not clear whether adaptation to an unfamiliar regional accent operates in the same way. Although some studies have shown that listeners are able to adapt to different accents within the same language after only a short amount of exposure (e.g., Maye et al., in press), others have shown that listeners do not always alter their perceptual representations when listening to a non-native regional accent even if they are highly familiar with that accent (Evans and Iverson, 2004, 2007). In this study, we further explored perceptual adaptation to different accents by comparing the time course of adaptation to an unfamiliar regional accent with adaptation to foreign- accented speech. Listeners identified sentences in noise produced in either an unfamiliar regional accent (Glaswegian) or foreign-accented speech (Spanish-accented English). Preliminary results suggest a different pattern of adaptation for each accent: although listeners show greater adaptation to foreign- accented speech, they perform more poorly with foreign-accented speech overall and the rate of adaptation is slower.

1pSCc16. Production of Parisian French front rounded vowels by second-language learners. Erika S. Levy (Teachers College, Columbia University, Biobehavioral Sciences, Box 180, 525 W120th St., New York, NY 10027, USA, elevy@tc.columbia.edu), Franzo Law (CUNY Graduate Center, 365 5th Avenue, Program in Speech-Language-Hearing Sciences, New York, NY 10016, USA, flaw@gc.cuny.edu)

This study examined the effects of language experience and consonantal context on the production of Parisian French (PF) vowels by American English (AE) learners of French. A repetition task was performed, involving French vowels /y-œ-i-a-u/ uttered by a native speaker of Parisian French (PF) in bilabial /bVp/ and alveolar /dVt/ contexts embedded in the nonsense word/phrase /raCVCa/. Three groups of native AE speakers participated: speakers without French experience (NoExp), speakers with formal French experience (ModExp), and speakers with formal and extensive immersion experience (HiExp). Production accuracy was assessed by native PF listeners' judgments and by acoustic analysis. Native PF listeners identified second-language (L2) learners' productions more accurately as a function of speakers' increased language experience, although /u/, /y/ and /œ/, even produced by the HiExp group, were frequently misidentified. A consonantal context effect was revealed, including /u/ being misidentified more often in alveolar context than in bilabial context by all three groups. Overall, all groups distinguished front rounded /y/ from /u/ in production, but often in a non-native manner, e.g., producing /y/ as /ju/. Individual differences, interactions between consonantal context and vowels, as well as implications for the perception-production link in L2 learning, are discussed.

1pSCc17. Development of assisting system for learning Chinese aspirated sounds. Akemi Hoshino (Toyama College of Maritime Technology, Ebie, Neria, 933-0293 Imizu, Toyama Prefecture, Japan, hoshino@toyama-cmt.ac.jp), Jianwu Dang (Japan Advanced Institute of Science and Technology, 1-1 Asahidai, Nomi, 923-1292 Ishikawa, Japan, jdang@jaist.ac.jp), Akio Yasuda (Tokyo University of Marine Science and Technology, 2-1-6 Etchujima, 135-8533 Tokyo, Japan, yasuda@kaiyodai.ac.jp)

Chinese aspirates are generally difficult for Japanese to pronounce and perceive. In order to assist Japanese students to learn Chinese, the authors attempt to build a system to automatically evaluate the pronunciation of Chinese aspirates by Japanese students. To do so, this study analyzed 21 single-vowel syllables of six different Chinese aspirates, bilabial, alveolar, velar, palatal, retroflex, and dental using two evaluation parameters: the voice onset time (VOT) and mean breathing power during VOT. The speech materials were uttered by nine Japanese students and nine native Chinese speakers. It is found that for a give aspirate, the longer the VOT is, the better the score is, as is generally said. But we found that an aspirate with a larger breathing power acquires good mark even with a shorter VOT in a certain range of VOT. The testing results showed that a combination of these two parameters can distinguish aspirated and unaspirated sounds quite well. To achieve an assisting system, we developed a method to automatically detect the VOT. To detect the burst of an aspirate, a filter bank was used to measure signal energy in frequency domain, and the burst timing was determined.

1pSCc18. Articulatory perturbation due to ultrasound imaging: an acoustic analysis. Rachael-Anne Knight (City University, Department of Language and Communication Science, Northampton Square, EC1V 0HB London, UK, knight@city.ac.uk), Christina Villafana Dalcher (City University, Department of Language and Communication Science, Northampton Square, EC1V 0HB London, UK, cvdalcher@mac.com), Mark J. Jones (University of Cambridge, Phonetics Lab, Department of Linguistics, Raised Faculty Building, Sidgwick Avenue, CB3 9DA Cambridge, UK, markjjones@hotmail.com)

A safe, non-invasive imaging technique which captures articulatory movements in real time is the Holy Grail of articulatory analysis. Ultrasound imaging of the tongue seems suitable, albeit for a single articulator. However, ultrasound requires positioning a probe under the chin which may inhibit jaw movement. It is well known that speakers compensate rapidly for similar articulatory perturbations such as bite-blocks. Consequently, the images obtained by ultrasound may show compensatory articulations due to jaw inhibition, rather than natural articulations. This study assesses the effects of articulatory compensation during ultrasound imaging using acoustic analysis. The experiment compares acoustic data from three speech conditions: probe-free, probe held manually, probe fixed non-manually. It is hypothesised that sounds requiring a low jaw position, such as low vowels, velars, and velarised laterals, will be worst affected. High jaw sounds such as /s/ and /i/ are also assessed. Any differences between conditions are assumed to be due to compensation for jaw immobility rather than learned segment-specific register effects and are therefore unlikely to diminish as the subjects relax. Variability may diminish, however, as compensatory strategies become more practised. We expect to find some effects on certain segments, but that manual probe holding allows for more natural speech.

1pSCc19. Cortical mechanisms of speech perception in noise in elderly listeners. Edward R. Lee (Northwestern University, 860 Hinman Ave., Apartment 715, Evanston, IL 60202, USA, EdwardLee86@gmail.com), Patrick C. Wong (Northwestern University, 2240 Campus Drive, Evanston, IL 60208, USA, pwong@northwestern.edu), Sumitrajit Dhar (Northwestern University, 2240 Campus Drive, Evanston, IL 60208, USA, s-dhar@northwestern.edu), Geshri M. Gunesekera (Northwestern

University, 2240 Campus Drive, Evanston, IL 60208, USA, geshri-g@northwestern.edu), Rebekah A. Abel (Northwestern University, 2240 Campus Drive, Evanston, IL 60208, USA, r-abel@northwestern.edu)

The present study examines the cerebral hemodynamics (measured by fMRI) associated with listening to speech in noise in elderly listeners with relatively normal peripheral hearing. We asked subjects to identify single words in quiet and in two multi-talker babble noise conditions (+20 and -5 dB SNRs). The behavioral results indicated that subjects performed similarly between the Quiet and +20 SNR conditions, both in accuracy and reaction time, but were less accurate and responded slower in the -5 SNR condition. There were performance-independent and SNR-dependent effects in the brain. A contrast of the +20 SNR and Quiet conditions revealed bilateral (especially left) auditory and prefrontal activation in noise despite equal behavioral performance (performance-independent but noise-dependent activations). As noise increased and behavioral performance decreased (as in the -5 SNR condition), activation in these regions increased. These results reveal a cortical network involving acoustic analysis, working memory, and auditory attention associated with speech perception in noise by the elderly. [Work supported by NIH.]

1pSCc20. Computer simulations of intraoral pressure patterns during voiced stop consonant production. Jorge C. Lucero (Univ. Brasilia, Dept. Mathematics, 70910-900 Brasilia - DF, Brazil, lucero@unb.br), Laura L. Koenig (Haskins Labs. and Long Island Univ., Brooklyn, New York, NY 11201-8423, USA, koenig@haskins.yale.edu)

Several past studies have used laryngeal and/or upper vocal tract models to explore aerodynamic control during production of obstruent consonants, yet many aspects of such control remain unclear. Of particular interest in this work is how varying laryngeal and vocal tract dimensions such as occur among men, women, and children influence phonatory behavior and the time course of intraoral pressure (Pio) increase during voiced stop consonant production. To maintain phonation during a voiced stop closure, Pio must remain below the subglottal pressure. Physiological and modeling studies indicate that adult speakers actively increase supraglottal volumes during voiced stops, which slows the rate of Pio increase. Speakers with smaller vocal tracts may either be less successful in slowing the rate of Pio buildup, or else may perform more extreme volumetric changes to achieve similar end results. The current study uses data recently collected on voicing and Pio during stop production in men, women, and children. We use a modified two-mass model of the vocal folds coupled to a model of the upper vocal tract to reproduce the observed Pio patterns, and explore how the behavior of the system reflects differences in anatomical and physiological dimensions. [Work supported by MCT/CNPq-Brazil.]

1pSCc21. The production of Mandarin and American English vowels by Mandarin-speakers. Jia-Shiou Liao (Department of Applied Foreign Languages, Chung Shan Medical University, No.100, Sec. 2, Dah-Ching St., 402 Taichung, Taiwan, jsliao@csmu.edu.tw)

This study examines whether there is any correspondence between how Mandarin-speakers pronounce Mandarin vowels and how they pronounce those vowels' English equivalents and non-equivalents. Twenty Mandarin graduate students, who spoke English as a second language and had stayed continuously in America for at least two years, produced a series of American English vowels in /hVd/ contexts from a randomly ordered list. To approximate English syllable structure, they also read a list of /hVdV/ syllables containing Mandarin vowels in the first syllable. The vowel in the second syllable is always a schwa. First- (F1) and second-formant (F2) values of each Mandarin and English vowel were analyzed. The statistical results suggest that the distances between the Mandarin corner vowels in the vowel space are similar to those between the English ones. The acoustic characteristics of the English vowels with Mandarin equivalents do not differ significantly from those equivalents. For the other English vowels, the formant values most often differ from those of their closest Mandarin equivalents in only one formant or in neither. For instance, Mandarin subjects do not distinguish English /u/ from the near-close near-back vowel in either formant - attributable to the absence of the near-close near-back vowel in Mandarin.

1pSCc22. The influence of the feature (sonorant) in lexical access in Spanish. Danny R. Moates (Ohio University, Department of Psychology, Porter Hall, Athens, OH 45701, USA, moates@ohio.edu), Emilia A. Marks (Ohio University, Department of Modern Languages, Athens, OH 45701, USA, markse@ohio.edu), Dario Barrera (Universidad de Sevilla, Facultad de Filologia, Departmento de Filologia Inglesa, Palos de la Frontera, s/n, 41004 Sevilla, Spain, dario@us.es)

Does the feature (sonorant) influence access to lexical entries? In current feature geometry, the feature (sonorant) is a root node feature, distinguishing resonants from obstruents. Marks, et al. (2002) demonstrated its influence in lexical access using the word reconstruction task in Spanish. Participants heard a nonword, e.g., dirmar, and were asked to change it into a real word (firmar) by changing just one consonant. Errors in recovering the correct word (firmar) were much higher when the word contained an obstruent that had been replaced with a resonant (nirmar) than when the word contained an obstruent that had been replaced by another obstruent (dirmar). Obstruent target words were easier to recover when the target segment and the replacing segment matched on the feature [sonorant]. Why do obstruents show this matching effect? The present study subdivided obstruents into stops and fricatives. Two experiments compared them separately to resonants in the word reconstruction task. Are fricatives alone or stops alone responsible for the observed obstruent effect? Results showed greater errors in the mismatch condition for both fricatives and stops, but significantly greater for fricatives than for stops, suggesting that the mismatch effect observed for obstruents is largely based on fricatives.

1pSCc23. Syllable production rate in conversational speech. Lawrence J. Raphael (Adelphi University, 1 South Avenue, Garden City, NY 11530, USA, raphael@adelphi.edu)

Most acoustic analyses of speech are based on samples obtained from carefully constructed corpora that are read or recited by subjects in a laboratory setting. Recently, speech scientists have attempted to obtain speech samples that are representative of a more casual, conversational style than might be obtained in the laboratory. One available and plentiful source of such speech samples can be found in ″talkradio″ shows in which listeners engage in phone conversations with radio hosts. Phone-in programs receive calls from thousands of callers each day across the continental United States. Moreover, the listeners who call generally speak in an essentially natural, unself-conscious manner, exhibiting a broad range of rates and emotional states. This paper reports the results of a study of syllable production rate from samples of speech obtained from a variety of types of phone-in programs, including those focusing on sports, politics and the arts. The data reveal that syllable production rates (in syllables per second) range from 3.05 to 7.50. Subjective judgements of speech rate by naive subjects were found to correlate only moderately with actual rates of syllable production.

1pSCc24. A temporally stable representation of power spectra of periodic signals and its application to F0 and periodicity estimation. Hideki Kawahara (Faculty of Systems Engineering, Wakayama University, 930 Sakaedani, 640-8510 Wakayama, Japan, kawahara@sys.wakayama-u.ac.jp), Masanori Morise (Faculty of Systems Engineering, Wakayama University, 930 Sakaedani, 640-8510 Wakayama, Japan, s055068@sys.wakayama-u.ac.jp), Toru Takahashi (Faculty of Systems Engineering, Wakayama University, 930 Sakaedani, 640-8510 Wakayama, Japan, tall@sys.wakayama-u.ac.jp), Ryuichi Nisimura (Faculty of Systems Engineering, Wakayama University, 930 Sakaedani, 640-8510 Wakayama, Japan, nisimura@sys.wakayama-u.ac.jp), Hideki Banno (Meijyo University, 501-1 Shiogamaguchi, Tenpakuku, 468-8502 Nagoya, Japan, banno@ccmfs.meijo-u.ac.jp), Toshio Irino (Faculty of Systems Engineering, Wakayama University, 930 Sakaedani, 640-8510 Wakayama, Japan, irino@sys.wakayama-u.ac.jp)

A unified framework for extracting F0 and periodicity is proposed based on a new formulation of STRAIGHT. Averaging power spectra, they are calculated using two time windows a half pitch period apart, yields a tempo-

rally stable power spectrum for periodic signals (TANDEM spectrum). Applying consistent sampling theory also yields computationally efficient implementaiton of spectral envelope estimation used in STRAIGHT (STRAIGHT spectrum). Normalized TANDEM spectrum by STRAIGHT spectrum only represents periodicity information and can be used to detect periodicity both in the base-band (for F0 extraction) and other frequency bands (for mixed mode excitation). This unified framework provides a basis to represent the complex modes of voice excitation and enables greatly realistic remaking of extreme vocal expressions. [Supported by Grant in aids for scientific research and CrestMuse project.]

1pSCc25. Construction of MRI-based three-dimensional atlas of the human tongue for tongue modeling. Chao-Min Wu (Dept. Electrical Engineering, National Central University, #300, Chung-Da Rd., 320 Chung-Li, Taiwan, wucm@ee.ncu.edu.tw), Sung-Yi Wang (Dept. Electrical Engineering, National Central University, #300, Chung-Da Rd., 320 Chung-Li, Taiwan, 945201073@cc.ncu.edu.tw)

The main purpose of this study is to build a MRI-based 3D tongue atlas for research on tongue morphometrics and physiological modeling of normal and disordered speech production. In this study, MRI data of 8 subjects (4 males and 4 females) were chosen from an orally-based MRI database of 20 male and 20 female college students without speech disorders. Sixteen landmarks were defined and selected from the 3D reconstructed MRI tongue images based on the subjects. Thin-plate spline analysis (TPS) was used to build a 3D tongue atlas for male and female subjects, respectively. Sagittal sections of the original MRI data were used to evaluate the accuracy of image registration and reconstruction. The resulted 3D tongue atlas was used to study subject-to subject, subject-to-atlas, and male-to-female morphometric variation. Preliminary results show the major difference among female subjects before and after the TPS analysis is in the area of tongue dorsum that is close to the velum and epiglottis, respectively. However, the major difference among male subjects is in the areas of tongue tip and body regardless of TPS analysis. In summary, our preliminary results imply that the 3D tongue atlas of female subjects show less subject-to-subject difference.

1pSCc26. Neural correlates on Chinese speech production: an fMRI study. Chao-Min Wu (Dept. Electrical Engineering, National Central University, #300, Chung-Da Rd., 320 Chung-Li, Taiwan, wucm@ee.ncu.edu.tw), Yi-Syuan Lin (Dept. Electrical Engineering, National Central University, #300, Chung-Da Rd., 320 Chung-Li, Taiwan, kenshin5718@yahoo.com.tw)

The aim of this study is to use functional magnetic resonance imaging (fMRI) method to find neural correlates on Chinese speech production. Three young normal adults (mean age 24 yrs) produced four tone Chinese characters ″ma1, ma2, ma3, and ma4″ in four ways: (A) normal speech, (B) mouthing speech, (C) unarticulated speech, (D) internal speech, and ″ma1, ma1, ma1, and ma1″ for the condition (E) normal speech. The fMRI results showed that the areas associated with the control of breathing for speech, vocalization, and hearing were the sensorimotor cortex, supplementary motor area, the superior temporal gyrus, the cerebellum, parietal association area, and the lingual gyrus. The areas associated with articulation were the sensorimotor cortex, the cerebellum, the inferior frontal gyrus, anterior and posterior cingulate gyrus, and the precuneus. The areas associated with tone variation were found in bilateral basal ganglia, hippocampal formation, and parietal association area, and the left pre-motor area, middle occipital gyrus, and the right cerebellum, superior temporal gyrus, and midbrain. Neural correlates of speech production and Chinese tone were all related to the cerebellum. In summary, our preliminary results showed the cerebellum plays an important role on Chinese speech production.

1pSCc27. Differences in the development of speech segmentation abilities in two French dialects. Thierry Nazzi (CNRS - Université Paris Descartes, 45 rue des Saints-Pères, 75006 Paris, France, thierry.nazzi@univ-paris5.fr), Karima Mersad (CNRS - Université Paris Descartes, 45 rue des Saints-Pères, 75006 Paris, France, crocnotekary@yahoo.fr),Galina Iakimova (CNRS - Université Paris Descartes, 45 rue des Saints-Pères, 75006 Paris, France, galina.iakimova@free.fr), Megha Sundara (UCLA Department of Linguistics, 3125 Campbell Hall, Los Angeles, CA 90095-1543, USA, megha.sundara@humnet.ucla.edu), Linda Polka (McGill University, School of Communication Sciences and Disorders, Beatty Hall, 1266 Pine Avenue West, Montreal, QC H3G 1A8, Canada, linda.polka@mcgill.ca)

Speech segmentation skills develop in infancy and are influenced by many phonological properties of the native language and, in particular, the prosodic structure of the infant's native language. Studies using the HPP task show that American English infants appear to favor a stress-based procedure (Jusczyk et al., 1999) whereas Parisian French infants favor a syllable-based procedure (Nazzi et al., 2006), in line with a prosodic-based bootstrapping account of segmentation abilities (Nazzi et al., 1998). However, in a study using different stimuli, Polka and Sundara (2003) found results that might suggest a developmental trajectory for Canadian French infants that does not rely on syllable-based segmentation. Given that the stimuli used in both studies on French were different, both research teams tested their infant populations (at 8, 12, and 16 months of age) with the stimuli originally used by the other team The results suggest a complex interaction between specific stimuli and infants' native dialect, thus providing for the first time data suggesting that word segmentation is dialect specific. We will discuss how these findings, together with acoustic analyses, show that early word segmentation is influenced by linguistic (rhythmic/syllabic, dialectal) prosodic cues, extra-linguistic (speech style) prosodic cues, and distributional cues.

1pSCc28. Effect of consonant gemination on vowel coarticulation. Maria-Gabriella Di Benedetto (University of Rome, Infocom Dept. Via Eudossiana 18, 00184 Rome, Italy, gaby@acts.ing.uniroma1.it), Daniele Domenicali (University of Rome, Infocom Dept. Via Eudossiana 18, 00184 Rome, Italy, dome@newyork.ing.uniroma1.it)

As well known V1CV2 structures are typically characterized by two different phenomena: the first vowel V1 spectral properties are affected by the presence and nature of the second vowel V2 (anticipatory effect), and V2 is influenced by the presence of the first one (cross-over effect). The intensity of anticipatory and the cross-over effects are language dependent and can vary significantly. Both effects have been observed in the past to be present in the Italian language through the analysis of VCV nonsense words. The Italian language has however a unique property, that is distinctive consonant gemination, i.e. consonant length is phonemic; two different words may thus differ by the sole presence or absence of gemination in one of this consonants. The Italian language offers therefore the ideal framework for analyzing the effect of gemination on across-consonant coarticulation. The object of this work is to analyze whether and how the presence of gemination may affect the acoustic properties of vowels in V1CCV2 words. First results of acoustic analysis of V1CV2 as well as their V1CCV2 counterparts, spoken by Italian native speakers, tend to show that gemination may have an effect on across-consonant coarticulation, with specific peculiarities for anticipatory vs. cross-over effects.

1pSCc29. Enhancement of voiced and voiceless stop categories in infant-directed speech to 11-month-old infants. Gina C. Cardillo (University of Washington, Dept. of Speech & Hearing Sciences, and Institute for Learning & Brain Sciences, Box 357988, Seattle, WA 98195, USA, ginacc@u.washington.edu), Jennifer R. Perry (University of Washington, Dept. of Speech & Hearing Sciences, and Institute for Learning & Brain Sciences, Box 357988, Seattle, WA 98195, USA, jperry3@u.washington.edu), Patricia K. Kuhl (University of Washington, Dept. of Speech & Hearing Sciences, and Institute for Learning & Brain Sciences, Box 357988, Seattle, WA 98195, USA, pkkuhl@u.washington.edu)

It has been proposed that infant-directed speech (IDS) increases the discriminability of phonetic categories by exaggerating the acoustic differences between phonetic units (Kuhl et al., 1997, Science). However, reports show conflicting results on whether this principle holds for consonants. The current study measured English /p/ /b/ /t/ /d/ in both IDS and adult-directed

speech (ADS) from connected speech in 27 mothers addressing their 11-month-old infants. Findings supported the exaggeration hypothesis. The mean VOT of /p/ was longer in IDS than ADS, and approached significance for /t/. The mean VOT difference between /p/ and /b/ was greater in IDS than in ADS. Similarly, when phonemes were grouped into voiceless and voiced categories, the difference between categories was significantly greater in IDS than ADS. We will discuss ways to measure AD-ID differences. [Work supported by NIH HD37954.]

1pSCc30. Speaker-specific patterns of token-to-token variability. Christine Mooshammer (Haskins lab and MIT Research Lab of Electronics, 300 George Street, Suite 900, New Haven, CT 06511, USA, tine@haskins.yale.edu), Pascal Perrier (ICP/GIPSA-lab, INPG, 46 Avenue Félix Viallet, 38031 Grenoble Cedex 01, France, Pascal.Perrier@gipsa-lab.inpg.fr), Susanne Fuchs (ZAS, Schuetzenstr. 18, 10117 Berlin, Germany, fuchs@zas.gwz-berlin.de)

One explanation for token-to-token variability is neural noise corrupting the motor commands. In a previous study using a two-dimensional tongue model, adding neural noise to motor commands was able to account for shapes and orientations of the dispersion ellipses of tongue positions for non-high vowels only. It was concluded that additional sources shaping lingual variability patterns of vowels should be examined: (a) stabilization of the tongue by lateral palate contact, (b) palate shape and (c) perceptual constraints due to the crowdedness of the vowel space. Variability patterns of three speakers of German were analyzed by means of EMMA, EPG, and formant frequencies. Only the most variable speaker used lingual-palatal contact to reduce lingual variability for high front vowels. The other two speakers achieved articulatory vowel targets in a very precise manner. A flat palate shape can explain the limited lingual variability of one of these two. Only for this speaker did the acoustic distance between vowel targets significantly limit acoustical variability with smaller Bark ellipsoid volumes in regions with closer neighbors. For the other precise speaker, neither palate shape nor perceptual demands were relevant. We conclude that the relative importance of the factors analyzed varies across speakers.

1pSCc31. Neural mechanism for understanding speakers' intentions: developmental analyses of children with and without communication disorders. Satoshi Imaizumi (The Prefectural Univ. of Hiroshima, 1-1 Gakuen-machi, 723-0053 Mihara, Japan, imaizumi@pu-hiroshima.ac.jp)

Ability to understand speakers' intentions through linguistic contents and affective prosody is examined for children between 5 and 12 years-old with and without communication disorders. Four types of spoken short phrases, expressing admiration, sarcasm, blame, and humor or joke, were presented. For each stimulus, the subjects were asked to choose between two cards, one with a written word ″praise″ and another with ″no praise″ accompanied by corresponding drawings. For children without any communication disorders, the percentage of the correct judgment of speaker intentions was high and stable for admiration and blame phrases which have congruent linguistic and affective valences. It was significantly low for 6-year-old children and increased with age for the sarcastic or joking phrases which have incongruent linguistic and affective valences. The percent correct was significantly lower for autistic children than normally developing children particularly for the phrases with incongruent valences. Although a significant difference was found between children with severe- and mild-hearing impairment, no significant difference was found in the percent correct between the congruent and incongruent phrases for them. Based on these results together with brain activation analyses using fMRI (Imaizumi et al., 2004, 2006), a model of neural mechanism for understanding speakers' intentions is discussed.

1pSCc32. Perception of two English front vowels by L1 Dutch speakers with different regional accents. Paola Escudero (University of Amsterdam, Institute of Phonetic Sciences, Spuistraat 210, 1012 VT Amsterdam, Netherlands, P.R.EscuderoNeyra@uva.nl),Ellen Simon(Ghent University, English Department, Rozier 44, 9000 Ghent, Belgium, Ellen.Simon@UGent.be)

This paper reports the results of a categorization task of the English vowels ″epsilon″ and ″ash″ by native speakers of Dutch. Dutch has only one member of the contrast (″epsilon″), the acoustic realization of which is subject to considerable regional variation (Adank et al., 2007). Previous research has shown that that there is asymmetrical lexical competition between English words containing ″epsilon″ and ″ash″ for native speakers of Dutch (Weber & Cutler, 2004; Escudero et al., in press). Weber & Cutler (2004) argue that ″epsilon″ is the dominant category for native speakers of Dutch, because it is phonetically closer to the L1 Dutch sound. The present study investigates whether the dominant category may vary depending on the speakers' L1 dialect by examining how two groups of Dutch-speaking participants from different dialect regions (the Randstad region in the Netherlands and East-Flanders in Belgium) perceive the English vowels ″epsilon″ and ″ash.″ Preliminary results indicate that participants from these two area's do indeed categorize English ″epsilon″ and ″ash″ differently as the result of the acoustic properties of their L1 vowel ″epsilon″ (F1, F2 and duration).

1pSCc33. Motor equivalent strategies in the production of /u/ in perturbed speech. Jana Brunner (Humboldt-Universität Berlin/Gipsa-lab, INP Grenoble, ZAS, Schützenstr. 18, 10117 Berlin, Germany, brunner@zas.gwz-berlin.de), Phil Hoole (Institut für Phonetik und Sprachverarbeitung, Schellingstr. 3, 80799 München, Germany, hoole@phonetik.uni-muenchen.de), Pascal Perrier (ICP/GIPSA-lab, INPG, 46 Avenue Félix Viallet, 38031 Grenoble Cedex 01, France, Pascal.Perrier@gipsa-lab.inpg.fr)

Several articulatory strategies are available during the production of /u/, all resulting in a similar acoustic output. For example, speakers can protrude the lips and compensate for that by widening the velar constriction. This study investigates whether speakers use this relation under perturbation. Five speakers were provided with palatal prostheses which were worn for two weeks. Speakers were instructed to make a serious attempt to produce normal speech. Their speech was recorded via EMA and acoustics several times over the adaptation period. Formant values of /u/-productions were measured. Velar constriction width and lip protrusion were estimated. For four speakers a correlation between constriction width and lip protrusion was found. A correlation between lip protrusion and F1 or F2 was rare and no correlation occurred between constriction size and either of the formants. The acoustic output was thus constant. The results show that under perturbation speakers use motor equivalent strategies. The correlation between constriction size and lip protrusion is stronger than in studies investigating unperturbed speech (e.g., Perkell et al., 1993). This could be because under perturbation speakers are inclined to try out several strategies in order to reach the acoustic target and the co-variability might thus be greater.

1pSCc34. Using sets of combs to control pitch estimation errors. Jean-Sylvain Lienard (LIMSI-CNRS, BP133, 91403 Orsay Cedex, France, jean-sylvain.lienard@limsi.fr), Claude Barras (LIMSI-CNRS, BP133, 91403 Orsay Cedex, France, claude.barras@limsi.fr), Francois Signol (LIMSI-CNRS, BP133, 91403 Orsay Cedex, France, francois.signol@limsi.fr)

We analyze the errors of a Pitch Estimation Algorithm using the Pitch Function (response of the periodicity estimator as a function of the frequency parameter F_c). The estimator's maximum response for a single signal of fundamental frequency F_0 is expected to occur for $F_c=F_0$. Actually the pitch function exhibits many secondary peaks which occasionally cause the errors. When several signals are mixed, secondary peaks of a signal may take over the main peak of the other. By taking as periodicity estimator the correlation of the spectrum module with a uniform infinite spectral comb of fundamental frequency F_c we show that each peak corresponds to a particular value of the ratio $F_c/F_0=p/q$ (p and q integers $\geqslant 1$). It follows that some secondary peaks can be canceled either by augmenting the comb with intermediary negative teeth, or by setting to zero some of its teeth. These modified combs can be viewed as linear combinations of uniform combs of different F_cs. The present study aims at precisely defining and combining the modified combs so that the main peaks of the new Pitch Function reliably

indicate the F_0s of the components. Examples are given on mixtures of voiced segments extracted from natural speech.

1pSCc35. Articulatory exaggerations during infant directed speech. Jordan R. Green (University of Nebraska, 318O Barkley Center, Lincoln, NE 68583-0738, USA, jgreen4@unl.edu), Ignatius Nip (San Diego State University, 5500 Campanile Dr., San Diego, CA 92182-1518, USA, inip@mail.sdsu.edu), Erin Wilson (Waisman Center, 1500 Highland Avenue, Madison, WI 53705-2280, USA, emhillman@wisc.edu), Antje Mefferd (University of Nebraska, 318O Barkley Center, Lincoln, NE 68583-0738, USA, amefferd@unlserve.unl.edu)

Although a growing body of literature suggests a principal role for observational learning in the acquisition of speech, the facial movements of infant directed speech (IDS) have rarely been studied. Identifying both the auditory and visual features of IDS is an essential step toward understanding the contribution of environmental stimulation to the development of speech and language. The current project uses three-dimensional motion capture technology to describe how parents modify their articulatory movements when communicating with their infants. The following three experimental questions will be addressed: (1) Do parents exaggerate articulatory gestures during IDS?; (2) If so, are there individual differences among parents in the degree of IDS?; and (3) Is there a strong association between acoustic and movement characteristics of IDS? Mouth movements were recorded from twenty-four mothers while speaking to their infants and to an unfamiliar adult. Mouth shapes during four target vowels were measured for differences in maximum vertical separation, maximum horizontal spread, and duration across speaking conditions. The result indicated that the majority of mothers exaggerated their lip movements when speaking to their infants. Speculation is made regarding the potential role of articulatory exaggerations in early speech learning.

1pSCc36. Evaluation of the Pitch Estimation Algorithms in the monopitch and multipitch cases. Francois Signol (LIMSI-CNRS, BP133, 91403 Orsay Cedex, France, francois.signol@limsi.fr), Claude Barras (LIMSI-CNRS, BP133, 91403 Orsay Cedex, France, claude.barras@limsi.fr), Jean-Sylvain Lienard (LIMSI-CNRS, BP133, 91403 Orsay Cedex, France, jean-sylvain.lienard@limsi.fr)

Reliably tracking the fundamental frequency F_0 of the components is an important step in the separation of superimposed speech signals. Several Pitch Estimation Algorithms are potentially usable and a rigorous evaluation method is needed in order to compare them. However, even in the monopitch case, many variations between them render such a comparison difficult . The extent of the F_0min-F_0max interval, the use of a priori information on the whole sequence or database, and above all the arbitrary setting of the voicing threshold, yield large differences in the results. These biases can be removed by setting the F_0 bounds to fixed values acceptable for many voices, by proceeding with the evaluation on a strictly frame-to-frame basis, and by fixing the voicing threshold in order to get an equal error rate for overvoiced and undervoiced frames. In the multipitch case any frame may exhibit 0, 1, or 2 valid voicings according to the coincidence between the voiced and unvoiced parts of both signals. This problem is treated by defining a similarity measure linking the PEA's hypotheses to the pitch values of the isolated signals. The proposed methodology is applied to several PEAs, using the Keele database in monopitch and multipich setups.

1pSCc37. An acoustic investigation of the Swedish child's acquisition of obstruent place of articulation. Jan Van Doorn (Umeå University, Department of Clinical Sciences, SE90187 Umeå, Sweden, jan.vandoorn@logopedi.umu.se), Fredrik Karlsson (Umeå University, Department of Language Studies, SE90187 Umeå, Sweden, fredrik.karlsson@ling.umu.se), Kirk P. Sullivan (Umeå University, Department of Language Studies, SE90187 Umeå, Sweden, kirk.sullivan@ling .umu.se)

Speech produced by children in the initial stages of development does generally not uphold as many phonetic distinctions as speech sounds produced by adults. A child's productions of different target words may therefore have similar acoustic properties and result in homonyms being perceived by the adult observer. This study presents a longitudinal investigation into the development of place of articulation from non-distinctive to distinctive productions in word-initial obstruents produced by 22 Swedish children (aged 18 - 48 months). The data was collected through monthly recordings, approximatelly one year per child. The acoustic correlates analysed were spectral diffuseness, spectral skewness and spectral tilt for plosives and spectral skewness, spectral kurtosis, spectral variance and F2 onset frequency for fricatives. The results show a developmental trend in spectral skewness that is indicative of a increasing number of acquired phonetic contrasts. Spectral tilt change, F2 onset frequency, spectral mean and spectral variance provide evicence of within-category refinement wich is argued to be caused primarilly by advancements in motor control.

1pSCc38. Nonlinear dynamics of speech categorization: critical slowing down and critical fluctuations. Leonardo Lancia (LPL, Aix-Marseille Université & CNRS, 29, avenue Robert Schuman, 13100 Aix-en-Provence, France, leonardo.lancia@lpl-aix.fr), Noel Nguyen (LPL, Aix-Marseille Université & CNRS, 29, avenue Robert Schuman, 13100 Aix-en-Provence, France, Noel.Nguyen@lpl-aix.fr), Betty Tuller (National Science Foundation, 4201, Wilson Boulevard, Arlington, VA 22230, USA, tuller@ccs.fau .edu)

The dynamical system view of speech perception assumes that speech categorization depends on both the acoustic properties of the incoming sound and the state of the perceptual system (indexed by the subject's responses to preceding sounds). Tuller and colleagues [1] systematically manipulated the order of presentation of stimuli from a ″say″-″stay″ continuum in a binary-choice word identification task. Listeners' responses were modeled using a nonlinear dynamical system whose point attractors were associated with perceptual categories. In the present study, we asked French speakers to categorize stimuli on a continuum from ″cèpe″ /sɛp/ to ″steppe″ /stɛp/. Our results provide support for two yet untested predictions from the model: the occurrence of a) critical slowing down and b) critical fluctuations . Critical slowing down relates to the increase in relaxation time that occurs as the system approaches points of instability. Critical fluctuations refer to the system's increased sensitivity to random fluctuations near the points of instability. [Work supported by the CNRS & French Ministry of Research, and by NSF.] [1] P. Case, B. Tuller, D. Mingzhou, and J.A.S. Kelso. Evaluation of a dynamical model of speech categorization. Perception and Psychophysics, **57**:977-988 (1995).

1pSCc39. The effects of vowel identification training on sentence-level speech recognition. Carolyn Richie (Communication Disorders, Butler University, 4600 Sunset Ave., Indianapolis, IN 46208, USA, crichie@butler .edu)

Recent work examined the effects of a novel computer-based approach to speech recognition training involving vowel identification [C. Richie, J. Acoust. Soc. Am. **121**, 3045 (2007)]. When vowel identification training was done under auditory-visual conditions with noise participants demonstrated modest improvements in sentence recognition, and when training was done under visual-only conditions participants failed to show improvements in sentence recognition. However, sentence recognition was assessed for the CID Everyday Sentences in terms of words correctly recognized. Improvements in speech recognition may have occurred following training on a level lower than the word, and gone unrecognized given this scoring method. The purpose of the present study is to determine whether vowel identification training leads to improvements in speech recognition on a test of sentence recognition, as measured by correct identification of consonants and vowels. These findings have implications for sentence recognition test scoring methods. The role of acoustics in improving speech recognition will also be discussed. (Supported by Butler University HAC grant #027096).

1pSCc40. An acoustic study on voiceless retroflex and dental sibilants of young native Min speakers in Taiwan. Yu-Ying Chuang (Graduate Institute of Linguistics, Grad. Inst. of Linguistics, National Taiwan Univ., 1,

Roosevelt Rd. Sec. 4, 106 Taipei, Taiwan, r95142001@ntu.edu.tw),Janice Fon (Grad. Inst. of Linguistics, National Taiwan Univ., 1, Roosevelt Rd. Sec. 4, 106 Taipei, Taiwan, jfon@ntu.edu.tw)

The Mandarin spoken in Taiwan is influenced by Min, a Southern Chinese dialect, in many perspectives. Due to the absence of retroflex sibilants in Min, previous studies claimed that retroflex sibilants are replaced by their dental counterparts. Recent studies, however, showed that retroflex and dental sibilants are actually distinguished. Such contradictory result was due to the fact that different speaker groups were targeted at - one on older generation, acquiring Min as L1, whereas the other on younger generation, acquiring Min as L2. Since age and the acquisition order of Min were involved, it was unknown which factor affected the realization of retroflex and dental sibilants more. To clarify this point, we targeted at the younger generation that acquired Min as L1. Acoustic measurements were taken on all sibilants. Results showed that retroflex and dental sibilants had distinctive realization, suggesting age factor to be more determent. Gender effect was found significant, in which females showed a greater distinction than males. Moreover, retroflex sibilants pronounced in syllables were significantly different from those in sentences. Future studies could be done on the other group - older generation, acquiring Min as L2. Also, whether the frequency of using Min plays a role awaits further exploration.

1pSCc41. A comparison of native speaker and American adult learner Vietnamese lexical tones. Allison Blodgett (University of Maryland College Park, Center for Advanced Study of Language, 7005 52nd Ave, College Park, MD 20742, USA, ablodgett@casl.umd.edu), Jessica Bauman (University of Maryland College Park, Center for Advanced Study of Language, 7005 52nd Ave, College Park, MD 20742, USA, jbauman@hesp.umd.edu), Anita Bowles (University of Maryland College Park, Center for Advanced Study of Language, 7005 52nd Ave, College Park, MD 20742, USA, abowles@casl.umd.edu), Lykara Charters (University of Maryland College Park, Center for Advanced Study of Language, 7005 52nd Ave, College Park, MD 20742, USA, lykarac@mac.com), Anton Rytting (University of Maryland College Park, Center for Advanced Study of Language, 7005 52nd Ave, College Park, MD 20742, USA, crytting@casl.umd.edu), Jessica Shamoo (University of Maryland College Park, Center for Advanced Study of Language, 7005 52nd Ave, College Park, MD 20742, USA, jshamoo@casl.umd.edu), Matthew Winn (University of Maryland College Park, Department of Hearing & Speech Sciences, 0100 Lefrak Hall, College Park, MD 20742, USA, mwinn@hesp.umd.edu)

This study introduces a modification of the traditional carrier sentence elicitation task, provides new native speaker data regarding aspects of pitch and voice quality in Vietnamese lexical tones, and provides an empirical description of non-native speaker errors in tone production. Participants produce a series of three-word utterances in response to target words that appear individually on a computer screen in one of four colors. In this way, participants actively describe a changing event, while critical components remain constant: the identity of the word preceding the target, the target position (utterance medial), and the target's focus structure. Native speaker results are consistent with existing descriptions of fundamental frequency contours and creakiness. In addition, they provide evidence supporting claims that breathiness can occur in two different tones: the falling tone (huyen) and curve tone (hoi). Non-native speaker results suggest that adult learners struggle with voice quality distinctions and pitch shape.

1pSCc42. Lip protrusion and constriction in anticipation in English and French. Aude Noiray (Haskins Laboratories, 300 George St, New Haven, CT 06511, USA, aude.noiray@haskins.yale.edu), Lucie Ménard (Département de linguistique et de didactique des langues, Université du Québec à Montréal, Case postale 8888, succursale Centre-ville, Montréal, QC H3C 3P8, Canada, menard.lucie@uqam.ca), Marie-Agnès Cathiard (Centre de Recherche sur l'Imaginaire (CRI), Université Stendhal, Grenoble 3, BP 25, 38040 Grenoble cedex 9, France, Marie-Agnes .Cathiard@u-grenoble3.fr),Christian Abry(Centre de Recherche sur l'Imaginaire (CRI), Université Stendhal, Grenoble 3, BP 25, 38040 Grenoble cedex 9, France, christian.abru@u-grenoble3.fr)

Though lip constriction is acoustically the most robust parameter for rounding, most studies on anticipatory coarticulation relied on the investigation of protrusion via EMG, optoelectrical systems or audiovisual processing. These various methods produced inconsistent anticipatory profiles across studies or even speakers. The Movement Expansion Model (MEM) of Abry and Lallouache has explained vocalic anticipatory coarticulation in four French adults and eight children via lip constriction, showing idiosyncratic behaviours, i.e. personal regression slopes but with a lawful variability validated by high correlation coefficients. In order to describe global anticipatory movement, the current study included measures of both protrusion and constriction over time. Four American English and four Canadian French adults were audio visually recorded, uttering [iC[n]u] sequences, in which C[n] corresponded to a varying number of intervocalic consonants. Lip protrusion was measured via an Optotrak system, and constriction via a Lip-Shape Tracker (from ICP Grenoble). We found that when tested on lip area control, English speakers joined French speakers in a regular MEM temporal pattern, displaying their own anticipatory behaviour, with personal regression slope or expansion coefficient.

1pSCc43. The contribution of vowel production to the intelligibility and accentedness of nonnative speech. Jessica E. Alexander (Dept. of Psychology, Emory University, 532 Kilgo Cir, Atlanta, GA 30322, USA, jessica.alexander@emory.edu), Sabrina K. Sidaras (Dept. of Psychology, Emory University, 532 Kilgo Cir, Atlanta, GA 30322, USA, ssidara@emory.edu), Lynne C. Nygaard (Dept. of Psychology, Emory University, 532 Kilgo Cir, Atlanta, GA 30322, USA, lnygaar@emory.edu)

The present study investigated the extent to which the perception of accentedness and intelligibility in nonnative speech depends on the specific acoustic realization of vowels produced by nonnative speakers. Twelve native speakers of Korean were recorded producing both word- and sentence-length English utterances. Acoustic analyses, including measures of vowel duration and formant frequencies, were conducted on tokens of individual English vowels identified from the word-length utterances. Vowel tokens were selected from a variety of phonetic contexts and were compared to productions of the same vowels produced in the same contexts by native English speakers. A separate set of native English-speaking listeners judged accentedness and intelligibility from the sentence-length utterances. The results showed that both the duration and spectral characteristics of Korean-accented vowels were related to overall sentence intelligibility and ratings of perceived accentedness. These findings suggest that the detailed acoustic realization of the temporal and spectral structure of non-native vowels contributes to global measures of perceived accentedness and overall intelligibility.

1pSCc44. Word-initial voiceless geminate stops: production and perception. Rachid Ridouane (Laboratoire de Phonétique et Phonologie-UMR7018 CNRS/Sorbonne Nouvelle, 19 rue des Bernardins, 75005 Paris, France, rachid.ridouane@univ-paris3.fr), Pierre Halle (Laboratoire de Phonétique et Phonologie-UMR7018 CNRS/Sorbonne Nouvelle, 19 rue des Bernardins, 75005 Paris, France, pierre.halle@univ-paris5.fr)

Quantity contrasts (i.e., singleton vs geminate consonants, short vs long vowels) are common in the languages of the world. Yet, most singleton-geminate contrasts occur in word-medial position. Languages that allow gemination in other than word-medial position (word-initially or word-finally) are quite few. Even less frequent is the occurrence in the languages of the world of word-initial voiceless geminate stops. Pattani Malay (Abramson, 1986), Turgovian Swiss German (Kraehenmann, 2003), Tashlhiyt Berber (Ridouane, 2007), are the only documented languages that allow singleton-geminate contrasts word-initially for all native consonants, including both voiced and voiceless plosives. In this work we deal with word-initial voiceless geminate stops in Tashlhiyt Berber and present results from 3 experiments: 1) a production study including acoustic and electropalatographic measurements 2) a native-listener experiment with labelling and discrimination, and 3) a cross-language perceptual experiment, with listeners of

two languages differing in germination: Italian (in which gemination only occurs word-medially) and French (in which gemination only occurs between words in continuous speech).

1pSCc45. Inter-speaker variability and the articulatory-acoustic relations in German and English /sh/. Susanne Fuchs (ZAS, Schuetzenstr. 18, 10117 Berlin, Germany, fuchs@zas.gwz-berlin.de), Martine Toda (CNRS & ENST, 46, rue Barrault, 75634 Paris, France, martinetoda@yahoo.co.jp)

The aim of this study is to investigate speaker-specific articulatory-acoustic relations and their potential causes in the realisation of /sh/. By means of electropalatographic and acoustic data for 12 German and 12 English native speakers (6 males and 6 females for each language), we obtained the following results: 1) relatively invariant COG values of the frication noise among the subjects, 2) huge inter-speaker variability in the articulatory place of articulation, especially for the males. We suggest that in the realisation of /sh/ motor equivalence principles can be used speaker-dependently. In particular, the length of palatal channel, the size of the front cavity (including its sublingual portion) as well as lip protrusion are the relevant articulatory parameters involved in the adjustment of the frication noise. Speaker-specific articulatory strategies will be discussed in the light of the formant transition characteristics, palatal morphology, and the prototypical articulatory patterns will be illustrated by means of acoustic modelling.

1pSCc46. Pitfalls of spectrogram readings of flaps. Minjung Son (Yale University and Haskins Labs, 300 George St. Suite 900, New Haven, CT 06511, USA, son@haskins.yale.edu)

Several acoustic studies have revealed stable characteristics of the speech signal for rhotics, whereas articulatory studies have found different articulatory strategies across speakers for producing these segments (Ladefoged and Maddison, 1996; Tiede et al., 2004). However, no study has showed that the phonologically reduced flap gesture, which is argued to be a lateral in the underlying representation, can sometimes fail to be reflected in the acoustic correlates of an articulatory event. Using electromagnetic midsagittal articulometry (Perkell et al., 1992), a case study has been conducted for Korean. Productions of two Seoul-Korean speakers were collected using real words in the within-word condition. The subjects read target words within a single accentual phrase, as in Jun (1993), and repeated eight times. Each target word (/ili/ and /ala/) appeared in its own distinct natural sentence at two speech rates (fast and comfortable). A total of 32 tokens were available for analysis. Tongue tip gestures were examined simultaneously with spectrograms. Results from one speaker indicated that sometimes no acoustic correlates of the tongue tip gesture for a flap were present (6.3% of productions) although articulation was obviously produced [Work supported by NIH DC00403.]

1pSCc47. Clicks with noisy accompaniment in West !Xoon. Sven Grawunder (Max Planck Institute for Evolutionary Anthropology, Deutscher Platz 6, 04103 Leipzig, Germany, grawunder@eva.mpg.de), Christfried Naumann (Max Planck Institute for Evolutionary Anthropology, Deutscher Platz 6, 04103 Leipzig, Germany, naumann@eva.mpg.de)

The current study is concerned with ingressive stops (clicks) with a noisy accompaniment exemplified by data from West !Xoon, a Taa variety (″!Xóõ″, Tuu/Southern Khoisan) spoken in Namibia. Within the obstruent system of West !Xoon, we describe (1) aspirated clicks, (2) clicks followed by a laryngeal fricative, (3) clicks with an aspirated uvular accompaniment, and (4) clicks followed by a uvular fricative. In previous analysis for the variety of East !Xoon (Traill and Ladefoged, 1994), (2) were analysed as series of ″delayed aspiration″, while the contrast between (1) and (3) was ignored. A novelty discovery are prenasalized ″voiced″ clicks followed by [h], the voiced counterparts of clicks with ″delayed aspiration″, which are probably absent in East !Xoon. We present an acoustic analysis of alveolar and palatal clicks based on field data of 6 speakers (3 male /3 female), where for each click type plus noise accompaniment three tokens in #CV context had been recorded repeatedly. As descriptive parameters served durational measures of burst length, cluster length, length of aspiration delay, and spectral measures of burst and friction parts. In opposite to the previous distinction our findings suggest a clear 3-way distinction of clicks (1-3) with noisy accompaniment.

1pSCc48. Blind source separation and directional audio synthesis for binaural auralization of multiple sound sources using microphone array recordings. Banu Gunel (I-Lab Multimedia and DSP Research Group, Centre for Communication Systems Research, University of Surrey, GU2 7XH Guildford, UK, B.Gunel@surrey.ac.uk), Huseyin Hacihabiboglu (I-Lab Multimedia and DSP Research Group, Centre for Communication Systems Research, University of Surrey, GU2 7XH Guildford, UK, h.hacihabiboglu@surrey.ac.uk), Ahmet Kondoz (I-Lab Multimedia and DSP Research Group, Centre for Communication Systems Research, University of Surrey, GU2 7XH Guildford, UK, A.Kondoz@surrey.ac.uk)

Microphone array signal processing techniques are extensively used for sound source localisation, acoustical characterisation and sound source separation, which are related to audio analysis. However, the use of microphone arrays for auralisation, which is generally related to synthesis, has been limited so far. This paper proposes a method for binaural auralisation of multiple sound sources based on blind source separation (BSS) and binaural audio synthesis. A BSS algorithm is introduced that exploits the intensity vector directions in order to generate directional signals. The directional signals are then used in the synthesis of binaural recordings using head related transfer functions. The synthesised recordings subsume the indirect information about the auditory environment conveying the source positions and the acoustics similar to dummy head recordings. Test recordings were made with a compact microphone array and a dummy head in different indoor environments. Subjective listening tests were performed to compare the synthesized recordings with the actual ones for their performance in providing presence, spaciousness and envelopment.

1pSCc49. Bilinguals' and monolinguals' reaction-time in two language contexts: evidence for the double phonetic representation in bilinguals. Adrian Garcia-Sierra (University of Washington, Institute for Learning and Brain Sciences, Box 357988, Seattle, WA WA 98195-7988, USA, gasa@u.washington.edu), Craig Champlin (University of Texas, 1 University Station A1100, Austin, TX 78712-0114, USA, champlin@austin.utexas.edu)

The time between the presentation of a stimulus and the response given to it is occupied by a series of mental operations reflecting the decision perse. Reaction-time (RT) can be thought as the duration of the mental operations behind making a decision. Small RT values involve less mental operations than larger RT values. In speech categorization tasks, sounds with clear phonetic membership produce small RT values, and ambiguous speech sounds produce large RT values. In the present investigation a Go-No-Go task was implemented to assess RT from Spanish-English bilinguals (N=27) and English monolinguals (N=27) in two language contexts. Participants were asked to identify the speech sound ″ta″ from a 10 token speech continuum varying from -20 to +25 ms of VOT. It was expected that bilinguals, but not monolinguals, would perceive +VOT stimuli as clear representations of 't' (faster RT) in the Spanish language context, but as ambiguous representations of 't' in the English language context. The results confirmed the expectations. That is, language contexts affected the speed by which mental operations were produced in bilinguals. This outcome is in agreement with the idea that bilinguals possess a double phonemic representation. Challenges and limitations of the present study are discussed.

1pSCc50. Is there a sensitive period for representation of phoneme sequences? Mary Anne Welton (University of Prince Edward Island, 550 University Ave, Charlottetown, PE C1A 4P3, Canada, mwelton@upei.ca), Annabel J. Cohen (University of Prince Edward Island, 550 University Ave, Charlottetown, PE C1A 4P3, Canada, acohen@upei.ca)

A key issue in development of speech perception and production concerns the possible existence of an early sensitive period that facilitates language acquisition. Spoken language acquisition entails representation of grammatical sequences of phonemes. In a two-phase experiment, 120 participants in three age groups (pre-adolescents, adolescents, young adults) were presented with 64 words, 16 each of English, English pronounceable

non-words, Spanish, and Mandarin. The task was to determine if the word was English. All age groups performed well, indicating that the words had been attended. A subsequent surprise recognition phase presented 64 words again, one half of which were old and one half new. Participants judged whether each word had previously been presented. Here performance overall was poorest for Spanish and Mandarin, and children performed relatively more poorly on English non-words as compared to the older groups, but showed no age-relative disadvantage for Chinese. Arguing that evidence for a sensitive period arises if children perform relatively better than older participants on foreign words as compared to English words or English non-words, the recognition results are consistent with the proposal of a sensitive period for phoneme sequence representation. The paradigm provides a new way of examining the sensitive period hypothesis. (supported by NSERC)

1pSCc51. A detailed biomechanical finite element tongue model. Reiner F. Wilhelms-Tricarico (Rewtnode, 27 Old Bay Road, Belchertown, MA 01007, USA, rewtnode@gmail.com), Maureen Stone (Vocal Tract Visualization Lab, Depts. of Biomedical Sciences and Orthodontics, University of Maryland Dental School, 650 W. Baltimore St., Baltimore, MD 21201, USA, mstone@umaryland.edu), Mark Carlson (MSC.Software Professional Services, 4332 Brookside Avenue, Minneapolis, MN 55436, USA, mark.carlson@mscsoftware.com), Paul Buscemi (Restore Medical, Inc, 2800 Patton Rd, Roseville, MN 55113, USA, pbuscemi@restoremedical.com)

For research on surgical modifications of the tongue, e.g., implants for treatment of sleep apnea, we built a detailed finite element model of the human tongue, to experimentally estimate and investigate muscle activations corresponding to observed movement data, and to study possible effects of tissue modifications. Most of the extrinsic and all intrinsic muscles of the tongue are represented as parametrized volumes within the tongue, and muscle fiber directions are specified by a tangent in curvilinear coordinate systems of parametric solids that overlay each muscle region. Fiber regions of different muscles may overlap, for example, for the transverse and vertical intrinsic muscles. Mixed Ogden type hyper-elastic models of strain energy density are used to represent passive tissue properties, and active contraction in muscle fibers is emulated by changing externally specified activation parameters in an anisotropic component of the strain energy density. The activation can vary over time and in its spatial distribution over a muscle, which is accomplished by specifying center point and spread of a Gaussian distribution in the muscle region. The tongue model is realized as a finite element implementation with large displacement/large strain calculations using incompressible 8-node elements in a commercial FE code (Marc by MSC-Software).

1pSCc52. Stable patterns of articulatory movements across inter-subject variability. Patrizia Bonaventura (Case Western Reserve University, 11206 Euclid Ave, Room 405, Cleveland, OH 44106, USA, pxb72@case.edu), Paul Taylor (Case Western Reserve University, 11206 Euclid Ave, Room 405, Cleveland, OH 44106, USA, paul.taylor@case.edu)

The goal of the present study was to test whether models of portions of curves, representing movements of the crucial articulator for production of place in syllables containing labiodental and alveolar consonants ('iceberg' portions of demisyllables), that had previously been found to be stable across different prosodic conditions (Bonaventura, 2003,2005, 2006; Bonaventura and Fujimura, 2007), a) remained stable across different subjects pronunciations, for each consonantal class b) were significantly different for the two different consonantal movements. Curves were previously extracted from microbeam articulatory data. Curve fitting models were obtained, by using a best fit fourth order polynomial, from 592 curves representing lower lip displacement for production of [f] in 'five' (3 subjects) and from 299 curves representing tongue tip displacement for production of [n] in 'nine' (3 subjects). Coefficients were statistically compared; results showed a) significant difference for all coefficients between subjects pronouncing same consonant, except for the 3rd coefficient, both in initial and final demisyllable, representing stability of slope around a position threshold. These results might indicate stable patterns across inter-subject variability; b) coefficients were significantly different for [f] vs [n] models across speakers, within initial vs. final demisyllable, possibly indicating properties of an identifiable articulatory gesture.

MONDAY AFTERNOON, 30 JUNE 2008 ROOM 343, 1:00 TO 2:20 P.M.

Session 1pSPa

Signal Processing in Acoustics: Sound Reproduction and Source Separation

William L. Martens, Cochair
McGill University, Schulich School of Music, 555 Sherbrooke Street West, Montreal, QC H3A 1E3, Canada

Jamie A. Angus, Cochair
University of Salford, 12 Lister Way, York, YO30 6NL, UK

Contributed Papers

1:00

1pSPa1. HRTF modeling in due consideration variable torso reflections. Markus Guldenschuh (Institute of Electronic Music and Acoustics, Inffeldgasse 10/3, 8010 Graz, Austria, markusgu@sbox.tugraz.at), Alois Sontacchi (Institute of Electronic Music and Acoustics, Inffeldgasse 10/3, 8010 Graz, Austria, sontacchi@iem.at), Franz Zotter (Institute of Electronic Music and Acoustics, Inffeldgasse 10/3, 8010 Graz, Austria, zotter@iem.at), Robert Höldrich (Institute of Electronic Music and Acoustics, Inffeldgasse 10/3, 8010 Graz, Austria, hoeldrich@iem.at)

Head related transfer functions (HRTFs) describe the physical path from an acoustical source to the ears. It can be gained within the relation of two measurements. The first will give the reference sound pressure in the virtual middle of the head the second has to be done in both ears. In literature exhaustive investigations concerning the idealized location of the second position can be found. Beyond that measurements with various artificial heads and human-beings considering various source directions (azimuth and elevation) with different angular resolutions have been undertaken. The obtained HRTFs exhibit, with subject to the examined source position, frequency dependent magnitude and phase. These complex transfer functions are caused by various reflections, diffractions, pressure superelevation, and shadowing, respectively. Reflections are caused form pinna, head and torso, too. Heretofore during determination of the transfer functions the influence of various head-torso arrangements have not be considered. Within this paper the differences which will be caused due to different head-torso angles will be highlighted. Beyond that a numerical model based on interpolation using spherical harmonics will be presented. By the aid of that model the

integration within an existing binaural resynthesis model can be realized and perceptual differences within a dynamic system can be investigated.

1:20

1pSPa2. Soundscape source extraction using wavelet-based sparse representations. Oliver Bunting (University of York, Department of Electronics, Heslington, YO10 5DD York, UK, ob103@ohm.york.ac.uk), David Chesmore (University of York, Department of Electronics, Heslington, YO10 5DD York, UK, edc1@ohm.york.ac.uk)

As part of the EPSRC Instrument for Soundscape Recognition, Identification and Evaluation (ISRIE) project, the work described here aims to extract sources from a soundscape, with the aim of improving the signal to interference ratio to aid automatic identification and classification. The paper will describe the project's background and aim. Results using directional audio coding (dirAC) to separate sparse signals will be presented. This method has been shown to have successfully separated two speakers at known positions from a virtual B-format soundscape. An extension of this method using the dual-tree complex wavelet transform will also be presented, which improves the sparsity of the time-frequency representation. Initial results for spatially known sources will be presented. It is expected that some results from current work on localising and tracking sources in a B-format soundscape will be presented.

1:40

1pSPa3. Instrument for Soundscape Recognition, Identification and Evaluation (ISRIE): Signal Classification. Jon Stammers (University of York, Department of Electronics, Heslington, YO10 5DD York, UK, js185@york.ac.uk), David Chesmore (University of York, Department of Electronics, Heslington, YO10 5DD York, UK, edc1@ohm.york.ac.uk)

ISRIE is a collaborative project between the universities of York and Newcastle and ISVR in Southampton. The work being undertaken at York is in its second year and focuses on signal separation and classification. Developing novel methods for classifying urban and other sounds into distinct categories (such as transportation, industrial, human, animal, etc.) is the focus of this project. The classification system will consist of two main parts: a feature extractor and a classifier. Both time and time-frequency domain techniques have been considered for feature extraction and it is anticipated that a combination of domains will be required for this complex task. To date only simple classifiers have been implemented and development is now focussed on syntactic pattern recognition. The project background and an overview of the techniques involved will be presented along with preliminary results for the classification of urban and other sounds using syntactic methods.

2:00

1pSPa4. Real-time acoustic blind signal separation system based on the spatio-temporal gradient analysis. Kenbu Teramoto (Saga University, 1-Honjo, 8408502 Saga, Japan, tera@me.saga-u.ac.jp), Md. Tawhidul Islam Khan (Saga University, 1-Honjo, 8408502 Saga, Japan, khan@me.saga-u.ac.jp)

This paper presents an autonomous directivity microphone system for the blind source separation based on the newly proposed spatio-temporal gradient algorithm. The blind source separation technique principally uses no a priori knowledge about parameters of convolution, filtering, nor mixing. In the simplest case of the blind source separation problems, the observed mixing signals are the linear combinations of unknown source signals which are mutually and statistically independent and contain zero mean. The proposed blind signal separation algorithm utilizes the linearity among the four signals: (1) the sound pressure, (2) x, (3) y, and (4) z-directional particle velocities, all of which are governed by the wave equation and the equation of motion. The proposed method, therefore, has an ability to simplify the convoluted blind source separation problems into the instantaneous blind source separation problems over the spatio-temporal gradient space. Several acoustical experiments have been performed with acceptable performance of the proposed method of blind source separation. A sensor for measuring the particle velocity of acoustic signal has been used in the experiment.

MONDAY AFTERNOON, 30 JUNE 2008 ROOM 343, 4:00 TO 7:00 P.M.

Session 1pSPb

Signal Processing in Acoustics: Acoustical Nondestructive Evaluation, Ultrasonics, and Imaging I

Grace A. Clark, Cochair
Lawrence Livermore National Laboratory, 7000 East Ave., L-130, Livermore, CA 94550, USA

Ning Xiang, Cochair
Rensselaer Polytechnic Institute, Greene Building, School of Architecture, 110 8th Street, Troy, NY 12180, USA

Contributed Papers

4:00

1pSPb1. Signal analysis in acoustic microscopy for nondestructive inspection of varnish layers on metal substrates. Sebastian Brand (University of Halle, Magdeburger St. 22, 06112 Halle, Germany, Sebastian.Brand@medizin.uni-halle.de), Peter Czuratis (SAM TEC GmbH, Gartenstrasse 133, 0553 Aalen, Germany, p.czurratis@stec-germany.com), Kay Raum (Martin Luther University of Halle-Wittenberg, Dept. of Orthopedics, Q-BAM Group, Magdeburger Str. 22, 06097 Halle, Germany, kay.raum@medizin.uni-halle.de)

For preventing corrosion and for surface protection metallic objects are commonly finished with layers of varnish. The integrity of the varnish and potential defect propagation influence the durability of the metal and hence are a measure for the quality of the finishing. Scanning acoustic microscopy provides high axial and lateral resolution, a sufficient penetration depth and is nondestructive. The goal of this work was the development of a method for detection and evaluation of delaminations of varnish layers on metallic surfaces. Investigated were samples containing one and two layers of varnish. One group contained priming only whereas the second group contained varnish on top of the undercoat. The surface integrity of the finishing was destroyed by a scratch through all finishing layers. Defect aging was then performed by exposing the samples to a corrosion-friendly atmosphere. Scanning acoustic microscopy combined with signal analysis was performed for investigating the connectivity between the finishing layers and the substrate. A robust numerical deconvolution technique has been adapted and optimized to enable the separation of strongly overlapping pulses. Echoes originated at the substrate and the finishing layers have been localized and layer thicknesses/distances were estimated. Delaminated spots of the finishing were successfully evaluated using the method developed during this study.

4:20

1pSPb2. Structural noise characterization and flaw detection in austenitic stainless steels using ultrasonic signals, wavelet analysis and significance testing. Mohamed Khelil (ENSIM - LAUM, Université du Maine, rue Aristote, 72085 Le Mans, France, mohamed.khelil@univ-lemans.fr), Jean-Hugh Thomas (ENSIM - LAUM, Université du Maine, rue Aristote, 72085 Le Mans, France, jean-hugh.thomas@univ-lemans.fr), Rachid El Guerjouma (ENSIM - LAUM, Université du Maine, rue Aristote, 72085 Le Mans, France, Rachid.El_Guerjouma@univ-lemans.fr), Laurent Simon (LAUM, CNRS, Université du Maine, Lab. d'Acoustique Université du Maine, UMR CNRS 6613, 72085 Le Mans Cedex 9, France, Laurent.Simon@univ-lemans.fr), Malika Boudraa (USTHB Faculté d'électronique et d'informatique, BP 32, El-Alia, 16031 Alger, Algeria, mk .boudraa@yahoo.fr)

The aim of this study is to characterize the structural noise in order to better detect flaws in several heterogeneous materials (steels, welding, composites œ) using ultrasonic waves. For this purpose, a continuous wavelet transform is applied to ultrasonic Ascan signals acquired using an ultrasonic Non Destructive Testing (NDT) device. The time-scale representation provided, which highlights the temporal evolution of the spectral content of the Ascan signals, is relevant but can lead to misinterpretation. The problem is to identify if each pattern from the wavelet representation is due to the structural noise or a flaw. To solve it, a detection technique based on statistical significance testing in the time-scale plane is used. Typical structural noise signals are then described using an autoregressive model which seems relevant according to the spectral content of the signals. The approach is tested on experimental signals, obtained by ultrasonic NDT of metallic materials (austenitic stainless steel) then of a welding in this steel and indeed enables to separate various components from the signal that is two kinds of structural noises and flaw echoes.

4:40

1pSPb3. Flaw detection and thin materials thickness measurement using time frequency and high resolution algorithms. Redouane Drai (Image and signal processing laboratory. Welding and NDT Centre, Route de Dely-Ibrahim, BP 64, Chéraga, 16035 Alger, Algeria, drai_r@yahoo.fr), Mohamed Khelil (ENSIM - LAUM, Université du Maine, rue Aristote, 72085 Le Mans, France, mohamed.khelil@univ-lemans.fr), Fouzia Megherbi (Welding and Control Research Center, Route de Dely-Ibrahim, B.P 64, Chéraga, 16035 Algiers, Algeria, fmegherbi@yahoo.fr), Abdelsaalam Benammar (Image and signal processing laboratory. Welding and NDT Centre, Route de Dely-Ibrahim, BP 64, Chéraga, 16035 Alger, Algeria, abs_benammar@yahoo.fr)

Several techniques of signal processing were introduced in ultrasonics NDT field. In thin samples the reflected signals are overlapping thus making detection of defects in these samples and accurate measurements impossible. It is thus necessary to enhance the visibility of the defect echo by signal processing techniques. In this context, we develop signal processing tools allowing detecting and locating the imperfections present in these materials. In this paper, we contribute by the development of some signal processing techniques based on time frequency and high resolution algorithms in order to enhance the resolution of flaw detection and to measure thin materials thickness. 1- We propose to implement temporal versions of methods known as high resolution like MUSIC, Root MUSIC and Eigen vectors method. These methods allow frequencies extraction in the case of the complex signals drowned in noise. 2- We apply time-frequency algorithms based on STFT, Wigner-Ville, Gabor transform on thin materials thickness measurement. A comparative study is carried out between all of these algorithms and is applied in separation of closer flaw echoes and thin materials thickness measurement. Satisfactory results are obtained with Gabor transform in measurement of few tenth (0.1) mm.

5:00

1pSPb4. Investigation of damage mechanisms of composite materials: multivariable analysis based on temporal and wavelet features extracted from acoustic emission signals. Anne Marec (ENSIM - LAUM, Université du Maine, rue Aristote, 72085 Le Mans, France, anne.marec.etu@univ-lemans.fr), Jean-Hugh Thomas (ENSIM - LAUM, Université du Maine, rue Aristote, 72085 Le Mans, France, jean-hugh.thomas@univ-lemans.fr), Rachid El Guerjouma (ENSIM - LAUM, Université du Maine, rue Aristote, 72085 Le Mans, France, Rachid .El_Guerjouma@univ-lemans.fr)

The aim of this work is the analysis of damage development and time-to-failure mechanisms within fibre-matrix composite materials in order to assess their remaining lifetime using in situ ultrasonic sensors. Thus Acoustic Emission (AE), which represents the generation of transient ultrasonic waves in a material under load, is used to discriminate the different damage mechanisms in composite materials. In this work, unsupervised pattern recognition analyses (fuzzy c-means) associated with a principal component analysis are used for classifying the AE events. A cluster analysis of AE data is achieved and the resulting clusters are correlated to the damage mechanisms of the material under investigation. This method gives good results on complex composite materials such as glass fibre/polyester cross-ply composites, sheet molding compound (SMC), concretes. Furthermore, AE signals of heterogeneous materials are not stationary. Thus, time-scale or time-frequency methods (continuous and discrete wavelet transforms) are used to determine new relevant descriptors from AE signals. These new descriptors are introduced in the clustering process to provide a better characterization and discrimination of the different damage mechanisms.

5:20

1pSPb5. Ultrasonic structural health monitoring by multiple-input-single-output minimum variance processing. Jeffrey Krolik (Duke University, ECE Dept. Hudson Hall 130, P.O. Box 90291, Durham, NC 27708, USA, jk@ee.duke.edu), Granger Hickman (Duke University, ECE Dept. Hudson Hall 130, P.O. Box 90291, Durham, NC 27708, USA, gwh@ee.duke.edu), Lawrence Carin (Duke University, ECE Dept. Hudson Hall 130, P.O. Box 90291, Durham, NC 27708, USA, lcarin@ee.duke.edu), Jennifer E. Michaels (Georgia Institute of Technology, Van Leer Electrical Engineering Building, Atlanta, GA 30332, USA, jennifer.michaels@ece.gatech.edu)

This work concerns ultrasonic detection and localization of defects in platelike metal structures such as airfoils. In previous work, MIMO delay-and-sum beamforming has been used to image these defects using change-detected ultrasonic signals between a sparse array of transmitters and receivers. However, mismatch of medium dispersion and unknown scattering properties of the defects can lead to significant imaging artifacts. To reduce imaging artifacts and sidelobes, a multiple-input-single-output (MISO) minimum variance (MV) approach is proposed here. MV-MISO imaging involves electronically scanning a transmit beam over the area of interest while, at each point being imaged, virutal transmit nulls are adaptively steered in the directions of interfering scatterers. For each imaging cell, this is achieved by adjusting transmit weights to minimize the variance of signals received at a single receiver subject to the constraint of achieving constant insonification. Using a model of dispersive Lamb wave propagation, the proposed algorithm has been successfully applied to change-detected data gathered with a six-sensor transmit-receive array coupled to a thin aluminum plate with artificial defects (e.g., drilled holes).

5:40

1pSPb6. An accurate distance measurement by calibration of doppler-shift for ultrasonic sonar sensing. Hirata Shinnosuke (Tokyo Institute of Technology, 4259 Nagatutamati, Midori-ku, 226-8502 Yokohama, Japan, hirata.s.ab@m.titech.ac.jp), Minoru K. Kurosawa (Tokyo Institute of Technology, 4259 Nagatutamati, Midori-ku, 226-8502 Yokohama, Japan, mkur@ip.titech.ac.jp), Takasi Katagiri (Sutekina Inc., 200 14 Akaho, 399-4117 Komagane, Japan, takashi.katagiri@primemotion.com)

Ultrasonic distance measurement with the pulse-echo method is based upon the determination of the time of flight of ultrasonic waves. The pulse-compression technique, which involves the calculation of the cross-

correlation function between the transmitted and the reflected waves, is the conventional method for improving the resolution of the measurement. The calculation of a cross-correlation operation requires high-cost digital signal processing, however. This paper presents a new sensor signal processing method of the pulse-compression technique using a delta-sigma modulated single-bit digital signal. The proposed method consists of three parts: an analyzing operation of the doppler-shifted frequency, a cross-correlation operation by single-bit signal processing, and a smoothing operation accomplished by a moving average filter. For the pulse-compression technique, this method reduces the calculation cost of digital signal processing. Since the frequency of the linear chirp signal is doppler-shifted, the distance from the moving transmitter to the moving object cannot be accurately measured in the pulse-compression technique. To solve this problem, the analyzing operation of the doppler-shifted frequency is used to calibrate the transmitted ultrasonic wave, thus effectively improving the accuracy of the measurement.

6:00

1pSPb7. Image processing and wavelets transform for sizing of weld defects using ultrasonic TOFD images. Ahmed Kechida (Image and Signal Processing Laboratory. Welding and NDT Centre, Route de Dely-Ibrahim, BP 64, Chéraga, 16035 Alger, Algeria, Abs_benammar@yahoo.fr), Redouane Drai (Image and Signal Processing Laboratory. Welding and NDT Centre, Route de Dely-Ibrahim, BP 64, Chéraga, 16035 Alger, Algeria, drai_r@yahoo.fr), Abdelsaalam Benammar (Image and Signal Processing Laboratory. Welding and NDT Centre, Route de Dely-Ibrahim, BP 64, Chéraga, 16035 Alger, Algeria, abs _benammar@yahoo.fr)

Ultrasonic time-of-flight diffraction (TOFD) is rapidly gaining prominence as a reliable nondestructive testing technique for weld inspection in steel structures, providing highly accurate positioning and sizing of flaws. A number of signal and image processing tools have been specifically developed for use with TOFD data and adapted to function autonomously without the need for continuous intervention, configuring automatically according to the nature of the data and the data acquisition settings. This paper presents the results of several innovative procedures based on Multiresolution analysis such as wavelet transforms and texture analysis for detecting edges of planar defects. The approach is based on the decomposition by packets of wavelets of the image while taking into account of the underimage content textural after each level of decomposition. The reconstruction of the image is done by eliminating the underimages of poor textural information and at the end the segmented image is got by a binarisation operation done on the image rebuilt histogram. The automation of sizing and positioning of weld flaws in TOFD data as an essential stage of a comprehensive TOFD inspection and interpretation aid is developed and implemented. Key words: Ultrasonic Time-Of-Flight Diffraction., Texture Analysis, Wavelet Transform.

6:20

1pSPb8. Temporal approach of the synthetic aperture imaging using Hadamard matrix. Frédéric Mosca (Ixsea, 46 Quai François Mitterrand, 13600 La Ciotat, France, fmo@ixsea.com), Jean-Marie Nicolas (Ecole Nationale Supérieure des Télécommunication de Paris, Telecom ParisTech, Département TSI, 46 rue Barrault, 75634 Paris Cedex 13, France, nicolas@enst.fr), Laurent Kopp (IXwaves, 220 rue Albert Caquot, 06560 Sophia Antipolis, France, laurent.kopp@ixwaves.com), Mathieu Couade (Supersonic Imagine, Les Jardins de la Duranne, bât E, 510, rue René Descartes, 13857 Aix-en-Provence, France, mathieu.couade @supersonicimagine.fr)

The synthetic aperture imaging is a very promising solution in the well-known compromise between contrast and frame rate. Indeed this method leads to the measurement of each transmitter/receiver impulse response of the system. From this fact, synthetic aperture imaging reach the transmit/receive focus imaging quality for the cost in frame rate of the number of antenna's elements. The main inconvenient of this method is the very low signal to noise ratio provided. Indeed, using only one transmitter per sequence leads to a very poor penetration. To correct this, a method using spatial Hadamard sequences has been introduced. For each of this Hadamard sequence, a Hadamard beam is generated in the medium. By a temporal approach, some interesting properties of those beams are highlighted and a method using those properties is proposed. Some experiments have been done using those properties and the results show an important improvement of the frame rate for a very small cost in contrast.

6:40

1pSPb9. Elastic-wave reverse-time migration imaging with a new vector-imaging condition. Huseyin Denli (Los Alamos National Laboratory, Mail Stop D408, Los ALamos, NM 87544, USA, denli@lanl.gov), Lianjie Huang (EES-11 (Geophysics) - Los Alamos National Laboratory, MS D443, Los Alamos, NM 87545, USA, ljh@lanl.gov)

With increasing computing capability, the use of elastic waves in three-dimensional subsurface imaging is becoming more feasible. However, the research in this area is still in the embryonic stage. In conventional seismic imaging, multicomponent data are decomposed into compressional and shear components, and solutions of the acoustic-wave equation are used to process each component independently. Such an imaging technique, however, cannot correctly handle elastic-wave conversions/couplings in complex regions, which is critically important for high-resolution and reliable imaging. In this paper, we develop elastic reverse-time migration imaging, applying a finite-difference solution to the pure elastic-wave equation in heterogeneous media. We implement numerical reverse-time migration imaging in a scheme similar to time-reversal acoustics in the laboratory. To correctly handle polarizations of compressional- and shear-waves during imaging, we also develop a novel vector-imaging condition for elastic-wave reverse-time migration. We use synthetic reflection data to demonstrate that, compared with the conventional imaging condition, our new vector-imaging condition increases image resolution and reduces image artifacts. The new imaging algorithm can significantly improve our capability to image complex subsurface structures.

Session 1pUW

Underwater Acoustics, Acoustical Oceanography, and ECUA: Seabed and Sea Surface Interaction Measurements and Modeling

Peter H. Dahl, Cochair
Applied Physics Laboratory, University of Washington, 1013 NE 40th St, Seattle, WA 98105, USA

Michael A. Ainslie, Cochair
TNO Defence, Security and Safety, Oude Waalsdorperweg 63, The Hague, 2597 AK, Netherlands

Invited Paper

1:00

1pUW1. Fine-grained sediment layers: an acoustic lens for sub-bottom sediment processes and structures. Charles W. Holland (Penn State University/Applied Research Lab, Applied Science Bldg., State College, PA 16804, USA, cwh10@psu.edu)

In many coastal and deep water regions, there is a layer of fine-grained sediment (e.g., clay and silty-clay) over coarser grained sediments or rock. This layer may range from scales of centimeters to hundreds of meters thick. Fine-grained sediments typically have a sound speed less than that of the interstitial fluid (i.e., overlying water column) with modest attenuation and thus act as a refracting lens for the acoustic field as it interacts with sub-bottom structures. The presence of fine-grained sediments frequently opens an effective window for acoustically probing very small-scale processes within the sediment. The presence of fine-grained sediments also has a profound impact on seabed reflection and scattering, hence propagation, reverberation, and clutter. The effect of fine-grained sediment layers (along with concomitant sub-bottom processes) on reflection and scattering is discussed using both theory and measurements. [Research supported by ONR OA321.]

Contributed Paper

1:20

1pUW2. A parametric study of interactions between acoustic signals reflected by the seafloor. Samuel Pinson (Ecole Navale/Irenav, BP 600, 29240 Brest Armées, France, samuel.pinson@ecole-navale.fr), Laurent Guillon (Ecole Navale/Irenav, BP 600, 29240 Brest Armées, France, guillon @ecole-navale.fr)

This paper deals with the study of broadband acoustic signals reflected by the seafloor and recorded on a vertical array in shallow water areas. Only the first bottom reflected path is considered here. In previous studies (see e.g., Guillon and Holland, JASA, **122**, 2974), two different aspects of the ″coherence″ of these signals were examined (the maximum of the cross-correlation coefficients and the phase of the cross-spectra) and it was shown that these parameters are sensitive to the geoacoustic nature of the seafloor. These results show that the interactions between signals can be used efficiently for improving geoacoustic inversion schemes or for transmission loss predictions. Before going to such applications, a detailed parametric study is needed to investigate the sensitivity of the interactions measurement to various parameters (range, geoacoustic structure,...). This is done using a numerical model, based on the spherical wave decomposition of plane waves, that simulates the signals reflected by the seafloor. The parametric study lead shows the relative importance of the various parameters and gives indications for the possibility of inverting these parameters.

Invited Paper

1:40

1pUW3. Mid-frequency bottom interaction measurements off the New Jersey continental shelf. Jee Woong Choi (Dept. of Environmental Marine Sciences, Hanyang Univ., 1271, Sa-3-dong, Sangrok-gu, 426-791 Ansan, Republic of Korea, choijw@hanyang.ac.kr), Peter H. Dahl (Applied Physics Laboratory, University of Washington, 1013 NE 40th St, Seattle, WA 98105, USA, dahl@apl.washington.edu)

Two kinds of bottom interaction measurements conducted in waters 80 m deep off the North American continental shelf as part of Shallow Water 06 (August, 2006) are discussed. In each, acoustic signals were recorded on two, colocated vertical line arrays of length 1.4 m, one at depth 25 m, and other at depth 50 m. The source was deployed at depth 40 m from the R/V Knorr that could either be positioned or towed at rate 0.1 m/s. The first, ″bottom reflection″ is interpreted as a measure of the modulus of the plane wave reflection coefficient as functions of frequency (1-20 kHz) and grazing angle associated with the discrete set of ranges (50-300 m). The second represents a ″move-out″ type measurement with source towed away from the receiver, and reflection at continuous angles associated with the 50-300 m range. Frequency range was 1-2 kHz, and as the source was 5 m off the bottom, spherical wave effects are

investigated. Both measurements were carried out over the same four directions originating from the receiver, each separated by 90 degrees. Physical processes responsible for the observations in each case are discussed and modeled. [Supported by ONR, with partial support from Hanyang University.]

Contributed Paper

2:00

1pUW4. Analysis of acoustic backscattering from the ocean bottom using radiative transfer theory. Jorge E. Quijano (NEAR Lab-Portland State University, 1900 SW 4th Avenue, Suite 160, Portland, OR 97201, USA, jorgeq@pdx.edu), Lisa M. Zurk (NEAR Lab-Portland State University, 1900 SW 4th Avenue, Suite 160, Portland, OR 97201, USA, zurkl @cecs.pdx.edu)

Radiative Transfer (RT) theory is a heuristic formulation for analysis of wave propagation in random media based on the principle of conservation of energy rather than on the solution of the wave equation. The theory has been applied to electromagnetics and more recently to ultrasound and seismics, and it has the advantage of being computationally tractable for complex random environments. In this paper the RT formulation is proposed for the problem of layered ocean bottom sediment with random scatterers. The volume backscattering level from tenuous media is obtained by solving the RT equation at each individual layer and by applying the corresponding reflection and transmission coefficients at the rough boundaries. Simulations of the backscattered acoustic intensity from a finite layer with elastic spherical scatterers are presented. The results obtained from the RT equation are compared to those based on the wave equation. Single frequency steady state solutions are considered for different cases of sediment attenuation and layer thickness. The flexibility of the RT method is demonstrated by showing the individual effect of propagating longitudinal and shear waves in the elastic sediment. It is proved that the contribution of shear waves in consolidated sediments is considerable.

Invited Paper

2:20

1pUW5. Determination of seabed scattering law from long range reverberation. Christopher H. Harrison (NATO Undersea Research Centre, Viale San Bartolomeo 400, 19138 La Spezia, Italy, harrison@nurc.nato.int)

Reverberation degrades sonar performance, and often the dominant cause in shallow water is scattering from the seabed. Usually scattering is weaker at low angles than at high whereas, in contrast, sound propagates better at low angles than at high. This, in turn, affects the range-dependence of signal-to-reverberation which influences the choice of source level. A better understanding of this scattering angle dependence (or scattering law) offers the potential of improved discrimination of targets against this reverberation background. This paper will discuss an experimental technique for deducing the scattering angle dependence and backscattering strength from long range reverberation (out to 25 km) measured on a vertical line array (VLA). Well-sampled near simultaneous angle-dependent propagation measurements out to comparable ranges are used to separate the propagation effects without the need for any modeling. Applying the technique to the Malta Plateau (during BOUNDARY2003 and BOUNDARY2004), first the method appears to work, and second it suggests that the scattering law is close to Lambert when the seabed is flat.

Contributed Paper

2:40

1pUW6. Underwater stereo-photographic measurement of small scale roughness: limits to spatial correlation accuracy. Gaetano Canepa (NATO Undersea Research Centre, Viale San Bartolomeo 400, 19126 La Spezia, Italy, canepa@nurc.nato.int), Eric Pouliquen (NATO ACT, 7857 Blandy Road, Suite 100, Norfolk, 23551-2490, USA, pouliquen@act.nato.int), Anthony P. Lyons (Applied Research Laboratory, The Pennsylvania State University, P.O. Box 30, State College, 16804, USA, apl2@psu.edu)

In recent years stereo-photogrammetry measurements of seafloor small scale roughness have been reported in the literature. Stereo-photogrammetry algorithm consists of a comparison between areas (windows) belonging to corresponding regions of a pair of photos. This comparison may be performed numerically or by human eyes using a photogrammetric stereocomparator. The results of this process are then converted in an array of seafloor heights. Until now underwater stereo-photographic data are given with no quantitative measurement of the positions and position correlation lengths errors: this work addresses this problem applying the results to the SAPHO system (Seafloor Automatic PHOtogrammetry) developed at NURC. It is shown that positional error estimates for stereo-photographic systems must take into account not only line/matrix resolution and system geometry but also the effects of comparison window size and image quality. A method by which this can be achieved is described. It is also shown that the stereo-photographic systematic error has an important effect when the purpose of the measurement is to determine seafloor correlation length or power spectral density for acoustic scattering estimation.

Invited Paper

3:00

1pUW7. Bubbles at the top and bottom of the water column: the acoustical effects, and the use of acoustics to measure them. Timothy G. Leighton (Institute of Sound and Vibration, Univ. of Southampton, University Road, Highfield, SO17 1BJ Southampton, UK, T.G.Leighton@soton.ac.uk), David Coles (National Physical Laboratory, Hampton Road, TW11 OLW Teddington, UK, dc@isvr.soton.ac.uk), Michael A. Ainslie (TNO Defence, Security and Safety, Oude Waalsdorperweg 63, 2597 AK The Hague, Netherlands, michael.ainslie@tno.nl), Paul R. White (Institute of Sound and Vibration, Univ. of Southampton, University Road, Highfield, SO17 1BJ Southampton, UK, prw@isvr.soton.ac.uk)

Bubbles of atmospheric gas can be entrained by breaking waves at the top of the water column: this bubble population is dynamic, and will evolve through the effects of buoyancy, gas exsolution and dissolution, and the fragmentation and coalescence of bubbles. These processes are important to ambient noise, sonar operation, and the overall gas budget of the planet. At the base of the water column, methane bubbles can occur in marine sediments, a phenomenon important to the global methane budget, to the petrochemical industry, and to the stability of the sediment (e.g., for civil engineering purposes). This paper examines the acoustical effects of both of

these populations, and the ways in which acoustics can be used to measure them. Data will be presented from field trials, including measurements of gassy marine sediments in UK waters, and of wave-generated bubble clouds measured by an 11 m spar buoy deployed from 16th June to 18th July 2007 at a distance of 400 miles off the west coast of Portugal.

3:20-3:40 Break

Contributed Paper

3:40

1pUW8. The effect of wind-generated bubbles on sea-surface backscattering at 940 Hz. Robbert Van Vossen (TNO Defence, Security and Safety, Oude Waalsdorperweg 63, 2597 AK The Hague, Netherlands, robbert.vanvossen@tno.nl), Michael A. Ainslie (TNO Defence, Security and Safety, Oude Waalsdorperweg 63, 2597 AK The Hague, Netherlands, michael.ainslie@tno.nl)

Predictions of sea-surface backscattering strength are needed for sonar performance modelling. Such predictions are hampered by two problems. First, measurements on surface backscattering are not available at small grazing angles. These are of special interest to low-frequency active sonar since these mainly contribute to long range propagation. Second, existing theoretical models underestimate the surface backscattering strength at larger grazing angles. We investigate whether wind-generated bubbles can explain this deficit. Thus, we develop a theoretical description which includes the effect of refraction and scattering of sound by wind-generated bubbles. We compare the theoretical surface backscattering predictions to Critical Sea Test measurements. These are a set of backscattering measurements for different wind speeds, and grazing angles are in the range between 5 and 30 degrees. The comparison shows that a good fit can be obtained between the theoretical predictions and the surface backscattering measurements, depending on the population density of resonant bubbles. This indicates that wind-generated bubbles significantly contribute to rough-surface back-scattering. The bubble backscattering contribution is dominant at large wind speeds and also at small grazing angles.

Invited Paper

4:00

1pUW9. Quasi-deterministic forward scattering from the sea surface. Grant Deane (Scripps Inst. Oceanography, Univ. Califiornia, San Diego, La Jolla, CA 92093, USA, gdeane@ucsd.edu), James Preisig (Woods Hole Oceanographic Institution, Bigelow 404, MS#9, Woods Hole, MA 02543, USA, jpreisig@whoi.edu), Chris T. Tindle (Physics Department, University of Auckland, Bag 92019, 1010 Auckland, New Zealand, c.tindle@auckland.ac.nz)

Gravity waves create focal regions and caustics in sound forward-scattered from the sea surface. Focal regions are associated with rapid variations in amplitude and Doppler shift, which can impact the performance of underwater communications systems and sonars operated near the shore. Single-bounce focal regions consist of a superposition of up to 3 micro-paths, each of which is associated with its own amplitude, time delay, and Doppler shift. Focal regions move systematically through the water column as the wave propagates. Studies of these effects in near-shore ocean experiments and a laboratory flume have shown that a quasi-deterministic analysis of wave scattering can lead to valuable insights about the underlying scattering process. [Work supported by ONR.]

Contributed Papers

4:20

1pUW10. Multipath reflection from surface waves. Chris T. Tindle (Physics Department, University of Auckland, Bag 92019, 1010 Auckland, New Zealand, c.tindle@auckland.ac.nz), Grant Deane (Scripps Inst. Oceanography, Univ. Califiornia, San Diego, La Jolla, CA 92093, USA, gdeane@ucsd.edu), James Preisig (Woods Hole Oceanographic Institution, Bigelow 404, MS#9, Woods Hole, MA 02543, USA, jpreisig@whoi.edu)

A tank experiment was conducted at Scripps Institution of Oceanography to measure reflection of underwater sound from surface waves. Short pulses at a nominal 200 kHz were transmitted beneath surface waves of wavelength 0.7 m to a receiver at 1.2 m range. The surface wave crests act as curved mirrors for underwater sound and lead to focussing and caustics in the surface reflected pulses. The locations of the foci and caustics move steadily as the wave progresses and lead to rapid variation of amplitude, phase and arrival time of the received pulses. Wavefront modeling has been used to calculate theoretical waveforms for the measured surface wave shape. The theory shows there are typically three distinct reflected eigenrays beneath a wave crest and they interfere to give rapid variation of the received signal. The theory gives good agreement with the details of the time dependent interference of the surface reflected pulses. [Work supported by ONR.]

4:40

1pUW11. Observations and modeling of angular compression and vertical spatial coherence in sea surface forward scattering. Peter H. Dahl (Applied Physics Laboratory, University of Washington, 1013 NE 40th St., Seattle, WA 98105, USA, dahl@apl.washington.edu)

Measurements and modeling of vertical spatial coherence and related angular spreading associated with forward scattering from the sea surface are presented. The van Cittert-Zernike theorem is used in the modeling. The measurements were conducted in waters 80 m deep off the North American continental shelf (Shallow Water 06, Aug. 2006). Acoustic signals were recorded on a moored array system (MORAY) consisting of three arrays (each 1.4 m): two vertical line arrays at depth 25 m and 50 m, and one horizontal array at depth 27 m. The source (1-20 kHz) was deployed at depth 40 m from the R/V Knorr, at ranges 50-500 m from the MORAY. Conditions were characterized by a downward-refracting profile, e.g., sound speed going from 1530 m/s at the surface to 1490 m/s at depth 25 m. Refraction modifies the vertical angular vertical spread due to scattering, which can understood from Snell's law. The Snell mapping is smooth, and a Taylor expansion around the mean grazing angle provides a functional relation between the angular variance near the surface and that at the receiver associated with scattering. The latter is measurably compressed owing to refraction, an effect mirrored in the spatial coherence data. [Research support from ONR.]

5:00

1pUW12. Unperturbed normal mode method for forward surface scattering. Frank S. Henyey (Applied Physics Laboratory, University of Washington, 1013 NE 40th St, Seattle, WA 98105, USA, frank@apl.washington.edu), Eric Thorsos (Applied Physics Laboratory, University of Washington, 1013 NE 40th St, Seattle, WA 98105, USA, eit @apl.washington.edu)

A technique is presented that uses an expansion in unperturbed modes to calculate acoustic scattering from ocean surface waves in a shallow water waveguide. The basic formalism as well as a useful extension to account for the difference between the water column and the domain in which the modes

are calculated. The coupling between the modes due to the waves is local at the ocean surface, unlike the coupling of local modes. Numerical examples of the calculation are given for both a sinusoid surface wave and a random surface wave with a typical wind driven spectrum.

5:20

1pUW13. Sonic-boom noise under a wavy air-water interface. Adam M. Fincham (University of Southern, Aerospace & Mechanical Engineering, 854 W Downey Way, Los Angeles, CA 90089-1191, USA, afincham@usc.edu), Tony Maxworthy (University of Southern, Aerospa & Mechanical Engineering, 854 W Downey Way, Los Angeles, CA 90089-1191, USA, maxworth@usc.edu), Hsien K. Cheng (University of Southern, Aerospace & Mechanical Engineering, 854 W Downey Way, Los Angeles, CA 90089-1191, USA, afincham@usc.edu), Charles P. Griffice (The Aerospace Corporation, System Planning and Engineering, El Segundo, CA 90245-4691, USA, Charles.P.Griffice@aero.org), Johnson C. Wang (The Aerospace Corporation, System Planning and Engineering, El Segundo, CA 90245-4691, USA, Johnson.C.Wang@aero.org), John R. Edwards (U. S. Air Force, Air Force Space Command, 483 N. Aviation Blvd., El Segundo, CA 90245-2808, USA, John.Edwards@LOSANGELES.AF.MIL), Adel A. Hashad(U. S. Air Force, Air Force Space Command, 483 N. Aviation Blvd., El Segundo, CA 90245-2808, USA, Adel.Hashad@LOSANGELES.AF.MIL)

Recent investigations of the underwater sound field produced by sonic booms show that the latter's interaction with surface waves can strongly alter the sound level, frequency range, and signal waveform reaching the deeper part of the ocean. Unlike conclusions from studies based on the flat-ocean model of Sawyers [1] which indicate little effects at depth beyond one signature length, the interaction of sonic-boom waves with a surface-wave train can generate nonevanescent, downward propagating waves which, owing to their lower spatial-attenuation rate, overwhelm the otherwise primary (flat-ocean) wave field. Theoretical results [2] substantiate and elucidate the significant differences between flat and wavy surfaces in waveform characteristics and their audibility in deep, and moderately deep water. Here we report on an extensive series of laboratory experiments performed specifically to validate this theoretical model and to ascertain the distinct differences in wave-field characteristics between a wavy and flat interface. The experimental measurements confirm the theoretical findings, showing the predicted differences between the sound fields measured under wavy and flat air-water interfaces stimulated by a passing sonic boom. [1] Sawyers, K. H. J. Acoust. Soc. Am., **44**(2), 523 - 524, (1968) [2] Cheng, H. K. and Lee, C. J., J. Fluid Mech. **514**, 281-312 (2004).

Session 2aAAa

Architectural Acoustics: Acoustics of Concert Halls II

Takayuki Hidaka, Cochair
Takenaka R&D Institute, 1-5-1, Otsuka, 270-1395 Inzai, Chiba, Japan

Daniel E. Commins, Cochair
Commins Acoustics Workshop, 15 rue Laurence Savart, Paris, 75020, France

Contributed Papers

8:00

2aAAa1. Acoustical design consideration for the new IFEZ concert hall. Jin Yong Jeon (Hanyang University, Department of Architectural Engineering, 133-791 Seoul, Republic of Korea, jyjeon@hanyang.ac.kr), Yong Hee Kim (Hanyang University, Department of Architectural Engineering, 133-791 Seoul, Republic of Korea, kimyonghee@gmail.com), Shin-Ichi Sato (Hanyang University, Department of Architectural Engineering, 133-791 Seoul, Republic of Korea, s_sato@mac.com)

The design of a new concert hall for the Incheon Free Economic Zone (IFEZ) Arts Center in Korea is in progress. The hall is supposed to be the home of the Asia Philharmonic Orchestra. It has over 1,700 seats, including 150 choirs. A vineyard seating arrangement will be applied, but the seats around the stage area will be minimized in order to form a solid stage enclosure. Lateral walls are designed for each seating block to increase acoustical intimacy. Average width between lateral walls has been designed to be less than 15 m, and every seat is arranged within 7.5 m to the closest lateral wall. All lateral walls are designed to be inclined to lead first reflections and to improve spatial impression at the audience area. Diffusers are functionally installed to the effective reflecting surfaces from the source on stage. The design considerations are investigated through both computer simulation and scale modelling.

8:20

2aAAa2. Objective and subjective analysis of acoustical response in newly renovated Palais Moncalm, Quebec City, Canada. Jean-Philippe Migneron (Lab. d'acoustique, École d'architecture, 1, Côte de la Fabrique, Vieux Séminaire, Université Laval, Québec, QC G1K 7P4, Canada, jean-philippe.migneron.1@ulaval.ca), Jean-Gabriel Migneron (Lab. d'acoustique, École d'architecture, 1, Côte de la Fabrique, Vieux Séminaire, Université Laval, Québec, QC G1K 7P4, Canada, jgmigneron@hotmail.com), Jean-François Hardy (Lab. d'acoustique, École d'architecture, 1, Côte de la Fabrique, Vieux Séminaire, Université Laval, Québec, QC G1K 7P4, Canada, jean-francois.hardy.1@ulaval.ca)

To celebrate the 75th anniversary of Palais Montcalm, the building has been almost entirely rebuilt to convert it into the House of Music. The main room, named Salle Raoul-Jobin, has been designed specifically for the resident chamber orchestra: Les Violons du Roy. Collaboration between acoustical consultant, Larry S. King, and architect Jacques Plante of MUSE consortium results in a 979 seats concert hall with variable acoustic to accommodate different kinds of musical events. Since reopening in March 2007, the general acoustic has been enthusiastically acclaimed by professionals, by world known musicians, and by the public. The principal objective of this study is to characterize acoustical response of the room with various adjustments of wall curtains and motorized canopy. This important reflective area is software-controlled in a range of 3 meters depending on musical needs. Acoustical objective parameters, such as reverberation time, early decay time, impulse response or C80 factor will be analyzed and compared to musical subjective perception of a few instruments played at multiple positions on stage and for different listening locations.

8:40

2aAAa3. New design tendencies in modern concert hall design. Alban A. Bassuet (Arup Acoustics, 155 avenue of the americas, New York, NY 10013, USA, alban.bassuet@arup.com)

New concert hall design trends are emerging as seen from recently completed halls around the world and recent international architectural competitions. Analyzing the current situation, the paper starts by differentiating the acoustical characters of major traditional concert hall forms such as the large shoe-box, the Vineyard and the surround hall. It discusses in particular the balance of acoustical energy that characterize these different basic hall shapes, the sensation of intimacy in relation to the listener's distance to the performance area and the different early reflection patterns inherent from these hall shapes. As an example of modern concert halls design tendencies, the paper then describes a design option chosen by Arup Acoustics for the Paris Concert Hall Architectural design competition with Zaha Hadid architect. The paper describes the development of the form and shape of the hall in response to the brief, the concept chosen for the design of sending/receiving surfaces to improve the early reflection ″efficiency″ and ″stability″ and the use of an overhead reflector to improve the balance between soloist and orchestra and the balance between the orchestra and the reverberation in the hall.

9:00

2aAAa4. Acoustic design and evaluation of a multi-purpose hall of a new conference centre. Attila Balázs Nagy (Kotschy Bt., Álmos vezér u. 4, 2045 Törökbálint, Hungary, nagyab@hit.bme.hu), Ferenc Tamás (Kotschy Bt., Álmos vezér u. 4, 2045 Törökbálint, Hungary, tamas.ferenc@kotschy.hu), András Kotschy (Kotschy Bt., Álmos vezér u. 4, 2045 Törökbálint, Hungary, bandi@kotschy.hu)

At Forum Acusticum 2005 the building and room acoustic design of a new Conference Centre was presented. Since then the construction work has been finished and the Centre is now open. The Conference Centre itself is a multi-functional building, having three wings of different functions. The Main Hall of the Centre is a room for 750 people which can be extended with adjacent section rooms for 1100 persons, giving a total volume of 14000 m^3. It was designed to host conferences, lectures, and - most of the time - to be used as a concert hall. The extremely different acoustical demands of being a concert hall and a lecture room had been fulfilled with appropriate room acoustic design and with variable acoustics by employing a DCR (Digital Control of Reverberation) system. In this paper we give a report on the achieved acoustical performance of the Main Hall of the Conference Centre. We have performed extensive room acoustic measurements in the Main Hall, the results of which are compared to the designed values and are presented in this paper. The design of the DCR system is discussed in a different paper.

9:20

2aAAa5. Renovation of the concert hall The Doelen: A case study on the impact of a stage canopy on stage and room acoustics. Margriet R. Lautenbach (Peutz BV, PO Box 696, 2700 AR Zoetermeer, Netherlands, m.lautenbach@zoetermeer.peutz.nl), Martijn Vercammen (Peutz, De Grippen 1124, 6605 TA Wijchen, Netherlands, m.vercammen@mook.peutz.nl), Klaus-Hendrik Lorenz-Kierakiewitz (Peutz BV, Kolberger Strasse 19, D-40599 Duesseldorf, Germany, khl@peutz.de)

When opened in 1966, the main concert hall in De Doelen, Rotterdam, the Netherlands, was provided with six canopies above the stage platform. Their function was twofold: to provide a large part of the audience with early reflections; to create good ensemble conditions for the musicians on stage. Despite good reviews after the opening, a few years later the canopies were removed to get rid of unwanted reflections at the recording microphones positions just below the canopy. Since then, a significant percentage of the orchestra is unhappy about the acoustic conditions on stage. During the design process of the renovation, possibilities to re-introduce a stage canopy are investigated. Objective acoustic parameters obtained by carrying out measurements in the hall as well as in a 1:10 scale model and by calculations with a ray-tracing computer model are examined. Parallel, three questionnaire rounds gave an impression about the musicians' subjective judgement about the stage acoustics. In this paper the acoustic differences of three situations (without canopy, with original canopies and with new canopy design) and the search for an optimal balance between improving the stage acoustics without altering room acoustical conditions in the audience are discussed.

Invited Paper

9:40

2aAAa6. Evaluation of virtual acoustic stage support for musical performance. Wieslaw Woszczyk (McGill University, Schulich School of Music, 555 Sherbrooke Street West, Montreal, QC H3A 1E3, Canada, wieslaw@music.mcgill.ca), William L. Martens (McGill University, Schulich School of Music, 555 Sherbrooke Street West, Montreal, QC H3A 1E3, Canada, wlm@music.mcgill.ca)

The effects of performance space acoustics on musical performance can be evaluated most effectively by eliminating the influence of powerful non-auditory factors, such as the visual appearance of the performance space. To allow for such relatively unbiased evaluations, a virtual acoustic stage support system was set up for a live musical performance, and the performer was asked to make blind comparisons between a variety of architectural acoustic simulations. While results support the broad generalization that the preferred reverberation time for acoustical stage support depends upon the piece of music to be performed, it was also clear that preferences strongly depended upon performers' aural familiarity with architectural acoustic spaces in which they had considerable experience in previous performances. After some exposure to descriptive analysis techniques, performers could explain their preferences in terms of the perceptual characteristics that differed between presented aural architectures.

TUESDAY MORNING, 1 JULY 2008 ROOM 253, 8:00 TO 9:00 A.M.

Session 2aAAb

Architectural Acoustics and Noise: Low Frequency Absorption: Mechanisms, Measurement Methods and Application II

Peter D'Antonio, Cochair
RPG Diffusor Systems, Inc., 651-C Commerce Drive, Upper Marlboro, MD 20774, USA

Christian Nocke, Cochair
Akustikbüro Oldenburg, Katharinenstr. 10, Oldenburg, 26121, Germany

Contributed Papers

8:00

2aAAb1. Effects of Low-frequency Absorption on Perceived Tightness of Bass Imagery in Music Reproduction. William L. Martens (McGill University, Schulich School of Music, 555 Sherbrooke Street West, Montreal, QC H3A 1E3, Canada, wlm@music.mcgill.ca)

In order to enable unbiased observation of the effects of low-frequency absorption on auditory imagery associated with multichannel loudspeaker reproduction, binaural recordings were made of surround sound program material that was reproduced over full-range loudspeakers located in a room that was specially constructed to allow for variation in low-frequency acoustical treatment. These recordings were then presented via headphones to allow for double-blind comparison of the variation in auditory imagery associated with selected changes in room acoustics while holding listener and loudspeaker locations constant. Several perceptual attributes were examined, but the listeners were able to make the most clear distinctions between auditory spatial images in terms of the attribute identified as the ″perceived tightness of bass imagery.″ Analysis of the signals presented to the listeners' ears in these binaurally-reproduced multichannel music samples showed that the tightest bass imagery was associated with high values of interaural coherence, with lower values producing more ″muddy″ bass imagery. [Work supported by Canada Foundation for Innovation.]

8:20

2aAAb2. Acoustical tests of custom-made, low-cost bass absorptive treatment for small rooms. Ioana Pieleanu (Acentech Incorporated, 33 Moulton Street, Cambridge, MA 02138, USA, ipieleanu@acentech.com), Jeffrey Fullerton (Acentech Incorporated, 33 Moulton Street, Cambridge, MA 02138, USA, jfullerton@acentech.com), Marc Choiniere (University of Nebraska, 101A Peter Kiewit Institute, Omaha, NE 68182, USA, mchoiniere@gmail.com)

Small music classrooms, practice rooms or small budget recording studios and control rooms are a few of the numerous applications where low frequency absorption is sought and necessary for a well-balanced acoustical spectrum. Often, low frequency absorption is achieved by using pre-engineered products, such as tuned panel resonators. Unfortunately, the cost of these pre-engineered products can be excessive for small budget projects,

or projects that involve a large number of such spaces. For these applications, more affordable, custom-made low frequency absorbers are desired. Several types of custom-made treatments were physically tested, to determine if the degree of low frequency absorption they provide would make them an effective replacement for the pre-engineered counterparts. The test samples included glass fiber panels mounted as corner traps, custom-made plywood panel resonators and others. The testing was conducted in a space comparable in size to a small studio room/control room, or a medium practice room. This presentation describes the test method and measurement results.

8:40

2aAAb3. The importance of bass clarity in pop and rock venues. Niels W. Adelman-Larsen (Flex Acoustics, Diplomvej 377, 2800 Lyngby, Denmark, nwl@flexac.com), Eric R. Thompson (Centre for applied hearing research, Technical University of Denmark, DTU, Bygn. 352, 2800 Lyngby, Denmark, et@oersted.dtu.dk)

High levels of bass sound have been shown to stimulate the part of the brain that controls such basic instincts as sexual desire and hunger [Todd, 2000]. In rock and pop music, the bass frequencies from 40-125 Hz get amplified to very loud levels. Easily half of the electrical power of the PA and monitor system goes to these 1.5 octaves. A recent survey [Adelman-Larsen et al., 2007] showed that the most important subjective parameter for a rock and pop music hall to score a high rating was 'bass clarity' which correlated with a coefficient of 0.74 to 'overall impression'. Informal discussions with audio engineers and bass players give the perspective that artificial reverberation is rarely, if ever, added to bass-frequencies. In fact the ideal hall should be as dry as possible at low-frequencies. In the mid-treble frequency range, sound absorption, and thereby 'clarity', is easily obtained through the presence of the audience that absorbs 4-6 times more mid/high frequency sound energy than bass sound energy. In the low-frequency range 'clarity' is not so easily obtained. This paper discusses the challenge in depth and proposes design solutions.

TUESDAY MORNING, 1 JULY 2008 ROOM 202/203, 8:20 A.M. TO 12:40 P.M.

Session 2aAAc

Architectural Acoustics and Engineering Acoustics: Acoustics and Electroacoustics of Small Rooms

Jiri Tichy, Cochair
Pennsylvania State University, 5552 N. Citation Road, Toledo, OH 43615, USA

Mendel Kleiner, Cochair
Chalmers Rm. Acoust. Group, Dept. of Appl. Acoust., Chalmers Univ. of Technology, Gothenburg, 41296, Sweden

Invited Papers

8:20

2aAAc1. Investigation of Bonello criteria as a practical tool in small room acoustics. Todd Welti (Harman International Industries, Inc., R&D Group, 8500 Balboa Blvd, Northridge, CA 91329, USA, twelti@harman.com)

The Bonello criteria are often used as an objective metric for assessing room dimensions with respect to modal response. In reality, the modal response is not simply a property of the room dimensions, but is quite dependent on source/receiver locations as well. The legitimacy of Bonello's criteria when used in rooms with typical subwoofer and seating configurations has not been well investigated. In this study, a room model is used to calculate room responses for a large number of combinations of room dimensions, subwoofer positions, and seating locations. The Bonello criteria are evaluated for each combination and compared to perceptually relevant criteria such as flatness and seat to seat consistency of the calculated acoustical responses.

8:40

2aAAc2. Region of control for low frequency modal equalisation in small listening rooms. Aki Mäkivirta (Genelec Oy, Olvitie 5, FIN-74100 Iisalmi, Finland, aki.makivirta@genelec.com)

Small-size listening rooms are characterized by sparse modal density with pronounced spectral colouration when the decay times at low frequencies are large. Various active approaches for reducing the modal decay time have been suggested in the literature. A review of the salient principles of these approaches is given. Active control of the modal decay time at the primary listening position by using the primary radiator for control is demonstrated and evaluated for performance. The locality and size of the region of control, and the amount of control achieved, are studied in light of the experiment. Effect of the modal equalizer filter to the perceived response flatness, audibility of low frequency resonances, and the required amount of modal equalization are discussed in light of the experiment.

9:00

2aAAc3. Improving room acoustics at low frequencies with multiple loudspeakers and time based room correction. Sofus Birkedal Nielsen (Aalborg University, Fredrik Bajers Vej 7 B, 9220 Aalborg Ø, Denmark, sbn@es.aau.dk), Adrian Celestinos (Oticon A/S, Kongebakken 9, 2765 Smørum, Denmark, adc@oticon.dk)

Small and medium size rectangular rooms are often used for sound reproduction. These rooms have substantial acoustical problems at low frequencies primarily caused by the reflections from the room boundaries. The spatial variation in sound pressure level (SPL) can be up to 30 dB in a room at low frequencies, and appear not only at modal frequencies. The problem is an acoustical issue in time, and should therefore be analyzed in the time-domain, instead of the traditional steady state frequency domain. The construction of a finite-difference time-domain approximation program (FDTD) has lead to a simple and untraditional solution called CABS (Controlled Acoustical Bass System) that makes use of multiple loudspeakers. With the proper placement of low frequency loudspeakers, CABS can create a plane wave from the front wall which will be absorbed by additional low frequency loudspeakers at the back wall. With the back wall reflection removed a homogeneous sound field will be created in the whole room at low frequencies. Simulations and measurements of normal size listening rooms show that 4 loudspeakers are enough to even the sound field in a room. The CABS system is controlled by a developed DSP system.

9:20

2aAAc4. Applications of a plane wave based room correction system for low frequencies using multiple loudspeakers. Adrian Celestinos (Oticon A/S, Kongebakken 9, 2765 Smørum, Denmark, adc@oticon.dk), Sofus Birkedal Nielsen (Aalborg University, Fredrik Bajers Vej 7 B, 9220 Aalborg Ø, Denmark, sbn@es.aau.dk)

When low frequency sound is radiated inside small listening spaces by loudspeakers, large uniformities occur over the sound field. This is due to the multiple reflection and diffraction of sound on the walls and different objects in the room. A developed system named Controlled Acoustically Bass System (CABS) produces uniform sound field at low frequencies. This is performed by utilizing loudspeakers at the front wall and extra loudspeakers at the opposite wall, processed to remove the rear-wall reflection of a rectangular room. Effectiveness of CABS on different room scenarios has been evaluated by using a computer simulation program based on the Finite Difference Time Domain Method (FDTD). CABS has been simulated in a small car cabin and in an irregular room. Non-ideal placement of loudspeakers in CABS have been evaluated. The influence of utilizing CABS with different types of loudspeakers has been evaluated by simulations and measurements.

9:40

2aAAc5. Active Sound Field Equalization. Akira Omoto (Kyushu University, 4-9-1, Shiobaru, Minamiku, 815-8540 Fukuoka, Japan, omoto@design.kyushu-u.ac.jp), Hisaharu Suzuki (Kyushu University, 4-9-1, Shiobaru, Minamiku, 815-8540 Fukuoka, Japan, hisaha@souldsp.jp), Akihiro Kakiuchi (Kyushu University, 4-9-1, Shiobaru, Minamiku, 815-8540 Fukuoka, Japan, kakirikakki @hotmail.com)

Dominant acoustic modes often result in the inevitable non-uniform distribution of the acoustic quantities such as sound pressure, especially in the small sized enclosure. In our study, active control technique is thus introduced to overcome the adverse effects of such modes. Instead of the squared sound pressure which is normally adopted in active noise control, the quantity to be controlled is selected as the weighted values of acoustic intensities or the acoustic impedances in rectangular directions such as x, y and z measured at plural points. The reasonably selected combinations of weights yield the control outputs which can alter the directions of propagating waves and result in reducing the complicated standing waves. Further, results of numerical simulations suggest that the well balanced arrangement of the primary and the secondary sources can 'rectify' the propagating direction and result in the uniform distributions of sound pressure. The strategies used in this study have possibilities of realizing useful controller for active sound field equalization.

10:00

2aAAc6. Different approaches for efficient finite element modelling of absorbers in small rooms. Marc Aretz (RWTH Aachen University, Institute for Technical Acoustics, Neustraße 50, 52066 Aachen, Germany, Marc.Aretz@akustik.rwth-aachen.de)

The FEM is a powerful tool for the numerical simulation of sound fields in enclosures. It accounts for the modal characteristics of the sound field, which are dominant at frequencies below the Schroeder frequency and it is also possible to model the mutual coupling between airborne and structure borne sound fields, when an appropriate structure model is implemented. When applying the FEM to complex room acoustics applications, like e.g. a control room in a recording studio, it is a challenging task to specify realistic boundary conditions. Different kinds of acoustical absorbers like Helmholtz resonators, plate absorbers and complex layered porous absorbers are found in these environments. While it is possible in principle to use complex and exhaustive models for these acoustical absorbers, it is often computationally much more efficient to use acoustic impedances or two-port network FEM elements to represent the fluid structure interactions. In the course of this study we compare different approaches for the modelling of Helmholtz resonators (without and without flow resistance), since it has proven very costly in terms of computation time to explicitly model every single hole in the resonator boxes. The simulation results are compared with results measured in a model room.

10:20-10:40 Break

10:40

2aAAc7. Direct and modal frequency response analysis of sound fields in small rooms by finite element method. Reiji Tomiku (Faculty of Engineering, Oita University, Dannoharu 700, 870-1192 Oita, Japan, tomiku-reiji@cc.oita-u.ac.jp), Toru Otsuru (Faculty of Engineering, Oita University, Dannoharu 700, 870-1192 Oita, Japan, otsuru@cc.oita-u.ac.jp), Noriko Okamoto (Faculty of Engineering, Oita University, Dannoharu 700, 870-1192 Oita, Japan, nokamoto@cc.oita-u.ac.jp), Yuka Kurogi (Faculty of Engineering, Oita University, Dannoharu 700, 870-1192 Oita, Japan, kurogi@cc.oita-u.ac.jp)

In this paper, sound pressures are computed by two techniques using finite element method. One is a technique by solving the system of linear equations directly (direct analysis) and the other is a technique by modal superposition (modal analysis). To confirm the accuracy of the direct analysis, sound pressures obtained by the technique are compared with those obtained by the modal analysis in a room with the volume of 10 m^3. Then, as in the modal analysis, two methods are employed: one is a simplified method based on a real eigenvalue problem assuming that the damping matrix, [C], has orthogonality; and another is the method based on complex eigenvalue problem. Those obtained by the direct analysis are in good agreement with those obtained by the two kinds of modal analyses regardless of absorption conditions, even if the analysis is carried out at the frequency close to an eigen frequency. Next, diffuseness of sound field below 315 Hz in a room, which is used in the measurement of ISO140-3, is investigated by the direct analysis from the viewpoint of mean sound pressure level measurements.

11:00

2aAAc8. The effect of diffusers on low frequency modes. Jamie A. Angus (University of Salford, 12 Lister Way, YO30 6NL York, UK, j.a.s.angus@salford.ac.uk)

Small listening rooms are becoming prevalent, due to the availability of production facilities on personal computers, and the financial pressures faced by the industry. In these rooms, modal behaviour at low frequencies significantly affects the quality of the reverberant decay, due to their non-diffuse nature compared with other frequencies. Diffusion and absorption can help and may be a useful way of improving the low frequency performance of such rooms. This paper discusses the properties of these rooms at low frequencies, in particular the effect of diffusing boundaries on the modal behaviour of such rooms. The paper will first discuss what is meant by a mode and modal decay. It will then go on to examine the effect of diffusing boundaries on the frequency and density of modes. In particular, it will examine the effect of the scale of the diffuser on its efficacy in this task. For ease of visualisation this will be done using a two dimensional model and, for accuracy a finite element, element simulation. The effect of going to three dimensions on the results will also be discussed. Finally, the effect of absorption based diffusing boundaries will be examined.

11:20

2aAAc9. Power output regularization in the active reproduction of sound fields in rooms. Nick Stefanakis (National Technical University of Athens, School of Electrical and Computer Engineering, Heroon Polytechniou 9, 157 73 Athens, Greece, nstefan@mobile.ntua.gr), Sotiris Dalianis (National Technical University of Athens, School of Electrical and Computer Engineering, Heroon Polytechniou 9, 157 73 Athens, Greece, dalias@central.ntua.gr), Tilemachos Karatzas (National Technical University of Athens, School of Electrical and Computer Engineering, Heroon Polytechniou 9, 157 73 Athens, Greece, tilkar6@hotmail.com), George Cambourakis (National Technical University of Athens, School of Electrical and Computer Engineering, Heroon Polytechniou 9, 157 73 Athens, Greece, gcamb@cs.ntua.gr)

In this paper we address the problem of using a multi-channel active control system in order to reproduce a harmonic sound field in a large part of the volume of a reverberant room. The problems associated with the calculation of the inverse system matrix are confronted by introducing a term that is proportional to the sound power-output of the system in the cost function that is obtained by the multiple point method. Simulation results show that this technique results to a better conditioning of the system matrix at low frequencies, comparing to other traditional regularization techniques. Moreover, it is shown that this method can be employed to increase the spatial robustness of the control sensor array inside the listening room.

11:40

2aAAc10. Low-frequency response in active acoustic practice rooms. Ronald Freiheit (Wenger Corporation, 555 Park Drive, Owatonna, MN 55060, USA, ron.freiheit@wengercorp.com)

Integrating active (virtual) acoustics into relatively small practice rooms to create a sense of envelopment is critical to the satisfaction of the musicians using these spaces for learning. The number of speakers and their locations play an important role in minimizing the ability to localize to the sources supporting this sense of envelopment. Equally important is the frequency response required for the speakers used in these applications, to more accurately simulate the acoustics of a performance environment. Excessive high frequencies increase the ability to localize and decrease the sensation of a larger space, since the air in larger spaces naturally absorbs many high frequencies. Another challenge is creating the sense of envelopment for instruments in the bass region (125Hz octave band and below) by providing enough low-frequency energy response. Work will be presented on low-frequency response desired to satisfy a sampling

of solo cello players using active acoustic practice rooms. The optimal sources for these low frequencies - single or multiple - will be discussed. Updated information will also be provided on the sound field coverage in active rooms with extended low-frequency response.

Contributed Papers

12:00

2aAAc11. Active playback of acoustic quadraphonic sound events. Domenico Stanzial (Italian National Research Council, FSSG-CNR Lab Acustica, c/o Fondazione Cini, Isola di San Giorgio Maggiore, 30124 Venezia, Italy, domenico.stanzial@cini.ve.cnr.it), Giorgio Sacchi (Physics Department - University of Ferrara, V. Saragat, 44100 Ferrara, Italy, giorgio.sacchi@student.unife.it), Giuliano Schiffrer (Physics Department - University of Ferrara, V. Saragat, 44100 Ferrara, Italy, schgln@unife.it)

The reproduction in a given confined space - such as a cinema hall or a smaller room - of a sound event previously recorded in a completely different acoustical environment is an interesting and still open acoustical problem. A new method for hi-fi audio playback based on the general solution of the acoustic inverse problem is here pourposed. A feed-forward control based on overdetermination of conditions at active contours - i.e. loudspeakers - in order to obtain an optimal stable solution via least square approach is here proposed. This is easily possible even for complex configurations thanks to acoustic quadraphony, the application of sound intensimetry to audio technology developed in the last years within the IST-2-511316-IP European project denominated IP-RACINE. After a short explanation of the model theory, the experimental application to the simplest case of 1-D confined field is presented and some obtained results are shown.

12:20

2aAAc12. Acoustics in a small control room. Sergio Beristain (Mexican Institute of Acoustics, P.O. Box 12-1022, Narvarte, 03001 Mexico, D.F., Mexico, sberista@hotmail.com)

Acoustics in small rooms is allways a problem, particularly at the low frequency range, because of their size and the fact that there is very limited space to install all the acoustic materials needed in order to obtain the desired acoustic response, but when an electroacoustic system has to be employed as it is the case in a small Control Room for a small recording studio, matters become even worse. First of all, the space is further reduced in order to accomodate the required sound system, and with the presence of hard to control low resonant frecuencies, which can be excited at any moment during any recording session, it can be produced highly different sound presure levels at those frequencies, changing the timbre of sounds. Some measurement results are presented.

TUESDAY MORNING, 1 JULY 2008 ROOM 253, 9:20 A.M. TO 1:00 P.M.

Session 2aAAd

Architectural Acoustics and Noise: Acoustics and Privacy in Healthcare Facilities I: Emerging Policy Around the World

David M. Sykes, Cochair
ANSI S12 Workgroup 44 and the Joint ASA/INCE/NCAC Subcommittee on Healthcare Acoustics & Speech Privacy, 23 Buckingham Street, Cambridge, MA 02138, USA

Kerstin Persson Waye, Cochair
Dept. of Environ. Medicine, The Sahlgrenska Acad. of Gothenburg Univ., Box 414, Gothenburg, 405 30, Sweden

Invited Papers

9:20

2aAAd1. Waves of change: global policies & their impacts on the acoustics profession. David M. Sykes (ANSI S12 Workgroup 44 and the Joint ASA/INCE/NCAC Subcommittee on Healthcare Acoustics & Speech Privacy, 23 Buckingham Street, Cambridge, MA 02138, USA, david.sykes@remington-partners.com)

In a decade, five waves of change swept across the globe stimulating new interest in acoustics. This session examines their effects on the EU, North America and Japan. The Internet caused the first wave-the EU's privacy Directive 9546EC drove nations everywhere to develop privacy laws, many covering ″Speech Privacy.″ A second wave, in 2000 when the ″tech bubble″ burst, produced laws to improve financial accountability and forcing organizations to find ways to shield their leaders. A third wave arose in 2001 with the increase in terrorism, producing a surge in security laws that challenge the right to privacy enshrined in the 1948 Declaration of Human Rights. The fourth wave is demographic: racing to build healthcare facilities for ″boomers,″ this giant industry is now wrestling with a ″noise epidemic″ resulting from decades of neglecting the health effects of noise. The fifth wave came from the ″green″ movement-the concept of ″indoor environmental quality″ has renewed interest in noise as a pollutant. How countries balance such concerns as state security, citizen privacy and human health will be decided by courts but these five waves have catalyzed demand for understanding, insight, expertise, standards, codes, manpower and solutions from the acoustical profession.

9:40

2aAAd2. Developing acoustical policies around in EU countries. Katrin Bergmark (Saint-Gobain Ecophon AB, Box 500, 26061 Hyllinge, Sweden, katrin.bergmark@ecophon.se), Marc R. Janssen (Saint-Gobain Ecophon AB, Box 500, 26061 Hyllinge, Sweden, marc.janssen@ecophon.se)

According to research, noise levels in hospitals worldwide have increased. At the same time, the awareness of the negative effects of noise on patients and healthcare staff has grown. To manage or eliminate noise in hospitals, standards and policies are a great help. An overview of international standards will be presented, showing various parameters and differences in values and angles of approach, e.g based on activity or room type. To further optimize the content, and stimulate the use of the standards, some countries have even defined healthcare specific standards. These can support the planning and the evaluation of the sound environment in those premises. New insights from research and case studies, as well as emerging laws, provide opportunities or even force us to extend the existing content of standards to meet future demands. Suggestions for that include extension of the amount of parameters, such as decrease of sound pressure level (ΔSPL) and parameters addressing privacy (PI, AC). Finally, revision of standards provides opportunities for end users to increase their understanding and interest in acoustic and to supply possibilities to define the desired quality of the sound environment.

10:00

2aAAd3. Effects of healthcare acoustics on medical outcomes. Roger Ulrich (Texas A&M University, Department of Architecture, 3137 TAMU, College Station, TX 77843, USA, rulrich@archmail.tamu.edu)

Although considerable research has examined detrimental effects of noise on patient sleep quality in healthcare buildings, few studies have investigated the extent to which noise may worsen other types of patient clinical outcomes. Studies are also scarce concerning the effects of noise and poor acoustics on healthcare staff. The presentation describes a prospective controlled study conducted with colleagues in Sweden that examined the impact of higher versus lower noise levels, and longer in contrast to shorter reverberation times, on several patient and staff outcomes in a hospital coronary critical care unit (CCU). Acoustics were altered during the study period by changing the ceiling tiles throughout the CCU from sound-reflecting tiles to sound-absorbing tiles of similar appearance. Regarding patients, an improved acoustics environment significantly reduced physiological stress, increased satisfaction with quality of care, improved sleep quality, and lessened incidence of costly re-hospitalizations following discharge. Better acoustics also improved speech intelligibility, and healthcare staff experienced reduced work demands and less pressure and strain. The discussion concludes by outlining research directions, including the need for more outcomes studies to enable development of a strong business case for better healthcare acoustics.

Contributed Papers

10:20

2aAAd4. Influence of intenesive coronary care acoustics on the quality of care and phyiological state of patients. Inger Hagerman (Dept of Cardiology, Karolinska University Hospital, M52, Huddinge, 141 86 Stockholm, Sweden, inger.hagerman@karolinska.se), Gundars Rasmanis (Dept of Cardiology, Karolinska University Hospital, M52, Huddinge, 141 86 Stockholm, Sweden, gundars.rasmanis@karolinska.se), Vanja Blomkvist (Dept of Cardiology, Karolinska University Hospital, M52, Huddinge, 141 86 Stockholm, Sweden, vanja.blomkvist@pubcare.uu.se), Roger Ulrich (Texas A&M University, Department of Architecture, 3137 TAMU, College Station, TX 77843, USA, rulrich@archmail.tamu.edu), Töres Theorell (Dept of Cardiology, Karolinska University Hospital, M52, Huddinge, 141 86 Stockholm, Sweden, tores.theorell@stressforskning.su.se)

Background unstable coronary disease is a stressful situation and environmental influences may increase stress mechanisms important for the cardiovascular status. Aim to evaluate acoustic influence on patients with coronary artery disease and to test if the effects of poor sound absorption on work environment affects quality of care and medical status of patients. Methods 94 patients admitted to the intensive coronary heart unit for chest pain evaluation participated. Patient groups were recruited during bad and good acoustic conditions respectively. Blood pressure, pulse amplitude, heart rate and heart rate variability were monitored. Patients were asked to fill in a questionnaire about the quality of the care and a follow up of re-hospitalisation and mortality was made at 1 and 3 months. Results good and bad acoustics differed significantly with respect to pulse amplitude in acute myocardial infarction and unstable angina pectoris groups, with lower values at night during the good acoustics period. Re-hospitalisations were higher for the bad acoustics group. During the good acoustics period patients considered the staff attitude much better than during the bad acoustics period. Conclusion, bad acoustics environment during acute illness may have important physiological effects of importance for rehabilitation.

10:40

2aAAd5. The future of UK hospital design. Adrian Popplewell (Arup Acoustics, St Giles Hall, Pound Hill, CB3 0AE Cambridge, UK, adrian.popplewell@arup.com)

The importance of acoustic conditions within hospitals is highlighted by recent research indicating that patient recovery times are significantly influenced by the noise levels within wards. Added to this are concerns about speech privacy and confidentiality, patient and staff comfort, communication between patient and doctor, and the effects of vibration on sensitive medical equipment, all of which makes the acoustic design a key parameter in any hospital development. This paper will discuss the practical issues associated with the implementation of the current national guidance on hospital acoustics (Health Technical Memorandum 2045) and the new, currently unpublished replacement, Health Technical Memorandum 08-01. The experiences of the author with several large Private Finance Initiative projects, designed to the current standard, have illustrated the practical difficulties of fully complying with all its requirements and the design solutions which can be adopted. Speech privacy and confidentiality has been a critical issue in developing the new design standard. With Arup Acoustics as key contributors to this document, and acoustic designers of one of the first major projects in the UK to comply with this standard, the author is in a prime position to be able to assess the practical and technical implications of the future guidance.

11:00-11:20 Break

11:20

2aAAd6. Development of 'sound and vibration design guidelines for health care facilities'. Kurt Rockstroh (Steffian Bradley Architects, 100 Summer Street, Boston, MA 02110, USA, kurtr@steffian.com)

"The Guidelines for Design & Construction of Healthcare Facilities" is utilized by the majority of the United States and its federal agencies involved in funding health care projects. As part of the development of the 2010 Edition of "The Guidelines" a joint subcommittee of ASA, INCE, NCAC and the Health Guidelines Revision Committee was formed to develop sound and vibration guidelines. This presentation will explain the collaborative process used to develop, publicize, review and formally vote acceptance of the sound and vibration guidelines. The presentation will also outline the major components of the new guidelines.

11:40

2aAAd7. Acoustics in green buildings: refining the concept of environmentally quality while improving occupant health and productivity synergistically. Sholem Prasow (Teknion Furniture Systems, 1150 Flint Rd., Thornhill, ON L3T 4 M9, Canada, sholem .prasow@teknion.com)

Environmental Quality has always been a keystone of the green building movement. The concept has evolved from "Indoor Air Quality", for example, in the first version of LEED seven years ago to a much broader and enriched concept - a concept that fully embraces Acoustics - today. This paper explores the evolution of Environmental Quality in both general and health care environments, and demonstrates the emerging role of Acoustics as an equal partner with Air Quality and Lighting as determinants of both health and productivity in the built environment. Specific references will be made to LEED rating systems and to emerging acoustical design requirements within LEED.

12:00

2aAAd8. Getting noise and speech privacy issues heard in design of healthcare facilities. Anjali Joseph (The Center for Health Design, 1850 Gateway Blvd., Suite 1083, Concord, CA 94520, USA, ajoseph@healthdesign.org)

Hospitals are extremely noisy, and noise levels in most hospitals far exceed recommended guidelines. The high ambient noise levels, as well as peak noise levels in hospitals, have serious impacts on patient and staff outcomes ranging from sleep loss and elevated blood pressure among patients to emotional exhaustion and burnout among staff. Poorly designed acoustical environments can pose a serious threat to patient confidentiality if private conversations between patients and staff or between staff members can be overheard by unintended listeners. At the same time, a poor acoustical environment impedes effective communication between patients and staff and between staff members by rendering speech and auditory signals less intelligible or detectable. This has serious implications for patient safety. A well-designed acoustical environment is critical in addressing these problems related to noise and communication of information. The purpose of this presentation is to examine how different aspects of sound - noise, speech privacy, speech intelligibility, and music - impact patient and staff outcomes in healthcare settings and the specific environmental design strategies that can be used to improve the acoustical environment of healthcare settings.

12:20

2aAAd9. Noise confounds in functional MRI research and potential solutions. Marc J. Kaufman (McLean Hospital, 115 Mill St., Brain Imaging Center, Belmont, MA 02478, USA, kaufman@mclean.harvard.edu), Blaise D. Frederick (McLean Hospital, 115 Mill St., Brain Imaging Center, Belmont, MA 02478, USA, BBFrederick@mclean.harvard.edu), Eric E. Ungar (Acentech Inc, 33 Moulton St., Cambridge, MA 02138, USA, eungar@ACENTECH.com), Jonathan D. Kemp (Acentech Inc, 33 Moulton St., Cambridge, MA 02138, USA, jdkemp@acentech.com), David M. Sykes (ANSI S12 Workgroup 44 and the Joint ASA/INCE/NCAC Subcommittee on Healthcare Acoustics & Speech Privacy, 23 Buckingham Street, Cambridge, MA 02138, USA, david.sykes@remingtonpartners.com)

High field functional MRI (fMRI) is becoming a neuroscience research technique of choice because it is noninvasive and can reveal brain circuitry regulating sensory, motor, and cognitive functions. Unfortunately, rapid scan fMRI results in high noise levels (100-140 dB) that can alter auditory, visual, and pain system function, and also can induce stress, which itself modulates brain responses to various stimuli. These effects can confound fMRI data interpretation. A number of solutions for this problem have been proposed including modifying MRI scanner hardware to reduce noise output, an expensive proposition limited to willing manufacturers, and modifying fMRI pulse sequences to reduce noise output, which is effective within certain limitations. Another approach is to develop acoustic noise isolating equipment that separates subjects from noise. This passive approach confers maximum flexibility because it is both hardware- and fMRI scan sequence-independent. We present initial data documenting efficacy of first generation acoustic noise isolating equipment for animal fMRI studies. As nearly 25% of patients referred for clinical MRIs refuse scans because they are stressful, acoustic noise isolating equipment scaled for clinical MRI scanner use may decrease stress and increase patient compliance, thereby decreasing morbidity and mortality, and improve MRI center workflow.

12:40

2aAAd10. Experimental study on applicability of sound masking system in medical examination room. Kanako Ueno (Institute of Industrial Science, University of Tokyo, Komaba 4-6-1, Meguro-ku, 153-8505 Tokyo, Japan, ueno@iis.u-tokyo.ac.jp), Hyojin Lee (Institute of Industrial Science, University of Tokyo, Komaba 4-6-1, Meguro-ku, 153-8505 Tokyo, Japan, leehj@iis.u-tokyo.ac.jp), Shinichi Sakamoto (Institute of Industrial Science, University of Tokyo, Komaba 4-6-1, Meguro-ku, 153-8505 Tokyo, Japan, sakamo@iis.u-tokyo.ac.jp), Atsuko Ito (Center for Advanced Sound Technologies, Yamaha, 203 Matsunokijima, 4380192 Iwata, Shizuoka, Japan, atsuko1_ito@gmx.yamaha.com), Mai Fujiwara (Center for Advanced Sound Technologies, Yamaha, 203 Matsunokijima, 4380192 Iwata, Shizuoka, Japan, mai_fujiwara@gmx.yamaha.com), Yasushi Shimizu (Center for Advanced Sound Technologies, Yamaha, 203 Matsunokijima, 4380192 Iwata, Shizuoka, Japan, yasushi_shimizu@gmx.yamaha.com)

Recently, speech privacy to avoid oral information leakage in healthcare facilities has become an important issue. This study investigated effectiveness of sound masking system in regard to masking efficiency, annoyance and its influence on speech conversation for medical examination rooms in an experimental approach. Considering actual application, two adjacent medical examination rooms partitioned by a low sound insulation wall in a typical healthcare facility were selected as an experimental field and sound masking system was temporally installed. In the rooms, acoustic environment was measured and reproduced in an anechoic room with a 3-D sound field simulation system using a 6-ch sound recording/reproduction technique. In the simulated acoustic condition, subjective tests were designed to quantify the masking efficiency and annoyance caused by the masking sound. The annoyance test was conducted in listening condition (with high attention to the sound) and in talking condition (with low attention). As a result, mixed maskers composed by water stream, synthesized speech signals, and steady state noise showed high performance in both aspect of masking efficiency and annoyance.

TUESDAY MORNING, 1 JULY 2008 ROOM 252B, 10:20 A.M. TO 1:00 P.M.

Session 2aAAe

Architectural Acoustics, Musical Acoustics, Physical Acoustics, and Noise: Acoustics of Opera Houses I

Robin Glosemeyer Petrone, Cochair
918 16th St., Apt 3, Santa Monica, CA 90403, USA

Roberto Pompoli, Cochair
Engineering Dept. - Univ. of Ferrara, Via Saragat, 1, Ferrara, 44100, Italy

Invited Papers

10:20

2aAAe1. Generous opera house acoustics for lyric and symphonic performances. Daniel E. Commins (Commins Acoustics Workshop, 15 rue Laurence Savart, 75020 Paris, France, d.commins@comminsacoustics.com)

It is believed that a short acoustic response is needed in an opera house to guarantee good intelligibility of lyrics. Some of the best opera houses have a relatively long reverberation time associated to good clarity. They are more suitable to symphonic concerts than ″damped″ rooms. The recently opened 1350-seat Grand Théâtre de Provence in Aix-en-Provence, France, is an example of an opera house with a long response and good clarity. An adequate orchestra shell and proper permanent acoustical treatment of the stage tower lead to suitable acoustical parameters in the symphony configuration. The measurements show that in an opera house of this capacity, it is possible to create conditions compatible with opera, symphony, chamber music and recitals. The rich opera configuration sound generates mostly positive reactions. Most concert goers consider that this room is now the reference for the region. One must note however that this approach is risky since the values that are considered ideal for opera must be stretched far. It may lead to excessive reverberation and even to unwanted reflections. This target requires genuine investigations, from early concept to final design, using the most advanced prediction and modeling techniques. The design of larger rooms under the same principle requires even more care.

10:40

2aAAe2. Opera House Reverberation Times - Design Considerations. Eckhard Kahle (Kahle Acoustics, 188 avenue Molière, 1050 Brussels, Belgium, kahle@kahle.be), Thomas Wulfrank (Kahle Acoustics, 188 avenue Molière, 1050 Brussels, Belgium, twulfrank@kahle.be), Yann Jurkiewicz (Kahle Acoustics, 188 avenue Molière, 1050 Brussels, Belgium, yjurkiewicz@kahle.be), Brian F. Katz (LIMSI-CNRS, B.P. 133, 91403 Orsay, France, brian.katz@limsi.fr)

The intimacy of many historic European Opera Houses, especially of the traditional Italian style, is highly cherished and many of these halls are considered to be among the best halls acoustically. From an acoustical point of view the generally small dimensions - often combined with a moderate seat count - provide excellent source presence and clarity. On the other hand, the corresponding small volume leads to short reverberation times, and in recent decades higher reverberation times have been preferred and asked for by clients and audiences in many countries. Ideas will be presented on how this apparent dilemma between the preference for small dimensions (for intimacy, source presence and definition) and increased volume (in order to create longer reverberation times) can be addressed.

11:00

2aAAe3. The ″Teatro di San Carlo″ in Naples and its smaller clone ″Teatro Verdi″ in Salerno. Raffaele Dragonetti (DETEC, University of Naples Federico II, Piazzale Tecchio 80, 80125 Naples, Italy, dragonet@unina.it), Carmine Ianniello (DETEC, University of Naples Federico II, Piazzale Tecchio 80, 80125 Naples, Italy, ianniell@unina.it), Francesco Mercogliano (DETEC, University of Naples Federico II, Piazzale Tecchio 80, 80125 Naples, Italy, francesco.mercogliano@unina.it), Rosario A. Romano (DETEC, University of Naples Federico II, Piazzale Tecchio 80, 80125 Naples, Italy, rosroman@unina.it)

The Teatro di San Carlo in Naples (Italy) is a well preserved baroque-type theatre. It was opened in 1737 and flourished up to a destructive fire. Nine months after the disastrous event the San Carlo was rebuilt completely as it was and reopened in 1817. It is still praised for its sound quality for opera performance. The Teatro Verdi was conceived by the Municipality of Salerno (Italy) in 1843. However, the ″querelles″ of local parties delayed much its construction so that it could be opened only in 1872. The architects who designed the Teatro Verdi were influenced very much by the successful Teatro di San Carlo and tried to copy the older and not-far-one in a smaller scale. The Verdi has undergone few minor changes during its life and is used also for opera shows. The main halls of the two are in a scale about 1:5. This paper reports a comparison of their acoustical features in terms of objective room-acoustics parameters accepted for opera-house sound quality. Acoustic measurements were performed with the same instrumentation set. Similarities and differences are discussed.

11:20

2aAAe4. Teatro 'La Fenice', Venice --- The secrets of the acoustical reconstruction of the destroyed theater according to historical and modern requirements. Jürgen Reinhold (Müller BBM GmbH, Robert Koch Strasse 11, D 82152 Planegg/München, Germany, Juergen.Reinhold@MuellerBBM.de)

The reconstruction of this artistically and architecturally very important opera house that was completely destroyed by a fire and which was famous throughout the world not least for its excellent acoustical qualities, was a brilliant challenge also for an acoustician. The historical planning requirements - complete reconstruction ″as it was; where it was″ - the latest findings in room acoustics as well as a huge number of ″modern″ requirements are to be brought in line. The theatre hall as heart of the Teatro ″La Fenice″ was reconstructed in its classical horseshoe shape with five tiers in pure wooden construction. Modern standard specifications had to be met for ventilation and air conditioning, the installation of a modern stage machinery as well as an improved safety and fire prevention concept. Furthermore the space allocation plan had to be extended by the integration of new rehearsal rooms and technical equipment rooms. From the point of view of building and room acoustics this was a very complex task - if in addition the cramped conditions of the Teatro ″La Fenice″ in Venice are taken into consideration. The lecture provides an insight into the building and room acoustical planning, its realization and the achieved acoustical results.

11:40

2aAAe5. The acoustics of the Beijing National Grand Theatre of China. Isabelle Schmich (CSTB, 24, Rue Joseph Fourier, 38400 Saint Martin D'Hères, France, isabelle.schmich@cstb.fr), Paul Chervin (CSTB, 24, Rue Joseph Fourier, 38400 Saint Martin D'Hères, France, paul.chervin@cstb.fr), Zhu Xiangdong (School of Architecture, Tsinghua University, Room 104, Centre Main Building, 100084 Beijing, China, zxd@abcd.edu.cn), Yan Xiang (School of Architecture, Tsinghua University, Room 104, Centre Main Building, 100084 Beijing, China, yx@abcd.edu.cn), L Guo-Qi (The National Grand Theatre, 2, Chang an sast street, 100031 Beijing, China, liguoqi@fujisound.com)

The National Grand Theatre of China opened in December 2007 in Beijing. It is a complex of three performance halls: the Opera (2400 seats), the Concert Hall (2000 seats) and the Theatre (1100 seats). These three halls are covered by a super-ellipsoidal shell made out of titanium and glass. The history of the acoustic design evolution from the winning of the competition in 1999 by the Architect Paul Andreu to the final construction will be retraced including the preliminary design, the acoustic simulations and auralisations. The acoustic design of each hall will be presented with its specifications and detailed particularities. Final acoustic measurements have been done in the three empty halls and in the occupied concert hall. The results and acoustic criteria will be discussed. In addition, a subjective evaluation has been done with psychoacoustic questionnaires and the results will be presented and analysed.

Contributed Papers

12:00

2aAAe6. Acoustical design and scale model test for the opera house of Zhongshan city. Shuo Xian Wu (State Key Laboratory of Subtropical Building Science, South China University of Technology, 381 Wushan Street, 510640 Guangzhou, China, arshxwu@scut.edu.cn), Yue Zhe Zhao (State Key Laboratory of Subtropical Building Science, South China University of Technology, 381 Wushan Street, 510640 Guangzhou, China, arzhyzh@scut.edu.cn)

The opera house of Zhongshan City in Guangdong province of China is the performing art center of the city. It was completed in Oct. 2005. It has 1400 seats including 833 stall seats and another 484 seats on two levels of balcony. The volume of the auditorium is 12000m3 and the V/N is 9.1m3 per seat. The main purpose of the building is for the performances of opera and ballet. Some music and conference events are also to be held there. Therefore, the occupied reverberation time at medium frequencies is set to be 1.6s and its background noise level has to meet NR-20. During the acoustical design, a 3D computer simulation model established with ODEON software and a 1:20 scale model was made to analyze the sound fields of the auditorium with and without a music shell on the stage. After the completion of the building, an acoustics test was taken. Several performances show that its acoustics reaches a quite high level and has won high praises.

12:20

2aAAe7. Subjective Assessments of Acoustical Environments for Un-assisted Traditional Peking Opera Performances. Wei-Hwa Chiang (National Taiwan University of Science and Technology, 43, sec. 4 Keelung Rd, Taiwan, 106 Taipei, Taiwan, edchiang1224 @hotmail.com), Wei Lin (National Taiwan University of Science and Technology, 43, sec. 4 Keelung Rd, Taiwan, 106 Taipei, Taiwan, D9313001@mail.ntust.edu.tw), Ya-Jhen Yu (National Taiwan University of Science and Technology, 43, sec. 4 Keelung Rd, Taiwan, 106 Taipei, Taiwan, ianmelody@hotmail.com)

The prevalence of Western performing arts has impacted on how traditional Peking opera is performed. It is, however, necessary to preserve and pass on traditional Peking opera for it integrates the essence of Chinese

opera. The research has been conducted regarding subjective assessment of the acoustical environment for traditional Peking opera. Recording of dry sound sources was also performed. Sound strength and listening direction were found to be the principle factors that determined evaluation for overall impression while reverberation time is less important. The 6000 m3 can be used as the upper limit for room volume when a thrust stage is used.

12:40

2aAAe8. Considerations about the acoustical properties of Teatro Nuovo in Spoleto after the restauration works. Alessandro Cocchi (University, DIENCA Dept. Facoltà di Ingegneria, Viale Risorgimento 2, 40136 Bologna, Italy, alessandro.cocchi@mail.ing.unibo.it), Marco Cesare Consumi (University, DIENCA Dept. Facoltà di Ingegneria, Viale Risorgimento 2, 40136 Bologna, Italy, marcocesare.consumi@mail.ing.unibo.it),Ryota Shimokura(AIST, 1-8-31 Midorigaoka, Ikeda, 563-8577 Osaka, Japan, ryota.shimokura@aist.go.jp)

In 2003 the municipality of Spoleto decided to stop the performances within the Teatro Nuovo, among the others also of ″Two World Annual Festival″, as it was necessary to modify some material, repair the floor, refurbish pictures and so on: the first author was charged with all the acoustical aspects and he decided to perform extensive acoustical measurements. During this measurement campaign, a flutter echo was detected in the stalls, so it became necessary to detect the origin of this problem, then to find some modification able to remove this problem: we have already presented our studies on this subject, from which a new design of the orchestra pit was derived. For fire safety reasons it was necessary also to remove some elastic panels from the boxes, and an acoustically equivalent technical solution was adopted. Even the stalls floor was removed and a new solution was adopted incorporating the heating plant and an acoustical solution. In this paper we will present the results of measurements performed after the opening of the theatre (a typical Italia Opera House of the end of the Eighteen Century) and some consideration about the acoustical results so obtained.

TUESDAY MORNING, 1 JULY 2008 ROOM 342B, 8:00 A.M. TO 1:20 P.M.

Session 2aAB

Animal Bioacoustics and ECUA: Animal Bioacoustic Censusing I

Marie A. Roch, Cochair
San Diego State University, Dept. of Computer Science, San Diego, CA 92182-7720, USA

Cédric Gervaise, Cochair
E3I2 - EA3876, 2 rue François Verny, Brest Cedex, 29806, France

Invited Papers

8:00

2aAB1. Passive acoustic detection of grouper sound production. David Mann (University of South Florida, College of Marine Science, 140 7th Ave. S., St. Petersburg, FL 33701, USA, dmann@marine.usf.edu), James Locascio (University of South Florida, College of Marine Science, 140 7th Ave. S., St. Petersburg, FL 33701, USA, locascio@marine.usf.edu), Michelle Schärer (University of Puerto Rico-Mayaguez, Department of Marine Sciences, Isla Magueyes, La Parguera, 00667 Lajas, Puerto Rico, m_scharer@hotmail.com), Chris Koenig (Florida State University, Coastal and Marine Laboratory, St. Teresa Beach, FL 32358, USA, koenig@bio.fsu.edu), Michael Nemeth (University of Puerto Rico-Mayaguez, Department of Marine Sciences, Isla Magueyes, La Parguera, 00667 Lajas, Puerto Rico, michaelnemeth@hotmail.com), Misty Nelson (University of South Florida, College of Marine Science, 140 7th Ave. S., St. Petersburg, FL 33701, USA, mnelson@marine.usf.edu), Felicia Coleman (Florida State University, Coastal and Marine Laboratory, St. Teresa Beach, FL 32358, USA, coleman@bio.fsu.edu), Richard Appeldoorn (University of Puerto Rico-Mayaguez, Department of Marine Sciences, Isla Magueyes, La Parguera, 00667 Lajas, Puerto Rico, rappeldo@uprm.edu)

Passive acoustic recordings were used to study the behavior of red hind (*Epinephelus guttatus*) at spawning aggregation sites off of Puerto Rico and Mona Island, and goliath grouper (*Epinephelus itajara*) and red grouper (*Epinephelus morio*) on the West Florida Shelf. The sounds produced by each species were unique, low-frequency pulsed sounds and associated with reproductive-related behavior. Male red hind produced sounds composed of a series of pulses that graded into a tonal-like sound, mostly during territorial patrolling. Long-term acoustic recorder (LARS) data from the west coast of Puerto Rico and Mona Island showed similar diel periodicities of sound production of red hind, but had different monthly peaks in sound production. Goliath grouper sounds consisted of low-frequency individual pulses (50-100 Hz) that are consistent with sounds produced by a large fish, and showed lunar periodicity in sound production. Peaks in sound production occurred nightly after midnight, but sounds were also produced throughout the day. Sound production and spawning by red grouper was recorded using a remotely operated vehicle (ROV) at depths of 80-100 m. Passive acoustic techniques can provide synoptic, long-term time series of sound production associated with reproductive activities of soniferous species at widely spaced sites.

8:20

2aAB2. The value of acoustic technologies for monitoring bird migration. Andrew Farnsworth (Cornell Laboratory of Ornithology, 420 E 54th St, 38J, New York, NY 10021, USA, af27@cornell.edu)

Many North American species of birds give distinctive flight calls during nocturnal migration. Monitoring these calls can be a powerful method for studying the timing and magnitude of migration, as well as for confirming the presence of individual species and

potentially for quantifying passage rates. Recent technological advances in acoustic monitoring, such as increased processor speeds of computers, automated detection software, increased data storage capacities, and a comprehensive identification guide, permit recording of the vocalizations of passing migrants over entire nights for entire migration seasons, thus yielding data on species composition, migration timing and routing, and the magnitude of migration traffic. I will discuss several recent studies that have used acoustic technologies to monitor nocturnal migration, presenting data on species composition and relative abundance. Additionally, I will present some recent approaches to addressing quantification of passing migrants by their calls. I will also discuss wider applications of this technology beyond the realm of North American migrant species.

Contributed Papers

8:40

2aAB3. Automatic detection of short time periodic bird calls in realistic monitoring scenarios. Daniel Wolff (Department of Computer Science III, University of Bonn, Roemerstr. 164, 53117 Bonn, Germany, wolffd@bonn.edu), Klaus H. Tauchert (Humboldt-University Berlin, Institute of Biology, Invalidenstr. 43, 10115 Berlin, Germany, klaus.tauchert@gmx.de), Karl H. Frommolt (Humboldt-University Berlin, Museum für Naturkunde, Tierstimmenarchiv, Invalidenstr. 43, 10115 Berlin, Germany, karl-heinz.frommolt@rz.hu-berlin.de), Rolf Bardeli (Department of Computer Science III, University of Bonn, Roemerstr. 164, 53117 Bonn, Germany, bardeli@iai.uni-bonn.de), Frank Kurth (FGAN-FKIE, Abteilung KOM, Neuenahrer Str. 20, 53343 Wachtberg-Werthhoven, Germany, kurth@fgan.de), Michael Clausen (Department of Computer Science III, University of Bonn, Roemerstr. 164, 53117 Bonn, Germany, clausen@iai.uni-bonn.de)

In this contribution, we propose a method for the automatic detection and localisation of bird calls featuring simple as well as highly repetitive structures. Reporting from a research project focused at computer aided acoustical monitoring, a detector for Locustella luscinoides (Savi's Warbler) is presented, performing reliably even on highly distorted recordings. In cooperation with the Animal Sound Archive at the Humboldt University, Berlin, this detector was incorporated into a multimodal censusing method combining GPS-data and automatically annotated audio recordings to perform line mapping. An evaluation of the proposed techniques for unsupervised monitoring purposes was also performed on 20 hours of multichannel recordings from Lake Parstein, a cane brake area in Germany. Finally, exemplifying the discriminative potential of the underlying features, we will point out the application to other members of the Warbler family as well as the detection of cricket and toad sounds.

9:00

2aAB4. Animal censusing using seismic cues: techniques used for African elephants. Jason D. Wood (Beam Reach Marine Science and Sustainability School, 7044 17th Ave NE, Seattle, WA 98115, USA, jason@beamreach.org), Caitlin E. O'Connell-Rodwell (Stanford University, Department of Otolaryngology, Head and Neck Surgery, Stanford, 94305, USA, ceoconnell@stanford.edu), Simon L. Klemperer (Stanford University, Department of Geophysics, Stanford, 94305, USA, sklemp@stanford.edu)

Counting populations of animals has proven to be difficult and inexact for species that are difficult to detect visually. A growing number of researchers have successfully turned to detecting animals by their acoustic signals in order to count their numbers. To predict the number of animals present a regression line is generated from the relationship between such measures as calling rate and the number of animals documented visually during that recording by the researcher. Depending on the communication system of the species in question, a significant amount of the variation in calling rate can be attributed to other factors such as group behavior rather than the number of individuals present. For species where these other sources of variation are high it may be more appropriate to use acoustic cues to detect and count the number of animals. This paper will present techniques used to detect and estimate elephant numbers from geophone recordings of their footfalls; cues that are a byproduct of their locomotion and are thus not as dependent on group behavior.

Invited Papers

9:20

2aAB5. Species identification and measurement of activity in odontocete species of Palmyra Atoll by acoustic monitoring. Simone Baumann (Scripps Institution of Oceanography- UCSD, 9500 Gilman Dr. #0205, La Jolla, CA 92093, USA, sbaumann@ucsd.edu), John A. Hildebrand (Scripps Institution of Oceanography- UCSD, 9500 Gilman Dr. #0205, La Jolla, CA 92093, USA, jhildebrand@ucsd.edu), Sean M. Wiggins (Scripps Institution of Oceanography- UCSD, 9500 Gilman Dr. #0205, La Jolla, CA 92093, USA, swiggins@ucsd.edu), Hans-Ulrich Schnitzler (Eberhard-Karls-Universität Tübingen, Zool. Institut, Abt. Tierphysiologie, Auf der Morgenstelle 28, 72076 Tübingen, Germany, hans-ulrich.schnitzler@uni-tuebingen.de)

Acoustic monitoring has been used to study odontocete presence at Palmyra Atoll, a remote island in the Northern Line Islands chain. Long-term recordings of high-frequency, broadband acoustic data have become possible with recent technological advances. A High-frequency Autonomous Recording Package (HARP) has been developed which samples at 200 kHz with a duty cycle of 1/4 for up to seven months. This instrument has recorded since October 2006 at Palmyra Atoll. Visual and acoustic surveys were conducted around Palmyra Atoll using a four-element towed hydrophone array sampling real-time at 200 kHz to obtain species-specific acoustic data. These data are used as reference for automatic detection algorithms applied on the long-term recordings. To date, acoustically and visually detected odontocetes include bottlenose dolphins (Tursiops truncatus), spinner dolphins (Stenella longirostris), melon-headed whales (Peponocephala electra) and beaked whales of the genus Mesoplodon. The long-term HARP data reveal acoustic activity primarily at night time and predominantely odontocete clicks. Both the beaked as well as the melon-headed whales are present year round and show a distinct daily acoustic activity cycle.

9:40

2aAB6. Distribution patterns of delphinids in the California Current Ecosystem observed through acoustic monitoring of species-specific echolocation clicks. Erin M. Oleson (Scripps Institution of Oceanography- UCSD, 9500 Gilman Dr. #0205, La Jolla, CA 92093, USA, eoleson@ucsd.edu), Melissa S. Soldevilla (Scripps Institution of Oceanography- UCSD, 9500 Gilman Dr. #0205, La Jolla, CA 92093, USA, msoldevilla@ucsd.edu), John Calambokidis (Cascadia Research Collective, 218 1/2 W. 4th Ave., Olympia, WA 98501, USA, calambokidis@cascadiaresearch.org), Curtis Collins (Naval Postgraduate School, 833 Dyer Road, Rm 328,

Monterey, CA 93943, USA, Collins@nps.edu),Sean M. Wiggins (Scripps Institution of Oceanography- UCSD, 9500 Gilman Dr. #0205, La Jolla, CA 92093, USA, swiggins@ucsd.edu), John A. Hildebrand (Scripps Institution of Oceanography- UCSD, 9500 Gilman Dr. #0205, La Jolla, CA 92093, USA, jhildebrand@ucsd.edu)

Visual surveys along the U.S. west coast conducted in the 1980s-90s suggested that Pacific white-sided and Risso's dolphins likely undergo annual movement between California during winter-spring, and Oregon-Washington in the summer-fall. Using high-frequency autonomous acoustic recordings within the southern California, central California, and Washington regions of the California Current System, we evaluated the seasonal occurrence of these dolphin species through detection of their echolocation clicks. The clicks of Pacific white-sided and Risso's dolphins are characterized by a unique combination of local frequency peaks for each species, providing a statistically robust means of identification from autonomous acoustic records. Based on these unique spectral characters, we extracted periods of clicking by each species from concurrently sampled coastal and shelf/slope locations off southern California and Washington, and a single offshore site off central California. The number of hours that each species was heard per day was quantified and compared among seasons and regions. Both species were heard year-round at shelf/slope sites off southern California and Washington; however their patterns of occurrence at coastal sites differed somewhat. Our results indicate year-round presence of Pacific white-sided and Risso's dolphins in some regions, suggesting that the seasonal distribution of these species may have recently changed.

10:00-10:20 Break

Contributed Papers

10:20

2aAB7. Radial distance sampling with passive acoustics: The prospect of estimating absolute densities of cetaceans from static acoustic datalogger data. Jakob Tougaard (National Environmental Research Institute, University of Aarhus, Frederiksborgvej399, DK-4000 Roskilde, Denmark, jat@dmu.dk)

Recording animal vocalisations with a static acoustic datalogger can be viewed as a form of point transect sampling and results analysed within the framework of distance sampling theory. The key element is the radial detection function, which specifies the probability of detecting a vocalisation as a function of distance from the datalogger. This function can be modelled theoretically or preferably determined experimentally and from it the efficient radial detection distance can be determined. Radial detection functions were determined for two different harbour porpoise dataloggers (T-PODs, version 1 and version 3) by means of concurrent visual tracking of porpoises. 52% and 82% of the porpoises within 100 m from the T-PODs were detected by the V1 and V3 T-POD, respectively and 11% and 30%, respectively were detected between 100 and 200 m from the T-PODs. Effective detection radius (EDR) was 97 m and 150 m for the two T-PODs, respectively. Porpoises echolocate almost continuously. If it is assumed that silent periods rarely exceeds 1 minute in duration an average detection rate on the version 3 T-POD for the study site of 2.7 detection positive minutes per hour can be converted into a density estimate of 0.69 porpoises/km^2.

10:40

2aAB8. Computer-aided detection of non-stereotyped bowhead whale calls in the presence of seismic airgun signals. Aaron Thode (Marine Physical Laboratory, Scripps Institution of Oceanography, 9500 Gilman Dr, MC 0238, La Jolla, CA 92093-0238, USA, athode@ucsd.edu), Delphine Mathias (Marine Physical Laboratory, Scripps Institution of Oceanography, 9500 Gilman Dr, MC 0238, La Jolla, CA 92093-0238, USA, delphine.mathias@gmail.com), Miles McLennan (Greeneridge Sciences, Inc., 4512 Via Huerto, Santa Barbara, CA 93110, USA, billm @greeneridge.com), Charles R. Greene (Greeneridge Sciences, Inc., 4512 Via Huerto, Santa Barbara, CA 93110, USA, cgreene@greeneridge.com)

In 2007 thirty-five autonomous recording packages were deployed over a 150 mile swath in the Beaufort Sea to monitor the annual migration of the bowhead whale (Balaena mysticetus) population during seismic exploration activities. Over 1350 days worth of acoustic data were gathered, generating a need for computer-aided assistance in detecting calls. Bowhead whales produce over ten types of frequency modulated calls, and the frequency range, duration, and fine structure of individual calls vary considerably even within each call type, creating difficulties when using simple matched-filtering or spectrogram correlation. Numerous airgun signals also display frequency-modulated structure, complicating the challenge. In this presentation a three-stage process is presented for detecting arbitrary bowhead whale calls in the presence of seismic airgun signals, implemented in JAVA and MATLAB, with components extracted from the industry-supported PAMGUARD software package. The first stage runs several ″energy-based″ detectors simultaneously across multiple frequency bands to capture events, and a second stage analyzes the timing of these detections to remove regular periodic sequences, such as those expected from airguns. The final stage attempts to trace contours on spectrograms. Both genetic algorithms and direct optimization are used to optimize the program's 21 input parameters. [Work supported by Shell Exploration and Production Company].

Invited Papers

11:00

2aAB9. Comparison of feature extraction methods for the identification of odontocete species based upon echolocation clicks. Marie A. Roch (San Diego State University, 5500 Campanile Dr, Dept of Computer Science, San Diego, CA 92182-7720, USA, marie.roch@sdsu.edu), Holger Klinck (Alfred Wegener Institute, P.O. Box 120161, 27515 Bremerhaven, Germany, holger.klinck@awi.de), David K. Mellinger (Oregon State Univ. and NOAA, 2030 SE Marine Science Dr., Newport, OR 97365, USA, David.Mellinger@oregonstate.edu), Melissa S. Soldevilla (Scripps Institution of Oceanography- UCSD, 9500 Gilman Dr. #0205, La Jolla, CA 92093, USA, msoldevilla@ucsd.edu), John A. Hildebrand (Scripps Institution of Oceanography- UCSD, 9500 Gilman Dr. #0205, La Jolla, CA 92093, USA, jhildebrand@ucsd.edu)

Recent work by several groups has shown that odontocete echolocation clicks contain information that can be used to detect or identify specific species. In this study, we compare the relative performance of cepstral and wavelet features on various Pacific Ocean species of odontocetes. Comparison of features within different systems is often complicated by the large number of variables unrelated to feature extraction that change between systems. By experimenting within a proven state of the art classification framework, it is possible to make meaningful comparisons of feature extraction performance with respect to common machine learning algorithms such as neural networks, support vector machines, and Gaussian mixture models.

11:20

2aAB10. Long-term Passive Acoustic Monitoring of Delphinids in the Southern California Bight. Melissa S. Soldevilla (Scripps Institution of Oceanography- UCSD, 9500 Gilman Dr. #0205, La Jolla, CA 92093, USA, msoldevilla@ucsd.edu), John A. Hildebrand (Scripps Institution of Oceanography- UCSD, 9500 Gilman Dr. #0205, La Jolla, CA 92093, USA, jhildebrand@ucsd.edu), Sean M. Wiggins (Scripps Institution of Oceanography- UCSD, 9500 Gilman Dr. #0205, La Jolla, CA 92093, USA, swiggins@ucsd.edu), Marie A. Roch (San Diego State University, 5500 Campanile Dr, Dept of Computer Science, San Diego, CA 92182-7720, USA, marie.roch@sdsu.edu)

Spectral characteristics of clicks are described for five species of delphinids in the Southern California Bight (long-beaked common dolphins, Delphinus capensis, short-beaked common dolphins, Delphinus delphis, Risso's dolphins, Grampus griseus, Pacific white-sided dolphins, Lagenorhynchus obliquidens, and bottlenose dolphins, Tursiops truncatus). Recent technological advancements allow long-term, broadband (100 kHz bandwidth), passive acoustic monitoring from autonomous sea-floor mounted instruments. The ability to record higher frequencies allows study of a broader range of odontocete vocalizations including echolocation clicks. To determine whether delphinid species could be identified by their clicks, concurrent ship-based visual and acoustic surveys were conducted. We find that clicks from Pacific white-sided and Risso's dolphins contain spectral peaks and notches that are unique and consistent for each species. These spectral patterns are also apparent in long-term autonomous acoustic recordings throughout the Southern California Bight. Utilizing this spectral classification method, we examine of diel, seasonal, and habitat use patterns of acoustically active Risso's and Pacific white-sided dolphins. The ability to monitor animals through the night provides insight into distinct diel patterns of acoustic activity for both species while the high temporal resolution acoustic data can be used to relate oceanographic time series to dolphin activity.

Contributed Papers

11:40

2aAB11. Sound production and spawning by black brum (Pogonias cromis) in southwest Florida. James Locascio (University of South Florida, College of Marine Science, 140 7th Ave. S., St. Petersburg, FL 33701, USA, locascio@marine.usf.edu), Ernst Peebles (University of South Florida, College of Marine Science, 140 7th Ave. S., St. Petersburg, FL 33701, USA, epeebles@marine.usf.edu), David Mann (University of South Florida, College of Marine Science, 140 7th Ave. S., St. Petersburg, FL 33701, USA, dmann@marine.usf.edu)

We used the Long Term Acoustic Recording System (LARS) to investigate patterns of sound production in spawning aggregations of black drum (Pogonias cromis) during 2004 - 2006 in southwest Florida. Our purposes were to document trends in black drum sound production on daily and seasonal time scales and to investigate the temporal and quantitative relationships between egg production and sound production. Sound production was strongly diel, beginning near dusk and lasting for several hours. Sound production occurred from October through April and peaked in February-March, consistent with prior descriptions of the spawning season for this species based on the gonado-somatic index (GSI). To investigate the relationship between sound production and egg production, surface plankton tows were conducted hourly between 1600 - 0400 on two consecutive nights while continuous underwater acoustic recordings were made. This was done five times between January and April, 2006. Neither the timing nor quantity of sound production was correlated with egg production on a nightly basis. These results indicate that patterns in sound production are not useful for predicting patterns in egg production by black drum on a daily scale but do provide accurate characterization of spawning behavior on a seasonal basis.

12:00

2aAB12. Nearest-neighbor techniques for automated monitoring of nocturnal flight calls. Harold Figueroa (Cornell University, Bioacoustics Research Program, 159 Sapsucker Woods Road, Ithaca, NY 14850, USA, harold.figueroa@gmail.com), Andrew Farnsworth (Cornell Laboratory of Ornithology, 420 E 54th St, 38J, New York, NY 10021, USA, af27@cornell.edu)

Flight-calls are short vocalizations used primarily during nocturnal flight. Their observation provides a means for studying the timing, location, and composition of nocturnal migrations. As part of a three-year study the Cornell Lab of Ornithology is using autonomous recorders to sample flight-calls of nocturnal migrants in the Northeastern US. The resulting tens of thousands of hours of recording, make software-assisted detection and classification essential. Automatic processing and human evaluation have yielded a considerable collection of flight-calls, 5-1000 examples for ~100 species. The many-class classification problem, along with the availability of many examples from most of the classes, and established (condensation and editing) and recent (metric-trees) techniques used in prototype-based classification nearest-neighbor techniques, have led us to develop nearest-neighbor based techniques and software to assist in the analysis of this data. We will present classification results on two examples, a set of thrushes (genera Catharus and Hylocichla, family Turdidae) consisting of six species and wood-warblers (family Parulidae) consisting of 48 species. The thrush flight-calls are visually and aurally distinctive, usually 100-400 ms in duration and occupy and the 2-5 kHz band. Wood-warbler flight-calls are typically between 20-100 ms in duration and occupy the 5-10 kHz, and are difficult for many experienced observers to distinguish.

Invited Paper

12:20

2aAB13. Sperm whale monitoring with a deep acoustic platform: Results from NEMO ONDE experiment and way ahead. Gianni Pavan (CIBRA - Università di Pavia, Via Taramelli 24, 27100 Pavia, Italy, gianni.pavan@unipv.it)

Within the INFN NEMO Project on the underwater detection of high energy neutrino, a deep hydrophone station, named ONDE (Ocean Noise Detection Experiment), has been deployed on the seafloor 21 km offshore Catania (Sicily, Italy), at 2000 m depth. Acoustic data recorded in 2005 and 2006 provided long term information on the underwater noise and a huge amount of sperm whales' detections that indicate a presence of the species higher than previously believed. Only few sightings are available for the previous years and scarce literature is available for the area. With ONDE, in year 2005 sperm whales were detected in 117 of the 231 recorded days and in 31 of the 83 days in year 2006. Clicks were the most common vocalizations recorded. Chirrups and codas (dominated by the 3+1 pattern) were present frequently, but creaks, possibly indicating feeding actions, were seldom heard. The whales were often detected, solitary or in groups, for time segments of only a few hours. This, with the low rate of creaks, may mean they were just in transit. Based on these results, a new project named (Listening Into the Deep Ocean) has been set with INGV to create a Mediterranean wide network by upgrading existing underwater seismic detectors with broadband acoustic sensors.

Contributed Paper

12:40

2aAB14. Detection and classification of call types in the vocalizations of north-east pacific blue whales. Jack McLaughlin (University of Washington, 1013 NE 40th St, Seattle, WA 98105-6698, USA, jackm@apl.washington.edu), Nicolas Josso (GIPSA-lab, dep. DIS, 961, rue de la Houille Blanche, 38402 St Martin d'Hères, France, nicolas.josso@gispa-lab.inpg.fr), Cornel Ioana (GIPSA-lab, dep. DIS, 961, rue de la Houille Blanche, 38402 St Martin d'Hères, France, cornel.ioana @gipsa-lab.inpg.fr)

Characterization of marine mammal vocalizations is an essential part of any program of marine mammal monitoring as well as being of great help for furthering understanding of subjects such as underwater communication, sonar, etc. The vocalizations of the North-East Pacific (NEPAC) blue whales are known to be made of at least three different call types: the A call, the B call and the C call. This study aims at the development of a wholly automatic process of detection and classification for the two most common call types of the NEPAC population which are the A call and the B call. We created one template for the A call and one for the B call in order to extract features with matched filtering operations. We show that a simple Gaussian Mixture Model classifier can be used to accurately track and identify the call types in 24-hour long records. The proposed methodology is applied to real data sets recorded by seismic sensors.

Invited Paper

1:00

2aAB15. Experience with VoxNet: a rapidly-deployable acoustic monitoring system for bio-acoustic studies. Lewis Girod (MIT/CSAIL, 32G-918, 32 Vassar St, Cambridge, MA 02139, USA, girod@nms.csail.mit.edu), Michael Allen (Cogent Computing ARC, Coventry University, Coventry, UK, allenm@lecs.cs.ucla.edu), Travis Collier (UCLA Dept. of Biology, 3563 Boelter Hall, Los Angeles, CA 90095, USA, travc@taylor0.biology.ucla.edu), Daniel T. Blumstein (UCLA Dept. of Biology, 3563 Boelter Hall, Los Angeles, CA 90095, USA, marmots@ucla.edu), Deborah Estrin (UCLA Dept. of Biology, 3563 Boelter Hall, Los Angeles, CA 90095, USA, destrin@cs.ucla.edu), Charles Taylor (UCLA Dept. of Biology, 3563 Boelter Hall, Los Angeles, CA 90095, USA, taylor @biology.ucla.edu)

Terrestrial bioacoustic census is a difficult problem because of propagation characteristics, obstructions, the diversity of bioacoustic sources, and the impact of noise. To address this problem we have developed VoxNet, a complete hardware and software platform for distributed acoustic monitoring applications. Each VoxNet node is a portable, self-contained processor with a small four-channel acoustic array. Using a distributed set of VoxNet nodes, a forested habitat can be monitored and the behavior of animals can be recorded and analyzed acoustically. In this work we present our experiences applying VoxNet to bioacoustic census. This work is based on data collected using the system during a deployment in Chiapas, Mexico at the Chajul Biological Field Station. The Chajul station is located in a region of dense rain forest and is home to Mexico's most diverse ecosystem. Using VoxNet in this harsh environment, we obtained census estimates based on observation of bird calls.

Session 2aAOa

Acoustical Oceanography and ECUA: Marine Ecosystem Acoustics II

Kenneth G. Foote, Cochair
Woods Hole Oceanographic Institution, Woods Hole, MA 02543, USA

Olav R. Godoe, Cochair
Institute of Marine Research, PO Box 1870, Bergen, 5817, Norway

Invited Papers

8:00

2aAOa1. Spawning Behaviour and Spatial Distribution of Atlantic Herring on Georges Bank Revealed by Ocean Acoustics Waveguide Remote Sensing. Purnima Ratilal (Northeastern University, 302 Stearns Center, Rm 311, 360 Huntington Ave, Boston, MA 02115, USA, purnima@ece.neu.edu), Zheng Gong (Northeastern University, 302 Stearns Center, Rm 311, 360 Huntington Ave, Boston, MA 02115, USA, zgong@ece.neu.edu), Daniel Cocuzzo (Northeastern University, 302 Stearns Center, Rm 311, 360 Huntington Ave, Boston, MA 02115, USA, dcocuzzo@ece.neu.edu), Mark Andrews (Northeastern University, 302 Stearns Center, Rm 311, 360 Huntington Ave, Boston, MA 02115, USA, Andrews.mar@neu.edu), Srinivasan Jagannathan (Massachusetts Institute of Technology, Room 5-435, 77 Massachusetts Avenue, Cambridge, MA 02139, USA, jsrini@mit.edu), Ioannis Bertsatos (Massachusetts Institute of Technology, Room 5-435, 77 Massachusetts Avenue, Cambridge, MA 02139, USA, ibertsat@mit.edu), Tianrun Chen (Massachusetts Institute of Technology, Room 5-212, 77 Massachusetts Avenue, Cambridge, MA 02139, USA, trchen@mit.edu), Hector Pena (Institute of Marine Research, PO Box 1870, 5817 Bergen, Norway, hector.pena@imr.no), Ruben Patel (Institute of Marine Research, PO Box 1870, 5817 Bergen, Norway, ruben.patel@imr.no), Olav R. Godo (Institute of Marine Research, PO Box 1870, 5817 Bergen, Norway, olav.rune.godoe@imr.no), J. Michael Jech (NOAA/Northeast Fisheries Science Center, 166 Water Street, Woods Hole, MA 02543, USA, michael.jech@noaa.gov), Thomas C. Weber (University of New Hampshire, Ctr. for Coastal and Ocean Mapping, 24 Colovos Road, Durham, NH 03824, USA, weber@ccom.unh.edu), Nicholas Makris (Massachusetts Institute of Technology, Room 5-212, 77 Massachusetts Avenue, Cambridge, MA 02139, USA, makris@mit.edu)

An ocean acoustics waveguide remote sensing (OAWRS) system was deployed in the Gulf of Maine, near Georges Bank to image Atlantic herring and other fish populations from Sep-Oct 2006. OAWRS provides spatially unaliased imaging of herring over wide areas, spannning over 100 km diameter. Migration and spawning behaviour of Atlantic herring was observed using OAWRS over several diurnal periods, including massive movements on and off the bank to spawn. Measurements made simultaneously with a conventional fish-finding echosounder (CFFS) and a multibeam sonar provide the depth distribution and local 3D morphology respectively of the herring schools in the water column. Concurrent trawl surveys provide identification of the fish species. Measurements mades by OAWRS and CFFS systems are highly correlated. Examples will be provided of the co-registration between the two systems over a one week period. Calibration of the OAWRS system using CFFS estimates of fish population densities along with a full-field scattering model that takes into account both coherent and incoherent scattering from a fish group is discussed. The fish swimbladder is modelled as a spheroidal bubble. Resonance scattering behaviour of herring is observed in the OAWRS system with significant changes in scattering amplitude over the 300 Hz to 1.5 kHz frequency range of the OAWRS system.

8:20

2aAOa2. Passive acoustic mapping of marine biological choruses. Gerald D'Spain (Marine Physical Lab, Scripps Institution of Oceanography, 291 Rosecrans St., San Diego, CA 92106, USA, gld@mpl.ucsd.edu), Heidi Batchelor (Marine Physical Lab, Scripps Institution of Oceanography, 291 Rosecrans St., San Diego, CA 92106, USA, heidi@mpl.ucsd.edu), Catherine Berchok (Marine Physical Lab, Scripps Institution of Oceanography, 291 Rosecrans St., San Diego, CA 92106, USA, cberchok@ucsd.edu)

Since underwater sound is a critical aspect of the ocean environment for marine animals, passive acoustic recordings provide important information on marine habitats. Conversely, because biological sounds can be a dominant component of the ocean sound field, knowledge of their characteristics is important for assessing sonar system performance. This presentation summarizes the properties of three biological choruses observed in experiments off the southern California coast. Measurements were made with large aperture, well-filled hydrophone arrays, yielding highly resolved estimates of the chorus directionality. The first chorus generated energy in the 200-800 Hz band, occurred predominantly at night in spring and summer, and displayed an unusual spatiotemporal pattern where the region of chorusing periodically propagated upcoast over 25 km of coastline at nearly 1.5 km/sec. The other two choruses occurred in the 1-10 kHz frequency band and come from slowly-moving, or fixed, sources at, or near, the ocean bottom. One chorus was present only on two consecutive nights during a summer experiment, whereas the second occurred at all times throughout the 10-day duration of a late winter experiment. Numerical models predict some of the characteristics of the choruses. [Work supported by the Office of Naval Research].

8:40

2aAOa3. Understanding potential effects of using active sonar to study marine ecosystems. Mardi C. Hastings (Penn State University, Applied Research Laboratory, 801 North Quincy Street, Suite 120, Arlington, VA 22203-1708, USA, mch26@psu.edu)

Biological organisms can suffer various kinds of effects when exposed to high intensity sound. Active sonar systems used to investigate marine ecosystems typically have source levels exceeding 220 dB re: 1 μPa at 1 m, which are high enough to have an effect on organisms in relatively close proximity. Although these systems operate at frequencies from the low kilohertz to megahertz ranges that are not usually associated with potentially harmful effects in the marine environment, fundamental interactions with sound occur at various biological scales that strongly depend on the size of the organism with respect to acoustic wavelengths. These effects range from subtle changes in behavior to various types of trauma that can result in temporary or permanent hearing loss, or in hemorrhage or even mortality. Examples from the literature will be used to illustrate the basic relationships between biological effects of sound and the size and structure of marine organisms, as well as potential concerns associated with using active sonar to study the marine environment.

9:00

2aAOa4. How toothed whales echolocate to find and capture prey in the deep ocean. Peter Tyack (Woods Hole Oceanographic Institution, Applied Ocean Physics & Engineering Dept., Woods Hole, MA 02543, USA, ptyack@whoi.edu), Mark Johnson (Woods Hole Oceanographic Institution, Applied Ocean Physics & Engineering Dept., Woods Hole, MA 02543, USA, majohnson@whoi.edu), Peter T. Madsen (University of Aarhus, Biological Sciences, Zoophysiology, C. F. Møllers Allé, Building 1131, DK-8000 Aarhus, Denmark, peter.madsen@biology.au.dk), Walter M. Zimmer (NATO Undersea Research Centre, Viale San Bartolomeo 400, 19126 La Spezia, Italy, walter@nurc.nato.int), Natacha A. Soto (University of La Laguna, BIOECOMAC Department of Animal Biology, 38207 La Laguna, Spain, naguilar@ull.es)

Sperm and beaked whales dive to feed on squid and deepwater fish. We have attached sound-and-orientation recording tags to study how these whales use echolocation to forage at depth. Tagged whales are usually silent when starting a dive, but start producing echolocation clicks at a few hundred meters depth, shallower than the depth at which they feed, suggesting that descending whales scan the deep layers where they will feed. Once sperm or beaked whales encounter prey, they switch from regular search clicks to a buzz of rapid clicks. Tags on beaked whales not only record outgoing clicks, but also echoes from prey at ranges out to 10-20 m. Beaked whales produce clicks every 0.2-0.4 sec when searching. Echoes from several targets are often detected after each beaked whale click. Beaked whales will pass by many targets before selecting one. Whales may switch from the search clicks to a buzz as they close within a body length of the prey. Sperm and beaked whales have an angular acceleration at the end of the buzz, which probably indicates turning to catch the prey.

9:20

2aAOa5. Hypotheses regarding exploitation of bubble acoustics by cetaceans. Timothy G. Leighton (Institute of Sound and Vibration, Univ. of Southampton, University Road, Highfield, SO17 1BJ Southampton, UK, T.G.Leighton@soton.ac.uk), Paul R. White (Institute of Sound and Vibration, Univ. of Southampton, University Road, Highfield, SO17 1BJ Southampton, UK, prw@isvr.soton.ac.uk), Daniel C. Finfer (Institute of Sound and Vibration, Univ. of Southampton, University Road, Highfield, SO17 1BJ Southampton, UK, d.c.finfer@soton.ac.uk)

Bubbles are the most acoustically active naturally occurring entities in the ocean, and cetaceans are the most intelligent. Having evolved over tens of millions of years to cope with the underwater acoustic environment, cetaceans may have developed extraordinary techniques from which we could learn. This paper outlines some of the possible interactions, ranging from the exploitation of acoustics by humpback whales (Megaptera novaeangliae) in bubble nets to trap prey, to techniques by which coastal dolphins (e.g. of the genus Cephalorhynchus) could successfully echolocate in bubbly water (a hypothesis which has led to the development of a man-made sonar which can penetrate bubble clouds, and a range of possibilities for homeland security).

9:40

2aAOa6. Marine ecosystem acoustics: contributions of sonar technology. Kenneth G. Foote (Woods Hole Oceanographic Institution, Woods Hole, MA 02543, USA, kfoote@whoi.edu)

Sonar is considered in the widest sense as an acoustic system consisting of a transmitter and receiver of underwater sound. It may be monostatic, bistatic, or multi-static; narrowband or broadband; with one or more fixed, rotating, or electronically formed beams. Transducers may be mounted on hulls of vessels and autonomous underwater vehicles, fixed structures, or seafloor; towed; or suspended. Spatial scales may be sampled from millimeters to thousands of kilometers; corresponding temporal scales vary from a fraction of a second, as in target-tracking, to seasons, as in observing animal migration. Several sonar types are described. Contributions of sonar technology to ecosystem studies, both actual and potential, are noted. These include, for example, fine-scale surveying of pelagic and semi-demersal fish by scientific echo sounder; mapping of the three-dimensional structure of fish aggregations and bathymetry by multibeam sonar; quantification of benthic egg beds of the squid Loligo opalescens by sidescan sonar; and large-scale surveying of swimbladdered fish by parametric sonar. Each of these sonar systems has potential for detection, quantification, and classification of marine organisms, as well as for characterization of the habitat, hence yielding the kind of information that is required for ecosystem assessment and management.

10:00

2aAOa7. Use of broadband active acoustics to study marine organisms. Timothy K. Stanton (Woods Hole Oceanographic Institution, Applied Ocean Physics & Engineering Department, 98 Water Street, MS #11, Woods Hole, MA 02543, USA, tstanton@whoi.edu), Dezhang Chu (NOAA/NMFS/NWFSC/FRAMD, Montlake Blvd., E. Seattle, WA 98112, USA, dchu@whoi.edu)

Broadband signals inherently have more information than narrowband signals. In essence, they have more ″channels″ of information due to the wider range of frequencies spanned. It is therefore advantageous to use broadband signals in active acoustic studies of marine organisms and to apply techniques that best exploit the broadband nature of the signals. In this presentation, a brief background on the use of narrowband systems for studying marine organisms by these authors and other investigators is given. Limitations to those studies are outlined, with arguments made for the use of broadband acoustics. The past twenty years of studies centered at the Woods Hole Oceanographic Institution are subsequently reviewed in which broadband signals are used both in the laboratory and field to study a variety of organisms-- swimbladder-bearing fish and three major anatomical categories of zooplankton. The analyses are divided broadly into two major categories-- time and frequency domain-- for various types of analyses, including pulse compression processing and spectral analysis. Results are first shown based on studies, one organism at a time, in the laboratory. Those laboratory approaches are then applied to ocean studies of fish and large zooplankton using a new towed instrument spanning the frequency range 1.7 kHz - 100 kHz.

TUESDAY MORNING, 1 JULY 2008 ROOM 342A, 10:40 A.M. TO 6:40 P.M.

Session 2aAOb

Acoustical Oceanography, Underwater Acoustics, Signal Processing in Acoustics, and ECUA: Geoacoustic Characterization of the Ocean Bottom and Geoacoustic Inversion I

Peter Gerstoft, Cochair
Marine Physical Laboratory, Scripps Institute of Oceanography, 8602 La Jolla Shores Drive, La Jolla, CA 92093-0238, USA

Dag Tollefsen, Cochair
Norwegian Defence Research Establishment (FFI), Box 115, Horten, 3191, Norway

Invited Papers

10:40

2aAOb1. Characterization of seabed geo-acoustic structure for a shallow water environment. David Knobles (Applied Research Laboratories, UT at Austin, P. O. Box 8029, Austin, TX 78713, USA, knobles@arlut.utexas.edu)

Full-field inversion methods over large frequency bands and spatial scales attempt to exploit the sensitivity of the frequency and spatial dependence of the acoustic field of the properties to the seabed. A comprehensive set of broadband impulsive and narrowband tonal acoustic recordings in the 5-3000 Hz band from two L-arrays separated by 20 km were made in a shallow water area on the New Jersey continental shelf during the Shallow Water 2006 (SW06) experiment. In addition, surface ship of opportunity passages on both arrays were recorded along with noise during the passage of tropical storm Ernesto. Reverberation and transmission loss data in the 25-9200 Hz band from explosive sources were also collected at a nearby site prior to the SW06 experiment. Numerous full-field geoacoustic inversion methods and analyses of all these acoustic data with supporting range and azimuth-dependent geo-physical measurements are employed to characterize the seabed properties. For example, the analyses of these data permit inferences about the frequency-dependence of the seabed sound speed and attenuation to be made. The overlapping data types act to reduce the intrinsic ambiguities associated with inversion, quantify the spatial variability, and serve as independent validation.

11:00

2aAOb2. Effect of ocean sound speed uncertainty on matched-field geoacoustic inversion. Chen-Fen Huang (Department of Marine Environmental Informatics/National Taiwan Ocean University, 2 Pei-Ning Road, 202 Keelung, Taiwan, chenfen@mail.ntou.edu.tw)

The effect of ocean sound speed uncertainty on matched field geoacoustic inversion is investigated using data from the SW06 experiment along a nearly range-independent bathymetric track. Significant sound speed differences were observed at the source and receiving array and several environmental parameterizations were investigated for the inversion including representing the ocean sound speed at both source and receivers with empirical orthogonal function (EOF) coefficients. A GA-based global optimization method was applied to the candidate environmental models. Then, a Bayesian inversion technique was used to quantify uncertainty in the environmental parameters for the best environmental model, which included an EOF description of the ocean sound speed.

11:20

2aAOb3. Quantifying the uncertainty of geoacoustic parameter estimates in a dynamic environment using oceanographic data. Ross Chapman (University of Victoria, 3800 Finnerty Rd, Vcitoria, BC V8W 3P6, Canada, chapman@uvic.ca), Yong-Min Jiang (University of Victoria, 3800 Finnerty Rd, Vcitoria, BC V8W 3P6, Canada, minj@uvic.ca)

This paper presents results of Bayesian matched field geoacoustic inversion in a temporally and spatially varying shallow water environment. The acoustic data were collected by a vertical line array at ranges of 1, 3 and 5 km in the SW06 (Shallow Water 06) experiment carried out in August 2006. The sound speed profiles measured at the array and at the source positions during the experiment showed significant variation in the thermocline in the middle part of the water column. The resulting uncertainty in the sound speed profile in the water impacts the performance of matched field inversion methods in estimation of geoacoustic model parameters. In previous work, an effective sound speed profile was estimated in the inversion, based on empirical orthogonal functions (EOFs) derived from a limited number of sound speed profiles measured at the time of the experiment. This paper explores the effect of using a larger number of profiles measured over several days in the SW06 experiment to include a greater diversity of ocean conditions in generating the EOFs. The inversion results for the two approaches are compared in terms of marginal probability distributions of the estimated geoacoustic parameters. (Work supported by Office of Naval Research).

11:40

2aAOb4. Short range geoacoustic inversion with a vertical line array. Yong-Min Jiang (University of Victoria, 3800 Finnerty Rd, Vcitoria, BC V8W 3P6, Canada, minj@uvic.ca), Ross Chapman (University of Victoria, 3800 Finnerty Rd, Vcitoria, BC V8W 3P6, Canada, chapman@uvic.ca), Peter Gerstoft (Marine Physical Laboratory, Scripps Institute of Oceanography, 8602 La Jolla Shores Drive, La Jolla, CA 92093-0238, USA, gerstoft@ucsd.edu)

During the SW06 (Shallow Water 06) experiments, short range geoacoustic inversion experiments were carried out at a source-receiver range of 230 m to determine the sea bed properties at fine spatial scales. Acoustic signals were collected at 16 hydrophones on a vertical line array from source depths of 15-65 m in 10 m intervals. For this experimental geometry, the angular coverage for reflectivity versus grazing angle is 7-25°. This paper combines the information extracted from low-frequency (100-900 Hz) and mid-frequency (1500-4500 Hz) LFM signals transmitted from the same source position to estimate multi-layered geoacoustic models. The model parameterization was based on the number of resolved sub-bottom reflections in the data. An inversion approach using adaptive simplex differential evolution was applied to the data to invert for the sub-bottom sound speeds and layer thicknesses. The temporal variation of the water column sound speed profile was included in the inversion. The estimated sound speeds are consistent with the range-averaged profile that was estimated previously from longer range data for the same radial path from the array. (Work supported by Office of Naval Research).

12:00

2aAOb5. Does a depth variable sound-speed profile matter for SW06 geoacoustic inversion? Alexandra Tolstoy (ATolstoy Sciences, 1538 Hampton Hill Circle, McLean, VA 22101, USA, atolstoy@ieee.org)

This work will discuss the effects of depth variability for a sound-speed profile with regard to goeacoustic inversion on some simulated SW06 ″data″. First, broadband (400-800 Hz) simulated ″data″ are generated using RAM_PE (by Collins) in the time domain for some short range (less than 1 km) SW06 scenarios. Next, the first 4 boundary reflection arrivals (from surface, bottom, surface-bottom, bottom-surface) are studied as a function of source range and depth, phone depth, and sound-speed variability. Finally, we examine the effects of sound-speed depth variability on geoacoustic inversion via MFP. We note that knowledge of array phone locations has a large impact on inversion capabilities.

12:20

2aAOb6. Three dimensional geoacoustic inversion on the New Jersey shelf. Megan S. Ballard (Penn. State University, P.O. Box 30, State College, PA 16804, USA, msd200@psu.edu), K.m. Becker (Penn. State University, P.O. Box 30, State College, PA 16804, USA, kmbecker@psu.edu)

Perturbative inversion, based on a linearized relationship between sound speed in the sediment and modal eigenvalues, is applied to data from the Shallow Water Experiment 2006. Data were collected by towing a low-frequency sound source out and back along radials, spanning a 90 degree angular sector, from a common receiver location. Range-dependent estimates of horizontal wave numbers are obtained along each of the radials using high-resolution signal processing techniques capable of detecting and localizing changes in sub-bottom properties, and that are particularly sensitive to changes in layer structure. Wave number estimates at each range are used in a linearized inversion algorithm to estimate local sediment properties. Locations of the R-reflector and other layering information are used as a priori information in the inversion algorithm. The additional information both constrains the solution of an otherwise ill-posed problem and emphasizes the layered structure of the sediment. These methods have been shown to yield accurate estimates of the sound speed profile deep into the sediment using very few perturbations to the forward model. Combining the local inversion results, a three-dimensional map of sediment sound speed structure is obtained for a 25 km2 region of the seafloor. [Supported by NDSEG and ONR]

12:40

2aAOb7. Experimental verification of range-dependent inverse method for geoacoustic parameters from modal dispersion data. Subramaniam Rajan (Scientific Solutions, Inc, 99 Perimeter Road, Nashua, NH 03063, USA, srajan@scisol.com), K.m. Becker (Penn. State University, P.O. Box 30, State College, PA 16804, USA, kmbecker@psu.edu)

The procedure for determining the sediment compressional wave speed profile from modal dispersion data in a range-independent case is well documented in the literature. In this paper, the procedure developed for the range-independent case is extended to cover the range-dependent case. In this procedure the region under investigation is divided into discrete range intervals and the sediment characteristics at each range interval estimated assuming that the sediment properties of each range interval are range independent. The approach has been demonstrated to yield range-dependent sediment properties when applied to synthetic data generated for an experiment consisting of multiple source/receiver combinations. During the Shallow Water Experiment 2006, broadband data transmitted by a single source were measured on multiple receivers. These data are used here to estimate range-dependent properties of the sediment. The results obtained in this manner are compared with inversion results obtained for the same region by other investigators who employed different approaches for estimating the geoacoustic properties. [Work supported by ONR, Ocean Acoustics].

1:00-2:00 Lunch Break

Invited Paper

2:00

2aAOb8. Modal inversion using the acoustic field emitted by a moving source and measured on a vertical line array of hydrophones. K.m. Becker (Penn. State University, P.O. Box 30, State College, PA 16804, USA, kmbecker@psu.edu), Megan S. Ballard (Penn. State University, P.O. Box 30, State College, PA 16804, USA, msd200@psu.edu)

As part of the Shallow Water Experiment 2006 (SW06), a low-frequency continuous wave acoustic source was towed out and back along radials from a fixed vertical line array of hydrophones. The resulting modal pressure field, measured on synthetic range apertures created by the relative source motion, is used to derive input data to inversion algorithms for estimating bottom properties. The inversion algorithms considered are based on well established relationship between modal eigenvalues and geoacoustic properties of the sediment. In this talk, linear inversion methods based on modal input data will be reviewed for their application to the SW06 data. The first step in these methods is the accurate estimation of modal eigenvalues from the pressure field data. For a moving source, theory predicts a Doppler shift along with frequency spreading proportional to both the transmitted frequency and tow speed. Propagating modes and their corresponding modal eigenvalues are predicted to correspond with the Doppler shifted frequencies. An emphasis of this work is on Doppler shift as an observable in the data and properly accounting for it in inversion. Sediment sound speeds estimated from data are consistent with sandy sediments found in the experimental area. [Work supported by ONR and NDSEG]

Contributed Paper

2:20

2aAOb9. Geoacoustic inversion using combustive sound source signals. Gopu R. Potty (University of Rhode Island, Department of Ocean Engineering, Narragansett Bay Campus, Narragansett, RI 02882, USA, gopu@uri.edu), James H. Miller (University of Rhode Island, Department of Ocean Engineering, Narragansett Bay Campus, Narragansett, RI 02882, USA, miller@egr.uri.edu), Preston S. Wilson (The University of Texas, Mechanical Engineering Department, Austin, TX 78712, USA, pswilson@mail.utexas.edu), James F. Lynch (Woods Hole Oceanographic Institution, 98 Water Street, Bigelow 203A, MS-11, Woods Hole, MA 02543, USA, jlynch@whoi.edu), Arthur Newhall (Woods Hole Oceanographic Institution, 98 Water Street, Bigelow 203A, MS-11, Woods Hole, MA 02543, USA, anewhall@whoi.edu)

In the summer of 2006, Combustive Sound Sources (CSS) were deployed in shallow waters off New Jersey during the Shallow Water experiment (SW 06). The depth of these sources were 26 m in water depths of the order of 100 m. CSS are low frequency broadband sound sources and suitable for modal dispersion based inversion. CSS data collected on various receivers (Single Hydrophone Receiving Units (SHRU), Vertical Line Array, etc.) will be used for the inversions. The inversions are based on an iterative scheme using a new time-frequency analysis technique (dispersion based short-time Fourier transform) in which each time-frequency tiling is adaptively rotated in the time-frequency plane, depending on the local wave dispersion. Data from various receivers will be used to investigate the spatial variation in compressional wave speed. Compressional wave attenuation will also be estimated using modal amplitude ratios. Inversion results will be validated by comparing the data with model predictions. [Work supported by the Office of Naval Research]

Invited Paper

2:40

2aAOb10. Tomographic and bottom geoacoustic inversions using Genetic Algorithms and a statistical characterization of the acoustic signal. Michael Taroudakis (University of Crete & FORTH/IACM, Vassilika Vouton, P.O.Box 1385, 711 10 Heraklion, Greece, taroud@iacm.forth.gr), Costas Smaragdakis (University of Crete, Dept of Mathematics, Knossou Ave, 71409 Heraklion, Greece, kesmarag@gmail.com)

The paper deals with the problem of estimation of the parameters of the water column and/or the sea bed, using measurements of the acoustic field due to a known source at a certain point in the water column. Following the work by Taroudakis et al. (JASA 119, 1396-1405 (2006)) the acoustic signal is characterized using the statistics of the wavelet sub-band coefficients, which obey a certain statistical law, described by an Alpha-Stable distribution. Thus, the signal observables are the set of the parameters of the appropriate distributions at the various levels of the signal decomposition. In this work an inversion procedure based on a Genetic Algorithm and the statistical characterization of the acoustic signal, is described. The quality of a certain population of candidate model parameters (properties of the water columns and/or the sea-bed) is evaluated using the Kullback-Leibler divergence (KLD) of the wavelet sub-band coefficient distributions, between the measured and simulated acoustic signals. Following an appropriate population regeneration procedure, the final population is described by an a-posteriori statistical distribution of the model parameters, indicating among the others their sensitivity in the inversion procedure. Very good inversion results have been observed in simulated shallow water environments.

Contributed Paper

3:00

2aAOb11. Dispersion curve estimation with partcile filters for geoacoustic inversion. Ivan Zorych (Department of Mathematical Sciences, New Jersey Institute of Technology, 323 M L King Blvd, Newark, NJ 07102, USA, zorych@gmail.com), Zoi-Heleni Michalopoulou (Department of Mathematical Sciences, New Jersey Institute of Technology, 323 M L King Blvd, Newark, NJ 07102, USA, michalop@njit.edu)

In this work we extend our particle filtering method for dispersion curve extraction from spectrograms of acoustic signals that have propagated in underwater environments, the goal being to obtain accurate representation of modal dispersion for geoacoustic inversion. The approach combines particle filtering with modeling of sound propagation in ocean environments to track dispersion curves of multimodal signals in noisy environments. In addition to providing connected modal ″trajectories″ that facilitate the computation of maximum a posteriori estimates of modal arrival times, the method provides posterior probability distributions for arrival times, quantifying errors that are then propagated into the geoacoustic inversion process. The method, thus, allows the calculation of posterior probability distributions of geoacoustic parameters. We present results from both synthetic and real data from the Gulf of Mexico experiment. [Work supported by ONR.]

Invited Paper

3:20

2aAOb12. Geoacoustic characterization of the seafloor from a subbottom profiler applied to the BASE'07 experiment. Gwladys Theuillon (SHOM, 13 rue du Chatellier, CS 92803, 29228 Brest cedex 2, France, gwladys.theuillon@shom.fr), Yann Stephan (SHOM, 13 rue du Chatellier, CS 92803, 29228 Brest cedex 2, France, yann.stephan@shom.fr)

The most recent subbottom profilers present good performances in term of signal to noise ratio, resolution and penetration. These devices can thus be used to infer quantitatively the geoacoustic parameters of the seafloor. We have previously developed inversion methods which aim to estimate absorption, reflection, penetration, impedance contrast and micro-roughness in sediments from the SBP 120 subbottom profiler, manufactured by Kongsberg. These methods have been tested against real data and geoacoustic parameters derived from the SBP 120 are fully coherent with in situ measurements, which tends to confirm the possibility of seafloor characterization with subbottom profilers. In this work, the inversion methods are applied to a set of data acquired on the Malta Plateau during BASE'07 experiment. Geoacoustic parameters results are presented and discussed. They are in good agreement with the a priori knowledge of sediment properties in the area.

3:40-5:20 Posters

Lecture sessions will recess for presentation of poster papers on various topics in acoustics. See poster sessions for topics and abstracts.

Invited Paper

5:20

2aAOb13. Bayesian model parameterization selection for seabed reflection-coefficient inversion. Jan Dettmer (University of Victoria, School of Earth and Ocean Sciences, Victoria, BC V8W 3P6, Canada, jand@uvic.ca), Stan E. Dosso (University of Victoria, School of Earth and Ocean Sciences, Victoria, BC V8W 3P6, Canada, sdosso@uvic.ca), Charles W. Holland (Penn State University / Applied Research Lab, Applied Science Bldg., State College, PA 16804, USA, cwh10@psu.edu)

This paper considers Bayesian inversion of seabed reflection-coefficient data for multi-layer geoacoustic models; in particular, the important issue of determining appropriate model parameterizations (e.g., number of layers, sound speed and density variations within layers). A poor model parameterization can lead to unreasonable inversion results. In particular, under-parameterization can introduce theory error in the inversion, causing biased results. However, more complex models always fit the data better. Therefore, parameterization quality cannot be quantified only in terms of data misfit, and Occam's razor is commonly applied to prefer simple parameterizations. In a Bayesian framework, Occam's razor is inherently included through Bayesian evidence. Bayesian inversion can be associated with two levels of inference. The first level assumes a specific model parameterization, and quantifies the data information content. This paper focuses on the second level: using Bayesian evidence to compare different model parameterizations. To this end, Gibbs sampling is applied, including full error covariance estimation, to sample the posterior probability density (PPD) for various parameterizations. Bayesian evidence is then computed from the PPD samples by numerical integration (reverse importance sampling).

Contributed Papers

5:40

2aAOb14. Combined inversion of mid-frequency propagation and reverberation sonar data. Peter Louring Nielsen (NURC, Viale S. Bartolomeo 400, 19126 La Spezia, Italy, nielsen@nurc.nato.int), Christopher H. Harrison (NATO Undersea Research Centre, Viale San Bartolomeo 400, 19138 La Spezia, Italy, harrison@nurc.nato.int)

Sonar performance predictions in shallow-water regions are strongly dependent on a good knowledge of the geoacoustic and scattering properties of the seabed. The bottom properties are probably the most difficult parameters to determine, but inversion of measured acoustic data to infer the geoacoustic and scattering properties is a feasible technique. One of these techniques relies on inverting: (1) propagation data to estimate local bottom properties and (2) long-range reverberation data providing effective bottom properties over larger areas. A matched-field inversion approach is applied to propagation and reverberation data received on a towed horizontal array during the BASE'04 experiment conducted on the Malta Plateau, Mediterranean Sea. A total of 30 transmissions along a 10-km track were used to capture eventual range-dependent bottom properties. The inversion algorithm is composed of efficient prediction tools which can provide environmental parameter estimates within tactical time frames for in-situ sonar performance predictions. The experimental set-up mimics a mid-frequency active sonar system using only the suite of sensors available on the vessel towing the sonar system; also known as the through-the-sensor technique. The impact on sonar performance utilizing the environmental characterization approach is shown for various experimental scenarios and seasons. [Research sponsored by NURC and the BOUNDARY Partners].

6:00

2aAOb15. Reverberation inversion for seabed properties. Stan E. Dosso (University of Victoria, School of Earth and Ocean Sciences, Victoria, BC V8W 3P6, Canada, sdosso@uvic.ca), Peter Louring Nielsen (NURC, Viale S. Bartolomeo 400, 19126 La Spezia, Italy, nielsen@nurc.nato.int), Christopher H. Harrison (NATO Undersea Research Centre, Viale San Bartolomeo 400, 19138 La Spezia, Italy, harrison @nurc.nato.int)

This paper applies nonlinear inversion to reverberation and/or propagation data recorded on a towed horizontal array for geoacoustic and scattering properties of the seabed. A Bayesian inversion approach is applied to estimate properties of the posterior probability density, such as the maximum a posteriori (most-probable) model, 1-D and 2-D marginal probability distributions, and covariance/correlation matrices, providing optimal parameter estimates and quantifying parameter uncertainties and inter-relationships. Of particular interest is quantifying the information content of different combinations of data (e.g., reverberation or propagation data; joint inversion of reverberation and propagation data) to resolve seabed parameters, and understanding strong parameter inter-relationships (correlations) which, in some cases, act as the limiting factor in resolving geoacoustic/scattering parameters. The inversion is also applied to shallow-water reverberation and propagation data recorded in Mediterranean Sea.

6:20

2aAOb16. Local bottom characterization using an autonomous underwater vehicle. Peter Louring Nielsen (NURC, Viale S. Bartolomeo 400, 19126 La Spezia, Italy, nielsen@nurc.nato.int), Charles W. Holland (Penn State University/Applied Research Lab, Applied Science Bldg., State College, PA 16804, USA, cwh10@psu.edu)

In the past decade the usage of autonomous underwater vehicles (AUV) to sample properties of the underwater environment has increased. The advantages of using platforms are their autonomy and that operations can be performed covertly. In 2007, the CLUTTER'07 experiment was conducted on the Malta Plateau with the main aim of characterizing the underwater environment. An AUV was deployed at a particular site on the Plateau to demonstrate the feasibility to infer bottom properties using such an autonomous platform. The AUV was equipped with 2 sound sources covering a frequency band 800-3500 Hz, and the transmitted signals were acquired on a bottom moored vertical array. The mission of the AUV was to perform a linear track of ~1000 m passing the vertical array as close as possible while transmitting every second from the sound sources. This experimental configuration is similar to the move-out or wide-angle reflection measurements. The received signals are inverted for geoacoustic properties using both matched-field techniques and processed for direct bottom reflection properties. The results obtained are compared to independent findings from different experiments using various types of equipment at different seasons in the same area. [Research sponsored by NURC, ONR OA321 and the CLUTTER Partners]

TUESDAY MORNING, 1 JULY 2008 ROOM 352B, 8:00 A.M. TO 2:40 P.M.

Session 2aBB

Biomedical Ultrasound/Bioresponse to Vibration and Physical Acoustics: Ultrasound Contrast Agents for Imaging I

Charles C. Church, Cochair
University of Mississippi, NCPA, 1 Coliseum Drive, University, MS 38677, USA

Ayache Bouakaz, Cochair
INSERM U930, 2, Bvd Tonnelle, Tours Cedex 9, 37044, France

Invited Paper

8:00

2aBB1. Ultrasound and microbubble interaction. Nico De Jong (Erasmus MC, Dr Molewaterplein 50 room Ee2302, 3015GE Rotterdam, Netherlands, n.dejong@erasmusmc.nl)

Ultrasound contrast agent (UCA) bubble response to ultrasound (US) is still the subject of several studies, since it determines the power of medical diagnostic imaging modalities. Generally, bubbles are studied using optical or acoustical methods, both having their specific advantages, in an environment that mimic the clinical practice as good as possible (small-diameter capillaries, red blood cells, blood viscosity). Acoustical observations could provide a better insight in the acoustical scattering of bubbles, which determines the final efficacy of contrast-enhanced diagnostic US imaging, and are better suitable to determine the properties of populations of bubbles. Optical observations allow for easier characterization of fewer bubbles and a more detailed characterisation in case where bubbles vibrate non spherically, which is expected for bubbles nearby a wall or red blood cells. In this presentation, we show optical recordings of the various bubble responses with the ultrahigh speed Brandaris-128 camera, and discuss the clinical implications of our findings.

8:20

2aBB2. Nonlinear pulsing schemes for the detection of ultrasound contrast agents. Michalakis A. Averkiou (University of Cyprus/Dept. of Mech. Engineering, 75 Kallipoleos Str., 1678 Nicosia, Cyprus, maverk@ucy.ac.cy), Christophoros Mannaris (University of Cyprus/Dept. of Mech. Engineering, 75 Kallipoleos Str., 1678 Nicosia, Cyprus, mannaris@ucy.ac.cy), Matthew Bruce (SuperSonic Imagine, Les Jardins de la Duranne - Bât. E, 510, rue René Descartes, F - 13857 Aix-en-Provence, France, matt.f.bruce@gmail.com), Jeffry Powers (Philips Medical Systems, 22100 Bothell Everett Hwy, Bothell, WA 98021, USA, jeff.powers@philips.com)

Ultrasound contrast agents are used in cardiology for the assessment of myocardial perfusion and in radiology for the detection and characterization of tumors. One widely used approach of imaging contrast agents is to use a low Mechanical Index (*MI*) nonlinear imaging technique to avoid bubble destruction and image both the macro- and micro-circulation in real-time. Various pulsing schemes are employed for the detection of nonlinear echoes from contrast microbubbles. The objective of this paper is to evaluate the various pulsing schemes for low *MI* imaging of contrast microbubbles and better understand their similarities and differences. The pulsing schemes considered are pulse inversion, power modulation, and their combination. Emphasis is placed on identifying whether nonlinearity due to propagation in tissue may be discriminated from nonlinearity due to scattering from bubbles. Bubble destruction (use of high *MI*) and tissue motion were not considered in this work. The evaluation of the different pulsing schemes was performed with numerical simulations from well established theoretical models and experimental data from microbubbles in tissue phantoms and human tissues.

8:40

2aBB3. Contrast agent response to chirp reversal. Anthony Novell (INSERM U930, CHRU Bretonneau, 37044 Tours Cedex 9, France, anthony.novell@etu.univ-tours.fr), Sander Van Der Meer (Physics of Fluids, University of Twente, P.O. Box 217, 7500 AE Enschede, Netherlands, s.m.vandermeer@utwente.nl), Michel Versluis (Physics of Fluids, University of Twente, P.O. Box 217, 7500 AE Enschede, Netherlands, m.versluis@utwente.nl), Nico De Jong (Erasmus MC, Dr Molewaterplein 50 room Ee2302, 3015GE Rotterdam, Netherlands, n.dejong@erasmusmc.nl), Ayache Bouakaz (INSERM U930, 2, Bvd Tonnelle, 37044 Tours Cedex 9, France, bouakaz@med.univ-tours.fr)

We investigate an excitation approach for contrast agents based on chirps. This technique, named chirp reversal, consists in transmitting an up sweep frequency chirp (UPF) followed by a down sweep frequency chirp (DNF). Simulations using a modified Rayleigh-Plesset equation were carried out. Chirps with center frequencies from 1.4 MHz to 2 MHz, pressures from 50 kPa to 200 kPa and frequency bandwidths from 30% to 65% were considered. High speed optical observations and acoustical measurements were performed using individual contrast bubbles of radii from 1 μm to 5 μm and a diluted solution of contrast agent respectively. Simulations showed differences between bubbles' oscillations following UPF and DNF chirps in terms of amplitude and duration. Maximal differences occurred for bubbles that were around 80% and 140% of the resonance size. Bubbles at resonance or far away from resonance provided identical responses to UPF and DNF chirps. Larger bandwidths and higher acoustic pressures accentuate further the difference between the UPF and DNF responses. These findings were confirmed through optical data and acoustical measurements. The results reveal the potential of chirp reversal for contrast agent detection.

9:00

2aBB4. Dual-frequency insonation of single microbubbles. Marcia Emmer (Erasmus MC, Ee2302, P.O. Box 2040, 3000 CA Rotterdam, Netherlands, m.emmer@erasmusmc.nl), Hendrik J. Vos (Biomedical Engineering, Erasmus MC, P.O. Box 2040, 3000 CA Rotterdam, Netherlands, H.J.Vos@ErasmusMC.nl),Nico De Jong(Erasmus MC, Dr Molewaterplein 50 room Ee2302, 3015GE Rotterdam, Netherlands, n.dejong@erasmusmc.nl)

Radial modulation imaging is a new medical imaging technique based on dual-frequency insonation of ultrasound contrast agents. The difference in echo between a high frequency 'imaging' pulse transmitted at either the compression or rarefaction phase of a low frequency 'modulating' pulse is detected by regular correlation techniques. Little is however known about the contrast agent microbubble dynamics in a dual-frequency ultrasound field, which were investigated in this study. Using a high-speed camera system, the radial excursions of single phospholipid-coated microbubbles were recorded. The microbubbles were simultaneously insonified with 2.5 cycles pulse at 0.5 MHz and 30 kPa and a 32 cycles pulse at 3.75 MHz and 80 kPa. The microbubbles studied had diameters ranging from 1.1 - 5.2 μm. Microbubbles smaller than 1.4 μm frequently showed shrinkage. Microbubbles larger than 2.6 μm showed low ($<$ 8 dB) or no amplitude modulation of the high frequency radial excursion. Microbubbles with diameters between 1.4 and 2.6 μm showed high amplitude modulation (up to 25 dB) and strong compression-only oscillation, which both may be explained by nonlinear shell properties. The observed behaviour is beneficial for the detection of contrast agents.

9:20

2aBB5. Sub-harmonic response from polymer-shelled contrast agents with a 40-MHz excitation. Jeffrey A. Ketterling (Frederic L. Lizzi Center for Biomedical Engineering, Riverside Research Institute, 156 William St., New York, NY 10038, USA, ketterling@rrinyc.org), Jonathan Mamou (Riverside Research Institute, 156 William St., 9th Floor, New York, NY 10038, USA, mamou@rrinyc.org)

There is a growing interest in using acoustic contrast agents with high-frequency ultrasound ($>$ 15 MHz) in order to better visualize microcirculation. Experiments were performed with polycaprolactone-shelled agents (POINT Biomedical, San Carlos, CA) having mean diameters of 0.56, 1.1, and 3.4 μm. The agents were heavily diluted in filtered water and injected through a 200 μm channel into the focal zone of a 40-MHz transducer that had a focal length of 12 mm and an outer diameter of 6 mm. Backscatter signals from single agents were digitized using tone bursts of 5 to 20 cycles at peak-negative pressures of 0.6 to 6.3 MPa. 1000 valid single-bubble backscatter events at each exposure condition were digitized and then analyzed for 20-MHz subharmonic content. The data showed that the subharmonic response was initiated between 5 and 10 cycles and the likelihood of a subharmonic event increased as the number of cycles increased. A subharmonic backscatter response was most likely at 3.9 MPa for the 3.4 μm agent and 1.7 MPa for the 0.56 and 1.1 μm agents. The increased pressure for subharmonic activity for larger agent was consistent with its larger size.

9:40

2aBB6. Combined optical and acoustical characterization of single ultrasound contrast agent microbubbles. Jeroen Sijl (Physics of Fluids, University of Twente, P.O. Box 217, 7500 AE Enschede, Netherlands, j.sijl@utwente.nl), Timo Rozendal (Physics of Fluids, University of Twente, P.O. Box 217, 7500 AE Enschede, Netherlands, t.rozendal@student.utwente.nl), Hendrik J. Vos (Biomedical Engineering, Erasmus MC, P.O. Box 2040, 3000 CA Rotterdam, Netherlands, H.J.Vos@ErasmusMC.nl), Benjamin Dollet (Physics of Fluids, University of Twente, P.O. Box 217, 7500 AE Enschede, Netherlands, benjamin.dollet@univ-rennes1.fr), Nico De Jong (Erasmus MC, Dr Molewaterplein 50 room Ee2302, 3015GE Rotterdam, Netherlands, n.dejong@erasmusmc.nl), Detlef Lohse (Physics of Fluids, University of Twente, P.O. Box 217, 7500 AE Enschede, Netherlands, d.lohse@utwente.nl), Michel Versluis (Physics of Fluids, University of Twente, P.O. Box 217, 7500 AE Enschede, Netherlands, m.versluis@utwente.nl)

Contrast enhancement in medical ultrasound imaging is provided by the non-linear characteristics of coated microbubbles used as Ultrasound Contrast Agents (UCA). Optical time-resolved observations of the UCA mi-

crobubble dynamics have revealed new non-linear bubble behavior such as ″compression only″ and ″thresholding″ behavior. Up to now, the contributions of such behavior to the non-linear acoustic response of UCA microbubbles is not known. Theoretically, the sound emission of an oscillating microbubble is derived from the unsteady Bernoulli equation and mass conservation assuming incompressible and irrotational flow. An experimental validation of this relation between the radial dynamics and the sound emission of a microbubble is not straightforward. We present a combined optical and acoustical setup to characterize individual BR-14 (Bracco Research S.A., Geneva, Switzerland) UCA microbubbles. The bubbles were isolated in a capillary fiber by an active flow control. During insonation the radial response of the single microbubble was recorded with the Brandaris ultra high-speed camera while the resulting acoustic response was measured with an accurately calibrated sensitive transducer. The sound emission calculated from the measured radius-time curves gives excellent quantitative agreement with the directly measured sound emission for both the linearly oscillating microbubbles and bubbles displaying ″compression-only″ and ″thresholding″ behavior, which indeed resulted in a strong non-linear sound emission.

Invited Paper

10:00

2aBB7. Secondary Bjerknes forces between ultrasound contrast agent microbubbles. Michel Versluis (Physics of Fluids, University of Twente, P.O. Box 217, 7500 AE Enschede, Netherlands, m.versluis@utwente.nl), Valeria Garbin (Physics of Fluids, University of Twente, P.O. Box 217, 7500 AE Enschede, Netherlands, v.garbin@tnw.utwente.nl), Benjamin Dollet (Physics of Fluids, University of Twente, P.O. Box 217, 7500 AE Enschede, Netherlands, benjamin.dollet@univ-rennes1.fr), Leen Van Wijngaarden (Physics of Fluids, University of Twente, P.O. Box 217, 7500 AE Enschede, Netherlands, l.vanwijngaarden@tnw.utwente.nl), Nico De Jong (Erasmus MC, Dr Molewaterplein 50 room Ee2302, 3015GE Rotterdam, Netherlands, n.dejong@erasmusmc.nl), Detlef Lohse (Physics of Fluids, University of Twente, P.O. Box 217, 7500 AE Enschede, Netherlands, d.lohse@utwente.nl)

Acoustic radiation forces arise on UCA microbubbles from pressure gradients in the ultrasound pressure field. The ultrasound wave emitted by an oscillating UCA microbubble and experienced by a neighboring bubble results in the so-called secondary Bjerknes force. Typically, only the (time) averaged value of the secondary Bjerknes force is estimated from experiments. Here, the ability to resolve in time the radial dynamics of UCAs and the evolution of their relative distances, allows us to obtain a quantification of the instantaneous secondary Bjerknes force. Two bubbles were selected and confined within two separate optical traps and positioned away from the sample chamber wall prior to insonation. The radius-time curves and distance-time curves were then extracted from high-speed optical recordings. The camera fully resolved the alternating attractive-repulsive features of the secondary Bjerknes force in time. The effect of the time averaged secondary Bjerknes force results in a net attraction of the two bubbles, with a typical observed displacement of 1-2 μm, with an instantaneous peak value of the secondary Bjerknes force of up to 10^{-6} N. We predict the mutual interaction of the two coated bubbles in their translation with an accuracy better than 10%.

10:20-10:40 Break

Contributed Paper

10:40

2aBB8. Mathematical models for contrast bubble dynamics. Charles C. Church (University of Mississippi, NCPA, 1 Coliseum Drive, University, MS 38677, USA, cchurch@olemiss.edu), John S. Allen (University of Hawaii-Manoa, Department of Mechanical Engineering, Holmes Hall Room 302, Honolulu, HI 96822, USA, alleniii@hawaii.edu)

Theoretical investigation of the acoustic responses of albumin-encapsulated microspheres began over fifteen years ago when Albunex, the first agent approved for clinical use in the US, was still in development. Since that time, the number of potential ultrasound contrast agents has grown considerably. Depending on the agent, the shell may comprise a layer of proteins, synthetic polymers, surfactants, or lipids with a thickness from a few nm to 500 mm and surrounding air, sulfur hexafluoride, perfluorocarbon, or other gas. A thorough understanding of the interaction between ultrasound pulses and contrast microbubbles is essential for the successful clinical application of a particular agent. In this talk, the behavior of various contrast agents will be discussed, and appropriate models for each will be described. The basis for each of these theories is a free bubble model ″supplemented″ by the effect of the encapsulating shell. The differences among these models lie primarily in their treatment of the encapsulating layer and, to some extent, the surrounding medium. Comparisons among models will include predictions of radial responses, thresholds for bubble destruction, and clinically significant acoustic properties (resonance frequency, scattering strength, nonlinearity, etc.). [Supported by NIH 2 RO1 EB000350-04A2 (CCC) and by NIH 2 G12RR003061-21 (JSA).]

Invited Papers

11:00

2aBB9. Ultrasound contrast agents: from concept to clinical use. François Tranquart (INSERM U930, 2, Bvd Tonnelle, 37044 Tours Cedex 9, France, tranquart@med.univ-tours.fr), Ayache Bouakaz (INSERM U930, 2, Bvd Tonnelle, 37044 Tours Cedex 9, France, bouakaz@med.univ-tours.fr), Aurore Bleuzen (INSERM U930, 2, Bvd Tonnelle, 37044 Tours Cedex 9, France, bleuzen@chu-tours.fr), Peggy Palanchon (INSERM U930, 2, Bvd Tonnelle, 37044 Tours Cedex 9, France, palanchon@med.univ-tours.fr), Jean-Michel Correas (Hopital Necker, 75015 Paris, France, jean-michel.correas@nck.ap-hop-paris.fr)

Contrast ultrasound imaging techniques are of interest for almost every clinical application in all organs including not only liver and kidney but also superficial organs and brain or lungs. This technique is mainly powerful in terms of lesion detection and characterization especially for liver with diagnostic value greater than 90%. This was the case for all categories of lesions (with values nearly 100% for liver metastases, FNH) but the accuracy was slightly lower for HCC. Specific recommendations were established by EFSUMB for the use of contrast agents in liver, pancreas, kidney, trauma and brain imaging for a proper and safe use to improve diagnosis accuracy. On the other hand, contrast-enhanced ultrasound may be used in evaluating response to therapy. The follow-up of vascularization under specific targeted treatments offers the capacity to early diagnose positive or negative local response for an adaptation of therapeutic way

before or in absence of tumour size changes. This non invasive method could be repeated without adverse events early after starting this therapy in order to depict local response or recurrence for a better adaptation of dose with a strong impact on cost and limitation of adverse events.

11:20

2aBB10. Dynamics of microbubbles targeted to surfaces: numerical and experimental modelling. Richard Manasseh (CSIRO, Fluid Dynamics Group, PO Box 56, Highett, VIC 3190 Melbourne, Australia, Richard.Manasseh@csiro.au), Edward Payne (University of Melbourne, Department of Mechanical & Manufacturing Engineering, Parkville, VIC 3010 Melbourne, Australia, Edward.Payne@csiro.au), Andrew Ooi (University of Melbourne, Department of Mechanical & Manufacturing Engineering, Parkville, VIC 3010 Melbourne, Australia, a.ooi@unimelb.edu.au)

Numerical calculations and illustrative experiments are presented on the volumetric oscillations of microbubbles on and near surfaces. There is a considerable theoretical and experimental literature on the acoustic interactions of bubbles. In the present study, the surface was represented by a mirror-image bubble and the nonlinear frequency response calculated by integrating acoustically coupled sets of Rayleigh-Plesset-like equations. A significant shift was found in the peak nonlinear response frequency of a bubble targeted onto a surface. This effect is increased when other bubbles are nearby on the surface. Owing to the asymmetric influence of the surface, experimental images were dominated by shape-mode instabilities, making optical determination of the peak nonlinear response frequency difficult. Moreover, it was found that even if bubbles are separated by only a small fraction of the sound wavelength, time delays owing to the finite speed of sound have a surprisingly significant influence. Calculations on the symmetric mode of mutual oscillation showed that the introduction of time delays significantly modified harmonics of the spectrum.

11:40

2aBB11. Echogenic liposomes for image-guided drug delivery. Christy K. Holland (University of Cincinnati, Biomedical Engineering, MSB, 231 Albert Sabin Way, Cincinnati, OH 45267-0586, USA, Christy.Holland@uc.edu), David D. McPherson (University of Texas Health Science Center, 6431 Fannin St., MSB 1.252, Houston, TX 77030, USA, David.D.McPherson@uth.tmc.edu)

Echogenic liposomes (ELIP) are under development to enable ultrasound-controlled drug delivery. Ultrasound-triggered release of hydrophilic and lipophilic agents was assessed from circulating ELIP in vitro using color Doppler ultrasound (6 MHz). Calcein, or recombinant tissue plasminogen activator (rt-PA), both hydrophilic agents, or papaverine, a lipophilic agent, were each loaded into ELIP and diluted in 0.5% bovine serum albumin. Ultrasound-triggered release of calcein, rt-PA or papaverine from ELIP was determined relative to detergent and untreated controls. Calcein concentration was measured by fluorimetry and release of rt-PA was assayed with a chromogenic substrate and a spectrophotometric method. Papaverine concentration was quantified by absorbance spectrophotometry and the amount of papaverine associated with P-ELIP was determined using a spin column filtration technique. Dynamic changes in echogenicity were assessed with low output B-mode ultrasound (0.04 MI) as mean digital intensity. Treatment with color Doppler ultrasound resulted in a statistically significant amount of calcein and rt-PA release from liposomes ($p < 0.01$), but did not induce papaverine release ($p > 0.05$). The differential efficiency of ultrasound-mediated pharmaceutical release from ELIP for water-soluble and lipid-soluble compounds suggests that water-soluble drugs are better candidates for the design and development of ultrasound-controlled drug delivery systems.

Contributed Papers

12:00

2aBB12. Ultrasound contrast agents in an in vivo murine melanoma model. François Tranquart (INSERM U930, 2, Bvd Tonnelle, 37044 Tours Cedex 9, France, tranquart@med.univ-tours.fr), Ayache Bouakaz (INSERM U930, 2, Bvd Tonnelle, 37044 Tours Cedex 9, France, bouakaz@med.univ-tours.fr), Sophie Serriere (INSERM U930, 2, Bvd Tonnelle, 37044 Tours Cedex 9, France, serrie_s@med.univ-tours.fr)

The purpose of the study was to test different types of microbubble contrast agents (SonoVue®, Definity® and targeted microbubbles against vascular endothelial growth factor receptors (KDR, antiCD31)) to quantify angiogenesis. After SonoVue® and Definity® injections, a strong, rapid and heterogeneous signal enhancement was detected in all tumors. According to the tumor size, the quantification of the perfused area revealed major inter-individual variations. Three groups of animals bearing tumors, following SonoVue® administration, were arbitrarily constituted to compare various sonographic parameters such as AUC, mTT, etcœ. The tumoral size increase seemed negatively correlated to a decrease in all quantified parameters. Non linear acoustic signal from microbubbles targeted to the molecular site was determined by an ultrasound-based destruction-reperfusion scheme. In tumor-bearing mice, an increase of the retention time (>10 minutes) was revealed following KDR and antiCD31 targeted microbubbles administrations when compared to the retention time of non targeted microbubbles. The amount of remaining targeted bubbles remains always lower than non specific agents. Results showed that quantitative contrast-enhanced ultrasound imaging could be an effective method for monitoring angiogenesis process in mice and so could be used for the follow-up of tumours under specific treatment.

12:20

2aBB13. Ultrasound contrast imaging of angiogenisis in a murine tumor model. Olivier Lucidarme (CHU Pitié-Salpétrière, 47-83 Boulevard de l'Hôpital, 75651 Paris, France, olivier.lucidarme@psl.aphp.fr), Laurent Taillade (Laboratoire d'Imagerie Paramétrique, 15 rue de l'Ecole de Médecine, 75006 Paris, France, laurenttaillade2@yahoo.fr), Aymeric Guibal (Laboratoire d'Imagerie Paramétrique, 15 rue de l'Ecole de Médecine, 75006 Paris, France, guibala@hotmail.com), Sebastien Mule (Lab d'Imagerie Fonctionnelle, 91 Boulevard de l'Hôpital, 75634 Paris, France, Sebastien.Mule@imed.jussieu.fr), Eva Comperat (CHU Pitié-Salpétrière, 47-83 Boulevard de l'Hôpital, 75651 Paris, France, eva.comperat@psl.aphp.fr), Yasmina Badachi (Laboratoire d'Imagerie Paramétrique, 15 rue de l'Ecole de Médecine, 75006 Paris, France, yasmina.badachi@gmail.com), Erwan Jouannot (Laboratoire d'Imagerie Paramétrique, 15 rue de l'Ecole de Médecine, 75006 Paris, France, Erwan.Jouannot@sanofi-aventis.com), Olivier Rixe (CHU Pitié-Salpétrière, 47-83 Boulevard de l'Hôpital, 75651 Paris, France, olivier.rixe@psl.aphp.fr), Lori Bridal (Laboratoire d'Imagerie Paramétrique, 15 rue de l'Ecole de Médecine, 75006 Paris, France, bridal @lip.bhdc.jussieu.fr)

Microvascularization modifications should precede tumor size-changes during anti-angiogenic therapy. We applied contrast functional ultrasound imaging (fUSI) to detect changes in Wilms tumors with anti-angiogenic treatment (Bevacizumab). Human Wilms tumor cells was grafted in left kidney of 32 mice. Once tumors had >5mm diameter, mice received : placebo, N=14; Bevacizumab for 21days, N=11; and Bevacizumab for 10days followed by placebo for 11days, N = 7. On days -1, +1, +9, +14 and +21

with respect to treatment start, fUSI was performed (CPS mode, SonoVue). Linear time intensity curves were obtained from regions in kidney cortex and matched-depth of tumor for first bolus passage and 50s following acoustic destruction of contrast. Excised tumor weight decreased with increased treatment duration: 3.7+/-1.8 g (placebo), 2.3+/-1.9 g (Bevacizumab-10days, placebo-11days), 1.4+/-0.7 g (Bevacizumab-21 days) [$p<0.05$]. Area under the bolus-passage curve (AUC) and the plateau intensity of the destruction-reperfusion were greater from D+9 to D+21 [$p<0.04$] in the placebo than Bevacizumab-21day. For the group treated during the first 10 days, fUSI values were comparable to those of the treated group until D+14, then increased to become slightly superior to those of the placebo group by D+21. Noninvasive fUSI demonstrated revascularization after suspension of anti-VEGF therapy.

12:40-1:40 Lunch Break

Invited Paper

1:40

2aBB14. Violent cavitation from optically configured microbubble pairs. Paul A. Campbell (University of Dundee, Ewing 1-6, Carnegie Physics Laboratory, Main Campus, DD1 4HN Dundee, UK, p.a.campbell@dundee.ac.uk)

The mutual interaction between two cavitating microbubbles was investigated using a novel optical trapping arrangement. This approach facilitated development of arbitrary, stable, and initial spatial configurations for two-bubble systems. Critically, exercising optical control over such a binary system can effectively isolate it from resident bubble populations during insonation. This ensures that any early stage dynamical evolution of the system is dominated by the mutual interaction of the two bubbles in view, rather than any extraneous influence arising from 'cross-talk'. In circumstances where the bubbles are located far from a rigid boundary, we observed, using high speed microphotography at framing rates of over 1MHz, that the action of secondary radiation forces leads to mutual bubble attraction often followed by the development of violent microjetting. Microbubble coalescence, with subsequent fragmentation could be observed, and the generation of short-lived anti-bubbles can often occur also. Finally, when cells are present as confluent monolayers on rigid substrates, the statistics for microbubble outcome and dynamics are modified somewhat. I will relate statistics to the parameter space that we interrogated, which included: inter-bubble spacing; relative bubble radii; and individual bubble stand-off parameters.

Contributed Papers

2:00

2aBB15. Nonlinear propagation in microbubble cloud, does it make the distal myocardium appear brighter or darker? Meng-Xing Tang (Imperial College London, Dept. of Bioengineering Engineering, South Kensington, SW7 2AZ London, UK, mengxing.tang@ic.ac.uk), Robert Eckersley (Imperial College London, Imaging Sciences Department, Hammersmith Campus, Du Cane Road, W12 0HS London, UK, r.eckersley@ic.ac.uk)

A number of questions remain in contrast ultrasound imaging regarding the complex interaction between bubbles, US and tissue. E.g. in contrast echocardiography for perfusion imaging, it is sometimes difficult to interpret the images for the myocardium distal to the probe. Due to US nonlinear propagation through the bubble-filled chamber, the distal part can appear artefactually brighter or darker in e.g. Pulse Inversion images. Although tissue at target is likely to increase in brightness in contrast specific images when nonlinear propagation happens, it is less clear for microbubbles. This work tries to gain better understanding of this by investigating how nonlinear propagation of ultrasound pulses can change the appearance of microbubbles and tissues in Pulse Inversion images by altering their acoustic response. A series of specifically designed simulations and experiments were performed. The results show that nonlinear propagation can have a significant impact on the appearance of tissue containing bubbles, and this varies with insonating frequency and pressure. These results suggest the mechanism involves a balance between a reduction in nonlinear bubble scattering after propagation against an increase in the nonlinear tissue scattering. Consequently the deeper tissues containing bubbles may appear brighter or darker depending on the relative contribution of these two effects.

2:20

2aBB16. Frequency dependence of kidney injury induced by contrast-aided diagnostic ultrasound. Douglas Miller (University of Michigan, Department of Radiology, Ann Arbor, MI 48109-0553, USA, douglm@umich.edu), Chunyan Dou (University of Michigan, Department of Radiology, Ann Arbor, MI 48109-0553, USA, chunyand@umich.edu), Roger C. Wiggins (University of Michigan, Department of Internal Medicine (Nephrology), Ann Arbor, MI 48109, USA, rwiggins@med.umich.edu)

Glomerular capillary hemorrhage (GCH) induced in rat kidneys by contrast aided diagnostic ultrasound was examined as a function of ultrasonic frequency. The right kidneys of anesthetized rats mounted in a water bath were exposed to image pulse sequences at 1 s intervals during intravenous infusion of diluted ultrasound contrast agent. Diagnostic ultrasound (DUS) scanners were utilized for exposure at 1.5, 2.5, 3.2, 5.0 and 7.4 MHz. A laboratory exposure system (LES) was used to simulate DUS exposure at 1.0, 1.5, 2.25, 3.5, 5.0 and 7.5 MHz at relatively high peak rarefactional pressure amplitudes (PRPAs). The exposed kidneys were removed and fixed for histology. GCH was measured by counting glomeruli with blood in the urinary (Bowman's) space on histological sections. The percentage of GCH at a fixed exposure frequency showed a rapid rise with PRPA above an apparent threshold. The threshold values were approximately proportional to the ultrasound frequency, with proportionality constants of 0.5 MPa/MHz for DUS and 0.6 MPa/MHz for LES exposures. The increasing thresholds with increasing frequency limited the GCH effect for contrast aided DUS, and no GCH was seen for DUS at 5.0 or 7.4 MHz for the highest available PRPAs.

Session 2aEAa

Engineering Acoustics, Underwater Acoustics, and ECUA: Sonar Transducer Design and Modeling II

John B. Blottman, Cochair
Naval Undersea Warfare Center, Division Newport, 1176 Howell Street, Newport, RI 02841-1708, USA

Pascal Mosbah, Cochair
IEMN dpt ISEN, UMR CNRS 8520, Lille, France

Invited Papers

8:00

2aEAa1. Acoustic array interactions in the time domain. George W. Benthien (511 Savoy Street, San Diego, CA 92106, USA, benthien@cox.net)

In this paper I discuss the computation of acoustic array interactions in the time domain. Acoustic array interactions in the time domain are expressed in terms of mutual impulse response functions. The mutual impulse response between a pair of array elements is the acoustic force on the first element of the pair due to an acceleration impulse of the second with all other elements held rigid. The mutual response functions are calculated in the frequency domain using the boundary element program CHIEF and then Fourier transformed to the time domain. As the convergence in the frequency domain can be very slow, I introduce modified impulse response functions that converge much faster in the frequency domain and are simply related to the desired impulse response functions. This approach reduces the range of frequencies required in the CHIEF computations and gives better accuracy in the initial time period. Transient results are presented for an array of simple transducer elements. The mutual impulse response functions are combined with the transducer element equations to yield a system of differential-integral equations of delay type. A solution procedure for equations of this type is presented.

8:20

2aEAa2. Exact model of Langevin transducers with internal losses. D. D. Ebenezer (Naval Physical and Oceanographic Laboratory, Thrikkakara, 682021 Kochi, India, tsonpol@vsnl.com), P. A. Nishamol (Naval Physical and Oceanographic Laboratory, Thrikkakara, 682021 Kochi, India, dd_ebenezer@yahoo.com)

An exact method is presented to analyze classical Langevin transducers with internal losses. The transducers consist of an axially polarized piezoelectric cylinder sandwiched between two elastic cylinders. All three cylinders are of the same diameter. Exact solutions to the exact equations of motion of the piezoelectric and elastic cylinders and the Gauss electrostatic condition are used. Complex piezoelectric and elastic coefficients are used to model internal losses. For each cylinder, the first set of solutions contains Bessel functions that form a complete set in the radial direction. The second and third sets contain trigonometric functions that form complete sets in the axial direction. They are used to represent fields that are symmetric and anti-symmetric with respect to the plane midway between the ends of the cylinder, respectively. The interface and boundary conditions are satisfied by using the orthogonal properties of the functions. Transducers with identical elastic cylinders at the ends as well as those with a light head mass and a heavy tail mass are analyzed. Numerical results are presented to illustrate the input electrical admittances of transducers. They are compared with those obtained using ATILA - a finite element package for the analysis of sonar transducers.

8:40

2aEAa3. Numerical acoustic modeling code applied to sonar transducers and arrays: review and perspectives. Gerard Vanderborck (Thales Underwater Systems SAS, Acoustic Department, 525 route des Dolines, BP 157, 06903 Sophia Antipolis Cedex, France, gerard.vanderborck@fr.thalesgroup.com)

In this paper a review based on several examples of Thales Underwater Systems (TUS) design and modeling of transducers will be presented: several examples like wide band free flooded ring flextensional and bender transducers, high frequency transducers with thermal analysis modeling included, will be discussed. An approach of the problem of the mutual impedance computation appearing in array modeling will be also presented. Tus used since several decades FEM - BEM codes to design acoustic transducers and arrays. The perspectives in transducer and array modeling will be indicated like the possibility to take into account the non-linearities in the material, the time dependent problem and the use of new kind of piezoelectric material will be also discussed. Specific aspect of single crystal transducers modeling will be presented. The increase of the computing power will also permit to take into account the complex problem of the interaction between transducers in an array (mutual impedances). We will conclude on complex ultra wide band antenna (based on strong transducers interactions) optimization and the associated modeling architecture issues.

9:00

2aEAa4. Finite element analysis simulations of a piezoelectric cymbal actuator using atila software. Thomas Tremper (Micromechatronics Inc., 200 Innovation Blvd, Suite 155, State College, PA 16803, USA, ttremper@mmech.com), Alfredo Vazquez Carazo (Micromechatronics Inc., 200 Innovation Blvd, Suite 155, State College, PA 16803, USA, avc@mmech.com), Kenji Uchino (Micromechatronics Inc., 200 Innovation Blvd, Suite 155, State College, PA 16803, USA, kenjiuchino@mmech.com)

The piezoelectric ultrasonic cymbal actuator is a well known flextensional type actuator. Because of the actuator's geometry, the small movements of the piezoelectric ceramic are amplified by the flextensional structure. Simulation of this device was performed using Atila finite element software, which is specially suited for piezoelectric devices. This study will focus on some of the necessary parameters to accurately simulate cymbal actuators and other piezoelectric actuators. The simulations discussed will be compared to actual experimental data. Based on the experimental results the simulations will be reexamined and modifications will be made to increase the models accuracy. Employing this iterative process will promote increased accuracy in future simulations, which would therefore decrease development time and increase productivity.

Contributed Papers

9:20

2aEAa5. Underwater tensor sensors based on optical fiber bragg gratings. Francois M. Guillot (Georgia Institute of Technology, Mechanical Engineering, 771 Ferst Drive, Atlanta, GA 30332-0405, USA, francois.guillot@me.gatech.edu), David H. Trivett (Georgia Institute of Technology, Mechanical Engineering, 771 Ferst Drive, Atlanta, GA 30332-0405, USA, david.trivett@me.gatech.edu), Peter H. Rogers (Georgia Institute of Technology, Mechanical Engineering, 771 Ferst Drive, Atlanta, GA 30332-0405, USA, peter.rogers@me.gatech.edu)

This paper deals with the development a new type of low-noise underwater tensor sensor aimed at improving the performance and the design of directional arrays. The transducer can be configured either as a particle velocity sensor (dipole) or as fluid shear sensor (quadrupole). The sensing principle of the device relies on the interference signal from two Bragg gratings written on the same fiber, and illuminated by a tunable, narrowband light source. The gratings are a few centimeters apart, and they each reflect a portion of the incident light. The fiber is epoxied to two spacers separated by a small gap situated between the gratings. This assembly is then adhered to two plates connected by a hinge, which is located below the gap. One plate is held rigidly and the tip of the other (free) plate experiences transverse vibrations, when ensonified. These vibrations produce periodic gap length changes, which modulate the interference signal from the two gratings. The modulation is related to the amplitude of the sound wave and is monitored with a photodetector. A noise analysis will be presented and the performance of prototype sensors will be discussed.

9:40

2aEAa6. Beampattern optimization for a conformal projecting array of transducers with baffle effect and mutual coupling among elements. Yuanliang Ma (Institute of Acoustic Engineering, Northwestern Polytechnical University, 710072 Xi'an, China, ylma@nwpu.edu.cn), Zhengyao He (Institute of Acoustic Engineering, Northwestern Polytechnical University, 710072 Xi'an, China, hezhengyao@163.com)

Beampattern optimization for projecting arrays is much more challenging in comparison with receiving arrays, particularly for conformal projecting arrays. It is because the array elements have to work in resonance state for efficient projecting and the variation of radiation impedance has strong effect on the array performance. The radiation impedance for each element is determined by a lot of factors, i.e, the element position, baffle property, mutual coupling and velocity weighting vector of the array. Thus beampattern optimization for a projecting conformal array must take into account all these factors. One thing makes the topic more difficult that the mutual impedance for each element is changeable along with the weighting vector change. In this paper a global solution approach is formulated and a boundary element model combined with transducer equivalent circuits is developed. The driving voltage weighting vector is deduced through an optimization algorithm. Computer simulation together with experiments are conducted for a 14-element conformal array. The results agree well. The multiple beampatterns formed within a wide observation sector exhibit uniform beamwidth and low sidelobes. The source level for each beam is maximized in constraint of the maximum driving voltage of array elements being constant.

10:00

2aEAa7. Advanced Single Crystal Piezoelectric Transducers for Naval Sonar and Medical Ultrasound Applications. Wesley Hackenberger (TRS Technologies, Inc., 2820 East College Avenue, State College, PA 16801, USA, wes@trstechnologies.com), Jun Luo (TRS Technologies, Inc., 2820 East College Avenue, State College, PA 16801, USA, jun@trstechnologies.com), Kevin Snook (TRS Technologies, Inc., 2820 East College Avenue, State College, PA 16801, USA, kevin@trstechnologies.com)

Single crystal piezoelectrics have received much attention due to their very high piezoelectric and electromechanical coupling coefficients. Naval sonar and medical ultrasound transducers, fabricated from this material, exhibit unprecedented increases in bandwidth, source level, and sensitivity compared to ceramic based devices. In this paper we report many new developments in the growth and manufacture of single crystals. These include increased diameter ($> 3''$) crystal boules, improved compositional uniformity, increased thermal stability, and minimized surface damage. Manufacturing improvements are being applied to a broad range of crystal transducer applications. For navy sonar systems, crystals are resulting in very high bandwidths ($> 100\%$) for transducer sizes that are 1/2 the resonating length and 1/4 the weight of ceramic counterparts with equivalent (or often lower) source level. Manufacturing improvements such as high tensile strength, achieved by precision polishing crystal surfaces, are enabling new transducer operational regimes not possible with ceramic. In particular, single crystal 1-3 composite projectors show promise for achieving high source level in a compact, integrated system designs. Single crystals are also enabling new applications in medical ultrasound including very broadband and extremely high frequency transducers. Further improvements are expected in the near future.

10:20-10:40 Break

10:40

2aEAa8. Design of a phase array ultrasonic sensor using vibration decoupled concept. Chia-Yu Lin (National Taiwan University, Rm.433, Institute of Applied Mechanics, No.1, Sec.4, Roosevelt Rd., 10617 Taipei, Taiwan, cylinx@mems.iam.ntu.edu.tw), Chih-Chiang Cheng (National Taiwan University, Rm.433, Institute of Applied Mechanics, No.1, Sec.4, Roosevelt Rd., 10617 Taipei, Taiwan, cccheng@nbm.ntu.edu.tw), Wen-Jong Wu (Department of Engineering Science and Ocean Engineering, National Taiwan University, Rm.433, Institute of Applied Mechanics, No.1, Sec.4, Roosevelt Rd., 10617 Taipei, Taiwan, wjwu@ntu.edu.tw), Chuin-Shan Chen (Department of Civil Engineering, National Taiwan University, Rm.433, Institute of Applied Mechanics, No.1, Sec.4, Roosevelt Rd., 10617 Taipei, Taiwan, dchen@ntu.edu.tw), Jay Shieh (Department of Material Science and Engineering, National Taiwan University, Rm.433, Institute of Applied Mechanics, No.1, Sec.4, Roosevelt Rd., 10617 Taipei, Taiwan, jayshieh@ntu.edu.tw), Chih-Kung Lee (National Taiwan University, Rm.433, Institute of Applied Mechanics, No.1, Sec.4, Roosevelt Rd., 10617 Taipei, Taiwan, cklee@mems.iam.ntu.edu.tw)

Phase array ultrasonic sensors have been used widely to generate higher directional radiating patterns in which piezoelectric units are distributed

sparsely in space. In this study, we present a novel design of a phase array ultrasonic sensor based on the concept of vibration decoupling. Decoupling is achieved by careful design of source aperture, and such design allows piezoelectric units tightly located in the same structure. The phase array sensor is designed herein as a cylinder with a dumbbell shape groove to decouple vibration, and finite element analysis is used to optimize the design. Two piezoelectric discs are adhered on the bottom plate of the sensor whereby desirable wave generation and detection are controlled adaptively. By electrical steering, the sensor thus operates as a dipole mode. Finally, prototypes of the sensor are made and experiments are conducted to verify simulation results.

11:00

2aEAa9. Nonlinear multifrequency transmitter for seafloor characterization. Lucilla Di Marcoberardino (Institut Jean le Rond D'Alembert, UMR 7190, 2 Place de la Gare de Ceinture, 78210 Saint Cyr L'Ecole, France, lucilladm@hotmail.com), Jacques Marchal (Institut Jean le Rond D'Alembert, UMR 7190, 2 Place de la Gare de Ceinture, 78210 Saint Cyr L'Ecole, France, jmarchal@ccr.jussieu.fr), Pierre Cervenka (Institut Jean le Rond D'Alembert, UMR 7190, 2 Place de la Gare de Ceinture, 78210 Saint Cyr L'Ecole, France, cvk@ccr.jussieu.fr)

In the underwater context, it is known that the frequency diversity provides essential information to derive the nature of the seafloor. This presentation deals with a new concept based on a transmitter that generates simultaneously several harmonic frequencies. Our final objective is to assert the feasibility of a multi-frequency tool whose desirable characteristics could be specified for applications such as detection of sunken oil slicks, sediment characterization, or surveys before cable or pipe laying. The acoustic beams are generated through the harmonic components of a shock wave radiated by an antenna driven at a high level. The source is unique in time and space so that the multi-frequency responses are inherently perfectly matched. A numerical model based on a generalized KZK equation has been developed to estimate the saturated fields. Measurements of the first harmonic fields obtained in our outdoor tank facility are compared with simulations.

11:20

2aEAa10. Modeling the acoustic radiation force in piezoelectrically driven micro fluidic chambers using ATILA. Karl Fisher (Lawrence Livermore National Laboratory, 7000 E Avenue, Brentwood, CA 94513, USA, fisher34@llnl.gov)

A procedure is demonstrated to quantitatively evaluate the acoustic radiation forces in micro fluidic particle manipulation chambers. Typical estimates of the acoustic pressure and the acoustic radiation force are based on an analytical solution for a simple 1-dimensional standing wave pattern. The complexities of a typical micro fluidic channel limit the usefulness of this approach. By leveraging finite element approaches, and a generalized equation for the acoustic radiation force, channel designs can be investigated in two- and three-dimensions. Calculations and experimental observations are in good agreement. This work was performed under the auspices of the U.S. Department of Energy by University of California, Lawrence Livermore National Laboratory under Contract W-7405-Eng-48.

11:40

2aEAa11. Equivalent circuit models derived from finite element models using structural dynamics techniques. Julien Bernard (Thales Underwater Systems, 525 route des Dolines BP 157 Valbonne Parc d'Activités de Sophia Antipolis, 06903 Sophia Antipolis Cedex, France, julien.bernard@fr.thalesgroup.com)

Electroacoustic transducers can be divided into an active part, the driver, and a passive part, the structure. The driver ensures electromechanical transduction, while the structure performs various mechanical and acoustical functions, such as support, shock and pressure protection, and impedance transformation. For design purposes, one often needs an equivalent circuit model which gives a relationship between the acoustic characteristics of the overall device and that of its components. Transducer equivalent circuits are usually either physical or modal. Physical equivalent circuits lend themselves to the treatment of a transducer as an assembly, but in general yield frequency dependant parameters. Modal equivalent circuits are more adequate for resonant transducers, but describe transducers as a whole. This works shows how these two types of equivalent circuits can be obtained from a full finite element model by using common structural dynamics techniques: substructuring and modal expansion. It also shows that a third, hybrid type of equivalent circuit can be obtained by using a component mode synthesis technique derived from the Craig-Bampton method. This hybrid equivalent circuit combines the advantages of physical and modal equivalent circuits, enabling to express transducer modal parameters in terms of driver and structure modal parameters.

12:00

2aEAa12. Acoustic field calculation for a compact barrel-stave flextensional transducer array. Zhengyao He (Institute of Acoustic Engineering, Northwestern Polytechnical University, 710072 Xi'an, China, hezhengyao@163.com), Chao Sun (Institute of Acoustic Engineering, Northwestern Polytechnical University, 710072 Xi'an, China, csun@nwpu.edu.cn)

The boundary element method together with the finite element method is used to calculate the radiated acoustic field of a compact array of barrel-stave flextensional transducers. At first, the surface vibration displacement distribution of one barrel-stave transducer is obtained by the finite element method using the commercial software ANSYS. The calculation results are then imported into the boundary element calculation software SYSNOISE. At the frequency of 1400Hz, the radiated acoustic field and radiation impedance are calculated by the boundary element method for a planar array which is composed of three identical barrel-stave flextensional transducers uniformly distributed on a circle with spacing much less than half wavelength. The calculation results show that the mutual interactions among elements are significant for the compact array. The mutual radiation resistance between two transducers is close to the self-radiation resistance of the transducers. And the transmitting source level of the 3-element array is 8.7dB higher than that of one transducer if the surface vibration velocities of the transducers in the array are the same as that of one transducer. The proposed technique can be used to predict the performance of a transmitting transducer array at the stage of preliminary design.

12:20

2aEAa13. Finite Element Modeling of 2-D Transducer Arrays. Hind Mestouri (ISEN Brest (Institut Supérieur de l'Electronique et du Numérique), 20, rue Cuirassé Bretagne, C.S. 42807, 29228 Brest, France, hind.mestouri@isen.fr), Alain Loussert (ISEN Brest (Institut Supérieur de l'Electronique et du Numérique), 20, rue Cuirassé Bretagne, C.S. 42807, 29228 Brest, France, alain.loussert@isen.fr), Gilles Keryer (ISEN Brest (Institut Supérieur de l'Electronique et du Numérique), 20, rue Cuirassé Bretagne, C.S. 42807, 29228 Brest, France, gilles.keryer@isen.fr)

Active sonar detects objects underwater by sending out sound waves in pulses, scientists could measure the time it takes these pulses to travel through the water, reflect off of an object, and return to the ship. There are a number of factors limiting the performance of low frequency transducer arrays for active sonar systems including the crosstalk and housing interactions which affects the directivity pattern and the sensitivity. Many important issues in transducer arrays design, such as crosstalk, cannot be accurately studied using analytic method due to the complexity of the partial differential equations involved. Finite element method is the only appropriate way to gain more detailed information. In this paper, a 2-D finite element model is constructed to analyze the crosstalk and structure interactions, using ATILA code and GiD graphical interface, of transducer arrays, consists of six active piezoceramic bars, and developed for shallow water use. The directivity pattern strongly depends on the transducer size versus wavelength, each transducer elements interacts directly with its neighbour and indirectly with the other elements, and the radiated acoustic power may considerably vary from one element to another. It is shown that crosstalk and housing interactions can be reduced through the use of different inter-element materials and housing characteristics.

Session 2aEAb

Engineering Acoustics: Acoustic Evaluation I

David Brown, Chair
BTech Acoustics, LLC and Universtity of Massachusetts Dartmouth, ATMC, Electro-Acoustics Research Laboratory and ECE Dept., 151 Martine St, Fall River, MA 02723, USA

Contributed Papers

8:00

2aEAb1. Measurement of Sound Velocity in Water Using Optical Probe and Acoustical Holography. Takeshi Ohbuchi (University of Tsukuba, 1-1-1 Tennoudai, 305-8573 Tsukuba, Japan, ohbuchi@aclab.esys.tsukuba.ac.jp), Koichi Mizutani (Tsukuba Univ., Tsukuba Science City, 305-8573 Ibaraki, Japan, mizutani@esys.tsukuba.ac.jp), Naoto Wakatsuki (Tsukuba Univ., Tsukuba Science City, 305-8573 Ibaraki, Japan, wakatuki@iit.tsukuba.ac.jp), Hiroyuki Masuyama (Toba National College of Maritime Technology, 1-1 Ikegami-cho, 517-8501 Toba, Japan, masuyama@toba-cmt.ac.jp)

We propose a method for a determination of a three-dimensional sound velocity using optical computerized tomography (O-CT) and near-field acoustical holography (NAH) for measuring a phase object. Ultrasonic waves affect a phase of the light passing through radiated sound fields. The zeroth order diffraction light including sound pressure information is acquired by an avalanche photodiode. Eighteen projections are acquired by rotational scanning, and each projection along the optical axis is obtained by single linear scanning and electronically quadrature-detected as the complex amplitude. The complex sound fields are reconstructed by O-CT in a region of 40×40 mm^2. Then the sound field on another plane is propagated using NAH from the acquired sound fields, and the sound field on the same plane is reconstructed by O-CT. Comparing the phase of propagated and reconstructed sound fields in wavenumber domain, we can obtain the sound velocity in three dimensional space in a region of $30 \times 30 \times 10$ mm^3. The experimental results are in agreement with the reference value measured by another mean.

8:20

2aEAb2. Influence of a load on the nonlinear behavior of a piezoelectric rod under high sinusoidal voltages. Denis Parenthoine (Lussi, Université F Rabelais de Tours, 40, rue de la Chocolaterie, 41000 Blois, France, parenthoine_denis@yahoo.fr), Lionel Haumesser (Lussi, Université F Rabelais de Tours, 40, rue de la Chocolaterie, 41000 Blois, France, lionel.haumesser@univ-tours.fr), François Vander Meulen (Lussi, Université F Rabelais de Tours, 40, rue de la Chocolaterie, 41000 Blois, France, vandermeulen@univ-tours.fr), Louis-Pascal Tran-Hhuu-Hue (Lussi, Université F Rabelais de Tours, 40, rue de la Chocolaterie, 41000 Blois, France, tran@univ-tours.fr)

At high levels of excitation, appear, in piezoelectric devices, nonlinear phenomena which can adversely affect the quality of the applications to which they are devoted. It is, in particular, true in non-destructive evaluation, where the generation of harmonics in the ultrasonic tranducer can make inacurrate measurements in materials. In a previous work, third-order constants in a piezoceramic rod of PZT-21 under high sinusoidal electric fields have been evaluted from the analysis of second harmonic generation in the mechanical displacement. All these measurements have been performed under condition of complete free stress. In order to allow a better understanding of the nonlinear behavior of the transducer, various loads, are, now, applied at one end of the piezoceramic rod. Velocity masurements performed by a laser probe at the free end of the active element provides then informations about the nonlinear behavior of the system. Influence of load on the linear and nonlinear behavior of the piezoelectric rod is then studied in the case of an aluminium bar, and in the case of more nonlinear materials. Results are compared both experimentally and theoritically in loaded and unloaded configurations.

8:40

2aEAb3. Uncertainty of Acoustical Material Characteristic Measurements. Samir N. Gerges (Federal University of Santa Catarina (UFSC), Campus Universitario - Trindade, 88040-900 Florianopolis, Brazil, samir@emc.ufsc.br), Peter K. Giesbrecht (Federal University of Santa Catarina (UFSC), Campus Universitario - Trindade, 88040-900 Florianopolis, Brazil, samir@emc.ufsc.br)

The experimental determination of the acoustic properties of sound absorption materials depends on numerous factors. The accuracy level in the determination of each property depends, for example, on the measurement apparatus and the type of material. The objective of this work is to present a study about the main sources of uncertainty in the measurement of properties such as sound absorption coefficient, acoustic impedance, flow resistivity and porosity. The uncertainties of the measurement apparatus of each property are quantified. The uncertainty of the materials heterogeneity is also assessed and its individual contribution highlighted. Important aspects of the Standards ASTM C 522 and ISO 10534-2, which present, respectively, recommendations and a procedure for flow resistivity and sound absorption measurements, are discussed. The methodology to calculate the uncertainty of each property is discussed with emphasis on the relevancy of each uncertainty source.

9:00

2aEAb4. Design and implementation of a three-dimensional seven microphone vector intensity probe with low and high frequency compensations. Khalid Miah (University of Texas, P.O. Box 7155, Austin, TX 78713, USA, miah@mail.utexas.edu), Elmer Hixson (Univ. of Texas, ECE Dept., 1 University Station 0803, Austin, TX 78712-0240, USA, ehixson@mail.utexas.edu)

A seven microphone vector intensity probe has been designed and implemented in this report with low and high frequency compensations. Measurements from plane wave tube and anechoic chamber are used for overall system calibration with corrected gain and phase mismatch errors. Measured and calculated intensity level from both plane wave tube and anechoic room settings showed close agreement with each other in comparison to separate low and high frequency components of the array. Particle velocity vectors and pressures determined for calculating intensity were also used to calculate sound power and total energy density components of various sources. This microphone array vector intensity probe is then used to explore various sound source identification and localization problems.

9:20

2aEAb5. Application of contrast optimisation autofocus to flexible ultrasonic arrays for non-destructive testing. Alan J. Hunter (University of Bristol, Queen's Building, University Walk, BS8 1SY Bristol, UK, a.hunter@bristol.ac.uk), Bruce W. Drinkwater (University of Bristol, Queen's Building, University Walk, BS8 1SY Bristol, UK,

b.drinkwater@bristol.ac.uk),Paul D. Wilcox(University of Bristol, Queen's Building, University Walk, BS8 1SY Bristol, UK, p.wilcox@bristol.ac.uk)

Flexible ultrasonic arrays are used for imaging within objects with complicated geometries for non-destructive testing and evaluation (NDT/NDE), e.g., thick-walled pipes, weld caps, etc. We consider the application of autofocus techniques (routinely used in synthetic aperture sonar (SAS)) to this engineering problem. A flexible ultrasonic array is functionally similar to a wide-beam, stripmap SAS with a single transmitter and receiver. Unfortunately, there are few autofocus algorithms available for this configuration. Popular algorithms, such as echo/image correlation, PGA, DPCA, etc., are better suited for use with a narrow-beam or multiple-receiver SAS. However, contrast optimisation is a more general technique that is well suited to the single transmitter/receiver geometry. In this presentation, we describe our implementation of contrast optimisation autofocus and show experimental results using a flexible array prototype.

9:40

2aEAb6. Inspection of complex components with flexible phased array transducer. Olivier Casula (CEA/LIST, bat 611, 91191 Gif sur Yvette, France, olivier.casula@cea.fr), Gwenael Toullelan (CEA/LIST, bat 611, 91191 Gif sur Yvette, France, gwenael.toullelan@cea.fr), Philippe Dumas (ZA, rue des Savourots, 70190 Voray-sur-l'Ognon, France, philippe.dumas@imasonic.com)

Non destructive testing techniques using ultrasonic methods are often carried out in contact. But, the inspection performances are limited to regular surfaces. Thus, surface irregularities lead to thickness variations of the coupling layer that result in beam distortions and losses of sensitivity. In the context, CEA/LIST has designed flexible phased-array techniques for compensating the surface irregularities and fitting the surface. The independent piezoelectric elements composing the radiating surface are mechanically assembled to build an articulated structure. An embedded profilometer measures the local surface distortion allowing to compute the optimized delay laws and to master the characteristics of the focus beam. Those delay laws computed by the UT-acquisition system are applied in real-time to the piezoelectric elements. To evaluate inspection method capabilities, CEA/LIST develops a simulation software for non destructive testing, CIVA, able to simulate realistic configurations in particular with complex 2D and 3D applications. Matrix flexible phased-array probes have been designed and manufactured in collaboration with IMASONIC. This paper sums up examples of inspections in complex geometries where these flexible probes have been successfully used. Moreover, the data are reconstructed thanks to CIVA tools and allow to locate and size the flaw in the part.

10:00-10:20 Break

10:20

2aEAb7. Characterization of laminated glasses by means of an inversion method using Finite Elements. Jorge Frances Monllor (DFISTS. Univ. de Alicante, Carretera de Sant Vicent del Raspeig s/n, 03690 San Vicente del Raspeig, Spain, jfmonllor@ua.es), Jaime Ramis Soriano (DFISTS. Univ. de Alicante, Carretera de Sant Vicent del Raspeig s/n, 03690 San Vicente del Raspeig, Spain, jramis@ua.es), Jesús Alba Fernandez (Escola Politècnica Superior de Gandia, Universitat Politècnica de València, Crtra Natzaret-Oliva s/n, 46730 Gandia, Spain, jesalba@fis.upv.es), Enrique E. Segovia Eulogio (Depto Ing. Construcción. Univ. de Alicante, Carretera de Sant Vicent del Raspeig s/n, 03690 San Vicente del Raspeig, Spain, Enrique.Gonzalo@ua.es), Jenaro Vera Guarinos (DFISTS. Univ. de Alicante, Carretera de Sant Vicent del Raspeig s/n, 03690 San Vicente del Raspeig, Spain, jenaro@dfists.ua.es)

The experimental determination of elastic modules and loss factor in laminated glass components is of great interest in building acoustics since at present there are a lot of building systems using these types of devices. This makes it necessary to predict the transmission losses in a partition. Even though described in regulation, the process is not exempt from serious difficulties. In this work we present a method in order to obtain the parameters mentioned above for a laminated glass composed of a sequence of isotropic layers by solving the model-based inverse problem for frequency admittance experimentally obtained. The parameter that best describes the mechanical constants of material of the layers is obtained by minimizing the discrepancy between the real numerically and numerically predicted waveform. This is done using an iterative optimization. A sensitivity study of the parameters uncertainty is performed in order to establish the feasibility of this technique.

10:40

2aEAb8. Detection of Shallow Underground Buried Object Using Air Vibration Probe. Yuji Sato (Tsukuba Univ., Tsukuba Science City, 305-8573 Ibaraki, Japan, yuji@aclab.esys.tsukuba.ac.jp), Tomohiro Okamura (Univ. of Tsukuba, 1-1-1 Tennodai, 305-8573 Tsukuba, Japan, mizutani@esys.tsukuba.ac.jp), Koichi Mizutani (Tsukuba Univ., Tsukuba Science City, 305-8573 Ibaraki, Japan, mizutani@esys.tsukuba.ac.jp), Naoto Wakatsuki (Tsukuba Univ., Tsukuba Science City, 305-8573 Ibaraki, Japan, wakatuki@iit.tsukuba.ac.jp)

An air vibration probe is a device to measure an acoustic impedance using acoustic delay line oscillation. The frequency is changed when the acoustic impedance is changed. If some objects are varied, the frequency is expected to be changed in the case of the shallow underground detection. The advantage of this device is that it can detect the underground object easily without any contacts or destructions. Two experiments were practiced to study the relation among the frequency, the space between the probe and the ground, and the depth of object. The space was changed with the buried objects in various depths. The frequency became higher when the space became wider. In addition, the frequency was changed more obviously when the space was narrower. The probe scanned the buried objects in the fixed space. The objects were buried in various depths. The frequency became high when the object was buried shallower. In conclusion, the air vibration probe can detect the buried object because the frequency became high when something was buried.

11:00

2aEAb9. Ultrasonic Airflow Meter in Greenhouse Using Acoustic Reflection against Wall. Ikumi Saito (Tsukuba Univ., Tsukuba Science City, 305-8573 Ibaraki, Japan, saitou@aclab.esys.tsukuba.ac.jp), Naoto Wakatsuki (Tsukuba Univ., Tsukuba Science City, 305-8573 Ibaraki, Japan, wakatuki@iit.tsukuba.ac.jp), Koichi Mizutani (Tsukuba Univ., Tsukuba Science City, 305-8573 Ibaraki, Japan, mizutani@esys.tsukuba.ac.jp), Limi Okushima (National Institute for Rural Engineering, 2-1-6 Kannondai, 305-8609 Tsukuba, Japan, limi@affrc.go.jp)

In this paper, we described an ultrasonic airflow meter in a greenhouse using an acoustic reflection against a wall. The ultrasonic airflow meter is available for measuring the spatial mean wind velocity and direction, which consists of two sound probes and the wall of the greenhouse. Use of sound probes has advantage that the airflow accumulated along sound paths from a loudspeaker to a microphone is obtained in contrast to point measurements. The wind velocity and direction are calculated from time of flights (TOFs) of direct and reflected signals. The wind velocity and direction were measured in a greenhouse of 7.2 m $\times$ 29.0 m under factitious winds generated from two large electric fans located at the one side of the greenhouse. In addition, we detected air convection generated from two pairs of fans. These were measured every 20 seconds for 120 minutes. Regarding the measurement; by the proposed airflow meter and a reference; by a conventional one, their mean wind velocities were 0.12 and 0.15 (m/s), respectively. The presented airflow meter using the acoustic reflection against the wall is convenient to measure the wind velocity and direction in large-size facilities such as the greenhouse.

11:20

2aEAb10. An alternative and industrial method using low frequency ultrasound enabling to measure quickly tortuosity and viscous characteristic length. François Fohr (Centre de Transfert de Technologie du Mans, 20, rue Thalès de Milet, 72000 Le Mans, France, ffohr@cttm-lemans.com), Damien Parmentier (Centre de Transfert de Technologie du Mans, 20, rue Thalès de Milet, 72000 Le Mans, France,

dparmentier@cttm-lemans.com),Bernard R. Castagnede(Laboratoire d'Acoustique de l'Université du Maine, Avenue Olivier Messiaen, 72085 Le Mans, France, bernard.castagnede@univ-lemans.fr), Michel Henry (Laboratoire d'Acoustique de l'Université du Maine, Avenue Olivier Messiaen, 72085 Le Mans, France, michel.henry@univ-lemans.fr)

In the past, several different methods have been proposed in order to determine tortuosity and characteristic lengths, using various physical approaches. For instance, the BET (from S. Brunauer, P. Emmett and E. Teller) method used the adsorption of argon molecules within the surface of the pores to measure thermal characteristic length (or the so-called specific surface). Ultrasonic methods, during the two last decades, were efficiently implemented to measure these parameters, using large frequency bandwidth, different gazes including helium, and varying static pressures. The most standard and well-known method relies on phase spectrum measurements performed over short bursts, by plotting the inverse of the squared velocity as a function of the inverse of the square root of the angular frequency. Unfortunately, this method is quite sensitive on noise during the unwrapping procedure. We here propose a much simplier and efficient method, which is very robust with noisy signals, working at one single frequency, in most cases around 40 kHz. Measurements have been done onto a specific bench developped at CTTM, with some calibrated glass beads, enabling to recover the expected values of the physicalparameters. This method is particularly well suited for industrial and ″on line″ applications.

11:40

2aEAb11. A new impedance tube for large frequency band measurement of absorbing materials. Jean Christophe Le Roux (CTTM, 20, rue Thales de Milet, 72000 Le Mans, France, jcleroux@cttm-lemans.com), Jean-Pierre Dalmont (Laboratoire d'Acoustique de l'Université du Maine, Avenue Olivier Messiaen, 72085 Le Mans, France, Jean-Pierre.Dalmont@univ-lemans.fr), Bruno Gazengel (Laboratoire d'Acoustique de l'Université du Maine, Avenue Olivier Messiaen, 72085 Le Mans, France, bruno.gazengel@univ-lemans.fr)

The standard two microphones technique does not allow the measurement of absorbing materials characteristics at low frequency. Moreover, to cover a range from 100 to 6000 Hz two experiments have to be done with two different sample diameters. By using a sensor with a known volume velocity source developed by the LAUM together with the CTTM, it is demonstrated that the impedance can be obtained from 10 to 6000 Hz by performing only one measurement with a single material sample. Results showing the behaviour of some materials at low frequency are presented. On the other hand a comparison is done with classical Kundt tube results.

12:00

2aEAb12. An experimental study of Sound Transmission Loss (STL) measurement techniques using an impedance tube. Behrooz Yousefzadeh (Univ. of Tehran, School of Mechanical Engineering, 1439957131 Tehran, Iran, behrooz.j.y@gmail.com), Mohammad Mahjoob (Univ. of Tehran, School of Mechanical Engineering, 1439957131 Tehran, Iran, mmahjoob@ut.ac.ir), Nader Mohammadi (Univ. of Tehran, School of Mechanical Engineering, 1439957131 Tehran, Iran, nmohamady@ut.ac.ir), Ali Shahsavari (Univ. of Tehran, School of Mechanical Engineering, 1439957131 Tehran, Iran, shervin.shahsavari@gmail.com)

A comparison between the two sound transmission loss (STL) measurement techniques using an impedance tube (i.e. two-load method and anechoic termination method) is presented. A modified B&K type 4206 impedance tube has been designed and built. STL tests have been carried out for three homogeneous and isotropic materials with disk-type test samples of identical diameters and different thicknesses. In addition, the results have been compared with those of the classical and more reliable method of two-room. For both methods, the effect of downstream (tube termination) boundary conditions have been completely studied. The two-load method yields results which matches with two-room measurements, especially when the two boundary conditions are considerably different. The anechoic termination method, on the other hand, is significantly dependant on the termination boundary conditions.

TUESDAY MORNING, 1 JULY 2008 AMPHI MAILLOT, 8:00 TO 10:40 A.M.

Session 2aMUa

Musical Acoustics and Physical Acoustics: Brass Instrument Acoustics I

Thomas Moore, Cochair
Rollins College, Department of Physics, Winter Park, FL 32789, USA

Joël Gilbert, Cochair
Laboratoire d'Acoustique de l'Université du Maine, Avenue Olivier Messiaen, Le Mans, 72085, France

Invited Paper

8:00

2aMUa1. Does mass matter? Examining a concrete didjeridu. Noam Amir (Tel Aviv University, Dept. of Communications Disorders, Sheba Medical Center, 52621 Tel Hashomer, Israel, noama@post.tau.ac.il)

The influence of wall material on the acoustics of musical wind instruments has been debated widely. While this has been examined for some western instruments, it has been barely touched upon regarding the Australian didjeridu. This is very interesting, considering that didjeridus vary enormously in materials and dimensions. Indeed, musicians and manufacturers alike often have very definite opinions concerning the influence of material type and thickness on instrument quality. As a first step towards examining this issue, we conducted a blind test involving three cylindrical didjeridus of identical internal dimensions: all three shared a basic structure of identical plastic tubing. However, a cement casing was cast on the exterior of one of these, bringing its weight to 17 kilograms. The three

instruments were fixed to a stationary wooden frame, then covered so that only the mouthpieces were visible. 32 players of varying expertise were allowed to play each instrument for as long as they wished, and then asked to judge which instrument was different from the other two. Results indicate that the responses were random, regardless of player level. Further research will be necessary to show whether this holds for noncylindrical bores and different internal finishings.

Contributed Paper

8:20

2aMUa2. Relationships among subjective assessments and measured physical properties in the didjeridu. John Smith (University of New South Wales, Music Acoustics, School of Physics, NSW 2052 Sydney, Australia, john.smith@unsw.edu.au), Guillaume Rey (University of New South Wales, Music Acoustics, School of Physics, NSW 2052 Sydney, Australia, guimms@free.fr), Joe Wolfe (University of New South Wales, Music Acoustics, School of Physics, NSW 2052 Sydney, Australia, J.Wolfe@unsw.edu.au)

Traditional didjeridus are unusual and ancient lip-valve instruments with an irregular bore that is largely constructed by termites eating the interiors of small eucalypt trees. This produces instruments with a broad range of bore geometries with many details not immediately apparent to a player. They are therefore well-suited for examining relationships between subjective assessments by players and their measured physical properties. In this study, seven experienced players assessed 38 didjeridus that spanned a wide range of quality, pitch and geometry. A control group of 11 plastic cylindrical pipes were also studied. Eight subjective parameters (backpressure, clarity, resonance, loudness, overtones, vocals, speed, and overall quality) were assessed and the ranking of each instrument correlated with measurements of their geometry and acoustic input impedance spectrum. A strong result of these experiments was the finding that the ranked quality of a didjeridu correlated negatively with the magnitude of its acoustic input impedance, particularly in the frequency range from 1 to 2 kHz. Maxima in the impedance of the player's vocal tract would have a greater effect on instruments with a low impedance, thus favouring the production of the varying spectral peaks or formants in the sound envelope that characterise this instrument.

Invited Papers

8:40

2aMUa3. A psychoacoustical investigation into the effect of wall material on the sound produced by lip-reed instruments. James W. Whitehouse (Acoustics Research Group, DDEM, MCT Faculty, Open University, Walton Hall, MK7 6AA Milton Keynes, UK, j.w.whitehouse@open.ac.uk), David B. Sharp (Acoustics Research Group, DDEM, MCT Faculty, Open University, Walton Hall, MK7 6AA Milton Keynes, UK, d.sharp@open.ac.uk)

In order to investigate whether a lip-reed instrument's material of manufacture plays a significant role in determining the timbre of the notes it produces, tests have been conducted on five post horns. These post horns have identical geometry but are manufactured from different copper alloys. Using a laser Doppler vibrometer, the structural resonances of each instrument have been established and the wall vibrations induced in each instrument when artificially blown have been measured. In this paper, these measurements are compared with findings from a series of blindfold playing tests carried out using professional musicians and with listening tests comprising notes produced by the different instruments.

9:00

2aMUa4. More experimental evidence favouring the hypothesis of significant wall vibration influence on radiated horn sound. Wilfried Kausel (Inst. f. Wiener Klangstil, Univ. f. Music, Anton von Webernplatz 1, A-1030 Vienna, Austria, kausel@mdw.ac.at), Alexander Mayer (Inst. f. Wiener Klangstil, Univ. f. Music, Anton von Webernplatz 1, A-1030 Vienna, Austria, mayer@mdw.ac.at)

The question whether wall vibrations of wind instruments do or can affect the radiated sound has not been finally answered yet. Instrument makers and musicians make a strong claim that wall thickness, material and conditioning are crucial factors for sound quality and response of wind instruments, while acousticians rather tend to question that claim. Recent experiments on horns are presented favoring the hypothesis that wall vibrations do matter. Although horn sound in general appears to change quite significantly when wall vibrations, particularly those of the bell, are dampened during artificial playing, it becomes more and more evident that more than one single mechanism has to be considered to explain the whole phenomenon. Radiation of the bell as multi-pole will add directivity and strengthen higher harmonics while absorption by the wall will rather weaken them. Dynamic interaction between air column and oscillating bore profile theoretically depends on broken symmetry. Feedback of structural resonances to the oscillating lips can be avoided by decoupling the mouthpiece from the instrument. Experiments and statistical evaluation have been laid out in order to exclude or identify certain mechanisms as well as possible artifacts like changes of mouthpiece position, bore or acoustical environment caused by damping forces.

9:20

2aMUa5. Design and manufacturing of an artificial marine conch by bore optimisation. Jef Petiot (Ecole Centrale Nantes - IRCCyN, 1 rue de la Noe, BP 92101, 44321 Nantes, France, jean-francois.petiot@irccyn.ec-nantes.fr), Francois Tavard (Ecole Centrale Nantes - IRCCyN, 1 rue de la Noe, BP 92101, 44321 Nantes, France, francois.tavard@eleves.ec-nantes.fr)

The marine conch is a traditional instrument of the brass family. The resonator is made of the inner shape of the shell, with which the lips of the player interact by the way of a hole pierced in the extremity of the shell. Several notes can be played with this instrument. Unfortunately, the marine conch has become very rare and expensive. In order to build an artificial conch (by injection moulding), we studied the acoustics property of a natural conch. This paper is dedicated to the description of the measurements we made on the conch, and to the presentation of the method used to design the bore. Firstly, the input impedance of the natural conch was measured. Secondly, the size of the bore of the natural conch was assessed by the way of pictures and image processing tools. An initial bore of the artificial

conch was designed with a CAD software, by taking into account manufacturing constraints. We developed next an optimisation procedure to improve the harmonicity of the artificial conch. Finally, an artificial conch was next manufactured by rapid prototyping. As a result, we noticed that the artificial conch manufactured can clearly be used as an interesting musical instrument.

Contributed Paper

9:40

2aMUa6. A design strategy for brass instruments. Robert W. Pyle (S. E. Shires Co., 11 Holworthy Place, Cambridge, MA 02138, USA, rpyle @post.harvard.edu)

This paper describes the processes being used to design a C trumpet. Since ″one size fits all″ is not a good approach for high-quality brass instruments, one of the goals is to create a basic design that, with minor variations, can be tailored to meet the needs of a variety of players. There are other goals, secondary to playing quality but nonetheless desirable. These include appearance and mechanical reliability (″fit and finish″), ease of manufacture (consistent quality at minimal possible cost), and ease of repair (accidents will happen, alas!). Existing instruments provide input data to the design process by way of physical dimensions, acoustic input impedance, and players' judgements. Computer modeling helps to predict the effect on intonation of changes of bore contour. Feedback from top professional players is essential to refine the design, especially the ″black magic″ aspects like brace placement and even the type of solder used to assemble the instrument.

Invited Paper

10:00

2aMUa7. Characterisation of brass musical instrument designs using the brassiness parameter. Arnold Myers (University of Edinburgh, Reid Concert Hall, Bristo Square, EH8 9AG Edinburgh, UK, am@ed.ac.uk)

Recent work has established a ″brassiness″ parameter as a measure of the support given over the sounding length of a brass instrument to non-linear propagation in sound production. This parameter is a function of the geometry (bore profile) of an instrument, and provides a useful means of relating the timbral characters to the designs of the various kinds of brass instrument. The geometries of over 1000 brass instruments belonging to museums worldwide and to individual musicians have been measured to determine the values of their brassiness parameter. Comparisons of these enable not only a more precise taxonomy but also provide a tool for studying the evolution of instrument design. This paper explores both the taxonomic analysis of the whole brasswind field and also gives examples of the use of brassiness in historical research.

Contributed Paper

10:20

2aMUa8. Influence of acoustic waveguides lengths on self-sustained oscillations: Theoretical prediction and experimental validation. Nicolas Ruty (Département Parole & Cognition, GIPSA-lab, 46, avenue Félix Viallet, 38031 Grenoble Cedex, France, nicolas.ruty@gipsa-lab.inpg.fr), Xavier Pelorson (Département Parole & Cognition, GIPSA-lab, 46, avenue Félix Viallet, 38031 Grenoble Cedex, France, pelorson@icp.inpg.fr), Annemie Van Hirtum (Département Parole & Cognition, GIPSA-lab, 46, avenue Félix Viallet, 38031 Grenoble Cedex, France, annemie.vanhirtum@gipsa-lab.inpg.fr)

Human vocal folds and lips of brass instruments players produce self-sustained oscillations due to the interaction between airflow, acoustic waveguides and deformable tissues. This interaction is commonly modelled as a distributed one or two mass-spring system coupled with a simple airflow and acoustic description. This study focuses on the influence of the acoustic waveguide length on the resulting self-sustained oscillation characteristics, i.e. the minimum pressure required to sustain oscillations, the oscillation frequency. Both fixed and varying waveguide lengths are considered. Theoretical predictions with the simplified interaction model are compared to experimental data obtained with a deformable in-vitro replica suitable to produce self-sustained oscillations in presence of an upstream (12, 24 or 32cm) and downstream (varying from 0 up to 235cm) acoustic waveguide. The current study shows the strong influence on the minimum pressure regardless the waveguide length. In addition the waveguide length is shown to impose the resonance frequency for waveguide length superior to 40cm. A rapid change in waveguide length introduces bifurcations between different oscillation regimes.

Session 2aMUb

Musical Acoustics: Interaction Between Instrument and Instrumentalist I

Gary Scavone, Cochair
Schulich School of Music, McGill University, 555 Sherbrooke Street West, Montreal, QC H3A 1E3, Canada

Xavier Boutillon, Cochair
Laboratoire de Mécanique des Solides, Ecole Polytechnique, Palaiseau Cedex, 91128, France

Invited Papers

11:00

2aMUb1. Motor control in drumming: Influence of movement pattern on contact force and sound characteristics. Sofia Dahl (Institute of Music Physiology and Musicians' Medicine, Hanover University of Music and Drama, Hohenzollernstr. 47, 30161 Hannover, Germany, dr.sofia.dahl@gmail.com), Eckart Altenmüller (Institute of Music Physiology and Musicians' Medicine, Hanover University of Music and Drama, Hohenzollernstr. 47, 30161 Hannover, Germany, altenmueller@hmt-hannover.de)

Whereas wind instrumentalists and string players have a continuous control of the acoustic sound parameters during playing, a percussionists' direct contact with the instrument is limited to a few milliseconds. The player has no possibilities to adjust grip or dampening during the actual contact. Whatever timbre and sound level the player is aiming for therefore has to be integrated in the entire striking gesture. How can the player control the complex interaction between drumstick and drumhead? In order to investigate how the players' grip and striking gestures influence the sound characteristics of drum strokes we recorded movements, audio, contact time and contact force during drumming. Different instructions were given with the intention to influence how the player's grip controlling the drumstick. ″Normal″ strokes were allowed to freely rebound from the drumhead. For ″controlled″ strokes the player was asked to control the ending position of the drumstick, stopping it as close as possible to the drumhead after the stroke. Preliminary analysis showed that the instructions influenced contact force, contact time, and perceptual ratings of the strokes. Further results and implications will be discussed.

11:20

2aMUb2. Two dimensional finger-string interaction in the concert harp. Jean-Loic Le Carrou (Laboratoire d'Acoustique de l'Université du Maine, Avenue Olivier Messiaen, 72085 Le Mans, France, jean-loic.le_carrou@univ-lemans.fr), Elio Wahlen (LAUM, CNRS, Université du Maine, Lab. d'Acoustique Université du Maine, UMR CNRS 6613, 72085 Le Mans Cedex 9, France, elio@elio.de), Emmanuel Brasseur (LAUM, CNRS, Université du Maine, Lab. d'Acoustique Université du Maine, UMR CNRS 6613, 72085 Le Mans Cedex 9, France, emmanuel.brasseur@univ-lemans.fr), Joël Gilbert (Laboratoire d'Acoustique de l'Université du Maine, Avenue Olivier Messiaen, 72085 Le Mans, France, joel.gilbert@univ-lemans.fr)

The sound of the concert harp partly depends on the way the string is plucked. The vibrating string is brought into a state of initial conditions by the finger-string interaction and then oscillates according to two transverse planes. In order to understand the plucking action of the concert harp, a one-dimensional model of this interaction has been developed in a previous paper [Le Carrou et al, Proc. ISMA (2007)]. The parameters of this model were deduced from measurements of the string's and finger's trajectories. The aim of the present paper is to extend this model to a more realistic one, including a two-transverse trajectory for each one of the interaction's elements. To do so, a special experiment with a high-speed camera, which films the interaction, is set up. Specific image processing, based on edges detection, helps to automatically track both objects' positions. The results show that the finger-string interaction takes place in two planes and permits us to obtain the parameters of the two-dimensional model for the finger-string interaction.

11:40

2aMUb3. The modern violin bow in off-string action. Knut Guettler (Norwegian Academy of Music, P.O.Box 5190 Majorstuen, 0302 Oslo, Norway, knut.guettler@nmh.no)

The convex camber of the modern Tourte-model bow permits off-string stroke techniques to be performed with resulting clean and crisp attacks. This paper discusses how different bow-, string-, and bowing parameters must combine in order for this to be achieved. Of particular interest are the geometrical changes imposed on the bow stick during bouncing strokes. A good spiccato bow is characterized by a stick that feels ″lively″, even when the bouncing is low or the hairs are not leaving the string at all. With lesser-quality bows the player has to work harder (on the lower-pitched double bass even sometimes synchronously ″shake″ the bow stick in the string-length plane) in order to induce sufficient stick oscillation. Included in this study are measurements of finger action on bow sticks of different quality.

Contributed Paper

12:00

2aMUb4. Observations on bow changes in violin performance. Matthias Demoucron (IRCAM, 1 Place Igor Stravinsky, 75004 Paris, France, demoucron@ircam.fr), Anders Askenfelt (Dept. of Speech, Music and Hearing, Royal Institute of Technology (KTH), Lindstedtsvägen 24, SE-100 44 Stockholm, Sweden, andersa@speech.kth.se), René E. Causse (IRCAM, 1 Place Igor Stravinsky, 75004 Paris, France, causse @ircam.fr)

Players of bowed instruments commonly separate notes by changing the direction of the bow motion (″bow changes″). The separation can be made more or less pronounced (detaché - portato - martellato). In contrast, long notes, requiring more than a full bow stroke, are played by making the bow changes as inaudible as possible. Acceptable bow changes require accurate control and coordination of a set of bowing parameters, in particular bow speed, bow force and bow-bridge distance. Long practice is required before optimal control is achieved. Detailed descriptions of basic bowing gestures such as bow changes are of great interest for various fields of violin-related studies, including realistic control of synthesis algorithms. We present recent measurements that provide an accurate description of the evolution of bow speed, acceleration and bow force during bow changes at the tip and the frog, respectively. Using these data for controlling a synthesis algorithm, we will discuss how modifications of the parameters influence the bow-string interaction and resulting string vibrations. The simulations are used to model efficient implementations of bow changes.

Invited Paper

12:20

2aMUb5. Extraction of lumped clarinet reed model parameters from numerically synthesised sound. Vasileios Chatziioannou (Sonic Arts Research Centre, Queen's University Belfast, BT7 1NN Belfast, UK, vchatziioannou01@qub.ac.uk), Maarten Van Walstijn (Sonic Arts Research Centre, Queen's University Belfast, BT7 1NN Belfast, UK, m.vanwalstijn@qub.ac.uk)

Fluid dynamical analysis and time-domain modelling of a single reed-mouthpiece-lip system can be used to inform the formulation of a lumped model of the woodwind excitation mechanism. Coupling this lumped model to a model of the instrument bore enables computationally efficient generation of sustained oscillations, using a small number of physical parameters that define the instrument and the way the player controls them. As such, the embouchure of the player as well as the geometry of the system is taken into account. In this paper, an attempt is carried out to use the numerically generated sound as an input to an inversion algorithm for the reed-mouthpiece-lip system. Assuming that the reed motion is proportional to the pressure difference across it, a relationship can be established between the pressure and the total flow inside the mouthpiece that allows a first estimation of the physical parameters using standard optimisation techniques. Currently we are undertaking efforts to apply the inversion to data measured under real playing conditions, i.e. effectively capturing player gesture information in the form of physical control parameters.

12:40-1:40 Lunch Break

Contributed Paper

1:40

2aMUb6. How to play the first bar of *Rhapsody in Blue*. Jer-Ming Chen (University of New South Wales, Music Acoustics, School of Physics, NSW 2052 Sydney, Australia, jerming@phys.unsw.edu.au), John Smith (University of New South Wales, Music Acoustics, School of Physics, NSW 2052 Sydney, Australia, john.smith@unsw.edu.au), Joe Wolfe (University of New South Wales, Music Acoustics, School of Physics, NSW 2052 Sydney, Australia, J.Wolfe@unsw.edu.au)

The two-and-a-half octave glissando opening Gershwin's *Rhapsody in Blue* is one of the great icons of 20th century music and one of the best known bars in music. Expert clarinettists combine unusual fingerings with even more unusual configurations of their vocal tract to achieve a nearly continuous rise in pitch. Using a novel method [1], we incorporated an acoustic impedance measurement head within a clarinet mouthpiece, allowing us to study the player's vocal tract at various stages in the glissando. We measured and compared vocal tract impedance spectra with the corresponding clarinet impedance spectra for the fingering used at that pitch. Partially uncovering an open finger-hole raises the frequency of clarinet impedance peaks in the lower register, thereby allowing smooth increases in the playing pitch. In the upper register, however, resonances in the clarinettist's vocal tract are manipulated to be comparable with those in the clarinet for frequencies in this range. Thus the pitch in the higher section of the glissando is largely controlled by smoothly varying a resonance of the player's vocal tract. [1] Chen, JM. Smith, J. and Wolfe, J., (2008) ''Experienced saxophonists learn to tune their vocal tracts''. Science, (in press).

Invited Papers

2:00

2aMUb7. Evaluating Vocal-Tract Influence in the Production of Saxophone Multiphonics. Gary Scavone (Schulich School of Music, McGill University, 555 Sherbrooke Street West, Montreal, QC H3A 1E3, Canada, gary@music.mcgill.ca), Antoine Lefebvre (Schulich School of Music, McGill University, 555 Sherbrooke Street West, Montreal, QC H3A 1E3, Canada, antoine.lefebvre2@mail.mcgill.ca), Andrey R. Da Silva (Schulich School of Music, McGill University, 555 Sherbrooke Street West, Montreal, QC H3A 1E3, Canada, andrey.dasilva@mail.mcgill.ca)

A new approach for the analysis of vocal-tract influence in single-reed woodwind instruments during performance was recently reported (Scavone et. al., 2008). Two types of vocal-tract influence were observed. When the downstream air column provides only weak support of a given note, players can use a strong and narrow-bandwidth upstream resonance to override the reed vibrations, such as when pitch bending or playing extended register notes. Performers can also use a more wide-bandwidth upstream resonance to affect subtle timbre variations when playing notes over the full range of the instrument. The research reported here addresses the performance of multiphonic tones, for which the results of the previously mentioned study were less conclusive. While it is clear that upstream influence is involved in the production of multiphonics, we are interested in determining whether performers must support a specific intermodulation component or a wider bandwidth range of components for proper production. The latest results of this research will be reported.

2:20

2aMUb8. A study of flute control parameters. Benoit Fabre (Institut Jean Le Rond d'Alembert / LAM (UPMC / CNRS / Ministère Culture), 11, rue de Lourmel, 75015 Paris, France, fabreb@ccr.jussieu.fr), Nicolas Montgermont (Institut Jean Le Rond d'Alembert / LAM (UPMC / CNRS / Ministère Culture), 11, rue de Lourmel, 75015 Paris, France, montgermont@lam.jussieu.fr), Patricio De La Cuadra (Centro de Investigación en Tecnologias de Audio (CITA), Universidad Católica de Chile, Alameda 340, Oficina 13, Casilla 114-D Santiago, Chile, pcuadra@uc.cl)

The sound of musical instruments played in self-sustained oscillations can be interpreted as a sounding transposition of the player's gesture. The playing of wind instruments requires expert control of the blowing that may be difficult to grasp and to measure because it induces only very little motion of the player, as opposed to string or keyboard instruments. In the case of instruments of the flute family, the player seems to control mainly the air jet velocity for mode selection. Flutes in which the air jet is formed between the lips also allow for a control of the total jet flow by the player, through lip adjustments. We present measurements carried on several players, in different playing conditions. The score includes technical exercises such as scales and short musical excerpts from the flute repertoire. Time evolutions of the control parameters are analysed, based on pressure and geometrical measurement, in the framework of the current knowledge on the sound production in flutes, such as jet instability. The control over different parameters will be discussed, both for basic technical exercises and in a musical melodical context.

Contributed Paper

2:40

2aMUb9. Acoustical analysis of timbral modulations on the flute as controlled by phonetic gestures. Maryse Lavoie (Laboratoire informatique, acoustique et musique, Faculté de musique, Université de Montréal, C.P. 6128, succursale Centre-Ville, Montréal, QC H3C 3J7, Canada, maryse.lavoie@umontreal.ca), Caroline Traube (Laboratoire informatique, acoustique et musique, Faculté de musique, Université de Montréal, C.P. 6128, succursale Centre-Ville, Montréal, QC H3C 3J7, Canada, caroline.traube@umontreal.ca), Marie-Hélène Breault (Observatoire international de la création et des cultures musicales (OICCM), Faculté de musique, Université de Montréal, C.P. 6128, succursale Centre-Ville, Montréal, QC H3C 3J7, Canada, mhbreault@yahoo.ca)

The purpose of this project is to study the control of timbre on the flute by varying articulatory parameters (i.e. embouchure) which correspond to distinct phonetic gestures. The main goal is to compare the production of a specific timbral modulation on the flute and its vocal reproduction (diphthong) by means of acoustical analyses of these sounds. The recordings of timbral modulations performed on the flute (e.g. by increasing the mouth opening) and reproduced vocally as diphthongs (e.g. [u] -> [a] transition) have been analyzed acoustically for intensity as well as for the first two formant trajectories. The results of the formant analyses as presented in an F1-F2 plane reveal the cardinal vowel triangle and confirm a correlation between the flute timbre modulations and the vocal diphthongs corresponding to the underlying phonetic gestures. In addition, a listening test has shown that flutists are able to perceive and recognize these timbral modulations from the sound alone.

Invited Papers

3:00

2aMUb10. Lip control of brass instruments. Donald M. Campbell (Edinburgh University, 4201 JCMB, Kings Buildings, Mayfield Road, EH9 3JZ Edinburgh, UK, d.m.campbell@ed.ac.uk)

Brass instruments are frequently described in the acoustics literature as ″lip reed″ instruments, emphasising the fact that the sounding mechanism of this instrumental class is flow modulation by the vibration of the player's lips. As well as providing the source of sound, the lips act as the major interface through which the performer controls the intonation, dynamics, articulation and timbre of the performance. Indeed, on instruments such as the natural trumpet and the alphorn, the player's lips form the only control interface. This paper reviews recent studies which have examined the vibrational properties of brass players' lips, the types of motion which they undergo when playing different instruments, and the nature of the interaction between the lips and the instrument. It also considers the extent to which current physical models of the lips are capable of encompassing these control processes.

3:20

2aMUb11. Vocal tract interactions in saxophone performance. Jer-Ming Chen (University of New South Wales, Music Acoustics, School of Physics, NSW 2052 Sydney, Australia, jerming@phys.unsw.edu.au), John Smith (University of New South Wales, Music Acoustics, School of Physics, NSW 2052 Sydney, Australia, john.smith@unsw.edu.au), Joe Wolfe (University of New South Wales, Music Acoustics, School of Physics, NSW 2052 Sydney, Australia, J.Wolfe@unsw.edu.au)

Although acousticians have debated the importance of the vocal tract in reed instrument performance, expert saxophonists report adjusting their vocal tract for advanced techniques including *altissimo* playing, subtone playing, bugling and multiphonics. Using a novel method [1], we incorporated an acoustic impedance head within a saxophone mouthpiece to study the vocal tract directly during playing. For fingerings above the first register, the operating peak in the saxophone's input impedance decreases with increasing pitch, falling to below 20 MPa.s.m^{-3} after 2.7 octaves, thus ending the standard range that is readily available to amateurs. Above this, in the *altissimo*, professional saxophonists produce peaks in the impedance of their tracts of about 20 to 40 MPa.s.m^{-3}, which they tune to select the desired note. The crossover of the relative magnitudes of saxophone and tract impedance peaks coincides with the transition from standard to *altissimo* register. While professionals use the vocal tract thus for other extended effects, inexperienced players do not tune their tract resonances and are unable to produce advanced effects. [1] Chen, JM. Smith, J. and Wolfe, J., (2008) ''Experienced saxophonists learn to tune their vocal tracts''. Science, (in press).

Contributed Paper

3:40

2aMUb12. Reproducibility of piano playing. Nicolas Principeaud (Laboratoire d'Acoustique Musicale, 11 rue de Lourmel, 75015 Paris, France, nicolas.principeaud@free.fr), Xavier Boutillon (Laboratoire de Mécanique des Solides, Ecole Polytechnique, 91128 Palaiseau Cedex, France, boutillon@lms.polytechnique.fr)

Mechanically, piano playing consists in giving to the hammer a certain escapement velocity at a certain time - t_e, v_e - by means of a traditional keyboard and piano action. Numerous replacement systems for the keyboard, action or even for the pianist's finger have been proposed. They implicitly raise the question of the accuracy with which the (t_e, v_e) information must be coded or reconstructed. The precision with which pianists are able to reproduce their playing sheds some light on this question. At this end we have asked several concert pianists to play the same passage several times with the highest reproducibility level they could achieve. The experiment was done on a traditional grand piano equipped with the Yamaha Disklavier system, used as a measurement tool for the escapement velocity of the hammers. The beginnings of a fugue by Bach and a study by Debussy were recorded. Results show that the reproducibility varies highly from note to note and can be as good as approximately 1%. Additional tests on auditors show that deviations on note amplitudes are not perceived unless they reach a level which turns out to be significantly higher than the reproducibility level achieved by the pianists.

TUESDAY MORNING, 1 JULY 2008 ROOM 250A, 8:00 A.M. TO 8:00 P.M.

Session 2aNSa

Noise, Physical Acoustics, and EURONOISE: Aeroacoustics II

Philip J. Morris, Cochair
Penn State University, 233C Hammond Building, University Park, PA 16802, USA

Christophe Bailly, Cochair
Ecole Centrale de Lyon, 36, avenue Guy de Collongue, LMFA, Ecully, 69134, France

Contributed Papers

8:00

2aNSa1. Source location prediction of subsonic isothermal jet flows. Juan Battaner-Moro (Institute of Sound and Vibration Research, University of Southampton, University Road, SO17 1BJ Southampton, UK, jpb@isvr.soton.ac.uk), Mahdi Azarpeyvand (Institute of Sound and Vibration Research, University of Southampton, University Road, SO17 1BJ Southampton, UK, ma@isvr.soton.ac.uk), Rod Self (Institute of Sound and Vibration Research, University of Southampton, University Road, SO17 1BJ Southampton, UK, rhs@isvr.soton.ac.uk)

The location of jet noise sources is a far from trivial problem that is of great importance for both understanding the noise production and radiation mechanisms and also for finding new jet noise reduction strategies. This paper presents comparisons of theoretical results with data for a number of jets. The theory used is based on the MGBK method but including a novel time scale based on the rate of energy transfer through the turbulent cascade. This new technique has been shown to give a number of advantages over existing models. The experimental results were obtained using the Polar Correlation Technique and were made at QinetiQ's Jet Noise Facility in the UK as part of the EU FP6 programme CoJeN. The high resolution jet noise images resulted from using a 64 microphone polar arc array set at two reference angles, namely 60 and 90 degrees to the jet axis. Comparisons with experimental data are made for coplanar and short cowl nozzles at different working conditions for predictions from different theoretical models. It is shown that the best agreement is obtained for the prediction methodology using the energy transfer rate timescale

8:20

2aNSa2. A hybrid method for jet noise predictions based on Large Eddy Simulation and Reynolds-Averaged Navier-Stokes simulations. Guillaume Bodard (Snecma Villaroche, Rond point René Ravaud, 77550 Moissy-Cramayel, France, guillaume.bodard@snecma.fr), Christophe Bailly (Ecole Centrale de Lyon, 36, avenue Guy de Collongue, LMFA, 69134 Ecully, France, christophe.bailly@ec-lyon.fr)

A hybrid jet noise prediction method combining steady and unsteady flow calculations is discussed. The main objective is to merge advantages of each technique to obtain a robust acoustic prediction tool, which will be able to correctly evaluate design and installation effects such as chevron nozzles or jet-pylon interaction for instance. The low-frequency component of acoustic spectra is computed using large-eddy simulations and the integral formulation derived by Ffowcs-Williams & Hawkings (1969, Phil. Trans. Roy. Soc. Lond., vol. 264). The high-frequency component associated with fine scale turbulence is obtained thanks to Tam & Auriault's mixing noise theory (1999, AIAA Journal, vol. 37) from Reynolds-Averaged Navier-Stokes simulations. The oral presentation will detail the two methods, the LES simulations for subsonic round single and coaxial jets, and the matching between the two approaches to get a complete picture of the acoustic spectra.

8:40

2aNSa3. Efficiency of optimized microjets on realistic nozzles. Alexandre Vuillemin (Snecma, Etablissement de Villaroche Sud, Rondpoint René Ravaud - Réau, 77550 Moissy-Cramayel, France, alexandre.vuillemin@snecma.fr)

Even if chevrons nozzles are an efficient way to reduce jet noise during take off, they also decrease performances during cruise. An innovative way to avoid this decrease is the use of active devices that could be switch off after take off, such as microjets nozzles. Snecma led test campaigns at Martel Facility (LEA/CEAT) to optimize microjets settings (geometric and thermodynamic parameters) and to characterize their efficiency on both 2D axisymmetric and chevrons nozzles. Acoustic and PIV measurements were done on a single stream hot jet with and without external flow, and on a double stream hot jet with pylon.

9:00

2aNSa4. Numerical investigation of the effect of nonlinear propagation distortion on helicopter noise. Penelope Menounou (University of Patras, Department of Mechanical and Aeronautical Engineering, Rion, 26504 Patras, Greece, menounou@mech.upatras.gr), Panagiotis

Vitsas(University of Patras, Department of Mechanical and Aeronautical Engineering, Rion, 26504 Patras, Greece, pvitsas@upnet.gr)

Nonlinear propagation distortion causes energy to be shifted to the high frequency end of the spectrum. This leads to underestimation of the noise levels at high frequencies. The effect has been demonstrated in the case of aircraft noise, but less attention has been given to helicopters. In the present work, the effect of nonlinear propagation distortion on helicopter noise is demonstrated based on measured data for low-speed descent and numerical calculations that predict the noise level away from the helicopter with and without nonlinear effects. It is shown that (i) for some frequency bands the difference between linear and nonlinear calculations can be as high as 8 dB, (ii) frequencies between 1000 and 3000 Hz are more affected, and (iii) the effect is highly directional depending on the receiver location around the helicopter. It is further shown that nonlinear effects manifest themselves differently than in the case of aircraft noise and that they depend on the specific helicopter noise mechanism. More specifically, the following helicopter-specific noise source types are investigated with regards to nonlinear effects: advancing Blade Vortex Interaction (BVI) noise vs retreating BVI noise, High Speed Impulsive noise, and BVI vs Very Impulsive noise.

Invited Papers

9:20

2aNSa5. Recent developments in helicopter rotor noise prediction. Kenneth S. Brentner (Penn State University, 233C Hammond Building, University Park, PA 16802, USA, ksb16@psu.edu)

Prediction of discrete frequency noise for rotorcraft in steady flight has reached a high level of sophistication and understanding. The primary challenge in such rotor noise predictions is the accurate determination of the loading on and flow field around the blades. Although current rotor noise prediction tools have been demonstrated for steady flight conditions, the utility of rotorcraft comes from their unique ability to hover and maneuver. Such maneuvers often occur near the ground in close proximity to people. This paper describes an initial study to characterize maneuver noise. A maneuver noise prediction system has been developed, which consists of a flight simulation code, free-vortex wake code, and a maneuver noise prediction code, loosely coupled together. One of the key aspects of this system is the ability to investigate the additional noise caused during the transition from one flight state to another. Several maneuvers including turns, accelerations, and pop-up/popdown maneuvers were considered. Significant increases in the low-frequency noise can occur, depending on how aggressive the maneuver is performed. The status of advanced research on predicting acoustic scattering of the rotor noise by the aircraft and the first-principles prediction of rotor broadband noise will also be presented.

9:40

2aNSa6. Aeroacoustic research complex for aircraft source noise characterization. Micah Downing (Blue Ridge Research and Consulting, 13 1/2 W. Walnut St., Asheville, NC 28801, USA, micah.downing@blueridgeresearch.com), Robert McKinley (Air Force Research Laboratory, AFRL/RHCB, 2610 Seventh St., Bldg 441, Wright-Patterson AFB, OH 45433, USA, Robert.McKinley@wpafb.af.mil), John Hall (Air Force Research Laboratory, AFRL/RHCB, 2610 Seventh St., Bldg 441, Wright-Patterson AFB, OH 45433, USA, John.Hall@wpafb.af.mil), Frank Mobley (Air Force Research Laboratory, AFRL/RHCB, 2610 Seventh St., Bldg 441, Wright-Patterson AFB, OH 45433, USA, Frank.Mobley@wpafb.af.mil), Michael James (Blue Ridge Research and Consulting, 13 1/2 W. Walnut St., Asheville, NC 28801, USA, michael.james@blueridgeresearch.com)

Aircraft noise has been traditionally measured with either a few ground-based microphones or a linear ground-plane array of microphones. These techniques capture one-dimensional and/or two-dimensional characteristics of aircraft flight noise. The US Air Force Research Laboratory has started the construction of a 3-dimensional measurement facility at White Sands Missile Range in New Mexico. This facility, the Aeroacoustic Research Complex (ARC), will allow aircraft to fly through the array, collecting fully 3D acoustic data. ARC is initially being developed in two phases The first phase includes two 91.4 m tall towers separated by 244 m and will focus on noise from rotary wing and UAV aircraft. The second phase will add two 366 m tall towers separated by 610 m and will focus on large and high performance fixed wing aircraft. This facility will allow more accurate characterization of in-flight noise directivity by providing synchronized 3-dimensional magnitude & spectral acoustical signatures from 50+ microphones. ARC responds to a critical need for validation of existing predictive acoustic models. Such models are used for aircraft design, survivability, nonlinear acoustic propagation research and assessing noise exposure to residents living adjacent to airfields.

10:00-10:20 Break

Contributed Papers

10:20

2aNSa7. Lateral directivity of aircraft noise. Walter Krebs (Empa, Ueberlandstrasse 128, 8600 Duebendorf, Switzerland, walter.krebs@empa.ch), Georg Thomann (Empa, Ueberlandstrasse 128, 8600 Duebendorf, Switzerland, georg.thomann@empa.ch)

A three-dimensional model was developed to characterise the directional sound emission of different aircraft. The model is based on spherical harmonics and defines the directional spectral sound pressure level at a reference distance. The parameters of the model are derived from acoustic measurements on real aircraft traffic. With the help of this model different physical effects on sound propagation and sound impact are analysed. Variations with respect to a rotational symmetric sound emission are outlined and compared to the engine installation corrections proposed in the revised Doc 29 3rd edition. In addition the influence of the ground effect on A-weighted sound levels is analysed for different receiver heights and ground impedances.

10:40

2aNSa8. Sonic booms, spectral analysis, and diffraction by buildings. Victor W. Sparrow (Penn State, Graduate Program in Acoustics, 201 Applied Science Bldg., University Park, PA 16802, USA, vws1@psu.edu)

An analysis has been performed upon conventional and low-amplitude N-wave sonic boom data taken by NASA outside two houses in June 2006 and July 2007. The buildings were one-floor residences which were carefully instrumented with strategically-placed, multiple microphones. The incident sonic booms had a substantial variation in rise times, most likely due to atmospheric effects. Previous work using the June 2006 data [Sparrow, Klos, and Buehrle, J. Acoust. Soc. Am. 122 (5, Pt. 2) 3084] revealed maximum pressure loads near the ground and wall facing the incident boom. A new spectral analysis of the individual booms now confirms that the diffraction of sound over the house tops is substantially affected by the spectral content of each boom. These results indicate that the pressure loading of homes due to conventional or low-amplitude sonic boom will be affected by

both the spectral content of each boom's rise phase and each house's exterior geometry. [Work supported by NASA.]

11:00

2aNSa9. Identification of aerodynamic sound sources: the key problem in noise control. Alexander Fedorchenko (Independent Researcher/Consultant, Dm. Ul'yanov Str. 27/12-1-50, 117449 Moscow, Russian Federation, fedorchenko@mail.com)

Despite the recent advances in the noise control technology, the key mechanisms of aerodynamic sound emission remained poorly studied. The ″well-recognized″ methods of TCAA did not lead to any breakthrough in this topical problem, and what seems most disappointing, the family of ″acoustic analogies″ is still used by many for definition of aerodynamic noise sources, though the sufficient set of mathematical proofs has been given by the author that this model is wrong. Experimental approaches aimed at localization of aerodynamic noise sources, including the method of acoustic imaging via using a microphone array, are considered, and their inherent limitations are pointed out. Unfortunately, no current experimental technique enables one to measure instantly all sound sources and sound disturbances inside the zone of generation, and so the latter is often regarded as a kind of ″black box″. The two-medium nonlinear theory of aerodynamic sound, based on the original decomposition of each flow variable into two components, for unsteady background flow and for acoustic field, has been created, that promotes better comprehension of the noise generation phenomena and opens new ways in flow/noise control. The main properties of this theory are now indicated in comparison with the most detrimental delusions originated from ″acoustic analogies″.

Invited Paper

11:20

2aNSa10. Direct aeroacoustic simulations based on domain decompositions. Jens Utzmann (University of Stuttgart, Institute for Aerodynamics and Gasdynamics, Pfaffenwaldring 21, 70569 Stuttgart, Germany, utzmann@iag.uni-stuttgart.de), Claus-Dieter Munz (University of Stuttgart, Institute for Aerodynamics and Gasdynamics, Pfaffenwaldring 21, 70569 Stuttgart, Germany, munz@iag.uni-stuttgart.de)

For CAA, an accurate and feasible direct simulation that considers both the generation of sound within the flow and its propagation into the far-field is hard to realize with one numerical method in a single computational domain. On the other hand, a direct approach contains automatically the interaction of the acoustic perturbations with the flow-field, a property which lacks the popular acoustic analogy models. The proposed method is basically a direct simulation, but it simplifies the problem that has to be solved for individual regions in the computational domain. The idea is to use a non-overlapping domain decomposition method where the equations, methods, grids and even the time steps are adapted to meet the local requirements. Inside the coupling framework, high-order solvers from different classes of methods are available: On unstructured grids, a reconstructed ADER finite volume method (ADER-FV) is used for linear and nonlinear problems, as well as a discontinuous Galerkin method. On structured grids, the ADER-FV and the ADER-FD method are efficiently implemented for nonlinear (FV) and linear (FV, FD) problems. These high-order accuracy methods ensure excellent wave propagation capabilities throughout the entire computational domain. In the subdomains, the Navier-Stokes, Euler and the linearized Euler equations are solved.

Contributed Papers

11:40

2aNSa11. Direct Noise Computation in subsonic and transonic flows. Frédéric Daude (LaMSID UMR EDF/CNRS, 1 avenue du Général de Gaulle, 92141 Clamart, France, frederic-externe.daude@edf.fr), Thomas Emmert (LaMSID UMR EDF/CNRS, 1 avenue du Général de Gaulle, 92141 Clamart, France, tommem@gmail.com), Philippe Lafon (EDF, 1, avenue du Général de Gaulle, 92141 Clamart, France, Philippe.lafon@edf.fr), Fabien Crouzet (EDF, 1, avenue du Général de Gaulle, 92141 Clamart, France, fabien.crouzet@edf.fr), Christophe Bailly (Ecole Centrale de Lyon, 36, avenue Guy de Collongue, LMFA, 69134 Ecully, France, christophe.bailly@ec-lyon.fr)

In order to model flow phenomena involving interactions between aerodynamics and acoustics, it is necessary to use Direct Noise Computation (DNC) instead of hybrid methods that are not suitable to take into account the feedback of acoustics on the flow. The methods that are now available in the field of Computational AeroAcoustics (CAA) allows us to deal with DNC in realistic configurations. The numerical code SAFARI (Simulation of Aeroacoustics in Fluids And with Resonance and Interactions) has been developed for this goal. The set of equations are the compressible 3-D Navier-Stokes equations. High order finite difference schemes are used. Multidomain capabilities are implemented in order to deal with complex geometries. Block decomposition is used in order to take advantage of parallel processing on large clusters Validation cases are presented: diffraction by a cylinder, shock tube. Results on realistic configurations are also shown: ducted cavity, transonic sudden enlargment, airfoil interactions.

12:00

2aNSa12. Asymptotic expressions for the directivity of round jets. Ricardo E. Musafir (UFRJ / COPPE, Universidade Federal do Rio de Janeiro, 21941-972 Rio de Janeiro, Brazil, rem@serv.com.ufrj.br)

Expressions for the directivity of round jets, in the high and low frequency limits, are derived, based on solutions of Lilley's equations. Two different forms of the equation in what concerns source terms representation are considered, along with general point sources of the appropriate type (i.e., equivalent stress and force sources and also, when necessary, volume sources), which are assumed to be statistically axisymmetric. Effects of mean shear and temperature gradients are accounted for, as well as of source movement. The expressions are compared with earlier ones, based on a plug flow model. The differences in the resulting expressions due to the choice of source description, which are relevant for hot jets, are discussed and used to derive a form consistent with both representations. Comparison with experimental data is also presented.

12:20

2aNSa13. Investigations of roughness-generated TBL sound using coupled physical-computational experiments in conjunction with theoretical development. William Blake (Naval Surface Warfare Center (Ret.), 6905 Hillmead Road, Bethesda, MD 20817, USA, hydroacoustics@aol.com), Ki-Han Kim (Office of Naval Research, Randolph St., Arlington, VA 22202, USA, kihan.kim@navy.mil), Michael Goody (Naval Surface Warfare Center (Ret.), 6905 Hillmead Road, Bethesda, MD 20817, USA, michael.goody@navy.mil), Meng Wang (University of Notre Dame, Departmernt of Aerospace and Mechanical Engineering, Notre Dame, MD 46556, USA, m.wang@nd.edu), William J. Devenport (Virginia Tech, Aerospace and Ocean Engineering, 224E Randolph Hall, Blacksburg, VA 24061, USA, devenport@vt.edu), Stewart A. Glegg (Florida Atlantic University, Department of Ocean Engineering, Boca Raton, VA 33431, USA, glegg@oe.fau.edu)

Sound produced by turbulent-boundary layers (TBL) over rough walls is being studied in a series of physical-computational experiments. At issue is the development of a knowledge of how the wall elements generate flow dipoles which directly determines how the sound is described in terms of dependent variables. The considered mechanisms include dipoles at the

roughness elements due to their shed wakes, distributed surface dipoles due to convecting turbulence impinging onto elements, Rayleigh-like scattering into sound of aerodynamic pressures of hydrodynamic wave numbers of flow above the roughness. The LES of rough-wall TBL consists of ″numerical″ experiments being used to isolate the separate mechanisms. These simulations are benchmarked with analysis and with matching physical experiments on rough wall patches in which identical geometries of wall roughness and identical Reynolds numbers are used. In the physical measurements, array-based measurements of the radiated sound are being used to characterize the directivity and magnitude of the sound and to relate the sound to aerodynamic wall pressure and to classical characteristics of the turbulent boundary layer. The LES produces comparison for both radiated sound and detailed flow structure around the roughness elements. This project is funded by the Office of Naval Research, Washington, D.C., USA.

12:40-2:00 Lunch Break

Contributed Paper

2:00

2aNSa14. Experimental investigation of sound from flow over a rough surface. Michael Goody (Naval Surface Warfare Center (Ret.), 6905 Hillmead Road, Bethesda, MD 20817, USA, michael.goody@navy.mil), Jason Anderson (Naval Surface Warfare Center (Ret.), 6905 Hillmead Road, Bethesda, MD 20817, USA, Jason.M.Anderson@navy.mil), Devin Stewart (Naval Surface Warfare Center (Ret.), 6905 Hillmead Road, Bethesda, MD 20817, USA, Devin.Stewart@navy.mil), William Blake (Naval Surface Warfare Center (Ret.), 6905 Hillmead Road, Bethesda, MD 20817, USA, hydroacoustics@aol.com)

Measurements of radiated noise and unsteady surface pressures have been carried out in order to better understand the mechanism for sound production from flow over a rough surface. In order to investigate scaling relationships, the flow speed, roughness height, geometry and element distribution were varied systematically. When considered in total, previous investigations do not present a consistent picture of the scaling behavior of roughness noise, or the underlying physical mechanism. They have reported roughness noise levels that scale on flow velocity, roughness height, and fetch area and have indicated that the sound production may be dipole or quadrupole in nature. Prevailing analytical models assume that both dipole and quadrupole sources are present. The scaling of roughness noise for large roughness height has not been investigated previously and is part of the current study. A recent developed scattering model (dipole) developed by Glegg et al is interrogated using detailed measurements of the roughness element height distribution, turbulent boundary layer properties, and array-based radiated sound levels.

Invited Paper

2:20

2aNSa15. On the sound generated by boundary-layer vorticity. Umberto Iemma (University Roma Tre, via vasca navale 79, 00146 Rome, Italy, u.iemma@uniroma3.it), Luigi Morino (via vasca navale 79, 00146 Roma, Italy, l.morino@uniroma3.it), Roberto Camussi (University Roma Tre, via vasca navale 79, 00146 Rome, Italy, camussi@uniroma3.it), Giovanni Caputi Gennaro (University Roma Tre, via vasca navale 79, 00146 Rome, Italy, gcaputi@uniroma3.it)

Turbulent boundary layers generate broadband noise as the effect of vortical-disturbances scattering into acoustic waves. The paper presents a formulation for evaluating of acoustic pressure in the field in terms of the transpiration velocity, here defined in terms of vorticity and closely related to Lighthill equivalent source. Specifically, the formulation used allows one to obtain, in the frequency domain, a matrix relationship between the transpiration velocity at a number of points on the body surface (those arising from boundary-element discretization) and the pressure at given points in the irrotational region. From this, the relationship between the corresponding PDF is easily obtained using the Wiener-Khintchine theorem. The paper will include the general formulation, validating numerical results, and comparison with experimental data. The inverse problem, that is, determining the source intensity on the body surface from field noise (in particular, the invertibility of the operator), will be also addressed.

Contributed Papers

2:40

2aNSa16. A numerical study on multimode sound propagation in lined ducts and radiation to the far field. Rie Sugimoto (ISVR, University of Southampton, Highfield, SO17 1BJ Southampton, UK, rs@isvr.soton.ac.uk), R Jeremy Astley (ISVR, University of Southampton, Highfield, SO17 1BJ Southampton, UK, rja@isvr.soton.ac.uk), Claire R. McAleer (ISVR, University of Southampton, Highfield, SO17 1BJ Southampton, UK, crm@soton.ac.uk), Iansteel Achunche (ISVR, University of Southampton, Highfield, SO17 1BJ Southampton, UK, ia1@isvr.soton.ac.uk)

In previous articles, the authors developed a hybrid scheme for analysing bypass duct noise, in which a numerical analysis using finite element method for in-duct propagation and an analytic radiation code with fully represented effects of bypass shear layer are coupled. Such procedure permits detailed study on the interaction between duct configurations, such as geometry and acoustic liner impedances, and modal propagation and attenuation, and also the effects on the radiation pattern, within practical timescale and at modest computational cost. The scheme has been applied to realistic aero-engine bypass ducts and has been integrated with an optimisation programme. The numerical results obtained so far have revealed that for ducts with acoustic liners highly attenuated modes are not necessarily those with high mode angles, which is contrary to general anticipation. The aim of the study in the current paper is to understand the physics behind this phenomenon and its effect on the radiation to the far field. Detailed investigation on modal attenuation is performed by using the hybrid scheme. The effect of modal power distribution at the duct exit on the directivity pattern of the radiated noise to the far field is also discussed.

3:00

2aNSa17. Modeling of sound propagation in nonuniform waveguides. Wenping Bi (Laboratoire d'Acoustique de l'Université du Maine, UMR CNRS 6613, AV. O. Messiaen, 72085 Le Mans, France, wenping.bi@univ-lemans.fr), Vincent Pagneux (Laboratoire d'Acoustique de l'Université du Maine, UMR CNRS 6613, AV. O. Messiaen, 72085 Le Mans, France, vincent.pagneux@univ-lemans.fr), Denis Lafarge (Laboratoire d'Acoustique de l'Université du Maine, Avenue Olivier Messiaen, 72085 Le Mans, France, denis.lafarge@univ-lemans.fr), Yves Aurégan (Laboratoire d'Acoustique de l'Université du Maine, Avenue Olivier Messiaen, 72085 Le Mans, France, yves.auregan@univ-lemans.fr)

Sound propagation in waveguides is modeled by a Multimodal Method. The waveguides geometries may involve bends, variable cross-sections, or their combinations. The waveguide boundaries may involve axially or circumferentially nonuniform impedance conditions or acoustically rigid

conditions. Uniform flow may also be included for a simple uniform geometry. The pressure (displacement potential for uniform flow) is expanded in terms of the modes of acoustically rigid waveguides and an additional function that carries the information about the impedance boundary. The rigid waveguide modes and the additional function are known a priori so that calculations of the true modes of waveguides with impedance boundary, which are difficult, are avoided. By matching the pressure and axial velocity (displacement potential and axial derivative for uniform flow) at the interface between different axially uniform segments, scattering matrices are obtained for each individual segment; these are then combined to construct a global scattering matrix for multiple segments. After calculating the scattering matrix, the transmitted and reflected sound fields or intensities may be obtained for any kind of modal sources. The method allows modeling sound propagation in waveguides with axially and circumferentially nonuniform impedance boundaries up to dimensionless frequency K=70 in just hours on a personal computer, which advantageously compares with other techniques.

3:20

2aNSa18. An Active Network Representation to Predict the Flow Noise Characteristics of Corrugated Ducts. Wim De Roeck (K.U.Leuven - Dept. of Mechanical Engineering, Celestijnenlaan 300B - bus 2420, 3001 Heverlee, Belgium, wim.deroeck@mech.kuleuven.be),Vasilisa Solntseva (Andreev Acoustics Institute, Shvernik, 4, Moscow, 117036 Moscow, Russian Federation, mironov@akin.ru), Wim Desmet (K.U.Leuven - Dept. of Mechanical Engineering, Celestijnenlaan 300B - bus 2420, 3001 Heverlee, Belgium, Wim.Desmet@mech.kuleuven.be)

In this paper, an active network representation is used to numerically predict and gain more insight in the internally generated flow noise sources in corrugated ducts (the active bi-port component) as well as to describe the acoustic transmission characteristics of this type of application (the passive bi-port components) in the presence of a non-uniform mean flow. For this purpose a numerical approach is chosen, using compressible Large Eddy Simulations (LES) to predict the noise generation mechanisms and Linearized Euler Equations (LEE) with a plane pulse excitation to obtain the transmission characteristics for these components. The accuracy of the active network component determination is increased by separating the aerodynamic and the acoustic fluctuating field of the LES using both an aerodynamic/acoustic splitting technique and multiple plane mode-matching strategies. In this way, a numerical method is proposed to analyze the flow-acoustic behavior of corrugated tubes, which can be generally used for all types of duct system applications.

3:40-5:20 Posters

Lecture sessions will recess for presentation of posters on various topics in acoustics. See poster sessions for topics and abstracts.

Contributed Papers

5:20

2aNSa19. Validation of a hybrid method of aeroacoustic noise computation applied to internal flows. Mélanie Piellard (Delphi Thermal, Avenue de Luxembourg, 4940 Bascharage, Luxembourg, melanie.piellard@delphi.com), Christophe Bailly (Ecole Centrale de Lyon, 36, avenue Guy de Collongue, LMFA, 69134 Ecully, France, christophe .bailly@ec-lyon.fr)

A hybrid method of aeroacoustic noise computation based on Lighthill's acoustic analogy is first validated, and then applied to investigate the noise radiated by a low Mach number flow through a diaphragm in a duct. The simulation method is a two-step hybrid approach relying on Lighthill's acoustic analogy, assuming the decoupling of noise generation and propagation. The first step consists in an incompressible Large Eddy Simulation of the turbulent flow field, during which the Lighthill's source term is recorded. In the second step, a variational formulation of Lighthill's Acoustic Analogy using a finite element discretization is solved in the Fourier space. The validation of this method is briefly presented: a general validation is performed on the case of two corotating vortices in a medium at rest; the exit of turbulent structures from the computational domain is accounted for by a spatial filtering; and a study of spatial interpolation from the CFD mesh to the acoustic mesh shows an acceptable level of error. This method is applied to a three-dimensional diaphragm with low Mach number flow, showing good agreement with both experimental results and Direct Noise Computation performed by Gloerfelt & Lafon (Computers & Fluids, 2007).

5:40

2aNSa20. Numerical strategies for investigation of gust-airfoil interaction. Florent Margnat (Arts et Métiers Paris Tech - Sinumef Lab, 151 bd de l'Hopital, 75013 Paris, France, florent.margnat@paris .ensam.fr), Thomas Le Garrec (Arts et Métiers Paris Tech - Sinumef Lab, 151 bd de l'Hopital, 75013 Paris, France, thomas.le-garrec@paris .ensam.fr), Djaafer Fedala (Lab. d'Energétique et de Mécanique des Fluides Interne, Arts et Métiers ParisTech, 151 boulevard de l'Hôpital, 75013 Paris, France, djaafer.fedala@paris.ensam.fr),Xavier Gloerfelt(Arts et Métiers Paris Tech - Sinumef Lab, 151 bd de l'Hopital, 75013 Paris, France, xavier.gloerfelt@paris.ensam.fr), Smaine Kouidri (LIMSI-CNRS, BP 133, 91403 Orsay Cedex, France, smaine.kouidri@limsi.fr)

The noise generated by the interaction between a gust and an airfoil in a uniform flow is investigated. This problematic is of major industrial interest, regarding fans, turbomachinery, or wind turbine applications. A two-dimensional symmetric Joukowski-type airfoil is immersed without incidence in a flow at Mach number 0.5, disturbed by a harmonic gust at 45° of incidence (4th CAA Workshop on Benchmark Problems, 2004). Our methodology is first to perform a high-order direct resolution of Euler's equations of the disturbed flow over the airfoil and the associated acoustic emission, which is taken as a reference simulation. Second, the near aerodynamic field is simulated with Fluent 6.3 solver based on finite volume method with second-order schemes. The aerodynamic data thus obtained are used for far field acoustic prediction, based on Ffowcs Williams and Hawkings analogy. Finally, following another hybrid approach, the noise is predicted by using integral formulations with source field from the DNS. The aim of the study is to provide insight into the efficiency and validity of these numerical strategies commonly used. Comparisons with results of the CAA workshop are given, covering various wavenumbers values.

6:00

2aNSa21. A stochastic source model for turbulent noise prediction including sweeping time dynamics. Malte Siefert (German Aerospace Center, Lilienthalplatz 7, 38108 Braunschweig, Germany, malte.siefert@dlr.de), Roland Ewert (DLR/Institute of Aerodynamics and Flow Technology, Lilienthalplatz 7, 38108 Braunschweig, Germany, Roland .Ewert@dlr.de)

We extend a low-cost computational aeroacoustic approach by taking into account temporal effects of the modeled turbulent flow. As the noise production is determined by the turbulent frequency spectrum rather than the wavenumber spectrum, temporal properties of the turbulent flow play a role in many cases. We focus on the most dominant temporal effect, on sweeping, i. e. the advection of inertial range structures by the energy containing large scales. By introducing a feedback-mechanism of the turbulent field onto itself, we are able to incorporate this effect in the fast random particle method, which was successfully applied to different cases such as

slat noise, jet noise and others. It is shown that sweeping reproduces important properties of spatio-temporal correlations of the turbulent flow, which are not grasp by most turbulence-models. The influence on the sound generation will be discussed for aeroacoustic simulations of jet and trailing edge noise.

6:20

2aNSa22. Aeroacoustic simulation based on linearized Euler equations and stochastic sound source modelling. Hervé Dechipre (Volkswagen AG, Brieffach 1777, 38436 Wolfsburg, Germany, herve.dechipre@volkswagen.de), Michael Hartmann (Volkswagen AG, Brieffach 1777, 38436 Wolfsburg, Germany, michael.Hartmann2@volkswagen.de), Jan W. Delfs (DLR/Institute of Aerodynamics and Flow Technology, Lilienthalplatz 7, 38108 Braunschweig, Germany, jan.delfs@dlr.de), Roland Ewert (DLR/Institute of Aerodynamics and Flow Technology, Lilienthalplatz 7, 38108 Braunschweig, Germany, Roland.Ewert@dlr.de)

In order to continually improve passenger car acoustic comfort, effective methods are needed to simulate the noise generated by external flows as well as the noise produced by duct flows in HVAC systems. The present paper illustrates the use of two methods based on the Linearized Euler equations and derivatives thereof to compute the acoustic field. The two methods implemented in the DLR's aeroacoustic code PIANO are the introduction of a perturbation (vortex) in the flow and the stochastic sound source modelling by Ewert. The application considered by this study is the noise produced by a flat plate in a two-dimensional duct at a thickness related Reynolds number of 1300. Different sizes and edge shapes of the flat plate have been tested. The simulations show a good agreement of the results obtained by the two methods as well as the existence of a vortex street behind the plate corresponding to a Strouhal number of 0.18. It could be shown computationally, that even in the absence of the classical Aeolian tone generation (pure broadband turbulence related trailing edge noise generation) resonance type phenomena occur in the duct. The computed modes for the different configurations show encouraging correlations with the Parker-type modes or resonance phenomena described by Koch.

6:40

2aNSa23. Active Perturbation on Vortex-Induced Acoustic Resonance. Li Cheng (Hong Kong Polytechnic University, Hung Hom, Hong Kong, Hong Kong, mmlcheng@polyu.edu.hk), Y Zhou (Hong Kong Polytechnic University, Hung Hom, Hong Kong, Hong Kong, mmyzhou@polyu.edu.hk), Ming Ming Zhang (Hong Kong Polytechnic University, Hung Hom, Hong Kong, Hong Kong, mingming@jhu.edu)

Flow-induced acoustic resonance results from strong interactions between unsteady separated flows and the acoustic modes of a cavity. This work explores the feasibility of using piezoelectric-actuator-based perturbation technique in the control of vortex-induced noise through systematic experimental studies. A thick rectangular plate was used as the vortex generator and placed upstream of a cavity. Curved piezo-ceramic actuators were embedded in a slot on the top side of the plate to provide a perturbation to the flow. Uncontrolled flow-acoustic interaction was first examined to provide a baseline for comparison. Results show that noises induced by flow separation from the thick rectangular plate and the wall ahead of the cavity have very different critical flow velocities so that their effects can be well separated. Open-loop control tests indicate that vortex-induced acoustic resonance can be successfully controlled using the proposed technique. Analyses suggest that the convection of votices separated from the leading edge along the plate surface was accelerated by the surface perturbation, which interacted vigorously with the formation of the dominant trailing edge vortex, thus weakening the vortex strength in the wake of the plate. This weakened vortex strength substantially alters the flow-acoustic interaction, resulting in a significant impairment of vortex-induced acoustic resonance. (Supported by Research Grants Council of HKSAR. PolyU 5132/07E)

7:00

2aNSa24. Sound amplification in a lined duct with flow: PIV measurements. David Marx (Laboratoire d'Etudes Aerodynamiques - CNRS, Bat K, 40 avenue du recteur Pineau, 86022 Poitiers, France, david.marx@lea.univ-poitiers.fr), Yves Aurégan (Laboratoire d'Acoustique de l'Université du Maine, Avenue Olivier Messiaen, 72085 Le Mans, France, yves.auregan@univ-lemans.fr), Helène Bailliet (Laboratoire d'Etudes Aerodynamiques - CNRS, Bat K, 40 avenue du recteur Pineau, 86022 Poitiers, France, helene.bailliet@lea.univ-poitiers.fr), Jean-Christophe Valière (Laboratoire d'Etudes Aérodynamiques (LEA), Université de Poitiers, ENSMA, CNRS, Bat K, 40 avenue du recteur Pineau, 86022 Poitiers, France, jean-christophe.valiere@lea.univ-poitiers.fr)

An experimental investigation of the acoustic behavior of a liner in a rectangular channel with grazing flow has been conducted. The liner is a locally reacting structure. When increasing the velocity of the grazing flow the transmission coefficient increases at resonance frequency. The transmission coefficient can even become larger than 1 meaning that acoustical energy is produced by the liner. This amplification of the sound wave is accompanied by an increase in the stationary pressure drop induced by the liner (up to 300%). This effect is attributed to a modification of the flow induced by the acoustic wave. Thus, the flow is measured using Particle Image Velocimetry (PIV) imaging technique and a comparison of velocity maps with and without sound amplification is performed. Some differences occur and will be presented.

7:20

2aNSa25. Acoustic PIV: Measurement of the acoustic particle velocity using synchronized PIV-technique. André Fischer (German Aerospace Center (DLR), Mueller-Breslau-Str. 8, 10623 Berlin, Germany, andre.fischer@dlr.de), Emilie Sauvage (Ecole Polytechnique de l'Univerité d'Orléans, 8 rue Léonard de Vinci, 45072 Orléans, France, milie.sauvage@gmx.net), Ingo Roehle (German Aerospace Center (DLR), Mueller-Breslau-Str. 8, 10623 Berlin, Germany, ingo.roehle@dlr.de)

This paper outlines a technique for measuring the acoustic particle velocity and the flow field simultaneously by applying synchronized particle image velocimetry (PIV). As test set-up a squared acrylic glass chamber was chosen. One side of the test section is connected to a loudspeaker, which allows a sinusoidal excitation of the chamber. To point out constrains of this method the investigation includes an analysis of excitation amplitude and frequency as well as the effect of the mean flow magnitude. Therefore a small PC fan can be mounted inside the test section to produce an adjustable mean flow. It can be shown that for a low number of averaged images (80) reasonable results can be achieved up to a certain level of fan rotation speed. Beyond this level the turbulence sensitivity increases and more images are necessary for the calculations. However, the acoustic particle velocity can be computed in the presence of turbulent flow. The presented method called acoustic PIV is a non intrusive technique, applied successfully in measuring acoustic particle velocity fields over a wide range of conditions.

7:40

2aNSa26. A finite element method for time harmonic acoustics in arbitrary flows. Anne-Sophie Bonnet- Ben Dhia (CNRS, ENSTA - 32 Boulevard Victor, 75 015 Paris, France, bonnet@ensta.fr), Jean-Francois Mercier (CNRS, ENSTA - 32 Boulevard Victor, 75 015 Paris, France, jmercier@ensta.fr), Florence Millot (CERFACS, 42 avenue Gaspard Coriolis, 31 057 Toulouse, France, millot@cerfacs.fr), Sebastien Pernet (CERFACS, 42 avenue Gaspard Coriolis, 31 057 Toulouse, France, pernet@cerfacs.fr)

The reduction of noise in aeronautics motivates an intensive research in aeroacoustics. In particular, there is a need for efficient tools to simulate acoustic propagation in a mean flow. We are interested here by solving the linearized problem in the frequency domain, by a finite element method able to take into account general geometries and flows. To our knowledge, only

the potential case has been completely handled. Recently, a new approach has been developed and validated in the case of a parallel shear flow: it relies on a regularized formulation of Galbrun's equation, well-suited for a discretization by Lagrange finite elements, combined with Perfectly Matched Layers. A drawback of the method comes from the additional term of regularization, which requires the evaluation of an oscillating integral, coupling all degrees of freedom located on the same streamline. This difficulty can be avoided by replacing this non-local term by its Low-Mach approximation We show here how to extend this Low-Mach approach to the case of a non parallel flow. Numerical experiments are done. In the case of a potential mean flow, a good agreement with the exact approach is observed, even for quite large Mach numbers.

TUESDAY MORNING, 1 JULY 2008 ROOM 251, 8:00 TO 10:00 A.M.

Session 2aNSb

Noise, Biomedical Ultrasound/Bioresponse to Vibration, ASA Committee on Standards, and EURONOISE: Session in Honor of Henning von Gierke

Paul Schomer, Cochair
Schomer and Associates, Inc., 2117 Robert Drive, Champaign, IL 61821, USA

Brigitte Schulte-Fortkamp, Cochair
TU Berlin, Institute of Fluid Mechanics and Engineering Acoustics, Einsteinufer 25, Sekr. TA 7, Berlin, D-10587, Germany

Invited Papers

8:00

2aNSb1. Where do we stand on standards for noise? William Lang (Noise Control Foundation, 29 Hornbeck Ridge, Poughkeepsie, NY 12603, USA, lang1ww@gmail.com)

Almost 40 years ago, Henning von Gierke organized and chaired a symposium at the ASA Cleveland meeting with the above title. The chairs of nine writing groups of the ANSI-predecessor working on methods for the measurement and rating of noise presented summaries of their tasks and their progress in 1968. If a symposium on the same theme were to be held today, there would be reports from fifty-four working groups of ANSI Accredited Standards Committees on Acoustics (S1), Bioacoustics (S3), and Noise (S12). These committees are cornerstones of the ASA standards program. As the first ASA Standards Director, Henning revitalized the Society's standards program to become the productive organization it is today. The progress in standardization in America during the past four decades is a tribute to his foresight and participation. He also contributed to international standardization as the leader of the U.S. delegation to ISO TC/43 (Acoustics) and its subcommittee on noise (SC1), and for three decades he chaired ISO TC/108/SC4 on human exposure to mechanical shock and vibration. Trained as an engineer, Henning was a leader of national and international standardization efforts to relate the mechanical energy in sound waves to the responses of the human organism.

8:20

2aNSb2. Henning E. von Gierke and human biodynamics. Anthony J. Brammer (Ergonomic Technology Center, Univ. of Connecticut Health Center, 263, Farmington Ave., Farmington, CT 06030, USA, brammer@uchc.edu)

In addition to his well-known involvement in protecting humans from exposure to excessive noise, Dr. Henning E. von Gierke was deeply involved in protecting humans from exposure to excessive mechanical shocks, impacts and vibration. From exploring the limits of survivability during the landing phase of space and aircraft capsules to the more everyday issues of occupational exposure to vibration, he provided scientific insight into problems and leadership in developing solutions. While most of Henning's contributions are buried in past literature, the spirit of his efforts lives on in a review chapter published in Harris' Shock and Vibration Handbook that I have had the privilege to co-author with him through two editions, now extending back more than a decade. The challenge of encompassing the original content of his contribution while introducing the results of more recent research has, so far, yielded a composition that he has endorsed. Henning's involvement and interests in human biodynamics will be illustrated by examples taken from this work.

8:40

2aNSb3. Service to his fellow men. Richard McKinley (AFRL, Wright-Patterson Air Force Base, Dayton, OH 45433-7901, USA, richard.mckinley@wpafb.af.mil)

Henning Von Gierke's life of service followed in the footsteps of his family legacy. This presentation will focus on Henning's 50 years of research at the Air Force Research Laboratory at Wright-Patterson Air Force Base, Dayton, Ohio and the recollections of Henning gathered from 20+ hours of video interviews. Henning's life and his research were dedicated to helping mankind. Beginning with his dissertation on noise produced by jet flow and continuing with the accomplishments of his division at the Air Force Research Laboratory his contributions to acoustics were outstanding. His contributions include the Air Force hearing conservation program, the EPA levels document, the BENOX report, the development of Bionics in the 1960's, car airbag research in the 60's, testing of the

original 7 US astronauts, human limits of survival for impact, human limits of performance in vibration, pioneering work in hearing protector modeling, bone conduction, and microwave hearing, speech communication, as well as his extensive work in American National Standards and international standards. His contributions have in one way or another affected nearly everyone. He was a great researcher and a great mentor. He will be missed by his colleagues at the Air Force Research Laboratory and around the world.

Contributed Paper

9:00

2aNSb4. Henning von Gierke, leader, consensus builder, mentor, and friend. Alice H. Suter (Alice Suter & Associates, 575 Dogwood Way, Ashland, OR 97520, USA, ahsuter@charter.net)

Over his long and illustrious career, Henning von Gierke has had an enormous effect on public policy in noise and vibration, not only because he was active in the field for more than half a century, but because of his intense dedication, his persistence, and his unique, almost legendary ability to build consensus. EPA's Office of Noise Abatement and Control could not possibly have produced its Criteria and Levels documents in response to the timeframe imposed by Congress without Henning's leadership. Those of us who were lucky enough to be mentored by him were able to accomplish more than we ever could have without his guidance. In addition to his invaluable assistance in my doctoral program, I knew him as ASA's Standards Director, then President of ASA, chairman of interagency task forces, chairman of several standards committees, and participant in numerous international activities. He was always willing to share the burden of work and to encourage the rest of us to forge ahead in an effort to make the world a quieter and healthier place.

Invited Papers

9:20

2aNSb5. Dr. Henning von Gierke—My mentor, everyone's mentor. Paul Schomer (Schomer and Associates, Inc., 2117 Robert Drive, Champaign, IL 61821, USA, schomer@SchomerAndAssociates.com)

Dr. Henning von Gierke was a leading force in acoustics for a majority of the 20th century. He led in human response to noise AND vibration and its assessment. He was a leading force in the US government and in the National Academy of Science (NAS) Committee on Hearing and Bioacoustics (CHABA). He was a leader in hearing assessment and conservation, and in Standards. And to many working in these various areas, he was a mentor, a confidant, and a friend. Mentoring did not stop at the doors of his laboratory, but rather, his mentoring extended to the world. He was a mentor to me in my first years after graduation when we developed the C-weighted procedure for the assessment of large-amplitude impulse noise, and in the development of related Standards and NAS studies. He thrust me into ISO work and CHABA studies, and, later, he chose me to succeed him as ISO delegation chair in acoustics and noise. Not enough can be said about Henning's impact on noise and vibration research and policy in the USA and in the world, and on the expanded reach of Henning's influence through the many like me that he mentored.

9:40

2aNSb6. Henning von Gierke's continuing contribution: Underwater whole-body vibration. Sarah Gourlie (Applied Research Laboratories, The University of Texas, P.O. Box 8029, Austin, TX 78713-8029, USA, sarah.gourlie@gmail.com), Mark F. Hamilton (Applied Research Laboratories, The University of Texas, P.O. Box 8029, Austin, TX 78713-8029, USA, hamilton@mail.utexas.edu)

Henning von Gierke was a leader in the characterization of human response to sound and vibration and in the development of international standards in this area. One focus of his research was using a multidisciplinary approach to create biodynamic models for whole-body vibration with the aim of predicting and preventing injury in vehicles. The focus of this presentation is whole-body vibration underwater with the aim of predicting discomfort or possibly injury to divers from low-frequency sonar. The frequency range of interest is 40-80 Hz, which encompasses the resonance of human lung. For this purpose, a biodynamic model developed by von Gierke to simulate thoracic, abdominal, and spinal responses to different vibrational excitations in air [H. E. von Gierke, J. Acoust. Soc. Am. 50, 1397 (1971)] is adapted for underwater conditions. It is assumed that the diver is neutrally buoyant and will therefore experience whole-body acceleration equal to the particle acceleration produced by the sound field in the absence of the diver. Emphasis is placed on determining the appropriate source distribution on the body as well as adjusting von Gierke's model to accommodate the decrease in lung compressibility with diver depth and mass loading on the chest. [Work supported by ONR.]

Session 2aNSc

Noise and EURONOISE: Physical and Psychophysical Evaluation of Vehicle Exterior Noise I

Paul Donavan, Cochair
Illingworth & Rodkin, Inc., 505 Petaluma Blvd. South, Petaluma, CA 94952, USA

Hugo Fastl, Cochair
AG Technische Akustik, MMK, TU München, Arcisstr. 21, München, 80333, Germany

Invited Papers

8:00

2aNSc1. Low speed exterior vehicle voise and the effect of pavement type. Paul Donavan (Illingworth & Rodkin, Inc., 505 Petaluma Blvd. South, Petaluma, CA 94952, USA, pdonavan@illingworthrodkin.com)

For operating conditions of cruise and moderate acceleration, the exterior noise emission of light vehicles is typically dominated by tire/pavement noise at speeds of 50 km/h or greater. At a test speed of 56 km/h, it has been found that pavement type can create a 10 dB or more variation in tire/pavement noise. This has significant implications for both community noise and vehicle noise emission testing. In this paper, the results tire/pavement noise measurements for over 40 different pavements in Europe and the United States are reported. These pavements include research surfaces, existing roadways, and ISO 10844 passby test surfaces. Measurements were conducted using an on-board sound intensity methodology that has been correlated to cruise-by noise levels. These results are discussed in terms of the revisions being considered for the newly revised ISO 362 passby test procedure and the ISO 10844 test surface specification. Additionally, a case history of community traffic noise reduction achieved by use of a quieter pavement is reviewed to demonstrate the importance of the pavement in low speed vehicle noise emissions.

8:20

2aNSc2. Noise source mapping for trucks, part 1: development and design. Kenneth J. Plotkin (Wyle Laboratories Inc., 241 18th Street S., Suite 701, Arlington, VA 22202, USA, kenneth.plotkin@wylelabs.com), Yuriy Gurovich (University of Mississippi, NCPA, 1 Coliseum Drive, University, MS 38677, USA, yuriy.gurovich@wylelabs.com), William Blake (Naval Surface Warfare Center (Ret.), 6905 Hillmead Road, Bethesda, MD 20817, USA, hydroacoustics@aol.com), Paul Donavan (Illingworth & Rodkin, Inc., 505 Petaluma Blvd. South, Petaluma, CA 94952, USA, pdonavan@illingworthrodkin.com)

Mapping and quantifying noise sources on trucks under actual operating conditions on the road are important for traffic noise modeling and mitigation. The purpose of this study is to develop a practical truck noise source localization technique using acoustic beamforming. An experimental 70+ microphone elliptical array was designed and fabricated for truck testing. Beam-forming software was developed and implemented using a computerized data acquisition system. Proof-of-concept tests were performed at low-speed and high-speed truck testing facilities for a representative sample of trucks with widely different characteristics to validate the measurement system performance. The measurement system design parameters were verified experimentally, and certain improvements to the system were recommended for future implementation based on the field experience. The developed beam-forming measurement system provided adequate noise mapping and localization for various noise sources on trucks, stationary and moving with the speed up to 50 mph. The results of the proof-of-concept testing presented in an accompanying paper (Part 2) confirm that the developed microphone array, data acquisition system and beam-forming software performed generally as expected and required no major adjustments. This ongoing project is funded by the National Cooperative Highway Research Program of the Transportation Research Board of the National Academies, USA.

8:40

2aNSc3. Noise source mapping for trucks, Part 2: Experimental results. William Blake (Naval Surface Warfare Center (Ret.), 6905 Hillmead Road, Bethesda, MD 20817, USA, hydroacoustics@aol.com), Kenneth J. Plotkin (Wyle Laboratories Inc., 241 18th Street S., Suite 701, Arlington, VA 22202, USA, kenneth.plotkin@wylelabs.com), Yuriy Gurovich (University of Mississippi, NCPA, 1 Coliseum Drive, University, MS 38677, USA, yuriy.gurovich@wylelabs.com), Paul Donovan (505 Petaluma Blvd, South, Petaluma, VA 94952, USA, pdonovan@illingworthrodkin.com)

The elliptical array described in the previous paper (Part 1) was deployed road-side at a test track for measuring the sound emitted from trucks during passby. Measurements were made on various truck models in various operating states with and without trailers. Extensive spherical-source calibrations confirmed the array's beamforming at both on-normal and steering angles (to 45°); they also disclosed the magnitudes of ground reflection paths for localized sources at different elevations. In all cases, the array output was computationally inverted to produce two-dimensional spatial maps of source levels in the side profile of the truck. In the cases of stationary trucks, the source maps were correlated with simultaneously-obtained intensity maps. Comparisons verified that the array-based source maps for the trucks ranked sound sources of disparate levels in the same order as did the sound power levels deduced from the sound intensity data. Acoustic source maps obtained during truck passbys were then used to provide time-histories and spatial distributions of sources and source paths from the engine, muffler, tires, and certain body components. This project is funded by the National Cooperative Highway Research Program of the Transportation Research Board of the National Academies, USA.

9:00

2aNSc4. Vehicle exterior noise from the view point of new experts. Brigitte Schulte-Fortkamp (TU Berlin, Institute of Fluid Mechanics and Engineering Acoustics, Einsteinufer 25, Sekr. TA 7, D-10587 Berlin, Germany, brigitte.schulte-fortkamp@tu-berlin.de)

The combination of physical and psycho- acoustical measurements with scientific evaluation of perceptual responses to environmental noise, known as Soundscaping, is an essential method for assessing and actualizing environments. Empirically, the perception of sounds and their evaluation will be explored under the premise of combining human judgment and physical factors. In a recent Soundscape Project, environmental noise perception and evaluation in a defined urban area were investigated in detail. Classical measurements and open, narrative, but issue-centred interviews with residents were carried out, and those interviews allowed the interviewed persons to set their own focus on certain aspects concerning the development of a public space in Berlin. Method and procedure will be discussed in detail to introduce to the New Expert Concept. The Soundscape Project is a module of the Project ″Nauener Platz - Remodelling for Young and Old″ in the framework of the research program ″Experimental Housing and Urban Development (ExWoSt)″ of the ″Federal Ministry of Transport, Building, and Urban Affairs (BMVBS)″ by the ″Federal Office for Building and Regional Planning (BBR)″. It is related to the fields of research (ExWoSt) concerned with ″Innovation of Urban Neighbourhoods for Families and the Elderly″. The project executing organization is the Regional Office Berlin-Mitte.

9:20

2aNSc5. Significance of Psychoacoustic Aspects for the Evaluation of Vehicle Exterior Noise. Klaus Genuit (HEAD acoustics GmbH, Ebertstrasse 30a, 52134 Herzogenrath, Germany, klaus.genuit@head-acoustics.de)

For 25 years acoustic engineers have been using specific measurement technologies and analyses to determine sound quality of vehicle interior noise. However, with regard to exterior vehicle noise only standard measurements, e.g. the A-weighted sound pressure level (ISO 362), have been used and interpreted so far. Extensive knowledge and experiences concerning the evaluation of interior noise are still unutilized for an advanced assessment of vehicle exterior noise. Within EU research projects, such as SVEN or QCity, exterior noise was investigated, methods established and psychoacoustic analyses carried out. The relevance of vehicle exterior noise with respect to perceived product quality was underestimated for a long time. Today, manufacturers recognize the importance of exterior noise beyond the annoyance perspective. Vehicle exterior noise conveys an impression of product quality. By optimizing the product sound quality manufacturers can compete against others and meet increased requirements. Customers prefer vehicle sounds which match their expectations, which also applies to the exterior sound of a vehicle. The acoustical fingerprint of a vehicle - inside and outside - provides enormous marketing opportunities. This paper shows how the knowledge of sound quality analyses with regard to interior noise can be transferred to the evaluation of exterior vehicle noise.

9:40

2aNSc6. Rating the Dieselness of engine-sounds. Hugo Fastl (AG Technische Akustik, MMK, TU München, Arcisstr. 21, 80333 München, Germany, fastl@mmk.ei.tum.de), Bernhard Priewasser (AG Technische Akustik, MMK, TU München, Arcisstr. 21, 80333 München, Germany, bernhard@prie.de), Markus Fruhmann (AG Technische Akustik, MMK, TU München, Arcisstr. 21, 80333 München, Germany, Markus.Fruhmann@gmx.de), Herbert Finsterhölzl (BMW Group, Knorrstr. 147, 80788 München, Germany, herbert.finsterhoelzl@bmw.de)

Sounds of idling Diesel engines were rated according to their Dieselness with two different psychoacoustic methods. On the one hand, a yes/no procedure was used. Subjects were presented sounds of two seconds duration and had to answer by yes or no to the following question: Does this sound stem from a Diesel engine? Histograms were calculated and a hypothesis was put forward as follows: The more positive answers are given to a specific sound, the larger is the Dieselness of this sound. On the other hand, the method of paired comparison was used, applying a kind of Bradley-Terry-Luce (BTL) procedure. Results are discussed with respect to the psychophysical method used and possible differences in ratings by expert versus naive listeners. Finally, psychoacoustic data are compared to predictions of Dieselness calculated by four different algorithms.

10:00

2aNSc7. Perceptive temporal features of train passbys. Jonathan Terroir (Laboratoire MRTE - UCP, 5, mail Gay-Lussac, Neuville-sur-Oise, 95031 Cergy-Pontoise Cedex, France, jterroir@u-cergy.fr), Catherine Lavandier (Laboratoire MRTE - UCP, 5, mail Gay-Lussac, Neuville-sur-Oise, 95031 Cergy-Pontoise Cedex, France, catherine.lavandier@u-cergy.fr)

This work deals with characterization of temporal features linked to train passages which may act upon annoyance. Two varying parameters in the recordings have been selected: distance from the railway (7.5 meters, 50 and 100 meters) and train category (four types of French trains). A first series of psychoacoustic tests are carried out in order to mainly extract temporal aspects which could be important for sound perception. To avoid the level saliency, a preliminary equalization has been made on L_{A5}. The selection of perceptive factors is carried out through a multidimensional analysis (INDSCAL). Dissimilarity tests highlight several dimensions: train category, slope of the level increase linked to train arrival and passage length. In addition to the dissimilarity between two stimuli estimation, subjects have to choose the one they prefer and explain their answers. The verbalization task helps illustrate multidimensional analysis axis. A second series of tests, designed with recordings varying on two independent parameters (the level and the slope of the temporal evolution) makes it possible to compare perceptive variations on temporal effects to loudness.

10:20

2aNSc8. Synthesis of pass-by railway noise. Shafiquzzaman Khan (Kungliga Tekniska Hogsklan, Department of Aeronautical and Vehicle Engineering, SE - 10044 Stockholm, Sweden, Shafik@kth.se), Mohite Ulhas (Indian Institute of Technology Roorkee, Graduta Student, Dept. of Mech. & Ind. Engg, 247667 Roorkee, India, goelvfme@iitr.ernet.in), Virendra Goel (Indian Institute of Technology Roorkee, Graduta Student, Dept. of Mech. & Ind. Engg, 247667 Roorkee, India, goelvfme@iitr.ernet.in)

Pass-by railway noise is one of the main problems in the community. Typically pass-by railway noise is estimated using Leq or Lden in dB(A) and often these methods do not reflect the listener perceptual overview. It is therefore necessary to reduce the pass-by railway noise by synthesizing the noise characters into various segments. The segments could be based on the physical properties of rail vehicles like rolling, traction, pantograph, cooling system noise, etc. There are few other segments which are also based on the perceptual view of the pass-by railway noise like squeaking, rattling or beating (tadak, tadak). In this study only a few of the physical characteristics of the railway noises are examined. The idea of synthesization is to determine what segments in the noise characters are annoying. And thereby make a virtual pleasant pass-by railway sound. Several pass-by noises from Swedish rail vehicles were recorded using binaural technology according to ISO 3095. Recorded noise signals were then analyzed with the help of spectrogram analysis using Matlab. The results of the studies indicate that the rolling noise and broadband noise are most annoying for the long distance passenger rail vehicles.

TUESDAY MORNING, 1 JULY 2008 ROOM 251, 10:20 A.M. TO 4:00 P.M.

Session 2aNSd

Noise and EURONOISE: Environmental Noise Mapping II

Kenneth Cunefare, Cochair
Woodruff School of Mechanical Engineering, The Georgia Inst. of Technol., Atlanta, GA 30332-0405, USA

Gaetano Licitra, Cochair
ARPAT - Dept. Firenze, Via Porpora, 22, Firenze, 50144, Italy

Invited Papers

10:20

2aNSd1. Managing Risk by Utilising an Integrated Approach to Quality Assurance During Strategic Noise Mapping. Simon J. Shilton (Acustica Ltd, Trident One, Styal Road, M22 5XB Manchester, UK, simon.shilton@acustica.co.uk), Alan Štimac (DARH2 Acoustics & Civil Eng. Ltd., Ljubicin prolaz 3, HR-10430 Samobor, Croatia, alan@darh2.hr), James Trow (Hepworth Acoustics Ltd, 5 Bankside, Crosfield Street, WA1 1UP Warrington, UK, james.trow@hepworth-acoustics.co.uk), Nathan Archer (Hepworth Acoustics Ltd, 5 Bankside, Crosfield Street, WA1 1UP Warrington, UK, nathan.archer@hepworth-acoustics.co.uk), Vincent Hii Jiu Ta (Hepworth Acoustics Ltd, 5 Bankside, Crosfield Street, WA1 1UP Warrington, UK, vincent.hii@hepworth-acoustics.co.uk), Nigel Jones (Extrium Ltd, Calverley House, 55 Calverley Road, TN1 2TU Tunbridge Wells, UK, nigel.jones@extrium.co.uk)

With the proclamation of the Directive on Environmental Noise (2002/49), the process of noise mapping and action planning has begun around Europe. As the development of strategic noise maps is arguably a new experience for many end-users, the first round of noise mapping could potentially lead to uncertainties within many aspects of the process. Noise maps represent a baseline for the implementation of noise management systems and any systematic errors within the noise maps could reduce the effective implementation of the whole management system. The extensive range of data inputs required in strategic noise mapping are usually obtained from different data sources or base datasets and as such, cataloguing with the use of metadata is key. The implementation of a quality assurance system is imperative to maintain consistency between technicians and within multi-disciplinary teams. It is also essential to ensure the control of processes and the ability to review inputs, intermediaries and deliverables. A similar approach may also be applied to calculation and post processing of noise levels. This paper presents collective experience of the implementation of quality assurance procedures used in several EU countries during the successful completion of projects within the first round of mapping.

10:40

2aNSd2. A methodology for mapping neighbourhood impacts. Ronny Klaeboe (Institute of Transport Economics, Gaustadalleen 21, 0349 Oslo, Norway, rk@toi.no), Erik Engelien (Statistics Norway, Oterveien 23, N-2225, 2225 Kongsvinger, Norway, erik.engelien@ssb.no), Margrete Steinnes (Statistics Norway, Oterveien 23, N-2225, 2225 Kongsvinger, Norway, margrete.steinnes@ssb.no)

A methodology for the spatial analysis of environmental impacts in urban areas and social gradients is presented. The methodology is computational intensive and requires access to geographically located data at the dwelling level. Neighbourhood information is harvested to provide contextual information, and a spatial smoothing technique used to provide powerful visualisations of residential and neighbourhood impacts. By focussing on impacts rather than exposures, the construction of accumulative non-monetarised and monetarised indicators of impacts such as disability adjusted life years (DALY) and health costs is facilitated. Since the residential dwelling location is, or can be made, the focal point for social, dwelling, environment, neighbourhood, and transportation related indicators, a rich network of information in a uniform format is available for construction of novel indicators. By focussing on neighbourhoods rather

than individual dwellings, privacy is enhanced while maintaining useful level of detail for involving the public and politicians in local planning. By combining information on social status and environmental exposures, questions on whether transportation related impacts are distributed fairly and whether social inequity is increased or decreases as a result of a particular measure can be addressed. The methodology is not applicable to rural areas and low probability events.

11:00

2aNSd3. Noise emissions at intersections: comparing microscopic and macroscopic traffic simulation approaches. Bert De Coensel (Ghent University - Department of Information Technology, Sint-Pietersnieuwstraat 41, 9000 Ghent, Belgium, bert.decoensel@intec.ugent.be), Dick Botteldooren (University Ghent - Department Information Technology, Sint-Pietersnieuwstraat 41, 9000 Gent, Belgium, dick.botteldooren@intec.ugent.be), Luc Dekoninck (Ghent University - Department of Information Technology, Sint-Pietersnieuwstraat 41, 9000 Ghent, Belgium, luc.dekoninck@intec.ugent.be), Dominique Gillis (Ghent University - Department of Civil Engineering, Krijgslaan 281 S8, 9000 Ghent, Belgium, dominique.gillis@ugent.be), Dirk Lauwers (Ghent University - Department of Civil Engineering, Krijgslaan 281 S8, 9000 Ghent, Belgium, dirk.lauwers@ugent.be)

Environmental noise mapping often involves the use of traffic simulation software. In most cases, traffic flows are simulated in a macroscopic way, considering only traffic flow parameters averaged over road segments. This approach does not allow to correctly account for the typical deceleration and acceleration patterns of traffic at intersections, which influence local noise emissions. Microscopic traffic simulation models, which model each vehicle individually, incorporate these dynamic effects. However, they require much larger amounts of input data for calibration, and are therefore less suited to map large areas. In this paper, we investigate the possible influence of the choice of simulation detail on simulated traffic flow parameters and, as a consequence, on noise emissions near intersections. As a case study, several types of road intersections under various traffic demand and traffic composition conditions are considered. Simulation results are obtained using a microscopic (Paramics) as well as a mesoscopic (MaDAM) and a macroscopic (OmniTRANS) traffic simulation model, and predicted traffic flow parameters and noise emission values are compared between these approaches.

Contributed Papers

11:20

2aNSd4. Environmental Noise Directive - results of noise mapping in Germany. Matthias Hintzsche (Federal Environment Agency, Woerlitzer Platz 1, 06844 Dessau-Rosslau, Germany, matthias.hintzsche@uba.de)

The Environmental Noise Directive intends the development of a concept to avoid, prevent or reduce on a prioritised basis the harmful effects, including annoyance, due to exposure to environmental noise and to inform the public on environmental noise and its effects. In a first step noise maps were made for all agglomerations and for all major roads, major railways and major airports. This noise maps are the basics for noise action plans. These plans have the target to prevent and to reduce environmental noise where necessary to preserve environmental noise quality where it is good. The results of the first round for noise mapping in Germany will be presented.

11:40

2aNSd5. Noise mapping of public roads in Norway: New calculation tool based on the Nord2000 Road Engineering Method. Ingunn Milford (Norwegian Public Roads Administration, Brynsengfaret 6A, P.O .Box 8142 Dep., N-0033 Oslo, Norway, ingunn.milford@vegvesen.no)

To comply with requirements in the Directive 2002/49/EC on environmental noise (END) and to national guidelines on land use and transport noise, the Norwegian Public Roads Administration has developed the calculation tool called NorStoy, which is composed of two main modules: 1. A calculation module with the Nord2000 Road Engineering Method algorithms. 2. An ArcGIS module to arrange the input data, delimit the calculation area, locate the calculation points and report the results. Nord2000 Road Engineering Model was completed in 2006, in cooperation with the Nordic countries. The model has very much in common with the coming joint European Harmonoise model. The challenge in using these models is to obtain an acceptable calculation time. To prevent NorStoy from stopping every time insufficient data occurs, we use default values based on either a typical mean value or the nearest registered value. At this time preparing input data is quite time consuming. We are able to produce the noise maps for the EC directive, but NorStoy is not yet an efficient tool for noise mapping in general. The development of NorStoy is still in progress.

12:00

2aNSd6. The national noise map of the Netherlands A trend in exposure since 1990. Rik Van Haaren (DHV, P.O. box 1132, 3800BC Utrecht, Netherlands, rik.vanhaaren@dhv.com)

Noise maps according to the environmental noise directive have been provided by several actors in the Netherlands. The results of the noise maps show the significance of each of the source types, as well as the distribution within and outside agglomerations. In the Netherlands 2.7 million people are exposed to noise levels above 55 dB(A). In some cases up to 4000 people are exposed to level higher than 75 dB(A). In the night period 2.3 million people are exposed to noise levels higher than 50 dB(A). Road noise is the dominant source for annoyance and sleep disturbance. Within agglomerations road noise is responsible for 88% of the highly annoyed population. Major roads, outside agglomerations, contribute less than 10% to the total annoyance due to road traffic. Railways are a second source in producing annoyance and sleep disturbance. 57% of the high annoyance due to railways is produced outside agglomerations. The results of the noise maps for road traffic noise have been compared with results for a selection of cities in 1990. The results show that the total number of exposed people has increased. However, the exposition to the higher bands has decreased.

12:20

2aNSd7. Noise Mapping and Noise Scoring - Software Techniques and Result Presentation. Wolfgang Probst (DataKustik GmbH, Gewerbering 5, 86926 Greifenberg, Germany, wolfgang.probst@datakustik.com)

Noise scoring is based on noise level maps and on exposure distribution. Different techniques can be used to develop the areal distribution of these values and to present them as coloured maps. Especially more complex ratings that are not only based on an exposure level and on population densities need relatively complex procedures to develop them from noise maps. It must be taken into account that there are two important steps in this procedure: One is the calculation of the noise score itself and the other is the presentation as coloured map to detect and focus on Hot Spots. Different techniques have been developed, were integrated in the software and have been applied in the frame of the QCity project. The consequences of different parameter settings are presented and discussed. The second step is the assignment of colours to a given scale of result values and even this simple process must be handled carefully to transport the needed information.

Contributed Papers

2:00

2aNSd8. The Milan agglomeration Strategic Noise Map. Giovanni Zambon (Department of Environmental Sciences of the University of Milano - Bicocca, Piazza della Scienza, 1, 20126 Milan, Italy, giovanni.zambon@unimib.it), Simone Radaelli (Department of Environmental Sciences of the University of Milano - Bicocca, Piazza della Scienza, 1, 20126 Milan, Italy, s.radaelli@unimib.it)

The aim of this paper is to describe the procedure used for the Milan agglomeration Strategic Noise Mapping, as defined by Environmental Noise Directive (2002/49/EC). City of Milan is a complex case study because of the presence of a plurality of sources: road traffic, railway traffic (also tram traffic) and aircraft noise (Linate airport). The assessment method is based on the guidelines contained in the ″Good Practice Guide for Strategic Noise Mapping and the Production of Associated Data on Noise Exposure″ (WG-AEN). The study of noise generated from several sources was carried out with the integrated use of both numerical models and Geographic Information Systems (GIS). Numerical models allow us to estimate of noise levels in large areas near to a specific noise source and GIS enable the efficient acquisition, management and elaboration of geo-referenced data representative of territory, sources and buildings. By means of the study of specific GIS application it was possible to predict the global noise exposure for overall sources, by overlapping the noise maps of the single noise sources.

2:20

2aNSd9. Budapest Noise Mapping Project I. - Experiences. András Muntag (Enviroplus Kft., Telepy u. 3., 1096 Budapest, Hungary, muntaga@zajan.hu), Mihály Berndt (Enviroplus Kft., Telepy u. 3., 1096 Budapest, Hungary, berndt@mgx.hu)

The Hungarian capital Budapest, and their agglomeration have recently finished their first strategic noise map. According to the Hungarian noise regulations and to the European Directive 2002/49/EC, this is a legal obligation. The main part of the costs was supported by the EU. The preparation of the strategic noise maps based on a computer model and describing the present noise situation of the municipalities, should be seen as the first step to build a true noise information and management system, based on the computer model initially developed. The main parameters of the project were the planned area 1100 qkm, number of dwellings 440 thousand, length of the mapped roads ca. 2000 km This paper based on the experience of 23 municipal noise maps - Budapest and other 22 settlements in the agglomeration. We successfully finished the project on time - the results (all maps) can be found on the internet-page: http://terkep.budapest .hu/website/zajterkep The first paper deals with the technical experiences of the project.

2:40

2aNSd10. Budapest Noise Mapping Project II. - Results. Mihály Berndt (Enviroplus Kft., Telepy u. 3., 1096 Budapest, Hungary, berndt@mgx.hu), András Muntag (Enviroplus Kft., Telepy u. 3., 1096 Budapest, Hungary, muntaga@zajan.hu)

The Hungarian capital Budapest, and their agglomeration have recently finished their first strategic noise map. According to the Hungarian noise regulations and to the European Directive 2002/49/EC, this is a legal obligation. The main part of the costs was supported by the EU. The preparation of the strategic noise maps based on a computer model and describing the present noise situation of the municipalities, should be seen as the first step to build a true noise information and management system, based on the computer model initially developed. The main parameters of the project were the planned area 1100 qkm, number of dwellings 440 thousand, length of the mapped roads ca. 2000 km This paper is based on the experience of 23 municipal noise maps - Budapest and other 22 settlements in the agglomeration. We successfully finished the project on time - the results (all maps) can be found on the internet-page: http://terkep.budapest .hu/website/zajterkep The second paper shows the results of the project.

3:00

2aNSd11. The Port of Livorno noise mapping experience. Mario Morretta (Sintesis - Enginering and Consulting S.r.l., via Martin Luther King, 15, 57128 Livorno, Italy, mario.morretta@sintesis.toscana.it), Andrea Iacoponi (ARPAT - Dipartimento di Livorno, via Marradi, 114, 57128 Livorno, Italy, a.iacoponi@arpat.toscana.it), Fabrizio Dolinich (Sintesis - Enginering and Consulting S.r.l., via Martin Luther King, 15, 57128 Livorno, Italy, fabrizio.dolinich@gmail.com)

Livorno Municipality and its seaport are requested to produce the strategic noise map according to the European Directive only in 2012. However Livorno Port Authority, following the principle of environmental sustainability and in coherence with its EMAS status, started the investigation about the interaction between the noise generated by port activities and the nearby city. This analysis has been carried out within the Life funded project NoMEPorts, whose goal is to develop and provide tools and expertise to European ports for implementing their strategic noise maps, by means of a collaborative mapping of 8 Port Authority technical representatives from all around Europe. The work presented outlines in detail the process followed in performing the noise mapping of the Livorno port area and the port-city interface area, focusing in the problems encountered in the data collection, in port noise model building steps and in the consequent solutions adopted. The paper also talks about the result obtained by showing the noise maps in six detail levels and reports about the action plan proposed. As a result this experience emphasises the importance of noise maps as a powerful tool for decision-makers in port planning.

3:20

2aNSd12. Strategic Noise Mapping of the City of Ljubljana, Slovenia. Alan Štimac (DARH2 Acoustics & Civil Eng. Ltd., Ljubicin prolaz 3, HR-10430 Samobor, Croatia, alan@darh2.hr), Aleš Globevnik (A-PROJEKT Natasa Kepe-Globevnik s.p., Vinarje 110b, SI-2000 Maribor, Slovenia, aprojekt@siol.net), Dinko Stipanicev (DARH2 Acoustics & Civil Eng. Ltd., Ljubicin prolaz 3, HR-10430 Samobor, Croatia, dinko@darh2.hr), Lilijana Kuhelj (Environmental Agency of the Republic of Slovenia, Vojkova 1B, SI-1000 Ljubljana, Slovenia, lilijana.kuhelj@gov .si)

Currently Ljubljana is the only agglomeration according to the definition of the directive 2002/49/EC in Slovenia. For this agglomeration, separate noise maps not only for road and rail traffic but also for industrial sources were made. As for the first phase of preparation there is no precise methodology stated for representing industrial noise sources in strategic noise maps regarding END and following the vision of other EU countries, only industrial plants classified as IPPC installations were taken into consideration of noise mapping. Short term noise measurements around industrial plants conducted according to ISO 1996 during previous three years were used as reverse engineering techniques for the determination of sound power levels of industrial plants. Elaboration of road and rail traffic noise maps required development of perfect acoustical model with 3D terrain modelling including all possible obstacles (barriers, walls, bridges, viaducts, etc.). For calibration of noise maps more then 30 measurements were performed following the standard DIN 45642. During all stages of elaborating noise maps, quality assurance procedures were performed with a view to estimate accuracy of the results. Strategic noise maps of the agglomeration performed at municipal level of Ljubljana will be used mainly for drawing up action plans and spatial planning of areas with different noise levels allowed.

3:40

2aNSd13. Mixed Industry and Traffic Noise Mapping. Céline Boutin (Acouphen Environnement, Campus de la DOUA, 66, BD Niels Bohr, BP 52132, 69603 Villeurbanne, France, celine.boutin @acouphen-environnement.com), Alexis Bigot (Acouphen Environnement, Campus de la DOUA, 66, BD Niels Bohr, BP 52132, 69603 Villeurbanne, France, alexis.bigot@acouphen-environnement.com)

The authors have a large experience on Noise Mapping of both transportation sources and industrial plants. This paper provides examples of Noise Maps for Communities of different sizes with road, railway and industrial sources. The difficulties to estimate Noise Emission from industrial sites are discussed. Recommandations are provided. A Methodology to create the Industry data base for a Noise Map with a large number of industrial sites in the territory is presented. It is shown how Noise Maps can be an attractive tool to be used in the Environmental Management System of the Plant Manager to communicate on the Plant environmental integration and Noise Abatement Plan.

TUESDAY MORNING, 1 JULY 2008 ROOM 252A, 11:00 A.M. TO 3:20 P.M.

Session 2aNSe

Noise and EURONOISE: General Topics in Noise I

Contributed Papers

11:00

2aNSe1. Comparison of International Standards for Measuring Sound Power in Tool-Machines. Jose A. Ballesteros (Universidad de Castilla-La Mancha, Campus Universitario, 16071 Cuenca, Spain, Josea.Ballesteros@uclm.es), Marcos D. Fernandez (Universidad de Castilla-La Mancha, Campus Universitario, 16071 Cuenca, Spain, Marcos.Fernandez@uclm.es), Samuel Quintana (Universidad de Castilla-La Mancha, Campus Universitario, 16071 Cuenca, Spain, Samuel.Quintana@uclm.es), Ivan Suarez (Universidad de Castilla-La Mancha, Campus Universitario, 16071 Cuenca, Spain, ivan.suarezcasal@gmail.com), Laura Rodriguez (Universidad de Castilla-La Mancha, Campus Universitario, 16071 Cuenca, Spain, Laura .Rodriguez@uclm.es)

Industrial noise is one of the most important contaminant agents in the industrialised countries due to its effects on health. Sound power is used in order to characterize the noise emitted by the machines because it does not depend on aspects like place or distance of the measurement. These measurements are handled by international standards like UNE-EN ISO 374x and UNE-EN ISO 9614-x. The advantages and disadvantages of each one of these standards have been evaluated after making a representative number of measurements in several types of tool-machines and then, a set of recommendations have been derived to choose the best standard depending on the machine that is going to be measured.

11:20

2aNSe2. Activated Resonance Systems as Silencers and Sound Absorbers. Philip Leistner (Fraunhofer IBP, Nobelstrasse 12, 70569 Stuttgart, Germany, philip.leistner@ibp.fraunhofer.de)

A great variety of classical resonance systems is used for sound absorption and attenuation in technical systems. Apart from other requirements such as minimum size, high reliability and low costs the acoustic efficiency can be fulfilled in a wide range. However, the performance is limited and focused on a certain frequency band. These restrictions can significantly be overcome by activation. A very clear system comprises a membrane (mass) and a rear air volume (spring) which can be assembled by using a conventional loudspeaker in front of a cassette. Even the 'passive' system is causing a respectable sound attenuation also at low frequencies. The activation is based on a microphone close to the membrane the signal (according to the exciting sound pressure) of which is linearly amplified and fed back to the loudspeaker. A lot of details have to be considered prior to the real applicability of such an activated resonator. But the remarkable benefits can be documented for numerous practical scenarios. Theoretical and experimental results are based on a sophisticated model of the resonant structure and its acoustic environment. Additionally, several practical challenges, e.g. the presences of turbulent air flow or high temperatures, can be solved by using specific modifications.

11:40

2aNSe3. Sound radiation of the end of cylindrical duct application on industrial stacks. Thierry Simoneau (Acoustique & Conseil, 17-19 rue des Grandes Terres, 92508 Rueil-Malmaison, France, ts@acoustique-conseil .com)

In order to determine the sound field emitted by the top end of an industrial stack, a study of the acoustical radiation of unbaffled semi-infinite cylindrical duct ends was conducted. Firstly, the main publications on the subject were studied. A calculation model of the radiation directivity of the end of a chimney, based on H. Levine and J. Schwinger's results for the fundamental mode and on the Geometrical Theory of Diffraction for the modes of superior order, was established. In order to validate the model, measurements on scaled model were made in an anechoic chamber. Tallying between theoretical and experimental results is very good, especially at low frequencies, where the number of radiating modes is low. Moreover, measurements on a real size industrial site have been made. They also show satisfying tallying between the theory and experimentation.

12:00

2aNSe4. Austrian investigation on the influence of sound leakage in noise reducing devices. Marco Conter (Arsenal Research, Giefinggasse 2, 1210 Vienna, Austria, marco.conter@arsenal.ac.at), Manfred Haider (Arsenal Research, Giefinggasse 2, 1210 Vienna, Austria, manfred .haider@arsenal.ac.at)

Noise barriers are the most widely used means for road traffic noise abatement. Sound absorption and sound insulation are the key properties for noise barrier elements. The standard method of determining these properties by reverberation room measurements has recently been complemented by an in-situ method following CEN/TS 1793-5, also known as Adrienne method. This method allows flexible assessment of the acoustic performance of noise barriers in almost arbitrary places by means of mobile measurement equipment. Using the possibility to perform in-situ measurements the authors have investigated the presence of sound leakage due to structural imperfections which limit the sound insulation performance of noise barriers. This paper summarizes the results of Austrian research on different kinds of barriers regarding the difference in sound insulation between measurements carried out in front of the supporting post (where leakage is likely to occur) and in the middle of the barrier. A statistical correlation of the data was also performed.

12:20

2aNSe5. A study of twenty-one cases of low-frequency noise complaints. Christian Sejer Pedersen (Acoustics, Aalborg University, Fredrik Bajers Vej 7 B5, 9220 Aalborg Ø, Denmark, cp@acoustics.aau.dk), Henrik Møller (Acoustics, Aalborg University, Fredrik Bajers Vej 7 B5, 9220 Aalborg Ø, Denmark, hm@acoustics.aau.dk), Kerstin Persson Waye (Dept. of Environ. Medicine, The Sahlgrenska Acad. of Gothenburg Univ., Box 414, 405 30 Gothenburg, Sweden, kerstin.persson-waye@amm.gu.se)

From 203 cases of low-frequency complaints a random selection of twenty-one previously unsolved cases were investigated. The main aim of the investigation was to answer the question whether the annoyance is caused by an external physical sound or by a physically non-existing sound, i.e. low-frequency tinnitus. Noise recordings were made in the homes of the complainants, and the complainants were exposed to these in blind test listening experiments. Furthermore, the low-frequency hearing function of the complainants was investigated, and characteristics of the annoying sound was matched. The results showed that some of the complainants are annoyed by a physical sound (20-180 Hz), while others suffer from low-frequency tinnitus (perceived frequency 40-100 Hz). Physical sound at frequencies below 20 Hz (infrasound) is not responsible for the annoyance - or at all audible - in any of the investigated cases, and none of the complainants has extraordinary hearing sensitivity at low frequencies. For comparable cases of low-frequency noise complaints in general, it is anticipated that physical sound is responsible in a substantial part of the cases, while low-frequency tinnitus is responsible in another substantial part of the cases.

12:40-2:00 Lunch Break

Contributed Papers

2:00

2aNSe6. Measuring low-frequency noise indoors. Steffen Pedersen (Acoustics, Aalborg University, Fredrik Bajers Vej 7 B5, 9220 Aalborg Ø, Denmark, stp@acoustics.aau.dk), Henrik Møller (Acoustics, Aalborg University, Fredrik Bajers Vej 7 B5, 9220 Aalborg Ø, Denmark, hm@acoustics.aau.dk), Kerstin Persson Waye (Dept. of Environ. Medicine, The Sahlgrenska Acad. of Gothenburg Univ., Box 414, 405 30 Gothenburg, Sweden, kerstin.persson-waye@amm.gu.se)

At low frequencies, the sound pressure level may vary 20-30 dB in a room due to standing waves. For assessment of annoyance, mainly areas with the highest occurring levels are relevant, since persons present in such areas are not helped by the existence of lower levels in other areas. The level that is exceeded in 10% of the volume of a room L_{10} is proposed as a rational and objective target for a measurement method. In Sweden and Denmark rules exist for measuring low-frequency noise indoors. The performance of these procedures was investigated in three rooms. The results from the Swedish method were close to the L_{10} target, but, due to a doubtful use of C-weighting in the scanning, it may give too low results in case of complex sounds. The Danish method was found to have a high risk of giving results substantially below the target, unless complainants can precisely appoint measurement positions, where the sound is loudest/most annoying - which they often cannot. An alternative method using measurements in four three-dimensional corners of the room is proposed. This easy and straightforward method seems to give reliable results close to the proposed target.

2:20

2aNSe7. The use of communication device in background noise. Esko Toppila (Finnish Institute of Occupational Health, P.O:Box 486, 33101 Tampere, Finland, esko.toppila@ttl.fi), Pekka Airre (FIOH, P.O.Box 486, 33101 Tampere, Finland, erkko.airo@ttl.fi), Pekka Olkinuora (FIOH, Topeliuksenkatu 41, 00250 Helsinki, Finland, pekka.olkinuora@ttl.fi)

Communication devices are used more and more often in industrial premises. We have evaluated how the users experience these device in a call center ($N=41$), in a low noise warehouse ($N=67$) and in a noisy ($L>80$ dB) warehouse ($N=25$). For all subjects the same questionnaire was sent. The questionnaire contained questions were about the quality of communications device and self-evaluated hearing symptoms. The self-evaluated speech intelligibility was lowest in the high background environments. Still in the call center five persons and five in the silent warehouse had great difficulties with speech intelligibility. All these persons evaluated that they have always difficulties when communicating with people. In the noisy environments this relationship was not found. The need to rise the voice was highest in the warehouses ad did not depend on the background noise. Tinnitus was more frequent among process industry workers. The results suggests that lowered hearing function cause problems in low background noise. The self-evaluated nuisance depends on the complexity of the communication. The quality of the communication channel may also play a vital role in the communication problems especially for workers with hearing problems.

2:40

2aNSe8. Phase spectral processing for improved time-domain soft microphone based noise estimation. Ioannis Paraskevas (T.E.I. Piraeus / Department of Electronics, 250, Thivon str., GR-12244 Athens-Aigaleo, Greece, paraskevas@env.aegean.gr), Maria Rangoussi (T.E.I. Piraeus / Department of Electronics, 250, Thivon str., GR-12244 Athens-Aigaleo, Greece, mariar@teipir.gr), Stylianos M. Potirakis (T.E.I. Piraeus / Department of Electronics, 250, Thivon str., GR-12244 Athens-Aigaleo, Greece, spoti@teipir.gr), Stylianos Savvaidis (T.E.I. Piraeus / Department of Electronics, 250, Thivon str., GR-12244 Athens-Aigaleo, Greece, ssavaid@teipir.gr)

'Soft Microphones' (SM) constitute a cost-effective, yet quality alternative to the multiple microphones measurement, in applications related to noise mapping. SM offer a solution of great interest to real field applications, e.g., industrial plants. The SM approach, proposed in previous work of the authors, is based on the estimation of the noise signal and the calculation of noise levels over a set of points within the space of interest. To this end, a novel, frequency domain method was introduced and verified in a real field, textile plant experiment, with satisfactory results. However, in order to expand the use of SM from accurate noise mapping to a full Active Noise Control application, it is necessary to obtain accurate noise signal estimates in the time rather than the frequency domain. Further research into the deconvolution step of the proposed method reveals that discontinuities, appearing across the phase spectrum of the estimated signals, cause ambiguities that affect the deconvolution process. We propose here the use of the Hartley transform phase spectrum, which conveys fewer discontinuities as compared to its Fourier Transform counterpart, while it allows for a discontinuities compensation scheme. Experimental results verify that phase spectrum preprocessing provides accurate time domain signal estimates.

3:00

2aNSe9. Research into the improvement of the management of helicopter noise in the UK. David C. Waddington (Acoustics Research Centre, School of Computing, Science & Engineering, University of Salford, M5 4WT Salford, UK, d.c.waddington@salford.ac.uk), Paul Kendrick (Acoustics Research Centre, School of Computing, Science & Engineering, University of Salford, M5 4WT Salford, UK, p.kendrick@salford.ac.uk), Geoff Kerry (Acoustics Research Centre, School of Computing, Science & Engineering, University of Salford, M5 4WT Salford, UK, g.kerry@salford.ac.uk), Matthew Muirhead (QinetiQ Ltd, Cody Technology Park, Ively Road, GU14 0LX Farnborough, UK, mmuirhead@qinetiq.com), Ray Browne (QinetiQ Ltd, Cody Technology Park, Ively Road, GU14 0LX Farnborough, UK, rwbrowne@qinetiq.com)

Helicopter noise has a negative impact on the quality of life for many people. Effected populations are not just those living close to heliports, but include those exposed to noise from helicopters used by emergency services, the military, and commercial companies. One problem identified in the UK is that it is often difficult to complain about helicopter noise, since it is un-

clear which organisation is responsible for dealing with the complaint. Consequently, the Department for Environment, Food and Rural Affairs (Defra, UK) has commissioned research to summarise the following: i. the nature and extent of the concern about helicopter noise in the UK. ii. rules and regulations governing operations. iii. existing procedures for handling complaints. This stage of the project will produce a detailed report into the improvement of the management of helicopter noise. Also to be produced is a short non-technical guide including the means of redress for perceived disturbance. This paper will report on the findings of this project. [Work funded by Defra, UK]

TUESDAY MORNING, 1 JULY 2008 AMPHI HAVANE, 8:00 A.M. TO 12:40 P.M.

Session 2aPAa

Physical Acoustics: Acoustics of Porous Media II

Walter Lauriks, Cochair
Lab. ATF, Katholieke Universiteit Leuven, Celestijnenlaan 200D, Leuven, B-3001, Belgium

Keith Attenborough, Cochair
Open University, Department of Design, Development, Materials and Environment, Walton Hall, Milton Keynes, MK7 6AA, UK

Contributed Papers

8:00

2aPAa1. Sensitivity analysis and non linear parameters estimation of porous materials from normal sound coefficient absorption measurements. Mohammed Garoum (Ecole Supérieure de Technologie de Salé, Laboratoire Energétique Matériaux et Environnement, Avenue du Prince Héritier, BP 227, 10000 Salé, Morocco, garoum1@yahoo.fr), Rachida Idchabani (Ecole Supérieure de Technologie de Salé, Avenue du Prince Héritier, BP 227, Salé, Morocco, idchabani@mcinet.gov.ma), Mohammed Tajayouti (Ecole Supérieure de Technologie de Salé, Avenue du Prince Héritier, BP 227, Salé, Morocco, mtajayouti@gmail.com), Mohammed Rhachi (Ecole Supérieure de Technologie de Salé, Laboratoire Energétique Matériaux et Environnement, Avenue du Prince Héritier, BP 227, 10000 Salé, Morocco, mrhachi@hotmail.com), Antonio Moreno (Instituto de Acústica, CSIC, 144 Callé Serrano, 28006 Madrid, Spain, amoreno@ia.cetef.csic.es)

In literature, various models have been proposed in order to predict characteristic impedance Zc and wave number kc of porous materials. To use these models their involved nonacoustical parameters (i. e. flow resistivity, tortuosity porosityœ) are usually measured. Unfortunately measurements require specialised equipments and are often difficult on loose porous materials leading most often to erroneous values. Moreover, the inverse estimation of theses parameters from experimental data is not an easy task as believed. This is due to the non linearity of models and the presence of some parameters with weak and/or linearly dependent influences. In this work an approach based on the tradeoff between magnitude and linear independence of the sensitivity matrix components is presented in order to achieve an efficient ranking of parameters according to their inherent ease of estimation. Next this approach is associated to Genetic Algorithms to minimize the least squares norm between measured and modelled normal sound absorption coefficient. For five widely used models in literatures, the application of the proposed inverse estimation procedure on loose granular cork and vegetable fibres, shows that, unlike classical gradient approaches methods, better estimation has been obtained.

8:20

2aPAa2. Characterization of an acoustic ceramic liner in a subsonic flow by mean of Laser Doppler Velocimetry. Romain Pethieu (ONERA, 2, av. Edouard Belin - BP 4025 - Cedex 4, 31055 Toulouse, France, romain .pethieu@onecert.fr)

As aircraft traffic constantly increases, serious efforts are made to reduce engine noise. Among them, the design of high performance absorbing materials (liners) placed on the nacelle's internal walls is an exciting challenge. Optimizing these media requires to know the mechanisms of acoustical propagation near them in the conditions encountered in jet engines: high speed hot shear flows. Particular interest is being granted to the influence of the grazing flow in contact with the liners. This is due to its known effects on the liners characteristics: efficiency of absorption and frequency resonance. This influence is remarkable for those configurations based on perforated plates. Therefore, a testing method based on non-intrusive measurements has been developed at ONERA. This technique consists in measuring acoustic velocities by laser Doppler velocimetry to determine acoustic quantities under grazing turbulent high-speed flow, thanks to an Eulerian-Lagrangian description of the perturbations. Experimental activity is performed on a honeycomb material, via the achievement of acoustical pressure and intensity fields, for different Mach numbers. Moreover, these measurements bring into evidence a coupling between acoustical modes and hydrodynamic modes (from Kelvin-Helmholtz instability) which modify the material acoustical behaviour.

8:40

2aPAa3. The effect of mechanical elasticity on the surface impedance of a organic/inorganic composite aerogel. Winny Dong (California State Polytechnic University, 3801 West Temple Avenue, Chemical and Materials Engineering, Pomona, CA 91768, USA, winnydong@csupomona.edu), Wayland Dong (Veneklasen Associates, 1711 Sixteenth Street, Santa Monica, CA 90404, USA, wdong@veneklasen.com), Tanya Faltens (California State Polytechnic University, 3801 West Temple Avenue, Chemical and Materials Engineering, Pomona, CA 91768, USA, tafaltens@csupomona.edu), Elizabeth Scott (California State Polytechnic University, 3801 West Temple Avenue, Chemical and Materials Engineering, Pomona, CA 91768, USA, escott@csupomona.edu), Travis Thompson (California State Polytechnic University, 3801 West Temple Avenue, Chemical and Materials Engineering, Pomona, CA 91768, USA, trthompson@csupomona.edu)

Previous reports on the acoustical properties of monolithic silica aerogels have indicated that although the material's high porosity, pore tortuosity, and surface area contribute to a low sound velocity in the material, the rigid matrix of the aerogel exhibit a high reflection coefficient. Work by Forest et al. and others have shown that using granules instead of silica aerogel monoliths, the acoustical properties can be significantly enhanced. We report the acoustic properties of a polydimethylsilicate (PDMS)/silica composite aerogel that has both high surface area and a mechanically elastic matrix. Both monoliths and granules are studied. The surface impedance (at normal incidence) as a function of open porosity, pore size distribution, surface area, elasticity, and granule size will be reported.

9:00

2aPAa4. Numerical modeling of transient poroelastic waves in the low frequency range. Guillaume Chiavassa (Ecole Centrale Marseille MSNM-GP, Technopole de Chateau-Gombert, 13013 Marseille, France, guillaume.chiavassa@ec-marseille.fr), Bruno Lombard (Laboratoire de Mécanique et d'Acoustique LMA, 31 chemin Joseph Aiguier, 13402 Marseille, France, lombard@lma.cnrs-mrs.fr), Joel Piraux (Laboratoire de Mécanique et d'Acoustique LMA, 31 chemin Joseph Aiguier, 13402 Marseille, France, piraux@lma.cnrs-mrs.fr)

A numerical method is proposed to simulate the propagation of transient poroelastic waves across heterogeneous media, in the low frequency range. A velocity-stress formulation of Biot's equations is followed, leading to a first-order differential system. The latter is splitted in two parts: a propagative one discretized by a fourth-order ADER scheme, and a diffusive one solved analytically. Near sources and interfaces, a space-time mesh refinement is implemented to capture the small scales of evolution of the diffusive slow compressional wave. Lastly, an immersed interface method is implemented to accurately model the jump conditions at interfaces between the different media. Numerical experiments in one and two dimensions are shown, with porous/porous or fluid/porous interfaces. Comparisons with analytical solutions confirm the efficiency of the approach. [1] G. Chiavassa, B. Lombard, J. Piraux, Numerical modeling of 1-D transient poroelastic waves in the low-frequency range, soumis au J. Comput. Appl. Math., (2007), disponible sur http://hal.archives-ouvertes.fr/hal-00193103/fr/

9:20

2aPAa5. On the scattering of a plane wave by porous sound-absorbing strip. Alex De Bruijn (Independent Acoustical Consultant, Schonenvaardersstraat 18014, 7418 CC Deventer, Netherlands, alex.bruijn@planet.nl)

The analysis concerning the scattering of a plane wave by a porous sound-absorbing strip embedded in an infinite sound-hard surface is most relevant for the evaluation of measurements with respect to absorbing materials tested in a reverberation room. This diffraction phenomenon around the edges leads to an additional sound absorption, the so-called edge effect. This extra absorption can be analyzed and computed - among other well-known methods - by using a spatial Fourier field expansion just on the absorbing strip. The field in the space above the reflecting surface can be put into a contour integral of an angular spectrum in the complex plane or -in other words- a superposition of plane waves with complex angles of incidence. Matching both field representations leads to the solution of the unknown coefficients of the Fourier expansion and hence to the amplitudes of the total diffracted field. It would be interesting to compare these results with diffraction data obtained via an alternative technique: the Finite-Difference Time-Domain method using the direct Euler equations, also within the porous sound-absorbing material. The paper will show the data for the field amplitudes obtained by both methods and will discuss the agreement and differences.

9:40

2aPAa6. Analysis of porous plate/water layered structures by means of the transition terms method. Ferroudja Belhocine (LOMC FRE CNRS 3102, Université du Havre, Place Robert Schuman, 76610 le Havre, France, ferroudja.belhocine@univ-lehavre.fr), Serge Derible (LOMC FRE CNRS 3102, Université du Havre, Place Robert Schuman, 76610 le Havre, France, serge.derible@univ-lehavre.fr), Cole Franklin (1241 East dyer road, Santa Ana, CA 92672, USA, colesfranklin@yahoo.com)

This paper is devoted to the study of water-saturated porous plate/water layered structures by means of the transition terms defined from the reflection and transmission coefficients R and T as follows: $TT_{sym}=(1-(R+T))/(2i)$, $TT_{asym}=(1-(R-T))/(2i)$. They are the eigenvalues of the scattering matrix of the water-immersed structure and are directly connected with its symmetric or antisymmetric vibrations. The N porous plates associated in our structures obey Biot's theory which is first used to calculate the reflection and transmission coefficients of a unique water-saturated plate. An induction on N process allows to find the reflection and transmission coefficients of a given N plate/water-layer structure. The plates used in the experiments at normal incidence are 5mm thick. The reflection and transmission coefficients of sets of 1, 2, 3, and 4 water immersed plates, separated from each other by a 1cm water gap, are measured thanks to two wideband transducers with central frequency 0.5MHz. There are good agreements between the calculated and experimental transition terms which exhibit the symmetric and antisymmetric resonances of the structures. They obey the Breit-Wigner resonant form which characteristics can be obtained

10:00

2aPAa7. On the adsorption-desorption relaxation time of carbon in very narrow ducts. Timothy J. Mellow (Nokia, Nokia House, Summit Avenue, GU14 0NG Farnborough, UK, tim.mellow@nokia.com), Olga Umnova (University of Salford, Acoustics Research Centre, Newton Building, M5 4WT Salford, UK, o.umnova@salford.ac.uk), Konstantinos Drossos (University of Southampton: Institute of Sound and Vibration Research, University Road, Highfield, SO17 1BJ Southampton, UK, kd806@soton.ac.uk), Keith Holland (University of Southampton: Institute of Sound and Vibration Research, University Road, Highfield, SO17 1BJ Southampton, UK, krh@isvr.soton.ac.uk), Andrew Flewitt (University of Cambridge: Centre for Advanced Photonics and Electronics, 9, JJ Thomson Ave., CB3 0FA Cambridge, UK, ajf@eng.cam.ac.uk), Leo Kärkkäinen (Nokia Research Center, Itämerenkatu 11 - 13, 00180 Helsinki, Finland, leo.m.karkkainen@nokia.com)

Loudspeakers generally have boxes to prevent rear wave cancellation at low frequencies. However, the stiffness of the air in a small box reduces the diaphragm's excursion at low frequencies. Hence the size of the box is generally a compromise between low frequency performance and practicality. Activated carbon has been found to increase the apparent size of a given box through adsorption of the air molecules when the pressure increases and likewise desorption when it decreases. However, the exact viscous effects in the granular structure are difficult to model. Thus it is impossible determine the high frequency limit due to the natural adsorption/desorption relaxation time in the absence of viscous losses. In this study, a tube model is presented which takes into viscous and thermal losses with boundary slip together with adsorption. Impedance measurements are performed on an array of 12 million holes, each 2 micrometers in diameter, etched in a 0.5 mm thick silicon wafer so that the viscous and thermal losses can be verified against the model without adsorption. Impedance measurements are then performed on an array of holes coated with graphite in order to create an activated carbon-like structure, thus enabling the adsorption/desorption relaxation time to be evaluated.

10:20

2aPAa8. Acoustic pulse attenuation and transmission in rigid porous media: Experimental investigation and numerical simulations. Diego Turo (University of Salford, Acoustics Research Centre, Newton Building, M5 4WT Salford, UK, d.turo@pgr.salford.ac.uk), Olga Umnova (University of Salford, Acoustics Research Centre, Newton Building, M5 4WT Salford, UK, o.umnova@salford.ac.uk)

This paper presents an investigation on acoustic pulse attenuation and transmission in rigid porous media. Transmission measurements of acoustic pulses through porous material with a rigid frame were performed using an appropriate standing wave tube. A vertical tube was built to make measurements on granular materials. The influence of pulse duration, layer thickness and material microstructure on the transmission has been investigated. Numerical time domain simulations based on two different semi-empirical models with one and two viscous relaxation times, respectively, were performed to compare with existing data. First, material microstructure and pulse durations were adapted to investigate the influence of viscous and inertial effects on pulse propagation separately. The simultaneous contribution of both viscous and thermal effects was then investigated. In the finite difference time domain (FDTD) model, different approaches are used to correctly simulate the pulse transmission through a porous layer. Accuracy and computational time required for the numerical methodologies have been compared and their advantages and drawbacks applied to this particular case shown.

10:40-11:00 Break

11:00

2aPAa9. On the influence of the micro-geometry on sound propagation through periodic array of cylinders. Rodolfo Venegas (University of Salford, Acoustics Research Centre, Newton Building, M5 4WT Salford, UK, R.G.VenegasCastillo@pgr.salford.ac.uk), Olga Umnova (University of Salford, Acoustics Research Centre, Newton Building, M5 4WT Salford, UK, o.umnova@salford.ac.uk)

Sound propagation in rigid porous media has been widely studied by using macroscopical models. These models make use of averaged quantities in which the microscopic details of the porous media geometry are represented by macroscopical parameters and, in a certain way, the influence of the microscopic geometry is not directly identified. In this paper, homogenization theory and finite element method are used for solving the full microscopic dynamic flow and dynamic heat problems for a porous medium modelled as an idealized geometry consisting of a periodic array of cylinders. Different cross-section shapes of the cylinders (circular, ellipsoidal and square cross-section shapes) and a wide range of porosity values are considered. The influence of the microscopic features of the porous media on dynamic permeability and dynamic compressibility is also studied.

11:20

2aPAa10. Acoustic emission before avalanches in granular media. Vincent Gibiat (Université Paul Sabatier, PHASE, 118, route de Narbonne, 31062 Toulouse cedex 9, France, gibiat@cict.fr), Eric Plazza (Université Paul Sabatier, PHASE, 118, route de Narbonne, 31062 Toulouse cedex 9, France, ericvpp@hotmail.com), Pierre De Guibert (Université Paul Sabatier, PHASE, 118, route de Narbonne, 31062 Toulouse cedex 9, France, dguibert@cict.fr)

Avalanches of granular media are mainly characterized by the observation and the measurement of the main angles of avalanche corresponding first to the movement of isolated beads and to the whole movement of a great part of the grains. These characterisations do not give any information about the rearrangements of the grains inside the layer of granular beads. As any movement of a grain produces a deformation of the structure it is quite normal to expect for a sound that will propagate inside the granular medium. We present an experimental study of the precursors of avalanches on spherical granular glass beads and silica aerogels in powder (size of grains less than 80 micrometers). Acoustic emission has been recorded with two piezoelectric transducers placed on the lower part of the material layer. Our results show clearly that before any movement on the upper part of the beads layer, so for an angle less than the first angle of avalanche, movements inside the material produce pulsed sounds that can be recorded. Theses vibrating events are occurring more and more when the angle is increasing until the first angle of avalanche where acoustic emission becomes intense.

11:40

2aPAa11. On heterogeneous blankets: Analytical solution for the interaction between masses and poro-elastic layers. Kamal Idrisi (Virginia Tech, Mechanical Engineering, 143 Durham 0238, Blacksburg, VA 24061, USA, idrisi@vt.edu), Andreas Wagner (Virginia Tech, Mechanical Engineering, 143 Durham 0238, Blacksburg, VA 24061, USA, andreasw@vt.edu), Marty Johnson (Virginia Tech, Mechanical Engineering, 143 Durham 0238, Blacksburg, VA 24061, USA, martyj@vt.edu), David Bartylla (Virginia Tech, Mechanical Engineering, 143 Durham 0238, Blacksburg, VA 24061, USA, bartylla@vt.edu)

There has been substantial research over the last five decades on control of aircraft cabin noise. One new passive approach is the heterogeneous (HG) blanket where a traditional acoustic blanket treatment is altered by adding mass inhomogeneities into the poro-elastic/viscoelastic layers. These masses act like distributed vibration absorbers and can be used to reduce vibration and sound transmission by targeting modes of the fuselage. The natural frequency of a mass inhomogeneity is determined by the mass itself and by the effective stiffness of the porous layer due to the mass/poro interaction. An experimental 1st order approach to predict the effective stiffness based on the shape of the mass inhomogeneities is reviewed. An analytical model for poro-elastic media proposed by Allard et al. was simplified for low frequencies and is used to validate and extend the 1st order approach. It is shown that the effective stiffness depends on mass shape, the foam thickness and material constants such as the modulus of elasticity and Poisson's ratio. Furthermore the model can be used to calculate the stress and displacements fields in the blanket in order to give further insight into the behaviour of the HG blankets.

12:00

2aPAa12. Influence of boundary slip on the acoustical properties of microfibrous absorbents. Olga Umnova (University of Salford, Acoustics Research Centre, Newton Building, M5 4WT Salford, UK, o.umnova@salford.ac.uk), David Tsiklauri (University of Salford, Acoustics Research Centre, Newton Building, M5 4WT Salford, UK, d.tsiklauri@salford.ac.uk), Rodolfo Venegas (University of Salford, Acoustics Research Centre, Newton Building, M5 4WT Salford, UK, R.G .VenegasCastillo@pgr.salford.ac.uk)

In the past decades a variety of new highly porous materials with unusually small pores have been manufactured. In aerogels, for instance, pores can be less than 20 nm in diameter. The conventional models have to be modified when applied to describe acoustical properties of those materials. The non-slip condition on a pore surface is no longer valid and needs to be replaced by the Knudsen boundary condition. In attempt to provide an insight into the behaviour of microfibrous materials, an analytical model has been developed, which accounts for the boundary slip in a medium consisting of rigid parallel fibres assuming different directions of sound propagation with respect to fibres. It has been shown that the presence of the boundary slip leads to a significant change in model predictions. For instance, in a material with fibre radius 80 nm and 95% porosity the sound speed decreases and attenuation increases by more than 20% compared to the values obtained assuming no boundary slip. The effect is stronger for smaller size fibres, lower porosity values and for sound propagating parallel to fibres. Numerical computations have been performed to simulate oscillatory flow around the cylindrical fibres assuming Knudsen boundary conditions and the results have been compared with the analytical model predictions

12:20

2aPAa13. Time-Resolved Spectroscopy of Water confined in Vycor. Riccardo Cucini (European Lab. for Non-Linear Spectroscopy (LENS), Univ. di Firenze, via Nello Carrara 1, 50019 Sesto Fiorentino (Fi), Italy, cucini@lens.unifi.it), Andrea Taschin (European Lab. for Non-Linear Spectroscopy (LENS), Univ. di Firenze, via Nello Carrara 1, 50019 Sesto Fiorentino (Fi), Italy, taschin@lens.unifi.it), Paolo Bartolini (European Lab. for Non-Linear Spectroscopy (LENS), Univ. di Firenze, via Nello Carrara 1, 50019 Sesto Fiorentino (Fi), Italy, bart@lens.unifi.it), Renato Torre (European Lab. for Non-Linear Spectroscopy (LENS), Univ. di Firenze, via Nello Carrara 1, 50019 Sesto Fiorentino (Fi), Italy, torre@lens .unifi.it)

We present measurements on water confined in Vycor 7930 by heterodyne-detected transient grating experiments (HD-TG) [1]. We studied the acoustic wave propagation, the thermal diffusion and the liquid viscous flow through the pores as a function of temperature (-15 - 90 °C) and of the exchanged q-vector (0.63 - 2.5 μm^{-1}). The data show interesting aspects due partly to the confinement effects and partly to the peculiarities of bulk water. Acoustic results are compared with the predictions of the Biot theory finding a good agreement only for the sound velocity data, while the predictions for the acoustic wave attenuation is poor as just reported in [2]. Our technique is able to induce a thermal grating inside the sample. The analysis of the data requires an extension of the Biot theory, that takes into account the temperature variations. Surprisingly, our data show that the acoustic oscillation are not affected by the temperature. The induced thermal grating is also used to analyze the viscous flow of water inside the pores and the thermal diffusion. [1] Time-resolved spectroscopy of complex liquids, edited by Torre R. (Springer, New York) 2008 [2] A. Taschin, R. Cucini, P. Bartolini, R. Torre, Europhys. Lett., in press.

Session 2aPAb

Physical Acoustics: Diffraction of Waves on Periodical Structures: Acoustic, Ultrasonic, and Acousto-Optical Diffraction Phenomena I

Nico F. Declercq, Cochair
Georgia Tech Lorraine - G.W. Woodruff School of ME, UMI Georgia Tech - CNRS 2958, 2 rue Marconi, Metz, 57070, France

Nataliya Polikarpova, Cochair
M.V. Lomonosov Moscow State University, Department of Physics, Moscow, 119991, Russian Federation

Invited Papers

8:00

2aPAb1. Spectral instruments based on acousto-optical tunable filters: advantages and prospects. Vladislav Pustovoit (Scientific Technological Center of Unique Instrumentation of RAS, ul.Butlerova, 15, 117342 Moscow, Russian Federation, np@ckbup.dol.ru), Vitold Pozhar (Scientific Technological Center of Unique Instrumentation of RAS, ul.Butlerova, 15, 117342 Moscow, Russian Federation, aoslab@ckbup.dol.ru)

A review of modern spectral techniques and instruments using acousto-optical tunable filters (AOTF) is presented. New approaches for spectrometers and spectral systems development are considered. The following instruments are described: a series of compact spectrometers and spectrophotometers of ultra-violet, visible, and infra-red ranges for Raman, fluorescence, and absorption spectroscopy for various applications, including out-of-door measurements; spectroradiometers for environment monitoring (open air, Earth surface, subsurface and depth seawater), specialised spectral equipment for industrial monitoring (microelectronics, alcoholometry), imaging spectral devices, time-resolve fluorescent spectrometers, and instruments for differential spectroscopy. Also some fundamental problems of AOTF-based spectroscopy are considered: spectrogram correction of instrument function distortions, ultimate spectral resolution of different methods, modulation techniques for instrument function synthesizing, optimization of measurement procedures, including adaptive algorithms. Basic trends of the past 30 years of AOTF-based spectroscopy development are formulated. The most promising ideas are discussed.

8:20

2aPAb2. Advances in acousto-optic devices based on frequency intermodulations suppression. Valeriy V. Proklov (IRE RAS, 11 Mokhovaya str., build.7, 125009 Moscow, Russian Federation, proklov@mail.cplire.ru), Sergey Antonov (IRE RAS, 11 Mokhovaya str., build.7, 125009 Moscow, Russian Federation, olga-ant@yandex.ru), Yury Rezvov (IRE RAS, 11 Mokhovaya str., build.7, 125009 Moscow, Russian Federation, rezvov@newmsk.tula.net), Alexander Vainer (IRE RAS, 11 Mokhovaya str., build.7, 125009 Moscow, Russian Federation, sawashi@yandex.ru)

The limitative influence of the frequency intermodulation effect on the most important parameters in a big family of acousto-optic (AO) devices is well known. The proposed presentation deals with new principles and related technical tools to perform significant suppression of the inherent intermodulation effects within broadband AO devices. The different AO interaction mechanisms in solids offering the intermodulations decrease have been considered. On this basis there were theoretically established and experimentally verified facilities to design a few types of advanced AO devices for a wideband signal processing with the extended spurious free dynamic range, as well as for a flexible laser beam forming with extremely high efficiency and etc.

Contributed Paper

8:40

2aPAb3. Periodically non-homogeneous acoustic beams and their application in acousto-optics. Vladimir I. Balakshy (Dept. of Physics, M.V.Lomonosov Moscow State Univ., Vorobyevy Gory, Bldg. 1, 119991 Moscow, Russian Federation, balakshy@phys.msu.ru), Bogumil B. Linde (Inst. of Exper. Physics, Univ. of Gdańsk, Ul. Wita Stwosza, Bldg. 57, 80-952 Gdańsk, Poland, fizbl@univ.gda.pl)

Light diffraction by ultrasonic waves is of great interest in the view of both fundamental physics and diverse applications. Acousto-optic devices are used for modulation of optical wave parameters, for optical information processing in real time, etc. In the given research, basic attention has been focused on the analysis of characteristics of anisotropic acousto-optic cells in which acoustic waves are excited by means of a phased array of transducers. Current technology makes it possible to create easily such transducers with antiphase excitation of adjacent elements of the array. The directional diagram of this composite transducer consists of several lobes whose spatial orientation varies with frequency. This peculiarity results in changing the Bragg condition. In the case of the anisotropic acousto-optic diffraction, every branch of the Bragg angle frequency dependence is split into several curves. This opens up new possibilities for optimization of acousto-optic devices. In this work, we have analyzed amplitude, frequency and angular characteristics of the phased transducer cells depending on crystal cut and transducer parameters. In particular, it has been shown that, in spite of a noticeable phase mismatch between interacting waves, the diffraction efficiency can approach 100%.

Invited Paper

9:00

2aPAb4. Differential properties of acousto-optical tunable filters in phase-modulation mode. Vitold Pozhar (Scientific Technological Center of Unique Instrumentation of RAS, ul.Butlerova, 15, 117342 Moscow, Russian Federation, aoslab@ckbup.dol.ru), Vladislav Pustovoit (Scientific Technological Center of Unique Instrumentation of RAS, ul.Butlerova, 15, 117342 Moscow, Russian Federation, np@ckbup.dol.ru), Sergey Beryoza (Scientific Technological Center of Unique Instrumentation of RAS, ul.Butlerova, 15, 117342 Moscow, Russian Federation, bruce_lee_22@mail.ru)

Tailoring the transmission function of acousto-optical tunable filters (AOTF) via acoustic waves control is one of the most challenging tasks, which is promising for optical spectroscopy applications. In our early work it was theoretically predicted and experimentally demonstrated that collinear AOTF with fast periodic phase manipulation exhibits differential properties, in particular capability of detection spectrum derivatives. In the report, the form of the instrument function of such AOTF was measured with use of Ne-lamp linear spectrum. Comparison to theoretically calculated function shows rather good agreement. Also the form of window of equivalent differential filter was determined and proved to be quite similar to AOTF classical window. Advantages of using this differential detection technique are considered. Its applicability to fluorescence spectroscopy is discussed.

Contributed Papers

9:20

2aPAb5. Quasicollinear acoustooptic tunable filters based on KDP single crystal. Vladimir Molchanov (Technological State Univ., Moscow Steel and Alloys Institute, Leninsky prospect, 4, 119049 Moscow, Russian Federation, v_molchanov@smtp.ru), Sergei Chizhikov (Technological State Univ., Moscow Steel and Alloys Institute, Leninsky prospect, 4, 119049 Moscow, Russian Federation, aocenter@mail.ru), Oleg Makarov (Molecular Technology GmbH, Rudower Chaussee 29-31, 12489 Berlin, Germany, moltech@mt-berlin.com)

The paper is devoted to the theoretical and experimental investigation of acoustooptical tunable filters, based on quasicollinear geometry of light-sound interaction in KDP single crystal. This geometry uses the effect of acoustic anisotropy in KDP, as well as peculiarities of acoustic wave reflections from the free boundary of KDP crystal. The mathematical approach for determination of optical and consructional characteristics of the filters is elaborated. Different types of quasicollinear filters are considered. The filters are intended for UV-VIS regions of optical radiation. The experimental acoustooptical filter was designed and investigated. Typical tunable spectral band is 220-500 nm, the spectral resolution doesn't exceed 0.1 nm in UV region of spectra. The experimental data are in a good agreement with the predicted one. This research is supported by RFBR grants # 07-02-12238 and # 07-02-01195.

9:40-10:00 Break

10:00

2aPAb6. Surface profile investigations by means of acousto-optic technique. Boris S. Gurevich (Scientific Instruments, Rizhsky prospekt 26, 190103 St. Petersburg, Russian Federation, bgurevich@mail.ru), Valentine V. Shapovalov (Intelligent Software Systems, Nevsky pr. 190, 193317 St. Petersburg, Russian Federation, Shapovalov@incomsys.ru), Sergey V. Andreyev (Scientific Instruments, Rizhsky prospekt 26, 190103 St. Petersburg, Russian Federation, svan51@mail.ru), Andrey V. Belyaev (Institute for analytical instrumentation RAS, Rizhsky pr. 26, 190103 St. Petersburg, Russian Federation, bgurevich@mail.ru), Ilya A. Kolesov (Intelligent Software Systems, Nevsky pr. 190, 193317 St. Petersburg, Russian Federation, ilkak@mail.ru)

Acousto-optic tunable filters (AOTF) represent a very strong tool in different kinds of investigations where high rate light wavelength variations are required. The rough surfaces profile investigation is among the problems which can be solved partially by this way. Our investigations have been connected with use of AOTF and lens components with strong chromatic aberration. One of the problems was to choose the z-distance resolving power criterion. The proposed criterion is defined by the admissible probability to miss information unit regarding the object characterization in z-distance. In our experiments we used the specially elaborated AOTF based on tellurium dioxide crystal with transmission bandwidth of several nm, depending on the central wavelength position. Also we have used the lenses fabricated with tellurium dioxide because this material provides high chromatic aberrations. The results of experiments are discussed from the point of view of the AOTF possibilities to increase the z-distance resolving power in comparison with existing systems. The 90%-probability distinguishing of defocusing while electric frequency variation of 200 kHz, can be considered as serious advantage. The device improvement can be attained by means of the noise level decreasing to the level taking place for electric frequency of 94 MHz.

10:20

2aPAb7. Transformation of Acoustic Modes in Case of Arbitrary Reflection in Acousto-Optic Crystals. Nataliya Polikarpova (M.V. Lomonosov Moscow State University, Department of Physics, Leninskie gory 1 bldg. 2, Division of Oscillations, 119991 Moscow, Russian Federation, polikarp@phys.msu.ru), Vitaly Voloshinov (M.V. Lomonosov Moscow State University, Faculty of Physics, Vorob'evy Gory, MSU, 119991 Moscow, Russian Federation, volosh@phys.msu.ru), Nico F. Declercq (Georgia Tech Lorraine - G.W. Woodruff School of ME, UMI Georgia Tech - CNRS 2958, 2 rue Marconi, 57070 Metz, France, nico .declercq@me.gatech.edu)

The phenomenon of unusual reflection of plane elastic waves is examined in the crystalline compounds of tellurium and mercury. It is predicted and registered in experiments that energy flow of one of the reflected waves may propagate practically in a back direction with respect to an incident energy flow. This phenomenon is observed in the materials with a strong anisotropy of elastic properties. In the case of inclined incidence, the reflection may take place strictly in the back direction with respect to the intrinsic energy flow. Moreover, all incident elastic energy may be reflected in a form of a back elastic wave. The analysis was carried out for all exisiting cases of inclined incidence in the crystals. It was proved that relative intensity of the unusually reflected wave might be close to a unit in a wide variety of incidence and cut angles in the crystals. A comparative analysis of the effect in new anisotropic materials and in the well-known crystals has been carried out. Since the crystals under investigation possess relatively high magnitudes of acousto-optic figure of merit, e.g. paratellurite and calomel, principal results of the research are of significance in development of new generations of acousto-optic devices.

10:40

2aPAb8. Optimization of KDP-based acousto-optic imaging filters. Konstantin B. Yushkov (Moscow State University, Phisical Faculty, Leninskie Gory, 119991 Moscow, Russian Federation, protonoa@mail.ru)

Acousto-optic devices can perform spatial and spectral tunable filtration of light with the use of anisotropic Bragg diffraction. In the near UV range

of spectrum, KDP single crystals provide the highest acousto-optic figure of merit among uniaxial crystals. The report is devoted to the problem of optimization of the filter parameters in order to maximize angle aperture of the instruments. It was found that the maximum angle aperture of wide angle tunable acousto-optic filters is equal to 3 degrees in air at output of the KDP crystals. This magnitude of the angle aperture is limited by a narrow deflection angle of light in KDP that is due to a relatively low birefringence of the material. The investigation showed that the diffraction efficiency of light depends on the dimensions of the acousto-optic cell, i.e. linear aperture and length of a piezoelectric transducer. A discussion on trade-off between transmission coefficient and the spatial resolution in the filter is presented in the report.

11:00

2aPAb9. Acousto-optic collinear diffraction of arbitrary polarized light. Sergey Mantsevich (Dept. of Physics, M.V.Lomonosov Moscow State Univ., Vorobyevy Gory, Bldg. 1, 119991 Moscow, Russian Federation, manboxx@mail.ru), Vladimir I. Balakshy (Dept. of Physics, M.V .Lomonosov Moscow State Univ., Vorobyevy Gory, Bldg. 1, 119991 Moscow, Russian Federation, balakshy@phys.msu.ru)

Acousto-optic collinear diffraction of light is a type of light scattering interesting as a physical phenomenon and important from practical point of view. This type of diffraction is used in tunable acousto-optic filters. In this case, the incident light has to be linearly polarized along one of the acousto-optic crystal anisotropy axes. If the incident light is not primordially polarized, a polarizer should be disposed at the input of the acousto-optic cell. Unfortunately, this leads to loss of half the light power. The present work is devoted to theoretical and experimental investigation of collinear acousto-optic interaction peculiarities that arise when the incident optical beam is not polarized. It is shown that the output diffraction spectrum in the general case contains four components which have different polarization and frequency. Beating of these components leads to modulation of light intensity passed through the output analyzer. In this work, dependences of modulation components amplitudes on frequency and power of the acoustic wave are examined for different polarizer and analyzer orientations.

Invited Paper

11:20

2aPAb10. Ultrasonic diffraction grating spectroscopy: particle size measurements and investigation of the inertial model for attenuation. Margaret Greenwood (Pacific Northwest National Laboratory, P. O. Box 999, Mailstop K5-26, Richland, Wa, WA 99352, USA, margaret.greenwood@pnl.gov)

The experimental setup consists of a unit with a grating machined on the surface of the unit. Send and receive transducers are placed at equal angles to the grating surface that is in contact with a slurry. The transmitted beam of spectral order $m = 1$ reaches an angle of 90° at the so-called critical frequency, where it becomes an evanescent wave that interacts with particles in the slurry. As a result of this interaction, the signal in the receive transducer exhibits a dependence upon particle size of the slurry. Data will be presented for slurries of polystyrene spheres, ranging in size from 45 μm to 467 μm, as a function of the volume fraction. The velocity of sound is also determined from the critical frequency. The distributions will be compared with the viscous and inertial models. The results show that larger particle sizes can be understood in terms of the inertial model, while the smaller sizes can be explained as a result of scattering. Also, arguments will be presented to show that this technique can probe the inertial model, without the simultaneous observation of scattering effects. Such studies can improve the theoretical interpretation of standard attenuation measurements.

Contributed Paper

11:40

2aPAb11. Non-reciprocity of acousto-optic interaction at high acoustic frequencies. Yury Dobrolenskiy (M.V. Lomonosov Moscow State University, Faculty of Physics, Vorob'evy Gory, MSU, 119991 Moscow, Russian Federation, dobrolenskiy@phys.msu.ru), Vitaly Voloshinov (M.V. Lomonosov Moscow State University, Faculty of Physics, Vorob'evy Gory, MSU, 119991 Moscow, Russian Federation, volosh@phys.msu.ru), Yury Zyuryukin (Saratov State Technical University, Politechnicheskaja str., 77, 410054 Saratov, Russian Federation, phys@sstu.ru)

Modern acousto-optic (AO) tunable filters have reached the values of spectral resolution exceeding 104 and operate with acoustic frequencies up to a few gigahertzes. At such high frequencies and such narrow bandwidths, there appear effects so far neglected. Among them there is non-reciprocity of AO interaction. It consists in the fact that acoustic frequency of light diffraction by ultrasound is different when optic beams propagate in directions opposite to each other. In the present research, the new effect has been studied theoretically and experimentally for the example of collinear AO diffraction. Theoretical analysis and calculations related to particular AO materials have shown that the effect is essential at acoustic frequencies about 1 GHz and higher. The value of the non-reciprocal shift of acoustic frequency can be as high as the frequency bandwidth of the filter. The effect has also been registered and investigated experimentally in a sample of lithium niobate crystal. The experimental data has totally confirmed the theoretical analysis. Therefore, it has been proved that the non-reciprocal effect influences the parameters of AO diffraction and, consequently, operation of AO filters at high frequencies. On the other hand, one can design devices, e.g. directional couples, exactly based on the non-reciprocity.

Invited Paper

12:00

2aPAb12. Critical cone channelling in directly bonded wafers. Evgeny Twerdowski (Institute of Experimental Physics II, University of Leipzig, Linnéstr. 5, 04103 Leipzig, Germany, twerdowski@physik.uni-leipzig.de), Moritz Von Buttlar (Institute of Experimental Physics II, University of Leipzig, Linnéstr. 5, 04103 Leipzig, Germany, vbuttlar@physik.uni-leipzig.de), Reinhold Wannemacher (Institute of Experimental Physics II, University of Leipzig, Linnéstr. 5, 04103 Leipzig, Germany, wannemacher@physik.uni-leipzig.de), Wolfgang Grill (Institute of Experimental Physics II, University of Leipzig, Linnéstr. 5, 04103 Leipzig, Germany, grill@physik.uni-leipzig.de)

Directly bonded semiconductor wafers have been investigated using ultrasonic transmission tomography and imaging of the phonon focusing patterns at ultrasonic frequencies. Beside of total disbonds, several bonded wafers contained defects that are fully transparent to normally incident waves of longitudinal polarization, and are fully opaque to those of transverse polarization. These defects, which are due to slip boundary conditions at the wafer-wafer interface, generate an additional acoustic mode by mode conversion at the interface. The additional mode is clearly observable in the experimental phonon focusing patterns and is indicative of the critical cone

channelling phenomenon, which is caused by the generation of pseudo-surface and head waves at weakly bonded solid-solid interfaces. The effect is also expected to be present in the case of weakly-bonded isotropic materials. Since the strong pseudo-surface wave resonance exists only in the case of boundary conditions that allow for the relative displacement of the two adjoining media along the interface, the critical cone channelling effect can serve as a measure of the type and quality of the bond.

Contributed Papers

12:20

2aPAb13. Sound waves in 3D periodic granular materials. Orion Mouraille (UTwente, Multi Scale Mechanics, P.O.Box 217, 7500 AE Enschede, Netherlands, o.j.p.mouraille@utwente.nl), Stefan Luding (UTwente, Multi Scale Mechanics, P.O.Box 217, 7500 AE Enschede, Netherlands, s.luding@utwente.nl)

The sound propagation mechanisms inside dense granular matter, even for periodical structures, are challenging the attempts to describe it because of the discrete nature of the material. Phenomena like dissipation, scattering, and dispersion are hard to predict based on the material state and/or properties and vice-versa. We propose here a simulation method using dynamic discrete elements in order to get more insight in this problem. The small perturbation created on one side of a dense, static regular packing of grains is examined during its propagation and when it arrives at the opposite side. Both longitudinal and shear perturbation are studied and an interesting wave-acceleration is observed [1]. Moreover the rotational degree of freedom permits to observe the role of rotations in the wave propagation. The control of the inter-particle forces like, contact potential, cohesion and friction make possible to observe the effect of these micro-parameters on the macro-behavior (at the wave scale). Long term goal is to predict the large-scale macroscopic material behavior from the microscopic structure and material parameters. [1] O. Mouraille, W A Mulder and S. Luding: Sound wave acceleration in granular materials, J. Stat. Mech. (2006) P07023.

12:40

2aPAb14. Bragg light diffraction in nontransparent crystals. Farkhad Akhmedzhanov (Navoi State Mine Institute, 27a Yuzhnaya Street, 210100 Navoi, Uzbekistan, farkhad2@yahoo.com)

As is well known, in absolutely transparent crystals an acoustooptical interaction is lacking. In this connection's acoustooptical investigations are presented greatest interest in optical range, in which the crystal is not transparent. In order to carry out similar experiments, it is necessary to use the crystal with a small light absorption coefficient at applied wavelength. The main problem is selection of an appropriate buffer crystal that the light beam can penetrate into sample by Bragg angle at required frequency. At present work the acoustooptical properties of Si crystal were investigated at light wavelength 632.8 nm. Dy_2S_3 crystals were used as a buffer sample. It was detected the diffracted light intensity is much more powerful in comparison with that for $LiNbO_3$ crystals. Acoustooptical efficiency M2 (it is defined the acoustic-optical quality of material) has been calculated from the values of optic coefficients and elastic constants for appropriate directions of sound and light. The results of executed investigations have shown the possibility of determination of acoustooptical properties of nontransparent crystals by Bragg diffraction method. At that rate, the very high intensity of diffracted light can be obtained in comparison with that in transparent crystals.

1:00-2:00 Lunch Break

Invited Paper

2:00

2aPAb15. Theory of resonant acoustic transmission through subwavelength apertures. Johan Christensen (Universidad Autónoma de Madrid, Departamento de Física Teórica de la Materia Condensada, Facultad de Ciencias, C-V, 28049 Madrid, Spain, johan.christensen@uam.es), Luis Martín-Moreno (Universidad de Zaragoza, Departamento de Física de la Materia Condensada, Instituto de Ciencia de Materiales de Aragón, C/ Pedro Cerbuna 12, 50009 Zaragoza, Spain, lmm@unizar.es), Francisco Jose García-Vidal (Universidad Autónoma de Madrid, Departamento de Física Teórica de la Materia Condensada, Facultad de Ciencias, C-V, 28049 Madrid, Spain, fj.garcia@uam.es)

The discovery of the phenomenon of extraordinary optical transmission through a two-dimensional array of subwavelength holes in a metallic film has opened a new line of research within optics. The key role played by surface plasmons in transferring light efficiently from the input side of the metal film to the output region was soon realized. This fundamental knowledge enabled extension of this surface-plasmon ability to achieve extraordinary optical transmission and strong collimation of light in a single hole surrounded by a finite periodic array of indentations. Here, we show how these ideas developed for electromagnetic radiation can be transferred to other classical waves such as acoustic waves.

Contributed Papers

2:20

2aPAb16. Theoretical and experimental ultrasonic investigation of a thin plate with regions of different periodic double-corrugations. Sarah W. Herbison (Georgia Tech Lorraine - G.W. Woodruff School of ME, UMI Georgia Tech - CNRS 2958, 2 rue Marconi, 57070 Metz, France, sherbison@gatech.edu), Nico F. Declercq (Georgia Tech Lorraine - G.W. Woodruff School of ME, UMI Georgia Tech - CNRS 2958, 2 rue Marconi, 57070 Metz, France, nico.declercq@me.gatech.edu)

In order to provide a qualitative measurement of the depth of periodic double-corrugations existing on both sides of a thin plate, theoretical and experimental ultrasonic techniques have been applied. The aesthetic galvanized steel sheets under investigation contain many regions of periodic double-corrugations, each region with a different corrugation depth. An ultrasonic technique is investigated as a means to improve existing optical testing techniques in quality and speed. Theoretical simulations using the theory of diffraction from periodically corrugated surfaces have been employed to obtain reflection spectra to facilitate qualitative observations regarding the depth of the corrugation in the different regions. Experiments to obtain reflection spectra correlate well with the theoretical simulations, and show the application of ultrasound to the qualitative measurement of the corrugation depth. Because the wavelengths necessary to make the investigations produce Lamb waves, some difficulty lies in the generation of diffracted bulk waves and Lamb waves. The research shows that correlations between theory and experiments exist, but they can only be obtained after thorough simulations that do not produce easy to apply rules of thumb.

2:40

2aPAb17. BEM analysis of plane waves scattered from periodic surfaces. Mahesh Bansal (Institute of Technical Acoustics, Tech. Univ. Berlin, Einsteinufer 25, 10587 Berlin, Germany, mbansal.iitk @gmail.com), Wolfgang Ahnert (Ahnert Feistel Media Group, Arkonastr. 45-49, 13189 Berlin, Germany, wahnert@ada-acousticdesign.de), Stefan Feistel (Ahnert Feistel Media Group, Arkonastr. 45-49, 13189 Berlin, Germany, sfeistel@afmg.eu)

Periodic surfaces like stairs, seats and repetitive designs on walls are very common and integral part of room acoustics. Effective simulation of the sound field inside enclosures requires the investigation of scattering from such periodic surfaces. In this work, we perform BEM analysis to calculate the scattering coefficients of different samples. For comparison purposes we also introduce a simple point-source based model to calculate the scattered wave fronts. Both approaches are implemented in a computational tool called EASE Scatterer. The incident plane waves are considered at various angles and scattered waves computed in both models are then compared with the measured data. It is found that while the point-source model can give reasonable asymptotic results, the BEM model matches with the measurement data significantly better in quantity and quality. Moreover, a study by varying the number of periods for the given sample is also performed.

3:00

2aPAb18. Diffraction phenomena associated with a composite plate containing an interior periodically corrugated interface. Sarah W. Herbison (Georgia Tech Lorraine - G.W. Woodruff School of ME, UMI Georgia Tech - CNRS 2958, 2 rue Marconi, 57070 Metz, France, sherbison@gatech.edu), Nico F. Declercq (Georgia Tech Lorraine - G.W. Woodruff School of ME, UMI Georgia Tech - CNRS 2958, 2 rue Marconi, 57070 Metz, France, nico.declercq@me.gatech.edu)

The interest in the study and applications of phononic crystals has naturally lead to the investigation of other novel periodic structures. The present work examines the case of a plate constructed of two solid layers of differing elastic properties separated by a periodically corrugated interface. It is shown how the dispersion curves are influenced by the internal corrugated interface and how they evolve as a function of the magnitude of this corrugation. Internal diffraction effects alter the dispersion properties and thus have an important effect on the composite when it is used as an acoustic filter. These effects are also important for the transmission and reflection of sound when the composite is used as a panel or when it is the intention to generate Lamb waves to investigate the composite plate nondestructively.

3:20

2aPAb19. Multiple scattering of acoustic waves from two transversely isotropic cylinders. Sina Sodagar (Faculty of Mechanical Engineering, K. N. Toosi University of Technology, Pardis St., Molla Sadra Ave., Vanak Sq., Postal code 1999143344, 16579 Tehran, Iran, ssodagar@alborz.kntu.ac.ir), Farhang Honarvar (Faculty of Mechanical Engineering, K. N. Toosi University of Technology, Pardis St., Molla Sadra Ave., Vanak Sq., Postal code 1999143344, 16579 Tehran, Iran, honarvar @mie.utoronto.ca), Anthony N. Sinclair (Department of Mechanical Engineering, University of Toronto, 5 King's College Road, Toronto, ON M5S 1A4, Canada, sinclair@mie.utoronto.ca)

The study of the interaction of acoustic waves with cylindrical structures has numerous applications including the ultrasonic nondestructive testing of materials. The scattered pressure field from a submerged cylinder contains valuable information about its physical properties. Scattering of acoustic waves from single cylindrical components including solid cylinders, shells, and multilayered cylinders has been of interest during the past two decades. These studies include theoretical modeling, numerical calculations, and experimental measurements of the scattered field of these objects. The more complex problem of multiple scattering from a grating of cylindrical components has also been considered during the past few years. These studies usually deal with either rigid or isotropic cylindrical objects. In this paper, the mathematical modeling for the scattering of plane acoustic waves from two adjacent infinite anisotropic solid cylinders will be presented. The type of anisotropy considered is transverse isotropy (hexagonal symmetry). The mathematical model accounts for the effects of the scattered filed of each cylinder on the total resultant pressure field. Numerical calculations are used to verify the validity of the developed mathematical model.

3:40-5:20 Posters

Lecture sessions will recess for presentation of poster papers on various topics in acoustics. See poster sessions for topics and abstracts.

Contributed Papers

5:20

2aPAb20. Phononic crystals in the diffraction regime. Vincent Laude (Institut FEMTO-ST/CNRS, 32 avenue de l'Observatoire, 25044 Besançon cedex, France, vincent.laude@femto-st.fr), Sarah Benchabane (Institut FEMTO-ST/CNRS, 32 avenue de l'Observatoire, 25044 Besançon cedex, France, sarah.benchabane@femto-st.fr), Abdelkrim Khelif (Institut FEMTO-ST/CNRS, 32 avenue de l'Observatoire, 25044 Besançon cedex, France, abdelkrim.khelif@femto-st.fr)

Phononic crystals are periodic composite materials exhibiting amazing wave propagation properties. In many works, complete band gaps are being looked for, i.e. the materials constituting the phononic crystal and its lattice arrangement are chosen such that propagation for all waves within a prescribed frequency range is forbidden. In other studies, the phononic crystal is considered a metamaterial, the anisotropic spatial dispersion of which can be tuned, and in which negative refraction can even be observed under certain circumstances. Such effects are usually considered in the sub-diffraction regime, i.e. below some critical onset frequency. In this work, we specifically examine phononic crystals in the diffraction regime. Indeed, the boundaries of a finite size phononic crystal embedded in a host propagation medium can be viewed as diffraction gratings, as we show. We will specifically consider two cases: two-dimensional phononic crystals composed of steel rods in water, and two-dimensional phononic crystals for surface acoustic waves achieved by etching cylindrical holes in a solid substrate.

5:40

2aPAb21. Methods to investigate the possibilities of using a three element periodic structure to suppress the transmission of energy in an elastic tube. Ole Holst-Jensen (Minus10dB, Stokrosevej 29, 8330 Beder, Denmark, ole.holst@minus10db.dk), Sergey Sorokin (Univ. of Aalborg, Institute for mechanical engineering, Pontoppidanstraede 101, 9220 Aalborg East, Denmark, svs@ime.aau.dk)

In industrial applications, such as pump and compressor systems, pipe vibrations can exceed an acceptable level. Periodically spaced masses added to the piping are an appropriate method of attenuation, and investigations to develop valid prediction models and measurement techniques has been initiated in the Danish Makunet network. The present investigation concern the effect of three masses attached periodically to a pipe of small diameter. The pipe is small enough that it can be treated as a beam. The masses are eccentric to the center of the beam, to achieve a large change in the moment of inertia by the added elements. The theoretical model is formulated as a system of boundary equations, which describe propagation of flexural, axial and torsion waves within each segment of a tube between periodic elements. An exact solution of this system is obtained and the power transfer is dramatically reduced in some frequency 'stop bands' regardless the excitation conditions. Transfer impedance measurements between the force input and the acceleration on selected positions are used to find the insertion loss due to the application of the periodic elements, showing good agreement with theory.

6:00

2aPAb22. Diffraction influence on the SAW tag characteristics. Boris V. Sveshnikov (Lebedev Research Center in Physics, 23, Lenin Av., 119991 Moscow, Russian Federation, bvs@ieee.org)

The diffraction of acoustic beams may influence notably on the responses of the SAW based RFID systems. In order to prevent such an influence one cannot increase the tag acoustic aperture too much because of ohmic loss in a transponder. On the other hand, usually the tag length should be large enough. There is a very specific and unique feature of the acousto-electric scattering of SAW beam on the coding sequence of the reflective metal electrodes placed on a piezoelectric substrate. The point is that the SAW itself is formed by two coupled sub-systems, namely: elastic displacements and electric field. Both of them are scattered on every discontinuity because of two kinds of the boundary condition perturbation: electric shorting beneath electrodes and mass-loading effect. A uniform metal electrode scatters differently from each other the ″elastic″ and ″electric″ subsystems with non-uniform wave-front caused by diffraction. The closed form expressions are found, allowing us to describe consistently the mentioned phenomena. Their numerical analysis has been added by the analytical one in case of parabolic approximation of the crystal slowness curve. The synthesis algorithm of SAW tags with high capacity is proposed taking into account the diffraction effect in a natural way.

6:20

2aPAb23. Frequency-domain diffraction for edges of arbitrary length with efficient numerical integration. Peter Svensson (Norwegian Univ. of Science and Technology, O.S. Bragstads plass 2B, Dept. of Electronics and Telecommunications, NO-7491 Trondheim, Norway, svensson@iet.ntnu.no), Paul Calamia (Rensselaer Polytechnic Institute, Greene Bldg., 110 8th St., Troy, NY 12180, USA, calamp@rpi.edu)

Frequency-domain edge diffraction from an infinite wedge insonified by a point source has been widely studied, with various analytical solutions dating back nearly a century. In this talk we present an alternative frequency-domain solution which can be used for finite as well as infinite edges. The expression, given as a line integral along the diffracting edge, is derived from an analytical time-domain expression presented in [U. P. Svensson et al., J. Acoust. Soc. Am. 106, 2331-2344 (1999)]. The new formulation is shown to be equivalent to an exact, analytical, contour-integral formulation for the infinite wedge via a variable transformation. Results for various finite and infinite edge cases will be presented, and numerical integration using an efficient quadrature method for highly oscillatory integrals will also be discussed.

6:40

2aPAb24. Acoustic cloaking by two-dimensional sonic crystals. Daniel Torrent (Politechnic University of Valencia, Wave Phenomena Group. Department of Electronic Engineering, C/ Camino Vera s.n, ES-46022 Valencia, Spain, datorma1@upvnet.upv.es), José Sanchez-Dehesa (Polytechnic University of Valencia, Cami de Vera s/n, 46022 Valencia, Spain, jsdehesa @upvnet.upv.es)

It has been previously shown that a two dimensional sonic crystal made of a periodic arrangement of solid cylinders in air behaves in the low frequency limit (homogenization) like an acoustic metamaterials with anisotropic effective density and isotropic effective bulk modulus [D. Torrent and J. Sanchez-Dehesa, New J. Phys. February 2008]. Here, the homogenization method is extended to the case of sonic crystals with two types of cylinders in the unit cell, and analytical expressions for the anisotropic effective density are then obtained. Moreover, it will be shown how these new acoustic metamaterials can be used to physically realize the solution for the acoustic cloaking proposed by Cummer and Schurig [New. J. Phys., vol. 9, 45, 2007] [Work supported by MEC of Spain.]

TUESDAY MORNING, 1 JULY 2008 ROOM 352A, 8:00 A.M. TO 7:00 P.M.

Session 2aPAc

Physical Acoustics: Outdoor Sound Propagation and Uncertainties I

Keith Wilson, Cochair
U.S. Army Cold Regions Research and Engineering Laboratory, 72 Lyme Road, Hanover, NH 03755-1290, USA

Michel C. Berengier, Cochair
Laboratoire Central des Ponts et Chaussées, Centre de Nantes - Route de Bouaye, BP 4129, Bouguenais cedex, 44341, France

Invited Papers

8:00

2aPAc1. Expected mean in an environmental noise measurement and its related uncertainty. Marco Paviotti (European Commission, via e. fermi, 1, 21020 Ispra, Italy, marco.paviotti@jrc.it), Stylianos Kephalopoulos (European Commission, via e. fermi, 1, 21020 Ispra, Italy, Stylianos.Kephalopoulos@jrc.it)

In the context of the implementation of the Environmental Noise Directive 2002/49/EC a study on noise measurement uncertainty was developed. In performing any noise measurement average, there might be assumptions over the distribution and independency of the samples. In a concrete example dealing with environmental noise, this might be the case of a series of measurements of a constant noise source like an industrial plant or a fluctuating noise source like road traffic. Using a series of 1 day Leq in the first case, or a series of 15 minutes samples in the second case, the average of these values is usually considered as the expected mean, however, the error caused by the specific selection of the samples is not evaluated. Statistically speaking, before establishing an average value, at least the lognormal distribution of the samples and the effect of adding-up several uncertainties should be evaluated. This article will focus on the formulas to be used and will discuss differences in assessing the expected mean for normally distributed values, or for lognormally distributed, and will suggest an approach to properly add-up all uncertainties related to an environmental noise measurement campaign.

8:20

2aPAc2. Criterion to select meteorological factors to evaluate uncertainties in sound propagation. Panu Maijala (VTT, Tekniikankatu 1, 33101 Tampere, Finland, Panu.Maijala@vtt.fi)

Most of the environmental factors have some effect on sound propagation outdoors. Many of these factors can be properly implemented to a sound propagation model. However, it is not easy to handle sound scattering due to the turbulence, and at the same time, the turbulence is the most important source of uncertainties. Concurrently with the studies of turbulence models we have developed a concept to get an estimate of the excess attenuation using a state-of-the-art physical model and to evaluate the uncertainties using a statistical model. This statistical model is based on two years continuous measurements using extensive acoustical and meteorological measurement facilities and producing over 100 factors hourly. Many meteorological factors had a strong and significant correlation with the excess attenuation, but between each other too. To avoid instable model due to the collinearity many factors were abandoned. In this paper the criterion and methods to select best explaining factors and to form this statistical model are considered.

8:40

2aPAc3. Methodological and metrological benchmarks for determining experimental values of meteorological parameters. Benoit Gauvreau (Laboratoire Central des Ponts et Chaussées, Centre de Nantes - Route de Bouaye, BP 4129, 44341 Bouguenais cedex, France, benoit.gauvreau@lcpc.fr)

Outdoor sound propagation is largely influenced by meteorological conditions: mean refraction, intermittency and atmospheric turbulence. Thus, acoustic engineers and scientists have to rigorously characterize those propagation conditions through several parameters, both for numerical predictions (input data) and for operational reports (impact studies). One of these influent parameters is the well-known (and widely used) effective vertical sound speed gradient, which depends on spatial and temporal mean values of wind and temperature between source and receiver. However, the experimental characterization of wind and temperature (and next sound speed) vertical profiles remains delicate: it requires accurate meteorological devices and adapted measuring methods. At this purpose, an experimental campaign has been carried in 2007 on a perfectly flat and open ground, in order to quantify the confidence, uncertainty and spreading of such parameter values for different time scales. This campaign involved different meteorological devices: instrumented towers, classical sensors, 3D sonic anemometers, etc. The benchmark results will be presented and next analysed in terms of metrological and methodological requirements for acousticians in charge of environmental studies for standard organizations and/or scientific institutes.

9:00

2aPAc4. Sources and potential influences of uncertainty in ground impedance measurements and estimations. Shahram Taherzadeh (The Open University, Faculty of Mathematics, Computing and Technology, Walton Hall, MK7 6AA Milton Keynes, UK, s.taherzadeh@open.ac.uk), Keith Attenborough (Open University, Department of Design, Development, Materials and Environment, Walton Hall, MK7 6AA Milton Keynes, UK, Keith.Attenborough@ioa.org.uk)

Knowledge of acoustic impedance of ground surface is essential for determining noise levels outdoors. At distances up to a few hundred metres from the source ground effect may be the dominant factor. The short-range measurement of sound level spectra from an omni-directional source has been used as a standard method to deduce the acoustic impedance spectrum of ground surfaces (e.g. ANSI S1.18, 1999). However, there remain a number of uncertainties in such measurement methods. For example, at low frequencies the difficulties in fitting theoretical or phenomenological models to short range data may result is a large uncertainty in predictions of sound levels at larger distances. Another source of uncertainty is the variability of the acoustic impedance of apparently uniform ground. Another potential influence on predictions of long term equivalent noise levels is seasonal variation. This paper discusses the extent and potential influences of such uncertainties in measured and deduced ground impedance spectra.

9:20

2aPAc5. Facing the challenge of calculating outdoor sound propagation using a 3D multi domain approach based on linear euler equations. Fabrice Junker (EDF, 1, avenue du Général de Gaulle, 92141 Clamart, France, fabrice.junker@edf.fr), Fabien Crouzet (EDF, 1, avenue du Général de Gaulle, 92141 Clamart, France, fabien.crouzet@edf.fr), Philippe Lafon (EDF, 1, avenue du Général de Gaulle, 92141 Clamart, France, Philippe.lafon@edf.fr)

Solving the Linear Euler Equations (LEE) is the reference method that allows to take into account all the phenomena involved in Outdoor Sound Propagation. However, the huge size of the problems to be treated is still a great limitation to the practical application of this method. The concept of multi domain computations associated with the use of massively parallel computers now pushes the limits away. The code SAFARI, recently developed by EDF, solves LEE with high order numerical schemes on structured grids. To deal with complex and large geometries, a multi domain approach is used. The computational domain is composed of several partially overlapping grids (overset grids). Computations are parallelized by domain decomposition to be runned on cluster facilities. The presentation means to show the capability of SAFARI to deal with propagation over realistic 3D domains. The strategy used to carry out the calculations is detailed. The new perspectives of this kind of method are finally given.

9:40

2aPAc6. Computing the parameter sensitivities of outdoor sound propagation in a random environment. Chris L. Pettit (U.S. Naval Academy, Aerospace Engineering Dept., 590 Holloway Rd., MS 11-B, Annapolis, MD 21402, USA, petitcl@usna.edu), Keith Wilson (U.S. Army Cold Regions Research and Engineering Laboratory, 72 Lyme Road, Hanover, 03755-1290, USA, D.Keith.Wilson @erdc.usace.army.mil)

Computational forecasts of near-ground sound levels are compromised by uncertainty (e.g., randomness) and error (e.g., grid resolution) in the atmosphere and terrain representations, and by simplified or incorrect physics. For an incompletely known environment, a model's predictive power cannot be assessed without first quantifying the sensitivity of its forecasts to the full range of every parameter. Knowledge of these sensitivities throughout the spatial domain also is essential for effectively investing data-gathering resources to support sound propagation forecasts. Sensitivity analysis therefore is central to raising the relevance of computational acoustics in practical applications. These considerations should motivate practitioners of computational acoustics to adopt a consistent framework for sensitivity and uncertainty analyses. Topics to be discussed include: (1) standard uncertainty taxonomies in computational mechanics, (2) why uncertainty about a parameter should be distinguished from sensitivity of a model to that parameter, (3) sources of uncertainty in the near-ground acoustics, (4) a sampling-based sensitivity analysis framework that facilitates estimating typical and extreme values of sensitivities at each point in the spatial domain (i.e., full-field sensitivities), (5) factors to be aware of when applying sensitivity analysis to forecasts of near-ground sound propagation, and (6) ways of representing sensitivity estimates to facilitate insight.

10:00-10:20 Break

10:20

2aPAc7. Field experiments on the influences of wind speed and direction on outdoor sound propagation over flat ground. Takatoshi Yokota (Kobayasi Institute of Physical Research, 3-20-41 Higashi-Motomachi Kokubunji, 185-0022 Tokyo, Japan, t-yokota@kobayasi-riken.or.jp), Koichi Makino (Kobayasi Institute of Physical Research, 3-20-41 Higashi-Motomachi Kokubunji, 185-0022 Tokyo, Japan, makino@kobayasi-riken.or.jp), Kohei Yamamoto (Kobayasi Institute of Physical Research, 3-20-41 Higashi-Motomachi Kokubunji, 185-0022 Tokyo, Japan, yamamoto@kobayasi-riken.or.jp), Yasuaki Okada (Faculty of Science and Technology, Meijo University, 1-501 Shiogamaguchi Tempaku-ku, 468-8502 Nagoya, Japan, okada@ccmfs.meijo-u.ac.jp), Koichi Yoshihisa (Faculty of Science and Technology, Meijo University, 1-501 Shiogamaguchi Tempaku-ku, 468-8502 Nagoya, Japan, yosihisa@ccmfs .meijo-u.ac.jp)

The influences of wind on outdoor sound propagation are investigated both by field experiments and numerical simulations. At first, measurements of sound propagation at a distance of 160 m were carried out under various wind speed and direction. The relationship between vector wind speed and the variation of sound pressure level has been examined not only for the up/down wind conditions but also for the cross wind conditions. Secondly, the short term sound fluctuations were investigated by the use of a high energy impulsive sound generator and a loud speaker as sound sources. Sound propagation up to 300 m was examined with frequency range from 16 Hz to 4 kHz octave band. Finally, the sound speed profiles in the measurement field were estimated by two methods; one was based on the time interval during the sound propagation from the source to the receivers, the other was based on the wind speed at height of 0.6 m, 1.2 m, 2.4 m and 4.8m, and the temperature. By using those sound speed profiles, the excess attenuation was calculated by the PE method. The measured and the calculated values have been compared and the methods to estimate the influences due to wind condition have been discussed.

10:40

2aPAc8. Variation in measured sound level as a function of propagation environment and distance. Michelle E. Swearingen (Norwegian Defense Research Establishment/US Army, Postboks 25, 2027 Kjeller, Norway, michelle.swearingen@ffi.no), Morten Huseby (Norwegian Defense Research Establishment/US Army, Postboks 25, 2027 Kjeller, Norway, Morten.Huseby@ffi.no), Michael J. White (US Army Engineer Research and Development Center, 2902 Newmark Drive, Champaign, IL 61826, USA, Michael.J.White @usace.army.mil)

The propagation environment exerts a large influence on the range of received levels of impulsive events. This talk focuses on the variation in excess attenuation over durations of less than approximately 15 minutes. Data are presented for greatly different measurement distances (25 m to 7 km) and propagation environments (sparse vegetation to forested), illustrating the effects of distance and terrain cover on sounds from a propane cannon and an artillery source. Over sparse vegetation 7 km from an artillery source, the received CSEL varied 11 dB within a 12-minute duration. In measurements up to approximately 300 m from the source, variation in received level (both peak and SEL) was less than 1 dB within the forest, and much more in the open. The control of the forest canopy on the micrometeorology seems to explain the effect.

11:00

2aPAc9. The revision of the French method for road traffic noise prediction. Guillaume Dutilleux (Lab. Régional des Ponts et Chaussées, 11, rue Jean Mentelin, BP 9, 67035 Strasbourg Cedex 2, France, Guillaume.Dutilleux@equipement.gouv.fr), Jérôme Defrance (CSTB, 24 rue Joseph Fourier, 38400 Saint-Martin-d'Hères, France, jerome.defrance@cstb.fr), Benoit Gauvreau (Laboratoire Central des Ponts et Chaussées, Centre de Nantes - Route de Bouaye, BP 4129, 44341 Bouguenais cedex, France, benoit.gauvreau@lcpc.fr), Francis Besnard (Lab. Reg. Régional des Ponts et Chaussées de l'Est Parisien, Rue de l'égalité prolongée, BP 34, 93352 Le Bourget, France, francis.besnard@equipement.gouv.fr)

A revision of the French method for road traffic noise prediction (NMPB-Routes-2008) has been released. The major principles of NMPB-Routes-2008 are outlined. The most important modifications regarding the source are the reduction of its height and the introduction of two different spectra. In this complete revision, the main change is the replacement of the ISO 9613-2 - based ground attenuation formula in downward conditions by the formula for ground attenuation in homogeneous conditions of NMPB-Routes-1996

with corrected heights in order to take into account the mean curvature of rays (refraction) and its spreading (turbulence). The revised NMPB adds an attenuation term for an occasional cutting embankment. Regarding diffraction the Δdif formula is now suitable for low height barriers. The validation of the revised NMPB with respect to experiment is presented. It is based on measurement campaigns on 6 sites with complex geometries and shows that the predicted noise levels obtained from the revised NMPB are significantly closer to experimental results than in the case of the original method.

11:20

2aPAc10. Long range propagation of high speed train noise: Sound level variations before and after the pass-bys. Benjamin Cotte (Ecole Centrale de Lyon, LMFA, UMR CNRS 5509, Université de Lyon, Bât. KCA, 36 Avenue Guy de Collongue, 69134 Lyon, France, benjamin.cotte@ec-lyon.fr), Philippe Blanc-Benon (Ecole Centrale de Lyon, LMFA, UMR CNRS 5509, Ecully, 69134 Lyon, France, Philippe.Blanc-Benon@ec-lyon.fr), Franck Poisson (SNCF DIR, 45, rue de Londres, 75379 Paris, France, franck.poisson@sncf.fr), Cora Cremezi-Charlet (UIC, 16,rue J. Rey, F-75015 Paris, France, cremezi@uic.asso.fr)

It has been observed relatively frequently that high speed train (TGV) noise could be heard tens of seconds before or after the actual train pass-bys. This study is aimed at characterizing this phenomenon and the conditions in which it occurs, both experimentally and numerically. Acoustic measurements of TGV pass-bys have been performed under controlled conditions. A relatively strong wind was blowing from the South during the experiment. The measurements show that the TGV noise can be heard before the pass-bys when the TGV was coming from the South (same wind and train directions), and after the pass-bys when the TGV was coming from the North (opposite wind and train directions). This noise is relatively low in frequency (around 400 Hz), and corresponds to propagation distances that can exceed 1 km. Levels associated with this phenomenon can vary significantly over short time intervals (5-10 minutes), which raises the issue of the representativeness of TGV measurements at long ranges. It will be shown using numerical prediction methods (parabolic equation in the frequency domain, linearized Euler equations in the time domain) that these acoustic variations are mostly due to variations in the meteorological conditions between the pass-bys.

11:40

2aPAc11. A model based monitoring system for aircraft noise. Frank Van Den Berg (TNO - Science and Industry, Stieltjesweg 1, 2628 CK Delft, Netherlands, Frank.vandenBerg@tno.nl), Arno R. Eisses (TNO, Stieltjesweg 1, P.O.Box 155, 2600 AD Delft, Netherlands, Arno.Eisses@tno.nl), Pieter J. Van Beek (TNO, Stieltjesweg 1, P.O.Box 155, 2600 AD Delft, Netherlands, Pieter.vanBeek @tno.nl)

A new approach for an airport noise monitoring system is presented that comprises not only a number of measuring stations, but also a dedicated sound propagation model and an aircraft noise emission model. This approach enables estimation of noise levels in the whole area around the airport and not only at the location of the measuring stations. An additional advantage is that the locations of the measuring stations can be chosen more freely. Traditionally the measuring stations must be located near residential areas where the influence of other noise sources (such as cars or wind) cannot be eliminated. Better locations can be found that yield more reliable data and therefore more reliable noise levels. To update the sound propagation model frequently, the measuring stations not only measure noise levels, but also other parameters, like temperature and wind profile. The sound emission of the aircraft is derived from a directional aircraft noise emission model. A tool was developed to visualize the power of combining data and models in this model-based monitoring system. The use of models opens possibilities for interesting applications such as i) short term noise forecasts, ii) scenario studies with various aircraft distributions and iii) enforcement of noise limits.

Contributed Papers

12:00

2aPAc12. The variability of acoustical turbulence in the atmospheric boundary layer. Sylvain Cheinet (ISL, 5 Rue du General Cassagnou, BP 70034, 68301 Saint-Louis, France, sylvain.cheinet@isl.eu)

Outside sound propagation is affected by small-scale turbulence in the atmospheric boundary layer through refractive processes. These effects modulate the performance of acoustical sensors, and are at the basis of the atmospheric remote sensing by sodar. Previous studies have documented the impact of a mean turbulence profile or a statistical distribution of turbulence. In this study, we use a high-resolution atmospheric model called LES to reveal the spatial and temporal variability of the small-scale turbulence. First, we introduce some standard results on the role of various eddy sizes on acoustical propagation. Second, we discuss the methodology to derive the acoustical refractive index fluctuations from LES data. Third, we analyze the LES prediction in the case of a fair-weather boundary layer, emphasizing the impact of large-scale convective organization. Finally, we discuss some challenges in attempting to predict the acoustical turbulence from present-day weather forecasts.

12:20

2aPAc13. Sound propagation in areas with a complex meteorology: a meteorological-acoustical model. Frits Van Der Eerden (TNO - Science and Industry, Stieltjesweg 1, 2628 CK Delft, Netherlands, frits.vandereerden@tno.nl), Frank Van Den Berg (TNO - Science and Industry, Stieltjesweg 1, 2628 CK Delft, Netherlands, Frank.vandenBerg@tno .nl)

Long range sound propagation is largely affected by the vertical wind and temperature gradients. These gradients are more complicated in areas where the meteorology can be complex, such as: coastal areas, islands, and lake districts. Furthermore, the gradients usually vary as a function of the horizontal distance, for instance at water-land crossings near a coast or a lake. As a result the sound propagation in these areas cannot be calculated with ″standard″ acoustic models, such as the ISO 9613 or Harmonoise engineering model. By using an advanced meso-scale meteorological model, which is using large-scale weather forecast data, and an acoustical model, that incorporates horizontal and vertical meteorological variations, long range sound propagation in such complex areas is calculated. In this paper

we present two applications of this hybrid meteorological-acoustical calculation scheme: i) propagation of impulse noise in a coastal area, and ii) propagation of industrial noise in a rural area with a lake. For the coastal area sound level contours have been calculated as a function of the meteorology for a complete year. For the lake area the effect of the lake on the sound propagation is demonstrated.

12:40-2:00 Lunch Break

Contributed Papers

2:00

2aPAc14. Horizontal wave number spectra of atmospheric acoustic fields in range-dependent environments. Kenneth E Gilbert (National Center for Physical Acoustics, University of Mississippi, University, MS 38677, USA, kgilbert@olemiss.edu), Xiao Di (National Center for Physical Acoustics, University of Mississippi, University, MS 38677, USA, xiaodi@olemiss.edu), Santosh Parakkal (National Center for Physical Acoustics, University of Mississippi, University, MS 38677, USA, sparakka @olemiss.edu)

The parabolic equation (PE) is a powerful method for computing sound propagation in range-dependent environments. However, the PE gives only the total field, with no information on the horizontal wave number spectrum of the acoustic field. In many situations, e.g., for propagation over irregular terrain, the horizontal wave number spectrum is valuable for analyzing the modal content of the acoustic field. For example, one might want to know the strength of the surface wave component at different ranges. A spectral decomposition method developed by Gilbert and Evans for ocean acoustics is applied here to atmospheric propagation over irregular terrain. This paper shows that for a PE field $p(z)$ at range r, the horizontal wave number spectrum $\phi(\kappa,z)$ can be obtained directly and efficiently by solving a one-dimensional elliptic equation that uses the field $p(z)$ as a source term. The derivation of the spectral decomposition equation is given along with a numerical method for solving it. Examples are presented and discussed for propagation over irregular terrain. [Research supported by the U. S. Army TACOM-ARDEC at Picatinny Arsenal, New Jersey]

2:20

2aPAc15. Numerical modeling of sonic boom propagation from hypersonic aircraft. Alexandra Loubeau (Institut Jean Le Rond d'Alembert, Université Pierre et Marie Curie, Boites 161 et 162, 4 place Jussieu, 75252 Paris Cedex 05, France, loubeau@lmm.jussieu.fr), François Coulouvrat (Institut Jean Le Rond d'Alembert, Université Pierre et Marie Curie, Boites 161 et 162, 4 place Jussieu, 75252 Paris Cedex 05, France, coulouvr@ccr.jussieu.fr)

A numerical study of sonic boom propagation from hypersonic aircraft is performed including the effects of nonlinearity, atmospheric absorption and dispersion, and atmospheric stratification. A second-order split-step algorithm, which alternates application of nonlinearity in the time domain and complex absorption in the frequency domain, allows for a faster convergence of results with fewer range steps than with conventional first-order algorithms. Nonlinearity is calculated using the potential, the integral of the pressure, as proposed by Burgers and later applied to sonic booms by Hayes et al. This method, an alternative to Landau's law of equal areas, efficiently locates the shock position by selecting the maximum potential in multivalued regions. Definition of atmospheric absorption at high altitudes is important for modeling the propagation of sonic booms from hypersonic aircraft. Some aspects of an extended absorption model by Sutherland and Bass are adopted, therefore, which extend absorption predictions above the 20 km limit of the current ISO and ANSI standards. The study is completed using the meteorological conditions at two locations, Le Havre, France and Edwards Air Force Base, CA, USA, over the course of a year. [Work supported by European Union through ATLLAS AST5-CT-2006-030729, meteorological data provided by ECMWF.]

2:40

2aPAc16. Road noise: characterization and estimation of uncertainty due to meteorological effects. David Ecotiere (Lab. Régional des Ponts et Chaussées, 11, rue Jean Mentelin, BP 9, 67035 Strasbourg Cedex 2, France, david.ecotiere@equipement.gouv.fr)

Meteorological effects can lead to important temporal fluctuations of the sound level in outdoor sound propagation. These fluctuations lead to sound level uncertainties that are rarely estimated. A method based on the coupling of a model of sound propagation and a temporal micrometeorological model is used to quantify sound level fluctuations only due to meteorological fluctuations, over a very long period (typ. 10-30 years). Some statistical analysis are presented: diary or seasonal fluctuations, influence of the duration of observation on the accuracy of the estimation of a LAeq. A semi-analytical method is also proposed for characterizing the uncertainty of the sound level of a distribution of punctual sources. An application to a road noise source is presented.

3:00

2aPAc17. A numerical study of sound propagation over urban canyons. Martin Schiff (Division of Applied Acoustics, Chalmers University of Technology, 41296 Göteborg, Sweden, schiff@student.chalmers.se), Maarten Hornikx (Applied Acoustics, Chalmers University of Technology, Sven Hultins Gata 8a, SE-41296 Gothenburg, Sweden, maarten.hornikx@chalmers.se), Jens Forssén (Division of Applied Acoustics, Chalmers University of Technology, 41296 Göteborg, Sweden, jens .forssen@chalmers.se)

Because quiet areas in dense urban environments are important, there is high interest in propagation to areas shielded from direct road traffic noise. Sound levels in shielded areas are strongly influenced by distant sources, so intermediate propagation factors such as metrology, screening, and intermediate canyons must therefore be addressed in a realistic propagation model. A numerical investigation of sound propagation across the open tops of intermediate urban canyons has been performed, using the Parabolic Equation and Equivalent Sources methods. Results have been collected for various canyon geometries, and the influence of multiple canyons, canyon/rooftop absorption, variable rooftop height, and correlated versus uncorrelated source models has been investigated. By characterizing the ″insertion loss″ of canyons intermediate to the source and receiver, the influence of these intermediate canyons could be addressed simply, without the overhead of a detailed numerical calculation.

3:20

2aPAc18. A validation test for the Acoustic Footprint Mission Planning System. Doru Velea (QinetiQ North America, Technology Solutions Group, 12030 Sunrise Valley Dr., Suite 400, Reston, VA 20191, USA, dvelea@plansys.com), Troy D. Schultz (Wyle Laboratories Inc., 241 18th Street S., Suite 701, Arlington, VA 22202, USA, troy.schultz@wylelabs.com), Kenneth J. Plotkin (Wyle Laboratories Inc., 241 18th Street S., Suite 701, Arlington, VA 22202, USA, kenneth.plotkin@wylelabs.com), Andy Rogers (QinetiQ North America, Technology Solutions Group, 12030 Sunrise Valley Dr., Suite 400, Reston, VA 20191, USA, arogers@plansys.com)

QinetiQ North America, Technology Solutions Group (QNA) and Wyle Laboratories have integrated two mature, proprietary technologies into a prototype Acoustic Footprint Mission Planning System. Wyle's Noise Model Simulation (NMSim) uses validated linear noise propagation routines in combination with ray-tracing algorithms based on weather data provided by QNA's Precision Airdrop System (WindPADS) to predict the time his-

tory of spectral noise levels from a flying aircraft at any number of user-defined receptor locations. Through interpolation over a ground-based receptor grid, the impact of noise propagated through a stratified atmosphere may be quantified in terms of audibility at any point inside the acoustic footprint. Weather data for the NMSim ray-tracing routines is extracted from the WindPADS three-dimensional forecast of wind, pressure, temperature and humidity in the atmosphere as a function of time. The three-dimensional field is the result of physical and dynamic assimilation of forecast and measured atmospheric data, with wind-forcing by the underlying terrain. This paper describes the results of a validation test performed at Yuma Proving Ground, AZ. It is shown that the noise propagation model predictions agree satisfactorily with the measurements of a C-130 cargo plane. [Work supported by Natick Soldier Center.]

3:40-5:20 Posters

Lecture sessions will recess for presentation of poster papers on various topics in acoustics. See poster sessions for topics and abstracts.

Contributed Papers

5:20

2aPAc19. Modal probabilistic analysis. Christophe Heinkele (ENTPE/DGCB, Rue Maurice Audin, 69518 Vaulx-en-Velin, France, heinkele@entpe.fr), Claude-Henri Lamarque (rue Maurice Audin, 69100 Vaulx-en-Velin, France, lamarque@entpe.fr)

In this paper, we first recall a method for estimating the numerical Probability Density Function (PDF) with Parzen-Rosenblatt estimators of experimental data (like the sound absorption coefficient with the Kundt's tube). Then we focus on the model of Mikki which is used as a predictive tool. We are interested then in inversing the model and in identifying the 3 parameters (q,σ,ϕ) of Mikki's model. But we want to go further and to identify from the estimated PDF directly the PDF of the 3 parameters. We explain first when it is possible, then we give some examples to illustrate the method. This work allows for evaluating the robustness of a model from experimental data.

5:40

2aPAc20. An experimental evaluation of a new approach to aircraft noise modelling. Foort De Roo (TNO Science and Industry, Stieljesweg 1, 2628CK Delft, Netherlands, foort.deroo@tno.nl), Erik Salomons (TNO Science and Industry, Stieljesweg 1, 2628CK Delft, Netherlands, erik.salomons@tno.nl)

Common engineering models for aircraft noise, such as INM, yield noise levels by interpolation of Noise Power Distance (NPD) tables. In the European project Imagine (2004 2006), a different approach was proposed: the source is characterized by an emission spectrum and the received noise spectrum is calculated by subtracting the propagation attenuation spectrum from this emission spectrum. This is the usual approach for noise mapping of most noise sources. The aircraft emission spectrum is a function of (downward) emission direction, so each aircraft is represented by a hemisphere of emission spectra. This has been described by Butikofer in Acta Acustica 93 (2007). As hemisphere emission data are not yet available for all aircraft types, a 'reverse engineering' scheme was developed within Imagine to derive first order estimates of hemispheres from NPD tables. To gain experience with this approach, we have performed an experiment near Amsterdam airport. Various types of data were collected for a set of aircraft departures, including noise data at eleven positions and flight data. The Imagine approach was used to calculate noise contours, and noise spectra at the eleven positions. The differences between measured and calculated spectra may be used as a basis for improving the first order estimates of the hemispheres.

6:00

2aPAc21. Sound propagation in a street canyon: A study by modal decomposition. Adrien Pelat (Laboratoire d'Acoustique de l'Université du Maine, Avenue Olivier Messiaen, 72085 Le Mans, France, adrien.pelat.etu@univ-lemans.fr), Simon Félix (Laboratoire d'Acoustique de l'Université du Maine, Avenue Olivier Messiaen, 72085 Le Mans, France, simon.felix@univ-lemans.fr), Vincent Pagneux (Laboratoire d'Acoustique de l'Université du Maine, UMR CNRS 6613, AV. O. Messiaen, 72085 Le Mans, France, vincent.pagneux@univ-lemans.fr), Christophe Ayrault(LAUM, CNRS, Université du Maine, Av. O. Messiaen, 72085 Le Mans, France, christophe.ayrault@univ-lemans.fr), Olivier Richoux (Laboratoire d'Acoustique de l'Université du Maine, Avenue Olivier Messiaen, 72085 Le Mans, France, olivier.richoux@univ-lemans.fr)

An urban, U-shaped, street canyon being considered as an open waveguide in which the sound may propagate, one is interested in a multimodal approach to describe the sound propagation within. The key point in such a multimodal formulation is the choice of the basis of local transversal modes on which the acoustic field is projected. For a classical waveguide, with a simple and bounded cross-section, a complete orthogonal basis can be analytically obtained. The case of an open waveguide is more difficult, since no such a basis can be exhibited. However, an open resonator, as displays for example the U-shaped cross-section of a street, presents resonant modes with complex eigen frequencies, owing to radiative losses. This work first presents how to numerically obtain these modes and, then, how they can be used as a basis for the modal decomposition of the sound field in a street canyon. Results are compared with experimental measurements on a scale model.

6:20

2aPAc22. Acoustical waves propagation in rough walls street. Bertrand Lihoreau (Laboratoire d'Acoustique de l'Université du Maine, Avenue Olivier Messiaen, 72085 Le Mans, France, bertrand.lihoreau@univ-lemans.fr), Simon Félix (Laboratoire d'Acoustique de l'Université du Maine, Avenue Olivier Messiaen, 72085 Le Mans, France, simon.felix@univ-lemans.fr), Claude Depollier (Laboratoire d'Acoustique de l'Université du Maine, Avenue Olivier Messiaen, 72085 Le Mans, France, claude.depollier@univ-lemans.fr)

We present a method for the numerical calculation of a sound wave propagating in a two dimensional rough-sided street. Is this situation, the wave is subject to multiple scattering at the two boundaries. The propagation is governed by a parabolic equation. We show that the amplitude of a pulse may be expressed as the fractional Fourier transform of the incident pulse, and that the order of the transformation is related to the distance between the source and the point of observation. Numerical simulations are proposed as illustration of this model and are compared to experimental results.

6:40

2aPAc23. A high-density infrasound array of particle velocity sensors in the Netherlands. Arnout Tim Van Zon (Royal Netherlands Meteorological Institute (KNMI), PO Box 201, 3730 AE De Bilt, Netherlands, zon@knmi.nl), Laeslo G. Evers (Royal Netherlands Meteorological Institute (KNMI), PO Box 201, 3730 AE De Bilt, Netherlands, evers@knmi.nl)

A small aperture, High-Density Infrasound Array (HDIA) is being operated by the Royal Netherlands Meteorological Institute (KNMI). This 80 sensor array is part of the geophysical application within LOFAR, i.e. an astronomical low-frequency array in the Netherlands. HDIA occupies an area of 100 by 100 meter, so about the size of a noise reducer used in infrasound arrays for verification purposes. HDIA will be able to estimate the wind-noise correlation length, which has implications for noise reducer design. Of the 80 instruments, 74 are Microflowns. These measure particle velocity and have a directional sensitivity. If two of them are closely spaced, then the azimuth of the incoming sound wave can be calculated from the

amplitude ratio. The field setup has 37 elements, each containing a pair of Microflowns. Six elements also have a pressure microphone. We will present the first results of using the vector properties of the particle velocity to estimate the direction of arrival (DOA) of events. These will be compared with DOA-estimates from beamforming of 1) the pressure data, 2) the particle velocity data and 3) pressure data of a nearby 6-element microbarometer array. Furthermore, the observed correlation length of wind will be discussed.

TUESDAY MORNING, 1 JULY 2008 ROOM 362/363, 8:00 A.M. TO 1:20 P.M.

Session 2aPAd

Physical Acoustics: Photoacoustics I

Gerald Diebold, Cochair
Department of Chemistry, Brown University, Providence, Rhode Island 02912, USA

Christ Glorieux, Cochair
Lab. ATF, Katholieke Universiteit Leuven, Celestijnenlaan 200D, Leuven, B-3001, Belgium

Invited Papers

8:00

2aPAd1. On the optical generation and detection of high frequency ultrasounds: thermal and non-thermal processes. Pascal Ruello (LPEC/UMR 6087/CNRS/Université du Maine, Avenue Olivier Messiaen, 72085 Le Mans Cedex 09, France, pascal.ruello@univ-lemans.fr), Philippe Babilotte (LPEC/UMR 6087/CNRS/Université du Maine, Avenue Olivier Messiaen, 72085 Le Mans Cedex 09, France, philippe.babilotte.etu@univ-lemans.fr), Shuo Zhang (INSP - UMR 7588 CNRS & Université Pierre et Marie Curie, 140 Rue de Lourmel, 75015 Paris, France, Shuo.Zhang@insp.jussieu.fr), Denis Mounier (LPEC/UMR 6087/CNRS/Université du Maine, Avenue Olivier Messiaen, 72085 Le Mans Cedex 09, France, denis.mounier@univ-lemans.fr), Jean-Marc Breteau (LPEC/UMR 6087/CNRS/Université du Maine, Avenue Olivier Messiaen, 72085 Le Mans Cedex 09, France, jean-marc.breteau@univ-lemans.fr), Mathieu Edely (LPEC/UMR 6087/CNRS/Université du Maine, Avenue Olivier Messiaen, 72085 Le Mans Cedex 09, France, mathieu.edely@univ-lemans.fr), Patrick Laffez (Université François Rabelais, Tours, IUT Blois, 6, place Jean Jaures, 41029 Blois, France, patrick.laffez@univ-tours.fr), Alain Bulou (LPEC/UMR 6087/CNRS/Université du Maine, Avenue Olivier Messiaen, 72085 Le Mans Cedex 09, France, alain.bulou@univ-lemans.fr), Bernard Perrin (INSP - UMR 7588 CNRS & Université Pierre et Marie Curie, 140 Rue de Lourmel, 75015 Paris, France, bernard.perrin@insp.jussieu.fr), Vitali Gusev (LPEC/UMR 6087/CNRS/Université du Maine, Avenue Olivier Messiaen, 72085 Le Mans Cedex 09, France, vitali.goussev@univ-lemans.fr)

We report on the results of the generation and detection by femtosecond laser pulses of the acoustic waves at frequencies of tens to hundreds GHz in semiconductors and in oxides compounds exhibiting phase transition. We focus first on the generation mechanisms involved to achieve opto-acoustic transformations. Particular attention will be paid to the cases where classical thermal effects (thermoelastic coupling) drive the mechanism of generation of acoustic phonons and those where non-thermal effects become significant and sometimes dominant sources of acoustic phonons field. In the latter cases, we will especially focus on the phonons generation based on photo-induced modifications of microscopic internal electric fields (potential deformation) and also on the use of photoexcited carriers dynamics (carriers recombination) as a tuning parameter of the photo-generated ultrasounds spectrum. Secondly, we give the examples demonstrating that the choice of optical frequency for ultrasound detection influences not only the amplitude of the detected signal but provides an opportunity to detect separately high or low frequencies in the spectrum of ultrasounds. This study was supported by CPER and ANR project No. BLAN06-3-136284.

8:20

2aPAd2. Optical detection of longitudinal and shear acoustic waves with laser picosecond acoustics. Osamu Matsuda (Division of Applied Physics, Graduate School of Engineering, Hokkaido University, 060 8628 Sapporo, Japan, omatsuda@eng.hokudai.ac.jp), Oliver B. Wright (Division of Applied Physics, Graduate School of Engineering, Hokkaido University, 060 8628 Sapporo, Japan, olly@eng.hokudai.ac.jp), David H. Hurley (Materials Characterization Department, Idaho National Laboratory, P.O.Box 1625, Idaho Falls, ID 83415-2209, USA, David.Hurley@inl.gov), Vitali Gusev (LPEC/UMR 6087/CNRS/Université du Maine, Avenue Olivier Messiaen, 72085 Le Mans Cedex 09, France, vitali.goussev@univ-lemans.fr), Ken'Ichi Shimizu (University Chemical Laboratory, Keio University, 4-1-1 Hiyoshi, Kohoku-ku, 223-8251 Kanagawa, Japan, shimizuk@econ.keio.ac.jp)

The absorption of picosecond light pulses in a medium can generate sub-THz acoustic waves. These cause a transient optical reflectance change that can be monitored by delayed probe light pulses. This technique, termed laser picosecond acoustics, can be used for the nondestructive evaluation of the physical properties of thin films and substrates. This paper describes a general method for quantitative analysis of such reflectance changes. It is applicable to multiple anisotropic layers that may be opaque or transparent. Longitudinal or shear acoustic waves propagating along the stacking direction of the multilayers modulate the dielectric permittivity anisotropically and inhomogeneously through the photoelastic effect, through local rotation, or through the surface and interface displacements. We describe how the optical reflectance for obliquely incident probe light can be calculated for the modulated medium.

We then demonstrate the method with reference to experimental results for a sample consisting of a silica film on a zinc substrate in which both longitudinal and shear acoustic waves are generated and detected. The analysis yields the film thickness, sound velocity, and photoelastic tensor components, for example. The method is also applicable to various light scattering problems involving the inhomogeneous modulation of optical properties such as in photothermal experiments.

Contributed Papers

8:40

2aPAd3. Experimental studies of generation and propagation of high frequency acoustic waves in various solid materials using ultraviolet picosecond laser pulses. Eirini Tzianaki (Department of Electronics, Technological Educational Institute of Crete, Romanou 3, 73133 Chania, Greece, i.tzianaki@mail.chania.teicrete.gr), Michael Tatarakis (Department of Electronics, Technological Educational Institute of Crete, Romanou 3, 73133 Chania, Greece, m.tatarakis@chania.teicrete.gr), Makis Bakarezos (Department of Music Technology and Acoustics, Technological Educational Institute of Crete, 1 E. Daskalaki Str., 74100 Rethymnon, Greece, bakarezos@stef.teicrete.gr), Maria Elefteriou (Department of Music Technology and Acoustics, Technological Educational Institute of Crete, 1 E. Daskalaki Str., 74100 Rethymnon, Greece, marel@physics.uoc.gr), Nektarios Papadogiannis (Department of Music Technology and Acoustics, Technological Educational Institute of Crete, 1 E. Daskalaki Str., 74100 Rethymnon, Greece, npapadogiannis@stef.teicrete.gr), Spyros Kazianis (Department of Physics, University of Ioannina, 45110 Ioannina, Greece, skaziannis@in.gr), Costas Kosmidis (Department of Physics, University of Ioannina, 45110 Ioannina, Greece, kkosmidis@uoi.gr), Andreas Lyras (Department of Physics, University of Ioannina, 45110 Ioannina, Greece, alyras@uoi.gr)

The generation of high frequency acoustic waves by picosecond laser pulses in the ultraviolet region and their detection by optical interferometric schemes, is presented. The two main acoustical modes, longitudinal and shear are clearly apparent in the time resolved spectra of solid materials, for various absorbing energies, extending from the thermoelastic to the ablative regime. The ultraviolet light is strongly absorbed by insulator materials like Pyrex and thus strong elastic waves are produced. From the time separation of the longitudinal waves we have deduced values for the speed of sound in various materials and of different thickness, that are in very good agreement with those reported in the literature. Also the time bandwidth of the sound waves is measured and significant differences, originating from different sample thickness, are apparent.

9:00

2aPAd4. Effect of photoacoustic generation mechanisms on transient grating measurements of thin films on silicon. Alexei A. Maznev (Department of Applied Physics, Hokkaido University, Kita 13 Nishi 8, Kita-ku, 060-8628 Sapporo, Japan, alexei.maznev@gmail.com)

Laser induced transient gratings technique is widely used for non-contact measurements of surface acoustic waves (SAWs). One major application of such measurements is characterization of thin films used in microelectronics. A peculiar phenomenon has been observed in transient gratings measurements of thin films on a silicon substrate: if the film is transparent, there is a systematic discrepancy between the measured and expected SAW velocity values that cannot be accounted for by instrumental errors. However, as soon as the sample is coated by an opaque metal film, the discrepancy disappears. In this presentation, we will show that the origin of the effect is in the competition of thermal and electronic mechanisms of the optical generation of sound in silicon. We will also describe another effect of the same origin observed on very thin semi-transparent metal films: at a certain film thickness, the SAW signal vanishes as the thermal expansion of the film and the contraction of silicon caused by photoexcited carriers cancel each other.

9:20

2aPAd5. Thickness measurement of submicron metal coatings on transparent substrate by laser optoacoustic method. Ivan Pelivanov (International Laser Center of Moscow State University, Vorob'yovy Gory, 1, 119992 Moscow, Russian Federation, pelivanov@ilc.edu.ru), Daria Kopylova (International Laser Center of Moscow State University, Vorob'yovy Gory, 1, 119992 Moscow, Russian Federation, dskopylova@mail.ru), Nataliya Podimova (Moscow State University, MSU, 1, building 2, GSP-2, Leninskiye Gory, 119992 Moscow, Russian Federation, npodymova@mail.ru), Alexander Karabutov (Moscow State University, MSU, 1, building 2, GSP-2, Leninskiye Gory, 119992 Moscow, Russian Federation, akarabutov@gmail.com)

New nondestructive method for measurement of the thickness of submicron metal coatings on a transparent dielectric substrate is developed. Theoretical background includes the consecutive solution of the thermal and acoustic problems. The experimental part is based on the measurement of frequency dependence of the laser-ultrasound excitation efficiency on the metal coating thickness for the system where the coating is covered by a transparent liquid. Three chrome coatings of various thicknesses (0.2, 0.3 and 0.6 micrometers) deposited on a quartz substrate were tested experimentally. A rough estimate of their thickness was obtained from the sputtering time. Two different experimental modes were used: forward mode (laser pulses irradiate the metal film through the substrate, excited acoustical transients are detected in the liquid) and backward mode (both laser irradiation of the film and detection of excited acoustical transients are performed in the liquid). Spectral dependencies of the thermo-optical transformation efficiency were calculated analytically and obtained experimentally for both signal detection modes. The values of the film thicknesses were determined by the least squares fitting of the theoretical curves to experimental data. It is demonstrated, that the developed optoacoustic method can be used for metal coatings thickness measurement in the range of 50 nm - 5 microns with inaccuracy of 50 nm.

9:40-10:00 Break

Invited Papers

10:00

2aPAd6. Acoustic phenomena in porous media studied by transient grating spectroscopy: a critical test of the Biot theory. Riccardo Cucini (European Lab. for Non-Linear Spectroscopy (LENS), Univ. di Firenze, via Nello Carrara 1, 50019 Sesto Fiorentino (Fi), Italy, cucini@lens.unifi.it), Andrea Taschin (European Lab. for Non-Linear Spectroscopy (LENS), Univ. di Firenze, via Nello Carrara 1, 50019 Sesto Fiorentino (Fi), Italy, taschin@lens.unifi.it), Paolo Bartolini (European Lab. for Non-Linear Spectroscopy (LENS), Univ. di Firenze, via Nello Carrara 1, 50019 Sesto Fiorentino (Fi), Italy, bart@lens.unifi.it), Renato Torre (European Lab. for Non-Linear Spectroscopy (LENS), Univ. di Firenze, via Nello Carrara 1, 50019 Sesto Fiorentino (Fi), Italy, torre@lens.unifi.it)

The propagation of sound in a porous solid filled by a liquid can be described by a phenomenological model introduced by M. A. Biot, that is still extensively used to predict the essential acoustic properties of a wide variety of porous media. Nevertheless testing of the Biot theory at ultra/hypersonic frequencies and in porous media with nanometric scale heterogeneities remains an open issue. We

studied the propagation of acoustic waves in two liquid-filled porous glasses by heterodyne detected transient grating experiments [1]. A test of the Biot theory is presented under two new regimes, namely, for a new frequency range up to 1.3 GHz and for porous media with nanometric scale heterogeneities [2]. We show that the Biot theory describes the sound velocity data correctly, but does not account for the acoustic attenuation. We suggest that the acoustic damping is mainly due to the dissipation mechanisms intrinsic of the matrix and the liquid which are not accounted for in the theory. [1] Time-resolved spectroscopy of complex liquids, edited by Torre R. (Springer, New York) 2008. [2] A. Taschin, R. Cucini, P. Bartolini, R. Torre, Europhys. Lett. In press.

10:20

2aPAd7. Laser ultrasonic study of Lamb wave propagation in different film loading configurations. Xiaodong Xu (Modern Acoustics, Institute of Acoustics, Nanjing University, 210093 Nanjing, China, xdxu@nju.edu.cn), G. Shkerdin (Laboratorium voor Akoestiek en Thermische Fysica - Departement Natuurkunde en Sterrenkunde - Katholieke Universiteit Leuven, Celestijnenlaan 200D, B-3001 Leuven, Belgium, shkerdin@yahoo.com), Christ Glorieux (Lab. ATF, Katholieke Universiteit Leuven, Celestijnenlaan 200D, B-3001 Leuven, Belgium, christ.glorieux@fys.kuleuven.be)

A study is performed concerning the propagation Lamb waves in technologically and scientifically interesting configurations. In a first configuration a thin film was loaded with different liquids on its two sides. Three experimental laser ultrasonic configurations, line excitation with scanning detection, grating excitation with single point detection, and grating excitation with scanning probe beam, were implemented. All experimental results were found to be consistent between experimental methods and with theoretical predictions. The configuration can be implemented in monitoring applications where elastic properties of liquids that are kept in containers can be determined via the outside container wall. In a second configuration laser excited and detected Lamb waves in a rubber-metal bi-layer were used to determine the highly damped elastic properties of rubber.

Contributed Papers

10:40

2aPAd8. Zero-group velocity modes and local vibrations of an elastic plate. Claire Prada (Laboratoire Ondes et Acoustique, ESPCI, Université Paris 7, CNRS, 10 rue Vauquelin, 75005 Paris, France, claire.prada-julia@espci.fr), Dominique Clorennec (Laboratoire Ondes et Acoustique, ESPCI, Université Paris 7, CNRS, 10 rue Vauquelin, 75005 Paris, France, dominique.clorennec@espci.fr), Daniel Royer (Laboratoire Ondes et Acoustique, ESPCI, Université Paris 7, CNRS, 10 rue Vauquelin, 75005 Paris, France, daniel.royer@espci.fr)

Elastic plates or cylinders can support guided modes with zero group velocity (ZGV) at a nonzero value of the wave number. The conditions required for the existence of ZGV Lamb modes in isotropic plates are discussed. It is shown that these modes appear in a range of Poisson's ratio over the value for which the cut-off frequency curves of modes belonging to the same family intercept, i.e for a bulk wave velocity ratio equal to a rational number. An interpretation of this phenomenon in terms of a strong repulsion between a pair of modes having a different parity in the vicinity of the cutoff frequencies is given. Using laser-based ultrasonic techniques, we experimentally investigate some properties of these ZGV Lamb modes: resonance, backward wave propagation, interference between backward and forward waves. Experiments performed with materials of various Poisson's ratio demonstrate that the resonance spectrum of an unloaded elastic plate, locally excited by a laser pulse, is dominated by the ZGV Lamb modes. From these local resonance frequencies, thickness variations can be measured accurately and material properties like the Poisson's ratio, bulk acoustic wave velocities or material attenuation can be determined without any mechanical contact.

11:00

2aPAd9. Mechanical contacts probed with picosecond ultrasonics. Thomas Dehoux (Division of Applied Physics, Graduate School of Engineering, Hokkaido University, 060-8628 Sapporo, Japan, dehoux@eng.hokudai.ac.jp), Motonobu Tomoda (Division of Applied Physics, Graduate School of Engineering, Hokkaido University, 060-8628 Sapporo, Japan, mtomoda@eng.hokudai.ac.jp), Oliver B. Wright (Division of Applied Physics, Graduate School of Engineering, Hokkaido University, 060 8628 Sapporo, Japan, olly@eng.hokudai.ac.jp)

We investigate the contact between a thin metal film and a ball bearing indented to nanometre depths using picosecond ultrasonics. The area of contact is acoustically imaged to micron spatial resolution using GHz acoustic pulses produced by ultrashort pulsed optical excitation of the film through a transparent substrate. In particular, acoustic echoes are detected through transient optical reflectance changes that are monitored by probe optical pulses. In this way we image the acoustic reflection coefficient at the interface between the film and the indenter. In addition, by imaging the arrival time of the acoustic echoes we determine the penetration profile of the indenter to nanometre precision. Furthermore, imaging the transient thermoreflectance gives a different means for measuring the contact area through spatial variations in thermal diffusion. We thus demonstrate that picosecond ultrasonics and thermoreflectance provide powerful tools for the non-contact evaluation of mechanical contacts. These techniques could be applied to the in situ characterization of contact interfaces between machine elements.

Invited Paper

11:20

2aPAd10. Photoacoustic imaging and laser-ultrasonics using Fourier domain reconstruction methods. Peter Burgholzer (Upper Austrian Research, Hafenstr. 47, 4020 Linz, Austria, peter.burgholzer@uar.at), Thomas Berer (Upper Austrian Research, Hafenstr. 47, 4020 Linz, Austria, thomas.berer@uar.at), Bernhard Reitinger (Upper Austrian Research, Hafenstr. 47, 4020 Linz, Austria, bernhard.reitinger@uar.at), Robert Nuster (Karl-Franzens-Universität Graz, Universitätsplatz 5, 8010 Graz, Austria, ro.nuster@uni-graz.at), Günther Paltauf (Karl-Franzens-Universität Graz, Universitätsplatz 5, 8010 Graz, Austria, guenther.paltauf@uni-graz.at)

Laser-ultrasonics as well as photoacoustic imaging use optically generated acoustic waves detected at the sample surface to image its interior. In laser-ultrasonics a laser pulse is absorbed at the sample surface generating an ultrasound pulse that propagates into the sample, is subsequently reflected at internal structures, and finally detected at the surface by an interferometer. In photoacoustic imaging ultrasound is generated by heating of light-absorbing structures inside of an optical semitransparent sample. The goal in photoacoustic imaging is to recover the spatial distribution of the absorbed energy density inside the sample from the acoustic pressure signals measured outside the sample (photoacoustic inverse problem). Fourier reconstruction is based on the decomposition into plane waves and is a fast and efficient method used in photoacoustic imaging. Interpolation is needed when signal Fourier components are mapped to

source Fourier components. We have shown that the synthetic aperture focusing technique (SAFT) in frequency domain, which needs no interpolation, and the Fourier reconstruction method are mathematically equivalent if the step size of the spatial discretization goes to zero. Both imaging methods are compared using simulated data and measurement data acquired with our interferometer set-up. This work has been supported by the Austrian Science Fund (FWF), project P18172-N02 and project L418-N20.

Contributed Papers

11:40

2aPAd11. Stroboscopic interferometric full-field imaging of laser-induced surface acoustic waves. Bart Sarens (Laboratorium voor Akoestiek en Thermische Fysica - Departement Natuurkunde en Sterrenkunde - Katholieke Universiteit Leuven, Celestijnenlaan 200D, B-3001 Leuven, Belgium, bart.sarens@fys.kuleuven.be), Osamu Matsuda (Division of Applied Physics, Graduate School of Engineering, Hokkaido University, 060 8628 Sapporo, Japan, omatsuda@eng.hokudai.ac.jp), Xiaodong Xu (Modern Acoustics, Institute of Acoustics, Nanjing University, 210093 Nanjing, China, xdxu@nju.edu.cn), Georgios Kalogiannakis (Laboratorium voor Akoestiek en Thermische Fysica - Departement Natuurkunde en Sterrenkunde - Katholieke Universiteit Leuven, Celestijnenlaan 200D, B-3001 Leuven, Belgium, Georgios.Kalogiannakis@vub.ac.be), Robbe Salenbien (Lab. ATF, Katholieke Universiteit Leuven, Celestijnenlaan 200D, B-3001 Leuven, Belgium, robbe.salenbien@fys.kuleuven.be), Renaud Côte (Lab. ATF, Katholieke Universiteit Leuven, Celestijnenlaan 200D, B-3001 Leuven, Belgium, renaud.cote@fys.kuleuven.be), Christ Glorieux (Lab. ATF, Katholieke Universiteit Leuven, Celestijnenlaan 200D, B-3001 Leuven, Belgium, christ.glorieux@fys.kuleuven.be)

Surface acoustic waves (SAW) have the interesting property that they specifically interact with surface and sub-surface regions, rendering them suitable for non-contact investigation of sub-surface properties and heterogeneities. Transmission, reflection and diffraction effects of SAW propagation are analysed in order to reveal information on the region over which they propagate. Laser excitation allows to efficiently excite SAW with short wavelengths, enhancing both the lateral and the depth resolution. Typically information on the waves is collected by scanning a part of the surface of interest with a fast laser probe, using the surface displacement or slope as a real time witness of the wave field. Here we present results obtained by a full field imaging technique [1], in which the sample is repetitively excited by a pulsed pump laser, and the wave displacement field is stroboscopically gathered by illuminating the sample surface with an electronically delayed pulsed probe laser, whose displacement induced optical path variations are visualized by interferometrically analyzing it. In this work, the technique is applied on different samples, varying the geometry of the pump laser beam pattern, the interferometric configuration, and the heterogeneities of the sample. [1] ″Phase mask-based interferometer: operation principle, performance, and application to thermo-elastic phenomena″, C. Glorieux, J.D. Beers, E.H. Bentefour, K. Van de Rostyne and K.A. Nelson, Rev. Sci. Instrum. **75**(9), 2906-2920 (2004).

12:00

2aPAd12. Laser-ultrasonic defectoscope with focused transducer. Alexander Karabutov (Moscow State University, MSU, 1, building 2, GSP-2, Leninskiye Gory, 119992 Moscow, Russian Federation, akarabutov@gmail.com), Nataliya Podimova (Moscow State University, MSU, 1, building 2, GSP-2, Leninskiye Gory, 119992 Moscow, Russian Federation, npodymova@mail.ru)

The novel focused laser-ultrasonic transducer for ultrasonic microscopy of constructive materials is presented. Short and sharp ultrasonic pulse is produced by optoacoustic effect - excitation of ultrasound by absorption of nanosecond laser pulse in special layer. Absorbing layer is integrated with the wide-band ultrasonic receiving system into common unit - laser-ultrasonic transducer. Ultrasound beam is focused by acoustical lens with relatively low numerical aperture (convergence angle - 15°, focal distance - 20 mm). An acoustic impedance of the lens matches that of the laser-ultrasonic transducer. The duration of the irradiated ultrasonic pulse was ~0.1 μs. The focused laser-ultrasonic transducer was mounted on 3-D linear translation system. The object under control and the transducer was placed in a tank with distilled water. The transducer was moved across the object with 2.5 μm step. The caustic of the probe ultrasonic beam was analyses by sliding the transducer across sharp beard of a knife. The reflected ultrasonic signal was recorded by 12-bit ADC. The diameter of the focal area was 0.53 mm. The length of caustic of ultrasonic was 28 mm. The amplitude of the probe ultrasonic pulse was ~20 kPa at laser energy 0.1 mJ. The dynamic range of ultrasonic trace measurement exceeded 90 dB.

12:20

2aPAd13. Acoustic waves generated by a laser point pulse in a micrometric fiber. Damien Segur (LMP, UMR CNRS 5469, Université Bordeaux I, 351, cours de la Libération, 33405 Talence, France, d.segur@lmp.u-bordeaux1.fr), Alexander Shuvalov (LMP, UMR CNRS 5469, Université Bordeaux I, 351, cours de la Libération, 33405 Talence, France, a.shuvalov@lmp.u-bordeaux1.fr), Yong Dong Pan (Institute of Acoustics, Tongji University, 200092 Shangai, China, ypan@mail.tongji.edu.cn), Nikolay Chigarev (LPEC/UMR 6087/CNRS/Université du Maine, Avenue Olivier Messiaen, 72085 Le Mans Cedex 09, France, Nikolay.Chigarev@univ-lemans.fr), Clément Rossignol (LMP, UMR CNRS 5469, Université Bordeaux I, 351, cours de la Libération, 33405 Talence, France, c.rossignol@lmp.u-bordeaux1.fr), Bertrand Audoin (LMP, UMR CNRS 5469, Université Bordeaux I, 351, cours de la Libération, 33405 Talence, France, b.audoin@lmp.u-bordeaux1.fr)

Having emerged in the 1980s, the laser ultrasonics technique with its non-contact generation and detection process overpasses the difficulties of coupling piezoelectric transducers with curved surfaces. To date, the authors [1] have been interested in acoustic generation for cylinders opaque at a given laser wavelength and for the acoustic source located at the cylinder surface. In this presentation, assuming point focusing of the laser pulses, we propose a three-dimensional (3D) semi-analytical model for acoustic waves generation and propagation in a partly transparent isotropic cylinder. First, the radial displacement at any position on the free surface is derived, in a 3D Fourier domain, for an inner point source. The response to a volume-source distribution along a radius is obtained as a convolution of the above Green function with the corresponding source distribution caused by optical absorption. Three inverse transforms are then applied to obtain the radial displacement at the cylinder surface. Picosecond ultrasonics experiments are performed on different micrometric fibers and compared with calculated waveforms for different optical absorptive properties. References [1] Y.D. Pan, C. Rossignol and B. Audoin, Appl. Phys. Lett. **82**, 4379 (2003).

12:40

2aPAd14. Simulations of Thermally Induced Photoacoustic Wave Propagation Using a Pseudospectral Time-Domain Method. Yae-Lin Sheu (Dept. Electrical Engineering, National Taiwan University, No.1, Sec. 4, Roosevelt Road, 106 Taipei, Taiwan, b88901147@ntu.edu.tw), Pai-Chi Li (Institute of Biomedical Electronics and Bioinformatics, National Taiwan University, No.1, Sec. 4, Roosevelt Road, 106 Taipei, Taiwan, paichi@cc.ee.ntu.edu.tw)

Physical models used to evaluate thermally induced photoacoustic waves in biomedical applications are mostly approximations based on certain hypotheses, such as the thermal and stress confinements, for the sake of obtaining analytical results. On the other hand, using numerical methods to solve the general photoacoustic wave equations gives detailed information of wave phenomena without making as many assumptions. The photoacoustic wave generated by thermal expansion involves the heat conduction theorem and the state, continuity, and Navier-Stokes equations. In this study a numerical approach was developed in 2.5D axis-symmetric cylindrical coordinates using a pseudospectral time-domain (PSTD) scheme. The method is efficient for large scale simulations in that only two grids for the smallest

wavelength are required, where in conventional methods 10~20 grids are typically needed. The numerical techniques include Berenger's perfectly matched layers (PMLs) for free wave simulations, and linear-perturbation analytical solutions are used to validate the simulation results. The numerical results using 2 grids for the minimum wavelength in simulation domain agree with theory to within an error of 7×10^{-3} in the absolute differences. On the other hand, conventional methods such as finite-difference time-domain method requiring 10 grids result in an error of 1.3×10^{-3}.

Invited Paper

1:00

2aPAd15. Laser ultrasonic study of Lamb wave propagation in different film loading configurations. Xiaodong Xu (Modern Acoustics, Institute of Acoustics, Nanjing University, 210093 Nanjing, China, xdxu@nju.edu.cn), G. Shkerdin (Laboratorium voor Akoestiek en Thermische Fysica - Departement Natuurkunde en Sterrenkunde - Katholieke Universiteit Leuven, Celestijnenlaan 200D, B-3001 Leuven, Belgium, shkerdin@yahoo.com), Christ Glorieux (Lab. ATF, Katholieke Universiteit Leuven, Celestijnenlaan 200D, B-3001 Leuven, Belgium, christ.glorieux@fys.kuleuven.be)

A study is performed concerning the propagation Lamb waves in technologically and scientifically interesting configurations. In a first configuration a thin film was loaded with different liquids on its two sides. Three experimental laser ultrasonic configurations, line excitation with scanning detection, grating excitation with single point detection, and grating excitation with scanning probe beam, were implemented. All experimental results were found to be consistent between experimental methods and with theoretical predictions. The configuration can be implemented in monitoring applications where elastic properties of liquids that are kept in containers can be determined via the outside container wall. In a second configuration laser excited and detected Lamb waves in a rubber-metal bi-layer were used to determine the highly damped elastic properties of rubber.

TUESDAY MORNING, 1 JULY 2008 ROOM 241, 8:00 A.M. TO 8:00 P.M.

Session 2aPPa

Psychological and Physiological Acoustics and ASA Committee on Standards: Applications of Psychoacoustics I

Patricia Davies, Cochair
Ray W. Herrick Lab., School of Mechanical Engineering, Purdue Univ., 140 S. Martin Jischke Drive, West Lafayette, IN 47907-2031, USA

Hugo Fastl, Cochair
AG Technische Akustik, MMK, TU München, Arcisstr. 21, München, 80333, Germany

Invited Papers

8:00

2aPPa1. Determination of filtering parameters for dichotic-listening binaural hearing aids. Yôiti Suzuki (R.I.E.C., Tohoku University, 2-1, Katahira, Aoba-ku, 980-8577 Sendai, Japan, yoh@ais.riec.tohoku.ac.jp), Atsunobu Murase (Panasonic Shikoku Electronics Co., Ltd, 600, Saedo-cho, Tsuzuki-ku, 224-8539 Yokohama, Japan, murase.atsunobu@jp.panasonic.com), Motokuni Itoh (Matsushita Electric Industrial Co., Ltd, 600, Saedo-cho, Tsuzuki-ku, 224-8539 Yokohama, Japan, ito.gempo@jp.panasonic.com), Shuichi Sakamoto (R.I.E.C., Tohoku University, 2-1, Katahira, Aoba-ku, 980-8577 Sendai, Japan, saka@ais.riec.tohoku.ac.jp)

Sensorineural hearing-impaired people have difficulty in hearing sounds not only because of the increased hearing threshold, but also because of their reduced dynamic range of hearing (loudness recruitment), as well as the large and extensive masking resulting from the reduced frequency selectivity, especially masking by which middle-frequency and high-frequency components are masked by the intense low-frequency component, the so-called upward spread of masking. Dichotic listening, listening to complementary filtered speech signals given to the two ears, has been proposed to cope with these problems. We introduce a dichotic listening technique for binaural hearing aids and the relationship between the effect of this technique and auditory characteristics of hearing-impaired people. The results of listening tests imply that some relationship exists between the width of the auditory filter and the effect of this technique. Moreover, intelligibility test results obtained using the low-frequency-boosted sounds suggest that this dichotic listening reduced the upward spread of masking. We are applying this technique to hearing aid systems and have begun evaluating the performance of this hearing aid.

8:20

2aPPa2. Binaural auralization based on spherical-harmonics beamforming. Wookeun Song (Brüel & Kjær Sound & Vibration Measurement A/S, Skodsborgvej 307, DK-2850 Nærum, Denmark, wksong@bksv.com), Wolfgang Ellermeier (Institut für Psychologie, Technische Universität Darmstadt, Alexanderstraße 10, D-64283 Darmstadt, Germany, ellermeier@psychologie.tu-darmstadt.de), Jørgen Hald (Brüel & Kjær Sound & Vibration Measurement A/S, Skodsborgvej 307, DK-2850 Nærum, Denmark, JHALD@bksv.com)

The binaural auralization of a 3D sound field using spherical-harmonics beamforming (SHB) techniques was investigated and compared with the traditional method using a dummy head. The new procedure was verified by comparing simulated room impulse responses with directly measured ones both monaurally and binaurally. The objective comparisons show that there is good agreement in the frequency range between 0.1 to 6.4 kHz. Psychoacoustic attributes of multi-channel reproduced sounds were measured in a listening experiment to validate the method subjectively. The results show that subjective ratings of the width, spaciousness and preference of different audio reproduction modes auralized based on SHB were not significantly different from those obtained for dummy head measurements. Thus binaural synthesis using SHB may be a useful tool to reproduce a 3D sound field binaurally while saving considerably on measurement time because head rotation can be simulated based on a single recording.

8:40

2aPPa3. Simulation of wave field synthesis. Florian Völk (AG Technische Akustik, MMK, TU München, Arcisstr. 21, 80333 München, Germany, florian.voelk@mytum.de), Josef Konradl (AG Technische Akustik, MMK, TU München, Arcisstr. 21, 80333 München, Germany, koj@mmk.ei.tum.de), Hugo Fastl (AG Technische Akustik, MMK, TU München, Arcisstr. 21, 80333 München, Germany, fastl@mmk.ei.tum.de)

Wave field synthesis utilizes a large number of loudspeakers to generate a desired wave field. It therefore is necessary to drive each speaker with an independent signal, which requires as many amplifier and soundcard channels as there are loudspeakers. These enormeous hardware costs make research and development very expensive and time consuming. Additionally, different rooms influence the wave field synthesis arrays in different ways. For this reason a simulation technique is of advantage which permits the evaluation of the perceived properties of arbitrary wave field synthesis configurations without the need to physically construct them. This paper proposes a simulation system capable to simulate wave field synthesis systems in different rooms based on physical measurements of one loudspeaker in each room. The techniques used are presented, and possiblities as well as limits of the system are discussed.

9:00

2aPPa4. The next generation of artificial heads. Janina Fels (Institute of Technical Acoustics, RWTH Aachen University, Neustr. 50, 52056 Aachen, Germany, Janina.Fels@akustik.rwth-aachen.de), Michael Vorlaender (Institute of Technical Acoustics, RWTH Aachen University, Neustr. 50, 52056 Aachen, Germany, mvo@akustik.rwth-aachen.de)

Standardised artificial heads are vital means when it comes to describing the binaural transmission from the sound field into the ear canal or rather the eardrum. In recent years numerous fields of application were created ranging from room acoustics, to product sound design or telecommunications, all based on the well-known KEMAR standard IEC TR 959. In the meantime, however, it has become a well-known fact, that a) specific artificial heads with natural heads or replicas in hearing experiments are superior to standard artificial heads as far as the quality of spatial hearing is concerned and that b) the standardised heads do not comply with the dimensions of an average population (the standard heads are too small). In this contribution first of all today's situation will be assessed and then a possible way will be outlined that could lead to a new future artificial head standard. This includes an adequate match with adult population for various continents, and also new approaches such as children-size artificial heads to measure and fit hearing aids or for new measurement techniques for classroom acoustics.

9:20

2aPPa5. Auditory memory and evaluation of environmental sounds. Sonoko Kuwano (Graduate School of Human Sciences, Osaka University, 1-2 Yamadaoka, 565-0871 Suita, Osaka, Japan, kuwano@see.eng.osaka-u.ac.jp), Seiichiro Namba (2-7-5-604 Obana, 666-0015 Kawanishi, Hyogo, Japan, QZW00041@nifty.com), Tohru Kato (Otemon Gakuin University, 2-1-15 Nishiai, 567-8502 Ibaraki, Osaka, Japan, tkatou@res.otemon.ac.jp)

A series of experiments were conducted concerning the memory of environmental sounds. Twelve kinds of sound were presented with soft background noise of about 6 min to participants. They were asked to recall or recognize the sound sources and to judge the loudness of the recalled or recognized sounds some period after they listened to the sounds. The recalled or recognized loudness was examined in relation to the length of the period between the presentation of sounds and the judgment of loudness, the method to measure the memory, LAeq of each sound source, etc. The results suggest that it is possible to judge the loudness of the memorized sounds and that the judgments seems reliable.

9:40

2aPPa6. Comparison of subjective impression of copy machine noise between Japanese, American and German participants. Tatsuya Furukawa (Ricoh Co., Ltd., 16-1 Shinei-cho, Tsuzuki-ku, 224-0035 Yokohama, Japan, furukawa@rdc.ricoh.co.jp), Osamu Takehira (Ricoh Co., Ltd., 16-1 Shinei-cho, Tsuzuki-ku, 224-0035 Yokohama, Japan, osamu.takehira@nts.ricoh.co.jp), Masaki Nagamiya (Ricoh Co., Ltd., 16-1 Shinei-cho, Tsuzuki-ku, 224-0035 Yokohama, Japan, masaki.nagamiya@nts.ricoh.co.jp), Sonoko Kuwano (Graduate School of Human Sciences, Osaka University, 1-2 Yamadaoka, 565-0871 Suita, Osaka, Japan, kuwano@see.eng.osaka-u.ac.jp), Seiichoro Namba (Graduate School of Human Sciences, Osaka University, 1-2 Yamadaoka, 565-0871 Suita, Osaka, Japan, namba.seiichiro@nifty.com), Hugo Fastl (AG Technische Akustik, MMK, TU München, Arcisstr. 21, 80333 München, Germany, fastl@mmk.ei.tum.de)

Psychological evaluations of copy machine noise are in progress to lower acoustical noise and to avoid disturbing the office environment. Psychological experiments were made for Japanese, American and German participants to examine cultural differences in sensitivity to copy machine noise using the Semantic Differential. Seventeen copy machine and laser printer sounds were used for the experiments. The results were analyzed statistically. The experiments revealed that, just as with Japanese, Americans and Germans were mostly sensitive to ″sound pressure levels.″ However, the second influential factor for Japanese participants was ″impulsiveness″ but ″sharpness″ for Americans and Germans. Evaluation formulas for ″pleasing″ noise using physical values were decided for each country. This suggests that copy machine noise will be evaluated without psychological experiments. The information gathered will possibly be used to adapt copy machine noise to levels that are comfortable to users in different countries.

10:00

2aPPa7. Applications of psychoacoustics to information technology products. Willem M. Beltman (Intel Corporation, 2111 NE 25th Avenue, M/S JF2-86, Hillsboro, OR 97124, USA, willem.m.beltman@intel.com), Rina A. Doherty (Intel Corporation, 5200 NE Elam Young Parkway, Hillsboro, OR 97124, USA, rina.a.doherty@intel.com), Eric Salskov (University of Twente, Dept. Mechanical Engineering, P.O. Box 217, 7500 AE Enschede, Netherlands, eric.salskov@intel.com), Philip J. Corriveau (University of Twente, Dept. Mechanical Engineering, P.O. Box 217, 7500 AE Enschede, Netherlands, philip.j.corriveau@intel.com), Doug Gabel (Intel Corporation, 2111 NE 25th Avenue, M/S JF2-86, Hillsboro, OR 97124, USA, doug.gabel@intel.com), Eric Baugh (Intel Corporation, 15400 NW Greenbrier Parkway, Beaverton, OR 97006, USA, eric.baugh@intel.com)

Emerging usage models for computing devices require low acoustic noise, for example in home entertainment systems. Studies have shown that not only the overall level, but also the psychoacoustic aspects matter. This paper provides an overview of testing techniques that are used in the information technology industry and outlines two specific case studies. First, an extensive subjective psychoacoustic study was designed and conducted in multiple geographies to determine the aspects of sound that best describe the annoyance to sound from information technology products in a home type environment. Over 200 participants in four countries participated in this carefully controlled experiment and rated typical steady state sounds on a 5 point annoyance scale. The relevant sound quality metrics were extracted and geographical variations quantified. Second, in a paired comparison study the influence of modulation on annoyance was investigated by superimposing different frequency and amplitude modulated sounds onto a baseline sound. The results indicate that modulation can have a significant effect on subjective perception.

10:20-10:40 Break

10:40

2aPPa8. Identification of transient events from a hard disk drive using non-stationary loudness. Dave Ali (Western Digital, 5863 Rue Ferrari, San Jose, CA 95127, USA, dave.ali@wdc.com)

The Hard Disk Drive (HDD) industry has been pushed so much to lower its limits of acoustic emissions by OEMs and customers that the levels of most HDDs flirt with the threshold of hearing and in some cases go below. With these much reduced levels come different problems and complaints from customers, namely transient events; latching, de-latching, spin up, spin down, etc. The difference in amplitude and duration of these events typically stand out to the human ear above the steady state nature of the HDD during idle and sometimes when it's active. This paper shows a method of characterizing these events with confidence to help in designing a better product for the industry.

11:00

2aPPa9. Automotive tire/road sound quality. Gabriella Cerrato Jay (Sound Answers Inc, 4856 Alton Drive, Suite 100, Troy, MI 48085, USA, gabriella.cerratojay@soundanswers.net), Todd Freeman (Sound Answers Inc, 4856 Alton Drive, Suite 100, Troy, MI 48085, USA, todd.freeman@soundanswers.net), Chris Raglin (Cooper Tire & Rubber Company, 701 Lima Avenue, Findlay, OH 45840, USA, caraglin@coopertire.com), Timothy Carson (IAC North America, 47785 W Anchor CT, Plymouth, MI 48170, USA, tcarson@iacna.com)

Tire/road noise and sound quality are increasingly important factors for customer satisfaction. As vehicle interior sound levels decrease, the noise from tires and their interaction with the road become more noticeable. Both tire and vehicle manufacturers need to assess as early as possible the impact of any tire-vehicle combination on perceived interior sound quality. In this paper, we describe two projects in which psychoacoustics concepts were applied to help, on one hand, tire manufacturers to screen for designs likely to generate poor sound quality in vehicle, and, on the other hand, vehicle manufacturers to measure the impact of road noise and interior acoustic treatment on speech transmission in the cabin. In both projects, the activities were driven by the understanding of the psychoacoustic features of tire/road noise and by the need to improve customer satisfaction.

Contributed Paper

11:20

2aPPa10. Acoustical aspects of travel comfort in the aircraft cabin. Ingo Baumann (Oldenburg University, Institute of Physics - Acoustics, Carl-von-Ossietzky Str. 9-11, 26111 Oldenburg, Germany, ingo @aku.physik.uni-oldenburg.de), Sandra Buss (Oldenburg University, Institute of Physics - Acoustics, Carl-von-Ossietzky Str. 9-11, 26111 Oldenburg, Germany, sandra@aku.physik.uni-oldenburg.de), Nils Freese (Oldenburg University, Institute of Physics - Acoustics, Carl-von-Ossietzky Str. 9-11, 26111 Oldenburg, Germany, nils_f@aku.physik.uni-oldenburg.de), Volker Mellert (Oldenburg University, Institute for Physics, 26111 Oldenburg, Germany, volker.mellert@uni-oldenburg.de), Reinhard Weber (Oldenburg University, Institute of Physics - Acoustics, Carl-von-Ossietzky Str. 9-11, 26111 Oldenburg, Germany, Reinhard.Weber@uni-oldenburg.de)

In several European projects tests were conducted during real flights and in aircraft simulators in order to identify important parameters of travel comfort. Physical environmental, physiological and questionnaire data were measured and investigated with respect to human perception. Besides numerous intrinsic quantities affecting health, well-being and awareness of ambience defined measurable environmental parameters influence flight and cabin crews' as well as passengers' perception, psychology and physiology. Sound and vibration are relevant environmental parameters with impact on passenger and crew. Other important influence is caused by e.g. air quality, pressure, local climate. Statistical analysis of the collected data reveals significant correlations between environment and human response for selected groups of test persons. A specific acoustic comfort is not well defined but part of common well-being and comfort. The demand for a general human response model is discussed, which relates ambience and perception.

Invited Papers

11:40

2aPPa11. The influence of speed bumps on perceived annoyance. Anna Preis (Institute of Acoustics, Adam Mickiewicz University, Unultowska 85, 61-614 Poznan, Poland, apraton@amu.edu.pl), Tomasz Kaczmarek (Institute of Acoustics, Adam Mickiewicz University, Unultowska 85, 61-614 Poznan, Poland, tomek@spl.ia.amu.edu.pl), Barbara Griefahn (Institute for Occupational Physiology, Ardeystr. 67, 44139 Dortmund, Germany, griefahn@ifado.de), Truls Gjestland (O.S. Bragstads plass 2, N-7464 Trondheim, Norway, Truls.Gjestland@sintef.no)

Recently, several attempts to use speed bumps as a noise reduction method have been made. Objective analyses of the effect of speed bumps on noise have been shown to result in a rather small reduction of noise. In the present paper the influence of speed bumps on perceived annoyance is investigated. The annoyance rating of a situation in which a passenger car approaches with constant velocity, then decelerates, crosses the bump, accelerates, and then recedes at a constant speed was compared with a car pass-by at a constant velocity without a bump. Three different velocities were analyzed: 40, 50 and 60 km/h, and two types of driving conditions: normal, and aggressive. Listeners judged their annoyance for all the investigated scenarios using the ICBEN scale (0-10) for annoyance assessment. Objective analyses showed a significant reduction of LAeqT in the bump situation for all tested velocities, and for both driving conditions. The results of this psychoacoustic experiment show no effect of the bump on annoyance rating for normal driving conditions. However, in aggressive driving conditions the bump resulted in a significant increase in annoyance. In the light of these results, speed bumps cannot be considered as a noise reduction method.

12:00

2aPPa12. The Adequate Sound Levels for Acoustic Signs for Visually Impaired in the Sound Environment with Ambient Musics from shops. Katsuya Yamauchi (Faculty of Engineering, Nagasaki University, 1-14 Bunkyo-machi, 852-8521 Nagasaki, Japan, yamauchi@cis.nagasaki-u.ac.jp), Koji Nagahata (Faculty of Symbiotic Systems Science, Fukushima University, 1 Kanayagawa, 960-1296 Fukushima, Japan, nagahata@sss.fukushima-u.ac.jp), Mari Ueda (Faculty of Human-Environment, Kyushu University, 6-19-1 Hakozaki, Higashik-ku, 812-8581 Fukuoka, Japan, mari-u@gsd.design.kyushu-u.ac.jp), Shin-Ichiro Iwamiya (Kyushu University, 4-9-1 Shiobaru, Minami-ku, 815-8540 Fukuoka, Japan, iwamiya@design.kyushu-u.ac.jp)

Providing auditory signs for the visually impaired is one of the most effective ways to support their orientation and mobility. Although the use of such sounds by the visually impaired has been revealed qualitatively, the acoustical properties of ideal sound-designs for them have not known sufficiently, even a basic property such as the sound level of these sounds. On the other hand, the advertising sounds from shops such as ambient musics are the one of the typical sounds in the Japanese downtown. These sounds also disturb their sound information listening and make their mobility difficult. Our previous studies revealed the adequate sound levels of acoustic signs under the road traffic noise environment. This study discusses the the effect of the ambient musics from shops on the adequate sound levels of acoustic signs through the psychoacoustical experiment. The results showed that the difference between the adequate sound level of acoustic signs and the environmental noise levels are larger than that under the road traffic noise environment. This trend is thought to be attributed to the frequency characteristics of the acoustical signs and the environmental noise.

12:20

2aPPa13. An algorithm modelling the Irrelevant Sound Effect (ISE). Sabine J. Schlittmeier (Work, Environmental and Health Psychology, Catholic University of Eichstaett-Ingolstadt, Ostenstr. 26-28, 85072 Eichstaett, Germany, sabine.schlittmeier@ku-eichstaett.de), Tobias Weissgerber (AG Technische Akustik, MMK, TU München, Arcisstr. 21, 80333 München, Germany, tobias@p-weissgerber.de), Stefan Kerber (AG Technische Akustik, MMK, TU München, Arcisstr. 21, 80333 München, Germany, stefan@ihr.mrc.ac.uk), Hugo Fastl (AG Technische Akustik, MMK, TU München, Arcisstr. 21, 80333 München, Germany, fastl@mmk.ei.tum.de), Juergen Hellbrueck (Work, Environmental and Health Psychology, Catholic University of Eichstaett-Ingolstadt, Ostenstr. 26-28, 85072 Eichstaett, Germany, juergen.hellbrueck@ku-eichstaett.de)

Verbal short-term memory capacity is reduced significantly during certain background sounds. Remembering a series of digits is significantly impaired by speech or music with prominent staccato passages whereas, for example, music with prominent legato passages does not disturb performance in comparison to silence. This so-called Irrelevant Sound Effect (ISE) occurs although the background sounds are irrelevant with respect to the digit sequences to be remembered. Until now, a multitude of cognitive psychological experiments explored the ISE and collected behavioral performance data during different sound conditions. The talk presents an algo-

rithm which models performance data in ISE experiments, i.e. the detrimental impact of background sounds on memory performance. The data base of this algorithm is about 50 background sounds and corresponding performance data, which have been collected in cognitive psychological experiments at the KU Eichstaett-Ingolstadt. The algorithm is based on the instrumental measuring of the hearing sensation fluctuation strength and is able to reconstruct the performance results in about 90% of cases within the interquartile ranges. The algorithm will be discussed within the scope of cognitive short-term memory models, which claim to explain the ISE and with respect to practical implications.

12:40-2:00 Lunch Break

Invited Papers

2:00

2aPPa14. Fusion and masking threshold of a tone in narrowband noise. Hans Hansen (IRCAM - Sound Perception & Design, 1 place Igor Strawinsky, 75004 Paris, France, Hans_Hansen@gmx.de), Reinhard Weber (Oldenburg University, Institute of Physics - Acoustics, Carl-von-Ossietzky Str. 9-11, 26111 Oldenburg, Germany, Reinhard.Weber@uni-oldenburg.de)

When comparing different pitch phenomena, it is not clear whether the expression pitch strength points towards a unique perceptive phenomenon or object. As many studies concentrate on one special phenomenon, the question, what is actually judged, seems only implicitly answered. Kubovy and Van Valkenburg (2001) define a perceptual object as ″that what is susceptible to figure-ground segregation″. Pitch plays a major role in these grouping processes. In this context the judgment of pitch strength refers to two perceptual cases. The first one is the pitch strength of a tone-in-noise, i.e. the case where the pitch is linked to a separate contour within the narrowband noise (NBN), while the second is the pitch strength of tonal noise. Here, the noise evokes a pitch sensation that is not related to a separate object. In order to explore the transition from case /1 tone-in-noise to case /2 tonal noise, the identification threshold hearing a tone in NBN centered on the tone is determined in a lab experiment. This segregation or fusion threshold is compared to the measured masking threshold for center frequencies 250-4000 Hz octave-wise at 60 dB SPL noise level. The bandwith of the NBN is varied from 50-250 Hz accordingly.

2:20

2aPPa15. Are absolute thresholds and loudness judgements influenced by different colours? Daniel Menzel (AG Technische Akustik, MMK, TU München, Arcisstr. 21, 80333 München, Germany, menzel@tum.de), Elias Faccinelli (AG Technische Akustik, MMK, TU München, Arcisstr. 21, 80333 München, Germany, fac@mmk.ei.tum.de), Hugo Fastl (AG Technische Akustik, MMK, TU München, Arcisstr. 21, 80333 München, Germany, fastl@mmk.ei.tum.de)

Previous experiments showed that images of differently colored trains and sports cars can influence the loudness ratings given by subjects via free magnitude estimation. Red vehicles caused subjects to rate the loudness of simultaneously presented train or car sounds higher relative to green vehicles. To investigate whether these loudness differences correspond to shifts in absolute threshold, subject's threshold in quiet was measured via Békésy-tracking while viewing red, green, and neutral color patches. Also, the influence of color on the loudness of broadband noise was measured using a method of adjustment, in which subjects had to adjust the level of a test sound until it was perceived as loud as a reference sound. In both cases, no influence of color on either absolute threshold or loudness perception measured via adjustment could be found. These results support the hypothesis that, compared to previously used methods like magnitude estimation, methods that require subjects to concentrate on the auditory stimulus do not seem to be as applicable for measurements of audio-visual interactions.

2:40

2aPPa16. An efficient masking model for audio coding exploiting spectro-temporal masking. Steven Van De Par (Philips Research Europe, Digital Signal Processing (MS WO02), High Tech Campus 36, 5656 AE Eindhoven, Netherlands, steven.van.de.par@philips.com), Jeroen Koppens (Philips Research Europe, Digital Signal Processing (MS WO02), High Tech Campus 36, 5656 AE Eindhoven, Netherlands, jeroen.koppens@philips.com), Armin Kohlrausch (Philips Research Europe, Digital Signal Processing (MS WO02), High Tech Campus 36, 5656 AE Eindhoven, Netherlands, armin.kohlrausch@philips.com), Werner Oomen (Philips Research Europe, Digital Signal Processing (MS WO02), High Tech Campus 36, 5656 AE Eindhoven, Netherlands, werner .oomen@philips.com)

Perceptual audio coding achieves part of its coding efficiency by spectrally shaping the quantization noise such that it is masked by the audio signal to be encoded. In order to determine how much quantization noise is allowed within each frequency band and time interval a masking model is used to predict a masking curve specifying the maximally allowed quantization noise level within each frequency band. In most audio coders only spectral masking properties of the audio signal are used. The model by Dau et al. [J. Acoust. Soc. Am. 99, Vol. 3615, 1996] provides an interesting approach to also model temporal masking. Since this model operates as an artificial observer it only predicts whether the quantization noise is audible or not in the presence of the audio signal. In order to determine the most efficient quantization noise shape, the encoder needs to iteratively adapt the noise shape and evaluate each option with the model. This implies a highly computational complex encoding algorithm. In this contribution we will present an efficient masking model based on the Dau et al. model that only requires a single evaluation of the input signal to determine the maximally allowed noise level within each frequency band.

3:00

2aPPa17. Factor analyses of critical-band-filtered speech of British English and Japanese. Kazuo Ueda (Perceptual Psychology Unit, Kyushu University, 4-9-1 Shiobaru, Minami-ku, 815-8540 Fukuoka, Japan, ueda@design.kyushu-u.ac.jp), Yoshitaka Nakajima (Perceptual Psychology Unit, Kyushu University, 4-9-1 Shiobaru, Minami-ku, 815-8540 Fukuoka, Japan, nakajima@design.kyushu-u.ac.jp)

Two-hundred sentences of British English and Japanese, each uttered by 10 native speakers (5 females and 5 males) in each language, were analyzed through 20 bands of critical band filters. Smoothed power fluctuations derived from the filters were submitted to principal component analyses followed by varimax rotation. The first three factors explained 34-37% of variance. One of the factors exhibited two peaks along frequency axis in the standardized scores and two of the factors showed one peak for each. These three factors divided the whole frequency range of speech sound into four bands. The structure of the factors and frequency bands was essentially the same across the two languages. These frequency bands can be used for speech perception in general, because intelligible noise-vocoded speech sounds can be synthesized with the frequency bands.

Contributed Paper

3:20

2aPPa18. A Structuralistic Approach to Acoustic-Auditory Functions of Meaning. Ute Jekosch (Chair of Communication Acoustics, TU Dresden, Helmholtzstr. 10, 01069 Dresden, Germany, ute.jekosch@tu-dresden.de), Ercan Altinsoy (Chair of Communication Acoustics, TU Dresden, Helmholtzstr. 10, 01069 Dresden, Germany, ercan.altinsoy@ias.et.tu-dresden.de), Sebastian Merchel (Chair of Communication Acoustics, TU Dresden, Helmholtzstr. 10, 01069 Dresden, Germany, sebastian.merchel@tu-dresden.de)

In this paper we introduce a methodology of semio-acoustics to get information on how human listeners associate meaning to acoustic-auditory events. We concentrate on identifying cues in the auditory stream listeners base the association of meaning on as well on modelling major characteristics of the reference system of meaning. The methodology we use is closely related to structuralism, an approach that has its origins in semiotics. In principle, structuralism differentiates between creating functions, carrying functions and changing functions of systems of meaning. We concentrate on carrying and changing functions here using the following procedure: a sign-carrier (in our case an acoustic-auditory event the association of meaning is based on) is decomposed into sub-units. By a minimal pair analysis we investigate carrying and changing functions of acoustic-auditory features with regard to the associated meaning. We will introduce the methodology used and discuss first results of a pilot study.

3:40-5:20 Posters

Lecture sessions will recess for presentation of poster papers on various topics in acoustics. See poster sessions for topics and abstracts.

Contributed Papers

5:20

2aPPa19. Optimization of a dual recognition tasks for speech quality assessment. Virginie Durin (France Télécom, 2 avenue Pierre Marzin, 22300 Lannion, France, virginie.durin@orange-ftgroup.com), Laetitia Gros (France Télécom, 2 avenue Pierre Marzin, 22300 Lannion, France, laetitia.gros@orange-ftgroup.com)

This paper deals with perceptive test methodologies to assess speech quality of telecommunication systems. Faced with drawbacks of typical methodologies recommended by ITU-T, a new way to assess speech quality is investigated. The new approach requires collecting reaction times and performances when subjects are achieving tasks involving degraded speech signals; it is shown that reactions times lengthen and performances decrease in a specific task when quality is impaired. The proposed task is a dual task with a digit recognition memory task and a letter recognition task. Three different quality levels are applied to audio signals describing digits and letters. Different experimental designs are examined to reinforce the effect of speech quality on performances and reaction times. The results show significant differences of performances and reaction times between the three quality levels, depending on the experimental design.

5:40

2aPPa20. Electronic pass-through hearing protection and directional hearing restoration integrated in a helmet. Wouter K. Vos (TNO, Kampweg 5, 3769ZG Soesterberg, Netherlands, wouter.vos@tno.nl), Adelbert W. Bronkhorst (TNO, Kampweg 5, 3769ZG Soesterberg, Netherlands, adelbert.bronkhorst@tno.nl), Jan A. Verhave (TNO, Kampweg 5, 3769ZG Soesterberg, Netherlands, jan.verhave@tno.nl)

Compared to standard earplugs, electronic pass-through earplugs provide better sound localisation. Provided that the bandwidth is sufficiently wide and the earplugs do not change the shape of the pinnae. However, when a helmet is worn that partially or completely covers the ears, the directional hearing capability is diminished. We attempt to restore directional hearing when wearing a helmet by attaching a microphone array to the helmet. The signals from the microphone array are filtered with Finite Impulse Response (FIR) filters to recreate an individual or generic open-ear Head Related Transfer Function (HRTF). The filters are designed by minimisation of an error measure in the frequency domain. The error measure incorporates both the log magnitude and the phase differences between the original and the recreated HRTF. The global minimum is found using modern optimisation techniques like Particle Swarm Optimisation (PSO) or Differential Evolution (DE). The total system is evaluated with subject experiments. Participants have to localise sounds and rate the quality of sounds. Independent variables are the number of microphones that should be used and their positions on the helmet.

6:00

2aPPa21. How many psycho-acoustic attributes are needed? Torben Holm Pedersen (Delta Acoustics & SenseLab, Venlighedsvej 4, 2970 Hørsholm, Denmark, thp@delta.dk), Nick Zacharov (Delta Acoustics & SenseLab, Venlighedsvej 4, 2970 Hørsholm, Denmark, nvz@delta.dk)

Sounds may be characterized by objective perceptive attributes (for which there may exist physical metrics) or by subjective (affective or connotative) attributes. This paper will deal with the perceptive attributes. Within product sound quality the metrics for classical the psycho-acoustic attributes (loudness, sharpness, roughness and fluctuation strength) -maybe supplemented with tone and impulse prominence- are often used as the only attributes to characterize the sounds. But are these 4-6 attributes or dimensions sufficient to characterize a sound? Within room acoustics and reproduced sound many other attributes are used and in the language around 100 direct sound describing words may be found. This paper will give an overview over attributes used within different acoustic areas. The latter part of the paper will discuss the role of sensory evaluation methods as a means to systematically developing attributes for the objective qualification and quantification of sound characteristics.

6:20

2aPPa22. Noise perception of wall-hung gas boilers. Patrick Chevret (01dB-Metravib, 200 Chemin des Ormeaux, 69578 Limonest Cedex, France, patrick.chevret@01db-metravib.com), Anne Coulon (CETIAT, Domaine Scientifique de la Doua, 25 avenue des Arts, BP 2042, F-69603 Villeurbanne cedex, France, anne.coulon@cetiat.fr), François Bessac (CETIAT, Domaine Scientifique de la Doua, 25 avenue des Arts, BP 2042, F-69603 Villeurbanne cedex, France, francois.bessac@cetiat.fr), Etienne Parizet (Laboratoire Vibrations Acoustique, Insa Lyon, 25 bis, av. J. Capelle, 69621 Villeurbanne Cedex, France, etienne.parizet@insa-lyon.fr)

The aim of this study is to assess the quality image for domestic wall-hung gas-fired boilers, based on their noise. Nine boilers were recorded using an acoustic manikin in a hemi-anechoic room, for different operating conditions. Two of these operating conditions (maximum heat input, hot water tapping) were first studied. Five-second sequences were presented (through headphones) to sixty listeners using the mixed assessment method allowing for the comparison between signals. Analyses showed several assessment strategies: according to listeners, the relevant noise parameters could be the loudness, the sharpness or the presence of tonal components. A second experimental phase focused on tonal components by artificially modifying some sounds to offer a relevant perceptive indicator. The results of this second experiment will also be presented.

Invited Papers

6:40

2aPPa23. Methodological aspects in the determination of the auditory filters and critical band at low and mid-frequencies. Carlos A. Jurado (Acoustics, Aalborg University, Fredrik Bajers Vej 7 B5, 9220 Aalborg Ø, Denmark, cjo@es.aau.dk), Henrik Møller (Acoustics, Aalborg University, Fredrik Bajers Vej 7 B5, 9220 Aalborg Ø, Denmark, hm@acoustics.aau.dk), Christian Sejer Pedersen (Acoustics, Aalborg University, Fredrik Bajers Vej 7 B5, 9220 Aalborg Ø, Denmark, cp@acoustics.aau.dk)

In order to evaluate loudness or audibility of complex sounds, knowledge of the auditory filter characteristics is necessary. At low frequencies, where both the threshold of hearing and dynamic range become considerably frequency dependent, care must be taken to account for this both in the psycho-acoustical model and the methodological approach. To account for variation in hearing sensitivity at low frequencies, equal loudness contours have been used to weight the stimuli accordingly. At mid and high frequencies, threshold of hearing curves have been used. These stimuli weightings can be applied before or after the experiment, normally being applied afterwards. Due to the non-linear characteristics of the cochlear amplifier, it is arguable whether post-experimental weighting is a proper approach, or whether at low frequencies there will be any difference between pre or post stimuli weighting. Listening experiments are then to be performed to test possible differences in pre or post filtering the stimuli. The most appropriate approach will then be discussed. Measurements will be done at low and mid frequencies. To obtain accurate auditory filter estimates, individual ELC or threshold curves will be determined. Methods such as the notched-noise method and the classical band-widening approach will be tested with these conditions.

7:00

2aPPa24. Effect of recording/playback technique and experimental method on assessments of noise. Emine Çelik-Christensen (Aalborg University / Rockwool International A/S, Rockwool International, Building Knowledge Center, Hovedgaden 584, Entrance C, 2640 Hedehusene, Denmark, emine.christensen@rockwool.com), Kerstin Persson Waye (Dept. of Environ. Medicine, The Sahlgrenska Acad. of Gothenburg Univ., Box 414, 405 30 Gothenburg, Sweden, kerstin.persson-waye@amm.gu.se), Henrik Møller (Acoustics, Aalborg University, Fredrik Bajers Vej 7 B5, 9220 Aalborg Ø, Denmark, hm@acoustics.aau.dk)

The study investigated possible effects of recording/playback technique and experimental method on assessments of annoyance, loudness and unpleasantness. A possible effect of exposure duration was also studied. Sounds were recorded with two different techniques: monophonic and binaural (dummy-head technique). In addition, they were reproduced with three different techniques: monophonic recordings presented through a loudspeaker system, binaural recordings presented through closed (circum-aural) and completely open (free-of-the-ear headphones. The study adopted three psychometric methods for collecting responses from test-subjects. Fifty-four subjects participated, and three types of sounds were used: everyday restaurant sound, road traffic sound and ventilation sound dominated by low frequencies. Each sound was played back at three different levels. The results show that there is no significant main effect of recording and playback technique for any of the three perceptual attributes; however, significant interactions between techniques and sounds were found. Since the effect of recording and playback technique differs depending on sound, this finding is of importance for future design of experiments and interpretation of results. The results also show that long-term annoyance and unpleasantness are poorly predicted by short-duration methods.

Contributed Papers

7:20

2aPPa25. Relation between the overall unpleasantness of a long duration sound and the one of its event6: application to a delivery truck. Emilie Geissner (Laboratoire Vibrations Acoustique - INSA Lyon, 25 bis avenue Jean Capelle, Bâtiment Saint-Exupéry, F-69621 Villeurbanne cedex, France, emilie.geissner@insa-lyon.fr), Etienne Parizet (Laboratoire Vibrations Acoustique, Insa Lyon, 25 bis, av. J. Capelle, 69621 Villeurbanne Cedex, France, etienne.parizet@insa-lyon.fr)

The goal of this study was to investigate the link between the unpleasantness assessment of an unstationary long duration sound composed of several distinct sound events and the corresponding judgments of each of those events. For that purpose, a sound sequence of a delivery truck was evaluated by 16 listeners during a test in laboratory: first, subjects had to continuously quantify the perceived unpleasantness of the sequence by moving a sliding cursor along a five levels graduated scale and then give a global rating by using the same scale. In a second step, listeners had to express their overall judgment of unpleasantness for eight samples of the delivery sequence. As previously shown for loudness by Kuwano and Namba (1985), the global rating of the unpleasantness of long sound could not be estimated by the arithmetic mean of the continuous assessment. It also appeared that the overall judgment corresponds to the arithmetic mean on the local values of unpleasantness of each main sound event. This last result was similar to the conclusions of Hellbrück et al. (2001) for the loudness scaling of traffic noise.

7:40

2aPPa26. Just noticeable differences of loudness and sharpness for earth moving machines. Francesca Pedrielli (CNR-Imamoter, via Canal Bianco 28, 44100 Ferrara, Italy, f.pedrielli@imamoter.cnr.it), Eleonora

Carletti(CNR-Imamoter, via Canal Bianco 28, 44100 Ferrara, Italy, e.carletti@imamoter.cnr.it), Camilla Casazza (CNR-Imamoter, via Canal Bianco 28, 44100 Ferrara, Italy, c.casazza@imamoter.cnr.it)

This paper describes some results of a research concerning the improvement of the noise climate at the operator station of construction machines during real working conditions. Binaural noise signals were previously recorded and then used in subjective listening tests aimed at identifying the set of acoustic and psychoacoustic parameters which affect the auditory perception of these signals with respect to the annoyance sensation. Results showed that loudness and sharpness are the parameters best correlated to the annoyance. In order to verify the efficacy of some noise control solutions in improving the operator comfort conditions, the next necessary step is to build a specific metrics able to show the minimum differences in these parameters which are subjectively perceived. This paper describes the results of specific listening tests carried out in order to evaluate the differential thresholds of loudness and sharpness by the Method of Limits. The test was repeated at two different signal presentation levels. The loudness value of each original stimulus was varied by interval steps of 0,3 sone, while the Sharpness by interval steps of 0,02 acum. At this moment in time, the data analysis is still in progress and the ultimate results will be presented in the manuscript.

Session 2aPPb

Psychological and Physiological Acoustics: Auditory Perception and Signal Processing by Prostheses I

Huanping Dai, Cochair
Univ. of Arizona, Speech, Language and Hearing Science, Tucson, AZ 85721, USA

Birger Kollmeier, Cochair
Universität Oldenburg, Medizinische Physik, Carl-von-Ossietzky Str. 9-11, Oldenburg, 26111, Germany

Invited Papers

8:00

2aPPb1. Advantages and disadvantages of fast and slow compression in hearing aids. Brian Moore (University of Cambridge, Department of Experimental Psychology, Downing Street, CB2 3EB Cambridge, UK, bcjm@cam.ac.uk)

Compression is used in hearing aids to compensate for the effects of loudness recruitment. However, there is no consensus about the ″best″ compression speed. The theoretical advantages and disadvantages of slow and fast compression will be discussed. Studies comparing the relative merits of slow and fast compression have led to a great variety of outcomes. It is argued, following the work of Gatehouse and colleagues, that this is partly the result of a failure to consider individual differences and the auditory ecology of each individual. It is argued that listening in the dips of a fluctuating background sound, such as a competing talker, depends on the ability to process the temporal fine structure (TFS) of sounds, as represented in patterns of phase locking in auditory neurons. For people with a good ability to process TFS, fast compression can amplify sounds in the dips, increasing the effectiveness of dip listening. However, for people with a poor ability to process TFS, envelope cues may be critical for speech intelligibility and fast compression may disrupt such cues. It is proposed that a test of the ability to process TFS might be useful for selecting compression speed for an individual.

8:20

2aPPb2. Dynamic compression in hearing aids based on an auditory model. Volker Hohmann (Carl von Ossietzky Universität Oldenburg, Ammerländer Heerstraße 114-118, 26111 Oldenburg, Germany, volker.hohmann@uni-oldenburg.de)

A multichannel dynamic compression algorithm is proposed that uses a novel nonlinear auditory filterbank which aims at effectively describing the basilar membrane (BM) response to arbitrary signals. It is based on a linear Gammatone filterbank, a subsequent instantaneous compression stage and a frequency-synthesis stage. In order to model the linear response to off-frequency tones and suppression effects from signals below the characteristic frequency (low-side suppression) the compression characteristics is controlled in each filter band by the deviation of the current sub-band instantaneous frequency from the band's center frequency. If the deviation is small, on-frequency components are prominent, and full gain and compression is applied. If the deviation is large, off-frequency components are prominent, and gain and compression is reduced. Simulations of responses to sinusoids as a function of frequency and level at a fixed BM place (i.e., within a fixed filter band) and for all filter bands (i.e., BM excitation patterns) show good correspondence with psychoacoustical excitation pattern models. Responses to two-tone stimuli quantitatively simulate psychoacoustical two-tone suppression. Likewise, nonlinear growth of simultaneous masking is quantitatively modeled. First results show that speech reception in modulated noise may be improved by the system for a subgroup of hearing-impaired subjects.

8:40

2aPPb3. Speech perception in fluctuating noise with signals compensated for hearing loss. Joost M. Festen (VU University Medical Center, de Boelelaan 1117, 1081 HV Amsterdam, Netherlands, jm.festen@vumc.nl)

For speech reception in noise normal-hearing listeners gain from masker modulations up to about 12 dB depending on rate, duty cycle, and depth of the modulations. Listeners with sensorineural hearing loss need a better signal-to-noise ratio to improve signal quality as a compensation for their auditory deficits. Generally, a larger compensation is needed for fluctuating interferences leading to

reduction or even absence of release from masking for modulated maskers. With the Speech Intelligibility Index adapted for modulated maskers, SIImod [Rhebergen and Versfeld, J. Acoust. Soc. Am. 117, 2181-92 (2005)] it is shown that these elevated thresholds are needed to compensate not only reduced hearing sensitivity but also impaired auditory and non-auditory processing. After frequency-dependent compensation for hearing loss as offered by a hearing aid, more of the speech is presented at impaired frequency regions. As a consequence the effect of a hearing aid on speech intelligibility will be less than predicted by SIImod. Speech reception thresholds in noise are affected by peripheral spectro-temporal processing (bottom-up) and by cognitive processing capabilities, like working memory (top-down). Effects of cognitive processing on speech perception are found especially in fluctuating noise as this masker presents a more complex and demanding environment than steady noise.

9:00

2aPPb4. Signal processing algorithms for speech in fluctuating noise. Peggy Nelson (University of Minnesota, 164 Pillsbury Drive SE, Minneapolis, MN 55455, USA, peggynelson@umn.edu), Janet Rutledge (University of Maryland Baltimore County, 1000 Hilltop Circle, Baltimore, MD 21250, USA, jrutledge@umbc.edu), Juan Carlos Tejero-Calado (University of Malaga, Boulevar Louis Pasteur 35, Campus de Teatinos - Complejo Tecnologico, 29071 Malaga, Spain, jctejero@uma.es)

Fluctuating background noise is a significant problem for listeners with sensorineural hearing loss (SNHL). Data indicate that fluctuating noise significantly affects both speech understanding and satisfaction with hearing aids. Listeners with SNHL do not take advantage of momentary dips in the noise and thus to not experience release from masking in fluctuating noise, as normal-hearing listeners do. Our results have shown that listeners with SNHL obtain about half of the masking release of their normal-hearing counterparts, and that this masking release is generally related to the audibility of the speech in the noise dips. Current slow-acting amplitude compression is based on the level of the background noise and does not improve the audibility of speech in the dips of fluctuating noise. Fast-acting multiband compression can improve audibility but may produce unwanted artifacts. Fast-acting algorithms based on spectral peaks shows potential for maximizing the audibility of speech in fluctuating noise to improve speech intelligibility, with limited artifact. Portions of this work are supported by the University of Minnesota and Starkey Laboratories.

9:20

2aPPb5. Signal processing in hearing aids: results of the HEARCOM project. Jan Wouters (ExpORL, Dept. Neurosciences, K.U. Leuven, Herestraat 49 bus 721, O. & N2, B-3000 Leuven, Belgium, jan.wouters@med.kuleuven.be), Heleen Luts (ExpORL, Dept. Neurosciences, K.U. Leuven, Herestraat 49 bus 721, O. & N2, B-3000 Leuven, Belgium, heleen.luts@med.kuleuven.be), Koen Eneman (ExpORL, Dept. Neurosciences, K.U. Leuven, Herestraat 49 bus 721, O. & N2, B-3000 Leuven, Belgium, koen.eneman@med.kuleuven.be), Ann Spriet (ESAT/SISTA, K.U. Leuven, Kasteelpark Arenberg 10, B-3001 Leuven, Belgium, ann.spriet@esat.kuleuven.be), Marc Moonen (ESAT/SISTA, K.U. Leuven, Kasteelpark Arenberg 10, B-3001 Leuven, Belgium, marc.moonen@esat.kuleuven.be), Michael Büchler (University Hospital, 8091 Zürich, Switzerland, michael.buechler@usz.ch), Norbert Dillier (University Hospital, 8091 Zürich, Switzerland, norbert.dillier@usz.ch), Wouter A. Dreschler (AMC, Clinical and Experimental Audiology, 1105 Amsterdam, Netherlands, w.a.dreschler@amc.uva.nl), Matthias Froehlich (Siemens Medical Solutions SAT, 91058 Erlangen, Germany, Matthias.froehlich@siemens.com), Giso Grimm (Carl von Ossietzky Universität Oldenburg, Ammerländer Heerstraße 114-118, 26111 Oldenburg, Germany, giso.grimm@vegri.net), Volker Hohmann (Carl von Ossietzky Universität Oldenburg, Ammerländer Heerstraße 114-118, 26111 Oldenburg, Germany, volker.hohmann@uni-oldenburg.de), Rolph Houben (AMC, KNO-Audiologie, 1105 Amsterdam, Netherlands, a.c.houben@amc.uva.nl), Arne Leijon (KTH, Royal Institute of Technology, 10044 Stockholm, Sweden, arne.leijon@ee.kth.se), Anthony Lombard (University of Erlangen, 91058 Erlangen, Germany, lombard@nt.e-technik.uni-erlangen.de), Dirk Mauler (Ruhr University of Bochum, 44780 Bochum, Germany, dirk.mauler@ruhr-uni-bochum.de), Henning Puder (Siemens Medical Solutions SAT, 91058 Erlangen, Germany, henning.puder@siemens.com), Michael Schulte (Hoerzentrum Oldenburg, 26129 Oldenburg, Germany, M.Schulte@hoerzentrum-oldenburg.de), M Vormann (Hoerzentrum Oldenburg, Hoerzentrum Oldenburg, 26129 Oldenburg, Germany, matthias.vormann@web.de)

Digital hearing aids of today allow the application of advanced signal processing strategies. In recent years a number of promising signal processing approaches have been designed and developed. However, most of these different evolutions have been evaluated only in a limited way. Within the framework of the HEARCOM EU-research project a number of signal enhancement techniques have been further developed and evaluated based on a representative set of real-life recordings and physical performance measures. Different auditory profiles, representing common categories of hearing aid users, have been taken into account. A selection of 5 of these signal enhancement techniques (single-channel noise suppression, blind source separation, dereverberation, multi-microphone adaptive processing, feedback reduction) has been implemented on a single common hard- and software test platform, the Master Hearing Aid (MHA). These signal processing strategies have been evaluated perceptually based on speech reception thresholds, listening effort and preference rating, at 5 different test-sites for a number of speech-and-noise listening scenarios. Fifty normal hearing subjects and 100 hearing aid users according to 2 auditory profiles, took part in this study.

9:40

2aPPb6. Model-based objective assessment of noise reduction systems for hearing aids. Birger Kollmeier (Universität Oldenburg, Medizinische Physik, Carl-von-Ossietzky Str. 9-11, 26111 Oldenburg, Germany, birger.kollmeier@uni-oldenburg.de), Rainer Huber (Kompetenzzentrum HörTech, Marie-Curie-Str. 2, 26129 Oldenburg, Germany, Rainer.Huber@HoerTech.de), Thomas Rohdenburg (Universität Oldenburg, Medizinische Physik, Carl-von-Ossietzky Str. 9-11, 26111 Oldenburg, Germany, thomas.rohdenburg@uni-oldenburg.de), Rainer Beutelmann (Universität Oldenburg, Medizinische Physik, Carl-von-Ossietzky Str. 9-11, 26111 Oldenburg, Germany, rainer.beutelmann@uni-oldenburg.de), Volker Hohmann (Carl von Ossietzky Universität Oldenburg, Ammerländer Heerstraße 114-118, 26111 Oldenburg, Germany, volker.hohmann@uni-oldenburg.de)

Since the ultimative goal of hearing-aid development is the (subjective) judgment of the individual hearing-impaired listener, time-consuming tests with the end user are indispensable. However, time- and effort-saving objective methods to assess the potential benefit of different versions and parameter sets of hearing aid algorithms are gaining importance. This contribution reviews perception-model-based approaches to predict the hearing-impaired judgement and speech reception performance achieved with various noise reduction

schemes. The perceptual similarity measure PSM evaluates the similarity between a tested condition and an ″ideal″ reference condition not on the physical level, but rather on the perceptual level at the output of a perception model for the individual hearing-impaired listener. The binaural extention of the SII approach uses a binaural preprocessing stage followed by a speech intelligibility index (SII)-based prediction scheme capable of predicting the relative benefit of binaural signal presentation and signal enhancement in complex spatial signal and noise source configurations. Both model-based schemes can be combined to assess the effect of noise reduction algorithms (such as adaptive beamformers) and to optimize their respective performance for different acoustical situations.

Contributed Papers

10:00

2aPPb7. Quantifying and modeling the acoustic effects of compression on speech in noise. Koenraad S. Rhebergen (AMC - Dept. of Clinical and Experimental Audiology, AMC, Clinical and Experimental Audiology, 1105 Amsterdam, Netherlands, k.s.rhebergen@amc.uva.nl), Niek J. Versfeld (AMC - Dept. of Clinical and Experimental Audiology, Meibergdreef 9, 1105AZ Amsterdam, Netherlands, n.j.versveld@amc.uva.nl), Wouter A. Dreschler (AMC, Clinical and Experimental Audiology, 1105 Amsterdam, Netherlands, w.a.dreschler@amc.uva.nl)

In this presentation a method is proposed that is able to separate a speech signal out of a noise signal after processing of the signal through wide-dynamic-range compression (WDRC). This technique reconstructs the speech signal and noise signal sample by sample separately using the gain factor of the WDRC, and can be used to quantify the acoustic effects of WDRC in noise. It will be shown that this technique is more accurate than a frequently used inversion technique, because the method is not affected by phase shifts that introduce distortion products in the reconstructed speech signal. As a result, the acoustic effects of WDRC can be measured more accurately. In addition, this reconstruction method allows modeling the speech intelligibility after non-linear signal processing in the Speech Intelligibility Index. With the aid of Speech Reception Threshold data it will be shown that this approach can give a good account for most existing data.

10:20

2aPPb8. Acoustical frequency discrimination and pitch matching in bimodal and hybrid hearing. Uwe Baumann (Univ. of. Frankfurt - ZHNO - Audiologische Akustik, Theodor-Stern-Kai 7, Haus 8D, 60590 Frankfurt a.M., Germany, uwe.baumann@kgu.de), Tobias Rader (Univ. of. Frankfurt - ZHNO - Audiologische Akustik, Theodor-Stern-Kai 7, Haus 8D, 60590 Frankfurt a.M., Germany, tobias.rader@kgu.de), Silke Helbig (Univ. of. Frankfurt - ZHNO - Audiologische Akustik, Theodor-Stern-Kai 7, Haus 8D, 60590 Frankfurt a.M., Germany, silke.helbig@kgu.de), Wolfgang Gstöttner (Univ. of. Frankfurt - ZHNO - Audiologische Akustik, Theodor-Stern-Kai 7, Haus 8D, 60590 Frankfurt a.M., Germany, a.jan@em.uni-frankfurt.de)

Frequency discrimination and pitch matching of implantees using combined electric and acoustic stimulation in either the same ear (EAS) or the opposite ear (bimodal condition) was assessed by means of adaptive procedures. EAS patients received either the MED-EL standard electrode or the recently introduced FLEX design with reduced diameter. Acoustic JNDF in EAS patients ranged from close to normal to grossly abnormal compared to a group of matched SNHL listeners. The median JNDF was 7.1% in the SNHL and 7.5% in the EAS group. There was no statistically significant difference in terms of JNDF between both groups of listeners. Frequency mapping was studied by means of an adjustment method where subjects were instructed to control the pitch of an acoustically presented sinusoid in reference to electrical stimulation. The findings demonstrate that the insertion of an intra-cochlear electrode does not significantly hamper the average frequency discrimination ability in EAS patients.

Invited Paper

10:40

2aPPb9. Combining hearing aids and cochlear implants to solve the cocktail party problem. Fan-Gang Zeng (University of California Irvine, 364 Med Surge II, Irvine, CA 92697, USA, fzeng@uci.edu)

The cocktail party problem refers to the difficulty in speech recognition in noise that a hearing-impaired listener must face in daily life. Combining a hearing aid with a cochlear implant can provide complementary information that may have a great potential to solve this problem. On one hand, a hearing aid may provide low-frequency temporal fine structure cues that are not conveyed by a cochlear implant. On the other hand, a cochlear implant can provide high-frequency temporal envelope cues that are not effectively delivered by a hearing aid. This talk will provide psychophysical and speech recognition evidence for combining hearing aids and cochlear implants to solve the cocktail party problem. One interesting finding along this line of research is that in many important functional tasks, the hearing aid and cochlear implant combination provides a more effective solution than bilateral cochlear implants. Another interesting finding is that the fundamental frequency cue alone can significantly improve speech perception in noise, especially when the noise is a competing voice. The latter finding suggests that combining a tactile aid and a cochlear implant can potentially achieve the same benefit as combining a hearing aid and a cochlear implant in patients with no residual acoustic hearing.

Session 2aPPc

Psychological and Physiological Acoustics: Binaural Perception by Hearing-Aid Wearers

Sridhar Kalluri, Cochair
Starkey Hearing Research Center, 2150 Shattuck Ave, Suite 408, Berkeley, CA 94704, USA

Michael A. Akeroyd, Cochair
MRC Institute of Hearing Research, Glasgow Royal Infirmary, 16 Alexandra Parade, Glasgow, G31 2ER, UK

Invited Paper

11:20

2aPPc1. Binaural function and its benefits for wearers of hearing aids. Sridhar Kalluri (Starkey Hearing Research Center, 2150 Shattuck Ave, Suite 408, Berkeley, CA 94704, USA, sridhar_kalluri@starkey.com), Brent Edwards (Starkey Hearing Research Center, 2150 Shattuck Ave, Suite 408, Berkeley, CA 94704, USA, brent_edwards@starkey.com)

Hearing-aid design has been predicated traditionally on improving the reception of speech in background noise, a goal that has, at least in part, been successfully attained. Despite the advances, hearing-aid wearers continue to have difficulty in complex acoustic environments and in auditory tasks where normal-hearing listeners benefit greatly from binaural hearing. In order to improve hearing-aid wearers' performance in such challenging conditions, recent research has begun examining the effects of hearing aids on binaural perception. Interest in the topic is heightened by the rapidly approaching prospect of bilateral hearing aids that communicate wirelessly and thereby allow implementation of more complex signal-processing algorithms than currently possible. This talk will review binaural function and its benefits, with particular emphasis on the aspects that hearing aids can affect. The talk will also speculate on which hearing-aid algorithms can affect binaural perception.

Contributed Paper

11:40

2aPPc2. Auditory localization with linear and compression hearing aids. Helen J. Simon (Smith-Kettlewell Eye Research Institute, 2318 Fillmore St., San Francisco, CA, CA 94115, USA, helen@ski.org), E. William Yund (VAMC, 150 Muir Road, Martinez, CA 94553, USA, yund@ebire.org), Harry Levitt (Advanced Hearing Concepts, PO Box 610, Bodega Bay, CA 94923, USA, harrylevitt@earthlink.net)

The question of how well hearing-impaired individuals can localize sound (with or without amplification) is still not fully resolved. This study was designed to compare sound localization with two types of hearing-aid (HA) processing, wide dynamic range multichannel compression (WDRMCC) and linear amplification (LA) with compression limiting, during the first 32 weeks of HA use. HAs from two different manufacturers were included to compare different digital signal processing implementations, (1) fast Fourier transform (FFT), necessitating a 10 ms delay, and (2) non-FFT signal processing with a shorter time delay (~1 ms). We found an initial degradation of sound localization, relative to original unaided performance, for both WDRMCC and LA in both FTT and non-FTT platforms. We found no difference between WDRMCC and LA processing. However, sound localization with non-FFT platform improved consistently throughout 32 weeks of HA use and was better than the original unaided measurements at 16 and 32 weeks. In contrast, localization with the FFT platform showed no consistent change throughout the 32-week test period and remained inferior to original unaided performance. The continuing localization problems present for the FFT, but not the non-FFT, implementations of LA and WDRMCC may be due to its 10-ms processing delay.

Invited Papers

12:00

2aPPc3. Effects of noise type and location on binaural benefit in asymmetric directional fittings. Benjamin Hornsby (Vanderbilt University, Room 8310 Medical Center East, South Tower, 1215 21st Ave. South, Nashville, TN 37232-8242, USA, ben.hornsby@vanderbilt.edu)

The benefits of bilateral directional processing for improving speech understanding in noise are well documented. However, these fittings are not universally accepted by hearing aid wearers. Research suggests that an asymmetric fitting (omnidirectional in one ear-/directional in the other) may provide benefit in noise comparable to symmetric directional fittings (directional in both ears). This study evaluated factors that may affect the relative benefit provided by an asymmetric directional fitting. Specific factors evaluated included noise configuration, reverberation and noise type. Twenty individuals with mild-moderate SNHL participated. Aided speech understanding in cafeteria babble was assessed in bilateral omnidirectional and directional modes and in an asymmetric mode in four (4) different noise configurations. Measures were made in both an anechoic and reverberant (RT ~620 ms). In a second experiment the effects of noise type were evaluated by comparing performance in symmetric and asymmetric modes in both steady state noise and cafeteria babble. Results suggest that noise configuration has a significant effect on the relative benefit provided by asymmetric fittings. No significant differences due to noise type were observed. Individual differences in bilateral directional benefit also appear to have a significant effect on the reduction in benefit resulting from an asymmetric fitting.

12:20

2aPPc4. Speech-in-noise enhancement and sound localization with improved binaural hearing instruments. Jan Wouters (ExpORL, Dept. Neurosciences, K.U. Leuven, Herestraat 49 bus 721, O. & N2, B-3000 Leuven, Belgium, jan.wouters@med.kuleuven.be), Simon Doclo (ESAT/SISTA, K.U. Leuven, Kasteelpark Arenberg 10, B-3001 Leuven, Belgium, simon.doclo@esat.kuleuven.be), Marc Moonen (ESAT/SISTA, K.U. Leuven, Kasteelpark Arenberg 10, B-3001 Leuven, Belgium, marc.moonen@esat.kuleuven.be), Tim Van Den Bogaert (ExpORL, Dept. Neurosciences, K.U. Leuven, Herestraat 49 bus 721, O. & N2, B-3000 Leuven, Belgium, tim.vandenbogaert@med.kuleuven.be)

Multi-microphone noise reduction schemes have become standard in commercial hearing aids and cochlear implants. Recent studies with bilateral hearing aids have shown that common adaptive directional microphone systems tend to distort localization cues, leading to inappropriate and reduced spatial awareness for bilateral hearing aid users. Here we show that binaural multi-microphone signal processing based on multi-channel Wiener filter (MWF) are capable of combining noise reduction with the preservation of directional hearing. Physical simulations and perceptual results from 10 listeners have been studied for different noise source scenarios, in different reverberant conditions, and for a number of signal processing schemes using up to 4 microphone inputs (2 each side). An overview is given of the localization performance and the speech reception benefits in these different listening conditions for the different noise reduction strategies. An adaptive directional microphone system (ADM) is used as a reference system. Signal processing based on MWF does, unlike ADM, provides a combination of noise reduction and preservation of spatial awareness. Moreover, in some conditions it even offers an improved spatial release from masking. The MWF outperforms the ADM in terms of localization and noise reduction if signals are not arriving from the most forward field of view.

12:40-2:00 Lunch Break

Invited Papers

2:00

2aPPc5. Interaction between stimulus and compression type in precedence situations with hearing aids. Bernhard U. Seeber (MRC Institute of Hearing Research, Science Rd / University Park, NG7 2RD Nottingham, UK, seeber@ihr.mrc.ac.uk), Cheryl Eiler (Starkey Hearing Research Center, 2150 Shattuck Ave, Suite 408, Berkeley, CA 94704, USA, cheryl_eiler@starkey.com), Sridhar Kalluri (Starkey Hearing Research Center, 2150 Shattuck Ave, Suite 408, Berkeley, CA 94704, USA, sridhar_kalluri@starkey.com), Ervin R. Hafter (University of California, Department of Psychology, 3210 Tolman Hall, Berkeley, CA, CA 94720-1650, USA, hafter@berkeley.edu), Brent Edwards (Starkey Hearing Research Center, 2150 Shattuck Ave, Suite 408, Berkeley, CA 94704, USA, brent_edwards@starkey.com)

Multiband compression in hearing aids has the potential to interfere with binaural perception by altering binaural cues. We compared binaural precedence in patients fitted with compression hearing aids or linear hearing aids and tested one month later with a variety of stimuli. In an open field environment simulated in an anechoic chamber, subjects localized the direction of a leading sound accompanied by a lagging copy played from a different direction. Precedence, defined by a strong influence of the first sound, was found in 6/7 of the subjects when the stimulus was a sentence, but in only 4/7 when it was a high-pass or a wideband burst of noise. The fact that increasing the noise-bandwidth to include low frequencies did not produce precedence in the two patients who had shown it with a sentence may indicate a need for them to accumulate information through the successive pseudo onsets in the speech-envelope. The choice of amplification, compressive or linear, did not significantly affect precedence for any sound, except for one subject who showed weak influence of compression with the high-pass noise. We conclude that although compression might alter interaural level cues, for most, especially with long sounds, localization dominance appears unimpaired.

2:20

2aPPc6. Effect of hearing aids on distance perception. Michael A. Akeroyd (MRC Institute of Hearing Research, Glasgow Royal Infirmary, 16 Alexandra Parade, G31 2ER Glasgow, UK, maa@ihr.gla.ac.uk)

The two primary auditory cues to distance in rooms are the overall level of the sounds received by the listener and the ratio of the level of the direct sound to the reverberant sounds. In previous work we have demonstrated that hearing-impaired listeners showed no overall deficits in the ability to use the overall-level cue, but they did have deficits in the ability to use the direct-to-reverberant cue [M. Akeroyd, S. Gatehouse, and J. Blaschke, J. Acoust. Soc. Am., 121, 1077-1089 (2007)]. These deficits would be expected to contribute to the auditory disability suffered by the listeners. But both of these auditory cues are level cues, as they require some measurement of intensity, and so they would be expected to be affected adversely by the amplitude compression found in most modern hearing aids. Initial results from an experiment measuring the just-noticeable difference (JND) for changes in distance (at 2 m and 5 m) with experienced hearing-aid users suggest, however, that their JNDs are no different to those of unaided but impaired listeners. If confirmed by the final results, this surprising result may be interpretable if listeners have acclimatized to the effects of their aids on level.

2:40

2aPPc7. Binaural hearing abilities of bilaterally fitted hearing aid users assessed using objective and subjective outcome measures. Thomas Behrens (Eriksholm Research Centre, Oticon A/S, 243 Kongevejen, 3070 Snekkersten, Denmark, tbs@oticon.dk), Tobias Neher (Eriksholm Research Centre, Oticon A/S, 243 Kongevejen, 3070 Snekkersten, Denmark, ton@oticon.dk)

Aided spatial hearing in the hearing impaired remains a rather sparsely explored topic. Therefore we do not know enough about the ability of the hearing impaired to exploit auditory cues for spatial hearing. In an attempt to advance our knowledge the following

experiment was set up. A group of 21 experienced hearing aid users took part in a test using modern completely in the canal hearing aids in the field for at least 7 weeks. After acclimatization to the devices they were tested on a number of outcome measures. These included spatial unmasking, an interview administered selection of questions from the Speech Spatial and Qualities of hearing scale, and a baseline speech in noise measure. Spatial unmasking was assessed using three concurrent female talkers, with the target talker always presented directly ahead and the maskers presented either at +/- 50 degrees or both at 180 degrees. This presentation will provide results from the study described above along with possible relations to auditory and non-auditory predictors of spatial hearing performance.

Contributed Paper

3:00

2aPPc8. The effect of binaural processing techniques on speech quality ratings of assistive listening devices in different room acoustics conditions. Johan Odelius (Luleå University of Technology, Dept Human Work Sciences, Div of Sound and Vibration, SE-97187 Luleå, Sweden, johan.odelius@ltu.se), Örjan Johansson (Luleå University of Technology, Dept Human Work Sciences, Div of Sound and Vibration, SE-97187 Luleå, Sweden, orjan.johansson@ltu.se)

External microphone systems, referred to as assistive listening devices (ALD), are used in classrooms for hearing impaired students. The objective is to investigate the effect of binaural processing techniques in different room acoustic conditions. A listening experiment was conducted with 10 normal hearing adults. Response variables were judgements of clarity, pleasantness, listening effort and overall speech quality. Design variables were binaural processing, room acoustics and ALD bandwidth. Stimuli were generated using the room acoustic modelling software CATT Acoustic. Three speech sources, two male voices and one female voice, were placed at a table in the centre of a room and one Brown noise source was placed in one corner of the room. Microphones were placed 0.5 m in front of each speech source. Target source was a random choice of one of the two male voices. The binaural processing was utilized by a simple HRTF filtering. Depending on the angle to the source from a fictitious listening position at the table, corresponding interaural time difference (ITD) and the interaural level difference (ILD) was applied to the signal. Stimuli were presented by loudspeakers using cross-talk cancellation. The hypothesis is that binaural processing will give a significant improvement in speech quality.

TUESDAY MORNING, 1 JULY 2008 ROOM 242B, 8:00 TO 10:40 A.M.

Session 2aSAa

Structural Acoustics and Vibration and EURONOISE: Vibration and Radiation from Complex Structural Systems II

David Feit, Cochair
Applied Physical Sciences Corp., Ste. 300, 2 State St., New London, CT 06320, USA

Jean-Louis Guyader, Cochair
INSA de Lyon - LVA, Bâtiment St. Exupéry, 25 bis avenue Jean Capelle, Villeurbanne Cedex, F-69621, France

Contributed Papers

8:00

2aSAa1. On the comparison of symmetric and unsymmetric formulations for experimental vibro-acoustic modal analysis. Morvan Ouisse (FEMTO-ST UMR CNRS, 23 chemin de l'Epitaphe, 25000 Besançon, France, morvan.ouisse@univ-fcomte.fr), Emmanuel Foltete (FEMTO-ST Applied Mechanics, 24 chemin de l'épitaphe, 25000 Besançon, France, emmanuel.foltete@univ-fcomte.fr)

The classical u-p formulation for vibro-acoustic problems is very convenient for experimental vibro-acoustic modal analysis since the physical variables are directly those which are measured by operators. In this particular context, the objective is to identify from experimental measurements a reduced model which has the same behaviour as the measured one. The complex mode shapes which are identified using this technique must satisfy a properness condition. When they do not verify it, they should be modified to be able to represent the behaviour of a physical system. Some techniques have been proposed in order to develop a strategy to obtain the modified eigenshapes, but this is a quite difficult point because of the unsymmetric topology of the equations. In this paper, a symmetric formulation is used in order to be able to directly apply the classical methodology which has been developed for structural modal analysis to obtain the physical reduced system. The methodology is described and compared with the u-p formulation, in terms of efficiency and precision, in particular when some absorbing devices are considered. All results are first presented on an ideal numerical test-case, and applications on experimental data are finally shown.

8:20

2aSAa2. Numerical modeling of Panphonics's G1 flat loudspeaker. Krisztián Gulyás (Budapest University of Technology and Economics, BME Dept. of Telecommunications, Magyar tudósok körútja 2, H-1117 Budapest, Hungary, gulyas@hit.bme.hu), Fülöp Augusztinovicz (Budapest University of Technology and Economics, BME Dept. of Telecommunications, Magyar tudósok körútja 2, H-1117 Budapest, Hungary, fulop@hit.bme.hu)

The basic idea behind AABC (Active Acoustic Barrier Control) is to reduce the sound radiation of a structure acoustically without influencing the vibration behavior of the structure. The large surface acoustic polymer material actuator/sensor systems are primarily meant to form the actuator/sensor system for the AABC concept. The main component of this package is a special active device: the rEMA - revised Elastic Mass Actuator based on the Panphonics' G1 panel loudspeaker element. This paper deals with the modeling and the low-frequency performance issues of the G1 flat loudspeaker. The aim was to create an accurate mathematical model to understand the operational principles of the loudspeaker, and then this model was used to optimize its low-frequency performance. Due to the special

structure and the optimization tasks, a new numerical method was developed to model special multi-layer coupled vibro-acoustics systems based on the Finite Difference and Boundary Element Method. The investigation focuses on the mechanical behavior of the panel and describes the sound radiation properties also. The performed work was a part of the research of the project InMAR (Intelligent Materials for Active Noise Reduction) which was funded by the European Union.

8:40

2aSAa3. Metrology and prediction for integrating a subsystem on a vehicle: Application to a fan system attached to the front end of a car. Marie-Hélène Moulet (CEVAA, Technopole du Madrillet, 2 Rue Joseph Fourier, 76800 Saint Etienne du Rouvray, France, mh.moulet@cevaa.com), Saul Mapagha (CEVAA, Technopole du Madrillet, 2 Rue Joseph Fourier, 76800 Saint Etienne du Rouvray, France, s.mapagha@cevaa.com), Vincent Martin (Institut Jean Le Rond d'Alembert, UMR CNRS 7190, UPMC, 2 Place de la Gare de Ceinture, 78210 Saint-Cyr l'Ecole, France, vmartin@ccr.jussieu.fr)

The car industry must satisfy physical acoustic and vibratory objectives in order to comply with safety and comfort norms. Among others, efforts entering the chassis should be limited. When a host structure is excited by a vibratory system, called subsystem, it also vibrates and may radiate an acoustic field. Usually, the subsystem is first tested on a bench and the question is then to deduce the efforts entering the chassis from those entering the test bench. Globalising notions of impedance already made evident via deformable structure configurations are used presently through measurements in a technological configuration, the complexity of which does not allow modelling. The case of a fan system attached to the front end of a car is under study. Some metrological conclusions, as well as more dedicated ones concerning the fan system itself, will be given. Finally, on the calculation and prediction sides, expected properties that are not satisfied (such as symmetry in measured matrices) are seen to be of no great consequence in the present case.

9:00

2aSAa4. Numerical study of the transition to chaos in nonlinear forced vibrations of plates. Cédric Camier (ENSTA, Chemin de la Hunière, 91761 Palaiseau cedex, France, cedric.camier@ensta.fr), Cyril Touze (ENSTA, Chemin de la Hunière, 91761 Palaiseau cedex, France, cyril.touze@ensta.fr), Olivier Thomas (CNAM, 2, rue Conté, 75003 Paris, France, olivier.thomas@cnam.fr), Stefan Bilbao (University of Edinburgh, Room 7306B, JCMB, King's Bldgs., Mayfield Rd., EH9 3JZ Edinburgh, UK, sbilbao@staffmail.ed.ac.uk)

Geometrically nonlinear vibrations of free edge circular plates subjected to a harmonic excitation are discussed. Particularly, transition from periodic to chaotic motion is observed when increasing the amplitude of the forcing. The present work is devoted to reproduce numerically these highly nonlinear behaviours. The temporal integration of such dynamics, including instabilities and chaotic regimes, is not straight forward because a stiff problem with a very large number of dofs is at hand. Consequently, numerical instabilities are observed when typical Runge-Kutta schemes are applied. To settle the matter, two methods have been tested and compared. They both rely on a modal approach applied to the von Kármán's model for large amplitude vibrations of plate. For the first one, the energies of the plates are expressed at the continuous level. The Hamiltonian of the system is then derived and discretized using the eigenmodes. The Hamiltonian formulation ensures the conservation of energy. An implicit time discrete scheme is then chosen to approximate the equations of motion. For the second one, the Gear's BDF method, implemented in the IMSL Fortran library, is used to integrate the nonlinear oscillator equations.

9:20

2aSAa5. Numerical investigations into the squeal propensity of a railway disc brake. Olivier Chiello (INRETS, Transport and Environment Lab., 25 avenue François Mitterrand, 69675 Bron cedex, France, olivier.chiello@inrets.fr), Xavier Lorang (SNCF, Innovative & Research Dept., 45 rue de Londres, 75379 Paris, France, xavier.lorang@sncf.fr)

This paper comes within the scope of a research program concerning with the reduction of the squeal noise generated by high power railway disc brakes. It focuses on the numerical results provided by a finite element model of the brake including unilateral contact and Coulomb friction at the disc/pad interfaces. In particular, the dynamic stability of the sliding equilibrium is investigated by performing a complex eigenvalue analysis of the linearized equations verified by the structural displacement fields. Complex eigenvalues and complex modes are used to estimate the squeal propensity of the brake in a given frequency range. The effect of various mechanical and geometrical parameters is studied in order to better understand the mechanism leading to the system instability.

9:40

2aSAa6. Three dimensional orthogonality of the Lamb modes in layered plates of elastic and viscoelastic materials and their implementation to the far field evaluation. Dmitry Zakharov (LMP, UMR CNRS 5469, Université Bordeaux I, 351, cours de la Libération, 33405 Talence, France, dmitrii.zakharov@gmail.com)

The 3D guided waves in the linearly viscoelastic laminates are considered. On the plate surfaces any of the homogeneous boundary conditions are allowed, e.g., the Lamb waves, waves in clamped plates, etc. are taken into account. The fundamental property of these waves is their generalized orthogonality, which is deduced and discussed. The applications of the orthogonality relations for solving some particular boundary value problems are suggested. A method for the exact calculation of the far field caused by an acoustic source of a finite size is suggested. The only restriction is that the distance required must exceed the longitudinal radius of the source. The obtained results can be used for evaluating the fields radiated by ultrasonic transducers of arbitrary aperture and by other realistic sources.

10:00

2aSAa7. Sound Radiation of a Large Truck Oil Pan: Estimation and Experimental Investigation. Olaf Heintze (German Aerospace Center (DLR), Institute of Composite Structures and Adaptive Systems, Lilienthalplatz 7, 38108 Braunschweig, Germany, olaf.heintze@dlr.de), Volker Wittstock (Physikalisch-Technische Bundesanstalt, Bundesallee 100, 38116 Braunschweig, Germany, volker.wittstock@ptb.de), Carl Fredrik Hartung (Volvo Technology Corporation, Götaverksgatan 10, 405 08 Göteborg, Sweden, carl.fredrik.hartung@volvo.com)

The oil pan of large diesel engine trucks has been identified as a significant contributor to their external noise radiation. This undesired broadband noise is caused by the oil pan's structural vibration and can not be treated effectively by passive measures especially in the low frequency regime up to 500Hz. In order to address this challenge, an active structural acoustic control system consisting of structural sensors and actuators is suitable to alter the oil pans vibrations in a sound reducing manner. A first step is however to classify the broadband sound radiation such that it allows for a proper and efficient sound power estimation resulting from structural measurements. Therefore, an acoustical model was set up based on a geometrical surface scan of a serial production large truck oil pan mounted in a laboratory test stand. This model served for the numerical computation of a set of principle velocity patterns contributing independently to the active sound power, where its hybrid estimation has been performed employing additionally the measured structural response of the oil pan assembly due to a shaker excitation. Finally, the sound power radiation of the test stand has been measured in a reverberation room to validate this hybrid estimation.

10:20

2aSAa8. Sound propagation on a high pressure gas pipe. Rolf Schirmacher (Müller-BBM, Robert-Koch-Straße 11, 82110 Planegg, Germany, Rolf.Schirmacher@MuellerBBM.de), Robert Baars (M+P raadgevende ingenieurs B.V., Visserstraat 50, 1431 GJ Aalsmeer, Netherlands, robertbaars@mp.nl)

At a two stage high pressure gas compressor with intermediate cooler, the cooler radiate a tone at the compressor rotational frequency of approx. 160 Hz. For the design of noise reduction devices, the mechanism of sound propagation in between the compressor an the cooler on a DN 400 steel pipe with 24 mm wall thickness and 160 Bar internal gas pressure was to be determined. By non-invasive vibration measurements on the pipe, the dominance of the fluid borne sound (natural gas) over the structure borne sound was found. Later, pressure measurements in the pipe clearly approved this result. The concepts upon which the measurements and data evaluation were based (propagating modes of coupled system, wave separation, etc) as well as the results are presentend.

TUESDAY MORNING, 1 JULY 2008 ROOM 243, 8:00 A.M. TO 12:20 P.M.

Session 2aSAb

Structural Acoustics and Vibration and EURONOISE: General Topics in Structural Acoustics and Vibration II

Wolfgang Kropp, Cochair
Chalmers University of Technology, Division of Applied Acoustics, Gothenburg, SE-41296, Sweden

Sean Wu, Cochair
Wayne State University, 5050 Anthony Wayne Dr., Detroit, MI 48202, USA

Contributed Papers

8:00

2aSAb1. Wavelet-based data processing for comparative study of noncontact measurement techniques for vibroacoustics. Dan Borza (National Institute of Applied Sciences of Rouen, INSA Rouen, LMR, Ave l'Universite, BP8 76800 Rouen, France, dan.borza @insa-rouen.fr), Ioana Nistea (Institut National des Sciences Appliquées de Rouen, BP8 avenue de l'Université, 76801 Saint-Etienne du Rouvray, France, ioana.nistea@insa-rouen.fr)

In vibration analysis of structures complex measurement information is required in order to perform modal analysis, therefore the choice of the measurement technique to be applied is essential. Non contact measurements are preferred to classical transducer based methods, mainly due to the absence of influence upon the structure under test. The various techniques available today in vibroacoustics produce results which are quite different in terms of spatial and temporal resolution or measured quantities and therefore a choice has to be made of the experimental tool best adapted for different fields of research (acoustics, mechanical structures, dynamics). In this paper, we present a comparative study of several optical, acoustical and numerical techniques for vibration measurement or simulation, namely Digital Speckle Interferometry, Laser Doppler Vibrometry and a FE model. The tests were made for the free and the forced vibrations of a highly dumped, non-metallic plate. In the data processing stage, discrete wavelet decomposition has been applied on the experimental data in order to match up the spatial maps of vibration amplitudes.

8:20

2aSAb2. Analysis of the acoustic signals backscattered by a tube using the time-frequency representations. Mustapha Laaboubi (Ibn Zohr University, FS Agadir, 80000 Agadir, Morocco, laaboubi @gmail.com), Elhoucien Aassif (Ibn Zohr University, FS Agadir, 80000 Agadir, Morocco, aassif@hotmail.com), Rachid Latif (ESSI - ENSA, BP 1136, Ibn Zohr University, 80000 Agadir, Morocco, latif@ensa-agadir.ac.ma), Gerard Maze (LAUE, Université du Havre, Place Robert Schuman, F-76610 Le Havre, France, gerard.maze @univ-lehavre.fr),Dominique Decultot(LOMC FRE 3102 CNRS Groupes Ondes Acoustiques, Université du Havre (IUT), Place Robert Schuman, 76610 Le Havre, France, dominique.decultot@univ-lehavre.fr), Ali Moudden (Ibn Zohr University, FS Agadir, 80000 Agadir, Morocco, ali_moudden@yahoo.fr), Abdelilah Dariouchy (LMTI, univirsté ibn zohr Faculté des Sciences LMTI bp 8106, 80000 Agadir, Morocco, abdelilah _dariouchy@yahoo.fr)

The normal excitation of a tube immersed in water by the acoustic plane wave, circumferential waves are generated inside the shell. These circumferential waves, standing form stationary waves on the circumference of the tube for some frequencies. These stationary waves, constituting resonances of the tube which are perfectly visible on the backscattered spectrum. Moreover, the studies carried out on the diffusion of a plane acoustic wave by target were based primarily on the use of the monodimensional methods (Temporal domain and/or frequencial domain). To exceed the disadvantages of these methods, in this work, we used the time-frequency representations such as the Short-Term Fourier Transform (STFT), Wigner-Ville Distribution (WVD) and Wavelet Transform method. These representations are applied to a theoretical signal backscattered by a tube of aluminium, copper and steel with radii ratio b/a = 0.95 (a is the external radius, and b the internal radius). From the time-frequency images obtained we have visualized the dispersion of circumferential waves (S0, A1, S1,œ) and identified these different waves. This analysis permits to compare between these time-frequency representations. And also we have compared between the cut-off frequencies of circumferential waves obtained from these representations and those computed by the proper modes theory of the vibration.

8:40

2aSAb3. Weak radiator design using dimples. D. Chih-Chun Cheng (National Chung Cheng University, Dept. of Mechanical Engineering, 160, San-Hsing, Ming-Hsiung, 621 Chia-Yi, Taiwan, imeccc@ccu.edu.tw), Wen-Nan Cheng (National Chung Cheng University, Dept. of Mechanical Engineering, 160, San-Hsing, Ming-Hsiung, 621 Chia-Yi, Taiwan, zzs1003@hotmail.com), Cary H. Koopmann (Pennsylvania

State University, Dept. of Mechanical and Nuclear Engineering, 157 Hammond Building, University Park, PA 16802, USA, ghk@engr.psu.edu)

A design method for achieving minimum radiation of sound from a beam by creating cylindrical dimples on its surface is presented. Two strategies of determining the dimple size and its location on the beam are presented. The first is based on the optimization method, in which the dimple size and its location are the design variables. The design variables that minimize the sound power are obtained directly using an optimization subroutine. The second is to synthesize the beam's weak radiator mode using a set of dimples, in which the mode shape of the dimpled beam is a close fit to the beam's weak radiator mode. As a comparison in sound power reduction between these strategies, numerical results for a simply supported beam in a rigid baffle excited by a harmonic force are presented.

9:00

2aSAb4. Estimation for vibration mode of membrane by NAH method. Nabilah Ibrahim (Shibaura Institute of Technology, 3-7-5, Toyosu, Koto-ku, 135-8548 Tokyo, Japan, m107068@sic.shibaura-it.ac.jp), Hideo Shibayama (Shibaura Institute of Technology, 3-7-5, Toyosu, Koto-ku, 135-8548 Tokyo, Japan, sibayama@sic.shibaura-it.ac.jp), Toru Itakura (Shibaura Institute of Technology, 3-7-5, Toyosu, Koto-ku, 135-8548 Tokyo, Japan, m106009@sic.shibaura-it.ac.jp)

Near Field Acoustic Holography (NAH) is the method of measuring sound information on the radiant surface in the near field as a hologram. By use the technique, we can visualize the vibration of the radiant surface. Thus, we can easily understand the object of the acoustic conditions in acoustic image processing. We made the measurement on one side of the drum using array microphone while the driven source is attached to the other side. In addition, the measurement is not touched on the vibrating membrane surface. This paper describes the estimated results of the vibration mode on the vibration membrane of a drum. And this is possible by apply it to the vibration controlling field for detecting the sound structure on the membrane.

9:20

2aSAb5. Computing high frequency vibrations of polygonal plates by the Image Source Method. Jacques Cuenca (LAUM, CNRS, Université du Maine, Lab. d'Acoustique Université du Maine, UMR CNRS 6613, 72085 Le Mans Cedex 9, France, Jacques.Cuenca.etu@univ-lemans.fr), François Gautier (Laboratoire d'Acoustique de l'Université du Maine, Avenue Olivier Messiaen, 72085 Le Mans, France, francois.gautier@univ-lemans.fr), Laurent Simon (LAUM, CNRS, Université du Maine, Lab. d'Acoustique Université du Maine, UMR CNRS 6613, 72085 Le Mans Cedex 9, France, Laurent.Simon@univ-lemans.fr)

The aim of this paper is to show that the Image Source Method (ISM) can be used for predicting medium and high frequency vibrations of arbitrarily shaped polygonal plates with controllable precision. Modeling the vibrations of polygonal plates by ISM consists in superposing the contributions of elementary image sources, which allows the plate boundary conditions to be satisfied. For particular plate shapes leading to a spatially periodic pattern of image sources, it is shown that ISM allows the exact computation of the Green's function by means of a Poisson summation formula. For arbitrarily polygonal plates, a criterion for truncating the image source generation process is examined and used as a control parameter for the precision of the estimations. The given examples show that the results are in good agreement with exact analytical solutions for simple plate shapes and with results obtained by the finite element method for more complex shapes. The convergence towards reference solutions as the number of image sources is increased is investigated. The main advantage of the method is that the accuracy is improved with structural damping and with frequency for a given number of image sources.

9:40

2aSAb6. Estimation of received acoustic levels in the near-field of a ship. Christopher Barber (Penn State University, PO Box 30, State College, PA 16804-0030, USA, cbarber@psu.edu)

Measured acoustic levels at the face of a receiver in close proximity to a ship in shallow water can differ substantially from the levels predicted by applying standard propagation models to a source level determined from a far-field radiated noise measurement. At distances typical of mine-ship engagements, the dimensions of the source (ship) can be large with respect to range, ocean depth and acoustic wavelength, and the ship cannot be approximated as a single point source, nor is the receiver necessarily located outside the acoustic near field. Direct free-field measurements of ship radiated noise at short range are problematic, so that the received acoustic level in the near-field of a ship must be estimated from other available information. Options for generating such estimates are presented, including a hybrid approach combining empirically-derived transfer functions, a virtual distributed-source representation of the ship, and in-situ hull vibration measurements. The potential for computational methods such as BEM - FEM and measurements such as Nearfield Acoustic Holography to provide an improved understanding of the vibration sources, structural responses, radiation mechanisms and propagation paths associated with the radiated noise field of realistic ship structures is also explored. (Work sponsored by ONR Code 331).

10:00

2aSAb7. Some notes on the sound reduction index of pax cabins panels on cruise ships. Marco Biot (DINMA, University of Trieste, Via Valerio, 10, 34100 Trieste, Italy, biot@units.it), Francesco De Lorenzo (Fincantieri SpA, Passeggio S. Andrea, 6, 34100 Trieste, Italy, Francesco.Delorenzo@fincantieri.it)

The issue of comfort of passenger ships has became in the last years of paramount importance; in this context the noise and vibration control plays a leading role. The concept of comfort on board is subjective and it is impossible to define it with simple formula. On the other hand, a few number of significant parameters is commonly used to characterize the level of comfort on board of ships, and the sound insulation index in one of the most important. As known, it has a paramount importance in defining the contractual comfort on board of ships. The report is related with the problem of setting up the sound insulation index for pax cabins, specifically in relation to the nature and characteristics of the panels between cabins.

10:20-10:40 Break

10:40

2aSAb8. Acoustic and vibration measurements of NASA spacesuits. Durand R. Begault (NASA Ames Research Center, Mail Stop 262-2, NASA ARC, Moffett Field, CA 94035, USA, Durand.R.Begault@nasa.gov), James L. Hieronymus (NASA Ames Research Center, Mail Stop 262-2, NASA ARC, Moffett Field, CA 94035, USA, JimH@riacs.edu), Bernard D. Adelstein (NASA Ames Research Center, Mail Stop 262-2, NASA ARC, Moffett Field, CA 94035, USA, Bernard.D.Adelstein@nasa.gov)

Research was conducted to examine interactions between acoustic signals and mechanical factors relevant to the design of improved auditory displays and noise mitigation for future NASA Spacesuits. Data were collected at NASA Johnson Space Center for the current Mark III advanced prototype surface suit during walking, walking with arm motion, and while seated. Measurements were made using multiple microphones (both head mounted and helmet mounted) and a tri-axial accelerometer to evaluate the effects of suit-borne vibration on overall background noise. Footfall impacts were found to create temporary depolarization of condenser microphone signals, and microphone positioning had a strong effect on signal-noise ratio, partially due to the effect of the helmet enclosure. The results indicate noise mitigation and signal conditioning strategies for improving lunar suit audio voice communications under extra-vehicular (EVA) conditions. Funded by a directed research program of NASA's Space Human Factors Engineering project and by NASA-JSC's Constellation EVA system audio group.

11:00

2aSAb9. Influence of material properties on sound radiation for flat loudspeakers. Jaime Ramis Soriano (DFISTS. Univ. de Alicante, Carretera de Sant Vicent del Raspeig s/n, 03690 San Vicente del Raspeig, Spain, jramis@ua.es), Jesús Alba Fernandez (Escola Politècnica Superior de Gandia, Universitat Politècnica de València, Crtra Natzaret-Oliva s/n, 46730 Gandia, Spain, jesalba@fis.upv.es), Jorge Frances Monllor (DFISTS. Univ. de Alicante, Carretera de Sant Vicent del Raspeig s/n, 03690 San Vicente del Raspeig, Spain, jfmonllor@ua.es), Jorge P. Arenas Bermudez (Universidad Austral de Chile, Institute of Acoustics, 567 Valdivia, Chile, jorgep.arenas@gmail.com)

This work aims to analyze numerically, analytically and experimentally, the influence on sound power radiated, frequency response, and directionality of different materials in flat loudspeakers. Concerned experimental setup, the excitation force consists in a shaker which his mechanical characteristics are completely known. Finite Element Method has been used to simulate this configuration .The analytical model used couples the electrical, mechanical and acoustical system of the panel. The parameters of the panel material which we are focused are elastic modulus and loss factor. The analytical formalism serves as the basis to study the structural and vibrational behaviour of the system that also is analyzed with experimental results. The results obtained from different materials and different excitation position serves as basis for optimum configuration in this type of speakers.

11:20

2aSAb10. Acoustical Effectiveness of Damping Coating. Raymond Fischer (Noise Control Engineering Inc, 799 Middlesex Tnpk, Billerica, MA 01821, USA, rayf@noise-control.com), Leonid Boroditsky (Noise Control Engineering Inc, 799 Middlesex Tnpk, Billerica, MA 01821, USA, leob@noise-control.com)

Damping coatings have again become popular in the shipbuilding industry to reduce onboard and underwater noise. Understanding of the actual effectiveness of damping tiles applied to ship structures is important for noise prediction during the design stage and for optimizing noise control. The commonly held opinion that energy loss is proportional to loss factor values is not confirmed by tests conducted on actual structures. This paper discusses differences between loss factors measured on the Oberst beam and on two-dimensional real structures. The paper shows how loss factor change may influence transmission loss, radiation efficiency and acceptance. The results of loss factor measurements in different conditions including water-loaded media are demonstrated. influences of resonant and non- resonant modes on damping tile effectiveness is discussed. Corrections for SEA noise prediction algorithms, taking into account results of this research, are proposed.

11:40

2aSAb11. On the prediction of absorption coefficient of porous materials with Finite Elements. Sabine Langer (TU Braunschweig, Institute of Applied Mechanics, Spielmannstr. 11, 38106 Braunschweig, Germany, s.langer@tu-bs.de), Meike Wulkau (TU Braunschweig, Institute of Applied Mechanics, Spielmannstr. 11, 38106 Braunschweig, Germany, m.wulkau@tu-bs.de)

The absorption coefficient gives the relation between incited and reflected sound power on a surface and is a measure for the damping properties of materials. Experimentally it can be investigated by using the impedance tube for perpendicular incitation and the echo chamber in the case of a diffuse sound field as is known. To optimize the sound absorption properties of materials in the pre-prototype stage, numerical simulation can support the design of materials. A detailed finite element simulation based on Biots Theory for poroelastic-media is used to predict the absorption coefficient of materials with open-pored surfaces. Prospects and limits of this strategy are discussed.

12:00

2aSAb12. Ground-borne vibration case studies in residential constructions. James Perry (Cerami & Associates, 404 Fifth Avenue, New York, NY 10018, USA, jperry@ceramiassociates.com)

Case studies are examined for several new high-rise residential and hotel buildings proposed for construction over or near underground and surface transit systems. Baseline vibration measurements were taken on grade and existing building structures and projected against standard functional vibration criteria (ANSI S3.29 / ISO 2631 2). Through post-construction testing and client feedback, the vibration and structure-borne noise impacts were field verified. Study results offer insight into the correlation between these vibration criteria and the subjective human perceptions of various sensitivities. Further items of discussion include the relative effects of various architectural constructions, building types, and applications as well as mitigating sound and vibration controls.

Session 2aSAc

Structural Acoustics and Vibration and EURONOISE: Source Characterization in Structure Borne Noise Problems I

Evan Davis, Cochair
The Boeing Company, P.O. Box 3707, Seattle, WA 98124, USA

Charles Pezerat, Cochair
Laboratoire Vibrations Acoustique - INSA Lyon, 25 bis avenue Jean Capelle, Bâtiment Saint-Exupéry, Villeurbanne cedex, F-69621, France

Invited Papers

11:00

2aSAc1. Structure-borne sound transmission from machines into ribbed structures. Barry M. Gibbs (University of Liverpool, School of Architecture, Abercromby Square, L693BX Liverpool, UK, bmg@liv.ac.uk), Andreas R. Mayr (Stuttgart University of Applied Sciences, Schellingstrasse 24, 70174 Stuttgart, Germany, andreas.mayr@hft-stuttgart.de)

The total structure-borne sound power of an installed machine is a function of the source activity and mobility, and the receiver mobility, at each contact and for each component of excitation. The data and computational requirements for prediction therefore are large. Manufacturers view their products as single entities and desire corresponding single values of source strength. A laboratory reception plate measurement procedure has been proposed which yields single equivalent values of source strength and source mobility. The source data, in combination with an estimate of the single equivalent value of receiver mobility, yields the approximate total installed power. The accuracy of the estimate is dependent on the spatial variation in contact conditions over the connections. In addition, phase information has been lost in the simplification. Case studies are described for multiple contact sources on a non-homogeneous plate (a timber-joist floor) where the approximate estimates of structure-borne power are compared with exact values obtained from full mobility formulations.

11:20

2aSAc2. Time domain identification of loads on plate-like structures using an array of acoustic velocity sensors. Quentin Leclere (Laboratoire Vibrations Acoustique - INSA Lyon, 25 bis avenue Jean Capelle, Bâtiment Saint-Exupéry, F-69621 Villeurbanne cedex, France, quentin.leclere@insa-lyon.fr), Charles Pezerat (Laboratoire Vibrations Acoustique - INSA Lyon, 25 bis avenue Jean Capelle, Bâtiment Saint-Exupéry, F-69621 Villeurbanne cedex, France, charles.pezerat@insa-lyon.fr)

The FAT (Force Analysis Technique) method has been developped to identify loads on beams or plates from the knowledge of their flexural displacements. The method is based on a local discretisation of the differential operator of the studied structure : all derivatives of the displacement field are assessed at a given point from a finite difference scheme. The estimation of the operator gives as an output the value of the force distribution. Up to now, applications of the FAT method have been made in the frequency domain, scanning the studied structure with accelerometers or with a laser vibrometer, and using phase references to get the phase relation between different points. The aim of the present study is to show that the FAT method allows to identify loads in the time domain. This operation requires the simultaneous measurement of at least 13 points on the plate, that can be realized without contact using an array of acoustic velocity sensors in the very near field of the plate. The method has been applied on a plate excited by an acoustic diffuse field. The identified force distribution is compared to the parietal acoustic pressure measured in the reverberant room.

11:40

2aSAc3. Measurements of the bending moment at boundaries of a structure. Simon Chesne (LaMCoS - INSA-Lyon - CNRS UMR5259, 18-20, rue des Sciences, Bâtiment Jean d'Alembert, F-69621 Villeurbanne, France, simon.chesne@insa-lyon.fr), Baptiste Chomette (LaMCoS - INSA-lyon - CNRS UMR5259, 18-20, rue des Sciences, Bâtiment Jean d'Alembert, F-69621 Villeurbanne, France, baptiste.chomette@insa-lyon.fr), Charles Pezerat (Laboratoire Vibrations Acoustique - INSA Lyon, 25 bis avenue Jean Capelle, Bâtiment Saint-Exupéry, F-69621 Villeurbanne cedex, France, charles.pezerat@insa-lyon.fr)

In the vibration transmission process, the part due to the moment excitation is often neglected, because of the difficulty to measure them, even if these terms are sometimes important. Indeed, several studies show that the influence of the moment in structure borne power transmission can be higher than simple force. Moment measurement or identification is an old problem especially at boundaries. It has been mainly investigated in mobility methods. In fact, bending moment expression can be seen as spatial derivatives of displacements. These derivatives can be approximated from measured displacements but two major difficulties appear: derivatives are highly sensitive to measurement errors and the usual methods used to obtain them (finite differences, modal approach, etc.) are not well adapted at boundary points. In this paper, three different moment identification methods are investigated where the considered structure is a beam. Both of these approaches are already developed by authors, the third method is based on the use of particular mechanical and electric setups of piezoelectric patches. These 3 methods are numerically and experimentally implemented allowing us to compare and discuss on results.

12:00

2aSAc4. Characterisation of structure borne sound sources from measurement in-situ. Andrew Elliott (University of Salford, Acoustic Research Centre, Newton Building, M5 4WT Salford, UK, a.s.elliott@pgr.salford.ac.uk), Andy T. Moorhouse (University of Salford, Acoustic Research Centre, Newton Building, M5 4WT Salford, UK, a.t.moorhouse@salford.ac.uk)

In-situ source characterisation methods are those which involve measurements made whilst source and receiver are coupled as they would be in a real installation. Potentially in-situ source characterisation may account for the physical reality lost in the ″black box″ approach. There are other potential benefits such as ease of measurement. In this work a structure borne sound source is characterised using in-situ measurements of blocked force and coupled mobility. Promising results from the method have been presented previously. Further to this, an extension of the method allowing the use remote measurement positions has been developed. Using reciprocity, the extended method will further ease measurement for situations where access poses a problem. The extended method is outlined and some preliminary validation results are presented.

12:20

2aSAc5. General model of a structure-borne sound source and its application to shock vibration. Yuri Bobrovnitskii (Mechanical Engineering Research Institute, 4, M. Kharitonievky Str., 101990 Moscow, Russian Federation, yuri@imash.ac.ru), Tatiana Tomilina (Mechanical Engineering Research Institute, 4, M. Kharitonievky Str., 101990 Moscow, Russian Federation, tatiana@imash.ac.ru)

One of the well-known models of structure-borne sound sources is described by the quantities defined at the source-receiving structure interface: by the matrix of the source impedances or mobilities and by the vector of the blocked forces or free velocities. Together with the receiver impedances or mobilities it allows one to predict the vibration field in the receiver and to develop and examine candidates for source characterization. In this paper, it is shown analytically that this model is valid when the sound is generated inside the source by a kinematic excitation as well as by force excitation or their combination and, thus, it represents a rather general model with wide range of applications. Most attention is paid to its peculiarities and limitations when applied to shock sources. Results are illustrated by the data measured in the shock tests of some scientific space instruments.

TUESDAY MORNING, 1 JULY 2008 ROOM 240, 8:20 TO 10:40 A.M.

Session 2aSCa

Speech Communication: Speech Technology II

Indranil Dutta, Chair

Rice University, Center for the Study of Languages, MS #36, 6100 Main St., Houston, TX 77005, USA

Contributed Papers

8:20

2aSCa1. Evaluation of acoustic environments using deteriorated speech sound. Yoshiki Nagatani (Nara Medical University, 840 Shijo-cho, 634-8522 Kashihara, Japan, naramed-u@nagatani.ne.jp), Takefumi Sakaguchi (Nara Medical University, 840 Shijo-cho, 634-8522 Kashihara, Japan, t-saka@naramed-u.ac.jp), Hiroshi Hosoi (Nara Medical University, 840 Shijo-cho, 634-8522 Kashihara, Japan, hosoi@naramed-u.ac.jp)

Aged or hearing-impaired people require better acoustical environments for higher QOL. Many methods of evaluating the quality of speech in acoustical environments have been developed. However, since they mainly focus on quality of speech in bad conditions (e.g. environments with huge noise or long reverberation), they are not suited for evaluations in generic environments such as normal houses or public facilities for aged people. For instance, the scores of D value (deutlichkeit) or speech transmission index (STI) are too high and not sensitive enough to refer to such environments. The intelligibility test using normal speech sounds cannot clarify the differences between different room environments because the intelligibility scores reach almost 100 percent in ordinary room environments. Therefore, we proposed a new evaluation method using deteriorated speech sounds. In this method, signal-processed speech sounds are presented to trial subjects under target sound environments. In this study, Japanese monosyllabic speech sounds convoluted by the impulse responses of room reverberations were presented through a headphone in order to simulate the architectural acoustic environments. As a result, it was shown that this new method could detect the small difference of sound environments, which the conventional methods could hardly evaluate.

8:40

2aSCa2. Measurement of Speech Intelligibility Using Low Level Output - Threshold Efficient S/N Ratios. Christos Nestoras (London South Bank University, FESBE, Borough Road, SE1 0AA London, UK, nestorasc@gmail.com), Stephen Dance (London South Bank University, FESBE, Borough Road, SE1 0AA London, UK, dances@lsbu.ac.uk)

Excessive background noise levels or perhaps annoyance due to a high test signal level are the main reasons for having a low signal to noise ratio (S/N) or low level output during a measurement session. A significant error, in this sense, can be introduced in the resulting data since the measurement technique requires, among others, a minimum S/N ratio for an accurate result. A validation is presented of low level output intelligibility measurements in an attempt to establish a point of reference for the verification of data accuracy for a given space. An indication of the functions taking place in this respect could be obtained through practical experimentation. Results are reported here.

9:00

2aSCa3. Vowels recognition using mellin transform and plp-based feature extraction. Mahdi Jamaati (Technical University of Shahrood, 12345 Shahrood, Iran, mahdi.jamaati@gmail.com), Hossein Marvi (Technical University of Shahrood, 12345 Shahrood, Iran, h_marvi@shahroodut.ac.ir), Milad Lankarany (Technical University of Shahrood, 12345 Shahrood, Iran, milad.lankarany@gmail.com)

Feature extraction for speech recognition is a subject of majer interest today. Different feature have been investigated in speech recognition systems. The scale transform is a particular restriction of the Mellin transform. The key property of the scale transform is the scale invariance .The mel frequency(MFCC) and perceptual linear predicate (PLP) have usually reported to have yielded good performance. In this paper, a new method is presented which combines feature extracted from mellin transform with the plp features. To evaluate the performance of the proposed features the comparative tests with the lpc features, MFCC and PLP were performed on the vowels based speech recognition system. Preliminary experiment show that this approach posses promissing result.

9:20

2aSCa4. A system for automatic detection and correction of detuned singing. Michał Lech (Gdansk University of Technology, Multimedia Systems Department, 11/12 Gabriela Narutowicza Street, 80-952 Gdansk, Poland, mlech@sound.eti.pg.gda.pl), Bozena Kostek (Gdansk University of Technology, Multimedia Systems Department, 11/12 Gabriela Narutowicza Street, 80-952 Gdansk, Poland, bozenka@sound.eti.pg.gda.pl)

The aim of the paper is to show a system engineered for automatic detection and correction of detuned singing. For this purpose, existing methods of fundamental frequency detection and pitch correction are reviewed. In addition, main characteristics of some existing detuning systems are presented. As algorithms for fundamental frequencies detection and pitch correction, the fast autocorrelation and HPS (Harmonic Product Spectrum), and the modified phase vocoder and PSOLA (Pitch-Synchronous Overlap-Add) are chosen and examined. Four possible combinations of the algorithms are reviewed not only in the context of fundamental frequency detection and pitch shifting correctness but also with regard to the quality of the resulting singing signal. Experiments are performed on both male and female singing samples consisting of a variety of tones and various articulations. Basing on the obtained results, it is concluded that the HPS and PSOLA algorithms are the optimum choice as means to correct detuned singing. In addition, listening tests are performed in order to confirm objective measurements of pitch detection and correction. The system is implemented in JAVA. Conclusions are drawn and proposals of improvements are provided.

9:40

2aSCa5. Spectrotemporal and f0 evidence for a theory of enhancement. Indranil Dutta (Rice University, Center for the Study of Languages, MS #36, 6100 Main St., Houston, TX 77005, USA, indranil.dutta@rice.edu)

According to Keyser & Stevens, 2006, apart from universal features that are utilized to calculate motoric instructions, there is a second parallel and language-specific process called enhancement, where additional motoric instructions are processed for the enhancement of the saliency of features that are in danger of being obliterated. The ″Standard View″ on the distinction between voiced stops (VS) and voiced aspirated stops (VAS) in Hindi proposes that the breathy-murmured release following VAS is sufficient to make the contrast between the VS and VAS (Ladefoged & Maddieson, 1996). Hence, audible distinctions between VAS and VS during closure (CD/VLT) are not relevant in maintaining the contrast. Results from our studies show that CD is a relevant cue in making a distinction between aspirated and unaspirated stops. Spectral intensity measures show that speakers employ different glottal configurations to obtain the breathy/modal voicing contrast. VLT durations are inversely correlated with f0, such that longer VLT for VAS leads to further lowering of f_0. This evidence suggests that f_0 perturbations, differences in the durations of closure, and nature and extent of aspiration, all contribute in making the four-way stop contrast possible in Hindi, in support of a theory of enhancement.

10:00

2aSCa6. A Statistical Prosodic Model for Voice Conversion. Jan Schwarz (Institute for Circuit and System Theory, Christian-Albrechts-University of Kiel, Kaiserstrasse 2, 24143 Kiel, Germany, js@tf.uni-kiel.de), Ulrich Heute (Institute for Circuit and System Theory, Christian-Albrechts-University of Kiel, Kaiserstrasse 2, 24143 Kiel, Germany, uh@tf.uni-kiel.de)

Nowadays Text-to-Speech (TTS) systems adapt the output voice to the user and the corresponding application. The aim is a personalisation. Thereby, the user is set into familiar surroundings, increasing the TTS acceptance. For example, an e-mail client that may read the incoming messages with the synthesised voice sounding like that of the sender. Such a personalised TTS system is costly; so, voice-conversion (VC) techniques are used to save resources. VC transforms the voice of a ''source speaker'' in such a way that the converted voice sounds like that of another ''target speaker''. This voice sounds only natural, if it includes all features relevant for the true target voice. Here, a main problem is the mapping of the prosody which is one of the essential features. This contribution introduces a statistical prosodic model for voice conversion. It is based on Gaussian-Mixture Models (GMM), trained for the pitch and the duration of diphones. To ensure sufficient data for the GMM training, seven diphone classes are separated as related to the international phonetic alphabet. The suitability for VC as well as limitations, necessary extensions (stress) and problems are pointed out.

10:20

2aSCa7. Modelling acoustic parameters of prosody for read and acted-speech synthesis. Milan Rusko (Institute of Informatics of the Slovak Academy of Sciences, Dubravska cesta 9, 845 07 Bratislava, Slovakia, milan.rusko@savba.sk), Marián Trnka (Institute of Informatics of the Slovak Academy of Sciences, Dubravska cesta 9, 845 07 Bratislava, Slovakia, trnka@savba.sk), Sakhia Darjaa (Institute of Informatics of the Slovak Academy of Sciences, Dubravska cesta 9, 845 07 Bratislava, Slovakia, utrrsach@savba.sk), Richard Kováč (Institute of Informatics of the Slovak Academy of Sciences, Dubravska cesta 9, 845 07 Bratislava, Slovakia, richard.kovac@savba.sk), Juraj Hamar (Philosophical Faculty, Comenius University, Gondova 2, 818 01 Bratislava, Slovakia, juraj.hamar@chello.sk)

The prosody model is one of the most important parts of every speech synthesizer, influencing mainly its naturalness. The intonation contour and phoneme lengths (together with speech quality) bear a great deal of extralinguistic and paralinguistic information contained in the synthesized speech. The features reflecting personality, mood and emotions of the speaker are in strong interaction with those reflecting speech styles. Anyway the appropriate choose of prosody model and training material can make it possible to create special model for every speaking style. The paper presents our approach to modelling of acoustic parameters of prosody in two different speech styles in Slovak. Our model is based on Classification and regression trees (CARTs). It uses independent CART for phoneme lengths and three CARTs for fundamental frequency (F0) at the beginning, centre, and end of every syllable. Two hours of read speech were used for training a model of read speech. The recordings of a puppet player were used to train a model of acted speech. The models were implemented in the Kempelen 2.2 unit selection Slovak speech synthesizer. The listening tests have shown that the models are capable of modelling significant amount of the differences of the two speaking styles.

Session 2aSCb

Speech Communication: How do Physical and Motor Knowledge Matter to Speech Perception?

Carol A. Fowler, Cochair
Haskins Laboratories, 300 George St, Suite 900, New Haven, CT 06511, USA

Mikko Sams, Cochair
Helsinki University of Technology, Lab. of Computational Engineering, Cognitive Science and Technology, Otakaari 5A, 02150 Espoo ('Magnet house'), Finland

Invited Papers

8:20

2aSCb1. Action-based multisensory integration in striking events. Bruno L. Giordano (Centre for Interdisciplinary Research in Music Media & Technology (CIRMMT) - Schulich School of Music - McGill Univ., 555 Sherbrooke Street West, Montreal, QC H3A1E3, Canada, bruno.giordano@music.mcgill.ca), Stephen McAdams (Centre for Interdisciplinary Research in Music Media & Technology (CIRMMT) - Schulich School of Music - McGill Univ., 555 Sherbrooke Street West, Montreal, QC H3A1E3, Canada, smc@music.mcgill.ca), Paolo Crosato (Dept. of Information Engineering, Univ. of Padova, Via G. Gradenigo 6/A, 35131 Padova, Italy, jimbobaus@virgilio.it), Federico Avanzini (Dept. of Information Engineering, Univ. of Padova, Via G. Gradenigo 6/A, 35131 Padova, Italy, avanzini@dei.unipd.it), Carmine Casciato (Centre for Interdisciplinary Research in Music Media & Technology (CIRMMT) - Schulich School of Music - McGill Univ., 555 Sherbrooke Street West, Montreal, QC H3A1E3, Canada, casciato@music.mcgill.ca), Stephen Sinclair (Centre for Interdisciplinary Research in Music Media & Technology (CIRMMT) - Schulich School of Music - McGill Univ., 555 Sherbrooke Street West, Montreal, QC H3A1E3, Canada, sinclair@music.mcgill.ca), Marcelo M. Wanderley (Centre for Interdisciplinary Research in Music Media & Technology (CIRMMT) - Schulich School of Music - McGill Univ., 555 Sherbrooke Street West, Montreal, QC H3A1E3, Canada, marcelo.wanderley@mcgill.ca)

Many theories of multisensory integration focus on action-independent perception. This approach has limited ecological validity, because under everyday conditions we frequently act upon multisensory events through motor behavior. We present a novel methodology for the study of multisensory integration in action-directed perception, focusing on striking events. Observers repeatedly hit a virtual object with a target striking velocity, and are presented with various types of sensory information about the striking event: auditory and/or haptic and/or visual. For each of the experimental trials, they initially receive feedback on the tracking of the target striking velocity. In a second phase, feedback is eliminated. In a third phase, the sensory properties of the striking event are changed. We quantify the extent to which a variation in each of the sensory modalities disrupts performance in the tracking of the target striking velocity. Multisensory dominance hierarchies are inferred from the comparison of the patterns of performance disruption in unimodal and multisensory contexts.

8:40

2aSCb2. Amodal specification of talker-specific motor behavior. Lawrence D. Rosenblum (University of California, Riverside, Department of Psychology, 900 University Ave., Riverside, CA 92521, USA, rosenblu@citrus.ucr.edu)

There is substantial evidence that the speech perception function incorporates information for articulatory motor behavior. Research over the last 15 years has shown that speech perception also uses information for talker-specific motor behavior. Interestingly, this research reveals that talker information can facilitate speech perception whether it is apprehended through auditory or visual speech (lipread) means. The multimodal nature of these effects could mean that the talker-specific properties used by the system are amodal and motoric-or gestural-in nature. Evidence for this proposition-that talker-specific facilitation of speech is based on amodal specification of gestural style-will be discussed. This evidence includes findings that isolated talker-specific phonetic information, available both optically and acoustically, can be informative about talker identity to the degree that it supports cross-modal talker matching. Other evidence shows that the talker familiarity gained through one modality can facilitate perception of speech in the other. Finally, recent evidence reveals that speech perceivers will align to (inadvertently imitate) talker-specific properties of utterances they are asked to shadow, whether that speech is presented auditorily or visually. These results suggest that some of the 'motor knowledge' bearing on speech perception takes the form of talker-specific gestural properties, amodally specified.

9:00

2aSCb3. Cross-modal synchrony perception reveals aspects of categorical perception. Armin Kohlrausch (Philips Research Europe, Digital Signal Processing (MS WO02), High Tech Campus 36, 5656 AE Eindhoven, Netherlands, armin.kohlrausch@philips.com), Rob L. Van Eijk (Technische Universiteit Eindhoven, Human-Technology Interaction, P.O. Box 513, 5600 MB Eindhoven, Netherlands, r.l.j.v.eijk@tue.nl), Steven Van De Par (Philips Research Europe, Digital Signal Processing (MS WO02), High Tech Campus 36, 5656 AE Eindhoven, Netherlands, steven.van.de.par@philips.com), James F. Juola (University of Kansas, Department of Psychology, 1415 Jayhawk Blvd., Lawrence, KS KS 66045, USA, juolas@ku.edu), Michael Vitevich (University of Kansas, Department of Psychology, 1415 Jayhawk Blvd., Lawrence, KS KS 66045, USA, mvitevit@ku.edu)

The phenomenon of ″categorical perception″ has played an important role in speech research. When a specific (combination of) feature(s) of a speech stimulus is varied along a physical dimension, categorical perception is reflected by two observations: (1) the percept of the sound changes abruptly from one category to another, e.g., from ″ba″ to ″da″ to ″ga″ for changes in formant transition frequencies, and (2) physical changes of a given amount lead to more easily perceivable differences for stimuli close to a category boundary, compared to stimuli in the center of a category. In this talk, I present data about audio-visual synchrony perception, which indicate that perceived synchrony also reveals properties of categorical perception. Depending on the physical delay between the auditory and visual component, the percept changes from ″audio first,″ to ″synchronous″ to ″video first.″ When measuring sensitivity to changes in audio-visual delays, we observe that the thresholds are small for stimuli at the transitions between the earlier determined categories, while they are larger for stimuli within a category.

9:20

2aSCb4. Do we perceive articulatory gestures when we listen to speech? Pierre Divenyi (VA Northern Calif. Health Care Syst. and East Bay Inst. for Research and Education, Bldg. R4, 150 Muir Rd., Martinez, CA 94553, USA, pdivenyi@ebire.org), Adam Lammert (VA Northern Calif. Health Care Syst. and East Bay Inst. for Research and Education, Bldg. R4, 150 Muir Rd., Martinez, CA 94553, USA, alammert@ebire.org)

Articulatory synthesis methods, classic and contemporary, have demonstrated that it is possible to generate speech from an ensemble of functions derived from articulatory gestures. Such gesture-to-waveform transforms suggest that, inversely, the speech signal should be also decomposable into the same set of gesture, or gesture-like, functions. These functions vary slowly in time and their association with the speech waveform (words as well as sentences) can be established by machine learning algorithms. In a recent study at our laboratory, listeners were asked to type the word or the sentence they heard, with speech (degraded in diverse ways) as the stimulus. The subjects' responses were synthesized, time-aligned with the stimulus, and decomposed into a set of eight gestures, as specified by the Haskins Laboratories TADA system (http://www.haskins.yale.edu/tada_download/index.html). When the running distance between input and response gesture functions is calculated, results indicate a significant degree of gesture information transmitted even during severely degraded speech segments, suggesting that the perceptual system may track speech via underlying functions similar to gestures. Epochs at which this running distance estimate fails, i.e., exceeds a certain threshold, may be considered to signal periods during which insufficient bottom-up information had to be supplemented using higher-order linguistic knowledge.

9:40

2aSCb5. Hearing the tongue and lips of vowel gestures: A new differential paradigm. Jean-Luc Schwartz (ICP-GIPSA, INPG, 46 Av. Félix Viallet, 38031 Grenoble, France, schwartz@icp.inpg.fr), Nathalie Vallée (ICP-GIPSA, INPG, 46 Av. Félix Viallet, 38031 Grenoble, France, vallee@icp.inpg.fr), Sonia Kandel (LPNC, Université Pierre Mendès-France - BP 47, 38040 Grenoble, France, Sonia.Kandel@upmf-grenoble.fr)

It is an old question to know to what extent a listener can recover the articulatory dimensions of a speaker's gesture. In the case of vocalic configurations, a number of experiments have been done on expert phoneticians, showing that vowel height can be reasonably well estimated from the sound, but the front-back and lip rounding dimensions are much less well recovered. However, almost nothing has been done on naive listeners, due to the difficulty to perform absolute estimations in the lack of explicit phonetic knowledge. In the past years, we have developed an original paradigm, exploiting differential rather than absolute estimations. We show that French listeners, even naïve, are able to discriminate to a certain extent which vowel in a given pair has a higher vs. lower or more front vs. more back tongue position, or more or less rounded lips. From these data, we have elaborated an algorithm enabling to estimate what are the internal representations of vowel height, frontness and rounding, and correlated these representations with acoustic parameters, F1, F2-F1 and F'2 in Barks appearing to play a key role in the auditory recovery of these three motor dimensions.

10:00

2aSCb6. Mathematical Evidence For Motor Theories of Speech Perception. Gordon Ramsay (Haskins Laboratories, 300 George Street, New Haven, CT 06511, USA, ramsay@haskins.yale.edu)

Theories of speech perception have often proposed, controversially, that recovery of phonological information from the acoustic signal necessarily requires implicit knowledge of the physical processes underlying speech production. Most of the evidence supporting this hypothesis has been derived empirically from experiments in speech perception. In this paper, we show that many of the basic ideas underlying motor theories of speech perception can also be derived mathematically from first principles, using classic results in stochastic nonlinear filtering theory. Two key results, the Duncan-Mortenson-Zakai and Fujisaki-Kallianpur-Kunita theorems, show that the optimal state estimator for any partially-observed nonlinear stochastic dynamical system always takes the form of a ″matched filter″, which is itself a nonlinear stochastic dynamical system, the structure of which mimics, and resonates with, the structure of the original. Interpreting this in the context of speech perception, recovery of phonological information from sound produced by a human vocal tract necessarily involves construction of an internal model of the processes implicated in speech production. A key prediction, which we explore, is that any such model need not reproduce all the details of these processes, but is only required to predict the lawful conditional correlation between gesture and sound.

Session 2aSCc

Speech Communication: Speech Recognition in Noisy Environments

Olivier Siohan, Cochair
Advanced Large Vocabulary Speech Recognition, IBM Watson Research Center, Yorktown, NY 10598, USA

Georges Linares, Cochair
Université d'Avignon et des Pays de Vaucluse, Laboratoire Informatique d'Avignon, 339, chemin des Meinajaries, Agroparc BP 1228, 84911 Avignon Cedex 9, France

Contributed Paper

10:40

2aSCc1. Speech recognition with body-conducted speech using differential acceleration. Masashi Nakayama (Hiroshima City University / National Institute of Advanced Industrial Science and Technology, 3-4-1 Ozuka-Higashi, Asa-Minami-Ku, 731-3194 Hiroshima, Japan, m.nakayama @aist.go.jp), Shunsuke Ishimitsu (Hiroshima City University / National Institute of Advanced Industrial Science and Technology, 3-4-1 Ozuka-Higashi, Asa-Minami-Ku, 731-3194 Hiroshima, Japan, ishimitu @hiroshima-cu.ac.jp), Seiji Nakagawa (National Institute of Advanced Industrial Science and Technology (AIST), 1-8-31 Midorigaoka, 563-8577 Ikeda, Osaka, Japan, s-nakagawa@aist.go.jp)

Speech-recognition rates decrease in noisy environments. The body-conducted speech, conducted in solids such as body and skins, has a noise-robust characteristics and can be served for recognition systems even in 98 dBSPL-noise (-20 dBSNR) environments. However, the body-conduction could not capture high frequency sounds. Conventional methods for the improvement in sound quality of body-conducted speeches needs both speeches and body-conducted speeches. In this paper, a new body-conducted speech retrieval technique in sound quality without a speech signal itself is proposed. First, high-frequency components in the body-conducted speech were emphasized using differential acceleration. Second, conventional noise reduction method was adopted to make a clear body-conducted speech from a retrieval speech which contains constant noise. The recognition experiments using the proposed method showed that it improved recognition rate in all speakers.

Invited Paper

11:00

2aSCc2. Exploiting confidence measures for missing data speech recognition. Christophe Cerisara (LORIA UMR 7503, Campus Scientifique, 54506 Vandoeuvre-lès-Nancy, France, Christophe.Cerisara@loria.fr)

Automatic speech recognition in highly non-stationary noise, for instance with a competing speaker or background music, is an extremely challenging and still unsolved problem. Missing data recognition is a robust approach that is well adapted to this kind of noise. A standard missing data technique consists in marginalizing out, from the observation likelihoods computed during decoding, the contribution of the spectro-temporal fragments that are dominated by noise. However, such an approach can hardly be applied to advanced parameterization domains that do not separate speech from noise frequencies, such as the cepstrum or ETSI AFE. We propose in this work to extend this technique to such parameterization domains, and not only to spectrographic-like front-ends as it was the case before. This is realized by masking the observations that favor erroneous decoding paths, instead of masking the features that are dominated by noise. These new missing data ″masks″ are now estimated based on speech recognition confidence measures, which can be considered as indicators of the reliability of decoding paths. A first version of this robust algorithm is evaluated on the French broadcast news ESTER corpus.

Contributed Paper

11:20

2aSCc3. An MTF-based blind restoration of temporal power envelopes as a front-end processor for automatic speech recognition systems in reverberant environments. Xugang Lu (Japan Advanced Institute of Science and Technology, 1-1, Asahidai, Nomi, 923-1292 Sendai, Japan, xugang@jaist.ac.jp), Masashi Unoki (JAIST, 1-1 Asahidai, 923-1292 Nomi, Japan, unoki@jaist.ac.jp), Masato Akagi (Japan Advanced Institute of Science and Technology, 1-1, Asahidai, Nomi, 923-1292 Sendai, Japan, akagi@jaist.ac.jp)

To reduce speech degradation in reverberant environments, we previously proposed a modulation transfer function (MTF) based method for speech dereverberation. It is based on the MTF relation that the sub-band temporal power envelope of reverberant speech can be represented as the convolution between temporal power envelopes of clean speech and the room impulse response. Therefore, the sub-band power envelope of clean speech can be estimated using inverse MTF filtering without measuring the room impulse response. We tested the effectiveness of this method as a front-end for automatic speech recognition (ASR) in both artificial and real reverberant environments. Reverberant speech signals were created by simple convolution of clean speech (AURORA-2J) and artificially-produced or real room impulse responses. The relative spectral filtering of the auditory-power-spectrum based method was used as a baseline. Compared with the baseline, our proposed method had 36.64% and 21.68% improvements in error reduction rate for artificial reverberant environments (reverberation times from 0.2 to 2.0 s) and real reverberant environments (43 reverberant impulse responses), respectively. These results indicate that our proposed method can be used as a robust front-end for ASR. [Work supported by a Grant-in-Aid for Science Research from the Japanese Ministry of Education (No. 18680017).]

Invited Paper

11:40

2aSCc4. Front-end processing of a distant-talking speech interface for control of an interactive TV system. Maurizio Omologo (Fondazione Bruno Kessler - IRST, Via Sommarive, 18, Povo, 38050 Trento, Italy, omologo@fbk.eu)

This work addresses a research activity being conducted for the development of a user-friendly interface for the access to a virtual smart assistant enabling the interaction with TV-related digital devices and infotainment services. In the given scenario, the users can speak in a natural and comfortable way, not encumbered by any hand-held or head-mounted microphone. The environment is typically a living room, equipped with digital TV, Hi-Fi audio devices, etc., and populated by a group of people (e.g., family members). Among the most challenging issues involved in this scenario are a multi-microphone front-end for an effective processing of the given acoustic scene, an Acoustic Echo Cancellation (AEC) component to compensate the sound produced by loudspeakers, and a multi-modal distant-talking spoken dialogue system. As far as the front-end is concerned, multiple speaker localization, speech activity detection, speaker identification, and speech recognition will have to perform accurately even when AEC is applied to the given microphone array. The paper aims to present preliminary results of this research, which is being conducted under the European Project DICIT.

Contributed Paper

12:00

2aSCc5. Speaker adaptation combined with missing data reconstruction. Ulpu Remes (Adaptive Informatics Research Centre, Helsinki University of Technology, P.O. Box 5400, 02015 Espoo, Finland, ulpu.remes@tkk.fi), Kalle J. Palomäki (Adaptive Informatics Research Centre, Helsinki University of Technology, P.O. Box 5400, 02015 Espoo, Finland, kalle.palomaki@tkk.fi), Mikko Kurimo (Adaptive Informatics Research Centre, Helsinki University of Technology, P.O. Box 5400, 02015 Espoo, Finland, mikko.kurimo@tkk.fi)

Missing data methods offer an attractive framework for automatic speech recognition (ASR) under time-varying and unpredictable noise conditions. The motivation for the methods comes from the human speech perception and auditory scene analysis, studies on which have suggested that the more intense sound components in an auditory scene dominate the neural response to the scene. The missing data methods developed for ASR divide the noisy speech signal to speech and noise dominated regions. Speech components in the noise dominated regions are viewed as missing but may be reconstructed based on the observed components. Missing data methods have performed well in previous studies with noise corrupted speech but have not become a standard in ASR. Especially considering ASR on large vocabularies, the methods have a disadvantage: it is not straightforward to combine them with common speaker adaptation methods such as constrained maximum likelihood linear regression (CMLLR). In this work, we investigate efficient ways to combine missing data reconstruction with speaker adaptation in large vocabulary ASR task with speech data recorded in noisy real-world environments. The experiments show that speaker adaptation combined with the missing data reconstruction can improve the missing data approach in noisy large vocabulary ASR.

Invited Paper

12:20

2aSCc6. An efficient frame selection approach to variable frame rate analysis for noise robust speech recognition. Zheng-Hua Tan (Department of Electronic Systems, Aalborg University, Niels Jernes Vej 12, 9220 Aalborg, Denmark, zt@es.aau.dk), Børge Lindberg (Department of Electronic Systems, Aalborg University, Niels Jernes Vej 12, 9220 Aalborg, Denmark, bli@es.aau.dk)

This paper presents a low-complexity, effective variable frame rate (VFR) analysis method that conducts frame selection on the basis of a posteriori signal-to-noise ratio (SNR) weighted energy distance. It has two characteristics. First, energy distance (instead of cepstral distance) is used to make it computationally efficient and thus enable a finer granularity in search as compared with cepstral distance criterion. Secondly, SNR weighting is used to emphasize the reliable regions in noisy speech signals. In terms of frame selection, it is experimentally found that the method is able to assign a higher frame rate to fast changing events such as consonants, a lower frame rate to steady regions like vowels and no frames to silence, even for very low SNR signals. The VFR method is applied to speech recognition in noisy environments to improve noise robustness. Being a method that takes effect in the time-domain, it is moreover combined with spectral- and cepstral-domain techniques to gain further improvement. Experiments are conducted on the Aurora 2 database, which is the TI digits database artificially distorted by adding different noises, and very encouraging results are obtained.

Session 2aSCd

Speech Communication: Speech Perception I

Mirjam Broersma, Chair
Radboud University Nijmegen, PO Box 9104, Nijmegen, 6500 HE, Netherlands

Contributed Papers

11:00

2aSCd1. Phonological specificity of vowels and consonants in 20-month-olds' word representations. Anders Højen (Univ. of Southern Denmark, Dept. Lang. Communication, Campus Vej 55, 5230 Odense, Denmark, anders@andershojen.dk), Thomas O. Madsen (Univ. of Southern Denmark, Dept. Lang. Communication, Campus Vej 55, 5230 Odense, Denmark, tom@language.sdu.dk), Werner Vach (Univ. of Southern Denmark, Dept. Lang. Communication, Campus Vej 55, 5230 Odense, Denmark, werner.v@stat.sdu.dk), Torkil Østerbye (Univ. of Southern Denmark, Dept. Lang. Communication, Campus Vej 55, 5230 Odense, Denmark, oesterbye@sdu.dk), Karina F. Christensen (Univ. of Southern Denmark, Dept. Lang. Communication, Campus Vej 55, 5230 Odense, Denmark, kf@language.sdu.dk), Hans Basbøll (Univ. of Southern Denmark, Dept. Lang. Communication, Campus Vej 55, 5230 Odense, Denmark, hba@language.sdu.dk), Sueli Caporali (Univ. of Southern Denmark, Dept. Lang. Communication, Campus Vej 55, 5230 Odense, Denmark, s.caporali@widex.com), Dorthe Bleses (Univ. of Southern Denmark, Dept. Lang. Communication, Campus Vej 55, 5230 Odense, Denmark, bleses @sdu.dk)

At the onset of word learning around the age of 12 months, infants are highly capable of perceiving native phonological distinctions. However, required to make word-object associations, infants sometimes fail to perceive certain phonological distinctions. The present study used an inter-modal preferential looking technique to examine Danish 20-month-olds' sensitivity to mispronunciations involving either a vowel or a consonant in familiar words. Each mispronounced word could be ″reconstructed″ to either of two familiar Danish words. By way of example, the English nonword ″bock″ can be turned into either ″rock″ or ″book″ depending on whether the mispronunciation is perceived to be in the first consonant or in the vowel. The results so far indicate that the infants were not differentially sensitive to vowel vs. consonant mispronunciations. This result, in turn, suggests that vowels and consonants do not differ in constraining lexical access to familiar words in Danish 20-month-olds.

11:20

2aSCd2. Perceptual asymmetries induced by category learning. Laurent Bonnasse-Gahot (CAMS-EHESS, 54 bd Raspail, 75270 Paris Cedex 06, France, lbg@ehess.fr)

This paper takes an information-theoretic approach to study the perceptual consequences of the neural encoding of categories (e.g. vowels). We focus on two well-known psychophysical phenomena: *categorical perception*, characterized by greater cross-category than within-category discrimination, and *perceptual magnet effect*, stating that perceptual space is wrapped around prototypical instances of a given category, leading to a better ability to discriminate stimuli near non-prototypical exemplars of a category than near prototypical ones. Introducing a perceptual distance based on the Kullback-Leibler distance between the patterns of activity evoked by two stimuli, we show that both categorical perception and prototypical effects emerge from maximizing information contained in the neural representation about a set of categories. We discuss the relations between these two psychophysical phenomena and show that they go in hand with another kind of asymmetric effect. The discriminability between a category prototype and a non-prototype is not symmetric, depending on which stimuli serves as a referent. Non-prototypical stimuli are judged closer to prototypical exemplars than the reverse. Quantitative and qualitative comparisons with experimental data and previous theoretical work are presented and discussed.

11:40

2aSCd3. Order effects and peripherality: a cross-linguistic perceptual study using an [i]-[e] articulatory continuum. Charalampos Karypidis (UMR 7018, CNRS / Univ. Paris III, 19, rue des Bernardins, 75005 Paris, France, ch_karypidis@yahoo.com), Antonia Colazo-Simon (UMR 7018, CNRS / Univ. Paris III, 19, rue des Bernardins, 75005 Paris, France, simonantonia@hotmail.com), Angelica V. Costagliola (UMR 7018, CNRS / Univ. Paris III, 19, rue des Bernardins, 75005 Paris, France, angelicacostagliola@yahoo.it), Cirineu Cecote Stein (UMR 7018, CNRS / Univ. Paris III, 19, rue des Bernardins, 75005 Paris, France, cirineustein@uol.com.br), Gilles Guglielmi (ARP / UFRL Univ. Paris VII - Denis Diderot, 30, rue du Chateau des Rentiers, 75013 Paris, France, gillesgug@yahoo.fr)

This paper attempted to provide further evidence on whether peripherality is a universal bias triggering stimulus order effects. Participants from four linguistic systems - Brazilian Portuguese, Salentinian Italian, French and Spanish - participated in the study. In Experiment 1, listeners identified as /i/ or /e/ the ten stimuli of a continuum prepared with an articulatory model. Experiment 2 consisted in an AX 'same-different' discrimination task including pairs of stimuli differing in one or two steps along the continuum. Discrimination was better when the more peripheral stimulus was presented second in a pair. However, these order effects were found mainly within the /i/ category and only for Italian and French. Experiment 3 was a replication of Experiment 2, except that two modifications were introduced: a. identical pairs were added, and b. one- and two-step pairs were separately examined. Order effects were again found but, this time, they covered a wider area of the continuum. Peripherality alone was not able to account for order effects. The role of focalization was later discussed.

12:00

2aSCd4. Perception of an infrequent assimilation: Labial-to-alveolar assimilation in German. Holger Mitterer (Max Planck Institute for Psycholinguistics, Wundtlaan 1, 6525 XD Nijmegen, Netherlands, holger .mitterer@mpi.nl)

In German (and many languages) the alveolar nasal /n/ can assimilate to [m] if followed by a labial (e.g. 'in Berlin' ← ″i[m] Berlin″). In a German spontaneous speech corpus (KielCorpus), one also finds a few cases in which an /m/ followed by an alveolar consonant surfaces as [n] (e.g., 'samstag' ← ″sa[n]stag″, Engl. Saturday). Four experiments investigated whether there is a similar pre-lexical compensation process for these labial-to-alveolar assimilations as previous research uncovered for alveolar-to-labial assimilations. This turns out to be the case: German and Dutch listeners-the latter potentially unfamiliar with this type of assimilation-tend to perceive the assimilated [n] in ″sanstag″ as /n/ if presented in isolation (″an″), but as /m/ if presented with minimal context (″ansta″). For German listeners, this context effect is larger if they hear the complete word ″sanstag″, introducing an additional lexical bias to perceive the [n] as /m/. Finally, phonetic detail such as transitions of the [s] fricative pole are also important: If the assimilated ″an″ is spliced into another /s/-initial syllable by the same speaker, the context effect is reduced. Perceiving infrequent assimilations seems therefore similar to perceiving frequent assimilations.

12:20

2aSCd5. Nonnative listeners prefer perceptual cues they know from their L1: Dutch listeners use vowel duration less than English listeners for English final /v/-/f/. Mirjam Broersma (Radboud University Nijmegen, PO Box 9104, 6500 HE Nijmegen, Netherlands, mirjam.broersma@mpi.nl)

Two 2AFC experiments investigated Dutch and English listeners' use of preceding vowel duration for the English nonword-final /v/-/f/ contrast. Like English, Dutch has a /v/-/f/ contrast, but unlike English, Dutch has no final /v/. Dutch listeners therefore have no native language experience with the use of preceding vowel duration as a final voicing cue. Previous research showed that Dutch listeners used preceding vowel duration less than English listeners when it was invariable in the experiment (Broersma, 2005, JASA, 117, 3890-3901). The present results show that they also used it less when it was varied. An 11-step fricative voicing continuum from a natural /v/ to a natural /f/ and a 7-step vowel duration continuum from a long (originally /v/-preceding) to a short (originally /f/-preceding) vowel were created. In Experiment 1, all steps of the fricative voicing continuum were combined with one long and one short vowel. In Experiment 2, all steps of the vowel duration continuum were combined with the /v/ and /f/ endpoints and with one ambiguous fricative. In both experiments, Dutch listeners used fricative voicing more and vowel duration less than English listeners did. Thus, the nonnative listeners especially used the perceptual cues they knew from their native language.

TUESDAY MORNING, 1 JULY 2008 ROOM 343, 8:00 TO 10:20 A.M.

Session 2aSPa

Signal Processing in Acoustics, Physical Acoustics, Biomedical Ultrasound/Bioresponse to Vibration, and Underwater Acoustics: Overview of Time Reversal in Acoustics I

David Chambers, Cochair
Lawrence Livermore Natl. Lab., L-333, 7000 East Ave., Livermore, CA 94550, USA

Claire Prada, Cochair
Laboratoire Ondes et Acoustique, ESPCI, Université Paris 7, CNRS, 10 rue Vauquelin, Paris, 75005, France

Invited Papers

8:00

2aSPa1. An overview of time-reversal acoustics. Mathias Fink (Laboratoire Ondes et Acoustique, ESPCI, Université Paris 7, CNRS, 10 rue Vauquelin, 75005 Paris, France, mathias.fink@espci.fr)

Time-reversal invariance is a very powerful concept in physics. In the field of acoustics where time reversal invariance occurs, time-reversal experiments may be achieved simply with arrays of transmit-receive transducers, allowing an incident wave field to be sampled, recorded, time-reversed and re-emitted. Time reversal mirrors (TRMs) may be used to study random media and chaotic reverberating structures. Common to these complex media is a remarkable robustness exemplified by observations that the more complex the medium between the probe source and the TRM, the sharper the focus. TRMs open the way to new signal processings that interest imaging, detection, telecommunications and therapy. Time reversal mirrors have plenty of applications including ultrasonic therapy and medical imaging, non destructive testing, telecommunications, underwater acoustics, seismology, sound control, home automation. An overview of these fields will be presented.

8:20

2aSPa2. Ocean acoustic time reversal. William A. Kuperman (MPL, Scripps Institution of Oceanography, University of California, San Diego, La Jolla, CA 92093-0238, USA, wkuperman@ucsd.edu)

A series of ocean acoustic time experiments have been jointly conducted in the last ten years by the NATO Undersea Research Centre and the Marine Physical Laboratory. The experiments demonstrated a robustness of the ocean acoustic time reversal mirror process similar to that found in more controlled, ultrasonic laboratory experiments. Results from these experiments have pointed to potential applications to SONAR signal processing methods and to acoustics communications. In addition, the experimental procedures themselves have yielded data that provide further understanding of the ocean acoustic environment and the increased stability of time reversal process over one way propagation in a fluctuating medium.

Contributed Paper

8:40

2aSPa3. 2004 M6.0 Parkfield earthquake characterization using Time Reversal. Carene Larmat (EES-11 (Geophysics) - Los Alamos National Laboratory, MS D443, Los Alamos, NM 87545, USA, carene@lanl.gov), Paul A. Johnson (EES-11 (Geophysics) - Los Alamos National Laboratory, MS D443, Los Alamos, NM 87545, USA, paj@lanl.gov), Lianjie Huang (EES-11 (Geophysics) - Los Alamos National Laboratory, MS D443, Los Alamos, NM 87545, USA, ljh@lanl.gov)

Time reversal has proved to be a robust source location method in acoustics and is now being developed for a number of seismic applications. One problem of particular interest is locating sources where the signal-to-noise ratio is small. These include small earthquakes (<M5.5) or atypical seismic sources with a small seismic energy radiation (e.g., tremor, slow earthquakes). Time reversal has been shown to be very robust and work in the presence of poor data, low signal to noise ratio, etc. We present a prototype study showing the power of time reversal, using seismic data from the 2004 M6.0 Parkfield earthquake, which is the world's best recorded event to date and thus one of the most studied. The back-propagation of recorded seismic data in a 3D Earth velocity model is numerically carried out. We show that the reconstructed reverse wave-field exhibits clear focusing at the source point but also displays a four-lobe radiation pattern for each type of rebroadcast waves (body, surface), which is consistent with the known source mechanism: a right-lateral strike slip along the almost-vertical San Andrea fault.

Invited Paper

9:00

2aSPa4. Time reversal and subwalength focal spot. Julien De Rosny (Laboratoire Ondes et Acoustique, ESPCI, Université Paris 7, CNRS, 10 rue Vauquelin, 75005 Paris, France, julien.derosny@espci.fr), Arnaud Tourin (Laboratoire Ondes et Acoustique, ESPCI, Université Paris 7, CNRS, 10 rue Vauquelin, 75005 Paris, France, arnaud.tourin@espci.fr), Geoffroy Lerosey (Laboratoire Ondes et Acoustique, ESPCI, Université Paris 7, CNRS, 10 rue Vauquelin, 75005 Paris, France, geoffroy.lerosey@espci.fr), Mathias Fink (Laboratoire Ondes et Acoustique, ESPCI, Université Paris 7, CNRS, 10 rue Vauquelin, 75005 Paris, France, mathias.fink@espci.fr)

When a wave is time-reversed inside a homogeneous medium, the focal spot width at best equals half a wavelength. This limit comes from the loss of evanescent wave during propagation. An analysis of the time reversed field in terms of the Green's function formalism shows that in order to get a finer spot, not only the field has to be time reversed but also the initial source. In such a case, an acoustic sink is obtained. Experimental results are presented. Then we show two methods to obtain subwavelength focal spot without time-reversed source. The first method consists of setting the time reversal mirror in the near field of the initial source. Despite the evanescent wave transmission, we will see that subwavelength focusing is only observed for a special time-reversal mirror. The second method consists of surrounding the initial source by many scatterers. In such a case, the evanescent waves emitted by the initial source are converted into propagating ones. During the time reversal step, back-conversion occurs that leads to a sub wavelength focal spot. Thanks to this principle, a focal spot of a thirtieth of a wavelength has been reported in the case an electromagnetic experiment.

Contributed Papers

9:20

2aSPa5. Model-based time reversal method for photoacoustic imaging of heterogeneous media. Peter Burgholzer (Upper Austrian Research, Hafenstr. 47, 4020 Linz, Austria, peter.burgholzer@uar.at), Hubert Gruen (Upper Austrian Research, Hafenstr. 47, 4020 Linz, Austria, huber.gruen@uar.at), Robert Nuster (Karl-Franzens-Universität Graz, Universitätsplatz 5, 8010 Graz, Austria, ro.nuster@uni-graz.at), Günther Paltauf (Karl-Franzens-Universität Graz, Universitätsplatz 5, 8010 Graz, Austria, guenther.paltauf@uni-graz.at), Markus Haltmeier (University of Innsbruck, Technikerst. 21a/2, 6020 Innsbruck, Austria, markus.haltmeier@uibk.ac.at)

In photoacoustic (also called optoacoustic or thermoacoustic) tomography acoustic pressure waves are generated by illumination of a semitransparent sample with pulsed electromagnetic radiation. Subsequently the waves propagate towards the detection surface enclosing the sample. The inverse problem consists of reconstructing the initial pressure sources from those measurements. In certain applications of photoacoustic imaging one has to deal with media with spatially varying sound velocity, e.g. bones in soft tissue. Image reconstruction without any compensation of this effect leads to a poor image quality. It is therefore essential to develop reconstruction algorithms that take spatially varying sound velocity into account and are able to reveal small structures in acoustically heterogeneous media. A model-based time reversal reconstruction method is presented that is capable of reconstructing the initial pressure distribution despite variations of sound speed. This reconstruction method calculates the time reversed field directly with a second order embedded boundary method by retransmitting the measured pressure on the detector positions in reversed temporal order. Numerical simulations and experiments with phantoms consisting of areas with spatially varying sound velocity are presented.

9:40

2aSPa6. The effects of transducers on the time reversal process in solids. Brian E. Anderson (EES-11 (Geophysics) - Los Alamos National Laboratory, MS D443, Los Alamos, NM 87545, USA, bea@lanl.gov), Michele Griffa (EES-11 (Geophysics) - Los Alamos National Laboratory, MS D443, Los Alamos, NM 87545, USA, mgriffa@lanl.gov), Paul A. Johnson (EES-11 (Geophysics) - Los Alamos National Laboratory, MS D443, Los Alamos, NM 87545, USA, paj@lanl.gov)

Every experimental implementation of Time Reversal (TR) involves the use of transducers to convert wave motion, whether mechanical or acoustical, into electrical signals, and vice versa. Practical considerations of transducers are not included in the basic theory of time reversal, which is based on idealized point-like sources. These considerations include temporal ring down at a narrowband transducer resonance, the finite size of the transducer giving rise to directivity, and the impedance contrast between the transducer and the medium. The effects of these considerations on the TR process will be characterized by presenting data from various TR experiments.

10:00

2aSPa7. Estimation of guided waves from cross-correlations of diffuse Wavefields for passive Structural Health Monitoring. Adelaide Duroux (Georgia Institute of Technology, School of Mechanical Engineering, 771 Ferst Drive, NW, Atlanta, GA 30332-0405, USA, adelaide.duroux@gatech.edu), Karim G. Sabra (Georgia Institute of Technology, School of Mechanical Engineering, 771 Ferst Drive, NW, Atlanta, GA 30332-0405, USA, karim.sabra@me.gatech.edu), Massimo

Ruzzene(Georgia Institute of Technology, School of Aerospace Engineering, 270 Ferst Drive, Atlanta, GA 30332-0150, USA, massimo .ruzzene@ae.gatech.edu), Vin Sharma (Georgia Institute of Technology, School of Aerospace Engineering, 270 Ferst Drive, Atlanta, GA 30332-0150, USA, vin.sharma@millenniumdynamics.com), James Ayers (Georgia Institute of Technology, School of Aerospace Engineering, 270 Ferst Drive, Atlanta, GA 30332-0150, USA, jayers3@gatech.edu)

Recent theoretical and experimental studies in a wide range of applications (ultrasonics, underwater acoustics, seismicœ) have demonstrated that Green's functions (impulse responses) can be extracted from cross-correlation of diffuse fields using only passive sensors. The technique, whose validity is supported by a physical argument based on time-reversal invariance, effectively uses a correlation process between the point source and points located in the focal zone. Indeed, the coherent noise source distributions can be considered as a time-reversal mirror and the cross-correlation operations gives the field measured at one receiver after refocusing on the other receiver. Passive-only reconstruction of coherent Lamb waves (80-200 kHz) in an aluminum plate and thickness comparable to aircraft fuselage and wing panels will be presented. In particular, the influence of the noise source characteristics (location, frequency spectrum) on the signal-to-noise ratio the emerging coherent waveform will be investigated using a scanning laser Doppler velocimeter. This study suggests the potential for a structural health monitoring method for aircraft panels based on passive ultrasound imaging reconstructed from diffuse fields.

Session 2aSPb

Signal Processing in Acoustics, Biomedical Ultrasound/Bioresponse to Vibration, and Underwater Acoustics: Time Reversal Methods for Array Imaging and Signal Processing I

David Chambers, Cochair
Lawrence Livermore Natl. Lab., L-333, 7000 East Ave., Livermore, CA 94550, USA

Claire Prada, Cochair
Laboratoire Ondes et Acoustique, ESPCI, Université Paris 7, CNRS, 10 rue Vauquelin, Paris, 75005, France

Invited Papers

10:40

2aSPb1. The detection and characterization of buried resonant targets by iterative, single-channel time reversal. Ronald A. Roy (Boston University, Dept. of Aerosp. and Mech. Eng., 110 Cummington St., Boston, MA 02215, USA, ronroy@bu.edu), Zachary J. Waters (Boston University, Dept. of Aerosp. and Mech. Eng., 110 Cummington St., Boston, MA 02215, USA, zjwaters@bu.edu), Benjamin R. Dzikowicz (Naval Surface Warfare Center, Panama City Division, Code HS-11, 100 Vernon Ave., Panama City, FL 32407, USA, benjamin.dzikowicz@navy.mil), R. Glynn Holt (Boston University, Dept. of Aerosp. and Mech. Eng., 110 Cummington St., Boston, MA 02215, USA, rgholt@bu.edu)

A technique for detecting buried resonant targets is described in which enhanced signal-to-noise ratio and convergence to a narrowband signal is achieved using the iterative time reversal of backscattered echo returns. [Waters et al., J. Acoust. Soc. Am. 122, 3023 (2007).] The center frequency of the converged-upon signal is typically a resonance frequency of the target and thus could be used for classification and identification purposes. This technique could offer a straightforward means for enhancing target return levels in a noisy or cluttered environment using existing SONAR systems. The procedure consists of exciting the transducer with a broadband pulse, digitizing the echo return windowed about the target, reversing the data stream in time, and using this signal as the source waveform for the next interrogation pulse. We report results derived from a multi-pronged investigation that includes numerical modeling, high-frequency (100 kHz - 2 MHz) scaled tank experiments employing both free-field and buried targets, and mid-frequency (20 kHz -200 kHz) buried target experiments run in a shallow pond. [Work supported by The Office of Naval Research and the Center for Subsurface Sensing and Imaging Systems (NSF ERC Award No. EEC-9986821).]

11:00

2aSPb2. Green's function estimation in speckle using the FDORT method. Jean-Luc Robert (Philips Research, 345 Scarborough Road, Briarcliff Manor, NY 10510, USA, jean-luc.robert@philips.com), Mathias Fink (Laboratoire Ondes et Acoustique, ESPCI, Université Paris 7, CNRS, 10 rue Vauquelin, 75005 Paris, France, mathias.fink@espci.fr)

The FDORT method (French acronym for Decomposition Of the Time Reversal Operator using Focused beams) is a Time Reversal based method that can detect point-scatterers in a heterogeneous medium and extract their Green's function. It is particularly useful when focusing in a heterogeneous medium. In this presentation, the theory of the FDORT method is generalized to random media (speckle), and it is shown that it is possible to extract Green's functions from speckle signal using this method. Therefore it is possible to achieve a good focusing even if no point scatterers are present. Moreover, a link is made between FDORT and the Van Cittert Zernike theorem. We deduce from this interpretation that the normalized first eigenvalue of the Focused Time Reversal Operator is a well-known

focusing criterion. The concept of an equivalent virtual object is introduced, that allows the random problem to be replaced by an equivalent deterministic problem and leads to an intuitive understanding of FDORT in speckle. Applications to aberration correction are presented. The reduction of the variance of the Green's function estimate is discussed.

Contributed Papers

11:20

2aSPb3. Separation of single and multiple scatterring: Application to the ultrasonic detection of a target embedded in a diffusive medium. Alexandre Aubry (Laboratoire Ondes et Acoustique, ESPCI, Université Paris 7, CNRS, 10 rue Vauquelin, 75005 Paris, France, alexandre.aubry@espci.fr), Arnaud Derode (Laboratoire Ondes et Acoustique, ESPCI, Université Paris 7, CNRS, 10 rue Vauquelin, 75005 Paris, France, arnaud.derode@ujf-grenoble.fr)

We present a new imaging technique dedicated to the detection of a target embedded in a strongly scattering medium. Classical imaging techniques such as echography fail in this kind of configuration because of multiply scattered echoes and aberration distorsions. The experimental set up consists in an array of programmable transducers placed in front of a collection of steel rods randomly distributed. The slab thickness is three times the mean free path. Behind this strongly diffusive slab, we set an echogene steel cylinder that we want to detect and localize. The impulse responses between each couple of transducers are measured and form the interelement matrix. Our technique separates the single-scattered echoes from the multiple scattering background. This is possible because of a deterministic coherence of single-scattering signals along the antidiagonals of the array response matrix, whatever the distribution of scatterers. Once this operation is performed, the detection of the target is achieved by applying the DORT method (French acronym for decomposition of the time reversal operator). The quality of detection is assessed theoretically with Random Matrix Theory and shown to be, by far, better than what is obtained with echography and the classical DORT method.

11:40

2aSPb4. Time reversal processing to forward scattering waves of underwater targets. Yoshiaki Tsurugaya (NEC @Corp., 1-10 @Nissin-cho, Fuchu, 183-8501 Tokyo, Japan, y-tsurugaya@bp.jp.nec.com), Toshiaki Kikuchi (National Defence Academy, 39-21 Uhoyabe 4-chome, Yokosuka, 238-0024 Kanagawa, Japan, ADS01881@nifty.com), Koichi Mizutani (Tsukuba Univ., Tsukuba Science City, 305-8573 Ibaraki, Japan, mizutani@esys.tsukuba.ac.jp)

This paper presents the detection of underwater targets using a time reversal. When a target exists between a sound source and a time reversal array in shallow water, the time reversal array receive the sound waves from the sound source and the waves scattering by the target. If the time reversal processing to them is carried out and they are re-transmitted from the time reversal array, it will be thought that they are converged at the position of the sound source and the target. However, since the waves converging at the sound source have a high level, the waves converging at the target position are usually masked by the high level sounds. Then, we cannot observe the waves converged at the target. We eliminate only the high level sounds from the sound fields. In each array element, the signals in case of non target are subtracted from the signals including the target. As a result of subtraction, the components of the scattering wave by the target are left on the array elements. The time reversal fields of the scattering wave are constructed by radiating the components of the scattered waves from each element again.

12:00

2aSPb5. Super-resolution imaging of active sound and vibrational sources using a time-reversal sink. Eric Bavu (Univ. de Sherbrooke, Mechanical Engineering Depart., 2500 Boulevard de l'Université, Sherbrooke, QC J1K 2R1, Canada, eric.bavu@usherbrooke.ca), Alain Berry (Univ. de Sherbrooke, Mechanical Engineering Depart., 2500 Boulevard de l'Université, Sherbrooke, QC J1K 2R1, Canada, alain.berry @usherbrooke.ca), Jean-Dominique Polack (Institut Jean le Rond d'Alembert, Laboratoire d'Acoustique Musicale, 11, rue de Lourmel, 75015 Paris, France, polack@ccr.jussieu.fr), Vincent Gibiat (Université Paul Sabatier, PHASE, 118, route de Narbonne, 31062 Toulouse cedex 9, France, gibiat@cict.fr), Charles Besnainou (Institut Jean le Rond d'Alembert, Laboratoire d'Acoustique Musicale, 11, rue de Lourmel, 75015 Paris, France, chbesnai@ccr.jussieu.fr)

Theory and experiments of super-resolution focusing using a time-reversal sink have been investigated in high-frequency regime [Rosny and Fink, Phys. Rev. Lett. **89**] and in audible range [Bavu, Besnainou, Gibiat, Rosny and Fink, Act. Acoust., **93**]. This technique, generalized to the case acoustic and vibrational imaging of active sources, allows super-resolution imaging and provides a new method of characterization of active sources in a known background medium. This imaging technique involves a measurement in the background medium using an array, and the simulation of the backpropagating-field in a fictive medium. An ideal numerical time-reversal sink (NumTRAS) is then used to refine results and obtain high-contrast, high-resolution imaging of initial sources. The algorithm has been validated in parallel supercomputer simulations, in both vibrational and acoustics fields and has been used to detect active vibrational sources in a clamped Mindlin plate and active sound sources in an anechoic room. All results show high-resolution imaging capabilities when compared with classical time-reversal backpropagation. NumTRAS provides an alternative to other imaging and source detection techniques, such as acoustic holography and beamforming. Beyond the applications of acoustic and vibrational nondestructive evaluation of industrial structures, NumTRAS has applications in evaluation of musical structures and is being tested to detect and characterize moving sources.

12:20

2aSPb6. Invariants of the time reversal operator for an elastic target in a water waveguide. Franck D. Philippe (Laboratoire Ondes et Acoustique, ESPCI, Université Paris 7, CNRS, 10 rue Vauquelin, 75005 Paris, France, franck.philippe@espci.fr), Claire Prada (Laboratoire Ondes et Acoustique, ESPCI, Université Paris 7, CNRS, 10 rue Vauquelin, 75005 Paris, France, claire.prada-julia@espci.fr), Julien De Rosny (Laboratoire Ondes et Acoustique, ESPCI, Université Paris 7, CNRS, 10 rue Vauquelin, 75005 Paris, France, julien.derosny@espci.fr), Jean-Gabriel Minonzio (Laboratoire Ondes et Acoustique, ESPCI, Université Paris 7, CNRS, 10 rue Vauquelin, 75005 Paris, France, jean-gabriel.minonzio@espci.fr), Mathias Fink (Laboratoire Ondes et Acoustique, ESPCI, Université Paris 7, CNRS, 10 rue Vauquelin, 75005 Paris, France, mathias.fink@espci.fr)

Detection and characterization of a target in shallow water is an active field of research. In general, in a waveguide, the dispersion is such that the frequency signature of a target cannot be extracted from a single backscatterd signal unless the waveguide properties as well as the target's position are known (Mignerey et al., JASA 1992 and Yang et al., JASA 1994). We propose to apply the Decomposition of the Time-Reversal Operator method to recover the target's signature in an unknown waveguide. Using a modal theory, we show that provided the target is far from the boundaries of the guide the first singular value of the time reversal operator is proportional to its signature. Using the same approach, the second singular value is shown to be proportional to the second derivative of the angular dependant form function which is a relevant parameter for target identification. Ultrasonic laboratory experiments are presented that confirm these theoretical results.

Session 2aUW

Underwater Acoustics and ECUA: Fifty Years of Progress in Sonar Acoustic Research: The Role of NURC/SACLANTCEN

Henrik Schmidt, Cochair
MIT, 77 Massachusetts Ave, 5-204, Cambridge, MA 02139, USA

Finn B. Jensen, Cochair
NATO Undersea Research Centre, Viale San Bartolomeo 400, La Spezia, 19126, Italy

8:40-9:00 Director's Welcome

Invited Papers

9:00

2aUW1. Saclant ASW Research Centre contributions to underwater acoustics during the first sixteen years of its existence: Personal records. Robert Laval (1 rue Emile Duclaux, 75015 Paris, France, robert-laval@wanadoo.fr)

In less than one year the NATO Undersea Research Centre, previously called Saclant ASW Research Centre, will celebrate its 50th anniversary. I had the great privilege to be one of the first scientists joining the Centre in 1959 and to work there until 1975. The main purpose of the research conducted in underwater acoustics was to reach a physical understanding of the different processes of sound propagation, including multipath effects, transformations introduced by a multilayered bottom and random scattering by the volume inhomogeneities and by the surface and bottom roughness. Experiments at sea first conducted from the research ships Aragonese and then Maria Paolina used explosives charges and active sonars FM pulses as sound sources. The digital analysis equipment, which had been designed to record, process and facilitate the interpretation of the received signals, had no equivalent at the time. The Centre has been a very active platform of intercommunications for most of the civilian and military organizations, which were involved in this discipline. The result of this continuous exchange of ideas has facilitated the harmonization of the research programs in the different NATO countries and has greatly contributed to the creation of a large international research community in underwater acoustics.

9:20

2aUW2. Shallow water environmental acoustics at NURC/SACLANTCEN. William A. Kuperman (MPL, Scripps Institution of Oceanography, University of California, San Diego, La Jolla, CA 92093-0238, USA, wkuperman@ucsd.edu)

The Centre has a long tradition of studying shallow water acoustics. The research has been experimental and theoretical, the latter effort often involving either using or developing models. Examples include innovations such as the concept of the optimum frequency of an acoustic channel, first measured and then precisely explained with modeling, to, for a recent example, the utilization of ocean ambient noise based on its special properties. Consequently, the Centre has continued to remain at the leading-edge for a half century. The common goals at the Centre that provided the impetus for the progression of research are presented. Then a brief historical review of a selection of the contributions the Centre has made in shallow water acoustics is given.

9:40

2aUW3. Seafloor studies at NURC/SACLANTCEN: The first 50 years (1959-2008). Michael Richardson (Naval Research Laboratory, Marine Geosciences Division, Stennis Space Center, MS 39529-5004, USA, Mike.Richardson@nrlssc.navy.mil)

Characterization of the seafloor has always been one of the central research themes at NURC/SACLANTCEN. These studies, reviewed in this presentation, generally supported acoustic measurement and modeling programs. Motivation for bottom-interacting acoustic research began with the deep-water ASW programs of the 1960s and 1970s (long-range propagation, reflection, and bottom loss measurements) and slowly evolved into support for high-frequency, shallow-water MCM programs of the 1990s and 2000s (acoustic propagation within sediments, penetration into and scattering from the sediment surface). Seafloor characterization has included scales appropriate for plate tectonics to sub-mm scale sediment microstructure used to statistically characterize sediment heterogeneity for high-frequency acoustic studies. Although collection and analysis of sediment cores has been the dominate methods of seafloor characterization, direct in situ measurements and remote acoustic characterization has often been used. Seafloor studies were first rate, cutting edge research as demonstrated by quality and quantity of peer-reviewed publications by NURC/SACLANTCEN scientists and their post-SACLANTCEN research careers. The excellent engineering department made possible the development of unique acoustic and seafloor sampling equipment. Ship support for seafloor studies has always been a NURC/SACLANTCEN advantage that has attracted many scientists to multi-national, multi-institutional experiments and symposia.

10:00

2aUW4. My personal perspective of sonar research at the NATO Undersea Research Centre. Peter Wille (Kitzeberger Strasse 31, 24226 Heikendorf, Germany, p.c.wille@t-online.de)

As the first German Director of the NATO Undersea Research Centre I was contemporary to the fall of the Berlin Wall in November 1989 and the unification of Germany in October 1990, the breathtaking termination of the Cold War without bloodshed. NATO's Undersea Research Centre, thirty years of age when the Berlin Wall fell, has been a key player and focal point of a most important and demanding field of defense research. It has been exemplary in combining customer oriented applied research on sonar concepts up to system demonstrators with basic research to understand, to model and to predict the variability of the ocean environment, the most difficult challenge of successful surveillance and reconnaissance. Some unique capabilities enable the Centre to serve the nations and the NATO commands: Above all, the ability to attract first class scientists to work together at the Centre for a few years and then return to their home countries, forming an ever growing international network of intense scientific cooperation. The advanced sea trial related technology and data treatment realized by a capable and flexible technical staff is no less decisive. The many high-ranking visitors, scientific, military and political underline the international standing of the Centre.

10:20-10:40 Break

10:40

2aUW5. 19 years in the SCNR for NURC: A recollection. Leif Bjørnø (UltraTech Holding, Stendiget 19, DK-2630 Taastrup, Denmark, prof.lb@mail.dk)

I joined the SCNR for NURC by January 1st 1980 and left it again by the end of 1998. This period, on which I will concentrate my talk, includes the toughest period of the ″Cold War″ up to 1989 and the period after, when money to NURC became sparse and new ways of funding had to be found. This presentation will emphasize some of the highlights in NURC's contributions to Underwater Acoustics, ASW, MCM and to engineering aspects of underwater research. These highlights include for instance towed arrays, underwater acoustic modelling, MILOC, the MCM and the REA programmes, time-reverse underwater acoustics, operations research and engineering of underwater instruments. These important contributions over 19 years were supervised by 10 chairmen of the SCNR and by 6 directors, all putting their special fingerprint, closely related to their personality, on the course of NURC's development. A few humoristic features and experiences from the 19 years will briefly be referred to.

11:00

2aUW6. The Centre: It's Impact on Ocean Science---Past, Present and Future. David Bradley (Pennsylvania State University, Post Office Box 30, State College, PA 16804-0030, USA, dlb25@psu.edu)

The Centre (NATO Undersea Research Centre) was formed in 1959, in response to the (then) clear Soviet Union expansion of submarine operations and consequent threat to the NATO Alliance. It began as an experiment to provide a ″water leveling″ of ASW capability to the Nations of the Alliance. The combination of multi-national staff, on site for 3-5 years for the most part; together with the resident staff, has made this ″experiment″ an incredible success. The contributions to this success come in two parts: Specific work and scientific progress on site at the Centre and equally importantly, continued international collaboration upon return to one's Nation. The primary purpose of this presentation is to provide some ″data″ to illustrate both the impact of the Centre on Ocean Science and it's role within the Alliance. Given the rather specific circumstances that lead to the creation of the Centre, the question should be (and is) asked: ″Should the experiment end?″ The simple answer is: ″NO!″ The Centre is poised to have an even more critical international role in the future: The knowledge and stewardship of vital marine resources.

11:20

2aUW7. NURC/SACLANTCEN contributions to sonar signal processing and ASW systems research. Douglas Abraham (CausaSci LLC, PO Box 5892, Arlington, VA 22205, USA, abrahad@ieee.org)

The NATO Undersea Research Centre (NURC) was established in 1959 as the SACLANT ASW Research Centre and tasked with providing scientific research and technical analysis in the area of antisubmarine warfare (ASW) to NATO nations. This presentation will review NURC's contributions to sonar acoustic research in the areas of sonar signal processing and ASW systems. These contributions span at-sea testing and experimentation of novel sonar system concepts to algorithm development and theoretical advances in sonar signal processing. The diversity of expertise across fields such as oceanography, acoustics, signal processing, systems, and operations research brought by international scientists into the cauldron of a small, focused research centre with world-class technicians, engineers, and at-sea capabilities produced innovative, interdisciplinary research. [Supported by the Office of Naval Research Code 321US under contract number N0001407C0092]

11:40

2aUW8. NURC/SACLANTCEN milestone experiments toward solving inverse problems in ocean acoustics. Jean-Pierre Hermand (Université libre de Bruxelles (U.L.B.) - Environmental hydroacoustics lab, av. Franklin D. Roosevelt 50, CP 194/5, 1050 Bruxelles, Belgium, jhermand@ulb.ac.be)

This paper reviews milestone experiments conducted by Saclant Undersea Research Centre to support the development and validation of techniques for obtaining and taking into account environmental information in sonar. The experiments brought together underwater acousticians, geophysicists and oceanographers with the aim to collect comprehensive acoustic and environmental ground-truth data. Environmental-adaptive signal processing was first demonstrated in a deep water area (WESTSARDINIA'89&90). From ducted propagation measurements, a model-based matched filter (MBMF) receiver that fully incorporates the physics of wave propagation determined a source range, depth and Doppler. For environmental inversion the broadband extension of matched-field processing

was investigated in a shallow water area south of Elba island (YELLOWSHARK'94&95). Geoacoustic properties of the sea bottom were determined by finding the best fit between predicted and observed sound fields at multiple frequencies using genetic search algorithms. The same inversion results were obtained by MBMF processing of broadband linearly-frequency-modulated signals enabling the use of an array of a few hydrophones instead of a dense and large vertical array. This motivated the development of drifting acoustic buoys which were tested successfully over the southern continental shelf off Marettimo island, Sicily (ENVERSE'97&98). A recent experiment demonstrated an integrated concept of Rapid Environmental Assessment (MREA/BP'07) using sparse arrays of hydrophones and pressure/temperature sensors, hand-deployed from small vessels.

Session 2pAAa

Architectural Acoustics and ASA Committee on Standards: Comparison of US and European Standards in Building/Room Acoustics I

Kenneth P. Roy, Cochair
Armstrong Building Products, 2500 Columbia Ave, Lancaster, PA 17603, USA

Eddy Gerretsen, Cochair
TNO Science and Industry, Stieljesweg 1, Delft, 2628CK, Netherlands

Invited Papers

2:00

2pAAa1. Building acoustics standards in the USA - ASTM and ISO. Sean D. Browne (Armstrong World Industries, 2500 Columbia Avenue, Lancaster, PA 17604, USA, sdbrowne@armstrong.com), Kenneth P. Roy (Armstrong Building Products, 2500 Columbia Ave, Lancaster, PA 17603, USA, kproy@armstrong.com)

In the US most architectural design and acoustical performance specifications are based on the ASTM International standards for Construction/Building & Environmental Acoustics. Those standards are developed as a responsibility of ASTM International committee E 33 on Building & Environmental Acoustics. The US is of course a participating member in the development of ISO standards through the American National Standards Institute (ANSI), and this participation relative to standards in architectural acoustics is within ISO TC 43 SC2 which deals with building acoustics. The actual ISO standard development and voting responsibilities in the US rests with the ANSI Technical Advisory Group (TAG) to ISO TC43 SC2 which is delegated to ASTM International committee E 33.06 International Standards. This paper will present the process whereby international participation is involved in the development of both ASTM and ISO standards from the US perspective.

2:20

2pAAa2. Prediction models for building performance - European need and world wide use. Eddy Gerretsen (TNO Science and Industry, Stieljesweg 1, 2628CK Delft, Netherlands, eddy.gerretsen@tno.nl)

The development of the unified European market made it necessary to create CE-marking to indicate a certain performance of products. For building products the performance had to enable the fulfilment of essential requirements by buildings, constructed with those products. This made it essential for acoustic requirements to standardize predictions models: the link between acoustic product performance and building performance. In the mean time all six parts of that standard (EN 12354) have been published and are used. Some parts have also been published as ISO standard (ISO 15712) indicating the wider interest in the subject. To be of use in Europe and elsewhere it is important that all types of building structures are covered and indeed work is going on to extend the models to lighter building elements, even more common outside Europe than within. Furthermore, a very important aspect of prediction models is the input data, hence an increased need of standards to determine product performance in an appropriate way. This is even more an item of world wide interest. So the existing standards, the current developments for improvement and the identified need for product standards will be addressed.

2:40

2pAAa3. Comparison of ASTM and ISO sound absorption test methods. Marsha S. Bischel (Armstrong Building Products, 2500 Columbia Ave, Lancaster, PA 17603, USA, msbischel@armstrong.com), Kenneth P. Roy (Armstrong Building Products, 2500 Columbia Ave, Lancaster, PA 17603, USA, kproy@armstrong.com), Joan V. Greenslade (Armstrong Building Products, 2500 Columbia Ave, Lancaster, PA 17603, USA, jvgreenslade@armstrong.com)

A series of planned experiments has been conducted in which the differences between ASTM C423 and ISO 354 have been compared. These experiments focused on the differences in the two test methods, with the goal of identifying and understanding differences in the ultimate test results. A variety of acoustical ceiling tiles were tested in the same NVLAP-certified facility, generating data that cover a broad range of acoustical performance. The factors examined were: the effect of sample size on absorption; the effect of

plenum depth on measured absorption; and the differences between the SAA and α_w curves resulting from the two test methods. The results of these experiments will then be used to identify areas in which additional research is needed if harmonization of the two standards is to occur.

Contributed Papers

3:00

2pAAa4. Evaluation of standards for transmission loss tests. Matthew Cassidy (Queen's University Belfast, School of Mechanical and Aerospace Engineering, Ashby Building, Stranmillis Road, BT9 5AH Belfast, UK, mcassidy06@qub.ac.uk), Richard K. Cooper (Queen's University Belfast, School of Mechanical and Aerospace Engineering, Ashby Building, Stranmillis Road, BT9 5AH Belfast, UK, R.Cooper@qub.ac.uk), Richard Gault (Queen's University Belfast, School of Mechanical and Aerospace Engineering, Ashby Building, Stranmillis Road, BT9 5AH Belfast, UK, r.gault@qub.ac.uk), Jian Wang (Queen's University Belfast, School of Mechanical and Aerospace Engineering, Ashby Building, Stranmillis Road, BT9 5AH Belfast, UK, j.wang@qub.ac.uk)

FG Wilson, a generator set manufacturer in Larne, UK, (part of the CAT Electric Power Division), has an acoustics facility for obtaining noise emission of current products, future developments and research. A wall between a hemi-anechoic chamber and a reverberation room contains an aperture which is used for testing canopy panels to determine their sound transmission loss. Two different standard procedures for transmission loss testing are compared; the J1400, and ISO 15186. Tests were carried out on both to determine which is most feasible for the company to use. The J1400 is a variation of the ASTM E90 which uses the same method but is specifically for a reverberation room to hemi-anechoic chamber. A known 'limp' material, chosen to be lead, is used to obtain a transmission loss correction. ISO 15186 is based on a sound intensity method. A microphone on the source side recorded the sound pressure levels, and an intensity mapping was done on the receiving side, from which transmission loss was calculated. Two tests were completed; a lead sheet, and a steel plate. Both standards showed an acceptable accuracy in relation to the mass law.

3:20

2pAAa5. Evaluation of Metrics for Field Airborne Sound Isolation. Wayland Dong (Veneklasen Associates, 1711 Sixteenth Street, Santa Monica, CA 90404, USA, wdong@veneklasen.com), John Loverde (Veneklasen Associates, 1711 Sixteenth Street, Santa Monica, CA 90404, USA, jloverde@veneklasen.com)

ASTM E336 and ISO 140 define several metrics describing airborne sound isolation for field measurements of wall and floor/ceiling assemblies. The current standards include provisions for the measurements of an apparent sound power reduction (ASTC and R'_w), a non-normalized noise reduction (NIC and $D_{n,w}$), and a normalized noise reduction (NNIC and $D_{nT,w}$). In a previous paper [LoVerde and Dong, J. Acoust. Soc. Am. 119, 3219 (2006)], the relationships between these metrics were reviewed. The desired metric for isolation in residential uses is discussed, specifically whether it should be based on sound power and related to the performance of the partition system (ASTC and R'_w), or based on sound pressure and related to the acoustic isolation between spaces (NNIC or NIC or ISO equivalents). The analysis indicates that the sound pressure-based metric is preferred. Since power and pressure-based airborne sound metrics have small differences in field tested assemblies in most cases, it appears engineers have assumed that ASTC (and R'_w) correlates with isolation. Field tests where this assumption does not hold are presented. In these cases, the power metric provides an inaccurate assessment of the acoustic isolation and can lead to engineering evaluations inconsistent with actual performance.

3:40-5:20 Posters

Lecture sessions will recess for presentation of poster papers on various topics in acoustics. See poster sessions for topics and abstracts.

Invited Papers

5:20

2pAAa6. The adaptation of the façade sound insulation requirements in the Belgian standard. Bart Ingelaere (BBRI, rue du Lombard, 42, B-1000 Brussel, Belgium, bart.ingelaere@bbri.be), Lieven De Geetere (Belgian Building Research Institute, Lombardstraat 42, B-1000 Brussel, Belgium, lieven.de.geetere@bbri.be), Gerrit Vermeir (Lab. ATF, Katholieke Universiteit Leuven, Celestijnenlaan 200D, B-3001 Leuven, Belgium, Gerrit.Vermeir@bwk.kuleuven.be), Manuel Vandamme (BBRI, rue du Lombard, 42, B-1000 Brussel, Belgium, manuel.vandamme@bbri.be)

In a previous paper, a draft of the new Belgian requirements for the sound insulation in dwellings in the prNBN S01-400-1 was presented. During the public enquiry, there was protest of the architectural associations against the façade sound requirements and this part of the draft had to be revised. Architects complained that it would become almost impossible to build even smaller projects without the help of acoustical engineers, what would increase building costs. The building market for dwellings is mainly a liberal market of an individual architect working for a single family, and only the intervention of a structural engineer is usual. The façade requirements are expressed as a function of the outdoor noise and concern the finished building. Architects found the relation of these requirements with the performance of the façade elements as can be calculated by EN 12 354-3:2000 too complicated. A simplified approach was developed and got the approval of the building sector and will be detailed in the presentation. Due to federal law on ″the obligatory use of good craftsmanship in building″, requirements in standards in Belgium are obligatory. The new standard will be of application from the 15th of February 2008.

5:40

2pAAa7. Latinoamerican perspective of acoustical standards - the Chilean approach. Kenneth P. Roy (Armstrong Building Products, 2500 Columbia Ave, Lancaster, PA 17603, USA, kproy@armstrong.com), Micaelina Campos (Armstrong Building Products, 2500 Columbia Ave, Lancaster, PA 17603, USA, mcampos@armstrong.com)

A review will be made of current acoustical standards in several countries of Latinoamérica: Brasil, Mexico, Costa Rica, Argentina, Chile, and Perú. Federal standards will be discussed relative to typical end user approaches to meeting requirements. Additionally, press articles warning of health concerns related to acoustics will be presented. Most Latinoamerican acoustical standards include measure-

ments of exterior noise, but do not mention interior noise requirements as mandatory. Brazilian standards establish overall maximum noise levels for different areas, but do not mention acoustical testing of materials. However, this is changing as a multi-professional team in Mexico is working to definition the acoustical coefficients required for ceilings and walls. And, this team is also working to establish levels of acoustical comfort in different office spaces. Most countries in Latinoamerica have federal institutions that deliver technical standards for the building industry. In Chile, we have the ″Instituto Nacional de Normalizacion″(National Standards Institute), and they base their standards on the ISO standards. In 2006 they have delivered many acoustical standards and regulations, including those on transmission loss for private housing including social housing parameters. They are planning to work on standards for Healthcare and School segments.

6:00

2pAAa8. A special procedure to guarantee sound isolation in dwellings. Wilhelmus Beentjes (Lichtveld Buis & Partners, Postbus 1475, 3430 BL Nieuwegein, Netherlands, beentjes@lbp.nl)

Brochures of projects for newly build dwellings and apartments create many expectations about the various qualities of the new buildings. This also concerns the quality of the sound isolation. But what happens if the quality is not as one expected and one cannot come to an agreement with the contractor? Where can one get one's rights. In the Netherlands we therefore have the Guarantee Institute Housing (In Dutch GIW). This organisation guarantees that the building fulfills the requirements of the Dutch Building Decree. In this paper the procedure will be explained in a few cases . The topics can vary from airborne- and impact sound insulation between buildings, the sound insulation of facades to the sound levels produced by domestic installations. What are the possibilities to improve the sound isolation if the measured values do not fulfill the guaranteed values?

Contributed Paper

6:20

2pAAa9. Analysis and comparison of acoustic insulation in dwellings and buildings, recently build. Leonardo Meza (Pontificia Universidad Católica de Chile, Av. Vicuña Mackena 4860, Macul, 7820436 Santiago, Chile, lmezam@uc.cl)

At this work the acoustic quality of new dwellings is analyzed from acoustic insulating measurements taken in both single-family dwellings and buildings. Through this work is intended to conduct a case study in order to know the acoustic quality of dwellings built after the year 2001, which fulfill the in force regulations called Basic Standards for Building. Therefore, acoustic insulation tests where realized in-situ in sitting rooms and bedrooms of the dwellings. We performed a total of 30 trials according to the ISO standard measure 140-5. This work is part of an investigation that will continue with the implementation of the Basic Document HR Code Technical Construction in Spain, which recently entered into force, so that this future will be how to compare the real benefits obtained with the implementation of this new regulation, to make a new campaign measures in dwellings built fulfilling this new regulation.

TUESDAY AFTERNOON, 1 JULY 2008 ROOM 242B, 2:00 TO 3:40 P.M.

Session 2pAAb

Architectural Acoustics, Musical Acoustics, Physical Acoustics, and Noise: Acoustics of Opera Houses II

Robin Glosemeyer Petrone, Cochair
918 16th St., Apt 3, Santa Monica, CA 90403, USA

Roberto Pompoli, Cochair
Engineering Dept., Univ. of Ferrara, Via Saragat, 1, Ferrara, 44100, Italy

Contributed Papers

2:00

2pAAb1. Sound-focusing effects in the plan of horse-shoe shaped opera theatres. Gino Iannace (Built Environment Control Laboratory Ri.A.S., Second University of Naples, Abazia di S. Lorenzo, 81031 Aversa, Italy, gino.iannace@unina2.it), Elvira Ianniello (DIMEC - University of Salerno, via Ponte don Melillo, 84084 Fisciano, Italy, gino.iannace@unina2.it)

An acoustical feature reported specifically for Italian-style opera houses is the non uniformity of early sound in the stalls. The curvature of the lower part of the lateral walls produces a sort of partial wave-guiding effect, like the well known ″whispering gallery″ effect, that is responsible of the concentration of early sound energy at seats located back in the stalls when the sound source radiates from the foreground of the stage floor. As much of the global room impression depends on the early part of the impulse response it can be supposed that the perceived sound quality of singers' voice and instrumentalists' music performing on the stage will be much different if the listener seats in the last rows with respect to different locations in the stalls. This paper reports an objective analysis on this subject based on measurements carried out in the stalls of a baroque-type theatre. Relevant computer simulations were also implemented.

2:20

2pAAb2. Opera Performance in a Broadway Roadhouse. Dawn Schuette (Threshold Acoustics, 53 W. Jackson Blvd, Suite 1734, Chicago, IL 60604, USA, dschuette@thresholdacoustics.com)

The John A. Williams Theatre at The Cobb Energy Centre for the Performing Arts is a facility that was designed to accommodate touring, large-

scale musical theatre productions, such as presentations of off-Broadway shows, as its primary revenue source. The 2750-seat space has recently received rave reviews, not just for its amplified music capabilities but for non-amplified opera presented by the Atlanta Opera, the first resident company in the facility. This paper discusses how the room form as well as fixed and adjustable acoustic elements in the space have allowed it to be successful for its various uses being conscious of its construction budget limitations. [Work completed while author was employed as a Principal Consultant at Kirkegaard Associates.]

2:40

2pAAb3. Acoustics of a selection of famous 18th century opera houses: Versailles, Markgräfliches, Drottningholm, Schweitzingen. Alban A. Bassuet (Arup Acoustics, 155 avenue of the americas, New York, NY 10013, USA, alban.bassuet@arup.com)

This paper presents the analysis of the acoustical measurements conducted in 8 renowned baroque Opera Houses located in France and Germany. Still in authentic condition to their time of usage, and incorporating the historical changing scenery system (shutter and groove), these Houses have undergone little renovations. The acoustical analysis investigates the performances of these great Houses using energy parameters, balance between stage and orchestra parameters, 3D intensity plots, new spatial distribution parameters and timbre frequency analysis. The objective of the study is to deduce (for the Constellation Project) design targets for a medium size Opera House against these benchmarks and also to revisit the use of the lateral changing scenery system as used in the Baroque era, as an original scenery design concept for a new House. The paper presents the unique qualities of the rooms, illustrates some of acoustical benefits of the 18th century Opera House design characteristics, discusses some differences in the design approach between the Italian and the French traditions and proposes new perspectives for modern Opera Houses design.

3:00

2pAAb4. The Ellie Caulkins Opera House: A study in simplified predictive modeling. Robert Mahoney (Robert F Mahoney & Associates, 310 Balsam Avenue, Boulder, CO 80304, USA, rfm@rfma.com)

Recent advances in predictive modeling and experience in understanding and interpreting the significance of the data provided by such models have given rise to a spate of wonderful new performance spaces. However the models - whether computer models or physical scale models - demand an investment in time, money and organizational resources that are not always available due to the funding and political climate surrounding some projects. In order to secure public funding for the Ellie Caulkins Opera House in Denver, CO USA, the architectural design team had to combine elements of modeling from both the recent past and decades ago in order to present to public authorities a definitive and detailed design and an equally firm estimate of construction costs quickly and with little investment. This paper discusses how the predictive techniques of the last half-century were synthesized to provide a confident estimate of the proposed design's acoustical character as well as definitive construction information.

3:20

2pAAb5. Opera House Acoustics - Case Studies of Renovations. Mark Holden (JaffeHolden, 114a Washington St, Norwalk, CT 06854, USA, mholden@jaffeholden.com)

In the Unites States, there has been a rapid increase in the number and type of perfomance halls built and renovated in the last 10 years. New Opera Houses are few, however three significant Opera Houses have been renovated by our firm, including the Seattle Opera House, The Houston Grand Opera House, and the Kennedy Center Opera House in Washington DC, home of the National Opera. This paper will discuss, compare and contrast approaches to pit design, wall shaping and ceiling shaping, materials for surfaces and orientation and distribution of acoustic volume. Design calculations and completed measurement data, where applicable, will be presented.

TUESDAY AFTERNOON, 1 JULY 2008 ROOM 243, 2:00 TO 7:00 P.M.

Session 2pAAc

Architectural Acoustics and Noise: Acoustics and Privacy in Healthcare Facilities II: Emerging Research Around the World I

William J. Cavanaugh, Cochair
Cavanaugh Tocci Associates, Inc., 327F Boston Post Road, Sudbury, MA 01776, USA

Kerstin Persson Waye, Cochair
Dept. of Environmental Medicine, The Sahlgrenska Academy of Gothenburg Univ., Box 414, Gothenburg, 405 30, Sweden

Invited Papers

2:00

2pAAc1. AIA/FGI interim acoustical guidelines for health care facilities. Gregory C. Tocci (Cavanaugh Tocci Associates, Inc., 327F Boston Post Road, Sudbury, MA 01776, USA, gtocci@cavtocci.com), William J. Cavanaugh (Cavanaugh Tocci Associates, Inc., 327F Boston Post Road, Sudbury, MA 01776, USA, wcavanaugh@cavtocci.com)

Currently, noise is one of, if not the most prominent complaint of hospital care by patients and staff. In response to a growing concern for sound in hospitals and other types of healthcare facilities, the Facility Guidelines Institute (FGI) of the American Institute of Architects (AIA) has asked for assistance in incorporating acoustical guidelines into their Guidelines for the Design and Construction of Health Care Facilities. A group of 40 acoustical consultants and persons from the architectural and medical professions were assembled to develop the resulting 32-page document entitled ″Interim Sound and Vibration Design Guidelines for Hospital and Healthcare Facilities.″ The document divides the variety of health care facility acoustical design issues into 6 sections as follows 1) site exterior noise, 2) interior finishes, 3) room noise levels, 4) sound isolation and speech privacy, 5) electroacoustics and alarms, and 6) building vibration. The presentation will provide an overview of the Interim Guides as they are expected to be adopted into the 2010 issue of the AIA/FGI Guidelines for the Design and Construction of Health Care Facilities.

2:20

2pAAc2. Relating the hospital sound environment to occupant psychological and physiological response. Kerstin Persson Waye (Dept. of Environ. Medicine, The Sahlgrenska Acad. of Gothenburg Univ., Box 414, 405 30 Gothenburg, Sweden, kerstin.persson-waye@amm.gu.se), Erica Ryherd (Woodruff School of Mechanical Engineering, Georgia Institute of Technology, Atlanta, GA 30332-0405, USA, erica.ryherd@me.gatech.edu), Berit Lindahl (School of Health and Sciences, Borås University College, 501 90 Borås, Sweden, berit.lindahl@hb.se), Ingegerd Bergbom (Institute of Health and Caring Sciences, The Sahlgrenska Academy at Göteborg University, PO Box 457, 405 30 Göteborg, Sweden, ingegerd.bergbom@fhs.gu.se)

Examining the relationship between specific acoustical characteristics of noise and occupant response is a fundamental step in determining the current hospital soundscape. Hospitals should be conducive to patient recovery and safety as well as employee health and productivity. Therefore, the sound environment that occupants are exposed to should be attended to from a health standpoint. Previous research on hospital patients has indicated negative effects of hospital sounds such as sleep disturbance, cardiovascular response, increased incidence of rehospitalization, extended hospital stay, and increased dosages of pain medication. There is some evidence that overall levels of hospital noise may impact staff mental efficiency, short-term memory and stress. A series of studies are currently being conducted by the authors to evaluate the modern hospital soundscape and the associated psycho-physiological responses of occupants, incorporating both quantitative and qualitative approaches. One phase in which detailed sound measurements, staff evaluations, and patient physiological measurements were conducted in a general intensive care unit will be highlighted, focusing also on methodological aspects related to physiological measurements. This phase also includes evaluation of patient ICU delirium, a condition that may negatively impact patient health and length of stay in the hospital. [Work supported by ASA and Swedish FAS].

2:40

2pAAc3. Quantifying the noise environment: effects of the wearer's voice on body-mounted noise dosimeter measurements. Steve Ryherd (Chalmers Rm. Acoust. Group, Dept. of Appl. Acoust., Chalmers Univ. of Technology, 41296 Gothenburg, Sweden, srryherd@arpeggioacoustics.com), Kerstin Persson Waye (Dept. of Environ. Medicine, The Sahlgrenska Acad. of Gothenburg Univ., Box 414, 405 30 Gothenburg, Sweden, kerstin.persson-waye@amm.gu.se), Mendel Kleiner (Chalmers Rm. Acoust. Group, Dept. of Appl. Acoust., Chalmers Univ. of Technology, 41296 Gothenburg, Sweden, mendel.kleiner@chalmers.se), Erica Ryherd (Woodruff School of Mechanical Engineering, Georgia Institute of Technology, Atlanta, GA 30332-0405, USA, erica.ryherd@me.gatech.edu)

The purpose of this project was to investigate the effects of the wearer's voice as a dominant sound source on body-mounted noise dosimeters in medium-level acoustic environments. Noise dosimeters provide a convenient method of quantifying an occupant's acoustical exposure. In recent years, interest in personal noise exposure has expanded beyond a necessary safety measure used in industrial settings to be used as a means of documenting a person's exposure to sound pressure levels in lower level environments like hospitals and schools. This study quantifies the contribution of the wearer's voice to the dosimeter measurement in sixteen different office conditions. Statistical analysis was used to determine the effects of the following experimental variables on the measured levels: 1) the type of room in which the measurement is taken, 2) the type of background noise present, 3) the level of background noise. Preliminary statistical results suggest significant main effects of the experimental variables with no significant interaction effects. The statistical effect of the subject's hearing level was also considered. The results of this study can improve the interpretation of dosimeter measurements in medium-level environments and may provide further motivation for alternate methods of quantifying sound pressure levels associated with body-mounted measurements.

3:00

2pAAc4. Acoustics in the Environment of Care: An Interdisciplinary Harvard Medical School Research Project. Joanne Solet (Harvard Medical School, 25 Shattuck Street, Boston, MA 02115, USA, joanne_solet@hms.harvard.edu), Andrew Carballeira (Cavanaugh Tocci Associates, Inc., 327F Boston Post Road, Sudbury, MA 02421, USA, acarballeira@cavtocci.com), Orfeu Buxton (Harvard Medical School, 25 Shattuck Street, Boston, MA 02115, USA, orfeu@hms.harvard.edu), Grace Wyshak (Harvard Medical School, 25 Shattuck Street, Boston, MA 02115, USA, unknown@unknown.com)

Noise in hospitals and healthcare facilities is a growing concern. Anticipating the wave of aging baby-boomers, the US healthcare industry is committed to significant construction and renovation over the next decade. New construction guidelines from the American Institute of Architects/Facility Guidelines Institute and the LEED-based ″Green Guide for Healthcare″ recognize improved acoustical conditions as vital to quality of care quality. To set these specific standards for acoustical performance in healthcare facilities, clinical evidence is needed on the impact of the acoustical environment on patients. An interdisciplinary team of Harvard Medical School faculty and acoustical engineers, in concert with public policy professionals, have designed and implemented a simulation methodology to test acoustic disruption of sleep in human subjects. This research collaboration uses soundscapes derived from recordings made in real healthcare environments, and then quantifies the human response to them. The methodology also enables virtual design changes with corresponding subject exposure to acoustically improved environments. Studies of the human sleep response using this methodology are providing objective evidence for establishing and validating design and construction standards to integrate improved acoustics with healthcare facility design.

3:20

2pAAc5. Speech privacy in healthcare buildings:review of early studies and current procedures for analysis. William J. Cavanaugh (Cavanaugh Tocci Associates, Inc., 327F Boston Post Road, Sudbury, MA 01776, USA, wcavanaugh@cavtocci.com), Gregory C. Tocci (Cavanaugh Tocci Associates, Inc., 327F Boston Post Road, Sudbury, MA 01776, USA, gtocci@cavtocci.com)

Studies on speech privacy problems in buildings, including healthcare facilities, since the mid-1950s, have convincingly shown that a person's sense of acoustical privacy is directly related to the intelligability of the intruding speech in adjacent spaces [Cavanaugh et al, ″Speech Privacy in Buildings″ J. Acoust. Soc. Am. **34**, 475-492 (1962)]. Both in laboratory and in real-world settings people feel they have adequate ″confidential″ privacy when the articulation index (AI) of the intruding speech is 0.05 or less. Higher values of AI, up to

about 0.15, are acceptable for less demanding tasks, i.e. ″normal″ or ″everyday″ privacy. The analysis procedure quantifies each of the significant variables involved and compares summations of these metrics with response data from prior case histories both to predict and, in the case of existing situations, to evaluate speech privacy conditions. In the mid-1960s independent review of the analysis method showed that sufficient accuracy is preserved if A-scale metrics are used in place ofmore cumbersome frequency-based metrics. later in the 1960s the method was successfully applied to open plan spaces although achieving confidential levels of speech privacy in such spaces proved difficult. Lessons leared in applying this relatively simple analysis method over the years are discussed.

3:40-5:20 Posters

Lecture sessions will recess for presentation of poster papers on various topics in acoustics. See poster sessions for topics and abstracts.

Invited Papers

5:20

2pAAc6. New Measurement Procedure and Rating Categories for Speech Privacy of Closed Rooms. John S. Bradley (National Research Council, 1200 Montreal Rd, Ottawa, ON K1A 0R6, Canada, john.bradley@nrc-cnrc.gc.ca), Brad N. Gover (National Research Council, 1200 Montreal Rd, Ottawa, ON K1A 0R6, Canada, Brad.Gover@nrc-cnrc.gc.ca)

A procedure for assessing the speech privacy of enclosed rooms is described based on measured level differences between room-average levels in the room and levels at spot receivers 0.25 m from the outside boundaries of the room. The procedure is not sensitive to the acoustics of the receiving space, assesses conditions at more sensitive listening positions, and can describe variations in speech privacy due to weaker elements such as doors. The arithmetic average of the level differences over speech frequencies from 160 to 5k Hz is used to determine uniform-weighted signal-to-noise ratios found to indicate the audibility and intelligibility of transmitted speech (J. Acoust. Soc. Am. 116 (6) 3480-3490 (2004)). The degree of speech privacy is related to the speech levels in the room, the measured transmission characteristics and ambient noise levels outside the room. The probability of transmitted speech being audible or intelligible to eavesdroppers is related to the likelihood of louder speech in the meeting room. The measured statistics of speech levels in a large number of meeting rooms have been used to describe categories of speech privacy of rooms ranging from minimal privacy to situations where transmitted speech would be very rarely audible.

5:40

2pAAc7. Evaluation of Speech Privacy Index and Noise Isolation Class rating of medical examination rooms and comparison with predictions. Steve Pettyjohn (The Acoustics & Vibration Group, Inc., 5700 Broadway, Sacramento, CA 95820-1852, USA, spettyjohn@acousticsandvibration.com)

The Health Insurance Portability and Accountability Act of 1996 (HIPAA) set speech privacy requirements for medical related information without defining speech privacy for all situations. Areas of special concern for medical organizations are examination rooms because of the need to exchange information between patient and care giver. These rooms are usually constructed in groups with up to three walls common to other examination rooms and a fourth wall next to a corridor. Each adjacency can pose special problems because of construction and position of the equipment in the room. Medical groups are attempting to design and build examination rooms to achieve what they perceive as acceptable levels of privacy while staying within budget and waiting for definitions and requirements. This study provides results of NIC and SPI tests of examination rooms for two medical groups using several different designs. A comparison is given between measured and predicted values based on wall heights and construction details. The wall designs ranged from standard products and construction to employing specialized products, but with only partial height walls. All rooms employed acoustical tile ceilings rather than hard lids. Construction details were found to be the major factor affecting SPI.

Contributed Papers

6:00

2pAAc8. Prediction of speech privacy between rooms. Jukka S. Keränen (Finnish Institute of Occupational Health, Lemminkäisenkatu 14-18 B, 20520 Turku, Finland, jukka.keranen@ttl.fi), Petra Virjonen (Finnish Institute of Occupational Health, Lemminkäisenkatu 14-18 B, 20520 Turku, Finland, petra.virjonen@gmail.com), Valtteri O. Hongisto (Finnish Institute of Occupational Health, Lemminkäisenkatu 14-18 B, 20520 Turku, Finland, valtteri.hongisto@ttl.fi)

The main purpose of sound insulation is usually to provide an appropriate level of speech privacy between rooms. However, the desired privacy is not always reached if, e.g. the background noise level of receiving room has not been considered or rooms are very small. This is often the case in dwellings and office rooms. Thus, sound reduction index does not correlate well with speech privacy. The aim of this study is to present a simple and validated model to predict the speech privacy between two arbitrary rooms when basic room and wall parameters are known. Speech privacy was described using Speech Transmission Index, STI. STI can be determined when the speech effort, room dimensions, early decay times of the rooms and background noise level of the reception room are known. The model was validated in several cases. The model is useful when economic optimization is appreciated. It can lead to major reductions or increments of conventional recommendations for R_w value, especially, when room dimensions are unusual or the rooms have special purposes. The optimization is very easy using a web-based software.

6:20

2pAAc9. A systematic review on the influence of noise on patients' sleep in the Intensive Care Units. Hui Xie (School of Architecture, University of Sheffield, Western Bank, S10 2TN Sheffield, UK, h.xie@sheffield.ac.uk), Jian Kang (School of Architecture, University of Sheffield, Western Bank, S10 2TN Sheffield, UK, j.kang@sheffield.ac.uk)

Noise level in the Intensive Care Units (ICU) often ranges far above the recommended standards. Patients in the ICUs are usually critically ill, making them more susceptible to the unfavorable environment in the hospital. Several objective and subjective methods have been used for the sleep measurement in previous intensive care studies, which showed that the sleep of ICU patients is remarkably and extraordinarily disrupted. While a number of

factors may affect sleep in the ICUs, many earlier studies reported that noise is one of the most common causes for disturbed nocturnal sleep among ICU patients, although some other studies also suggested that noise in the hospital environment is not the most frequent cause of patients' awakenings. Moreover, patients would become accustomed to noise accompanied with their hospital stay. In this paper, a systematic review is given to the influence of noise on patients' sleep in the ICUs, and some strategies to improve the sleep quality are also discussed.

Invited Paper

6:40

2pAAc10. Vibration effects in healthcare facilities. Anthony Nash (Charles M. Salter Associates, 130 Sutter, 5th Floor, San Francisco, CA 94104, USA, anthony.nash@cmsalter.com)

In the USA, the principal rating system for ″green″ buildings is named, ″Leadership in Energy and Environmental Design″ (LEED). There is now a proposed LEED rating system for healthcare facilities as described in a ″pilot draft″ document that was released for public comment in November 2007. This document, in turn, cites the 2006 AIA/AHA Draft Interim Sound and Vibration Design Guidelines. These AIA/AHA Guidelines focus on both the human perceptual effects of vibration as well as the control of structure-borne noise. This paper addresses another aspect of vibration in healthcare facilities - the effects of vibration upon sensitive diagnostic equipment installed on floors above grade. Such equipment may include magnetic resonance imagers, surgical microscopes, and computed tomography (CT) scanners, some of which do not have specific vibration limits provided by the manufacturer. The obvious need for attaining low-level building vibration may conflict with other design constraints imposed on modern healthcare facilities as architects and engineers strive for lightweight floor bays having widely-spaced support columns. This paper reviews the generic vibration design criteria found in the AIA/AHA Guidelines and discusses them in light of several case studies.

TUESDAY AFTERNOON, 1 JULY 2008 P2-B, LEVEL 2, 3:40 TO 5:20 P.M.

Session 2pAAd

Architectural Acoustics and Noise: Acoustics of Open-Plan Spaces II (Poster Session)

Kenneth P. Roy, Cochair
Armstrong Building Products

Valtteri Hongisto, Cochair
Finnish Institute of Occupational Health

All posters will be on display from 3:40 p.m. to 5:20 p.m. To allow contributors an opportunity to see other posters, contributors of odd-numbered papers will be at their posters from 3:40 p.m. to 4:30 p.m. and contributors of even-numbered papers will be at their posters from 4:30 p.m. to 5:20 p.m.

Contributed Papers

2pAAd1. Acoustic Design for Open Plan Spaces. Björn Hellström (ÅF-Ingemansson AB, Box 47321, SE-100 74 Stockholm, Sweden, Bjorn.Hellstrom@afconsult.com), Erling Nilsson (Saint-Gobain Ecophon AB, Box 500, SE-260 61 Hyllinge, Sweden, erling.nilsson @ecophon.se), Björn Berthelsen (Saint-Gobain Ecophon AB, Box 500, SE-260 61 Hyllinge, Sweden, bjorn.berthelsen@ecophon.se)

In an ongoing Nordic cooperation project (Nordic Innovation Center - Sound Design of Open-Plan Offices) the acoustical conditions in open-plan spaces are investigated (see also the adjacent paper Room Acoustical Measures for Open Plan Spaces). The project's starting point is that acoustic qualities in terms of communication, orientation, comfort and privacy are crucial for open-plan spaces. Therefore, beside acoustic parameters, the aim is to develop methodologies in order to measure and specify such qualities. Beside site analyses, one major methodological tool concerns the development of a questionnaire, intended to be utilized as a compliment to acoustic measurements, and thereby function as a tool for design measures of large open-plan offices. Its purpose is to aid acousticians as well as architects and designers to identify different types of acoustic design criteria. The questionnaire covers not only the perception of the sound environment, but also psychosocial criteria, architectural design and the furnishing of the workplace. These qualitative criteria will be discussed and suitable parameters for design and evaluation of open-plan spaces will be suggested.

2pAAd2. Adaptive sound masking. Robert Chanaud (Secure Sound, 3044 Chaco Circle, Prescott, AZ 86305, USA, 3044sound@cableone .net), Ronald Zuydervliet (STCSound, Drususlaan 20, 6932NS Westervoort, Netherlands, ronald@STIsound.com)

Because activity sound levels vary widely during the day in open offices, fixed level sound masking spectra do not keep employees free of distractions. Programmed level control, time scheduling that permits hourly changes in level, is considerably better, but requires pre-knowledge of the activity. An adaptive masking system detects and responds to activity sound, both human and nonhuman, to provide constancy of privacy as opposed to constancy of masking level. These systems use several sound detectors in an area, average the sound level from them, and develop a running table of percentile levels with a given sensitivity. Two percentile levels (L10 and L99) are used to separate the masking from the activity sound. The system acts to continually keep the difference between them constant. The advantage of adaptive masking will be shown by comparison with other methods. The distraction potential will be discussed in terms of dB-minutes. The overall design of these systems will be discussed and examples of experience with existing systems will be given.

Session 2pAAf

Architectural Acoustics, Musical Acoustics, Physical Acoustics, and Noise: Acoustics of Opera Houses III (Poster Session)

Robin Glosemeyer Petrone, Cochair

Roberto Pompoli, Cochair
Engineering Dept. - Univ. of Ferrara

All posters will be on display from 3:40 p.m. to 5:20 p.m. To allow contributors an opportunity to see other posters, contributors of odd-numbered papers will be at their posters from 3:40 p.m. to 4:30 p.m. and contributors of even-numbered papers will be at their posters from 4:30 p.m. to 5:20 p.m.

Contributed Papers

2pAAf1. Diagnosis of an historical performance hall: case study. Maud Serra (Peutz & Associés, 10 rue des Messageries, F75010 Paris, France, m.serra@peutz.fr)

The Opera of Vichy is an historical Italian style performance hall. Initially solely devoted to opera performance, the economical trends have pushed towards concert and theatre. A first major refurbishment was performed in the 1990s and prior to that a diagnosis of that hall was performed in order to characterize the acoustics of the facility prior to actual work being carried out. While the historical preservation constraints did not allow for much acoustical work to be performed, the hall proved to be quite decent. However, in order to improve the intelligibility for theatre purposes, a new diagnosis was recently carried out so as to support the relevant computer simulations. After a brief reminder of the historical background of the project, this paper submits the diagnosis procedure that was followed, as well as its main conclusions regarding the fitness of the hall for the various performances. It turns out that such a diagnosis can be a convincing tool in order to help both the design team and the end user understand the implications - and the limitations too!- of the existing facility and its possible developments.

2pAAf2. Acoustics of new and renovated Russian opera houses: Decade 1998-2007. Michael Lannie (MNIIP, Acoustic Lab., 2-nd Brestskaja Str, 29a, 123056 Moscow, Russian Federation, mlannie@mail.ru)

Four new opera houses have been built in Russia and two existing opera houses have been fully renovated during the last 10 years. New chairs were installed and new materials were used on the inner surfaces of the renovated theatres. All the opera houses are not very large and the biggest one has 1200 seats. The plan of the two theatres has a horse-shoe form that is typical for old classic opera houses. The other three theatres have plans which are close to rectangular and one renovated theatre has a semicircular form of the back walls behind the stalls and the large balcony. The subject of the presentation is the acoustic design of these theatres. The results of the acoustic measurements which have been done in the halls are going to be discussed as well. Acoustics of the recently opened fully renovated Moscow academic musical theatre for 1100 seats is going to be presented in a more substantial way.

2pAAf3. The influence of the stage layout on the acoustics of the auditorium of the Grand Theatre in Poznan. Anna Sygulska (Poznan University of Technology, ul. Nieszawska 13C, 60-965 Poznan, Poland, annasygulska@wp.pl)

The paper concerns the influence of the stage layout on the acoustic properties of the auditorium of the Grand Theatre in Poznan. An experimental investigation and a numerical calculation were carried out. During the experimental investigation three cases were analyzed. Firstly, the stage was prepared for a concert (acoustical shell), secondly in had sets for the ″Wedding of Figaro″, and thirdly it was empty. The reverberation time and the acoustic pressure distribution were analyzed. The research was done by the interrupted noise method and by the true impulsive sources (pistol shots). The modified ray method was used in numerical calculations of acoustic field parameters. It turned out that the light weight structures (materials used in construction of stage sets and acoustical shell) had only decorative function and their influence on the acoustics of the auditorium opera theatre is small. Moreover, the investigation proved that the distribution of the sound pressure level in the auditorium is asymmetrical. It is because of the geometrical asymmetry of the stage (only one side wing). An acoustical correction of the stage was suggested i.e. applying of slided acoustics walls to separate the stage from the background and the side wing.

2pAAf4. Resonant cavities and acoustics vases in Italian Opera Houses; the ″Teatro Principal″ of Valencia and the eighteenth century treatises about theatres. Arturo Barba Sevillano (Grup d'Acustica Arquitectònica, Ambiental i Industrial, E.T.S.I.I, Univ. Politécnica de Valencia, Camino de Vera, s/n, 46022 Valencia, Spain, arbarse@doctor.upv.es), Alicia Giménez (Grup d'Acustica Arquitectònica, Ambiental i Industrial, E.T.S.I.I, Univ. Politécnica de Valencia, Camino de Vera, s/n, 46022 Valencia, Spain, agimenez@fis.upv.es), Radu Lacatis (Grup d'Acustica Arquitectònica, Ambiental i Industrial, E.T.S.I.I, Univ. Politécnica de Valencia, Camino de Vera, s/n, 46022 Valencia, Spain, rala1@doctor.upv.es), Rosa Cibrián (Facultad de Medicina, Univ. de Valencia, Av. Blasco Ibáñez, 15, 46010 Valencia, Spain, rosa.m.cibrian@uv.es)

This paper describes the research job carried out at Polytechnic University of Valencia -Spain- about resonant cavities placed under the orchestra pits of Italian Opera Houses, and others acoustics mechanisms like this one. The Teatro Principal of Valencia was built following the project developed by the Italian architect Felipe Fontana in 1774 and it opened its doors in 1832. Fifteen years ago, in the last architectonic intervention in this theatre, almost a hundred of acoustic vases were found in one of those resonant cavities. What acoustics role they accomplish? How they ″functioned″? This was the starting point to study this kind of artifices, throughout the eighteenth century European treatises about theatres and in our Teatro Principal.

2pAAf5. CARMEN® in the Norwich Theatre Royal, UK. Christophe Rougier (CSTB, 24, Rue Joseph Fourier, 38400 Saint Martin D'Hères, France, christophe.rougier@cstb.fr), Isabelle Schmich (CSTB, 24, Rue Joseph Fourier, 38400 Saint Martin D'Hères, France,

isabelle.schmich@cstb.fr),Paul Chervin(CSTB, 24, Rue Joseph Fourier, 38400 Saint Martin D'Hères, France, paul.chervin@cstb.fr), Paul Gillieron (Paul Gillieron Acoustic Design, 130 Brixton Hill, SW2 1RS London, UK, paul@pgacoustics.org)

Since 1999 the CARMEN® system has been installed in several halls in Europe. The last installation took place in November 2007 at the Norwich Theatre Royal. This classical stage venue has been completely refurbished to become a multipurpose hall with 1280 seats and a single very deep balcony. To fulfil the different acoustic requirements for each performance type (from speech drama to symphonic music) it was decided to install an electroacoustic Reverberation Enhancement System. CARMEN® is a regenerative one which is based upon the virtual wall principle. It can increase the Reverberation Time (RT) of a hall up to 100% and adapt the acoustics to each performance. The installed system has been tuned with 6 configurations: Theatre, Chamber Music, Opera, Concerto, Symphony, and Chorus. The RT of the empty hall now ranges from 1.1s without CARMEN® to 2.2s in the Chorus preset. A brief description of the CARMEN® principle will be presented first. Then the tuning of the different configurations in the hall will be described. Empty hall measurements have been done and the measured acoustic criteria will be analysed. The deep balcony of the Norwich Theatre Royal separates it into two slightly coupled volumes. This particularity will be discussed.

2pAAf6. Italian opera house Mantua's Teatro Scientifico acoustical parameters measurements' comparison between Neumann KU 100 and Schoeps KFM 6 binaural recording systems. Franco Policardi (University, DIENCA Dept. Facoltà di Ingegneria, Viale Risorgimento 2, 40136 Bologna, Italy, franz@nemail.it), Ryota Shimokura (AIST, 1-8-31 Midorigaoka, Ikeda, 563-8577 Osaka, Japan, ryota.shimokura@aist.go.jp), Marco C. Consumi (University, DIENCA Dept. Facoltà di Ingegneria, Viale Risorgimento 2, 40136 Bologna, Italy, marco.cesare@mail.ing.unibo.it), Alessandro Cocchi (University, DIENCA Dept. Facoltà di Ingegneria, Viale Risorgimento 2, 40136 Bologna, Italy, alessandro.cocchi@mail.ing.unibo.it)

From the dawning of modern acoustics, researchers tryed to develop useful measurement techniques to describe acoustical field. Sound field measurement improvement's first endeavours implementing microphone capsule miniaturization technology date back to the thirtyes of the past century. Long human perception reproduction path through recording technique came to the attempt to position transducers similarly to the human natural hearing system, frequently obtaining as alluring results as difficult comparison among them and reapply. This paper describes processes, first results and comparison between as much as possible identical acoustical measurement sessions in Mantua's Teatro Scientifico opera house using Neumann KU 100 and Schoeps KFM 6 binaural recording systems at the same time.

TUESDAY AFTERNOON, 1 JULY 2008 P2-B, LEVEL 2, 3:40 TO 5:20 P.M.

Session 2pAAg

Architectural Acoustics: Acoustics of Concert Halls II (Poster Session)

Takayuki Hidaka, Cochair
Takenaka R&D Institute

Daniel Commins, Cochair
Commins Acoustics Workshop

All posters will be on display from 3:40 p.m. to 5:20 p.m. To allow contributors an opportunity to see other posters, contributors of odd-numbered papers will be at their posters from 3:40 p.m. to 4:30 p.m. and contributors of even-numbered papers will be at their posters from 4:30 p.m. to 5:20 p.m.

Contributed Papers

2pAAg1. Measuring absorption coefficients of open ceilings in multi-purpose halls. Yong Hee Kim (Hanyang University, Department of Architectural Engineering, 133-791 Seoul, Republic of Korea, kimyonghee@gmail.com), Hye Mi Lee (Hanyang University, 133-791 Seoul, Republic of Korea, ymihoo@daum.net), Jin Yong Jeon (Hanyang University, Department of Architectural Engineering, 133-791 Seoul, Republic of Korea, jyjeon@hanyang.ac.kr)

This paper investigates the acoustical characteristics of open ceilings in multi-purpose halls using a 1:25 scale model. A steel truss, duct system, catwalk and opening were selected for the major components of open ceilings from a field survey of 17 existing halls. Absorption characteristics of the equipped ceilings with the 1:25 scale model were measured in a reverberation chamber according to ISO 354. It was found that different volume and materials of the ceiling spaces cause the composite decay characteristics to be similar to those of coupled room effects. Results showed that the absorption coefficients of an empty ceiling with 50% opening and 6 m of depth are 0.2-0.3 above 500 Hz. Adding steel trusses to the ceiling increases the absorption coefficient by 0.1 at 125-2,000 Hz; ducts and catwalks with steel trusses yield an increase in the absorption coefficient at high frequencies. The average absorption coefficients of the various composite ceiling structures were 0.19 to 0.61.

2pAAg2. Singers' preferences for acoustical characteristics of concert halls. Kathleen Stetson (Rensselaer Polytechnic Institute, Greene Bldg., 110 8th St., Troy, NY 12180, USA, kstetson@post.harvard.edu), Jonas Braasch (Rensselaer Polytechnic Institute, Greene Bldg., 110 8th St., Troy, NY 12180, USA, braasj@rpi.edu)

It is the goal of acousticians aiding in concert hall design to create an ideal acoustical environment for experiencing music. To this end, parameters have been developed to quantify the listener's experience in a hall, and while many contribute positively toward listener satisfaction, they only tell part of the story. In reality, the experience of a listener is dependent on the quality of the performance occurring in the hall in addition to the acoustics; even great performers can only perform their best when in comfortable environments conducive to their art. Yet only one widely used parameter,

Stage Support, considers a performer's acoustical needs, and this metric only applies to instrumentalists playing in ensemble. This study examines the unexplored case of a solo singer in a concert hall, augmenting the little existing research on this subject as a first step toward a new parameter. Subjective responses from a survey given to a number of experienced singers and the preferences of singers for acoustical aspects of various virtual concert halls, auralized real-time as the singers sang, are examined. The limitations in using typical acoustical measurement techniques to capture data for voice self-perception are discussed.

2pAAg3. The Temporal and Spectral characteristics of Gamelan Sunda Music. I Gde Nyoman Merthayasa (Institute of Technology Bandung, Dept. of Engineering Physics - ITB, Jln. Ganesha no. 10, 40132 Bandung, Indonesia, ignmerth@tf.itb.ac.id), Bayu Pratomo (Institute of Technology Bandung, Dept. of Engineering Physics - ITB, Jln. Ganesha no. 10, 40132 Bandung, Indonesia, rah_220@yahoo.com)

In order to design a dedicated Concert hall for Gamelan Sunda, first of all, it is important to determine the temporal and spectral parameters of Gamelan Sunda Music (Degung Musics). Gamelan Sunda's music compositions are strongly affected by the sound envelope and timbre. The fundamental frequencies of instrument keys also affect the musical scale, notes placings and the communication between the musical ensembles. The acoustical parameters of the anechoic studio recorded sound waves has been analyzed to determine the acoustical parameters. The sound envelopement factors have been compared with the note configuration in the musical composition, in order to analyze the influence of the sound envelopement to the music composition. In addition, the effective duration of the autocorrelation has also been analyzed to determine the preffered reverberation time in the proposed Concert hall for Gamelan Sunda.

2pAAg4. Diffuser design for both auditorium and stage acoustics in concert halls. Jae Ho Kim (Hanyang University, 133-791 Seoul, Republic of Korea, nosaer4@gmail.com), Yong Hee Kim (Hanyang University, Department of Architectural Engineering, 133-791 Seoul, Republic of Korea, kimyonghee@gmail.com), Jin Yong Jeon (Hanyang University, Department of Architectural Engineering, 133-791 Seoul, Republic of Korea, jyjeon@hanyang.ac.kr)

This study investigates the effect of the shapes and the locations of diffusers on acoustical characteristics, both in the audience area and on the stage, using a 1:50 scale model. Random-incidence scattering coefficients of the diffusers were measured in a reverberation chamber together with the RT, EDT, C80, G and ST1 of the model hall. The results show that an appropriate design of diffusers in halls affects the sound field of both the auditorium and the stage of the hall. It was also found that the effective number of surface reflections at a receiver position actually quantifies the sound diffusion. Through instillation of omni-directional diffusers close to stage walls, the number of reflected rays increases not only in the audience area but also in the stage area.

2pAAg5. New (stage) parameter for conductor's acoustics? Elisabeth W. Van Den Braak (DHV Building and Industry, Larixplein 1, 5616 VB Eindhoven, Netherlands, bertie.vandenbraak@dhv.com), Laurentius C. Van Luxemburg (LeVeL Acoustics BV, De Rondom 10, 5612 AP Eindhoven, Netherlands, l.c.j.v.luxemburg@tue.nl)

During fine-tuning of the stage acoustics of the main auditorium of Casa da Musica, designed by the Office for Metropolitan Architecture, in Porto (Portugal) we were confronted with conflicting comments with respect to the acoustic effect of different canopy positions. The well known stage parameters, ST and CS, did not point out a difference in results for the different canopy positions, while the conductor's experience did. So we carried out several measurements and tried to find a parameter that could clarify the contradictory experiences of the musicians and the conductor. We needed a parameter that correlated with the 'transversely support over the stage' instead of or additional to the known parameters. It was also not clear to what degree the commonly used parameters describe the acoustics at the conductor's position. This study aims at proposing a new (stage) parameter as well as trying to find out more about the 'conductor's acoustics'. In the main auditorium (CdM) the newly defined parameter seems to describe the musicians' and conductor's experiences on the hearing 'ensemble' on stage even better than the known stage parameters. The same measurements have been carried out in other halls in order to check the validity of this new parameter.

2pAAg6. On the interaction between double basses and the stage floor. Knut Guettler (Norwegian Academy of Music, P.O.Box 5190 Majorstuen, 0302 Oslo, Norway, knut.guettler@nmh.no), Anders Askenfelt (Dept. of Speech, Music and Hearing, Royal Institute of Technology (KTH), Lindstedtsvägen 24, SE-100 44 Stockholm, Sweden, andersa@speech.kth.se), Anders Buen (Brekke & Strand akustikk as, Hovfaret 17, 0275 Oslo, Norway, Anders.Buen@bs-akustikk.no)

Double bassists unanimously claim the importance of a compliant stage floor for producing a warm and nuanced orchestra sound. However, in the limited number of reports studying the stage floor's contribution to radiated sound no clear conclusion has been reached. The present study, based on measurements of three concert halls and three double basses, points at some measurable features that should be considered when trying to settle the question: (1) With a compliant floor the velocity transfer between the bass bridge and floor is often higher than 0 dB in the low-frequency range. In these cases the bass largely acts as a mass (viewed from the end pin) while the floor acts like a spring. (2) The floor properties affect the bridge mobility in the low-frequency range. (3) Below the Helmholtz resonance, around 60 Hz, the radiation of the bass corpus falls about 40 dB within one octave while the ratio between the input power at the bridge and the power transferred to the floor via the end pin has been observed to boost from 3 to 40% in the same range. (4) The effect of a compliant floor may be more pronounced for the player than for the audience.

2pAAg7. Historical and chronological evolution of the concert hall acoustics parameters. Radu Lacatis (Grup d'Acustica Arquitectònica, Ambiental i Industrial, E.T.S.I.I, Univ. Politécnica de Valencia, Camino de Vera, s/n, 46022 Valencia, Spain, rala1@doctor.upv.es), Alicia Giménez (Grup d'Acustica Arquitectònica, Ambiental i Industrial, E.T.S.I.I, Univ. Politécnica de Valencia, Camino de Vera, s/n, 46022 Valencia, Spain, agimenez@fis.upv.es), Arturo Barba Sevillano (Grup d'Acustica Arquitectònica, Ambiental i Industrial, E.T.S.I.I, Univ. Politécnica de Valencia, Camino de Vera, s/n, 46022 Valencia, Spain, arbarse@doctor.upv.es), Salvador Cerdá (Grup d'Acustica Arquitectònica, Ambiental i Industrial, E.T.S.I.I, Univ. Politécnica de Valencia, Camino de Vera, s/n, 46022 Valencia, Spain, salcerjo@mat.upv.es), José Romero (Grup d'Acustica Arquitectònica, Ambiental i Industrial, E.T.S.I.I, Univ. Politécnica de Valencia, Camino de Vera, s/n, 46022 Valencia, Spain, romerof@fis.upv.es), Rosa Cibrián (Facultad de Medicina, Univ. de Valencia, Av. Blasco Ibáñez, 15, 46010 Valencia, Spain, rosa.m.cibrian@uv.es)

The present paper examines the historical evolution of the concert halls acoustic parameters, in the international field. From the beginnings of twentieth century, the acoustic parameters have had a continuous evolution, covering more and more aspects of the concert hall acoustics qualification. Since the bibliography about these is fragmented, we performed in this article, a global and updated presentation on the chronology and the evolution of the studied parameters. Considering the great variety of the same, we presents the appearance of each parameter, located in decades, who has proposed them and, where is possible, indicates articles or publications where they have been presented for the first time. Thus, the historical presentation of the majority of the acoustic parameters of concert halls, it optimizes and can be useful for future research as a central platform in a bibliographical study. The presentation of the same is also grouped according to quality criteria.

2pAAg8. Designing a desirable medium-sized multipurpose hall using ODEON. Jason Duty (Charles M Salter Associates, Inc., 130 Sutter St, Suite 500, San Francisco, CA 94104, USA, jason.duty@cmsalter.com), Hari V. Savitala (Charles M Salter Associates, Inc., 130 Sutter St, Suite 500, San Francisco, CA 94104, USA, hari.savitala@cmsalter.com)

This presentation focuses on using the room acoustics program ODEON for modeling a desirable medium-sized multipurpose hall (400-600 seats). A sampling of medium-sized halls was taken and impulse response measurements were conducted with drapes deployed and retracted. In each hall, the

same configurations were modeled in ODEON. Acoustical parameters, such as T20, T30, C50, C80, were used to check the agreement of the model to the measurements. A systematic approach was then used to adjust model parameters to match the real-world measurements. These results and modifications are presented to better understand how to accurately model and design medium-sized multipurpose halls.

2pAAg9. The acoustical design of rehearsal rooms for orchestra and choir in the Teatro Lirico in Cagliari. Andrea Farnetani (Engineering Dept. - Univ. of Ferrara, Via Saragat, 1, 44100 Ferrara, Italy, andrea.farnetani@unife.it), Nicola Prodi (Engineering Dept. - Univ. of Ferrara, Via Saragat, 1, 44100 Ferrara, Italy, nicola.prodi@unife.it), Roberto Pompoli (Engineering Dept. - Univ. of Ferrara, Via Saragat, 1, 44100 Ferrara, Italy, roberto.pompoli@unife.it)

The acoustical conditions of rehearsal rooms are of primal importance during the training process of an orchestra or a choir. For this reason these spaces should be specifically designed to allow the musicians to clearly ear themselves and each other. At the same time an appropriate sound level should be maintained to avoid extensive exposure to high levels, which is a risk seldom lamented among musicians. Notwithstanding the peculiar role of these rooms in the musical production process, their acoustical requirements are still not sufficiently clarified. In particular the most effective parameters to employ and the best ranges to adopt need further investigations. This work reports the final acoustical optimization of the orchestra and choir rehearsal rooms in the Teatro Lirico in Cagliari (Italy). The comparison between the acoustical parameters before and after the refurbishment will be shown and discussed, with a focus on the difference between the sound level generated by the performer himself and by the others.

2pAAg10. The influence of the source directivity on the measurement uncertainty. Renzo Vitale (Institute of Technical Acoustics, Templergraben 55, 52056 Aachen, Germany, renzo.vitale@akustik.rwth-aachen.de), Ingo Witew (Institute of Technical Acoustics, Templergraben 55, 52056 Aachen, Germany, Ingo.Witew@akustik.rwth-aachen.de)

Modelling can play a key role in assessing the measurement uncertainties, as specified in the ″Guide to the expression of Uncertainty in Measurements″ (GUM). A model is presented that is used to quantify the influence of the source directivity on the measurement uncertainty. On the grounds of image sources and radiosity methods the propagation of sound in rooms is simulated. In this model the characteristics of dodecahedron sound sources are implemented with their statistical properties and characteristics. In Monte Carlo Simulations these two core concepts are combined and the results are compared with measurement results. This comparison allows a quality assessment of the model. In a conclusion the input quantities that affect the measurement uncertainty that is introduced by the source directivity are identified.

2pAAg11. Establishment a methodology for an objective-subjective acoustic analysis in a multifunctional hall: Paraninfo of the Polytechnic University of Valencia. Radu Lacatis (Grup d'Acustica Arquitectònica, Ambiental i Industrial, E.T.S.I.I, Univ. Politécnica de Valencia, Camino de Vera, s/n, 46022 Valencia, Spain, rala1@doctor.upv.es), Alicia Giménez (Grup d'Acustica Arquitectònica, Ambiental i Industrial, E.T.S.I.I, Univ. Politécnica de Valencia, Camino de Vera, s/n, 46022 Valencia, Spain, agimenez@fis.upv.es), Salvador Cerdá (Grup d'Acustica Arquitectònica, Ambiental i Industrial, E.T.S.I.I, Univ. Politécnica de Valencia, Camino de Vera, s/n, 46022 Valencia, Spain, salcerjo@mat.upv.es), Rosa Cibrián (Facultad de Medicina, Univ. de Valencia, Av. Blasco Ibáñez, 15, 46010 Valencia, Spain, rosa.m.cibrian@uv.es), José Romero (Grup d'Acustica Arquitectònica, Ambiental i Industrial, E.T.S.I.I, Univ. Politécnica de Valencia, Camino de Vera, s/n, 46022 Valencia, Spain, romerof@fis.upv.es), Arturo Barba Sevillano (Grup d'Acustica Arquitectònica, Ambiental i Industrial, E.T.S.I.I, Univ. Politécnica de Valencia, Camino de Vera, s/n, 46022 Valencia, Spain, arbarse@doctor.upv.es)

This study presents a methodology for the acoustic analysis, from a comprehensive study of a multifunctional hall, of the Polytechnic University of Valencia, as a pilot hall in a Spanish Coordinated Project. The acoustic parameters studied were those who the most acoustics experts consider of interest. In the objective measures were use the equipment and methods conforming to ISO 3382. The questionnaire used to analyze the subjective response has been patented in Spain, by the research group that developed the project. The correlation between objective and subjective results, along with the accurate simulation of the hall provides a valid tool for design, restoration and improvements the enclosures where the sound quality is preferred.

2pAAg12. Relationship between room shape and acoustics of rectangular concert halls. Andrzej K. Klosak (Institute of Building Materials and Structures, Faculty of Civil Eng., Cracow University of Technology, Warszawska 24, 31-155 Cracow, Poland, andrzej.klosak@pk.edu.pl), Anders C. Gade (Dept. of Acoustic Technology, Technical University of Denmark, Building 352, DK 2800 Lyngby, Denmark, acg@oersted.dtu.dk)

Extensive acoustics computer simulations have been made using Odeon computer simulation software. In 24 rectangular rooms representing ″shoebox″ type concert halls with volumes of 8 000 m^3, 12 000 m^3 and 16 000 m^3 from 300 to 850 measurements positions have been analysed. Only room averaged objective measures are considered here, in particular Clarity (C_{80}), Strength (G) and Early Lateral Energy Fraction (LF_{80}). Results from simulations have been compared with regression models created based on real hall measurements. In general, simulated results of C_{80} and G are found to be in good agreement with regression models. Divergences are found in LF_{80} behaviour; these have been associated with influence of proportions of rectangular halls. Updated formula for predicting of LF_{80} in rectangular halls has been proposed, which takes into the account both width and length of hall.

Session 2pAAh

Architectural Acoustics and Noise: Low Frequency Absorption: Mechanisms, Measurement Methods and Application III (Poster Session)

Peter D'Antonio, Cochair
RPG Diffusor Systems, Inc.

Christian Nocke, Cochair
Akustikbüro Oldenburg

All posters will be on display from 3:40 p.m. to 5:20 p.m. To allow contributors an opportunity to see other posters, contributors of odd-numbered papers will be at their posters from 3:40 p.m. to 4:30 p.m. and contributors of even-numbered papers will be at their posters from 4:30 p.m. to 5:20 p.m.

Contributed Papers

2pAAh1. Sound absorption control at low frequencies in the new symphonic concert Hall of VillaPrado Valladolid. Victoria Chavez Thielemann (University of Chile & Xu Acoustique, 17, rue Danton, 94270 Le Kremlin Bicêtre, France, v.chavez@yahoo.fr)

In large concert halls for symphonic orchestras the sound absorption control at low frequencies is a compromise between acoustics and architecture. In general the architectural approach is imposed over acoustical wills. In this way the acoustician must adapt his work to the architectural choice of finishing materials. Commonly is the case of the wood material's choice (usage of thin wood panels in medium density), whose architectural expression is related to orchestra instruments and to the visual warmth. Today the acoustical trend is to obtain in concert halls the appropriate acoustical ″warmth″. As convention, this acoustical quality in a concert hall is related to the bass sound spotlessness, and an appropriate strength of the bass tones arriving to the audience. In this context we will present the solutions and constructive compromises realised in the auditorium of Villa Prado in the way to obtain the desired warmness. This concert hall has a ″shoe box″ shape, an audience capacity of 1720 seats and it was made completely - walls, ceiling - in wood panels (architect: R. Bofiil, acoustician: XuAcoustique, inaugurated in April 2007, Spain).

2pAAh2. Signal analysis in the sound absorption measurement procedure: The importance of time subtraction and reference surface corrections. Paolo Guidorzi (DIENCA - Univ. of Bologna, Viale Risorgimento 2, 40136 Bologna, Italy, paolo.guidorzi@mail.ing.unibo.it), Massimo Garai (DIENCA - Univ. of Bologna, Viale Risorgimento 2, 40136 Bologna, Italy, massimo.garai@mail.ing.unibo.it)

The sound absorption coefficient measurement (following ISO 13472-1 normative) of highly absorbing materials, which are tipically employed in room acoustic correction, presents some inherent difficulties. These materials present highly sound absorption coefficient indeed, but usually low sound insulation index and are installed over highly reflective surfaces. This leads to some measurement problems, partially solved by means of the reference surface method. In this work some measurement examples on the same materials but with different contour conditions are analyzed and the improvements on the results, due to reference surface normalization and time domain subtraction of free field response, are discussed.

Session 2pAAi

Architectural Acoustics and ASA Committee on Standards: Comparison of US and European Standards in Building/Room Acoustics II (Poster Session)

Kenneth P. Roy, Cochair
Armstrong Building Products

Eddy Gerretsen, Cochair
TNO Science and Industry

All posters will be on display from 3:40 p.m. to 5:20 p.m. To allow contributors an opportunity to see other posters, contributors of odd-numbered papers will be at their posters from 3:40 p.m. to 4:30 p.m. and contributors of even-numbered papers will be at their posters from 4:30 p.m. to 5:20 p.m.

Contributed Paper

2pAAi1. Sound Insulation Requirements in Hospitals: Comparisons and case studies. Simone Secchi (Univ. of Florence, Via San Niccolò 89/a, 50125 Florence, Italy, simone.secchi@taed.unifi.it), Gianfranco Cellai (Univ. of Florence, Via San Niccolò 89/a, 50125 Florence, Italy, gianfranco.cellai@unifi.it), Elisa Nannipieri (Univ. of Florence, Via San Niccolò 89/a, 50125 Florence, Italy, elisa.nannipieri@taed.unifi.it), Giorgio Raffellini (Univ. of Florence, Via San Niccolò 89/a, 50125 Florence, Italy, giorgio@studioraff.it)

Italian and EU regulations for sound insulation of hospitals are very hard to be satisfied. Especially with reference to sound insulation from outside noise, the simultaneous presence of important sound sources (refrigerating units, fans and others) and of sensitive receivers (the patients) imposes high requirements for façade sound insulation. Moreover, the necessity to assure high values of natural lighting in interiors imposes the use of large windows on façades. By using the tabular estimation model defined by annex B of the European Norm 14351 for the calculation of the performance of windows and the model of EN 12354-3 for the performance of façades, it is easy to show that the limiting values defined by the Italian Law can be achieved only with a perfect realisation of the building construction. In the paper the comparison between EU regulations for hospitals is shown. Moreover, different case studies of hospital buildings are analysed either with a theoretical approach or with measures carried out in site.

Session 2pAAj

Architectural Acoustics and Musical Acoustics: Surround Sound Acoustics II (Poster Session)

Anthony Hoover, Cochair
McKay Conant Hoover Inc.

Alexander Case, Cochair
Fermata Audio and Acoustics

Etienne Corteel, Cochair
Sonic Emotion

All posters will be on display from 3:40 p.m. to 5:20 p.m. To allow contributors an opportunity to see other posters, contributors of odd-numbered papers will be at their posters from 3:40 p.m. to 4:30 p.m. and contributors of even-numbered papers will be at their posters from 4:30 p.m. to 5:20 p.m.

Contributed Papers

2pAAj1. Directivity control with Wave Field Synthesis: implications for live music performances. Terence Caulkins (Arup, 155 Ave of the Americas, New York, NY 10013, USA, terence.caulkins@arup.com), Etienne Corteel (Sonic Emotion, Eichweg, 6, CH-8154 Oberglatt, Switzerland, etienne.corteel@sonicemotion.com), Joseph Sanson (IRCAM, 1 Place Igor Stravinsky, 75004 Paris, France, joseph.sanson@ircam.fr), Olivier Warusfel (IRCAM, 1 Place Igor Stravinsky, 75004 Paris, France, Olivier .Warusfel@ircam.fr)

Loudspeaker room interaction has a large impact on the perception of surround sound, especially in the context of ″mixed concert″, in which a loudspeaker system is used to synthesize virtual instruments that share the acoustic space of the stage with real musicians. Loudspeakers excite the listening environment in a way that differs from real instruments since, by design, they tend to exhibit constant directivity characteristics as a function of frequency. Moreover, real instruments exhibit radiation patterns that vary according to pitch, fingering and expressive movements. We present an approach based on Wave Field Synthesis which enables a control of radiation properties of the loudspeaker system which can be dynamically monitored in real time. Applications and potential perceptual impacts are discussed, focusing on the possibility of using directivity control to vary the excitation of the concert hall in order to monitor early reflections level and direct/reverberant energy ratio associated to virtual sources.

2pAAj2. Acoustic Radiation Properties of Dynamic Loudspeaker Arrays versus Multiactuator Panels for Wave Field Synthesis. Basilio Pueo (University of Alicante, Signals, Systems and Telecommunications, Cta San Vicente del Raspeig s/n, E-03690 Alicante, Spain, basilio@ua.es) , José J. Lopez (Tech. Univ. of Valencia, Camino de Vera S/N, 46021 Valencia, Spain, jjlopez@dcom.upv.es)

Wave Field Synthesis (WFS) is a spatial sound rendering technique that generates a true sound field using loudspeaker arrays. Dynamic loudspeaker arrays, that were used since the beginning of WFS, is the technology employed in most prototypes. Alternatively, Distributed Mode Loudspeakers can be used to build arrays for WFS, also known as Multiactuator Panels (MAPs). For that purpose, multiple vibrating exciters are attached to a single flat panel of a light and stiff material, creating bending waves that are then radiated as sound fields. An analysis of the radiation properties and spatial performance of such loudspeaker arrays for WFS reproduction is presented in this paper. Wave fields have been interpreted in the wavenumber domain, where the source radiation is decomposed into plane waves for arbitrary angles of incidence. Then, measurement and analysis of the radiation performance, evaluation of the spatial aliasing frequency and associated sampling artefacts for both linear loudspeaker arrays are addressed. In addition, parameters that can modify spatial aliasing artifacts, such as truncation effects caused by the array geometry or array directivity are also discussed. Simulations and experiment results are discussed through several case studies, comparing dynamic loudspeaker arrays and MAPs in WFS operation.

2pAAj3. Acoustical design of multichannel audio listening environments. Timothy Gulsrud (Kirkegaard Associates, 954 Pearl Street, Boulder, CO 80302, USA, tgulsrud@kirkegaard.com)

The acoustical design of spaces for surround sound music production raises issues concerning room size and shape, loudspeaker placement, and placement of sound-absorbing and sound-diffusing finishes that require different solutions than for 2-channel stereo listening environments. Design and construction of a new room for multichannel audio, rather than renovating a room originally conceived for a 2-channel stereo loudspeaker system, presents an opportunity to address the issues from first principles. This paper presents a case study of the design, construction, and commissioning of a new audio control room for multichannel classical music recording, and discusses unique solutions to the critical issues for these listening environments. The use of a computer model as a design tool and in situ measurements in the completed room are also discussed.

2pAAj4. Effects of practical loudspeaker characteristics on virtual acoustic imaging systems. Xiaojun Qiu (Key Laboratory of Modern Acoustics and Institute of Acoustics, Nanjing University, 210093 Nanjing, China, xjqiu@nju.edu.cn), Michael Vorlaender (Institute of Technical Acoustics, RWTH Aachen University, Neustr. 50, 52056 Aachen, Germany, mvo@akustik.rwth-aachen.de)

Loudspeakers used in virtual acoustic imaging systems are usually considered as monopoles in the models; however, it is only an approximation at low frequency range, and practical loudspeaker boxes behave complex directivity in mid to high frequency range and almost only radiate in the front direction above a certain frequency. Some studies have taken into account of the frequency response characteristics of the loudspeakers in virtual acoustic imaging systems, and others have considered their directivity characteristics separately. This paper presents a complete model of a virtual acoustics imaging system which takes account of both the temporal and spatial characteristics of the sound sources, and the effects of practical loudspeaker characteristics on virtual acoustic imaging systems are studied.

Session 2pAAk

Architectural Acoustics: Case Studies and Design Approaches

Bryon Harrison, Cochair
124 South Boulevard, Oak Park, IL, 60302 USA

Witew Jugo, Cochair
Institut für Technische Akustik, RWTH Aachen University Neustrasse 50, 52066 Aachen, Germany

Contributed Papers

5:20

2pAAk1. Towards a classification of the ″sonic character″ of the architectural space. Fausto E. Rodriguez-Manzo (Departamento de Procesos y Tecnicas, CyAD, Universidad Autonoma Metropolitana-Azcapotzalco, Av. San Pablo 180, Edificio H-PB, Col. Reynosa Tamaulipas, Delegacion Azcapotzalco, 02200 Mexico, D.F., Mexico, rfme@correo.azc.uam.mx)

Today it is well-known that an architectural space can be compared with a musical instrument. One of the main characteristics of a musical instrument is its timbre, which makes unique the sound produced by it. We can understand this timbre as the sound quality of the instrument that is produced due to the specific physical characteristics of the instrument. In an architectural space these concepts of timbre and sound quality could be applied through the concept of ″sonic character″ of the space. The ″sonic character″ of the architectural space is the sound personality of the space due to the specific physical or architectural characteristics of it. Understanding this concept in architecture could be of great importance to architectural design purposes since this could be the way by which sound can be embodied in an integral way of designing architectural spaces. This paper presents a proposal for the classification of the ″sonic character″ of the architectural space as an important step of a research towards a better understanding of the need of taking into account the sound as an essential component of the architectural space. The presentation includes also some architectural space examples to improve the understanding of this important concept.

5:40

2pAAk2. High Environmental Quality (HQE), the GIAc/ADEME approach. Eric Gaucher (Acoustique & Conseil, 17-19 rue des Grandes Terres, 92508 Rueil-Malmaison, France, eg@acoustique-conseil.com)

The ″Haute Qualité Environnementale″ HQE concept is increasingly important for French building. The French acoustics consultants association, GIAc, has been working, with the ADEME's support in order to define acoustically a building that aims to be HQE. The approach is to come back to the analysis of a building acoustics situation: the activity developed in a room generates a sound which can disturb activities held in surrounding rooms. In return, this very activity requires quietness to be held in adequate conditions. If we define rules allowing quantification of this aggressivity and sensitivity, we can deduce the insulation criteria corresponding to the quality we are looking for. The main advantage of this method is the homogeneity it induces on the different criteria, which were usually defined independently one from the other. Many present situations show that the equilibrium between acoustic criteria is at least as important as their absolute values. Even though this approach has not been included in the QEB reference book, it can be used to validate the absolute values, to extend the qualification to other kinds of rooms, and also to adapt objective criteria to different situations.

6:00

2pAAk3. Auditory sketching as a tool in architectural design education. Tim Frank (Georgia Institute of Technology, College of Architecture, Atlanta, GA 30332-0155, USA, timothy.frank@coa.gatech.edu), Selen Okcu (Georgia Institute of Technology, College of Architecture, Atlanta, GA 30332-0155, USA, okcuse@yahoo.com)

Architectural spaces are perceived through embodied experiences that are made up of both visual and non-visual stimuli. However, the conventional means that a designer uses to depict non -visual stimuli such as aural phenomena contain a visual bias. We have introduced a new aural drawing system called, ″Auditory Sketching″ as a way for design students to visualize the auditory fields that structure one's perception of architectural space. The Auditory Sketching procedure requires that the design student first mediate aural perceptions linguistically through meticulous observation during which they are encouraged to define aural qualities within the space such as notes, tones, clusters, bands, and pitches that would be difficult to capture using a graphic system of notation. Using this written language as a guide for graphic expression, they explore different ways of expressing these time and space notations with ink pens; creating an auditory system of 'tones' by building up marks in different ways: hatching, layering up, scribbling, etc. The eventual translation of aural perception into graphic patterns is crucial because designers need to visualize the sound in order to consider it a significant medium of architecture that they can define and shape.

Invited Paper

6:20

2pAAk4. Concepts & Methods in Architectural Acoustics from the Classical Period to the Enlightenment. Adam Di Angelo (Rensselaer Polytechnic Institute, Greene Bldg., 110 8th St., Troy, NY 12180, USA, diangelo@secondstation.com), Paul Calamia (Rensselaer Polytechnic Institute, Greene Bldg., 110 8th St., Troy, NY 12180, USA, calamp@rpi.edu)

Herein is presented a critical examination of the early concepts in architectural acoustics in the western world. This study suggests that the historical extent of architectural acoustics is much more sophisticated than is generally considered. The presentation focuses on specific contributors and their discoveries in the nascent art of architectural acoustics. Among those studied are Marcus Vitruvius Pollio, the ancient Roman architect responsible for the tome De Architectura; German polymath Athanasius Kircher who delicately balanced empirical science with magic to explain acoustical phenomena in his two books, the Phornugia Nova and the encyclopedic Musurgia

Universalis; and English architects-cum-scientists Sir Samuel Morland and Sir Robert Hooke whose wide and varied research often entered into acoustics. In the works of these gentlemen are elegant, precocious, and sometimes absurd revelations on the science of sound and surface.

Contributed Paper

6:40

2pAAk5. Acoustic characterization of rehabilitated cloisters. Antonio P. Carvalho (FEUP - Laboratory of Acoustics, R. Dr. Roberto Frias, P-4200-465 Porto, Portugal, carvalho@fe.up.pt), Silvia R. Vilela (FEUP - Laboratory of Acoustics, R. Dr. Roberto Frias, P-4200-465 Porto, Portugal, ec01199@fe.up.pt)

This paper presents the results of field measurements in eight rehabilitated cloisters of old monasteries in Portugal (length: 20 to 35 m and height: 3.3 to 6.3 m) regarding their acoustic behavior to two objective parameters: RT and RASTI. The goal is to characterize the acoustic effect of the rehabilitation done on theses spaces to adapt them to new uses. All these cloisters had recently their galleries' openings to the central yard closed with glass panels. Simple formulas were obtained that relate among the objective acoustic parameters and between the acoustic and architectural parameters. This paper also presents the variation on the RASTI and RT average values resulting of the rehabilitation work done on these buildings.

TUESDAY AFTERNOON, 1 JULY 2008 ROOM 342B, 2:20 TO 7:00 P.M.

Session 2pABa

Animal Bioacoustics, Underwater Acoustics, Acoustical Oceanography, Signal Processing in Acoustics, and ECUA: Animal Sonar Systems I

James A. Simmons, Cochair
Brown University, Department of Neuroscience, Box G-LN, Providence, RI 02912, USA

Michel Andre, Cochair
Laboratori d'Aplicacions Bioacústiques, Universitat Politècnica de Catalunya, avda. Rambla Exposició s/n, Vilanova i la Geltrú, 08800, Spain

Invited Paper

2:20

2pABa1. The echolocating bat controls the direction and distance of its acoustic gaze. Cynthia Moss (University of Maryland, Department of Psychology, Biology-Psychology 2123M, College Park, MD 20742, USA, cmoss@psyc.umd.edu), Kaushik Ghose (University of Maryland, Department of Psychology, Biology-Psychology 2123M, College Park, MD 20742, USA, kghose@umd.edu), Annemarie Surlykke (University of Southern Denmark, Institute of Biology, Campusvej 55, -DK-5230 Odense, Denmark, ams@biology.sdu.dk)

Echolocation is an active sensing system that depends upon the dynamic interplay between auditory information processing and adaptive motor control. The echolocating bat produces ultrasonic vocalizations and uses information contained in the returning echoes to build a three-dimensional auditory representation of its surroundings. The timing, bandwidth, and duration of echolocation signals used to probe the environment directly impact the information available to the bat's acoustic imaging system. In turn, the bat's auditory representation of space guides its actions--ear movements, head aim, flight path, and the features of subsequent sonar vocalizations. This talk will summarize the bat's adaptive vocal behavior as it engaged in complex spatial tasks. The bat's 3D flight path was recorded with high-speed stereo IR video; its sonar signals were recorded with a microphone array that permitted reconstruction of the emission pattern. The sonar emission pattern of the big brown bat, *Eptesicus fuscus*, is directional, but broad enough to collect echo information from objects within a 60-90 deg cone, which would enable simultaneous inspection of objects in the frontal plane. Here, we report that bats encountering a complex environment shifted the direction and distance of their sonar gaze to inspect closely spaced obstacles and targets sequentially.

2:40

2pABa2. Simulating bat sonar using vector sound intensity. Robert Hickling (Sonometrics Inc., 8306 Huntington Road, Huntington Woods, MI 48070-1643, USA, sonometrics@comcast.net)

In general bats use ultrasound to determine their surroundings and to detect flying insects. Generally the beam width of ultrasonic signals emitted by bats is too wide to distinguish closely-spaced objects and the receiving pattern of bats' ears is similar (J. A. Simmons, ″Directionality of biosonar broadcasts and reception by the ears″, Tutorial Lecture, ASA Spring Meeting, 2002). To locate an object requires knowing both distance and direction. Distance can be readily determined using time-of-flight. How a bat determines direction is less clear. In this presentation, an ultrasonic device is demonstrated that measures both distance and direction (R. Hickling, ″Method and Apparatus for Echolocation″ US Patent No. 7,054,226, May 2006). This uses a combination of a pulsed ultrasonic source and a vector sound-intensity probe. The probe has four ultrasonic receivers at the vertices of a regular tetrahedron and determines direction from the sound-intensity vector, using finite-difference approximations and the cross-spectral formulation. The frequencies of the echoes received by the probe have to be heterodyned down to lower frequencies for accuracy in the finite-difference approximations. Echolocation data using the device are presented.

3:00

2pABa3. An autocorrelation model of bat sonar. Lutz Wiegrebe (Biocenter, University of Munich, Großhaderner Str. 2, 82152 Munich, Germany, lutzw@lmu.de)

Their sonar system allows echolocating bats to navigate with high skill through a complex, three-dimensional environment at high speed and low light. The auditory analysis of the echoes of their ultrasonic sounds requires a detailed comparison of the emission and echoes. Here an auditory model of bat sonar is introduced and evaluated against a set of psychophysical phantom-target, echo-acoustic experiments. The model consists of a relatively detailed simulation of auditory peripheral processing in the bat, Phyllostomus discolor, followed by a functional module consisting of a strobed, normalised, autocorrelation in each frequency channel. The model output is accumulated in a sonar image buffer. The model evaluation is based on the comparison of the image-buffer contents generated in individually simulated psychophysical trials. The model provides reasonably good predictions for both temporal and spectral behavioural sonar processing in terms of sonar delay, roughness, and phase sensitivity and in terms of sensitivity to the temporal separations in two-front targets and the classification of spectrally divergent phantom targets.

3:20

2pABa4. Object-oriented echo perception and cortical representation in the bat Phyllostomus discolor. Uwe Firzlaff (Biocenter of the Ludwig-Maximilians University of Munich, Großhaderner Str. 2, 82152 Planegg-Martinsried, Germany, firzlaff@zi.biologie.uni-muenchen.de)

Echolocating bats can identify three-dimensional objects exclusively through the analysis of acoustic echoes of their ultrasonic emissions. However, objects of the same structure can differ in size and the auditory system must achieve a size-invariant, normalized object representation for reliable object recognition. In this talk both the neural representation in the auditory cortex and the behavioral classification of echoes of complex virtual objects that vary in object size are described. Electrophysiological experiments revealed a population of units in the auditory cortex of the bat Phyllostomus discolor which showed an object-size invariant response (14/109 units, 13%). These units respond preferentially to echoes from objects in which echo duration (encoding object depth) and echo amplitude (encoding object surface area) co-varies in a meaningful manner. The electrophysiological results are corroborated by the results of a phantom-target playback experiment, in which it is shown that P. discolor spontaneously classifies most scaled versions of objects according to trained standards. These results indicate that at the level of the bat's auditory cortex, an object-oriented rather than a stimulus-parameter oriented representation of echoes is achieved. This work was supported by the Volkswagen Foundation (I/79782)

3:40-5:00 Posters

All sessions will recess for presentation of poster papers on various topics in acoustics. See poster sessions for topics and abstracts.

Invited Papers

5:00

2pABa5. Absolute target range and target range profile in separate computational compartments: Synthetic aperture echolocation. James A. Simmons (Brown University, Department of Neuroscience, Box G-LN, Providence, RI 02912, USA, james_simmons@brown.edu)

Echolocating big brown bats emit wideband (20-100 kHz) FM sounds and perceive target range from echo delay with an accuracy determined by echo relative bandwidth (Q). They distinguish among target shapes by echo spectra, but they perceive shape in terms of distances to different parts (glints), or the target's range profile. Shape resolution based on glint delay differences extracted from target interference spectra is in fractions of millimeters. The bat's flight velocity is about 5 m/s, so that echo delay changes continuously during production of broadcasts and then again during reception of echoes, smearing and displacing delay estimates for target ranging by several hundred microseconds. Previous workers have identified a particular distance at which smearing is minimal, but it is not known whether this ″distance of focus″ has significance for the bat. However, perception of target shape is based on a spectral representation that is only slightly distorted by the bat's motion, and it is kept in separate computational path from absolute delay until after absolute delay is determined, whereupon it is attached to absolute delay to place the target's image in an approximate spatial position. The bat's system achieves synthetic aperture imaging of shape while avoiding motion-related blurring.

5:20

2pABa6. Vocal motor control in horseshoe bats - a bottom-up approach. Kota Kobayasi (UCLA, Dept. Physiol. Sci., Box 951606, Los Angeles, CA 90095, USA, kobayash@ucla.edu), Steffen Hage (UCLA, Dept. Physiol. Sci., Box 951606, Los Angeles, CA 90095, USA, hage@ucla.edu), Jie Ma (UCLA, Dept. Physiol. Sci., Box 951606, Los Angeles, CA 90095, USA, majie@ucla.edu), Walter Metzner (UCLA, Dept. Physiol. Sci., Box 951606, Los Angeles, CA 90095, USA, metzner@ucla.edu)

Most animals constantly adjust the spectrotemporal composition of their vocalizations depending on the information content intended to be conveyed by these signals. Whereas most studies focus on the sensory processing of spectrotemporal features of vocalizations in various vertebrates, it is still widely unknown how vocal motor structures in the brain adjust these call parameters. We used

echolocation and acoustic communication behaviors in horseshoe bats to analyze the neurobiological and biomechanical basis for the motor control of their vocalizations. Results from pharmacological studies of the vocal motor nucleus, the nucleus ambiguus, lead us to developed a novel model for call frequency control by vocal motor neurons. Neurophysiological recordings combined with pharmacological manipulations at the single cell level in spontaneously vocalizing bats substantiated this model. Biomechanical properties of the larynx were also found to aid in call frequency control: Altering tracheal air flow in an isolated larynx preparation resulted in two distinct frequency bands that were non-harmonically related and reflected the main frequency components of echolocation pulses and communication signals, respectively. In addition, changes in air pressure revealed transitions from periodic to chaotic that occurred within a single signal cycle, giving rise to spectral features observed in horseshoe bat communication signals.

5:40

2pABa7. Echolocation-like pulse emission for communication by Japanese horseshoe bats, Rhinolophus ferrumequinum nippon. Hiroshi Riquimaroux (Faculty of Engineering, Doshisha Univ., 1-3 Miyakodani Tatara, 610-0321 Kyotanabe, Japan, hrikimar@mail.doshisha.ac.jp), Ryota Shimazawa (Faculty of Engineering, Doshisha Univ., 1-3 Miyakodani Tatara, 610-0321 Kyotanabe, Japan, bte0060@mail4.doshisha.ac.jp), Shizuko Hiryu (Faculty of Engineering, Doshisha Univ., 1-3 Miyakodani Tatara, 610-0321 Kyotanabe, Japan, shiryu@mail.doshisha.ac.jp)

It has been reported that the bats communicate with conspecifics by various types of vocalizations, which are different from echolocation pulses. However, we have found pulses used for communication, which were emitted when a bat walked to another individual, appeared to be very similar to those for echolocation. Data have shown two evidences. First, the bats never approached another one without emitting pulses. Second, the bats emitted echolocation-like pulses whose CF2 frequency sequentially changed during the approaching behavior. Such pulses were never emitted by an isolated bat. The changes in CF2 frequency were clearly different from Doppler-shift compensation. If this frequency shift was caused by Doppler-shift compensation, the bat should be moving as fast as 1-5 m/s in the cage. Thus, we suggest that these CF2 frequency shifts may play an important role for communication during the approaching behavior to a conspecific animal. [The research supported by a grant to RCAST at Doshisha Univ. from MEXT and by the Innovative Cluster Creation Project promoted by MEXT.]

Contributed Paper

6:00

2pABa8. A model of range discrimination of multiple objects by using the linear period modulation signal. Ikuo Matsuo (Tohoku Gakuin University, Tenjinzawa 2-1-1, Izumi-ku, 9813193 Sendai, Japan, matsuo@cs.tohoku-gakuin.ac.jp)

Using the echolocation, bats can capture moving objects in 3D space. The big brown bats, Eptesicus fuscus, emit the linear period modulation sound and can identify objects with an accuracy of less than a millimeter. The delay separation of three or more closely spaced objects can be determined through analysis of the echo spectrum. However, delay times cannot be properly correlated with objects using only the echo spectrum because the sequence of delay separations cannot be determined without information on temporal changes in the interference pattern of the echoes. We previously proposed the model to determine delays of multiple objects from the echoes by using the linear frequency modulation sound. In order to extract the temporal changes, Gaussian chirplets with a carrier frequency compatible with bat emission sweep rates were used. In this paper, we examined the effect of the window's shape which was changed to extract the temporal changes dependent on delays of multiple objects by using the linear period modulation sound.

Invited Paper

6:20

2pABa9. Acoustic focussing: how flying bats control spatial distribution of Doppler-ranging errors by signal sweep rate. Marc W. Holderied (School of Biological Sciences, University of Bristol, Woodland Road, BS8 1UG Bristol, UK, marc.holderied@bristol.ac.uk)

Echolocating bats obtain three-dimensional images of their surroundings in complete darkness by emitting sonar signals and evaluating returning echoes. When flying close to objects, bats risk collision and therefore depend on the accuracy of images - particularly in the perceived distance of obstacles, which is coded by the time delay between call and echo. Yet, during flight, such accuracy is perturbed first because bats call and receive echoes at different positions and second because echoes are modified by Doppler shifts. The spatial distribution of such ranging errors is range dependent - objects at one particular distance from the bat have zero ranging errors, while ranging-errors increase for closer or more distant objects. Interestingly, this distance of zero ranging error depends on signal design, in particular sweep rate. By adjusting signal design flying bats could shift this distance adaptively to their target of interested. Because this has similarities with focusing (i.e. accommodation) in vision, this distance is called distance of focus (DOF). We will present examples for actual distances of focus of different bat species in different behavioural contexts, such as search flight, obstacle avoidance and target approach. DOF gives a novel perspective to the adaptive relevance of frequency modulated sonar signals.

Contributed Paper

6:40

2pABa10. Passive acoustic localization techniques of Eastern Pacific grey whales. Jennifer L. Wladichuk (University of Bath, Dept. Mechanical Engineering, Claverton Down, BA2 7AY Bath, UK, jlw23@bath.ac.uk), William M. Megill (University of Bath, Dept. Mechanical Engineering, Claverton Down, BA2 7AY Bath, UK, enswmm@bath.ac.uk), Philippe Blondel (University of Bath, Department of Physics, Claverton Down, BA2 7AY Bath, UK, pyspb@bath.ac.uk)

Eastern Pacific grey whales (Eschrichtius robustus) apparently do not actively echolocate, yet still they thrive in shallow water environments where visibility is much reduced. Along their migration route and in their feeding grounds these whales are exposed to high levels of ambient noise, highly-turbid waters and many underwater obstacles. To test possible passive acoustic localization mechanisms (e.g. Acoustic Daylight Imaging and Passive Synthetic Aperture), we made extensive acoustic measurements during comprehensive field studies of these whales on their summer feeding grounds in British Columbia (Canada). In combination with visual observations of the whales and their behaviours, we investigated the acoustical sources available to the whales when navigating within a feeding bay. First, we measured ambient noise levels to construct the acoustic landscape around the whales. Second, we investigated how sound is altered when objects such as kelp beds and rocks are present. We also measured acoustic changes induced by direct, controlled modifications of the near-shore environment. The aim of this research is to understand how grey whales might be finding their way around, and what impact, if any, increased levels of ambient noise might have on the whales' ability to find food and navigate within the feeding grounds.

TUESDAY AFTERNOON, 1 JULY 2008 P3-C, LEVEL 3, 3:40 TO 5:20 P.M.

Session 2pABb

Animal Bioacoustics and ECUA: Animal Bioacoustic Censusing II (Poster Session)

Marie Roch, Cochair
San Diego State University

Cédric Gervaise, Cochair
E3I2 - EA3876

All posters will be on display from 3:40 p.m. to 5:20 p.m. To allow contributors an opportunity to see other posters, contributors of odd-numbered papers will be at their posters from 3:40 p.m. to 4:30 p.m. and contributors of even-numbered papers will be at their posters from 4:30 p.m. to 5:20 p.m.

Contributed Papers

2pABb1. Acoustic detection of beaked whales from autonomous recording buoys. Antón Arias (Departamento de Zoología y Antropología Física, Facultad de Biología, Universidad Complutense de Madrid, 28040 Madrid, Spain, amarias@estumail.ucm.es), Mark Johnson (Woods Hole Oceanographic Institution, Applied Ocean Physics & Engineering Dept., Woods Hole, MA 02543, USA, majohnson@whoi.edu), Natacha Aguilar Soto (Univ. de La Laguna, Department of Animal Biology, 38256 La Laguna (Tenerife), Spain, naguilar@ull.es), Peter T. Madsen (University of Aarhus, Biological Sciences, Zoophysiology, C. F. Møllers Allé, Building 1131, DK-8000 Aarhus, Denmark, peter.madsen@biology.au.dk), Peter Tyack (Woods Hole Oceanographic Institution, Applied Ocean Physics & Engineering Dept., Woods Hole, MA 02543, USA, ptyack@whoi.edu), Bertel Møhl (University of Aarhus, Biological Sciences, Zoophysiology, C. F. Møllers Allé, Building 1131, DK-8000 Aarhus, Denmark, bertel.moehl@biology.au.dk)

Beaked whales are among the least known cetaceans but may be especially vulnerable to mid-frequency sonars. Effective implementation of passive acoustic monitoring (PAM) of beaked whale vocalizations may help both to study the biology of these elusive species and to mitigate human impacts. Here we report results of a feasibility study of PAM performed off El Hierro (Canary Islands) where there are coastal resident populations of two species of beaked whales. An acoustic recording system, comprising a GPS-equipped buoy with an archival acoustic tag (Dtag) suspended 200m below, was deployed in an area with visual coverage from land. The DTAG recorded broadband acoustic data sampled at 96 kHz along with timing and position information from the GPS. The buoy was deployed on 6 days and clicks were clearly detectable in all recordings. A majority of these were confirmed to be beaked whale clicks by comparison against sounds previously recorded from the same species. Visual sightings were then compared against acoustic detections to develop a methodology for estimating the probability of detection as a function of distance and group size. Results demonstrate the effectiveness of sonobuoy-type PAM systems for beaked whales and the possibility for low-cost tests of acoustic detection models.

2pABb2. Automated real-time detection of cetaceans at the Station ALOHA Cabled Observatory. Julie N. Oswald (Univ. of Hawaii, P.O. Box 1106, Kailua, HI 96734, USA, oswald.jn@gmail.com), Whitlow W. Au (Univ. of Hawaii, P.O. Box 1106, Kailua, HI 96734, USA, wau@hawaii.edu), Fred K. Duennebier (Univ. of Hawaii, Dept. of Geology and Geophysics, 2525 Correa Rd., Honolulu, 96822, USA, fred@soest.hawaii.edu)

Hawaiian waters support a wide variety of cetacean species, however, little is known about their occurrence in offshore waters. A cabled ocean bottom observatory located at Station ALOHA (Station ALOHA Cabled Observatory - ACO) provides a unique opportunity to study the occurrence of cetaceans in real-time and over long time scales at a deep ocean research site located 100 km north of Oahu. A retired electro-optical telecommunications cable provides power and broadband Ethernet communications capability to

the ACO, allowing real-time continuous acoustic monitoring. The ACO has been operational since February 2007 and includes a hydrophone with a bandwidth of 0.01Hz to 40kHz. Automated methods for detection and identification of cetacean calls have been developed and data are processed in nearly real-time. Several cetacean species have been detected, including: dolphins and humpback, minke, fin, and sperm whales. The relationship between the occurrence of different species and changes in the environment has been explored using near-monthly shipboard oceanographic observations collected at Station ALOHA. In addition, seasonal trends in the occurrence of minke whales, a species that has been especially difficult to study using visual methods due to their cryptic behavior, have been examined.

2pABb3. Validating passive acoustic monitoring data loggers by visual observations. Line A. Kyhn (National Environmental Research Institute, University of Aarhus, Frederiksborgvej399, DK-4000 Roskilde, Denmark, lky@dmu.dk), Jakob Tougaard (National Environmental Research Institute, University of Aarhus, Frederiksborgvej399, DK-4000 Roskilde, Denmark, jat@dmu.dk), Mats Amundin (Kolmardens Djurpark & Biology Dep., Inst. of Physics, Chemistry and Biology, Linkoping University, Kolmardens Djurpark, SE-61892 Kolmarden, Sweden, MATS.AMUNDIN @KOLMARDEN.COM), Joanna Stenback (Kolmardens Djurpark & Biology Dep., Inst. of Physics, Chemistry and Biology, Linkoping University, Kolmardens Djurpark, SE-61892 Kolmarden, Sweden, JOANNA .STENBACK@GMAIL.COM), Jonas Teilmann (National Environmental Research Institute, University of Aarhus, Frederiksborgvej399, DK-4000 Roskilde, Denmark, jte@dmu.dk), Daniel Wennerberg (Kolmardens Djurpark & Biology Dep., Inst. of Physics, Chemistry and Biology, Linkoping University, Kolmardens Djurpark, SE-61892 Kolmarden, Sweden, daniel .wennerberg@gmail.com)

The use of passive acoustic monitoring (PAM) is increasingly used as a monitoring tool in e.g environmental impact assessments. However, very few studies have focused on validating PAM data against independent observations which is critical in order to compare data from different studies and areas, and over time. In August 2007 we tested two types of odontocete PAM equipment: version 5 T-PODs (Chelonia, U.K.) and PCL's (Aquatec, Lochborough, UK) by comparing acoustic detections to visual theodolite tracings of wild harbour porpoises. Eight T-PODs with known detection thresholds and four PCLs were mounted in four clusters. Detection thresholds of the T-PODs varied from 117 to 125dB re 1µPapp. Based on visual tracks of 28 porpoises it is shown that detection ranges correlated inversely with detection threshold. However, PAM-detection also strongly depended on the angle between the swim track of porpoises and the line to the data logger. Some porpoises were not detected despite swimming within 20m of the nearest data logger. It was not possible to distinguish between recordings from one and more than one animal on the PAM-recordings, despite that the number of animals was known from the corresponding tracks. All in all, the results showed good correspondence between PAM recordings and visual tracings, as well as among PAM recordings.

2pABb4. Data Handling of a Perennial Acoustic Observatory in the Antarctic Ocean. Lars Kindermann (Alfred Wegener Institute, P.O. Box 120161, 27515 Bremerhaven, Germany, lars.kindermann@awi.de), Holger Klinck(Alfred Wegener Institute, P.O. Box 120161, 27515 Bremerhaven, Germany, holger.klinck@awi.de), Ilse Catharina Van Opzeeland (Alfred Wegener Institute, P.O. Box 120161, 27515 Bremerhaven, Germany, Ilse .Van.Opzeeland@awi.de)

In December 2005, 4 broadband hydrophones were deployed through boreholes under the 100m thick floating ice shelf near Atka Bay, Antarctica. Since then, more than 10,000 hours of underwater sounds have been recorded, containing marine mammal vocalizations and the unique background sounds generated by ice and the occasional ship. These records from this pristine region are analyzed in terms of the local noise budget, the behaviour of marine mammals and anthropogenic impacts. The observatory is energetically self-sufficient and connected by a 15km WLAN link to the year-round manned German Neumayer Base, where a leased satellite line allows live streaming of highly compressed audio to http://icecast.awi.de. While the recording device is capable of four channels / 192kHz / 24Bit, this cannot be transferred continuously through the WLAN and satellite link, so a multi-stage automatic buffering and selection scheme is implemented to allow for both, continuous coverage and high quality recordings of selected events. About two terabytes per year are automatically streamed into the petabyte data storage of the World Data Centre for Marine Environmental Data, hosted by AWI, where they are analysed and prepared for publishing under an open access license.

2pABb5. Development of a prototype electronic tag for studying the migratory behaviour of marine species. Prajas John (Department of Electronics, Cochin University of Science & Technology, Thrikkakara, 682 022 Ernakulam, India, prajas@cusat.ac.in), Jinto George (Department of Electronics, Cochin University of Science & Technology, Thrikkakara, 682 022 Ernakulam, India, jintokg@cusat.ac.in), Supriya M. Hariharan (Department of Electronics, Cochin University of Science & Technology, Thrikkakara, 682 022 Ernakulam, India, supriya @cusat.ac.in), Saseendran Pillai (Department of Electronics, Cochin University of Science & Technology, Thrikkakara, 682 022 Ernakulam, India, prspillai@cusat.ac.in)

Archival electronic tags can be used as standalone data loggers for sampling the ocean for gathering the environmental parameters and studying the migratory patterns of marine species, identifying their feeding and spawning grounds, etc. A prototype archival electronic tag for monitoring the ocean parameters like temperature, pressure and light intensity has been developed. A digital temperature sensor is used to sample the temperature from the tag's surroundings, while a micro machined piezoresistive silicon digital pressure sensor, which is capable of measuring absolute pressure levels upto 14 bars, provides the depth information. One of the important parameters to be measured is the geolocation of the species, which is computed from the ambient light intensities recorded by the digital light sensor in the tag. These parameters can be sampled and recorded in the memory at preset time intervals, as set at the time of deployment of the tag. This minuaturised tag provides the temperature data with 13 bit resolution, while the pressure and light intensity values have 15 bit resolutions. When used in fisheries studies, the size of the device has to be miniaturised, so that by way of attaching such devices, the normal behaviour of the species remain unaffected.

Session 2pABc

Animal Bioacoustics, Noise, and ECUA: Anthropogenic Noise Effects on Animals II (Poster Session)

Michael Stocker, Cochair
Ocean Conservation Research

Jonathan Gordon, Cochair
Sea Mammal Research Unit

All posters will be on display from 3:40 p.m. to 5:20 p.m. To allow contributors an opportunity to see other posters, contributors of odd-numbered papers will be at their posters from 3:40 p.m. to 4:30 p.m. and contributors of even-numbered papers will be at their posters from 4:30 p.m. to 5:20 p.m.

Contributed Papers

2pABc1. Discovery of Sound in the Sea website: Educational and media resources. Kathleen Vigness Raposa (Marine Acoustics, Inc., 809 Aquidneck Ave., Middletown, RI 02842, USA, kathleen.vigness@marineacoustics.com), Gail Scowcroft (University of Rhode Island, Graduate School of Oceanography, Narragansett, RI 02882, USA, gailscow@gso.uri.edu)

The scientific community and the public have become increasingly aware of, and concerned about, underwater sound. There is growing interest in learning about sources and uses of underwater sound, and potential effects of sound on the marine environment. Underlying this interest, however, is a need to provide scientific information at a level appropriate for the general public and for educational and media professionals that communicate with the public. The ″Discovery of Sound in the Sea″ website (http://www.dosits.org) provides scientific content introducing the physical science of underwater sound and how people and animals use sound to accomplish various tasks. In addition, it has recently been expanded to include three major resource sections: (1) Media Resources, (2) Teacher Resources, and (3) Student Resources. The Media Resources include a Facts & Myths quiz, Frequently Asked Questions, and PDF reprints of a tri-fold pamphlet and a 12-page educational brochure highlighting the content of the website. The Teacher and Student Resources include structured tutorials, educational games, and PowerPoint presentations. These resource sections provide easy, efficient access to timely information on the science of underwater sound and the current state of knowledge of the effects of underwater sound on marine mammals and fishes.

2pABc2. The effects of noise emanating from an adjoining architectural space on beluga whale audition in an aquarium exhibit. Katie Starke (University of Connecticut, 70 Pinney Hill Rd., #95, Willington, CT 06179, USA, kathryn.starke@uconn.edu), Peter Scheifele (University of Cincinnati, French-East 345A, Cincinnati, OH 45221, USA, scheifpr@UCMAIL.UC.EDU)

Aquaria must have regulations regarding the intensity levels of anthropogenic noise that make their way into their captive belugas' tank, thus affecting the animals' ability to hear and vocalize naturally. My research focuses on the sound transmission across the acrylic and cement boundary that separates the beluga tank from the ballroom in the Georgia Aquarium. This ballroom hosts many social events which are often accompanied by high levels of noise that cross the barrier into the animal enclosure. I focus on the intensity range of 90-100dBA and experiment with a variety of frequencies, specifically those that are included in the range of beluga hearing. Though the data will be specific to the Georgia Aquarium, the results will apply to all aquaria that keep beluga whales, as high intensity sound will always travel through the exhibit boundaries and affect the animals living on the other side.

Session 2pABd

Animal Bioacoustics, Underwater Acoustics, Acoustical Oceanography, Signal Processing in Acoustics, and ECUA: Animal Sonar Systems II (Poster Session)

James Simmons, Cochair
Brown University

Michel Andre, Cochair
Laboratori d'Aplicacions Bioacústiques, Universitat Politècnica de Catalunya

All posters will be on display from 3:40 p.m. to 5:20 p.m. To allow contributors an opportunity to see other posters, contributors of odd-numbered papers will be at their posters from 3:40 p.m. to 4:30 p.m. and contributors of even-numbered papers will be at their posters from 4:30 p.m. to 5:20 p.m.

Contributed Paper

2pABd1. An area sensitive to apparent acoustic motion in the auditory cortex of the bat Phyllostomus discolor. Susanne Hoffmann (Biocenter of the Ludwig-Maximilians University of Munich, Großhaderner Str. 2, 82152 Planegg-Martinsried, Germany, hoffmann@zi.biologie.uni-muenchen.de), Uwe Firzlaff (Biocenter of the Ludwig-Maximilians University of Munich, Großhaderner Str. 2, 82152 Planegg-Martinsried, Germany, firzlaff@zi.biologie.uni-muenchen.de), Gerd Schuller (Biocenter of the Ludwig-Maximilians University of Munich, Großhaderner Str. 2, 82152 Planegg-Martinsried, Germany, gschuller@lmu.de)

The processing of apparent acoustic motion was investigated in neurons in the auditory cortex of anaesthetized bats (*Phyllostomus discolor*). Apparent motion in the horizontal plane was generated by presenting pairs of pure tones with different interaural intensity differences (IIDs) and temporal separations, i.e. inter-pulse intervals (IPIs). Thus the spatial extent, motion direction and velocity of motion changed for each stimulus pair. A complete stimulus matrix consisted of 81 IID-combinations in the range between -40 to +40 dB IID and was randomly presented via earphones with ten repetitions for up to five different IPIs (6.25 to 150 ms). Thirty percent (71) of the 236 extracellularly recorded cortical single cells or small neuronal clusters showed facilitatory responses to acoustic motion compared to static stimulation and were classified as motion sensitive. With decreasing IPI, all motion sensitive neurons changed their azimuthal receptive field in size or spatial position. Twenty two percent (15) of them preferred small movements in the frontal area at very short IPIs. Most interestingly, the motion sensitive neurons were almost exclusively (97 %) found in the dorsal area of the caudal part of the auditory cortex indicating that this cortical area is specifically involved in the processing of acoustic motion.

Session 2pAOa

Acoustical Oceanography and ECUA: Marine Ecosystem Acoustics III (Poster Session)

Kenneth Foote, Cochair
Woods Hole Oceanographic Institution

Olav Godoe, Cochair
Institute of Marine Research

All posters will be on display from 3:40 p.m. to 5:20 p.m. To allow contributors an opportunity to see other posters, contributors of odd-numbered papers will be at their posters from 3:40 p.m. to 4:30 p.m. and contributors of even-numbered papers will be at their posters from 4:30 p.m. to 5:20 p.m.

Contributed Papers

2pAOa1. An acoustic finite-element model to study sonar interactions with marine mammals. Gonzalo R. Feijoo (Woods Hole Oceanographic Institution, Woods Hole, MA 02543, USA, gfeijoo@whoi.edu), Kenneth G. Foote (Woods Hole Oceanographic Institution, Woods Hole, MA 02543, USA, kfoote@whoi.edu)

A computer model based on the finite-element method (FEM) is being developed to study the interaction of sonar signals with marine mammals. This model solves the Helmholtz equation in a computational box that includes the animal and the surrounding medium, water. The FEM code has been validated with analytical solutions for scattering of a plane wave by a fluid sphere over a range of parameters and frequencies of interest. The same FEM code has been applied to a 142-cm-long specimen of the common dolphin (*Delphinus delphis*); internal pressure and displacement fields have been computed. The animal is represented in the computer model by a set of tissue groups whose acoustic properties, density and sound speed, are taken from the literature. The geometry of each tissue group was constructed from segmented computerized tomography images. Results are presented for harmonic signals in the 1-10 kHz frequency range. [Work supported by NOPP through ONR award N000140710992.]

2pAOa2. Mid-frequency pelagic imaging multi-beam sonar. Christopher D. Jones (Applied Physics Laboratory, University of Washington, 1013 NE 40th Street, Seattle, WA 98105, USA, cjones@apl.washington.edu)

A unique circular array multi-beam sonar is used to investigate volumetric imaging of pelagic marine environments. Imaging of a radial volume of the ocean up to a kilometer in range and at 8-12kHz will be discussed, focusing mainly on the imaging of large aggregations of fish in shallow water. Several imaging geometries are presented including backscatter imaging in a shallow water waveguide used to resolve the two-dimensional horizontal structure of large fish schools, and the autonomous deployment of the sonar in a fixed location to create a time series of images and observations of variability over a 24 hour period. The potential for new imaging geometries will be explored including vertical profiling to create volumetric images of different pelagic zones in the ocean. Operational issues related to specific scientific question, and signal processing issues related to circular arrays will be discussed. Preliminary field data will be presented.

2pAOa3. Using multi-angle reflections to enhance ecosystem characterization. Jules S. Jaffe (Scripps Institution of Oceanography, Marine Physical Laboratory, 8820 Shellback Way, La Jolla, CA 92093, USA, jules@mpl.ucsd.edu),Olav R. Godo(Institute of Marine Research, PO Box 1870, 5817 Bergen, Norway, olav.rune.godoe@imr.no), Hector Pena (Institute of Marine Research, PO Box 1870, 5817 Bergen, Norway, hector.pena@imr.no), Ben Maurer (Scripps Institution of Oceanography, Marine Physical Laboratory, 8820 Shellback Way, La Jolla, CA 92093, USA, bmaurer@ucsd.edu)

Improved knowledge about target tilt can be used to improve acoustic estimates of abundance and to gain insights into the behavioural patterns of exploited marine species. This is because tilt angle strongly affects backscatter, especially at high frequencies. In order to estimate tilt, a dual-transducer system for synchronous observation of marine organisms at two angles (0o and 9o) at 38 kHz was tested. Data was characterized via the ″angle response″; the area backscatter from one transducer divided by the sum of both. This metric was computed for layers of small planktonic organisms as well as fish. While the angle response is almost negligible for small organisms at night and slightly in favour of the tilted transducer during day, there is a significant angle response from fish in layers. A theoretical model supports the idea that this effect is due swimbladder tilt. Backscatter from 13 schools of horse mackerel was also analyzed. Although no statistically significant difference was observed, the variability indicate that the angle response is highly dynamic and dependent on the actual behaviour of the school at time of observation. Further studies are planned to improve upon data collection as well as the theoretical aspects of interpretation.

2pAOa4. Application of multiple angle acoustic scatter to remote fish classification. Paul L. Roberts (University of California San Diego, Electrical and Computer Engineering Department, 9500 Gilman Dr., La Jolla, CA 92093, USA, plrobert@ucsd.edu), Jules S. Jaffe (Scripps Institution of Oceanography, Marine Physical Laboratory, 8820 Shellback Way, La Jolla, CA 92093, USA, jules@mpl.ucsd.edu)

Observation of broadband acoustic scatter from fish at multiple angles has the potential to offer advantages for remote classification in cases where the species exhibit differences in size and or body shape, and animal orientation is unknown or difficult to estimate. However, the total angular coverage of the observations, available bandwidth, and the inter- and intra-species variability in size can significantly influence classification accuracy. These parameters are investigated using laboratory data collected from ten different fish species using a linear array of receivers and a single transmitter with an effective angular coverage of up to 25 degrees with a 3 degree sampling increment. Results indicate that when the species exhibit significant differences in length, even two observations covering only 10 degrees are sufficient to obtain an 80 percent improvement in classification accuracy over a single observation angle. This holds true for a wide range of animal

orientations. As inter-species size similarity increases, and intra-species size variability increases, more observations covering a larger range of angles are required to maintain a similar improvement in classification accuracy.

2pAOa5. Simultaneous acoustic observations of turbulence and zooplankton. Tetjana Ross (Dalhousie University, Department of Oceanography, 1355 Oxford Street, Halifax, NS B3H 4JI, Canada, tetjana.ross@dal.ca), Isabelle Gaboury (Jasco Research, Suite 432 - 1496 Lower Water Street, Halifax, NS B3J 1R9, Canada, isabelle.gaboury@gmail.com), Rolf Lueck (Rockland Scientific International Inc., 520 Dupplin Road, Victoria, BC V8Z 1C1, Canada, rolf @rocklandscientific.com)

Models and laboratory experiments show that zooplankton may locate food more easily in turbulent waters, but whether plankton seek or avoid turbulence in the ocean is an open question. It is difficult to measure turbulence and plankton simultaneously and with the necessary spatial resolution using traditional methods (nets and airfoil shear sensors). Acoustics is commonly used to survey zooplankton abundance and recent studies have shown that stratified turbulence can also be a significant source of sound scatter. This may seem like more of a complication than a boon for those aiming to use acoustics to observe plankton in turbulence. We present acoustic data, however, that show that at least under certain circumstances, zooplankton and turbulence can be observed simultaneously with a single 307 kHz sounder. The different natures of the two targets (discrete targets versus a volume effect) allow them to be distinguished. The key is sampling the same targets at multiple ranges and having low enough concentrations that there is no more than one animal within the beam at the closest ranges.

2pAOa6. Potential influence of shells on multibeam backscatter imagery within the Te Matuku Marine Reserve, New Zealand. Alexandre C. Schimel (Univ. of Waikato - Coastal Marine Group, Ruakura Satellite Campus, PB3105 Hamilton, New Zealand, alex.schimel@gmail.com), David Johnson (MetOcean Solutions Ltd, 3/17 Nobs Line, PO Box 441 New Plymouth, New Zealand, d.johnson@metocean.co.nz), Terry Healy (Univ. of Waikato - Coastal Marine Group, Ruakura Satellite Campus, PB3105 Hamilton, New Zealand, t.healy@waikato.ac.nz), Peter J. McComb (MetOcean Solutions Ltd, 3/17 Nobs Line, PO Box 441 New Plymouth, New Zealand, p.mccomb@metocean.co.nz), Brett Beamsley (MetOcean Solutions Ltd, 3/17 Nobs Line, PO Box 441 New Plymouth, New Zealand, b.beamsley@metocean.co.nz), Dirk Immenga (Univ. of Waikato - Coastal Marine Group, Ruakura Satellite Campus, PB3105 Hamilton, New Zealand, d.immenga@waikato.ac.nz)

Backscatter imagery from a KONGSBERG EM3000 multibeam echosounder (300kHz) has been analyzed to investigate its potential for benthic habitat mapping. A MATLAB code has been developed to process both bathymetry and coregistered echo-strength, which includes a simple correction to remove the typical multibeam echo strength swathe contrast introduced by the backscatter incident-angle dependence. Although the correction algorithm does completely remove the effect, it is sufficient to generate maps of suitable quality for further analysis. The processing code was applied to a dataset from a survey performed on two sites in the Tamaki Strait, New Zealand, in August 2007, including a section of the Te Matuku marine reserve. Within the marine reserve, a 400m2 area displays a strong reflectivity that contrasts with its surroundings while a past ground-truth data collection shows the full area is dominated by mud with only some differences in shell fragments distribution. Hypotheses to explain the origin of this reflectivity contrast are formulated and verified against past sediment and benthic survey results with emphasis on the potential influence of shells on multibeam backscatter. The potential of multibeam surveying for detecting the coverage of shells patches in benthic habitat mapping is discussed.

2pAOa7. Acoustic methods for water mass delineation in coastal marine ecosystems. John Proni (AOML/NOAA, 4301 Rickenbacker Cswy, Miami, FL 33149, USA, john.proni@noaa.gov), Jack Stamates (AOML/NOAA, 4301 Rickenbacker Cswy, Miami, FL 33149, USA, Jack.Stamates@noaa.gov), Thomas Carsey (AOML/NOAA, 4301 Rickenbacker Cswy, Miami, FL 33149, USA, thomas.p.carsey@noaa.gov), Jia-Zhong Zhang (AOML/NOAA, 4301 Rickenbacker Cswy, Miami, FL 33149, USA, Jia-Zhong.Zhang@noaa.gov), Chris Sinigalliano (AOML/NOAA, 4301 Rickenbacker Cswy, Miami, FL 33149, USA, Christopher.Sinigalliano@noaa.gov), Kevin Sullivan (AOML/NOAA, 4301 Rickenbacker Cswy, Miami, FL 33149, USA, Kevin.Sullivan@noaa .gov)

Acoustical methods play an important role in the in the study of nutrient sources for coral reef ecosystems in the south Florida coastal ocean. Many nutrients released into the coastal ocean are released in distinct water masses such as inlet discharge plumes, wastewater outfall discharge plumes, and hurricane-induced re-suspensions. Using water column acoustic backscatter profiles, obtained via either ship-borne instrumentation or in-situ instrumentation, multidimensional images of nutrient bearing water masses are derived. Said images are of assistance in the design of chemical and biological sampling efforts. Examples of water mass imaging will be presented as well as the use of such images in the design of water quality sampling programs. Using a combination of acoustic backscatter, Doppler current profilers, nutrient (nitrate, nitrite, silica, phosphate, ammonia) samples and microbiological (fecal, protozoa, viruses) samples, flux estimates of said quantities may be made for inlet discharges. Results will be presented for a south Florida inlet having an average net seaward discharge of approximately 200 million gallons per day. Selected acoustic images of treated waste water effluent plumes will be presented and compared with plume spatial distributions inferred from conservative plume tracer studies.

2pAOa8. Acoustic data from platforms of opportunity as fuel for ecosystem models. Nils Olav Handegard (Institute of Marine Research, C. Sundtsgt 64, Nordnes, 5817 Bergen, Norway, nilsolav@imr.no), Olav Rune Godoe (Institute of Marine Research, C. Sundtsgt 64, Nordnes, 5817 Bergen, Norway, olavrune@imr.no), Patrick Lehodey (Collecte Localisation Satellites, 8-10, rue Hermès, Parc Technologique du Canal, 31520 Ramonville Saint-Agne, France, plehodey@cls.fr)

Echo sounders are a widely used tool for observing marine ecosystems. Traditionally, rigid designed surveys are used to integrate biomass to a global estimate, which is coupled to traditional stock assessment models. More recently, the focus has shifted from single species assessment to an ecosystem approach, taking into account ecosystem function and dynamics. As a response, several ecosystem models have been developed. The data requirements for these models are different than for the traditional models, and new sensors and platforms have been developed as a response to this need. However, examples on how to integrate these observations with these new models are scarce. We propose a state-space observation-space approach, and compare the results from a vertically structured eco-system model with observations from an echo sounder positioned at the Mid Atlantic ridge. We argue that this approach is less vulnerable to assumptions in the data analysis process, and discuss adequate observations regimes for these models.

Session 2pAOb

Acoustical Oceanography and ECUA: Acoustical Oceanography of Polar Environments II (Poster Session)

Peter N. Mikhalevsky, Cochair
Science Applications International Corporation

Hanne Sagen, Cochair
Nansen Environmental and Remote Sensing Center

All posters will be on display from 3:40 p.m. to 5:20 p.m. To allow contributors an opportunity to see other posters, contributors of odd-numbered papers will be at their posters from 3:40 p.m. to 4:30 p.m. and contributors of even-numbered papers will be at their posters from 4:30 p.m. to 5:20 p.m.

Contributed Papers

2pAOb1. The factors that influence the design of an underwater acoustic modem for Arctic missions. Andrew M. Smerdon (Aquatec Group Ltd, High Street, RG27 8NY Hartley Wintney, UK, asmerdon@aquatecgroup.com)

As summer Arctic sea ice cover continues to reduce, there is a growing need to monitor the ice-ocean interface to aid in understanding and quantifying Arctic climate change. As part of the DAMOCLES EU 6th Framework programme, several subsea elements of a new Arctic Ocean observing system will be deployed in the Arctic Ocean during 2008. To ensure that the observing system is effective, it is essential that measured data from the ocean environment be delivered in a timely fashion for assimilation with data sets from the ice surface and atmosphere. As several of the observing platforms are drifting freely in the water below the ice, there is a need to communicate data to the surface using underwater acoustic techniques. We discuss the factors that influence the specification of an acoustic modem to achieve this data transfer. These include development of standards for data transfer and storage processes, standby power considerations, logistics of establishing a communication link, and under-ice acoustics.

2pAOb2. High-frequency broadband acoustic scattering for investigating double- diffusive convection. Tetjana Ross (Dalhousie University, Department of Oceanography, 1355 Oxford Street, Halifax, NS B3H 4JI, Canada, tetjana.ross@dal.ca), Andone Lavery (Woods Hole Oceanographic Institution, Applied Ocean Physics & Engineering Department, 98 Water Street, MS #11, Woods Hole, MA 02543, USA, alavery@whoi.edu)

Polar regions, with their supercooled and relatively fresh surface water, are highly susceptible to the diffusive regime of double-diffusive convection (DDDC). The fluxes associated with DDDC can play a significant role in their heat/buoyancy budgets. The use of high-frequency acoustics as a tool to map the extent and evolution of DDDC in the ocean is explored through a series of laboratory 200-300 kHz broadband acoustic backscattering measurements. Pulse compression signal processing allows centimeter-scale interface thicknesses to be rapidly and remotely measured, and the evolution, and ultimate merging, of multiple centimeter-scale interfaces to be observed. Combining the acoustically measured interface thicknesses with knowledge of the relatively-constant temperatures within the surrounding layers allows the estimation of DDDC fluxes. Thus, broadband acoustics offers a rapid and remote method to infer fluxes, without the need for time-consuming microstructure measurements, suggesting that this technique could benefit field studies of DDDC. Using simple models to extrapolate to the thermohaline steps typically found associated with DDDC in polar regions, diffusive-convection interfaces are predicted to scatter at measurable levels in many areas. Narrowband (120 and 200 kHz) acoustic backscattering observations of two scattering layers in the Western Antarctic Peninsula support this prediction.

2pAOb3. Acoustic contributions to marine ecosystem studies. Andrzej J. Orlowski (Sea Fisheries Institute in Gdynia, Kollataja 1, 81-332 Gdynia, Poland, orlov@mir.gdynia.pl)

Since the early 1970s, acoustic data collected in a form of calibrated measurements of integrated echo energy have been applied by the Sea Fishery Institute in Gdynia to observe the relationships among fish distribution and marine environment. Measurements were collected primarily with scientific echo sounders operating at 38kHz, 24h a day, and stored in the form of standardized intervals of sailed distance and depth for comparison with values of selected environmental parameters, measured concurrently. Acoustic, biological, and hydrological data were transferred to the complex data base, enabling spatial correlation and four-dimensional analyses of relationships characterising a wide range of the marine organism behaviour. Selected methods and standards of comparison are described to explain how to improve the recognition of relationships between three-dimensional spatial environmental gradients and fish distribution. Results of several case studies, including the influence of hydrologic and seabed characteristics, illustrate the practical application and validity of the methods. Particular attention is given to indicators of the dependence of local fish biomass density on temperature structure in the sea and diel cycles of fish behaviour. Animations of time-dependent processes, modelled on the collected data, will be included as a new tool for marine ecosystem analysis.

2pAOb4. Estimation of macrophytes using single-beam and multibeam echosounding for environmental monitoring of arctic fjords (Kongsfjord, West Svalbard Island). Aleksandra Kruss (Institute of Oceanology Polish Academy of Sciences, Powstancow Warszawy 55, 81-712 Sopot, Poland, kruss@iopan.gda.pl), Philippe Blondel (University of Bath, Department of Physics, Claverton Down, BA2 7AY Bath, UK, pyspb@bath.ac.uk), Jaroslaw Tegowski (Institute of Oceanology Polish Academy of Sciences, Powstancow Warszawy 55, 81-712 Sopot, Poland, tegowski@iopan.gda.pl), Jozef Wiktor (Institute of Oceanology Polish Academy of Sciences, Powstancow Warszawy 55, 81-712 Sopot, Poland, wiktor@iopan.gda.pl), Agnieszka Tatarek (Institute of Oceanology Polish Academy of Sciences, Powstancow Warszawy 55, 81-712 Sopot, Poland, derianna@iopan.gda.pl)

This paper presents results of a study on the spatial distribution and biomass of macrophytobentos in a fjord of Arctic Svalbard. Kongsfjord represents a periglacial environment with intense morphodynamic processes and rapidly progressing changes in the biotic environment, making it one of the most promising areas to research climate impact on ecosystems. The main objective was to provide an acoustic tool for the evaluation of benthic habitats. The 2007 field survey included systematic, co-registered, single-beam and multibeam echosounder measurements. Acoustic observations were verified by biological samplings and observations for the classification

algorithm development and verification. Analyses of acoustic signals scattered on bottoms covered by algae indicate the good quality of the data recorded, providing a map of phytobenthos distribution and biomass estimation in Kongsfjord. The algorithms designed and tested for processing single- and multibeam data allow extracting the morphological forms of the bottom and determine the areas covered by algae. This survey was the first instance where a multibeam imager was used to map macrophytes in an Arctic environment, in a wide variety of depths and ranges. Comparing the two types of echosounders was a great opportunity to understand the visualisation of macrophytes by multibeam systems and their identification.

TUESDAY AFTERNOON, 1 JULY 2008 P3-C, LEVEL 3, 3:40 TO 5:20 P.M.

Session 2pAOc

Acoustical Oceanography, Underwater Acoustics, Signal Processing in Acoustics, and ECUA: Geoacoustic Characterization of the Ocean Bottom and Geoacoustic Inversion II (Poster Session)

Peter Gerstoft, Cochair
Marine Physical Laboratory, Scripps Institute of Oceanography

Dag Tollefsen, Cochair
Norwegian Defence Research Establishment (FFI)

All posters will be on display from 3:40 p.m. to 5:20 p.m. To allow contributors an opportunity to see other posters, contributors of odd-numbered papers will be at their posters from 3:40 p.m. to 4:30 p.m. and contributors of even-numbered papers will be at their posters from 4:30 p.m. to 5:20 p.m.

Contributed Papers

2pAOc1. Extracting Green's functions from noise correlation of SW06 data. Laura Brooks (Marine Physical Laboratory, Scripps Institute of Oceanography, 8602 La Jolla Shores Drive, La Jolla, CA 92093-0238, USA, lbrook02@gmail.com), Peter Gerstoft (Marine Physical Laboratory, Scripps Institute of Oceanography, 8602 La Jolla Shores Drive, La Jolla, CA 92093-0238, USA, gerstoft@ucsd.edu)

Ambient noise was recorded on an L-shaped array during the SW06 (Shallow Water 2006) sea trials. The data were cross-correlated in order to approximate the Green's function, and subsequently the acoustic travel time, between hydrophone pairs. Examination of the individual noise spectra and their mutual coherence revealed that the coherently propagating noise is dominated by frequencies less than 100 Hz. Both time and frequency domain preprocessing techniques, and their effect upon the resulting correlation, were investigated. Times corresponding to the envelope peak of the noise cross-correlation time-derivative are in agreement with both the expected direct, and surface reflected, inter-hydrophone travel times.

2pAOc2. Single parameter description of seafloors for shallow oceans. Adrian D. Jones (Defence Science and Technology Organisation, P.O Box 1500, 5111 Edinburgh, Australia, bearjones@chariot.net.au), Graham J. Day (Defence Science and Technology Organisation, P.O Box 1500, 5111 Edinburgh, Australia, Graham.Day@dsto.defence.gov.au), Paul A. Clarke (Defence Science and Technology Organisation, P.O Box 1500, 5111 Edinburgh, Australia, Paul.Clarke@dsto.defence.gov.au)

For a shallow ocean, sound transmission beyond short range is dominated by seafloor interactions at small grazing angles, for which the loss in dB on each bottom reflection may be approximated by a function F dB/radian which is linear with grazing angle. Acoustic inversion techniques have been shown to be able to obtain the value of F for a particular frequency. The suitability of this single parameter F as a seafloor descriptor has now been studied for an extensive range of seafloor types. It is shown that the phase-incoherent transmission loss (TL) obtained using the parameter F is not greatly different to TL predicted using complete knowledge of a particular seafloor, for a shallow ocean. Further, if the phase angle for a seafloor reflection is linked to the parameter F via a simple approximation, the phase-coherent properties of the shallow water interference field may be estimated to an accuracy which is surprising. This paper reviews the relevant theory and presents comparisons between TL predicted using full geoacoustic parameters versus TL based on the single parameter, for both uniform half-space and layered seafloor types.

2pAOc3. On some possibilities and properties of matched-field geoacoustic inversion in shallow water. Alexander Zharikov (M.V. Lomonosov Moscow State University, Faculty of Physics, Alexander Zharikov, ul. Simonovskiy val 14, kv. 58, 115088 Moscow, Russian Federation, alexandr-j@yandex.ru), Pavel Kravchun (Moscow State University, Faculty of Physics, Department of Acoustics, Box 15, 125130 Moscow, Russian Federation, gedackt@mail.ru)

The aim of this paper is to estimate possibilities of matched-field geoacoustic inversion (MFI) in shallow water, and to recommend optimal arrangements of signal source and hydrophone array in variety of particular environments. We assumed ocean to be range independent with bottom consisting of homogeneous liquid layers. Sound fields were calculated as superposition of normal modes and continuous spectrum for tonal point source and vertical line array. MFI based on Bartlett processor was used. Possibilities of MFI were characterized by MFI penetration depth, sensitivity to various bottom parameters and non-uniqueness of inverted data. These characteristics were analysed as functions of frequency and the source depth and range for different values of sound attenuation in sediments and for various sound-speed profiles. To estimate possibilities of MFI in real ocean conditions, influence of array tilt and inadequacy of geoacoustic model were analysed. The influence of continuous spectrum was also discussed. Among the major results, optimal source ranges corresponding to the maximum penetration depth of MFI were calculated, and high influence of attenuation in sediments on possibilities of MFI was revealed.

2pAOc4. A mixin algorithm for geoacoustic inversion. Hefeng Dong (Dept. of Electron. & Teleco., Norwegian Univ. of Science and Technology, NO-7491 Trondheim, Norway, dong@iet.ntnu.no), Arne Johannes

Jenssen(Norwegian Defense Research Establishment, NO-3191 Horten, Norway, Arne-Johannes.Jenssen@ffi.no)

Shear wave velocities in the sediment can be inverted by using the dispersion curves of interface wave. It can be done by use of an algorithm based on singular value decomposition (SVD). This method can only invert the shear wave velocities and requires knowledge of the thicknesses and densities of the sediment layers. This paper presents a new algorithm for inversion of geoacoustic parameters based on dispersion curves that we have coined ″mixin inversion″. Mixin inversion combines SVD and global search using genetic algorithm (GA). The GA searches the depths and densities by doing a shear wave velocity inversion with SVD for each of its parameter values. This algorithm can be applied on cases where the depths, densities and shear wave velocities of the sediments are unknown. The advantage is that it is faster than pure GA since the search space is much smaller and it can be applied on cases where pure SVD inversion fails because necessary information about depths and densities is not known.

TUESDAY AFTERNOON, 1 JULY 2008 ROOM 352B, 2:40 TO 7:00 P.M.

Session 2pBBa

Biomedical Ultrasound/Bioresponse to Vibration: Ultrasound Contrast Agents for Therapy I

Tyrone Porter, Cochair
Boston University, 110 Cummington Street, Boston, MA 02215, USA

Eleanor Stride, Cochair
University College London, Department of Mechanical Engineering, Torrington Place, London, WC1E 7JE, UK

Invited Papers

2:40

2pBBa1. Acceleration of ultrasonic tissue heating by microbubble agent. Shin-Ichiro Umemura (Tohoku University, Aoba 6-6-05, Aramaki, Aoba-ku, 980-8579 Sendai, Japan, sumemura@ecei.tohoku.ac.jp), Shin Yoshizawa (Tohoku University, Aoba 6-6-05, Aramaki, Aoba-ku, 980-8579 Sendai, Japan, syoshi@ecei.tohoku.ac.jp), Kazuaki Sasaki (Tokyo University of Agriculture and Technology, 3-5-8 Saiwai-cho, Fuchu, 183-0054 Tokyo, Japan, skazuaki@cc.tuat.ac.jp), Ken-Ichi Kawabata (Hitachi Central Research Laboratory, 1-280, Higashi-Koigakubo, Kokubunji, 185-8601 Tokyo, Japan, kenichi.kawabata.ap@hitachi.com)

Ultrasound in the existence of microbubbles, whether they have been generated by acoustic cavitation or administered into the body, is known to induce bioeffects normally through mechanical or sonochemical mechanisms. Recently, it is reported that ultrasonic tissue heating can be accelerated several times by an administered microbubble agent. A microbubble, subjected to ultrasonic pressurein the frequency range of its resonanance converts the acoustic energy to heat through its volume oscillation. The acoustic power converted to heat by a microbubble through viscous heating was numerically calculated, and it was predicted that tissue ultrasonic absorption would be doubled if a microbubble agent is delivered to the tissue at a concentration in the order of 100 microbubbles /mg. Exteriorized murine kidneys were exposed to focused ultrasound at 3.2 MHz in degassed saline and the tissue temperature change was measured. Optison at a dose of 0.2 ml /kg multiplied the temperature elevation induced by ultrasonic exposure by several times. In order to use this effect to treat a deep-seated tumor, microbubbles should be somehow delivered to the tumor selectively. A novel method of selective delivery, in which nano liquid particles are administered and converted into microbubbles by ultrasonic stimulation, will also be discussed.

3:00

2pBBa2. Ultrasound contrast agents pushing drug delivery: high speed optical observations. Annemieke Van Wamel (Erasmus MC, Dr Molewaterplein 50 room Ee2302, 3015GE Rotterdam, Netherlands, Annemieke@ieee.org), Klazina Kooiman (Erasmus MC, Dr Molewaterplein 50 room Ee2302, 3015GE Rotterdam, Netherlands, k.kooiman@erasmusmc.nl), Nico De Jong (Erasmus MC, Dr Molewaterplein 50 room Ee2302, 3015GE Rotterdam, Netherlands, n.dejong@erasmusmc.nl)

Ultrasound-activated-microbubbles can cause transient non-lethal sonoporation of cells. Studies of influx of cell-membrane impermeable-dye, genetic materials, and nanoparticles have confirmed that the action of ultrasound-microbubbles on the cell-membrane is to alter both the cell-permeability. The sonoporation action of ultrasound-contrast-agent on cells lies in the fact that microbubbles oscillate while irradiated with ultrasound resulting in a mechanical-deformation of the cells. Oscillation microbubbles nearby cells have been optically recorded using a microscope and a high-speed camera. This camera is able to record the MHz oscillation microbubbles and therefore the interaction between oscillation microbubbles and cells. Micro-mechanical forces generated by the oscillating microbubble may also be used to locally 'push' the drugs into the cells. Ultrasound-activated-microbubbles are able to transiently increase the vascular-endothelial-layer permeability. These features may be used for future ultrasound-guided drug-delivery-systems. Next to increasing the drugs internalization, microbubbles can also be used as drug/particle carrier. Drug-loaded contrast-agents can be intentionally ruptured by diagnostic ultrasound. Using microbubbles to carry drugs to targets sites and rupturing the microbubbles by localized ultrasound energy, will result in a high local concentration of drugs. High-speed-optical-recordings of ultrasound-contrast-agent induced cell and vascular-endothelial-layer permeability will be demonstrated. Furthermore, recordings of ultrasound-controlled drug-delivery using pay-loaded ultrasound-contrast-agents will be shown.

3:20

2pBBa3. Characterization and Optimization of Ultrasound-induced Molecular Delivery In Vivo. Elisa Konofagou (Dept. of Biomedical Engineering, Columbia Univ., 351 Engineering Terrace MC 8904, 1210 Amsterdam Ave., New York, NY 10027, USA, ek2191@columbia.edu), James Choi (Dept. of Biomedical Engineering, Columbia Univ., 351 Engineering Terrace MC 8904, 1210 Amsterdam Ave., New York, NY 10027, USA, jjc2132@columbia.edu), Shougang Wang (Dept. of Biomedical Engineering, Columbia Univ., 351 Engineering Terrace MC 8904, 1210 Amsterdam Ave., New York, NY 10027, USA, sw2401@columbia.edu), Barclay Morrison (Dept. of Biomedical Engineering, Columbia Univ., 351 Engineering Terrace MC 8904, 1210 Amsterdam Ave., New York, NY 10027, USA, bm2119@columbia.edu), Mark Borden (Dept. of Biomedical Engineering, Columbia Univ., 351 Engineering Terrace MC 8904, 1210 Amsterdam Ave., New York, NY 10027, USA, mb2910@columbia.edu)

Current treatments of neurological and neurodegenerative diseases are limited due to the lack of a truly noninvasive, transient, and regionally selective brain drug delivery method. The brain is particularly difficult to deliver drugs to because of the blood-brain barrier (BBB). Over the past few years, we have been developing methods that combine Focused Ultrasound (FUS) and microbubbles in order to noninvasively, locally and transiently open the BBB so as to treat neurodegenerative diseases. In this paper, we will focus on the characterization of the type of molecular delivery that can be induced through the opened BBB. More specifically, we willl characterize important properties of the BBB opening such as its size and permeability using fluorescence and MR imaging techniques, respectively. The role of the microbubble type, size and concentration on the BBB diffusion properties, its reversibility and the pressure threshold for the opening will also be described in vivo. Finally, results will be shown in both non-transgenic (normal) and transgenic (Alzheimer's) mice in order to determine the variability of the properties of the opened BBB in the presence and absence of disease.

3:40-5:20 Posters

Lecture sessions will recess for presentation of poster papers on various topics in acoustics. See poster sessions for topics and abstracts.

Invited Papers

5:20

2pBBa4. Echogenic liposomes for vasoactive gas delivery and inhibition of intima hyperplasia in atheroproliferative disease. Huang Shaoling Huang (MSB 1.246, 6431 Fannin St., Houston, TX 77030, USA, Shaoling.Huang@uth.tmc.edu), David D. McPherson (University of Texas Health Science Center, 6431 Fannin St., MSB 1.252, Houston, TX 77030, USA, David.D.McPherson@uth.tmc.edu), Christy K. Holland (University of Cincinnati, Biomedical Engineering, MSB, 231 Albert Sabin Way, Cincinnati, OH 45267-0586, USA, Christy.Holland@uc.edu)

Our group has developed targeted echogenic liposomes (ELIP) for targeted ultrasound enhancement of atheroma as well as targeted therapeutic delivery. Nitric oxide (NO) has potent biological activities but is too labile for in-vivo vascular delivery. We have developed a methodology to entrap NO, cause local prolonged release and retain NO effect. NO-loaded ELIP were injected into the common carotid artery after balloon injury. Fourteen days later, the carotids were removed. Administration of NO-ELIP resulted in $51 \pm 6\%$ inhibition of intimal thickening when compared with controls. Using a 6.0 MHz clinical Doppler diagnostic ultrasound system, we (Smith et al) have identified the optimal pressure threshold (MI 0.08) for NO diffusion from ELIP. Using these parameters we have enhanced vascular permeability of drugs and stem cells to help stabilize atherosclerotic plaques. We have developed a novel method for encapsulating NO into ELIP demonstrating their capacity for NO delivery, inhibition of intimal hyperplasia and controlled gas diffusion with ultrasound. This methodology provides a new approach for delivering a variety of bioactive gases to target tissues, which otherwise would have negligible effects when administered systemically.

5:40

2pBBa5. Echogenic liposomes for molecular targeted therapeutic delivery. David D. McPherson (University of Texas Health Science Center, 6431 Fannin St., MSB 1.252, Houston, TX 77030, USA, David.D.McPherson@uth.tmc.edu), Shaoling Huang (University of Texas Health Science Center, 6431 Fannin St., MSB 1.252, Houston, TX 77030, USA, Shaoling.Huang@uth.tmc.edu), Christy K. Holland (University of Cincinnati, Biomedical Engineering, MSB, 231 Albert Sabin Way, Cincinnati, OH 45267-0586, USA, Christy.Holland@uc.edu)

Our group has developed targeted echogenic liposomes (ELIP) that can entrap therapeutics and release them at the target site. A key therapeutic is t-PA (tissue plasminogen activator). We have demonstrated entrapment and release following ultrasound application with t-PA effect on clot dissolution. We have demonstrated that t-PA can act as a targeting agent. Thus this drug can be both a targeting agent and a lytic agent minimizing the development of complicated formulations required for targeting and lysis. We have entrapped glitazones and demonstrated release following ultrasound application with drug effect by suppressing vascular hyperplasia. We have demonstrated that ultrasound with our ELIP can enhance delivery of agents into all areas of the atheroma, including the intima, media, the loose and dense adventitia. Heretofore these regions close to the arterial media have been impenetrable using standard intravenous drug therapy. These projects are helping to develop our echogenic immunoliposomes to; optimize targeted contrast delivery into vascular beds that are poorly penetrable by standard imaging agents; and optimize local release and concentration of therapeutics at the site of interest. This will ultimately help to direct therapeutic delivery, increase local effect, while minimizing the systemic effects of drugs and genes.

6:00

2pBBa6. Enhancement of microbubble mediated gene delivery by simultaneous exposure to ultrasonic and magnetic fields. Eleanor Stride (University College London, Department of Mechanical Engineering, Torrington Place, WC1E 7JE London, UK, e_stride@meng.ucl.ac.uk), Colin Porter (The Institute of Cancer Research, Gene Therapy Group, Section of Cell and Molecular Biology, 237 Fulham Road, SW3 6JB London, UK, colin.porter@icr.ac.uk), Ana-Garcia Prieto (University College London, London Centre for Nanotechnology, 17-19 Gordon Street, WC1H 0AH London, UK, a.prieto@ucl.ac.uk), Quentin Pankhurst (University College London, London Centre for Nanotechnology, 17-19 Gordon Street, WC1H 0AH London, UK, q.pankhurst@ucl.ac.uk)

It has been shown in previous studies that ultrasound mediated gene delivery can be greatly enhanced by the presence of contrast agent microbubbles and that transfection efficiency is highly dependent upon both bubble/cell separation and the ultrasound field parameters. It has also been shown that gene delivery can be promoted by exposing cells to a magnetic field in the presence of DNA conjugated to magnetic nanoparticles. The aim of this work was to investigate whether it was possible to combine the advantages of both these techniques. It was found that transfection of Chinese hamster ovary cells by naked plasmid DNA was enhanced by simultaneous exposure to ultrasound (40-cycle sinusoidal pulses, centre frequency 0.5-3MHz, peak negative pressure 0.25-1.5MPa, repetition frequency 1kHz for 10s) and a uniform magnetic field (3-5Nm-3) in the presence of two different microbubble/nanoparticle preparations. The first consisted of phospholipid-coated microbubbles mixed with micelles containing magnetic nanoparticles; the second of microbubbles which were themselves magnetically active. These preparations were found to be much more effective than either magnetic micelles or phospholipid-coated microbubbles alone. The mechanisms underlying these observations in terms of microbubble dynamics, the sensitivity to the ultrasound parameters and their significance for potential therapeutic applications will be discussed.

6:20

2pBBa7. Acoustic properties of multifunctional nano/microbubbles used in ultrasonography and ultrasound-mediated chemotherapy. Natalia Rapoport (University of Utah, 72 S. Central Campus Dr. room 2646, Department of Bioengineering, Salt Lake City, UT 84112, USA, natasha.rapoport@utah.edu), Kwon-Ho Nam (University of Utah, 72 S. Central Campus Dr. room 2646, Department of Bioengineering, Salt Lake City, UT 84112, USA, kwonho@gmail.com), Zhonggao Gao (University of Utah, 72 S. Central Campus Dr. room 2646, Department of Bioengineering, Salt Lake City, UT 84112, USA, zggao@yahoo.com), Douglas A. Cristensen (University of Utah, 72 S. Central Campus Dr. room 2646, Department of Bioengineering, Salt Lake City, UT 84112, USA, christen@ee.utah.edu), Anne M. Kennedy (University of Utah, 72 S. Central Campus Dr. room 2646, Department of Bioengineering, Salt Lake City, UT 84112, USA, Anne.Kennedy@hsc.utah.edu)

Multifunctional nano/microbubbles were developed that combine properties of drug carriers, ultrasound imaging contrast agents, and enhancers of ultrasound-mediated drug delivery. At room temperature, the formulations comprised perfluoropentane (PFP) nanodroplets stabilized by biodegradable diblock copolymers. The nanodroplets converted into nano/microbubbles upon heating or ultrasound irradiation. The acoustic properties of the droplets and corresponding bubbles depended on the type of the bubble stabilizing copolymer. Two different copolymers were tested, poly(ethylene oxide)-co-poly(L-lactide) (PEG-PLLA) and poly(ethylene oxide)-co-polycaprolactone (PEG-PCL). For the same quantitative composition, the PEG-PLLA-stabilized bubbles demonstrated higher inertial cavitation threshold and coalescence propensity than PEG-PCL-stabilized bubbles. Nanobubble tendency to coalescence is advantageous for using PEG-PLLA bubbles as tumor-targeted contrast agents.On the other hand, a lower cavitation threshold for PEG-PCL-stabilized bubbles is useful for ultrasound-mediated drug delivery. The drug doxorubicin (DOX) was localized in the bubble walls; it was released from the bubbles in response to sonication by therapeutic ultrasound, which resulted in a significant degree of drug tumor-targeting and effective tumor chemotherapy.

6:40

2pBBa8. Trans-blood-brain barrier delivery of compounds at pharmacologically relevant molecular weights in the hippocampus of mice using Focused Ultrasound. James Choi (Dept. of Biomedical Engineering, Columbia Univ., 351 Engineering Terrace MC 8904, 1210 Amsterdam Ave., New York, NY 10027, USA, jjc2132@columbia.edu), Shougang Wang (Dept. of Biomedical Engineering, Columbia Univ., 351 Engineering Terrace MC 8904, 1210 Amsterdam Ave., New York, NY 10027, USA, sw2401@columbia.edu), Yao-Sheng Tung (Dept. of Biomedical Engineering, Columbia Univ., 351 Engineering Terrace MC 8904, 1210 Amsterdam Ave., New York, NY 10027, USA, yt2235@columbia.edu), Barclay Morrison (Dept. of Biomedical Engineering, Columbia Univ., 351 Engineering Terrace MC 8904, 1210 Amsterdam Ave., New York, NY 10027, USA, bm2119@columbia.edu), Elisa Konofagou (Dept. of Biomedical Engineering, Columbia Univ., 351 Engineering Terrace MC 8904, 1210 Amsterdam Ave., New York, NY 10027, USA, ek2191@columbia.edu)

Molecular engineering has recently contributed immensely to the development of neuropharmaceuticals. However, most of these compounds are greater than 400 Da, which are too large to traverse the brain's natural defense, the blood-brain barrier (BBB). In this study, molecular delivery at pharmacologically relevant molecular weights through a Focused Ultrasound (FUS) induced BBB opening was investigated. The left hippocampus of mice (n=13) was sonicated (frequency: 1.525MHz, pressure: 0.64MPa, duty cycle: 20%, duration: 1-min) in vivo through the intact skin and skull following intravenous injection of microbubbles (SonoVue®; 25μl). After sonication, otherwise BBB-impermeable fluorescent-tagged dextrans at various molecular weights were administered intravenously. Ex vivo fluorescent microscopy determined BBB opening by a significant increase in fluorescence in the left over the right hippocampus. The threshold for the molecular weights allowed through the hippocampal BBB was between 70k and 2,000k Da. Smaller compounds (i.e., 3k Da) were more spatially uniformly deposited throughout the hippocampus than larger (i.e., 70k Da) compounds. In conclusion, dextrans at neuropharmaceutically-relevant sizes were deposited in the left hippocampus of mice. This study thus demonstrates that FUS-induced BBB opening could allow neuropharmaceuticals previously impermeable to the BBB, such as inhibitors and antibodies, to target tissue they were designed to treat.

Session 2pBBb

Biomedical Ultrasound/Bioresponse to Vibration: Ultrasound Contrast Agents for Therapy II (Poster Session)

Tyrone Porter, Cochair
Boston University

Eleanor Stride, Cochair
University College London, Department of Mechanical Engineering, Torrington Place, London WC/E 7JE, UK

All posters will be on display from 3:40 p.m. to 5:20 p.m. To allow contributors an opportunity to see other posters, contributors of odd-numbered papers will be at their posters from 3:40 p.m. to 4:30 p.m. and contributors of even-numbered papers will be at their posters from 4:30 p.m. to 5:20 p.m.

Contributed Papers

2pBBb1. Comparison of Spectral and Temporal Criteria for Inertial Cavitation Collapse. Mathieu Santin (Laboratoire d'Imagerie Paramétrique, 15 rue de l'Ecole de Médecine, 75006 Paris, France, santin@lip.bhdc.jussieu.fr), Alexander Haak (University of Illinois at Urbana-Champaign, Beckman Institute, 405 N Mathews, Urbana, IL 61801, USA, ahaak@uiuc.edu), Lori Bridal (Laboratoire d'Imagerie Paramétrique, 15 rue de l'Ecole de Médecine, 75006 Paris, France, bridal@lip.bhdc.jussieu.fr), William D. O'Brien, Jr. (University of Illinois at Urbana-Champaign, Beckman Institute, 405 N Mathews, Urbana, IL 61801, USA, wdo@uiuc.edu)

Dilute solutions of Optison and Definity were studied using a passive cavitation detector (PCD) with a 2.8-MHz transmitter and 13-MHz receiver. The dilution was such that each received signal should, on average, arise from a single microbubble. Several hundred microbubble responses were acquired at each of three rarefactional pressures (1.6+/-0.2, 2.0+/0.2 and 2.4+/-0.2 MPa). Each microbubble response was grouped with signals presenting post-excitation emissions (100% Inertial Cavitation-Collapse) or those with no evidence of post-excitation emission (0% IC-Collapse). For each incident pressure, we compared discrimination of 100% and 0% IC-Collapse groups with peak-voltage, broadband noise (12-17.6 MHz) and power at the fundamental, 2^{nd}, 3^{rd}, and 4^{th} harmonic peaks. In addition to increased peak-voltage and broadband noise, spectra from 100% IC-Collapse groups consistently presented increased 2^{nd}, 3^{rd} and 4^{th} harmonics compared to the 0% IC-Collapse group. Throughout the studied pressure range, best separation between 0% and 100% IC-Collapse groups was obtained with peak-voltage (4.7+/-1.8dB), broadband noise (4.4+/-1.8dB) and 4^{th} harmonic (5.6+/-2.2dB) for Optison. For Definity, all harmonics (2^{nd} to 4^{th}) increased strongly for the 100% IC-Collapse group (on the order of 6 dB) as well as peak-voltage (5.3+/-1.2dB) and broadband noise (5.8+/-2dB). Results should contribute to relating PCD criteria and IC activity.

2pBBb2. Extraction of green fluorescent proteins with sonoporation. Kadija Kaddur (INSERM U930, 2, Bvd Tonnelle, 37044 Tours Cedex 9, France, kadija.kaddur@etu.univ-tours.fr), Anthony Delalande (CNRS-UPR4301, Centre de Biophysique Moléculaire, 45071 Orléans Cedex 2, France, anthony.delalande@cnrs-orleans.fr), François Tranquart (INSERM U930, 2, Bvd Tonnelle, 37044 Tours Cedex 9, France, tranquart@med.univ-tours.fr), Patrick Midoux (CNRS-UPR4301, Centre de Biophysique Moléculaire, 45071 Orléans Cedex 2, France, patrick.midoux@cnrs-orleans.fr), Chantal Pichon (CNRS-UPR4301, Centre de Biophysique Moléculaire, 45071 Orléans Cedex 2, France, pichon@cnrs-orleans.fr),Ayache Bouakaz(INSERM U930, 2, Bvd Tonnelle, 37044 Tours Cedex 9, France, bouakaz@med.univ-tours.fr)

The mechanism of permeabilization with sonoporation is not understood but the recurrent hypothesis assumes the formation of pores in the cell membrane. The aim of our study is to comfort this assumption by investigating whether ultrasound (US) and microbubbles could also facilitate outward transport of molecules across the plasma membrane through these probable pore formations. Stably transfected Hela-GFP cells were used and insonified with a 1 MHz unfocused transducer in presence of BR14 microbubbles (Bracco Research, Geneva) at different acoustic parameters. The percentage of Hela-GFP cells and the mean cell fluorescence intensity (FI) were measured by flow cytometry to evaluate the GFP release. While US alone did not affect the cells, the addition of BR14 microbubbles induced a significant decrease of FI and the percentage of Hela-GFP cells. A reduction of more than 50% of FI and GFP + cells was achieved between 400-600 kPa and 40-75 % of duty cycle during 2 minutes insonation. However a progressive recovery of Hela-GFP cells percentage and FI post-insonation has been observed which indicates a viable situation of Hela-GFP permeabilized cells allowing a restoration of GFP cell content. These results comfort pore formation hypothesis allowing transmembrane transport following molecular concentration gradient.

2pBBb3. Blood-brain barrier disruption using a diagnostic scanner and Definity in mice. Kristin Frinkley (Biomedical Engineering, Duke Univ., 136 Hudson Hall, Durham, NC 27708, USA, kdf2@duke.edu), Gabriel Howles-Banerji (Center for In Vivo Microscopy, Duke Univ., 141D Bryan Res Bldg., Durham, NC 27710, USA, gabriel.howles@duke.edu), Yi Qi (Center for In Vivo Microscopy, Duke Univ., 141D Bryan Res Bldg., Durham, NC 27710, USA, yi.qi@duke.edu) , G. Allan Johnson (Center for In Vivo Microscopy, Duke Univ., 141D Bryan Res Bldg., Durham, NC 27710, USA, gaj@orion.duhs .duke.edu), Kathryn Nightingale (Biomedical Engineering, Duke Univ., 136 Hudson Hall, Durham, NC 27708, USA, kathy.nightingale@duke.edu)

Objective: To quantify localized disruption of the blood-brain barrier (BBB) in a murine model using focused, diagnostic ultrasound (at higher frequencies than previously studied) and contrast agent and to explore the optimal parameters for opening without causing irreversible damage. Methods: Definity (US contrast) and Magnevist (MR contrast) were injected before a custom ultrasound transmission sequence. The volume of tissue over which the BBB disruption allowed Magnevist to enter the brain was quantified by the contrast in T1-weighted MR images. Results: Preliminary results suggest increased BBB opening with decreased time between Definity injection and insonification. A range of typical diagnostic frequencies (e.g. 5-8 MHz) has shown BBB disruption, with maximum contrast occur-

ring at 5.7 MHz. Increasing pressure had an apparent threshold for visible opening, while increasing F/# led to a larger region of BBB opening and increasing duty cycle produced more contrast. Histology showed blood cell extravasation from B-mode imaging (MI=1.5, duty cycle=0.4%), but no damage was noted after the low-pressure, custom sequences. Conclusions: This study has shown the ability of a diagnostic ultrasound system and contrast agent to open the BBB for nanometer-scale particles (possibly drugs) and examined the effects of various parameters on this opening.

TUESDAY AFTERNOON, 1 JULY 2008 P3-B, LEVEL 3, 3:40 TO 5:20 P.M.

Session 2pBBc

Biomedical Ultrasound/Bioresponse to Vibration and Physical Acoustics: Ultrasound Contrast Agents for Imaging II (Poster Session)

Charles C. Church, Cochair
University of Mississippi

Ayache Bouakaz, Cochair
INSERM U930

All posters will be on display from 3:40 p.m. to 5:20 p.m. To allow contributors an opportunity to see other posters, contributors of odd-numbered papers will be at their posters from 3:40 p.m. to 4:30 p.m. and contributors of even-numbered papers will be at their posters from 4:30 p.m. to 5:20 p.m.

Contributed Papers

2pBBc1. Influence of a rigid boundary on the resonance of an ultrasound contrast agent. Marie-Christine Pauzin (CNRS - LMA, 31 Chemin Joseph Aiguier, 13009 Marseille, France, pauzin@lma.cnrs-mrs.fr), Serge Mensah (Laboratory for Mechanics and Acoustics CNRS, 31 chemin Joseph Aiguier, 13009 Marseille, France, mensah@lma.cnrs-mrs.fr), Jean-Pierre Lefebvre (Laboratory for Mechanics and Acoustics CNRS, 31 chemin Joseph Aiguier, 13009 Marseille, France, lefebvre@lma.cnrs-mrs.fr)

Recent experimental studies showed that the behavior of an Ultrasound Contrast Agent (UCA) is strongly modified when located close or targeted to a vessel wall. Asymmetrical oscillations can occur and the frequency response differs from those of free UCA. To design new techniques for diagnostic or therapeutic applications with UCA, it is important to have a better knowledge of the acoustic behavior and the dynamics of UCA in vessels. We used a finite element model (FEM) to focus on how the resonance frequency is affected by a boundary. A FEM had been first developed with COMSOL Multiphysics to calculate the pressure field scattered by two types of spherical objects (air microbubble or UCA with a viscoelastic shell) immersed in an unbounded liquid. The results obtained with the FEM being coherent with analytical models, a rigid boundary was then added to study its influence on the frequency responses of both objects. We observed a decrease of the resonance frequency of both objects when they are close to the boundary. This behavior is in good agreement with experimental results found in literature. The model has been used to perform parametrical studies (distance to the wall, UCA radius, shell parameter...).

2pBBc2. Simulation of the oscillation dynamics and translational motion of ultrasound contrast agents. Alexander Teterev (Belarus State University, 4, Nezavisimosti Ave., 220030 Minsk, Belarus, Teterev@bsu.by), Larisa Rudak (Belarus State University, 4, Nezavisimosti Ave., 220030 Minsk, Belarus, rudak@bsu.by), Natalia Misuchenko (Belarus State University, 4, Nezavisimosti Ave., 220030 Minsk, Belarus, misuchenko@bsu.by)

A numerical model has been developed to simulate the oscillatory dynamics and the translational motion of both free and encapsulated bubbles in an ultrasound field. The model allows for the compressibility of the surrounding liquid and the bubble shell, which makes it possible to model the bubble dynamics at high acoustic pressures. Simulations can be carried out either by solving Rayleigh-Plesset-type equations, or in the hydrodynamic approximation taking into account the rheological properties of the liquid and the shell, or by a combined method. In the latter case, the gas pressure at the bubble surface, which is found from the gas-dynamic problem, is used as an input parameter for Rayleigh-Plesset-type equations at every time layer. The resulting radius of the bubble is then used as the boundary condition for the gas-dynamic equations. The model is a handy and flexible tool to investigate the effect of different factors on the oscillatory dynamics of the bubble, such as the thickness of the bubble shell, the rheological properties of the shell, and the translational displacement of the bubble. Using the developed model, the resonance frequency and translational displacement of contrast agents were numerically estimated.

2pBBc3. Improvement of the GMM-AR classification of multiframe contrast ultrasound images using gaussian filter. Bilal Ghazal (Univ. of Balamand Lebanon and Univ. of Claude Bernard France, Main Road Abdel Halim Ghazal bldg Kab-Elias Bekaa, 00961 Kab-elias, Lebanon, bilalghazal00@hotmail.com), Maha Khachab (Univ. of Balamand, Biomedical Dept., El Koura, 00961 Tripoli, Lebanon, maha.khachab@balamand.edu.lb), Denis Friboulet (Université de Lyon, 43 boulevard du 11 Novembre 1918, 69622 Villeurbanne, France, denis.friboulet@creatis.insa-lyon.fr), Chafic Mokbel (Univ. of Balamand, Biomedical Dept., El Koura, 00961 Tripoli, Lebanon, chafic.mokbel@balamand.edu.lb), Christian Cachard (Université de Lyon, 43 boulevard du 11 Novembre 1918, 69622 Villeurbanne, France, christian.cachard@creatis.insa-lyon.fr)

Despite the use of contrast agents that enhance the visualization of vascular zones, the backscattered signals from the contrast agent and tissue are still close which prevents the direct wide ultrasonic use in diagnosis. Thus, it was necessary to implement image-processing techniques that enhance the contrast echo and have the capability of classification. We have applied a new approach based on the autoregressive model where an image of prediction errors is calculated in the first phase. Then, a Gaussian filter is applied in order to model well afterward both agent and tissue behaviors by a Gaussian mixture model. The Agent to Tissue Ratio (ATR)factor and Fisher cri-

terion are adopted to compare the performance of this method with existing techniques as the harmonic and B mode techniques. The experiments conducted have shown the advantages of our proposed approach where an increasing of ATR and Fisher are recorded. In fact, our ATR attains 19.20 dB which represents a good improvement in comparison with B mode (9.50 dB) and Harmonic technique (12.13 dB). Whereas Fisher, the parameter of classification feasibility, it reaches 2.01 which matches an excellent amelioration with respect the mentioning techniques with 0.97 and 1.00 respectively.

2pBBc4. Finite difference time domain numerical simulation of ultrasonic propagation in coated contrast agents. Galaz Belfor (Université Paris 6, Laboratoire d'Imagerie Paramétrique, 15, rue de l'Ecole de Médecine, 75006 Paris, France, bgalaz@fisica.usach.cl), Guillaume Haiat (CNRS, Laboratoire de Recherches Orthopédiques, 10, Avenue de Verdun, 75010 Paris, France, haiat@univ-paris12.fr), Taulier Nicolas (Université Paris 6, Laboratoire d'Imagerie Paramétrique, 15, rue de l'Ecole de Médecine, 75006 Paris, France, Nicolas.Taulier@lip.bhdc.jussieu.fr), Urbach Wladimir (Université Paris 6, Laboratoire d'Imagerie Paramétrique, 15, rue de l'Ecole de Médecine, 75006 Paris, France, urbach@lps.ens.fr)

Acoustic wave propagation in solutions of ultrasound contrast agents (UCA) designed for in situ drug delivery remains unclear due to the complex interaction between ultrasound and the coated particles (mode conversion, scattering, multiple reflections). To address this problem, two-dimensional Finite Difference Time Domain numerical simulations of ultrasound transmission and reflection were performed in solutions of an aqueous suspension of spheres made of fluid surrounded by a polymeric capsule. Simulations were made for particle concentrations equivalent ranging from 2 to 87 mg/ml. For each concentration 15 aqueous solutions with randomly located particles were considered. The speed of sound c, the attenuation coefficient and the integrated backscattered coefficient were computed from the transmitted and backscattered signals. The values of c decrease from 1498 m/s to 1432 m/s when the concentration increases, in good agreement with an effective medium model. The attenuation coefficient at 5 MHz is an increasing function of the concentration, from 0.05 to 1.2 dB/cm. The integrated backscattered coefficient increases with the concentration for low concentration values but decreases for high concentration (with a maximum value for a concentration of about 50 mg/ml). Our numerical simulations successfully mimic experimental results of ultrasound propagation in solutions of UCA.

2pBBc5. Photoacoustical evaluation of thermal response of microbubbles. Angelo Biagioni (Sapienza Università di Roma, Via A. Scarpa, 14, 00161 Rome, Italy, angelo.biagioni@uniroma1.it), Adriano Alippi (Sapienza Università di Roma, Via A. Scarpa, 14, 00161 Rome, Italy, adriano.alippi@uniroma1.it), Andrea Bettucci (Sapienza Università di Roma, Via A. Scarpa, 14, 00161 Rome, Italy, andrea.bettucci @uniroma1.it), Annunziata D'Orazio (Sapienza Università di Roma, Via A. Scarpa, 14, 00161 Rome, Italy, annunziata.dorazio @uniroma1.it), Massimo Germano (Sapienza Università di Roma, Via A. Scarpa, 14, 00161 Rome, Italy, massimo.germano@uniroma1.it), Daniele Passeri (Sapienza, Università di Roma, Via A. Scarpa, 14, 00161 Rome, Italy, daniele.passeri@uniroma1.it)

Photoacoustic technique has emerged as a tool for the study of liquid, gel, suspension behaviour and has been recently employed in a number of new biomedical applications. In the present paper, a new photoacoustic sensor is presented which was designed and realized to analysing photoacoustic signals from solution filled with microbubbles, usually used as contrast agents in echotomography imaging. The device is a closed cell where photothermal expansion in acqueous solution samples causes the deflection of a thin membrane closing a short pipe 0.7 mm by radius. The overall set up acts as a Helmoltz resonator, where the solution in the pipe is the mass oscillating under the driving force produced by the alternating expansion of the solution in the cell body. Displacement of the membrane was measured using a laser probe interferometer, whereas photoacoustic signal was generated by chopping a laser light beam impinging into the solution through a glass window in the cell. The response of the cell filled with shelled microbubble solution was investigated with respect to water behaviour, at the cell resonance frequency and for different temperatures.

2pBBc6. Frequency response of bubble pulsations in tubes with arbitrary wall impedance. Todd A. Hay (Applied Research Laboratories, The University of Texas, P.O. Box 8029, Austin, TX 78713-8029, USA, haymaker@mail.utexas.edu), Theresa Y. Cheung (Applied Research Laboratories, The University of Texas, P.O. Box 8029, Austin, TX 78713-8029, USA, cheung.ty@gmail.com), Mark F. Hamilton (Applied Research Laboratories, The University of Texas, P.O. Box 8029, Austin, TX 78713-8029, USA, hamilton@mail.utexas.edu), Yurii A. Ilinskii (Applied Research Laboratories, The University of Texas, P.O. Box 8029, Austin, TX 78713-8029, USA, yura@arlut.utexas.edu)

A model is presented for the linear pulsation of a small bubble in a tube with locally reactive walls but with otherwise arbitrary wall impedance. The model is based on the normal mode expansion of the Green's function presented by Morse and Ingard [*Theoretical Acoustics* (McGraw-Hill, 1968), Eq. (9.2.10)]. The specific case of a cylindrical tube is considered. For a bubble that is located in the center of the tube and that is small compared with both tube diameter and wavelength, the radiation impedance on the bubble is given by a summation of the normal modes evaluated in the center of the tube. From the radiation impedance, the frequency response of the bubble to an applied sound field is obtained. For tube walls that are either rigid of pressure release, the solution agrees with the frequency response calculated using the method of images for a square tube having the same cross-sectional area. In tubes with hard walls the resonance frequency decreases as tube radius decreases because of radiation damping. In tubes with very soft walls the radiation damping is negligible below the cutoff frequency of the lowest mode, and the resonance frequency increases slightly as tube radius is decreased.

2pBBc7. New theoretical models for lipid-shelled ultrasound contrast agents. Alexander A. Doinikov (Belarus State University, 11 Bobruiskaya Street, 220030 Minsk, Belarus, doinikov@bsu.by)

Analysis of existing theoretical models for lipid-coated contrast agents is presented. A general theoretical approach to the development of zero-thickness encapsulation models, allowing the testing of different rheological laws for encapsulation, is proposed. Based on available experimental data, analysis of the rheological behavior of encapsulating lipid shells is made. The problems of the existing models, such as the dependence of shell parameters on the initial bubble radius and the ″compression-only″ behavior, are discussed. Physical explanations for the observed effects and new theoretical models for their simulation are offered. In particular, it is shown that the inclusion of nonlinear shell viscosity allows one to model the ″compression-only″ behavior. It is also very important to select an appropriate rheological law describing the dependence of the shell viscosity on the shear rate. A correct choice reduces considerably the spread of the experimentally estimated values of the shell parameters and makes them look more ordered. Whereas with an inappropriate rheological law, the experimental data may look rather chaotic.

2pBBc8. Non-linear extensions to shell models of ultrasound contrast agents: theory and experiment. Nikos A. Pelekasis (Dept. Mechanical Engineering, University of Thessaly, Pedion Areos, 38334 Volos, Greece, pel@uth.gr), Kostas Tsiglifis (Dept. Mechanical Engineering, University of Thessaly, Pedion Areos, 38334 Volos, Greece, kotsigl@uth.gr), Benjamin Dollet (Physics of Fluids, University of Twente, P.O. Box 217, 7500 AE Enschede, Netherlands, benjamin.dollet@univ-rennes1.fr), Nico De Jong (Erasmus MC, Dr Molewaterplein 50 room Ee2302, 3015GE Rotterdam, Netherlands, n.dejong@erasmusmc.nl), Detlef Lohse (Physics of Fluids, University of Twente, P.O. Box 217, 7500 AE Enschede, Netherlands, d.lohse@utwente.nl), Michel Versluis (Physics of Fluids, University of Twente, P.O. Box 217, 7500 AE Enschede, Netherlands, m.versluis @utwente.nl)

The standard UCA models, characterized by the area dilatation modulus and viscosity of the encapsulating membrane, are extended in order to account for deviations from linear material behaviour and for non-spherical

pulsations. The former effect is captured by introducing a parameter that measures the degree of membrane softness, whereas the latter is modelled by introducing a bending elasticity. Lipid shells exhibit the phenomenon of 'thresholding behavior' where excursions in the relative area dilatation are measured only beyond a critical sound amplitude. Treating the lipid shell as strain softening reproduces this non-linear behaviour which can be further optimized by controlling the shell softness parameter. Such a tuning can be used to estimate the degree of softness for the contrast agent BR-14. Stability analysis allowing for shape distortions provides an estimate for the bending elasticity that reproduces the experimentally observed threshold for growth of surface modes. Phase diagrams are constructed for BR-14, based on high-speed optical observations and stability analysis. Both experiment and numerical analysis exhibit a smaller variation between the stability threshold of subsequent shape modes in the case of UCA's, as compared to free bubbles. Numerical simulations reproduce the experimentally observed saturation of growing shape modes for pre-stressed UCA's.

TUESDAY AFTERNOON, 1 JULY 2008 P3-B, LEVEL 3, 3:40 TO 5:20 P.M.

Session 2pBBd

Biomedical Ultrasound/Bioresponse to Vibration and Engineering Acoustics: High-Intensity Focused Ultrasound Metrology and Standards II (Poster Session)

Peter Kaczkowski, Cochair
Center for Industrial and Medical Ultrasound, Applied Physics Lab.

Gail Ter Haar, Cochair
Institute of Cancer Research

All posters will be on display from 3:40 p.m. to 5:20 p.m. To allow contributors an opportunity to see other posters, contributors of odd-numbered papers will be at their posters from 3:40 p.m. to 4:30 p.m. and contributors of even-numbered papers will be at their posters from 4:30 p.m. to 5:20 p.m.

Contributed Papers

2pBBd1. Simultaneous measurement of pressure and temperature in a focused ultrasound field with a fiber optic hydrophone. Michael S. Canney (Center for Industrial and Medical Ultrasound, Applied Physics Lab., University of Washington, 1013 NE 40th St., Seattle, WA 98105, USA, mcanney@u.washington.edu), Michael R. Bailey (Center for Industrial and Medical Ultrasound, Applied Physics Lab., University of Washington, 1013 NE 40th St., Seattle, WA 98105, USA, bailey@apl.washington.edu), Vera A. Khokhlova (Center for Industrial and Medical Ultrasound, Applied Physics Lab., University of Washington, 1013 NE 40th St., Seattle, WA 98105, USA, vera@acs366.phys.msu.ru), Oleg A. Sapozhnikov (Center for Industrial and Medical Ultrasound, Applied Physics Lab., University of Washington, 1013 NE 40th St., Seattle, WA 98105, USA, oleg@acs366.phys.msu.ru), Lawrence A. Crum (Center for Industrial and Medical Ultrasound, Applied Physics Lab., University of Washington, 1013 NE 40th St., Seattle, WA 98105, USA, lac@apl.washington.edu)

The characterization of high intensity focused ultrasound (HIFU) fields is important for both clinical treatment planning as well as for regulation of HIFU medical devices. In previous work, we have used a 100-μm fiber optic probe hydrophone (FOPH) to measure pressure waveforms from a 2-MHz HIFU source with 42-mm aperture and 44-mm focal length. The formation of shock waves with peak positive pressure of up to 80-MPa were measured and modeled in transparent tissue-mimicking gel phantoms and boiling was achieved in milliseconds [Canney MS, et al., J. Acoust. Soc. Am., 120:3110 (2006)]. In this work, the FOPH was also used to measure temperature changes in tissue phantoms from HIFU at peak focal intensities of 5000-20,000 W/cm^2. Temperature measurements were obtained by first low-pass filtering the voltage signal measured from the FOPH to remove the acoustic part of the measurement. Then, calibration of voltage to temperature was performed using results from a separate calibration experiment. Experimental measurements were compared with numerical modeling using a KZK-type model for acoustic propagation coupled with a heat transfer model. In summary, temperatures of 100°C were measured at the HIFU focus in milliseconds, in agreement with modeling [Work supported by NIH DK43881, NSBRI SMS00402, and RFBR.]

2pBBd2. Visualization of transducer fields using a two-dimensional acousto-optic sensor. Charles Pergantis (US Army Research Laboratory, Aberdeen Proving Ground, Abredeen, MD 21005-5069, USA, cpergan@arl.army.mil), Jaswinder Sandhu (Santec Systems, Inc., 716 South Milwaukee Ave., Wheeling, IL 60090, USA, j-sandhu@santecsystems.com), Witold Popek (Santec Systems, Inc., 716 South Milwaukee Ave., Wheeling, IL 60090, USA, w-popek@santecsystems.com)

In this paper we will report on the use of a novel two-dimensional acousto-optic (2D AO) sensor as a simple, fast and cost-effective method of mapping transducer fields, which could be useful for quality control and quality assurance (QC/QA) of diagnostic and therapeutic transducers. This capability could be particularly useful for monitoring power output of therapeutic transducers prior to administering ultrasound based thermo-therapy treatment. It may also provide a quick tool for determining beam position and other transducer field characteristics such as propagation angle, beam diameter, divergence, and cross-sectional uniformity. Current standard transducer field mapping practices requires point-by-point scanning over a ball reflector or a hydrophone to map the transducer field. This approach is tedious, requiring hours of scanning time to generate the full cross-sectional and axial field distributions. The 2D AO system could overcome some of the drawbacks of current conventional scanning methodologies.

2pBBd3. Uncertainty Evaluation of Effective Radiation Area of Ultrasound Transducers: Preliminary Results of Inmetro's Laboratory of Ultrasound. Andre V. Alvarenga (Laboratory of Ultrasound - Inmetro, Av. N. Sra. das Gracas, 50, predio 1 - Xerem, 25250-020 Duque de Caxias - Rio de Janeiro, Brazil, avalvarenga@inmetro.gov.br), Rodrigo Costa-Felix (Laboratory of Ultrasound - Inmetro, Av. N. Sra. das Gracas,

50, predio 1 - Xerem, 25250-020 Duque de Caxias - Rio de Janeiro, Brazil, rpfelix@inmetro.gov.br)

According to the ″Guide to the Expression of Uncertainty of Measurement″ (GUM), on calculation of the uncertainty of a given measurement it is necessary to take into account two types of uncertainty: Type A and Type B. Type A uncertainty is obtained from the statistical analysis of a series of observations, while Type B comes from sources that can not be evaluated considering statistical analysis, but can be obtained from previous measurements, knowledge on the behaviour of the measuring equipment, manufacturer's specifications, and data from certificates or handbooks. Herein, the Effective Radiation Area (ERA) of ultrasound transducers has been estimated at Inmetro's Laboratory of Ultrasound using an acoustic pressure field mapping system. ERA calculation protocol developed was based on Standard IEC 61689. Besides, the Type A uncertainty was estimated from 4 repetitions of the full procedure for the determination of ERA, and Type B one was estimated from the mathematical model for ERA calculation, obtained based on IEC 61689 and the GUM. Initial tests using US transducer of 1.0 MHz and 2.25 MHz indicated an expanded uncertainty inferior to 7.0%. This preliminary result encourages further research and development in order to increases frequency range to be assessed.

TUESDAY AFTERNOON, 1 JULY 2008 P3-B, LEVEL 3, 3:40 TO 5:20 P.M.

Session 2pBBe

Biomedical Ultrasound/Bioresponse to Vibration: High-Intensity Focused Ultrasound II (Poster Session)

Lawrence Crum, Cochair
Center for Industrial and Medical Ultrasound, Applied Physics Lab.

Jean Yves Chapelon, Cochair
INSERM, U556

All posters will be on display from 3:40 p.m. to 5:20 p.m. To allow contributors an opportunity to see other posters, contributors of odd-numbered papers will be at their posters from 3:40 p.m. to 4:30 p.m. and contributors of even-numbered papers will be at their posters from 4:30 p.m. to 5:20 p.m.

Contributed Papers

2pBBe1. High intensity ultrasound activation of coagulation factors. Stuart B. Mitchell (Applied Physics Laboratory, University of Washington, 1013 NE 40th Street, Seattle, WA 98105, USA, sbmitch@u.washington.edu), Noemie C. Juaire (Center for Industrial and Medical Ultrasound, Applied Physics Lab., University of Washington, 1013 NE 40th St., Seattle, WA 98105, USA, noemiej@apl.washington.edu), Yak-Nam Wang (Applied Physics Laboratory, University of Washington, 1013 NE 40th Street, Seattle, WA 98105, USA, ynwang@apl.washington.edu)

Although it has been demonstrated that High Intensity Focused Ultrasound (HIFU) can induce vascular cauterization, acoustic hemostasis technology has not been successful in making the transition from proof-of-concept to clinical settings. One reason for this lack of acceptance is the limited understanding of the fundamental mechanisms involved in ultrasound-vessel and ultrasound-blood interactions. The aim of this research was to investigate the hematological and biochemical mechanisms which are influenced by HIFU induced coagulation. HIFU was used to induce coagulation in an in vitro hematological flow system and in animal models. The flow circuit and in vivo arteries were instrumented with flow probes and thermocouples in the treatment region. Physiological parameters were recorded throughout the in vivo experiments. Blood samples were drawn for analysis prior to, during, and immediately following each HIFU treatment. Clotting time, complete blood count, and biochemical analysis were performed immediately and citrated samples were immediately centrifuged and frozen for future analysis. Results indicate that HIFU can change local and systemic levels of thombin/anti-thrombin complex (TAT) and tissue plasminogen activator (tPA), as well as induce changes in activated clotting time (ACT). These results indicate that HIFU can induce coagulation via the coagulation cascades (TAT) and that normal hematological response to thrombus formation is unaffected.

2pBBe2. Dynamical focusing method for high-intensity ultrasound applications. Andrey Rybianets (Ultrashape Ltd., New Industrial Park, POB 80, 20692 Yoqneam, Israel, arybyanets@gmail.com)

New method for direct synthesis of dynamically focused acoustic field suitable for HIFU applications is proposed. The method is based on the continuous cyclic generation of different focal patterns at optimal repetition frequency by simultaneous applying of ″M″ different frequency signals to ″N″ sectors of spherically shaped sectored transducer array. The HIFU transducer arrays comprising a spherical piezoceramic cap with back electrode divided circumferentially into ″N″ regular or specially shaped sectors were designed and tested. The sectors were simultaneously powered by ″M″ ($M \leqslant N$) sinus or burst drive signals with different frequencies from 6 dB bandwidth of the transducer. Calculation and modeling of acoustic field patterns for different array configurations and frequencies sets were performed. Acoustic pressure in focal planes was measured in water using calibrated hydrophone and 3D acoustic scanning system. In vitro experiments on different tissues confirming the advantages of dynamical focusing method were performed. The benefits of the method are creating bigger treated tissue volumes and enhancement of the cavitational, mechanical or thermal influences due to coincidence of the repetition frequency with a specific resonance/relaxation times for tissue and/or for cavitation ″cloud″. Applications of the method for ultrasonic therapy, hyperthermia, and body aesthetics were considered.

2pBBe3. Delivery of antibacterial-nanoparticles into dentinal tubules with high intensity focused ultrasound. Siew Wan Fong (Institute of High Performance Computing, 1 Science Park Road, #01-01 The Capricorn, 117528 Singapore, Singapore, fongsw@ihpc.a-star.edu.sg), Annie Shrestha (Department of Restorative Dentistry, Faculty of Dentistry,

National University of Singapore, 5 Lower Kent Ridge road, 119074 Singapore, Singapore, g0600129@nus.edu.sg), Zhilong Shi (Department of Chemical and Biomolecular Engineering, National University of Singapore, 10 Kent Ridge Crescent, 119260 Singapore, Singapore, chesz@nus.edu.sg) , Boo Cheong Khoo (National University of Singapore, Dept of Mechanical Engineering, 10 Kent Ridge Crescent, 119260 Singapore, Singapore, mpekbc@nus.edu.sg), Anil Kishen (Department of Restorative Dentistry, Faculty of Dentistry, National University of Singapore, 5 Lower Kent Ridge road, 119074 Singapore, Singapore, rsdak@nus.edu.sg)

High-Intensity-Focused-Ultrasound (HIFU) when applied clinically often result in the formation of cavitation bubbles in the nearby fluid or tissue which collapse with high-speed jets and can be utilized for particle delivery. Bacteria residing in anatomical complexities and dentinal tubules resist conventional disinfection procedures during root canal treatment. This study aims is to evaluate the efficacy of jet flow produced by collapsing cavitations to push antibacterial nanoparticles into the areas inaccessible to conventional treatment. Eight dentin blocks of $8x3x1.5mm^3$ were prepared from the root region of freshly extracted single rooted tooth samples and divided into two groups: (1) Control and (2) Nanoparticles. The samples were placed in sterile deionized water and nanoparticles suspension (1mg/ml) for groups 1 and 2 respectively. HIFU at 27 kHz for two minutes was employed. The samples were then sectioned to expose the dentinal tubules and viewed under field emission scanning electron microscopy and Energy Dispersive X-ray analysis to ascertain the depth of penetration of the nanoparticles. The findings from this study suggested that HIFU treatment resulted in the significant penetration and coating of the dentinal tubules with nanoparticles. HIFU can be used as a potential tool for the delivery of antibacterial nanoparticles to disinfect the root canals.

2pBBe4. The effect of high intensity focussed ultrasound (HIFU) on pH responsive PEGylated micelles. Moira J. Smith (Chemical Engineering Department, Cambridge University, New Museums Site, CB2 3RA Cambridge, UK, mjs224@cam.ac.uk), Mark E. Eccleston (Chemical Engineering Department, Cambridge University, New Museums Site, CB2 3RA Cambridge, UK, mark.eccleston@vivamer.com), Nigel K. Slater (Chemical Engineering Department, Cambridge University, New Museums Site, CB2 3RA Cambridge, UK, nigel_slater@cheng.cam.ac.uk)

The effect of HIFU on pH responsive PEGylated micelles was investigated. Micelles can be used as drug carrier vehicles reducing unwanted drug toxicity. HIFU is able to release drugs from the circulating micelles, as well as improving intracellular uptake of both micelle-encapsulated and free drugs non-invasively. Large molecules generally enter cells by endocytosis. Endosomes gradually become acidic and fuse with enzyme containing lysosomes degrading the endosomal contents and preventing them from reaching their intracellular target. Using pH responsive polymers enables endosomes to be distrupted, releasing their contents into the cytoplasm before degradation occurs. Addition of poly(ethylene glycol), referred to as PEGylation, prolongs circulatory half-life and reduces degradation within the bloodstream. HIFU did enable release of encapsulated molecules from the modified micelles, and the micelles were taken up by H69 human carcinoma cells in vitro. Further work will investigate optimization of the micelles to maximize encapsulated drug release. The combined approach of using both pH responsive PEGylated micelles and HIFU to deliver drugs would provide more accurate targeting of therapies allowing higher therapeutic doses to be administered, reduce unwanted side effects and give patients a higher quality of life.

2pBBe5. The interaction of microbubbles with high intensity pulsed ultrasound. Siew Wan Fong (Institute of High Performance Computing, 1 Science Park Road, #01-01 The Capricorn, 117528 Singapore, Singapore, fongsw@ihpc.a-star.edu.sg), Evert Klaseboer (Institute of High Performance Computing, 1 Science Park Road, #01-01 The Capricorn, 117528 Singapore, Singapore, evert@ihpc.a-star.edu.sg), Boo Cheong Khoo(National University of Singapore, Dept of Mechanical Engineering, 10 Kent Ridge Crescent, 119260 Singapore, Singapore, mpekbc@nus.edu.sg)

High intensity pulsed ultrasound when interacting with microbubble contrast agents is potentially useful for biomedical applications such as drug delivery, cancer treatment and tissue ablation. To establish a fundamental understanding of the interaction between a microbubble with a sound wave, numerical simulations are performed using the Boundary Element Method (BEM). Bubble dynamics in terms of shape changes in time, maximum bubble radius obtained, jet velocity and translational movement of the bubble center is studied. The effect of varying ultrasound intensity and initial bubble size is examined as well. One important result is the determination of the conditions under which a clear high speed jet will be formed in the microbubble when it is hit by a specific sound wave. The jet is crucial to the success of the biomedical applications mentioned. Also, it is shown that one cycle of ultrasound consisting of a single negative part followed by a single compressive part would be the optimized wave form because collateral damage by re-expanding remnants of a collapsed microbubble by the subsequent negative pressure wave is prevented. The BEM model has greater computational efficiency in terms of speed and storage space over other full domain methods because only surface meshing is needed.

2pBBe6. A passive array technique for cavitation mapping during HIFU treatment. Miklós Gyöngy (University of Oxford, Medical Engineering Unit, 43 Banbury Road, OX2 6PE Oxford, UK, miklos.gyongy@jesus.ox.ac.uk), Manish Arora (University of Oxford, Medical Engineering Unit, 43 Banbury Road, OX2 6PE Oxford, UK, manish.arora@eng.ox.ac.uk), Alison Noble (University of Oxford, Wolfson Medical Vision Laboratory, Department of Engineering, OX13PJ Oxford, UK, noble@robots.ox.ac.uk), Constantin C. Coussios (University of Oxford, Medical Engineering Unit, 43 Banbury Road, OX2 6PE Oxford, UK, constantin.coussios@eng.ox.ac.uk)

During exposure of tissue to HIFU, cavitation has been shown to enhance the rate of heat deposition in tissue and could provide an effective means of treatment monitoring. However, cavitation activity occurring prefocally or growing unstable around the focal region is known to impede safe and effective treatment delivery. A combined computational and experimental approach is being applied to develop a passive array-based technique for mapping cavitation activity in real-time, using a novel cross-correlation algorithm to combine single-channel information received by an imaging array co-axial to the HIFU transducer. The cavitation maps produced in this manner were validated using two single-element 15-MHz focused PCDs during continuous-wave insonation of a polyacrylamide-based tissue mimicking material by 1.1 MHz HIFU. Initial experiments have shown bubble cloud movement towards the HIFU transducer, in agreement with previously reported observations. Future work will involve applications of advanced imaging techniques to achieve a high spatiotemporal resolution, which is essential because of the unstable nature of cavitation activity and the requirement that treatment be well localized.

2pBBe7. Quantitative assessment of thermal dose using photographic measurements of tissue discoloration. Gavriel Speyer (Center for Industrial and Medical Ultrasound, Applied Physics Lab., University of Washington, 1013 NE 40th St., Seattle, WA 98105, USA, gavriel@u.washington.edu), Peter Kaczkowski (Center for Industrial and Medical Ultrasound, Applied Physics Lab., University of Washington, 1013 NE 40th St., Seattle, WA 98105, USA, peter@apl.washington.edu), Andrew Brayman (Center for Industrial and Medical Ultrasound, Applied Physics Lab., University of Washington, 1013 NE 40th St., Seattle, WA 98105, USA, brayman@apl.washington.edu), Marilee Andrew (Center for Industrial and Medical Ultrasound, Applied Physics Lab., University of Washington, 1013 NE 40th St., Seattle, WA 98105, USA, marilee@apl.washington.edu), Steven Kargl (Applied Physics Laboratory, University of Washington, 1013 NE 40th Street, Seattle, WA 98105, USA, kargl@troutmask

.apl.washington.edu),Lawrence A. Crum(Center for Industrial and Medical Ultrasound, Applied Physics Lab., University of Washington, 1013 NE 40th St., Seattle, WA 98105, USA, lac@apl.washington.edu)

High Intensity Focused Ultrasound (HIFU) is rapidly gaining widespread clinical use in China, and is undergoing regulatory evaluation in Europe and the US for many target diseases. Nevertheless, tools for therapy planning, monitoring, and assessment remain at a rudimentary level. In particular, measurement of thermal dose in tissues exposed with HIFU has not been sufficiently quantitative to make detailed comparisons with numerical simulations, required for validation of therapy planning models. Indeed, model validation is complicated by high sensitivity of the results to small changes in parameter values and by the general difficulty of performing geometrical registration with sufficient precision to meaningfully compare millimeter scale features typical of HIFU lesions. Our work uses photographic measurement of visible tissue discoloration so that it can be used to accurately and rapidly quantify HIFU-induced bioeffects at scales of several centimeters for comparison with the prior therapy plan. Precise comparison between nonlinear acoustic simulation and macroscopic lesion data indicates that a newly defined ″blanching index″ is nearly linearly proportional to the logarithm of predicted thermal dose over a very wide range of exposure, including well below the 240 minute (at 43 degrees) necrotic threshold up to about 10,000 minutes.

Session 2pBBf

Biomedical Ultrasound/Bioresponse to Vibration: Quantitative Ultrasound Methods for Diagnosis and Therapy II (Poster Session)

Jonathan Mamou, Cochair
Riverside Research Institute

Geneviève Berger, Cochair
LIP, CNRS, Paris, France

All posters will be on display from 3:40 p.m. to 5:20 p.m. To allow contributors an opportunity to see other posters, contributors of odd-numbered papers will be at their posters from 3:40 p.m. to 4:30 p.m. and contributors of even-numbered papers will be at their posters from 4:30 p.m. to 5:20 p.m.

Contributed Papers

2pBBf1. Liver fibrosis identification by spectral slope of the backscattering curve. Mahmoud Meziri (Univ Badji Mokhtar Annaba, Bp 12 Sidi- Amar Wilaya Annaba, 23000 Annaba, Algeria, mmahmouddz@yahoo.fr), Wagner C. Pereira (Biomedical Engineering Program - COPPE, Federal University of Rio de Janeiro, CEP. 21.941-972 Rio de Janeiro, Brazil, wagner@peb.ufrj.br), Naceur Tiah (Univ Badji Mokhtar Annaba, Bp 12 Sidi- Amar Wilaya Annaba, 23000 Annaba, Algeria, nac_tiah@yahoo.fr), Naamane Remita (Univ 20 Aout 55 Skikda, BP 24, 21000 Skikda, Algeria, n.remita@yahoo.fr), Bouzid Boudjema (Univ 20 Aout 55 Skikda, BP 24, 21000 Skikda, Algeria, boudjema_b@yahoo.fr), Pascal Laugier (Université Paris 6, Laboratoire d'Imagerie Paramétrique, 15, rue de l'Ecole de Médecine, 75006 Paris, France, laugier@lip.bhdc.jussieu.fr)

Ultrasonic tissue characterization is primarily based on radio-frequency (RF) signals. Different studies have demonstrated that the RF signals are closely linked to tissue structures. The processing of these signals using spectral methods has shown the possibility of deriving quantitative parameters (attenuation and backscattered coefficients) and also of providing a means to estimate the elementary properties of tissue (scatterer size, concentration, periodicity) by evaluating spectral parameters (slope, intercept etc). We have estimated the spectral slope of the average backscattering curve to test its potential in the discrimination of fibrosis stages (F0, F1, F2, F3, and F4, METAVIR scale) from 20 in-vitro human liver samples, insonified at 20 MHz. The slope estimations were (dB/MHz): 0.95,0.24 (F0), 1.15,0.43 (F1), 1.20,0.26 (F3) and 1.07,0.33 (F4). The Kolmogorov-Smirnov test ($p>0.05$) indicated that the slope alone cannot discriminate all fibrosis groups (as well as the other mentioned parameters). When associated to integrated backscattered coefficient, discriminant analysis has correctly classified 80% of liver samples ($p<0.0000$). The misclassification resulted from some F0 samples grouped as F4 or vice-versa, which agrees with our previous results that suggested some parameter overlapping for normal and cirrhotic hepatic tissue. Nevertheless, combination of these parameters can help the diagnosis of liver fibrosis.

2pBBf2. Ultrasonic method to define human serum blood total protein and protein fractions. Anna Klemina (Dept. of Acoustics, Radiophysical Faculty, Nizhny Novgorod State University, 23 Gagarin Ave., 603950 Nizhny Novgorod, Russian Federation, klemina@rf.unn.ru)

Research of ultrasonic characteristics of biological liquids for purposes of medical diagnostics is the important task. Ultrasonic method to define total protein and protein fractions - albumin, αl -, α2 -, β -, γ - globulin's of human serum blood is discussed. This method is based on the precise measurements of velocity and absorption of ultrasonic waves in serum blood and its modified solutions under different temperatures from range (15-40)0C. The measurements of ultrasonic velocity and absorption in samples serum blood fulfils by means of method ultrasonic interferometer constant length or resonator method. The precision of relative measurements of velocity by means of this method is 10-5 and absorption is 10-3, temperature stability is the order of 10-3 0C. Protein fractions define by means of decision of linear system of equations where in the character of unknown components consider these protein fractions. Comparison of data of different patient obtained by traditional electrophoreses method with data of ultrasonic method shows very high correlation of all protein fractions and total protein. This work was supported by RFBR and Leading Scientific Schools grants.

2pBBf3. Evaluation of performance in some ultrasonic procedures for non-invasive thermal estimation into hyperthermia phantoms. Ivonne Bazan (CINVESTAV, Dpto. Ingen. Electrica, Mexico DF, Mexico,

ibazan@cinvestav.mx),Antonio Ramos(Instituto de Acustica CSIC, Serrano 144, 28006 Madrid, Spain, aramos@ia.cetef.csic.es), Monica Vazquez (UNAM, IIMAS, Mexico DF, Mexico, moni260577 @yahoo.com.mx), Arturo Vera (CINVESTAV, Dpto. Ingen. Electrica, Mexico DF, Mexico, arvera@cinvestav.mx), Lorenzo Leija (CINVESTAV, Dpto. Ingen. Electrica, Mexico DF, Mexico, lleija@cinvestav.mx)

To dispose of a precise and non-invasive temperature measurement over the treated area becomes very important during hyperthermia treatments, in order to make possible an optimization of their healing effects. A performance analysis of some previously reported ultrasonic techniques, which were proposed for non-invasive temperature estimation, is made in this work over phantoms mimicking human tissues. A first technique is based on discrete scattering modeling for tissue characterization and spectral analysis of frequency distributions related to average scatters spacing [R. Seip & E.S. Ebbini]. Other technique uses certain relations between tissue temperature changes and time-shifts in echoes due to thermally induced sound velocity changes and expansions [R. Maass-Moreno & C.A. Damianou]. And finally, the third procedure analyzed here, is a recently proposed alternative, based on phase demodulation processing, to estimate the indirect effects of echoes time-shifts in the phase domain [M. Vázquez, A. Ramos, et al.]. The three options are analyzed for the same simulated & measured multi-pulse echo patterns, looking for detecting possible advantages and inconveniences in each case. Finally, some improvement paths over the basic estimation methods are also explored.

2pBBf4. Sensitivity study of the acoustic nonlinearity parameter for measuring temperatures during High Intensity Focused Ultrasound treatment. Koen W. Van Dongen (Lab. of Acoustical Imaging and Sound Control, Faculty of Applied Sciences, Delft Univ. of Technology, PO Box 5046, 2600 GA Delft, Netherlands, K.W.A.vanDongen@tudelft.nl), Martin D. Verweij (Lab. of Electromagnetic Research, Faculty of Electrical Engineering, Mathematics and Computer Science, Delft Univ. of Technology, Mekelweg 4, 2628 CD Delft, Netherlands, m.d.verweij@tudelft.nl)

The aim of High Intensity Focused Ultrasound (HIFU) is to locally increase the temperature in a body. For an adequate application of the treatment it is important to measure non-invasively the temperature profiles in the heated region. Most efficiently, this is done with the same modality as being used for heating. Consequently, the preferred measuring method should rely on the temperature dependence of an acoustic medium parameter. The goal of this study is to determine which parameter is most sensitive to temperature changes. To find the most suitable parameter, the temperature dependence of the speed of sound (SOS), the density of mass and the acoustic nonlinearity parameter B/A are compared for water. The temperature dependence of the SOS and the mass density are obtained by interpolating values found in literature. Since measured values of the B/A parameter are only known for a few coarsely distributed temperature values, it has been synthesised from a two-dimensional function describing the SOS versus temperature and pressure. It turns out that the B/A parameter is far more sensitive for temperature changes than the other parameters. Comparison with measured B/A values confirms the idea that nonlinear acoustics is a favourite candidate to measure temperature profiles.

2pBBf5. The scattering of sound by a moving sphere in a stratified liquid. Jason Bach (Georgia Tech Lorraine - G.W. Woodruff School of ME, UMI Georgia Tech - CNRS 2958, 2 rue Marconi, 57070 Metz, France, jsbach82@yahoo.com), David Ku (Georgia Tech Lorraine - G.W. Woodruff School of ME, UMI Georgia Tech - CNRS 2958, 2 rue Marconi, 57070 Metz, France, david.ku@me.gatech.edu), Nico F. Declercq (Georgia Tech Lorraine - G.W. Woodruff School of ME, UMI Georgia Tech - CNRS 2958, 2 rue Marconi, 57070 Metz, France, nico.declercq@me.gatech.edu)

The interaction of sound with a sphere and the Doppler shift caused by scatterers in motion are well described in the literature. A numerical study is performed on the interaction of sound with a moving sphere and with multiple moving spheres. The study shows how the reflected sound fields are influenced by the relative motion and relative position of the spheres. The aim of the research is to discover efficient acoustic methods to detect and characterize moving spheres at different levels of complexity determined by the number of spheres, their relative velocities and the velocity of the surrounding liquid. At a first stage the interaction of sound with a single sphere in a stratified fluid flow is investigated. The research is performed in the framework of the use of ultrasound for biomedical applications.

2pBBf6. Two coupling media method for ultrasonic velocity measurement in biological tissues. Jérôme Mathieu (IES - Univ. Montpellier 2, place Eugène Bataillon, cc 082, 34095 Montpellier Cedex 5, France, mathieu@lain.univ-montp2.fr), Audrey Leydier (IES - Univ. Montpellier 2, place Eugène Bataillon, cc 082, 34095 Montpellier Cedex 5, France, leydier@lain.univ-montp2.fr)

Measuring the ultrasonic velocity in soft materials, especially in biological tissues, is never easy. One of the main problems is that the thickness of the sample in test is badly defined. From time-of-flight measurement method uncertainties in the thickness induce important uncertainties in experimental results. This causes that the ultrasonic velocity is often a poor criteria whereas it could be a good one. This paper brings a new method to measure the ultrasonic velocity in soft materials without knowing the sample thickness The main idea of this method is to use two different coupling media for making two relative time-of-flight measurements. The comparison of these two measurements gives the ultrasonic velocity in the sample in test. Furthermore, this comparison can give the local sample thickness of the sample. The uncertainty calculi show up that the effect on the thickness uncertainties is drastically reduced by using this new ultrasound method. This method is validated on reference samples, in silicon. Before concluding, some experimental results obtained with mouse skin samples are presented.

2pBBf7. Ultrasound elasticity assessment of in vivo human achilles tendons during a quick-release exercise. Marielle Defontaine (LUSSI, 10 Bd Tonellé, 37032 Tours, France, defontai@med.univ-tours.fr), Mourad Bentahar (ENSIM - LAUM, Université du Maine, rue Aristote, 72085 Le Mans, France, Mourad.Bentahar@univ-lemans.fr), Francis Canon (CNRS UMR6600, Centre de Recherche de Royallieu - UTC, 60 200 Compiègne, France, francis.canon@utc.fr)

An ultrasound (US) axial transmission technique has been developed to assess in vivo real time tendon biomechanical properties during calibrated exercises. The US propagation velocity changes are indeed related to the tendon visco-elasticity variations. We propose to monitor the propagation velocity changes during a very short period of time corresponding to the tendon/muscle complex release just after a sub-Maximal Voluntary isometric Contraction (MVC). This measurement is repeated for several sub-MVC amplitudes. The propagation velocity variations, linearly related to the torque measurements, allow to estimate a stiffness index, essentially due to the Series Elastic Component of the Achilles tendon. This study has been performed in collaboration with the UMR 6600 (UTC, France), and we have used the Ergometer they developed a few years ago. The US device is composed of a 1.8 MHz US probe (1 emitter, 20 receivers), and an electronic module (Althaïs Technologies, France) allowing real time and synchronous acquisitions of US RF signals and auxiliary inputs (Torque, angular position). Four healthy subjects were asked to develop several submaximal voluntary isometric contractions, and the sole was suddenly released (sub MVC to relaxed state, 2s, 2kHz). This protocol was repeated two times with foot and probe repositioning.

2pBBf8. Carotid Inter-adventitial Distance based Vascular Age and Heart Disease Risk Estimation from B mode Ultrasound. Jayaraj Joseph (Indian Institute of Technology, ESB 313 ; Dept. of Electrical Engineering, IIT Madras, 600036 Chennai, India, jayaraj85@yahoo .com), Kishore Kumar (Indian Institute of Technology, ESB 313 ; Dept. of Electrical Engineering, IIT Madras, 600036 Chennai, India, kishorekumar015@yahoo.co.in), V Jayashankar (Indian Institute of Technology, ESB 313 ; Dept. of Electrical Engineering, IIT Madras, 600036 Chennai, India, jshankar@ee.iitm.ac.in)

A method to estimate the risk of heart disease in a person, based on diagnostic ultrasound is proposed here. The ″vascular age″ obtained from carotid ultrasound is very commonly used as a measure of cardiac health. Existing methods of vascular age estimation make use of the Carotid Intima Media Thickness (CIMT) measurements to arrive at an estimate of the vascular age. Recent work has demonstrated that the carotid inter adventitial

distance (CAD) has a direct relation with the risk of coronary heart disease in persons. It has also been demonstrated that CAD correlates better to a number of risk factors accounting for heart disease than the CIMT. Hence, we propose a method to estimate vascular age based on CAD. B mode images of the carotid artery are analyzed to find out the carotid inter adventitial distance. The vascular age is estimated from carotid diameter using a statistical model developed based on the Atherosclerosis Risk In Communities Limited access database. This vascular age is then used to modify standard risk assessment procedures like the Framingham risk equation to give a better estimate of coronary heart disease risk. A comparison of the method with the CIMT based method is also performed.

2pBBf9. Effect of inclination of articular surface on ultrasonic surface reflection and surface roughness in diagnosing cartilage degeneration. Erna Kaleva (University of Kuopio, Department of Physics, POB 1627, FI-70211 Kuopio, Finland, erna.kaleva@uku.fi), Simo Saarakkala (University of Kuopio, Department of Physics, POB 1627, FI-70211 Kuopio, Finland, simo.saarakkala@uku.fi), Juha Töyräs (Kuopio University Hospital, POB 1777, 70211 Kuopio, Finland, Juha.Toyras@kuh.fi)

High-frequency Quantitative Ultrasound Imaging is a potential method for detecting early osteoarthrotic changes in articular cartilage. However, uncontrolled inclination of the ultrasound transducer or the curvature of the cartilage surface can jeopardize the reliability of the method. Visually intact and mechanically degraded osteochondral bovine patellae samples were imaged using a scanning acoustic microscope equipped with a 50 MHz ultrasound transducer. The surfaces of the sample and transducer were adjusted to a known relative inclination in three sequential scans (0, 2 and 5 degrees). Surface reflection was evaluated in time and frequency domains and surface roughness in time domain as a function of the inclination. Inclination of the surface of the sample had a greater effect on the reflection than on the roughness value. Despite the inclination-induced error, the degraded sample could be distinguished from the intact one at all inclinations with both the reflection and roughness parameters. However, as the inclination affected the reflection parameters significantly more, their reliability at greater inclinations is questionable. Furthermore, the proportion of scattering vs. reflection may change as a function of inclination. Provided that the amount of scattering varies against cartilage surface fibrillation, this can affect the reliability of ultrasound diagnostics significantly.

2pBBf10. Acoustothermometrical control during hyperthemia of biological objects. Andrej Anosov (Institute for Radio-Engineering and Electronics of the RAS, Starosadskij per, 8, 101000 Moscow, Russian Federation, aanosov@atom.ru), Aleksandr Kazanskij (Institute for Radio-Engineering and Electronics of the RAS, Starosadskij per, 8, 101000 Moscow, Russian Federation, kazansky@ihome.ru), Anton Sharakshane (Institute for Radio-Engineering and Electronics of the RAS, Starosadskij per, 8, 101000 Moscow, Russian Federation, iva@hotmail.ru)

A number of acoustothermometrical experiments modelling hyperthermia of biological objects was carried out. After that the first preliminary acoustothermometrical measurement of laser hyperthermia of human tissues was conducted. In all experiments the changes of the thermal acoustic radiation intensity in 1.4-2.2 MHz region were controlled during both the heating and the cooling of the object (about 8-10 minutes) with the help of set of acoustothermometers. As model objects we used the beef liver and glycerin water solution in which plasticine was placed. We reconstructed the 2-D inner temperature distribution by using acoustothermometrical experimental data, i.e. we calculated position, size and temperature of thermal source. The object surface temperature was controlled with the help of IR-thermograph. Acoustothermometrical measurements were carried out during laser hyperthemia of mammary and thyroid glands for seven patients. Obtained data allowed us to estimate inner temperature changes which were a result of laser hyperthemia.

2pBBf11. Measurement of dynamic shear modulus in soft solids using laser vibrometry. Maria Y. Izosimova (Center for Industrial and Medical Ultrasound, Applied Physics Lab., University of Washington, 1013 NE 40th St., Seattle, WA 98105, USA, maria.izossimova@mail.ru),Alexandr I. Korobov (Dept. of Acoustics, Physics Faculty, M.V. Lomonosov Moscow State University, Leninskie gory 1, 119991 Moscow, Russian Federation, akor@acs465a-1.phys.msu.ru), Ekaterina V. Prokhorova (Center for Industrial and Medical Ultrasound, Applied Physics Lab., University of Washington, 1013 NE 40th St., Seattle, WA 98105, USA, e-v-p@rambler.ru), Oleg A. Sapozhnikov (Center for Industrial and Medical Ultrasound, Applied Physics Lab., University of Washington, 1013 NE 40th St., Seattle, WA 98105, USA, oleg@acs366.phys.msu.ru)

Shear modulus is an important property of biological tissue and can be imaged for diagnostic purposes. A related application involves the acquisition of precise shear modulus measurements in excised soft tissue. Because the mechanical properties of tissue are frequency-dependent, it is important to develop methods that characterize the elasticity of soft solids at various frequencies. Here, two methods of measuring shear modulus are presented that employ laser vibrometry. At low frequencies (1-10 Hz), the tissue sample is fixed between plates so that the displacement of one plate induces a shear strain. Vibrometer measurements of the plate displacement define the induced strain so that shear modulus can be deduced if the applied shear force is known. At higher frequencies (0.1-10 kHz), the sample lays flat on a surface and an impulsive force is applied to the exposed surface. Using the vibrometer to measure displacements along the exposed surface enables estimation of the surface wave speed and the implied shear modulus. To demonstrate the capabilities of these techniques, experiments were performed using plastisol tissue phantom samples. These experiments indicated a shear modulus that was 50% greater at high frequencies (300 Hz) than at low frequencies (10 Hz). Work supported by RFBR.

2pBBf12. Applying Genetic Algorithms to Optimise Breast Ultrasound Images Segmentation Procedure Based on Morphological Operators. Andre V. Alvarenga (Laboratory of Ultrasound - Inmetro, Av. N. Sra. das Gracas, 50, predio 1 - Xerem, 25250-020 Duque de Caxias - Rio de Janeiro, Brazil, avalvarenga@inmetro.gov.br), Wagner C. Pereira (Biomedical Engineering Program - COPPE, Federal University of Rio de Janeiro, CEP. 21 .941-972 Rio de Janeiro, Brazil, wagner@peb.ufrj.br), Antonio F. Infantosi (Biomedical Engineering Program - COPPE, Federal University of Rio de Janeiro, CEP. 21.941-972 Rio de Janeiro, Brazil, afci@peb.ufrj.br), Carolina M. Azevedo (Brazilian National Cancer Institute - INCa, Praça da Cruz Vermelha, 23, 20230-130 Rio de Janeiro, Brazil, azevedocma@bol.com.br)

Ultrasound (US) image segmentation is a complex problem due its textural nature. To address this difficulty, different segmentation procedures have been described to support radiologists in recognising abnormal US-image areas. This work proposes a procedure, based on Genetic Algorithms (GA) and Morphological Operators (MO), to segment breast tumours on ultrasound images. Each chromosome represents a complete image processing sequence, composed of MOs and structuring elements (SE). The GA generates 500 chromosomes of 93 genes, where the three first genes summed indicate the number of performed operations, the following 45 genes represent the operations' sequence, and the last 45, the SE-disk diameter (in pixel). The best segmentation sequence (best chromosome) is selected using an objective function, based on the weighted sum of the number of false-positive and false-negative pixels. The gold standards are the tumour contours depicted by an experienced radiologist. Twenty images are used to train the GA procedure, and the best chromosome tested with 40 different images. The performance of the procedure is assessed using the overlap ratio among the obtained segmentation and the gold standard. All tested images present an area overlap ratio superior to 70%. This initial result encourages us to go further by increasing the number of images.

2pBBf13. Measuring physiological properties of lymphoedemous tissues by ultrasound: theoretical foundations. Paul E. Barbone (Boston University, 110 Cummington St, Boston, MA 02215, USA,

barbone@bu.edu),Ricardo Leiderman(Federal University of Rio de Janeiro, Program of Mechanical Engineering, Ilha do Fundo, 21945-970, P.B. 68509 Rio de Janeiro, Brazil, leider@mecanica.coppe.ufrj.br), Jeff Bamber (Institute of Cancer Research, 15 Cotswold Road, Belmont, Sutton, SM2 5NG Surrey, UK, jeff.bamber@icr.ac.uk), Gearoid Berry (Institute of Cancer Research, 15 Cotswold Road, Belmont, Sutton, SM2 5NG Surrey, UK, gearoid.berry@icr.ac.uk), Assad A. Oberai (Rensselaer Polytechnic Institute, Mechanical, Aerospace and Nuclear Engineering, 5048 JEC, 110 8th Street, Troy, NY 12180, USA, oberaa@rpi.edu), Yixiao Zhang (Rensselaer Polytechnic Institute, Mechanical, Aerospace and Nuclear Engineering, 5048 JEC, 110 8th Street, Troy, NY 12180, USA, zhangy12@rpi.edu)

Roughly one in four breast cancer survivors report some degree of arm oedema. Lymphoedema is a build-up of excess lymph fluids in the tissues. Persistent lymphoedema leads to pain, diminished limb function, increased risk of infection, soft tissue fibrosis, and severe cases can be grossly disfiguring. From a mechanics perspective, the lymphoedemous tissue may be thought of as a two phase composite, consisting of both fluid and solid phases. Here we discuss the use of composites mixture theory to model the mechanics of lymphoedemous tissues. By treating the tissue as a fluid-solid composite, rules-of-mixtures may be used to estimate the effective moduli in terms of the properties of the individual components and their respective volume fractions in these two states. The mechanical properties of the tissue may be measured in vivo using a generalization of the methods of ultrasound elasticity imaging. We discuss how the measured ''effective stiffness'' depends upon whether the tissue is drained or undrained, and how ultrasound may be used to measure these properties. Thus we explore the possibility of evaluating volume fractions and component properties of the individual tissue phases from ultrasound elasticity imaging.

2pBBf14. Multilayered non-invasive temperature estimation from backscattered ultrasound. Cesar A. Teixeira (University of Algarve, Faculty of Sciences and Technology, Campus de Gambelas, 8005-139 Faro, Portugal, cteixei@gmail.com), Maria Graça Ruano (University of Algarve, Faculty of Sciences and Technology, Campus de Gambelas, 8005-139 Faro, Portugal, mruano@ualg.pt), António Ruano (University of Algarve, Faculty of Sciences and Technology, Campus de Gambelas, 8005-139 Faro, Portugal, aruano@ualg.pt), Wagner C. Pereira (Biomedical Engineering Program - COPPE, Federal University of Rio de Janeiro, CEP. 21.941-972 Rio de Janeiro, Brazil, wagner@peb.ufrj.br)

A major drawback on the application of thermal therapies is the lack of reliable knowledge about temperature in the region under treatment. The most attractive approach is non-invasive temperature estimation (NITE) strategies and, among them, techniques based on backscattered ultrasound (BSU) are a convenient choice for its portability and simplicity. Using BSU some methods have been proposed for temperature estimation basically for homogeneous media, and simple operating situations. More complex scenarios can be explored by non-linear approaches. In this work, a methodology based on neural networks is presented for temperature estimation in a multilayer phantom. A three-layer gel-based phantom was heated at eight intensities, between 0.30 and 2.0 W/cm^2 (at 1MHz) for 15 minutes. Temperature and BSU signals were acquired from five spatial-points at each 10 seconds. Temporal echo-shifts, induced by temperature change, were computed from the BSU signals, and used as model's input information. Neural models were developed to estimate temperature at four intensities. Then models were validated in data including all the intensities. The best model presents a maximum absolute error of 0.43 °C for untrained situations. To the best of our knowledge this is the first NITE approach in multilayered media.

TUESDAY AFTERNOON, 1 JULY 2008 ROOM 353, 2:00 TO 7:00 P.M.

Session 2pEAa

Engineering Acoustics: Silicon Microphones

James West, Cochair
Johns Hopkins University, Department of Electrical Engineering, 3400 North Charles Street, Baltimore, MD 21218, USA

Gerhard Sessler, Cochair
Darmstadt University of Technology, Merckstrasse 25, 64283 Darmstadt, Germany

Invited Paper

2:00

2pEAa1. Overcoming Scaling Problems in Miniaturized Silicon Microphones. Sung B. Lee (Knowles Acoustics, 1151 Maplewood Dr, Itasca, IL 60143, USA, sung.lee@knowles.com), David E. Schafer (Knowles Acoustics, 1151 Maplewood Dr, Itasca, IL 60143, USA, dave.schafer@knowles.com), Peter V. Loeppert (Knowles Acoustics, 1151 Maplewood Dr, Itasca, IL 60143, USA, pete.loeppert@knowles.com)

In 2008 it is projected that global demand for mobile devices will reach 1.2 billion units. Compared to electronic gadgets from 2002 when 430 million cell phones were sold world wide, these devices are smaller, have more features, and will generally be priced lower. In order to keep up with designers and manufacturers who relentlessly pursue efficient use of space at lower cost, it is required that component manufacturers pursue the same goal. For a microphone manufacturer like Knowles, this led to the introduction of world's

first commercialized surface-mountable microphone, the SiSonic™ microphone, in 2002. MEMS technology is used to manufacture the complex miniaturized components used in SiSonic™ microphone. Straightforward miniaturization of microphone diaphragms made of silicon, a common material in MEMS technology, instead of traditional diaphragm materials leads to poor performing microphones. To take advantage of MEMS technology without sacrificing microphone performance we developed the free plate technology. In this presentation we discuss the use of free plate technology to overcome difficulties related to miniaturization in MEMS.

Contributed Paper

2:20

2pEAa2. Silicon microphones: a commercial success? and what comes next? Stephen C. Thompson (Applied Reearch Laboratory, The Pensylvania State University, P.O. Box 30, State College, PA 16804, USA, sct12@psu.edu)

The first silicon microphone commercial product was introduced to the market in late 2005. As of early 2008 the cumulative production is well over a half billion units and the production rates continue to rise. To date the acoustical performance of these microphones is only as good as that of the of the lowest priced miniature electret microphones. Yet acoustical systems manufacturers often prefer silicon microphones because they are compatible with automated insertion and wave soldering assembly methods. Silicon microphones are also more environmentally stable in sensitivity than are electrets which may be important in matched microphone applications. Current research activities are investigating methods to reduce the internal noise improve matching tolerances, and further reduce manufacturing costs. This paper will review the current state of silicon microphones in commercial manufacture, and will survey some of the areas of current research in an attempt to suggest some possible directions of future market development.

Invited Paper

2:40

2pEAa3. Optimization of miniaturized silicon microphones using a two-wafer approach. Jianmin Miao (Nanyang Technological University, School of Mechanical and Aerospace Engineering, 50 Nanyang Avenue, 639798 Singapore, Singapore, mjmmiao@ntu.edu.sg), Chee Wee Tan (Nanyang Technological University, School of Mechanical and Aerospace Engineering, 50 Nanyang Avenue, 639798 Singapore, Singapore, cheewee@ntu.edu.sg), Zhihong Wang (Nanyang Technological University, School of Mechanical and Aerospace Engineering, 50 Nanyang Avenue, 639798 Singapore, Singapore, ezhwang@ntu.edu.sg)

A two-wafer concept is proposed for the fabrication of silicon microphones with emphasis on deep reactive ion etching and wafer bonding techniques. For miniaturized sensor structures with an air gap of 1-2 microns, the viscous damping effect dominates the dissipation mechanism, which can have an adverse influence on the microphone performance, namely frequency response characteristic and mechanical-thermal noise. Therefore, an optimum microphone performance has its origin in a well-designed backplate structure. A silicon backplate with carefully placed acoustic slots and holes is attached to a silicon nitride/metal-based diaphragm. An impediment to achieve high sensitivity is the residual stress that is presented in the diaphragms. Besides the process optimization of less stress silicon nitride layer and the introduction of corrugated diaphragm, an investigation is carried out to determine the effects of sputtering parameters of Cr/Au metal electrode film (thickness, sputtering process pressure and process power) on the residual stress of silicon nitride/metal diaphragm. Details of modeling, fabrication and experimental results will be presented.

Contributed Papers

3:00

2pEAa4. Piezoelectric Cantilevers for Low-Noise Silicon Microphones. Robert Littrell (University of Michigan, 2250 G G Brown Bldg, 2350 Hayward St., Ann Arbor, MI 48109, USA, rlittrel@umich.edu), Karl Grosh (University of Michigan, 2250 G G Brown Bldg, 2350 Hayward St., Ann Arbor, MI 48109, USA, grosh@umich.edu)

Microphones fabricated using microelectromechanical systems (MEMS) technology are one of the fastest growing applications of MEMS. Capacitive sensing has been the dominant detection principle used in MEMS microphones. Piezoelectric sensing, however, offers advantages including simpler accompanying circuitry and the possibility for simpler fabrication. Piezoelectric microphones have been limited primarily by a high noise floor, typically at least an order of magnitude higher than, otherwise similar, capacitive microphones. We present a low noise piezoelectric cantilever microphone to overcome the main limitation of previously constructed piezoelectric microphones. Aluminum Nitride (AlN) has been selected as the piezoelectric material because its piezoelectric coupling coefficient, in combination with its electric permittivity, and its piezoelectric loss coefficient enable low-noise devices. Through both mechanical and electrical optimization, models indicate that by combining several short, thin cantilevers made exclusively of Molybdenum and AlN, microphones with a die size of 1mm x 1mm, 10 kHz bandwidth, 2mV/Pa sensitivity, and noise floor below 40 dBA can be constructed using a simple 4 mask process. Analytical and numerical models and experimental results will be presented.

3:20

2pEAa5. A low-noise biomimetic differential microphone. Ronald N. Miles (State University of New York, PO 6000, Vestal Parkway East, Binghamton, NY 13902-6000, USA, miles@binghamton.edu), Quang T. Su(State University of New York, PO 6000, Vestal Parkway East, Binghamton, NY 13902-6000, USA, be83190@binghamton.edu), Weili Cui (State University of New York, PO 6000, Vestal Parkway East, Binghamton, NY 13902-6000, USA, weilicui@yahoo.com), Stephen A. Jones (State University of New York, PO 6000, Vestal Parkway East, Binghamton, NY 13902-6000, USA, saj0716@gmail.com), F. Levent Degertekin (Georgia Institute of Technology, G. W. Woodruff School of Mechanical Engineering, 801 Ferst Dr. NW, Atlanta, GA 30332-0405, USA, levent.degertekin@me.gatech.edu), Baris Bicen (Georgia Institute of Technology, G. W. Woodruff School of Mechanical Engineering, 801 Ferst Dr. NW, Atlanta, GA 30332-0405, USA, baris@gatech.edu), Caesar Garcia (Georgia Institute of Technology, G. W. Woodruff School of Mechanical Engineering, 801 Ferst Dr. NW, Atlanta, GA 30332-0405, USA, caesar@gatech.edu), Neal A. Hall (Georgia Institute of Technology, G. W. Woodruff School of Mechanical Engineering, 801 Ferst Dr. NW, Atlanta, GA 30332-0405, USA, nahall@alumni.utexas.net)

A miniature differential microphone is described that has a noise floor that is substantially lower than that of existing devices of comparable size. The sensitivity of a differential microphone suffers as the distance between the two pressure sensing locations decreases, resulting in an increase in the input sound pressure-referred noise floor. In the microphone described here, the two sources of microphone internal noise, the diaphragm thermal noise and the electronic noise, are minimized by a combination of novel diaphragm design and the use of low-noise optical sensing. The differential microphone diaphragm measures 1 mm by 2 mm and is fabricated out of polycrystalline silicon. The diaphragm design is based on the coupled ears of the fly Ormia ochracea. The sound pressure input-referred noise floor of this miniature differential microphone has been measured to be less than 36 dBA.

Contributed Paper

5:20

2pEAa6. Thin film thermo-viscous damping in miniature condenser microphones. Thierry Le Van Suu (Laboratoire d'Acoustique de l'Université du Maine, Avenue Olivier Messiaen, 72085 Le Mans, France, thierry.levansuu@univ-lemans.fr), Petr Honzik (CVUT v Praze, Fakulta Elektrotechnická, K13137 Katedra Radioelektroniky - Technická 2, 166 27 Praha 6, Czech Republic, Petr.Honzik@lf1.cuni.cz), Stephane Durand (Laboratoire d'Acoustique de l'Université du Maine, Avenue Olivier Messiaen, 72085 Le Mans, France, stephane.durand@univ-lemans.fr), Nicolas Joly (Laboratoire d'Acoustique de l'Université du Maine, Avenue Olivier Messiaen, 72085 Le Mans, France, nicolas.joly@univ-lemans.fr), Zdeněk Škvor (CVUT v Praze, Fakulta Elektrotechnická, K13137 Katedra Radioelektroniky - Technická 2, 166 27 Praha 6, Czech Republic, skvorzdn@feld.cvut.cz), Michel Bruneau (Laboratoire d'Acoustique de l'Université du Maine, Avenue Olivier Messiaen, 72085 Le Mans, France, michel.bruneau@univ-lemans.fr)

The thermo-viscous damping due to the thin fluid film between the membrane and the backing electrode strongly influences both the sensitivity of the condenser microphones in the lower frequency range and the upper limit of the frequency bandwidth. Nowadays, most of the MEMs microphones use a perforated backing electrode while some authors suggest that a continuously curved backing electrode could enhance their performances (among avantages in the design when etching). The present paper provides two kinds of modeling for such microphones with a tapered fluid film: the first one lies on Kirchhoff-network analysis (neglecting cross-coupling between elements) whereas the second one is based upon the direct resolution of the set of basic equations (including heat transfer phenomena). The results are presented and discussed for both models in the cases of flat, parabolic, and stepped shapes backing electrode. Finally, the pressure field in the fluid film, computed (for an axisymmetrical configuration) using the abovementioned models, is compared to the one computed with a new FEM formulation taking into account both viscous and thermal phenomena in the boundary layers.

Invited Paper

5:40

2pEAa7. Miniature diffraction-based optical MEMS microphones with integrated optoelectronics. Levent Degertekin (Georgia Institute of Technology, G. W. Woodruff School of Mechanical Engineering, 801 Ferst Dr. NW, Atlanta, GA 30332-0405, USA, levent@gatech.edu), Kamran Jeelani (Georgia Institute of Technology, G. W. Woodruff School of Mechanical Engineering, 801 Ferst Dr. NW, Atlanta, GA 30332-0405, USA, gtg804t@mail.gatech.edu), Shakeel Qureshi (Georgia Institute of Technology, G. W. Woodruff School of Mechanical Engineering, 801 Ferst Dr. NW, Atlanta, GA 30332-0405, USA, shakeel@ece.gatech.edu), Paul Hasler (Georgia Institute of Technology, School of Electrical and Cumputer Engineering, 777 Atlantic Drive NW, Atlanta, GA 30332-0250, USA, phasler@ece.gatech.edu), Baris Bicen (Georgia Institute of Technology, G. W. Woodruff School of Mechanical Engineering, 801 Ferst Dr. NW, Atlanta, GA 30332-0405, USA, baris@gatech.edu), Weili Cui (State University of New York, PO 6000, Vestal Parkway East, Binghamton, NY 13902-6000, USA, weilicui@yahoo.com), Quang T. Su (State University of New York, PO 6000, Vestal Parkway East, Binghamton, NY 13902-6000, USA, be83190@binghamton.edu), Ronald N. Miles (State University of New York, PO 6000, Vestal Parkway East, Binghamton, NY 13902-6000, USA, miles@binghamton.edu)

Diffraction-based optical interferometric sensing has been shown to be a low-noise displacement detection method for MEMS microphones. For this method to be useful in many important applications such as hearing aids, it needs to be packaged in a small volume and should have power consumption levels suitable for operation with a battery. In this talk, we describe miniature, packaged optical microphones that use solid state vertical cavity surface emitting lasers (VCSELs) as light sources and custom designed photodetectors. The package carries silicon chips with two micromachined biomimetic differential microphones as well as an omnidirectional microphone. It is made by 3-D laser stereo lithography process and has dimensions suitable for behind-the-ear hearing aids. With this configuration, the input referred noise floor for the differential microphone is measured as 42.6dBA, limited by the VCSEL intensity noise in this particular case. In addition to miniature packaging, an optoelectronic chip including VCSEL pulser, photodetectors, transimpedance amplifiers and 1 bit Sigma-Delta ADC has been implemented in 1.5V, 0.35u CMOS technology. The second order ADC structure providing 14-bits of theoretical resolution with 64 over sampling ratio and 20 kHz input signal is described and initial characterization results are presented.

Contributed Papers

6:00

2pEAa8. On determination of microphone response and other parameters by a hybrid experimental and numerical method. Salvador Barrera-Figueroa (Danish Fundamental Metrology, Matematiktorvet 307, 2800 Kgs. Lyngby, Denmark, sbf@dfm.dtu.dk), Finn Jacobsen (Acoustic Technology Department, Technical University of Denmark, Ørsted Plads, B352, DK-2800 Lyngby, Denmark, fja@oersted.dtu.dk), Knud Rasmussen (Danish Fundamental Metrology, Matematiktorvet 307, 2800 Kgs. Lyngby, Denmark, kra@dfm.dtu.dk)

Typically, numerical calculations of the pressure, free-field and random-incidence response of a condenser microphone are carried out on the basis of an assumed displacement distribution of the diaphragm of the microphone; the conventional assumption is that the displacement follows a Bessel function. This assumption is probably valid at frequencies below the resonance frequency. However, at higher frequencies the movement of the membrane is heavily coupled with the damping of the air film between membrane and back plate, and with resonances in the back chamber of the microphone. A solution to this problem is to measure the velocity distribution of the membrane by means of a non-contact method, such as laser vibrometry. The measured velocity distributions can be used together with a numerical formulation such as the Boundary Element Method for estimating the microphone response and other parameters such as the acoustic centres. In this work, a hybrid method is presented. The velocity distributions of condenser Laboratory Standard microphones were measured using a laser vibrometer. This measured velocity distribution was used for estimating the microphone responses and parameters. The agreement with experimental data is good. This method can be used as an alternative for validating the parameters of the microphones determined by classical calibration techniques.

6:20

2pEAa9. Diffraction based optical MEMS microphones and accelerometers with active electrostatic force feedback. Baris Bicen (Georgia Institute of Technology, G. W. Woodruff School of Mechanical Engineering, 801 Ferst Dr. NW, Atlanta, GA 30332-0405, USA, baris@gatech.edu), Caesar Garcia (Georgia Institute of Technology, G. W. Woodruff School of Mechanical Engineering, 801 Ferst Dr. NW, Atlanta, GA 30332-0405, USA, caesar@gatech.edu), Neal A. Hall (Georgia Institute of Technology, G. W. Woodruff School of Mechanical Engineering, 801 Ferst Dr. NW, Atlanta, GA 30332-0405, USA, nahall@alumni.utexas.net), Murat Okandan (Sandia National Laboratories, New Mexico, PO Box 5800, Albuquerque, NM 87185-1080, USA, mokanda@sandia.gov), Weili Cui (State University of New York, PO 6000, Vestal Parkway East, Binghamton, NY 13902-6000, USA, weilicui@yahoo.com), Quang T. Su (State University of New York, PO 6000, Vestal Parkway East, Binghamton, NY 13902-6000, USA, be83190@binghamton.edu), Ronald N. Miles (State University of New York, PO 6000, Vestal Parkway East, Binghamton, NY 13902-6000, USA, miles@binghamton.edu), Levent Degertekin (Georgia Institute of Technology, G. W. Woodruff School of Mechanical Engineering, 801 Ferst Dr. NW, Atlanta, GA 30332-0405, USA, levent@gatech.edu)

Diffraction-based optical displacement detection method and its use in low noise micromachined microphones have been shown earlier. [Hall et al., J. Acoust. Soc. Am. **118**, 3000-3009 (2005), Garcia et al., J. Acoust. Soc. Am. **121**, 3155 (2007)]. In these devices, the integrated electrostatic port of the sensor is uncoupled from the integrated optical sensing. This structure enables one to use this port for sensitivity tuning, self characterization, and active control to adjust the device dynamics. Given that the displacement noise of integrated optical sensor is below the thermal-mechanical noise of the mechanical structure, one can implement force feedback methods such as active Q-control, or adjust device stiffness without adding substantial noise to the system. We implemented micromachined optical microphones and accelerometers with integrated optoelectronics integrated in a 1.5mm**3** volume. We present experimental results on force feedback Q-control of low noise omnidirectional, and biomimetic directional optical microphones, as well as adjusting the stiffness of accelerometers to improve their frequency response. [Work supported by NIH Grant 5R01DC005762-03 and the Catalyst Foundation.]

Invited Paper

6:40

2pEAa10. Piezoelectric silicon microphones for aeroacoustics applications. Mark Sheplak (University of Florida, 231 MAE-A Building, PO Box 116250, Gainesville, FL 32611-6250, USA, sheplak@ufl.edu)

This talk presents the development of several microelectromechanical systems (MEMS)-based piezoelectric measurement microphone technologies for aeroacoustic applications. Piezoelectric MEMS microphones offer the promise of reducing cost, improving performance, and increasing mounting flexibility over existing conventional microphone technologies. Specifically, a microphone with no external power requirement has a key advantage for a large-channel count, widespread deployment. The modeling and design aspects of these devices are reviewed. First, the electroacoustic transduction is predicted via piezoelectric composite plate theory. Lumped element models are then synthesized to describe the dynamic characteristics of the microphone diaphragm and the cavity/vent structure. Constrained nonlinear design optimization using a sequential quadratic programming scheme is then performed to determine the microphone design parameters. From a fabrication perspective, the main drawback to silicon-micromachined piezoelectric devices is material integration and compatibility with standard micromachining. Several different device structures and fabrication approaches will be discussed in this talk. Representative results from a lead zirconate-titanate-based device will then be presented. Finally, unresolved technical issues are summarized for future sensor development.

Session 2pEAb

Engineering Acoustics and Signal Processing in Acoustics: Microphone Array Signal Processing II (Poster Session)

Gary Elko, Cochair
mh acoustics LLC

Walter Kellermann, Cochair
Univ. of Erlangen—Nuremburg

All posters will be on display from 3:40 p.m. to 5:20 p.m. To allow contributors an opportunity to see other posters, contributors of odd-numbered papers will be at their posters from 3:40 p.m. to 4:30 p.m. and contributors of even-numbered papers will be at their posters from 4:30 p.m. to 5:20 p.m.

Contributed Papers

2pEAb1. Advanced Processing of Microphone Array Data for Engineering Applications. Sandro Guidati (HEAD acoustics GmbH, Ebertstrasse 30a, 52134 Herzogenrath, Germany, claudia.erens@head-acousitcs.de)

Microphone arrays are tools for the localisation and quantification of sound sources. The use of the technology is strongly related to the progresses in computer technology. For a long time the application was limited to military or scientific use. The focus of the systems designed for industrial applications lies on fast setup and basic evaluation (e.g. delay-and-sum beamforming). The resulting boundaries are mainly a limited dynamic range and the limitation to free field environments. Although a wide range of algorithms for advanced evaluation has been developed, only few of them are integrated in industrial systems. This is mainly due to the fact that these algorithms require considerably longer computation time, expert knowledge and the integration of additional hardware. This paper presents techniques for almost real-time processing of microphone array data including multi-band beamforming, coherence/incoherence filtering and the integration of measured source characteristics for the application in strongly reverberant environments. By combining the signals of multiple cameras it is possible to detect the distance between the array and a three dimensional source distribution increasing the accuracy of the localisation and quantification.

2pEAb2. Instrumentation Synchonization Techniques for Large Microphone Arrays. Kurt Veggeberg (National Instruments, 11500 N. Mopac C, Austin, TX 78759, USA, kurt.veggeberg@ni.com)

In many acoustic measurement applications, there is a need to correlate data acquired from different systems or synchronize systems together with precise timing. Signal Based and Time Based are the two basic methods of synchronizing instrumentation. In Signal Based synchronization, clocks and triggers are physically connected between systems. Typically this provides the highest precision synchronization. In many acoustic applications size and distance constrains physically connecting the systems needed for making measurements though the inter-channel phase information of simultaneously sampled signals is crucial. In Time Based synchronization, system components have a common reference of what time it is. Events, triggers and clocks can be generated based on this time. This is an overview of how you can use a variety of time references including GPS, IEEE-1588, and IRIG-B to correlate and synchronize measurements anywhere in the world with absolute timing with and without a direct connection between the measurement systems. The level of precision of the variety of methods that can be used for timestamping, generating a trigger at a user specified time as well as synchronizing multiple instrumentation types is covered. Specific applications where this has been applied to large microphone arrays will be described.

2pEAb3. Differential microphone array for speech recognition. Philippe Martin (Ecole Polytechnique Fédérale de Lausanne, EPFL STI LEMA, Station 11, CH 1015 Lausanne, Switzerland, philippe.martin@epfl.ch), Hervé Lissek (Ecole Polytechnique Fédérale de Lausanne, EPFL STI LEMA, Station 11, CH 1015 Lausanne, Switzerland, herve.lissek@epfl.ch), John Dines (IDIAP, Rue du Simplon 4, 1920 Martigny, Switzerland, john.dines@idiap.ch)

Speech recognition applications embedded on a PDA are already available on the market. The usual hardware for this kind of system is a single microphone mounted on the PDA, giving good results within quiet environments. Though, the recognition rate falls drastically as the signal to noise ratio decreases. Arrays of microphones are then particularly interesting, allowing the discrimination of useful sounds sources within parasitic ones, thanks to an improved directivity pattern. In speech recognition applications on PDA, a trade-off is to be found on an array small enough to guarantee the ergonomics of the whole system, while operating on a bandwidth covering the frequency range of human voice, from 300 Hz up to 6 kHz and low distortion ratio. Differential arrays are well adapted to fulfill these specifications, since they are known to be robust and allow small dimensions for a high directivity index. The performances could be improved by the addition of adaptive post-filtering and noise reduction algorithms. This work describes the design and the implementation of a recording device dedicated to speech recognition applications on PDA, based on overlapping differential arrays. The assessment of its performances in a noisy environment is carried out and show the system efficiencies.

2pEAb4. Speech separation based on law of causality. Kensaku Fujii (University of Hyogo, 2167 Shosha, 671-2280 Himeji, Japan, fujiken@eng.u-hyogo.ac.jp), Hirofumi Nakano (University of Hyogo, 2167 Shosha, 671-2280 Himeji, Japan, er06j025@steng.u-hyogo.ac.jp), Mitsuji Muneyasu (Kansai University, 3-3-35 Yamate-cho, 564-8680 Suita, Japan, muneyasu@ipcku.kansai-u.ac.jp)

This paper proposes a microphone array system separating speech signals, based on a different principle from independent component analysis (ICA). This system applies linear prediction error filters to microphone outputs, and using the prediction errors, adjusts the coefficients of adaptive filters. In this case, only the prediction errors satisfying the low of causality become available for the adjustment; consequently, this system can steer a null toward a direction satisfying it. The permutation problem discussed in

ICA can be thereby avoided. This system also can compensate the separated speech signals by using adaptive filters, and finally, can provide high quality speech signals. This paper moreover verifies the performance of the proposed system by using speech signal data measured in an ordinary room. This result shows that the proposed system works well even in reverberation environment.

2pEAb5. Time-Shift Sensor Noise Suppression Algorithm. Alain De Cheveigne (CNRS, Universite Paris 5, Ecole Normale Superieure, 29 rue d'Ulm, 75230 Paris, France, alain.de.cheveigne@ens.fr)

We propose a new method to remove sensor noise from multichannel data recordings. Each channel is projected on the span of the time-shifted neighboring channels, and replaced by its projection. Noise specific to any sensor is attenuated, whereas any signal component that loads more than one sensor is preserved. The inclusion of a range of time shifts allows the method to compensate for any delay or convolutional mismatch in the signal paths between sensors. The method is expected to be of use for microphone arrays to reduce sensor-specific noise, e.g. thermal noise, wind noise, or overloading. The new method extends a previous method for sensor noise suppression in physiological recordings (EEG, MEG), that performed the same operation without the delays.

2pEAb6. Acoustic payload on an aerostat detects and locates transient sources. Michael V. Scanlon (US Army Research Laboratory, AMSRD-ARL-SE-SA, 2800 Powder Mill Road, Adelphi, MD 20783-1197, USA, mscanlon@arl.army.mil), Christian Reiff (US Army Research Laboratory, AMSRD-ARL-SE-SA, 2800 Powder Mill Road, Adelphi, MD 20783-1197, USA, creiff@arl.army.mil), Latasha Solomon (US Army Research Laboratory, AMSRD-ARL-SE-SA, 2800 Powder Mill Road, Adelphi, MD 20783-1197, USA, lsolomon@arl.army.mil)

The US Army Research Laboratory (ARL) has conducted experiments using acoustic sensor arrays suspended below tethered aerostats to detect and localize transient signals from mortars, artillery, and small arms fire. The airborne acoustic sensor array calculates an azimuth and elevation to the originating transient, and immediately cues a collocated imager to capture the remaining activity at the site of the acoustic transient. This single array's vector solution defines a ground-intersect region or grid coordinate for threat reporting. Unattended ground sensor (UGS) systems can augment aerostat arrays by providing additional solution vectors from several ground-based acoustic arrays to perform a 3D triangulation on a source location. The aerostat array's advantage over ground systems is that it is not as affected by diffraction and reflection from man-made structures, trees, or terrain, and has direct line-of-sight to most events. Helicopter detection and tracking algorithms can also be implemented.

TUESDAY AFTERNOON, 1 JULY 2008 P3-C, LEVEL 3, 3:40 TO 5:20 P.M.

Session 2pEAc

Engineering Acoustics: Acoustic Evaluation II (Poster Session)

All posters will be on display from 3:40 p.m. to 5:20 p.m. To allow contributors an opportunity to see other posters, contributors of odd-numbered papers will be at their posters from 3:40 p.m. to 4:30 p.m. and contributors of even-numbered papers will be at their posters from 4:30 p.m. to 5:20 p.m.

Contributed Papers

2pEAc1. Mechanism detection of stress corrosion cracking by acoustic emission and effect of manufacturing process on AE signals. Hossein Heidary (Polytechnic of Tehran, AmirKabir University of Technology, Department of Mechanical Engineering, NDT Lab., 424 Hafez Ave, 15875-4413 Tehran, Iran, hosseinheidary@gmail.com), Amir Refahi Oskouei (Polytechnic of Tehran, AmirKabir University of Technology, Department of Mechanical Engineering, NDT Lab., 424 Hafez Ave, 15875-4413 Tehran, Iran, amir.refahi@cic.aut.ac.ir), Mehdi Ahmadi (Polytechnic of Tehran, AmirKabir University of Technology, Department of Mechanical Engineering, NDT Lab., 424 Hafez Ave, 15875-4413 Tehran, Iran, ahmadin@cic.aut.ac.ir)

Stress corrosion cracking could occur wherever a specific corrodent and sufficient tensile stresses coexist. In the objective to monitor online the SCC on real structures, it seems reasonable to characterize and recognize acoustic emission during static U-bend tests. The present study is concerned with static tests on 304 stainless steels in two different media (5% HCl and 5% H2SO4) in order to find a criterion to distinguish, the two different mechanism of SCC (anodic dissolution and hydrogen embrittlement) by characteristic parameters and waveform analysis of AE signals. In the next stage, effect of residual stress on stress corrosion cracking in chloride solution has been studied. Three samples have been prepared: one of them was stress relieved; the second one was made sensitive to SCC by heat treatment and the last one was cold worked by rolling. Cumulative count, amplitude distribution and waveform analysis were selected as AE-parameters. AE with amplitudes ranging from 39 to 65 dB with different counts and energy occurred during SCC of SS-304 at room temperature. According to the results, acoustic emission is able to be used as robust technique for mechanism detection of SCC. In addition it can be used to measure the effect of residual stress in manufacturing process on SCC.

2pEAc2. Underground Sonar Using Shear Waves -Resolution improvement Using Pulse Compression and Dynamic Focusing-. Hiraku Kawasaki (Toin University of Yokohama, 1614 Kurogane-cho, Aoba-ku, 225-8502 Yokohama, Japan, hot.hu2.feel.good@gmail.com), Tsuneyoshi Sugimoto (Toin University of Yokohama, 1614 Kurogane-cho, Aoba-ku, 225-8502 Yokohama, Japan, tsugimot@cc.toin.ac.jp)

In order to detect the buried relics and ruins at shallow depth, a method by using shear waves has proposed. The effect of the pulse compression processing is examined for improving the underground imaging resolution. Using a super-magnetostriction vibrator which can change waveforms and use high frequency waves, we generate both chirp waves and high frequency waves. To confirm the resolution of underground images, pulse compression is simulated. And, to confirm the lateral resolution, dynamic focusing is simulated in our laboratory. Then, its exploration experiment is carried out where the buried position has already known. The axial resolutions are smaller than 0.2m when the range of start and stop frequencies are more

than 700Hz in the simulation. And the underground images obtained from exploration experiment confirm that the images by the pulse compression have almost the same axial resolution as by the result of the simulation.

2pEAc3. PVB mechanical constants characterization in laminated glasses using low frequency ultrasound. Jaime Ramis Soriano (DFISTS. Univ. de Alicante, Carretera de Sant Vicent del Raspeig s/n, 03690 San Vicente del Raspeig, Spain, jramis@ua.es), Jorge Frances Monllor (DFISTS. Univ. de Alicante, Carretera de Sant Vicent del Raspeig s/n, 03690 San Vicente del Raspeig, Spain, jfmonllor@ua.es), Jesús Alba Fernandez (Escola Politècnica Superior de Gandia, Universitat Politècnica de València, Crtra Natzaret-Oliva s/n, 46730 Gandia, Spain, jesalba@fis.upv.es), Enrique E. Segovia Eulogio (Depto Ing. Construcción. Univ. de Alicante, Carretera de Sant Vicent del Raspeig s/n, 03690 San Vicente del Raspeig, Spain, Enrique.Gonzalo@ua.es), Jenaro Vera Guarinos (DFISTS. Univ. de Alicante, Carretera de Sant Vicent del Raspeig s/n, 03690 San Vicente del Raspeig, Spain, jenaro@dfists.ua.es)

To predict the behaviour of a partition made of laminated glasses, it's necessary to know the parameters of the layers composing it. These types of devices are composed by monolithic glass and an intermediate muffling layer usually made of PVB. In this study, we present a method to find the mechanical constants of PVB in laminated glasses. Mechanical constants characterization in these materials is studied using a model-based inverse problem and the data obtained from an ultrasonic transmission setup: a numerical simulation of the system is proposed using a lineal finite elements model of the ultrasonic propagation on the multilayered solid. Parameters are obtained by minimizing divergences between experimental and numerically predicted waveform.

2pEAc4. Ultrasonic Technique for the Quality Control of Water Containing Clay. Adil Hamine (Ibn Zohr University, FS Agadir, 80000 Agadir, Morocco, adil.hamine@Gmail.com), Bouazza Faiz (Ibn Zohr University, FS Agadir, 80000 Agadir, Morocco, faizbou@hotmail.com), Driss Izbaim (Ibn Zohr University, FS Agadir, 80000 Agadir, Morocco, driss_izbaim@yahoo.fr),Ali Moudden(Ibn Zohr University, FS Agadir, 80000 Agadir, Morocco, ali_moudden@yahoo.fr)

In this work a new method is developed to control the stopping water using an ultrasonic technique. This technique allows controlling the presence of clay grains by measuring the attenuation of the ultrasonic waves. The dimension of clay grains used in this study is about 10 μm. For slurries with different weight percent of clay 1% or less, high sensitivity is gained by analyzing attenuation measurements. At high clay concentrations, sufficient sensitivity is obtained by analyzing data from a simple transmission. The experimental results show that the sound attenuation due to particles varies linearly with mass fraction.

2pEAc5. Acoustic Computerized Tomography for Temperature Distribution Measurement in Rectangular Space. Ayumu Minamide (Grad. Sch. of Sys. Inf. Eng., Univ. of Tsukuba, 1-1-1, Tennodai, 305-8573 Tsukuba, Japan, minamide@aclab.esys.tsukuba.ac.jp), Naoto Wakatsuki (Tsukuba Univ., Tsukuba Science City, 305-8573 Ibaraki, Japan, wakatuki@iit.tsukuba.ac.jp), Koichi Mizutani (Tsukuba Univ., Tsukuba Science City, 305-8573 Ibaraki, Japan, mizutani@esys.tsukuba.ac.jp)

In this research, we propose an improved algorithm of Acoustic Computerized Tomography to measure temperature distribution in rectangular space. Temperature distribution measurement is used in various fields, such as, air-conditioning control in offices, temperature control in greenhouse. If acoustic transducers are fixed, they are ordinarily arranged at equal intervals on a circle. However, it is difficult to take circular arrangements of transducers in the rectangular spaces. Thus, we devise to arrange the transducers on a rectangle. Therefore, a problem is occurs that projection data could not be obtained at equal angular intervals. To solve this problem, we propose non-uniform angular interval Back-Projection to weight the projection data with respect to its angular intervals. We confirm usefulness of the proposed method by numerical simulations. In the simulations, 24-acoustic transducers are arranged at equal intervals on a rectangle whose aspect ratio is two. By using the proposed method, the shape approaches to the given temperature distribution, and RMS error of the reconstructed distribution to the given distribution decreases about 25 % compared to the error of conventional CT.

Session 2pEAe

Engineering Acoustics, Underwater Acoustics, Signal Processing in Acoustics, and ECUA: Sensor Technologies for Autonomous Acoustic Sensing Systems II (Poster Session)

Henrik Schmidt, Cochair
MIT

Andrea Caiti, Cochair
University of Genova

All posters will be on display from 3:40 p.m. to 5:20 p.m. To allow contributors an opportunity to see other posters, contributors of odd-numbered papers will be at their posters from 3:40 p.m. to 4:30 p.m. and contributors of even-numbered papers will be at their posters from 4:30 p.m. to 5:20 p.m.

Contributed Papers

2pEAe1. High Accuracy Multisensor Hydroacoustic System for Models of Trawl Geometry Measurements. Jacek Marszal (Gdansk University of Technology, Narutowicza 11/12, 80-952 Gdansk, Poland, marszal@eti.pg.gda.pl)

The new high accuracy multisensor hydroacoustic system for models of trawl geometry measurements was designed for developing the construction of cod trawl net for the Baltic fishery. The system consist of 20 miniature hydrophones attached by the light-gauge cables to the measuring microprocessor device and notebook computer. The pulse excitation at high frequency and correlation digital signal processing make it possible to obtain high resolution of measurements. Additionally each of hydrophones is equipped with the thermistor which is used to calculate the local sound velocity and enable precision calibration of obtained measururing data. This method of calibration is particularly important for measurements investigated in the surface water layer with the high temperature gradient. The construction details, the measuring signal processing algorithms as well as examples of obtained data and the accuracy verification will be presented in the paper.

2pEAe2. Ultra-deep low-frequency sub-bottom profiler for AUV and ROV. Yves Le Gall (IFREMER, BP 70, 29280 Plouzané, France, Yves.Le.Gall@ifremer.fr), Anne Pacault (IFREMER, BP 70, 29280 Plouzané, France, Anne.Pacault@ifremer.fr),Frédéric Mosca(Ixsea, 46 Quai François Mitterrand, 13600 La Ciotat, France, fmo@ixsea.com), Gilles Greninguey (Ixsea, 46 Quai François Mitterrand, 13600 La Ciotat, France, ggr@ixsea.com), Marcel Vial (Ixsea, 46 Quai François Mitterrand, 13600 La Ciotat, France, mvi@ixsea.com), Jean-Claude Aissa (Ixsea, 46 Quai François Mitterrand, 13600 La Ciotat, France, jca@ixsea.com)

Acoustical techniques for ultra-deep sub-bottom exploration are still little investigated. IXSEA and IFREMER have launched in 2006 the development of a new deep-sea low-frequency sub-bottom profiler, working up to 6000 meters depth. Based on the Janus-Helmholtz broadband technology, two acoustic sources have been modelled, achieved and in-tank and at-sea measured : a single transducer working in the [1.8, 6.2 kHz] frequency band, and a three-transducer array operating in the [2, 8 kHz] frequency band. In both cases, vertical resolution is better that 20 cm. Comparison between finite element modelling and in-tank measurements is presented, together with the specific constraints linked to very-deep water and AUV mounting. Power electronics and impedance matching unit have been specifically optimised to deliver a sound level of 190 dB (ref. 1 μPa @ 1 m), with 48 VDC supply voltage and 250 W available electric power. The receiving part is made up of a three-hydrophone array with a loss of sensitivity lower than 1 dB between 0 and 600 bar. This ultra-deep light system has been mounted on an IFREMER's AUV and the first results at sea are presented and discussed.

Session 2pEAf

Engineering Acoustics and Psychological and Physiological Acoustics: Hearing Aid Engineering II (Poster Session)

Daniel Warren, Cochair
Knowles Electronics

Stefan Launer, Cochair
Phonak AG

All posters will be on display from 3:40 p.m. to 5:20 p.m. To allow contributors an opportunity to see other posters, contributors of odd-numbered papers will be at their posters from 3:40 p.m. to 4:30 p.m. and contributors of even-numbered papers will be at their posters from 4:30 p.m. to 5:20 p.m.

Contributed Papers

2pEAf1. Two-input two-output speech enhancement with binaural spatial information using a soft decision mask filter. Satoshi Hongo (Faculty of Design and Computer Applications, Miyagi National College of Technology, 48, Nodayama, Medeshima Shiote, 981-1239 Natori, Japan, hongo@miyagi-ct.ac.jp), Ai Sasaki (R.I.E.C., Tohoku University, 2-1, Katahira, Aoba-ku, 980-8577 Sendai, Japan, asasaki@ais.riec.tohoku.ac.jp), Shuichi Sakamoto (R.I.E.C., Tohoku University, 2-1, Katahira, Aoba-ku, 980-8577 Sendai, Japan, saka@ais.riec.tohoku.ac.jp), Junfeng Li (Japan Advanced Institute of Science and Technology, 1-1, Asahidai, Nomi, 923-1292 Ishikawa, Japan, junfeng@jaist.ac.jp), Yôiti Suzuki (R.I.E.C., Tohoku University, 2-1, Katahira, Aoba-ku, 980-8577 Sendai, Japan, yoh@ais.riec.tohoku.ac.jp)

A two-input two-output speech enhancement method that preserves binaural spatial information in the output is effective for realizing a comfortable auditory communication system. Such a system benefits from the noise reduction capability provided by the signal processing technology, in addition to the binaural processing of the human auditory system. We investigated a two-input two-output speech enhancement method that calculates soft decision mask filters to attenuate a noisy time-frequency bin. The soft decision mask filter is estimated for each direction of arrival (DOA) based on a target noise ratio calculated using an adaptive filter that cancels the target signal. Results of computer simulations show that the proposed method has superior capabilities for maintaining spatial information in the two-output signals and for segregating the target signal in arbitrary azimuth and elevation DOA.

2pEAf2. Improvement of speech intelligibility by audio hearing systems. Hannes Seidler (Clinic of ORL, Dept. of Medicine, TU Dresden, Fetscherstrasse 74, 01307 Dresden, Germany, Hannes.Seidler@tu-dresden.de)

All hearing aids and cochlea implants have algorithm to improve the speech intelligibility. The idea is to share human speech and noise to find different ratings. The result should be easier to understand by impaired people. On the market there are big efforts to recognize speech and to separate it from noise. In this field we can notice a remarkable progress in the last years. But the reverberant sound in rooms or noise from same direction like the signal need a lot of work to suppress them effective. The simplest way seems to be to gets the original speech signal direct from the source and to processes it individual in hearing devices. Induction loop systems as well as wireless infrared or radio frequency systems are used in churches, cinemas, theatres and conference rooms. But the available systems are very different in costs and benefit for management and clients. If these systems are used there is a considerable improvement of speech intelligibility. The presentation will show the level of most used external audio hearing systems, their possibilities to improve the signal to noise ratio, the speech transmission index (STI) and the benefit for hearing aid or cochlear implant users.

Session 2pEAg

Engineering Acoustics, Underwater Acoustics, and ECUA: Sonar Transducer Design and Modeling III (Poster Session)

John Blottman, Cochair
Naval Undersea Warfare Center, Division Newport

Pascal Mosbah, Cochair
IEMN dpt ISEN

All posters will be on display from 3:40 p.m. to 5:20 p.m. To allow contributors an opportunity to see other posters, contributors of odd-numbered papers will be at their posters from 3:40 p.m. to 4:30 p.m. and contributors of even-numbered papers will be at their posters from 4:30 p.m. to 5:20 p.m.

Contributed Papers

2pEAg1. Finite element and boundary element modeling of multimodal arrays. Julien Bernard (Thales Underwater Systems, 525 route des Dolines BP 157 Valbonne Parc d'Activités de Sophia Antipolis, 06903 Sophia Antipolis Cedex, France, julien.bernard@fr.thalesgroup.com)

Modern active sonar arrays exhibit the following characteristics: low operating frequency, large number of transducers, small transducer spacing compared to wavelength, and in some cases, multimodal transducers. This results in strong, complex acoustic interaction phenomena which can involve both a large number of array elements and multiple transducer modes. To predict the performance of such arrays, this paper presents a modeling approach which is both accurate and computationally economical. First, the generic equivalent circuit for an array of multimodal transducers is described. The field of application of such a model, the definition of the parameters, and the characteristics which can be calculated from it are provided. Second, the computation of the equivalent circuit parameters is performed using commercial finite element and boundary element codes. Specifically, a method is described to compute the mechanical, electrical, self and mutual radiation parameters of the various transducer modes. Finally, the methodology is applied to a 12 element volumetric array of flextensional transducers, with both $\lambda/2$ and $\lambda/4$ spacings.

2pEAg2. The design of a wideband and widebeam piston transducer in a finite closed circular baffle. Zekeriyya Sahin (Aselsan A.S., Mehmet Akif Ersoy Mah. 16.Cad. no:16, Macunkoy, 06370 Ankara, Turkey, zsahin@aselsan.com.tr), Hayrettin Koymen (Bilkent Univ., Dept. of Electrical and Electronics Engineering, 06800 Ankara, Turkey, koymen@ee.bilkent.edu.tr)

The design of a high power piezoelectric underwater transducer operating at frequency range 45kHz-85kHz with acoustic power capability in excess of 150W is described. The transducer consists of two back-to-back elements. Each element is formed by stacked PZT-4 ceramic rings, a matching and a steel backing layer, and placed in a finite rigid circular baffle. We investigate the dependence of bandwidth and beamwidth to the combination of piston and baffle radii, a and b, respectively. With a ka of 2.45 (k:wave number) and b/a ratio of 2, the transducer resonates at 65kHz with 70% bandwidth and has a beamwidth of 60° at each half space. We show that when two transducers are placed at right angles spatially and driven in parallel, we can obtain an omnidirectional beam pattern horizontally in the lower frequency band. The beam pattern exhibits two dips in each quadrant at the higher end of the frequency band, which are within 7 dB. We also investigated power handling capability of the transducer from thermal point of view using finite element analysis. The input impedance measurements agree well with the numerical results within the pass band.

2pEAg3. A lossy, one-dimensional, linear systems model for piezoelectric transducers containing opposing zones of polarization. Sivaram Nishal Ramadas (Institute of Sound and Vibration Research, University of Southampton, University Road, Highfield, S017 1BJ Southampton, UK, nishal@ieee.org)

Inversion layer transducers (ILT), consisting of two or more active, piezoelectrically opposed regions along their thickness direction, have attracted considerable interest in the recent past, due to the potential for wide bandwidth and even harmonic sensitivity. However, design and manufacture of such ILT devices are not straightforward due to the large number of degree of freedom involved. This paper presents the development of a lossy, computationally efficient analytical model to design ILT configuration. The mathematical formulation for a generalized linear systems model, applicable to arbitrary ILT configurations is presented. The model describes multiple active and passive layers, including zones of variable piezoelectric polarization, matching layers and bondlines. The model is extended further to include mechanical wave absorption in both the active transducer element and the propagating channel, and the effect of such frequency dependant loss on the operational characteristics of an ILT device is reported. Several simulation results are shown to demonstrate the feasibility of the approach together with a comparisonal analysis to conventional finite modeling techniques and experimental evaluations. The results indicate clearly that such approximate analytical techniques can be used effectively to design optimal ILT configurations.

2pEAg4. An analytical model for piezoelectric/elastic axisymmetric bender disks radiating in water. Raphaël Lardat (Thales Underwater Systems, 525 Route des Dolines, BP 157, 06930 Sophia Antipolis cedex, France, raphael.lardat@fr.thalesgroup.com)

Flextensional transducers have been widely studied for low frequency SONAR application due to the low celerity of the flexion wave. In this work, we will describe in detail a complete analytical model for an axisymmetric disk made of one elastic plate on which two piezoelectric disks of smaller radius have been reported on each side. The model, starting from flexural axisymmetric theory and from the piezoelectric equations, finally comprises local radiation impedance and mutual coupling with neighboring disks. In particular, we will explain the continuity conditions that are to be imposed at the external radius of the piezoelectric disk. We also show how to include a radiation force opposed and proportional to the normal velocity

inside the analytical solution given by a fourth order differential equation. The described model is then able to compute a large number of parameters such as Eigen modes, harmonic admittance, radiated pressure, coupling coefficient and static and dynamic stresses. The validity of the model is assessed by comparison to solutions of the coupled problem in water using classical FEM/BEM. We will show an extremely good agreement enabling us to use this simple model for geometry optimization and design improvement.

TUESDAY AFTERNOON, 1 JULY 2008 P2-D, LEVEL 2, 3:40 TO 5:20 P.M.

Session 2pMUa

Musical Acoustics and Physical Acoustics: Brass Instrument Acoustics II (Poster Session)

Thomas Moore, Cochair
Rollins College

Joël Gilbert, Cochair
Laboratoire d'Acoustique de l'Université du Maine

All posters will be on display from 3:40 p.m. to 5:20 p.m. To allow contributors an opportunity to see other posters, contributors of odd-numbered papers will be at their posters from 3:40 p.m. to 4:30 p.m. and contributors of even-numbered papers will be at their posters from 4:30 p.m. to 5:20 p.m.

2p TUE. PM

Contributed Papers

2pMUa1. Pedal notes of brass instruments, a mysterious regime of oscillation. Joël Gilbert (Laboratoire d'Acoustique de l'Université du Maine, Avenue Olivier Messiaen, 72085 Le Mans, France, joel.gilbert@univ-lemans.fr), Pierre Aumond (Lab. d'Acoustique Université du Maine, UMR CNRS 6613, 72085 Le Mans Cedex 9, France, pierre .aumond.etu@univ-lemans.fr)

In reed and brass instruments, sound is produced by self-sustained mechanical oscillations driven by an airflow coming from a pressure supply such as the player's lungs. Most of the time, the fundamental frequency of a periodic oscillation is close to, and mainly controlled by one given acoustic mode. Even though, these oscillations are the result of a complex non-linear coupling between all the acoustic modes and the mechanical valve. The pedal note, which is the lowest note that can be sounded on a brass instrument, is well-known as a counter-example. Eighty years ago, Bouasse did an experiment by replacing the brass mouthpiece by a reed mouthpiece on a brass instrument, and obtained a pedal note a fifth below! An elementary model dedicated to both cane-reed and lip-reed instruments can be used. In order to investigate the sound production of pedal notes, a simulation method based on modal decomposition of bore and reed dynamics has been carried out. Then, the periodic solutions of this model are obtained, and the mysterious oscillation regimes of Bouasse experiment are discussed.

2pMUa2. Nonlinear effects in the propagation of outgoing and reflected pulses inside a trombone. Pablo L Rendón (CCADET, Universidad Nacional Autónoma de México, Ciudad Universitaria, 04510 Mexico, Mexico, pablo.rendon@ccadet.unam.mx), Felipe Orduña-Bustamante (CCADET, Universidad Nacional Autónoma de México, Ciudad Universitaria, 04510 Mexico, Mexico, felipe.orduna@ccadet.unam.mx), Jacques Sorrentini (Institut Fresnel, UMR 6133 CNRS, Campus de Saint Jérôme, Av. Escadrille Normandie 13397, Cedex 20 Marseille, France, jacques.sorrentini@ec-marseille.fr), Antonio Pérez-López (CCADET, Universidad Nacional Autónoma de México, Ciudad Universitaria, 04510 Mexico, Mexico, antonio.perez@ccadet.unam.mx)

While sound propagation in a trombone can be generally quite properly described by linear models, it is commonly acknowledged that the ″brassiness″ of sound produced at high amplitudes is associated to nonlinear effects. Whether these effects are due principally to propagation inside a long, narrow pipe, or to the production of sound at the mouthpiece is still unclear. We present experimental measurements taken both from a long, narrow tube, and an actual slide trombone from which it is observed that the scale of nonlinear effects seems to be greater for outgoing pulses than for the reflected pulses at the open end of the trombone or tube. A theoretical model is also proposed, based on weakly nonlinear perturbations of linear theory, and is validated both by experimental results and by numerical simulations. The results indicate that both the amplitude and the shape of the initial perturbation produced at the trombone mouthpiece have an effect on the scale of propagation nonlinearity present inside the trombone resonator, and thus also on the ″brassy″ quality of sound.

2pMUa3. External sound radiation of vibrating trombone bells. Guillaume Nief (Laboratoire d'Acoustique de l'Université du Maine, Avenue Olivier Messiaen, 72085 Le Mans, France, guillaume .nief.etu@univ-lemans.fr), François Gautier (Laboratoire d'Acoustique de l'Université du Maine, Avenue Olivier Messiaen, 72085 Le Mans, France, francois.gautier@univ-lemans.fr), Jean-Pierre Dalmont (Laboratoire d'Acoustique de l'Université du Maine, Avenue Olivier Messiaen, 72085 Le Mans, France, Jean-Pierre.Dalmont@univ-lemans.fr), Joël Gilbert (Laboratoire d'Acoustique de l'Université du Maine, Avenue Olivier Messiaen, 72085 Le Mans, France, joel.gilbert@univ-lemans.fr)

The issue of the influence of bell vibrations on the sound of brass instruments is still debated. For such instruments, external sound field is the superposition of the sound field resulting from acoustic oscillations of the air column and the sound field resulting from direct radiation of the bell and walls. The aim of this paper is to quantify the bell contribution with respect to the air column one, and to examinate the conditions for which the former may become audible. For this purpose, the structural modes of a trombone bell are identified using an experimental modal analysis. For each mode shape, the radiation efficiency is computed using a model of the radiated sound based on a distribution of equivalent monopoles. A critical frequency is defined for the bell and allows us to determine at which condition a given structural mode is radiating. Measurements of the sound power radiated by a trombone excited by an harmonic acoustic source are carried out when the bell is free to vibrate and when bell vibrations are damped. Comparison between the two configurations is analyzed using the developed model and is used to quantify the sound power due to bell vibrations.

2pMUa4. Acoustic radiation of wind instruments resonators. Bastien Mallaroni (Laboratoire de Mécanique et d'Acoustique - CNRS, 31 chemin Joseph Aiguier, 13402 Marseille, France, mallaroni@lma.cnrs-mrs.fr), Pierre-Olivier Mattei (Laboratoire de Mécanique et d'Acoustique - CNRS, 31 chemin Joseph Aiguier, 13402 Marseille, France, mattei@lma.cnrs-mrs.fr), Philippe Herzog (Laboratoire de Mécanique et d'Acoustique - CNRS, 31 chemin Joseph Aiguier, 13402 Marseille, France, herzog@lma.cnrs-mrs.fr)

Optimization of the acoustic radiation of wind instruments resonators may be based on the study of finite length circular ducts radiating in unbounded medium, as this is a model realistic enough, but which allows advanced analytics developments. Our approach is based on the calculation of resonance frequencies of such a simplified wind instrument. These are the complex frequency singularities of the operator describing the global resonator/external fluid system. A Newton's method is used to search for the singularities of the multimodal Green's function of the duct. This is obtained by the product of impedance matrices which relate pressure and velocity between two abscissae inside the duct. A variable coupling factor is introduced with external acoustic radiation, described by a multimodal radiation impedance based on the Zorumski formulation. Examples of variation of the resonance frequencies with this coupling factor will be given. Surprisingly, regular variations of the coupling lead to non regular evolution of the resonances. Physical interpretation of this behaviour will be discussed.

2pMUa5. Transient behaviour of human and artificial brass players' lips. Samuel Stevenson (Edinburgh University, 4201 JCMB, Kings Buildings, Mayfield Road, EH9 3JZ Edinburgh, UK, samuel.stevenson@ed.ac.uk), Donald M. Campbell (Edinburgh University, 4201 JCMB, Kings Buildings, Mayfield Road, EH9 3JZ Edinburgh, UK, d.m.campbell@ed.ac.uk), John Chick (Edinburgh University, 4201 JCMB, Kings Buildings, Mayfield Road, EH9 3JZ Edinburgh, UK, john.chick@ed.ac.uk), Joël Gilbert (Laboratoire d'Acoustique de l'Université du Maine, Avenue Olivier Messiaen, 72085 Le Mans, France, joel.gilbert@univ-lemans.fr), Stefan Bilbao (University of Edinburgh, Room 7306B, JCMB, King's Bldgs., Mayfield Rd., EH9 3JZ Edinburgh, UK, sbilbao@staffmail.ed.ac.uk)

It is widely accepted that the starting transient is an extremely significant perceptual feature of musical sound. For players, the ease with which a note can be started on a particular instrument is also of great importance. However, until recently research has concentrated on the analysis of steady state sounds rather than the study of the starting behaviour of the instrument. The work reported here uses a high speed camera to capture the motion of lip reeds during the starting transient. Simultaneous recordings are made of the pressure signals generated in the mouthpiece of the instrument and radiated from the bell. Preliminary results on human players, already presented, have been extended and supplemented by measurements using an artificial mouth in order to separate effects due to the instrument from those dependent on the expertise of a particular human player. Computational simulations have been compared to these experimental findings.

2pMUa6. Tristan trumpet or English horn? Robert W. Pyle (S. E. Shires Co., 11 Holworthy Place, Cambridge, MA 02138, USA, rpyle@post.harvard.edu), Sabine K. Klaus (National Music Museum, The University of South Dakota, PO Box 190, Landrum, SC 29356, USA, sabineklaus@alltel.net)

In Act III of his opera "Tristan und Isolde", Richard Wagner wrote an instrumental tune to be (apparently) played by a shepherd. This was originally scored for, and is customarily played by, an off-stage cor anglais. Wagner indicated that he would have preferred some form of wooden trumpet, similar to a small-scale alphorn. A few such instruments have been built. These are pitched in 4-foot C, with a pear-shaped bell similar to that of the cor anglais, and a single metal whole-tone valve. The Utley Collection at the National Music Museum, The University of South Dakota, has two such instruments: one made by Gebrüder Alexander (Mainz), formerly used in the National Opera in Prague (Volkstheater), the other a copy of a trumpet by Martin Lehner, Munich, in the possession of the Staatsoper Dresden, made by Andreas Schöni and Rainer Egger (Bern and Basel). We will compare sound spectra of the Tristan trumpet with that of the cor anglais. We will also compare the acoustic input impedance of the Tristan trumpet with that of an ordinary trumpet of the same pitch.

2pMUa7. Harmonicity of trumpet modes. Peter L. Hoekje (Baldwin-Wallace College, 275 Eastland Rd., Berea, OH 44017, USA, phoekje@bw.edu), Michael Attaway (Richardson ISD, 400 S. Greenville Ave., Richardson, TX 75081, USA, michael_attaway@hotmail.com)

The mouthpiece on a brass instrument is generally removable but constitutes an important part of the whole instrument. In the frequency domain, it can be considered to provide a frequency dependent equivalent length that increases with frequency up to the Helmholtz resonance frequency f_{pop} of the mouthpiece itself. Geometrical changes that affect the total volume or the f_{pop} of the mouthpiece will affect the harmonicity of the nearly harmonic normal modes of the instrument. Using heterodyne filter analysis, the development of the frequency components and their amplitudes were measured for low trumpet notes, both for repeated attacks of short notes and for sustained note crescendos from pianissimo to fortissimo. The measurements were repeated after the mouthpiece was modified to improve the harmonicity of the normal modes. During both attack and crescendo tests, the modified mouthpiece was associated generally with more stable frequencies of the partials and more even development of the amplitudes of the partials.

2pMUa8. The influence of braces on the playability of trumpets. Alexander Mayer (Inst. f. Wiener Klangstil, Univ. f. Music, Anton von Webernplatz 1, A-1030 Vienna, Austria, mayer@mdw.ac.at), Rainer Egger (Blechblas-Instrumentenbau Egger, Turnerstrasse 32, 4058 Basel, Switzerland, info@eggerinstruments.ch), Gregor Widholm (Inst. f. Wiener Klangstil, Univ. f. Music, Anton von Webernplatz 1, A-1030 Vienna, Austria, Widholm@mdw.ac.at)

The influence of braces on the playability, response and sound properties of the trumpet is an intense discussed subject for players and instrument makers. In addition to the problem of finding the proper position of the braces, inserted braces can produce stress between the instruments tubes. In this paper the influence of the tube stress is investigated. To ensure an adjustable and reproducible stress between the trumpet tubes special adjustable braces in conjunction with a force monitor are used. The results of blind playing tests are compared with spectral analysis of the played sounds. In addition, the acoustic input impedance, the wall vibrations and the transfer function of the instrument are investigated.

Session 2pMUb

Musical Acoustics: Edge Tone and Flue Pipes II (Poster Session)

Shigeru Yoshikawa, Cochair
Kyushu University

Judit Angster, Cochair
Fraunhofer Institute for Building Physics

All posters will be on display from 3:40 p.m. to 5:20 p.m. To allow contributors an opportunity to see other posters, contributors of odd-numbered papers will be at their posters from 3:40 p.m. to 4:30 p.m. and contributors of even-numbered papers will be at their posters from 4:30 p.m. to 5:20 p.m.

Contributed Papers

2pMUb1. Vortex sound of the flute and its interpretation. Andreas Bamberger (Physics Institute University Freiburg, Hermann-Herder-Str. 3, 79104 Freiburg, Germany, bamberger@physik.uni-freiburg.de)

The flute as an example of flue instruments is investigated for its properties of the jet-labium interaction at 1kHz. The jet and the externally excited acoustic flow in the embouchure especially near the labium is recorded with endoscopic Particle-Image-Velocimetry. Extracting the vorticity the data allows us to calculate the vortex sound according to M. How (1975) . The far field acoustic power of the flute is measured as well and compared with the vortex sound power, which matches in sign and magnitude up to a factor 2 for different sound levels. The non-trivial interpretation of the sound production is based on the near cancellation of the two vortex layers of the jet along its path except near the labium. In order to gain insight of the interplay of the different ingredients of the vortex sound power the coriolis force, the acoustic field and their phase relation are determined. Scaling of laws for these quantities as a function of the jet velocity/pressure of the standing wave are deduced and compared with the acoustic power dependence. A comparison with recently available numerical simulations (ISMA 2007) is discussed.

2pMUb2. Experimental investigation of the aeroacoustic coupling of self-sustained tones to non-planar modes of a resonator. Martin Glesser (CNRS - LMA, 31 Chemin Joseph Aiguier, 13009 Marseille, France, glesser@lma.cnrs-mrs.fr), Vincent Valeau (Laboratoire d'Etudes Aérodynamiques (LEA), Université de Poitiers - ENSMA - CNRS, Bâtiment K, 40 Avenue du Recteur Pineau, F-86022 Poitiers, France, vincent.valeau@lea.univ-poitiers.fr), Anas Sakout (LEPTIAB Université de La Rochelle, Avenue Michel Crépeau, 17042 La Rochelle Cedex 01, France, asakout@univ-lr.fr)

Recent studies have shown that a jet-slot oscillator (ie, an aeroacoustic self-sustained source consisting of the impingement of the vortical structures of a plane jet on a slotted plate) can be coupled to non-planar modes of the flow-supply duct. This phenomenon occurs in the particular case where the jet-exit and the obstacle are misaligned in the spanwise direction. This paper presents an experimental investigation of the excited modes as a function of the plate inclination angle, and of the distance between the jet-exit and the slot. It is shown that: (i) the vortex-tubes spanwise morphology is governed by the nature of the transverse excited modes, and (ii) the vortices tend to impinge on the inclined obstacle almost in phase in the spanwise direction, in order to enhance the coherence of the interaction along the slot. Moreover, an elementary analytical model of the resonant acoustic field shows that the ratio between the transverse and planar modes amplitudes is tuned by the system in order to keep this coherence maximum. The existence of a so-called ″opposed transverse mode″ is also shown, generating vortices with an inclination angle opposed to the plate inclination angle.

2pMUb3. Open and closed loop characterization of an air-jet reflection amplifier. John C. Price (University of Colorado, Department of Physics, 390 UCB, Boulder, CO 80309-0390, USA, john.price@colorado.edu)

Our laboratory has embarked on an effort to understand the steady-state behavior of a Yamaha YRT-304B tenor recorder. The instrument is split at the head-joint, and both sides are studied with a multi-microphone reflectometer using sinusoidal excitation. For the head joint, data is obtained versus frequency, blowing pressure, and excitation amplitude. We have two goals: First, to use our open-loop reflectometry data to understand the internal acoustic spectrum of the assembled instrument, as a function of blowing pressure and fingering; and second, to provide a well-defined set of open-loop observables for comparison with hydrodynamic calculations of the air-jet dynamics. This particular instrument is attractive for several reasons: it disassembles at a straight cylindrical section of the bore, and so is easily coupled to straight waveguide; it is large enough for accurate reflection coefficient and internal pressure measurements; it can be studied closed-loop as a complete instrument; and it represents a fiducial geometry that is readily available to any laboratory.

Session 2pMUc

Musical Acoustics: Acoustic Measurements on Wind Instruments II (Poster Session)

Noam Amir, Cochair
Tel Aviv University

David B. Sharp, Cochair
Open Univeristy

All posters will be on display from 3:40 p.m. to 5:20 p.m. To allow contributors an opportunity to see other posters, contributors of odd-numbered papers will be at their posters from 3:40 p.m. to 4:30 p.m. and contributors of even-numbered papers will be at their posters from 4:30 p.m. to 5:20 p.m.

Contributed Papers

2pMUc1. Sound power level measurement of Sheng, a Chinese wind instrument. Yue Zhe Zhao (State Key Laboratory of Subtropical Building Science, South China University of Technology, 381 Wushan Street, 510640 Guangzhou, China, arzhyzh@scut.edu.cn), Shuo Xian Wu (State Key Laboratory of Subtropical Building Science, South China University of Technology, 381 Wushan Street, 510640 Guangzhou, China, arshxwu@scut.edu.cn), Jian Zhen Qiu (State Key Laboratory of Subtropical Building Science, South China University of Technology, 381 Wushan Street, 510640 Guangzhou, China, qjianzhen@gmail.com), Li Ling Wu (Dept. of Musicology, Xinghai Conservatoire of Music, 510500 Guangzhou, China, wushijun@scut.edu.cn), Hong Huang (Dept. of Musicology, Xinghai Conservatoire of Music, 510500 Guangzhou, China, yyxyhuanghong@163.com)

Sheng is one of the Chinese traditional wind instruments. But its sound power level has never been carefully measured. In this paper, the sound power measurements of Sheng were performed for the first time in a reverberation chamber according to ISO standard and Chinese national standard. Two qualified musicians performed on their own instruments in the center of the reverberation chamber. The radiated sound energy and the dynamic ranges of the Sheng were investigated by four channel acoustic measuring equipments. Typical sound power values were obtained through averaging and the results were reported in this paper. It was showed that the mean forte sound power level can reach up to 98dB with a dynamic range of 22.5dB when music scale was performed. The method discussed here is valuable for the sound power measurements of other musical instruments. The measurement of the sound power radiated by national musical instruments lays foundations for the investigation into the acoustics of national music halls.

2pMUc2. Measurements of woodwind tone-hole parameters using a double impedance head method. Paul Dickens (University of New South Wales, Music Acoustics, School of Physics, NSW 2052 Sydney, Australia, PDickens@resmed.com.au), Yakov Kulik (University of New South Wales, Music Acoustics, School of Physics, NSW 2052 Sydney, Australia, ykulik@phys.unsw.edu.au), Joe Wolfe (University of New South Wales, Music Acoustics, School of Physics, NSW 2052 Sydney, Australia, J.Wolfe@unsw.edu.au)

A woodwind tone hole is often represented as a T-junction with a shunt and series impedance. We measured the frequency dependence of the series and shunt impedances of open and closed tone holes using a pair of impedance heads, one on either side of a symmetric section of short bore pipe with a finger hole, and each calibrated on resonance-free loads. The shunt impedance is most accurately measured when the hole is located at a pressure antinode (speakers in phase) and the series impedance at a pressure node (speakers in anti-phase). We use both conditions, in this way, to measure series and shunt impedances for all frequencies studied. Pipes with the same length and diameter, but having wall thicknesses 1.5-5.0 mm and tone hole diameters 1.5-15.0 mm were used. For open holes, results are compared with calculations and results measured using other methods. The results for holes closed with fingers are also used to calculate the effective length of finger intrusion. Examples of the inclusion of the results into woodwind models are given.

2pMUc3. Investigation of clarinet reed auto-oscillations with digital Fresnel holography. Denis Mounier (LPEC/UMR 6087/CNRS/Université du Maine, Avenue Olivier Messiaen, 72085 Le Mans Cedex 09, France, denis.mounier@univ-lemans.fr), Pascal Picart (Laboratoire d'Acoustique de l'Université du Maine, Avenue Olivier Messiaen, 72085 Le Mans, France, pascal.picart@univ-lemans.fr), Julien Leval (Laboratoire d'Acoustique de l'Université du Maine, Avenue Olivier Messiaen, 72085 Le Mans, France, julien.leval.etu@univ-lemans.fr), Francis Piquet (Laboratoire d'Acoustique de l'Université du Maine, Avenue Olivier Messiaen, 72085 Le Mans, France, francis.piquet@univ-lemans.fr), Jean-Pierre Boileau (Laboratoire d'Acoustique de l'Université du Maine, Avenue Olivier Messiaen, 72085 Le Mans, France, jean-pierre.boileau@univ-lemans.fr), Thomas Guimezanes (Laboratoire d'Acoustique de l'Université du Maine, Avenue Olivier Messiaen, 72085 Le Mans, France, thomas.guimezanes@univ-lemans.fr), Jean-Pierre Dalmont (Laboratoire d'Acoustique de l'Université du Maine, Avenue Olivier Messiaen, 72085 Le Mans, France, Jean-Pierre.Dalmont@univ-lemans.fr)

This paper describes a full field digital holographic method for studying the cinematic of the vibration of the clarinet reed in playing conditions in an artificial mouth. Since many years, LAUM is interested in studying musical instruments and particularly the clarinet. The behaviour of such an instrument is particularly complex because it depends on aerodynamics, contact between reed and beak, and interaction with the lip of the musician. Thus, visualisation of the full movement of the reed in playing conditions is necessary to better understand physics of the clarinet. However, free oscillations have high amplitude of several hundreds of micrometers, thus corresponding to several thousand times the laser wavelength. The analysis of the movement is performed by a laser tracking of the vibration. It is demonstrated that it is possible to reconstruct a synthetic high amplitude deformation of auto-oscillations encoded with digital Fresnel holograms. The setup is applied to the auto-oscillation of the clarinet reed in a synthetic mouth. Tracking of the vibration is performed by using the pressure signal delivered by the mouth. Experimental results show the four steps of the reed movement and especially emphasize the shocks of the reed on the mouthpiece.

Session 2pMUd

Musical Acoustics: Interaction Between Instrument and Instrumentalist II (Poster Session)

Gary Scavone, Cochair
Schulich School of Music, McGill University

Xavier Boutillon, Cochair
Laboratoire de Mécanique des Solides

All posters will be on display from 3:40 p.m. to 5:20 p.m. To allow contributors an opportunity to see other posters, contributors of odd-numbered papers will be at their posters from 3:40 p.m. to 4:30 p.m. and contributors of even-numbered papers will be at their posters from 4:30 p.m. to 5:20 p.m.

Contributed Papers

2pMUd1. Chest wall dynamics and respiratory muscle recruitment during flute playing. Isabelle Cossette (McGill University, 555, Sherbrooke St, Montréal, QC H3A 1E3, Canada, isabelle.cossette1@mcgill.ca), Pierpaolo Monaco (McGill University, 555, Sherbrooke St, Montréal, QC H3A 1E3, Canada, pierpal@yahoo.it), Andrea Aliverti (Politecnico di Milano, Dipartimento di Bioingegneria, P.zza Leonardo da Vinci, 32, 20133 Milano, Italy, andrea.aliverti@polimi.it), Peter Macklem (PO Box 250, Lansdowne, ON K0E 1L0, Canada, peter.macklem @gmail.com)

Respiratory parameters and sound were recorded during professional flute playing in order to assess what physiological processes were associated with the control of sound production that results in 'breath support' which in turn is associated with high quality playing. Four standing young professional flautists played flute excerpts with different technical requirements with and without breath support. Recordings included optoelectronic plethysmographic measurements of chest wall volume (Vcw) and its compartments, surface electromyography of the scalene, lateral abdominal, rectus abdominus, parasternal and sternocleidomastoid muscles, mouth pressure, and sound. Flow was estimated from differentiating Vcw during playing. Comparison in between various types of playing were performed. Results showed that flute support entails antagonistic contraction of non-diaphragmatic inspiratory muscles that tends to hold the rib cage at higher lung volume during long legato phrase playing. This relieves the expiratory muscles from the task of producing the right mouth pressure, especially at the end of the phrases, so they can contribute more to the finer control of mouth pressure modulations required for high quality playing.

2pMUd2. A concise overview of present knowledge of bowed-string gestures and their acoustical consequences. Knut Guettler (Norwegian Academy of Music, P.O.Box 5190 Majorstuen, 0302 Oslo, Norway, knut .guettler@nmh.no)

During the few years of our young millennium the picture of what happens acoustically when the bow is drawn across the string has become considerably more complete. A few surprises emerged along the way: the bow's position on the string does not seem to influence the spectral envelope-and different from what Schelleng predicted-there seems to be no clear correlation between minimum bow force and the bow speed. The intention of this presentation is to give a brief survey of related studies and their results, as well as pointing out some of the blank spots still remaining on the canvas.

Session 2pMUe

Musical Acoustics and Speech Communication: Singing Voice and Source-Filter Interaction

Brad Story, Cochair
University of Arizona, Dept. of Speech and Hearing Sciences, 1131 E. 2nd Street, Tucson, AZ 85721-0071, USA

Nathalie Henrich, Cochair
Département Parole & Cognition, GIPSA-lab, 46, avenue Félix Viallet, Grenoble Cedex, 38031, France

Contributed Paper

5:20

2pMUe1. How whisper and croak phonation affect vocal tract resonances. Yoni Swerdlin (University of New South Wales, Music Acoustics, School of Physics, NSW 2052 Sydney, Australia, yoniswerdlin@hotmail.com), John Smith (University of New South Wales, Music Acoustics, School of Physics, NSW 2052 Sydney, Australia, john.smith@unsw.edu.au), Joe Wolfe (University of New South Wales, Music Acoustics, School of Physics, NSW 2052 Sydney, Australia, J.Wolfe @unsw.edu.au)

The whisper and croak modes of phonation provide convenient broad band excitation of the vocal tract and thus give relatively precise information about tract resonances. How closely do the measured resonances for these mechanisms approximate those of normal speech? We measured the frequencies of the first four resonances (R1-R4) in normal, whisper and croak phonation. Subjects produced pairs of these phonations in the same vocal gesture. Formants were used to measure the frequencies (R1-R4) for the non-periodic phonations and broad band excitation at the mouth was used to measure them with similar precision in normal speech. For R1 to R4 respectively, whispering raised the resonant frequencies by 255±90 Hz (92)*, 115±105 Hz (119)*, 125±125 Hz (109)* and 75±120 Hz (118)*, (mean ± standard deviation (n), asterisks show significance at the 5% level). These values, and their decrease with increasing frequency, are consistent with the effect of the increased glottal opening in whispering only if the increased opening is large. A supra-glottal narrowing in the tract could also help raise the frequencies of resonance. Croak phonation raises the resonant frequencies respectively by 45±50 Hz (121)*, 10±60 Hz (124), 65±120 Hz (109)* and 15±110 Hz (108).

Invited Papers

5:40

2pMUe2. Vocal folds and ventricular bands in interaction: comparison between 'in vivo' measurements and theoretical predictions. Lucie Bailly (Département Parole & Cognition, GIPSA-lab, 46, avenue Félix Viallet, 38031 Grenoble Cedex, France, Lucie.Bailly@gipsa-lab.inpg.fr), Nathalie Henrich (Département Parole & Cognition, GIPSA-lab, 46, avenue Félix Viallet, 38031 Grenoble Cedex, France, Nathalie.Henrich@gipsa-lab.inpg.fr), Xavier Pelorson (Département Parole & Cognition, GIPSA-lab, 46, avenue Félix Viallet, 38031 Grenoble Cedex, France, pelorson@icp.inpg.fr), Joël Gilbert (Laboratoire d'Acoustique de l'Université du Maine, Avenue Olivier Messiaen, 72085 Le Mans, France, joel.gilbert@univ-lemans.fr)

Period-doubling occurrences have been found during singing phonations such as Mongolian *Kargyraa* throat singing or Sardinian *A Tenore* Bassu singing. The combined vibrations of vocal folds and ventricular bands have been observed during the production of such low-pitch bass-type sounds. The present study aims at better understanding the physical interaction between the ventricular-bands vibration and the vocal-folds self-sustained oscillations. In this paper, the vibratory properties of both vocal folds and ventricular bands in interaction are analysed on a professional singer by means of acoustical, electroglottographic signals and synchronized glottal images obtained by high-speed cinematography. Using the detected glottal and ventricular areas, the aerodynamic behavior of the laryngeal system is simulated using a simplified aerodynamic modelling previously validated ″in vitro″ on vocal-folds and ventricular-bands replica. An estimate of the subglottal pressure along with the ventricular aperture extracted from the ″in vivo″ data allows a theoretical prediction of the glottal aperture. The ″in vivo″ measurements of the glottal aperture are then compared to the simulated estimations. The influence of the subglottal pressure is also discussed.

6:00

2pMUe3. Longitudinal voice source and acoustic analysis of English girl cathedral choristers. David M. Howard (University of York, Department of Electronics, Heslington, YO10 5DD York, UK, dh@ohm.york.ac.uk)

Since 1998, the authors have been recording girl choristers who sing at Wells Cathedral in England to enable a longitudinal quantitative exploration of voice development for girls aged between 8 and 16 who are involved in professional choral singing on a daily basis. The recordings are made of their acoustic output and the output from an electrolaryngograph for a series of vocal tasks including speaking and singing. Changes have been observed on a longitudinal basis for larynx closed quotient (the percentage of each cycle for which the vocal folds remain closed), long-term average spectra as well as in the overall spectral coverage in terms of frequency and dynamic ranges. Evidence of observations will be presented and their implications will be discussed with reference to source-filter interaction as appropriate.

Contributed Papers

6:20

2pMUe4. Phonetograms of laryngeal source parameters for different vowels and laryngeal mechanisms. Sylvain Lamesch (IJLRA-LAM, 11, rue de Lourmel, 75015 Paris, France, lamesch@lam.jussieu.fr), Boris Doval (LIMSI-CNRS, B.P. 133, 91403 Orsay Cedex, France, boris.doval@limsi.fr), Michèle Castellengo (IJLRA-LAM, 11, rue de Lourmel, 75015 Paris, France, castel@ccr.jussieu.fr)

This paper explores how the laryngeal source is adjusted by the singer when the sung vowel changes. As the source parameter adjustments may depend on intensity and pitch, comparisons are done through phonetograms computed for each vowel. Distinction is made in the phonetograms between the two main laryngeal mechanisms (M1 and M2). Male and female subjects were recorded producing crescendos and decrescendos from C3 to C5 on /a/, /i/ and /o/ in order to obtain a reduced phonetogram for each vowel and each laryngeal mechanism. Sound, electroglottographic signals and vertical larynx position (VLP) were recorded. Investigations were done on the open quotient and the VLP. The results show a smaller vocal dynamic on /i/ (and in a smaller extent on /o/) in each laryngeal mechanism, and differences on the intensity low limit of the highest part of the M1-phonetogram. Clear tendencies about the larynx position were measured. They are similar for both laryngeal mechanisms, but differ among singers. The Oq seems to be lower on /i/ than on /a/ and /o/ for M1 productions.

6:40

2pMUe5. Resonance strategies and glottal behaviour in the two main laryngeal mechanisms for professional operatic singers. Nathalie Henrich(Département Parole & Cognition, GIPSA-lab, 46, avenue Félix Viallet, 38031 Grenoble Cedex, France, Nathalie.Henrich@gipsa-lab.inpg.fr), John Smith (University of New South Wales, Music Acoustics, School of Physics, NSW 2052 Sydney, Australia, john.smith@unsw.edu.au), Joe Wolfe (University of New South Wales, Music Acoustics, School of Physics, NSW 2052 Sydney, Australia, J.Wolfe@unsw.edu.au)

In lyrical singing, two principal laryngeal mechanisms are used to produce all the notes across the singer's tessitura. Laryngeal mechanisms M1 and M2 are characterised by a greater and lesser vibrating mass respectively. Different timbres between the two are at least partly explained by their different glottal behaviours. However, different adjustments of the vocal-tract resonances, which can also contribute to different timbres, may also be involved, but have been neglected. We studied seven professional operatic singers, who produced sustained vowels at the same pitch using both laryngeal mechanisms. Vocal-tract resonances were directly measured during phonation, by broadband acoustic excitation at the mouth. Glottal behaviour and laryngeal movement were measured indirectly with an electroglottograph. As expected, we measured lower values of open quotient and higher sound pressure levels in M1 than in M2. In most cases, the first two vocal-tract resonances were characterised by lower frequencies in M2 than in M1. In the singer's formant region, similar resonance-frequency values were found for both laryngeal mechanisms. The effect on the sound spectrum of an open-quotient increase together with a first-formant decrease may be modelled by source-filter theory. The theoretical and measured amplitudes of the first two harmonics will be compared.

Invited Paper

7:00

2pMUe6. Chest, head and whistle registers in an untrained female singer analyzed by videokymography, strobolaryngoscopy and sound spectrography. Jan G. Svec (Palacky University Olomouc, Faculty of Science, Dept. Experimental Physics, Laboratory of Biophysics, Tr. Svobody 26, CZ-771 46 Olomouc, Czech Republic, svecjan@vol.cz), Johan Sundberg (KTH, Department of Speech, Music and Hearing, Lindstedtsvägen 24, SE-100 44 Stockholm, Sweden, jsu@csc.kth.se), Stellan Hertegard (Karolinska University Hospital Huddinge, Dept. Logopedics and Phoniatrics, SE-141 86 Stockholm, Sweden, Stellan.Hertegard@ki.se)

There has been a lack of objective data on the singing voice registers, particularly on the so called ″whistle″ register, occurring in the top part of the female pitch range, which is accessible only to some singers. This study offers unique strobolaryngoscopic and high-speed (7812.5 images/s) videokymographic data on the vocal fold behavior of an untrained female singer capable of producing three distinct voice qualities, i.e., the chest, head and whistle registers. The sound was documented spectrographically. The transition from chest to head register, accompanied by pitch jumps, occurred around tones B4-C#5 (500-550 Hz) and was found to be associated with a slight decrease in arytenoids adduction, resulting in decrease of the closed quotient. The register shifts from head to whistle, also accompanied by pitch jumps, occurred around tones E5-B5 (670-1000 Hz) without any noticeable changes in arytenoids adduction. Some evidence was found for the vocal tract influence on this transition. The mechanism of the vocal fold vibration in whistle register was found principally similar to that at lower registers: vibrations along the whole glottal length and vertical phase differences (indicated by sharp lateral peaks in videokymography) were seen on the vocal folds up to the highest tone G6 (1590 Hz).

Contributed Paper

7:20

2pMUe7. Sopranos' secondo passagio: a resonance adjustment and/or a laryngeal transition to the whistle voice? Maeva Garnier (University of New South Wales, Music Acoustics, School of Physics, NSW 2052 Sydney, Australia, maeva.garnier@gmail.com), Nathalie Henrich (Département Parole & Cognition, GIPSA-lab, 46, avenue Félix Viallet, 38031 Grenoble Cedex, France, Nathalie.Henrich@gipsa-lab.inpg.fr), John Smith (University of New South Wales, Music Acoustics, School of Physics, NSW 2052 Sydney, Australia, john.smith@unsw.edu.au), Joe Wolfe (University of New South Wales, Music Acoustics, School of Physics, NSW 2052 Sydney, Australia, J.Wolfe@unsw.edu.au)

How are glottal source and vocal tract involved in the sopranos' passagio around E5? This pilot study investigates a legit soprano singing C5 to C6 with a lyrical technique and C5 to D7 in a ″light″ voice. On (de)crescendi and glissandi over the passagio, we observed clear bifurcations from ″light″ to lyrical mode, with discontinuous changes in f0, larynx vertical position, amplitude and shape of the electroglottographic signal. No such discontinuities occurred from C5 to D7 within the ″light″ mode. We established phonetograms of both modes and characterised differences in voice quality (Spectrum, Harmonicity, Open quotient). For [oe] in both modes, this singer tunes the first vocal tract resonance (R1) to f0 over the passagio. For a free vowel, a single and strong resonance is observed in the ″light″ mode, which may correspond to the merging of R1 and R2 and which is tuned to 2 f0 below C6, then to f0 until F6. Above F#6, two resonances are observed again and R2 is tuned to f0. All these observations suggest that, for this singer, the secondo passagio may correspond to both a resonance adjustment and a transition from the second laryngeal mechanism to the third, also called whistle voice.

Session 2pNSa

Noise, ASA Committee on Standards and EURONOISE: Sound Quality Tools and Applications I

Wade R. Bray, Cochair
HEAD acoustics, Inc., 6964 Kensington Road, Brighton, MI 48116, USA

Klaus Genuit, Cochair
HEAD acoustics GmbH, Ebertstrasse 30a, Herzogenrath, 52134, Germany

Etienne Parizet, Cochair
Laboratoire Vibrations Acoustique, Insa Lyon, 25 bis, av. J. Capelle, Villeurbanne Cedex, 69621, France

Invited Papers

2:00

2pNSa1. How loud is low frequency noise? Norm Broner (Sincliar Knight Merz, 590 Orrong Road, Armadale, 3143 Melbourne, Australia, nbroner@skm.com.au)

When it comes to assessing noise, the conventional wisdom is that the loudness of a sound will correlate well with its perceived annoyance. On this basis, the A-weighted sound pressure level is also assumed to correlate with the potential percieved annoyance of a sound. This might well be a reasonable assumption for mid range frequency sounds. But for low frequency sounds, particularly below 63 Hz, the assumption that loudness is correlated highly with perceived annoyance breaks down. Indeed, while loudness adaptation may occur for low frequency sound, the annoyance can increase with time. Thus, with time, the annoyance may keep increasing while the apparent loudness decreases!

2:20

2pNSa2. Metric assessment of subjective annoyance due to low frequency aircraft noise. Kathleen Hodgdon (Applied Research Laboratory, The Pennsylvania State University, P.O. Box 30, State College, PA 16804, USA, kkh2@psu.edu), Matthew L. Nickerson (IBM, 3039 Corwallis Road, Durham, NC 27709, USA, mlnicker@us.ibm.com), Anthony A. Atchley (The Graduate Program in Acoustics, The Pennsylvania State University, PO Box 30, State College, PA 16804, USA, atchley@engr.psu.edu), Thomas Gabrielson (The Graduate Program in Acoustics, The Pennsylvania State University, PO Box 30, State College, PA 16804, USA, tbg3@psu.edu)

A low frequency noise study was conducted at the Pennsylvania State University to investigate human response to the low frequency content of aviation noise. Metric assessment included level based and loudness metrics, including time-varying loudness. Current predictive noise models and metrics may underestimate the impact of low-frequency noise produced by aviation noise. Assessing the role of low frequency noise on human response will facilitate understanding how this type of noise can impact communities. Indoor recordings of aircraft arrivals and departures at Washington Dulles International Airport made in 2004 were used to assess subjective noise annoyance. These recordings and low-frequency variants of these recordings were reproduced for subjects through the Gulfstream Supersonic Acoustic Signature Simulator II (SASS II); the signatures were then rated for annoyance. Subjective judgments were statistically analyzed and compared against objective metrics that were calculated for each signature. Results are shown that all things being equal higher levels of low-frequency content in aircraft noise can result in increased annoyance in subjects. The C-weighted sound exposure level was found to correlate well with the subjective annoyance response.

2:40

2pNSa3. Sound character ratings by experienced and naive listeners. Reinhard Weber (Oldenburg University, Institute of Physics - Acoustics, Carl-von-Ossietzky Str. 9-11, 26111 Oldenburg, Germany, Reinhard.Weber@uni-oldenburg.de), Hans Hansen (IRCAM - Sound Perception & Design, 1 place Igor Strawinsky, 75004 Paris, France, Hans_Hansen@gmx.de)

In the frame of a cross-cultural study on pitch perception of tones in noise, two different groups of participants took part in the listening tests in France. Trained in psycho-acoustic evaluation tasks, members of the laboratory belonged to the first group, whereas the second one consisted of naïve students. 25 stimuli with different tone-to-noise ratios were presented via headphones and, using a semantic differential of 14 adjective pairs, the participants made their judgements on common seven step scales. For both listening groups a PCA of the results led to the same three orthogonal dimensions of the perceptual spaces. They were identified in accordance to Namba's findings as 'pleasant', 'metallic' and 'powerful' factors with an interesting difference: For the trained, the 'metallic' factor, preferably describing the sound character, explained the largest amount of total variance as first factor. The 'pleasant' factor as 'evaluation' dimension took the second place and the 'powerful' factor ranked behind. However, the order of the first two factors was reversed for the untrained listeners. For them the variance of 'pleasant' factor was a bit higher compared to the 'metallic' factor. So the variance in sound character judgements was higher for the trained compared to the untrained listeners.

Contributed Papers

3:00

2pNSa4. Optimising the value of sound quality evaluations by observing assessors' driving strategies. Sebastiano S. Giudice (WMG, University of Warwick, Gibbet Hill Road, CV47AL Coventry, UK, S.D.Giudice@warwick.ac.uk), Paul Jennings (WMG, The University of Warwick, International Manufacturing Centre, CV4 7AL Coventry, UK, paul.jennings@warwick.ac.uk), Rebecca Cain (WMG, The University of Warwick, International Manufacturing Centre, CV4 7AL Coventry, UK, R.Cain.1@warwick.ac.uk), Garry Dunne (Jaguar & LandRover, Jaguar Engineering Center Abbey Road, Whitley, CV3 4LF Coventry, UK, gdunne@jaguar.com), Mark Allman-Ward (Sound Evaluations Ltd, 18 Walsworth Road, Hitchin, Hertfordshire, SG49SP Hitchin, UK, mallman@soundevaluations.com), Roger Williams (Sound Evaluations Ltd, 18 Walsworth Road, Hitchin, Hertfordshire, SG49SP Hitchin, UK, rwilliams@soundevaluations.com)

Traditionally vehicle sound evaluations have been conducted either whilst driving a car or by auditioning fixed test conditions in a listening room. On-road testing provides the right context but the results are often inconsistent and unrepeatable. Furthermore it is not possible to evaluate prototype sounds or carry out back-to-back comparisons. In-room evaluations improve the statistical confidence, but the context of the assessments is unrepresentative. Interactive NVH vehicle simulators enable assessments to be performed in a setting representative of real appraisals. Accurate sounds can now be generated in real-time, and assessors can adopt a driving strategy that allows their own interpretation of the attributes. The benefits include the opportunity to understand how preferences are formed by assessors, albeit with added complexities. Different assessors may be associating their preferences on different operating conditions which have different acoustical properties. Therefore for engineers to identify the key features that influence perception they need to be able to relate the driving strategies with the subjective preferences. This paper reports on new observational methods which capture assessors' decision making strategies. It demonstrates how these help in relating subjective preferences to vehicle operating conditions and how to design a structured evaluation to reduce sources of experimental error.

3:20

2pNSa5. Perception of simple sounds from an emotional point of view. Anders Sköld (Chalmers University of Technology, Division of Applied Acoustics, Sven Hultinsgata 8a, 41296 Gothenburg, Sweden, anders.skold@chalmers.se), Penny Bergman (Chalmers University of Technology, Division of Applied Acoustics - Chalmers Room Acoustics Group, Sven Hultins gata 8a, 41296 Gothenburg, Sweden, penny@chalmers.se), Daniel Vastfjall (Chalmers University of Technology, Division of Applied Acoustics - Chalmers Room Acoustics Group, Sven Hultins gata 8a, 41296 Gothenburg, Sweden, daniel.vastfjall@psy.gu.se), Andreas Colebring (Chalmers University of Technology, Division of Applied Acoustics, Sven Hultinsgata 8a, 41296 Gothenburg, Sweden, andreas.colebring@gmail.com)

In sound perception the focus often lies in the cognitive aspect of the sound. We argue that the emotional aspect has to be added to get a fuller picture of sound perception. By using emotions as parameter in design of auditory alerts, one can reach a more accurate reaction to the alert. In this paper we studied the emotional connection to some attributes, common in music psychology, that are possible to describe by simple parameters. Short stimuli were created from these parameters in a factorial test design. The sounds were presented over headphones, with same signal fed to both ears, to 30 participants. The participants were asked to rate level of valence and activation, using a pictorial scale (SAM). Statistical differences was mostly found in ratings of activation, but differences were also shown in valence ratings. Results will be discussed in relation to theories of sound perception as well as music psychology.

3:40-5:00 Posters

Lecture sessions will recess for presentation of poster papers on various topics in acoustics. See poster sessions for topics and abstracts.

Contributed Paper

5:00

2pNSa6. Emotional bias for the perception of rising tones. Ana Tajadura-Jiménez (Chalmers University of Technology, Division of Applied Acoustics, Sven Hultinsgata 8a, 41296 Gothenburg, Sweden, ana.tajadura@chalmers.se), Aleksander Väljamäe (Laboratory for Synthetic Perceptive, Emotive and Cognitive Systems (SPECS) - Universitat Pompeu Fabra, Ocata 1, 08003 Barcelona, Spain, aleksander.valjamae@iua.upf.edu), Daniel Vastfjall (Chalmers University of Technology, Division of Applied Acoustics - Chalmers Room Acoustics Group, Sven Hultins gata 8a, 41296 Gothenburg, Sweden, daniel.vastfjall @psy.gu.se)

Sounds with rising and falling intensity are often perceived, respectively, as approaching or receding sound sources. Research has shown the existence of biases both at perceptual and neural levels towards approaching versus receding sounds. It has been suggested that these effects might be accounted to a greater biological salience of approaching sounds. In the present study we investigated whether this asymmetry could be also explained by emotional theories. Approaching and receding tones, followed by neutral, negative or positive photographs, were presented. Participants were required to make a speeded three-alternative forced choice (3AFC) task regarding their feelings towards the photographs. Reaction times (RTs) to this task, together with self-reported valence (pleasantness) and arousal (activation) ratings for the photographs were collected. In addition, participants' electrodermal activity (EDA) and facial electromyography (EMG) when listening to the sounds were measured. Participants responded faster to photographs preceded by approaching tones, especially for photographs with a negative emotional content. Both the intensity range and the period of intensity change of the sounds had a significant effect in RTs. Taken together, these results suggest that approaching sounds induce a greater emotional response on listeners, which might modulate subsequent attentional and perceptual processes.

Invited Papers

5:20

2pNSa7. Survey of sound quality research and applications in the information technology industry. Terry Baird (Hewlett-Packard Co., 11311 Chinden Blvd, Boise, ID 83714, USA, terry.baird@hp.com)

Traditionally, emission sound power level has been the key attribute measured and reported for describing IT equipment acoustic performance. More recently, designers and manufacturers of IT equipment have come to realize that customer satisfaction or annoyance is not dictated by sound power alone, but is dependent on many sound quality attributes as well. Additionally, sound power level tends

to be a poor indicator of equipment condition or component degradation where other tools are required for diagnosis and characterization. This paper reviews key research and trends over the last several years using psychoacoustic principles and analyses, as well as case studies of specific applications in the IT sector.

5:40

2pNSa8. Identification and Classification of Noise Patterns. Roland Sottek (HEAD acoustics GmbH, Ebertstrasse 30a, 52134 Herzogenrath, Germany, claudia.erens@head-acoustics.de)

Sound quality evaluation is a challenge due to spectral and temporal structures of noise. Tonal components, howling sounds and modulated signals are often the cause of customer complaints. Thus, besides frequency-weighted level like dB(A) or loudness, additional parameters are required. Besides time-varying loudness, other psychoacoustic parameters like sharpness and roughness can be used for sound quality evaluation. Sharpness considers the amount of high frequency components of a noise, and roughness evaluates modulation characteristics. In addition, a metric combining modulation spectral analysis with loudness calculation has been introduced. Some years ago, a ″Hearing Model″ was developed with the intention of explaining and describing psychoacoustic effects. Applying the Hearing Model to sound quality tasks allows evaluating the spectral and temporal patterns of a sound (″Relative Approach″ analysis) where absolute level or loudness is often without significance. The Relative Approach analysis emphasizes all relevant signal components concerning human auditory perception: tonal and transient signals. For extracting and evaluating individual patterns further signal-processing steps are necessary. The paper presents different methods for effective sound quality evaluation of noise and their application to several examples.

6:00

2pNSa9. The Calibration and Validation of a Binaural Room Scanning System Used for Subjective Evaluation of Automotive Audio Systems. Sean E. Olive (Harman International Industries, Inc., R&D Group, 8500 Balboa Blvd, Northridge, CA 91329, USA, solive@harman.com), Todd Welti (Harman International Industries, Inc., R&D Group, 8500 Balboa Blvd, Northridge, CA 91329, USA, twelti@harman.com)

Binaural room scanning (BRS) is a method of capturing the acoustical response of audio systems in rooms and automotive cabins as a set of binaural impulse responses that are stored and later reproduced through head-tracking headphones. All BRS systems have errors that without careful calibration limit their usefulness for subjective measurements of sound quality. This paper discusses a method for calibrating and testing a proprietary BRS system based on how well it reproduces listeners' preference ratings of different automotive audio systems made in situ. A group of trained listeners gave preference ratings for 5 different equalizations of a high quality automotive audio system made both in situ and through the BRS capture/playback system. The tests were repeated in mono and stereo using 6 individualized listener calibrations. The results can be summarized as follows: there were no significant differences in preferences between the in situ and BRS-based evaluations for either the mono or stereo tests. A significant interaction was found between the different equalizations and individualized calibrations that were largely confined to 1 particular listener calibration. The results suggest that a generalized BRS calibration may provide sufficiently accurate preference measurements of audio system sound quality.

Contributed Papers

6:20

2pNSa10. Head and torso simulators for acoustic measurements. Gunnar Rasmussen (G.R.A.S. Sound & Vibration A/S, Skovlytoften 33, 2840 Holte, Denmark, gr@gras.dk)

Head and torso simulators which reproduce the acoustical effect of a median human adult, including diffraction and direction-dependent transformation from free field to the ear drum as well as allow for objective testing of sound systems involving hearing aids, headphones, earphones, telephones, mobile phones, headsets and sound quality type of measurements may be realized based on different philosophies. It may be based on geometrically simplified shape or mean values of individuals. The geometrically simplified shape will appear like no human being. The mean values may result in non human like features, while average anthropometric dimensions of an adult human may offer data closer to a subjective test. Especially the shape of the pinna may often be critical to test of earphones and headphones as well as mobile phones. Subjective tests on groups of people may be supplemented with objective tests on a manikin for reference and quality control purposes. Variations in pinna size may have significant influence on the measurement of earphones as well as leakage in telephone testing. The influence of the dress worn may also be of significance especially for the head related transfer function and on the directional response in the middle frequency range.

6:40

2pNSa11. Capturing blocked-entrance binaural signals from open-entrance recordings. Dorte Hammershøi (Acoustics, Aalborg University, Fredrik Bajers Vej 7 B5, 9220 Aalborg Ø, Denmark, dh@es.aau.dk), Pablo F. Hoffmann (Acoustics, Aalborg University, Fredrik Bajers Vej 7 B5, 9220 Aalborg Ø, Denmark, pfh@es.aau.dk), Søren K. Olesen (Acoustics, Aalborg University, Fredrik Bajers Vej 7 B5, 9220 Aalborg Ø, Denmark, sko@es.aau.dk), Per Rubak (Acoustics, Aalborg University, Fredrik Bajers Vej 7 B5, 9220 Aalborg Ø, Denmark, pr@es.aau.dk)

Binaural recordings enable us to capture all sound attributes including spatial information, room effect, and source characteristics in a given environment. It has been shown that blocked-entrance binaural recordings provide advantages over open-entrance recordings, primarily because the blocked-entrance recordings is not influenced by the ear canal acoustics of the individual for which it is recorded. However, blocking the ear canal for recoding imposes an obvious disruption to normal hearing conditions, which may be unacceptable for applications in which binaural audio capturing is desired but without interfering the individual's hearing and doing. In this work we propose a strategy for the recording of binaural audio with minimal hearing interference, and for transforming these recordings to blocked-entrance versions that are more suitable for analysis and reproduction of binaural audio in a more general context. To this purpose, equalization filters are derived from the ratio between blocked and open ear canal transfer functions. Different transfer-function measuring techniques and inverse filtering methods are evaluated.

Invited Paper

7:00

2pNSa12. PsySound3: a program for the analysis of sound recordings. Densil Cabrera (University of Sydney, Faculty of Architecture, Design and Planning, NSW 2006 Sydney, Australia, densil@usyd.edu.au), Sam Ferguson (University of Sydney, Faculty of Architecture, Design and Planning, NSW 2006 Sydney, Australia, samferguson@ihug.com.au), Farhan Rizwi (Empirical Musicology Group, University of New South Wales, NSW 2052 Sydney, Australia, farhan.rizwi@unswalumni.com), Emery Schubert (Empirical Musicology Group, University of New South Wales, NSW 2052 Sydney, Australia, E.Schubert@unsw.edu.au)

This paper demonstrates the sound analysis software PsySound3, which was written by the authors. The software currently includes a range of DSP-based analysis techniques (e.g., spectrum, cepstrum, autocorrelation, Hilbert transform, sound level meter emulator), as well as implementations of psychoacoustical algorithms often associated with sound quality (e.g., loudness, sharpness, loudness fluctuation, roughness, pitch, binaural attributes). In some cases, PsySound3 makes available multiple models of the one auditory attribute - for example it implements dynamic and static loudness models using Erb- and Bark-based auditory filters. The program is extensible, and so has the potential to allow researchers to share their analysis models using a common interface. PsySound3 is written in Matlab, and is also available as a stand-alone program. The software is freely available from www.psysound.org.

Contributed Papers

7:20

2pNSa13. Hartis, a re-synthesis tool for vehicles sound design. Gaylord Desoeuvre (GIST, 62 bis avenue André Morizet, 92100 Boulogne Billancourt, France, gaylord.desoeuvre@ext.mpsa.com), Florent Richard (PSA Peugeot Citroën, Centre Technique de Vélizy, Route de Gisy, 78943 Vélizy-Villacoublay, France, florent.richard@mpsa.com), Vincent Roussarie (PSA Peugeot Citroën, Centre Technique de Vélizy, Route de Gisy, 78943 Vélizy-Villacoublay, France, vincent.roussarie@mpsa.com), Marie Céline Bezat (PSA Peugeot Citroën, Centre Technique de Vélizy, Route de Gisy, 78943 Vélizy-Villacoublay, France, marieceline.bezat@mpsa.com)

For more than thirty years, the main goal for the automotive acoustic engineer was the car's noise level reduction. Within new customers' behaviours, the car manufacturers have now to put products sound quality at the same level as its aesthetic qualities or ergonomics. To improve customer's satisfaction, one solution is to increase sensory coherence and perceived quality by controlling the sound identity and character of a vehicle. To reach this new objective, the Research Department of PSA Peugeot Citroën is developing his own sound design software HARTIS [1] (HArmonics Real TIme Synthesis). HARTIS is a complete re-synthesis tool useful in many stages of vehicle sound design process. In this paper we first present the last version of HARTIS fully interfaced for an easy use in project teams. The second part of the paper presents new integrated module that deals with impulsional noise for diesel application and other sources models. Each type of source can be controlled and filtered to recreate different driving situation. References [1] Sound design in car passenger compartment Process and tool for the control of engine sound character. V. Roussarie, F. Richard, Journées du Design Sonore 2004.

7:40

2pNSa14. Ride quality and noise in high speed elevators. Mauro Pierucci (San Diego State University, 5500 Campanile drive, San Diego, CA 92182-3020, USA, mpierucci@mail.sdsu.edu), Michael Frederick (San Diego State University, 5500 Campanile drive, San Diego, CA 92182-3020, USA, mike.frederick-1@nasa.gov)

Ride quality in an elevator is the latest ″hot topic″ in elevator design and construction. In skyscrapers being built in Asia, Dubai and the US, the new elevators travel close to and beyond 10m/s. The rides to the highest floors will last well over one minute. From a comfort point of view, it is important that the ride be as smooth and quiet as possible. There are many factors that influence the vibration of the elevator and the concomitant noise. In this paper we will examine the sudden forces that the elevator experiences as it passes each floor. The side forces on the elevator are caused by the asymmetric flow field about the elevator cab. The pressure and streamline flow field was evaluated by using the CFD code FLUENT. Comparison between the numerical and the measured results are given and the pressure disturbances caused by the passage of the elevator and its appendages are discussed together with some solutions to alleviate the pressure disturbances.

Session 2pNSb

Noise, Physical Acoustics, and EURONOISE: Aeroacoustics III (Poster Session)

Philip Morris, Cochair
Penn State University

Christophe Bailly, Cochair
Ecole Centrale de Lyon

All posters will be on display from 3:40 p.m. to 5:20 p.m. To allow contributors an opportunity to see other posters, contributors of odd-numbered papers will be at their posters from 3:40 p.m. to 4:30 p.m. and contributors of even-numbered papers will be at their posters from 4:30 p.m. to 5:20 p.m.

Contributed Papers

2pNSb1. Nonlinear propagation of spark-generated N-waves in atmosphere: theoretical and experimental assessment of the shock front structure. Petr V. Yuldashev (Center for Industrial and Medical Ultrasound, Applied Physics Lab., University of Washington, 1013 NE 40th St., Seattle, WA 98105, USA, petr@acs366.phys.msu.ru), Mikhail V. Averiyanov (Center for Industrial and Medical Ultrasound, Applied Physics Lab., University of Washington, 1013 NE 40th St., Seattle, WA 98105, USA, misha@acs366.phys.msu.ru), Vera A. Khokhlova (Center for Industrial and Medical Ultrasound, Applied Physics Lab., University of Washington, 1013 NE 40th St., Seattle, WA 98105, USA, vera@acs366.phys.msu.ru), Oleg A. Sapozhnikov (Center for Industrial and Medical Ultrasound, Applied Physics Lab., University of Washington, 1013 NE 40th St., Seattle, WA 98105, USA, oleg@acs366.phys.msu.ru), Ollivier Sebastien (Ecole Centrale de Lyon, LMFA, UMR CNRS 5509, Ecully, 69134 Lyon, France, Sebastien.Ollivier@ec-lyon.fr), Philippe Blanc-Benon (Ecole Centrale de Lyon, LMFA, UMR CNRS 5509, Ecully, 69134 Lyon, France, Philippe .Blanc-Benon@ec-lyon.fr)

Extensive outdoor and laboratory-scale experiments on sonic boom propagation in turbulent atmosphere have shown that shock wave amplitude and rise time are important parameters responsible for sonic boom annoyance. However, accurate measurement of the shock front structure with standard microphone remains a challenge due to the broadband spectrum of the N-wave shock front. In this work the experimental setup utilizing a spark source has been designed and built to investigate nonlinear N-wave propagation in homogeneous medium. Short duration (30μs) and high amplitude (1 kPa) spherically divergent N-waves were generated. In addition to acoustic measurements with 1/8″ B&K microphones, the shadowgraphy method using short duration flash lamp (20 ns) and CCD camera was employed to assess the shock front structure at different distances from the spark. It is shown that the shock rise time measured by the shadowgraphy method was in a good agreement with the theoretical predictions and it was 10 times shorter than in microphone measurements. The widening of the shock in acoustic measurements was therefore due to the limited bandwidth of the microphone. The combination of modeling, acoustic and optical measurements provided an accurate calibration of the shock wave measuring system. [Work supported by RFBR and INTAS.]

2pNSb2. Doppler effect in aeroacoustics. Jean Varnier (ONERA, 29 avenue de la Division Leclerc, 92320 Châtillon, France, jean.varnier@onera .fr)

Doppler effect in aeroacoustics The prediction of acoustic fallout caused at the ground level by aircraft in flight or by launchers at take-off sets the problem of the distortion of the emitted sound spectrum by the Doppler effect. Former studies applied to this problem use a geometrical formalism based on simplifying hypotheses such as homogeneous atmosphere, rectilinear trajectory and constant velocity of the sound source. Other studies consider the supersonic case using a model of spherical waves inside the Mach cone. These approaches are in fact not well adapted to the real cases, and the literature does not give many practical examples concerning this topic. In this study, we propose a new time approach of the Doppler effect that allows to avoid the complexity of the geometrical models and to take into account real atmosphere, curvilinear trajectories or accelerations of moving sound sources. This model allows to easily calculate the frequency shift and the change of acoustic level of the signal recorded at a given hearing point, in both cases of subsonic and supersonic sound sources. We present a first validation of this method applied to signals recorded in Kourou during the atmospheric phase of Flight 521 of Ariane 5.

2pNSb3. Noise computation of an axisymmetric free jet using general purpose CFD code. Péter Tóth (Dep. of Fluid Mechanics, Budapest Univ. of Technology and Economics, Bertalan Lajos street 4-6, 1111 Budapest, Hungary, toth@ara.bme.hu), Máté Márton Lohász (Dep. of Fluid Mechanics, Budapest Univ. of Technology and Economics, Bertalan Lajos street 4-6, 1111 Budapest, Hungary, lohasz@ara.bme.hu)

The increasing interest in the noise prediction of the turbulent flows is leading the general purpose Computational Fluid Dynamics (CFD) software developers to integrate noise predicting methods into their code. However the aeroacoustic simulation of free shear flows, where the mean source of noise is the turbulent fluctuations in the free space is challenging with a general purpose CFD application. The aim of this work is to investigate the capabilities of commercial CFD software in the field of noise prediction of free shear flows. The important acoustical properties of a low Reynolds number, low Mach number axisymmetric (2D) jet is computed by means of hybrid Computational Aeroacoustic method using Fluent. The noise source is computed without modeling instantaneously using the compressible solver of the code, and the far field acoustical data is evaluated by the Ffowcs-Williams-Hawkings acoustical analogy. The results is compared to the Direct Numerical Simulation of [Jiang2004 J. Sound Vib.] in terms of frequency spectra in the far field and directivity pattern of the jet.

2pNSb4. Application of RANS modelling and LES to the prediction of noise from a simple cold propane jet. Tanya Stanko (The University of Leeds, School of Process, Environmental and Materials Engineering, LS2 9JT Leeds, UK, pmtss@leeds.ac.uk), Michael Fairweather (The University of Leeds, School of Process, Environmental and Materials Engineering, LS2 9JT Leeds, UK, M.Fairweather@leeds.ac.uk), Mohamed Pourkashanian (The University of Leeds, School of Process, Environmental

and Materials Engineering, LS2 9JT Leeds, UK, m.pourkashanian @leeds.ac.uk), Derek Ingham (The University of Leeds, School of Process, Environmental and Materials Engineering, LS2 9JT Leeds, UK, D.B.Ingham @leeds.ac.uk)

Numerical simulation, combining computational fluid dynamic and acoustic models, is useful as an aeroacoustic tool that is effective in identifying components or surfaces that generate significant amounts of noise, and can thereby provide opportunities for early design changes. In this work, numerical solutions of a cold turbulent jet of propane issuing from a circular nozzle are used to provide velocity information at a Reynolds number of 68,000. Predictions provided by large eddy simulation are compared with Reynolds-averaged Navier-Stokes solutions derived using a second-moment turbulence closure, as well as with experimental data available in the literature. Reasonable agreement with data is found, and these solutions are used subsequently as the basis for noise predictions. The first acoustic model employed is based on Lighthill's theory using the Goldstein broadband noise source formalisation that postulates axisymmetric turbulence superposed on the mean flow. The second approach is based on Ffowcs-Williams and Hawkings theory which implies that the far field sound is computed from an integral formulation with all quantities evaluated on a control surface, with the control surface itself assumed to enclose all nonlinear flow effects and noise sources. The simulation results reported in this paper confirm previous experimental works presented in the literature demonstrating that jet noise is modified by inlet conditions.

2pNSb5. Uncertainties of Measured and Calculated Aircraft Noise and Consequences in Relation to Noise Limits. Georg Thomann (Empa, Ueberlandstrasse 128, 8600 Duebendorf, Switzerland, georg.thomann@empa .ch)

The uncertainties of measuring and calculating aircraft noise have been analysed in a thesis at the ETH Zurich. The thesis provides information and methods for estimating uncertainties. It shows possibilities for handling these uncertainties and provides guidance to legal and administrative bodies on how to deal with such uncertainties when applying the legal noise limits. To estimate the uncertainties of calculations and measurements the Swiss aircraft noise calculation program FLULA2 and a great deal of measured data have been analysed. Using radar data it is possible to achieve a standard uncertainty of the calculated Leq between 0.5 dB for day-time and 1.0 dB for night-time. The analyses also show that the uncertainty of measurements at automated stations is in the same order of magnitude as the calculations. Therefore the annual calculations and measurements of aircraft noise show no significant deviations. Furthermore with FLULA2 it is possible to present the uncertainty at a confidence level of 90%. It is now up to administrative and legal bodies to set up rules on how to account for uncertainties of calculations in evaluating noise situations close to the legal noise limits.

2pNSb6. Acoustic test facility for aero engine fans. Yuri Khaletskiy (Central Institute of Aviation Motors, 2, Aviamotornaya Str., 111116 Moscow, Russian Federation, noise@ciam.ru), Victor Mileshin (Central Institute of Aviation Motors, 2, Aviamotornaya Str., 111116 Moscow, Russian Federation, mileshin@ciam.ru), Rollan Shipov (Central Institute of Aviation Motors, 2, Aviamotornaya Str., 111116 Moscow, Russian Federation, noise@ciam.ru)

The facility for acoustic tests of aero engine fans in conditions of anechoic chamber is created in Central Institute of Aviation Motors (Moscow). The facility is designed for testing models of single rotating fans and counter rotating fans. The measurements of the sound are carried out in forward and rearward semi-spheres simultaneously. Design features of the anechoic chamber and its acoustic performance are presented. Also a fan drive system and systems of acoustic and aerodynamic measurements are described. In particular fan rotor max rotation frequency makes up 13,000 rpm at each shaft max power 2.5 MW. The rig acquisition system allows checking in real time results of complete three-octave analysis of machine noise on all 24 channels in a measurement frequency range of 0œ80 kHz.

2pNSb7. Nonlinear Propagation of Screech Noise. Jothi Punekar(School of Engineering and Materials, Queen Mary, University of London, 327 Mile End Road, E1 4NS London, UK, j.punekar@qmul.ac.uk), Eldad Avital (School of Engineering and Materials, Queen Mary, University of London, 327 Mile End Road, E1 4NS London, UK, e.avital@qmul.ac.uk)

This study investigates the non-linear propagation of screech noise emitted by supersonic jets. Supersonic jet noise consists of three components: mixing, broadband and screech noise. In order to generate broadband and screech noise the jet has to expand imperfectly, meaning shock waves are formed inside the potential core and interact with the surrounding shear layer. The feedback between the generated noise and the nozzle cause the screech noise pattern. It is associated with high frequency (annoying to the human ear). Near field screech noise obtained from Large Eddy Simulation (LES) of circular supersonics jets is investigated using the Burgers equation, taking into account thermo-viscous effects. The Burgers equation is commonly used to investigate non-linear propagation effects. The initial screech signal is found to consist of two main frequency modes. Significant nonlinear effects appear during propagation although the pressure amplitude is no more than a few percentages of the ambient pressure. Saw tooth waves are generated and the amplitude is found to decrease as 1/sqrt(t) for low viscous medium according to Lighthill' 'bunching' theory. Further high frequencies are also generated. Finally, geometrical attenuation is discussed by transforming the plane wave propagation to cylindrical form.

2pNSb8. Instability wave control in a subsonic round jet. Georgy Faranosov (TsAGI, Acoustic Division, 17, Radio str, 105005 Moscow, Russian Federation, georgefalt@rambler.ru)

It is generally accepted that one of the main sources of acoustic radiation from a turbulent jet is due to spatial instability wave packets propagating downstream within the jet. This approach has enabled to explain and predict the principal features of sound radiated by a supersonic jet. Therefore the problem of noise control for the jet could be considered as a problem of instability wave control. Instability wave developed in the tone-excited jet issued from axisymmetric, semi-infinite duct is considered. The flow field in the vicinity of the nozzle edge is investigated for the purpose of identifying instability wave parameters. Instability wave turned out to be damped completely on the condition that the amplitude and the phase of the external forcing are chosen in accordance with those of the instability wave. The robust strategy of instability wave experimental suppression based on the near field measurements is formulated. Similar problem in two-dimensional case was recently analyzed in Kopiev & Faranosov (Acoust. Phys. 2008, V.54, N.2).

2pNSb9. Decomposition of the Lighthill source term and analysis of acoustic radiation from mixing layers. Florent Margnat (Arts et Métiers Paris Tech - Sinumef Lab, 151 bd de l'Hopital, 75013 Paris, France, florent.margnat@paris.ensam.fr), Véronique Fortuné (Univ. Poitiers, CNRS Laboratoire d'Etudes Aérodynamiques, Bat. K - 22 avenue du recteur Pineau, 86022 Poitiers, France, veronique.fortune@lea.univ-poitiers.fr), Peter Jordan (Univ. Poitiers, CNRS Laboratoire d'Etudes Aérodynamiques, 43, rue de l'Aérodrome, 86036 Poitiers, France, peter.jordan@lea.univ-poitiers.fr), Yves Gervais (Laboratoire d'Etudes Aérodynamiques (LEA), Université de Poitiers - ENSMA - CNRS, Bâtiment K, 40 Avenue du Recteur Pineau, 86022 Poitiers, France, yves.gervais@lea.univ-poitiers.fr)

Acoustic radiation from jet flow has been studied extensively by means of theoretical, experimental and numerical approaches over the past decades. Unfortunately, the mechanisms responsible for the production of sound by unbounded turbulence in subsonic flows remain unclear. For advancing our fundamental understanding of these mechanisms, the development of specific analysis tools is needed. Our study is based on a decomposition of the Lighthill source term, which is known to contain all the existing links between the fluid flow and the acoustic field. Ten subterms are written with the help of physically meaningful quantities such as velocity, density, dilatation and vorticity. The methodology is tested through the two-dimensional compressible mixing layer flow in spatial development, at a Reynolds number of 400 and a Mach number of 0.25. A direct numerical simulation of the flow and its acoustic radiation is performed and used as a reference solution.

Acoustic field generated by each source terms is predicted computing the integral solution of Lighthill's equation. Effect of the compressibility on the balance between the contribution of major subterms is of key importance. Directivity and convective effects are identified as well.

2pNSb10. Acoustic and aerodynamic dissipations induced by a sound wave-impacted Helmholtz resonator. Jean-Michel Roche (ONERA, BP 72 - 29 avenue de la Division Leclerc, 92322 Châtillon, France, jean-michel.roche@onera.fr), Laurent Leylekian (ONERA, BP 72 - 29 avenue de la Division Leclerc, 92322 Châtillon, France, laurent.leylekian@onera.fr), François Vuillot (ONERA, BP 72 - 29 avenue de la Division Leclerc, 92322 Châtillon, France, francois.vuillot@onera.fr)

The purpose of the work introduced herein is to study the dissipation of the acoustic energy carried by sound waves, by a Helmholtz resonator. Two-dimensional direct numerical simulations (DNS) are performed with the CEDRE code, a Navier-Stokes equations solver developed by Onera, for a resonator with a 0.8 × 0.8 mm square opening. The incident sound pressure level (SPL) varies between 100 dB and 150 dB: it is checked that when the SPL is low, the acoustic energy is dissipated in the resonator opening by viscous wall friction, whereas when the SPL is high, the acoustic energy is converted in kinetic energy carried by micro-vortices induced at the opening mouths. However, when the SPL takes intermediate values, both mechanisms coexist. Thus, for each case, we aim at splitting the aeraoacoustic field into respective acoustic and aerodynamic contributions, and at evaluating the ratio between these two distinct mechanisms in order to quantify their relative weight on the global dissipation. Our results are compared with those obtained by Tam et al. for the same geometry. A three-dimensional study for a Helmholtz resonator with a cubic opening is eventually considered.

2pNSb11. The multiple side-branch system as a model for a corrugated pipe. Devis Tonon (Technische Universiteit Eindhoven, CC.2.25, N-LAAG, Postbus 513, 5600 MB Eindhoven, Netherlands, d.tonon@tue.nl), Stefan Belfroid (TNO Science and Industry, Stieltjesweg 1 PO Box 155, 2600 AD Delft, Netherlands, stefan.belfroid@tno.nl), Jan F. Willems (Technische Universiteit Eindhoven, CC.2.25, N-LAAG, Postbus 513, 5600 MB Eindhoven, Netherlands, J.F.H.Willems@tue.nl), Avraham Hirschberg (Technische Universiteit Eindhoven, CC.2.25, N-LAAG, Postbus 513, 5600 MB Eindhoven, Netherlands, a.hirschberg@tue.nl)

Corrugated pipes are used as flexible risers in offshore natural gas production and for vacuum cleaners. Such pipes can display whistling. As theoretical models are available to predict the aero-acoustical behaviour of closed side branches [1], we consider a row of equally spaced closed side branches along a pipe, as a model for a corrugated pipe. We consider side branches with a diameter D and depth L equal to the main pipe diameter, placed at a distance of three diameters from each other. For systems of 11 or 12 side branches the lowest resonance modes are reasonably well predicted by assuming $n(\lambda/2)$ standing wave modes with an effective speed of sound c_{eff}[2]. Whistling is observed for the n=2 and n=3 modes with a pressure fluctuation amplitude $p'/(\rho_0 c_0 U_0)=O(2\times10^{-2})$ similar to that observed for sharp edges corrugations in a corrugated pipe (with ρ_0 the fluid density, c_0 the speed of sound and U_0 the main flow velocity). The Strouhal number of these oscillations is $Sr_D=(f\cdot D)/U_0\simeq0{,}70$. This is higher than typical values observed for corrugated tubes [3]. References: [1] J.C. Bruggeman et al., J. Sound and Vibration 1991 **150**(4) 371-393. [2] J.W. Elliot, in ″Lecture Notes on the Mathematics of Acoustics″ M.C.M. Wrigth, Imperial College Press, London (2005). [3] S. Belfroid et al., ASME paper PVP2007-26503.

2pNSb12. The sound wave reflection from the corrugated plane streamlined by the low Mach number shear flow (generalized Miles mechanism). Mikhail Mironov (Andreev Acoustics Institute, Shvernik, 4, Moscow, 117036 Moscow, Russian Federation, mironov@akin.ru), Ivan Belyaev (Central Aerohydrodynamics Institute (TsAGI), Acoustic Division, 17 Radio str., 105005 Moscow, Russian Federation, belyaev_iv@bk.ru), Vasilisa Solntseva (Andreev Acoustics Institute, Shvernik, 4, Moscow, 117036 Moscow, Russian Federation, mironov@akin.ru)

The plane sound wave reflection from the periodically corrugated plane streamed by the parallel shear flow is studied. The incident wave scatters on corrugations and gives both the mirror reflected sound wave and two inhomogeneous nonpropagating in the normal to the plane direction waves. One of the inhomogeneous waves goes in the same direction along the plane of the flow and the second one in the opposite direction. The first inhomogeneous wave interacts with critical layer of flow according to Miles mechanism (which was originally applied to the generation of surface waves by the wind (JFM: 1957, 1959)) and reflects from this layer back to the plane. After that this inhomogeneous wave scatters from the corrugated plane and gives some additional part to the mirror reflected sound wave. The total reflection coefficient of sound wave appeared to be more than 1. The angle dependence of the reflection coefficient is analyzed. The equivalent impedance is calculated. The obtained amplification is compared with thermal and viscous surface losses

2pNSb13. On a stability of the shear flow with a tangential discontinuity in the presence of a small scatterer. Nikolay Kanev (Andreev Acoustics Institute, Shvernik, 4, Moscow, 117036 Moscow, Russian Federation, nikolay.kanev@mail.ru), Mikhail Mironov (Andreev Acoustics Institute, Shvernik, 4, Moscow, 117036 Moscow, Russian Federation, mironov@akin.ru)

It is well known a tangential discontinuity of velocity in the shear flow is unstable. That instability is convective i.e. all disturbances of the tangential discontinuity grow exponentially but they are carried away by the flow downstream so that after all the amplitude of sound field generated by the tangential discontinuity will decrease at any fixed point. In the presented paper we consider the problem when a small scatterer is placed near the tangential discontinuity. It appears this system can be absolutely unstable under the definite position of the scatterer. It means that the appearance of any disturbance of the tangential discontinuity will result in rising of the amplitude of sound field at every point of space. The cause of absolute instability is a feedback provided by the scatterer and the type of instability does not depend on the size of the scatterer. An absolutely unstable system behaves as an autogenerator and radiates tone or multitone sound. So the obtained result explains the possible mechanism of noise generation in systems with tangential discontinuities and gives some hints about noise control in such systems.

2pNSb14. Spectral attenuation of sound in dilute suspensions with nonlinear particle relaxation. Max Kandula (ASRC, Mailstop ASRC-5211, NASA Kennedy Space Center, Kennedy Space Center, FL 32899, USA, max.kandula-1@ksc.nasa.gov), Michael Lonergan (NASA, Kennedy Space Center, Mailstop NE-M1, Kennedy Space Center, FL 32899, USA, michael.lonergan-1@ksc.nasa.gov)

Theoretical studies on the dissipation and dispersion of sound in two-phase suspensions have been briefly reviewed. Previous studies (theory of Temkin & Dobbins, JASA, Vol. 40, No. 2, pp. 314-324, 1966,) on the sound attenuation in particle-laden flows under Stokesian drag and conduction-controlled heat transfer have been extended to accommodate the nonlinear drag and heat transfer. It has been shown that for large particle-to-fluid density ratio, the particle Reynolds number bears a cubic relationship with {\omega}{\tau},where {\omega} is the circular frequency and {\tau}the Stokesian particle relaxation time. This dependence leads to the existence of a peak value in the linear absorption coefficient occurring at a finite value of {\omega}{\tau}. Comparison of the predictions with the test data of Norum (AIAA-2004-2976) for the spectral attenuation of sound with water injection in a perfectly expanded supersonic jet (Mach number of 1.45) shows a satisfactory trend of the proposed theory. It is found that the nonlinear particle relaxation processes (particle drag and heat transfer) are primarily responsible for reduction in the linear absorption coefficient of sound at high frequencies.

2pNSb15. Aeroacoustic simulation of automotive ventilation outlets. Jean-Luc Adam (Renault SAS, 1 avenue du golf, 78288 Guyancourt, France, jean-luc.adam@renault.com), Denis Ricot (Renault SAS, 1 avenue

du golf, 78288 Guyancourt, France, denis.ricot@renault.com),Flavien Dubief (Renault SAS, 1 avenue du golf, 78288 Guyancourt, France, flavien.dubief@renault.com), Christine Guy (Ligeron, Les Algorithmes Bâtiment Euclide, 91194 Saint Aubin, France, christine.guy@ligeron.com)

In this work we have numerically studied aeroacoustics of automotive ventilation outlets. Simulations are performed with the CFD software PowerFLOW based on Lattice Boltzmann method (LBM). Low dissipative LBM scheme enables to compute aeroacoustic sources generated by turbulence fluctuations and to propagate them in the same simulation. In a first step we validate the ability of LBM for propagating acoustic waves in ducts and radiating them at open end terminations. In a second step, aeroacoustic simulations on automotive vents will be presented and compared with experimental data obtained from a DoE (Design of Experiment). This DoE is based on an idealized outlet with variing parameters (number and lenght of grid blades, grids spacing ...) which gives 18 distinct geometrical configurations. All these configurations have been simulated with PowerFLOW and measured with a new test facility (built in the Renault Research Department). The large number of tested geometries and the statistical analysis of the DoE give an accurate idea of the capability of PowerFLOW, and more generally LBM, to correctly simulate the generation and propagation of aeroacoustic sources for a complex geometry. Results will be presented and discussed.

2pNSb16. Increase of sound proofing of air duct. Igor Shubin (Research Institute of Building Physics (NIISF RAABS), 21, Lokomotivny pr., 127238 Moscow, Russian Federation, marina_niisf@mail.ru), Vladimir Gusev (Research Institute of Building Physics (NIISF RAABS), 21, Lokomotivny pr., 127238 Moscow, Russian Federation, marina_niisf@mail.ru), Marina Pestereva (Research Institute of Building Physics (NIISF RAABS), 21, Lokomotivny pr., 127238 Moscow, Russian Federation, marina_niisf@mail.ru)

One of ways of noise protection from transit air duct is increase of sound insulation of air duct by different acoustical materials. The main interest of this work is in comparative analysis of acoustic efficiency different thermal insulation materials for use as sound insulation coverings. The report contains analysis of the distribution of noise through round and rectangular air ducts. There was discovered different tipes of thermal insulation materials such as easy made foam materials and fibrous materials. Tests are executed in the reverberation chamber. The received results have shown advantage of a fibrous material.

2pNSb17. On the correlation of the acoustic signal of microphones mounted on a flat plate to the turbulence of an impinging jet. Christoph Reichl (Arsenal Research - Austrian Research Centers, Giefinggasse 2, 1210 Wien, Austria, Christoph.Reichl@arsenal.ac.at), Michelle Boeck (Arsenal Research - Austrian Research Centers, Giefinggasse 2, 1210 Wien, Austria, michelle.boeck@arsenal.ac.at), Wolfgang Tilser (Arsenal Research - Austrian Research Centers, Giefinggasse 2, 1210 Wien, Austria, wolfgang.tilser@arsenal.ac.at), Hermann Lang (Arsenal Research - Austrian Research Centers, Giefinggasse 2, 1210 Wien, Austria, hermann.lang@arsenal.ac.at), Klaus Haindl (AKG Acoustics GmbH, Lemboeckgasse 21-25, 1230 Wien, Austria, HaindlK@akg.com), Friedrich Reining (AKG Acoustics GmbH, Lemboeckgasse 21-25, 1230 Wien, Austria, ReiningF@akg.com), Martin Opitz (AKG Acoustics GmbH, Lemboeckgasse 21-25, 1230 Wien, Austria, OpitzM@akg.com)

An axial symmetric fan driven by a brushless actuator with variable frequency is used to generate a turbulent circular jet leading to typical core-velocities of around 10 m/s (Re = 99000). The jet impinges on a flat plate. Turbulence is generated using different sets of turbulence generators in the pipe consisting of meshes, rods, cubes and spikes. The turbulent flow field downstream of the pipe outlet is measured using two-axis hot wire anemometry with a temporal resolution of a minimum of 48 kHz. The CTA probe is positioned using an automated three-axis traversing system. 12 Microphones are mounted on a flat plate and are used to capture the wall pressure fluctuations. CFD calculations are performed for the different turbulence generators and are compared to the acoustic and CTA signals. An important aspect of the work is the simultaneous recording of both the CTA- and the acoustic signals in the experimental and numerical approach. This allows for the calculation of correlation patterns between turbulence and the acoustic signals of the plate mounted microphones.

Session 2pNSc

Noise, ASA Committee on Standards, and EURONOISE: Comparing Noise Regulations and Codes in USA and Europe (Poster Session)

Robert Bruce, Cochair
CSTI, 15835 Park Ten Place, Suite 105, Houston, TX 77084-5131, USA

Wolfgang Probst, Cochair
DataKustik GmbH, Gewerbering 5, 86926 Greifenberg, Germany

All posters will be on display from 3:40 p.m. to 5:20 p.m. To allow contributors an opportunity to see other posters, contributors of odd-numbered papers will be at their posters from 3:40 p.m. to 4:30 p.m. and contributors of even-numbered papers will be at their posters from 4:30 p.m. to 5:20 p.m.

Contributed Papers

2pNSc1. Noise limits and noise levels along motorways in Europe. Wiebe Alberts (Rijkswaterstaat: Centre for Transport and Navigation, Postbus 5044, 2600 GA Delft, Netherlands, wiebe.alberts@rws.nl)

Environmental noise caused by traffic is one of the main local environmental problems in Europe. The National Road Authorities (NRA's), combined in the Conference of European Directors of Roads (CEDR), are aware of the environmental noise problem along their motorways. One of the main objectives of CEDR is to facilitate knowledge sharing on noise abatement issues among European NRA's. The CEDR noise group has made a comprehensive questionnaire survey on how the CEDR member states handle noise issues. The paper focuses on the part of the survey on noise limits and noise levels along motorways throughout Europe. It will deal with the: - status of noise limits; - noise indicators to express noise limits; - noise limits (outdoor and indoor) for motorways; - noise models to calculate noise levels. Due to the use of different noise indicators and different noise calculation models, the comparison of noise levels and noise limits along motorways in Europe is complicated to say the least. The only way to solve this problem is to have and to use a European noise model for road traffic based on the outcome of the HARMONOISE/IMAGINE projects.

2pNSc2. Origins of the modern noise ordinance in the County of San Diego, California. John C. Bennett (6110 Loukelton Circle, San Diego, CA 92120, USA, jc.bennett@cox.net)

An unofficial history of the origins of San Diego County's noise regulations has been compiled as an investigative tool to review current and future zoning schemes in this jurisdiction. These regulations date back to the 1970's and overlap with the development of city regulations. The focus of the history is the acoustical aspect of their development. A general discussion of performance standards is included in a comparison with similar regulations in two other California jurisdictions developed within the last five years. Some practical similarities and differences with European regulations in local jurisdictions are identified to encourage an open discussion in this session.

2pNSc3. Implementation of the noise directive in music and entertainment sector in Finland. Esko Toppila (Finnish Institute of Occupational Health, P.O:Box 486, 33101 Tampere, Finland, esko.toppila@ttl.fi), Pekka Olkinuora (FIOH, Topeliuksenkatu 41, 00250 Helsinki, Finland, pekka.olkinuora@ttl.fi), Pekka Airre (FIOH, P.O.Box 486, 33101 Tampere, Finland, erkko.airo@ttl.fi)

In the noise directive (2003/10/EC) the member countries were obliged to develop codes of conduct for the music and entertainment sector. In Finland the code of conduct was adopted into use in February 2007. According to this code of conduct the workers in the music and entertainment sector consist of performers (musicians, singers, conductors and actors), staff exposed to music (waiters,...) and teacher who teach music in schools. Guidelines were designed based on the worker group and the type of employment. In this approach the performers, who actually produce the ″noise″, must be able to monitor the sound levels in real time. Restaurants and music halls design the protective actions for other staff based on the assumption that predefined sound level is not exceeded the premises. The same principle is applied to schools. For temporary staff there must be hearing protectors available. Also the need for damping and use of quieter instruments is recognised. The code of conduct give the principles for the hearing conservation, but for the music and entertainment sector direct application of the principles is too complicated. Implementation examples are needed for all exposure patterns. This work is going on now in Finland.

Session 2pNSd

Noise, ASA Committee on Standards, and EURONOISE: Sound Quality Tools and Applications II (Poster Session)

Wade Bray, Cochair
HEAD acoustics, Inc.

Klaus Genuit, Cochair
HEAD acoustics GmbH

Etienne Parizet, Cochair
Laboratoire Vibrations Acoustique, Insa Lyon

All posters will be on display from 3:40 p.m. to 5:20 p.m. To allow contributors an opportunity to see other posters, contributors of odd-numbered papers will be at their posters from 3:40 p.m. to 4:30 p.m. and contributors of even-numbered papers will be at their posters from 4:30 p.m. to 5:20 p.m.

Contributed Papers

2pNSd1. Two-level description of environmental sounds: comparison and generalization of 4 timbre studies. Antoine Minard (IRCAM - UMR CNRS 9912, Equipe Perception et Design Sonores, 1, place Igor Stravinsky, 75004 Paris, France, antoine.minard@ircam.fr), Patrick Susini (IRCAM - UMR CNRS 9912, Equipe Perception et Design Sonores, 1, place Igor Stravinsky, 75004 Paris, France, susini@ircam.fr), Nicolas Misdariis (IRCAM - UMR CNRS 9912, Equipe Perception et Design Sonores, 1, place Igor Stravinsky, 75004 Paris, France, misdarii@ircam.fr), Guillaume Lemaitre (IRCAM - UMR CNRS 9912, Equipe Perception et Design Sonores, 1, place Igor Stravinsky, 75004 Paris, France, lemaitre@ircam.fr), Stephen McAdams (Centre for Interdisciplinary Research in Music Media & Technology (CIRMMT) - Schulich School of Music - McGill Univ., 555 Sherbrooke Street West, Montreal, QC H3A1E3, Canada, smc@music.mcgill.ca), Etienne Parizet (Laboratoire Vibrations Acoustique, Insa Lyon, 25 bis, av. J. Capelle, 69621 Villeurbanne Cedex, France, etienne.parizet@insa-lyon.fr)

The purpose of this study is to propose a scheme of environmental sound description based on the comparison and generalization of 4 timbre studies of diverse environmental sounds. In the medium term, the aim is to make the indexing and classification processes of this kind of sound automatic, which is essential for sound content-based searching and browsing methods using perceptual models of environmental sounds. First, we inventoried the stimuli, experiments and perceptual results of these 4 studies. Then, we experimentally identified 3 main environmental sound categories that constitute this overall sound dataset: impact sounds, motor sounds and instrument-like sounds. We developed an efficient tool that predicts these categories according to only two acoustic features calculated on the signal. However, because of the specificities of the sound production of these three categories, each of them has its own timbre space. Therefore, we finally used perceptually relevant acoustic features to explain these timbre spaces, according to the main acoustic characteristics that define each sound class. We found that timbral brightness is a common feature used to discriminate sounds in all classes, while other particular features are specifically used within each class. [Work partially supported by the SamplerOrchestrator project of the ANR program]

2pNSd2. Relations between acoustic parameters and perceptual properties: an approach by regressions tree applied to car door closure sounds. Marie Céline Bezat (PSA Peugeot Citroën, Centre Technique de Vélizy, Route de Gisy, 78943 Vélizy-Villacoublay, France, marieceline.bezat@mpsa.com), Vincent Roussarie (PSA Peugeot Citroën, Centre Technique de Vélizy, Route de Gisy, 78943 Vélizy-Villacoublay, France, vincent.roussarie@mpsa.com), Richard Kronland-Martinet (CNRS-LMA, 31, chemin Joseph Aiguier, 13402 Marseille, France, kronland@lma.cnrs-mrs.fr), Solvi Ystad (CNRS-LMA, 31, chemin Joseph Aiguier, 13402 Marseille, France, ystad@lma.cnrs-mrs.fr)

The aim of this study is to identify perceptually pertinent parameters for the evaluation of car door closure sounds. For this purpose, door closing sounds are finely decomposed into perceptual properties: analytical properties (which are obtained thanks to sensory analysis), natural properties (linked to perception of sources and events) and evocations. The acoustic characterisation of the sound is then processed by means of an analysis-synthesis model which aims, not at reproducing the exact replica of the door closing sounds, but to synthesize sounds that preserve perceptual properties with a reduced number of signal parameters. The model consists in decomposing the sound in several independent impact sources, each impact being modelled by a set of gains and damping factors in frequency bands. Listening tests on controlled sounds are then carried out to observe the effects of acoustic parameters on the perceptual properties. The complex relations between acoustic parameters and perceptual properties are finally established via regressions tree analyses.

2pNSd3. Acoustic feedback of control elements in cars. Alexander S. Treiber (Heilbronn University, Max-Planck-Str. 39, 74081 Heilbronn, Germany, treiber@hs-heilbronn.de), Gerhard Gruhler (Heilbronn University, Max-Planck-Str. 39, 74081 Heilbronn, Germany, gruhler@hs-heilbronn.de)

Due to the complexity of modern car's on-board systems, car manufacturers tend to use menu based user interfaces. These interfaces offer a relatively low number of control elements for a large number of functions. Optimization of both haptical and acoustical feedback of the remaining control elements can improve both acceptance and security of operation. Since cars nowadays are no longer sold simply as technical but as lifestyle products it is crucial for the success that the potential customer perceives every single aspect of the car to be valuable. Obvious examples are exterior design and material quality. Since the user interface of the car can be judged even before a test drive the feeling of buttons and switches is a key aspect. This work presents the results of a jury test which is part of an ongoing research project focused on acoustical feedback. Subjects were asked to judge both

recordings of real control elements as well as synthesized signals which were presented on purpose-built hardware. Based on the subjective results the recorded signals were analyzed in order to identify spectral features which correlate with the subject's responses.

2pNSd4. Influence of time-varying booming noise on automotive comfort. Florent Richard (PSA Peugeot Citroën, Centre Technique de Vélizy, Route de Gisy, 78943 Vélizy-Villacoublay, France, florent.richard@mpsa.com), Francois Costes (PSA Peugeot Citroën, Centre Technique de Vélizy, Route de Gisy, 78943 Vélizy-Villacoublay, France, francois.costes@free.fr), Vincent Roussarie (PSA Peugeot Citroën, Centre Technique de Vélizy, Route de Gisy, 78943 Vélizy-Villacoublay, France, vincent.roussarie@mpsa.com)

Noise level reduction is the main preoccupation for acoustic engineers in the automotive industry. Huge progresses were made during the past decades thanks to the use of acoustic materials and specific intake or exhaust silencers. In the future, vehicles will have to be lighter and engines optimized to ensure very low energy consumption. This sets new compromises between mass, performances and acoustics, in particular for booming noise that can be very affected by mass reduction or exhaust modifications. Acoustic specifications must therefore be optimized to guarantee customer's comfort in spite of these new constraints. In this paper, we study the impact of time-varying booming noise on customer's comfort on acceleration sound samples. We performed several customer tests to evaluate the impact of different time-varying booming profiles on comfort and to find out an acceptability threshold for booming.

TUESDAY AFTERNOON, 1 JULY 2008 P2-A, LEVEL 2, 3:40 TO 5:20 P.M.

Session 2pNSe

Noise and EURONOISE: General Topics in Noise II (Poster Session)

All posters will be on display from 3:40 p.m. to 5:20 p.m. To allow contributors an opportunity to see other posters, contributors of odd-numbered papers will be at their posters from 3:40 p.m. to 4:30 p.m. and contributors of even-numbered papers will be at their posters from 4:30 p.m. to 5:20 p.m.

Contributed Papers

2pNSe1. Measurement of the acoustic pressure distribution occurring around an aerial substation adjacent to apartment buildings. Sebastian Borucki (Technical University of Opole, ul. Miko^{3}ajczyka 5, 45-271 Opole, Poland, s.borucki@po.opole.pl), Tomasz Boczar (Technical University of Opole, ul. Miko^{3}ajczyka 5, 45-271 Opole, Poland, t.boczar@po.opole.pl), Andrzej Cichon (Technical University of Opole, ul. Miko^{3}ajczyka 5, 45-271 Opole, Poland, a.cichon@po.opole.pl)

The subject matter of the research work presented in this paper refers to the measurements of the values of the acoustic pressure levels (noise) occurring around a main feeding-point aerial substation adjacent to apartment buildings. The paper presents the values of the noise accompanying the particular power devices, mainly transformers, during their regular operation. The main aim of this research work was the comparison and assessment of the acoustic pressure values measured with the permissible values defined by environmental standards binding in Poland. The research analysis carried out proved that during a long-term operation of power appliances installed in substations the acoustic pressure level that they emit into the environment is not constant but is subject to changes. Thus the increase of the noise level above the permissible values can be the cause of violation of environmental standards. Due to a significant increase of people's awareness and readiness to claim their rights, the main consequence of violating the standards is a growing number of claims. Therefore it is imperative that the level of the acoustic pressure be monitored during routine tests, especially around high-power transformers.

2pNSe2. Investigation and application of theoretical acoustic field model evaluating the change of environmental conditions. Robertas Mikalauskas (Kaunas University of Technology, K.Donelaicio str. 73, LT-44029 Kaunas, Lithuania, robertas.mikalauskas@ktu.lt), Vitalijus Volkovas (Kaunas University of Technology, K.Donelaicio str. 73, LT-44029 Kaunas, Lithuania, tsdi@ktu.lt)

The effectiveness of the means used to reduce the noise depends on many factors. One of the main factors is the sources which generates acoustic field. In industrial premises there are many sources, their impact to acoustic field differs, and the source may also change due to environmental conditions. Therefore the task of the creation of the mobile noise reduction means, their rational arrangement and control becomes more and more relevant. In this case theoretical modeling of interaction of acoustic noise control systems with environment has significant importance for creating such systems. This paper provides acoustic field model using FEM, which imitates changing conditions of real industrial premise, evaluates the effectiveness and application possibilities of the mobile noise reduction system. It also provides the comparison of the results of theoretical experiment with experimental results. The results showed that with the help of the model mobile noise reduction system can be modeled, their effectives might be evaluated considering the change of sources and reflection planes, and the structural model of the investigative room can be supplemented with acoustic noise reduction means - noise reduction screens, selecting their geometric dimensions, arrangement in the space and selecting the materials and predicting the values of acoustic field parameters in the real object point under consideration.

2pNSe3. Effects of personal stereo use: pilot results from 20 university students. Eric De Santis (Acoustics, Aalborg University, Fredrik Bajers Vej 7 B5, 9220 Aalborg Ø, Denmark, ems@es.aau.dk), Rodrigo Ordoñez (Acoustics, Aalborg University, Fredrik Bajers Vej 7 B5, 9220 Aalborg Ø, Denmark, rop@es.aau.dk), Karen Reuter (Acoustics, Aalborg University, Fredrik Bajers Vej 7 B5, 9220 Aalborg Ø, Denmark, kr@es.aau.dk), Dorte Hammershøi (Acoustics, Aalborg University, Fredrik Bajers Vej 7 B5, 9220 Aalborg Ø, Denmark, dh@es.aau.dk)

Modern personal stereo systems have the ability to store thousands of music files in small, relatively low-cost, compact devices. The popularity and widespread presence of the MP3 player cannot go unnoticed in contemporary society. Given a sufficient noise level and listening duration, consumers are at risk of developing a noise-induced hearing loss. A study into the effects of personal stereo use will be carried out with the intention of investigating common noise exposure levels in realistic settings, user listening habits and the hearing status in a group of listeners. Noise exposure levels are to be obtained by using the manikin technique described in the ISO

11904-2 standard. The questionnaire to be presented to interested participants is designed to report personal stereo listening habits and to screen subjects for the hearing status evaluation. The hearing status of selected subjects will be evaluated through the use of conventional and possibly extended high-frequency audiometry, transient-evoked otoacoustic emissions and distortion product otoacoustic emission fine structures.

2pNSe4. Classroom noise in schools containing children learning English as a second language. Gina Ramirez (5924 N. Campbell Avenue, Chicago, IL 60659, USA, gina.ramirez@loop.colum.edu)

This study analyzes the acoustics of two elementary schools containing both native English speaking children and large English learning populations, to determine if facilities are best being utilized acoustically. As stated by the ASA, children learning English require a more favorable signal-to-noise ratio and should thus be instructed in quieter learning environments. The study examined at least 20 classrooms in each facility by measuring ambient noise level and reverberation time by methodologies outlined in the ANSI S12.60 (2002) standard. Creating a noise mapping allowed for the evaluation of each school based on utilization of pre-existing facilities. Based on preliminary results all classrooms tested failed to meet the maximum A-weighted steady background noise level specified in the standard furthermore schools placed English learning students in environments that were up to 10 dB louder than classrooms used for native English speaking students, demonstrating that more attention to ambient noise level and its effect on speech intelligibility is needed when planning the layout of learning facilities containing large English learning populations. The ongoing analysis of the data aims at assessing the impact of the measured acoustical environments in terms of perceived intelligibility by using a survey tool among the student population.

Session 2pNSf

Noise, Computational Acoustics, and EURONOISE: Time-Domain Modeling Methods in Acoustics I (Poster Session)

Paul Calamia, Cochair
Rensselaer Polytechnic Institute

Maarten Hornikx, Cochair
Applied Acoustics, Chalmers University of Technology

All posters will be on display from 3:40 p.m. to 5:20 p.m. To allow contributors an opportunity to see other posters, contributors of odd-numbered papers will be at their posters from 3:40 p.m. to 4:30 p.m. and contributors of even-numbered papers will be at their posters from 4:30 p.m. to 5:20 p.m.

Contributed Papers

2pNSf1. Optimization of compact finite difference method for wave acoustic simulation. Hideo Tsuru (Nittobo Acoustic Engineering, 1-21-10 Midori Sumida-ku, 130-0021 Tokyo, Japan, tsuru@noe.co.jp), Reima Iwatsu (Tokyo Denki University, Kanda-Nishikicho 2-2, Chiyoda-ku, 101-8457 Tokyo, Japan, iwatsu@cck.dendai.ac.jp)

Recently, the finite difference method, a tool for wave acoustic simulations, can be applied to practical analysis. However, the numerical dispersion which makes propagation speed in simulations change according to the wave length, is a severe problem to maintain high accuracy in the analysis. The numerical error accompanied by the time integration hinders to carry out an accurate simulation. An examination of a compact finite difference scheme which can approximate differentiation precisely on a comparatively large grid spacing was made. It was shown that the adjusting the coefficients in the compact finite difference scheme can simulate a wave propagation accurately with a small amount of computation. The improvement method of the time integration was also discussed. The possibility of improvement of accuracy through a multi-step integration is shown.

2pNSf2. Time-domain modeling of porous media acoustics. David K. Wilson (U.S. Army Engineer Research and Development Center, 72 Lyme Rd., Hanover, NH 03755-1290, USA, D.Keith.Wilson@usace.army.mil), Sandra L. Collier (U.S. Army Research Lab, Attn: AMSRD-ARL-CI-EE, 2800 Powder Mill Rd., Adelphi, MD 20783, USA, sandra.collier@us.army.mil), Vladimir E. Ostashev (NOAA/Earth System Research Laboratory, 325 Broadway, Boulder, CO 80305, USA, vladimir.ostashev@noaa.gov),David H. Marlin(U.S. Army Research Lab, Attn: AMSRD-ARL-CI-EE, 2800 Powder Mill Rd., Adelphi, MD 20783, USA, dmarlin@arl.army.mil), David F. Aldridge (Sandia National Laboratories, PO 5800, MS 0750, Albuquerque, NM 87185-0750, USA, dfaldri@sandia.gov), Neill P. Symons (Sandia National Laboratories, PO 5800, MS 0750, Albuquerque, NM 87185-0750, USA, npsymon@sandia.gov)

Sound waves propagating in porous media are subject to strong dissipation and dispersion. This paper elaborates upon several recent publications by the authors regarding the time-domain description of these effects. The foundation is a relaxational description of the viscous and thermal dissipation in a rigid porous medium, which is shown to possess an exact, analytical conversion from the frequency to the time domain. The complex density and bulk modulus operators transform to temporal convolutions between a causal response function and the acoustic field variables. When the convolutions are neglected, the equations reduce to the well known Zwikker-Kosten phenomenological model. The relaxation function can be inverted to provide an equivalent time-domain formulation from the complex volume and compressibility operators. Although a direct time-domain transformation of the specific impedance from the relaxation model has not been found, an accurate broadband approximation thereof can be transformed. The resulting time-domain boundary condition (TDBC) describes the absorptive and reactive response of the material. The response of the boundary decays slowly, as the inverse square root of time, but efficient numerical procedures are formulated that allow the TDBC to be approximated with a small number of recursive filters.

Session 2pNSg

Noise and EURONOISE: EU Projects for Aircraft Noise Reduction I (Poster Session)

Dominique Collin, Chair
Snecma - Safran Group

All posters will be on display from 3:40 p.m. to 5:20 p.m. To allow contributors an opportunity to see other posters, contributors of odd-numbered papers will be at their posters from 3:40 p.m. to 4:30 p.m. and contributors of even-numbered papers will be at their posters from 4:30 p.m. to 5:20 p.m.

Contributed Papers

2pNSg1. Effect of curvature on the scattering coefficients of Herschel-Quincke tubes. Benjamin Poirier (Université de Technologie de Compiègne, Centre de Recherche Royallieu, BP20529, 60205 Compiègne, France, bpoirier@utc.fr), Jean-Michel Ville (Université de Technologie de Compiègne, Centre de Recherche Royallieu, BP20529, 60205 Compiègne, France, jean-michel.ville@utc.fr), Cédric Maury (Université de Technologie de Compiègne, Centre de Recherche Royallieu, BP20529, 60205 Compiègne, France, cedric.maury@utc.fr), Félix Foucart (Université de Technologie de Compiègne, Centre de Recherche Royallieu, BP20529, 60205 Compiègne, France, felix.foucart@utc.fr)

The concept of Herschel-Quincke (HQ) tubes has been known since the beginning of the 20th century and was shown to be of interest to reduce tonal and broadband noise from turbofan engine. To help to understand the physical phenomena underlying the HQ concept, Hallez & Burdisso have developed a 3D theoretical model. The 3D modelling technique considers the tubes-inlet interfaces as finite piston sources that couple the acoustic field inside a hard-walled duct with the acoustic field within the HQ tubes. This model makes a geometrical approximation by considering the tube as a straight duct whereas in reality it corresponds to a curved duct. In this paper, a model is presented which takes into account the curvature of the bend by integrating two differential equations for the pressure and velocity in the bend, projected on the local transverse modes. Results of some typical coefficients of the scattering matrix [S] deduced from the curved HQ model are compared with the 3D straight tube model, the experimental results and the numerical results. The curvature is shown to modify the HQ resonances and then have to be taken into account in the analytical formulation.

2pNSg2. Assessment of noise impacts of the air traffic. Katrin Ohlau (Universität Stuttgart / IER, Heßbrühlstraße 49a, 70565 Stuttgart, Germany, katrin.ohlau@ier.uni-stuttgart.de), Peter Bickel (Universität Stuttgart/IER, Heßbrühlstraße 49a, 70565 Stuttgart, Germany, peter.bickel@ier.uni-stuttgart.de), Rainer Friedrich (Universität Stuttgart/IER, Heßbrühlstraße 49a, 70565 Stuttgart, Germany, rainer.friedrich@ier.uni-stuttgart.de)

Against the background of the generally increasing traffic and especially the expansion plans in doubling the air traffic until 2020, this paper presents an assessment of noise effects of air traffic and underlines its future meaning. In several projects including the EC funded projects HEATCO (Developing Harmonised European Approaches for Transport COsting and Project Assessment), GRACE (Generalisation of Research on Accounts and Cost Estimation) and ASSET (ASsessing SEnsitiveness to Transport), methodologies for assessing noise including aircraft noise have been developed, improved and applied. The methodologies focus on the impact pathway approach, i.e. first noise levels are estimated, and then level- response functions are applied to calculate health impact and annoyance level distributions. Afterwards it is evaluated by transforming the impacts into monetary levels. Our studies for assessing annoyance have been carried out with the contingent valuation method. Results of the monetary valuation will be shown for the airports Frankfurt, Hamburg, Berlin-Tegel, Düsseldorf, Köln/Bonn, München and Stuttgart. The total air traffic noise costs for Germany range from EUR 150 million to EUR 1200 million per year.

2pNSg3. Efficiency of shielding effect on installed double stream nozzles. Sébastien Aeberli (SNECMA - groupe SAFRAN, Villaroche - Rond-point R. Ravaud, 77550 Moissy-Cramayel, France, sebastien.aeberli@snecma.fr)

In spite of acoustic improvements on jet noise brought by innovative technologies such as chevrons, a way to ensure important acoustic gains is to optimize the power plant integration on aircrafts in order to benefit of the shielding effect due to wing, empennage and fuselage surfaces. In this presentation, these effects are illustrated thanks to a jet noise test campaign at 1/10th scale in an anechoic chamber as part of a European project. This campaign gives a better understanding of shielding effect by a wing and also of the acoustic impact of pylon azimutal direction on two representative BPR 9 nozzles (Baseline - smooth - and Low Noise - with chevrons). The efficiency of shielding effect on jet noise sources in these configurations is assessed.

Session 2pNSh

Noise and EURONOISE: Action Planning and Global Solutions for Urban Noise II (Poster Session)

Klaus Genuit, Cochair
HEAD acoustics GmbH

Itziar Aspuru Soloaga, Cochair
Labein-Tecnalia

All posters will be on display from 3:40 p.m. to 5:20 p.m. To allow contributors an opportunity to see other posters, contributors of odd-numbered papers will be at their posters from 3:40 p.m. to 4:30 p.m. and contributors of even-numbered papers will be at their posters from 4:30 p.m. to 5:20 p.m.

Contributed Papers

2pNSh1. A proposal for doing a touch of anova with noise levels. Michel Maurin (INRETS-LTE, case 24, 69 675 Bron cedex, 69 500 Bron, France, maurin@inrets.fr)

Because noise levels are logarithm of additive variables, the usual numerical processings are not suitable for them (mind $60+60\neq120$). Then one has to deal with them differently, following some other syntaxic rules which may be called in a general way the ″logic of levels″. Of course this question is correctly resolved with the ″energetic mean″ but it fails as soon as one has to deal with variances of levels or covariances with other variables (data analysis, linear regressions, œ). Some (necessarily) approximate compromises may be developped between the logic of levels and the arithmetical logic, (transforming variables in statistics for instance). Here we introduce a new statistic, the h-dispersion, which is not a variance but has many properties of variance, and very fortunatly takes account of the logarithmic status of data. This new compromise may be employed for levels in some cases of design of experiments, such as one-way cases and comparisons ″before-after″ in relation to acoustics operations for instance, and also more or less for two-ways cases. It remains approximate (a syntaxic compromise), but in any time this is an improvement in comparison with a crude ANOVA on levels.

2pNSh2. Study of the surface traffic inside the Cluj-Napoca urban agglomeration. Geamilia Solea (Technical University of Cluj-Napoca, Faculty of Machines Design; Department of Mechanics and Computer Programming, B-dul Muncii; Nr. 103-105, 400 641 Cluj-Napoca, Romania, marylandprod@gmail.com),Mariana Arghir(Technical University of Cluj-Napoca, Faculty of Machines Design; Department of Mechanics and Computer Programming, B-dul Muncii; Nr. 103-105, 400 641 Cluj-Napoca, Romania, marianaarghir@yahoo.com), Dan Borza (National Institute of Applied Sciences of Rouen, INSA Rouen, LMR, Ave l'Universite, BP8 76800 Rouen, France, dan.borza@insa-rouen.fr), Mariana Runcan (National Institute of Applied Sciences of Rouen, INSA Rouen, LMR, Ave l'Universite, BP8 76800 Rouen, France, mariruncan@yahoo .com)

The environment's protection is one of the most actual problems, because of the fact that pollution is a major danger for planet life. The environment's pollution is caused because some pollution agents are in too large a quantity for a long time and they become dangerous for human health, for the flora, for the fauna and for the constructions too. The pollution sources can be classified as natural and artificial sources. The quality of the environment from a specific area at a certain time can be determined by: a) the air quality; b) the water quality; c) the soil quality; d) the health level of the population; e) the decrease of animals and plants species that are accounted for. In the paper there are given the urban traffic on the principal routes inside the Cluj-Napoca municipality. The traffic is the constituent part of the research activity of the national project having the destination the monitoring of the noise and vibrations into an urban agglomeration, applied to the Cluj - Napoca town. This study is the first step for the ″noise map″ asked for by the Romania integration in the European Union for the team researchers of TUCN under the the direction of Dr. Mariana Arghir.

Session 2pNSi

Noise and EURONOISE: Railway Noise and Vibration I (Poster Session)

Richard Carman, Cochair
Wilson, Ihrig & Associates

Franck Poisson, Cochair
SNCF DIR

David Thompson, Cochair
Inst. of Sound and Vibration

All posters will be on display from 3:40 p.m. to 5:20 p.m. To allow contributors an opportunity to see other posters, contributors of odd-numbered papers will be at their posters from 3:40 p.m. to 4:30 p.m. and contributors of even-numbered papers will be at their posters from 4:30 p.m. to 5:20 p.m.

Contributed Papers

2pNSi1. On effectiveness of vibration isolation using super-elastic rail support combined with booted sleeper or floating slab. Tianxing X. Wu (Shanghai Jiao Tong University, School of Mechanical Engineering, 800 Dong Chuan Road, 200240 Shanghai, China, txwu@sjtu.edu.cn)

Ground vibration or structure vibration of viaduct due to railway traffic can be reduced by use of super-elastic rail support, booted sleeper and floating slab to isolate vibration transmission from the track to the infrastructure. In this study modeling in the frequency domain of track structure dynamics and wheel/rail interaction is carried out. Wheel/rail interaction and transmission to the infrastructure of the interaction force due to a relative displacement excitation are simulated. The effectiveness of vibration isolation is analyzed for booted sleeper or floating slab combined with super-elastic rail fastener. It is found that the combination of super-elastic rail fastener with booted sleeper or floating slab can effectively reduce the wheel/rail interaction force in the medium frequencies, compared with the booted sleeper or floating slab track using usual rail pad. The combination also shows better ability to block vibration transmission from the track to the infrastructure in the medium and high frequencies.

2pNSi2. Overview of Railway Noise Control in Europe. Jakob Oertli (Swiss Federal Railways, Schanzenstrasse 5, 3000 Bern, Switzerland, jakob.oertli@sbb.ch)

European and national legislation, increasing freight traffic, political pressure and many more factors contribute to make noise an issue of increasing importance for the railways. This paper provides an overview of railway noise abatement efforts throughout Europe. Different countries in Europe have adopted varying noise abatement strategies, ranging from an emphasis on infrastructure based measures to a combination of rolling stock measures with noise barriers. Important in the current European discussion is the development and retrofitting of freight wagons with K- and LL-brake blocks. To support this retrofitting a wide variety of incentives, such as differential track access charges, operational restrictions or direct subsidies are being discussed. The current efforts by the European Commission, the International Union of Railways (UIC), the Community of European Railways (CER) and other international organisation to promote silent railways are presented.

2pNSi3. A guideline for prediction and control of noise in railroads maintenance activities. Sergio Luzzi (Vie En.Ro.Se. Ingegneria, Via Stibbert, 1, 50134 Florence, Italy, sergio.luzzi@vienrose.it)

In railroads routine maintenance as well as emergency maintenance can be represented by the acoustic point of view as a system of classified yard activities, including catalogued single and grouped noise sources, that is moved along the tracks areas. RFI (Rete Ferroviaria Italiana), the Italian National Railway Company, has provided a guideline for the correct evaluation of noise impact on receivers surrounding the yards, which can be adapted to many situations fitting the specific national law and local regulations disposals about noise assessment, prediction and reduction in temporary activities. Starting from their long term experience, the authors have developed a method for the production of local reports on maintenance railroad yard activities based on the modelling of standard scenarios. Each machinery employed in yards (for superstructure laying or repairing, electric traction, etc,) has been measured and characterized as noise source or as part of a noise sources system (emission box). The noise propagation scenarios are then build using an MS Excel based adaptation software. This methodology represents the technical and procedural architecture of the guideline which provides materials for the management of all the different typologies of maintenance yards operating on the RFI railroad network.

2pNSi4. Railway vibration mitigation - An innovative concept. Frederic Le Corre (Alstom Transport, TGS Engineering - 33, rue des Bateliers, 93400 Saint-Ouen, France, frederic.le-corre@transport.alstom.com), Christine Charles (Alstom Transport, TGS Engineering - 33, rue des Bateliers, 93400 Saint-Ouen, France, christine.charles@transport.alstom.com), Marcel Girardi (Alstom Transport, TGS Engineering - 33, rue des Bateliers, 93400 Saint-Ouen, France, marcel.girardi@transport.alstom.com)

These last decades, rail transportation has known an amazing development. Hence, the resulting pollution on people living alongside lines or above underground lines has become a crucial subject of consideration. The disturbance has two origins: the direct noise or vibration from the railway traffic and the noise produced by vibration of the building walls, the so-called re-radiated noise. Noise and vibration excitation is essentially due to wheel and rail roughness at the contact point. From this excitation point, the track acts as a filter of vibrations. Hence, spectrum of emitted vibrations can be controlled with the design of railway track. Providing vibration mitigation with the track is now commonly encountered, especially on urban projects (LRT MRT). This is usually achieved by introducing an adequate resilient layer to provide the required attenuation. Alstom Transport and Sateba are developing a system to mitigate vibrations. This system called AFST is based on the booted sleeper system. After a complete analysis of critical parameters, a special design has been drawn. The resulting antivibratile solution is a high-performance system suiting areas where vibration mitigation and/or attenuation of re-radiated noise are required.

2pNSi5. Noise and vibrations at tram track intersection. Stjepan Lakusic (University of Zagreb, Faculty of Civil Engineering, Kaciceva 26, 10000 Zagreb, Croatia, laki@grad.hr), Marijan Bogut (KONCAR - Electrical Engineering Institute, Fallerovo setaliste 22, 10000 Zagreb, Croatia, mbogut@koncar-institut.hr), Visnja Tkalcevic Lakusic (University of Zagreb, Faculty of Civil Engineering, Kaciceva 26, 10000 Zagreb, Croatia, visnjat@grad.hr)

In urban areas noise and vibration due to public traffic diminish the quality of life. In Zagreb, tram traffic is the most important form of public transport. Tram network has 120 km of the tracks and 190 trams are used for passengers transport every day. In the movement of the vehicle over track, the interaction between the wheel and track plays the most important role in the field of noise and vibrations. The increasing of noise and vibrations are particularly emphasized at track intersection where a given number of track switches and crossings are installed. This paper presents an experimental study of noise and ground vibrations through the passage of three types of tram vehicles. The measurements were done on the tram intersection with the highest traffic volume in Zagreb's tram network. Two types of track construction were analyzed, discrete and continuous rail fastening system. During the track reconstruction at this intersection, the existing discrete rail fastening system was replaced with a continuous. Because of that, the measurements were carried before and after reconstruction at the same test points. Test results have showed significant reductions of noise and vibrations at track intersection in the case of continuous rail installation.

2pNSi6. Numerical and analytical models for high speed train pantograph radiated noise prediction. Massimo Viscardi (Dept. of Aerospace Engineering - University of Naples, Via Claudio, 21, 80125 Naples, Italy, massimo.viscardi@unina.it), Michele Iadevaia (Dept. of Aerospace Engineering - University of Naples, Via Claudio, 21, 80125 Naples, Italy, miadevaia@inwind.it), Salvatore Melchionna (Dept. of Aerospace Engineering - University of Naples, Via Claudio, 21, 80125 Naples, Italy, s.melchionna@active-group.it), Leonardo Lecce (Dept. of Aerospace Engineering - University of Naples, Via Claudio, 21, 80125 Naples, Italy, leonardo@unina.it)

The present work deals with the development and comparison of an analytical and numerical models for the evaluation of the noise radiated from a pantograph of an high speed train. Under the numerical point of view, a simplified model has been developed for the pantograph; the model that substructures the problem approaching a complex structure as a combination of simple components, has been derived from a similar aeronautical problem (landing gear noise) but has been self-modified to adapt the formulation to the specific problem. The output of the model is the radiated noise level and spectra as a function of the pantograph speed. The CFD numerical model has been developed for the pantograph based upon a commercial code; only the upper part of the system has been herein simulated because it was addressed as the main noise source during previous laboratory acoustic tests. As an output of the model, the radiated noise has been derived with special reference to two main speed to which experimental data could be referred. Analytical and numerical results will be within the paper discussed and compared to highlight the single approach's advantage and drawbacks. At the and of the paper, some line experimental results will be also introduced and discussed.

TUESDAY AFTERNOON, 1 JULY 2008 P2-A, LEVEL 2, 3:40 TO 5:20 P.M.

Session 2pNSj

Noise and EURONOISE: Noise, Structure Borne Noise from Building Technical Equipment, and Ground Borne Noise from Railways I (Poster Session)

James Nelson, Cochair
Wilson, Ihrig and Associates, Inc.

Michel Villot, Cochair
CSTB

All posters will be on display from 3:40 p.m. to 5:20 p.m. To allow contributors an opportunity to see other posters, contributors of odd-numbered papers will be at their posters from 3:40 p.m. to 4:30 p.m. and contributors of even-numbered papers will be at their posters from 4:30 p.m. to 5:20 p.m.

Contributed Papers

2pNSj1. Low frequency noise reduction from building technical equipment: A case study. Kathleen Kondylas (NEVA Associates Noise Control, 15 Beck Street, Newburyport, MA 01950, USA, kondylas@earthlink.net), Chris R. Fuller (Virginia Tech, 131 Durham Hall, Blacksburg, VA 24061, USA, christopher.r.fuller@nasa.gov), Joseph A. King (DuPont, 5401 Jefferson Davis Highway, Richmond, VA 23234, USA, joseph.a.king@usa.dupont.com), Natalia Levit (DuPont, 5401 Jefferson Davis Highway, Richmond, VA 23234, USA, natalia.v.levit@usa.dupont.com)

Mechanical equipment (fans, chillers, motors) produces airborne and structure-borne noise with a significant low frequency component. However, in many applications, mitigation of the low frequency noise requires implementation of significant mass barrier in combination with an air space. This work presents case studies on the use of a novel lightweight and thin acoustical material to mitigate low frequency noise from mechanical equipment. This advanced material, based on patented distributed absorber technology, was used to treat the metal housing of the mechanical equipment. The novel material effectively increased transmission loss of the metal housing below 300 Hz. The total noise reduction was 10-14 dB (A) with 5 dB improvement over typical flexible acoustical blankets below 300 Hz.

2pNSj2. Experimental and numerical study of the ground transmission of structure-borne sound generated by trams. Guillaume Coquel (RATP - CSTB, 13, Rue Jules Vallès, 75547 Paris Cedex 11, France,

guillaume.coquel@cstb.fr),Philippe A. Jean(CSTB, 24 rue JosephFourier, 38400 Saint-Martin-d'Hères, France, philippe.jean@cstb.fr), Michel Villot (CSTB, 24 rue Joseph Fourier, 38400 Saint-Martin-d'Hères, France, michel.villot@cstb.fr)

The increase of railway traffic in urban areas leads to developments in modelling and understanding the propagation of structure borne sound through soil, foundation and structure. Vibration propagation through the ground, is still not well known. The present paper focuses on the propagation of trams vibrations (20-250Hz) in the ground and the energy transmission to the structure. In the first part, calculations performed using a 2D code based on a FEM/BEM approach are compared to measurements performed on a test site. The railway excitation is produced with a vibrator in order to recreate a line of uncorrelated forces. Soil properties are evaluated by an analysis of surface waves. Both bending and in-plane waves are measured on the structure. The ratio of the soil velocity over the structure velocity is computed in order to evaluate the accuracy of the computation. A 2,5D modelisation is also performed in order to evaluate the effect of a point source on the velocity fields on the soil and on the structure. In the second part, a parametric study using the 2D code is performed on typical cases in order to evaluate the modification of vibration transmission from the ground to the foundation.

2pNSj3. A parametric study on the isolation of ground-borne noise and vibrations in a building using a coupled numerical model. Péter Fiala (Budapest University of Technology and Economics, BME Dept. of Telecommunications, Magyar tudósok körútja 2, H-1117 Budapest, Hungary, fiala@hit.bme.hu), Shashank Gupta (KU Leuven, Department of Civil Engineering, Kasteelpark Arenberg 40, B-3001 Leuven, Belgium, shashank.gupta@bwk.kuleuven.be), Geert Degrande (KU Leuven, Department of Civil Engineering, Kasteelpark Arenberg 40, B-3001 Leuven, Belgium, geert.degrande@bwk.kuleuven.be), Fülöp Augusztinovicz (Budapest University of Technology and Economics, BME Dept. of Telecommunications, Magyar tudósok körútja 2, H-1117 Budapest, Hungary, fulop@hit.bme.hu)

Underground traffic induced vibrations and noise in buildings are a major environmental concern in urban areas. To quantify these vibrations a numerical prediction model has been developed and validated. A coupled FE-BE model is used to compute the incident ground vibrations due to the passage of a train in the tunnel. A dynamic soil-structure interaction model is used to determine the vibration levels of the building. The soil-structure interaction problem is solved by means of a 3D boundary element method for the soil coupled to a 3D finite element method for the structural part. An acoustic 3D spectral finite element method is used to predict the acoustic response. The coupled numerical model is used to quantify the efficiency of vibration and noise mitigation measures at different stages of the vibration propagation chain. Vibration isolation with a floating slab track is modeled on the source side, base isolation is incorporated in the structure model, and a box-within-box arrangement is considered for the isolation of re-radiated noise in the building's rooms. The insertion gain of the three methods is compared using the model of a multi-story portal frame office building subjected to ground-borne vibrations from an underground railway line.

TUESDAY AFTERNOON, 1 JULY 2008 P2-A, LEVEL 2, 3:40 TO 5:20 P.M.

Session 2pNSk

Noise and EURONOISE: Physical and Psychophysical Evaluation of Vehicle Exterior Noise II (Poster Session)

Paul Donavan, Cochair
Illingworth & Rodkin, Inc.

Hugo Fastl, Cochair
AG Technische Akustik, MMK, TU München

All posters will be on display from 3:40 p.m. to 5:20 p.m. To allow contributors an opportunity to see other posters, contributors of odd-numbered papers will be at their posters from 3:40 p.m. to 4:30 p.m. and contributors of even-numbered papers will be at their posters from 4:30 p.m. to 5:20 p.m.

Contributed Papers

2pNSk1. Questionnaire survey on vehicle horn use. Masahiko Takada (Omihachiman Community Medical Center, 1379 Tsuchida-cho, 523*0082 Omihachiman, Japan, takada@design.kyushu-u.ac.jp), Yoko Fukuda (Foster Electric Company, Limited, 512 Miyazawa-cho, Akishima City, 196-8550 Tokyo, Japan, yoko_19831228@yahoo.co.jp), Shin-Ichiro Iwamiya (Kyushu University, 4-9-1 Shiobaru, Minami-ku, 815-8540 Fukuoka, Japan, iwamiya@design.kyushu-u.ac.jp)

The Japanese Road Traffic Law provides that a vehicle horn should be utilized in the dangerous situation or the place where the horn sign was installed. However, drivers are frequently seen to use their vehicle's horn as a signal in the situations when they pass each other. Given such situations, the mentioned above law is likely to become a law in name only. Therefore, a questionnaire survey was carried out to ascertain the current circumstance of a vehicle horn use. The respondents were asked the latest or last remembered case of horn use in various situations of both their driving or as pedestrians. With regards to an experience of being tooted at by another driver, the questionnaire included questions concerning place, traffic volume, the aim of the horn use, time pattern of horn tooting, respondent's mental reaction when tooted at by another driver, etc. As a result, drivers mostly had negative mental reactions (i.e., startled, noisy and irritating) by long toots. Pedestrians' negative mental reactions were mainly aroused by horn use calling another's attention to something or to inform of a danger. Furthermore, nearly 40 percent of the respondents were discontented with the volume and the sound quality of horn.

2pNSk2. Sound Quality Evaluation for the Axle Gear Noise in the vehicle. Hyun Ho Lee (Inha University, Mechanical Engineering, 253 Yonghyun Dong, 402-751 Inchon, Republic of Korea, hyunho0424@naver

.com),Ho Wuk Kim(Inha University, Mechanical Engineering, 253 Yonghyun Dong, 402-751 Inchon, Republic of Korea, mowugi@gmail.com) , Sang Kwon Lee (Inha University, Mechanical Engineering, 253 Yonghyun Dong, 402-751 Inchon, Republic of Korea, sangkwon@inha.ac.kr)

A gear whine sound due to the axle system is one of the most important sound qualities in a sport utility vehicle (SUV). In the previous works about the gear whine sound, it was known that it is difficult to evaluate the gear whine sound objectively by using the only A-weighted sound pressure level because of the masking effect. In this paper, for the objective evaluation of the axle-gear whine sound, the characteristics of the axle-gear whine sound is at the first investigated based on the synthetic sound technology and the new objective evaluation method for the axle-gear whine sound is developed by using the sound metrics, which is the psychoacoustic parameters, and the artificial neural network (ANN) used for the modeling of the correlation between objective evaluation and subjective evaluation. This model is successfully applied the objective evaluation of the axle-gear whine sound for real sport utility vehicles and the output of the model are compared with subjective evaluation. The results have a good correlation over 90 per cent.

2pNSk3. Effect of coolant temperature on combustion and combustion noise fluctuations in a Diesel engine at idle conditions. Matthieu Gazon (Coria CNRS UMR6614, Site Universitaire du Madrillet, Avenue de l'Université BP12, 76801 St Etienne du Rouvray, France, gazon@coria.fr) , Jean Bernard Blaisot (Coria CNRS UMR6614, Site Universitaire du Madrillet, Avenue de l'Université BP12, 76801 St Etienne du Rouvray, France, Jean-Bernard.Blaisot@coria.fr), Nicolas Duclaux-De-L'Estoille (Renault SAS, 1 Allée Cornuel, 91510 Lardy, France, nicolas.duclaux-de-lestoile @renault.com), Shanjin Wang (Renault SAS, 67, rue des Bons Raisins, 92508 Rueil Malmaison, France, shanjin.wang@renault.com)

At idle conditions, the cycle-to-cycle fluctuations in Diesel engines lead to combustion noise variations that could be annoying for people, even if the mean level is low, and the cold start condition is one of the worst cases. This study focuses on the effect of injection parameters (duration and timings) and the effect of coolant temperature on combustion characteristics and on the combustion noise. A Direct Injection Diesel engine (four cylinders, 16 valves) equipped with a common-rail injection system and piezoelectric injectors was used. The coolant temperature is changed at idle from the ambient temperature to the temperature at normal working conditions. The combustion is analysed in terms of rate of heat release and combustion noise through the measurement of the cylinder pressure. The results show the dependency of the combustion behavior on the increase of coolant temperature at constant engine adjustment parameters. It is also shown that acting on adjustment parameters can modify the combustion behavior and, consequently, the cycle-to-cycle fluctuations. A trade-off between combustion noise and engine emissions can thus be reached.

2pNSk4. Sound perception of urban delivery trucks. Florence Manca-Demirdjian (Laboratoire Vibrations Acoustique - INSA Lyon, 25 bis avenue Jean Capelle, Bâtiment Saint-Exupéry, F-69621 Villeurbanne cedex, France, florence.manca@gmail.com), Etienne Parizet (Laboratoire Vibrations Acoustique, Insa Lyon, 25 bis, av. J. Capelle, 69621 Villeurbanne Cedex, France, etienne.parizet@insa-lyon.fr)

The study deals with the annoyance of urban delivery trucks noises. Sound sequences of two lorries were recorded during a typical delivery : a commercial one and a prototype specially designed to reduce sound emissions. Various sources could be heard during these sequences (engine, doors, hydraulic rear doors). These recordings (the duration of which being more than 5 minutes) were evaluated by subjects in a sound proofed room by two methods. The first one was a continuous assessment of sequences : the listeners had to continuously assess their annoyance by moving a cursor sliding along a five levels graduated scale (from ″not at all annoying″ to ″extremely annoying″). The second one was an overall evaluation (using the same scale) of each event of the sequences (for example : the arrival of the truck, or the closing of the driver's door, etc...). The comparison of the results obtained from these two methods for both lorries will be presented, as well as the reduction of the annoyance could be realized on the prototype.

Session 2pNSl

Noise and EURONOISE: Environmental Noise Mapping III (Poster Session)

Kenneth Cunefare, Cochair
The Georgia Inst. of Technol.

Gaetano Licitra, Cochair
ARPAT - Dept. Firenze

All posters will be on display from 3:40 p.m. to 5:20 p.m. To allow contributors an opportunity to see other posters, contributors of odd-numbered papers will be at their posters from 3:40 p.m. to 4:30 p.m. and contributors of even-numbered papers will be at their posters from 4:30 p.m. to 5:20 p.m.

Contributed Papers

2pNSl1. Low frequency noise impact of road traffic in the Netherlands. J. Jabben (RIVM, A. van Leeuwenhoeklaan 9, 3720 BA Bilthoven, Netherlands, jan.jabben@rivm.nl), Eric Schreurs (RIVM, A. van Leeuwenhoeklaan 9, 3720 BA Bilthoven, Netherlands, eric.schreurs@rivm.nl)

Current traffic noise impact assessments are usually based on broadband A-weighted noise indicators. A more complete picture and better correlation with annoyance and health effects may result from indicators that include temporal aspects and frequency character. These aspects are currently under investigation at RIVM. This paper gives an evaluation of low frequency noise impact from road traffic in the Netherlands. The results are based on low frequency noise maps covering the entire road network. In particular the effectiveness of various types of noise control measures, such as noise barriers or walls, porous asphalt layers and reduction of noise emission, with regards to low frequency impact were studied. The results indicate for low frequency noise levels, powertrain noise and freight traffic in general, are of major importance for environmental quality.

2pNSl2. In Situ Characterization and Noise Mapping of Ships Moored in the Port of Venice. Antonino Di Bella (Dept. Technical Physics - University of Padova, Via Venezia 1, 35131 Padova, Italy, antonino.dibella@unipd.it), Andrea Tombolato (Studio di Acustica, Via Tripoli 16, 35141 Padova, Italy, tombolato@acusticapd.191.it), Stefano Cordeddu (Studio di Acustica, Via Tripoli 16, 35141 Padova, Italy, cordeddu@acusticapd.191.it), Emanuele Zanotto (Autorità Portuale di Venezia, Porto Commerciale - Molo A - Fabbricato 448, 30175 Marghera, Italy, emanuele.zanotto@port.venice.it), Marco Barbieri (Autorità Portuale di Venezia, Porto Commerciale - Molo A - Fabbricato 448, 30175 Marghera, Italy, marco.barbieri@port.venice.it)

The acoustical characterization and the mapping of noise emitted from ships were carried out on behalf of the Venice Port Authorithy in the frame of the European Project NoMEPorts (Noise Management in European Ports). According to the Directive 2002/49/CE (END), different noise sources (like roads, railways, aircraft, industrial sites, ports) have to be considered and mapped separately; so, in the first step, the acoustical characterization of ships is required. Annex IV of the Directive, in particular, establishes that the strategic noise maps for agglomerations shall put a special emphasis on the noise emitted by, inter alia, industrial activities, including ports. Three kinds of ships were investigated, using the Italian technical standards UNI 10855 and UNI 11143: 1. inland navigation ships (along wharves); 2. ferries (along wharves and when maneuvering); 3. cruises (along wharves and when maneuvering). As for the maneuvering, it could be said that a supplementary noise indicator is needed, as the END, Annex I, forsees in the case the average number of noise events in one or more of the day periods is very low (for example, less than one noise event an hour).

2pNSl3. Mapping urban noise quota generated by a transport service. Sergio Luzzi (Vie En.Ro.Se. Ingegneria, Via Stibbert, 1, 50134 Florence, Italy, sergio.luzzi@vienrose.it)

The paper refers to a recent noise mapping experience, regarding the determination of quotas generated by urban transport services in complex areas. The first results of this study have been presented at Euronoise 2006 in Tampere and at Transport Noise 2006 congress in Saint Petersburg. Now the study is completed. Italian Law established that noise levels produced by buses, coaches and trams, must respect noise limits of area and road buffers classification. Public and Private transport companies are directly requested to point out their specific contributions levels and action plans for the reduction of those levels. At the same time, data for 2002/49/EC Directive have to be collected by them and given to authorities in agreement with formats and standards. The original methodology of source analysis, noise mapping and action planning studied and experienced by the authors in the Florentine area, applies a multi-variable couple-checking algorithm for the optimal choice of critical sites, to the whole road network of each company, reducing the number of calculations and conducting measurement campaigns only for the chosen critical ″pivot″ scenarios. Noise contribution quotas, generated by bus and coach traffic on linear sources and road systems, have been investigated and considered in models.

2pNSl4. Uncertainty of noise mapping software. Jacek Wierzbicki (AGH University of Science and Technology, Al. Mickiewicza 30, 30-059 Kraków, Poland, wierzbic@agh.edu.pl), Wojciech Batko (AGH University of Science and Technology, Al. Mickiewicza 30, 30-059 Kraków, Poland, batko@agh.edu.pl)

Noise map is a tool to come to noise policy and especially to an action plan. The most important question connected with noise mapping realized by computational methods is about reliability of results. It is closely connected with quality of input data and calculation algorithms and their parameters. An influence of elements location, buildings height and number of vehicles accuracy on calculated results was considered in first stage. Before implementation of Harmonoise/Imagine P2P algorithms there are differences between various software. The paper presents first results from investigations with two commercial prediction programs. The absolute accuracy (uncertainty) of predicted by software sound levels is very difficult to quantify because an uncertainty in the measurements. The main result of

investigations is a table of differences in sound level calculations related to variation of input data (geometry of objects and acoustic parameters) and calculation algorithm.

2pNSl5. Noise mapping of major roads in Milan District. Alessandro Bisceglie (Department of Environmental Sciences of the University of Milano - Bicocca, Piazza della Scienza, 1, 20126 Milan, Italy, alessandro.bisceglie@unimib.it), Giovanni Zambon (Department of Environmental Sciences of the University of Milano - Bicocca, Piazza della Scienza, 1, 20126 Milan, Italy, giovanni.zambon@unimib.it), Fabrizio Artom (Phoneco S.r.l., Via San Cristoforo 84, 20090 Trezzano Sul Naviglio, Italy, artom@phoneco.it), Mattia Viganò (Phoneco S.r.l., Via San Cristoforo 84, 20090 Trezzano Sul Naviglio, Italy, vigano@phoneco.it), Franco Bertellino (Microbel s.r.l., via Livorno 60, 10144 Torino, Italy, franco.bertellino@microbel.it), Marco Longoni (Provincia di Milano, Corso di Porta Vittoria 27, 20122 Milano, Italy, m_longoni@provincia.milano.it)

The paper deals with noise map calculation, according to the first deadline of the END (Environmental Noise Directive, 2002/49/EC), for Milan district major roads. The roads with more than six million vehicle passages per year have been estimated to cover 405 km out of 1090 km total. Noise emission has been calculated from peak hour flow data for each segment of the whole road network and from some local traffic direct measurements. A statistical method to assign mean flow values to each road segment has been used, according to Italian reference periods. These data enable to use an acoustic model on a wide area with several line sources in order to obtain noise propagation maps of Lden and Lnight indicators. A procedure to estimate people exposed to different noise levels, as required by the END, has been also studied. Through a geographic information system it has been possible to intersect population input data (demographic density for different areas, buildings use type and buildings volumetric data) and noise mapping data. Every step of the procedure has been carried out complying with WG-AEN Good Practice Guide recommendations, on the basis of the best available data in Milan district.

2pNSl6. 3D noise map of an hospital and noise sources evaluation. Paulo J. Sequeira Goncalves (EST / Instituto Politecnico de Castelo Branco, Av Empresario, 6000-767 Castelo Branco, Portugal, pgoncalves@est.ipcb.pt)

This paper presents the tri-dimensional acoustical characterization of Castelo Branco Hospital. Traffic and air conditioning machines produce noise that influences the Hospital and the buildings nearby. The results are presented in two dimensions at a height of four meters above the ground and in the vertical direction to access the noise levels in the building floors. For the construction of the model were used and compared to types of measurements of vehicles counting, for characterization of the traffic noise. The first approach was performed at every hour during the 24 hours of the day, by counting periods of 10 minutes. In the second approach counting was performed for 30 minutes on six time intervals, identified by inquiries to the nearby population and by a 24 hour noise measurement. The air conditioning machines were modelled using the Portuguese norm, NP EN ISO 3744. Correlation results taken from the two previous approaches and the noise measurements used to validate the Cadna/A model showed values of 0.87 and 0.85. Since they are very similar, one can conclude that both approaches can be used in practice. Taking the economical factor, the second approach is preferable because it takes less time to be performed.

2pNSl7. Management of the Tourist & Entertainment Noise Using Noise Mapping Technique. Alan Štimac (DARH2 Acoustics & Civil Eng. Ltd., Ljubicin prolaz 3, HR-10430 Samobor, Croatia, alan@darh2.hr), Aleš Globevnik (A-PROJEKT Natasa Kepe-Globevnik s.p., Vinarje 110b, SI-2000 Maribor, Slovenia, aprojekt@siol.net), Lilijana Kuhelj (Environmental Agency of the Republic of Slovenia, Vojkova 1B, SI-1000 Ljubljana, Slovenia, lilijana.kuhelj@gov.si)

In countries with strong orientation in tourism and entertainment, especially during summer months, noise problems are always present. This paper represents some applications of noise mapping techniques for the management of tourist & entertainment noise that were conducted in Croatia and Slovenia. The noise mapping techniques were applied for the prediction of noise levels on several places inside the cities of Varaždin and Pola (Croatia) including famous Roman amphitheatre, and in the city of Nova Gorica (Slovenia) especially during entertainment live-shows (concerts, movie festival etc). Such approach enables the city authorities to prepare the base for the implementation of noise policy with introducing such a system that would represent background documents for providing criteria of setting out areas on one side intended to entertainment and quiet areas on the other. For the daily activities in areas that are the most attractive for tourists, noise-modelling techniques have been used for predicting noise emitted from pubs and bars including terraces and loudspeakers. Such approaches have been used by city authorities to establish technique for ″fixed quotas″ that will be able to designate maximum area of terraces concerning number of seating places in relation with the type of bar/pub and noise emission.

2pNSl8. Managing Input Data Uncertainty within Strategic Noise Mapping by Utilising Data Schema Specifications. Simon J. Shilton (Acustica Ltd, Trident One, Styal Road, M22 5XB Manchester, UK, simon.shilton@acustica.co.uk), Nigel Jones (Extrium Ltd, Calverley House, 55 Calverley Road, TN1 2TU Tunbridge Wells, UK, nigel.jones@extrium.co.uk), James Trow (Hepworth Acoustics Ltd, 5 Bankside, Crosfield Street, WA1 1UP Warrington, UK, james.trow@hepworth-acoustics.co.uk)

With the proclamation of the Directive on Environmental Noise (2002/49), the process of noise mapping and action planning has begun around Europe. Large scale wide area noise modelling requires an extensive range of data inputs. The requirements for these inputs are driven by several factors, including the noise calculation methodologies, noise mapping software system, GIS and the deliverables set out within the Directive and recommended Reporting Mechanism. Utilising a staged approach to project design led to the development of detailed noise mapping data schema specifications prior to the collation of input datasets for the calculation process. The data schema may be used throughout the mapping project as a framework to manage dataset concatenation, data capture or the use of defaults and GPGv2 Toolkits to infill data gaps. They also enable data preprocessing guidelines to be passed to non-acoustic GIS specialists, and help to guide and catalogue data processing steps. This paper presents experience gained whilst developing a number of noise mapping data schema specifications and their implementation within successful projects during the first round of mapping. Railway noise mapping is used as an example of how a data schema may be used to develop solutions to technical problems as well as coordinate data capture.

2pNSl9. On railway noise modelling - an approach to the european interim method. J. Luis Bento Coelho (CAPS, Instituto Superior Técnico, TU Lisbon, Av. Rovisco Pais, P-1049-001 Lisbon, Portugal, bcoelho@ist.utl.pt), Diogo Alarcão (CAPS, Instituto Superior Técnico, TU Lisbon, Av. Rovisco Pais, P-1049-001 Lisbon, Portugal, diogo.alarcao@ist.utl.pt)

Railway noise results from a number of sources, with airborne and structure borne transmission mechanisms being responsible for the noise radiation and propagation. The European Directive 2002/49/EC requires the drawing of noise maps for areas near major transport infrastructures. The Portuguese Noise Act of 2007 further requires the drawing of noise maps for all transport infrastructures. This paper reports on our experience on noise mapping of the major Portuguese railway lines. The interim calculation model RMR96/SRMII, recommended in Directive 2002/49/EC, was adopted for the prediction of the railway noise, where a 1/1 octave band noise spectrum curve fitting approach was followed. Details on the implementation, adaptation and validation of the calculation procedure are reported. Emphasis on the required data such as train categories, superstructure, and speed profiles will be given. Examples and results for a number of major railway lines will be presented.

2pNSl10. Is DNL appropriate for airport noise zoning? Jules G. Slama (UFRJ, Av. Horacio Macedo, 2030, Centro de Tecnologia, Bl. G, Sala 204, Cidade Universitária, 21941-914 Rio de Janeiro, Brazil, julesslama@yahoo.com.br), Félix A. Mora-Camino (Ecole Nationale de l'Aviation Civile, 7 avenue Edouard-Belin BP 54005, 31055 Toulouse, France, felix.mora@enac.fr), Teo C. Revoredo (UFRJ, Av. Horacio Macedo, 2030, Centro de Tecnologia, Bl. G, Sala 204, Cidade Universitária, 21941-914 Rio de Janeiro, Brazil, teorevoredo@yahoo.com.br)

The use of the DNL metric in airport noise zoning is based in the works of Schultz, that were later improved by Fidell. The basic idea is to use the percentage of highly annoyed people as a parameter to organize the area around airports. In urban zoning it is recommended to use the equivalent sound level LAEQ, which uses different criteria to day and night periods to define the land use. With regards to airport noise one may use LAD and LAN metrics which are the equivalent sound levels determined for day and night period, respectively. In this case, the maximum levels chosen to the establishment of the zoning are based on the land use. It is possible, through a simple equation, to determine the DNL level associated to a LAD, LAN pair. The inverse problem, however, has not a unique solution, once this relation depends on the number of daily and night flights of the airport. Thus, the use of DNL in airport noise zoning may lead to completely different results for different airports. Exemples are presented and discussed for two main brazilian airports: Recife and Congonhas.

TUESDAY AFTERNOON, 1 JULY 2008 P2-A, LEVEL 2, 3:40 TO 5:20 P.M.

Session 2pNSm

Noise and EURONOISE: Noise Mapping Techniques and Uncertainties II (Poster Session)

Wolfgang Probst, Chair
DataKustik GmbH, Gewerbering 5, Griefenberg, 86926, Germany

All posters will be on display from 3:40 p.m. to 5:20 p.m. To allow contributors an opportunity to see other posters, contributors of odd-numbered papers will be at their posters from 3:40 p.m. to 4:30 p.m. and contributors of even-numbered papers will be at their posters from 4:30 p.m. to 5:20 p.m.

Contributed Papers

2pNSm1. Strategic noise mapping in slovak republic. Milan Kamenicky (Norsonic Slovensko s.r.o., Letisko M.R. Stefanika 63, 82001 Bratislava, Slovakia, kamenicky@norsonic.sk), Peter Petrak (AkusTech s.r .o., Lubovnianska 14, 85107 Bratislava, Slovakia, akustech@akustech.sk)

In the EU there is an ongoing process of strategic noise mapping and action planning. The goal is to determine the noise produced by the main noise sources - road, rail and air transport and industrial facilities and the exposure caused by them in densely populated agglomerations. Subsequently it is necessary to consider possibilities, how to reduce additional increase of noise levels in the environment. Authors participated in the strategic noise map development process and this paper comprises the information about the measurement and calculation results of traffic and industrial noise in Bratislava and in the slovak republic. Presentation of strategic noise maps and actions plans in Slovakia.

2pNSm2. Mapping of noise caused by military airplane operation. Milan Kamenicky (Norsonic Slovensko s.r.o., Letisko M.R. Stefanika 63, 82001 Bratislava, Slovakia, kamenicky@norsonic.sk), Peter Petrak (AkusTech s.r.o., Lubovnianska 14, 85107 Bratislava, Slovakia, akustech@akustech.sk)

Noise from military airplane operations is a serious problem in affected surroundings of military airports. Usually, military airplane noise emission data are not available in databases of common programs, which causes problems in noise load modeling. In such cases it is necessary to obtain emission data by measurement. Measurement must be performed in modes which are not used in ordinary airplane operation. Based on these measurements, acoustic emission data will be processed in the required form according to a used mathematical model. This paper will include examples of acoustic data acquisition and their utilization in mapping of noise load caused by military airplane operations in the surroundings of military airports. Also, verification of data acquired by prediction and measurement in the airport surrounding ordinary airplane operations will be present.

2pNSm3. Effect of limitations of ray-tracing software on predicting community from petrochemical plants. Frank Brittain (Bechtel, Corp., 2255 Peavine Valley Road, Reno, NV 89523, USA, fhbritta@bechtel.com), Marlund Hale (Advanced Engineering Acoustics, 663 Bristol Ave., Simi Valley, CA 93065, USA, noisedoc@aol.com)

Ray-tracing software has proven to be a valuable and powerful tool to predict community noise from outdoor petrochemical and power plants. Accurate predictions are necessary to determine noise reductions needed to meet regulations and/or project noise limits, and then to determine individual equipment noise limits, select add-on noise controls, and confirm the plant will comply with its noise limits. Modeling using ray-tracing software is much more powerful and versatile than a spreadsheet model, which had often been used. Ray tracing and similar image source software have many limitations, particularly for outdoor petrochemical and power plants. To effectively use ray-tracing software, the user needs to understand those limitations. For example, ray tracing does not adequately predict for configurations where distances are significant compared to the wave length of sound, reflections from dense pipe racks, or screening by pipelines and equipment. This paper identifies and discusses some of the limitations of ray-tracing software for predicting community noise. Examples are given. This paper emphasizes limitations of ray-tracing methodology, and not those arising from atmospheric effects.

Session 2pNSn

Noise and EURONOISE: Railway Noise and Vibration II

Richard A. Carman, Cochair
Wilson, Ihrig & Associates, 5776 Broadway, Oakland, CA 94618, USA

Franck Poisson, Cochair
SNCF DIR, 45, rue de Londres, Paris, 75379, France

David Thompson, Cochair
Institute of Sound and Vibration Research, University Road, Highfield, Southampton S017 1BJ, UK

Invited Papers

5:20

2pNSn1. The railway noise reductions achieved in the Silence project. Franck Poisson (SNCF DIR, 45, rue de Londres, 75379 Paris, France, franck.poisson@sncf.fr), Pierre Etienne Gautier (SNCF DIR, 45, rue de Londres, 75379 Paris, France, pierre-etienne .gautier@sncf.fr)

The European project Silence is dedicated to the reduction of railway and roadway noise in urban areas. Within the framework of the subproject E and G, the reduction of the railway noise is addressed. Source ranking of state of the art rolling stocks has been carried out. Then, the Diesel engine, the exhaust, the cooling unit, the electrical engine, the wheels and the track have been optimised by the manufacturers and prototypes have been constructed. The most promising have been selected through laboratory measurement to be installed on the trains and trams. Last measurement campaigns have been carried out to characterise the combination of optimised rolling stocks running on optimised track. Then, relevant reductions of the pass-by noise have been achieved for electrical and Diesel multiple unit trains, freight trains and trams. In the same time, a software called VAMPPASS has been developed in subproject B to simulate the time signal of a train pass-by. The paper focuses on the results of the last measurement campaigns which validate the noise reduction achieved on the global pass-by noise of several rolling stocks and tracks. A comparison with the reduction predicted by VAMPPASS will be also presented. Some improvement of the solutions will be also addressed.

5:40

2pNSn2. Principles for selection of rail fastening systems for control of railway noise and vibration. Stephen J. Cox (Pandrol Rail Fastenings Ltd, 63 Station Road, KT15 2AR Addlestone, UK, s.cox@pandrol.com)

Railways generate noise and vibration as trains pass along the track. It is usually ultimately noise that causes annoyance to those above or alongside the track, but this noise is often generated as a result of vibrations transmitted along and away from the track. Examples of ground-borne vibration at the surface above railway tunnels; airborne noise from trains passing at grade; and noise from trains passing over structures such as viaducts and bridges are each considered in turn. The selection of suitable rail fastening systems, and in particular their stiffness, to control each of these problems is discussed. This often requires compromise - for example, reduction of the noise emitted from the rail may suggest a high stiffness, while reduction of noise from the supporting structure may require a low stiffness. These considerations lead to different solutions to different problems. Some general conclusions are drawn as to how, and to what extent, each of the different types of railway noise and vibration problem may be addressed by modifications to the track fastening system.

6:00

2pNSn3. Cost-effectiveness of railway noise measures in practice. Chiel Roovers (ProRail, P.O. Box 2038, Department VMJB, Railway Noise Knowledge Centre, NL-3500 GA Utrecht, Netherlands, Chiel.Roovers@prorail.nl)

The Dutch noise nuisance law enforces railinframanager ProRail to take noise measures when railway transport is growing, new lines are built or changes are made to the existing lines. Also, measures are taken by the Dutch government at existing ″hotspots″. At the moment the toolbox of measures includes noise barriers, sleeper renewal, raildampers, acoustic grinding and façade insulation. The life-cycle costs of these measures have been derived from recent projects. This paper focuses on the evaluation of the cost-effectiveness of these measures in typical situations where the choice of the application of noise mitigation measures was made recently. In what circumstances is it considered to be appropriate to take measures, and how much money will be available? Are source measures like raildampers more cost-effective compared to noise barriers? The introduction of a track-access-charge system which differentiates on the noise emission of trains concludes this paper.

6:20

2pNSn4. Comparing railway noise prediction results for passenger trains using various models. Malgorzata Reiter (Gdansk University of Technology, Multimedia Systems Department, 11/12 Gabriela Narutowicza Street, 80-952 Gdansk, Poland, reiter.m@sound.eti.pg.gda.pl), Bozena Kostek (Gdansk University of Technology, Multimedia Systems Department, 11/12 Gabriela Narutowicza Street, 80-952 Gdansk, Poland, bozenka @sound.eti.pg.gda.pl)

Railway noise modeling is a requirement for all European countries. Under the European Directive on the Assessment and Management of Environmental Noise, 2002/49/EC all member states were obliged to create strategic noise maps of the major railways by June 30th, 2007. Some of the participating states have their own national schemes dedicated to noise prediction. For those not having their own noise prediction model, the recommendation is to use the Dutch SRM II Model. The most important assessment criterion is an inaccuracy value, which is defined as a difference between the result calculated based on a model and the actual measurements under the same atmospheric conditions simulated. Therefore, it is essential to check out which of the main calculation schemes produces most accurate results. Therefore, all above models were implemented numerically and calculations of the noise maps were performed with the use of: Schall 03 developed in Germany, Dutch SRM II and the Nordic model engineered in Norway. Those models were tested employing sample passenger trains data exploited in Gdansk, Poland. Noise maps were drawn in CadnaA software and then were compared to the field noise measurement test results.

6:40

2pNSn5. Dynamic wheel/rail forces induced by trams at low frequencies. Olivier Chiello (INRETS, Transport and Environment Lab., 25 avenue François Mitterrand, 69675 Bron cedex, France, olivier.chiello@inrets.fr), Marc Maldonado (Research Inst. of Civil Eng. and Mech., UMR CNRS 6183, 1 rue de la Noë, 44321 Nantes Cedex 3, France, marc.maldonado@ec-nantes.fr)

This work is part of various experimental and theoretical investigations into the noise and the vibrations caused by trams in Nantes, France. It focuses on the problem of the low frequency vibrations induced in the track and the ground and particularly on the excitation mechanism at the wheel-/rail interface. In order to estimate the corresponding dynamic wheel/rail forces, axle-box vibrations have been measured on a carrying bogie in various vehicle and track configurations. Additionally, a specific instrument has been used to measure the rail unevenness at large wavelengths likely to excite the vehicle/track system in the low frequency range. Finally, the vertical receptance of the different tracks has been measured by using an impact hammer. In the paper, all these experimental results are presented and the validity of a simple vehicle/track interaction model is discussed.

7:00

2pNSn6. A fast time-domain model for wheel/rail interaction demonstrated for the case of impact forces caused by wheel flats. Astrid Pieringer (Chalmers University of Technology, Division of Applied Acoustics, SE-41296 Gothenburg, Sweden, astrid.pieringer@chalmers .se), Wolfgang Kropp (Chalmers University of Technology, Division of Applied Acoustics, SE-41296 Gothenburg, Sweden, wolfgang.kropp @chalmers.se)

The prediction of impact forces caused by wheel flats requires the application of time-domain models that are generally more computationally demanding than are frequency-domain models. In this paper, a fast time-domain model is presented to simulate the dynamic interaction between wheel and rail, taking into account the non-linear processes in the contact zone. Track and wheel are described as linear systems using impulse-response functions that can be precalculated. The contact zone is modelled by non-linear contact springs, allowing for loss of contact. This general model enables the calculation of the vertical contact forces generated by any kind of roughness excitation between wheel and rail. Here, the model is adapted to the excitation caused by wheel flats by introducing the irregular wheel shape as a form of extreme roughness. A brief parameter study is presented to demonstrate the functioning of the model. The results from the model are discussed and compared with results from literature.

7:20

2pNSn7. Testing a new rail roughness measurement standard. Chris J. Jones (Institute of Sound and Vibration Research, Univeristy of Southampton, Highfield, SO17 1BJ Southampton, UK, cjcj@isvr.soton.ac.uk), Fabien Létourneaux (SNCF - Agence d'Essai Ferroviaire, 21 avenue Salvador Allende, F-94407 Vitry-Sur-Seine, France, fabien.letourneaux@sncf .fr), Pascal Fodiman (SNCF - Direction Générale Déléguée Infrastructure, 34 rue du Commandant Mouchotte, 75699 Paris Cedex 14, France, pascal .fodiman@sncf.fr)

Railway rolling noise arises from the combined roughness of the wheel and rail surfaces. The rail roughness is therefore an important parameter in the assessment of train pass-by noise. The Technical Specifications for Interoperability (TSI's) in Europe require noise to be measured on a 'reference track' the conditions of which are controlled. A spectral limit for the rail roughness is a major part of that control. The TSIs needed a new standard for rail roughness measurement so the CEN commissioned TC 256 Working Group 3 to draft one. The final draft of the new standard is now complete and will soon be published. This paper describes a 'road test' that was part of the standard development process. This test involved asking eight teams from all over Europe with seven different instruments to measure roughness at the same site, independently making their own interpretation of the standard. The paper outlines the aims of the new standard and describes the road test. It presents results and conclusions of the test that have been used already to improve the standard. Consideration had to be made of how railhead defects are treated and how different measurement technologies are used.

7:40

2pNSn8. Brake noise measurements on mixed freight trains with composite brake blocks. Erwin H. Jansen (TNO Science and Industry, PO Box 155, 2600 AD Delft, Netherlands, erwin.jansen@tno.nl), Michael G. Dittrich (TNO Science and Industry, PO Box 155, 2600 AD Delft, Netherlands, michael.dittrich@tno.nl), Erik L. Sikma (Lloyd's Register Rail Europe B.V., PO Box 2016, 3500 GA Utrecht, Netherlands, erik.sikma @lrrail.com)

In the Netherlands, the noise emission of shunting yards, which are often located in urban areas, are a source of disturbance. The noise emission of shunting yards is legislated in terms of maximum allowable equivalent sound pressure levels and peak noise levels of the façade of residences. Brake noise is known to be a major contributor to the total sound emission of shunting yards, in particular from trains with cast-iron block brakes. Within the scope of the Dutch Innovation Programme on Noise Reduction, the rolling noise reducing effect of alternative composite block brakes, such as LL and K blocks, was successfully demonstrated. Additionally, the effect of composite brake blocks on braking noise was studied. For this purpose, noise measurements were conducted on mixed freight trains according to the applicable protocols. Measurements were conducted on trains slowing down from a speed of 30 km/h to a standstill and trains passing-by with brake systems applied. Some composite brake blocks show a considerable reduction of both braking pass-by levels and peak noise levels. Results are presented. If squeal noise is absent, braking noise of most considered brake blocks show a speed dependency similar to that for rolling noise.

Session 2pNSo

Noise and EURONOISE: Noise, Structure Borne Noise from Building Technical Equipment, and Ground Borne Noise from Railways II

James Nelson, Cochair
Wilson, Ihrig & Associates, Inc., 5776 Broadway, Oakland, CA 94618, USA

Michel Villot, Cochair
CSTB, 24 rue Joseph Fourier, Saint-Martin-d'Hères, 38400, France

Invited Papers

5:20

2pNSo1. Prediction method for structure borne noise generated in buildings by tools such as drills. Michel Villot (CSTB, 24 rue Joseph Fourier, 38400 Saint-Martin-d'Hères, France, michel.villot@cstb.fr), Philippe A. Jean (CSTB, 24 rue Joseph Fourier, 38400 Saint-Martin-d'Hères, France, philippe.jean@cstb.fr)

Tools such as drills generate structure borne noise which propagate in the building structure and radiate loud noise even in rooms far from the source. This paper presents a method for predicting this type of noise, frequent in buildings under construction or renovation. First the structural power injected by the tool to the receiving structure (floors or walls) is estimated from field measurements of the vibrational (bending) energy stored in the receiving plate. Then the vibration propagation through the building structures and the noise radiated in the receiving room is estimated using Statistical Energy Analysis (SEA), where both bending and in plane waves are taken into account. Comparisons between predictions and results measured in an apartment building under construction show that SEA gives quite acceptable results down to 1/3 octave 50 Hz for structure borne sound sources such as drills.

5:40

2pNSo2. Structure borne sound source data of building service equipments for EN 12354 part 5 - Round Robin measurements. Christian Simmons (Simmons Akustik & Utveckling, Krokslätts Fabriker 1, 43137 Mölndal, Sweden, info@simmons.se)

At the conference, results will be presented of a round robin test where sound pressure levels and vibration data have been measured in 7 sites using two laundry machines and one heating compressor as sources. The vibrations are determined as transversal vibration levels of the concrete slabs (with the structural loss factors) according to a draft standard prEN 15657-1, as well as relative levels compared to the standardized tapping machine (ISO 140-8). The purpose is to study whether these data may be applied to predict structure borne sound in nearby spaces, according to the draft standard prEN 12354 parts 5 and 2, with a reasonable accuracy as compared to the measured sound pressure levels. The variations in space and time will be monitored carefully to observe any modal coincidence and whether the time and spatial average is the best descriptor of these types of source.

6:00

2pNSo3. A combined approach for base isolation design. Albano Neves E Sousa (IST, Department of Civil Engineering and Architecture, Av. Rovisco Pais, 1, 1049-001 Lisbon, Portugal, albano.nsousa@civil.ist.utl.pt), Luís Guerreiro (IST, Department of Civil Engineering and Architecture, Av. Rovisco Pais, 1, 1049-001 Lisbon, Portugal, luisg@civil.ist.utl.pt), Rui Gomes (IST, Department of Civil Engineering and Architecture, Av. Rovisco Pais, 1, 1049-001 Lisbon, Portugal, ruigomes@civil.ist.utl.pt)

New buildings in the vicinity of underground railway lines should be protected against noise and vibrations induced by railway traffic. In the present paper a case study is presented. A 2D FEM model of the tunnel, ground and building was built in order to identify the transfer function of vibration from the tunnel to building foundations. A 3D model of the building was built, including not only structural elements, but also other non structural walls, in order to identify the transfer function of vibration from foundations to walls and floors. As the impedance of heavy walls and floors is much higher than the acoustic impedance of air, the numerically assessed vibration fields of walls and floors were used to calculate sound fields in rooms by means of natural mode analysis. The vibration and sound fields were then compared with comfort criteria in order to design a base isolation system. With this combined approach, the analysis was performed up to 170 Hz, which is more than one can usually do with integrated 3D models.

6:20

2pNSo4. Variance in predicted structure borne sound power due to simplified characterisation of the source. Tomos A. Evans (University of Salford, Acoustic Research Centre, Newton Building, M5 4WT Salford, UK, t.a.evans@pgr.salford.ac.uk), Andy T. Moorhouse (University of Salford, Acoustic Research Centre, Newton Building, M5 4WT Salford, UK, a.t.moorhouse@salford.ac.uk)

Theoretically the structure borne sound power transmission from a vibration source to a receiving structure can be predicted using the mobility method. In order for all the power transmission mechanisms to be accounted for the source and receiver mobility matrices must contain the mobilities for all degrees of freedom (three translational and three rotational) for each contact point and the transfer mobilities between; each contact point, each degree of freedom and each degree of freedom at each contact point. In practice reliable

measured data for some degrees of freedom is difficult to obtain, so simplified source characterisation methods are required, for example using only certain degrees of freedom. The novel contribution of this paper is to investigate the variance in the predicted structure borne sound power transmission calculated when some degrees of freedom are missing, and when the source is approximated as a single equivalent excitation. The investigation was carried out using numerical simulations of simplified source and receiver structures.

6:40

2pNSo5. Uncertainties and repeatability of the Reception Plate Method. Lieven De Geetere (Belgian Building Research Institute, Lombardstraat 42, B-1000 Brussel, Belgium, lieven.de.geetere@bbri.be), Bart Ingelaere (BBRI, rue du Lombard, 42, B-1000 Brussel, Belgium, bart.ingelaere@bbri.be), Pieter Schevenels (Lab. ATF, Katholieke Universiteit Leuven, Celestijnenlaan 200D, B-3001 Leuven, Belgium, pieter.schevenels@bwk.kuleuven.be)

The Reception Plate Method (RPM) as proposed by CEN/TC126/WG7 in prEN 15657-1 estimates the structure-borne sound power injected from a (high mobility) vibrating source into a (low mobility) building structure. In the near future, a round-robin test is planned to investigate repeatability and reproducibility issues of the RPM. As a preparation of this round-robin, uncertainties of the RPM are studied using the standard ISO tapping machine, placed on a 4 feet table on a reception plate. The injected power into the reception plate is calculated using different methods. The influence of the source position, accelerometer positions and airborne excitation are investigated, together with repeatability tests. Also, differences in injected power between two different brands of the ISO tapping machine will be studied. Finally, in-situ installed structure-borne sound power level will be predicted using prEN 12354-5 and compared to measurements on a simple building structure.

7:00

2pNSo6. Investigation of a vibro-acoustic reciprocal method to derive the contact forces of building equipment. Pieter Schevenels (Lab. ATF, Katholieke Universiteit Leuven, Celestijnenlaan 200D, B-3001 Leuven, Belgium, pieter.schevenels@bwk.kuleuven.be), Arne Dijckmans (Lab. ATF, Katholieke Universiteit Leuven, Celestijnenlaan 200D, B-3001 Leuven, Belgium, arne.dijckmans@bwk.kuleuven.be), Peter J. Van Der Linden (Qsources BVBA, Ketelwinning 38, 3293 Diest, Belgium, info@qsources.be), Gerrit Vermeir (Lab. ATF, Katholieke Universiteit Leuven, Celestijnenlaan 200D, B-3001 Leuven, Belgium, Gerrit.Vermeir@bwk.kuleuven.be)

Structure-borne sound caused by installations can be derived from the injected structure-borne sound power into the connected building element. Theoretically, this is as simple as summing the products of force and velocity at each contact point of the installation. The velocity can be well approximated by the velocity measured close to the contact point. But to measure the force, installation and building element would have to be separated to insert a force sensor. This is generally impractical or even impossible. In this paper, a method is analyzed to derive the force between an installation and a building element in a vibro-acoustic reciprocal way. First, a dedicated volume sound source is placed in an adjacent room and the transfer function of its volume acceleration with the acceleration of the building element is determined. Next, the sound pressure is measured at the source's position while the installation is operating. Since most installations have an important lower frequency contribution, below 50 Hz, the sound source must cover this frequency range with sufficient level. Moreover, an accurate measure of the in-situ volume acceleration of the used source is required. Finally, the method is compared to other methods that approximate the injected structure-borne sound power.

Contributed Papers

7:20

2pNSo7. Building Isolation Design for Noise Critical Applications. George P. Wilson (Wilson, Ihrig & Associates, Inc., 5776 Broadway, Oakland, CA 94618, USA, gwilson@wiai.com)

Because it is a complex, multi-degree-of-freedom system, the success of a building isolation installation depends on careful selection of a number of design factors. The new Toronto Opera House, the Four Seasons Centre for the Performing Arts, opened in June 2006, is located directly adjacent to a surface light rail trackway and to a subway rail transit system. The results characterized as ″the quietest Opera House in the world″ demonstrate that groundborne noise and vibration is not a factor precluding the use of a noisy site for a noise-sensitive facility. Measurement of the existing groundborne noise provided the basis to determine the required noise reduction. Very stiff and massive foundation elements with stiff and massive structure directly above the isolation bearings allows the isolation design to be simplified to a single-degree-of-freedom system for deriving the performance of the isolation at low frequencies. Natural rubber bearings with thickness adjusted to achieve a specific amount of insertion loss for the structure-borne noise can be used to determine the expected performance at frequencies above 50-80 Hz. Isolation system design parameters for the new 2000-seat Opera House Performance Hall and graphical results from vibration and noise projections and tests are presented.

7:40

2pNSo8. Ground vibration requirements in vehicle projects. Janne Färm (Bombardier Transportation Mainline and Metros Division, Östra Ringvägen 2 MLN/TSSV, 721 73 Västerås, Sweden, janne.farm@se.transport.bombardier.com), Siv Leth (Bombardier Transportation Centre of Competence Acoustics and Vibration, Östra Ringvägen 2 CoC AcV, 721 73 Västerås, Sweden, siv.leth@se.transport.bombardier.com), Philipp Rüst (Bombardier Transportation Bogie Division, Zürcherstrasse 39 Postfach 414, 8401 Winterthur, Switzerland, philipp.ruest@ch.transport.bombardier.com)

The climate is right for trains and the environmental targets regarding noise and vibration have to be met to enhance the competitiveness of rail over other forms of transport. Ground vibration is one part that needs to be further addressed. Customer requirements on ground vibration are often included in vehicle contracts even if the vehicle is only one part of the system determining the ground vibration at the receiver point. For the design of new lines there is a need for a better optimization of overall generation of noise and vibration where both the infrastructure and vehicle parameters are included. An overview of the diversity of ground vibration requirements in different vehicle projects is given and the relation to a number of vehicle and track parameters. The potential conflict between ground vibration reduction and increased airborne noise generation is analyzed for particular examples. The background analysis clearly points out the need for a standardization regarding both setting and evaluation of requirements. There is also a need for developing one commonly used, widely accepted, validated prediction tool for ground vibration. It should facilitate engineering level decision making and allow assessment of mitigation measures.

Session 2pPAa

Physical Acoustics: Nonlinear Acoustics in Earthquake Processes and Other Earth Processes I

Paul A. Johnson, Cochair
EES-11 (Geophysics) - Los Alamos National Laboratory, MS D443, Los Alamos, NM 87545, USA

Fabrice Cotton, Cochair
Université Joseph Fourier, Laboratoire de Géophysique Interne et Tectonophysique, CNRS, BP53, France

Invited Papers

2:00

2pPAa1. Stick-slip dynamics of a granular medium. Alberto Petri (Institute of Complex Systems - CNR, via del Fosso del Cavaliere 100, 00133 Rome, Italy, alberto.petri@isc.cnr.it), Andrea Baldassarri (Dipartimento di Fisica -Università di Roma La Sapienza, P.le Aldo Moro 5, 00186 Rome, Italy, andrea.baldassarri@roma1.infn.it), Fergal Dalton (Institute of Complex Systems - CNR, via del Fosso del Cavaliere 100, 00133 Rome, Italy, fergal.dalton@isc.cnr.it), Giorgio Pontuale (Institute of Complex Systems - CNR, via del Fosso del Cavaliere 100, 00133 Rome, Italy, giorgio.pontuale@isc.cnr.it), Stefano Zapperi (CNR-INFM, S3, Dipartimento di Fisica - Universita' di Modena e Reggio Emilia, via Campi 213/A, 41100 Modena, Italy, stefano.zapperi@roma1.infn.it)

Under certain limits, granular materials share many features with fluids and solids. Most of the time, however, they exhibit peculiar features which originate in the non-equilibrium and dissipative character of the grain dynamics. We have investigated the dynamics of a granular medium in a channel, when subject to continuous shear stress from a plate connected to a motor by an elastic spring. We have shown [1] that the statistical features of granular stick-slip dynamics are not simply Gaussian and that [2] can be described in a quantitative way by a simple stochastic equation. Extant work, such as the statistical properties of friction in solid-on-solid systems, further suggests that a large class of driven instabilities can be described in terms of similar general mechanisms. The intensity of the acoustic signals emitted by the granular medium during the slip events displays a non trivial correlation with the plate velocity. [1] F. Dalton et al., Phys. Rev. Lett. 95, 138001 (2005) [2] A. Baldassarri et al., Phys. Rev. Lett. 96, 118002 (2006)

2:20

2pPAa2. Monitoring changes in crustal properties with seismic noise. Michel Campillo (LGIT - CNRS - Université Joseph Fourier, Maison des Géosciences, 1381 rue de la Piscine, BP 53, 38041 Grenoble, France, Michel.Campillo@obs.ujf-grenoble.fr), Florent Brenguier (Laboratoire de Sismologie IPGP, 4 place Jussieu, 75252 Paris, France, fbrengui@ipgp.jussieu.fr), Celine Hadziioannou (LGIT Université Joseph Fourier/CNRS, Maison des Géosciences Domaine Universitaire, 38041 Grenoble, France, eline.hadziioannou@ujf-grenoble.fr), Nikolai Shapiro (Laboratoire de Sismologie IPGP, 4 place Jussieu, 75252 Paris, France, nshapiro@ipgp.jussieu.fr), Eric Larose (LGIT - CNRS - Université Joseph Fourier, Maison des Géosciences, 1381 rue de la Piscine, BP 53, 38041 Grenoble, France, Eric.Larose@obs.ujf-grenoble.fr)

The seismic noise is a continuous source of waves due to the interaction between the solid Earth and its fluid envelopes. Theoretically, the time correlation of the field measured at two distant points allows retrieving the Green function between the points for a random distribution of sources or in presence of a diffuse field. We use this property and study the stability of the correlation functions. We show that the velocity measurements made with correlations are very stable. Using doublet analysis, we found that that we can monitor relative velocity changes smaller than 10^{-4}. We present applications to the forecast of volcanic eruptions and to the monitoring of an active fault.

Contributed Paper

2:40

2pPAa3. Force fluctuations in granular disks near the jamming threshold. Robert E. Ecke (Los Alamos National Laboratory, Center for Nonlinear Studies, MS-B258, Los Alamos, NM 87545, USA, ecke@lanl.gov), Mahesh Bandi (Los Alamos National Laboratory, Condensed Matter and Thermal Physics, MS-K764, Los Alamos, NM 87545, USA, mbandi@lanl.gov), Michael K. Rivera (Los Alamos National Laboratory, Condensed Matter and Thermal Physics, MS-K764, Los Alamos, NM 87545, USA, mkrivera@lanl.gov)

We study experimentally the force fluctuations felt by a probe disk as it is dragged at a nominally constant rate through a two-dimensional bidisperse system of randomly packed photo-elastic disks. As the packing fraction increases from loose packing to a value where the disks are jammed, lines of connected force - stress chains - develop that couple the entire domain. We consider the transition from an unjammed state with no long range force distribution to a jammed state with stress chains spanning the system size. We characterize this transition using the measured force fluctuations and the determination of stress chains as visualized by the photo-elastic disks. Length and time scales obtained from these measurements are used to describe both the transition to jamming and the nature of the jammed state. The reorganization of disks and the force fluctuations have a stick-slip character in the jammed state.

Invited Paper

3:00

2pPAa4. Rheology and mobility in a sono-fluidized granular packing. Eric Clement (Laboratoire PMMH, ESPCI, 10 rue Vauquelin, 75231 Paris Cedex 5, France, erc@ccr.jussieu.fr), Gabriel Caballero (Laboratoire PMMH, ESPCI, 10 rue Vauquelin, 75231 Paris Cedex 5, France, g.a.caballerorobledo@tnw.utwente.nl), Chay Goldenberg (Laboratoire PMMH, ESPCI, 10 rue Vauquelin, 75231 Paris Cedex 5, France, chayg@pmmh.espci.fr)

Dynamics near jamming (glassy phase, aging, memory effects and intermittency) shows amazing analogies among a variety of very different systems (colloids, dense suspensions, foams, granular materials). Recently, several proposals have emerged with the aim of describing in a general and unified way this behavior. With the purpose of testing experimentally some of these ideas, we performed several experimental studies on dry granular materials under vibration. We found that even with a weak level of vibration, such as sound injection, the behavior of granular matter is changed dramatically. We directly observe that the grains undergo a sub diffusive collective dynamics on a very long time scale which results on global compaction effects. In this regime, we have studied the rheology of an intruder moving in the bulk as a function of the level of energy injected, the driving velocity and the shape of the moving object. We also present a simple model to account for the observed behavior.

Contributed Paper

3:20

2pPAa5. Irreversible interaction of sound waves with dense granular matter. Jérôme Laurent (Université Paris-Est Marne la Vallée, 5 Bd. Descartes, 77454 Marne la Vallée, France, jerome.laurent@univ-mlv.fr), Thomas Brunet (Université Paris-Est Marne la Vallée, 5 Bd. Descartes, 77454 Marne la Vallée, France, Thomas.Brunet@insp.jussieu.fr), Xiaoping Jia (Université Paris-Est Marne la Vallée, 5 Bd. Descartes, 77454 Marne la Vallée, France, jia@univ-mlv.fr)

In this talk, we will describe quantitatively the irreversible interaction between sound and the granular medium under low confining pressure ($<$ 0.1 MPa). Both resonance measurement and pulsed wave propagation show that as the acoustic pressure goes up to a few percent of the confining pressure, the dynamic bulk modulus and shear one can be reduced to 10% and 20%, respectively. This observation of modulus softening is qualitatively in agreement with the prediction by a model based on the Mindlin hysteretic nonlinearity at the grain contact level. Beyond certain thresholds of acoustic amplitude, the irreversible sound-granular matter interaction is accompanied by continue or intermittent sample compactions. No visible grain motion is observed at this stage; however the multiply scatted shear waves [1] allow probing a significant evolution of the contact networks, which coincide with slow recovery of elastic moduli. This work may have the implication for better understanding the physical origin of dynamic triggering of the fault core [2]. [1] X. Jia, ″Coda-like multiple scattering of elastic waves in dense granular media,″ Phys. Rev. Lett. 93, 154303 (2004) [2] P.A. Johnson & X. Jia, ″Nonlinear dynamics, granular media and dynamic earthquake triggering,″ Nature 437, 871-874 (2005)

3:40-5:20 Posters

Lecture sessions will recess for presentation of poster papers on various topics in acoustics. See poster sessions for topics and abstracts.

Contributed Papers

5:20

2pPAa6. Acoustic emissions for the prediction of avalanches. Pierre De Guibert (Université Paul Sabatier, PHASE, 118, route de Narbonne, 31062 Toulouse cedex 9, France, dguibert@cict.fr), Vincent Gibiat (Université Paul Sabatier, PHASE, 118, route de Narbonne, 31062 Toulouse cedex 9, France, gibiat@cict.fr), Eric Plazza (Université Paul Sabatier, PHASE, 118, route de Narbonne, 31062 Toulouse cedex 9, France, ericvpp@hotmail.com)

Although we know well enough the main zones where occur avalanches, the main difficulty results in forecasting avalanches because of the constant evolution of the snow coat. The coat, composed of various slopes have different properties according to the weather conditions not only during falls but also after. Weather modifications after snow falls generate instability of slopes which create stress, fissure and failure states. These different states generate acoustic emissions whose parameters can lead to forecast avalanches. The aim is to detect in situ these precursors, that initiate a low frequency signal. We have settled an experiment to monitor and register this signal. It includes two geophones to detect the acoustic signals, an acquisition system, one aerial of temperature sensor and a wireless connection to a deported PC. The system is controlled by ADSL in our offices. It will be shown on examples that any movement of the snow cap provides a signal. The rate of repetition of these elementary signals is the indication of an increasing instability of the snow precursor to an avalanche. By comparing the acoustic signals to temperature variation evolution of the snow pack we could define an alarm degree allowing to secure the area.

5:40

2pPAa7. The effect of acoustic waves on stick-slip behaviour in sheared granular media, with implications to earthquake processes. Paul A. Johnson(EES-11 (Geophysics) - Los Alamos National Laboratory, MS D443, Los Alamos, NM 87545, USA, paj@lanl.gov), Heather Savage (University of California, Department of Earth and Planetary Science, Santa Cruz, CA 95064, USA, hsavage@ucsc.edu), Matt Knuth (University of Wisconsin, Department of Geology and Geophysics, Madison, WI 53707, USA, mwknuth@wisc.edu), Joan Gomberg (US Geological Survey, University of Washington, Department of Earth and Space Sciences, Box 351310, Seattle, WA 98195-1310, USA, gomberg@usgs.gov), Robert Behringer (Duke University, Department of Physics, Durham, NC 27708, USA, bob@phy.duke.edu), Chris Marone (Pennsylvania State University, Department of Earth and Planetary Science, University Park, PA 16802, USA, cjm@geosc.psu.edu)

We are studying the effects of acoustic waves on sheared granular material, with two goals in mind: one is to understand the intriguing physics that arises in this experimental system, and the other is to see if such experiments offer insight into earthquake processes, in particular the phenomenon where one earthquake triggers another nearby, or distant, earthquake ('dynamic earthquake triggering'). We conducted laboratory experiments of stick-slip in granular media using a double-direct, shear apparatus, while applying low amplitude vibration as well as pulsed waves. We find that vibration and pulses significantly perturb the shearing behaviour of the granular material, and that the manifestation of vibration is extremely complex, including strong material memory of the acoustic perturbation, that persists. We note that the wave disturbance must take place near the critical point, where the granular material is near failure, otherwise no effect is observed. Also, horizontal loads on the system can eliminate the effect if they arelarge ($\geq$4-5 MPa).

Invited Paper

6:00

2pPAa8. Observations and models of dynamic earthquake triggering. Joan Gomberg (US Geological Survey, University of Washington, Department of Earth and Space Sciences, Box 351310, Seattle, WA 98195-1310, USA, gomberg@usgs.gov), Paul A. Johnson (EES-11 (Geophysics) - Los Alamos National Laboratory, MS D443, Los Alamos, NM 87545, USA, paj@lanl.gov)

Seismologists have long accepted the idea that step-function perturbations to the deformation field acting on a fault can change its likelihood of, or 'trigger', failure as fault slip. We review the observations that have lead to the very recent recognition that transient perturbations (e.g., associated with seismic waves) also affect failure probabilities, and more broadly, observations of the spatial and temporal variations in both triggering deformations and triggered responses. Many of these cannot be explained by conventional models of earthquake nucleation, requiring consideration of ideas developed in other disciplines, such as those describing and explaining nonlinear dynamic elasticity from rock-mechanics. In addition to the scientific challenges, these observations and models significantly impact earthquake forecasts and hazard assessments. We focus on observations of natural earthquakes and from the rock-mechanics laboratory, and some of the explanatory models that we and others have proposed. While many of these observations and models are just being vetted now, even newer ones related to slow aseismic fault slip and non-volcanic tremor (seismic radiation that scales very differently from that from earthquakes) may lead to substantive modifications and advances. We conclude with a few tantalizing examples as a prelude to a companion presentation.

Contributed Paper

6:20

2pPAa9. Dynamic asperity failure triggering during the rupture process? Carene Larmat (EES-11 (Geophysics) - Los Alamos National Laboratory, MS D443, Los Alamos, NM 87545, USA, carene@lanl.gov)

Dynamic triggering by the transient deformations associated with seismic waves has been proposed as an alternative mechanism for inducing aftershocks in contrast to the Coulomb stress. This idea is supported by observations of triggered seismicity like for the Mw=7.3 Landers earthquake (1992), the Mw=7.1 Hector Mine (1999), and after the Mw=7.4 Izmit earthquake for which small events began in Greece immediately after the passage of the mainshock surface waves (Brodsky et al., 2000). Gomberg et al. (2003) conducted a rigorous analysis of aftershock distribution for 15 mainshocks and showed that most of the triggered events are located in the rupture direction which corresponds to a maximum of the radiated seismic energy. Another argument is the fact that the correctly scaled amplitude of the dynamic deformations are consistent with laboratory observations of failure processes (Gomberg & Johnson, 2005). Finally, work by Felzer and Brodsky (2006) indicates that aftershocks are due to dynamic triggering rather than quasistatic stress changes. Thus instabilities can be triggered as aftershocks as well as at remote distances by seismic waves, suggesting asperities located on the mainshock fault may fail due to transient strains. In this study, we propose to explore that hypothesis.

TUESDAY AFTERNOON, 1 JULY 2008 ROOM 362/363, 2:20 TO 7:20 P.M.

Session 2pPAb

Physical Acoustics: Nonlinear Acoustics of Unconsolidated Granular Media I

Paul A. Johnson, Cochair
EES-11 (Geophysics) - Los Alamos National Laboratory, MS D443, Los Alamos, NM 87545, USA

Vitali Gusev, Cochair
LPEC/UMR 6087/CNRS/Université du Maine, Avenue Olivier Messiaen, Le Mans Cedex 09, 72085, France

Invited Papers

2:20

2pPAb1. Strongly nonlinear behavior of granular chains and granular composites. Vitali F. Nesterenko (University of California, San Diego, 9500 Gilman Drive, Department of Mechanical and Aerospace Engineering, La Jolla, CA 92093-0411, USA, vnesterenko@ucsd.edu), Eric B. Herbold (University of California, San Diego, 9500 Gilman Drive, Department of Mechanical and Aerospace Engineering, La Jolla, CA 92093-0411, USA, eherbold@gmail.com), David J. Benson (University of California, San Diego, 9500 Gilman Drive, Department of Mechanical and Aerospace Engineering, La Jolla, CA 92093-0411, USA, dbenson@ucsd.edu), Jeonghoon Kim (University of California, San Diego, 9500 Gilman Drive, Materials Science and Engineering Program, La Jolla, CA 92093, USA, jek008@ucsd.edu), Chiara Daraio (California Institute of Technology, Aeronautics (GALCIT) and Applied Physics, Pasadena, CA 91125, USA, daraio@caltech.edu)

Strongly nonlinear behavior of granular phononic crystals composed of stainless steel cylinders and PTFE spheres is considered experimentally and numerically. The tenability of phononic band gap in this two-mass prestressed chain was investigated. The results show that the phononic band gap exists within audible frequency regime (20–20,000 Hz) and can be tuned by changing the value of prestress. Influence of the weak and strong nonlinearity on the propagation of signals with frequencies inside band gap was investigated. The mechanical properties of reactive materials (e.g., high density mixtures of polytetraflouroethylene (PTFE), aluminum (Al) and

tungsten (W) powders) where unconsolidated granular packing of metal particles plays significant role in the dynamic behavior was investigated. It was found that dynamic strength can be tailored by changing the morphology of the particles and porosity. Cold isostatically pressed PTFE-Al-W powder composites with fine metallic particles and a higher porosity exhibited higher ultimate compressive strength than less porous composites having equivalent mass ratios with coarse W particles. Based on the numerical analysis it was concluded that a mesoscale force chains between the fine metallic particles are responsible for this unusual phenomenon. This work was supported by the NSF DCMS03013220 and by MURI ONR N00014-07-1-0740.

2:40

2pPAb2. Elastic waves in one-dimensional unconsolidated medium with Hertz nonlinearity. Alexandr I. Korobov (Dept. of Acoustics, Physics Faculty, M.V. Lomonosov Moscow State University, Leninskie gory 1, 119991 Moscow, Russian Federation, akor@acs465a-1.phys.msu.ru), Maria Y. Izosimova (Center for Industrial and Medical Ultrasound, Applied Physics Lab., University of Washington, 1013 NE 40th St., Seattle, WA 98105, USA, maria.izossimova@mail.ru), Yurii A. Brazhkin (Dept. of Acoustics, Physics Faculty, M.V. Lomonosov Moscow State University, Leninskie gory 1, 119991 Moscow, Russian Federation, akor@acs465a.phys.msu.su), Elizaveta Sovetskaya (Dept. of Acoustics, Physics Faculty, M.V. Lomonosov Moscow State University, Leninskie gory 1, 119991 Moscow, Russian Federation, akor@acs465a.phys.msu.su)

Results of experimental study of elastic longitudinal harmonic wave's propagation in one-dimensional unconsolidated medium are presented. A 1-D chain of identical pre-pressed beads is used as an experimental model. To describe elastic properties of such medium the Hertz model is used. Presence of periodical structure causes elastic waves to be dispersive in such medium and to have a cutoff frequency. A cutoff frequency depends not only on material's elastic properties and beads' geometrical sizes but also on pre-press value. Velocity dependence on frequency of longitudinal harmonic wave of small magnitude is measured experimentally, and dispersion curves are built under different pre-press value. Pre-press value is regulated with applied external static force along chain axis. Measured dispersion dependences are in good agreement with theoretically calculated ones. Dispersion impedes observation of higher harmonics generation in such chain. Therefore to study nonlinear properties of 1-D structure, velocity dependence on longitudinal wave amplitude were investigated. The wave velocity depends not only on its magnitude but also on pre-press value on beads. It was experimentally shown the one-dimensional chain of elastic beads is a medium with dispersion, linear and nonlinear properties to be controlled with the applied external static force. Work supported by RFBR.

Contributed Papers

3:00

2pPAb3. Breathing in Granular Chains and Conversion of Wave Energy to Useful Forms. Surajit Sen (State University of New York at Buffalo, Dept of Physics, SUNY-Buffalo, Buffalo, NY, Buffalo, NY 14260-1500, USA, sen@nsm.buffalo.edu)

Estimates suggest that a meter of a wave front carries ~ 100 kW of power. A significant amount of renewable energy is hence dissipated across the time scale of minutes as surface gravity waves dissipate on any beach. Given that the majority of the world population lives near the ocean, it makes sense to explore the conversion of wave energy into electrical energy. Here we consider a new concept - that of a potentially scalable system that converts wave energy into energy in mechanical pulses and then to voltage drops. The envisioned system would exploit the well studied physics of nonlinear repulsion between elastic grains encased in cylinders to continuously convert the incident wave energy into dispersionless energy bundles, which can be subsequently converted to stress pulses in a piezo-electric slab. The key points involved in the concept will be presented.

3:20

2pPAb4. Wave propagation in wetted Hertzian granular chains: analysis of a single contact dynamics. Stéphane Job (Supméca Paris, 3 rue Fernand Hainaut, 93407 Saint-Ouen Cedex, France, stephane.job@supmeca.fr), Francisco Santibañez (Univ. de Santiago de Chile - Dept. de Fisica, Avenida Ecuador 3493, Casilla 307, Correo 2, Santiago de Chile, Chile, fsantibanez@fisica.usach.cl), Francisco Melo (Univ. de Santiago de Chile - Dept. de Fisica, Avenida Ecuador 3493, Casilla 307, Correo 2, Santiago de Chile, Chile, fmelo@usach.cl)

A one-dimensional dry granular medium, a chain of beads which interact via the nonlinear Hertz potential, exhibits strongly nonlinear behaviors. When such an alignment contains some viscous fluid between grains, it exhibits new interesting features. We report some recent experiments, analysis and numerical simulations concerning nonlinear wave propagation in dry and wet chains of spheres. We consider first a monodisperse chain as a reference case. We then analyze how the pulse characteristics are modified in the presence of an interstitial viscous fluid. The fluid not only induces dissipation but also strongly affects the intergrain stiffness: in a wet chain, wave speed is enhanced and characteristic pulse duration is shorter. Our observations are in a satisfactory agreement with ultrasound propagation measurements in 3D wetted granular beds reported in the literature. Recent experiments performed with a single sphere colliding a wall covered by a thin film of fluid allowed us to determine the rheology of the contact dynamics, and confirmed that a complex elastohydrodynamic interaction takes place close to solids contact.

3:40-5:00 Posters

Lecture sessions will recess for the presentation of poster papers in various topics in acoustics. See poster sessions for topics and abstracts.

Invited Paper

5:00

2pPAb5. Dynamic effective mass of granular media. David L. Johnson (Schlumberger-Doll Research, One Hampshire St., Cambridge, MA 02139, USA, johnson10@slb.com)

We report an experimental and theoretical investigation of the frequency-dependent effective mass, $M(\omega)$, of loose granular particles which occupy a rigid cavity to a filling fraction of 48%. We demonstrate that this is a sensitive and direct way to measure those properties of the granular medium that are the cause of the changes in acoustic properties of structures containing grain-filled cavities. The dominant features of $M(\omega)$ are a sharp resonance and a broad background, which we analyze within the context of simple models as well as with molecular dynamic simulations. We find that: a) These systems may be understood in terms of a height-dependent and diameter-dependent effective sound speed ($\sim$ 130 m/s) and an effective viscosity ($\sim 2\times 10^4$ Poise). b) There is a dynamic Janssen effect in the sense that, at any frequency, and depending on the method of sample preparation, approximately one-half of the effective mass is borne by the side walls of the cavity and one-half by the bottom. c) On a fundamental level, dissipation is dominated by adsorbed films of water at grain-grain contacts in our experiments, not by global viscous damping.

Contributed Paper

5:20

2pPAb6. Mechanisms of acoustic absorption in weakly wet granular media. Thomas Brunet (Université Paris-Est Marne la Vallée, 5 Bd. Descartes, 77454 Marne la Vallée, France, Thomas.Brunet@insp.jussieu.fr), Xiaoping Jia (Université Paris-Est Marne la Vallée, 5 Bd. Descartes, 77454 Marne la Vallée, France, jia@univ-mlv.fr), Pierre Mills (Université Paris-Est Marne la Vallée, 5 Bd. Descartes, 77454 Marne la Vallée, France, mills@univ-mlv.fr)

Multiply scattered elastic waves provide a sensitive probe for studying the viscoelastic properties of a granular medium at the length scale of grains. Based on a diffusion model, we can infer the structural and viscoelastic properties of the material from the fitting parameters such as the diffusion constant D and quality factor Q. In this work, we characterize quantitatively the acoustic dissipation occurring at the grain contacts by measuring the Q factor in different granular samples. We focus a particular attention on the effects of on the internal loss by adding a small amount of liquid in the granular medium ($\sim$0.05%). Using the Hertz-Mindlin contact theory we have identified two different mechanisms of acoustic absorption: frictional and viscous dissipations.

Invited Papers

5:40

2pPAb7. Static and dynamic nonlinear behaviors of unconsolidated granular media. Zhiqu Lu (University of Mississippi, NCPA, 1 Coliseum Drive, University, MS 38677, USA, zhiqulu@olemiss.edu), James M. Sabatier (University of Mississippi, NCPA, 1 Coliseum Drive, University, MS 38677, USA, sabatier@olemiss.edu)

Unconsolidated granular media such as sands, soils, and glass beads, exhibit astonishing static and dynamic nonlinear behaviors that are quite different from those of elastic materials such as liquids and crystalline solids. They can generally classified as mesoscopic hysteretic nonlinear materials since hysteresis is a universal phenomenon for these materials. In order to understand the mechanism and to quantify the nonlinearity of unconsolidated granular materials, a series of studies have been conducted on re-molded unconsolidated soils. The systematic research consists of three parts: (1) a triaxial cell test with pre-defined stress-paths and sound speed measurement, focusing on the exploration of the role of hysteresis in both linear and nonlinear acoustics; (2) the phase shift method, using non-classical nonlinear acoustic theory to measure the hysteretic nonlinearity parameter; (3) the study of fluid effects on the hysteretic nonlinearity parameter. The study reveals many static and dynamic nonlinear behaviors of soils, including: nonlinear stress/strain relationship, hysteresis loop, end-point memory, much greater dynamic elastic modulus than static elastic modulus, strain-amplitude dependence of elastic modulus, linear resonant frequency shift and phase shift relationships against strain, extremely high values of the hysteretic nonlinearity parameter, harmonics generation, and moisture effects.

6:00

2pPAb8. Acoustic waves in granular materials. Stefan Luding (UTwente, Multi Scale Mechanics, P.O.Box 217, 7500 AE Enschede, Netherlands, s.luding@utwente.nl), Orion Mouraille (UTwente, Multi Scale Mechanics, P.O.Box 217, 7500 AE Enschede, Netherlands, o.j.p.mouraille@utwente.nl)

The numerous sound propagation mechanisms in granular materials are rather complex and strongly depend on the material micro-scale parameters, such as inter-particle friction or damping. The use of DEM (Discrete Element Simulations) allows us to tune these parameters and hence to understand their influence. In both regular (crystal-like) and polydisperse (sand-like) systems of spheres, a small perturbation is created on one side of the simulation box and examined during its propagation and on arrival at the opposite side. Starting from a regular packing, a tiny size variation comparable to the typical contact deformation already changes sound propagation considerably [1]. The transmission spectrum becomes discontinuous, i.e., a lower frequency band is transmitted well, while higher frequencies are not, mainly due to scattering effects. Furthermore, the wave propagation and transmission properties are studied on fully polydisperse, frictional and cohesive packings under increasing load until breakage of the material [2]. [1] O. Mouraille and S. Luding, Sound wave propagation in weakly polydisperse granular materials, Ultrasonics, submitted. [2] O. Mouraille, O. Herbst and S. Luding, Testing cohesive and frictional granular materials with the discrete element model, in preparation.

6:20

2pPAb9. Acoustic wave propagation in granular systems. Ellak Somfai (University of Warwick, Department of Physics and Centre for Complexity Science, CV4 7AL Coventry, UK, E.Somfai@warwick.ac.uk), Jean-Noel Roux (Laboratoire des Materiaux et des Structures du Genie Civil, Institut Navier, 2 allee Kepler, Cite Descartes, 77420 Champs-sur-Marne, France, jean-noel.roux@lcpc.fr), Jacco H. Snoeijer (University of Bristol, Department of Mathematics, University Walk, BS8 1TW Bristol, UK, jacco.snoeijer@bristol.ac.uk), Martin Van Hecke (Universiteit Leiden, Kamerlingh Onnes Laboratory, P.O. Box 9504, 2300RA Leiden, Netherlands, mvhecke@lorentz.leidenuniv.nl), Wim Van Saarloos (Universiteit Leiden, Kamerlingh Onnes Laboratory, P.O. Box 9504, 2300RA Leiden, Netherlands, saarloos@lorentz.leidenuniv.nl)

We present numerical simulations of acoustic wave propagation in granular systems consisting of particles interacting with the three-dimensional Hertz-Mindlin force law. The response to a short mechanical excitation on one side of the system is found to be a propagating coherent wavefront followed by random oscillations made of multiply scattered waves. We find that the coherent wavefront is insensitive to details of the packing: force chains do not play an important role in determining this wavefront. The coherent wave has a well defined velocity, which is roughly compatible with the predictions of macroscopic elasticity, and its amplitude and width depend as a power law on distance. As there is at present no theory for the broadening and decay of the coherent wave, we numerically and analytically study pulse-propagation in a one-dimensional chain of identical elastic balls. The results for the broadening and decay exponents of this system differ significantly from those of the disordered packings. We briefly discuss the eigenmodes of the system and effects of damping are investigated as well.

Contributed Papers

6:40

2pPAb10. Localization of sound in a three-dimensional elastic network. John H. Page (Dept. of Physics and Astronomy, Univ. of Manitoba, Winnipeg, MB R3T 2N2, Canada, jhpage@cc.umanitoba.ca), Hefei Hu (Dept. of Physics and Astronomy, Univ. of Manitoba, Winnipeg, MB R3T 2N2, Canada, hefeihu2@uiuc.edu), Anatoliy Strybulevych (Dept. of Physics and Astronomy, Univ. of Manitoba, Winnipeg, MB R3T 2N2, Canada, anatoliy@physics.umanitoba.ca), Sergey Skipetrov (Université Joseph Fourier, Laboratoire de Physique et Modélisation des Milieux Condensées/CNRS, Maison des Magistères, 38042 Grenoble, France, Sergey.Skipetrov@grenoble.cnrs.fr), Bart Van Tiggelen (Université Joseph Fourier, Department of Applied Physics, Hokkaido University, 060-8628 Sapporo, Japan, Bart.Van-Tiggelen@grenoble.cnrs.fr)

A long standing question in physical acoustics has been whether or not the Anderson localization of sound can be demonstrated unambiguously in three dimensions. Here we address this question by reporting evidence for the localization of ultrasonic waves in a three-dimensional granular network of weakly sintered aluminum beads. In the upper part of the intermediate frequency regime, where the ultrasonic wavelength is comparable with the sizes of the pores and beads, the intensity time-of-flight profile of the multiply scattered waves exhibits non-exponential decay, which may be construed as a slowing down of the diffusion coefficient with propagation time and is consistent with predictions for localized waves. We use a quasi point source and detector to demonstrate how localization cuts off the transverse spreading of the multiply scattered waves, an effect, which we call 3D transverse localization, that has not been observed previously for any type of wave. These results are interpreted using recent theoretical predictions based on the self-consistent theory of the dynamics of localization, allowing the localization length to be determined. Further evidence is obtained from intensity statistics, which reveal a Thouless conductance g less than unity. These results unambiguously demonstrate the localization of sound in this system.

7:00

2pPAb11. Surface elastic waves in granular media under gravity and their relation to booming avalanches. Lénaïc Bonneau (Laboratoire PMMH, ESPCI, 10 rue Vauquelin, 75231 Paris Cedex 5, France, bonneau@pmmh.espci.fr), Bruno Andreotti (Laboratoire PMMH, ESPCI, 10 rue Vauquelin, 75231 Paris Cedex 5, France, Andreotti@pmmh.espci.fr), Eric Clement (Laboratoire PMMH, ESPCI, 10 rue Vauquelin, 75231 Paris Cedex 5, France, erc@ccr.jussieu.fr)

Due to the nonlinearity of Hertzian contacts, the speed of sound c in granular matter is expected to increase with pressure as P1/6. A static layer of grains under gravity is thus stratified so that the bulk waves are refracted toward the surface. The reflection at the surface being total, there is a discrete number of modes (both sagittal plane and transverse ones) localized close to the free surface. The shape of these modes and the corresponding dispersion relation are investigated in the framework of an elastic description taking into account the main features of granular matter: the nonlinearity between stress and strain and the existence of a yield transition. We show in this context that the surface modes localized at the free surface exhibit a waveguide effect related to the nonlinear Hertz contact. Sound propagation measurements in a laboratory scale channel as well as in the field (slip face of a singing dune), will be presented and compared to the theoretical predictions. Finally, these results will be used to constrain the possible dynamical mechanisms at the origin of booming avalanches.

Session 2pPAc

Physical Acoustics: Diffraction of Waves on Periodical Structures: Acoustic, Ultrasonic and Acousto-Optical Diffraction Phenomena II (Poster Session)

Nico Declercq, Cochair
Georgia Tech Lorraine - G.W. Woodruff School of ME

Nataliya Polikarpova, Cochair
M.V. Lomonosov Moscow State University, Department of Physics

All posters will be on display from 3:40 p.m. to 5:20 p.m. To allow contributors an opportunity to see other posters, contributors of odd-numbered papers will be at their posters from 3:40 p.m. to 4:30 p.m. and contributors of even-numbered papers will be at their posters from 4:30 p.m. to 5:20 p.m.

Contributed Papers

2pPAc1. Information losses minimization in spectral devices based on acousto-optic Bragg cells. Boris S. Gurevich (Scientific Instruments, Rizhsky prospekt 26, 190103 St. Petersburg, Russian Federation, bgurevich@mail.ru), Simon B. Gurevich (A.F. Ioffe Physical-Technilcal Institute RAS, Politekhnicheskaya, 26, 194021 St. Petersburg, Russian Federation, sbgurevich@mail.ru), Sergey V. Andreyev (Scientific Instruments, Rizhsky prospekt 26, 190103 St. Petersburg, Russian Federation, svan51@mail.ru), Andrey V. Belyaev (Institute for analytical instrumentation RAS, Rizhsky pr. 26, 190103 St. Petersburg, Russian Federation, bgurevich@mail.ru)

Spectral devices such as spectrophotometers are intended, as many other devices, for information transmission and processing. Hence, they can be characterized by specific information characteristics such as information transmission capability and information capacity, which can be connected with some physical and technical parameters of the devices. The use of acousto-optic components in these devices introduce some peculiarities in information transmission and processing in spectrophotometers. We have considered the information transmission limitations based on signal and noise in acousto-optic Bragg cells. The spectral resolving power is also considered as one of decisive characteristics influencing on acousto-optic spectral device transmission capability.

2pPAc2. Theoretical study of the diffraction fields generated by a fluid-loaded plate with two-surface corrugation. Sarah W. Herbison (Georgia Tech Lorraine - G.W. Woodruff School of ME, UMI Georgia Tech - CNRS 2958, 2 rue Marconi, 57070 Metz, France, sherbison@gatech.edu), Nico F. Declercq (Georgia Tech Lorraine - G.W. Woodruff School of ME, UMI Georgia Tech - CNRS 2958, 2 rue Marconi, 57070 Metz, France, nico.declercq@me.gatech.edu)

A renewed interest has recently emerged in the study of the interaction of elastic waves with periodic structures, including periodically corrugated surfaces. From prior theoretical and experimental studies of the diffracted fields generated by such surfaces, it is well known that periodically corrugated surfaces can be used to generate ultrasonic surface waves, which are especially important in the field of ultrasonic non-destructive evaluation. In general, anomalies appear in the reflection and transmission spectra due to the presence of the corrugation, and these anomalies can be correlated with the surface waves generated. The present work has extended the theory of diffraction on periodically corrugated surfaces to the case of a fluid-loaded plate with both sides corrugated. The unique filtering effects and diffraction phenomena that can be achieved with such a structure are examined and related to the creation of surface and plate waves.

2pPAc3. 2D-ultrasonic tomography using first-order Born and canonical approximations. Philippe Lasaygues (Laboratory for Mechanics and Acoustics CNRS, 31 chemin Joseph Aiguier, 13009 Marseille, France, lasaygues@lma.cnrs-mrs.fr),Loic Le Marrec(Institute of Mathematical Research of Rennes IRMAR, Campus de Beaulieu, 35042 Rennes, France, loic.lemarrec@univ-rennes1.fr), Thierry Scotti (CNRS - LMA, 31 Chemin Joseph Aiguier, 13009 Marseille, France, scotti@lma.cnrs-mrs.fr)

This paper deals with the two-dimensional image reconstruction of an elastic tubes using ultrasonic tomographic method based on first-Born approximation and a canonical approximations. The latter improvement makes it possible to extend the scope of tomography from lower impedance contrast media to higher impedance contrast situations, even when the ultrasonic propagation is greatly perturbed by the difference in acoustic impedance between the scatterer and the surrounding medium. The strategy used to solve this problem was based on comparisons between the experimental diffracted field and the canonical solution approached as a forward problem. The algorithm adopted, using the analytical solution to the local forward problem and an iterative process to recover the unknowns, is fast enough to yield real-time information about the shape. A single frequency does not suffice to determine the real solution as the global minimum of the cost function, and the inversion is improved by using all the frequencies present in the broadband of the transducers. The method presented is robust and is not perturbed by the experimental measurements or small errors in the material properties. The results are most promising. This method gives an image with an error, which is lower than the wavelength.

2pPAc4. Light interaction with leaky acoustic wave radiation in YX-LiTaO3. Paulius Kazdailis (Vilnius Univ., Dept. of Radiophysics, Saulëtekio al. 9, LT-10222 Vilnius, Lithuania, paulius.kazdailis@ff.vu.lt), Romualdas Rimeika (Vilnius Univ., Dept. of Radiophysics, Saulëtekio al. 9, LT-10222 Vilnius, Lithuania, romualdas.rimeika@ff.vu.lt), Daumantas Ciplys (Vilnius Univ., Dept. of Radiophysics, Saulëtekio al. 9, LT-10222 Vilnius, Lithuania, daumantas.ciplys@ff.vu.lt)

The theoretical model and experimental studies of 633 nm laser light interaction with radiation from leaky surface acoustic waves (LSAW) at various frequencies in YX-lithium tantalate (LiTaO3) are presented. The acousto-optic diffraction with and without polarization rotation has been observed. The values of BAW propagation angle and of the corresponding velocity have been calculated and compared to the ones extracted from the experiment. The differences of the light diffraction process in YX-lithium tantalate from the one in ZX-lithium niobate have been pointed. The potential of the described acousto-optic interaction for applications in light control devices and acoustic wave probing has been demonstrated.

2pPAc5. Scattering of ultrasonic waves in randomly layered materials. Michal Pakula (Université Paris 6, Laboratoire d'Imagerie Paramétrique, 15, rue de l'Ecole de Médecine, 75006 Paris, France, michalp@ukw.edu.pl), Mieczyslaw Cieszko (Institute of Environmental

Mechanics and Applied Computer Science, Kazimierz Wielki University in Bydgoszcz, ul. Chodkiewicza 30, 85-064 Bydgoszcz, Poland, cieszko@ukw.edu.pl), Jozef Kubik (Institute of Environmental Mechanics and Applied Computer Science, Kazimierz Wielki University in Bydgoszcz, ul. Chodkiewicza 30, 85-064 Bydgoszcz, Poland, kubik@ukw.edu.pl)

The goal of the paper is the proposal of a new macroscopic description of scattering of elastic waves at internal inhomogeneities of the material. Within the studies the microscopic inhomogeneity of the medium is modeled as the alternately arranged two kinds of elastic layers of random thicknesses and different mechanical properties. Calculations of the acoustical characteristics of such medium (reflection and transmission coefficients) are performed in two stages: (i) first the problem of interaction of plane harmonic wave with the half space of the randomly layered medium for the case of normal wave incidence is analyzed; (ii) then the interaction of the harmonic wave with the slice composed of randomly layered structure is considered. Such approach allowed to derive analytical relations for the phase velocity of wave propagation and attenuation as the explicit functions of frequency, stochastic structural parameters of the medium and material properties of layers. The obtained formulas are helpful for interpretation of experimental ultrasonic data and may serve for identification of the characteristic size of material inhomogeneity based on the measured wave parameters like frequency dependent phase velocity, attenuation as well as backscattering coefficient.

2pPAc6. Design of III-Nitride multi-layer structures for optical and surface acoustic wave interaction. Samuel Dupont (IEMN CNRS 8520 DOAE, Université de Valenciennes et du Hainaut Cambrésis Le Mont Houy, 59313 Valenciennes, France, samuel.dupont@univ-valenciennes .fr), Jean-Claude Kastelik (IEMN CNRS 8520 DOAE, Université de Valenciennes et du Hainaut Cambrésis Le Mont Houy, 59313 Valenciennes, France, jean-claude.kastelik@univ-valenciennes.fr), Victor Y. Zhang (IEMN-CNRS, Av. Poincare, Cite Scientifique, B.P. 60069, 59652 Villeneuve d'Ascq Cedex, France, victor.zhang@iemn.univ-lille1 .fr), Federica Causa (Dept. of Electronic and Electrical Engineering, Univ. of Bath, BA2 7AY Bath, UK, f.causa@bath.ac.uk), Qingbin Meng (Dept. of Electronic and Electrical Engineering, Univ. of Bath, BA2 7AY Bath, UK, Q.Meng@bath.ac.uk), Jayanta Sarma (Dept. of Electronic and Electrical Engineering, Univ. of Bath, BA2 7AY Bath, UK, J.Sarma@bath.ac.uk)

Research efforts into Surface Acoustic Waves (SAW) devices built on III-Nitrides has recently significantly intensified because of the increasing availability of good-quality epitaxial material. Owing to their strong piezoelectricity and high acoustic velocity, high-Al-content materials are of particular interest in high-speed applications (GHz electronics). For optoelectronics applications III-Nitrides cover a wide range of wavelengths from ultra-violet (AlN) to blue (GaN) to infra-red (InN); thus providing great flexibility in the choice of operating wavelength. III-Nitrides, therefore, become particularly attractive for the development of acousto-optic modulators where the SAW is used to create a controllable (moving) optical grating, causing the diffraction of the Optical Guided Wave (OGW). The interaction is governed by the momentum and energy conservation and importantly by the field overlap of the two waves. We present here design guidelines and modelling results for the development of III-Nitride-based multi-layer structures to support both OGW and SAW. The purpose of this study is to attempt to optimise the device efficiency compared to single GaN-layer structures typically used in the literature where only the SAW characteristics are optimised.

2pPAc7. Short access time acousto-optic deflector based on two cascaded Paratellurite devices. Nabil Ouail (IEMN CNRS 8520 DOAE, Université de Valenciennes et du Hainaut Cambrésis Le Mont Houy, 59313 Valenciennes, France, nabil.ouail@univ-valenciennes.fr), Jean-Claude Kastelik (IEMN CNRS 8520 DOAE, Université de Valenciennes et du Hainaut Cambrésis Le Mont Houy, 59313 Valenciennes, France, jean-claude.kastelik@univ-valenciennes.fr),Michel Pommeray(IEMN CNRS 8520 DOAE, Université de Valenciennes et du Hainaut Cambrésis Le Mont Houy, 59313 Valenciennes, France, michel.pommeray @univ-valenciennes.fr), Samuel Dupont (IEMN CNRS 8520 DOAE, Université de Valenciennes et du Hainaut Cambrésis Le Mont Houy, 59313 Valenciennes, France, samuel.dupont@univ-valenciennes.fr)

Acousto-optic deflectors (AODs) are used in many applications requiring optical scanning devices with various specifications regarding access time, resolution and wavelength. High time-bandwidth products can be achieved with AODs made in a tellurium dioxide (TeO2) crystal. As paratellurite crystals are available with relatively large dimensions, the time-bandwidth product can be increased by enlarging the optical aperture. However, the access time is increased which is not suitable for random access scanning mode. A new laser scanning system is then presented based on two wide-band paratellurite acousto-optic deflectors. Anisotropic interactions take place under two different tangential phase matching (TPM) configurations in such a way that the acousto-optic bandwidths add up. The optical arrangement of the two cascaded AODs is detailed. The feasibility of such a cascade deflection system has been demonstrated for the green wavelength $\lambda = 514$ nm of an argon laser. The total frequency bandwidth is $\Delta ft = 100$ MHz, equally distributed between the two acousto-optic deflectors. The total angular scan at the output is $\Delta\theta t = 4.5$ ° leading to more than 120 resolvable spots for a 1 mm truncated Gaussian beam and a short access time (as low as 1.5 μs).

2pPAc8. Peculierities of acoousto-optic interaction in nanodimensional laser heterostructures. Liudmila Kulakova (Ioffe Physico-Technical Institute RAS, Polytekhnicheskaya 26, 194021 St. Petersburg, Russian Federation, L.Kulakova@mail.ioffe.ru)

In the report, we present results of study of acousto-optic and acousto-electron interactions in active and optical resonator regions of nanodimensional laser heterostructures. It was established that an ultrasonic wave introduced into a laser heterostructure produces modulation of the laser radiation frequency with a period equal to that of the acoustic wave. The static and dynamic analysis of the spectral parameters change under the ultrasonic strain has been fulfilled. The appreciable contribution of the acousto-optic interaction (comparable with the acousto-electron), resulting in the modulation in time of the positions of the heterolaser optical resonator lines was found out. The assumption about basic influence of quasi-two dimensional configuration of the laser optical resonator on the photoelastic properties causing unexpectedly large acousto-optic efficiency is stated.

2pPAc9. 3D Simulation of periodic surface wave inter-digital transducer using finite element/boundary element analysis. Sylvain Ballandras (CNRS FEMTO-ST, 32 Avenue de l'Observatoire, 25044 Besançon, France, sylvain.ballandras@femto-st.fr), William Daniau (CNRS FEMTO-ST, 32 Avenue de l'Observatoire, 25044 Besançon, France, william.daniau@femto-st.fr), Mikaël Wilm (Imasonic, ZA rue des Savourots, 70190 Voray/Ognon, France, mikael.wilm@imasonic.com), Alexandre Reinhardt (CEA-LETI, 17 rue des Martyrs, 38054 Grenoble, France, alexandre.reinhardt@cea.fr), Raphaël Lardat (Thales Underwater Systems, 525 Route des Dolines, BP 157, 06930 Sophia Antipolis cedex, France, raphael.lardat@fr.thalesgroup.com), William Steichen (THALES Safare, 525 Route des Dolines, 06560 Sophia Antipolis, France, william.steichen @fr.thalesgroup.com)

Spectacular advances have been made during the past years in the development of surface acoustic wave thanks to technology improvements but also to a strong effort in the modelling and design of such devices, taking into account their actual structure to benefit from second order effects (for instance the influence of the metal strip shape used in inter-digital transducers on the wave propagating under periodic gratings). In this paper, we present a 2D-periodic 3D-simulation approach to compute the spectral response of one period of a surface wave transducer, accounting for the actual shape of the electrodes as well as realistic guiding conditions and acoustic properties of the propagation surface. The idea consists in meshing the inhomogeneous part of the transducer, i.e. the electrodes and the bus bar, as well as a thin layer of the substrate to match the finite element section with

surface boundary elements simulating the acoustic contribution of the substrate (propagation and radiation). Periodic boundary conditions are applied in both surface direction, allowing for the exploitation of spectral Green's function-based boundary elements, but additional absorbing conditions are added in the transverse direction (from both part of the bus bars) to suppress any unwanted modes generated by the mesh.

2pPAc10. Acoustic wave scattering from infinite cylinders made from functionally graded materials. Jalil Jamali (Faculty of Mechanical Engineering, K. N. Toosi University of Technology, Pardis St., Molla Sadra Ave., Vanak Sq., Postal code 1999143344, 16579 Tehran, Iran, ja_ja032@yahoo.com), Farhang Honarvar (Faculty of Mechanical Engineering, K. N. Toosi University of Technology, Pardis St., Molla Sadra Ave., Vanak Sq., Postal code 1999143344, 16579 Tehran, Iran, honarvar@mie.utoronto.ca), Mohammad Hasan Naei (Faculty of Mechanical Engineering, K. N. Toosi University of Technology, Pardis St., Molla Sadra Ave., Vanak Sq., Postal code 1999143344, 16579 Tehran, Iran, mhnaei@ut.ac.ir)

Functionally graded materials (FGM's) are superheat-resistive materials which show attractive properties in many applications including furnace liners. FGM's consist of two distinct materials, for example a ceramic and a metal alloy. These two materials are mixed such that the composition of each material changes continuously along a specific direction resulting in a continuous change of microstructure along that direction. The change in microstructure induces chemical, material, and microstructural gradients, and makes functionally graded materials different in behavior from homogeneous materials and traditional composites. In this paper, the scattering of an incident plane acoustic wave from an infinite solid cylinder made from functionally graded materials is studied. Expressions are derived for the far-field scattered pressure generated by illumination of the infinite FGM cylinder by an infinite plane acoustic wave. The propagation direction of the incident wave can make an arbitrary angle with the normal to the cylinder axis. The mathematical equations are derived and numerical results for cylinders made from specific functionally graded materials are presented at different incidence angles.

2pPAc11. Pendellösung phenomenon in two-dimensional sonic crystals. Mitko Angelov (Politechnic University of Valencia, Wave Phenomena Group. Department of Electronic Engineering, C/ Camino Vera s.n, ES-46022 Valencia, Spain, mitan@doctor.upv.es), Daniel Torrent (Politechnic University of Valencia, Wave Phenomena Group. Department of Electronic Engineering, C/ Camino Vera s.n, ES-46022 Valencia, Spain, datorma1@upvnet.upv.es), Francisco Cervera (Politechnic University of Valencia, Wave Phenomena Group. Department of Electronic Engineering, C/ Camino Vera s.n, ES-46022 Valencia, Spain, fcervera@fis.upv.es), José Sanchez-Dehesa (Polytechnic University of Valencia, Cami de Vera s/n, 46022 Valencia, Spain, jsdehesa@upvnet.upv.es)

The phenomenon of ″Pendelösung″ oscillations, which is well known in X-ray diffraction [P.P. Ewald, Phys. Z. **14**, 465 (1913); Ann. Phys. **54**, 519 (1917); Rev. Mod. Phys. **37**, 189 (1965)] is predicted here and experimentally verified for the case of two-dimensional sonic crystals made of hexagonal arrays of fluidlike cylindrical bars embedded in water. The dependence of diffraction intensity is studied as a function of layer thickness; i.e., of the layer number N. Nearly periodic oscillations have been observed at specific frequencies and the oscillation period is also a function of the frequency. The periodic behaviour is evidence of the exchange of energy between two modes in the sonic crystal. [Work supported by MEC of Spain.]

2pPAc12. Sound diffraction in periodic surfaces in ancient architectural structures. Jorge Antonio Cruz Calleja (Instituto Pólitecnico Nacional, Av Santa Ana No. 1000 col. San Francisco Culhuacan, Del Coyoacan, 04430 México, Mexico, jorgeacruzc@hotmail.com)

In this work is analyzed the sound diffraction in architectural structures caused by periodic surfaces. Is studied the sound interaction with architectural structures using different types of sources, materials and sizes. The apparently scattering effect of the staircases in ancient constructions (like the staircase of the Kukulcan pyramid in Chichen Itza), that allows the speech communication to large distances and the spatial filter effect using the glide repetition pitch theory are also analyzed (Is the Chirp echo of the ancient prehispanic pyramids an intentional effect?). Computational models of the phenomenon and real measurements were used to establish the phenomena physics principles.

Session 2pPAd

Physical Acoustics: Outdoor Sound Propagation and Uncertainties II (Poster Session)

Keith Wilson, Cochair
U.S. Army Cold Regions Research and Engineering Laboratory

Michel Berengier, Cochair
Laboratoire Central des Ponts et Chaussées

All posters will be on display from 3:40 p.m. to 5:20 p.m. To allow contributors an opportunity to see other posters, contributors of odd-numbered papers will be at their posters from 3:40 p.m. to 4:30 p.m. and contributors of even-numbered papers will be at their posters from 4:30 p.m. to 5:20 p.m.

Contributed Papers

2pPAd1. Lossy propagation of the Gulfstream Quiet Spike. Joe Salamone (Gulfstream Aerospace, 500 Gulfstream Rd., M/S R-01, Savannah, GA 31402, USA, joe.salamone@gulfstream.com)

The Gulfstream Quiet Spike is a telescoping nose extension with multiple segments of decreasing diameter intended to reduce the outdoor loudness of a sonic boom. This work examines the influence of the atmosphere on a propagated sonic boom signature for this device. First, atmospheric data, averaged by season, has been collected as a function of latitude to reasonably bound the range of meteorological conditions. These atmospheric profiles are subsequently input to nonlinear, lossy propagation code that computes the primary sonic boom carpet for a supersonic aircraft in steady, level flight. This code is an augmented implementation of the KZK model equation for one-dimensional propagation. The confluence of shocks generated by the Quiet Spike remains distinct and do not coalesce, as intended per the design. The amplitudes, rise times and spacing of the shocks from the individual spike segments are strongly governed by dispersion and attenuation. Loudness levels calculated from the resulting ground signatures show an observable change of over 4 dB at certain azimuths due to the various atmospheric conditions. Based on these results, minor design changes are recommended to improve the acoustic performance of the Gulfstream Quiet Spike.

2pPAd2. Practical analysis of the influence of basic meteorological phenomena on the long-term noise level. Barbara Joanna Lebiedowska (Warsaw University of Technology, ul. Lukasiewicza 17, 09-400 Plock, Poland, barbara_lebiedowska@yahoo.fr)

Current regulations on the prognosis of the acoustic climate outdoors require that meteorological conditions should be examined as part of long-term noise level calculations. The impact of meteorological conditions on the noise level was analysed using simulation calculations performed with NMPB-96 method and Mithra software. Their aim was to determine the relationship between the value of these influences and the distance between the receiver point and the noise source and its height above the ground.The distance between a source and the built-up area varied. A number of its locations in relation to the built-up area ranging between 200m and 4 000 m were considered. The built-up area consisted of a row of 11-storey buildings ca. 600 m long. The ground floor height and the floor height were accepted to be 3.5 m and 3.0 m, respectively. Calculations were performed for various meteorological conditions: from P=0 (homogenous conditions) to P=1.0, increasing by every 0.1. The receiver point was located 2 m away from the façade at varying heights: from the lowest point positioned at 5 m to the highest point at 27.5 m, increasing by 2.5 m, which corresponds to the median position of each successive storey, from first floor to tenth floor.

Session 2pPAe

Physical Acoustics: Phononic Crystals II (Poster Session)

Pierre Deymier, Cochair
University of Arizona

Jérôme Vasseur, Cochair
IEMN, UMR CNRS 8520

All posters will be on display from 3:40 p.m. to 5:20 p.m. To allow contributors an opportunity to see other posters, contributors of odd-numbered papers will be at their posters from 3:40 p.m. to 4:30 p.m. and contributors of even-numbered papers will be at their posters from 4:30 p.m. to 5:20 p.m.

Contributed Papers

2pPAe1. Advances in acoustics of liquid crystals. Olga Kapustina (Institute of Acoustics, 4 Shvernik Street, 117036 Moscow, Russian Federation, oakapustina@yandex.ru)

Advances in the fundamental problem of the orientation transition in liquid crystals produced by acoustical action are considered. The theoretical models to describe a variety of liquid crystals orientation transitions in acoustic fields for the homeotropically and planar oriented layers which were developed in the framework of the Leslie-Ericksen hydrodynamics and the new methodology based on the ideas of non-equilibrium thermodynamics and nonlinear hydrodynamics are discussed and are substantiated experimentally. The orientation phenomena in liquid crystals were classified and the physical factors defining a kind of transition (threshold or non-threshold type) and a choice of approach correct to describe adequately the experimental data on a new molecular arrangement induced by acoustical action were established. Among them a macrostructure type of liquid crystals layer, a layer thickness-viscous wavelength in liquid crystal ratio, an angle between the medium optical axe (the liquid crystal director) and the line of acoustical wave propagation, a sound intensity, a type of acoustical boundary conditions at the layer edges. The modern ideas on the distortion peculiarities of liquid crystals above a certain threshold of the structure instability under non-stationary dynamic action on the liquid crystal layer of sound-induced oscillating flows for a wide frequency band were considered.

2pPAe2. SH-wave propagation and localization anomalies in semi-infinite 1D magnetic phononic crystal. Tetyana V. Laptyeva (Donetsk Institute for Physics and Technology, 72, R. Luxemburg str., 83114 Donetsk, Ukraine, lapteva@mail.fti.ac.donetsk.ua), Sergey V. Tarasenko (Donetsk Institute for Physics and Technology, 72, R. Luxemburg str., 83114 Donetsk, Ukraine, tarasen@mail.fti.ac.donetsk.ua), Olga S. Tarasenko (Donetsk Institute for Physics and Technology, 72, R. Luxemburg str., 83114 Donetsk, Ukraine, tarasen@mail.fti.ac.donetsk.ua), Vladimir M. Yurchenko (Donetsk Institute for Physics and Technology, 72, R. Luxemburg str., 83114 Donetsk, Ukraine, yurch@mail.fti.ac.donetsk.ua)

At the present, the composite magnetic materials with a superstructure (magnetic photonic crystals) are actively investigated in view of conditions of electromagnetic wave transmission. Some of these materials are acoustically continuous media and, then, can be considered as magnetic phononic crystals (MPC). However, the dynamic acoustic peculiarities of such structures have been disregarded. Theoretical investigation of SH-wave propagation in the gyrotropic and nongyrotropic semi-infinite one dimensional magnetic phononic crystals (1D MPC) is presented here. We have taken into account magnetoelastic interaction and the commensurability a wavelength and 1D MPC period. The transfer matrix method allowed us to determine the specific features of volume SH-wave localization and propagation near the rigid interface of 1D MPC and nonmagnetic medium. In particular, the necessary conditions of existence and dispersion relations for three types of shear surface acoustic waves localized near the external surface of 1D MPC have been found. This type of elastic excitation are exists also for a case when elastic properties of MPC components are identical. The conditions of reflectionless transmission of volume SH-waves through a finite 1D MPC have been determined.

2pPAe3. Zone center phonons in thalium fluoroborate. Hem Chandra Gupta (Indian Institute of Technology, Physics Department, 110016 New Delhi, India, hcgupta@physics.iitd.ac.in), Jaya Singh (Indian Institute of Technology, Physics Department, 110016 New Delhi, India, hcgupta @physics.iitd.ac.in)

The study of phonons in thalium fluoroborate is very important in order to understand the phenomenon of phase transition in perchlorates and fluoroborates.Few studies of structural phase transition have been made of perchlorates and fluoroborates with a higher thalium ion, but their zone center phonons have not been investigated thoroughly. In order to understand the above, the Raman and the infrared frequencies of thalium fluoroborate have been investigated for the first time theoretically in its orthorhombic phase of space group Pnma. A short range force constant model (SRFCM) as well as rigid ion model (RIM) with stretching and bending force constants has been applied to obtain the zone center Raman and infrared phonons. The calculated values of Raman and infrared phonons are in very good agreement with the available observed values. The effect of these calculated interatomic force constants on the phase transition of thalium fluoroborate is discussed.

2pPAe4. Study of full band gaps and propagation of acoustic waves in two-dimensional piezoelectric phononic plates. Jin-Chen Hsu (Institute of Applied Mechanics, National Taiwan University, No. 1, Sec. 4, Roosevelt Road, 106 Taipei, Taiwan, hsu@ndt.iam.ntu.edu.tw), Tsung-Tsong Wu (Institute of Applied Mechanics, National Taiwan University, No. 1, Sec. 4, Roosevelt Road, 106 Taipei, Taiwan, wutt@ndt.iam.ntu.edu.tw)

Acoustic wave propagation in periodic structures composed of multi-constituents, namely the phononic crystals (PCs), has received much attention in the past decade. Recently, PCs constructed in the form of plate structures with two-dimensional lattices have been investigated, and some important phenomena, such as the full band-gap and waveguiding effects, induced by the periodicities of the phononic plates were reported. One of the virtues using Lamb waves is to perfectly confine the acoustic energy within the plate thickness and guided in structures with only 2D lattices rather than 3D lattices; however, the additional free surfaces derive much more complicated characteristics which are still awaiting study further. In this study, we

investigate the band-gap and propagation properties of waves in two-dimensional phononic plates that consist of either elastic or piezoelectric materials by employing a revised full 3D plane wave expansion (PWE) method and so on. To apply the PWE method efficiently, Fourier expansions are performed in the thickness direction for an imaginary 3D periodic structure by stacking the phononic plates and vacuum layers alternatively. Moreover, effects of piezoelectricity, lattices, and filling ratios on band gaps are discussed.

2pPAe5. Shannon Entropy as a Characterization Tool in Acoustics. Helios Sanchis-Alepuz (Polytechnic University of Valencia, Cami de Vera s/n, 46022 Valencia, Spain, hesana@alumni.uv.es), José Sanchez-Dehesa (Polytechnic University of Valencia, Cami de Vera s/n, 46022 Valencia, Spain, jsdehesa@upvnet.upv.es)

Shannon entropy [1] was introduced as a measure of the uncertainty associated with a random variable and initially it was used to quantify the information contained in a binary message. In this work, a definition of Shannon's information entropy is introduced in acoustics, defined in terms of the displacement field, as a measure of the localization of resonant modes. As an example, it is applied to study the avoided crossing appearing in the resonant Zener-like phenomenon in ultrasonic superlattices made of two different fluidlike metamaterials. It is shown that acoustic Shannon entropy gives a correct physical insight of the localization effects taking place and manifest the informational exchange of the involved acoustic states in the narrow region of parameters where the avoided crossing occurs. Results for ultrasonic structures consisting of alternating layers of polymethylmethacrylate (Plexiglas) and water cavities, in which the acoustic Zener effect were recently demonstrated [2], are also reported. It is concluded that Shannon entropy is a useful tool to characterize localization effects in acoustical systems. [1] C.E. Shannon, Bell Sys. Tech. J. 27, 623 (1948). [2] H. Sanchis-Alepuz, Yu.A. Kosevich, and J. Sanchez-Dehesa, Phys. Rev. Lett. 98 134301 (2007).

2pPAe6. Acoustic wave band gaps in triangular and honeycomb two-dimensional phononic crystals. Fu-Li Hsiao (Institute of Optical Sciences, National Central University, 320 Jung-Li, Taiwan, flhsiao@ios.ncu.edu.tw), Abdelkrim Khelif (Institut FEMTO-ST/CNRS, 32 avenue de l'Observatoire, 25044 Besançon cedex, France, abdelkrim.khelif@femto-st.fr), Boujemaa Aoubiza (Institut FEMTO-ST/CNRS, 32 avenue de l'Observatoire, 25044 Besançon cedex, France, boujemaa.aoubiza@univ-fcomte.fr), Abdelkrim Choujaa (Institut FEMTO-ST/CNRS, 32 avenue de l'Observatoire, 25044 Besançon cedex, France, abdelkrim.choujaa@femto-st.fr), Hanane Moubchir (Institut FEMTO-ST/CNRS, 32 avenue de l'Observatoire, 25044 Besançon cedex, France, hanane.moubchir@femto-st.fr), Chii-Chang Chen (Institute of Optical Sciences, National Central University, 320 Jung-Li, Taiwan, trich@ios.ncu.edu.tw), Vincent Laude (Institut FEMTO-ST/CNRS, 32 avenue de l'Observatoire, 25044 Besançon cedex, France, vincent.laude @femto-st.fr)

The ultrasonic band gap properties of phononic crystals composed of arrays of steel cylinders immersed in water and arranged according to square, triangular or honeycomb lattices are compared theoretically and experimentally. In all three cases, complete band gaps are obtained, and the conditions of existence are identified by observing the complete band gap width as a function of the size of the inclusions. However, the measured transmission spectra reveal in the hexagonal symmetry cases (triangular and honeycomb lattices) the existence of deaf bands that cause strong attenuation in the transmission, with no band gap being involved. Band gaps and deaf bands are identified by comparing band structure computations for the infinite phononic crystal, obtained by a periodic-boundary finite element method (FEM), with transmission simulations for the finite phononic crystal, obtained using the finite difference time domain (FDTD) method. The possibility of managing phononic wave guides within a defect line channel inside an otherwise perfect triangular lattice phononic crystal is further demonstrated experimentally.

2pPAe7. Shock waves in nanomechanical resonators. Robert H. Blick (University of Wisconsin-Madison, Electrical and Computer Engineering, 1415 Engineering Drive, Madison, WI 53705, USA, blick@engr.wisc.edu), Florian W. Beil (University of Munich, Center for NanoScience, Geschwister Scholl Platz 1, 80539 Munich, Germany, beil_florian@bah.com), Achim Wixforth (University of Augsburg, Universitaetstrasse 1, 86135 Augsburg, Germany, achim.wixforth@physik .uni-augsburg.de), Werner Wegscheider (University of Regensburg, Fakultaet fuer Physik, 93040 Regensburg, Germany, werner.wegscheider @physik.uni-regensburg.de), Dieter Schuh (University of Regensburg, Fakultaet fuer Physik, 93040 Regensburg, Germany, dieter.schuh @physik.uni-regensburge.de), Max Bichler (Technical University of Munich, Coulombweg 1, 86748 Garching, Germany, max.bichler@wsi.tum.de)

The dream of every surfer is an extremely steep wave propagating at the highest speed possible. The best waves for this are would be shock waves, but are very hard to surf. In the nanoscopic world the same is true: the surfers in this case are electrons riding through nanomechanical devices on acoustic waves. Naturally, this has a broad range of applications in sensor technology and for communication electronics for which the combination of an electronic and a mechanical degree of freedom is essential. But this is also of interest for fundamental aspects of nano-electromechanical systems (NEMS), when it comes to quantum limited displacement detection and the control of phonon number states. Here, we study the formation of shock waves in a NEMS resonator with an embedded two-dimensional electron gas using surface acoustic waves. The mechanical displacement of the nanoresonator is read out via the induced acoustoelectric current. Applying acoustical standing waves we are able to determine the anomalous acoustocurrent. This current is only found in the regime of shock wave formation. We ontain very good agreement with model calculations.

2pPAe8. Experimental measurements of the band structure of Lamb waves in phononic lattices. Bernard Bonello (CNRS and Paris VI University, INSP - 140 rue de Lourmel, 75015 Paris, France, bernard.bonello@insp.jussieu.fr), Thomas Brunet (CNRS and Paris VI University, INSP - 140 rue de Lourmel, 75015 Paris, France, thomas.brunet@insp.jussieu.fr), Jiu-Jiu Chen (CNRS and Paris VI University, INSP - 140 rue de Lourmel, 75015 Paris, France, chen99nju@gmail .com)

We have measured the band structure of Lamb waves propagating in 2D phononic crystals. Different cases were investigated. First we have studied the phononic film deposited on a homogeneous substrate. The phononic film is made of cylindrical iron scatterers embedded into a copper background; the substrate is a 700 μm silicon plate. The propagation is along the crystallographic direction [100] of Si. At low filling fraction, a frequency band gap for the antisymmetric mode arises at reduced Brillouin edge. At high filling fraction, a band gap opens also on the symmetric branch. We have also studied the case of phononic slabs with very high contrast between the scatterers and the matrix. The samples are made of 200 μm silicon plates with air holes lattices drilled throughout. Whatever the symmetry of the lattice, square of centered rectangular, broad band gaps open at first and second reduced Brillouin zone edges. Experimental data are then compared to theoretical predictions obtained using a plane wave expansion method.

2pPAe9. Order/disorder transition for ultrasonic propagation in 2D scatterer arrays. Alice Bretagne (Laboratoire Ondes et Acoustique, ESPCI, Université Paris 7, CNRS, 10 rue Vauquelin, 75005 Paris, France, alice.bretagne@espci.fr), Arnaud Tourin (Laboratoire Ondes et Acoustique, ESPCI, Université Paris 7, CNRS, 10 rue Vauquelin, 75005 Paris, France, arnaud.tourin@espci.fr), Mathias Fink (Laboratoire Ondes et Acoustique, ESPCI, Université Paris 7, CNRS, 10 rue Vauquelin, 75005 Paris, France, mathias.fink@espci.fr)

Recently, intriguing phenomena in quantum mechanics, such as the Aharonov-Bohm effect [P. Roux et al., Phys. Rev. Lett. 79, 3170 (1997)], weak localization in disordered media [A. Tourin et al., Phys. Rev. Lett. 79, 3637 (1997)] and maybe one of the most striking, tunnelling [S. Yang et al., Phys. Rev. Lett. 88, 104301 (2002)], have been revisited using acoustic waves. The advantages of using ultrasound for such studies lie in the macroscopic character of samples and the possibility of directly measuring the

phase of the wavefield. Here we explore propagation of MHz-ultrasound in a medium which is either ordered or disordered in the two transverse dimensions (x,y) but invariant in the propagation direction (z). An equivalent scheme has been recently used in optics to demonstrate transverse localization of light [T. Schwartz et al., Nature 446, 52 (2007)]. Our samples are made of a parallel arrangement of cylindrical scatterers (0.8mm in diameter) embedded in a PVA matrix. In the ordered case, the probe beam undergoes ballistic transport. In the disordered case transport becomes diffusive and as the sample length increases the wave tends to be laterally confined.

2pPAe10. Experimental and theoretical investigations of focusing of ultrasonic waves by two-dimensional flat phononic crystals. Alexey Sukhovich (Universidad de Murcia, Dept. of Physics and Astronomy, Univ. of Manitoba, Winnipeg, MB R3T 2N2, Canada, alexei@physics.umanitoba.ca), John H. Page (Dept. of Physics and Astronomy, Univ. of Manitoba, Winnipeg, MB R3T 2N2, Canada, jhpage@cc.umanitoba.ca), Bassam Merheb (University of Arizona, Materials Science and Engineering Department, Mines Bldg., P.O. Box 210012, Tucson, AZ 85721, USA, bassam@merheb.net), Jérôme Vasseur (IEMN, UMR CNRS 8520, avenue Poincaré, BP 60069, 59652 Villeneuve d'Ascq, France, jerome.vasseur@univ-lille1.fr), Pierre Deymier (University of Arizona, Materials Science and Engineering Department, Mines Bldg., P.O. Box 210012, Tucson, AZ 85721, USA, deymier@u.arizona.edu)

We compare experimental and theoretical results demonstrating focusing of sound fields emitted by subwavelength sources using two-dimensional flat phononic crystals. Our phononic crystals are made of stainless steel rods assembled in a triangular crystal lattice and immersed in a liquid. Focusing is achieved due to negative refraction of ultrasonic waves propagating through the crystal, which is realized at the frequencies corresponding to the 2nd band, where the group velocity and wave vector are antiparallel. High quality images are obtained experimentally with a methanol-filled phononic crystal surrounded by water, in which the source and detecting transducers are located. Excellent resolution approaching the diffraction limit is achieved for the frequency at which the equifrequency contours inside the crystal match those in water. Our experimental results are compared with theoretical predictions by the Finite Difference Time Domain (FDTD) method. Good agreement is observed for the width of the focal spot in the direction parallel to the crystal surface, while along the perpendicular direction, we find experimentally that the focal spot is narrower and closer to the crystal surface than in the theoretical predictions.

2pPAe11. Complete band gap in the phonon spectra of compact ceramics. Evgenii I. Salamatov (Physical-Technical Institute UrB RAS, 132 Kirov str., 426000 Izhevsk, Russian Federation, salam@otf.pti.udm.ru)

The processes of sound propagation in inhomogeneous systems have long the focus of researchers attention. The new interest in this problem i last years has been inspired by the appearance of artificial elastic periodic structures - phononic crystals. Since the lattice parameter artificial phononic crystals is about several millimetres the complete bandgap is assumed to lie in the megahertz range. It is of fundamental importance for modern radio equipment to obtain phononic crystals with forbidden bandgap in the gigahertz range, which requires generation of phononic lattices with the period of the order of tens and hundreds nanometers. The author believes nanoceramics compacted from a superfine powder in a special way to be very promising systems for the generatio such phononic lattices. In this work the phonon spectra of the model two-dimensional ceramics numerically calculated using the finite-difference time-domain (FDTD) method. To interpret the results, the analytical expressions obtained for an elastic limit are used, which enables formalization of the conditions necessary for the appearance of a gap in a phonon spectrum. The possibility of creation of bulk acoustic waves resonators is discussed.

2pPAe12. A Transient Grating approach to elastic wave and thermal propagation in a 2D free-standing micrometric phononic crystal. Iacopo Malfanti (European Lab. for Non-Linear Spectroscopy (LENS), Univ. di Firenze, via Nello Carrara 1, 50019 Sesto Fiorentino (Fi), Italy, malfanti@lens.unifi.it),Renato Torre(European Lab. for Non-Linear Spectroscopy (LENS), Univ. di Firenze, via Nello Carrara 1, 50019 Sesto Fiorentino (Fi), Italy, torre@lens.unifi.it), Paolo Bartolini (European Lab. for Non-Linear Spectroscopy (LENS), Univ. di Firenze, via Nello Carrara 1, 50019 Sesto Fiorentino (Fi), Italy, bart@lens.unifi.it), Andrea Taschin (European Lab. for Non-Linear Spectroscopy (LENS), Univ. di Firenze, via Nello Carrara 1, 50019 Sesto Fiorentino (Fi), Italy, taschin@lens.unifi.it), Francesco Vita (via Brecce Bianche, 1, 60131 Ancona, Italy, f.vita@univpm.it), Francesco Simoni (via Brecce Bianche, 1, 60131 Ancona, Italy, f.simoni@univpm.it)

We investigate the phonon propagation in a 2D phononic crystal (with typical dimensions on the micrometric scale) by means of a transient grating (TG) heterodyne detected experiment. In a TG experiment both a temperature and a density grating are induced by means of optical techniques. The relaxation dynamics of the induced grating are then monitored live-time over 6 temporal decades with a probe beam. Our sample is a freestanding 100 micrometer thick polymer matrix with empty rods (filled with gas) arranged in a triangular lattice. Evidence of the presence of two different bulk wave acoustic modes are experimentally found. The excited acoustic modes show a correlation with the orientation of the sample with respect to the induced grating wave vector, while the thermal properties show a significant dependence on the magnitude of the induced grating wave vector.

2pPAe13. Thermal shifting of phononic bandgaps in barium strontium titanate-based structures. Kwok Lung Jim (Department of Applied Physics and Materials Research Centre, The Hong Kong Polytechnic University, Hunghom, Kowloon Hong Kong, China, jim.kl@polyu.edu.hk), Chi Wah Leung (Department of Applied Physics and Materials Research Centre, The Hong Kong Polytechnic University, Hunghom, Kowloon Hong Kong, China, apleung@inet.polyu.edu.hk), Chung Loong Choy (Department of Applied Physics and Materials Research Centre, The Hong Kong Polytechnic University, Hunghom, Kowloon Hong Kong, China, scclchoy@inet.polyu.edu.hk), Helen L. W. Chan (Department of Applied Physics and Materials Research Centre, The Hong Kong Polytechnic University, Hunghom, Kowloon Hong Kong, China, apahlcha@inet.polyu.edu.hk)

Phononic crystals, which are structures with periodic variations of density and/or sound velocities, can exhibit phononic bandgaps where propagation of acoustic waves is forbidden. The ability of phononic crystals to manipulate sound, in a similar manner which photonic crystal control light, makes them particularly useful for applications such as acoustic filters or very efficient waveguides. Since the positions of the phononic bandgaps depend solely on the densities and the sound velocities of the constituent materials, it is expected that a modulation in the densities and/or sound velocities of the constituent materials would result in a phononic bandgap shift. It is known that ferroelectric ceramic, such as barium strontium titanate (BST), will undergo a ferroelectric-to-paraelectric phase transition across the Curie temperature. During the phase transition, there is a large variation in the sound velocities of BST which result in a shift of the phononic bandgaps. In this work, we calculated the phononic bandstructures of BST-based structures by the plane-wave expansion method and showed that the phononic bandgaps can be shifted thermally.

2pPAe14. Nondiffractive propagation of sound in sonic crystals. Isabel Perez-Arjona (IGIC - Universitat Politècnica de València, Cra. Nazaret-Oliva S/N, E-46730 Gandia, Spain, iparjona@upvnet.upv.es), Victor Sánchez-Morcillo (IGIC - Universitat Politècnica de València, Cra. Nazaret-Oliva S/N, E-46730 Gandia, Spain, victorsm@fis.upv.es), Víctor Espinosa (IGIC - Universitat Politècnica de València, Cra. Nazaret-Oliva S/N, E-46730 Gandia, Spain, vespinos@fis.upv.es), Kestutis Staliunas (Departament de Fisica i Enginyeria Nuclear, Colom 11, 08222 Terrassa (Barcelona), Spain, Kestutis.Staliunas@icrea.es), Javier Redondo (IGIC - Universitat Politècnica de València, Cra. Nazaret-Oliva S/N, E-46730 Gandia, Spain, fredondo@fis.upv.es)

In this work we present the study of the nondiffractive propagation regime of ultrasonic waves in a two-dimensional periodic acoustic media (sonic crystal) both from the theoretical and the experimental point of view. An analytical treatment of this regime sonic wave propagation is presented, which allows evaluating the parameters of the nondiffractive regime, just as

the minimum size of the nondiffractively propagating acoustic beam. Experimentally, we report on the first experimental demonstration of the subdiffractive propagation (self-collimation) of an ultrasound beam in a sonic crystal formed by steel cylinders in water. The experimental measurements show a good agreement with the theoretical predictions, where the effect of the finite size of the crystal was also considered. The preliminary results on self-collimation of sound in three-dimensional sonic crystal, in progress at the present moment, will be also presented.

TUESDAY AFTERNOON, 1 JULY 2008 P3-A, LEVEL 3, 3:40 TO 5:20 P.M.

Session 2pPAf

Physical Acoustics: Acoustics of Porous Media III (Poster Session)

Walter Lauriks, Cochair
Lab. ATF, Katholieke Universiteit Leuven

Keith Attenborough, Cochair
Open University

All posters will be on display from 3:40 p.m. to 5:20 p.m. To allow contributors an opportunity to see other posters, contributors of odd-numbered papers will be at their posters from 3:40 p.m. to 4:30 p.m. and contributors of even-numbered papers will be at their posters from 4:30 p.m. to 5:20 p.m.

Contributed Papers

2pPAf1. In-situ measurement of interface permeability. Lin Lin (Universisty Of Maine, 5711 Boardman Hall, Orono, ME 04469, USA, lin.lin@umit.maine.edu), Michael Peterson (Universisty Of Maine, 5711 Boardman Hall, Orono, ME 04469, USA, michael.peterson @maine.edu), Alan Greenberg (Univesity of Colorado, 427 UCB Dept. of Mechanical engineering, Boulder, CO 80309, USA, Alan.Greenberg @colorado.edu), Benjamin McCool (ExxonMobil Research and Engineering Company, 1545 Route 22 East, Annandale, NJ 08801, USA, Benjamin .a.mccool@exxonmobil.com)

Permeability of a porous interface is important for many areas of research and technology ranging from transport of nutrients in marine sediments to produce separations in bio-pharmaceuticals. Biot theory has shown that porous materials are able to support the propagation of two longitudinal waves: fast and slow wave. By measuring the propagation threshold of the slow longitudinal wave when the wave number is higher than the critical wave number kcr, we can obtain the intrinsic permeability of a porous interface. The ability to sense permeability change due to differences in pore size and fluid viscosity is demonstrated. The measurement is compared to an exact solution for kcr as well as previously published analytical solutions. This technique for measuring permeability has been shown in a model material and can now be extended to a wide range of materials of scientific and technical importance.

2pPAf2. Sound absorption of advanced textile materials. Ivan Bolkovac (Faculty of EE and Computing, Unska 3, Department of Electroacoustics, HR-10000 Zagreb, Croatia, ibolkovac@gmail.com), Hrvoje Domitrovic (Faculty of EE and Computing, Unska 3, Department of Electroacoustics, HR-10000 Zagreb, Croatia, hrvoje.domitrovic@fer .hr), Martina Bozic (Faculty of textile technology, University of Zagreb, Ljubijska 51a, 10000 Zagreb, Croatia, martina.bozic.ttf@gmail.com)

Today's acoustic applications demand an ever greater array of materials used for acoustic treatment of spaces for both professional or non-professional use. Elements like absorbers, diffusers and silencers are met with increasingly strict demands, both aesthetic and functional. That is the reason why we were interested in acoustic qualities (absorption coef.) of different kinds of textile materials that could be used in building or finishing such elements. Textile materials range from conventional to high-performance textiles. The latter, with their advanced qualities (both acoustic and mechanical) promise a much wider area of application and further specialized use, both as stand-alone elements or their parts.

2pPAf3. Influence of sound absorption on close proximity noise of porous pavement. S. E. Paje (Laboratory of Acoustics Applied to Civil Engineering (LA2IC), Universidad de Castilla-La Mancha, Department of Applied Physics, 13071 Ciudad Real, Spain, santiago.exposito@uclm .es), Moises Bueno (Laboratory of Acoustics Applied to Civil Engineering (LA2IC), Universidad de Castilla-La Mancha, Department of Applied Physics, 13071 Ciudad Real, Spain, moises.bueno@uclm.es), Urbano Viñuela (Laboratory of Acoustics Applied to Civil Engineering (LA2IC), Universidad de Castilla-La Mancha, Department of Applied Physics, 13071 Ciudad Real, Spain, urbano.vinuela@uclm.es), Fernando Terán (Laboratory of Acoustics Applied to Civil Engineering (LA2IC), Universidad de Castilla-La Mancha, Department of Applied Physics, 13071 Ciudad Real, Spain, fernando.teran@uclm.es)

The main objective of this research is to correlate sound absorption of a new bituminous porous pavement (air void content 21%) with the close proximity noise. Different core samples were taken from a porous road surface. The normal incidence sound absorption spectra were measured for these samples using the two-microphone impedance tube. Noise levels close to the tire/pavement contact patch were measured continuously in a georeferenced way, when the test vehicle was rolling. The emission properties of the porous surface as a function of vehicles speed are analyzed in the acoustic frequency range showing different behaviors for the relationships between noise levels and speed. An abrupt variation in the relationship between the coefficient B and frequencies below 1 kHz was observed ($Lcp = A + B \cdot \log(V)$). This feature could be highly influenced by sound absorption mechanism, particularly noticeable for a non-clogged porous surface with a high content of air voids.

2pPAf4. Physico-chemical properties and ultrasonic characterization of calcium phosphate ceramics. Daniela Predoi (National Institute of Materials Physics, Atomistilor 105 bis, 77123 Magurele, Romania,

dpredoi_68@yahoo.com),Serge Derible(LOMC FRE CNRS 3102, Université du Havre, Place Robert Schuman, 76610 le Havre, France, serge.derible@univ-lehavre.fr), Hugues Duflo (LOMC FRE CNRS 3102, Université du Havre, Place Robert Schuman, 76610 le Havre, France, hugues.duflo@univ-lehavre.fr), Mihai Valentin M. Predoi (University Politechnica of Bucharest, Department of Mechanics, 060032 Bucharest, Romania, predoi@cat.mec.pub.ro), Cristian Catalin Petre (University Politechnica of Bucharest, Department of Mechanics, 060032 Bucharest, Romania, cristian.petre@promteh.ro)

Calcium phosphate compounds have been studied for biomedical applications due to their chemical and structural similarity to the mineral phase of bone and tooth. The composition, physical and chemical properties, crystal size and morphology of synthetic apatite are extremely sensitive to preparation conditions and sometimes it resulted into non- stoichiometric calcium deficient hydroxyapathite (Hap) powders. The present paper refers to calcinations of calcium phosphate ceramics at 800 and 1000^{o}C. The effect of heat treatment were investigated by X-ray diffraction (XRD), Fourier transform infrared (FTIR), differential thermal analysis (DTA) and thermal gravimetric analysis (TGA). FTIR spectra showed the presence of various $PO_4$3- and OH-groups present in the powders. Powders compacted and sintered at 800 and 1000^{o}C showed an increase in density. The main objective of the paper is a comparison of the results obtained by the previous methods to those obtained using the ultrasonic air-coupling technique. Modulated ultrasonic signals of 500 kHz central frequency have been transmitted through the calcium phosphate ceramics specimens. Correlation between signals allowed some conclusions concerning density, porosity and preparation temperature influence on these specimens. These comparisons and correlation of methods, allow a better characterisation of such important materials

2pPAf5. Ultrasonic monitoring of hardening concrete. Julien Bue (Institut Jean le Rond D'Alembert / UMR 7190, 2 Place de la Gare de Ceinture, 78210 Saint Cyr L'Ecole, France, julien.bue@wanadoo.fr), Frederic Cohen Tenoudji (Institut Jean le Rond D'Alembert / UMR 7190, 2 Place de la Gare de Ceinture, 78210 Saint Cyr L'Ecole, France, fcohentenoudji@yahoo.fr)

Monitoring results of velocities and attenuations of compressional and transverse ultrasonic waves in hardening concrete using short pulse through-transmission are presented. A fluid concrete is a highly attenuating heterogeneous medium, composed of several phases and granular classes. Different attenuation mechanisms are considered in order to account for experimental results: high impedance mismatch between air layers and solid-fluid clusters at early ages, Energy loss by viscous dissipation and wave scattering by heterogeneities (Rayleigh scattering at low frequencies, single or multi diffusion scatterings at intermediate and high frequencies) during the beginning of hardening. At early ages, the medium may be described as composed of a succession of large slabs of fresh concrete separated by very thin slabs of air. Attenuation is then computed from the effective transmission coefficient of this medium. This model is in good agreement with experiments. During the beginning of hardening, the medium may be seen as composed of big particles immersed in an effective medium formed by the ensemble of the particles of lesser granular sizes and water. Then, the Rayleigh scattering model at low frequencies and the multiple diffusion model predictions at intermediate frequencies are in good agreement with experiments.

2pPAf6. Flow resistivity profile inversion for a porous medium. Claude Depollier (Laboratoire d'Acoustique de l'Université du Maine, Avenue Olivier Messiaen, 72085 Le Mans, France, claude.depollier@univ-lemans.fr), Naima Sebaa (Laboratoire d'Acoustique de l'Université du Maine, Avenue Olivier Messiaen, 72085 Le Mans, France, naima.sebaa@univ-lemans.fr), Mouna Naas (Laboratoire d'Acoustique de l'Université du Maine, Avenue Olivier Messiaen, 72085 Le Mans, France, mouna.naas.etu@univ-lemans.fr), Bernard R. Castagnede (Laboratoire d'Acoustique de l'Université du Maine, Avenue Olivier Messiaen, 72085 Le Mans, France, bernard.castagnede@univ-lemans.fr), Zine Fellah (CNRS-Laboratoire de Mécanique et d'Acoustique, 31 Chemin Joseph Aiguier, 13402 Marseille, France, fellah@lma.cnrs-mrs.fr), Walter Lauriks (Lab. ATF, Katholieke Universiteit Leuven, Celestijnenlaan 200D, B-3001 Leuven, Belgium, Walter.Lauriks@fys.kuleuven.be)

Predictions for the low frequency sound waves propagation in a porous medium needs the knowledge of the flow specific resistance of the medium. We present a scheme for the flow resistivity profile inversion for a layered medium. In the framework of the fluid equivalent model a closed-form relation of the resistivity profile with the Fourier transform of the reflection is derived. It provide a straightforward way to perform the reconstruction of the profile. The result show a strong correlation between the flow resistivity profile and the reflection coefficient in this model. Some numerical simulations are given as examples of the applicability of this scheme.

2pPAf7. Wave equation in non-integer-dimensional porous media. Claude Depollier (Laboratoire d'Acoustique de l'Université du Maine, Avenue Olivier Messiaen, 72085 Le Mans, France, claude.depollier@univ-lemans.fr), Jean-Baptiste Legland (Laboratoire d'Acoustique de l'Université du Maine, Avenue Olivier Messiaen, 72085 Le Mans, France, jean-baptiste.legland.etu@univ-lemans.fr)

Over some range of scales, porous media display properties of fractals. It particular both pore sizes and pore-interfaces exhibit the fractal characteristics. One of the fascinating interests of fractals is their capability to model objects with complicate structure. This is due to an important property of fractal objects that their structure is characterized by a small number of parameters. One of them is the fractal dimension which tells how the fractal fills the space in which it lies. Very early, fractal concept has been incorporated in the study of porous media to investigate various phenomena as flow in porous media, pores and fractures of geological media. We present generalized Biot's wave equations for a fractional dimensional system of 3-spatial coordinates used as an effective description of porous media. Some specific examples are given as an application of this model.

2pPAf8. Investigation of the limp model validity for porous materials. Olivier Doutres (Laboratoire d'Acoustique de l'Université du Maine, Avenue Olivier Messiaen, 72085 Le Mans, France, olivier.doutres.etu@univ-lemans.fr), Nicolas Dauchez (Laboratoire d'Acoustique de l'Université du Maine, Avenue Olivier Messiaen, 72085 Le Mans, France, nicolas.dauchez@univ-lemans.fr), Jean Michel Genevaux (Laboratoire d'Acoustique de l'Université du Maine, Avenue Olivier Messiaen, 72085 Le Mans, France, jean-michel.genevaux@univ-lemans.fr), Olivier Dazel (Laboratoire d'Acoustique de l'Université du Maine, Avenue Olivier Messiaen, 72085 Le Mans, France, olivier.dazel@univ-lemans.fr)

A new criterion to test the validity of using the limp model for porous materials is proposed. The limp model is derived from the poroelastic Biot model assuming that the frame has no bulk stiffness. Being an equivalent fluid model accounting for the motion of the frame, it has fewer limitations than the usual equivalent fluid model assuming a rigid frame. A criterion is derived to identify the porous materials for which the limp model can be used. This criterion relies on a new parameter, the Frame Stiffness Influence (FSI) based on porous material properties. The critical values of FSI under which the limp model can be used, are determined using a 1D analytical modeling for three boundary sets: absorption of a porous layer backed by a rigid wall, radiation of a vibrating plate covered by a porous layer and transmission loss of a double leaf panel filled in by a porous layer. Compared with other criteria, the criterion associated with FSI provides information in a wider frequency range and can be used for configurations which include vibrating plates.

2pPAf9. An index to quantify the through-thickness symmetry of sound absorbing materials. Yacoubou Salissou (Groupe d'Acoustique de l'Université de Sherbrooke, 2500, Boul. de l'Université, Département de génie mécanique, Sherbrooke, QC J1K-2R1, Canada, Yacoubou.Salissou

@USherbrooke.ca),Raymond Panneton(Groupe d'Acoustique de l'Université de Sherbrooke, 2500, Boul. de l'Université, Département de génie mécanique, Sherbrooke, QC J1K-2R1, Canada, raymond.panneton @usherbrooke.ca)

In this work, an extension of the theoretical formulation of the transfer matrix to non symmetrical sound absorbing porous materials is carried out. From this extension, an index of asymmetry is proposed and discussed. This index allows one to quantify the through-thickness asymmetry of a sound absorbing porous material. This index may be used for quality control or to assess the symmetry of the material in terms of its acoustic properties (absorption, reflection, impedance, propagation constant). To validate the application of the index of asymmetry, samples made up from two layers of porous materials are studied. Each so-constructed two-layered sample is seen as an equivalent asymmetrical single porous layer with a sudden change in its physical properties. The acoustic properties of each sample are then measured in the direct and inverted configurations (i.e., when both sides of the sample are facing successively the incident wave). Their values are compared in terms of the asymmetry index of the equivalent single layer. From these tests, an index value is suggested. Above this value, the acoustic properties of a sound absorbing material should be considered as being not symmetrical.

2pPAf10. Ultrasonic critical angle reflectometry applied to porous nuclear fuel mechanical characterization. Vivian Cereser Camara (Université Montpellier II, Place Eugène Bataillon, 34095 Montpellier, France, cereser@lain.univ-montp2.fr), Didier Laux (Université Montpellier II, Place Eugène Bataillon, 34095 Montpellier, France, laux@lain .univ-montp2.fr), Gilles Despaux (Université Montpellier II, Place Eugène Bataillon, 34095 Montpellier, France, despaux@lain.univ-montp2 .fr), Daniel Baron (EDF, CEA Cadarache, 13108 St Paul Lez Durance, France, daniel.baron@edf.fr)

An ultrasonic reflectometer working from 2 to 10 MHz on zones around 4 mm has been built in order to assess in a non destructive way the reflection coefficient R(θ, f) as a function of incident angle and frequency. Many experiments were performed on various materials (glass, aluminium,…) showing that with this goniometer and the related signal processing it is possible to assess very accurately R(θ, f) for bulk or thin samples (Lamb modes). Longitudinal and shear velocities (VL, Vs) deduced from R(θ, f) have been used to determine the elastic moduli E and G which values match very favourably with literature. Hence the Ultrasonic Critical angle Reflectometry is a powerful tool for materials characterization. In a second step, this device has been used on civil power plants fuel (UO2) with various volume fraction of porosity. The elastic moduli obtained are in good agreement with the literature data. The relations between VL, VS and the porosity (p) on the one hand, and E and G with p on the other hand will be presented and discussed. In particular, a link between these relations and the pores morphology (deduced with numerical simulations) will be pointed out.

2pPAf11. Hybrid inversion technique for predicting geometrical parameters of porous materials. Paresh Shravage (Dipartimento di Ingegneria - University of Ferrara, Via Saragat 1, 44100 Ferrara, Italy, paresh.shravage@unife.it), Paolo Bonfiglio (Dipartimento di Ingegneria - University of Ferrara, Via Saragat 1, 44100 Ferrara, Italy, paolo.bonfiglio @unife.it), Francesco Pompoli (Dipartimento di Ingegneria - University of Ferrara, Via Saragat 1, 44100 Ferrara, Italy, francesco.pompoli@unife.it)

In prediction of acoustical behavior of porous materials, five geometrical parameters play a very important role, but some of these geometrical properties are very difficult to measure directly. So many authors have suggested different inversion strategies for getting these properties from directly measured both characteristic and surface properties of the material using standing wave tube. These approaches can be divided in two different categories: analytical (based on the limit behaviour of the bulk properties) and minimization based methods (which make use of searching algorithms to determine the best solution that minimizes a cost function calculated by means of a prediction model). Recent studies have shown the reliability of the analytical methods for the determination of the airflow resistivity and the minimization based approach by using genetic algorithms for getting the other physical parameters. Consequently, a hybrid inversion technique can be proposed for the complete calculation of the geometrical quantities and here it is presented in detail. Moreover the paper compares the results from the hybrid approach with the experimentally measured parameters and the values of the five parameters obtained by using genetic algorithms. Finally, the paper presents the effect of both inversion techniques on acoustical properties using Johnson-Allard-Champoux model.

2pPAf12. Absorption and dispersion of acoustical waves in synthetic and natural compressed fibrous materials. Bernard R. Castagnede (Laboratoire d'Acoustique de l'Université du Maine, Avenue Olivier Messiaen, 72085 Le Mans, France, bernard.castagnede @univ-lemans.fr), Bruno Brouard (Laboratoire d'Acoustique de l'Université du Maine, Avenue Olivier Messiaen, 72085 Le Mans, France, bruno.brouard@univ-lemans.fr), Claude Depollier (Laboratoire d'Acoustique de l'Université du Maine, Avenue Olivier Messiaen, 72085 Le Mans, France, claude.depollier@univ-lemans.fr), Olivier Dazel (Laboratoire d'Acoustique de l'Université du Maine, Avenue Olivier Messiaen, 72085 Le Mans, France, olivier.dazel@univ-lemans.fr), Denis Lafarge (Laboratoire d'Acoustique de l'Université du Maine, Avenue Olivier Messiaen, 72085 Le Mans, France, denis.lafarge@univ-lemans.fr)

When a fibrous slab is compressed along its thickness, there are some changes in the basic physical parameters which describe the propagation of sound waves. For instance during compression, the acoustical resistivity and the tortuosity increase, while at the same time the porosity as well as the viscous and thermal characteristic lengths diminish. For a 1-D compression along the thickness of the porous layer, these changes are decribed by straightforward linear equations, as long as the compression ratio is kept small (e.g. between 1 and 5). Such simple expressions are derived theoretically on the base of conservation principles relying on some fundamental metrology indicators. Next, the influence of these changes on the 5 fundamental physical properties of any porous networks are studied numerically on the dispersion and attenuation curves versus frequency, in the frame of the ″equivalent-fluid″ model [4]. Finally, experiments are performed in order to check some of these predictions on various felt fibrous materials having different compression ratio.

2pPAf13. Acoustic properties of partly saturated porous soils. Kirill V. Horoshenkov (University of Bradford, School of Engineering, Design and Technology, BD7 1DP Bradford, UK, k.horoshenkov@Bradford .ac.uk), Mostafa H. Mohamed (University of Bradford, School of Engineering, Design and Technology, BD7 1DP Bradford, UK, m.h.a.mohamed@Bradford.ac.uk), Siow N. Ting (University of Bradford, School of Engineering, Design and Technology, BD7 1DP Bradford, UK, s.n.ting@bradford.ac.uk)

Controlled experiments are performed on soil samples saturated with different types of liquid such as water and oil to determine the relations between the degree of saturation, type of saturated liquid and the acoustic surface admittance. These experiments are conducted using a Buchner funnel attached directly to an acoustic impedance tube. The results show a very sensitive dependence of the acoustic admittance upon the degree of saturation irrespective of the liquid present. It is found that the relationship between the volumetric water content and the real part of the surface admittance in the frequency range of 500 - 1000 Hz can be expressed using a logarithmic equation. The coefficients of the proposed equation can be determined using a soil property called ″uniformity coefficient″ and the acoustic admittance of dry soil. Results of volumetric water content obtained using the proposed equation are validated using those obtained from an independent test. The results of the validation exercise demonstrate that the proposed relations can be used to determine very accurately the volumetric water content within soil from the acoustical data. The accuracy of the acoustically measured degree saturation is found to be within 2.0%.

Session 2pPAg

Physical Acoustics: Photoacoustics II (Poster Session)

Gerald Diebold, Cochair
Brown Univ.

Christ Glorieux, Cochair
Lab. ATF, Katholieke Universiteit Leuven

All posters will be on display from 3:40 p.m. to 5:20 p.m. To allow contributors an opportunity to see other posters, contributors of odd-numbered papers will be at their posters from 3:40 p.m. to 4:30 p.m. and contributors of even-numbered papers will be at their posters from 4:30 p.m. to 5:20 p.m.

Contributed Papers

2pPAg1. Fiber Bragg grating applied pulsed photoacoustic detection technique for online monitoring concentration of liquid. Atsushi Yarai (Osaka Sangyo University, 3-1-1 Nakagaito, 574-8530 Daito, Osaka, Japan, yarai@osaka-sandai.ac.jp), Takuji Nakanishi (Osaka Sangyo University, 3-1-1 Nakagaito, 574-8530 Daito, Osaka, Japan, a.yarai@ieee.org)

The need for real-time monitoring of the concentration of raw liquids and wastewater flowing in ducts is one of the significant process controls in chemical plants. A concentration sensor applicable to acidic fluids, however, has not been practically developed because of the maintenance required to sustain performance due to the metal erosion of the electrode from the acidity. To overcome this problem, we propose the fiber Bragg grating applied pulsed photoacoustic (PA) detection technique for online monitoring concentration of liquid. In our technique, optical fiber made of quartz is used for the PA signal generation and detection, for which a 0.6-mm-diameter step index fiber and Bragg grating composed of single mode fiber are used as an object, respectively, so that our metal-free sensor head is not only of small size but is also maintenance-free. The concentration of dye (Rhodamine 6G) dissolved into distilled water was measured to estimate the capability. A Q-switched frequency doubled Nd:YAG laser was used as the PA exiting beam, which is fed to the PA sensor through the fiber. It was experimentally confirmed that the detection linearity was significantly obtained in a concentration range from a few ppm to approximately 200 ppm.

2pPAg2. Film thickness determination by laser ultrasonics. Michaël Lemaire (Institut d'Electronique de Microélectronique et de Nanotechnologie, Département Opto-Acousto-Electronique (UMR CNRS 8520), Université de Valenciennes et du Hainaut-Cambrésis, Le Mont-Houy, 59313 Valenciennes cedex 9, France, Michael.Lemaire@meletu.univ-valenciennes.fr), Frédéric Jenot (Institut d'Electronique de Microélectronique et de Nanotechnologie, Département Opto-Acousto-Electronique (UMR CNRS 8520), Université de Valenciennes et du Hainaut-Cambrésis, Le Mont-Houy, 59313 Valenciennes cedex 9, France, frederic.jenot@univ-valenciennes.fr), Mohammadi Ouaftouh (Institut d'Electronique de Microélectronique et de Nanotechnologie, Département Opto-Acousto-Electronique (UMR CNRS 8520), Université de Valenciennes et du Hainaut-Cambrésis, Le Mont-Houy, 59313 Valenciennes cedex 9, France, mohammadi.ouaftouh@univ-valenciennes.fr), Wei Jiang Xu (Institut d'Electronique de Microélectronique et de Nanotechnologie, Département Opto-Acousto-Electronique (UMR CNRS 8520), Université de Valenciennes et du Hainaut-Cambrésis, Le Mont-Houy, 59313 Valenciennes cedex 9, France, weijiang.xu@univ-valenciennes.fr), Marc Duquennoy (Institut d'Electronique de Microélectronique et de Nanotechnologie, Département Opto-Acousto-Electronique (UMR CNRS 8520), Université de Valenciennes et du Hainaut-Cambrésis, Le Mont-Houy, 59313 Valenciennes cedex 9, France, Marc.Duquennoy@univ-valenciennes.fr), Mohamed Ourak (Institut d'Electronique de Microélectronique et de Nanotechnologie, Département Opto-Acousto-Electronique (UMR CNRS 8520), Université de Valenciennes et du Hainaut-Cambrésis, Le Mont-Houy, 59313 Valenciennes cedex 9, France, Mohamed.Ourak@univ-valenciennes.fr), Renaud Côte (Lab. ATF, Katholieke Universiteit Leuven, Celestijnenlaan 200D, B-3001 Leuven, Belgium, renaud.cote@fys.kuleuven.be), Robbe Salenbien (Lab. ATF, Katholieke Universiteit Leuven, Celestijnenlaan 200D, B-3001 Leuven, Belgium, robbe.salenbien@fys.kuleuven.be), Bart Sarens (Laboratorium voor Akoestiek en Thermische Fysica - Departement Natuurkunde en Sterrenkunde - Katholieke Universiteit Leuven, Celestijnenlaan 200D, B-3001 Leuven, Belgium, bart.sarens@fys.kuleuven.be), Walter Lauriks (Lab. ATF, Katholieke Universiteit Leuven, Celestijnenlaan 200D, B-3001 Leuven, Belgium, Walter.Lauriks@fys.kuleuven.be), Christ Glorieux (Lab. ATF, Katholieke Universiteit Leuven, Celestijnenlaan 200D, B-3001 Leuven, Belgium, christ.glorieux@fys.kuleuven.be)

The thickness of films deposited on substrates is crucial for their thermal, electrical, optical behaviour. These properties are essential in thin film applications, especially in the field of microelectronics. In this study, we are interested in thickness determination of silver and gold films deposited by evaporation on a silicon substrate by using an ultrasonic non-destructive technique. In particular, the well-known laser ultrasonic technique is used to generate and detect the surface acoustic waves. Results obtained by two complementary methods allowing a non-contact measurement in a large bandwidth (from 5 MHz to 200 MHz) are presented, and the dispersion of the Rayleigh wave propagation velocity is analyzed to determine the film thickness.

2pPAg3. Photoacoustic metrology of nanoimprint polymers. Timothy Kehoe (Tyndall National Institute, Lee Maltings, University College Cork, Prospect Row, Cork, Ireland, tim.kehoe@tyndall.ie), Juerg Bryner (ETH Zurich, Institute of Mechanical Systems, Dept. of Mechanical and Process Engineering, CH 8092 Zurich, Switzerland, bryner@imes.mavt.ethz.ch), Jacqueline Vollmann (ETH Zurich, Institute of Mechanical Systems, Dept. of Mechanical and Process Engineering, CH 8092 Zurich, Switzerland, vollmann@imes.mavt.ethz.ch), Clivia Sotomayor Torres (Tyndall National Institute, Lee Maltings, University College Cork, Prospect Row, Cork, Ireland, clivia.sotomayor@tyndall.ie), Laurent Aebi (ETH Zurich, Institute of Mechanical Systems, Dept. of Mechanical and Process Engineering, CH 8092 Zurich, Switzerland, aebi@imes.mavt.ethz.ch), Juerg

Dual(ETH Zurich, Institute of Mechanical Systems, Dept. of Mechanical and Process Engineering, CH 8092 Zurich, Switzerland, juerg.dual@imes.mavt.ethz.ch)

Nanoimprint lithography (NIL) is an alternative lithography method for patterning of thin polymer films using a rigid stamp, which is being developed as desired minimum feature sizes reduce to the scale of tens of nanometres. To characterise nanoimprinted structures, there is a need for more convenient and non-destructive wafer-scale metrologies to complement scanning electron microscopy and atomic force microscopy. The photoacoustic method, with a resolution in the range of 10 nm, and normally used to measure metal and dielectric layer thicknesses and physical properties, has been used for the first time to study nanoimprinting polymer layers. A good signal was obtained from the top and the bottom interfaces of two polymers, mr-I PMMA 75k300 and mr-NIL 6000.3, with thicknesses ranging from 100 to 500 nm. From the measured time of flight of the acoustic wave, and modelling physical parameters of the polymers, thicknesses calculated agree well with those measured by profilometry. The measurements are performed on a short pulse laser pump-probe setup, where bulk wave packets are excited and detected using near infrared laser pulses of less than 100 fs duration. The entire experimental setup is also simulated numerically.

2pPAg4. Line-focus beam photoacoustic imaging of surface and undersurface defect simulated on a planar specimen. Tsutomu Hoshimiya (Tohoku Gakuin University, 13-1, Chuo 1, 985-8537 Tagajyo, Japan, tpth@tjcc.tohoku-gakuin.ac.jp), Mika Hatake-Yama (Tohoku Gakuin University, 13-1, Chuo 1, 985-8537 Tagajyo, Japan, hatakemail@yahoo.co.jp)

A theoretical formulation of photoacoustic (PA) imaging with a line-focus beam (LFB) for surface and undersurface simulated defect was performed. Equivalence between 2D surface defect photoacoustic tomography (PAT) and X-ray CT was derived. PAT imaging experiment was carried out A second harmonics of a LD-pumped YAG laser was used as a LFB. The laser power was 45mW. The length and width of a laser beam on a specimen was 25 mm times 0.65mm The measured area was 27mm x 27mm, while the reconstructed area was 18mm x 18mm. 64 times 64 resolution image was reconstructed from the rotation and translation scanning. Reconstructed PA image agreed with the PA image obtained with a point-focus PA imaging. The frequency dependence of thermally diffused image agreed well with the theoretical prediction (thermal diffusion length is inversely proportional to the square root of modulation frequency) Under surface PAT image was obtained by a thermal wave diffraction formula, and the simulated image agreed well with the experimental data.

2pPAg5. Generation of Acoustic Wavelength Shorter Than 10nm By Means Of Nonlinear Acoustic. Shuo Zhang (INSP - UMR 7588 CNRS & Université Pierre et Marie Curie, 140 Rue de Lourmel, 75015 Paris, France, Shuo.Zhang@insp.jussieu.fr), Emmanuel Péronne (INSP - UMR 7588 CNRS & Université Pierre et Marie Curie, 140 Rue de Lourmel, 75015 Paris, France, emmanuel.peronne@insp.jussieu.fr), Laurent Belliard (INSP - UMR 7588 CNRS & Université Pierre et Marie Curie, 140 Rue de Lourmel, 75015 Paris, France, lbelliar@ccr.jussieu.fr), Bernard Perrin (INSP - UMR 7588 CNRS & Université Pierre et Marie Curie, 140 Rue de Lourmel, 75015 Paris, France, bernard.perrin@insp.jussieu.fr)

As the size of the structure decrease toward the nanoscale, their acoustic properties get closer to the THz range. Traditional techniques based on piezoelectric transducer or the Brillouin diffusion can hardly reach the adequate frequency range. However, if we tightly focus short optical pulses, we can expect to generate high frequencies due to nonlinear effect during the propagation of the acoustic pulses. Moreover, such small source could be used to image buried structures. We have developed an pump-probe experiment based on a Ti:Sa oscillator using microscope objectives and 2 axis displacement stage to study nonlinear propagation and diffraction of acoustic wave in 3 dimension. We have studied 356-μm thick GaAs substrate and have demonstrated the generation of acoustic longitudinal wavelength as short as 10 nm. Due to the acoustic dispersion during the propagation, acoustic solitons are observed for high excitation power. Thanks to the use of interferometric detector, the acoustic pulses are characterized in great details. Such experimental development can help us to study the properties of transmission and reflection of buried nanosystem such as single quantum well or phonon nanocavities.

2pPAg6. The theoretical analyse of the surface acoustic waves propagated on the surface of the bulk materials with subsurface defect. Xiaodong Xu (Modern Acoustics, Institute of Acoustics, Nanjing University, 210093 Nanjing, China, xdxu@nju.edu.cn), Ran Ding (Nanjing University, P.O.Box44#, Pukou Campus, 210089 Nanjing, China, snail_dr@hotmail.com), Christ Glorieux (Lab. ATF, Katholieke Universiteit Leuven, Celestijnenlaan 200D, B-3001 Leuven, Belgium, christ.glorieux@fys.kuleuven.be), Xiaojun Liu (Modern Acoustics, Institute of Acoustics, Nanjing University, 210093 Nanjing, China, xjliu@nju.edu.cn)

A theoretical model based on finite element method is used to analyse the properties of surface acoustic wave (SAW) propagated on the surface of the bulk materials with subsurface defect. The simulation results reveal the modes conversion between SAW and Lamb wave at the border of the defect and explain the diffusion properties of SAW propagated on the bulk material with subsurface defect. The modes conversion and wave reflection at the border of the defect are theoretically explained why there are a lot of riffles after the SAW passed through Al sample with circle subsurface defect, which detected by laser ultrasonic method. The relationships between the wavelength of wave and the physical state of the defect in the bulk material are also fully described in theoretical simulation.

2pPAg7. LED-based Stroboscopic Schlieren System. Kalle Hanhijärvi (Electronics Research Unit, University of Helsinki, P.O.Box 64 (Gustaf Hällströmin katu 2), FIN-00014 Helsinki, Finland, kalle.hanhijarvi@helsinki.fi), Ivan Kassamakov (Electronics Research Unit, University of Helsinki, P.O.Box 64 (Gustaf Hällströmin katu 2), FIN-00014 Helsinki, Finland, ivan.kassamakov@helsinki.fi), Juha Aaltonen (Electronics Research Unit, University of Helsinki, P.O.Box 64 (Gustaf Hällströmin katu 2), FIN-00014 Helsinki, Finland, juha.aaltonen@helsinki.fi), Edward Hæggström (Electronics Research Unit, University of Helsinki, P.O.Box 64 (Gustaf Hällströmin katu 2), FIN-00014 Helsinki, Finland, edward.haeggstrom@helsinki.fi)

A stroboscopic Schlieren system is proposed to characterize acoustic fields in transparent media. Schlieren imaging has been used to visualize beam profiles of ultrasonic transducers mostly in liquids. The method is sensitive to gradients in refractive index, and can thus be used with solids and fluids. A stroboscopic illumination synchronized with the ultrasonic vibration (controllable phase delay between the illumination and the ultrasonic drive signal), allows obtaining an image of a propagating tone burst. An LED source provides relatively fast response time for high measurement bandwidth. Incoherent light doesn't suffer from unwanted interference, as with laser sources. Our setup employs two 90° off-axis parabolic mirrors. Non-reflected light is blocked with spatial filtering which is achieved with a knife-edge, placed at the focal point of the focusing mirror. We first present a time-averaged Schlieren image of the acoustic field of a 7.5 MHz focusing transducer, as a proof-of-principle result. Then a custom-built LED-based stroboscopic illumination system is used to visualize wave propagation in water emitted by a high power 20 kHz transducer. Schlieren imaging is useful in applications, where non-contact characterization of acoustic fields is necessary.

2pPAg8. Stroboscopic White Light Interferometry for Dynamic Characterization of Capacitive Pressure Sensors. Ivan Kassamakov (Electronics Research Unit, University of Helsinki, P.O.Box 64 (Gustaf Hällströmin katu 2), FIN-00014 Helsinki, Finland, ivan.kassamakov@helsinki.fi), Kalle Hanhijärvi (Electronics Research Unit, University of Helsinki, P.O.Box 64 (Gustaf Hällströmin katu 2), FIN-00014 Helsinki, Finland, kalle.hanhijarvi@helsinki.fi), Juha Aaltonen (Electronics Research Unit, University of Helsinki, P.O.Box 64

(Gustaf Hällströmin katu 2), FIN-00014 Helsinki, Finland, juha.aaltonen@helsinki.fi), Lauri Sainiemi (Micro and Nanosciences Laboratory, Helsinki University of Technology, P.O.Box 3500, FI-02015 TKK, Finland, lauri.sainiemi@tkk.fi), Kestutis Grigoras (Micro and Nanosciences Laboratory, Helsinki University of Technology, P.O.Box 3500, FI-02015 TKK, Finland, kestas.grigoras@tkk.fi), Sami Franssila (Micro and Nanosciences Laboratory, Helsinki University of Technology, P.O.Box 3500, FI-02015 TKK, Finland, sami.franssila@tkk.fi), Anu Kärkkäinen (VTT Technical Research Centre of Finland, P.O.Box 1000, FIN-02044 VTT, Finland, anu.karkkainen@vtt.fi), Edward Hæggström (Electronics Research Unit, University of Helsinki, P.O.Box 64 (Gustaf Hällströmin katu 2), FIN-00014 Helsinki, Finland, edward .haeggstrom@helsinki.fi)

Scanning white light interferometry (SWLI) is a well-established method for accurate static out-of-plane 3-D profiling of micromechanical devices. Periodic displacement can be measured using stroboscopic illumination synchronized to an arbitrary phase angle of the sample oscillation. We modified an existing SWLI setup for dynamic MEMS characterization. A two-channel function generator drives the sample and the stroboscopic illumination, and controls the inter-channel phase. A phosphorous white light LED or single-color LED is used as light source. Currently our shortest stroboscopic pulse is 50 ns. We measured the out-of-plane displacement of a thermal microbridge fabricated on SOI wafer with 20 nm accuracy. The microbridge was driven with sinusoidal and square wave signals (1 Hz - 960 Hz). The stroboscopic duty cycles were 0.1% - 5%. We also characterize the vibration modes of the membrane of a capacitive pressure sensor. Stroboscopic SWLI is useful for nanoscale profile measurements of periodic oscillations.

2pPAg9. Laser-generated narrow-band ultrasonic wave for detection of subsurface defect. Ran Ding (Nanjing University, P.O.Box44#, Pukou Campus, 210089 Nanjing, China, snail_dr@hotmail.com), Xiaodong Xu (Modern Acoustics, Institute of Acoustics, Nanjing University, 210093 Nanjing, China, xdxu@nju.edu.cn)

Laser ultrasonics employs laser beams to excite ultrasound. Spatial and/or temporal modulated intensity of laser on the surface of the specimen (aluminum) can serve to narrow the band of the generated ultrasound around the desired central frequency and meanwhile obtains higher signal-noise ratio. In the present work, we use Computer Generated Holograms (CGHs) to spatial-modulate the laser beam. CGHs provide flexibility of adjustment of the intensity profile of the laser on the specimen and the online reconstruction of CGHs by digital and electronic devices helps to reduce the complexity of the experimental system and is promising in detection of subsurface defect and depth profiling as the surface acoustic waves penetrate into the solids a depth proportional to the wavelength. Discussion was carried out between experimental results and a theoretical model which based on finite element analysis.

2pPAg10. Laser-Ultrasonic Measurement of Stress in Metal. Aleksei Podolsky (Moscow State University, MSU, 1, building 2, GSP-2, Leninskiye Gory, 119992 Moscow, Russian Federation, uzh@yandex .ru), Vladimir Koshkin (Moscow State University, MSU, 1, building 2, GSP-2, Leninskiye Gory, 119992 Moscow, Russian Federation, uzh@ya.ru), Viktor Bel'Ko (Moscow State University, MSU, 1, building 2, GSP-2, Leninskiye Gory, 119992 Moscow, Russian Federation, uzh@ya.ru), Andrei Fetisov (Moscow State University, MSU, 1, building 2, GSP-2, Leninskiye Gory, 119992 Moscow, Russian Federation, uzh@ya.ru), Alexander Karabutov (Moscow State University, MSU, 1, building 2, GSP-2, Leninskiye Gory, 119992 Moscow, Russian Federation, akarabutov@gmail.com)

Stress in metal was investigated by acousto-elastic effect. The dependence of longitudinal ultrasonic wave velocity on transverse stress was considered. A laser-ultrasonic defectoscope was used for precise ultrasonic velocity measurement. Optoacoustic transducer provides laser excitation and piezoelectric wide-band detection of ultrasonic pulse. The accuracy of the measurement exceeded 0.1% for 2 mm thick metal sample. Samples in the form of plates with the thickness of 2 to 4 mm made of aluminum and titanium alloys and stainless steel were tested. The samples were loaded quasistatically, the load was changing from zero to yield point stress. Load, deformation and velocity of ultrasound were measured. It is shown that the velocity changes significantly with the load. Some features of the velocity change under tensile stress are presented. The possibility of the local residual stress measurement with the laser-ultrasonic technology is discussed.

2pPAg11. Application of nonlinear laser photoacoustic technique to crack detection. Jacek Zakrzewski (LPEC/UMR 6087/CNRS/Université du Maine, Avenue Olivier Messiaen, 72085 Le Mans Cedex 09, France, jzakrzew@fizyka.umk.pl), Nikolay Chigarev (LPEC/UMR 6087/CNRS/Université du Maine, Avenue Olivier Messiaen, 72085 Le Mans Cedex 09, France, Nikolay.Chigarev@univ-lemans.fr), Vincent Tournat (LPEC/UMR 6087/CNRS/Université du Maine, Avenue Olivier Messiaen, 72085 Le Mans Cedex 09, France, vincent.tournat@univ-lemans .fr), Denis Mounier (LPEC/UMR 6087/CNRS/Université du Maine, Avenue Olivier Messiaen, 72085 Le Mans Cedex 09, France, denis.mounier@univ-lemans.fr), Vitali Gusev (LPEC/UMR 6087/CNRS/Université du Maine, Avenue Olivier Messiaen, 72085 Le Mans Cedex 09, France, vitali.goussev@univ-lemans.fr)

Nonlinear acoustics is a promising method for non-destructive testing (NDT) as it allows to improve the sensitivity and contrast of defects detection. The application of contactless laser photoacoustic technique for the tasks of nonlinear acoustics looks very promising. Meanwhile, real examples of industrial systems using nonlinear photoacoustics are still absent. In this work nonlinear photoacoustic response of artificially prepared cracks has been studied. Acoustic vibrations have been excited through the loASAHGRcal heating caused by the absorption of a focused beam of visible or near-infrared laser radiation. Several methods have been applied for the detection of surface displacement including piezo-transducers, air-coupled transducers and optical laser interferometry. It has been shown, that nonlinear acoustic response increases drastically when both pump and probe points are localized near the crack. For this reason, the last two methods allowing local probing look very promising. Two dimensional scans of generation and detection points on the sample surface could be used to obtain the images of crack at new spectral components induced by crack nonlinearity. The goal of this work is to find optimal methods of the excitation and detection of nonlinear photoacoustic response of the crack. It should make the technique attractive for the industrial applications.

2pPAg12. Looking for shear waves in glass forming liquids. Thomas Pezeril (Massachusetts Institute of Technology, 77 Mass. Avenue, room 6-026, Cambridge, MA 02215, USA, pezeril@mit.edu), Christoph Klieber (Massachusetts Institute of Technology, 77 Mass. Avenue, room 6-026, Cambridge, MA 02215, USA, cklieber@mit.edu), Stephane Andrieu (Laboratoire de Physique des Matériaux UMR7556, Université H. Poincaré/Nancy I, 54506 Vandoeuvre, France, stephane.andrieu@lpm .u-nancy.fr), Keith Nelson (Massachusetts Institute of Technology, 77 Mass. Avenue, room 6-026, Cambridge, MA 02215, USA, kanelson@mit .edu)

The ability of the generation of picosecond shear acoustic pulses in solids using ultrashort optical pulses have been employed to look for high frequency shear waves in glass forming liquids. As a transducer we used a canted iron thin film deposited on a glass substrate. The strong shear efficiency of generation provided by this kind of samples allowed the study of several glass forming liquids. As a first try, we have detected shear brillouin scattering in m-toludine at 100K, that is below the glass transition temperature, at a frequency of 9 GHz. Then, we observed shear waves propagating at room temperature in glycerol at frequencies below 50 GHz.

Session 2pPAh

Physical Acoustics and Signal Processing in Acoustics: Acoustic Landmine Detection II (Poster Session)

James Sabatier, Cochair
University of Mississippi

Keith Attenborough, Cochair
Open University

All posters will be on display from 3:40 p.m. to 5:20 p.m. To allow contributors an opportunity to see other posters, contributors of odd-numbered papers will be at their posters from 3:40 p.m. to 4:30 p.m. and contributors of even-numbered papers will be at their posters from 4:30 p.m. to 5:20 p.m.

Contributed Papers

2pPAh1. Vector surface velocity measurement using contour scanning laser vibrometers for the detection of landmines. Patrick F. O'Malley (Catholic University, 620 Michigan Ave, Washington, DC 20064, USA, 68omalley@cua.edu), Woods J. Teresa (Catholic University, 620 Michigan Ave, Washington, DC 20064, USA, 59woods@cua.edu), Joseph F. Vignola (Catholic University, 620 Michigan Ave, Washington, DC 20064, USA, vignola@cua.edu), John A. Judge (Catholic University, 620 Michigan Ave, Washington, DC 20064, USA, judge@cua.edu), Jacek Jarzynski (Catholic University, 620 Michigan Ave, Washington, DC 20064, USA, jjarzynski@comcast.net)

Much work has been done studying the detection of buried landmines using acoustic excitation and measuring the vibration response of the ground using Laser Doppler Vibrometry (LDV). We examine the benefits of measuring the full three-dimensional velocity response of the ground surface when a landmine is present. Three-dimensional velocity measurements provide a richer data set for identification of buried targets and avoid potential errors associated with projecting the surface velocity vector onto a single laser line of sight direction. We present results of a study conducted using landmines buried in sand in a laboratory environment. The data were obtained using a novel five-axis laser vibrometry system, which uses a single point LDV system to measure the surface of the sand from multiple angles at each measurement location. Data will be presented showing the consequences of a buried landmine on the three-dimensional velocity response of a contoured ground surface.

2pPAh2. Scattering of a buried circular membrane imbedded in a rigid substrate in a layered fluid waveguide. Michelle B. Mattingly (Physics Dept., United States Naval Academy, Chauvenet Hall Room 295, 572 C Holloway Road, Annapolis, MD 21402, USA, mini_matisick@hotmail.com) , James L. Buchanan (Mathematics Dept., United States Naval Academy, 572 C Holloway Road, Annapolis, MD 21402, USA, jlb@usna.edu), Reza Malek-Madani (Mathematics Dept., United States Naval Academy, 572 C Holloway Road, Annapolis, MD 21402, USA, mm@usna.edu), Murray S. Korman (Physics Dept., United States Naval Academy, Chauvenet Hall Room 295, 572 C Holloway Road, Annapolis, MD 21402, USA, korman @usna.edu)

A study of mathematical modeling of the buried landmine detection problem involves wave propagation in a layered waveguide in the presence of a flush mount buried circular target. In this study, emphasis is placed on acoustic to seismic coupling of an airborne CW point source located over an iso-velocity fluid layer. The top plate of the buried landmine is modeled as a circular elastic membrane stretched flush over a cylindrical cavity in a rigid substrate beneath the fluid layer. The finite fluid layer affords a manageable study of the modal resonances in the waveguide system with and without the target. The Helmholtz equation is solved in the atmospheric layer using cylindrical coordinates and a point source. The homogeneous Helmholtz equation is used in the fluid layer. Green's function techniques involving vibrations of the membrane are incorporated into the boundary conditions. Results of the closed form normal mode solution will be presented in a MATLAB™ user interface; describing the effects of frequency, depth, density, sound, absorption, including radius and elastic parameters of the membrane. Comparison of the results (involving the fluid surface particle velocity profiles across the target) will be made with experiments reported in the literature to evaluate its usefulness.

2pPAh3. Nonlinear scattering of a surface wave by an object buried in soil. Evgenia A. Zabolotskaya (Applied Research Laboratories, The University of Texas, P.O. Box 8029, Austin, TX 78713-8029, USA, zhenia@arlut.utexas.edu), Yurii A. Ilinskii (Applied Research Laboratories, The University of Texas, P.O. Box 8029, Austin, TX 78713-8029, USA, yura@arlut.utexas.edu), Mark F. Hamilton (Applied Research Laboratories, The University of Texas, P.O. Box 8029, Austin, TX 78713-8029, USA, hamilton@mail.utexas.edu)

Nonlinear scattering of a surface wave by an object buried in soil is investigated theoretically. The object is supposed to be excited by a monochromatic seismic wave and its pulsations are considered to be nonlinear. Specific features of soil are taken into account, namely, shear modulus less than compressibility modulus and anomalously high nonlinearity. Two analytical approaches are applied. One is based on theory of elasticity and the other is based on fluid mechanics. The two approaches yield identical results for the second harmonic in the scattered field. The second harmonic is evaluated in the near field where the medium can be considered as incompressible. The analysis is performed with perturbation theory for small displacement amplitudes in the soil. The second harmonic is also investigated with an asymptotic expression obtained from the general equation for the second harmonic generated by a pulsating object in a compressible medium. The equation is expanded for a small object at distances that are small compared with a wavelength. The influence of a stress-free boundary on the scattered field is evaluated using Green's functions. [Work supported by ONR.]

2pPAh4. Numerical simulations of resonant granular layers. Joseph A. Turner (University of Nebraska, Dept. of Engineering Mechanics, W317.4 NH, Lincoln, NE 68588, USA, jaturner@unl.edu), Florin Bobaru (University of Nebraska, Dept. of Engineering Mechanics, W317.4

NH, Lincoln, NE 68588, USA, fbobaru2@unl.edu),Kitti Rattanadit (University of Nebraska, Dept. of Engineering Mechanics, W317.4 NH, Lincoln, NE 68588, USA, kittir@bigred.unl.edu)

A coupled Discrete Element Method-Finite Element Method (DEM-FEM) model is developed and implemented for simulating the dynamic response of a dry granular layer on top of an elastic beam. The implementation is first validated against the quasi-static results for spherical particles which are compared with well-bonded effective-medium models. In the dynamic regime however, the effective-medium analytical result differs from experimental values in terms of the dependence of particle size. The simulations developed are used to understand the discrepancy between the theory and the experiments. The first resonance of the system is examined with respect to particle size using a variety of particle sizes and a frequency sweep input. The particle size dependence observed experimentally is reproduced in the simulations only through inclusion of cohesive forces between the particles. Rolling resistance and friction between particle is shown to be of minor importance. This new modeling tool offers promise for understanding the dynamic interactions of granular materials. [Work supported by ARL]

Session 2pPAi

Physical Acoustics: Nonlinear Acoustics of Unconsolidated Granular Media II (Poster Session)

Paul Johnson, Cochair
EES-11 (Geophysics) - Los Alamos National Laboratory

Vitali Gusev, Cochair
LPEC/UMR 6087/CNRS/Université du Maine

All posters will be on display from 3:40 p.m. to 5:20 p.m. To allow contributors an opportunity to see other posters, contributors of odd-numbered papers will be at their posters from 3:40 p.m. to 4:30 p.m. and contributors of even-numbered papers will be at their posters from 4:30 p.m. to 5:20 p.m.

Contributed Papers

2pPAi1. Low-frequency acoustoelasticity in glass beads saturated with water using a nonlinear wave-coupling technique. Guillaume Renaud (LUSSI, 10 Bd Tonellé, 37032 Tours, France, guillaume.renaud28@etu.univ-tours.fr), Samuel Callé (LUSSI, 10 Bd Tonellé, 37032 Tours, France, calle_s@med.univ-tours.fr), Jean-Pierre Remenieras (LUSSI, 10 Bd Tonellé, 37032 Tours, France, remenier@med.univ-tours.fr), Marielle Defontaine (LUSSI, 10 Bd Tonellé, 37032 Tours, France, defontai@med.univ-tours.fr)

To study ″non-classical″ acoustical nonlinearities in cracked materials, we developed a nonlinear (NL) wave coupling technique. Propagation velocity and amplitude of short high-frequency (HF, 600 kHz) bursts are modulated as result of nonlinear interaction with a low-frequency (LF, 3 kHz) wave. Time Of Flight Modulation (TOFM) is indeed related to both elasticity and density variations. Because high acoustic nonlinearities in glass beads have been reported, we applied our technique to glass beads with different diameters (hundreds micrometers). A small container is filled up with glass beads saturated with water and placed below the LF source. The large HF to LF ratio (200) and the small sample size (6 cm) compared to the LF wavelength in water (50 cm) allow: 1) to measure instantaneous Time Of Flight Modulation (TOFM) and attenuation as functions of the instantaneous LF pressure, 2) to consider the LF pressure field a quasi-static hydrostatic variation of the ambient pressure in the medium. The LF pressure amplitude in water is approximately 10 kPa. Different TOFM and NL attenuation behaviors in tension and in compression, as well as different hysteresis patterns, are observed. The influence of the LF pressure amplitude is discussed.

2pPAi2. Sound in a linear array of magnetic spheres. J. Carlos Ruiz-Suarez (CINVESTAV-IPN, Antigua Carretera a Progreso Km 6, 97310 Merida, Mexico, cruiz@mda.cinvestav.mx), Florent Malloggi (PMMH-ESPCI Paris, 10 Rue Vaquelin, 75005 Paris, France, F.G.J.Malloggi@tnw.utwente.nl),Osvaldo Carvente(CINVESTAV-IPN, Antigua Carretera a Progreso Km 6, 97310 Merida, Mexico, ocarven@yahoo.com.mx), Jose Cruz-Damas (CINVESTAV-IPN, Antigua Carretera a Progreso Km 6, 97310 Merida, Mexico, josia.damas@gmail.com), Felipe Pacheco (CINVESTAV-IPN, Antigua Carretera a Progreso Km 6, 97310 Merida, Mexico, fpacheco@mda.cinvestav.mx)

We study the propagation of sound in a chain of strongly magnetized spheres. The strong dipole-dipole magnetic force allows us to hold the chain in different positions to evaluate the effect gravity produces on sound transmission. This strong cohesion permits us also to insert in the chain a periodical array of impurities and study the effect this array has in the transmission. A well defined gap of frequencies, where no sound propagation exists, is observed. We investigate as well square lattices, and look into the effects dipole anisotropy causes to sound propagation. Finally, we study the effects produced by vacancies.

2pPAi3. Linear and non linear acoustic waves in macroscopically inhomogeneous unconsolidated granular crystals. Aurélien Merkel (LPEC/UMR 6087/CNRS/Université du Maine, Avenue Olivier Messiaen, 72085 Le Mans Cedex 09, France, aurelien.merkel.etu@univ-lemans.fr), Xavier Jacob (LPEC/UMR 6087/CNRS/Université du Maine, Avenue Olivier Messiaen, 72085 Le Mans Cedex 09, France, xavier.jacob@univ-lemans.fr), Vincent Tournat (LPEC/UMR 6087/CNRS/Université du Maine, Avenue Olivier Messiaen, 72085 Le Mans Cedex 09, France, vincent.tournat@univ-lemans.fr), Vitali Gusev (LPEC/UMR 6087/CNRS/Université du Maine, Avenue Olivier Messiaen, 72085 Le Mans Cedex 09, France, vitali.goussev@univ-lemans.fr)

Ordered unconsolidated structure of spherical beads in the absence of external loading except the gravity field constitutes a macroscopically inhomogeneous and strongly nonlinear phononic crystal. We report the experimental and theoretical investigation of linear and nonlinear acoustic phenomena in these granular crystals of finite thickness along the gravity

direction. In particular the dependence of the resonance frequencies on the thickness of the crystal (the number of layers) is evaluated. The linear transmission of acoustic waves from the bottom to the free surface of the granular crystal exhibits complicated features. It is compared to the linear transmission through the same structure but with a macroscopically homogeneous static stress. Some frequency regions of the acoustic response function are shown to be insensitive to the transition from an inhomogeneous static stress (gravity induced) to a homogeneous one (additional external load). The nonlinear acoustic phenomena of resonance frequency shift and resonance curve broadening with increasing amplitude of acoustic oscillations are observed. It allows to measure the nonlinear parameters of the crystal for different amounts of layers, accounting for the absolute particle velocity amplitude detected at the free surface with a laser vibrometer. Corresponding theoretical models describing the acoustic eigenmodes in macroscopically homogeneous and inhomogeneous granular crystals are developed.

TUESDAY AFTERNOON, 1 JULY 2008 P3-A, LEVEL 3, 3:40 TO 5:20 P.M.

Session 2pPAj

Physical Acoustics: Nonlinear Acoustics in Earthquake Processes and Other Earth Processes II (Poster Session)

Paul Johnson, Cochair
EES-11 (Geophysics) - Los Alamos National Laboratory

Fabrice Cotton, Cochair
Université Joseph Fourier

All posters will be on display from 3:40 p.m. to 5:20 p.m. To allow contributors an opportunity to see other posters, contributors of odd-numbered papers will be at their posters from 3:40 p.m. to 4:30 p.m. and contributors of even-numbered papers will be at their posters from 4:30 p.m. to 5:20 p.m.

Contributed Papers

2pPAj1. Elastic-anisotropic properties of rocks along the Finnish Drill Hole (OKU) section in the depth range down to 1 km. Mikhail Kovalevskiy (Geological Institute of Kola Science Centre of Russian Academy of Sciences, 14, Fersman St., 184209 Apatity, Russian Federation, koval@geoksc.apatity.ru)

The Finnish drill hole OKU was drilled in the south-eastern Baltic Shield (Finland). The drill hole limiting depth is 2516m. The goal of investigations was determination of elastic and non-elastic characteristics of 14 rock samples taken within 1.0km depth. The determinations were done on the basis of the latest improvement of the acoustopolarization method with devices for determining elastic properties [1]. The study of the rock sample properties from the drill hole section showed that they are all elastic anisotropic and pertain to the transverse-isotropic and orthorhombic symmetry types. A slight change in the compression and shear wave velocities with depth can be observed. The effect of linear acoustic anisotropic absorption has been registered in the samples. The nature of this effect manifestation is related to the presence of microcracks of the natural character. The effect of depolarization of shear waves was registered in some samples which suggests the presence of the angular unconformity between the directions of the LAAA elements and elastic symmetry elements. The pattern of change in the anisotropy factors for compression and shear waves with depth is manifested in a similar way. REFERENCES 1. Gorbatsevich F.F. Acoustopolariscopy of rocks. Apatity, Acad. Sciences, 1995, 204 p.

2pPAj2. Generation and Evolution of Cavitation in Magma under Decompression Waves. Valeriy K. Kedrinskiy (Lavrentyev Institute of Hydrodynamics, Siberian Division of the Russian Academy of Sciences, Lavrentyev prospect 15, 630090 Novosibirsk, Russian Federation, kedr@hydro.nsc.ru), Maxim N. Davydov (Lavrentyev Institute of Hydrodynamics, Siberian Division of the Russian Academy of Sciences, Lavrentyev prospect 15, 630090 Novosibirsk, Russian Federation, davydov @hydro.nsc.ru)

It's considered that presence of the dissolved water (with concentration up to 5-7 % (wt.)) and viscosity of magma play one of the key roles in volcanic processes. According to the geophysical data, both a character and a structure of explosive volcano eruptions are defined by dynamics of cavitation development and the viscosity increasing orders during the diffusion of the dissolved gas from magma in bubbles. This paper represents a full system of the equations, including the kinetics of phase transitions, which allows us to describe dynamics of a magma melt state in a gravity field behind the front of a decompression wave. The problem is solved numerically, using a known expression for the nucleation frequency as a function of current concentration of gas dissolved in magmatic melt. The notion of diffusion zones which arise around cavitation nuclei is introduced. The latter allow us to define real density of cavitation kernels generated in an unit of magmatic melt volume as a result of phase transitions behind a rarefaction-wave front. The dynamics of the size distribution of cavitation bubbles along a magma-melt column (1km height) and also of the magma viscosity changing dynamically vs. a concentration of dissolved water are investigated. (RFBR 06-01-00317a financial support).

2pPAj3. Features of acoustic emission at various influences on rock samples. Alexander S. Voznesenskiy (Moscow State Mining University, Leninskiy Prospect 6, 119991 Moscow, Russian Federation, al48@mail.ru), Sergey V. Viljamov (Moscow State Mining University, Leninskiy Prospect 6, 119991 Moscow, Russian Federation, serjo@mail.ru)

In the report special features of acoustic emission (AE) in the rock samples during its deforming, loading, dissolving and heating are discussed. The AE-activity and spectral characteristics of AE at the frequency band from on 30 kHz up to 500 kHz versus time at various influence stages and forms are analyzed. For example the amplitudes at the frequencies 30-90 kHz during deforming of carnallite are higher than these ones during its

dissolving. It means the cracks at the deforming are about 4-10 mm and these ones at the dissolution are about 1-3 mm. These results can be used for the recognition of influence forms and stages.

2pPAj4. Formation of ripples on sand surface as result of nonlinear interaction of sound waves and wind drift particles. Nora A. Vilchinska (LAA-Latvian Acoustics Association, 3 Kurzemes pr, LV-1064 Riga, Latvia, vilcinska@hotmail.com)

The phenomenon speaks within the limits of nonlinear acoustics, considering it as amplification of surface acoustic waves (SAWs) by drift of carriers. Interaction and amplification of SAWs, borne from falling sand particles on dry sand surface and drift sand particles under wind action, is responsible for the first ripple forming on a dry sand flat surface. SAWs interact with drift sand particles in the moment, when the velocity of drift is equal to velocity of a sound propagation. The sound wave acts on drifting particles so that sand grains, a little bit advancing wave, will be braked, and lagging behind be accelerated. Particles will gather in a phase of a wave - take place grouping of particles and ripple forming. The distance between groups is a ripples wave length λ. Experimental in-situ are measured weak sound field on frequencies 25 Hz in just forming sand massif, and near surface velocity of sand drug under wind action. Measured ripples wave lengths λ are in good agreement with measured diapason of wind velocitys. Measurements were carried out on the sand beach of the gulf of Riga, Latvia. Theoretically the phenomenon speaks within the limits of nonlinear acoustics or within the limits of nonlinear mechanic.

2pPAj5. A numerical study of the onset of granular avalanches. Lydie Staron (Institut Jean le Rond d'Alembert, 4 place Jussieu, case 161-162, 75252 Paris Cedex 05, France, staron@lmm.jussieu.fr)

Granular media can either exist in a jammed state, in which their behaviour can be seen as solid-like, or they can exist in a dilute state and flow as a fluid would. In this contribution, we are interested in the mechanisms prevailing in the transition between solid-like and fluid-like behaviour, specifically in the case of the onset of granular avalanches. Therefore, discrete numerical simulations of granular flows are carried out. The focus is set on the analysis of the stick-slip dynamics preceeding the trigger of the avalanche; the existence of precursors to the flow, and their distribution in space and time will be investigated.

TUESDAY AFTERNOON, 1 JULY 2008 P3-A, LEVEL 3, 3:40 TO 5:20 P.M.

Session 2pPAk

Physical Acoustics: Sonic, Ultrasonic, and Megasonic Cleaning II (Poster Session)

Ralph Muehleisen, Cochair
Illinois Institute of Technology

Claus-Dieter Ohl, Cochair
University of Twente

All posters will be on display from 3:40 p.m. to 5:20 p.m. To allow contributors an opportunity to see other posters, contributors of odd-numbered papers will be at their posters from 3:40 p.m. to 4:30 p.m. and contributors of even-numbered papers will be at their posters from 4:30 p.m. to 5:20 p.m.

Contributed Paper

2pPAk1. Ultrasonic cleaning of submerged membranes for drinking water applications. Sonja Lauterborn (TU Darmstadt, Institut WAR, Petersenstraße 13, 64287 Darmstadt, Germany, s.lauterborn@iwar.tu-darmstadt.de), Wilhelm Urban (TU Darmstadt, Institut WAR, Petersenstraße 13, 64287 Darmstadt, Germany, w.urban@iwar.tu-darmstadt.de)

Ultrasonic cleaning of membranes used in water purification and waste water treatment is under investigation for avoiding fouling and scaling on the membranes. So far chemicals are used, but their use is under scrutinity for safety, waste removal and health issues. Chemicals often even do not solve the cleaning problem durably. For applications in the part of drinking water treatment it is necessary to ensure the filtered water is really clean. Therefore in the presented experiment the outflow is constantly controlled by turbidity measurements and by using a particle counter in an online system. A pilot plant for sonication of submerged membranes to produce drinking water from surface water was constructed and placed at the Rhine water works in Biebesheim. It could be shown that sonication with 130 kHz when backflushing the membranes only works with following air overflow. Then the permeability keeps high. No damage of the membranes occurs like often has been found in former studies. Only 30 seconds of sonication after 30 min of filtration are enough to keep high performance of the membranes. Thus energy demand is low, which is a pre-condition for an economical use in technical applications.

Session 2pPAl

Physical Acoustics: Mathematical and Numerical Methods II (Poster Session)

All posters will be on display from 3:40 p.m. to 5:20 p.m. To allow contributors an opportunity to see other posters, contributors of odd-numbered papers will be at their posters from 3:40 p.m. to 4:30 p.m. and contributors of even-numbered papers will be at their posters from 4:30 p.m. to 5:20 p.m.

Contributed Papers

2pPAl1. Finite element modelling of thermoviscous acoustics in closed cavities. Nicolas Joly (Laboratoire d'Acoustique de l'Université du Maine, Avenue Olivier Messiaen, 72085 Le Mans, France, nicolas.joly @univ-lemans.fr)

A numerical methodology is presented to compute the acoustic field in a closed domain filled by a thermoviscous fluid, using the finite element method. The formulation based upon temperature variation and particle velocity is well suited for both (i) modelling the acoustic, thermal and viscous effects in the fluid bulk and (ii) accounting for the non-slip and thermal boundary conditions on the solid. The set of coupled equations presents usual scalar- and vector- operators for finite element modelling. Due to the development of thin thermal- and viscous- boundary layers compared to the acoustic wavelength, very different scales are present in the computed fields: the finite-element mesh needs to be dramatically refined along the direction normal to the boundary, while a coarse mesh is often sufficient along the directions parallel to the boundary, and far from the boundaries. The optimised mesh is obtained iteratively, using a loop procedure computing (a) the thermoviscous solution, (b) the metric map suited for this field, and (c) the unstructured anisotropic adapted mesh based on this metric, until convergence. Results are presented for two-dimensional and axisymmetric three-dimensional applications, illustrating thermoviscous effects for various geometries of cavities.

2pPAl2. Wave propagation in stratified fluid flows: Application of the Stroh formalism to Lagrangian acoustic perturbations. Olivier Poncelet (LMP, UMR CNRS 5469, Université Bordeaux I, 351, cours de la Libération, 33405 Talence, France, o.poncelet@lmp.u-bordeaux1 .fr), Mélanie Ottenio (INRETS - Univ. Claude Bernard Lyon 1, UMR-T 9406, Laboratoire de Biomecanique et Mecanique des Chocs, 25, Avenue Francois Mitterand, 69675 Bron, France, melanie.ottenio@inrets.fr)

We consider the problem of harmonic waves propagating in non uniform fluid flows in presence of either solid interfaces (elastic walls), or jumps of mechanical properties or jumps of fluid convection-speed. The acoustic field is described by taking into account Lagrangian perturbations referred to an Eulerian frame related to the moving fluid. In contrast to the case of eulerian perturbations, the lagrangian description enables us to introduce the acoustical displacement in the problem and therefore to write the continuity conditions in a simple and unambiguous way: normal acoustical displacement is always continuous through an interface between either solids or (moving) fluids; the normal acoustical stress is also continuous in most of the practical cases (boundary layers, vibrating walls). We express the wave equation as an ordinary differential system by making use of the Stroh formalism from which analytical and semi-analytical results can be obtained for any arbitrary profile of the flow properties. This formalism, coupled with Peano-Neumann series expansion and Frobenius power series, enable us to compute modes dispersion in elastic ducts, and reflective properties of a mixing layer in between two fluids in relative motion. Some analytics on those problems is provided.

2pPAl3. Treatment of the asymptotic behaviour of the piezolectric Green's function for finite element/boundary element analysis of surface waveguides. Sylvain Ballandras (CNRS FEMTO-ST, 32 Avenue de l'Observatoire, 25044 Besançon, France, sylvain.ballandras@femto-st .fr), Michel Lenczner (CNRS FEMTO-ST, 32 Avenue de l'Observatoire, 25044 Besançon, France, michel.lenczner@femto-st.fr), Thierry Larroche (CNRS FEMTO-ST, 32 Avenue de l'Observatoire, 25044 Besançon, France, thierry.larroche@femto-st.fr)

The simulation of surface waveguides has been dramatically improved by the combination of analytic description of piezoelectric materials using surface Green's function and numerical approaches sur as plane wave expansion, finite diffrence, finite element, etc. A lot of work has been dedicated to treat the singularities of such Green's function generally derived in the spectral domain. An interesting approach consists in using the Green's function which relates the surface stresses to the displacements which is particularly well-suited for mixed finite element/boundary element formulations. This Green's function does not exhibit any pole but presents an asymptotic behavior which tends to infinity along increasing wavenumber values, which prevents the computation of its Fourier transform. In this work, we show how this difficulty can be overcome and we propose a formulation in which the Green's function is factorized in order to change its asymptotic behaviour to a form allowing for Fourier transform computation for non periodic problems and an analytic treatment of its asymptotic behaviour for the simulation of periodic structures. Examples are provided to show the interest of the proposed approach in terms of computation delays and precision.

2pPAl4. 'Maxwellian' macroscopic acoustics and acoustic metamaterials. Denis Lafarge (Laboratoire d'Acoustique de l'Université du Maine, Avenue Olivier Messiaen, 72085 Le Mans, France, denis.lafarge@univ-lemans.fr), Aroune Duclos (Laboratoire d'Acoustique de l'Université du Maine, Avenue Olivier Messiaen, 72085 Le Mans, France, aroune.duclos@univ-lemans.fr)

For electromagnetic wave propagation it was found that there exist composite media exhibiting strong spatial dispersion. This has raised the question of the relevance of the spatial dispersion in the characterization of the new metamaterials. The present communication intends to show that exactly the same problematic occurs in acoustics when considering long-wavelength acoustic wave propagation in a fluid in presence of solid obstacles of any arbitrary shape. When these obstacles resemble ″Helmholtz″ resonators the macroscopic equivalent medium may exhibit strong spatial dispersion. It is demonstrated that the corresponding Macroscopic Acoustics, which may be worked out in detail, is very similar to the general nonlocal Maxwellian Macroscopic Electrodynamics. This raises the question of the relevance of the spatial dispersion in the characterisation of porous materials, and specifically the question of the possible design of acoustic metamaterials exhibiting enhanced absorption due to spatial dispersion.

2pPAl5. Theoretical proof of acoustic source property single definition in liquid and solid. Leo Zagorskiy (Moscow Mining Institute, Lenin Street, 6, 16-14, Settl. Vugi, 140004 Luybertsy, Russian Federation, ZAGORSKIY_LEV@MAIL.RU)

The problem of acoustic waves property sourse single definition consists in unknown density and elastic modules of the medium. The Green's function definition is difficult as well as the real sourse isn't point and has the

time dependence. In the early author's papers Green's function had been defined by using Levitan's polynomials. In the liquid or solid medium it is necessary for that to know only the first eigen values and shear or P-wave velocity at the first step from the free surface. It provides to calculate amplitudes of first mode of SH waves, α and β - the limits of lacunas in the spectrum. The time function of not moving sourse F is defined from the equation F* G≡U, where U is displacement, G- Green's function, * denominates rolling up. That equation is solved by direct and inverse fast Fourie transform. The further definition of source's location from the direct task for P or S body waves with defined velocity isn't hard by using modern finite element method. The rounding of the fronts gives the location of the sourse.

TUESDAY AFTERNOON, 1 JULY 2008 P2-C, LEVEL 2, 3:40 TO 5:20 P.M.

Session 2pPPa

Psychological and Physiological Acoustics: General Topics in Psychological and Physiological Acoustics I (Poster Session)

Elizabeth Strickland, Cochair
Purdue University

Armin Kohlrausch, Cochair
Philips Research Europe

Alain De Cheveigne, Cochair
CNRS, Universite Paris 5, Ecole Normale Superieure

All posters will be on display from 3:40 p.m. to 5:20 p.m. To allow contributors an opportunity to see other posters, contributors of odd-numbered papers will be at their posters from 3:40 p.m. to 4:30 p.m. and contributors of even-numbered papers will be at their posters from 4:30 p.m. to 5:20 p.m.

Contributed Papers

2pPPa1. Detection and Cortical Representations of the Break in Interaural Correlation of Narrowband Noises Are Affected by Center Frequency and Interaural Delay. Ying Huang (Dept. of Psychology, Peking Univ., 5 Yeheyuan Road, Haidian District, 100871 Beijing, China, innhuang@gmail.com), Lingzhi Z. Kong (Dept. of Psychology, Peking Univ., 5 Yeheyuan Road, Haidian District, 100871 Beijing, China, konglingzhi@gmail.com), Silu Fan (Graduate School of the Chinese Academy of Sciences, 100049 Beijing, China, slfan@gucas.ac.cn), Xihong H. Wu (Dept. of Machine Intelligence, Speech and Hearing Research Center, 2 Science Building, Peking Univ., 5 Yeheyuan Road, Haidian District, 100871 Beijing, China, wxh@cis.pku.edu.cn), Liang Li (Dept. of Psychology, Peking Univ., 5 Yeheyuan Road, Haidian District, 100871 Beijing, China, liangli@pku.edu.cn)

When either broadband or narrowband arbitrary noises presented at the two ears are correlated, a fused noise image is perceived inside the head if the interaural interval (interaural time difference, ITD) is sufficiently short, indicating that acoustic-waveform information can be binaurally integrated. At both the perceptual level and neurophysiological level, this study investigated whether the binaural integration of correlated noises is affected by center frequency (for narrowband noise) and ITD. Results of the psychophysical experiment show that the duration threshold for detecting a break in correlation (BIC) in the correlated noises at the two ears was higher for high-frequency noises than for low-frequency noises, and dramatically elevated with the increase of the ITD from 0 to 4 ms. Moreover, the ITD-induced threshold elevation was much larger for high-frequency narrowband noises than for low-frequency narrowband noises. Results of the neurophysiological experiments show that the cortical components of scalp event-related potentials to the BIC were markedly modulated by both the center frequency (for narrowband noise) and ITD. Thus, temporal integration of acoustic waveform details of correlated noises at the two ears is both frequency and ITD dependent. Supported by the National Natural Science Foundation of China.

2pPPa2. Object-related negativity indexes perception of sounds beyond the echo threshold. Lisa D. Sanders (Univ. of Massachusetts, Department of Psychology, Tobin Hall, Amherst, MA 01003, USA, lsanders@psych.umass.edu), Benjamin Zobel (Univ. of Massachusetts, Department of Psychology, Tobin Hall, Amherst, MA 01003, USA, benjaminzobel@yahoo.com), Rachel Keen (University of Virginia, Department of Psychology, P. O. Box 400400, Charlottesville, VA 22904-4400, USA, rachelkeen@virginia.edu), Richard L. Freyman (Univ. of Massachusetts, Dept. of Communication Disorders, 358 N. Pleasant St., Amherst, MA 01003, USA, rlf@comdis.umass.edu)

The ability to isolate a single sound source among concurrent sources and reverberant energy is crucial for understanding the auditory world. The precedence effect describes an experimental finding that when listeners are presented with identical sounds from two locations with a short onset asynchrony, they report hearing a single source with a location dominated by the lead sound. We recently showed that event-related potentials (ERPs) elicited by click pairs differ for trials on which listeners do and do not report hearing the lag sound as a separate source. Specifically, when participants report hearing two sounds, we observe a negativity between 100 and 250 ms, previously termed the object-related negativity (ORN). These results indicate that the precedence effect reflects top-down cognitive influence over early neurosensory processing. Additionally, the study provides support for the claim that the ORN, initially reported for sounds perceived as two concurrent pitches, indexes auditory object perception. The effects on the ORN of repeating identical click pairs, a condition that has previously been shown to

increase echo thresholds, will also be discussed in the context of listeners forming complex models of room acoustics based on what they hear in a specific setting.

2pPPa3. Improving source localisation in multi-source, reverberant conditions: exploiting local spectro-temporal location cues. Heidi Christensen (University of Sheffield, Regent Court, Dept. of Computer Science, 211 Portobello Road, s1 4dp Sheffield, UK, h.christensen@dcs.shef.ac.uk), Ning Ma (University of Sheffield, Dept. of Computer Science, Regent Court, 211 Portobello Street, S1 4DP Sheffield, UK, n.ma@dcs.shef.ac.uk), Stuart N. Wrigley (University of Sheffield, Regent Court, Dept. of Computer Science, 211 Portobello Road, s1 4dp Sheffield, UK, s.wrigley@dcs.shef.ac.uk), Jon Barker (University of Sheffield, Dept. of Computer Science, Regent Court, 211 Portobello Street, S1 4DP Sheffield, UK, j.barker@dcs.shef.ac.uk)

This paper examines the use of binaural cues for estimating the location of individual sources in multi-source acoustic mixtures. In most environments, location cues such as interaural time difference (ITD) and interaural intensity difference (IID) are rendered unreliable by noise due to competing sources and reverberation. We propose a method that examines spectro-temporal regions where such effects are minimised. Source location is estimated by combining two processing stages. First, following [Christensen et al, Interspeech (2007)], as pitch cues are generally less affected by noise, a multi-pitch estimation and tracking algorithm is used to identify local spectro-temporal 'fragments' in which the SNR is high. Second, the confidence of ITD and IID estimates arising from each time-frequency 'pixel' is estimated based on interaural coherence [Faller and Merimaa, J. Acoust. Soc. Am. 116, 3075--3089 (2004)] and reverberation estimation [Heckmann et al, Int. Conf. Int. Robots and Systems (2006)]. A location estimate is then constructed by integrating suitably weighted cues from each pixel within the fragment. Experiments are carried out on a large corpus of multi-speaker data, mixed from binaural recordings in a real, reverberant environment. The fragment based processing is shown to provide significant improvements when compared to competitive baseline approaches.

2pPPa4. The effect of spectral overlap on sensitivity to interaural time differences. Christopher A. Brown (Arizona State University, Dept. of Speech & Hearing Science, P.O. Box 870102, Tempe, AZ 85287-0102, USA, c-b@asu.edu), William A. Yost (Arizona State University, Dept. of Speech & Hearing Science, P.O. Box 870102, Tempe, AZ 85287-0102, USA, William.Yost@asu.edu)

Cochlear implant users who have some residual low-frequency hearing in both their implanted and unimplanted ears may have access to interaural time differences (ITDs), which could provide a cue for sound source segregation. Speech intelligibility has been shown in simulation to improve under these conditions. However, implant patients who stand to benefit from ITDs may have a significant asymmetry in the configuration of loss in the low-frequency region. It is unknown how a difference in corner frequency of loss across ears will affect ITD sensitivity. As a first step toward characterizing this relationship, the present study measured ITD just-noticeable differences (JNDs) of bands of noise that varied in the amount of spectral overlap across ears in five normal-hearing listeners. In one ear, the center frequency was 250 Hz, and the bandwidth was either 1/3 or 2/3 octaves. In the other ear, the center frequency was 250, 281, 315, 354, 397, or 794 Hz, and the bandwidth was 1/3 or 2/3 octaves. Results showed that although ITD JNDs increased as spectral overlap decreased, ITDs were only detectable so long as some spectral overlap was present.

2pPPa5. Perception of speaker's facing angle. Hiroaki Kato (ATR Cognitive Information Science Laboratories, 2-2-2 Hikaridai, Seika-cho Soraku-gun, 619-0288 Kyoto, Japan, kato@atr.jp), Hironori Takemoto (ATR Cognitive Information Science Laboratories, 2-2-2 Hikaridai, Seika-cho Soraku-gun, 619-0288 Kyoto, Japan, takemoto@atr.jp), Ryouichi Nishimura (National Institute of Information and Communications Technology/ATR Cognitive Information Science Laboratories, 2-2-2 Hikaridai, Seika-cho, 619-0288 Kyoto, Japan, ryou@atr.jp)

In pursuit of an ultimately realistic human-to-human telecommunication technology, the ability to auditorily perceive the facing direction of a human speaker was explored. A male speaker sat on a pivot chair in an anechoic chamber and spoke a short sentence (about 5 seconds) while facing either of eight azimuth angles (0=listener's direction, 45, 90, 135, 180, 225, 270, or 315 degrees) and either of three elevation angles (0=horizontal direction, -45, or 45 degrees). The azimuth angles were set solely by turning the pivot chair. Twelve blindfolded listeners heard the spoken sentence at a distance of either 1.2 or 2.4 meters from the speaker and were asked to indicate the speaker's facing angle. In separate sessions, the speaker changed facing angles while speaking and the listeners indicated the perceived direction of horizontal movement (clockwise or counter-clockwise) or vertical movement (up or down). Overall results showed that the listeners were more accurate in indicating the movement of the speaker than in simply indicating the facing angles. Effective acoustic cues were then discussed on the basis of the transfer characteristics from the speaker's mouth to the listener's ears measured by the cross-spectral method using the speaker's own voice.

2pPPa6. Auditory capture in a spatial cueing task. Marieke Van Der Hoeven (TNO, Kampweg 5, 3769ZG Soesterberg, Netherlands, marieke.vanderhoeven@tno.nl), Adelbert W. Bronkhorst (TNO, Kampweg 5, 3769ZG Soesterberg, Netherlands, adelbert.bronkhorst@tno.nl)

This study examined how an auditory non-informative spatial cue influences detection and localization of auditory targets. In a go-no go task subjects attended a centrally placed loudspeaker surrounded by 6 other loudspeakers and were asked to respond only to centre targets. The cue came from one of the loudspeakers and preceded the target tone with an SOA of 100 or 400 ms. A baseline condition with a spatially diffuse cue was included, using out-of-phase presentation through two loudspeakers. Results show that, compared to the baseline, cues shortened reaction times at small cue-target angles (up to 7°) and increased them at larger angles. At the shortest SOA, the reaction time difference was up to 80 ms. Furthermore, cueing seems to have no effect on sound localization: false alarms were normally distributed around the hits. These findings demonstrate that strong auditory capture effects occur that depend on cue-target distance.

2pPPa7. Spatiotemporal interactions between audition and vision. Adelbert W. Bronkhorst (TNO, Kampweg 5, 3769ZG Soesterberg, Netherlands, adelbert.bronkhorst@tno.nl), Thomas Koelewijn (Vrije Universiteit, van der Boechorststraat 1, 1081 BT Amsterdam, Netherlands, T.Koelewijn@psy.vu.nl), Erik Van Der Burg (Vrije Universiteit, van der Boechorststraat 1, 1081 BT Amsterdam, Netherlands, E.van.der.Burg@psy.vu.nl)

It is well known that spatial auditory cues can affect performance on spatial visual tasks. One example is crossmodal cueing: response times for a visual spatial discrimination task are shortened when the location of the visual stimuli is cued auditorily, and prolonged when an invalid location is cued. Another example is auditory support of visual search: we normally find lower search times for visual items when the location of the target item is indicated by an auditory cue. In our research we have explored two questions: one related to crossmodal cueing, and the other to audiovisual search. In our crossmodal cueing paradigm we have looked at the interaction between (exogenous) cueing and endogenous information given before each trial. In this way we wanted to determine whether auditory cues are able to capture visual attention even when this attention has already been focused endogenously. In our audiovisual search paradigm we have studied whether nonspatial auditory cues, presented simultaneously with the visual target item, are able to improve visual search. Because of the temporal synchrony, the auditory stimuli do not act as actual cues but they are probably fused with the visual stimuli into an integrated percept.

2pPPa8. The acoustical bright spot and the erroneous localization of tones by human listeners. Brad Rakerd (Michigan State University, Dept. of Communicative Sciences and Disorders, East Lansing, MI 48824, USA,

rakerd@msu.edu),Zach Ryan(Michigan State University, Dept. of Physics and Astronomy, East Lansing, MI 48824, USA, ryanzach@msu.edu), Eric Macaulay (Michigan State University, Dept. of Physics and Astronomy, East Lansing, MI 48824, USA, macaula5@msu.edu), William M. Hartmann (Michigan State University, Dept. of Physics and Astronomy, East Lansing, MI 48824, USA, hartmann@pa.msu.edu)

In free-field sound localization experiments, human listeners estimated the locations of sine tones originating at 13 loudspeakers that spanned a range of azimuths from 0 degrees (straight ahead) to 90 degrees (extreme right). During the experiments the tone amplitudes and phases were measured in the listener's ear canals. Because of the acoustical bright spot, measured interaural level differences (ILD) were found to be a nonmonotonic function of azimuth at frequencies above about 1000 Hz. In source identification experiments at 1500 Hz, there was no correlation between estimated location and the interaural phase difference. There was high correlation with ILD, causing listeners to make large localization errors for azimuths greater than about 55 degrees. In a second experiment, listeners judged the direction of movement of sounds from one source to another. Errors in the second experiment could be well predicted from the localization responses in the source identification experiment. The ear canal measurements showed that, in principle, listeners could localize successfully by using the levels in the two ears independently. However, localization performance remained poor even after extensive training. Work supported by the NIDCD, grant DC00181.

2pPPa9. Human cortical responses to change in sound lateralization suggest non-topographical coding of interaural time differences. David A. Magezi (MRC Institute of Hearing Research, University Park, NG7 2RD Nottingham, UK, david.magezi@ihr.mrc.ac.uk), Katrin Krumbholz (MRC Institute of Hearing Research, University Park, NG7 2RD Nottingham, UK, katrin@ihr.mrc.ac.uk)

It is generally assumed that interaural time differences (ITDs) are coded by a parametric array of finely tuned ITD channels (topographic code). An alternative theory is that ITD is coded by a rate code, which involves only one channel in each hemisphere, broadly tuned to the contralateral hemispace. The aim of the current study was to investigate ITD coding in humans by using electroencephalography (EEG) with a continuous stimulation paradigm (CSP). In this paradigm, a test sound, with a given ITD, is immediately preceded by an appropriately matched control sound with a different ITD. At the transition from the test to the control sound, only neural elements that respond to the test but not the control ITD would be expected to be activated. Thus, the size of the transition response would be assumed to be determined by the degree of overlap between the neural responses to the control and test ITDs. The pattern of results was found to be inconsistent with the topographic model, and thus lend support to the hemispheric channel model.

2pPPa10. Both prime length and prime position affect the spatial release of nonsense speech from informational masking. Zhigang Yang (Dept. of Psychology, Peking Univ., 5 Yeheyuan Road, Haidian District, 100871 Beijing, China, synrhine@163.com), Jing Chen (Dept. of Machine Intelligence, Speech and Hearing Research Center, 2 Science Building, Peking Univ., 5 Yeheyuan Road, Haidian District, 100871 Beijing, China, chenj@cis.pku.edu.cn), Qiang Huang (Dept. of Machine Intelligence, Speech and Hearing Research Center, 2 Science Building, Peking Univ., 5 Yeheyuan Road, Haidian District, 100871 Beijing, China, QIANG.HUANG@SPREADTRUM.COM), Ying Huang (Dept. of Psychology, Peking Univ., 5 Yeheyuan Road, Haidian District, 100871 Beijing, China, innhuang@gmail.com), Xihong H. Wu (Dept. of Machine Intelligence, Speech and Hearing Research Center, 2 Science Building, Peking Univ., 5 Yeheyuan Road, Haidian District, 100871 Beijing, China, wxh@cis.pku.edu.cn), Yanhong Wu (Dept. of Psychology, Peking Univ., 5 Yeheyuan Road, Haidian District, 100871 Beijing, China, wuyh@pku.edu.cn), Liang Li (Dept. of Psychology, Peking Univ., 5 Yeheyuan Road, Haidian District, 100871 Beijing, China, liangli@pku.edu.cn)

When masking speech is present, pre-presentation of early part of nonsense target speech improves recognition of the rest of target speech, indicating a content and/or voice priming effect (Freyman et al., 2004; Yang et al., 2007). Here, we examined both the prime-length effect and the prime-position effect on recognition of nonsense target speech with twelve syllables and three keywords. Target speech started 1 sec. after the onset of two-talker masking speech. The results show that a longer prime with 10 syllables (including the 1st and 2nd keywords) significantly improved recognition of the last (3rd) keyword in target speech. However, when the 1st four syllables (including the 1st keyword) were pre-presented, recognition of either the 2nd or 3rd keyword was not improved. Interestingly, when the 2nd four syllables (including the 2nd keyword) were pre-presented, recognition of the 1st but not the 3rd keyword was significantly improved. Thus under speech-on-speech masking conditions, both the prime length and the prime position in the sentence influence the priming effect on recognition of target speech, and listeners contribute more attentional resource to the initial part of target speech. Supported by the National Natural Science Foundation of China.

2pPPa11. Masking release based on fine-grain temporal pitch cues in speech-like stimuli - mechanisms and implications for the cocktail-party phenomenon. Nicholas R. Clark (MRC Institute of Hearing Research, University Park, NG7 2RD Nottingham, UK, n.clark@ihr.mrc.ac.uk), Katrin Krumbholz (MRC Institute of Hearing Research, University Park, NG7 2RD Nottingham, UK, katrin@ihr.mrc.ac.uk)

One of the most important cues for segregating wanted from unwanted sounds when listening in noisy environments is temporal regularity (or harmonicity), which gives rise to the perception of pitch. This study measured masked signal detection thresholds when both the signal and the masker are complex tonal stimuli similar to speech. Detection was considerably easier when the pitch of the masker differed from that of the signal. A control experiment involving non-simultaneous masking revealed that this pitch-based release from masking was not due to spectral differences between the signal and the masker. A second experiment investigated the effect of a pitch difference between the signal and the masker on the audibility of certain perceptual features of the signal when the signal is presented at a supra-threshold level. Two features were used that are known to be particularly important for speech perception: amplitude modulation and spectral profile related to formant frequencies. The supra-threshold tasks enabled to quantify the unmasking effect of pitch on the processing of these features over and above the effect on the signal detection threshold. The results provide new insights into the low-level processes involved in the cocktail-party phenomenon. Acknowledgement: Work supported by the Medical Research Council.

2pPPa12. Perceptual sensitivity to high-frequency interaural time differences created by rustling sounds. Lutz Wiegrebe (Biocenter, University of Munich, Großhaderner Str. 2, 82152 Munich, Germany, lutzw@lmu.de)

ITDs are recruited to localize sounds in azimuth. ITDs can be extracted from low-frequency sounds or from the envelopes of high-frequency, complex sounds. Studies of the latter have included amplitude-modulated or transposed tones. A recent study showed that not the degree of envelope fluctuation, as quantified by the envelope 4th moment, determines sensitivity to envelope ITDs but the envelope spectrum and with it the interaural cross-correlation function of the auditory envelopes provide a good description of envelope ITD sensitivity. Here we use a different class of high-frequency stimuli, namely noise stimuli generated with different degrees of roughness which resemble natural rustling sounds. Stimuli are generated with a Gaussian-noise carrier and an aperiodic, rectangular modulator of statistically different duty cycle. The results show that ITD sensitivity increases both with increasing roughness and increasing bandwidth of the rustling sounds. While the effect of bandwidth on ITD sensitivity is in line with previous conclusions, the effect of roughness is not. ITD sensitivity for rustling sounds elicited ITD thresholds as low as 32 μs, i.e., considerably lower than reported in previous studies with transposed stimuli. The data show that high-frequency rustling sounds provide strong temporal localization cues which the auditory system can effectively exploit.

2pPPa13. Lateralization of binaural stimuli with independent fine-structure and envelope-based temporal disparities. Mathias Dietz (Carl von Ossietzky Universität Oldenburg, Ammerländer Heerstraße 114-118, 26111 Oldenburg, Germany, mathias.dietz@uni-oldenburg.de), Stephan D. Ewert (Carl von Ossietzky Universität Oldenburg, Ammerländer Heerstraße 114-118, 26111 Oldenburg, Germany, stephan.ewert@uni-oldenburg.de), Volker Hohmann (Carl von Ossietzky Universität Oldenburg, Ammerländer Heerstraße 114-118, 26111 Oldenburg, Germany, volker.hohmann@uni-oldenburg.de)

A computational model for the lateralization of binaural stimuli, motivated by recent physiological findings in the literature and psychoacoustic data is presented. The model is based on the evaluation of the interaural phase difference (IPD). In the model, IPDs are separately assessed for the stimulus' fine-structure and envelope. Psychoacoustic measurements were conducted and compared to model predictions. Sinusoidally amplitude modulated 1-kHz tones with a modulation frequency of 25, 50, and 100 Hz were employed. The IPD of the fine-structure and the envelope IPD were independently matched with an interaural level difference or were traded against each other. Lateralization increased for increasing IPDs up to 135° of either the fine-structure or envelope independent of the modulation frequency. However, trading a fine-structure IPD with an opposing envelope IPD revealed a most persistent fine-structure IPD at 45°. The data could be modeled assuming a physiological distribution of the best IPDs of binaural neurons clustered around 45°. The model was also utilized to correctly predict the perceived lateralization of critical stimuli from literature. Individual differences in the perceptual salience of envelope and fine-structure cues, also known from the literature, could be modeled by a personal weighting coefficient for the fine-structure cue.

2pPPa14. A binaural advantage in the subjective modulation transfer function with simple impulse responses. Eric R. Thompson (Centre for applied hearing research, Technical University of Denmark, DTU, Bygn. 352, 2800 Lyngby, Denmark, et@oersted.dtu.dk), Torsten Dau (Centre for applied hearing research, Technical University of Denmark, DTU, Bygn. 352, 2800 Lyngby, Denmark, tda@oersted.dtu.dk)

The speech transmission index (STI) has been a popular method for predicting speech intelligibility in rooms. It is based on the magnitude of the modulation transfer function, which can be derived from the impulse response of the room and the background noise levels. However, it does not take into account that humans listen with two ears. There can be large interaural phase differences in the modulation transfer functions, which can create detectable interaural level difference fluctuations. Measurements were made to determine whether these interaural modulation phase differences can be used to enhance the detectability of sinusoidal intensity modulations imposed on a broadband noise carrier and then convolved with simple, dichotic impulse responses. The results show that there can be a significant advantage to listening with two ears over listening with just one. Some further investigations were made to determine whether this advantage in signal detection can also be used as an advantage for speech intelligibility.

2pPPa15. Temporal weighting of interaural level differences in high-rate click trains. Christopher Stecker (Dept. of Speech and Hearing Sciences, University of Washington, 1417 NE 42nd St, Seattle, WA 98105, USA, cstecker@u.washington.edu)

When high-carrier-frequency stimuli are amplitude modulated at rates above ~200 Hz, lateralization based on envelope interaural time differences (ITD) becomes dominated by onset ITD. The role of onset cues in interaural-level-difference (ILD) processing, however, is less well understood. Although theoretical predictions suggest that onset dominance should have similar effects upon ILD as upon ITD, some experimental data suggest that ILD processing retains greater sensitivity during post-onset segments of a high-rate stimulus. In this study, subjects lateralized ILDs carried by trains of 16 Gaussian-filtered clicks (carrier frequency 4000 Hz) that varied in interclick interval (ICI) from 2 to 10 ms (modulation rate 100-500 Hz). ILDs of individual clicks in each train were randomly perturbed. Multiple linear regression of listener responses onto the perturbed ILD values was used to generate temporal weighting functions (TWFs) that describe how a listener's sensitivity to ILD changes over the stimulus duration. The resulting TWFs were compared to predictions from models of onset dominance as well as to TWFs measured for ITD and in free-field conditions. The results have implications for binaural processing of high-rate pulsatile stimuli experience by users of bilateral cochlear implants.

2pPPa16. Modeling the precedence effect in inferior colliculus neurons using converging excitatory and inhibitory inputs. Jing Xia (Boston University Hearing Research Center, 677 Beacon Street, Boston, MA 02215, USA, xiajing0928@hotmail.com), Andrew Brughera (44 Cummington St., Boston, MA 02215, USA, brughera@bu.edu), H Steven Colburn (44 Cummington St., Boston, MA 02215, USA, colburn@bu.edu), Barbara Shinn-Cunningham (Boston University Hearing Research Center, 677 Beacon Street, Boston, MA 02215, USA, shinn@cns.bu.edu)

Responses of a population model of low-frequency inferior colliculus (IC) neurons to a pair of broadband clicks were evaluated. IC inputs came from Hodgkin-Huxley models of medial superior olive (MSO) and cochlear nucleus bushy cells driven by a stochastic auditory nerve model. Each IC cell received converging inputs that were excitatory from ipsilateral MSO and inhibitory from contralateral MSO. Convergence of multiple excitatory, ipsilateral MSO inputs with similar interaural time difference (ITD) tuning improved ITD sensitivity and reduced the influence of MSO onset responses caused by monaural, rather than binaural, coincidences. Inhibition that lasted over several milliseconds suppressed IC responses to the lagging click. The effect of the inhibition depended on the ITD tuning of the excitation and inhibition converging on a given IC neuron. With appropriate convergence, the IC population showed no response to the lagging click at short delays, and responded to the lagging click but did not encode its ITD at intermediate delays. Only at longer inter-click delays did IC responses show sensitivity to the lagging click ITD, consistent with the perceptual phenomenon of the precedence effect. [Work supported by NSF and NIH].

2pPPa17. Relationship between reading and language ability and auditory temporal processing measured with the precedence effect. Cynthia M. Zettler (University of Wisconsin, Waisman Center, 1500 Highland Ave, Madison, WI 53705, USA, zettler@waisman.wisc.edu), Rose A. Sevcik (Georgia State University, Dept of Psychology, University Plaza, Atlanta, GA 30303, USA, psyras@langate.gsu.edu), Robin D. Morris (Georgia State University, Dept of Psychology, University Plaza, Atlanta, GA 30303, USA, psyrdm@langate.gsu.edu), Mary Ann Romski (Georgia State University, Dept of Psychology, University Plaza, Atlanta, GA 30303, USA, mromski@gsu.edu), Colleen O'Rourke (Georgia State University, Dept of Psychology, University Plaza, Atlanta, GA 30303, USA, corourke@gsu.edu), Marsha G. Clarkson (Georgia State University, Dept of Psychology, University Plaza, Atlanta, GA 30303, USA, mclarkson@gsu.edu)

Processing of timing information by the auditory system contributes to numerous abilities, including spatial hearing and higher-order language and reading skills. However, relationships among these abilities are poorly understood. The present study was aimed at investigating potential common mechanisms that involve timing. Auditory timing was measured by click stimuli presented via two loudspeakers at a rate of 1.5/sec. Fourteen-ms clicks were presented from one (single-source condition) or two (dual-source condition) loudspeakers. In the latter condition, the onset of one loudspeaker was delayed relative to the other by 5, 10, 20, 50, 100, 200, or 400 ms. Seventy-five naïve adults (mean age 21.23 years) listened to the auditory stimuli and were asked to identify the source of the leading sound. Additionally, all participants completed a battery of language and reading measures. Results on the auditory task revealed that performance was significantly above chance on single-source trials, dropped at short delays, and improved with increasing delay. The mean threshold for correctly identifying the source of the sound was 43.48 ms. A significant correlation ($p < .05$) found between this threshold and a measure of word identification suggests a relationship between timing required for auditory localization and timing required for reading ability.

2pPPa18. Lateralization of unidirectional frequency sweeps at high frequencies. I-Hui Hsieh (University of California, Department of Cognitive Sciences, Irvine, CA 92697, USA, ihsieh@uci.edu), Kourosh

Saberi(University of California, Department of Cognitive Sciences, Irvine, CA 92697, USA, saberi@uci.edu)

The ability to lateralize FM sweeps at high frequencies was investigated in a 2IFC 2-down 1-up adaptive design. Four conditions were examined in which the unidirectional FM stimulus swept either up or down in frequency, and either linearly or logarithmically between 3 and 8 kHz with the onset frequency roved by 15% on each presentation. The signal was an interaural delay in the waveform's fine-structure and hence its instantaneous frequency. The waveforms to the left and right ears had simultaneous envelopes and were filtered with the inverse of the headphone transfer functions to eliminate frequency-dependent interaural level differences. Results showed that sweep durations exceeding 25ms produce near-chance performance. Thresholds monotonically improved with increasing sweep rate to a lower asymptote of approximately 100 microseconds. Counterintuitive reversals of lateral position percepts were observed for down-sweeps which were inconsistent with lateralization based on envelope outputs of frequency-matched filters.

2pPPa19. The localization of multiple simultaneous sounds is mediated by attention. Brian D. Simpson (AFRL, 2610 Seventh Street, WPAFB, OH 45433, USA, Brian.Simpson@wpafb.af.mil), Douglas S. Brungart (AFRL, 2610 Seventh Street, WPAFB, OH 45433, USA, douglas.brungart@wpafb.af.mil), Robert H. Gilkey (Wright State University, Department of Psychology, 335 Fawcett Hall, Dayton, 45435, USA, gilk@wright.edu), Nandini Iyer (AFRL, 2610 Seventh Street, WPAFB, OH 45433, USA, nandini.iyer@wpafb.af.mil), James T. Hamil (Ohio State University, Department of Electrical Engineering, Columbus, 43210, USA, hamil.3@osu.edu)

Real-world listening experiences suggest that listeners possess a much greater ability to recover spatial information from multiple simultaneous sounds than would be predicted from the results of most multisource listening experiments. Recent data from our laboratory are consistent with these real-world experiences, and indicate that listeners can reliably report the location of a sound that has been deleted from a multisource scene. However, performance degrades as the number of competing sounds increases, and it is unclear if this 'set size effect' arises from changes in signal-to-noise ratio (SNR) related to the number of competing sources, or from attentional constraints that limit the number of simultaneous sources that can be monitored. In this study, SNR was held roughly constant by fixing the number of competing sources at 8, and the 'relevant set size' was varied by displaying on a visual monitor, prior to an observation interval, a list of 1,2,3,4,6, or 8 environmental sounds, one of which was the target sound (the sound that would be deleted). The ability to localize this target sound decreased as the relevant set size increased, suggesting that the ability to monitor complex auditory scenes is mediated by attentional constraints.

2pPPa20. Better-ear listening strategies for normal-hearing and hearing-impaired individuals. William M. Whitmer (GN Auditory Research Laboratory, 2601 Patriot Blvd, Chicago, IL 60026, USA, whitmerb@beltone.com), Maureen Coughlin (GN Auditory Research Laboratory, 2601 Patriot Blvd, Chicago, IL 60026, USA, mcoughlin@gnresound.com), Jeff Bondy (GN Auditory Research Laboratory, 2601 Patriot Blvd, Chicago, IL 60026, USA, jbondy@gnresound.com), Andrew Dittberner (GN Auditory Research Laboratory, 2601 Patriot Blvd, Chicago, IL 60026, USA, adittberner @gnresound.com)

The current study was designed to examine how hearing-impaired (HI) listeners use better-ear listening. Better-ear performance was initially assessed for normal-hearing (NH) and HI participants using a connected-speech recognition test at two signal-to-noise-ratio (SNR) levels presented over insert earphones. Test conditions consisted of monaural, symmetric and asymmetric combinations of better and worse SNR conditions. SNRs were different for NH and HI groups. Stimuli were presented at each participant's most comfortable level; to account for audibility with HI participants, stimuli were spectrally shaped based on audiometric data. A second experiment investigated the role of spatial information using recordings of the same stimuli presented in a sound-dampened chamber at the same SNR differences, with the speech signal at 0° azimuth/elevation, and uncorrelated babble presented from eight speakers at the corners of the chamber. Listening strategies between NH and HI groups were similar across experiments; neither group consistently used an optimal listening strategy. Results will be discussed in terms of hearing-impaired pathologies, rehabilitation and amplification strategies.

2pPPa21. Numerical Analysis of the Effects of Pinna Shape and Position on the Characteristics of Head-Related Transfer Functions. Yukio Iwaya (R.I.E.C., Tohoku University, 2-1, Katahira, Aoba-ku, 980-8577 Sendai, Japan, iwaya@riec.tohoku.ac.jp), Yôiti Suzuki (R.I.E.C., Tohoku University, 2-1, Katahira, Aoba-ku, 980-8577 Sendai, Japan, yoh@ais .riec.tohoku.ac.jp)

There are distinctive notches and peaks in Head-Related Transfer Functions (HRTFs). Some of them are considered as important cues in the perception of the elevation angle and thus the roles of these peaks and notches should be clarified. It is known that the characteristics of HRTFs are deeply related to listener's anthropometry. It is thus naturally expected that frequencies of the peaks and notches also change according to the individuality of listeners' anthropometry. Therefore, in this study, effects of ear shapes and positions on frequency positions of the peaks and notches are examined by numerical analyses. The analysis was performed with boundary element method (BEM). A three-dimensional model of a dummy-head was constructed with a three-dimensional laser scanner and HRTFs of the model were numerically computed with a BEM solver. The model was modified on some features as follows: 1) pinna position, 2) pinna size, 3) angle of pinna toward listener's head, and 4) existence of wrinkles of pinna. HRTFs of the modified models were also computed. From the comparison among the results of calculation, several systematic changes were found. For example, the frequency position of notches around 8 kHz is shifted toward lower frequency as the size of pinna increases.

2pPPa22. Are interaural time and level cues processed by separate or integrated networks in the human auditory cortex? Barrie A. Edmonds (MRC Institute of Hearing Research, University Park, NG7 2RD Nottingham, UK, barrie@ihr.mrc.ac.uk), Katrin Krumbholz (MRC Institute of Hearing Research, University Park, NG7 2RD Nottingham, UK, katrin @ihr.mrc.ac.uk)

Listeners use two cues to localise the position of a sound source in the horizontal plane: interaural time differences (ITDs) and interaural level differences (ILDs). It is thought that these two cues are encoded separately at the level of the brainstem, but are likely to be combined at higher levels in order to produce a representation of sound azimuth. In the current study, we used electro-encephalography (EEG) to investigate whether the cortical representation of a stimulus containing both ITDs and ILDs reflects separate processing of ITDs and ILDs or a combined code for perceived sound location. Stimuli were presented over headphones using a continuous stimulation paradigm; a diotic control sound was presented for 1.5 seconds followed immediately by a dichotic test sound for 250 milliseconds. Evoked responses were recorded for test stimuli containing an ITD only, an ILD only, or both an ITD and an ILD indicating either the same or opposite source azimuths. When the two cues were in opposition, the stimuli were perceived as central and were indistinguishable from the diotic control sound. However, they still elicited a strong cortical response. This suggests that ITDs and ILDs are encoded separately in the auditory cortex.

Session 2pPPb

Psychological and Physiological Acoustics and ASA Committee on Standards: Applications of Psychoacoustics II (Poster Session)

Patricia Davies, Cochair
Ray W. Herrick Lab., School of Mechanical Engineering, Purdue Univ.

Hugo Fastl, Cochair
AG Technische Akustik, MMK, TU München

All posters will be on display from 3:40 p.m. to 5:20 p.m. To allow contributors an opportunity to see other posters, contributors of odd-numbered papers will be at their posters from 3:40 p.m. to 4:30 p.m. and contributors of even-numbered papers will be at their posters from 4:30 p.m. to 5:20 p.m.

Contributed Papers

2pPPb1. Loudspeaker sound quality: comparison of assessment procedures. Vincent Koehl (LISyC EA 3883, 6 avenue Victor Le Gorgeu, CS 93837, 29238 Brest Cedex 3, France, vincent.koehl @univ-brest.fr), Mathieu Paquier (LISyC EA 3883, 6 avenue Victor Le Gorgeu, CS 93837, 29238 Brest Cedex 3, France, mathieu.paquier@univ-brest.fr)

In listening tests involving different loudspeakers and aimed at assessing the sound quality of these sound-reproducing systems, the level is generally adjusted to compensate for differences in sensitivity. The loudness sensation must be alike for each system under test. Because of the non-stationary nature of the musical signals used as test material in loudspeaker ratings, loudness assessment by using the current models (Zwicker, Mooreœ) remains slightly inaccurate. In practice, loudness is often equalized by ear by the experimenter. This study deals with the comparison of various test procedures. The first experiment was a paired comparison of loudspeakers where short-duration stimuli were presented to listeners for preference ratings. In the second experiment, the same listeners were allowed to switch, at any time, from one loudspeaker to another one so that the proposed stimuli were longer. In both experiments the loudness was equalized by the experimenter. However, under normal listening conditions, the listener is usually free to adjust by himself the reproduction level. At last, in a third experiment, the listeners had the opportunity, at any time, to not only to switch from one system to another one, but also to adjust the loudness of the stimuli.

2pPPb2. Study of the perceptive space linked to dashboard tapping sounds. Francois Montignies (Renault Technocentre, FR TCR LAB 252, 1 avenue du Golf, 78288 Guyancourt Cedex, France, francois.montignies @insa-lyon.fr), Etienne Parizet (Laboratoire Vibrations Acoustique, Insa Lyon, 25 bis, av. J. Capelle, 69621 Villeurbanne Cedex, France, etienne .parizet@insa-lyon.fr)

It was observed that dashboard tapping sounds can be produced by customers exploring static vehicles. To master the perceived quality of the dashboard, a global sound design process has thus been engaged. The specific aim of the present study was to identify the acoustical and technological characteristics being major determinants in the discrimination of the sounds and in the evaluation of the sound sources. 47 sounds were used for a perceptive test in laboratory. They were recorded in 22 vehicles by hand-tapping on different dashboard parts. In a same session, each subject performed 3 different tasks: categorisation (free sorting of sounds), description (free verbalisations) and evaluation (the score of a freely selected prototype was attributed to the whole group). Data analysis took advantage of the combination of various multidimensional analysis techniques, already used in psychoacoustics or sensory analysis. This low-cost methodology allowed us to describe a wide range of product samples with complementary psychological data. Results will help us to propose a sound metric which represent the evaluation of dashboard quality evoked by the sound. Furthermore, they give first hypotheses for the technological variables that could be decisive in the design process.

2pPPb3. Perceptual pitch compensation for low frequency bandwidth extension. Kim Seung (So. EECS/EE at Seoul National University, INMC, 132-302 Seoul National University, 599 Gwanangno, Gwanak-gu, 151-742 Seoul, Republic of Korea, bandwalk@acoustics.snu .ac.kr), Koeng-Mo Sung (Applied Acoustics Lab., INMC, 132-302, Seoul National University, San 56-1, Sillim-dong, Kwanak-gu, 151-742 Seoul, Republic of Korea, kmsung@snu.ac.kr)

As the size of speakers decreases with miniaturization of audio devices and thickness of TV, there is increased demand to ensure low-frequency sound quality. Psychoacoustics bandwidth extension for low-frequency has been applied to recent audio devices. A perceptual pitch does not correspond with fundamental frequency of missing fundamental, because the perceptual pitch is heard highly than desirable fundamental frequency. Consequently, the algorithm compensating perceptual pitch with difference is needed. This paper describes the algorithm compensating the difference using mel scale curve, and the listening test result of sound source applying the algorithm in comparison with sound source applying conventional algorithm.

2pPPb4. Towards an hearing threshold prediction model in car noise. Jean-François Sciabica (PSA Peugeot Citroën, Centre Technique de Vélizy, Route de Gisy, 78943 Vélizy-Villacoublay, France, jean-francois.sciabica @mpsa.com), Florent Richard (PSA Peugeot Citroën, Centre Technique de Vélizy, Route de Gisy, 78943 Vélizy-Villacoublay, France, florent.richard@mpsa.com), Vincent Roussarie (PSA Peugeot Citroën, Centre Technique de Vélizy, Route de Gisy, 78943 Vélizy-Villacoublay, France, vincent.roussarie@mpsa.com)

Sound design is an important challenge at PSA Research Center. Engine noise is rich in harmonics and interacts with aerodynamic and road noise. In this context, comprehension of masking phenomenon is indispensable to obtain a good description of sound attributes like roughness and booming. In this paper, we present a study about interaction between engine harmonics and road and aerodynamic noise. Thresholds for the detection of one harmonic in noise are firstly measured as a function of noise level. We propose also a prediction model for thresholds as a linear function of noise level in critical band. Results were compared to data available in the literature. Secondly, masking of harmonics by a harmonic and noise is measured. The

masker frequency is 100 Hz and its level varies from 65 to 85 dB SPL in 5 dB steps. Noise level is 80dB SPL. Masking patterns are traced for 8 frequencies (50 to 225 Hz).

2pPPb5. The noise induced harmful effects assessment using psychoacoustical noise dosimeter. Jozef Kotus (Gdansk University of Technology, Multimedia Systems Department, 11/12 Gabriela Narutowicza Street, 80-952 Gdansk, Poland, joseph@sound.eti.pg.gda.pl), Bozena Kostek (Gdansk University of Technology, Multimedia Systems Department, 11/12 Gabriela Narutowicza Street, 80-952 Gdansk, Poland, bozenka@sound.eti.pg.gda.pl), Andrzej Czyzewski (Gdansk University of Technology, Multimedia Systems Department, 11/12 Gabriela Narutowicza Street, 80-952 Gdansk, Poland, andcz@sound.eti.pg.gda.pl), Krzysztof Kochanek (The Institute of Physiology and Pathology of Hearing, Pstrowskiego 1, 01-943 Warsaw, Poland, k.kochanek@ifps.org.pl), Henryk Skarzynski (The Institute of Physiology and Pathology of Hearing, Pstrowskiego 1, 01-943 Warsaw, Poland, h.skarzynski@ifps.org.pl)

A new way of assessment of noise-induced harmful effects on human hearing system was presented in the paper. Employing the developed psychoacoustical noise dosimeter the new indicators of noise harmfulness were verified on the basis of hearing examinations and noise measurement results. The indicators were based on some psychoacoustical properties of the human hearing system and, at the same time, on evaluation of the time and frequency characteristics of noise. Additionally, time properties of the Temporary Threshold Shift are calculated during the noise exposure. The evaluation of the proposed indicators were conducted on the basis of hearing examinations in the real noise exposure situations and also on the basis of simulation results employing standard test signals (such as: white, pink and brown noise). The standard noise dose analysis results were also presented for the purpose of comparison. The performed analysis and obtained results confirmed correctness and practical usefulness of the proposed indicators.

2pPPb6. Subjective and objective evaluation of localisation accuracy in wave field sysnthesis. Joseph Sanson (IRCAM, 1 Place Igor Stravinsky, 75004 Paris, France, joseph.sanson@ircam.fr), Etienne Corteel (Sonic Emotion, Eichweg, 6, CH-8154 Oberglatt, Switzerland, etienne.corteel@sonicemotion.com), Olivier Warusfel (IRCAM, 1 Place Igor Stravinsky, 75004 Paris, France, Olivier.Warusfel@ircam.fr)

Wave Field Synthesis (WFS) is a holophonic technique that relies on the reproduction of physical properties of sound fields in an extended listening area. Limitations of this technique are due to approximations regarding the mathematical basis and have been studied in [Ber88] [dB04]. The synthesis remains correct up to a corner frequency referred to as the spatial aliasing frequency and inside an area limited by the length of the WFS array and the position of the virtual sources. A Multichannel Equalization filter (MEQ) is applied to the driving limentation signals of the loudspeakers, as described in [Cor06]. The aim of the present study is to evaluate localisation in WFS depending on both listening and source positions. An objective analysis of the binaural signals is compared to the results of a localisation task for which spatialised high-pass filtered white noises served as stimuli. The results of the psycho-acoustic test are compared to the binaural localisation cues, namely ITD (interaural time differences) and ILD (interaural level differences). Above the aliasing frequency, ITD and ILD are conflicting and ILD errors account in most cases for the perceptual errors.

2pPPb7. Analysis of everyday sounds which are extremely annoying for children with autism. Örjan Johansson (Luleå University of Technology, Dept Human Work Sciences, Div of Sound and Vibration, SE-97187 Luleå, Sweden, orjan.johansson@ltu.se), David Lindegren (Luleå University of Technology, Dept Human Work Sciences, Div of Sound and Vibration, SE-97187 Luleå, Sweden, david.lindegren@gmail.com)

Extreme sensitivity to noise is a problem that almost all autistic children suffer from. A sound that is extremely annoying does not need to be loud. However, the characteristics and temporal variations of these sounds are sparsely investigated. The aim of this study is to increase the knowledge about these extremely annoying sounds so they can be avoided by better design criteria for classrooms and venues like that. By interviewing teachers and parents a number of everyday sounds were identified and binaurally recorded. Examples are vacuum cleaners, ventilation noise, washing machines and pouring water. Detailed psychoacoustic analyses of this type of sounds were achieved by a listening test procedure in three parts. First 16 children composed different types of vacuum cleaner sounds trying to minimize annoyance in two different tests, a) keeping original sound pressure level. b) adjusting to acceptable loudness. In the second part, teachers working with autistic children performed a listening test to evaluate some of the composed sounds from part 1 and modified versions of them. The third part was performed by children to validate the results. The results showed that Roughness, Loudness and an index defined as High frequency tonality were the most important characteristics.

2pPPb8. Application of psychoacoustic tests for the evaluation of acoustical characteristics of Bartók Béla Concert Hall in Palace of Arts, Budapest. Zsuzsanna Alabardos (St Stephan King Technical School of Music Arts, Columbus u.11, H-1143 Budapest, Hungary, alabardos.zsuzsanna@aratokft.hu), Eva Arato-Borsi (Arato Acoustics Ltd, Mezo u.7, H-1038 Budapest, Hungary, arato.eva@aratokft.hu)

The objective characterisation of the subjective listening effect of single number quantities are well known in concert halls such: reverberation time, clarity, centre time, lateral energy fraction and so on. The Bartók Béla Concert Hall in the Palace of Arts in Budapest has been inaugurated at 15th of March 2005. The acoustic consultant office of the hall was ARTEC Ltd. A set of objective measurements has been carried out in the Concert Hall and a series of listening tests were accomplished. Results of the experiment show clear correlations in the relationship of architectural and room acoustical parameters. Apart from the important conclusions, there are some questions revealed.

2pPPb9. Parametric quality prediction for IP-based audio. Alexander Raake (Deutsche Telekom Laboratories, Berlin Institute of Technology, Ernst-Reuter-Platz 7, 10587 Berlin, Germany, alexander.raake @telekom.de), Marieneige Garcia (Deutsche Telekom Laboratories, Berlin Institute of Technology, Ernst-Reuter-Platz 7, 10587 Berlin, Germany, marie-neige.garcia@telekom.de), Bernhard Feiten (T-Systems Enterprise Services GmbH, Goslarer Ufer 35, 13437 Berlin, Germany, bernhard.feiten@telekom.de), Sebastian Möller (Deutsche Telekom Laboratories, Berlin Institute of Technology, Ernst-Reuter-Platz 7, 10587 Berlin, Germany, sebastian.moeller@telekom.de)

Different multimedia services are more and more transmitted over a common network infrastructure, e.g. using the Internet Protocol (IP). Examples are the widespread voice over Internet Protocol (VoIP), and Internet Protocol Television (IPTV). The streaming of pure audio over IP even has a longer tradition, with applications such as internet radio. For an efficient development, planning and monitoring of such services, models can be used that predict user-perceived quality based on technical service characteristics. Speech quality models for telephony are among the most advanced ones in this context, with different model types like the signal-based PESQ (ITU-T Rec. P.862, 2001) or the parametric E-model (ITU-T Rec. G.107, 2005). In this paper, we describe a parametric approach for predicting the quality of IP-based audio. The main parameters are the audio codec, codec bitrate, packet loss characteristics and the audio content. We base our considerations on own listening tests conducted in the framework of IPTV quality assessment, on approaches and test data described in the literature and on complementary knowledge from the fields of speech and video quality models. In this context, we identify similarities and discrepancies between different types of services in the light of a common model framework.

Session 2pPPc

Psychological and Physiological Acoustics: Loudness, from Controlled Stimuli to Environmental Sounds I (Poster Session)

Jeremy Marozeau, Cochair
Northeastern University

Sabine Meunier, Cochair
CNRS-LMA

All posters will be on display from 3:40 p.m. to 5:20 p.m. To allow contributors an opportunity to see other posters, contributors of odd-numbered papers will be at their posters from 3:40 p.m. to 4:30 p.m. and contributors of even-numbered papers will be at their posters from 4:30 p.m. to 5:20 p.m.

Contributed Paper

2pPPc1. Effect of reverberation on loudness perception. Andrew Raimond (Reading University, Department of Psychology, RG6 6AL Reading, UK, a.raimond@reading.ac.uk), Anthony J. Watkins (Reading University, Department of Psychology, RG6 6AL Reading, UK, syswatkn@rdg.ac.uk)

Stimuli with a slow-attack/fast-decay (S-F) envelope are judged to be louder than stimuli with a temporally-reversed, equal-energy version of the same envelope (fast-attack/slow-decay or F-S). It may be that the energy in the tails of F-S stimuli is discounted from loudness judgments because it is perceptually attributed to room reverberation. Here we examine the characteristics of real-room reverberation that affect loudness perception, particularly the way that reverberant tails tend to be de-correlated at the two ears. Our experiments used reverberation from real-room measurements of binaural room impulse responses (BRIRs). We ask if the perceived reduction in loudness of F-S stimuli relative to S-F stimuli is still apparent with dichotic sounds processed by the BRIRs.

Session 2pPPd

Psychological and Physiological Acoustics: Integrated Approaches to Auditory Scene Analysis II (Poster Session)

Mounya Elhilali, Cochair
Johns Hopkins University

Daniel Pressnitzer, Cochair
CNRS UMR 8158; Univ. Paris Descartes; Ecole Normale Supérieure

All posters will be on display from 3:40 p.m. to 5:20 p.m. To allow contributors an opportunity to see other posters, contributors of odd-numbered papers will be at their posters from 3:40 p.m. to 4:30 p.m. and contributors of even-numbered papers will be at their posters from 4:30 p.m. to 5:20 p.m.

Contributed Papers

2pPPd1. The ability of temporally integrating acoustic waveforms is associated with release of speech from informational masking under reverberant conditions. Liang Li (Dept. of Psychology, Peking Univ., 5 Yeheyuan Road, Haidian District, 100871 Beijing, China, liangli@pku.edu.cn), Ying Huang (Dept. of Psychology, Peking Univ., 5 Yeheyuan Road, Haidian District, 100871 Beijing, China, innhuang@gmail.com), Qiang Huang (Dept. of Machine Intelligence, Speech and Hearing Research Center, 2 Science Building, Peking Univ., 5 Yeheyuan Road, Haidian District, 100871 Beijing, China, QIANG.HUANG@SPREADTRUM.COM), Xun Chen (National Key Lab. on Machine Perception, Peking Univ., 5 Yiheyuan Road, 100871 Beijing, China, Xun.Chen@sonyericsson.com), Xihong H. Wu (Dept. of Machine Intelligence, Speech and Hearing Research Center, 2 Science Building, Peking Univ., 5 Yeheyuan Road, Haidian District, 100871 Beijing, China, wxh @cis.pku.edu.cn)

Perceptual integration of the sound wave directly emanating from the source with reflections of the source needs both bridging temporal gaps and calculating correlations between sound waves. In this study, we examined whether the temporal integration of source/reflection signals is frequency dependent and associated with speech unmasking under simulated reverberant conditions. In Experiment 1, a break in correlation (BIC) between correlated wideband or narrowband noises at the two ears was detectable even when an interaural interval (IAI) was introduced. The longest IAI varied markedly across listeners. In wideband noise, it could be up to 21 ms; in narrowband noise, it decreased as the center frequency was increased. In Experiment 2, when the interval between target speech and its single-reflection simulation (inter-target interval, ITI) was reduced from 64 to 0 ms, intelligibility of target speech was markedly improved under the speech-masking condition but not the noise-masking condition. The longest effective ITI under the speech-masking condition significantly correlated with the longest IAI for detecting the BIC in low-frequency ($<$ or $=$ 400 Hz) narrowband noises. Thus the frequency-dependent temporal integration of sound-waveform signals is critical for releasing speech from informational masking in reverberant environments. Supported by the National Natural Science Foundation of China.

2pPPd2. A computational model for auditory scene analysis. Maria E. Niessen (University of Groningen, Dept. Artificial Intelligence, P.O. Box 407, 9700 AK Groningen, Netherlands, m.niessen@ai.rug.nl), Ronald A. Van Elburg (University of Groningen, Dept. Artificial Intelligence, P.O. Box 407, 9700 AK Groningen, Netherlands, r.van.elburg@ai.rug.nl), Dirkjan J. Krijnders (University of Groningen, Dept. Artificial Intelligence, P.O. Box 407, 9700 AK Groningen, Netherlands, j.d.krijnders@ai.rug.nl),Tjeerd C. Andringa (University of Groningen, Dept. Artificial Intelligence, P.O. Box 407, 9700 AK Groningen, Netherlands, t.andringa@ai.rug.nl)

Primitive auditory scene analysis (ASA) is based on intrinsic properties of the auditory environment. Acoustic features such as continuity and proximity in time or frequency cause perceptual grouping of acoustic elements. Various grouping attributes have been translated into successful signal processing techniques that may be used in source separation. A next step beyond primitive ASA is source identification through schema-based ASA. We present a computational model for ASA that is inspired by models from cognitive research. It dynamically builds a hierarchical network of hypotheses, which is based on (learned) knowledge of the sources. Each hypothesis in the network, initiated by bottom-up evidence, represents a possible sound event. The network is updated for each new input event, which may be any sound in an unconstrained environment. The analysis of new input events is guided by knowledge of the environment and previous events. As a result of this adaptive behavior, information about the environment increases and the set of possible hypotheses decreases. With this method of continuously improving sound event identification we make a promising advance in computational ASA of complex real-world environments.

2pPPd3. Pitch-based streaming of vowel sequences, speech-in-speech segregation, and frequency selectivity. Etienne Gaudrain (Laboratoire Neurosciences Sensorielles, Comportement, Cognition, UMR 5020, Université Lyon 1 - CNRS, 50 av. Tony Garnier, 69366 Lyon Cedex 07, France, egaudrain@gmail.com), Nicolas Grimault (Laboratoire Neurosciences Sensorielles, Comportement, Cognition, UMR 5020, Université Lyon 1 - CNRS, 50 av. Tony Garnier, 69366 Lyon Cedex 07, France, ngrimault@olfac.univ-lyon1.fr), Eric W. Healy (University of South Carolina, Speech Psychoacoustics Laboratory, Department of Communication Sciences and Disorders, William Brice Bldg., 1621 Greene St., Columbia, SC 29208, USA, ewh@sc.edu), Jean-Christophe Béra (INSERM U556, 151 cours Albert Thomas, 69424 Lyon Cedex 03, France, jean-christophe .bera@ec-lyon.fr)

Simultaneous and sequential segregation are described as the base mechanisms for auditory scene analysis and are likely to be involved in concurrent speech segregation. However, speech-in-noise perception has been found to be uncorrelated to simultaneous segregation, but related to pure-tone fusion threshold. This study aimed to clarify the relationship between pitch-based speech-in-speech segregation, pitch-based streaming and frequency selectivity. Twenty-five listeners with close to normal hearing were involved. Auditory filter widths were derived from a notched-noise method. Speech-in-speech perception was measured using words presented in a time reversed single talker background, with various pitch differences between

target and masker. The streaming performance was measured using an objective order-naming task on vowel sequences. The results showed a correlation between frequency selectivity and performance in speech-in-speech perception suggesting that intelligibility relies on simultaneous masking. A correlation was also found between the effect of pitch on speech-in-speech perception and the effect of pitch on streaming performance. However, no correlation was found between streaming and frequency selectivity. These latter results suggest that pitch-based segregation probably relies on pitch discrimination which is only weakly correlated to frequency selectivity.

2pPPd4. Speech- synchronized visual cues release speech from informational masking. Mengyuan Y. Wang (Dept. of Psychology, Peking Univ., 5 Yeheyuan Road, Haidian District, 100871 Beijing, China, motoluto@163.com), Jingyu Y. Li (Dept. of Machine Intelligence, Speech and Hearing Research Center, 2 Science Building, Peking Univ., 5 Yeheyuan Road, Haidian District, 100871 Beijing, China, lijy@cis.pku.edu.cn), Ying Huang (Dept. of Psychology, Peking Univ., 5 Yeheyuan Road, Haidian District, 100871 Beijing, China, innhuang@gmail.com), Yanhong Wu (Dept. of Psychology, Peking Univ., 5 Yeheyuan Road, Haidian District, 100871 Beijing, China, wuyh@pku.edu.cn), Xihong H. Wu (Dept. of Machine Intelligence, Speech and Hearing Research Center, 2 Science Building, Peking Univ., 5 Yeheyuan Road, Haidian District, 100871 Beijing, China, wxh@cis.pku.edu.cn), Liang Li (Dept. of Psychology, Peking Univ., 5 Yeheyuan Road, Haidian District, 100871 Beijing, China, liangli@pku.edu.cn)

Visual speech information, such as lipreading cues, can assist listeners to segregate a target voice from competing voices (Helfer and Freyman, 2005). However, because signals contained in lipreading are multidimensional, it is not clear whether a simple visual cue, such as the light flash that is synchronous to the onset of each syllable in target speech, is sufficient to release target speech from noise or speech masking. In this study, when target speech was of a constant rate, the speech-synchronized light flash had no effects on speech recognition under either speech or noise masking condition. However, when the rate of target speech was artificially manipulated unstable or an intense noise burst occurred in the middle of the target sentence, the speech-synchronized light flash improved speech recognition when the two-talker speech masker but not the speech-spectrum noise masker was co-presented. These data suggest that only when the rate of target speech cannot be predicted and the masker is speech, speech-synchronized visual cues play a role in helping listeners attend to the target voice and follow the stream of target speech, leading to a release of target speech from informational masking. Supported by the National Natural Science Foundation of China.

2pPPd5. Phonemic restoration with hearing-impaired listeners. Deniz Baskent (Starkey Hearing Research Center, 2150 Shattuck Ave, Suite 408, Berkeley, CA 94704, USA, deniz_baskent@starkey.com), Cheryl Eiler (Starkey Hearing Research Center, 2150 Shattuck Ave, Suite 408, Berkeley, CA 94704, USA, cheryl_eiler@starkey.com), Brent Edwards (Starkey Hearing Research Center, 2150 Shattuck Ave, Suite 408, Berkeley, CA 94704, USA, brent_edwards@starkey.com)

Baskent et al. (ISAAR 2007) showed that simulated undershoot that may happen due to release from hearing-aid compression may reduce phonemic restoration by normal-hearing (NH) listeners. Phonemic restoration was measured as the increase in recognition of interrupted speech when the silent intervals were filled with loud noise bursts. These results would be more crucial for hearing-impaired (HI) listeners who might encounter such problems in real life as hearing-aid users. However, it has not been previously shown if HI listeners benefit from phonemic restoration similar to NH listeners. Factors such as adverse effects of background noise on speech perception and increased forward masking observed with HI listeners might affect phonemic restoration. The present study explored phonemic restoration with mildly and moderately HI listeners with a method similar to the previous study. NH listeners participated as the control group. Perception of speech interrupted at rates of 1.5 and 2.2 Hz was measured with silent intervals and with noise bursts filling the silent intervals. The preliminary results showed that many HI listeners, especially with mild hearing loss, were able to benefit from phonemic restoration. However, in each subject group, there were a small number of listeners who did not show any benefit.

2pPPd6. Effect of lip movement cues on auditory streaming of concurrent speech. Aymeric Devergie (Université Lyon 1, UMR 5020 CNRS, 50 av. T. Garnier, 69366 Lyon cedex 07, France, aymeric.devergie@olfac.univ-lyon1.fr), Nicolas Grimault (Laboratoire Neurosciences Sensorielles, Comportement, Cognition, UMR 5020, Université Lyon 1 - CNRS, 50 av. Tony Garnier, 69366 Lyon Cedex 07, France, ngrimault@olfac.univ-lyon1.fr), Frédéric Berthommier (Gipsa-lab UMR 5216, 46 avenue Félix Viallet - INPG, F - 38031 Grenoble cedex, France, frederic.berthommier@gipsa-lab.inpg.fr), Etienne Gaudrain (Laboratoire Neurosciences Sensorielles, Comportement, Cognition, UMR 5020, Université Lyon 1 - CNRS, 50 av. Tony Garnier, 69366 Lyon Cedex 07, France, egaudrain@gmail.com), Eric W. Healy (University of South Carolina, Speech Psychoacoustics Laboratory, Department of Communication Sciences and Disorders, William Brice Bldg., 1621 Greene St., Columbia, SC 29208, USA, ewh@sc.edu)

Lip reading is known to induce audio-visual integration processes that enhance speech-in-speech intelligibility. Recent work in auditory scene analysis [see Gaudrain et al., Acoustic'08] found correlations between sequential segregation performance and intelligibility of speech-in-speech. Our working hypothesis is that an audiovisual binding process is involved in speech understanding in multi-talker situations. However, the potential effect of audio-visual integration on auditory stream segregation remains unclear. A single previous study [Gaudrain et al., J. Acoust. Soc. Am. 122, 3065 (2007)] found that lip movements congruent with the presentation of vowels may enhance segregation. In this paradigm, audio-visual sequences of vowels with alternating low and high fundamental frequencies have been generated, in which the lip movements are paired with the second ones. The current experiment is built to test further the potential effect of visual cues on segregation. As in the previous study, lips movements were either steady (control condition), open-closed (rhythm condition) or congruent with each particular vowel. Moreover, a congruent but asynchronous audio-visual condition has been introduced as a new control. This is expected to disrupt the audiovisual binding process. Results are interpreted as an evaluation of the contribution of visual cues in Cocktail Party situations.

2pPPd7. Modelling the temporal response of the auditory nerve to the pitch of complex tones in reverberation. Lowel P. O'Mard (Centre for the Neural Basis of Hearing, The Physiological Laboratory, Downing Street, CB2 3EG Cambridge, UK, lpo21@cam.ac.uk), Mark Sayles (Centre for the Neural Basis of Hearing, The Physiological Laboratory, Downing Street, CB2 3EG Cambridge, UK, ms417@cam.ac.uk), Ian M. Winter (Centre for the Neural Basis of Hearing, The Physiological Laboratory, Downing Street, CB2 3EG Cambridge, UK, imw1001@cam.ac.uk)

A computational model of the auditory nerve has been used to investigate the effect of reverberation on the response to the fundamental frequency (F0) of frequency-swept harmonic complexes. The model used a computationally efficient dual resonance non-linear (DRNL) model of basilar membrane frequency selectivity. The DRNL architecture comprises two parallel filter paths providing linear and non-linear responses. The model successfully reproduced the results of a physiological investigation using the same stimuli in a population of single units from the ventral cochlear nucleus (VCN). In particular the effect of reverberation was dependent upon unit best frequency, F0 and source-to-receiver distance. The model results suggest that the effects of reverberation observed at the level of the VCN are already present in the auditory periphery. The use of the model has also enabled us to examine the effect of hearing impairment by the removal of the non-linear path response. This simulation of a sensorineural hearing loss accentuated the loss of the temporal representation of F0 in the presence of reverberation.

2pPPd8. Blind source separation and sound source localization on time-frequency domain considering time lag information. Shogo Ueda (Department of Architecture, Tokyo University of Science, 1-3 Kagurazaka, Shinjuku-ku, 162-8601 Tokyo, Japan, shogo_0604@yahoo.co.jp), Fumio Sasaki (Department of Architecture, Tokyo University of Science, 1-3 Kagurazaka, Shinjuku-ku, 162-8601 Tokyo, Japan, fsasaki@rs.kagu.tus.ac.jp), Osamu Tanaka (Department of Architecture, Tokyo University of Science, 1-3 Kagurazaka, Shinjuku-ku, 162-8601 Tokyo, Japan, otanaka@rs.kagu.tus.ac.jp), Masahito Yasuoka (Department of Architecture, Tokyo University of Science, 1-3 Kagurazaka, Shinjuku-ku, 162-8601 Tokyo, Japan, shogoarc@ybb.ne.jp)

The blind source separation and sound source localization based on independent component analysis on time-frequency domain considering time lag information between source signals and observation signals are conducted. The formulation based on the independency of time-frequency domain and the linearity of source signal is presented. The method which can be conducted not only the separation of source signals but also the specification of location of source signals is proposed through the consideration of time lags. Using this method, it can be analyzed even if observation signals include an intermittent noise, under the assumption of some independency of source signals. First of all, the number of source signals is specified through the quotient of complex valued time-frequency information of two observation signals. Next, the locations of source signals are specified using the relationship of relative time lags between source signal and observation signal. Then, the source signals are obtained by use of the Fourier information. The numerical test is conducted to confirm our method, and then the locations of source signals and source signals are obtained by high accuracy.

Session 2pPPe

Psychological and Physiological Acoustics: Cochlear Implants: Going Beyond the Envelope II (Poster Session)

Bernhard Seeber, Cochair
MRC Institute of Hearing Research

H Steven Colburn, Cochair
Boston University

All posters will be on display from 3:40 p.m. to 5:20 p.m. To allow contributors an opportunity to see other posters, contributors of odd-numbered papers will be at their posters from 3:40 p.m. to 4:30 p.m. and contributors of even-numbered papers will be at their posters from 4:30 p.m. to 5:20 p.m.

Contributed Papers

2pPPe1. Perception of speech and environmental sounds in cochlear implant patients. Valeriy Shafiro (Rush University Medical Center, Dept. Communication Disorders, 600 S. Paulina Str., 1015 AAC, Chicago, IL 60612, USA, valeriy_shafiro@rush.edu), Brian Gygi (East Bay Institute for Research and Education, 150 Muir Road 151-I, Martinez, CA 94552, USA, bgygi@ebire.org), Min-Yu Cheng (Rush University Medical Center, Dept. Communication Disorders, 600 S. Paulina Str., 1015 AAC, Chicago, IL 60612, USA, min-yu_cheng@rush.edu), Megan Mulvey (Rush University Medical Center, Dept. Communication Disorders, 600 S. Paulina Str., 1015 AAC, Chicago, IL 60612, USA, megan_mulvey@rush.edu), Blythe Holmes (Rush University Medical Center, Dept. Communication Disorders, 600 S. Paulina Str., 1015 AAC, Chicago, IL 60612, USA, blythe_holmes@rush.edu)

Limited research has investigated cochlear implant (CI) patients' ability to perceive environmental sounds. In this study, environmental sound perception was assessed with a large-item test composed of 40 sound sources, each represented by four different tokens. The relationship between speech and environmental sound perception and the role of working memory and basic auditory abilities was examined based on patient performance on a battery of speech tests (HINT, CNC, and individual consonant and vowel tests), tests of basic auditory abilities (audiometric thresholds, gap detection, temporal pattern and temporal order tests), and a backward digit recall test. Twelve postlingually deaf adult CI patients, having 1-5 years of implant experience participated. The results indicate substantially reduced ability to identify common environmental sounds in CI patients. Speech test scores correlated strongly with the scores on the environmental sound test. Both speech and environmental sound tests moderately correlated with gap detection, temporal order test and backward digit recall test. However, the correlation between speech and environmental sounds changed little after partialling out the variance due to other variables. These results suggest that speech and environmental sounds may overlap considerably in their perceptual processing, being largely independent of peripheral limitations that may affect both sound classes.

2pPPe2. Intelligibility of interrupted speech in normal-hearing listeners and cochlear implantees. Dan Gnansia (Univ Paris Descartes, CNRS, Ecole Normale Superieure, DEC, 29 rue d'Ulm, 75005 Paris, France, dan.gnansia@ens.fr), Vincent Pean (MXM / Neurelec, 2729 Chemin St Bernard, 06224 Vallauris Cedex, France, vpean@neurelec.com), Christian Lorenzi (Univ Paris Descartes, CNRS, Ecole Normale Superieure, DEC, 29 rue d'Ulm, 75005 Paris, France, lorenzi@ens.fr)

The intelligibility of a target speech signal is substantially degraded in the presence of a competing talker in cochlear implantees. The current study aimed to test whether this degradation is caused by an inability to i) make use of the partial target speech information glimpsed into the competing talker ″valleys″, and ii) fuse perceptually those successive glimpses into coherent speech streams. This hypothesis was tested by assessing the intelligibility of periodically interrupted vowel-consonant-vowel (VCV) signals pronounced by a male (F0=113 Hz) and female (F0=216 Hz) speaker in normal-hearing listeners and implantees. A 4-Hz square-wave modulator with random phase was used to interrupt periodically each signal. The interrupted VCVs from each speaker were either presented alone (Experiment 1) or interleaved (Experiment 2: the two speakers were alternated). In experiment 1, the mean identification score calculated for each voice was about 90% in normal-hearing listeners, and 40% in implantees. In experiment 2, the mean identification score corresponding to correct identification of both voices was about 50% in normal-hearing listeners, but at chance

level in implantees. Taken together, these data suggest that implantees can make use of partial speech information, but cannot organize this partial speech information into coherent streams.

2pPPe3. Electrode Discrimination and the effect on Speech Perception for Adults with Cochlear Implants. Debi A. Vickers (UCL Ear Institute, 332-336 Gray's Inn Road, WC1X 8EE London, UK, d.vickers@ucl.ac.uk), Leah Meerton (UCL Cochlear Implant Team, 332-336 Gray's Inn Road, WC1X 8EE London, UK, leah.meerton@royalfree.nhs.uk)

Zwolan et al (1997) showed that electrode discrimination can have an effect on speech perception for adult cochlear implant users with the Nucleus Mini 22 multi-channel device. The purpose of this study was to evaluate electrode discrimination in subjects using different implant systems and speech processing strategies to observe the effect that switching off undiscriminable electrodes has on speech perception. 17 postlingually deafened adults were tested; they used either a Nucleus 24 device (either using SPEAK or ACE processing strategies) or an Advanced Bionics HiRes cochlear implant (either using HiRes or HiRes120 strategies). Only electrodes that were activated in the subjects' clinical maps were tested in the electrode discrimination task. Electrode discrimination was performed using standard clinical software at comfortable listening level and pairs of electrodes that scored less than 60% were deemed undiscriminable. One of the undiscriminable pair was switched off and the electrode selected was determined from the results of the other electrode pairs. Performance was evaluated prior to and immediately after switch off and at a follow up appointment 1 month later. Zwolan T, Collins L and Wakefield G (1997). J. Acoust. Soc. Am. **102** (6), 3673-3685.

TUESDAY AFTERNOON, 1 JULY 2008 P2-C, LEVEL 2, 3:40 TO 5:20 P.M.

Session 2pPPf

Psychological and Physiological Acoustics: Auditory Perception and Signal Processing by Prostheses II (Poster Session)

Huanping Dai, Cochair
University of Arizona

Birger Kollmeier, Cochair
Universität Oldenburg, Medizinische Physik

All posters will be on display from 3:40 p.m. to 5:20 p.m. To allow contributors an opportunity to see other posters, contributors of odd-numbered papers will be at their posters from 3:40 p.m. to 4:30 p.m. and contributors of even-numbered papers will be at their posters from 4:30 p.m. to 5:20 p.m.

Contributed Papers

2pPPf1. A model for predicting hearing aid benefit. Michael Nilsson (Sonic Innovations, 2795 East Cottonwood Parkway, Suite 660, Salt Lake City, UT 84121, USA, mnilsson@sonici.com), Victor Bray (Sonic Innovations, 2795 East Cottonwood Parkway, Suite 660, Salt Lake City, UT 84121, USA, vbray@sonici.com)

A 'large n' database was created incorporating demographic information as well as speech-recognition-in-noise measurements from several hundred subjects who participated in field trials with wearable DSP hearing aids. Performance measures were obtained across multiple hearing aid styles (CIC to BTE) with multiple signal processing technologies (multi-channel compression, digital noise reduction, directionality). The database was previously analyzed using various regression techniques (results presented at AAS-2005, IHCON-2006, AAS-2007). The current analysis includes additional parameters that were not in the earlier models and uses a more robust statistical analysis. Aided speech-understanding-in-noise can be predicted based on factors of (a) unaided thresholds for tones (b) unaided thresholds for speech in quiet, (c) unaided thresholds for speech in noise, (d) hearing aid technology, and (e) subject age. We conclude that a model for hearing aid benefit can be used as a new tool for evidence-based management of hearing aid clients. Patient parameters may be entered into the model to serve as a basis for prediction of benefit in speech-understanding-in-noise using various forms of amplification treatment.

2pPPf2. Temporal manipulations in multi-channel compression effecting sound quality and performance. Michael Nilsson (Sonic Innovations, 2795 East Cottonwood Parkway, Suite 660, Salt Lake City, UT 84121, USA, mnilsson@sonici.com), Michelle Hicks (Sonic Innovations, 2795 East Cottonwood Parkway, Suite 660, Salt Lake City, UT 84121, USA, mhicks@sonici.com), Robert Ghent (Sonic Innovations, 2795 East Cottonwood Parkway, Suite 660, Salt Lake City, UT 84121, USA, bghent@sonici.com), Victor Bray (Sonic Innovations, 2795 East Cottonwood Parkway, Suite 660, Salt Lake City, UT 84121, USA, vbray@sonici.com)

Multi-channel compression (in four or more compression channels) is expected in modern hearing aids, but compression temporal characteristics vary without an understanding of what is optimal and why. This study takes a 16 channel system using linearly spaced compressors with minimal overlap and evaluates sound quality ratings and speech recognition performance with the HINT in quiet and noise with various attack and release settings in a 2 x 2 x 2 design. The first variable is the relationship between attack and release times, with asymmetric time constants (attack faster than release) or symmetric time constants (attack and release set the same). The second variable is the relationship of time constants across frequency channels, with uniform settings across frequencies, or frequency dependent time constants (faster settings for higher frequencies with shorter wavelengths). The third variable is absolute speed, with fast or slow time constants. No characteristics other than the temporal settings of the compressor were changed between conditions. Results will be presented showing optimal settings for

sound quality as well as speech recognition. The interaction between compression characteristics and additional signal processing, such as single-microphone noise reduction, will be discussed.

2pPPf3. Speech Intelligibility in Virtual Environments Simulating an Asymmetric Directional Microphone Configuration. Lorenzo Picinali (De Montfort University, Music, Technology and Innovation Research Centre, LE1 9BH Leicester, UK, lorenzo@limsi.fr), Silvano Prosser (Dipartimento di Audiologia, Università degli Studi di Ferrara, Corso Giovecca 203, 44100 Ferrara, Italy, prssvn@unife.it), Antonio Mancuso (DICO-LIM, Università degli Studi di Milano, Via Comelico, 39, 20135 Milano, Italy, knmbm@tin.it), Giancarlo Vercellesi (DICO-LIM, Università degli Studi di Milano, Via Comelico, 39, 20135 Milano, Italy, giancarlo.vercellesi@dico.unimi.it)

The benefit of directional processing and binaural listening in terms of speech intelligibility for frontal sound sources has been well documented in recent and past studies. Nevertheless, only the 20% of the situations in real life present a speaker located exactly in the frontal position. Different attempt have been done so far in order to allow, manually or automatically, a change in the directional pattern of the hearing aid, but the results of these studies are far from being satisfying. The purpose of this study is to explore the advantages brought by the asymmetric directional microphone configuration of hearing aids in terms of speech intelligibility for frontal, lateral and rear sound sources in noisy environments, and in terms of the quality of the ″spatial perception″ of the surrounding sound-scape. Through a 3D Ambisonic virtual environment manipulation, the presence of two microphones (the two hearing aids) is simulated in a noisy environment with a speech sound source. The listeners are presented with the signal recorded from the two simulated microphones, calibrated with symmetrical and asymmetrical directional patterns, and played through a pair of headphones. The speech intelligibility is measured for all the directional microphones configurations and for all the speech sound source positions.

2pPPf4. Simulation of an electro-acoustic implant (EAS) with a hybrid vocoder. Fabien Seldran (Univ. Lyon 1 - Lab. Neurosciences, Service Pr Collet, Pavillon U, Hôpital Edouard Herriot, F-69003 Lyon, France, fseldran@yahoo.fr), Eric Truy (Hôpital Edouard Herriot, Service ORL, Place d'Arsonval, 69003 Lyon, France, eric.truy@chu-lyon.fr), Stéphane Gallégo (Univ. Lyon 1 - Lab. Neurosciences, Service Pr Collet, Pavillon U, Hôpital Edouard Herriot, F-69003 Lyon, France, iakhoun@olfac.univ-lyon1.fr), Christian Berger-Vachon (Univ. Lyon 1 - Lab. Neurosciences, Service Pr Collet, Pavillon U, Hôpital Edouard Herriot, F-69003 Lyon, France, iakhoun@olfac.univ-lyon1.fr), Lionel Collet (Univ. Lyon 1 - Lab. Neurosciences, Service Pr Collet, Pavillon U, Hôpital Edouard Herriot, F-69003 Lyon, France, iakhoun@olfac.univ-lyon1.fr), Hung Thai-Van (Univ. Lyon 1 - Lab. Neurosciences, Service Pr Collet, Pavillon U, Hôpital Edouard Herriot, F-69003 Lyon, France, iakhoun@olfac.univ-lyon1.fr)

Electroacoustic stimulation (EAS) is indicated for hearing impaired patients with enough residual hearing in low frequencies and severe hearing loss in high frequencies. We aimed at simulating the speech intelligibility provided by EAS with a hybrid vocoder model. The French Fournier word set was used in this study. We therefore tested several parameters on 24 normal hearing adults. First, the boundary between acoustic and electric stimulation frequency areas (Fc) was taken at 500, 707, 1000 and 1414Hz. Second, we assessed the effect of electrical stimulation channel numbers (1 to 4). Third, we tested the effect of background noise with a cocktail party noise at -6, 0 and +6 dB SNR. It appeared that the 3 electrical channels & 707 Hz Fc condition produced normal-hearing-like results (at least in quiet). In noisy auditory scene, 4 electrical channels & 500 Hz Fc could produce fair speech intelligibility. [Work supported by CNRS, Lyon1 University and Medel].

2pPPf5. Cartilage conduction hearing aid for the patient with atresia auris. Takefumi Sakaguchi (Nara Medical University, 840 Shijo-cho, 634-8522 Kashihara, Japan, t-saka@naramed-u.ac.jp), Osamu Saito (Department of Otorhinolaryngology, Nara Medical University, 840 Shijo-cho, 634-8522 Kashihara, Japan, osam0502@yahoo.co.jp), Hiroshi Hosoi (Nara Medical University, 840 Shijo-cho, 634-8522 Kashihara, Japan, hosoi@naramed-u.ac.jp)

Although bone conduction hearing aid is considered to be better to compensate the hearing loss of the patients who have atresia auris, some of these patients tend to wear air conduction hearing aid because of the feeling of tightness when wearing bone conduction haring aid. We expected cartilage conduction would reduce feeling of tightness compared to bone conduction, and improve compensation compared to air conduction. In this study, we report the result of the basic studies performed to evaluate the usefulness of cartilage conduction hearing aid. Patient who has atresia auris participated in the hearing test. Stimuli were presented to the patient by means of two types of transmitter. One was piezoelectric transducer placed on antilobium, another one was insertion earphone. We found that the hearing threshold of the patient improved about 25 dB or greater when the transducer was located on antilobium compared to the result when insertion earphone was used. These results suggest that the cartilage conduction hearing aid can be an option of the hearing aid for the patient who has atresia auris which is better than air conduction hearing aid in compensating their hearing, and more comfortable to wear compared to the bone conduction hearing aid.

2pPPf6. Verifying the attenuation of earplugs in situ: variability of transfer functions among human subjects. Annelies Bockstael (Ghent University, De Pintelaan 185 2P1, 9000 Gent, Belgium, annelies.bockstael@ugent.be), Dick Botteldooren (University Ghent - Department Information Technology, Sint-Pietersnieuwstraat 41, 9000 Gent, Belgium, dick.botteldooren@intec.ugent.be), Bart Vinck (Ghent University, De Pintelaan 185 2P1, 9000 Gent, Belgium, bart.vinck@ugent.be)

The use of in situ measurements of hearing protectors' (HPD's) attenuation following the MIRE-protocol (Microphone In Real Ear) is increasing. The attenuation is hereby calculated from the difference in sound levels outside the ear and inside the ear canal behind the HPD. Custom-made earplugs have been designed with an inner bore that allows inserting a miniature microphone. A thorough understanding of the difference, henceforth called 'transfer function', between the sound pressure of interest at the eardrum and the one measured at the inner bore of the HPD is indispensable for optimizing this technique and extending its field of application. Of particular interest is the variation of these transfer functions among humans. This was checked experimentally on 19 subjects. Differences in sound pressure were measured at the HPD's inner bore, by the MIRE-microphone, and at the eardrum by inserting an extra tube microphone in the ear canal. All transfer functions showed a comparable shape, however variability was substantial for the exact frequency and amplitude of the resonance peaks. The link between this variability and the morphology of the individual's HPD and ear canal was addressed using FDTD-simulations (Finite-Difference Time-Domain) of the outer ear canal occluded by an earplug with inner bore.

Session 2pPPg

Psychological and Physiological Acoustics: Loudness, from Controlled Stimuli to Environmental Sounds II

Jeremy Marozeau, Cochair
Northeastern University, 360 Huntington Ave - 106A Forsyth Building - SLPA, Institute for Hearing, Speech & Language, Boston, MA 02115, USA

Sabine Meunier, Cochair
CNRS-LMA, 31, chemin Joseph Aiguier, Marseille, 13402, France

Invited Papers

5:20

2pPPg1. Does induced loudness reduction explain contextual effects in loudness judgment? Lawrence E. Marks (John B. Pierce Laboratory, 290 Congress Avenue, New Haven, CT 06519, USA, MARKS@JBPIERCE.ORG)

Briefly presenting an inducing tone of 70-80 dB can substantially reduce the loudness of a subsequent test tone at or near the inducer's frequency, a phenomenon called Induced Loudness Reduction (ILR). The study of ILR emerged from earlier observations on differential contextual effects in loudness judgment: Tones of a given SPL and frequency were judged softer when presented as part of an ensemble of high rather than low SPL tones at the same frequency, relative to judgments of loudness of tones at a different sound frequency. At first, these effects of stimulus context on loudness judgment were assumed to reflect decisional processes, that is, to reflect biases in loudness judgment. On the other hand, ILR is often assumed to reflect a depression in the intensity response of the auditory system. While it is tempting to explain differential contextual effects in loudness judgment wholly in terms of ILR, the properties of ILR and the properties of contextual effects may not be identical, leaving open a possible role for decisional processes as well as sensory processes in contextual effects, and perhaps also in ILR, in both laboratory and 'real-world' settings.

5:40

2pPPg2. The effects of induced loudness reduction on tone-burst otoacoustic emissions. Michael Epstein (Northeastern University, 360 Huntington Ave - 106A Forsyth Building - SLPA, Institute for Hearing, Speech & Language, Boston, MA 02115, USA, m.epstein@neu.edu), Jeremy Marozeau (Northeastern University, 360 Huntington Ave - 106A Forsyth Building - SLPA, Institute for Hearing, Speech & Language, Boston, MA 02115, USA, marozeau@gmail.com)

Induced loudness reduction (ILR) is a phenomenon by which the loudness of a sound is reduced when it is preceded by a higher-level sound (inducer). Because the effects of ILR can last for at least several minutes after exposure to an inducer, many clinical and laboratory test procedures may be unintentionally confounded. However, little is known about the physiologic manifestation of ILR or how it might affect clinical tests. The present study examined whether ILR could be observed in otoacoustic emission measurements, which have been shown to correlate well with loudness. Otoacoustic emissions were measured monaurally in 12 normal-hearing listeners in response to a 1 kHz 70 dB SPL tone-burst stimulus before and after a series of 1 kHz 90 dB SPL tone-burst inducers. Additionally, otoacoustic emissions were measured in two control conditions in which ILR was not expected to occur. For most listeners, the level of otoacoustic emissions decreased after inducer exposure and did not decrease in the control conditions. The results indicate that at least some component of ILR is likely to arise as a cochlear process and that although the observed effects are small, ILR may affect measures beyond just loudness judgments.

6:00

2pPPg3. Modelling categorical loudness perception for arbitrary listeners and sounds. Birger Kollmeier (Universität Oldenburg, Medizinische Physik, Carl-von-Ossietzky Str. 9-11, 26111 Oldenburg, Germany, birger.kollmeier@uni-oldenburg.de), Jens E. Appell (Universität Oldenburg, Medizinische Physik, Carl-von-Ossietzky Str. 9-11, 26111 Oldenburg, Germany, jens.appell@offis.de), Jesko Verhey (Universität Oldenburg, Medizinische Physik, Carl-von-Ossietzky Str. 9-11, 26111 Oldenburg, Germany, jesko.verhey@uni-oldenburg.de), Volker Hohmann (Carl von Ossietzky Universität Oldenburg, Ammerländer Heerstraße 114-118, 26111 Oldenburg, Germany, volker.hohmann@uni-oldenburg.de)

While ″classical″ loudness models predict loudness in sone using the concepts of Stevens' compressive power law, (subdivided) categorical loudness perception after Heller follows the compressive logarithmic Weber-Fechner law. To bridge the gap between both approaches, this contribution reviews various steps towards a loudness model that predicts categorical loudness (in categorical units, CU) for normal and hearing-impaired listeners for arbitrary sounds. It uses a (modified) classical loudness model for stationary signals to derive the loudness in sone and a nonlinear transformation from sone to CU. This transformation is approximated by a cubic polynomial equation wich is derived from categorical loudness data of 84 normal-hearing subjects. The model parameters are further set to predict the standard isophones that are in good agreement with the equal loudness level contours derived from categorical loudness data. Also, the model predicts the loudness functions near threshold both for normal and hearing-impaired listeners and can be extended to predict duration-dependent loudness perception. Since categorical loudness can be measured more easily and directly than loudness in sone, the current modelling approach can be experimentally tested and can be used in various applications, such as, e.g. hearing aid processing and fitting procedures.

6:20

2pPPg4. Binaural loudness summation in and out of the laboratory. Mary Florentine (Northeastern University, 360 Huntington Ave - 106A Forsyth Building - SLPA, Institute for Hearing, Speech & Language, Boston, MA 02115, USA, florentin@neu.edu), Michael Epstein (Northeastern University, 360 Huntington Ave - 106A Forsyth Building - SLPA, Institute for Hearing, Speech & Language, Boston, MA 02115, USA, m.epstein@neu.edu)

Textbooks state that a tone presented binaurally is louder than the same tone presented monaurally. This is called Binaural Loudness Summation, BLS. Recent data and classroom demonstrations of BLS using speech stimuli from a visually present talker yield much less BLS than previously reported. Are conclusions about BLS drawn from tones presented via earphones in the laboratory applicable to live- voice speech in a room? To answer this question, eight normal listeners were presented three types of stimuli [monitored live voice (MLV) spondees, recorded spondees, and tones] monaurally and binaurally across a wide range of levels. The same stimuli were presented via earphones and loudspeakers. Loudness was measured using magnitude estimation. Results show that the amount of BLS was significantly less for MLV spondees than for tones or recorded spondees. It was also significantly less for loudspeaker presentation than for earphone presentation. The amount of BLS was least for MLV spondees presented via loudspeakers. Results indicate that BLS in loudspeaker conditions is significantly less than BLS in typical laboratory test conditions using earphones. A new phenomena-called ″Binaural Loudness Constancy″-will be described that may result from expectations about loudness of a visually present talker. [Work supported by NIH-NIDCD grant R01DC02241]

6:40

2pPPg5. Loudness asymmetry ratings between accelerating and decelerating car sounds. Patrick Susini (IRCAM - UMR CNRS 9912, Equipe Perception et Design Sonores, 1, place Igor Stravinsky, 75004 Paris, France, susini@ircam.fr), Stephen McAdams (Centre for Interdisciplinary Research in Music Media & Technology (CIRMMT) - Schulich School of Music - McGill Univ., 555 Sherbrooke Street West, Montreal, QC H3A1E3, Canada, smc@music.mcgill.ca)

Loudness change has been studied for tones with linearly varying levels revealing an asymmetry depending on the direction of change (increasing vs. decreasing) and the range of levels (high vs. low). Different assumptions were proposed to explain this asymmetry in favour of linearly increasing sounds. Teghtsoonian et al. (2005) and, more recently, Susini et al. (2006) explain that loudness of an increasing sound is influenced by the end level. Neuhoff (1999) describes this result by a survival advantage for detecting an approaching sound source. Whatever the assumption is, the results show that loudness judgments for abstract sounds (1000-Hz tones) and synthetic vowel sounds were significantly higher for increasing ramps. Those results are compared here with continuous and global ratings obtained on everyday sounds such as accelerating and decelerating car sounds with a same duration (43 s), but with different temporal functions and range of levels. Global loudness judgments made after the end of the sound are significantly higher for accelerating than decelerating car sounds, but are judged on average similar using continuous judgments. In addition, an increase in the speed (acceleration) is evaluated primarily in terms of its level at the end. These results confirm the previous studies.

Contributed Papers

7:00

2pPPg6. Temporal weighting in loudness judgments of time-varying sounds containing a gradual change in level. Daniel Oberfeld (Dept. of Psychology, Johannes Gutenberg-Universitaet Mainz, Staudingerweg 9, 55128 Mainz, Germany, oberfeld@uni-mainz.de)

Two experiments studied how listeners weight the level information from different portions of a noise consisting of ten temporal segments, the levels of which were sampled independently from a normal distribution. If a gradual increase in level (″fade-in″) is imposed on the first few segments in such a sound, temporal weights in global loudness judgments in a one-interval paradigm show a delayed primacy effect [Oberfeld and Plank, Fortschritte der Akustik - DAGA2005, 227-228 (2005)]. The maximum weight is assigned to the first segment presented at the full level, while the weights assigned to the fade-in segments are close to zero. In Experiment 1, a similar pattern of weights was observed in a two-interval paradigm. Thus, listeners do not use intensity information from the fade-in segments even when making within-trial comparisons. In Experiment 2, the first three segments gradually decreased rather than increased in level (i.e., the first segment had the highest level). Listeners gave near exclusive weight to the first segment. The results are compatible with a tendency to assign greater weight to loud elements [Lutfi and Jesteadt, J. Acoust. Soc. Am. 120, 3853-3860 (2006)] rather than with segmentation of the noise into a ″gradually changing″ and a ″stable″ part.

7:20

2pPPg7. Magnitude judgments of loudness change for discrete, dynamic, and hybrid stimuli. Jesse D. Flint (Binghamton University (SUNY), Department of Psychology, Binghamton, NY 13902-6000, USA, jdflint@binghamton.edu), Richard E. Pastore (Binghamton University (SUNY), Department of Psychology, Binghamton, NY 13902-6000, USA, pastore@binghamton.edu),Jeremy R. Gaston(Binghamton University (SUNY), Department of Psychology, Binghamton, NY 13902-6000, USA, jgaston1@binghamton.edu)

Recent investigations of loudness change across dynamically varying stimuli have identified differences between increasing versus decreasing power that depends upon stimulus complexity and intensity range [e.g., Canévet, Acustica, 62, 2136-2142 (1986); Neuhoff, Nature, 395(6698), 123-124, (Sep 1998)]. Some explanations of these findings are based upon known psychophysical effects [Teghtsoonian, Teghtsoonian & Canévet, Perception & Psychophysics, 67(4), 699-712 (2005)], whereas others posit qualitative differences in the perception of discrete laboratory and dynamic natural sound structures (Neuhoff, 1998). For discrete, static stimuli, the relationship between loudness and power is dependant upon a number of factors, including frequency, intensity range, perceptual anchoring, temporal order, and integration of power across time. The current investigation examines listener perception of loudness for sound structures that vary systematically from discrete to dynamic changes in power, allowing evaluation of the contributions of static versus dynamic change, as well as other factors in the perception of loudness change within complex stimuli. Relevant methodology, as well as commonalities and differences with predictions of traditional psychophysics, are discussed.

7:40

2pPPg8. Loudness of impulsive sounds as a function of duration: a parametric study of the effect of level and frequency. Sabine Meunier (CNRS-LMA, 31, chemin Joseph Aiguier, 13402 Marseille, France, meunier@lma.cnrs-mrs.fr), Guy Rabau (CNRS-LMA, 31, chemin Joseph Aiguier, 13402 Marseille, France, rabau@lma.cnrs-mrs.fr)

Loudness of brief signals increases when signal duration increases up to about 100 ms, this increase is called temporal summation. The question examined in this study is to determine how loudness change as a function of

duration. Literature shows different results that lead to different conclusions: when duration increases (i) the loudness increases in direct proportion to energy (intensity x duration); (ii) the loudness increases faster than energy; (iii) the loudness increases slower than energy. We have shown, in previous experiments, that loudness change with duration can follow either (i) or (ii) depending on signal level. The present study provides a parametric examination of this question. Loudness was measured for signals whose energy was kept constant while the duration was varied. The parameters of the experiment were the signal frequency and level. The results allow us to explain part of the discrepancies found in literature. Moreover, the results of this study are used into a model of impulsive sounds that calculate with a good precision the loudness of environnemental short-duration sounds.

TUESDAY AFTERNOON, 1 JULY 2008 ROOM 252B, 2:00 TO 8:00 P.M.

Session 2pSAa

Structural Acoustics and Vibration and EURONOISE: Acoustic Imaging in Confined Space I

Earl G. Williams, Cochair
Naval Research Laboratory, 4555 Overlook Ave, Washington, DC 20375, USA

Alexandre Garcia, Cochair
CNAM, 292 rue Saint Martin, Paris, 75003, France

Invited Papers

2:00

2pSAa1. Analysis of enclosed sound fields using spherical microphone array processing. Boaz Rafaely (Ben-Gurion University of the Negev, Department of Electrical and Computer Engineering, 84105 Beer-Sheva, Israel, br@ee.bgu.ac.il)

Enclosed sound fields in rooms and auditoria are characterized by multiple reflections in addition to the direct sound. The spatial and temporal manner in which sound propagates from the sound source to a listener determines the acoustics of the enclosed space. Recent studies showed that spherical microphone arrays and associated array processing can be used effectively in the experimental study of the acoustics of auditoria. The main advantages presented are the true three-dimensional analysis and the effectiveness of array processing in the spherical harmonics domain. Spherical microphone array design issues will first be reviewed in this work, in particular concerning the design of open-sphere arrays useful in room acoustics analysis with high spatial resolution. Then, beam-forming methods will be presented which can facilitate identification of individual room reflections, and computation of directional room impulse responses. Finally, the use of optimal array processing methods will be presented which facilitates improved sound field analysis.

2:20

2pSAa2. Resolution improvement of beamformers using spherical microphone array. Jean-Claude Pascal (ENSIM - LAUM, Université du Maine, rue Aristote, 72085 Le Mans, France, Jean-Claude.Pascal@univ-lemans.fr), Jing-Fang Li (Visual VibroAcoustics, 51 rue d'Alger, 72000 Le Mans, France, jingfang.li@visualvibroacoustics.com)

Spherical microphone array has been studied for various applications. In enclosed space, spherical array eliminates forward-backward grating lobes occurring in two-dimensional arrays. Beamforming and spherical harmonic decomposition are both used to map the distribution of source strength. The two approaches show similar performance at frequencies where the upper spherical harmonic order equals the product of the wave number and sphere radius. However, at lower frequencies, processing using spherical harmonics maintains the same directivity while the spatial resolution for delay-and-sum beamformer deteriorates. It has been shown that the scattering of sound by a rigid sphere improves the directivity of the same open sphere microphone beamformer, by increasing the path length travelled by incident sound. This paper concerns focused beamformer using rigid and open sphere. The concept of statistically optimized array processing (SOAP) is applied to adapt to a particular interior geometry, considering the scattered field in case of rigid sphere. The regularization process makes it possible to use a model of partially coherent sound field in the enclosed space. A deconvolution post-processing based on the knowledge of the actual steering vector leads to an efficient and robust solution to improve considerably the resolution of the source strength distribution.

2:40

2pSAa3. Measurement of low-frequency sources in non-anechoic room using near-field acoustic holography. Manuel Melon (CNAM, 292 rue Saint Martin, 75003 Paris, France, melon@cnam.fr), Christophe Langrenne (CNAM, 292 rue Saint Martin, 75003 Paris, France, christophe.langrenne@cnam.fr), Alexandre Garcia (CNAM, 292 rue Saint Martin, 75003 Paris, France, garcia@cnam.fr), Philippe Herzog (Laboratoire de Mécanique et d'Acoustique - CNRS, 31 chemin Joseph Aiguier, 13402 Marseille, France, herzog@lma.cnrs-mrs.fr)

Low frequency (20 Hz-200 Hz) measurements of sound sources are rather difficult to perform because free field conditions can not be easily achieved properly. Moreover, some industrial sources have to be measured in situ. In such a case, a Field Separation Method (FSM) can be used to subtract the pressure field reflected by walls of the testing room from the measured data. This approach required the knowledge of both acoustic pressure and velocity on a closed surface surrounding the source. In this paper, a spherical harmonic expansion of measured data is used to solve the problem. The proposed method is applied to the measurement of the frequency response

of a closed box subwoofer tested under various conditions: in a room with variable reverberation time (6.4 s to 0.6 s). Theoretical frequency response of the subwoofer is also calculated using the Thiele and Small model. Results show a good agreement between separated data and simulations. The influences of the measurement distance and of the measurement point number required on the separation process are discussed.

3:00

2pSAa4. Vector intensity reconstructions in a volume surrounding a rigid spherical measurement array. Earl G. Williams (Naval Research Laboratory, 4555 Overlook Ave, Washington, DC 20375, USA, earl.williams@nrl.navy.mil), Kazuhiro Takashima (Nittobo Acoustic Engineering Co., Ltd., 1-21-10, Midori, Sumida-Ku, 130-0021 Tokyo, Japan, taka@noe.co.jp)

An approach is presented that provides a prediction of the vector intensity field throughout a volume exterior to a rigid spherical measurement array consisting of 31 flush mounted microphones. The theory is based on spherical harmonic expansions of the measured field with the radial variation of the near-field pressure obtained using the Greens function with vanishing normal derivative at the rigid sphere surface. Experimental results with rigid spherical arrays of differing radii are presented using multiple incoherent sources. Successful intensity reconstructions are obtained over a volume three times the sphere radius up to a frequency of 1.5 kHz that clearly reveal the locations and levels of the two sources. This volumetric intensity probe is very similar mathematically to one described recently by the author (EGW) that used 50 microphones in an open array. The latter was used successfully inside an aircraft cabin in flight to uncover sources of noise. This work was supported by the US Office of Naval Research and Nittobo Acoustic Engineering Co. Ltd.

3:20

2pSAa5. A boundary element method for near-field acoustical holography in bounded noisy environment. Christophe Langrenne (CNAM, 292 rue Saint Martin, 75003 Paris, France, christophe.langrenne@cnam.fr), Manuel Melon (CNAM, 292 rue Saint Martin, 75003 Paris, France, melon@cnam.fr), Alexandre Garcia (CNAM, 292 rue Saint Martin, 75003 Paris, France, garcia @cnam.fr)

This paper presents a boundary element method to recover free field conditions from noisy bounded space situations. The proposed approach is based on the Helmholtz integral formulation and requires the knowledge of double layer pressure fields on two parallel closed surfaces surrounding the source. First, the outgoing and ingoing pressure fields are separated. Then, the incident field scattered by the tested source is subtracted from the outgoing field to estimate the pressure field which would have been radiated in free field. The method had been numerically tested and an experimental example is given here. The source is a rectangular box with seven loudspeakers mounted on it driven by bandwith limited white noise. The source is put at 0.4 m from the ground of a semi-anechoïc room. The ground plays a disturbant role because it produces secondary sources. The results show the effectiveness of the method particularly at frequencies where stationary waves between the ground and the underside of the box exist.

3:40-5:20 Posters

Lecture sessions will recess for presentation of poster papers on various topics in acoustics. See poster sessions for topics and abstracts.

Invited Papers

5:20

2pSAa6. Acoustically invisible cylinder. Yuri Bobrovnitskii (Mechanical Engineering Research Institute, 4, M. Kharitonievky Str., 101990 Moscow, Russian Federation, yuri@imash.ac.ru)

Coatings of new type recently proposed by the author (Acoustical Physics, 2007, vol. 53, N5, pp. 535-545) are applied to bodies of cylindrical geometry to reduce reflection or scattering of sound and thus to make them undetectable by imaging systems. Such a coating, called as a coating with extended reaction, represents a periodic set of small elements with coupling between the neighboring elements. Appropriate choice of the coupling parameters makes its efficiency much higher than that of commonly used coatings. In the present paper, it is shown by computer simulation that a rather simple coating of this type can reduce the back-scattered pressure amplitude more than 40 dB (with respect to the rigid cylinder) practically at all frequencies. Considerable reduction of the scattered power can also be achieved in a low frequency range. The width of this range and the reduction index depend on the number of couplings introduced into the coating.

5:40

2pSAa7. Acoustic source identification in an enclosed space using the inverse phased beam tracing at medium frequencies. Jeong-Guon Ih (KAIST, Dept. of Mechanical Engineering, Science Town, 305-701 Daejeon, Republic of Korea, J.G.Ih@kaist.ac.kr), Cheol-Ho Jeong (Acoustic Technology, DTU Elektro, Technical University of Denmark, Building 352, Ørsted plads, DK-2800 Kgs. Lyngby, Denmark, chj@oersted.dtu.dk)

When the source is enclosed by room surfaces, it is not easy, though not totally impossible, to apply conventional modal methods for source identification. This is because there are too many complicated wave interferences and effects of wall impedance, in particular at medium frequencies. The phased beam tracing method was suggested as a fast and efficient acoustic simulation tool at the medium frequencies in an enclosure, which overcomes the defects of geometrical acoustics techniques. In this study, the phased beam tracing method, implemented in its inverse form, was applied to the identification of the acoustic sources inside a chamber. In the simulation

tests, spherical and rectangular shaped sources operating in a room were taken as examples. When the source pressure distribution was reconstructed by this numerical inverse technique, the sound power spectrum radiated from the source could be estimated by eliminating the contribution from surface reflections. Reconstruction error was investigated by the Monte Carlo simulation in terms of the signal-to-noise ratio.

Contributed Papers

6:00

2pSAa8. Noise source characterisation using patch impedance technique. G Pavić (INSA de Lyon - LVA, Bâtiment St. Exupéry, 25 bis avenue Jean Capelle, F-69621 Villeurbanne Cedex, France, goran.pavic @insa-lyon.fr), Nicolas Totaro (INSA de Lyon - LVA, Bâtiment St. Exupéry, 25 bis avenue Jean Capelle, F-69621 Villeurbanne Cedex, France, nicolas.totaro@insa-lyon.fr)

A novel approach of an environment-independent sound source characterisation is discussed. The source is defined via a suitable enveloping interface surface by its blocked sound pressure and its surface impedance. Both the blocked pressure and the impedance are discretised using the averaging patch concept. Such a definition avoids singularity of point acoustic impedance and is suitable for numerical as well as experimental implementation. The characterisation of a source by the patch concept allows for the acoustical sub-structuring, which in turn enables the prediction of the sound field created by the source coupled to an arbitrary environment. Numerical simulations are presented which demonstrate the feasibility of the approach. It is hoped that the proposed approach can serve as a universal tool for noise synthesis of complex equipment incorporating noise sources.

6:20

2pSAa9. Local patch acoustic holography methods in enclosed spaces. Zdenek Havranek (Brno University of Technology, UAMT-FEEC, Kolejni 4, 61200 Brno, Czech Republic, havranek@feec.vutbr.cz),Ludvik Bejcek (Brno University of Technology, UAMT-FEEC, Kolejni 4, 61200 Brno, Czech Republic, bejcek@feec.vutbr.cz)

The paper compares reconstruction accuracy and computational cost of three patch acoustic holography algorithms applicable in the enclosed spaces for prediction of sound field near sources. Algorithms under investigation were DL-SONAH, IBEM and classical NAH with spatial transformations and hologram aperture enlargement. All of the selected algorithms take an advantage of using double layer microphone array for measurement of sound pressure field. The reconstruction accuracy of all algorithms is determined by using of simple 3D model of curved radiating surface on the basis of calculation of difference between true acoustic quantity (pressure, velocity or intensity) values very close to the surface and predicted sound field at same positions. All these methods use different calculation procedure to obtain predicted sound field near source surface, thus comparison of effectiveness of these algorithms including prediction accuracy-to-computational cost ratio is useful to determination their applicability in practice. Results of prediction error and calculation time including regularization with different parameter choice methods (L-curve, GCV, etc., are presented and compared. Initial comparison of the selected methods confirms shorter calculation time in non-element based methods, especially in NAH with transformations, while reconstruction error is in the same order.

Invited Papers

6:40

2pSAa10. Identification of source velocities with Inverse Patch Transfer Functions method. Mathieu Aucejo (INSA de Lyon - LVA, Bâtiment St. Exupéry, 25 bis avenue Jean Capelle, F-69621 Villeurbanne Cedex, France, mathieu.aucejo@insa-lyon.fr), Nicolas Totaro (INSA de Lyon - LVA, Bâtiment St. Exupéry, 25 bis avenue Jean Capelle, F-69621 Villeurbanne Cedex, France, nicolas.totaro@insa-lyon.fr), Jean-Louis Guyader (INSA de Lyon - LVA, Bâtiment St. Exupéry, 25 bis avenue Jean Capelle, F-69621 Villeurbanne Cedex, France, jean-louis.guyader@insa-lyon.fr)

The identification of source velocities remains an important problem in noise control. For this purpose, several methods were developed such as Near-field Acoustic Holography (NAH) or inverse Boundary Elements Method (iBEM). An alternative method, based on the double measurement of pressure and particle velocity fields surrounding the source is presented. This method has been developed in the SILENCE European project framework. In this method, called inverse Patch Transfer Functions method (iPTF), measurement and identification surfaces are divided into elementary areas called patches. Then, source velocities are computed from acoustic field and inversion of impedances matrices obtained by FEM. Theoretically, this method presents two main advantages: it can be applied to sources with complex 3D geometries and measurements can be carried out in a non-anechoic environment, even in the presence of other sources. In the present paper, theoretical background of iPTF is exposed and results are presented on a source with simple geometry (an L-shaped plate) and discussed.

7:00

2pSAa11. Detection of acoustic radiating areas of a generic helicopter cabin by beamforming. Gérard Martin (ONERA, 2 avenue Edouard Belin, BP 4025, 31055 Toulouse, France, Gerard.Martin@onecert.fr), Frank Simon (ONERA, 2 avenue Edouard Belin, BP 4025, 31055 Toulouse, France, Frank.Simon@onecert.fr), Daniel Biron (ONERA, 2 avenue Edouard Belin, BP 4025, 31055 Toulouse, France, Daniel.Biron@onecert.fr)

Improvement of the helicopter internal noise is essential to decrease the fatigue effects of passengers. This requires having a metrological tool, able to give information on acoustic radiating areas in cabin in order to target appropriate acoustic passive or active solutions. In this context, the authors have shown, in previous papers, capability of modified beamforming using a cross-shaped array of microphones, associated with an acoustic mask, to localize isolated sources in a generic composite helicopter cabin (VASCo), thus, in spite of free field's hypothesis. The present paper deals with the feasibility of this measurement method to identify main acoustic pressure areas radiated by an helicopter mechanical deck whose vibration is generated by gear box beams between 800 and 5000 Hz. This configuration is performed, thanks to simulations and experiments on a sandwich composite panel of VASCo, excited by 4 cor-

related shakers. It appears that beamforming can be used to identify main acoustic area coming from the radiating of many coupled vibration modes. Nevertheless, the dynamic range decreases with the number of pressure anti-nodes and it is necessary to introduce an inverse method to reject the ghost images and to reconstruct amplitude and phase of synthesized sources.

Contributed Papers

7:20

2pSAa12. 3D localization of acoustic sources with a spherical array. Karim Haddad (Brüel & Kjær Sound & Vibration Measurement A/S, Skodsborgvej 307, DK-2850 Nærum, Denmark, khaddad@bksv.com), Jørgen Hald (Brüel & Kjær Sound & Vibration Measurement A/S, Skodsborgvej 307, DK-2850 Nærum, Denmark, JHALD@bksv.com)

This paper describes a technique dedicated for the localization of acoustic sources in all directions and in the far-field. Classical beamforming techniques based on planar arrays provides an acoustic map restricted to a limited aperture, but a spherical array does not have such a limitation since there is no preferential direction. In this processing called Spherical Harmonics Beamforming, the sound field on the sphere is decomposed with spherical harmonics functions, and then a corrected summation gives the acoustic contribution from a given direction. We have used a rigid spherical array, which has the advantage that cabling of microphones and integrated cameras can be hidden inside the sphere. A rigid surface also provides better numerical stability in connection with Spherical Harmonics Beamforming. In this study, this technique is evaluated in connection with the resolution and the dynamic range. Simulated and experimental results are presented.

7:40

2pSAa13. Near-field Acoustic Holography for partial measurements inside complex structures. Nicolas Valdivia (Naval Research Laboratory, 4555 Overlook Ave, Washington, DC 20375, USA, valdivia@pa.nrl.navy.mil), Earl G. Williams (Naval Research Laboratory, 4555 Overlook Ave, Washington, DC 20375, USA, earl.williams@nrl.navy.mil)

Near-field acoustical holography (NAH) requires the measurement of the near-field pressure field over a closed surface in order to recover the acoustic field on a nearby conformal surface. Very often we encounter applications where pressure measurements are available only over a patch of the measurement surface. In these cases the strict NAH theory does not hold, but still there are techniques that have been developed to overcome this difficulty. The best-known technique for planar surfaces is patch NAH and, recently proposed, for arbitrarily shaped surfaces patch IBEM and patch ESM. It was found in a recent study by the authors that these techniques will be affected by the problem of back-source contamination for interior NAH, but it was showed that this problem could be overcome by the use of ″Cauchy″ measurements. In this work we will compare the reconstruction of the acoustic field from patch based techniques with the technique that uses Cauchy measurements, and discuss the problem of back-source contamination in more detail. We use a cylindrical surface excited by a point force as an example to validate our results. This work was supported by the US Office of Naval Research.

TUESDAY AFTERNOON, 1 JULY 2008 P2-B, LEVEL 2, 3:40 TO 5:20 P.M.

Session 2pSAb

Structural Acoustics and Vibration and EURONOISE: Source Characterization in Structure Borne Noise Problems II (Poster Session)

Evan Davis, Cochair
The Boeing Company

Charles Pezerat, Cochair
Laboratoire Vibrations Acoustique - INSA Lyon

All posters will be on display from 3:40 p.m. to 5:20 p.m. To allow contributors an opportunity to see other posters, contributors of odd-numbered papers will be at their posters from 3:40 p.m. to 4:30 p.m. and contributors of even-numbered papers will be at their posters from 4:30 p.m. to 5:20 p.m.

Contributed Papers

2pSAb1. The significance of cross-order terms in interface mobilities for structure-borne sound source characterization. Hannes A. Bonhoff (Berlin Institute of Technology, Einsteinufer 25, TA7, 10587 Berlin, Germany, hannes.bonhoff@tu-berlin.de), Björn A. Petersson (Berlin Institute of Technology, Einsteinufer 25, TA7, 10587 Berlin, Germany, b.a.t.petersson@tu-berlin.de)

For the characterization of structure-borne sound sources and the description of the associated transmission process, the source descriptor and coupling function were introduced. The concept of source descriptor and coupling function can be reformulated by incorporating the interface mobilities. The applicability for source-receiver assemblies with a multi-point or continuous connection is thereby granted. The accuracy of the results and consequently the validity of this approach, however, depends on the significance of the so-called cross-order terms. Such cross-order terms consist of force orders and cross-order interface mobilities. In recent theoretical and experimental work, the influence of cross-order interface mobilities as well as the distribution of force-orders have been investigated. Based on this knowledge, the significance of the cross-order terms is assessed in the present contribution.

2pSAb2. Measurement of force and moment mobilities using a finite difference technique. Andrew Elliott (University of Salford, Acoustic Research Centre, Newton Building, M5 4WT Salford, UK, a.s.elliott@pgr.salford.ac.uk), G Pavić (INSA de Lyon - LVA, Bâtiment St. Exupéry, 25 bis avenue Jean Capelle, F-69621 Villeurbanne Cedex, France, goran.pavic@insa-lyon.fr), Andy T. Moorhouse (University of Salford, Acoustic Research Centre, Newton Building, M5 4WT Salford, UK, a.t.moorhouse@salford.ac.uk)

Measuring only force mobilities it is possible to derive a moment mobility without the need for an externally applied moment. The method uses finite differences of both forces and velocities about a central point. In this way pure forces and moments can be extracted as can pure velocities and angular velocities. There are, however, errors associated with finite difference techniques. In this case the purity of the extracted quantities depends on the area over which they are measured and its significance in terms of wavelength. Meanwhile experimental errors such as noise dictate that the area is sufficiently large to provide differences which are incorruptible. The paper aims to quantify the finite difference error in a general way free of situation specifics.

TUESDAY AFTERNOON, 1 JULY 2008 P2-B, LEVEL 2, 3:40 TO 5:20 P.M.

Session 2pSAc

Structural Acoustics and Vibration and EURONOISE: Acoustic Imaging in Confined Space II (Poster Session)

Earl Williams, Cochair
Naval Research Laboratory

Alexandre Garcia, Cochair
CNAM

All posters will be on display from 3:40 p.m. to 5:20 p.m. To allow contributors an opportunity to see other posters, contributors of odd-numbered papers will be at their posters from 3:40 p.m. to 4:30 p.m. and contributors of even-numbered papers will be at their posters from 4:30 p.m. to 5:20 p.m.

Contributed Papers

2pSAc1. Experimental feasibility of in-duct sound source reconstruction. Teresa Bravo (Université de Technologie de Compiègne, Centre de Recherche Royallieu, BP20529, 60205 Compiègne, France, teresa.bravo-maria@utc.fr), Cédric Maury (Université de Technologie de Compiègne, Centre de Recherche Royallieu, BP20529, 60205 Compiègne, France, cedric.maury@utc.fr)

Due to the expected air transport growth and stringent environmental regulations, there is a strong need to develop noise reduction techniques at acceptable cost in the aeronautical sector. A sound characterisation of the aero-acoustic sources in the nacelle acoustic duct problem plays a crucial role. In this study, it is shown how the liners optimized impedances strongly depend on the noise source characteristics under both tonal and broadband excitation conditions, and in the latter case, for varying degree of correlations between the random source strengths. The limitations for source identification methods, such as pointwise model-based inverse techniques, have been studied. These methods are able to provide reliable models of equivalent sound sources from a limited number of in-duct measurements, but require a priori knowledge of the source location. The performance of such techniques are compared with two different approaches, namely the use of focussed in-duct beamforming techniques to locate the unknown sources, and a decomposition of the assumed source strengths into angular Fourier series for both the location and the determination of the source amplitudes. Experimental results are presented for the location and the reconstruction of the particle velocity spectrum of wall-mounted compression drivers from in-duct measurements.

2pSAc2. Vector intensity measurement with a rigid spherical microphone array in a vehicle cabin. Kazuhiro Takashima (Nittobo Acoustic Engineering Co., Ltd., 1-21-10, Midori, Sumida-Ku, 130-0021 Tokyo, Japan, taka@noe.co.jp), Hiroshi Nakagawa (Nittobo Acoustic Engineering Co., Ltd., 1-21-10, Midori, Sumida-Ku, 130-0021 Tokyo, Japan, nakagawa@noe.co.jp), Earl G. Williams (Naval Research Laboratory, 4555 Overlook Ave, Washington, DC 20375, USA, earl.williams@nrl.navy.mil)

Measurement results showing intensity vector reconstructions using a rigid spherical microphone array in a vehicle cabin are presented. The measurement equipment developed by Nittobo was used in previous demonstrations to visualize the acoustic field using a beamforming technique superimposed on a picture from an on-board camera. In the present study intensity reconstructions are shown and are successful in locating and quantifying sources, demonstrating the usefulness of this technique in an enclosed space like a vehicle cabin, aircraft cabin, small room, etc. This work was supported by the US Office of Naval Research and Nittobo Acoustic Engineering Co. Ltd.

2pSAc3. An improved method of visualizing the energy flow: the Rayleigh wave. Cleon E. Dean (Physics Department, Georgia Southern University, P. O. Box 8031, Statesboro, GA 30460-8031, USA, cdean@GeorgiaSouthern.edu), James P. Braselton (Department of Mathematical Sciences, Georgia Southern University, P.O.B. 8093, Statesboro, GA 30460-8093, USA, jbraselton@GeorgiaSouthern.edu)

A variety of ways of visualizing the energy flux or elastodynamic Poynting vector field are demonstrated including gridded vector field, color coding, and other methods for the simple example of a Rayleigh wave. In particular an improved version of a technique shown at the 8th International Conference on Theoretical and Computational Acoustics, ICTCA 2007 is demonstrated [David M. F. Chapman, ″Visualizing acoustic energy flow into the seabed using energy streamlines,″ Eighth International Conference on Theoretical and Computational Acoustics, ICTCA 2007, Heraklion, Crete, GREECE, 2-5 July 2007.]. The improved streamline method shows both the direction and the intensity of the energy flow.

Session 2pSAd

Structural Acoustics and Vibration and EURONOISE: Vibration and Radiation from Complex Structural Systems III (Poster Session)

David Feit, Cochair
Applied Physical Sciences Corp.

Jean-Louis Guyader, Cochair
INSA de Lyon - LVA

All posters will be on display from 3:40 p.m. to 5:20 p.m. To allow contributors an opportunity to see other posters, contributors of odd-numbered papers will be at their posters from 3:40 p.m. to 4:30 p.m. and contributors of even-numbered papers will be at their posters from 4:30 p.m. to 5:20 p.m.

Contributed Papers

2pSAd1. Implementation of the high order asymptotic models of linings and coatings to the SAW spectra evaluation. Dmitry Zakharov (LMP, UMR CNRS 5469, Université Bordeaux I, 351, cours de la Libération, 33405 Talence, France, dmitrii.zakharov@gmail.com), Alexander Shuvalov (LMP, UMR CNRS 5469, Université Bordeaux I, 351, cours de la Libération, 33405 Talence, France, a.shuvalov@lmp.u-bordeaux1.fr), Olivier Poncelet (LMP, UMR CNRS 5469, Université Bordeaux I, 351, cours de la Libération, 33405 Talence, France, o.poncelet@lmp.u-bordeaux1.fr)

High order asymptotic models of the relatively thin linings and coatings are used to reduce the problem dimension when dealing with a reasonable frequency range. The essential point consists in the use of asymptotic expansion for the internal stress and strain state of a laminate, subjected to the tight conditions at least on one of its faces, i.e., the conditions formulated for the displacements. The respective algorithm, based on it, is shorter than for the direct evaluation of the SAW spectra. It can be implemented to the calculation of Rayleigh waves or Lamb waves in layered media. Numerical examples are presented with both asymptotical and numerical evaluation of error.

2pSAd2. Plate Sound Radiation Prediction in Machines Using Multiple Input Techniques. Armand Nejade (Institut National de Recherche et de Sécurité (INRS), Ave. de Bourgogne, B.P. 27, F-54501 Vandoeuvre Cedex, France, armand.nejade@inrs.fr)

In systems with various types of noise sources, the characterization and ranking of each source may require a different approach. Also, one of the main challenges in such investigations, consists of isolating each source from the influence of the others. Often in the machines, the constituting plates are efficient radiators whose specific contributions need to be properly determined. In this presentation, we describe a method of plate radiation characterization using multiple input techniques. These techniques have frequently been used in case of discrete sources such as, for instance, vehicle engine cylinders where the pressure variations are modelled as the inputs. This application differs from the traditional ones by the fact that the inputs are now, the elements of a continuous medium. Here the surface of a plate is meshed, each element is taken as a sub-source and consequently, the plate is modelled as an assembly of sub-sources. The plate contributions at the operational modes, are then obtained through vibration measurements and therefore, are not affected by the noise from the other sources. Investigations on structures of various geometries and materials have so far, demonstrated the efficiency of this type of application.

2pSAd3. Forced vibrations of a cylindric panel with regular orthogonal system of stiffeners. Leonid A. Lazarev (Central Aerohydrodynamic Institute (TsAGI), 17, Radio Str., 105005 Moscow, Russian Federation, leonidl74@mail.ru), Boris M. Efimtsov (Central Aerohydrodynamic Institute (TsAGI), 17, Radio Str., 105005 Moscow, Russian Federation, efimtsov@prob-lab.ru)

Forced vibrations of a cylindrical panel freely supported in contour, with regular orthogonal system of stiffeners (typical of aircraft fuselage structure) are investigated. The connection of all three components of displacement of the skin and of discrete stiffeners as well as of the respective elastic and inertial forces and moments are taken into account in the case of excitation by normal and tangential forces. This connection can be described correctly at joint application of the recreptance method and the method of space-harmonics. The task of forced vibrations is solved directly except the procedure of solving the task in terms of eigen-values. Some illustrative examples of the aircraft fuselage panel by a concentric harmonic force are presented. They demonstrate a high efficiency of applying this combined method. Potential possibilities of using this combined method for solving the tasks related to vibrations of a framed skin modeling the aircraft fuselage section and to the sound field in the volume bounded by it are considered.

2pSAd4. Optimisation of building vibration isolation by means of numerical methods. Fülöp Augusztinovicz (Budapest University of Technology and Economics, BME Dept. of Telecommunications, Magyar tudósok körútja 2, H-1117 Budapest, Hungary, fulop@hit.bme.hu)

Ground-borne vibrations pose a steadily increasing environmental problem in densely populated areas of large cities. Although not the cheapest, the application of resilient elements in the construction of new buildings is an effective and viable method. Obviously, experimentation with parameters and placement of the isolators is not possible in this case. Therefore, a careful and watchful optimization of the static and dynamic characteristics of the supporting elements is a must. The proposed paper gives an overview of the vibration isolation design and reports on the expected effect of some basic design versions of a typical multi-storey building. Standard structural finite element method is used as a basic design tool, but a number of vibro-acoustic aspects are also considered and treated. Experimental results as well as comparisons of measurements and predictions will be reported too.

2pSAd5. Refracto-vibrometry - a novel method for visualizing sound waves in transparent media. Lothar Zipser (HTW University of Applied Sciences, Friedrich-List-Pl. 1, D-01069 Dresden, Germany, zipser @et.htw-dresden.de), Heinz H. Franke (HTW University of Applied Sciences, Friedrich-List-Pl. 1, D-01069 Dresden, Germany, zipser@et.htw-dresde.de)

For optimization of new sonic techniques, for development of acoustic sensors or for understanding of complex sonic phenomena it is often desirable to visualize the generation and distribution of the invisible sound waves. A novel method for measuring and visualizing the sound waves in transparent media was developed and tested by the authors. This non-contact method is based on a scanning laser-Doppler vibrometer. It can be used for measuring and visualizing sound fields in gases, fluids and even pellucid solid objects. The variation of the optical refractive index n of transparent media, caused by the sound waves is used as measuring effect. This justifies the denomination ″refracto-vibrometry″. The paper describes the theoretical fundamentals and the technical equipment required for the novel method. As examples, the generation and radiation of sound in air, water and transparent solid objects are presented. The animation of the results as videos is very impressive and instructive. In research, education and system design refracto-vibrometry has a large potential to make acoustics clearer and more feasible for application.

2pSAd6. Influence of the pre-stress state on the wave propagation in a shearable Timoshenko beam. Nicolas Bideau (Institute of Mathematical Research of Rennes IRMAR, Campus de Beaulieu, 35042 Rennes, France, nicolas.bideau@univ-rennes1.fr), Polynice Eyi-Assoumou (Institut de Recherche Mathématique de Rennes, Université de Rennes 1, Campus de Beaulieu, 35042 Rennes, France, polynice.eyi-assoumou @univ-rennes1.fr), Loic Le Marrec (Institute of Mathematical Research of Rennes IRMAR, Campus de Beaulieu, 35042 Rennes, France, loic.lemarrec@univ-rennes1.fr), Lalaonirina Rakotomanana (Institut de Recherche Mathématique de Rennes, Université de Rennes 1, Campus de Beaulieu, 35042 Rennes, France, lalaonirina.rakotomanana-ravelonarivo @univ-rennes1.fr)

It is very common to use pre-stressed beam models in the structure design. However in the nonlinear domain, the modal analysis remains difficult especially when shearability is taken into account. This work aims to study the natural vibrations of pre-stretched nonlinear shearable Timoshenko beam using Cosserat continuum mechanics. In this paper, a three dimensional nonlinear beam model is first developed. Then we analyse waves which are superimposed on a finite pre-stretch state. Namely, analytical dispersion relations are given for different values of pre-strech. The complete spectrum, including propagating and evanescent traction/compression, shear and bending modes, of a pre- stretched shearable beam is calculated through dispersion pattern. Spectrum strongly depends on initial pre-stress value. A significant qualitative and quantitative difference with the classical Timoshenko beam theory is pointed out even for small pre-stretch values.

2pSAd7. Temporal prediction of the acoustic radiation of vibrating structures: subjective evaluation of a simplified approach. Nacer Hamzaoui (LVA, INSA de Lyon, Bat. Saint-Exupéry, 25 bis avenue Jean Capelle, 69621 Villeurbanne, France, nacer.hamzaoui @insa-lyon.fr), Juliette Pierangelo (LVA, INSA de Lyon, Bat. Saint-Exupéry, 25 bis avenue Jean Capelle, 69621 Villeurbanne, France, juliette.pierangelo@insa-lyon.fr), Antoine Levy (LVA, INSA de Lyon, Bat. Saint-Exupéry, 25 bis avenue Jean Capelle, 69621 Villeurbanne, France, antoine.levy@insa-lyon.fr)

The goal of the approach presented in this paper is to predict the noise radiated by vibrating structures with acquired vibratory measurements, in the temporal field, on their surface. In the frequential field this prediction is based on the resolution of the Kirchhoff integral equation, which requires a lot of computing time and is thus limited to low and intermediate frequencies; the boundary element method (BEM) is used for the resolution. Simplifications were already brought to low ($<$ Flim1) and to high ($>$ Flim2) frequencies, leading to a simple calculation of a fast integral. The limiting frequencies (Flim1 and Flim2) depend on the structure dimensions and its position towards the observation point. In this paper we will present an approach developed in the temporal field in which a complete calculation (BEM) is avoided by choosing a minimal distance in order to have Flim1 = Flim2 and use only the simplified calculations. The vibratory data is measured in the temporal field and the studied structure is a parallelepipedic box excited by two mechanical excitation pots which excite one or two faces. The acoustic pressures calculated in the temporal field will be confronted with measurements, by using similarity subjective tests and integrating a variation of the principal parameters intervening in this approach.

2pSAd8. Radiation efficiency of natural modes of plates with beam stiffeners. Andreas Rousounelos (Loughborough University, Department of Aeronautical and Automotive Engineering, Ashby Road, LE11 3TU Loughborough, UK, a.rousounelos@lboro.ac.uk), Stephen J. Walsh (Loughborough University, Department of Aeronautical and Automotive Engineering, Ashby Road, LE11 3TU Loughborough, UK, S.J.Walsh@lboro.ac.uk), Victor V. Krylov (Loughborough University, Department of Aeronautical and Automotive Engineering, Ashby Road, LE11 3TU Loughborough, UK, V.V.Krylov@lboro.ac.uk)

In this paper, the radiation efficiency of the natural modes of finite plates with attached beams is considered. Firstly, the scattering of flexural waves, by the beams and the boundaries, in the plate is considered. The reflection and transmission coefficients along with the near-field coefficients of the beam are used to calculate the vibration field of the plate, by taking into account an infinite number of reflections from the boundaries. A wavenumber transform of the vibration velocity field is used to calculate the sound power and the radiation efficiency. Numerical results are presented, for a number of attached beams, and show that the beams introduce ripples in the radiation efficiency curve, below a certain frequency. The amplitude of the ripples is controlled by the mass and the torsional stiffness of the attached beams whereas the stiffness of the beam has little influence. The results are compared with measurements of the radiation efficiency of plates with attached beams.

2pSAd9. Virtual statistical energy analysis for vibroacoustic industrial prediction. Gérard Borello (InterAC, 10 impasse Borde-Basse, ZA. La Violette, 31240 L'Union, France, gerard.borello@interac.fr), Laurent Gagliardini (PSA Peugeot Citroën, Route de Gisy, 78943 Vélizy-Villacoublay Cedex, France, laurent.gagliardini@mpsa.com), Denis Thenail (PSA Peugeot Citroën, Route de Gisy, 78943 Vélizy-Villacoublay Cedex, France, denis.thenail@mpsa.com)

In the mid-frequency range (200-2000 Hz), difficulty is encountered when modeling car body vibroacoustic interactions, mainly due to the complexity of automotive design. Analytical Statistical Energy Analysis (ASEA) is efficient to bring to the fore regions of interest regarding NVH design but was proven to be accurate only above 2000 Hz. To overcome ASEA limitations at lower frequencies, Virtual SEA (VSEA) technique was introduced to translate the dynamic information contained in a finite element (FE) model into an SEA model. Any FE model, whatever its complexity, can thus be processed thanks to an automatic sub-structuring algorithm and a built-in VSEA modal synthesis solver, fast leading to robust numerical SEA model. VSEA also addresses structure-borne noise problems by coupling structural VSEA subsystems to analytical acoustic subsystems through a virtual wave number. Investigation of damping and trim treatment effects on mixed acoustic and structural subsystems are thus possible. While reviewing VSEA theory, industrial application cases will be presented.

2pSAd10. Noise Prediction for a Pumping Loop using the Noise Synthesis Technology Approach. Henri Pepin (CETIM, 52 Avenue Felix Louat, 60300 Senlis, France, henri.pepin@cetim.fr), Axel Hass (52, avenue Félix Louat, 60304 Senlis, France, Axel.Haas@cetim.fr)

A collective project involving the french manufacturers of industrial pumps and valves is dedicated to the noise prediction in pumping plants. This paper presents a methodology based on virtual acoustic prototyping, and specifically on the noise synthesis technology (NST). Prediction of radiated noise in particular locations, such as operator stations or contractual specifications, allows us to control from the conception stage if the industrial plant will meet the prescribed noise criteria (regulations or user specifications). In addition, related noise control recommendations can be

achieved by comparison of data obtained from the individual response of the components and their interaction. This methodology does not work as an absolute predictive process, and thus requires experimental validation. Components are taken into account by establishing their detailed vibroacoustic characteristics (technical data or measurements); in the present work on a simplified pumping loop, selected components are a centrifugal pumping unit, an open pipe circuit and several type of valves. Vibroacoustic and hydroacoustic measurements have to be adjusted according to the NST requirements. Comparison of the NST results with experimental data show a wide validity domain, covering the 100-10kHz third-octave range.

2pSAd11. Design of air springs for improved frequency response characteristics using computational fluid dynamics. Grace R. Kessenich (IPTRADE, Inc, 1 Gateway Center Suite 601, Newton, MA 02458, USA, grace.kessenich@iptrade.com), Allan D. Pierce (College of Enginering, Boston University, 110 Cummington St, Boston, MA 02215, USA, adp@bu.edu), Baruch Pletner (IPTRADE, Inc, 1 Gateway Center Suite 601, Newton, MA 02458, USA, baruch.pletner@iptrade.com)

High performance air springs can be limited as vibration isolation devices by aeroacoustic cavity resonances. Such systems require detailed knowledge of their frequency response over all frequencies of interest. Transient computational fluid dynamics (CFD) simulations can derive quantitative magnitude and phase data early in the design cycle, before manufacturing. CFD models are unaffected by ambient noise, resonances from other sources, and sensor sensitivity, major experimental concerns. Unlike analytical methods, CFD modeling is applicable to complex as well as simple geometries. The modeling methodology is illustrated in the present study with 2D and 3D simulations of three different prototypical chambers. A chamber wall section, representing a piston, is moved with a sinusoidal displacement at constant frequency. Measurement of the magnitude and phase from the resulting sinusoidal force on this surface provides one point of a frequency response. By running multiple simulations over a wide frequency range, the null and resonant frequencies are readily apparent. Comparison with analytical predictions for simple geometries validates this technique. Insertion of porous membranes in the air spring cavity is modeled and is shown to be an effective method for mitigating aeroacoustic effects on air spring performance. Simulations provide crucial information for membrane parameter and placement optimization.

TUESDAY AFTERNOON, 1 JULY 2008 P2-B, LEVEL 2, 3:40 TO 5:20 P.M.

Session 2pSAe

Structural Acoustics and Vibration and EURONOISE: General Topics in Structural Acoustics and Vibration III (Poster Session)

Wolfgang Kropp, Cochair
Chalmers University of Technology

Sean Wu, Cochair
Wayne State University

All posters will be on display from 3:40 p.m. to 5:20 p.m. To allow contributors an opportunity to see other posters, contributors of odd-numbered papers will be at their posters from 3:40 p.m. to 4:30 p.m. and contributors of even-numbered papers will be at their posters from 4:30 p.m. to 5:20 p.m.

Contributed Papers

2pSAe1. The investigation on sound souce indentification in semi-space by NAH. Dejiang Shang (Harbin Engineering University, College of Underwater Acoustic Engineering, 150001 Harbin, China, chizhafengyun1979@126.com), Yongwei Liu (Harbin Engineering University, College of Underwater Acoustic Engineering, 150001 Harbin, China, chizhafengyun1979@126.com)

The near field acoustic holography (NAH) theory model in semi-space has been constructed on the foundation of NAH theory in full-space. The technique of semi-space acoustic field reconstruction by NAH has been developed on Fast Fourier Transform Algorithm. This method has considered the water surface as soft boundary condition. The equivalent free sound field can be acquired if the measured sound field has been handled dissymmetrically by the principle of the mirror. This method can overcome the disadvantages of the boundary element method which can be used to resolve the problems of sound source identification in semi-space, such as the using of the semi-space Green function, complex transformation matrix calculation, more time consummation and singularity solution existence. This method has been verified by numerical calculation and by experiment respectively. The experimental frequency is between 3 and 10 kHz. The distance between the hologram plane and source plane is 3 centimeter. The results show that it's an efficiency way to deal with the problem of sound source identification in semi-space.

2pSAe2. An analysis of the modes of wave propagation in cylindrical shells. Yu-Cheng Liu (Graduate Institute of the Mechanical & Aeronautical Engineering, Feng Chia University, No. 100 Wenhwa Rd., Seatwen, 40724 Taichung, Taiwan, p9245215@fcu.edu.tw), Yun-Fun Hwang (Electroacoustic Graduate Program, No. 100 Wenhwa Rd., Seatwen, 40724 Taichung, Taiwan, yfhwang@fcu.edu.tw), Jin-Huang Huang (Department of Mechanical and Computer-Aided Engineering, No. 100 Wenhwa Rd., Seatwen, 40724 Taichung, Taiwan, jhhuang@fcu.edu.tw)

Similar to a recent paper by Karczub [J. Acoust. Soc. Am., Vol. 119(6), 3553-3557, 2006], this work utilizes a symbolic math solution to obtain analytical solutions for the dispersion relation in a thin circular cylindrical shell. Analyses on the propagating wave mode shapes are particularly emphasized. The analytical solutions provide a straightforward calculation for all four branches of the dispersion curves, and the cumbersome numerical root searching technique is avoided. The dispersion relations for the breathing and torsional modes (n=0 circular harmonic), which were neglected by

Karczub, are included. Mode shapes that characterize the types of wave that are predominantly transversal, longitudinal, circumferential, or in any combination of the three are analyzed in considerable detail. Effects by thickness and Poisson ratio variations are considered and examined. The cutoff frequencies for the higher order propagating modes are compared among the various orders of circular harmonics, from n = 0 to 10. Finally, comparison among several shell theories in the dispersion relation prospective, which is directly related to their accuracy in predicting the vibratory resonant frequencies of a finite shell, is also included in the discussion.

2pSAe3. Influence of Constructional Parameters Of Small Reciprocating Compressors on Sound Power Emissions. Peter J. Kral (Vienna University of Technology, Institute for Engineering Design and Logistics Engineering, Getreidemarkt 9/E307, 1230 Vienna, Austria, peter.kral@tuwien.ac.at)

Noise in the environment is an increasing problem in industrial countries and is often strongly restricted by governmental laws. Therefore reducing sound levels must be one target in every design process. This paper describes in detail the influence of constructional parameters on the total sound power emitted by a small reciprocating compressor (V_H=159 m^3) with reed valves. Measurements (sound power levels, sound pressure levels, FFT-analysis, time-signal analysis) on a test bed situated in an anechoic room by varying the operating conditions - for example - rotational speed, maximum pressure, and suction terms, were done. Additionally sound power measurements with regard to reed valve parameters (thickness of the reed, area of the inlet and outlet port of the valve plate, material of the valve plate) were achieved. Theoretically researches with the aid of computational methods (FEM-Analysis with Ansys, Calculations with MatLab) are presented and show very good accordance compared to the sound level measurements. These results should lead to a better understanding of the causal connection between constructional (valve) parameters/operating conditions and the resulting sound power emissions. Finally the differentiation of airborne and structure born noise may be helpful to minimize the noise emissions of compressors already within the design process.

2pSAe4. Modelling of the hydro and aero acoustic sources in piping. Véronique Villouvier (EDF/R&D, 1 avenue du Général de Gaulle, 92141 Clamart, France, veronique.villouvier@edf.fr)

In the industrial piping networks, various components are crossed by flows, generally in air or in water. The pressure fluctuations generated locally close to these singularities are propagated then in all the network and can lead to important vibrations of the structures. A research program based on many laboratory tests made it possible to highlight a hydroacoustic modelling of the butterfly valves in the low frequencies domain. The model, which describes the acoustic sources, generated by the turbulence, has a general applicability. In this paper, one presents the application of this model to orifices (openings and slits) working in air and in water. These various orifices were studied from an acoustic point of view on different test loops and for several hydraulic conditions (flow rate and head loss). These experimental cases were then simulated using the source model of turbulence noise, associated to the transfer matrix of each singularity, which is determined by another way. The comparison between these calculations and the corresponding measurements makes it possible to consolidate the general character of the model of turbulence noise for singularities in piping.

2pSAe5. Hydroacoustic modeling of the butterfly valves - some industrial applications. Véronique Villouvier (EDF/R&D, 1 avenue du Général de Gaulle, 92141 Clamart, France, veronique.villouvier@edf.fr)

The French PWR units include a large number of control valves which are sometimes at cavitation working for certain operating conditions. The very high excitations which are then created may lead to the cracking of some small lines located nearby. These devices have been tested on laboratory test loops. An hydroacoustic behaviour model has been set up on the basis of very precise identifications obtained from numerous experimental tests. The model obtained describes the acoustic transfers through the valve and the sources generated by turbulence and cavitation in the low frequency domain, according to the main operating parameters: aperture, flow rate, cavitation number, upstream pressure and diameter. Hydraulic and vibratory measurements were carried out on several Residual Heat Removal circuits for many control configurations. When this circuit is functioning under certain conditions, the two valves which regulate the hot and cold flow rates operate according to a cavitation system. The hydroacoustic valve model is used to simulate of the valves under the hydraulic conditions of measurements. The results are compared at the vibratory levels recorded on site. The model also makes it possible to determine the optimal operating conditions in order to limit the vibrations of the circuit.

2pSAe6. Use of noise and vibration signal for detection and monitoring of cavitation in kinetic pumps. Jan Černetič (University of Ljubljana, Faculty of Mechanical Engineering, Aškerčeva 6, 1000 Ljubljana, Slovenia, jan.cernetic@fs.uni-lj.si), Jurij Prezelj (University of Ljubljana, Faculty of Mechanical Engineering, Aškerčeva 6, 1000 Ljubljana, Slovenia, jurij.prezelj@fs.uni-lj.si), Mirko Čudina (University of Ljubljana, Faculty of Mechanical Engineering, Aškerčeva 6, 1000 Ljubljana, Slovenia, mirko.cudina@fs.uni-lj.si)

Cavitation in kinetic pumps causes lowering performance, mechanical damage and increase of vibrations and noise. Therefore, it is important to detect inception and development of cavitation phenomenon in the pump. This paper deals with signals of vibrations and noise, which will be used for detection and monitoring of cavitation in kinetic pumps, and also to prevent the effect of cavitation in the pump and pumping system. When the cavitation is increasing, the flowing conditions are changing, which leads to an increase of vibrations of the pump and emitted noise in the surroundings. Because vibrations and noise are transferred from the pump through its casing, the signal is non-uniformly distorted due to transfer losses and structure of the casing surfaces. Even so, it is possible to determine development of cavitation phenomena from the measured signal. Noise and vibrations are increasing steadily, but in some specific frequency ranges the signal is more pronounced than in other part of the spectrum. Experimental results have shown that when the cavitation is fully developed, the measured signals at a characteristic frequency or range of frequencies start to decrease. This characteristic frequency or band of frequency is discussed in this paper, and also comparison between theoretical expectations and measurement results was performed.

2pSAe7. The wavelet analysis the acoustic emission signals generated by multi-source partial discharges. Andrzej Cichon (Technical University of Opole, ul. Miko^{3}ajczyka 5, 45-271 Opole, Poland, a.cichon@po.opole.pl), Sebastian Borucki (Technical University of Opole, ul. Miko^{3}ajczyka 5, 45-271 Opole, Poland, s.borucki@po.opole.pl), Tomasz Boczar (Technical University of Opole, ul. Miko^{3}ajczyka 5, 45-271 Opole, Poland, t.boczar@po.opole.pl)

Within the research work, the results of which are presented in this paper, a comparative analysis of the acoustic emission (AE) signals generated by multi-source partial discharges (PDs) was carried out. The research investigations were carried out in a model system in which PDs were generated with two spark-gaps. A spark-gap in the surface system and a point-plane spark-gap were used due to the fact that these are the most commonly occurring PD forms in power transformers. The AE signals were registered with a contact transducer placed on the external part of the tub. The analysis in the time-frequency domain using a short-time Fourier transform (STFT) was carried out for the AE signals generated by PDs. The results of the analysis are shown in the form of two- and three-dimensional spectrograms of the power spectral density and three-dimensional spectrograms of the amplitude spectrum.

2pSAe8. Using wavelet transform to locate acoustic emission source in composite plate with one sensor. Amir Refahi Oskouei (Polytechnic of Tehran, AmirKabir University of Technology, Department of Mechanical Engineering, NDT Lab., 424 Hafez Ave, 15875-4413 Tehran, Iran, amir.refahi@cic.aut.ac.ir), Mehdi Ahmadi (Polytechnic of Tehran,

AmirKabir University of Technology, Department of Mechanical Engineering, NDT Lab., 424 Hafez Ave, 15875-4413 Tehran, Iran, ahmadin@cic.aut.ac.ir)

In this paper a new method for locating the AE source with one sensor is presented. When acoustic emission signals propagate in wave-guided, they have multi-mode and dispersion characteristics. The separation of the modes at the sensors could make it possible to extract the exact information about the source that produced the waves. Based on the modal nature of AE, it can be understood that a good location would have two methods to determine the arrival times. One is determined on the same part of the waves (not only the same mode, but also the same frequency) at all sensors. The other is determined on the different modes at one sensor, which makes it possible to reduce the number of sensors needed. First, through modal analysis of the propagation of elastic waves in a thin plate, the dispersion characteristics of the modes are predicted. Second, the wavelet transform theory is briefly outlined and its application in elastic waves is explained. It is shown that by using the peak of the magnitude of the wavelet transform, the arrival times of the different modes can be determined. Additionally, experiments were undertaken using a lead break on the edge of the plate. These demonstrated the feasibility of the one sensor linear location scheme.

2pSAe9. Effect of boundary restraints on sound radiation. Wen Li (Wayne State University, Department of Mechanical Engineering, 5050 Anthony Wayne Dr., Detroit, MI 48202, USA, wli@wayne.edu)

This study is focused on the effect of boundary restraints on the sound radiation from a rectangular plate. The modal and acoustic characteristics of square plates are studied for different restraining stiffnesses and configurations. It is shown that the modes of the restrained plates can be considerably different from those for the familar simply supported boundary condition, so are the corresponding modal radiation efficiencies. The proposed method generally applies to the plates elastically restrained along any edge(s) and for any stiffness values. The acoustic calculations are also valid for any acoustic wavenumber, instead of only for some extreme acoustic-/structural wavenumbers as in other investigations.

2pSAe10. Progress in Primary Calibration of Acoustic Emission Sensors. Jiri Keprt (Brno University of Technology, UAMT-FEEC, Kolejni 2906/4, 61200 Brno, Czech Republic, keprt@feec.vutbr.cz), Petr Benes (Brno University of Technology, UAMT-FEEC, Kolejni 2906/4, 61200 Brno, Czech Republic, benesp@feec.vutbr.cz)

The paper reviews the background of the primary calibration of acoustic emission sensors and the determination of uncertainty by this calibration. There are discussed the aims and the purpose of the primary calibration and main sources of uncertainty in practical usage of calibration results. The comparison of the results of the both method is presented. The shape of calibration characteristics corresponds well up to 500 kHz. The calculation of the uncertainty in the reciprocity and step function calibration is closely described. The problem of propagation of uncertainty in the fast fourier algorithm was solved. Uncertainty of measurement by primary calibration is determined and presented in the paper. The uncertainty in reciprocity calibration of UT 1000 in range from 60 kHz to 285 kHz was $\pm$3dB and from 285 kHz to 1 MHz up to $\pm$8 dB and the same results in the calibration by step function. The calculation of the uncertainty includes all the presumable sources. Such as variation of input coefficient of reciprocity parameter, impact of thickness of glass capillary Also the main problems, that were solved and have to be solved, are presented.

2pSAe11. High-speed electronic speckle pattern interferometry of a struck flat plate. Thomas Moore (Rollins College, Department of Physics, Winter Park, FL 32789, USA, tmoore@rollins.edu), Daniel Zietlow (Rollins College, Department of Physics, Winter Park, FL 32789, USA, dzietlow@rollins.edu), Christopher Gorman (Rollins College, Department of Physics, Winter Park, FL 32789, USA, cgorman@rollins.edu)

An electronic speckle pattern interferometer capable of imaging 33,000 frames per second has been used to study the transient motion of a flat plate which was struck at a point near the edge. Multiple interferograms, each with an exposure time of 25 microseconds, were combined to construct a video of the plate motion that can be used for both qualitative and quantitative analysis. The interferograms reveal the expected evolution of the bending waves created when a thin circular plate is struck near the edge; however, anomalous displacement of the surface of the plate is also observed. This unusual displacement of the surface takes the form of a transverse wave that precedes the motion directly attributable to the normal propagation of the initial bending wave.

2pSAe12. The Investigation on Measuring the Reflection Coefficient of Materials in Semi-space by Spatial Fourier Transforms. Yongwei Liu (Harbin Engineering University, College of Underwater Acoustic Engineering, 150001 Harbin, China, chizhafengyun1979@126.com), Dejiang Shang (Harbin Engineering University, College of Underwater Acoustic Engineering, 150001 Harbin, China, chizhafengyun1979@126.com), Qi Li (Harbin Engineering University, College of Underwater Acoustic Engineering, 150001 Harbin, China, chizhafengyun1979@126.com)

A new method using SFT (Spatial Fourier Transforms) has been investigated to measure reflection coefficient at arbitrary angles of incidence by NAH(Near-field Acoustical holography) in semi-space. The paper gives an experimental verification of this method. The experimental frequency is from 3 kHz to 10 kHz. The size of test steel plate is 1.6m$\times$1.5m,the size of hologram surfaces is 1.32m$\times$1.14m, the distance between two hologram surface and the test material is about 2cm, the distance between sound source and water surface is about 4cm. The measured results are generally in good agreement with the theoretical value; the mean-square error of data is below 0.06. The experimental results show that this method eliminates the effect of the scattered sound field of the water surface completely. Because the sound source and the test material are set near the water surface during the experiment, it is very easy to set the measuring system, and this is very useful in practice.

2pSAe13. Optimizing the Dynamic Behaviour of a Large Portal Robot. Christian R. Koenig (University of Bremen, Badgasteiner Str. 1, FZB - Room 2140, 28359 Bremen, Germany, chkoenig@uni-bremen.de), Markus Kochmann (University of Bremen, Badgasteiner Str. 1, FZB - Room 2140, 28359 Bremen, Germany, kochmann@uni-bremen.de), Jan Ohlendorf (University of Bremen, Badgasteiner Str. 1, FZB - Room 2140, 28359 Bremen, Germany, johlendorf@uni-bremen.de), Dieter H. Müller (University of Bremen, Badgasteiner Str. 1, FZB - Room 2140, 28359 Bremen, Germany, ml@biba.uni-bremen.de), K.-D. Thoben (University of Bremen, Badgasteiner Str. 1, FZB - Room 2140, 28359 Bremen, Germany, tho@biba.uni-bremen.de)

The object under investigation in this work is a portal robot used for the production of large fibre reinforced structures. The achieved product quality and the production speed of the device are influenced by the vibration and the damping behaviour of the system. The required process time is determined by kinematic parameters, i.e. speed and acceleration of the system and the dead time required for the vibration level to decay to a threshold level given by the required precision of process. In the first step, a Design of Experiments is used in order to identify the ideal combination of acceleration and speed. At this optimum, the sum of the drive time and the dead time reaches a minimum for a given precision. In the second step, an experimental Modal Analysis is performed in order to identify the potential for an optimization of the structure.

2pSAe14. Evaluation of hand-transmitted vibration exposure on basis of a questionnaire. Rauno Pääkkönen (Finnish Institute of Occupational Health, P.O:Box 486, 33101 Tampere, Finland, rauno.paakkonen@ttl.fi), Riitta Sauni (Finnish Institute of Occupational Health, P.O:Box 486, 33101 Tampere, Finland, riittta.sauni@ttl.fi), Jukka Uitti (Finnish Institute of Occupational Health, P.O:Box 486, 33101 Tampere, Finland, jukka.uitti@ttl.fi), Esko Toppila (Finnish Institute of Occupational Health, P.O:Box 486, 33101 Tampere, Finland, esko.toppila@ttl.fi)

We made a survey to see if metal workers had symptoms caused by vibration. The vibration exposure over lifetime was also asked. The cumulative HAV dose was calculated as a HAV index determined on the basis of the questionnaire, in which jobs, tools and active work time (hours/day, days/week, moths/year) had been requested. An index, I, describing the total

HAV exposure was determined by I= a8h2 x y x d, where I = cumulative exposure index (m2ad/s4), y = exposure time in years (a), and d = annual exposure time in days. The exposure of metal workers varied 1-5 m/s2, and the average was 2.4 m/s2. The limit value of European directive 5 m/s2 is not usually exceeded. However, there is a wide unaccuracy area that needs to be cleared one way or another. We also connected symptoms and exposure on statistical level. The total exposure times did not differ significantly in these groups, but, when the daily HAV exposure was taken into account in the calculation of the cumulative index, the difference was statistically significant.

2pSAe15. Experimental investigation of the acoustic black hole effect for vibration damping in elliptical plates. François Gautier (Laboratoire d'Acoustique de l'Université du Maine, Avenue Olivier Messiaen, 72085 Le Mans, France, francois.gautier@univ-lemans.fr), Jacques Cuenca (LAUM, CNRS, Université du Maine, Lab. d'Acoustique Université du Maine, UMR CNRS 6613, 72085 Le Mans Cedex 9, France, Jacques.Cuenca.etu@univ-lemans.fr), Victor V. Krylov (Loughborough University, Department of Aeronautical and Automotive Engineering, Ashby Road, LE11 3TU Loughborough, UK, V.V.Krylov@lboro.ac.uk), Laurent Simon (LAUM, CNRS, Université du Maine, Lab. d'Acoustique Université du Maine, UMR CNRS 6613, 72085 Le Mans Cedex 9, France, Laurent.Simon@univ-lemans.fr)

It is well known that flexural waves in beams or plates slow down if their thickness decreases. A beam or a plate with a decreasing thickness in the vicinity of one of their boundaries can be designed so that the travel time needed for a wave to reach the edge becomes infinite. Thus, the reflection coefficient associated with the corresponding region is zero. This effect is referred to as the acoustic black hole effect. The use of 'acoustic black holes' in combination with thin damping layers for wedges of power-law profile has been theoretically and experimentally studied by V.V. Krylov and R.E.T.B. Winward (JSV 300 (2007) 43-49). The aim of this paper is to show experimentally the acoustic black hole effect in a two-dimensional configuration comprising an elliptical plate with a pit of power-law profile placed in one of its focuses. The elliptical shape of the plate induces a focalization of waves towards the black hole, which is observed by means of scanning laser vibrometry. Comparison of input mobility measurements for plates with and without black hole shows the reduction in vibrational level induced by the black hole effect.

2pSAe16. Characterising elastic layers as non-lightly damped SDOF systems for the reduction of impact transmission noise. Francisco Simon (Instituto de Acústica (CSIC), C/ Serrano 144, 28006 Madrid, Spain, psimon@ia.cetef.csic.es), David K. Anthony (Instituto de Acústica (CSIC), C/ Serrano 144, 28006 Madrid, Spain, iaca344@ia.cetef.csic.es)

There is a wealth of literature dealing with modal determination of lightly damped viscous systems, however there is relatively little reported for medium and heavily damped systems or with non-viscous damping. The most commonly reported and applied methods have significant errors in the determination of both modal frequency and damping ratio for systems with high damping. For the lightly damped case simplification can be often conveniently made to allow the performance of each method to be studied theoretically, however for the non-lightly damped case this is not possible and the analysis must proceed on a heuristic basis. For the application modal parameter determination of elastic floor layers designed to reduce building transmission noise by impact testing, traditional and new methods of modal parameter determination for non-lightly are presented and heuristically evaluated for both viscous and non-viscous SDOF systems. It is also shown the performance often depends on the type of damping. This either must be known a priori or can be gleaned by comparing results from different methods.

2pSAe17. Eigenvalue imaging method for subsurface defects detection. Kenbu Teramoto (Saga University, 1-Honjo, 8408502 Saga, Japan, tera@me.saga-u.ac.jp)

This paper proposes the eigenvalue imaging method to be independent of frequency and phase velocity and to characterize the Lamb-wave field. Lamb-waves play important roles in NDE fields. Being placed on the surface of a plate, a sound source excites several kinds of waves: (a) pressure and shear waves, (b) a Rayleigh wave, and (c) symmetric and anti-symmetric Lamb-waves traveling along the plate. The first two waves are utilized for traditional ultrasonic techniques such as pulse-echo methods. In contrast to these classical techniques, in which the wavelength is shorter than the plate thickness, the Lamb-wave has the advantage of propagating over large area. The variation of the Lamb-wave velocity, however, causes difficulties for interpretation of observed signals. It is important, therefore, to establish the crack detection criterion independent of local wave numbers. This paper proposes a novel imaging method which utilizes the 3rd and 4th eigenvalues of the covariance matrix, which is defined over the 4- dimensional vector space which is spanned by following components: (1) a vertical displacement, (2) its particle velocity, (3) the orthogonal pair of out-of-plane strains. This study shows that the 3rd eigenvalue detects a wave scattered by defects and the 4th one has an ability to localize defects.

Session 2pSCa

Speech Communication: Speech Perception II

Souhila Messaoud-Galusi, Chair
University College London, Wolfson House, Department of Phonetics and Linguistics, 4 Stephenson Way, London, NW1 2HE, UK

Contributed Papers

2:00

2pSCa1. Cue switching in the perception of approximants: Evidence from two English dialects. Rachael-Anne Knight (City University, Department of Language and Communication Science, Northampton Square, EC1V 0HB London, UK, knight@city.ac.uk), Christina Villafana Dalcher (City University, Department of Language and Communication Science, Northampton Square, EC1V 0HB London, UK, cvdalcher@mac.com), Mark J. Jones (University of Cambridge, Phonetics Lab, Department of Linguistics, Raised Faculty Building, Sidgwick Avenue, CB3 9DA Cambridge, UK, markjjones@hotmail.com)

A surprising dissimilarity is attested in the perception of approximants by speakers of American and Standard Southern British English. Eighteen subjects (6 AE and 12 SSBE) performed an identification task in which they judged whether stimuli were more like /r/ or /w/. The stimuli comprised five sounds, copy-synthesised from a source /r/, where the values of F2 and F3 we adjusted to fall between the frequencies typical for [″turned r″] and [w]. The only significant difference between the two dialect groups' performance occurred with a token in which F3 was at a frequency typical for /r/ and F2 was lowered to that of /w/. AE and SSBE speakers identified this token as /r/ 90% and 59% of the time, respectively. This is unexpected as /r/ in both dialects is characterised by a low F3. However, the difference may be due to the existence of the 'labiodental' variant of /r/ in SSBE. As this variant does not have a low F3, SSBE speakers must tolerate a wider diversity of /r/-types than AE speakers. Therefore, the /r/ category in SSBE may be becoming increasingly defined by F2, rather than F3, which also has implications for the future production of /r/ in this accent

2:20

2pSCa2. Dialectal effects in the perception of vowels produced by first and second language speakers: North Carolinian versus Southern Welsh listeners. Ricardo Augusto Hoffmann Bion (SISSA - Cognitive Neuroscience, VL Stock 2/2, 34135 Trieste, Italy, ricardobion@gmail.com), Paola Escudero (University of Amsterdam, Institute of Phonetic Sciences, Spuistraat 210, 1012 VT Amsterdam, Netherlands, P.R.EscuderoNeyra@uva.nl), Geoffrey Stewart Morrison (Australian National University, School of Language Studies, Building 110, ACT 0200 Canberra, Australia, geoff.morrison@anu.edu.au)

This paper investigated the effect of listeners' regional origin on the perception of vowels. Listeners from North Carolina and South Wales were presented with natural tokens of the four English vowels /i/, /I/, /E/ and /{/ which were produced by L1 and L2 speakers. Randomization tests revealed a significant difference between the listener groups' confusion matrices. Examination of the confusion matrixes suggested that the dialectal differences were primarily in the vowel contrasts /I/-/E/ and /E/-/{/. In order to explore these findings, logistic regression models were fitted to each listener group's responses (predictor variables in the models were initial and final formant values and duration). Territorial maps based on the logistic regression models indicated that there was a substantial difference in the locations of the /E/-/{/, and a smaller difference in the location of the /I/-/E/ boundary.

2:40

2pSCa3. Is there evidence of an allophonic mode of speech perception in dyslexic children. Souhila Messaoud-Galusi (University College London, Wolfson House, Department of Phonetics and Linguistics, 4 Stephenson Way, NW1 2HE London, UK, souhila@phon.ucl.ac.uk), Valerie Hazan (University College London, Wolfson House, Department of Phonetics and Linguistics, 4 Stephenson Way, NW1 2HE London, UK, val@phon.ucl.ac.uk), Stuart Rosen (UCL, Wolfson House, 4, Stephenson Way, NW1 2HE London, UK, stuart@phon.ucl.ac.uk)

Recent studies have suggested that dyslexics perceive phonemic categories in a less categorical fashion than individuals of average reading ability due to increased within-category discrimination ('allophonic' mode of perception). In the present study, 62 dyslexic and 51 typically-developing (TD) children aged between 6;6 and 13;7 years old were tested on the perception of a /pi-bi/ continuum using an adaptive identification task presented in clear and in background noise, and a fixed-level discrimination task presented in clear. They also undertook a battery of tests of reading, IQ, phonological awareness, phonological short-term memory and word perception in noise. The gradient of the identification function was significantly weaker for the dyslexic than TD group in clear, but the two groups did not differ in the noisy condition. In the discrimination test, there was no evidence of increased within-category discrimination in the dyslexic group but the TD group showed better cross-category discrimination. These results do not support the existence of an allophonic model of speech perception in dyslexic children. Also, they do not support the view that dyslexic children are more affected by noise as a result of more poorly specified phonemic categories. [Work supported by Wellcome Trust].

3:00

2pSCa4. fMRI evidence for central auditory processing of speech in deaf infants under sedation. Scott K. Holland (Cincinnati Children's Hospital Medical Center, Imaging Research Center, 3333 Burnet Ave, Cincinnati, OH 45229, USA, scott.holland@cchmc.org), Prasanna Karunanayaka (Cincinnati Children's Hospital Medical Center, Imaging Research Center, 3333 Burnet Ave, Cincinnati, OH 45229, USA, KAR4RP@cchmc.org), Akila Rajagopal (Cincinnati Children's Hospital Medical Center, Imaging Research Center, 3333 Burnet Ave, Cincinnati, OH 45229, USA, RAJA7Y@cchmc.org), Kristen Smith (Cincinnati Children's Hospital Medical Center, Imaging Research Center, 3333 Burnet Ave, Cincinnati, OH 45229, USA, SMIJ6D@cchmc.org)

Functional MRI (fMRI) performed in infants with congenital hearing loss provides evidence that auditory language stimulation produces activation of the central auditory system in the brain. Babies are normally sedated for clinical MRI scans. With IRB approval we have added a 10 minute fMRI scanning procedure to clinically indicated MRI scans in infants with severe to profound hearing impairment (n=18) or normal hearing (n=22). Sedation is performed according to clinical guidelines at our institution using either Propofol ((200-250 mcg/kg/min i.v.) or pentobarbital (5 mg/kg orally). fMRI scanning is performed using Echo-planar gradient echo acquisitions on a 3 Tesla clinical MRI system while a mothers voice reads stories to the babies at a sound level 10 dB above the measured hearing threshold. Brain activation is measured in primary auditory cortex and planum temporale speech recognition areas. Results in the normal hearing group of infants demonstrates that the central auditory system is stimulated by speech in in-

fants, although sedation does attenuate brain activation in a dose dependent manner. Central auditory and language activation is also detected in hearing impaired infants with levels of activation correlating to measured hearing thresholds.

3:20

2pSCa5. Left parietal activation during the production of pointing in several modalities: prosodic focus, syntactic extraction, digital- and ocular- pointing. Hélène Loevenbruck (Speech and Cognition Department, GIPSA-lab, 46 avenue Félix Viallet, 38031 Grenoble, France, Helene.Loevenbruck@gipsa-lab.inpg.fr), Coriandre Vilain (Speech and Cognition Department, GIPSA-lab, 46 avenue Félix Viallet, 38031 Grenoble, France, coriandre.vilain@gipsa-lab.inpg.fr), Francesca Carota (Centre de Neuroscience Cognitive, 67, Boulevard Pinel, 69675 Bron, France, Francesca.Carota@isc.cnrs.fr), Monica Baciu (Laboratoire de Psychologie et NeuroCognition, UFR Sciences de l'Homme et de la Société, BP47, 38040 Grenoble, France, monica.baciu@upmf-grenoble.fr), Christian Abry (Centre de Recherche sur l'Imaginaire (CRI), Université Stendhal, Grenoble 3, BP 25, 38040 Grenoble cedex 9, France, christian.abru@u-grenoble3.fr), Laurent Lamalle (Plateforme régionale IRM 3Tesla, IFR n° 1, RMN Biomédicale : de la cellule à l'homme, CHU de Grenoble, BP 217, 38043 Grenoble Cedex 9, France, Laurent.Lamalle@ujf-grenoble.fr), Cédric Pichat (Laboratoire de Psychologie et NeuroCognition, UFR Sciences de l'Homme et de la Société, BP47, 38040 Grenoble, France, cedric.pichat@upmf-grenoble.fr), Christoph Segebarth (Grenoble Institut de Neurosciences, CHU de Grenoble - B.P. 217, 38043 Grenoble, France, csegebar@ujf-grenoble.fr)

Deixis, or pointing, is the ability to draw the viewer/listener's attention to an object, a person, a direction or an event. Pointing is gradually acquired by children, first with the eyes, then with the finger, then with intonation and finally with syntax. The crucial role of digital pointing in language acquisition suggests that all modalities of pointing may share a common cerebral network. An fMRI study of the production of multimodal pointing was carried out on 15 subjects. Subjects were scanned during the execution of index finger pointing gestures, eye pointing gestures, prosodic pointing (focus) and syntactic pointing (extraction). The results of a random effect group analysis show that the left superior parietal lobule (BA 7) was activated in all three digital, ocular and prosodic pointing but not in syntactic pointing. These results indicate that pointing in different modalities may recruit the left superior parietal lobule, with ocular pointing more anterior than prosodic pointing, itself more anterior than digital pointing. A grammaticalisation process is suggested to explain the lack of parietal activation in syntactic pointing.

TUESDAY AFTERNOON, 1 JULY 2008 ROOM 250B, 2:00 TO 3:40 P.M.

Session 2pSCb

Speech Communication: Speech Articulation I

Helen M. Hanson, Chair
Union College, 807 Union St., Schenectady, NY 12308, USA

Contributed Papers

2:00

2pSCb1. Acoustic cues to the voicing contrast in coda stops in the speech of 2-year-olds learning American English. Helen M. Hanson (Union College, 807 Union St., Schenectady, NY 12308, USA, hansonh@union.edu), Stefanie Shattuck-Hufnagel (Massachusetts Institute of Technology, Research Laboratory of Electronics, Speech Communication Group, 77 Massachusetts Ave., Cambridge, MA 02139, USA, stef@speech.mit.edu)

Developing a model of how children acquire the phonological feature contrasts and phonetic cues of their adult speech community requires a detailed understanding of how production changes during development. Earlier studies based on listening provided an initial estimate of these patterns; recent instrumental studies of the acoustic and articulatory details of production during development have revealed some surprises, including covert contrasts between distinctive feature categories (e.g., Scobbie et al., 1996) and of incomplete acquisition of adult feature-cue patterns (Imbrie, 2005), which can be difficult for adults to hear. Few instrumental studies, however, have focused on the child's cue patterns for coda consonants (although see Song and Demuth, in press). Our study of cues to the feature [voice] for coda stops used quantitative acoustic analyses of tokens from the Imbrie corpus of 2-year-old speech to compare child productions with those of their adult caretakers. Results show that a) many children produce a noisy region at the end of the vowel for voiceless codas (in duck, cup) but a long strong voice bar during closure for voiced codas (in bug, tub), and b) these cues may be exaggerated versions of the feature cues of their adult caretakers.

2:20

2pSCb2. Are acoustic and articulatory changes of speech produced in noise only related to the increase in vocal intensity? Maeva Garnier (University of New South Wales, Music Acoustics, School of Physics, NSW 2052 Sydney, Australia, maeva.garnier@gmail.com), Nathalie Henrich (Département Parole & Cognition, GIPSA-lab, 46, avenue Félix Viallet, 38031 Grenoble Cedex, France, Nathalie.Henrich@gipsa-lab.inpg.fr), Danièle S. Dubois (CNRS, LCPE/LAM 11 rue de Lourmel, 75015 Paris, France, ddubois@ccr.jussieu.fr)

Speech acoustics and articulation are modified in speech produced in noisy environments. Is this simply a result of the increase in vocal intensity or may these modifications be some communicative strategies to increase audiovisual intelligibility? We recorded a first acoustic database with ten speakers and a second acoustic and articulatory database with three speakers, for quiet and for two kinds of background noise. We first verified previous observations about speech modifications in noise and observed that some are not strongly correlated to the increase in vocal intensity and cannot be entirely explained by previous models of vocal effort. We also made additional observations. Pitch does not only rise in noise but also extends its dynamic. For female speakers, pitch not only rises but also fits spectrum ″holes″ of cocktail-party noise. Speech modifications are not only global

over the whole utterance but also specific to some of its units. Articulatory modifications consist not only of an amplification of lip movements, but also correspond to an enhancement of the potentially visible contrast between vowels. Lastly, some articulatory changes may be compensation for formant modifications induced by the increase in vocal intensity, rather than a consequence of it.

2:40

2pSCb3. Muscle saturation effect in /i/ production: Counterevidence from a 3D biomechanical model of the tongue. Stéphanie Buchaillard (ICP/GIPSA-lab, INPG, 46 Avenue Félix Viallet, 38031 Grenoble Cedex 01, France, stephanie.buchaillard@gipsa-lab.inpg.fr), Pascal Perrier (ICP/GIPSA-lab, INPG, 46 Avenue Félix Viallet, 38031 Grenoble Cedex 01, France, Pascal.Perrier@gipsa-lab.inpg.fr), Yohan Payan (TIMC-IMAG, Pavillon Taillefer, Faculté de Médecine, 38706 La Tronche cedex, France, yohan.payan@imag.fr)

Numerous works suppose the existence of a saturation effect to facilitate the control of the constriction area when producing vowel \i\. This study exploits a 3D biomechanical Finite Element model of the vocal tract to evaluate the effectiveness of this assumption. The model includes the tongue and its major muscles, represented as a hyperelastic body, inserted in the oral cavity including jaw, palate, pharyngeal walls and hyoid bone. Muscles activations are controlled with the lambda model (Equilibrium-Point Hypothesis). After determining a set of possible motor commands to generate vowel \i\, the impact of local variations of these commands on tongue shape was studied. The main tongue muscles motor commands were independently modified (by $\pm 2\%$, 5%, 8% around their values at target) and the effect on the tongue shape and on the acoustic signal was studied. The simulations showed a global stabilization of the tongue body, thanks to the palatal contacts, but also variability in the alveolar groove due to the anterior genioglossus activation. Though extremely localized, this variation has an important impact on the constriction size and, then, on the acoustic signal. Consequently, a specific control of the articulatory variability could be necessary to explain experimental data for vowel \i\.

3:00

2pSCb4. Compensatory tongue patterns in glossectomy patients. Emi Murano (University of Maryland Dental School, 650 W Baltimore St. #8402, Department of Biomedical Sciences, Baltimore, MD 21201, USA, emurano@umaryland.edu), Maureen Stone (Vocal Tract Visualization Lab, Depts of Biomedical Sciences and Orthodontics, University of Maryland Dental School, 650 W. Baltimore St., Baltimore, MD 21201, USA, mstone@umaryland.edu), Xiaofeng Liu (The Johns Hopkins University, 3400 N Charles Street, 105 Barton Hall, Baltimore, MD 21218, USA, xiaofeng@jhu.edu), Jiachen Zhuo (University of Maryland Medical System, 22 South Greene Street, Department of Diagnostic Radiology, Baltimore, MD 21201, USA, JZHUO@umm.edu), Andrew Salama (University of Maryland Dental School, 650 W Baltimore St. #8402, Department of Biomedical Sciences, Baltimore, MD 21201, USA, asalama@umm.edu), Rao Gullapalli (University of Maryland Medical System, 22 South Greene Street, Department of Diagnostic Radiology, Baltimore, MD 21201, USA, RGULLAPALLI@umm.edu), Robert Ord (University of Maryland Dental School, 650 W Baltimore St. #8402, Department of Biomedical Sciences, Baltimore, MD 21201, USA, rord@umm.edu), Jerry Prince (The Johns Hopkins University, 3400 N Charles Street, 105 Barton Hall, Baltimore, MD 21218, USA, prince@jhu.edu)

To examine the effects of glossectomy surgery on tongue deformation strategies, a unique combination of data was used, including internal tongue strain patterns from tagged-cine-MRI and detailed muscle architecture from high-resolution MR images. Two glossectomy patient groups were studied and compared to normal controls. They differed in the type of reconstruction after cancer excision: primary closure or reconstruction with forearm flap. All patients included in this study had the same tumor type (Squamous Cell Carcinoma), size (T1 and T2) and location (unilateral mid-third of oral tongue). The tongue developed distinct deformation strategies that move the remaining tongue tissue, the flap and the scar tissue. Compensatory patterns such as pivot points and areas of rigidity will be shown and discussed. These appear to be compensatory strategies to optimize speech output after surgery. This presentation is based on viewing the tongue as a muscular hydrostat, which provides the basis for hypotheses about the formation and release of areas of rigidity within the tongue. The rigidity might be a way to simplify sound-specific strategies for moving the tongue and controlling changes in its shape in normal and patient subjects. Supported by NIH K99DC009279, and R01DC01758 from the NIDCD.

3:20

2pSCb5. Statistical identification of critical, dependent and redundant articulators. Philip J. Jackson (University of Surrey, Centre for Vision, Speech and Signal Processing, GU2 7XH Guildford, UK, p.jackson@surrey.ac.uk), Veena D. Singampalli (University of Surrey, Centre for Vision, Speech and Signal Processing, GU2 7XH Guildford, UK, v.singampalli@surrey.ac.uk)

An automatic method for identifying critical, dependent and redundant roles in speech articulation is presented. Critical articulators are identified using the Kullback-Leibler divergence between phone-specific and model pdfs, which are initialised to the grand pdfs for each articulator. Model pdfs of critical and dependent articulators, those significantly correlated with the critical ones, are updated accordingly for both 1D and 2D cases, as long as the divergence exceeds the threshold. Those unaffected are termed redundant. Algorithm performance is evaluated on the MOCHA-TIMIT database by comparison with phonetic features. Results are also given for an exhaustive search, and principal component analysis of articulatory fleshpoints. Implications of being able to extract phonetic constraints automatically from articulatory recordings are discussed.

Session 2pSCc

Speech Communication: General Topics in Speech Communication II (Poster Session)

Yukari Hirata, Cochair
Colgate University, Dept. of East Asian Lang. and Lit., 13 Oak Dr., Hamilton, NY 13346, USA

James Hillenbrand, Cochair
Western Michigan University, Dept. Speech Path. and Aud., 1903 W. Michigan Ave., Kalamazoo, MI 49008, USA

Natasha Warner, Cochair
University of Arizona, MPI NIjmegen, Dept. of Linguistics, Box 210028, Tucson, AZ 85721, USA

All posters will be on display from 3:40 p.m. to 5:20 p.m. To allow contributors an opportunity to see other posters, contributors of odd-numbered papers will be at their posters from 3:40 p.m. to 4:30 p.m. and contributors of even-numbered papers will be at their posters from 4:30 p.m. to 5:20 p.m.

Contributed Papers

2pSCc1. A grouping approach to harmonic complexes. Dirkjan J. Krijnders (University of Groningen, Dept. Artificial Intelligence, P.O. Box 407, 9700 AK Groningen, Netherlands, j.d.krijnders@ai.rug.nl), Maria E. Niessen (University of Groningen, Dept. Artificial Intelligence, P.O. Box 407, 9700 AK Groningen, Netherlands, m.niessen@ai.rug.nl), Tjeerd C. Andringa (University of Groningen, Dept. Artificial Intelligence, P.O. Box 407, 9700 AK Groningen, Netherlands, t.andringa@ai.rug.nl)

Humans seem to perform sound-source separation for quasi-periodic sounds, such as speech, mostly on harmonicity cues. To model this function, most machine algorithms use a pitch-based approach to group the speech parts of the spectrum. In these methods the pitch is obtained either explicitly, in autocorrelation methods, or implicitly, as in harmonic sieves. If the estimation of pitch is wrong, the grouping will fail as well. In this paper we show a method that performs harmonic grouping without first calculating the pitch. Instead a pitch estimate is associated with each grouping hypothesis. Making the grouping independent of the pitch estimate makes it more robust in noisy settings. The algorithm obtains possible harmonics by tracking energy peaks in a cochleogram. Co-occuring harmonics are compared in terms of frequency difference. Grouping hypotheses are formed by combining harmonics with similar frequency differences. Consistency checks are performed on these hypotheses and hypotheses with compatible properties are combined into harmonic complexes. Every harmonic complex is evaluated on the number of the harmonics, the number of subsequent harmonics and the presence of a harmonic at the pitch position. By using the number of subsequent harmonics octave errors are prevented. Multiple concurrent harmonic complexes can be found as long as the spectral overlap is small.

2pSCc2. The role of generalization in learning perceptual contrasts. Meghan Sumner (Stanford University, Department of Linguistics, Margaret Jacks Hall, Stanford, CA 94305-2150, USA, sumner@stanford.edu)

Understanding spoken language is a difficult task. Variation caused by accents make this task even more daunting. This project examines the generalization of novel phonetic cues by listeners of non-native speech. Native speakers of English were trained on Korean-English pronunciations of minimal pairs with word-final contrasts (e.g., bed - bet). While native English speakers rely on vowel duration to cue a final voicing contrast, native Korean speakers of English do not produce a vowel duration contrast, but use a different distinguishing phonetic cue (e.g., voicing into closure duration). Listeners were trained on a subset of minimal pairs ending in final stops (bet - bed). Following successful training, listeners participated in an immediate or long-term form priming task. Four conditions included: Trained Identity (bet - bet), Trained Non-identity (bed - bet), Novel Non-identity, Trained Rime (wet - wed), and Novel Non-identity, Novel Rime (beat - bead). Preliminary results show episodic treatment of words in the immediate priming task, but generalization to novel forms in the long-term priming task. These data suggest that early learning is mediated by episodic representations - learning proceeds episodically until sufficient information is available to support a more abstract generalization.

2pSCc3. Vocalizations of deaf infants before and after cochlear implantation. Mary K. Fagan (Indiana University School of Medicine, Riley Research Wing 044, 699 West Drive, Indianapolis, IN 46202, USA, mkfagan@indiana.edu)

Critical aspects of spoken language depend on perceiving and understanding speech sounds. For deaf infants, however, neither sound perception nor awareness of the sound-making consequences of their actions is available. The goal of this study was to uncover and document early, measurable effects of hearing loss on infant vocalization and changes in these behaviors following cochlear implantation. Participants were 8 deaf infants, 7-11 months old, and 8 infants with cochlear-implants, 12-20 months old and 1-6 months post-implantation. Dependent variables include number of vocalizations, mean vocalization duration, and mean frequency before and after cochlear implantation and in relation to reduplicated babble onset and word production. Post-implant changes in vocal behaviors may have clinical implications for decisions regarding age of implantation and auditory habilitation as well as for understanding post-implant variability.

2pSCc4. Contrastive Focus in Taiwan Mandarin. Ho-Hsien Pan (Dept. of Foreign Languages and Literatures, National Chiao Tung University, 1001 TA Hsueh Road, 300 Hsinchu, Taiwan, hhpan@faculty.nctu.edu.tw), Hui-Ying Tsou (Dept. of Foreign Languages and Literatures, National Chiao Tung University, 1001 TA Hsueh Road, 300 Hsinchu, Taiwan, hytsou@ms11.hinet.net), Wan-Ting Huang (Dept. of Foreign Languages and Literatures, National Chiao Tung University, 1001 TA Hsueh Road, 300 Hsinchu, Taiwan, caissybelle@yahoo.com.tw)

This study investigated the production and perception of given, new, and contrastive information in Taiwan Mandarin. Spontaneous dialogues elicited through a game were analyzed to access the acoustical parameters marking different information structures. In perceptual studies, two perceptual experiments, (1) a dialogue history experiment, of which listeners identified the questions preceding the sentences, and (2) a pair comparison experi-

ment, of which subject compared sentence with same wording but different information structures were used. The stimuli were either natural utterances form elicited spontaneous dialogues or resynthesized utterances with conflicting duration and f0 cues swapped from utterances of different information structures. Preliminary results of production experiments showed that duration elongation is a more consistent cue for marking narrow and contrastive foci than f0 range expansion. Listeners performed better in the pair comparison experiments than in the dialogue history experiment. For nature utterances, listeners were able to identify sentences with given information, given versus new information, and given versus contrastive information, but were not able to identify utterances with more than two contrastive foci. Listeners' performances declined when resynthesized utterances with conflicting duration and f0 cues were presented. When presented with conflicting cues, listeners relied more on durational than f0 cues.

2pSCc5. Comparison of Japanese expressive speech perception by Japanese and Taiwanese listeners. Chun-Fang Huang (Japan Advanced Institute of Science and Technology, 1-1, Asahidai, Nomi, 923-1292 Sendai, Japan, chuang@jaist.ac.jp), Donna Erickson (Showa University of Music, 808 Sekiguchi, Atsugi, 243-8521 Kanagawa, Japan, EricksonDonna2000@gmail.com), Masato Akagi (Japan Advanced Institute of Science and Technology, 1-1, Asahidai, Nomi, 923-1292 Sendai, Japan, akagi@jaist.ac.jp)

Language is an important tool in speech communication. Even without the understanding of one language, we can still judge the expressive content of a voice, such as happiness or sadness. However, sometimes misunderstanding of emotional communication occurs. It is not clear what the common/different features are that help or hinder people with different culture/native-languages background in making judgments about the expressivity of speech. In order to explore this question, we focus on Japanese and Taiwanese listeners perception of Japanese expressive speech utterances. We used the perceptual model proposed by [Huang and Akagi, InterSpeech 2005; 2007], which involves a concept called ″semantic primitives″-- adjectives for describing voice perception. This concept simplifies and clarifies the discussion of common/different features in terms of acoustic cues and expressive speech perception categories. Using this model, we found some common/different features in the perception of expressive speech. Specifically, our results suggest that there may be primary and secondary semantic primitives associated with acoustic speech characteristics which are involved in the perception of expressive speech, and that people from different cultures/native-language background tend to use the same primary semantic primitives in perceiving expressive speech but different secondary ones.

2pSCc6. Acoustic analysis of the vocal tract during vowel production by finite-difference time-domain method. Hironori Takemoto (ATR Cognitive Information Science Laboratories, 2-2-2 Hikaridai, Seika-cho Soraku-gun, 619-0288 Kyoto, Japan, takemoto@atr.jp), Parham Mokhtari (ATR Cognitive Information Science Laboratories, 2-2-2 Hikaridai, Seika-cho Soraku-gun, 619-0288 Kyoto, Japan, parham@atr.jp), Tatsuya Kitamura (Konan University, Okamoto 8-9-1, Higashinada, 658-8501 Kobe, Japan, t-kitamu@konan-u.ac.jp)

An acoustic simulator based on the finite-difference time-domain (FDTD) method was evaluated by acoustic measurements on solid models of the vocal tract. Three-dimensional vocal tract (3D VT) shapes for a male subject during production of the five Japanese vowels were measured by magnetic resonance imaging. Transfer functions of the 3D VT shapes were computed by the acoustic simulator. The accuracy of the finite-difference algorithm was second-order in time and fourth-order in space. From the same 3D VT shapes, solid models were made of epoxide resin by a stereolithographic technique, and their acoustic transfer functions were measured using a time-stretched pulse signal. The calculated and measured spectra were compared up to 8 kHz. Although locations of major poles and zeros were common between calculated and measured spectra, the calculated spectra showed a larger number of small zeros, possibly caused by underestimation of VT acoustic losses in the simulation. However, the lower four formants were simulated remarkably accurately, with a mean absolute error of only 2.2 % compared with the acoustic measurements. These facts indicated that the acoustic simulator can reasonably account for acoustic phenomena within the VT.

2pSCc7. Speech intelligibility determined with various tests presented against noise. Edward Ozimek (Umultowska 85, 61-614 Poznan, Poland, ozimaku@amu.edu.pl), Dariusz Kutzner (Umultowska 85, 61-614 Poznan, Poland, konsbol@wp.pl), Anna Warzybok (Umultowska 85, 61-614 Poznan, Poland, a_warzybok@poczta.onet.pl)

The paper describes three Polish tests for assessment of speech intelligibility under noisy conditions: the matrix test, the sentence test and the digit triplet test. The matrix test contains semantically unpredictable sentences of fixed syntactical structures. This test is very useful for long-term intelligibility measurements and is applicable for subjects with profound hearing loss or cochlear implants users. The sentence test comprises utterances taken from everyday speech and aims at clinical speech intelligibility measurements. The digit triplet test contains sequences of three digits that are spoken separately and is aimed at screening measurements, especially via telephone. The statistical and phonemic properties of the tests are analyzed and compared. The correlation between results obtained in the respective tests and the tests applicability are also discussed.

2pSCc8. Consonants, but not vowels, prime lexical decision following masked priming. Boris New (CNRS - Université Paris Descartes, 71 Avenue Edouard Vaillant, 92100 Boulogne-Billancourt, France, boris.new@univ-paris5.fr), Veronica Araujo (CNRS - Université Paris Descartes, 71 Avenue Edouard Vaillant, 92100 Boulogne-Billancourt, France, veronica.cruzaraujo@gmail.com), Nathalie Bour (CNRS - Université Paris Descartes, 71 Avenue Edouard Vaillant, 92100 Boulogne-Billancourt, France, psynat93@hotmail.com), Thierry Nazzi (CNRS - Université Paris Descartes, 45 rue des Saints-Pères, 75006 Paris, France, thierry.nazzi@univ-paris5.fr)

Recently, Nespor et al (2003) have argued that consonants play a more important role at the lexical level than vowels. This proposal has received direct support from studies showing that 16/20/30-month-old infants are better at processing specific consonantal than vocalic information while learning new words (Nazzi, 2005; Nazzi & New, 2007). This proposal is also supported, although indirectly, by studies on adults. Adults have been found to rely more on consonants than on vowels when asked to transform a nonword into a real word (Cutler et al., 2000). Moreover, adults presented with a continuous stream of syllables are able to segment it into ″lexical units″ by relying on consonantal but not vocalic information (Bonatti et al., 2005). In our study, we directly investigate this issue using a visual masked priming lexical decision task (an oral version being currently implemented). The test items are bisyllabic (CVCV or VCVC) and trisyllabic (CVCVCV or VCVCVC) words, which are presented following four different primes: identity (e.g., joli-joli), unrelated (vabu-joli), same consonants (jalu-joli) and same vowels (vobi-joli). Priming was found for the identity and same consonants conditions, not for the same vowels condition, supporting the privileged role of consonants at the lexical level.

2pSCc9. Frequency importance function of Mandarin Chinese speech. Jing Chen (Dept. of Machine Intelligence, Speech and Hearing Research Center, 2 Science Building, Peking Univ., 5 Yeheyuan Road, Haidian District, 100871 Beijing, China, chenj@cis.pku.edu.cn), Tianshu S. Qu (Dept. of Machine Intelligence, Speech and Hearing Research Center, 2 Science Building, Peking Univ., 5 Yeheyuan Road, Haidian District, 100871 Beijing, China, qutianshu@cis.pku.edu.cn), Xihong H. Wu (Dept. of Machine Intelligence, Speech and Hearing Research Center, 2 Science Building, Peking Univ., 5 Yeheyuan Road, Haidian District, 100871 Beijing, China, wxh@cis.pku.edu.cn), Qiang Huang (Dept. of Machine Intelligence, Speech and Hearing Research Center, 2 Science Building, Peking Univ., 5 Yeheyuan Road, Haidian District, 100871 Beijing, China, QIANG

.HUANG@SPREADTRUM.COM),Ying Huang(Dept. of Psychology, Peking Univ., 5 Yeheyuan Road, Haidian District, 100871 Beijing, China, innhuang@gmail.com), Liang Li (Dept. of Psychology, Peking Univ., 5 Yeheyuan Road, Haidian District, 100871 Beijing, China, liangli@pku.edu.cn), Huisheng S. Chi (Dept. of Machine Intelligence, Speech and Hearing Research Center, 2 Science Building, Peking Univ., 5 Yeheyuan Road, Haidian District, 100871 Beijing, China, chi@pku.edu.cn)

The speech intelligibility index (SII) theory objectively assesses speech intelligibility, and the frequency-importance function (FIF), which reflects the relative importance of various frequency bands to speech intelligibility for various languages, occupies the central part of the theory. However, the FIF has not been examined for tonal Chinese Mandarin speech. In this study, considering the characteristics of Mandarin speech, 50 phonemically-balanced one-syllable words were selected as the speech stimuli from the speech corpus ″A Method for Calculating Articulation Index (GB/T 15508-1995)″, which meets the National Standards of China, and the 1/3 octave FIF was measured and computed with the Fletcher's method. The results show that spectrum regions with frequencies 2000-4000 Hz are more important in Chinese speech than those in English speech. The results predicted by SII model with the new FIF fit the result of human psychophysical studies well, which indicate that the new FIF model is effective and appropriate for assessing the intelligibility of Mandarin speech even when a steady-state noise masker is co-presented. [Supported by the NSFC 60435010; 60535030; 60605016; 30670704]

2pSCc10. Arabic Diagnostic Rhyme Test using minimal pairs. Bachir Boudraa (USTHB Faculté d'électronique et d'informatique, BP 32, El-Alia, 16031 Alger, Algeria, b.boudraa@yahoo.fr), Malika Boudraa (USTHB Faculté d'électronique et d'informatique, BP 32, El-Alia, 16031 Alger, Algeria, mk.boudraa@yahoo.fr), Bernard Guerin (INPG, Avenue Félix Viallet, 38031 Grenoble, France, Bernard.Guerin@enserg.fr)

In this paper, we try to adapt to Arabic the diagnostic rhyme test (DRT) developed by Voiers for English and adapted to French by Peckels & Rossi. DRT is specific to each language and is essential to subjective assessments of coders and synthesizers. Six Arabic pertinent dimensions are used which are acuteness, compactness, tenseness, stridence, nasality and flatness. 72 monosyllabic meaningful pairs of words called minimal pairs have been developed. The apprehensibility of every attribute is tested in each of six vowel contexts. Every feature has been repeated six times and has been paired twice with every vowel.

2pSCc11. A fascinating personage in the history of phonetics: The phonetics and the politics of Elise Richter. Natasha Warner (University of Arizona, MPI NIjmegen, Box 210028, Dept. of Linguistics, Tucson, AZ 85721-0028, USA, nwarner@u.arizona.edu)

Elise Richter (1865-1943) was the first woman lecturer or professor in Austria or Germany, and she was also an experimental phonetician and even an experimental phonologist. Richter's career was delayed by the roles allowed for women at the time, and the end of her career, and her life, came about through the Nazis' policies toward Jews. Richter began her scientific work in Romance philology, but decided to seek explanations for historical sound change in phonetics. This led her to a productive career in experimental phonetics, and she even applied phonetic methods to study questions of phonological structure. Richter was a leader in exploring new methods and bringing together questions across widely differing fields. Although her specific experimental findings were superseded with time, Richter's refusal to be constrained by the limits of a field led her to ideas that have become current in phonetics just recently. In addition to her scientific career, Richter was politically active, both in working to expand women's opportunities and in general politics. This poster presents a new perspective on Richter's contributions to phonetics and on her view of feminism. Furthermore, it makes new observations of a parallel between Richter's political activities and her scientific work.

2pSCc12. The role of tongue articulation for /s/ and /z/ production in whispered speech. Hirohide Yoshioka (University of Tsukuba, 1-4-5 Shinmei, Urawa, 336-0023 Saitama, Japan, hirohide-y@mtc.biglobe.ne.jp)

Although the timing of the initiation and cessation of vocal fold vibrations is crucial to characterize the voiced and voiceless cognates, other cues, such as the duration of preceding vowels, the patterns of the formant transitions in the following vowels, and the period of stop closure, may also play important roles in performing these distinctions. The present study is to further investigate the role of tongue articulatory movements during voiced and unvoiced consonant production, specifically when the vocal folds do not vibrate during the production of fricative consonants, /s/ and /z/ in whispered speech. A normal Japanese speaker served as the subject. The palato-lingual contact patterns during the intervocalic consonant /s/ and /z/ in whispered speech were recoded using dynamic electro-palatography. The results show that the area of palato-lingual contact is clearly wider during /z/ production than /s/ production; the opening for fricative turbulent noise production is narrower and longer for /z/ than for /s/. In addition, the contact pattern is unstable for /s/ production.

2pSCc13. Production and perception of V1V2 described in terms of formant transition rates. René Carré (Laboratoire Dynamique du Langage, UMR 5596, CNRS, Université Lyon 2, 14 Avenue Marcelin Berthelot, 69363 Lyon cedex 07, France, recarre@wanadoo.fr)

Vowels can be produced with static articulatory configurations leading to stable formant frequencies (targets). Here, an algorithm computes area functions according to the criterion of minimal deformation leading to maximal acoustic variations. Within this evolutionary dynamics, the deformations of the tube are not performed to reach targets, unknown during the process, but to move in the acoustic space in order to increase acoustic contrast. The corresponding formant trajectories in the acoustic space can be described in terms of formant transition rates. For example, following this dynamic approach, to produce [ae] from [a], the transition rates of F1 and F2 are necessary and sufficient to represent [e] and at the very beginning of the transition and throughout the transition there is sufficient information to detect [e]. This assertion means that the transition duration is more or less constant. Studies of V1V2 production and perception characterized by their formant transition rates are presented. Such a representation leads to new interpretations of vowel reduction, coarticulation, perceptual overshoot, hyper and hypo speech, normalization.

2pSCc14. The effect of facal dynamics on infant perception of adult-directed speech in noise. Linda Polka (McGill University, School of Communication Sciences and Disorders, Beatty Hall, 1266 Pine Avenue West, Montreal, QC H3G 1A8, Canada, linda.polka@mcgill.ca), Robin Panneton (Virginia Polytechnic Instit. & State Univer., Williams Hall, Blacksburg, VA 24061-0436, USA, Panneton@vt.edu), Jessica Versele (Virginia Polytechnic Instit. & State Univer., Williams Hall, Blacksburg, VA 24061-0436, USA, Versele@vt.edu)

Recently Polka and Rvachew (in press) found that 6- to 8-month-old infants discriminated a native contrast(″bu″ - ″gu″) when familiarized and tested with syllables presented in quiet, but not when familiarized with syllables mixed with a competing noise, even when testing was conducted in quiet. Because the competing noise (segments of cricket and bird song) did not create energetic masking, infant failure to encode the familiarization syllable was due to a disruption in attention to the speech stream. Importantly, in this study, infants watched a checkerboard while listening to syllables spoken in an adult-directed (AD) style. The current study investigated if the addition of a dynamic face facilitates infants' speech processing in the same task. Six-month-olds were habituated to repetitions of the native syllable ″ba″ mixed with the same noise but these infants saw and heard syllables produced in AD style. Following habituation, infants were presented familiar (repetitions of ″ba″) and novel test trials (repetitions of ″ga″). Infants failed to show syllable discrimination as indexed by a reliable preference for

the novel test trials. These findings show that a dynamic face producing AD speech does not engage infant attention to speech enough to support syllable discrimination in noise.

2pSCc15. Voicing offsets and onsets in relation to intraoral pressure values in lingual obstruents of German. Laura L. Koenig (Haskins Labs. and Long Island Univ., Brooklyn, New York, NY 11201-8423, USA, koenig@haskins.yale.edu), Susanne Fuchs (ZAS, Schuetzenstr. 18, 10117 Berlin, Germany, fuchs@zas.gwz-berlin.de)

Phonation requires that tracheal pressure remain higher than intraoral pressure (Pio). In obstruent consonants, a major constriction in the upper vocal tract yields an increase in Pio, inhibiting phonation. The degree of Pio increase in consonants varies as a function of laryngeal and supraglottal apertures. Voiceless stops involve a rapid buildup and discharge of Pio, whereas fricatives involve more gradual changes in Pio. This work quantifies phonation offsets and onsets in German obstruents in relation to the Pio at these times. Pio signals were recorded via a pressure transducer affixed to the posterior end of an EPG palate while 9 speakers of standard German produced intervocalic voiceless consonant sequences (stops, fricatives, affricates, and clusters). Past theoretical work suggests that phonation offsets and onsets will show a hysteresis effect, with onsets requiring higher driving pressures than offsets. Of particular interest here is whether the extent of hysteresis differs among stops, fricatives, and obstruent sequences. Data on intraoral pressure change will also be compared with EPG data to explore how supraglottal constrictions affect Pio, and thus, phonation.

2pSCc16. Magnetic Resonance investigation of palatalized stop consonants and spirants in Russian. Galina Y. Kedrova (Moscow State Lomonosov University, GSP-2, Leninskije Gory, MGU, 1st Humanities, R. 983, Centre for New Technologies in Humanities, 119992 Moscow, Russian Federation, kedr@philol.msu.ru), Nikolay V. Anisimov (Moscow State Lomonosov University, GSP-2, Leninskije Gory, MGU, 1st Humanities, R. 983, Centre for New Technologies in Humanities, 119992 Moscow, Russian Federation, kedr@philol.msu.ru), Leonid M. Zaharov (Moscow State Lomonosov University, GSP-2, Leninskije Gory, MGU, 1st Humanities, R. 983, Centre for New Technologies in Humanities, 119992 Moscow, Russian Federation, kedr@philol.msu.ru), Yurij A. Pirogov (Moscow State Lomonosov University, GSP-2, Leninskije Gory, MGU, 1st Humanities, R. 983, Centre for New Technologies in Humanities, 119992 Moscow, Russian Federation, kedr@philol.msu.ru)

The research in question is aimed at the experimental MRI-investigation of articulatory gestures corresponding to the palatalized Russian stop consonants [p'], [t'], [k'], [b'], [d'], [g'] and spirants [s'], [z'] [h'] countered with their non-palatalized counterparts [p], [t], [k], [b], [d], [g], [s], [z] [h] in Russian speech production. An experimental dataset was based upon 2D MR-images, audio- and video recordings taken from 4 native speakers of Russian (3 males and 1 female) producing VCCV sequencies (Russian pseudo-words with the second vowel stressed) containing Russian consonants under investigation in the vocalic contexts [a]_[a] and [a]_[i]. All speaking subjects had standard pronunciation and were without any perceptible articulation disease. MRI investigation of the Russian consonantal phonemes was based upon admitted procedures and techniques though expanded with several new original methods elaborated by the Russian team of experimentalists. Experimental data was collected through several MRI sessions (done in a month and in a year with participation of the same speaking subjects), ensuring thereby credibility and robustness of the experimental results. A detailed analysis of the whole dataset of MR-images of palatalised Russian consonants countered with their non-palatalized counterparts revealed special articulatory pattern of palatalisation in Russian.

2pSCc17. Duration of Japanese singleton and geminate obstruents in two- to four-mora words. Yukari Hirata (Colgate University, 13 Oak Drive, Department of East Asian Languages and Literatures, Hamilton, NY 13346, USA, yhirata@mail.colgate.edu), Hiroaki Kato (ATR Cognitive Information Science Laboratories, 2-2-2 Hikaridai, Seika-cho Soraku-gun, 619-0288 Kyoto, Japan, kato@atr.jp), Keiichi Tajima (Hosei University, 2-17-1 Fujimi, Chiyoda-ku, 102-8160 Tokyo, Japan, tajima@hosei.ac.jp)

Hirata and Whiton [J. Acoust. Soc. Am. 118, 1647-1660 (2005)] found an invariant durational structure for Japanese stop quantity distinction in two- and three-mora words across different speaking rates. The present study examined whether their finding extends to include fricative and affricate quantity distinctions and three- and four-mora words. Stimuli were stop, fricative, and affricate contrasts in four types of words, including (1) a long vowel (e.g., ka.so.o vs. ka.s.so.o), (2) a moraic nasal (e.g., ji.se.n vs. ji.s.se .n), (3) CV sequence (e.g., ho.so.ku vs. ho.s.so.ku), and (4) shorter words (e.g., i.shi vs. i.s.shi), spoken in isolation at three speaking rates by four native Japanese speakers. Duration of contrasting obstruents, words, and the interval between the onsets of the first and the second vowels (VOI) was measured. Results indicated durational patterns similar to those found previously for stop contrasts. In addition, duration of words, regardless of their segmental composition, reflected well the number of moras they contained. Finally, the ratio of the contrasting obstruent to the word and the ratio of the VOI to the mean mora duration were useful in classifying the singleton and geminate categories across rates. [Supported by Grant-in-Aid for Scientific Research, JSPS]

2pSCc18. Effects of hand gesture and lip movements on auditory learning of second language speech sounds. Spencer Kelly (Colgate University, 13 Oak Drive, Department of Psychology, Hamilton, NY 13346, USA, skelly@mail.colgate.edu), Yukari Hirata (Colgate University, 13 Oak Drive, Department of East Asian Languages and Literatures, Hamilton, NY 13346, USA, yhirata@mail.colgate.edu), Jen Simester (Colgate University, 13 Oak Drive, Department of Psychology, Hamilton, NY 13346, USA, jsimester@gmail.com), Jackie Burch (University of Rochester, 585 Elmwood Ave., Box 645, Rochester, NY 14642, USA, Jaclyn_Burch @mail.urmc.rochester.edu), Emily Cullings (Colgate University, 13 Oak Drive, Department of East Asian Languages and Literatures, Hamilton, NY 13346, USA, ecullings@mail.colgate.edu), Jason Demakakos (Colgate University, 13 Oak Drive, Department of Psychology, Hamilton, NY 13346, USA, jdemakakos@mail.colgate.edu)

Previous research found that auditory training helps native English speakers to perceive phonemic vowel length distinction in Japanese, but that their performance has never reached native levels (Hirata et al., 2007). Given that multimodal information, such as hand gesture and lip movements, influences semantic aspects of language processing and development (Kelly et al., 2002), we examined whether this multimodal information helps to improve native English speakers' ability to perceive Japanese vowel length distinction. Forty-five native English speakers participated in one of three types of training: (1) audio alone; (2) audio with hand gestures; and (3) audio with lip movements and hand gestures. Before and after training, participants were given phoneme perception tests that measured their ability to distinguish between short and long vowels in Japanese, e.g., /kato/ versus /kato:/. Our original prediction was that more modalities in training would result in greater learning. Although all three groups improved from pre- to post-test, there were no significant differences among the three training groups. Unlike the original prediction, hand gestures and lip movements did not seem to augment learning of difficult sound distinctions. We will discuss possible benefits and limitations of using multimodal information in second language speech learning.

2pSCc19. MRI-based 3-D vocal tract acoustic analysis of an American English lateral sound. Xinhui Zhou (Speech communication lab, Institute of systems research and department of electrical and computer engineering, University of Maryland, College Park, MD 20742, USA, zxinhui @umd.edu), Carol Y. Espy-Wilson (Speech communication lab, Institute of systems research and department of electrical and computer engineering, University of Maryland, College Park, MD 20742, USA, espy

@glue.umd.edu),Mark Tiede(Haskins lab and MIT Research lab of electronics, 300 George street suite 900, New Haven, CT 06511, USA, tiede@haskins.yale.edu), Suzanne Boyce (Department of communication sciences and disorders, University of Cincinnati, Mail location 0394, Cincinnati, OH 45267, USA, boycese@email.uc.edu)

The lateral sound /l/ in American English involves a complex articulatory configuration that includes one or two lateral channels along the sides of the tongue, and sometimes a lingual-alveolar contact. The acoustic characteristics of /l/ consist of a third formant (F3) that is close in frequency to the F3 of the adjacent vowel(s), but is often considerably weaker in amplitude. Generally, there is relatively weak energy in the F3-F5 region. The articulatory-acoustic relationship is not well understood. Previous studies did not consider the 3-D vocal tract model and the area function extraction was based on some assumed model. In this study, we constructed a 3-D vocal tract geometry based on magnetic resonance images from one subject during sustained production of syllabic dark /l/ (as in ″pole″), and performed finite-element analysis. The harmonic analysis showed that the frequency response of the 3-D vocal tract is comparable in many ways to the spectrum of the acoustic signal, suggesting good agreement between the actual and reconstructed vocal tracts. A pole-zero pair is found in F3-F4 region, which may explain the weak energy level in this frequency region. Application of the 3-D wave propagation property to vocal tract area function extraction will also be discussed. [Research supported by NIH.]

2pSCc20. The acoustics of yer and non-yer vowels [e] and [o] in Slovak. Stefan Benus (Constantine the Philosopher University, Stefanikova 67, 94901 Nitra, Slovakia, sbenus@ukf.sk)

Yers of Slavic languages are vowels that alternate with zero and historically developed from high short lax vowels. In Slovak, both front and back yers were preserved and surface as [e] and [o] respectively. For example, the second [o] in kotol 'cauldron-Nom-Sg' is a yer because it disappears with adding a suffix vowel: kotla 'cauldron-Gen-Sg'. Compare with a non-yer [o] in kostol 'church-Nom-Sg', kostola 'church-Gen-Sg'. Traditional phonological accounts of this difference (e.g. Rubach 1993) assume that yer vowels are underlyingly different from non-yer vowels and merge with [e] and [o] through a phonological process. Therefore, these accounts predict that yer and non-yer vowels should be phonetically identical since they enter the phonetic component already merged as [e] or [o]. The results of our acoustic experiments show that yer vowels are phonetically different from non-yer vowels. The most salient differences were observed in the first formant and duration: yers have lower F1 than non-yers, and for some subjects they are also shorter. This finding supports the view that the phonetic component has access to deep phonological alternations and that phonetics-phonology is a single cognitive system in which the components have different granularities and interact bidirectionally.

2pSCc21. Behavioral and physiological correlates of language preference. Megha Sundara (UCLA Department of Linguistics, 3125 Campbell Hall, Los Angeles, CA 90095-1543, USA, megha.sundara@humnet.ucla.edu), Christine Kitamura (MARCS Auditory Laboratories, Bankstown Campus, Building 1, University of Western Sydney, Locked Bag 1797, 1797 Penrith South DC NSW, Australia, c.kitamura@uws.edu.au), Thierry Nazzi (CNRS - Université Paris Descartes, 45 rue des Saints-Pères, 75006 Paris, France, thierry.nazzi@univ-paris5.fr)

With increasing experience listening to language, infants' sensitivity to the patterns of their native language becomes more specialized. In monolingual, hearing infants, this tuning-in into the native language has been demonstrated in an elegant experiment. Hayashi et al. (2001) tested Japanese-learning infants between 4 and 14 months on their preference for listening to Japanese when compared to English. Not surprisingly, Japanese-learning infants preferred to listen to Japanese over English. Critically, the magnitude of this native language preference increased linearly from 4- to 14-months. In this study, we replicated and extended Hayashi et al.'s results. We tested 65 Australian-English learning infants aged 3 - 16 months on their preference for Australian-English compared to Japanese sentences. Our results confirm the findings of Hayashi et al.: Australian-English hearing infants' prefer their native language, and this preference increases linearly with age. We also tested preference when the same infants heard Australian-English and German sentences. English and German are rhythmically similar, while differing in segmental characteristics. Results indicate that similar to early language discrimination, rhythmic distance affects the emergence of language preference. We are currently analysing concomitant heart rate measured from these infants when they were listening to native and non-native sentences.

2pSCc22. Improvement of speech recognition thresholds by spectral modulation enhancement. Chang Liu (University of Texas, Dept. of Comm. Sci. & Dis., 1 University Station A1100, Austin, TX 78712, USA, changliu@mail.utexas.edu), David A. Eddins (University of Rochester, Department of Otolaryngology, Rochester, NY 14618, USA, David_Eddins @URMC.Rochester.edu)

Our previous studies have shown that vowel identification in noise was significantly improved by spectral enhancement resulting from modifications in the spectral modulation domain. The present study investigates whether spectral enhancement results in improved speech recognition in background competition. Speech recognition thresholds (SRT) were measured in a long-term speech shaped (LTSS) noise and in multi-talker babble using NU-6 words with and without spectral enhancement for young normal-hearing listeners. Results indicated that SRTs were significantly reduced, by 2.2 dB, in LTSS noise and in babble when speech sounds were spectrally enhanced between 2.0 and 2.5 cycles/octave, while no significant changes in SRTs occurred for enhancement between 1.5 and 2 cycles/octave or between 1.5 and 2.5 cycles/octave. Spectral modulation transfer functions were also measured for each listener. Linear regression analyses showed that SRT improvement was moderately correlated with modulation detection thresholds at a spectral modulation frequency of 0.5 cycles/octave. Thus, it appears that better modulation detection at low spectral modulation frequencies is associated with greater improvement in word recognition in background competition.

2pSCc23. Perception of sinewave vowels. James M. Hillenbrand (Western Michigan University, Dept of Speech Path & Aud., 1903 W. Michigan Ave., Kalamazoo, MI 49008, USA, james.hillenbrand@wmich.edu), Michael J. Clark (Western Michigan University, Dept of Speech Path & Aud., 1903 W. Michigan Ave., Kalamazoo, MI 49008, USA, michael.clark@wmich.edu)

There is a significant body of research examining the intelligibility of sinusoidal replicas of naturally spoken utterances. Discussion has followed about what the sinewave speech phenomenon might imply about the auditory and perceptual mechanisms that are involved in phonetic recognition. However, this work has typically been conducted using meaningful and syntactically well formed sentences, making it unclear what the relative contributions are of higher level, top-down processes as opposed to lower level auditory and phonetic mechanisms. The simple purpose of this study was to measure vowel intelligibility using sinusoidal replicas of naturally spoken /hVd/ syllables. The sinusoidal signals were modeled after 300 utterances selected from a database of 1,668 syllables spoken by men, women, and children [Hillenbrand, Getty, Clark, and Wheeler, J. Acoust. Soc. Am., 97, 3099-3111 (1995)]. Listeners consisted of 74 students enrolled in an introductory phonetics course. Recognition rates for the sinusoidal vowels averaged 55%, with considerable variability across listeners. This figure is substantially lower than the ~95% intelligibility (measured in several earlier studies) of the naturally spoken signals upon which the sinusoidal replicas were modeled. Attempts to improve performance using three different training methods met with modest success, with post-training recognition rates rising by ~5-12 percentage points, depending on the training method.

2pSCc24. Complexity of acoustic-production-based models of speech perception. Geoffrey Stewart Morrison (Australian National University, School of Language Studies, Building 110, ACT 0200 Canberra, Australia, geoff.morrison@anu.edu.au)

Discriminant analysis models trained on acoustic vowel production data have been found to have significant correlation with listeners' perception. Two regularised discriminant analysis models were trained on monolingual speakers' vowels. One model was trained on North Central Peninsular Span-

ish vowel tokens, and the other on Western Canadian English vowel tokens. For each language the model which resulted in the lowest cross-validated classification error rate was close to the least complex model possible, i.e., close to linear discriminant analysis using the variances of each acoustic variable but not the covariances between variables. In order to make cross-language vowel perception predictions the Spanish model was used to classify English vowel tokens and the English model was used to classify Spanish vowel tokens. Results suggest that monolingual North Central Peninsular Spanish listeners would assimilate most tokens of Western Canadian English /i/ and /I/ to Spanish /i/ and /e/ respectively, and thus for this combination of dialects, Spanish-speaking learners of English would not be expected to have difficulty with the English /i/-/I/ contrast.

2pSCc25. Letter sound and letter name recognition for automated literacy assessment of young children. Shrikanth Narayanan (University of Southern California, 3740 McClintock Ave, EEB430, Los Angeles, CA 90089-2561, USA, shri@sipi.usc.edu), A Kazemzadeh (University of Southern California, 3740 McClintock Ave, EEB430, Los Angeles, CA 90089-2561, USA, kazemzad@usc.edu), Matthew Black (University of Southern California, 3740 McClintock Ave, EEB430, Los Angeles, CA 90089-2561, USA, Matthew.Black@usc.edu), Joseph Tepperman (University of Southern California, 3740 McClintock Ave, EEB430, Los Angeles, CA 90089-2561, USA, tepperma@usc.edu), Sungbok Lee (University of Southern California, 3740 McClintock Ave, EEB430, Los Angeles, CA 90089-2561, USA, sungbokl@usc.edu), Abeer Alwan (University of California, 405 Hilgard Ave, Los Angeles, CA 90095, USA, alwan@ee.ucla.edu)

Evaluations of letter naming and letter sounding are commonly used to measure a young child's growing reading ability, since performance in them is well-correlated with future reading development. Assessing a child's oral reading skills requires teachers, as well as technologies that attempt to automate such assessment, to form an item-level accept/reject decision based on speech cues and prior knowledge of the child's literacy level and linguistic background. With data collected from 171 K-2 children, both learners and native speakers of American English, we designed and evaluated an automated letter naming assessment method using a simple word-loop HMM decoding for the word-level letter names. The automated accept/reject evaluation performance, 81.9%, approached the agreement of human raters, 83.2% (0.62 kappa). However, the task where children must produce the sound that the letter represents was more difficult: English orthography allows one-to many letter-to-sound mapping, teachers showed less agreement in their assessment (80.9%, 0.55 kappa), and the brief durations of some of the letter sounds made it difficult to distinguish them from each other and from background noises. Phone-level HMM based evaluation accuracy was 58.2%. Preprocessing the recordings into speech, silence, and noise improved these results, especially for plosive sounds. [Supported by NSF]

2pSCc26. Neighbors as competitors: Phonological analysis of spoken word recognition errors. Adam Buchwald (NYU, 665 Broadway, Suite 910, New York, NY 10012, USA, buchwald@nyu.edu), Robert A. Felty (Indiana University - Speech Research Laboratory, 1101 E 10th St., Dept. of Psychology, Bloomington, IN 47401, USA, robfelty@indiana.edu), David B. Pisoni (Indiana University - Speech Research Laboratory, 1101 E 10th St., Dept. of Psychology, Bloomington, IN 47401, USA, pisoni@indiana.edu)

Theories of speech perception and spoken word recognition widely assume that phonetically similar words compete for selection during lexical access. These competitors - called lexical neighbors - are classically defined as differing by a single segment, with little attention paid to other levels of phonological structure such as featural content or syllabic structure. This paper reports on analyses of over 15,000 word recognition errors made on a representative sample of the lexicon (N=1428) that includes the same variety of syllable structures, lengths, and lexical frequencies that exists in the English lexicon. The analyses reveal that competitors share segmental information as has been previously suggested, but that the classic definition of neighbor cannot capture the level at which featural and syllabic properties of the target constrain the error responses. We will discuss several analyses on these issues and discuss the implications for our understanding of the organization of the lexicon. [Work supported by NIH-NIDCD R01 00111 and T32 00012]

2pSCc27. The prosody of second position clitic placement and focus in Croatian. Kristine Yu (Dept. of Linguistics, University of California, 3125 Campbell Hall, Los Angeles, CA 90095, USA, krisyu@humnet.ucla.edu)

Since Browne 1974, the placement of second position clitics in Bosnian-/Croatian/Serbian has inspired debate about interaction at the syntax-phonology interface. The placement of these clitics can alternate quite freely: either after the first phonological word or after the first syntactic constituent. While it's generally agreed that prosodic phonology, in addition to morphosyntax, plays a role in clitic placement in Bosnian/Croatian/Serbian, the prosodic patterns for the different placements have not been studied acoustically. In addition, it has been suggested that clitic placement and pragmatic focus may interact (Bošković 2001), but this has not been systematically studied. We recorded adult Zagreb Croatian speakers producing subject noun phrases with initially stressed trisyllabic adjectives and nouns in transitive sentences. We varied clitic placement (after the first word or first constituent) and focus domain (broad focus, and narrow focus on adjective, noun, both the adjective and the noun, or the entire noun phrase) and controlled for dialect and pitch accents. Preliminary results from three speakers indicate that gross differences in prosodic patterns occur only as a function of focus domain but not clitic placement. Further work will confirm if these patterns hold for more speakers and if clitic placement is correlated with finer-grained prosodic differences.

2pSCc28. English /r/-/l/ pronunciation training for Japanese speakers. Kota Hattori (University College London, Department of Phonetics and Linguistics, 4, Stephenson Way, NW1 2HE London, UK, k.hattori@ucl.ac.uk), Paul Iverson (University College London, Department of Phonetics and Linguistics, 4, Stephenson Way, NW1 2HE London, UK, p.iverson@ucl.ac.uk)

Previous studies have demonstrated that perceptual training improves both perception and production by adult second-language (L2) learners. The present study examined whether production training likewise improves both perception and production. Japanese speakers underwent ten sessions of production training for English /r/ and /l/. The training combined three methods: (1) subjects received audio-visual examples and pronunciation instructions for /r/ and /l/; (2) they produced mono syllables (i.e., /ra/ and /la/) and minimal-pair words, with online feedback about their formant frequencies using a real-time spectrogram as well as pronunciation feedback from an instructor; and (3) they made recordings of minimal-pair words and compared them to ″enhanced″ versions of these recordings (i.e., signal-processed versions with the correct F3 frequencies and transition durations). All participants completed a battery of pre/post training tests (i.e., English /r/-/l/ identification, discrimination, perceptual mapping of best exemplars, and production). The preliminary results indicate that this training approach improves production; the results will be further discussed in terms of its effect on perception and the underlying representation of these categories.

2pSCc29. Production of American English [eI] and [ɛ] by Mandarin speakers: mono- vs. disyllabic words. Chung-Lin Yang (Dept. of Linguistics, Indiana Univ.-Bloomington, Memorial Hall 322, Bloomington, IN 47405, USA, cy1@indiana.edu)

Mandarin productions of English tense vs. lax vowels are difficult for English speakers to differentiate (Chen et al. 2006). In this study the production of American English [eI] and [ɛ] by Mandarin and American participants was investigated. The target vowels were embedded in monosyllabic and disyllabic words with a stop-V-voiceless stop context in carrier sentences of variable length. There were two formant measurements for each vowel (20% after the onset and before the end of the vowel). In the monosyllabic condition, Mandarin speakers' performance was similar to American speakers in duration and formant values except that [eI] started too low. However, in the disyllabic condition, Mandarin speakers' formants for [eI] and [ɛ] were overlapped and there was no significant durational distinction between [eI] and [ɛ]. One possible account for this difference is that

when producing a disyllabic word, Mandarin speakers tend to shorten the vowel duration of the first syllable to compensate for the production of the following syllable. The difference in syllable conditions may reflect a tendency that Chinese regularizes word durations regardless of the number of syllables. Reference: Chen, Y. et al. (2006). Vowel production by Mandarin speakers of English. Clinical linguistics and phonetics, 15, 427-440

2pSCc30. A numerical analysis of fluctuations in pressure wave within the larynx using two-dimensional asymmetrical vocal folds model. Hideyuki Nomura (Dept. of Electronic Eng., Univ. of Electro-Communications, 1-5-1, Chofugaoka, 182-8585 Chofu-shi, Japan, nomu@ee.uec.ac.jp), Tomoo Kamakura (Dept. of Electronic Eng., Univ. of Electro-Communications, 1-5-1, Chofugaoka, 182-8585 Chofu-shi, Japan, kamakura@ee.uec.ac.jp), Tetsuo Funada (Div. of Electronic Eng. and Computer Sci., Kanazawa Univ., Kakuma-machi, 920-1192 Kanazawa-shi, Japan, funada@t.kanazawa-u.ac.jp)

Numerical simulations of pathological voice production and estimations of pressure wave fluctuations are performed based on a two-dimensional asymmetrical vocal folds (VFs) model. The asymmetrical VFs model takes into account of geometrical asymmetries (the thickness, effective depth of vibration region, and lateral rest position) and mechanical asymmetries (the Young's modulus, density, and viscosity of VF tissues). Simulation results based on the asymmetrical VFs model show that the left and right VFs vibrate with a phase difference. Obtained pressure waves within the larynx and vocal tract indicate fluctuations of fundamental frequency, amplitude, and waveform. In order to quantitatively evaluate the fluctuations, the coefficient of variation of the fundamental frequency, the coefficient of variation of the amplitude, and the harmonic-to-noise ratio are estimated. With increasing the VF asymmetries, especially on the effective depth and the density of VF elements, remarkable fluctuations are observed not only at the glottis but also in the regions downstream of the glottis and faraway from the glottis. This suggests that the estimation of fluctuation in pressure wave is useful for the diagnosis of pathological VFs.

2pSCc31. Differential effects of the phonemes on identification of previously unknown speakers. Kanae Amino (Dept. of Electrical and Electronics Engineering, Sophia University, 7-1 Kiyoi-cho, Chiyoda-ku, 102-8554 Tokyo, Japan, amino-k@sophia.ac.jp), Takayuki Arai (Dept. of Electrical and Electronics Engineering, Sophia University, 7-1 Kiyoi-cho, Chiyoda-ku, 102-8554 Tokyo, Japan, arai@sophia.ac.jp)

In perceptual speaker identification, it is known that the identification accuracy depends on the contents of the stimuli presented to the listeners. In our previous experiments, we found that the stimuli containing a nasal sound are effective for human speaker identification, and that coronal sounds are more effective than labial ones. This tendency was observed in the identifications of both familiar and previously unknown speakers. In this present study, we investigated the effects of the speech contents again, by focusing on the vowels in CV monosyllabic stimuli. Through the experiment we obtained several findings: 1) stimuli containing a nasal gained significantly higher accuracy compared to stimuli with only oral sounds; 2) coronal sounds were more effective than labial sounds; 3) palatalisation caused an improvement in performance; and 4) back vowels were more effective than front vowels significantly. These results can be explained by speaker-specific morphologies of the nasal cavity and the paranasal sinuses, and also of the pharyngeal cavity. We will also show analyses and discussions on the acoustical properties of the stimuli and the performance differences among the subjects. [Work supported by Sophia University Open Research Centre from MEXT.]

2pSCc32. Coarticulation in CV sequences: Locus Equation data. Simone Graetzer (University of Melbourne, Royal Parade, Parkville Victoria, 3010 Melbourne, Australia, n.graetzer@pgrad.unimelb.edu.au)

Background: Speech sounds are known to be influenced by the context in which they occur, and to be produced in an overlapping way. These processes are referred to by the term ″coarticulation″. Objective: The aim of the study was to compare the magnitude of anticipatory coarticulation of oral voiceless plosives by following vowels in four Australian languages, Arrernte, Burarra, Gupapuyngu, and Warlpiri. Methods: The corpus consists of approximately six hundred isolated real words spoken by eight female adult speakers of the four languages. Locus equations are calculated for intervocalic consonants /p,c,t,tr,k/ (where ″/tr/″ represents a voiceless oral retroflex plosive) and all following vowels in consonant-vowel sequences. Measurement points are 0.1 and 0.5 into the vowel. The relationship between these two measurement points is linear and is expressed as a locus equation. The slope of the fitted line associated with the equation is a measure of the magnitude of coarticulation of the consonant by the following vowels. Results: There was a general tendency towards relatively highly coarticulated bilabial and velar plosives, weakly coarticulated retroflex plosives, and moderately coarticulated alveolar plosives. Results were variable for palatal plosives. These results are for the most part in accordance with findings for other Australian languages.

2pSCc33. Lexical analysis of spoken word recognition errors. Robert A. Felty (Indiana University - Speech Research Laboratory, 1101 E 10th St., Dept. of Psychology, Bloomington, IN 47401, USA, robfelty@indiana.edu), Adam Buchwald (NYU, 665 Broadway, Suite 910, New York, NY 10012, USA, buchwald@nyu.edu), David B. Pisoni (Indiana University - Speech Research Laboratory, 1101 E 10th St., Dept. of Psychology, Bloomington, IN 47401, USA, pisoni@indiana.edu)

In speech perception and spoken word recognition, a lexical ″neighbor″ of a target word is a phonetically similar word that competes with the target during lexical access. A commonly-used definition is that neighbors differ from one another by a single segment. While this basic definition accounts for many results of lexical decision and word recognition tasks among monosyllabic words, it also suggests that approximately half of the words in the English lexicon are hermits (words without neighbors). To generate a more inclusive definition of neighbor, we created a representative sample of the lexicon (N=1428) to examine spoken word recognition errors, and we used the incorrectly selected competitors as a means of indexing ″neighbor″ status. Analysis of over 15,000 errors reveals several patterns: (1) Errors tend to be of higher frequency than the target word; (2) Less than 1/3 of the errors were neighbors according to the traditional definition of neighborhood density; and (3) Errors differed in phonetic similarity more as the S/N ratio decreased. We use these data to test several alternative definitions of ″neighbor″ and their ability to predict actual word recognition errors. [Work supported by NIH-NIDCD R01 00111 and T32 00012]

2pSCc34. Articulatory constaints on coarticulation in fricatives as a function of tongue involvement. Carole E. Gelfer (William Paterson University, 300 Pompton Road, Wayne, NJ 07470, USA, gelferc@wpunj.edu), Fredericka Bell-Berti (St. John's University, 8000 Utopia Parkway, Queens, NY 11439, USA, bellf@stjohns.edu)

Numerous studies have shown coarticulatory effects of vowel rounding on the spectra of sibilants. However, the extent to which the tongue contributes to coarticulation is not clear because most studies have used only fricatives whose constriction is formed with the tongue. This study examines the effects of vowel environment on coarticulation in fricatives under two conditions: when the constriction is formed with the tongue (i.e., [s]) and when it is not (i.e., [f]), paired with the English vowels occurring at the extremes of the vowel quadrilateral. Preliminary results for adult native speakers of American English suggest that in the absence of tongue constraint (i .e., [f]), there is a greater effect of vowel context on the fricative spectrum. This result reinforces the importance of considering the freedom of an articulator to anticipate an upcoming gesture when examining the extent of coarticulation.

2pSCc35. Acquisition of rhythm: evidence from spontaneous L2 speech. Irina Shport (University of Oregon, Department of Linguistics, 1290, Eugene, OR 97403, USA, ishport@uoregon.edu)

This study examined the acquisition of Japanese rhythm by comparing the rhythmic characteristics of elicited spontaneous speech of English learners in the setting of an oral proficiency test. Two metrics for the quantification of speech rhythm that have been shown to reliably discriminate rhythmic classes in both L1 and L2 speech (White and Mattys, 2007) were utilized for the analysis - 1) the proportion of vowel intervals within the sentence (%V), and 2) the standard deviation of vowel intervals divided by the

mean vowel interval duration and multiplied by 100 (VarcoV). A difference in the rhythm scores of novice-mid and intermediate-high learners of Japanese was found. Furthermore, the learners' scores were significantly different from Japanese native speakers' scores, suggesting that speakers start acquiring speech rhythm relatively early, but they are still short of the target at the intermediate level of proficiency. By comparing the obtained scores with scores of stress-timed languages, such as English, the difference in the scores may be attributed to an L1 transfer into the rhythmic organization of the L2 speech.

2pSCc36. Effects of training, style, and rate of speaking on speech perception of young people in reverberation. Nao Hodoshima (Dept. of Electrical and Electronics Engineering, Sophia University, 7-1 Kiyoi-cho, Chiyoda-ku, 102-8554 Tokyo, Japan, n-hodosh@sophia.ac.jp), Takayuki Arai (Dept. of Electrical and Electronics Engineering, Sophia University, 7-1 Kiyoi-cho, Chiyoda-ku, 102-8554 Tokyo, Japan, arai@sophia.ac.jp), Kiyohiro Kurisu (TOA Corporation, 2-1 Takamatsu-cho, Takarazuka, 665-0043 Hyogo, Japan, kurisu_kiyohiro@toa.co.jp)

Because of the difficulty of listening to speech in reverberation (e.g. train stations or airports), we need to find characteristics of intelligible speech sounds that are appropriate for announcements over loudspeakers in public spaces. This study investigated the effects of training (seven talkers who have received speech training or not), style (conversational/clear) and rate (normal/slow) of speaking on speech perception of young people in simulated reverberant environments. The talkers were instructed to speak nonsense words embedded within a carrier sentence clearly or normally in an anechoic room, and listening tests were carried out with young people in simulated reverberant environments. Results showed that correct rates significantly differed among the talkers, but no difference in correct rates was found between the two speaking rates, and conversational speech had significantly higher correct rates than clear speech. Casual inspections of the stimuli indicate that vowels are enhanced as well as consonants in clear speech so that clear speech had lower correct rates than conversational speech due to increased reverberant masking in clear speech compared to conversational speech. [Work supported by Sophia University Open Research Center from MEXT.]

2pSCc37. Prosody in French theatrical declamation traced backwards in time. George Brock-Nannestad (Patent Tactics, Resedavej 40, DK-2820 Gentofte, Denmark, pattac@image.dk)

Listening to early recordings of a French theatrical personality, such as Sarah Bernhardt, the emphatic emission of words is very noticeable. It is sometimes ascribed to Bernhardt's theatrical mannerisms, but possibly also caused by an erroneous speed of reproduction. But even at correct speed, huge variations in intenseness are very noticeable. Literature does not give a clear indication whether this manner of performance was considered deviating at the time (ca. 1900). New research into the original handwritten patent documents of Édouard-Léon Scott (filed 1857 and 1859) has analyzed his method of recording the performance of the human voice. Scott documented the performance of a complete stanza from a French play, and looking at his graphical output and interpretation it becomes clear that the prosody of Mme. Bernhardt was already in place in 1859. Having identified the French play, even earlier descriptions of the prosodic approach in French declamation were found. The paper also discusses the patents of Édouard-Léon Scott and his desire for the use of his invention, which was different from that of his manufacturer, Rudolph Koenig. Furthermore, the prosodic documentation will be demonstrated, and a historically informed reproduction of a recording by Sarah Bernhardt will be presented.

2pSCc38. Articulatory coordination in German and English onset and coda clusters. Marianne Pouplier (Institute of Phonetics and Speech Processing, University of Munich, 80799 Munich, Germany, pouplier@phonetik.uni-muenchen.de), Stefania Marin (Institute of Phonetics and Speech Processing, University of Munich, 80799 Munich, Germany, stefania.marin@gmail.com)

Articulatorily, onset consonants differ from coda consonants in their spatial as well as their temporal characteristics in that onsets exhibit greater spatial displacement and are generally less variable than codas. As to their temporal organization, it has been claimed that onsets, but not codas exhibit a so-called c-center organization in which all consonant gestures of a cluster are organized as a single complex structure with respect to the vowel, while consonant clusters in codas have been hypothesized to be organized sequentially [Browman & Goldstein 1988 Phonetica]. While some studies have confirmed the c-center hypothesis for onsets but not codas, others found a c-center organization for both onset and coda consonants. The current study uses German and English onset and coda clusters to test systematically the c-center hypothesis on the basis of EMA data. Results for both languages indicate that a c-center organization may be observed in both onset and coda position, yet it does not appear consistently for all clusters. Also cross word-boundary clusters may exhibit c-center organization, possibly indicating resyllabification.

2pSCc39. Acoustic consequences of gestural intrusion errors. Stefania Marin (Institute of Phonetics and Speech Processing, University of Munich, 80799 Munich, Germany, stefania.marin@gmail.com), Marianne Pouplier (Institute of Phonetics and Speech Processing, University of Munich, 80799 Munich, Germany, pouplier@phonetik.uni-muenchen.de), Jonathan Harrington (Institute of Phonetics and Speech Processing, University of Munich, 80799 Munich, Germany, jmh@phonetik.uni-muenchen.de), Susanne Waltl (IPS, LMU, Schellingstr. 3/II, 80799 München, Germany, susanne@phonetik.uni-muenchen.de)

An increasing number of studies have elicited speech errors in articulatory experiments, and thus evaluated errors on the basis of their articulatory properties, yet there has been no study that relates the articulatory variability observed in errors to the acoustic consequences. The present study aims to evaluate the acoustic properties of errorful/error-free [k] and [t] stimuli with known articulatory configurations (and articulatorily categorized as errorful/error-free), and determine the extent to which articulatory errors have acoustically observable consequences. The most frequent error observed in the articulatory data is an intrusion of a second gesture, resulting in a simultaneous presence of both tongue tip and tongue body gestures during production of [k] or [t]. Spectral analysis of these stimulis' bursts shows that [k] and [t] are differently affected by intrusion gestures: intrusion errors during intended [k] tokens are more robustly grouped with error-free [k] across speakers, while intrusion errors during intended [t] tokens are more variable, some being acoustically like [t], some like [k], and some like neither category, matching previous perceptual results (Pouplier & Goldstein 2004, Journal of Phonetics). These results will be discussed in the context of different timing patterns between the two co-occurring gestures during intrusion errors.

2pSCc40. Embodiment, not imitation, leads to the replication of timing phenomena. Piers Messum (112 Warner Road, SE5 9HQ London, UK, p.messum@gmail.com)

In many languages, a spoken vowel is shorter before phonologically voiceless consonants than before voiced ones. In West Germanic languages, including English, tense and lax vowels have different lengths and there is a characteristic 'stress-timed' rhythm. For these phenomena and some others, it is generally assumed that time is the controlled variable for production, and that children replicate these speech behaviors through the reproduction of timing patterns abstracted from the adult input (i.e. by imitation). The developmental data does not support these assumptions, and an imitative mechanism would present a young speaker with a highly complex challenge. Instead, these behaviors are more plausibly the result of the embodiment of speech. Embodiment goes beyond laryngeal and articulatory function. A child's speech breathing is not a scaled-down version of the adult model but a distinctly different skill, and one that must be learnt during speech production. Similarly, the aerodynamic setting of child speech differs significantly from that of adults. The constraints that these factors impose become manifest in speech as changes in timing, but these changes are epiphenomenal, not modelled directly. Phenomena particular to West Germanic languages reflect the style of speech breathing these languages require of a child.

2pSCc41. Investigating the perception of noise-vocoded speech - an individual differences approach. Carolyn McGettigan (University College London, Institute of Cognitive Neuroscience, 17 Queen Square, WC1N 3AR London, UK, c.mcgettigan@ucl.ac.uk), Stuart Rosen (UCL, Wolfson House, 4, Stephenson Way, NW1 2HE London, UK, stuart@phon.ucl.ac.uk), Sophie K. Scott (University College London, Institute of Cognitive Neuroscience, 17 Queen Square, WC1N 3AR London, UK, sophie.scott@ucl.ac.uk)

We used a cochlear implant simulation (noise-vocoded speech) to investigate speech recognition and perceptual learning in normal-hearing adult speakers of English. In two separate sessions (1-2 weeks apart), 28 listeners were tested on recognition of noise-vocoded Sentences, Words, and isolated segments (Consonants and Vowels). There was evidence of significant perceptual learning that survived until Session 2 for all tasks. An individual differences analysis of Session 1 data suggested two independently-varying 'levels' of processing at work in the initial perception of the distorted speech stimuli - a 'top-down' listening mode making use of contextual and lexical information, and a 'bottom-up' mode focussed on acoustic-phonetic discriminations. By Session 2, a more generalised listening mode emerged, reflecting listeners' consolidation of basic sound-to-representation mappings. Further exploration of Consonant and Vowel confusion data (using Information Transfer analyses) suggested that better speech recognition performance may be achieved through more efficient use of the preserved cues to duration and voicing in noise-vocoded stimuli, but that listeners failed to take full advantage of such information. We conclude that training regimes involving directed attention to specific features, such as vowel length, may help to improve performance with noise-vocoded speech.

2pSCc42. Speed-curvature relations in speech production: a multilingual experimental and modeling study. Pascal Perrier (ICP/GIPSA-lab, INPG, 46 Avenue Félix Viallet, 38031 Grenoble Cedex 01, France, Pascal.Perrier@gipsa-lab.inpg.fr), Susanne Fuchs (ZAS, Schuetzenstr. 18, 10117 Berlin, Germany, fuchs@zas.gwz-berlin.de)

Regularities in the relations between tangential velocity and trajectory curvature have been found in a number of human movements. They were formalized in the 1/3 power law [Viviani and Terzuolo, Neuroscience 7: 431-437, 1982]. Viviani and colleagues also found that modifying the speed-curvature relations would influence the perception of synthetic movements in terms of naturalness and classification. Hence, these relations could be at the core of the perception-action link in human movements. In this paper, tongue movement collected from speakers of French, German and Mandarin are analyzed. They are compared with data from simulations using a biomechanical tongue model, which is controlled on a target-to-target basis. Our results for experimental data and simulations are very similar. It is found that the 1/3 power law offers a fair description of the velocity-curvature relations when a large amount of movements are considered together. However, a refined analysis of individual movements reveals that the exceptions to this law are numerous. It is concluded that the velocity-curvature relation is not controlled in speech movements, and that the 1/3 power law only accounts for general characteristics of movements, which could arise from dynamical properties of the articulators.

2pSCc43. Vowel spaces in Swedish children with cochlear implants. Tina Ibertsson (Lund University, Dept. Logopedics, Phoniatrics & Audiology, University Hospital, SE-221 85 Lund, Sweden, Tina.Ibertssont@med.lu.se), Birgitta Sahlén (Lund University, Dept. Logopedics, Phoniatrics & Audiology, University Hospital, SE-221 85 Lund, Sweden, Birgitta.Sahlen@med.lu.se), Anders Lofqvist (Lund University, Dept. Logopedics, Phoniatrics & Audiology, University Hospital, SE-221 85 Lund, Sweden, Anders.Lofqvist@med.lu.se)

This study analyzed vowel productions of Swedish children with cochlear implants, capitalizing on the rich vowel system of Swedish with nine vowels. Minimal word pairs were used as linguistic material. A group of 12 children with CI (mean age 184 months, range 144-229 months), and a group of children with normal hearing (mean age 105 months, range 103-118 months) were recruited. The age at implantation of the CI was 79 months (range 31-155 months). The first two formants were measured for each vowel. To estimate the vowel space, the average Euclidean distance in the F1-F2 plane between each vowel and the mean first and second formant frequencies of all the vowels was calculated for each child. The results show a significantly smaller vowel space for the children with a cochlear implant. However, there was no overall significant correlations between the vowel space and measures of speech recognition and vowel production in the CI group. Although the present results show that speech recognition ability affects intelligibility and vowel production, the vowel space may not be a suitable measure for assessing speech production in this population. [Work supported by the Sunnderdahl Disability Foundation.]

2pSCc44. Detection of obstruent consonant landmark for knowledge based speech recgonition system. Jung-In Lee (Yonsei University, 134 Sinchon-dong, Seodaemun-gu, 120-749 Seoul, Republic of Korea, junginida@dsp.yonsei.ac.kr), Jeung-Yoon Choi (Yonsei University, 134 Sinchon-dong, Seodaemun-gu, 120-749 Seoul, Republic of Korea, jychoi @yonsei.ac.kr)

Obstruent consonant landmarks are detected using spectral energy difference profiles. This study expands upon previous work by Liu. A[J. Acoust. Soc. Am. 100, 3417-3430, 1996]. The proposed algorithm detects four types of landmarks : [stop closure], [stop release], [fricative closure] and [fricative release], where affricates are detected by combining [stop closure], [fricative closure] and [fricative release]. In addition to finding abrupt changes in energy differences, we use energy contours, relative energy and spectral center of gravity differences. This method results in improved performance particularly for CV obstruents. Overall detection rates for stop closure and release are 76.9% and 85.7% for obstruent landmarks in TIMIT, and fricatives yield 82.2% and 83.6% respectively. For strident fricatives, the figures are 94.7% and 93.6%.

2pSCc45. Acoustic-phonetic features for stop consonant place detection in clean and telephone speech. Jung-Won Lee (Yonsei University, 134 Sinchon-dong, Seodaemun-gu, 120-749 Seoul, Republic of Korea, jaesuk2002@dsp.yonsei.ac.kr), Jeung-Yoon Choi (Yonsei University, 134 Sinchon-dong, Seodaemun-gu, 120-749 Seoul, Republic of Korea, jychoi @yonsei.ac.kr)

This work classifies voiceless stop consonant place in CV tokens of English using burst release cues for clean (TIMIT) and telephone speech (NTIMIT). We compared the performance of cepstral coefficients to acoustic phonetics-motivated features such as center of gravity, burst amplitude and relative difference of formant amplitudes. In clean speech, cepstral coefficients resulted in better classification. However, for test data from NTIMIT, acoustic phonetic-based features outperformed cepstral coefficients, particularly if models were trained on clean speech. In addition, augmenting cepstral coefficients with acoustic phonetic-based measurements resulted in the best performance. These findings suggest that cepstral coefficients are able to model speech in a given environment in finer detail, whereas acoustic phonetic-based features are more robust to changes in environment, so that combining both types of measurements leads to the best performance.

2pSCc46. Vowel place detection for a knowledge-based speech recognition system. Sukmyung Lee (Yonsei University, 134 Sinchon-dong, Seodaemun-gu, 120-749 Seoul, Republic of Korea, pooh390@dsp.yonsei.ac.kr), Jeung-Yoon Choi (Yonsei University, 134 Sinchon-dong, Seodaemun-gu, 120-749 Seoul, Republic of Korea, jychoi @yonsei.ac.kr)

This work aims to detect vowel place as part of a knowledge-based speech recognition system. Vowel place was classified into 6 groups based on tongue advancement [Front/Back] and height [High/Mid/Low]. Experiments were performed using 300 /hVd/ utterance data from Hillenbrand [J. Acoust. Soc. Am. 97, 3099-3111] and 6600 TIMIT vowels. Features used include fundamental frequency (F0) and formant value (F1~F3), where formant measurements were classified into separate groups using F0 measurements. The nearest class was found using a simple Mahalanobis distance measure, and yielded a 91.5% classification rate for the /hVd/ data.

The results for the TIMIT data were 64.4%, and error analysis with regard to adjacent segment manner and place was carried out to observe the effects of coarticulation, which was not observed in the /hVd/ data.

2pSCc47. Cross-modal perceptual learning of spectrally degraded speech: Behavioral and neuroimaging studies. Frank Eisner (University College London, Institute of Cognitive Neuroscience, 17 Queen Square, WC1N 3AR London, UK, f.eisner@ucl.ac.uk), Carolyn McGettigan (University College London, Institute of Cognitive Neuroscience, 17 Queen Square, WC1N 3AR London, UK, c.mcgettigan@ucl.ac.uk), Stuart Rosen (UCL, Wolfson House, 4, Stephenson Way, NW1 2HE London, UK, stuart@phon.ucl.ac.uk), Andrew Faulkner (UCL, Wolfson House, 4, Stephenson Way, NW1 2HE London, UK, andyf@phon.ucl.ac.uk), Sophie K. Scott (University College London, Institute of Cognitive Neuroscience, 17 Queen Square, WC1N 3AR London, UK, sophie.scott@ucl.ac.uk)

We investigated normal-hearing listeners' ability to adapt to a speech signal that simulates aspects of the stimulation received from a cochlear implant. The training materials were spoken sentences which were spectrally degraded by noiseband-vocoding and shifted upwards in frequency. A control condition consisted of spectrally inverted, unintelligible versions of these stimuli. Participants listened passively to these sentences, and on each trial received visual feedback which could be either a written version of the sentence or a video of the talker who originally produced it. Learning under both feedback conditions was relatively fast: Subjects improved on average by 25% on keyword recognition scores after 100 trials. No learning effects were observed in the control condition. We further used functional magnetic resonance imaging to investigate which cortical areas may be recruited during learning. A comparison of degraded and learnable sentences with the unlearnable control stimuli showed activity in the left superior temporal sulcus both during passive listening and receiving feedback. In contrast, the left inferior frontal gyrus was activated only when subjects were receiving feedback in the learnable condition. These results suggest that the inferior frontal gyrus plays an important role in integrating acoustic-phonetic processing with externally provided feedback.

2pSCc48. Robust harmonic grouping by octave error correction. Hedde Van De Vooren (University of Groningen, Dept. Artificial Intelligence, P.O. Box 407, 9700 AK Groningen, Netherlands, h.van.de.vooren@ai.rug.nl), Renante R. Violanda (University of Groningen, Dept. Artificial Intelligence, P.O. Box 407, 9700 AK Groningen, Netherlands, R.Violanda@ai.rug.nl), Tjeerd C. Andringa (University of Groningen, Dept. Artificial Intelligence, P.O. Box 407, 9700 AK Groningen, Netherlands, t.andringa@ai.rug.nl)

Harmonic grouping is a frequently applied technique in computational auditory scene analysis and automatic speech recognition systems. However, grouping is easily disrupted by noise and reverberation. For instance, a noise induced signal component positioned roughly between two harmonics, might undesirably be assigned to the harmonic complex (HC) as well. This results in an octave error: harmonics in an HC are assigned to harmonic numbers twice as high as the correct values. We propose a cost function based method to correct these octave errors. This function is designed to, on the one hand, improve the balance between odd and even harmonic numbers, and, on the other hand, minimize the amount of signal components to be rejected. As a preprocessing step we applied short-time Fourier analysis to derive an instantaneous frequency representation from which we obtained the signal components. We used these as input for our harmonic grouping algorithm to obtain the HCs. Then we selected the optimal solution from the cost function and modified the composition of the HCs accordingly. As long as enough harmonics are sufficiently above the local noise level, this octave error correction mechanism works well for various sorts of harmonic sounds including speech.

2pSCc49. A cross-language familiar talker advantage? Susannah Levi (University of Michigan, 440 Lorch Hall, 611 Tappan Street, Ann Arbor, MI 48109, USA, svlevi@umich.edu), Stephen Winters (University of Calgary, Social Sciences Bldg. Room 820, Department of Linguistics, Calgary, AB T2N 1N4, Canada, swinters@basesproduced.com), David B. Pisoni (Indiana University - Speech Research Laboratory, 1101 E 10th St., Dept. of Psychology, Bloomington, IN 47401, USA, pisoni@indiana.edu)

Previous research has shown that familiar talkers are more intelligible than unfamiliar talkers. In the current study, we tested the source of this familiar talker advantage by manipulating the type of talker information available to listeners. Two groups of native English listeners were familiarized with the voices of five German-English bilingual talkers; one group learned the voices from German stimuli and the other from English stimuli. Thus, English-trained listeners had access to both language-independent and English-specific talker information, while German-trained listeners had access to language-independent and German-specific talker information. After three days of voice learning, all listeners performed a word recognition task in English. Consistent with previous findings, English-trained listeners found the speech of familiar talkers to be more intelligible than unfamiliar talkers, as measured by whole words and phonemes correct. In contrast, German-trained listeners showed no familiar talker advantage, suggesting that listeners must have knowledge of talker-specific, linguistically relevant information to elicit the familiar talker advantage and that knowledge of language-independent talker information - such as size and shape of the vocal tract - does not facilitate speech perception.

2pSCc50. Prosodic effects on articulatory coordination in initial consonant clusters in German. Lasse Bombien (Institut für Phonetik und Sprachverarbeitung, Schellingstr. 3, 80799 München, Germany, lasse@phonetik.uni-muenchen.de), Christine Mooshammer (Haskins lab and MIT Research lab of electronics, 300 George street suite 900, New Haven, CT 06511, USA, tine@haskins.yale.edu), Phil Hoole (Institut für Phonetik und Sprachverarbeitung, Schellingstr. 3, 80799 München, Germany, hoole@phonetik.uni-muenchen.de), Barbara Kuehnert (Laboratoire de Phonétique et Phonologie - UMR 7018 CNRS - Paris 3, 19, rue des Bernadins, 75005 Paris, France, barbara.kuhnert@univ-paris3.fr)

This study examines how articulatory coordination in heterorganic initial consonant clusters is modulated by prosodic condition. Extending the paradigm of articulatory strengthening at domain edges to clusters, we provide EPG data of 7 speakers as well as EMA data of two speakers including domain-initial clusters (/kl/, /kn/ and /sk/) in different prosodic positions, varying the strength of the preceding boundary and the position of lexical stress. (e.g. 'Claudia vs. Klau'sur, i.e. stressed vs. unstressed target cluster). The results show that C1 was consistently lengthened at higher boundaries, but only if the cluster was preceded by a clear pause. C2 was only weakly and inconsistently affected. There were no effects on the spatial domain at all. No consistent effects of lexical stress were found for either C1 or C2. Regarding overlap of C1 and C2 there was a tendency, albeit quite weak, in the direction of more overlap at the lower boundary levels and in unstressed condition. However, differences in timing between segmentally different clusters were consistent and much larger than boundary and stress effects. Especially for /kl/ vs. /kn/ we find that the lateral's timing to /k/ is much closer than the nasal's.

2pSCc51. Hierarchical approach to voice activity detection in realistic environmental noise. Jörg-Hendrik Bach (Universität Oldenburg, Medizinische Physik, Fakultät V, 26111 Oldenburg, Germany, j.bach@uni-oldenburg.de), Jörn Anemüller (Universität Oldenburg, Medizinische Physik, Fakultät V, 26111 Oldenburg, Germany, joern.anemueller @uni-oldenburg.de)

The automatic identification of acoustic objects, particularly speech, in adverse backgrounds can pose a difficult problem. In this work, the problem of speech detection in different backgrounds is tackled using a hierarchical decision tree: The root node provides a coarse classification of the noise background, while the next nodes are optimised to detect speech in one particular background each. The results of this approach are compared to the ITU G729B standard VAD and to a binary classifier trained on speech vs a mixture of the backgrounds. The features employed are amplitude modulation spectra of the signals (Kollmeier & Koch, 1993) that represent the modulation content of a signal as a two-dimensional (modulation-frequency vs centre frequency) spectral pattern. The best features for classification at

each node are selected independently (node-specific) using a sequential floating forward search algorithm. The statistical learner is an open source support vector machine (Chang & Lin, 2001).

2pSCc52. Visual Influences on Alignment to Voice Onset Time. Kauyumari Sanchez (University of California, Riverside, Department of Psychology, 900 University Ave., Riverside, CA 92521, USA, ksanc004@student.ucr.edu), Rachel M. Miller (University of California, Riverside, Department of Psychology, 900 University Ave., Riverside, CA 92521, USA, rmill002@ucr.edu), Lawrence D. Rosenblum (University of California, Riverside, Department of Psychology, 900 University Ave., Riverside, CA 92521, USA, rosenblu@citrus.ucr.edu)

In speech alignment, interlocutors inadvertently imitate aspects of each others utterances. Alignment also occurs when talkers are asked to shadow (identify out loud) recorded words heard over headphones. For example, the voice onset time (VOT) of consonants produced by subjects will be greater when shadowing heard words whose consonants have been modified to have extended VOTs [K. Shockley, et al., Percept. Psychophys. 66, 422 (2004)]. An experiment was conducted to test whether alignment to VOT has a purely acoustic basis. For this purpose, visual speech tokens composed of a face articulating /ba/ syllables at three different rates, were each dubbed onto a series of seven audio /ba/ syllables varying in VOT. Subjects were asked to simply shadow the audiovisual /ba/s. Results revealed that both the visible syllable rate and audio VOT of the stimuli influenced the VOTs of the shadowers' produced syllables. The implications of these results for theories of alignment, audiovisual integration, and the perceptual primitives of speech are discussed.

2pSCc53. The '[+English]' effect in acquisition of English as a second language: Novel- category biases in second language perception and production. Kenneth De Jong (Indiana University, 322 Memorial Hall, 1021 E. 3rd Street, Bloomington, IN 47405, USA, kdejong@indiana.edu), Yen-Chen Hao (Indiana University, 322 Memorial Hall, 1021 E. 3rd Street, Bloomington, IN 47405, USA, yehao@indiana.edu), Hanyong Park (Indiana University, 322 Memorial Hall, 1021 E. 3rd Street, Bloomington, IN 47405, USA, hanypark@indiana.edu), Noah H. Silbert (Indiana University, 322 Memorial Hall, 1021 E. 3rd Street, Bloomington, IN 47405, USA, nosilber@indiana.edu)

Silbert & de Jong (JASA, 122: 3092) investigated correlations between response bias and segment frequency in a number of previously published segment identification data sets. In general, bias tends to be positively correlated with frequency. When applied to second language (L2) learning, this pattern predicts biases toward identifying novel L2 categories as L1 categories, since the number of instances of L1 categories far outweighs those of novel categories in learners' experience. Nagao, Lim, & de Jong (2003, ICPhS) confirm this: Japanese listeners tend to label ambiguous English coda consonants as onsets. However, younger and less experienced learners of English tend to label ambiguous tokens as codas; they tend toward using the novel category even though it is less frequent in their experience. This paper reports experiments in which Korean EFL learners identified English obstruents and in which they produced them. Cases of novel category response bias are observed in identification, and less so in production. Such novel category effects suggest a model in which novel categories serve, in part, as indicators of the L2 itself and stand out as response options in L2 identification tasks. These effects are likely counteracted by motor difficulties in L2 production tasks.

2pSCc54. Study on voice quality parameters for anger degree estimation. Yoshiko Arimoto (Tokyo University of Technology, Graduate School of Bionics, Information and Media Science, Faculty of MS, Iida labolatory, 1404-1 Katakura, Hachioji, 192-0982 Tokyo, Japan, ar@mf.teu.ac.jp), Sumio Ohno (Tokyo University of Technology, 1404-1 Katakura, 192-0982 Hachioji, Japan, ohno@cc.teu.ac.jp), Hitoshi Iida (Tokyo University of Technology, 1404-1 Katakura, 192-0982 Hachioji, Japan, iida@media.teu.ac.jp)

With great advance of automatic speech recognition (ASR) systems and a voice command system are demanded to be more sensitive to user's intention or emotion. These systems currently process linguistic information, but not process nonlinguistic information or paralinguistic information which users expressed during dialogs. For that reason, computers can obtain less information about a user through a dialog than human listeners can. If computers will recognize user's emotions conveyed by acoustic information, more appropriate response can be made toward users. For realization of emotion recognition, we have continued our study on anger degree estimation by both prosodic features and segmental features with anger utterances which were recorded during two kinds of pseudo-dialogs. This report focuses on only segmental features related to voice quality and examines them for capabilities to estimate anger degree. The first cepstral coefficient of anger utterances has been analyzed to obtain acoustic parameters related to spectral tilt in our previous works. In addition to the previous voice quality parameters, features related to amplitude of formants and harmonics were extracted from the same anger utterances as that in the previous works. Comparisons were made with the previous parameters to evaluate estimation accuracy of each voice quality parameters.

2pSCc55. Identification of place of articulation and voicing in white and babble noise. Magnus Alm (Norwegian University of Science and Technology, Psychology Dept, NO 7491 Trondheim, Norway, magnusal@stud.ntnu.no), Dawn Behne (Norwegian University of Science and Technology, Psychology Dept, NO 7491 Trondheim, Norway, dawn.behne@svt.ntnu.no)

Previous research shows that white noise influences the degree auditory and visual modalities are used in audio-visual (AV) speech perception. This study assesses identification of voicing and place of articulation (POA) in the infrequently studied natural babble noise. Incongruent monosyllabic AV stimuli were presented to 15 young adults in white and babble noise at 0 and -12 dB SNR where voicing stimuli differed in voicing and voicing structure and POA stimuli differed in POA and POA structure. In white noise POA stimuli received fewer audio responses than in babble whereas voicing stimuli received more audio responses in white noise than in babble. Voiced syllables received more audio responses than voiceless. Findings suggest that differences in noise type for POA and voicing identification are attributable to discrepancies in acoustical attributes of noise and target stimuli. In voicing identification, the spectral transition between aspiration (stabile signal) and voicing (fluctuating signal) is less distinct in the fluctuating babble noise than in the flat power white noise. Voiceless consonants are more spectrally similar to white noise than voiced consonants, making the latter more auditorily accessible. Visual cues aid voicing identification, but only when POA is visually salient and auditorily susceptible to the noise type.

2pSCc56. A comparison of task and non-task related variability in speech production and acoustics, with implications to speech perception. Khalil Iskarous (Haskins Laboratories, 300 George St, New Haven, CT 06511, USA, iskarous@haskins.yale.edu)

Task Dynamics provides a way of testing whether production goals are acoustic or articulatory. According to this theory, during the production of a segment, the vocal tract can be divided into locations where a task is specified and locations where no task is specified. The goal is for articulators to synergetically achieve the constriction in the task location. Articulatory variability in the non-task locations is permitted due to overlap. However, articulatory activity in both task and non-task locations affects the area function and acoustic output. Therefore it is possible that an articulatory synergy stabilizes an articulatory task variable, without stabilizing the acoustics, evidence that the goal is articulatory. An experiment on the articulation and acoustics of /Vd/ in Ameican English by 26 subjects, using the Wisconsin Xray Microbeam database, shows that there is a synergy between jaw and tongue tip that explains 79% of the variability in articulator locations. This synergy stabilizes the position of the tongue tip in the alveolar region. But the formant transitions and bursts are highly variable, since the back of the tongue and jaw assume positions consistent with the preceding vowel-evidence that the goal is articulatory. (Funded by NIH DC-02717).

2pSCc57. Evaluation of a simplified phonetic annotation scheme for disordered speech. Kathleen Murray (Head and Neck Surgery, Drexel University College of Medicine, Department of Otolaryngology - Head and Neck Surgery, 1721 Pine Street, Philadelphia, PA 19103, USA, kathleen.murray@drexel.edu), David Graff (Linguistic Data Consortium, 3600 Market St. Suite 810, Philadelphia, PA 19104-2653, USA, graff@ldc.upenn.edu), Yolanda D. Heman-Ackah (Head and Neck Surgery, Drexel University College of Medicine, Department of Otolaryngology - Head and Neck Surgery, 1721 Pine Street, Philadelphia, PA 19103, USA, Phillyvoicemd@aol.com), Robert T. Sataloff (Head and Neck Surgery, Drexel University College of Medicine, Department of Otolaryngology - Head and Neck Surgery, 1721 Pine Street, Philadelphia, PA 19103, USA, rtsataloff@phillyent.com)

Attempts to train a computer to mimic a vocal pathology expert's perception of perceivable voice problems have had limited success. A recent study successfully used a Cepstrum-based calculation (CPPs) to detect dysphonic speech, but it made significant false negative and false positive errors [1]. Appropriate training data could improve calculation accuracy, but logistical and legal issues from the medical domain render large amounts of detailed, consistent training data difficult to produce. A simple scheme has been developed based on labeling one point in time for each of a few vowels in a read statement. Calculations from [1] and [2], centered on neighborhoods of these vowels will augment the CPPs classifier. The annotation scheme will be evaluated with respect to its ability to assist a classifier to automatically predict perceptual labels [1] from data, and practicalities such as inter/intra-annotator agreement. 1. Heman-Ackah, Y.D., Heuer, R.J., Michael, D.D., Ostrowski, R., Horman, M., Baroody, M., Hillenbrand, J.M., and Sataloff, R.T. (2003). ″Cepstral peak prominence: A more reliable measure of dysphonia,″ Annals of Otology, Rhinology, and Laryngology, 112, 324-333. 2. ″Perceived Level of Noise by Mark VII and Decibels (E)″ S. S. Stevens, J. Acoustical Soc. Am. v. 51(2, part 2) 1972. pp. 575-602.

2pSCc58. Neural correlates of speech and non-speech processing: Role of language experience in brain activation. Alexis N. Bosseler (University of Washington, Dept. of Speech & Hearing Sciences, and Institute for Learning & Brain Sciences, Box 357988, Seattle, WA 98195, USA, bosseler@u.washington.edu), Toshiaki Imada (University of Washington, Dept. of Speech & Hearing Sciences, and Institute for Learning & Brain Sciences, Box 357988, Seattle, WA 98195, USA, imada@u.washington.edu), Elina Pihko (BioMag Laboratory, Helsinki University Central Hospital, 00029 Helsinki, Finland, pihko@biomag.hus.fi), Jyrki Mäkelä (BioMag Laboratory, Helsinki University Central Hospital, 00029 Helsinki, Finland, jyrki.makela@hus.fi), Samu Taulu (Elekta-Neuromag Oy, 22 Elimäenkatu, 00510 Helsinki, Finland, samu@squid.neuromag.fi),Antti Ahonen(Elekta-Neuromag Oy, 22 Elimäenkatu, 00510 Helsinki, Finland, antti.ahonen@elekta.com), Patricia K. Kuhl (University of Washington, Dept. of Speech & Hearing Sciences, and Institute for Learning & Brain Sciences, Box 357988, Seattle, WA 98195, USA, pkkuhl@u.washington.edu)

In adults, neural responses to the acoustic properties of native and non-native speech sounds differ. Recent magnetoencephalography (MEG) studies indicate that two regions of the brain, the superior temporal area and inferior parietal area (Broca's), in both the left and right hemispheres, may contribute to how the adult brain responds to the acoustic properties of speech. The aim of the present study was to investigate neural activation in adults when listening to native and non-native speech, and to non-speech analogs of speech. We used MEG to examine activation of the superior temporal and inferior parietal areas. Native speakers of Finnish were presented with Finnish (/pa/ and /ta/) and Chinese (/t ″looped c″ ″superscript h″ i/ and /″looped c″ i/) syllables, and sine-wave replicas of /pa/ and /ta/, in a passive oddball paradigm. Our analysis examines the properties of localized neural activities to determine how activation of sensory and motor speech areas differs for speech and non-speech, and the role of language experience in brain activation.

2pSCc59. Why words do not have a psychological alphabet. Robert F. Port (Indiana University, 330 Memorial Hall, Bloomington, IN 47405, USA, port@indiana.edu)

Linguists and psychologists share a powerful intuition that the psychological form of language (in memory) employs letter-like units for spelling words and any other linguistic material. However evidence accumulating over the decades shows that memory for linguistic material actually consists of continuous-time representations containing much more information than we thought, plus there are episodic representations with much redundancy. So Liberman's /di/ and /du/ share nothing in their representation. There need not be an abstract /d/ in the memory representations of language. Our intuition that a letter-like representation is necessary for speech perception and production turns out to be shared only with literate people. Because we cultivate our reading and writing skills, we bias our brains (and consciousness) to model speech using something like letters (e.g, phones) - either from an orthographic or a technical alphabet. So our conscious experience of language is shaped by our cultural tradition of training children to hear speech as letters and letters as speech - all to exploit the technology of literacy. When we can overcome this education-based bias toward phones and phonemes, we will discover the phonemic emperor has no supporting evidence. Linguistic material in memory is richly detailed - relative to what an alphabet represents.

Session 2pSPa

Signal Processing in Acoustics: Beamforming, Localization, and Tracking I

Michael Roan, Cochair
Virginia Tech, 917 Village Way North, Blacksburg, VA 24060, USA

Natalia Sidorovskaia, Cochair
Department of Physics, University of Louisiana, UL BOX 44210, Lafayette, LA 70504-4210, USA

Contributed Papers

2:00

2pSPa1. Acoustic vector-sensor array beamforming based on fourth-order cumulants. Tingting Li (College of Underwater Acoustic Engineering, Harbin Engineering University, 150001 Harbin, China, liqiaocheng@hrbeu.edu.cn), Xiukun Li (College of Underwater Acoustic Engineering, Harbin Engineering University, 150001 Harbin, China, xiukun_li@yahoo.com.cn)

Abstract: Some high-resolution direction-of-arrival (DOA) estimation methods, such as the MUSIC method, have been developed based on vector-sensor array. However, these high-resolution methods suffer from serious drawbacks. Indeed, they are not able to estimate coherent signals and sensitive to calibration errors. Mainly to overcome these limitations and in particular to satisfy practical engineering application, vector-sensor array beamforming based on fourth-order cumulants is adopted in this paper. The main interest in using fourth-order cumulants instead of second-order ones in vector-sensor array processing application is the aperture extension property of higher-order cumulants, which makes it possible to increase both the resolution and the number of sources to be processed from a given array, and suppress the Gaussian noise. Based on this method, smaller size of array and higher accuracy of DOA estimation can be realized, besides, this method is less sensitive to the coherence of the signals and calibration errors, which makes it possible to work well in engineering application. The results of computer simulation and analysis of data from outfield trials show that this method excels traditional direct estimation and can improve estimation capability of vector-sensor arrays.

2:20

2pSPa2. Robust array pattern synthesis with uncertain manifold vector. Shefeng Yan (Department of Electronics and Telecommunications, Norwegian University of Science and Technology, O.S. Bragstads plass 2A, 7491 Trondheim, Norway, sfyan@ieee.org)

The knowledge of the array manifold vectors of an acoustic array can be imprecise, which is often the case in practice. This may cause undesirably high sidelobes for a nominal optimal beamformer where the array manifold vectors are assumed to be known exactly. Although the norm constraint on beamformer weights can be imposed to improve the robustness of the optimal beamformer, it is not clear how to choose the optimal constrained parameter based on the known level of uncertainty of the array manifold vectors. A pattern synthesis approach to arbitrary arrays with robustness against array manifold vectors errors is developed. Our technique optimizes the worst-case performance by minimizing the worst-case sidelobe level while maintaining a distortionless response to the worst-case signal steering vector. The parameters can be optimally chosen based on the uncertainty of the array manifold vector. The robust beamformer problem is shown to be convex, which can be efficiently solved using second-order cone programming. A simple lower bound on how much worse the robust optimal beamformer will be compared to the nominal one is also derived. Computer simulations show better performance of the proposed robust beamformer.

2:40

2pSPa3. Analytical prediction of sample eigenvector quality deterioration in large arrays due to SNR or sample size constraints. Raj Nadakuditi (MIT, Department of Mathematics, 77 Massachusetts Avenue, Cambridge, MA 02139, USA, raj@mit.edu), Arthur B. Baggeroer (MIT, Department of Mathematics, 77 Massachusetts Avenue, Cambridge, MA 02139, USA, abb@boreas.mit.edu)

It is well-known that subspace-based estimation methods in adaptive array processing suffer a rapid degradation in performance as either the signal-to-noise ratio (SNR) or the number of available snapshots drops below a certain threshold value. In the large system, relative large sample size limit, one can use random matrix theory to analytically predict this threshold and the degradation in the ''quality'' of the corresponding subspace estimates. In certain settings, one observes a ″phase transition″ phenonemon so that if the signals are too weak or there are insufficient number of snapshots or both, the subspace estimates are, statistically speaking, noise-like. We discuss the implication of these results for the subspace based detection of signals in white and colored noise using large arrays and illustrate the accuracy of the predictions with numerical simulations.

3:00

2pSPa4. Efficient Replica Generation for Space Time Adaptive Processing of Acoustic Signals. Neena Imam (Oak Ridge National Laboratory, 1 Bethel Valley Road, Oak Ridge, TN 37831-6015, USA, imamn@ornl.gov), Jacob Barhen (Oak Ridge National Laboratory, 1 Bethel Valley Road, Oak Ridge, TN 37831-6015, USA, barhenj@ornl.gov), Michael Traweek (Office of Naval Research, 875 North Randolph Street, Arlington, VA 22203, USA, Mike.Traweek@navy.mil)

This paper addresses an innovative method for real-time replica generation using generalized Green's function for Space Time Adaptive Processing (STAP) technology for sonar applications. In hypothesis processing for STAP algorithms, the first step is to generate replicas for various target hypothesis such as the infinite-range fixed-direction (IRFD) target hypotheses or the tracking (trajectory) hypotheses. Once generated, these replicas are used in multiple steps of the STAP algorithm for computing system parameters such as the signal to noise ratio. Replicas are traditionally precomputed or hard-wired due to computational load constraints. Such a precomputation precludes direct application of array shape corrections, and limits the ability to process arbitrary target trajectories. W propose to use a generalized Green's function for efficient and ultra-fast real-time generation of replicas on multi-core processors Specifically, for an arbitrary target trajectory $r_T(t_i)=[x_T(t_i),\ y_T(t_i),\ z_T(t_i)]$, arbitrary receive array trajectory $r_{R(k)}(t_i)=[x_{R(k)}(t_i), y_{R(k)}(t_i), z_{R(k)}(t_i)]$, $(k=1,...,N_{EL})$, arbitrary vector of frequencies in homogeneous acoustic medium $f=[f_1 f_2,....,f_n,...]$, and sound speed c_0, we can write $G[r_T(t_i),r_{R(k)}(t_i),f_n|c_0]= \exp[j(2\pi f_n/c_0)|\ r_{R(k)}(t_i)-\ r_T(t_i)\ |]/\ |\ r_{R(k)}(t_i)-\ r_T(t_i)\ |$ In terms of rationale, this is the simplest possible replica set for any STAP algorithm. The efficient implementation of the generalized Green's function on a multi-core processor will allow real-time adjustment-/modification of acoustical target tracking resulting in improved numerical accuracy and time performance.

3:20

2pSPa5. Beam-forming with progressive focalisation. Gaetano Caronna (Università La Sapienza - Dept. Fisica Tecnica, Via Eudossiana 18, 00184 Roma, Italy, gaetano.caronna@uniroma1.it), Pierluigi Testa (Università La Sapienza - Dept. Fisica Tecnica, Via Eudossiana 18, 00184 Roma, Italy, pierluigi.testa@uniroma1.it)

This investigation is aiming to detect and track a moving target using its acoustic emissions and applying a new beam-forming approach. An original algorithm of medium computational complexity is reported that is capable of locating, with good accuracy, the direction of an acoustic source with only a few microphones. This algorithm circumvents the known localisation ambiguities due to the unwanted ″grating lobes″, by using all spectral content of the acoustic source and progressively and narrowly focusing its beam in the direction of the target. The algorithm starts by locating the direction of the target with low angular resolution, using only low frequency components of the acoustic emissions; in this way, no grating lobes occur even with only a few microphones. Then, the angular resolution is increased by processing higher frequencies of the spectrum, but profiting of the information on the angular position achieved in the previous stages. Some algorithmic means are introduced to increase the performance of the algorithmic against environmental noise. This scheme is described in detail. Some experimental tests are included and discussed.

TUESDAY AFTERNOON, 1 JULY 2008 P3-C, LEVEL 3, 3:40 TO 5:20 P.M.

Session 2pSPb

Signal Processing in Acoustics: Beamforming, Localization, and Tracking II (Poster Session)

Michael Roan, Cochair
Virginia Tech

Natalia Sidorovskaia, Cochair
Department of Physics, University of Louisiana

All posters will be on display from 3:40 p.m. to 5:20 p.m. To allow contributors an opportunity to see other posters, contributors of odd-numbered papers will be at their posters from 3:40 p.m. to 4:30 p.m. and contributors of even-numbered papers will be at their posters from 4:30 p.m. to 5:20 p.m.

Contributed Papers

2pSPb1. Particles filter applied in the real-time bearings-only tracking problem of a sonar target. Cleide V. Rodrigues (Ipiru 2 Ilha do Governador, 21931-095 Rio de Janeiro, Brazil, clevital@hotmail.com), William Soares-Filho (Ipiru 2 Ilha do Governador, 21931-095 Rio de Janeiro, Brazil, wsoaresf@hotmail.com)

The development of a passive sonar tracking system in real-time needs algorithms each time more accurate and that can be able to follow rapid changes in the signal characteristics. In a bearings-only tracking problem, the bearing model is a nonlinear function of the target states. Nowadays, methods that deal with nonlinear and non-Gaussian estimation are receiving great attention. Particles filter is one of these methods. Particles filters are Sequential Monte Carlo methods that represent the required probability density function as a set of random samples. This present paper describes the particles filter application in the bearings-only tracking problem. Real data of targets are displayed in energy versus bearing graphics obtained in an operational naval environment. These data were used with the Sampling Importance Resampling algorithm (SIR). The particles filter is formulated in the Cartesian coordinates and then are transformed to modified polar coordinates. Results are compared with Kalman Extended Filter and the effectiveness and limitations of SIR algorithm for tracking target using a bearing/time record are examined.

2pSPb2. Tracking of underwater acoustic tone sources with linear antenna arrays. Denis Orlov (Institute of Applied Physics of the Russian Academy of Sciences, 46 Ulyanov Street, 603950 Nizhny Novgorod, Russian Federation, denis@hydro.appl.sci-nnov.ru), Alexander Rodionov (Institute of Applied Physics of the Russian Academy of Sciences, 46 Ulyanov Street, 603950 Nizhny Novgorod, Russian Federation, alexr@hydro.appl.sci-nnov.ru)

Track determination is a necessary task for a variety of underwater measurement applications, such as measurement of acoustic fields of ships. The use of linear antenna arrays provides great advantages for measurements and tracking. The investigated ship may be equipped by a special sound source of either pulse or tone signal utilized for tracking. The work considers two scenarios involving the case of a tone source. The scenarios are conditioned by parameters of the array and the source, which may vary depending on task. When a source is of relatively high frequency (several thousands Hz), tracking can be based on the dependence of the Doppler frequency shift and bearing on time; in this case, the parameters to be estimated are the ones of the whole track (velocity, traverse instant, etc.). If the source frequency is relatively low (up to 300 Hz), the array is large (greater than a typical distance from the source to the array aperture), the array focusing ability allows to perform the determination of ″instant″ locations of the source at various

instances; estimating of parameters of the track as a whole is then based on the set of the obtained coordinates. The developed methods have been successfully tested using a large amount of experimental data.

2pSPb3. Robust beamforming and beamspace DOA estimation using measured array manifold of arbitrary geometry acoustic array. Yixin Yang (Institute of Acoustic Engineering, Northwestern Polytechnical University, 710072 Xi'an, China, yxyang@nwpu.edu.cn), Chao Sun (Institute of Acoustic Engineering, Northwestern Polytechnical University, 710072 Xi'an, China, csun@nwpu.edu.cn)

The acoustic diffraction of array supporting structure will result in the large difference of the amplitude and phase response of each hydrophone, which leads to the distortion of beampattern. A method for obtaining the array manifold of arbitrary geometry acoustic array is proposed in this paper. We measured the array response vector in many directions with a fixed angular step in anechoic water tank. The array response vectors were smoothed to eliminate the measurement system error. Using these smoothed array response vectors, the robust beampattern of arbitrary geometry array is obtained via beam synthesis method. A 16 element volumetric acoustic array was constructed and tested in an anechoic water tank. Robust low sidelobe beampatterns based on the measured manifold were formed, and then the beamouputs were used to apply to beamspace high resolution DOA estimation methods. The experimental results show that our method can suppress noise and interferences outside the beam coverage regions, and get high resolution DOA estimation results. When the array geometry has some distortion, the weighting vectors of beamforming can still work well to form good beampatterns, and then get accurate DOA estimation results. This verifies the effectiveness of our proposed method.

TUESDAY AFTERNOON, 1 JULY 2008 P3-C, LEVEL 3, 3:40 TO 5:20 P.M.

Session 2pSPc

Signal Processing in Acoustics: Acoustical Nondestructive Evaluation, Ultrasonics, and Imaging II (Poster Session)

Grace Clark, Cochair
Lawrence Livermore National Laboratory

Ning Xiang, Cochair
Rensselaer Polytechnic Institute

All posters will be on display from 3:40 p.m. to 5:20 p.m. To allow contributors an opportunity to see other posters, contributors of odd-numbered papers will be at their posters from 3:40 p.m. to 4:30 p.m. and contributors of even-numbered papers will be at their posters from 4:30 p.m. to 5:20 p.m.

Contributed Papers

2pSPc1. Identification of Noise Emission in a Gear Unit. Ales Belsak (University of Maribor, Faculty of Mechanical Engineering, Smetanova ulica 17, 2000 Maribor, Slovenia, ales.belsak@uni-mb.si), Jurij Prezelj (University of Ljubljana, Faculty of Mechanical Engineering, Aškerčeva 6, 1000 Ljubljana, Slovenia, jurij.prezelj@fs.uni-lj.si)

Today it is very important to ensure a stable production without unscheduled outages. To achieve this objective it is required to use advanced production technologies, to ensure adequate maintenance of mechanical systems and to monitor the condition of a device or machine. Reliable and accurate operation of machines and devices with as few outages as possible is desired. The significance of a life cycle design of machines and devices is growing. Possible damages in gear units can be defined by means of monitoring acoustic emission. A crack in the tooth root is usually indicated by significant changes in tooth stiffness. A difference in dynamic responses of an undamaged gear and of a damaged gear can be noted. The possibility of the use of an acoustic method in the field of condition diagostics is dealt with. The noises produced by a gear unit have been analysed, the noise sources within a gear unit have been determined and the corresponding time-frequency analysis of these sources have been performed, using an acoustic camera.

2pSPc2. Detection of Ultrasonic closer flaws using Nonlinear signal processing. Abdessalem Benammar (Image and signal processing laboratory. Welding and NDT Centre, Route de Dely-Ibrahim, BP 64, Chéraga, 16035 Alger, Algeria, Abs_benammar@yahoo.fr), Redouane Drai (Image and signal processing laboratory. Welding and NDT Centre, Route de Dely-Ibrahim, BP 64, Chéraga, 16035 Alger, Algeria, drai_r@yahoo.fr), Ahmed Kechida (Image and signal processing laboratory. Welding and NDT Centre, Route de Dely-Ibrahim, BP 64, Chéraga, 16035 Alger, Algeria, Abs_benammar@yahoo.fr), Abderrezak Guessoum (Image and signal processing laboratory. Welding and NDT Centre, Route de Dely-Ibrahim, BP 64, Chéraga, 16035 Alger, Algeria, Abs _benammar@yahoo.fr)

The ultrasonic flaw detection is an important problem in the nondestructive evaluation (NDE) of materials. In order to successfully detect and classify flaw echoes from high scattering grain echoes, an efficient and robust method is required. In this paper, a method using split-spectrum processing (SSP) combined with a neural network (NN) has been developed and applied on the ultrasonic signals to perform the detection of closer echoes. SSP can display signal diversity and is therefore able to provide the signal feature vectors for signal classification. The neural network (NN) performs

highly complex nonlinear mapping by which signals can be classified according to their feature vectors. Therefore, the combination of SSP and NN (SSP-NN) presents a powerful technique for ultrasonic NDE. The SSP is achieved by using Gaussian bandpass filters. Then, an adaptive three layer neural network using a backpropagation learning process is applied to perform the classification processing of frequency diverse data. The SSP-NN method has been tested using both simulated and experimental ultrasonic signals, and the results show that SSP-NN has good sensitivity in the detection of ultrasonic closer flaws echoes drowned in the noise.

2pSPc3. Quantitative Ultrasonics for Inclusion and Pore Characterization of Steel Billets. Ville Kananen (Univ. of Helsinki / Dept. of Physical Sciences, POB 64 (Gustaf Hällströmin katu 2), 00014 Helsinki, Finland, ville.kananen@helsinki.fi), Joona Eskelinen (Univ. of Helsinki / Dept. of Physical Sciences, POB 64 (Gustaf Hällströmin katu 2), 00014 Helsinki, Finland, joona.eskelinen@helsinki.fi), Edward Hæggström (Electronics Research Unit, University of Helsinki, P.O.Box 64 (Gustaf Hällströmin katu 2), FIN-00014 Helsinki, Finland, edward .haeggstrom@helsinki.fi)

We present ultrasonic quantitative inclusion and pore characterization in bearing steel 100Cr6. A 9.5MHz focused transducer (14cm focal length, 6.3MHz bandwidth) scanned across the top surface of immersed $22*12*6cm^3$ production samples (8pcs). Automatic pre-processing was employed to detect inclusions in samples. Recorded RF-data were analyzed. Continuous wavelet transform and cross-correlation were applied to measured and registered RF-signals from known (verified by SEM) inclusions and pores. This allowed characterizing the echoes by shape from wavelet coefficients (WC) and cross-correlation coefficients: the echo is a superposition of the reflection from the inclusion front and back surface, whereas pores exhibit no back surface echo due to their large acoustic impedance mismatch. Fourier transform allows characterizing echo RF-signals by frequency content. Dissimilarities -signal phase and WCs- in echo characteristics between different inclusion and pore classes allows quantitative inclusion and pore characterization. We discriminate three classes: oxide-inclusions (aluminium-oxides, calcium-aluminates), sulphides (manganese-sulphide), and pores. We also estimate inclusion size, position, and orientation. Rolled (reduction ratio 4 and 10) and unrolled production samples are characterized. The instrument functionality was validated by blind tests using SEM. Inclusion distributions in different classes of steel 100Cr6 and classification probabilities are presented. Our software saves sample preparation and image analysis work.

2pSPc4. Digital High Frequency Coded Imaging System. Marcin Lewandowski (Institute of Fundamental Technological Research, Swietokrzyska 21, 00-049 Warsaw, Poland, mlew@ippt.gov.pl), Andrzej Nowicki(Institute of Fundamental Technological Research, Swietokrzyska 21, 00-049 Warsaw, Poland, anowicki@ippt.gov.pl)

Coded transmission is an approach to solve the inherent compromise between penetration and resolution required in ultrasound imaging. It is universally acknowledged that this technique gives major improvement in SNR. A novel high frequency (20-35 MHz) ultrasound real-time imaging system for research and evaluation was developed. The digital programmable coder-digitizer module based on the field programmable gate array (FPGA) supports arbitrary waveform coded transmission and RF echoes sampling up to 200 MSPS, as well as real-time streaming of digitized RF data via a high speed USB interface to the PC. All RF and image data processing were implemented in the software. A novel balanced software architecture using CPU and GPU processing supports real-time processing and display at rates up to 30 frames/sec. The system was used to acquire data for sine burst and 16-bit Golay code excitation using a single element scanning head with thick film focused spherical transducer 25 MHz center frequency and 56% system bandwidth. SNR gain for the Golay codes (referenced to single burst) of 15 dB for 20 MHz and 16 dB for 35 MHz were obtained. In water the axial resolution for both single burst and the Golay codes was the same FWMH=20 ns at 20 MHz and FWMH=15 ns at 35 MHz.

2pSPc5. Wavelet threshold enhancement by an energetic characterization of ultrasonic signal Ndt analysis. Fairouz Bettayeb (Research Center on Welding and Control, CSC, Route de Delly Brahim, Bp: 64. Chéraga, 16800 Algiers, Algeria, fairouz_bettayeb@email .com)

In ultrasonic NDE of industrial components, the visibility of flaw echoes is corrupted by noise due to multiple scattering. Grain boundaries can reach the size of the same order of magnitude than discontinuities to be detected, becoming scatters of ultrasonic noise and could be confused with defect indications. Many studies have been conducted on the use of the wavelet theory for ultrasonic signal de-noising, but nothing has been done on the structural noise features and its analyzing wavelet function. In the framework of the automation of the ultrasonic signal analysis project, we have followed the exploration of the wavelet theory, from the continuous transforms to the discrete ones, and the experiments give us some ambivalent results. So for a best threshold control, our idea was directed to the investigation of the noise analyzing function. In this work the noise features were extracted by an energetic smoothing algorithm that allows the exploration of the noise analyzing function; by which the random nature of the noise in the spatial domain is bypassed. The energetic characterization of the noise and the defects allows an improved filtering process. The new smoothing algorithm performs an accurate signal reconstruction in an interesting computing time.

Session 2pSPd

Signal Processing in Acoustics and Physical Acoustics: Biomedical Applications of Time-Reversal II (Poster Session)

Oleg Sapozhnikov, Cochair
Center for Industrial and Medical Ultrasound, Applied Physics Lab.

Mickael Tanter, Cochair
Laboratoire Ondes et Acoustique

All posters will be on display from 3:40 p.m. to 5:20 p.m. To allow contributors an opportunity to see other posters, contributors of odd-numbered papers will be at their posters from 3:40 p.m. to 4:30 p.m. and contributors of even-numbered papers will be at their posters from 4:30 p.m. to 5:20 p.m.

Contributed Papers

2pSPd1. Time reversal elastography in soft solids. Thomas Gallot(LGIT Université Joseph Fourier/CNRS, Maison des Géosciences Domaine Universitaire, 38041 Grenoble, France, thomas.gallot@obs.ujf-grenoble .fr), Stefan Catheline (LOA, Université Paris 7 Denis Diderot, ESPCI, 10 rue Vauquelin, 75005 Paris, France, stefan.catheline@espci.fr), Nicolas Benech (Science University of Montevideo, 11400 Montevideo, Uruguay, nbenech@fisica.edu.uy), Javier Brum (Science University of Montevideo, 11400 Montevideo, Uruguay, jbrum@fisica.edu.uy), Carlos Negreira (Science University of Montevideo, 11400 Montevideo, Uruguay, carlosn@fisica.edu.uy), Philippe Roux (LGIT - CNRS - Université Joseph Fourier, Maison des Géosciences, 1381 rue de la Piscine, BP 53, 38041 Grenoble, France, philippe.roux@obs.ujf-grenoble.fr)

One channel time-reversal (TR) experiments allow focalization of waves in reverberant cavities. According to Rayleigh criteria, the focal spot width is directly related to wavelength and therefore depends on the mechanical properties of the medium. Thus the general idea of this work is to extract quantitative estimations of these mechanical properties from TR experiments. They were performed inside 3D soft solid cavities (gelatin based phantoms). An external source creates mechanical waves in the audible frequency range and one component of the vectorial field is measured as function of time by ultrasonic techniques developed in elastography. The wavelength information of shear waves, that dominates the vectorial field, is deduced from TR experiments. The advantage is that the technique works with sources of any shape and with any time dependence. This robustness as regard to shear wave source allows to think about many applications in the medical field, including deep or moving organs. Examples of elasticity image will be shown in inhomogeneous soft tissues.

2pSPd2. Time Reversal Acoustic focusing with random reverberator. Laurent Fillinger (Artann Laboratories/ Stevens Institute of Technology, 711 Hudson St, Hoboken, NJ 07030, USA, laurent.fillinger@artannlabs .com), Alexander Sutin (Stevens Institute of Technology, Castle Point on Hudson, Hoboken, NJ 07030, USA, asutin@stevens.edu), Armen Sarvazyan (Artann Laboratories, 1753 Linvale-Harbourton, Lambertville, NJ 08350, USA, armen@artannlabs.com)

Time Reversal Acoustic (TRA) focusing system based on an external reverberator can provide good focusing with minimum side lobes even with a few transducers. The focusing ability of such system can be increased using reverberator with rough boundaries or by adding internal random scatterers. The experiments were conducted with a reverberator made of a polyethylene bottle filled with water and a single piezoceramic disk attached externally to its wall. Experiments demonstrated that inserting in the bottle random hard scatterers or altering of the bottle surface significantly decreases the size of the focused spot and the level of side lobes. The new pseudo-impulse method of TRA focusing allowed suppressing piezotransducer resonances and provided formation of short wide band signals. The ability of such TRA focusing system based on random reverberator to form simultaneously multiple focuses and produce focal spots of the complex shape has been demonstrated. The application of binary radiation regime led to several fold increasing of the amplitude of the focal spot while the focal structure practically was not affected. Applications of such random focusing system for medical imaging and HIFU treatment is discussed.

Session 2pSPe

Signal Processing in Acoustics, Acoustical Oceanography, and ECUA: Bayesian Signal Processing I (Poster Session)

Zoi-Heleni Michalopoulou, Cochair
Department of Mathematical Sciences, New Jersey Institute of Technology

Simon Godsill, Cochair
Dept. of Engineering, University of Cambridge, Trumpington St., CB2 1PZ Cambridge, UK

All posters will be on display from 3:40 p.m. to 5:20 p.m. To allow contributors an opportunity to see other posters, contributors of odd-numbered papers will be at their posters from 3:40 p.m. to 4:30 p.m. and contributors of even-numbered papers will be at their posters from 4:30 p.m. to 5:20 p.m.

Contributed Papers

2pSPe1. Continuous estimation of VTL from vowels using a linearly VTL-covariant speech feature. Christian Feldbauer (Centre for the Neural Basis of Hearing, Department of Physiology, Development and Neuroscience, University of Cambridge, Downing Site, CB23EG Cambridge, UK, feldbauer@tugraz.at), Jessica J. Monaghan (Centre for the Neural Basis of Hearing, Department of Physiology, Development and Neuroscience, University of Cambridge, Downing Site, CB23EG Cambridge, UK, jjmm2@cam.ac.uk), Roy D. Patterson (Centre for the Neural Basis of Hearing, Department of Physiology, Development and Neuroscience, University of Cambridge, Downing Site, CB23EG Cambridge, UK, rdp1@cam.ac.uk)

Vowel sounds encode information about the speaker's vocal tract length (VTL) as well as vowel type. This paper shows how VTL can be estimated on a frame-by-frame basis from vowels to facilitate speaker tracking and make automatic speech recognition (ASR) more robust in multi-speaker environments. The algorithm is based on a new, VTL-covariant speech feature that encodes the size information linearly. The paper shows that this new speech feature is better suited for VTL estimation than the more traditional cepstral coefficients. The VTL estimation is based on a Gaussian mixture model that was trained on the speech material of speakers with known body height but unknown VTL. Research supported by the Austrian Science Fund (FWF) [J2541-N15], EOARD [FA8655-05-1-3043], and the UK-MRC [G0500221].

2pSPe2. A sequential Bayesian approach to vertical slice tomography of a shallow water environment. Olivier Carrière (Université libre de Bruxelles (U.L.B.) - Environmental hydroacoustics lab, av. Franklin D. Roosevelt 50, CP 194/5, 1050 Bruxelles, Belgium, ocarrier@ulb.ac.be), Jean-Pierre Hermand (Université libre de Bruxelles (U.L.B.) - Environmental hydroacoustics lab, av. Franklin D. Roosevelt 50, CP 194/5, 1050 Bruxelles, Belgium, jhermand@ulb.ac.be)

A major challenge of acoustic tomography in shallow water environments is to track physical features that are highly variable in time and space and to properly account for sound interaction with the subbottom. In a previous work an extended Kalman filter (EKF) scheme was proposed to track the sound-speed field variations in a vertical slice of the water column for known bottom geoacoustic parameters. Although the results were encouraging, it was shown that some biases were encountered when using the standard EKF, principally because of the high nonlinearity between the observations (the multi-frequency pressure field) and the environmental parameters (here the sound-speed field). In this paper, we show that Ensemble Kalman or sequential Monte Carlo filtering significantly enhance the estimation of the sound-speed field, for both range-independent and range-dependent cases. Reproducible results show that the temporal variations are well tracked, even in presence of measurement noise and model uncertainty. Furthermore the sampling approach allows to increase the time interval between successive measurements, which is an advantage from an operational viewpoint. The performances of the different nonlinear filters are also discussed.

2pSPe3. Source localization and tracking in a waveguide via sequential bayesian estimation. Kevin Cockrell (MIT, 77 Mass Ave, 5-204, Cambridge, MA 02139, USA, cockrell@mit.edu), Henrik Schmidt (MIT, 77 Mass Ave, 5-204, Cambridge, MA 02139, USA, henrik@mit.edu)

This talk addresses the problem of sequentially estimating the location of a moving acoustic source in a waveguide, given a series of acoustic field measurements from an array. The approach taken, in it's most general form, is known as sequential Bayesian estimation. A well known special case of sequential Baysian estimation is the Kalman filter. However, the Kalman filter is only optimal when the relationship between the measured parameters and the ones to be estimated is linear with Gaussian noise. Given the highly non-linear relationship between the acoustic source location and the measured acoustic field, other approaches must be taken. The performance and computational feasibility of various approaches, such as grid-based methods, will be explored using simulated data.

2pSPe4. The role of reproducing densities in a joint likelihood approach to multi-sensor detection and estimation. Michael Roan (Virginia Tech, 917 Village Way North, Blacksburg, VA 24060, USA, mroan@vt.edu), Elizabeth Hoppe (Virginia Polytechnic Institute and State University, 141 Durham Hall, Blacksburg, VA 24060, USA, ehoppe@vt.edu)

In this work, a Bayesian, joint estimation-detection approach is used for computation of sufficient statistics and development of a general multi-sensor information fusion architecture. An approach borrowed from sequential Bayesian processing is used to compute prior densities for joint Bayesian estimation-detection. In this approach, a posteriori densities calculated at one sensor become priors at the next sensor after a coordinate transformation that transforms the outputs of each sensor to a common reference frame for all sensors. Reproducing prior densities are used to simplify the Bayesian iteration scheme and reduce communications requirements. The framework that is developed is equally applicable to networks where all sensors communicate with a centralized detection and estimation processor as well as those networks where sensors relay information from point to point.

We anticipate using Bayesian iteration to convert posterior information into prior information on the next data gather cycle, iterate on estimates by exchanging information between sensors, i.e., ″turbo likelihood fusion,″ and having the central decision maker decide when sensors should or should not communicate, depending on a cost criterion which combines information gain versus communication energy expenditure. Simulation are used to show detection and estimation performance under various conditions of sensor position and orientation uncertainty.

TUESDAY AFTERNOON, 1 JULY 2008 P3-C, LEVEL 3, 3:40 TO 5:20 P.M.

Session 2pSPf

Signal Processing in Acoustics, Biomedical Ultrasound/Bioresponse to Vibration, and Underwater Acoustics: Time Reversal Methods for Array Imaging and Signal Processing II (Poster Session)

David Chambers, Cochair
LLNL

Claire Prada, Cochair
Laboratoire Ondes et Acoustique

All posters will be on display from 3:40 p.m. to 5:20 p.m. To allow contributors an opportunity to see other posters, contributors of odd-numbered papers will be at their posters from 3:40 p.m. to 4:30 p.m. and contributors of even-numbered papers will be at their posters from 4:30 p.m. to 5:20 p.m.

Contributed Papers

2pSPf1. Isolation of backscattering resonances of a thin spherical shell using iterative time reversal. Zachary J. Waters (Boston University, Dept. of Aerosp. and Mech. Eng., 110 Cummington St., Boston, MA 02215, USA, zjwaters@bu.edu), Benjamin R. Dzikowicz (Naval Surface Warfare Center, Panama City Division, Code HS-11, 100 Vernon Ave., Panama City, FL 32407, USA, benjamin.dzikowicz@navy.mil), R. Glynn Holt (Boston University, Dept. of Aerosp. and Mech. Eng., 110 Cummington St., Boston, MA 02215, USA, rgholt@bu.edu), Ronald A. Roy (Boston University, Dept. of Aerosp. and Mech. Eng., 110 Cummington St., Boston, MA 02215, USA, ronroy@bu.edu)

The backscattering spectrum of thin spherical shells show resonance peaks due to several different physical processes including high frequency Lamb wave excitation and low frequency modal ringing [Kaduchak et al., J. Acoust. Soc. Am. 97, 2699-2708 (1995)]. These different processes can be isolated in both time and frequency by using simulated iterative time reversal. This is accomplished by windowing in the time domain and/or filtering in the frequency domain. Iterative time reversal techniques developed for buried target detection [Waters et al., J. Acoust. Soc. Am. 122, 3023 (2007)] are applied to the partial wave series solution for the backscattering of plane acoustic waves by a thin-walled spherical shell. Tank experiments are performed to verify theoretical results. Targets loaded with both water and sediment are considered. Understanding the relationship between the time reversal window's size/position and the dominant target scattering mechanisms is key to the development of time reversal as a detection and identification technique. [Work supported by The Office of Naval Research.]

2pSPf2. The Decomposition of the Time Reversal Operator with virtual transducers. Jean-Luc Robert (Philips Research, 345 Scarborough Road, Briarcliff Manor, NY 10510, USA, jean-luc.robert@philips.com), Mathias Fink (Laboratoire Ondes et Acoustique, ESPCI, Université Paris 7, CNRS, 10 rue Vauquelin, 75005 Paris, France, mathias.fink@espci.fr)

The FDORT method (French acronym for Decomposition Of the Time Reversal Operator using Focused beams) is a variant of the DORT method using focused transmits instead of single element transmits. An intuitive interpretation of the method is presented here. It is shown that the FDORT method is equivalent to a DORT method with two different arrays: the actual array and a virtual array whose transducers are located at the foci of the transmits. By changing the focal depth, it is possible to change the position of the virtual array and thus obtain different information. An application to aberration correction in a far field phase screen model will be presented.

2pSPf3. Reconstruction of temporal invariants of the time-reversal operator for communication in shallow water. Franck D. Philippe (Laboratoire Ondes et Acoustique, ESPCI, Université Paris 7, CNRS, 10 rue Vauquelin, 75005 Paris, France, franck.philippe @espci.fr), Thomas Folégot (NATO Undersea Research Center, Viale San Bartolomeo 400, 19126 La Spezia, Italy, folegot@nurc.nato.int), Claire Prada (Laboratoire Ondes et Acoustique, ESPCI, Université Paris 7, CNRS, 10 rue Vauquelin, 75005 Paris, France, claire.prada-julia@espci.fr), Mathias Fink (Laboratoire Ondes et Acoustique, ESPCI, Université Paris 7, CNRS, 10 rue Vauquelin, 75005 Paris, France, mathias.fink@espci.fr)

Time-reversal techniques allow focusing in waveguides with application for detection or telecommunication (Kupperman et al., J. Acoust. Soc. Am. **103**(1), 25-40, (1998)). It has been shown that the DORT method (French acronym for Decomposition of the Time Reversal Operator) can be used to achieve detection and selective focusing on pointlike scatterers in a waveguide (Mordant et al., J. Acoust. Soc. Am. **105**, 2634-2642 (1999)). However, the decomposition is done in frequency domain providing eigenvectors $V(\omega)$ of undetermined phase. In order to achieve temporal focusing, it is necessary to built 'temporal eigenvectors' V(t) as an appropriate combination of the eigenvectors $V(\omega)$. Due to dispersion, the reconstruction of the temporal eigenvectors is difficult in waveguides. One solution was proposed by Mordant et al., using the symmetry of the array response matrix and assuming continuous frequency dependence of the invariants. However this method does not work if eigenvalues crossings occur. Furthermore, it cannot be applied to distinct arrays of transmitters and receivers. We propose a simple method to reconstruct the temporal invariants by using the back propagation of eigenvector in free space. Application to data from a laboratory experiment and from the DOREV 2005 shallow water experiment are presented.

2pSPf4. Modeling time-reversal focusing in a multiple scattering medium. Kevin J. Haworth (University of Michigan, Department of Radiology, Kresge III, R3320, Ann Arbor, MI 48109-0553, USA, khaworth@umich.edu), Jeffrey B. Fowlkes (University of Michigan, Department of Radiology, Kresge III, R3320, Ann Arbor, MI 48109-0553, USA, fowlkes@umich.edu), Paul L. Carson (University of Michigan, Department of Radiology, Kresge III, R3320, Ann Arbor, MI 48109-0553, USA, pcarson@umich.edu), Oliver D. Kripfgans (University of Michigan, Department of Radiology, Kresge III, R3320, Ann Arbor, MI 48109-0553, USA, greentom@umich.edu)

Time-reversal acoustics has been shown to be effective at focusing sound through high-order multiple-scattering media. In addition to signals being refocused, large amplitudes via pulse compression have also been observed. Previously, a statistical model was developed to simulate a time-reversal experiment where an impulse is sent into the scattering medium and the entire response is time-reversed [A. Derode et al., J. App. Phys. 85, 6343-6352 (1999)]. The high-order multiple-scattering process is modeled as a shot noise process. Again postulating a shot noise process the model has been extended to allow for arbitrary input functions and arbitrary windowing before time-reversal. The model has been shown to accurately predict the variance and expectation value of ensembles of simulated data. The analytical model is also tied directly to the governing physical processes, which is useful in attempting to optimize refocused signals. This extension is motivated by a desire to achieve high-amplitude long-pulse focusing, as would be useful in thermal therapies and radiation force experiments. However, the model can find application beyond this specific end-point. The model, it's physical implications, and several time-reversal simulations will be presented.

2pSPf5. Spectral properties of the backscattering matrix in random scattering media. Alexandre Aubry (Laboratoire Ondes et Acoustique, ESPCI, Université Paris 7, CNRS, 10 rue Vauquelin, 75005 Paris, France, alexandre.aubry@espci.fr), Arnaud Derode (Laboratoire Ondes et Acoustique, ESPCI, Université Paris 7, CNRS, 10 rue Vauquelin, 75005 Paris, France, arnaud.derode@ujf-grenoble.fr)

We investigate, both experimentally and theoretically, the spectral properties of the backscattering operator in random media. The experimental set up consists in an array of 64 programmable ultrasonic transducers placed in front of a random scattering medium. The impulse responses between each couple of transducers are measured and form the interelement matrix.The evolution of the singular values with time and frequency is computed by means of a short-time Fourier analysis. Our aim is to compare the mean distribution of the singular values with the predictions of Random Matrix Theory (RMT). Two kinds of random media have been investigated: a highly scattering medium in which multiple scattering predominates and a weakly scattering medium. In both cases, residual correlations that may exist between matrix elements are shown to be a key parameter. The mean distribution of singular values exhibits, surprisingly, very different behaviors in the single and multiple scattering regimes. The agreement between experimental results and RMT predictions is found to be very good in both cases. The results are applied to the detection of a target embedded in a random scattering medium with the DORT method.

TUESDAY AFTERNOON, 1 JULY 2008 P3-C, LEVEL 3, 3:40 TO 5:20 P.M.

Session 2pSPg

Signal Processing in Acoustics, Physical Acoustics, Biomedical Ultrasound/Bioresponse to Vibration, and Underwater Acoutics: Overview of Time Reversal in Acoustics II (Poster Session)

David Chambers, Cochair
LLNL

Claire Prada, Cochair
Laboratoire Ondes et Acoustique

All posters will be on display from 3:40 p.m. to 5:20 p.m. To allow contributors an opportunity to see other posters, contributors of odd-numbered papers will be at their posters from 3:40 p.m. to 4:30 p.m. and contributors of even-numbered papers will be at their posters from 4:30 p.m. to 5:20 p.m.

Contributed Paper

2pSPg1. Numerical modeling of the effects of finite size transducers for time reversal acoustics in solid media. Michele Griffa (EES-11 (Geophysics) - Los Alamos National Laboratory, MS D443, Los Alamos, NM 87545, USA, mgriffa@lanl.gov), Brian E. Anderson (EES-11 (Geophysics) - Los Alamos National Laboratory, MS D443, Los Alamos, NM 87545, USA, bea@lanl.gov), Paul A. Johnson (EES-11 (Geophysics) - Los Alamos National Laboratory, MS D443, Los Alamos, NM 87545, USA, paj@lanl.gov)

Time Reversal Acoustics (TRA) has been shown to be very robust not only in fluids but also in solid bounded media. The most relevant limitations to the Time Reversal Process (TRP) in solid specimens are the co-existence of several propagation modes, mode conversion at each interface (inhomogeneities or boundaries), attenuation mechanisms and the multidimensional nature of the propagating wave fields. Additional limitations arise in practical applications, for example for Non Destructive Evaluation purposes, when the Time Reversal Mirror (TRM) piezoelectric transducers are usually attached to the surface of the solid. We have investigated the role of the finite size of the TRM transducers and their sensitivity to only certain components of the incident wave fields in the TRP when they are attached to the surface of the sample under study. We have developed a theoretical analysis and performed numerical simulations and laboratory experiments in order to examine the robustness of TRA in solid media, including where the TRM is composed of finite size elements attached to the specimen surface. The results lead to useful information about the efficiency of the TRP as well as the optimization of the TRM setup in terms of transducer size.

Session 2pSPh

Signal Processing in Acoustics: Advances in Acoustic Sensors and Networks for Defense Applications I

Brian G. Ferguson, Cochair
Defence Science and Technology Organisation, PO Box 44, Pyrmont NSW, Sydney, 2009, Australia

Pierre Naz, Cochair
ISL, 5 rue du Général Cassagnou, 68300 Saint Louis, France

Contributed Papers

5:00

2pSPh1. Acoustic signal processing methods for detecting intrusions and threats in the battlespace. Brian G. Ferguson (Defence Science and Technology Organisation, PO Box 44, Pyrmont NSW, 2009 Sydney, Australia, Brian.Ferguson@dsto.defence.gov.au), Kam W. Lo (Defence Science and Technology Organisation, PO Box 44, Pyrmont NSW, 2009 Sydney, Australia, Kam.Lo@dsto.defence.gov.au)

The processing of acoustic sensor data enables the detection, classification, localization and tracking of intrusions and threats in the battlespace. Initially, passive acoustic signal processing methods that are used in unattended ground sensor networks and onboard uninhabited aerial vehicles are reviewed. These methods process radiated noise (acoustic signature) data generated by sources of military interest and extract tactical information on air and ground vehicles as well as direct (rifle) and indirect (artillery/mortar) fire weapons. Examples of applying various passive acoustic signal processing methods to real sensor data collected during field experiments are presented. The tactical parameter estimates derived from these acoustic methods are then compared with ground truth data. Next, the application of active sonar signal processing to the automatic detection and tracking of a fast inshore watercraft in a cluttered harbor environment is demonstrated using real data. The air bubbles associated with wakes from high-speed surface craft are highly reflective of incident high frequency sonar signal transmissions. Finally, various high frequency active sonar methods that use both real and synthetic apertures to image sea mines are reviewed and demonstrated.

5:20

2pSPh2. Networking and Fusion of Disparate Acoustic Sensors for Battlespace Applications. Tien Pham (US Army Research Laboratory, 2800 Powder Mill Road, Attn: AMSRD-ARL-SE-SA, Adelphi, MD 20783-1197, USA, tien.pham1@us.army.mil), Gene Whipps (US Army Research Laboratory, 2800 Powder Mill Road, Attn: AMSRD-ARL-SE-SA, Adelphi, MD 20783-1197, USA, gene.whipps@us.army.mil)

A network of distributed acoustic sensor systems on the ground and/or in the air can be used effectively for autonomous and remote intelligence, surveillance, and reconnaissance (ISR) applications. However interoperability of disparate sensor systems is a major challenge for current coalition force applications. Specifically, a network of acoustic sensor nodes can exhibit heterogeneity in a variety of dimensions. At the sensor-level, the acoustic sensors can vary in their types (e.g., cardioid vs. omni-direction) and in their responsiveness to transient and continuous sources. At the node-level, the acoustic systems can vary in their array configuration, platform mobility, node reactiveness (e.g., timeliness of response), and information processing and output. At the network-level, the acoustic systems can vary in their communication protocols and access mediums. Current R&D efforts within the US-UK International Technology Alliance seek to develop a ″sensor fabric″ technology to seamlessly connect disparate systems for networked sensing applications. Results from a recent field experiment to detect and locate moving ground targets, weapon firings, and explosions via a network of disparate acoustic sensor systems and sensing platforms (e.g., PDA's, workstations, motes and unattended ground sensor systems) are presented.

5:40

2pSPh3. Performace Bounds for a Multi-Array Network Approach to Gunfire Detection and Localization. Michael Roan (Virginia Tech, 917 Village Way North, Blacksburg, VA 24060, USA, mroan@vt.edu), Elizabeth Hoppe (Virginia Polytechnic Institute and State University, 141 Durham Hall, Blacksburg, VA 24060, USA, ehoppe@vt.edu), Marty Johnson (Virginia Tech, Mechanical Engineering, 143 Durham 0238, Blacksburg, VA 24061, USA, martyj@vt.edu)

Acoustics-based gunfire detection and sniper localization have become important in both military and civilian sectors. For the case of rifle fire, most current localization algorithms rely on estimating parameters using the projectile's cone-shaped shockwave and the muzzle blast. Previous studies have attempted to quantify shockwave detection performance as a function of range for various approaches such as wavelet matched filtering for the ″N″ shaped shockwave. Accurately detecting the shockwave is important because the shockwave shape can be used to determine bullet trajectory if the bullet velocity is known. A second layer of direction of arrival (DOA) estimation can be added by using the time difference of arrival between the shockwave and the muzzle blast. These DOA methods require a two step process of detection and estimation. In this work, a signal model is developed for a network of microphone arrays that receives the acoustic waveform generated by supersonic projectiles. The best-case localization performance of the multi-array network is quantified via the Cramer-Rao lower bound on the error in estimating shooter position. Results are illustrated using simulated data to generate CRLB ellipses on shooter position estimation error and via live fire experiments using several calibers and a multi-array network of microphones.

6:00

2pSPh4. Automated Identification of Vehicles using Acoustic Signal Processing. Naoko Evans (University of York, Department of Electronics, Heslington, YO10 5DD York, UK, ne502@ohm.york.ac.uk), David Chesmore (University of York, Department of Electronics, Heslington, YO10 5DD York, UK, edc1@ohm.york.ac.uk)

Automated identification of unauthorised intruding vehicles approaching protected infrastructure is becoming increasingly important for security purposes. This three-year project, which is now in its second year, aims to develop a real-time acoustic vehicle type recognition system that will be predominantly composed of three main parts; acoustic signal pre-processing, feature extraction, and decision making (or classification). The main study area covers various signal processing techniques in time, time-frequency and potentially frequency domains with signal classification implemented using a range of artificial intelligence techniques such as artificial neural networks. So far the focus has been on time domain signal processing and neural network classification. Whilst the work is at an early stage, the time domain methods such as Time Domain Signal Coding (TDSC) and Co-Occurrence Matrix combined with neural networks have already shown some promise. The presentation will introduce the project, describe methodologies involved as well as the results to date for the novel acoustic identification of categories of vehicles.

6:20

2pSPh5. Source detection and tracking in 3-D space using efficient subspace methods. Colin Barnhill (Johns Hopkins University, 3400 N. Charles St, Baltimore, MD 21218, USA, shaolin_cb@yahoo.com)

This presentation will demonstrate the versatility and robustness of a MUSIC-based subspace algorithm for acoustic source detection and tracking. The new algorithm (MUSIC3D) is designed for use with spherical arrays and performs three dimensional source detection and tracking. MUSIC3D operates on a spherical decomposition of the received array signals which results in its high efficiency. Spherical decomposition of the array signals allows for data reduction, frequency selection, and direct subspace calculations. The appeal of the MUSIC3D algorithm is that it offers a large variety of implementations which can be tailored for specific environments, signal sources or noise sources. Source tracking is accomplished through a combination of a Kalman-based filter and the MUSIC3D algorithm.

6:40

2pSPh6. Optimal estimation of aircraft noise with four microphones in a spatial configuration. Nico Roosnek (Roosnek Research & Development, Vlaskamp 82, 2592 AC The Hague, Netherlands, nico@roosnek.nl)

By using all time shifts between the arrivals of the acoustic signal at the four microphones - in a spatial configuration - the source direction is obtained. The used correlation technique reduces significantly noise from other sources and the error in the estimated level of noise from the tracked aircraft/source. By taking into account a motion model for the source, the history of that motion and the measured acoustic data a very robust sound monitor system is obtained. The sensitivity for other sources, wind and rain noise is greatly reduced - theoretically almost unlimited - in comparison with classical monitor systems. Four aircraft can be tracked simultaneously. Another system capability is the estimation of the true flightpath with a system error depending on the system configuration and the environmental conditions. Using this path information the soundscape can be calculated by inter- and extrapolation. The design goal of the system is truly met!

Session 2pUWa

Underwater Acoustics and ECUA: Auralization of Sonar Signals

Paul C. Hines, Cochair
Defence R&D Canada - Atlantic, P.O. Box 1012, Dartmouth, NS B2Y3Z7, Canada

Paul R. White, Cochair
Institute of Sound and Vibration, Univ. of Southampton, University Road, Highfield, Southampton, SO17 1BJ, UK

Invited Papers

2:00

2pUWa1. Active sonar clutter and auralization. Douglas Abraham (CausaSci LLC, PO Box 5892, Arlington, VA 22205, USA, abrahad@ieee.org)

Target-like false alarms generically termed clutter are the primary hindrance to active sonar in shallow water operational areas. Clutter can arise from a myriad of sources with geologic, biologic and anthropogenic origin. The clutter-source echoes are often determined by automatic signal processing to be target-like and therefore potentially of interest. These numerous false alarms consume either the sonar operator's time or flood automated data and information processing algorithms. Aural analysis of clutter echoes (auralization) can increase active sonar performance through improved operator or algorithmic classification. An overview of active sonar clutter is presented with a focus on the role of auralization for clutter reduction. [Supported by the Office of Naval Research Code 321US under contract number N0001407C0092]

2:20

2pUWa2. Insights to dolphin sonar discrimination capabilities with human listening experiments. Whitlow W. Au (Univ. of Hawaii, P.O. Box 1106, Kailua, HI 96734, USA, wau@hawaii.edu), Caroline M. Delong (Brown University, Box 1953, Providence, RI 02912, USA, Caroline_Delong@brown.edu)

Dolphins have a very keen sonar system that is able to make fine discriminations between complex targets such as proud and buried mines. To understand the cues that dolphins use for fine target discrimination, human listening experiments have been conducted with echoes from real targets using a simulated broadband dolphin echo-ranger. Echoes are stretched in time to translate the echoes into the human auditory range. The human performance is usually as accurate as the dolphin, with the additional benefit of being able to get feedback on cues used. Various types of discrimination and detection experiments have been conducted paralleling dolphin sonar experiments. Discrimination of material composition of cylinders and spheres, detection of target in clutter and cylinder wall thickness difference discrimination experiment have been performed. The human listeners performed as well or better than the dolphins at the task of discriminating between a standard target and comparison targets. Click pitch, echo duration, time-separation pitch and timbre are some of the cues used by human listeners to discriminate targets. Dolphins may use some of the same echo features as humans. Human listening studies can quickly identify salient combinations of echo features that permit object discrimination and also help refine dolphin experiments.

2:40

2pUWa3. Similarity-Based Perceptual Feature Identification for Active Sonar Signal Classification. Scott M. Philips (MIT Lincoln Laboratory, 244 Wood Street, Lexington, MA 02420-9108, USA, scott.philips@ll.mit.edu), James W. Pitton (Office of Naval Research Global, Blenheim Crescent, West Ruislip, Middlesex, HA4 7HL London, UK, jpitton@onrglobal.navy.mil)

In many acoustic signal processing applications human listeners are able to outperform automated processing techniques, particularly in the identification and classification of acoustic events. This paper develops a framework for employing perceptual information from human listening experiments to improve automatic classification of active sonar signals. We focus on the identification of new signal features that are able to predict the human performance observed in formal listening experiments. Using this framework, our newly identified features have the ability to elevate automatic classification performance closer to the level of human listeners. We develop several new methods for learning a perceptual feature transform from human similarity measures. In addition to providing a more fundamental basis for uncovering perceptual features than previous approaches, these methods also lead to a greater insight into how humans perceive sounds in a dataset. We also develop a new approach for learning a perceptual distance metric. This metric is shown to be applicable to modern kernel-based techniques used in machine learning and provides a connection between the fields of psychoacoustics and machine learning.

3:00

2pUWa4. Auditory-motivated techniques for detection and classification of passive sonar signals. Guy J. Brown (University of Sheffield, Dept. of Computer Science, Regent Court, 211 Portobello Street, S1 4DP Sheffield, UK, g.brown@dcs.shef.ac.uk), Robert W. Mill (University of Sheffield, Dept. of Computer Science, Regent Court, 211 Portobello Street, S1 4DP Sheffield, UK, r.mill@dcs.shef.ac.uk), Simon Tucker (University of Sheffield, Dept. of Information Studies, Regent Court, 211 Portobello Street, S1 4DP Sheffield, UK, s.tucker@dcs.shef.ac.uk)

Hydrophone arrays used to make passive sonar recordings are becoming increasingly complex, thus placing great demands on sonar operators who are required to identify transient and tonal events. Machine hearing systems can mitigate this problem, by performing initial classification and detection of passive sonar signals based on perceptually relevant principles. We describe two such systems. In the first system, transient sounds are characterised using measures of timbre and acoustic pattern. Acoustic features relating to timbre were identified by a multidimensional scaling study, in which human listeners judged the similarity of transient sonar sounds. The perceptual features give improved classification performance compared to commonly-used statistical measures derived from the power spectrum. The second system is an auditory-motivated approach to narrowband detection, which is based on information in zero-crossing intervals rather than signal power. This is motivated by the observation that the fine time structure of an acoustic stimulus is preserved by the phase locking of auditory nerve fibres. We show that a power detector outperforms the interval detector when the signal is centred on the analysis filter. However, when the signal frequency deviates from the centre of the analysis band, interval-based detection improves and power-based detection worsens.

3:20

2pUWa5. Auditory models and nonlinear filterbanks in underwater auralization. Stefan Bleeck (National Physical Laboratory, Hampton Road, TW11 OLW Teddington, UK, bleeck@gmail.com), Paul D. Fox (National Physical Laboratory, Hampton Road, TW11 OLW Teddington, UK, pf@isvr.soton.ac.uk), Paul R. White (Institute of Sound and Vibration, Univ. of Southampton, University Road, Highfield, SO17 1BJ Southampton, UK, prw@isvr.soton.ac.uk), Niamh O'Meara (National Physical Laboratory, Hampton Road, TW11 OLW Teddington, UK, niamh17@gmail.com)

Mammals like dolphins and humans have the ability to distinguish between different objects by listening to their scattered signals. We explore this phenomenon by evaluating the ″Auditory Image Model″ (AIM), a biologically inspired model of the human auditory system from the outer ear up to central processing. AIM aims to simulate the spectral analysis of the basilar membrane, the neural encoding and the temporal integration performed by the auditory system. Simulated scattered signals from the same object objects of different sizes and different objects of same size subjected to an incident pulse were analysed numerically with AIM, simulating the response of the human auditory system. The resulting neuronal activity patterns were analysed in two independent dimensions using the filter centre frequency and the relative timing intervals of the responses. The results are interpreted globally as reflecting the size and the shape/properties of the object respectively. We show for a series of calibration stimuli that the model can distinguish between same objects of different size and different objects of the same size. We also discuss how a nonlinear model of the basilar membrane, performing a Gammachirp/Mellin transformation, may act as a possible feature extraction tool for classification methods

3:40-5:20 Posters

Lecture sessions will recess for presentation of poster papers on various topics in acoustics. See poster sessions for topics and abstracts.

5:20

2pUWa6. What it is like to be a bat: A sonar system for humans. Cameron Morland (Boston University, Dept. of Cognitive and Neural Systems, 677 Beacon St., Boston, MA 02215, USA, cjmorlan@bu.edu), David Mountain (Boston University, Biomedical Engineering Dept., 44 Cummington St., Boston, MA 02215, USA, dcm@bu.edu)

Echolocation is a method of perceiving the world by emitting noises then listening to the reflections of these noises off objects in the world. It is used by animals for hunting and navigation. Some visually impaired humans use echolocation as part of their orienting repertoire. This work describes a device designed to enhanced one's existing echolocation ability. The device repeatedly emits an inaudible, ultrasonic ''click'', several times per second. Each click reflects off surfaces; this reflection is detected by head-mounted microphones. Computer processing converts the signals into audible signals, which are presented to the user over custom open-ear earphones. ILD, ITD, HRTF, and Doppler shifts in the reflections allow the user to distinguish the location and size/surface properties of objects. The spatial cues presented by our device match those used to localize ordinary audible objects. The auditory ''image'' generated in this way causes objects in the world to seem to emit sounds, and for objects with different shapes/textures to have subtly different sounds. A prototype has been constructed. Simple detection of objects and open spaces is readily possible, as well as Doppler-based gross surface texture. Further refinement in the areas of emission design, spectral spatialization, externalization, and miniaturization is required.

5:40

2pUWa7. Modeling the mechanism and neural substrate for aural categorization of sonar echoes. Jason E. Summers (U.S. Naval Res. Lab., Acoust. Div., Code 7142, 4555 Overlook Ave. SW, Washington, DC 20375, USA, jason.summers@nrl.navy.mil), Charles F. Gaumond (U.S. Naval Res. Lab., Acoust. Div., Code 7142, 4555 Overlook Ave. SW, Washington, DC 20375, USA, charlie.gaumond@nrl.navy.mil), Derek Brock (U.S. Naval Res. Lab., Acoust. Div., Code 7142, 4555 Overlook Ave. SW, Washington, DC 20375, USA, derek.brock@nrl.navy.mil), Ralph N. Baer (U.S. Naval Res. Lab., Acoust. Div., Code 7142, 4555 Overlook Ave. SW, Washington, DC 20375, USA, ralph.baer@nrl.navy.mil)

Previously, human perception of impulsive active-sonar echoes was investigated through paired-comparison ratings and multidimensional scaling (MDS). In the resulting MDS configuration, stimuli formed clusters representing aurally distinct categories. An interpretation is presented which suggests that dissimilarity judgments reflect separate processes for within- and between- category comparisons. The process of categorization is not based on decision boundaries in a low- dimensional space of ordinal-scale perceptual features, while within-category judgments do reflect such features. A class-specific paradigm seems appropriate as a model of human categorization: signals are compared to category archetypes, each described by a set of features that may be unique to that category. Regardless of the specific mechanism, listeners must carry out categorization on a particular signal representation: the neural substrate of the process. The suitability of various temporal, spectral, and time-frequency signal representations are investigated through observing categories formed by hierarchical clustering. A signal-processing model of the spectrotemporal receptive fields of the auditory cortex and the processing of the auditory periphery [T. Chi et al., J. Acoust. Soc. Am. **118**, 887-906 (2005)] is shown to yield good agreement with human categorization. Techniques for feature selection from this representation are discussed. [Work supported by ONR.]

6:00

2pUWa8. Automatic classification of vocalizations with Gaussian Mixture Models and Hidden Markov Models. Judith C. Brown (MIT Media Lab, 37 Indian Ridge Rd, Natick, MA 01760, USA, brown@media.mit.edu), Paris Smaragdis (Adobe Systems Inc., 275 Grove St., Newton, MA 02466, USA, paris@media.mit.edu)

The automatic classification of marine mammal sounds is very attractive as a means of assessing massive quantities of recorded data, freeing humans and offering rigorous and consistent output. Calculations on a set of vocalizations of Northern Resident killer whales using Dynamic Time Warping have been reported recently. [Brown, J. C., and P.J.O. Miller, ''Automatic classification of killer whale vocalizations using dynamic time warping,'' J. Acoust. Soc. Am. 122, 1201-1207, (2007).] Since this method requires the time-consuming pre-processing measurement of the frequency contours, we have explored the use of Gaussian Mixture Models (GMM) and Hidden Markov Models (HMM). These methods can be applied directly to time-frequency decompositions of the recorded signals. Calculations have been made on a set of 75 calls previously classified perceptually into 7 call types. Preliminary results give an agreement of roughly 85% agreement with the perceptual classification for the GMM and over 90% for an HMM.

6:20

2pUWa9. Incorporation of acoustic level analysis with sonar operator workstation workflow using hierarchical hidden Markov models. Justin Nevitt (Naval Research Laboratory, 4555 Overlook AVE SW, Washington, DC 20375, USA, justin.nevitt@nrl.navy.mil), James Ballas (Naval Research Laboratory, 4555 Overlook AVE SW, Washington, DC 20375, USA, james.ballas@nrl.navy.mil)

Future Anti Submarine Warfare (ASW) systems will be highly automated, and utilize multiple sonar signal processing, non-acoustic information, off platform information, and environmental information to maximize the detection, tracking, and classification of undersea threats. Recently, a hidden Markov model (HMM) was developed to describe and characterize the workflow strategies that expert sonar operators used during the IUSW-21 (Integrated UnderSea Warfare for the 21st Century) Sea Test. Abandoning the normative workflow designed into the system, the sonar operators developed and utilized unanticipated strategies to gather evidence to confirm or disconfirm automated classifications or to manually classify contacts. The workflow included detailed visual inspection of and listening to the sonar return. This initial HMM did not include a characterization of the auditory processing. Hidden Markov models are well suited to this purpose. Adding this component to the operator workflow was achieved by a hierarchical HMM which represents the acoustic processing as an embedded HMM in the overall workflow HMM. The resulting model is not just an operator workflow but defines a system processing model that could be used as a framework to develop automated processing of selected components.

Session 2pUWb

Underwater Acoustics and ECUA: Sonar System and Transducer Calibration Methodology I

Kenneth G. Foote, Cochair
Woods Hole Oceanographic Institution, Woods Hole, MA 02543, USA

Stephen P. Robinson, Cochair
National Physical Laboratory, Hampton Road, Teddington, TW11 OLW, UK

Invited Papers

2:00

2pUWb1. The sonar equations: definitions, dimensions and units of individual terms. Michael A. Ainslie (TNO Defence, Security and Safety, Oude Waalsdorperweg 63, 2597 AK The Hague, Netherlands, michael.ainslie@tno.nl)

The passive and active sonar equations are reviewed with regard to the definitions of individual terms and their units. It is shown on the one hand that ambiguities exist in conventional definitions that can lead to misinterpretation, and on the other that under special conditions correction terms are needed that are not included in the standard equations. Revised definitions are proposed that remove the need for some of the correction terms and reduce the likelihood of misunderstanding. Particular emphasis is placed on the terms 'propagation loss' and 'source level' for both active and passive sonar. For example, the effect on changes in impedance between the source and receiver of the sound is considered in the case of passive sonar, and between the source, receiver and scatterer of sound in the case of active sonar.

2:20

2pUWb2. Validation of primary hydrophone calibrations by inter-laboratory comparisons and by independent calibration methods. Stephen P. Robinson (National Physical Laboratory, Hampton Road, TW11 OLW Teddington, UK, Stephen.Robinson@npl.co.uk), Peter D. Theobald (National Physical Laboratory, Hampton Road, TW11 OLW Teddington, UK, pdt @npl.co.uk)

A description is presented of two approaches which may be used to validate primary calibration methods for hydrophones and transducers. Firstly, a comparison may be made with another independent absolute calibration method, preferably one based on a different physical principle (and therefore with few common sources of uncertainty). Secondly, an inter-laboratory comparison of calibrations may be undertaken between different institutes operating at a similar level. This paper describes the results of such exercises for free-field calibration of hydrophones in the range from 1 kHz to 500 kHz. Firstly, two independent calibration methods are compared: the three-transducer reciprocity method and a method based on optical interferometry. The differences observed in the results are typically less than 0.5 dB, which is of the same order as the overall uncertainties of each of the methods. Secondly, the results are shown of a recent international comparison of hydrophone calibrations involving institutes from Canada, China, Germany, Russia, South Africa, UK, and USA. Here, the agreement was generally within quoted uncertainties, the results generally lying within a ± 0.5 dB band for frequencies up to 300 kHz. A discussion is given of the general sources of uncertainties in the calibrations.

2:40

2pUWb3. Phase calibration of hydrophone and its application in the reconstruction of underwater acoustic waveforms. Yuebing Wang (Hangzhou Applied Acoustics Research Institute, 96 Huaxing Road, 310012 Hangzhou, China, wang_yuebing@tom.com), Shui Li (Hangzhou Applied Acoustics Research Institute, 96 Huaxing Road, 310012 Hangzhou, China, lishui9861@163.com), Yongjun Huang (Hangzhou Applied Acoustics Research Institute, 96 Huaxing Road, 310012 Hangzhou, China, pink2701@126.com)

Abstract: In this paper, both the reciprocal method and the optical method for the calibration of plural sensitivities of hydrophones are reviewed firstly. Then an experimental system is introduced in which with a 1.5MHz focusing transducer acting as a position indicator, phase responses of hydrophones can be calibrated easily and accurately. Measurements are carried out for different types of hydrophones and results are given in the frequency range 20kHz to 400kHz. Finally, with the plural responses of hydrophones included in the construction for the transfer function of the receiving system, acoustic waveforms produced by a projector are reconstructed in wide band from received signals, and a few conclusions are summarized from the experiment.

3:00

2pUWb4. The hydrophone free-field calibration in the non-anechoic water tank using continuous radiation mode. Alexander Isaev (VNIIFTRI, Mendeleevo, 141570 Moscow, Russian Federation, isaev@vniiftri.ru), Anton Matveev (VNIIFTRI, Mendeleevo, 141570 Moscow, Russian Federation, matveev@vniiftri.ru)

Anechoic chambers are used at free-field measurements in acoustic. Quality of the anechoic chamber estimate by comparing the dependence of sound pressure with distance between a projector and the receiver with the inversely proportional law. Creation of an anechoic water tank is a difficult technical problem. Therefore measurements in a water tank usually use tone burst radiation technique. In a non-anechoic water tank it is possible to provide free-field conditions at a continuous radiation mode. It is achieved by using a signal with the distributed spectrum and mathematical processing of results of measurements. The measurement procedure and results of free field calibration of this method are considered in the paper. Efficiency of measuring procedure was estimated by a check of the inversely proportional law in conditions of a non-anechoic water tank.

3:20

2pUWb5. Calibration of vector sensors. Joseph A. Clark (NSWCCD, Code 7340, 9500 MacArthur Blvd., West Bethesda, MD 20817-5000, USA, joseph.a.clark1@navy.mil)

Vector sensors that combine a hydrophone and a triaxial arrangement of accelerometers in a neutrally buoyant package are currently being used for underwater radiated noise measurements and other applications. Precise amplitude and phase calibration is required to obtain high quality measurements. A basic procedure that has been used successfully to calibrate measured radiated noise spectra in one-third-octave and narrowband formats will be described. Results of validation experiments that compared vector sensor measurements with other reference data will be presented. An iterative calibration scheme for improving the performance of a vector sensor employed as part of an active sonar system will also be presented.

3:40-5:20 Posters

Lecture sessions will recess for the presentation of poster sessions on various topics in acoustics. See poster sessions for topics and abstracts.

Invited Papers

5:20

2pUWb6. Array gain degradation due to nearby bubbles. Richard Lee Culver (ARL Penn State, PO Box 30, State College, PA 16804, USA, rlc5@psu.edu), Mario F. Trujillo (ARL Penn State, PO Box 30, State College, PA 16804, USA, mft10@psu.edu)

Signal-to-noise ratio (SNR) is signal power divided by noise power, usually expressed in dB (SNR = 20*log10(Psig/Pnoise). Array gain (AG) is the increase in SNR at an array output relative to that at a single element. AG assumes spatially-compact signals embedded in spatially-diffuse noise or interference. When the array is steered in the direction of a signal, AG is maximum when the signal is fully coherent across the array (i.e. the signals add in phase for all elements) while the noise or interference is incoherent across the array (i.e. adds with random phase). For an acoustic array operating in the ocean, we would like to understand the degree to which nearby bubbles degrade AG. Scattering by bubbles represents interference at the array. Bubble attenuation can also degrades array performance by attenuating the signal of interest, but that is separate from AG degradation. Previously we applied the single scattering approximation of Ishimaru (1977, Chap. 6) and found that scattering from bubbles very close to the array can generate correlated interference, thereby decreasing AG. Here we validate the theory using in-water measurements of AG as the distance of from the array to the bubbles varies. Work sponsored by Office of Naval Research, Code 321 Undersea Signal Processing.

5:40

2pUWb7. A method for calibrating hydrophones immersed in sandy sediment. Gary B. Robb (National Oceanography Centre, University of Southampton Waterfront Campus, European Way, SO14 3ZH Southampton, UK, gbor199@noc.soton.ac.uk), Gary Hayman (National Physical Laboratory, Hampton Road, TW11 OLW Teddington, UK, Gary.Hayman@npl.co.uk), Peter D. Theobald (National Physical Laboratory, Hampton Road, TW11 OLW Teddington, UK, pdt@npl.co.uk), Victor F. Humphrey (Institute of Sound and Vibration, Univ. of Southampton, University Road, Highfield, SO17 1BJ Southampton, UK, vh@isvr.soton.ac.uk), Stephen P. Robinson (National Physical Laboratory, Hampton Road, TW11 OLW Teddington, UK, Stephen.Robinson@npl.co.uk), Timothy G. Leighton (Institute of Sound and Vibration, Univ. of Southampton, University Road, Highfield, SO17 1BJ Southampton, UK, T.G.Leighton@soton.ac.uk), Justin K. Dix (National Oceanography Centre, University of Southampton Waterfront Campus, European Way, SO14 3ZH Southampton, UK, jkd@noc.soton.ac.uk), Angus I. Best (National Oceanography Centre, University of Southampton Waterfront Campus, European Way, SO14 3ZH Southampton, UK, aib@noc.soton.ac.uk)

Hydrophones are frequently used as receivers for in situ sediment acoustic experiments. At present, processing techniques use receiver sensitivities measured from water-based calibrations. It is, however, accepted that the receive sensitivity will depend on the medium surrounding the hydrophone, particularly at frequencies close to the transducer's resonance frequency. To assess this affect, a series of calibrations were performed over the frequency range of 10 to 200 kHz on two types of hydrophones (with cylindrical and spherical elements) inserted into degassed sandy sediment. Sensitivities were measured using a modified three-transducer reciprocity technique, which uses a co-linear arrangement to allow the sediment attenuation to be omitted from the sensitivity calculation. The insertion of the hydrophones into the sediment reduced the measured receive sensitivities by a maximum value of 3.8 dB with respect to the equivalent water-based calibrations. The co-linear arrangement adopted allowed the transmission between the outer devices to be recorded with and without the central hydrophone present. Repeat measurements indicated that the sediment disturbance associated with the removal of the central hydrophone caused sensitivity differences of less than 1.2 dB, while the inclusion of the central hydrophone caused a shadowing effect which increased sensitivities by between 1.3 to 4.0 dB.

6:00

2pUWb8. Standard-target method of calibrating active sonars: principles, applications, benefits. Kenneth G. Foote (Woods Hole Oceanographic Institution, Woods Hole, MA 02543, USA, kfoote@whoi.edu)

The standard-target method of calibrating active sonar involves suspending a target at a known position in a sonar beam, insonifying it with a known signal, measuring the scattered pressure field, and relating this to the scattering properties of the target. These properties are known a priori for standard targets, rendering the calibration primary. Repetition of the procedure for different relative sonar-target positions can enable determination of directional and nearfield characteristics. Following a review of standard-target calibration principles, the method is illustrated for both narrowband and broadband scientific echo sounders and multibeam sonars, with operating frequencies in the range 18-3200 kHz. Applications to sidescan sonar and to low-frequency parametric sonars and other mid-frequency sonars in the nominal range 1-10 kHz have not yet been developed, but are evidently feasible given preliminary standard-target designs, which are described. In every case, the standard targets are of a proven manageable size, with immersion weight less than 200 N. Benefits of standard-target calibration, including accuracy, operational convenience, and cost-effectiveness, among others, are emphasized. The method, which is useful for both quantitative and qualitative imaging applications, extends to borehole acoustic sensors and medical ultrasonic devices.

Contributed Paper

6:20

2pUWb9. Calibration of broadband active acoustic systems using a single standard spherical target. Timothy K. Stanton (Woods Hole Oceanographic Institution, Applied Ocean Physics & Engineering Department, 98 Water Street, MS #11, Woods Hole, MA 02543, USA, tstanton@whoi.edu), Dezhang Chu (NOAA/NMFS/NWFSC/FRAMD, Montlake Blvd., E. Seattle, WA 98112, USA, dchu@whoi.edu)

When calibrating a broadband active acoustic system with a single standard target such as a sphere, the inherent resonances associated with the scattering by the sphere pose a significant challenge. In this research, a method is developed which completely eliminates the source of resonances through isolating and exploiting the echo from the front interface of a sphere. This echo is relatively insensitive to frequency over a wide range of frequencies, lacking resonances, and relatively insensitive to small changes in material properties and, in the case of spherical shells, shell thickness. The research builds upon the concept of using this echo for calibration in the work of Dragonette et al. (J. Acoust. Soc. Am. 69, 1186-1189 (1981)). This current work generalizes that of Dragonette by 1) incorporating a pulse compression technique to significantly improve the ability to resolve the echo, and 2) rigorously accounting for the scattering physics of the echo so that the technique is applicable over a wide range of frequencies and material properties of the sphere. The utility of the new approach is illustrated through application to data collected at sea with an air-filled aluminum spherical shell and long broadband chirp signals (30-105 kHz).

TUESDAY AFTERNOON, 1 JULY 2008 P3-C, LEVEL 3, 3:40 TO 5:20 P.M.

Session 2pUWd

Underwater Acoustics and ECUA: Sonar System and Transducer Calibration Methodology II (Poster Session)

Kenneth Foote, Cochair
Woods Hole Oceanographic Institution

Stephen Robinson, Cochair
National Physical Laboratory

All posters will be on display from 3:40 p.m. to 5:20 p.m. To allow contributors an opportunity to see other posters, contributors of odd-numbered papers will be at their posters from 3:40 p.m. to 4:30 p.m. and contributors of even-numbered papers will be at their posters from 4:30 p.m. to 5:20 p.m.

Contributed Paper

2pUWd1. Low frequency hydrophone calibration with using tensometric pressure sensor. Alexander Isaev (VNIIFTRI, Mendeleevo, 141570 Moscow, Russian Federation, isaev@vniiftri.ru), Alexander Shchelkunov (VNIIFTRI, Mendeleevo, 141570 Moscow, Russian Federation, for_my_reg@mail.ru)

Usually when calibrating a hydrophone in an acoustic coupler the piezoelectric hydrophones use an auxiliary transducer. Widely applicable reciprocity calibration is high-ly accurate, but difficult in realization and laborious. The method of comparison with a reference transducer is more simple and quick, but less accurate. In the paper the method of low frequency hydrophone calibration using the auxiliary transducer with a flat frequency response up to 3 kHz is considered. The auxiliary transducer is calibrated accurately by changing the water column in the acoustic coupler. It finally allows us to calibrate measuring hydrophones more accurately too. The measuring equipment on the basis of tensometric pressure sensor type MPX 5010 is considered.

Session 2pUWe

Underwater Acoustics and ECUA: Geoacoustic Sediment Modeling I (Poster Session)

Nicholas Chotiros, Cochair
Applied Research Laboratories, University of Texas

Jean-Pierre Sessarego, Cochair
Laboratory for Mechanics and Acoustics CNRS

All posters will be on display from 3:40 p.m. to 5:20 p.m. To allow contributors an opportunity to see other posters, contributors of odd-numbered papers will be at their posters from 3:40 p.m. to 4:30 p.m. and contributors of even-numbered papers will be at their posters from 4:30 p.m. to 5:20 p.m.

Contributed Papers

2pUWe1. Estimating the frequency dependent behavior of marine sediment sound speeds using low frequency aircraft sound. Alireza Amiri-Simkooei (Acoustic Remote Sensing Group, Delft Institute of Earth Observation and Space Systems, Delft University of Technology, Kluyverweg 1, 2629 HS Delft, Netherlands, a.amirisimkooei@tudelft.nl), Mirjam Snellen (Acoustic Remote Sensing Group, Delft Institute of Earth Observation and Space Systems, Delft University of Technology, Kluyverweg 1, 2629 HS Delft, Netherlands, m.snellen@tudelft.nl), Dick G. Simons (Delft University of Technology, P.O. Box Postbus 5048, 2600 GA Delft, Netherlands, d.g.simons@tudelft.nl), Michael Buckingham (Marine Physical Lab, Scripps Institution of Oceanography, UCSD, 9500 Gilman Dr. M/C 0238, La Jolla, CA 92093-0238, USA, mjb@mpl.ucsd.edu)

For investigating the dispersion behavior of sediment sound speeds, broadband sound speed measurements are required. Sediment sound speed dispersion models predict the largest sound speed variations typically at low frequencies. Aircraft fly-over noise acquired on receivers placed in sediment proved to be a promising approach towards broadband low-frequency measurements. Since the magnitude of the Doppler-shift depends on sound speed at the receiver position, the observed Doppler-shift can be used to derive the sound speed. We propose a new approach using the entire time series instead of employing only the two observed frequencies at approaching and departing. It is based on a model for received signals, accounting for the Doppler-shifted frequency. By maximizing the match between modeled and measured time series as a function of sound speed and frequency in a least-squares framework, estimates of the frequency-dependent sound speed are obtained. The method is applied to data acquired at receivers placed in air, water and sediment. Statistical tests indicate that the marine sediment sound speed depends indeed on frequency, i.e. sound speed decreases significantly below 300 Hz. A comparison is made with a modified viscous fluid model from which realistic values for the geotechnical parameters of the considered sediment were obtained.

2pUWe2. Imaging of Large-Scale Sediment Transport Dynamics with Multibeam Sonar. Stephen M. Simmons (University of Leeds, School of Earth and Environment, University of Leeds, LS29JT Leeds, UK, s.m.simmons@leeds.ac.uk), Dan R. Parsons (University of Leeds, School of Earth and Environment, University of Leeds, LS29JT Leeds, UK, parsons.daniel@btinternet.com), Jim L. Best (Departments of Geology and Geography and Ven Te Chow Hydrosystems Laboratory, 1301 W. Green St., University of Illinois, Urbana, IL 61801, USA, jimbest@uiuc.edu), Chris Malzone (Reson Inc., Goleta, Santa Barbara, CA 93117, USA, CMalzone @reson.com), Gareth M. Keevil (University of Leeds, School of Earth and Environment, University of Leeds, LS29JT Leeds, UK, g.keevil@see.leeds .ac.uk)

Multibeam Echo-Sounder (MBES) systems have developed rapidly over recent decades and are routinely deployed to provide high-resolution bathymetric imaging. Modern data handling and storage technologies have facilitated the logging of the back-scatter information previously discarded by these systems. This paper develops a novel methodology to exploit this logging capability to quantify the concentration and dynamics of suspended sediment within the water column. This development provides a multipurpose tool for the holistic surveying of sediment transport by imaging suspended sediment concentration, associated flow structures and providing concurrent high-resolution bathymetry. This paper presents the results obtained from the deployment a RESON 7125 MBES in the field, with the aim of examining the dynamics of suspended sediment transport over dune bedforms and in the region of flow mixing between large rivers of significantly different suspended sediment concentration. Results from controlled tank tests are also presented, obtained using different types and mixes of sediment. The results demonstrate the capability of MBES systems to successfully resolve the contrast in suspended sediment concentrations. The large sets of data recorded in the two-dimensional MBES swath enables the real-time monitoring of suspended sediment transport and related flow processes on a scale previously unrealisable with single-beam acoustic systems.

2pUWe3. The influence of topography on sidescan sonar images. Dietmar Bürk (GKSS Research Centre, Max-Planck-Str. 1, Institute for Coastal Research, 21502 Geesthacht, Germany, dietmar.buerk @gkss.de), Ingo Klaucke (IFM-GEOMAR, Leibniz-Institute of Marine Sciences, Wischhofstraße 1-3, 24148 Kiel, Germany, iklaucke@ifm-geomar .de)

The backscattering signal on sidescan sonar images is to a large degree dependent on the incident angle of the acoustic beam onto the seafloor. As sidescan sonar systems are often used for mapping seafloor lithologies, it is necessary to reduce or even remove the effect of different backscattering strengths caused by varying incidence angles. This study evaluates the influence of seafloor morphology on the acoustic backscattering signal of the deep-towed IFM-GEOMAR DTS-1 sidescan sonar system. Data used are from the Pacific continental slope offshore Nicaragua in a water depth between 800 and 2400 metres. There authigenic carbonate patches formed by cold fluid venting are imaged with a high backscattering level. The carbonates are often located on top or on the flanks of mound structures with a strong morphology. The specific DTS-1 backscattering function is determined on normal, uniform seafloor sediment, and then applied in a new processing algorithm to the raw data of two test areas. The change in amplitude strength when considering seafloor morphology is calculated. The topographic influence on the backscattering signal can be quite significant when

imaging mound structures. Nevertheless the high backscatter on mounds is not completely removed, leading to the conclusion that it originates from a different seafloor lithology and roughness.

2pUWe4. Theoretical justification of a coherent forward model for subbottom profiler data inversion. Sandrine Rakotonarivo (Laboratoire E3I2, ENSIETA, 2, rue François Verny, 29806 Brest, France, rakotosa@ensieta.fr), Michel Legris (Laboratoire E3I2, ENSIETA, 2, rue François Verny, 29806 Brest, France, legrismi@ensieta.fr), Rozenn Desmare (Institut de Recherche de l'Ecole Navale, IRENav, BP 600, 29240 Brest Armées, France, desmare@ecole-navale.fr), Frédéric Jean (IXSEA, 46, quai François Mitterrand, 13600 La Ciotat, France, frj@ixsea.com)

Subbottom profiling systems measure and identify sediment layers that exist below the sediment/water interface. Nowadays, very-high resolution chirp profilers provide calibrated wideband signals which may enable quantitative seabed characterisation. In literature, sediment classification is based on attenuation and reflectivity estimation and backscattering models used for the inversion consider plane wave propagation through layered homogeneous attenuated bottom. But this bottom modelling may be in contradiction with the emitted spherical front wave and core samples observations which point out a heterogeneous structure of marine subbottom. Therefore, impacts of profiler features, geometry measurement and subbottom structure (layering, attenuation, rugosity, and volumetric inhomogeneity) on backscattering signal are all reviewed in this paper. This analysis shows that classical model of wave coherent propagation through layered homogeneous attenuated media offers the best compromise between its accuracy and inversion possibility, if bottom heterogeneities are insignificant (Rayleigh scatterers). For bigger heterogeneities (Rayleigh parameter close to unity), coherent backscattering still prevails though wave propagation is affected by scattering. In this case, the same coherent forward model is used with modified reflectivity and transmission coefficients. Then, sensitiviy and inversion possibility of the coherent bottom backscattering model are discussed.

2pUWe5. Use of dual methods to infer methane bubble populations in gassy sediments: Inversion of combination-frequency data. Agni Mantouka (Institute of Sound and Vibration, Univ. of Southampton, University Road, Highfield, SO17 1BJ Southampton, UK, am2@isvr.soton.ac.uk), Timothy G. Leighton (Institute of Sound and Vibration, Univ. of Southampton, University Road, Highfield, SO17 1BJ Southampton, UK, T.G.Leighton@soton.ac.uk), Gary B. Robb (National Oceanography Centre, University of Southampton Waterfront Campus, European Way, SO14 3ZH Southampton, UK, gbor199@noc.soton.ac.uk), Angus I. Best (National Oceanography Centre, University of Southampton Waterfront Campus, European Way, SO14 3ZH Southampton, UK, aib@noc.soton.ac.uk), Justin K. Dix (National Oceanography Centre, University of Southampton Waterfront Campus, European Way, SO14 3ZH Southampton, UK, jkd@noc.soton.ac.uk),Zygmunt Klusek(Institute of Oceanography, Polish Academy of Science, P.O. Box 148 Sopot, Poland, klusek@iopan.gda.pl), Paul R. White (Institute of Sound and Vibration, Univ. of Southampton, University Road, Highfield, SO17 1BJ Southampton, UK, prw@isvr.soton.ac.uk)

Bubbles can dramatically change the acoustic properties of their host medium even if they are present in very small amounts. This paper describes the combination-frequency component of tank and field measurements taken using a device which measures bubbles in marine sediments using multiple acoustic techniques (allowing the results of the various techniques to be compared). The combination-frequency method uses the nonlinear scattering property of bubbles when insonified by two primary frequencies. For low void fractions, there is a monotonic relationship between the scattered field and the population of bubbles resonant at either of the primary frequencies or combination of these and/or their subharmonics. This principle is used to infer the bubble size distribution. In contrast to the case of gas bubbles in water, in marine sediments the shear properties of the host medium must be incorporated into the model for the bubble dynamics and a new model for this is presented. This model is then inverted to obtain the bubble size distribution. The predictions of this method were compared with the method of inversion of propagation data (detailed in a companion paper), obtained from in situ experiments on the South coast of England.

2pUWe6. Comparisons of Biot and grain-shearing theories: sound speed, attenuation and acoustic impedance. Brian T. Hefner (Applied Physics Laboratory, University of Washington, 1013 NE 40th St, Seattle, WA 98105, USA, hefner@apl.washington.edu), Kevin L. Williams (Applied Physics Laboratory, University of Washington, 1013 NE 40th St, Seattle, WA 98105, USA, williams@apl.washington.edu)

The comparison of sediment sound speed and attenuation measurements to predictions has been the primary method used to test Biot theory and the grain-shearing model. Examples of data/model comparisons will be shown. Subsequent refinements made to these models result in similar predictions for sound speed and attenuation. However, the underlying physics is substantially different suggesting other, more indirect means for discriminating between sediment propagation theories. One technique that has received recent attention is the measurement of forward scattering from the sediment interface. Model predictions of these measurements depend not only the sound speed and attenuation, but also on the acoustic impedance of the medium. Examination of the physics incorporated into Biot Theory shows that the ^{3}effective density^{2} seen by the acoustic wave is lower than the bulk density, thus lowering the acoustic impedance. This results in a difference in the predicted flat surface reflection coefficient for Biot-type models as compared to grain-shearing models. The flat surface reflection coefficients derived from experiment will be compared with predictions using the Biot model and the viscosity grain shearing (VGS) model for a sand sediment. The validity of obtaining reflection coefficients using forward scattering from rough surfaces will also be discussed. [Work supported by ONR.]

Session 2pUWf

Underwater Acoustics, Signal Processing in Acoustics, and ECUA: Acoustic Vector Fields and Sensor Processing I (Poster Session)

Kevin Smith, Cochair
Naval Postgraduate School/Naval Undersea Warfare Center

Jean-Pierre Hermand, Cochair
Université libre de Bruxelles (U.L.B.) - Environmental hydroacoustics lab

All posters will be on display from 3:40 p.m. to 5:20 p.m. To allow contributors an opportunity to see other posters, contributors of odd-numbered papers will be at their posters from 3:40 p.m. to 4:30 p.m. and contributors of even-numbered papers will be at their posters from 4:30 p.m. to 5:20 p.m.

Contributed Papers

2pUWf1. Vector-phase methods of bottom reflecting properties research in shallow shelf area. Elena Ermolaeva (Moscow Lomonosov State University, Leninskie Gory, Physics Faculty, 119992 Moscow, Russian Federation, ermolaeva@phys.msu.ru), Boris Goncharenko (Moscow Lomonosov State University, Leninskie Gory, Physics Faculty, 119992 Moscow, Russian Federation, goncharenko@phys.msu.ru), Valery Gordienko (Moscow Lomonosov State University, Leninskie Gory, Physics Faculty, 119992 Moscow, Russian Federation, gordienko@phys.msu.ru)

It is known, that parameters of bottom have essential influence on the signal propagation in the shallow water. Variation of the attenuation coefficient can amount to tens dB. Therefore, research of bottom properties and its structure (first of all - thickness and acoustics parameters of alluvial soil) is actual problem, especially at low frequencies. Using of receivers, which record both sound pressure and its gradient make it easier to solve this problem in a number of cases. The following methods are considered: impedance method, which is based on direct measurement of relation between pressure and vertical component of oscillatory velocity in one point on the water/bottom boundary; method, which is based on measuring phase difference between pressure and horizontal or vertical component of particle velocity; method in which additive combination of sound pressure and vertical component of oscillatory velocity are used. The essence of the last method consists in formation of minima of reception system directional characteristic in the direction at the signals extending from surface to bottom and reflected from bottom. The suggested methods of acoustic characteristics research of a ground repeatedly have been checked in shallow shelf area of the Baltic and the Black seas, and also in conditions of shallow inland water areas.

2pUWf2. Geoacoustic Inversion Based on a Vector Hydrophone Array. Fenghua Li (National Laboratory of Acoustics, Institute of Acoustics, Chinese Academy of Sciences, No 21, Beisihuanxilu, 100080 Beijing, China, lfh@mail.ioa.ac.cn), Renhe Zhang (National Laboratory of Acoustics, Institute of Acoustics, Chinese Academy of Sciences, No 21, Beisihuanxilu, 100080 Beijing, China, zrh@mail.ioa.ac.cn)

Vector sensor has attracted much attention in recent years. However, there are few papers involving in geoacoustic inversion from vector sensor. In this research, a geoacoustic inversion scheme employing a vector hydrophone array has been developed based on the fact that vector hydrophone can provide more acoustic field information than traditional pressure hydrophones. The inversion scheme is the combination of the Matched Field Processing and the difference of transmission losses between pressure and velocity. The advantages of this method are that it can decrease the uncertainty of the inverted sediment sound speed and the inversion of the sediment attenuation is independent on the source level. [Work supported by the National Natural Science Foundation of China under Grand No. 10574136].

2pUWf3. Underwater low frequency sound field simulation with the digital waveguide mesh method. Shengchun Piao (College of Underwater Acoustic Engineering, Harbin Engineering University, 145 Nantong Street, 150001 Harbin, China, shengchunpiao@hrbeu.edu.cn), Lingai Tian (Hangzhou Applied Acoustics Research Institute, 96 Huaxing Road, 310012 Hangzhou, China, tianling_ai@hrbeu.edu.cn), Jing Yang (College of Underwater Acoustic Engineering, Harbin Engineering University, 145 Nantong Street, 150001 Harbin, China, bambooyang7@163.com)

Digital waveguide mesh method has been widely used to model musical instruments and simulation for room acoustics. In this paper, this method was applied to calculation the acoustic vector fields in the Pekeris waveguide. After introducing a boundary condition treatment method for the ocean bottom in the digital waveguide mesh, the acoustic pressure and particle velocity fields are calculated in spatial and temporal dimensions. Using these calculation results, the waveforms for the received signals and distribution of acoustic intensity in the underwater sound channel can also be obtained. Numerical simulation shows that the digital waveguide mesh method can be used to simulate the low frequency two-dimensional acoustic vector fields in shallow water and this method is easy to applied to three-dimensional acoustic fields calculation.

Session 2pUWg

Underwater Acoustics and ECUA: High Frequency Variability I (Poster Session)

Marcia Isakson, Cochair
Applied Research Laboratories, University of Texas

Thomas Folégot, Cochair
NATO Undersea Research Center

All posters will be on display from 3:40 p.m. to 5:20 p.m. To allow contributors an opportunity to see other posters, contributors of odd-numbered papers will be at their posters from 3:40 p.m. to 4:30 p.m. and contributors of even-numbered papers will be at their posters from 4:30 p.m. to 5:20 p.m.

Contributed Paper

2pUWg1. Correcting bathymetry measurements for water sound speed effects using inversion theory. Jelle De Plaa (Delft Institute of Earth Observation and Space Systems, Delft University of Technology, Kluyverweg 1, 2629 HS Delft, Netherlands, j.deplaa@tudelft.nl), M. Snellen (Delft Institute of Earth Observation and Space Systems, Delft University of Technology, Kluyverweg 1, 2629 HS Delft, Netherlands, M.Snellen@tudelft.nl), Dick G. Simons (Delft University of Technology, P.O. Box Postbus 5048, 2600 GA Delft, Netherlands, d.g.simons@tudelft.nl)

We present a method to accurately estimate the bathymetry and water sound speed in shallow waters using overlapping swaths obtained from a Multi-Beam Echo Sounder (MBES). The method is designed to correct the errors in the bathymetry manifested mainly in the outer beams of the MBES. The errors are caused by deviations in sound speed, which occur, for example, in estuaries where fresh river water mixes with seawater. Simulations show that we are able to simultaneously estimate the mean sound speed and the bathymetry. This is accomplished by minimizing the differences between the MBES measurements in the overlap region using a Levenberg-Marquardt optimization routine. We also present an application of the method to real data obtained at the fairway to the harbour of Rotterdam, The Netherlands. Analysis shows that the inverted sound speed agrees well with the measured sound speed at the transducer. However, the uncertainties are larger when the track-to-track distance is ~2 times the depth. Therefore, we also discuss the optimal distance between sailed tracks. The method appears to be a promising tool for the accurate mapping of sea floors in shallow-water areas with a complex sound-speed profile.

Session 3aAAa

Architectural Acoustics: Case Studies and Design Approaches I

Bryon Harrison, Cochair
124 South Boulevard, Oak Park, IL, 60302

Witew Jugo, Cochair
Institut für Technische Akustik, RWTH Aachen University, Neustrasse 50, 52066 Aachen, Germany

Contributed Papers

8:00

3aAAa1. Acoustic and audience response analyses of eleven Venetian churches. Davide Bonsi (The Acoustics Lab., Fondazione Scuola di San Giorgio, Isola di San Giorgio Maggiore, I-30124 Venezia, Italy, davide.bonsi@scuoladisangiorgio.it), Malcolm Longair (Cavendish Lab., University of Cambridge, JJ Thomson Avenue, CB3 0HE Cambridge, UK, pjg47@cam.ac.uk), Philip Garsed (Dept. of Engineering, University of Cambridge, Trumpington Street, CB2 1PZ Cambridge, UK, msl1000@hermes.cam.ac.uk), Raf Orlowski (Arup Acoustics, St Giles Hall Pound Hill, CB3 0AE Cambridge, UK, Raf.Orlowski@arup.com)

A research project has been carried out by the University of Cambridge (UK), Arup Acoustics (Cambridge, UK) and the Fondazione Scuola di San Giorgio-CNR (Venice, Italy) with the purpose of investigating the relationship between music and the architectural spaces within which it was performed in the context of Venetian vocal polyphony during the 16th century. The most representative churches (San Marco, Parish churches, hospitals and monasteries) were selected for this study and the music was performed within them by the Choir of St John's College of Cambridge University. Members of the audience completed questionnaires assessing the acoustic qualities of the spaces. The results of the audience and expert scores were then statistically analyzed and correlated with a set of room acoustic indices which had been measured in the same locations. In the present paper technical aspects of the experiments and the data analysis will be illustrated. The principal conclusions were as follows: 1. There is a strong correlation between the subjective impression of reverberance with EDT and T30 and musical clarity with C80; 2. A grouping of the churches by typology was found by analysing the reverberation times; 3. The poor quality of clarity was assessed for churches with longest EDT for the performance of music involving polyphony.

8:20

3aAAa2. A Comparative Study of Four Concert Halls in Istanbul: Correlation of Subjective Evaluation with Objective Acoustic Parameters. Nurgun Bayazit Tamer (Istanbul Technical University, Taskisla Taksim Istanbul, 34437 Istanbul, Turkey, nurgun@itu.edu.tr), Anil Vural (Istanbul Technical University, Taskisla Taksim Istanbul, 34437 Istanbul, Turkey, vuralanist@yahoo.com)

In the studies of room acoustics, the parameters that are taken into consideration while evaluating the acoustic performance of a hall are examined in two sections: objective acoustic parameters which can be measured and calculated and, subjective acoustic parameters which define the impacts of a hall's acoustical qualities over the audiences. During the first half of the century, the reverberation time was considered to be the most important objective acoustic parameter which defined the acoustic quality of a hall. But, the later studies indicated that this parameter wasn't sufficient alone to define a subjective evaluation. Consequently, studies have been made to define the subjective influence on people from the acoustic performance of a hall. In this study, it has been attempted to define the statistical correlation between the subjective evaluation of the acoustic characteristics of the four concert halls, which was done by the members of orchestra together with the ordinary concert-goers, and their objective acoustic parameters are explained. The detailed objective acoustic parameters are presented for measurements in four concert halls in Istanbul. The halls are used by many different performances, from concerts to ballet or opera. The measured octave band quantities are RT, EDT, G,C80 and D50.

8:40

3aAAa3. Computer modelling and simulation of sound field in 24 rectangular concert halls. Andrzej K. Klosak (Institute of Building Materials and Structures, Faculty of Civil Eng., Cracow University of Technology, Warszawska 24, 31-155 Cracow, Poland, andrzej.klosak@pk.edu.pl)

Extensive acoustics computer simulations has been made using Odeon computer simulation software. From 300 to 850 measurements positions have been analysed in 24 rectangular rooms representing ″shoe-box″ type concert halls with volumes of 8 000m^3, 12 000m^3 and 16 000m . In total 14 000 receiver positions have been analysed. For each receiver position eight objective measures have been calculated, in particular Reverberation Time (T_{30}), Early Decay Time (EDT), Clarity (C_{80}), Strength (G, G_{early}, G_{late}), Early Lateral Energy Fraction (LF_{80}) and Late Lateral Strength (G_{LL}). Most of measures have been calculated in six octave bands from 125Hz to 4000Hz. Extensive amount of generated data required developing of new methods for processing, comparing and graphical presentation of results. Those methods together with description of modelling and simulation procedures are described in this paper.

9:00

3aAAa4. Improvement of acoustic conditions in a historical interior by means of a DSP-controlled sound-reinforcement system. Tadeusz Fidecki (F. Chopin Academy of Music, Okolnik 2, 00-368 Warszawa, Poland, fidecki@chopin.edu.pl), Andrzej Miskiewicz (F. Chopin Academy of Music, Okolnik 2, 00-368 Warszawa, Poland, misk@chopin.edu.pl), Jan Zera (Centr. Inst. for Labour Prot. - Natl. Res. Inst., Czerniakowska 16, 00-701 Warsaw, Poland, jazer@ciop.pl)

Stringent building conservation requirements in historical interiors pose substantial limitations in acoustical treatment and sound reinforcement systems used to secure proper sound quality. This presentation discusses the means undertaken to improve the acoustic conditions in the historic Great Ballroom of the Royal Castle in Warsaw. Originally, the room was too reverberant (T_{30} = 2.9 s at 500 Hz) what resulted in a lack of clarity of performed music and poor speech intelligibility (STI < 0.3). A precise laser scan of the interior was made to obtain input data for a computer acoustic model of the room. This model was used for selection of a DSP-controlled sound reinforcement system to improve listening conditions for speech and music. [Work supported by the Polish Ministry of Science and Higher Education, grant No. R17 004 02].

9:20

3aAAa5. On the acoustics of a specifically designed library discussion room with corrugated ceiling. Nico F. Declercq (Georgia Tech Lorraine - G.W. Woodruff School of ME, UMI Georgia Tech - CNRS 2958, 2 rue Marconi, 57070 Metz, France, nico.declercq@me.gatech.edu), Katrien Dewijngaert (Georgia Tech Lorraine - G.W. Woodruff School of ME, UMI Georgia Tech - CNRS 2958, 2 rue Marconi, 57070 Metz, France, declercq@ieee.org), Katelijn Vanderhaeghe (Georgia Tech Lorraine - G.W. Woodruff School of ME, UMI Georgia Tech - CNRS 2958, 2 rue Marconi, 57070 Metz, France, declercq@ieee.org), Patricia Verleysen (Ghent University, Mechanics of Materials and Structures, Sint-Pietersnieuwstraat 41, 9000 Ghent, Belgium, Patricia.Verleysen@ugent.be)

There is a discussion room at the library of Viipuri in Finland where the ceiling has been especially designed to enhance the acoustics and make every position within the room acoustically equivalent. In other words no matter where a speaker is standing, he is supposed to be heard equally well all over the room. For that purpose a corrugated ceiling has been constructed that must distribute sound optimally, at least from the point of view of a ray theoretical analysis. The numerical study presented here shows that the corrugation is such that the ray approach is not exactly valid and a plane wave expansion technique shows that the acoustics is much worse than it is supposed to be. A detailed description of the sound distribution as a function of the position of the sound source and the receiver is presented. The acquired knowledge is important for future construction of similar rooms.

9:40

3aAAa6. Acoustic climate inside a canteen and mitigation solutions. Giuseppe Marsico (APAT, Via Vitaliano Brancati 48, 00144 Rome, Italy, giuseppe.marsico@apat.it), Giovanni Brambilla (CNR Institute of Acoustics, Via del Fosso del Cavaliere 100, 00133 Rome, Italy, giovanni.brambilla@idac.rm.cnr.it), Salvatore Curcuruto (APAT, Via Vitaliano Brancati 48, 00144 Rome, Italy, salvatore.curcuruto @apat.it), Monica Clapiz (Via Edoardo Jenner 102, 00151 Rome, Italy, mony.c@libero.it), Rinaldo Betti (APAT, Via Vitaliano Brancati 48, 00144 Rome, Italy, rinaldo.betti@apat.it), Michele Riccardi (APAT, Via Vitaliano Brancati 48, 00144 Rome, Italy, michele.riccardi@apat.it)

The acoustic environment inside a canteen is an important feature to guarantee speech intelligibility and speech privacy, as well as to reduce the exposure levels. Unfortunately this aspect is not always properly taken into account as others, like cleanliness. This paper describes the case-study of the canteen at the National Agency for Environmental Protection (APAT), having a capacity of 220 seats. The acoustic environment has been characterized by measuring the main acoustic descriptors for speech intelligibility (Reverberation Time, STI, C80 and D50) and evaluating the noise exposure levels for the users. The comparison of the results with the recommended values showed a bad situation, especially in the speech frequency range, which requires acoustic corrections to improve the quality of the acoustic environment. To identify these corrections a numerical model of room acoustics, implemented on a commercial software, has been used to evaluate the effects produced by different corrections. The proposed correction improves the acoustic performances up to a good level, without modifying the structural parts and existing walls. Moreover, the solution allows to maintain the hall's usability without obstructing user mobility, screening natural lighting and reducing number of seats.

10:00

3aAAa7. Cost Benefit Analysis of Acoustic Treatments for Entertainment Venues. David M. Borgeaud (Environmental Resources Management Australia Pty Ltd, Level1, 60 Leichhardt Street, Spring Hill QLD, 4000 Brisbane, Australia, david.borgeaud@erm.com)

Fortitude Valley, in Brisbane City, Australia is an inner city area combining retail, commercial, residential, and entertainment uses. It has been the starting point for several major Australian bands. To address the increase in apartments in the Valley, the Brisbane City Council has developed a noise policy (called The Valley Music Harmony Plan) using entertainment precincts with specific noise criteria within the Valley, to allow informed decisions to be made regarding future development while minimising potential noise conflicts. An earlier paper by the Author has addressed the ambient noise mapping undertaken for the Valley, and this paper discusses the results of the cost benefit study undertaken into the acoustic treatment of selected venues. The purpose of this work was to provide Council with information on both the feasibility of treating the entertainment venues to reduce noise emissions and the order of cost for the treatments. The study of four venues found that attenuation of 3 - 22dB(A) or 1 - 17dB(C) could be achieved with asociated costs ranging from $30,000 to over $400,000 (Australian dollars). The costing work provided invaluable knowledge in the development of the Valley Music Harmony Plan.

10:20-10:40 Break

10:40

3aAAa8. Open-air theatre in the centre of the city: Acoustic design and noise environment control. Nicolaos Barkas (Democritus University of Thrace/ Greece, Vas. Sofias street 1, Department of Architecture, 67100 Xanthi, Greece, nbarkas@arch.duth.gr)

The municipal open-air Garden Theatre of Thessaloniki has for decades been located in the biggest urban park of the city next to a busy crossroads, where five major traffic roads meet. The intensification of traffic noise over the years led to the degradation of its use. In 1997, the organisation of the Cultural Capital of Europe served as a springboard for a study conducted by the author on redesigning the theatre. The design comprised a variety of arrangements, such as the rotation of the auditorium according to the results of the noise environment study, the choice of a closed plan in the type of the Greek-Roman Odeion, the sinking of the theatre space and the construction of barriers and shades. Various problems (such as archaeological findings, existence of big trees inside the auditorium, high level of underground water) and budget cuts during the design and construction, led to restricted execution of the planned architectural interventions. This paper deals with the design parameters that optimise acoustic function and maximise sound protection in an urban, open-air theatre and includes an analysis of the theatre's initial state, acoustic proposals and an assessment of the final applications.

11:00

3aAAa9. New acoustic test chambers at the University of Palermo. Marco Gullo (DREAM, Univ. of Palermo, Viale delle Scienze, Edificio 9, 90128 Palermo, Italy, mgullo@dream.unipa.it), Armando La Pica (DREAM, Univ. of Palermo, Viale delle Scienze, Edificio 9, 90128 Palermo, Italy, lapica@unipa.it), Giuseppe Rodono' (DREAM, Univ. of Palermo, Viale delle Scienze, Edificio 9, 90128 Palermo, Italy, rodon@unipa.it), Vincenzo Vinci (DREAM, Univ. of Palermo, Viale delle Scienze, Edificio 9, 90128 Palermo, Italy, vincenzo_vinci @hotmail.it), Vincenzo Conti (DREAM, Univ. of Palermo, Viale delle Scienze, Edificio 9, 90128 Palermo, Italy, conti@csai.unipa.it)

Acoustic test chambers at the University of Palermo have been completed after a design optimization of existent building structures. A unique building houses five reverberation chambers, differently coupled each other in order to achieve a large flexibility on testing procedures, and offices for the staff. Main measurements offered to national and international standards include determination of sound power, sound insulation and sound absorption. Reverberation chambers present peculiar geometries in order to achieve the desidered sound fields. Chambers structure and layout within the whole building, housing all the acoustic facilities, has been designed in order to achieve strong sound insulation requirements. The present work describes design solutions and reportes preliminary results from a large, still running, validation in order to characterize the chamber acoustic behaviour. Design targets and objective achievements are listed and commented.

11:20

3aAAa10. Design and construction of an acoustic lab facility. Douglas Winker (ETS-Lindgren, 1301 Arrow Point Drive, Cedar Park, TX 78763, USA, douglas.winker@ets-lindgren.com)

This paper will discuss the design and construction of a new acoustic lab facility. The lab consists of a hemi anechoic chamber and a reverberation chamber suite. The hemi anechoic chamber was designed to obtain a 0 dBA

noise floor in the frequency range of interest. It features a 200 cubic meter volume inside the wedges. To achieve the design goals, several aspects were considered including ambient levels, vibration isolation, HVAC noise, and free field performance. The design solutions for each of these areas will be presented. The reverb chamber suite consists of two reverberation chambers designed to perform transmission loss tests and sound absorption testing. The source chamber has an internal volume of 214 cubic meters and the receive room has an internal volume of 418 cubic meters. Design considerations will be discussed including vibration isolation, wall panel design, and diffuser placement. Additionally, the design and construction of the transmission loss coupling will be addressed.

11:40

3aAAa11. Measurements of existing modular construction classroom acoustics in the Midwestern United States. Norman Philipp (University of Nebraska - Lincoln, 1110 S. 67th St., Omaha, NE 68182-0681, USA, nphilipp@mail.unomaha.edu), Lily M. Wang (University of Nebraska - Lincoln, 1110 S. 67th St., Omaha, NE 68182-0681, USA, LWang4@UNL.edu)

Modular construction classrooms in the United States currently total more than 300,000 units, with 37% nationally of all public schools utilizing portable classrooms, according to the Modular Building Institute and a 2007 survey of Public School Principals conducted by the National Center for Education Statistics. Given this ever growing number there is a desire to improve their acoustics to meet ANSI S12.60-2002 guidelines for classroom acoustics. This paper gives a survey of existing acoustic conditions of relocatable classrooms currently in use in the Midwestern United States. Data to be presented include reverberation times, interior/exterior noise reduction, and site noise measurements. The results of these measurements and additional qualitative surveys will aid in understanding the performance of modular classrooms and assist in drafting a standard for them to supplement the guidelines in ANSI S12.60-2002.

12:00

3aAAa12. The influence of the scattering coefficient on the reverberation time. Franz Huber (Ziviltechnikerbüro Dipl. - Ing. Franz Huber, Neumühl 44, A-3250 Wieselburg, Austria, fh@zthuber.at), Thomas Bednar (University of Technology, Karlsplatz 13/206, A-1040 Vienna, Austria, thomas.bednar@tuwien.ac.at)

The reverberation time is still seen as an important measure of quality in architectural acoustic. The absorption coefficient is to be considered as the largest influencing factor on the reverberation time. The formulas after Sabine and Eyring give us the opportunity to calculate the reverberation time, when the absorption coefficients are known. In contrast to this, is the investigation of the influence of the scattering coefficient on the reverberation time a relatively new field for research. In this study the reverberation time for a ″shoebox″ was simulated, where the parameters were the values of the absorptions coefficient and the scattering coefficient and the even and uneven distribution of the absorption coefficient. The results of the simulation were compared with the results from the formulas by Sabine and Eyring. The simulations indicate a significant influence of the scattering coefficient on the reverberation time especially at low absorption coefficients. You can see by comparing the results of the simulation with the results of the formulas by Sabine and Eyring, that the theoretical formulas assume a minimum of scattering coefficient. It shows that the variation of the scattering coefficient is a possibly way to influence the reverberation time.

12:20

3aAAa13. Air Absorption Error in Room Acoustical Modeling. Remy H. Wenmaekers (LeVeL Acoustics BV, De Rondom 10, 5612 AP Eindhoven, Netherlands, r.h.c.wenmaekers@tue.nl), Constant C. Hak (Technische Universteit Eindhoven, De Rondom 10, 5612 AP Eindhoven, Netherlands, c.hak@inter.nl.net), Heiko J. Martin (Eindhoven University of Technology, Den Dolech 2, BWK/BPS, 5600 MB Eindhoven, Netherlands, h.j.martin@tue.nl), Laurentius C. Van Luxemburg (LeVeL Acoustics BV, De Rondom 10, 5612 AP Eindhoven, Netherlands, l.c.j.v.luxemburg@tue.nl)

Most statistical and ray-tracing computer models take into account the absorption of sound by air when calculating the reverberation time. Extensive research by many scientist lead to the standardized calculation model for pure tone air absorption. The phenomenon was discovered from a room acoustical point of view by Sabine, while the further development of the calculation model took place in the fields of physics and environmental noise. As a result, several parameters and units are used for the same phenomenon. However, air absorption is calculated for pure tones, while room acoustics calculations are performed for frequency bands. Most computer models use the center frequency of the normalized frequency bands to calculate the air absorption by the pure tone method. Frequency band reverberation measurements under laboratory and practical conditions show that errors larger than the JND are made in calculating the air absorption by this 'center frequency method'. No literature is found that provides an accurate air absorption calculation for frequency bands.

Session 3aAAb

Architectural Acoustics: Prediction Methods in Building Acoustics I

Berndt Zeitler, Cochair
NRC - Institute for Research in Construction, 1200 Montreal Road, Building M-27, Ottawa, ON K1A 0R6, Canada

Catherine Guigou-Carter, Cochair
CSTB, 24, rue Joseph Fourier, Saint Martin D'Hères, 38400, France

Contributed Papers

8:00

3aAAb1. FEM based prediction model for the impact sound level of floors. Andreas Rabold (Technische Universität München, Fakultät für Bauingenieur- und Vermessungswesen, Arcisstraße 21, 80290 München, Germany, rabold@bv.tum.de), Alexander Düster (Technische Universität München, Fakultät für Bauingenieur- und Vermessungswesen, Arcisstraße 21, 80290 München, Germany, duester@bv.tum.de), Ernst Rank (Technische Universität München, Fakultät für Bauingenieur- und Vermessungswesen, Arcisstraße 21, 80290 München, Germany, rank@bv.tum.de)

Up to now the research and development in the field of building acoustics is based mainly on experiments. The consequence of this approach is that the development and optimization of a new building component is a very tedious and expensive task. A considerably reduction of these costs could be achieved, if the optimization relying on experiments would be replaced - at least to some extent - by a computational approach. Common prediction models of the impact sound level from lightweight floors are based on measured impact sound level data for the component parts under consideration. These models are very useful for the evidence of performance of known building components, but they are not suited for the development of new components. An alternative approach in this context is the application of the finite element method (FEM). Based on a FE model, a modal- and spectral analyses provides the framework for an optimization of the building component. This contribution will present the overall approach consisting of the three-dimensional modeling of a lightweight-floor and the excitation source (tapping machine), the subsequent modal- and the spectral-analyses and the computation of the radiated sound from the floor.

8:20

3aAAb2. Human footsteps induced floor vibration. Delphine Bard (Lund University, Division of Engineering Acoustics, John Ericsson väg 1, 221 00 Lund, Sweden, delphine.bard@acoustics.lth.se), Julia Sonnerup (Lund University, Division of Structural Mechanics, John Ericsson väg 1, 221 00 Lund, Sweden, julia.sonnerup@byggmek.lth.se), Göran Sandberg (Lund University, Division of Structural Mechanics, John Ericsson väg 1, 221 00 Lund, Sweden, goran@byggmek.lth.se)

The generation of the impact sound by the act of the human walk involves two factors, the characters of the footfall and the shape of the induced floor deflection. The footfall noise is created by the impact excitation and the characters of the footfall depend on the foot-ware: the heels and the frequencies of the footfall. The shape of the floor deflection depends rather on the geometrical walking pattern and the construction of the floor structure. In this investigation, the vibration patter of the light-weight construction floor is created by the same walking object, a male with common height. The excitation from the person to the floor in the FE simulations is a function of the length of the foot and the weight of the walking object. The geometrical time history is of the foot step allows it to have different directions in the room. Since the excitation is assumed to be deterministic, differences between the excitation frequencies are estimated from the video records. The goal of this investigation is to determine the difference of the floor structure deflections between two different walking paths: one is perpendicular to the bearing beams and the other is the diagonal path.

Invited Papers

8:40

3aAAb3. Vibration of a rib-reinforced floor/ceiling structures with irregularities. Hyuck Chung (The University of Auckland, Department of Mathematics, Private Bag 92019, 1001 Auckland, New Zealand, hyuck@math.auckland.ac.nz), Colin Fox (Department of Physics, The University of Otago, 730 Cumberland Street, P O Box 56, 9010 Dunedin, New Zealand, fox@physics.otago.ac.nz)

This paper describes mathematical modelling procedure of the rib-reinforced floor/ceiling structures, which are made up of components with irregular shapes and physical parameters. Exact determination of the vibration of a composite structure becomes impossible beyond the low-frequency range because one cannot determine all the necessary parameters of the components. Even if every possible parameter of the structure is known, the results from such deterministic model would not represent the real behaviour of the structure. Therefore, the prediction model in the mid- to high-frequency range must include the effects of the irregularities. We show how the power spectra of the irregular features of each component can be included in the model. The model gives statistical estimates of the solutions, which can give appropriate mean and variance of the vibration of the structure for the given severity of the irregularities.

9:00

3aAAb4. Parameter survey of a rib stiffened wooden floor using sinus modes model. Lars-Göran Sjökvist (Acoustic Technology Department, Technical University of Denmark, Ørsted Plads, B352, DK-2800 Lyngby, Denmark, lars-goran.sjokvist@sp.se), Jonas Brunskog (Dept. of Acoustic Technology, Technical University of Denmark, Building 352, DK 2800 Lyngby, Denmark, jbr@oersted.dtu.dk), Finn Jacobsen (Acoustic Technology Department, Technical University of Denmark, Ørsted Plads, B352, DK-2800 Lyngby, Denmark, fja@oersted.dtu.dk)

In buildings built with new techniques there exists a need for better understanding of their acoustical performance. The development of large wooden houses slows down by the uncertainty and costly testing that have to be performed many times before gaining good

results. A greater understanding of the sound insulation for lightweight buildings have the possibility to speed up the development of new techniques and in the end give tenants better quality of life. This study uses Fourier sinus series to calculate the vibrations on a rib stiffened plate. The beams are modelled as line forces and moments that reacts onto the plate vibrations. A parameter study is performed with the aim to identify the most important parameters and their behaviour. The preliminary results show that the attenuation of the system is by far most evident in the direction across the beams. The influence from the basic input parameters on the attenuation is then studied. And it is preliminary shown that the placement of the excitation force within a bay actually is irrelevant for the calculated attenuation.

9:20

3aAAb5. The modelling of vibration transmission through plate/beam structures typical of lightweight buildings. Laurent Galbrun (Heriot-Watt University, School of the Built Environment, EH14 4AS Edinburgh, UK, l.g.u.galbrun@hw.ac.uk)

Vibration transmission through plate/beam structures typical of lightweight buildings is examined in this paper. Modelling difficulties are analysed and related to the several modelling choices available, including connection type, beam modelling, modal properties and material properties. A number of key experiments carried out on structures made of one or more parallel plates attached to a single beam are discussed, and the applicability and limitations of fundamental theories are identified through the use of Statistical Energy Analysis (SEA) models. It is shown that the interrelation between the various modelling factors can lead to complex models. The systems for which existing models can be used are identified, as well as those for which more complex models need to be developed.

Contributed Papers

9:40

3aAAb6. Approximation of single equivalent mobilities of timber joist floors. Andreas R. Mayr (Stuttgart University of Applied Sciences, Schellingstrasse 24, 70174 Stuttgart, Germany, andreas.mayr@hft-stuttgart.de), Barry M. Gibbs (University of Liverpool, School of Architecture, Abercromby Square, L693BX Liverpool, UK, bmg@liv.ac.uk)

To estimate the structure-borne sound power of vibrational active machines or components two source quantities, corresponding to the source activity and mobility, and one receiver quantity, the mobility, are usually required. A practical, laboratory-based measurement procedure for the characterisation of mechanical installations has recently been proposed, which yields single equivalent values of source strength and source mobility. In order to predict the power in the installed condition, an estimate of the receiver mobility also is required, again, for practical reasons, in the form of a single equivalent value. This paper considers the single equivalent receiver mobilities for lightweight building structures - timber joist floors. The value obtained is in the form of the average magnitude of the effective mobilities over the contact points. A simple prediction method is proposed for point- and transfer mobilities (both are required to yield the effective mobility at each contact) based on infinite beam and infinite plate behaviour. Estimates for point-, transfer- and single equivalent receiver mobilities are discussed and compared with measured data.

10:00

3aAAb7. Towards a prediction of the sound transmission from lightweight stairs. Jochen Scheck (Stuttgart University of Applied Sciences, Schellingstrasse 24, 70174 Stuttgart, Germany, jochen.scheck@hft-stuttgart.de), Barry M. Gibbs (University of Liverpool, School of Architecture, Abercromby Square, L693BX Liverpool, UK, bmg@liv.ac.uk), Andreas Drechsler (University of Applied Sciences, Schellingstr. 24, 70174 Stuttgart, Germany, andreas.drechsler@hft-stuttgart.de), Heinz-Martin Fischer (University of Applied Sciences, Schellingstr. 24, 70174 Stuttgart, Germany, heinz-martin.fischer@hft-stuttgart.de)

The sound transmission from lightweight stairs which are connected to separating walls often gives rise for complaints. One reason for this is that at present there is no prediction method available. Treating the stair as an active component in a similar manner like vibrating machines stairs can be characterised as structure-borne sound sources. The source data then can be used to predict the sound transmission in buildings using parts of EN 12354. Following this approach investigations on a timber stair have been carried out in a staircase test facility. Based on a full characterisation by contact free velocity and mobility and in-situ measurement using an indirect method, more practical methods like the reception plate method and a characterisation based on a reference power calibration are investigated. The source data obtained was used to predict the sound transmission in buildings.

10:20

3aAAb8. Prediction of the impact sound transmission from lightweight stairs in buildings based on a simplified laboratory characterisation. Andreas Drechsler (University of Applied Sciences, Schellingstr. 24, 70174 Stuttgart, Germany, andreas.drechsler@hft-stuttgart.de), Jochen Scheck (Stuttgart University of Applied Sciences, Schellingstrasse 24, 70174 Stuttgart, Germany, jochen.scheck@hft-stuttgart.de), Heinz-Martin Fischer (University of Applied Sciences, Schellingstr. 24, 70174 Stuttgart, Germany, heinz-martin.fischer@hft-stuttgart.de)

Based on a simplified laboratory characterisation of lightweight stairs the normalized impact sound pressure level in buildings can be predicted using parts of EN 12354. For the characterisation an approach is followed where the stair is treated as an active component with respect to an external excitation (e.g. by the tapping machine). The laboratory characterisation was performed for a timber stair and the normalized impact sound pressure level was predicted for different building situations. The various transmission paths via the separating and flanking walls were investigated and compared to the prediction according to EN 12354. Within the presentation the proceeding will be outlined and the restrictions are discussed. By comparison of measured and calculated values some references for the accuracy of the method are obtained.

10:40-11:00 Break

Invited Paper

11:00

3aAAb9. Impedance of standard impact sources and their effect on impact sound pressure level of floors. Berndt Zeitler (NRC - Institute for Research in Construction, 1200 Montreal Road, Building M-27, Ottawa, ON K1A 0R6, Canada, berndt.zeitler@nrc-cnrc.gc.ca), Trevor Nightingale (NRC - Institute for Research in Construction, 1200 Montreal Road, Building M-27, Ottawa, ON K1A 0R6, Canada, Trevor.Nightingale@nrc-cnrc.gc.ca)

This paper reports on a systematic study of the Impact Sound Pressure Level (ISPL) due to different standard sources (ISO hammer box, Ball, and ″Bang Machine″) when applied to a wood-joist floor-ceiling construction with and without various floor toppings. Measurement data show that for each floor, the ISPL was different for each source. Not surprising since the blocked force for each source is different. But, after applying corrections for the applied force the ISPL's remain different, suggesting problems since the sources simulate the same human walking activity. Perhaps more importantly, the rank of topping effectiveness (which is simply the difference in ISPL with and without the topping) was different for the three sources. Measurements of the drive point impedance of sources and floors are presented to explain this behaviour and to recognise that the power injected is not just related to the applied force, but also a function the impedance match (or miss-match) between the source and floor. The paper shows using a simple model, it is possible to predict ISPL's for any source if the forces and impedances are known, and using this model floor treatment effectiveness can be correctly ranked by each of the three standardised sources.

Contributed Papers

11:20

3aAAb10. Conversion of floor impact sound levels in apartment buildings. Pyoung Jik Lee (Hanyang University, Department of Architectural Engineering, 133-791 Seoul, Republic of Korea, pyoungjik@daum.net), Shin-Ichi Sato (Hanyang University, Department of Architectural Engineering, 133-791 Seoul, Republic of Korea, s_sato@mac.com), Jin Yong Jeon (Hanyang University, Department of Architectural Engineering, 133-791 Seoul, Republic of Korea, jyjeon@hanyang.ac.kr)

A procedure to convert the floor impact sound level of the bang machine as well as the tapping machine into that of the impact ball was suggested. Because the bang machine has been the only standard heavy-weight impact source for a long time in Japan and Korea, much of its data is available. The conversion factor of the sound pressure level between the impact ball and other standard impact sources was applied to the sound pressure level of a bang machine and a tapping machine. In addition, a conversion method using a correlation analysis between the sound pressure level of impact ball and that of other standard impact sources at each octave band was also investigated. Results indicate that bang machine and tapping machine data can be successfully converted into impact-ball data, in the case of box-framed type, reinforced concrete structures.

11:40

3aAAb11. A simplified approach to impact sound insulation rating without using a tapping machine. Ming Li (Acoustics Research Centre, School of Architecture, The University of Auckland, 1010 Auckland, New Zealand, mli072@ec.auckland.ac.nz), George Dodd (Acoustics Research Centre, School of Architecture, The University of Auckland, 1010 Auckland, New Zealand, mli072@ec.auckland.ac.nz)

The aim of this study is to investigate a simplified approach for obtaining ratings of impact insulation of floors which requires only airborne sound measurements and correction factors depending on the particular type of floor finish. One third octave frequency-dependent correction factors have been obtained by processing published results of both airborne and impact insulation on floors. The uncertainty of predicted Ln,w values using correction factors shows a good agreement with ISO recommended limits. The proposed technique has value in reducing the cost and effort for field insulation measurements. Further work is underway to refine the method and to extend the range of constructions for which we have correction factor.

12:00

3aAAb12. Reciprocity and the Prediction of the Apparent Sound Reduction Index for Lightweight Structures According to EN12354. Jeffrey Mahn (University of Canterbury, Department of Mechanical Engineering, Private Bag 4800, 8140 Christchurch, New Zealand, jma251@student.canterbury.ac.nz), John Pearse (University of Canterbury, Depart-ment of Mechanical Engineering, Private Bag 4800, 8140 Christchurch, New Zealand, john.pearse@canterbury.ac.nz)

EN12354 makes use of reciprocity to cancel the radiation efficiency terms from the equations used to predict the apparent sound reduction index. The use of reciprocity works well for the application of EN12354 to massive, concrete structures with diffuse wave fields and with critical frequencies below the frequency range of interest. However, lightweight constructions may have critical frequencies above the frequency range of interest and may not support diffuse wave fields. The use of reciprocity for application to lightweight structures may introduce errors into the predictions. This study investigates the uncertainty introduced into the predictions of the apparent sound reduction index of lightweight constructions due to the use of reciprocity.

12:20

3aAAb13. Innovative building systems to improve the acoustical quality in lightweight masonry constructions: Application of resilient joints at junctions - PART 1: Analysis of the experimental results. Charlotte Crispin (BBRI, rue du Lombard, 42, B-1000 Brussel, Belgium, charlotte.crispin@bbri.be), Bart Ingelaere (BBRI, rue du Lombard, 42, B-1000 Brussel, Belgium, bart.ingelaere@bbri.be), Gerrit Vermeir (Lab. ATF, Katholieke Universiteit Leuven, Celestijnenlaan 200D, B-3001 Leuven, Belgium, Gerrit.Vermeir@bwk.kuleuven.be)

The more severe acoustic requirements imposed by the new Belgian standard for dwellings are a real challenge for the building professionals (architects, contractors, building elements manufacturers and suppliers, œ) and more particularly for the market of lightweight materials. An important brick producer in partnership with the BBRI has succeeded to propose efficient acoustic solutions for these kinds of materials by treating in particular the flanking transmission. Indeed, to obtain high sound insulations, the structural transmission paths of noise through the flanking walls cannot be neglected any more. By the application of resilient rubber interlayers at the junctions, these transmission paths are nearly eliminated. A large number of measurements was carried out in order to study in detail the effect of these flexible joints on the sound transmission. These measurements were made in a specially designed laboratory where vibration reduction indexes can be measured for all types of connections and for different loads. We present, in this paper, the measurement campaign and the analysis of the results.

12:40-1:40 Lunch Break

Contributed Paper

1:40

3aAAb14. Innovative building systems to improve the acoustical quality in lightweight masonry constructions: Application of resilient joints at junctions - PART 2: Study cases modelled according to the standard 12354-1 (2000). Charlotte Crispin (BBRI, rue du Lombard, 42, B-1000 Brussel, Belgium, charlotte.crispin@bbri.be), Bart Ingelaere (BBRI, rue du Lombard, 42, B-1000 Brussel, Belgium, bart.ingelaere@bbri.be), Debby Wuyts (BBRI, rue du Lombard, 42, B-1000 Brussel, Belgium, debby.wuyts@bbri.be)

An important brick manufacturer in partnership with the BBRI has succeeded to propose efficient acoustic solutions for this kind of lightweight materials by treating the flanking transmission using flexible interlayers at junctions and foundations. A large measurement campaign has been carried out to study the efficiency of the resilient joint and to provide a prediction model on airborne sound insulation in brickwork constructions. The prediction model used is based on the standard 12354-1 but was adapted in order to take into account higher orders for the flanking transmission paths. This adapted model thus allowed to study different applications of the flexible joint and their contribution to the improvement of the global sound insulation. This paper presents a discussion on the calculation model, the input data and some early results.

Invited Papers

2:00

3aAAb15. Direct and flanking sound transmission of solid gypsum walls - practical experience and numerical prediction. Andreas Ruff (Stuttgart University of Applied Sciences, Schellingstrasse 24, 70174 Stuttgart, Germany, andreas.ruff@hft-stuttgart.de), Heinz-Martin Fischer (University of Applied Sciences, Schellingstr. 24, 70174 Stuttgart, Germany, heinz-martin.fischer@hft-stuttgart.de)

In modern multi storey buildings gypsum blocks are often used for solid inner walls without static requirements. However, these relatively light walls with a mass per unit area of about 90 kg/m^2 are not connected rigidly to the adjacent building elements. They are decoupled with elastic interlayers made of bitumen, cork or polyethylene foam. These elastic interlayers have a significant influence on the direct and the flanking sound transmission of the gypsum walls. For this reason the decoupled walls have to be considered different to rigidly connected walls. Within a recent research project there was an extensive investigation into the direct and the flanking sound transmission of gypsum walls in different test facilities in the laboratory. For several kinds of elastic interlayers the sound reduction index of gypsum walls was measured in the test stand for direct sound transmission. The vibration reduction index was investigated in a test facility for flanking transmission as well as in different building situations. The measured values are used as input data for the prediction model according EN 12354-1. The overall sound reduction index calculated with this prediction model is compared with the results measured in the buildings.

2:20

3aAAb16. Some practical aspects of the prediction of structure-borne sound caused by house-hold equipment. Eddy Gerretsen (TNO Science and Industry, Stieljesweg 1, 2628CK Delft, Netherlands, eddy.gerretsen@tno.nl)

Sound levels in rooms due to service equipment in the building can be an important reason for disturbance and more so in light weight building structures. Though the recently published draft standard prEN 12354-5 gives a framework for the prediction of the structure-borne sound as caused by this type of sources, there is still a lot to be studied and developed. That is certainly the case for light weight building structures. Some possibilities to simplify the indicated models have been studied and experimental data has been gathered for house hold equipment, taking a washing machine as an example, applied both in a 'heavy' and in a 'light weight' building. Various possibilities to apply substitution methods to characterise such a source as structure-borne sound source have been tried and compared.

Contributed Papers

2:40

3aAAb17. An hybrid method for sound transmission through opened windows. Philippe A. Jean (CSTB, 24 rue Joseph Fourier, 38400 Saint-Martin-d'Hères, France, philippe.jean@cstb.fr), Michel Villot (CSTB, 24 rue Joseph Fourier, 38400 Saint-Martin-d'Hères, France, michel.villot@cstb.fr)

An hybrid model for the calculation of sound transmission between apartments when windows are opened is presented. It is an extension of Kropp's model for balconies (integral/modal/wave approach). Two rectangular rooms are set in a baffle with rectangular openings. A point source is placed in one room and sound attentation between rooms is computed. The external field may include the ground and a nearby building by means of a combined image source approach to compute a Green function in the integral description at the openings. Results are validated against BEM and published measurements. SEA is employed to assess the importance of vibration transmission relative to airborne transmission through the external medium.

3:00

3aAAb18. Directional distribution of acoustic energy density incident to a surface under reverberant condition. Cheol-Ho Jeong (Acoustic Technology, DTU Elektro, Technical University of Denmark, Building 352, Ørsted plads, DK-2800 Kgs. Lyngby, Denmark, chj@oersted.dtu.dk), Jeong-Guon Ih (KAIST, Dept. of Mechanical Engineering, Science Town, 305-701 Daejeon, Republic of Korea, J.G.Ih@kaist.ac.kr)

Most of acoustic measurements presume ideal conditions: one ideal condition is a diffuse and reverberant field. In a practical situation, diffuse sound field in a reverberation chamber can not be achieved. In particular, the directional diffusion which means the uniform angular distribution of incident direction can not be satisfied. Angle dependency of incident energy density was simulated by the phased beam tracing simulation. Various results were found by changing room shape and source position, and number of sources. Acoustic energy generally decreases with the angle of incidence. This result can be used as a weighting function for the calculation of sound transmission index and random incidence absorption coefficient.

Invited Paper

3:20

3aAAb19. Exposure of building roofs to road traffic noise; consequences on the field performance of skylights. Michel Villot (CSTB, 24 rue Joseph Fourier, 38400 Saint-Martin-d'Hères, France, michel.villot@cstb.fr), Philippe A. Jean (CSTB, 24 rue Joseph Fourier, 38400 Saint-Martin-d'Hères, France, philippe.jean@cstb.fr)

In this paper, the exposure to road traffic noise of building roofs is studied both theoretically and experimentally. First, the incident field is estimated using a BEM approach, taking into account the sound diffraction on the roof edge. The theoretical results show significant differences in noise exposure between roofs and vertical façades, particularly with relatively tall buildings; these differences are then confirmed by field measurements. The grazing incidence of the sound fields on roofs raises the question of the acoustic performances of skylights in real situation, as opposed to their laboratory performances measured under diffuse sound field; this problem is experimentally investigated by laboratory measurements of glazing under different angles of incidence, using a big size plane wave generator.

WEDNESDAY MORNING, 2 JULY 2008 ROOM 342B, 8:00 TO 10:00 A.M.

Session 3aABa

Animal Bioacoustics, Underwater Acoustics, Acoustical Oceanography, Signal Processing in Acoustics, and ECUA: Animal Sonar Systems III

James Simmons, Cochair
Brown University, Dept. of Neuroscience, Box G-LN, Providnece, RI 02912, USA

Michel Andre, Cochair
Laboratori, d' Aplicacions Bioacútques, Universitat Politècnica de Catalunya, avda. Rambla Exposicío s/n, 08800 Vilanova, la Geltrú, Spain

Contributed Papers

8:00

3aABa1. Localization of brief sounds by a bottlenose dolphin. Gennadi L. Zaslavski (University Authority for Applied Research, RAMOT, Tel-Aviv University, str. Gordon 51 app 7, 42442 Netanya, Israel, gennadi .zaslavski@gmail.com)

Spatial hearing in dolphins is believed to be similar to that in humans. The same binaural phenomenon known for humans is used to explain sound localization in dolphins. However, the ability of a bottlenose dolphin to localize a sound in the vertical plane as accurate as in the horizontal plane appears to undermine binaural phenomenon concept in dolphin sonar. We found that directionality of the bottlenose dolphin transmit beam could account for most results on the bottlenose dolphin underwater object localization. In this paper passive localization and spatial discrimination of brief signals by a bottlenose dolphin is examined. The bottlenose dolphin was found capable of discriminating clicks with different intensity as well as a click and brief noise pulse simultaneously transmitted via transducers separated in azimuth by less than 1°. The dolphin was also able to discriminate a lead from a lag noise pulse at the transducer azimuth separation as small as 0.3°-0.4° and the lag delay as small as 20 microseconds. The results are discussed with regard to the bottlenose dolphin auditory time resolution and so called precedence effect phenomenon well known for the binaural system of humans.

8:20

3aABa2. The interaction of emitted pulses and echoes in a whale's biosonar: A partial contribution to biosonar automatic gain control. Alexander Y. Supin (Institute of Ecology and Evolution, 33 Leninsky Prospect, 119071 Moscow, Russian Federation, alex_supin@mail.ru), Paul E. Nachtigall (University of Hawaii, Hawaii Institute of Marine Biology, P.O. Box 1106, Kailua, HI 96734, USA, nachtiga@hawaii.edu), Marlee Breese (University of Hawaii, Hawaii Institute of Marine Biology, P.O. Box 1106, Kailua, HI 96734, USA, mbreese@hawaii.edu)

In a false killer whale Pseudorca crassidens, echo perception thresholds were measured using a go/no-go psychophysical paradigm and one-up-one-down staircase procedure. Electronically synthesized echoes were triggered by whale-emitted echolocation pulses, and the echo amplitudes were presented proportional to the triggering biosonar pulse amplitudes, thus imitating the basic feature of real target echoes. Echo thresholds were measured in terms of attenuation relative to the source level of the biosonar pulses. The echo threshold dependence on echo delay was investigated. With increasing echo delay, the threshold echo attenuation decreased from -49.3 dB at 2 ms to -79.5 dB at 16 ms, with a regression slope of -31.5 dB per delay decade. At delays longer than 16 ms, the threshold remained nearly constant around -80.4 dB. This echo threshold dependence on delay is interpreted as a release from forward masking by the preceding emitted pulse. This release may well compensate for the echo level decrease with distance which is from 20 to 40 dB per distance decade, depending on target properties. This compensation may keep the echo sensation level independent of, or little dependent on, target distance. Supported by Office of Naval Research (USA), Ministry of Science and Education (Russian Federation).

8:40

3aABa3. Investigation into the possible role of dolphins' teeth in sound reception. Sabine Graf (University of Bath, Dept. Mechanical Engineering, Claverton Down, BA2 7AY Bath, UK, sg283@bath.ac.uk), William M. Megill (University of Bath, Dept. Mechanical Engineering, Claverton Down, BA2 7AY Bath, UK, enswmm@bath.ac.uk), Philippe Blondel (University of Bath, Department of Physics, Claverton Down, BA2 7AY Bath, UK, pyspb@bath.ac.uk), Sally E. Clift (University of Bath,Dept. Mechanical Engineering, Claverton Down, BA2 7AY Bath, UK, enssec@bath.ac.uk)

Odontocetes use active sonars for echolocation, navigation and socialisation. These sonars are characterised by narrow transmission and reception directivity patterns, over a variety of ranges. There is physiological

and behavioural evidence to suggest that dolphins hear the echoes of their high-frequency clicks through their lower jaws. Current theory suggests that sound is transmitted through a thin region at the base of the jaw into a waveguide leading to the ear. The angular precision predicted by this theory is however much less than dolphins have been observed behaviourally to be able to do. A novel hypothesis is that the teeth of the dolphin's lower jaw act as an end-fire sonar array. This paper will start by putting these competing hypotheses into their context, presenting bioacoustics in the ocean, dolphin echolocation physiology and acoustic behaviour, and the mechanical properties of bones and teeth. This information is used to model the reception of different sounds by bottlenose dolphins (tursiops truncatus) with each possible mechanism, investigating the variations with nerve delay, the role of the jaw relative to the teeth, and the resulting changes in frequency sensitivity and directivity. The results can then be compared with observations of behavioural patterns.

9:00

3aABa4. Acoustic behavior of echolocating porpoises during prey capture. Stacy Deruiter (Woods Hole Oceanographic Institution, Applied Ocean Physics & Engineering Dept., Woods Hole, MA 02543, USA, deruiter@mit.edu), Alexander Bahr (MIT, 32 Vassar St., Room 32-331, Cambridge, MA 02139, USA, abahr@mit.edu), Marie-Anne Blanchet (Fjord&Bælt / University of Southern Denmark, Margrethes Plads 1, 5300 Kerteminde, Denmark, marie@fjord-baelt.dk), Sabina Hansen (Fjord&Bælt / University of Southern Denmark, Margrethes Plads 1, 5300 Kerteminde, Denmark, sabina@fjord-baelt.dk), Jakob Kristensen (Fjord&Bælt / University of Southern Denmark, Margrethes Plads 1, 5300 Kerteminde, Denmark, jakob@fjord-baelt.dk), Peter T. Madsen (University of Aarhus, Biological Sciences, Zoophysiology, C. F. Møllers Allé, Building 1131, DK-8000 Aarhus, Denmark, peter.madsen @biology.au.dk), Peter Tyack (Woods Hole Oceanographic Institution, Applied Ocean Physics & Engineering Dept., Woods Hole, MA 02543, USA, ptyack@whoi.edu), Magnus Wahlberg (Fjord&Bælt / University of Southern Denmark, Margrethes Plads 1, 5300 Kerteminde, Denmark, magnus @fjord-baelt.dk)

Porpoise echolocation has been studied in target detection experiments using stationed animals and steel spheres as targets, but little is known about the acoustic behavior of free swimming porpoises as they echolocate for prey. Here we used archival tags (modified Dtags) recording audio (400 kHz, 16-bit stereo sampling rate) and animal movements (depth, heading, 3D pitch and roll, and acceleration) to study echolocation in trained porpoises catching fish. The prey capture experiments were conducted with and without suction cups covering the porpoises' eyes. Without the eye cups, the porpoises could use both echolocation and vision to locate and ingest their prey, but with eye cups they could use only echolocation. Our data show that time to prey capture is about 27% greater with eye cups (T-test, $p<0.01$). They also allow us to describe and compare prey capture in the two experimental conditions, including analysis of the animals' detailed movements and echolocation behavior leading up to and following prey capture events.

9:20

3aABa5. Biosonar model for obtaining fine target structure in complex targets. John R. Buck (UMass Dartmouth, ECE Dept, 285 Old Westport Rd, N. Dartmouth, MA 02740-2300, USA, johnbuck@ieee.org)

Bats use echolocation to discriminate targets with multiple glints in which the glints are much closer together in time than the integration time of the bat auditory system. This indicates the bats cannot be using purely time-domain processing to image the target. It is likely that the bats exploit cues such as spectral peaks and notches due to the interference between the glints at specific frequencies. However, these interference patterns quickly grow complicated as the number of glints increases. The cepstrum is a signal processing algorithm designed to identify these interference intervals. We previously demonstrated that simple two-glint targets can be accurately resolved using a time-varying version of the cepstrum, or cepstrogram. This talk will present an algorithm for interpreting the evolution of cepstral peaks across a target with many glints to estimate the inter-glint intervals. This algorithm has the desirable quality of processing the data causally as it is received, and thus is possible to implement in real time. The performance of the algorithm will be evaluated using experimental data from an ultrasonic bat simulator. [Work supported by US Office of Naval Research]

Invited Paper

9:40

3aABa6. Acoustics of shape recognition by a dolphin in a cross-modal matching-to-sample paradigm. Matthias Hoffmann-Kuhnt (Acoustic Research Laboratory, National University of Singapore, 12A Kent Ridge Road, 119223 Singapore, Singapore, mahoku@nus.edu.sg), Mandar A. Chitre (Acoustic Research Laboratory, National University of Singapore, 12A Kent Ridge Road, 119223 Singapore, Singapore, mandar@arl.nus.edu.sg), Paul J. Seekings (Acoustic Research Laboratory, National University of Singapore, 12A Kent Ridge Road, 119223 Singapore, Singapore, paul@arl.nus.edu.sg), Grant Abel (Ocean Park Hong Kong, Aberdeen, 118336 Hong Kong, Hong Kong, grant.abel@oceanpark.com.hk)

A pacific bottlenose dolphin was trained in a two-alternative cross-modal matching-to-sample paradigm. The animal was able to inspect complex PVC-pipe shapes through echolocation or vision but never through both senses simultaneously. Acoustic data was collected through a 3-channel high-frequency recording system while the dolphin performed one of the following tasks: (1) match a complex shape with its sonar only (pure echoic matching), (2) match from vision to echolocation and (3) match from echolocation to vision. Simultaneously, synchronized in-air and underwater video was recorded documenting the approach path of the dolphin to either the sample object or to the alternative objects. The collected data was analyzed for type of click signals used, the frequency range of the emitted clicks, number of clicks emitted before a successive match and variations of click type with different objects.

Session 3aABb

Animal Bioacoustics and ECUA: Odontocete Acoustics I

David K. Mellinger, Cochair
Oregon State Univ. and NOAA, 2030 SE Marine Science Dr., Newport, OR 97365, USA

Michel Andre, Cochair
Laboratori d'Aplicacions Bioacústiques (Universitat Politècnica de Catalunya), avda. Rambla Exposició s/n, Vilanova i la Geltrú, 08800, Spain

Invited Paper

10:20

3aABb1. Annotated odontocete recordings for developing automated detection and classification methods. David K. Mellinger (Oregon State Univ. and NOAA, 2030 SE Marine Science Dr., Newport, OR 97365, USA, David.Mellinger@oregonstate.edu), Holger Klinck (Oregon State Univ. and NOAA, 2030 SE Marine Science Dr., Newport, OR 97365, USA, Holger.Klinck@oregonstate.edu), Sara Heimlich (Oregon State Univ. and NOAA, 2030 SE Marine Science Dr., Newport, OR 97365, USA, Sara.Heimlich@oregonstate.edu), Sharon Nieukirk (Oregon State Univ. and NOAA, 2030 SE Marine Science Dr., Newport, OR 97365, USA, Sharon.Nieukirk@oregonstate.edu)

A free archive has been developed for research in automatic detection/classification of cetacean sounds. The archive contains many datasets, with each dataset comprising recordings and metadata for a given species and geographic area. This archive differs from other sound archives in three important respects: (1) Recordings are annotated to indicate where in time and frequency the sounds of a given species occur. These annotations are done manually to remove the bias of any automatic detection system. (2) The archive deliberately includes poor-quality recordings, recordings encountered in any realistic detection/classification application. (3) Since performance of detection/classification methods depends heavily on the SNR of target sounds, the archive includes each vocalization's SNR so performance can be effectively represented. Until recently, most recordings in the archive were of baleen whales [Mellinger and Clark, Applied Acoustics 67(11), 2006]. However, datasets for toothed whales and dolphins are now being incorporated. Initial efforts have been focused on beaked whales because of high interest for management and because of the difficulty of visual detection. To date, recordings of Cuvier's, Blainville's, Baird's, and Arnoux's beaked whales have been entered into the archive, as have those of bottlenose whales, pilot whales, and some delphinid species. Further contributions are welcomed.

Contributed Papers

10:40

3aABb2. Dynamic tracking of free-swimming whale groups using digital acoustic recording tags. Charles White (University of Rhode Island, Department of Ocean Engineering, Narragansett Bay Campus, Narragansett, RI 02882, USA, cwhite@oce.uri.edu), James H. Miller (University of Rhode Island, Department of Ocean Engineering, Narragansett Bay Campus, Narragansett, RI 02882, USA, miller@egr.uri.edu), Gopu R. Potty (University of Rhode Island, Department of Ocean Engineering, Narragansett Bay Campus, Narragansett, RI 02882, USA, gopu@uri.edu), Mark Johnson (Woods Hole Oceanographic Institution, Applied Ocean Physics & Engineering Dept., Woods Hole, MA 02543, USA, majohnson@whoi.edu)

Understanding the group behavior of free-swimming whales is critical to the management and conservation of many whale species. Moreover, understanding how whales coordinate their activities could serve as a model for improving the communication and navigation systems of underwater robots and autonomous underwater vehicles (AUVs). One method for studying the group behavior of free-swimming whales involves simultaneously attaching acoustic recording tags to multiple animals within a close-swimming conspecific group. Acoustic recording tags can sample an animal's acoustic environment simultaneously with other physical parameters such as diving depth and acceleration. In this paper, methods are presented for dynamically tracking whales that vocalize regularly such as odontocetes using the DTAG, a digital acoustic recording tag developed by the Woods Hole Oceanographic Institution. A trilateration model is reviewed for tracking groups of whales that include three or more tagged whales using time of flight data and results are given from applying this model to a novel data set of three simultaneously diving and cross-audible short-finned pilot whales (Globicephala macrorhyncus). A new model is subsequently proposed for tracking whale groups that include only two tagged whales using a generalization of multilateration and data captured by stereo DTAGs.

11:00

3aABb3. Spatial confirmation of vocal communication between a killer whale calf and its natal family. Scott Veirs (Beam Reach Marine Science and Sustainability School, 7044 17th Ave NE, Seattle, WA 98115, USA, scott@beamreach.org), Val Veirs (Colorado College, Department of Physics, Colorado Springs, CO 80903, USA, vveirs@coloradocollege.edu), Jason D. Wood (Beam Reach Marine Science and Sustainability School, 7044 17th Ave NE, Seattle, WA 98115, USA, jason@beamreach.org)

We recorded an interchange of vocal signaling between a four-year-old Southern Resident killer whale and its natal family members (mother and brother). This information was recorded on a 30-m-long linear array of hydrophones that was towed behind our electric motor powered research vessel. Over the course of about 1/2 hour we recorded signals from these isolated orcas about 500 m offshore of San Juan Island, WA. Surface locations of the orcas were documented with visual accounts, photographs, video, and - during the latter portion of the encounter - with a hand-bearing compass. During a six minute interval of the recording we have localized ~70 vocalizations that we can associate with the surface positions of either the juvenile or the mother-brother pair (they were close together). The central three minutes of this interval document an event in which the juvenile left the family group, swam toward our vessel, approached it within about 10m, turned abruptly away during a rapid call-response sequence with the

mother and/or brother, and then rejoined the natal group. This rare event informs killer whale vocal development, repertoire, communication, and active space.

11:20

3aABb4. Killer whales (Orcinus orca) and Bell Laboratories: What can information theory tell us about the communication system of this species? Kenna D. Lehmann (University of California, Dept. of Evolution and Ecology, Davis, CA 95616, USA, kdlehmann@ucdavis.edu), Jason D. Wood (Beam Reach Marine Science and Sustainability School, 7044 17th Ave NE, Seattle, WA 98115, USA, jason@beamreach.org)

In the 1950's Shannon and Weaver developed information theory as a statistical tool to determine the structure and organization within communication systems. More recently information theory has been applied to the study of animal communication. We gathered acoustic recordings of the Southern Resident killer whales in the inland waters of Washington State, USA, and British Columbia, Canada, from both land based and boat based acoustic arrays. Recorded calls were categorized using the accepted call catalog for this population. In this paper we will present our results from applying various Shannon entropies to the documented call sequences. One notable result is that the call repertoire is more redundant than is ideal to convey the maximum amount of information. This may be a result of their particular social system and behavioral ecology, or may be an indication of the amount of noise present in their acoustic environment. Comparisons will also be made with measures of information theory in other species.

11:40

3aABb5. Whistle repertoire of captive bottlenose dolphins, Tursiops truncatus. Rebeca M. Lopez-Rivas (UNAM, Facultad de Ciencias, Depto. Física, Lab Acústica, Circuito exterior s/n, Cd. Universitaria, 04510 México, D.F., Mexico, rmlopez.rivas@gmail.com), Volker B. Deecke (University of British Columbia, Marine Mammal Research Unit, Vancouver, BC V6T 1Z4, Canada, deecke@zoology.ubc.ca), Carmen Bazúa Durán (UNAM, Facultad de Ciencias, Depto. Física, Lab Acústica, Circuito exterior s/n, Cd. Universitaria, 04510 México, D.F., Mexico, bazua@servidor.unam.mx)

The whistle repertoire of bottlenose dolphins has been poorly described in the literature, thus little information is known to support the hypothesis that whistles are used by dolphins to communicate. In this study, whistles emitted by four captive bottlenose dolphins housed in two aquaria in Mexico City were recorded to analyze the whistle repertoire and whistle emission rate for each aquarium. The whistle repertoire was described using human and automated categorizations. Results show that whistle emission rate and the whistle repertoire are both larger for the two dolphins that are more active and which are housed in the same aquarium. As for whistles shared in the repertoire of both aquaria, these are very few, probably because dolphins of the two aquaria were captured in different oceans and are of different ages, besides of the different activities that dolphins can perform in each aquarium. Additionally, all four dolphins could use similar whistles for a specific activity, like ″swimming″, while different whistles were used for another specific activity, like ″observing″. These results show that dolphins use whistles selectively, supporting the hypothesis that whistles may be used to communicate information for particular situations. [Work supported by PAPIIT, UNAM & CoNaCyT]

12:00

3aABb6. Unsupervised clustering of whistle-sounds of bottlenose dolphins (Tursiops truncatus). Sebastian V. Huebner (Pestalozzistrasse 5, 14482 Potsdam, Germany, sebastian@sejona.de)

An unsupervised symbolic clustering algorithm for whistles of bottlenose dolphins (Tursiops truncatus) was tuned on an artificial data set containing 12 ideal synthetic signature whistles. Afterwards approximately 25,000 representations of natural whistles were clustered with the tuned algorithm. Recordings were made from a group of twelve adult semi-free living animals in Eilat (Israel). Obtained clusters were evaluated with the help of their individual compression rates. The clustering algorithm perfectly converged on all twelve artificial whistle types. Also, automatic whistle extraction produced good representations of both artificial and natural whistles, but clustering of natural whistles provided low support for the signature whistle hypothesis: The six most frequent induced whistle types could be interpreted as slight variations of only two signature whistles. Also, a great variety of different but rare types in automatically generated clusters could be observed. Results suggest that certain aspects of the group behavior are manifest in the frequency whistle types occur.

12:20

3aABb7. Acoustic studies of dolphins in their natural habitat: Challenges and successes. Katherine Kim (HLS Research, Inc., 3366 N. Torrey Pines Ct., Ste. 310, La Jolla, CA 92037, USA, Katherine.Kim@HLSResearch.com), Paul Hursky (HLS Research, Inc., 3366 N. Torrey Pines Ct., Ste. 310, La Jolla, CA 92037, USA, paul.hursky@hlsresearch.com), Michael B. Porter (HLS Research, Inc., 3366 N. Torrey Pines Ct., Ste. 310, La Jolla, CA 92037, USA, michael.porter@hlsresearch.com), John A. Hildebrand (Scripps Institution of Oceanography- UCSD, 9500 Gilman Dr. #0205, La Jolla, CA 92093, USA, jhildebrand@ucsd.edu), Elizabeth Henderson (Scripps Institution of Oceanography- UCSD, 9500 Gilman Dr. #0205, La Jolla, CA 92093, USA, e0hender@ucsd.edu), John Calambokidis (Cascadia Research Collective, 218 1/2 W. 4th Ave., Olympia, WA 98501, USA, calambokidis@cascadiaresearch.org), Erin Falcone (Cascadia Research Collective, 218 1/2 W. 4th Ave., Olympia, WA 98501, USA, EFalcone@cascadiaresearch.org)

Acoustic methods for studying marine mammals is a research area of great potential, with applications which include population estimation, spatial distribution, behavioral studies, and the effects of anthropogenic noise on animals. Until recently, much of the acoustic research on free-ranging animals has focused on mysticetes and sperm whales; however, concern over highly-publicized dolphin strandings has raised interest in other odontocetes. From acoustic and signal processing perspectives, dolphins pose numerous new challenges: They typically aggregate in pods composed of tens or hundreds of individuals, often vocalizing simultaneously, and their calls are highly variable and high-frequency. Detection algorithms will be presented which are robust (or, conversely, can be fine-tuned) to these variable calls and have been automated to overcome the ordinarily labor-intensive analysis requirements of such large data sets. Historically, acoustic studies of marine mammals used relatively simple sensor systems comprised of one or few hydrophones. In our studies, multiple sensor systems were deployed. Doing so enabled the utilization of array and co-array processing techniques for improved localization estimation which, like our detection algorithms, were fully automated. They also raised important deployment considerations due to the acoustic propagation physics as well as challenges in call association between different systems.

12:40

3aABb8. Narrow band high frequency clicks from Hourglass dolphins (Lagenorhynchus cruciger). Line A. Kyhn (National Environmental Research Institute, University of Aarhus, Frederiksborgvej399, DK-4000 Roskilde, Denmark, lky@dmu.dk), Jakob Tougaard (National Environmental Research Institute, University of Aarhus, Frederiksborgvej399, DK-4000 Roskilde, Denmark, jat@dmu.dk), Magnus Wahlberg (Fjord&Bælt / University of Southern Denmark, Margrethes Plads 1, 5300 Kerteminde, Denmark, magnus@fjord-baelt.dk), Kristian Beedholm (Institute of Biology, University of Southern Denmark, Campusvej 55, 5230 Odense M, Denmark, beedholm@mail.dk), Peter T. Madsen (University of Aarhus, Biological Sciences, Zoophysiology, C. F. Møllers Allé, Building 1131, DK-8000 Aarhus, Denmark, peter.madsen@biology.au.dk)

The source properties of toothed whale echolocation clicks are essential for evaluating the performance of biosonar systems. However, such data only exist for a small number of free ranging toothed whale species. Here we present a quantitative analysis of the first recordings of echolocation sounds from hour glass dolphins (Lagenorhynchus cruciger) made in the Drake Strait. Recordings were made with a vertical array of four broadband, calibrated hydrophones that allows for acoustic localization and source parameter derivation. Only apparent on-axis clicks were used for analysis. Hour glass dolphins produce clicks with a mean peak and centroid frequency around 128kHz, a narrow, mean RMS bandwidth of 10kHz with no energy below 100kHz and a mean signal duration of 161μs. Echolocation clicks of hour glass dolphins are thus of the high frequency narrow band-

width type (NBHF type) found in porpoises, a few delphinids of the Cephalorhynchus genus and the pygmy sperm whale Kogia breviceps, but are strikingly different from other dolphins. Acoustic convergence from vastly different genera and ecotypes suggest that evolution of NBHF clicks are adaptations to special auditory processing or acoustic crypsis rather than to habitat.

WEDNESDAY MORNING, 2 JULY 2008 ROOM 342A, 8:00 TO 11:20 A.M.

Session 3aAO

Acoustical Oceanography, Underwater Acoustics, Signal Processing in Acoustics, and ECUA: Geoacoustic Characterization of the Ocean Bottom and Geoacoustic Inversion III

Peter Gerstoft, Cochair
Marine Physical Laboratory, Scripps Institute of Oceanography, 8602 La Jolla Shores Drive, La Jolla, CA 92093-0238, USA

Dag Tollefsen, Cochair
Norwegian Defence Research Establishment (FFI), Box 115, Horten, 3191, Norway

Invited Papers

8:00

3aAO1. Location of Targets and Scatterers with Ambient Noise. Christopher H. Harrison (NATO Undersea Research Centre, Viale San Bartolomeo 400, 19138 La Spezia, Italy, harrison@nurc.nato.int)

By placing a vertical array in an ambient noise field and forming an upward and downward beam one obtains two time series which can be cross-correlated to reveal a sub-bottom profile of the seabed [Siderius, et al., J. Acoust. Soc. Am., 120, 1315-1323, (2006)]. Here the cross-correlation approach is extended to the location in range and bearing of a point target. An experiment was designed using floats and weights mounted (and dismounted) on the same cable as the vertical array. Careful measurements were made of the location of all likely floats, ballast weights, array terminations, and so on. After suitable coherent averaging, peaks were seen at delays (correlation offsets) agreeing with the reflector positions and were shown to be absent when reflectors were removed. An implication for geoacoustic inversion is that, in priciple, the technique can be used to explore scattering as well as reflection properties of layers. A simple extension of the theory developed in [Harrison and Siderius, J. Acoust. Soc. Am., (2007), accepted] is used to explain the amplitudes of the reflections. The approach differs from ″acoustic daylight″ principally in determining a target range.

8:20

3aAO2. Wide-area geoacoustic inversion using distant ship noise. Altan Turgut (Naval Research Laboratory, Acoustics Division, Code 7120, Washington, DC 20375, USA, altan.turgut@nrl.navy.mil)

Broadband (50-500 Hz) noise data from fast-traveling surface ships in the vicinity of a VLA and a bottomed HLA are used to estimate the geoacoustic properties on the New Jersey Shelf. Matched-field inversion of geometric and geoacoustic parameters are presented by using twenty days of ship noise data, collected during the RAGS03 winter experiment. Noise data from different ships at different ranges provided robust geoacoustic inversions for both VLA and bottomed HLA data. Acoustic propagation tracks are determined from the HLA beamforming results and a 3-D geoacoustic parameter map is constructed. The constructed geoacoustic parameter map shows good agreement with the results from chirp sonar inversion and acoustic probe measurements, indicating silty seafloor sediments on the outer-shelf area and sandy sediments on the inner-shelf area. Efficiency of the 3-D geoacoustic inversion and extension to range-dependent inversions at longer ranges are also discussed. [Work supported by ONR.]

8:40

3aAO3. Doppler Geo-Spectroscopy in the Makai Experiment. David R. Barclay (Marine Physical Lab, Scripps Institution of Oceanography, UCSD, 9500 Gilman Dr. M/C 0238, La Jolla, CA 92093-0238, USA, dbarclay@mpl.ucsd.edu), Michael Buckingham (Marine Physical Lab, Scripps Institution of Oceanography, UCSD, 9500 Gilman Dr. M/C 0238, La Jolla, CA 92093-0238, USA, mjb@mpl.ucsd.edu)

Using data collected during the 2005 Makai experiment, acoustic parameters of a coral-sand seabed were obtained using the Doppler spectroscopy inversion technique. A light aircraft was used as a low frequency (80 - 400 Hz) sound source over an isovelocity shallow water channel. A microphone near the ocean surface and a hydrophone near the seabed were used to record the Doppler spreading of each harmonic of the aircraft's engine and propeller. In the water column, spectral peaks with the greatest up and down Doppler shifts are associated with the shallow equivalent rays of normal modes. The least mean squares (LMS) adaptive filter was used to track and enhance the frequency of these propagating modes. The inversion relies on a full wave number spectral model of a moving source in

a three-layer waveguide. The Doppler shifted modes in the water column are observed in the data and simulated in the model. The comparison of the two, in symphony with the aircraft's signal in the air, returns the geoacoustic parameters of the seabed. The inversion was performed on numerous over-flights and the results were averaged to show statistical confidence. Work supported by ONR.

Contributed Papers

9:00

3aAO4. Geoacoustic inversion in the frequency range 0.8-1.6 kHz with drifting sparse arrays during MREA/BP'07 experiment. Jean-Claude Le Gac (NATO Undersea Research Center, Viale San Bartolomeo 400, 19126 La Spezia, Italy, legac@nurc.nato.int), Jean-Pierre Hermand (Université libre de Bruxelles (U.L.B.) - Environmental hydroacoustics lab, av. Franklin D. Roosevelt 50, CP 194/5, 1050 Bruxelles, Belgium, jhermand@ulb.ac.be), Sergio Jesus (ISR, Universidade do Algarve, PT-8005-139 Faro, Portugal, sjesus@ualg.pt)

In order to evaluate properly the acoustic propagation characteristics in shallow water environments, it is well established that appropriate knowledge of the acoustic properties of the seabottom is required. In the last decade, full-field geoacoustic inversion techniques have been demonstrated to provide adequate methodologies to assess those properties. However, several of the developed techniques may suffer a lack of adequacy to the design of low-frequency active sonar systems (LFAS) for which the assessment of seabottom characteristics are drawn. For instance most matched-field inversion techniques demonstrated so far use acoustical signals at much lower frequencies than those of the sonar. Furthermore, some of the techniques may be difficult to be handled in an ″operationally relevant context″ since they are based on relatively complex designed systems such as highly instrumented vertical line arrays spanning the whole water column. In this paper, we investigate the potential of medium-frequency acoustical signals (0 .8-1.6 kHz) received at several ranges on a field of drifting sparse arrays, eventually reduced to a couple of hydrophones, for spatially-coherent geoacoustic inversion purposes. The experimental datasets of the Maritime Rapid Environmental Assessment MREA/BP'07 sea trial south of Elba Island in the Mediterranean Sea are used to support this study.

9:20

3aAO5. Using offshore seismic surveys as acoustic sources of opportunity for geoacoustic inversion. Alec J. Duncan (Curtin University of Technology, Centre for Marine Sci & Tech, GPO Box U1987, 6845 Perth, WA, Australia, A.J.Duncan@curtin.edu.au), Alexander Gavrilov (Curtin University of Technology, Centre for Marine Sci & Tech, GPO Box U1987, 6845 Perth, WA, Australia, a.gavrilov@cmst.curtin.edu.au), Tao Hu (Institute of Acoustics, Chinese Academy of Science, PostBox 2712, NO.21, Bei-Si-huan-Xi Road, 100080 Beijing, China, hutao76@yahoo.com.cn)

Commercial offshore seismic surveys involve the use of powerful acoustic sources consisting of arrays of airguns. These sources produce frequent, loud, impulsive sounds at precisely timed intervals, at accurately known positions during surveys that may last for several months. By deploying a low-cost acoustic receiving system in the vicinity of such a survey scientists can acquire high quality data for geoacoustic inversion experiments in an extremely cost-effective manner. This paper discusses the various factors that must be considered when using such data for geoacoustic inversion, including the prediction of source spectra and array directionality, and provides some examples.

9:40-10:00 Break

10:00

3aAO6. Geo-acoustic inversion with adaptive beamformed data. Steven A. Stotts (Applied Research Laboratories/The University of Texas, 10000 Burnet Rd, Austin, TX 78758, USA, stotts@arlut.utexas.edu), Robert A. Koch (Applied Research Laboratories/The University of Texas, 10000 Burnet Rd, Austin, TX 78758, USA, koch@arlut.utexas.edu)

Geo-acoustic inversion with matched field replicas constructed by adaptive techniques lacks robustness, because localizations with such techniques are sensitive to model mismatch [Soares, Jesus, and Coelho, J. Acoust. Soc. Am. 122, 3391-3404 (2007)]. Instead of adapting the matched field weights, inversion with adaptive beam-formed (ABF) plane wave sub-aperture data produces accurate source localizations for ships of opportunity [Stotts and Hawkins, J. Acoust. Soc. Am. 118, 1857 (2005)]. Model inputs to the matched-field cost function are evaluated at sub-aperture phase centers in this approach. The main purpose of this talk is to demonstrate the robustness and accuracy of solutions obtained from geo-acoustic inversion using plane wave ABF data. Improvements over either single element or conventional plane wave beam-formed (CBF) sub-aperture data for geo-acoustic inversions and simultaneous geo-acoustic inversions/source localizations using a source of opportunity in real data containing interferers will be demonstrated.

10:20

3aAO7. Geoacoustic inversion with recreational boat noise. A. Vincent Van Leijen (Netherlands Defence Academy, P.O. Box 10 000, 1780 CA Den Helder, Netherlands, av.v.leijen@nlda.nl)

During the MREA07 sea trials various experiments involved geoacoustic inversion with sound sources of opportunity. A particular experiment that focussed on exploiting the self noise of autonomous vehicles suffered from interfering noise due to increased boating activity in the weekend. In this work the same data is re-examined to study the potential of recreational boats as sound sources for geoacoustic inversion. Even though recreational boats are non cooperative sound sources, in the sense that weekend traffic does not sail predefined tracks and navigational logging is absent, various boats swarm out and cover large areas thus acting as a distributed set of sound sources. A typical small boat signature counts numerous harmonics of narrowband tones that cover the frequency spectre from 100 Hz up to 2 kHz. With these tones matched field inversion and traditional Doppler techniques are used to find an initial geometry of the experiments and these results are fine tuned during the final geoacoustic inversion of a locally range-independent model of a coastal environment. Results of inversions with recreational boating sounds are shown to match with previous analysis results with self noise of autonomous vehicles, bottom grab samples and seismic data.

10:40

3aAO8. Geoacoustic uncertainties in matched-field inversions of ship-noise data. Dag Tollefsen (Norwegian Defence Research Establishment (FFI), Box 115, 3191 Horten, Norway, dag.tollefsen@ffi.no), Stan E. Dosso (University of Victoria, School of Earth and Ocean Sciences, Victoria, BC V8W 3P6, Canada, sdosso@uvic.ca)

This paper applies geoacoustic inversion to ship-noise data recorded on a horizontal array deployed on the seafloor in an experiment conducted by FFI in the Barents Sea. A Bayesian matched-field inversion method is employed which quantifies geoacoustic uncertainties and allows for quantitative comparisons of results from different data sets. Estimates of sediment parameters and their uncertainties were obtained by inversions of low-frequency narrowband data from a quiet research ship at source-array ranges of 1-6 km and different orientations with respect to the array, as well as from a merchant ship at ranges of 6-8 km. Multiple, independent data segments are included in the inversion and shown to significantly reduce geoacoustic parameter uncertainties. The effect of the state of prior information on the ship track (e.g., well known or unknown) on geoacoustic information content is also examined. Estimates of the sound-speed profile and density of sediment are compared with results from inversion of data from a towed controlled-source, and with reference values from other geophysical data collected in the area.

11:00

3aAO9. Optimal source tracking in an unknown ocean environment. Michael J. Wilmut (University of Victoria, School of Earth and Ocean Sciences, Victoria, BC V8W 3P6, Canada, mjwilmut@uvic.ca), Stan E. Dosso (University of Victoria, School of Earth and Ocean Sciences, Victoria, BC V8W 3P6, Canada, sdosso@uvic.ca)

This paper develops and compares two approaches to localizing and tracking a low-level acoustic source when ocean environmental properties are unknown. Both approaches are based on a Bayesian formulation in which source and environmental parameters are considered random variables constrained by noisy acoustic data and by prior information on parameter values (e.g., physical limits for water-column and seabed properties) and on inter-parameter relationships (e.g., limits on horizontal and vertical source speed). One approach is based on determining the source track and environmental parameters that maximize the posterior probability density (PPD) using adaptive hybrid optimization. A key to solving this challenging problem efficiently is that the Viterbi algorithm is applied to compute the highest-probability source track for each environmental realization considered in the optimization-this provides the optimal track while requiring the optimization is applied only to environmental parameters. The second approach involves integrating the PPD over unknown environmental parameters to represent source-track information as a series of joint marginal probability surfaces over range and depth. The Viterbi algorithm is applied to extract the optimal track from these surfaces. For realistic environmental models (e.g., more than a dozen unknown parameters), the integration is carried out using efficient Markov-chain Monte Carlo methods.

WEDNESDAY MORNING, 2 JULY 2008 ROOM 352B, 8:00 TO 10:40 A.M.

Session 3aBBa

Biomedical Ultrasound/Bioresponse to Vibration and Physical Acoustics: Shock Waves in Medicine

Robin O. Cleveland, Cochair
Boston University, Dept. of Aerosp. and Mech. Eng., 110 Cummington St., Boston, MA 02215, USA

Oleg A. Sapozhnikov, Cochair
Center for Industrial and Medical Ultrasound, Applied Physics Lab., University of Washington, 1013 NE 40th St., Seattle, WA 98105, USA

Invited Paper

8:00

3aBBa1. Short- and long-delay tandem shock waves for application in medicine. Achim M. Loske (Universidad Nacional Autónoma de México, Centro de Física Aplicada y Tecnología Avanzada, AP 1-1010, 76000 Querétaro, Mexico, loske@fata.unam.mx), Francisco Fernandez (Universidad Nacional Autónoma de México, Centro de Física Aplicada y Tecnología Avanzada, AP 1-1010, 76000 Querétaro, Mexico, francisco@fata.unam.mx), Miguel De Icaza (Universidad Nacional Autónoma de México, Centro de Física Aplicada y Tecnología Avanzada, AP 1-1010, 76000 Querétaro, Mexico, icaza@fata.unam.mx), Guillermo Canseco (Universidad Nacional Autónoma de México, Centro de Física Aplicada y Tecnología Avanzada, AP 1-1010, 76000 Querétaro, Mexico, gcanseco@fata.unam.mx)

Long-delay tandem shock waves with an inter-pulse delay between about 200 and 500 microseconds have shown to enhance fragmentation of artificial kidney stones during in vitro and in vivo extracorporeal shock wave lithotripsy (SWL) in the past. Cell-permeabilization and inactivation of bacteria using tandem shock waves have also been proposed. The purpose of this research was to study the influence of short-delay (less than 50 microseconds) tandem shock waves on cavitation induced damage to kidney stones during SWL. A multipurpose piezoelectric shock wave generator was designed to generate shock waves at variable delays. The effect of short- and long-delay dual-pulse shock waves on the surface of artificial kidney stones was evaluated by microscopy. An adequate selection of delays was possible by means of a numerical model and high speed photography. Stone fragmentation was compared to that of standard (single-pulse) shock waves. Our results indicate that specific combinations of short- and long-delay tandem shock waves could improve damage to kidney stones by acoustic cavitation.

8:20

3aBBa2. Correlation of vasoconstriction and kidney protection during shock wave lithotripsy. Michael R. Bailey (Center for Industrial and Medical Ultrasound, Applied Physics Lab., University of Washington, 1013 NE 40th St., Seattle, WA 98105, USA, bailey@apl.washington.edu), Marla Paun (Center for Industrial and Medical Ultrasound, Applied Physics Lab., University of Washington, 1013 NE 40th St., Seattle, WA 98105, USA, paun@u.washington.edu), Rajash K. Handa (Department of Anatomy and Cell Biology, Indiana University School of Medicine, 635 Barnhill Dr. MS5055, Indianapolis, IN 46202, USA, rhanda@iupui.edu), Sujuan Gao (Department of Medicine, Division of Biostatistics, Indiana University School of Medicine, 410 West 10th Street, Suite 3000, Indianapolis, IN 46202, USA, sgao@iupui.edu), Lynn R. Willis (Department of Pharmacology, Indiana University School of Medicine, 635 Barnhill Dr. MS5055, Indianapolis, IN 46202, USA, willisl@iupui.edu), Bret A. Connors (Department of Anatomy and Cell Biology, Indiana University School of Medicine, 635 Barnhill Dr. MS5055, Indianapolis, IN 46202, USA, connors@anatomy.iupui.edu), James A. McAteer (Department of Anatomy and Cell Biology, Indiana University School of Medicine, 635 Barnhill Dr. MS5055, Indianapolis, IN 46202, USA, mcateer @anatomy.iupui.edu), Andrew P. Evan (Department of Anatomy and Cell Biology, Indiana University School of Medicine, 635 Barnhill Dr. MS5055, Indianapolis, IN 46202, USA, aevan@iupui.edu)

Kidney injury in lithotripsy can lead to long-term adverse effects, so minimizing injury is beneficial. We have found that injury is significantly reduced when shock wave (SW) administration is halted briefly- 3-minutes-early in treatment. Previous studies have shown that SWs stimulate renal blood vessels to constrict. Therefore, we tested the idea that vasoconstriction mediates SW-induced protection of the kidney. Doppler ultrasound was used to measure resistive index (RI), a ratio of systolic and diastolic velocities, indicating vasoconstriction. RI was determined for single intralobar arteries in targeted porcine kidneys treated by standard versus protection protocols (2,000SW, uninterrupted vs 500SW-3-min pause-2,000SW) using a Dornier-HM3 lithotripter (2Hz, 24kV). Significant differences in RI from baseline within a group and between groups at various time points were determined using mixed-effect models for repeated measures with Holm's step-down method for multiple comparison adjustment. All animals had similar baselines. Sham pigs (no-SWs) showed no significant change in RI. The protection protocol produced a significant rise ($p<0.05$, $n=8$) in RI 15 minutes into treatment, while the standard protocol did not yield a significant rise ($p<0.05$, $n=7$) until 45 minutes after treatment. Thus, the treatment protocol shown to protect against injury, induces early vasoconstriction. [NIH-DK43881, NSBRI-SMS00402]

8:40

3aBBa3. Fundamental study of shock induced acceleration of cell growth by plane shock waves. Masaaki Tamagawa (Kyushu Institute of Technology, Hibikino 2-4, Wakamatsu-ku, 808-0196 Kitakyushu, Japan, tama@life.kyutech.ac.jp)

This paper describes effects of shock waves on cells to certificate the angiogenesis by shock wave in the clinical application. Especially, the effects of plane shock waves without cavitation bubbles on the endothelial cells are investigated by experiments and computation. In the experiments, the plane shock waves using shock tube apparatus are applied to the endothelial cells. The peak pressure working on the cells in the test case is 0.4 MPa, which is under disintegration level for endothelial cells. After working shock waves on suspended cell, the disintegration and growth rate are measured. It is found that the initial growth rate of the shock-worked cells are clearly higher than that of control ones. As for the effect of rise time of working shock waves, to change the rise time of shock wave, Air and He gas are used as driver gas in the shock tube. As a result, the shorter rise time brings higher growth rate. In the computation, to check the effects of rise time on the pressure and stress distribution on the cells, fluid and structural interaction model are analyzed. The result shows that shorter rise time makes high stress level distribution on the cell membrane.

9:00

3aBBa4. Beamwidth measurement of single lithotripter shock waves. Wayne Kreider (Center for Industrial and Medical Ultrasound, Applied Physics Lab., University of Washington, 1013 NE 40th St., Seattle, WA 98105, USA, wkreider@u.washington.edu), Michael R. Bailey (Center for Industrial and Medical Ultrasound, Applied Physics Lab., University of Washington, 1013 NE 40th St., Seattle, WA 98105, USA, bailey@apl.washington.edu), Jeffrey A. Ketterling (Frederic L. Lizzi Center for Biomedical Engineering, Riverside Research Institute, 156 William St., New York, NY 10038, USA, ketterling@rrinyc.org)

New lithotripters with narrower foci and higher peak pressures than the original Dornier HM3 electrohydraulic lithotripter have proven to be less effective and less safe. Hence, accurate measurements of the focal characteristics of lithotripter shock waves are important. The current technique for measuring beamwidth requires collection of single-point measurements over multiple shock waves, thereby introducing error as a result of any shock-to-shock variability. This work reports on the construction of a hydrophone array sensor and on array measurements of individual lithotripter shock waves. Beamwidths for an electrohydraulic lithotripter with a broad-focus, HM3-style reflector and a narrow-focus, modified reflector were measured using both new and worn electrodes as well as two different electrical charging potentials. The array measured the waveform, beamwidth, and focal location of individual shock waves. The HM3-style reflector produced repeatable focal waveforms and beam profiles at an 18-kV charging potential with both new and worn electrodes. Accordingly, these measurements agreed with averaged point measurements acquired under the same conditions. However, a lack of consistency in the measured focal locations and beam profiles at 23 kV underscores the value in obtaining beam profile measurements from individual shock waves. Work supported by Riverside Research Institute, NIH DK43881, and NSBRI SMS00402.

9:20

3aBBa5. Numerical simulation of shock wave generation and focusing in shock wave lithotripsy. Jeffrey Krimmel (California Institute of Technology, 1200 E. California Blvd, Pasadena, CA 91125, USA, jkrimmel @caltech.edu), Tim Colonius (California Institute of Technology, 1200 E. California Blvd, Pasadena, CA 91125, USA, colonius@caltech.edu)

Shock wave lithotripsy is a procedure where focused shock waves are fired at kidney stones in order to pulverize them. Lithotripters with different source mechanisms and reflector shapes (or lenses) are in clinical use, but prediction of focal region pressure is made difficult by nonlinearity and cavitation. We report on development of a numerical simulation framework aimed at accurate prediction of focal region pressures and bubble dynamics. Shock wave generation and beam focusing are simulated via the Euler equations with MUSCL-type shock-capturing scheme and adaptive mesh refinement (AMR). Electrohydraulic, electromagnetic, and piezoelectric-array lithotripters are modeled with axisymmetric geometries. In the electrohydraulic case, an expanding bubble model simulates spark firing. In the piezoelectric case, a boundary condition prescribing the motion of individual elements is used. Calculated peak pressures and pulse widths agree well with experimental data for the electrohydraulic and electromagnetic lithotripters. For the piezoelectric case, peak pressures are increasingly overpredicted by the model when more elements are fired, and reasons for this discrepancy will be discussed. Finally, we compare the spatial and temporal characteristics of the focal pressure fields for several clinical lithotripters in the context of observed stone comminution efficacy and tissue damage. This work is supported by NIH grant PO1 DK043881 and ONR Grant N00014-06-1-0730.

9:40

3aBBa6. Effect of elastic waves in the metal reflector on bubble dynamics at the focus of an electrohydraulic lithotripter. Oleg A. Sapozhnikov (Center for Industrial and Medical Ultrasound, Applied Physics Lab., University of Washington, 1013 NE 40th St., Seattle, WA 98105,

USA, oleg@acs366.phys.msu.ru),Wayne Kreider(Center for Industrial and Medical Ultrasound, Applied Physics Lab., University of Washington, 1013 NE 40th St., Seattle, WA 98105, USA, wkreider@u.washington.edu), Michael R. Bailey (Center for Industrial and Medical Ultrasound, Applied Physics Lab., University of Washington, 1013 NE 40th St., Seattle, WA 98105, USA, bailey@apl.washington.edu), Vera A. Khokhlova (Center for Industrial and Medical Ultrasound, Applied Physics Lab., University of Washington, 1013 NE 40th St., Seattle, WA 98105, USA, vera@acs366.phys.msu.ru), Francesco Curra (Center for Industrial and Medical Ultrasound, Applied Physics Lab., University of Washington, 1013 NE 40th St., Seattle, WA 98105, USA, fcurra@apl.washington.edu)

In extracorporeal electrohydraulic lithotripters, a hemi-ellipsoidal metal reflector is used to focus a spherical wave generated by an electrical discharge. The spark source is positioned at one of the ellipsoid foci (F1); this makes the reflected wave focused at the other focus (F2). Despite the common assumption that the reflector behaves as a rigid mirror, the true reflection phenomenon includes the generation and reverberation of elastic waves in the reflector, which reradiate to the medium. Although these waves are much lower in amplitude than the specularly reflected wave, they may influence cavitation at F2. To explore such effects, waves in water and a brass reflector were modeled in finite differences based on the linearized equations of elasticity. The bubble response was simulated based on a Rayleigh-type equation for the bubble radius. In addition, the role of acoustic nonlinearity was estimated by numerical modeling. It is shown that the elastic waves in the reflector give rise to a long ″ringing″ tail, which results in nonmonotonic behavior of the bubble radius during its inertial growth after shock wave passage. This numerical result is qualitatively confirmed by experimental observations of bubble behavior using high-speed photography. Work supported by NIH-DK43881, NSBRI-SMS00402, NIH-DK075090, and RFBR.

10:00

3aBBa7. Elastic waves in human kidney stones: Shear dominates spall in shock wave lithotripsy. Robin O. Cleveland (Boston University, Dept. of Aerosp. and Mech. Eng., 110 Cummington St., Boston, MA 02215, USA, robinc@bu.edu), Haibiao Luo (Boston University, Dept. of Aerosp. and Mech. Eng., 110 Cummington St., Boston, MA 02215, USA, hluo@bu.edu), James C. Williams (Indiana Univ. School of Medicine, 635 Barnhill Dr, Indianapolis, IN 46202, USA, williams@anatomy.iupui.edu)

We investigated the role of shear waves and spall in the fragmentation of human kidney stones. Seven human kidney stones, approximately 5 mm in diameter, were scanned with micro computed tomography to obtain a 3D representation that was imported into an elastic wave code. The code was initialized with a lithotripsy waveform and the evolution of stresses and strains was tracked through space and time. The evolution of the principal stress indicated that reflection from the distal surface of the stone (spallation) did not induce large tensile stresses ($<$40 MPa) due to the curved geometry of the proximal and distal surfaces. Instead as the shock wave in the fluid passed the mid-section of the stone there was efficient coupling into shear waves which then propagated into the interior of the stone and generated the largest regions of high tensile stress ($>$60 MPa). The results indicate that for the human stones studied here shear waves generated at the stone periphery are more important than spall in generating high tensile stress. These data suggest that the focal width of a lithotripter needs to be larger than the stone in order to generate large stresses. [Work supported by NIH DK43881 and DK59933].

10:20

3aBBa8. Damage potential of single-bubble collapse in shockwave lithotripsy. Eric Johnsen (California Institute of Technology, 1200 E. California Blvd, Pasadena, CA 91125, USA, johnsen@stanford.edu), Tim Colonius (California Institute of Technology, 1200 E. California Blvd, Pasadena, CA 91125, USA, colonius@caltech.edu)

In shockwave lithotripsy, the combined effect of focused shockwaves and cavitation pulverizes kidney stones. Although cavitation is known to play an important role in stone comminution, the underlying mechanism is not fully understood. The goal of the present study is to quantify the potential damage caused by Rayleigh collapse (RC) and shock-induced collapse (SIC) of a single bubble near a stone. A high-order accurate, quasi-conservative, shock- and interface-capturing scheme [E. Johnsen and T. Colonius, J. Comput. Phys. 2006] is employed to simulate both phenomena. A high-speed re-entrant jet forms during the collapse and hits the distal side of the bubble, thereby generating a water-hammer pressure wave. A high pressure is measured along the stone surface upon the impact of this wave, thus providing potential for erosion. In SIC, this pressure may reach 1 GPa and bubbles within approximately 15 initial radii generate a pressure higher than the incoming pulse. In addition, by using the present results as time-dependent boundary conditions for an elastic wave propagation code, it is shown that a tension large enough to lead to failure may be achieved within small stones or fragments. This work is supported by NIH grant PO1 DK043881 and ONR Grant N00014-06-1-0730.

Session 3aBBb

Biomedical Ultrasound/Bioresponse to Vibration and Physical Acoustics: Light and Sound for Medical Imaging and Therapy I

Ronald A. Roy, Cochair
Boston University, Dept. of Aerosp. and Mech. Eng., 110 Cummington St., Boston, MA 02215, USA

Emmanuel Bossy, Cochair
Laboratoire Photons et Matière, ESPCI/CNRS, 10 rue Vauquelin, Paris Cedex 05, 75231, France

Invited Papers

11:00

3aBBb1. Photoacoustic imaging for characterising the structure and function of vascular networks. Paul C. Beard (University College London, Gower Street, London, WC1E 6BT London, UK, pbeard@medphys.ucl.ac.uk)

Photoacoustic imaging is a new non invasive soft tissue imaging method in which low energy nanosecond pulses of visible or near infrared (NIR) laser light are used to excite subsurface ultrasound waves. The distinguishing advantage of the technique is that provides the high contrast and spectroscopic based specificity of optical techniques along with the high spatial resolution of ultrasound. Haemoglobin represents the most important source of naturally occurring photoacoustic contrast due its relatively strong optical absorption in the visible and NIR making the technique particularly well suited to imaging blood vessels. In addition, functional information can be provided by obtaining images at multiple wavelengths and applying a spectroscopic analysis to quantify the concentrations of endogenous chromophores such as oxy and deoxyhaemoglobin. These attributes make the technique well suited to studying a wide range of tissue abnormalities such as tumours and other pathologies characterised by changes in the structure and oxygenation status of the vasculature. A novel optical ultrasound imaging system has been developed and used to obtain 3D images of the superficial vascular anatomy of the mouse brain, skin and implanted tumours and demonstrate the spectroscopic capability of the technique.

11:20

3aBBb2. The role of ultrasound and photoacoustic imaging in laser therapy of cancer. Stanislav Y. Emelianov (Applied Research Laboratories, The University of Texas, P.O. Box 8029, Austin, TX 78713-8029, USA, emelian@mail.utexas.edu)

Laser therapy is an alternative cancer treatment approach when traditional surgery cannot be used to remove small, poorly defined lesions embedded within vital organs. For example, in photothermal laser therapy, a localized temperature increase to cause tumor necrosis is achieved by using a continuous wave laser and molecular targeted and optically tuned photoabsorbers. However, for laser therapy to be successful, it is necessary to identify the presence of photoabsorbers in the tumor prior to therapy, to monitor the spatio-temporal temperature changes during therapy, and, finally, to identify thermal/mechanical damage and tumor destruction after therapy. To guide laser therapy, we developed a combined ultrasound/photoacoustic imaging system and bioconjugated nanoabsorbers. In our approach, ultrasound imaging is utilized to identify the anatomy of the tumor while photoacoustic imaging is used to ensure the presence of targeted nanoparticles before therapy. Both ultrasound and photoacoustic imaging techniques are then used to monitor temperature during therapy, ensuring tumor necrosis and protection of the surrounding healthy tissue. Finally, ultrasound and elasticity imaging is used to confirm thermal damage and cancer destruction. The results of our studies indicate that photoacoustic and ultrasound imaging can be used to effectively guide laser therapy.

11:40

3aBBb3. Photoacoustic cancer imaging. Wiendelt Steenbergen (University of Twente /Institute for Biomedical Technology, PO Box 217, NL-7500 AE Enschede, Netherlands, w.steenbergen@utwente.nl)

Photoacoustics, or optoacoustics, involves ultrasound imaging based on ultrasound generated by absorption of light by tissue chromophores such as blood and melanin. Ultrasound is generated when pulsed or intensity modulated light is used which locally deposits a sufficient amount of energy in a sufficiently short time to cause an efficient generation of internal stress in the tissue. When this stress relaxes, an ultrasound wave is emitted which can be detected at the surface of the tissue. On the basis of these ultrasound waves, a threedimensional image the internal distribution of absorption can be constructed. We will discuss various technical implementations of the technique, and will illustrate various medical applications. A particularly important application field is oncology: in cancer, the presence of blood vessels is essential for the tumor to grow and spread. We will show results of photoacoustic imaging performed on small animals with implanted tumors. It appears, that measurement speed is a key issue in obtaining images with sufficient quality. Furthermore, we will show results obtained with our photoacoustic mammoscope on patients with breast cancer.

12:00

3aBBb4. Theory and applications of frequency domain photoacoustic microscopy. Todd W. Murray (Boston University, 110 Cummington Street, Aerospace and Mechanical Engineering, Boston, MA 02215, USA, twmurray@bu.edu), Suraj Bramhavar (Boston University, 110 Cummington Street, Aerospace and Mechanical Engineering, Boston, MA 02215, USA, suraj10@bu.edu), Ashwin Sampathkumar (Boston University, 110 Cummington Street, Aerospace and Mechanical Engineering, Boston, MA 02215, USA, suraj10@bu.edu), Bruno Pouet (Bossa Nova Technologies, 606 Venice Boulevard, Venice, CA 90291, USA, Bpouet@BossaNovaTech.com)

In frequency domain photoacoustic microscopy, the pulsed laser source used for ultrasound excitation in conventional photoacoustic imaging is replaced by a low power, amplitude modulated laser source. The acoustic signals are detected using an interferometer or contact transducer, coupled to a RF lock-in amplifier or vector network analyzer. The detection bandwidth reduction afforded by this technique allows for a significant improvement in signal-to-noise ratio (SNR) over systems using pulsed laser excitation. In this paper, the method of frequency domain photoacoustic microscopy is reviewed and compared to the pulsed-laser based approach. Methods for processing the frequency domain data to extract the information of interest are discussed, along with the effects of measurement bandwidth and frequency resolution. A new technique to optically downshift acoustic signals detected using an optical interferometer to a fixed intermediate frequency is presented, which allows for the detection of high frequency (100's of MHz- GHz) acoustic signals using low frequency, low cost detection electronics. Several applications of frequency domain photoacoustic microscopy are presented including the inspection of thin films and environmental barrier coatings and the photothermal operation of nano-electro-mechanical systems. Finally, potential applications of this technique for the characterization of biological media are discussed.

Contributed Papers

12:20

3aBBb5. Photoacoustic microscopy for high-resolution imaging. Wolfgang Bost (Fraunhofer IBMT, Ensheimer Strasse 48, 66386 Sankt Ingbert, Germany, wolfgang.bost@ibmt.fhg.de), Robert M. Lemor (Fraunhofer IBMT, Ensheimer Strasse 48, 66386 Sankt Ingbert, Germany, robert.lemor@ibmt.fhg.de)

Photoacoustics is a hybrid technology based on the photoacoustic effect that detects absorbed photons ultrasonically. Photoacoustic imaging combines ultrasonic resolution with high contrast due to light absorption depending on the physiology of the examined biological tissue. The resolution of conventional systems is not sufficient for in-vitro measurements of small tissue samples or individual cells. In this work, we present a high-resolution photoacoustic microscopy platform based on the SASAM acoustic microscope that allows high resolution imaging on living cells. The system based on an inverted optical microscope consists of a laser source for optical multi wavelength excitation (diode- and solid-state-laser) which emits nanosecond laser pulses with a wavelength in the near infrared spectrum (optical window). It allows the usage of different ultrasound transducers in the frequency range up to 300MHz. In addition to the photoacoustic imaging mode, all common optical modalities are implemented. Pure acoustic imaging mode is used for reference imaging. The developed photoacoustic microscopy platform is a system for high-quality volumetric imaging in different scanning modes. 3D offline reconstruction is possible based on the presented 2D imaging. The system was characterized by in-vitro measurements with a lateral resolution better than 100μm in the confocal mode.

12:40

3aBBb6. Acoustic signals from gold nanoparticles irradiated with pulsed lasers. Constantin Ungureanu (Faculty of Science and Technology (TNW), Biophysical Engineering Group (BPE), Twente University, 7500AE Enschede, Netherlands, c.ungureanu@tnw.utwente.nl), Tamara Van Weperen (University Twente, Building Meander, 7500 AE Enschede, Netherlands, t.m.vanweperen@student.utwente.nl), Jeroen Sijl (Physics of Fluids, University of Twente, P.O. Box 217, 7500 AE Enschede, Netherlands, j.sijl@utwente.nl), Raja Rayavarapu (Faculty of Science and Technology (TNW), Biophysical Engineering Group (BPE), Twente University, 7500AE Enschede, Netherlands, R.Rayavarapu@tnw.utwente.nl), Srirang Manohar (University of Twente, Biophysical Engineering Group (BPE), Faculty of Science and Engineering (TNW), P.O. Box 217, 7500 AE Enschede, Netherlands, s.manohar@tnw.utwente.nl), Michel Versluis (Physics of Fluids, University of Twente, P.O. Box 217, 7500 AE Enschede, Netherlands, m.versluis@utwente.nl), Ton G. Van Leeuwen (Univ. of Twente, P.O. Box 217, 7500 AE Enschede, Netherlands, a.g.j.m.vanleeuwen@tnw.utwente.nl)

Photoacoustic imaging is a new imaging technique, which enables imaging of living tissue with high resolution. The technique analyses ultrasound pulses generated when absorbing structures in tissue are irradiated with pulsed light. Due to the phenomenon of plasmon resonance gold nanoparticles possess high optical absorption coefficients which makes them potential contrast agents in photoacoustics. Further, the heat generated around these particles when irradiated with pulsed light can lead to nonlinear effects including bubble formation. The acoustic signals produced by gold nanoparticles in the linear thermoelastic and non-linear regimes are expected to have specific acoustic signatures. In this study, we investigate the acoustic signals generated by two sets of gold spheres having 25 nm and 60 nm diameter irradiated by laser pulses with increasing incident fluence rates. We identify and discuss the differences in acoustic signals belonging to the thermoelastic expansion regime and the non-linear regime. Finally, the experimental results are compared with different theoretical models available in literature.

1:00-1:40 Lunch Break

Invited Papers

1:40

3aBBb7. Imaging tissue and wavefront control: Application to acousto-optics and photoacoustics. François Ramaz (Laboratoire Photons et Matière, ESPCI/CNRS, 10 rue Vauquelin, 75231 Paris Cedex 05, France, francois.ramaz@espci.fr), Emmanuel Bossy (Laboratoire Photons et Matière, ESPCI/CNRS, 10 rue Vauquelin, 75231 Paris Cedex 05, France, emmanuel.bossy@espci.fr), Vincent Loriette (Laboratoire Photons et Matière, ESPCI/CNRS, 10 rue Vauquelin, 75231 Paris Cedex05, France, vincent.loriette@espci.fr), Sylvain Gigan (Laboratoire Photons et Matière, ESPCI/CNRS, 10 rue Vauquelin, 75231 Paris Cedex 05, France, sylvain.gigan@espci.fr), Albert-Claude Boccara (Laboratoire Photons et Matière, ESPCI/CNRS, 10 rue Vauquelin, 75231 Paris Cedex 05, France, boccara@optique.espci.fr)

Although optical waves do not exhibit the same ability to be manipulated as e.g. electromagnetic waves up to a few GHz or acoustic waves, for which field emitters-detectors are available, various tools are nevertheless available in the optical domain which open the path to tricks which can be used in the context of sound-light detection. In the purely optical domain, one knows the impact of deformable mirrors led to adaptive optics which is now coupled to OCT for retinal examination. Real time holography leads to complex wavefront synthesis and are useful in acousto-optics (AO) to monitor very complex speckle field distributions. Phase conjugation which is in certain conditions equivalent to time reversal, starts to be used for wavefront retrieval after propagation in turbid media, one can think to use it for AO signal monitoring; moreover matrices of spatial light modulators allow to control light not only spatially but also in the frequency domain and open the field to new astonishing experiments. We will discuss a few applications and perspectives offered by these new devices to the field of biomedical imaging.

2:00

3aBBb8. Optoacoustics for biomedical sensing, monitoring, and imaging. Rinat O. Esenaliev (University of Texas Medical Branch, 301 University Blvd., Galveston, TX 77555-0456, USA, riesenal@utmb.edu)

Optoacoustics can provide diagnostic information with high optical contrast and ultrasound resolution. It is based on detection of broadband ultrasound induced by short optical pulses and utilizes absorption contrast in tissues. We proposed and developed sensing, monitoring, and imaging optoacoustic systems for in a variety of biomedical applications including pulsed laser tissue ablation, accurate measurement of tissue optical properties, tumor detection, monitoring of tissue hyperthermia, coagulation, freezing, and important blood parameters such as oxygenation and hemoglobin concentration. Recently, we built a novel, portable, multi-wavelength optoacoustic system which includes optical parametric oscillator operating in the range from 680 to 2400 nm and sensitive, broadband optoacoustic probes developed in our laboratory. We tested the system performance in animal and clinical studies. We monitored continuously and in real time cerebral blood oxygenation and total hemoglobin concentration. Direct probing of blood vessels with high contrast and resolution allowed for monitoring of these parameters with accuracy approaching that of the standard invasive techniques. Results on other important clinical applications of the optoacoustic technique will be presented as well.

Contributed Papers

2:20

3aBBb9. Photoacoustic tomography with a single detector in a reverberant cavity. Ben Cox (University College London, Gower Street, London, WC1E 6BT London, UK, bencox@mpb.ucl.ac.uk), Paul C. Beard (University College London, Gower Street, London, WC1E 6BT London, UK, pbeard@medphys.ucl.ac.uk)

In biomedical photoacoustic tomography (PAT), acoustic pulses, generated by the absorption of pulses of near-infrared light, are recorded on an array of ultrasound detectors, and the measured pressure time series are subsequently transformed into an image of the absorbed optical energy density within the tissue. For high resolution imaging, large-area detector arrays with a high density of sensitive, small elements are required. Such arrays can be expensive, so reverberant-field PAT is proposed as a means of obtaining PAT images using smaller arrays or even a single detector. By recording the reflections from a reverberant cavity surrounding the detector(s), in addition to the primary acoustic waves, sufficient information can be captured to allow a PAT image to be reconstructed, without the requirement for a large-area array. Image reconstruction, time reversal, non-uniqueness, and related ideas in quantum chaos will be discussed.

2:40

3aBBb10. Detection of elastic and optical contrasts in tissue mimicking phantoms based on the interaction of coherent laser light and transient displacements caused by the acoustic radiation force. Khalid Daoudi (Laboratoire Photons et Matière, ESPCI/CNRS, 10 rue Vauquelin, 75231 Paris Cedex 05, France, khalid.daoudi@espci.fr), Emmanuel Bossy (Laboratoire Photons et Matière, ESPCI/CNRS, 10 rue Vauquelin, 75231 Paris Cedex 05, France, emmanuel.bossy@espci.fr), Mickael Tanter (Laboratoire Ondes et Acoustique, ESPCI, Université Paris 7, CNRS, 10 rue Vauquelin, 75005 Paris, France, michael.tanter@espci.fr),Mathias Fink(Laboratoire Ondes et Acoustique, ESPCI, Université Paris 7, CNRS, 10 rue Vauquelin, 75005 Paris, France, mathias.fink@espci.fr), Albert-Claude Boccara (Laboratoire Photons et Matière, ESPCI/CNRS, 10 rue Vauquelin, 75231 Paris Cedex 05, France, boccara@optique.espci.fr)

We recently demonstrated experimentally the possibility to optically detect transient perturbations generated by the acoustic radiation force, applied several centimetres deep in a tissue-mimicking phantom [Bossy *et al*., APL **90**(17), 2007]. We proposed a detection scheme based on the transient decorrelation (millisecond time scale) of optical speckle patterns formed by coherent laser light that propagates through the phantom during the application of the radiation force. We demonstrated that this approach allows to detect optical contrasts embedded several centimetres deep in the phantom, based on the time-evolution of the correlation coefficient during the transient motion of the medium. In the present work, we demonstrate that this approach also allows the detection of shear mechanical contrast. Moreover, the shape of the observed decorrelation curve provides a way to discriminate between an optical contrast and a shear mechanical contrast. We are now currently investigating the feasibility of detecting with spatial resolution the propagation of a shear wave, based on its effect on localized acousto-optic interaction.

3:00

3aBBb11. Hybrid photoacoustic - ultrasound transmission parameter imaging in a miniature photoacoustic imager. Srirang Manohar (University of Twente, Biophysical Engineering Group (BPE), Faculty of Science and Engineering (TNW), P.O. Box 217, 7500 AE Enschede, Netherlands, s.manohar@tnw.utwente.nl), Rene G.

Willemink(University of Twente, Signals and Systems Group (SaS), Faculty of Electrical Engineering, Mathematics and Computer Sciences (EWI), P.O. Box 217, 7500AE Enschede, Netherlands, G.H.Willemink@utwente.nl), Johan C. Van Hespen (University of Twente, Biophysical Engineering Group (BPE), Faculty of Science and Engineering (TNW), P.O. Box 217, 7500 AE Enschede, Netherlands, J.C.G.vanhespen@utwente.nl), Ton G. Van Leeuwen (Univ. of Twente, P.O. Box 217, 7500 AE Enschede, Netherlands, a.g.j.m.vanleeuwen@tnw.utwente.nl)

Photoacoustic imaging is based on detecting laser pulse induced ultrasound transients from absorbing structures in tissue. The technique combines the advantages of a high optical absorption exhibited by tumors for example with the high resolution possible with ultrasound. A conventional photoacoustic imager operating in a CT geometry comprises a light source, an ultrasound detector array and a coupling medium usually water between the subject under investigation and detector. The imaging protocol usually consists of obtaining projections at angles around the subject. Recently we reported a method of measuring the local speed-of-sound variations by the addition of an absorber to the conventional imager, arranged between the light source and subject. This generates an ultrasound signal which interacts with the subject which can then be detected at the far-end by the detector. This allows the measurement of the integrated speed-of-sound (SOS) at projections around the subject leading to the formation of SOS images. In this article we discuss further analysis of the ultrasound obtained at projections to obtain images of the acoustic attenuation as well. In addition conventional photoacoustic images of the subject are also formed. The principle is demonstrated on well-characterized phantoms and we discuss the potential applications of this technique.

Session 3aEAa

Engineering Acoustics and Signal Processing in Acoustics: Transducers and Signal Processing for the Oil and Gas Industry I

Fernando Garcìa-Osuna, Cochair
Schlumberger, Sugar Land, TX, USA

Benoit Froelich, Cochair
Etudes et Productions Schlumberger, 1, rue Becquerel, BP 202, Clamart, 92142, France

Contributed Paper

8:00

3aEAa1. Sonic gas analyzer for hydrogen and methane. Steven Garrett (Penn State, Applied Research Laboratory, PO Box 30, State College, PA 16804, USA, sxg185@psu.edu)

In the late-1800s, Germans used a ″methane whistle″, known as a *Schlagwetterpfeife*, to determine the presence of hydrogen or methane in the air that was circulated in mines. This paper describes a modern version of that concept that should be suitable for safety-related applications in mines, sewers, garages that shelter hydrogen or methane-powered vehicles, etc. A compact, self-resonant standing wave tube, 2 cm in diameter and 3 cm long, is capped at both ends by two small electrodynamic speakers. The cylindrical copper resonator has two slits at the mid-plane to allow a 25 mm fan to continuously sample the air which is brought to the resonator's temperature after being drawn along the outside of the resonator body. Variation in the resonator's temperature is compensated electronically by an integrated-circuit temperature sensor that produces one microampere per Kelvin. The sensor can measure the concentration of hydrogen to an accuracy of better than ± 30 ppm or methane to $\pm 0.02\%$ in air using phase-locked loop frequency tracking electronics and a voltage-controlled oscillator. Concentration data will be presented for several different gas mixtures and will be compared to concentrations determined by other techniques (*e.g.*, thermal conductivity gauges).

Invited Papers

8:20

3aEAa2. Cylindrical ultrasonic array for borehole applications. Kenneth Liang (Schlumberger-Doll Research, One Hampshire Street, Cambridge, MA 01775, USA, kliang@boston.oilfield.slb.com), Gérard Fleury (Imasonic, 15 rue Alain Savary, 25000 Besançon, France, Gerard.Fleury@imasonic.com), Benoit Froelich (Etudes et Productions Schlumberger, 1, rue Becquerel, BP 202, 92142 Clamart, France, bfroelich@clamart.oilfield.slb.com), Jean-Luc Guey (Imasonic, 15 rue Alain Savary, 25000 Besançon, France, jean-luc.guey@imasonic.com), Pascal Schoeb (Statice Etudes & Developpement, 9, rue Thomas Edison, 25000 Besançon, France, p.schoeb@statice.com)

A cylindrical ultrasonic array has been developed for operating environments that can reach extremes of 175 C and 20,000 psi. The array is a key component of the PharUSIT* (Phased Array Ultrasonic Transducer for Inspection of Tubing), a research demonstrator developed for borehole applications. The full array consists of 800 elements (10 rings of 80 elements each) and can provide a whole range of beam-forming versatilities and capabilities in 3-D, such as variable focusing, beam steering, electronic scanning, etc, all accomplished without mechanical movements. Special piezo-composites have been developed for the transduction layer, and new polymeric composites have been formulated for the backing material. The center frequency was chosen to be about 500 kHz to accommodate attenuation of the propagation media. A novel technique utilizing custom flexible circuit provides electrical connections between the array and the front-end electronics. Special fabrication processes have been developed to construct the array in a cylindrical geometry. A customized testing protocol has been implemented to demonstrate the survivability of the array technology and to evaluate

the performance characteristics of individual elements under high-temperature/high-pressure conditions. The unique experimental setup will be presented. Data from electroacoustic measurements such as electrical impedance, bandwidth, sensitivity, angular directivity, and inter-element cross-talks will be shown. *EC GROW project PharUSIT (GIRD-CT-2002-000689)

8:40

3aEAa3. Acoustic modeling for designing sonic logging tools. Toshihiro Kinoshita (Schlumberger K.K., 2-2-1 Fuchinobe, 229-0006 Sagamihara, Japan, tkinoshi@fuchinobe.oilfield.slb.com), Hiroshi Hori (Schlumberger K.K., 2-2-1 Fuchinobe, 229-0006 Sagamihara, Japan, hori@fuchinobe.oilfield.slb.com)

Formation acoustic properties such as velocity and attenuation provide useful information regarding rock type and formation fluid. Sonic logging is one of the principal measurements to evaluate the presence of hydrocarbons in the well and to enable an efficient and safe production of oil. Unfortunately the sonic measurement is affected by the tool itself. Suppressing or attenuating the tool wave, which propagates along the logging tool and is received by the sensors, is directly related to the accuracy of the answer products. In order to improve the measurement quality and to increase the efficiency of logging operations, the structure of sonic logging tools must be well understood. A sonic tool with known effects is decidedly more complex and acoustic modeling incorporating the tool structure details is becoming essential to better sonic tool design. The methodology of numerical modeling used to predict the response of a sonic tool is to be presented.

9:00

3aEAa4. Extracting dispersion curves of acoustic data with continuous wavelet transform. Henri-Pierre Valero (Schlumberger Doll Research, 1 Hampshire Street - MD- B 213, Cambridge, MA 02139, USA, hvalero@boston.oilfield.slb.com), Sandip Bose (Schlumberger Doll Research, 1 Hampshire Street - MD- B 213, Cambridge, MA 02139, USA, bose1@boston.oilfield.slb.com), Suchin Aeron (Boston University College of Engineering, One Sherborn Street, Boston, MA 02215, USA, shuchin@bu.edu)

Group and phase velocity (i.e. dispersion) of acoustic data carry important information about the acoustic state of the rock and are important tools for interpretation and for quantitative inversion. In this paper we propose an approach to automatically extract the velocity dispersion (group and phase) of acoustic waves received by an array of receivers without the use of any physical model, user inputs or supervision. The first step consists in applying the continuous wavelet transform to the waveforms recorded by each receiver. Then, the peak on the modulus map is used to determine the time locus of the energy of each mode as a function of frequency. At each frequency, a method of data association is used to find the corresponding loci for all receivers. A straight line is fit to these loci and its slope is used as an estimate for the group velocity at that frequency. Moreover the rate of change of the phase of the complex wavelet coefficients at the locations corresponding to this best-fit straight line can be used to compute an estimate of the phase slowness at the same frequency. Repeating this for all frequencies and all separated modes of interest yields the desired dispersion curves for these modes.

Contributed Paper

9:20

3aEAa5. Small scale adaptation of the seismic full waveform inversion method - Application to civil engineering applications. Francois Bretaudeau (LCPC, Centre de Nantes BP4129, 44341 Bouguenais, France, francois.bretaudeau@lcpc.fr), Donatienne Leparoux (LCPC, Centre de Nantes BP4129, 44341 Bouguenais, France, donatienne.leparoux @lcpc.fr), Odile Abraham (LCPC, Centre de Nantes BP4129, 44341 Bouguenais, France, odile.abraham@lcpc.fr)

Full Waveform Inversion (FWI) is a very general multi-parameters quantitative imaging method originally developed to obtain high resolution images of velocities and attenuation in the natural underground media. FWI promises interesting performances for civil engineering applications like cavity detection. Performances of the FWI method in seismic exploration are difficult to quantify because in real experimentations, the properties of the media are not known. Furthermore, characteristics of the source and coupling of receivers are not controlled. In order to quantify the performances of FWI and its adaptability to near subsurface applications, small scale physicals models are realized and a non-contact laser ultrasonic laboratory is dedicated to simulate seismic reflection measurement configurations at ultrasonic scale. Seismograms well reproduce real scale data in terms of waveforms and repartition of energy. A FWI algorithm developed by Geosciences Azur and applied in geological investigation is used. The direct part of the algorithm uses a frequency domain finite difference modelisation. The inverted model is obtained by using a Gauss-Newton method of optimization. Results of inversion of multi-receivers and multi-sources data obtained from simple physical models are presented.

Invited Paper

9:40

3aEAa6. Simulating Sonic Scanner responses in an interactive Web-based High Performance Computing environment. Valery Polyakov (Schlumberger Doll Research, 1 Hampshire Street - MD- B 213, Cambridge, MA 02139, USA, valp@computer .org), Henri-Pierre Valero (Schlumberger Doll Research, 1 Hampshire Street - MD- B 213, Cambridge, MA 02139, USA, hvalero@boston.oilfield.slb.com), Dzevat Omeragic (Schlumberger Doll Research, 1 Hampshire Street - MD- B 213, Cambridge, MA 02139, USA, omeragic@boston.oilfield.slb.com), Raymond L. Kocian (Schlumberger Doll Research, 1 Hampshire Street - MD- B 213, Cambridge, MA 02139, USA, rkocian@boston.oilfield.slb.com), Tarek M. Habashy (Schlumberger Doll Research, 1 Hampshire Street - MD- B 213, Cambridge, MA 02139, USA, thabashy@boston.oilfield.slb.com), Jahir Pabon (Schlumberger Doll Research, 1 Hampshire Street - MD- B 213, Cambridge, MA 02139, USA, jahir@boston.oilfield.slb.com)

Sonic Scanner logging tool collects a wealth of data about the geological formation. The drawback of this is that we are now discovering new features on the acoustic logs that have never been observed before; only rigorous modeling can help properly interpret the data. Invariably, it is difficult to learn quickly how to run a modeling code, set the parameters properly, and be able to detect possible errors in the input. In addition, complex modeling requires high power computing resources, which are not always easily accessible the user. To address these problems we developed a multi-tier Web-based log modeling environment where the Sonic Scanner simulator is

easily accessible from the common Web browser. The user builds the model in an intuitive AJAX-like interface and submits the simulation to a remote High Performance Cluster. The computed waveforms are played back in the browser using Scalable Vector Graphics in a variety of customizable displays. The Web application is easily available to any user with an Internet access. In addition, a programmatically accessible Web service is available to application developers who desire to build their own interpretation applications using the Sonic Scanner simulator engine.

WEDNESDAY MORNING, 2 JULY 2008 ROOM 353, 10:20 A.M. TO 3:40 P.M.

Session 3aEAb

Engineering Acoustics: Ultrasonic Acoustic MEMS I

F. Levent Degertekin, Cochair
Georgia Institute of Technology, G. W. Woodruff School of Mechanical Engineering, 801 Ferst Dr. NW, Atlanta, GA 30332-0405, USA

Dominique Certon, Cochair
Lab. LUSSI Inserm U930 CNRS FRE 2448 Univ. François Rabelais, 10, Boulevard Tonnellé, Tours, 37032, France

Contributed Paper

10:20

3aEAb1. Micro-viscometer using acoustic wave absorption in micro-chamber and channel. Sungjoon Choi (Postech, San 31, Hyoja-Dong, Namgu, 790-784 Pohang, Republic of Korea, csjangel@postech.ac.kr), Wonkyu Moon (Postech, San 31, Hyoja-Dong, Namgu, 790-784 Pohang, Republic of Korea, wkmoon@postech.ac.kr), Geunbae Lim (Postech, San 31, Hyoja-Dong, Namgu, 790-784 Pohang, Republic of Korea, limmems@postech.ac.kr)

A micro-viscometer is designed for real-time measurement on the viscosity change of biomaterial including DNA or RNA, etc. It is composed of two chambers and several micro-channels connecting between them. Each chamber has a PZT unimorph membrane for generating and sensing the sound waves. Namely, one is regarded as an actuator, the other as a sensor. Micro-channels, which have the large attenuation of acoustic waves caused by wall effect, are applied to the micro-viscometer for increasing viscosity effect. When the actuator is driven at a resonance frequency under the condition of continuous flowing of liquid through an inlet/outlet hole, the sensor can detect the amplitude differences caused by viscosity change. Therefore, it is possible to measure the viscosity change in real time by detecting the signal change of sensor. The micro-viscometer can be also applied to the integration kit such as LOC (Lab-On a Chip) to detect whether DNA is amplified by micro-PCR (Polymerase Chain Reaction) and it will give a first opportunity for experimentally evaluating the viscosity effect on the propagation of acoustic waves in micro-channel. [Research supported by MRCnd of DAPA]

Invited Paper

10:40

3aEAb2. Use of rapid protyping techniques in transducer manufacture. David Hutchins (University of Warwick, School of Engineering, CV4 7AL Coventry, UK, D.A.Hutchins@warwick.ac.uk), Duncan R. Billson (University of Warwick, School of Engineering, CV4 7AL Coventry, UK, drb@eng.warwick.ac.uk), Robert J. Bradley (University of Warwick, School of Engineering, CV4 7AL Coventry, UK, R.J.Bradley@warwick.ac.uk), Kwok S. Ho (University of Warwick, School of Engineering, CV4 7AL Coventry, UK, K.S.Ho@warwick.ac.uk)

This paper will describe the use of a rapid protyping technique, known as micro-sterolithography, for the manufacture of ultrasonic transducers. There are two main types to be described. The first is a MEMS-type capacitive transducer, this being an example of a capacitive micromachined ultrasonic transducer (CMUT). This can be made with all the main structural elements fabricated from polymers, so that no silicon processing is required. Experiments have investigated the properties of these devices, operating in air, water, and in contact with a metal surface. The technique has also been used to make electromagnetic acoustic transducers (EMATs), by forming the main structure from polymers and including a metal coil. These are interesting developments, which may have application to the fabrication of many types of acoustic MEMS devices.

11:00

3aEAb3. Design, fabrication and characterisation of piezoelectric micromachined ultrasonic transducers. Anne-Christine Hladky-Hennion (IEMN, UMR CNRS 8520, avenue Poincaré, BP 60069, 59652 Villeneuve d'Ascq, France, Anne-Christine.Hladky@isen.fr), Didace Ekeom (Microsonics, 39 rue des Granges Galand, 37550 Saint Avertin, France, didace.ekeom@microsonics.fr), Fabrice Duval (IEMN, UMR CNRS 8520, avenue Poincaré, BP 60069, 59652 Villeneuve d'Ascq, France, fa_duval@yahoo.fr), Eric Cattan (IEMN, UMR CNRS 8520, avenue Poincaré, BP 60069, 59652 Villeneuve d'Ascq, France, Eric.Cattan@univ-valenciennes.fr)

Micro-machined ultrasonic transducers (MUT) are investigated for phased arrays in high frequency acoustic imaging to overcome resolution and frequency limits of bulk PZT transducers currently used. The advantage of structures on silicon substrate is that transducers could be integrated with the electronics of the system. From a design point of view, finite element (FEM) codes are commonly used to model MUT, but to take into account the fluid surrounding the device radiation, scattering and the inter-mutual acoustic influence of the MUT arrays cells - the boundary element method (BEM) coupled with the finite element method is advantageously used. This paper describes the design, the fabrication and the characterisation of bending mode circular piezoelectric membranes, with operating frequency around 10 MHz. The devices are based on a PZT (lead zirconate titanate) film 1 μm thick supported by a membrane of polysilicon, 2 μm thick and SiO2, 500 nm thick. The PZT thin film was deposited following a sol-gel route. Fully-supported membranes as well as suspended cells are considered with a view to increase the resonant frequency and decrease the cross coupling between cells.

11:20

3aEAb4. Capacitive micromachined ultrasonic transducers for generation of highly directional sound with a parametric array. Ira O. Wygant (E. L. Ginzton Laboratory, Stanford University, Stanford, CA 94305, USA, iwygant@stanford.edu),Mario Kupnik(E. L. Ginzton Laboratory, Stanford University, Stanford, CA 94305, USA, kupnik@stanford.edu), Jeffry C. Windsor (Applied Research Laboratories, The University of Texas, P.O. Box 8029, Austin, TX 78713-8029, USA, jwindsor@arlut.utexas.edu), Wayne M. Wright (Applied Research Laboratories, The University of Texas, P.O. Box 8029, Austin, TX 78713-8029, USA, wwright@arlut.utexas.edu), Mark S. Wochner (Applied Research Laboratories, The University of Texas, P.O. Box 8029, Austin, TX 78713-8029, USA, mwochner@mail.utexas.edu), Goksen G. Yaralioglu (E. L. Ginzton Laboratory, Stanford University, Stanford, CA 94305, USA, goksenin@gmail.com), Mark F. Hamilton (Applied Research Laboratories, The University of Texas, P.O. Box 8029, Austin, TX 78713-8029, USA, hamilton@mail.utexas.edu), Butrus (pierre) T. Khuri-Yakub (E. L. Ginzton Laboratory, Stanford University, Stanford, CA 94305, USA, pierreky@stanford.edu)

Capacitive micromachined ultrasonic transducers (CMUTs) with vacuum-sealed cavities have been fabricated and used to project directional sound using parametric arrays. The wafer bonding approach used to fabricate the CMUTs provides good control over device dimensions, a single-crystal silicon membrane that has predictable mechanical properties, and the capability to fabricate CMUTs with large-diameter membranes and deep cavities. The fabricated CMUTs are about 8 cm in diameter and comprise 284 circular membranes, each 4 mm in diameter. Testing of CMUTs with 40-μm and 60-μm-thick membranes shows they have center frequencies of 46 kHz and 55 kHz and 3-dB bandwidths of 1.9 kHz and 5.3 kHz, respectively. With application of DC bias voltages of 380 V and 350 V and an AC excitation of 200 V peak-to-peak, the devices generate effective source levels of 139 dB and 131 dB (re 20 μPa), respectively. We used the CMUT design with a 60-μm-thick membrane to produce 5 kHz sound at 3 m with a 6-dB beamwidth of 8.7 deg and a sound pressure level of 58 dB. The results demonstrate that large-area CMUTs, which produce high pressure ultrasound, can be fabricated for transmitting directional sound with parametric arrays. [Work supported by DARPA.]

Invited Papers

11:40

3aEAb5. A finite element tool for the analysis and the design of capacitive micromachined ultrasonic transducer (cMUT) arrays for medical imaging. Alessandro Caronti (Dept. of Electronic Engineering, University Roma Tre, via della Vasca Navale, 84, 00146 Roma, Italy, caronti@uniroma3.it), Giosue' Caliano (Dept. of Electronic Engineering, University Roma Tre, via della Vasca Navale, 84, 00146 Roma, Italy, giosue.caliano@uniroma3.it), Philipp Gatta (Dept. of Electronic Engineering, University Roma Tre, via della Vasca Navale, 84, 00146 Roma, Italy, gatta@uniroma3.it), Cristina Longo (Dept. of Electronic Engineering, University Roma Tre, via della Vasca Navale, 84, 00146 Roma, Italy, clongo@uniroma3.it), Alessandro Savoia (Dept. of Electronic Engineering, University Roma Tre, via della Vasca Navale, 84, 00146 Roma, Italy, savoia@uniroma3.it), Massimo Pappalardo (Dept. of Electronic Engineering, University Roma Tre, via della Vasca Navale, 84, 00146 Roma, Italy, pappalar@uniroma3.it)

The fabrication technology of capacitive micromachined ultrasonic transducers (cMUTs) is now mature enough to exploit the potential of this new generation of electro-acoustic transducers in the field of diagnostic medical imaging and non-destructive evaluation. Converting a demonstrator into a commercial product often requires many design and process refinements, and sometimes significant modifications to the fabrication process. Because each design-fabrication-and-test cycle is time-consuming and costly, the development of a modeling tool for the computer simulation of cMUTs is an essential aid to reduce the time to market and costs. Much effort has been put by researchers to develop more and more accurate and smart simulation tools, that advanced from the standard equivalent circuit modeling with lumped parameters to more powerful techniques based on the finite element method (FEM). This paper aims to give an overview of the most ordinary modeling approaches used for the simulation of cMUTs. It is shown that the pulse-echo operation of cMUT arrays for medical imaging applications can be analysed by a set of FEM models developed using a commercial software. The important aspects of the cMUT operation, including electro-mechanical-acoustical coupling and nonlinear effects in transmission, are taken into account.

12:00

3aEAb6. Wafer bonded, local oxidation defined, capacitor micromachined ultrasonic transducers for medical applications. Butrus (pierre) T. Khuri-Yakub (E. L. Ginzton Laboratory, Stanford University, Stanford, CA 94305, USA, pierreky@stanford.edu), Kwan Kyu Park (E. L. Ginzton Laboratory, Stanford University, Stanford, CA 94305, USA, kwankyup@stanford.edu), Hyunjoo Jenny Lee (E. L. Ginzton Laboratory, Stanford University, Stanford, CA 94305, USA, hyunjoo@stanford.edu), Mario Kupnik (E. L. Ginzton Laboratory, Stanford University, Stanford, CA 94305, USA, kupnik@stanford.edu), Omer Oralkan (E. L. Ginzton Laboratory, Stanford University, Stanford, CA 94305, USA, ooralkan@stanford.edu)

We present a technology for making capacitive micromachined ultrasonic transducers (CMUTs) that is based on direct wafer bonding of silicon on insulator wafer (SOI), and where the vertical dimensions and geometry of the CMUT are defined by local oxidation (LOCOS). The advantages of this approach for making CMUTs is the excellent control, no only over the membrane properties, but also over the shape and dimensions of the cavity. We demonstrated the ability to make devices with cavities in the 10s of nanometer range which enables devices up to a frequency of 100 MHz. The devices exhibit reduced charging where we measure a voltage shift of 0.03 V for devices cycled in and out of collapse at 50 V. The devices also have reduced parasitic capacitance as thicker oxides are grown in the regions of the SOI bond to the membrane. These are typically the regions that contribute most to the parasitic capacitance. Finally, because of the reduced charging, it is possible to operate these devices in and out of collapse which results in higher output pressure than devices operating in conventional mode. Hence, these CMUTs are much more predictable and reproducible in their operation and performance.

Contributed Paper

12:20

3aEAb7. Acoustic microelectromechanical viscometer. Arthur Ballato (US Army Communications-Electronics R&D Center, AMSRD-CER-CS, Fort Monmouth, NJ 07703-5201, USA, Arthur.Ballato@us.army.mil)

Current dynamic techniques for measuring fluid shear viscosities using quartz, or other piezoelectrics, rely on the resonator surface being exposed to a measurand bath whose extent greatly exceeds the penetration depth of the evanescent shear mode excited by the active element. This configuration allows the effect of the loading parameters to be expressed concisely. Perturbation of the electrical equivalent circuit parameters of the resonator by the fluid loading permits calculation of the mass density - shear viscosity product. In this paper, we explore the interesting, albeit more complicated situation where the separation between the resonator and a confining wall is less than the penetration depth of the fluid occupying the intervening region. It turns out that the resonator perturbation in this case is a sensitive function of the separation. This important fact permits extreme miniaturization, since for gases between 200K and 400K, pressures between 0.01 to 100 atm, and frequencies between 10 MHz and 1 GHz, the penetration depth varies from micrometers to nanometers. Variations in the spacing is effected by using a second, nonresonant piezoelectric as the wall. Micro-electro-mechanics (MEMS) versions of viscometers and associated types of fluid sensors are thereby enabled.

12:40-2:00 Lunch Break

Contributed Papers

2:00

3aEAb8. Thin Film Piezoelectric MEMs Devices. Mareike Dr. Klee (Philips Research Laboratories, High Tech Campus 4, 5656 AA Eindhoven, Netherlands, mareike.klee@philips.com), Henk Boots (Philips Research Laboratories, High Tech Campus 4, 5656 AA Eindhoven, Netherlands, henk.boots@philips.com), Biju Kumar (Philips Research Laboratories, High Tech Campus 4, 5656 AA Eindhoven, Netherlands, biju.kumar@philips.com), Wilco Keur (Philips Research Laboratories, High Tech Campus 4, 5656 AA Eindhoven, Netherlands, wilco.keur@philips.com), Marco De Wild (Philips Research Laboratories, High Tech Campus 4, 5656 AA Eindhoven, Netherlands, marco.de.wild@philips.com), Peter Dirksen (Philips Research Laboratories, High Tech Campus 4, 5656 AA Eindhoven, Netherlands, peter.dirksen@philips.com), Klaus Reimann (NXP Research, HighTech Campus 4, 5656 AA Eindhoven, Netherlands, klaus.reimann@nxp.com), Olaf Wunnicke (NXP Research, HighTech Campus 4, 5656 AA Eindhoven, Netherlands, olaf.wunnicke@nxp.com), Christel Renders (NXP Research, HighTech Campus 4, 5656 AA Eindhoven, Netherlands, christel.renders@nxp.com), Harry Van Esch (Philips Research Laboratories, High Tech Campus 4, 5656 AA Eindhoven, Netherlands, harry.van.esch@nxp.com), Chris Van Heesch (Philips Research Laboratories, High Tech Campus 4, 5656 AA Eindhoven, Netherlands, chris.van.Heesch@philips.com), Georg Schmitz (Medical Engineering, University Bochum, 44680 Bochum, Germany, georg.schmitz@rub.de), Martin Mienkina (Medical Engineering, University Bochum, 44680 Bochum, Germany, martin.mienkina@rub.de), Michal Mleczko (Medical Engineering, University Bochum, 44680 Bochum, Germany, michal.mleczko@rub.de)

Thin film piezoelectric devices, processed in Si-related processes, are attractive for ultrasound transducers and piezoelectric switches. Thin film ultrasound transducer enable large bandwidth ($>$ 100%), high frequency operation. In piezoelectric micromachined ultrasonic transducers (PMUTs) the ultrasonic waves are generated by flexural motion of the membrane, which is coupled to strain in the piezoelectric film. We have investigated the piezoelectric properties of thin films for ultrasound transducers and piezoelectric switches. Thin film piezoelectric ultrasound transducers as well as piezoelectric switches have been designed, processed and characterized. Thin film piezoelectric devices with excellent quality and reliability have been realized.

2:20

3aEAb9. Increasing power-efficiency of a micro-machined pump transducer for a parametric transmitting array in air. Haksue Lee (Postech, San 31, Hyoja-Dong, Namgu, 790-784 Pohang, Republic of Korea, jolary@postech.ac.kr), Wonkyu Moon (Postech, San 31, Hyoja-Dong, Namgu, 790-784 Pohang, Republic of Korea, wkmoon@postech.ac.kr)

Parametric array applications in air, such as high directional loudspeaker system, have been studied with a large radiator (generally D$\geqslant$300mm) to generate high intensive sound beams required for nonlinear interactions. However, conventional transducer requires high electrical power because its electro-acoustic efficiency is too low due to an acoustic impedance mismatch. For mobile applications, a high efficient transducer is required. As an alternative pump transducer, a feasibility of a micro-machined ultrasonic transducer is studied. The efficiency can be improved by applying a thin-film membrane, overcoming the impedance mismatch. The efficiency of micro-machined transducer is simulated with a reduced dynamic model and compared with that of a conventional transducer. Two types of unimorph piezoelectric micro-machined ultrasonic transducers are designed and fabricated as small pump transducers for a ranging sensor and a loudspeaker. The

electro-acoustic efficiency and dynamic characteristics related with primary wave generation are mainly examined in this work. The radiation characteristics, directional beam patterns and axial pressure distributions, of primary and secondary waves are also measured and compared with theoretical results. Throughout this work, feasibility of the proposed pump transducer is shown, but further work is also required for practical applications. [Research supported by MRCnd and ADD-UD070054AD of DAPA]

2:40

3aEAb10. Ultraviolet detector based on a surface acoustic wave oscillator system with ZnO-nanostructure sensing material. Tsung-Tsong Wu (Institute of Applied Mechanics, National Taiwan University, No. 1, Sec. 4, Roosevelt Road, 106 Taipei, Taiwan, wutt@ndt.iam.ntu.edu.tw), Wei-Shan Wang (Institute of Applied Mechanics, National Taiwan University, No. 1, Sec. 4, Roosevelt Road, 106 Taipei, Taiwan, dainty@ndt.iam.ntu.edu.tw), Tai-Hsu Chou (Institute of Applied Mechanics, National Taiwan University, No. 1, Sec. 4, Roosevelt Road, 106 Taipei, Taiwan, deshi@ndt.iam.ntu.edu.tw),Yung-Yu Chen(Department of Mechanical Engineering, Tatung University, No. 40, Sec. 3, Chungshan N. Rd., 104 Taipei, Taiwan, yychen@ttu.edu.tw)

Recently, ultraviolet (UV) detectors based on surface acoustic wave (SAW) devices utilizing the acoustoelectric effect have been demonstrated. However, most of presented cases were based on semiconductor sensing films. Sensors with nanostructure sensing material not only possess high sensitivity but also accelerate response and recovery time due to their high surface-to-volume ratio and fast charge diffusion rate. In this paper, ZnO-nanostructure and a dual delay line SAW oscillator system are combined to develop a high precision UV detector. The UV detector is made of ZnO nanorod on a 128oYX-LiNbO3 based SAW device. The operating frequency is around 145MHz. The system is illuminated by a UV source consists of a Xe lamp and a monochromator, resulting in frequency shifts. The frequency shifts related to different light wavelengths and power are measured and discussed. Results show the ZnO-nanostructure based SAW oscillator is a promising candidate for a real-time and high precision UV detector.

Invited Paper

3:00

3aEAb11. Silicon Micromachined Energy Concentrating Acoustic Transducers for Biomedical Applications. Amit Lal (Cornell University, 118 Phillips Hall, School of Electrical and Computer Engineering, Ithaca, NY 14853, USA, lal@ece.cornell.edu), Abhishek Ramkumar (Cornell University, 118 Phillips Hall, School of Electrical and Computer Engineering, Ithaca, NY 14853, USA, ar339@cornell.edu), Muhamet Araz (Cornell University, 118 Phillips Hall, School of Electrical and Computer Engineering, Ithaca, NY 14853, USA, mka22@cornell.edu)

Silicon's high maximum ultrasonic particle velocity, high thermal conductivity, and low internal loss, make it an ideal material for for high-intensity ultrasonic actuators. We have designed and microfabricated silicon ultrasonic horns, which when actuated at their $\lambda/2$ longitudinal resonance (using ceramic PZT transducers) concentrate ultrasonic energy and magnify displacements. By incorporating microprobes at the high energy sites we have successfully demonstrated reduction of penetration force on biological tissues. We have also reported cardiac action potential measurement from multiple sites simultaneously within the heart wall by incorporating platinum electrodes on the microprobes. We have reported on mechanical and spatial characterization of seminiferous tubules in the testis in order to extract sperm for artificial insemination. We are currently exploring silicon ultrasonic horns in detecting testicular and prostate cancer in the early stages. In addition, silicon ultrasonic horns can be used for low power ultrasonic pumping and also atomization. By using bulk micromachining techniques an enclosed conduit is opened along the horn. Due to the highly amplified acoustic field at the tip, fluid enclosed in the channel can be atomized from the tip. Reversibly when the tip is immersed in fluid, fluid can also be pumped into the channel due to changing boundary conditions.

Contributed Paper

3:20

3aEAb12. Reproducibity and life duration assessment of cMUT transducers. Cyril Meynier (Vermon SA, 180 rue Général Renault, 37000 Tours, France, c.meynier@vermon.com), Dominique Certon (Lab. LUSSI Inserm U930 CNRS FRE 2448 Univ. François Rabelais, 10, Boulevard Tonnellé, 37032 Tours, France, dominique.certon@univ-tours.fr), Franck Teston (Lab. LUSSI Inserm U930 CNRS FRE 2448 Univ. François Rabelais, 10, Boulevard Tonnellé, 37032 Tours, France, franck.teston @univ-tours.fr), Guillaume Ferin (Vermon SA, 180 rue Général Renault, 37000 Tours, France, g.ferin@vermon.com)

Cmut-based transducers are often expected to be superior in terms of reproducibility to piezoelectric transducers due to the use of microelectronic technology instead of more traditional machining techniques. During the conventional (sacrificial-layer based) production process of cmut transducers, various process steps can display inhomogenities and uncertainty in flow rate, temperature profile, stochiometry, or other aspects, resulting in variations in layers thicknesses, gap height, and material properties, each having an impact on transducer performances. In this study, we choose to use impedance measurement technique as evaluation tool for the stability of the properties of cmut transducers. A large number of cMUT transducers with the same design, were characterized, allowing to compare their properties from wafer to wafer, and according to their position of origin in the wafer. The resistance of cmut transducers to temperature cycling was also investigated, using impedance and optical measurements control before and after a 3-days +60/-20°c test. The reliability was tested under a long-duration electroacoustic measurement, where a cMUT transducer was submitted to periodic large amplitude excitation, and its pulse-echo response recorded for several hours.

Session 3aMUa

Musical Acoustics and Speech Communication: Interdisciplinary Research on the Science of Singing: A Tribute to Johan Sundberg

Annabel J. Cohen, Cochair
University of Prince Edward Island, 550 University Ave, Charlottetown, PE C1A 4P3, Canada

Sten Ternstrom, Cochair
KTH, Department of Speech, Music and Hearing, Lindstedtsvägen 24, S-100 44 Stockholm, Sweden

Invited Papers

8:00

3aMUa1. Listener-oriented motor control: Comparing evidence from speech and singing. Björn Lindblom (Stockholm University, Universitetsvägen 10C, SE10691 Stockholm, Sweden, lindblom@ling.su.se)

Singing and speech make different use of the vocal tract but work in similar ways with respect to how sound production is controlled. A principle that they share is: output-oriented control. This mode of organization implies that the task of the motor system is defined in terms of the desired properties of the output sound, rather than in terms of motor processes. This claim is strongly supported by Johan Sundberg's experimental work on singing and by 'compensatory articulation' and 'hyper-speech', phenomena that remind us that, for speech, output-directed control is also readily acknowledged. Our comparative review of singin and speech will be placed in the context of the current debate on the 'invariance' and true nature of phonetic units: 'articulatory gestures' or 'auditory goals'?

8:20

3aMUa2. Methods for singing voice control and synthesis. Xavier Rodet (Ircam, 1, place I. Stravinsky, 75004 Paris, France, Xavier.Rodet@ircam.fr)

There are various methods to synthesize the singing voice. Whatever the method, in order to obtain high quality voice output, it is essential to respect the precise parameter values for the first three to five formants of the vowels. These parameters depend on many factors including the singer, note, vowel, vocal effort, etc. Articulation of the notes is achieved by variations of fundamental frequency, vibrato, vocal effort and eventually formant characteristics of the vowels. Finally, the succession of consonants and vowels also has to be taken into account and implemented. With the expertise of J. Sundberg, a method called Formant Waveform Synthesis and a program for the control of all the above mentioned variations, except consonants, were developed at Ircam in the 1980s. This program permitted high quality singing voice synthesis but without consonants. Another synthesis method is to is to concatenate units of recorded singing voice. This provides good consonant-to-vowel articulations. But it necessitates to transpose and change the duration of these units which often degrades the output quality and precise control over the formant characteristics is rather difficult. These various methods will be discussed and examples given.

8:40

3aMUa3. A developmental approach to voice science. Stefanie Stadler Elmer (University of Zürich, Dachsweg 8b, CH - 4410 Liestal, Switzerland, stefanie.stadler@access.uzh.ch)

Vocal development had been studied mostly with a focus on speaking, and only rarely, on singing. Traditional theories on singing development are often based on wrong premises, e.g. eurocentrism, and reliable analyses of singing are missing or selective. A new theory - inspired by the principles of Piaget's theory -, and a new methodology - based on acoustic measures - are proposed. The voice starts to organise at birth, and gradually adapts to the cultural surrounding and its conventions concerning language, music, and social rules. Vocal and musical behaviour are highly adaptive and constructive, and concern two symbolic systems: music and language. The child develops the voice by playing and imitating. The development proceeds from sensorimotor activities towards more and more conscious actions and thoughts. In order to study children's singing, computer aided programs were devised to analyse and represent pitch, timing, pitch qualities, and syllables. This method yields complex configurations of these parameters describing children's song singing. Detailed descriptions allow to reconstruct the strategies children apply to invent or learn new songs. The empirical results from children at various ages demonstrate that the focus on the analysis of the organisation of the vocal expression is a promising research strategy.

9:00

3aMUa4. Observing a chameleon: How to bridge a gap between the voice training and its scientific description. Jaan Ross (Koidu 122-61, 10139 Tallinn, Estonia, jaan.ross@ut.ee), Allan Vurma (Estonian Academy of Music and Theatre, Rävala Puiestee 16, 10143 Tallinn, Estonia, vurma@ema.edu.ee)

An overview of the authors' research on perception and production of singing voice as well as on the methods of voice training is presented. In the first study, a correlation was found for a group of voice students between the duration of training and the strength of the singer's formant, while the tone quality estimates were not significantly higher for students with longer practice years. In the second study we investigated possible acoustical correlates of the 'forward'/'backward' placing of a voice. A 'forward' placed voice may have higher F1, F2 and/or the singer's formant frequencies as well as a higher level of the singer's formant. In the third study we investigated the intonation accuracy in a cappella performance. There are considerable inter-individual differences between performers as to their adjustment of pitch level. The stability of intonation varies significantly both within a single rendition of the vocal exercise as well as between its consecutive renditions. There is a positive correlation between the deviation of a melodic interval from its equally tempered standard value and the number of out-of-tune judgments by the listeners. The dispersion of out-of-tune judgments is considerable, which suggests that listeners might have adopted different criteria for intonation accuracy.

9:20

3aMUa5. Rate of change of Fo in performance singing. Ronald C. Scherer (Bowling Green State University, Department of Physics and Astronomy, Bowling Green, OH 43403, USA, ronalds@bgnet.bgsu.edu), Nandhu Radhakrishnan (University of Missouri, 316 Lewis Hall, Department of Communication Science and Disorders, Columbia, MO 65211, USA, radhakrishnann@health.missouri.edu), Prakash Boominathan (Sri Ramachandra Medical College & Research Institute (DU), Dept. of Speech Language & Hearing Sciences, Porur, Chennai, 600 116 TamilNadu, India, Praxb77@yahoo.com), Haidee Tan (Bowling Green State University, 200 Health Center, Department of Communication Disorders, Bowling Green, OH 43403, USA, haideetan@hotmail.com)

Johan Sundberg has had a strong interest in the vocal behavior of singers of different styles and nationalities. This tribute talk emphasizes the voluntary change of rate of fundamental frequency in performance singing of ornaments and vibrato. The ″taan″ gestures from Northern Indian classical singing, the ″pulse patterns″ in Carnatic Southern Indian classical singing, and pitch change in classical western coloratura singing constitute the primary corpus for this study of Fo rate change. Rate of Fo change varied from approximately 20 to 120 ST/s for soprano pitch change, 8 to 20 ST/s for the Southern Indian pulse patterns, and 7 to 60 ST/s for the Northern Indian taan gestures. What these rates depend upon and rates from other ornaments will be discussed, as well as the relation to maximum Fo rates in the literature, performance needs, perceptual characteristics, and control.

9:40

3aMUa6. Singing out of tune: Disturbances of vocal performance in the general population. Simone Dalla Bella (Dept. of Cognitive Psychology, University of Finance and Management in Warsaw, Pawia Street 55, 01-030 Warsaw, Poland, sdallabella@vizja.pl)

Acoustical methods can provide a reliable and objective estimate of singing proficiency in the general population, in terms of pitch and temporal accuracy (e.g., Dalla Bella, Giguère, & Peretz, 2007). The majority, when asked to sing a well-known song at a slow tempo, are as proficient as professional singers. Nonetheless, some nonmusicians exhibit poor singing. This deficit is mostly limited to the pitch domain and sometimes is not accompanied by impaired perception. More recently singing proficiency was examined in nonmusicians with tasks extending beyond singing familiar melodies. Forty participants imitated single pitches, intervals, and short melodies; in addition, participants sung three well-known melodies at a spontaneous tempo and at a fixed slow tempo. Additional tasks (e.g., Montreal Battery of the Evaluation of Amusia) were carried out to assess participants' perceptual abilities. Acoustical analyses of vocal performance revealed that the majority of nonmusicians sung in tune and in time, thus confirming previous findings. Still, various patterns of poor singing emerged from the analyses of pitch and time accuracy (e.g., poor pitch singing with or without perceptual deficits). The relationship between perception and performance mechanisms in vocal production will be discussed.

10:00

3aMUa7. Hi-Fi voice: observations on the distribution of energy in the singing voice spectrum above 5 kHz. Sten O. Ternström (Kungliga Tekniska Högskolan, Dept. of Speech, Music & Hearing, Lindstedtsvägen 24, SE-100 44 Stockholm, Sweden, stern@kth.se)

Current audio technology enables the weak spectrum of the voice above 4-5 kHz to be studied reliably. It is known that energy in the 5-20 kHz range can be perceived even when it is 50 dB or more below the main voice spectrum peak. Also, these upper frequencies are conventionally emphasized in the production of popular vocal music; yet very few studies of the acoustic content of this range have been made. High fidelity recordings were made of singers sustaining vowels at varying levels of vocal effort. A general characterization of the two highest octaves (5-20 kHz) was sought. The prevalence of high-frequency energy, the variation of harmonics to noise over frequency, and the covariation with overall SPL were all highly variable, but several landmark features were identified. In addition to the commonly observed zero at 4-5 kHz, zeroes were often seen also around 6 and 12 kHz, as were clusters of resonances in the regions 7-10 kHz and 13-16 kHz. Harmonic energy was observed to over 16 kHz in strong female voices. The audibility of these features was assessed by listening tests with selective filtering. A feature-based nomenclature for these uppermost frequency bands is suggested.

10:20

3aMUa8. Advancing Interdisciplinary Research in Singing through a Shared Digital Repository. Annabel J. Cohen (University of Prince Edward Island, 550 University Ave, Charlottetown, PE C1A 4P3, Canada, acohen@upei.ca)

The domain of research in singing encompasses numerous disciplines, countless styles, and many lifespan stages of skill development. A comprehensive understanding of this domain would benefit from a vast digital repository for storing, accessing, and annotating recordings of singing in all its manifestations. A cross-cultural strategy for acquiring and storing the essential audio, audio-visual, and symbolic data parallels the Child Language Data Exchange System (CHILDES) developed and maintained by Brian MacWhinney (http://childes.psy.cmu.edu/) and used by hundreds of psycholinguistics researchers worldwide. A prototype of a digital repository for singing (http://vre.upei.ca/chimes) is under development using infrastructure at UPEI associated with a Canada Foundation for Innovation project on the enhancement of education through media. The database will support and be supported by an international team aiming to Advance Interdisciplinary Research in Singing (AIRS) on the following themes: (1) acquisition of singing (2) comparison of singing and speech acquisition (3) singing pedagogy (4) singing and intercultural understanding (5) singing and intergenerational understanding (6) singing and well-being. The breadth of the work of Johan Sundberg, an honoured member of this team, encompasses these themes and exemplifies the international, interdisciplinary scope of the initiative. (Supported by Canada Foundation for Innovation CFI).

WEDNESDAY MORNING, 2 JULY 2008 AMPHI MAILLOT, 11:00 A.M. TO 12:40 P.M.

Session 3aMUb

Musical Acoustics: Plucked Stringed Instruments I

François Gautier, Cochair
Laboratoire d'Acoustique de l'Université du Maine, Avenue Olivier Messiaen, Le Mans, 72085, France

Chris Waltham, Cochair
University of British Columbia, Department of Physics & Astronomy, Vancouver, BC V6T 1Z1, Canada

Contributed Papers

11:00

3aMUb1. A vibrating sitar string: Modeling the 3D dynamics of a plucked string impacting a spatial obstacle with friction. Chandrika P. Vyasarayani (University of Waterloo, Department of Systems Design Engineering, Waterloo, ON N2L 3G1, Canada, cpvyasar@engmail.uwaterloo.ca), Stephen Birkett (University of Waterloo, Department of Systems Design Engineering, Waterloo, ON N2L 3G1, Canada, sbirkett@real.uwaterloo.ca), John McPhee (University of Waterloo, Department of Systems Design Engineering, Waterloo, ON N2L 3G1, Canada, mcphee@real.uwaterloo.ca)

In some musical instruments of Indian origin, such as sitar, veena, or tambura, the string termination is a shallow curved (parabolic) bridge. The string is usually plucked obliquely and interacts with the bridge, thus producing a buzzing or ringing tone which is significantly different from stringed instruments with knife edge supports like guitar. The string is also not restricted to planar motion and friction between bridge and string plays an important role in damping the non-planar motion. A mathematical model is presented for simulating a 3D vibrating string as it impacts a curved obstacle with friction. The bridge is represented as a foundation model with nonlinear visco-elastic springs; multiple distributed spatial impacts occur between the bridge and string, however the locations of these are not known in advance so must be determined during the simulation. Galerkin approximation is used to reduce the partial differential equations of motion to a set of nonlinear ordinary differential equations. These equations have been solved numerically for different contact and friction conditions. Parametric studies show the effect of bridge geometry, impact damping, and friction on the bidirectional vibration behavior of the string subject to an oblique plucking idealized as an initial condition.

11:20

3aMUb2. Acoustical measurement of Indian musical instruments (vina-s): Towards greater understanding for better conservation. Sandie Le Conte (Musée de la Musique, 221 avenue Jean Jaures, 75019 Paris, France, sleconte@cite-musique.fr),Stéphane Vaiedelich(Musée de la Musique, 221 avenue Jean Jaures, 75019 Paris, France, svaiedelich@cite-musique.fr), Philippe Bruguiere (Musée de la Musique, 221 avenue Jean Jaures, 75019 Paris, France, pbruguiere@cite-musique.fr)

Among the Musée de la musique collection of non-Western musical instruments are some rare and delicate ones from India, which have been the subject of acoustical investigation for a greater understanding, and hence a better conservation. In the case of the vina-s, the vibration of the string (exciter) plucked by the musician is transmitted to the resonators made from gourd through a flat bridge thus giving the instrument a remarkably singular timber. Acoustical and vibrational measurements were applied in order to determine the acoustic properties of resonators. These techniques are based on gauging the radiated acoustical field triggered by a light impact or a frequency sweep. This analysis confirms the importance given by instrument makers to the painstaking choice of gourd resonators. Thanks to the estimation of resonant frequency - and from the vibrating length - it is possible to hypothesise on the type of strings used (the material, diameter and strain). In short, these analyses make it possible the diagnosis of the mechanical state of constituent elements. These descriptors could facilitate decisions to optimise the choice of gourds in the production of instruments (sitar, tampura) that have today taken on semi-industrial shades.

11:40

3aMUb3. The influence of plectrum thickness on the radiated sound of the guitar. Sandra Carral (University of Music and performing Arts, Anton-von-Webern-Platz 1, Gebäudeteil M, 2. Stock, A-1030 Vienna,Austria, carral@mdw.ac.at), Martin Paset (University of Music and performing Arts, Anton-von-Webern-Platz 1, Gebäudeteil M, 2. Stock, A-1030 Vienna, Austria, martin.paset@students.mdw.ac.at)

It is generally thought that the human ear is very sensitive to subtle changes in sounds. In the context of musical instruments, one important aspect to study is how much the physical attributes of any given instrument have to differ so that a human can perceive a difference in the produced

sound. In the case of the guitar, it is unquestionable that when the string is plucked at a particular position, some of the differences on the produced sound of the instrument are introduced by changes in how the player plucks the string (playing technique). However, given the wide variety of plectrum types, materials and thicknesses, it is hypothesised that the player is not the only parameter that influences the sound, but that the plectrum itself plays a significant role in the sound production. This paper presents a study whereby a guitar is played with three plectra of different thicknesses with an artificial plucking machine. The radiated sound is recorded, and subsequently analysed using the program SNDAN. Physical and psychoacoustical attributes of the sound are calculated from the resulting analysis. A thorough comparison of these results obtained for the three different plectra is presented and discussed.

12:00

3aMUb4. Acoustics of the French Baroque Lute. Nicholas Makris (Massachusetts Institute of Technology, Room 5-212, 77 Massachusetts Avenue, Cambridge, MA 02139, USA, makris@mit.edu)

Design innovations of the French baroque lute characterize the final plateau in the lutes' millennia long evolution in Europe before its eventual extinction at the end of the baroque period. They came with a dramatic increase in number of strings, a new tuning, the first physical description of string vibration, by Marin Mersenne, and led to the ″style brisee″ which became ubiquitous in baroque music. Compared to the violin, the lute experienced relatively large variations in design and construction material over its lifetime. The aesthetic effect of these variations on musical acoustics were and are often described in compelling but qualitative terms, even by players such as Aristotle and Constantjin Huygens. Here we will use fundamental theoretical principles to quantitatively analyze the acoustic effects of typical design and construction variations found in historic instruments, ranging from the material and thickness of sound boards, bracing and ribs, to rosette design and stringing. We will show how quantitative analysis can be reconciled with qualitative descriptions to help match lute design with desired sound quality.

12:20

3aMUb5. Vibrational Characteristics of Harp Soundboards. Chris Waltham (University of British Columbia, Department of Physics & Astronomy, Vancouver, BC V6T 1Z1, Canada, cew@phas.ubc.ca)

The musical quality of a harp depends on many factors, but key among these is the soundboard. This work sets out to define general vibrational qualities of a good harp soundboard. First, in order to understand the relationship between the vibrational behavior of a bare soundboard and that of the completed instrument, a 36-string harp was built from scratch. Measurements were made at each stage of construction and compared to finite-element calculations. The results showed how the bare soundboard properties affect those of the finished harp. Second, the soundboards of several harps of different sizes were assessed by measuring the admittances along the string bar. These data, and the views of the musicians who play the harps, showed that the most crucial relationship is that between the modal shapes and frequencies of the soundboard, and the position and pitches of the strings attached to it. This allows a general statement to be made about the vibrational qualities of a good soundboard, and suggests a recipe for improving poor soundboards.

WEDNESDAY MORNING, 2 JULY 2008 ROOM 250A, 8:00 TO 9:40 A.M.

Session 3aNSa

Noise, Physical Acoustics, and EURONOISE: Aeroacoustics IV

Philip J. Morris, Cochair
Penn State University, 233C Hammond Building, University Park, PA 16802, USA

Christophe Bailly, Cochair
Ecole Centrale de Lyon, 36, avenue Guy de Collongue, LMFA, Ecully, 69134, France

Contributed Papers

8:00

3aNSa1. Finite Volume Solvers and Moving Least Square Approximations for the Linearized Euler Equations on Unstructured Grids. Sofiane Khelladi (Lab. d'Energétique et de Mécanique des Fluides Interne, Arts et Métiers ParisTech, 151 boulevard de l'Hôpital, 75013 Paris, France, sofiane.khelladi@paris.ensam.fr), Xesús Nogueira (Group of Numerical Methods in Engineering, GMNI Dept. of Applied Mathematics, School of Civil Engineering, University of A Coruña, Campus de Elviña, 15071 A Coruña, Spain, xnogueira@udc.es), Farid Bakir (Lab. d'Energétique et de Mécanique des Fluides Interne, Arts et Métiers ParisTech, 151 Boulevard de l'Hôpital, 75013 Paris, France, farid.bakir @paris.ensam.fr), Luis Cueto-Felgueroso (Aerospace Computational Design Lab., Dept. of Aeronautics and Astronautics, Massachusetts Institute of Technology, 77 Massachusetts Avenue, Cambridge, MA 02139, USA, lcueto@mit.edu), Ignasi Colominas (Group of Numerical Methods in Engineering, GMNI Dept. of Applied Mathematics, School of Civil Engineering, University of A Coruña, Campus de Elviña, 15071 A Coruña, Spain, icolominas@udc.es)

This paper presents the application of a high-order finite volume scheme based on the Moving Least Squares approximations (FVMLS) to solve Linearized Euler Equations (EEL) on unstructured grids. The proposed method allows the direct reconstruction of the (convective) fluxes using compact stencils, and without introducing new degrees of freedom, which is a real advantage over the most popular existing high-order methods. This particularity confers to the proposed methodology a significant reduction in workload and memory storage capability. The proposed scheme is compared to a second-order accurate finite volume scheme with centered fluxes around a uniform flow, with absorbing and/or reflecting boundary conditions. Some test cases are used to illustrate the potential of the FVMLS approximations on acoustic wave propagation. The ultimate objective of our research action is to simulate acoustic wave propagation into confined geometries and complex flows provided by subsonic turbomachines.

8:20

3aNSa2. Weak Compressibility Method for Prediction of Fluid Noise Generation by Cavity Flow at Low Mach Number. Ming Zhu (ESI Group, 99 rue des Solets, BP 80112, 94513 Rungis, France, Ming.Zhu @esi-group.com), Kjell Herfjord (Statoil Hydro, P.O. Box 7190, 5020 Bergen, Norway, kjher@statoilhydro.com), Mustafa Megahed (ESI Group, Mergenthalerallee 15-21, 65760 Eschborn, Germany, mme@esi-group

.com),Argiris Kamoulakos(ESI Group, 99 rue des Solets, BP 80112, 94513 Rungis, France, Argiris.Kamoulakos@esi-group.com)

This paper presents the implementation and validation of a numerical simulation method that takes into account the air-borne acoustic wavepropagation within the turbulent flow solution at low Mach number, which is so-called weak compressibility, in order to cope with fully coupled aeroacoustics problems in a nonlinear system. An academic single 3D cavity case is used to validate the method in comparison with the experiment. The simulated results showed excellent agreement with the experimental data in regard to the acoustic pressure and frequency for the dominant peak of the sound pressure level (SPL) spectra over a wide speed range up to 55 meter per second. An industrial case of so-called singer riser in the system of ocean natural gas rig is studied using this method. There is fluid sound generation due to the interaction of the gas flow field with the pipe grooves. This sound causes strong resonance and vibration over the equipments on the gas rig platform therefore forces the gas producer to control the gas production rate. By using numerical simulation, the aero-acoustic behaviour of a gas flowing in a lab-scale corrugated pipe has been captured which provides deep insights of fluid sound generation mechanism of this singer riser. Experimental results are used to validate the numerical models.

8:40

3aNSa3. Transparent boundary condition for acoustic propagation in lined guide with mean flow. Emmanuel Redon (Université de Bourgogne, LRMA, 9, avenue Alain Savary, 21000 Dijon, France, Emmanuel .Redon@u-bourgogne.fr), Boureima Ouedraogo (Université de Bourgogne, LRMA, 9, avenue Alain Savary, 21000 Dijon, France, Boureima .Ouedraogo@u-bourgogne.fr), Anne-Sophie Bonnet-Ben Dhia (CNRS, ENSTA - 32 Boulevard Victor, 75 015 Paris, France, Anne-Sophie.Bonnet -Bendhia@ensta.fr), Jean-Francois Mercier (CNRS, ENSTA - 32 Boulevard Victor, 75 015 Paris, France, jmercier@ensta.fr), Colin Chambeyron (CNRS, ENSTA - 32 Boulevard Victor, 75 015 Paris, France, colin.chambeyron@ensta.fr)

A finite element analysis of acoustic radiation in an infinite lined guide with mean flow is studied. In order to bound the domain, transparent boundary conditions are introduced by means of a Dirichlet to Neumann (DtN) operator based on a modal decomposition. This decomposition is easy to carry out in a hard-walled guide. With absorbant lining, many difficulties occur even without mean flow. Since the eigenvalue problem is no longer selfadjoint, acoustic modes are not orthogonal with respect to the L2-scalar product. However, an orthogonality relation exists which permits writing the modal decomposition. For a lined guide with uniform mean flow, modes are no longer orthogonal but a new scalar product allows us to define the DtN operator. We consider first the case of an infinite rectangular two-dimensional lined guide with uniform mean flow in order to present the methodology. Then, some extensions will be presented: non-uniform two-dimensional geometries by calculating potential mean flow, and cylindrical axisymmetric three-dimensional problems with uniform mean flow.

9:00

3aNSa4. Sound radiation from annular jet ducts with impedance walls. João M. Oliveira (Instituto Superior Tecnico, Av. Rovisco Pais, 1049-001 Lisboa, Portugal, joliveira@ist.utl.pt)

An analytical model for sound radiation from a semi-infinite annular duct with cylindrical infinite centre section and carrying a jet issuing into an uniform mean flow is presented. The interior of the outer wall of the duct is allowed to have an acoustic impedance. This is an extension to a recent model where only rigid walls were considered. The unstable cylindrical vortex layer attached to the edge of the duct, between the jet and the uniform mean flow, is considered. The geometry considered aims to model a turbofan exhaust, where sound generated at the inlet propagates along the annular duct and refracts through the bypass jet before radiating into the far field. In this paper the effect of the acoustic impedance of the duct outer wall on the radiated acoustic field is studied.

9:20

3aNSa5. Acoustics of Low Mach Number Nozzles with Area Expansions. Fernando J. Lau (Instituto Superior Tecnico, Av. Rovisco Pais, 1049-001 Lisboa, Portugal, lau@ist.utl.pt), João M. Oliveira (Instituto Superior Tecnico, Av. Rovisco Pais, 1049-001 Lisboa, Portugal, joliveira@ist.utl.pt)

The acoustic wave equation for quasi-one-dimensional propagation is obtained, along a cylindrical duct with a significant area expansion and containing a low Mach number mean flow. The motivation is the study of the reflection in cross-sectional expanding area. The ray approximation, which holds only for wavelengths which are short compared with the length scales of the variation of the cross-section and mean flow velocity, is used as a factor to reduce the wave equation to a Schrodinger form, in a nozzle with a hyperbolic tangent expansion. The exact solutions are obtained, without restriction, as power series solutions around the middle of the duct; since this solution fails to converge at the two ends of the duct it is matched to the other solutions there, by application of the causality principle. In this way it is possible to calculate everywhere the pressure and velocity perturbation profiles, for both the transmitted and reflected waves, as well as the reflection and transmission coefficients. These are plotted as a function of the longitudinal coordinates along the duct for several values of the three dimensionless parameters in the problem, *viz.* (*i*) the area expansion ratio , *ii*) the Mach number of the mean flow at the central section and *iii*) the wavenumber.

Session 3aNSb

Noise and EURONOISE: Railway Noise and Vibration III

Richard A. Carman, Cochair
Wilson, Ihrig & Associates, 5776 Broadway, Oakland, CA 94618, USA

Franck Poisson, Cochair
SNCF DIR, 45, rue de Londres, Paris, 75379, France

David Thompson, Cochair
ISVR, University of Southampton, Highfields, SO17 1BT, UK

Contributed Papers

8:00

3aNSb1. Noise reduction of freight wagons achieved by LL-blocks implementation: Last investigations and results from IPG and NICOBB projects. Fabien Létourneaux (SNCF - Agence d'Essai Ferroviaire, 21 avenue Salvador Allende, F-94407 Vitry-Sur-Seine, France, fabien.letourneaux@sncf.fr), Jasper Peen (Lloyd's Register Rail Europe B.V., Catherijnesingel 33, PO Box 2016, 3500 GA Utrecht, Netherlands, jasper.peen@lrrail.com), Nicolas Meunier (Deutsche Bahn AG, Messungen Akustik (TZV12.1), Völckerstraße 5, D-80939 München, Germany, Nicolas.Meunier@bahn.de), Erwin H. Jansen (TNO Science and Industry, PO Box 155, 2600 AD Delft, Netherlands, erwin.jansen@tno.nl), Cora Cremezi-Charlet (UIC, 16,rue J. Rey, F-75015 Paris, France, cremezi@uic.asso.fr)

The high noise emission levels of freight wagons during rolling are mainly due to uneven wheel treads produced during the braking sequences when the vehicle is equipped with cast iron blocks. This has lead to the development of two types of composite brake shoes (K- and LL-blocks), which are far less aggressive to the wheel.It has been demonstrated that K-blocks achieve a noise reduction of about 10 dB but they are mainly dedicated, at term, to the new vehicles as their friction coefficient is very different to the cast iron one. LL-blocks are on the contrary especially designed for retrofit vehicles and do not require major modifications of the braking equipment. But as they were only very recently made available by the manufacturers due to difficulties in their development, noise efficiency of LL-blocks products is not well-established. This paper focuses on the noise reduction and noise emission values of freight vehicles equipped with LL-blocks. It aims at presenting on-going studies on this topic and at providing reliable and accurate results from different measurement campaigns carried out on a TSI reference track. This work is the result of a collaboration between the UIC project NICOBB and the Dutch Noise Innovation Programme.

8:20

3aNSb2. Measurements of curve squeal from Oslo's subway. Sigmund Olafsen (Brekke & Strand akustikk as, Hovfaret 17, N-0275 Oslo, Norway, so@bs-akustikk.no), Tore Killengreen (Brekke & Strand akustikk as, Hovfaret 17, N-0275 Oslo, Norway, tkn@bs-akustikk.no)

Curve squeal from the subway line at Brattlikollen, Oslo, has led to severe noise complaints through the years. Two important steps have been taken to reduce the problem. An automatic rail lubrication system has been installed on the critical spot, and Oslo's old subway trains (1300 series) are being replaced. One of the new trains (MX) has also been fitted with wheel dampers. Continuous measurements during 16 days and nights with 2238 train passages have been analyzed to verify the effectiveness of these steps to reduce noise. The main results are as follows: 1300 series trains without rail lubrication give severe curve squeal during 18% of the train passages. 1300 series trains with rail lubrication give severe curve squeal during less than 1% of the train passages MX trains give substantially less curve squeal than 1300 series trains, with or without lubrication The MX trains with wheel dampers gives no curve squeal, even without lubrication

8:40

3aNSb3. Reduction of Noise from Composite Steel/Concrete Aerial Structures by Damping Steel Plates. George P. Wilson (Wilson, Ihrig & Associates, Inc., 5776 Broadway, Oakland, CA 94618, USA, gwilson@wiai.com), Francis Kirschner (FGK Consulting, Inc., East Hills, Long Island, NY 11576, USA, francis516@aol.com)

Noise radiated from steel girders at bridges and aerial structures has been a long standing problem for steel wheel and rail systems. During the initial design period for the San Francisco Bay Area Rapid Transit System, a full scale model girder and deck was constructed in 1964 and tested with and without constrained layer damping on the steel girder plates. The radiated noise from 20 Hz to 150 Hz was reduced by 9 dB with full plate area damping. A test track installation in 1965 also showed about 9 dB reduction in wayside noise with the overall result within about 1 dB of the noise radiated by an all-concrete structure. Because full plate area constrained damping is expensive, a scheme with small area damping pads was developed in the 1970's and applied to composite steel/concrete aerial structures at the Atlanta rail transit system. The result was 9 to 10 dB reduction of low frequency radiated noise, allowing sound barrier walls at the outer edges of the decks to be fully effective in reducing overall wayside noise levels from trains. Drawings of the aerial structures and graphical results from vibration and noise tests are presented.

9:00

3aNSb4. Noise reduction applied to an engine cooling system for a diesel railway vehicle. Anders Frid (Bombardier Transportation, Östra Ringvägen 1, SE-72173 Vasteras, Sweden, anders.r.frid@se.transport.bombardier.com), Karl-Richard Fehse (Bombardier Transportation, Am Rathenaupark, 16761 Hennigsdorf, Germany, karl-richard.fehse@de.transport.bombardier.com)

In recent years there there has been growing attention to reduce the noise from rail traffic in urban areas. In or around stations and depots, noise from cooling systems and traction and auxiliary equipment normally dominates. New legislation setting noise limits for stationary and accelerating trains puts further emphasis on increased noise reduction of such sources. An experimental investigation has been carried out in which several design changes on a roof-mounted diesel engine cooler from the AGC (Autorail Grande Capacité) train have been assessed in laboratory and on a train. Even though this train is considered as a state-of-the-art product having very low noise emission, the engine cooler is identified as the dominating noise source when operating at its maximum capacity. The wide range of minor and major modifications tested includes different ways to guide the air flow into the fans, reduced tip clearance, absorption material in various positions

inside and outside the cooler. Also different fan types have been tried (an axial fan with swept blades and a radial fan). The work has been carried out within the 6th framework EU-project ″Silence″ (ref TIP4-CT-2005-516288)

9:20

3aNSb5. Upgraded BB64700 locomotives - Noise Management Plan during the redesign process. Sebastien Dalle (CETIM, 52, av. Felix Louat, 60300 Senlis, France, sebastien.dalle@cetim.fr)

To extend the working life of its BB 64700 locomotives, SNCF decided to upgrade a fleet of 19 tractive units. Priorities for the upgrading work include changing the motor and its cooling system, adding air conditioning to the cab while meeting new environmental obligations and improving cab acoustics. An acoustic model that combines calculations and experimental data is used as a platform to specify maximum allocated acoustic power to each system suppliers. The global approach to sub-structuring and acoustic synthesis is based on decomposition of the product in a main structure and several noise sources, and that their acoustic and vibration energy propagates via different identified transfer paths. The model, which is updated throughout the design process, serves as a decision tool to enable corrective action plans if a clause might be not respected. In the context of this project, measured noise levels on the upgraded locomotive meet SNCF specifications for interior and exterior acoustic according to the defined operating conditions (idling, max load traction).

9:40

3aNSb6. Noise reduction strategies for a light metro rail traction system. Nicola Rusciano (Dept. of Aerospace Engineering - University of Naples, Via Claudio, 21, 80125 Naples, Italy, nruscian@unina.it), Massimo Viscardi (Dept. of Aerospace Engineering - University of Naples, Via Claudio, 21, 80125 Naples, Italy, massimo.viscardi@unina.it), Stefano Ferraiuolo (Ansaldobreda, Via Argine, 80100 Naples, Italy, ferraiuolo .stefano@ansaldobreda.it)

Inside the paper the vibro-acoustic characterization of a light rail vehicle is presented, with special reference to the traction noise emission identification. As a first step , on board measurements and pass by measurements, were performed in order to separate traction noise from rolling noise; these test revealed the electrical engine, as the most relevant sources at low speed. The electrical engine has then been characterized during specific laboratory test and innovative noise control solution were proposed to be tested. The first one could be a modification of inverter algorithm; this trying to reduce the influence of most relevant acoustic tones. This approach is essentially based on a software modification of the PWM algorithm through which modify the engine's spectral response. The second possible tested approach involved the enclosure of the engine in a sort of semi-active skin panels co-located at short distance from the engine; it has been demonstrated that this approach, by the merging of passive and active peculiarities, potentially lead to a wide frequency range application area. Following laboratory tests, the PWM solution was also decided to be implemented during ″on board″ test; a wide set of experimental results will be presented and discussed.

10:00

3aNSb7. Tram noise emission: Spectral analysis of the noise source contributions. Marie-Agnès Pallas (INRETS, 25 av. F. Mitterrand, case 24, 69675 Bron, France, marie-agnes.pallas@inrets.fr), Joel Lelong (INRETS, 25 av. F. Mitterrand, case 24, 69675 Bron, France, lelong@inrets.fr), Roger Chatagnon (INRETS, 25 avenue F. Mitterrand, case 24, 69675 Bron, France, roger.chatagnon@inrets.fr)

In France we can assist to a wide development of tram networks for public transportation in main cities. At the same time arises questioning on the noise emission of trams and possible consequences for resident exposure. A French research project has been conducted for studying noise and vibration emission of trams : this paper concerns the description of the noise emission of passing-by trams. A measurement campaign was achieved on the city of Nantes network, involving two kinds of trams with distinct technologies and equipment, and tested on two types of tracks having different platform surfaces. Acoustic measurement included both a 2D-array for noise source identification and a microphone set for vertical directivity analysis. The dominant noise sources are mainly the bogie areas (powered bogies, unpowered bogies) and an extended noise source along the track and the lower part of the tram, all of them involving rolling noise. This paper focuses on the spectral description of the main sources. A parametric study is presented, pointing out the effect of speed, tram type and track type on the frequency distribution of the emitted noise.

Session 3aNSc

Noise, Computational Acoustics, and EURONOISE: Source Identification in Radiation and Scattering I

J. Stuart Bolton, Cochair
Ray W. Herrick Labs., School of Mech. Eng., Purdue University, 140 S. Martin Jischke Drive, West Lafayette, IN 47907-2031, USA

Peter Juhl, Cochair
Institute of Sensors, Signals and Electrotechnics, University of Southern Denmark, Niels Bohrs Allé 1, Odense S, 5230, Denmark

Invited Paper

8:00

3aNSc1. Spherical near field acoustic holography with microphones on a rigid sphere. Finn Jacobsen (Acoustic Technology Department, Technical University of Denmark, Ørsted Plads, B352, DK-2800 Lyngby, Denmark, fja@oersted.dtu.dk), Jørgen Hald (Brüel & Kjær Sound & Vibration Measurement A/S, Skodsborgvej 307, DK-2850 Nærum, Denmark, JHALD@bksv.com), Efrén Fernandez (Acoustic Technology Department, Technical University of Denmark, Ørsted Plads, B352, DK-2800 Lyngby, Denmark, efrenfer@hotmail.com), Guillermo Moreno (Acoustic Technology Department, Technical University of Denmark, Ørsted Plads, B352, DK-2800 Lyngby, Denmark, s051216@student.dtu.dk)

Spherical near field acoustic holography (SNAH) is a recently developed technique that makes it possible to reconstruct the sound field inside and just outside an acoustically transparent spherical surface on which the sound pressure is measured with an array of microphones with negligible scattering. Because of the versatile geometry of a sphere SNAH is potentially extremely useful for source identification. On the other hand a rigid sphere is somewhat more practical than an open sphere, and it is possible to modify the SNAH theory so that a similar sound field reconstruction can be made with an array of microphones flush-mounted on a rigid sphere. However, this approach is only valid if it can be assumed that the sphere has a negligible influence on the incident sound field, in other words if multiple scattering can be ignored, and this is not necessarily a good assumption when the sphere is close to a radiating surface. This paper describes the modified SNAH theory and examines the matter through simulations and experimentally.

Contributed Paper

8:20

3aNSc2. Applications of Near-field Acoustic Holography on Small Apertures. Rick Scholte (Eindhoven University of Technology, Dept. of Mechanical Engineering, Dynamics & Control, P.O. Box 513, 5600MB Eindhoven, Netherlands, r.scholte@tue.nl), Ines Lopez (Eindhoven University of Technology, Dept. of Mechanical Engineering, Dynamics & Control, P.O. Box 513, 5600MB Eindhoven, Netherlands, i.lopez@tue.nl), N.b. Roozen (Eindhoven University of Technology, Dept. of Mechanical Engineering, Dynamics & Control, P.O. Box 513, 5600MB Eindhoven, Netherlands, n.b.roozen@tue.nl), Henk Nijmeijer (Eindhoven University of Technology, Dept. of Mechanical Engineering, Dynamics & Control, P.O. Box 513, 5600MB Eindhoven, Netherlands, h.nijmeijer@tue.nl)

Small, finite measurement apertures are a major impediment for accurate and fast application of near-field acoustic holography (NAH). In theory, FFT-based NAH methods are very powerful and acquire extremely fast inverse calculations of the sound field. However, in practice the usually small amount of sensors in a measurement array limit the possibilities of classical implementations of NAH, especially near the edges of the array or measurement grid. An alternative method to, for example, spatial windowing, patch NAH, SONAH, etc. is the recently introduced border-padding technique. This method makes it possible to apply FFT-based NAH with a large increase of accuracy compared to the original methods, specifically at the measurement grid edges, while maintaining the high speed of the inverse process PNAH is known for. This work focuses on the application of border-padding and the practical implementation in a newly developed PNAH system. It illustrates a large variety of extended possibilities for PNAH that border-padding enables. Apart from the earlier introduced standard border-padding, experimental results are shown for a highly improved border-padding method. Measurements and calculations on industrial products illustrate the wide applicability of the presented method.

Invited Papers

8:40

3aNSc3. A study on regularization parameter choice in Near-field Acoustical Holography. Jesper Gomes (Brüel & Kjær Sound and Vibration Measurement A/S, Skodsborgvej 307, DK-2850 Nærum, Denmark, jgomes@bksv.com)

Regularization plays an important role in Near-field Acoustical Holography (NAH), and choosing the right amount of regularization is crucial in order to get a meaningful solution. An automated method such as the L-curve or Generalized Cross-Validation (GCV) is often used in NAH to choose a regularization parameter. These parameter choice methods (PCMs) are attractive, since they require no a priori knowledge about the noise. However, there seems to be no clear understanding of when one PCM is better than the other. This paper presents comparisons of three PCMs: GCV, L-curve and Normalized Cumulative Periodogram (NCP). The latter method is new within NAH and it is based on the Fourier transform of the residual vector. The methods are used in connection with three NAH methods: Statistically Optimized Near-field Acoustical Holography (SONAH), the Inverse Boundary Element Method (IBEM), and the

Equivalent Source Method (ESM). All combinations of the PCMs and the NAH methods are investigated using simulated measurements with different types of noise added to the input. Finally, the comparisons are carried out for a practical experiment. This aim of this work is to create a better understanding of which mechanisms that affect the performance of the different PCMs.

9:00

3aNSc4. Regularization method applied to deconvolution problem in Real-Time Acoustic Holography. Sebastien Paillasseur (ENSIM - LAUM, Université du Maine, rue Aristote, 72085 Le Mans, France, sebastien.paillasseur.etu@univ-lemans.fr), Jean-Hugh Thomas (ENSIM - LAUM, Université du Maine, rue Aristote, 72085 Le Mans, France, jean-hugh.thomas@univ-lemans .fr), Jean-Claude Pascal (ENSIM - LAUM, Université du Maine, rue Aristote, 72085 Le Mans, France, Jean-Claude.Pascal@univ-lemans.fr)

Near-field Acoustic Holography (NAH) [Maynard et Williams, 1985] is a measuring process for locating stationary sound sources from measurements made by an antenna of microphones positioned near the acoustic source plane. In order to characterize non-stationary sources, a new formulation has been introduced [Grulier, 2004] to propagate signals on a forward plane using a convolution product with an impulse response in the time-wavenumber domain. The purpose of this study is to solve the deconvolution problem in order to introduce the Real-Time Acoustic Holography and to test its accuracy. Taking the evanescent waves into account improves the spatial resolution of the solution but makes the deconvolution problem ″ill-posed″. Thus, the inverse of the impulse response is neither unique nor stable. Then, regularization methods that consist of giving an other constraint to the solution to solve this problem are studied. In particular, the standard Tikhonov regularization is used, which is based on the minimisation of the solution's energy, combined with generalized cross validation to estimate the regularization parameters. This method provides an image representation of the time dependent pressure of the source plane in order to localize and characterize the different sound sources.

9:20

3aNSc5. A comparison of SONAH and IBEM for near-field acoustic holography. Peter Juhl (Institute of Sensors, Signals and Electrotechnics, University of Southern Denmark, Niels Bohrs Allé 1, 5230 Odense S, Denmark, pmjuhl@sense.sdu.dk), Jesper Gomes (Brüel & Kjær Sound and Vibration Measurement A/S, Skodsborgvej 307, DK-2850 Nærum, Denmark, jgomes@bksv.com)

Among the popular techniques for acoustic source identification in complex environments are the Statistically Optimal Near Acoustic Holography (SONAH) and the Inverse Boundary Element Method (IBEM). These two methods are quite different regarding the underlying assumptions and the practical implementations: Whereas SONAH performs the back-propagation of the sound field to a plane surface; the IBEM has no restrictions on the radiating geometry. On the other hand, IBEM requires the generation of a surface mesh and a time consuming solution process. The present paper compares the performance of the two methods for a number of simulated test cases and studies the influence on the performance of the models when changing selected parameters. Finally, the performance of the methods is compared in a simple measurement setup.

9:40

3aNSc6. Precise localisation of noise source using statistically optimal beamforming and post -processing deconvolution. Jean-Claude Pascal (ENSIM - LAUM, Université du Maine, rue Aristote, 72085 Le Mans, France, Jean-Claude.Pascal@univ-lemans.fr), Jing-Fang Li (Visual VibroAcoustics, 51 rue d'Alger, 72000 Le Mans, France, jingfang.li@visualvibroacoustics.com), Xavier Carniel (Centre Technique des Industries Mécaniques (CETIM), 52, avenue Félix Louat, 60304 Senlis, France, Xavier.Carniel@cetim.fr), Axel Hass (52, avenue Félix Louat, 60304 Senlis, France, Axel.Haas@cetim.fr), Laurent Bollade (DYVA - DYnamique Vibration & Acoustique, 10 Rue Maryse Bastié, 69008 Lyon, France, laurent.bollade@dyva.fr)

Conventional data-independent beamforming with microphone array is widely used to locate sound sources and build acoustic model of equipments, engines and vehicles. The particularities of this technique are the use of a relatively few number of microphones and a simple signal processing. So, this technique is fast and easy to use. Other approaches using experimental data for computing the steering vector have been proposed to increase the resolution, for example, minimum variance method, and high-resolution methods. However these methods are often delicate to put in use in acoustic engineering where they are often reproached for lack of robustness in perturbed acoustic fields. Whereas, the most used methods nowadays are those by which the determination of the steering vector is data-independent. Among those methods we consider a method using a Statistically Optimal Array Processing (SOAP) completed by techniques of post-processing deconvolution, by which the resolution of the conventional beamforming is considerably increased, particularly at low frequencies. Some relevant indicators evaluate the performance of the proposed method by using perturbed data and by comparing between conventional and high-resolution beamformers. Examples of industrial measurements in a multi-sources environment demonstrate the practical interest of this technique.

10:00-10:20 Break

10:20

3aNSc7. Directional Recording and Analysis of Sounds from Musical Instruments. Franz Zotter (Institute of Electronic Music and Acoustics, Inffeldgasse 10 / 3, 8010 Graz, Austria, zotter@iem.at)

The sound of musical instruments doesn't radiate omni directionally into the sound field. Moreover, each component of the sound (e.g. a partial) can have its own directivity pattern which, in turn, may also vary over time. In general, the radiated sound in free space will have a different timbre at different locations around the sound source. In many cases the description of a particular radiation pattern contour may not be valid for other instruments, tones, playing techniques or even the same musical gesture on the same instrument. Consequently, this work focuses on the synchronous capture and analysis of musical sound sources with a spherical microphone array.

In order to analyze the directivity in its very detail, a spatial model for radiated sound is suggested. Assuming coherent signals, a common signal decomposition is applicable. The relations between the signal components yield the desired directivity patterns. Spherical harmonics interpolation between the discrete measurement points allows for the estimation of the radiation in a continuous angular space.

Contributed Paper

10:40

3aNSc8. Improving the localisation of sources based on shaped arrays with a reduced number of microphones. Lucille L. Lamotte (MicrodB, 7b allée Claude Debussy, 69130 Ecully, France, ll@microdb.fr), Quentin Leclere (Laboratoire Vibrations Acoustique - INSA Lyon, 25 bis avenue Jean Capelle, Bâtiment Saint-Exupéry, F-69621 Villeurbanne cedex, France, quentin.leclere@insa-lyon.fr)

The capacity of hardware today allows carrying out noise sources localisation without moving the microphone array at a limited financial and time cost. The single shot measurement processed with beamforming is comfortable for the user. But the quality of the results limits the interest of such systems: bad resolution, low dynamics and no quantitative levels. This article proposes complementary methods to beamforming to improve the results based on the same single measurement. First a near field beamforming algorithm is developed improving the resolution, and then an inverse method is applied based on the transfer function between the sources and the acoustic pressure at microphone positions or on the hologram in order to ″clean″ the localisation map and give quantitative results.

Invited Paper

11:00

3aNSc9. Array based measurement of radiated and absorbed sound intensity components. Jørgen Hald (Brüel & Kjær Sound & Vibration Measurement A/S, Skodsborgvej 307, DK-2850 Nærum, Denmark, JHALD@bksv.com), Jakob Mørkholt (Brüel & Kjær Sound & Vibration Measurement A/S, Skodsborgvej 307, DK-2850 Nærum, Denmark, jmorkholt@bksv.com), Pierre Hardy (Dassault Aviation, 80 quai marcel Dassault - Cédex 300, 92552 Saint Cloud, Cédex, France, Pierre.Hardy@dassault-aviation.com), Dominique Trentin (Dassault Aviation, 80 quai marcel Dassault - Cédex 300, 92552 Saint Cloud, Cédex, France, Dominique.Trentin @dassault-aviation.com), Martin Bach-Andersen (Ødegaard & Danneskiold-Samsøe A/S, Titangade 15, DK-2200 København Ø, Denmark, martin.bach-andersen@lr-ods.com), Graeme Keith (Ødegaard & Danneskiold-Samsøe A/S, Titangade 15, DK-2200 København Ø, Denmark, Graeme.Keith@lr-ods.com)

Calibration of energy flow models for cabin environments requires tools able to measure the energy flow between the sub-systems of the models. Here we shall specifically consider the energy flow between acoustic energy in the cabin and vibration energy in the panels. Sound intensity measurement, for example with a two-microphone intensity probe, can provide the total sound intensity at some distance from panels. It cannot resolve, how much of the intensity is due to radiation from the surface and how much is due to absorption of energy from the sound field. And it cannot provide the information right on the panel surface, leading to a degraded resolution. The ability to distinguish between radiated and absorbed intensity is important for energy flow modeling, and for identification of the areas where noise energy enters the cabin. The present paper describes some work done to measure the radiated and absorbed intensity components by the use of a double layer microphone array. Two measurements are performed: A measurement of surface absorption coefficient and an operational measurement. Non-locally reacting surfaces represent a particular challenge, the handling of which will be discussed. Results from both loudspeaker measurements and in-flight measurements will be presented.

Contributed Papers

11:20

3aNSc10. Cyclic Sound Intensity and Source separation from NAH measurements on a Diesel engine. Brice Lafon (Renault, 67 rue des Bons Raisins, CTR A03 3 37, 92500 Rueil Malmaison, France, brice.lafon @renault.com), Jerome Antoni (Université de Technologie de Compiègne, Centre de Recherche de Royallieu, rue Personne de Roberval, 60200 Compiègne, France, jerome.antoni@utc.fr)

Noise source separation and acoustic imaging are two research fields of interest in car industry. For this, RENAULT (French car manufacturer) and the University of Technology of Compiègne (UTC, France) are conducting an original study aiming to couple these fields to solve in an efficient way engine NVH problems. Previously, in the first part of this study, combustion noise separation on Diesel engine radiation was implemented from classical sound intensity measurements. The separation, based on Wiener filtering, was performed by taking advantage from the cyclostationary property of engine signals. The second part, presented here, aims to overcome the main shortcoming of the method: time-consuming measurements. Our method is then applied to Near-field Acoustic Holography that is faster and more adapted to an industrial context. Source separation is implemented to complete global radiation maps by specific-source radiation maps such as combustion and other sources radiating in low frequencies since NAH performs rather in low frequencies. Furthermore, the exploitation of cyclostationarity enables to define a cyclic sound intensity (an instantaneous intensity estimated during an average engine cycle). Then, radiation movies can be set to allow a precise location of a specific radiation emergence in space, in frequency and in crankshaft angle.

11:40

3aNSc11. Tire radiation in vehicle environment: A review of some source identification methods. Christophe Picard (PSA Peugeot Citroën, Route de Gisy, 78943 Vélizy-Villacoublay Cedex, France, christophe .picard3@mpsa.com), Matthieu Fiack (Segula Technologies for PCA, Route de Gisy, 78943 Vélizy-Villacoublay Cedex, France, matthieu .fiack1@ext.mpsa.com), Olivier Tanneau (Altran AIT for PCA, Route de Gisy, 78943 Vélizy-Villacoublay Cedex, France, tanneau77@hotmail .com), Olivier Sauvage (PSA Peugeot Citroën, Route de Gisy, 78943 Vélizy-Villacoublay Cedex, France, olivier.sauvage@mpsa.com), Laurent Gagliardini (PSA Peugeot Citroën, Route de Gisy, 78943 Vélizy-Villacoublay Cedex, France, laurent.gagliardini@mpsa.com)

The REBECA research project aims at defining new architectural concepts and reduction strategies of vehicle external noise emission regarding the international pass-by noise certification standard (ISO 362). The first task of the project is to qualify and quantify the major contributor of the external emission, the tires/road surface source. To this end, a 3D array composed of 164 microphones has been set up in the near and far field around vehicle. Measurements have been performed for several operational conditions with the use of a chassis dyno in a semi-anechoic chamber. A review and a comparison of some source identification methods has been led including experimental FRFs based on inverse techniques (Nelson), conventional and optimized beamforming approaches (Elias, Dougherty, Brooks and Humphreys, Ravetta) and inverse BEM method (Hamdi, Omrani). This

study permits to identify the more appropriate microphone array technique with respect to source identification robustness, power level and directivity radiation reconstruction in the far field.

12:00

3aNSc12. Large array optimization using a genetic algorithm and application to wide band moving sources imaging. Sébastien Debert (PSA-Peugeot-Citroën, Route de Gizy, CC : VV013 - Bât. 14, F-78943 Vélizy-Villacoublay Cedex, France, sebastien.debert@mpsa.com), François Ollivier (UPMC Univ Paris 06, CNRS UMR 7190 Institut Jean Le Rond D'Alembert, 2 Place de la Gare de Ceinture, 78210 Saint Cyr l'Ecole, France, frol@ccr.jussieu.fr)

In order to design a microphone array able to follow moving wide band acoustic sources, and improve the quality of the images obtained with a classical beam forming technique, numerical simulations were carried out. The various steps of the study are presented here. Searching the best design for a large microphone array, a simple genetic algorithm was developed. Considering a constant outer dimension of the array and technological constraints in order to design an adaptive array of 60 microphones, the algorithm selects among a large set several combinations of their positions. The functional being optimized is the directivity pattern, in terms of side lobes level. The genetic algorithm always converges to solutions comparable to a randomized set of microphones. Besides, taking advantage of symmetry properties of the array, an improvement of the speed of beamforming calculation was introduced. The optimum array being chosen, wide band moving sources were simulated and images were processed. In order to provide beam formed images with a constant resolution over the band a homotetic-balanced array of 120 microphones was assembled. Finally the dynamic of the images was significantly improved by performing a non-coherent image synthesis technique.

12:20

3aNSc13. Non stationary tire-road noise analysis using large array beam forming in the time and frequency domains. François Ollivier (UPMC Univ Paris 06, CNRS UMR 7190 Institut Jean Le Rond D'Alembert, 2 Place de la Gare de Ceinture, 78210 Saint Cyr l'Ecole, France, frol@ccr.jussieu.fr)

In the framework of the REBECA Project founded by the ADEME, one seeks to provide a description of the tire-road noise source from the exterior of the vehicle perspective. Far field acoustic imaging techniques were proposed to identify the sources. Therefore an optimised array of 120 microphones, 4 m in diameter, was modelled and built. Measurements of the noise produced by a car mounted on a roll were performed in a semi anechoïc room. The front car axle was driven at various constant speeds and to rising speeds as well. Beam formed images and point signals have been post-processed with a 125 kHz sampling rate in order to derive space and time analysis of the pressure field in the vicinity of the tire-roll contact point. The high rate movies processed clearly exhibit periodic phenomena generated around the contact point, while the tire structure borne source appears to be insignificant. Results of frequency and order analysis are also presented in this attempt to provide an interpretation of the tire/road contact noise in terms of source models.

WEDNESDAY MORNING, 2 JULY 2008 ROOM 253, 8:00 A.M. TO 1:00 P.M.

Session 3aNSd

Noise and EURONOISE: Tire-Road Noise from the Road Perspective I

Paul Donavan, Cochair
Illingworth & Rodkin, Inc., 505 Petaluma Blvd. South, Petaluma, CA 94952, USA

Fabienne Anfosso-Ledee, Cochair
Laboratoire Central des Ponts et Chaussées, BP 4129, Bouguenais Cedex, 44341, France

Invited Papers

8:00

3aNSd1. Tyre/road noise prediction: A comparison between the SPERoN and HyRoNE models - Part 1. Thomas Beckenbauer (Müller-BBM GmbH, Robert-Koch-Straße 11, 82152 Planegg, Germany, T.Beckenbauer@MuellerBBM.de), Philippe Klein (INRETS, 25 av. F. Mitterrand, case 24, 69675 Bron, France, philippe.klein@inrets.fr), Jean-François Hamet (INRETS, 25 av. F. Mitterrand, case 24, 69675 Bron, France, hamet@inrets.fr), Wolfgang Kropp (Chalmers University of Technology, Division of Applied Acoustics, SE-41296 Gothenburg, Sweden, wolfgang.kropp@chalmers.se)

The SPERoN and HyRoNE models predict the pass-by tyre/road noise of a passenger car from intrinsic characteristics of the road surface. Both models are hybrid: they combine statistical laws with physical models. With a computing time of a few minutes (very quick compared to full physical models), they provide operational tools for tyre/road noise prediction. Particular fields of interest are road surface optimisation with respect to noise at the laboratory scale, conformity of production of a new surface and acoustic monitoring of roads. They are now implemented as user-friendly stand-alone applications. The presentation will address the principles of the models, their performances and their respective main fields of application. Part 1 will address the principles of the models and their respective fields of application.

8:20

3aNSd2. Tyre/road noise prediction: A comparison between the SPERoN and HyRoNE models - Part 2. Philippe Klein (INRETS, 25 av. F. Mitterrand, case 24, 69675 Bron, France, philippe.klein@inrets.fr), Thomas Beckenbauer (Müller-BBM GmbH, Robert-Koch-Straße 11, 82152 Planegg, Germany, T.Beckenbauer@MuellerBBM.de), Jean-François Hamet (INRETS, 25 av. F. Mitterrand, case 24, 69675 Bron, France, hamet@inrets.fr), Wolfgang Kropp (Chalmers University of Technology, Division of Applied Acoustics, SE-41296 Gothenburg, Sweden, wolfgang.kropp@chalmers.se)

The SPERoN and HyRoNE models predict the pass-by tyre/road noise of a passenger car from intrinsic characteristics of the road surface. Both models are hybrid: they combine statistical laws with physical models. With a computing time of a few minutes (very quick compared to full physical models), they provide operational tools for tyre/road noise prediction. Particular fields of interest are road surface optimisation with respect to noise at the laboratory scale, conformity of production of a new surface and acoustic monitoring of roads. They are now implemented as user-friendly stand-alone applications. The presentation will address the principles of the models, their performances and their respective main fields of application. Part 2 will address the performances of the models.

8:40

3aNSd3. Experimental study of dynamical contact forces for tyre/road noise application. Julien Cesbron (Université d'Evry - Val d'Essonne, Laboratoire de Mécanique d'Evry, EA3332, 40, rue du Pelvoux, 91 020 Evry Cedex, France, cesbron.julien@neuf.fr), Fabienne Anfosso-Ledee (Laboratoire Central des Ponts et Chaussées, BP 4129, 44341 Bouguenais Cedex, France, fabienne.anfosso@lcpc.fr), Denis Duhamel (ENPC, UR Navier, 6 et 8 Avenue Blaise Pascal, Cité Descartes, Champs sur Marne, 77455 Marne la Vallée, France, duhamel@lami.enpc.fr), Hai Ping Yin (ENPC, UR Navier, 6 et 8 Avenue Blaise Pascal, Cité Descartes, Champs sur Marne, 77455 Marne la Vallée, France, yin@lami.enpc.fr), Donatien Le Houedec (Ecole Centrale de Nantes, GeM, 1 rue de la Noe, BP 92101, 44321 Nantes Cedex 3, France, Donatien.Lehouedec@ec-nantes.fr)

This paper deals with the experimental study of tyre/road contact forces in rolling conditions for tyre/road noise investigation. In situ measurements of contact forces and CPX noise levels were carried out for a slick tyre rolling on six different road surfaces at rolling speeds between 30 km/h and 50 km/h. Contact stresses were measured at a sampling frequency around 10000 Hz using a single array of digital pressure sensitive cells both in the transverse and in the longitudinal directions. The contact areas obtained during rolling were smaller than the one measured in statics. This could be due to an influence of the viscoelastic behavior of the rubber of the tyre tread during rolling. Additionally the global energy of the longitudinal contact forces at different speeds were in the same order for the six road surfaces, while their spectrums at different speeds were quite different. This may be explained by a spectral influence of the vibration of the tyre during rolling. Finally, the levels of longitudinal contact forces and CPX noise measured at 30 km/h were correlated. A high positive correlation was found around 800 Hz, which frequency could be directly linked to the road texture.

9:00

3aNSd4. Optimized thin layers for urban roads. Sigurd N. Thomsen (Danish Road Institute/Road Directorate, Guldalderen 12, 2640 Hedehusene, Denmark, snt@vd.dk), Hans Bendtsen (Danish Road Institute/Road Directorate, Guldalderen 12, 2640 Hedehusene, Denmark, hbe@vd.dk), Bent Andersen (Danish Road Institute/Road Directorate, Guldalderen 12, 2640 Hedehusene, Denmark, bea@vd.dk)

In the EU project SILENCE work has been carried out to optimize the noise reduction of different types of pavements for urban roads. The Danish Road Institute (DRI) participated in this work together with the Swedish National Road and Transport Research Institute (VTI) and BAST in Germany. Joint international development work has been carried out including laboratory experiments. The objective was to find pavements with promising noise reduction. It was decided to carry out a full scale field testing in some countries. DRI has in cooperation with the municipality of Copenhagen and the Colas road construction company tested series of SMA pavements and open graded pavements, optimized for noise reduction by using small aggregate size of 4 to 6 mm and by constructing a relatively high builtin air void. Eight different pavements were constructed in June 2007 on Kastrupvej in Copenhagen. DRI has conducted SPB and CPX noise measurements. An initial noise reduction for passenger cars of 4.3 dB in relation to a DAC 11 reference pavement has been achieved. It is planned to continue the measurements in the coming years in order to be able to analyse the long time acoustical and structural performance of these test pavements.

9:20

3aNSd5. Traffic noise levels after replacing the top of two-layer porous asphalt at Øster Søgade. Jørgen Kragh (Danish Road Institute/Road Directorate, Guldalderen 12, 2640 Hedehusene, Denmark, kragh@vd.dk), Hans Bendtsen (Danish Road Institute/Road Directorate, Guldalderen 12, 2640 Hedehusene, Denmark, hbe@vd.dk)

In 1999 three different types of two-layer porous asphalt pavement with 5 mm or 8 mm maximum aggregate in the top layer were built in a city street in Copenhagen. A section with dense asphalt concrete was built as a reference. The pavements have been monitored since then. The initial noise reduction of 6 - 7 dB compared with the noise level at the reference section has vanished over the years due to gradual clogging of the porosities in the pavement. After 8 years in service the drainage asphalt in the spring of 2007 was worn and ravelling had begun. The municipality of Copenhagen decided to have the top layer milled away and replaced by new porous asphalt with 8 mm maximum aggregate. This type had proven most durable, acoustically and structurally. Noise measurements were carried out in 2007 as part of the SILENCE project, both before and after replacing the top layer. The measurements showed that at two of the test sections most of the initial noise reduction was regained while this was not the case at the one test section that was thinnest (a total of 55 mm while the other were 70 mm and 90 mm, respectively).

Contributed Papers

9:40

3aNSd6. The effect of grinding and grooving on the noise generation of Portland Cement Concrete pavement. Tanya Wulf (Purdue Univ., 140 Martin Jischke Dr., Herrick Lab., West Lafayette, IN 47907, USA, twulf@purdue.edu), Tyler Dare (Purdue Univ., 140 Martin Jischke Dr., Herrick Lab., West Lafayette, IN 47907, USA, tdare@purdue.edu), Robert Bernhard (Purdue Univ., 140 Martin Jischke Dr., Herrick Lab., West Lafayette, IN 47907, USA, rbernhar@nd.edu)

In this investigation, studies have been done to understand the effects of various grinding and grooving parameters to investigate their effect on noise generation at the tire-pavement interface. Grinding uses diamond-infused blades that are closely-spaced such that the fins between the blade tracks break off exposing an entirely new surface. For grooving, the blades are more widely spaced such that the fins do not break off and the surface texture remains largely unchanged except for grooves that are used for moisture control. Both procedures, used independently or in combination, have an effect on the noise produced by the tire-pavement interaction. Variation of grinding parameters was shown to have as much as a 3 dB effect on noise generation. Variation in grooving parameters has a secondary effect, which allows grooves to be added to texture without overall effect on overall noise. This paper will illustrate the effects on noise of the different parameters, such as grinding depth, blade width, and blade spacing, for grinding and grooving.

10:00

3aNSd7. Monitoring 20 Silent Roads Over 10 Years In The Municipality Of Groningen. Wim Van Keulen (Vankeulen Advies BV, De Savornin Lohmanlaan 68, 5252 AJ Vlijmen, Netherlands, info @vankeulenadvies.nl)

The municipality of Groningen in the northern part of the Netherlands has a wide experience with the application of silent roads. This experience covers a period of about 20 tracks with 2-layered porous asphalt and various types of thin layers. These tracks have been and are monitored regularly. The obtained data from 10 years monitoring offer a vast amount of valuable information on noise reduction, durability, maintenance, costs, contracts and policy. The municipality of Groningen in the northern part of the Netherlands has a wide experience with the application of silent roads. This experience covers a period of about 20 tracks with 2-layered porous asphalt and various types of thin layers. These tracks have been and are monitored regularly. The obtained data from 10 years monitoring offer a vast amount of valuable information on noise reduction, durability, maintenance, costs, contracts and policy.

10:20-10:40 Break

10:40

3aNSd8. A quiet poroelastic road surface manufactured in a normal asphalt mixing plant. Nils-Åke Nilsson (Acoustic Control AB, Tumstocksvägen 1, SE-187 66 Taeby, Sweden, na.nilsson@acoustic.se), Nils Ulmgren (NCC Roads Sweden AB, R&D Center, Bryggervägen 13, SE194 36 Upplands Väsby, Sweden, nils.ulmgren@ncc.se), Ake Sandin (City of Goteborg, Traffic and Public Transport Authority, PO Box 2403, 403 16 Goteborg, Sweden, ake.sandin@trafikkontoret.goteborg.se)

A poroelastic road surface for low tire/road noise has been developed. It is manufactured using conventional asphalt mixing plants and conventional paving machines. Crumb rubber was added to the mix for attaining the desired elastic characteristics. The crumb rubber was subject to a long term pre-treatment before feeding it to the plant mixer. This ensures both long term durability and excellent adhesion to the binder. The crumb rubber grain size and amount in the mix has been carefully tuned to the aggregate grain size. By the pre-treatment of the crumb rubber the crumb rubber amount can be freely selected since it is not locked to the amount of binder (as for the hot bitumen pre-mixer technique) Single layer poroelastic road surface sections has been paved in Gothenburg. The reduction of noise relative to a SMA16 was found to be 4-6 dB(A) depending on the vehicle speed and amount of crumb rubber. The surface is almost unaffected by wear after 6 months winter traffic with studded tyres. Tuning the recipe for further increased reduction of the tire/road noise continues. Fundings from European Commission (project Quiet City Transport (QCITY)) is acknowledged.

Invited Paper

11:00

3aNSd9. Evaluation of the ASTM Standard Reference Test Tire for purposes of standardized measurement of on-bound tire/pavement noise. Paul Donavan (Illingworth & Rodkin, Inc., 505 Petaluma Blvd. South, Petaluma, CA 94952, USA, pdonavan @illingworthrodkin.com)

Currently in the US, efforts are underway to develop standard methods for on-board sound intensity (OBSI) measurement of tire-/pavement noise. Up until recently, the default standard tire was the Goodyear Aquatred 3 tire originally selected due to its apparent similarity to Tire A specified in the ISO CPX procedure. Because of longer-term availability, the ASTM Standard Reference Test Tire (SRTT) is the primary candidate for replacement of the Aquatred 3. Issues of concern for the SRTT include tire-to-tire variation, the relation of the SRTT to previously used reference tire, and the ″break-in″ period required for stable test tires. To address tire-to-tire variability, six SRTT's were tested on variety of asphalt (AC) and Portland cement concrete (PCC) surfaces. These included four new tires and two that had been in use for some time. Two of the new tires were retested with increasing use to examine any break-in period effect. For comparison, the older Aquatred 3 was also tested on these same surfaces using both OBSI and controlled pass-by measurements. The results of these measurements are presented along with their implication to for reference tire selection.

Contributed Papers

11:20

3aNSd10. Evaluation of effects of pavement characteristics on the OBSI levels using Principal Components Regression. Aybike Ongel (Kultur University, Ataköy Kampüsü Bakırköy, 34156 Istanbul, Turkey, aybikeongel@gmail.com), Erwin Kohler (Dynatest, University of California, Davis, CA 95616, USA, ekohler@dynatest.com), John Harvey (University of California, Civil and Environmental Engineering, Davis, CA 95616, USA, jtharvey@ucdavis.edu)

Tire/pavement noise is a major contributor to traffic noise at highway speeds. Tire/pavement noise is affected by different pavement properties. A study conducted in California measured the noise levels of different mix types and the mix characteristics affecting noise levels. In this study, tire-/pavement noise was measured using the on-board sound intensity (OBSI) method. Data was collected on four different types of pavement mixes: conventional open graded asphalt concrete (OGAC), rubberized asphalt concrete that are open graded (RAC-O), rubberized asphalt concrete that are gap graded (RAC-G), and dense graded asphalt concrete mixes (DGAC). A total of 72 field pavement sections were included in the study, all of which were less than 8 years old at the time of the measurements. This paper evaluates the pavement characteristics affecting noise levels using principal components regression. This technique was used due to the multicollinearity found among the variables. Two principal components were extracted from

the measured parameters such as air void content, gradation properties, pavement roughness, age, and pavement surface condition.

11:40

3aNSd11. Austrian experience with the backing board method for statistical pass-by measurements. Marco Conter (Arsenal Research, Giefinggasse 2, 1210 Vienna, Austria, marco.conter@arsenal.ac.at), Manfred Haider (Arsenal Research, Giefinggasse 2, 1210 Vienna, Austria, manfred.haider@arsenal.ac.at)

Traffic noise is one of the major environmental concerns within the countries of the European Union. 80 to 90% of the traffic noise pollution is generated by road traffic. The major part of the noise emitted by vehicles on roads in the mid- to high-speed range is nowadays due to tyre/road noise. It is generated by the interaction between tyre and road surface, and therefore the measurement of the typical noise emission is essential for the classification of pavements with regard to noise. The SPB method (Statistical Pass-By, ISO 11819-1) is nowadays the most widely used method to characterise road surfaces, but it is difficult to apply especially in the presence of roadside noise barriers. The backing board method, further developed within the EU Project SILENCE in the past years, offers a possibility to measure and to characterise surfaces also close to reflective objects and in urban environments. This paper describes the first Austrian experimental experience with the application of this variant of the SPB method.

12:00

3aNSd12. Acoustical characterisation and life-cycle of porous road surfaces. Beate Altreuther (Mueller-BBM GmbH, Robert-Koch-Str. 11, 82152 Planegg, Germany, beate.altreuther@muellerbbm.de), Wolfram Bartolomaeus (Bundesanstalt fuer Strassenwesen, Bruederstr. 53, 51427 Bergisch Gladbach, Germany, bartolomaeus@bast.de)

The German Federal Highway Research Institute (Bundesanstalt für Straßenwesen, BASt) is planning to develop an assessment procedure to characterize the acoustical properties of porous road surfaces. Final objective is to specify the life-cycle of these pavements with respect to their acoustical performance based on civil engineering properties. In 2007 comprehensive measurements of the acoustically relevant parameters absorption coefficient, air flow resistance and surface texture have been performed on a multitude of bavarian motorways with porous asphalt pavements of different types of construction and different ages. Additional measurements of the near-field rolling noise (CPX) as well as measurements of the statistical pass-by-noise (SPB) have been performed. From precedent projects for the sections under investigation there is an extensive database covering details on asphalt mixtures as well as the results of drill core investigations concerning void content, binder content etc. The results of the present investigation allow to draw new conclusions with respect to acoustical performance and durability of porous asphalt pavements. We gratefully acknowledge the project funding by the German Federal Ministry of Transport, Building and Urban Affairs (project No. FE 02.276/2006/LRB).

12:20

3aNSd13. DEUFRABASE: A German-French acoustic database on road pavements. Michel C. Berengier (Laboratoire Central des Ponts et Chaussées, Centre de Nantes - Route de Bouaye, BP 4129, 44341 Bouguenais cedex, France, Michel.Berengier@lcpc.fr), Bettina Droste(Bundesanstalt für Strassenwesen, Brüderstrasse 53, 51427 Bergisch Gladbach, Germany, droste@bast.de), Benoit Gauvreau (Laboratoire Central des Ponts et Chaussées, Centre de Nantes - Route de Bouaye, BP 4129, 44341 Bouguenais cedex, France, benoit.gauvreau@lcpc.fr), Denis Duhamel (ENPC, UR Navier, 6 et 8 Avenue Blaise Pascal, Cité Descartes, Champs sur Marne, 77455 Marne la Vallée, France, duhamel@lami.enpc.fr), Markus Auerbach (Bundesanstalt für Strassenwesen, Brüderstrasse 53, 51427 Bergisch Gladbach, Germany, m.auerbach@bast.de)

In the framework of a DEUFRAKO (German/French cooperation) project on the Prediction and Propagation of Rolling Noise (P2RN), it has been proposed to rank the different German and French road pavements with respect to noise for different long distance configurations representative of real road topographies, ground characteristics and meteorological situations. After identification of those typical 28 configurations, the attenuations between a reference point in the near field and several receiving points in the far field have been computed according to the most relevant and adapted modelling methods currently available. The main goal being the accuracy of the prediction and not the computation time, analytical (ray tracing) and numerical (BEM, Parabolic Equation) approaches have been implemented. In the following, a technique permitting to estimate day and night LAeq and Lden has been used to classify the various pavements for the whole configurations. All those results have been gathered in a common database (DEUFRABASE) which will be directly available on the website of the authors' Institutes. The paper deals with the description of the ranking procedures, how the database is implemented on the web and how to use it for road traffic noise prediction.

12:40

3aNSd14. Road noise characterization by Harmonoise procedures reviewed for the Italian case. Luca Alfinito (University of Pisa - Dept. of Civil Engineering, Via Diotisalvi, 2, 56100 Pisa, Italy, l.alfinito@arpat.toscana.it), Gaetano Licitra (ARPAT - Dept. Firenze, Via Porpora, 22, 50144 Firenze, Italy, g.licitra@arpat.toscana.it), Mauro Cerchiai (ARPAT - Dept. Pisa, Via V. Veneto, 27, 56127 Pisa, Italy, m.cerchiai@arpat.toscana.it), Lorenzo Magni (ARPAT - Dept. Pisa, Via V. Veneto, 27, 56127 Pisa, Italy, l.magni@arpat.toscana.it), Massimo Losa (University of Pisa - Dept. of Civil Engineering, Via Diotisalvi, 2, 56100 Pisa, Italy, losa@ing.unipi.it)

Several methods have been introduced to describe acoustical properties of road pavements in situ, such as the extended surface technique (Adrienne), the Statistical Pass-By and the Close Proximity methods. In general the aim of these techniques, normed in ISO standards, is to evaluate some indexes that may be representative of noise generation and propagation with respect to tyre-road interaction and surface absorption. In this paper we use results obtained in the LEOPOLDO project, that involves measurements carried out on many sites all over Tuscany Region characterized by typical conditions of Italian roads, to review the state-of-the-art of acoustical parameters in the modelling of road vehicles showed in the HARMONOISE documents. This task has been accomplished by comparing the theoretical results obtained from the HARMONOISE prediction method with the energy levels measured at the microphone locations close to the road borders, in order to apply corrections to the parameters influencing sound generation and propagation. As a consequence, we introduce a new parameter, related to transfer function between source and receiver sound energy levels, which involves directivity and ground reflection effects, obtaining a more suitable characterization of road surface acoustical behaviour.

Session 3aNSe

Noise, Structural Acoustics and Vibration, Signal Processing in Acoustics, and EURONOISE: Airframe Noise Measurement, Prediction, and Control I

Joe W. Posey, Cochair
NASA, Langley Research Center, MS 461, Hampton, VA 23681, USA

Denis Gely, Cochair
Département Simulation Numérique des écoulements et Aéroacoustique (DSNA), Onera, BP72 - 29 avenue de la Division Leclerc, 92320 Chatillon, France

Invited Paper

10:00

3aNSe1. Airframe noise prediction. Yueping Guo (Boeing, 5301 Bolsa Ave, Huntington Beach, CA 92647, USA, yueping.guo @boeing.com)

This presentation discusses the prediction of aircraft airframe noise, namely, the noise that is generated by non-propulsion components of aircraft, including the leaning edge slats, the side edges of flaps and the landing gears. An overview will be given on various methodologies, ranging from empirical prediction to more physics-based modeling to full-blown numerical simulation. The advantages of each method will be discussed and compared with each other to reveal the most suitable application domain of each method. Detailed discussions will be given to the physics-based modeling, such as the acoustic analogy, which is ranked in between empirical and numerical methods in various aspects, including accuracy, turn-around time, limitations on geometry and flow conditions, and applicability/ feasibility in practical design applications. Examples will be given to demonstrate the applications of acoustic analogy in both noise prediction and noise reduction treatment design. Critical elements of the method that can and need to be improved to further mature the method will also be identified and discussed, providing potential directions for future research and development.

Contributed Paper

10:20

3aNSe2. ONERA's activities on airframe noise numerical simulation. Eric Manoha (ONERA (French aerospace Center), CFD & Aeroacoustics Department, BP 72, 29 avenue de la division Leclerc, 92322 Chatillon Cedex, France, eric.manoha@onera.fr)

Airframe noise, or noise generated by flow around the airframe (high lift devices, landing gears and cavities), is a major contributor to the overall noise of large commercial aircraft in the approach phase. For several years, ONERA has been involved in the development of methodologies for the numerical simulation of airframe noise. These hybrid methods generally combine (i) CFD computations for the near field flow, including unsteady CFD techniques such as LES, DES and NLDE, and (ii) acoustic (CAA) propagation techniques in the mid- and far-field. A large range of acoustical methods is available for the propagation of sound waves in uniform or heterogeneous mean flows, either from the family of integral methods (Lighthill, FWH, BEM) or in the domain of (non-linear or linearized) Euler equations in perturbation. The key challenges of these hybrid methodologie are (i) the ad-hoc coupling between individual techniques and (ii) the availability of reliable and dedicated experimental database for the validation. The paper presents a survey of ONERA's activities in this field, with applications to (i) single symmetrical airfoil, (ii) high lift wing with deployed slat and flap, (iii) landing gears and (iv) cylindrical cavities.

Invited Papers

10:40

3aNSe3. Measurement techniques for airframe noise source identification. Ricardo A. Burdisso (Virginia Tech, Mechanical Engineering, 153 Durham 0238, Blacksburg, VA 24061, USA, rburdiss@vt.edu)

Despite the significant progress achieved over the last three decades, noise pollution generated by aircraft around airports is still an obstacle to the further growth of the aviation industry. The engines and airframe constitute the main sources of the overall aircraft noise. Airframe noise is as important as the engine noise on approach due to the engines operating at low thrust. High-lift devices and landing gears are the dominant airframe noise components. Many efforts have recently been devoted to accurately locate and control the specific components of the airframe noise. Experimental studies on airframe noise include full-scale flight tests, and tests conducted on isolated small-scale models in both hard-walled and anechoic wind tunnels. These experimental efforts on airframe noise have been greatly helped by the advent of the microphone phased array technology. This presentation will focus on microphone phased array measurement techniques, in particular for model scale testing in wind tunnels. Issues such as beamforming algorithms, data corrections, effect of flow and acoustic environment on the measurements (hard-wall vs anechoic tunnels), etc. will be discussed. Illustrative results from experimental measurements of landing gear and high lift devices performed at the Virginia Tech wind tunnel will also be presented.

11:00

3aNSe4. Reduction technologies and prediction of high lift noise. Jan W. Delfs (DLR/Institute of Aerodynamics and Flow Technology, Lilienthalplatz 7, 38108 Braunschweig, Germany, jan.delfs@dlr.de)

In the final approach phase airframe noise represents the ultimate aircraft noise barrier for future aircraft when equipped with quiet UHBR engines. This paper presents some of the main dependencies of high-lift noise sources on flow conditions as derived from extensive noise testing at DLR. Some successful reduction technologies for high-lift noise are discussed in view of their influence on the noise generation mechanisms. The remainder of the paper focusses on the numerical prediction of high-lift noise. The prediction concept as implemented in DLR's PIANO code is discussed. It is based on a two step approach, a) the computation of the time averaged turbulent flow field as a result of a CFD(=Computational Fluid Dynamics) simulation and b) the highly accurate CAA (=Computational Aeroacoustics) simulation of perturbations about this mean flow. The prediction relies on an advanced stochastic modelling of the turbulence related sources and thus avoids time consuming turbulence simulations. The method represents an accurate yet ″low cost″ prediction of high-lift noise. This is particularly important for real applications at flight (very high) Reynolds numbers and corresponding design trade-off studies, which typically require the computation of large numbers of configurations. Examples for such kind of applications are given.

Contributed Paper

11:20

3aNSe5. Acoustic characterization and noise reduction strategies for a general aviation aircraft. Nicola Rusciano (Dept. of Aerospace Engineering - University of Naples, Via Claudio, 21, 80125 Naples, Italy, nruscian@unina.it), Massimo Viscardi (Dept. of Aerospace Engineering - University of Naples, Via Claudio, 21, 80125 Naples, Italy, massimo.viscardi@unina.it)

This work concerns with the vibro-acoustic characterization of a general aviation aircraft with the objective of designing solutions to reduce the inside noise level during the flight; first of all a new passive insulation, and then verifying the possibility of an active noise control approach. The acoustic characterization was performed into two different step; in-flight acoustic and vibration measurements during a typical mission of the vehicle were initially measured, to characterize the acoustic levels and spectra elated to the different flight operations. Ground measurement were also performed to characterize the sound insulation properties of the aircraft structure. The next item was the partial re-design of the sound insulation pack for the vehicle by the use of innovative material; the choice of the best technical solution has been performed by the use of numerical prediction models and through experimental tests on modified samples of the aircraft structure. The in-flight acoustic and vibration measurement showed also the presence of dominant low frequencies tonal components related to the BPF's and upper harmonics. This situation suggested the possibility to implement an active noise control approach. All these activities will be herein presented and discussion of the main results will be performed within the paper.

Invited Paper

11:40

3aNSe6. On the reduction of flap side edge noise. Florence Hutcheson (NASA Langley Research Center, Hampton, VA 23681, USA, Florence.V.Hutcheson@nasa.gov), Thomas F. Brooks (NASA Langley Research Center, Hampton, VA 23681, USA, thomas.f.brooks@nasa.gov)

Results from flap side edge noise reduction experiments are presented. The test model used was a NACA 632-215 main-element airfoil with a half-span Fowler flap. The flap side edge was flat for the baseline configuration. The effect that small geometric variations of the flap edge have on the noise spectra is shown, and noise measurements from a ″continuous mold-line link″ (CML) flap configuration are presented. These measurements are compared to those obtained from the baseline flap. The results indicate that a large level of noise reduction is achieved using the CML flap. Finally, Particle Image Velocimetry (PIV) measurements of the flow in the region of a flap side edge are presented for a blowing flap configuration. In this active control approach, air was blown from small slots located along the side edge of the flap to weaken the vortex system that is present in that region of the flap. These measurements are presented to show the effects that the flap tip jets have on the structure of the flap side edge flow, and the potential that this blowing flap configuration has in reducing flap side edge noise.

Contributed Paper

12:00

3aNSe7. Landing gear noise assessment on Airbus aircraft. Nicolas Molin (Airbus France, 316 route de Bayonne, Acoustics and Environment Dept EDEA, 31060 Toulouse, France, nicolas.molin@airbus.com)

During the last two decades, airframe noise sources (high lift devices and landing gears) have become noticeable in new aircraft technology, especially during approach. Aircraft manufacturers need prediction tools, in order to include noise modelling at the early stages of aircraft design. Such tools can be developed on the basis of simple formulations. As long as the dominant features are preserved in the simplified problems, the solution is believed to behave correctly in terms of EPNdB. Such a model of landing gear noise prediction was developed in the late 1990s. It is based on the decomposition of a landing gear into different noise sources: the primary structure (massive elements) and the secondary structure (wire, pipes, œ), whose noise is estimated with existing classical source noise model fed with empirical constants based on wind tunnel test results. Airbus implemented this model into its total aircraft noise program and validated it with dedicated flight tests. As the model takes into account all main components with their geometry, it is well adapted to predict the impact of add-on treatment such as fairings on the gear or the impact of an advanced low noise gear with simplified geometry.

Invited Paper

12:20

3aNSe8. A design-oriented approach to landing gear noise prediction. Philip J. Morris (Penn State University, 233C Hammond Building, University Park, PA 16802, USA, pjm@psu.edu), Kenneth S. Brentner (Penn State University, 233C Hammond Building, University Park, PA 16802, USA, ksb16@psu.edu), Leonard V. Lopes (Penn State University, 233C Hammond Building, University Park, PA 16802, USA, lvl105@psu.edu)

Landing gear noise is one of the most important sources of airframe noise. But it is the most difficult to predict. The difficulty is that the landing gear is made up of components of substantially different scales. The small-scale features such as tubes and hoses are known to contribute to the landing gear noise, especially in the mid to high frequency range. Existing semi-empirical models are only reliable for the range of landing gear geometries for which test data are available. The present paper describes a component-based landing gear noise prediction model. The method uses an application of simple, fast, and scalable models called acoustic elements that are used to represent the complex landing gear geometry with a high level of geometric detail. Extensions to an earlier model developed by the authors is described, including the replacement of the original time domain approach with a frequency domain method. The local mean flow is also taken into account through the use of low-fidelity computational fluid dynamics simulations. Estimates of the effects of acoustic shielding are also described. Comparisons are made with available experimental data to demonstrate the capabilities of the method. Future improvements are also described.

WEDNESDAY MORNING, 2 JULY 2008 ROOM 251, 10:40 A.M. TO 12:40 P.M.

Session 3aNSf

Noise and EURONOISE: Soundscape in the Heritage of Urban and Natural Areas I

Bennett Brooks, Cochair
Brooks Acoust. Corp., 27 Hartford Turnpike, Vernon, CT 06066, USA

Giovanni Brambilla, Cochair
CNR Institute of Acoustics, Via del Fosso del Cavaliere 100, Rome, 00133, Italy

Invited Papers

10:40

3aNSf1. Modeling auditory attention focusing in multisource environments. Bert De Coensel (Ghent University - Department of Information Technology, Sint-Pietersnieuwstraat 41, 9000 Ghent, Belgium, bert.decoensel@intec.ugent.be), Dick Botteldooren (University Ghent - Department Information Technology, Sint-Pietersnieuwstraat 41, 9000 Gent, Belgium, dick.botteldooren@intec.ugent.be)

In this paper, a mathematical submodel for auditory attention focusing is discussed in the framework of our ongoing research towards a unified model for soundscape perception. The submodel implements a balance between top-down focusing, in which higher level cognition guides attention towards expected sources, and bottom-up focusing, in which attention is triggered by the noticing of sound events. Attention elasticity - the ability to switch attention between different environmental sounds - depends on the current context (natural, urban...) as well as on the current activity of the modeled individual. The soundscape perception model is applied to case studies of simulated sound exposure in open area and in environments with a mixture of natural and man-made sounds. A comparison of the simulation results with survey results shows that introducing a submodel for auditory attention focusing into our model for soundscape perception enhances its ability to predict the emergence of annoyance.

11:00

3aNSf2. SOUND-SCAPE: A framework for characterising positive urban soundscapes. Rebecca Cain (WMG, The University of Warwick, International Manufacturing Centre, CV4 7AL Coventry, UK, R.Cain.1@warwick.ac.uk), Paul Jennings (WMG, The University of Warwick, International Manufacturing Centre, CV4 7AL Coventry, UK, paul.jennings@warwick.ac.uk), Mags Adams (Acoustics Research Centre, University of Salford, Newton Building, Salford, M5 4WT Manchester, UK, M.D.Adams@salford.ac.uk), Neil Bruce (Acoustics Research Centre, University of Salford, Newton Building, Salford, M5 4WT Manchester, UK, N.S.Bruce@pgr.salford.ac.uk), Angus Carlyle (London College of Communication, University of the Arts, Elephant & Castle, SE1 6SB London, UK, angus_carlyle@yahoo.co.uk), Peter Cusack (London College of Communication, University of the Arts, Elephant & Castle, SE1 6SB London, UK, pcusack@btinternet.com), William Davies (Acoustics Research Centre, University of Salford, Newton Building, Salford, M5 4WT Manchester, UK, w.davies@salford.ac.uk), Ken Hume (School of Chemistry, Biological and Health Science, Manchester Metropolitan University, Chester Street, M1 5GD Manchester, UK, K.I.Hume@mmu.ac.uk), Christopher J. Plack (Psychology Department, Lancaster University, LA1 4YF Lancaster, UK, c.plack@lancaster.ac.uk)

People's assessments of urban soundscapes are dependent upon many factors. For example, perceptions of a soundscape may depend on the activity that the listener is doing and their associated listening state at the time. Temporal variations (daily, weekly, seasonal) can also affect perceptions of the soundscape, as can the type and usage of urban space, architectural characteristics and the cultural and historical setting. The context of listening is also a factor in terms of the cognitions that people bring to the listening situation by way

of memories, preferences, attitudes, values and meaning. In order to inform the planning process with regard to assessing and creating positive urban soundscapes, a framework is under development. The framework attempts to bring together all the influencing factors in urban soundscape assessment in a new and novel way, and considers how the identification of sources and the variety and mix of sources interact to produce a soundscape. The framework presented in this paper forms the basis of multi-disciplinary soundscape research in the EPSRC funded ″Positive Soundscapes Project″, which seeks to develop a rounded view of human perception of soundscapes by combining methods from several disciplines.

11:20

3aNSf3. Can urban squares be recognized by means of their Soundscape? Giovanni Brambilla (CNR Institute of Acoustics, Via del Fosso del Cavaliere 100, 00133 Rome, Italy, giovanni.brambilla@idac.rm.cnr.it), Maria Di Gabriele (Built Environment Control Laboratory Ri.A.S., Second University of Naples, Abazia di S. Lorenzo, 81031 Aversa, Italy, maria.digabriele@unina2.it), Luigi Maffei (Built Environment Control Laboratory Ri.A.S., Second University of Naples, Abazia di S. Lorenzo, 81031 Aversa, Italy, luigi.maffei@unina2.it), Patrizio Verardi (CNR Institute of Acoustics, Via del Fosso del Cavaliere 100, 00133 Rome, Italy, patrizio .verardi@idac.rm.cnr.it)

Squares have always played important functions in urban areas, being a reference place in the citizen's life. During last decades, road traffic noise has influenced the perception of the sonic environment in many squares. However, there are squares where historical and typical sound sources are still present. In both cases the sonic environment remains a feature of the square together with other factors, like the visual impact. The present paper deals with the above issue and describes an experiment aimed to study how the soundscape of a square can contribute to recognize the square itself. For this purpose some well known squares in Naples and Rome have been selected to cover a range of different characteristics. In each square binaural recordings and pictures have been taken simultaneously. Then the binaural recordings have been played back by headphone to a group of subjects in laboratory simultaneously to the display of the pictures of all squares on a screen. After listening each sound the subject was asked to choose among the pictures the one showing the square judged to have the sonic environment most appropriate to the sound just heard. The comparison between subjective responses and correct answers are in progress.

11:40

3aNSf4. Fountains as a natural component of urban soundscape. Catherine Semidor (GRECAU-ENSAPBx, Domaine de Raba, 33400 Talence, France, catherine.semidor@bordeaux.archi.fr), Flora Venot-Gbedji (GRECAU-ENSAPBx, Domaine de Raba, 33400 Talence, France, flora.venot@bordeaux.archi.fr)

Fountains play an important role in urban landscape as well as being a cultural mark in a city. They also have an environmental function. For example, their effect in the control of the microclimate is well known. The paper deals with the sound effects which big fountains located in large squares have on the urban soundscape of the area. In particular, we deal with how their natural character can change the global perception of the site. Indeed, the representation of water sounds is positively appreciated by most city-dwellers. Depending on their size and shape, they are able to give a quiet or a dynamic character to the site. But in the case of areas with a lot of traffic we ask ourselves what are the interactions with strong background noise level and others sound sources. GRECAU uses the soundwalk method to assess the acoustic environment. The following case studies, Plaza de Cataluna in Barcelona and Piazza Ferrari in Genoa, are two examples of such a situation. Some of the results we give here try to answer the previous questions.

12:00

3aNSf5. Contemporary soundscape of ancient theatres. Kalliopi Chourmouziadou (School of Architecture, University of Sheffield, Western Bank, S10 2TN Sheffield, UK, pepitahou@hotmail.com), Jian Kang (School of Architecture, University of Sheffield, Western Bank, S10 2TN Sheffield, UK, j.kang@sheffield.ac.uk)

Ancient drama is performed every summer in ancient theatres in the Mediterranean countries, especially in Greece. In many cases the performance conditions in terms of acoustics are poor, due to the effects of external noise sources. There is often a motorway constructed near an archaeological site, without careful consideration regarding the impact on the overall soundscape. Previous studies have demonstrated the effectiveness of purposely designed scenery on improving the internal acoustic conditions, and this study investigates the contribution of scenery to the improvement of the acoustic environment of ancient theatres in terms of reducing nearby traffic noise. The acoustic simulation for the theatre of Philippi, with scenery design in the form of a background wall in different sizes, suggests that there is a decrease in traffic noise by about 4dB. Further improvements have also been demonstrated with noise barriers of various heights and lengths. Different levels of traffic flow have been examined. It is expected that the results will be verified by on-site measurements and recordings of summer performances will be presented during the conference.

Contributed Paper

12:20

3aNSf6. Soundscape and California planning guidelines. Richard B. Rodkin (Illingworth & Rodkin, Inc., 505 Petaluma Boulevard South, Petaluma, 94952, USA, rrodkin@illingworthrodkin.com), Michael S. Thill (Illingworth & Rodkin, Inc., 505 Petaluma Boulevard South, Petaluma, 94952, USA, mthill@illingworthrodkin.com)

Community noise has been recognized as a significant environmental concern in California for more than 30 years. All cities and counties are mandated by state law to include a Noise Element as a part of the community's General Plan to provide ″a basis for comprehensive local programs to control and abate environmental noise and to protect citizens from excessive exposure.″ What is, and has been missing from this process, is how the soundscape in a particular setting may affect the compatibility of land uses there. Generalized noise and land use planning guidelines are no longer sufficient. Specific attention must be given to the development of guidelines and policies that address ″smart growth″ in and around urban and suburban transportation corridors, residential and agricultural interactions, mixed-use developments, industrial-to-residential conversions (e.g., the gentrification of traditionally industrial areas like ports). A new soundscape vocabulary must be introduced to describe the acoustical environments in these settings to facilitate other goals in land use planning. Examples are presented of specific communities where planning goals and traditional noise and land use compatibility guidelines were in conflict and how these were resolved.

Session 3aPAa

Physical Acoustics: Nonlinear Acoustics of Consolidated Materials and Non Destructive Testing I

Jim A. Tencate, Cochair
EES-11 (Geophysics) - Los Alamos National Laboratory, MS D443, Los Alamos, NM 87545, USA

Koen Van Den Abeele, Cochair
K.U.Leuven Campus Kortrijk, E. Sabbelaan 53, Kortrijk, 8500, Belgium

Contributed Papers

8:00

3aPAa1. Three wave mixing test of hyperelasticity in sedimentary rocks. David L. Johnson (Schlumberger-Doll Research, One Hampshire St., Cambridge, MA 02139, USA, johnson10@slb.com), Kenneth Winkler (Schlumberger-Doll Research, One Hampshire St., Cambridge, MA 02139, USA, kwinkler@boston.oilfield.slb.com), Ralph D'Angelo (Schlumberger-Doll Research, One Hampshire St., Cambridge, MA 02139, USA, dangelo2943@boston.oilfield.slb.com)

We report measurements of 3-wave mixing amplitudes on solids whose 3rd order elastic constants have also been measured by means of the elasto-acoustic effect. Because attenuation and diffraction are important aspects of our measurement technique we analyze our results using a frequency domain version of the KZK equation, modified to accommodate an arbitrary frequency dependence to the attenuation. We find that the value of β so deduced for polymethylmethacrylate (PMMA) agrees quite well with that predicted from the stress-dependent sound speed measurements, establishing that PMMA may be considered a hyperelastic solid, in this context. The β values of sedimentary rocks, though they are typically two orders of magnitude larger than e.g. PMMA's, are still a factor 3-10 less than those predicted from the elasto-acoustic effect. Moreover, these samples exhibit significant heterogeneity on a centimeter scale, which heterogeneity is not apparent from a measurement of the position dependent sound speed.

8:20

3aPAa2. Fatigue Damage Monitoring and Remaning Life Assessment using Nonlinear Vibro-Modulation Technique. Dimitri Donskoy (Stevens Institute of Technology, Dabvidson Lab., 711 Hudson Street, Hoboken, NJ 07030, USA, ddonskoy@stevens.edu), Alexander Chudnovsky (Univ. of Illinois at Chicago, Fracture Mechanics & Material Durability Lab., 842 W. Taylor Styreet, Room 2095 ERF, Chicago, IL 60607, USA, achudnov@uic.edu), Andrei Zagrai (New Mexico Institute of Mining and Technology, Department of Mechanical Engineering, 801 Leroy Pl., Weir Bld., Room 124, Socorro, NM 87801, USA, azagrai@nmt.edu), Edvard Golovin (Univ. of Illinois at Chicago, Fracture Mechanics & Material Durability Lab., 842 W. Taylor Styreet, Room 2095 ERF, Chicago, IL 60607, USA, egolovin@cs.com), Vinod Agarwala (Naval Air Systems Command, 48110 Shaw Road, Bldg. 2187/Suite 2373, Patuxent River, MD 20670, USA, vinod.agarwala@navy.mil)

Assessment of structural deterioration due to in-service and environmental loads is an essential element in ensuring safety, operability and long life of various structures and structural components. We applied vibro-acoustic modulation technique to monitor material degradation at the micro/meso scale before the onset of the macro-scale fracture. The technique explores nonlinear acoustic interaction of high frequency ultrasound and low frequency structural vibration at the site of the incipient damage. It is shown that micro/meso scale degradation increases the material nonlinearity leading to modulation of the high frequency ultrasonic signal by low frequency vibration, quantified by the nonlinear acoustic Damage Index (DI). Numerous tests with hundreds of test coupons proved high sensitivity of the developed technique to micro/meso scale fatigue damage accumulation. The study further demonstrated that the remaining life of the fatigued material can be predicted using phenomenological damage accumulation rule expressed through measured Damage Index. Work supported by NAVAIR.

8:40

3aPAa3. Thermal ageing evaluation with nonlinear elastic wave spectroscopy method of carbon fiber reinforced plastic composite plates. Faouzi Guenab (LOMC FRE-3102 CNRS Groupe Ondes Acoustique, Place Robert Schuman BP 4006, 76610 le Havre, France, guenab_faouzi@yahoo.fr), Hugues Duflo (LOMC FRE CNRS 3102, Université du Havre, Place Robert Schuman, 76610 le Havre, France, hugues.duflo@univ-lehavre.fr)

The excellent and specific properties of composite materials in the various fields such as aeronautics, transport, energy, the nuclear power and civil engineering led to the need of knowing their behaviours in presence of defect (crack, ageing, delamination...). Therefore, the aim of this paper is to study the thermal ageing of the carbon fibre reinforced composite plates, using their nonlinear behaviours. The method used to achieve this work is the NEWS method (Non-linear Elastic Wave Spectroscopy), where two alternatives of this one are used. The first one is SIMONRUS which involves a study of the nonlinear response of a single resonant mode of the plate according to various amplitudes of excitation. In this case, the nonlinear phenomena analysed are resonance frequency shift and damping characteristic of different level ageing of plate. The second one consists in studying the frequential response and the harmonics generated at the multiple of a resonance frequency f (at f, 2f, 3f...) caused by the ageing. Evolution of non linear effetcts are then correled to ageing duration

9:00

3aPAa4. Mesoscopic study of the enhancement of the nonlinearity of an ultrasonic wave in inhomogeneous media. André Moura (University of Heidelberg, Institute of Physical Chemistry, AK Hess, Im Neuenheimer Feld 253, 69120 Heidelberg, Germany, Moura@uni-heidelberg.de)

In quantitative nondestructive evaluation of materials it is not still clear why linear elastic waves often exhibit substantial nonlinearity when traveling through inhomogeneous medium, whereas this effect exists but remains minor in most homogeneous media. A current dominant thesis claims that when damaged, intact brittle materials become nonlinear mesoscopic elastic materials. Although this model is consistent with macroscopic observations in the framework of continuum mechanics, it eludes, however, a fundamental aspect, i.e., the detailed nature of the wave/microstructure interaction like scattering and transmission through microcrack. To construct a unified theory, from the mesoscopic to the macroscopic scale, that could take account altogether such so different mesoscopic elastodynamic effects is our objective. Toward this aim, many aspects of the wave/slit interaction are thoroughly analyzed among the clapping effect and nonlinear scattering, and experimental schemes are scheduled. At the current state of our knowledge, a first general postulate is claimed.

9:20

3aPAa5. A phase-pegistration acoustic method for nondestructive testing of porous materials. Valery M. Tsaplev (North-West State Technical University, 5, Millionnaya Street, 191186 Saint-Petersburg, Russian Federation, valery@lek.ru)

The well-known method of complex vibrator is modified for the purpose of meas-urements of complex elastic moduli (Young's and shear moduli) and corresponding values of internal friction, that change under the influence of different external factors. These external factors are: mechanical uniaxial compressive or tension stresses, temperature, electric and/or magnetic fields, etc. Different variants of phase-control methods in the self-excitation system of the complex vibrator are considered depending on the connection of the active piezoelec-tric bars: active external control or adaptive self-control at prescribed level of the in-put excitation level. The system contains the recording device to record quick changes of elastic and unelastic parameters of the test specimen. The system also contains the termostatic switch with the active control device to provide the specimen temperature control at prescribed algorithm. The method is used for the nondestructive testing of the acoustic properties of different materials under the influence of the stepwise applied mechanical stress.

9:40-10:00 Break

10:00

3aPAa6. Nonlinear-nonequilibrium wave propagation in sandstones. Donatella Pasqualini (Los Alamos National Laboratory, POBox 1663, Los Alamos, NM 87545, USA, dondy@lanl.gov), Jim A. Tencate (EES-11 (Geophysics) - Los Alamos National Laboratory, MS D443, Los Alamos, NM 87545, USA, tencate@lanl.gov), Salman Habib (Los Alamos National Laboratory, POBox 1663, Los Alamos, NM 87545, USA, habib@lanl.gov)

The transition from linear to nonlinear-nonequilibrium dynamical elasticity in rocks is of considerable interest in seismic wave propagation as well as in understanding the basic dynamical processes in consolidated granular materials. We have carried out a careful experimental investigation of this transition for Berea and Fontainebleau sandstones. These experiments have showed the existence of two strain regimes. At low strain (10-9 up to 10-7) the rocks behave elastically as classical (Landau-Lifshitz theory) nonlinear materials. At higher strains memory effects due to a driven nonequilibrium state complicate the characterization of the nonlinear behavior. The understanding of this second region is not trivial. The main focus of this work is to review the behavior of the low strain, nonlinear region and to report on new experiments meant to understand more about the behavior in the non-equilibrium regime.

Invited Paper

10:20

3aPAa7. Scattering of Rayleigh wave by microcrack with interacting faces. Alexey M. Lomonosov (General Physics Institute, Vavilova str. 38, 119991 Moscow, Russian Federation, lom@kapella.gpi.ru), Peter Hess (Physical Chemistry Institute, University of Heidelberg, Im Neuenheimer Feld 253, 69120 Heidelberg, Germany, peter.hess@urz.uni-heidelberg.de)

Scattering of short Rayleigh pulse by a partially closed surface-breaking microcrack is studied both experimentally and numerically. The microcrack was generated by a nonlinear surface wave with shock. In practice such type of cracks corresponds to fatigue or thermally generated ones. The crack was irradiated by a probe laser-generated Rayleigh. The scattered acoustic field at the surface, monitored by means of optical detector, consisted of the reflected and transmitted Rayleigh waves, longitudinal and shear acoustic waves excited by mode-conversions at the crack. Characteristic size of the crack was 50-100 μm, experimental bandwidth was 5-200 MHz. Scattering was simulated numerically in finite differences. For modeling the partially closed crack we proposed a simple one-parameter model, which takes into account weak interaction between the crack faces. It was shown, that interaction changes the predicted frequency-dependent transmission and reflection coefficients significantly. On the basis of fitting the simulated acoustic field to the measured one, the evaluation of the crack size has been performed. In this work frequency dependence of the following three parameters were employed for that purpose: transmission and reflection coefficients, and the time delay of the transmitted pulse. Obtained estimates were compared to the direct microscopic measurement of the crack.

Contributed Papers

10:40

3aPAa8. Finite element simulation of the linear and nonlinear interaction of progressive acoustic waves with a standing acoustic wave field. Ebrahim Lamkanfi (Ghent University, Sint-Pietersnieuwstraat 41, 9000 Ghent, Belgium, Ebrahim.Lamkanfi@ugent.be), Nico F. Declercq (Georgia Tech Lorraine - G.W. Woodruff School of ME, UMI Georgia Tech - CNRS 2958, 2 rue Marconi, 57070 Metz, France, nico.declercq@me.gatech.edu), Wim Van Paepegem (Ghent University, Sint-Pietersnieuwstraat 41, 9000 Ghent, Belgium, wim.vanpaepegem@ugent.be), Joris Degrieck (Ghent University, Sint-Pietersnieuwstraat 41, 9000 Ghent, Belgium, joris.degrieck@ugent.be)

Throughout the 20th century studies have been published on the scattering of sound by sound. It has been shown that a combination of nonlinear effects and diffraction effects exists. Approximate models have been developed and some have been verified by experiments. The report presents a finite element simulation of the effect and results in exact solutions for configuration under consideration. It is shown that, depending on the amplitude of the standing wave field, orthogonally incident sound waves diffract. A simplified model is developed for linear interactions, followed by a more realistic model incorporating nonlinear elastic effects. The study is performed in a liquid and also in a solid. Analysis is achieved by Fourier transformation and a comparison is made with diffraction laws governed by the grating equation. For simplicity a 2D model is presented that is extendible however to a 3D problem should that be necessary. Comparison with some of the earlier published approximate results is also performed. The study shows the detailed influence of the amplitude on the strength of the diffraction effect.

11:00

3aPAa9. Use of synchronous nonlinear interaction of flexural Lamb waves in NDT-application. Maria Y. Izosimova (Center for Industrial and Medical Ultrasound, Applied Physics Lab., University of Washington, 1013 NE 40th St., Seattle, WA 98105, USA, maria.izossimova@mail.ru), Alexandr I. Korobov (Dept. of Acoustics, Physics Faculty, M.V. Lomonosov Moscow State University, Leninskie gory 1, 119991 Moscow, Russian Federation, akor@acs465a-1.phys.msu.ru), Dmitrii Mekhedov (Center for Industrial and Medical Ultrasound, Applied Physics Lab., University of Washington, 1013 NE 40th St., Seattle, WA 98105, USA, akor@acs465a.phys.msu.ru)

Workability of synchronous nonlinear interaction of flexural Lamb waves in NDT-application is demonstrated. During experiments traveling and standing A_0 waves were used. Lamb waves are dispersive, so to provide synchronous nonlinear mode for traveling waves, non-collinear interaction of two waves with frequency f were realized in aluminum alloy plate with defects. In the area of waves' nonlinear interaction, traveling wave of $2f$ frequency appeared. Standing Lamb waves were excited with amplitude-modulated signal in a cylindrical resonator of aluminum plate. Carrier

frequency f and modulating frequency F≪f are equal to natural modes of the resonator. Spectrum of amplitude-modulated waves contained oscillations with frequencies *f*, *f+F*, and *f-F*. As a result of interaction, oscillation on heterodyne frequency *F* appeared in the plate and excited a natural mode. Amplitudes of traveling and standing waves on heterodyne frequencies depend on presence of defects in investigated area (non-classic nonlinearity). Spatial distribution of amplitudes of initial waves and ones on heterodyne frequency in samples were measured with laser vibrometer PolytecPSV300. In area containing heterogeneities, amplitude increase of waves on heterodyne frequencies was observed. The possibility to define the spatial distribution of defects using measurements of heterodyne wave amplitude distribution was shown experimentally. Work supported by RFBR.

Invited Papers

11:20

3aPAa10. Microdamage detection and monitoring using nonlinear elastic wave spectroscopy over a wide frequency range. Bart Van Damme (K.U.Leuven Campus Kortrijk, E. Sabbelaan 53, 8500 Kortrijk, Belgium, Bart.vandamme@kuleuven-kortrijk.be), Pierre-Yves Le Bas (EES-11 (Geophysics) - Los Alamos National Laboratory, MS D443, Los Alamos, NM 87545, USA, pylb@lanl.gov), Koen Van Den Abeele (K.U.Leuven Campus Kortrijk, E. Sabbelaan 53, 8500 Kortrijk, Belgium, koen.vandenabeele@kuleuven-kortrijk.be)

Innovative diagnostic techniques based on Nonlinear Elastic Wave Spectroscopy (NEWS) have been implemented for global inspection of microdamage in intact and damaged aeronautical components using low and high frequency sound waves. For low frequency analysis, we focused on the amplitude dependent analysis of the resonance behavior, both in time and frequency domain. Alternatively, we have analyzed the time-windowed interaction of a hammer impact with a high frequency continuous wave. The results of both techniques agree extremely well, and prove their potential for quick and global microdamage detection. For local inspection, we have implemented a combination of the traditional elastic wave time reversal technique with a phase coded pulse sequence selective excitation. Alternatively, sparse array tomographic reconstruction with NEWS pre-treatment could be used. The nonlinearity based imaging techniques are illustrated on aeronautical components, and discussed in terms of the feasibility and usefulness of the methodologies as new tools for microdamage imaging.

11:40

3aPAa11. Simulations of nonlinear ultrasonic NDT of plate-like structures. Marieke Geeraert (K.U.Leuven Campus Kortrijk, E. Sabbelaan 53, 8500 Kortrijk, Belgium, Marieke.Geeraert@student.kuleuven.be), Els Janssen (K.U.Leuven Campus Kortrijk, E. Sabbelaan 53, 8500 Kortrijk, Belgium, Els.Janssen@kuleuven-kortrijk.be), Steven Delrue (K.U.Leuven Campus Kortrijk, E. Sabbelaan 53, 8500 Kortrijk, Belgium, steven.delrue@kuleuven-kortrijk.be), Olivier Bou Matar (IEMN, UMR CNRS 8520, avenue Poincaré, BP 60069, 59652 Villeneuve d'Ascq, France, olivier.boumatar@iemn.univ-lille1.fr), Erik Blomme (Katholieke Hogeschool Zuid-West-Vlaanderen dept. VHTI, Doorniksesteenweg 145, 8500 Kortrijk, Belgium, Erik.Blomme@katho.be), Herbert De Gersem (K.U.Leuven Campus Kortrijk, E. Sabbelaan 53, 8500 Kortrijk, Belgium, Herbert.DeGersem@kuleuven-kortrijk.be), Koen Van Den Abeele (K.U.Leuven Campus Kortrijk, E. Sabbelaan 53, 8500 Kortrijk, Belgium, koen.vandenabeele@kuleuven-kortrijk.be)

Inclusions in materials generally affect the linear wave propagation characteristics of sound waves, observed through scattering, and reduced reflection or transmission with respect to pure materials. The smaller the inclusions, for a fixed ultrasonic frequency, the harder it is to interpret these observations. Therefore, zones of microdamage initiated from fatigue or thermal loading might not induce any linear scattering at all. Nevertheless, the damage information is definitely carried along within the propagating sound wave. In this case, however, it is necessary to investigate the spectral changes of the propagating sound waves, in the form of harmonics and intermodulation frequencies. This contribution reports on simulations of the nonlinear signatures arising in Lamb, Rayleigh and bulk wave propagation in media with localised microdamaged zones. The simulations are performed with a Finite Difference Time Domain solver accounting for microdamage though the inclusion of hysteretic nonlinear stress-strain relations at the microscale. Depending on the configuration it is possible to obtain one or more harmonic images of the defect, their number and relative position containing information about the location and depth of the defect. The simulations allow simple prediction of the response images in complicated experimental conditions.

Contributed Paper

12:00

3aPAa12. Fast and Slow Dynamics in Damaged Materials: Correlation to Acoustic Emission. Mourad Bentahar (ENSIM - LAUM, Université du Maine, rue Aristote, 72085 Le Mans, France, Mourad.Bentahar@univ-lemans.fr), Anne Marec (ENSIM - LAUM, Université du Maine, rue Aristote, 72085 Le Mans, France, anne.marec.etu@univ-lemans.fr), Rachid El Guerjouma (ENSIM - LAUM, Université du Maine, rue Aristote, 72085 Le Mans, France, Rachid.El_Guerjouma@univ-lemans.fr), Jean-Hugh Thomas (ENSIM - LAUM, Université du Maine, rue Aristote, 72085 Le Mans, France, jean-hugh.thomas@univ-lemans.fr)

Results are reported of the study of anomalous nonlinear fast dynamics (FD) and slow dynamics (SD) in damaged solids. Experimental observations characterizing FD and SD may be used to detect and eventually characterize induced damage of structural components. Here, we analyze the evolution of the non-linear dynamic behaviour of two polymer-based composites of different reinforcing elements as Sheet Moulding Compound (SMC) and Polymer Concrete (PC) as a function of their gradual damage. More particularly, non-linear FD and SD parameters (time and frequency shift) have been found to be very sensitive to damage creation and evolution for both materials. Besides,acoustic emission monitoring was performed and allowed to calculate the elastic energy released by SMC and PC at every damage stage. Interesting logarithm-like evolution of the followed non-linear parameters as a function of the calculated energy is found. A classification of the collected acoustic emission signals is proposed to understand the contribution of the different damage mechanisms to the evolution of the non-linear behaviour.

12:20-1:40 Lunch Break

1:40

3aPAa13. Chirp-coded excitation applied with advanced pulse inversion for nonlinear acoustics in complex steel samples. Serge Dos Santos (ENI Val de Loire, Université François Rabelais de Tours, LUSSI CNRS, rue de la Chocolaterie, 41034 Blois, France, serge.dossantos @univ-tours.fr), Thomas Goursolle (ENI Val de Loire, Université François Rabelais de Tours, LUSSI CNRS, rue de la Chocolaterie, 41034 Blois, France, thomas.goursolle@univ-tours.fr), Martin Drab (Czech Technical University in Prague, Trojanova 13, 120 00 Praha 2, Czech Republic, drab@kepler.fjfi.cvut.cz), Tomas Slunecko (ZD Rpety - DAKEL, Ohrobecka 408, 142 00 Praha 4, Czech Republic, drab@kepler.fjfi.cvut.cz)

Nonlinear acoustics for nondestructive testing is still an emergent technique in complex materials with localized cracks because linear effects can be cancelled using specific symmetries for the pre- and post-signal processing. The local nonlinear signature is accessible even in complex aeronautic structure by using the symmetry properties: i. e. time reversal invariance and pulse inversion associate to chirp-coded excitation. Excitation Symmetry Analysis Method [Dos Santos et al., JNLM, 2007] which is an extension of the pulse inverted method for extraction of third order nonlinearity is applied experimentally for the measurement of relative level of nonlinearity on a airplane steel bracket, on which visible crack was created by fatigue tests. This pre-processing method has been coupled to a 100-250 kHz bandwidth chirp-coded ultrasonic excitation, realized at various amplitude (A, $A/2$, $3^{1/2}A/2$, etc.), and performed with DAKEL IDK09 200 kHz PZT sensors. Signal processing based on correlation measurements, allow an extraction of the nonlinear signature versus fatigue level. Experiments and data processing have been conducted with a 12 bit DAKEL-DTR system in the bandwidth 80-800 kHz and compared with a continuous 4 channel acoustic emission device.

2:00

3aPAa14. Determination of symmetry relations between higher order material constants for the study of nonlinear acoustic properties of piezoelectric crystals of any symmetry class. Nico F. Declercq (Georgia Tech Lorraine - G.W. Woodruff School of ME, UMI Georgia Tech - CNRS 2958, 2 rue Marconi, 57070 Metz, France, nico.declercq@me.gatech.edu)

Each crystal is invariant under a given point symmetry operation. This results in relations between the different material property constants, such as second order elastic constants, second order piezoelectric constants and second order dielectric constants. Those relations are well reported in text books for the linear behavior of crystals. When nonlinear effects are studied, higher order constants play a significant role and their symmetry relations have only been reported in the literature for a limited number of crystal classes. The problem with higher order constants is that it is rather complicated and very time consuming to study the symmetry relations. This paper presents a newly developed semi-automatic computer program that is able to handle any kind of symmetry relation. Results are reported for all the different crystal classes for the higher order constants, i.e. third order elastic constants, third order piezoelectric constants, third order dielectric constants and electrostrictive constants. The results are important for the study of nonlinear properties of crystals and composites and will ease the experimental quantitative determination of all linear and nonlinear material constants of crystals.

2:20

3aPAa15. Nonlinearity, hysteresis, end-point memory, and congruence in sandstones. Kevin E. Claytor (Los Alamos National Laboratory, POBox 1663, Los Alamos, NM 87545, USA, ke.claytor@gmail .com), Joseph R. Koby (Los Alamos National Laboratory, POBox 1663, Los Alamos, NM 87545, USA, jkoby@lanl.gov), Jim A. Tencate (EES-11 (Geophysics) - Los Alamos National Laboratory, MS D443, Los Alamos, NM 87545, USA, tencate@lanl.gov)

Very low frequency stress-strain measurements on many rocks show definite and repeatable hysteresis loops. Much of the modeling of this behavior uses Preisach or Ising-like models adapted from models developed for magnetic systems which exhibit hysteresis. To date, the experimental data on many rocks showing end-point memory are noisy and only qualitative. The congruence property, in fact, has never been examined for rocks. Just how well does the behavior of a sandstone fit a Preisach model? To find the answer to this question, we performed a new set of careful stress-strain experiments on several sandstones to examine end-point memory (in detail) and also to see if the congruence property does indeed hold for these rocks. In addition we explored the dependence of measurement rate on the relaxation time of these rocks (the analog to magnetic aftereffect). For very slow measurement rates (low frequencies), hysteresis disappears, leaving only a simple nonlinear stress-strain curve.

2:40

3aPAa16. Foundations of the ultrasonic non-destructive method of determination of stresses in near-the-surface layers of solids. Alexander Guz (Institute of Mechanics, Nesterov str. 3, Kiev, 03057 Kiev, Ukraine, guz@carrier.kiev.ua)

The ultrasonic non-destructive method under consideration is intended for measurements of uniaxial and two axial stresses in the near-the-surface layers of relatively rigid materials (metals, alloys and similar material). This method is intended for measurements of the actual, assemble, operating, preload prestress and other stresses. Above mentioned stresses must be considered as initial or residual stresses taking into account the theory [1] under consideration. In this case the disturbances (displacements and stresses of the 3-D linearized theory [1] of elastic waves in bodies with initial or residual stresses) arise due to ultrasonic vibrations. Description of the non-destructive method under consideration and information on instruments and devices for measurements are presented. Some examples of non-destructive determination of stresses in near-the-surface layers of materials are presented also as applied to the residual stresses arising at electric welding and to the operating stresses arising at loading. Additional information is presented in monograph [1]. References: 1.Guz A.N. Elastic waves in bodies with initial (residual) stresses. Kiev: ″A.C.K.″ Publishers, 2004. – 672 p. (In Russian).

3:00

3aPAa17. Effect of Water Saturation on the Nonlinear Elastic Response of Concrete. Cédric Payan (LCND - Université de la Méditerranée, IUT Aix Provence, Avenue Gaston Berger, 13625 Aix en Provence Cedex, France, cedric.payan@univmed.fr), Vincent Garnier (LCND - Université de la Méditerranée, IUT Aix Provence, Avenue Gaston Berger, 13625 Aix en Provence Cedex, France, vincent.garnier@univmed.fr), Joseph Moysan (LCND - Université de la Méditerranée, IUT Aix Provence, Avenue Gaston Berger, 13625 Aix en Provence Cedex, France, joseph.moysan @univmed.fr)

Nonlinear interaction of a monochromatic elastic wave with a low frequency should be a good tool for non-destructive evaluation of existing concrete structures. This technique has already proofed efficient in detecting global damage. However, it is necessary to understand the influence of some structural parameters as porosity, stress state, or water saturation on the nonlinear processes. In this way, a thermodynamically based model containing all of them is presented in this paper. It is sustained by nonlinear interaction measurements in order to quantify the evolution of the nonlinear behaviour of concrete with water saturation state.

3:20

3aPAa18. The Parametric Array in Berea Sandstone, Revisted. Pierre-Yves Le Bas (EES-11 (Geophysics) - Los Alamos National Laboratory, MS D443, Los Alamos, NM 87545, USA, pylb@lanl.gov), Jim A. Tencate (EES-11 (Geophysics) - Los Alamos National Laboratory, MS D443, Los Alamos, NM 87545, USA, tencate@lanl.gov)

Previous measurements of the characteristics of the parametric array in sandstone by Johnson and Shankland [J. Geophys. Res., 94, 17729-17734 (1989)] were difficult to perform and, given the apparatus of the day, only qualitative. Since then, memory effects have been found to play a strong role in the dynamic behavior of rocks. This experimental study was performed to

find out how well the ″classical″ theory of nonlinear acoustics, i.e., all compressional waves with no memory effects, works at describing the parameteric array in a granular solid. An array of PZT disk transducers (every other one broadcasting one of two frequencies) was epoxied to a large block of Berea sandstone (1.2x0.4x0.4 m). The two primary frequencies were near 100kHz and chosen to produce a difference frequency around 15kHz. Using a scanning laser vibrometer (Polytec), several scans of the beampatterns were made at the opposite end of the rock and the results compared with calculations based on those commonly used for parametric arrays in water. A narrow beam generated from the two primaries was measured and the beampattern compared with those of the primaries. The agreement is surprisingly good using a beta of around 200 and a Q of about 50.

Session 3aPAb

Physical Acoustics: Acoustic Probes of Planetary Environments I

Andi Petculescu, Cochair
University of Louisiana, Department of Physics, PO Box 44210, Lafayette, LA 70504, USA

Martin C. Towner, Cochair
PSSRI, The Open University, Walton Hall, Milton Keynes, MK7 6AA, UK

Invited Paper

8:00

3aPAb1. The atmospheres of Mars, Venus and Titan: observed and modelled structures. Sebastien Lebonnois (Laboratoire de Meteorologie Dynamique, IPSL/CNRS, 4 place Jussieu, box 99, 75252 Paris Cedex 05, France, sllmd@lmd.jussieu.fr)

In our solar system, three bodies possess atmospheres presenting similar characteristics with our own environment: our neighbours Mars and Venus, and also Saturn's largest satellite Titan. The comparative study of these different atmospheric systems provides many insights on their respective behaviour, and helps understand the processes at work within these complex systems. In this review, the observed vertical and latitudinal structures of these atmospheres are presented, including their variability and seasonal evolution. Waves that have been observed are also shown, e.g., thermal tides, gravity waves. Global Climate Models that have been developed to study such atmospheric systems are also presented. Using these tools, production and role of the different waves present in each atmosphere may be studied.

Contributed Paper

8:20

3aPAb2. Bach on other planets or why acoustic sensors make sense in planetary science. Andi Petculescu (University of Louisiana, Department of Physics, PO Box 44210, Lafayette, LA 70504, USA, andi @louisiana.edu), Timothy G. Leighton (Institute of Sound and Vibration, Univ. of Southampton, University Road, Highfield, SO17 1BJ Southampton, UK, T.G.Leighton@soton.ac.uk)

The European Huygens probe, which landed on Titan in 2005, is the only planetary probe so far to incorporate passive and active acoustic sensing. Acoustic wave motion is intimately coupled with an atmosphere and thus can give first-hand information on that environment. Motivation for acoustic sensing in planetary atmospheres abounds: anemometry, turbulence measurements, soil characterization, sound generation by lightning, acoustics of liquid hydrocarbon flows, cryovolcanoes, dust devils, quantitative fluid spectroscopy, thermometry, atmospheric boundary layers etc. In this paper it is shown quantitatively how the environments of Mars, Venus, and Titan affect the generation and propagation of audible sound differently. To exemplify, a musical fragment with a rich frequency content was chosen (Bach's Toccata and Fugue in D-minor played by one of the authors) and passed through the three planetary ''filters.'' Appreciation of the nature of these sounds will inform the design of acoustic sensors for future space probes. Furthermore, a demonstration that the physics is sufficiently understood to predict these sounds indicates that the same understanding can be applied quantitatively to interpret alien sounds to estimate the environmental conditions.

Invited Papers

8:40

3aPAb3. Use of microphones to record windspeed and turbulence in planetary environments. Ralph D. Lorenz (JHU Applied Physics Lab, 11100 Johns Hopkins Road, Laurel, MD 20723, USA, ralph.lorenz@jhuapl.edu)

A major feature of any planetary acoustic measurement is noise due to ambient winds, or to the motion of the measurement platform through the air. Venera 13 and 14 recorded sound on the surface of Venus: the amplitude of the microphone signal was interpreted (by dynamic pressure scaling) to recover a windspeed. The Huygens probe at Titan also recorded sound levels during descent and on the surface with a passive microphone and an acoustic sounder. The author has made passive microphone measurements made on a rotating aerospace vehicle (an instrumented Frisbee) which show spin modulation and a variation with flight speed and angle of attack. He has also used microphones as a crude wind sensor on an array of 20 meteorological stations used to study dust devils in Arizona. All of these observations will be reviewed. Lessons learned for future planetary measurements, and prospects and methods for microphonic anemometry (especially with limited telemetry bandwidth) will be discussed.

9:00

3aPAb4. The Huygens Surface Science Package sound speed measurements and the methane content of Titan's atmosphere. A. Hagermann (PSSRI, Open University, Walton Hall, MK7 6AA Milton Keynes, UK, unknown@unknown.com), Martin C. Towner (PSSRI, The Open University, Walton Hall, MK7 6AA Milton Keynes, UK, m.c.towner@open.ac.uk), Philip D. Rosenberg (PSSRI, Open University, Walton Hall, MK7 6AA Milton Keynes, UK, p.d.rosenberg@open.ac.uk), James R. Garry (PSSRI, Open University, Walton Hall, MK7 6AA Milton Keynes, UK, jrcgarry@hotmail.com), Hakan Svedhem (European Space Agency, Keplerlaan 1, NL 2201 AZ Noordwijk ZH, Netherlands, hsvedhem@rssd.esa.int), Mark R. Leese (PSSRI, Open University, Walton Hall, MK7 6AA Milton Keynes, UK, m.r.leese@open.ac.uk), Brijen Hathi (PSSRI, Open University, Walton Hall, MK7 6AA Milton Keynes, UK, b.hathi@open.ac.uk), Ralph D. Lorenz (JHU Applied Physics Lab, 11100 Johns Hopkins Road, Laurel, MD 20723, USA, ralph.lorenz@jhuapl.edu), John C. Zarnecki (PSSRI, Open University, Walton Hall, MK7 6AA Milton Keynes, UK, j.c.zarnecki @open.ac.uk)

The Huygens probe descended through Titan's atmosphere in January 2005. On board was the Surface Science Package (SSP), a set of nine sensors, which included a speed-of-sound sensor. We present a detailed description of the SSP speed of sound measurements and report constraints on the methane content in Titan's lower atmosphere based on these measurements. After extensive instrument calibration and subsequent Bayesian analysis of the data, the most likely result derived from our measurements in Titan's lower atmosphere is a methane fraction of approximately 2% at 10 km, increasing to 3.5% at lower altitudes. These estimates are based on a binary composition. Our data show that any large scale variation of methane within the lower 11 km of Titan's atmosphere is unlikely. Within experimental and theoretical uncertainties, our estimates are lower than, but compatible with earlier estimates obtained from the mass spectrometry experiment.

9:20

3aPAb5. Waterfalls in space, and other problems of 'underwater' acoustics on a small planet. Timothy G. Leighton (Institute of Sound and Vibration, Univ. of Southampton, University Road, Highfield, SO17 1BJ Southampton, UK, T.G.Leighton @soton.ac.uk), Paul R. White (Institute of Sound and Vibration, Univ. of Southampton, University Road, Highfield, SO17 1BJ Southampton, UK, prw@isvr.soton.ac.uk), Daniel C. Finfer (Institute of Sound and Vibration, Univ. of Southampton, University Road, Highfield, SO17 1BJ Southampton, UK, d.c.finfer@soton.ac.uk)

Whilst extraterrestrial liquids do occur in the Solar System, today's acoustical oceanographers have fewer sites to which they can apply their experience of Earth's oceans than perhaps they would have had in the early Solar System, with its magma oceans. Possible sites are Saturn's moons Titan and Enceladus, and Jupiter's moon Europa. The ability to transfer our understanding of Earth's acoustical oceanography to other moons and planets is particularly valuable, given that current understanding is sufficient to undertake complex inversions to estimate Earth's ocean environmental parameters from relatively sparse, or even naturally-occurring, acoustical signals. However such transference should be done with care, as terms familiar in Earth's acoustical oceanography may not be correct on other worlds. For example, in a deep ocean on a small world (such as Europa), the hydrostatic pressure will not equal the product of the density, the depth, and the surface value of the acceleration due to gravity, since the latter can vary with depth, and because vertical lines are not parallel on a small planet. This paper explores two cases of transferring our terrestrial experience off world, to the ice seas of Europa, and to the methane lakes and waterfalls of Titan.

9:40-10:00 Break

10:00

3aPAb6. Acoustic Anemometry on Mars. Jean-Pierre Williams (California Institute of Technology, Division of Geological and Planetary Sciences, MC 150-21, Padadena, CA 91125, USA, jpierre@gps.caltech.edu), Ian McEwan (California Institute of Technology, Division of Geological and Planetary Sciences, MC 150-21, Padadena, CA 91125, USA, ijm@gps.caltech.edu)

Acoustic anemometers provide wind measurements with high sensitivity, temporal resolution, and accuracy, and are in many ways superior to the hot wire technique anemometers currently and previously flown to Mars. An anemometer is under development that employs an internal model of how sound is changed by a particular gas mixture with respect to wind speed and temperature to derive these values. This is done by measuring the transfer function (attenuation and phase versus frequency) of sound between two transducers with a very wide spread-spectrum signal and comparing this with its internal model. While sonic anemometry is the premier technique for research studies of winds on Earth, the acoustic properties differ substantially from atmosphere to atmosphere and it is not valid to assume that an existing terrestrial system can provide heritage for a planetary instrument. Further, current multi-gas acoustic models rely on constants derived from experiments performed in conditions far from the planetary application intended here. Since the parameters of the model must be well defined in our approach, the instrument's ability to accurately measure transfer functions will be used in experiments to improve our knowledge of the behavior of various calibrated gas mixtures over relevant temperatures and pressures.

10:20

3aPAb7. An ultrasonic anemometer for Mars. Colin Wilson (University of Oxford, Department of Atmospheric, Oceanic and Planetary Physics, OX1 3PU Oxford, UK, wilson@atmos.ox.ac.uk), Lee A. Davis (University of Warwick, School of Engineering, CV4 7AL Coventry, UK, lee.davis@warwick.ac.uk), David Hutchins (University of Warwick, School of Engineering, CV4 7AL Coventry, UK, D.A.Hutchins@warwick.ac.uk), Martin C. Towner (PSSRI, The Open University, Walton Hall, MK7 6AA Milton Keynes, UK, m.c.towner@open.ac.uk)

Ultrasonic anemometers are often used for studies of 3-D atmospheric turbulence on Earth, due to their robust calibration and fast operation ($>$10 Hz). The same qualities make ultrasonic anemometry attractive for use on Mars, where similar atmospheric turbulence is found. The low density of Martian atmosphere - a hundredth that of the Earth's - is problematic, because of the large acoustic impedance mismatch between the atmosphere and piezoelectric transducers. One solution to this problem is to use piezoelectric transduc-

ers with a hornlike resonator bonded to their front surface. Another solution is to use a capacitive membrane transducer instead. We report on performance of various ultrasonic transducers in carbon dioxide Martian pressures, and present an instrument design capable of meeting the stringent mass, power, and environmental requirements of the European ExoMars lander.

10:40

3aPAb8. Solid-fluid coupling on planets: from seismology to acoustics and beyond. Raphael F. Garcia (DTP-OMP Univ. Toulouse, 14 Avenue E. Belin, 31400 Toulouse, France, garcia@dtp.obs-mip.fr), Philippe Lognonné (IPGP, 4 avenue de Neptune, 94107 Saint Maur des Fossés, France, lognonne@ipgp.jussieu.fr), Giovanni Occhipinti (IPGP, 4 avenue de Neptune, 94107 Saint Maur des Fossés, France, ninto@ipgp.jussieu.fr)

On Earth, solid-fluid coupling is responsible for acoustic signals created by quakes or volcanic eruptions which have been observed by infrasonic sensors or through ionospheric perturbations produced by infrasounds. Similarly volcanic explosions, ocean surface waves and ocean internal gravity waves are producing seismic signals. A specific normal mode coupling theory has been developed for the whole solid/ocean/atmosphere Earth system in order to model these phenomena. Recent developments for the observation and modeling of the infrasonic waves created by quakes and tsunamis have focused on the ionospheric perturbations produced by the exponential amplification of vertically propagating infrasonic and gravity waves. On Earth, these tools are particularly interesting for the observation of seismic surface waves and tsunamis in the open ocean where sensors are not present. However, the interest is even stronger to infer the internal structure of planets for which the deployment of seismometers is almost impossible. Theoretical modeling of solid/atmosphere coupling on Venus is presented, including open questions concerning the attenuation of infrasounds by Venus atmosphere. An attempt to observe quake signals with VIRTIS instrument on board Venus Express ESA mission is also described. Finally, a mission analysis tool and other ideas for future planetary investigations of atmospheric acoustic normal modes are discussed.

WEDNESDAY MORNING, 2 JULY 2008 ROOM 352A, 8:00 A.M. TO 1:00 P.M.

Session 3aPAc

Physical Acoustics and Computational Acoustics: Combustion Noise and Thermo-Acoustics I

Tim Lieuwen, Cochair
School of Aerospace Engineering, Georgia Institute of Technology, Atlanta, Georgia 30332-0150, USA

Maria A. Heckl, Cochair
Keele University, Staffordshire, Newcastle-under-Lyme, ST5 5BG, UK

Rafael Piscoya, Cochair
Technische Fachhochschule Berlin, Univ. of Applied Sciences, Luxemburger Str. 10, Berlin, 13353, Germany

Invited Papers

8:00

3aPAc1. Sound production by partially premixed flames in a stagnation flow. Thierry Schuller (Ecole Centrale Paris, Laboratoire EM2C - CNRS, Grande-Voie des Vignes, 92295 Chatenay-Malabry, France, thierry.schuller@em2c.ecp.fr), Patrick Duchaine (Ecole Centrale Paris, Laboratoire EM2C - CNRS, Grande-Voie des Vignes, 92295 Chatenay-Malabry, France, patrick.duchaine@em2c.ecp.fr), Laurent Zimmer (Ecole Centrale Paris, Laboratoire EM2C - CNRS, Grande-Voie des Vignes, 92295 Chatenay-Malabry, France, laurent.zimmer@em2c.ecp.fr)

In the perspective of combustion noise reduction, understanding mechanisms of sound generation from combustion of non perfectly mixed reactants is a major challenge. Sound production is thus investigated for vortices impinging a flat laminar flame in a stagnation flow. Such a configuration helps to better understand sound production from turbulent flames. A study with different compositions of the main flow and surrounding gases - mixtures of nitrogen, air and methane - is carried out under the same mean flow and perturbations conditions. Time traces of radiated sound pressure and chemiluminescence emission from radical species present in the reaction zone are characterized together with detailed imaging of the flame and flow motions. Elements of classical combustion noise theory are used to identify the main noise sources when air or fuel is entrained by the vortex interacting with the flame.

8:20

3aPAc2. Flow field and acoustic characteristics of an acoustically forced burner impinging jet. Yang Zhang (The University of Manchester, School of Mechanical, Aerospace and Civil Engineering, George Begg Building, M60 1QD Manchester, UK, yang.zhang@manchester.ac.uk), Saad Hajim (The University of Manchester, School of Mechanical, Aerospace and Civil Engineering, George Begg Building, M60 1QD Manchester, UK, saad.hajim@manchester.ac.uk), Jason Bassi (The University of Manchester, School of Mechanical, Aerospace and Civil Engineering, George Begg Building, M60 1QD Manchester, UK, jason.bassi @manchester.ac.uk), S Farhat (The University of Manchester, School of Mechanical, Aerospace and Civil Engineering, George Begg Building, M60 1QD Manchester, UK, s.farhat@manchester.ac.uk)

The flow field and acoustic characteristics of a turbulent impinging jet from an impinging burner have been investigated experimentally. The effect of acoustically excited upstream flow with a range of driving frequencies from 0 to 3000Hz and use of perforated plate near the nozzle have been studied to achieve modifications to the near-field and far-field of the jet. The acoustic response of the burner to upstream acoustically excited flow under different geometry configurations was investigated in detail. The burner components were found to have a significant effect on the burner acoustic response, with overall damping and enhancement achieved over the full driving frequency range. The velocity flow field of the impinging jet, including spectra and rms data, were mapped from the burner nozzle to the plate with CTA measurements with three acoustic excitation frequencies and no excitation; 0Hz, 52.5Hz, 75Hz and 530Hz (within acoustic mode bands of burner).The results show that excitation frequencies of 52.5Hz and 75Hz were found to propagate all the way to the plate, whilst 530Hz dissipates near the nozzle exit. (Re = 16,200 , H/D = 3, nozzle velocity profile).

8:40

3aPAc3. Prediction of Self Excitation Frequencies and Amplitudes for a Model Gas Turbine Burner. Catherine Gardner (Queen Mary University of London, School of Engineering and Material Science, Mile End Road, E1 4NS London, UK, catherine .gardner@qmul.ac.uk), S. M. Reza Hosseini (Queen Mary University of London, School of Engineering and Material Science, Mile End Road, E1 4NS London, UK, s.m.hosseini@qmul.ac.uk), Chris J. Lawn (Queen Mary University of London, School of Engineering and Material Science, Mile End Road, E1 4NS London, UK, c.j.lawn@qmul.ac.uk)

Forced excitation of a swirl stabilised methane/air flame by acoustic waves at atmospheric pressure has been characterised in order to show that the frequencies and amplitudes where self-excitation occurs, but the natural limit cycle takes effect, can be predicted from these data. Chemiluminescent emission was therefore recorded to measure the Flame Transfer Function (FTF), as the flame was acoustically excited by two loud speakers. The experiments covered a wide range of frequencies and amplitudes with particular emphasis on the FTF at high amplitudes of excitation, where a non-linear response is often reported. The system was modelled by the 1D thermoacoustic element method, in which each acoustic element, such as a duct or a contraction, is described by a four-pole matrix. The flame is incorporated as another four-pole matrix that describes the measured flame transfer function. The solution of this set of equations without forcing predicts self-excitation frequencies and amplitudes that can be compared with the experimental data. The minimum magnitudes of the FTF for excitation may also be calculated. When proven at this small scale, the procedure will be applied to predict the limit cycling of actual installations from rig tests.

9:00

3aPAc4. Low-order modelling of unsteady flame behaviour in a spray combustor. David M. Arthur (University of Cambridge, Department of Engineering, Trumpington Street, CB2 1PZ Cambridge, UK, david.arthur@cantab.net), Ann P. Dowling (University of Cambridge, Department of Engineering, Trumpington Street, CB2 1PZ Cambridge, UK, apd1@cam.ac.uk), Stewart Cant (University of Cambridge, Department of Engineering, Trumpington Street, CB2 1PZ Cambridge, UK, rsc10@eng.cam.ac.uk)

The effect of mass flow rate perturbations on the stability of a liquid-fulled annular aeroengine gas turbine is investigated using a three-dimensional uRANS code. The simulations are performed on a single sector of an idealised annular gas turbine geometry. A Lagrangian fuel spray description is used with a Monte Carlo solution of Williams' spray equation. Broadband mass flow fluctuations are imposed at the combustor inlet and dilution ports, and the effect on heat release is quantifed using flame transfer functions. The excitation of inlet and dilution flows leads to signifcant unsteady combustion and the implications for self-excited oscillations are considered. The numerical results are then compared to a low-order model which is developed to account for the different physical mechanisms responsible for unsteady heat release when the inlet and dilution port air mass flow rates are perturbed. The low-order model is used to predict the possibility of self-excited oscillations as well as to investigate the potential of altering the phase and relative magnitude of the inlet and dilution port excitation as a possible means of controlling thermoacoustic oscillations.

9:20

3aPAc5. Mode switching of combustion instabilities associated with flame transfer function non-linearities. Daniel Durox (Ecole Centrale Paris, Laboratoire EM2C - CNRS, Grande-Voie des Vignes, 92295 Chatenay-Malabry, France, daniel.durox@em2c.ecp.fr), Nicolas Noiray (Ecole Centrale Paris, Laboratoire EM2C - CNRS, Grande-Voie des Vignes, 92295 Chatenay-Malabry, France, nicolas.noiray@em2c.ecp.fr), Thierry Schuller (Ecole Centrale Paris, Laboratoire EM2C - CNRS, Grande-Voie des Vignes, 92295 Chatenay-Malabry, France, thierry.schuller@em2c.ecp.fr), Sebastien Candel (Ecole Centrale Paris, Laboratoire EM2C - CNRS, Grande-Voie des Vignes, 92295 Chatenay-Malabry, France, sebastien.candel@em2c.ecp.fr)

Studies of combustion instabilities indicate that the frequency of oscillation changes during the growth of oscillations before a limit cycle is reached. It is also found that a system can switch from one mode to another when the amplitude exceeds a certain threshold. It is shown that these features can be linked to the flame response non-linearity. The analysis is carried out by examining combustion instabilities appearing on a multipoint injection burner, placed a the end of a cylindrical manifold. This element acts like a resonator and its length can be modified easily. Experiments indicate that mode switching takes place between two resonant modes of the cavity and this is shown to be caused by the non-linearity of the flame response. The phenomenon can be analyzed by considering the non-linear

evolution of the flame transfer function. It is possible to combine this information with a stability analysis of the burner, and define conditions which give rise to mode switching. It is found that this behavior is related to a change in phase difference between heat release rate fluctuations and velocity perturbations at the burner outlet. This phase shift takes place as the amplitude of oscillation increases.

9:40

3aPAc6. Impact of acoustic boundary conditions on confined combustion noise. Ammar Lamraoui (Ecole Centrale Paris, Laboratoire EM2C - CNRS, Grande-Voie des Vignes, 92295 Chatenay-Malabry, France, ammar.lamraoui@em2c.ecp.fr), Franck Richecoeur (Ecole Centrale Paris, Laboratoire EM2C - CNRS, Grande-Voie des Vignes, 92295 Chatenay-Malabry, France, franck.richecoeur@em2c.ecp.fr), Thierry Schuller (Ecole Centrale Paris, Laboratoire EM2C - CNRS, Grande-Voie des Vignes, 92295 Chatenay-Malabry, France, thierry.schuller@em2c.ecp.fr), Sébastien Ducruix (Ecole Centrale Paris, Laboratoire EM2C - CNRS, Grande-Voie des Vignes, 92295 Chatenay-Malabry, France, sebastien.ducruix@ecp.fr)

The noise produced by aircraft engines at take-off and landing can be very harmful for airport neighbors, an issue that became recently particularly crucial. While combustion instabilities, where a strong coupling between flames and acoustic modes of the combustion chamber cause very high levels of harmonic sound, the wide bandwidth noise emitted by confined flames in stable situations is less well-documented. It has been recently shown by Tran et al. (2007) that varying the burner upstream acoustic boundary condition was a very efficient method for damping combustion instabilities and creating ideal conditions for the study of combustion noise. In the present study, the noise level induced by stable combustion is investigated for various upstream conditions. The test bench consists in a swirl stabilized burner, connected to a rectangular combustion chamber, equipped with microphone ports for acoustic measurements. The 40 kW burner is composed of two identical stages fed with air and propane. A photomultiplier equipped with a narrow band filter measuring the CH^* spontaneous emission from the flame is used to study heat release fluctuations in the flame. Time-resolved measurements are carried out and spectral analysis of pressure measurements and light emissions are performed for various inlet impedances.

10:00-10:20 Break

10:20

3aPAc7. Green's function model for a Rijke tube with a distributed heat source. Maria A. Heckl (Keele University, Staffordshire, ST5 5BG Newcastle-under-Lyme, UK, m.a.heckl@keele.ac.uk)

A Rijke tube is an open-ended tube with a compact heat source (flame or hot gauze) inside. The heat source is commonly modelled by the "nτ law", which assumes a point source releasing heat at a rate that is proportional to the velocity (delayed by a time lag τ) at the heat source. The present paper aims to extend this model to include distributed heat sources. A distributed source is simulated by a row of point sources with individual heat release rates and time lags. The acoustic processes in the tube will be modelled by Lighthill's acoustic analogy equation, combined with a Green's function approach. The occurrence of thermo-acoustic instabilities will be predicted for different properties of the heat source. Geometrical complications in the tube, such as a blockage and a jump in cross-section, as well as a jump in mean temperature, will be taken into account.

10:40

3aPAc8. Experimental and Numerical Investigation of the Acoustic Response of Multi-slit Bunsen Burners. Philip De Goey (Eindhoven Univesity of Technology, Den Dolech 2, 5600 MB Eindhoven, Netherlands, l.p.h.d.goey@tue.nl), Victor Kornilov (Eindhoven Univesity of Technology, Den Dolech 2, 5600 MB Eindhoven, Netherlands, v.n.kornilov@tue.nl), Ronald Rook (Eindhoven Univesity of Technology, Den Dolech 2, 5600 MB Eindhoven, Netherlands, r.rook@tue.nl), Jan Ten Thije Boonkkamp (Eindhoven Univesity of Technology, Den Dolech 2, 5600 MB Eindhoven, Netherlands, tenthije@win.tue.nl)

Acoustic resonances in combustion systems like central heating boilers prohibit further technological advances in these systems. The design and construction is obstructed by acoustic problems because they are largely misunderstood, in spite of our increase in knowledge over the last decades. The flame often acts as an active element in the acoustic field, because the flame transfer function of acoustic waves has a large amplitude at low frequencies. Current models of the phase of the flame transfer function of Bunsen-type flames, based on kinematic behavior of the flame dynamics, completely miss the experimentally observed phase, unless the measured flow field is used in the model. In the current paper we analyze numerical results of the flame dynamics, flow field and flame transfer function found with a 2D detailed numerical model of the flow and structure of the flame on a multiple-slit burner. The model is validated with experiments of the flame dynamics (using chemiluminescence), flow dynamics (using PIV) and flame transfer function (using OH luminescence for the heat release fluctuations and heated wire probe for the acoustic distortions) on exactly the same configuration. A very good agreement is found which indicates the importance of predicting all the influences of the flow on the flame and vise-versa.

11:00

3aPAc9. Numerical prediction of interaction between combustion, acoustics and vibration in gas turbines. Artur Pozarlik (University of Twente, P.O. Box 217, 7500 AE Enschede, Netherlands, a.k.pozarlik@utwente.nl), Jim B. Kok (University of Twente, P.O. Box 217, 7500 AE Enschede, Netherlands, j.b.w.kok@utwente.nl)

The turbulent flame in the lean combustion regime in a gas turbine combustor generates significant thermo-acoustic instabilities. The flame can amplify fluctuations in the released heat, and thus in the acoustic field as well. The induced pressure oscillations will drive vibrations of the combustor walls and burner parts. Stronger fluctuating pressure results in stronger fluctuations in the wall structure. Due to fatigue the remaining life time of the hard ware will be reduced significantly. This paper investigates modeling of acoustic oscillations and mechanical vibrations induced by lean premixed natural gas combustion. The mutual interaction of the combustion processes, induced oscillating pressure field in the combustion chamber, and induced vibration of the liner walls are investigated with

numerical techniques. A partitioned procedure is used here: CFX-10 for the CFD analysis and Ansys-10 for the CSD analysis are coupled to give insight into a correlation between acoustic pressure oscillations and liner vibrations. These results will be compared with the available experimental data. The data are gathered in a purpose built 500 kW/5 bar premixed natural gas test rig.

11:20

3aPAc10. Influence of Temperature Gradients on the Sound radiated from Flames. Rafael Piscoya (Technische Fachhochschule Berlin, Univ. of Applied Sciences, Luxemburger Str. 10, 13353 Berlin, Germany, piscoya@tfh-berlin.de), Martin Ochmann (Technische Fachhochschule Berlin, Univ. of Applied Sciences, Luxemburger Str. 10, 13353 Berlin, Germany, ochmann@tfh-berlin.de)

The far field pressure of a turbulent flame can be determined using the standard boundary element method (BEM) if the sound pressure or its derivative is known at a closed surface (control surface) surrounding the flame, as long as the medium outside the control surface is homogeneous. If temperature gradients are present, the homogeneous Helmholtz equation is no more valid. In that case, the wave equation can be rewritten in form of an inhomogeneous Helmholtz equation with a source term that depends also on the unknown pressure. Using the ″Dual Reciprocity BEM″ the integral form of this wave equation can be solved involving only surface integrals, so that the sound field can still be computed from field values at the control surface. The cases under study consider a volume of hot gas with a temperature distribution that is prescribed or obtained from a CFD simulation. The influence of the temperature gradients on the sound field can be evaluated by comparison of characteristic quantities like sound power and radiation patterns, with and without temperature gradient.

11:40

3aPAc11. Localization of Sound Sources in Combustion Chambers. Christian Pfeifer (Institut für Strömungsmechanik und Technische Akustik, Technische Universität Berlin, Mueller-Breslau-Str. 8, 10623 Berlin, Germany, christian.pfeifer@pi.tu-berlin.de), Jonas P. Moeck (Institut für Strömungsmechanik und Technische Akustik, Technische Universität Berlin, Mueller-Breslau-Str. 8, 10623 Berlin, Germany, jonas.moeck@pi.tu-berlin.de), Lars Enghardt (DLR - German Aerospace Center, Mueller-Breslau-Str. 8, 10623 Berlin, Germany, lars.enghardt@dlr.de), Christian Oliver Paschereit (Institut für Strömungsmechanik und Technische Akustik, Technische Universität Berlin, Mueller-Breslau-Str. 8, 10623 Berlin, Germany, oliver.paschereit@tu-berlin.de)

To optimize the efficiency and to minimize the emissions of pollutants, modern combustion chambers for aeroengines or stationary gas turbines run in high temperature ranges with lean fuel-air mixtures. The disadvantage of this combustion mode is its susceptibility to the formation of thermoacoustic instabilities. These self-excited oscillations are an unacceptable noise source and, furthermore, they reduce the durability of the combustion chamber significantly. The focus of this paper is the localization of combustion noise sources in enclosed combustion chambers. This can be achieved using the acoustical nearfield information from pressure measurements with wall-flush mounted sensors. The spatially bounded region, where the sound sources are suspected, is discretized by a grid of monopole sources. A system of linear equations for the source strengths is built based on the relations between the sound sources and the sound pressure field, theoretically caused by the assumed sources of the grid. The source strengths are calculated by inverting the system of equations. A spatial variation of the source grid allows the scan of likely regions of sound sources to finally deduce their original distribution. Numerical simulation results will be shown to illustrate the potential and the limits of the proposed method.

12:00

3aPAc12. Computation of Indirect Combustion Noise by a CAA Method. Christoph Richter (Technische Universität Berlin, Sekr. MB1, Müller-Breslau-Str. 11, ISTA, 10623 Berlin, Germany, christoph.richter@tu-berlin.de), Frank H. Thiele (Technische Universität Berlin, Sekr. MB1, Müller-Breslau-Str. 11, ISTA, 10623 Berlin, Germany, Frank.Thiele@TU-Berlin.de)

Indirect combustion noise, which is generated by the acceleration of hot gases from a turbulent swirling flame, has become an important issue to understand turbo-machinery core noise. This indirect combustion noise it is dominated by a strong interaction of hydrodynamic and acoustic perturbations due to the transonic base flow in the turbine stages and combustion chamber exit nozzle. Current numerical simulation methods for the phenomenon based on compressible Large Eddy Simulation (LES) are very expansive. Thus LES applications are still limited to one design or few variations with immense computational costs. The most simple model fully covering indirect combustion noise, are the linearized non-isentropic Euler equations over an arbitrary mean flow. Therefore the gap between theory and LES is closed by a method adopted from Computational Aeroacoustics (CAA). It combines a high cost efficiency in terms of required points per wavelength with a high adaptability to realistic mean flow conditions. The CAA method is first validated with a simplified experiment and then applied to predict the acoustic properties of two model combustion chambers, one of them with transonic termination nozzle. By means of the acoustic intensity the sources of the noise are located.

12:20

3aPAc13. Study of oscillating regimes in air-staged diffusion flames. Javier Ballester (University of Zaragoza / LITEC, Centro Politecnico Superior, Maria de Luna, 3, 50018 Zaragoza, Spain, ballester@unizar.es), Ricardo Hernández (University of Zaragoza / LITEC, Centro Politecnico Superior, Maria de Luna, 3, 50018 Zaragoza, Spain, richard@litec.csic.es), Ana Sanz (University of Zaragoza / LITEC, Centro Politecnico Superior, Maria de Luna, 3, 50018 Zaragoza, Spain, anasanz@litec.csic.es)

The occurrence of fluctuating behaviours in air-staged diffusion flames was studied experimentally in a gas-fired furnace. Burner settings (swirl levels, air distribution) were systematically varied, leading to a broad range of flame characteristics and pollutant emissions. Pressure fluctuations reached significant amplitudes and displayed characteristic frequencies for certain operating conditions. However, heat release fluctuations (as estimated from OH^* chemiluminescence) were correlated with pressure only in a part of those cases. Therefore, thermo-acoustic coupling is thought to exist only under certain conditions, whereas other oscillating regimes are not ascribed to acoustic feedback but to changes in the location of the flame stabilization region. This conclusion was supported by the values of the Rayleigh index calculated for the different regimes. An enhanced tendency to the onset of thermo-acoustic instabilities was observed for highly staged flames.

12:40

3aPAc14. The acoustic wave propagation equation in a turbulent combusting flow. Jim B. Kok (University of Twente, P.O. Box 217, 7500 AE Enschede, Netherlands, j.b.w.kok@utwente.nl)

Sound generation by turbulent flames originates from the fluctuating heat release in the flame. The description of this fluctuating heat release and its effect on acoustics in turbulent flames is complicated due to the interaction of chemical reactions with turbulence, mixing and pressure fluctuations. In a turbulent flame the instantaneous density, velocity, pressure, temperature and species concentrations are determined by the transport equations for mass, momentum, enthalpy and species and by the equation of state. In the proposed paper an equation is formulated that describes the propagation of acoustic pressure fluctuations, and that determines the source terms. These source terms are compared with various terms derived in the literature. Significant differences are found between several approaches. An effort is made to come to a reliable and generally acceptable formulation. Subsequently events are ordered on basis of their typical time scale. That way source terms can be evaluated for the situation where the combustion is described with the use of time averaged chemical reaction progress variables and a mixture fraction variable. Subsequently the consequences of Reynolds and Favre averaging on these source terms and conservation of acoustical variables in a domain with turbulent flow are discussed.

WEDNESDAY MORNING, 2 JULY 2008 ROOM 362/363, 8:00 TO 9:20 A.M.

Session 3aPAd

Physical Acoustics: Ultrasonics: Material Characterization I

Bart Lipkens, Cochair
Western New England College, 1215 Wilbraham Road, Box S-5024, Springfield, MA 01119, USA

Nicolas Wilkie-Chancellier, Cochair
ECIME Université de Cergy-Pontoise, rue d'Eragny, Neuville-sur-Oise, 95031, France

Contributed Papers

8:00

3aPAd1. Frequency sweeping and fluid flow effects on particle trajectories in ultrasonic standing waves. Bart Lipkens (Western New England College, 1215 Wilbraham Road, Box S-5024, Springfield, MA 01119, USA, blipkens@wnec.edu), Jason Dionne (Western New England College, 1215 Wilbraham Road, Box S-5024, Springfield, MA 01119, USA, jdionne@flodesign.org), Michael Costolo (Physical Sciences Inc., 20 New England Business Center, Andover, MA 01810, USA, mac@psicorp.com), Edward Rietman (Physical Sciences Inc., 20 New England Business Center, Andover, MA 01810, USA, rietman@psicorp.com)

Particle concentration in ultrasonic standing waves by the acoustic radiation force is discussed. The acoustic radiation force is a function of the density and compressibility of the fluid and the suspended particles. A two-dimensional theoretical model is developed for particle trajectory calculations. An electro-acoustic model is used to predict the acoustic field in a resonator. The results of the linear acoustic model are used to calculate the acoustic radiation force acting on a particle suspended in the resonator. A particle trajectory model is developed that integrates the equation of motion of a particle subjected to a buoyancy force, a fluid drag force, and the acoustic radiation force. Computational fluid dynamics calculations are performed to calculate the velocity field. For a fixed frequency excitation, the particles are concentrated along the stable node locations of the acoustic radiation force. Through a periodic sweeping of the excitation frequency particle translation is achieved. Two types of frequency sweeps are considered, a ramp approach and a step-change method. Numerical results of particle trajectory calculations in a resonator with dimensions much larger than a typical wavelength are presented. A movie of experimental observations of particle trajectories is shown to illustrate the method.

8:20

3aPAd2. Elastic constants identification of anisotropic composite rectangular parallelepipeds. Thomas Delaunay (Université Montpellier II, Place Eugène Bataillon, 34095 Montpellier, France, delaunay@lain.univ-montp2.fr), Didier Laux (Université Montpellier II, Place Eugène Bataillon, 34095 Montpellier, France, laux@lain.univ-montp2.fr),Jean-Yves Ferrandis(Radio Application Division, NEC Corporation, Université Montpellier II, Place Eugène Bataillon, 34095 Montpellier, France, ferrandi@lain.univ-montp2.fr)

For many years, composite materials have been investigated due to their potential in many applications such as nuclear fuel. Nowadays, the improvement of structure conception and simulation requires many reliable properties, especially the entire elastic tensor. For these reasons, the implementation of simulation and characterization methods adapted to the geometry of samples and the high anisotropy degree of such materials are then crucial issues to developers and end users. The work presented here reports first macroscopic properties of two composites Duralumin/Air and Duralumin-/Tungsten Carbide) calculated using periodical homogenization method from elastic constants of each phase measured by high frequency acoustic microscopy. Then a resonant ultrasonic spectroscopy method is used to identify the entire elastic tensor. First, computation predicting the resonant frequencies and the mode shapes of free vibrations of cubes are presented. Excitation is then ensured by ultrasonic transducers and detection is performed by means of a laser vibrometer. A fit process of the theoretical frequencies on the measured data is then described. This method allows us to conclude about the accuracy of the homogenization method.

8:40

3aPAd3. Viscoelastic material monitoring using an acoustical cylindrical spectrometer. Nicolas Wilkie-Chancellier (ECIME Université de Cergy-Pontoise, rue d'Eragny, 95031 Neuville-sur-Oise, France, Nicolas.Wilkie-Chancellier@u-cergy.fr), Loic Martinez (ECIME Université de Cergy-Pontoise, rue d'Eragny, 95031 Neuville-sur-Oise, France, loic.martinez@u-cergy.fr), Pascal Griesmar (ECIME Université de Cergy-Pontoise, rue d'Eragny, 95031 Neuville-sur-Oise, France, pascal.griesmar@u-cergy.fr), Stéphane Serfaty (ECIME Université de Cergy-Pontoise, rue d'Eragny, 95031 Neuville-sur-Oise, France, stephane.serfaty@u-cergy.fr)

Acoustic sensors often have a plane geometry due to manufacturing constrains. In the present work, the cylindrical geometry is investigated with a normal incident beam in order to suppress the edge effects on mode conversion. The experimental setup uses an aluminium cylindrical shell. A

classical immersion transducer (2 MHz central frequency) sends a plane pulse wave on the shell at normal incidence. A second immersion transducer can turn around, enabling the observation of the waves scattered by the cylindrical shell. Previous works have shown that the acoustic field scattered by the shell as a rainbow structure enabling the acoustic spectrometry of the material poured inside the shell. From these results, the present study proposes an acoustical model linking the resonances parameters to the material ones, enabling the monitoring of time varying viscous materials. Several gelation monitoring experiments are performed and analysed using the proposed model. Results are in good agreement with quartz sensor measurements and offer a good alternative to wide frequency range measurements.

9:00

3aPAd4. Ultrasonic and photoacopustic investigations of water mixtures with dioxanes 1-3 & 1-4. Bogumil B. Linde (Inst. of Exper. Physics, Univ. of Gdańsk, Ul. Wita Stwosza, Bldg. 57, 80-952 Gdańsk, Poland, fizbl@univ.gda.pl), Anna K. Kiszel (Inst. of Exper. Physics, Univ. of Gdańsk, Ul. Wita Stwosza, Bldg. 57, 80-952 Gdańsk, Poland, ania_tczew84@wp.pl), Anna Sikorska (Inst. of Exper. Physics, Univ. of Gdańsk, Ul. Wita Stwosza, Bldg. 57, 80-952 Gdańsk, Poland, fizams@univ.gda.pl)

Ultrasonic velocities, densities and thermal effusivity dependence on concentration were measured in the mixtures of water with dioxanes 1-3 and 1-4 in the temperature range from 291.15 to 303.15 K. Adiabatic compressibilities were calculated from Laplace's equation based on the experimental results obtained. Variations of these values with concentration and temperature were studied. Structural interactions and the formation of a compact pseudo-stable structure at very low concentrations of these liquids were observed. The plots of the adiabatic compressibility versus the mole fraction of these molecules display two characteristic points at low concentrations: the intersection of the isotherms and their minimum. Such relations between adiabatic compressibility, concentration and temperature are usually attributed to the formation of pseudo-stable molecular structures. To formulate a model of local structures present in the investigated molecular systems it is indispensable to get an insight into hydration of molecules and the formation of hydrogen bonds. Therefore, the attention was focused particularly on these problems.

WEDNESDAY MORNING, 2 JULY 2008 ROOM 362/363, 9:20 A.M. TO 12:40 P.M.

Session 3aPAe

Physical Acoustics: Ultrasonics: NDT and Layered Systems I

Vincent Pagneux, Cochair
Laboratoire d'Acoustique de l'Université du Maine, UMR CNRS 6613, AV. O. Messiaen, Le Mans, 72085, France

Claire Prada, Cochair
Laboratoire Ondes et Acoustique, ESPCI, Université Paris 7, CNRS, 10 rue Vauquelin, Paris, 75005, France

Contributed Papers

9:20

3aPAe1. Thickness determination of a multilayered system of different materials by natural frequencies. Changzhi Zhou (Institute of Acoustics, Chinese Academy of Sciences, NO.21, Bei-Si-huan-Xi Road, 100080 Beijing, China, zcz@mail.ioa.ac.cn), Mingxuan Li (Institute of Acoustics, Chinese Academy of Sciences, NO.21, Bei-Si-huan-Xi Road, 100080 Beijing, China, lmx@mail.ioa.ac.cn), Jie Mao (Institute of Acoustics, Chinese Academy of Sciences, NO.21, Bei-Si-huan-Xi Road, 100080 Beijing, China, maojie@mail.ioa.ac.cn), Xiaomin Wang (Institute of Acoustics, Chinese Academy of Sciences, NO.21, Bei-Si-huan-Xi Road, 100080 Beijing, China, wangxiaomin@mail.ioa.ac.cn)

This paper is focusing on the relationship between the natural frequencies of a multilayered system of different isotropic elastic materials and the thickness of each layer. A relevant ultrasonic method for thickness determination of a multilayered system by natural frequencies has been developed. The natural frequencies are numerically calculated from the normally incident reflection coefficient of a ″steel-epoxy resin-aluminum-thin polymer″ structured lamination. Some natural frequencies are sensitive to one layer thickness in certain range while the others are invariable. This phenomenon is explained by the defined strain energy ratio, and used for our thickness inversion. The measured natural frequencies of a specimen show good agreement with the theoretical ones. All the natural frequencies are taken into account, and the simulated annealing method is employed for the thickness inverse calculation of the multilayered structure. The average relative errors of calculated thickness of the each layer are -0.7%, 35%, -1.3% and -6.1%, corresponding to the real values: 1957μm, 16μm, 1913μm and 54μm.

9:40

3aPAe2. Bonding quality evaluation of layered materials by guided wave dispersion. Young H. Kim (Korea Science Academy, 111 Backyangkwanmoonro, Busanjin-ku, 614-822 Busan, Republic of Korea, youngkim@paran.com), Minseok Bae (Korea Science Academy, 111 Backyangkwanmoonro, Busanjin-ku, 614-822 Busan, Republic of Korea, bms1991@empal.com), Sunhee Choi (Korea Science Academy, 111 Backyangkwanmoonro, Busanjin-ku, 614-822 Busan, Republic of Korea, cjtwo120@hanmail.net), Jisu Kim (Korea Science Academy, 111 Backyangkwanmoonro, Busanjin-ku, 614-822 Busan, Republic of Korea, boone90@hotmail.com), Seokchan Hong (Korea Science Academy, 111 Backyangkwanmoonro, Busanjin-ku, 614-822 Busan, Republic of Korea, charliehongn@hanmail.net)

Multi-layered materials have been widely used for high performance materials with advanced properties required for the critical parts of structures. The characteristics of bonding quality in multi-layered materials have been hot issue for a long time. The bonding quality was evaluated by using dispersion of guided wave. Broadband guided waves were generated at oblique incidence angle, and waves reflected at the edge of the specimen were detected by using a pulse-echo setup. The dispersion curves were obtained from edge-reflected leaky guided wave for various plates: Single layered plates of aluminum, copper and stainless steel, and double layered plates of aluminum-stainless steel cladding, epoxy-bonded aluminum-stainless and epoxy-bonded aluminum-copper. The aluminum-stainless steel cladding specimen showed similar dispersion for both sides, whereas epoxy-bonded specimens showed different dispersions which are similar to that of upper layer only. These results imply that the cladding specimen used in the

present work is well bonded, whereas epoxy-bonded specimens are acoustically isolated. The dispersion curve of guided wave has high potential to evaluate bonding quality of layered materials.

10:00

3aPAe3. Acoustical imaging with bending waves based on sparse inversion. Lars Hörchens (University of Technology Delft, Lorentzweg 1, 2628 CJ Delft, Netherlands, l.horchens@tudelft.nl), Diemer De Vries (University of Technology Delft, Lorentzweg 1, 2628 CJ Delft, Netherlands, d.devries@tudelft.nl)

Bending waves can be employed in the context of acoustical imaging for the detection of material defects or localization of vibration sources. The obtainable spatial resolution is limited by the minimal wavelength contained in the excitation signal. The evanescent part of the wave field can usually not be used for the imaging of sources at distances exceeding a wavelength. Therefore only the propagating part of the field can be employed, which means that the minimum size of the region where energy can be focused is in the order of half a wavelength due to the diffraction limit. If the recovery of vibration sources and reflections is posed as an inverse problem, regularization techniques can be applied in order to force a sparse solution. Preliminary results indicate that the assumption of a sparse source distribution can be used to resolve features significantly smaller than half a wavelength. The approach is therefore applied as a high-resolution imaging technique for bending wave fields.

10:20-10:40 Break

10:40

3aPAe4. An experimental method of corrugated surface reconstruction investigated in combination with finite-element simulation. Sarah W. Herbison (Georgia Tech Lorraine - G.W. Woodruff School of ME, UMI Georgia Tech - CNRS 2958, 2 rue Marconi, 57070 Metz, France, sherbison@gatech.edu), Ebrahim Lamkanfi (Georgia Tech Lorraine - G.W. Woodruff School of ME, UMI Georgia Tech - CNRS 2958, 2 rue Marconi, 57070 Metz, France, Ebrahim.Lamkanfi@ugent.be), Nico F. Declercq (Georgia Tech Lorraine - G.W. Woodruff School of ME, UMI Georgia Tech - CNRS 2958, 2 rue Marconi, 57070 Metz, France, nico.declercq@me.gatech.edu)

Current theory applied to ultrasonic diffraction from periodically corrugated surfaces is valid only in the far-field; it cannot be applied to determine the diffracted field within the surface corrugations themselves. Therefore, information regarding the corrugation is difficult to extract from experiments that are necessarily conducted in the far-field. The present work aims to simulate a potential experimental method for investigating the corrugations themselves. Using near-field results obtained from a finite-element code, the far-field diffraction is constructed as a series of time-harmonic plane waves. By back-propagating this diffracted field, information about the corrugations is obtained. Comparing the results of the back-propagated field to the field generated by the finite-element code shows the limitations of determining details of periodically corrugated surfaces from far-field experiments.

11:00

3aPAe5. Determination of the width of an axisymmetric deposit on a metallic pipe by means of Lamb type guided modes. Mustapha El Moussaoui (LOMC FRE 3102 CNRS Groupes Ondes Acoustiques, Université du Havre (IUT), Place Robert Schuman, 76610 Le Havre, France, elmoussm@univ-lehavre.fr), Farid Chati (LOMC FRE 3102 CNRS Groupes Ondes Acoustiques, Université du Havre (IUT), Place Robert Schuman, 76610 Le Havre, France, farid.chati@univ-lehavre.fr), Fernand Leon (LOMC FRE 3102 CNRS Groupes Ondes Acoustiques, Université du Havre (IUT), Place Robert Schuman, 76610 Le Havre, France, fernand.leon@univ-lehavre.fr), Aleksander Klauson (Tallinn University of Technology, Dept. of Mechanics, Ehitajate tee 5, 19086 Tallinn, Estonia, aklauson@staff.ttu.ee),Gerard Maze(LAUE, Université du Havre, Place Robert Schuman, F-76610 Le Havre, France, gerard.maze@univ-lehavre.fr)

The non-destructive evaluation of pipes using guided waves is extensively used for the detection and the size estimation of defects. The important number of investigations concerning with the interaction between a guided wave and a defect show the growing need to improve our knowledge of this phenomenon in order to detect and to characterize as well as possible the defect. This work is devoted to the evaluation of the width of an axisymmetric resin deposit coupled to the wall of a metallic tube by means of longitudinal modes S0, S1. To that end, we interest to damping of these modes provoked by the deposit. The study is carried out both from the numerical point of view and from the experimental point of view in considering a deposit of variable width. The finite element method is employed to model the propagation and the diffraction of Lamb-type waves. The experiment is based on the generation of axisymmetric waves on the section of a tube by a piezoelectric transducer. Measurements of temporal echoes reflected by the deposit and transmitted after the deposit are achieved. A mathematical law of the attenuation as function of the width is deduced for each wave.

11:20

3aPAe6. Scattering by a defect in an elastic waveguide: Coupling of finite elements and modal representations. Vahan Baronian (CNRS, ENSTA - 32 Boulevard Victor, 75 015 Paris, France, vahan.baronian@ensta.fr), Anne-Sophie Bonnet- Ben Dhia (CNRS, ENSTA - 32 Boulevard Victor, 75 015 Paris, France, bonnet@ensta.fr), Colin Chambeyron (CNRS, ENSTA - 32 Boulevard Victor, 75 015 Paris, France, colin.chambeyron@ensta.fr), Eric Luneville (ENSTA - CEA, 32 Boulevard Victor, 75 015 Paris, France, eric.luneville@ensta.fr)

The potentiality of guided ultrasonic waves in nondestructive testing is currently investigated. Indeed, guided waves can allow a rapid inspection of large areas and of non accessible parts of particular structures like plates or pipes, compared to conventional techniques. This work concerns the numerical finite element computation, in the frequency domain, of the diffracted wave produced by a defect (crack, heterogeneity, discontinuity, local bend etc.) located in an infinite elastic waveguide. The computational domain is chosen as a portion of the waveguide, containing the perturbation, and our purpose is to build transparent conditions on its artificial boundaries by using modal representations. This cannot be achieved in a classical way, due to nonstandard properties of elastic modes. However, a biorthogonality relation is established which allows to derive a transparent condition relating hybrids displacement/stress vectors. An original mixed formulation is then implemented, whose unknowns are the displacement field in the bounded domain and the normal component of the normal stresses on the artificial boundaries. Numerical validations are presented in the two-dimensional and three-dimensional cases.

11:40

3aPAe7. Interaction of elastic waves with dislocations. Agnes Maurel (LOA/ESPCI, 10 rue Vauquelin, 75005 Paris, France, agnes.maurel@espci.fr), Vincent Pagneux (Laboratoire d'Acoustique de l'Université du Maine, UMR CNRS 6613, AV. O. Messiaen, 72085 Le Mans, France, vincent.pagneux@univ-lemans.fr), Felipe Barra (Universidad de Chile, av. Blanco encalada, 0 Santiago, Chile, fbarra@uchile.cl), Fernando Lund (CIMAT, Universidad de Chile, 0 Santiago, Chile, flund@cimat.cl)

This work concerns the effective propagation of elastic waves in a medium filled with randomly placed dislocations. Multiple scattering theory is applied to derive the effective velocity and attenuation of the waves (both transverse and longitudinal) because of the effect of the dislocations. Our work is a generalization of Granato & Lucke theory since it takes into account the polarization of the elastic waves. Two principal results have been obtained, in connexion with experiments: 1) we have explained the different attenuations experimentally measured between longitudinal and transverse waves. The difference between the two values is obtained in quantitative agreement with no adjustable parameter. 2) we have offered a scenario for the frequency law in the attenuation measured in polycrystals (a combina-

tion of quadratic and quartic law). This has been done by taking into account the dislocations at the grain boundaries that can contribute to the attenuation process.

12:00

3aPAe8. Particle deposit formation during filtration characterisation using ultrasonic waves. Didier Laux (Université Montpellier II, Place Eugène Bataillon, 34095 Montpellier, France, laux@lain.univ-montp2.fr), Hugues Blasco (Université Montpellier II, Place Eugène Bataillon, 34095 Montpellier, France, blasco@lain.univ-montp2.fr), Jean-Yves Ferrandis (Radio Application Division, NEC Corporation, Université Montpellier II, Place Eugène Bataillon, 34095 Montpellier, France, ferrandi@lain.univ-montp2.fr), Julie Mendret (INSA Toulouse, Av de Rangueil, 31077 Toulouse, France, julie.mendret@insa-toulouse.fr), Christelle Guigui (INSA Toulouse, Av de Rangueil, 31077 Toulouse, France, guigui@insa-toulouse.fr), Corinne Cabassud (INSA Toulouse, Av de Rangueil, 31077 Toulouse, France, cabassub@insa-toulouse.fr), Philippe Schmitz (INSA Toulouse, Av de Rangueil, 31077 Toulouse, France, philippe.schmitz@insa-toulouse.fr)

Membranes filtration processes are widely used because of their ability to remove particles, colloidal species and micro-organisms from different liquids feeds. However an inherent process limitation is the membrane fouling due to deposition of suspended matter during filtration. Therefore the understanding of formation and transport properties of particle deposit responsible for membrane fouling is a necessary step to optimize membrane processes. These deposits are non homogeneous, highly porous and very thin (less than 500 μm). Thus, it is necessary to obtain local information in order to analyze and model the basic mechanisms involved in deposit formation and then to further predict process operation. As local parameters such as cake thickness and porosity are hardly reachable with conventional techniques, we propose in this paper the use of an ultrasonic echographic method. In a first step this method is validated on deposits of small glass balls. We show that the porosity and thickness of the deposit is in good agreement with theory. Then, the ultrasonic technique has been adapted on a filtration cell in order to give in line results during filtration. First results are presented and discussed.

12:20

3aPAe9. Single-sided air-coupled ultrasonic NDT of thick plates. Steven Delrue (K.U.Leuven Campus Kortrijk, E. Sabbelaan 53, 8500 Kortrijk, Belgium, steven.delrue@kuleuven-kortrijk.be), Pieter Lust (Katholieke Hogeschool Zuid-West-Vlaanderen dept. VHTI, Doorniksesteenweg 145, 8500 Kortrijk, Belgium, pieter.lust@katho.be), Jurgen Deveugele (Katholieke Hogeschool Zuid-West-Vlaanderen dept. VHTI, Doorniksesteenweg 145, 8500 Kortrijk, Belgium, jurgen.deveugele@katho.be), Erik Blomme (Katholieke Hogeschool Zuid-West-Vlaanderen dept. VHTI, Doorniksesteenweg 145, 8500 Kortrijk, Belgium, Erik.Blomme@katho.be), Olivier Bou Matar (IEMN, UMR CNRS 8520, avenue Poincaré, BP 60069, 59652 Villeneuve d'Ascq, France, olivier.boumatar@iemn.univ-lille1.fr), Koen Van Den Abeele (K.U.Leuven Campus Kortrijk, E. Sabbelaan 53, 8500 Kortrijk, Belgium, koen.vandenabeele@kuleuven-kortrijk.be)

Non-contact air-coupled ultrasonic inspection using single sided access to the material offers interesting possibilities for the development of ultrasonic in-line NDT-systems. This contribution reports observations and simulations obtained from a single-sided air-coupled pitch-catch configuration. The feasibility of the technique is demonstrated with respect to artificial defects in aluminium samples. Depending on the configuration it is possible to establish one or more ultrasonic images of the defect, their number and relative position containing information about the location and depth of the defect. The experiments are simulated using a spectral solution obtained within Comsol, and compared with a full 2D Finite Difference Time Domain simulation and a ray tracing (shadow) approach. The simulations allow simple prediction of the response images in more complicated experimental conditions.

WEDNESDAY MORNING, 2 JULY 2008 ROOM 351, 11:20 A.M. TO 12:40 P.M.

Session 3aPAf

Physical Acoustics: Ultrasonics: Industrial NDT I

Bertrand Nongaillard, Cochair
IEMN - DOAE, Université de Valenciennes, Le Mont - Houy, Valenciennes, 59313, France

Christophe Aristegui, Cochair
LMP, UMR CNRS 5469, Université Bordeaux I, 351, cours de la Libération, Talence, 33405, France

Contributed Papers

11:20

3aPAf1. Simple and versatile non-contact technique for measuring the interfacial tension of a liquid-liquid interface using pulsed acoustic radiation pressure. Bruno Issenmann (Bordeaux University - CPMOH, 351 cours de la Liberation, 33405 Talence Cedex, France, b.issenmann@cpmoh.u-bordeaux1.fr), Regis Wunenburger (Bordeaux University - CPMOH, 351 cours de la Liberation, 33405 Talence Cedex, France, r.wunenburger@cpmoh.u-bordeaux1.fr), Jean-Pierre Delville (Bordeaux University - CPMOH, 351 cours de la Liberation, 33405 Talence Cedex, France, jp.delville@cpmoh.u-bordeaux1.fr)

We present a versatile non-contact technique for measuring the interfacial tension of a liquid-liquid interface using the acoustic radiation pressure. This technique is based on the analysis of the shape of the time-dependent deformation of the liquid interface induced by the radiation pressure of a focused, pulsed ultrasonic beam. It combines a simple optical detection step and a novel analytical model of interface deformation dynamics that accurately takes into account interfacial, gravitational, as well as viscous effects in both weakly and highly viscous limits. The accuracy of this technique is experimentally demonstrated on liquid-air and liquid-liquid interfaces.

11:40

3aPAf2. Diffuse ultrasonic backscatter at oblique incidence for heterogeneous solids. Joseph A. Turner (University of Nebraska, Dept. of Engineering Mechanics, W317.4 NH, Lincoln, NE 68588, USA, jaturner@unl.edu), Goutam Ghoshal (University of Nebraska, Dept. of Engineering Mechanics, W317.4 NH, Lincoln, NE 68588, USA, goutamghoshal@rediffmail.com)

Diffuse ultrasonic backscatter techniques are useful for probing heterogeneous materials. They can be used to extract microstructural parameters and to detect flaws which cannot be detected by conventional ultrasonic

techniques. Such experiments, usually done using a modified pulse-echo technique, utilize the spatial variance of the signals as a primary measure of microstructure. Quantitative ultrasonic scattering models include components of both transducer beams as well as microstructural scattering information. Of particular interest for interpretation of many experiments is the propagation through a liquid-solid interface at normal and oblique incidence. Here, the Wigner distribution of the beam pattern of an ultrasonic transducer through a liquid-solid interface is used in conjunction with the stochastic wave equation to model this scattering problem within a single scattering formulism. The Wigner distribution represents a distribution in space and time of the spectral energy density as a function of wave vector and frequency. A Gaussian beam is used to model the transducer beam pattern. The scattered response in the time domain is then compared with experimental results for materials of common interest. These results are anticipated to impact ultrasonic nondestructive evaluation and characterization of heterogeneous media.

Invited Paper

12:00

3aPAf3. Model-based reconstruction methods of NDT ultrasonic array data. Pierre Calmon (CEA LIST, Centre de Saclay, F-91191 Gif sur Yvette, France, pierre.calmon@cea.fr), Ekaterina Iakovleva (CEA LIST, Centre de Saclay, F-91191 Gif sur Yvette, France, ekaterina.iakovleva@cea.fr), Alex Fidahoussen (CEA LIST, Centre de Saclay, F-91191 Gif sur Yvette, France, alex.fidahoussen@cea.fr), Guillemette Ribay (CEA LIST, Centre de Saclay, F-91191 Gif sur Yvette, France, guillemette.ribay@cea.fr)

Ultrasonic array techniques are more and more used in NDT applications because of their flexibility and of their adaptability to complex configurations. In addition they can provide richer data than conventional methods. An optimal exploitation of such data in the aim of localizing and characterizing the detected flaws requires the application of imaging and reconstruction techniques based on a direct modeling of the propagation of ultrasound from the transmitter to the receiver. The quantitative models for the propagation which are available in the CIVA software platform developed at CEA-LIST allow such direct modelling in parts of possibly complex geometries and materials. Different array data reconstruction methods based on the exploitation of these direct models have been studied and implemented in the plat-form. Thus, in this communication we present in particular algorithms derived of synthetic focusing approach. These algorithms exploit the time of flight identification and can be apply to any set of array data. We also present a reconstruction method based on the post-processing of the transfert matrix of the array and the application of MUSIC algorithm. We show and discuss results obtained with these methods both on simulated and experimental data.

Contributed Paper

12:20

3aPAf4. Low frequency composite acoustic sensor for highly absorbing media characterization. Alain Skaf (IEMN - DOAE, Université de Valenciennes, Le Mont - Houy, 59313 Valenciennes, France, alain.skaf@univ-valenciennes.fr), Georges Nassar (IEMN - DOAE, Université de Valenciennes, Le Mont - Houy, 59313 Valenciennes, France, gnassar@univ-valenciennes.fr), Fabrice Lefebvre (IEMN - DOAE, Université de Valenciennes, Le Mont - Houy, 59313 Valenciennes, France, Fabrice.Lefebvre@univ-valenciennes.fr), Bertrand Nongaillard (IEMN - DOAE, Université de Valenciennes, Le Mont - Houy, 59313 Valenciennes, France, Bertrand.Nongaillard@univ-valenciennes.fr)

Ultrasonic techniques are widely used in nondestructive testing and evaluation of media. But when media are highly absorbing, it becomes often impossible to operate at classical ultrasonic frequencies. In this work, we propose a low frequency acoustic device to characterize such highly absorbing media. This device is composed of a piezoelectric disc embedded in a metallic ring. The technique consists in bringing into resonance the entire structure. Firstly, we will study analytically and numerically the main resonance modes of the sensor, which are the flexion modes and the radial modes. The results of the modelization are compared to measurements obtained through an impedance analyzer. In a second part, we will use this model of sensor to characterize two different media. The first type consists of a series of polymer disks with different viscoelastic properties. Using radial modes of vibration, we will characterize these polymer disks through measurement of the acoustic velocity. After that, we will characterize using the flexion modes a very complex medium which present a highly absorbing phenomenon such as dough in the fermentation phase. The measurements show the aptitude of this technique to follow the evolution of the physical properties of complex media.

Session 3aPPa

Psychological and Physiological Acoustics and ASA Committee on Standards: Applications of Psychoacoustics III

Patricia Davies, Cochair
Ray W. Herrick Lab., School of Mechanical Engineering, Purdue Univ., 140 S. Martin Jischke Drive, West Lafayette, IN 47907-2031, USA

Hugo Fastl, Cochair
AG Technische Akustik, MMK, TU München, Arcisstr. 21, München, 80333, Germany

Contributed Papers

8:00

3aPPa1. Psychoacoustic evaluation of compression drives. Joan Cruanes Catala (Escola Politècnica Superior de Gandia, Universitat Politècnica de València, Crtra Natzaret-Oliva s/n, 46730 Gandia, Spain, joacrca@upvnet.upv.es), Jorge Frances Monllor (DFISTS. Univ. de Alicante, Carretera de Sant Vicent del Raspeig s/n, 03690 San Vicente del Raspeig, Spain, jfmonllor@ua.es), Jaime Ramis Soriano (DFISTS. Univ. de Alicante, Carretera de Sant Vicent del Raspeig s/n, 03690 San Vicente del Raspeig, Spain, jramis@ua.es), Jesús Alba Fernandez (Escola Politècnica Superior de Gandia, Universitat Politècnica de València, Crtra Natzaret-Oliva s/n, 46730 Gandia, Spain, jesalba@fis.upv.es)

The following work tries to be an approximation to the sound quality valuation of radiant systems, in concrete, the case of compression drives. This approach is realized from different perspectives: on one hand, an evaluation of the quality of these systems from the point of view of the psychoacoustic classic parameters described by Zwicker will be done. On the other hand, a perceptual model described by Moore and based on the human auditory system will be applied. Both models will be applied in signals registered on different commercial models of compression drives. The work also includes the accomplishment of a psychoacoustic experiment in which a hearing will realize a valuation of perceived quality. Finally, one will try to establish a correlation with the information obtained in the three mentioned approaches.

8:20

3aPPa2. A study of evaluating the button sounds. Shunsuke Ishimitsu (Hiroshima City University / National Institute of Advanced Industrial Science and Technology, 3-4-1 Ozuka-Higashi, Asa-Minami-Ku, 731-3194 Hiroshima, Japan, ishimitu@hiroshima-cu.ac.jp), Koji Sakamoto (Hiroshima City University, 3-4-1 Ozuka-Higashi, Asa-Minami-Ku, 731-3194 Hiroshima, Japan, koji_s@tm.ten.fujitsu.com), Takayuki Arai (Univ. of Hyogo, 2167, Shosha, 671-2280 Himeji, Japan, es07g001@steng.u-hyogo.ac.jp), Toshikazu Yoshimi (Pioneer Corp., 25-1, Nisimachi, Yamada, 350-8555 Kawagoe, Japan, toshikazu_yoshimi@post.pioneer.co.jp), Yuichi Fujimoto (Pioneer Corp., 25-1, Nisimachi, Yamada, 350-8555 Kawagoe, Japan, yuichi_fujimoto@post.pioneer.co.jp), Kenichi Kawasaki (Pioneer Corp., 25-1, Nisimachi, Yamada, 350-8555 Kawagoe, Japan, kenichi_kawasaki@post.pioneer.co.jp)

In recent years, much attention has been directed at the sound design which designs various sound treated as noise, such as automobile acceleration sound and cleaner sound, because the point of view sound is a part of products, has permeated. This research considered the sound design and its evaluation about 11 kinds of the button sounds. First, the impression was extracted by the SD method and relevance with time frequency analysis was investigated. Moreover, we also confirmed that an impression changed, when the sound of a bad impression is processed into the sound of a good impression using adaptive control.

8:40

3aPPa3. Factoring end-user expectations into the sound design process of computer keyboards. Romain Boulandet (Ecole Polytechnique Fédérale de Lausanne, EPFL STI LEMA, Station 11, CH 1015 Lausanne, Switzerland, romain.boulandet@epfl.ch), Hervé Lissek (Ecole Polytechnique Fédérale de Lausanne, EPFL STI LEMA, Station 11, CH 1015 Lausanne, Switzerland, herve.lissek@epfl.ch), Sylvain Sauvage (Logitech Europe S.A., Z.I. Moulin du choc D, CH 1122 Romanel/Morges, Switzerland, sylvain_sauvage@eu.logitech.com), Jacques Robert (Logitech Europe S.A., Z.I. Moulin du choc D, CH 1122 Romanel/Morges, Switzerland, jacques_robert@eu.logitech.com)

The poor acoustic comfort of usual commercial products is often perceived as annoying. Today, more and more companies have realized that sound can be an important component of product attributes and image. They are interested in having acoustic guidelines for enhancing their products sound quality. The objective of this research is to quantify the objective and subjective noise production of computer keyboards, and hence to translate the pleasantness in an objective way. Our strategy consists in developing both benchmarks and listening tests to ensure that sound design process never looses sight of the end-users expectations. The presented work proposes an original methodology to define what keystroke sound matches the image of a pleasant keyboard. We also approach what acoustic characteristics have a significant influence on the global appreciation of keystroke sounds. Good results have been obtained showing a strong correlation between perceptive cues and metrics.

Session 3aPPb

Psychological and Physiological Acoustics: Auditory Perception of Sound Source Properties I

John Neuhoff, Cochair
The College of Wooster, 930 College Mall, Wooster, OH 44691, USA

Anna Preis, Cochair
Institute of Acoustics, Adam Mickiewicz University, Unultowska 85, Poznan, 61-614, Poland

Invited Paper

8:00

3aPPb1. Non-visual identification of walking grounds. Bruno L. Giordano (Centre for Interdisciplinary Research in Music Media & Technology (CIRMMT) - Schulich School of Music - McGill Univ., 555 Sherbrooke Street West, Montreal, QC H3A1E3, Canada, bruno.giordano@music.mcgill.ca), Stephen McAdams (Centre for Interdisciplinary Research in Music Media & Technology (CIRMMT) - Schulich School of Music - McGill Univ., 555 Sherbrooke Street West, Montreal, QC H3A1E3, Canada, smc@music.mcgill.ca), Yon Visell (Centre for Interdisciplinary Research in Music Media & Technology (CIRMMT) - Schulich School of Music - McGill Univ., 555 Sherbrooke Street West, Montreal, QC H3A1E3, Canada, yon@cim.mcgill.ca), Jeremy Cooperstock (Centre for Intelligent Machines - CIRMMT - Dept. of Electrical and Computer Engineering - McGill Univ., 3480 University Street, Montreal, QC H3A 2A7, Canada, jer@cim.mcgill.ca), Hsin-Yun Yao (Centre for Intelligent Machines - McGill Univ., 3480 University Street, Montreal, QC H3A 2A7, Canada, hyyao@cim.mcgill.ca), Vincent Hayward (Centre for Intelligent Machines - McGill Univ., 3480 University Street, Montreal, QC H3A 2A7, Canada, hayward@cim.mcgill.ca)

We investigated the role of haptic, proprioceptive and auditory information in the non-visual identification of walking grounds. We selected four solid materials (e.g., marble) and four aggregate materials (e.g., fine gravel). Five observers identified the materials in each of four experimental conditions: multisensory, haptic, proprioceptive, and auditory. In the auditory condition, they were presented with walking sounds they produced. In the other conditions, observers walked blindfolded on the materials. In the haptic and proprioceptive conditions auditory information was masked. In the proprioceptive condition haptic information was masked. No masking took place in the multisensory condition. In all conditions, solids and aggregates were seldom confused, and aggregates were better identified than solids. Chance identification performance was observed only for solids in the presence of simultaneous haptic and auditory masking, suggesting a secondary role of proprioceptive information. In the proprioceptive condition, identification of aggregates was better than chance, suggesting a significant role of proprioception. Identification of aggregates was at its best in the haptic condition, and not in the multisensory condition, suggesting either an inconsistency of information between auditory and non-auditory channels, or conflicting cognitive strategies for the exploitation of these sources of information in multisensory contexts.

Contributed Paper

8:20

3aPPb2. The effect of tone envelope on sensory integration: support for the 'unity assumption'. Michael Schutz (University of Virginia, 102 Gilmer Hall, Charlottesville, VA 22904, USA, schutz@virginia.edu), Michael Kubovy (University of Virginia, 102 Gilmer Hall, Charlottesville, VA 22904, USA, kubovy@virginia.edu)

Research on the integration of auditory and visual sensory information consistently confirms the optimal integration hypothesis, according to which information is weighted according to its relative quality. Thus, since the auditory system has greater temporal resolution, this hypothesis predicts that visual information will not affect auditory judgments of duration. In conflict with this hypothesis, Schutz & Lipscomb (2007) report that percussionists use visual information to alter audience perception of note duration. To show that this discrepancy arises from the acoustic characteristics of percussive sounds, we paired visual information derived from a striking motion with pure tones exhibiting two types of envelopes: percussive (sharp onset followed by exponential decay) and flat (sharp onset to a fixed level, followed by sharp offset) envelopes. Visual information affected auditory duration judgments only for the tones with percussive envelopes (e.g. the sounds produced by a striking motion). As ratings of percussive tones were no more variable than ratings of flat tones, the difference cannot be explained by ″ambiguity″ of percussive-tone duration. In contrast to the notion of optimal integration, we conclude that envelope is an important acoustic cue for cross-modal integration and offers important information regarding event identification.

Invited Papers

8:40

3aPPb3. Subjective verification of simulation of a vehicle pass-by. Tomasz Kaczmarek (Institute of Acoustics, Adam Mickiewicz University, Unultowska 85, 61-614 Poznan, Poland, tomek@spl.ia.amu.edu.pl)

The simulation of a moving vehicle can be a very powerful tool for investigating the perception of vehicle motion (velocity, acceleration, road traffic annoyance studies etc). Before applying a simulated vehicle in psychoacoustic noise annoyance studies, one should perform a subjective validation of this tool. The present paper presents the subjective validation of simulation method created by the author. Real pass-by recordings were used to calculate the one-third octave power spectra of a vehicle. Based on these spectra, the simulated pass-bys were created. The simulation was validated in terms of annoyance level and perception of velocity by comparing (in

psychoacoustic experiment) the original pass-bys with their simulated replicas. Two types of engines - otto and diesel - were tested, for velocities ranging from 30-110 km/h. For velocities above 50 km/h, the annoyance of simulated pass-bys is very close to the original signal. For lower velocities, simulated pass-bys result in lower annoyance ratings. The solution to the problem would be a reconstruction of the tonal components from the exhaust system.

9:00

3aPPb4. Experimentation in physics-based sound modeling. Davide Rocchesso (IUAV University of Venice, Department of Art and Design, Dorsoduro 2206, 30123 Venezia, Italy, roc@iuav.it)

Since 2001, as part of the Sounding Object and CLOSED projects, we have been developing physics-based sound models for everyday events and processes. The procedure of describing a sound-producing phenomenon in physical terms, building a model, and accessing its parameters, easily gives the illusion of controlling sound production in the most effective and convenient way. For example, it is trivial to connect a force sensor to the rubbing pressure variable of a friction model. However, one soon realizes that it is often difficult to predict changes in perceived sound in response to physical changes, and that robust models are difficult to achieve. These issues can partially be addressed with experimental research in perception, psychophysics, and phenomenology. Although this approach is inherently time consuming, it will eventually lead to sound models whose parametric layout is more suitable to human manipulation and control. Conversely, in the practice of designers we find that problems are tackled by rapidly producing a multiplicity of attempts, or sketches, and by critically comparing them. In our practice of sound modelers, there are several examples where both approaches, the one based on experimental psychology and the one based on design, proved to be compelling and useful.

9:20

3aPPb5. Size from sound: Size estimates of balls dropped from various height. Massimo Grassi (Dipartimento di Psicologia Generale, via Venezia 8, 35131 Padova, Italy, massimo.grassi@unipd.it)

Three experiments investigated the perception of the size of a ball (i.e., a non sounding object) from the sound it produces when dropped upon a plate (i.e., a sounding object) from various heights. Experiment one: listeners estimated metrically the size of seven balls (Ø 1, 1.5, 2, 2.5, 3, 4, 5 cm) when dropped upon a baked clay plate from 6 cm of height. Experiment two: a new group of listeners estimate the size of the balls, however, balls could be dropped from either 6 cm or 12 cm of height. In the last experiment, balls could be dropped from either 3, 6 or 12 cm of height. In all experiments listeners received no foregoing information about the sound source event, such as the material of the balls, the material of the plate, etc. Overall, listeners' estimations matched veridically the actual size of the balls. However, in the second and third experiment, listeners' estimations were dependent on the height: balls were judged slightly larger when dropped from the highest heights.

Contributed Paper

9:40

3aPPb6. The texture of natural sounds. Tjeerd C. Andringa (University of Groningen, Dept. Artificial Intelligence, P.O. Box 407, 9700 AK Groningen, Netherlands, t.andringa@ai.rug.nl)

The texture, a spectro-temporal pattern, of many sound sources is a robust and characteristic perceptual property that listeners use for sound source recognition. The robustness of the texture ensures that we can recognize sound sources like a helicopter, flowing water, or a surf breaking on pebbles in a wide variety of acoustic environments. This robustness suggests that textures can be used for automatic source identification or environment classification. We introduce a method to determine the presence of sound textures associated with, for example, flat noise, pulsed noises (helicopter), sweep based textures (running water), and tonal noises (babble). The cumulative probability density of time-frequency fluctuations are matched with prototypical cumulative probability density functions (cpdf) with a running variant of the Kolmogorov-Smirnov test. Textures with a similar distribution as the target distribution, contribute approximately equally to all values of the cpdf. The flatness of this distribution is used as a distance measure. When the pdf's of the target textures do not overlap strongly, the method can determine the texture of time-frequency-regions as small as 100 ms by 6 semi-tones. This method can therefore also be used to determine the texture of the background.

Invited Papers

10:00

3aPPb7. 'Behavioral Relevance' as a guiding principle in investigating the perception of sound source properties. John Neuhoff (The College of Wooster, 930 College Mall, Wooster, OH 44691, USA, jneuhoff@wooster.edu)

Perceiving a sounding object is the result of a complex interaction between physical, physiological, and cognitive factors. However, early in the history of modern psychacoustics, the difficulty in generating complex, controlled, dynamic stimuli limited many investigations of auditory perception to monaural presentation of static sine wave tones or bursts of noise. Thus, very influential models of auditory processing were developed using sounds that are not frequently encountered in a natural listening environment. Although this approach was useful in developing models of the function of the peripheral auditory system, it was less so in developing models of auditory cognition and behavior. If one accepts the position that our perceptual abilities have evolved specifically to help us survive and deal with the stimuli that occur in a natural environment, perhaps it is not surprising that there are differences in processing naturally occurring stimuli and those that are more artificial. Recent paradigmatic shifts spurred by technical innovations have spawned more ecologically valid investigations of complex auditory perception and cognition that include the perception of sound source properties. The future for this approach is promising if ″behavioral relevance″ can serve a guiding principle.

10:20-10:40 Break

10:40

3aPPb8. Classification of everyday sounds: Influence of the degree of sound source identification. Olivier Houix (IRCAM - UMR CNRS 9912, Equipe Perception et Design Sonores, 1, place Igor Stravinsky, 75004 Paris, France, olivier.houix@ircam.fr), Guillaume Lemaitre (IRCAM - UMR CNRS 9912, Equipe Perception et Design Sonores, 1, place Igor Stravinsky, 75004 Paris, France, lemaitre@ircam.fr), Nicolas Misdariis (IRCAM - UMR CNRS 9912, Equipe Perception et Design Sonores, 1, place Igor Stravinsky, 75004 Paris, France, misdarii@ircam.fr), Patrick Susini (IRCAM - UMR CNRS 9912, Equipe Perception et Design Sonores, 1, place Igor Stravinsky, 75004 Paris, France, susini@ircam.fr)

Based on a review of everyday sound classification studies, we define three types of similarity that might underlie the formation of categories: acoustical similarity, related to the perception of the sound signal properties; causal similarity, related to the perception of the cause of the sound; semantic similarity, related to the meaning of the sounds. This study focuses on the influence of the degree of sound source identification on the type of similarity used during a free sorting task. Our hypothesis is that well-identified sounds will lead to categories based on causal or semantic similarities, while non-identified sounds will lead to categories based on acoustical similarity. First we measure the causal uncertainty of each sound of a set of kitchen sounds. We ask to participants to describe the cause of the sounds in order to measure the degree of identification for each sound. The results of a free sorting task on this sound corpus indicate that participants groups together sounds according to our assumptions. The classification of the well-identified sounds shows a clear distinction between classes of sound events (gas, liquid, solids, motor) confirming a taxonomy proposed in literature. [Work supported by the CLOSED project of the NEST program]

Contributed Paper

11:00

3aPPb9. Verbal imitations of sound events enable recognition of the imitated sound events. Karine Aura (Université de Toulouse II Le Mirail, Laboratoire Octogone-Lordat URI 41 56, IFR96, Pavillon de la Recherche, 5 allée Antonio Machado, 31058 Toulouse, France, aura@univ-tlse2.fr), Guillaume Lemaitre (IRCAM - UMR CNRS 9912, Equipe Perception et Design Sonores, 1, place Igor Stravinsky, 75004 Paris, France, lemaitre@ircam.fr), Patrick Susini (IRCAM - UMR CNRS 9912, Equipe Perception et Design Sonores, 1, place Igor Stravinsky, 75004 Paris, France, susini@ircam.fr)

We report a study investigating how verbal imitations of sound events might convey information enabling the recognition of the imitated sounds. We sampled twenty-eight sounds across a taxonomy of kitchen sounds, obtained from a previous experiment focused on the perceived properties of the causes of the sounds. First, we recorded speakers while imitating the sounds. They were specifically required not to use words. Then we selected the imitations of six speakers (three men, three women) imitating twelve sounds. Finally a group of twenty listeners performed a sorting task (they had to group together imitations thought to imitate the same events), and were asked to describe how they built each category. The categories of imitations, obtained from a hierarchical tree representation, fit very well with the categories of the original sound events. This suggests that speakers have succeeded in capturing the information sufficient to enable listeners to recognize the sound events. This is further confirmed by the analyses of the verbalizations. Phonetic analyses show that imitations grouped together share some phonetic similarities, yet the main similarities seem rather to be based on prosodic indexes (duration, intonation, rhythmic patterns). [This work is founded by the FP6 NEST Pathfinder European project CLOSED]

Invited Papers

11:20

3aPPb10. Auditory Perception of Silent Object Properties. Lawrence D. Rosenblum (University of California, Riverside, Department of Psychology, 900 University Ave., Riverside, CA 92521, USA, rosenblu@citrus.ucr.edu)

While much of what we consciously hear is based on sound sources, we also hear properties of objects that are themselves silent, but act to reflect and obstruct sound. A research program has been initiated to examine the degree to which listeners can judge properties of silent, sound-structuring objects. Results of this research have revealed impressive sensitivity to many of these properties. Thus far, this work has shown that (sighted) listeners have some ability to: a) determine the location, dimensions, and general shape of sound-obstructing panels; and b) identify various rooms based on how rooms structure emitted sounds; and c) determine their location in a room based on how the room structures sound at different positions. These results indicate that listeners are sensitive to ambient, as well as emitted acoustic properties, and call for a modified conception of human audition that takes into account these sensitivities.

11:40

3aPPb11. Evaluation and modification of listener decision strategy in human gait perception. Richard E. Pastore (Binghamton University (SUNY), Department of Psychology, Binghamton, NY 13902-6000, USA, pastore@binghamton.edu), Jesse D. Flint (Binghamton University (SUNY), Department of Psychology, Binghamton, NY 13902-6000, USA, jdflint@binghamton.edu), Jeremy R. Gaston (Binghamton University (SUNY), Department of Psychology, Binghamton, NY 13902-6000, USA, jgaston1@binghamton.edu)

Beyond obvious differences, there are many similarities in the challenges faced in studies of speech and natural (nonspeech) sounds. The source events are dynamic, complex and highly variable. Source properties map only statistically in the sounds produced, resulting in many acoustic properties that are only sometimes accurate indicators of specific source properties. Finally, beyond the nonlinear mapping of acoustic to perceptual properties, listeners vary in decision weights assigned to the perceived attributes of the sounds. Beginning with this complex conceptualization of source-sound-perception relationships, our research on the perception of human gait from walking sounds investigated the perception of walker posture. The current research extends this project on human gait perception, evaluating both the decision strategy of listener individual listeners and alternative approaches to improving that decision strategy. Implications for studying of both natural nonspeech and speech will be briefly discussed.

12:00

3aPPb12. Source Perception of Everyday and Self Produced Sounds: Factors in the Evolution of Human Auditory Cognitive Capability. James Ballas (Naval Research Laboratory, 4555 Overlook AVE SW, Washington, DC 20375, USA, james.ballas@nrl.navy.mil)

The everyday world was making meaningful sound well before language developed. Self-produced sound exhibits a tight binding between source event and interpretation. These assertions naturally prompt thoughts about the role of these types of sound in the evolution of human auditory capability, especially language. The recent resurgence in theorizing about the origin of language has included other human capabilities as potential generative factors (e.g., gestures), but there has been little discussion about the possible role of capability to process everyday and self-produced sound. This is surprizing given that recent neurocognitive research has supported common processing for speech and meaningful sound. Key attributes of language processing are the ability to interpret not just signs but symbols, and the ability to employ generative grammar processing to produce and interpret symbol strings. Association of sound events with causes and sequences, auditory representation of meaning, persistence of meaning under event and sequence variation, and persistence of event interpretations beyond what is currently present (temporal and spatial abstraction) are all fundamental requirements for these language attributes, and it is asserted that these capabilities might have developed to accurately perceive everyday and self-produced sound.

12:20

3aPPb13. Detection of missing modal frequencies. Christophe N. Stoelinga (University of Wisconsin-Madison, Department of Communicative Disorders, 1975 Willow drive, Madison, WI 53706, USA, stoelinga@wisc.edu), Robert A. Lutfi (University of Wisconsin-Madison, Department of Communicative Disorders, 1975 Willow drive, Madison, WI 53706, USA, ralutfi@wisc.edu)

The amount of information about a source that can be recovered from sound is naturally limited by the ear's ability to resolve individual modal frequencies unique to that source. To measure these limits, listeners were asked to detect, in a standard two-interval, forced-choice task with feedback, which of two sounds on each trial contained a missing partial. The frequencies of the partials corresponded to the ideal modes of a simply-supported, rectangular plate. Plate surface areas and height-wide ratios were chosen to produce the same bandwidths (125-1125, 250-2250 or 500-4500 Hz) for different numbers of partials (11, 16 or 24). Overall level of the sounds was roved to discourage detection based on simple level differences. Detection of five highly-practiced listeners was largely independent of the frequency of the lowest partial, being best for partials 1-3, 1-4 or 1-6 for 11, 16 or 24 partials in total, respectively. Mutual masking among the higher-number partials is given as the likely cause. The results are discussed in terms of their implications for the identification of rudimentary source attributes from sound. [Work supported by NIDCD grant 5 R01 DC006875].

WEDNESDAY MORNING, 2 JULY 2008 ROOM 241, 9:00 A.M. TO 12:40 P.M.

Session 3aPPc

Psychological and Physiological Acoustics, Architectural Acoustics, Noise, and Signal Processing in Acoustics: Jens Blauert and His Contributions

Ervin R. Hafter, Cochair
University of California, Department of Psychology, 3210 Tolman Hall, Berkeley, CA, CA 94720-1650, USA

Armin Kohlrausch, Cochair
Philips Research Europe, Digital Signal Processing (MS WO02), High Tech Campus 36, Eindhoven, 5656 AE, Netherlands

Invited Papers

9:00

3aPPc1. A means for comparing normal and impaired listeners in spatial hearing. Ervin R. Hafter (University of California, Department of Psychology, 3210 Tolman Hall, Berkeley, CA, CA 94720-1650, USA, hafter@berkeley.edu)

In our computer controlled Simulated Open Field Environment (SOFE), a computer generates simulated sources and echoes in an anechoic chamber. The SOFE has evolved over many years through ideas and hard work from a superb group of graduate students and post docs including Francoise Briolle, Tom Buell, Poppy Crum, Eric Jensen, Kourosh Saberi, Chris Stecker, Bernhard Seeber, and Miriam Valenzuela, as well as advice from such luminaries as Georg von Bekesy, Arnold Leiman and, of course, Jens Blauert. The ready use of Head Related Transfer Functions (HRTFs) with headphones raises the question, ″Why the SOFE?″ The answer is that each subject enters the environment with his or her natural HRTF and hearing apparatus intact, thus allowing comparisons between patients with cochlear implants or hearing aids, as well as listeners with normal hearing. Since its inception, this environment has been used to examine precedence, the role of relative level in echo suppression, multiple factors in auditory motion perception, and ventriloquism. This presentation will review some of the more interesting results.

9:20

3aPPc2. The salience of interaural temporal disparities (ITDs) conveyed by high-frequency signals is determined by the temporal features of their ongoing envelopes. Constantine Trahiotis (University of Connecticut Health Center, Departments of Neuroscience and Surgery (Otolaryngology), 263 Farmington Avenue, Farmington, CT 06030-3401, USA, tino@neuron.uchc.edu), Leslie R. Bernstein (University of Connecticut Health Center, Departments of Neuroscience and Surgery (Otolaryngology), 263 Farmington Avenue, Farmington, CT 06030-3401, USA, les@neuron.uchc.edu)

Many studies of binaural hearing reveal that envelopes of complex, high-frequency stimuli convey useful interaural time differences (ITDs). Envelope-based ITDs have, typically, been found to be less ″potent″ than those conveyed by low-frequency waveforms. When considering such findings, Blauert, in his classic textbook, noted that monaural, peripheral processing would result in 1) low-frequency inputs to the binaural processor that are essentially half-wave rectified versions of the input waveforms and 2) high-frequency inputs that are essentially full-wave rectified versions of only the envelopes of the input waveforms. Taking this into account, Blauert, echoing Colburn and Esquissaud (1976), surmised that low-frequency signals would ultimately convey ″more distinct time cues″ having greater ″transient features″ than would high-frequency signals and, therefore, be expected to provide more precise ITD information. By using high-frequency ″transposed″ stimuli having envelopes constructed to provide ″more distinct time cues″ we have shown in a variety of experimental contexts that the potency of envelope-based ITDs, can rival that measured with low-frequency stimuli. Our most recent experiments use ″raised sine stimuli″ in order to vary directly the temporal features of the envelope waveform including its ″sharpness,″ ″off-time,″ and interaural cross-correlation function. The new data will be discussed in terms of Blauert's insight.

9:40

3aPPc3. Cognitive influences on spatial hearing. Rachel Keen (University of Virginia, Department of Psychology, P. O. Box 400400, Charlottesville, VA 22904-4400, USA, rachelkeen@virginia.edu)

In reverberant rooms a listener perceives a sound coming from its source but simultaneously suppresses reflected sound or echoes. This phenomenon is known as the precedence effect because the preceding (original) sound is given heavier weight than its subsequent reflections. Our research has explored this perceptual process and found that listeners are sensitive to the acoustic information contained in the reflected sound even though it is ″suppressed″. Specifically, below echo-threshold information relevant to room acoustics (e.g., delay between lead and lag sounds, filtering of the echo's spectrum, presence or absence of an echo at a particular location) is processed by the listener and influences perception. Listeners' expectations about ongoing input can raise or lower echo threshold. Recent ERP data on listeners' responses to click pairs near echo threshold found that when listeners perceived lead and lag sounds as separate sources, a negativity between 100 and 250 ms was elicited, termed object-related negativity (ORN). When the same stimulus was heard as a single fused sound, no ORN was elicited. These findings suggest that higher-level cognitive processes exert top-down influences over early neurosensory processing.

10:00

3aPPc4. Modeling the Precedence Effect -- how we arrived where we are today. Jonas Braasch (Rensselaer Polytechnic Institute, Greene Bldg., 110 8th St., Troy, NY 12180, USA, braasj@rpi.edu)

Throughout his career, Jens Blauert was interested in further exploring the precedence effect, an auditory phenomenon that enables us to localize sounds in rooms and other enclosures. A series of models that were developed at Bochum's Institute of Communication Acoustics under his leadership have changed the way we think about the precedence effect. While this effect as a psychoacoustic phenomenon is known for its complexity -- for which Jens Blauert's talent to define precise terminology and listen critically came in handy -- the modeling aspects are equally challenging due to the non-linear nature of the underlying auditory processes. Blauert and Cobben's binaural model from 1978 was already able to simulate observations related to the precedence effect. A few years later, Blauert's doctoral student Werner Lindemann introduced a binaural model with specific stages to model the precedence effect. Since then, almost all approaches to simulate the precedence effect are based on inhibitory elements. In this talk, the evolution of this class of models over several student generations at Bochum will be described, and the fruitful scientific exchange with other institutions such as Steven Colburn's laboratory at Boston University will be highlighted as well.

10:20

3aPPc5. A History of Binaural Interaction Modeling - Walks with Jens Blauert. H Steven Colburn (44 Cummington St., Boston, MA 02215, USA, colburn@bu.edu), Suzanne Carr (44 Cummington St., Boston, MA 02215, USA, ruiwan@bu.edu), Rui Wan (44 Cummington St., Boston, MA 02215, USA, suzy@bu.edu)

Jens Blauert has been cut an impressively wide path through diverse areas of binaural and spatial hearing. He has consistently integrated viewpoints based on empirical results, intuitive interpretations, and mathematical and computational models of binaural interaction and spatial hearing. This talk focuses on the development of ideas about binaural interaction as represented in quantitative models and the strong influence that Blauert exerted on these models. These influences start with simple models of the extraction and use of interaural time and level differences, include mechanisms that incorporate complex interactions of these differences, and lead to models that are appropriate for the interpretation of complex acoustic scenes. Finally, some current modeling activities will be outlined and related to these historical developments. [Work supported by the US National Institutues of Health DC00100.]

10:40-11:00 Break

11:00

3aPPc6. Localization-based segregation of acoustic sources: Advantages and limitations. Pierre Divenyi (VA Northern Calif. Health Care Syst. and East Bay Inst. for Research and Education, Bldg. R4, 150 Muir Rd., Martinez, CA 94553, USA, pdivenyi@ebire.org)

It has been suggested [Divenyi, P., & Oliver, S.K., (1989), JASA 85, 2042-2052] that segregation of simultaneous pairs of sounds in the horizontal plane requires both resolution of the azimuthal separation between the sources, and correct assignment of each signal to the correct source. In fact, contrary to our a priori expectations, localization did not emerge as the dominant dimension underlying segregation of source pairs: its importance often fell behind that of segregation based on differences of spectral or temporal envelope structure, except for some listeners. Nevertheless, the possibility remains that these limitations can be attributed to localization dominance by one of the sources or both. The dual requirement of localization and signal-to-source assignment, in addition to reverberation, may represent a limiting factor for the role of localization in the cocktail-party effect.

Contributed Paper

11:20

3aPPc7. From binaural hearing to auralization: A triumph of Blauert's 40 years in room acoustics. Ning Xiang (Rensselaer Polytechnic Institute, Greene Building, School of Architecture, 110 8th Street, Troy, NY 12180, USA, xiangn@rpi.edu), Wolfgang Hess (Harman/Becker Automotive Systems, EG - Advanced Signal Processing, 76307 Karlsbad, Germany, WHess@harmanbecker.com)

In the late 60's when Jens Blauert's work on sound localization in the median plane was recognized by the psychoacoustics community, he had already started on a long journey from binaural-hearing research to many aspects of what nowadays is called Communication Acoustics. In addition to initiating many new research activities such as binaural auditory modelling, binaural technology, sound-quality, and speech synthesis, his unremitting endeavour in room acoustics has led to innovative developments in the fields of analysis and synthesis of auditory scenes. For example, binaural room-acoustics modelling, real-time dynamic room-impulse response processing, and auditory virtual environments (nowadays known as ″auralization″) were particularly driven by his work and his supervision of over 50 doctoral students. In this regard the first head-tracking and fast-convolution patent application was filed in the early 70's. Recently auditory models have been applied in auditory spatial evaluations of rooms and cars. Not only his excellent analytical skills and theoretical knowledge, but also his vision for transfer to practical applications in room acoustics and human-auditory spatial perception led to an outstanding life-work. This paper will highlight just a few of Jens Blauert's major contributions to room-acoustics.

Invited Papers

11:40

3aPPc8. Binaural technology for e.g. rendering auditory virtual environments. Dorte Hammershøi (Acoustics, Aalborg University, Fredrik Bajers Vej 7 B5, 9220 Aalborg Ø, Denmark, dh@es.aau.dk)

Jens Blauert's research up through the late 1960s and later, pioneered the field of binaural technology and auditory virtual environments. He mastered the measurement of head-related transfer functions (HRTFs) before the term was introduced, and his methods were standard for decades. While most acknowledge his efforts in understanding the binaural hearing and the significance of interaural differences, appreciation is also in place for his evaluation of localization with identical ear input signals. The relations between the hearing's ″directional″ bands and the transfer functions' ″boosted″ bands, helped mediate the understanding that if the transfer functions could be mastered, then important dimensions of the auditory percept could also be controlled. He early understood the potential of using the HRTFs and numerical sound transmission analysis programs for rendering auditory virtual environments. Jens Blauert participated in many European cooperation projects exploring this field (and others), among other the SCATIS project addressing the auditory-tactile dimensions in the absence of visual information.

12:00

3aPPc9. How can we model a quality event? Some considerations on describing quality judgment and prediction processes. Sebastian Möller (Deutsche Telekom Laboratories, Berlin Institute of Technology, Ernst-Reuter-Platz 7, 10587 Berlin, Germany, sebastian.moeller@telekom.de)

Jens Blauert has introduced a systemic view on a listener in an auditory experiment. This view helps to separate sound events from auditory events and from their descriptions, and to identify and describe the processes involved in such experiments. The notion has later been extended to listeners in a quality judgment situation by Jekosch and Raake, leading to the notion of a ″quality event″. On the one hand, knowledge of the involved processes is necessary to design appropriate measurement processes for, e.g., sound quality, transmission quality, auditory-scene quality, or product-sound quality. On the other hand, such knowledge enables us to define algorithms which estimate quality - or sub-aspects of it - in the system design process. The talk will mainly follow the second line and will identify components which are necessary for an algorithmic description of the processes involved in the formation of a quality event. Taking the example of telecommunication services, it will be shown which components of quality prediction models are already available, and which others are still out-of-reach and require further study.

12:20

3aPPc10. Semio-acoustics: a domain of communication acoustics. Ute Jekosch (Chair of Communication Acoustics, TU Dresden, Helmholtzstr. 10, 01069 Dresden, Germany, ute.jekosch@tu-dresden.de)

For user-oriented design of modern information and communication systems we investiate the perception of acoustic signals as sign carriers: How do listeners process acoustic/auditory events when they treat them as information carriers and which meaning do they associate with them? Sign carriers (in our case the acoustic signals) transport information across space and time. When being perceived, they are decoded, analyzed and interpreted with regard to their cultural meaning and their relevance for the actual living and commu-

nication situation. These processes are universal to a certain degree. It is the aim of our research in Dresden to investigate the fundamental structures and organisational principles underlying this assignment of meaning to acoustic and their accompanying auditory events. In this talk, some semio-acoustic paradigms will be introduced. As a Ph.D. student of Jens Blauerts' and as a post doc in his team, the semio-acoustic approach has developed as a logical continuation of his way of thinking, of his research approaches, and of his scientific goals, based on and fed by his basic statement: Communication acoustics is not conceivable without audition, and only if we are able to understand auditory events, and even cognitive processes, we are able to make use of acoustic communication and information technology in a user-friendly way.

WEDNESDAY MORNING, 2 JULY 2008 ROOM 252B, 8:00 TO 10:00 A.M.

Session 3aSAa

Structural Acoustics and Vibration, Computational Acoustics, and EURONOISE: Efficient Boundary Element Methods I

Ramani Duraiswami, Cochair
University of Maryland Institute for Advanced Computer Studies, 115 A.V. Williams Bldg, College Park, MD 20742, USA

Lothar Gaul, Cochair
Institute of Applied and Experimental Mechanics, University of Stuttgart, Pfaffenwaldring 9, Stuttgart, 70550, Germany

Invited Papers

8:00

3aSAa1. Vibroacoustic Simulation of Partly Immersed Bodies by a Coupled Fast BE-FE Approach. Dominik Brunner (Institute of Applied and Experimental Mechanics, University of Stuttgart, Pfaffenwaldring 9, 70550 Stuttgart, Germany, brunner@iam.uni-stuttgart.de), Michael Junge (Institute of Applied and Experimental Mechanics, University of Stuttgart, Pfaffenwaldring 9, 70550 Stuttgart, Germany, junge@iam.uni-stuttgart.de), Christian Cabos (Germanischer Lloyd, Vorsetzen 35, 20459 Hamburg, Germany, christian.cabos@gl-group.com), Lothar Gaul (Institute of Applied and Experimental Mechanics, University of Stuttgart, Pfaffenwaldring 9, 70550 Stuttgart, Germany, gaul@iam.uni-stuttgart.de)

Simulation of vibroacoustic behavior of submerged bodies necessitates dealing with fluid-structure coupled problems. In case of a high density of the fluid, the feedback of the acoustic pressure onto the structure cannot be neglected and a fully coupled system must be investigated. In this work, the finite element method (FEM) is used for the structural part. The commercial finite element package ANSYS is applied for setting up the mass and stiffness matrices. The boundary element method (BEM) is well suited for simulating the sound propagation in the unbounded exterior acoustic fluid domain. Here, the fast multipole method (FMM) is applied to overcome the known bottleneck of classical BE-methods. In the case of partly immersed bodies, Dirichlet boundary conditions on the fluid surface additionally have to be incorporated. This is done by applying a halfspace formulation. The extension of the FMM to this scenario is discussed. Iterative preconditioned solvers are employed and the numerical efficiency is discussed. The applicability of the coupling scheme is demonstrated using a realistic model problem.

8:20

3aSAa2. A half-space BEM for the simulation of sound propagation above an impedance plane. Haike Brick (TFH Berlin - University of Applied Sciences, FB II, Mathematics - Physics - Chemistry, Luxemburger Str. 10, 13353 Berlin, Germany, brick@tfh-berlin.de), Martin Ochmann (Technische Fachhochschule Berlin, Univ. of Applied Sciences, Luxemburger Str. 10, 13353 Berlin, Germany, ochmann@tfh-berlin.de)

The Boundary-Element-Method is a powerful tool for the simulation of sound radiation and scattering. Classically, it was developed for the free 3D-space, but it can be modified easily for half-space solutions as long as the half-space is delimited by a perfectly rigid or soft plane. In this case, the Green's function, the core of the BEM, can be derived from a simple image source ansatz, which however cannot be used for a more general impedance boundary condition. The alternative, an additional discretisation of a finite but large part of the plane leads to an enormous increase of the size of the set of equations. In this presentation, an appropriate Green's function will be introduced, which is able to describe the sound propagation above an impedance plane and is suitable for an implementation into a BEM code. It bases on the superposition of sound sources with complex source points. The numerical evaluation of this Green's function will be presented along with several test cases including sound radiation from burning flames above ground and tire-road noise. The computational costs of the developed ″Complex-Source-Point-BEM″ (CBEM) in comparison with a classical BEM together with a discretisation of the impedance plane will be discussed.

8:40

3aSAa3. Simulation of noise barrier insertion loss using the boundary element method. Holger Waubke (Austrian Academy of Sciences / Acoustics Research Institute, Wohllebengasse 12-14, 1040 Vienna, Austria, holger.waubke@oeaw.ac.at), Wolfgang Kreuzer (Austrian Academy of Sciences / Acoustics Research Institute, Wohllebengasse 12-14, 1040 Vienna, Austria, wolfgang.kreuzer@oeaw.ac.at), Zhensheng Chen (Austrian Academy of Sciences / Acoustics Research Institute, Wohllebengasse 12-14, 1040 Vienna, Austria, zhensheng.chen@oeaw.ac.at)

Within a project of the European Commission ″Calm Tracks & Routes″ the performances of different styles of noise barriers were investigated. Additionally new methods for increasing the absorption were investigated. A central theme was to investigate the mitigation of curved walls with high absorption coefficients, because studies made before the project gave the hint that noise barriers curved away from the source should give satisfying insertion loss. Due to the curvature the view in the landscape is hindered to a lesser degree compared to straight noise barriers. The investigation of the noise barriers was done by boundary element methods. An absorptive model for grassland was added and implemented into Green's functions. Due to the existence of smeared sources the application of the fast multipole method was not possible and the simulations were limited to the two-dimensional case. It became obvious that the distance of the source is important for the mitigation of curved noise barriers with respect to straight ones. Therefore different wall types and source positions were investigated. The results of the numerical simulation were compared to measurements in situ and in a large anechoic chamber.

9:00

3aSAa4. A GWBEM method for high frequency acoustic scattering. Emmanuel Perrey-Debain (Université de Technologie de Compiègne, Lab. Roberval UMR 6253, Dept. Acoustique, BP 60319, 60203 Compiègne, France, emmanuel.perrey-debain@utc.fr), Hadrien Bériot (Université de Technologie de Compiègne, Lab. Roberval UMR 6253, Dept. Acoustique, BP 60319, 60203 Compiègne, France, beriotha@gmail.com), Mabrouk Ben Tahar (Université de Technologie de Compiègne, Lab. Roberval UMR 6253, Dept. Acoustique, BP 60319, 60203 Compiègne, France, mabrouk.bentahar@utc.fr), Catherine Vayssade (Université de Technologie de Compiègne, Lab. Roberval UMR 6253, Dept. Acoustique, BP 60319, 60203 Compiègne, France, catherine.vayssade@utc.fr)

This paper considers the problem of scattering of a time-harmonic acoustic incident wave by a hard obstacle. The numerical solution to this problem is found using a Galerkin Wave Boundary Element Method (GWBEM) whereby the functional space is built as the product of conventional low order piecewise polynomials with a set of plane waves propagating in various directions. In this work we present strategies for finding the appropriate plane wave basis locally on each boundary element in order to deal efficiently with very irregularly meshed structures exhibiting both large smooth scattering surfaces as well as corners and small geometrical features. Numerical results clearly demonstrate that these improvements allow the handling of scatterers with complicated geometries while maintaining a low discretization level of 2.5 to 3 degrees of freedom per full wavelength.

9:20

3aSAa5. Fast multipole accelerated boundary element method (FMBEM) for solution of 3D scattering problems. Nail A. Gumerov (University of Maryland Institute for Advanced Computer Studies, 115 A.V. Williams Bldg, College Park, MD 20742, USA, gumerov @umiacs.umd.edu), Ramani Duraiswami (University of Maryland Institute for Advanced Computer Studies, 115 A.V. Williams Bldg, College Park, MD 20742, USA, ramani@umiacs.umd.edu)

Wideband FMBEM codes are challenging to implement since there are problems at both very low and high frequencies. Substantially different schemes for function representation and translation are efficient for low and high frequency ranges. We present a method which is suitable for solution both high and low frequency problems since it implements a switch between different representations and uses fast translation methods appropriate to each representation. For a high frequency problem the switch between representations may occur at some intermediate levels of hierarchical space subdivision of the FMM. We also present an FMM-based preconditioner used in the flexible GMRES iterative solver for scattering problems and discuss example problems computed in range $0.001<kD<200$, where k is the wave number and D is the size of the computational domain. The theoretical and experimental computational complexity of our algorithm is approximately $O((kD)^3)$ at large kD with relatively small asymptotic constant and the algorithm allows to solve problems with up to million nodes used for surface discretization in the range tested on a conventional personal computer.

9:40

3aSAa6. An efficient distributed BEM solver for acoustic and vibroacoustic analyses on a standard PC network. Paolo Di Francescantonio (STS, Via Dalmazia 30, 21100 Varese, Italy, pdifra@sts-web.it)

An efficient BEM approach that permit to solve large acoustic and vibroacoustic problems distributing analyses on a standard PC network is presented. The high efficiency is based on a mix of elements including: 1) A proprietary and high efficient communication and synchronization library (not MPI) 2) A Multi Domain Approach for reducing memory requirements and solution time 3) Efficient iterative solvers The proprietary communication / synchronization library permits to take full advantage of recent multi core PC, enabling to set up clusters with a large number of computing units with a reduced number of PC. A ″distributed memory″ approach permit to have available the sum of all the PCs RAM, ensuring the possibility to solve large and huge problems that cannot be faced with standard approaches. The Multi Domain approach permit to further reduce the memory requirements, while preserving all the required flexibility in terms of boundary condition and coupling with structural modes. Examples will be showed of large an huge analyses in different application fields including purely acoustics, and fully coupled structural-acoustic analyses.

Session 3aSAb

Structural Acoustics and Vibration, Computational Acoustics, and EURONOISE: Fluid—Structure Interaction I

Noureddine Atalla, Cochair
Univ. de Sherbrooke, Mechanical Engineering Depart., 2500 Boulevard de l'Université, Sherbrooke, QC J1K 2R1, Canada

Vicente Cutanda Henriquez, Cochair
Institute of Sensors, Signals and Electrotechnics, University of Southern Denmark, Niels Bohrs Allé 1, Odense S, 5230, Denmark

Stefan Schneider, Cochair
Laboratoire de Mécanique et d'Acoustique, UPR 7051 CNRS, 31,Chemin Joseph-Aiguier, Marseille, 13402, France

Invited Papers

10:40

3aSAb1. Practical modeling of acoustic losses in air due to heat conduction and viscosity. René Christensen (Oticon A/S, Kongebakken 9, 2765 Smoerum, Denmark, rch@oticon.dk), Peter Juhl (Institute of Sensors, Signals and Electrotechnics, University of Southern Denmark, Niels Bohrs Allé 1, 5230 Odense S, Denmark, pmjuhl@sense.sdu.dk), Vicente Cutanda Henriquez (Institute of Sensors, Signals and Electrotechnics, University of Southern Denmark, Niels Bohrs Allé 1, 5230 Odense S, Denmark, vch@sense.sdu.dk)

Accurate acoustics models of small devices with cavities and narrow slits and ducts should include the so-called boundary layer attenuation caused by thermal conduction and viscosity. The purpose of this paper is to present and compare different methods for including these loss mechanisms in analytical and numerical models. A simple circular geometry with a narrow tube has been used as a reference and is investigated both through measurements and the different models. The simulation methods compared are: i) traditional analytical approaches such as lumped parameter modelling and transmission line modelling, ii) numerical methods implemented into commercial packages, such as the low reduced frequency models as proposed by W. M. Beltman and implemented in ACTRAN and the linearized Navier-Stokes equations used in COMSOL Multiphysics, and iii) an implementation specifically made for this purpose using BEM and the full linearized model by M. Bruneau.

11:00

3aSAb2. An overview of models for viscothermal wave propagation, including fluid structure interaction. Willem M. Beltman (Intel Corporation, 2111 NE 25th Avenue, M/S JF2-86, Hillsboro, OR 97124, USA, willem.m.beltman@intel.com), Ysbrand H. Wijnant (University of Twente, Dept. Mechanical Engineering, P.O. Box 217, 7500 AE Enschede, Netherlands, Y.H.Wijnant@ctw.utwente.nl), Marten J. Nijhof (University of Twente, Dept. Mechanical Engineering, P.O. Box 217, 7500 AE Enschede, Netherlands, m.j.j.nijhof@ctw.utwente.nl)

In acoustics, the standard wave propagation models neglect the effects of viscosity and thermal conductivity. When waves propagate in narrow tubes or thin layers these simplifications might not be accurate. This paper presents an overview of models that take the effects of inertia, viscosity, thermal conductivity and compressibility into account. Based on the use of dimensionless parameters, three classes of models are outlined. The most important dimensionless parameter is the shear wave number, an unsteady Reynolds number that indicates the ratio between inertial and viscous effects. These viscothermal wave propagation models can be coupled to structural models to capture the fluid structure interaction. Analytical solutions can be found for these coupled analysis cases only for simple geometries and boundary conditions. For more complex geometries, numerical models were developed. Examples of applications of these models are also presented.

11:20

3aSAb3. A 3 dimensional finite element modeling of ″smart foam″ and its experimental validation. Pierre M. Leroy (Laboratoire de Mécanique et d'Acoustique - CNRS, 31 chemin Joseph Aiguier, 13402 Marseille, France, leroy@lma.cnrs-mrs.fr), Noureddine Atalla (Univ. de Sherbrooke, Mechanical Engineering Depart., 2500 Boulevard de l'Université, Sherbrooke, QC J1K 2R1, Canada, Nouredinne.Atalla@Usherbrooke.ca), Alain Berry (Univ. de Sherbrooke, Mechanical Engineering Depart., 2500 Boulevard de l'Université, Sherbrooke, QC J1K 2R1, Canada, alain.berry@usherbrooke.ca), Philippe Herzog (Laboratoire de Mécanique et d'Acoustique - CNRS, 31 chemin Joseph Aiguier, 13402 Marseille, France, herzog@lma.cnrs-mrs.fr)

The ″smart foam″ concept and design originate from the combination of passive dissipation of acoustic foams in the medium and high frequency range and the active absorption ability of piezoelectric actuators (generally PVDF) in the low frequency range. This results in a passive/active absorption control device that can efficiently operate over a broad range of frequencies. In this paper, a 3D finite element model of smart foam and its experimental validation are presented. The finite element model uses quadratic poroelastic elements with a (u,p) formulation, as well as elastic, fluid and piezoelectric elements. The weak integral formulation of the different

involved domains and their coupling conditions are presented. In particular, an isotropic and a simplified orthotropic model of poroelastic media are presented and compared. The fabrication of a prototype smart foam based on melamine foam with a curved, bonded PVDF film is discussed. Passive absorption and acoustic radiation of this prototype are measured in an impedance tube. The measured data are in good agreement with the numerical results, thereby validating the finite element model. This modeling tool constitutes a powerful platform to simulate and optimize various configurations of smart foams.

11:40

3aSAb4. Prediction of the sound field in anechoic rooms : comparison of two different approaches. François-Xavier Bécot (Matelys - Acoustique & Vibrations, 20/24 rue Robert Desnos, 69120 Vaulx-en-Velin, France, francois-xavier.becot @matelys.com), Stefan Schneider (Laboratoire de Mécanique et d'Acoustique, UPR 7051 CNRS, 31,Chemin Joseph-Aiguier, 13402 Marseille, France, schneider@lma.cnrs-mrs.fr), Luc Jaouen (Matelys - Acoustique & Vibrations, 20/24 rue Robert Desnos, 69120 Vaulx-en-Velin, France, luc.jaouen@matelys.com)

Despite the numerical advances, predicting the sound field in anechoic rooms is still challenging because it requires a fine modeling of the wall surface, acoustic properties and geometry, and the computation of the room sound field. It is proposed here to compare two innovative approaches to predict the performance of anechoic wedges, in particular to quantify the influence of porous frame motion, and to propose a numerically efficient model for the prediction of the sound field in anechoic room sounds at low frequencies. The first approach relies on the theory for modeling the sound propagation in double porosity media first presented by Olny & Boutin [J. Acoust. Soc. Am. 114 (1), 2003]. It has been shown that this approach could accurately predict the cut-off frequency of anechoic wedges. The interest is that this approach is numerically costless and that complex geometry could be considered. The second approach is based on the combination of FEM and BEM. It allows to predict the sound field in anechoic rooms. Compared to the previous approach, the latter one has the advantage of being able to identify structural effects inside the wedges and to propose an accurate prediction of the sound field in the room.

12:00

3aSAb5. Improvements on the directional characteristics of a calibration sound source using the Boundary Element Method. Vicente Cutanda Henriquez (Institute of Sensors, Signals and Electrotechnics, University of Southern Denmark, Niels Bohrs Allé 1, 5230 Odense S, Denmark, vch@sense.sdu.dk), Salvador Barrera-Figueroa (Danish Fundamental Metrology, Matematiktorvet 307, 2800 Kgs. Lyngby, Denmark, sbf@dfm.dtu.dk), Peter Juhl (Institute of Sensors, Signals and Electrotechnics, University of Southern Denmark, Niels Bohrs Allé 1, 5230 Odense S, Denmark, pmjuhl@sense.sdu.dk)

The project Euromet-792 aims to investigate and improve methods for secondary free-field calibration of microphones. In this framework, the comparison method is being studied at DFM in relation to the more usual substitution method of microphone calibration. The design of the sound source is of particular importance to achieve a sound field that reaches both microphones with the same level and that is sufficiently uniform at the microphone positions, in order to reduce the effect of misalignment. An existing sound source has been modeled using the Boundary Element Method, and the simulations have been used to modify the source and make it suitable for this kind of calibration. It has been found that a central plug, already present in the device, can be re-shaped in such a way that makes the sound field on the microphone positions more uniform, even at rather high frequencies. Measurements have been carried out in order to verify the goodness of this solution.

12:20

3aSAb6. Analysis of the resonance frequency shift in cylindrical cavities containing a sphere and its prediction based on the Boltzmann-Ehrenfest principle. Arturo Santillan (Universidad Nacional Autonoma de Mexico, Centro de Ciencias Aplicadas y Desarrollo Tecnologico, CCADET-UNAM, Circuito Exterior s/n, Cd. Universitaria, A. P. 70-186, 02510 Mexico, D.F., Mexico, arturo.orozco@ccadet.unam.mx), Vicente Cutanda Henriquez (Institute of Sensors, Signals and Electrotechnics, University of Southern Denmark, Niels Bohrs Allé 1, 5230 Odense S, Denmark, vch@sense.sdu.dk)

It is known that forces generated by high-level acoustic waves can compensate for the weight of small samples, which can be suspended in a fluid. To achieve this, a standing wave is created in a resonant enclosure, which can be open or closed to the external medium. This phenomenon, called Acoustic levitation, has numerous applications in containerless study and processing of materials. Although it is possible to levitate a sample for long periods of time, instabilities can appear under certain conditions. One of the causes of oscillational instabilities is the change of the resonance frequency of the cavity due to the presence of the levitated object. The Boltzmann-Ehrenfest principle is used to find an analytical expression for the resonance frequency shift in a cylindrical cavity produced by a small sphere, with $kr < 1$, where k is the wavenumber and r is the radius of the sphere. The validity of this expression has been investigated by means of the Boundary Element Method and experiments. In addition, the effect of the dispersion of the sound field by the sphere and the boundaries of the cavity on the resonance frequency shift has been analyzed using the BEM.

12:40-2:00 Lunch Break

Invited Paper

2:00

3aSAb7. A hybrid SEA/image sources approach for the prediction of the insertion loss of enclosures. Franck C. Sgard (IRSST, Service de la recherche, 505 Boulevard de Maisonneuve O, Montréal, QC H3A3C2, Canada, frasga@irsst.qc.ca), Hugues Nelisse (IRSST, Service de la recherche, 505 Boulevard de Maisonneuve O, Montréal, QC H3A3C2, Canada, hugnel@irsst.qc.ca), Noureddine Atalla (Univ. de Sherbrooke, Mechanical Engineering Depart., 2500 Boulevard de l'Université, Sherbrooke, QC J1K 2R1, Canada, Nouredinne.Atalla@Usherbrooke.ca), Celse Kafui Amedin (GAUS, Université de Sherbrooke - 2500 Bd de l'Université, Sherbrooke, QC J1K2R1, Canada, Celse-kafui.amedin@Usherbrooke.ca), Rémy Oddo (GAUS, Université de Sherbrooke - 2500 Bd de l'Université, Sherbrooke, QC J1K2R1, Canada, Remy.Oddo@USherbrooke.ca)

Enclosures are a classical solution to reduce the sound exposure of workers to the noise radiated by machinery. Their acoustic design can be achieved with the help of predictive tools based on simple analytical tools or sophisticated numerical deterministic models. However, there is no simple and fast tool allowing to account for the complexity of the enclosure configuration, capable of better simulating the non-diffuse nature of the field inside the enclosure and covering the typical frequency range [100Hz; 5000Hz]. This paper presents the development of such a tool for the prediction of the acoustic performance of enclosures. It is based on a hybrid model: the statistical energy analysis (SEA) for the sound transmission across the various elements of the enclosure and the method of image sources for the sound field inside the enclosure. The approach is validated by comparing calculation and experimental results carried out in a semi-anechoic room on rectangular and L-shape enclosures for several inner source locations. The effect of an opening is also investigated. The comparisons between the models and the experimental results show a good agreement for most of the tested configurations.

Contributed Papers

2:20

3aSAb8. Vibroacoustic interface conditions between prestressed structures and moving fluids. Fabien Treyssède (Nantes Atlantique University - LCPC, Division for Metrology and Instrumentation, Route de Pornic - BP 4129, 44341 Bouguenais, France, fabien.treyssede@lcpc.fr)

Many applications involve coupling between prestressed solids and fluids (possibly flowing). Typical problems might be given by vibroacoustics of fluid-filled pressurized cavities, wave propagation, dynamics and stability of pipes conveying fluids. The goal of this work is to investigate jump conditions that hold for small linear perturbations at any impermeable interfaces, slip or bonded, plane or not, between fluids and structures in the presence of initial flow and prestress. First, the mixed Eulerian-Lagrangian description is briefly recalled. It yields an interesting unification between existing formulations for inviscid fluids (Galbrun's equation) and solids (updated Lagrangian formulation). Based on conservative equations obtained from this description, interface conditions are derived in an elegant manner thanks to the concept of generalized functions in distribution theory. These conditions are written in terms of a curvilinear coordinate system attached to the interface. They are shown to coincide with a direct linearization of standard Eulerian jump conditions. General interface conditions for displacement, stress, heat flux and temperature are given. As an example, these conditions are applied to the analysis of elastoacoustic wave propagation inside an inviscid fluid-filled pressurized duct. The combined effects of slip, prestress and initial flow are briefly discussed.

2:40

3aSAb9. Experimental and numerical investigation of the dynamics in spatial fluid-filled piping systems. Jan Herrmann (Institute of Applied and Experimental Mechanics, University of Stuttgart, Pfaffenwaldring 9, 70550 Stuttgart, Germany, herrmann@iam.uni-stuttgart.de), Thomas Haag (Institute of Applied and Experimental Mechanics, University of Stuttgart, Pfaffenwaldring 9, 70550 Stuttgart, Germany, thomasshaag@gmx.de), Lothar Gaul (Institute of Applied and Experimental Mechanics, University of Stuttgart, Pfaffenwaldring 9, 70550 Stuttgart, Germany, gaul@iam.uni-stuttgart.de)

Hydraulic piping systems, such as fluid-filled break and fuel pipes in automotive applications, undergo strong acoustic excitation due to pressure pulsations of pump and valve operation. By fluid-structure coupling the sound transmission within the pipe may lead to a structural excitation of other car components causing excessive noise levels or even structural failure. In order to obtain a complete and reliable understanding of the wave propagation and vibration phenomena in spatial piping systems, a test rig is presented, consisting of a pressure source and a fluid-filled break pipe with an attached target structure. With this experimental setup, it is possible to quantify the acoustic sound transmission and to examine the dynamic behavior by transfer functions. The experimental results are compared with harmonic and transient finite element simulations employing efficient model order reduction techniques for the fluid-structure coupled system. This research focuses on the identification of hydraulic resonances and the optimal mounting of the fluid-filled break pipe in order to minimize the structure-borne sound induced on the target structure.

3:00

3aSAb10. Noise generation in an unstable boundary-layer flow over a flexible wall. Marie-Laure Gobert (IRENav, BP 600, 29240 Brest Armées, France, marie-laure.gobert@ecole-navale.fr), Uwe Ehrenstein (IRPHE, 49 rue Joliot-Curie, BP 146, 13384 Marseille Cedex 13, France, ehrenstein@irphe.univ-mrs.fr), Jacques Andre Astolfi (IRENav, BP 600, 29240 Brest Armées, France, astolfi@ecole-navale.fr), Patrick Bot (IRENav, BP 600, 29240 Brest Armées, France, bot@ecole-navale.fr), Jean Audet (Thales Underwater Systems, 525 route des Dolines, BP 157, 06903 Sophia Antipolis, France, Jean.Audet@fr.thalesgroup.com), Guillaume Oudot (DCNS Divison Navires Armés, Le Mourillon, BP 1306, 83076 Toulon cedex, France, guillaume.oudot@dcnsgroup.com)

The boundary-layer flow, for instance along a sonar dome, gives rise to hydrodynamic noise due to the pressure fluctuations. The prediction of the resulting self-noise received by the sonar antenna is based on models, which in general take only partially into account the flexibility of the dome wall. The present work readdresses the problem of hydrodynamic noise, considering the geometrically simplified model of a two-dimensional unstable boundary-layer flow along an elastic plate with clamped ends. The incompressible Navier-Stokes equations are fully coupled to the elastic plate model and the system is numerically solved for various plate materials. The unstable flow dynamics is analyzed with respect to the wall properties. The Fourier-transformed stress tensor is then used in the framework of Lighthill's analogy to determine the generated radiative sound, emphasizing the effect of wall-flexibility. This work is supported by Thales Underwater System and DCNS.

Session 3aSCa

Speech Communication: Speech Prosody and How it Relates to Segmental Aspects of Speech

Yi Xu, Cochair
University College London, Wolfson House, 4 Stephenson Way, London, NW1 2HE, UK

Hansjörg Mixdorff, Cochair
TFH Berlin University of Applied Sciences, Luxemburger Str. 10, Berlin, 13353, Germany

Invited Papers

8:00

3aSCa1. Segmental variability related to speech prosody - An articulatory-functional perspective. Yi Xu (University College London, Wolfson House, 4 Stephenson Way, NW1 2HE London, UK, yi.xu@ucl.ac.uk)

Just like in the tonal aspect, variability abounds in the segmental aspect of speech. Here I argue that segmental variability, similar to supra-segmental variability, can be understood from an articulatory- functional perspective. That is, two independent sources of segmental variability co-exist: a) multiple layers of communicative functions, and b) articulatory mechanisms of their encoding. From an articulatory perspective, much of the segmental variability arises from the nature of the syllable as a product of generating time markers, namely, synchronized onsets of consonant, vowel, tone and phonation register at the start of each syllable as recurrent events that serve like clock ticks to enable time tracking by both speakers and listeners. Such time marking results in complete overlap of initial consonant and the following vowel, which is responsible for most of the variability known as coarticulation, and sequential offset of coda components in a syllable, making them susceptible to deletion and merger. From a functional perspective, segments as supralaryngeal articulatory movements encode not only lexical contrast, but also other functional contrasts such as focus, grouping, attitude, etc. Like the tonal aspect of speech, these extra-lexical information are probably encoded as modification of segmental targets that have been lexically assigned.

8:20

3aSCa2. Prosodic Variation: Understanding Scope, Categoricity, and Recursion in Speech Production and Perception. Dani Byrd (Dept of Linguisitcs, University of Southern California, 3601 Watt Way, GFS 301, Los Angeles, CA 90089-1693, USA, dbyrd@usc.edu), Jelena Krivokapic (Department of Linguistics, Yale University, 370 Temple St, Room 204, PO Box 208366, New Haven, CT 06520-8366, USA, jelena.krivokapic@yale.edu)

Prosodic structure refers to the level of linguistic structure above the segmental level, namely prominence and phrasal organization. We will examine both articulatory and perceptual characteristics of phrasal organization, and their interrelation. An experiment using articulatory movement tracking examines how far in time remotely from a boundary the effect of the boundary extends. In a second experiment (Krivokapic 2007), we examine how structural properties of a range of prosodic boundaries are reflected in perception--specifically, whether boundary perception is categorical or gradient. A third study considers whether prosodic junctures of the same category type (e.g, an intonational phrase boundary) can, when embedded, give rise in articulation to boundary signatures of measurably different strengths. That is, we evaluate the possibility of recursive prosodic structures of the kind that Ladd (1996) postulates. Taken together, these experiments inform us about structurally induced variability. They provide the opportunity to evaluate standard assumptions about prosodic structure such as the question of boundaries as symbolic or temporal events, categoricity, and strict layering. Throughout, we will consider how the pi-gesture framework (Byrd & Saltzman 2003) offers theoretical insight regarding issues of prosodic representation and realization. [Supported by NIH]

Contributed Papers

8:40

3aSCa3. Temporal organization of prosodic and segmental features in spoken Japanese. Hiroya Fujisaki (University of Tokyo (Prof. emeritus), 3-31-12 Ebisu, Shibuya-ku, 150-0013 Tokyo, Japan, fujisaki@alum.mit.edu), Sumio Ohno (Tokyo University of Technology, 1404-1 Katakura, 192-0982 Hachioji, Japan, ohno@cc.teu.ac.jp)

It is apparent that prosodic and segmental features of speech must be temporally coordinated in order to produce a consistent and meaningful message. The precise mechanism for the coordination, however, has not been clear. The present study looks into this problem in the case of word accent in spoken Japanese. The speech material consisted of utterances of Japanese words that were identical in the word accent type, in the number of morae, in vowel constituents, but were different in consonantal constituents (including a 'null' consonant) at a certain intervocalic position. As for the prosodic features, the fundamental frequency contours were analyzed using the command-response model, and the onset and the offset of the extracted accent command were used as indices of prosodic timing. As for the segmental features, the formant frequency trajectories of the vowels were analyzed using another command-response model, which allowed extraction of the onset of the articulatory command for a vowel nucleus as an index of segmental timing. Comparison of the timings of these commands provides a means for quantitative analysis of the relationship between segmental and prosodic features of speech, and leads to an understanding of the underlying mechanism for their temporal coordination.

9:00

3aSCa4. Stress, focus, and the roots of segmental variation. Kenneth De Jong (Indiana University, 322 Memorial Hall, 1021 E. 3rd Street, Bloomington, IN 47405, USA, kdejong@indiana.edu)

de Jong (JASA, 1995) proposed a definition of linguistic stress as variation in the articulation of segmental material; stress is variation on the hypo- to hyper-articulation dimension (Lindblom, 1990) localized to the syllable.

This definition has suggested that the interaction of stress and segmental articulation will involve 1) linguistic conventionalization, since stress is a property of particular linguistic systems, 2) the structure of segmental contrasts, since hyper-articulation is driven by contrast enhancement, and 3) propensities in articulation, since hypo-articulation is driven by motor considerations. This paper reviews evidence for effects of linguistic conventionalization of stress. It further examines and compares the results of a number of experiments in segmental variation related to focus. Some dimensions of acoustic contrast, vowel quality, transition dynamics, and glottal timing, exhibit readily detectable and gradient variation as expected by a hyperarticulation model, and such variation is specific to the language's contrastive structure. Not all contrastive dimensions, however, are so affected, for example, noise associated with obstruent consonants. These patterns of results together suggest a functional interaction between the various speech gestures which may define a unit of speech at about the level of the syllable; the level which is the domain of expression of stress.

Invited Papers

9:20

3aSCa5. Close coupling or points of rendezvous? Connections between intonational events and the segmental grid. Hansjörg Mixdorff (TFH Berlin University of Applied Sciences, Luxemburger Str. 10, 13353 Berlin, Germany, mixdorff@tfh-berlin.de), Hartmut Pfitzinger (Christian-Albrechts-University, Leibnizstr. 10, 24118 Kiel, Germany, hpt@phonetik.uni-muenchen.de), Stefan Werner (University of Joensuu, PL111, 80101 Joensuu, Finland, stefan.werner@joensuu.fi)

The authors examine the connection between the fundamental frequency (f0) contour and the segmental grid, employing the Fujisaki model for decomposing an f0 contour into phrase and accent components. As shown in earlier work by the first author, accent commands are closely connected with the accented syllables of the constituent words of an utterance. They reflect the temporal alignment of intonational gestures by their on- and offset times, as well as the magnitude of the gestures by their amplitudes. Their timing relates to phonemic function, and the amplitudes are strongly correlated with the prominence of an accented syllable. In this study the authors attempt to model the intensity contour of an utterance as a concomitant of the articulatory gesture, namely by low-pass filtering pulsewise ″syllable commands″, yielding onset and offset points as well as amplitude values of the syllabic gestures and relate these data to the accent command data from the f0 tier. We examine the influence of phonemic distinctions on the alignment between the f0 contour and the segmental grid, as well as the influence of the intonational gesture on the realization of segments. The work is carried out on spontaneous American English speech data from the Buckeye corpus.

9:40

3aSCa6. Segmental effects on the prosody of voice quality. Hartmut Pfitzinger (Christian-Albrechts-University, Leibnizstr. 10, 24118 Kiel, Germany, hpt@phonetik.uni-muenchen.de)

Voice quality variability is due to supra-segmental influences but also to segmental factors like phoneme class, vowel quality, nasalization, airstream mechanism etc. These factors determine a rather unexplored micro-prosodic phenomenon: the phone-intrinsic voice quality which causes voice quality coarticulation and voice quality transitions in fluent speech. I subsume all these phenomena under the high-frequency components of prosody. Since high-frequency and low-frequency components (supra-segmentals) of voice quality prosody are superposed and thus encoded the main goal of this paper is to separate them and make both accessible to speech research. In 2003 a holistic voice quality parameter extractor was introduced by Mokhtari, Pfitzinger, and Ishi: It applies a principal components analysis to a database of glottal-flow waveforms for the purpose of later reconstructing and interpolating all underlying glottal-flow waveforms from just a few principal components. Recently, by applying this basic principle to a large corpus of manually segmented glottal-flow waveforms of 44 speakers I dramatically improved its applicability to any speech signals. The application of this version to a large speech database and subsequent high-pass and low-pass filtering of the resulting voice quality parameters yielded phone-intrinsic voice quality parameter sets as well as slowly varying meaningful voice quality parameter contours.

Session 3aSCb

Speech Communication: Speech Perception III

Eva Reinisch, Chair
Max Planck Institute for Psycholinguistics, Postbus 310, Nijmegen, 6500AH, Netherlands

Contributed Papers

8:40

3aSCb1. Lexical stress information modulates the time-course of spoken-word recognition. Eva Reinisch (Max Planck Institute for Psycholinguistics, Postbus 310, 6500AH Nijmegen, Netherlands, eva.reinisch@mpi.nl), Alexandra Jesse (Max Planck Institute for Psycholinguistics, Postbus 310, 6500AH Nijmegen, Netherlands, alexandra.jesse@mpi.nl), James M. McQueen (Max Planck Institute for Psycholinguistics, Postbus 310, 6500AH Nijmegen, Netherlands, james.mcqueen@mpi.nl)

Segmental as well as suprasegmental information is used by Dutch listeners to recognize words. The time-course of the effect of suprasegmental stress information on spoken-word recognition was investigated by tracking Dutch listeners' looks to arrays of four printed words on a computer screen as they listened to spoken sentences. Each target was displayed along with a competitor that did not differ segmentally in its first two syllables but differed in stress placement (e.g., 'CENtimeter' and 'sentiMENT'; capitals marking stressed syllables). The listeners' eye-movements showed that suprasegmental stress information is used to recognize the target before distinct segmental information is available. Furthermore, the presence of initial-syllable stress affected the degree to which words compete for recognition: Targets with non-initial stress ('sentiMENT') suffered from stronger competition than initially stressed targets ('CENtimeter'). Follow-up experiments showed that initial-syllable duration, as a cue to lexical stress, is not interpreted dependent on the speaking rate of the preceding carrier sentence. This still held when other stress cues like pitch and amplitude were removed. Rather, the speaking rate of the preceding carrier affected the speed of word recognition globally, even though the speaking rate of the target itself was not altered.

9:00

3aSCb2. Using pause durations to discriminate between lexically ambiguous words and dialog acts in spontaneous speeech. Rajdip Dhillon (Dept. of Linguistics, Yale Univ., 370 Temple St., Rm. 204, New Haven, CT 06520, USA, rajdip.dhillon@yale.edu)

Using multiparty conversations conducted in spontaneous Scottish English speech, this study examines whether pause durations can be used to discriminate between lexically ambiguous words pertaining to different dialog acts and, more generally, whether pause durations signal different types of dialog acts. Dialog acts describe the pragmatic functions of utterances and their detection requires attention to pragmatic function, syntax, prosody, surrounding context, and interaction between speakers. In this study, the dialog acts examined are 'floor grabbers', which are used by speakers to gain attention or to interrupt a current speaker who has the floor, and 'acceptance/agreements', which express agreement to or acceptance of a previous speaker's question, proposal, or statement. Experiments 1 and 2 examine pause durations following the lexical items 'right' and 'good' respectively when used as 'floor grabbers' or 'acceptance/agreements'. Experiment 3 examines pause durations following 'floor grabbers' and 'acceptance/agreements', regardless of the lexical item. Results of all three experiments indicate that pauses following 'floor grabbers' are significantly longer than those following 'acceptance/agreements'. This study shows that pause durations are in fact a reliable means of discriminating between lexically ambiguous words and distinguishing dialog acts. The study also sheds light on how stable pause usage is in spontaneous speech.

9:20

3aSCb3. Identification of talkers speaking emotional speech. Kyung Wha Kim (Forensic Science Div, Supreme Prosecutors' Office, 706 Banporo, Seocho-gu, 137-730 Seoul, Republic of Korea, savoix@spo.go.kr), Patrick C. Wong (Northwestern University, 2240 Campus Drive, Evanston, IL 60208, USA, pwong@northwestern.edu)

Identification of talkers speaking emotional speech is common in many communicative situations and forensic ″voice line ups″. However, emotional speech is auditorily and acoustically different from neutral speech, which may cause difficulty in talker identification. In this study, we examined how listeners identify different talkers speaking emotional or neutral voices, and how short-term training may benefit talker identification. Recordings were obtained from 10 male speakers speaking in angry and neutral voices. Within one session, listeners were first trained to identify the talkers, and their ability to generalize to untrained sentences spoken by the same talkers was tested. We found that while there was no significant difference in identifying neutral and angry voices, the ability to generalize to untrained sentences was more impaired with angry voices. The theoretical and forensic implications of these results are discussed. [Work supported by NIH and NSF]

9:40

3aSCb4. An fMRI-based structural equation model for natural language processing shows age-dependent changes in brain connectivity. Scott K. Holland (Cincinnati Children's Hospital Medical Center, Imaging Research Center, 3333 Burnet Ave, Cincinnati, OH 45229, USA, scott.holland@cchmc.org), Prasanna Karunanayaka (Cincinnati Children's Hospital Medical Center, Imaging Research Center, 3333 Burnet Ave, Cincinnati, OH 45229, USA, KAR4RP@cchmc.org), Elena J. Plante (Univ. Arizona, Dept. Speech and Hearing Sciences, P.O. Box 210071, Tucson, AZ 85721-0071, USA, eplante@U.Arizona.EDU), Vincent J. Schmithorst (Cincinnati Children's Hospital Medical Center, Imaging Research Center, 3333 Burnet Ave, Cincinnati, OH 45229, USA, Vince.Schmithorst@cchmc.org)

Structural Equation Modeling (SEM) or path analysis is a multivariate analytic tool that is used to test hypothesis about causal influences among measured or latent variables. When applied to functional neuroimaging (fMRI) data, SEM combines interregional covariance and neuroanatomy to investigate brain connectivity and the dynamic flow of information across neural networks. We have investigate Linear SEM or LSEM as a first step in estimating connection strengths from fMRI data in children during acoustic stimulation with stories in English. An average LSEM was constructed based on the concatenated fMRI data from N=313 children, age 5 to 18, listening to stories. Time courses from the fMRI data is used as input to the LSEM as computed in AMOS (v.5.1, SmallWaters, Corp. Chicago, IL) to yield an average model for the entire group. The LSEM path coefficients were examined between brain regions involved in auditory speech perception and language processing. Connectivities estimated by LSEM are significantly age dependent in some brain areas, while the connectivity coefficient between other brain regions is not a function of age.

Session 3aSCc

Speech Communication: Speech Articulation II

Yves Laprie, Chair
LORIA CNRS, 615 rue du Jardin Botanique, Bâtiment C, Villers-lès-Nancy, 54600, France

Contributed Papers

10:40

3aSCc1. Modeling formant pattern in fricative-vowel sequences. Martine Toda (CNRS & ENST, 46, rue Barrault, 75634 Paris, France, martinetoda@yahoo.co.jp), Shinji Maeda (CNRS & ENST, 46, rue Barrault, 75634 Paris, France, maeda@tsi.enst.fr)

MRI data indicate that there are two subject-dependent articulatory patterns in French post-alveolar sibilant fricative /'integral of'/. Each type of articulations can correspond to the Polish fricatives /'curled c'/ and /'underdotted s'/ on the basis of their articulatory similarity: palatalized for the former, and the presence of a sublingual cavity as well as lip protrusion for the latter. The F2 transitions, in part, reflect the acoustic contrast between these Polish fricatives, which exhibit a higher locus in the palatalized /'curled c'/ than in /'underdotted s'/. However, no systematic transitional characteristic could be found in French. We hypothesize that the subject-specific formant-cavity affiliation in the adjacent vowel /a/ and/or the difference of scale in vocal tract lengths manifest as the acoustic variation in French, whereas those VT morphological differences are articulatorily compensated in Polish to maintain the distinctiveness of these two post-alveolar fricatives. In order to assess this hypothesis, the F-patterns along /a 'integral of' a/ sequences are simulated for various vocal tract configurations. In calculations, the two different types of the fricative articulations are combined with the vocal-tract area functions appropriate for /a/ but different in shape and in size to taken into account for female and male speakers. The results will be discussed.

11:00

3aSCc2. Diffraction effects on speech phonemes during phonation. Vijayakumar V (Multimedia University, FOSEE, Jalan Air Keroh Lama, 75450 Melaka, Malaysia, vijaya@mmu.edu.my), Eswaran C (Multimedia University, Faculty of Information Technology, Cyberjaya Campus, 63100 Cyberjaya, Malaysia, eswaran@mmu.edu.my)

In this paper we will show how the ventricular fold modifies speech phonemes and also causes the shimmering of speech. Diffraction of sound waves at the ventricular fold which can be considered as a circular aperture, can modify the vocalized glottal sound spectrum reaching the pharyngx. Thus during phonation, speech phoneme spectra are essentially enveloped by Bessel functions. Since Bessel beams are known to be nondiffracting, this step ensures that the phonemes do not undergo further diffraction effects which can destroy the unique harmonic structure of the phonemes. Note that the wavelengths of sound waves and the dimensions of the human vocal tract appendages are of the same order of magnitude which mean that diffraction should be commonplace in the vocal tract if not for the initial packaging of the speech phoneme at the ventricular fold.

11:20

3aSCc3. Evaluation of phonetic constraints in acoustic-to-articulatory inversion. Yves Laprie (LORIA CNRS, 615 rue du Jardin Botanique, Bâtiment C, 54600 Villers-lès-Nancy, France, Yves.Laprie@loria.fr), Blaise Potard (LORIA CNRS, 615 rue du Jardin Botanique, Bâtiment C, 54600 Villers-lès-Nancy, France, Blaise.Potard@loria.fr), Anne Bonneau (LORIA CNRS, 615 rue du Jardin Botanique, Bâtiment C, 54600 Villers-lès-Nancy, France, Anne.Bonneau@loria.fr)

The objective is to evaluate phonetic constraints intended to guarantee the phonetic realism of vocal tract shapes generated by an articulatory model, i.e. here that of Maeda. The constraints are based on the relation between vocal tract shapes allowed for a vowel and formants frequencies of the vowel. They are speaker independent since they are derived from standard phonetic knowledge. We used them to reduce the number of solutions in acoustic-to-articulatory inversion. The impact of constraints has been investigated by comparing vocal tract shapes recovered by inverting five French vowels /i, e, a, u, y/ to those obtained by outlining articulator contours in X-ray images. To that purpose we used X-ray images (used by Maeda to elaborate his articulatory model) with the corresponding speech signal. The evaluation shows that unrealistic vocal tract shapes are penalized by constraints, that vocal tract shapes recovered through inversion are in very good agreement with X-ray images and that relevant articulatory variability is recovered when considering all vocal tract shapes corresponding to one vowel. These constraints thus complement the articulatory model very efficiently. Additionally, the inversion framework complemented by phonetic constraints is an efficient way of investigating the acoustic properties of an articulatory model.

11:40

3aSCc4. Acoustic-to-articulatory inversion of fricatives. Farid Feïz (LORIA CNRS, 615 rue du Jardin Botanique, Bâtiment C, 54600 Villers-lès-Nancy, France, Farid.Feiz@loria.fr), Blaise Potard (LORIA CNRS, 615 rue du Jardin Botanique, Bâtiment C, 54600 Villers-lès-Nancy, France, Blaise.Potard@loria.fr), Yves Laprie (LORIA CNRS, 615 rue du Jardin Botanique, Bâtiment C, 54600 Villers-lès-Nancy, France, Yves.Laprie@loria.fr)

The objective is to recover the vocal tract shape dynamics from the speech signal of vowels and fricatives. The method relies on the analysis-by-synthesis paradigm and is an extension of the method proposed by Ouni and Laprie which exploits a hypercubic articulatory table to represent the synthesis facet, i.e. Maeda's articulatory model. The first major modification is the use of parallelepiped instead of cubes. The new construction strategy only subdivides the articulatory space in the articulatory direction which gives rise to the strongest non-linearities. This enables a substantial reduction of the table size. The second major modification is the inversion of fricative sounds. In addition to the articulatory parameters the relative location of the noise source downstream the constriction is taken into account. This gives rise to three different articulatory codebooks, each corresponding to the relative position of the source with respect to the main constriction. This new inversion method has been evaluated on VCV sequences. It turns out that the correct vocal tract dynamics is recovered even if the constriction area is slightly underestimated. Input data are the first three formant frequencies but MFCC coefficients are now investigated since they render the high frequency region of fricative spectra better.

Session 3aSCd

Speech Communication: Prosody I

Volker Dellwo, Chair
UCL, Wolfson House, 4, Stephenson Way, London, NW1 2HE, UK

Contributed Papers

10:40

3aSCd1. Quantifying rhythm in running speech. Tristie Ross (Dept. of Linguistics, UCSD, 9500 Gilman Drive #0108, La Jolla, 92093-0108, USA, tross@ling.ucsd.edu), Naja Ferjan (Dept. of Linguistics, UCSD, 9500 Gilman Drive #0108, La Jolla, 92093-0108, USA, naja@ling.ucsd.edu), Amalia Arvaniti (Dept. of Linguistics, UCSD, 9500 Gilman Drive #0108, La Jolla, CA 92093-0108, USA, amalia@ling.ucsd.edu)

In the past decade several metrics that reflect the variability of vocalic and consonantal intervals in speech have been used to quantify the impressionistic division of languages into stress- and syllable-timed. Although all such metrics successfully separate prototypical languages, such as stress-timed English and syllable-timed Spanish, their results for other languages are less clear. The problem is related to the limited datasets used, which consist of either a small number of sentences per language elicited from several speakers, or longer stretches of speech elicited from one speaker per language. Here we elicited short sentences, story reading and spontaneous speech from several speakers of stress-timed English, syllable-timed Spanish, Korean, a hitherto unclassified language, and Greek, which has shown to resist classification. Our results show that different metrics yield different classifications for some languages, like Greek, while scores for the same language differ depending on speaking style. Taken all together these results cast doubt on the robustness and usefulness of the popular metrics and suggest that alternative ways of conceiving of speech rhythm that do not rely exclusively on timing but take relative prominence into account may ultimately be more successful in explaining speech rhythm.

11:00

3aSCd2. Temporal Organization of the Compounds in Standard Chinese. Eric Zee (Phonetics Lab, Dept. of Chinese, Translation and Linguistics, City University of Hong Kong, 83 Tat Chee Avenue, Kowloon Hong Kong, Hong Kong, eric.zee@cityu.edu.hk), Wai-Sum Lee (Phonetics Lab, Dept. of Chinese, Translation and Linguistics, City University of Hong Kong, 83 Tat Chee Avenue, Kowloon Hong Kong, Hong Kong, w.s.lee@cityu.edu.hk)

The study investigates the temporal organization of the bisyllabic, trisyllabic and quadrisyllabic compounds in Standard Chinese. Results of the analysis of the speech data from six speakers show that (a) the rime durations, the durations of the syllable-initial voiceless fricatives and the VOT of the syllable-initial voiceless aspirated stops and affricates are conditioned by the position of the component syllable in the compounds; (b) the rime duration decreases as the component syllable moves from the final toward the initial position in the compounds; (c) the mean duration of the rimes is longer in the final position than in the initial and medial positions; (d) the voiceless fricatives and the voiceless aspirated stops and affricates are shorter in the medial position than in the initial and final positions; (e) the cross-speaker variation is less in the rime duration than in the duration of the voiceless fricatives and VOT of the voiceless aspirated stops and affricates; and (f) no temporal patterns have been observed in the voiceless unaspirated stops and affricates. The results will be discussed in terms of articulatory programming and timing (Kozhevnikov and Chistovich, 1965; Allen, 1975). A temporal model of the compound production in Standard Chinese will be proposed.

11:20

3aSCd3. Second language rhythm and rhythm metrics. Naja Ferjan (Dept. of Linguistics, UCSD, 9500 Gilman Drive #0108, La Jolla, 92093-0108, USA, naja@ling.ucsd.edu),Tristie Ross(Dept. of Linguistics, UCSD, 9500 Gilman Drive #0108, La Jolla, 92093-0108, USA, tross@ling.ucsd.edu), Amalia Arvaniti (Dept. of Linguistics, UCSD, 9500 Gilman Drive #0108, La Jolla, CA 92093-0108, USA, amalia@ling.ucsd.edu)

Several metrics that reflect the variability of vocalic and consonantal intervals in speech have been shown to successfully discriminate between the rhythm of first and second language (L2) speakers producing short sentences of a given language. Here we elicited running read speech from native speakers of English, German and Italian speaking English. We hypothesized that the scores of German L2 speakers would be closer to the scores of native English speakers, since both English and German are stress-timed, and that the scores of Italian L2 speakers would exhibit greater differences from native English scores, since Italian is stress-timed. Our results show instead that the scores of some German speakers are less close to those of the native English speakers than the scores of some Italian speakers, a difference that cannot be attributed to fluency, proficiency level, or length of exposure to English. It is possible that these results reflect over-compensation of some sort by some L2 speakers, though a more likely explanation is that the popular metrics used to quantify speech rhythm may be unreliable or at least not sufficiently robust to be used with L2 data. Reasons why this may be so for L2 speech in particular are discussed.

11:40

3aSCd4. Influences of language typical speech rate on the perception of speech rhythm. Volker Dellwo (UCL, Wolfson House, 4, Stephenson Way, NW1 2HE London, UK, v.dellwo@ucl.ac.uk)

Human listeners can distinguish languages of different rhythmic classes (e.g. stress- and syllable-timed languages). The present study investigated the role of speech rate in this process. In experiment I, speech rate measurements (syllables/second) of read speech were performed in two stress-timed (English, German) and two syllable-timed languages (French, Italian). The results revealed that speech rate distinguishes as reliable between rhythmic class as previously proposed correlates of speech rhythm (%V, VarcoC and nPVI). For a perceptual task (experiment II) sentences from French and German were delexicalized by turning consonantal intervals into white noise and vocalic intervals into complex periodic tones. 18 listeners rated the regularity of the noise-tone sequences on a 13 point scale. The results revealed that listeners rated French stimuli as significantly more regular than English stimuli. It was further shown that the rate of noise-tone sequences was the best predictor for the regularity rating (faster sequences were perceived as more regular) compared to standard rhythm measures (%V, VarcoC and nPVI). Both experiments together show that a) syllable-timed languages are produced faster than stress-timed languages and b) listeners' perception of speech rhythm is highly influenced by these rate differences.

12:00

3aSCd5. Computing the fundamental frequency variation spectrum in conversational spoken dialogue systems. Kornel Laskowski (Carnegie Mellon University, 407 South Craig Street, Pittsburgh, PA 15213, USA, kornel@cs.cmu.edu), Matthias Wölfel (Universität Karlsruhe, am Fasanengarten 5, 76131 Karlsruhe, Germany, wolfel@ira.uka.de), Mattias

Heldner(KTH, Lindstedtsvägen 24, SE-100 44 Stockholm, Sweden, mattias@speech.kth.se), Jens Edlund (KTH, Lindstedtsvägen 24, SE-100 44 Stockholm, Sweden, edlund@speech.kth.se)

Continuous modeling of intonation in natural speech has long been hampered by a focus on modeling pitch, of which several normative aspects are particularly problematic. The latter include, among others, the fact that pitch is undefined in unvoiced segments, that its absolute magnitude is speaker-specific, and that its robust estimation and modeling, at a particular point in time, rely on a patchwork of long-time stability heuristics. In the present work, we continue our analysis of the fundamental frequency variation (FFV) spectrum, a recently proposed instantaneous, continuous, vector-valued representation of pitch variation, which is obtained by comparing the harmonic structure of the frequency magnitude spectra of the left and right half of an analysis frame. We analyze the sensitivity of a task-specific error rate in a conversational spoken dialogue system to the specific definition of the left and right halves of a frame, resulting in operational recommendations regarding the framing policy and window shape.

12:20

3aSCd6. A longitudinal study on vocal aging - Changes in F0, jitter, shimmer and glottal noise. Hideki Kasuya (International Univ. of Health and Welfare, 2600-1 Kita-kanemaru, 324-8501 Otawara, Japan, kasuyah@snow.ucatv.ne.jp),Hajime Yoshida(Yoshida Clinic, West 3, South 6, 096-8585 Nayoro, Japan, nort3381@north.hokkai.net), Hiroki Mori (Fac. of Engr., Utsunomiya Univ., 7-1-2 Yoto, 321-8585 Utsunomiya, Japan, hiroki@speech-lab.org), Hiroshi Kido (Tohoku Inst. of Technology, 35-1 Yagiyama Kasumicho, Taihaku-ku, 982-8557 Sendai, Japan, kidoh@tohtech.ac.jp)

A longitudinal study on vocal aging was conducted for voicing source parameters: fundamental frequency (F0), jitter (period perturbation quotient, PPQ), shimmer (amplitude perturbation quotient, APQ) and glottal noise (normalized noise energy in a high frequency band, NNEb). Acoustic analyses were made on the sustained phonations of the Japanese vowel /a/ of 20 males and 38 females with no laryngeal disease, which were recorded once every year over periods ranging from 11 to 19 years. The acoustic parameters measured were subjected to statistical regression analysis, where the longitudinal change of the parameters was evaluated by the t-test. Two males (10%) and 12 females (32%) showed significant falling in F0 ($P<0.05$) but no significant rising was observed. Five males (25%) and 12 females (32%) displayed a significant increase in APQ ($P<0.05$), whereas only six females (16%) and no male revealed significant changes in PPQ ($P<0.05$). Increase in NNEb was significant for seven males (35%) and 14 females (37%) ($P<0.05$). We conclude that 1) F0 falling is a more emblematic tendency of female vocal aging than male, 2) shimmer is a more observable indication of vocal aging than jitter, and 3) glottal noise in a high frequency region tends to increase with age.

WEDNESDAY MORNING, 2 JULY 2008 ROOM 343, 8:00 TO 10:40 A.M.

Session 3aSPa

Signal Processing in Acoustics and Physical Acoustics: Biomedical Applications of Time-Reversal II

Oleg A. Sapozhnikov, Cochair
Center for Industrial and Medical Ultrasound, Applied Physics Lab., University of Washington, 1013 NE 40th St., Seattle, WA 98105, USA

Mickael Tanter, Cochair
Laboratoire Ondes et Acoustique, ESPCI, Université Paris 7, CNRS, 10 rue Vauquelin, Paris, 75005, France

Invited Papers

8:00

3aSPa1. Time-Reversal Acoustics in Biomedical Engineering. Mathias Fink (Laboratoire Ondes et Acoustique, ESPCI, Université Paris 7, CNRS, 10 rue Vauquelin, 75005 Paris, France, mathias.fink@espci.fr), Gabriel Montaldo (Laboratoire Ondes et Acoustique, ESPCI, Université Paris 7, CNRS, 10 rue Vauquelin, 75005 Paris, France, gabriel.montaldo@espci.fr), Mickael Tanter (Laboratoire Ondes et Acoustique, ESPCI, Université Paris 7, CNRS, 10 rue Vauquelin, 75005 Paris, France, michael.tanter@espci.fr)

Time-reversal is a very powerful method for focusing through complex and heterogeneous media and shows very promising results in biomedical applications. In this presentation, we review some of the main applications investigated during the past decade. An iterative implementation of the time-reversal process allows tracking gallstones in real time during lithotripsy treatments. In this application domain, a smart exploitation of the reverberations in solid waveguides permits the focusing of high amplitude ultrasonic shock waves with a small number of transducers. Because time reversal is able to correct the strong distortions induced by the skull bone on ultrasonic propagation, this adaptive focusing technique allows brain ultrasonic therapy through the skull bone. Finally, time-reversal focusing guided by speckle noise can be implemented to correct distortion in medical ultrasonic imaging and recent results will be presented.

8:20

3aSPa2. A comparison of planar projection and time reversal techniques. Gregory Clement (Harvard Medical School, Focused Ultrasound Lab - BWH Radiology, 221 Longwood Ave RM 521, Boston, MA 02115, USA, gclement@hms.harvard.edu)

Planar projection methods, such as the angular spectrum approach, have been shown to rapidly relate fields between two planes in space/time, with only a single measurement plane needed to characterize an entire field. Variants of the method have been used for medical transducer characterization, as well as for HIFU treatment planning. Presently, a potential advantage of the approach is considered: Operating in the temporal frequency domain, backward planer projection (i.e. ″space reversal″) is invariant with respect to

the spatial dimension, even in the presence of anomalous dispersion. This ability can be contrasted with time reversal, which is violated in the presence of the absorption term. Time reversal is compared with planar back-projection under a varying set of conditions, including the presence of dispersive and nonlinear homogeneous and heterogeneous media. The specific case of a simulated impulsive signal from a 30-cm diameter piston radiator is directed through a 50-cm section of a tissue-like medium (B/A = 5 to 7, c = 1480 to 1600 m/s, ρ = 0.9 to 1.1 gm/cm3, α= 0.5 to 2 db/cm/MHz) over a range of pressures. Ability of backward projection to restore initiating signals is verified, provided that significant signal levels of all relevant frequencies can be reached at the initial plane.

8:40

3aSPa3. Nonlinear imaging of isoechogenic phantoms using selective phase conjugation of acoustic harmonics. Vladimir L. Preobrazhensky (IEMN, UMR CNRS 8520, avenue Poincaré, BP 60069, 59652 Villeneuve d'Ascq, France, vladimir .preobrajenski@iemn.univ-lille1.fr), Philippe Pernod (IEMN, UMR CNRS 8520, avenue Poincaré, BP 60069, 59652 Villeneuve d'Ascq, France, philippe.pernod@iemn.univ-lille1.fr), Leonid M. Krutyansky (WRC-GPI-RAS LEMAC, Vavilova street, 38, 119991 Moscow, Russian Federation, krut@orc.ru)

Selective phase conjugation of acoustic harmonics generated by an intense focused probing wave is applied for imaging of isoechogenic phantoms non detectable by the linear echography. The principle of imaging is based on the difference between the nonlinear properties of a phantom and its surrounding medium. As shown by theoretical modelling the analysis of the phase conjugate second harmonic 2ω of the probing wave provides an image contrast comparable with the relative difference between the nonlinear parameters of the phantom and its background. Second harmonic generation by the phase conjugate wave 2ω during its back propagation to the source of the probing wave provides an image contrast at the frequency 4ω even stronger than the difference of nonlinear parameters. These theoretical conclusions are confirmed by the experimental measurements carried out using 10MHz supercritical parametric phase conjugator. The objects were prepared with methanol water solutions of concentrations 20% and 60%. The solutions filling either a cavity in the agar gel or an acoustically transparent container immersed in water represented isoechogenic phantoms with weaker and stronger nonlinearities relatively to water. The contrast values of 2ω-images were measured as -14% and +10% respectively while for 4ω-images the contrast achieved -45% and +37%.

9:00

3aSPa4. Ultrasonic transducers for imaging and therapy based on time-reversal principles. Armen Sarvazyan (Artann Laboratories, 1753 Linvale-Harbourton, Lambertville, NJ 08350, USA, armen@artannlabs.com)

Focusing of ultrasonic waves is a fundamental aspect of most of the medical applications of ultrasound. There are three approaches in focusing acoustic energy: geometrical, using concave transducers and acoustic lenses, electronic, using phased arrays, and time-reversal (TR), which allows both spatial and temporal concentration of acoustic energy. The aim of this talk is to make comparative analysis of advantages and disadvantages of ultrasound focusing techniques, demonstrate unique capabilities of TR focusing in medical imaging, surgery and therapy. Examples of embodiments of ultrasonic focusing transducers utilizing TR method for various biomedical applications will be presented. TR ultrasonic transducers are comprised of a reverberation chamber, which could be either an aluminum block or a water filled volume of irregular shape, and one or several piezotransducers attached to or incorporated in the reverberator. Optimization of the TR transducers for a particular application is considered, including the geometry of the TR reverberator, shape, type and dimensions of the piezotransducers. Unique abilities of TR transducers to steer the focal spot in 3D, produce pulses with arbitrary waveforms in a wide frequency band and generate focal regions of arbitrary predefined shapes using simple means such as single channel system with one piezoelement will be demonstrated.

9:20

3aSPa5. Doppler ultrasonography using wave phase conjugation. Yuri Pyl'Nov (Moscow Institute of Radio Engineering, Electronics & Automation, Vernadsky prosp., 78, 119454 Moscow, Russian Federation, pylnov@yandex.ru), Nikolay Smagin (Moscow Institute of Radio Engineering, Electronics & Automation, Vernadsky prosp., 78, 119454 Moscow, Russian Federation, pylnov@yandex.ru), Philippe Pernod (IEMN, UMR CNRS 8520, avenue Poincaré, BP 60069, 59652 Villeneuve d'Ascq, France, philippe.pernod@iemn.univ-lille1.fr), Vladimir L. Preobrazhensky (IEMN, UMR CNRS 8520, avenue Poincaré, BP 60069, 59652 Villeneuve d'Ascq, France, vladimir.preobrajenski@iemn.univ-lille1.fr)

Ultrasound wave phase conjugation (WPC) is an efficient tool for velocimetry of flows due to its sensibility to the break of time reversal invariance of acoustic fields in moving media. The presence of flow leads to the non compensated Doppler phase shift of the backward phase conjugate wave relatively to the primary probing wave. This phase shift provides detection, diagnostics and velocimetry of flows and does not require the presence of any scatterers in a flow. Furthermore the phase shift of phase conjugate wave can be used in liquid flowmeters. As it was shown in previous works the sensitivity of liquid flowmeters using phase conjugate ultrasonic waves essentially increases by using nonlinear effects appearing during propagation of phase conjugate waves in a moving liquid. In the present paper we report the theoretical and experimental results on imaging of flow velocity distributions in tubes and phantoms of blood vessel. The scanning auto-confocal system based on parametric ultrasonic wave phase conjugator at 10MHz operation frequency is used in the experiments.The preliminary results of experimental measurements of velocity of vascular blood flow in soft tissues in vitro are discussed.

9:40

3aSPa6. Guiding of HIFU beams towards optical contrast agents by time-reversal of photoacoustic waves. Emmanuel Bossy (Laboratoire Photons et Matière, ESPCI/CNRS, 10 rue Vauquelin, 75231 Paris Cedex 05, France, emmanuel.bossy@espci.fr), Jean-François Aubry (Laboratoire Ondes et Acoustique, ESPCI, Université Paris 7, CNRS, 10 rue Vauquelin, 75005 Paris, France, jean-francois.aubry@espci.fr), Arik R. Funke (Laboratoire Photons et Matière, ESPCI/CNRS, 10 rue Vauquelin, 75231 Paris Cedex 05, France, arik.funke@espci.fr), Mathias Fink (Laboratoire Ondes et Acoustique, ESPCI, Université Paris 7, CNRS, 10 rue Vauquelin, 75005 Paris, France, mathias.fink@espci.fr), Albert-Claude Boccara (Laboratoire Photons et Matière, ESPCI/CNRS, 10 rue Vauquelin, 75231 Paris Cedex 05, France, boccara@optique.espci.fr)

This presentation will discuss the opportunity to use photoacoustics to guide high-intensity focused ultrasound (HIFU) in biological tissue. The photoacoustic effect consists in the emission of sound by an illuminated optically absorbing region, based on the thermoelastic expansion following the absorption of a light pulse. In the near-infrared range (700 nm to 900 nm), the absorption of light in biological tissue is relatively low, and multiply scattered photons can travel as deep as a few centimetres in tissue. Photoacoustic waves can therefore be generated deep in tissue, and have recently been used *in vivo* to perform passive acoustical imaging of optical absorbing features, such as blood vessels. We recently demonstrated on tissue-mimicking phantoms that photoacoustics could be coupled to time-reversal to automatically focus ultrasound towards an optical absorber [Bossy *et al.*, APL **89**(18), 2006]. We propose to further develop this approach to automatically guide HIFU therapy beams towards a targeted region labelled with an optically absorbing contrast agent. This presentation will discuss various aspects of such an approach, based on modelling and experimental results.

Contributed Papers

10:00

3aSPa7. Time Reversal Acoustic focusing using layered membranes structure. Yegor Sinelnikov (ProRhythm, 105 Comac St., Ronkonkoma, NY 11779, USA, yegor@prorhythm.com), Andrey Vedernikov (ProRhythm, 105 Comac St., Ronkonkoma, NY 11779, USA, vedernikov@prorhythm.com), Alexander Sutin (Stevens Institute of Technology, Castle Point on Hudson, Hoboken, NJ 07030, USA, asutin@stevens.edu), Armen Sarvazyan (Artann Laboratories, 1753 Linvale-Harbourton, Lambertville, NJ 08350, USA, armen@artannlabs.com)

In the recent years numerous Time Reversal Acoustic Focusing Systems (TRA FS) employing various reverberation chambers (″acoustic cavities″) accumulating acoustic energy in time were described in the literature. We propose an alternative reverberator composed of a liquid-filled volume comprising a series of spatially distributed membranes with varying thickness in the range from one quarter to half wavelength of ultrasound. Random spatial variation of ultrasound reflection from such membranes leads to randomization of acoustic field that highly improve Time Reversal focusing of the system. A theoretical model of reflections from nonuniform membranes is suggested to evaluate spatial and temporal characteristics of TRA focusing formed as a result of numerous reflections and reverberation of ultrasound propagating though the plurality of membranes. The dependence of focal structure and focused waveform was investigated for suggested structure and their focusing efficiency has been compared with that of the conventional reverberators. In the experiment, the membrane were made of Polyethylene Terephthalate or Nylon thermoformed films. Ultrasonic signals were radiated by transducers with frequency in the range from 3 to 10 MHz. Experiment demonstrated effective TRA focusing by membrane arrangement that can be used for ultrasound focusing and steering in various minimally-invasive biomedical applications.

10:20

3aSPa8. Time Reversed Elastic Waves within Soft Solids. Stefan Catheline (LOA, Université Paris 7 Denis Diderot, ESPCI, 10 rue Vauquelin, 75005 Paris, France, stefan.catheline@espci.fr), Carlos Negreira (Science University of Montevideo, 11400 Montevideo, Uruguay, carlosn@fisica.edu.uy), Nicolas Benech (Science University of Montevideo, 11400 Montevideo, Uruguay, nbenech@fisica.edu.uy), Javier Brum (Science University of Montevideo, 11400 Montevideo, Uruguay, jbrum@fisica.edu.uy)

When a scalar far-field wave is time reversed from the surface of a cavity, it starts to converge toward its initial point source location, then collapses and finally diverges. Without near field evanescent waves, the symmetric focus spot is limited by the Rayleigh criterion. We present an experimental observation of a time-reversal vectorial wave in the volume of a soft solid. The elastic field is measured using the transient elastography technique. It is observed that the time reversed far field wave collapses and gives birth to near field effects. Numerical computation based on elastodynamic Green's functions in a time-reversal cavity confirms and completes the experimental conclusions: the time symmetry with respect to collapse time is broken and the Rayleigh criterion is direction dependant; the spatial collapse is larger in the direction of the point body force than in the perpendicular direction. The authors anticipate that the method can be used for shear wave beam forming in soft tissues as well as to tissue elasticity assessment.

Session 3aSPb

Signal Processing in Acoustics: Filter Design, Detection, and Estimation I

Michael Roan, Cochair
Virginia Tech, 917 Village Way North, Blacksburg, VA 24060, USA

Jorge E. Quijano, Cochair
NEAR Lab-Portland State University, 1900 SW 4th Avenue, Suite 160, Portland, OR 97201, USA

Contributed Papers

11:00

3aSPb1. Wavelet filter bank based wide-band audio coder. Jan Nováček (Czech Technical University, Faculty of Electrical Engineering, Technicka 2, 16627 Prague, Czech Republic, novacj1@fel.cvut.cz)

New system for wide-band audio signals compression is presented. The system is based on a two stage wavelet filter bank principle. Special psychoacoustic model was designed for the system. Data compression is nowadays very topical issue. Due to the development of information technologies more sophisticated compression algorithms may be designed. Most of the present compression systems, e.g. MPEG, ATRAC or Vorbis, use a simple filter bank or DCT transformation. Both methods suffer from the origin of undesirable artefacts which are disturbing for the sound perception. Wavelet filter bank is used to suppress these artefacts and to increase data compression. Frequency dependant windowing function is used for improve of frequency resolution at low frequencies along with faster response at high frequencies. Wavelet transformation based coding algorithm can improve temporal masking effects over conventional perceptual coding algorithms for data compression.

11:20

3aSPb2. Investigation of a novel nonlinear detector of weak acoustic signals in noise. Julian L. Deeks (Institute of Sound and Vibration, Univ. of Southampton, University Road, Highfield, SO17 1BJ Southampton, UK, jd1@isvr.soton.ac.uk), Paul R. White (Institute of Sound and Vibration, Univ. of Southampton, University Road, Highfield, SO17 1BJ Southampton, UK, prw@isvr.soton.ac.uk)

Recent work has identified and explored a method of detecting weak signals in Gaussian noise, based on the response of a nonlinear system to small input perturbations. The technique is applicable to the detection of weak underwater acoustic signals in unwanted ambient sea noise. Much of the research to date has been carried out using a forced Duffing oscillator as the nonlinear system, with parameters selected so as to place the system at the point of transition from a chaotic state to a stable periodic state. The additive input perturbation, most commonly comprising a simulated single frequency embedded in Gaussian noise with a very low input SNR, has been found to initiate the transition as indicated by the appearance of a stable trajectory in phase space. The attendant increase in amplitude at the output of the detector, at or near to the signal frequency, constitutes a detection of that weak signal. This paper presents a quantitative investigation of the technique as applied to underwater acoustic signals (real and simulated), using receiver operating characteristics (ROC) as a measure of its performance. Both the Duffing system, and a more novel version of the technique using a forced Lorenz system, are investigated.

11:40

3aSPb3. Comparison of non linear system identification methods : the example of non linear propagation of acoustic waves in ducts. Antonin Novak (Laboratoire d'Acoustique de l'Université du Maine, Avenue Olivier Messiaen, 72085 Le Mans, France, antonin.novak.etu@univ-lemans.fr),Laurent Simon(LAUM, CNRS, Université du Maine, Lab. d'Acoustique Université du Maine, UMR CNRS 6613, 72085 Le Mans Cedex 9, France, Laurent.Simon@univ-lemans.fr), Joël Gilbert (Laboratoire d'Acoustique de l'Université du Maine, Avenue Olivier Messiaen, 72085 Le Mans, France, joel.gilbert@univ-lemans.fr), Pierrick Lotton (Laboratoire d'Acoustique de l'Université du Maine, Avenue Olivier Messiaen, 72085 Le Mans, France, Pierrick.Lotton@univ-lemans.fr), Frantisek Kadlec (CVUT, Department of Radioelectronic, Technická 2, 166 27 Praha 6, Czech Republic, kadlec@fel.cvut.cz)

The weakly non linear propagation of travelling acoustic waves in ducts is a well known problem leading to approximated analytical solutions. From an experimental point of view, the classical way for estimating the non linear parameters of propagation is to generate sine waves and to analyse the higher order harmonics as a function of the amplitude and the frequency of the excitation. In this work, new methods for estimating the non linear parameters of propagation are developed and compared to the sine excitation based method. The excitation signals associated to these new methods can be stationary noise or logarithmic chirps. For these excitation signals, the data processing is based on Multiple Input Single Output (MISO) direct path method. The comparison is made in terms of signal to noise ratio robustness and computation time. Experimental and theoretical results are also compared. We particularly show that a measurement using only one logarithmic chirp allows estimating accurate results for a broad band of amplitudes and frequencies. Associated computational time is then drastically reduced.

12:00

3aSPb4. The Use of Mel Cepstral Coefficients and Markov Models for the Automatic Identification, Classification and Sequence Modelling of Salient Sound Events Occurring During Tennis Matches. Gordon J. Hunter (Kingston University, Faculty of Computing, Information Systems and Mathematics, Penrhyn Road, KT1 2EE Kingston-upon-Thames, UK, G.Hunter@kingston.ac.uk), Krzysztof Zienowicz (Kingston University, Faculty of Computing, Information Systems and Mathematics, Penrhyn Road, KT1 2EE Kingston-upon-Thames, UK, zienowicz@btinternet.com), Ahmed I. Shihab (Kingston University, Faculty of Computing, Information Systems and Mathematics, Penrhyn Road, KT1 2EE Kingston-upon-Thames, UK, ais@kingston.ac.uk)

Some significant events in sports matches occur too quickly to be detected by conventional video. Audio signals, normally sampled at a much higher rate, provide a way to detect such short events. Here, we employ methods used in automatic speech recognition - templates of Mel Frequency Cepstral Coefficients (MFCCs) over several adjacent time windows, with Principal Components Analysis (PCA) - to identify and classify sound events : different tennis strokes, ball bounces, echos, speech and applause, occurring during tennis matches. Excellent success rates were achieved for both event detection (97.74 %) and correct classification (on average 98.64 % across all classes) of 1504 sound events in the available recordings. The successful classification rate varied between classes but no class had a success rate below 94%. This could be valuable to spectators, officials and coaches in tennis and other sports - including cricket, baseball and golf - or

to make video games (such as the Nintendo Wii) more realistic. We also model sequences of these events in both discrete (event oriented) and continuous time domains, using Markov and other models, to give our system predictive as well as reactive capability, help identify ″unusual″ or ″unexpected″ salient sounds and hopefully improve the correct classification rate for the classes where the performance was weakest.

12:20

3aSPb5. 3D Gabor analysis of transient space-time waves. Loic Martinez (ECIME Université de Cergy-Pontoise, rue d'Eragny, 95031 Neuville-sur-Oise, France, loic.martinez@u-cergy.fr), Nicolas Wilkie-Chancellier (ECIME Université de Cergy-Pontoise, rue d'Eragny, 95031 Neuville-sur-Oise, France, Nicolas.Wilkie-Chancellier@u-cergy.fr), Christ Glorieux (Lab. ATF, Katholieke Universiteit Leuven, Celestijnenlaan 200D, B-3001 Leuven, Belgium, christ.glorieux@fys.kuleuven.be)

Laser generation/detection methods allow the investigation of ultrasonic transient phenomena in both space and time dimensions. Used for the experimental investigation of surface wave propagation along a two dimensional medium, laser ultrasonics leads to three dimensional (3D) space-time signal collections. In order to extract the wave propagation information, the classical high resolution signal processing methods or 3D Fourier Transforms are not suitable to identify the transient and local aspect of wave propagation and mode conversion. In order to quantify these transient aspects in the Space-Time-Wave number-frequency domains, the 3D Gabor transform and some other suitable methods are presented. Their potential for the identification of the local and transient complex wave numbers is illustrated with the propagation of Lamb waves on a plane limited plate. The experimental results are in good agreement with the numerical simulations.

12:40

3aSPb6. Computer learning method for scattering junction identification. Adam Kestian (New York University, 77 Park Ave., apt 1214, Hoboken, NJ 07030, USA, apk240@nyu.edu), Agnieszka Roginska (New York University, 35 West Fourth St., Room 777, New York, NY 10012, USA, roginska@nyu.edu)

Acoustic reflectometry is a non-invasive, time-domain method of identifying the geometry of an acoustical space. A sound pulse is injected into a space and the resulting impulse response details particular changes of impedance, which is a result of a cross-sectional area change or an elbow/T-intersection. Each cause of reflection, known as a scattering junction, has a distinct reflection contour. Previous works were able to identify these scattering junctions via algorithms that attempt to extract particular contours from the impulse response. In the present study, the prominent reflections of the space are observed, isolated, and then compared to a training database of all possible scattering junctions. This method eliminates the necessity to create a contour identification algorithm, as scattering junctions are defined based on its most similar neighbors in the training database. Preliminary results suggest that this computer-learning algorithm can successfully identify reflection contours of a space with varying cross-sectional areas from those that were stored in the training database, which suggests that this method could be a more efficient and versatile alternative to previous identification processes.

WEDNESDAY MORNING, 2 JULY 2008 AMPHI BORDEAUX, 8:00 A.M. TO 12:40 P.M.

Session 3aUWa

Underwater Acoustics, Acoustical Oceanography, and ECUA: Impact of Environmental Variability on Mid-Frequency Sonar Performance

Dajun Tang, Cochair
Applied Physics Laboratory, University of Washington, 1013 NE 40th St, Seattle, WA 98105, USA

Paul C. Hines, Cochair
Defence R&D Canada - Atlantic, P.O. Box 1012, Dartmouth, NS B2Y3Z7, Canada

Peter Louring Nielsen, Cochair
NURC, Viale S. Bartolomeo 400, La Spezia, 19126, Italy

Invited Papers

8:00

3aUWa1. Operational Impacts of the Environment on Mid-Frequency Navy Sonar Systems In Shallow Water. Marcus M. Speckhahn (Planning Systems Inc., 3990 Old Town Avenue, Cabrillo Plaza, Suite A101, San Diego, CA 92110-2930, USA, marcus.speckhahn.ctr@navy.mil), Stephen C. Lingsch (Commander Naval Meteorology and Oceanography Command, 1100 Balch Boulevard, Stennis Space Center, MS 39529, USA, stephen.lingsch@navy.mil), Josette P. Fabre (Naval Research Laboratory, Code 7180, Stennis Space Center, MS 39529, USA, josie.fabre@nrlssc.navy.mil), Michael T. Garr (Naval Undersea Warfare Center, Code 1521, 1176 Howell Street, Newport, RI 02841, USA, michael.garr@navy.mil), Sandra K. Wetzel-Smith (Naval Mine and Anti-Submarine Warfare Command, 32444 Echo Lane, Suite 300, San Diego, CA 92147, USA, skw@spawar.navy.mil)

The coastal oceans represent a challenging domain for mid-frequency maritime Anti-Submarine Warfare (ASW) sonar systems to operate effectively. Information on the advantages and disadvantages of, as well as general tactical employment criteria for the prevalent types of active mid-frequency sonar systems found in the world's navies is provided. Operational performance of these systems, which include hull-mounted sonars, monostatic buoys and multistatic active systems, as well as dipping sonars, is always affected by shallow water environmental parameters. These acoustic and oceanographic factors include frequent bottom interactions of the transmitted acoustic energy, highly variable sound speed and noise fields, strong coastal currents and high levels of acoustic clutter. Accurate and timely four-dimensional sensor performance predictions and optimization recommendations can mitigate some of the negative impact of

the environment on sonar detection ranges. We discuss the trade-offs and assumptions made by modern computer-based tactical decision aids to deliver the most accurate environmental information balanced by the need to deliver these data in tactical time frames useful to the ASW mission planner and sonar operator at sea. We will also present thoughts on the quantification of acoustic uncertainty in support of ASW operations and the need for high-fidelity active sonar training systems.

8:20

3aUWa2. Quantifying ocean acoustic sensitivity to environmental uncertainty/variability. Stan E. Dosso (University of Victoria, School of Earth and Ocean Sciences, Victoria, BC V8W 3P6, Canada, sdosso@uvic.ca)

It is well known that acoustic data used in sonar applications are strongly influenced by physical parameters of the ocean environment. Environmental sensitivity studies are often based on a qualitative comparison of acoustic fields computed for a reference environmental model and for a perturbed model in which one or more parameters have been changed. The acoustic-field perturbation generally includes a component representing a spatial shift of the field (i.e., local field structure remains coherent, but shifts in range and/or depth) and a component representing a change to the shifted field. Hence, the field change at a fixed point can indicate high sensitivity in cases where the field structure changes little but is simply offset, which can conflict with an intuitive understanding of sensitivity. This paper quantifies sensitivity rigorously in terms of a statistical measure of the relative uncertainty of acoustic fields or transmission loss due to realistic uncertainty/variability in environmental parameters. Further, accounting for field shifts can provide a more meaningful sensitivity measure for many applications. The sensitivity of acoustic fields to the state of knowledge of the sound-speed profile, bathymetry, and seabed geoacoustic parameters is examined for both range-independent and range-dependent cases. [Funded by DRDC-Atlantic Rapid Environmental Assessment Project.]

8:40

3aUWa3. Tools and techniques to measure environmental parameters that improve mid-frequency sonar performance predictions. John C. Osler (Defence R&D Canada - Atlantic, P.O. Box 1012, Dartmouth, NS B2Y3Z7, Canada, john.osler@drdc-rddc.gc.ca), Sean Pecknold (Defence R&D Canada - Atlantic, P.O. Box 1012, Dartmouth, NS B2Y3Z7, Canada, sean.pecknold@drdc-rddc.gc.ca), Paul C. Hines (Defence R&D Canada - Atlantic, P.O. Box 1012, Dartmouth, NS B2Y3Z7, Canada, Paul.Hines@drdc-rddc.gc.ca)

The performance of mid-frequency active sonar systems in littoral waters depends upon several environmental factors and their variability in space and time. These factors include seabed scattering strength, bottom loss, and the water column sound speed profiles. DRDC Atlantic has developed experimental apparatus and techniques to measure these environmental parameters in order to enhance the accuracy of sonar performance estimates in the mid-frequency band, 1 to 10 kHz. Experiments have been conducted during sea-trials on the Scotian Shelf and Strataform area on the New Jersey Shelf. In some instances, these experiments have been in conjunction with international research partners to provide an inter-comparison between experimental techniques and/or a comparison of rapid environmental assessment techniques with more traditional, and time-consuming, methods. In this talk, we will demonstrate that predictions of sonar system performance improve when the environmental parameters obtained with these techniques are used, rather than parameters from archival sources.

Contributed Papers

9:00

3aUWa4. A comparison of methods for approximating acoustic uncertainty in underwater sound channels. Kevin R. James (Univ. of Michigan, 2010 Lay Auto Lab, Ann Arbor, MI 48109, USA, krjames @umich.edu), David R. Dowling (Univ. of Michigan, 2212 G. G. Brown Laboratory, Ann Arbor, MI 48109, USA, drd@umich.edu)

The accuracy and reliability of acoustic field calculations are often determined by uncertainty in environmental parameters. There are currently several approaches for predicting calculated-acoustic-field uncertainty arising from environmental uncertainties. This presentation outlines the current development of a method for predicting acoustic uncertainty based on correlations between variations in an uncertain parameter and spatial shifts within a calculated acoustic field. The results of this technique are compared with several other modern methods for predicting acoustic uncertainty such as direct sampling of environmental parameters, linearization and higher-order finite difference approaches, the adjoint method for approximating derivatives of the acoustic field with respect to environmental parameters, and polynomial chaos methods. The advantages and limitations of each technique are presented for range-independent shallow-ocean sound channels at nominal ranges of 1 to 10 km and frequencies from 100 Hz to 1 kHz. Comparisons of accuracy, computational speed, and applicability to particular uncertain parameters and field prediction routines are provided. Emphasis is placed on identifying the types of sound channel properties and environmental uncertainties for which each technique performs most reliably, as well as identifying situations for which current techniques are not yet adequate. [Sponsored by the Office of Naval Research, Code 321OA].

9:20

3aUWa5. Fluctuation of mid-frequency propagation in shallow water. Dajun Tang (Applied Physics Laboratory, University of Washington, 1013 NE 40th St, Seattle, WA 98105, USA, djtang@apl.washington.edu), Frank S. Henyey (Applied Physics Laboratory, University of Washington, 1013 NE 40th St, Seattle, WA 98105, USA, frank@apl.washington.edu), Kevin L. Williams (Applied Physics Laboratory, University of Washington, 1013 NE 40th St, Seattle, WA 98105, USA, williams@apl.washington.edu), Daniel Rouseff (Applied Physics Laboratory, University of Washington, 1013 NE 40th St, Seattle, WA 98105, USA, rouseff@apl.washington.edu), Peter H. Dahl (Applied Physics Laboratory, University of Washington, 1013 NE 40th St, Seattle, WA 98105, USA, dahl@apl.washington.edu), Zhongkang Wang (Hangzhou Applied Acoustics Research Institute, PO Box 1249, 310012 Hangzhou, China, zkwang@apl.washington.edu), Jorge E. Quijano (NEAR Lab-Portland State University, 1900 SW 4th Avenue, Suite 160, Portland, OR 97201, USA, jorgeq@pdx.edu), Jee Woong Choi (Dept. of Environmental Marine Sciences, Hanyang Univ., 1271, Sa-3-dong, Sangrok-gu, 426-791 Ansan, Republic of Korea, choijw@hanyang.ac.kr)

As part of the ONR-sponsored SW06 experiment, mid-frequency sound propagation was measured at ranges 1-10 km in the frequency band of 2-10 kHz in August, 2006. The water depth is 80 m and the source depth is 30 m, close to the minimum of a duct with a thermocline above and a warm salty water below. The receivers are clustered into two groups, one at 25 m depth, the other at 50 m. The region has active internal wave activity during this time. Because the source is near the axis of the sound channel, it is observed that propagation is dominated by trapped modes and behaves similar to

sound propagation in a deep water duct. Amplitude fluctuations and cross-frequency correlations are estimated. The scintillation index as a function of frequency and bandwidth is calculated.

9:40

3aUWa6. Active Tracking using the Invariance Extended Kalman Filter (IEKF). Lisa M. Zurk (NEAR Lab-Portland State University, 1900 SW 4th Avenue, Suite 160, Portland, OR 97201, USA, zurkl@cecs.pdx.edu), Chensong He (NEAR Lab-Portland State University, 1900 SW 4th Avenue, Suite 160, Portland, OR 97201, USA, zurkl@pdx.edu), Jorge E. Quijano (NEAR Lab-Portland State University, 1900 SW 4th Avenue, Suite 160, Portland, OR 97201, USA, jorgeq@pdx.edu), Christian Hempel (1176 Howell Street, Newport, RI 02841, USA, HempelCG@Npt.NUWC.Navy.Mil)

The pressure received from a moving source in a shallow water channel has a frequency dependent structure that is imposed by the propagation characteristics of the channel. While an exact description of this structure requires fine knowledge of the channel properties (including bottom composition), an approximate relationship which utilizes the so-called waveguide invariant can be used to describe the intensity variations as a function of frequency versus range. This relationship has been extensively explored and utilized for application to passive sonar systems. Recent work has demonstrated that a similar structure, called the active invariance, may be present in active sonar. In this paper the active invariance relationship is incorporated into an extended Kalman filter (EKF) to create a new tracking formulation called the Invariance EKF (IEKF). The IEKF differs from the conventional formulation by incorporating the time-dependent frequency content into both the state space representation and the update equations, where the relationship between target position and frequency is given by the active invariance expression. Performance of the IEKF relative to conventional approaches is explored with normal mode simulations and bistatic data collected in the Maltese channel. Sponsored by ONR-321US

10:00

3aUWa7. Comparison of sonar transmission models at mid-frequency for synthetic and real environments. Adrian D. Jones (Defence Science and Technology Organisation, P.O Box 1500, 5111 Edinburgh, Australia, bearjones@chariot.net.au), Janice S. Sendt (Thales Australia, 274 Victoria Road, 2116 Rydalmere, Australia, Janice.Sendt@au.thalesgroup.com), Alec J. Duncan (Curtin University of Technology, Centre for Marine Sci & Tech, GPO Box U1987, 6845 Perth, WA, Australia, A.J.Duncan@curtin.edu.au), Paul A. Clarke (Defence Science and Technology Organisation, P.O Box 1500, 5111 Edinburgh, Australia, Paul.Clarke@dsto.defence.gov.au), Zhiyong Zhang (Defence Science and Technology Organisation, P.O Box 1500, 5111 Edinburgh, Australia, Yong.Zhang@dsto.defence.gov.au), Han Vu (Defence Science and Technology Organisation, P.O Box 1500, 5111 Edinburgh, Australia, Han.Vu@dsto.defence.gov.au)

The suitability of sonar transmission loss models for application to the mid-range of acoustic frequencies has been studied by comparing the outputs from a number of models. Emphasis has been placed upon the requirements for models for circumstances relevant to both continental shelf and deep ocean zones within the Australian region. In particular, the ability to describe transmission in surface ducted environments for a deep ocean, and in a shallow ocean with both ducted and downward refracting environments has been considered. For the deep ocean case, a synthetic environment was selected, and the ability to describe duct trapping was examined. For the shallow ocean case, scenarios selected for comparison correspond with ocean tracks for which environmental parameters had been collected and received sound pressure time series measured. The subject transmission loss models are from a variety of types. To enable the most valid comparison, input parameters have been matched across models to the fullest extent. This paper presents the state of progress of this work, including a comparison of models amongst themselves and, for continental shelf scenarios, against measured transmission loss.

10:20-10:40 Break

10:40

3aUWa8. In ocean evaluation of low frequency active sonar systems. Karl Thomas Hjelmervik (FFI, Postboks 115, 3191 Horten, Norway, kth@ffi.no), Geir Helge Sandsmark (FFI, Postboks 115, 3191 Horten, Norway, ges@ffi.no)

Sonar performance measurements in the sea are always affected by uncontrollable and/or uncertain environmental conditions as sound speed variations, bottom topography or the acoustic properties of the sea floor. This paper presents a method to determine a sonar - target geometry which minimizes the uncertainty in target signal excess due to environmental variability. An acoustic model is used to estimate the signal excess for a large number of sound speed profiles measured in the relevant area. The results are compared seeking a target range and depth where the estimated signal excess is robust with respect to the variation of sound speed profiles to be expected in the actual area. Results from sea trials will be presented as well as simulated examples used to demonstrate the robustness or sensitivity of the signal excess to environmental changes at different test geometries.

11:00

3aUWa9. Effects of volume and boundary variability on the statistics of received signal frequency. Jeremy Joseph (ARL Penn State, PO Box 30, State College, PA 16804, USA, jmj269@psu.edu), Richard Lee Culver (ARL Penn State, PO Box 30, State College, PA 16804, USA, rlc5@psu.edu), Colin W. Jemmott (ARL Penn State, PO Box 30, State College, PA 16804, USA, cwj112@psu.edu)

The overall goal of our research is to incorporate statistical knowledge of received passive signal variability and uncertainty into the signal processing. To accomplish this goal we need to better understand the sources of this variability, which are due in part to propagation through the ocean channel. Propagation introduces significant variation in received signal parameters through rough surface and bottom scattering as well as volume inhomogeneities. This talk focuses on the variability introduced by these sources and its effect on the statistics of the frequency spectrum of the received signal. We consider low frequencies, for which theoretical predictions are compared with PE-based simulation results. Work supported by ONR Undersea Signal Processing Code 321US.

11:20

3aUWa10. Modeling higher order statistics of shallow water reverberation. Kevin D. Lepage (Naval Research Laboratory, 4555 Overlook Ave SW, Washington, DC 20375, USA, kevin.lepage@nrl.navy.mil)

The modeling of the higher moments of shallow water reverberation is addressed for problems where non-Rayleigh reverberation is caused by scattering from rough boundaries with non-Gaussian height distributions. Expressions for the first three spatial moments of exponentially height-distributed roughness are derived for both Gaussian and exponential correlation functions corresponding to Gaussian or von-Karman second order spectra. The bi and tri-spectra for these roughness distributions are also derived, and differences are highlighted between these results and the results that are obtained for Gaussian height-distributed higher order spectra. Finally results for the higher moments of reverberation pressure are derived for exponentially height-distributed bottom roughness with the Gaussian spatial correlation function in the presence of multipath as a function of time, bandwidth, and correlation length scale. [Work supported by ONR]

11:40

3aUWa11. Computational Predictions of sonar performance based on full wave acoustic propagation modeling. Michael Wolfson (Univ. of Washington, Applied Physics Lab., 1013 40 St NE, Seattle, WA 98105, USA, wolfson@apl.washington.edu)

For fishery acoustics, sonars offer the advantage of inferring the biomass of a given ocean volume at a lower operational cost of traditional echo-sounders, but wave guide effects which induce multi-pathing yield unknown variances in bio-mass estimates. A sonar performance model has recently been developed to assist in understanding this variance based on the para-

axial approximation to the acoustic wave equation. The model takes into account the geometry of the sonar deployment (source depth, transmit/receive beam patterns, pulse shape) and the acoustic environment (water column and geo-acoustic bottom) and creates a data base of two-way transfer functions for a chosen set of range-depth cells. Then, given a hypothetical aggregation or school of fish, each with its own target strength, as well as noise and reverberation levels, one can create intensity maps which can be used to perform sensitivity studies to ascertain the performance characteristics of a fishery sonar. This talk will discuss the theoretical development of the model, its constraints, and provide an example which highlights its potential for future work. The example will be in a shallow water (100 m) environment using acoustic frequencies of around 10 kilohertz for imaging aggregations of pelagic fish. The Naval Ocean Partnership Program is gratefully acknowledged for this work.

12:00

3aUWa12. Temporal and spatial coherence of low frequency acoustic modes in shallow water. Harry Deferrari (Univ. of Miami, 4600 Rickenbacker Causeway, Miami, FL 33149, USA, hdeferrari@rsmas.miami.edu), Hien B. Nguyen (Univ. of Miami, 4600 Rickenbacker Causeway, Miami, FL 33149, USA, hnguyen@rsmas.miami.edu), Jennifer Whylie (Univ. of Miami, 4600 Rickenbacker Causeway, Miami, FL 33149, USA, jwhylie@rsmas.miami.edu)

Three recently collected shallow water acoustic propagation data sets have common experimental parameters of fixed sources with multiple frequency m-sequence transmissions, HLA and VLA receptions, and detailed measurements of the ocean acoustic environments. In each case, broad band signals allow the separation of modes by arrival time and the computation of spatial and temporal coherency for individual modes of propagation thus eliminating the effects of multipath interference. Here, coherency estimates are compared for several ranges from 10 to 80 Km and depths of 80 to 250 m, frequencies from 100 to 1600 Hz and for a wide range of potential energy levels of the internal wave field. There are a number of consistent findings. Low order modes are more coherent than high order modes in both space and time. Low frequency signals respond deterministically and in proportion to internal wave fluctuations whereas higher frequencies are randomized and have saturated statistics. In between, phase wrapping occurs. The number of bottom interactions is shown to be a critical factor in coherence especially for frequencies of 800 Hz and above. At very long ranges out of plane arrivals introduce multipath interference even for single mode reception.

12:20

3aUWa13. Effects of internal waves on acoustic coherent communications during SW06. Aijun Song (University of Delaware, College of Marine and Earth Studies, S. College Street, Newark, DE 19716, USA, ajsong@udel.edu), Mohsen Badiey (University of Delaware, College of Marine and Earth Studies, S. College Street, Newark, DE 19716, USA, badiey@udel.edu), Arthur Newhall (Woods Hole Oceanographic Institution, 98 Water Street, Bigelow 203A, MS-11, Woods Hole, MA 02543, USA, anewhall@whoi.edu), James F. Lynch (Woods Hole Oceanographic Institution, 98 Water Street, Bigelow 203A, MS-11, Woods Hole, MA 02543, USA, jlynch@whoi.edu), Harry Deferrari (Univ. of Miami, 4600 Rickenbacker Causeway, Miami, FL 33149, USA, hdeferrari@rsmas.miami.edu)

During the SW06 experiment conducted east off the New Jersey continental shelf from July to September of 2006, internal wave surface expression and water temperature profiles were recorded when phase shift keying signals (PSK) were transmitted to study internal wave effects on coherent underwater acoustic communications at low to mid frequency bands. The collected communications data are processed using time reversal multichannel combining followed by a decision feedback equalizer. Due to the presence of internal waves, the acoustic channels show a time-varying property. Continuous channel updates prior to time reversal combining are required to combat fast channel fluctuations. The communications performance in terms of output signal-to-noise ratio exhibits significant change due to the internal waves. Further, the internal wave effects on the performance of coherent acoustic communications exhibit a frequency- and depth- dependency. The choices of receiver parameters also can be affected by the presence of internal waves.

WEDNESDAY MORNING, 2 JULY 2008 ROOM 341, 8:00 TO 10:20 A.M.

Session 3aUWb

Underwater Acoustics and ECUA: Sonar System and Transducer Calibration Methodology III

Kenneth G. Foote, Cochair
Woods Hole Oceanographic Institution, Woods Hole, MA 02543, USA

Stephen P. Robinson, Cochair
National Physical Laboratory, Hampton Road, Teddington, TW11 OLW, UK

Invited Paper

8:00

3aUWb1. Calibration of wideband systems, need for a standard. Manell E. Zakharia (French Naval Acadamey, BP 600, 29240 Brest-Armees, France, manell.zakharia@ecole-navale.fr)

Although wide band sonar system are becoming more and more popular, there is no unified standard method for their calibration. Most of the wideband systems are calibrated at multiple frequencies using single frequency methods. Although such calibrations give correct figures, these figures do not correspond to the real use of the systems and do not display properly the problems encountered while using such systems such as signal deformation due to the directivity pattern. For instance, the zeroes of directivity patterns that correspond to destructive interference at one frequency are spatially smeared even for a band of 10% and appear as spectral variations. We will show two examples of such calibration with increasing difficulty. The first case considers a wideband sounder covering two

octaves (20-80 kHz) and the second one a parametric array (primaries around 100 kHz and parametric generation from 10 to 20 kHz). In the second case, the difficulty is increased due to the factor of about ten between the primary and the secondary frequencies that are also associated to important level difference (about 40 dB). It requires a high linearity constraint of the whole calibration chain.

Contributed Paper

8:20

3aUWb2. Calibration of broadband sonar systems using multiple standard targets. Philip Atkins (University of Birmingham, Department of Electronic, Electrical and Computer Engineering, Edgbaston, B15 2TT Birmingham, UK, p.r.atkins@bham.ac.uk), David T. Francis (University of Birmingham, Department of Electronic, Electrical and Computer Engineering, Edgbaston, B15 2TT Birmingham, UK, francdti@adf.bham.ac.uk), Kenneth G. Foote (Woods Hole Oceanographic Institution, Woods Hole, MA 02543, USA, kfoote@whoi.edu)

A seven-octave active sonar system spanning the nominal frequency range 25-3200 kHz was deployed in Norwegian waters for the purpose of measuring the acoustic scattering characteristics of a range of marine organisms. This system transmitted linear frequency-modulated (LFM) signals in order to achieve good range resolution and to obtain spectral information on resolved targets. Total system performance was variously measured in situ and ex situ, depending on the particular octave band, using standard-target spheres. This enabled the frequency response of the entire system to be determined and the sidelobe level of the matched-filter receiver to be reduced. The effects of the deep nulls encountered in the backscattered spectrum of target spheres were partially reduced by using a string of up to six spheres of different sizes and material properties. Typical results will be presented showing that such calibration procedures are sensitive the relative alignment of the sonar-target and to sound-speed profile changes over the length of the string. [This work originated with EU RTD support through contract MAS3-CT95-0031.]

Invited Paper

8:40

3aUWb3. Measuring the equivalent beam angle of echo sounders with split-beam transducers. Lars Nonboe Andersen (Simrad, P.O. Box 111, 3191 Horten, Norway, lars.nonboe.andersen@simrad.com), Egil Ona (Institute of Marine Research, P.O.Box 1870 Nordnes, 5817 Bergen, Norway, egil.ona@imr.no), Geir Pedersen (Institute of Marine Research, P.O.Box 1870 Nordnes, 5817 Bergen, Norway, geir.pedersen@imr.no), Frank Tichy (Simrad, P.O. Box 111, 3191 Horten, Norway, frank.tichy@kongsberg.com), Even Borten Lunde (Simrad, P.O. Box 111, 3191 Horten, Norway, even.borten.lunde@kongsberg.com)

When trying to measure the numerical density of marine animal populations with scientific echo sounders, several technical system parameters are determined through a standard-target calibration. The acoustic scattering properties of standard targets are known *a priori*. In a typical standard-target calibration the system gain and the transducer beam pattern are estimated. The system gain parameter is used both when measuring volume backscattering strength and when measuring target strength. The calibrated beam pattern is currently used only for target strength estimation. However, measurements of mean volume backscattering strength also require knowledge of the effective sampling volume of the acoustic beam, namely the equivalent beam angle. This parameter is typically not determined during an ordinary echo sounder calibration. A method for measuring the equivalent beam angle and the transducer angle sensitivity of a specific split-beam transducer is described, and results from exemplary calibrations are presented. Changes in the calibration parameters as a function of environmental parameters, especially the sound speed in water, are discussed.

Contributed Paper

9:00

3aUWb4. Multibeam sonar calibration techniques. Christian De Moustier (UNH, Center for Coastal and Ocean Mapping, Chase Ocean Engineering Lab, 24 Colovos Road, Durham, NH 03824, USA, cpm@ieee.org), Barbara J. Kraft (UNH, Center for Coastal and Ocean Mapping, Chase Ocean Engineering Lab, 24 Colovos Road, Durham, NH 03824, USA, bjkraft@cisunix.unh.edu), Glenn McGillicuddy (UNH, Center for Coastal and Ocean Mapping, Chase Ocean Engineering Lab, 24 Colovos Road, Durham, NH 03824, USA, glennm@ccom.unh.edu)

The acoustic calibration facility at the University of New Hampshire's Chase Ocean Engineering Laboratory has been used to calibrate several transducer arrays from multibeam sonars that operate at 100 kHz and above. In each case, we mount the transducer array on a rotating colum and measure the array's transmit and receive characteristics with a reference transducers leased from the Naval Undersea Warfare Center, Newport RI. Our rotation angles are known to within 0.2° and our acoustic calibration measurements are repeatable to within 0.5 dB. After adjusting for measured impedance mismatches between the elements of the array, we determine the actual element separation as the ratio of physical spacing over acoustic wavelength, and we use this result to estimate the beam pointing accuracy of the sonar. The beamforming gain is then estimated for all beam directions from broadside to the full range of steering angles used by the sonar. This work is motivated by research efforts to obtain calibrated acoustic backscatter measurements from multibeam echo-sounder that are used for seafloor characterization applications or for detection and identification of targets in the water column.

Invited Papers

9:20

3aUWb5. A comparison of hydrophone near-field scans and optical techniques for characterising high frequency sonar transducers. Victor F. Humphrey (Institute of Sound and Vibration, Univ. of Southampton, University Road, Highfield, SO17 1BJ Southampton, UK, vh@isvr.soton.ac.uk), Stephen P. Robinson (National Physical Laboratory, Hampton Road, TW11 OLW Teddington, UK, Stephen.Robinson@npl.co.uk), Peter D. Theobald (National Physical Laboratory, Hampton Road, TW11 OLW Teddington, UK, pdt@npl.co.uk), Gary Hayman (National Physical Laboratory, Hampton Road, TW11 OLW Teddington, UK, Gary.Hayman@npl.co.uk), Martin P. Cooling (National Physical Laboratory, Hampton Road, TW11 OLW Teddington, UK, mc@isvr.soton.ac.uk)

Two potential methods of fully characterising the response of high frequency sonar transducers and arrays operating in the frequency range 100 kHz to 500 kHz are compared. In the first approach two-dimensional planar scans, with a spatial resolution of better than half a wavelength, are performed in the acoustic near-field using a small probe hydrophone. The measured two-dimensional data are propagated numerically using a Fourier Transform method to predict the far-field response. Alternatively the data can be back-propagated to re-construct the pressure distribution at the source, a powerful diagnostic technique which can identify defects in transducers and array elements. The second approach uses a scanning laser vibrometer to measure the velocity of the transducer surface; with the resulting velocity data also being used to predict the far-field response by numerical propagation. The two approaches are compared for a number of devices. Comparison of the propagated hydrophone near-field scan data with direct measurements at these ranges shows very good agreement, indicating the usefulness of the method for deriving far-field transducer responses from near-field measurements in laboratory tanks. The potential limitations introduced to the optical approach by the acousto-optic effect are discussed.

9:40

3aUWb6. Acousto-optic tomography for mapping of high-frequency sonar fields. Peter D. Theobald (National Physical Laboratory, Hampton Road, TW11 OLW Teddington, UK, pdt@npl.co.uk), Stephen P. Robinson (National Physical Laboratory, Hampton Road, TW11 OLW Teddington, UK, Stephen.Robinson@npl.co.uk), Gary Hayman (National Physical Laboratory, Hampton Road, TW11 OLW Teddington, UK, Gary.Hayman@npl.co.uk), Triantafillos Koukoulas (National Physical Laboratory, Hampton Road, TW11 OLW Teddington, UK, triantafillos.koukoulas@npl.co.uk)

This paper presents an acousto-optic method for tomographic mapping of acoustic fields generated by high-frequency sonar array transducers. The method uses a laser interferometer to measure the integrated refractive index change across the propagating acoustic wave generated by the transducer. An interferometer being a displacement or velocity measuring device, interprets this rate of change of optical path length as a displacement or velocity. Obtaining a series of these projections by scanning the laser beam or the transducer for a number of rotation angles of the transducer allow a two-dimensional plane of the acoustic field to be reconstructed using the techniques commonly used in X-ray Computed Tomography. Acousto-optic tomographic measurement results are presented for a 95 by 95 mm, 400 kHz 1-3 composite, 4 element sonar array transducer and are compared to conventional planar hydrophone scans obtained using a 1.5 mm probe hydrophone. The optical method allows measurement of the acoustic field without perturbing the field being measured, which can occur when using the planar hydrophone scanning method. Different tomographic geometries are considered, including parallel beam and fan-beam methods, with the advantages and disadvantages of each being discussed.

Contributed Paper

10:00

3aUWb7. Prediction for the acoustic field of a high frequency cylindrical transducer. Tiejian Xia (Hangzhou Applied Acoustics Research Institute, 401# Fuyang, Zhejiang, 311400 Fuyang, China, xiatiejian@263.net), Yuebing Wang (Hangzhou Applied Acoustics Research Institute, 96 Huaxing Road, 310012 Hangzhou, China, wang_yuebing@tom.com), Lisheng Zhou (Rensselaer Polytechnic Institute, Greene Building, School of Architecture, 110 8th Street, Troy, NY 12180, USA, lszhou@163.com), Qiang Liu (Hangzhou Applied Acoustics Research Institute, 401# Fuyang, Zhejiang, 311400 Fuyang, China, 715liuqiang@163.com)

The BEM software is implemented in the prediction of the acoustic field produced by a cylindrical transducer, the transducer consists of 1200 PZT pillars which are fixed on the surface of a 156-mm-diameter and 120-mm-height cylinder. The acoustic field around the transducer is measured at the frequency 120kHz using an optical vibrometer, the measured data are fed into the BEM software as the boundary condition, and the directivities of the transducer are forecasted in the vertical and horizontal planes. To verify the calculation, the acoustic field in the far field of the transducer is measured using a hydrophone, and good agreements between the prediction and the measurement convince that the BEM software can be used to predict acoustic fields of cylindrical transducers through distributions of acoustic fields measured in their near fields.

Session 3aUWc

Underwater Acoustics, Signal Processing in Acoustics, and ECUA: Acoustic Vector Fields and Sensor Processing II

Kevin B. Smith, Cochair
Naval Postgraduate School/Naval Undersea Warfare Center, Code PH/Sk, Department of Physics, Monterey, CA 93943, USA

Jean-Pierre Hermand, Cochair
Université libre de Bruxelles (U.L.B.) - Environmental hydroacoustics lab, av. Franklin D. Roosevelt 50, CP 194/5, Bruxelles, 1050, Belgium

Invited Papers

10:40

3aUWc1. Acoustic vector sensors and vector/tensor processing in ocean acoustics research. Gerald D'Spain (Marine Physical Lab, Scripps Institution of Oceanography, 291 Rosecrans St., San Diego, CA 92106, USA, gld@mpl.ucsd.edu)

Several passive sensor systems that simultaneously measure acoustic pressure and the three components of acoustic particle motion have been designed and deployed in seagoing experiments by the Marine Physical Lab over the past two decades. Descriptions of these sensor systems and results from applying various signal/array processing methods with these data are presented in this talk. Although vector sensors do not provide any additional information on the sound field than that obtained by a suitable number of properly placed hydrophones, they do provide estimates of the sound field's directional properties from a very compact package. Applications where available space is severely limited include autonomous underwater vehicles (AUV). Recent results from acoustic vector sensors installed in a flying wing underwater glider and inside a prop-driven AUV to quietly measure sounds in the ocean illustrate the benefits, and drawbacks, of the use of vector sensors on autonomous platforms. The extension of the signal/array processing approaches to tensor sensors indicates the promise of additional gain, if the sensor design challenges can be overcome. [Work supported by the Office of Naval Research].

11:00

3aUWc2. Robust Adaptive Vector Sensor Processing. Andrew J. Poulsen (Massachusetts Institute of Technology, 77 Massachusetts Avenue, Cambridge, MA 02139, USA, poulsen@mit.edu), Arthur B. Baggeroer (MIT, Department of Mathematics, 77 Massachusetts Avenue, Cambridge, MA 02139, USA, abb@boreas.mit.edu), Jonathan Paul Kitchens (MIT Lincoln Laboratory, 244 Wood Street, Lexington, MA 02420, USA, jonpaul@mit.edu), Jennifer A. Watson (MIT Lincoln Laboratory, 244 Wood Street, Lexington, MA 02420, USA, watson@ll.mit.edu)

A sizable literature exists on the theory of processing signals for many vector sensor array applications. In practice, however, mismatch and several noise processes can pose significant problems. If adaptive beamforming is also used, the ″snapshot″ issue potentially increases by a factor of four since each element in a vector sensor array consists of a scalar hydrophone and up to three spatially orthogonal particle motion sensors. Both of these sensor types have very different response and noise characteristics. Particle motion sensors are more sensitive to non-acoustic, motion-induced noise than hydrophones. In towed line array configuration, those sensors orthogonal to the direction of motion are exposed to higher intensities of flow noise at low frequencies than those coincident to the array axis. Similarly, different dipole sensors may be exposed to varying degrees of rotational mismatch. Sensors may also rest on the seafloor, creating asymmetries. Physical constraints also relate pressure and particle velocity measurements via conservation of momentum and mass equations. We examine adaptive processing methods customized to the unique characteristics of vector sensors. Array gain and other performance metrics in the presence of system mismatch and uncertainties is presented using common ocean noise models, including directional jamming, isotropic and surface noise.

11:20

3aUWc3. Using acoustic streamlines to visualize energy flow across boundaries. David M.F. Chapman (Scientific Consultant, 8 Lakeview Avenue, Dartmouth, NS B3A 3S7, Canada, dave.chapman@ns.sympatico.ca)

For spherical waves that radiate from a point source in a homogeneous fluid and propagate across a plane boundary into a dissimilar homogeneous fluid, the acoustic field may differ significantly from the geometric acoustics approximation if either the source or receiver is near the interface (in terms of acoustic wavelengths) or if the minimum-phase path is near the critical angle. Cross-boundary energy flow from a continuous-wave point source is visualized by tracing acoustic streamlines: those curves whose tangent everywhere is the average acoustic intensity vector. It is seen that the acoustic energy flow is not always in line with the ″Snell's law″ or minimum-phase ray path. Also, acoustic energy streamlines do not display unusual behaviour in the vicinity of the critical angle. Finally, it is shown that there exists a law of refraction of acoustic energy streamlines across density discontinuities, analogous to Snell's law of refraction of ray paths across sound speed discontinuities. Examples include water-to-seabed transmission and water-to-air transmission. [Work supported in part by ONR Code 32]

11:40

3aUWc4. Real time sound field visualization in the near field, far field and at absorbing surfaces. Hans-Elias De Bree (Microflown Technologies Inc., PO BOX 300, 6900 AH Zevenaar, Netherlands, debree@microflown.com), Emiel Tijs (Microflown Technologies Inc., PO BOX 300, 6900 AH Zevenaar, Netherlands, tijs@microflown.com), Tom Basten (TNO Science and Industry, Stieltjesweg 1, 2600 AD Delft, Netherlands, tom.basten@tno.nl)

The Microflown is a small sensor that is capable of measuring the acoustic particle velocity. In combination with a small pressure microphone it is possible to measure the complete sound field. If the sound field close to an acoustic material is measured it make sense to measure the particle velocity normal to the surface and the sound pressure. With this, the acoustic impedance and absorption can be measured in real time, and with a high spatial resolution. If the sound field of a sound radiating object is measured, the sound field can be obtained directly. Three applications include: direct acoustic camera, that is the real time display of the sound field (velocity, pressure, intensity). Holography that is the pressure, velocity reconstruction on the surface based on the measured sound field (and other places). And cabin interior noise mapping, that is the visualization of the interior noise perceived on a certain location. With three dimensional sound probes (sound pressure and particle velocity in three dimensions), sources in the free field can be found for both bearings as distance. Most recent developments are presented.

12:00

3aUWc5. Measurement of total sound energy density in enclosures at low frequencies. Finn Jacobsen (Acoustic Technology Department, Technical University of Denmark, Ørsted Plads, B352, DK-2800 Lyngby, Denmark, fja@oersted.dtu.dk)

Many acoustic measurements rely on determining the total sound energy in an enclosure; and this quantity is usually estimated by measuring the mean square pressure at a number of discrete positions. Almost 30 years ago it was shown theoretically that the normalised spatial variance of the total sound energy density (potential and kinetic) is one third of the normalised spatial variance of the potential energy density (the mean square pressure) in a reverberant sound field above the Schroeder frequency. About ten years later this prediction was confirmed experimentally. However, until recently measurement of the total sound energy density (in air) has required an elaborate arrangement based on finite different approximations using at least four matched pressure microphones; therefore the method has never come into use. However, with the advent of a three-dimensional particle velocity transducer it has become somewhat easier to measure total rather than only potential energy density in a sound field. This paper examines the spatial uniformity of potential, kinetic and total sound energy density in enclosures theoretically and experimentally with particular emphasis on the frequency range below the Schroeder frequency.

Contributed Papers

12:20

3aUWc6. On the usefulness of waterborne measurement of particle velocity in geoacoustic inversion. Jean-Pierre Hermand (Université libre de Bruxelles (U.L.B.) - Environmental hydroacoustics lab, av. Franklin D. Roosevelt 50, CP 194/5, 1050 Bruxelles, Belgium, jhermand@ulb.ac.be), Kevin B. Smith (Naval Postgraduate School/Naval Undersea Warfare Center, Code PH/Sk, Department of Physics, Monterey, CA 93943, USA, kbsmith@nps.edu)

Recent advances in sensor design have led to the development of receiving systems whose elements are vector sensors, i.e., sensors that simultaneously measure the acoustic pressure and fluid motion due to the propagation of acoustic energy at the sensor location. As such, arrays of vector sensors can provide more information about the sound field than arrays made of traditional hydrophones, and thus are attractive for various applications including the inversion for environmental properties. The fundamental question addressed by this paper is: does the use of acoustic vector data versus pressure-only data improve the results of an inversion scheme based on waterborne observations and matched field processing? To our knowledge no experimental data are available yet to allow a detailed comparison of performance between standard (pressure-only) arrays and vector sensor arrays for environmental inversions. For a preliminary study we will simulate the inversion of vector sensor data in the South Elba environment for which pressure-only inversion results and ground truth data are available following the Yellow Shark'94 and Blue Planet'07 experiments. Broadband signals received on fully-populated and sparse arrays will be considered.

12:40

3aUWc7. Characterization of the Near Scattered Acoustic Vector Field. Robert Barton (Naval Undersea Warfare Center, Code 1522 bldg1320, 1176 Howell st, Newport, RI 02841, USA, bartonrj@npt.nuwc.navy.mil), Kevin B. Smith (Naval Postgraduate School/Naval Undersea Warfare Center, Code PH/Sk, Department of Physics, Monterey, CA 93943, USA, kbsmith@nps.edu)

In this study, we investigate the properties of the scattered acoustic vector fields generated by simple geometric objects, including the infinite rigid plate, disk, and sphere. Analytical solutions are derived from acoustic target strength scattering models in the near field region. Of particular interest is the understanding of the characteristics of energy flow of the scattered acoustic vector field in the near to far-field transition region. We utilize the time and space separable instantaneous active and reactive acoustic intensity to investigate the relative phase properties of the scattered field. Numerical results are presented for the near region scattered acoustic vector field of simple objects in both two and three dimensions.

Session 3aUWd

Underwater Acoustics and ECUA: Geoacoustic Sediment Modeling II

Nicholas P. Chotiros, Cochair
Applied Research Laboratories, University of Texas, PO Box 8029, Austin, TX 78713-8029, USA

Jean-Pierre Sessarego, Cochair
Laboratory for Mechanics and Acoustics CNRS, 31 chemin Joseph Aiguier, Marseille, 13009, France

Invited Papers

11:20

3aUWd1. The Viscous-Grain-Shearing (VGS) theory of wave propagation in marine sediments. Michael Buckingham (Marine Physical Lab, Scripps Institution of Oceanography, UCSD, 9500 Gilman Dr. M/C 0238, La Jolla, CA 92093-0238, USA, mjb@mpl.ucsd.edu)

The grain-shearing (GS) theory of wave propagation in a marine sediment is based upon the idea that, as grains slide against one another, the dissipation becomes progressively stronger, a phenomenon known as strain hardening. The GS theory predicts a sound speed showing weak, logarithmic dispersion and an attenuation that scales linearly with frequency. At frequencies above about 10 kHz, such behavior matches the sound speed and attenuation data obtained during the SAX99 experiment in the Gulf of Mexico. But at lower frequencies, the measured dispersion curves show a lower sound speed and higher attenuation than predicted by the GS theory. A generalized version of the GS theory, designated the VGS theory, takes account of the effective viscosity of the molecularly thin layer of pore fluid between contiguous grains, which limits the degree of strain hardening that can occur during sliding. The VGS dispersion expressions are the same as those of the GS theory, except for the appearance of a simple algebraic function that has an effect only at low frequencies, below 10 kHz. The resultant VGS curves match the sound speed and attenuation measurements from SAX99 over the measurement frequency band from 1 to 400 kHz. (Research supported by ONR.)

11:40

3aUWd2. Analysis of acoustical transmission and reflection from a sandy stratified rough sediment using the grain shearing model. Laurent Guillon (Ecole Navale/Irenav, BP 600, 29240 Brest Armées, France, guillon@ecole-navale.fr), Vladislav Aleshin (LPEC/UMR 6087/CNRS/Université du Maine, Avenue Olivier Messiaen, 72085 Le Mans Cedex 09, France, aleshinv@mail.ru)

A number of applications, such as geoacoustic inversion or object detection, require an appropriate theoretical consideration of the sound reflection and transmission problem. The analysis we present here includes three essential aspects: account for a constitutive behavior of a saturated unconsolidated granular material, presence of vertical gradients in material properties, and roughness of the sediment surface. Accepting the Buckingham grain shearing model (see e.g. JASA, vol. 117, pp. 137-152) for the stress-strain relationship in the sediment, the gravity-induced variations of the longitudinal and shear rigidity can be described. The corresponding numerical solution for the plane interface is presented and the influence of infinite rigidity gradients at the surface is discussed. Another important contribution is provided by the interface roughness that considerably improves the penetration conditions. This problem is solved using a statistical treatment of a number of roughness realizations with a given spatial spectrum. The developed numerical tool enables to study the influence of all these factors and estimate the penetrated energy for different acoustical frequencies, roughness parameters, and grain sizes (This work was founded by DGA and Thales Underwater Systems).

12:00

3aUWd3. Bistatic scattering in sediments: comparison of model and scaled tank experiments at 238 kHz. Russell Howey (University of Bath, Department of Physics, Claverton Down, BA2 7AY Bath, UK, rph23@bath.ac.uk), Philippe Blondel (University of Bath, Department of Physics, Claverton Down, BA2 7AY Bath, UK, pyspb@bath.ac.uk)

Multiple-aspect scattering is increasingly used to investigate seabeds and objects, buried or not. However, high-frequency scattering processes on/in sediments need to be better understood, particularly when the structure and/or composition of these sediments is not fully homogeneous. Scaled tank experiments were conducted using the University of Bath facilities. A narrow acoustic beam (10° beamwidth) was generated by a transducer resonant at 238 kHz, imaging a silt seabed at 45°. Scattering angles varied between ~16° and ~70° (50 distinct values); bistatic angles varied 40° either side of in-plane with a 2.5° step (33 distinct values). Bottom returns were picked through two methods (automatic and manual) and converted into scattering strengths, accounting for the size of the scattering patch. This large dataset has been compared with the model of Jackson and Williams for bistatic scattering, intended for 10-100 kHz but successfully tested at 240 kHz by other workers. Recursive fitting of model parameters to the experimental values shows the influence of sediment variations (backed by microscopic measurements of actual grain size distributions) and the importance of even small tilts in the surface of the sediments. These results can be used to test the validity of extending this scattering model to higher frequencies.

12:20

3aUWd4. Dispersion and attenuation due to scattering from heterogeneities in the frame bulk and shear moduli of sand sediments. Brian T. Hefner (Applied Physics Laboratory, University of Washington, 1013 NE 40th St, Seattle, WA 98105, USA, hefner@apl.washington.edu), Darrell R. Jackson (Applied Physics Laboratory, University of Washington, 1013 NE 40th Street, Seattle, WA 98105, USA, drj@apl.washington.edu), Joseph Calantoni (Naval Research Laboratory, Marine Geosciences Division, Code 7440.3, Building 1005, MS 22217, USA, joec@nrlssc.navy.mil)

Previously, we presented the results of applying perturbation theory to the problem of fast compressional wave propagation through a Biot medium with heterogeneities in the frame bulk modulus (B. T. Hefner et al., J. Acoust. Soc. Am. 119, 3447 (2006)). It was found that the heterogeneities scattered energy into both the slow and fast compressional waves, thus increasing the attenuation of the fast compressional wave. This theory has since been generalized to account for heterogeneities in both the frame bulk and shear moduli. For the fast compressional wave, energy is now scattered into the shear wave as well as the fast and slow compressional waves, further increasing the attenuation of the coherent field. While shear wave propagation is unaffected by variations in the frame bulk modulus, scattering does occur when there are heterogeneities in the shear modulus. Energy in the shear wave is scattered into both shear and compressional waves as well. The generalized theory depends on the autocorrelation functions of both the shear and bulk moduli variations as well as the cross-correlation function between the moduli. Efforts are underway to estimate these statistics in simple random packings of spherical grains using discrete-element modeling. [Work supported by ONR.]

12:40-2:00 Lunch Break

Invited Papers

2:00

3aUWd5. Data-model comparisons for broadband sound speed and attenuation in sandy seabed. Ji-Xun Zhou (School of Mech. Eng., Georgia Institute of Technology, 771 Ferst Drive, Atlanta, GA 30332-0405, USA, jixun.zhou@me.gatech.edu), Xue-Zhen Zhang (School of Mech. Eng., Georgia Institute of Technology, 771 Ferst Drive, Atlanta, GA 30332-0405, USA, xuezhen.zhang@me.gatech.edu)

Sound speed and attenuation in sandy seabed were analyzed and reviewed from low-frequency (LF) acoustic measurements, conducted at 18 locations in different coastal zones around the world. [Zhou and Zhang, JASA 117(4), 2494 (2005) and 119 (5), 3447 (2006)]. The resultant sound speed and attenuation in a frequency range of 50-2000 Hz in sandy bottoms can be described equally well by the Biot-Stoll poro-elastic model, the Chotiros BICSQS model [JASA 116(4), 2011-2022 (2004)] or the Buckingham VGS model [JASA 122(3), 1486-1501(2007)]. The geophysical parameters were inverted from the best match between the LF data and each of these three geo-acoustic models. The values of the inverted geophysical parameters were reasonable based on both theoretical considerations and published experimental measurements. A combination of the LF field-inverted data with data from the SAX99 experiment and other recent high-frequency measurements offers a broadband reference data set of sound velocity and attenuation for sandy bottoms in shallow water over a frequency range of 50-400,000Hz. The data-model comparisons show that, with one set of adjustable input parameters, all three geo-acoustic models may perfectly match either the broadband velocity dispersion or broadband attenuation, but not both. These models generally either underestimate dispersion or overestimate LF attenuation. [Work supported by ONR.]

2:20

3aUWd6. Role of heterogeneity for sound speed and attenuation in unconsolidated ocean sediments. Jim G. Berryman (Lawrence Berkeley National Laboratory, 1 Cyclotron Road MS90R1116, Berkeley, CA 94720, USA, JGBerryman@LBL.GOV), Steven R. Pride (Lawrence Berkeley National Laboratory, 1 Cyclotron Road MS90R1116, Berkeley, CA 94720, USA, SRPride@LBL.GOV)

Although ocean sediments may have many types and degrees of heterogeneity, it has been determined that two-component models are tractable for poroelastic, thermoelastic, and thermoporoelastic studies. We have found in particular that a substantial part of the increased sound wave attenuation observed in both ocean sediments and laboratory glass-bead experiments above 50 kHz can be explained by such a two-component poroelastic model. Furthermore, the inclusion of thermal expansion and entropy effects into a generalized binary thermoporoelastic model provides an additional attenuation enhancement (though not as large --- by itself --- as the poroelastic enhancement) of a mathematically very similar type that is also relatively easy to model and understand. The paper will present this extended model as well as comparisons to available data.

2:40

3aUWd7. Frequency and grain size dependence of longitudinal wave velocity in granular marine sediments. Masao Kimura (Tokai Univ., 3-20-1 Orido, Shimizu-ku, 424-8610 Shizuoka, Japan, mkimura@scc.u-tokai.ac.jp)

Frequency dependence of longitudinal wave velocity in granular marine sediments is important in underwater acoustics. Also, the grain size dependence is significant for the identification of sediments. In this study, the measurements of the velocity of three kinds of sands with different grain sizes are carried out in the frequency ranges from approximately 5 kHz to 500 kHz in the laboratory. The velocity at a low frequency is measured by using an acoustic tube method. Time-of-flight method is used for the measurements of the velocity at higher frequencies. These measured results are compared with the calculated results by using the Biot-Stoll model and a modified gap stiffness model incorporated into the Biot model (BIMGS model). It is shown that the frequency and grain size dependence of velocity can be explained by using the BIMGS model.

3:00

3aUWd8. Biot-Stoll with squirt flow and shear (BICSQS) model: high-frequency correction. Nicholas P. Chotiros (Applied Research Laboratories, University of Texas, PO Box 8029, Austin, TX 78713-8029, USA, chotiros@arlut.utexas.edu)

The modeling of the grain to grain shear stiffness within the larger Biot-Stoll plus contact squirt flow and shear (BICSQS) model [N. P. Chotiros and M. J. Isakson, J. Acoust. Soc. Am. 116(4), 2011-2022, 2004] assumes Poiseuille flow, which must become invalid at high-frequencies. Specifically, the viscous shear drag term will be unphysically large. A correction is introduced based on Biot's solution for oscillatory flow between two parallel plane boundaries [M. A. Biot, J. Acoust. Soc. Am. 28, 179-191, 1956]. Although the original solution was derived for oscillatory fluid flow relative to stationary parallel plane boundaries, it can be readily adapted for oscillatory motion of the boundaries in opposite directions relative to the fluid, as in shear drag at the grain to grain contact. This correction extends the frequency range of the BICSQS model. Theoretical results, with and without the correction, will be compared. Work supported by the Office of Naval Research, Ocean Acoustics.

Contributed Paper

3:20

3aUWd9. Use of dual methods to infer methane bubble populations in gassy sediment: Inversion of propagation data. Gary B. Robb (National Oceanography Centre, University of Southampton Waterfront Campus, European Way, SO14 3ZH Southampton, UK, gbor199@noc.soton.ac.uk), Timothy G. Leighton (Institute of Sound and Vibration, Univ. of Southampton, University Road, Highfield, SO17 1BJ Southampton, UK, T.G.Leighton@soton.ac.uk), Agni Mantouka (Institute of Sound and Vibration, Univ. of Southampton, University Road, Highfield, SO17 1BJ Southampton, UK, am2@isvr.soton.ac.uk), Angus I. Best (National Oceanography Centre, University of Southampton Waterfront Campus, European Way, SO14 3ZH Southampton, UK, aib@noc.soton.ac.uk), Justin K. Dix (National Oceanography Centre, University of Southampton Waterfront Campus, European Way, SO14 3ZH Southampton, UK, jkd@noc.soton.ac.uk), Victor F. Humphrey (Institute ofSound and Vibration, Univ. of Southampton, University Road, Highfield, SO17 1BJ Southampton, UK, vh@isvr.soton.ac.uk), Zygmunt Klusek (Institute of Oceanography, Polish Academy of Science, P.O. Box 148 Sopot, Poland, klusek@iopan.gda.pl), Paul R. White (Institute of Sound and Vibration, Univ. of Southampton, University Road, Highfield, SO17 1BJ Southampton, UK, prw@isvr.soton.ac.uk)

The inversion of the acoustic properties of gassy sediments presents the optimum manner of determining the in situ distribution of sediment-based methane bubbles. An in situ device that measures both compressional wave attenuations and combination-frequency components in gassy sediment lying within 2 m of the seabed has been developed at the University of Southampton. This device was deployed at an inter-tidal site along the South coast of England. Compressional wave attenuations were measured from 10 to 100 kHz though the analysis of propagation signals transmitted from a variety of sources to a buried co-linear hydrophone array, with propagation distances spanning 0.5 to 2 m. Measured attenuations were inverted to infer in situ bubble size distributions using both established and new acoustic models for gassy sediment. The analysis and results of the combination-frequency component are described in a companion paper.

WEDNESDAY AFTERNOON, 2 JULY 2008 ROOM 242B, 2:00 TO 3:40 P.M.

Session 3pAA

Architectural Acoustics: Architectural Acoustics Potpourri I

David T. Bradley, Cochair
124 Raymond Avenue, Poughkeepsie, NY, 12604

Andrea Farnetani, Cochair
University of Ferrara, Via Saragat 1, 44100 Ferrara, Italy

Contributed Papers

2:00

3pAA1. Shape optimization of polygonal rooms for a correct modal distribution at low frequencies based on psychoacoustic criterion. Sergio Floody (Universidad Tecnologica de Chile INACAP, Brown Norte 290, Nunoa, 7790569 Santiago, Chile, sfloody@utc.cl), Rodolfo Venegas (University of Salford, Acoustics Research Centre, Newton Building, M5 4WT Salford, UK, R.G.VenegasCastillo@pgr.salford.ac.uk)

Resonances in small rooms may lead to inadequate frequency responses. In rooms, where the exigencies on the listening conditions are important, these resonances may cause non wanted coloration effects, which implies a non desirable sound quality. By choosing the right shape and dimensions it is possible to reduce the audible effects of these resonances. The presented methodology aims to determine the shape and size of small and medium polygonal-shaped rooms based on the finite element method for modeling the physical acoustic behavior of the room; a neural network for loudness estimation and genetic algorithm for estimating the optimal dimensions. A comparison with previous techniques used to choose the dimension of rectangular room is also presented.

2:20

3pAA2. The reflected sound field by curved surfaces. Martijn Vercammen (Peutz, De Grippen 1124, 6605 TA Wijchen, Netherlands, m.vercammen@mook.peutz.nl)

Many spaces have curved walls or ceilings. With improved building technology and new fashions in architecture (blobs) there is an increasing number of problems due to the acoustic reflections by these surfaces. Sound reflected by concave surfaces will concentrate in a narrow area. In practical applications of room acoustics these curved surfaces will be calculated with mirror imaging or ray tracing programs, in which the structure is modeled by flat segments. Alternative is a geometrical approach. Both methods do

not correspond to reality. The only valid calculation method is the calculation from a wave extrapolation method. It is shown that a theoretical correct solution of the sound field by curved surfaces is possible. A fairly simple expression for the sound pressure in the focal point is found and a more complicated description of the reflected sound field by small curved surfaces is presented. With these results the sound field in field applications can be calculated.

2:40

3pAA3. Calculation of temporal evolution of sound pressure levels in rooms, based on diffuse reflection. René Gamba (Gamba Acoustique, 2 rue de la découverte, BP 163, 31676 Labege Cedex, France, rene.gamba@acoustique-gamba.fr), Guillaume Cazard (Gamba Acoustique, 2 rue de la découverte, BP 163, 31676 Labege Cedex, France, guillaume.cazard@acoustique-gamba.fr), Claude Senat (Gamba Acoustique, 2 rue de la découverte, BP 163, 31676 Labege Cedex, France, claude .senat@acoustique-gamba.fr)

This paper describes a model which enables the temporal evolution of sound pressure levels in rooms to be calculated. It is built on the assumption that sound waves are totally scattered when reflected by the walls. This model prescribes the sampling of all the surfaces of the room and defines a process of time discretization, process which enables the temporal evolution of energetic exchanges between each sample to be known. Ultimately, the model allows the sound pressure level to be calculated in every point of the room for each time sample Δt (echograms). Thanks to the echograms, some useful criterias for room acoustic studies can be evaluated : reverberation time, EDT, D50, C80,... Measurements and calculations have been carried out for different kinds of rooms. We will describe them in the second part of this paper.

3:00

3pAA4. Sound absorption with fibre-free sintered aluminium in combination with thermally activated concrete slabs. Wouter Rottiers (Sonogamma, P.O.Box 49, Heverlee Ambassade, 3001 Leuven, Belgium, info@sonogamma.com)

Due to increasing ecological awareness and growing requirements of human well-being in working environments, contemporary interior design requires sustainable solutions. Consequently, cooling ceilings are an efficient alternative to conventional air conditioning systems with high energy demands. In order to maintain its thermal efficiency however, the ceiling surface must remain uncovered as much as possible. Conventional perforated or grooved acoustical materials allow for sound absorption only in combination with mineral wool or foam, thus presenting a thermal isolating barrier: they obviously decrease the performance of a thermal ceiling. Porous panels made of pure sintered aluminium offer a conductivity up to 96 kcl / mhC with a thermal radiation of 18.4 W / m^2K, combined with a broadband sound absorption up to $\alpha w = 0.7$ without the use of any additional thermally isolating material. The panels meet the environmental, hygienic and fire safety requirements: they are fibre-free, non-combustible (Euroclass A1), rust-, moisture- and chlorine-proof and can be recycled. The unvisible porosity does not give away the outstanding acoustical qualities. Available in several designs and any colour, the sheets are optically identical to a plain, matt aluminium panel. Several possible configurations are discussed.

3:20

3pAA5. Sound reduction of open noise screens. Jan Hardlooper (Cauberg-Huygen Consulting Engineers, Postbus 9222, 3007 AE Rotterdam, Netherlands, j.hardlooper@chri.nl)

Open noise screens consist of vertical absorbing screens with a depth of 1 meter, placed perpendicular to a building with a mutual distance of 1 meter. The screens are placed at a distance of approximately 1,5 meter. Open noise screens combine a sound reduction of 16 dB with a very open character for ventilation and daylight admittance. Measurements are carried out on a scale model (1:40) in a laboratory and in situ on a real size mock-up, built in a 40-ft container. The results of the mock-up are comparable to the laboratory results. Frequency analysis shows the acoustical principles of the screens and the influence of several parameters. A calculation model is developed tot predict the results for other configurations. The principle of open noise screens is successfully applied for 200 new dwellings in Amsterdam. Suggestions are given for applying open noise screens near highways and railroads, instead of traditional closed screens.

Session 3pAB

Animal Bioacoustics, Psychological and Physiological Acoustics, and ECUA: Auditory Brainstem Response and Behavior Correlation I

Elizabeth Brittan-Powell, Cochair
Dept of Psychology, University of Maryland, College Park, MD 20742, USA

Alexander Y. Supin, Cochair
Institute of Ecology and Evolution, 33 Leninsky Prospect, Moscow, 119071, Russian Federation

Invited Papers

2:00

3pAB1. Auditory brainstem responses in birds: How well do they compare to behavioral techniques for assessing hearing? Elizabeth Brittan-Powell (Dept of Psychology, University of Maryland, College Park, MD 20742, USA, bbrittanpowell@psyc.umd.edu), Bernard Lohr (Department of Biological Sciences, Northern Kentucky University, SC 204D, Nunn Drive, Highland Heights, AK 41099, USA, lohrb1@nku.edu), Isabelle Noirot (Dpt of Science/Oceanography, University of Liege, Bat B6c, 4000 Sart-Tilman, B-4000 Liege, Belgium, isa_noirot@hotmail.com), Robert Dooling (Dept of Psychology, University of Maryland, College Park, MD 20742, USA, dooling@psyc.umd.edu)

Behavioral methods are the gold standard for assessing hearing sensitivity in birds. In many cases, however, behavioral techniques are simply impractical. The non-invasive auditory brainstem response (ABR) represents perhaps the next best approach, and researchers are increasingly turning to the ABR to obtain estimates of hearing sensitivity, auditory system function and development. Our lab has evaluated hearing sensitivity in over 11 species of birds using the ABR, and for six of these species, we have also obtained auditory thresholds by behavioral conditioning methods. These data, along with other results from the literature on bird hearing, now allow general conclusions about the use of ABR as a tool for measuring auditory sensitivity in birds. Waveform morphology is highly conserved across orders of birds. Regardless of how threshold is defined, the ABR audiogram reliably reflects the frequency range of hearing and the shape of the behavioral audiogram. However, ABR thresholds are higher than behavioral thresholds by 20-30 dB but with some variation across species. Aside from audiograms based on simple detection thresholds for tone bursts, ABR methods in birds have also been useful in assessing auditory development, hearing impairment, recovery of function with hair cell regeneration, masked thresholds and aspects of spectral and temporal processing.

2:20

3pAB2. The Auditory Brainstem Response (ABR) Across Mammalian Species. Robert Burkard (University at Buffalo, Department of Rehabilitation Science, 511 Kimball Tower, Buffalo, NY 14214, USA, rfb@buffalo.edu)

The auditory brainstem response (ABR) has been reported in a variety of mammalian species. I have published ABR studies in mammalian species including humans, gerbils, cats, rats, bats, and mice. In many cases, the non-human work was designed to extend observations made in humans. I will discuss data that addresses the variability in the slope of the ABR latency/intensity function across animal species. I will compare ABRs in humans and in gerbils to stimulus manipulations such as click level, click rate, noiseburst risetime and level of masking noise. I will discuss the effects of high stimulus rates across age in the kitten/cat, and compare this to reports in humans from the literature. I will end by discussing my views of the advantages as well as the challenges of using animal models when interested in human normative or pathologic processes.

Contributed Paper

2:40

3pAB3. Arbitrary evoked potentials: using AEPs to measure hearing in fishes. David Mann (University of South Florida, College of Marine Science, 140 7th Ave. S., St. Petersburg, FL 33701, USA, dmann@marine.usf.edu), Randy Hill (University of South Florida, College of Marine Science, 140 7th Ave. S., St. Petersburg, FL 33701, USA, randyjhill@yahoo.com)

Auditory evoked potential (AEP) techniques have become commonly used to measure hearing of a wide variety of animals. However, there is no standard way of defining a threshold from auditory evoked potential data. There are two arbitrary factors affecting the precision of AEP data: the number of sweeps averaged together to detect the AEP, and the method of calculating a threshold from the AEP data. While these arbitrary factors do not invalidate comparative studies where these variables are standardized, different laboratories use different techniques. We describe sources of variation in estimating thresholds using evoked potential techniques using the goldfish as an example. There was little variation in AEP thresholds due to variation in electrode placement or in the method of arbitrarily assigning an AEP threshold. The largest variation was due to differences in the number of sweeps averaged. Under controlled conditions using the same goldfish in the same test tank with the same number of sweeps averaged, AEP's better predicted behavioral thresholds at high frequencies than low frequencies. Since averaging reduces uncorrelated background noise (neural and electrical), it should theoretically be possible to obtain AEP measurements below behavioral thresholds with enough sweeps averaged together.

Invited Papers

3:00

3pAB4. False killer whale hearing adjustment during echolocation measured with evoked potentials. Paul E. Nachtigall (University of Hawaii, Hawaii Institute of Marine Biology, P.O. Box 1106, Kailua, HI 96734, USA, nachtiga@hawaii.edu), Alexander Y. Supin (Institute of Ecology and Evolution, 33 Leninsky Prospect, 119071 Moscow, Russian Federation, alex_supin@mail.ru)

While much has been previously learned about the echolocation performance and characteristics of the outgoing signals of echolocating dolphins and small whales, we have measured hearing using evoked potentials during echolocation. We have found that: (1) the whale may hear her loud outgoing clicks and much quieter returning echoes at comparable levels, (2) the whale has protective mechanisms and hears her outgoing signals at a level about 40 dB lower than similar signals presented directly in front of her, (3) when echo return levels are lowered either by making the targets smaller or by placing the targets farther away - without changing the levels of her outgoing signals, the hearing of those echoes remains at almost the same level, (4) if targets are made much smaller and harder to echolocate, the animal will increase what she hears of her outgoing signal - as if to heighten overall hearing sensitivity to keep the echo level hearable, and (5) the animal has an active 'automatic gain control' mechanism in her hearing based on both forward masking that balances outgoing pulse intensity and time between pulse and echo and active hearing control. Overall, hearing during echolocation appears to be an actively changing process.

3:20

3pAB5. Temporal resolution in the hearing system and auditory evoked potentials. Kristian Beedholm (Institute of Biology, University of Southern Denmark, Campusvej 55, 5230 Odense M, Denmark, beedholm@mail.dk), Lee A. Miller (Institute of Biology, University of Southern Denmark, Campusvej 55, 5230 Odense M, Denmark, lee@biology.sdu.dk)

A popular type of investigation with auditory evoked potentials (AEP) consists of mapping the dependency of the envelope following response to the AM frequency. This results in what is called the modulation rate transfer function (MRTF). The physiological interpretation of the MRTF is not straight forward, but is often used as a measure of the ability of the auditory system to encode temporal changes. It is, however, shown here that the MRTF must depend on the waveform of the click-evoked AEP (ceAEP), which does not relate directly to temporal resolution. The theoretical relationship between the spectrum of the ceAEP and MRTF is such that the MRTF should be identical to the ceAEP if a 1/f weighting is applied to the ceAEP. Deviations from this relationship indeed reflect temporal resolution capabilities. We measured this in a harbour porpoise. Our devised stimulus was a sequence of 0.5 ms Hann weighted 130 kHz tone pips presented at an increasing rate (chirped) over a time span of 32 ms. The results reveal that the system's responsiveness declines roughly exponentially as a function of click rate with a rate constant of about -0.7 kHz and appears more rate limited than implied by traditional MRTF.

WEDNESDAY AFTERNOON, 2 JULY 2008 AMPHI MAILLOT, 1:40 TO 3:40 P.M.

Session 3pMUa

Musical Acoustics: Bowed and Keyboard Stringed Instruments I

Knut Guettler, Cochair
Norwegian Academy of Music, P.O.Box 5190 Majorstuen, Oslo, 0302, Norway

Claudia Fritz, Cochair
University of Cambridge, Music Faculty, West Rd, Cambridge, CB3 9DP, UK

Contributed Papers

1:40

3pMUa1. On the dynamics of the clavichord. Christophe D'Alessandro (LIMSI-CNRS, B.P. 133, 91403 Orsay, France, cda@limsi.fr)

The clavichord is generally considered as the most sensitive and subtle among keyboard instruments. The player/instrument interaction is very direct: the mechanism is reduced to as simple lever, allowing for a direct contact between the finger and string through the key. Key velocity, two string-tangent contact signals, radiated acoustic signal have been synchronously measured for about 10 dynamic nuances and all the notes of four instruments (a 51 notes unfretted instrument, after a German XVIIIth century model, a 51 notes fretted instrument after Hubert (1754), a 45 notes fretted instrument, after a German XVIIth century model, a 37 notes fretted instrument after a medieval model). The instruments can be portrayed in terms of dynamic range, tonal/spectral colour and sound decay time. As for the dynamics, there is some evidence for a linear relationship between sound pressure level and the velocity of the tangent; and an almost constant spectral richness independently of loudness (in contrast with e.g. the piano). A simple model of the tangent/string interaction is proposed. This model reproduces well the behaviour of experimental data, and it may explain why sound quality of the clavichord depends much on the player's ability.

2:00

3pMUa2. Couchet Harpsichord soundboard vibroacoustics behaviour: An application of the Impact Nearfield Acoustical Holography (IPNAH). Sylvie Le Moyne (UPMC Univ Paris 06, CNRS UMR 7190 Institut Jean Le Rond D'Alembert, 2 Place de la Gare de Ceinture, 78210 Saint Cyr l'Ecole, France, slemoyne@ccr.jussieu.fr), Sandie Le Conte (Musée de la Musique,

221 avenue Jean Jaures, 75019 Paris, France, sleconte@cite-musique.fr), François Ollivier (UPMC Univ Paris 06, CNRS UMR 7190 Institut Jean Le Rond D'Alembert, 2 Place de la Gare de Ceinture, 78210 Saint Cyr l'Ecole, France, frol@ccr.jussieu.fr)

The Music Museum in Paris recently acquired a harpsichord made by Ioannes Couchet in 1652 in Anvers. As a masterpiece this instrument is considered as a ″National Treasure″ and therefore protected. A challenging problematic has risen when its restoration was decided since the aim was to play this instrument again in concert. In the objectives of increasing our understanding of the harpsichord ageing, improve a numerical model currently in process and develop a diagnostic method for conservation, an experimental modal analysis of the soundboard was performed by processing its sound field. A non intrusive method, the Impact Planar Nearfield Acoustic Holography, was used. This technique, developed by the authors, implements the well known inverse method NAH on the basis of the acoustic impulse response field and is well adapted to modal analysis. NAH is performed here in unusual conditions compared to literature, as they are far from the ideal: unbaffled source, low sound pressure level, unusually large measurement distance, preponderance of evanescent waves. An additional challenge was to muffle strings, as they should not be removed nor slackened. However, a very satisfying modal decomposition for [30-1500Hz] bandwidth is obtained. Results are confronted with literature and an energetic analysis is proposed.

2:20

3pMUa3. What have they done to the Strads? John McLennan (University of New South Wales, Music Acoustics, School of Physics, NSW 2052 Sydney, Australia, jmcl1597@bigpond.net.au), Joe Wolfe (University of New South Wales, Music Acoustics, School of Physics, NSW 2052 Sydney, Australia, J.Wolfe@unsw.edu.au)

Almost every baroque violin, including those of Stradivarius etc, was extensively modified during the conversion to the romantic or modern configuration. What were the acoustic and playing changes? To answer this question, independently of the confounding factors of wood and manufacture, a baroque violin was made and subjected to acoustic and playing tests, before and after (i) replacement of the neck and fingerboard with longer, heavier more inclined parts, (ii) replacing gut with modern nylon-cored strings. Other changes were also made, including bridge style and position, bass bar and soundpost sizes and bow used. Loudness (Saunders plot) was not greatly changed, except for the E string with a long string length. Some acoustic features survived the changes, and professional baroque and modern style players reported that the instrument preserved some of its ″personality″. Comparisons were made with modern gut strings used by professional baroque players. As well as the acoustic differences, player assessments of bright/dull, full/thin, open/closed, ease of response, evenness, dynamic range are reported. Averaged over all ratings, the players ranked the romantic set up slightly better than the baroque (78% vs 71%).

2:40

3pMUa4. Perceptual studies of violin vibrato. Claudia Fritz (University of Cambridge, Music Faculty, West Rd, CB3 9DP Cambridge, UK, cf291@cam.ac.uk), Jim Woodhouse (University of Cambridge, Dept of Engineering, Trumpington St, CB2 1PZ Cambridge, UK, jw12@cam.ac.uk), Brian Moore (University of Cambridge, Department of Experimental Psychology, Downing Street, CB2 3EB Cambridge, UK, bcjm@cam.ac.uk), Ian Cross (University of Cambridge, Music Faculty, West Rd, CB3 9DP Cambridge, UK, ic108@cam.ac.uk)

Although it seems obvious to violinists that vibrato has a large influence on the perception of violin tone quality, published studies of violin vibrato have mainly concerned its influence on the sound from a scientific point of view, i.e. the characterisation of its time-frequency properties. Work will be described to explore the link between the perception of vibrato notes, the extent of frequency modulation and the level of damping of the resonance modes of the violin. Damping influences the ″peakiness″ of the frequency response function. The test methodology is based on liveliness ratings and triadic comparisons, where subjects have to select the most similar and the most different pair in each triad (presentation of three sounds). The sounds of the corpus are synthesised using sawtooth waves with frequency modulation, whose amplitude is varied, filtered through a set of admittances corresponding to a reference violin and two modified violins, one with the damping of all modes increased, the other one with the damping decreased.

3:00

3pMUa5. Performance comparison of violins through experimental force analyses. Enrico Ravina (University of Genoa - Centre of Research on Choral and Instrumental Music (MUSICOS), Via Opera Pia 15 A, 16145 Genova, Italy, enrico.ravina@unige.it), Paolo Silvestri (Univ. of Genoa - DIMEC, Via Opera Pia 15 A, 16145 Genova, Italy, p.silvestri@unige.it), Federico Lowenberger (Master Violinmaker, Via Marussig 13, 16100 Genova, Italy, info@baroqueviolins.com)

The paper describes the most recent experiments developed on violins with different mounting (baroque, classical, modern) and specifically oriented to the dynamic forces analysis in significant points of the instruments. The vibrational behaviour of the soundboards are strongly influenced by the dynamic forces transmitted from the bridge: they are related also to the tension of the strings. An original testbench conceived to forces measurement has been set up: tensions on strings, forces detected under the bridge and deformations on the fingerboard and on the tailpiece are, in particular, monitored by means not intrusive thin-film tactile pressure measurement devices, micro load cells and micro strain gauges. Mapping of forces and strains are acquired in real time playing the instrument; the paper reports comparisons between differently mounted violins, playing notes under different techniques: continuous (″tenuta″) , ghost (″strappata″), ″detachet″. Experiments are developed using different kind of strings (bowels, metallic,...). The results are used as input for experimental dynamic analyses and tests of the soundboard: in addition, they can be correlated to the acoustic response of the instrument.

3:20

3pMUa6. Shaping and understanding sound: Violin makers, musicians and scientists from Renaissance to Romantism. Anne Houssay (Cité de la musique, 221, avenue Jean Jaurès, 75019 Paris, France, ahoussay@cite-musique.fr)

The training of instrument-makers in Renaissance Italy is linked to a rediscovery of theoretical works on physics and sound as well as to some new tools and skills. Then, the development of physics in the seventeenth and eighteenth century lead the establishment of acoustic as a modern science, with the distinction of partials from harmonics. The ″western world″ has given explanations on vibrations, modes and then elasticity theories, some of which have been included into general knowledge. By times, links between scientists and makers have developed and have participated to the development of musical instruments. Traditional violin makers are craftspeople, and they construct instruments by choosing step by step between many possibilities from the drawing of the model and the choice of materials, to the cutting out of the shapes to create air volumes and vibrating facings. Their parameters are the dimensions, shapes, weight, elasticity, quality and duration of sounds and notes. The test for judging the results is the playing of the instrument by a very competent musician. We will explore, with a point of view of the historian of techniques how the meeting of different cultures and knowledge have transformed the instruments from the Renaissance to the begining of the 19th century.

Session 3pMUb

Musical Acoustics: Wind Instruments I

Seiji Adachi, Cochair
Fraunhofer Institute for Building Physics, Nobelstrasse 12, Stuttgart, 70569, Germany

Simon Félix, Cochair
Laboratoire d'Acoustique de l'Université du Maine, Avenue Olivier Messiaen, Le Mans, 72085, France

Contributed Papers

1:40

3pMUb1. Individual reed characteristics due to changed damping using coupled flow-structure and time-dependent geometry changing Finite-Element calculation. Rolf Bader (University of Hamburg, Institute of Musicology, Neue Rabenstr. 13, 20354 Hamburg, Germany, R_Bader@t-online.de)

The vibration of a reed of a saxophone is calculated using a 2D model of the mouth cavity, the mouth piece and the reed. The time-dependent Finite-Element calculation takes the flow-structure interaction into account and changes the geometry of the flow according to the reed vibration in time. The model is used to study the flow behaviour, pressure distribution, reed vibration and reaction to disturbances of the system. A constant pressure is assumed at the mouth cavity to simulate the pressure of the player's lungs. During the time-dependent process, an impulse is modeled at the end of the mouth piece travelling back from the end of the tube. The damping of the reed was changed to study the reed behaviour. Hard damped reeds show a simple and stable impulse behaviour causing a clear pressure impulse. When the damping is decreased, the impulse coming back from the end of the tube causes the reed not only to open and close but also to show additional vibrations caused by the interplay of the reed's eigenfrequencies and the pressure acting on the reed. These are more or less independent of the travelling impulse and so are a sound characteristic of the reed itself independent of the played note and used articulation.

2:00

3pMUb2. Aspects of vibrato and micromodulation in double reed instrument sounds. Michael Oehler (Institute for applied Musicology and Psychology, Saarstrasse 1A, 50677 Koeln, Germany, michael.oehler@iamp.info), Christoph Reuter (University of Cologne - Musicological Institute, Beethovenstrasse 4, 50674 Koeln, Germany, info@chr-reuter.de)

The perceived naturalness of real and synthesized oboe and bassoon vibrato sounds has been investigated in several perception experiments. The stimuli were generated by means of a currently developed synthesis and analysis framework for wind instrument sounds (first presented at 152nd ASA meeting), based on the pulse forming theory. The framework allows the control of amplitude and frequency parameters at different sound production levels. The stimuli were rated by 60 subjects from ″natural″ to ″unnatural″. A conducted ANOVA showed ($p<.01$) that the different types of modulation significantly affect the perceived naturalness of vibrato sounds: The synthesized stimuli with combined pulse width and cycle duration modulation (source modulation) are perceived as natural as the real sounds. The subsequently modulated synthesized stimuli (AM and/or FM near the end of the signal path) are perceived significantly less natural ($p<.01$). The results support the hypothesis, that source-affected timbre modulation is an important factor for the perceived naturalness of oboe and bassoon vibrato sounds. The use of the developed framework for wind instrument sounds is an alternative method to analyze (micro-)modulation effects. Further investigations may be useful for exploring new sound synthesis algorithms as well as for other experiments in the field of timbre research.

2:20

3pMUb3. The influence of the mean flow on the transmission properties of wind instruments. Andrey R. Da Silva (Schulich School of Music, McGill University, 555 Sherbrooke Street West, Montreal, QC H3A 1E3, Canada, andrey.dasilva@mail.mcgill.ca), Gary Scavone (Schulich School of Music, McGill University, 555 Sherbrooke Street West, Montreal, QC H3A 1E3, Canada, gary@music.mcgill.ca)

The influence of mean flow on the transmission properties of wind instruments has traditionally been neglected due to the range of Strouhal numbers in which this family of instruments normally operate. However, this topic has gained considerable interest among the musical acoustic community during the last decade due to the appearance of new outcomes in research on duct acoustics. Nevertheless, very few contributions have investigated the effect of the mean flow on the transmission properties by taking into account the physical characteristics and dynamic peculiarities of wind instruments. The goal of this work is to present a numerical investigation of the influence of the mean flow on the end correction and on the magnitude of the reflection coefficient for different geometries and Strouhal numbers normally found in wind instruments. The results suggest that, excepting for a few cases, the mean flow can indeed be neglected and the aforementioned transmission properties can be described by the quiescent flow theory.

2:40

3pMUb4. Effect of bending portions of the air column on the acoustical properties of a wind instrument. Simon Félix (Laboratoire d'Acoustique de l'Université du Maine, Avenue Olivier Messiaen, 72085 Le Mans, France, simon.felix@univ-lemans.fr), Cornelis J. Nederveen (Acacialaan 20, 2641 AC Pijnacker, Netherlands, cjnederv@xs4all.nl), Jean-Pierre Dalmont (Laboratoire d'Acoustique de l'Université du Maine, Avenue Olivier Messiaen, 72085 Le Mans, France, Jean-Pierre.Dalmont@univ-lemans.fr), Joël Gilbert (Laboratoire d'Acoustique de l'Université du Maine, Avenue Olivier Messiaen, 72085 Le Mans, France, joel.gilbert@univ-lemans.fr)

The need to keep long wind musical instruments compact imposes the bending of portions of the air column. Although manufacturers and players mention its effects as being significant, the curvature is generally not included in physical models and only a few studies, in only simplified cases, attempted to evaluate its influence. The aim of our study is to quantify the influence of the curvature by modelling the wave propagation in an air column with a multimodal formalism. In a duct with a circular cross-section and a finite curvature, two infinite sets of coupled first-order differential equations are constructed for the components of the pressure and axial velocity, projected on the local transverse modes. From these an impedance matrix is defined, which can be easily calculated, particularly when considering a duct with a piecewise constant curvature. Influence of the curvature on the input impedance, effective length, or playing frequencies is then quantified, displaying notably a dependence to frequency such that, compared to an equivalent straight tube, the shift in resonance frequencies in a tube with bent sections is not always positive, as generally stated. Results are independently corroborated by numerical - finite differences - computations.

3:00

3pMUb5. Numerical investigations of the bassoons aeroacoustic. Andreas Richter (Technische Universität Dresden, Institute for Aerospace Engineering, 01062 Dresden, Germany, andreas.richter4@tu-dresden.de), Roger Grundmann (Technische Universität Dresden, Institute for Aerospace Engineering, 01062 Dresden, Germany, roger.grundmann@tu-dresden.de)

Solving the compressible, unsteady Navier-Stokes equations allows us to track single traveling waves in conjunction with a nonuniform superposed mean flow. Significant physical phenomena like wave steepening, viscothermal losses and acoustic streaming can be investigated. This may be helpful to understand the acoustical characteristics of different geometries, especially in musical woodwind instruments. Since acoustic perturbations are usually small compared to the driving pressure, the solution demands high-order accuracy and appropriate boundary conditions. We present a collection of our numerical results based on two- and threedimensional simulations of the aeroacoustic behavior inside the bassoon. This includes both simulations of the whole instrument under real playing conditions and also numerical studies of subsections of the instrument like tone holes. Here especially viscothermal effects are analyzed. Nonlinear effects like acoustic streaming which is primarily present in the crook of the instrument are also investigated and discussed. Flow field measurements based on Particle Image Velocimetry and pressure measurements inside and outside the instrument are performed to validate the earned results and show a good agreement between measurements and numerical results.

3:20

3pMUb6. Analysis of the timbre of Slovak folk reed aerophones using source-filter model. Milan Rusko (Institute of Informatics of the Slovak Academy of Sciences, Dubravska cesta 9, 845 07 Bratislava, Slovakia, milan.rusko@savba.sk)

Bagpipes are the only group of traditional folk reed instruments that have survived in Slovak folk culture until now. Unlike Scottish highland pipe, gaita, cornemuse etc., all the types of Slovak bagpipes use single reeds in both chanters and drones. Moreover the horns of the drones are partly closed with a plate having only a small opening for air output and sound radiation. This forms a Helmholz-like resonator - acoustic filter having a strong influence on the acoustic and aesthetic properties of the sound. The ideal of the sound timbre of these pipes is ″less open″ (compare to open and closed vowels in speech) and, in spite of its relatively high loudness, ″less agressive″ in comparison to pipes with open horns. This paper presents our approach to study the ideal of sound timbre of the Slovak bagpipe using a source-filter all-pole model. To identify resonance frequencies/formants, we applied inverse filtering technique using discrete linear prediction. Some properties of the source (reed) were studied using parameters like amplitude qutient and open quotient. The possible relations between timbre of speech sounds (vowels) and the timbre of the sound of musical instruments are discussed.

WEDNESDAY AFTERNOON, 2 JULY 2008 ROOM 252A, 1:40 TO 3:40 P.M.

Session 3pNSa

Noise, ASA Committee on Standards, and EURONOISE: Sleep Disturbances and Other Health Effects

Lily M. Wang, Cochair
University of Nebraska - Lincoln, 1110 S. 67th St., Omaha, NE 68182-0681, USA

Barbara Griefahn, Cochair
Institute for Occupational Physiology, Ardeystr. 67, Dortmund, 44139, Germany

Jacques Lambert, Cochair
Laboratoire Transport et Environnement, INRETS, 25, Avenue François Mitterrand, F-69675 BRON cedex, France

Invited Paper

1:40

3pNSa1. Associations between road traffic noise level, road traffic noise annoyance and high blood pressure in the HYENA study. Wolfgang Babisch (Federal Environmental Agency, Corrensplatz 1, 14195 Berlin, Germany, wolfgang.babisch@uba.de), Danny Houthuijs (The National Institute For Public Health and Environmental Protection, PO Box 1, 3720 B A Bilthoven, Netherlands, danny.houthuijs@rivm.nl), Goran Pershagen (Institute of Environmental Medicine, Karolinska Institutet, Box 210, 17177 Stockholm, Sweden, goran.pershagen@ki.se), Klea Katsouyanni (Department of Hygiene and Epidemiology, Medical School, University of Athens, 75 Mikras Asias Str, 11527 Athens, Greece, kkatsouy@med.uoa.gr), Manolis Velonakis (Laboratory of Prevention, Nurses School, University of Athens, 123 Papadiamadopoulou St, 11527 Athens, Greece, evelonak@nurs.uoa.gr), Ennio Cadum (Piedmont Regional Environmental Protection Agency, Via Sabaudia 164, 10095 Grugliasco (TO), Italy, e.cadum@arpa.piemonte.it), Lars Jarup (Imperial College London, Norfolk Place, W2 1PG London, UK, l.jarup@imperial.ac.uk)

The HYENA study is a multi-centred study regarding the effects of aircraft noise and road traffic noise on blood pressure (BP) which was funded by the European Community. Study subjects were 4,861 males and females aged between 45 and 70 years, who had lived for at least 5 years in the vicinity of any of six major European airports. Aircraft noise contours and road traffic noise levels were modelled using the Integrated Noise Model (INM) and national calculation methods. The noise levels were linked to each participant's home address (most exposed façade) using graphical information systems (GIS). Noise annoyance was assessed using the 11-point ICBEN scale. High blood pressure was determined by measurements of systolic and diastolic blood pressure, anti-hypertensive medication and self-reported doctor diagnosed hypertension. The focus here is on the effects of road traffic noise. The road traffic noise level

(LAFm, 24 hours) and noise annoyance due to road traffic noise were both significantly associated with high blood pressure. The association between road traffic noise and high blood pressure was stronger for the road noise level than for the road noise annoyance (90th percentile vs. 10th percentile of the exposure distributions).

Contributed Paper

2:00

3pNSa2. Computing Number of People Awakened by Aircraft Operations Noise. Nicholas P. Miller (Harris Miller Miller & Hanson Inc., 77 South Bedford Street, Burlington, MA 01803, USA, nmiller@hmmh.com)

The acoustics literature documents a number of field studies in which aircraft noise was measured in people's bedrooms while their awakening was simultaneously monitored. Nearly all the field studies produced a dose-response relationship between noise and an awakening response. These dose-response relationships generally show good agreement with each other. Virtually without exception, however, these dose-response relationships pertain to (1) the indoor noise dose produced by a single aircraft flyover and (2) the chances that the noise dose will awaken an average person. These dose-response relationships are too limited for application to a full night of operations and to a realistic population of varying individual sensitivities to noise-induced awakenings. The dose-response relationships do not account for multiple aircraft exposures during the night or for person-to-person variation in how deeply different people sleep. This presentation first briefly reviews a method previously reported for applying the study data to a full night of operations, accounting for time of night and for individual sensitivity to awakening. It then compares percent of population awakened for realistic situations, and shows the effects of including or excluding time of night or individual sensitivities to awakening.

Invited Paper

2:20

3pNSa3. Determination of noise sensitivity within an internet survey using a reduced version of the Noise Sensitivity Questionnaire. Barbara Griefahn (Institute for Occupational Physiology, Ardeystr. 67, 44139 Dortmund, Germany, griefahn@ifado.de)

The Noise Sensitivity Questionnaire (NoiSeQ), that determines noise sensitivity as a moderator of annoyance globally and separately for different everyday activities is with 35 items too long for extended social surveys. This study aimed at the development of a shorter version. Using 429 questionnaires (266 women, 163 men, 16-74 yrs) three factor analyses were performed leading to the NoiSeQ-R that consists of the three subscales 'Sleep', 'Habitation', and 'Work' with 4 items each. The scores are normally distributed, internal consistency is $\alpha = 0.87$ and test-retest reliability varies between rtt = 0.66 and 0.74 depending on the time gaps that varied between 1 to 37 months. To test the validity the NoiSeQ-R was applied to a field study where 190 residents (102 males, 88 females, 17-80 years, median: 51 years) in the vicinity of a large airport rated their chronic annoyance (for the previous 12 months) and their actual annoyance hourly during four consecutive days. As expected, noise sensitivity did not correlate with the individual noise load but significantly with annoyance and with age. Thus the NoiSeQ-R, which is available in ten languages, is regarded as a reliable and valid instrument which can be easily applied in even extended surveys.

Contributed Paper

2:40

3pNSa4. A case study on the validation of models that predict the impact of aircraft noise on sleep. Sarah McGuire (Ray W. Herrick Lab., School of Mechanical Engineering, Purdue Univ., 140 S. Martin Jischke Drive, West Lafayette, IN 47907-2031, USA, mcguires@purdue.edu), Patricia Davies (Ray W. Herrick Lab., School of Mechanical Engineering, Purdue Univ., 140 S. Martin Jischke Drive, West Lafayette, IN 47907-2031, USA, daviesp@ecn.purdue.edu)

The impact of aircraft noise on sleep disturbance is not accurately assessed by cumulative noise metrics that are often used to predict community impact, such as L_{dn}, because sleep disturbance is highly dependent on the noise level of individual events. Most existing sleep disturbance models are dose-response relationships that relate the noise level of individual events, as measured by *SEL(A)* or $L_{A_{max}}$ to the percent awakened, and independence of responses to individual events is assumed. There are a few models that also incorporate additional parameters such as time of night and noise sensitivity, and some that predict the impact of noise on sleep structure. In order to determine whether a model should be used as a general aircraft noise sleep disturbance prediction tool, its performance in a variety of situations must be evaluated. Data was collected from a number of sleep disturbance studies and comparisons were made between responses and model predictions of awakenings and sleep stages. The sufficiency of the collected data for estimating the parameters of more complex models of sleep disturbance is also discussed.

Invited Paper

3:00

3pNSa5. Effects of a hearing aid noise management feature on user perception and performance under noise. Lauren M. Ronsse (University of Nebraska - Lincoln, 1110 S. 67th St., Omaha, NE 68182-0681, USA, lronsse@mail.unomaha.edu), Lily M. Wang (University of Nebraska - Lincoln, 1110 S. 67th St., Omaha, NE 68182-0681, USA, LWang4@UNL.edu)

This paper presents the effects of a hearing aid noise management feature on user perception and performance under noise. Hearing-impaired subjects were exposed twice to seven different noise signals which simulate common mechanical system noise, once with the noise management feature enabled and once disabled. The seven noise signals vary in terms of level and spectral quality, but are all within the range of background noise conditions found in commercial offices. Performance is gauged on three types of tests (math, verbal and typing), while subjective perception is measured via a subjective questionnaire. The results of this investigation will show if the hearing aid noise management feature reduces detrimental effects caused by background noise. Additionally, the data from hearing-

impaired subjects are compared to those from normal-hearing persons to assess if significant differences are present between the two groups. If so, they may lead to the development of different standards for noise criteria levels in spaces designed for the hearing-impaired. [Work supported by a Univ. of Nebraska Layman Award and an ASHRAE Graduate Student Grant-in-Aid]

Contributed Paper

3:20

3pNSa6. Noise and health in the Greater Rotterdam Area. Henk Wolfert (DCMR EPA, P.O. Box 843, sGravelandseweg 565, 3100AV Schiedam, Netherlands, henk.wolfert@dcmr.nl)

In the Greater Rotterdam Area a second study to Noise and Health has been carried out in 2007 and 2008. In 2003 a first study was carried out and that study reported that around 12 percent of the people living in the Greater Rotterdam Area were highly annoyed by noise mainly caused by traffic. The number of people sleep was disturbed and suffered high blood pressure were reported and amounted to 6 percent for sleep disturbance and 3 percent were suffering hypertension. The 2003 study took place within the regularly framework of the Rotterdam Regional Council of Governments Environmental Monitoring program, a program that reports yearly the environmental performance indicators in the Greater Rotterdam Area. Beside this yearly report a theme report is published. Last year's theme reports were published about Air Quality and Energy. In 2007 the board of this program decided that in 2008 the theme should be Noise and Health. The 2008 study is not only an update of the 2003 study but is more detailed and more comprehensive as well, and based on recent insights in health effects, caused by long lasting noise too.

WEDNESDAY AFTERNOON, 2 JULY 2008 ROOM 251, 2:00 TO 3:40 P.M.

Session 3pNSb

Noise, ASA Committee on Standards, and EURONOISE: Prominent Discrete Tones I

Robert Hellweg, Cochair
13 Pine Tree Road, Wellesley, MA 02482, USA

Lothar Schmidt, Cochair
Currenta GmbH & Co. OHG, Building F1, Dormagen, 41538, Germany

Invited Papers

2:00

3pNSb1. Comparison of various procedures for the assessment of prominent discrete tones using a large number of sound samples. Lothar Schmidt (Currenta GmbH & Co. OHG, Building F1, 41538 Dormagen, Germany, lothar.schmidt@currenta.de), Dirk Sagemuehl (Kattenbachstr. 77a, 51467 Bergisch-Gladbach, Germany, DSagemuehl@aol.com)

The procedures from the standards ISO 1996-2 and DIN 45681 as well as the two procedures (TNR and PR) from ISO 7779 are compared. In the first section, characteristic features of the procedures (e.g. signal analysis parameters, degree of automation and characteristics of the prominent discrete tone analysis) are compared. In the second section, the procedures are applied to approximately 70 sound samples. Besides natural sounds (e.g. from machines), synthetic sounds (e.g. peak in a trough) are also used. The results are compared against assessments of the sounds by human subjects. The results of the comparisons are discussed, with special attention paid to cases where significant deviations occur. The third section looks at the results of the comparisons under the aspect of requirements for a standard (e.g. robustness, precision). Overall it was determined that none of the procedures investigated provides optimal results for all sound samples.

2:20

3pNSb2. Prominent tones in noise - Proficiency testing among 30 laboratories of the ISO 1996-2 Annex C method and its predecessors. Torben Holm Pedersen (Delta Acoustics & SenseLab, Venlighedsvej 4, 2970 Hørsholm, Denmark, thp@delta.dk)

Since 1979 the Danish Environmental Protection Agency's Reference laboratory for noise measurements have arranged proficiency testing for the around 30 approved Danish laboratories that are measuring environmental noise. Many of these ″comparison measurements″ have included objective analysis of the prominence of audible tones according to the Joint Nordic Methods which are the predecessors and very similar to the method described in ISO 1996 part 2 Annex C. This paper gives examples on (computerized) analyses of the samples from these proficiency tests and states the uncertainties that can be expected when a number of laboratories with different experience and different types of equipment analyze the same samples. The samples will be available for future reference and can be downloaded from DELTA's homepage.

2:40

3pNSb3. Updates on Prominent Discrete Tone Procedures in ISO 7779, ECMA 74, and ANSI S1.13. Robert Hellweg (13 Pine Tree Road, Wellesley, MA 02482, USA, Hellweg@HellwegAcoustics.com)

There are two alternative procedures for determining if a tone is prominent, i.e. a ″prominent discrete tone″ in ISO 7779, ECMA 74 and ANSI S1.13: the Tone to Noise Ratio (TNR) method and the Prominence Ratio (PR) method. Both of these procedures have been used by the computer industry for more than a decade. Recent revisions to these procedures have refined the calculation of the critical bandwidth and modified the both procedures for low level tones. This paper describes these changes and the rationale behind them. Examples are presented that demonstrate the features of each procedure. The paper presents an overview on the applicability and limitations of each procedure.

3:00

3pNSb4. Issues in the evaluation of the tonality of nonstationary sounds containing time- varying harmonic complexes. Patricia Davies (Ray W. Herrick Lab., School of Mechanical Engineering, Purdue Univ., 140 S. Martin Jischke Drive, West Lafayette, IN 47907-2031, USA, daviesp@ecn.purdue.edu), Shashikant R. More (Ray W. Herrick Lab., School of Mechanical Engineering, Purdue Univ., 140 S. Martin Jischke Drive, West Lafayette, IN 47907-2031, USA, shashi@purdue.edu)

Nonstationary sounds that contain broadband noise and tone complexes whose fundamental frequency varies with time are encountered frequently. Aircraft flyovers and machines shifting operating speeds are examples. The tonalness of such sounds is a factor in how annoying they are. Most metrics used to quantify the tonalness of sounds have been developed for stationary sounds and are based on an analysis of spectra. Contributions from individual sinusoids are estimated and either summed or the maximum is taken. When sounds vary, spectral estimation can be problematic due to the conflicting needs to reduce the variance of the estimate, maintain high frequency resolution, and generate spectra at a rate where the varying tonal behavior can be tracked sufficiently. Harmonic complexes are often perceived holistically, having one dominant pitch, thus treating sinusoidal components independently and summing may not be appropriate. Tests conducted to analyze the tonalness of harmonic complexes in noise are described, and an analysis of aircraft flyovers is used to illustrate the issues that need to be addressed when estimating the tonalness of complex time-varying sounds.

3:20

3pNSb5. Implementation of ISO 1996-2 (2007) pure tone assessment in a sound level meter. Charles Greene (Brüel & Kjær, Skodsborgvej 307, 2850 Nærum, Denmark, cgreene@bksv.com), Douglas Manvell (Brüel & Kjær, Skodsborgvej 307, 2850 Nærum, Denmark, dmanvell@bksv.com), Matthias Scholz (Brüel & Kjær, Skodsborgvej 307, 2850 Nærum, Denmark, mscholz@bksv.com), Anne Lin Enggaard (Nordsjællands Akustik, Skræntevej 13, Holløselund, 3210 Vejby, Denmark, ale@nordsjaellandsakustik.dk)

Noise can be said to be tonal if it contains a distinguishable, discrete, continuous note. This may include a whine, hiss, screech, hum, etc., and any such subjective finding is open to discussion when reported. This is important when it is considered that the likelihood of a noise-provoking complaint depends on its relative level to background, and whether or not it has certain audible characteristics. Fortunately, ISO 1996-2 (2007) provides objective FFT (engineering) and 1/3-octave band (survey) assessment procedures to be used to verify the presence of audible tones if their presence is in dispute. Brüel & Kjær has implemented the methodology of ISO 1996-2 in relation to assessing the audibility of prominent discrete tones in environmental noise into its innovative 2250 and 2270 hand-held analysers. This paper describes the implementation in hand-held instrumentation.

Session 3pNSc

Noise and EURONOISE: Car Acoustics I

Luc Mongeau, Cochair
McGill University, 817 Sherbrooke St. West, Montreal, QC H3A 2K6, Canada

Virginie Maillard, Cochair
RENAULT, Groupe Acoustique, Technocentre, 1 avenue du Golf, 78288 Guyancourt Cedex, France

Contributed Paper

2:20

3pNSc1. Effects of notches on span wise correlation of surface pressure fluctuations downstream of a wall-mounted spoiler. Paloma Mejia (Purdue University, 140 S. Intramural Dr., West Lafayette, 47906, USA, umaphuyu@gmail.com), Jong Beom Park (McGill University, 817 Sherbrooke St. West, Montreal, QC H3A 2K6, Canada, jong.b.park @mail.mcgill.ca), Luc Mongeau (McGill University, 817 Sherbrooke St. West, Montreal, QC H3A 2K6, Canada, luc.mongeau@mcgill.ca)

Leading edge spoilers are widely-used for suppressing flow-induced cavity resonance such as buffeting due to open sunroofs in moving cars. Spoilers deflect the grazing flow over the opening into a region of greater flow velocity, thereby increasing the critical velocity. Notched spoilers have been observed to enhance resonance suppression while moving the flow reattachment region upstream, resulting in a decreased drag. The mechanisms involved in the effectiveness of the notched spoiler were investigated experimentally and numerically. Static and dynamic pressures on the surface behind a wall mounted notched spoiler were measured, and the spatial correlations of the measured pressures were compared to those for a spoiler without notches. The span wise pressure correlation was decreased by the presence of the notches, suggesting a breakdown of the span wise leading vortices predominantly responsible for the cavity excitation. Numerical flow simulations were performed using the lattice Boltzmann method (LBM) with turbulence modeling. Surface pressure results were compared with experimental data to better highlight surface pressure trends.

Invited Papers

2:40

3pNSc2. Simulation of vehicle interior wind noise at low frequencies: a case study. Robert Powell (Ford Motor Company, EVB, MD X-19, Rm 1EB08, 20800 Oakwood Blvd, Dearborn, MI 48121, USA, rpowell7@ford.com), Bijan Khatib-Shahidi (Ford Motor Company, EVB, MD X-19, Rm 1EB08, 20800 Oakwood Blvd, Dearborn, MI 48121, USA, bshahidi@ford.com)

Quietness of passenger vehicle interiors has become a critical-to-quality metric in designing modern passenger vehicles. At the same time, the necessity of bringing fresh designs to market quickly has greatly compressed the development time available to achieve the desired refinement of interior noise and vibration. This has forced manufacturers to place increasing responsibility on analytical simulations in developing countermeasures for noise problems. One aspect of car acoustics that has not received very much attention from the simulation community is the wind noise created by external air flow at speed. Significant contributions to interior loudness can come from underbody air flow, while improvements in simulation efficiency of Computational Fluid Dynamics (CFD) flow models and Finite Element Analysis (FEA) vehicle vibration and acoustic models now make it feasible to analytically simulate interior noise caused by wind excitation. This lecture describes a case study where existing vehicle models were adapted to first build a wind load case from CFD, and then to apply it in estimating and reducing interior noise in FEA. Topics to be covered include: spatial discretization of continuous panel pressures, application of random loads to deterministic vehicle FEA models and diagnostic imagery for visualizing noise and vibration responses.

3:00

3pNSc3. On the use of linear aero-acoustic models. Mats Abom (KTH-The Marcus Wallenberg Laboratory, Teknikringen 8, 100 44 Stockholm, Sweden, matsabom@kth.se)

The classical theory of aero-acoustics is based on Lighthills acoustic analogy which essentially leads to a wave equation with a source term defined by the flow field. This source term is assumed unaffected by the acoustic field and the resulting model can be seen as a linear model which, e.g., for duct acoustic problems can be formulated as an acoustic multi-port. Such linear aero-acoustic models can be applied to most aero-acoustic problems occurring in engineering practice with the exception of whistling, i.e., situations where the source term is affected by the acoustic field. At KTH this methodology has been applied to a number of applications over the years ranging from cooling and ventilation fans to flow generated noise from ducted orifices (valves) and air terminal devices. In this paper the experience from these works is summarized and the experimental techniques developed at KTH to characterize linear aero-acoustic sources are described. Recent efforts to extract linear aero-acoustic models from numerical calculations are also addressed.

Contributed Paper

3:20

3pNSc4. Modeling and characterization of rattle noise encountered in an automotive environment. Ludovic Desvard (Renault, Technocentre, 1 avenue du Golf, 78288 Guyancourt, France, ludovic.desvard@renault.com), Nacer Hamzaoui (LVA, INSA de Lyon, Bat. Saint-Exupéry, 25 bis avenue Jean Capelle, 69621 Villeurbanne, France, nacer.hamzaoui@insa-lyon.fr), Jean-Marc Duffal (Renault, Technocentre, 1 avenue du Golf, 78288 Guyancourt, France, jean-marc.duffal@renault.com)

In an automotive cockpit, rattle noises deal with all noise due to normal impacts which radiate as annoying noises for customers. The state of the art shows studies focused on one automotive subsystem, describing the specific associated physic. The method proposed, in this study, is to generate automotive rattle noises using simple geometries. The interest of this approach is to know all the parameters of the system (impact location, material, geometries, excitation...) and to precisely describe the physical phenomena related to the apparition of rattle noises. Firstly an experimental bench was proposed to generate rattle noises using simple geometries. These rattle noises are similar to those encountered in an automotive environment. This experimental approach allows to measure the vibrational behaviour and the radiated sound of the system under a random impact excitation. Then an analytical model, which describes the experimental approach, is developed to predict the radiated sound, knowing the displacement of the impactor. Numerical and experimental results are compared. Finally, thanks to the experimental approach, a database of rattle noises is created and used to find metrics to quantify the annoyance.

WEDNESDAY AFTERNOON, 2 JULY 2008 ROOM 351, 1:40 TO 3:40 P.M.

Session 3pPAa

Physical Acoustics: Quantum Acoustics I

Michel De Billy, Cochair
Institut Jean le Rond d'Alembert / UMR 7190, 2, place de la Gare de Ceinture, Saint Cyr l'Ecole, 78210, France

Walter Lauriks, Cochair
Lab ATF, Katholicke Universiteit Leuven, Celestijnenlaan 2000, Leuven, B-3001, Belgium

Contributed Papers

1:40

3pPAa1. Phonon dispersion in graphene. Leonid A. Falkovsky (Landau Institute for Theoretical Physics, Kosygina 2, 119334 Moscow, Russian Federation, falk@itp.ac.ru)

Taking into account constraints imposed by the lattice symmetry, we calculate analytically [1] the phonon dispersion for graphene with interactions between first and second neighbors. We find that the out-of-plane (bending) modes are not coupled with in-plane modes and described only with two force constants, one of which is determined by the corresponding Raman frequency and another by the smallest elastic constant C44. In contrast to calculations by Saito et al, we find the linear dispersion of the bending (out-of-plane) mode around the Γ point with a small but finite sound velocity $=1.57$ km/s. The sound velocity of this mode is very sensitive to small variations of the force constants. The sound velocities of in-plane modes are $=20.3$ km/s and $=13.1$ km/s. Because of the lack of information for graphene, we compare the present theory with experiments on graphite. The low phonon frequencies in the critical points turn out less than their values in graphite, since the atoms in graphene are more free to move in the out-of-plane direction in comparison with graphite. Accuracy of the comparison can be estimated using the value of the observed splitting of the ZA and ZO' modes in graphite which is around 130 1/cm. [1] L.A. Falkovsky, cond-mat/0702409.

2:00

3pPAa2. Mechanical (acoustic-like) wave propagation along a vortex array in the superconducting heterostructure. Bogdan T. Maruszewski (Poznan University of Technology, Institute of Applied Mechanics, ul. Piotrowo 3, 60-965 Poznan, Poland, bogdan.maruszewski@put.poznan.pl), Andrzej Drzewiecki (Poznan University of Technology, Institute of Applied Mechanics, ul. Piotrowo 3, 60-965 Poznan, Poland, andrzej.drzewiecki@put.poznan.pl),Roman Starosta(Poznan University of Technology, Institute of Applied Mechanics, ul. Piotrowo 3, 60-965 Poznan, Poland, roman.starosta@put.poznan.pl)

Magnetic flux can penetrate the type - II superconductor in the form of Abrikosov vortices (also called flux lines, flux tubes or fluxons) each carrying a quantum of magnetic flux. These tiny vortices of supercurrent tend to arrange themselves in a triangular or quadratic flux-line lattice. Since the vortices are formed by the applied magnetic field, around of each of them the supercurrent flows. Moreover, there also exist some Lorentz force interactions among them. Those interactions form an origin of an additional mechanical (stress) field occurring in the type-II superconductor. The paper deals with an analysis of elastic (acoustic-like) wave propagation solely along vortices in a heterostructure consisted of the superconducting layer put on the superconducting substrate. Dispersion and the amplitude distribution of those waves in the vortex field existing in that structure has been presented.

2:20

3pPAa3. Amplitude distribution of magnetoelastic waves propagating in a vortex field in a superconducting layer. Bogdan T. Maruszewski (Poznan University of Technology, Institute of Applied Mechanics, ul. Piotrowo 3, 60-965 Poznan, Poland, bogdan.maruszewski@put.poznan.pl), Andrzej Drzewiecki (Poznan University of Technology, Institute of Applied Mechanics, ul. Piotrowo 3, 60-965 Poznan, Poland, andrzej.drzewiecki@put.poznan.pl), Roman Starosta (Poznan University of Technology, Institute of Applied Mechanics, ul. Piotrowo 3, 60-965 Poznan, Poland, roman.starosta@put.poznan.pl)

Magnetic field enters the type - II superconducting body along a discrete arrangement of magnetic vortex lines. In the dynamic case when the magnetic field vary in time, around each such a line a supercurrent flows. So, the vortices interact one to another with the help of the Lorentz force forming this way a new mechanical field of elastic properties. Moreover, those lines arrange themselves in a triangular or quadratic lattice. Such a set is observed

if the intensity of the applied to the material magnetic field is close to its lower limiting value. The paper aims at investigating amplitude distributions of magnetoelastic waves propagating solely in the vortex field of the superconducting layer. Our attention have been focused on the applied magnetic field intensity influence on those amplitudes for various wave frequencies.

2:40

3pPAa4. Acoustical dissipation due to phonon-phonon interaction, thermoelastic loss and dislocation damping in MnO and CoO. Rishi Pal Singh (Banaras Hindu University, 221005 Varanasi, India, rishisingh80@rediffmail.com), Manish Pratap Singh (Banaras Hindu University, 221005 Varanasi, India, mps_bhu@yahoo.co.in), Rajendra Kumar Singh (Department of Physics, Banaras Hindu University, 221005 Varanasi, India, rksingh_17@rediffmail.com)

The temperature dependent acoustical dissipation due to phonon-phonon (p-p) interaction, thermo-elastic mechanism and dislocation damping due to screw and edge dislocations have been evaluated in MnO and CoO in fcc (NaCl-B1 type) phase, in a wide temperature range $50 \leqslant T \leqslant 500$K for longitudinal and shear modes of propagation along three crystallographic directions viz. <100>, <110> and <111>. Electrostatic and Born repulsive potentials were used to obtain second order and third order elastic constants (SOEC and TOEC), taking interactions up to next nearest neighbours.The SOEC and TOEC obtained at diffrent temperatures have been used to obtain gruneisen parameters and non-linearity or anisotropic parameters which in turn were used to evaluate (α/f2) for longitudinal and shear waves. Specific heat (as function of Debye temperature), hardness parameter, lattice parameter have been used as input data. It has been found that (α/f2) increases with temperature and the acoustical dissipation is mainly influenced by p-p interaction.The possible implications of results have been discussed.

3:00

3pPAa5. Numerical and experimental results on sonic band gaps in 1-D phononic crystals with a symmetric stub. Michel De Billy (Institut Jean le Rond d'Alembert / UMR 7190, 2, place de la Gare de Ceinture, 78210 Saint Cyr l'Ecole, France, mdebilly@univ-paris-diderot.fr), Anne-Christine Hladky-Hennion (IEMN, UMR CNRS 8520, avenue Poincaré, BP 60069, 59652 Villeneuve d'Ascq, France, Anne-Christine.Hladky@isen.fr), Jérôme Vasseur (IEMN, UMR CNRS 8520, avenue Poincaré, BP 60069, 59652 Villeneuve d'Ascq, France, jerome.vasseur@univ-lille1.fr), Bahram Djafari-Rouhani (IEMN, UMR CNRS 8520, avenue Poincaré, BP 60069, 59652 Villeneuve d'Ascq, France, Bahram.Djafari-Rouhani@univ-lille1.fr)

The wave propagation in periodic systems has received a great deal of attention during the last years. By analogy with the studies driven on photonic crystals, many works were conducted on phononic crystals. In this paper the propagation of elastic waves through a one dimensional chain of beads with grafted stubs is experimentally as well as numerically investigated. The results obtained by both approaches are well correlated and show that the stub introduces a dip in the spectral response of the chain. The numerical analysis shows that this dip is due to the excitation of a stub mode that cancels the transmission from one extremity of the chain to the other. The position and the shape of the dip in the response are related to the geometry and nature of the stub. The results show that it is possible to adjust the position of the dip and open potential applications of these structures for filtering or demultiplexing. Finally first results on periodically grafted stubs in the chain are presented.

3:20

3pPAa6. Evidence for vortex transport by surface acoustic waves in a high-Tc superconductor. Carsten Hucho (Paul-Drude-Institut, Hausvogteiplatz 5-7, 10117 Berlin, Germany, hucho@pdi-berlin.de), Munise Rakel (Paul-Drude-Institut, Hausvogteiplatz 5-7, 10117 Berlin, Germany, rakel@pdi-berlin.de), Arno Wirsig (Paul-Drude-Institut, Hausvogteiplatz 5-7, 10117 Berlin, Germany, wirsig@pdi-berlin.de), Fabian Jachmann (Paul-Drude-Institut, Hausvogteiplatz 5-7, 10117 Berlin, Germany, jachmann@pdi-berlin.de)

The interaction of surface acoustic waves (SAW) with the magnetic vortex system in YBa2Cu3O7 is investigated. A 100nm YBCO film is deposited on a piezoelectric substrate and structured for electrical 4-point measurements. Interdigital transducers are fabricated on the same substrate. When applying an external magnetic field perpendicular to the film surface a SAW-induced dc-voltage perpendicular to the acoustic sound-path is observed. This is interpreted as consequence of directed dragging of vortices by the SAW induced dynamic pinning structure [1]. The piezoacoustic wave acts as a conveyor for mobile flux quanta. Additional ac-dc-conversion as result of the nonlinear current-voltage characteristics close to the superconducting transition temperature can be resolved and separated. In order to observe the sound-induced vortex motion directly, the flux distribution is analyzed magnetooptically. Magnetooptic imaging allows for time resolved analysis of flux distribution. Quantitative analysis of changes in the magnetization distribution when acoustic driving fields are applied is carried out. The influence of piezoacoustic waves on the pinning properties and sound-induced depinning is discussed. [1] F. Jachmann and C. Hucho, Sol. State Comm., 142 (4) (2007), 212

Session 3pPAb

Physical Acoustics: General Topics in Nonlinear Acoustics I

Thomas Matula, Cochair
Center for Industrial and Medical Ultrasound, Applied Physics Lab., University of Washington, 1013 NE 40th St., Seattle, WA 98105, USA

Murray S. Korman, Cochair
Physics Dept., United States Naval Academy, Chauvenet Hall Room 295, 572 C Holloway Road, Annapolis, MD 21402, USA

Contributed Papers

2:00

3pPAb1. Atomization and deviation of cylindrical water jets in a transverse acoustic field. Jean-Baptiste Carpentier (Coria UMR 6614, avenue de l'Université, 76800 Saint-Etienne-du-Rouvray, France, jean-baptiste.carpentier@univ-rouen.fr), Françoise Baillot (Coria UMR 6614, avenue de l'Université, 76800 Saint-Etienne-du-Rouvray, France, baillot@coria.fr), Jean-Bernard Blaisot (Coria UMR 6614, avenue de l'Université, 76800 Saint-Etienne-du-Rouvray, France, blaisot@coria.fr), Christophe Dumouchel (Coria UMR 6614, avenue de l'Université, 76800 Saint-Etienne-du-Rouvray, France, dumouchel@coria.fr)

This work deals with a particular breakup mode experienced by cylindrical liquid jets when submitted to an intense transverse acoustic wave. Experiments on low speed water jets (< 1 m/s) of diameters 3 mm and 6 mm show that sound waves with a frequency ranging from 500 Hz to 1800 Hz can produce bulges along the jet. When the sound level is high enough, these bulges can trigger an effective atomization mechanism where the jet flattens as a liquid sheet before disintegrating. Sound field can also induce steady deviation of the jet. Both phenomena are theoretically studied. A first model, which treats bulges as outward marks of one particular mode of vibration of the liquid column, is proposed. This model leads to a criterion for the onset of atomization that satisfactorily agrees with experimental observations of the present work. A second analysis identifies deviations as radiation pressure effects. It predicts the direction of experimental deviations with success.

2:20

3pPAb2. Numerical and experimental observations of azimutal shock waves. Régis Marchiano (Institut Jean Le Rond d'Alembert, Université Pierre et Marie Curie, Boites 161 et 162, 4 place Jussieu, 75252 Paris Cedex 05, France, marchi@lmm.jussieu.fr), Jean-Louis Thomas (Centre National de la Recherche Scientifique, Institut des NanoSciences de Paris, Université Pierre et Marie Curie, 4 place Jussieu, 75252 Paris Cedex 05, France, thomasjl@ccr.jussieu.fr), Thomas Brunet (CNRS and Paris VI University, INSP - 140 rue de Lourmel, 75015 Paris, France, thomas.brunet@insp.jussieu.fr), François Coulouvrat (Institut Jean Le Rond d'Alembert, Université Pierre et Marie Curie, Boites 161 et 162, 4 place Jussieu, 75252 Paris Cedex 05, France, coulouvr@ccr.jussieu.fr)

Acoustical Vortices (AV) are acoustical beams with a phase singularity of screw type. They possess a phase with an helical structure which is winding around the axis of propagation. These twists of phase engender special properties such as the existence of an associated angular momentum and imply a coupling between the axial and transverse components of the beam. Propagation of AV of finite amplitude follows the classic rule of nonlinear acoustics. Beyond a shock formation distance, AV develop shocks, but the structure of the latters is noticeable. It will be shown by numerical simulations and experimental measurements, that the nonlinear propagation of AV gives birth to 3D shock waves: a classical shock in the direction of propagation plus an azimutal one in the transverse plane. The numerical simulation, based on an original algorithm solving the 3D Khokhlov-Zabolotskaya equation, is used to investigate the dynamic of the formation of the azimutal shock. Experimental observations made with ultrasonics in water confirm the existence of particular shock waves. Finally, a brief discussion of the potential applications will be proposed.

2:40

3pPAb3. Water flow generation owing to interaction between pulsing bubble and rigid wall. Alexey P. Drozhzhin (Lavrentyev Institute of Hydrodynamics SB RAS, Lavrentyev ave., 15, 630090 Novosibirsk, Russian Federation, ruslan@hydro.nsc.ru), Vyacheslav S. Teslenko (Lavrentyev Institute of Hydrodynamics SB RAS, Lavrentyev ave., 15, 630090 Novosibirsk, Russian Federation, vteslenko@academ.org)

Generating a directed water flow in periodic forming a non-symmetrical acoustic field was experimentally investigated in the work. Periodic acoustic wave field was formed with the help of a vapor-gas bubble pulsing in the hole of a thin diaphragm near a rigid wall. Alternate formation of two water flows moving in opposite directions was found. During the bubble growth stage the flow at velocity V1 was formed in the opposite direction of the plate, and during the bubble collapse stage the flow at velocity V2 was formed towards the plate. By changing the parameter $k=R/r$ where R was a distance from the hole center to the rigid wall, and r was a hole radius, the possibility to control average values V1 and V2 was shown. It was found that at $k=R/r=5.8$ $V1=V2$, at $k>5.8$ $V1>V2$, and at $k<5.8$ V1 was less than V2. It was shown that due to variation of the distance between a pulsing bubble and a rigid wall it was possible to control velocity V and direction of the total flow of water through the hole. The maximum value of velocity V reached 40 cm/s in the experiment.

3:00

3pPAb4. Nonlinear ultrasound fields simulation of harmonics from exponential and bessel beams sources. Hicham Jakjoud (Lab. Electrical Systems and Telecommunications, Faculté des Sciences et Techniques Gueliz B.P. 549, 40000 Marrakech, Morocco, hicham.jakjoud@gmail.com), Ahmed Chitnalah (Lab. Electrical Systems and Telecommunications, Faculté des Sciences et Techniques Gueliz B.P. 549, 40000 Marrakech, Morocco, chitnalah@fstg-marrakech.ac.ma), Noureddine Aouzale (Lab. Electrical Systems and Telecommunications, Faculté des Sciences et Techniques Gueliz B.P. 549, 40000 Marrakech, Morocco, aouzale.nour@gmail.com), Djilali Kourtiche (Lab. d'Instrumentation, Electronique de Nancy, UHP Nancy I, BP 239, 54506 Vandœuvre, 54506 Nancy, France, djilali.kourtiche@lien.uhp-nancy.fr)

It's well known that the harmonic imaging quality can be improved by using sources that radiate narrower and attenuated sidelobe beams. Hence we try to enhance the harmonics' cartography by studying different source's power distributions. We developed a numerical code, using the spectral method, in order to resolve the parabolic wave equation. The numerical results are compared to those given by other researchers in order to validate our algorithm. Two source's power distributions (exponential and Bessel beams) are studied and compared to the uniform case. The use of exponential source leads to harmonics diagrams without sidelobes neither nearfield oscillations. But the beam width is increasing with propagation. The Bessel

source presents a limited diffraction beam. The beam width is almost constant throughout the nearfield and the transition zone. The sidelobes have a weak level in the fundamental curves and they don't appear in the second harmonic ones.

3:20

3pPAb5. Experimental confirmation of the theory of acoustic radiation pressure applying on transparent interfaces. Bruno Issenmann (Bordeaux University - CPMOH, 351 cours de la Liberation, 33405 Talence Cedex, France, b.issenmann@cpmoh.u-bordeaux1.fr), Alice Nicolas (Laboratoire de Physique Matiere Condensee - Univ. Nice, Parc Valrose - 28, avenue Valrose, 06108 Nice Cedex 02, France, Alice .NICOLAS@unice.fr), Regis Wunenburger (Bordeaux University - CPMOH, 351 cours de la Liberation, 33405 Talence Cedex, France, r.wunenburger@cpmoh.u-bordeaux1.fr), Sébastien Manneville (Ecole Normale Supérieure de Lyon, 46 allée d'Italie, 69364 Lyon Cedex 07, France, sebastien.manneville@ens-lyon.fr), Jean-Pierre Delville (Bordeaux University - CPMOH, 351 cours de la Liberation, 33405 Talence Cedex, France, jp.delville@cpmoh.u-bordeaux1.fr)

Since Rayleigh and Brilloin, the acoustic radiation pressure has been the subject of several theoretical works, but of few quantitative tests. Whereas the radiation pressure acting on perfectly reflecting or perfectly absorbing solid targets is commonly used for the calibration of high intensity focused ultrasonic beams, it has never been quantitatively studied on acoustically transparent interfaces. Using an acoustically transparent liquid-liquid interface deformed by the radiation pressure of a focused, continuous wave beam, we have tested the theory of the acoustic radiation pressure acting on transparent interfaces for the first time. At large intensity, depending on the direction of propagation of the beam, we observe surprising interface shapes such as drop emitting jets and ″nipple-like″ deformations.

WEDNESDAY AFTERNOON, 2 JULY 2008 ROOM 241, 2:00 TO 3:40 P.M.

Session 3pPPa

Psychological and Physiological Acoustics: General Topics in Psychological and Physiological Acoustics II

Elizabeth Strickland, Cochair
Purdue University, 500 Oval Drive, West Lafayette, IN 47907, USA

Armin Kohlrausch, Cochair
Philips Research Europe, Digital Signal Processing (MS WO02), High Tech Campus 36, Eindhoven, 5656 AE, Netherlands

Alain De Cheveigne, Cochair
CNRS, Universite Paris 5, Ecole Normale Superieure, 29 rue d'Ulm, Paris, 75230, France

Contributed Papers

2:00

3pPPa1. A pair of spectral notches which plays a role as a spectral cue in the vertical localization, and it's application to estimation of sound source elevation from binaural signals. Kazuhiro Iida (Chiba Institute of Technology, 2-17-1 Tsudanuma, 275-0016 Narashino, Japan, kazuhiro.iida @it-chiba.ac.jp)

The author [Applied Acoustics, 68, 835-850 (2007)] proposed a parametric HRTF model for vertical sound localization. The parametric HRTF is recomposed only of the spectral peaks and notches extracted from the measured HRTF. The results of the median plane localization tests, which were carried out using the parametric HRTFs with various combinations of spectral peaks and notches, show that the pair of first and second notches (N1 and N2) above 5 kHz can be regarded as spectral cues. In this research, estimation of the elevation of sound source in the upper median plane by extracting N1 and N2 frequencies from binaural input signal was carried out. The kinds of sound sources were female voice, male voice, music, white noise, and pink noise. The results show that the estimation is accurate for almost of all the elevation and of all the kind of sound sources.

2:20

3pPPa2. Trading of intensity and interaural correlation cues in the perception of loudness. John F. Culling (Cardiff University, School of Psychology, Tower Building, Park Place, CF10 3AT Cardiff, UK, CullingJ@cardiff.ac.uk), Hannah G. Lewis (Cardiff University, School of Psychology, Tower Building, Park Place, CF10 3AT Cardiff, UK, lewishg @Cardiff.ac.uk)

When a signal is added to noise in the NoSπ binaural configuration, a reduction in interaural cross-correlation (IACC) occurs at the signal frequency. Increases in tone intensity produce decreases in IACC. Consistent with this relationship, direct manipulations of IACC can result in the perception of an added signal and progressive reduction in IACC produces progressive increases in the loudness of this signal [Culling et al. 2001 J. Acoust. Soc. Am. 110, 1020-1029]. In the present study, a narrow sub-band of noise (460-540 Hz) embedded within a broadband (0-3 kHz) diotic noise was manipulated in both intensity and IACC in a 3-interval, odd-one-out task. In the reference intervals, IACC was zero and the spectrum was flat. In the target interval, both the IACC and the intensity of the target band were incremented. These increases have opposing effects on loudness. Correct identification of the target interval followed a U-shape as a function of the size of intensity increment. The minimum of the function was at chance performance, indicating that the opposing cues were fully traded.

2:40

3pPPa3. A comparison between interaural level difference and interaural correlation uncertainty on binaural signal detection thresholds. Nicolas Le Goff (Technical University Eindhoven, Den Dolech 2, 5600 MB Eindhoven, Netherlands, n.legoff@tm.tue.nl), Armin Kohlrausch (Philips Research Europe, Digital Signal Processing (MS WO02), High Tech Campus 36, 5656 AE Eindhoven, Netherlands,

armin.kohlrausch@philips.com),Jeroen Breebaart(Philips Research Europe, Digital Signal Processing (MS WO02), High Tech Campus 36, 5656 AE Eindhoven, Netherlands, jeroen.breebaart@philips.com)

Experiments were performed to study the effect of the presence of interaural level differences (ILDs) on binaural detection abilities. The subjects had to detect an interaurally out-of-phase 500-Hz tone in the presence of a diotic noise masker that had a bandwidth of either 1 kHz, 100 Hz or 10 Hz. Experiments were conducted for both frozen and running-noise conditions and ILDs up to 30 dB were applied to both signal and masker. The results indicate an ILD dependency that varies with the bandwidth of the masker. Furthermore, with increasing ILDs, the difference in detection thresholds between frozen and running-noise conditions was larger for narrow-band noise conditions. Similar observations were made by previous investigations on the influence of reduced masker correlation. Both data sets are compared in order to find possible similarities in the mechanisms involved in the detection tasks.

3:00

3pPPa4. The effect of a speech target's motion on its recognition in the presence of simultaneous competing sentences. Wesley Grantham (Vanderbilt Bill Wilkerson Center, Department of Hearing and Speech Sciences, 1215 21st Avenue South, Room 8310, Nashville, TN 37232-8242, USA, d.wesley.grantham@vanderbilt.edu), Todd Ricketts (Vanderbilt Bill Wilkerson Center, Department of Hearing and Speech Sciences, 1215 21st Avenue South, Room 8310, Nashville, TN 37232-8242, USA, todd.a.ricketts@vanderbilt.edu), Daniel Ashmead (Vanderbilt Bill Wilkerson Center, Department of Hearing and Speech Sciences, 1215 21st Avenue South, Room 8310, Nashville, TN 37232-8242, USA, daniel.h.ashmead@vanderbilt.edu)

Prior knowledge of where to listen significantly improves speech recognition of target sentences presented in the presence of distracter sentences coming from different locations [G. Kidd et al., J. Acoust. Soc. Am. 118, 3804-3815 (2005)]. The present study extended the work of Kidd et al. by measuring the effect of a target's motion on its recognition when competing messages are present. In an anechoic chamber normal-hearing subjects were presented with three simultaneous sentences from the CRM corpus and were instructed to indicate key words from the target sentence (identified by a call-sign previously known to the subject). In the stationary condition the three sentences came from -60°, 0°, and +60° azimuth. In the moving condition, the target source moved during its on-time (e.g., from -60° to 0°) while the two distracter sentences were stationary (e.g., at ±60°). In both cases, subjects either knew in advance where the target would be (Certain Condition) or did not know (Uncertain Condition). It is hypothesized that motion of the target will result in a release from informational masking. That is, the detrimental effect of location uncertainty observed with the stationary targets will be reduced or eliminated when the target is moving.

3:20

3pPPa5. Frequency selectivity in diotic and dichotic masking conditions for normal-hearing and hearing-impaired listeners. Marc Nitschmann (Universität Oldenburg, Medizinische Physik, Carl-von-Ossietzky Str. 9-11, 26111 Oldenburg, Germany, marc.nitschmann@uni-oldenburg.de), Jesko Verhey (Universität Oldenburg, Medizinische Physik, Carl-von-Ossietzky Str. 9-11, 26111 Oldenburg, Germany, jesko.verhey@uni-oldenburg.de), Birger Kollmeier (Universität Oldenburg, Medizinische Physik, Carl-von-Ossietzky Str. 9-11, 26111 Oldenburg, Germany, birger.kollmeier@uni-oldenburg.de)

Previous studies argued that, for broadband maskers, the operational binaural critical bandwidth is similar to the monaural critical bandwidth. The aim of the present study was to test this hypothesis using the notched noise paradigm. Thresholds were measured for a diotic masker and a signal that was either in phase or had an interaural phase difference of 180 degrees. For comparison, thresholds were also measured for a broadband masker (without a notch) at various masker levels to account for possible level effects of the binaural masking level difference (BMLD). Normal-hearing and hard-of-hearing listeners with various degrees of sensorineural hearing impairment participated in the experiment. For all subjects, the thresholds decreased faster for the diotic than the dichotic signal as the notch width increased. The comparison with the data for the broadband masker indicated that this decrease of the BMLD is not due to the decrease of masker level within the auditory filter centered at the signal frequency. The thresholds can be predicted by an equalization-cancellation model assuming a slightly broader auditory filter in the dichotic masking condition. A possible realization of this different binaural auditory filter shape is adding to the on-frequency filter fractions of the adjacent filters.

Session 3pPPb

Psychological and Physiological Acoustics: General Topics in Psychological and Physiological Acoustics III

Elizabeth Strickland, Cochair
Purdue University, 500 Oval Drive, West Lafayette, IN 47907, USA

Armin Kohlrausch, Cochair
Philips Research Europe, Digital Signal Processing (MS WO02), High Tech Campus 36, Eindhoven, 5656 AE, Netherlands

Alain De Cheveigne, Cochair
CNRS, Universite Paris 5, Ecole Normale Superieure, 29 rue d'Ulm, Paris, 75230, France

Contributed Papers

2:00

3pPPb1. Effects on cochlear frequency selectivity after hypobaric pressure exposure. Jonas Brännström (Department of Audiology, Malmö University Hospital and Lund University, 205 05 Malmö, Sweden, jonas.brannstrom@skane.se), Jan Grenner (Department of Audiology, Lund University Hospital, 221 85 Lund, Sweden, jan.grenner@skane.se)

The effects of hypobaric pressure chamber exposure was measured in noise in ten patients with monaural fluctuating low-frequency hearing loss (FLFHL) such as Ménière's disease using psychophysical tuning curves (PTC), transiently evoked otoacoustic emissions (TEOAE), binaural pitch matches and speech recognition scores (SRS) in noise. In the literature, reversible hearing losses have been observed in about 50 % of the patients, but sometimes improved SRS can be observed in patients without hearing threshold improvement. This indicates possible effects of pressure treatment on cochlear frequency selectivity. The relative overpressure in the middle ear obtained after repeated exposures in hypobaric pressure chamber (total duration 18.5 to 28 minutes) was used to impose pressure gradients to the inner ear. The results indicated that the treatment effects were small, but slightly improved SRS in noise, TEOAEs emission strength and PTCs were observed after treatment. Pure tone hearing thresholds improved only for patients exposed to longer treatment durations. Subjective improvement at follow-up could not be predicted from the results. Although the effects were small, the data suggest that hypobaric pressure treatment may improve cochlear frequency selectivity in the affected ear in patients with monaural FLFHL.

2:20

3pPPb2. IPods listening levels on London Underground. Stephen Dance (London South Bank University, FESBE, Borough Road, SE1 0AA London, UK, dances@lsbu.ac.uk), Phil Wash (Bickerdike Allen Partners, 117-121 Salusbury Road, Queens Park, NW6 6RG London, UK, pwash @bickerdikeallen.com)

In the last 5 years the prevalence of the iPod/MP3 players has grown exponentially. The use of such in-earphones under urban conditions has been reported widely in the press at the anecdotal level. This study compared listening levels under quiet conditions and that representative of a London Underground train journey. Calibrated recordings of underground trains running in tunnels were played through loudspeakers in an anechoic chamber, whilst pop music or speech podcasts were played through the iBuds. Thirty-three participates listened to the iPod whilst a Binaural Head and Torso measured the noise levels through the in-earphones. The participants had time to adjust the volume setting on each occasion. A small audiometric study was undertaken for those participates with particularly high and low volume settings a week after the tests were completed. Results show very high volume settings were used when speech was played with the train noise.

2:40

3pPPb3. Assessment of hearing damage when listening to music through a personal digital audio player. Adriano Farina (Liceo Classico G.D. Romagnosi, Viale Maria Luigia 1, 43100 Parma, Italy, adriano @adrianofarina.it)

This study evaluates the sound pressure at the ears of users of personal digital audio players, equipped with in-ear earbuds. More than 50 devices were measured, provided by students aged 15/18. EN standard 50332 specifies the techniques for measuring the sound pressure level at the ears employing an head and torso simulator equipped with binaural microphones, when the gain control of the device is set to maximum. In this study, however, two measurmenets were performed on each device, one at maximum level, and another at the level at which the device had been left by the user after last listening. This way, on a statistical basis, it is possible to relate the effective exposure in daily usage with the maximum loudness of which the device is capable. Furthermore the study did also analyze the spectrum of the test signal: whilst the EN standard mandates for the IEC programme simulation noise, the analysis of thousands songs taken from the players under test revealed a slightly different spectrum, characterized by more boost at low frequencies and larger crest factor. The results of the study did show a relevant hearing risk for users of these personal digital audio players, which exceed noise exposure limits even when used for just one hour per day.

3:00

3pPPb4. The Healthy Benefits of Isolating Earphones. Jeremie Voix (Sonomax Hearing Healthcare Inc, 8375 Mayrand, Montreal, QC H4P 2E2, Canada, jvoix@sonomax.com), Cecile Le Cocq (Ecole de Technologie Superieure, 1100 Notre-Dame Ouest, Montreal, QC H4P 2E2, Canada, clecocq@mec.etsmtl.ca), Lee D. Hager (Sonomax Hearing Healthcare Inc, 8375 Mayrand, Montreal, QC H4P 2E2, Canada, lhager@sonomax.com)

With the ubiquitous presence of Personal Stereo Players (PSPs), namely iPods™ and the like, many hearing conservationists have raised concerns about the temporary and permanent hearing damages that could result from long exposure to loud music playback, especially among adolescents and teenagers. The crux of the problem can be identified as an overexposure of the auditory system. In order to reduce the dose received by the PSP listener, the playback level and/or the duration should be reduced. Assuming that the duration of the music playback experience is really up to the user, the remaining parameter is the music playback level. The purpose of this study is to first understand - from the available public and scientific literature - what factors are influencing the PSP playback level; and second, to investigate if the use of earphones featuring good attenuation of the ambient noise level would lead to a reduced playback level, hence a reduced dose and eventually less auditory damage. Other benefits on sound quality that are associated with isolating earphones will be presented in a third part. Finally the article will review other safety mechanisms that could be used in earphones and PSP to make them safe for the hearing.

3:20

3pPPb5. Potentiation of noise-induced hearing loss by aviation fuel exposure in rats. Laurence D. Fechter (Loma Linda VA Medical Center, Research Service (151), 11201 Benton Street, Loma Linda, CA 92357, USA, larry.fechter@va.gov), Caroline A. Gearhart (Loma Linda VA Medical Center, Research Service (151), 11201 Benton Street, Loma Linda, CA 92357, USA, caroline.gearhart@va.gov), Sherry Fulton (Loma Linda VA Medical Center, Research Service (151), 11201 Benton Street, Loma Linda, CA 92357, USA, sherry.fulton@va.gov), Yoon Hwan Kim (Dept Otolaryngology Cheongju St Mary's Hospital, 589-5 JuJung-Dong, SangDang-Gu, Cheong-Ju, 360-568 Chung-Buk, Republic of Korea, akeell@hanmail.net)

Clear standards have been established for workplace noise. These are designed to protect workers against noise-induced hearing loss. That occupational hearing loss still occurs despite such standards may reflect a variety of issues ranging from enforcement of standards, to adequacy of standards, and problems of noise assessment. An additional factor that influences susceptibility to noise-induced hearing loss is the presence of chemical contaminants in the workplace that render the auditory system especially vulnerable to noise. We report on the ability of aviation fuels to potentiate noise-induced hearing loss in laboratory rats. Subjects were exposed to JP-8 jet fuel, a synthetic fuel produced from coal using the Fischer-Tropsch method, or to clean air. Half of the subjects received a moderate noise exposure following fuel or air exposure. The noise exposure was designed to produce a temporary threshold shift. JP-8 + noise produced greater disruption of distortion product otoacoustic emissions as well as the auditory threshold than did noise alone. Supported by VA Rehabilitation Service grants and the American Petroleum Institute.

WEDNESDAY AFTERNOON, 2 JULY 2008 ROOM 240, 2:00 TO 3:40 P.M.

Session 3pSCa

Speech Communication: Phonetics

Joseph S. Perkell, Chair

Massachusetts Institute of Technology, Research Laboratory of Electronics, Room 36-511, 50 Vassar St., Cambridge, MA 02139-4307, USA

Contributed Papers

2:00

3pSCa1. Auditory and somatosensory goals for sibilants. Joseph S. Perkell (Massachusetts Institute of Technology, Research Laboratory of Electronics, Room 36-511, 50 Vassar St., Cambridge, MA 02139-4307, USA, perkell@mit.edu), Melanie L. Matthies (Massachusetts Institute of Technology, Research Laboratory of Electronics, Room 36-511, 50 Vassar St., Cambridge, MA 02139-4307, USA, matthies@bu.edu), Satrajit S. Ghosh (Massachusetts Institute of Technology, Research Laboratory of Electronics, Room 36-511, 50 Vassar St., Cambridge, MA 02139-4307, USA, satra@speech.mit.edu), Edwin Maas (Massachusetts Institute of Technology, Research Laboratory of Electronics, Room 36-511, 50 Vassar St., Cambridge, MA 02139-4307, USA, maas@bu.edu), Alexandra Hanson (Massachusetts Institute of Technology, Research Laboratory of Electronics, Room 36-511, 50 Vassar St., Cambridge, MA 02139-4307, USA, alex.hanson@gmail.com), Frank H. Guenther (Boston University, 677 Beacon Street, Boston, MA 02215, USA, guenther@cns.bu.edu), Harlan Lane (Massachusetts Institute of Technology, Research Laboratory of Electronics, Room 36-511, 50 Vassar St., Cambridge, MA 02139-4307, USA, lane@speech.mit.edu), Lucie Ménard (Département de linguistique et de didactique des langues, Université du Québec à Montréal, Case postale 8888, succursale Centre-ville, Montréal, QC H3C 3P8, Canada, menard.lucie@uqam.ca), Mark Tiede (Massachusetts Institute of Technology, Research Laboratory of Electronics, Room 36-511, 50 Vassar St., Cambridge, MA 02139-4307, USA, tiede@speech.mit.edu)

In prior studies [JSLHR 47, 1259-69, 2004; JASA 116, 2338-44, 2004], we found that speakers' auditory acuity for synthetic sibilant (/s/, /sh/) and vowel stimuli was correlated with the degree of acoustic contrast they produced. This outcome is consistent with the view that the articulatory movements underlying phonemic contrasts have auditory goals. There was also a cross-speaker relation between sibilant contrast and use of contact between the tongue tip and lower alveolar ridge for /s/ (but not /sh), indicating that such contact is a somatosensory goal for /s/. In the current study, another, larger group of subjects also showed relations between measures of auditory acuity and acoustic contrast for sibilants and vowels. To determine whether the idea of a somatosensory goal for /s/ would also be supported by a relation between acuity and contrast, we made measurements of somatosensory discrimination. Small plastic (JVP) domes with grooves of different spacing were pressed against each subject's tongue tip and the subject was asked to identify one of four possible orientations of the grooves. A wide range of individual performance was observed with a bias-corrected sensitivity measure. Correlations with produced sibilant contrast and further analyses will be reported. [Research supported by NIDCD, NIH.]

2:20

3pSCa2. Perceptual explanations of articulatory variability in the realisation of the nasal feature for the consonants. Jacqueline Vaissière (Laboratory of Phonetics and Phonology, 19 rue des bernardins, 75005 Paris, France, jacqueline.vaissiere@univ-paris3.fr)

This paper illustrates how the perceptual constraints explain the observed articulatory and aerodynamic inter-speakers and inter-languages variability between initial nasal consonants (/n/), and unreleased final consonants (/N/). In the case of /n/, only a short, well-defined region around the consonant release needs to be nasalized for the consonant to be perceived as nasal. In the case of /N/, because of the lack of a nasal release, a longer span is needed for deciphering the presence of nasalisation; contextual nasalization of the preceding vowel can be avoided, but in that case, the nasal murmur has to be long to be perceived (since the first part of the murmur is perceptually masked by the vowel), and/or /N/ has to be released. Such observations argue for the division of the nasal consonant into three parts, onset, murmur and release: the realisation of the nasal feature is aligned around the /N/ onset, and around the /n/ offset. It also argues for a better integration of the perceptual requirements and masking phenomena in modelling the observed variability. Finally, it shows that a feature can be realized very differently depending on the position of the phoneme in the syllable.

2:40

3pSCa3. Final consonant voicing and vowel height contrasts in whispered speech. Yana D Gilichinskaya (City University of New York, Graduate Center, 365 Fifth Avenue, New York, NY 10016, USA, ygilichinskaya@gc.cuny.edu), Winifred Strange (CUNY Graduate Center,

365 5th Avenue, Program in Speech-Language-Hearing Sciences, New York, NY 10016, USA, strangepin@aol.com)

Whispered speech is a naturally distorted speech signal. Whereas it preserves some characteristics of fully phonated speech, some important acoustic cues are removed, diminished or altered. The prominence of acoustic cues in whispered speech may change due to the physical properties of the whispered speech signal, i.e., decreased intensity, the absence of periodic vibration of the vocal folds, damping of F1, shift of the formants and flattening of the amplitude envelope. Such changes affect the acoustic cues both for vowels (e.g. vowel height) and consonants (e.g. voicing contrasts). The objective of the present project was to explore the acoustic cues for post-stressed syllable-final consonant voicing contrasts and the vowels preceding them in continuous whispered speech of American English speakers and to compare the results with those in fully phonated speech. The stimuli were recorded in the carrier sentence ″I'll utter /habVC/ off the list″. The consonant pairs included voiced/voiceless bilabial stops /b-p/ and labiodental fricatives /f-v/, each combined with 11 AE vowels /i, I, ″epsilon″, e, æ, a, ″turned-v″, o, ″open-o″, u, ″horseshoe″/. Preliminary results showed that vowels had longer duration in whispered speech than in fully phonated speech. Spectral dispersion, temporal contrastivness of vowels; F1, and vowel duration cues will be reported in the presentation.

3:00

3pSCa4. Production and perception of vietnamese short vowels. Nguyen Viet Son (MICA center HUT - CNRS/UMI2954 INP Grenoble, C10 Hanoi university of Technology, No1 Dai Co Viet street - Hai Ba Trung, 0084 Hanoi, Viet Nam, viet-son.nguyen@mica.edu.vn), René Carré (Laboratoire Dynamique du Langage, UMR 5596, CNRS, Université Lyon 2, 14 Avenue Marcelin Berthelot, 69363 Lyon cedex 07, France, recarre@wanadoo.fr), Eric Castelli (MICA center HUT - CNRS/UMI2954 INP Grenoble, C10 Hanoi university of Technology, No1 Dai Co Viet street - Hai Ba Trung, 0084 Hanoi, Viet Nam, Eric.Castelli@mica.edu.vn)

It is well known that vowels can be produced in isolation, acoustically stable in such a way that they are represented as points in the F1-F2-F3 space. Vietnamese language presents 13 vowels, however, Vietnamese can only pronounce 9 vowels [i, u, e, o, ω, a, σ, ε, γ] in isolated mode. A previous study showed that the 4 remaining vowels [α, δ, ν, ϵ] have the same acoustic characteristics (F1, F2, F3) as, respectively, the vowels [a, ε, σ, γ], but their dynamic characteristics (the rate of CV transitions) are clearly distinct. Measurements show us that vowels durations of [α, ν] are always shorter than the one of corresponding classical vowels [a, γ] and are not acoustically stable. For test perceptions (with 10 Vietnamese people), synthesized syllables [a-t] and [γ-t] with changing vowel duration are recognized as [α-t, ν-t] when then duration of initial vowel [a, γ] are 60% - 70% shorter. It means that the vowel duration is an important parameter that allows Vietnamese distinguishing the long vowels and short vowels in Vietnamese language. This paper further analyses the production of Vietnamese CV, including long vowels and short vowels in terms of duration, formant evolution and rate of C.V transitions.

3:20

3pSCa5. Acoustic properties of the interdental approximant in Kagayanen. Kenneth S. Olson (SIL International, 7500 W Camp Wisdom Rd, Dallas, TX 75236, USA, Ken_Olson@sil.org), Jeff Mielke (University of Ottawa, Arts Hall, 70 Laurier Ave East, Room 401, Ottawa, ON K1N 6N5, Canada, jmielke@uOttawa.ca)

This paper describes the acoustic properties of the interdental approximant, a rare speech sound reported to date only in a dozen languages in the Philippines. The measurements analyzed here are based on recordings of one female speaker of Kagayanen. The interdental approximant exhibits acoustic characteristics typical of semi-vowels: the formant pattern is similar to that of vowels, and the formant transitions with adjoining vowels have a long duration, usually 35 ms or more. The values of F2 and F3 are analogous to those of the Kagayanen [l], a prototypical voiced alveolar lateral; the only significant formant value difference between the two sounds involves F1: the interdental approximant has a mean of 508 Hz (n=9), whereas the mean for [l] is 368 Hz (n=9). On the other hand, while these two segments sound impressionistically similar, the interdental approximant differs acoustically from [l] in several other respects as well: there is no abrupt change in the formant pattern at the junctures with adjoining vowels, the higher formants (F6 and above) are not reduced in intensity, and F3 is not enhanced in intensity compared to semi-vowels.

WEDNESDAY AFTERNOON, 2 JULY 2008 ROOM 250B, 2:00 TO 3:40 P.M.

Session 3pSCb

Speech Communication: Prosody II

Marion Dohen, Chair

Speech and Cognition Department, GIPSA-lab, 46 avenue Félix Viallet, Grenoble, 38031, France

Contributed Papers

2:00

3pSCb1. Audiovisual perception of prosodic contrastive focus in whispered French. Marion Dohen (Speech and Cognition Department, GIPSA-lab, 46 avenue Félix Viallet, 38031 Grenoble, France, marion.dohen@gipsa-lab.inpg.fr), Hélène Loevenbruck (Speech and Cognition Department, GIPSA-lab, 46 avenue Félix Viallet, 38031 Grenoble, France, Helene.Loevenbruck@gipsa-lab.inpg.fr)

This study investigates the potential contribution of visual information in the audiovisual perception of prosodic contrastive focus in French. Contrastive focus is used to attract the listener's attention to a specific part of the utterance. Mostly conceived of as auditory/acoustic, it also has visible correlates which have been shown to be perceived. This study aimed at analyzing the interaction between audition and vision for the perception of prosodic focus by using a whispered speech paradigm. It was based on audiovisual recordings from 4 speakers wearing no facial markers. It combined performance assessment to reaction time measurements and confirmed and extended preliminary results obtained on 2 speakers wearing facial markers (needed for a parallel articulatory analysis). The results showed that adding vision to audition for the perception of prosodic focus can not only improve perception performances but can also reduce perceptual cognitive load. A further analysis suggested that the two modalities are integrated for the perception of prosodic focus. Visual only perception was facilitated for whispered speech suggesting an enhancement of visual cues. Moreover, the absence of facial markers did not impair perception. Therefore facial markers do not seem to enhance the relative importance/salience of visual cues.

2:20

3pSCb2. Effects of boundary tones on accent-related F0 peak alignment. Yen-Liang Shue (Univ. of California Los Angeles, Dept. of Electrical Engineering, 405 Hilgard Ave., Los Angeles, CA 90095, USA,

yshue@ee.ucla.edu),Markus Iseli(Univ. of California Los Angeles, Dept. of Electrical Engineering, 405 Hilgard Ave., Los Angeles, CA 90095, USA, iseli@ee.ucla.edu), Stefanie Shattuck-Hufnagel (Massachusetts Institute of Technology, Research Laboratory of Electronics, Speech Communication Group, 77 Massachusetts Ave., Cambridge, MA 02139, USA, stef@speech.mit.edu), Nanette Veilleux (Simmons College, Dept. of Computer Science, 300 The Fenway, Boston, MA 02115, USA, nanette.veilleux@simmons.edu), Sun-Ah Jun (Univ. of California Los Angeles, Dept. of Linguistics, 405 Hilgard Ave., Los Angeles, CA 90095, USA, jun@humnet.ucla.edu), Abeer Alwan (University of California, 405 Hilgard Ave, Los Angeles, CA 90095, USA, alwan@ee.ucla.edu)

Speakers sometimes delay the F0 peak of a high accent beyond the accented syllable (Silverman and Pierrehumbert, Papers in Laboratory Phonology I, 1990; Xu, Phonetica, 2001). Previous studies of factors affecting peak alignment focused on the phrasal position of the accented word and the segments of the accented syllable (Jilka and Möbius, Interspeech 2007). Shue et al. (Interspeech 2007) hypothesized that if an accented word also contains boundary tones, that could influence the position and height of the F0 peak. A test corpus controlling for vowel type, syllable number and position of the focused word, based on the utterances ″Dagada gave Anne a dada (daily)″ and ″A dada gave Anne dagadas (daily)″, was produced using four prosodically different contours, involving high (H*) and low (L*) pitch accents on either ″dagada″ or ″dada″, in declarative and interrogative forms eliciting different boundary tones. Analysis of five repetitions spoken by four male and four female native American English speakers reveals that for most speakers, the presence of boundary tones on the target word shifts the accent-related F0 peak earlier when other factors are held constant. Preliminary results suggest effects of boundary tone on H* F0 peak height as well.

2:40

3pSCb3. Double focus in general American English. Fang Liu (The University of Chicago, Department of Linguistics, 1010 E. 59th Street, Chicago, IL 60637, USA, liufang@uchicago.edu)

This study investigates the acoustic realization of double focus in statements and declarative questions in English. Five speakers produced eight sets of utterances with alternating focus (medial, final, or double) and sentence type (statement or declarative question) conditions. F0 analyses indicate that the effect of double focus on the global pitch range and the local pitch target is somewhat moderate when compared to that of single focus: 1) Post-focus pitch range suppression shows a smaller magnitude in double- than in medial-focused statements, 2) Post-focus pitch range raising is less dramatic in double- than in medial-focused questions, and it ends before the stressed syllable of the second focus in double-focused questions, in order to realize a rising pitch target for the on-focus stressed syllable, and 3) pitch targets of on-focus stressed syllables are more fully realized (i.e., showing steeper slopes or higher registers) in single- than in double-focused sentences. Duration analyses indicate that the length of the double-focused item is in between those of the corresponding single- and non-focused item, with the single-focused stressed syllable having the longest duration. These findings demonstrate a delicate balance among the realization of lexical stress, focus, and sentence type in English.

3:00

3pSCb4. Melodic prominences structures: exploring to what extent the speaker variability is spreading. Geneviève Caelen-Haumont (MICA Center, C10, Hanoi Universirty of Technology, 1 Dai Co Viet Str., Hai Ba Trung, Hanoi, Hanoi, Viet Nam, genevieve.caelen@mica.edu.vn)

Melodic prominences in speech have a deserved reputation of conveying a great part of variability, as they are greatly based on subjective impulse and feelings. We think that these specific contours are nevertheless relevant, and that their structure, while obeying to internal laws of regulation, allow also a range of speaker variability. Generally no specific tool was used to describe these FO contours with precision. An automatic analysis tool MELISM was then developed by Caelen-Haumont and Auran (2004) allowing accurate descriptions of F0 salience (melisms). This paper aims at 1° describing the MELISM tool, the automatic segmentation, the annotation, the melodic labelling of the melism structure it provides in the prosody domain 2° presenting the main results over 4 speaker exploring to what extent the speaker variability spreads. The melism structures are explored and analysed such as the whole variability is reduced through three major components (onset, nucleus, coda) and their respective subparts, where only the nucleus is the compulsory part. Statistics running on these structures put to light a set of interesting laws about the internal regulation of melisms but in the other side, the part devoted to the speaker variability.

3:20

3pSCb5. How prosody correlates with syntax: An observation on Sakizaya, an endangered Formosan language. Sally Chen (Grad. Inst. of Linguistics, National Taiwan Univ., 1, Roosevelt Rd. Sec. 4, 106 Taipei, Taiwan, d93142002@ntu.edu.tw), Wen-Chi Shen (Grad. Inst. of Linguistics, National Taiwan Univ., 1, Roosevelt Rd. Sec. 4, 106 Taipei, Taiwan, r94142007@ntu.edu.tw), Li-May Sung (Grad. Inst. of Linguistics, National Taiwan Univ., 1, Roosevelt Rd. Sec. 4, 106 Taipei, Taiwan, limay@ntu.edu.tw), Janice Fon (Grad. Inst. of Linguistics, National Taiwan Univ., 1, Roosevelt Rd. Sec. 4, 106 Taipei, Taiwan, jfon@ntu.edu.tw)

This pioneering study investigates the relationship between prosody and syntax of Sakizaya, an endangered Formosan language in eastern Taiwan. Both elicitation data and spontaneous data were collected from five informants (aged 48 to 74), in order to provide a more thorough sketch on this VSO language with clear case marking and voice systems. Preliminary results showed that in descriptive sentences, prosodic units and syntactic units do correlate with each other, depending on which of the four voices is used. (The four voices in Sakizaya: agent-, patient-, instrumental, and locative voices) However, once specific functions are imposed onto a sentence, they will override this ″default″ setting, and adopt corresponding prosodic patterns for the ease of communication. For example, in this language, the default position to receive a nuclear accent should be the ultimate syllable of a sentence; however, we observed an accent shift onto the penultimate syllable for yes/no questions, exclamations, as well as continuously progressive sentences. In negation sentences, pitch peaks are distinctively higher in the accented syllable of the negator (which posited sentence-initially), instead of the ultimate syllable in sentence-final position. Lastly, case markers and voice markers were found as preferred positions for speech planning and repair.

Session 3pSP

Signal Processing in Acoustics, Acoustical Oceanography, and ECUA: Model-Based Signal Processing I

Sean Lehman, Cochair
Lawrence Livermore Natl. Lab., Livermore, CA 94551, USA

Christian Pichot, Cochair
Antennas & Telecommunications Laboratory, University of Nice-Sophia Antipolis, France

Invited Papers

2:00

3pSP1. Model-based algorithms for detecting damage in ultrasonic nondestructive evaluation measurements. Grace A. Clark (Lawrence Livermore National Laboratory, 7000 East Ave., L-130, Livermore, CA 94550, USA, clark9@llnl.gov)

This work addresses the ″As-Built″ modeling problem in ultrasonic nondestructive evaluation (NDE), in which one is given measurements of a mechanical part before and after use. The condition of the ″as-built″ part (prior to use) is known, so that after the part has been used, it can be tested for damage. This enables a two-step model-based approach: (1) Given input-output measurements (A-Scans), estimate a dynamic prediction-error model of the ″as-built″ measurement(s) using system identification algorithms. The model is validated by testing the innovations (residuals) for statistical whiteness and then stored for future use. (2) Later, when testing the part for damage, the error between the measurement and the output of the stored model is tested against a short-term whiteness confidence interval test statistic. If the part passes the test, this implies that the model remains valid and the part is declared undamaged. If the part fails the test, this indicates a model mismatch, which means that the part's acoustic properties have changed, and the part is declared damaged. Performance of the algorithms is demonstrated using real measurements, receiver operating characteristic (ROC) curves and a confidence interval about the probability of correct classification.

2:20

3pSP2. Signal-based ray tracing modeling in complex tectonics. Paul Cristini (CNRS-UMR5212 Modélisation et Imagerie en Géosciences, UPPA BP115, 64013 Pau, France, paul.cristini@univ-pau.fr), Eric De Bazelaire (11, Route du Bourg, 64230 Beyrie-en-Béarn, France, edebaz@wanadoo.fr), Charles Revaux (50, Rue Lagardere, 64000 Pau, France, charles.revaux@wanadoo.fr)

The objective of this talk is to present a novel method which can perform the fast computation of the times of arrival of seismic waves which propagate between a source and an array of receivers in a stratified medium. This method combines signal processing concepts for the approximation of interfaces and wavefronts, and ray theory for the propagation of wavefronts. The main idea is to put in adequation the computations with the the precision and the resolution of the source signal in order to avoid unnecessary computational effort. This new approach leads to the redefinition and simplification of the model through which waves propagate. The modifications are governed by the spectral characteristics of the source signal. All rays are computed without any omission at a much lower cost in computing time than classical methods. In addition, we will show how to include surface waves such as head waves within the proposed method.

Contributed Papers

2:40

3pSP3. Imaging the earth's subsurface via regularized inversion. Robert Clapp (Stanford University, 397 Panama Mall, Geophysics Department, Stanford, CA 94305, USA, bob@sep.stanford.edu)

Modern seismic exploration geophysics attempts to construct a model of the earth's subsurface using measurements taken at the earth's surface. The recorded measurements comprise datasets with billions to trillions of samples. Despite the size of the datasets, models are often poorly sampled because of the complexity of the earth's subsurface. Therefore, the resultant model is poorly determined for many components. The massive size of our problems introduce additional limitations. We are limited to adjoint-based inversion methods, we can never afford to iterate to true convergence, and most importantly we make approximations to the physics in our operators. These limitations introduce spurious events when inverting. Significantly improved results can be obtained by incorporating regularization that incorporates a priori knowledge of the physics and geology into the inversion process.

3:00

3pSP4. Characterization of targets buried in disordered medium. Kamal Belkebir (Faculté St Jérôme, 13397 cedex 20 Marseille, France, kamal.belkebir@fresnel.fr), Faheem Ashraf (Faculté St Jérôme, 13397 cedex 20 Marseille, France, faheem.ashraf@fresnel.fr), Marc Saillard (Faculté St Jérôme, 13397 cedex 20 Marseille, France, marc.saillard@lseet.univ-tln.fr), Patrick Chaumet (Faculté St Jérôme, 13397 cedex 20 Marseille, France, patrick.chaumet@fresnel.fr)

We consider in this paper the problem of the determination of the permittivity profile of an unknown buried object from measurements of the electromagnetic scattered field. The target under test is assumed to be buried in one of the two involved media while the sources and the receivers are located in the other medium (limited-aspect data configuration). This ill-posed and non-linear inverse scattering problem is reformulated as an optimization problem that is solved iteratively. This method consists in building up a sequence of the parameter of interest by minimizing, at each iteration step, a cost functional representing the discrepancy between the data and

those that would be obtained with the best available estimation of the parameter. In addition, when clutter is present, the decomposition of the time reversal operator method is used to improve the signal-to-clutter ratio, since it allows us to synthesize a wave that focuses on the scatterer. The data associated with this incident field are included in the iterative minimization procedure.

Invited Paper

3:20

3pSP5. Underwater channel characterization using opportunity sources : a time-frequency-phase approach. Cornel Ioana (GIPSA-lab, dep. DIS, 961, rue de la Houille Blanche, 38402 St Martin d'Hères, France, cornel.ioana@gipsa-lab.inpg.fr), Arnaud Jarrot (Schlumberger Riboud Product Center, 1 rue Becquerel, 92140 Clamart, France, ajarrot@clamart.oilfield.slb.com), Cédric Gervaise (E3I2 - EA3876, 2 rue François Verny, 29806 Brest Cedex, France, cedric.gervaise@ensieta.fr), Andre Quinquis (Scientific Research and Innovation Division, DET/GESMA BP 42, 29240 Brest, France, andre.quinquis@dga.defense.gouv.fr), Jérôme I. Mars (GIPSA-lab, dep. DIS, 961, rue de la Houille Blanche, 38402 St Martin d'Hères, France, jerome.mars@gipsa-lab.inpg.fr)

Analyzing natural signals constitutes the main tool for characterization of physical phenomena. Underwater channel is an example of a natural environment potentially characterized by signals generated by various sources : underwater mammals, human activity noise, etc. In order to efficiently exploit the information from these signals two major problems should be addressed. First, since the signals are unknown or disturbed by unpredictable factors, we are deal with a blind processing context. That is, the lack of a priori hypothesis has to be considered. Generally, the signal has a complex shape characterized by multi-component non-linear time-frequency structures. The proposed solution consists in focusing our processing on non-parametric time-frequency analysis considering also fundamental signal items such as time-frequency energy and local phase analysis. The second problem is related to the complex connection between physical parameters of a phenomenon and parameters of signals characterizing this phenomenon. The proposed approach consists of combining the physical model with the information provided by a parametric representation of the signal. This framework helps to the definition of the concept of underwater passive tomography which provides the characterization of the underwater channel of interest by taking advantage of environmental signals : mammals vocalizations, motion sources, etc.

WEDNESDAY AFTERNOON, 2 JULY 2008 AMPHI BORDEAUX, 2:00 TO 3:20 P.M.

Session 3pUWa

Underwater Acoustics and ECUA: Fluctuations and Statistics

Barry J. Uscinski, Cochair
Cambridge University, Centre for Mathematical Sciences, Wilberforce Rd., Cambridge, CB3 0WA, UK

Kevin D. Lepage, Cochair
Naval Research Laboratory, 4555 Overlook Ave SW, Washington, DC 20375, USA

Contributed Papers

2:00

3pUWa1. Horizontal structure of acoustic intensity fluctuations in the ocean. Barry J. Uscinski (Cambridge University, Centre for Mathematical Sciences, Wilberforce Rd., CB3 0WA Cambridge, UK, bju1@cam.ac.uk), Jim Nicholson (QinetiQ Ltd., Winfrith Technology Centre, Dorchester, Dorset, DT2 8XJ Dorchester, UK, jrnicholson@qinetiq.com)

In April 1989 an acoustic experiment was performed over the abyssal plain south of Msderia in which transmissions were made, for about an hour, at 482, 680 and 740Hz from a ship steaming at 5kts to a receiving array towed by another ship 65km away travelling on a parallel course at the same speed. The signals arrived by two paths, an upper path trapped in the surface duct and a lower path via the main sound channel. This paper describes the experiment and analyses the intensity fluctuations in the signal received by the lower path. We investigate the horizontal structure of intensity fluctuations in the ocean when these are mainly due to internal waves. This aspect of such acoustic intensity fluctuations has received little attention until now. The experimental results are compared with theoretical predictions based on the parabolic moment equations for propagation and scattering in randomly irregular media, and on the stnadard Garrett-Munk model for ocean internal waves. The experimental results and theoretical predictions agree quite well but some new questions arise about the correlation of intensity fluctuations as the acoustis transmission frequency is varied.

2:20

3pUWa2. Evolution of the statistics of the unscattered component of low order acoustic modes as a function of range. Tarun K. Chandrayadula (George Mason University, 4400, University Drive, Fairfax, VA 22030, USA, tchandra@gmu.edu), Kathleen E. Wage (George Mason University, 4400, University Drive, Fairfax, VA 22030, USA, kwage@gmu.edu)

Scattering due to internal waves in the ocean causes the acoustic modes to exchange energy as they propagate. At a specific range, the mode signal consists of two components: the unscattered component is the energy that has propagated only in the designated mode and the scattered component contains the contributions from other modes. The unscattered component dominates the signal at short ranges, but decays to zero at longer ranges. If the unscattered component can be isolated from the scattered energy, it could be used in tomographic inversions. Signal processing techniques are needed to detect the unscattered component. A statistical model for the unscattered component that would help design signal processing techniques is currently unavailable. This talk describes a new model for the unscattered component that was developed using coupled mode and parabolic equation simulations. The model characterizes the statistics of the unscattered component using parameters such as frequency and time coherence. The characteristics of the unscattered component are then compared with the scat-

tered component. The implications of these results for the design of detectors is briefly discussed. [Work supported by ONR Ocean Acoustics Graduate Traineeship Award]

2:40

3pUWa3. Exact and approximate moments for dispersive pulse propagation. Leon Cohen (City University of New York, Hunter-Phyiscs, 695 Park Ave., New York, NY 10021, USA, leon.cohen @hunter.cuny.edu), Patrick Loughlin (University of Pittsburgh, 348 Benedum Engineering Hall, Dept. of Electrical & Computer Engineering, Pittsburgh, PA 15261, USA, loughlin@engr.pitt.edu)

We derive exact moments for pulse propagation in a dispersive medium. These moments are not only inherently interesting but clarify the validity of a recently proposed approximation scheme for wave propagation. The approximation method for pulse propagation is based on the Wigner position-wave/number representation and is very accurate, easy to apply, and moreover is physically illuminating. In particular one obtains the evolved approximate Wigner distribution from the initial Wigner distribution by a simple linear translation in phase space. Propagation with damping is also taken into account. We will show that the reason for the high accuracy of the approximation is that the important low order moments are exactly given by the approximation and that these low order moments preserve very well the basic shape of the pulse. Moreover, now that we understand why the approximation method works well, the approximation can be systematically improved. We give a number of specific examples of exactly calculable moments to illustrate the method and we compare exact and approximate moments. The work of PL is supported by The Research of LC was supported by AFOSR and the work of PL is supported by ONR (N00014-06-1-0009)

3:00

3pUWa4. Absolute intensities of acoustic shadow zone arrivals. Lora Van Uffelen (MPL, Scripps Institution of Oceanography, University of California, San Diego, La Jolla, CA 92093-0238, USA, lvanuffe@ucsd .edu), Peter Worcester (MPL, Scripps Institution of Oceanography, University of California, San Diego, La Jolla, CA 92093-0238, USA, pworcester@ucsd.edu), Matthew Dzieciuch (MPL, Scripps Institution of Oceanography, University of California, San Diego, La Jolla, CA 92093-0238, USA, mad@ucsd.edu)

Qualitative observations from bottom-mounted US Navy SOSUS receiving stations in the North Pacific reveal anomalously deep acoustic arrivals at travel times directly corresponding with timefronts expected to have turned much higher in the water column. The vertical structure of these shadow zone arrivals was studied during SPICEX, a long-range propagation experiment conducted from June to November 2004 in the North Pacific, utilizing moored sources 500 and 1000 km distant from two vertical line array receivers, which together virtually spanned the full ocean depth. Comparison of the measured absolute intensities of shadow zone arrivals with Monte Carlo parabolic equation simulations suggest that the amount of internal wave scattering associated with the standard Garrett-Munk (GM) internal wave spectrum is not adequate to account for the extent of scattering into the acoustic shadow evident in the experimental data, suggesting either that the GM spectrum is not an appropriate representation of the internal wave field or that some other mechanism, such as oceanic spice, may be also be contributing to the scattering.

WEDNESDAY AFTERNOON, 2 JULY 2008 ROOM 341, 2:00 TO 3:40 P.M.

Session 3pUWb

Underwater Acoustics and ECUA: Array Processing

David L. Bradley, Cochair
Pennsylvania State University, Post Office Box 30, State College, PA 16804-0030, USA

Claire Debever, Cochair
MPL, Scripps Institution of Oceanography, University of California, San Diego, La Jolla, CA 92093-0238, USA

Contributed Papers

2:00

3pUWb1. Effect of array element location on coherent inter-array processing. Claire Debever (MPL, Scripps Institution of Oceanography, University of California, San Diego, La Jolla, CA 92093-0238, USA, cdebever@ucsd.edu), William A. Kuperman (MPL, Scripps Institution of Oceanography, University of California, San Diego, La Jolla, CA 92093-0238, USA, wkuperman@ucsd.edu)

In the SWellEx-96 experiment, two 25-elements horizontal arrays, each of length 250 m, were moored 3.5 km apart [N.O. Booth et al, IEEE, JOE, 25, no 3, July 2000]. A broadband source (50 to 400 Hz tones) was towed from 1 km to 10 km away from the arrays. The data is processed using the simple conventional plane-wave beamformer for all the cases covering incoherent frequency and incoherent inter-array processing to coherent frequency and coherent inter-array processing as a function of source position relative to the arrays. The effect of noise and array element location mismatch on source localization and coherent processing gain is investigated. An attempt to improve array element localization is made using a self-focusing technique. [Work supported by ONR.]

2:20

3pUWb2. Longitudinal Correlation Improvement with Model-based Technique. Renhe Zhang (National Laboratory of Acoustics, Institute of Acoustics, Chinese Academy of Sciences, No 21, Beisihuanxilu, 100080 Beijing, China, zrh@mail.ioa.ac.cn), Fenghua Li (National Laboratory of Acoustics, Institute of Acoustics, Chinese Academy of Sciences, No 21, Beisihuanxilu, 100080 Beijing, China, lfh@mail.ioa.ac.cn)

Longitudinal correlation coefficient is one of the most important parameters for signal processing in ocean acoustics. Multi-path interference is an important effect on the decrease of the longitudinal correlation for low frequency sound propagation in shallow water. In this research, the Frequency-Phase-Shift Relationship (FPSR) between the Frequency Response Function (FRF) of sound propagation at two horizontally separated locations based on waveguide invariant is derived. The validity of the FPSR is demonstrated by both numerical simulations and data from two experiments. Experimental data also show that the decrease of the longitudinal correlation coefficient of low frequency signals from explosive source due to multi-path interference can be conquered significantly with the FPSR. [Work supported by the National Natural Science Foundation of China under Grand No 10734100].

2:40

3pUWb3. Performance analysis of GARCH based DOA estimation in SONAR. Hadi Amiri (Engineering Research Institute, Ministry of J-Agriculture, 13445-754 Tehran, Iran, h.amiri@ieee.org), Hamidreza Amindavar (Amirkabir University of Technology, Department of Electrical Engineering, 15914 Tehran, Iran, hamidami@aut.ac.ir), Mahmoud Kamarei (University of Tehran, Department of Electrical and Computer Engineering, 14395-515 Tehran, Iran, kamarei@ut.ac.ir)

In this paper we propose a new source localization method using additive noise modeling based on Generalized Autoregressive Conditional Heteroscedasticity (GARCH) time-series. In an actual application such as underwater acoustics, the measurement of additive noise in a natural environment shows that noise can sometimes be significantly non-Gaussian and nonstationary, and therefore, signal processing algorithms that are optimized for Gaussian noise, may degrade significantly in this environment. GARCH models are feasible for heavy tailed PDFs and time varying variances of stochastic process and also has flexible forms. We use a more realistic GARCH(1,1) based noise model in the Maximum Likelihood Approach for the estimation of Direction-Of-Arrivals (DOAs) of impinging sources. In the performance analysis of the method, we examine the suitability of the proposed method in a passive sonar using simulation methods with cramer-rao bound (CRB) and perturbaion appraoch such as gain, phase and sensors positions errors.

3:00

3pUWb4. Direct wave suppression using wavelet transform for bistatic sonar. Bo Lei (Institute of Acoustic Engineering, Northwestern Polytechnical University, 710072 Xi'an, China, lei.bo.thunder@gmail.com), Yuanliang Ma (Institute of Acoustic Engineering, Northwestern Polytechnical University, 710072 Xi'an, China, ylma@nwpu.edu.cn), Kunde Yang (Institute of Acoustic Engineering, Northwestern Polytechnical University, 710072 Xi'an, China, ykdzym@nwpu.edu.cn), Chao Sun (Institute of Acoustic Engineering, Northwestern Polytechnical University, 710072 Xi'an, China, csun@nwpu.edu.cn)

The bistatic sonar is often influenced by the direct wave, especially when the target approaches the baseline of the system. The direct wave is above 50dB higher than the scattering signal level. The paper analyzes the effect of the direct wave, and proposes a new method based on wavelet transform for direct wave suppression. The strong direct wave is well eliminated while maintaining the weak scattering signal almost unchanged. The basic idea is that the direct wave is firstly removed form the received signal after wavelet transform. Then the signal is reconstructed in time domain, finally the cross-correlation is achieved to shown the doppler frequency shift of the weak scattering signal. Computer simulation is given. The cross-correlations of the received signal for both before and after the direct wave suppression are compared. It shows that the influence of the direct wave is correctly removed, the time delay and Doppler frequency shift are shown in the figure and the target is detectable.

3:20

3pUWb5. Adaptive beamforming applied to underwater acoustic measurements. Denis Orlov (Institute of Applied Physics of the Russian Academy of Sciences, 46 Ulyanov Street, 603950 Nizhny Novgorod, Russian Federation, denis@hydro.appl.sci-nnov.ru), Iosif Fiks (Institute of Applied Physics of the Russian Academy of Sciences, 46 Ulyanov Street, 603950 Nizhny Novgorod, Russian Federation, fiks@hydro.appl.sci-nnov.ru), Galina Fiks (Institute of Applied Physics of the Russian Academy of Sciences, 46 Ulyanov Street, 603950 Nizhny Novgorod, Russian Federation, galya@hydro.appl.sci-nnov.ru), Pavel Korotin (Institute of Applied Physics of the Russian Academy of Sciences, 46 Ulyanov Street, 603950 Nizhny Novgorod, Russian Federation, monitor@hydro.appl.sci-nnov.ru), Victor Turchin (Institute of Applied Physics of the Russian Academy of Sciences, 46 Ulyanov Street, 603950 Nizhny Novgorod, Russian Federation, tvi@hydro.appl.sci-nnov.ru)

In many applications, such as measuring the underwater noise level of moving ships, underwater acoustic measurements face serious difficulties related to several factors, including low signal-to-noise ratio, effects of surface and bottom on signal, as well as complicated spatial structure of the sea interference. The increase of the measurement interference resistance, compared to the case of a single receiver (hydrophone), can be provided by the use of spatially distributed receiving systems (antenna arrays), which are able to suppress the interference due to their spatial selectivity. The present work is aimed at developing adaptive methods for underwater acoustic measurements with the use of vertical antenna arrays. The method must provide the maximum reduction of external interference keeping the given measurement accuracy, i.e., the result must coincide with the output of a single receiver in the absence of interference. From the point of view of synthesis of array systems, the originality of the presented approach is mainly in conjunction of measurement functionality of the antenna array and the maximum interference suppression. The results of numerical simulation and experimental testing under sea conditions show that the proposed adaptive methods provide high precision of measurements under strong and/or complex interference conditions.

Session 3pUWc

Underwater Acoustics and ECUA: Objects Scattering and Detection

Sven M. Ivansson, Cochair
Swedish Defence Research Agency, FOI Kista, Stockholm, SE-16490, Sweden

Ahmad Abawi, Cochair
HLS Research, Inc., 3366 N. Torrey Pines Ct., Ste. 310, La Jolla, CA 92037, USA

Contributed Papers

2:00

3pUWc1. Numerical design of Alberich anechoic coatings with superellipsoidal cavities of mixed sizes. Sven M. Ivansson (Swedish Defence Research Agency, FOI Kista, SE-16490 Stockholm, Sweden, sveni@foi.se)

Thin rubber coatings with cavities in a doubly periodic lattice are able to reduce reflections of underwater sound by redistributing normally incident energy such that absorption in the surrounding rubber is enhanced. For spherical scatterers, the anechoic effect can be studied numerically by the layer multiple-scattering method. In comparison to more flexible but also more computer intensitive methods, such as FEM modeling, there are two important advantages. An improved physical understanding of the anechoic effect can be achieved by simplified semianalytical analysis, and the high computational speed allows modern global optimization techniques to be applied for coating design. In this paper, the flexibility of the layer multiscattering method is improved by combination with an efficient algorithm for numerical computation of transition matrices for superellipsoidal scatterers. Extensions to mixtures of nonspherical scatterers of different types are also considered, in order to enhance the broad-band performance. Symmetry properties are used to reduce the size of the pertinent equation systems. Examples of numerical coating design for underwater acoustic applications are presented, using differential evolution algorithms for the optimization.

2:20

3pUWc2. Scattering from rotationally-symmetric objects using only free space Green's functions. Ahmad Abawi (HLS Research, Inc., 3366 N. Torrey Pines Ct., Ste. 310, La Jolla, CA 92037, USA, Abawi@HLSResearch.com), Michael B. Porter (HLS Research, Inc., 3366 N. Torrey Pines Ct., Ste. 310, La Jolla, CA 92037, USA, michael.porter@hlsresearch.com)

To compute scattering from an object, one has to solve the wave equation and impose the appropriate boundary conditions on the surface of the object. For objects for which the wave equation can be separated, like cylinders, spheres and spheroids, this problem can be solved analytically. For more general objects, methods like the finite element or boundary element techniques can be employed. The use of free space Green's functions offers another method for computation of scattering from a general-shaped object. This method, which is known as the method of field superposition or the virtual source technique, can be used to impose the appropriate boundary conditions on the surface of the object by using free space Green's function with complex amplitudes. These amplitudes are determined from a matrix equation that results when boundary conditions are imposed. In this paper we apply this technique to compute scattering from rotationally symmetric objects. These objects can be homogeneous solids or shells, filled with a homogeneous fluid. The versatility and robustness of the method is demonstrated by applying it to various objects in free space and in a waveguide.

2:40

3pUWc3. Modeling of underwater sonar barriers. Andrzej Elminowicz (R&D Marine Technology Centre, Ul. Dickmana 62, 81-109 Gdynia, Poland, andrzeje@ctm.gdynia.pl), Leonard Zajaczkowski (R&D Marine Technology Centre, Ul. Dickmana 62, 81-109 Gdynia, Poland, leonard@ctm.gdynia.pl)

Commonly used Diver Detection Sonar (DDS) are characterized by detection and tracking as well as intruder warning in limited range 300 m ÷ 600 m. A new approach to underwater protection is focused on multimonostatic, bistatic and multistatic active sonar barriers (ASB). This paper describes key features of a multi-monostatic (MM), bistatic (BS) and multistatic (MS) operation in the littoral beginning from system configuration, its performance and constraints. A new type of acoustic devices in a form of a transmitting/receiving module and its application in active sonar barriers (ASB) has also been presented. Coverages and ranges of barriers for various technical parameters, environmental conditions and wave propagation as well as modules location (including transducers' depth, azimuth and inclination) have been studied. The application of active sonar barriers (ASB), especially in protection systems, has been presented as barriers protecting docks, harbour basins, ships at piers or harbour entries. The new type of a monostatic/bistatic acoustic barrier in technology demonstrator form, has been designed and constructed. In order to display detection and localization of the small underwater objects as well as their tracking and classification the performance tests of the barrier will be conducted. The results of the tests will be attached to the paper.

3:00

3pUWc4. Wideband sonar system for autonomous surveys using REMUS. Chris Capus (Ocean Systems Laboratory, School of Eng. & Phys. Sciences, Heriot-Watt University, EH14 4AS Edinburgh, UK, C.Capus@hw.ac.uk), Yan Pailhas (Ocean Systems Laboratory, School of Eng. & Phys. Sciences, Heriot-Watt University, EH14 4AS Edinburgh, UK, Y.Pailhas@hw.ac.uk), Keith E. Brown (Ocean Systems Laboratory, School of Eng. & Phys. Sciences, Heriot-Watt University, EH14 4AS Edinburgh, UK, K.E.Brown@hw.ac.uk)

Many new roles are being proposed for Autonomous Underwater Vehicles (AUVs) to carry out hazardous tasks in harsh or remote locations and to free up valuable resources required for manned missions. These roles include marine environmental survey, target detection and classification and tracking of underwater pipes and cables. Suitable sensing and processing packages must be provided and building on recent wideband sonar research, the Ocean Systems Laboratory (OSL) is putting together a wideband system for deployment on board a REMUS AUV. The prototype sensor package comprises paired projectors and receivers mounted in a side-looking arrangement to provide complementary information to the standard REMUS sidescan modules. The sensor bandwidths cover a range from 30-130kHz similar to those used by the bottlenose dolphin. Data is gathered autonomously with a dedicated AMD Geode based PC104+ PC controlling a 4-channel 800kHz simultaneous sampling data acquisition module. Acquisition is triggered to coincide with mission requirements from a separate mission control PC on board the vehicle.

3:20

3pUWc5. A multistatic synthetic aperture sonar to detect a cylinder lying on a rough interface: experimental results. Caroline Herve (Laboratory for Mechanics and Acoustics CNRS, 31 chemin Joseph Aiguier, 13009 Marseille, France, herve@lma.cnrs-mrs.fr), Jean-Pierre Sessarego (Laboratory for Mechanics and Acoustics CNRS, 31 chemin Joseph Aiguier, 13009 Marseille, France, sessarego@lma.cnrs-mrs.fr), Régine Guillermin (Laboratory for Mechanics and Acoustics CNRS, 31 chemin Joseph Aiguier, 13009 Marseille, France, guillermin@lma.cnrs-mrs .fr), Françoise Schmitt (Groupe d'Electromagnétisme Appliqué, Pôle Scientifique et Technologique de l'Université Paris X Nanterre Site de Ville d'Avray, 50, rue de Sèvres, 92410 Paris Ville-d'Avray, France, fschmitt@u-paris10.fr), Franck Daout (Groupe d'Electromagnétisme Appliqué, Pôle Scientifique et Technologique de l'Université Paris X Nanterre Site de Ville d'Avray, 50, rue de Sèvres, 92410 Paris Ville-d'Avray, France, fdaout@u-paris10.fr)

Monostatic Synthetic Aperture Sonar (SAS) are high resolution systems for target imaging which are now of common use in the underwater acoustics domain. The objective of this work was to analyse what kind of information should be obtained from a multistatic SAS system. This idea has been applied in radar but very few works exist in the underwater acoustics domain. The applications could be detection and identification of buried mines or mines lying on the seabed and divers detection for harbour protection. These applications deal with the problem of target detection and identification near a rough surface. To show what can be obtained with a multistatic SAS processing, we have performed an experiment with a circular cylinder of 1 cm diameter lying on a rough interface made of sand grains of 1 mm diameter. Measurements were performed in a tank with both a multistatic and a monostatic SAS systems. The signal used to insonified the target area was a short impulse with a 2 MHz central frequency which corresponds to a ka about 40. Images of the cylinder in presence of clutter have been reconstructed with the matched filtering algorithm from monostatic and multistatic acquisitions and have been compared.

Awards Ceremony

Gilles A. Daigle
President, Acoustical Society of America

Luigi Maffei
President, European Acoustics Association

Jean Kergomard
President, Société Française d'Acoustique

Acoustical Society of America

Presentation of ASA Fellowship Certificates

Michael A. Akeroyd
Susanna B. Blackwell
Dick B. Botteldooren
Dani M. Byrd
Brian R. Glasberg
Larry E. Humes
Vera A. Khokhlova
Christophe D. Micheyl
Anthony P. Nash
John C. Osler
Subramaniam D. Rajan
Richard M. Stern
Brad H. Story
Lily M. Wang

2007 Research Grant in Speech Science of the American Speech-Language-Hearing Foundation to Mary K. Fagan

Medwin Prize in Acoustical Oceanography to Mark V. Trevorrow

Distinguished Service Citation to Charles E. Schmid

R. Bruce Lindsay Award to Tyrone M. Porter

Helmholtz-Rayleigh Interdisciplinary Silver Medal to James V. Candy

Gold Medal to Patricia K. Kuhl

European Acoustics Association

Award for Lifetime Achievements in Acoustics to Gunnar Rasmussen

Award for Contributions to the Promotion of Acoustics in Europe to the Federation of Acoustical Societies of Europe (FASE) 1971–1996

Award for Outstanding Recent Scientific Results Published in *Acta Acustica united with Acustica* to Catherine Guastavino, Brian F. G. Katz, Jean-Dominique Polack, Daniel J. Levitin, and Danièle Dubois

Société Française d'Acoustique

The French Medal to Vitalyi Gusev

The Foreign Medal to Walter Lauriks

Session 3eID

Plenary Session

Introduced by Dick Botteldooren, Ghent University, Belgium

5:40

3eID1. Binaural Hearing and Systems for SOund Reproduction. Philip A. Nelson (ISVR, University of Southampton, Highfield, SO171BJ Southampton, UK, P.A.Nelson@aoton.ac.uk), M. Park (ISVR, University of Sothamton, Highfield, SO171BJ Southamption, UK, unknown@unknown.com), Takashi Takeuchi (OPSODIS Limited, c/o ISVR, University of Southamption, Highfield, SO17 1BJ Southampton, UK, ff1@isvr.soton.ac.uk)

Recent developments in models of binaural hearing can be usefully adapted and extedned to provide design tools for engineers engaged in the design of systems for sound reproduction. The particular focus of the work described is upon the development of models that give good statistical predictions of human sound localisation, based upon knowledge of the fluctuating acoustic pressures at the ears. Such models can be applied successfully to the prediction of stereophonic image localisation and reveal a number of important features of localisation relevant to audio system design. Developments will also be described in loudspeaker based systems for binaural reproduction that are finding their way into practical use. Binaural hearing models can be used to provide a preliminary evaluation of the performance of alternative designs. Finally, a brief review will be presented of multi-channel loudspeaker-based systems aimed at "full field" sound reproduction. Again, models of localisation provide some useful guidance for the designers of such systems.

Introduced by William M. Hartmann, Michigan State University, USA

6:10

3eID2. Optoacoustics: Can ultrasound become the preferred modality for molecular imaging? Matthew O'Donnell (University of Washington, 371 Loew Hall, Box 352180, Seattle, WA 98195-2180, USA, odonnel@engr.washington.edu)

Optoacoustics can be used to image the distribution of optical absorption in tissue, combining the specificity and sensitivity of optical imaging with the high resolution and penetration of ultrasound imaging. It represents one of the most promising techniques for molecular imaging because the optical absorption of bioconjugated nanoparticles can greatly exceed that of tissue over a range of wavelengths in which light can penetrate multiple centimeters into the body. We have explored several types of nanoparticles conjugated to a range of antibodies targeted to several important biological systems. Here we discuss two potential applications of bioconjugated gold nanorods, one for cancer cell targeting and the other to identify inflamed endothelial cells signaling the early stages of atherosclerosis. Optoacoustic images of cell cultures and animal models demonstrate the sensitivity and specificity of these nanosystems for molecular imaging. To translate these experimental findings into a clinically acceptable molecular imaging modality, we have also explored integrated optical systems able to deliver the optical pulse for optoacoustic excitation and detect the resultant ultrasonic waves using an all-optical transducer. The basic operating principles of this device, and the prospects for ultrasound-based molecular imaging using it, will be discussed.

ACOUSTICAL SOCIETY OF AMERICA GENERAL ASSEMBLY

Acoustical Oceanography Prize Lecture

James H. Miller, Chair
Univ. of Rhode Island, Dept. of Ocean Engineering, Narragansett, RI 02882

Chair's Introduction–5:40

5:45

The use of moored inverted echosounders for monitoring near-surface processes. Mark Trevorrow (Defence R&D Canada Atlantic, 9 Grove St., PO Box 1012, Dartmouth, NS B2Y 3Z7, Canada, mark.trevorrow@drdc-rddc.gc.ca)

The near-surface ocean is a difficult place to conduct measurements of physical and biological processes. High-frequency inverted echo-sounders (IES), moored a short distance below the surface, provide a simple means for sustained, high-resolution monitoring. In particular, long duration deployments are useful in capturing transient events, such as storms or solitary wave trains, and placing their occurrence within the context of longer term trends. Lessons learned from use of these moored IES systems can be applied to modern ocean observatories. A number of long duration deployments of a self-contained 200kHz IES were made in the late 1990's. Three specific examples will be discussed. Firstly, an investigation of calibrated volume scattering from near-surface bubbles in the NE Pacific Ocean showed the frequent occurrence of vertical, plume-like structures drawn downwards up to 25 m. Within the plumes, the backscatter cross-section exhibited an exponential decay with depth, with e-folding scale in the range 0.5 to 2.5 m. Secondly, imaging of near-surface internal solitary waves was performed from a mooring near the Oregon coast, supplementing measurements made with nearby temperature sensors. These measurements showed some suggestion of scattering by turbulence. Thirdly, through the use of both backscatter intensity and echo statistics, a moored IES demonstrated quantitative monitoring of migratory zooplankton and fish populations.

Celebration of the 60th Anniversary of the French Acoustical Society

On June 25, 1948, the so-called "Groupement des Acousticiens de Langue Française" (GALF) was created, with its first President, Yves Rocard, and was transformed into the "Société Française d'Acoustique" (SFA) in 1986. SFA now has 830 members and is composed of 8 technical groups and 3 regional sections. It is one of the founding members of the European Acoustics Association (EAA).

The 60th anniversary will be focused on the presentation of the "White Book" of Acoustics in France, and the publishing of a DVD including the main part of the French journals in Acoustics since 1934.

Agenda

Opening by the current President of SFA and a former President (René-Guy Busnel)

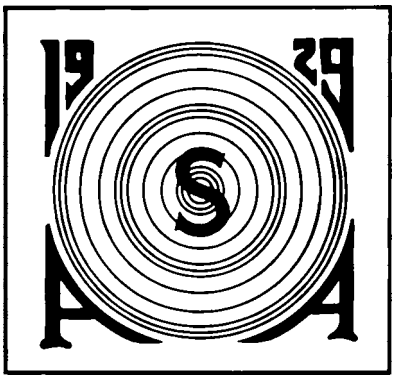
Acoustical French journals since 1934: Presentation of the DVD

The White Book of Acoustics in France in 2008

White Book: An example of the position of acoustics in an activity sector: The automotive industry

60 years of acoustics in France: An overview

ACOUSTICAL SOCIETY OF AMERICA
DISTINGUISHED SERVICE CITATION



Charles E. Schmid

2008

The Distinguished Service Citation is awarded to a present or former member of the Society in recognition of outstanding service to the Society.

PREVIOUS RECIPIENTS

Laurence Batchelder	1972	Frederick E. White	1987
Robert W. Young	1973	Daniel W. Martin	1989
Betty H. Goodfriend	1973	Murray Strasberg	1990
Gerald J. Franz	1974	William J. Cavanaugh	1994
Robert T. Beyer	1978	John C. Burgess	1996
Henning E. von Gierke	1978	Alice H. Suter	1997
R. Bruce Lindsay	1981	Elaine Moran	1999
William S. Cramer	1984	John V. Bouyoucos	2000
Stanley L. Ehrlich	1986	F. Avril Brenig	2000
Samuel F. Lybarger	1986	Thomas D. Rossing	2006



CITATION FOR CHARLES E. SCHMID

. . . for contributions as Executive Director of the Acoustical Society of America

PARIS, FRANCE • 2 JULY 2008

Charles Ernest Schmid grew up in East Williston, New York, about a 15-minute drive from the ASA's current headquarters in Melville. His father was an electrical engineer who ran the Shield Electric Company, which was founded by Charles's grandfather in 1909. They developed a process called thermo-welding for third rails for the Long Island Railroad and the New York City subway system. Charles's mother was a social worker who volunteered for the Red Cross. Long before the term "family values" became a cliché, Charles's parents were the genuine article, and they imparted those values to their children. His dad was a hard worker but tenderhearted and sometimes took in friends or relatives who were down on their luck. His mother was the practical one—very smart with a quick wit. Charles had one sibling, a younger sister Susan. There was much laughter in the Schmid household, and they had close and friendly relations with their neighbors and relatives. Summers were spent at their cottage on Fire Island, NY. There, Charles and Susan were free to roam—swimming, fishing, and clamming with their cousins and friends. It was an idyllic childhood for Charles, and that warmth and sense of optimism has carried over to his adult life.

At school Charles showed an early interest in mathematics, science, and history. Charles's great grandfather had emigrated from Ulm, Germany, "the city of artists and engineers," and that tradition apparently trickled down to Charles, who received a bachelor's degree in electrical engineering from Cornell University in 1963. Rowing was a big part of his undergraduate years. He still keeps in touch with fellow oarsmen, and can sometimes be found during lunch break taking a row in Eagle Harbor. Charles was also known on the Cornell campus for his 1929 Model-A Ford. It had a manifold heater and no defroster (you put your hand on the window to melt the ice) and a tendency to break down. It was truly an adventure to head off from Cornell in upstate New York to Long Island, especially during the winter.

After graduation from Cornell Charles moved to the seaside village of Stonington, Connecticut and went to work for Electric Boat designing sonar systems, where he participated in many submarine sea trials in the Atlantic and the Pacific. He also began working on his masters degree at the University of Connecticut and took courses in creative writing on the side. It was during this period that he met his wife Linda. Linda says that not only was he tall and nice looking, but by now he had ditched the old Model A and drove a red sports car!

Captivated by the natural beauty of the Pacific Northwest while on a sea trial there, Charles moved to Seattle in 1966 to work at Honeywell Marine Systems. He immediately joined the Seattle Mountaineers and learned glacier and rock climbing techniques, eventually leading seven climbs to the summit of Mt. Rainier, over 14,000 ft. This was one of the most productive times of Charles's life, working at Honeywell, helping to raise two children (Andrew and Jenny), and pursuing a PhD at the University of Washington. His dissertation was on computer recognition of musical instruments. When Charles finds any free time at an ASA meeting, he can often be found in a Musical Acoustics session.

Apparently the childhood memories of Fire Island remained with Charles because he and Linda found a place on Bainbridge Island, where they bought an old house that introduced Charles to the gentle arts of plumbing, wiring, and drywall hanging. On Bainbridge Island, Charles began community activities; he helped spearhead incorporation for Bainbridge Island and organized their new all-island government. (If you want to start a spirited conversation, just ask Charles what is happening in local politics on Bainbridge Island.)

In 1985, Charles took his interest in politics to Washington, DC as one of the first ASA Congressional Science and Engineering Fellows. The year in Washington, DC was a seminal one for Charles as he learned a new set of skills in his work to increase communications between scientists and Congress. A few years later, when the ASA announced an opening for its first Executive Director, Charles was an enthusiastic applicant. He assumed the position in 1990 and has held it ever since. Fortunately, Charles brought to the job of Executive Director qualities and skills he learned from his parents and

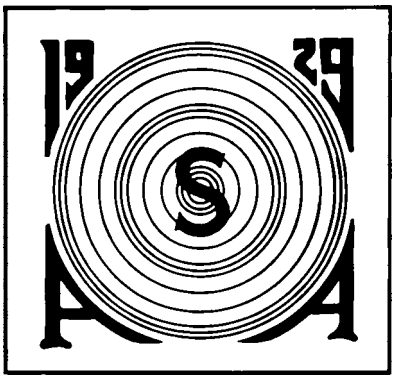
developed over a lifetime: love of family, leadership, imagination, problem solving, abundant energy, persistence and patience, a good memory and sense of history, and a tolerance for diverse viewpoints. The ASA Executive Director must ensure that the Society not only survives, but flourishes. Directing an organization that depends so much on an ever-changing cadre of volunteers requires diplomacy of a high order. Charles has thrived in this environment as few others could, and the Society has thrived as well.

Charles has made many contributions to our Society, and to acoustics. He has been a member of the Governing Board of the American Institute of Physics (AIP) since 1990, and was elected to its Executive Committee for five separate terms. Anyone who has attended a meeting of the AIP Board will quickly recognize the high regard with which he is held by his AIP peers. He is also a member of the International Commission for Acoustics and regularly attends meetings of other national and regional acoustical societies. Charles played an indispensable role in leading the Society to reach out beyond its geographical borders. In 1998, he helped organize a joint meeting of the ASA and the International Congress on Acoustics, followed by a meeting with the European Acoustics Association in Berlin in 1999, a joint meeting with the Mexican Institute of Acoustics and Federation of Iberoamerican Acoustics held in Cancun, Mexico in 2002, and in 1996 and 2006 the third and fourth joint meetings with the Acoustical Society of Japan in Hawaii. It is appropriate that Charles should be recognized for his service to acoustics worldwide at another international conference, Acoustics'08 in Paris.

LAWRENCE A. CRUM
WILLIAM M. HARTMANN
PATRICIA K. KUHL

ACOUSTICAL SOCIETY OF AMERICA

R. BRUCE LINDSAY AWARD



Tyrone M. Porter

2008

The R. Bruce Lindsay Award (formerly the Biennial Award) is presented in the Spring to a member of the Society who is under 35 years of age on 1 January of the year of the Award and who, during a period of two or more years immediately preceding the award, has been active in the affairs of the Society and has contributed substantially, through published papers, to the advancement of theoretical or applied acoustics, or both. The award was presented biennially until 1986. It is now an annual award.

PREVIOUS RECIPIENTS

Richard H. Bolt	1942	Ilene J. Busch-Vishniac	1987
Leo L. Beranek	1944	Gilles A. Daigle	1988
Vincent Salmon	1946	Mark F. Hamilton	1989
Isadore Rudnick	1948	Thomas J. Hofler	1990
J. C. R. Licklider	1950	Yves H. Berthelot	1991
Osman K. Mawardi	1952	Joseph M. Cuschieri	1991
Uno Ingard	1954	Anthony A. Atchley	1992
Ernest Yeager	1956	Michael D. Collins	1993
Ira J. Hirsh	1956	Robert P. Carlyon	1994
Bruce P. Bogert	1958	Beverly A. Wright	1995
Ira Dyer	1960	Victor W. Sparrow	1996
Alan Powell	1962	D. Keith Wilson	1997
Tony F. W. Embleton	1964	Robert L. Clark	1998
David M. Green	1966	Paul E. Barbone	1999
Emmanuel P. Papadakis	1968	Robin O. Cleveland	2000
Logan E. Hargrove	1970	Andrew J. Oxenham	2001
Robert D. Finch	1972	James J. Finneran	2002
Lawrence R. Rabiner	1974	Thomas J. Royston	2002
Robert E. Apfel	1976	Dani Byrd	2003
Henry E. Bass	1978	Michael R. Bailey	2004
Peter H. Rogers	1980	Lily M. Wang	2005
Ralph N. Baer	1982	Purnima Ratilal	2006
Peter N. Mikhalevsky	1984	Dorian S. Houser	2007
William E. Cooper	1986		



CITATION FOR TYRONE M. PORTER

. . . for contributions to ultrasound-guided drug delivery

PARIS, FRANCE • 2 JULY 2008

Tyrone Michael Porter was born in Detroit, Michigan on July 21, 1973. His parents, Dr. Elijah and Laverne Porter were teachers in the Detroit public school system. Elijah taught high school math early in his career and later served as Principal of Henry Ford High School and Laverne taught third through fifth grade at Vetal Elementary until their retirement a few years ago. Elijah and Laverne were strict disciplinarians and kept a close watch on Tyrone and his friends when they were teenagers. What Tyrone initially interpreted as an infringement of freedom was soon seen as a concern for his welfare, and he attributes much of his success in life to the important values he learned from his parents. Tyrone is a middle child with an older brother, Elijah Porter, II, and a younger sister, Dr. Dawne Jones. This birth order served as the quintessential training for Tyrone as a lively listener, a tolerant team-builder and a patient peacemaker. He continues to enjoy his role as proud uncle of five nephews and nieces. Tyrone is newly married to Dr. Monica Hall-Porter, and they reside in Roxbury, MA. Tyrone attended Renaissance High School in Detroit and graduated in 1991. While attending high school, Tyrone participated in the Detroit Area Pre-College Engineering Program, which served as a platform for pursuing a degree in engineering.

He left Michigan to attend Prairie View A&M University, a historically Black university in southeast Texas. While earning a Bachelor of Science degree in Electrical Engineering (Magna Cum Laude), Tyrone participated in several organizations, including the National Society of Black Engineers (NSBE) and Alpha Phi Alpha Fraternity. He was later named 2002 Graduate Student of the Year by NSBE, and now directs their Bioengineering Special Interest Group. At the NSBE 2007 national convention in Columbus, Ohio, he organized a special session entitled, Sound Therapy: Innovation in Biomedical Acoustics. As an undergraduate, Tyrone also co-founded Peers Advising, Counseling, and Teaching (PACT) to motivate high school students to strive for academic excellence and attend college. In 1996 he was featured in *USA Today* as one of the nation's top undergraduate engineering students, and was awarded a position on the Collegiate All Academic Team.

Tyrone was encouraged to pursue a doctoral degree in engineering and a career in higher education. He attended graduate school at the University of Washington (UW), where he was awarded the Doctor of Philosophy in Bioengineering in 2003. Tyrone came cheap as a graduate student, arriving at UW with a National Science Foundation Fellowship, and when that ran out, a fellowship sponsored by the United Negro College Fund (UNCF) and Merck. Tyrone was so well known at the UW that the three recommendation letters for the UNCF/Merck award came from his thesis advisor, and the Provost and the President of the University of Washington. As a graduate student, Tyrone co-founded the Minority Think Tank, a social-activist group created to discuss and develop solutions to common problems among underrepresented groups. During his graduate days, Tyrone was always organizing things from trips to Whistler for skiing to faculty-student softball games. As an outspoken proponent of social justice, he soon gained the attention of local politicians, and was regularly on the evening news and in the local paper with an articulate defense of affirmative action or equal opportunity.

For his dissertation, Tyrone helped to develop a new class of "smart" polymeric carriers that could destabilize biological membranes to enhance DNA or protein drug delivery. Tyrone worked on the novel idea that the synergistic effects of ultrasound and these polymeric carriers might be used to enhance their biofunctionality by triggering membrane destabilization. In this way, drug delivery might be stimulated with an on/off type of switch by application of an acoustic stimulus. This project embodied the spirit of interdisciplinary study and collaborative research that is the cornerstone of biomedical engineering. To be successful, he had to learn the fundamental concepts of acoustics, polymer chemistry, biochemistry and biology. Tyrone was so well known as a graduate student at the University of Washington that he was asked to serve on the Search Committee for a new President...a committee that included the founder of Costco Wholesale Corporation, the CEO of Recreational Equipment, Inc. (REI), and the CEO of Delta

Airlines. When he defended his dissertation, a lecture theater for over 200 people was reserved and it was nearly filled to capacity, including three Deans and a Vice Provost in attendance.

Tyrone was awarded the ASA's Frederick V. Hunt Postdoctoral Research Fellowship in Acoustics in 2003-04, which he chose to undertake at the University of Cincinnati. He worked with scientists in biomedical engineering, cardiology, biochemistry, and immunology to characterize the acoustic properties of echogenic liposomes, submicron-sized phospholipid vesicles that contain both gas and fluid. With antibody conjugation and drug incorporation, these liposomes can be used as novel targeted diagnostic and therapeutic ultrasound contrast agents. In addition to his scientific expertise, his sports acumen was legendary, and often led to rather heated and highly opinionated discussions on the merits of the Detroit Pistons versus anyone else. A detailed plan for the rehabilitation of the Cincinnati Bengals as a professional football team also resulted from these talks with his fellow researchers, as did some suggestions regarding recruitment ideas for the Reds.

At Boston University (BU), where he serves as a member of both the Department of Aerospace and Mechanical Engineering and the Department of Biomedical Engineering, Tyrone is crafting a world-class research program combining basic principles in chemistry, acoustics, and thermodynamics to develop novel drug delivery strategies for cancer therapy. He maintains research laboratories in both Departments and is forging true interdisciplinary collaborations involving team members with diverse interests and expertise. His research is currently focused on the development of targeted ultrasound contrast agents for image enhancement (molecular imaging), perfusion imaging, and image-guided drug delivery. Ultrasound-enhanced transport of drugs and genes across cell membranes and ultrasound-enhanced drug activity play an important role in this research.

At BU, Tyrone has been tasked with teaching the introductory dynamics course, which is a key college-wide curricular requirement populated by sizeable classes and students with diverse backgrounds. In this significant effort, Tyrone has acquitted himself extremely well, garnishing some of the finest teaching evaluations ever bestowed upon a freshman professor in the AME Department. Tyrone is destined to be a pedagogical star in a department populated with some of the best teachers in the BU College of Engineering. He is committed to the highest quality of education of students. His impeccable integrity and an infectious enthusiasm entice students to flock to him. Tyrone has the heart and heritage of an educator, and he will have a huge impact on younger people.

Tyrone has also been very active in the affairs of the ASA, having served on the Student Council, as a member of the organizing committee for the joint ASA/ICA meeting in Seattle in 1998, as one of the nine special presenters at ASA's 75th anniversary celebration, and as an organizer of several special sessions for the Technical Committee on Biomedical Ultrasound/Bioresponse to Vibration, of which he is also a member.

Tyrone Porter's parents, siblings, aunts and uncles, and a host of friends and colleagues are very proud of Tyrone's accomplishments and look forward to the exciting career that lies before him.

CHRISTY K. HOLLAND
RONALD A. ROY
LAWRENCE A. CRUM

ACOUSTICAL SOCIETY OF AMERICA

Helmholtz-Rayleigh Interdisciplinary Silver Medal in Signal Processing in Acoustics and Underwater Acoustics



James V. Candy

2008

The Silver Medal is presented to individuals, without age limitation, for contributions to the advancement of science, engineering, or human welfare through the application of acoustic principles, or through research accomplishment in acoustics.



CITATION FOR JAMES V. CANDY

. . . for contributions to signal processing and underwater acoustics

PARIS, FRANCE • 2 JULY 2008

We have all heard the saying "Them that can, do; them that can't, teach." We also know that one exception disproves the theory. In the case of Jim Candy, we have that exception. He is a born teacher with a highly creative mind. When one first meets him, he comes across as a rather unassuming person. But once he becomes interested in a problem, he dives into it with a tenacious passion until he solves it. The teacher in him comes through by his ability to use simple analogies drawn from his wealth of knowledge and ideas. His intuitive creativity is displayed in clever innovative solutions to complex problems.

Many of his creative solutions are based on his background in control theory and recursive estimation theory. When he joined the staff of the Lawrence Livermore National Laboratory, Dr. Candy quickly found himself dealing with problems in electromagnetics, lasers, nuclear physics, internal waves, nuclear fusion, ultrasonics, array processing and inverse problems in general. It was not long before he gained the reputation as the "go to" guy when there was a need for a new approach in modeling, classification, estimation and detection, regardless of the subject. And anyone who deals with him on a collaborative basis walks away all the richer for it.

James Vincent Candy was born in Astoria, New York, on January 21, 1944. He received a B.S. in Electrical Engineering from the University of Cincinnati in 1966, an M.S.E. in Electrical Engineering from the University of Florida in 1972, and a Ph.D. in Electrical Engineering in 1976, also from the University of Florida. During the period, from 1967 to 1971, he served as a Captain in the United States Air Force and from 1966 to 1967, he worked as an Engineer for the General Electric Company. In 1976, Dr. Candy began his employment with the University of California, Lawrence Livermore National Laboratory (LLNL) as a scientist for the Engineering Directorate. At present, he is Chief Scientist for the Engineering Directorate and an Adjunct Professor at the University of California, Santa Barbara.

He began working in the field of oceanic signal processing during a short-term assignment at the NATO SACLANT ASW Research Center in 1987. Since that time, he has developed the "Model-Based" approach to oceanic signal processing. This has produced a wealth of applications in underwater acoustic signal processing to localization, tracking, signal enhancement, sound-speed inversion, noise cancellation, sequential detection and internal wave signal processing. His work led to the Bayesian solution for dispersive wave propagation, most notably as applied to internal waves in imaging and detection applications.

This model-based approach to signal processing evolved from Jim's intimate knowledge of Bayesian statistics and the Kalman filter. This type of processor has been used in the area of optimum control for many years, but it was not until he pointed out that in principle, there is really no limit to the sophistication of the physical models one can use in these processors, that it was recognized that they had great value in areas outside of control theory. This insight has laid the framework for a general scheme for including a priori information, in the form of physical models, into basically any processing scheme. This provides a self-consistent Bayesian structure, that avoids many of the difficulties associated with the use of physical models, including the so-called "mismatch problem," that arises when the physical parameters are not well known. Dr. Candy has closely followed, applied and contributed to advances made in recent years in this field, including the Unscented Kalman Filter and the particle filter, which avoid some of the limitations of the original Kalman filter, such as its inability to handle the cases of nonlinearity and non-Gaussian statistics.

Jim is a former Director of the LLNL Center for Advanced Signal and Image Sciences. He has been an Adjunct Professor at San Francisco State University, University of Santa Clara, and the University of California, Berkeley Extension, teaching graduate courses in signal and image processing. He is a Fellow of the Acoustical Society of America (ASA), the Institute of Electrical and Electronics Engineers (IEEE), and was recently elected as a Life Member (Fellow) of Clare Hall College at the University of Cambridge in the UK.

He received the IEEE Distinguished Technical Achievement Award in 2002 for contributions of signal processing to oceanic engineering. Along with his many other publications, he has produced three texts: *Signal Processing: The Model-Based Approach, Signal Processing: The Modern Approach, and Model-Based Signal Processing and Bayesian Signal Processing: Classical, Modern and Particle Filtering Methods* (in press). He has conducted many short courses and tutorials on applied signal processing at meetings of the Acoustical Society of America and the Oceanic Engineering Society. He has also presented short courses in Applied Model-Based Signal Processing for the SPIE Optical Society. He is currently the Chair of the IEEE Technical Committee on Sonar Signal and Image Processing and was the Chair of the ASA Technical Committee on Signal Processing in Acoustics as well as an Associate Editor for Signal Processing for *JASA Express Letters* (JASA EL).

In addition to his technical accomplishments, Dr. Candy has been a mentor to many junior colleagues. His enthusiasm for signal processing in the ASA was contagious as he worked to bring the Signal Processing Committee into existence starting from an interdisciplinary technical group. He was its first Chair. He has also persuaded colleagues to become active members of the ASA and almost all of the active Society members from the Lawrence Livermore National Laboratory began their involvement through Jim's encouragement. His commitment and enthusiasm for acoustical signal processing is evidenced by the visibility of our Society at the Lawrence Livermore National Laboratory.

EDMUND J. SULLIVAN
WILLIAM M. CAREY

GOLD MEDAL
of the
Acoustical Society of America



Patricia K. Kuhl

2008

The Gold Medal is presented in the spring to a member of the Society, without age limitation, for contributions to acoustics. The first Gold Medal was presented in 1954 on the occasion of the Society's Twenty-Fifth Anniversary Celebration and biennially until 1981. It is now an annual award.

PREVIOUS RECIPIENTS

Wallace Waterfall	1954	Richard K. Cook	1988
Floyd A. Firestone	1955	Lothar W. Cremer	1989
Harvey Fletcher	1957	Eugen J. Skudrzyk	1990
Edward C. Wente	1959	Manfred R. Schroeder	1991
Georg von Békésy	1961	Ira J. Hirsh	1992
R. Bruce Lindsay	1963	David T. Blackstock	1993
Hallowell Davis	1965	David M. Green	1994
Vern O. Knudsen	1967	Kenneth N. Stevens	1995
Frederick V. Hunt	1969	Ira Dyer	1996
Warren P. Mason	1971	K. Uno Ingard	1997
Philip M. Morse	1973	Floyd Dunn	1998
Leo L. Beranek	1975	Henning E. von Gierke	1999
Raymond W. B. Stephens	1977	Murray Strasberg	2000
Richard H. Bolt	1979	Herman Medwin	2001
Harry F. Olson	1981	Robert E. Apfel	2002
Isadore Rudnick	1982	Tony F. W. Embleton	2002
Martin Greenspan	1983	Richard H. Lyon	2003
Robert T. Beyer	1984	Chester M. McKinney	2004
Laurence Batchelder	1985	Allan D. Pierce	2005
James L. Flanagan	1986	James E. West	2006
Cyril M. Harris	1987	Katherine S. Harris	2007
Arthur H. Benade	1988		



CITATION FOR PATRICIA K. KUHL

. . . for contributions to understanding how children acquire spoken language and for leadership in the Society.

PARIS, FRANCE • 2 JULY 2008

Patricia Katherine Kuhl was born and raised in St. Cloud, Minnesota, the second of five children of Joseph and Susan Kuhl. In high school, Pat was involved in many school activities, including the debate club, the honor society, and the basketball team. She was especially interested in music, showing great enthusiasm and talent for voice and piano. Luckily for the field of speech communication, Pat's parents stressed talking in addition to music. Every night before dinner in the Kuhl household, Pat's father unplugged the telephone so that the family could discuss the day's activities, the national political scene, and world affairs. Pat's father always read the newspaper before dinner, and expected the children to as well, so Pat read the papers before her father arrived home. Pat was always ready to debate her dad about anything and everything. For those of you who know Pat, she loves a lively discussion and is always prepared with facts as well as opinions.

Pat is married to Andrew Meltzoff, who along with Pat, is co-Director of one of the more visible research groups at the University of Washington–The Institute for Learning and Brain Sciences. Pat is also the Co-Director of another high-profile interdisciplinary research group on campus, an NSF Science of Learning Center–LIFE–which links neuroscience to education. Pat and Andy have enjoyed a long and productive collaboration in developmental cognitive science. According to Andy, the "best collaboration of all" was one that resulted in their daughter Katherine, who combines Andy's love of swimming and Pat's love of music. Katherine is one of the stars on the swim team at Trinity College in Connecticut and also had the singular distinction of participating in the first test of the acoustics in Seattle's Benaroya Hall by singing while former ASA President Cyril Harris, acoustical engineer for the Hall, dashed around taking measurements.

Pat completed her BA, MA, and Ph.D. degrees in Minnesota at St. Cloud State University and the University of Minnesota. Pat's interest in the development of speech perception in children began with her postdoctoral years at the Central Institute for the Deaf with James D. Miller. Those years led to a series of papers that examined the responses of mammals and children to speech. She established commonalities between mammals and human infants in their response to speech sounds, and, importantly, where their patterns of responses to speech stimuli diverged.

In the early 1980's, Pat's interest expanded beyond the auditory perception of speech to include studies of how infants integrate auditory and visual information about speech, and to the imitation of speech. Especially impressive has been Pat's insights into the future of speech research: She has consistently published important papers that inspire new lines of research, from her animal studies in the 70's and 80's, to her auditory-visual and imitation work in the 80s, to her work on language experience and its effects on learning in the early 90's, and her most recent work which is forging new territory using the tools of modern neuroscience. She has most recently worked to develop baby Magnetoenchephalography (MEG). The technique is completely safe, non-invasive, and noiseless, and Pat and her team worked with engineers in Helsinki to develop ways to track an infant's head movements so the baby's brain activities can be precisely located in the infant brain as the child listens to language or music, and processes complex social information. Pat has a unique talent for spotting where the next interesting finding may lie, and an ability to put together the resources and interdisciplinary research teams needed to conduct work that few others would be able to accomplish. She has forged collaborations with speech scientists from Japan, Taiwan, Sweden, Russia, Finland, Spain, China, France, and Mexico to study how language experience affects speech processing in adults and young children. Pat's students also come from many different countries, and a tour through her Institute introduces a visitor to students from Taiwan, Japan, China, Mexico, and Finland. Once trained, many of these students return to their native countries to set up speech research laboratories of their own.

Pat's research has had theoretical as well as practical impact. If you have ever tried to learn a new language as an adult, you soon recognize that it is difficult to pronounce certain sounds, or even to hear the relevant differences, while your children seem to pick

up foreign languages easily and speak without an accent. Pat has performed pioneering research in this field and learned from her studies with babies as young as 6 months that infants are born "citizens of the world" with regard to language. They can distinguish sounds from languages around the world, even if they have never heard them before. By the end of the first year of life, however, they become "language-specialists"—the ability to attend to native-language sounds increases substantially while the ability with foreign languages diminishes. Pat proposed the Native Language Neural Commitment Theory to account for this dramatic developmental change. The model shows that infants use computational abilities to "crack" the speech code and, interestingly, that infants' social skills may "gate" learning. She and her students showed that infants learn phonemes and words rapidly from a live foreign-language tutor at 9 months of age but that the same foreign-language material presented from a TV or audio-tape produces no learning. The finding has theoretical implications as well as implications for education and society.

Pat's research in acoustics has led to a number of singular honors: for example, she is a member of the American Academy of Arts and Sciences, the Rodin Academy, and the Norwegian Academy of Science and Letters. She was awarded the Silver Medal of the Acoustical Society of America in 1997, and the Kenneth Craik Research Award from Cambridge University in 2005. She received the University of Washington's Faculty Lectureship Award in 1998, and in 2007, she was awarded the University of Minnesota's Outstanding Achievement Award. Pat is a Fellow of the American Association for the Advancement of Science, the Acoustical Society of America, and the American Psychological Society.

Pat has also been an eloquent spokesperson for childhood learning and was one of six scientists invited to the White House in 1997 to make a presentation at President and Mrs. Clinton's Conference on "Early Learning and the Brain." In 2001 she was invited to make a presentation at President and Mrs. Bush's White House Summit on "Early Cognitive Development: Ready to Read, Ready to Learn." In 1999, she co-authored *The Scientist in the Crib: Minds, Brains, and How Children Learn*.

Pat has played an active role in the affairs of the Society for a number of years. She has served as an Associate Editor of the *Journal*, as a member of the Executive Council, and as a member or chair of several committees. Pat was cochair of the joint 135th meeting of the Acoustical Society of America and the 16th International Congress on Acoustics in 1998 as well as coeditor of its proceedings. She was cochair of the ASA's 75th Anniversary Celebration Committee with Leo Beranek in 2004. As part of the celebration, Pat organized a series of presentations by nine young investigators entitled "A Celebratory Look into the Future." She was elected the Society's Vice President in 1996, and in 1999 was the first woman elected President of the ASA. While President, Pat created the Student Council, one of the most successful presidential initiatives, and one that has generated great enthusiasm among our younger members.

The Gold Medal winners of the ASA are indeed a select group; they have been outstanding innovators and leaders in science and engineering and they have brought great recognition to our Society. Patricia Kuhl now joins this elite group and elevates its stature even more.

FREDERICKA BELL-BERTI
YANG ZHANG
PAUL IVERSON

EAA AWARD 2008

For lifetime achievements in acoustics

Gunnar Rasmussen



For his outstanding contribution in the field of acoustic measurements and instrumentation

Gunnar Rasmussen is a pioneer in the construction of acoustic instrumentation, particularly of pressure transducers and related devices. He was employed at Brüel & Kjær Denmark as an electronics engineer immediately after his graduation in 1950. After holding various positions in development, testing and quality control, he spent one year in the United States working for Brüel & Kjær in sales and service. After his return to Denmark in the mid-1950's he began the development of a new measurement microphone. This involved the invention of new methods for manufacturing microphone diaphragms in electro-galvanic deposited nickel, to replace the very corrosive aluminium foil diaphragms in use at that time. Also the mechanical construction was drastically simplified from more than 30 different parts to less than 10 parts. This resulted in superior mechanical stability, increased temperature and long term stability. The resulting one-inch pressure microphone soon became the *de facto* standard microphone for acoustical measurements.

The optimized mechanical design of the new generation of measurement microphones opened up the possibility for reducing the size of the microphones, first to a 1/2" microphone and then to 1/4" and 1/8" microphones with essentially the same superior mechanical, temperature and long term stability. Notably the 1/2" microphone is still the most widely used noise abatement tool today. Since the beginning of the 1960's, this microphone design has been preferred for all types of acoustic measurements and has formed the basis for the IEC 1094 series of international standards for measurement microphones.

Gunnar Rasmussen received the Danish Design Award in 1969 for his novel design of the microphones which were exhibited at the New York Museum of Modern Art. He also developed the first acoustically optimized sound level meter, where the shape of the body was designed to minimize the effect of reflections from the casing to the microphone. This type 2203 sound level meter was for many years seen as the archetype of sound level meters and its characteristic shape became the symbol of a sound level meter. It was also awarded the Danish Design Award in 1965.

Other major inventions and designs include the Delta Shear accelerometer, the dual piston pistonphone calibrator for precision calibration, the face-to-face sound intensity probe and hydrophones, occluded ears, artificial mouth, etc. Gunnar Rasmussen is also the author of numerous papers on acoustics and vibration and has served as chairman and vice-chairman of various international organizations and standard committees. In 1990 he received the CETIM medal for his contributions to the field of intensity techniques. He is also a Fellow of the Acoustical Society of America.

In 1994 Gunnar Rasmussen started his own company, G.R.A.S. Sound and Vibration. Started as a company specializing in precision outdoor microphones for permanent noise monitoring around airports, it is now one of the world's leading companies in acoustic front-ends and transducers forming a wide range of general purpose and specialized microphones, electro-acoustic measurement devices such as ear couplers, precision calibration tools and multi-dimensional sound intensity probes. After many years of rich and fruitful work, Gunnar Rasmussen is still very active with the design of new transducers and solutions. At the same time he is an indispensable partner in discussions of measurement standards, where he provides valuable input and help for younger colleagues who admire his deep knowledge and experience and acknowledge his kindness and modest character.

EAA wishes to honour Gunnar Rasmussen for his tremendous impact on acoustics, for being an example for generations of scientists and engineers dealing with acoustic measurements, for the expertise he has given to us all.

EAA AWARD 2008

For contributions to the promotion of Acoustics in Europe

FASE Federation of Acoustical Societies of Europe 1971-1996

Federation of Acoustical Societies of Europe
Fédération Européenne des Sociétés d'Acoustique
Europäische Föderation der akustischen Gesellschaften
Федерация Акустических Обществ Европы

For the establishment, organization and support of new platforms of cooperation, partnership and friendship among European acousticians

Probably very few people in Europe know that on 9 May 1950 the first move was made toward establishing the European Union. On that day in Paris, against the background of the threat of a Third World War engulfing Europe as a whole, French Foreign Minister Robert Schuman read to the international press a declaration calling upon France, Germany and other European countries to pool together their coal and steel production as "the first concrete foundation of a European federation."

Probably very few acousticians in Europe know that on 26 August 1968 during the 6th International Congress on Acoustics in Tokyo, the first move was made towards the creation of the European Acoustics Association (EAA). On that day in Tokyo, on the initiative of Prof. G. Kurtze and Prof. E. Zwicker, a semi-official meeting of the delegates of the European acoustical societies was organized in order to discuss the possibilities of founding the Federation of Acoustical Societies of Europe.

It took three more years to consult with different societies and to establish the main purposes of the new "learned society." Finally on 24 August 1971 in Budapest, representatives of 13 acoustical societies declared the foundation of FASE, the Federation of Acoustical Societies of Europe, and a provisional steering committee was elected.

On 5 May 1972, the first meeting of the FASE Council took place in Paris with the election of officers: Prof. J. Frenkiel (President), Prof. W. Furrer (Vice-President), Dr. F. Kolmer (Secretary), as well as the approval of a program of activities concerning the coordination of scientific acoustical events, information on possibilities of vacancies in acoustical institutions in Europe (universities, research institutes, firms, etc.) and a survey on education in acoustics in Europe.

During the next 25 years more European acoustical societies, academies of sciences and associations joined FASE, 7 Congresses on Acoustics and 12 Symposia on specific acoustic topics and in different European cities were organized, 25 Council meetings were held and more officers and members of the council were involved in these activities.

On a voluntary basis FASE has contributed to establish and sustain the contact between scientists in acoustics in the former Eastern Block countries and in Western Europe during a historical period in which travel and exchange of information was difficult. FASE has established fruitful collaboration, representing Europe, with international societies such as ICA, ASA, EEAA, ESCA, CEC, and ICSU. In 1986 FASE contributed to the publication of the volume *Noise Pollution* of the SCOPE (Scientific Committee on Problems of the Environment, ICSU) through Prof. A. Lara-Sáenz in collaboration with Prof. R.W.B. Stephens who called together 23 specialists in acoustics. FASE has promoted international journals and has organized surveys on education in acoustics.

During the development of the European Union it became necessary to build an association like an image of nations represented by their national societies rather than a group of societies, associations and academies of sciences. Accordingly, on 1 January 1997, with a natural process, FASE was integrated into the European Acoustics Association (EAA) which formally took the inheritance of FASE's purposes and activities.

The Federation of Acoustical Societies of Europe was not only the first and successful attempt of harmonization among acoustical societies in Europe but it also represented a generation of European acousticians, their knowledge and their efforts.

The award will be presented to Prof. Paul Françoise, Prof. Felix Kolmer and Prof. Andrés Lara-Sáenz on behalf of FASE.

EAA AWARD 2008

For outstanding recent scientific results published in ACTA ACUSTICA UNITED WITH ACUSTICA

The award for outstanding recent research is given to a team of researchers for their contribution in the field of acoustics with the strict requirement that they published their results in the EAA scientific journal ACTA ACUSTICA UNITED WITH ACUSTICA within three years prior to the date that the award is given. In 2008 this EAA award goes to:

Catherine Guastavino, Brian F. G. Katz,
Jean-Dominique Polack, Daniel J. Levitin, Danièle Dubois

For their work on linguistic exploration of verbal data as a methodology for exploring the cognitive processing of environmental sounds, first published in:

Ecological Validity of Soundscape Reproduction
ACTA ACUSTICA UNITED WITH ACUSTICA Vol. 91 (2005) 333 – 341

"A fundamental aim of psychoacoustics is to better understand how acoustic phenomena are perceived and represented at a cognitive level by individuals. Mental representations of sounds cannot be observed directly, but one way to study these representations empirically is through language, specifically, by analyzing how people talk about their sensory experiences." With these opening sentences the authors immediately point to the new line of thinking in psychoacoustics that they propose. Their methodology for digging into the cognitive level seems able to capture both the effect of *source events* and of the effect of *background noise*. Perception of environmental sound based on cognitive processes grounded in source recognition, have been well understood and can be studied using various methods. In environments with multiple sources, the soundscape is processed as a whole since source identification is hindered. The methodology proposed by the authors also allows the investigation of the perception of this background noise. In this case, mental representations related to both physical properties of the acoustic signal and semantic features and psychological effects can be identified.

In the awarded paper the authors apply the proposed methodology to investigate the ecological validity of reproduction of environmental soundscapes. They observed that ecological validity is easily obtained for sound events but that reproducing the urban background noise required immersive multichannel reproduction. This confirms existing knowledge on the cognitive processing of environmental sound. In later publications cited below the team applies their new methodology for exploring the meaning of urban soundscapes for its users and thus proves wider applicability of their methodology.

The awarded team goes beyond the classical paths of psychoacoustics and proposes a methodology for exploring mental representations of environmental sound. The novelty and potential impact of this approach were main motivations for the jury to select this work for the 2008 award for outstanding scientific results published in ACTA ACUSTICA UNITED WITH ACUSTICA.

The full paper can be downloaded from ACTA ACUSTICA UNITED WITH ACUSTICA ONLINE at www.ingentaconnect.com/content/dav/aaua.

Further reading

Dubois, D., Guastavino, C., and Raimbault, M. (2006). "A cognitive approach to urban soundscapes: Using verbal data to access everyday life auditory categories," Acta Acustica United with Acustica 92, 865–874.

Guastavino, C., (2006) "The Ideal Urban Soundscape: Investigating the Sound Quality of French Cities," Acta Acustica United with Acustica, 92, 945–951.

FOREIGN MEDAL 2007
of the
French Acoustical Society



Walter LAURIKS

The Foreign Medal is annually presented to a renowned scientist having strong relations with French acousticians

PREVIOUS RECIPIENTS

1966	BERANEK (USA)
1967	L. PIMONOW (Poland)
1968	SACERDOTE (Italy)
1969	FRENKIEL (Belgium)
1970	MALECKI (Poland)
1971	TARNOCZY (Hongrie) et KOBRYNSKI (Poland)
1972	FURRER (Switzerland)
1973	STEPHENS (United Kingdom)
1974	GRUTZMACHER (German)
1975	RYFFERT (Poland)
1976	LARA-SAENZ (Spain)
1977	BOSQUET (Belgium)
1978	A.STAN (Romania)
1979	TARABA (Czechoslovakia)
1980	WANG TE CHAO (China)
1981	INGERSLEV (Denmark)
1982	KURTOVIC (Yugoslavia)
1983	CREMER (Germany)
1984	LAUBER (Switzerland)
1985	DOAK (United Kingdom)

1986	MYNCKE (Belgium)
1987	KUTRUFF (Germany)
1988	W.G. MAYER (USA)
1989	J.E. FFOWCS WILLIAMS (United Kingdom)
1990	J. BLAUERT (Germany)
1991	G. WEINREICH (USA)
1992	O. B.WILSON (USA)
1993	Z. SKVOR (Czech Republic)
1994	F. FAHY (United Kingdom)
1995	L. BJØRNØ (Denmark)
1996	H. UBERALL (USA)
1997	HIRSCHBERG (The Netherlands)
1998	H. LEVINE (USA)
1999	W. LAUTERBORN (Germany)
2000	M. CAMPBELL (United Kingdom)
2001	O. LEROY (Belgium)
2002	G. DAIGLE (Canada)
2003	M. ROSSI (Switzerland)
2004	J. WOLFE (Australia)
2005	V. PREOBRAJENSKI (Russia)
2006	M. LOWE and P. CAWLEY (United Kingdom)



Walter Lauriks (born in 1961 in Reet – Belgium, married, 3 children) obtained a Master in Physics in 1983 and his Ph.D. in Physics in 1990, both at the University of Leuven (Belgium). Since then he worked as a research fellow at the Laboratory of Acoustics and Thermal Physics of the Department of Physics of the University of Leuven (K.U.Leuven), his main research area being sound propagation in elastic porous materials (also the subject of his Ph.D. thesis). He was responsible for multiple research projects in acoustics (among others for the Scientific Research Fund Flanders).

In 2005, Walter Lauriks became full professor and director of the Laboratory of Acoustics and Thermal Physics of the K.U.Leuven. At present, he is responsible for teaching different courses at the Faculty of Science and the Faculty of Engineering of the university: "Electricity and Magnetism", "Optics, Lasers and Acoustics" and "Physical Acoustics".
Until now, he supervised 13 PhD theses (as advisor or promotor) and he was 37 times Jury member of Ph.D. committees, both national and international.

Walter Lauriks has developed a close and fruitful collaboration with the Laboratoire d'Acoustique de l'Université du Maine (UMR CNRS 6613, Le Mans, France) for more than twenty years and more recently with the LMA (Marseille, France) mainly in the domain of acoustics of air saturated porous media. He pioneered research in this field. The results of these works have many implications, ranging from fundamental studies to Applied Architectural Acoustics and the metrology of sound absorbing porous media.

Walter Lauriks is main author or co-author of more than 100 publications in international peer-reviewed journals and more than 110 conference proceedings for international conferences. At different occasions, he was session organiser and/or session chairman at these conferences. He also contributed to 7 book chapters.

Since 1997, Walter Lauriks is Associate Editor Physical Acoustics "Acustica united with Acta Acustica". He is member of several scientific organisations: Société Française d'Acoustique, Acoustical Society of America, Association Belge des Acousticiens (board member), Netherlands Akoestisch Genootschap (Dutch Acoustical Society NAG, board member), IEEE, The American Association of Physics Teachers.

FRENCH MEDAL 2007
of the
French Acoustical Society



Vitalyi GUSEV

2007

The French Medal is annually presented to a French scientist, who has contributed significantly to the reputation of French acoustics.

PREVIOUS RECIPIENTS

1966	CANAC and P. CHAVASSE
1967	A. BARON
1968	R. LUCAS
1969	J. BRILLOUIN
1970	P. LIENARD
1972	R-G. BUSNEL
1973	T. VOGEL
1974	J-J. MATRAS
1975	R. CHOCHOLLE
1976	J. PUJOLLE
1977	R. SIESTRUNK
1978	E. LEIPP
1979	P. RAPIN
1980	M. BURGEAT
1981	A. DIDIER
1982	A. BERGASSOLI
1983	G. COMTE-BELLOT
1984	J. MATTEI (refused)
1985	R. LEHMANN
1986	P. LORAND

1987	P. FRANCOIS
1988	E. DIEULESAINT
1989	B. POIREE
1990	R. CARRE
1991	C. GAZANHES
1992	J-F. ALLARD
1993	M-C. BOTTE
1994	J-P. HATON
1995	J. RIPOCHE
1996	A.M. BRUNEAU
1997	J. POULIQUEN
1998	D. ROYER
1999	P. FILLIPI
2000	A. DANCER
2001	G. CANEVET
2002	P. GATIGNOL
2003	M. FINK
2004	M. BRUNEAU
2005	C. LESUEUR
2006	D. CATHIGNOL



Professor Vitalyi GUSEV received degrees of PhD (1982) and Dr. Sc. (1991) in Physics and Mathematics from Moscow State University (Russia). After several years of being researcher and assistant professor at the same university, he joined in 1990 the International Laser Centre at Moscow State University where he was associated professor. In 1998, he joined University of Maine in Le Mans (France) where he became professor in a national engineering school (ENSIM). He is now full professor of University of Maine at the highest grade and he is since 2006 the Senior member of the "Institut Universitaire de France" (Institute of French Universities) because of his outstanding research achievements.

Pr. Gusev is the recipient of several awards, including the Lenin Comsomol Prize in Science and Technology (1987, Russia), the distinction of the International Science Foundation (1994), Senior Prize of International Photoacoustic and Photothermal Association" (2004).

He was invited in several universities (Sapporo, Japan - Heidelberg, Germany - Brown, USA - Toronto Canada - Leuven, Belgium - Paris, France) as fellow, visiting scientist, visiting professor, etc. He gave more than 50 lectures and seminars as an invited speaker. He is member of international scientific committees, among them: International Congress on Ultrasonics, International Conference on the Emerging Technologies in Quantitative Nondestructive Testing, International Conference on Photoacoustic and Photothermal Phenomena...

He is the author of more than 400 scientific publications, among them more than 180 are in international scientific journals or are book chapters. He also published a book "Laser Optoacoustics" with A. Karabutov (translated from Russian into English in 1993 by the American Institute of Physics, New York, USA).

His fields of research can be summarised mainly as: photothermal and photoacoustic phenomena, picosecond ultrasonics, nonlinear acoustics, acoustics of micro-inhomogeneous media, thermoacoustics. He has made deep and original contributions in all of his fields of interest and even he had a pioneering role in tackling theoretically several challenging

Session 4aAAa

Architectural Acoustics: Architectural Acoustics Potpourri

David T. Bradley, Cochair
124 Raymond Avenue, Poughkeepsie, NY, 12604

Andrea Farnetani, Cochair
Engineering Dept. - Univ. of Ferrara, Via Saragat, 1, Ferrara, 44100, Italy

Contributed Papers

8:00

4aAAa1. Irregular sound absorbers work better. Bernard Sapoval (Ecole Polytechnique, PMC-Polytechnique Route de Saclay, 91128 Palaiseau, France, bernard.sapoval@polytechnique.edu), Anna Rozanova-Pierrat (Ecole Polytechnique, PMC-Polytechnique Route de Saclay, 91128 Palaiseau, France, anna.rozanova-pierrat@polytechnique.edu), Simon Félix (Laboratoire d'Acoustique de l'Université du Maine, Avenue Olivier Messiaen, 72085 Le Mans, France, simon.felix@univ-lemans.fr), Marcel Filoche (Ecole Polytechnique, PMC-Polytechnique Route de Saclay, 91128 Palaiseau, France, marcel.filoche@polytechnique.edu)

The diffraction and absorption of waves by a system with both absorbing properties and irregular geometry is an open physical problem. In the same time, irregular absorbers have been shown to be extremely efficient (1). A more reachable and closely related goal is the understanding of wave oscillations in confined systems containing an absorbing material with an irregular shape. From the theoretical point of view, the difficulty lies in the fact that part of the propagation occurs in a lossy material for which the wave operator is non-hermitian. It is found here that, in resonators containing an irregular shaped absorbent material, there appears a new type of localization. This phenomemon, that we call ''astride'' localization, describes the fact that these modes exist in both the lossless and the lossy regions. They are then both lossy and well coupled to sources in the air. A numerical computation of the time decay of acoustic energy shows that indeed sound absorbing devices work better when presenting a very irregular shape and that this is directly linked due to the existence of astride localisation. (1) Fractal Wall, product of Colas Inc., French patent N0-203404; U.S. patent 10/508,119.

8:20

4aAAa2. A brief review on micro-perforated sound absorbers. Christian Nocke (Akustikbüro Oldenburg, Katharinenstr. 10, 26121 Oldenburg, Germany, nocke@akustikbuero-oldenburg.de), Catja Hilge (Akustikbüro Oldenburg, Katharinenstr. 10, 26121 Oldenburg, Germany, hilge@akustikbuero-oldenburg.de), Jean-Marc Scherrer (Normalu S.A.S, Route du Sipes, 68680 Kembs, France, jmscherrer@barrisol.com)

The theory and design of microperforated panel sound-absorbing constructions have been introduced by D.-Y. Maa in 1975. Since then many variations of micro-perforated sound absorbing devices and materials have been introduced. Materials that have been used to be micro-perforated have been metal, wood, plastics and many others. A survey of different applications of micro-perforation will be presented. Examples shown in more detail are the development of stretched foils and metal as micro-perforated panels. Results of sound absorption measurements of various assemblies for normal and statistical incidence of sound will be shown and compared with theoretical predictions. Finally the potential of the micro-perforated sound absorber will be discussed.

8:40

4aAAa3. The vibration sound absorption theory of soft materials. Xin An Zhang (Xi'an Polytechnic University, 134#, Key Laboratary, 19 South Jin Hua Road, 710048 Xi'an, China, zxafafa@yahoo.com.cn)

During the past 2 years, a new theory has been established for soft materials that the vibration of materials brings the sound absorption, regardless whether they have pores in them or not. This theory is totally different from Classical theory, such as the Rayleigh model and the Zwikker and Kosten theory. Firstly, an empirical sound absorption coefficients formula of fibrous materials was found. Secondly, the theory sound absorption formula of thin fiber layers was obtained by the vibration sound absorption analysis and the applying of conservation law of energy. This formula agrees well with the empirical sound absorption formula of fibrous materials (mentioned above). Based on this achievment and applying classical laws of conservation of momentum and conservation of energy, the sound absorption theory formula of membrane (diaphragm) was also obtained, which have been well justified and also agree with the practice. This paper will review and discuss the main point about the vibration sound absorption theory and its establishment.

9:00

4aAAa4. The influence of absorption on statistical distribution of free path lengths in rooms. Dragana Sumarac Pavlovic (Faculty of Electrical Engineering, Bulevar Kralja Aleksandra 73, 11000 Belgrade, Serby, dsumarac@etf.bg.ac.yu), Miomir Mijic (Faculty of Electrical Engineering, Bulevar Kralja Aleksandra 73, 11000 Belgrade, Serby, emijic@etf.bg.ac.yu)

The ray tracing method in sound field simulation in a room allows the calculation of the free path lengths distribution (FPL) by superimposing all rays paths generated in the analysis. In room acoustics the statistical theory of sound field defined this distribution as an indicator of room geometrical properties which are independent of absorption. Accordingly, some commercial softwares for ray tracing simulation allow user to calculate that global distribution of FPL only. This paper is concerned with the analysis of the changes in the shape of FPL distribution as a consequence of nonuniform arrangement of absorption in room. Particularly is analysed the impact of absorptive auditorium in different global forms of the halls where all other interior surfaces are acoustically hard.

9:20

4aAAa5. The influence of geometrical features of rooms on their acoustic response - insight based on measurements in physical models. Miomir Mijic (Faculty of Electrical Engineering, Bulevar Kralja Aleksandra 73, 11000 Belgrade, Serby, emijic@etf.bg.ac.yu), Dragana Sumarac Pavlovic (Faculty of Electrical Engineering, Bulevar Kralja Aleksandra 73, 11000 Belgrade, Serby, dsumarac@etf.bg.ac.yu)

In a previous paper by the same authors, an analysis of the influence of geometrical features of rooms on their acoustic response was presented (Acta Acustica, Vol 93, 2007, 1012-1026). The analysis was based on ray tracing simulation. The results have shown that geometrical characteristics of rooms do influence reverberation time, and this influence is realised by the structure of sound energy paths through the room. It was concluded that

room geometry influences reverberation time both at macro and micro levels, and this influence cannot be separated. To validate these conclusions in a real sound field, additional measurements have been conducted in specially prepared physical models of rooms. In several models of different shapes selected from previous results, scaled 1:10, the changes of scattering were introduced by appropriate modifications of interior surfaces. The results have confirmed the previous study conclusions.

9:40

4aAAa6. Room acoustics prediction based on multiple linear regressions and artificial neural networks. Maria Ribeiro (FEUP/DEC, Rua Dr. Roberto Frias, 4200-465 Porto, Portugal, mribeiro@fe.up.pt), Fernando Martins (FEUP/DEC, Rua Dr. Roberto Frias, 4200-465 Porto, Portugal, fgm@fe.up.pt)

Room acoustic quality is known to be dependent on several objective variables that are expected to be well correlated with subjective impressions of the room acoustics as judged by musical experts. Although subjects have different preferences and overall judgments are based in different criteria, it can be said that listeners in their subjective evaluation would give preference to reverberance, clarity, intimacy or spaciousness attributes. In this study, reverberance and clarity, expressed respectively by T30/EDT and C80 objective values, were predicted by multiple linear regression and artificial neural networks using normalized original data and principal components as dependent variables. The results obtained by these approaches were compared with predicted values using a computer simulation program based on the physics of ray-tracing and with measured data. Room acoustical quality was also evaluated based on preferred values as suggested by some researchers.

10:00-10:20 Break

10:20

4aAAa7. Minimum BRIR grid resolution for dynamic binaural synthesis. Alexander Lindau (Department of Audio Communication, Technical University of Berlin, Sekr. EN-08, Einsteinufer 17c, 10587 Berlin, Germany, alexander.lindau@tu-berlin.de), Hans-Joachim Maempel (Department of Audio Communication, Technical University of Berlin, Sekr. EN-08, Einsteinufer 17c, 10587 Berlin, Germany, hans-joachim.maempel@tu-berlin.de), Stefan Weinzierl (Department of Audio Communication, Technical University of Berlin, Sekr. EN-08, Einsteinufer 17c, 10587 Berlin, Germany, stefan.weinzierl@tu-berlin.de)

Binaural synthesis of acoustical environments is based on binaural room impulse responses (BRIRs) measured with a certain grid of spherical coordinates separated by angles of typically between 1° and 15°. The resulting spatial resolution defines the size of the BRIR database as well as the duration of its measurement. Perceptual evaluations of datasets with a different spatial resolution using HRTFs (anechoic case) have been reported from. Most of these studies use the localization performance of listeners as a criterion; a more sensitive measurement for slight degradations in audio quality can be expected from a criterion-free comparison of datasets with different angular grids. Thus, to determine the minimum grid resolution required for dynamic binaural synthesis a listening test was performed. Following an adaptive 3AFC procedure, the spatial resolution of a recorded BRIR dataset was gradually lowered from a maximum of 1°/1° resolution until audible artefacts were introduced. This was done for a sound source located at 0°/0° presented with dynamical auralization in two degrees of freedom. To test for interaction effects the thresholds were derived independently for azimuth and elevation. The datasets used were acquired in an anechoic environment and in two rooms of different size and reverberation time.

10:40

4aAAa8. Optimum Room Acoustic Comfort™ (RAC™) can be achieved by using a selection of appropriate acoustic descriptors. Carsten Svensson (Saint-Gobain Ecophon AB, Box 500, SE-260 61 Hyllinge, Sweden, carsten.svensson@ecophon.se), Erling Nilsson (Saint-Gobain Ecophon AB, Box 500, SE-260 61 Hyllinge, Sweden, erling.nilsson@ecophon.se)

In order to create an optimum Room Acoustic Comfort™ (RAC™) in rooms it is important to consider a variety of different acoustic descriptors. These descriptors must match and facilitate for wanted human qualities such as ability to concentrate, reduced stress, clear speech etc. In this process it is important to consider the people, what they do (the activity) and what room they will be in. Today, when designing ordinary rooms from an acoustic perspective, mainly reverberation time (T20) is utilised - both in practice but also in building regulation and standards. Reverberation time (T20) only describe the later part of the decay curve, and therefore only partly mirror the wanted acoustic reality. Thus, based upon a large number of acoustic measurements, we suggest a ″cocktail″ of acoustic descriptors for ordinary rooms in buildings like schools, offices, health care premises etc. These descriptors have to cover both early and late decay, sound levels and speech quality. Our suggestions are Speech Clarity (C50), Speech Transmission Index (STI), Early Decay Time (EDT), Reverberation Time (T20) and Strength (G). Moreover, in open and long spaces we also suggest the acoustic descriptors Rate of Spatial Decay (DL2) and Excess of Sound Pressure Level (DLf).

11:00

4aAAa9. Distribution of Speech Intelligibility Metrics in Classrooms with Varied Signal to Noise (S/N) Ratios. Nurgun Bayazit Tamer (Istanbul Technical University, Taskisla Taksim Istanbul, 34437 Istanbul, Turkey, nurgun@itu.edu.tr)

In a classroom to provide adequate speech intelligibility is vital especially when young children are concerned. Room acoustical characteristics of classrooms like reverberation times and background noise mainly define the speech intelligibility in classrooms. Excessive background noise deteriorates the signal to noise ratio (S/N) and leads to reduction in learning efficiency. An extensive measurements study is being used in Istanbul Elementary Schools as part of a project. This paper explains the results of the investigation of the influence of varying signal to noise ratios on different speech intelligibility metrics. Background noise are includes external noises such as outdoor traffic noise, noise from playground or noise from adjacent classrooms. STI, RASTI, Alcon(%) values of 20 different classrooms in 20 different schools are measured in 9 different positions. The measurements were repeated in each classroom while windows were open and closed respectively. The object of the work was to systematically study the influence of the S/N ratio variations and reverberation time on the different speech intelligibility metrics. Finally to elucidate the effects of different absorption treatments achieving recommended reverberations on the measured speech metrics are also discussed.

11:20

4aAAa10. Speaker comfort and increase of voice level in lecture rooms. Jonas Brunskog (Dept. of Acoustic Technology, Technical University of Denmark, Building 352, DK 2800 Lyngby, Denmark, jbr@oersted.dtu.dk), Anders C. Gade (Dept. of Acoustic Technology, Technical University of Denmark, Building 352, DK 2800 Lyngby, Denmark, acg@oersted.dtu.dk), Gaspar Payà Bellester (C/ Sènia 1, 1er. C.P., 03640 Monòver Alacant, Spain, kansbarpb@gmail.com), Lilian Reig Calbo (Alacant, Spain, xusketa@hotmail.com)

Teachers often suffer health problems or tension related to their voice. These problems may be related to there working environment, including room acoustics of the lecture rooms which forces them to stress their voices. The present paper describes a first effort in finding relationships between the objectively measurable parameters of the rooms and the objective voice power produced by speakers. In rooms with different sizes, reverberation time and other physical attributes, the sound power levels produced by six speakers where measured while giving a short lecture. Relevant room acoustic parameters were also measured in the rooms and subjective impressions from about 20 persons who had experience talking in these rooms were collected as well. Analysis of the data revealed significant differences in the sound power produced by the speaker in the different rooms. It was also found that these changes were mainly related to the size of the room and to the gain or support produced by the room. To describe this quality, a new room acoustic quantity called 'room gain' is proposed.

11:40

4aAAa11. Measuring the mixing time in auditoria. Guillaume Defrance (Institut Jean le Rond d'Alembert, Laboratoire d'Acoustique Musicale, 11, rue de Lourmel, 75015 Paris, France, defrance@lam.jussieu.fr), Jean-Dominique Polack (Institut Jean le Rond d'Alembert, Laboratoire d'Acoustique Musicale, 11, rue de Lourmel, 75015 Paris, France, polack@ccr.jussieu.fr)

The goal of prediction, in Room Acoustics, is to synthesize the impulse responses (IRs) of a hall, in order to derive acoustic indices or to allow auralization. The process assumes the hall to be a time invariant linear system. Furthermore, the IR is known to behave stochastically when the sound field becomes diffuse, that is, after a certain time called mixing time. This study aims at characterizing the IR mixing time. Three methods are presented for visualizing and detecting the time evolution of the IR behaviour. The first one highlights the transition from early reflections to diffuse sound field by monitoring the phase evolution versus time. The two others exploit the gaussian distribution of pressure in a diffuse sound field, when the IR becomes statistical. These methods are applied to measurements, carried out in Salle Pleyel, and confirm the simple relationship found earlier between mixing time and volume.

THURSDAY MORNING, 3 JULY 2008 ROOM 243, 8:00 TO 9:20 A.M.

Session 4aAAb

Architectural Acoustics: Prediction Methods in Building Acoustics II

Berndt Zeitler, Cochair
NRC - Institute for Research in Construction, 1200 Montreal Road, Building M-27, Ottawa, ON K1A 0R6, Canada

Catherine Guigou-Carter, Cochair
CSTB, 24, rue Joseph Fourier, Saint Martin D'Hères, 38400, France

Invited Papers

8:00

4aAAb1. Prediction method for the acoustic performance of permanent form systems. Jean-Baptiste Chene (CSTB, 84, Avenue Jean-Jaurès, 77447 Marne-la-Vallée Cedex 2, France, jean-baptiste.chene@cstb.fr), Catherine Guigou-Carter (CSTB, 24, rue Joseph Fourier, 38400 Saint Martin D'Hères, France, catherine.guigou@cstb.fr)

Permanent form systems considered in this paper combine a layer of porous or fibrous material onto which a concrete layer is poured. Such systems allow the fulfillment of French thermal regulations. However, their acoustic performance is quite limited. Indeed, the acoustic performance of the concrete layer is usually reduced by the presence of the porous or fibrous layer. The modeling of such multi-layered structures submitted to acoustic excitation is discussed in this work. The behavior of such a system is investigated by using a wave approach based prediction tool. The porous layer is modeled following Biot's theory. The effect of the metallic anchors that connect the fiber and the concrete layers is also investigated. The acoustic performance of such systems is studied both experimentally and analytically. A parametric study is performed to identify the most determinant parameters. The model is thus used to obtain insight into the behavior of such systems in order to develop solutions that result in improved acoustic performance.

8:20

4aAAb2. The directivity of the forced radiation of sound from panels and openings including the shadow zone. John L. Davy (RMIT University, Applied Physics, GPO Box 2476V, 3001 Melbourne, Victoria, Australia, john.davy@rmit.edu.au)

This paper presents a method for calculating the directivity of the radiation of sound from a two dimensional panel or opening, whose vibration is forced by the incidence of sound from the other side. The directivity of the radiation depends on the angular distribution of the incident sound energy. For panels or openings in the wall of a room, the angular distribution of the incident sound energy is predicted using a physical model which depends on the sound absorption coefficient of the room surfaces. For an opening at the end of a duct, the sound absorption coefficient model is used in conjunction with a model for the directivity of the sound source in the duct. For angles of radiation approaching 90 degrees to the normal to the panel or opening, the effect of the diffraction by the panel or opening, or by the finite baffle in which the panel or opening is mounted, is included. A simple empirical model has been developed to predict the diffraction of sound into the shadow zone when the angle of radiation is greater than 90 degrees to the normal to the panel or opening. The method is compared with published experimental results.

Contributed Papers

8:40

4aAAb3. Numerical study of sound transmission loss using an indirect boundary element method. Matthew Cassidy (Queen's University Belfast, School of Mechanical and Aerospace Engineering, Ashby Building, Stranmillis Road, BT9 5AH Belfast, UK, mcassidy06@qub.ac.uk), Richard K. Cooper (Queen's University Belfast, School of Mechanical and Aerospace Engineering, Ashby Building, Stranmillis Road, BT9 5AH Belfast, UK, R.Cooper@qub.ac.uk), Richard Gault (Queen's University Belfast, School of Mechanical and Aerospace Engineering, Ashby Building, Stranmillis Road, BT9 5AH Belfast, UK, r.gault@qub.ac.uk), Jian Wang (Queen's University Belfast, School of Mechanical and Aerospace Engineering, Ashby Building, Stranmillis Road, BT9 5AH Belfast, UK, j.wang@qub.ac.uk)

The purpose of this study was to simulate transmission loss tests at the acoustic facilities of FG Wilson, Larne, UK. A hemi-anechoic chamber adjoins a reverberation room via a transmission plug where canopy panel sections are mounted for testing. Boundary element methods in LMS Virtual .Lab are used in conjunction with a baffle model to simulate the test facilities for transmission loss. On one side of this wall the reverberation room is modelled as a diffuse field using a series of defined plane waves, and on the other the hemi-anechoic chamber is represented as a free field. Experiments were carried out on a steel plate and lead sheet following the ISO 15186 standard for measurement of sound insulation using sound intensity. Source room sound pressure levels were recorded with a microphone, and an intensity probe was used to map the sound intensity field on the receiving side. Transmission loss for a frequency range was calculated as stated in the standard and compared with the results for the computational analysis. Comparison of the computational simulation with the experimental yielded a sufficient agreement.

Invited Paper

9:00

4aAAb4. Prediction of the Sound Transmission Loss of Multi-layered Small Sized Elements. Stefan Schoenwald (Eindhoven University of Technology, Den Dolech 2, BWK/BPS, 5600 MB Eindhoven, Netherlands, s.schoenwald@tue.nl), Eddy Gerretsen (TNO Science and Industry, Stieljesweg 1, 2628CK Delft, Netherlands, eddy.gerretsen@tno.nl), Heiko J. Martin (Eindhoven University of Technology, Den Dolech 2, BWK/BPS, 5600 MB Eindhoven, Netherlands, h.j.martin@tue.nl)

In this paper an improved method for the prediction of the sound transmission loss of multilayered finite structures, like glazing will be presented. The sound transmission loss of an infinite structure is predicted with a common transfer matrix as a function of the angle of the incident sound wave. Then Villiot's spatial windowing method is applied to take into account the finiteness of the element. Usually an ideal diffuse distribution of the incident sound power is assumed and the prediction results are integrated over all angles of incidence. The obtained prediction results tend to underestimate sound transmission loss due to the dominance of the small values for gracing incidence. Often simple ad-hoc corrections are used for improvement, like Beranek's field incidence, that fail for multilayered structures. Kang suggests that the incident sound power on a surface of a room generally is Gaussian distributed on the angle of incidence and introduces a weighting function for the integration of the prediction results over the angles of incidence. New in this paper is that spatial windowing as well as a Gaussian distributed sound power is considered for the prediction of the transmission loss. The results of the prediction are validated by experiment.

THURSDAY MORNING, 3 JULY 2008 ROOM 243, 10:00 A.M. TO 7:00 P.M.

Session 4aAAc

Architectural Acoustics: Measuring Methods and Uncertainty in Building Acoustics I

Brandon Tinianow, Cochair
Quiet Solution, 1250 Elko Dr., Sunnyvale, CA 94089, USA

Werner Scholl, Cochair
Physikalisch-Technische Bundesanstalt, Bundesallee 100, Braunschweig, 38116, Germany

Contributed Papers

10:00

4aAAc1. A new technique for the measurement of the normal incidence absorption coefficient using an impedance tube and a single microphone with fixed position. Cedric Vuye (Hogeschool Antwerpen, Dept. of Industrial Sciences, Paardenmarkt 92, BE-2000 Antwerpen, Belgium, c.vuye@ha.be), Steve Vanlanduit (Vrije Universiteit Brussel, Acoustics and Vibration Research Group, Dept. of Mechanical Engineering, Pleinlaan 2, BE-1050 Brussels, Belgium, Steve.Vanlanduit@vub.ac.be), Karl Van Nieuwenhuyse (Vrije Universiteit Brussel, Acoustics and Vibration Research Group, Dept. of Mechanical Engineering, Pleinlaan 2, BE-1050 Brussels, Belgium, karl.van.nieuwenhuyse@skynet.be), Patrick Guillaume (Vrije Universiteit Brussel, Acoustics and Vibration Research Group, Dept. of Mechanical Engineering, Pleinlaan 2, BE-1050 Brussels, Belgium, Patrick.Guillaume@vub.ac.be)

The normal incidence absorption coefficient of acoustic materials can be measured inside an impedance tube with different settings for the microphone(s). The two most widespread techniques are the standing wave method using a probe microphone and side-mounted two-microphone techniques. Errors that can occur here are related to phase mismatch between the two microphones and the knowledge of the exact locations of the (acoustic centre of the) microphones and test sample. These problems have (partially) been solved by, for example, calibrating the microphones by swapping them and calculating a calibration transfer function or by using one microphone techniques. In this article we will present a novel technique

which will also avoid the need for the knowledge of the exact microphone location by continuously moving the sample under test. Different results will be presented and compared to the traditional techniques.

10:20

4aAAc2. New method for measuring sound absorption coefficients in an industrial hall. Joël Ducourneau (Faculté de Pharmacie de Nancy, Université Henri Poincaré, 5, rue Albert Lebrun, BP 80403, 54001 Nancy, France, Joel.Ducourneau@pharma.uhp-nancy.fr), Vincent Planeau (Institut National de Recherche et de Sécurité (INRS), Ave. de Bourgogne, B.P. 27, F-54501 Vandoeuvre Cedex, France, vincent.planeau@secav.fr), Jacques Chatillon (Institut National de Recherche et de Sécurité (INRS), Ave. de Bourgogne, B.P. 27, F-54501 Vandoeuvre Cedex, France, jacques.chatillon @inrs.fr), Armand Nejade (Institut National de Recherche et de Sécurité (INRS), Ave. de Bourgogne, B.P. 27, F-54501 Vandoeuvre Cedex, France, armand.nejade@inrs.fr)

Predicting the sound pressure level at a workplace requires in-situ characterization of the facings. This work describes a new method for the measurement of the sound absorption coefficient of flat panels present in industrial halls. In such room, it is necessary to separate the echo coming from the studied panel from the others due to the entire reverberation. This separation has been achieved in space by an acoustic array and in time by an impulse sound source. The array processing uses a multipolar weighting to achieve a directivity constant with frequency and with attenuated side lobes. This weighting requires a limited number of microphones. The impulse source has been designed using the inverse impulse response from the emission system (equalizer, amplifier, loudspeaker). This inverse filtering technique allows equalizing the response of the emission system in order to radiate very short pulses. Sound absorption coefficient of several flat facings have been evaluated by mean of this new device in a semi-anechoic chamber and in an industrial hall designed for testing. The results show a good agreement with others techniques except at low frequencies for which the array length is too small and the absorption coefficients too low.

Invited Paper

10:40

4aAAc3. Measurement uncertainty of the sound absorption coefficient. Anna Izewska (Building Research Institute, Filtrowa Str.1, 00-611 Warsaw, Poland, a.izewska@itb.pl)

The standard ISO/IEC 17025:2005 on the competence of testing and calibration laboratories requires that these laboratories shall apply procedures for estimating the uncertainty of their measurement results. One of the possibility is to evaluate the budget of uncertainty, taking into account all components that contribute significant uncertainty to the final result. In case of the sound absorption coefficient measurement, carried out according to the standard EN ISO 354:2003, the overall uncertainty is first of all influenced by the reverberation times T1, T2 and the power attenuation coefficients m1 and m2, calculated according to the ISO 9613-1 standard and representing the climatic conditions in the reverberation room. In spite of very little difference between the values m1 and m2 representing the change of climatic conditions (usually, it is the case in laboratory), exponential form of the coefficient's function causes that the uncertainty of measurement results increase with frequency very fast. Particularly for the high frequencies, the values of uncertainty are so important that the evaluation of the sound absorption coefficient is practically not possible.

Contributed Papers

11:00

4aAAc4. A comparison of impulse-like sources to be used in reverberation time measurements. Marko Horvat (Faculty of EE and Computing, Unska 3, Department of Electroacoustics, HR-10000 Zagreb, Croatia, marko.horvat@fer.hr), Kristian Jambrosic (Faculty of EE and Computing, Unska 3, Department of Electroacoustics, HR-10000 Zagreb, Croatia, kristian.jambrosic@fer.hr), Hrvoje Domitrovic (Faculty of EE and Computing, Unska 3, Department of Electroacoustics, HR-10000 Zagreb, Croatia, hrvoje.domitrovic@fer.hr)

As a part of an extensive ongoing research on reverberation time measurements, efforts have been made to find an impulse-like source that will comply with certain demands concerning its spectral content and sound pressure levels it can provide. Although the relevant standards state that such kind of sources should be avoided due to the lack of measurement repeatability, their use has proved to be necessary due to inability of conventional omni-directional loudspeakers to provide adequate sound pressure levels, especially at the low end of the frequency range of interest, thereby ensuring sufficient dynamic range. Therefore, the emphasis of this investigation has been made on peak sound pressure levels and the amount of low frequency content each source is able to provide. The investigated sources include 6 mm and 8 mm pistols, firecrackers with different amount of explosive compound and explosive mixtures of acetylene gas.

11:20

4aAAc5. An Application of Time-Reversal Acoustics to Sound Insulation Measurements in Buildings. Doheon Lee (University of Sydney, Faculty of Architecture, Design and Planning, NSW 2006 Sydney, Australia, dlee7117@mail.usyd.edu.au), Densil Cabrera (University of Sydney, Faculty of Architecture, Design and Planning, NSW 2006 Sydney, Australia, densil@usyd.edu.au)

This paper considers the possible application of time reversal acoustics (TRA) to airborne sound insulation measurements in buildings. In TRA, an array of transducers is set up to form a time-reversal 'mirror' or 'cavity'. Using this array, the sound radiated from an initial source is collected and refocused spatially and temporally, thereby being reproduced at the initial source position with high signal-to-noise ratio (S/N). Most previous studies of TRA have been conducted underwater with ultrasonic sound sources, with only a few in the audible range in real buildings. The technique is best suited to non-dissipative systems, raising the question of whether any advantage could exist for transmission between rooms. This study applies TRA experimentally in the audible range using maximum length sequence signals for transmission between two rooms. Comparison is made between conventional measurements (with and without impulse response deconvolution) and TRA in terms of effective S/N and apparent level difference between the rooms. Substantially greater S/N is achieved using TRA, but the interpretation of measurements is not straightforward, and the technique is much more demanding than conventional measurements.

11:40

4aAAc6. Measuring Sound Insulation using Deconvolution Techniques. Constant C. Hak (Technische Universteit Eindhoven, De Rondom 10, 5612 AP Eindhoven, Netherlands, c.hak@inter.nl.net), Nicole H. Van Hout (LeVel Acoustics BV, De Rondom 10, 5612 AP Eindhoven, Netherlands, n.h.a.m.v.hout@tue.nl), Heiko J. Martin (Eindhoven University of Technology, Den Dolech 2, BWK/BPS, 5600 MB Eindhoven, Netherlands, h.j .martin@tue.nl)

To compare the acoustic performance of a building element with the given sound insulation requirements, measurements need to be done. Generally, a broadband noise source is used according to international standards. This method does not always work in practice due to high sound insulation values or high background noise levels. It is very inconvenient from a practical point of view or even impossible to perform an accurate sound insulation measurement for all frequency bands. A solution to this problem can be found in deconvolution techniques using mls or sweep signals. It is possible to increase the signal to noise ratio with these techniques by averaging mea-

surements and spreading out the spectral sound energy in time. As a result an efficient use of available sound power is possible. In a laboratory is investigated how to use mls or sweep signals as a source signal and deconvolution as a measurement technique to obtain the sound insulation under noisy conditions.

12:00

4aAAc7. Characterising a washing machine as a structure borne sound source on a lightweight floor. Matthias Lievens (Institute of Technical Acoustics, Neustraße 50, 52056 Aachen, Germany, mli@akustik.rwth-aachen.de)

The transfer of structure borne sound power depends on the mobility of the source and the receiver. If source and receiver are coupled through multiple points, the interaction between those points has to be accounted for. The force of a washing machine injected into a lightweight wooden floor is analysed to develop a simple measurement procedure for similar multiple point structure borne sound sources. A complete mobility model will be compared with a simplified model based on a reduced mobility matrix. The importance of different matrix components will be determined. Receiver structures used in real buildings will be investigated.

Invited Paper

12:20

4aAAc8. On the use of scaled models in building acoustics. Volker Wittstock (Physikalisch-Technische Bundesanstalt, Bundesallee 100, 38116 Braunschweig, Germany, volker.wittstock@ptb.de), Martin Schmelzer (Physikalisch-Technische Bundesanstalt, PTB, Working group 1.71 'Building Acoustics', Bundesallee 100, 38118 Braunschweig, Germany, martin.schmelzer@ptb.de), Christoph Kling (Physikalisch-Technische Bundesanstalt, PTB, Working group 1.71 'Building Acoustics', Bundesallee 100, 38118 Braunschweig, Germany, christoph.kling@ptb.de)

Experimental studies of physical effects in building acoustics are usually time consuming and expensive. This is mainly caused by the building costs but also by the experimental effort. It is thus desirable to have another method for the investigation of basic effects in building acoustics. Building acoustic problems are characterized by the interaction between airborne and structure-borne sound fields. It is therefore possible to use scaled models when both sound fields are treated correctly. This means that the wavelengths in the airborne and in the structure-borne sound fields have to be scaled in the same way. With a scaling factor of typically 1:8, the costs can be reduced drastically and nearly all model parameters can be changed separately. Due to these advantages, this technique is used at PTB's building acoustics group. This contribution gives an overview on the physical background of scaled models, reports on validation experiments and on several applications e.g. investigations of the influence of temperature and static pressure, damping effects, geometry influence on the sound insulation of walls, the measurement of the flanking transmission of walls and the measurement of suspended ceilings.

12:40-1:40 Lunch Break

Contributed Paper

1:40

4aAAc9. Influence of the source orientation on the measurement of acoustic parameters in a large reverberant cathedral. Miguel Arana (Public University of Navarre, Physics Department. Campus de Arrosadia, s/n, 31006 Pamplona, Spain, marana@unavarra.es), Ricardo San Martin (Public University of Navarre, Physics Department. Campus de Arrosadia, s/n, 31006 Pamplona, Spain, ricardo.sanmartin@unavarra.es), Maria Luisa San Martin (Public University of Navarre, Physics Department. Campus de Arrosadia, s/n, 31006 Pamplona, Spain, sanmartin@unavarra.es)

ISO 3382 standard describes both definitions and measurement procedures of different acoustic parameters derived from the room impulse response. Regarding to sound sources, most of the commercial dodecahedron loudspeakers comply with the maximum allowed directional deviations of the source specified in the standard. However, the influence of its specific orientation may affect the results obtained on some parameters more than their subjective just noticeable difference-jnd- at least in rooms with no high reverberation times. An interesting aim is to study such influence in function of the liveliness of the room. A detailed measurement set is been carrying out in a reverberant place (Cathedral of Tudela, Spain) with the objective to analyze the influence of the source's orientation-apart from its acoustic characterization. In addition to dodecahedron loudspeakers, pseudo-impulsive sources are been used in order to compare results from a statistical point of view. Results obtained will be compared with those obtained in several concert and theater rooms.

Invited Papers

2:00

4aAAc10. Measurement of reverberation time with rotating microphone in test chamber and its problems. Hiroshi Sato (National Institute of Advanced Industrial Science and Technology, Central 6, 1-1-1 Higashi, 305-8566 Tsukuba, Japan, sato.hiro@aist.go.jp), Junichi Yoshimura (Kobayasi Institute of Physical Research, 3-20-41 Higashi-Motomachi, Kokubunji, 185-0022 Tokyo, Japan, yoshi@kobayasi-riken.or.jp), Satoshi Sugie (Kobayasi Institute of Physical Research, 3-20-41 Higashi-Motomachi, Kokubunji, 185-0022 Tokyo, Japan, sugie@kobayasi-riken.or.jp), Takashi Koga (Kajima Technical Research Institute, 2-19-1 Tobitakyu, Chofu, 182-0036 Tokyo, Japan, tkoga@kajima.com), Emi Toyoda (Kobayasi Institute of Physical Research, 3-20-41 Higashi-Motomachi, Kokubunji, 185-0022 Tokyo, Japan, toyoda@kobayasi-riken.or.jp), Jongkwan Ryu (National Institute of Advanced Industrial Science and Technology, Central 6, 1-1-1 Higashi, 305-8566 Tsukuba, Japan, jongkwan-ryu@aist.go.jp)

When measurement of reverberation time is done in a test chamber to evaluate acoustical property of materials, spatial averaging of reverberation time should be done. Using microphone rotator is recognized as one of the tool to do spatial averaging. This study compares between three methods of spatial averaging of reverberation times measured in small rectangular test chamber (3m x 4m x 5m). The first method is averaging reverberation time measured at 5 of fixed position used as standard positions for testing, the second is at 72 fixed positions on the circle of microphone rotator, and the third is with microphone rotator (64 s/rotation). The result of comparison between three method revels that reverberation time measured by rotating microphone has more scatter than and presents different reverberation time from those measured by other method especially at lower frequency bands. Simulation of microphone rotation with

the decay curves measured at 72 fixed positions suggests that spatial distribution of steady state sound pressure level, rotation speed of microphone, and reverberation time of test chamber are key factors of errors. As a conclusion, the strict guideline for measurement of reverberation time with microphone rotator should be presented to minimize errors.

2:20

4aAAc11. Uncertainty in building acoustics. Werner Scholl (Physikalisch-Technische Bundesanstalt, Bundesallee 100, 38116 Braunschweig, Germany, werner.scholl@ptb.de), Volker Wittstock (Physikalisch-Technische Bundesanstalt, Bundesallee 100, 38116 Braunschweig, Germany, volker.wittstock@ptb.de)

In many countries, legal requirements exist with respect to the acoustical performance of buildings and building elements. Therefore information about the uncertainty of measured or predicted building acoustic properties is urgendly needed. The complexity of the problem becomes obvious taking sound recuction index R as an example: R represents the ratio of incoming and transmitted sound power of a building element. For practical reasons, the direct measurement of R is replaced by a spatiotemporally averaged sound pressure level difference in two limited rooms, adjusted by the absorption of the receiving room. In doing so, unwanted influences occur like modal effects, flanking transmission, structural power exchange between laboratory and specimen, deviation from ideal diffuse sound fields with unknown consequences etc. For economic reasons, often only one sample is tested and declared 'typical' for the whole family of products without regarding their spread. As a consequence, the uncertainty most often is felt to be too large to decide about the compliance with regulations but cannot be quantified. PTB in Germany has investigated the problem for the German authorities by calculation, evaluation of Round-Robin-tests und large measurement series in model houses. The results are presented in the talk.

Contributed Paper

2:40

4aAAc12. Uncertainty evaluation in field measurements of airborne sound insulation. Ranny L.X. Michalski (Inmetro / CNPq, Av. N. S. das Graças, 50, Xerém, Duque de Caxias, 25250-020 RJ, Brazil, ranny_xavier@yahoo.com.br), Daiana Ferreira (Inmetro / CNPq, Av. N. S. das Graças, 50, Xerém, Duque de Caxias, 25250-020 RJ, Brazil, dpferreira@inmetro.gov.br), Marco Nabuco (Inmetro / CNPq, Av. N. S. das Graças, 50, Xerém, Duque de Caxias, 25250-020 RJ, Brazil, nabuco@inmetro.gov.br), Paulo Massarani (Inmetro / CNPq, Av. N. S. das Graças, 50, Xerém, Duque de Caxias, 25250-020 RJ, Brazil, pmmassarani @inmetro.gov.br)

The Brazilian Committee of Civil Engineering presented a set of standards concerning the evaluation of the performance of several topics for buildings up to five floors. The acoustic performance is one of them. The standards are in approval process and measurements in real buildings will be necessary. Different professionals using different equipment will emit certificates establishing which levels of insulation a certain flat provides and its uncertainties. The expanded measurement uncertainty can provide the basis to compare different measurement results for a same building. The international Guide to the Expression of Uncertainty in Measurement, the ISO GUM, is the document that specifies how to determine and evaluate the uncertainty of a measurement result. The standards concerning sound insulation measurements are ISO 140 and ISO 18233. Uncertainty estimates are available only for the classical technique described in ISO 140, based in repeatability and reproducibility tests performed in laboratories. Field measurements present some characteristics that can contaminate the results, as time variance. Several independent measurements were carried out in a one flat building using ISO 18233 specifications and the ISO GUM was applied to obtain the uncertainty for measurement results of airborne sound insulation between rooms in situ.

Invited Paper

3:00

4aAAc13. Uncertainty of Receiving Space Volume in Field Measurements of Transmission Loss Under ASTM E336-05. Jonah Sacks (Acentech, 33 Moulton Street, Cambridge, MA 02138, USA, jsacks@acentech.com)

As acoustical consultants, we are frequently asked by our clients to measure the sound isolating performance of constructions in the field. While it is often preferable to report ″system-level″ performance ratings such as Noise Isolation Class, there are compelling benefits both to us and to our clients to measuring and reporting ″specimen-level″ performance ratings such as Apparent Sound Transmission Class, defined by ASTM E336-05 (and E413-04). The accuracy of such ratings depends on accurate assessment of the amount of acoustical absorption present in receiving spaces at the time of testing, arrived at by means of reverberation time measurements and physical measurement of receiving spaces. When a receiving space is irregular in shape, one may feel pressed to use creative judgment to estimate its effective volume, and such judgments can have large impacts on the reported results. We will discuss the challenges of measuring apparent transmission loss in the field, and the compelling reasons to conduct these measurements despite the challenges.

Contributed Paper

3:20

4aAAc14. Field measurements of acoustic performance in buildings: a Round Robin Test. Fabio Scamoni (Construction Technologies Institute of Italian National Research Council, Viale Lombardia, 49, 20098 San Giuliano Milanese (MI), Italy, Fabio.Scamoni@itc.cnr.it), Maurizio Bassanino (ARPA Lombardy - Air and Physical Agents, 3/1, Viale F. Restelli, 20124 Milan, Italy, M.BASSANINO@arpalombardia.it), Giuseppe Bruno (Lombardy Region - Environmental Quality, Via Pola, 14, 20124 Milan, Italy, giuseppe_bruno@regione.lombardia.it), Giovanni Zambon (Department of Environmental Sciences of the University of Milano - Bicocca, Piazza della Scienza, 1, 20126 Milan, Italy, giovanni .zambon@unimib.it)

This paper presents the experimental results of a round robin test performed on the same building by different teams working with three independent bodies: a research body, ITC-CNR, a university laboratory DISAT and the Regional Agency for Environment Protection of Lombardy, ARPA. A partition wall (the airborne sound insulation between rooms), a floor (the impact sound insulation between rooms) and a façade (the insulation of the façade against outdoor sound) were tested, using the measurement methods

given in the relevant parts of the ISO 140 series. The accuracy of acoustic measurement methods in buildings depends on many factors. In this round robin test, the situation (varying from straightforward rectangular rooms to half open spaces with all kind of shapes) and the construction details were kept fix. The analysis was aimed at investigating the influence of the operating condition of the equipment (repeatable settings) and the reproducibility, using different types of acoustic instrumentation and varying the method (choice of source and microphone positions). In particular the tolerance limits in the verification of the requirements of tender specifications were investigated.

3:40-5:00 Posters

Lecture sessions will recess for presentation of poster papers on various topics in acoustics. See poster sessions for topics and abstracts.

Invited Papers

5:00

4aAAc15. Handling of uncertainties for CE marking concerning Sound Transmission Loss of glazings. Marc Rehfeld (Saint Gobain Glass, CRDC, B.P. 40103, 60777 Thourotte Cedex, France, marc.rehfeld@saint-gobain.com)

A joint working group between CEN TC 126 (building acoustics) and CEN TC 129 (glass in building) has been created to handle the redaction of a test code, (give rules for CE marking) and particularly handle uncertainty problems. A round robin has been organised, at which 23 European labs have participated, and two configuration of double glazings have been tested: one with two monolithic glass components, the other with one monolithic and one highly damped laminate component. The paper will present the specifications and main results of this round robin, the questions that occurred concerning the possible ways to decrease uncertainty values, as well as the conclusions and decisions of the working group.

5:20

4aAAc16. Repeatability and reproducibility of field noise isolation testing. John Loverde (Veneklasen Associates, 1711 Sixteenth Street, Santa Monica, CA 90404, USA, jloverde@veneklasen.com), Wayland Dong (Veneklasen Associates, 1711 Sixteenth Street, Santa Monica, CA 90404, USA, wdong@veneklasen.com)

The reliability and precision of test measurements and methods are generally described in terms of repeatability and reproducibility. ASTM standards define and quantify these terms for noise isolation test methods in both laboratory and field conditions. Understanding these as reproducibility and repeatability of the measurement method, the authors extend the concept to the reproducibility and repeatability of a wall or floor/ceiling assembly design. Multiple instances of a floor/ceiling assembly on a multi-family residential project built by the same contractors is an example of design repeatability, while the same assembly design constructed on different projects is an example of design reproducibility. In a previous paper [LoVerde and Dong, J. Acoust. Soc. Am. 122, 2955 (2007)], definitions were suggested for field repeatability and reproducibility for Field Impact Insulation Class testing. Test data is presented to quantify the field repeatability and reproducibility of several assembly designs, which are compared to laboratory values. Field and laboratory repeatability and reproducibility of airborne noise isolation for a partition assembly are also examined.

5:40

4aAAc17. Analysis of uncertainty in building acoustic predictions using Monte-Carlo methods. Ralph T. Muehleisen (Illinois Institute of Technology, Civil, Architectural and Environmental Engineering, 3201 S. Dearborn St., Room 228, Chicago, IL 60616, USA, muehleisen@iit.edu)

One of the most common tasks in architectural acoustics is the prediction of the acoustic performance of some aspect of a building, such as the background sound level of a room, the reverberation time of an enclosure, or the sound transmission of a wall construction. The accuracy of a prediction is not only dependent upon the computation model, but also upon the accuracy of the data of the model. Because of the complicated, non-linear interaction of various inputs, assessing the accuracy of a prediction can be difficult. One way to provide more accurate predictors and estimate the error in the prediction of complicated, multiple input systems is to utilize the Monte-Carlo method. In this talk, the application of Monte-Carlo methods to building acoustic predictions is presented.

Contributed Papers

6:00

4aAAc18. Diffuseness and sound field distribution at room boundaries. Jean-Daniel Chazot (Université de Technologie de Compiègne, Lab. Roberval UMR 6253, Dept. Acoustique, BP 60319, 60203 Compiègne, France, jean-daniel.chazot@utc.fr), Jean-Louis Guyader (INSA de Lyon - LVA, Bâtiment St. Exupéry, 25 bis avenue Jean Capelle, F-69621 Villeurbanne Cedex, France, jean-louis.guyader@insa-lyon.fr)

In the present work, a classical modal analysis is used up to medium frequencies to study the sound field distribution, and its diffuseness, particularly at boundaries. Due to intensification zones at boundaries, the diffuse field distribution at room boundaries can not be assimilated to the distribution inside the room. Moreover, diffuseness at room boundaries, that is of interest for sound insulation measurement, is usually only related to an incidence angle while inside the room volume several descriptors such as a correlation function and the spatial uniformity are necessary to characterize a diffuse field. In this paper, we present a new descriptor adapted to characterize the sound field diffusivity at boundaries. This descriptor is called Boundary Diffuse Field Index. Its averaged value over a specific surface can be related to a limit incidence angle, and its standard deviation can be related to the spatial distribution over the surface. Finally, thanks to this descriptor, Sabine's assumptions of diffuse sound field are also evaluated in this study.

6:20

4aAAc19. Previous results on the evaluation of the influence of sound level meter case in diffuse field. Alfonso R. Molares (University of Vigo,E.T.S.I de Telecomunicación, Rúa Maxwell s/n, 36310 Vigo, Spain, amolares@gts.tsc.uvigo.es), Manuel A. Sobreira-Seoane (University of Vigo, E.T.S.I de Telecomunicación, Rúa Maxwell s/n, 36310 Vigo, Spain, msobre@gts.tsc.uvigo.es)

In order to evaluate the influence of the sound level meter case on real measurements, two different case geometries are tested using Boundary Element Method. Solving the coupled structural-acoustic problem by means of an iterative procedure, their correction curves are obtained for various angles of incidence and for diffuse field. The deviation due to the case is obtained by comparison against the result of the reference microphone. The results reveal that the influence of the case can be relevant at the middle frequency range with deviations that can exceed 0.4 dB under free-field conditions for normal incidence. At the time of writing this abstract the available results show that the deviation for diffuse field at middle frequencies can reach 0.2 dB, although further research is needed to evaluate the deviation at higher frequencies.

6:40

4aAAc20. Uncertainty analysis in acoustical modeling of room. Dominik Mleczko (Romera 17, 33-300 Nowy Sacz, Poland, dmleczko@agh.edu.pl)

For a long time there is a need in industry of acoustical modeling of rooms. It is necessary for new production room design, machine exchange, renovation or enlargement of production rooms, change in a production profile or acoustical room adaptation for acoustical work conditions improvement. In such cases modeling quality is essential and thanks to uncertainty analysis it is possible to quantitatively estimate the effect that input parameters value variation has on model behavior. The article presents general rules for sound pressure level prediction uncertainty calculation in a room. By partial uncertainty calculation analysis of input parameters influence on uncertainty prediction an effort was taken to find parameters with biggest influence on the prediction process. As an example an industrial production room is presented which was modeled to predict noise level on a work stands after it was expanded.

THURSDAY MORNING, 3 JULY 2008 ROOM 342B, 8:00 TO 10:20 A.M.

Session 4aABa

Animal Bioacoustics, Psychological and Physiological Acoustics, and ECUA: Auditory Brainstem Response and Behavior Correlation II

Elizabeth Brittan-Powell, Cochair
Dept of Psychology, University of Maryland, College Park, MD 20742, USA

Alexander Y. Supin, Cochair
Institute of Ecology and Evolution, 33 Leninsky Prospect, Moscow, 119071, Russian Federation

Invited Papers

8:00

4aABa1. Evoked-potential study of hearing directivity and sound-receiving apertures in dolphins. Vladimir V. Popov (Institute of Ecology and Evolution, 33 Leninsky Prospect, 119071 Moscow, Russian Federation, popov_vl@sevin.ru), Alexander Y. Supin (Institute of Ecology and Evolution, 33 Leninsky Prospect, 119071 Moscow, Russian Federation, alex_supin@mail.ru)

Positions of sound-receiving apertures were searched-for in bottlenose dolphins using the ABR technique. The receiving-area position was computed basing on ABR delays at various sound-source positions. Two acoustic apertures were revealed in such a way: for frequencies of 32 kHz and higher, the receiving area was located near a proximal part of the lower jaw (the mandibular acoustic window); for lower frequencies, the receiving area was located near the tympanic bulla. In another experimental series, AEP thresholds to near-field stimuli were measured with transducer positioning next to various points of the dolphin's head. Again, at stimulus frequencies of 32 kHz and higher, the lowest threshold area was next to the mandibilar acoustic window; at lower frequencies, the lowest threshold area was next to the bulla. The conclusion is that dolphins have at least two acoustic apertures differing in their frequency sensitivity. Directional sensitivity of these two apertures was investigated by measuring ABR thresholds at different frequencies and different sound source positions. At higher frequencies, the best-sensitivity direction estimated by ABR thresholds was near the head midline, at lower frequencies the best-sensitivity direction deviated laterally. These data were interpreted as indicating different axis directions of the two receiving apertures.

8:20

4aABa2. Tuning curves derived from auditory brainstem responses point to a defect in outer hair cells of hypothyroid mice. Edward Walsh (Boys Town National Research Hospital, 555 North 30th Street, Omaha, NE 68132, USA, walsh@boystown.org), Megan Korte (Boys Town National Research Hospital, 555 North 30th Street, Omaha, NE 68132, USA, kortem@boystown.org), Joann McGee (Boys Town National Research Hospital, 555 North 30th Street, Omaha, NE 68132, USA, mcgee@boystown.org)

Based on an analysis of ABR derived tuning curves, recent reports suggest that the mechanics of passive transduction in hypothyroid mice, although delayed developmentally, eventually become indistinguishable from normal animals, whereas the mechanics of active transduction remain grossly abnormal throughout life, raising the possibility that the outer hair cell system is at least partially responsible for abnormalities observed in mutant animals. Moreover, results of in vitro studies have shown that although OHCs are electro-

motile, they appear unable to withstand extensive voltage excursions in the whole cell voltage clamp environment; i.e., they appear fragile. These data led us to question the structural integrity of the OHC lateral wall in hypothyroid mice. Preliminary studies suggest that the cortical cytoskeleton is abnormal in at least some regions of the OHC lateral wall and preliminary confocal immunofluorescence images of the constituent proteins, f-actin and α-II spectrin, suggest that spectrin is either absent or expressed in very low levels in the cytoskeleton of OHCs harvested from the hypothyroid progeny of Tshr mutant dams. We suggest that a cytoskeletal defect involving the f-actin cross-linking protein, spectrin, might compromise the efficient transfer of force along the long axis of OHCs, effectively diminishing the power of active amplification.

Contributed Papers

8:40

4aABa3. Electrophysiological and behavioral measures of temporary threshold shift in a bottlenose dolphin (Tursiops truncatus). James J. Finneran (US Navy Marine Mammal Program, Space and Naval Warfare Systems Center, 53560 Hull St., Code 71510, San Diego, CA 92152, USA, james.finneran@navy.mil), Carolyn E. Schlundt (EDO Professional Services, 3276 Rosecrans St., San Diego, CA 92110, USA, carolyn.melka@edocorp.com), Brian K. Branstetter (US Navy Marine Mammal Program, Space and Naval Warfare Systems Center, 53560 Hull St., Code 71510, San Diego, CA 92152, USA, branstet@hawaii.edu), Randall L. Dear (Science Applications International Corporation, 4065 Hancock St., San Diego, CA 92110, USA, RANDALL.L.DEAR@saic.com)

Auditory evoked potentials are being increasingly applied to more advanced studies of marine mammal hearing, such as frequency selectivity, temporal processing, and temporary threshold shift (TTS). In this study, both behavioral and electrophysiological techniques were used to measure TTS in a bottlenose dolphin exposed to 20-kHz tones. Behavioral hearing thresholds were estimated using a modified staircase procedure and a whistle response. Electrophysiological thresholds were assessed using the multiple auditory steady-state response. Evoked potential stimuli consisted of seven frequency-modulated tones having carrier frequencies from 10-70 kHz and unique modulation rates. Tones were simultaneously presented and the evoked response at each modulation rate independently tracked to test hearing at all seven frequencies simultaneously. The behavioral and evoked response data both showed frequency-dependent patterns of TTS, with the largest shifts at 30 kHz; however, TTS measured using evoked potentials (up to 40-45 dB) was always larger than that observed behaviorally (19-33 dB). This discrepancy may be the result of the evoked response input-output function, which can be represented as the sum of two processes, a low threshold, saturating process and a higher threshold linear process, that react and recover to fatigue at different rates.

9:00

4aABa4. Directional sensitivity and hearing pathways in the beluga whale, Delphinapterus leucas. Aude Pacini (University of Hawaii, Hawaii Institute of Marine Biology, P.O. Box 1106, Kailua, HI 96734, USA, aude@hawaii.edu), Paul E. Nachtigall (University of Hawaii, Hawaii Institute of Marine Biology, P.O. Box 1106, Kailua, HI 96734, USA, nachtiga@hawaii.edu), T. Aran Mooney (University of Hawaii, Hawaii Institute of Marine Biology, P.O. Box 1106, Kailua, HI 96734, USA, mooneyt@hawaii.edu), Manuel Castellote (L'Oceanografic, C/. Junta de Murs i Valls, s/n, 46013 Valencia, Spain, mcastellote@oceanografic.org), Kristen A. Taylor (University of Hawaii, Hawaii Institute of Marine Biology, P.O. Box 1106, Kailua, HI 96734, USA, kristent@hawaii.edu), José-Antonio Esteban (Research Department, Parques Reunidos Valencia S. A. L'Oceanogràfic, Ciudad de las Artes y las Ciencias, 46013 Valencia, Spain, investigacion@oceanografic.org)

Although much variation exists in jaw morphology among species, odontocetes are believed to receive sound primarily through the pan bone region of the lower jaw. In order to further examine this jaw hearing hypothesis, we tested the head receiving sensitivity and directional hearing of a beluga whale, Delphinapterus leucas. Hearing measurements were conducted with a 9-yr-old female beluga using the auditory evoked potential technique. A preliminary audiogram indicated that the subject had very sensitive hearing (45-55dB from 32-80 kHz) and heard up to 128 kHz. The pathway investigation used a piezo-electric transducer to present the click stimuli, whereas the hearing directivity was measured in the far field, also using broadband clicks. Like the bottlenose dolphin, the subject had a region of high sensitivity around the pan bone region (78 dB), however, unlike the bottlenose dolphin, we found that the region of maximum sensitivity was at the tip of the lower jaw (75dB). The subject also proved to have highly directional hearing. This study supports the shaded receiver hypothesis and also shows that hearing pathway variations appear to exist among odontocete species and are at least partially dependent on head morphology.

9:20

4aABa5. Evoked potential and behavioral hearing thresholds in nine bottlenose dolphins (Tursiops truncatus). Carolyn E. Schlundt (EDO Professional Services, 3276 Rosecrans St., San Diego, CA 92110, USA, carolyn.melka@edocorp.com), James J. Finneran (US Navy Marine Mammal Program, Space and Naval Warfare Systems Center, 53560 Hull St., Code 71510, San Diego, CA 92152, USA, james.finneran@navy.mil), Brian K. Branstetter (US Navy Marine Mammal Program, Space and Naval Warfare Systems Center, 53560 Hull St., Code 71510, San Diego, CA 92152, USA, branstet@hawaii.edu), Randall L. Dear (Science Applications International Corporation, 4065 Hancock St., San Diego, CA 92110, USA, RANDALL.L.DEAR@saic.com), Dorian S. Houser (Biomimetica, 7951 Shantung Dr., Santee, CA 92071, USA, dhouser@spawar.navy.mil), Erica Hernandez (University of Southern Mississippi, Department of Psychology, 118 College Dr., Box 5025, Hattiesburg, MS 39406, USA, erica.hernandez@yahoo.com)

Auditory evoked potentials are popular for assessing hearing in marine mammals because they do not require the same access to and training of animals as behavioral methods; however, within-subject comparisons of behavioral and electrophysiological thresholds are still necessary to benchmark evoked potential results against the more universally accepted behavioral data. In this study, auditory thresholds were measured in nine dolphins using both behavioral and electrophysiological methods. Subjects included eight males and one female, ages 21-43 yrs. Some had a full-range of hearing and others exhibited high-frequency hearing loss. Tests were conducted in-air, in San Diego Bay, and/or in quiet pools. Hearing test stimuli included frequency-modulated, amplitude-modulated, or pure tones projected in the direct field or via a ″jawphone″ contact transducer. Comparisons reveal good agreement between the evoked potential and behavioral methods, particularly when the testing environments, stimulus delivery methods, and stimulus waveforms are similar. The results show that evoked potential thresholds obtained in a variety of conditions provide reasonable approximations to underwater sensitivity, especially with respect to the shape of the audiogram and the upper limit of hearing.

9:40

4aABa6. Interactions of frequency components of multi-component envelope following response in a beluga. Alexander Y. Supin (Institute of Ecology and Evolution, 33 Leninsky Prospect, 119071 Moscow, Russian Federation, alex_supin@mail.ru), Vladimir V. Popov (Institute of Ecology and Evolution, 33 Leninsky Prospect, 119071 Moscow, Russian Federation, popov_vl@sevin.ru)

The envelope-following response (EFR) in odontocetes is composed of overlapping ABRs produced by each cycle of rhythmic sound stimulus at a rate of a few hundred cycles per sec. It has been shown recently (Finneran et al., JASA 2007, 121: 1775) that a complex stimulus consisting of a few carriers modulated by different rates produces a complex EFR composed of components reproducing all the modulation rates. Using this technique, interactions between different components of complex EFR were investigated in a beluga whale Delphinapterus leucas. When all carriers of the complex stimulus were equalized by SPL, the interaction depended on both the SL of carriers (their level relative the threshold) and inter-carrier frequency spacing. Addition of components of higher SL (at low-threshold

frequencies) dramatically reduced the amplitudes of other EFR components, especially at short frequency spacing. The leading factor of this reduction was decreasing of the modulation depth of each of the carriers when the overall power of the stimulus increased by additional components. The threshold estimate of each carrier little depended on the number of components; however precision of threshold determination fell down with increasing the number of stimulus components due to the reduced amplitudes of EFR components.

10:00

4aABa7. Acoustic communication in Panthera tigris: A study of tiger vocalization and auditory receptivity revisited. Edward Walsh (Boys Town National Research Hospital, 555 North 30th Street, Omaha, NE 68132, USA, walsh@boystown.org), Douglas L. Armstrong (Henry Doorly Zoo, 3701 S. 10th, Omaha, NE 68107, USA, douga@omahazoo.com), Julie Napier (Henry Doorly Zoo, 3701 S. 10th, Omaha, NE 68107, USA, julie.napier@omahazoo.com), Lee G. Simmons (Henry Doorly Zoo, 3701 S. 10th, Omaha, NE 68107, USA, lsimmons@omahazoo.com), Megan Korte (Boys Town National Research Hospital, 555 North 30th Street, Omaha, NE 68132, USA, kortem@boystown.org), Joann McGee (Boys Town National Research Hospital, 555 North 30th Street, Omaha, NE 68132, USA, mcgee@boystown.org)

Preliminary findings reported at the 145th meeting of the Society suggested that confrontational tiger roars contain energy in the infrasonic portion of the electromagnetic spectrum. This discovery generally supported the proposition that free ranging individuals may take advantage of this capability to communicate with widely dispersed conspecifics inhabiting large territories in the wild. Preliminary ABR findings indirectly supported this view suggesting that although tigers are most sensitive to acoustic events containing energy in the 0.3 to 0.5 kHz band, they are most likely able to detect acoustic events in the near-infrasonic and infrasonic range based on the assumption that felid audiograms exhibit uniform shapes. In this study, the spectral content of territorial and confrontational roars was analyzed and relevant features of ABR based threshold-frequency curves were considered in relation to the acoustical properties of both roar types. Unlike the confrontational roar, infrasonic energy was not detected in the territorial roar; however, like the confrontational roar, peak acoustic power was detected in a frequency band centered on ~ 0.3 kHz. In addition, ABR recordings acquired in a double walled sound attenuating chamber recently installed at the Henry Doorly Zoo suggest that acoustic sensitivity is significantly underestimated under ″field″ conditions.

THURSDAY MORNING, 3 JULY 2008 ROOM 342B, 10:40 A.M. TO 1:00 P.M.

Session 4aABb

Animal Bioacoustics: Sound Production and Reception in Amphibious Marine Mammals

Jason Mulsow, Cochair
UCSC Institute of Marine Sciences, Long Marine Lab - University of California, 100 Shaffer Road, Santa Cruz, CA 95060, USA

Ronald J. Schusterman, Cochair
UCSC Institute of Marine Sciences, Long Marine Lab - University of California, 100 Shaffer Road, Santa Cruz, CA 95060, USA

Ian Boyd, Cochair
Sea Mammal Research Unit, Gatty Marine Laboratory, University of St Andrews, St Andrews, KY16 8LB, UK

Invited Papers

10:40

4aABb1. Vocal Learning in Pinnipeds: A Model System for Human Speech Evolution. William T. Fitch (Centre for Social Learning and Cognitive Evolution, University of St.Andrews, School of Psychology, KY16 9JP St.Andrews, Fife, UK, wtsf@st-andrews.ac.uk), Ronald J. Schusterman (UCSC Institute of Marine Sciences, Long Marine Lab - University of California, 100 Shaffer Road, Santa Cruz, CA 95060, USA, rjschust@ucsc.edu), Colleen Reichmuth (UCSC Institute of Marine Sciences, Long Marine Lab - University of California, 100 Shaffer Road, Santa Cruz, CA 95060, USA, coll@ucsc.edu), Marija Spasikova (Centre for Social Learning and Cognitive Evolution, University of St.Andrews, School of Psychology, KY16 9JP St.Andrews, Fife, UK, marija.spasikova@gmail.com), Daniel Mietchen (Structural Brain Mapping Group, University of Jena, PF 07737 Jena, Germany, daniel.mietchen@googlemail.com)

Vocal learning is limited to a small subset of vertebrates: including birds (songbirds, parrots, hummingbirds), and mammals (humans, cetaceans, pinnipeds, and probably elephants and bats). Intriguingly, in most of these species, vocal production involves functionally or mechanistically novel systems: the avian syrinx, the nasal bursae in odontocetes, and ultrasonic echolocation in bats. The novel neural circuitry that evolved to control these systems may provide a ″preadaptation″ for vocal learning. Only two known vocal learners - humans and seals - definitely use the standard vertebrate vocal production system (larynx and vocal tract). Our studies of vocal production in harbour seals verify a surprisingly human-like vocal production system, and the critical question remaining is what neural mechanisms underlie the control of the Phoca vocal system, and whether such ″human″ specializations as direct cortico-ambiguual connections are also found in seals. Pinniped investigations also open the door to molecular exploration of the genetic bases for neural innovations. In addition to these mechanistic questions, we discuss evolutionary questions. What functional forces might select for vocal learning in aquatic mammals? One hypothesis is that selection for control of breathing may provide a preadaptation for enhanced cortical vocal control, explaining its prevalence in marine mammals.

11:00

4aABb2. Sound production by pinnipeds can be modified by contingency learning. Ronald J. Schusterman (UCSC Institute of Marine Sciences, Long Marine Lab - University of California, 100 Shaffer Road, Santa Cruz, CA 95060, USA, rjschust@ucsc.edu), Colleen Reichmuth (UCSC Institute of Marine Sciences, Long Marine Lab - University of California, 100 Shaffer Road, Santa Cruz, CA 95060, USA, coll@ucsc.edu)

In contrast to terrestrial mammals, pinnipeds (seals, sea lions and walruses) have remarkable flexibility in the ways that they can learn to use and modify their amphibious sound emissions. The experiments that we will describe are drawn from captive studies which show that changes in sound production can occur as a result of contingency learning, using food as positive reinforcement. A range of specialized physiological and anatomical adaptations appear to play a critical role in controlling sound production in pinnipeds. These adaptations include breath-holding and buoyancy mechanisms, as well as fine muscular control of the mouth, lips and tongue that may be used primarily in feeding. The manipulation and modulation of air flow through these components of the vocal tract and associated super-laryngeal filters appears to be susceptible to some of the same reinforcing consequences that are routinely used to establish reliable control over motor behaviors, such as flipper waving, in operant conditioning contexts.

11:20

4aABb3. Inertial and cochlear constraints for high-frequency hearing in phocid and otariid pinnipeds. Sirpa Nummela (University of Helsinki, Department of Biological and Environmental Sciences, PO Box 65 (Viikinkaari 1), FI-00014 Helsinki, Finland, snummela@fastmail.fm), Simo Hemilä (University of Helsinki, Department of Biological and Environmental Sciences, PO Box 65 (Viikinkaari 1), FI-00014 Helsinki, Finland, simo.hemila@welho.com), Annalisa Berta (San Diego State University, Biology Department, LS 250, San Diego, CA 92182-4614, USA, aberta@sciences.sdsu.edu), Tom Reuter (University of Helsinki, Department of Biological and Environmental Sciences, PO Box 65 (Viikinkaari 1), FI-00014 Helsinki, Finland, tom.reuter@helsinki.fi)

In air-borne hearing, mammals rely on sound transmission through the tympanic membrane and middle ear ossicles between the surrounding air and the cochlea. The high-frequency hearing limit (HFHL) is determined by the ossicular inertia, and also by the cochlear sensitivity. Due to coevolution, the sensitivity ranges of the middle and inner ear structures generally overlap, and the roles of inertial and cochlear constraints for the HFHL are difficult to discern. For studying this question we considered anatomical and experimental data for two phocid and two otariid pinnipeds. While any detailed mechanism for pinniped underwater hearing remains unclear, an underwater HFHL exceeding that in air is possible. Published in-air and underwater audiograms provide an opportunity for comparing the roles of ossicular mass inertia and cochlear sensitivity in HFHL. Phocid ossicles are very heavy, and their inertia explains the lower HFHLs in air - according to underwater audiograms the phocid cochlea is sensitive to higher frequencies. Otariids have normal-sized mammalian ossicles, and their inertia should allow underwater hearing at higher frequencies than in air. However, the HFHL is approximately equal in air and water for otariids, hence their underwater HFHL is apparently set by the cochlea alone.

11:40

4aABb4. Evoked potential audiometry in sea lions. Jason Mulsow (UCSC Institute of Marine Sciences, Long Marine Lab - University of California, 100 Shaffer Road, Santa Cruz, CA 95060, USA, jmulsow@ucsc.edu), Colleen Reichmuth (UCSC Institute of Marine Sciences, Long Marine Lab - University of California, 100 Shaffer Road, Santa Cruz, CA 95060, USA, coll@ucsc.edu)

Auditory sensitivity in the otariid pinnipeds (sea lions and fur seals) has traditionally been studied using a relatively small number of trained subjects and psychophysical techniques. Recent refinement of auditory evoked potential techniques with odontocete cetaceans has elevated interest in adapting these methods for sea lion subjects, with the goal of increasing sample size and efficiency in audiometric studies. To date, several basic electrophysiological characteristics of the California sea lion (*Zalophus californianus*) auditory system have been described, and these findings have allowed for the development of more advanced techniques in investigations of sea lion hearing. Most notable is the recording of the envelope following response (EFR) evoked by narrow-band, sinusoidally amplitude-modulated tones. This method can provide significant advantages in the detection of low-amplitude electrophysiological signals in noise using Fourier analysis and objective statistical detection of responses. Currently, EFR audiometry in the California sea lion and Steller sea lion (*Eumetopias jubatus*) is proving to be a promising method for rapidly assessing the variation of hearing capabilities among individuals, including the detection of hearing loss.

12:00

4aABb5. Air and bone conduction evoked potential audiometry in the northern elephant seal. Dorian S. Houser (Biomimetica, 7951 Shantung Dr., Santee, CA 92071, USA, dhouser@spawar.navy.mil), Daniel Crocker (Sonoma State University, Department of Biology, 1801 East Cotati Avenue, Rohnert Park, CA 94928, USA, crocker@sonoma.edu), James J. Finneran (US Navy Marine Mammal Program, Space and Naval Warfare Systems Center, 53560 Hull St., Code 71510, San Diego, CA 92152, USA, james.finneran @navy.mil)

Elephant seals (*Mirounga angustirostris*) are the largest and most aquatic of the pinnipeds, spending up to eight months of the year at sea diving to depths as great as 1600 m. The pinna is absent in the elephant seal and the middle ear cavity and auditory canal are lined with a cavernous tissue, both of which are likely adaptations to deep diving. Elephant seals demonstrate a greater sensitivity to low frequency sounds than do other pinnipeds and an overall greater sensitivity to underwater sound than to airborne sound. The relative importance of sound conduction pathways in the elephant seal is undetermined, although it has been speculated that bone conduction pathways are important to underwater hearing in this species. To compare the sensitivity of the elephant seal to both air and bone conducted stimuli, auditory evoked responses were recorded in seals exposed to signals presented through headphones and via a bone vibrator. In comparison to airborne stimuli, bone conduction methods provide an opportunity to more effectively study sensitivity to low frequency sounds, but are challenged by a lack of reference equivalent threshold sound pressure levels. Future efforts should compare bone conduction and direct field audiometry results obtained within the same individual.

12:20

4aABb6. Preliminary Results of a Behavioral Audiometric Study of the Polar Bear. Ann E. Bowles (Hubbs-Sea World Research Institute, 2595 Ingraham Street, San Diego, CA 92109, USA, abowles@hswri.com), Megan A. Owen (Conservation and Research for Endangered Species, Zoological Society of San Diego, PO Box 120551, San Diego, CA 92112-0551, USA, mowen@sandiegozoo.org), Samuel L. Denes (Hubbs-Sea World Research Institute, 2595 Ingraham Street, San Diego, CA 92109, USA, sdenes@hswri.org), Stefanie K. Graves (Hubbs-Sea World Research Institute, 2595 Ingraham Street, San Diego, CA 92109, USA, sgraves@hswri.org), Jennifer L. Keating (Hubbs-Sea World Research Institute, 2595 Ingraham Street, San Diego, CA 92109, USA, jenniferlkeating@hotmail.com)

The hearing of polar bears is of great interest because little is known about hearing of large terrestrial carnivores, they are amphibious, their predatory habits differ from most bears, and there is an increasing need for data to manage anthropogenic noise in maternal denning habitat. Behavioral auditory thresholds were collected from two female polar bears at the San Diego Zoo (ZSSD) in 2006-2007, and are now underway with two females and a male at SeaWorld San Diego (SWSD). Thresholds were measured at 19 frequencies between 125 Hz and 31.5 kHz using shaped 500 ms tones, a 'go/no-go' response protocol, and staircase presentation order with catch trials. Holding areas in both facilities were sound-isolated to the extent practicable. Threshold measurements were limited by background noise below 5 kHz, but sensitivity could be measured to below 0 dB at higher frequencies. To date, the bears have detected sounds down to the noise floor from 125 Hz to about 14 kHz. Their sensitivity declines rapidly above 20 kHz. The results suggest that their auditory threshold functions are narrower or shifted to lower frequencies than those of small carnivores. [Supported by Polar Bears International, ZSSD, SWSD and the author's organizations]

12:40

4aABb7. Variation in pup vocalisations and mother-pup behaviour between harp seal whelping patches: effects of climate or geography? Ilse Catharina Van Opzeeland (Alfred Wegener Institute, P.O. Box 120161, 27515 Bremerhaven, Germany, Ilse.Van.Opzeeland@awi.de), Peter J. Corkeron (US NOAA, Northeast Fisheries Science Center, 166 Water Street, Woods Hole, MA 02543, USA, peter.corkeron@gmail.com), Denise Risch (US NOAA, Northeast Fisheries Science Center, 166 Water Street, Woods Hole, MA 02543, USA, drisch@whsun1.wh.whoi.edu), Gary B. Stenson (Dept of Fisheries and Oceans, P.O. Box 5667, St John's, NL A1C5X1, Canada, StensonG@DFO-MPO.GC.CA), Sofie Van Parijs (US NOAA, Northeast Fisheries Science Center, 166 Water Street, Woods Hole, MA 02543, USA, sofie.vanparijs@noaa.gov)

Harp seals breed in pack-ice, a substrate which can vary substantially between whelping patches depending on differing environmental and oceanographic conditions. This study demonstrates clear site differences in pup vocalizations and mother pup behaviour between Northeast (Greenland Sea) and Northwest (Canadian Front) Atlantic harp seal populations. Classification trees showed a distinctive split between Front and Greenland Sea pup vocalisations. No clear sex differentiation in vocalizations was present for pups at the Front; 42% (n = 12) of male and 38% (n = 13) of female calls could be attributed to a given individual. In the Greenland Sea, 55% (n = 42) of female vocalisations were attributed to individuals compared with only 8% for males (n = 47). In addition behavioural observations of mother pup pairs were conducted (Front, n = 58; Greenland Sea, n = 78). Greenland Sea pups were found to nurse more, and were more alert than Front pups. Female attendance patterns also differed between sites: females at the Front were more likely to attend their pups than those in the Greenland Sea. This marked difference in female presence between sites could have several origins such as variability in ice conditions, predation pressure, or female condition.

Session 4aAO

Acoustical Oceanography, Signal Processing in Acoustics, and ECUA: Adjoint Modeling for Geoacoustic Inversion

Paul Hursky, Cochair
HLS Research, Inc., 3366 N. Torrey Pines Ct., Ste. 310, La Jolla, CA 92037, USA

Jean-Pierre Hermand, Cochair
Université libre de Bruxelles (U.L.B.) - Environmental hydroacoustics lab, av. Franklin D. Roosevelt 50, CP 194/5, Bruxelles, 1050, Belgium

Invited Papers

11:00

4aAO1. Validation of adjoint-generated environmental gradients for the acoustic monitoring of a shallow water area. Matthias Meyer (Royal Netherlands Naval College (NLDA) - REA group, PO Box 10000, 1780 Den Helder, Netherlands, mmeyer@ulb.ac.be), Jean-Pierre Hermand (Université libre de Bruxelles (U.L.B.) - Environmental hydroacoustics lab, av. Franklin D. Roosevelt 50, CP 194/5, 1050 Bruxelles, Belgium, jhermand@ulb.ac.be), Mohamed Berrada (Laboratoire d'Océanographie et du Climat - Expérimentation et Approches Numériques, Université Pierre et Marie Curie, Tour 45-55 - 5ème étage - 4, place Jussieu, 75005 Paris, France, mohamed.berrada@locean-ipsl.upmc.fr), Mark Asch (Université de Picardie Jules Verne, LAMFA (CNRS UMR 6140), 33 Rue Saint Leu, 80039 Amiens, France, mark.asch@u-picardie.fr)

In the framework of the recent Maritime Rapid Environmental Assessment sea trial MREA07/BP'07 [Le Gac&Hermand, 2007] that was conducted in the same area south of the island of Elba as the earlier Yellow Shark trial (YS94), this paper examines the original YS94 acoustic data and the recent MREA07 oceanographic data to demonstrate adjoint-based acoustic monitoring of environmental parameters in Mediterranean shallow waters. First, adjoint-generated environmental gradients are validated for the application in geoacoustic inversion where the bottom acoustic parameters of the YS94 layered seabed are determined from the long-range waterborne propagation of a multi-frequency signal. Then, for the application in ocean acoustic tomography, the temporal variability of the MREA07/BP'07 oceanographic data is analyzed in terms of empirical orthogonal functions and the adjoint-based inversion scheme is used to track the time-varying sound speed profile of the experimental transect.

11:20

4aAO2. Variational assimilation of simulated ocean acoustic tomography data in an ocean model. Elisabeth Remy (Mercator-Ocean, Parc Technologique du Canal, 8-10 rue Hermès, 31520 Ramonville Saint Agne, France, eremy@mercator-ocean.fr), Fabienne Gaillard (LPO-IFREMER, BP 70, 29280 Plouzane, France, fabienne.gaillard@ifremer.fr), Jacques Verron (Laboratoire des Ecoulements Géophysiques et Industriels (LEGI), BP 53, 38041 Grenoble Cedex 9, France, verron@hmg.inpg.fr)

In the concept of large scale observing system for the ocean, ocean acoustic tomography is an original tool to monitor the ocean interior. Analysis of tomographic travel time using inversion gives an estimate of the temporal evolution of the heat content along the observed sections, an important quantity to monitor the ocean climate evolution. At lower scales than the cell size defined by the observational array, it is not possible to estimate the ocean temperature field without using other sources of information. A possible approach is to combine the tomographic observations with a numerical dynamical ocean model to obtain a complete description consistent with the data on a given time interval. We propose to explore a variational method using the adjoint technic to assimilate those integral data. We studied the case of a basin scale observational array, as the one deployed in the Mediterranean sea for the Thetis 2 experiment. Only travel time anomalies due to the sea water properties are considered. The ability of tomographic data to constrain the ocean model circulation is evaluated using simulated observations with a model solution. This approach called twin experiments, allows to compare the result after assimilation with the ''true'' solution.

Contributed Papers

11:40

4aAO3. Probabilistic PCA and Ocean Acoustic Tomography Inversion with an Adjoint Method. Mohamed Berrada (Laboratoire d'Océanographie et du Climat - Expérimentation et Approches Numériques, Université Pierre et Marie Curie, Tour 45-55 - 5ème étage - 4, place Jussieu, 75005 Paris, France, mohamed.berrada@locean-ipsl.upmc.fr), Fouad Badran (Laboratoire CEDRIC, Conservatoire National des Arts et Métiers, 292, rue Saint Martin, 75003 Paris, France, badran@cnam.fr), Sylvie Thiria (Laboratoire d'Océanographie et du Climat - Expérimentation et Approches Numériques, Université Pierre et Marie Curie, Tour 45-55 - 5ème étage - 4, place Jussieu, 75005 Paris, France, Sylvie.Thiria@locean-ipsl.upmc.fr)

We present an Ocean Acoustic Tomography (OAT) inversion in a shallow water environment. The idea is to determine the celerity c(z), z is depth, knowing the acoustic pressures caused by a multiple frequencies source and collected by a sparse receiver array. The variational approach minimizes a cost function which measures the adequacy between the measurements and their forward model equivalent. This method introduces also a regularisation term in the form $(c(z)-c_b)^t B^{-1}(c(z)-c_b)$, which supposes that c(z) follows an a priori normal law. To circumvent the problem of estimating B^{-1}, we propose to model the celerity vectors by a probabilistic PCA. In contrast to the methods which use PCA as a regularization method and filter the useful information, we take a sufficient number of axes which allow the modelization of useful information and filter only the noise. The probabilistic PCA intro-

duces a reduced number of non correlated latent variables η which act as new control parameters introduced in the cost function. This new regularization term, expressed as $\eta^t\eta$, reduces the optimization computation time. In the following we apply the probabilistic PCA to an OAT problem, and present the results obtained when performing twin experiments.

12:00

4aAO4. Geoacoustic Adjoint-Based Inversion via the Parabolic Equation. John S. Papadakis (Institute of Applied & Computational Mathematics, Foundation for Research and Technology-Hellas (FORTH), Vassilika Vouton, P.O. Box 1385, GR-71110 Heraklion, Greece, johnsp@iacm.forth.gr), Jean-Pierre Hermand (Université libre de Bruxelles (U.L.B.) - Environmental hydroacoustics lab, av. Franklin D. Roosevelt 50, CP 194/5, 1050 Bruxelles, Belgium, jhermand@ulb.ac.be), Evangelia T. Flouri (Institute of Applied & Computational Mathematics, Foundation for Research and Technology-Hellas (FORTH), Vassilika Vouton, P.O. Box 1385, GR-71110 Heraklion, Greece, flouri@iacm.forth.gr), Matthias Meyer (Royal Netherlands Naval College (NLDA) - REA group, PO Box 10000, 1780 Den Helder, Netherlands, mmeyer@ulb.ac.be)

In this paper an analytic method is exhibited for recovering the acoustic parameters of the sub-bottom region in the ocean. The acoustic propagation problem is modeled via the wide angle parabolic equation and the bottom boundary condition used is in the form of a Neumann to Dirichlet or Dirichlet to Neumann map. The sub-bottom region is assumed homogeneous or horizontally stratified with homogeneous layers. The inversion is modeled as an optimal control problem, and the solution is based on the adjoint method. Several cost functions are introduced which make use of the relative amplitude of the observed complex field. The method is applied to several test cases and satisfactory convergence of the inversion scheme is exhibited.

12:20

4aAO5. Adjoint modeling for Acoustic Inversion based on an Adjoint Parabolic Equation. John S. Papadakis (Institute of Applied & Computational Mathematics, Foundation for Research and Technology-Hellas (FORTH), Vassilika Vouton, P.O. Box 1385, GR-71110 Heraklion, Greece, johnsp@iacm.forth.gr), Evangelia T. Flouri (Institute of Applied & Computational Mathematics, Foundation for Research and Technology-Hellas (FORTH), Vassilika Vouton, P.O. Box 1385, GR-71110 Heraklion, Greece, flouri@iacm.forth.gr)

In this paper the acoustic propagation problem is modeled by the wide angle parabolic equation and the bottom boundary condition is in the form of a Neumann to Dirichlet map. We formulate the inversion as an optimal control problem, the control parameters being the sound speed in the water and the sound speed, density and attenuation in the bottom. Using the adjoint operator to the wide angle parabolic equation, an inversion scheme is derived for the acoustic parameters of the water column and the bottom region. The optimization approach used is the method of steepest decent. Several test cases are exhibited.

THURSDAY MORNING, 3 JULY 2008 ROOM 352B, 8:00 A.M. TO 12:20 P.M.

Session 4aBB

Biomedical Ultrasound/Bioresponse to Vibration: Theoretical and Computational Models of Ultrasonic Propagation in Bones I

James G. Miller, Cochair
Washington University, Physics Box 1105, 1 BrookingsDrive, St. Louis, MO 63130, USA

Pascal Laugier, Cochair
Université Paris 6, Laboratoire d'Imagerie Paramétrique, 15, rue de l'Ecole de Médecine, Paris, 75006, France

Invited Papers

8:00

4aBB1. Recent developments in modeling and measuring scattering from trabecular bone. Keith A. Wear (U.S. Food and Drug Administration, Center for Devices and Radiological Health, 10903 New Hampshire Ave, Bldg 62, Rm 3108, Silver Spring, MD 20993, USA, keith.wear@fda.hhs.gov)

Laboratories at the US Food and Drug Administration, the University of Paris and elsewhere have investigated scattering from trabecular bone. Recent analysis of data from 23 human femur samples in vitro suggests that the Faran Cylinder Model and the Weak Scattering Model accurately predict frequency dependence of backscatter coefficient. Shear mode conversion of incident longitudinal waves may be a significant source of scattering loss. Other recent work involves the effect of errors of attenuation measurements on backscatter coefficient estimates. Backscatter measurements must be compensated for attenuation in order to estimate backscatter coefficient. However, attenuation is often overestimated because it is often measured using phase sensitive receivers that exhibit phase cancellation artifacts. Recent analysis of data from 16 human calcaneus samples in vitro suggests that backscatter coefficient estimates that are based on phase sensitive attenuation compensation tend to overestimate 1) average magnitude of backscatter coefficient at 500 kHz by a factor of about 1.6 $\pm$ 0.3 (mean $\pm$ standard deviation) and 2) average exponent (n) of frequency dependence by about 0.34 $\pm$ 0.12 (where backscatter coefficient is assumed to be proportional to frequency to the nth power).

8:20

4aBB2. The fast wave propagation in bovine cancellous bone-experiments and simulation. Mami Matsukawa (Doshisha University, 1-3, Tatara Miyakodani, 610-0321 Kyotanabe, Japan, mmatsuka@mail.doshisha.ac.jp), Katsunori Mizuno (Doshisha University, 1-3, Tatara Miyakodani, 610-0321 Kyotanabe, Japan, dtg0151@mail4.doshisha.ac.jp), Yoshiki Nagatani (Nara Medical University, 840 Shijo-cho, 634-8522 Kashihara, Japan, naramed-u@nagatani.ne.jp)

Cancellous bone is comprised of a complicated network of trabeculae and has strong anisotropy and inhomogeneity. In the cancellous bone, two types of longitudinal waves, fast and slow waves, are observed when the waves propagate parallel to the trabeculae direction. Paying attention to the wave front of observed waves, we have experimentally made clear the effect of anisotropy on the fast wave speeds and shown interesting relation between the mean trabeculae length and wave speeds (Mizuno et. al., IEEE Trans., UFFC, accepted), making use of the microstructural indices of the measured bone. We then compared the experimental results of fast waves with the simulation studies, using the three dimensional X-ray CT data and the Finite-Difference Time-Domain (FDTD) method. In spite of the lack of attenuation effects in the simulation, we can find interesting correlation between the fast wave speeds obtained by experiments and simulation. In addition, the characteristic attenuation behaviors of fast wave were found in both experiments and simulations. Attenuation of fast wave is always higher in the initial state of propagation, regardless of propagation direction and samples.

Contributed Papers

8:40

4aBB3. Experimental confirmation of negative dispersion and Bayesian inversion of multimode propagation in a bone-mimicking phantom. Adam Q. Bauer (Washington University, Physics Box 1105, 1 Brookings Drive, St. Louis, MO 63130, USA, abauer@hbar.wustl.edu), Christian C. Anderson (Washington University, Physics Box 1105, 1 Brookings Drive, St. Louis, MO 63130, USA, canderson@wustl.edu), Karen R. Marutyan (Department of Radiology, Washington University, 1 Brookings Drive, St. Louis, MO 63130, USA, karenmarutyan@gmail.com), G Larry Bretthorst (Department of Radiology, Washington University, 1 Brookings Drive, St. Louis, MO 63130, USA, gbretthorst@wustl.edu), Keith A. Wear (U.S. Food and Drug Administration, Center for Devices and Radiological Health, 10903 New Hampshire Ave, Bldg 62, Rm 3108, Silver Spring, MD 20993, USA, keith.wear@fda.hhs.gov), Mark R. Holland (Washington University, Physics Box 1105, 1 Brookings Drive, St. Louis, MO 63130, USA, mrh@wuphys.wustl.edu), James G. Miller (Washington University, Physics Box 1105, 1 Brookings Drive, St. Louis, MO 63130, USA, james.g.miller@wustl.edu)

Previously we demonstrated using numerical simulations that negative dispersion observed in bone can result from the interference of two propagating modes, each of which exhibits positive dispersion, consistent with the Kramers-Kronig predictions. [J. Acoust. Soc. Am. 120, EL55-61 (2006)] One goal of the present study was to demonstrate this negative dispersion experimentally using the simplest example of a bone-mimicking phantom that is capable of producing two such interfering modes. An additional goal was to establish that, with the experimental data serving as input to a Bayesian approach to the inverse problem [J. Acoust. Soc. Am. 121, EL8-15 (2007)], reliable estimates of the underlying properties of the bone-mimicking phantom could be obtained from the measured signals. The phantom consisted of a flat and parallel PlexiglasTM plate into which a step discontinuity was milled. The phase velocity and attenuation coefficient (3 to 7 MHz) of the phantom were measured with a 0.25-inch piezoelectric receiver and calculated using both broadband and narrowband data. Negative dispersion was observed at specific spatial locations near the step where the attenuation coefficient rose approximately linearly with frequency. Results demonstrate that interference between modes can result in negative dispersion and that Bayesian inversion can yield underlying material properties.

9:00

4aBB4. Modeling of ″anomalous″ velocity dispersion in trabecular bone: effect of multiple scattering and of viscous absorption. Guillaume Haiat (CNRS, Laboratoire de Recherches Orthopédiques, 10, Avenue de Verdun, 75010 Paris, France, haiat@univ-paris12.fr), Alain Lhémery (Commissariat à l'Energie Atomique, Bat 611, LIST, CEA Saclay, 91191 Gif-sur-Yvette, France, alain.lhemery@cea.fr), Frederic Padilla (Université Paris 6, Laboratoire d'Imagerie Paramétrique, 15, rue de l'Ecole de Médecine, 75006 Paris, France, Frederic.Padilla@lip.bhdc.jussieu.fr), Pascal Laugier (Université Paris 6, Laboratoire d'Imagerie Paramétrique, 15, rue de l'Ecole de Médecine, 75006 Paris, France, laugier@lip.bhdc.jussieu.fr), Salah Naili (Université Paris 12, B2OA, 61, Avenue du Général de Gaulle, 94010 Créteil, France, naili@univ-paris12.fr)

Speed of sound is now widely used in the clinic to assess bone strength and susceptibility to fracture. Therefore, much effort has been spent on the understanding of ultrasonic wave propagation in trabecular bone, which is an attenuating composite material in which negative values of velocity dispersion have been measured, but remain poorly explained physically. In this work, the physical determinants of velocity dispersion are described with a 2D homogenization model of the wave propagation in trabecular bone. The medium is assumed to be constituted of infinite viscoelastic cylinders (trabeculae) immersed in a saturating viscoelastic matrix (marrow). The coupling between multiple scattering and absorption phenomena allows the computation of phase velocity and of dispersion as a function of bone properties. Negative values of velocity dispersion are predicted, in good agreement with experimental results obtained in phantoms mimicking trabecular bone. In trabecular bone, mostly negative but also positive values of velocity dispersion are predicted, which spans within the range of values measured experimentally. Scattering effects are responsible for the negative values of dispersion whereas the frequency dependence of the attenuation coefficient in bone marrow and/or in the trabeculae is shown to induce an increase of dispersion.

9:20

4aBB5. Effects of elastic properties on the wave propagation in cancellous bones - a simulation study -. Yoshiki Nagatani (Nara Medical University, 840 Shijo-cho, 634-8522 Kashihara, Japan, naramed-u@nagatani.ne.jp), Takashi Saeki (Doshisha University, 1-3, Tatara Miyakodani, 610-0321 Kyotanabe, Japan, dth0915@mail4.doshisha.ac.jp), Mami Matsukawa (Doshisha University, 1-3, Tatara Miyakodani, 610-0321 Kyotanabe, Japan, mmatsuka@mail.doshisha.ac.jp), Takefumi Sakaguchi (Nara Medical University, 840 Shijo-cho, 634-8522 Kashihara, Japan, t-saka@naramed-u.ac.jp), Hiroshi Hosoi (Nara Medical University, 840 Shijo-cho, 634-8522 Kashihara, Japan, hosoi@naramed-u.ac.jp)

For diagnosing osteoporosis, ultrasonic systems are considered a powerful tool, because ultrasonic waves strongly depend on the elasticity and structure of cancellous bones. We have reported the separation of longitudinal waves into fast and slow waves, a phenomenon that is strongly connected to the alignment of bone trabeculae.In order to understand this complicated wave propagation, we have simulated the wave propagations with the finite-difference time-domain (FDTD) method using three-dimensional X-ray CT images of actual cancellous bones. In this simulation, the effects of elastic properties in the solid portions are important. One idea is to adopt the experimentally observed ultrasonic properties of cortical bone. However, we should remind the possible problems like the elasticity difference between cancellous and cortical bones, individual differences, and anisotropy.

In this study, then, we have investigated the influences of elastic properties, Poisson's ratio, and densities of solid portion (trabeculae). As a result, we confirmed that the small changes give strong influences on not only the wave speed but also the amplitudes of fast and slow waves. The influence on the amplitudes seems to come from the changes of acoustic impedance of trabeculae. The results show the importance of elastic properties in the simulation.

9:40

4aBB6. Wave propagation in cancellous bone in terms of Biot's theory. Michal Pakula (Université Paris 6, Laboratoire d'Imagerie Paramétrique, 15, rue de l'Ecole de Médecine, 75006 Paris, France, michalp@ukw.edu.pl), Frederic Padilla (Université Paris 6, Laboratoire d'Imagerie Paramétrique, 15, rue de l'Ecole de Médecine, 75006 Paris, France, Frederic.Padilla@lip.bhdc.jussieu.fr), Mariusz Kaczmarek (Institute of Environmental Mechanics and Applied Computer Science, Kazimierz Wielki University, ul. Chodkiewicza 30, 85-064 Bydgoszcz, Poland, mkk@rose.man.poznan.pl), Pascal Laugier (Université Paris 6, Laboratoire d'Imagerie Paramétrique, 15, rue de l'Ecole de Médecine, 75006 Paris, France, laugier@lip.bhdc.jussieu.fr)

The paper is focused on modelling of wave propagation in cancellous bones using Biot's theory. Almost all required input mechanical and structural parameters for 31 pure femoral trabecular bone specimens were measured individually. Then frequency dependent wave parameters predicted by the model were compared with the results of ultrasonic tests performed on the same specimens. To compare the predictions to measurements, additional interactions of the plane harmonic wave with the slab of cancellous was considered. The most important finding is the significant contribution of the fluid/bone and bone/fluid boundaries on the global attenuation loss. The corrected values of attenuation coefficient are of the same order of magnitude compared to measured values. The theoretical results exhibit higher attenuation of fast wave compared to that of the slow wave in good agreement with experimental observations. Moreover the amplitude ratio of simulated time domain signals of both longitudinal waves (accordingly to the Biot's model with boundary corrections), are of the same order of magnitude compared to the amplitude ratio of experimental time records. However, an analysis in the frequency domain shows that the frequency content of the simulated pulses of the fast and slow wave differs from that observed in the experiments.

10:00

4aBB7. Experimental and numerical investigation of ultrasonic transmission through the skull bone and associated temperature rise. Mathieu Pernot (Laboratoire Ondes et Acoustique, ESPCI, Université Paris 7, CNRS, 10 rue Vauquelin, 75005 Paris, France, mathieu.pernot@espci.fr), Emmanuel Bossy (Laboratoire Photons et Matière, ESPCI/CNRS, 10 rue Vauquelin, 75231 Paris Cedex 05, France, emmanuel.bossy@espci.fr), Marie Muller (Laboratoire Ondes et Acoustique, ESPCI, Université Paris 7, CNRS, 10 rue Vauquelin, 75005 Paris, France, marie.muller@espci.fr), Christine Boué (Laboratoire Photons et Matière, ESPCI/CNRS, 10 rue Vauquelin, 75231 Paris Cedex 05, France, christine.boue@espci.fr), Jean-François Aubry (Laboratoire Ondes et Acoustique, ESPCI, Université Paris 7, CNRS, 10 rue Vauquelin, 75005 Paris, France, jean-francois.aubry@espci.fr), Mickael Tanter (Laboratoire Ondes et Acoustique, ESPCI, Université Paris 7, CNRS, 10 rue Vauquelin, 75005 Paris, France, michael.tanter@espci.fr), Mathias Fink (Laboratoire Ondes et Acoustique, ESPCI, Université Paris 7, CNRS, 10 rue Vauquelin, 75005 Paris, France, mathias.fink@espci.fr), Albert-Claude Boccara (Laboratoire Photons et Matière, ESPCI/CNRS, 10 rue Vauquelin, 75231 Paris Cedex 05, France, boccara@optique.espci.fr)

The feasibility of transcranial high-intensity focused-ultrasound (HIFU) therapy within the brain relies on the ability to transmit ultrasound through the skull bone at relatively high ultrasound power. Absorption of ultrasound through the skull bone may cause important temperature rises, and is therefore an important parameter to control. Ultrasonic measurements have shown that the ultrasound beam undergoes a significant attenuation when propagating through the skull, with values on the order of 10 to 20 dB/cm/MHz. To predict temperature rise from such values, it is fundamental to weigh the relative role of absorption to the total ultrasonic attenuation (scattering + absorption + specular reflection). In this work, two types of numerical simulations and experiments are performed to investigate this relative role. Through-transmission of 1 MHz ultrasound was performed numerically using a 3D Finite-Difference Time-Domain (FDTD) algorithm coupled to a 3D bone model obtained from high-resolution synchrotron microtomography, and compared to experimental measurements obtained with the same bone sample. Temperature rises were numerically simulated using the 3D bone model coupled to the heat equation, and compared to infrared thermography obtained experimentally while high-intensity ultrasound was propagating through the sample.

10:20-10:40 Break

10:40

4aBB8. Ultrasound simulation in the distal radius using clinical high-resolution CT images. Jonathan J. Kaufman (CyberLogic, Inc., 611 Broadway, Suite 707, New York, NY 10012, USA, jjkaufman@cyberlogic.org), Vincent Le Floch (Ecole Nationale Supérieure d'Arts et Métiers, Provence-Alpes-Cote-d'Azur, 13090 Aix-en-Provence, France, jjkaufman@cyberlogic.org), Donald J. McMahon (College of Physicians and Surgeons, Columbia University, 630 West 168th Street, New York, NY 10032, USA, jjkaufman@cyberlogic.org), Gangming Luo (CyberLogic, Inc., 611 Broadway, Suite 707, New York, NY 10012, USA, jjkaufman@cyberlogic.org), Adi Cohen (College of Physicians and Surgeons, Columbia University, 630 West 168th Street, New York, NY 10032, USA, jjkaufman@cyberlogic.org), Elizabeth Shane (College of Physicians and Surgeons, Columbia University, 630 West 168th Street, New York, NY 10032, USA, jjkaufman@cyberlogic.org), Robert S. Siffert (Mount Sinai School of Medicine, One Gustave L. Levy Place, New York, NY 10029, USA, jjkaufman@cyberlogic.org)

The overall objective of this research is to develop an ultrasonic method for non-invasive assessment of the distal radius. The specific objective of this study was to examine the propagation of ultrasound through the distal radius and determine the relationships between bone mass and architecture and ultrasound parameters. Twenty-six high-resolution peripheral-CT clinical images were obtained from a set of subjects that were part of a larger study on secondary osteoporosis. A single mid-section binary slice from each image was selected and used in the 2D simulation of an ultrasound wave propagating from the anterior to the posterior surfaces of each radius. Mass and architectural parameters associated with each radius, including total bone mass, volume fraction, trabecular number, and trabecular thickness were computed. Ultrasound parameters, including net time delay (NTD), broadband ultrasound attenuation (BUA), and ultrasound velocity (UV) were also evaluated. Significant correlations were found between NTD and total bone mass ($R2 = 0.92$), BUA and trabecular number ($R2 = 0.78$), and UV and trabecular bone volume fraction ($R2 = 0.82$). The study shows that ultrasound measurements are correlated with bone mass and architecture at the distal radius, and thus ultrasound may prove useful as a method for non-invasive assessment of osteoporosis and fracture risk.

11:00

4aBB9. Guided ultrasound wave propagation in cortical bone with microstructure using the gradient elasticity theory. Maria G. Vavva (University of Ioannina, Unit of Medical Technology and Intelligent Information Systems, Department of Computer Science and Department of Material Science and Engineering, GR 45110 Ioannina, Greece, mvavva@cc.uoi.gr), Vasilios C. Protopappas (University of Ioannina, Unit of Medical Technology and Intelligent Information Systems, Department of Computer Science and Department of Material Science and Engineering, GR 45110 Ioannina, Greece, vprotop@cc.uoi.gr), Leonidas N. Gergidis (University of Ioannina, Department of Material Science and Engineering, GR 45110 Ioannina, Greece, lgergidi@uoi.gr), Antonios Charalambopoulos (University of Ioannina, Department of Material Science and Engineering, GR 45110 Ioannina, Greece, acharala@cc.uoi.gr), Dimitrios I. Fotiadis (University of Ioannina, Unit of Medical Technology and Intelligent Information Systems, Department of Computer Science and Department of Material Science and Engineering, GR 45110

Ioannina, Greece, fotiadis@cc.uoi.gr),Demos Polyzos(University of Patras, Department of Mechanical Engineering and Aeronautics, GR 26500 Patras, Greece, polyzos@mech.upatras.gr)

Ultrasonic characterization of bone has been largely based on the linear theory of classical elasticity. However, the classical theory cannot adequately describe the mechanical behavior of materials with microstructure. In such materials, the stress state has to be defined in a nonlocal manner by employing theories, such as those proposed by Cosserat brothers, Mindlin (gradient elastic theory) and Eringen. In this study, we adopt the simplest form of gradient theory (Mindlin FormII) to model the cortical bone's microstructural effects in a macroscopic framework. The frequency characteristic equations are analytically derived for a bone plate (4mm thick, density 1.5 g/cm^3, bulk longitudinal velocity 4107 m/s). The plate is assumed free of stresses, as in the classical Lamb problem, and free of double stresses. The volumetric strain gradient energy coefficient, g (a measure of internal length), is equal to 10^{-4} and 10^{-5} m, i.e. of the order of the osteons size. The velocity dispersion curves of guided waves are numerically obtained using root-finding techniques and compared with those of the Lamb waves. It is shown that microstructure affects mode dispersion by inducing both material and geometrical dispersion. In conclusion, bone models with microstructure can contribute to the interpretation of in vivo measurements.

11:20

4aBB10. Investigation of the porous network as a determinant of the overall stiffness of cortical bone: Mori-Tanaka model vs. ultrasound propagation. Cécile Baron (Université Paris 6, Laboratoire d'Imagerie Paramétrique, 15, rue de l'Ecole de Médecine, 75006 Paris, France, norabelic@yahoo.fr), Quentin Grimal (Université Paris 6, Laboratoire d'Imagerie Paramétrique, 15, rue de l'Ecole de Médecine, 75006 Paris, France, quentin.grimal@lip.bhdc.jussieu.fr), Maryline Talmant (Université Paris 6, Laboratoire d'Imagerie Paramétrique, 15, rue de l'Ecole de Médecine, 75006 Paris, France, talmant@lip.bhdc.jussieu.fr), Pascal Laugier (Université Paris 6, Laboratoire d'Imagerie Paramétrique, 15, rue de l'Ecole de Médecine, 75006 Paris, France, laugier@lip.bhdc.jussieu.fr)

Assessing the effect of porosity on stiffness in cortical bone remains an important issue that has already been addressed with several models. The originality of the present work is to compare two models of cortical bone: one uses a realistic porous network (voxel 20 microns) reconstructed from synchrotron radiation tomography; the other considers cylindrical pores aligned in a single direction. In the first case, overall elastic properties are evaluated indirectly by means of finite difference time domain simulation of ultrasound bulk wave propagation at 1 MHz. In the second model, effective elasticity is calculated by means of a Mori-Tanaka scheme based on Eshelby solution for cylindrical inclusions with ellipsoidal cross section. Overall properties were evaluated with the two methods for 18 porosity values, each corresponding to a reconstructed bone volume. The diagonal stiffness coefficients of the overall bone material estimated with the two methods compared well. Results for the stiffness coefficient in the longitudinal bone direction are indistinguishable, which indicates that the detailed geometry and distribution of the pores have a negligible effect on the longitudinal stiffness. For the other stiffness coefficients, the Mori-Tanaka method slightly overestimates the stiffness compared to the wave propagation evaluation.

11:40

4aBB11. Numerical modelling and in-vitro studies of ultrasound signal loss across fractures in cortical bone mimics. Victor F. Humphrey (Institute of Sound and Vibration, Univ. of Southampton, University Road, Highfield, SO17 1BJ Southampton, UK, vh@isvr.soton.ac.uk), Simon P. Dodd (University of Bath, School of Management, Claverton Down, BA2 7AY Bath, UK, S.Dodd@bath.ac.uk), Sabina Gheduzzi (University of Bath, Centre for Orthopaedic Biomechanics, Dept. of Mechanical Engineering, BA2 7AY Bath, UK, S.Gheduzzi@bath.ac.uk), James L. Cunningham (University of Bath, Centre for Orthopaedic Biomechanics, Dept. of Mechanical Engineering, BA2 7AY Bath, UK, J.L.Cunningham@bath.ac.uk), Anthony W. Miles (University of Bath, Centre for Orthopaedic Biomechanics, Dept. of Mechanical Engineering, BA2 7AY Bath, UK, A.W.Miles@bath.ac.uk)

The propagation of 200 kHz ultrasonic waves along cortical bone mimics and across a simulated fracture has been investigated using a Finite Difference numerical model. The first arrival signal (FAS) transit time and peak amplitude have been calculated as a function of range at 200kHz in order to help understand the factors that determine the propagation across a fracture. The variation in the amplitude of the first peak of the reradiated wave is studied as a function of the gap width and shape. The results compare well with experimental measurements made in vitro using an axial transmission technique on cortical bone mimics and bovine cortical bone samples. The effects of various stages of the healing process have also been considered by introducing different fracture geometries into the plate model. Changing the geometry to an external callus with different mechanical properties causes the signal loss across the fracture to reduce significantly. The most significant changes are observed to occur from the initial inflammatory stage to the formation of a callus and in the remodelling stage after a significant reduction in the size of the callus has taken place.

12:00

4aBB12. The role of bone marrow on acoustic properties of cancellous bone - finite difference time domain modelling study. Antti S. Kallioniemi (University of Kuopio, POB 1627, 70211 Kuopio, Finland, antti.kallioniemi@uku.fi), Juha Töyräs (Kuopio University Hospital, POB 1777, 70211 Kuopio, Finland, Juha.Toyras@kuh.fi), Mikko Hakulinen (University of Kuopio, POB 1627, 70211 Kuopio, Finland, Mikko.Hakulinen@uku.fi), Jukka Jurvelin (University of Kuopio, POB 1627, 70211 Kuopio, Finland, Jukka.Jurvelin@uku.fi)

Quantitative ultrasound (US) parameters are related to structure and properties of cancellous bone. The effect of bone marrow on US propagation, *i.e.* absorption and scattering, is still poorly understood. However, substitution of fatty marrow with water is known to significantly affect the US parameters. The present study investigates the role of marrow on US parameters, using microtomography based 3D-finite difference time domain (FDTD) modelling. Eleven human cancellous bone samples were analysed with a micro-CT system (SkyScan 1072) to determine microstructure and morphology. Wave 3000 Pro software (Cyberlogic Inc.) was used for simulations. Models were created to simulate experimental US measurement geometry with focused 1MHz transducers. Simulations were repeated before and after replacing the marrow with water. The voxel size of the simulation mesh significantly affected sample structure and simulations. US attenuation and speed decreased and increased, respectively, when marrow was replaced with water ($p<0.01$). US reflection at sample surface and backscattering from internal structures increased ($p<0.01$) when marrow was replaced with water. Contribution of bone marrow was stronger in samples with low bone volume fraction. This implicates that inter-individual differences in the composition of marrow may significantly affect measured ultrasound parameters, especially when investigating osteoporotic bone with low density.

Session 4aEA

Engineering Acoustics: Sound Fields I

Raymond Kirby, Chair
Brunel University, School of Engineering and Design, Uxbridge, Middlesex, UB8 3PH, UK

Contributed Papers

8:00

4aEA1. A virtual headphone based on wave field synthesis. Klaus Laumann (Institut für Rundfunktechnik GmbH, Floriansmühlstraße 60, 80939 München, Germany, laumann@irt.de), Günther Theile (Institut für Rundfunktechnik GmbH, Floriansmühlstraße 60, 80939 München, Germany, theile@irt.de), Hugo Fastl (AG Technische Akustik, MMK, TU München, Arcisstr. 21, 80333 München, Germany, fastl@mmk.ei.tum.de)

The term ″virtual headphone″ refers to specially designed loudspeaker systems aiming for transmission characteristics equal to real headphones. Particularly of interest is the exact pre-filtering of the speaker signals to compensate the effect of head related transfer functions (HRTFs) between loudspeakers and ear canal. These so-called ″HRTF inverse filters″ are dependent on geometrical conditions and so they have to be updated with every head movement. In order to avoid problematic adaptive HRTF inverse filtering, the real loudspeakers are replaced by focussed sources generated according to the principles of Wave Field Synthesis (WFS). Head tracking controlled adjustment of driving functions allows easy source movement and thus fixed source positions in relation to the listener's ears, providing stable virtual headphone reproduction. A single static HRTF inverse filter network can be used. It is designed to ensure precise headphone equalization according to ITU-R BS.708 and offers accurate reproduction of e.g. binaural signals. A pilot study with a circular WFS array built in a panel above the listener's head has verified the functional capability of this concept.

8:20

4aEA2. Modelling sound propagation in a waveguide containing multiple obstacles. Raymond Kirby (Brunel University, School of Engineering and Design, Uxbridge, UB8 3PH Middlesex, UK, ray.kirby@brunel.ac.uk)

Acoustic waveguides often include relatively short area changes and/or complex non-uniform obstacles. Understanding the propagation of sound within such waveguides requires a detailed knowledge of the scattering of sound at each obstacle and how these obstacles interact with one another. Mathematically modelling sound propagation in waveguides containing multiple non-uniform obstacles is challenging, especially if one assumes that the waveguide is relatively large. Accordingly, a computationally efficient hybrid numerical method is presented here that uses the standard finite element method to model non-uniform obstacles, and maps this onto a wave-based modal solution that is used for uniform duct sections only. The hybrid method has the advantage, moreover, of removing the need to numerically enforce a non-reflecting boundary condition downstream of the obstacles, which is often encountered in studies that rely solely on the standard finite element method. In this way, transmission loss predictions for relatively large ducts and multiple obstacles may be generated efficiently, and predictions are presented here for two cylinders placed in a two-dimensional waveguide.

8:40

4aEA3. Sound generation by airflow in a pipe having a small internal cavity. Ulf Kristiansen (Acoustics group, Norwegian University of Science and Technology, O.S. Bragstads plass 2B, N-7491 Trondheim, Norway, ulf.kristiansen@iet.ntnu.no), Børge Nygård (Acoustics group, Norwegian University of Science and Technology, O.S. Bragstads plass 2B, N-7491 Trondheim, Norway, borge.b.nygaard@iet.ntnu.no)

Gas flow through corrugated pipes is known to excite strong acoustic resonances within the pipe. In an attempt to better understand the flow acoustic phenomena involved, we have investigated experimentally a short pipe (0.6m long and 0.04m diameter) having a single small (5mm long, 2.5mm deep) circumferential cavity. It was found that if placed close to the pipe's inflow end, strong acoustic resonances were generated. The experimental results were compared to a model based on describing-function theory. The model involves two transfer functions, one associated with the pipe resonator, and the other the shear layer above the cavity. These are combined to a feedback system. This model gives the frequencies generated and the acoustic pressure levels (to within a constant) for different flow velocities. Reasonable agreement was obtained between the experimental results and the model predictions.

9:00

4aEA4. Multi-modal acoustic propagation in pipes with arbitrary defects: theory and experiments. Raymond Kirby (Brunel University, School of Engineering and Design, Uxbridge, UB8 3PH Middlesex, UK, ray.kirby@brunel.ac.uk), Kirill V. Horoshenkov (University of Bradford, School of Engineering, Design and Technology, BD7 1DP Bradford, UK, k.horoshenkov@Bradford.ac.uk), Tareq Bin Ali (University of Bradford, School of Engineering, Design and Technology, BD7 1DP Bradford, UK, m.t.binali@Bradford.ac.uk)

Underground sewer systems are prone to flooding incidents caused by obstructions such as sediment deposits and wall deterioration. An efficient method for identifying and characterising these obstructions involves measuring the amplitudes of the reflected and transmitted acoustic normal modes excited by a point source in the sewer pipe. However, the behaviour of higher order modes in relatively large pipe work is often difficult to predict and interpret. In order to provide a greater physical insight into the measured data and to guide future experimental work, theoretical predictions have been developed and validated. The presented theoretical work is based on a finite element method and a mode matching technique. In this paper the predicted and measured sound fields are analysed for up to four acoustic modes reflected from two different obstacles (axisymmetric and non-axisymmetric) deposited in a 150 mm diameter uPVC pipe.

9:20

4aEA5. Benchmarking for acoustic simulation software. Alfonso R. Molares (University of Vigo, E.T.S.I de Telecomunicación, Rúa Maxwell s/n, 36310 Vigo, Spain, amolares@gts.tsc.uvigo.es), Manuel A. Sobreira-Seoane (University of Vigo, E.T.S.I de Telecomunicación, Rúa Maxwell s/n, 36310 Vigo, Spain, msobre@gts.tsc.uvigo.es)

The validation of acoustic simulation software is still an obscure and imprecise matter. Validation studies of commercial implementations are rarely provided by vendors which are reluctant to show their product weakness. On the contrary in open academic implementations validation studies are one of the keys to make them used, rather than marketing. However, they demand from users a high level of knowledge and imply, generally, so long calculation times that make them impractical for common industry purposes. The aim of this study is to contribute to clarify this point setting a simple benchmark to measure the accuracy and performance of different software pack-

ages for sound field calculations. The benchmark is presented by its application with two widely used commercial implementations of finite element method and with an open-source implementation of boundary element method developed at the Southern Denmark University. The validation is performed against analytical formulae and also against experimental results. In order to study the balance between accuracy and computational cost the results are finally presented in terms of relative error versus calculation time.

9:40

4aEA6. Spatialized additive synthesis. Charles Verron (Orange Labs, 2 avenue Pierre Marzin, 22307 Lannion, France, charles.verron @orange-ftgroup.com), Mitsuko Aramaki (CNRS - INCM and Université de Provence, 31, chemin Joseph Aiguier, 13402 Marseille, France, aramaki@lma.cnrs-mrs.fr), Richard Kronland-Martinet (CNRS-LMA, 31, chemin Joseph Aiguier, 13402 Marseille, France, kronland@lma .cnrs-mrs.fr), Grégory Pallone (Orange Labs, 2 avenue Pierre Marzin, 22307 Lannion, France, gregory.pallone@orange-ftgroup.com)

In virtual auditory environments, a spatialized sound source is typically simulated in two stages: first a ″dry″ monophonic signal is recorded or synthesized, and then spatial attributes (directivity, width and position) are applied by specific signal processing algorithms. In this paper, a unified analysis/spatialization/synthesis system is presented. It is based on the spectral modeling framework that analyses/synthesizes sounds as a combination of time-varying sinusoidal, noisy and transient contributions. The proposed system takes advantage of this representation to allow intrinsic parametric sound transformations, such as spatial distribution of sinusoids or diffusion of the noisy contribution around the listener. It integrates timbre and spatial parameters at the same level of sound generation, so as to enhance control capability and computational performance.

10:00

4aEA7. Notes on the reproduction of moving virtual sound sources. Jens Ahrens (Deutsche Telekom Laboratories, Ernst-Reuter-Platz 7, 10587 Berlin, Germany, jens.ahrens@telekom.de), Sascha Spors (Deutsche Telekom Laboratories, Ernst-Reuter-Platz 7, 10587 Berlin, Germany, sascha .spors@telekom.de)

Wave field synthesis and higher-order Ambisonics are two representatives of sound reproduction systems that are based upon the concept of physical recreation of a desired sound field. Conventional implementations of such systems typically reproduce moving virtual sound sources as a concatenation of static source positions that change over time. This approach introduces various artifacts which are reported in the literature to be strongly audible. It was recently shown by the authors that the explicit consideration of the physical properties of the sound field of moving sources in the reproduction algorithm avoids these artifacts. It thus allows for the accurate reproduction of the Doppler Effect. In practical implementations of such sound field reproduction systems unavoidable artifacts arise. These are mainly a consequence of sampling and truncation of the loudspeaker distribution and appear both for static and moving virtual sound sources. For static sources, they are well documented in the literature. We revisit these investigations and point out the particularities of these artifacts with respect to the time-variant property of the reproduced sound field.

10:20-10:40 Break

10:40

4aEA8. Loudspeakers simulation of sound environments for the car industry. Benoît Gauduin (Genesis S.A., Bâtiment Gérard Mégie, Domaine du Petit Arbois - BP 69, 13545 Aix-en-Provence Cedex 4, France, benoit.gauduin@genesis.fr), Sylvain Hourcade (Genesis S.A., Bâtiment Gérard Mégie, Domaine du Petit Arbois - BP 69, 13545 Aix-en-Provence Cedex 4, France, sylvain.hourcade@genesis.fr),Nathalie Le Hir(Renault, TCR/AVA 163, Technocentre, 78288 Guyancourt Cedex, France, nathalie.le-hir@renault.com), Gaël Guyader (Renault, TCR/AVA 163, Technocentre, 78288 Guyancourt Cedex, France, gael.guyader@renault .com)

Car manufacturers are strongly interested in sound quality: they need to understand the expectations of their customers in terms of engine sound signature, door closure noise, etc. ... In order to allow engineering teams of research departments to perform psychoacoustics tests under controlled and realistic conditions, GENESIS supplies high fidelity listening 3D simulators on loudspeakers. Based on binaural recordings, these simulators, called transaural, are calibrated to obtain the best fidelity in terms of spatial and spectral components. In this presentation, we will discuss the requirements regarding sound system and room installation and present the precision reachable in terms of frequency response. Measurements and results achieved on such systems will be shown, with a particular focus on the two systems built for RENAULT and GENESIS. Finally, in order to perform equivalent psychoacoustics tests on both RENAULT and GENESIS sites, we will develop the procedure of comparison and validation of both transaural systems.

11:00

4aEA9. Development of a simple and accurate approximation method for the Gaussian beam expansion technique. Wei Liu (Institute of Acoustics, Chinese Academy of Sciences, Bei-Si-Huan-Xi Road, 100080 Beijing, China, liuwei9811@gmail.com), Peifeng Ji (Institute of Acoustics, Chinese Academy of Sciences, Bei-Si-Huan-Xi Road, 100080 Beijing, China, jipeifeng@mail.ioa.ac.cn), Jun Yang (Institute of Acoustics, Chinese Academy of Sciences, Bei-Si-Huan-Xi Road, 100080 Beijing, China, junyang.ioa@gmail.com)

The calculation of the sound field can be greatly simplified by using the Gaussian beam expansion technique. The source distribution function is expressed as the superposition of a small number of Gaussian functions, and the expansion coefficients could be obtained by minimizing an object function in the spatial or k-space domain. In this paper, a fast algorithm is developed to determine the Gaussian function coefficients for a more accurate approximation. Two-stage procedures are employed in the proposed method. Firstly, two real coefficients are estimated by a simple search approach, and then the least mean square (LMS) algorithm is adopted for determining the optimal expansion coefficients. Finally, the presented method is evaluated in the case of calculation of sound fields radiated from a piston and a rectangular planar source. Simulation results show that, compared with the previous approaches, the developed scheme is simple to implement with high accuracy.

11:20

4aEA10. Determination of Condition for Fastest Negative Group Velocities of Lamb-Type Waves under each Density Ratio of Solid and Liquid Layers. Kojiro Nishimiya (Tsukuba Univ., Tsukuba Science City, 305-8573 Ibaraki, Japan, nishimiya@aclab.esys.tsukuba.ac.jp), Koichi Mizutani (Tsukuba Univ., Tsukuba Science City, 305-8573 Ibaraki, Japan, mizutani@esys.tsukuba.ac.jp), Naoto Wakatsuki (Tsukuba Univ., Tsukuba Science City, 305-8573 Ibaraki, Japan, wakatuki@iit.tsukuba.ac.jp), Ken Yamamoto (Kansai Univ., 3-3-35 Yamate-cho, 564-8680 Suita, Japan, ken @ipcku.kansai-u.ac.jp)

Lamb-type waves are coupling modes of leaky Lamb waves on a layer structure. The Lamb-type waves have complicated propagation characteristics more than ordinary Lamb waves on a uniform elastic plate. In the characteristics, we examine the negative group velocities. Generally, the negative group velocities of Lamb waves are slower than positive group velocities under the same condition. If the negative group velocities are applied to fabricating some new application, it is desired that the speeds of negative group velocities are comparable to those of positive group velocities. Consequently, we aim to obtain the faster negative group velocities. Lamb-type waves show more discriminative characteristics in negative group velocities than ordinary Lamb waves. In this research, we consider the Lamb-type waves in a solid/liquid/solid structure. It is de-

scribed the conditions for obtaining the fastest negative group velocities of Lamb-type waves. The conditions, which are the acoustical impedance ratio, are expressed as the function of the density ratio of solid and liquid layers. These results are verified by numerical calculations.

11:40

4aEA11. Acoustic characterization of thin polymer layers for Love mode surface acoustic waveguide. Laurent Robert (CNRS FEMTO-ST, 32 Avenue de l'Observatoire, 25044 Besançon, France, laurent.robert @femto-st.fr), Lamia El Fissi (CNRS FEMTO-ST, 32 Avenue de l'Observatoire, 25044 Besançon, France, lamia.elfissi@femto-st .fr), Jean-Michel Friedt (CNRS FEMTO-ST, 32 Avenue de l'Observatoire, 25044 Besançon, France, jmfriedt@femto-st.fr), Frederic Cherioux (CNRS FEMTO-ST, 32 Avenue de l'Observatoire, 25044 Besançon, France, frederic.cherioux@femto-st.fr), Sylvain Ballandras (CNRS FEMTO-ST, 32 Avenue de l'Observatoire, 25044 Besançon, France, sylvain.ballandras @femto-st.fr)

We investigate the use of thin (1-10 um) polymer films as guiding layer for Love mode surface acoustic wave sensors. Beyond the great gravimetric sensitivity provided by the polymer guiding layer resulting from the low acoustic velocity, the use of photoresists provide ecnonomical means of depositing guiding layers of optimal thicknesses compared to inorganic layer deposition processes (typically PECVD deposition of silicon dioxide lasting several hours). The limit of very thick ($>$ 100 um) layers provides means of propagating interface waves mostly insensitive to the environment (package-less sensors) whose properties only vary through modification of the bulk properties of the polymer. We here analyse the evolution of the properties of the guiding layer in terms of acoustic velocity and losses as a function of time (solvent evaporation following photoresist spin coating) and temperature (typical baking steps). The polymer films is deposited on AT-cut quartz patterned with interdigtated transducers for generating 40 um-wavelength shear waves converted to a guided Love mode in a delay line configuration. We complete the experimental results with data interpretation using a model of acoustic wave propagation yielding quantitative results including viscosity and density out of the velocity and insertion loss measurements, both for the guided Love mode and interface layers

12:00

4aEA12. From frequency to time domain: Signal features and physical characteristics for resonant acoustical systems. Samuel Rodriguez (Renault - Laboratoire PHASE, Centre Technique Renault - CTL L16 1 29, 1, allée Cornuel, 91510 Lardy, France, rodriguez.samuel@yahoo .fr), Vincent Gibiat (Université Paul Sabatier, PHASE, 118, route de Narbonne, 31062 Toulouse cedex 9, France, gibiat@cict.fr), Stephane Guilain (Renault - Laboratoire PHASE, Centre Technique Renault - CTL L16 1 29, 1, allée Cornuel, 91510 Lardy, France, stephane.guilain @renault.com), Alain Lefebvre (Renault - Laboratoire PHASE, Centre Technique Renault - CTL L16 1 29, 1, allée Cornuel, 91510 Lardy, France, alain.a.lefebvre@renault.com)

The determination of the impulse response or the reflection function of an acoustical system from data expressed in the frequency domain is not immediate. Signal processing from frequency domain to time domain should involve phenomena of large amplitude as oscillations known as ″ripple″ that does not correspond to any physical phenomenon. The ″ripple phenomenon″ will be analyzed from both a signal processing and a physical point of view with the help of simple duct acoustic examples. A map designed as a new time-frequency tool helps us to show that it cannot be removed in most cases without the use of processing techniques involving modifications in the computed signal. This work has been developed for the automotive research, but can be applied to musical acoustics or to any field connected with time domain exploration of acoustic cues.

12:20

4aEA13. Extension of Optimal Source Distribution principle. Takashi Takeuchi (OPSODIS Limited, c/o ISVR, University of Southampton, Highfield, SO17 1BJ Southampton, UK, tt@isvr.soton.ac.uk)

Binaural reproduction over loudspeaker requires system inversion which is often referred to as cross-talk cancellation. Such process is the major factor to degrade the quality of 3D sound reproduction but Optimal Source Distribution (OSD) provides simple and effective loudspeaker design principle and signal processing which enables lossless crosstalk cancellation process. OSD takes advantage of its physical property where in-phase and out-of-phase components of the binaural reproduction process are balanced, hence the bulk of the crosstalk cancellation is achieved by its loudspeaker design principle and natural interference in the sound field. It is also shown that the advantage of OSD is further enhanced by separating in-phase and out-of-phase components through its loudspeaker design.

Session 4aEDa

Education in Acoustics: Acoustics in the Public School Science Classrooms

Uwe J. Hansen, Cochair
Indiana State University, 64 Heritage Dr, Terre Haute, IN 47803, USA

Malte Kob, Cochair
RWTH Aachen, Dept. of Phoniatrics, Pedaudiology, and Communication Disorders, Pauwelsstr. 30, Aachen, 52074, Germany

Invited Papers

8:00

4aEDa1. Acoustics in the public school classroom. Uwe J Hansen (Indiana State Univwersity, 64 Heritage Dr, Terre Haute, IN 47803, USA, u-hansen@indstate.edu), Corinne Darvennes (Tennessee Tech Univ., Dept. of Mechanical Engineering, PO Box 5014, Cookeville, TN 38501, USA, cdarvennes@tntech.edu)

As mentioned in a DAGA 07 paper 1, physical science preparation in American schools often leaves something to be desired. In recent years the ASA Committee on Education in Acoustics has made an effort to participate in finding relief for that problem. Three approaches have been of some influence. 1. Teacher workshops; 2. Hands-on student sessions. 3. Secondary school curriculum input. Teacher workshops have emphasized music as a vehicle to introduce science in the elementary classroom. Hands-on student sessions have included about 20 acoustics experiments of varying degrees of sophistication for students both in high school physics classes and in elementary general science classes. Secondary curriculum input has included both, development of laboratory experiments in acoustics, and exposure to relatively low cost educational versions of computational software. Examples of teacher workshop content, a number of hands-on experiments, and some finite element calculations will be discussed. 1Musik: Zugang zur Wissenschaft in der Grundschule. Uwe J. Hansen, DAGA 2007, Stutgart pp. 171-172.

8:20

4aEDa2. Math and science partnership program in the Upper Cumberland districts of Tennessee. Corinne Darvennes (Tennessee Tech Univ., Dept. of Mechanical Engineering, PO Box 5014, Cookeville, TN 38501, USA, cdarvennes@tntech.edu)

The Mathematics and Science Partnership (MSP) program by the US Department of Education ″is intended to increase the academic achievement of students in mathematics and science by enhancing the content knowledge and teaching skills of classroom teachers. Partnerships between high-need school districts and the science, technology, engineering, and mathematics (STEM) faculty in institutions of higher education are at the core of these improvement efforts.″ This paper will present efforts in the Upper Cumberland districts of Tennessee to introduce engineering applications to Math and Science teachers in grades 8-12. The science teachers recruited represented the disciplines of Chemistry, Physics, and Physical Science. The 3-year program consisted of summer institutes, as well as bimonthly Saturday workshops. An overview of the program will be discussed. It will include background information about the Upper Cumberland region, Tennessee content standards related to acoustics, working with teachers, some of the hands-on activities that were used during summer workshops, and the equipment that was provided to the teachers.

8:40

4aEDa3. Teaching Communication Acoustics and Physiology at the girl's day. Malte Kob (RWTH Aachen, Dept. of Phoniatrics, Pedaudiology, and Communication Disorders, Pauwelsstr. 30, 52074 Aachen, Germany, mkob@ukaachen.de)

The girl's day is an annual event for young female pupils who wish to have their own experiences during a day in a potential future work place. In our department a team of 19 phoniatricians, speech therapists, phoneticians, engineers, audiometrists and assistants works on diagnosis and therapy of disorders of voice, speech, hearing and swallowing. For several years, our department has been visited by a group of 16 to 20 pupils who are guided in small groups through a sequence of stations with hands-on exercises in the field of voice and hearing acoustics. The experiments include the measurement of a voice range profile, recording and visualisation of voice signals, subjective and objective assessment of voice disorders, and listening tests. The experiences with organisation and feedback of the girl's days are reported.

Contributed Paper

9:00

4aEDa4. Investigating musical sound as a model for the scientific process. Andrew Piacsek (Central Washington University, Department of Physics, 400 E. University Way, Ellensburg, WA 98926, USA, piacsek@cwu.edu)

In recent years, science pedagogy at all levels has embraced active student learning, in which students are engaged in the process of discovery, rather than passively receiving information. One of the benefits of active learning in a science curriculum is that students have an opportunity to emulate scientists in their approach to producing knowledge. It is desirable that students at all levels, including those in primary and secondary schools, develop an understanding of (or at least an appreciation for) the scientific process, in addition to learning science content. Presented here is a description of a musical acoustics curriculum used at Central Washington University for non-science students, with emphasis on how the structure of the curriculum and the active-learning elements contribute to accomplishing the objectives of conceptual learning, problem-solving ability, and scientific thinking. An essential feature of this curriculum is the combination of guided and open scientific investigations by teams of students. Portions of this college curriculum have been successfully adapted to the high school classroom and to audiences of children as young as ten years of age. Because musical acoustics incorporates many fundamental topics in physics and engineering, and it is appealing and relevant to students of all ages, this topic can be a significant asset to any science curriculum.

Invited Paper

9:20

4aEDa5. Acoustics Modules Developed in the IIT Research Experience for Teachers Program. Ralph T. Muehleisen (Illinois Institute of Technology, Civil, Architectural and Environmental Engineering, 3201 S. Dearborn St., Room 228, Chicago, IL 60616, USA, muehleisen@iit.edu)

From 2004-2008, the Illinois Institute of Technology (IIT) received funding from the US National Science Foundation (NSF) to institute a program to bring K-12 (primary and secondary school) teachers into University research labs for a seven week summer program where teachers work with an IIT faculty Research Mentor and develop an educational module for their students based on their mentor's research. The module's goal is to introduce students to engineering design concepts, utilizing scientific inquiry techniques, and incorporating an ethics component and a design project. Additionally, the modules must be linked to the Illinois State Board of Education Learning Standards. In 2005, a teacher developed a module for teaching high school algebra, geometry, and physics using musical acoustics, culminating with a woodwind instrument design project. In 2006, a teacher developed a module for a 3rd grade science class that explores the basics of sound and hearing, culminating in a noise control design project. This paper will present and discuss these two acoustic teaching modules. This project was supported by NSF grant EEC-0502174.

9:40-10:00 Break

Contributed Papers

10:00

4aEDa6. Inquiring activities on the acoustic phenomena at the classroom using sound card in personal computer. Young H. Kim (Korea Science Academy, 111 Backyangkwanmoonro, Busanjin-ku, 614-822 Busan, Republic of Korea, youngkim@paran.com)

Inquiring activities on acoustic phenomena have been carried out in the classroom of a high school for highly gifted children. Instead of expensive instruments such as function generators and oscilloscopes, sound cards, installed in a personal computer, were employed for the generation and detection of sound. The stereo function of the sound card offered two sound sources, so that phenomena of interference and beats can be realized in the classroom. The record function of the sound card offered detection of sound, permitting frequency spectrum analysis of sounds from two tuning forks or the sound from a moving fork. Using sound card, a lot of acoustic phenomena can be demonstrated in the classroom. In addition, sound from Rijke tube, which is a typical theromacoustic phenomena, was analyzed by using a sound card. Popup sound of a wine bottle and breaking of wine glasses, which are related to resonace and standing waves, were also investigated. Curiosity of students was greatly increased through a series of inquiring activities with sound cards, so that they were completely absorbed in research on acoustics.

10:20

4aEDa7. Ur[ban]sonate: Echoes of twentieth-century sound art in the urban elementary classroom. Kevin N. Summers (101 Woodbine Ave., Apt. 305, Syracuse, NY 13206, USA, knsummers@hotmail.com), Jason E. Summers (ARiA Consulting LLC, 1222 4th St. SW, Washington, DC 20024, USA, jesummers@alumni.kenyon.edu)

The sonic arts provide a variety of cross-disciplinary entry points into the traditional lower-elementary curriculum. The exploration of sound poetry provides students with a workspace to deconstruct the connection between written and spoken language; phonemes; phonics; voiced, unvoiced, stressed and unstressed letter sounds and blends. Kurt Schwitters's ″Ursonate,″ the music and scores of John Cage, various other sound art works and Deep Listening (TM) techniques provide a bridge to the study of acoustic sound and serve to validate/contextualize students' desires to creatively explore physical phonemes such as the relationship of pitch to frequency of vibration. After creating symbolic representations of sounds, writing sound poems and creating musical instruments, students synthesize learned material by scoring and directing the performance of original sound art pieces.

10:40

4aEDa8. Acoustics in the partial deaf student school music classrooms. Filiz Bal Kocyigit (Karabuk University, 232. Str. No: 5/5 Ilkbahar Mah., Cankaya, 06550 Ankara, Turkey, filizbkocyigit@yahoo.com), Kubra Sevim X. Gulec (Karabuk University Fine Arts and Design Faculty, Safranbolu, 78600 Karabuk, Turkey, kubsev@gmail.com)

Music schools need some special acoustical design for good education. If this is also for children with disabilities, the effect is more important. Research is about musical education for partially hearing disabled children. At this point architectural acoustic design acquires importance. This is not only in the shape of the room but also in using covering materials and other solutions. The question is whether architectural acoustics solutions can affect the music education of partially hearing disabled children or not. Here the first discussion is whether we need some additional components of good classrom acoustics for partially hearing disabled children in the American National Standards Institute Standard S12.60 2002 for clasroom acoustics, and the cost impact of the Standard. Childhood hearing loss is a widespread problem with significant impact, an invisible condition resulting in communication problems that can ultimately interfere with learning and social development. Included are audio files that illustrate that even a mild hearing loss can have a significant impact on a child's ability to understand the teacher. Especially children with a partial hearing loss need a more lively room to amplify the instrument sound for improved hearing capacity.

11:00

4aEDa9. The energy flow for a spherical acoustic lens: ray vs. wave methods. Cleon E. Dean (Physics Department, Georgia Southern University, P. O. Box 8031, Statesboro, GA 30460-8031, USA, cdean@GeorgiaSouthern.edu), James P. Braselton (Department of Mathematical Sciences, Georgia Southern University, P.O.B. 8093, Statesboro, GA 30460-8093, USA, jbraselton@GeorgiaSouthern.edu)

A simple classroom demonstration consists of a weather balloon filled with carbon dioxide, a sound source, and a microphone. Since the speed of sound is slower in carbon dioxide than in air at room temperature and pressure, the balloon acts as a positive spherical acoustic lens. The accuracy of ray methods in locating the acoustic focus versus a full blown wave solution approach is probed. This problem presents particular difficulties if the sound source lies in the near field region. The sound emitter is treated as a dipole source equivalent to a rigid oscillating sphere of small size and amplitude of motion relative to the scatterer. The energy flux around the balloon is visualized by both ray methods and by the acoustic Poynting vector field. The geometrical ray results and the acoustic Poynting vector field resulting from the wave solution are compared.

THURSDAY MORNING, 3 JULY 2008 ROOM 202/203, 11:20 TO 12:20 P.M.

Session 4aEDb

Education in Acoustics: Take 5's

Uwe J Hansen, Cochair
Indiana State University, 64 Heritage Dr, Terre Haute, IN 47803, USA

Malte Kob, Cochair
RWTH Aachen, Dept. of Phoniatrics, Pedaudiology, and Communication Disorders, Pauwelsstr. 30, Aachen, 52074, Germany

Thomas D. Rossing, Cochair
Stanford University, CCRMA, Department of Music, Stanford, CA 94305, 26464 Taaffe Rd, Los Altos Hills, CA 94022, USA

For a Take-Five session no abstract is required. We invite you to bring your favorite acoustics teaching ideas. Choose from the following: short demonstrations, teaching devices, or videos. The intent is to share teaching ideas with your colleagues. If you can, bring a brief, descriptive handout with enough copies for distribution. Spontaneous inspirations are also welcome. You sign up at the door for a five-minute slot before the session starts. If you have more than one demo, sign up for non-consecutive slots.

Session 4aMU

Musical Acoustics: Virtual Musical Instruments I

Julius O. Smith, Cochair
Stanford Univ., Center for Computer Research in Music and Acoustics (CCRMA), Dept. of Music, Stanford, CA 94305-8180, USA

Antoine Chaigne, Cochair
ENSTA, Chemin de la Hunière, Palaiseau, 91761, France

Invited Papers

8:00

4aMU1. Interacting with virtual musical instruments at the junction nodes. Cumhur Erkut (Helsinki University of Technology (TKK), Lab. Acoustics and Audio Signal Processing, P.O. Box 3000, FI-02015 TKK Espoo, Finland, Cumhur.Erkut@tkk.fi), Antti Jylhä (Helsinki University of Technology (TKK), Lab. Acoustics and Audio Signal Processing, P.O. Box 3000, FI-02015 TKK Espoo, Finland, antti.jylha@tkk.fi), Matti Karjalainen (Helsinki University of Technology (TKK), Lab. Acoustics and Audio Signal Processing, P.O. Box 3000, FI-02015 TKK Espoo, Finland, matti.karjalainen@tkk.fi)

Sound synthesis by block-based physical modeling of musical instruments separates the tasks of component modeling and managing their interactions. The components are the exciters or the resonators, and their interactions are managed by explicit interaction blocks, which are obtained from the physical continuity and energy conservation rules. Well-known examples of the interactors include the wave- digital adaptors and the digital waveguide scattering junctions. When the virtual instruments need to be interfaced to the outside environment with sensors and actuators for bidirectional interaction, it is advantageous to reformulate the interactors to accept and provide signal inputs and outputs, respectively. In this contribution, we refer to these elements as nodes, introduce different types of nodes, and discuss their interconnection.

8:20

4aMU2. Block based physical modeling for virtual musical instruments. Rudolf Rabenstein (University Erlangen-Nürnberg, Cauerstr.7, D-91058 Erlangen, Germany, rabe@LNT.de)

A variety of methods for physical modeling sound synthesis has been developed so far, mostly for single sound objects like strings, plates, etc. However, complex virtual musical instruments require not only advanced models but also methods for combining one or more sound objects with excitation mechanisms and resonating structures. This presentation shows how to derive modeling blocks from basic physical laws and how to connect them in a physically meaningful way. The first step is to establish a physical model of a dynamical structure in terms of potential and flow variables, like force and velocity. It is important to observe also the boundary conditions because firstly they shape the spectrum of the vibrating structure and thus the timbre of the sound and secondly they determine the exchange of energy with the environment. The second step is the discretization of the physical model. This procedure is shown for the functional transformation method, which delivers discrete-time models with direct access to the parameters of the physical model and which reproduces the original sound spectrum. In the last step, the resulting modeling blocks are connected by scattering elements which reflect energy back into the model or transmit it to neighboring blocks.

8:40

4aMU3. Cymbal Synthesis. Stefan Bilbao (University of Edinburgh, Room 7306B, JCMB, King's Bldgs., Mayfield Rd., EH9 3JZ Edinburgh, UK, sbilbao@staffmail.ed.ac.uk)

Time domain sound synthesis based on a physical model of the cymbal presnts special problems, due to the need for a strongly nonlinear model of shell vibration. When standard numerical methods such as finite difference schemes are employed, various computational issues arise; among these are numerical stability, a proper treatment of numerical boundary conditions, which are nontrivial at the free edge and center of the the cymbal, and the extra concern of working in polar coordinates. Coupling with mallet and bow models, possibilities for increased computational efficiency using spectral methods, and general strengths and weaknesses of difference methods in this context will be discussed.

9:00

4aMU4. Passive admittance synthesis for sound synthesis applications. Balázs Bank (University of Verona, Ca' Vignal 2, strada le Grazie 15, 37134 Verona, Italy, bank@mit.bme.hu), Matti Karjalainen (Helsinki University of Technology (TKK), Lab. Acoustics and Audio Signal Processing, P.O. Box 3000, FI-02015 TKK Espoo, Finland, matti.karjalainen@tkk.fi)

In physics-based sound synthesis, it is in general possible to incorporate a mechanical or acoustical admittance/impedance in the form of a digital filter. Examples include modeling of the termination of a string or a tube. However, when digital filters are fitted to measured admittance or impedance data, care has to be taken that the resulting filter corresponds to a passive mechanical or acoustical

system, otherwise the stability of the instrument model is at risk. This paper presents a simple method for designing inherently passive admittance or impedance filters. The admittance/impedance is composed as a linear combination of positive real (PR) functions, and the weights are determined by a constrained least squares optimization. The resulting filter is a parallel set of second-order sections. For wave-based modeling, such as digital waveguides (DWGs) or wave digital filters (WDFs), the admittance/impedance is converted to a reflectance filter. The parallel filter structure is retained during conversion. As an example, a guitar model based on DWG approach is presented, using mechanical admittance measurements of a guitar bridge behavior. The model is implemented as an efficient real-time sound synthesis algorithm.

9:20

4aMU5. Modal parameter estimation for shape-changing geometric objects. Cynthia Maxwell (Center for New Media and Audio Technologies, 1750 Arch Street, Berkeley, CA 94720, USA, cynthia@code404.com)

As a novel advancement in interactive sound synthesis, we would like to change the shape of a finite element model of an instrument and hear how the sound changes in real-time. Traditional modal synthesis methods require computing a new eigendecomposition for each geometric change -- a costly computation using today's hardware. However, by using the modes computed for one geometry to estimate modal frequencies for other nearby geometries, we can instantly hear the effects of changing the instrument shape on the sound produced. In this talk, we describe the process of estimating resonant frequencies of an instrument by combining information about the modes of similar instruments. We also propose a method for transferring the modal information from one finite element mesh to another. This method is used in situations where severe modifications to the object's geometry distort the finite element mesh and require an entirely new mesh to be created. We also describe the balance between computational speed and numerical accuracy of the computed resonances.

9:40

4aMU6. Applications of passivity theory to the active control of acoustic musical instruments. Edgar Berdahl (Stanford Univ., Center for Computer Research in Music and Acoustics (CCRMA), Dept. of Music, Stanford, CA 94305-8180, USA, eberdahl@ccrma.stanford.edu), Guenter Niemeyer (Stanford Univ., Mech. Eng., Bldg. 530, Stanford, CA 94305, USA, gunter.niemeyer@stanford.edu), Julius O. Smith (Stanford Univ., Center for Computer Research in Music and Acoustics (CCRMA), Dept. of Music, Stanford, CA 94305-8180, USA, jos@ccrma.stanford.edu)

The dynamic behavior of any acoustic musical instrument can be modified by closing a feedback loop around even a single sensor and actuator. The ultimate goal is to make the acoustics of the instrument programmable by way of a digital feedback controller, while the instrument retains its tangible form. In this talk, we describe a class of controllers that are applicable to passive acoustic musical instruments, and we present sound examples from laboratory experiments on a vibrating string. First, we briefly introduce positive real functions. Next, we design positive real controllers allowing the quality factor and resonant frequency of instrument modes to be individually controlled. Because positive real controllers are passive, they are stable if the instrument is passive. This means that neither a full instrument model nor complete state measurements are required. Finally, we describe a class of simple passive nonlinear controllers that can emulate various kinds of friction, stiffening and softening springs, etc. Passivity of these controllers follows from the local passivity of the controller components. Controller parameters may often be tweaked so that the controllers are no longer passive but still perform useful functions, such as bowing emulation.

10:00-10:20 Break

Contributed Papers

10:20

4aMU7. Vibrating-String Coupling Estimation from Recorded Tones. Nelson Lee (Stanford Univ., Center for Computer Research in Music and Acoustics (CCRMA), Dept. of Music, Stanford, CA 94305-8180, USA, nalee@stanford.edu), Julius O. Smith (Stanford Univ., Center for Computer Research in Music and Acoustics (CCRMA), Dept. of Music, Stanford, CA 94305-8180, USA, jos@ccrma.stanford.edu)

Coupling of vibrational polarizations in a single string, for an instrument such as the acoustic guitar, produces psychoacoustically significant effects such as beating and two-stage decay (Weinreich, JASA v62 n6). Previous considerations of string coupling phenomena appear not to have addressed the practical problem of calibrating computational models based on recorded tones. In this work, we take a data-driven approach using measured data from a vibrating string from an acoustic guitar, the motion of the string in two orthogonal planes, and formulate a regularized least-squares problem for computing the coupling between the measurements. Such a formulation ensures that the resulting coupling is physically admissible, in that the resulting coupling factors do not generate energy, and are easily found as the problem is convex. Well-studied algorithms for solving convex problems, such as interior-point and gradient descent methods can be used and are widely available in the form of open-source libraries.

10:40

4aMU8. Sound synthesis of circular plates by finite differences. Kevin Arcas (ENSTA, Chemin de la Hunière, 91761 Palaiseau, France, arcas@ensta.fr), Antoine Chaigne (ENSTA, Chemin de la Hunière, 91761 Palaiseau, France, antoine.chaigne@ensta.fr), Stefan Bilbao (University of Edinburgh, Room 7306B, JCMB, King's Bldgs., Mayfield Rd., EH9 3JZ Edinburgh, UK, sbilbao@staffmail.ed.ac.uk)

This paper shows a method for simulating linear flexural vibrations of circular plates by finite differences (FD) for the purpose of sound synthesis. The vibrations are assumed to follow the Kirchhoff-Love model. In order to solve the continuous problem numerically, the equations are approximated in space and time by FD methods. Two schemes are presented and compared; depending on the coordinate system used for the grid, rectangular and polar, respectively. Cartesian FD are not easily adaptable to circular boundary conditions and generic conservative boundary conditions cannot be found. On the contrary, polar FD allow to find well-adapted conservative boundary conditions. With a polar grid, the distance between consecutive gridpoints decreases from the edge to the center. As a consequence the stability of the algorithm depends on the minimum radius of the grid, where this distance is the smallest. Because of this highly restrictive stability condition, numerical dispersion is high and the high-frequency content of the spectrum is badly reproduced. To avoid this problem an implicit polar FD

scheme has been developed which yields simulations with acceptable numerical dispersion. The accuracy of the algorithm is estimated by computing the ratio between numerical and analytic eigenfrequencies in a simple case.

11:00

4aMU9. Digital algoritm for sound synthesis: Realism and complexity for creativity. Joël Bensoam (IRCAM, 1, place Igor Stravinsky, 75004 Paris, France, bensoam@ircam.fr)

Modalys, a sound synthesis software developed at Ircam for research and musical applications, make it possible to build virtual instruments based on physical models in order to obtain the broadest range of expressive variations in the instrument in response to intuitive controls. An instrument, as a complex structure, is described by the mechanical/acoustical interactions of its components (strings, tubes, soundboard, 3D FEM objects...). New research has recently been carried out in two directions: On one hand, a generic digital algorithm able to treat a large class of non linear interaction models (lip-reed, contact and friction, aero-acoustics jets, etc) was built. Based on a Gauss-Siedel strategy, this algorithm is used indifferently regardless of the modeled structure's complexity and guaranties convergence and robustness of the whole sound synthesis. On the other hand, efforts are made to infer from measurements the physical parameters needed for the sound synthesis (geometric or gesture parameters for example). Due to the lack of a complete analytical formulation (digital algorithm), derivative based methods to solve inverse problem (Newton, gradient, etc) are not allowed. Evolution Strategy (ES), especially for multiobjective optimization, are then investigated.

11:20

4aMU10. Application of Volterra series to simulate dynamics of a Reissner beam. David Roze (IRCAM, 1, place Igor Stravinsky, 75004 Paris, France, david.roze@ircam.fr), Thomas Hélie (IRCAM, 1, place Igor Stravinsky, 75004 Paris, France, thomas.helie@ircam.fr), Joël Bensoam (IRCAM, 1, place Igor Stravinsky, 75004 Paris, France, bensoam @ircam.fr)

Sound synthesis of strings needs the use of nonlinear models to provide realistic sounds according to the amplitude and the method of excitation (pluck, bow...). In order to include coupling between the different degrees of freedom, the Reissner beam model will be used to simulate nonlinear dynamics of a string. Expression of equilibrium of Reissner beams using Lie groups and algebra allows us to write an exact, simple formulation including nonlinearities due to large strains. This work aims to apply Volterra series method to this formulation in order to perform simulation of a Reissner beam at a given order of nonlinearity. Volterra series requires a rewriting of the model with well-defined boundary and initial conditions and interconnection laws of the series adapted to the variables (vector and matrix). Once the linear part isolated and studied (calculation of the Green function, and therefore of the first kernel), nonlinear terms must be organized to define a recurent relation and solve the kernel equation. Finally, it can be possible to identify a structure of simulation using instantaneous sums and products of outputs of linear filters.

11:40

4aMU11. Singing Integrals or wind instruments modeling using Boundary Integral Equations. Umberto Iemma (University Roma Tre, via vasca navale 79, 00146 Rome, Italy, u.iemma@uniroma3.it)

The paper deals with the modeling of woodwind musical instruments using a Boundary Integral Equation (BIE) formulation. Specifically, the BIE is used to model the acoustic response of the instrument bore, and is numerically solved by means of a Boundary Element Method (BEM). The latter takes advantage of an analytical solution for the calculation of the BEM coefficients, thus allowing for the representation of the problem as an open-domain problem. This peculiarity avoids the use of approximated boundary conditions at the open end of the pipe. The formulation is used to: evaluate the input impedance of the resonating air column; identify the frequency dependent transfer function relating the inflow of the instrument with the signal measured at a specified location (the Reed-To-Microphone transfer function); extend the analysis to a realistic performing environment to obtain the ″Reed-To-Listener″ transfer function. Standard techniques are used to take into account the interaction of the bore with the nonlinear exciting device. Numerical results are obtained for single-reed instruments in terms of tuning properties, convergence of solution, directivity patterns, and simple synthesized sounds. Issues related to the possibility of real-time simulations are briefly addressed. Specifically, the identification of digital filters from the calculated transfer functions is investigated, and some preliminary numerical result included.

12:00

4aMU12. An approach and technique for acoustic modelling of contact. Matthias Rath (Technische Universität Berlin, Deutsche Telekom Laboratories, Quality and Usability Lab, Ernst-Reuter-Platz 7, 10587 Berlin, Germany, matthias.rath@telekom.de)

Vibration of solid objects can often be modelled by modal description, which exists when certain operators in a differential equation are linear. Discrete-time algorithms can represent the behaviour of ″modal objects″ without artefacts, *exact* (with precision of finite computer architecture), if based on analytical solution, *not* numeric approximation. In particular, the energy associated with the state of the system is then preserved and the algorithm stable. A scenario of two objects interacting only during contact, however, is non-linear: a non-zero linear function cannot be zero in a half-space of the system's state-space. Existing computational models are based on *approximate*, numeric solution and cannot guaranty stability in situations with longer contact phases, such as rolling or sliding. General principle of our approach is: although any possible term for the interaction force must be non-linear, it may be *piecewise-linear*, and during each linear phase the whole system (of interacting solids) may be simulated by modal description. The question of ″switching″ between the different phases is here critical but may be solved in a way that assures control over the system's energy. Our implemented new contact model is stable in any condition and overcomes artefacts found with previous techniques.

Session 4aNSa

Noise and EURONOISE: EU Projects for Aircraft Noise Reduction II

Dominique Collin, Chair
Snecma - Safran Group, Centre de Villaroche, Direction R&T / UC, Moissy Cramayel, 77550, France

Invited Papers

8:00

4aNSa1. European Aircraft Noise Research Network (X3-Noise). Dominique Collin (Snecma - Safran Group, Centre de Villaroche, Direction R&T / UC, 77550 Moissy Cramayel, France, dominique.collin@snecma.fr)

The X3-NOISE Coordination Action, through its network structure and comprehensive workplan involving expert groups, scientific workshops, stakeholder seminars and a common information system, addresses the aircraft noise challenges set by the ACARE 2020 Vision. To this end, X3-Noise undertakes the elaboration and coordination of research strategies, the dissemination of results and the integration of European research activities in the field of air transport related to noise. Over 4 years, the project involves 32 partners from 20 countries (FR, UK, ES, NL, BE, DE, SE, IT, PL, HE, HU, CZ, LT, IE, PT, RO, CH, UA, EG, BR), combining the complementary skills and expertise of industry partners, SMEs, university and research establishments to cover the whole field of interest. The international co-operation aspects of the research agenda to be developed through the project activity are further reinforced by the participation of 3 partners from Ukraine, Egypt and Brazil acting as Focal Points at Regional level.

8:20

4aNSa2. The EU FP6 research project PROBAND - Objectives and first results. Lars Enghardt (DLR - German Aerospace Center, Mueller-Breslau-Str. 8, 10623 Berlin, Germany, lars.enghardt@dlr.de)

Fan broadband noise is a major aircraft noise challenge now and in the future will be even more important. Novel low-noise engine architectures, such as ultra-high-bypass-ratio engines and lower-speed fans, can help address jet noise and fan tone noise, but previous EC-funded programmes have shown they are unlikely to reduce significantly fan broadband noise without improved understanding of the source mechanisms. PROBAND will accomplish a major technical leap in providing industry with an improved understanding of the broadband noise source mechanisms, with validated broadband noise prediction methods, and with low fan broadband noise concepts. PROBAND will exploit the noise technology and methodology acquired in EC-funded projects and national programmes, to develop methods to allow the design of a fan system that will generate sufficiently low broadband noise to meet the EU noise level targets. This will be achieved by: 1. Developing a better understanding of broadband noise generation mechanisms using advanced experimental and computational techniques. 2. Developing and validating improved prediction methods using conventional computational fluid dynamics, and integrating them into industrial codes. 3. Exploring new prediction strategies using advanced computational techniques 4. Developing low broadband fan noise concepts.

8:40

4aNSa3. SILENCE(R): A major step towards aircraft noise reduction. Eugène J. Kors (Snecma, Etablissement de Villaroche Sud - UE, Rond-point René Ravaud - Réau, 77550 Moissy-Cramayel cedex, France, eugene.kors@snecma.fr)

From 2001 up to 2007, SILENCE(R) has focused on the development of aircraft noise reduction technologies. As an European Union project coordinated by Snecma, SILENCE(R) brought together some 50 companies (including Airbus, Rolls-Royce, MTU Aero Engines and Snecma), research centers and universities. The overall budget was 112 million euros. Combined with innovative low-noise operational procedures studied at the same time, SILENCE(R) has achieved an impressive 5 dB noise reduction. This meets the medium-term objective of the European Commission's R&D Framework Programs, and marks a significant advance towards ACARE's research goal of a 10 dB reduction in aircraft noise by 2020. SILENCE(R) carried out successful tests of more than 35 prototypes to check 10 noise reduction technology concepts. These included several advanced low noise fan rotors, as well as components for a complete low-noise nacelle (negatively scarfed intake, ″squid″ nozzle fitted with high frequency liner), flight tested on an Airbus A320. Flight tests were also carried out on an Airbus A340 with landing gear fitted with aerodynamic fairings.

Contributed Papers

9:00

4aNSa4. TIMPAN - Technologies to IMProve Aiframe Noise. Stephane Perrin Decroux (Airbus France S.A.S, 316, route de Bayonne BP M0112/4, 31060 Toulouse, France, stephane.perrin-decroux@airbus.com)

TIMPAN is a 3-year Strategic Targeted Research Project of the 6th European Framework Programme, Priority ″Aeronautics and Space″, launched in 2006. It addresses the community noise reduction objective for commercial aircraft by focusing on main airframe noise sources: landing gear and high-lift devices - responsible, on recent aircraft, for about half of the total noise in approach situation. TIMPAN addresses both sources, within 3 main tasks: 1) Landing gear activity: investigation of both innovative low noise technologies on bluff body structures and the improvement of advanced low noise main gear design, as outcome from previous EC Technology Platform SILENCE(R). 2) High lift device activity: study of both innovative concepts based on flow control technologies and mid-term noise reduction solutions as absorptive wing leading edge treatments and high-lift settings optimization through computational aero-acoustic methods. 3) Technology evaluation: aims to prepare the exploitation phase by evaluating the noise reduction technologies under consideration in terms of noise benefit, integration, cost and performance. TIMPAN brings together 14 actors from the European aeronautics industry including aircraft manufacturers (Airbus and Dassault Aviation), landing gear manufacturers (Messier-Dowty and Messier Bugatti), key research institutes (DLR, ONERA, NLR, EADS-IW), universities (University of Southampton, Technical University of Braunschweig) and SMEs (ATECA, Free Field Technologies).

9:20

4aNSa5. Passive and active designs for noise and vibrations reduction in aircraft cabins. Vincent Marant (Acusttel - Acústica y Telecomunicaciones SL, Pol. Ind. Benieto, C/ Transport n° 12, 46702 Gandía (Valencia), Spain, vmarant@acusttel.com), Antonio Reig Fabado (Universidad Politécnica de Valencia, Camino de Vera s/n, 46022 Valencia, Spain, areig@fis.upv.es), Juan Luís Aguilera De Maya (Acusttel - Acústica y Telecomunicaciones SL, Pol. Ind. Benieto, C/ Transport n° 12, 46702 Gandía (Valencia), Spain, jlaguilera@acusttel.com), José Christian Donayre Ramírez (Acusttel - Acústica y Telecomunicaciones SL, Pol. Ind. Benieto, C/ Transport n° 12, 46702 Gandía (Valencia), Spain, cdonayre@acusttel.com)

Within the sixth European Commission framework programme, the main objective of the SEAT project initiated in September, 2006, consists of the development of a radically new concept, where the aircraft passenger comfort is considered at the highest level. Smart reactive seats and an interior environment able to detect on real time physiological and psychological changes in the passenger conditions will be developed. These data will be analysed and the appropriate parameters, like noise and vibration levels, temperature or air ventilation, will be adapted. Moreover, each passenger will be able to create his own configuration, with his personal entertainment and work characteristics. The project is focussed on the questions previous to the integration of the system, that is above all the creation of a more healthy and comfortable travel environment by means of noise and vibration reduction, as well as specific climatic controls. In this paper, the first passive and active designs under development are presented.

Invited Paper

9:40

4aNSa6. Reducing aircraft noise during approach and departure by efficient operations. Robert J. De Muynck (National Aerospace Laboratory NLR, Anthony Fokkerweg 2, 1059CM Amsterdam, Netherlands, demuynck@nlr.nl)

Reducing the noise from aircraft around airports is a serious challenge. Apart from making the noise source, the aircraft, more silent, by advanced engines and aerodynamics, additional noise reduction can be achieved by moving the noise source away, as well as by a more silent operation of the aircraft. One of these innovative approach procedures is the Continuous Descent Approach. The principle is that aircraft approaching an airport follow a continuous descent profile at low thrust setting instead of making gradual altitude steps. The higher altitude and the lower thrust of the aircraft allow decreasing significantly noise exposure around the airport. First results show considerable noise reduction from 3dB to 8dB compared to conventional practices. Additionally, this procedure allows reducing fuel consumption and emissions. To make CDA procedures operationally feasible however, efforts are needed to develop *CDA operating procedures so that they can be flown in busy traffic *improved onboard systems to fly the CDA *accurate planning and sequencing tools for air traffic controllers *better interaction and interoperability between aircraft and air traffic control systems The presentation will discuss progress made in EU projects such as Sourdine II, OPTIMAL and ERAT.

Session 4aNSb

Noise, ASA Committee on Standards, and EURONOISE: Measurement of Occupational Noise Exposure I

William J. Murphy, Cochair
National Institute for Occupational Safety and Health, 4676 Columbia Parkway, Mailstop C-27, Cincinnati, OH 45226-1998, USA

Beat W. Hohmann, Cochair
Suva, Physics Section, Roesslimattstrasse 39, P.O. Box 4358, Luzern, CH-6002, Switzerland

Invited Paper

8:00

4aNSb1. Measurement strategies according to the new ISO/DIS 9612. Jürgen Maue (BGIA - Institut for Occupational Safety and Health, Alte Heerstraße 111, D-53757 Sankt Augustin, Germany, juergen.maue@dguv.de)

The European Directive 2003/10/EC on noise protection at the workplace has given the impact for the revision of the ISO 9612 describing the measurement and assessment of occupational noise. The ISO/TC 43 ″Acoustics″ decided that the revision should only contain requirements for the determination of the noise exposure for the purpose of assessing potential hearing damage. Meanwhile a new Draft ISO/DIS 9612 has been presented, which gives a detailed description of three alternative measurement strategies for the determination of the noise exposure level. Moreover the standard provides a method for estimating the uncertainty of the results. The measuring strategies, called ″task based measurements″, ″job based measurements″ and ″full day measurements″ are illustrated and compared to each other. The choice of the appropriate strategy is explained, depending on the complexity of the work situation and the movements of the worker doing his job. Based on practical experience some comments are given, which may help to reduce time and effort of measurements. The evaluation of measurement uncertainties is explained in a few words.

Contributed Paper

8:20

4aNSb2. Effective protection of the sense of hearing is prevented by ISO1999 noise standard. Gerald Fleischer (Liebig University School of Medicine, Aulweg 123, 35392 Giessen, Germany, gerald.fleischer@gmx.net)

To determine auditory performance in a simple way, pure-tone audiometry is being used. While health-related diagnostics is generally becoming more and more refined, ISO1999 is demanding rather rudimentary procedures. Both, frequency range and number of test frequencies are reduced, making it impossible to use modern and effective analytical tools such as pattern recognition. There is a clear relation between pressure-time-history of impulses and the details of the resulting auditory damage. But this relation can only be recognized if the restrictions of this standard are being ignored. Typical examples of audiograms from a large data base will be presented, showing simultaneously the data according to ISO1999 and in more modern ways. It will also be demonstrated how useful the tool of pattern recognition can be, for analysis of damages, as well as for preventive measures.

Invited Paper

8:40

4aNSb3. Comparison of impulse noise damage risk criteria using the Albuquerque blast overpressure walkup study data. William J. Murphy (National Institute for Occupational Safety and Health, 4676 Columbia Parkway, Mailstop C-27, Cincinnati, OH 45226-1998, USA, wjm4@cdc.gov), Amir Khan (National Institute for Occupational Safety and Health, 4676 Columbia Parkway, Mailstop C-27, Cincinnati, OH 45226-1998, USA, amk1@cdc.gov), Peter B. Shaw (National Institute for Occupational Safety and Health, 4676 Columbia Parkway, Mailstop C-27, Cincinnati, OH 45226-1998, USA, pbs3@cdc.gov)

The 1968 CHABA recommendations to limit impulsive noise exposure to levels below 140 dB SPL form the basis of current United States occupational and military standards. The U.S. military standard, MIL-STD-1474D, estimates the number of allowable shots to which a person may be exposed using peak level, B-duration, for varying levels of hearing protection usage. The European Union upper limit peak exposure action level is 137 dB C-weighted for the unprotected ear and 140 dB C-weighted for the protected ear. The U.S. Army blast overpressure studies in the early 1990's investigated the effects on the hearing of soldier subjects of simulated weapon blasts with varied levels and A-durations. The hearing thresholds of the subjects were tested before and after exposure to blasts. Exposures ranged from 6 shots to 100 shots per day and levels from 173 to 195 dB peak SPL. As judged by information criteria (AIC, BIC), the L_{Aeq8} index with unprotected data yielded the best fit to logistic models; all the indices produced a better fit with unprotected data than with protected data. Other metrics including the MIL-STD-1474D and the Auditory Hazard Assessment Algorithm for Human were evaluated and will be presented in this paper.

Contributed Papers

9:00

4aNSb4. Reconstruction of acoustic field horizontal layer in diffusive ambience. Arunas Pozera (Kaunas University of Technology/Technological Systems Diagnostics Institute, Kestucio st. 27, 3004-LT Kaunas, Lithuania, arunas.pozera@stud.ktu.lt), Vitalijus Volkovas (Kaunas University of Technology, K.Donelaicio str. 73, LT-44029 Kaunas, Lithuania, tsdi@ktu.lt)

This study introduces a method how to minimize the number of acoustic measurements in the diffusive ambience in order to reconstruct the horizontal layer of primary acoustic field. This reconstruction means determination of the level of the sound pressure at any point of surface, e.g. worker's occupational place, where there are a lot of sound sources. A mathematical modeling, based on regularity of sound spread, is used in the study. The elements of active experiment are applied in the research, the adequacy of mathematical model is evaluated by Fisher criterion, and the mathematical model of horizontal layer of the acoustic field is based on the polynomial of the regressive equation. The results are compared to the measurements received in the real experiment. This study also pays great attention to local and the EU legal regulations about the noise standards at the worker's occupational place and the measures to be taken to lower the noise level. The device of sound measurement INVESTIGATOR type 2260 and MAPLE 11 mathematics software tool have been used in the research.

9:20

4aNSb5. An experimental investigation of the measurement uncertainties in the assessment of exposure to noise in a working environment according to ISO 9612. Marco Nabuco(Inmetro / CNPq, Av. N. S. das Graças, 50, Xerém, Duque de Caxias, 25250-020 RJ, Brazil, nabuco@inmetro.gov.br), Ana Claudia Fiorini (Catholic University of São Paulo - Audiology Dept., Rua Ministro Godoy, 969 - Perdizes, 05014-001 São Paulo, Brazil, acfiorini@pucsp.br), Gilberto Fuchs (GROM Acustica e Automação, Rua Indiana, 343 - Apt° 11 - Broklin, 04562-000 São Paulo, Brazil, gilberto@grom.com.br)

The Brazilian regulation for workplace noise evaluation requires a comparison between the measured noise levels and the noise limits listed on a table. The table establishes the maximum work hours per day for each measured sound level. As in some other countries, the Brazilian table shows limit values with a resolution of 1 dB(A) and considers a 5 dB(A) exchange rate. The measured uncertainty is unknown. The use of type 2 equipment for instance can mean, theoretically, a uncertainty of 3 dB(A). In Brazil it is not possible to estimate the impact of the measurement uncertainty on the costs of compensations paid due to noise exposure. It is also very difficult to assess the number of workers that are receiving unfair compensations or are not receiving any due to inaccurate noise exposition measurements. However it is possible to assure that the amount of money can reach incredible numbers in our country. This paper presents an experimental study of the uncertainty calculated on the ISO 9612 basis for different sound signals, in different workplaces, emitted by different noise sources. The main purpose is to show how important it can be to estimate the uncertainty for each measurement.

Invited Paper

9:40

4aNSb6. Simple evaluation of occupational noise exposure without measurements. Beat W. Hohmann (Suva, Physics Section, Roesslimattstrasse 39, P.O. Box 4358, CH-6002 Luzern, Switzerland, beat.hohmann@suva.ch)

In almost any country, employers must assess the noise exposure of the employees. But for small and medium-sized enterprises (SMEs), individual noise measurements are hardly feasible. Therefore, since almost 30 years, Suva publishes noise level tables, which list typical noise levels of many tools and machines. These 66 noise level tables cover almost any branch of the industry. Moreover, they include shooting noise, music, and so on. However, most SMEs were not able to calculate their workers' long-term noise exposure. Therefore, based on Suva's extensive database, typical noise exposure levels for occupations and activities were calculated. The new type of noise level tables includes now the typical noise exposures for the different occupations. Moreover, since 2007, the noise level tables also indicate the measures to be taken. Therefore, SMEs do not have to put their efforts into the determination of noise exposure but can start immediately to protect the workers against noise-induced hearing loss. The list of the noise level tables available (in French, German and Italian language) and the noise level tables themselves may be found at: www.suva.ch/waswo/86005

Contributed Papers

10:00

4aNSb7. A comparison of two active-speaker-detection methods suitable for usage in noise dosimeter measurements. Fredric Lindstrom (Dept. of Environ. Medicine, The Sahlgrenska Acad. of Gothenburg Univ., Box 414, 405 30 Gothenburg, Sweden, fredric.lindstrom @amm.gu.se), Keni Ren (Umea University, Dept. of Applied Physics and Electronics, Teknikhuset, Box 414, 901 87 Umea, Sweden, renkeni@gmail.com), Kerstin Persson Waye (Dept. of Environ. Medicine, The Sahlgrenska Acad. of Gothenburg Univ., Box 414, 405 30 Gothenburg, Sweden, kerstin.persson-waye@amm.gu.se), Haibo Li (Umea University, Dept. of Applied Physics and Electronics, Teknikhuset, Box 414, 901 87 Umea, Sweden, haibo.li@tfe.umu.se)

Measuring noise exposure in a working environment is often done by using standard noise dosimeters. This method is suitable for the evaluation of many working environments. However, in some situations the worker uses his/her voice a large amount during the day, e.g. teachers in a preschool environment. Thus, in these situations regular dosimeter measurements will not correspond to the actual noise exposure. In order to provide correct measurements, methods that can detect when the workers own voice is active are required. This paper presents a study of two such methods originating from voice research; the binaural and the throat microphone methods. The methods are compared using a receiver operating characteristics based method, where the performance is assessed by the Probability-of-failure measure, i.e. the percentage of own voice that the method failures to detect correctly. The evaluation is performed in a lab environment as well as in real field conditions in a preschool. The results of the study show that both methods can be successful in a controlled low noise (<45dBA) environment (Probability-of-failure <0.1% for both methods), while in the preschool environment, the throat microphone method (Probability-of-failure <0.1%) is more suitable than the binaural method (Probability-of-failure >6%).

10:20-10:40 Break

10:40

4aNSb8. Recovery of distortion product otoacoustic emissions (DPOAE) after impulse vs. continuous equal-energy exposures. Miguel Angel Aranda De Toro (Acoustics, Aalborg University, Fredrik Bajers Vej 7 B5, 9220 Aalborg Ø, Denmark, maat@es.aau.dk), Rodrigo Ordoñez (Acoustics, Aalborg University, Fredrik Bajers Vej 7 B5, 9220 Aalborg Ø, Denmark, rop@es.aau.dk), Karen Reuter (Acoustics, Aalborg University, Fredrik Bajers Vej 7 B5, 9220 Aalborg Ø, Denmark,

kr@es.aau.dk),Dorte Hammershøi(Acoustics, Aalborg University, Fredrik Bajers Vej 7 B5, 9220 Aalborg Ø, Denmark, dh@es.aau.dk)

The correct assessment of impulse noise from occupational environments for hearing-conservation purposes is still a controversial issue. Currently, no universally accepted standard defines impulse noise accurately nor does a standard method exist to measure impulses. Moreover, current impulse-damage risk-criteria suffer from lack of empirical data needed to quantify impulse noise exposures and assess potential damage. In this experiment human subjects are exposed to binaural recordings of noises from industrial environments. Stimuli consist of impulse noise, continuous noise, and combinations of impulse and continuous noise. Noise exposures are normalized to have the same energy ($L_{Aeq,8h}$= 80dB). The effects in the hearing of the subjects are monitored by measuring the recovery of the distortion product otoacoustic emissions (DPOAE) with high-time resolution. The results can be used to investigate the validity of current assessment methods and descriptors of the temporal characteristics of sound exposures and their relation to the temporal effects produced on the human hearing as well as investigating selected issues that may lead to possible improvements or alternative measuring methods. [Work supported by the Danish Research Council for Technology and Production.]

Invited Paper

11:00

4aNSb9. ″Real world″ noise exposure beneath hearing protectors : a scattered international practise. Pierre Canetto (INRS - Institut National de Recherche et de Sécurité, Avenue de Bourgogne BP No 27, 54501 Vandoeuvre, France, pierre.canetto@inrs.fr), Nicolas Trompette (INRS - Institut National de Recherche et de Sécurité, Avenue de Bourgogne BP No 27, 54501 Vandoeuvre, France, nicolas.trompette@inrs.fr)

Assessing occupational noise exposure ″beneath″ Hearing Protection Devices (HPD) is a topical subject. Standardized methods allow to calculate the exposure by using the HPD attenuation. The HPD attenuations declared by manufacturers are much higher from the ″real-world″ ones. To reduce this difference, some ″compensation″ methods are proposed. The methods and their rules vary a lot from one country to another. The ″derating″ rmethod reduces the declared values from a certain amount, according to the HPD kind. ″Double-labelling″ method uses attenuation values measured in laboratory with untrained subjects. ″Statistical range enlargement″ widens the statistical confidence of the laboratory-test results. All these methods propose a global solution: the reasons due to human behaviour (mainly bad HPD wearing) , products quality, and the difference between laboratory and industrial situations are mixed. This ″blind″ approach could be considered as endorsing the lack of workers' training, and could impede the progress in HPD developments. But a ″short-term″ answer to the problem is needed. It should allow to build a more relevant medium-term answer, which could be worked out possibly on an international scale.

Contributed Papers

11:20

4aNSb10. A comparison of earmuff protection measured in real-world and laboratory conditions. Emil Kozlowski (Centr. Inst. for Labour Prot. - Natl. Res. Inst., Czerniakowska 16, 00-701 Warsaw, Poland, emkoz@ciop.pl), Ewa Kotarbinska (Warsaw Univ. of Technology Inst. of Radioelectronics, Nowowiejska 15/19, 00-665 Warsaw, Poland, Ewa .Kotarbinska@ire.pw.edu.pl)

It has been well known and that noise protection provided by earmuffs in real-world conditions is lower than measured by a laboratory standardized REAT test. In this study, earmuff protection was tested by simultaneous measurement of the L_{Aeq} under and outside the earmuffs in 91 industrial workplaces and in the laboratory. In all cases, the L_{Aeq} measured under the earmuffs was compared with the level predicted according to the EN 458 standard, by an octave-band method for calculating the A-weighted SPL under the hearing protector. The L_{Aeq} levels measured under the earmuffs in real-world conditions were by more than 3 dB(A) and 15 dB(A) higher than predicted by the octave-band method, respectively in 65% and 17% of cases. The main causes of worse protection at workplaces were worn-out earmuffs due to prolonged usage (33%), improper way of wearing earmuffs (15%), or the use of eye-glasses (8%). The data show that attenuation values measured by the REAT method overestimate by 1-5 dB the earmuff protection obtained in real-world conditions. [Work supported by the Polish Ministry of Labour and Social Policy, grants 4.S.03 and 3.S.02].

11:40

4aNSb11. Empirical evaluation using impulse noise of the level-dependency of various passive earplug designs. Elliott H. Berger (E-A-R / Aearo Technologies, 7911 Zionsville Rd., Indianapolis, IN 46268-1657, USA, eberger@compuserve.com), Pascal Hamery (French German Institut of Saint Louis (ISL), 5 rue du Général Cassagnou, 68301 Saint-Louis, France, hamery@isl.tm.fr)

An objective in the development of hearing protection devices (HPDs) has been the design of a passive earplug that provides modest or no attenuation at low sound levels, with greater protection at high sound levels. This raises the issue of not only how to construct such a device, but also how to evaluate it. There is the related question of whether conventional HPDs are actually level independent. Passive level dependency is typically accomplished via an orifice that causes sound transmission to decrease as input level increases. We utilized an impulsive noise source (explosives) with peak levels from 110 to 190 dB SPL to measure the insertion loss of a variety of commercially available and developmental earplugs. The tests were conducted at frontal incidence in a reflection-free outdoor environment using the Institute of Saint-Louis acoustical test fixture specifically constructed for HPD attenuation measurements. Conventional foam and premolded earplugs exhibited attenuation that was essentially constant with level, whereas the best of the level-dependent designs provided attenuation that increased by about 25 dB over the 80-dB range of test impulse levels. This latter design has been successfully utilized since 2000 in the Combat Arms™ Plug widely fielded in the U. S. Military.

Invited Paper

12:00

4aNSb12. Impulse and continuous noise reduction of tactical hearing protection systems. Richard McKinley (AFRL, Wright-Patterson Air Force Base, Dayton, OH 45433-7901, USA, richard.mckinley@wpafb.af.mil), Brian Hobbs (AFRL, Wright-Patterson Air Force Base, Dayton, OH 45433-7901, USA, brian.hobbs@wpafb.af.mil), Karl Buck (French German Institut of Saint Louis (ISL), 5 rue du Général Cassagnou, 68301 Saint-Louis, France, karl.buck@isl.eu), Dean Hudson (AFRL, Wright-Patterson Air Force Base, Dayton, OH 45433-7901, USA, harvey.hudson@wpafb.af.mil)

Tactical hearing protectors are devices designed to protect the wearer from high levels of impulse noise while providing some ambient listening and communication capability. Many of these devices also provide some attenuation of continuous noise. The efficacy of these types of devices depends on the amount of impulse noise protection and continuous noise protection, the quality of the ambient listening capability, and the intelligibility of the speech communication capability. This paper will describe the peak noise reduction of approximately 1 ms duration impulses with peak levels at 165 dB and 195 dB, for several earplugs and earmuffs. The frequency dependent reduction of impulse noise measured using an acoustic test fixture (the French German Research Institute at Saint Louis Head). Generally the data show higher levels of impulse noise reduction with earplugs than with earmuffs. Additionally, continuous noise attenuation was measured using human subjects performing the ANSI S12.6 Real Ear At Threshold (REAT) test. High speed (20k frames/sec) video will show the dynamic motion of typical tactical hearing protection earplugs and earmuffs when stimulated with a 195 dB impulse.

Contributed Papers

12:20

4aNSb13. Sound path(s) to the ear protected by double hearing protection. Karl Buck (French German Institut of Saint Louis (ISL), 5 rue du Général Cassagnou, 68301 Saint-Louis, France, karl.buck@isl.eu), Pascal Hamery (French German Institut of Saint Louis (ISL), 5 rue du Général Cassagnou, 68301 Saint-Louis, France, hamery@isl.tm.fr), Richard McKinley (AFRL, Wright-Patterson Air Force Base, Dayton, OH 45433-7901, USA, richard.mckinley@wpafb.af.mil)

Studies have shown that the attenuation performance of double hearing protection is limited by bone or tissue conduction. We present the first results of a program to determine the different paths of the sound to the ear when a person is protected by double hearing protection. In order to determine the contribution of the noise signal passing by secondary sound paths (bone or tissue conduction) into the volume of the ear canal behind the earplug, identical tests have been performed on humans and artificial heads. Time delay and attenuation through the hearing protection (NR) were measured on the ipsi- and contra-lateral side of the head. The measurements show differences in time delay and attenuation between artificial heads and humans which indicate that the main transmission mechanism is different. They also give a strong indication that the path of the acoustic signal depends on the angle of arrival when using double HP. This may partly explain the poor sound localization performance when using double HP that was reported by Brungart (2002). The single HP, and the double HP were then used in a sound localization experiment. The localization performance of these conditions will be presented along with the related parameters.

12:40

4aNSb14. Prediction of impulsive noise waveform under an earmuff worn by a real user. Rafal Mlynski (Centr. Inst. for Labour Prot. - Natl. Res. Inst., Czerniakowska 16, 00-701 Warsaw, Poland, rmlynski@ciop.pl), Jan Zera (Centr. Inst. for Labour Prot. - Natl. Res. Inst., Czerniakowska 16, 00-701 Warsaw, Poland, jazer@ciop.pl)

For the assessment of hearing damage risk caused by impulsive noise, it is important to know the impulse waveform a user is exposed to under the hearing protector. In this study, a complex transmittance of an earmuff was used to predict the waveform under a hearing protector. Earmuff's transmittance was calculated from impulses recorded outside and under the hearing protector, for a real user, as transmittance of the equivalent FIR filter. The transmittance determined in that way was then used to predict the impulse waveforms under the earmuffs produced in response to various outside impulses. Accuracy of predictions was assessed by a comparison of peak SPL, L_{Aeq8}, A, C, or D duration of the impulse waveforms calculated and measured under the earmuffs. Results obtained for a real user were compared with the measurements made with the use of an artificial test fixture (ATF, ISO 4869-3). [Work supported by Polish grants R18004304 (MNiSzW) and 3.S.03 (MPiPS)].

Session 4aNSc

Noise, Computational Acoustics, and EURONOISE: Time-Domain Modeling Methods in Acoustics II

Paul Calamia, Cochair
Rensselaer Polytechnic Institute, Greene Bldg., 110 8th St., Troy, NY 12180, USA

Maarten Hornikx, Cochair
Applied Acoustics, Chalmers University of Technology, Sven Hultins Gata 8a, Gothenburg, SE-41296, Sweden

Invited Papers

8:00

4aNSc1. Time domain modeling of acoustic propagation with acoustic wave propagator and absorbing boundary conditions. Jan H. Ehrlich (FWG Underwater Acoustics and Marine Geophysics Research Institute, Klausdorfer Weg 2-24, 24148 Kiel, Germany, janehrlich@bwb.org)

The acoustic wave propagator (AWP) is the application of the time evolution operator on the acoustic wave equation for stationary systems in a polynomial expansion of Chebychev polynomials. It allows to increase the time step by more than one order of magnitude compared to finite difference time domain (FDTD) codes. In contrast to other implementations of the AWP the spatial differentiation is carried out with finite difference techniques because this allows the use of the perfectly matched layer formulation as absorbing boundary conditions. The formulation includes the direct implementation of acoustic sources with sinusoidal time evolution. Other sources can be synthesized by their Fourier components. For the calculation of large areas the explicit formulation of a large system matrix can be avoided by calculating the propagation equations for each time step at row and column level repeatedly which reduces memory requirements notably. This procedure and the suitability of the finite difference approach for parallelization makes the extension to fully three dimensional calculations possible. Examples for benchmark problems with sound propagation in air and water are given.

8:20

4aNSc2. A time domain boundary element method for compliant surfaces. Jonathan A. Hargreaves (University of Salford, M5 4WT Manchester, UK, j.a.hargreaves@salford.ac.uk), Trevor J. Cox (University of Salford, Acoustics Research Centre, Newton Building, M5 4WT Salford, UK, t.j.cox@salford.ac.uk)

The best way of representing compliant surfaces in time domain prediction models, such as the transient Boundary Element Method (BEM), is currently unresolved. This is not true of frequency-domain, time-invariant models, where the common practice is to represent the characteristics of a material by its surface impedance. A BEM may be used to predict the scattering of sound, and reduces the problem of modelling a volume of air to one involving surfaces conformal to the obstacles. Surface impedance is a convenient concept for inclusion in the frequency domain BEM as it abstracts the obstacle's characteristics into a property of the conformal surface. The time domain BEM predicts transient scattering of sound, and is usually solved in an iterative manner by marching on in time from known initial conditions. For surface impedance data to be utilised it must be Fourier transformed from a frequency dependent multiplication into a temporal convolution. This approach typically yields convolution kernels which involve future sound, hence is not compatible with time-marching solvers. In this paper an alternative time domain representation of compliant locally reacting materials is proposed to overcome this problem, and its implementation and limitations discussed.

8:40

4aNSc3. Stability behaviour and results of a transient boundary element method for exterior radiation problems. Michael Stütz (Technische Fachhochschule Berlin, Univ. of Applied Sciences, Luxemburger Str. 10, 13353 Berlin, Germany, stuetz@tfh-berlin.de), Martin Ochmann (Technische Fachhochschule Berlin, Univ. of Applied Sciences, Luxemburger Str. 10, 13353 Berlin, Germany, ochmann@tfh-berlin.de)

Based on the Helmholtz integral equation, a boundary element method in time domain (TD-BEM) can be formulated. Because of instability issues, this method is rarely used in numerical acoustics. The stability and accuracy of the method for exterior radiation problems is investigated using some simple examples. A connection between the internal resonances of the closed structure and the instable behaviour of the method is assumed, but it is mathematically unproven. Numerical evidence of this connection is presented. Because of the sparse structure of the resulting system matrix, the use of iterative solvers is advantageous. The performances of different solvers are compared with respect to stability and numerical costs. For testing purposes, the acoustic radiation from an open turbulent flame is calculated and compared with results of a frequency domain BEM calculation.

9:00

4aNSc4. Analytical validation of time-step interpolation in transient insular nodal analysis. Tom De Rybel (The University of British Columbia, Department of Electrical and Computer Engineering, 2332 Main Mall, Vancouver, BC V6T 1Z4, Canada, tomr@ece.ubc.ca), José Marti (The University of British Columbia, Department of Electrical and Computer Engineering, 2332 Main Mall, Vancouver, BC V6T 1Z4, Canada, jrms@ece.ubc.ca), Murray Hodgson (The University of British Columbia, Department of Electrical and Computer Engineering, 2332 Main Mall, Vancouver, BC V6T 1Z4, Canada, mhodgson@interchange.ubc.ca)

The transient insular nodal analysis method (TINA) combines elements from the finite differences (FD) and transmission-matrix methods (TLM) in one unified approach. In contrast to existing TLM-FD methods, TINA uses time-decoupled cells, avoiding the need for solving large system matrices. The time-decoupled cells allow for easy parallelisation, and the solution of large systems in detail. Due to the use of an exact transmission-line model in the cells, wave propagation can be computed without the need for discretisation of the equations, nor the use of prediction, yielding an unconditionally stable method. Boundary conditions are implicit, and are solely defined by the wave speed and characteristic impedance of the medium. One key difference with the TLM method is how cells whose transmission time is not an integer multiple of the simulation time step are integrated in the simulation. These mismatches occur due to the the varying wave speeds of the different media in the cells. In TINA, the match is obtained through interpolation, as opposed to the stub-matching methodology employed in TLM. In this paper, we will demonstrate the validity of the interpolation approach analytically, as well as compare the TINA method to a theoretical case.

9:20

4aNSc5. An eigenfunction expansion method to efficiently evaluate spatial derivatives for media with discontinuous properties. Maarten Hornikx (Applied Acoustics, Chalmers University of Technology, Sven Hultins Gata 8a, SE-41296 Gothenburg, Sweden, maarten.hornikx@chalmers.se), Roger Waxler (University of Mississippi, NCPA, 1 Coliseum Drive, University, MS 38677, USA, rwax@olemiss.edu)

Pseudo-Spectral methods are often used as an alternative to the Finite Difference Time Domain (FDTD) method to model wave propagation in heterogeneous moving media. The FDTD method is robust and accurate but is numerically expensive. Pseudo-Spectral methods make use of the wavelike nature of the solution to obtain more efficient time-domain algorithms. The most straightforward of the Pseudo-Spectral methods is the Fourier method in which a spatial Fourier transform is used to evaluate the spatial derivatives in the wave equation. Whereas this method is accurate for a weakly heterogeneous moving medium, it degenerates for media with discontinuous properties. The eigenfunction expansion method presented here is a way to accurately and efficiently evaluate spatial derivatives in media with interfaces. As in the Fourier method, transforms may be calculated using FFT's and spatial sampling is limited only by the Nyquist condition. The performance of the method is shown in a time-domain implementation for media with discontinuous density and sound speed.

9:40

4aNSc6. Optimal tree canopy shape for improving downwind noise barrier efficiency. Timothy Van Renterghem (University Ghent - Department Information Technology, Sint-Pietersnieuwstraat 41, 9000 Gent, Belgium, Timothy.Van.Renterghem@intec.Ugent.be), Dick Botteldooren (University Ghent - Department Information Technology, Sint-Pietersnieuwstraat 41, 9000 Gent, Belgium, dick.botteldooren@intec.ugent.be)

The presence of a row of trees behind a highway noise barrier significantly reduces the screen-induced refraction of sound by wind. In this paper, the influence of quantitative tree properties, such as the pressure resistance coefficient of the canopy and the distribution of biomass over height, was studied numerically. Three computational models were involved. First, computational fluid dynamics (CFD) software is used to accurately predict the wind fields. The finite-difference time-domain (FDTD) method is then used to simulate sound propagation in the direct vicinity of the noise barrier in combination with trees. In a last step, the Parabolic Equation (PE) method is used to predict sound fields at larger distances. As a general conclusion, it was found that coniferous trees are superior to deciduous trees to improve downwind noise barrier efficiency.

10:00

4aNSc7. Green roofs to enhance quiet sides. Timothy Van Renterghem (University Ghent - Department Information Technology, Sint-Pietersnieuwstraat 41, 9000 Gent, Belgium, Timothy.Van.Renterghem@intec.Ugent.be), Dick Botteldooren (University Ghent - Department Information Technology, Sint-Pietersnieuwstraat 41, 9000 Gent, Belgium, dick.botteldooren@intec.ugent.be)

In this paper, the finite-difference time-domain method is used to study sound propagation over a green roof in an urban situation. Sound propagation between adjacent city canyons is considered, and the focus is on the reduction of the sound pressure level in the non-exposed canyon due to the presence of a vegetated (green) roof. Numerical calculations have been conducted for both intensive and extensive green roofs, showing that an important reduction of the sound pressure level in the shielded canyon can be achieved, compared to a rigid roof. In case of an extensive green roof, there is a strong dependence on the substrate layer thickness; a maximum reduction of 10 dB at the octave band of 1000 Hz was found. For intensive green roofs, the influence of the substrate layer thickness is limited.

Session 4aNSd

Noise and EURONOISE: Car Acoustics II

Luc Mongeau, Cochair
McGill University, 817 Sherbrooke St. West, Montreal, QC H3A 2K6, Canada

Virginie Maillard, Cochair
RENAULT, Groupe Acoustique, Technocentre, 1 avenue du Golf, 78288 Guyancourt Cedex, France

Invited Paper

8:00

4aNSd1. Trim FEM simulation of a dash and floor insulator cut out modules with structureborne and airborne excitations. Arnaud Duval (Faurecia AST, Center of Acoustic Technology, Dämmstoffwerk 100, 38524 Sassenburg, Germany, arnaud.duval@faurecia.com), Julien Baratier (Faurecia AST, Center of Acoustic Technology, Dämmstoffwerk 100, 38524 Sassenburg, Germany, julien.baratier@faurecia.com), Christian Morgenstern (Faurecia AST, Center of Acoustic Technology, Dämmstoffwerk 100, 38524 Sassenburg, Germany, christian.morgenstern@faurecia.com), Ludovic Dejaeger (Faurecia AST, Center of Acoustic Technology, Dämmstoffwerk 100, 38524 Sassenburg, Germany, ludovic.dejaeger@faurecia.com), Norimasa Kobayashi (Toyota Motor Corporation, 1, Toyota-cho, 471-8572 Toyota, Aichi, Japan, koba@nori.tec.toyota.co.jp), Hiroo Yamaoka (Toyota Motor Corporation, 1, Toyota-cho, 471-8572 Toyota, Aichi, Japan, yamaoka@giga.tec.toyota.co.jp)

During a vehicle development, measurements on cut out modules in large coupled reverberant rooms are often carried out in the middle and high frequency range in order to optimize the insulation performance of the trims (Transmission Loss). Using optimal controlled mounting conditions, we have been able to extend the frequency range to the low frequencies in order to validate trim FEM models of a dash and floor insulator modules with structureborne and airborne excitations. Both coupled response with movable concrete cavities (structureborne excitation) and Transmission Loss with the coupled reverberant rooms (airborne excitation) have been measured and simulated for various types of insulators on the same setup, without any change on the mounting conditions. An additional movable absorbing environment in the large reception room has been deployed in order to carry out laser vibrometer (skeleton velocity) and p-u probes (particle velocity and intensity) measurements on the surface of the trims. By incorporating the maximal treatment mock-ups of the cut out modules as additional trims in the models, we have obtained good correlation results between measurements and simulations for both bare and trimmed configurations for a dash and floor insulators with structureborne and airborne excitations.

Contributed Papers

8:20

4aNSd2. Practical aspects of implementing car interior active noise control systems. Rolf Schirmacher (Müller-BBM, Robert-Koch-Straße 11, 82110 Planegg, Germany, Rolf.Schirmacher@MuellerBBM.de), Roland Lippold (Müller-BBM, Robert-Koch-Straße 11, 82110 Planegg, Germany, Roland.Lippold@MuellerBBM.de), Frank Steinbach (Müller-BBM, Robert-Koch-Straße 11, 82110 Planegg, Germany, Frank.Steinbach@MuellerBBM.de), Florian Walter (Müller-BBM, Robert-Koch-Straße 11, 82110 Planegg, Germany, Florian.Walter@MuellerBBM.de)

When implementing real-world, close-to-production active noise control (ANC) systems for car interiors, many aspects far beyond textbook theory have to be taken into consideration -- many of which might also be left out for first demonstrator systems. Due to the predominant role of robustness and reliability, any kind of uncertainty in the system has to be considered carefully. Among others, the uncertainties and changes of the acoustical environment, e.g. due to temperature changes, number of passengers, open windows and also of system components, e.g. loudspeakers and microphones have to be measured and/or modeled. This also gives some new insight into the acoustical environment inside cars at low frequencies. In addition, the quality of input data (e.g., the update rate for rpm information) is of major importance for the acoustical performance in terms of noise reduction. Finally, stability analyses and robustness calculations must be extended to incorporate uncertainties as well as time domain effects even for more or less freqency domain problems like engine noise. This requires to re-formulate feed-forward systems as feed-back systems and calculate system responses. Measurement results on the interior acoustics (and its uncertainty) as well as additional developments on ANC system robustness will be presented.

8:40

4aNSd3. Fluctuations under turbulent flows: Enhanced methods for separation of propagative wavenumbers from wall pressure dataset. Sébastien Debert (PSA-Peugeot-Citroën, Route de Gizy, CC : VV013 - Bât. 14, F-78943 Vélizy-Villacoublay Cedex, France, sebastien.debert@mpsa.com), Marc Pachebat (PSA-Peugeot-Citroën, Route de Gizy, CC : VV013 - Bât. 14, F-78943 Vélizy-Villacoublay Cedex, France, marc.pachebat@mpsa.com), Vincent Valeau (Laboratoire d'Etudes Aérodynamiques (LEA), Université de Poitiers - ENSMA - CNRS, Bâtiment K, 40 Avenue du Recteur Pineau, F-86022 Poitiers, France, vincent.valeau@lea.univ-poitiers.fr), Yves Gervais (Laboratoire d'Etudes Aérodynamiques (LEA), Université de Poitiers - ENSMA - CNRS, Bâtiment K, 40 Avenue du Recteur Pineau, 86022 Poitiers, France, yves.gervais@lea.univ-poitiers.fr)

This work is a part of a more general study on automobile interior noise due to acoustic and aerodynamic wall-pressure fluctuations. Using experimental data of wall-pressure fluctuations measured with a microphone array beneath several kinds of flows, a wave-number analysis based on recently developed signal processing methods -- the spatial Empirical Mode Decomposition (sEMD) and the Ensemble Empirical Mode Decomposition (E-EMD) -- is carried out, in order to separate acoustic and aerodynamic pressure fluctuations. In opposition with an existing classical method previously used, based on the spatial correlogram, these methods do not require a stationary uniform flow. A turbulent boundary layer on a flat plate and a detached/reattached flow downstream three different forward-facing steps are tested, with flow velocities from 0 to 40 $m.s^{-1}$, with or without a well-controlled artificial acoustic source. The sEMD method is first used as a wavenumber filter, and is shown to improve the detection of acoustic fluc-

tuations of about 5 dB on classical wavenumber (k,f) representations. The E-EMD method is developed in order to decompose the (x,t) representation to make possible the separation of the acoustic and aerodynamic components, regardless of the stationarity or the uniformity of the flow.

9:00

4aNSd4. Stochastic modeling of the vibro-acoustic behavior of production cars. Laurent Gagliardini (PSA Peugeot Citroën, Route de Gisy, 78943 Vélizy-Villacoublay Cedex, France, laurent.gagliardini@mpsa.com), Jean-Francois Durand (Université Paris-Est, Laboratoire de Mécanique, 5 bd Descartes, 77454 Marne-la-Vallée, France, jean-francois.durand@astrium.eads.net), Christian Soize (Université de Marne la Vallée, 5, Boulevard Descartes, 77454 Marne la Vallée, France, soize@univ-mlv.fr)

Production cars -as any industrial product- are subject to various causes of variability including process uncertainties or product diversity. Many authors have shown that vibroacoustic problems sensitivity to small uncertainties increases dramatically with frequency until only statistical approaches remain relevant in the high frequency range. Moreover, modeling uncertainties due to numerous model simplifications induce similar dispersion effects on the computed responses. Both kind of uncertainties may be addressed when using a non-parametric stochastic modeling, based on the random matrices theory. Such a modeling, appears to be very practicable for industrial vibroacoustic problems while relying on a strong mathematical background. In a first part, the application of the non-parametric modeling of uncertainties to vibro-acoustics problems will be addressed. Stochastic aspects are controlled by only 7 dispersion parameters that provide most of the dynamic behaviors that can be observed experimentally. A Monte-Carlo simulation is performed to provide converged statistics of the stochastic problem solution. In a second part, the dispersion parameters are identified so that the stochastic model fits experimental data. Frequency Response Functions of 25 production vehicles were measured for this purpose and compared to the computed results in the low frequency range ($<$200 Hz).

9:20

4aNSd5. Improved spectrofilter applied to diesel engine noise : combustion and mechanical noise separation. Laurent Pruvost (Laboratoire Vibrations Acoustique, Insa Lyon, 25 bis, av. J. Capelle, 69621 Villeurbanne Cedex, France, laurent.pruvost@insa-lyon.fr), Quentin Leclere (Laboratoire Vibrations Acoustique - INSA Lyon, 25 bis avenue Jean Capelle, Bâtiment Saint-Exupéry, F-69621 Villeurbanne cedex, France, quentin.leclere@insa-lyon.fr), Etienne Parizet (Laboratoire Vibrations Acoustique, Insa Lyon, 25 bis, av. J. Capelle, 69621 Villeurbanne Cedex, France, etienne.parizet@insa-lyon.fr)

For engineers working on alternative fuels and diesel engine sound quality, being able to separate combustion noise and mechanical noise would be of prime interest. This separation can be attempted using a spectrofilter (also called Wiener filter) when in-cylinder pressure signals can be recorded. The major drawback of the spectrofilter is its unability to separate correlated sources like combustion and piston slap. An upgraded version of the spectrofilter can be computed. Its computation just requires to consider only the random parts of the engine signals. Actually, considering these random parts artificially uncorrelates the noise sources. Highly correlated signals have been synthesised and successfully separated by the upgraded spectrofilter. When dealing with real-life engine noise, the quality of the separation cannot be judged directly since the signals to separate are unknown. The spectrofilter's causality and stability have been used as criteria to judge its quality. These two criteria both confirmed the superiority of the spectrofilter computed using the random parts of the signals. A synchronous averaging step is required to estimate the signals random parts. This estimation has been found to depend on the phase-locking strategy.

9:40

4aNSd6. Prediction of the Excitation Force Based on the Dynamic Analysis for Flexible Model of a Powertrain. Yoon Sug Kim (Inha University, Mechanical Engineering, 253 Yonghyun Dong, 402-751 Inchon, Republic of Korea, black_boxter@hanmail.net), Sung Jong Kim (Inha University, Mechanical Engineering, 253 Yonghyun Dong, 402-751 Inchon, Republic of Korea, kimsungjong@gmail.com),Min Geun Song(Inha University, Mechanical Engineering, 253 Yonghyun Dong, 402-751 Inchon, Republic of Korea, somiku@hanmail.net), Sang Kwon Lee (Inha University, Mechanical Engineering, 253 Yonghyun Dong, 402-751 Inchon, Republic of Korea, sangkwon@inha.ac.kr)

The powertrain is one of the import sources for the interior noise. In order to predict the interior noise due to a powertrain, the experimental method is has been used based on the TPA (transfer path analysis). Although this experimental method is a useful tool for the identification of the noise source and the transfer path due to the powertrain, it is difficult to modify the structure of a powertrain by using the experimental method for the reduction of vibration and noise. In order to solve this problem, the paper presents the noble approach for the prediction of interior noise caused by the vibration of the powertrain based on the hybrid TPA (transfer path analysis) technology. Therefore, the vibration of the powertrain in a vehicle is numerically analyzed by using FEM (finite element method). The vibration of the other part in a vehicle is investigated by using the experimental method based on VATF (vibrato-acoustic transfer function) analysis. These two methods are combined for the prediction of interior noise caused by powertrain. This paper present the prediction of the excitation force of the powertrain to the vehicle body based on numerical simulation.

10:00-10:20 Break

10:20

4aNSd7. Sound quality evaluation of air-conditioning sounds in a vehicle using psychoacoustic parameters. Ryota Nakasaki (Utsunomiya Univ., Calsonickansei Corp., 7-3 Sakae-cho, Tochigi-ken, 327-0816 Sano-shi, Japan, ryota_nakasaki@ck-mail.com), Takaharu Ogata (Utsunomiya Univ., 7-1-2 Yoto, Tochigi-ken, 321-8585 Utsunomiya-shi, Japan, mt076508@ced.is.utsunomiya-u.ac.jp), Hiroshi Hasegawa (Utsunomiya Univ., 7-1-2 Yoto, Tochigi-ken, 321-8585 Utsunomiya-shi, Japan, hasegawa@is.utsunomiya-u.ac.jp), Yukio Ozeki (Utsunomiya Univ., Calsonickansei Corp., 7-3 Sakae-cho, Tochigi-ken, 327-0816 Sano-shi, Japan, ryota_nakasaki@ck-mail.com), Masaharu Onda (Utsunomiya Univ., Calsonickansei Corp., 7-3 Sakae-cho, Tochigi-ken, 327-0816 Sano-shi, Japan, ryota_nakasaki@ck-mail.com), Masao Kasuga (Utsunomiya Univ., 7-1-2 Yoto, Tochigi-ken, 321-8585 Utsunomiya-shi, Japan, kasuga@is.utsunomiya-u.ac.jp)

With recent developments of noise reduction technologies from mechanical components of a vehicle, air-conditioning systems become a major noise source in the compartment of a vehicle. To improve quietness in the compartment further, it is important not only to reduce the sound pressure level (SPL), but also to improve the sound quality. In this study, we tried to evaluate the air-conditioning sounds from a viewpoint of sound quality. First, we carried out a subjective evaluation experiment using some evaluation words that represent characteristics of the air-conditioning sounds. As a result of a factor analysis, noting that the air-conditioning sounds can be explained by three factors of ″rough,″ ″space″ and ″refreshing.″ ″Rough factor″ has strong correlation with the SPL, however, ″space factor″ and ″refreshing factor″ have little correlation with SPL. Next, to investigate parameters that correlate with these factors, we carried out an experiment to evaluate the air-conditioning sounds using the psychoacoustic parameters of loudness and sharpness. As a result, noting that ″rough″ factor strongly correlates with loudness, ″space″ and ″refreshing″ factors correlate with sharpness. This result shows that it is possible to evaluate the air-conditioning sounds a viewpoint of sound quality by using the sharpness that is different from SPL.

10:40

4aNSd8. Low noise truck study for distribution in urban areas. Nicolas Blairon (Volvo 3P, 99 route de Lyon, 69802 Saint - Priest, France, nicolas.blairon@volvo.com), Bruno Carton (Volvo 3P, 99 route de Lyon, 69802 Saint - Priest, France, bruno.carton@volvo.com)

Today, vehicle noise is identified in opinion pools as one of the main annoyance source in urban areas. To face this issue, truck manufacturers are today developing low noise vehicles in order to allow their customer to deliver goods in urban areas during night. An acoustic research program has

been launched by Volvo 3P (Volvo Trucks, Renault Trucks and Mack Trucks): the LUT project as Low Noise Urban Truck. The partners of the project are Michelin, the Institut National des Sciences Appliquées de Lyon (INSA) - a French university - and Marmonier - a noise shield manufacturer. This project has been founded by ADEME The target in terms of noise reduction is ambitious because the low noise truck will emit an acoustic power four times lower than today's vehicles in specific rolling conditions! Methods and tools have been developed to analyze the vehicle noise sources in urban conditions and define acoustic solutions to reduce the main vehicle noise sources.

11:00

4aNSd9. Operational transfer path analysis: Comparison with conventional methods. Martin Lohrmann (Müller-BBM Vibroakustik Systeme, Robert Koch Strasse 13, 82152 Planegg / München, Germany, MLohrmann@MuellerBBM-vas.de)

Transfer Path Analysis describes how sound and vibration propagates through complex structures. The correct determination of transfer coefficients between sources and receivers is essential for a high quality analysis. Conventional methods use artificial excitations (forces or volume velocities) to evaluate transfer functions. Therefore, they do not consider the influence of different load conditions on the transfer function behaviour of complex structures. In a second step, operational data (vibrations or sound pressures) are applied to the transfer functions to calculate the different path contributions. In order to overcome these restrictions, transfer coefficients can be evaluated directly from operational data. Thus, the actual load conditions are taken into account and the quality of transfer characteristics is improved. The relation between simultaneously measured data of sources and receivers can be derived by statistical methods. Principal Component Analysis is used to separate the total signal into individual path contributions, while operating on airborne and structure-borne contributions simultaneously. Operating in the time-domain gives direct access to auralisation and in-depth analysis of dominant path contributions. This new single-step approach has been proven to generate more precise analysis results within a much shorter testing time.

11:20

4aNSd10. A transversal substructuring modal method for the acoustic analysis of dissipative mufflers with mean flow. José Albelda (Dept. Ingeniería Mecánica y de Materiales. Univ. Politécnica de Valencia, Camino de Vera, s/n, 46022 Valencia, Spain, jalbelda@mcm.upv.es), Francisco D. Denia (Dept. Ingeniería Mecánica y de Materiales. Univ. Politécnica de Valencia, Camino de Vera, s/n, 46022 Valencia, Spain, fradegu1@mcm.upv.es) , F. Javier Fuenmayor (Dept. Ingeniería Mecánica y de Materiales. Univ. Politécnica de Valencia, Camino de Vera, s/n, 46022 Valencia, Spain, ffuenmay@mcm.upv.es), Manuel J. Martínez (Dept. Ingeniería Mecánica y de Materiales. Univ. Politécnica de Valencia, Camino de Vera, s/n, 46022 Valencia, Spain, mamarbor@doctor.upv.es)

This work presents a modal approach to evaluate the transversal modes and wavenumbers for dissipative mufflers with mean flow. The method is based on the division of the transversal section of the muffler into subdomains, for which two simple sets of modes are considered. The first set of modes satisfies the condition of zero pressure at the common boundary between subdomains, while the second fulfils the condition of zero derivative in the direction normal to this boundary. From these sets, a substructuring procedure is applied that provides the final modes of the complete cross section, considering the presence of absorbent material, a perforate and mean flow. The technique avoids iterative schemes associated with the nonlinear characteristic equation found, for instance, in the analytical modelling of perforated dissipative circular mufflers. Once the final transversal modes have been calculated, the mode matching technique is applied at the geometrical discontinuities to completely define the acoustic field inside the muffler. The acoustic attenuation is then predicted by means of the transmission loss. Comparison with finite element calculations and results available in the literature show good agreement. The attenuation of some selected mufflers is analysed, including the effect of the perforate and the mean flow.

11:40

4aNSd11. Prediction of sound transmission through automotive door seal systems. Bertrand Andro (Renault, Technocentre, 1 avenue du Golf, 78288 Guyancourt, France, bertrand.andro@renault.com), Sébastien Chaigne (Renault, Technocentre, 1 avenue du Golf, 78288 Guyancourt, France, sebastien.chaigne@renault.com), Alpha Diallo (Renault, Technocentre, 1 avenue du Golf, 78288 Guyancourt, France, alpha.diallo@renault.com), Matthieu Mermet (CEMEF, 1, rue Claude Daunesse, 06904 Sophia Antipolis, France, matthieu.mermet-renexter@renault .com)

In automotive industry the door seal systems is an important contributor to vehicle interior noise in the middle and high frequency range. The aim of the study was to develop a numerical model in order to predict the sound transmission loss through elastomeric seals. At the early stage of the development process, this type of numerical tool is very interesting to investigate the influence of the design parameters of the seal. Two steps were necessary: a static analysis to calculate the seal shape after compression (door closure event), an acoustic analysis based on dynamic parameters to determine the sound transmission. Finite element methods were used for both steps (commercial softwares). These two steps were validated experimentally for two types of geometry, different compression ratios and loading cases. One original contribution of the paper concerns the determination of a valid nonlinear model for the static part and of a good approximation of the dynamic behavior of the elastomer's Young modulus. Finally, a sensibility analysis was performed in order to evaluate the influence of the design parameters of the door seal system such as the compression ratio or the dynamic parameters.

12:00

4aNSd12. Quantification of structural damping of a multi-layered windshield at low and medium frequencies. Manuel Etchessahar (PSA Peugeot Citroën, Route de Gisy, 78943 Vélizy-Villacoublay Cedex, France, manuel.etchessahar@mpsa.com), Laurent Gagliardini (PSA Peugeot Citroën, Route de Gisy, 78943 Vélizy-Villacoublay Cedex, France, laurent .gagliardini@mpsa.com)

Structural damping is known as one of the most efficient design variable in order to reduce structure-borne noise. At low and medium frequencies (100-500 Hz), the vibro-acoustic behavior of the car is essentially governed by large panels as windshield, roof or front panel for example. In order to improve the car body design regarding cost, weight, performances and reliability, one must have a good understanding of the damping performances of these large panels submitted to various operating conditions. In a previous paper, the authors have proposed an improved method for structural damping numerical assessment of structural elements with non uniform damping using a stochastic distribution of input forces. In the present paper, this method is applied to quantify the structural damping of a multi-layered windshield at low and medium frequencies. Effects of the geometry, of the viscoelastic properties of the PVB layer and of the windshield glue bead on the total damping properties will be studied.

Session 4aNSe

Noise and EURONOISE: Noise from Wind Power Projects I

Eddie Duncan, Cochair
Resource Systems Group (RSG), 55 Railroad Row, White River Junction, VT 05001, USA

Kerstin Persson Waye, Cochair
Dept. of Environ. Medicine, The Sahlgrenska Acad. of Gothenburg Univ., Box 414, Gothenburg, 405 30, Sweden

Invited Paper

10:20

4aNSe1. Improving sound propagation modeling for wind power projects. Eddie Duncan (Resource Systems Group (RSG), 55 Railroad Row, White River Junction, VT 05001, USA, eduncan@rsginc.com), Kenneth Kaliski (Resource Systems Group (RSG), 55 Railroad Row, White River Junction, VT 05001, USA, kkaliski@rsginc.com)

Sound propagation from wind power projects can be modeled in the same manner as other more common outdoor noise sources, but are these models suited to wind turbines' uniquely high source heights, operating under high wind conditions, and various degrees of terrain ruggedness. In ″Propagation Modeling Parameters for Wind Turbines″ (K. Kaliski and E. Duncan, Proceedings of Institute of Noise Control Engineers NOISECON 2007), the effects of ground attenuation and various adjustments for wind conditions on sound propagation modeling were discussed. This paper continues the discussion and explores the accuracy of existing sound propagation modeling methods for wind power projects including ISO 9613 and other standards. Model data for wind power projects and the implications of various terrain and ground coverage will be discussed.

Contributed Papers

10:40

4aNSe2. A review of the use of different noise prediction models for windfarms and the effects of meteorology. Graham Parry (ACCON UK Limited, Unit B, Fronds Park, Frouds Lane, Aldermaston, RG7 4LH Reading, UK, graham.parry@accon-uk.com)

As a result of involvement in a specific wind farm development at Guestwick, Norfolk and a requirement to determine the efficacy of competing noise prediction models a review of the potential impacts of a six-turbine wind farm was carried out. The paper considers the results of comparing three specific noise prediction methods and algorithms and determines the extent to which adherence to either one of the methodologies could result in relatively large differences in predicted noise levels under varying wind conditions and accordingly the potential for differing conclusions being reached as to the acceptability of the wind farm with respect to the ETSU-R-97 assessment methodology. The paper also examines other noise modelling research carried out on behalf of ETSU.

11:00

4aNSe3. Noise Impact of Wind Farms: Uncertainties due to wind data reference at 10m. David Slaviero (Acouphen Environnement, Campus de la DOUA, 66, BD Niels Bohr, BP 52132, 69603 Villeurbanne, France, david.slaviero@acouphen-environnement.com), Alexis Bigot (Acouphen Environnement, Campus de la DOUA, 66, BD Niels Bohr, BP 52132, 69603 Villeurbanne, France, alexis.bigot@acouphen-environnement.com)

Noise impact prediction or measurement of Wind Farms requires wind reference data at 10 meters. From data collected on more than 200 Farms in France, over the last 5 years, this paper shows that, in the sampling of noise and meteolological data for noise prediction and assessment, differences in the wind profil from one site to another, in the period of the day (day, night) can lead to different estimations of emission data selection and impact assessment. Different parameter studies are presented both with regard to the effect on impact studies and farms impact monitoring and control. The work presented is in accordance with the project of acoustic standard for the assessment of noise impact of Wind Farms under study in France.

Invited Papers

11:20

4aNSe4. Models of natural background noise and masking of wind turbine noise. Karl Bolin (KTH/MWL, Teknikringen 8, SE100 44 Stockholm, Sweden, kbolin@kth.se)

Wind turbine (WT) noise limits adjusted to background noise levels are used in several countries among others Britain and France. To determine the background noise level extensive measurements at locations near the proposed WT site are performed. This paper present methods to avoid these measurements in woodland and coastal areas, it also include a pre-study concerning the audibility of WT noise when mixed with background noise. A prediction model for noise from vegetation is described. This has been coupled to wind field simulations and fluctuations of vegetation noise can therefore be predicted. Measurements and a model for sea wave noise are also presented. Furthermore the paper present results from psycho acoustic tests with 8 subjects. These involve hearing thresholds and partial loudness when WT noise is mixed with background noise. These are compared to two loudness models. Two different WT sounds have been used as stimuli. The first sound is from a single WT and the second sound is from a WT park. Results show how natural background noises influence the audibility of WT noise and could be used as a tool to optimize the power generated from WTs without causing disturbance among nearby residents.

11:40

4aNSe5. Criteria for wind farm noise: Lmax and Lden. Frits Van Den Berg (University of Groningen - Science & Society Group, Nijenborgh 4, 9747AG Groningen, Netherlands, fvdberg@ggd.amsterdam.nl)

Wind turbine noise limits are based on either the highest sound immission level (Lmax) or several sound immission levels for a series of wind speed classes (Lmax,v). As yet no procedure has been proposed to determine the day-evening-night sound level (Lden) that is now commonly used in the European Union for all noise sources. Wind speed dependent rating wind turbine noise levels Lr,v can be predicted based on climatological data. This has been verified by measurements over a nine month period for a wind farm at a coastal location in the Netherlands. From these measurements also the long term average sound level Lden can be determined. Lden can also be determined from previously published wind speed measurements at an inland location over one year. The procedure shows that for a wind turbine or wind farm the Lden can be derived from Lmax by taking into account the regional climatology.

12:00

4aNSe6. Response to wind turbine noise in the Netherlands. Eja Pedersen (Occupational and Environmental Medicine, Göteborg University, PO Box 100, SE-405 30 Göteborg, Sweden, eja.pedersen@set.hh.se), Jelte Bouma (Northern Centre for Healthcare Research, University Medical Centre Groningen, PO Box 30001, 9700 RB Groningen, Netherlands, j.bouma@med.umcg.nl), Roel Bakker (Northern Centre for Healthcare Research, University Medical Centre Groningen, PO Box 30001, 9700 RB Groningen, Netherlands, R.H.Bakker@med.umcg.nl), Frits Van Den Berg (University of Groningen - Science & Society Group, Nijenborgh 4, 9747AG Groningen, Netherlands, fvdberg@ggd.amsterdam.nl)

A cross-sectional study with the objective to explore the impact of wind turbine noise on people living in the vicinity of wind farms was carried out in the Netherlands in 2006. A postal questionnaire assessing response to environmental exposures in the living area, including wind turbine noise, was answered by 725 respondents (response rate: 37%). Immission levels of wind turbine noise outside the dwelling of each respondent were calculated in accordance with ISO-9613. The risk for being annoyed by wind turbine noise outdoors increased with increasing sound levels ($rs = 0.501$, $n = 708$, $p<0.001$). The risk for annoyance was decreased for respondents who could not see wind turbines from their dwelling and for respondents who benefited economically from the turbines. No statistically significant correlations between immission levels of wind turbine noise and health or well-being were found. However, noise annoyance due to wind turbine noise was associated with stress symptoms, psychological distress and lowered sleep quality.

12:20

4aNSe7. Laboratory assessment of noise annoyance from large wind turbines. Steffen Pedersen (Acoustics, Aalborg University, Fredrik Bajers Vej 7 B5, 9220 Aalborg Ø, Denmark, stp@acoustics.aau.dk), Henrik Møller (Acoustics, Aalborg University, Fredrik Bajers Vej 7 B5, 9220 Aalborg Ø, Denmark, hm@acoustics.aau.dk)

An investigation of the annoyance from the wind turbine noise, to which neighbors may be exposed, is carried out. The aim is to obtain dose-response relationships and to uncover if specific noise components (e.g. low-frequencies) are primary contributors to the annoyance. In the experiments, sounds recorded close to large wind turbines are filtered (and levels adjusted accordingly) to represent indoor and outdoor positions at the neighbors' dwellings and played back in the laboratory. Challenges relating to the recording and transformation of sounds are discussed. The exposure technique is a combination of an advanced low-frequency chamber that can reproduce the frequency range 2-250 Hz (with uniform distribution in the room) and additional loudspeakers for the higher frequencies. The listening test is a randomized design. The stimuli, of 10 minute duration, are presented at three levels and in combinations of filtered versions (low- and mid-frequency) such that the influence of low-frequency tonal components and level fluctuations is investigated. 25 subjects are exposed to the stimuli while reading a novel and afterwards they rate annoyance on a visual analog scale.

Session 4aNSf

Noise and EURONOISE: Fan Noise and Low-Mach Number Rotating Blade Noise I

Scott C. Morris, Cochair
Notre Dame, 109 Hessert Laboratory, University of Notre Dame, Notre Dame, IN 46556, USA

Michel Roger, Cochair
Ecole Centrale de Lyon, 36 Avenue Guy de Collongue, Centre Acoustique, Ecully, 69134, France

Contributed Papers

10:40

4aNSf1. Overview of turbofans noise prediction methods based on CFD computations. Cédric Morel (Snecma, Site de Villaroche, Rond-Point René Ravaud, 77550 Moissy-Cramayel, France, cedric.morel @snecma.fr), Benoit Farvacque (Snecma, Site de Villaroche, Rond-Point René Ravaud, 77550 Moissy-Cramayel, France, benoit.farvacque@snecma .fr)

Overview of turbofans noise prediction methods based on CFD computations The constant trend to increase bypass ratio in turbofan aircraft engines has led to an increase of the relative contribution of rotors to the overall engine noise. There is therefore a need for efficient and accurate prediction tools to achieve a silent design of the rotor components. Here is given an overview of the different aeroacoustic methods investigated by Snecma and used for prediction of tone interaction noise, broadband interaction noise and broadband fan self noise. Different levels of methods refinement, from various analytical models to steady and unsteady CFD, will be compared in terms of accuracy of prediction and computational cost. Examples of implementation of these methods on conventional turbofan and counter-rotating fan configurations will be presented.

11:00

4aNSf2. Benchmark of fan noise propagation tools. Jacky Mardjono (SNECMA Villaroche, 77550 Moissy Cramayel, France, jacky .mardjono@snecma.fr)

Various propagating codes based on different formulations have been developed over the last years to simulate the fan noise propagation into the nacelle of a turbofan engine and its radiation in the Far field. The abilities of the ACTRAN softwares (Potential formulation / FEM), SPACE (Linearised EULER equations / DGM) and ICARE (Rays-tracing method) to simulate typical industrial configurations in the frequential domain have been evaluated based on measurements carried out at the RACE acoustic test facility on a fan model at 1/2 scale. The results of the computations carried out with each of these codes on intake and exhaust configurations (axisymmetric assumption) in hard wall and lined duct will be compared to the measured far field directivities. These comparisons will be discussed depending on the establishment of patterns (sources types, mean flows types, boundaries conditions) considered in the simulations of each of these codes. The impacts of the considered convected mean flow types (Uniform, Euler, NS,...) and the capacities of these codes to predict noise attenuation of the treatments will be investigated in particular.

11:20

4aNSf3. Comparative helicopter noise analysis in static and in-flight conditions. Doris Novak (University of Zagreb, Vukeliceva 4, 10000 Zagreb, Croatia, doris.novak@fpz.hr)

Rotary wing aircraft, i.e. helicopter, is a source of intense noise, external and internal alike, in conclusion becoming serious environmental and health issue. The generated noise is in some aspects similar to propeller noise in fixed wing aircraft (airplane), while differing in main noise source alignment in respect to the relative airflow: in helicopters, both rotors, i.e. main and tail, that produce forces necessary for flight, are inline with the direction of flight, while in airplanes rotor(s) are perpendicular to it. Another distinctive noise in helicopters, well known as ″slapping″, comes from the rotor cutting its own wake/vortex air inflow, especially while descending. In this article main helicopter noise sources will be discussed and most significant results of various static and in-flight noise measurements on two different types of helicopters will be presented and analyzed.

11:40

4aNSf4. Validation of Thickness and Loading Noise Codes by Isom's Formula Applied to Subsonic Axial and Centrifugal Fans. Sofiane Khelladi (Lab. d'Energétique et de Mécanique des Fluides Interne, Arts et Métiers ParisTech, 151 boulevard de l'Hôpital, 75013 Paris, France, sofiane.khelladi@paris.ensam.fr), Djaafer Fedala (Lab. d'Energétique et de Mécanique des Fluides Interne, Arts et Métiers ParisTech, 151 boulevard de l'Hôpital, 75013 Paris, France, djaafer.fedala@paris.ensam.fr), Farid Bakir (Lab. d'Energétique et de Mécanique des Fluides Interne, Arts et Métiers ParisTech, 151 Boulevard de l'Hôpital, 75013 Paris, France, farid.bakir@paris.ensam.fr), Robert Rey (Lab. d'Energétique et de Mécanique des Fluides Interne, Arts et Métiers ParisTech, 151 Boulevard de l'Hôpital, 75013 Paris, France, robert.rey@paris.ensam.fr)

The thickness noise predicted by the Ffowcs Williams and Hawkings (FW&H) equation depends on the normal velocity v_n which is very sensitive to the meshing size. Isom showed that in far field a monopolar source is equivalent to a dipolar source induced by a uniform distribution of the load on the entire moving surface. Consequently, the calculation of the thickness noise becomes completely independent of the normal velocity v_n. Its expression, as suggested by Farassat, is for any moving surfaces. The main objective of this paper is to determine a specific expression of Isom's thickness noise in time and frequency domains for axial and centrifugal subsonic fans. The scope of the proposed expression of Isom's thickness noise is threefold: (1) highlight the effect of each geometrical parameter of the fan on the overall thickness noise, (2) a fast computational mean and low memory storage capability since the acoustic pressure in frequency domain is calculated for only one blade, and (3) a benchmark test of consistency for thickness and loading noise codes in both time and frequency domains when using the free field solution of FW&H's equation.

12:00

4aNSf5. Prediction of the tonal noise radiation of an axial flow fan located downstream of a Bluff Body. Richard Gault (Queen's University Belfast, School of Mechanical and Aerospace Engineering, Ashby Building, Stranmillis Road, BT9 5AH Belfast, UK, r.gault@qub.ac.uk), Richard K. Cooper (Queen's University Belfast, School of Mechanical and Aerospace Engineering, Ashby Building, Stranmillis Road, BT9 5AH Belfast, UK,

R.Cooper@qub.ac.uk),Jian Wang(Queen's University Belfast, School of Mechanical and Aerospace Engineering, Ashby Building, Stranmillis Road, BT9 5AH Belfast, UK, j.wang@qub.ac.uk), Christophe Schram (LMS International, Researchpark Z1, Interleuvenlaan 68, 3001 Leuven, Belgium, Christophe.Schram@lmsintl.com)

This paper investigates the tonal noise radiated by a subsonic axial flow fan when installed downstream of a bluff body. Typically industrial axial flow fans operate in cluttered environments, and are usually driven through direct coupling from an engine. For this investigation, the fan is located in a knife-edged shroud and placed downstream of a bluff body having representative dimensions of a typical engine. Axial flow fans in general radiate broadband and discrete frequency noise, the latter of which modelling efforts are maturing. The numerical simulation is based on the aero-acoustic analogy where the unsteady flow is first computed using CFD and then passed to a BEM solver to compute the acoustic radiation. URANS and DES methods are examined for the turbulence modelling. The time-varying force on a single blade in the CFD solver over one complete rotation is used to construct the equivalent fan source in the BEM model. Experimental measurements of Sound Pressure Level are performed in a hemi-anechoic chamber, and a comparison between numerical predictions made. This numerical procedure can be used to further aid designers in understanding the effects of fan tonal noise in cluttered environments.

Invited Papers

12:20

4aNSf6. Near-field scattering of ducted fan noise using a boundary element method. Christophe Schram (LMS International, Researchpark Z1, Interleuvenlaan 68, 3001 Leuven, Belgium, Christophe.Schram@lmsintl.com)

The noise emitted by rotating machinery is a concern in many applications, such as aeroengines, wind turbines, and cooling devices for IC engines or electronic appliances. A specific derivation of the Ffowcs Williams and Hawkings analogy for the tonal noise emitted by a fan was presented by Goldstein (1976), under the assumption that the listener is placed in the acoustical and geometrical far field. That formulation accounts for the modulation of the Doppler frequency shift during the fan revolution, but neglects near field effects. This work presents the application of an alternative derivation, introduced by Roger (2007), which preserves the near-field features of the sound field. This analytical method is compared with a second method in which the fan is modelled by a fixed azimuthal distribution of dipoles. A validation is performed for the case of a generic fan located in an infinite circular duct. The sound field within the duct is obtained by two means: i) calculating the sound field emitted by the fan, modelled by the above mentionned approaches, and scattered by the duct through the application of a Boundary Element Method, ii) computing the sound field by projecting the source in the duct modes.

12:40

4aNSf7. LES prediction of wall-pressure fluctuations and noise of a low-speed airfoil. Meng Wang (University of Notre Dame, Departmernt of Aerospace and Mechanical Engineering, Notre Dame, MD 46556, USA, m.wang@nd.edu), Stéphane Moreau (Valeo Thermal Systems, rue Louis Normand, 8, 78321 La Verrière, France, stephane.moreau@valeo.com), Gianluca Iaccarino (Stanford University, Dept. of Mechanical Engineering, Stanford, CA 94305, USA, jops@ctr.stanford.edu), Michel Roger (Ecole Centrale de Lyon, 36 Avenue Guy de Collongue, Centre Acoustique, 69134 Ecully, France, michel.roger@ec-lyon.fr)

The wall-pressure fluctuations and noise of a low-speed airfoil are computed using large-eddy simulation (LES). The results are compared with experimental measurements made in an open-jet anechoic wind-tunnel at Ecole Centrale de Lyon. To account for the effect of the jet on airfoil loading, a RANS calculation is conducted in the full wind-tunnel configuration, which provides velocity boundary conditions for the LES in a smaller domain within the potential core of the jet. The flow field is characterized by an attached laminar boundary layer on the pressure side and a transitional and turbulent boundary layer on the suction side. The predicted unsteady surface pressure field shows reasonable agreement with the experimental data in terms of frequency spectra and coherence in the trailing-edge region. In the nose region, characterized by unsteady separation and transition to turbulence, the wall-pressure fluctuations are highly sensitive to small perturbations and difficult to predict or measure with certainty. The LES, in combination with the Ffowcs Williams and Hall solution to the Lighthill equation, also predicts well the radiated trailing-edge noise. A finite-chord correction is derived and applied to the noise prediction, which is shown to improve the overall agreement with the experimental sound spectra.

1:00-2:00 Lunch Break

Contributed Papers

2:00

4aNSf8. The influence of the design parameters of centrifugal fans on the difference between outlet and inlet noise levels. Mikhail Y. Liberman (MOVEN Co., 17 Plekhanova str., 24/30 Zemlyanoi val str., apt. 27, 111141 Moscow, Russian Federation, mikhail.liberman@yahoo.com)

The operation of the industrial centrifugal fans is accompanied by the air-borne noise generation thanks to such phenomenon as: vortex formation within blade channels of impeller (because of flow separation in channel) and interactions between vortex wakes (at outlet of impeller) and cut-off of fan casing. Sound waves, which are formed at outlet of blade channels and within fan casing, propagate as through outlet side of casing, as in opposite direction: through rotating blade channels of impeller and inlet cone of casing. As it follows from theoretical analysis and experimental research the noise levels at outlet side of centrifugal fan are higher than noise levels at inlet of fan (as for broadband as for tonal noise), because of noise reduction, which is caused by sound wave propagation through inhomogeneous channel, consisted of impeller and inlet cone of casing. The efficiency of the noise reduction depends on the design parameters of impeller and casing. In particular, according to results of research the difference between levels of noise, radiated from outlet and inlet sides of fan, depend on: shape of blade channels, relation between width of casing and impeller.

2:20

4aNSf9. Prediction of flow induced noise in rotating devices using nonmatching grids. Jens Grabinger (Univ. Erlangen-Nuremberg, Dept. of Sensor Technology, Paul-Gordan-Str. 3/5, 91052 Erlangen, Germany, jens.grabinger@lse.eei.uni-erlangen.de), Branimir Karic (University Erlangen-Nuremberg, Institute of Fluid Mechanics, Cauerst. 4, 91058 Erlangen, Germany, branimir.karic@lstm.uni-erlangen.de), Simon Triebenbacher (Univ. Erlangen-Nuremberg, Dept. of Sensor Technology, Paul-Gordan-Str. 3/5, 91052 Erlangen, Germany, simon.triebenbacher @lse.eei.uni-erlangen.de), Manfred Kaltenbacher (Univ. Erlangen-Nuremberg, Dept. of Sensor Technology, Paul-Gordan-Str. 3/5, 91052 Erlangen, Germany, manfred.kaltenbacher@lse.eei.uni-erlangen.de), Stefan

Becker(University Erlangen-Nuremberg, Institute of Fluid Mechanics, Cauerst. 4, 91058 Erlangen, Germany, stefan.becker@lstm.uni-erlangen .de), Reinhard Lerch (Univ. Erlangen-Nuremberg, Dept. of Sensor Technology, Paul-Gordan-Str. 3/5, 91052 Erlangen, Germany, reinhard.lerch@lse .eei.uni-erlangen.de)

With increasing number of electrical devices, e.g. air conditioning systems, used in homes and offices, noise pollution is becoming a more and more relevant topic. A large amount of this noise is generated by turbulent flows and laminar flows at leading and trailing edges, where mainly tonal noise is generated. The objective of our contribution is to investigate shape optimizations of rotating devices in order to reduce their noise levels. For this purpose, we conduct a simulation of the turbulent flow in a ventilator. The acoustic source terms are obtained from the fluid dynamics solution by using Lighthill's acoustic analogy. The acoustic domain is decomposed into a rotating part and a fixed part. The coupling between these two parts is enforced at their interface by a mortar finite element method, which uses Lagrange multipliers in order to ''glue'' the geometrically independent parts together. The mortar method takes into account the movement of the rotating part through a moving nonmatching grid, that is recomputed at each time step.

2:40

4aNSf10. Trailing edge noise computation of a fan blade profile. Julien Christophe (von Karman Institute, Chausee de Waterloo, 72, 1640 Rhode-Saint-Genese, Belgium, christju@vki.ac.be), Jerome Anthoine (von Karman Institute, Chausee de Waterloo, 72, 1640 Rhode-Saint-Genese, Belgium, anthoine@vki.ac.be), Stéphane Moreau (Valeo Thermal Systems, rue Louis Normand, 8, 78321 La Verrière, France, stephane.moreau@valeo .com)

In problem involving noise generated by fans or high-lift devices in uniform stationary flow, trailing edge noise has a primary interest. This paper proposes to study the trailing edge noise produced by a Controlled-Diffusion (CD) airfoil specially developed for automotive engine cooling by Valeo. A LES flow computation is realised through the Fluent solver 6.3 for a Reynolds number based on the chord of 1.5×10^5 and an angle of attack of 8 degrees. This computation is compared to pressure and velocity measurements performed at ECL (France) and obtained by measurement techniques involing pressure probes and hot-wire anemometry. Amiet's theory using surface pressure spectra around the airfoil trailing-edge region is used to obtain far field acoustic predictions that are compared to microphone measurements.

3:00

4aNSf11. Optimization problem for the automatic positioning of flow obstructions to control tonal fan noise. Anthony Gerard (Univ. de Sherbrooke, Mechanical Engineering Depart., 2500 Boulevard de l'Université, Sherbrooke, QC J1K 2R1, Canada, Anthony.Gerard@USherbrooke .ca), Alain Berry (Univ. de Sherbrooke, Mechanical Engineering Depart., 2500 Boulevard de l'Université, Sherbrooke, QC J1K 2R1, Canada, alain.berry@usherbrooke.ca), Patrice Masson (Univ. de Sherbrooke, Mechanical Engineering Depart., 2500 Boulevard de l'Université, Sherbrooke, QC J1K 2R1, Canada, Patrice.Masson@USherbrooke.ca)

Tonal noise from subsonic axial fans can be controlled by adding obstructions in the downstream or upstream flow field of the rotor. These obstructions must be located with care to create secondary circumferential modes of the blade unsteady lift of equal magnitude but opposite in phase with the primary unsteady lift modes responsible for the tonal noise. The general optimization problem of controlling N circumferential modes using N obstructions with 2 degrees of freedom or 2N obstructions with 1 degree of freedom is first posed. This optimization problem can be greatly simplified using nB-perdiodic obstructions (where B is the number of blade) designed to control the most radiating mode of the blade unsteady lift at frequencies n×BPF. In this case, the control of each frequency is uncoupled and a single error microphone in the axis of the fan can be used to globally control the selected frequencies.

3:20

4aNSf12. Axial fan noise: Towards sound prediction based on numerical unsteady flow data - a case study. Hauke Reese (Ansys, Birkenweg 14a, 64295 Darmstadt, Germany, hauke.reese@ansys .com), Thomas Carolus (Institute of Fluid- and Thermodynamic, University of Siegen, Paul-Bonatz-Str. 9-11, 57068 Siegen, Germany, thomas .carolus@uni-siegen.de)

Objective of this work is to evaluate modern numerical methods for predicting flow induced fan noise. A generic fan assembly is investigated consisting of a low pressure axial impeller (diameter 0.3 m, hub to tip ratio of 0.45) including an optional turbulence generator. The flow field is simulated with different state of the art unsteady computational fluid dynamic methods. All results are compared with each other and with hot wire flow velocity and surface pressure measurements. From the numerical data, the relevant dipole sound sources, i.e. the unsteady forces on the fan blades are derived. Eventually both, a free field formulation in the time domain (acoustical analogy by FFOWCS WILLIAMS and HAWKINGS), and a boundary element formulation in the frequency domain (SYSNOISE®) are employed to predict the radiated sound field based on the numerical source data. The acoustical results are compared and contrasted with measurements.

3:40-5:20 Posters

Lecture sessions will recess for presentation of poster papers on various topics in acoustics. See poster sessions for topics and abstracts.

Contributed Papers

5:20

4aNSf13. Aeroacoustic Computation of Ducted-Fan Broadband Noise Using LES Data. Gabriel Reboul (ONERA, 29 avenue Division Leclerc, 92320 Châtillon, France, gabriel.reboul@onera.fr), Cyril Polacsek (ONERA, 29 avenue Division Leclerc, 92320 Châtillon, France, cyril.polacsek@onera.fr), Serge Lewy (ONERA, 29 avenue Division Leclerc, 92320 Châtillon, France, serge.lewy@onera.fr), Sebastien Heib (ONERA, 29 avenue Division Leclerc, 92320 Châtillon, France, sebastien.heib@onera.fr)

Following large efforts to reduce tone noise during the last decades in modern high-bypass ratio turbofans, fan broadband noise reduction has become now an industrial priority. A hybrid computational method providing source-to-far-field predictions of broadband noise due to rotor-stator interaction is presented. The acoustic model is based on the loading term of the FWH (Ffowcs Williams and Hawkings) equation with a modal Green's function valid for an infinite annular duct, and a Kirchhoff approximation for the free-field radiation. The aerodynamic sources on the airfoils required by the model are expected to be directly issued from a LES (Large Eddy Simulation) computation. The method is applied to a simplified configuration tested in a laboratory rig. The first part of the study is concerned with the assessment of in- duct acoustic field. Usual assumptions about coherence and energy distribution between the acoustic modes are analyzed. PSD (Power Spectrum Density) are calculated through several ways. The second part is focused on the ability to generate an equivalent PSD by means of equivalent source distributions. The purpose is to validate a practical way for coupling LES with Computational Aero-Acoustics Euler solver, in order to include realistic geometry and mean flow effects.

5:40

4aNSf14. Improvements of a parametric model for fan broadband and tonal noise. Antoine Moreau (DLR - German Aerospace Center, Mueller-Breslau-Str. 8, 10623 Berlin, Germany, antoine.moreau@dlr.de), Lars Enghardt (DLR - German Aerospace Center, Mueller-Breslau-Str. 8, 10623 Berlin, Germany, lars.enghardt@dlr.de)

The fan of an aero-engine is one of the most significant noise sources of civil aircraft. The purpose of the present work is to provide a tool for fan noise prediction, which can be integrated into the design process of innovative fans. Fan noise is predicted by means of an analytic model. A single noise source is considered: the rotor-stator interaction noise due to rotor blade wakes impinging onto the stator vanes. This source is known to be the major source of fan broadband and tonal noise. The formula for the sound power is based on the single airfoil theory in far field developed by Amiet. It accounts for the effect of subsonic compressible flow and source non-compactness. The model accounts for fan parameters such as geometry (blade and vane count, chord length, rotor-stator gap) and flow parameters (mean velocities, wake and turbulence characteristics). Future work will investigate a more detailed description of the sound field based on an acoustic modal approach, in which each frequency component of the sound spectrum is decomposed into a distribution of duct acoustic modes.

6:00

4aNSf15. Turbulence ingestion fan noise predictions using an advanced turbulence correlation model. Scott C. Morris (Notre Dame, 109 Hessert Laboratory, University of Notre Dame, Notre Dame, IN 46556, USA, s.morris@nd.edu)

The generation of sound by an isolated rotating blade row results from the interaction of the blades with turbulence in the approach flow. The relationship between the unsteady velocity field and the sound produced can be expressed directly in terms of the two point velocity correlation function of the approach flow field. It is often assumed that the turbulent flow can be approximated by a number of simplifying assumptions, such as homogeneous, isotropic flow. However, in the frequency range of interest for a number of applications these assumptions are not valid, and their use can lead to significant errors in the prediction of generated sound. The present work will describe a method for using advanced models of two-point velocity correlations and outline new experimental results that validate this approach.

6:20

4aNSf16. Investigation into the effect of altering incoming gust shape to far field noise radiation in Amiet's theory. Michael Bilka (von Karman Institute, Chausee de Waterloo, 72, 1640 Rhode-Saint-Genese, Belgium, bilka@vki.ac.be), Jerome Anthoine (von Karman Institute, Chausee de Waterloo, 72, 1640 Rhode-Saint-Genese, Belgium, anthoine@vki.ac.be)

Noise prediction for turbulent interactions with fan-blades or high-lift devices has been continuously developed for the last thirty years. A benchmark solution to this problem is Amiet's theory for acoustic radiation from an airfoil in a turbulent stream. In most aerodynamic theories the incoming gust is assumed to be sinusoidal, which is also the case for the theory of Amiet. This assumption affects the derivation of the unsteady lift function which is used to propagate the noise to the far-field. This paper proposes to show the effect of altering the shape of the incoming gust by assuming a Gaussian function. This analysis will then be compared to the case of the sinusoidal gust as well as to acoustic measurements of an airfoil placed in a jet taken in the VKI semi-anechoic chamber.

6:40

4aNSf17. Aeroacoustics of a low Mach number tip-gap flow. Julien Grilliat (Ecole Centrale de Lyon, 36, av. Guy de Collongue, 69134 Lyon, France, julien.grilliat@ec-lyon.fr), Marc C. Jacob (Ecole Centrale de Lyon, 36, av. Guy de Collongue, 69134 Lyon, France, marc.jacob@ec-lyon.fr)

A thorough experimental study was performed in several campaigns in the anechoic wind tunnel of the Ecole Centrale de Lyon on a single airfoil at a low Mach number to investigate the tip leakage flow and the associated broadband noise. The influence of the inflow velocity, the airfoil angle of attack and the gap size were characterized and hence an extensive data set was obtained. Both near field aerodynamic and far field acoustic features of this configuration were recorded. Statistical post-processing of the data highlighted some of the governing parameters of this jet-like flow configuration and two different noise generation mechanisms. Some scaling laws were derived from the experimental data which gave also inputs for semi-analytical far field noise prediction models relying on the theory for linearised unsteady aerodynamics around a slender airfoil. The underlying sound generation mechanism is the scattering of the tip clearance flow perturbations by the airfoil trailing edge. The aerodynamic perturbation is described as a gust with a spanwise distribution that is concentrated near the gap region. The models are presented and compared to experimental results and CFD calculations. This work has been funded by the European Community as part of the 6th Framework Project PROBAND n° AST4-CT-2005-012222.

Session 4aPAa

Physical Acoustics: Thermoacoustics I

Steven Garrett, Cochair
Penn State, Applied Research Laboratory, PO Box 30, State College, PA 16804, USA

Philippe Blanc-Benon, Cochair
Ecole Centrale de Lyon, LMFA, UMR CNRS 5509, Ecully, Lyon, 69134, France

Invited Papers

8:00

4aPAa1. Recent progress on thermoacoustic heat engines and refrigerators. Ercang Luo (Technical Institute of Physics and Chemistry, CAS, Beiyitiao Rd., Zhongguancun St., P.O.Box 2711, 100080 Beijing, China, Ecluo@cl.cryo.ac.cn)

In this talk, recent progress on thermoacoustic heat engines and refrigerators developed at the Technical Institute of Physics and Chemistry (TIPC), Chinese Academy of Sciences (CAS), is covered, which mainly includes three aspects: (i) Energy-focused thermoacoustic-Stirling heat engines (EF-TASHE) by using tapered resonators are highlighted for both low-frequency (~50Hz) and medium-frequency (~300Hz) operation; (ii) A thermoacoustically driven two-stage pulse tube cryocoolers capable of achieving liquid hydrogen temperature (~20K) is described. In addition, a 300 Hz compact thermoacoustically driven pulse tube cryocooler operating below 80K is also covered. In this part, an acoustical pressure amplifier is highlighted; (iii) A heat-driven thermoacoustic refrigeration system with double thermoacoustic-Stirling configuration for room temperature cooling is reported. This system is able to provide a cooling power of more than 300 W at -20°C, showing good prospect as an alternative of CFC refrigeration. Finally, consideration and prospect for future development are forecasted.

8:20

4aPAa2. Study of a thermoacoustic-Stirling engine. Hassan Tijani (Energy research Centre of the Netherlands (ECN), Westerduinweg 3, 1755 LE Petten, Netherlands, tijani@ecn.nl), Simon Spoelstra (Energy research Centre of the Netherlands (ECN), Westerduinweg 3, 1755 LE Petten, Netherlands, spoelstra@ecn.nl), Gaelle Poignand (Energy research Centre of the Netherlands (ECN), Westerduinweg 3, 1755 LE Petten, Netherlands, poingnand@ecn.nl)

During the last decade most efforts in thermoacoustics have been focused on the development and understanding of the traveling-wave thermoacoustic systems. These systems get much attention because they employ the inherently efficient Stirling cycle. This makes them much more efficient that the standing-wave counter parts which are intrinsically irreversible. A 1 kW thermal power thermoacoustic-Stirling engine is designed and performance measurements are performed. The engine incorporates a compact acoustic network to create the traveling-wave phasing necessary to operate in a Stirling cycle. The acoustic network consists of a regenerator unit, an acoustic compliance and a feedback inertance. The design, construction and performance measurements of the traveling-wave thermoacoustic engine will be presented and discussed.

8:40

4aPAa3. Low operating temperature integral thermo acoustic devices for solar cooling and waste heat recovery. Kees De Blok (Aster Thermoakoestische Systemen, Smeestraat 11, NL 8194 LG Veessen, Netherlands, c.m.deblok@aster-thermoacoustics.com)

Utilizing low temperature differences from solar vacuum tube collectors or waste heat in the range 70-200 °C seems to be the most promising field of applications for thermoacoustic systems. At these reduced temperatures overall system performance is increasingly affected by the ratio between amplified (useful) power and acoustic power stored in the resonance circuitry. Well known is that this ratio can be improved by deploying multiple regenerator units (hex-reg-hex). However, in commonly used torus or coaxial bypass configurations the correct timing (real and high acoustic impedance) is hardly realized inside more than two regenerator units (soft spot). Acoustic losses in the standing wave resonator account for another fundamental limitation because of the relatively low transferred power at a given pressure amplitude. Therefore a novel acoustic geometry will be presented in which a high and near real impedance can be maintained in even more than two regenerator units and in which acoustic feedback is performed by a true traveling wave. This approach improves the overall performance of integral thermoacoustic systems. Details and experimental results of a solar driven thermoacoustic cooler and ongoing work on thermoacoustic tri-generation utilizing exhaust gas of a standard gas-engine will be presented.

9:00

4aPAa4. Commercial thermoacoustic products and next-step developments in acoustic cooling. John Corey (CFIC-Qdrive, 302 Tenth St., Troy, NY 12180, USA, jcorey@cficinc.com), Philip Spoor (CFIC-Qdrive, 302 Tenth St., Troy, NY 12180, USA, pspoor@cficinc.com)

CFIC-Qdrive committed to development and commercialization of thermoacoustic energy conversion devices in 1999, by combining the newly developed acoustic perspective and tools developed at Los Alamos with a deep well of Stirling-cycle experience to achieve a total physics model with both inertial and viscous behavior of the working fluid. Such acoustic-Stirling devices combine the mechanical simplicity, robustness, and efficiency. Focusing first on refrigeration for cryogenics; this work has led to a family of standard products that have found uses worldwide, from air-quality sampling and oil refinery support to military aviation oxygen liquefaction. This paper details the basic operation of these acoustic- Stirling products and the key technological elements that make them viable and attractive in cryogenics; then examines the implications for less-cold uses like food-storage and air-conditioning; with a discussion of achievable performance in accessible applications. We review the work now underway to develop devices to meet those opportunities with environmentally benign cooling of superior performance.

9:20

4aPAa5. Generating electricity from burning wood using Thermo-acoustics for use in developing countries. Paul H. Riley (University of Nottingham, Room 1211 Tower Block, School of Electrical and Electronic Engineering, NG7 2RD Nottingham, UK, paul.riley@nottingham.ac.uk), Mark Johnson (University of Nottingham, Room 1211 Tower Block, School of Electrical and Electronic Engineering, NG7 2RD Nottingham, UK, mark.johnson@nottingham.ac.uk)

SCORE is a wood burning stove that will cook food, generate electricity and cooling for use in developing countries by means of thermoacoustics. The consortium of Nottingham (Lead), Manchester, Queen Mary, Imperial and City universities with the charity Practical Action, believe that the very demanding cost targets can be achieved by using thermo-acoustic technology due to the no-moving-part design. Standing wave and travelling wave designs are being evaluated with support from Los Alamos Laboratories in the US. The presentation will concentrate on the stove requirements and needs of the developing world and how this affects the thermo-acoustic and mechanical design. Results from mathematical modelling and measurements from an early demonstrator will be presented. More information can be found at Http://www.score.uk.com. The £2M Score research project is funded by EPSRC, a UK government agency.

9:40

4aPAa6. Recent developments on heat to electricity thermoacoustic conversion. Guadalupe Huelsz (UNAM, Privada Xochicalco Temixco Centro, Temixco Morelos, 62580 Temixco, Mexico, ghl@cie.unam.mx), Miguel Piñeirua (UNAM, Privada Xochicalco Temixco Centro, Temixco Morelos, 62580 Temixco, Mexico, mipim@cie.unam.mx), Alfonso A. Castrejon-Pita (UNAM, Privada Xochicalco Temixco Centro, Temixco Morelos, 62580 Temixco, Mexico, aacp@atm.ox.ac.uk), Fabrisio Gomez (UNAM, Privada Xochicalco Temixco Centro, Temixco Morelos, 62580 Temixco, Mexico, flgog@cie.unam.mx)

In this work we present recent developments for the conversion of heat into electricity based on the combined effects of a thermoacoustic prime mover coupled to a magnetohydrodynamic generator where different working fluids can be optimally chosen for each process. We consider the acoustically produced oscillatory motion of a liquid drop confined into a horizontal squared cross section capillary tube as a possible flow configuration for the system. We investigated the energy losses of the system and concluded that this system would be a convenient configuration for small systems. [Work supported by CONACYT 25116 project]

10:00-10:20 Break

Contributed Paper

10:20

4aPAa7. Fundamental study of a loop-tube-type thermoacoustic cooling system using heat energy from condensed sunlight. Shin-Ichi Sakamoto (Faculty of Engineering, Doshisha Univ., 1-3 Miyakodani Tatara, 610-0321 Kyotanabe, Japan, ssakamot@mail.doshisha.ac.jp), Shintaro Komiya (Faculty of Engineering, Doshisha Univ., 1-3 Miyakodani Tatara, 610-0321 Kyotanabe, Japan, bte1031@mail4.doshisha.ac.jp), Naoki Miya (Faculty of Engineering, Doshisha Univ., 1-3 Miyakodani Tatara, 610-0321 Kyotanabe, Japan, dtg0144@mail4.doshisha.ac.jp), Jiro Senda (Faculty of Engineering, Doshisha Univ., 1-3 Miyakodani Tatara, 610-0321 Kyotanabe, Japan, jsenda@mail.doshisha.ac.jp), Yoshiaki Watanabe (Faculty of Engineering, Doshisha Univ., 1-3 Miyakodani Tatara, 610-0321 Kyotanabe, Japan, kwatanab@mail.doshisha.ac.jp)

The feasibility of implementation of a sunlight-based loop-tube-type thermoacoustic cooling system is investigated. Sunlight is condensed using a 0.60 m diameter Fresnel lens and irradiated to the high-temperature heat exchanger. Then, the temperature of heat exchanger is risen. This heat energy from condensed sunlight is applied to the driving hear energy of the loop-tube-type thermoacoustic cooling system. The total length of the loop tube is 3300 mm, and a gaseous mixture of He and Ar (50% / 50%) is used as the working fluid. A 50-mm-long ceramic honeycomb is used for the stack. The channel radius of the prime mover stack is 0.45 mm; that of the heat pump is 0.35 mm. The cooling point temperature falls from 29°C to -4.3°C before sunlight is irradiated to the high-temperature heat exchanger. Consequently, a temperature drop of 33.3°C is achieved using sunlight. Result obtained in this experiment underscores the feasibility of implementation of a sunlight-based loop-tube-type thermoacoustic cooling system.

Invited Paper

10:40

4aPAa8. Geometry effects and scaling in thermoacoustics. Jos Zeegers (Eindhoven University of Technology, Den Dolech 2, 5612 AZ Eindhoven, Netherlands, j.c.h.zeegers@tue.nl)

Current work at TU Eindhoven on thermoacoustics will be discussed. The end effects of the geometry of a stack on the performance of thermoacoustic machines will be shown. End effects and the formation of vortices is an issue that contributes to enhanced convective losses at the stack ends. Influence of Reynolds and Strouhal numbers on the oscillatory flow field in the stack are studied. It is possible to plot Sr and Re number diagrams in which various zones can be identified that display characteristic flow patterns. Furthermore the influence of the type of regenerator material is studied in traveling wave engines. Performance of honeycomb material of high-density pores is compared with wire screen regenerators in a thermoacoustic motor. As a last point the effects of downscaling to miniature systems is discussed. Limits of how far the size of a thermoacoustic cooler can be downscaled before conduction effects limit the performance are relevant.

Contributed Papers

11:00

4aPAa9. Suppression of harmonics in a high frequency standing-wave thermoacoustic engine. Wei Dai (Technical Institute of Physics and Chemistry, CAS, Beiyitiao Rd., Zhongguancun St., P.O.Box 2711, 100080 Beijing, China, dwpeng@yahoo.com), Bo Yu (Technical Institute of Physics and Chemistry, Chinese Academy of Sciences, Zhongguancun BeiYiTiao 2, Hai Dian, 100080 Beijing, China, yubo@mail.ipc.ac.cn), Guoyao Yu (Technical Institute of Physics and Chemistry, Chinese Academy of Sciences, Zhongguancun BeiYiTiao 2, Hai Dian, 100080 Beijing, China, gyyao@cl.cryo.ac.cn), Ercang Luo (Technical Institute of Physics and Chemistry, CAS, Beiyitiao Rd., Zhongguancun St., P.O.Box 2711, 100080 Beijing, China, Ecluo@cl.cryo.ac.cn)

A thermoacoustic engine converts heat into acoustic power and could be used to driven a cooler for refrigeration purposes or to drive a piston for electric power generation. Due to non-linear effects inside the system, higher order harmonics could be generated which may deteriorate the thermal performance of the whole system. In this report, a 500Hz standing wave thermoacoustic engine has been built. The occurrence of higher order acoustic oscillations has been closely observed. A series of experiments has been done to investigate the influence of resonance tube configuration on this phenomenon. The influence on the related thermal performance is also reported.

11:20

4aPAa10. Energy conversion efficiency improvement of a thermoacoustic cooling system - The influence of a lamination mesh on cooling effect-. Atsushi Sakaguchi (Faculty of Engineering, Doshisha Univ., 1-3 Miyakodani Tatara, 610-0321 Kyotanabe, Japan, dth0165@mail4.doshisha.ac.jp), Shin-Ichi Sakamoto (Faculty of Engineering, Doshisha Univ., 1-3 Miyakodani Tatara, 610-0321 Kyotanabe, Japan, ssakamot@mail.doshisha.ac.jp), Yoshiyuki Tsuji (Faculty of Engineering, Doshisha Univ., 1-3 Miyakodani Tatara, 610-0321 Kyotanabe, Japan, dtg0925@mail4.doshisha.ac.jp), Yoshiaki Watanabe (Faculty of Engineering, Doshisha Univ., 1-3 Miyakodani Tatara, 610-0321 Kyotanabe, Japan, kwatanab@mail.doshisha.ac.jp)

It was generally considered that energy conversion efficiency of a thermoacoustic cooling system was improved by increasing proportion of a thermal boundary layer in the stack. Thinning down a channel radius of the stack is required to increase the thermal boundary layer per unit area. A ceramic stack is difficult to satisfy this requirement. To satisfy this requirement, we propose to use a lamination mesh which is formed by piled up a stainless mesh. Since the lamination mesh has complex channel, the effect of changing the mesh number on the cooling effect is obscure. The experiments were carried out by changing the mesh number and the insertion position of the stack using the straight acoustic tube to measure the cooling effect. From the experimental results, changing mesh number causes the distribution shift of the phase difference between pressure and particle velocity. The insertion position of the stack for which the maximum temperature decrease come close to center of the acoustic tube. This is corresponded to a result using the ceramic stack. It suggests that a same design method, which is used in case of applying the ceramic stack, can be adapted to the lamination mesh.

11:40

4aPAa11. Scalability of Thermoacoustic Refrigerator. Ehab Abdel-Rahman (The American University, 211 Science Building, 113 Kasr El Aini St., P.O. Box 2511, 11511 Cairo, Egypt, ehab_ab@aucegypt.edu)

The uses of thermoacoustic effect are the conversion of heat onto acoustic wave by thermoacoustic prime mover and pumping heat by acoustic wave using a thermoacoustic refrigerator. Thermoacoustic refrigerator is a good alternative to conventional vapor compression device. It can be very compact, using a minimum of uncomplicated, economical components. It can also provide variable cooling capacity and scalability to different sizes in ways that conventional vapor compression technology is not capable of. We are investigating the minimum size of a thermoacoustic refrigerator that can meet the cooling requirement for different applications. The coefficient of performance (COP) of small thermoacoustic refrigerators is in the range of 20% of the ideal (Carnot cycle) COP, which is actually better than similarly scaled vapor compression coolers which is at about 10%. The efficiency of thermoacoustic refrigerator can be improved by better designing of its components. In this paper the effect of components design on the performance of thermoacoustic refrigerator is discussed. The scalability of such devices is also investigated.

12:00

4aPAa12. Advanced flow measurements in thermoacoustic systems. Arganthaël Berson (Ecole Centrale de Lyon, LMFA, UMR CNRS 5509, Ecully, 69134 Lyon, France, arganthael.berson@ec-lyon.fr), Philippe Blanc-Benon (Ecole Centrale de Lyon, LMFA, UMR CNRS 5509, Ecully, 69134 Lyon, France, Philippe.Blanc-Benon@ec-lyon.fr)

One of the bottlenecks for the conception of highly efficient thermoacoustic systems is the poor performances of heat exchangers. A better understanding of both aerodynamical and thermal phenomena that occur at the interface between the stack and the heat exchangers is necessary for the improvement of heat transport between these components, especially at high acoustic amplitudes that are required for industrial applications. To this end, a specific Particle Image Velocimetry (PIV) method has been developed and measurements are performed within a standing-wave thermoacoustic refrigerator model driven at high drive ratios (up to 5%). Vortex streets are observed behind the plates of a single stack at high acoustic level. The flow is characterized using advanced vortex analysis tools and dimensionless numbers. Vortices also appear within the gap between the stack and the heat exchangers. They will influence heat transport as was previously shown in numerical simulations from the literature. Moreover, as a first step toward enthalpy flux measurements, cold and hot wire anemometry methods are developed specifically for temperature and velocity measurements in oscillating flows. First results with these techniques will be presented and compared to available numerical and analytical models. This work is supported by ANR (project MicroThermAc NT051_42101).

Invited Paper

12:20

4aPAa13. Powerful, efficient, robust, electro-acoustic transducers. John Corey (CFIC-Qdrive, 302 Tenth St., Troy, NY 12180, USA, jcorey@cficinc.com)

The STAR™ resonant, reciprocating transducer began as a lightweight linear alternator design for a space-power free-piston Stirling engine in the early 1990's. It has since been developed into a range of commercially available motors and alternators with rated powers from 100 to over 10,000 watts (acoustic). As motors, these are acoustic pressure drivers with unlimited operating life and typical transduction efficiencies of 80-90 percent. This paper explains the electrodynamics and operation of these moving- magnet Lorentz-force devices and the unique geometric configuration that has allowed scaling over such a wide range. We discuss the design and function of the unique single-degree-of-freedom flexure suspension that enables both the compact geometry and unlimited service life without wear. Data is presented from a large sample of units placed in service during the last decade, demonstrating the durability and performance of these remarkable devices.

12:40-1:40 Lunch Break

Invited Paper

1:40

4aPAa14. Recent developments in miniaturization of thermoacoustic devices. Pierrick Lotton (Laboratoire d'Acoustique de l'Université du Maine, Avenue Olivier Messiaen, 72085 Le Mans, France, Pierrick.Lotton@univ-lemans.fr), Guillaume Penelet (Laboratoire d'Acoustique de l'Université du Maine, Avenue Olivier Messiaen, 72085 Le Mans, France, guillaume.penelet@univ-lemans.fr), Etienne Gaviot (Laboratoire d'Acoustique de l'Université du Maine, Avenue Olivier Messiaen, 72085 Le Mans, France, etienne.gaviot@univ-lemans.fr), Stephane Durand (Laboratoire d'Acoustique de l'Université du Maine, Avenue Olivier Messiaen, 72085 Le Mans, France, stephane.durand@univ-lemans.fr), Lionel Camberlein (Laboratoire d'Acoustique de l'Université du Maine, Avenue Olivier Messiaen, 72085 Le Mans, France, lionel.camberlein@univ-lemans.fr), Philippe Blanc-Benon (Ecole Centrale de Lyon, LMFA, UMR CNRS 5509, Ecully, 69134 Lyon, France, Philippe.Blanc-Benon@ec-lyon.fr), Michel Bruneau (Laboratoire d'Acoustique de l'Université du Maine, Avenue Olivier Messiaen, 72085 Le Mans, France, michel.bruneau@univ-lemans.fr)

This talk will present a review of recent works on thermoacoustic devices miniaturization conducted at Laboratoire d'Acoustique de l'Universite du Maine (LAUM), in collaboration with Laboratoire de Mecanique de Fluides et d'Acoustique (LMFA). A part of these works deals with new designs allowing higher compactness of devices. As an example, a compact non-resonant thermoacoustic refrigerator will be described, and experimental results obtained on a prototype will be presented. Another part of these works deals with the miniaturization of each element of a thermoacoustic device, especially the stack and the acoustic source. The acoustical and thermal sensors used to control these small devices have also to be miniaturized. Some specific actuators and sensors designed for miniaturized thermoacoustic refrigerators will be presented. Finally, potential applications of these miniaturized devices will be discussed.

Contributed Papers

2:00

4aPAa15. Miniaturation of thermoacoustic refrigerators. Yan Li (Eindhoven Univ. of Tech, Applied Physics, Low Temperature Physics, Cascade 3.13, PO Box 513, 5600MB Eindhoven, Netherlands, yan.li@tue.nl)

The possibility to miniature thermoacoustic refrigerators is theoretically investigated. Both standing-wave and traveling-wave systems are considered. In the consideration of standing-wave refrigerators, a system consisting of a resonator tube (50 cm) with a closed end and a PVC stack (length 5 cm) is taken as a reference. Helium is used at a mean pressure of 10 bars and an amplitude of 1 bar. The operating frequency is 1 kHz. The variation of the performance of the refrigerator when scaled down in size is computed under the prerequisites that the temperature difference over the stack or the energy flux or energy flux density are fixed. The analytical results show, as expected, that there is a limitation for scaling-down of a standing-wave thermoacoustic refrigerator due to heat conduction. Similar scaling trends are also shown in traveling-wave refrigerators. The traveling-wave reference system consists of a feedback inertance tube of 0.567 m long, inside diameter 78 mm, a compliance volume of 2830 cm^3 and a 24 cm thermal buffer tube. The regenerator is sandwiched between two heat exchangers. The system is operated at 125 Hz and filled with 30 bar helium gas. Again, the thermal conductance forms a practical limitation in down-scaling.

2:20

4aPAa16. Nonlinear effects in standing-wave types of thermoacoustic devices. Paul Aben (Eindhoven University of Technology, Den Dolech 2, 5612 AZ Eindhoven, Netherlands, p.c.h.aben@tue.nl), Jos Zeegers (Eindhoven University of Technology, Den Dolech 2, 5612 AZ Eindhoven, Netherlands, j.c.h.zeegers@tue.nl)

In order to create high amplitudes ($p'/p_0 > 10\%$) for a relatively low frequency range (between 5 and 125 Hz), a large subwoofer is connected to a resonator tube by an exponential horn. A parallel-plate stack, with various plate thicknesses and separations, can be placed at different positions in the resonator tube. The position of the subwoofer membrane, the voltage and current of the subwoofer, as well as the pressure at six different positions in the resonator is measured. The measurements are in good agreement with simulations. Using a multi-microphone method the transfer matrix of a stack is determined experimentally. Using a PIV method a 2-D velocity field between and around the stack plates is measured. The vortex shedding at the end of stack plates is studied in particular. The amplitude, frequency, plate thickness, plate separation and plate-ending shape are varied. Also the streaming velocity field is studied. Small asymmetries in the geometry have a huge influence on the streaming velocity.

2:40

4aPAa17. Intensity measurement of a periodic acoustic shock wave in a resonator. Tetsushi Biwa (Dept. of Mechanical Systems and Design, Tohoku Univ., Aramaki 6-6-01, Aoba-ku, 980-8579 Sendai, Japan, biwa@amsd.mech.tohoku.ac.jp), Taichi Yazaki (Aichi Univ. Education, Igaya, 448-8542 Kariya, Japan, tyazaki@auecc.aichi-edu.ac.jp)

A periodic shock wave of a gas column is formed in a duct, when the gas column is sinusoidally driven near the resonance frequency. This phenomenon has been one of the fundamental problems in nonlinear acoustics and has been studied extensively both theoretically and experimentally. In this work, we study the nonlinear effect leading to the shock formation through measurements of the acoustic intensity. A gas column of atmospheric air is filled in a resonator with a length of 1.15 m and internal radius of 10.5mm, and driven by an oscillating piston at 144.4 Hz near the fundamental resonance frequency. Pressure and axial acoustic particle velocity of the gas column are measured as a function of the resonator axis using small pressure transducers and a laser Doppler velocimeter. We show the spatial distribution of the acoustic intensity associated with the fundamental and the second modes, from which we show the nonlinear interaction between these oscillating modes.

3:00

4aPAa18. Transition to turbulence and acoustic Rayleigh streaming in thermoacoustic devices. Helene Baillet (Laboratoire d'Etudes Aérodynamiques (LEA), Université de Poitiers, ENSMA, CNRS, Bat K, 40 avenue du recteur Pineau, 86022 Poitiers, France, helene.baillet@lea.univ-poitiers.fr), Jean-Christophe Valière (Laboratoire d'Etudes Aérodynamiques (LEA), Université de Poitiers, ENSMA, CNRS, Bat K, 40 avenue du recteur Pineau, 86022 Poitiers, France, jean-christophe.valiere@lea.univ-poitiers.fr), Solenn Moreau (Laboratoire d'Etudes Aérodynamiques (LEA), Université de Poitiers, ENSMA, CNRS, Bat K, 40 avenue du recteur Pineau, 86022 Poitiers, France, solene.moreau@lea.univ-poitiers.fr), David Marx (Laboratoire d'Etudes Aerodynamiques - CNRS, Bat K, 40 avenue du recteur Pineau, 86022 Poitiers, France, david.marx@lea.univ-poitiers.fr)

Thermoacoustic engines and refrigerators with practical levels of heating or pumping power must generally operate at high pressure amplitudes. When used to describe the behavior of such high-amplitude thermoacoustic devices, the well-established foundations of thermoacoustics, based on the acoustic approximation, reach their limits. It is necessary to gain a deeper understanding of the high-amplitude phenomena in order to improve the performances of thermoacoustic devices, and efforts of several research groups have been directed towards this goal over the last decade. In this presentation, we will consider recent advances in the understanding of some of the gas-dynamics phenomena leading to limitation of devices performances, namely transition to turbulence and acoustic Rayleigh streaming. The common point for these phenomena is that they owe their origin in the dynamic of oscillating flows in very near wall regions, so that their quantification implies measurements of acoustic particle velocity in adverse conditions. Recent progresses in Laser techniques used to perform such measurements will therefore also be reviewed.

3:20

4aPAa19. PIV contribution for measuring acoustic and streaming flow in thermoacoustic systems, using phase average dynamics. Diana Baltean Carlès (LIMSI-CNRS, BP 133, F-91403 Orsay, France, baltean@limsi.fr), Philippe Debesse (LIMSI-CNRS, BP 133, F-91403 Orsay, France, debesse@limsi.fr), François Lusseyran (LIMSI-CNRS, BP 133, F-91403 Orsay, France, francois.lusseyran@limsi.fr), Maurice-Xavier François (LIMSI-CNRS, BP 133, F-91403 Orsay, France, mxf@limsi.fr)

The present study deals with the experimental challenge of the measurement of the velocity field generated by a thermoacoustic wave. The system consists in a cylindrical standing-wave resonator, filled with gas confined at high mean pressure, driven by a thermoacoustic prime-mover. The axial and radial components of fluid velocity are measured using Particle Image Velocimetry (PIV) with an optical flow technique. The average cycle of acoustic oscillation of the velocity field is reconstructed from a temporally under-sampled set of PIV snapshots, using an embedding method for building out a suitable phase space based on Singular Value Decomposition (SVD). This reconstruction allows us to extract both oscillation component of the velocity field (with the harmonic content) and time-averaged component of velocity (streaming flow). The measurements are confirmed using a second experimental procedure, based on a classical phase-averaged method: velocity measurements are synchronized with the pressure signal, the fundamental time period being decomposed in 16 phases. The measurements are repeated for different values of the drive ratio (acoustic pressure/mean pressure). The results are compared with available theory. Different experimental methods used in measuring the velocity field in thermoacoustic systems are analysed and compared with the present method.

3:40-5:00 Posters

Lecture sessions will recess for presentation of poster papers on various topics in acoustics. See poster sessions for topics and abstracts.

Invited Papers

5:00

4aPAa20. Interactive analysis, design, and teaching for thermoacoustics using DeltaEC. William C. Ward (Los Alamos National Laboratory, MS C914, Los Alamos, NM 87545, USA, ww@lanl.gov), Greg W. Swift (Los Alamos National Laboratory, MS C914, Los Alamos, NM 87545, USA, swift@lanl.gov), John P. Clark (Los Alamos National Laboratory, MS C914, Los Alamos, NM 87545, USA, jpclark@stanford.edu)

The 2008 release of the Los Alamos thermoacoustics code, DeltaEC, is distinctly different from the text-based program that was first made available in 1993. The physics captured by ″Design Environment for Low-Amplitude Thermoacoustic Energy Conversion″ has been steadily extended over the years. Toroids and other acoustic network topologies are now possible, along with superimposed steady flow, time-averaged pressure gradients, gas diodes, Gedeon streaming, thermoacoustic mixture separation, and resonator vibration solutions. Eight different stack pore geometries are supported, and a powerful algebraic user language allows complex, custom results to be derived without source code revisions at Los Alamos. Over the last year, the numerical methods of DeltaEC were condensed into a FORTRAN computational core and wrapped with a Python-based graphical user interface to provide modern interactive features: a multi-model tabbed interface, colorizing editors, scaled schematics, and 2D plotter windows. An intricate model can now be divided into interlinked sub-models that can be solved independently (and consistently). In addition to providing usability and new capabilities, the Python front end makes the legacy code more maintainable, extensible, and verifiable. The latest download of DeltaEC is available to all researchers at www.lanl.gov/thermoacoustics/.

5:20

4aPAa21. Design road-map for thermoacoustic refrigerators. Kaveh Ghorbanian (Sharif Univ. of Technology, Dept. of Aerospace Engineering, Azadi Street, 14588-89694 Tehran, Iran, ghorbanian@sharif.edu), Hemed Hosseini (Sharif Univ. of Technology, Dept. of Aerospace Engineering, Azadi Street, 14588-89694 Tehran, Iran, hamed_hosseiny20042000@yahoo.com), Mahmoud Jafargholi (Sharif Univ. of Technology, Dept. of Aerospace Engineering, Azadi Street, 14588-89694 Tehran, Iran, mahmoud.jafargholi @gmail.com)

The main purpose of this work is to develop a road-map to enhance the design procedure and performance analysis of thermoacoustic refrigerators (TAR). The basic mechanism of TAR is very simple and is based on the wave interaction processes of gas particles with their surrounding environment. As known, the performance of a TAR system is highly dependent to the number of gas particles involved in the process. The essential components of TAR include a sound generating device, a resonance tube, a stack of plates, and heat exchangers. In this paper, the parameters influencing the performance of a TAR system are grouped into four blocks: (I) Operation (drive ratio, operating frequency), (II) Fluid (Prandtl number), (III) Geometry (blockage ratio, tube diameter, stack length, stack positioning), and (IV) Material. A parametric study is executed to determine the optimized design of a TAR system for fixed Block II and IV scenario. First, an analysis is made on obtaining the optimum number of gas particles to be involved in the process. Then, based on this, an optimization approach is carried out to identify the best drive ratio, blockage ratio, stack positioning, stack length, and resonance tube diameter. Finally, results are compared with experimental data.

Contributed Paper

5:40

4aPAa22. Thermoacoustics in random fibrous materials. Carl R. Jensen (The University of Mississippi - NCPA, 1 Coliseum Drive, University, MS 38677, USA, crjensen@olemiss.edu), Richard Raspet (National Center for Physical Acoustics, University of Mississippi, University, MS 38677, USA, raspet@olemiss.edu), Henry E. Bass (The University of Mississippi - NCPA, 1 Coliseum Drive, University, MS 38677, USA, pabass @olemiss.edu)

Current approaches to acoustics in fibrous and porous materials use fitting parameters to match theoretical models to measured values for the material's complex compressibility and wavenumber. In effect, these models treat the material as though it were composed of an array of rigid capillary tubes; they have proven accurate in fitting the model to data for various different porous materials such as wools and foams. However, these models do not address thermoacoustic heat transfer when the material is put under a static temperature gradient. A direct simulation has been performed using a three-dimensional thermal fluid solver to calculate both the acoustic properties and the thermoacoustic properties of a random fibrous material. The results of the simulation will be compared to experimental results for complex compressibility and wavenumber [Tarnow, H., J. Acoust. Soc. Am., 97(4) ,2272-81] as well as a proposed extension to porous theory that incorporates thermoacoustics [Roh et al., J. Acoust. Soc. Am., 121(3), 1413-22]. [Work supported by U.S. Army Space & Missile Defense Command.]

Invited Paper

6:00

4aPAa23. Numerical study of the performance of thermally isolated thermoacoustic-stacks in the linear regime. Antonio Piccolo (Dept. of Civil Engineering - Univ. of Messina, Contrada di Dio, Villaggio S.Agata, 98100 Messina, Italy, apiccolo@unime.it), Giuseppe Pistone (Dept. of Matter Physics and Advanced Physical Technologies - Univ. of Messina, Contrada di Dio, Villaggio S.Agata, 98100 Messina, Italy, pistone@unime.it)

A simplified calculus model to investigate on the transverse heat transport near the edges of a thermally isolated thermoacoustic stack in the low acoustic Mach number regime is presented. The proposed methodology relies on the well known results of the classical linear thermoacoustic theory which are implemented into an energy balance calculus-scheme through a finite difference technique. Details of the time-averaged temperature and heat flux density distributions along a pore cross-section of the stack are given. It is shown that a net heat exchange between the fluid and the solid walls takes place only near the edges of the stack plates, at distances from the ends not exceeding the peak-to-peak particle displacement amplitude. The structure of the mean temperature field within a stack plate is also investigated; this last results not uniform near its terminations giving rise to a smaller temperature difference between the plate

extremities than that predicted by the standard linear theory. This result, when compared with experimental measurements available in literature, suggests that thermal effects localized at the stack edges may play an important role as sources of the deviations found between linear theory predictions and experiments at low and moderate Mach numbers.

Contributed Paper

6:20

4aPAa24. Time-domain modelling of thermoacoustic devices: Reflections from the stack. Stig Kleiven (Chalmers University of Technology, Division of Applied Acoustics, SE-41296 Gothenburg, Sweden, stig.kleiven@chalmers.se), Krister Larsson (Chalmers University of Technology, Division of Applied Acoustics, SE-41296 Gothenburg, Sweden, kl@ta.chalmers.se), Wolfgang Kropp (Chalmers University of Technology, Division of Applied Acoustics, SE-41296 Gothenburg, Sweden, wolfgang.kropp@chalmers.se)

Thermoacoustic devices are today mainly simulated using frequency-domain models. Contrary to frequency-domain models, time-domain models may include time-varying boundary conditions and time varying effects. Furthermore, effects like reflections from the stack can be visualised which, in turn, can improve the understanding. The primary aims were: (1) to study the initial behaviour of the acoustic field in a thermoacoustic device using a time-domain method; and (2) to compare the results from the simulations with experiments. Since time-domain techniques are computational expensive, the detailed Finite-Difference Time-Domain (FDTD) method are combined with the quicker Equivalent Source Method (ESM). The acoustic field in the stack, only including viscous effects, was modelled using the FDTD method, and the ESM was used outside the stack. The experimental setup consisted of a loudspeaker connected to a circular tube containing a ceramic stack with rectangular pores. From the results of both the simulations and the experiments, clear reflections from the stack were seen. Since these reflections influence the total acoustic field in thermoacoustics devices, time-domain methods provide useful tools for further development of thermoacoustic devices.

Invited Paper

6:40

4aPAa25. Cooling load and coefficient of performance of thermoacoustic refrigerators: the role of the working fluid. Cila Herman (Johns Hopkins University, 3400 N. Charles Street, Baltimore, MD 21218, USA, cherman.jhu@gmail.com)

Thermoacoustic refrigeration is a technology that uses mechanical energy in the form of sound waves to drive a heat pumping process that offers an environmentally safe, relatively low maintenance alternative to vapor compression refrigeration. Improving the design of the thermoacoustic core, composed of the stack plates and heat exchangers, may have the potential to bring thermoacoustic technology closer to commercial use. The stack plates have been analyzed to increase efficiency (expressed in terms of the coefficient of performance, COP) but in some applications a very high efficiency can lead to a smaller cooling load. The thermoacoustic stack was analytically optimized for maximum heat transfer (cooling load) and coefficient of performance (COP) for a range of working fluids of interest. Different noble gas mixtures were analyzed as the working fluid and helium was found to produce the highest cooling load because of its low molecular weight. The thermoacoustic stack plate center location, length, thickness and spacing were analyzed and optimum values to maximize cooling load and COP were found to exist for the specific input parameters considered. These optimization techniques may be used to design devices where maximum cooling load is more desirable than high efficiency.

Contributed Papers

7:00

4aPAa26. van der Waal gaz and direct simulation for thermoacoustics. Alain Fontaine (Université Paul Sabatier, PHASE, 118, route de Narbonne, 31062 Toulouse cedex 9, France, fontaine@cict.fr), Marie-Catherine Mojtabi (Univ. Paul Sabatier, PHASE, 118 route de Narbonne, 31062 Toulouse Cedex 9, France, cmojtabi@cict.fr), Abdelkader Mojtabi (IMFT, Allée du Professeur Camille Soula, 31400 Toulouse, France, mojtabi@cict.fr), Jean-Louis Breton (Univ. Paul Sabatier, PHASE, 118 route de Narbonne, 31062 Toulouse Cedex 9, France, breton@cict.fr), Vincent Gibiat (Université Paul Sabatier, PHASE, 118, route de Narbonne, 31062 Toulouse cedex 9, France, gibiat@cict.fr)

Thermoacoustic refrigerators work with high amplitube acoustic waves and lead to high thermal local gradient near the stack. In order to understand nonlinear thermoacoustic effects, an acoustic plane wave is propagated in a model with a specific geometry. It is a two-dimensional channel with adiabatic walls, including two conductive plates whose thickness is not regarded as null.The fluid is supposed to be a real gaz with thermodynamic properties described by a van der Waals law. A two-dimensional direct numerical model for compressible flow is used to investigate unsteady dynamic and energetic behaviours in the channel. This model relies on a finite volume formulation of the mass, momentum and energy equations for compressible flow. Thermal equilibrium between gaz and plates is assured by a Dirichlet boundary condition for the interface temperature and a thermal conduction equation in the plate. Adiabatic walls are described by a Neumann boundary condition for the temperature on the wall. The acoustic wave is generated at the input. Perfectly Matched Layer (PML) is used on input and output as a boundary condition to deal with wave reflections. Numerical investigation will be presented and compared with linear classical model.

7:20

4aPAa27. Modeling and simulation of Taconis oscillations in a framework of the boundary-layer theory. Nobumasa Sugimoto (Osaka University, Department of Mechanical Science, Graduate School of Engineering Science, Toyonaka, 560-8531 Osaka, Japan, sugimoto@me.es.osaka-u.ac.jp), Dai Shimizu (Osaka University, Department of Mechanical Science, Graduate School of Engineering Science, Toyonaka, 560-8531 Osaka, Japan, shimizu@mars.me.es.osaka-u.ac.jp)

This paper develops a simplified one-dimensional model to simulate numerically the onset of Taconis oscillation in a helium-filled, quarter-wavelength tube in cryogenics. Introducing a boundary layer on the tube wall, nonlinear fluid-dynamical equations are averaged over the cross-section of the acoustic main-flow region outside of the boundary layer. The boundary layer gives rise to memory effects, which are taken into account in the form of half-order derivatives. For a smooth temperature distribution of the tube wall, an initial and boundary-value problem of the equations derived is solved numerically for evolution of a small disturbance. The boundary condition at the open end neglects radiation and requires the excess pressure to vanish, while the condition at the closed end takes account of the boundary layer. When the ratio of the temperature at the closed end to the one at the open end exceeds a critical value, the initial helium column becomes unstable to grow in amplitude and stationary self-excited Taconis os-

cillations of finite amplitude emerge. It is shown that even the first-order boundary-layer theory can describe such an evolution of a small unstable disturbance into self-excited oscillations.

7:40

4aPAa28. Numerical model of boundary layer effects in Rayleigh streaming. Brian Tuttle (Penn State, 412 W Foster Ave, State College, PA 16801, USA, btuttle@psu.edu), Victor W. Sparrow (Penn State, Graduate Program in Acoustics, 201 Applied Science Bldg., University Park, PA 16802, USA, vws1@psu.edu)

In thermoacoustic devices such as the pulse-tube refrigerator, efficiency is diminished by the formation of a second-order mean velocity known as Rayleigh streaming. This flow emerges from the interaction of the working gas with the wall of the tube in a thin boundary layer. This research develops a numerical model to investigate Rayleigh streaming in straight and tapered tubes. Since the accuracy of the model depends on the correct representation of boundary layer effects, special consideration is given to the computation of thermal and viscous boundary layers including finite difference methods, computational grid refinement, and exaggeration of physical parameters for testing of boundary layers at low grid resolution. The model also allows for the inclusion or exclusion of temperature-dependent viscosity and thermal conductivity terms, the effects of which will be examined. [Work supported in part by the Office of Naval Research.]

THURSDAY MORNING, 3 JULY 2008 ROOM 351, 8:00 A.M. TO 7:40 P.M.

Session 4aPAb

Physical Acoustics: Ultrafast Acoustics I

David H. Hurley, Cochair
Materials Characterization Department, Idaho National Laboratory, P.O.Box 1625, Idaho Falls, ID 83415-2209, USA

Clément Rossignol, Cochair
LMP, UMR CNRS 5469, Université Bordeaux I, 351, cours de la Libération, Talence, 33405, France

Invited Paper

8:00

4aPAb1. Coherent phonons in semiconductor superlattice under DC electrical bias. Anthony Kent (University of Nottingham, School of Physics and Astronomy, University Park, NG9 3JE Nottingham, UK, anthony.kent@nottingham.ac.uk), Ryan Beardsley (University of Nottingham, School of Physics and Astronomy, University Park, NG9 3JE Nottingham, UK, ppxrb1@nottingham.ac.uk), Andrey Akimov (University of Nottingham, School of Physics and Astronomy, University Park, NG9 3JE Nottingham, UK, andrey.akimov@nottingham.ac.uk), Mohamed Henini (University of Nottingham, School of Physics and Astronomy, University Park, NG9 3JE Nottingham, UK, mohamed.henini@nottingham.ac.uk)

Resonant pumping of superlattices SLs by femtosecond laser pulses results in the generation of coherent phonons with frequency centred approximately on s/d_{SL}, where s is the speed of longitudinal sound and d_{SL} is the SL period. The phonons can be detected by measuring the changes in reflectance of time-delayed probe pulses. To date, measurements have been made on nominally undoped SLs, and phonon frequencies are typically in the range 100 GHz - 1 THz. The motivation for these studies is that such hypersound could be used for acoustic probing of nanostructures. Here we describe the generation and detection of coherent phonons in a doped and electrically-biased SL. The studied SL consisted of 50×(6 nm GaAs and 4 nm AlAs), uniformly doped with Silicon to density 2×10^{22} m^{-3}. Pump-probe measurements were made at $\lambda\sim770$ nm on an optical MESA at $T=12$K. At zero bias, we observed a similar phonon spectrum as previously observed in comparable but undoped SLs, with a mode at ~ 450GHz. Under applied bias this mode increased in amplitude, and the decay time was also increased. We discuss these observations in terms of the effects of the bias on the coherent phonon generation and detection process and also the possibility of coherent phonon amplification occurring in the structure.

Contributed Papers

8:20

4aPAb2. Acoustic Bloch oscillations, Wannier-Stark ladders and negative refraction in ultra- and hypersonic superlattices. Yuriy A. Kosevich (Semenov Institute of Chemical Physics Russian Academy of Sciences, ul. Kosygina 4, 119991 Moscow, Russian Federation, yukosevich @yahoo.com)

A new and very efficient ultrasonic superlattice is realized for the study of such fundamental effects of quantum transport in a perturbed periodic potential as acoustic Bloch oscillations, Wannier-Stark ladders and resonant Landau-Zener tunneling. The acoustic equivalent of the Wannier-Stark ladders is employed in a set of water cavities, with a gradient of the thicknesses, in a simple water-solid multilayer system. Bloch oscillations in different acoustic minibands are observed as time-resolved oscillations of the transmisssion of ultasonic pulses with corresponding spectral positions and widths. Acoustic Bloch oscillations with different temporal periods for the pulses centered in two neighboring acoustic minibands are observed. Experimental observations are in very good agreement with the transfer-matrix simulations [1]. The propagation of acoustic pulse in an even acoustic miniband in orthogonal or oblique with respect to the superlattice axis direction will result in negative refraction and Bloch oscillations of acoustic pulse with ″negative effective mass″, which can be visualized by mapping out of acoustic pressure field. Hypersonic phononic structures, which can be fabricated with the use of interference lithography, render possible the obser-

vation of all the abovementioned acoustic phenomena in the hypersound frequency range. 1. H. Sanchis-Alepuz, Yu. A. Kosevich, and J. Sanchez-Dehesa, 2007, Phys. Rev. Lett. v. 98, 134301.

8:40

4aPAb3. Strain wave induced electron transport in superlattices. Anthony Kent (University of Nottingham, School of Physics and Astronomy, University Park, NG9 3JE Nottingham, UK, anthony.kent@nottingham.ac.uk), Daivid Fowler (University of Nottingham, School of Physics and Astronomy, University Park, NG9 3JE Nottingham, UK, daivid.fowler@nottingham.ac.uk), Mohamed Henini (University of Nottingham, School of Physics and Astronomy, University Park, NG9 3JE Nottingham, UK, mohamed.henini@nottingham.ac.uk), Mark Greenaway (University of Nottingham, School of Physics and Astronomy, University Park, NG9 3JE Nottingham, UK, ppxmg@nottingham.ac.uk), Alexander Belanov (University of Nottingham, School of Physics and Astronomy, University Park, NG9 3JE Nottingham, UK, alexander.belanov@nottingham.ac.uk), Mark Fromhold (University of Nottingham, School of Physics and Astronomy, University Park, NG9 3JE Nottingham, UK, mark.fromhold@nottingham.ac.uk)

We show that propagating high-amplitude coherent strain pulses, generated by ultrafast optical excitation of a metal film can induce a charge current in a GaAs/AlAs superlattice (SL). The studied SL had a period of of 12.5 nm and a miniband width of 12 meV. It was grown by MBE on a 0.35 mm-thick semi-insulating GaAs substrate, and a 100 micron device MESA fabricated. On the other side of the substrate a 100 nm-thick Al film was deposited. A coherent picosecond strain pulse was generated opposite the device by exciting the Al film with 40 fs, 800 nm pulses from a 5 KHz, 2.5 mJ Ti:Sapphire amplifier. A strong current pulse from the device was observed about 80 ns after the laser pulse was incident on the Al film, this time delay being equal to the time of flight of longitudinal polarized strain pulses across the GaAs substrate. We attribute the current pulse to electrons that are confined and dragged along by the potential generated by the strain wave. Theoretical calculations show that this ″wave dragging″ effect in the presence of the SL potential can give rise to the generation of ultra-high (THz) frequency electron dynamics.

9:00

4aPAb4. Thickness dependence of the acoustical response of ultra-thin metallic films studied by Colored Picosecond Ultrasonics. Arnaud Le Louarn (IEMN-CNRS, Cité Scientifique - Avenue Poincaré, BP 60069, 59652 Villeneuve d'Ascq Cedex, France, arnaud.lelouarn@isen.fr), Arnaud Devos (IEMN-CNRS, Cité Scientifique - Avenue Poincaré, BP 60069, 59652 Villeneuve d'Ascq Cedex, France, arnaud.devos@isen.fr), Clément Rossignol (LMP, UMR CNRS 5469, Université Bordeaux I, 351, cours de la Libération, 33405 Talence, France, c.rossignol@lmp.u-bordeaux1.fr)

We have previously demonstrated [1,2] that a connection exists between Colored Picosecond Ultrasonic (CPU) experiments and electronic structure of metallic thin films. Indeed, a strong change of the detected acoustic echoes is observed when the laser is tuned around an interband transition wavelength. This connection suggests that CPU can be an useful tool for measuring interband transitions in thin metallic films. Surprisingly, by doing such a measurement on a series of ultra-thin Aluminium films, we observed a significant shift of the transition (from 880 to 970 nm) as the film thickness is reduced (from 400 to 120 A). We will discuss the origin of the phenomenon and propose some applications to the characterization of ultra-thin metallic films. [1] A. Devos and C. Lerouge, Phys. Rev. Lett. 86, 2669 (2001) [2] A. Devos and A. Le Louarn, Phys. Rev. B 68, 045405 (2003)

9:20

4aPAb5. Monochromatic high frequency coherent phonons propagation with superlattice transducers. Agnès Huynh (INSP - UMR 7588 CNRS & Université Pierre et Marie Curie, 140 Rue de Lourmel, 75015 Paris, France, agnes.huynh@insp.jussieu.fr), Maria Florencia Pascual Winter (INSP - UMR 7588 CNRS & Université Pierre et Marie Curie, 140 Rue de Lourmel, 75015 Paris, France, Florencia.PascualWinter@insp.jussieu.fr), Bernard Perrin (INSP - UMR 7588 CNRS & Université Pierre et Marie Curie, 140 Rue de Lourmel, 75015 Paris, France, bernard.perrin@insp.jussieu.fr), Bernard Jusserand (INSP - UMR 7588 CNRS & Université Pierre et Marie Curie, 140 Rue de Lourmel, 75015 Paris, France, Bernard.Jusserand@insp.jussieu.fr), Aristide Lemaitre (LPN, CNRS route de Nozay, 91460 Marcoussis, France, Aristide.Lemaitre@lpn.cnrs.fr), Alejandro Fainstein (Centro Atomico Bariloche & Instituto Balseiro, C. N. E. A., 8400 S. C. de Bariloche, Argentina, afains@cab.cnea.gov.ar)

The availability of efficient and compact phonons transducers in the THz range would be very interesting for phonons spectroscopy, acoustic microscopy and study of vibrational and electronic properties of nanostructures. Thanks to epitaxial growth of semiconductors multilayers, high quality phononic nanostructures with standard semiconductors, such as superlattices (SL) and nanocavities can be obtained for the GHz and THz transduction. Picosecond ultrasonics experiments have been performed in transmission geometry with pump and probe incident on opposite sides of the substrate, allowing discoupling acoustic generation and detection processes. By these means, we have shown independently that SL are very efficient high frequency monochromatic phonon generators and detectors. We report on experiments where two superlattices have been grown on the opposite sides of a substrate: a first SL with uniform layer thickness over the whole surface sample is used as a generator; the other one, used as the detector, presents a thickness gradient and the location of the detection is chosen in order to have the best matching with the emitted frequency. This setup is used to study the propagation of monochromatic high frequency coherent phonons as a function of temperature.

9:40

4aPAb6. Progress on coherent generation of terahertz acoustic phonons by resonant absorption of nanosecond-pulsed far-infrared laser radiation in silicon doping superlattices. Thomas E. Wilson (Marshall University, Department of Physics, One John Marshall Drive, Huntington, WV 25755-2570, USA, wilsont@marshall.edu)

We report progress on experiments to generate and detect coherent terahertz acoustic phonons. Coherent phonons are generated[1] in a silicon-doping superlattice by the absorption of grating-coupled high peak-power cavity-dumped far-infared laser radiation[2]. The superlattice period is chosen to match the phonon wavelength at the excitation frequency of the laser radiation. The phonons propagate across the Si:B substrate and are detected by a novel superconducting granular aluminium/palladium bilayer microbolometer[3] with sub-nanosecond resolution. The phonon spectrum is obtained by piezo-phonon spectroscopy[4] via the boron impurities in the silicon substrate. (1) P. Ruden and G.H. Dohler, ″Anistropy Effects and Optical Excitation of Acoustic Phonons in n-i-p-i Doping Superlattices″, Solid State Commun. 45 (1), 23 (1983). (2) T.E. Wilson, ″A High-Power NH3 Laser Pumped in a Three-Mirror CO2 Laser Cavity with Optically-Switched Cavity-Dumping″, International Journal of Infrared and Millimeter Waves 14 (2), 303 (1993). (3) T E Wilson, ″Fabrication and characterization of granular aluminum/palladium bilayer microbolometer″, Meas. Sci. Technol. 18 N53-N59 (2007). (4) S. Roshko and W. Dietsche, ″Phonon Spectroscopy in High Magnetic Fields: The B+ Center in Si″, Solid State Comm. 98(5), 453 (1996).

10:00-10:20 Break

10:20

4aPAb7. Escape time of an acoustic nanocavity mode. Maria Florencia Pascual Winter (INSP - UMR 7588 CNRS & Université Pierre et Marie Curie, 140 Rue de Lourmel, 75015 Paris, France, Florencia.PascualWinter@insp.jussieu.fr), Guillermo Rozas (Centro Atomico Bariloche & Instituto Balseiro, C. N. E. A., 8400 S. C. de Bariloche, Argentina, rozasg@ib.cnea.gov.ar), Alejandro Fainstein (Centro Atomico Bariloche & Instituto Balseiro, C. N. E. A., 8400 S. C. de Bariloche, Argentina, afains@cab.cnea.gov.ar), Bernard Jusserand (INSP - UMR 7588 CNRS & Université Pierre et Marie Curie, 140 Rue de Lourmel, 75015 Paris, France, Bernard.Jusserand@insp.jussieu.fr), Bernard Perrin (INSP - UMR 7588 CNRS & Université Pierre et Marie Curie, 140 Rue de Lourmel, 75015

Paris, France, bernard.perrin@insp.jussieu.fr),Aristide Lemaitre(LPN, CNRS route de Nozay, 91460 Marcoussis, France, Aristide.Lemaitre@lpn.cnrs.fr)

We present a study of the escape time of a 1 THz nanocavity phonon mode as a function of the Q-factor of the cavity. We compare results from picosecond acoustics and high resolution Raman scattering experiments, the latter obtained by means of a Fabry-Perot/triple-additive spectrometer tandem. A nanocavity consists of a GaAs spacer enclosed by two acoustic GaAs/AlAs Bragg mirrors. The number of periods of the inner mirror varies from sample to sample, spanning a range $64<Q<2470$. This means that the cavity mode tunnels through the inner mirror to the substrate at theoretical time intervals that vary from 64 to 2470 ps for the different samples. An optic AlGaAs/AlAs Bragg mirror was grown between the substrate and the inner acoustic mirror in order to allow for the observation of the cavity mode in a backscattering configuration of the Raman experiments, otherwise forbidden by symmetry. At room temperature we observe escape times that vary from 65 to 278 ps. The theoretical values match the experimental results if a 3.0-GHz-wide lorentzian convolution is included to account for broadening effects. Possible explanations for this broadening will be discussed, as well as low temperature results.

Invited Papers

10:40

4aPAb8. Measurement of the velocity dispersion and attenuation in a liquid metal at GHz frequencies. Oliver B. Wright (Division of Applied Physics, Graduate School of Engineering, Hokkaido University, 060 8628 Sapporo, Japan, olly@eng.hokudai.ac.jp), Bernard Perrin (INSP - UMR 7588 CNRS & Université Pierre et Marie Curie, 140 Rue de Lourmel, 75015 Paris, France, bernard.perrin@insp.jussieu.fr), Osamu Matsuda (Division of Applied Physics, Graduate School of Engineering, Hokkaido University, 060 8628 Sapporo, Japan, omatsuda@eng.hokudai.ac.jp), Vitali Gusev (LPEC/UMR 6087/CNRS/Université du Maine, Avenue Olivier Messiaen, 72085 Le Mans Cedex 09, France, vitali.goussev@univ-lemans.fr)

Ultrashort optical pulses are used to excite and interferometrically detect picosecond longitudinal acoustic pulses in thin films of liquid mercury sandwiched between sapphire plates. By analysing consecutive acoustic echoes we derive the dispersion of the ultrasonic attenuation and sound velocity for this liquid at frequencies up to 10 GHz. Two types of optical detection, from the same side of the film as the excitation light and from the opposite side to the excitation light, are presented. Significant effects of structural relaxation are observed and are compared to a simple model that indicates the presence of picosecond relaxation times in mercury.

11:00

4aPAb9. Pulse laser induced wave propagation in graded media and focusing devices. Jacqueline Vollmann (ETH Zurich, Institute of Mechanical Systems, Dept. of Mechanical and Process Engineering, CH 8092 Zurich, Switzerland, vollmann@imes.mavt.ethz.ch), Juerg Bryner (ETH Zurich, Institute of Mechanical Systems, Dept. of Mechanical and Process Engineering, CH 8092 Zurich, Switzerland, bryner@imes.mavt.ethz.ch), Laurent Aebi (ETH Zurich, Institute of Mechanical Systems, Dept. of Mechanical and Process Engineering, CH 8092 Zurich, Switzerland, aebi@imes.mavt.ethz.ch), Jurg Dual (ETH Zurich, Institute of Mechanical Systems, Dept. of Mechanical and Process Engineering, CH 8092 Zurich, Switzerland, dual@imes.mavt.ethz.ch)

Near-infrared-laser pulses having durations of 100 fs are used to excite elastic waves thermoelastically propagating in a sub-THz frequency range. The elastic waves interact with inhomogeneities and carry information to the surface. The arrivals of the elastic pulses at the surface lead to transient changes of the optical reflectance which are monitored with short laser pulses which have a defined and controlled time delay relative to the initial pulses. Two activities of the research group are presented: The reflection and transmission behavior of acoustic waves propagating in graded media shows a frequency dependent nature and can therefore be used for filtering purpose. Time-boundary value problems are solved for various gradients with a finite-difference method. Results of the numerical simulation are presented and compared with laser-acoustic measurements. A 'classical' photoacoustic set-up provides an in-depth resolution of about 5 nm whereas the lateral resolution is in the order of 5 to 10 microns. To enhance the lateral resolution of the pump-probe technique, the elastic wave propagation along structures with arbitrary tip-like geometries consisting of orthotropic material is analyzed. With such structures representing ultrasonic lenses, the elastic energy is focused to a spot size given by the sharpness of the tip thereby leading to a higher lateral resolution.

Contributed Papers

11:20

4aPAb10. Acoustic dynamics in glasses in the mesoscopic range. Giulio Monaco (ESRF, 6, rue Horowitz, 38043 Grenoble, France, gmonaco@esrf.fr)

The investigation of the high-frequency acoustic excitations in glasses and of their connection to the universal anomalies in the thermal properties remains a largely debated topic. For instance, one interpretation is based on the observation that the high-frequency acoustic dynamics in simulated harmonic glasses shares the same main features as those found in experiments on real glasses [1]. Another interpretation is based on the observation that both acoustic dispersion and attenuation measured in glasses and in the corresponding poly-crystals are indistinguishable [2]. A further interpretation is based on the observation that in some glasses the high-frequency acoustic attenuation increases as a power of q with an exponent of four or larger up to frequencies corresponding to the Boson peak [3]. Here, I will discuss the above approaches on the basis of recent inelastic x-ray scattering results on the high-frequency acoustic dynamics of glasses. [1] G. Ruocco et al., Phys. Rev. Lett. 84, 5788 (2000). [2] A. Matic et al., Phys. Rev. Lett. 93, 145502 (2004). [3] B. Rufflè et al., Phys. Rev. Lett. 96, 045502 (2006).

11:40

4aPAb11. Perspectives on spatial dispersion in cubic crystals provided by neutron scattering, phonon imaging, picosecond laser ultrasound and lattice dynamics models. Arthur G. Every (School of Physics, University of the Witwatersrand, PO Wits 2050 Johannesburg, South Africa, arthur.every@wits.ac.za), Kudakwashe Jakata (School of Physics, University of the Witwatersrand, PO Wits 2050 Johannesburg, South Africa, Kudakwashe.Jakata@students.wits.ac.za)

Spatial dispersion is the variation of acoustic wave speed with wavelength, and sets in when the wavelength approaches the natural scale of length of a medium, or lattice spacing in the case of a crystal. The first onset of dispersion can be treated within the context of continuum mechanics by the incorporation of third and fourth order spatial derivatives of the displacement field in the elastic wave equation. These additional terms yield corrections to the phase velocity which in general are quadratic in the spatial frequency k. This paper will survey the experimental techniques that give one access to the coefficients in these expansions, in particular inelastic neutron scattering, ballistic phonon imaging and picosecond laser ultrasound. The main emphasis of the paper will be on deriving the numerical values of the

dispersion coefficients for four cubic crystals, Si, Ge, GaAs and InSb, from published neutron scattering data and demonstrating how modified continuum elastodynamics with these values of the coefficients is able to account well for the available dispersive phonon images of these crystals. Comparison will be made with values for the dispersion coefficients that have been obtained from laser ultrasound measurements and from lattice dynamics models.

12:00

4aPAb12. High frequency ultrasonic waves in metals and dielectrics. Maria Eleftheriou (Department of Music Technology and Acoustics, Technological Educational Institute of Crete, 1 E. Daskalaki Str., 74100 Rethymnon, Greece, marel@physics.uoc.gr), Makis Bakarezos (Department of Music Technology and Acoustics, Technological Educational Institute of Crete, 1 E. Daskalaki Str., 74100 Rethymnon, Greece, bakarezos@stef.teicrete.gr), Andreas Lyras (Department of Physics, University of Ioannina, 45110 Ioannina, Greece, alyras@uoi.gr), Costas Kosmidis (Department of Physics, University of Ioannina, 45110 Ioannina, Greece, kkosmidis@uoi.gr), Michael Tatarakis (Department of Electronics, Technological Educational Institute of Crete, Romanou 3, 73133 Chania, Greece, m.tatarakis@chania.teicrete.gr), Nektarios Papadogiannis (Department of Music Technology and Acoustics, Technological Educational Institute of Crete, 1 E. Daskalaki Str., 74100 Rethymnon, Greece, npapadogiannis@stef.teicrete.gr)

We theoretically study the generation of high frequency ultrasonic waves by short laser pulses, as well as their propagation, in metals and dielectrics. For this purpose, we employ a theoretical model that applies to both cases of materials. In the case of the dielectric the theoretical model is reduced properly. We compute key physical quantities of the lattice deformation such as the temperature, the strain and the displacement of the bulk while we compare the obtained results for the two different abovementioned types of materials. The dependence of these quantities on the generating laser intensity and pulse duration is investigated, revealing interesting differences in their behavior.

12:20

4aPAb13. Imaging of 3D acoustic wave-fronts by means of picosecond laser ultrasonics in GaAs substrate. Emmanuel Péronne (INSP - UMR 7588 CNRS & Université Pierre et Marie Curie, 140 Rue de Lourmel, 75015 Paris, France, emmanuel.peronne@insp.jussieu.fr), Laurent Belliard (INSP - UMR 7588 CNRS & Université Pierre et Marie Curie, 140 Rue de Lourmel, 75015 Paris, France, lbelliar@ccr.jussieu.fr), Shuo Zhang (INSP - UMR 7588 CNRS & Université Pierre et Marie Curie, 140 Rue de Lourmel, 75015 Paris, France, Shuo.Zhang@insp.jussieu.fr), Clément Rossignol (LMP, UMR CNRS 5469, Université Bordeaux I, 351, cours de la Libération, 33405 Talence, France, c.rossignol@lmp.u-bordeaux1.fr), Bernard Perrin (INSP - UMR 7588 CNRS & Université Pierre et Marie Curie, 140 Rue de Lourmel, 75015 Paris, France, bernard.perrin@insp.jussieu.fr)

Picosecond ultrasonic experiments are widely used as pump-probe technique using longitudinal acoustic pulses and measuring time dependence of the signal. We present an experiment which combines an interferometer with the control of the pump-probe spatial overlap. Such set-up can perform a new kind of bulk phonon imaging based on ultrafast optical generation and detection scheme. When ultrafast acoustic longitudinal wave propagate in crystals they generate coherent transverse acoustic wave by diffraction. Transverse waves are known to give rise to phonon focusing patterns. The imaging of such patterns in time and space allowed us to partially reconstruct the wave front surface of bulk acoustic wave in crystals. The data may be viewed as 2D slices of the 3D acoustic wavefront revealing the basic anisotropy of the solid with unprecedented micronic lateral and in-depth resolution. Measurements are carried out in a 356 μm-thick GaAs sample as an example, but many different experimental conditions are compatible with the present set-up. This technique provides a new way to perform phonon energy and phonon polarisation dependent experiment with high frequency phonons.

12:40-1:40 Lunch Break

Contributed Paper

1:40

4aPAb14. Surface acoustic waves propagating on microstructured phononic crystals. Dieter M. Profunser (Division of Applied Physics, Graduate School of Engineering, Hokkaido University, 060 8628 Sapporo, Japan, dieter@profunser.net), Oliver B. Wright (Division of Applied Physics, Graduate School of Engineering, Hokkaido University, 060 8628 Sapporo, Japan, olly@eng.hokudai.ac.jp), Osamu Matsuda (Division of Applied Physics, Graduate School of Engineering, Hokkaido University, 060 8628 Sapporo, Japan, omatsuda@eng.hokudai.ac.jp), Yukihiro Tanaka (Division of Applied Physics, Graduate School of Engineering, Hokkaido University, 060 8628 Sapporo, Japan, yuki@eng.hokudai.ac.jp), Abdelkrim Khelif (Institut FEMTO-ST/CNRS, 32 avenue de l'Observatoire, 25044 Besançon cedex, France, abdelkrim.khelif@femto-st.fr), Vincent Laude (Institut FEMTO-ST/CNRS, 32 avenue de l'Observatoire, 25044 Besançon cedex, France, vincent.laude@femto-st.fr), Sarah Benchabane (Institut FEMTO-ST/CNRS, 32 avenue de l'Observatoire, 25044 Besançon cedex, France, sarah.benchabane@femto-st.fr)

We investigate the interaction between high frequency surface acoustic waves and periodic microstructured patterns that form phononic crystals. The experimental method combines an optical pump-probe setup with interferometric detection and provides picosecond temporal and micron spatial resolutions. Surface acoustic waves with frequency components up to 1.3 GHz are imaged in real-time propagating over the periodic metamaterial. We used a DRIE (deep reactive ion etching) process to fabricate 2D air-silicon phononic crystals in the form of a square lattice. We present real-time animations of surface acoustic waves scattered by the phononic crystals. In particular we describe the frequency and angular dependence of the surface acoustic wave reflection from a 2D phononic crystal boundary. Fourier analysis allows us to reveal details of the acoustic band structure including gaps. The presence of such phononic band gaps enables us to visualize surface acoustic waves in waveguides, cavities and other phononic circuits at GHz frequencies.

2:00

4aPAb15. Nanoacoustic waves in nanomaterials. Jaap I. Dijkhuis (Utrecht University, Ornsteinlaboratorium, Princetonplein 1, 3508TA Utrecht, Netherlands, j.i.dijkhuis@phys.uu.nl), Peter J. Van Capel (Utrecht University, Ornsteinlaboratorium, Princetonplein 1, 3508TA Utrecht, Netherlands, p.j.s.vancapel@phys.uu.nl)

We discuss the formation and detection of acoustic soliton trains in crystal slabs. High-amplitude amplitude strain pulses are generated by impact of intense femtosecond optical pulses on a metallic film and injected into the crystal slab. Nonlinear acoustic propagation leads to the formation of shock fronts (N-waves), that, in absence of viscous damping and by virtue of dispersion, may develop into soliton trains at the leading edge and high frequency tails at the trailing edge. Interferometric pump-probe optical experiments are discussed to directly detect the ultrafast surface displacements when a soliton is reflected at the surface of the crystal slab. Finally, we experimentally prove that these acoustic solitons are capable of impulsively exciting THz transitions in electronic centers in solids. The coherent terahertz acoustic pulse trains are applied to manipulate the optical response of two-dimensional excitons in a III-V quantum well on the ultrafast timescale. By virtue of the deformation potential, the coherent exciton emission becomes strongly ″chirped″ when the acoustic pulse train passes the quantum well. This yields the prospect to perform pump-probe terahertz acoustic experiments with nanoacoustic waves in semiconductor nanomaterials.

2:20

4aPAb16. Phonons rectification in picosecond laser ultrasonics. Bernard Perrin (INSP - UMR 7588 CNRS & Université Pierre et Marie Curie, 140 Rue de Lourmel, 75015 Paris, France, bernard.perrin@insp.jussieu.fr), Shuo Zhang (INSP - UMR 7588 CNRS & Université Pierre et Marie Curie, 140 Rue de Lourmel, 75015 Paris, France, Shuo.Zhang@insp.jussieu.fr), Laurent Belliard (INSP - UMR 7588 CNRS & Université Pierre et Marie Curie, 140 Rue de Lourmel, 75015 Paris, France, lbelliar@ccr.jussieu.fr), Emmanuel Péronne (INSP - UMR 7588 CNRS & Université Pierre et Marie Curie, 140 Rue de Lourmel, 75015 Paris, France, emmanuel.peronne @insp.jussieu.fr)

In standard ultrafast acoustic experiments very short coherent acoustic pulses are generated by the absorption of a femtosecond laser pulse in a thin metallic transducer deposited on the sample. Subsequently the acoustic pulses and the heat generated in the transducer cross the sample and are partially transmitted in the underlaying substrate. At low temperature, heating of the metallic transducer gives rise to the emission of incoherent phonons wave packets which propagate ballistically over large distances in the substrate. We report on a series of experiments which demonstrate the acoustic rectification [1-3] of these wave packets as they propagate through large GaAs or Si substrates. [1] B. Perrin, J. de Phys. **C8** (1979) 216. [2] S. M. Avanesyan, V. E. Gusev, Solid State. Commun. **54** (1985) 1065. [3] B. Perrin, E. Péronne, L. Belliard, Ultrasonics, **44** (2006) 1277.

2:40

4aPAb17. Optical characterization of the acoustic response in a nanostructure using the transient reflection matrix formalism. Denis Mounier (LPEC/UMR 6087/CNRS/Université du Maine, Avenue Olivier Messiaen, 72085 Le Mans Cedex 09, France, denis.mounier@univ-lemans.fr), Pascal Picart (Laboratoire d'Acoustique de l'Université du Maine, Avenue Olivier Messiaen, 72085 Le Mans, France, pascal.picart@univ-lemans.fr), Pascal Ruello (LPEC/UMR 6087/CNRS/Université du Maine, Avenue Olivier Messiaen, 72085 Le Mans Cedex 09, France, pascal.ruello@univ-lemans.fr), Jean-Marc Breteau (LPEC/UMR 6087/CNRS/Université du Maine, Avenue Olivier Messiaen, 72085 Le Mans Cedex 09, France, jean-marc.breteau@univ-lemans.fr), Vitali Gusev (LPEC/UMR 6087/CNRS/Université du Maine, Avenue Olivier Messiaen, 72085 Le Mans Cedex 09, France, vitali.goussev@univ-lemans.fr)

The transient reflectometry and transient interferometry are the most commonly used techniques of picosecond acoustics for the study of isotropic planar stratified nanostructures. Nevertheless when anisotropy is present in the sample, the standard techniques have to be completed by transient polarimetry. The reflection properties of an anisotropic sample at oblique incidence are completely determined by the 2x2 reflection matrix (RM): R=[rpp,rps;rsp,rss]. Considering that the transient acoustic phenomena induce a perturbation ΔR of the reflection matrix, we demonstrate that the transient reflection matrix (TRM): $\Delta R \cdot R^{-1}$, where R^{-1} is the inverse of the reflection matrix, can be completely determined experimentally using the three techniques: transient reflectometry, interferometry and polarimetry (TRIP). In particular, the off-diagonal components of the TRM can be determined by transient polarimetry measurements only. Moreover, theoretical calculations of the TRM point up the close relation between the off-diagonal components of the TRM and the presence of a shear strain wave propagating perpendicularly to the free surface of the sample. Experimental results using the transient polarimetry technique will be presented to support the theoretical prediction of the TRM formalism.

3:00

4aPAb18. Picosecond ultrasonics in a single biological cell. Bertrand Audoin (LMP, UMR CNRS 5469, Université Bordeaux I, 351, cours de la Libération, 33405 Talence, France, b.audoin@lmp.u-bordeaux1.fr), Clément Rossignol (LMP, UMR CNRS 5469, Université Bordeaux I, 351, cours de la Libération, 33405 Talence, France, c.rossignol@lmp.u-bordeaux1.fr), Nikolay Chigarev (LMP, UMR CNRS 5469, Université Bordeaux I, 351, cours de la Libération, 33405 Talence, France, n.chigarev@lmp.u-bordeaux1.fr), Marie-Christine Durrieu (INSERM U577, Université Victor Segalen Bordeaux 2, 146, rue Léo-Saignat, Case 45, 33076 Talence, France, durrieumc@bordeaux.inserm.fr), Fabien Guillemot (INSERM U577, Université Victor Segalen Bordeaux 2, 146, rue Léo-Saignat, Case 45, 33076 Talence, France, fabien.guillemot@bordeaux.inserm.fr), Guillaume Forget (Laboratoire de Biomatériaux et Reparation Tissulaire, INSERM U 577, Université Bordeaux 2, 146, rue Léo-Saignat, 33076 Bordeaux, France, guillaume.forget@bordeaux.inserm.fr)

The picosecond ultrasonic technique has been developed during the last 20 years due to permanent interest in the study of mechanical properties of nano- and micro-layers made of metals and semiconductors used in solid state physics and microelectronics. The technique relies on generation, propagation and detection of ultra-short acoustic waves by femtosecond laser pulses. Important advan-

tages of these techniques are the absence of direct contact to the sample and extremely high frequency range. In this presentation, the picosecond ultrasonics technique is applied to generate and detect acoustic waves with a frequency as high as 15 GHz in a single biological cell. Hypersound velocity and attenuation can thus be mapped in the cell with the small lateral resolution provided by optics, ie 1μm. In addition to single cell imaging, the sensitivity of the measurements to cell compressibility suggests promising perspectives in the field of biology. An application to the analysis of mouse cells grafting on biomaterials will illustrate the potentialities for quantitative evaluation of implants bio compatibility.

Contributed Paper

3:20

4aPAb19. Parallel detection for picosecond ultrasonics. Richard Smith (University of Nottingham, School Electrical and Electronic Engineering, University Park, NG7 2RD Nottingham, UK, richard.j.smith@nottingham.ac.uk), Mike Somekh (University of Nottingham, School Electrical and Electronic Engineering, University Park, NG7 2RD Nottingham, UK, mike.somekh@nottingham.ac.uk), Steve Sharples (University of Nottingham, School Electrical and Electronic Engineering, University Park, NG7 2RD Nottingham, UK, steve.sharples@nottingham.ac.uk), Roger Light (University of Nottingham, School Electrical and Electronic Engineering, University Park, NG7 2RD Nottingham, UK, roger.light@nottingham.ac.uk), Nicholas Johnston (University of Nottingham, School Electrical and Electronic Engineering, University Park, NG7 2RD Nottingham, UK, Nicholas.Johnston@nottingham.ac.uk), Mark Pitter (University of Nottingham, School Electrical and Electronic Engineering, University Park, NG7 2RD Nottingham, UK, mark.pitter@nottingham.ac.uk)

Picosecond laser ultrasonics is a powerful technique for measurement and diagnosis of micro- and nano-scale structures. Unfortunately the data acquisition speeds are slow, this is a major drawback for widespread acceptance and usually makes imaging impractical. We are engaged in a program to accelerate the data capture rate by parallel acquisition of the incoming signals. This involves electronic developments as well as optical design. In order to parallelise the electronics we have used two approaches (i) a modified commercial camera and (ii) a custom built CMOS array detector. These approaches use an integrating camera which by application of suitable algorithms can perform the task of parallel lock in detection. Modulation depths below 1 part in 106, over 512 pixels can be readily detected with the commercial detector and smaller modulation depths are possible with the custom detector on account of the large well depth and hence high signal to noise. We also discuss the novel optical detection configurations that allow parallel detection of ultrasonic waves with ultrasonic wavelengths below the optical diffraction limit. Results are presented that show image acquisition rates orders of magnitude faster than normally possible with picosecond ultrasonic systems. Prospects for ultrahigh resolution optical resolution are discussed.

3:40-5:00 Posters

Lecture sessions will recess for presentation of poster papers on various topics in acoustics. See poster sessions for topics and abstracts.

Contributed Paper

5:00

4aPAb20. Acoustic phonon generation by intrinsically localized vibrational modes in double-helices of DNA macromolecules and transition from inter-strand energy exchange to nonlinear self-trapping. Yuriy A. Kosevich (Semenov Institute of Chemical Physics Russian Academy of Sciences, ul. Kosygina 4, 119991 Moscow, Russian Federation, yukosevich@yahoo.com), Alexander V. Savin (Semenov Institute of Chemical Physics Russian Academy of Sciences, ul. Kosygina 4, 119991 Moscow, Russian Federation, asavin@center.chph.ras.ru), Voislav L. Golo (Department of Mechanics and Mathematics, Lomonosov Moscow State University, 119992 Moscow, Russian Federation, voislav.golo@gmail.com), Yuriy S. Volkov (Department of Mechanics and Mathematics, Lomonosov Moscow State University, 119992 Moscow, Russian Federation, yu.volkov@gmail.com)

We study ultrafast dynamics of intrinsically localized vibrational modes (breathers) in a double helix of two weakly coupled chains of nonlinear oscillators. With this we model nonlinear dynamics of DNA-type macromolecules, which can be studied by means of femtosecond infrared pump-probe laser spectroscopy similar to the case of protein α-helices [1]. We show that there are two regimes of coupled breathers: the time-periodic wandering of low-amplitude breather between the chains, and the one-chain-localization (self-trapping) of high-amplitude breather. We also find bound states of two breathers, localized in different chains, with different positions in the chains. The helix symmetry of the system results in a specific chiral mode which accomplishes the interaction between torsional and longitudinal acoustic modes in the constituent chains. In both nonlinear regimes, the inter-strand energy exchange gives rise to acoustic phonon generation in the coupled chains, and the generation is much stronger in the wandering-breather regime. Ultrafast acoustic phonon generation can be detected by means of optoacoustics, which can therefore provide a tool to study in time domain the inter-strand energy exchange and the transition to nonlinear self-trapping in DNA-type macromolecules. 1. J. Edler, R. Pfister, V. Pouthier, C. Falvo, and P. Hamm, 2004, Phys. Rev. Lett. v. 93, 106405.

Invited Papers

5:20

4aPAb21. Coherant acoustic excitation of nanostructures probed with asynchronous optical sampling. Thomas Dekorsy (University Konstanz, Fach M700, Fachbereich Physik, 78457 Konstanz, Germany, thomas.dekorsy@uni-konstanz.de)

We report the high-sensitivity detection of coherent acoustic excitation in semiconductor heterostructures and metallic nanostructures by using high-speed asynchronous optical sampling. Asynchronous optical sampling is based on two tunable femtosecond Ti: sapphire lasers with slightly different repetition rates close to 1 GHz. This new technique provides the performance of an all-optical oscilloscope for coherent excitations in a pump-probe set-up without any mechanically moving part. A time delay of 1 ns is scanned with a frequency of 10 kHz and a time resolution of 100 fs. Investigations on coherent zone-folded phonons in semiconductor superlattices and nanoscale metallic structures are discussed. For the latter the influence of the substrate on the damping of acoustic excitations is investigated in detail.

5:40

4aPAb22. Opto-acousto-optic evaluation of the physical properties of nanoporous materials. Charfeddine Mechri (Université du Maine, avenue O. Messiaen, 72085 Le Mans, France, cmechri@hotmail.com), Pascal Ruello (LPEC/UMR 6087/CNRS/Université du Maine, Avenue Olivier Messiaen, 72085 Le Mans Cedex 09, France, pascal.ruello@univ-lemans.fr), M Nsenkoue (Université du Maine, avenue O. Messiaen, 72085 Le Mans, France, m.nsenkoue@univ-lemans.fr), Denis Mounier (LPEC/UMR 6087/CNRS/Université du Maine, Avenue Olivier Messiaen, 72085 Le Mans Cedex 09, France, denis.mounier@univ-lemans.fr), Jean-Marc Breteau (LPEC/UMR 6087/CNRS/Université du Maine, Avenue Olivier Messiaen, 72085 Le Mans Cedex 09, France, jean-marc.breteau@univ-lemans.fr), Mathieu Edely (LPEC/UMR 6087/CNRS/Université du Maine, Avenue Olivier Messiaen, 72085 Le Mans Cedex 09, France, mathieu.edely@univ-lemans.fr), Y Minhao (Université du Maine, avenue O. Messiaen, 72085 Le Mans, France, y.minhao@univ-lemans.fr), Alain Gibaud (Université du Maine, avenue O. Messiaen, 72085 Le Mans, France, alain.gibaud@univ-lemans.fr), I Povey (Tyndall National Institute, University College Cork, Prospect Row, 115 Cork, Ireland, i.povey@tyndall.ie), M Pemble (Tyndall National Institute, University College Cork, Prospect Row, 115 Cork, Ireland, m.pemble@tyndall.ie), Sergei Romanov (Tyndall National Institute, University College Cork, Prospect Row, 115 Cork, Ireland, sergei.romanov@tyndall.ie), Mikhail Baklanov (IMEC, Kapeldreef 75, B-3001 Leuven, Belgium, baklanov@imec.be), P Verdonck (IMEC, Kapeldreef 75, B-3001 Leuven, Belgium, verdonck@imec.be), Vitali Gusev (LPEC/UMR 6087/CNRS/Université du Maine, Avenue Olivier Messiaen, 72085 Le Mans Cedex 09, France, vitali.goussev@univ-lemans.fr)

The porous materials with the characteristic dimensions of the pores from few nanometers up to a few hundred of nanometers find applications in microelectronic industry (as low-k materials), in photovoltaics and for developing of effective chemical sensors. When the pores are ordered in a spatially periodic structure, these systems present photonic and/or phononic properties which are of a prime interest in applied optics and telecommunication (light and/or phonons spectrum control). Here we report how the methods of picosecond laser ultrasonics based on the generation and detection by lasers of the acoustic waves with frequencies in the band of 10 GHz - 1 THz (with the lengths of hundreds of nanometers down to few nanometers) are applied for the evaluation of the mechanical and optical properties of these materials.

6:00

4aPAb23. Nanoscale objects as promising high frequency acoustic transducers in picosecond acoustics. Arnaud Devos (IEMN-CNRS, Cité Scientifique - Avenue Poincaré, BP 60069, 59652 Villeneuve d'Ascq Cedex, France, arnaud.devos@isen.fr)

Twenty year ago, H. Maris opened up the field of nanoscale acoustics by demonstrating the opportunity of using ultrashort optical pulses for generating and detecting high frequency acoustic waves. Roughly, an optical pulse is converted in a picosecond acoustic pulse through the optical absorption in a thin metallic layer. Since then, this so-called picosecond ultrasonics has known a larger and larger success all around the world. Up to now, picosecond ultrasonics meets two main limitations. First it is difficult to reach the THz range using the usual way of producing the acoustic pulse. Second, in the common geometry only longitudinal waves are excited by the laser. Here we present some results showing that nanoscale objects could help in overcoming both difficulties. We first show that semiconductor quantum dots can be a very efficient emitter of coherent phonons whose frequency can be higher than those obtained in metallic thin films. Second we show that 2D arrays of nanosize metallic dots offers a way of generating and detecting high frequency surface acoustic waves.

6:20

4aPAb24. Nanoultrasonics based on piezoelectric semiconductor nanolayers. Chi-Kuang Sun (Naional Taiwan University, 1, Section 4, Roosevelt Road, 10617 Taipei, Taiwan, sun@cc.ee.ntu.edu.tw)

In this presentation, we will review our recent work on the development of nanoultrasonics based on piezoelectric semiconductor nanolayers. Through epitaxial growth of multiple or single piezoelectric semiconductor layers with a period on the order of 10 nm, nanoacoustic waves with a frequency of 1 terahertz and a wavelength of 10 nm can be excited and measured with femtosecond optical pulses. Using temperal coherent and spatial nonlinear optical controls, we are able to synthesize nanoacoustic waveforms and generate a lateral acoustic spot on the order of 100 nm without the need of the near-field optical techniques. In this presentation, we will also discuss the potential use of this terahertz acoustic source for various nanoacoustic applications, including nanoultrasonic imaging.

6:40

4aPAb25. Photoelastic transduction in photo-phononic nanodevices. Alejandro Fainstein (Centro Atomico Bariloche & Instituto Balseiro, C. N. E. A., 8400 S. C. de Bariloche, Argentina, afains@cab.cnea.gov.ar), Bernard Jusserand (INSP - UMR 7588 CNRS & Université Pierre et Marie Curie, 140 Rue de Lourmel, 75015 Paris, France, Bernard.Jusserand@insp.jussieu.fr), Maria Florencia Pascual Winter (INSP - UMR 7588 CNRS & Université Pierre et Marie Curie, 140 Rue de Lourmel, 75015 Paris, France, Florencia .PascualWinter@insp.jussieu.fr), Norberto Daniel Lanzillotti Kimura (Centro Atomico Bariloche & Instituto Balseiro, C. N. E. A., 8400 S. C. de Bariloche, Argentina, lanzilln@ib.cnea.gov.ar), Guillermo Rozas (Centro Atomico Bariloche & Instituto Balseiro, C. N. E. A., 8400 S. C. de Bariloche, Argentina, rozasg@ib.cnea.gov.ar), Bernard Perrin (INSP - UMR 7588 CNRS & Université Pierre et Marie Curie, 140 Rue de Lourmel, 75015 Paris, France, bernard.perrin@insp.jussieu.fr), Agnès Huynh (INSP - UMR 7588 CNRS & Université Pierre et Marie Curie, 140 Rue de Lourmel, 75015 Paris, France, agnes.huynh@insp.jussieu.fr), Aristide Lemaitre (LPN, CNRS route de Nozay, 91460 Marcoussis, France, Aristide.Lemaitre@lpn.cnrs.fr)

We will discuss the new possibilities that semiconductor superlattices and acoustic nanocavities open for the controlled manipulation of quasi-monochromatic acoustic waves in the terahertz range. Playing with the specific electronic properties of quantum wells constituting acoustic nanodevices allows to selectively generate or detect phonons with a specific spatial distribution of the deformation along the acoustic device propagation axis. We could for instance demonstrate the selective generation of cavity phonons at resonance with cavity excitonic transitions or the increased photoelastic coupling of folded acoustic modes in mirrors when the number of nodes of the acoustic mode coincide with the one of the dominantly resonant excitonic transition. We also used the combination of photonic and phononic cavities to ensure phase matching with cavity phonons in the standard detection scheme corresponding to transient reflectivity

in the time domain or Raman backscattering in the frequency domain. Photonic cavities moreover provide a strong increase of the internal optical fields by quality factors up to 100 typically, resulting in high enhancements of the transduction efficiency of monochromatic phonons to the benefit of the envisioned high speed modulation of optoelectronic properties of coupled photo-phononic nanodevices.

Contributed Papers

7:00

4aPAb26. Thermomechanical behavior of surface acoustic waves in ordered arrays of nanodisks studied by near-infrared pump-probe diffraction experiments and finite element simulations. Claudio Giannetti (Università Cattolica del Sacro Cuore, via dei Musei 41, I-25121 Brescia, Italy, c.giannetti@dmf.unicatt.it), Francesco Banfi (Università Cattolica del Sacro Cuore, via dei Musei 41, I-25121 Brescia, Italy, f.banfi@dmf.unicatt.it), Damiano Nardi (Università Cattolica del Sacro Cuore, via dei Musei 41, I-25121 Brescia, Italy, dnardi@dmf.unicatt.it), Bernard Revaz (Département de Physique Theorique, Universitè de Genève, 24 Quai Ansermet, CH-1211 Genève, Switzerland, bernard.revaz@gmail.com), Gabriele Ferrini (Università Cattolica del Sacro Cuore, via dei Musei 41, I-25121 Brescia, Italy, gabriele@dmf.unicatt.it), Paolo Vavassori (Dipartimento di Fisica - Univeristà di Ferrara, via dell'università, I-44100 Ferrara, Italy, vavassori@fe.infn.it), Vitali Metlushko (Department of Electrical and Computer Engineering, University of Illinois at Chicago, Chicago, IL 60607, USA, vmetlush@ece.uic.edu), Fulvio Parmigiani (Dipartimento di Fisica, Università degli Studi di Trieste and Sincrotrone Trieste, Basovizza, I-34012 Trieste, Italy, fulvio@dmf.unicatt.it)

The ultrafast thermal and mechanical dynamics of a two-dimensional lattice of metallic nanodisks has been studied by near-infrared pump-probe diffraction measurements over a temporal range spanning from 100 fs to several nanoseconds. The experiments demonstrate that in these systems a surface acoustic wave (SAW), with a wave vector given by the reciprocal periodicity of the two-dimensional array, can be excited by ~120 fs Ti: sapphire laser pulses. We unambiguously show that the observed SAW velocity shift originates from the mechanical interaction between the SAWs and the nanodisks, while the correlated SAW damping is due to the energy radiation into the substrate. In order to clarify the interaction between the nanodisks and the substrate, numerical calculations of both the elastic eigenmodes and the time-dynamics of the system, following the impulsive heating excitation by the laser, are performed. Simulations based on finite-elements analysis, together with a wavelet analysis of our experimental data, suggest the opening of a band-gap at the centre of the super-Brillouin zone. The modes at the centre of the super-Brillouin zone are excited following laser excitation, as opposed to thermal population, of the elastic modes.

7:20

4aPAb27. High frequency acoustics in nanostructures by spontaneous Brillouin light scattering. Tim Still (Max Planck Institute for Polymer Research, Ackermannweg 10, 55128 Mainz, Germany, still@mpip-mainz.mpg.de), Markus Retsch (Max Planck Institute for Polymer Research, Ackermannweg 10, 55128 Mainz, Germany, retsch@mpip-mainz.mpg.de), Revekka Sainidou (Instituto de Óptica - CSIC, Serrano 121, 28006 Madrid, Spain, rsainid@io.cfmac.csic.es), Ulrich Jonas (Max Planck Institute for Polymer Research, Ackermannweg 10, 55128 Mainz, Germany, jonas@mpip-mainz.mpg.de), George Fytas (Department of Materials Science and Technology, University of Crete and Forth, 71110 Heraklion, Greece, fytas@mpip-mainz.mpg.de)

We report on the dispersion of high frequency (GHz) acoustic excitations in three-dimensional colloidal crystalline or amorphous assemblies of sub-micron particles in different matrices by Brillouin light scattering (BLS) in order to explore the phononic and elastic properties of nanostructured materials. In air, we record eigenmodes of the individual particles, which are shown to be independent from the crystallinity and the composition of the sample but sensitively depend on the particle architecture (e.g core/shell silica/PMMA, hollow spheres) and their mechanical properties at nanoscale. In fluid matrices, the dispersion relations are recorded. We demonstrate the occurence of two hypersonic phononic band gaps of different nature. One is a Bragg gap appearing only in crystalline samples, the other one is a particle resonance-induced hybridization gap, which appears in crystalline samples along with the Bragg gap and alone in amorphous samples. Furthermore, we investigate the influence of filling fraction, crystallinity and monodispersity of size on the hypersonic behaviour of our samples.

Session 4aPAc

Physical Acoustics, Acoustical Oceanography, and Biomedical Ultrasound/Bioresponse to Vibration: Acoustically Activated Bubble Dynamics and Applications I

Erich C. Everbach, Cochair
Swarthmore College, 500 College Avenue, Engineering Department, Swarthmore, PA 19081, USA

Joachim Holzfuss, Cochair
Institute of Applied Physics, TU Darmstadt, Schlossgartenstr. 7, Darmstadt, 64289, Germany

Invited Papers

8:00

4aPAc1. Bubbles, surfactants, shape oscillations, optical levitation, and light scattering: a survey. Philip L. Marston (Washington State University, Physics and Astronomy Department, Pullman, WA 99164-2814, USA, marston@wsu.edu), David B. Thiessen (Washington State University, Physics and Astronomy Department, Pullman, WA 99164-2814, USA, thiessen@wsu.edu)

Research emphasizing relatively slow aspects of bubble dynamics will be summarized. Though the attention is mainly on acoustically levitated bubbles larger than the size for monopole resonance, early experiments on stable optical levitation of gas bubbles in water [J. Acoust. Soc. Am. 83, 970-975 (1988)] will also be noted as well as fundamental aspects of light scattering by bubbles [J. Opt. Soc. Am. and/or Applied Optics (1979-1991)]. Modulated radiation pressure was demonstrated to be an effective way for mode-specific excitation of shape oscillations of acoustically levitated bubbles [J. Acoust. Soc. Am. 93, 706-713 (1993)]. The damping of shape oscillations was demonstrated to be strongly influenced by the presence of insoluble or soluble surfactants [J. Fluid Mech. 300, 149-167 (1995); Phys. Rev. Let. 75, 2686-2689 (1995); J. Acoust. Soc. Am. 102, 3372-3377 (1997)]. A convenient way of measuring the damping was to use laser beam extinction to monitor freely decaying shape oscillations. This technique was sufficiently sensitive to reveal the strong dependence of the damping on surface elasticity. Even for clean bubbles, an improved analysis of the damping was needed. [Sponsored in part by NASA and by ONR.]

8:20

4aPAc2. Measuring the Extreme Conditions Created During Cavitation. Kenneth S. Suslick (University of Illinois at Urbana-Champaign, 600 S. Mathews Av., Urbana, IL 61801, USA, ksuslick@uiuc.edu)

Extreme temperatures and pressures are produced through acoustic cavitation: the formation, growth and collapse of bubbles in a liquid irradiated with high intensity ultrasound. Single bubbles have generally been assumed to give higher temperature conditions than bubble clouds, but confirmation from the single buble sonoluminescence (SBSL) emission spectra have been problematic because SBSL typically produces featureless emission spectra that reveal little about the intra-cavity physical conditions or chemical processes. Here we present definitive evidence of the existence of a hot, highly energetic plasma core during SBSL. From a luminescing bubble in sulfuric acid, excited state to excited state emission lines are observed both from noble gas ions (Ar+, Kr+, and Xe+) and from neutral atoms (Ne, Ar, Kr, and Xe). The excited states responsible for these emission lines range from 8.3 eV (for Xe) to 37.1 eV (for Ar+) above the ground state. Observation of emission lines allows for identification of intra-cavity species responsible for light emission; the energy levels of the emitters indicate the plasma generated during cavitation is comprised of highly energetic atomic and ionic species.

8:40

4aPAc3. Nonlinear dynamics of sonoluminescing bubbles. Joachim Holzfuss (Institute of Applied Physics, TU Darmstadt, Schlossgartenstr. 7, 64289 Darmstadt, Germany, Joachim.Holzfuss@physik.tu-darmstadt.de)

The current work focuses on the acoustical and nonlinear dynamical aspects of sonoluminescence (SBSL). Several hydrodynamical instabilities in parameter space are analyzed in detail numerically. Their occurrence in experiments is discussed especially in the context of period doubled unisotropic light emission. The acoustical emissions during stable and unstable oscillations show characteristics of shock waves. The emitted sound generates a complex acoustic environment in the driving cell leading to backreactions to the bubble. Characteristic dynamical effects during unstable sonoluminescence are clarified. Chemical processes during high temperature and high pressure, spatial translations, gas diffusion, the highly nonlinear bubble oscillations and acoustic emissions are attributed to oscillations and modulations of bubble dynamics outside the range of stable SBSL. In particular reasons for quasiperiodic oscillations with incommensurate frequencies in different setups are found.

9:00

4aPAc4. Bubble-bubble interaction in disperse bubble clouds. Andrew J. Szeri (University of California, 6119 Etcheverry Hall, Berkeley, CA 94720-1740, USA, andrew.szeri@berkeley.edu), Jean O. Toilliez (University of California, 6119 Etcheverry Hall, Berkeley, CA 94720-1740, USA, toilliez@me.Berkeley.EDU), Chris Heckman (University of California, 6119 Etcheverry Hall, Berkeley, CA 94720-1740, USA, checkman@berkeley.edu), Parastou Eslami (University of California, 6119 Etcheverry Hall, Berkeley, CA 94720-1740, USA, peslami20@berkeley.edu)

Disperse bubble fields driven by pressure waves feature effects of time delays associated with the finite speed of travel of the driving acoustic wave, and the finite travel time of pressure waves between bubbles. The relative spatial arrangement of bubble nuclei in a disperse field, and the direction of the incoming pressure wave, both influence the cavitation behavior of a cloud of nuclei. In this paper, we consider the dynamics of a disperse field of bubble nuclei driven by a strong rarefaction, such as one sees in shock wave lithotripsy. We make comparisons to experimental work published in J. I. Iloreta, A. J. Szeri, Y. Zhou, G. Sankin and P. Zhong, Assessment of shock wave lithotripters via cavitation potential, Physics of Fluids 19, 086103 (2007). Bubble-bubble interactions are the key ingredient to resolving a mystery concerning the extent of cavitation bubble growth.

9:20

4aPAc5. The effects of sonication on bacteria. Timothy J Mason (Sonochemistry Centre, Coventry University, Priory Street, CV1 5FB Coventry, UK, t.mason@coventry.ac.uk), L Paniwnyk (Sonochemistry Centre, Coventry University, Priory Street, CV1 5FB Coventry, UK, apx077@coventry.ac.uk), E Joyce (Sonochemistry Centre, Coventry University, Priory Street, CV1 5FB Coventry, UK, apx077@coventry.ac.uk)

High power ultrasound at frequencies around 20kHz is capable of killing bacteria and for many years has been standard technique in microbiology for the disruption of living cells to release their contents. So successful is this effect that ultrasound has been studied as a possible method for water disinfection. The energies required for using ultrasound alone are high but commercial equipment is available and is often used for disinfection in conjunction with other techniques such as ozonation or uv irradiation. Now evidence is emerging that is possible to induce effects on bacteria other than kill by modifying the acoustic energy entering the suspension (Ultrason. Sonochem. 10:315, 2003). This can be done by altering the duration of exposure, the acoustic power used or the frequency of the ultrasound. In this way sonication can lead to such effects as deagglommeration, enhanced reaction to biocides and gene transfer (Nucleic Acids Res. 35:e129, 2007).

9:40

4aPAc6. Cavitational activity in bacterial biofilms exposed to 1 MHz ultrasound. Erich C. Everbach (Swarthmore College, 500 College Avenue, Engineering Department, Swarthmore, PA 19081, USA, ceverba1@swarthmore.edu), Roby Velez (Swarthmore College, 500 College Avenue, Engineering Department, Swarthmore, PA 19081, USA, rvelez1@swarthmore.edu), Amy C. Vollmer (Swarthmore College, 500 College Avenue, Biology Department, Swarthmore, PA 19081, USA, avollme1@swarthmore.edu)

An exposure system was previously developed to quantify destruction of bacterial biofilms by 1 MHz c.w. ultrasound at 0.8 MPa peak-to-peak acoustic pressure amplitude (JASA 122(5):3052, 2007). Bacterial killing is quantified via confocal microscopy using florescent E. Coli and image processing. Recently, a passive detector of inertial and stable cavitation was included, relying upon the presence and character of acoustic emissions. The detector, a PVDF array placed on the microscope slide forming the base of the exposure chamber, produces a proxy measure of cavitational activity during ultrasound exposure. Acoustic pressure thresholds for biofilm destruction and cavitational activity suggest that inertial and stable cavitation both play a role in biofilm destruction by ultrasound.

10:00-10:20 Break

10:20

4aPAc7. Bubbles in piezo-acoustic inkjet printing. Detlef Lohse (Physics of Fluids, University of Twente, P.O. Box 217, 7500 AE Enschede, Netherlands, d.lohse@utwente.nl), Roger Jeurissen (Physics of Fluids, University of Twente, P.O. Box 217, 7500 AE Enschede, Netherlands, r.j.m.jeurissen@tnw.utwente.nl), Jos De Jong (University of Twente, P.O. Box 217, Department of Science and Technology, 7500 AE Enschede, Netherlands, jos.dejong@tnw.utwente.nl), Michel Versluis (Physics of Fluids, University of Twente, P.O. Box 217, 7500 AE Enschede, Netherlands, m.versluis@utwente.nl), Herman Wijshoff (Oce Technology, P.O. Box 101, 5900 MA Venlo, Netherlands, herman.wijshoff@oce.com), Marc Van Den Berg (Oce Technology, P.O. Box 101, 5900 MA Venlo, Netherlands, marc.van.den.berg@oce.com), Hans Reinten (Oce Technology, P.O. Box 101, 5900 MA Venlo, Netherlands, hans.reinten@oce.com)

Ink-jet printing is considered as the hitherto most successful application of microfluidics. A notorious problem in piezo-acoustic ink-jet systems is the formation of air bubbles during operation. They seriously disturb the acoustics and can cause the droplet formation to stop. We could show by a combination of acoustical detection and high-speed visualization that the air-bubbles are entrained at the nozzle and then grow by rectified diffusion. Experimental results on the droplet velocity as a function of the equilibrium radius R0 of the entrained bubble are presented, too. Surprisingly, the droplet velocity shows a pronounced maximum around R0=17 micrometer before it sharply drops to zero around R0=19 micrometer. A simple one-dimensional model is introduced to describe this counterintuitive behavior which turns out to be a resonance effect of the entrained bubble. We show that the bubble counteracts the pressure buildup necessary for the droplet formation. The channel acoustics and the air bubble dynamics are modeled. It is crucial to include the confined geometry into the model: The air bubble acts back on the acoustic field in the channel and thus on its own dynamics. This two-way coupling limits further bubble growth and thus determines the saturation size of the bubble.

Contributed Papers

10:40

4aPAc8. The acoustic excitation mechanism of bubbles released from a nozzle. Grant Deane (Scripps Inst. Oceanography, Univ. Califiornia, San Diego, La Jolla, CA 92093, USA, gdeane@ucsd.edu), Helen Czerski (Scripps Inst. Oceanography, Univ. Califiornia, San Diego, La Jolla, CA 92093, USA, hczerski@ucsd.edu)

At the moment of their formation, bubbles emit a short pulse of sound. Bubble noise is associated with sound from a variety of natural processes, including whitecaps, waterfalls, breaking surf and rain. A number of acoustic excitation mechanisms for bubble noise have been proposed, including the increase in internal pressure of the bubble associated with the Laplace pressure, hydrostatic pressure effects, shape mode to volume mode coupling, and a fluid jet associated with the collapse of the neck of air formed during bubble creation. Using bubbles released from a nozzle as a model system, we have determined that sound production is excited by a sudden decrease in bubble volume driven by the collapse of the neck of gas joining the bubble to its parent. A simple analytical model of neck collapse driven by surface tension energy is in agreement with high speed photographic measurements, and sufficient to explain the details of acoustic excitation. [Work supported by ONR and NSF]

11:00

4aPAc9. Characterizing microbubble interactions with ultrasound using flow cytometry. Thomas Matula (Center for Industrial and Medical Ultrasound, Applied Physics Lab., University of Washington, 1013 NE 40th St., Seattle, WA 98105, USA, matula@apl.washington.edu), Jarred Swalwell (Center for Industrial and Medical Ultrasound, Applied Physics Lab., University of Washington, 1013 NE 40th St., Seattle, WA 98105, USA, jarred@u.washington.edu)

Characterizing the fundamental interaction of ultrasound with microbubbles is challenging because of the small spatial and temporal scales. High speed optical imaging is perhaps the most well-known method, as it provides direct information about their response. Although the image is in a plane, the image quality can be sufficient to obtain important information about bubble response. However, high-speed cameras are expensive, data is very limited, and difficult to process. We previously showed how light scattering can be used to obtain similar information - volume oscillations, destruction, even shell properties. Light scattering can be an inexpensive method for probing microbubbles. The difficulties with light scattering (also with optical imaging) are alignment and signal/noise. In this talk we will describe a technique to use commercially-available light-scattering systems to investigate the interaction of pulsed ultrasound with microbubbles. In particular, we developed a technique to insonify microbubbles flowing through the focal region of a flow cytometer. Attached to the quadrature side of a flow cuvette is a small piezoelectric transducer, driven in pulsed mode at various voltages to induce a bubble response. The light scattered from the bubbles can be used for sizing, destruction thresholds, and to assess volume oscillations. Funded by NIH #5R01EB000350

Invited Paper

11:20

4aPAc10. Determination of cavitation bubble lifetimes using bubble-bubble coalescence data. Franz Grieser (Department of Chemical and Biomolecular Engineering, The University of Melbourne, Parkville, Victoria, 3010 Melbourne, Australia, franz@unimelb.edu.au), Devi Sunartio (Department of Chemical and Biomolecular Engineering, The University of Melbourne, Parkville, Victoria, 3010 Melbourne, Australia, franz@unimelb.edu.au), Muthupandian Ashokkumar (Department of Chemical and Biomolecular Engineering, The University of Melbourne, Parkville, Victoria, 3010 Melbourne, Australia, masho@unimelb.edu.au)

The effect that surface-active solutes, such as aliphatic alcohols and sodium dodecylsulfate, have on the extent of bubble coalescence in liquids under different sonication conditions has been investigated by measuring the volume change of the solution following a period of sonication. The data obtained led to the conclusion that SDS does not reach equilibrium adsorption level at the bubble/solution interface. On this basis, a method is proposed for estimating nonequilibrium surface excess values for solutes that do not fully equilibrate with the bubble/solution interface during sonication. For the case of SDS in the presence of excess NaCl, the method was further employed to estimate the maximum lifetime of bubbles in a multibubble field. Data obtained from this study suggests that an acoustic bubble in a multibubble field has a finite lifetime, and that this lifetime decreases with increasing applied frequency, ranging from up to 0.35 ± 0.05 ms for 213 kHz to 0.10 ± 0.05 ms for 1062 kHz. These estimated lifetimes equate to a bubble in a multibubble field undergoing an upper limit of 50-200 oscillations over its lifetime for applied acoustic frequencies between 200 kHz and 1 MHz.

Contributed Papers

11:40

4aPAc11. Interpretation of the pressure waves radiated by oscillating bubbles. Karel Vokurka (Technical University of Liberec, Physics Department, Studentska 6, 461 17 Liberec, Czech Republic, karel.vokurka @tul.cz), Silvano Buogo (CNR-Istituto di Acustica 'O,M.Corbino', Via del Fosso del Cavaliere, 100, 00133 Rome, Italy, silvano.buogo@idac.rm.cnr.it)

An oscillating bubble is an excellent acoustic radiator. In a pressure wave emitted by the oscillating bubble information about the bubble properties and behavior is present. Hence, when using a suitable method, this information could be extracted and used to improve our understanding of the physical processes accompanying the bubble oscillations. However, to be able to extract this information, a number of prerequisites must be met. First, the measuring apparatus should be able to record a faithful copy of the pressure wave. Second, a large, statistically representative set of pressure records must be available for the analysis. Third, a suitable method must be used to analyze the recorded waves. All these requirements will be discussed in detail at the conference. Presented results are based on experience gained during evaluation of a large set of pressure records obtained recently in experiments with spark generated bubbles. [Work has been partly supported (K.V.) by the Czech Ministry of Education as the research project MSM 46747878501.]

12:00

4aPAc12. Dynamics and radiation of single cavity in an abnormal compressible bubbly media. Valeriy K. Kedrinskiy (Lavrentyev Institute of Hydrodynamics, Siberian Division of the Russian Academy of Sciences, Lavrentyev prospect 15, 630090 Novosibirsk, Russian Federation, kedr @hydro.nsc.ru)

The equation of a pulsation of a single cavity in the equilibrium (on pressure) bubbly medium was suggested. The state of such medium is described by Lyakhov's equation which at the condition of pressure equilibrium in the both phases (gas/liquid) becomes essentially simpler. The numerical analysis of features of cavity dynamics and the acoustic losses was executed. The notion ″acoustic losses″ mean a radiation generated by cavity. The analysis of radiation parameters was restricted by the vicinity of cavity wall from a liquid side. The studies of cavity behavior, the structure and

amplitude of a radiation have shown that the degree of a cavity compression by a stationary shock wave goes down when the volumetric concentration of gas phase K in the medium increases. The amplitude of pulsation essentially decrease and function R(t) (radius cavity vs. time) asymptotically (without oscillations) tends to the equilibrium state when K is equal approximately 3%. The equilibrium state is defined by amplitude of an incident shock wave and does not depend on K-value. The structure of a radiation wave takes the ″soliton″ form, its amplitude is essentially lesser and the width is much more in the comparison with corresponding parameters for a single-phase liquid. (RFBR 06-01-00317a financial support).

12:20-1:40 Lunch Break

Contributed Papers

1:40

4aPAc13. Equilibrium state of a multi-size bubble population in a liquid. Svetlana Kovinskaya (Mechmath LLC, 14530 Bluebird Trail, Prior Lake, MN 55372, USA, mechmath@mechmath.com)

A propagation of a linear pressure wave in the liquid with multi-size bubble population is investigated. The wave in the bubbly mixture is modeled as wave in the waveguide interacting with distributed resonators having different resonance frequencies. Each bubble sub-population has the frequency range of effective influence on the wave propagation. This range is started from the resonance frequency of the individual bubble and ended in dependency on the partial void fraction of this sub-population. Mutual influence of sub-populations leads to additional sound attenuation that in essence is a Landau damping. The dispersive equation for the propagating wave lets introduce a criterion for the equilibrium state of the bubbly mixture with multi-size bubble population. The equilibrium distribution which meets this criterion is found analytically. It is shown that the equilibrium distribution is an exact result from the resonant acoustical absorption theory. This theory is employed to find the bubble distribution from measured attenuation of the acoustical wave with assumption that only resonating bubbles contribute attenuation at the frequency of their resonance (neglecting off-resonance contributions). The deviation from the equilibrium contributes Landau damping into the resonant absorption. A dependency of Landau damping on the bubble size distribution is presented.

2:00

4aPAc14. Optical measurements of the hot spot and incandescent shock from high pressure cavitation in water. Robert Hiller (Impulse Devices, Inc., 13366 Grass Valley Av. Unit H, Grass Valley, CA 95945, USA, asa@roberthiller.com), D. Felipe Gaitan (Impulse Devices, Inc., 13366 Grass Valley Av. Unit H, Grass Valley, CA 95945, USA, gaitan@impulsedevices.com)

Spontaneous acoustic cavitation in water at static pressure up to 300 bar has been experimentally investigated. Cavities are initiated by negative pressure and then collapse due to both acoustic pressure and shock waves reflected from the inner surface of the spherical resonator. The implosions result in intense (Mbar) shock waves and bright (1 nJ) light flashes which last from 5 to 40 nanoseconds. The optical spectrum of the flash is measured with a grating monochromator and intensified array detector for high wavelength resolution (~5 nm) but slow time resolution, and with a multiple-anode microchannel plate photomultiplier tube along with bandpass filters for fast time resolution (~1 ns) but poor wavelength resolution. The spectrum is generally broad-band and featureless, matching roughly to a Planck spectrum at 5000 to 8000K. The spectral and temporal structure of the flashes is matched to hydrocode simulations. The model suggest the flashes are due to a shell of hot, opaque, shocked water which surrounds and obscures the central hot core. (SMDC contract W9113M-07-C-0178)

2:20

4aPAc15. Investigation of bubble dynamics and sonoluminescence in megasonic fields. Andrea Otto (Göttingen University, Friedrich-Hund-Platz 1, 37077 Göttingen, Germany, aotto@physik3.gwdg.de), Till Nowak (Göttingen University, Friedrich-Hund-Platz 1, 37077 Göttingen, Germany, tnowak@physik3.gwdg.de), Robert Mettin (Göttingen University, Drittes Physikalisches Institut, Friedrich-Hund-Platz 1, 37077 Göttingen, Germany, R.Mettin@physik3.gwdg.de), Frank Holsteyns (SEZ AG, SEZ-Strasse 1, 9500 Villach, Austria, F.Holsteyns@at.sez.com),Alexander Lippert (SEZ AG, SEZ-Strasse 1, 9500 Villach, Austria, A.Lippert@at.sez.com)

Cavitation bubble motion and bubble structures in water are investigated for standing wave fields in the megasonic range by high-speed imaging. Larger degassing bubbles and small bubbles with high translation speeds can be resolved. Groups of bubbles arrange in lines or arrays, as reported earlier by Miller [Miller, JASA 62, 1977]. Additional, sonoluminescence is measured in overall long-term and phase-resolved (gated) long-term exposures. Several distinct luminescing islands can be detected. The findings seem to be strongly related to the standing wave nature of the pressure field in our setup. Conclusions on bubble distributions and for cleaning applications are drawn.

2:40

4aPAc16. Development of an acoustics-based instrument for bubble measurement in liquids. Georges L. Chahine (Dynaflow, Inc., 10621-J Iron Bridge Rd, Jessup, MD 20794, USA, glchahine@dynaflow-inc.com), Xiongjun Wu (Dynaflow, Inc., 10621-J Iron Bridge Rd, Jessup, MD 20794, USA, xiongjun@dynaflow-inc.com), Xiaozhen Lu (Dynaflow, Inc., 10621-J Iron Bridge Rd, Jessup, MD 20794, USA, xiaozhen@dynaflow-inc.com)

The acoustic bubble spectrometer (ABS) is an acoustics-based device that provides bubble size distribution in a bubbly liquid through measurement at various frequencies of the sound speed and attenuation and solution of an inverse problem. Acoustic bursts of varying frequencies are emitted by one hydrophone and detected by another. A PC and data boards control signal generation, detection, signal processing, inverse problem solution, and results display. Extensive validation experiments were conducted against high speed-video optical measurements. The two methods give very close results for void fractions up to 3e-3, with the ABS possessing the significant advantage of enabling near real-time measurements. The field of application is being expanded to media other than water, and the technique improved to detect larger void fractions, with the help of numerical simulations of nonlinear behavior of bubble clouds in acoustic fields.

3:00

4aPAc17. An acoustic resonator for determining the void fraction of bubbly mercury flows. Ronald A. Roy (Boston University, Dept. of Aerosp. and Mech. Eng., 110 Cummington St., Boston, MA 02215, USA, ronroy@bu.edu), Christopher E. Ormonde (Boston University, Dept. of Aerosp. and Mech. Eng., 110 Cummington St., Boston, MA 02215, USA, chrisceo@bu.edu), Parag V. Chitnis (Boston University, Dept. of Aerosp. and Mech. Eng., 110 Cummington St., Boston, MA 02215, USA, pchitnis@bu.edu), Robin O. Cleveland (Boston University, Dept. of Aerosp. and Mech. Eng., 110 Cummington St., Boston, MA 02215, USA, robinc@bu.edu), R. Glynn Holt (Boston University, Dept. of Aerosp. and Mech. Eng., 110 Cummington St., Boston, MA 02215, USA, rgholt@bu.edu)

An acoustic resonator for measuring free-gas void fraction of a helium-mercury mixture is investigated. We employ a vertical, stainless steel cylindrical waveguide with a 5.08-cm i.d., a 1.27-cm wall thickness, a 40-cm length, and pressure-release boundary conditions at both ends. A bubble injection flow loop produces 2-phase mixtures of varying void fraction that flows upwards through the tube, spills over, and recirculates. The resonator is driven from the top by a 2.54-cm diameter circular piston affixed to an

electrodynamic shaker. A hydrophone mounted 1 cm above the tube bottom is used to measure the frequency response of the system. Sound speed is inferred by assuming a linear dependence of axial mode number on mode frequency, and void fraction is calculated assuming a mixture sound speed for a bubble population with maximum sized much smaller than the resonant sizes in the modal frequency range (Wood's limit). The system was validated using non-bubbly water and water-air mixtures of different void fractions. Void fraction measurements for Helium-Mercury mixtures will be presented. [Supported by the ORNL Spallation Neutron Source, which is managed by UT-Battelle, LLC, under contract DE-AC05-00OR22725 for the U.S. Department of Energy.]

3:20

4aPAc18. Cavitation bubbles as microfluidic actuators. Claus-Dieter Ohl (University of Twente, P.O. Box 217, Department of Science and Technology, 7500 AE Enschede, Netherlands, c.d.ohl@utwente.nl), Rory Dijkink (University of Twente, Physics of Fluids, Building Meander, Postbus 217, 7500 AE Enschede, Netherlands, r.j.dijkink@tnw.utwente.nl), Zwaan Ed (University of Twente, Physics of Fluids, Building Meander, Postbus 217, 7500 AE Enschede, Netherlands, e.v.zwaan@casema.nl), Séverine Le Gac (University of Twente, BIOS The Lab-on-a-Chip group, 7500 AE Enschede, Netherlands, S.LeGac@ewi.utwente.nl), Albert Van Den Berg (University of Twente, BIOS The Lab-on-a-Chip group, 7500 AE Enschede, Netherlands, A.vandenBerg@ewi.utwente.nl), Kinko Tsuji (Shimadzu Europa GmbH, 47269 Duisburg, Netherlands, kts@shimadzu.de)

In this talk we give an overview on the usage of single cavitation bubbles to pump, mix, and manipulate cells in microfluidics. The bubbles are generated with a laser pulse in optically transparent lab-on-a-chip devices. The bubble pulsations is inherently fast, thus although the characteristic dimensions are small high Reynolds numbers flow can be achieved. Experiments show that depending on the channel height 2-dimensional or 3-dimensional fluid flow is generated. Interestingly, there exists a regime which can be described with the Laplace equation, thus it is essentially a potential inviscid flow. We will present the current work (of others and our group) on cavitation assisted pumping using the jetting effect, mixing flows through the creation of vorticity, and the interaction of a bubble with suspension cells. The first results on the latter promise a fruitful future for biologic relevant applications in integrated lab-in-chip devices.

3:40

4aPAc19. Ultrasonic synthesis of enzyme coated microbubbles. Muthupandian Ashokkumar (Department of Chemical and Biomolecular Engineering, The University of Melbourne, Parkville, Victoria, 3010 Melbourne, Australia, masho@unimelb.edu.au), Francesca Cavalieri (Department of Chemical and Biomolecular Engineering, The University of Melbourne, Parkville, Victoria, 3010 Melbourne, Australia, masho@unimelb.edu.au), Franz Grieser (Department of Chemical and Biomolecular Engineering, The University of Melbourne, Parkville, Victoria, 3010 Melbourne, Australia, franz@unimelb.edu.au)

Gas-filled polymer coated microbubbles are intrinsically ultrasound responsive systems and when tailored with targeting features are promising candidates for smart drug delivery. We have ultrasonically synthesised stable, versatile, biodegradable and biocompatible microbubbles using the enzyme, lysozyme. The synthesis of lysozyme microbubbles has been achieved by sonicating an aqueous solution containing denatured lysozyme. The microbubbbles have been characterised using a number of imaging techniques such as, SEM, AFM and light microscopy. We have observed that the experimental parameters such as, length of sonication, DTT concentration and denaturisation time deeply affect the yield and the size of the microbubbles. We have also investigated the secondary structure and the enzymatic activity of lysozyme coated microbubbles. The lysozyme microbubbles have retained their enzymatic antimicrobial activities.

4:00-5:20 Posters

Lecture sessions will recess for presentation of poster papers on various topics in acoustics. See poster sessions for topics and abstracts.

Contributed Papers

5:20

4aPAc20. Modeling of the effect of boundaries on ultrasound contrast agent microbubbles response. Benjamin Dollet (Physics of Fluids, University of Twente, P.O. Box 217, 7500 AE Enschede, Netherlands, benjamin.dollet@univ-rennes1.fr), Leen Van Wijngaarden (Physics of Fluids, University of Twente, P.O. Box 217, 7500 AE Enschede, Netherlands, l.vanwijngaarden@tnw.utwente.nl), Nico De Jong (Erasmus MC, Dr Molewaterplein 50 room Ee2302, 3015GE Rotterdam, Netherlands, n.dejong@erasmusmc.nl), Detlef Lohse (Physics of Fluids, University of Twente, P.O. Box 217, 7500 AE Enschede, Netherlands, d.lohse@utwente.nl), Michel Versluis (Physics of Fluids, University of Twente, P.O. Box 217, 7500 AE Enschede, Netherlands, m.versluis@utwente.nl)

Ultrasound contrast agents are coated microbubbles currently extensively studied to target endothelial cells, for local drug delivery. It is therefore important to distinguish acoustically free-floating bubbles from bubbles located close, or targeted to blood vessels. Here, we propose a theoretical study to understand the effect of boundaries on bubble response to ultrasound. We consider the hydrodynamic interaction of a single bubble with a wall, including all possible bubble motions: volumetric oscillations, translation, and nonspherical deformations. We also include the friction in the viscous boundary layer along the wall. We derive the coupled equations of the bubble dynamics using a Lagrangian approach. We predict the bubble response to ultrasound, as a function of various parameters (applied frequency and amplitude, bubble size and coating, bubble/wall distance). We show that our new model predicts a decrease of the resonance frequency as a bubble gets closer to a wall, in agreement with experiments. We reproduce correctly the observed decrease of oscillation amplitude for a close close to the wall, showing that it is due to the coupling between oscillation and translation rather than the friction in the boundary layer. The threshold for nonspherical oscillations is also discussed and compared to experimental measurements.

5:40

4aPAc21. Experimental investigation of the effect of heating rate on pre-existing gas nuclei in a viscoelastic medium. Ian Webb (University of Oxford, Medical Engineering Unit, 43 Banbury Road, OX2 6PE Oxford, UK, ian.webb@eng.ox.ac.uk), Manish Arora (University of Oxford, Medical Engineering Unit, 43 Banbury Road, OX2 6PE Oxford, UK, manish.arora@eng.ox.ac.uk), Stephen Payne (University of Oxford, Dept. of Engineering Science, Parks Road, OX1 3PJ Oxford, UK, stephen.payne@eng.ox.ac.uk), Ronald A. Roy (Boston University, Dept. of Aerosp. and Mech. Eng., 110 Cummington St., Boston, MA 02215, USA, ronroy@bu.edu), Constantin C. Coussios (University of Oxford, Medical Engineering Unit, 43 Banbury Road, OX2 6PE Oxford, UK, constantin.coussios@eng.ox.ac.uk)

Inertial cavitation is known to play a key role in thermal HIFU therapy, both from the point of view of treatment safety and delivery, and as a potential tool for treatment monitoring. However, bubble behaviour in rapidly changing temperature fields remains poorly understood. Using a theoretical model, we have previously shown that, for a given initial bubble radius, a critical heating rate exists, above which the bubble will grow, and below which it will dissolve. In order to test this hypothesis, an electrical resistor embedded in 0.5% Xanthan Gum solution is used to impose a known temperature profile, measured by an array of thermocouples, on a series of embedded bubbles. An optical arrangement employing a 10 Megapixel CCD and a macro lens is used to image the bubbles within the gel at sufficient resolution for accurate sizing. The radius-time profiles for a range of bubble

sizes are thus extracted using image analysis techniques, allowing comparison with model predictions and subsequent refinement of the theoretical model. Future work will focus on the incorporating the effects of acoustic excitation, such as rectified diffusion, to develop a unified model of bubble behaviour in viscoelastic media under the effect of a HIFU field.

6:00

4aPAc22. Damage to single biological cells induced by laser-induced tandem microbubbles. Georgy Sankin (Duke University, Department of Mechanical Engineering and Materials Science, Durham, NC 27708, USA, gns@duke.edu), Fang Yuan (Duke University, Department of Mechanical Engineering and Materials Science, Durham, NC 27708, USA, fang.yuan@duke.edu), Pei Zhong (Duke University, Department of Mechanical Engineering and Materials Science, Durham, NC 27708, USA, pzhong@duke.edu)

Recent studies have highlighted the potential for using laser-induced micro-cavitation in lab-on-a-chip devices. Shear stress in a liquid can be controlled and significantly enhanced by bubble-bubble interaction, providing new options for in situ cell treatment. Two micro-bubbles (10 μs life time) are generated in a 25-μm liquid layer using 5 ns tandem laser pulses delivered through the objective of a microscope. Bubble-bubble interaction in nearly two-dimensional flow is observed using high-speed video cameras. Two liquid micro-jets moving in opposite directions can be generated when the second bubble is produced at the maximum size of the first one. The jet velocity is estimated about 35 m/s. Particle imaging velocimetry reveals vortex flow motion around the oscillating bubble lasting for about 200 μs. Cell lyses produced by jetting from asymmetric oscillation of tandem microbubbles are investigated at various bubble-cell distances and compared with the results from single symmetric bubble oscillation. The interaction of tandem microbubbles can produce microjetting, leading to damage of adjacent single biological cells.

6:20

4aPAc23. Introduction of a compliant gas-layer serves to mitigate damage to solid surfaces from the collapse of cavitation bubble clouds. Parag V. Chitnis (Boston University, Dept. of Aerosp. and Mech. Eng., 110 Cummington St., Boston, MA 02215, USA, pchitnis@bu.edu), Nicholas J. Manzi (Boston University, Dept. of Aerosp. and Mech. Eng., 110 Cummington St., Boston, MA 02215, USA, nmanzi@bu.edu), Robin O. Cleveland (Boston University, Dept. of Aerosp. and Mech. Eng., 110 Cummington St., Boston, MA 02215, USA, robinc@bu.edu), Ronald A. Roy (Boston University, Dept. of Aerosp. and Mech. Eng., 110 Cummington St., Boston, MA 02215, USA, ronroy@bu.edu), R. Glynn Holt (Boston University, Dept. of Aerosp. and Mech. Eng., 110 Cummington St., Boston, MA 02215, USA, rgholt@bu.edu)

The collapse of transient bubble clouds near a boundary was investigated. Transient cavitation bubbles were created using a shock-wave lithotripter. A porous ceramic disk (flow-pressure 7.5psi) was placed at the lithotripter focus. Air was forced through the disk to alter the boundary condition at the ceramic disk's proximal face. Gas pressure below 7.5psi resulted in a ceramic disk partially filled with fluid (rigid boundary); gas pressure over 7.5psi resulted in active bubbling at the proximal face (compliant boundary). Cavitation dynamics of bubble clouds near ceramic disks were studied for varying gas pressures (0-10psi). Images of the collapse were obtained from a high-speed camera. Additionally, a passive cavitation detector (3.5MHz focused transducer) was aligned with the lithotripter focus. Both the images and the acoustic measurements indicated that bubble clouds near a rigid boundary collapse onto the boundary, forming a re-entrant liquid jet whose impact leads to surface erosion. When a compliant boundary is introduced, bubble clouds collapse away from the surface, thus mitigating cavitation damage. The damage to the ceramic disks was quantified using micro-CT imaging. [Supported by the ORNL Spallation Neutron Source, which is managed by UT-Battelle, LLC, under contract DE-AC05-00OR22725 for the U.S. Department of Energy.]

6:40

4aPAc24. Stability and simulations of pulsating contrast agents. Nikos A. Pelekasis (Dept. Mechanical Engineering, University of Thessaly, Pedion Areos, 38334 Volos, Greece, pel@uth.gr), Kostas Tsiglifis (Dept. Mechanical Engineering, University of Thessaly, Pedion Areos, 38334 Volos, Greece, kotsigl@uth.gr)

The encapsulating membrane of ultrasound contrast agents, UCA's, is treated as a viscoelastic thin shell whose deviation from linear Hookean behavior is modeled as a strain softening or strain hardening effect via a parameter measuring the degree of membrane softness. As the amplitude of sound increases it controls the shift in resonance frequency until it hits the forcing frequency in which case an abrupt increase in the microbubble response takes place. Only strain softening shells exhibit this behavior. Deviations from sphericity are modeled via an additional parameter, namely the scalar bending modulus. This parameter controls static buckling of the shell, the onset of parametric instability and dynamic buckling. In this fashion phase diagrams can be constructed for a specific UCA that map regions of subharmonic growth of shape modes. Stability analysis and numerical simulations are employed in order to capture the onset, growth and break-up or saturation of shape modes. The above two parameters are added to the area dilatation modulus and viscosity of the membrane in order to construct a model that can be used to design new agents that behave optimally in different diagnostic or therapeutic modalities.

7:00

4aPAc25. Acoustic characterization of an ultrasound surgical transmitter in the linear and nonlinear regime of working. Antonio Petosic (Faculty of Electrical Engineering and Computing, Unska 3, 10000 Zagreb, Croatia, antonio.petosic@fer.hr), Bojan Ivančević (Faculty of Electrical Engineering and Computing, Unska 3, 10000 Zagreb, Croatia, bojan.ivancevic@fer.hr), Dragoljub Svilar (Brodarski Institut, Avenija Većeslava Holjevca bb, 10000 Zagreb, Croatia, dsvilar@hrbi.hr)

The method for measurement of a derived acoustic power of an ultrasound surgical transducer has been suggested in the free field conditions. The pressure field of the transmitter, immersed in depth of quater wavelength and vibrating at the fundamental frequency (≈25kHz), has been measured with calibrated hydrophone at different excitation levels. In the linear regime, the transmitter has been theoretically described as an acoustic dipole, the source parameters have been found and good agreement between theoretical and experimental results is obtained. When transmitter is excitated at higher excitation levels, the nonlinear behaviour in loading medium appears, with strong cavitation activity. In the averaged power spectrum of the recorded acoustic pressure signal, is evident the presence of harmonics (n·f), subharmonics (f/q), ultraharmonics (n·f/q) of excitation frequency. The spatial pressure distribution of each discrete frequency component in the free acoustic field has been measured and its contribution to total acoustic power has been calculated. The total acoustic power in the cavitation noise signal is estimated integrating the averaged pressure power spectrum with appropriate contributions of each frequency component in the signal.

Session 4aPPa

Psychological and Physiological Acoustics: General Topics in Psychological and Physiological Acoustics IV

Elizabeth Strickland, Cochair
Purdue University, 500 Oval Drive, West Lafayette, IN 47907, USA

Armin Kohlrausch, Cochair
Philips Research Europe, Digital Signal Processing (MS WO02), High Tech Campus 36, Eindhoven, 5656 AE, Netherlands

Alain De Cheveigne, Cochair
CNRS, Universite Paris 5, Ecole Normale Superieure, 29 rue d'Ulm, Paris, 75230, France

Contributed Papers

8:00

4aPPa1. Circumaural transducer arrays for binaural synthesis. Raphaël Greff (A-Volute, 4120 route de Tournai, 59500 Douai, France, raphael.greff@a-volute.com), Brian F. Katz (LIMSI-CNRS, B.P. 133, 91403 Orsay, France, brian.katz@limsi.fr)

Binaural cues such as the interaural time and level differences are the primary cues for estimation of the lateral position of a sound source, but are not sufficient to determine elevation or the exact position on the ″cone of confusion″. Spectral content of the head-related transfer function (HRTF) provides cues that permit this discrimination, notably high frequency peaks and notches created by diffraction effects within the pinnae. For high quality binaural synthesis, HRTFs need to be individualized, matching the morphology of the listener. Typical means for this are to measure or calculate the HRTF of the listener, but these lengthy and costly methods are not feasible for general public applications. This paper presents a novel approach for HRTF individualization, separating the head and torso effect from that of the pinnae. The head/torso component is numerically modelled while the pinnae component is created using a multiple transducer array placed around each pinna. The philosophy of this method consists in trying to excite the correct localization cues provided by the diffraction of the reconstructed wave front on the listener's own pinnae. Simulations of HRTF reconstruction with various array sizes and preliminary auditory localization tests are presented.

8:20

4aPPa2. Interaural-time-difference sensitivity to acoustic temporally-jittered pulse trains. Matthew J. Goupell (Austrian Academy of Science / Acoustics Research Institute, Wohllebengasse 12-14, 1040 Vienna, Austria, matt.goupell@gmail.com), Piotr Majdak (Austrian Academy of Science / Acoustics Research Institute, Wohllebengasse 12-14, 1040 Vienna, Austria, piotr@majdak.com), Bernhard Laback (Austrian Academy of Science / Acoustics Research Institute, Wohllebengasse 12-14, 1040 Vienna, Austria, Bernhard.Laback@oeaw.ac.at)

Bandpass-filtered pulse trains in acoustic hearing have been used to understand the high-rate pulse trains used in electrical stimulation strategies. In a left-right discrimination test, sensitivity to interaural time differences (ITD) in 600-pulses-per-second (pps) periodic pulse trains and aperiodic (temporally-jittered) pulse trains was tested with six normal-hearing listeners. It was found that jitter significantly and systematically increased ITD performance. A second experiment using 1200-pps pulse trains was performed to show that listeners were not solely benefiting from the longest interpulse intervals and thus the instances of reduced rate by adding jitter. To better understand the effect of jitter, the output of a basilar membrane model and a higher-level physiologically-based model was observed. Results from the modeling were reminiscent of an effect called ″release from binaural adaptation″ where the binaural system is reactivated by a temporal irregularity and this release possibly occurs at the level of the cochlear nucleus or lower. These results help understand pulse-rate limitations of ITD in cochlear-implant listeners.

8:40

4aPPa3. From sounds to melodies: Memory for sequences of pitch and loudness. Marion Cousineau (CNRS UMR 8158; Univ. Paris Descartes; Ecole Normale Supérieure, 29 rue d'Ulm, 75005 Paris, France, mcousineau@ens.fr), Daniel Pressnitzer (CNRS UMR 8158; Univ. Paris Descartes; Ecole Normale Supérieure, 29 rue d'Ulm, 75005 Paris, France, Daniel.Pressnitzer@ens.fr), Laurent Demany (CNRS UMR 5227; Univ. Victor Segalen, 146 rue Léo Saignat, 33076 Bordeaux, France, laurent.demany@psyac.u-bordeaux2.fr)

In order to understand speech or appreciate music, listeners have to process and remember patterns of sounds that vary along many perceptual dimensions. Here we investigated the perception of pitch sequences and loudness sequences, using a psychophysical method that uncouples discriminability and memory capacity. Pitch could be produced by either resolved or unresolved harmonics. Random sequences were constructed for which a single attribute (pitch or loudness) could take only two different values. These values were selected individually for each participant to produce equal discriminability (d') for isolated sounds. The participants then had to perform Same-Different judgments on pairs of sequences of two, four or eight elements each. We found that performance decreased rapidly with the number of elements for the loudness and pitch of unresolved harmonics conditions. With sequences of four and eight elements, performance was markedly better for the pitch of resolved harmonics condition. These findings show that short-term auditory memory capacity changes with the type of attribute that is varied within a sequence. For pitch, resolved harmonics yield a higher capacity than do unresolved harmonics; this could explain part of the difficulties encountered by cochlear implant users when listening to music.

9:00

4aPPa4. Local-pitch identification accuracy depending on the trajectory of frequency-modulated tones. Yuki Hiruma (School of Media Science, Tokyo Univ. of Technology, 1404-1 Katakuracho, Hachioji, 192-0982 Tokyo, Japan, m01043572a@mss.teu.ac.jp), Kiyoaki Aikawa (School of Media Science, Tokyo Univ. of Technology, 1404-1 Katakuracho, Hachioji, 192-0982 Tokyo, Japan, aik@media.teu.ac.jp)

Local-pitch identification accuracies were analyzed for frequency-modulated (FM) tones. The problem was whether every portion of a continuous sound was perceived at the same accuracy or not. Psychophysical experiments revealed that the local-pitch identification accuracies were significantly different among the nodes of continuous FM tones. Also, the accuracies were dependent on the frequency trajectory shape. The stimuli included two types of piecewise-linear FM tones of up-down-up and down-up-down glide sequences. Each tone had four nodes; the initial, two intermediate points, and the final. The duration of each linear glide was 100 ms. The frequency range was between 1000 and 1500 Hz. A pair of FM tone was presented with one-second interval. The frequency was shifted up or down at one of the nodes in either of the tones. The shift amounts were 0%,

4%, and 8%. The subjects were requested to answer whether two pitch sequences were the same or different. The pitch identification accuracy was low at the initial for both types of FM tones. The accuracy at the final was highest for the up-down-up tone. The intermediate high frequency node showed the highest accuracy for the down-up-down tone. These results indicated that the local-pitch identification accuracies were trajectory-dependent.

9:20

4aPPa5. Pitch discrimination: Combination of information across frequency. Hedwig E. Gockel (MRC CBU, 15 Chaucer Rd., CB2 7EF Cambridge, UK, hedwig.gockel@mrc-cbu.cam.ac.uk), Robert P. Carlyon (MRC CBU, 15 Chaucer Rd., CB2 7EF Cambridge, UK, bob.carlyon@mrc-cbu.cam.ac.uk), Christopher J. Plack (Psychology Department, Lancaster University, LA1 4YF Lancaster, UK, c.plack@lancaster.ac.uk)

Performance (d') for fundamental frequency (F0) discrimination was measured for two complex tones (A and B) presented either individually or simultaneously. The objective was to investigate how information is combined in pitch processing. For most subjects, tones A and B were filtered from 1350-1650 and 3300-4200 Hz, respectively, such that both contained only unresolved components (components were added in sine phase). The tones had identical nominal F0s of 75 Hz, and the difference in F0 between the two intervals of a 2AFC trial was the same for A and B. When A and B were tested individually, performance was equal for the two tones (d' value ~ 1). For some subjects, to achieve equal d' for the two tones, all components were added in alternating phase, F0 was increased to 90 Hz, and tones A and B were filtered from 1375-1875 and 3900-5400 Hz, respectively. Presenting the tones simultaneously should increase d' by a factor of 1.41, if information from both were combined optimally. The results showed no increase in d' above that measured for the individual tones for three subjects, and only a very small improvement for another three subjects (factor of about 1.1) [supported by EPSRC Grant EP/D501571/1].

9:40

4aPPa6. The role of compression in forward masking by Schroeder-phase complexes. Magdalena Wojtczak (University of Minnesota, Department of Psychology, 75 E. River Road, Elliott Hall N218, Minneapolis, MN 55455, USA, wojtc001@umn.edu), Andrew J. Oxenham (University of Minnesota, Department of Psychology, 75 E. River Road, Elliott Hall N218, Minneapolis, MN 55455, USA, oxenham@umn.edu)

Waveforms with flat temporal envelopes can produce more forward masking than waveforms with more modulated, or peakier, temporal envelopes after auditory filtering, even when the rms amplitude of the two waveforms is equal. This has been explained in terms of basilar-membrane nonlinearity, which can result in a higher rms amplitude for the flatter than for the peakier temporal waveform after compression. Here, forward masking was measured as a function of the phase curvature of two Schroeder-phase complexes, one with components around the signal frequency (on-frequency masker) and the other with components well below the signal frequency (off-frequency masker). The experiment tested the hypothesis that since the basilar-membrane response to the off-frequency complex at the signal-frequency place is presumably linear, masking should not depend on the phase curvature of the complex, whereas compression of the on-frequency masker should produce phase-dependent thresholds, with the minimum corresponding to the peakiest internal representation of the masker. The results replicate prominent phase effects using on-frequency maskers, but also show some phase effects with off-frequency maskers, which are not predicted by our current understanding of basilar-membrane compression. Other possible influences, such as efferent effects and neural compression, are considered. [Supported by NIH grant R01DC03909].

10:00

4aPPa7. Additivity of auditory masking using Gaussian-shaped tones. Bernhard Laback (Austrian Academy of Science / Acoustics Research Institute, Wohllebengasse 12-14, 1040 Vienna, Austria, Bernhard.Laback@oeaw.ac.at), Peter Balazs (Austrian Academy of Science / Acoustics Research Institute, Wohllebengasse 12-14, 1040 Vienna, Austria, peter.balazs@oeaw.ac.at), Gwenael Toupin (Austrian Academy of Science / Acoustics Research Institute, Wohllebengasse 12-14, 1040 Vienna, Austria, toupin@kfs.oeaw.ac.at), Thibaud Necciari (CNRS-LMA, 31, chemin Joseph Aiguier, 13402 Marseille, France, necciari@lma.cnrs-mrs.fr), Sophie Savel (CNRS-LMA, 31, chemin Joseph Aiguier, 13402 Marseille, France, savel@lma.cnrs-mrs.fr), Sabine Meunier (CNRS-LMA, 31, chemin Joseph Aiguier, 13402 Marseille, France, meunier@lma.cnrs-mrs.fr), Solvi Ystad (CNRS-LMA, 31, chemin Joseph Aiguier, 13402 Marseille, France, ystad@lma.cnrs-mrs.fr), Richard Kronland-Martinet (CNRS-LMA, 31, chemin Joseph Aiguier, 13402 Marseille, France, kronland@lma.cnrs-mrs.fr)

Both temporal and spectral masking have been studied extensively in the literature. Mostly, they have been regarded as separate phenomena. Very little is known about the interaction between these two effects, i.e. masking in the time-frequency domain. Data on the time-frequency spread of masking evoked by a single Gaussian-shaped tone pulse are presented in an accompanying study at the same conference (Necciari et al.). The current study gathers data on the additivity of masking by up to four, approximately equally effective Gaussian maskers (ERB=600 Hz), separated either along the time or the frequency axis. For temporal separation, the amount of masking increases with the number of maskers, with excess masking (exceeding linear additivity) of up to 25 dB. For frequency separation (preliminary data) excess masking amounts up to 15 dB, and the higher-frequency masker (relative to the target) contributes more to the additivity than the lower-frequency maskers. Experiments with multiple maskers combining both temporal and frequency separation are underway. Combined with the single maker data, these data may serve as a basis for modeling time-frequency masking effects in complex signals. Work partly supported by OEAD (WTZ project AMADEUS) and ANR

10:20-10:40 Break

10:40

4aPPa8. Auditory masking using Gaussian-windowed stimuli. Thibaud Necciari (CNRS-LMA, 31, chemin Joseph Aiguier, 13402 Marseille, France, necciari@lma.cnrs-mrs.fr), Sophie Savel (CNRS-LMA, 31, chemin Joseph Aiguier, 13402 Marseille, France, savel@lma.cnrs-mrs.fr), Sabine Meunier (CNRS-LMA, 31, chemin Joseph Aiguier, 13402 Marseille, France, meunier@lma.cnrs-mrs.fr), Solvi Ystad (CNRS-LMA, 31, chemin Joseph Aiguier, 13402 Marseille, France, ystad@lma.cnrs-mrs.fr), Richard Kronland-Martinet (CNRS-LMA, 31, chemin Joseph Aiguier, 13402 Marseille, France, kronland@lma.cnrs-mrs.fr), Bernhard Laback (Austrian Academy of Science / Acoustics Research Institute, Wohllebengasse 12-14, 1040 Vienna, Austria, Bernhard.Laback@oeaw.ac.at), Peter Balazs (Austrian Academy of Science / Acoustics Research Institute, Wohllebengasse 12-14, 1040 Vienna, Austria, peter.balazs@oeaw.ac.at)

This study investigates auditory masking with Gaussian-windowed tones as target and masker stimuli. On the purpose of developing a time-frequency masking model, such stimuli minimize the time-frequency uncertainty. Also, as proposed by van Schijndel *et al.* (1999), they activate a single spectro-temporal observation window of the auditory system. The study presented here measured auditory masking with Gaussian-windowed stimuli with an ERB of 600 Hz and an effective duration of 9.6 ms. The masker was centered at 4 kHz. Its level was 60 dB SL. Four experiments were conducted. (1) Absolute thresholds for Gaussian-windowed and 300-ms-sinusoidal targets were measured and compared for 11 frequencies. (2) Masking patterns were obtained with targets of various frequency separations from the masker. (3) Forward masking functions with 4-kHz targets were measured at 5 temporal separations. (4) Forward masking was measured for different frequency separations between masker and target. These data are compared with those typically obtained with stimuli that are broader either in the frequency or time domain. A modelling attempt is made. A companying article

on multiple masker additivity based on the present results is presented at the same conference (Laback *et al.*). *Work partly supported by EGIDE (PAI Amadeus) and the ANR.*

11:00

4aPPa9. Gaussian-noise discrimination as a tool to investigate auditory object formation. Tom L. Goossens (Technische Universiteit Eindhoven, Den Dolech 2, 5600 MB Eindhoven, Netherlands, tomgoos@gmail.com), Steven Van De Par (Philips Research Europe, Digital Signal Processing (MS WO02), High Tech Campus 36, 5656 AE Eindhoven, Netherlands, steven.van.de.par@philips.com), Armin Kohlrausch (Philips Research Europe, Digital Signal Processing (MS WO02), High Tech Campus 36, 5656 AE Eindhoven, Netherlands, armin.kohlrausch@philips.com)

In the present study we show that, in a same/different experiment, listeners are good at discriminating 50-ms Gaussian-noise tokens with a spectral range of 350-850 Hz. However, when an identical 200-ms noise fringe, with the same statistical properties as the 50-ms target tokens, is appended to both target tokens, listeners show very poor discrimination performance. Apparently, these identical fringes cannot be ignored and these extra non-informative fringes impair the discrimination of the target tokens. It seems that a target token and the appended fringe form one auditory object and that access to subparts of these tokens is not possible. When a perceptual cue is introduced that can lead to the segregation of the target token and noise fringe, e.g., a temporal gap between target and fringe, the ability to discriminate improves implying that the non-informative noise can be (partly) ignored when it is part of a different auditory object than the target token. This method is used as a new approach to investigate the influence of cues such as spectral range, level, interaural level difference, and interaural time delay, on the formation of auditory objects.

11:20

4aPPa10. Evidence for Poisson processes in change detection. Christian Kaernbach (Institut für Psychologie, Universität Kiel, Olshausenstr. 62, 24098 Kiel, Germany, chris2008@kaernbach.de)

Comparisons between two stimuli (e.g., ″which stimulus was louder?″) and change detection (″same or different?″) are often assumed to operate on the same decision basis. In the Gaussian signal detection theory, each of the two stimuli to be compared is transformed into a number, and the comparison is then made between these two numbers. If both stimuli are well above absolute threshold, the numbers to be compared have to be large, which motivates the use of normal distributions. The present study tests this assumption by measuring same-different ROC curves for the detection of small changes in the intensity of sinusoids. In contrast to previous studies, change detection was measured not only when the possible direction of change was a priori unknown, but also in two conditions where changes had a fixed direction. The obtained ROCs are asymmetric. This points to Poisson processes with low means. Moreover, the sensitivity to increments was significantly higher than the sensitivity to decrements. The results put into question the Gaussian theory of sensory comparisons and change detection.

11:40

4aPPa11. Low level auditory processing of simple and complex sounds in autism. Anna C. Bonnel (McGill University, Faculty of Educational and Counselling Psychology, 3700 McTavish Street, Montreal, QC H3A1Y2, Canada, anna.bonnel@mail.mcgill.ca), Stephen McAdams (Centre for Interdisciplinary Research in Music Media & Technology (CIRMMT) - Schulich School of Music - McGill Univ., 555 Sherbrooke Street West, Montreal, QC H3A1E3, Canada, smc@music.mcgill.ca), Bennett K. Smith (Centre for Interdisciplinary Research in Music Media & Technology (CIRMMT) - Schulich School of Music - McGill Univ., 555 Sherbrooke Street West, Montreal, QC H3A1E3, Canada, bennett.smith@music.mcgill.ca), Armando Bertone (McGill University, Faculty of Educational and Counselling Psychology, 3700 McTavish Street, Montreal, QC H3A1Y2, Canada, armando.bertone@mcgill.ca), Jake A. Burack (McGill University, Faculty of Educational and Counselling Psychology, 3700 McTavish Street, Montreal, QC H3A1Y2, Canada, jake.burack@mcgill.ca), Valter Ciocca (University of British Columbia, School of Audiology and Speech Sciences, 5804 Fairview Avenue (J.M. Mather Building), Vancouver, AB V6T 1Z3, Canada, vvciocca@audiospeech.ubc.ca), Laurent Mottron (Pervasive Developmental Disorders Clinic, Riviere-des-Prairies Hospital and Fernand Seguin Research Center, University of Montreal, Montreal, QC H3C 3J7, Canada, mottronl@istar.ca)

The documented dissociation between enhanced and diminished auditory processing performance in autistic listeners may be linked to the neural complexity required to process auditory stimuli. To test this hypothesis, four discrimination experiments were designed targeting pitch, spectral envelope, vocal timbre, and loudness. A range of pure- and complex-tone stimuli, with or without frequency or amplitude modulation, varied along spectral and temporal dimensions. An adaptive procedure was used to assess the auditory discrimination thresholds of groups of high-functioning participants with autism (HFA), Asperger syndrome (ASP), and typically developing individuals (TDs). Our research question was whether increasing the level of spectral and/or temporal complexity would have a detrimental impact on autistic listeners' ability to discriminate between acoustic stimuli. Preliminary results suggest that auditory discrimination performance of the latter group is not as dependent on levels of spectro-temporal complexity as originally predicted. The results will be interpreted in the context of current perceptually based models of enhanced and diminished perceptual functioning in autism.

12:00

4aPPa12. Roughness detection in fricative-like noise and tone stimuli. Jonathan Pincas (University of Surrey, GU2 7XH Guildford, UK, jon@pincas.co.uk), Philip J. Jackson (University of Surrey, Centre for Vision, Speech and Signal Processing, GU2 7XH Guildford, UK, p.jackson@surrey.ac.uk)

Audio (spectral) and modulation (envelope) frequencies both carry information in a speech signal. While low modulation frequencies (2-20Hz) convey syllable information, higher modulation frequencies (80-400Hz) allow for assimilation of perceptual cues, e.g., the roughness of amplitude-modulated noise in voiced fricatives, considered here. Psychoacoustic 3-interval forced-choice experiments measured AM detection thresholds for modulated noise accompanied by a tone with matching fundamental frequency at 125Hz: (1) tone-to-noise ratio (TNR) and phase between tone and noise envelope were varied, with silence between intervals; (2) as (1) with continuous tone throughout each trial; (3) duration and noise spectral shape were varied. Results from (1) showed increased threshold (worse detection) for louder tones (40-50dB TNR). In (2), a similar effect was observed for the in-phase condition, but out-of-phase AM detection appeared immune to the tone. As expected, (3) showed increased thresholds for shorter tokens, although still detectable at 60ms, and no effect for spectral shape. The phase effect of (2) held for the short stimuli, with implications for fricative speech tokens (40ms-100ms). Further work will evaluate the strength of this surprisingly robust cue in speech.

12:20

4aPPa13. Measurement of equal-loudness contours using eardrum pressure as reference signal. Sebastian Schmidt (Institute of Communication Acoustics, Ruhr-Universität Bochum, IC 1/142, Universitätsstr. 150, 44780 Bochum, Germany, sebastian.schmidt@rub.de), Herbert Hudde (Institute of Communication Acoustics, Ruhr-Universität Bochum, IC 1/142, Universitätsstr. 150, 44780 Bochum, Germany, herbert.hudde@rubr-uni-bochum.de)

Equal-loudness contours represent the relationship of loudness perception and sound pressure at the ear. Usually, the reference pressure is defined with a standardised calibration procedure. Individual ear canal characteristics significantly influence the contours, resulting in peaks and notches. By

choosing the eardrum pressure as reference for the perception measurements, individual ear canal features are cancelled, when loudness and pressure are related. Thus, flatter contours can be achieved. Finite-element simulations of the sound field in the canal have shown that signals at remote positions may differ significantly from the eardrum pressure. Thus, to achieve eardrum related measurements, it is necessary to insert probe microphones sufficiently deep into the canal. However, the desired signal has to be estimated from a distance, since measurements directly at the drum are not practical. A method is shown to determine both the probe tip distance and the transformation terms to calculate the drum pressure estimate. In this contribution, the results of equal-loudness contour measurements are discussed. The positioning and transformation processes are verified by simulations with one-dimensional and finite-element models and experiments.

THURSDAY MORNING, 3 JULY 2008 ROOM 242A, 8:40 A.M. TO 7:00 P.M.

Session 4aPPb

Psychological and Physiological Acoustics: General Topics in Psychological and Physiological Acoustics V

Elizabeth Strickland, Cochair
Purdue University, 500 Oval Drive, West Lafayette, IN 47907, USA

Armin Kohlrausch, Cochair
Philips Research Europe, Digital Signal Processing (MS WO02), High Tech Campus 36, Eindhoven, 5656 AE, Netherlands

Alain De Cheveigne, Cochair
CNRS, Universite Paris 5, Ecole Normale Superieure, 29 rue d'Ulm, Paris, 75230, France

Contributed Papers

8:40

4aPPb1. A fast FFT-based integral-equation solver for simulation of elastoacoustic wave propagation in human head. Elizabeth Bleszynski (Monopole Research, 739 Calle Sequoia, Thousand Oaks, CA 91360, USA, elizabeth@monopoleresearch.com), Marek Bleszynski (Monopole Research, 739 Calle Sequoia, Thousand Oaks, CA 91360, USA, marek@monopoleresearch.com), Thomas Jaroszewicz (Monopole Research, 739 Calle Sequoia, Thousand Oaks, CA 91360, USA, tomek@monopoleresearch.com)

We describe formulation, implementation, and representative applications of a fast integral-equation solver for modeling wave propagation in inhomogeneous visco-elastic and visco-acoustic media (e.g. in biological tissues). The present approach is an extension of our work on fast integral equation solvers in pure acoustics. It is based on Lippmann-Schwinger (L-S) integral equations. It incorporates: (i) FFT-based compression of the stiffness matrix and the corresponding fast iterative method resulting in the solution complexity proportional to the number of unknowns, and ability to solve problems of several million unknowns, (ii) piecewise-linear basis functions supported on tetrahedra, representing displacement field, and corresponding efficient algorithms for evaluation of Galerkin matrix elements, (iii) rigorous two-stage solution scheme applicable to scatterers composed of high contrast materials and consisting of transforming the L-S equations into a system of two well-conditioned problems (conventional solution schemes, when applied to such scatterers, lead to stiffness matrix of large condition number). We present applications of the developed approach to simulation of elastic wave propagation in realistic models of the human head, with the goal of comparing sound transmission through the normal auditory airways and through bone conduction, and in the presence and absence of noise-protective devices. This work is supported by the Air Force Office of Scientific Research.

9:00

4aPPb2. Towards a transfer function used to adjust audio for bone-conduction transducers. Raymond M. Stanley (Georgia Institute of Technology, Georgia Tech, School of Psychology, 654 Cherry St, Atlanta, GA 30332-0170, USA, rms@gatech.edu),Bruce N. Walker(Georgia Institute of Technology, Georgia Tech, School of Psychology, 654 Cherry St, Atlanta, GA 30332-0170, USA, bruce.walker@psych.gatech.edu)

Bone-conduction transducers may effectively replace normal air-conduction headphones in cases where the ears need to be plugged, or else remain unoccluded. However, sounds designed to be presented via air conduction need to be adjusted to maintain optimal perception via bone conduction. This study sought to find bone-to-air amplitude and phase shifts, as preliminary data for a complete transfer function between the bone-conduction and air-conduction pathway. The variability or stability of the shift data can indicate the feasibility of making effective adjustments to sounds to account for the bone-conduction pathway. Listeners cancelled air-conducted and bone-conducted tone pairs by method of adjustment at three frequencies (500, 3150, and 8000 Hz). The amplitude adjustments were relatively consistent, while the phase adjustments were quite variable. Further analysis revealed that the variability in phase adjustments came from differences between people, but were relatively consistent within a person. Together, these data suggest that generalized adjustments for the bone-conduction pathway may not be effective, but that individualized adjustments may be both necessary and potentially quite effective. These results can be extended to continuous transfer functions applied to sounds before they are presented via bone-conduction transducers (″bonephones″) in an auditory display.

9:20

4aPPb3. Variability of hearing protection devices attenuation as a function of source location. Hugues Nelisse (IRSST, Service de la recherche, 505 Boulevard de Maisonneuve O, Montréal, QC H3A3C2, Canada, hugnel@irsst.qc.ca), Marc-André Gaudreau (École de Technologie Supérieure, Département de Génie Mécanique, 1100, rue Notre-Dame Ouest, Montreal, QC H3C 1K3, Canada, gaudream@cdrummond.qc.ca), Jérémie Voix (École de Technologie Supérieure, Département de Génie Mécanique, 1100, rue Notre-Dame Ouest, Montreal, QC H3C 1K3, Canada, jvoix@jerevox.com), Jérôme Boutin (IRSST, Service de la recherche, 505 Boulevard de Maisonneuve O, Montréal, QC H3A3C2, Canada, jerbou@irsst.qc.ca), Frédéric Laville (École de Technologie Supérieure,

Département de Génie Mécanique, 1100, rue Notre-Dame Ouest, Montreal, QC H3C 1K3, Canada, Frederic.Laville@etsmtl.ca)

It is of common knowledge, and well documented, that laboratory-measured noise attenuation values of most hearing protection devices (HPD) exceed significantly the attenuation values obtained in real-world workplace environments. Various reasons may explain such discrepancies (lack of training, wearing time, lack of comfort, bad fitting, noise environments, etc.) but very few of them have been studied in details due to the complexity of the problem. This study focuses on the variability of the attenuation of HPDs as a function of the location of the noise source. Laboratory measurements were performed where subjects, wearing a HPD and facing a loudspeaker, were asked to rotate slowly on a rotating chair to simulate different angular positions of the head relative to the source. The protected and unprotected sound pressure signals for both ears were recorded as time signals using miniature microphones placed respectively inside and outside the HPD (F-MIRE technique). The microphones signals were processed to obtain attenuation values for the different angular positions. Results for different type of HPD (ear-muffs and ear-plugs) are presented and discussed.

9:40

4aPPb4. Assessment of exposure to impulsive and continuous noise by auditory brainstem response. Jan Zera (Centr. Inst. for Labour Prot. - Natl. Res. Inst., Czerniakowska 16, 00-701 Warsaw, Poland, jazer@ciop.pl), Krzysztof Kochanek (The Institute of Physiology and Pathology of Hearing, Pstrowskiego 1, 01-943 Warsaw, Poland, k.kochanek@ifps.org.pl), Adam Pilka (The Institute of Physiology and Pathology of Hearing, Pstrowskiego 1, 01-943 Warsaw, Poland, a.pilka@ifps.org.pl), Rafal Mlynski (Centr. Inst. for Labour Prot. - Natl. Res. Inst., Czerniakowska 16, 00-701 Warsaw, Poland, rmlynski@ciop.pl)

The aim of the work was to measure the wave V latency or thresholds in the auditory brainstem responses (ABRs) produced by impulsive and continuous noise. A forward-masking paradigm was used in which the ABR was evoked by a 4-kHz tone pip. The tone pip was masked by a preceding 201-ms or 501-ms interval of click trains or band-pass noise presented at various levels. The inter-click interval ranged from 20 ms (50 clicks/s) to 100 ms (10 clicks/s). The center frequencies of the noise bands ranged from 250 to 4000 Hz. Results show that changes in wave V latency may be used as an indicator of the equivalence of the effect of various kinds of noise on the human auditory system. [Work supported by the Polish Ministry of Science and Higher Education, grant 4T07B00428].

10:00

4aPPb5. Evaluation of auditory processing disorder and auditory efferent system functionality in adult dyslexics: towards a unification theory of auditory-language processing impairments? Michel Hoen (Laboratoire d'Etude des Mécanismes Cognitifs (EMC). EA 3082 CNRS, Université Lumière Lyon 2, 5, Avenue Pierre Mendès-France, 69676 Bron Cedex, France, Michel.Hoen@univ-lyon2.fr), Claire Grataloup (Laboratoire Dynamique du Langage (DDL), UMR 5596 CNRS, Université de Lyon et Lyon 2, Institut des Sciences de l'Homme - 14 avenue Berthelot, 69363 Lyon Cedex 07, France, Claire.Grataloup@pse.unige.ch), Evelyne Veuillet (Univ. Lyon 1 - Lab. Neurosciences, Service Pr Collet, Pavillon U, Hôpital Edouard Herriot, F-69003 Lyon, France, iakhoun@olfac.univ-lyon1.fr), Hung Thai-Van (Univ. Lyon 1 - Lab. Neurosciences, Service Pr Collet, Pavillon U, Hôpital Edouard Herriot, F-69003 Lyon, France, iakhoun@olfac.univ-lyon1.fr), Lionel Collet (Univ. Lyon 1 - Lab. Neurosciences, Service Pr Collet, Pavillon U, Hôpital Edouard Herriot, F-69003 Lyon, France, iakhoun@olfac.univ-lyon1.fr), Fanny Meunier (Laboratoire Dynamique du Langage (DDL), UMR 5596 CNRS, Université de Lyon et Lyon 2, Institut des Sciences de l'Homme - 14 avenue Berthelot, 69363 Lyon Cedex 07, France, fanny.meunier@univ-lyon2.fr)

In a recent paper, Veuillet et al., (2007) suggested that some auditory processing mechanism could be impaired in children with dyslexia. They reported a link between children's ability to perceive phonemic boundaries and the physiological functionality of their medial olivocochlear system (MOC), an auditory efferent pathway functioning under central control. In the present experiment, we extended this observation by comparing speech-in-speech comprehension performances in a group of control participants (N=40) and a group of adults who had been diagnosed dyslexic as children (N=49). Confirming the idea that patients with dyslexia present auditory processing disorders (APD), we show that adult dyslexics exhibit greater difficulty in comprehending speech in noise. Data moreover suggest a link between speech-in-noise comprehension difficulty and the MOC functionality in these participants. More precisely, it appears that the absolute functionality of the left and right MOC bundles does not differ in dyslexic patients compared to controls. What appears to be differing is the functional asymmetry in the MOC functionality between both ears, normal readers showing a classical functional asymmetry, while dyslexic adults show an absence of, or reduced functional asymmetry between MOC bundles. These results will be discussed in the context of current models of APD and Dyslexia.

10:20-10:40 Break

10:40

4aPPb6. Training of English vowel perception by Finnish speakers to focus on spectral rather than durational cues. Maria Uther (Brunel University, School of Social Sciences, UB8 3PH Uxbridge, UK, maria.uther@brunel.ac.uk), Sari Ylinen (Cognitive Brain Research Unit, University of Helsinki, PO BOX 9, 00014 Helsinki, Finland, sari.ylinen@helsinki.fi), Antti Latvala (Cognitive Brain Research Unit, University of Helsinki, PO BOX 9, 00014 Helsinki, Finland, antti.latvala@helsinki.fi), Reiko Akahane-Yamada (ATR Promotions, Human Information Sciences Laboratory, -2-2 Hikaridai Keihanna Science City, Seika-cho, Soraku-gun, 619-0288 Kyoto, Japan, yamada@atr.jp), Paul Iverson (University College London, Department of Phonetics and Linguistics, 4, Stephenson Way, NW1 2HE London, UK, p.iverson@ucl.ac.uk)

This study used the High-Variability Phonetic Training (HVPT) technique to train Finnish speakers to distinguish English vowels. It was found that Finnish speakers tend to use durational cues (which are phonemically relevant in their own language) to make a vowel category distinction rather than the relevant spectral cues. We used duration-modified stimuli with a HVPT program to 'force' the use of spectral cues. We focused on the /i/ (as in 'feet') vs /I/ (as in 'fit') vowel contrast and tested behavioural performance using a perceptual identification task. We also measured the Mismatch negativity (MMN) component of auditory event-related potential (ERP) before and after the training to look at changes in brain responses. The worst pre-test performance was for the 'modified duration' condition (i.e. where the learner had no choice but to rely on spectral cues). There were also asymmetries in vowel perception in both behavioural and MMN tasks, with the detection of /i/ being more difficult compared to the detection of /I/. Nevertheless, training did result in marked improvement of the most problematic contrasts for Finnish speakers.

11:00

4aPPb7. Effects of voice familiarity and age on perceptual organization of sound from two competing talkers. Ingrid S. Johnsrude (Queen's University, Dept Psychology, 62 Arch Street, Kingston, ON K7L 3N6, Canada, ingrid.johnsrude@queensu.ca), Allison Mackey (The Rotman Research Institute, Baycrest, 3560 Bathurst Street, 938, Toronto, ON M6A 2E1, Canada, allison.mackey@hotmail.com), Elizabeth M. Alexander (Queen's University, Dept Psychology, 62 Arch Street, Kingston, ON K7L 3N6, Canada, 3ema@queensu.ca), Heather Macdonald (Queen's University, Dept Psychology, 62 Arch Street, Kingston, ON K7L 3N6, Canada, hpmacdonald@gmail.com), Robert P. Carlyon (MRC CBU, 15 Chaucer Rd., CB2 7EF Cambridge, UK, bob.carlyon@mrc-cbu.cam.ac.uk)

We used the Coordinate Response Measure (CRM) procedure (Bolia et al, 2000) to examine whether a non-acoustic characteristic of speech -voice familiarity- can affect a listener's ability to separate competing voices. We tested 27 listeners, aged 45-79, with their spouse's and two novel voices (other listeners' spouses). Couples had been living together at least 18 years. On each trial, two different talkers produced two of four callsigns (one being the target 'Baron'), two of four colours and two of eight numbers, and the participant responded by indicating the colour-number combination to which 'Baron' was told to go. We tested three conditions: spouse-voice target phrase with a novel-voice masker phrase (F/N); novel-voice target with

spouse-voice masker (N/F); novel-voice target with (different) novel-voice masker (N/N). Compared to N/N, performance was significantly better in F/N, and, crucially, N/F conditions, indicating that listeners can exploit learned characteristics of a masking voice to help them track a novel voice. Furthermore, whereas the younger participants (under 60) benefited from having a familiar voice as target or as masker, the older group (over 60) benefited only when the familiar voice was the focus of attention, suggesting that the ability to use voice familiarity to segregate sounds changes with age.

11:20

4aPPb8. Detection threshold and prominence of background music with interfering speech. Mark M. Houben (TNO, Kampweg 5, P.O. Box 23, 3769 ZG Soesterberg, Netherlands, mark.houben@tno.nl)

Spoken radio and television messages are often accompanied by background music. When automating identification of broadcast music for handling copyright exploitation, it may be questioned to what extent music at very low sound levels should be taken into account. Should it just be perceivable by listeners who attend to the speech, or should the music be present more prominently? We studied detection and level of prominence of music with interfering speech. For this, Dutch radio and television broadcasts were recorded and speech fragments without background music were selected. To the fragments, music was added with various level differences between speech and music. Subjects were presented with these stimuli and answered a random generic question about the speech after each stimulus. As a second task, the prominence of the background music had to be scored on a scale (including 'not present'). Results show that, on average, 50% of the music is detected if the level of the music is 45 dB lower than the speech. A threshold based on a criterion of 'moderate prominence' results in a level difference of 26 dB. This level happens to coincide with a detection threshold of 95%.

11:40

4aPPb9. Emotion and meaning in interpretation of sound sources. Penny Bergman (Chalmers University of Technology, Division of Applied Acoustics - Chalmers Room Acoustics Group, Sven Hultins gata 8a, 41296 Gothenburg, Sweden, penny@chalmers.se), Daniel Vastfjall (Chalmers University of Technology, Division of Applied Acoustics - Chalmers Room Acoustics Group, Sven Hultins gata 8a, 41296 Gothenburg, Sweden, daniel.vastfjall@psy.gu.se), Niklas Fransson (Chalmers University of Technology, Division of Applied Acoustics, Sven Hultinsgata 8a, 41296 Gothenburg, Sweden, niklas.fransson@psy.gu.se), Anders Sköld (Chalmers University of Technology, Division of Applied Acoustics, Sven Hultinsgata 8a, 41296 Gothenburg, Sweden, anders.skold@chalmers.se)

Research regarding the perception of sound focuses in large on the acoustical properties of the sound. We argue that, for a more complete picture of sound perception, one must take the non-physical properties into account. By changing the emotional descriptor of a sound the perception in terms of level of annoyance will change. The present study investigates how a priming picture placing the origin of the sound in either a positive or negative environment affects the level of annoyance to same sound. Three different sounds were used in the experiment, all based on pink noise. The participants were, in the beginning of each sound, exposed to a picture telling where the sound originated. The picture was either a positive environment (a picture of a waterfall) or a negative environment (a picture of a larger factory). While listening to the sounds the participants completed different performance tasks. In the end of each sound the participants rated the level of annoyance. Results show that the annoyance ratings are significantly lower when primed with a positive picture. Results also indicate that for more attention demanding tasks this correlation is stronger. The findings are discussed in relation to theories of sound perception.

12:00

4aPPb10. Fast Detection for Natural Animal Sounds. Clara Suied (CNRS - UPMC UMR 7593, Pavillon Clérambault, Hôpital de la Salpêtrière, 47, Bd de l'Hôpital, 75013 Paris, France, clara.suied@ircam.fr), Marie Magnin (IRCAM - UMR CNRS 9912, Equipe Perception et Design Sonores, 1 place Igor Stravinsky, 75004 Paris, France, magnin.marie@gmail.com), Sabine Langlois (Renault, 1 avenue du golf, 78288 Guyancourt, France, sabine.langlois@renault.com), Patrick Susini (IRCAM - UMR CNRS 9912, Equipe Perception et Design Sonores, 1, place Igor Stravinsky, 75004 Paris, France, susini@ircam.fr), Stephen McAdams (Centre for Interdisciplinary Research in Music Media & Technology (CIRMMT) - Schulich School of Music - McGill Univ., 555 Sherbrooke Street West, Montreal, QC H3A1E3, Canada, smc@music.mcgill.ca)

Human listeners seem remarkably good at identifying complex and natural sounds. Relatively little attention, however, has been paid to the simple detection of such sounds. The present experiments measured the time course of sound detection in human listeners. Two categories of sounds were used: a train of 1-kHz pure tone pulses varying along an Inter Onset Interval dimension (termed here ″IOI″ sounds) and animal call sound samples. All sounds were equalized in loudness in a preliminary experiment. The task consisted of a simple reaction time, in which listeners were presented with interleaved IOI and animal sounds and had to manually press a button as fast as possible when they heard any stimulus. Two main results were observed. First, reaction times were significantly shorter for IOIs of 50, 33 and 25 ms than for an IOI of 100 ms, with no significant differences between IOIs of 33 and 25 ms, highlighting a threshold at 33 ms. Second, average reaction times were significantly shorter for animal sounds than for IOI sounds. Differences in terms of spectral content and temporal modulation characteristics might explain part of these effects. These results also suggest a fast detection advantage for natural animal sounds.

12:20-2:00 Lunch Break

Contributed Papers

2:00

4aPPb11. The effect of postural information on the perceived velocity of moving sound sources. Shuichi Sakamoto (R.I.E.C., Tohoku University, 2-1, Katahira, Aoba-ku, 980-8577 Sendai, Japan, saka@ais.riec.tohoku.ac.jp), William L. Martens (McGill University, Schulich School of Music, 555 Sherbrooke Street West, Montreal, QC H3A 1E3, Canada, wlm@music.mcgill.ca), Yôiti Suzuki (R.I.E.C., Tohoku University, 2-1, Katahira, Aoba-ku, 980-8577 Sendai, Japan, yoh@ais.riec.tohoku.ac.jp)

In this study, the effect of postural information on the perceived velocity of moving sound sources was investigated. Auditory information was presented via five surround speakers and five subwoofers. Two sounds were presented first in front of participants, and then these moved past them toward the rear. At the same time, rearward pitch motion was presented via a motion platform on which participants were situated. Duration of stimulus was 8 s. Initial distance of sound sources was set to 2.0, 4.0, 6.0, 8.0 and 10.0 m. Amplitude of pitch variation was 0, 0.2, 0.4, 1.0 and 2.0 degrees. Participants made magnitude estimates for speed of moving sound images, and judgment of goodness of movement matching between both auditory and postural information. The resulting speed magnitude estimates showed that pivot magnitude significantly affected the estimated velocity of sound sources except when velocity of sound sources was extremely high. Moreover, participants judged the multimodal match to be poor when the velocity of the moving sound sources was extremely high or low. These results suggest that the strongest multimodal interaction occurs when auditory information and postural variation are well matched, and are consistent with self motion.

2:20

4aPPb12. Auralization of an orchestra with phase-shifted string sections. Michelle C. Vigeant (Univ. of Nebraska - Lincoln, Architectural Eng. Program, 1110 S. 67th St., Omaha, NE 68182-0681, USA, michelle.vigeant@gmail.com), Lily M. Wang (University of Nebraska - Lincoln, 1110 S. 67th St., Omaha, NE 68182-0681, USA, LWang4@UNL.edu)

Orchestra auralizations have been created in ODEON using multi-channel individual instrument anechoic recordings of two symphonies; however, only one or two string instruments were recorded to represent each string section. To simulate the chorus effect of an entire string section more accurately, the anechoic tracks of the single string instruments have been mixed with other versions of the same signal, each with some phase shift in time. Two groups of phase shifts were used: one with shorter delays of up to 23 ms, and one with longer delays of up to 47 ms. A maximum of seven differently phase-shifted signals were combined with the original to create a final anechoic recording for use in the auralizations, depending on the number of players each source represented. Using paired comparisons, test subjects were asked to identify the auralization that sounded most similar to the experience of listening to an orchestra in an actual concert hall: one having none, short or long phase-shifts. Results show that subjects have difficulty differentiating between these three types of auralizations, indicating that phase shifting may not be required for such multi-source multi-channel orchestra auralizations. [Work supported by the National Science Foundation.]

2:40

4aPPb13. Individual differences in auditory localization of real sources in the horizontal plane. Sophie Savel (CNRS-LMA, 31, chemin Joseph Aiguier, 13402 Marseille, France, savel@lma.cnrs-mrs.fr)

Recent studies on spatial hearing showed that individual variability is greater with virtual sources than with real ones, but that sensorial feedback provides an efficacious and rapid learning procedure. This study evaluated the degree of inter-individual variability with real sound sources in the absence of feedback. Fifty normal-hearing listeners, aged 18-62, either left- or right handed, participated. The experiment was conducted in an anechoic room. One of twelve loudspeakers placed in the frontal horizontal plane and hidden by a curtain emitted a train of low-pass pulses. Listeners had to indicate the estimated direction of that source by placing a pointer on a screen. No feedback was given to them. Each listener completed 480-720 trials. Results indicated that variability between individual was great in both resolution in bias. Precisely, individuals differed (1) in the size of their maximum error, (2) in the azimuthal region in which this maximum error occurred, and (3) in the spatial symmetry of their performance. Indeed, 25% of the listeners showed significant left-right differences in their performance, these differences always favoring the left side of space. Such asymmetries have been noticed earlier but attributed to greater front-back confusions on the right, which cannot explain the present results.

3:00

4aPPb14. Investigating effects of spatially disparate visual stimuli on auditory localization in VR environments. Khoa-Van Nguyen (IRCAM, 1 Place Igor Stravinsky, 75004 Paris, France, nguyen@ircam.fr), Clara Suied (CNRS - UPMC UMR 7593, Pavillon Clérambault, Hôpital de la Salpêtrière, 47, Bd de l'Hôpital, 75013 Paris, France, clara.suied@ircam.fr), Isabelle Viaud-Delmon (CNRS - UPMC UMR 7593, Pavillon Clérambault, Hôpital de la Salpêtrière, 47, Bd de l'Hôpital, 75013 Paris, France, ivd@ext.jussieu.fr), Olivier Warusfel (IRCAM, 1 Place Igor Stravinsky, 75004 Paris, France, Olivier.Warusfel@ircam.fr)

Investigating the time and spatial constraints under which visual and auditory stimuli are perceived as a unique percept or as spatially coincident has been a topic of numerous researches in neuroscience. However, these findings have been derived up to now in extremely simplified stimulation context consisting in the combination of elementary auditory and visual stimuli usually displayed in dark and anechoic conditions. The present experiment is conducted in a VR environment using a stereoscopic passive screen and binaural audio rendering. Auditory stimuli are displayed on headphones using individualized head-related transfer functions and visual stimuli are integrated in a visual background in order to convey visual perspective. The experiment investigates the effect of a spatially disparate visual stimulus on the auditory localization judgments (crossmodal bias), as well as the relation between the magnitude of the crossmodal bias and the perception of a unified bi-modal stimulus. The present study will indicate whether previous findings (Hairston et al., Journal of Cognitive Neuroscience, 2003) still hold in more complex audio-visual contexts such as those offered by VR environments.

3:20

4aPPb15. The Role of Auditory-Visual Integration in Object Recognition. Clara Suied (CNRS - UPMC UMR 7593, Pavillon Clérambault, Hôpital de la Salpêtrière, 47, Bd de l'Hôpital, 75013 Paris, France, clara.suied@ircam.fr), Nicolas Bonneel (REVES/Inria Sophia-Antipolis, 2004 route des lucioles, BP 93, FR-06902 Sophia Antipolis, France, Nicolas.Bonneel@sophia.inria.fr), Isabelle Viaud-Delmon (CNRS - UPMC UMR 7593, Pavillon Clérambault, Hôpital de la Salpêtrière, 47, Bd de l'Hôpital, 75013 Paris, France, ivd@ext.jussieu.fr)

Combining auditory and visual information about the same external event enhances perception and behavioural performance. Numerous factors have been shown to contribute to the integration of visual and auditory stimuli, like spatial or semantic relationships between the two stimuli. We studied the influence of spatial disparity between the auditory and the visual stimuli on bimodal object recognition in a go/no-go task, under realistic virtual environment. Participants were asked to react as fast as possible to a target object, presented in the visual and/or the auditory modality, and to inhibit a distractor object. Reaction times were significantly shorter for semantically congruent bimodal stimuli than would be predicted by independent processing of information about the auditory and the visual targets. Moreover, reaction times were significantly shorter for semantically congruent bimodal stimuli (i.e. visual and auditory targets) than for semantically incongruent bimodal stimuli (i.e. target represented in only one sensory modality). Importantly, these results were not altered by a large spatial disparity between the auditory and the visual targets. Altogether our findings suggest that rules governing multisensory integration vary according to the purpose for which auditory and visual stimuli are combined.

3:40-5:20 Posters

Lecture sessions will recess for presentation of poster papers on various topics in acoustics. See poster sessions for topics and abstracts.

5:20

4aPPb16. Why is sharp-limited low-frequency noise extremely annoying? Detlef Krahé (Univ. of Wuppertal, Rainer-Gruenter-Str. 21, 42119 Wuppertal, Germany, krahe@uni-wuppertal.de)

Sharp-limited low-frequency noise having only weak components of higher frequencies, such as noise of an air condition or traffic noise attenuated by a thick window, has a very annoying effect on persons also at low levels. The strong fluctuation, which is specific to this kind of sound, is a frequently used explanation for this effect possibly caused by adaptation in the inner ear. Another or additional explanation could be a strong synchronism in the activities on the nerve fibers. Computer models of the auditory system show this synchronism. If some components at higher frequencies are added, the synchronism disappears and the noise is judged less uncomfortable. This raises the question, if noise protection resulting in a sound as described can not be even counterproductive. Differently sharp-limited sounds are investigated by an auditory model. The results are compared with results of judgment by hearing.

5:40

4aPPb17. Comparison of subjective and objective evaluation methods for audio source separation. Josef Kornycky (I-Lab Multimedia and DSP Research Group, Centre for Communication Systems Research, University of Surrey, GU2 7XH Guildford, UK, J.Kornycky@surrey.ac.uk), Banu Gunel (I-Lab Multimedia and DSP Research Group, Centre for Communication Systems Research, University of Surrey, GU2 7XH Guildford, UK, B.Gunel@surrey.ac.uk), Ahmet Kondoz (I-Lab Multimedia and DSP Research Group, Centre for Communication Systems Research, University of Surrey, GU2 7XH Guildford, UK, A.Kondoz@surrey.ac.uk)

The evaluation of audio separation algorithms can either be performed objectively by calculation of numerical measures, or subjectively through listening tests. Although objective evaluation is inherently more straightforward, subjective listening tests are still essential in determining the perceived quality of separation. This paper aims to find relationships between objective and subjective results so that numerical values can be translated into perceptual criteria. A generic audio source separation system was modelled which provided varying levels of interference, noise and artifacts. This enabled a full spread of objective measurement values to be obtained. Extensive tests were performed utilising the output synthesised by this separation model. The relationships found were presented and the factors of prime importance were determined.

6:00

4aPPb18. An exploration of attentional monitoring of isochronous asynchronous streams in deviant detection and sensorimotor synchronization. Martine Turgeon (Lancaster University, Psychology Department, Fylde College, LA1 4YF Lancaster, UK, m.turgeon@lancaster.ac.uk)

Past studies of auditory selective attention focused on location and/or pitch cues in stream segregation. In this study, two perceptually-segregated streams competed for attention in a perceptual-judgment task based on timbre cues and a sensorimotor task (tapping to the sounds of one stream). Both streams shared the same temporal structure (isochronous 100-ms events at 1.67 Hz) but were asynchronous (target-distractor asynchronies of -200, -100, 100, 200 ms), differed in pitch (712 or 1000 Hz) and could share or not their perceived location (diotic vs. dichotic). Deviants were amplitude modulated at 25 or 50 Hz and varied in temporal envelopes. Attentional filtering (distracting stream constant) was done using a discrimination task requiring pressing one of two keys upon hearing one of two deviants (Experiment 1) and a synchronization task requiring selective tapping to the high-pitch or low-pitch sounds (Experiment 3). Attentional monitoring (distracting stream varies) required maintaining attention to the same stream upon hearing slow-modulated deviants and switching attention to the other stream upon hearing the fast-modulated deviants. This was done for the discrimination task (Experiment 2) and synchronization task (Experiment 4). Perceptual and perceptuo-motor results suggest attentional-filtering and attentional-monitoring costs. Surprisingly, the mere presence of a non-concurrent stream in a different frequency band interferes with deviant-discrimination and synchronization-tapping performance.

6:20

4aPPb19. Normalization in count-comparison model of interaural time difference decoding. Ville Pulkki (Helsinki University of Technology, P.O .Box 5400, 02015 TKK, Finland, Ville.Pulkki@tkk.fi)

Recent neurophysical studies suggest that binaural decoding is based on count comparison for both ITD and ILD. In such mechanisms, the neural signals are stronger in the auditory pathways leading to the ipsilateral hemisphere when a signal is presented earlier, or with higher level, to the contralateral ear. A computational model is described implementing binaural cue decoding based on count-comparison principles for ITD decoding, which is assumed to occur in medial superior olive (MSO). Pooled response of MSO is modeled as running multiplication between inputs, which are derived from ear canal signals with GTFB filtering and phase-locked impulse generator. The contralateral and ipsilateral inputs to MSO are then convolved with different responses. The model output corresponds well to neurophysiological results. In the earlier version of the model, the MSO output was normalized only with the contralateral signal, as suggested by the neuroanatomy. It has been later found out that the output of MSO model depends on ILD, which is in contradiction with psychoacoustics studies. In this study, it is proposed that the ipsilateral input to MSO is self-normalized, which provides ILD-independent ITD decoding.

6:40

4aPPb20. Representation of Harmonic Sounds in the Helix of the Lateral Lemniscus. Gerald Langner (Neuroacoustics, TUD, Zool. Institut, Schnittspahnstr. 3, 64287 Darmstadt, Germany, gl@bio.tu-darmstadt.de), Claudia Simonis (Schnittspahnstr. 3, 64287 Darmstadt, Germany, simonis@bio.tu-darmstadt.de), Antje Sauck (Schnittspahnstr. 3, 64287 Darmstadt, Germany, antjesalg@freenet.de), Ralf Galuske (Schnittspahnstr. 3, 64287 Darmstadt, Germany, galuske@mpih-frankfurt.mpg.de)

The percept of pitch of harmonic sounds is based on temporal processing. This explains also our ability to recognize harmonic relationships between different sounds, because as a result of a neuronal correlation analysis in the auditory midbrain neurons are tuned not only to a certain pitch but to a certain degree also to integer multiples of that pitch. The responses to harmonics of a pitch are suppressed within 30 ms after signal onset by inhibition with the likely source being the ventral nucleus of the lateral lemniscus (VNLL). An investigation of spatial representation of periodicity information with the 2-Deoxyglucose method in gerbils showed that low pitch is represented dorsally and high pitch ventrally along the length-axis of the VNLL. Three-dimensional computer reconstructions of the VNLL (program AMIRA) gave evidence for a helical periodicity map with 7 to 8 turns, reminiscent of the pitch helix known from music psychology. Moreover, the spatial organization of the VNLL suggests that it is organized as a double-helix representing musical octaves and fifths. Reconstructions of the VNLL of Nissl-stained human brains gave evidence of a similar organization and therefore of a similar functional role of the VNLL for pitch processing in humans.

Session 4aSAa

Structural Acoustics and Vibration, Computational Acoustics, and EURONOISE: Fluid—Structure Interaction II

Noureddine Atalla, Cochair
Univ. de Sherbrooke, Mechanical Engineering Depart., 2500 Boulevard de l'Université, Sherbrooke, QC J1K 2R1, Canada

Vicente Cutanda Henriquez, Cochair
Institute of Sensors, Signals and Electrotechnics, University of Southern Denmark, Niels Bohrs Allé 1, Odense S, 5230, Denmark

Stefan Schneider, Cochair
Laboratoire de Mécanique et d'Acoustique, UPR 7051 CNRS, 31,Chemin Joseph-Aiguier, Marseille, 13402, France

Contributed Papers

8:00

4aSAa1. Fluid-structure interaction and computational aeroacoustics of the flow past a thin flexible structure. Frank Schäfer (University Erlangen-Nuremberg, Institute of Fluid Mechanics, Cauerst. 4, 91058 Erlangen, Germany, frank.schaefer@lstm.uni-erlangen.de), Thomas Uffinger (University Erlangen-Nuremberg, Institute of Fluid Mechanics, Cauerst. 4, 91058 Erlangen, Germany, thomas.uffinger@lstm.uni-erlangen.de), Stefan Becker (University Erlangen-Nuremberg, Institute of Fluid Mechanics, Cauerst. 4, 91058 Erlangen, Germany, stefan.becker@lstm.uni-erlangen.de), Jens Grabinger (Univ. Erlangen-Nuremberg, Dept. of Sensor Technology, Paul-Gordan-Str. 3/5, 91052 Erlangen, Germany, jens.grabinger@lse.eei.uni-erlangen.de), Manfred Kaltenbacher (Univ. Erlangen-Nuremberg, Dept. of Sensor Technology, Paul-Gordan-Str. 3/5, 91052 Erlangen, Germany, manfred.kaltenbacher@lse.eei.uni-erlangen.de)

In many technical applications the interaction between a fluid flow and a thin flexible structure leads to the generation of acoustic noise which is caused by flow induced structural vibrations. Examples for such applications are coverings and panelings of cars and airplanes. In many cases the generated noise is unwanted so that noise reduction is a topic of major interest. In the present work we investigate the acoustic field resulting from the interaction of a thin flexible structure with a turbulent flow field by means of numerical simulation. Two different model configurations are considered: one is the flow over a flexible plate, in the second case the flexible plate is located in the wake of a square cylinder. The major aim of this work is to provide a better understanding of the noise generation processes in these flow cases. The numerical methodology applied is utilized for a decomposition of the acoustic field into one part generated by the structural vibrations and another part which is due to stream noise. Finally, comparisons to experimental data available at our institute are provided.

8:20

4aSAa2. An Equivalent-Acoustic Finite Element Method for Modeling Sound Absorbing Materials. Donald J. Nefske (General Motors R&D Center, Vehicle Development Research Laboratory, 30500 Mound Rd., Warren, MI 48090-9055, USA, DNefske@aol.com), Shung H. Sung (General Motors R&D Center, Vehicle Development Research Laboratory, 30500 Mound Rd., Warren, MI 48090-9055, USA, Shung.H.Sung@gm.com)

An equivalent-acoustic finite element method is developed for modeling sound absorbing materials, such as seats and interior trim in the automobile passenger compartment. The equivalent-acoustic method represents the sound absorbing material using acoustic finite elements with frequency-dependent material properties determined from the measured acoustic impedance of sound absorbing material samples. Solution of the equivalent-acoustic model within the Nastran computer capability and coupling of the model with an acoustic finite element model of a surrounding enclosure, such as the passenger compartment, are developed. The accuracy of the equivalent-acoustic method is assessed for modeling a sound absorbing material in a one-dimensional impedance tube, a foam layer in a rectangular box enclosure, and an automotive seat in a semi-reverberant enclosure.

8:40

4aSAa3. Finite element modelling of transient elastic wave propagation in an inhomogeneous anisotropic fluid/solid multilayer medium: A time-domain method. Guillaume Haiat (CNRS, Laboratoire de Recherches Orthopédiques, 10, Avenue de Verdun, 75010 Paris, France, haiat@univ-paris12.fr), Salah Naili (Université Paris 12, B2OA, 61, Avenue du Général de Gaulle, 94010 Créteil, France, naili@univ-paris12.fr), Quentin Grimal (Université Paris 6, Laboratoire d'Imagerie Paramétrique, 15, rue de l'Ecole de Médecine, 75006 Paris, France, quentin.grimal@lip.bhdc.jussieu.fr), Maryline Talmant (Université Paris 6, Laboratoire d'Imagerie Paramétrique, 15, rue de l'Ecole de Médecine, 75006 Paris, France, talmant@lip.bhdc.jussieu.fr), Christophe Desceliers (Université de Marne la Vallée, 5, Boulevard Descartes, 77454 Marne la Vallée, France, christophe.desceliers@univ-mlv.fr), Christian Soize (Université de Marne la Vallée, 5, Boulevard Descartes, 77454 Marne la Vallée, France, soize@univ-mlv.fr)

The axial transmission technique is used clinically for cortical bone assessment. However, ultrasonic propagation in this multiscale medium remains unclear, in particular because of the heterogeneous nature of cortical bone. The aim of this work is to evaluate the effect of spatial gradients of elastic moduli on the ultrasonic response of the bone structure. Therefore, a 2D finite element time-domain method is developed to simulate transient wave propagation in a three-layer medium constituted of an inhomogeneous transverse isotropic solid layer sandwiched between two acoustic fluid layers and excited by an acoustic linear source located in one fluid layer delivering broadband ultrasonic pulses. The model couples the acoustic propagation in both fluid media with the elastodynamic response of the solid. The conditions of continuity are used to model the fluid-structure interaction. A constant spatial gradient of material properties in the direction perpendicular to the layer is considered in the solid structure. In the presence of a gradient, the first arriving signal (FAS) velocity depends on the average material properties when the thickness is smaller than the wavelength (guided wave modes) whereas the FAS velocity depends on the velocity at the surface when the thickness is larger than the wavelength (lateral wave).

9:00

4aSAa4. Dynamic behavior analysis of vehicle acoustic trim using FEM. Norimasa Kobayashi (Toyota Motor Corporation, 1, Toyota-cho, 471-8572 Toyota, Aichi, Japan, koba@nori.tec.toyota.co.jp), Yoshihisa Uno (Toyota Motor Corporation, 1, Toyota-cho, 471-8572 Toyota, Aichi, Japan, yoshi@uno.tec.toyota.co.jp), Hiroo Yamaoka (Toyota Motor Corporation, 1, Toyota-cho, 471-8572 Toyota, Aichi, Japan, yamaoka@giga.tec.toyota.co.jp)

Multilayer vehicle acoustic trim containing poroelastic materials affects noise and vibration phenomena not only in the high-frequency range but also in the low and mid-frequency range. However, there are few established technology to analyze the vehicle model which includes the characteristics of the trim. In this paper, a methodology for the analysis of multilayer acoustic trim within a vehicle FEM model is derived based on Biot theory. Using this methodology, dynamic vibration, radiation and absorption behavior of three types of multilayer trim including conventional isolative type, absorptive type and isolative type with absorptive top layer backed by rectangular metal plates are analyzed. The trim model is also applied to a vehicle FEM model and its effects on interior sound pressure level are validated with experimental data.

9:20

4aSAa5. Noise reduction prediction of Ariane 5 fairing with acoustic protection made of porous-elastic material. Slaheddine Frikha (ESI France, 99 rue des Solets, Parc des affaires SILIC - BP 80112, 94513 Rungis, France, slaheddine.frikha@esi-group.com), Mohamed Ali Hamdi (ESI GROUP & UTC, 20, Rue Du Fonds Pernant, 60471 Compiègne, France, Mohamed-Ali.Hamdi@esi-group.com), Philippe Roux (CNES, Rond Point de L'Espace, 91 023 Courcouronnes, France, philippe.roux@cnes.fr), Lassen Mebarek (ESI GROUP & UTC, 20, Rue Du Fonds Pernant, 60471 Compiègne, France, Lassen.Mebarek@esi-group.com), Abderrazak Omrani (ESI GROUP & UTC, 20, Rue Du Fonds Pernant, 60471 Compiègne, France, Abderrazak.Omrani@esi-group.com)

ESI Group (Formerly STRACO) has been involved during the last two decades in the numerical prediction of noise reduction index of ARIANE 5 fairing. During the 1990's, STRACO developed an axi-symmetric, boundary element model of the fairing where the fairing protection made of distributed Helmholtz Resonator is modeled by equivalent local impedance. Recently, the fairing acoustic protection has been replaced by a foam-made insulator. Such porous materials are widely used by transportation industries to improve the payload acoustic comfort. In collaboration with automotive industry, ESI group developed RAYON-VTM, a powerful tool allowing the predicting of fully trimmed vehicle vibroacoustic response up to 500 Hz. RAYON VTM model the porous-elastic material using a 3D Finite Element (PEM), based on the Modified-Biot-Equations. This new module of RAYON software has been applied to predict the vibroacoustic response of the ARIANE 5 fairing allowing a detailed modeling of the acoustic protection. A fully 3-D model of the fairing has been developed. The results show the influence of intrinsic modeling of the porous-elastic protection as well as the influence of non-axi-symmetric details usually neglected in the axi-symmetric approach.

9:40

4aSAa6. Influence of solid phase elasticity in poroelastic liners submitted to grazing flows. Benoit Nennig (Université de Technologie de Compiègne, Lab. Roberval UMR 6253, Dept. Acoustique, BP 60319, 60203 Compiègne, France, benoit.nennig@utc.fr), Jean-Daniel Chazot (Université de Technologie de Compiègne, Lab. Roberval UMR 6253, Dept. Acoustique, BP 60319, 60203 Compiègne, France, jean-daniel.chazot@utc.fr), Emmanuel Perrey-Debain (Université de Technologie de Compiègne, Lab. Roberval UMR 6253, Dept. Acoustique, BP 60319, 60203 Compiègne, France, emmanuel.perrey-debain@utc.fr), Mabrouk Ben Tahar (Université de Technologie de Compiègne, Lab. Roberval UMR 6253, Dept. Acoustique, BP 60319, 60203 Compiègne, France, mabrouk.bentahar@utc.fr)

In the present work, we study the sound propagation in a duct treated with a poroelastic liner exposed to a grazing flow. Acoustic propagation in the liner and in the fluid domain is respectively governed by Biot's model and Galbrun's equation. Here, the coupling between Galbrun's and Biot's equation is carried out with a mixed pressure-displacement FE. On one hand, a mixed formulation is used in Galbrun's equation to avoid numerical locking. And on the other hand, in poroelastic media, the description of both phases involves the displacement of the solid phase and the pressure in the fluid phase. In addition of using the complete Biot's model, simplified models are also tested. A fluid equivalent model that does not take into account solid phase elasticity and a model that neglects only the shear stress are hence used. These two simplified models enable to evaluate the contributions of the compressional and shear waves in the solid phase. Finally, validity of each simplified model in the specific case of a liner exposed to a grazing flow is discussed for different materials.

10:00-10:20 Break

10:20

4aSAa7. An Evolutionary Optimization Method applied to Absorbing Poroelastic Systems. Francisco Silva (Unité de Mécanique (UME), ENSTA, Chemin de la Hunière, 91761 Palaiseau, France, francisco-ilson.dasilva@ensta.fr), Renato Pavanello (Depart. of Computational Mechanics - FEM - Unicamp, POBOX 6122, Rua Mendeleiev, s/n - Cidade Universitária, 13083-970 Campinas, Brazil, pava@fem.unicamp.br)

Poroelastic materials can be used in engineering applications such as: noise control of automobiles, acoustical insulation systems for aircrafts, industrial, environmental and domestic sound quality control, etc. The insulating systems must be as light as possible and the acoustic absorption in the low frequency domain must be maximized for certain gaps. Topology Optimization is frequently used to design structures and acoustic systems in a large range of engineering applications. In this work, we propose one method to maximize the absorbing performance of insulation poroelastic systems using a coupled finite element model and Evolutionary strategies. The goal is find the best distribution of poroelastic material on insulating systems. The absorbing performance of the poroelastic material samples in a Kundt tube is simulated using a coupled poroelastic and acoustic finite element model. The Biot-Allard Coupled Model is used to represent the foam material. The porous material model is coupled to a waveguide using a modal superposition technique. A sensitivity number indicating the optimum locations for porous material removing is derived and used in a numerical hard kill scheme. The sensitivity number is used to form an evolutionary poroelastic optimization (EPO) algorithm which is verified though numerical examples.

10:40

4aSAa8. Acoustic frequency wave propagation and fluid-loading in composite sandwich panels. Jennifer F. Crossley (Swansea University Engineering Department, Singleton Park, SA2 0DS Swansea, UK, 437441@swansea.ac.uk), Johann Sienz (Swansea University Engineering Department, Singleton Park, SA2 0DS Swansea, UK, J.Sienz@swansea.ac.uk)

Composite sandwich panels comprising glass fibre reinforced epoxy skins with nomex honeycomb cores have found application as aircraft interior fixtures and partitions. This is due to their low density combined with static strength and stiffness. In this complex acoustic and vibration environment however, the same properties can lead to unwanted sound transmission through the structure. We analyse, in this paper, fluid-loading of such a panel by an acoustic fluid using an elementary theory which has been developed in the study of structural dynamics and vibration, based on a generalisation of Timoshenko theory for homogeneous beams. The dispersion relations derived from this theory, with and without fluid-loading terms, are used to quantify the effect of fluid-loading by air on shear and flexural waves at acoustic frequencies in such stiff, lightweight structures. The most appropriate method of fluid-structure coupling to be applied in modelling an internal acoustic field enclosed by such a structure is discussed.

11:00

4aSAa9. A formulation based on modal optimization for predicting sound radiation from fluid-loaded aircraft structures. Olivier Collery (Airbus France - Acoustics and Environment Department, 316 route de Bayonne, F-31060 Toulouse Cedex 09, France, olivier.collery @insa-lyon.fr), Jean-Louis Guyader (INSA de Lyon - LVA, Bâtiment St. Exupéry, 25 bis avenue Jean Capelle, F-69621 Villeurbanne Cedex, France, jean-louis.guyader@insa-lyon.fr)

This study is led in the context of understanding sound transmission through fluid-loaded aircraft structures with non-uniform damping. The fluid/structure coupling is here highlighted. Classic approaches using modal radiation impedances to formulate the fluid/structure coupling do lead to complexity and are computationally time-consuming. A method defining rigorously this coupling and avoiding the calculation of the modal radiation impedances is proposed. This method aims at developing a simple formulation taking advantage of current technical progress in optimization algorithms. Sound radiation from a simply supported, baffled, fluid-loaded plate excited mechanically or acoustically is here solved in optimizing the modal amplitudes so that they fit the governing equation with fluid loading. To perform this optimization, a sampling of the plate into observation points is first done, then a modal decomposition into in vacuo modes is led. Comparison with results from the literature over [10-1000Hz] for 3 reference cases of steel plate immersed in air (critical frequencies equal to fC1=1 .2kHz and fC2=12kHz) show excellent agreement within 1dB. The simplicity and computation time allow an extension to non-uniform damped aircraft structures and a prediction over a large frequency band. As perspectives, results from multi-layered plates with a local damping patch are presented.

THURSDAY MORNING, 3 JULY 2008 ROOM 252B, 11:40 A.M. TO 7:00 P.M.

Session 4aSAb

Structural Acoustics and Vibration and EURONOISE: Distributed Active Noise and Vibration Control I

Kenneth Cunefare, Cochair
Woodruff School of Mech. Eng., The Georgia Inst. of Technol., Atlanta, GA 30332-0405, USA

Manuel Collet, Cochair
FEMTO-ST UMR CNRS, 23 chemin de l'Epitaphe, Besançon, 25000, France

Invited Papers

11:40

4aSAb1. Smart panels with active wedges. Paolo Gardonio (ISVR, University of Southampton, Highfield, SO17 1BJ Southampton, UK, pg@isvr.soton.ac.uk), Yohko Aoki (ISVR, University of Southampton, Highfield, SO17 1BJ Southampton, UK, ya@isvr.soton.ac.uk), Stephen J. Elliott (ISVR, University of Southampton, Highfield, SO17 1BJ Southampton, UK, sje@isvr.soton .ac.uk)

This paper presents an experimental study comparing the vibration and sound radiation control performance obtained from six different rectangular panels with various geometries of active wedge. Each panel is equipped with sixteen triangular piezoceramic actuators along the panel border and accelerometer sensors located at the top vertex of the triangular actuators. These sensor-actuator pairs are used to implement decentralized velocity feedback loops that produce active damping on the plate. The primary objective of this paper is to investigate the effect of the size and geometry of the triangular actuators on stability and control performance. Narrow frequency band measurements highlight that vibration reductions at the first few resonant frequencies are significantly improved by increasing the height of the triangular actuators. However, the increase of the height also results in spillover effects at frequencies higher than around 700Hz. In contrast, an increase of the base length of the triangular actuators improves the overall control performance up to 1 kHz without increasing the spillover effect.

12:00

4aSAb2. A new hybrid passive/active cell to realize a complex impedance boundary condition. Marie-Annick Galland (Centre Acoustique du LMFA, Ecole Centrale de Lyon, 36 avenue Guy de Collongue, 69134 Ecully cedex, France, marie-annick.galland@ec-lyon.fr), Jean-Baptiste Dupont (Centre Acoustique du LMFA, Ecole Centrale de Lyon, 36 avenue Guy de Collongue, 69134 Ecully cedex, France, jean-baptiste.dupont@ec-lyon.fr)

Hybrid passive/active cells previously developed at the LMFA have proved their efficiency for global noise reduction. A hybrid cell combines passive absorbent properties of a porous layer and active control at its rear face. Active control is mainly used to increase absorption at low frequencies by cancelling the imaginary part of the surface impedance presented by the absorber. A specific decentralized control algorithm allowed realizing large panels to reduce multi-tone noise radiated by a flow duct. Generally, the design of such absorbers starts by determining the optimal impedance for the targeted application, defined as that which, for each frequency, produces the highest reduction. However, in many cases results show that this optimal impedance is complex and that both real and imaginary parts are frequency dependent. This paper investigates the potential of a new hybrid absorber intended to realize any of impedance. The new cell uses one microphone on each side of a resistive cloth. Normal velocity can then be deduced by a simple pressure difference, which allows an easy synthesis of the error signal. First experiments carried out in a standing wave tube are described and different control strategies are examined, allowing us to validate this promising concept.

12:20

4aSAb3. The performance trade off of decentralised, distributed and centralised controllers. Oliver N. Baumann (Institute of Sound and Vibration Research, University of Southampton, Highfield, SO171BJ Southampton, UK, onb@isvr.soton.ac.uk), Kenneth Frampton (ISVR, University of Southampton, Highfield, SO17 1BJ Southampton, UK, kdf@soton.ac.uk), Paolo Gardonio (ISVR, University of Southampton, Highfield, SO17 1BJ Southampton, UK, pg@isvr.soton.ac.uk)

Direct velocity feedback control of structures is well known to increase structural damping and thus reduce vibration. In multichannel systems the way in which the velocity signals are used to inform the actuators ranges from decentralised controller through distributed or clustered controllers to the fully centralised controller. The objective of distributed controllers is to exploit the anticipated performance advantage of the centralised controller whilst maintaining the ease of implementation and robustness of the decentralised controller. It has been observed, however, that in many vibration control systems the centralised controller struggles to perform significantly better than a decentralised controller. This paper compares a number of distributed controllers and optimisation techniques for the reduction of kinetic energy and radiated sound power and identifies the conditions under which the centralised and distributed controllers offer a significant performance advantage.

12:40

4aSAb4. Reduced models for elastoacoustic problems with intelligent interfaces. Mohamed Ichchou (Centre Acoustique du LMFA, Ecole Centrale de Lyon, 36 avenue Guy de Collongue, 69134 Ecully cedex, France, mohamed.ichchou@ec-lyon.fr), Aida A. Kacem (Centre Acoustique du LMFA, Ecole Centrale de Lyon, 36 avenue Guy de Collongue, 69134 Ecully cedex, France, aida.hadj-kacem@ec-lyon.fr)

Effective and predictive noise and vibration modelling and design tools as well as efficient and high-performance materials are essential to produce world-leading products with regards to the noise and vibration quality. In one hand, the modern trend towards virtual design and prototyping requires good analysis and modelling tools in the entire noise frequency band. In another hand, new passive, adaptive or active materials offer improved technologies issues for the vibration and noise treatment. However, there is still a lack of efficient numerical tools in the low frequency band, and an absence of tools in the mid-frequency range. Moreover, although new materials potential can be demonstrated in prototype structures, their performances are still insufficient in integrated applications. To bring advances in noise and vibration treatment using new materials, the challenge is to be capable of supporting specific aspects related to advanced materials and virtual prototyping methods. An essential requirement for this is a multi-disciplinary analysis and coupled simulation tools where effects on a very different scale need to be interconnected. The paper proposes reduced models of elastoacoustic problems with localised intelligent interface. The main focus is development of fast simulation tool for the design of new systems. Theoretical as well as numerical experiments are offered in this work.

1:00-2:00 Lunch Break

Invited Papers

2:00

4aSAb5. Decentralised active control of single - frequency panel vibrations using piezoelectric actuator - sensor pairs. Alain Berry (Univ. de Sherbrooke, Mechanical Engineering Depart., 2500 Boulevard de l'Université, Sherbrooke, QC J1K 2R1, Canada, alain.berry@usherbrooke.ca), Philippe Micheau (Univ. de Sherbrooke, Mechanical Engineering Depart., 2500 Boulevard de l'Université, Sherbrooke, QC J1K 2R1, Canada, Philippe.Micheau@USherbrooke.ca), Rémi Louviot (Univ. de Sherbrooke, Mechanical Engineering Depart., 2500 Boulevard de l'Université, Sherbrooke, QC J1K 2R1, Canada, remi.louviot@usherbrooke.ca), Yvonnick Brunet (Univ. de Sherbrooke, Mechanical Engineering Depart., 2500 Boulevard de l'Université, Sherbrooke, QC J1K 2R1, Canada, yvonnick.brunet@usherbrooke.ca)

This paper addresses active control of the bending response of a panel using independent PZT (piezoceramic) actuator - PVDF (piezopolymer) sensor pairs distributed on the panel. Previous work showed that under the assumption of collocated, dual actuator - sensor pairs, decentralised static gain control is stable due to plant matrix passivity at all frequencies. However, duality is not guaranteed for collocated PZT - PVDF pairs because of the coupling of piezoelectric transducers with both bending and extensional modes of the panel. Moreover, the spatially local nature of PZT actuator to PVDF sensor transfers on the panel can lead to a diagonal - dominant FRF matrix but is detrimental to global control of the panel vibration or acoustic radiation; hence, a non-diagonal dominant plant matrix is more likely to result in global control for this problem. In the case of single-frequency disturbance, stability analysis shows that plant matrix passivity is only required at the disturbance frequency and that a phase - shift compensation, identical for all independent units, can ensure stable decentralized control. Guidelines for the design of decentralised PZT - PVDF pairs are provided, with the objective of global vibroacoustic control of a panel.

2:20

4aSAb6. Broad-Band Vibration Attenuation in Plates With Periodic Arrays of Shunted Piezoelectric Patches. Massimo Ruzzene (Georgia Institute of Technology, School of Aerospace Engineering, 270 Ferst Drive, Atlanta, GA 30332-0150, USA, massimo.ruzzene@ae.gatech.edu), Luca Airoldi (Dipartimento di Ingegneria Aerospaziale, Via La Masa 34, 20156 Milano, Italy, luca.airoldi@gmail.com)

Periodic arrays of shunted piezoelectric patches are employed for the control of waves propagating over the surface of plate structures. The shunted piezoelectric patches act as sources of impedance mismatch, which yield interference phenomena resulting from the interaction between incident, reflected and transmitted waves produced by the mismatch. The impedance mismatch corresponding to the shunted piezos can be tuned to achieve strong attenuation over frequency bands which are defined by the shunting circuit connected to the patches. Broad-band vibration attenuation can be achieved through the application of series and parallel of multiple resonant

circuits, or through the implementation of negative capacitance configurations. The ability of plates with periodic shunted piezoelectric patches to attenuate vibrations over extended frequency bands is demonstrated numerically, through Finite Element models of the considered electromechanical structures. The effect of number of patches and of their periodic distributions is investigated together with the analysis and the comparison of performance achieved with various shunting strategies.

2:40

4aSAb7. Use of head mounted microphone arrays for active control. Marty Johnson (Virginia Tech, Mechanical Engineering, 143 Durham 0238, Blacksburg, VA 24061, USA, martyj@vt.edu)

There has been an effort recently to create head mounted or user worn microphone arrays. These arrays pose challenges in their design and characterization but can be used for a number of different purposes. Initially these arrays were intended for sound source localization and natural hearing restoration (where the hearing of a user whose ears are obstructed by an encapsulating helmet or headset is restored). Once in place, and assuming the user is wearing headphones, these arrays can be used for a number of different applications including voice isolation for communication, focused listening and noise cancellation. Specifically this paper investigates the use of these arrays for the active control of noise both at the user's ears and in the communications/voice signals sent from the user. A numerical study, using both data generated numerically and experimentally, demonstrates that large reductions in noise can be achieved using adaptive active control methods.

3:00

4aSAb8. Active control of multimodal tonal noise propagated in circular duct with axial subsonic mean flow until M=0.3. Martin Glesser (CNRS - LMA, 31 Chemin Joseph Aiguier, 13009 Marseille, France, glesser@lma.cnrs-mrs.fr), Emmanuel Friot (Laboratory for Mechanics and Acoustics CNRS, 31 chemin Joseph Aiguier, 13009 Marseille, France, friot@lma.cnrs-mrs.fr), Muriel Winninger (CNRS - LMA, 31 Chemin Joseph Aiguier, 13009 Marseille, France, winninger@lma.cnrs-mrs.fr), Cédric Pinhède (CNRS - LMA, 31 Chemin Joseph Aiguier, 13009 Marseille, France, pinhede@lma.cnrs-mrs.fr), Alain Roure (CNRS - LMA, 31 Chemin Joseph Aiguier, 13009 Marseille, France, roure@lma.cnrs-mrs.fr)

As new generation of aircraft engine with lower blade passing frequency appeared in the 1990's, the fan tones radiated from the inlets had become one of the dominant source of sound. Efforts have then been made to develop active noise control. Encouraging results have been obtained but the physical limitation of the fan tones reduction have not been clearly determined, owing mainly to the complexity of the experimental rigs. This paper present an experimental investigation of the control of multimodal tonal noise propagated in circular duct in presence of a mean flow ($M \leqslant 0.3$). A laboratory wind tunnel has been implemented for this purpose. Two limiting factors for the sound reduction are underlined: (i) the degradation of the secondary transfer matrix conditioning as the number of propagating modes increases in the duct and (ii) the degradation of the hypothesis of the time-invariance of the system to control as the flow velocity is increased. The effect of those limiting factors on the control efficiency are evaluated.

Contributed Paper

3:20

4aSAb9. New prospects in implementing distributed control strategies for mechanical structures optimization. Manuel Collet (FEMTO-ST UMR CNRS, 23 chemin de l'Epitaphe, 25000 Besançon, France, manuel.collet@univ-fcomte.fr)

The research activities in the fields of smart materials and structures today are very important and represent a large potential for the technological innovations. New methods are now available which allow active transducers and their driving electronics to be directly integrated in otherwise passive structures. Today the main research challenge deals with the development of new multi-functional structures integrating their own electro-mechanical controlling systems. In the past few years, a technological revolution has occurred in the fields of integrated MEMS that offers new opportunities for smart structures design and optimization. By using such as integrated active or hybrid distributed set of electromechanical transducers, we could also control the material's intrinsic mechanical behavior for building new desired functionalities. We can also speak of ″integrated distributed smart structures″. Through two examples, this paper aims at showing what can be the main advantages in developing such of integrated distributed control strategies in comparison with passive and ″classical″ active systems. The adopted point of view takes also into consideration energy balance assessments, absolute efficiency and of course robustness. The first introduced example deals with the vibroacoustic impedance control of tube for wave power flow cancellation. The second one treats of the optimization of hybrid shunted piezoelectric distributed patches for mechanical power flow control.

3:40-5:20 Posters

Lecture sessions will recess for presentations of poster papers on various topics in acoustics. See poster sessions for topics and abstracts.

Contributed Papers

5:20

4aSAb10. Online adaptive distributed control of vibro-acoustic systems. Kenneth Frampton (ISVR, University of Southampton, Highfield, SO17 1BJ Southampton, UK, kdf@soton.ac.uk)

One of the primary difficulties in distributed, real-time vibro-acoustic control is the difficulty of high-bandwidth network communication of sensor data. The necessary communications rate has proven overwhelming to existing communications protocols. In order to overcome this limitations an adaptive control technique has been developed that requires only occasional inter-node communication of sensor data in order to maintain optimal performance. The technique is based on iterative feedback tuning (IFT) which has the advantage of not requiring a system model. In this system, each control node collects its sensor data over a period of time. The data is then communicated to other nodes in the system. Once a node has received the required sensor data the local adaptation algorithm is initiated. Local feedback gains are adjusted based on an estimate of the cost function gradient and the new control law is implemented until the next adaptation cycle. This work presents the theory behind this adaptive control technique and simulation results of the control performance are presented. It is demonstrated that this approach to distributed control can perform as well as model based optimal distributed control, and nearly as well as centralized control.

5:40

4aSAb11. Damping of a device with piezoelectric materials and negative capacitance electrical circuits. Christian S. Granger (IEMN, 41 boulevard Vauban, 59046 Lille, France, christian.granger@isen.fr), Anne-Christine Hladky (IEMN, UMR CNRS 8520, avenue Poincaré, BP 60069, 59652 Villeneuve d'Ascq, France, anne-christine.hladky@isen.fr), Jean-Claude Debus (IEMN, 41 boulevard Vauban, 59046 Lille, France, jean-claude.debus@isen.fr)

In this paper, the damping of a device is obtained by a transfer of the vibratory energy into electrical energy and then into thermal energy (dissipation in an electrical resistance). The transfer is carried out by using piezoelectric materials (PZT piezoelectric plates, macro fibre composite MFC) and it is improved by charging the piezoelectric materials by an electrical circuit having a negative capacitance impedance. Two devices are considered: a clamped plate, witch is a academic case, and a large aluminium plate (0.85m×0.78m×2mm). The optimal position and the geometry of the ceramics are determined using an analytical method and a numerical method with the help of the ATILA finite element code. The equivalent electrical circuit of the device is conceived. Damping of the device charged by the electrical circuits is measured using a laser vibrometer. Damping can be performed on a given frequency range, covering several bending modes, by using several ceramics on the plate and several external electrical circuits, connected to the active material. Finally, tests in an anechoic chamber show the efficiency of the device for the reduction of the noise transmitted through the plate.

6:00

4aSAb12. Decentralized control of sound radiation using a high-authority/low-authority control strategy with anisotropic actuators. Noah H. Schiller (NASA Langley Research Center, 2 North Dryden Street, Hampton, VA 23681, USA, noah.h.schiller@nasa.gov), Randolph H. Cabell (NASA Langley Research Center, 2 North Dryden Street, Hampton, VA 23681, USA, randolph.h.cabell@nasa.gov), Chris R. Fuller (Virginia Tech, 131 Durham Hall, Blacksburg, VA 24061, USA, christopher.r.fuller@nasa.gov)

This paper describes a combined control strategy designed to reduce sound radiation from stiffened aircraft-style panels. In particular, the control approach uses robust active damping in addition to high-authority LQG control. Active damping is achieved using direct velocity feedback with triangularly shaped strain actuators and point velocity sensors [P. Gardonio and S.J. Elliott, JASA 117(4), 2046-2064 (2005)]. However unlike previous work, anisotropic actuators are used since they outperform traditional isotropic actuators in this application. While active damping is simple and robust, stability is guaranteed at the expense of performance. Therefore, this approach is often referred to as low-authority control. In contrast, LQG control strategies can achieve substantial reductions in sound radiation. Unfortunately, the unmodeled interaction between neighboring control units can destabilize decentralized control systems. Numerical simulations show that combining active damping and decentralized LQG control can be mutually beneficial. In particular, augmenting the in-bandwidth damping supplements the performance of the LQG control strategy and reduces the destabilizing interaction between neighboring control units. Therefore, the performance of the combined system can be better than the sum of each individual strategy.

6:20

4aSAb13. An impedance matching technique for active-passive vibration control. Jonas L. Svensson (Chalmers University of Technology, Division of Applied Acoustics, SE-41296 Gothenburg, Sweden, jonas.svensson@chalmers.se), Patrik B. Andersson (Chalmers University of Technology, Division of Applied Acoustics, SE-41296 Gothenburg, Sweden, patrik.andersson@chalmers.se), Wolfgang Kropp (Chalmers University of Technology, Division of Applied Acoustics, SE-41296 Gothenburg, Sweden, wolfgang.kropp@chalmers.se)

Impedance matching techniques have shown potential for active vibration control of structures in bending. Such structures are commonly described by Euler-Bernoulli theory. Previous studies concerning impedance matching of these structures have only considered scalar quantities. However, for an Euler-Bernoulli beam four field variables are involved which implies that a scalar impedance is insufficient. The purpose of this study is therefore to expand the technique to include full 2x2 matrices. This is achieved by first deriving the reflection matrix as a function of the characteristic impedance matrices of an Euler-Bernoulli beam and an arbitrary termination impedance. An active impedance load is then introduced in order to manipulate the reflection matrix. A theoretical example is given where the approach is utilized to match the junction between an Euler-Bernoulli beam and a sandwich composite. This proposed active-passive damping configuration employs active control to enclose all incident power in the sandwich composite. Results show that the active impedance load is responsible for the main part of the power absorption over a broad frequency range.

6:40

4aSAb14. Hybrid Foams for passive/active control of transmission loss of panels. Morvan Ouisse (FEMTO-ST UMR CNRS, 23 chemin de l'Epitaphe, 25000 Besançon, France, morvan.ouisse@univ-fcomte.fr), Manuel Collet (FEMTO-ST UMR CNRS, 23 chemin de l'Epitaphe, 25000 Besançon, France, manuel.collet@univ-fcomte.fr)

Absorbing materials are widely used in transport industry. Classical foams can efficiently improve transmission loss of panels, but only in the higher frequency range. For the lower part of the frequency range, structural active control can be a good strategy to reduce the vibratory level and induced noise. Trying to take advantage of those two points is the objective of the development of hybrid foams. Many practical and scientific aspects are related to their design: which passive material should be used? Which active material, and what shapes should be better? In order to understand the basics of the hybrid foams, some specific multiphysics models are developed, including vibro-acoustic modelling of foams, coupled with elasto-dynamics for structural parts and piezo-elastic models for active parts. The objective of the strategy is to try to take advantage of distributed actuators within the foam in order to modify the energy transmission path. The physical strategy is presented in the paper, together with the full description of the model, with numerical results. The main difficulty for the numerical part is the very high number of degrees of freedom which are required by the model. Some model reduction strategies are then investigated.

Session 4aSCa

Speech Communication: Acoustics of Speech Production: Aeroacoustics and Phonation

David A. Berry, Cochair
The Laryngeal Dynamics Laboratory, Division of Head & Neck Surgery, David Geffen School of Medicine at UCLA, 31-24 Rehab Center, 1000 Veteran Ave., Los Angeles, 90095-1794, USA

Xavier Pelorson, Cochair
Département Parole & Cognition, GIPSA-lab, 46, avenue Félix Viallet, Grenoble Cedex, 38031, France

Invited Papers

8:40

4aSCa1. Implications of the fluctuating drag force voice source. Richard S. McGowan (CReSS LLC, 1 Seaborn Place, Lexington, MA 02420, USA, rsmcgowan@earthlink.net), Michael S. Howe (College of Engineering, Boston Univ., 110 Cummington Street, Boston, MA 02215, USA, mshowe@bu.edu)

A recently published paper on the aeroacoustics of the voice source calculates the acoustic source of voice caused by fluctuation drag forces [Howe, M. S. and McGowan, R. S., J. Fluid Mech., 592, 367-92]. There are two extensions to this calculation that will be presented: 1) inclusion of the ventricular folds downstream of the vocal folds, and 2) the fluid-structure interaction at the vocal folds. For the ventricular folds, the effect of tissue shape on the drag forces will be investigated in terms of the shape's effect on the relation between the Lamb vector and the Kirchoff vector. Regarding the fluid-structure interaction at the vocal folds, the two-mass model will be examined in light of the recently published calculation of drag forces. [Work supported by grant NIDCD-004688 to Dr. G. S. Berke of UCLA.]

9:00

4aSCa2. Investigation of the mechanisms of voicing offset. Anna Barney (ISVR, Univ. of Southampton, SO17 1BJ Southampton, UK, ab3@soton.ac.uk), Luis Jesus (Escola Superior de Saúde da Universidade de Aveiro, Universidade de Aveiro, Campus Universitário de Santiago, 3810-193 Aveiro, Portugal, lmtj@ua.pt), Ricardo Santos (Escola Superior de Saúde da Universidade de Aveiro, Universidade de Aveiro, Campus Universitário de Santiago, 3810-193 Aveiro, Portugal, ricardo.santos@ua.pt)

During voiced speech the source of sound production arises from the vibrations of the vocal folds within the larynx. In order to terminate these vibrations it is necessary either to adduct the vocal folds to produce a forced closure or to reduce the pressure drop across them to below a threshold level. A reduction in pressure drop might be achieved by reducing the sub-glottal pressure, by increasing the supra-glottal pressure or by abduction of the folds. Two human subjects were asked to achieve phonation offset by each of these strategies in turn. Acoustic and EGG signals measured on the subjects were compared with the output of a simple theoretical vocal fold model. A further comparison was made with corresponding signals recorded during the production of selected short phrases by a European Portuguese speaker; a language where devoicing of both vowels and voiced consonants is particularly prevalent.

9:20

4aSCa3. Numerical study of volume sources associated with displacement flow during phonation. Jong Beom Park (McGill University, 817 Sherbrooke St. West, Montreal, QC H3A 2K6, Canada, jong.b.park@mail.mcgill.ca), Luc Mongeau (McGill University, 817 Sherbrooke St. West, Montreal, QC H3A 2K6, Canada, luc.mongeau@mcgill.ca)

The glottal displacement flow is a volume flow induced by the motion of the vocal folds in the absence of transglottal pressure. This source may eventually contribute to the radiated sound, in particular during glottal opening. The volume source strength was numerically computed for a time-varying rigid M5 geometry, and decomposed into monopole and dipole components. The air mass entrained by the dipole moment was found to have a length equivalent to the glottal dimension based on the net force exerted on the fluid by the vocal folds wall. The dipole moment, associated with asymmetric geometries and/or motion, is significant even for the case of motion of a incompressible deformable solid with constant volume, but having a time-varying shape.

9:40

4aSCa4. Aeroacoustic production of speech sounds. Michael Krane (ARL Penn State, PO Box 30, State College, PA 16804-0030, USA, mhk5@only.arl.psu.edu)

Speech sound production is described in terms of its essential physics by focusing on the aeroacoustics of jets in the vocal tract. Aeroacoustic theory is used to show that the primary sources of sound may be expressed in terms of unsteady aerodynamic forces on the vocal tract walls, especially where a jet is formed, and where the jet performs a strong interaction with the walls. The theory further clarifies which details of jet structure and vocal tract geometry contribute to sound production. This information is used to guide useful

approximations concerning the aerodynamics. With the assistance of measurement, these approximations are used to develop a model of the sound source in the time and frequency domains. The contribution of jet structure and vocal tract geometry to sound source characteristics is then discussed. Model predictions of the resulting acoustic field are compared to acoustic measurements.

Contributed Papers

10:00

4aSCa5. Increasing the complexity of glottal flow models: in-vitro validation for steady flow conditions. Julien Cisonni (Département Parole & Cognition, GIPSA-lab, 46, avenue Félix Viallet, 38031 Grenoble Cedex, France, julien.cisonni@gipsa-lab.inpg.fr), Annemie Van Hirtum (Département Parole & Cognition, GIPSA-lab, 46, avenue Félix Viallet, 38031 Grenoble Cedex, France, annemie.vanhirtum@gipsa-lab.inpg.fr), Xiao Yu Luo (Dept. of Mathematics, Univ. of Glasgow, University Gardens, G12 8QW Glasgow, UK, x.luo@maths.gla.ac.uk), Xavier Pelorson (Département Parole & Cognition, GIPSA-lab, 46, avenue Félix Viallet, 38031 Grenoble Cedex, France, pelorson@icp.inpg.fr)

Quasi one-dimensional glottal flow descriptions predict vocal folds oscillations characteristics which are qualitatively relevant to in-vitro and in-vivo experimental data. The current paper considers the resolution of the 2D Navier-Stokes equations in order to obtain a refined description of the flow phenomena adapted to more realistic glottal geometry. The pressure and flow rate predictions obtained from quasi one-dimensional flow models and the resolution of the 2D Navier-Stokes equations are examined for steady flows within a rigid glottis. The models predictions are validated against in-vitro measurements performed on rigid constriction replicas comparable to the geometrical conditions of the glottis and mounted in a suitable set-up. The confrontation between the experimental and computed data tends to show that the accuracy of the estimated pressures increases with the complexity of the flow model whereas the inverse tendency can be observed for the estimated flow rates. A focus is made on the flow separation point which is predicted by the resolution of the Navier-Stokes equations and appears to be a crucial parameter of the quasi one-dimensional flow models. The use of a variable separation criterion obtained from the 2D flow modelling in the quasi one-dimensional models makes the different models predictions more similar.

10:20

4aSCa6. Calculation model of the influence of the vocal fold shape on the vocal fold oscillation form. Andreas Gömmel (RWTH Aachen, Civil Engineering Dept., Structural Statics and Dynamics, Mies-van-der-Rohe-Str. 1, 52064 Aachen, Germany, goemmel@lbb.rwth-aachen.de), Christoph Butenweg (RWTH Aachen, Civil Engineering Dept., Structural Statics and Dynamics, Mies-van-der-Rohe-Str. 1, 52064 Aachen, Germany, butenweg@lbb.rwth-aachen.de), Malte Kob (RWTH Aachen, Dept. of Phoniatrics, Pedaudiology, and Communication Disorders, Pauwelsstr. 30, 52074 Aachen, Germany, mkob@ukaachen.de)

Vocal fold (VF) oscillation is driven by fluid-structure interaction effects. A possible way of modeling these effects is the finite-element (FE) method. The presented FE model consists of two coupled domains: A fluid domain representing the air, and a structural domain representing the VFs. In principle, each of the domains is a stand-alone simulation model. In the current implementation a thin three-dimensional frontal slice of the vocal folds and the sub- and supraglottal areas is modeled. Flow calculation is done using the standard Navier-Stokes equations. The air is modeled as a transient, viscous, and laminar flow. Constant physiologic values of pressure are used as driving force. For structural analysis, linear volume elements are used. There are two different models which differ in the VF shape. The first one is an assumed shape of a normal voice while the second shape was measured at an excised larynx and resembles more a falsetto voice. The results support two observations and assumptions: During normal phonation the VF touch each other in a constantly changing converging and diverging shape while during the more falsetto-like phonation, no converging/diverging shape is visible and no closure occurs.

10:40-11:00 Break

11:00

4aSCa7. Intraglottal pressure distributions for oblique glottal angles. Ronald C. Scherer (Bowling Green State University, Department of Physics and Astronomy, Bowling Green, OH 43403, USA, ronalds@bgnet.bgsu.edu)

Asymmetric vocal fold oscillation occurs for both normal and pathological phonation. The pressures on the right and left glottal walls receive different pressures when the glottis is oblique, as we have shown previously. Different driving forces may affect the motion, although to what extent is not yet known. We have continued empirical modeling of various oblique glottal shapes using a Plexiglas model (M5), and report the findings of those studies. In general, an oblique glottis tends to receive higher pressures on the more convergent side, and the cross-channel pressure differences may shift polarity between upstream and downstream sections. The effects on intraglottal pressures for a wide range of obliquity, minimal glottal diameter, transglottal pressure, and included glottal angle will be shown and discussed relative to potential oscillatory effects. [supported by NIH R01DC03577]

11:20

4aSCa8. Separated flow behavior in an in-vitro rigid model of the laryngeal channel. Denisse Sciamarella (CNRS, Bâtiment 508, Université Paris-Sud, 91403 Orsay, France, denisse@limsi.fr), Elisa Chisari (LFD, Facultad de Ingenieria, Universidad de Buenos Aires, Av. Paseo Colon 850, C1063ACV Buenos Aires, Argentina, elisachisari@gmail.com), Guillermo Artana (LFD, Facultad de Ingenieria, Universidad de Buenos Aires, Av. Paseo Colon 850, C1063ACV Buenos Aires, Argentina, gartana@fi.uba.ar), Lucie Bailly (Département Parole & Cognition, GIPSA-lab, 46, avenue Félix Viallet, 38031 Grenoble Cedex, France, Lucie.Bailly@gipsa-lab.inpg.fr), Xavier Pelorson (Département Parole & Cognition, GIPSA-lab, 46, avenue Félix Viallet, 38031 Grenoble Cedex, France, pelorson@icp.inpg.fr)

Flow through an in-vitro rigid model of the scaled-up laryngeal channel is measured using pressure sensors and visualized using the Schlieren technique for different geometrical configurations. Three downstream flow-conditions are considered: steady, quasi-impulsive and periodical using an electromechanical device controlling the inflow and producing the cyclic jet emerging from the glottis. The separated flow behavior in the presence of a ventricular constriction (″false vocal folds″) is also examined. Direct theoretical flow predictions and numerical simulations are proposed to quantify the aerodynamic impact involved by the ventricular bands on the pressure distribution. Two parameters are investigated: the aperture of the ventricular bands and the distance between the vocal folds and the ventricular bands. The influence of both parameters are measured and compared to the theoretical outcome.

11:40

4aSCa9. Aeroacoustic measurements in a vocal tract model. Daniel J. Leonard (ARL Penn State, PO Box 30, State College, PA 16804-0030, USA, djl239@psu.edu), Michael Krane (ARL Penn State, PO Box 30, State College, PA 16804-0030, USA, mhk5@only.arl.psu.edu)

An experiment to clarify the relation between turbulent jet structure, vocal tract wall shape and the resulting sound is described. A life-scale model of the vocal tract (18cm length, 2.6cmx2.6cm square cross-section), fabricated from clear cast acrylic is used. A jet, formed at a constriction, passes over or against a simple obstacle, generating sound. Correlated aerodynamic and acoustic measurements are used to determine the transfer function between the obstacle and the measurement location outside the model and the aeroacoustic source spectrum. For comparison the source spectrum is also estimated using the model described in Krane (JASA, 2005), using aerodynamic measurements as empirical input.

12:00

4aSCa10. Influence of vocal fold stiffness on phonation characteristics at onset in a body-cover vocal fold model. Zhaoyan Zhang (School of Medicine, University of California, 31-24 Rehab Center, 1000 Veteran Ave., Los Angeles, CA 90095-1794, USA, zyzhang@ucla.edu), Juergen Neubauer (School of Medicine, University of California, 31-24 Rehab Center, 1000 Veteran Ave., Los Angeles, CA 90095-1794, USA, jneubauer @mednet.ucla.edu)

The influence of the body and cover stiffnesses on phonation onset and the resulting vibration pattern was investigated in a body-cover continuum model of the vocal folds. An eigenvalue analysis was performed to obtained phonation onset characteristics. The analysis showed that, with increasing body-cover stiffness ratio, both the phonation threshold pressure and frequency (normalized by the Young's modulus and wave speed of the cover layer, respectively) first increased rapidly and then gradually approached a plateau. For a given glottal resting opening, a soft vocal fold body led to a larger prephonatory glottal opening, which had an negative effect on phonation onset pressure, and for certain vocal fold geometries, led to a local minimum in the phonation threshold pressure as a function of the body stiffness. Although the phonation threshold pressure was low for a vocal fold configuration with both a soft cover and a soft body, the vocal fold vibration at onset exhibited a significant whole-body vertical motion and a low sound production efficiency, and therefore it may not be desirable for voice production. For a large body-cover stiffness ratio, this vertical motion was suppressed and vibration was restricted to the cover layer and the medial surface, resulting in a more effective flow modulation and a better sound production efficiency.

12:20

4aSCa11. Modeling of voice registers and bifurcation theory. Marco Zemke (Institute for Theoretical Biology, Invalidenstraße 43, 10115 Berlin, Germany, marco.zemke@biologie.hu-berlin.de), Isao Tokuda (Japan Advanced Institute of Science and Technology, 1-1 Asahidai, Nomi-shi, 923-1292 Ishikawa, Japan, isao@jaist.ac.jp), Hanspeter Herzel (Institute for Theoretical Biology, Invalidenstraße 43, 10115 Berlin, Germany, h.herzel @biologie.hu-berlin.de)

The exact definition of registers in the human voice is still under debate. Especially the quantitative analysis of transitions between these registers have not been investigated in much detail yet. Experiments show different kinds of voice instabilities that appear close to the transition from chest to falsetto register. These instabilities include abrupt jumps between the two registers exhibiting hysteresis, aphonic episodes, subharmonics and chaos. To model these phenomena we start with a three mass cover model of the human larynx which can vibrate in chest and falsetto like patterns. We extend our model to a four mass body-cover polygon model with a supraglottal resonator. We more realistic make use of bifurcation theory to understand how small smooth changes of parameter values can cause sudden qualitative changes in the dynamical behavior of the larynx. Experiments with excised human larynges and untrained singers show comparable coexistence of both registers in a extended parameter region. Our study suggests that voice range profiles can be generalized as two dimensional bifurcation diagrams.

12:40-2:00 Lunch Break

Contributed Papers

2:00

4aSCa12. Theoretical and experimental results of phonation threshold pressure vs. oscillation frequency of the vocal folds. Jorge C. Lucero (Univ. Brasilia, Dept. Mathematics, 70910-900 Brasilia - DF, Brazil, lucero@unb.br), Annemie Van Hirtum (Département Parole & Cognition, GIPSA-lab, 46, avenue Félix Viallet, 38031 Grenoble Cedex, France, annemie.vanhirtum@gipsa-lab.inpg.fr), Nicolas Ruty (Département Parole & Cognition, GIPSA-lab, 46, avenue Félix Viallet, 38031 Grenoble Cedex, France, nicolas.ruty@gipsa-lab.inpg.fr), Julien Cisonni (Département Parole & Cognition, GIPSA-lab, 46, avenue Félix Viallet, 38031 Grenoble Cedex, France, julien.cisonni@gipsa-lab.inpg.fr), Xavier Pelorson (Département Parole & Cognition, GIPSA-lab, 46, avenue Félix Viallet, 38031 Grenoble Cedex, France, pelorson@icp.inpg.fr)

The dynamical principles of the vocal fold oscillation at phonation were set forth by Titze (I. R. Titze, J. Acoust. Soc. Am. **83**, 1536-1552 , 1988), by representing motion of the tissues as a surface wave propagating in the direction of the airflow. An important result of his work was an equation for the phonation threshold value of lung pressure, defined as the minimum value required to initiate the vocal fold oscillation. Titze's model assumed a small time delay for the mucosal wave to travel along the vocal folds, with the consequence that the phonation threshold pressure results independent of the oscillation frequency. Here, we consider an extension of his model for an arbitrary time delay. Our results show that the threshold pressure increases with oscillation frequency following a $x/\sin(x)$ law. We investigate the validity of the theoretical equation by comparing it with pressure measures from a mechanical replica of the vocal folds, under various configurations. In general, the equation shows good agreement with the experimental data, and may find applications for building empirical relations of glottal aerodynamics, and for clinical studies of phonation. [Work supported by CAPES-Brazil]

2:20

4aSCa13. Physical modelling of Vowel-Stop-Vowel sequences. Claire Brutel-Vuilmet (GIPSA-Lab, INPG, 46 Av. Felix-Viallet, 38031 Grenoble, France, claire.brutel-vuilmet@gipsa-lab.inpg.fr), Xavier Pelorson (Département Parole & Cognition, GIPSA-lab, 46, avenue Félix Viallet, 38031 Grenoble Cedex, France, pelorson@icp.inpg.fr), Annemie Van Hirtum (Département Parole & Cognition, GIPSA-lab, 46, avenue Félix Viallet, 38031 Grenoble Cedex, France, annemie.vanhirtum @gipsa-lab.inpg.fr), Susanne Fuchs (ZAS, Schuetzenstr. 18, 10117 Berlin, Germany, fuchs@zas.gwz-berlin.de)

The physical phenomena involved in the production of vowel sounds are now well described and several effective physical models have been developed. On the contrary, only a few studies concern the physical aspects of the production of consonant sounds (fricatives, stops...) or the production of vowel-consonant-vowel sequences. Indeed, more complex acoustical and aerodynamical mechanisms should be considered (generation of aeroacoustical sources, dynamical description...). In this contribution, we focus on the production of vowel-stop-vowel sequences. A stop sound is produced after a complete occlusion of the vocal tract. In an intervocalic context, the closure entails an increase of the intraoral pressure, which results in the cessation of the vocal folds vibration. The opening is quickly followed by the generation of an aeroacoustical source, and entails a decrease of the intraoral pressure, which results in the resumption of the vocal folds motion. A physical model able to describe these aerodynamical observations and to predict the evolution of the intraoral pressure during the closure gesture is first detailed. Different interesting results are discussed (influence of the closure time, influence of the closure position, coordination of the different sources...). And a confrontation between theoretical results and experimental data is presented.

2:40

4aSCa14. Analysis of frication noise modulation from a physical model. Anna Barney (ISVR, Univ. of Southampton, SO17 1BJ Southampton, UK, ab3@soton.ac.uk), Philip J. Jackson (University of Surrey, Centre for Vision, Speech and Signal Processing, GU2 7XH Guildford, UK, p.jackson @surrey.ac.uk)

A physical model, built to investigate the aeroacoustic properties of voiced fricative speech, was used to study the amplitude modulation of the

turbulence noise it generated. The amplitude and fundamental frequency of glottal vibration, relative positions of the constriction and obstacle, and the flow rate were varied. Measurements were made from pressure taps in the duct wall and the sound pressure at the open end. The high-pass filtered sound pressure was analyzed in terms of the magnitude and phase of the turbulence noise envelope. The magnitude and phase of the observed modulation was related to the upstream pressure. The effects of moving the obstacle with respect to the constriction are reported (representative of the teeth and the tongue in a sibilant fricative respectively). These results contribute to the development of a parametric model of the aeroacoustic interaction of voicing with turbulence noise generation in speech.

3:00

4aSCa15. Towards sibilant /s/ modelling: preliminary computational results. Xavier Grandchamp (Département Parole & Cognition, GIPSA-lab, 46, avenue Félix Viallet, 38031 Grenoble Cedex, France, xavier.grandchamp@gipsa-lab.inpg.fr), Annemie Van Hirtum (Département Parole & Cognition, GIPSA-lab, 46, avenue Félix Viallet, 38031 Grenoble Cedex, France, annemie.vanhirtum@gipsa-lab.inpg.fr), Xavier Pelorson (Département Parole & Cognition, GIPSA-lab, 46, avenue Félix Viallet, 38031 Grenoble Cedex, France, pelorson@icp.inpg.fr), Kazunori Nozaki (Cyber Media Center, Osaka University Cybermedia, 5-1 Mihogaoka Ibaraki, 567-0047 Osaka, Japan, nozaki@cmc.osaka-u.ac.jp), Shinji Shimojo (Cyber Media Center, Osaka University Cybermedia, 5-1 Mihogaoka Ibaraki, 567-0047 Osaka, Japan, shimojo@cmc.osaka-u.ac.jp)

Acoustic effects of the turbulence in human sounds production is generally accepted in the case of fricatives. Nevertheless, this phenomenon is not taken into account in physical modelling of the speech production. Steady flow in a uniform two dimensional channel with a one side triangular obstacle has been simulated using Large Eddy Simulation for different Reynolds numbers. The used geometrical and flow characteristics are severe simplifications of the human articulators during the production of the sibilant /s/. The impact of different geometrical configurations of the downstream obstacle representing the teeth on the computational results is searched in order to detect the aeroacoustic sources produced by turbulent flow, crucial in /s/ production.

3:20

4aSCa16. The Influence of Constriction Geometry on Sound Generation in Fricative Consonants. Gordon Ramsay (Haskins Laboratories, 300 George Street, New Haven, CT 06511, USA, ramsay@haskins.yale.edu)

Sound generation in fricative consonants is traditionally supposed to depend only on the Reynolds Number, usually defined in terms of the constriction area and the volume velocity at the constriction. The potential influence of the detailed three-dimensional geometry of the constriction is often ignored, even though previous empirical studies have shown this to have an important effect on the spectral shape of the source and the overall sound strength. At present, the physical processes governing turbulent jet formation and aeroacoustic source generation in fricative consonants are not fully understood. In this paper, we use large-eddy simulations of three-dimensional viscous incompressible flow to visualize the development of the turbulent flow field and aeroacoustic source distribution in an elliptical duct representing the vocal tract, for elliptical, laminar, and grooved constriction shapes that share the same cross-sectional area function. By contrasting results for these geometries, we test the hypothesis that turbulent jet formation is determined largely by the shape of the boundary layer where flow separates at the exit of the constriction, and that the perimeter of the constriction, rather than the cross-sectional area, may therefore be a more appropriate parameter for characterizing properties of the aeroacoustic source.

THURSDAY MORNING, 3 JULY 2008 ROOM 250B, 8:40 A.M. TO 12:00 NOON

Session 4aSCb

Speech Communication: Neurobiology of Speech Perception

Paul Iverson, Cochair
University College London, Department of Phonetics and Linguistics, 4, Stephenson Way, London, NW1 2HE, UK

Christophe Pallier, Cochair
Cognitive Neuroimaging Unit INSERM 562, CEA/Neurospin, bat 145, point courier 156, Gif/Yvette, 91191, France

Invited Papers

8:40

4aSCb1. Involvement of Auditory Cortex in Speech Production. Frank H. Guenther (Boston University, 677 Beacon Street, Boston, MA 02215, USA, guenther@cns.bu.edu)

In addition to their role in speech perception, the auditory cortical areas of the superior temporal lobe are important for the formation and maintenance of motor commands for speech production. Using a combination of neural network modeling, neuroimaging, and auditory perturbation experiments, we have characterized the network of brain regions involved in auditory feedback control of segmental aspects of speech. This network involves auditory error cells in bilateral posterior superior temporal cortex which become active when the current auditory feedback mismatches the auditory target for the current speech sound. Projections from these auditory cortical areas to the right hemisphere ventral premotor areas, then on to primary motor cortex, transform perceived auditory errors into corrective movement commands for the speech articulators. The DIVA model of speech production produces a close quantitative fit to acoustic data collected during unexpected auditory perturbation of speech and during sensorimotor adaptation to sustained auditory perturbations. Neuroimaging results motivate a modification of the model to include right ventral premotor cortical areas in the auditory feedback circuit for speech production. [Work supported by NIDCD, NSF.]

9:00

4aSCb2. Motor regions contribute to speech perception: awareness, adaptation and categorisation. Matthew H. Davis (MRC CBU, 15 Chaucer Rd., CB2 7EF Cambridge, UK, matt.davis@mrc-cbu.cam.ac.uk), Ingrid S. Johnsrude (Queen's University, Dept Psychology, 62 Arch Street, Kingston, ON K7L 3N6, Canada, ingrid.johnsrude@queensu.ca), Alexis G. Hervais-Adelman (Centre for the Neural Basis of Hearing, Department of Physiology, Development and Neuroscience, University of Cambridge, Downing Site, CB23EG Cambridge, UK, alexis.hervais-adelman@mrc-cbu.cam.ac.uk), Jack C. Rogers (MRC Cognition and Brain Sciences Unit, 15 Chaucer Road, CB2 7EF Cambridge, UK, jack.rogers@mrc-cbu.cam.ac.uk)

Functional imaging and TMS studies show that motor and premotor cortex responds to heard speech though the functional significance of this response is unclear. Three recent fMRI studies, showing modulation of motor responses to heard speech in the absence of overt spoken or manual responses, may shed light on how regions typically associated with speech production contribute to perception. (1) Motor activity remains robust during light anaesthetic sedation, but is obliterated for deeply sedated participants who are no longer aware of speech. (2) Motor cortex responds more to distorted yet intelligible noise-vocoded words than to clear speech or unintelligible noise. This neural correlate of listening effort is also observed for ″clear-then-vocoded″ presentations that enhance perceptual adaptation compared to a matched ″vocoded-then-clear″ condition that doesn't enhance adaptation. (3) During paired priming of audio-morphed syllables we see a greater response to acoustic changes that cross phonological category boundaries compared to acoustically-equivalent within-category changes. Additional responses to between-category pairs extend to motor regions, suggesting that neural correlates of categorical perception include regions involved in speech production. These findings illustrate how perceptual awareness, adaptation and categorisation of speech all engage motor regions. Implications for neurobiological accounts of speech perception will be discussed.

9:20

4aSCb3. From Speech to Language: Mapping the Auditory Comprehension Network. Jonas Obleser (Max Planck Institute of Human Cognitive and Brain Sciences, Stephanstrasse 1A, 04103 Leipzig, Germany, jonas@obleser.de)

Speech comprehension is a complex perceptual and cognitive task that is fulfilled in a surprisingly robust manner. I will present a series of studies that aim at disentangling the interaction of sensory/acoustic and cognitive/linguistic factors driving the speech comprehension system: (i) How does the system in its entirety deal with noise at the auditory entry level? (ii) Which are key contextual influences that aid speech comprehension when the signal quality drops, and (iii) what is the functional circuitry within and across auditory cortex that copes with comprehension difficulties? Main results include: 1. Comprehension of intermediate signal quality based on semantic predictability engages a left- hemispheric, widely distributed array of brain structures. Also, functional connectivity amongst these areas appears enhanced. 2. Signal intelligibility gates and enables the expected semantic effects (cloze probability; BA44 BOLD response and EEG N400), whereas semantic effects shape the intelligibility modulation in anterolateral temporal cortex. 3. The angular gyrus (BA 39) enhances difficult yet successful speech comprehension whereas left posterior STG reflects higher computational effort (either poor signal quality or low cloze probability) in speech comprehension. Behavioural, EEG and fMRI data will be presented, and themes of (bi-)laterality and bottom-up/top-down directionality will be re-visited along the way.

9:40

4aSCb4. An fMRI study of subliminal priming of spoken words. Christophe Pallier (Cognitive Neuroimaging Unit INSERM 562, CEA/Neurospin, bat 145, point courier 156, 91191 Gif/Yvette, France, christophe@pallier.org), Sid Kouider (Laboratoire de Sciences Cognitives et Psycholinguistique, Ecole Normale Supérieure, 29 rue d'Ulm, 75005 Paris, France, sid.kouider@ens.fr), Vincent De Gardelle (Laboratoire de Sciences Cognitives et Psycholinguistique, Ecole Normale Supérieure, 29 rue d'Ulm, 75005 Paris, France, gardelle@biologie.ens.fr)

Repetition priming has been widely used to study spoken and written word recognition. Its physiological counterpart is repetition suppression, a reduction in neural activity resulting in a measurable decrease of the fMRI signal. By varying the representational level at which the repetition occurs, one can determine which properties are encoded in a given brain area, and which are not. We will report on an fMRI experiment using subliminal auditory priming of spoken words. Subliminal priming has been used, for example, by Dehaene et al. to study visual word recognition. Our experiment employs a technique developped by Kouider & Dupoux that allows subliminal presentation of auditory stimuli using temporal compression and forward masking. The participants perform a lexical decision task on the target item, which is preceded by a subliminal prime that can be phonetically identical or different from the target, and spoken or not by the same speaker. A fast-event related paradigm is used where each prime-target pair is presented during silent gaps between the acquisitions. The planned analyses will seek to identify the brain regions showing subliminal repetition suppression to word repetition regardless of speaker change, as well as other areas sensitive to speaker change regardless of linguistic content.

Contributed Paper

10:00

4aSCb5. The neural bases of normalising for accented speech: A repetition suppression functional magnetic resonance imaging study. Patti Adank (F.C. Donders Centre for Cognitive Neuroimaging, Kapittelweg 29, 6525EN Nijmegen, Netherlands, patti.adank@fcdonders.ru.nl), Peter Hagoort (F.C. Donders Centre for Cognitive Neuroimaging, Kapittelweg 29, 6525EN Nijmegen, Netherlands, peter.hagoort@fcdonders.ru.nl)

A repetition suppression fMRI paradigm was employed to explore the neuroanatomical substrates of normalisation for accented speech in spoken sentence processing. Sentences were produced in two accents: in Standard Dutch and an artificial accent of Dutch. In the experiment, participants listened to two sentences presented in quick succession. The second sentence was either spoken by the same speaker in the same accent, by the same speaker in a different accent, by a different speaker in the same accent, or by a different speaker in a different accent. This design allowed us to study neural responses to a change in speaker only, a change in accent only and a change in accent and speaker. Results showed small effects for a change of speaker only in right Superior Temporal Gyrus (STG). A change of accent only showed extensive activations in left and right STG and Superior Temporal Sulcus (STS). Finally, a change of speaker and accent showed extensive activations in left and right STG and STS, and increased activity in left Inferior Frontal Gyrus (IFG). The results indicate that normalisation processes for accented speech recruit a wide neural network. The role of left IFG in normalisation processes will be discussed.

10:20-10:40 Break

Invited Papers

10:40

4aSCb6. Streams of processing and hemispheric asymmetries in speech perception. Sophie K. Scott (University College London, Institute of Cognitive Neuroscience, 17 Queen Square, WC1N 3AR London, UK, sophie.scott@ucl.ac.uk)

Studies in non-human primates have indicated that, as in the visual system, there are (at least) two streams of processing in the auditory system. These pathways are associated with different types of auditory processes - an anterior 'what' pathway and posterior 'how/where' pathway(s). In this talk I will use these neurophysiological theories as a framework for interpreting findings from a range of PET and fMRI studies of human speech perception and production, and present evidence that the anterior 'what' pathway in humans shows hierarchical processing of the speech signal, reflecting a move from acoustic/phonetic processing to a more abstract representation in the anterior superior temporal sulcus. In contrast, posterior auditory areas in humans are associated with sensory/motor interactions in speech, and with aspects of working memory processing. I will address how these systems are differentially recruited when speech perception is made difficult, due to different types of masking noise. Finally, I will outline differences in the processing of speech in left and right auditory areas.

11:00

4aSCb7. The temporal analysis of spoken language. David Poeppel (University of Maryland, 1401 Marie Mount Hall, College Park, MD 20742, USA, dpoeppel@umd.edu)

The (concurrent) construction of syllabic and phonemic representations forms the basis for creating interpretable representations of speech; therefore we look here to temporal attributes commensurate with their acoustic implementation. Based on a distributed model of the functional anatomy of speech perception (Hickok & Poeppel 2007) and on the assumption that the perception of speech requires multi-time resolution analysis (Poeppel 2003), electrophysiological data are shown that illustrate how auditory cortex makes use of one specific temporal mechanism, the processing of phase (Luo & Poeppel 2007). We hypothesized that the phase pattern of cortical rhythms associated with modulation rates mediating intelligible speech provide an encoding mechanism. We observed that the phase of the theta band response generated in auditory cortex tracks sentence-level acoustics with the sensitivity and specificity necessary for neuronal encoding. The data are consistent with the view that a ~200 ms temporal window (period of theta oscillation) segments the incoming signal, resetting and sliding to track speech dynamics. This hypothesized mechanism for cortical speech analysis is based on the stimulus-induced modulation of inherent cortical rhythms and provides supporting evidence implicating the syllable as a computational primitive for the representation of spoken language.

11:20

4aSCb8. ERPs and speech sound perception - possibilities and restrictions. Maija S. Peltola (University of Turku, Department of Phonetics, FIN-20014 Turku, Finland, maija.peltola@utu.fi)

Speech sound perception is a complex combination of attention independent and attention dependent processes which both contribute to the final goal of understanding the spoken message. The preattentive level has become more accessible to research and event related potentials (ERPs) can easily be used to study the automatic processing of the speech signal. In particular, the mismatch negativity (MMN) response offers a tool for investigating the manner in which speech sounds are encoded as neural representations. Cross-linguistic studies revealing different kinds of representations in native speakers of different languages form the core for further studies, which have shown the plasticity of the brain in forming new representations for non-native sounds in various types of learning environments. However, despite all these promising advances there are still some restrictions connected both with the methodology available and the conclusions that can be reached on the basis of the occasionally contradicting results. Also, since results obtained by using attention independent and dependent methods are not always compatible, some potentially significant results may never reach the attention that they deserve, even if this incompatibility may be one of the keys into the understanding of the complicated mechanisms underlying speech sound perception.

Contributed Paper

11:40

4aSCb9. Cognitive control skills and speech perception after short-term second language experience during infancy. Barbara Conboy (University of Washington, Dept. of Speech & Hearing Sciences, and Institute for Learning & Brain Sciences, Box 357988, Seattle, WA 98195, USA, bconboy@u.washington.edu), Jessica Sommerville (University of Washington, Dept. of Speech & Hearing Sciences, and Institute for Learning & Brain Sciences, Box 357988, Seattle, WA 98195, USA, sommej@u.washington.edu), Patricia K. Kuhl (University of Washington, Dept. of Speech & Hearing Sciences, and Institute for Learning & Brain Sciences, Box 357988, Seattle, WA 98195, USA, pkkuhl@u.washington.edu)

Previous research has linked increasing cognitive abilities to reductions in sensitivity to nonnative phonemes toward the end of the first year, but found no association between cognitive skills and native speech perception (Conboy et al., 2006; Lalonde & Werker, 1995). The present study examined cognitive abilities and brain activity to second-language (L2) phoneme contrasts in infants who had short-term experience with the L2: we predicted better cognitive skills in infants with better discrimination of the L2 contrast. Seventeen infants from monolingual English homes completed event-related potential (ERP) speech perception testing and nonlinguistic tasks requiring attentional flexibility, memory, and inhibitory control at 11 months, after twelve Spanish play sessions from 9.5 - 10.5 months. An ERP oddball paradigm assessed discrimination of English and Spanish contrasts

(English: voiced /da/ vs. voiceless-aspirated [tha]; Spanish: prevoiced /da/ vs. voiceless-unaspirated /ta/). Infants showed broad mismatch negativity (MMN) discriminatory responses to both contrasts. Larger Spanish MMN amplitudes were linked to better performance on cognitive tasks (detour-reaching object-retrieval and the A not B task) (Fisher's exact test, $p=.01$), suggesting a role for specific cognitive abilities in the early stages of phonetic learning. There was no association between English MMN amplitudes and cognitive skills.

THURSDAY MORNING, 3 JULY 2008 ROOM 343, 8:00 TO 10:20 A.M.

Session 4aSPa

Signal Processing in Acoustics, Acoustical Oceanography, and ECUA: Model-Based Signal Processing II

Sean Lehman, Cochair
Lawrence Livermore Natl. Lab., Livermore, CA 94551, USA

Christian Pichot, Cochair
Antennas & Telecommunications Laboratory, University of Nice-Sophia Antipolis, France

Contributed Paper

8:00

4aSPa1. Water column tomographic inversion with a network of drifting buoys. Sergio Jesus (ISR, Universidade do Algarve, PT-8005-139 Faro, Portugal, sjesus@ualg.pt), Cristiano Soares (ISR, Universidade do Algarve, PT-8005-139 Faro, Portugal, csoares@ualg.pt), Nelson Martins (ISR, Universidade do Algarve, PT-8005-139 Faro, Portugal, nmartins@ualg.pt)

The estimation of ocean environmental properties by means of the inversion of acoustic signals has in several occasions been performed using a single vertical array of acoustic receivers, with a towed acoustic source as an attempt to ensure a rapid spatial coverage of the area of interest, as only a single ocean transect is ″seen″ at each time. Ideally, one would like to obtain an instantaneous picture of the complete area (volume) under observation. However, the resulting acoustic observations, hence environmental estimates, are not simultaneous in time. Using multiple acoustic receiving arrays appears to be a natural step towards both increasing the spatial coverage, and obtaining simultaneous environmental estimates of different ocean transects. It also gives a higher chance to capture spatial transient features, as for example solitons. Using multiple receiver arrays represents the addition of a new spatial dimension at the receiving end and opens up the number of possibilities to a Nx2D or full 3D view of the ocean. Taking support on the data set of the RADAR'07 experiment (July 9 - 16, 2007) where data was simultaneously collected on three vertical arrays, this paper explores space coherent processing of the several receiving arrays and Nx2D or 3D environmental constrained water coloumn matched-field inversion.

Invited Paper

8:20

4aSPa2. Model based echo processing architectures for sonar target classification. Manell E. Zakharia (French Naval Acadamey, BP 600, 29240 Brest-Armees, France, manell.zakharia@ecole-navale.fr)

The discrimination between man-made and natural targets is faced to the problem of setting up appropriate processing architectures that extract relevant and robust parameters that could be used for classification. To be robust, signal models have to be associated to physical models and echo parameters have to be associated to physical ones. Several models already published are investigated: bright spots, generalized bright spots, resonances. Associated processing architectures are presented: matched filter, bank of filters, AR modeling. Their performance are compared on experimental data set obtained in tank. The discriminating performance are compared in the case of shells (man-made) and solid targets (natural) of the same shape insonified in a random incidence (monostatic). Following a detailed description of echo formation mechanisms in the time-frequency plane, an explicit time-frequency architecture is presented: the time-frequency filtering. Finally a new (all chirp) model based on velocity dispersion of surface waves ,is proposed that could reduce the number of discriminating parameters and be robust to minor changes of shell characteristics.

Contributed Papers

8:40

4aSPa3. Automatic Acoustics Measurement of Audible Inspirations in Pathological Voices. Eduardo Castilllo-Guerra (University of New Brunswick, P.O. Box 4400, 15 Dineen Dr., D36 Head Hall, Fredericton, NB E3B 5A3, Canada, ecastill@unb.ca), Williams Lee (University of New Brunswick, P.O. Box 4400, 15 Dineen Dr., D36 Head Hall, Fredericton, NB E3B 5A3, Canada, wlee@unb.ca)

Audible inspiration (AI) is a type of speech perturbation commonly heard in pathologic voices. This acoustic parameter is used in conjunction with other acoustic observations to assess different types of pathologic conditions of speech associated with neurological or vocal cord disorders. However, the perception of this speech perturbation is often very subjective and difficult to appraise in a quantitative and consistent form. This work reports an algorithm to estimate the severity of this perturbation using time-frequency characteristics. The algorithm is based on a linear combination of the frequency of occurrence, the duration and the intensity of the inspirations. An algorithm to segment the AIs in conversational speech is proposed. The AI index was first evaluated with the Massachusetts Eye and Ear Infirmary Voice Database and then with two other databases containing recording from motor speech disorders. The segmentation algorithms was 90% effective detecting the audible inspirations and the AI index showed a high correlation (80.8%) with respect to the average perceptual judgment obtained from three judges with experience evaluating disordered speech.

9:00

4aSPa4. Comparative Study of Wideband Subspace Direction of Arrival (DOA) estimation methods. Sheraz Khan (Laboratoire Ondes et Acoustique, ESPCI, 10 rue Vauquelin, 75231 Paris, France, sheraz.khan @polytechnique.edu)

Signal subspace Methods like ESPRIT, MUSIC and MATRIX PENCIL, provides high resolution Direction Of Arrival (DOA) estimation in comparison to traditional Delay and Sum and Capon methods, which are limited by sensor spacing. However underwater Acoustics signals are inherently wideband in nature and most of these Subspace methods works on narrowband signals. Currently modified version of these methods for wideband signals are emerging. These methods are broadly classified as Coherent and Incoherent methods depending upon how signals of different frequencies have been merged. Performances of these methods are evaluated using extensive Monte-Carlo simulations under various protocols by comparing there Mean Square Error in DOA estimation and by their respective resolution power. This comparison study is also complemented with real acoustic data from public domain.

9:20

4aSPa5. Application of statistical methods in underwater signal classification. Brett E. Bissinger (ARL Penn State, PO Box 30, State College, PA 16804, USA, beb194@psu.edu), Richard Lee Culver (ARL Penn State, PO Box 30, State College, PA 16804, USA, rlc5@psu.edu), Nirmal K. Bose (ARL Penn State, PO Box 30, State College, PA 16804, USA, bkn@engr.psu.edu), Colin W. Jemmott (ARL Penn State, PO Box 30, State College, PA 16804, USA, cwj112@psu.edu)

The overall goal of our work is to utilize knowledge of the ocean environment to improve sonar detection and classification performance. Source classification and localization in the underwater environment is a challenging problem in part because propagation through the space- and time-varying medium introduces multipath, variability, and decorrelation to the signal. Traditional underwater signal classification has relied on parametric methods such as the likelihood ratio tests. Recent research has explored nonparametric methods like maximum entropy and maximum likelihood with favorable results. This talk considers other, more contemporary nonparametric methods, e.g. principle component analysis, independent component analysis and support vector machines, and compares their structure and performance with previous results. Work supported by Office of Naval Research Undersea Signal Processing.

9:40

4aSPa6. Estimation of acoustic directivity from microphone array measurements using parametric models. Jean Bulté (ONERA, BP 72 - 29, avenue de la division Leclerc, 92322 Châtillon, France, jean.bulte@onera.fr),Vincent Fleury(ONERA, BP 72 - 29, avenue de la division Leclerc, 92322 Châtillon, France, vincent.fleury@onera .fr), Renaud Davy (ONERA, BP 72 - 29, avenue de la division Leclerc, 92322 Châtillon, France, renaud.davy@onera.fr)

In this paper, we are interested in recovering the far-field acoustic pattern of a directive source from signals recorded in the near-field by an array of microphones with a reduced spatial extent. This question is particularly relevant in small test facilities where far-field acoustic measurements can not be carried out. A two-step approach is suggested. Firstly, the characteristics of sources are estimated from near-field measurements. Secondly, these characteristics are used to estimate the far-field radiation pattern. The main difficulty of this problem mainly resides in the first step. Due to the reduced spatial extent of the array, much information is lost about source characteristics, which mathematically leads to solve an ill-posed inverse problem. Our approach consists in using a parametric model based on physical assumptions, which has the virtue of regularizing the estimation problem. The suggested method is firstly evaluated with simulations, and then applied to experimental data recorded during aeroacoustic tests with a subsonic jet in an anechoic wind tunnel. It is shown that comparison between far-field measurements and estimated far-field pattern are in good agreement.

10:00

4aSPa7. A volumetric interferometric synthetic aperture sonar reconstruction algorithm. Michael Hayes (University of Canterbury, Private Bag 4800, 8022 Christchurch, New Zealand, michael.hayes @canterbury.ac.nz), Peter T. Gough (University of Canterbury, Private Bag 4800, 8022 Christchurch, New Zealand, peter.gough@canterbury.ac.nz)

Interferometric synthetic aperture sonar (InSAS) bathymetric reconstruction is an inverse problem that is often simplified to a time delay estimation problem. This uses a simple system model of a continuous scattering surface with single scatterer per resolution cell. This model is violated by layover, multiple scattering, occlusions, or sea-surface multipath producing artefacts in the reconstructed image. While some artefacts, such as from occluded shadow regions, can be rejected by using a threshold on the correlation coefficient, this does not work in general. Moreover, since each pixel is reconstructed independently it is difficult to improve the reconstruction by adding prior information. In this paper we propose a reconstruction algorithm using a probabilistic volumetric model; similar to those used for photometric 3-D scene reconstruction from multiple cameras. While significantly slower than time delay estimation methods, the bathymetric reconstruction can be improved due to better scene modelling and the incorporation of priors such as surface continuity. Furthermore, an advantage of a volumetric model is that correction for the footprint shift is implicit. We demonstrate the algorithm using both simulated and real data.

Session 4aSPb

Signal Processing in Acoustics, Acoustical Oceanography, and ECUA: Bayesian Signal Processing II

Zoi-Heleni Michalopoulou, Cochair
Department of Mathematical Sciences, New Jersey Institute of Technology, 323 M L King Blvd, Newark, NJ 07102, USA

Simon J. Godsill, Cochair
Trumpington Street, Cambridge, CB21PZ, UK

Invited Papers

10:40

4aSPb1. An Overview of Bayesian Computational methods for audio signal processing. Simon J. Godsill (Trumpington Street, CB21PZ Cambridge, UK, sjg@eng.cam.ac.uk), Ali-Taylan T. Cemgil (Trumpington Street, CB21PZ Cambridge, UK, atc27@eng.cam.ac.uk), Paul Peeling (Trumpington Street, CB21PZ Cambridge, UK, php23@cam.ac.uk)

In this talk we describe Bayesian computational models and methods for inference about noisy audio signals, with the aim of performing tasks such as musical trnscription, source separation, automated annotation with content descriptors, noise reduction and object-based coding. The models are structured models of non-stationary sparsity in audio sources, usually expressed in the time-frequeny plane. The computational inference methods are based around Monte Carlo techniques including the particle filter for rapid on-line inference and Markov chain Monte Carlo for batch problems of higher compleixity. Examples will be given from the spheres of source separation, multiresolution noise reduction, denoising and intetrpolation of missing batches from audio. We will also describe their use for acoustical analysis of the properties of a musical instrument, focusing on the parameters of inharmonicity in struck or plucked strings.

11:00

4aSPb2. Bayesian approach to signal detection, source localization and ocean environmental parameter estimation. Loren W. Nolte (Duke University, Department of Electrical and Computer Engineering, Durham, NC 27708, USA, lwn@ee.duke.edu)

From a Bayesian perspective, signal detection, source localization and ocean environmental parameter estimation algorithms can be viewed as simultaneous signal processing operation. In these cases, the likelihood function provides a mechanism for incorporating physical models of the ocean environment. In addition, one can incorporate uncertainties of source location and ocean environmental parameters a priori, rather than dealing with them ″after the processing″, and this approach also provides a posteriori probabilities of these source and ocean parameters as outputs of the processing. In addition to affecting the structure of optimal signal processing algorithms, these uncertainties affect how well one can spatially localize the source of sound, or the accuracy with which one can estimate the ocean environmental parameters. In passive and active sonar detection, these uncertainties, along with the knowledge of the ocean physics that has been incorporated in the likelihood function, determine detection performance. In particular, this paper will illustrate how signal detection theory can provide quantitative upper bounds of sonar detection performance on the receiver operating characteristic (ROC) as a function of the amount of uncertainty in ocean environmental parameters, source location, and signal-to-noise ratio.

11:20

4aSPb3. Desoloing for musical accompaniment systems. Lawrence J. Raphael (Adelphi University, 1 South Avenue, Garden City, NY 11530, USA, raphael@adelphi.edu)

I discuss ongoing work for musical accompaniment systems in which we remove the soloist from a full recording for soloist and accompanying ensemble (e.g. a concerto), leaving just the accompaniment. I will discuss briefly the score matching problem, which generates a correspondence between a symbolic music representation and the audio. Using this score match, straightforward masking leads to usable source separation results, since the nature of the accompaniment problem partially compensates for the damage done by masking. However, I will discuss methods of improving this separation process involving imputing unobserved audio. The presentation will include a live demonstration of the accompaniment system.

11:40

4aSPb4. Bayesian linear regression onto data-driven dictionaries with application to music transcription. Cédric Févotte (CNRS-Telecom ParisTech, 37-39, rue Dareau, 75014 Paris, France, fevotte@tsi.enst.fr)

In this work, we describe a linear regression technique where features of the dictionary (the collection of explanatory variables) are learnt from the data itself. Our Bayesian setting allows to add regularization constraints on both the explanatory variables and the regressors that fit physical properties of sound. More precisely, smoothness constraints can be imposed on the first ones while time-

persistency and/or sparse constraints can be imposed on the second ones. When applied to music, we observe that the retrieved explanatory variables bear a semantic value and that the overall process yields a compact data-driven object-based transcription of the original signal.

12:00

4aSPb5. Bayesian formant tracking using conditionally linear Gaussian models. Patrick Wolfe (Harvard University, Harvard University - SEAS, 33 Oxford St Rm MD-129, Cambridge, MA 02138-2901, USA, patrick@seas.harvard.edu)

Formants play a central role in the perception and analysis of speech. In this presentation we describe Bayesian approaches to estimating vocal tract resonances from speech waveforms, formulated as a statistical model-based tracking problem. In particular, approaches by Deng and colleagues have shown the promise of an extended Kalman filtering approach based on a robust linearization of the formant-to-cepstrum map. We describe recent extensions to model inter- as well as intra-formant correlation, and detail efficient inference schemes that preserve conditional Gaussianity. A database of formant trajectories provides a notion of ground truth by which estimator performance can be evaluated, and which demonstrates the efficacy of our approach relative to contemporary benchmark tools for formant analysis.

12:20

4aSPb6. Bayesian tracking and geoacoustic inversion. Stan E. Dosso (University of Victoria, School of Earth and Ocean Sciences, Victoria, BC V8W 3P6, Canada, sdosso@uvic.ca), Michael J. Wilmut (University of Victoria, School of Earth and Ocean Sciences, Victoria, BC V8W 3P6, Canada, mjwilmut@uvic.ca)

This paper describes a Bayesian approach to two related inverse problems in underwater acoustics: localizing/tracking an acoustic source when ocean environmental properties are unknown, and determining environmental properties using acoustic data from an unknown (moving) source. The goal of this work is not simply to estimate values for source and/or environmental parameters, but to determine parameter uncertainty distributions, thereby quantifying the state of knowledge and information content of the inversion. A common formulation is applied for both problems in which source parameters (location and spectrum) and environmental parameters are considered unknown random variables constrained by noisy acoustic data and by prior information on parameter values (e.g., physical limits for environmental properties) and on inter-parameter relationships (limits on horizontal and vertical source speed). Given the strong nonlinearity of the inverse problem, marginal posterior probability densities are computed numerically using efficient Markov-chain Monte Carlo importance sampling methods. Source tracking results are represented by joint marginal probability distributions over range and depth, integrated over unknown environmental parameters. The approach is illustrated with two examples representing tracking a quiet submerged source and geoacoustic inversion using noise from an unknown ship-of-opportunity. In both cases, source, seabed, and water-column parameters are unknown.

12:40-2:00 Lunch Break

Invited Papers

2:00

4aSPb7. Geoacoustic Environment Tracking Using Kalman and Particle Filters. Peter Gerstoft (Marine Physical Laboratory, Scripps Institute of Oceanography, 8602 La Jolla Shores Drive, La Jolla, CA 92093-0238, USA, gerstoft@ucsd.edu), Caglar Yardim (Marine Physical Laboratory, Scripps Institute of Oceanography, 8602 La Jolla Shores Drive, La Jolla, CA 92093-0238, USA, cyardim@ucsd.edu), William Hodgkiss (MPL, Scripps Institution of Oceanography, University of California, San Diego, La Jolla, CA 92093-0238, USA, wsh@mpl.ucsd.edu)

This paper addresses the problem of tracking the geoacoustic environmental parameters such as the sound speeds in water, sediment and the bottom, sediment attenuation, density and thickness. The tracking is based on using acoustic measurements within an extended Kalman (EKF), unscented Kalman (UKF), and particle filter (PF) framework. The acoustic field is computed using a normal mode code which introduced a varying degree of nonlinearity depending on the environmental parameter of interest. Posterior Cramer-Rao lower bounds (PCRLB) are used to compute the tracking performances of the filters, including the filter efficiencies, divergence statistics, and computational complexities. The results showed that some of the parameters such as the water column parameters can be tracked by Kalman filters, however, the tracking performance of the Kalman filters was limited by the highly nonlinear relation between the sediment/bottom parameters and the acoustic field and non-Gaussian densities of these parameters. Particle filters proved to be very promising in tracking sediment layer parameters, even in the abruptly changing environments.

2:20

4aSPb8. Inference and learning in gamma chains for Bayesian audio processing. Ali Taylan Cemgil (University of Cambridge, Trumpington street, CB2 1PZ Cambridge, UK, atc27@cam.ac.uk), Onur Dikmen (Bogazici University, Dept. of Computer Engineering, 80815 Istanbul, Turkey, onuro@boun.edu.tr)

Statistical description of complex phenomena encountered in many applications requires construction of nonstationary models. A first step in analysis of such nonstationary sources involves typically a traditional time-frequency analysis Short time Fourier transform. In all these techniques, the underlying implicit assumption is that the process is piecewise stationarity, however dependencies across frequency bands or time frames are not explicitly characterised. Here, we investigate a class of prior models, called Gamma chains, for modelling such statistical dependencies in the time-frequency representations of signals. In particular, we model the prior variance of transform coefficients using Markov chains, trees and fields of inverse Gamma random variables. This model class is Markovian and conditionally conjugate, so standard inference methods like Gibbs sampling, variational Bayes or sequential Monte Carlo can be applied

effectively and efficiently. We also show how hyperparameters, that determine the coupling between prior variances of transform coefficients, can also be optimised. We discuss the pros and cons of various inference schemata (variational Bayes, Gibss sampler and particle filtering) in terms of complexity and optimisation performance for this model class. We illustrate the effectiveness of our approach in audio denoising and single channel audio source separation applications.

2:40

4aSPb9. A nonlinear frequency-domain beamformer for underdetermined speech mixtures. Michael Davies (University of Edinburgh, ICDOM, Kings Buildings, Mayfield Road, EH9 3JL Edinburgh, UK, mike.davies@ed.ac.uk), Mohammad Dmour (University of Edinburgh, Institute for Digital Communications, School of Engineering & Electronics, Alexander Graham Bell Building, Kings Buildings, Mayfield Road, EH9 3JL Edinburgh, UK, m.dmour@ed.ac.uk)

Extraction of a target speech source from among multiple interfering speech sources is challenging when there are fewer microphones than sources (the underdetermined case). Existing speech source separation techniques often suffer from artifacts as well as performance deterioration in reverberant environments, and in some cases also need to estimate the number of sources present. This paper introduces a frequency-domain non-linear beamformer that can perform speech source separation of underdetermined mixtures, is reasonably artifact free and does not require prior knowledge of the number of speakers. Our approach models the data via a Gaussian mixture distribution in the observation domain, which can be learned using the expectation maximization (EM) algorithm. A non-linear distortionless beamformer is then developed, based on this model. Simulations of the non-linear beamformer in underdetermined mixtures with room reverberation confirm its capability to successfully separate speech sources with virtually no artifacts.

3:00

4aSPb10. Bayesian model selection applied to room-acoustic energy decay analysis. Tomislav Jasa (Institute fur Neuroinformatik ETH/UNIZ, Winterthurerstrasse 190, 8057 Zurich, Switzerland, jasa@ini.phys.ethz.ch), Ning Xiang (Rensselaer Polytechnic Institute, Greene Building, School of Architecture, 110 8th Street, Troy, NY 12180, USA, xiangn@rpi.edu)

The previous work of Xiang et al. [Xiang & Goggans, J. Acoust. Soc. Am. 110 (2001), pp. 1415-1424; 113 (2003), pp. 2685-2697; Xiang & Jasa, J. Acoust. Soc. Am. 120 (2006) pp.3744-3749] successfully applied the Bayesian formulism to estimate multiple decay parameters from Schroeder decay functions measured or calculated in acoustically coupled spaces. In this work we consider a more difficult problem of determining the correct decay model in the presence of energy decay data within the Bayesian framework. We will compare the Annealing/Thermodynamic algorithm [Neal, R. M., Statistics and Computing 11 (2001), pp. 125-139], the Nested Sampling algorithm [Silvia & Skilling, Data Analysis: A Bayesian Tutorial, Oxford Science Publications (2006)], and a combined Variational/Markov Chain Monte Carlo approach in order to determine the correct decay model. The advantages/shortcomings of these methods are discussed in the context of the decay model selection and parameter estimation using experimentally measured data from real coupled spaces.

3:20

4aSPb11. Efficient Bayesian inference for multiple pitch estimation of music audio. Emmanuel Vincent (INRIA Rennes Bretagne Atlantique, Campus de Beaulieu, 35042 Rennes Cedex, France, emmanuel.vincent@irisa.fr)

Multiple pitch estimation consists of estimating the number of active notes and their fundamental frequencies on each time frame of a music signal. This is a core problem for several applications, including score transcription and source separation. Bayesian harmonic models are a promising approach, since they allow the joint exploitation of various priors on the model parameters. However existing Bayesian inference methods often rely on specific prior distributions and remain computationally demanding for realistic data. We propose a generic inference method based on adaptive factorization of the joint posterior that allows the application of such models to real-world data. We evaluate the results for the task of multiple pitch estimation using different levels of factorization.

3:40

4aSPb12. Bayesian single channel blind speech dereverberation using Monte Carlo methods. James R. Hopgood (Institute for Digital Communications, The University of Edinburgh, School of Engineering and Electronics, Alexander Graham Bell Building, The King's Buildings, Mayfield Road, EH9 3JL Edinburgh, UK, James.Hopgood@ed.ac.uk), Christine Evers (Institute for Digital Communications, The University of Edinburgh, School of Engineering and Electronics, Alexander Graham Bell Building, The King's Buildings, Mayfield Road, EH9 3JL Edinburgh, UK, c.evers@ed.ac.uk), Judith Bell (Heriot Watt University, School of Engineering and Physical Sciences, Riccarton, EH14 4AS Edinburgh, UK, j.bell@hw.ac.uk)

Audio signals in confined spaces exhibit reverberation due to reflections off surrounding obstacles. Moreover, the signal is distorted by noise, usually modeled as an additive signal observed within the room, independent of the microphone's location, and unaffected by the acoustics. Reverberation and noise cause significant deterioration of audio quality and intelligibility to signals recorded in acoustic environments. Bayesian blind dereverberation infers knowledge about the system by exploiting the statistical properties of speech and the acoustic channel. In the Bayesian framework, the reverberant and noisy signal can be enhanced by processing it either sequentially using online methods or in a batch using offline methods. This paper compares several distinct Bayesian approaches for single-channel blind speech dereverberation. These include Markov chain Monte Carlo methods for batch processing, and sequential Monte Carlo (particle filtering) methods for online processing. In the batch method, static parametric models are used for modeling the statistics of the speech and channel. Optimal parameter estimates are then used to enhance the observed signal. In the sequential approach, the clean speech signal is considered itself an unknown state. Various dynamical models and optimal sampling strategies are discussed for state estimation. The results demonstrate the superiority of the sequential method.

Session 4aUWa

Underwater Acoustics, Acoustical Oceanography, and ECUA: Impact of Internal Waves on Shallow Water Propagation

James F. Lynch, Cochair
Woods Hole Oceanographic Institution, 98 Water Street, Bigelow 203A, MS-11, Woods Hole, MA 02543, USA

Thomas Folégot, Cochair
NATO Undersea Research Center, Viale San Bartolomeo 400, La Spezia, 19126, Italy

Invited Paper

8:00

4aUWa1. Spatial and temporal sound field fluctuations due to propagating internal waves in shallow water. Mohsen Badiey (University of Delaware, College of Marine and Earth Studies, S. College Street, Newark, DE 19716, USA, badiey@udel.edu), Boris Katsnelson (Voronezh State University, 1, Universitetskaya sq., 394006 Voronezh, Russian Federation, katz@phys.vsu.ru), James F. Lynch (Woods Hole Oceanographic Institution, 98 Water Street, Bigelow 203A, MS-11, Woods Hole, MA 02543, USA, jlynch@whoi.edu)

Fluctuating three dimensional acoustic wave propagation in shallow water presents a challenge due to the anisotropic nature of the environment. Temporal and spatial changes in the water column caused by the passage of internal waves are among the the primary causes of the anisotropy. Three main mechanisms for the acoustic field variations have been determined: 1) adiabatic propagation,. 2) horizontal refraction, and 3) mode coupling. All these mechanisms provide different characteristics of the sound fluctuations, and depend on the angle between the internal wave direction and the source receiver propagation path, as well as frequency and mode number. In a recent multi-institutional shallow water experiment (SW06) a series of source-receiver positions were created to examine the effects of 3D environmental fluctuations on the propagation of low to mid frequency (0.05-3 kHz) broadband acoustic signals while extensive environmental observations were made. These recent observational results confirm the above theoretical hypothesis. Work supported by ONR-321OA and RFBR.

Contributed Papers

8:20

4aUWa2. Sound intensity variations in the presence of shallow-water internal waves passing through acoustic track. Jing Luo (University of Delaware, College of Marine and Earth Studies, S. College Street, Newark, DE 19716, USA, luojing@udel.edu), Mohsen Badiey (University of Delaware, College of Marine and Earth Studies, S. College Street, Newark, DE 19716, USA, badiey@udel.edu), Entin A. Karjadi (College of Marine and Earth Studies, University of Delaware, Newark, DE 19716, USA, karjadi@udel.edu), Boris Katsnelson (Voronezh State University, 1, Universitetskaya sq., 394006 Voronezh, Russian Federation, katz@phys.vsu.ru), Alexander Tshoidze (Voronezh State University, 1, Universitetskaya sq., 394006 Voronezh, Russian Federation, tshoidze@phys.vsu.ru), James Moum (College of Oceanic and Atmospheric Sciences, Oregon State University, 104 COAS Administration Bldg, Corvallis, OR 93371, USA, jmoum@coas.oregonstate.edu), James F. Lynch (Woods Hole Oceanographic Institution, 98 Water Street, Bigelow 203A, MS-11, Woods Hole, MA 02543, USA, jlynch@whoi.edu)

Fluctuations of low frequency pulses (LFM signals in 270-330 Hz band) in the presence of internal solitary wave (ISW) packet during the SW06 experiment are analyzed to quantify the interaction of sound with ISW field. Three situations during approximately 2 hours (20:30 - 22:30 GMT of August 17, 2006) are considered: a period when ISW was absent, a period when ISW started to intersect the acoustic track, and a period when ISW occupied the acoustic track. The propagation direction, velocity, and amplitude of the ISW were estimated from the on-board radar images recorded by two research vessels along with temperature records of sensors moored at the source, at the receiver, and between the source-receiver track. Modeal and frequency filtering of received pulses was carried out as well as analysis of temporal variations of the field depth distribution. This analysis allows us to identify two different acoustic fluctuation mechanisms: horizontal refraction and adiabatic variability, and it confirms the previously proposed theory on the sound field fluctuations due to ISW. Work was supported by ONR and RFBR.

8:40

4aUWa3. Short-range acoustic propagation through non-linear internal waves. Daniel Rouseff (Applied Physics Laboratory, University of Washington, 1013 NE 40th St, Seattle, WA 98105, USA, rouseff@apl.washington.edu), Dajun Tang (Applied Physics Laboratory, University of Washington, 1013 NE 40th St, Seattle, WA 98105, USA, djtang@apl.washington.edu), Kevin L. Williams (Applied Physics Laboratory, University of Washington, 1013 NE 40th St, Seattle, WA 98105, USA, williams@apl.washington.edu), James Moum (College of Oceanic and Atmospheric Sciences, Oregon State University, 104 COAS Administration Bldg, Corvallis, OR 93371, USA, jmoum@coas.oregonstate.edu), Zhongkang Wang (Hangzhou Applied Acoustics Research Institute, PO Box 1249, 310012 Hangzhou, China, zkwang@apl.washington.edu)

During the Shallow Water 2006 Experiment (SW06), mid-frequency acoustic transmission data were collected on a vertical array over a continuous 7-hour period at range 550 m. The relatively short range was deemed desirable for studying the effects of internal waves; individual waves in a packet of nonlinear internal waves might be isolated between the acoustic source and receiver. Of present interest are data immediately before, during and after the passage of a non-linear internal wave on 18 August 2006. Among other features, the data show a new acoustic path being generated as the internal wave passes the acoustic source. A ray-based model is developed for the observed effect that uses as input nearby oceanographic measurements. [Work supported by ONR.]

9:00

4aUWa4. Intensity fluctuations of mid-frequency sound signals passing through moving nonlinear internal wave in experiment sw06. Boris Katsnelson (Voronezh State University, 1, Universitetskaya sq., 394006 Voronezh, Russian Federation, katz@phys.vsu.ru), Valery Grigorev (Voronezh State University, 1, Universitetskaya sq., 394006 Voronezh, Russian Federation, grig@box.vsi.ru), James F. Lynch (Woods Hole Oceanographic Institution, 98 Water Street, Bigelow 203A, MS-11, Woods Hole, MA 02543, USA, jlynch@whoi.edu), Dajun Tang (Applied Physics Laboratory, University of Washington, 1013 NE 40th St, Seattle, WA 98105, USA, djtang@apl.washington.edu)

Fluctuations of an intensity of the broadband pulses are studied in mid-frequency area (2 - 4.5 kHz) propagating in the shallow water in the presence of intensive internal waves (IW) moving approximately along an acoustic track. Theory elaborated earlier predicts that in this case specific features of fluctuations are provided by modes coupling (for low frequency sound) or ray scattering (high frequency area) and depend on direction of propagation of signals relative wave front of IW. The corresponding research was carried out during multi-institutional experiment sw06 in New Jersey shelf. We analyze temporal dependence of intensity for the sequence of the sound pulses radiated from the R/V Knorr during approximately one hour - 15:31 -16:20 GMT (August 13, 2006) and received by two separate single hydrophone units (SHRUs) placed at different distance from the source (~4 km and ~12 km). The corresponding acoustic tracks had a little different directions relative wave front of IW. Properties of IW were established using temperature records of sensors in different locations. It is shown that frequency spectra of fluctuations for these SHRUs have different predominating frequencies in accordance with mentioned directions of acoustic tracks. Results of measurements are compared with theoretical estimations and demonstrate good consistency.

9:20

4aUWa5. Simultaneous nearby measurements of acoustic propagation and high-resolution sound speed structure containing internal waves. Frank S. Henyey (Applied Physics Laboratory, University of Washington, 1013 NE 40th St, Seattle, WA 98105, USA, frank@apl.washington.edu), Kevin L. Williams (Applied Physics Laboratory, University of Washington, 1013 NE 40th St, Seattle, WA 98105, USA, williams@apl.washington.edu), Dajun Tang (Applied Physics Laboratory, University of Washington, 1013 NE 40th St, Seattle, WA 98105, USA, djtang@apl.washington.edu)

On two occasions during the SW06 experiment, towed CTD chain measurements were made close to an acoustic propagation path. The acoustic path was 1 km long, oriented roughly in the direction of propagation of large nonlinear internal waves. On the first occasion, large nonlinear internal waves were absent, and on the second occasion, they were present. The CTD chain was towed in loops around the acoustic path, roughly 200 m on either side of the path. On the first occasion, 17 loops were made in about 5.5 hr, and on the second occasion, 7 loops were made in about 2.5 hr. Throughout these time periods, acoustic transmissions between 2 kHz and 10 kHz were carried out. The acoustic environment on the path is estimated by space and time interpolation between the tows on the two sides of the path. The acoustic data is compared with propagation modeling in this environment.

9:40

4aUWa6. The effects of non-linear internal wave curvature on acoustic propagation. Timothy Duda (Woods Hole Oceanographic Institution, 98 Water Street, Bigelow 107, MS-12, Woods Hole, MA 02543, USA, tduda@whoi.edu), James F. Lynch (Woods Hole Oceanographic Institution, 98 Water Street, Bigelow 203A, MS-11, Woods Hole, MA 02543, USA, jlynch@whoi.edu), Ying-Tsong Lin (Woods Hole Oceanographic Institution, 98 Water Street, Bigelow 107, MS-12, Woods Hole, MA 02543, USA, ytlin@whoi.edu), Arthur Newhall (Woods Hole Oceanographic Institution, 98 Water Street, Bigelow 203A, MS-11, Woods Hole, MA 02543, USA, anewhall@whoi.edu), Hans Graber (RSMAS - University of Miami, 4600 Rickenbacher Causeway, Miami, FL 33149, USA, hgraber@rsmas.miami.edu), Micheal Caruso (RSMAS - University of Miami, 4600 Rickenbacher Causeway, Miami, FL 33149, USA, mcaruso@rsmas.miami.edu)

It is well known that coastal nonlinear internal waves can have curved wavefronts, due to either being generated at a "point source" such as a submarine canyon or valley or due to the wave being refracted by large scale water column or bathymetric features. We will explore the first case here, with the emphasis on circular wave fronts. Three cases of acoustic propagation in the vicinity of a circular wavefront will be considered: 1) the source within a soliton train, 2) the source in front of the soliton train, and 3) the source behind the soliton train. Simple geometric forms are presented showing how the curved wavefronts can lead to mode number and frequency dependent dispersion and shadowing effects. Work sponsored by Office of Naval Research.

10:00

4aUWa7. The effects of the internal waves on the statistic characteristics of the sound fields in the 2001 ASIAX South China Sea Experiment. Lixin Wu (National Laboratory of Acoustics, Institute of Acoustics, Chinese Academy of Sciences, NO.21, Bei-Si-huan-Xi Road, 100080 Beijing, China, wlx@mail.ioa.ac.cn), Jun Wang (National Lab. of Acoustics, Institute of Acoustics, Chinese Academy of Sciences, NO.21, Bei-Si-huan-Xi Road, 100080 Beijing, China, wangj@mail.ioa.ac.cn), Shaoqiang Wang (National Lab. of Acoustics, Institute of Acoustics, Chinese Academy of Sciences, NO.21, Bei-Si-huan-Xi Road, 100080 Beijing, China, wsq@mail.ioa.ac.cn), James F. Lynch (Woods Hole Oceanographic Institution, 98 Water Street, Bigelow 203A, MS-11, Woods Hole, MA 02543, USA, jlynch@whoi.edu), Timothy Duda (Woods Hole Oceanographic Institution, 98 Water Street, Bigelow 107, MS-12, Woods Hole, MA 02543, USA, tduda@whoi.edu)

Internal waves are one of primary sources of ocean variations in shallow water. The temporal-spatial stability of sound channel may be degraded by the activities of internal waves. We present analyses of statistic characteristics observed in acoustic signals transmitted by two 400Hz sources moored as part of ASIAEX 2001 South China Sea (SCS) experiment. One source was 31.3 km offshore from the receiving array, and the other was 20.6 km alongshore from the array. Time series of signal intensity measured at individual phones of a 16-element vertical line array and a 32-element horizontal line array. temporal-spatial correlations were observed from 2 May to 17 May 2001. The temporal-spatial decorrelation scales are closely related to internal wave properties. The largest internal wave, especially solitary wave packets, are the principal contributors to reduction of the temporal-spatial decorrelation scales. We also present elementary analyses of higher-order statistics (HOS), such as bispectrum, bicoherency coefficients, etc.

10:20-10:40 Break

10:40

4aUWa8. Observed acoustic arrival structure and intensity variability induced by transbasin nonlinear internal waves in the South China Sea basin. Chingsang Chiu (Naval Postgraduate School, Department of Oceanography, 833 Dyer Road, Rm 328, Monterey, CA 93943-5738, USA, chiu@nps.edu), D. Benjamin Reeder (Naval Postgraduate School, Department of Oceanography, 833 Dyer Road, Rm 328, Monterey, CA 93943-5738, USA, dbreeder@nps.edu), Christopher Miller (Naval Postgraduate School, Department of Oceanography, 833 Dyer Road, Rm 328, Monterey, CA 93943-5738, USA, cwmiller@nps.edu), Justin Reeves (Naval Postgraduate School, Department of Oceanography, 833 Dyer Road, Rm 328, Monterey, CA 93943-5738, USA, jmreeves@nps.edu), Steve Ramp (Naval Postgraduate School, Department of Oceanography, 833 Dyer Road, Rm 328, Monterey, CA 93943-5738, USA, sramp@nps.edu), Yiing-Jang Yang (Naval Academy, Department of Marine Science, P.O. Box 90175, Tsoying Kaohsiung, Taiwan, yjyang@cna.edu.tw), Ruey-Chang Wei (National Sun Yat-sen University, 70 Lien-Hai Road, Institute of Undersea Technology, 804 Kaohsiung City, Taiwan, rcwei@mail

.nsysu.edu.tw),Chifang Chen(National Taiwan University, Dept. of Engineering Science and Ocean Engineering, University No. 1 Roosevelt Road, Section #4, Taipei, Taiwan, chifang@ntu.edu.tw)

During the 2005-2006 Windy Island Nonlinear Soliton Experiment (WISE), large-amplitude internal waves were observed by in situ oceanographic sensors to propagate eastward from the Luzon Strait, through the deep basin, onto the shelf and Dongsha Plateau of the South China Sea year round except winter. In a parallel effort to measure the effects of these transbasin internal waves on long-range, low-frequency sound propagation, an acoustic source with a center frequency of 400-Hz and bandwidth of 100-Hz was moored on the west side of the deep basin transmitting a phase-modulated m-sequence signal every 15 min from February to October 2006. These periodic transmissions were recorded by a receiver moored ~166 km to the east of the source. The recording was processed to give the arrival structure of a pulse and its temporal changes over the eight-month period. The observed temporal variability in the arrival structure and in the acoustic intensity were analyzed using time-series techniques and models with emphasis to elucidate the connection to the observed sound speed variability induced by the nonlinear transbasin internal waves. Results from the analysis are presented and discussed. [The research is sponsored by the US ONR and the Taiwan NSC.]

11:00

4aUWa9. Spatial and temporal coherence of low-frequency acoustic field in shallow water: Experimental results. Lianghao Guo (National Laboratory of Acoustics, Institute of Acoustics, Chinese Academy of Sciences, NO.21, Bei-Si-huan-Xi Road, 100080 Beijing, China, glh2002@mail.ioa.ac.cn), Zaixiao Gong (National Laboratory of Acoustics, Institute of Acoustics, Chinese Academy of Sciences, NO.21, Bei-Si-huan-Xi Road, 100080 Beijing, China, gzx@mail.ioa.ac.cn), Lixin Wu (National Laboratory of Acoustics, Institute of Acoustics, Chinese Academy of Sciences, NO.21, Bei-Si-huan-Xi Road, 100080 Beijing, China, wlx@mail.ioa.ac.cn), Xilu Li (National Laboratory of Acoustics, Institute of Acoustics, Chinese Academy of Sciences, NO.21, Bei-Si-huan-Xi Road, 100080 Beijing, China, glh2002@mail.ioa.ac.cn)

Spatial and temporal coherence of acoustic field has very important effects on applications of underwater acoustics. In this paper, recent experimental results of low-frequency signal coherence in shallow water are presented. For signals with low frequencies of 100~500Hz in shallow water, the vertical correlation has no distinct depth dependence, but it has obvious range dependence. The horizontal correlation length is greater than 40 wavelengths, the temporal correlation length is greater than 510s at frequency of 475Hz and greater than 1800s at frequency of 150Hz. These experimental results show that low-frequency acoustic field has strong spatial coherence and temporal stability in shallow water. [Work supported by the National Natural Science Foundation of China under Grant No.10734100]

11:20

4aUWa10. Temporal correlation of MFP with the presence of internal waves. Zhenglin Li (Haikou Acoustic Lab. & National Lab. of Acoustics, Inst. of Acoustics, Chinese Academy of Sciences, 63 Binghaidadao, 570105 Haikou, China, lzhl@mail.ioa.ac.cn), Guihua Ji (Haikou Acoustic Lab. & National Lab. of Acoustics, Inst. of Acoustics, Chinese Academy of Sciences, 63 Binghaidadao, 570105 Haikou, China, jgh@mail.ioa.ac.cn), Qiongxing Dai (Haikou Acoustic Lab. & National Lab. of Acoustics, Inst. of Acoustics, Chinese Academy of Sciences, 63 Binghaidadao, 570105 Haikou, China, dqx66@163.com)

Internal wave is a dominant source of ocean uncertainties in shallow waters. The ability of passive source localization may be degraded due to mismatch between model predictions and measurements caused by the activities of internal waves. Using ocean environment measurements from an experiment, the effects of Garrett-Munk and solitary internal waves on the temporal correlation of matched-field processing (MFP) in shallow water for sources with different frequencies and different depths are numerically investigated. It is shown that the temporal correlation of MFP decreases as the amplitude of solitons or the average energy density of linear internal waves increased. For a source with lower frequency or located below the thermocline, the temporal correlation of MFP is less affected by internal waves, and the length of which is longer. Moreover, the effects of the range between solitons and source on the temporal correlation of MFP are relatively small.

11:40

4aUWa11. Observations of noise generated by nonlinear internal waves on the continental shelf during the SW06 experiment. Andrey N. Serebryany (Woods Hole Oceanographic Institution, 98 Water Street, Bigelow 203A, MS-11, Woods Hole, MA 02543, USA, aserebryanyy@whoi.edu), Arthur Newhall (Woods Hole Oceanographic Institution, 98 Water Street, Bigelow 203A, MS-11, Woods Hole, MA 02543, USA, anewhall@whoi.edu), James F. Lynch (Woods Hole Oceanographic Institution, 98 Water Street, Bigelow 203A, MS-11, Woods Hole, MA 02543, USA, jlynch@whoi.edu)

As part of the Shallow Water 2006 (SW06) experiment, simultaneous measurements of coastal internal wave oceanography and ocean acoustics were made over a two month period in late summer. The generation of noise by nonlinear internal waves propagating on the shelf during the SW06 experiment was observed, and is reported upon here. Three main types of noise were observed: bed noise, mid-column noise and noise from the sea surface. Surface noise is created due to an enhancement of surface wave breaking in the convergence zone created by the internal waves. Strong broadband bed noise was observed during the moments of internal wave passage above a horizontal array of hydrophones lying on the bottom. Appearance of bed noise in the form of several spikes we observed coinciding with the strongest bottom currents created by internal wave orbital currents. For the case of breaking internal waves, the near-bed spike-like noise disappeared and mid-column noise of a different character was seen instead. Mechanisms of the various types noise generation will be discussed. Work sponsored by ONR.

12:00

4aUWa12. Applying the Data Nullspace Projection Method to a Geoacoustic Bayesian Inversion in a Randomly Fluctuating Shallow-Water Ocean. James F. Lynch (Woods Hole Oceanographic Institution, 98 Water Street, Bigelow 203A, MS-11, Woods Hole, MA 02543, USA, jlynch@whoi.edu), Ying-Tsong Lin (Woods Hole Oceanographic Institution, 98 Water Street, Bigelow 107, MS-12, Woods Hole, MA 02543, USA, ytlin@whoi.edu), Arthur Newhall (Woods Hole Oceanographic Institution, 98 Water Street, Bigelow 203A, MS-11, Woods Hole, MA 02543, USA, anewhall@whoi.edu)

Bayesian inversion techniques which are commonly used in geoacoustic inversion can suffer the effects of uncertain water-column fluctuations. To reduce these effects, one could also invert for the fluctuating water-column parameters; however, there are issues with this approach. One obvious problem is that the dimensions of parameter space will increase, so that Bayesian inversion may not be efficient. Another issue arises from the temporal and spatial randomness and variability of the water-column parameters; this requires extra effort in handling the randomness and variability in the inversion procedure. In this paper, we propose another approach to the problem. The data nullspace projection method, which has been applied to perturbative inversion, is extended to Bayesian inversion using acoustic modal wavenumbers and group velocities. The idea of this method is to project acoustic data onto a subspace that is insensitive to uncertain water-column fluctuations, and use the projected data to invert for bottom properties. The advantage of this approach is that we do not need to invert for water-column parameters, so that the inversion requires less operations than the previous approach. A numerical simulation demonstrates the feasibility of the projection approach. It is then applied to real data collected in the SW06 experiment.

12:20

4aUWa13. Acoustic propagation modeling in the presence of environmental uncertainty. Yu Yu Khine (USNRL, 4555 Overlook Ave SW, Washington, DC 20375, USA, yuyu.khine@nrl.navy.mil), Steven

Finette(USNRL, 4555 Overlook Ave SW, Washington, DC 20375, USA, steven.finette@nrl.navy.mil), Roger Oba (USNRL, 4555 Overlook Ave SW, Washington, DC 20375, USA, roba@wave.nrl.navy.mil)

Due to incomplete knowledge of ocean environments, this research incorporates environmental uncertainty into an acoustic model representing wave propagation in order to quantitatively represent the uncertainty of the acoustic field. The waveguide considered here has a spatially varying, uncertain sound speed distribution with a known correlation length. Karhunen-Loeve and polynomial chaos expansions are used to represent the uncertainty in the environment and acoustic field, respectively, in a narrow- angle parabolic wave equation. In this two-dimensional model, the water depth is 150 m and propagation is over a range of 20 km. The environmental uncertainty term in the wave equation is assumed to vary randomly in the range direction, and is characterized by an exponentially decaying correlation function. An implicit finite difference scheme is used to solve a set of coupled differential equations for the stochastic envelope function at different source frequencies in the range of a few hundred Hz. The simulated results will include probability density functions at selected spatial locations in the waveguide, first and second moments of the field, and these results will be compared with those obtained independently from Monte Carlo samplings from the same ocean environment. Work supported by ONR.

12:40-1:40 Lunch Break

Contributed Papers

1:40

4aUWa14. New Numerical Computation of Acoustic Propagation in the Ocean in the Presence of Internal Waves is 1000 Times Faster than Traditional Split-Step Fourier Approaches. Alfred R. Osborne (University of Torino, Dipartimento di Fisica Generale, Via Pietro Giuria 1, 10124 Torino, Italy, al.osborne@gmail.com)

A new numerical model for acoustic propagation based upon the large angle parabolic type equations is found to execute about 1000 times faster than the FFT split step algorithm. The approach is applied to the imaging and nonlinear filtering of internal waves in shallow water regions for 3-dimensional propagation of acoustic waves. For appropriate array placement one can construct the inverse problem and hence the internal wave field from the acoustic measurements themselves. The unique nonlinear filtering method allows one to filter out the internal waves from the density field and hence to realized acoustic wave propagation in the absence of the internal waves. The hyperfast acoustic model has some of the following characteristics: (1) The work can be extended to the fully 3-dimensional Helmholtz equation. (2) The method is a kind of multi-dimensional Fourier analysis which exactly solves the wave equations (PE, large angle PEs and Helmholtz)) so that the acoustic wave does not degrade with range as with more traditional numerical integrations. (4) Multi-dimensional Fourier transforms can be used to nonlinearly filter acoustic signals in a wide range of applications and hence the approach is quite robust to interference from background acoustic noise.

2:00

4aUWa15. Modeling probability density functions for acoustic propagation through internal waves in shallow water environments. Kevin D. Lepage (Naval Research Laboratory, 4555 Overlook Ave SW, Washington, DC 20375, USA, kevin.lepage@nrl.navy.mil)

Acoustic propagation through internal waves is shallow water introduces randomness to the acoustic field in that internal waves are generally incompletely measured and are therefore best understood as random realizations of a stochastic process. Due to the physics of internal waves these environmental perturbations are expressed in a finite number of modes, each of which affects acoustic propagation differently. As acoustic propagation in shallow water is itself confined into modes, a matrix of interaction strengths for both the accumulated phase and the mode coupling may be derived which can be integrated forward along the acoustic path to account for the accumulation of uncertainty. A powerful ansatz for solving this problem is a Polynomial Chaos (PC) expansion of the complex modal amplitudes in the random variables which are the internal wave amplitudes. In this work the PC technique is used to derive the probability density functions of the complex modal amplitudes in the presence of a homogeneous internal wave field, showing good agreement with Monte-Carlo results. The pdfs of the complex modal amplitudes can then be combined to obtain the pressure field pdf as well as various statistics of interest such as the scintillation index. [Work supported by ONR]

2:20

4aUWa16. A modified dnoidal model for internal solitary waves and its effect on sound transmission. Shaoqiang Wang (National Lab. of Acoustics, Institute of Acoustics, Chinese Academy of Sciences, NO.21, Bei-Si-huan-Xi Road, 100080 Beijing, China, wsq@mail.ioa.ac.cn), Lixin Wu (National Laboratory of Acoustics, Institute of Acoustics, Chinese Academy of Sciences, NO.21, Bei-Si-huan-Xi Road, 100080 Beijing, China, wlx@mail.ioa.ac.cn), Changqing Hu (Shanghai Acoustics Lab., Chinese Academy of Sciences, No.456, Xiao-Mu-Qiao Road, Xu-Hui District, 200032 Shanghai, China, hchq@mail.ioa.ac.cn)

A new solution of KDV equation in the form of dnoidal function is developed in this paper. Based on this new solution, a modified solution of KDV equation with slowly varying parameters in the form of dnoidal function is derived. Numerical simulation shows that the wave pockets scale of the modified solution is only 1/5 to the solution in the reference (JASA, 108 (3), pp 957-972), and also the equilibrium positions are different. Comparing the solutions with slowly varying parameters with the published data of internal solitary waves in the ocean indicates that the modified solution is better for the description of the dnoidal wave. Based on the modified solution of KDV equation with slowly varying parameters, a modified model for dnoidal wave is given and its effect on sound transmission is discussed in this paper.

Session 4aUWb

Underwater Acoustics and ECUA: Determination of Acoustic Properties of Materials for Sonar Applications I

Kenneth G. Foote, Cochair
Woods Hole Oceanographic Institution, Woods Hole, MA 02543, USA

Stephen P. Robinson, Cochair
National Physical Laboratory, Hampton Road, Teddington, TW11 OLW, UK

Invited Papers

8:00

4aUWb1. Phase change measurement, sound speed and attenuation determination from underwater acoustic panel tests. Jean Piquette (Naval Undersea Warfare Center, 1176 Howell Street, Newport, RI 02841, USA, paoleroae@npt.nuwc.navy.mil), Anthony Paolero (Naval Undersea Warfare Center, 1176 Howell Street, Newport, RI 02841, USA, paoleroae@npt.nuwc.navy.mil), Robert Drake (Naval Undersea Warfare Center, 1176 Howell Street, Newport, RI 02841, USA, Drakerm@npt.nuwc.navy.mil)

Material measurements in underwater acoustics are employed regularly for characterization of materials used as acoustic windows. Various techniques have been developed to measure the acoustic attenuation magnitudes of materials. Recently, there has been increased interest in window configurations of complex geometries and of phase response of that material to an acoustic wave. This latter phase parameter can be of high significance for acoustic devices composed of an array of elements. Thus, the phase response of the attenuation is needed to properly characterize material performance on the overall system. This translates into a primary need to measure the complex acoustic attenuation of panels at various angles of incidence. This paper summarizes the methodology to measure the complex attenuation of materials. Case examples of test materials measured will be presented; comparisons to theoretical response will be provided. Considerations given to rigging and required acoustic settling times are discussed. Expansion of the methodology that incorporates a causal relationship between the measured phase response and attenuation to the sound speed of the material will be developed. The model relating these parameters and their implementation via an iterative least squares fitting of the parameters to the measurement data will be discussed.

8:20

4aUWb2. The underwater acoustic testing of modest sized panel materials using a multi-element array technique in a laboratory test vessel. Michael J. Martin (QinetiQ Ltd, Rm 1146, Bldg A7, Cody Technology Park, Ively Road, GU14 0LX Farnborough, UK, mjmartin1@qinetiq.com), Stephen P. Robinson (National Physical Laboratory, Hampton Road, TW11 OLW Teddington, UK, Stephen.Robinson@npl.co.uk), John Smith (DSTL, Rm 14, Bldg 352, Porton Down, SP4 0JQ Salisbury, UK, jdsmith@dstl.gov.uk), Victor F. Humphrey (Institute of Sound and Vibration, Univ. of Southampton, University Road, Highfield, SO17 1BJ Southampton, UK, vh@isvr.soton.ac.uk)

The underwater acoustic properties of materials can be assessed in panel form via a simple single hydrophone measurement technique which is ideally conducted on large test panels in open water. Alternatively measurements may be conducted in a laboratory test vessel which is capable of simulating ocean conditions. However, physical limitations imposed by the constraints of the vessel, including a reduction in test panel dimensions, require modification of the traditional technique to allow measurements to be made down to low kilohertz frequencies. This can be achieved by, in addition to a directional source, the use of a directional receiver in the form of a planar multi-hydrophone array. The technique is described and illustrated with measurements of reflection loss and insertion loss between 1 kHz and 7 kHz performed on a test panel in a pressure vessel through changing hydrostatic pressure from ambient to 2.8 MPa. The efficacy of this technique is considered with simulated multi-hydrophone array measurements on a scaled panel in an open tank.

8:40

4aUWb3. Panel transmission measurements: The influence of the non plane wave nature of the incident field. Victor F. Humphrey (Institute of Sound and Vibration, Univ. of Southampton, University Road, Highfield, SO17 1BJ Southampton, UK, vh@isvr.soton.ac.uk), John Smith (DSTL, Rm 14, Bldg 352, Porton Down, SP4 0JQ Salisbury, UK, jdsmith@dstl.gov.uk)

For reasons of cost and practicality, laboratory measurements of the acoustic transmission and reflection properties of materials for use in underwater applications are typically performed on samples of limited dimensions - and with the source and receiver separated by relatively short distances - resulting in a non planar measurement field. The influence of this on the resulting measurements is investigated in this paper. In particular, for low frequency measurements the influence of the evanescent wave contributions can become significant. In this paper two alternative approaches are used to evaluate the transmission properties. The first method decomposes the incident spherical wave into its plane wave components and integrates the resulting transmitted waves numerically to evaluate the transmitted field. The second approach uses an asymptotic expansion of the field in terms of wave front curvature: bounds are then

placed on the error in this expansion at low frequency using thin plate theory. Results are compared and contrasted for measurements in the frequency range 1 to 60 kHz for panels of simple elastic materials (steel and Perspex (polymethylmethacrylate)). In addition the nature and significance of the modes of the panel for evanescent waves are considered. The consequences for laboratory measurements are also outlined.

9:00

4aUWb4. Comparisons of the dynamic moduli of various polymers. John Smith (DSTL, Rm 14, Bldg 352, Porton Down, SP4 0JQ Salisbury, UK, jdsmith@dstl.gov.uk)

To fully characterise the elastic properties of a homogeneous, isotropic material, two independent elastic constants are needed, usually the bulk and shear moduli. For the types of polymers used in sonar applications, these moduli are typically both frequency and temperature dependent. Of particular interest is the position (in frequency and temperature) of peak loss tangent, which is related to the glass transition temperature through the free volume concept. Although there exists in the literature a lot of data on the dynamic shear (and Young's) modulus for various polymers, data on dynamic bulk modulus is scarcer, due to the difficulty of the measurement. This paper reviews the current literature on the dynamic moduli of various polymers, with particular regard to the relationship between the peak loss tangents of the bulk and shear moduli. Simple relaxation models are studied to give insight on the factors affecting the peak of the loss tangent and new measurements on a nitrile-butadiene rubber compound are presented.

9:20

4aUWb5. Pulse tube measurement of bulk modulus of visco-elastic composite materials: Theory and practice. Peter R. Brazier-Smith (Thales, Ocean House, Somerset, BA8 0DH Templecombe, UK, peter.brazier-smith@uk.thalesgroup.com), Allan R. Clark (Thales, Ocean House, Somerset, BA8 0DH Templecombe, UK, allan.clark@uk.thalesgroup.com)

A method for the determination of the bulk moduli and loss factors of micro-voided composite materials is presented. The method requires that the reflection and transmission coefficients of a tile of uniform thickness are determined in both amplitude and phase as functions of frequency. Reduction to the bulk modulus and loss factor then proceeds by using the analytic properties of a function of a complex variable derived from the reflection and transmission coefficients. A pulse tube is used for the determination of the complex reflection and transmission coefficients. Although other measurement techniques are available, the pulse tube has proved to be versatile in covering a large range of the frequency-temperature master curve for typical composite materials used in underwater acoustics. It achieves this versatility by using an anti-freeze/water mixture as the medium following which measurements can be made over a range of different temperatures.

Contributed Papers

9:40

4aUWb6. Determining dynamic viscoelastic properties without time-temperature shifting. Walter M. Madigosky (Catholic University of America, Department of Physics, Washington, DC, DC 20064, USA, wmadigosky@yahoo.com), Gilbert F. Lee (NSWCCD, 9500 McArthur Boulevard, Bethesda, MD 20817, USA, gilbert.f.lee@navy.mil), Jan M. Niemiec (NSWCCD, 11798 Fox Rest Court, New Market, MD 21774, USA, jan301@comcast.net)

A novel unbiased procedure to analyze dynamic mechanical data of rheologically simple viscoelastic polymers by modeling the data with the Havriliak and Negami (HN) equation is described. The real and imaginary parts of the HN equation are used to solve for the global frequency-time dependent parameter ($\omega\tau$) for all the data thereby uniquely determining the time- temperature shift function. Displaying the experimental data in the form of a wicket or Argand diagram provides initial estimates for the HN parameters. An unbiased error analysis is performed to minimize the difference between experimental and calculated complex viscoelastic values. Finally the characteristic relaxation time, τb> <0>, is determined by minimizing the error between the calculated data and experimental data at the reference temperature <T> <0> . Using this procedure, the complete master curve is generated without the need for overlapping frequency data and the procedural error and operator bias associated with time-temperature shifting is eliminated. The technique can also generate a complete frequency spectrum from isochronal temperature scans such as those obtained from a torsion-pendulum, rheovibron or a Dynamic Mechanical Analyzer (DMA) apparatus, which is not otherwise possible.

10:00

4aUWb7. A new integral equation method for elastic composites. Natasha J. Willoughby (The University of Manchester, School of Mathematics, Oxford Road, M13 9PL Manchester, UK, Natasha.J.Willoughby @student.manchester.ac.uk), William J. Parnell (The University of Manchester, School of Mathematics, Oxford Road, M13 9PL Manchester, UK, William.Parnell@manchester.ac.uk), I David Abrahams (The University of Manchester, School of Mathematics, Oxford Road, M13 9PL Manchester, UK, David.Abrahams@manchester.ac.uk)

A new integral equation approach to elastodynamic homogenization has been proposed [1] to determine the effective properties of periodic fibre reinforced composite materials in the case of SH wave propagation. When all the fibres are aligned in the same direction and considered infinite in extent, the microstructure is two-dimensional. The integral equation method is based on Navier's equations of elasticity in integral equation form, and uses the notion of separation of scales and averaging to find explicit expressions for the effective properties in a convenient form. Here we discuss an extension to the in-plane problem: the response of periodic fibre reinforced composites to time harmonic (low frequency) P/SV wave propagation. For simplicity, we assume all fibres are identical and of circular cross-section, and that both host and fibre phases are isotropic; additionally we restrict attention to lattice geometries which result in, at most, orthotropic elastic symmetry. The governing equations are presented and the effective quasi-static material properties are determined via the integral equation methodology. Results are presented for the effective material properties and compared with existing methods. [1] W.J. Parnell and I.D. Abrahams. ″A new integral equation approach to elastodynamic homogenization″. Submitted to Proc. Roy. Soc. A, 2007.

10:20-10:40 Break

10:40

4aUWb8. Velocity dispersion analysis of acoustic scattering wave from elastic shells. Cao Zhengliang (State Key Lab Ocean Acoustics, Hangzhou Appl Acous Res Inst, Rm 1510 No 96 HuaXing Rd, 310012 Hangzhou, China, caozhengliang@yahoo.com), Du Shuanping (State Key Lab Ocean Acoustics, Hangzhou Appl Acous Res Inst, Rm 1510 No 96 HuaXing Rd, 310012 Hangzhou, China, skldusp@tom.com), Zhou Shihong (State Key Lab Ocean Acoustics, Hangzhou Appl Acous Res Inst, Rm 1510 No 96 HuaXing Rd, 310012 Hangzhou, China, shih_zhou@yahoo.com.cn), Cong

Weihua(State Key Lab Ocean Acoustics, Hangzhou Appl Acous Res Inst, Rm 1510 No 96 HuaXing Rd, 310012 Hangzhou, China, cwhfrj@hzcnc .com)

In recent years the analysis of velocity dispersion of circumferential waves (or surface waves), excited by an incident plane wave to an elastic cylindrical or spherical shell, has theoretically provided valuable insight into the underlying mechanisms of scattering. In the present study, an approach of velocity dispersion analysis on acoustic scattering wave is advanced for the data induced by a spectral bandwidth signal. The method, based on a signal processing technique in time-frequency domain, is examined with simulating waveforms scattered from an elastic spherical and cylindrical shell respectively by linear frequency-modulated signal. In addition, the forward scattering waves of an elastic cylindrical shell filled with fluid is obtained by a line horizontal array in laboratory waveguide, and the results of velocity dispersion is compared with that of theoretical calculation. [Work supported by the National Natural Science Foundation of China (Grant No. 10704068)]

11:00

4aUWb9. Experimental study of piezoelectret foams as underwater sensors. Michael Haberman (The University of Texas, Applied Research Laboratories, 10000 Burnet Road, Austin, TX 78758, USA, haberman@arlut.utexas.edu),Steven Embleton(The University of Texas, Applied Research Laboratories, 10000 Burnet Road, Austin, TX 78758, USA, steve.embleton@arlut.utexas.edu)

This work explores the use of piezoelectret foams (PF) as acoustic sensors for underwater applications. PF material (Emfit Ltd.) provides an intriguing alternative to piezoelectric ceramics and piezopolymers due to their low density, minimal thickness, and potential for easily creating sensors of complex geometries. The foams consist of a continuous polymer containing electrically polarized elliptical voids. Typical density, thickness, and low frequency receive voltatge sensitivity (RVS) values of these foams are 300 kg/m3, 80 μm, and -175 dB re 1V/μPa, respectively. This work presents experimentally obtained RVS of piezoelectret sensors with rigid and pressure release backing. The results show PF sensor RVS is comparable to conventional sonar transducers at low ambient pressures with RVS degradation as ambient pressure increased. The results are compared with theoretical predictions using microelectromechanical mean field theory and equivalent circuit models. Theoretical predictions explain the observed sensitivity degradation due to void closure caused by the applied pressure. To overcome the performance degradation, two pressure tolerant sensor design concepts are proposed and tested. The designs aim to employ PF elements for high ambient pressure applications while leveraging foam density and thickness to create lightweight, low profile sensors.

THURSDAY MORNING, 3 JULY 2008 ROOM 342A, 8:00 TO 10:40 A.M.

Session 4aUWc

Underwater Acoustics and ECUA: Geoacoustic Sediment Modeling III

Nicholas P. Chotiros, Cochair
Applied Research Laboratories, University of Texas, PO Box 8029, Austin, TX 78713-8029, USA

Jean-Pierre Sessarego, Cochair
Laboratory for Mechanics and Acoustics CNRS, 31 chemin Joseph Aiguier, Marseille, 13009, France

Contributed Papers

8:00

4aUWc1. Measuring grain roughness for the purpose of high-frequency acoustic modeling. Kevin Briggs (Naval Research Laboratory, Marine Geosciences Division, Stennis Space Center, MS 39529-5004, USA, kbriggs@nrlssc.navy.mil), Allen Reed (Naval Research Laboratory, Marine Geosciences Division, Stennis Space Center, MS 39529-5004, USA, areed@nrlssc.navy.mil), Richard Ray (Naval Research Laboratory, Oceanography Division, Stennis Space Center, MS 39529-5004, USA, Ricky.Ray@nrlssc.navy.mil), Michael Richardson (Naval Research Laboratory, Marine Geosciences Division, Stennis Space Center, MS 39529-5004, USA, Mike.Richardson@nrlssc.navy.mil)

Grain roughness and packing may be important sediment properties for newer acoustic models. We present Scanning Electron Stereomicroscopic imagery of natural sand grains of varying shape and roughness for evaluation of potential grain interactions of individual grains. The grain shape and presence of microasperities will determine the probability of the contact with surrounding grains being a point or a broader area. Moreover, the use of a micro-roughness power spectrum in characterizing the sand grain roughness may be appropriate. Grain contact information is an essential starting point for developing and evaluating acoustic models that address acoustic losses at high frequencies. This information provides the basis to understand contact mechanics, such as grain slip and frame dilation, during insonification. Because media frame stiffness depends, at the grain scale, on the number and type of grain-to-grain contacts, ultimately we would like to characterize sand sediments with imagery identifying such grain contact information. The natural shapes of grains, their variations, and their packing density present a variety of non-ideal (point) contacts. X-ray micro-focus Computed Tomography shows great promise for documenting of the number and size (area) of grain contacts within grain aggregations, and a demonstration of these data will also be presented.

8:20

4aUWc2. An in situ sediment sound speed measurement platform: Design, operation and experimental results. Jie Yang (Applied Physics Laboratory, University of Washington, 1013 NE 40th Street, Seattle, WA 98105, USA, jieyang@apl.washington.edu), Dajun Tang (Applied Physics Laboratory, University of Washington, 1013 NE 40th St, Seattle, WA 98105, USA, djtang@apl.washington.edu), Kevin L. Williams (Applied Physics Laboratory, University of Washington, 1013 NE 40th St, Seattle, WA 98105, USA, williams@apl.washington.edu)

A unique Sediment Acoustic-speed Measurement System (SAMS) was developed to directly measure sediment sound speed. The system consists of ten fixed sources and one receiver. In a typical deployment, the SAMS is deployed from a ship that is dynamically positioned. The sources are arranged just above the sea bottom and the receiver is drilled into the sediment with controlled steps by a vibro-core. The maximal sediment penetration depth is 3 meters. At each receiver depth, the 10 sources transmit to the receiver at different angles in the frequency range of 2-35 kHz, providing 10 estimates of sound speed through time-of-flight measurements from the known source-to-receiver geometry. SAMS was deployed three times during

the recent Shallow Water Experiment 2006 (SW06) on the New Jersey shelf at 80 m water depth. Preliminary results of sediment sound speed are 1618 ± 11, 1598 ± 10, and 1600 ± 20 m/s at three separate deployment locations. Little dispersion in sediment sound speed was observed. (Work supported by ONR)

8:40

4aUWc3. Estimating sediment speed and attenuation with sub-bottom reflections. Kunde Yang (Institute of Acoustic Engineering, Northwestern Polytechnical University, 710072 Xi'an, China, ykdzym@nwpu.edu.cn), Ross Chapman (University of Victoria, 3800 Finnerty Rd, Vcitoria, BC V8W 3P6, Canada, chapman@uvic.ca), Yuanliang Ma (Institute of Acoustic Engineering, Northwestern Polytechnical University, 710072 Xi'an, China, ylma@nwpu.edu.cn)

An inversion method based on sub-bottom reflection is investigated using LFM data collected by a Vertical Linear Array from the SW06 experiment. The distance between the LFM source and the array is about 230m. After extracting the impulse response with matched filter from the received signal, the sub-bottom reflections were found to be strong. The chirp sonar survey nearby the experiment site showed that there is a prominent shallow sub-bottom R reflector with about 20 m depth (based on 1500 m/s). The relative arrival time and amplitude of the sub-bottom reflection signals were used to estimate the sound speed and the attenuation of the sediment. Because the direct arrivals in the water were influenced strongly by the internal wave, the first bottom reflection was applied as the reference path to calculate the relative arrival time and absorption loss in sediment. The sediment attenuation was estimated by assuming that it had linear frequency dependence. The estimated values of the sediment sound speed and attenuation were compared with matched field geoacoustic inversion results published by other research group.

9:00

4aUWc4. Shear wave speed increases with depth to the one-sixth power in sandy/silty marine sediments. Allan D. Pierce (College of Enginering, Boston University, 110 Cummington St, Boston, MA 02215, USA, adp@bu.edu), William M. Carey (College of Enginering, Boston University, 110 Cummington St, Boston, MA 02215, USA, wcarey@bu.edu)

Gravity holds the sediment's particles in loose contact; the strength varies with depth. The distribution in shapes, sizes, and orientations is presumed independent of depth. Each particle is subject to several contact forces, and also to a buoyancy force exerted by the surrounding water. An externally imposed shear stress results in distortions in the individual grains, the nature and magnitudes of which depend on the contact areas between the grains, which in turn depend on depth. A derivation making use of fundamdental mechanics, the theory of elasticity, and Hertz's theory of contact yields shear modulus G as a dimensionless quantity times $g^{1/3}(\rho_s\text{-}\rho_w)^{1/3}E^{2/3}d^{1/3}$, where d is depth into the sediment and E is the elastic modulus of the solid material in the grains. The dimensionless quantity depends on Poisson's ratio and porosity. The shear speed $(G/\rho_{av})^{1/2}$ consequently varies with depth as $d^{1/6}$. The prediction is consistent with data reported in the past by Stoll, Yamamoto, and Hamilton; the discrepancy of the theoretical prediction of 0.167 with experimentally derived exponents of the order of 0.25, although not viewed as significant, is discussed, and it is suggested that such may be caused by the variation of porosity with depth.

9:20

4aUWc5. Measuring attenuation and velocity within unconsolidated lacustrine sediments, using high-resolution seismic data. Luke J. Pinson (National Oceanography Centre, University of Southampton Waterfront Campus, European Way, SO14 3ZH Southampton, UK, ljwp101@soton.ac.uk), Timothy J. Henstock (National Oceanography Centre, University of Southampton Waterfront Campus, European Way, SO14 3ZH Southampton, UK, then@noc.soton.ac.uk), Justin K. Dix (National Oceanography Centre, University of Southampton Waterfront Campus, European Way, SO14 3ZH Southampton, UK, jkd@noc.soton.ac.uk), Jonathan M. Bull (National Oceanography Centre, University of Southampton Waterfront Campus, European Way, SO14 3ZH Southampton, UK, jmb1@noc.soton.ac.uk), Angus I. Best (National Oceanography Centre, University of Southampton Waterfront Campus, European Way, SO14 3ZH Southampton, UK, aib@noc.soton.ac.uk)

We present estimates of in-situ compressional-wave attenuation and velocity within the uppermost 30 m of unconsolidated lacustrine sediments within Lake Windermere (U.K.), using high-resolution seismic data acquired with Boomer and Chirp sources. The wide frequency bandwidth of the Chirp source allows attenuation to be examined over a frequency range of approximately 2-9 kHz, and by using a spectral ratio technique incorporating robust re-weighted least squares regression, the apparent quality factor of sediments can be accurately and precisely determined. A 60 m multi-channel streamer used with the Boomer source allows interval velocities between target reflectors to be obtained. Models relating quality factor to mean grain-size distinguish between coarse grain-dominated and clay-dominated sediments. The interval velocities improve the classification of the sediment sequences to clays, laminated silts & sands, and coarse sand and gravel deposits. The results are evaluated against geological and core data.

9:40

4aUWc6. Environmental effects on frequency behavior of modal attenuation coefficients for sandy bottoms. Wendy Saintval (University of Miami, RSMAS, 4600 Rickenbacker Causeway, Miami, FL 33149, USA, wsaintval@hotmail.com), William M. Carey (College of Enginering, Boston University, 110 Cummington St, Boston, MA 02215, USA, wcarey@bu.edu), Allan D. Pierce (College of Enginering, Boston University, 110 Cummington St, Boston, MA 02215, USA, adp@bu.edu), James F. Lynch (Woods Hole Oceanographic Institution, 98 Water Street, Bigelow 203A, MS-11, Woods Hole, MA 02543, USA, jlynch@whoi.edu), William L. Siegmann (Rensselaer Polytechnic Institute, 110 8th Street, Troy, NY 12180, USA, siegmw@rpi.edu)

The modal attenuation coefficients (MACs) can be determined using a recent simplification of Biot theory [A.D. Pierce *et al.*, J. Acoust. Soc. Am. **114**, 2345 (2003)]. Numerical calculations use sandy bottom sediments and isospeed, linear, and piecewise linear water profiles, which are simplifications that preserve key features of those obtained in experiments off the New Jersey Shelf. The calculations indicate the importance of downward refracting profiles and the strength of near-interface gradients for increasing energy loss. Principal characteristics of the MACs that are observed from the calculations include: increases with interface gradient, reordering of least attenuated modes, and variations of the frequency power-law exponents of the MACs from f^1 to f^4 at frequencies up to 2 kHz. Evidence of the behavior observed in the calculations is in good agreement with previous analysis of results in Gulf of Mexico experiments [F. Ingenito, J. Acoust. Soc. Am. **53**, 858--863 (1973)], for profiles that were classified as weakly downward refracting or nearly isospeed. [Work partially supported by ONR.]

10:00

4aUWc7. What is the spatial volume involved for wave reflection from flat and curved interfaces? Paul Cristini (CNRS-UMR5212 Modélisation et Imagerie en Géosciences, UPPA BP115, 64013 Pau, France, paul.cristini@univ-pau.fr), Nathalie Favretto-Cristini (CNRS-UMR5212 Modélisation et Imagerie en Géosciences, UPPA BP115, 64013 Pau, France, nathalie.favretto@univ-pau.fr), Eric De Bazelaire (11, Route du Bourg, 64230 Beyrie-en-Béarn, France, edebaz@wanadoo.fr)

The spatial region in the vicinity of the interface which actually affects the interface response, and hence the reflected wavefield, is of particular interest for the characterization of reflectors. This region represents a volume of integration of properties above and beyond the interface whose maximum lateral extent corresponds to the lateral extent of the Interface Fresnel Zone (IFZ), and whose maximum vertical extent is equal to a thickness we evaluate approximately for subcritical incidence angles and for the case of a plane homogeneous interface. The maximum vertical extent may be greater than the seismic wavelengths for subcritical incidence angles close to the critical angle and for strong impedance contrast at the interface. The whole part of reflector which actually affects the reflected wavefield is then larger than described by previous estimates which considered only the spatial region beyond the interface. In addition to the case of a flat interface, we also discuss the change in the characteristics of this part of the reflector as a function of the interface curvature.

10:20

4aUWc8. Laboratory sound speed measurements on high water content sediment samples. Vanessa A. Martin (Laboratoire GeM (et EDF), UMR CNRS 6183 - Institut de Recherche en Génie Civil et Mécanique, IUT de St Nazaire - département Génie Civil - 58 rue Michel Ange, 44600 Saint Nazaire, France, vanessa.martin@univ-nantes.fr), Alain Alexis (Laboratoire GeM (et EDF), UMR CNRS 6183 - Institut de Recherche en Génie Civil et Mécanique, IUT de St Nazaire - département Génie Civil - 58 rue Michel Ange, 44600 Saint Nazaire, France, alain.alexis@univ-nantes.fr), Vincent Martin (Institut Jean Le Rond d'Alembert, UMR CNRS 7190, UPMC, 2 Place de la Gare de Ceinture, 78210 Saint-Cyr l'Ecole, France, vmartin@ccr.jussieu.fr)

Laboratory measurements of sound speed in fluid viscous materials are known to be difficult, especially for frequencies of a few kHz. An experimental set up which allows such measurements is developed. Tests are run on sediment samples of various lengths (5cm - 20cm), all water-saturated but with different water contents (or densities). When sound speed only depends on the water content over a narrow frequency bandwidth, its estimation originates from time-of-flight measurements on samples of different lengths. It will appear that the water content does play a significant role on the speed of sound. When sound speed depends on frequency (dispersive waves) due to the sediment viscoelastic behaviour, the dependency can be taken into account. An analysis according to the sample length will be given to characterize the sound dispersion for different water contents. It will be shown that both the above studies on the experimental campaign yield sound speed estimations against sample lengths under various hypotheses. In these conditions, the estimation leads to information about saturated sediment behaviour.

THURSDAY MORNING, 3 JULY 2008 ROOM 362/363, 8:00 A.M. TO 1:00 P.M.

Session 4aUWd

Underwater Acoustics and ECUA: Propagation and Reverberation

David L. Bradley, Cochair
Pennsylvania State University, Post Office Box 30, State College, PA 16804-0030, USA

Kevin D. Lepage, Cochair
Naval Research Laboratory, 4555 Overlook Ave SW, Washington, DC 20375, USA

Contributed Papers

8:00

4aUWd1. Sound focusing and scanning in shallow water with background internal wave field. Andrey A. Lunkov (Moscow State Technical University n.a. N.E. Bauman, 2nd Baumanskaya 5, 107005 Moscow, Russian Federation, landr2004@mail.ru), Sergey A. Pereselkov (Voronezh State University, 1 Universitetskaya Sq., 394006 Voronezh, Russian Federation, pereselkov@yandex.ru)

Sound field focusing and scanning with focal spot are investigated for shallow water and long distances (up to 30km). It is studied the availability of horizontal and vertical scanning for controlling long-range low-frequency bottom reverberation as well. These researches are carried out by using numerical modeling for typical acoustic waveguides including random ones with background internal waves. The acoustic field is focused with vertical array by phase conjugation of sound wave from probe source placed at preset point. Horizontal scanning with the focal spot is performed by radiation frequency tuning. It is demonstrated that the best feasibility for scanning and hence for controlling bottom reverberation takes place for the regular waveguide under winter conditions when sound speed depends on depth only slightly and background internal waves are nonexistent practically. As an example for these conditions we can control the bottom reverberation on interval~ 5km in the neighborhood of preset point. In summer for near bottom sound waveguide the range of distances for which it is practicable is much narrower even without internal waves. For the waveguide with intense background internal waves the control of long-range bottom reverberation becomes impossible. The work was supported by RFBR Project 05-02-16842.

8:20

4aUWd2. An optimized source transmission scheme based on pressure sensitivity kernels. Kaustubha Raghukumar (MPL, Scripps Institution of Oceanography, University of California, San Diego, La Jolla, CA 92093-0238, USA, kaus@mpl.ucsd.edu), Bruce Cornuelle (MPL, Scripps Institution of Oceanography, University of California, San Diego, La Jolla, CA 92093-0238, USA, bdc@ucsd.edu),William Hodgkiss(MPL, Scripps Institution of Oceanography, University of California, San Diego, La Jolla, CA 92093-0238, USA, wsh@mpl.ucsd.edu), William A. Kuperman (MPL, Scripps Institution of Oceanography, University of California, San Diego, La Jolla, CA 92093-0238, USA, wkuperman@ucsd.edu)

A first-order Born approximation is used to obtain the pressure sensitivity of the received signal to small changes in medium sound speed. The pressure perturbation to the received signal caused by medium sound speed changes is expressed as a linear combination of single-frequency sensitivity kernels weighted by the source signal in the frequency domain. This formulation is used to optimize the pressure sensitivity kernel to give a new source transmission that can produce a focal spot and at the same time, to have less sensitivity to sound speed fluctuations than time-reversal. The formulation allows for a trade-off between quality of focal spot and sensitivity to environmental fluctuations. The optimized new source transmission uses knowledge of the medium statistics and is related to the regularized inverse filter.

8:40

4aUWd3. Passive phase conjugation processing to forward scattering waves by target in shallow water. Yoshiaki Tsurugaya (NEC @Corp., 1-10 @Nissin-cho, Fuchu, 183-8501 Tokyo, Japan, y-tsurugaya@bp.jp.nec.com), Toshiaki Kikuchi (National Defence Academy, 39-21 Uhoyabe 4-chome, Yokosuka, 238-0024 Kanagawa, Japan, ADS01881@nifty.com), Koichi Mizutani (Tsukuba Univ., Tsukuba Science City, 305-8573 Ibaraki, Japan, mizutani@esys.tsukuba.ac.jp)

This paper describes the detection of an underwater target using a passive phase conjugation processing. It is assumed that a sound source and an array are disposed in shallow water, and a target exists between them. The traveling wave from the sound source and the scattered wave from the target are received by the array. However, they are received almost simultaneously. In addition, because the level of the traveling wave is considerably larger than that of the scattered wave, the detection of the scattered wave is

difficult. Then, the traveling wave components are removed from the signals received in the array. And, the passive phase conjugation processing is given to the signals. The signal to which the passive phase conjugation is processed is similar with the signal radiated from the target. The signal radiated from the target relates to the sound wave that enters at the position of the target from the sound source for the small target. The sound wave that enters at the position of the target is uniquely decided depending on the condition of the propagation environment and the sound source. Therefore, the result that the passive phase conjugation is processed contains the position information of the target.

9:00

4aUWd4. Efficient time reversal by Lanczos iterations. Assad A. Oberai (Rensselaer Polytechnic Institute, Mechanical, Aerospace and Nuclear Engineering, 5048 JEC, 110 8th Street, Troy, NY 12180, USA, oberaa@rpi.edu), Gonzalo R. Feijoo (Woods Hole Oceanographic Institution, Woods Hole, MA 02543, USA, gfeijoo@whoi.edu), Paul E. Barbone (Boston University, 110 Cummington St, Boston, MA 02215, USA, barbone@bu.edu)

Time reversal methods have seen many applications in underwater acoustics, medical ultrasound, nondestructive evaluation, and several non-acoustics applications. Techniques to target and/or locate individual scatterers are based upon using iterative time-reversal. From a mathematical perspective, iterative time reversal is akin to the power method of extracting eigenvectors of the scattering operator. As such, standard iterative time-reversal inherits the limitations of the power method. For example, iterative time-reversal converges slowly in the presence of multiple scatterers of similar strength and has difficulty identifying weaker scatterers. On the other hand, Lanczos iterations surmount these difficulties, and tend to converge faster than the power method, even when the latter works well. In this contribution we show how Lanczos iterations can be adapted to time-reversal iteration. This allows the strongest eigenvectors of the scattering operator to be measured with greater accuracy and in many fewer iterations than required by standard time-reversal. We describe how this algorithm may be implemented in a practical situation and build a new time-reversal method around it. We apply this method to some numerical examples to demonstrate its effectiveness and compare its performance with the more traditional time-reversal iterations.

9:20

4aUWd5. Specific features of surface reverberation in shallow water with focused sound field. Valeriy G. Petnikov (A.M. Prokhorov General Physics Institute, 38 Vavilov str., 119991 Moscow, Russian Federation, petniko@kapella.gpi.ru), Sergey A. Pereselkov (Voronezh State University, 1 Universitetskaya Sq., 394006 Voronezh, Russian Federation, pereselkov @yandex.ru)

The specific features of long-range low-frequency (230 Hz) surface reverberation using vertical radiating array are studied in the framework of numerical experiment. We assume that the array focuses a sound field at different distances from ruffled surface in shallow water. Focusing is carried out by using a time-reversal mirror at a distance 10 - 30 km from radiating array. We consider sound focusing and surface reverberation in the presence of developed wind waves for acoustic waveguide common to shallow water for different seasons. The feasibility of surface reverberation suppression is estimated by sound focusing in the central region of the waveguide including the region located below thermocline. The results of numerical modeling are compared with the similar results obtained before for bottom reverberation. The work was supported by RFBR Project 05-02-16842.

9:40

4aUWd6. Active sonar discrimination of water-column objects from bottom clutter using waveguide invariant modeling of distributed backscatter. Jeffrey Krolik (Duke University, ECE Dept. Hudson Hall 130, PO Box 90291, Durham, NC 27708, USA, jk@ee.duke.edu), Ryan Goldhahn (Duke University, ECE Dept. Hudson Hall 130, PO Box 90291, Durham, NC 27708, USA, rag15@ee.duke.edu), Granger Hickman (Duke University, ECE Dept. Hudson Hall 130, PO Box 90291, Durham, NC 27708, USA, gwh@ee.duke.edu)

The ability to differentiate water-column returns from clutter discretes due to backscatter from bottom features is critical to improving the detection performance in active sonar. Previous approaches include the use of statistical feature-based classifiers and physics-based depth estimation. Such methods are typically challenged by the convolutive effect of both uncertain multipath propagation and complex scattering characteristics in sonar returns. In previous work, we used waveguide invariant theory to model frequency-selective fading observed in distributed backscatter from the ocean bottom. In particular, the short-time energy spectrum of backscatter from the sea bottom at a given range can be well estimated along striations in time-frequency energy predicted by waveguide invariant theory. In this paper, we present a statistic which tests the observed frequency-selective fading of the short-time energy spectrum for a range cell under test against the spectrum predicted by waveguide invariant theory for a bottom feature using neighboring ranges and frequency bins. Results are presented for discrimination of a water column target versus bottom clutter using data simulated via a normal mode propagation model with environmental parameters from the Malta Plateau. Receiver operating characteristic analysis is performed showing good discrimination of equal energy targets from clutter. [Work supported by ONR].

10:00

4aUWd7. Using a dispersive source signal to generate a dispersive field in a nondispersive medium. Shane C. Walker (MPL, Scripps Institution of Oceanography, University of California, San Diego, La Jolla, CA 92093-0238, USA, shane@mpl.ucsd.edu), William A. Kuperman (MPL, Scripps Institution of Oceanography, University of California, San Diego, La Jolla, CA 92093-0238, USA, wkuperman@ucsd.edu)

In typical treatments, dispersion is considered to be a property of the medium. For example, a free space, static, homogeneous medium is dispersionless while gravity waves, particularly in the case of surface waves in a deep body of water, exhibit dispersion. Here it is shown that dispersion in the field can also result from dispersion in the source signal. As a demonstration, a dispersive source signal is shown to introduce dispersion in a dispersionless medium. Consequently, through proper design of the source signal, it is possible to tailor the resulting field dispersion to suit a variety of applications. Here potential applications to imaging in complex media are discussed. Simulation and experimental results are presented.

10:20-10:40 Break

10:40

4aUWd8. Equivalence of the waveguide invariant and two path ray theory methods for range prediction based on Lloyd's mirror patterns. Daphne Kapolka (Naval Postgraduate School, 13693 Tierra Spur, Salinas, CA 93908, USA, dkapolka@nps.edu)

For shallow, range-independent environments where the sound is dominated by low-order modes, the constant which characterizes the modal interference pattern, the waveguide invariant, is approximately equal to one. The speed of a contact which maintains a constant course and speed as it passes through its closest point of approach (CPA) can be determined from the asymptotic behavior of its tonal frequencies from the Doppler shift. This information can be used along with the change in broadband striation frequencies in a Lloyd's mirror pattern over time to extract the range of the contact as it transits through CPA. If instead of using normal mode theory, the Lloyd's mirror pattern is derived as the coherent interference between a straight-line direct and surface-reflected path, a relationship between the striation frequencies and time of a crossing contact can also be derived. This relationship can be shown to be identical to the result obtained from the nor-

mal mode approach when the value of the waveguide invariant is equal to one. Thus, the same equations can be used to extract range information from a Lloyd's mirror pattern regardless of contact range as long as the environmental conditions support a waveguide invariant close to one.

11:00

4aUWd9. Analytical Time Domain Analysis of an Acoustic Waveguide. Hüseyin Ö. Sertlek (The Scientific and Technological Research Council of Turkey, Marmara Research Center, Information Technologies Institute, Gebze, 41400 Kocaeli, Turkey, ozkan.sertlek@bte.mam.gov.tr), Serkan Aksoy (Gebze Institute of Technology, Electronics Engineering Department, Çayırova, Gebze, 41400 Kocaeli, Turkey, saksoy@gyte.edu.tr)

A new analytical time domain Normal Mode solution for one layer acoustic channel in two dimensional Cartesian coordinates is presented in this paper. The method is based on the separation of variables technique for the time domain wave equation. Dirichlet boundary condition is applied on the upper and lower boundaries of the channel. Klein-Gordon equation is obtained and solved by using the Green function. The fundamental advantage of this new technique is not necessary to use the Fourier Transformation to obtain time domain response of arbitrary acoustical source signal in the waveguide. In order to validate the obtained results, first of all, the Fast Fourier Transform is applied to the time domain analytical data, then, the comparisons are given between KRAKEN program and a new analytical time domain Normal Mode solution in the sense of Transmission Loss relating to ranges. The excellent agreement is obtained between the results.

11:20

4aUWd10. Application of the Mode Matching Technique to Fluid - Solid Layered Acoustic Problems. Hüseyin Ö. Sertlek (The Scientific and Technological Research Council of Turkey, Marmara Research Center, Information Technologies Institute, Gebze, 41400 Kocaeli, Turkey, ozkan.sertlek@bte.mam.gov.tr), Serkan Aksoy (Gebze Institute of Technology, Electronics Engineering Department, Çayırova, Gebze, 41400 Kocaeli, Turkey, saksoy@gyte.edu.tr), Deniz Bolükbas (The Scientific and Technological Research Council of Turkey, Marmara Research Center, Information Technologies Institute, Gebze, 41400 Kocaeli, Turkey, deniz.bolukbas@bte.mam.gov.tr), Sevgi Akgün (The Scientific and Technological Research Council of Turkey, Marmara Research Center, Information Technologies Institute, Gebze, 41400 Kocaeli, Turkey, sevgi.akgun @bte.mam.gov.tr)

An application of Mode Matching technique for analyzing interactions between range dependent fluid-solid layers in two dimensional cylindrical coordinates is presented by using Normal Mode method. The transmission loss for fluid-solid medium with semi-infinite bottom layer is calculated for range-dependent bottom profiles. The bottom solid half space is divided independent vertical regions due to different bottom parameters for simulation of the real acoustic environment. The transition between the independent vertical regions is ensured by using Mode Matching technique with Normal Mode method. The attenuation of acoustic wave modes in a range dependent two layered fluid-solid medium due to absorption of the lower semi-infinite solid layer is calculated. In order to validate the obtained results in the sense of Transmission Losses, Parabolic Equation program (RAM) is used for different transition cases. The good agreement is found between the results which can be used for realistic Sonar simulators.

11:40

4aUWd11. The comparative analysis of two solutions of Pekeris boundary problem. Nadezhda Zlobina (Institute of Marine Technology Problems, Sukhanov str., 5à, 690950 Vladivostok, Russian Federation, zlobina@marine.febras.ru), Boris Kasatkin (Institute of Marine Technology Problems, Sukhanov str., 5à, 690950 Vladivostok, Russian Federation, bigcezar@mail.ru)

The solution of the reduced Pekeris boundary problem, satisfying to the generalized radiation condition on an impedance interface is obtained. Mode part of the solution is presented by series expansion on the total system of regular normal waves, of generalized normal waves and of leakage normal waves. The principle of the continuous continuation of the obtained solution in physical half-space with validity of boundedness condition is formulated. Expansion of the solution on physical half-space in a class of generalized functions is constructed. The obtained generalized solution includes canonical series expansion on the set of eigenfunctions of both conjugate operators corresponding an initial not self-conjugate boundary problem, the associated eigenfunctions of a waveguide with two soft boundaries, the associated eigenfunctions of a waveguide with upper soft boundary and lower rigid boundary and a set of spherical components. Results of the comparative analysis of the classical solution and generalized solution are given.

12:00

4aUWd12. Parabolic Wavelet Technique to Numerical Modelling of Sallow Water Acoustic. Mostafa Bakhoday Paskyabi (Research Engineering Institute, 16th Kilometers of Old Road Of Tehran-Karaj, Control Engineering Group, Agricultural Engineering Institute, 13445-754 Tehran, Iran, bakhoda@guilan.ac.ir), Seyed Taha Mortazavi (Research Engineering Institute, 16th Kilometers of Old Road Of Tehran-Karaj, Control Engineering Group, Agricultural Engineering Institute, 13445-754 Tehran, Iran, t_mortazavi@yahoo.com)

In this paper, parabolic equation (PE) model is applied for environment of slowly varying with range and azimuth in a region of Persian Golf. This method is currently the most used to study propagation in non-stratified media. Due to required accuracy for a gridding step comparable with the wavelength, the computation load is very heavy. To overcome this disadvantage, we develop the weak form of PE formulation by the use of Deslauier-Daubuc interpolating wavelet (DDW) basis functions. The formulation is similar to combination of conventional Finite Element Method (FEM) and split step technique except that, here DDW basis is used for approximating in depth to reduce the cost of computations and to increase the accuracy of method by the use of multi-resolution structure of wavelets. The localized and circulant representations of depth differential operators based on DDW connection coefficients allow efficient imposition of boundary values and circumvent some disadvantages of the traditional PE. Furthermore, details of bottom boundary imposing and some disadvantages of approach are presented. Numerical experiments are performed to study two layers water-bottom environment with none-smooth sediment interface to some canonical standard test problems in comparison with solutions obtained by conventional PE method.

12:20

4aUWd13. Studying converted waves in shallow marine environment. Nihed El Allouche (Delft University of Technology, P.O. Box Postbus 5048, 2600 GA Delft, Netherlands, n.elallouche@tudelft.nl), Guy G. Drijkoningen (Delft University of Technology, P.O. Box Postbus 5048, 2600 GA Delft, Netherlands, g.g.drijkoningen@tudelft.nl), Willem Versteeg (Ghent University, Krijgslaan 281, S8, 9000 Ghent, Belgium, willem.versteeg@ugent.be), Dick G. Simons (Delft University of Technology, P.O. Box Postbus 5048, 2600 GA Delft, Netherlands, d.g.simons @tudelft.nl)

For many years, waves converted from compressional to shear mode have been successfully applied in hydrocarbon exploration to image and characterize the subsurface. Since shear-waves propagate with a velocity that is dependent on the shear modulus and are thus directly related to the shear strength of the sediment, they are very useful for geotechnical purposes. Generally, P-wave reflection amplitudes contain S-wave information but Riedel et al. (2001) showed that these reflections are not very sensitive to this. An alternative approach is to obtain S-wave information directly from converted waves. However, it is not clear whether these waves can be applied for geotechnical aims. The main focus will be on understanding the dependence of mode conversion on the seismic properties. In this study, we investigate the possibility of acquiring converted waves in marine unconsolidated sediments. From our numerical experiments we found that the conversion is maximal at two angles where the smallest angle appears to be more favorable in the environment of interest. Furthermore, we show how and where converted waves can be observed on a seismogram and the optimum field configuration to acquire them.

12:40

4aUWd14. Conservative initial-boundary value problems for the Wide-Angle PE in waveguides with variable bottoms. Dimitra Antonopoulou (Department of Applied Mathematics, University of Crete, 71409 Heraklion, Greece, danton@tem.uoc.gr), Vassilios Dougalis (Mathematics Department, University of Athens, 15784 Zografou, Greece, doug@math.uoa.gr), Frederic Sturm (Laboratoire de Mécanique des Fluides et d'Acoustique (UMR CNRS 5509), Ecole Centrale de Lyon, Centre acoustique, 36, avenue Guy de Collongue, 69134 Ecully Cedex, France, frederic.sturm@ec-lyon.fr), George Zouraris (Department of Applied Mathematics, University of Crete, 71409 Heraklion, Greece, zouraris @math.uoc.gr)

We consider the third-order, Claerbout-type Wide-Angle Parabolic Equation (PE) in the context of Underwater Acoustics in a cylindrically symmetric medium consisting of water over a soft bottom B of range-dependent topography. There are strong indications, that the initial-boundary value problem for this equation with just a homogeneous Dirichlet boundary condition on B, may not be well-posed, for example when B is downsloping. In previous work we proposed an additional bottom boundary condition that, together with the zero field condition on B, yields a well-posed problem. In the present paper we continue our investigation of additional bottom boundary conditions that yield well-posed, physically correct problems. Motivated by the fact that the solution of the wide-angle PE in a domain with horizontal layers conserves its L2 norm in the absence of attenuation, we seek additional boundary conditions on a variable-topography bottom, that yield L2- conservative solutions of the problem. We identify a family of such boundary conditions after a range-dependent change of the depth variable that makes B horizontal. We discretize the continuous problems by second-order accurate Crank-Nicolson type finite difference schemes, and show, by means of numerical experiments, that the new models yield accurate simulations of the acoustic field in standard, wedge-type domains with upsloping and downsloping bottoms.

THURSDAY MORNING, 3 JULY 2008 ROOM 341, 11:40 A.M. TO 7:40 P.M.

Session 4aUWe

Underwater Acoustics and ECUA: Tank Experiments I

Raymond J. Soukup, Cochair
U.S. Naval Res. Lab., Acoust. Div., Code 7142, 4555 Overlook Ave. SW, Washington, DC 20375, USA

Jean-Pierre Sessarego, Cochair
Laboratory for Mechanics and Acoustics CNRS, 31 chemin Joseph Aiguier, Marseille, 13009, France

Invited Papers

11:40

4aUWe1. Tank experiment: The ultrasonic approach to ocean physics. Philippe Roux (LGIT - CNRS - Université Joseph Fourier, Maison des Géosciences, 1381 rue de la Piscine, BP 53, 38041 Grenoble, France, philippe.roux@obs.ujf-grenoble.fr)

Acoustic/elastic waves ranging from a few kHz to a few MHz are nowadays easy to emit/receive through the use of ″key in hands″ multi-channel systems. These systems provide the instantaneous amplitude and phase of the deterministic wave propagating in the medium with a dynamic larger than 90 dB in some cases (16-bit amplitude sampling). The use of a large number of channels (at least 64) is mandatory to simultaneously investigate the spatial and temporal aspect of wave propagation in complex media. The advantage of a laboratory-scaled ocean model relies in the ease with which it can be build, modified, and/or controlled over time. Finally, the trend in ocean wave physics is now to study the dynamics of such medium (internal waves, turbulent flow, sensor motion) that requires the use of a real-time acquisition system. Examples of the types of analog experiments that could be carried out with a laboratory-scaled system are the study of nonuniform doppler shifted fields in reverberant environments, ocean acoustic tomography and similar inverse problems, coherent communications in complex moving environments, etc. After the description of the equipment, we give more specific examples of potential experiments to illustrate the versatility of the laboratory set-up.

12:00

4aUWe2. Tank experiments of sound propagation over a tilted bottom: Comparison with a 3-D PE model. Alexios Korakas (Laboratoire de Mécanique des Fluides et d'Acoustique (UMR CNRS 5509), Ecole Centrale de Lyon, Centre acoustique, 36, avenue Guy de Collongue, 69134 Ecully Cedex, France, alexis.korakas@ec-lyon.fr), Frederic Sturm (Laboratoire de Mécanique des Fluides et d'Acoustique (UMR CNRS 5509), Ecole Centrale de Lyon, Centre acoustique, 36, avenue Guy de Collongue, 69134 Ecully Cedex, France, frederic.sturm@ec-lyon.fr), Jean-Pierre Sessarego (Laboratory for Mechanics and Acoustics CNRS, 31 chemin Joseph Aiguier, 13009 Marseille, France, sessarego@lma.cnrs-mrs.fr), Didier Ferrand (Laboratoire de Mécanique et d'Acoustique (UPR CNRS 7051), 31, chemin Joseph Aiguier, 13402 Marseille Cedex 20, France, ferrand@lma.cnrs-mrs.fr)

We present results of tank experiments of long-range acoustic propagation over a wedge-shaped oceanic bottom. Previous work investigated the propagation of broadband pulses in a range-independent configuration showing good agreement between experimental results and model predictions [Korakas et al., Proceedings of UAM 2007 (Heraklion, Crete, Greece, 25-29 June 2007)]. As a follow-up, preliminary experiments were carried out considering a tilted bottom. Non-negligible 3-D effects were observed and proved to compare favorably with numerical predictions obtained running a parabolic equation based code [Sturm et al., Proceedings of UAM 2007]. In the

present work we continue the investigation of the wedge-like environment. Additional series of experimental measurements are performed. Received signals are recorded on a very fine spatial grid. Then, the measured data are processed using matched field processing. In our inversion algorithm, the replica are provided by a fully three-dimensional parabolic equation code. The technical aspects of the inversion procedure used (e.g., CPU time) are discussed.

12:20

4aUWe3. Laboratory investigations of the detection and characterization of buried targets by iterative, single-channel time reversal. Zachary J. Waters (Boston University, Dept. of Aerosp. and Mech. Eng., 110 Cummington St., Boston, MA 02215, USA, zjwaters@bu.edu), Benjamin R. Dzikowicz (Naval Surface Warfare Center, Panama City Division, Code HS-11, 100 Vernon Ave., Panama City, FL 32407, USA, benjamin.dzikowicz@navy.mil), R. Glynn Holt (Boston University, Dept. of Aerosp. and Mech. Eng., 110 Cummington St., Boston, MA 02215, USA, rgholt@bu.edu), Ronald A. Roy (Boston University, Dept. of Aerosp. and Mech. Eng., 110 Cummington St., Boston, MA 02215, USA, ronroy@bu.edu)

Due to the dynamic nature of the shallow water environment, targets are often buried beneath the seafloor, hindering their detection and identification by acoustic methods. Using iterative time reversal with a single channel transducer [Waters et al., J. Acoust. Soc. Am. 122, 3023 (2007)], the monostatic return from a buried resonant target is enhanced, yielding convergence to a narrowband waveform characteristic of the dominant mode in the target's scattering response. Scaled laboratory experiments are performed with a broadband (Q~2) transducer operating in the 0.5-2 MHz frequency range. Solid and evacuated metallic spheres used as targets are buried beneath a layer of simulated sediment. Images generated by scanning the transducer laterally in two dimensions over an area of sediment containing multiple targets show enhancement of different modes in a single target's scattering response and test the selectivity between targets of differing type. Experiments with the transducer positioned at normal and non-normal incidence, quantify the enhancement in the signal-to-noise ratio of target returns as a function of window size and position. [Work supported by The Office of Naval Research and the Center for Subsurface Sensing and Imaging Systems (NSF ERC Award No. EEC-9986821).]

12:40-2:00 Lunch Break

Invited Papers

2:00

4aUWe4. Detection and classification of a cylindrical target partially or completely buried in thin sand/water mixture by time-frequency representation. Gerard Maze (LAUE, Université du Havre, Place Robert Schuman, F-76610 Le Havre, France, gerard.maze@univ-lehavre.fr), Dominique Decultot (LOMC FRE 3102 CNRS Groupes Ondes Acoustiques, Université du Havre (IUT), Place Robert Schuman, 76610 Le Havre, France, dominique.decultot@univ-lehavre.fr), Katia Cacheleux (LOMC FRE 3102 CNRS Groupes Ondes Acoustiques, Université du Havre (IUT), Place Robert Schuman, 76610 Le Havre, France, katia.cacheleux@univ-lehavre.fr), Romain Liétard (LOMC FRE 3102 CNRS Groupes Ondes Acoustiques, Université du Havre (IUT), Place Robert Schuman, 76610 Le Havre, France, romain.lietard@univ-lehavre.fr)

Numerous papers show that it is possible to characterize an air-filled cylindrical shell immersed in water from a time-frequency representation. The time scattered signal is constituted by echoes related to the reradiation of waves circumnavigating around the cylindrical target. For particular frequencies, these echoes make resonances which characterize this target. In first part, the scattered signal is calculated, the cylindrical shell is in water or in a medium with characteristics similar to the mixture sand/water used for the experimental measurements. In second part, the cylindrical shell is partially or completely buried in a thin sand/water mixture. It is insonified in normal or oblique incidence relatively to the interface water/mixture. The impulse time scattered signal is plotted and it is treated with a time-frequency representation. The comparison between the theoretical and experimental time-frequency representations shows us that it is possible to detect and classify the object buried in thin sand/water mixture.

2:20

4aUWe5. Acoustic radiation of low frequency flexural vibration modes in a submerged plate. Dominique Decultot (LOMC FRE 3102 CNRS Groupes Ondes Acoustiques, Université du Havre (IUT), Place Robert Schuman, 76610 Le Havre, France, dominique.decultot@univ-lehavre.fr), Romain Liétard (LOMC FRE 3102 CNRS Groupes Ondes Acoustiques, Université du Havre (IUT), Place Robert Schuman, 76610 Le Havre, France, romain.lietard@univ-lehavre.fr), Farid Chati (LOMC FRE 3102 CNRS Groupes Ondes Acoustiques, Université du Havre (IUT), Place Robert Schuman, 76610 Le Havre, France, farid.chati@univ-lehavre.fr), Gerard Maze (LAUE, Université du Havre, Place Robert Schuman, F-76610 Le Havre, France, gerard.maze@univ-lehavre.fr), Aleksander Klauson (Tallinn University of Technology, Dept. of Mechanics, Ehitajate tee 5, 19086 Tallinn, Estonia, aklauson@staff.ttu.ee)

In some submarine structures, the acoustic radiation of vibrations at the neighbourhood of sonar equipment limits their use. So the aim of this study is to understand the process of acoustic radiation of a submerged plate subjected to a vibration. For the low frequency domain, only two types of wave can propagate: the first antisymmetric Lamb wave (A0) and the first symmetric Lamb wave (S0). When the plate is immersed in water the A0 wave is modified and the new wave is named A wave. In this work, experimental and numerical analysis of vibration modes in a plate are carried out. The studied rectangular plate of thickness 10 mm is made of steel. Its length and width are respectively 1.0 m and 0.5 m. The plate is partially immersed in water (90%). Flexural vibrations are generated by a shaker normally connected to the emerging plate part. The applied signal is one sinusoidal period at a frequency which is under the critical frequency. Relations between the admittance of the plate and the radiated pressure in water are highlighted.

2:40

4aUWe6. Inverse problems in sound radiation of complex structures from measurements in a large acoustic tank. Earl G. Williams (Naval Research Laboratory, 4555 Overlook Ave, Washington, DC 20375, USA, earl.williams@nrl.navy.mil), Brian H. Houston (Naval Research Laboratory, 4555 Overlook Ave, Washington, DC 20375, USA, houston@code7136.nrl.navy.mil), Nicolas Valdivia (Naval Research Laboratory, 4555 Overlook Ave, Washington, DC 20375, USA, valdivia@pa.nrl.navy.mil), Peter C. Herdic (SFA Inc., Suite 405, Crofton, MD 21114, USA, herdic@code7136.nrl.navy.mi)

The Laboratory for Structural Acoustics (LSA) at NRL consists of an indoor cylindrical tank (17 m dia. by 15 m deep) filled with ~ 1 million gallons of deionized water. Key features include: 1) vibration isolation, 2) active temperature control, and 3) anechoic materials. This unique laboratory is instrumented with sophisticated mechanical, electronic and optical systems, that include large work-space in-water robotic scanners to generate nearfield acoustical holography (NAH) databases. We discuss such a database consisting of the underwater near-field pressure measured on a two-dimensional surface conformal to an internally driven complex structure floating at the air-water interface. Various inverse approaches are discussed to image the normal velocity and intensity of the structure at its interface to the fluid, as well as the total power radiated, revealing mechanisms of radiation related to the internal structure. These inverse approaches consist of the equivalent source method compared with the well established Fourier acoustics methods of NAH. This work was supported by the US Office of Naval Research.

3:00

4aUWe7. Broadband elastic scattering by fiberglass spherical shells and plates measured in a water tank: Acoustic inversion and wave analysis. Alessandra Tesei (NATO Undersea Research Centre, Viale San Bartolomeo 400, 19126 La Spezia, Italy, tesei@nurc.nato.int), Paul D. Fox (National Physical Laboratory, Hampton Road, TW11 OLW Teddington, UK, pf@isvr.soton.ac.uk), Gary B. Robb (National Oceanography Centre, University of Southampton Waterfront Campus, European Way, SO14 3ZH Southampton, UK, gbor199@noc.soton.ac.uk)

Spherical shells and plane plates made of different types of fiberglass (either random or textured) were measured in the backscatter direction, suspended in a water tank in a broadband frequency range between 30 and 350 kHz. The range of ka for the spheres was approximately 8 to 90, with the fd range for the plates approximately 0.15 to 1.75 MHz*m. The aim of the study was to investigate the effects of the fiber type on the object signature, as the frequency and the type of fiber layers vary. Inversion of the material parameters was conducted on the basis of the object's temporal echo. In particular, the estimate of material loss is crucial to determine at what frequency elasticity becomes irrelevant to the object's global response. The spherical shells were measured either void or filled with different materials (liquid and solid) in order to evaluate the contribution of the shell-borne elastic waves with respect to sound scattered from the interior of the object. Elastic wave analysis and analytical modeling tools were used to support the physical interpretation of the measured responses from the different objects.

3:20

4aUWe8. Modal analysis of resonances of an elliptic elastic cylinder immersed in water. Fernand Leon (LOMC FRE 3102 CNRS Groupes Ondes Acoustiques, Université du Havre (IUT), Place Robert Schuman, 76610 Le Havre, France, fernand.leon@univ-lehavre.fr), Farid Chati (LOMC FRE 3102 CNRS Groupes Ondes Acoustiques, Université du Havre (IUT), Place Robert Schuman, 76610 Le Havre, France, farid.chati@univ-lehavre.fr), Jean-Marc Conoir (Institut Jean Le Rond d'Alembert-UMR CNRS 7190, Université Paris 6, tour 55-65, 4 place Jussieu, 75005 Paris, France, conoir@lmm.jussieu.fr)

Considerable work has been done on the scattering by cylindrical objects having a circular cross section. The modal formalism based on the theory of elasticity has been developed for studying the acoustic scattering by these elastic cylinders immersed in water. In particular, it has been demonstrated, in normal incidence, that the eigenfrequencies of a circular cylinder can be determined from a resonance spectrum. These eigenfrequencies correspond to circumferential waves that form a resonance when a phase matching along a closed path is obtained. Each eigenfrequency is characterized by a given mode n, i.e., the number of wavelengths spanning the circumference. Comparatively, little attention has been devoted to the more general case of the noncircular cylindrical cylinders such as the elliptical elastic cylinders. For these objects, we have been developed a modal formalism based on the theory of elasticity. From the results obtained theoretically and experimentally, we show how to obtain a resonance spectrum, independently of the azimuth incident angle and of the radii ratio (minor radius and major radius) so that the eigenfrequencies can be determined. We present also a modal analysis of resonances as function of the azimuth incident angle and of the radii ratio.

3:40-5:20 Posters

Lecture sessions will recess for the presentation of poster papers on various topics in acoustics. See poster sessions for topics and abstracts.

5:20

4aUWe9. Estimation of some geoacoustic parameters of a tank experiment by match field processing. Panagiotis Papadakis (IACM-FORTH, N. Plastira 100, 70 013 Vassilika Vouton, Greece, panos@iacm.forth.gr), Michael Taroudakis (University of Crete & FORTH/IACM, Vassilika Vouton, P.O.Box 1385, 711 10 Heraklion, Greece, taroud@iacm.forth.gr), Jean-Pierre Sessarego (Laboratory for Mechanics and Acoustics CNRS, 31 chemin Joseph Aiguier, 13009 Marseille, France, sessarego@lma.cnrs-mrs.fr), Patrick Sanchez (Laboratoire de Mécanique et d'Acoustique (UPR CNRS 7051), 31, chemin Joseph Aiguier, 13402 Marseille Cedex 20, France, patrick.sanchez@eoures.com)

The work deals with an inversion procedure for the estimation of geometrical and environmental parameters of a simulated shallow water environment. Two of the most significant parameters in a shallow water environment affecting the acoustic field in long range acoustic propagation are the sound speed of the sediment and the depth of the water column. The accurate estimation of these parameters is perhaps the most important task in scaled laboratory experiments. Therefore, the calibration phase of such an experiment involves the estimation of these parameters, preferably using acoustical techniques, regardless the final scope of the experiment. The present work describes an inversion procedure based on standard match field processing. The acoustic signal used was a short gaussian shaped pulse and it was recorded at a certain distance from the source and for several depths in the water column. The spectrum of the recorded signal was obtained using FFT and the complex acoustic field at the central frequency was calculated. The estimated values of the water depth and the sound speed in the sand which was used to simulate the sea-bed, were found in accordance with the observed modal structure of the acoustic field.

5:40

4aUWe10. High frequency propagation in and scattering from water-saturated granular sediments: Laboratory study. Anatoliy N. Ivakin (Applied Physics Laboratory, University of Washington, 1013 NE 40th Street, Seattle, WA 98105, USA, ivakin@apl.washington.edu), Jean-Pierre Sessarego (Laboratory for Mechanics and Acoustics CNRS, 31 chemin Joseph Aiguier, 13009 Marseille, France, sessarego@lma.cnrs-mrs.fr)

Acoustic properties of water-saturated granular sediments at frequencies from 150 kHz to 8 MHz were studied in controlled laboratory conditions using broadband transducers. Two samples of medium sand sediments, with the same mean grain size, but with different width of the size distribution, were taken for the study, degassed, and their surface was flattened. Another sample of sediments was composed of glass beads of the same grain size. The main difference of glass beads from sand grains was their shape. Backscattering strength at normal and oblique incidence and reflection coefficient at normal incidence were measured for the three samples. The reflection experiments were made for different thicknesses of the samples, so that reflections from both first and second interfaces of the sediment layer were measured. This allowed also estimating sound speed and attenuation in the sediments. The results obtained for the three chosen types of the sediments were compared to demonstrate effects of the grain size distribution width and the grain shape on acoustic properties of the sediment. [Work supported by ONR and CNRS].

6:00

4aUWe11. A time domain model of scattering from small discrete volume particles: Tank validation. Gaetano Canepa (NATO Undersea Research Centre, Viale San Bartolomeo 400, 19126 La Spezia, Italy, canepa@nurc.nato.int), Jean-Pierre Sessarego (Laboratory for Mechanics and Acoustics CNRS, 31 chemin Joseph Aiguier, 13009 Marseille, France, sessarego@lma.cnrs-mrs.fr), Alessandra Tesei (NATO Undersea Research Centre, Viale San Bartolomeo 400, 19126 La Spezia, Italy, tesei@nurc.nato.int), Régine Guillermin (Laboratory for Mechanics and Acoustics CNRS, 31 chemin Joseph Aiguier, 13009 Marseille, France, guillermin@lma.cnrs-mrs.fr), Raymond J. Soukup (U.S. Naval Res. Lab., Acoust. Div., Code 7142, 4555 Overlook Ave. SW, Washington, DC 20375, USA, soukup@abyss.nrl.navy.mil)

A model of the time domain scattering from small discrete volume particles is presented here with an experimental validation. The model was implemented on the backbone of the BORIS-3D model which originally included only surface scattering and volume scattering from small perturbation of the volume density and sound speed. The proposed model adds discrete volume scattering and simulates both monostatic and bistatic configurations. The experimental validation was performed in a tank of the CMRS/LMA Laboratory (Laboratoire de Mécanique et d'Acoustique) using an in-house produced silicon plate (with a flat upper interface) in which 10% of the volume embeds spherical glass beads 1 mm in diameter. The characteristics of this plate was well known; in particular, the amplitude of the volume backscattering (as a function of the scattering angle) has already been presented. In this work, we are particularly interested in the time domain evolution of the scattered echo. The results of this study show a very good agreement between simulated and experimental data in both amplitude and time evolution shape.

6:20

4aUWe12. Backscattering From Scale Models of Elastic Ocean Bottoms with Power-law Roughness. Raymond J. Soukup (U.S. Naval Res. Lab., Acoust. Div., Code 7142, 4555 Overlook Ave. SW, Washington, DC 20375, USA, soukup@abyss.nrl.navy.mil), Edward L. Kunz (U.S. Naval Res. Lab., Acoust. Div., Code 7142, 4555 Overlook Ave. SW, Washington, DC 20375, USA, kunz@abyss.nrl.navy.mil), Gaetano Canepa (NATO Undersea Research Centre, Viale San Bartolomeo 400, 19126 La Spezia, Italy, canepa@nurc.nato.int), Harry J. Simpson (U.S. Naval Res. Lab., Acoust. Div., Code 7142, 4555 Overlook Ave. SW, Washington, DC 20375, USA, harry.simpson@nrl.navy.mil), Jason E. Summers (U.S. Naval Res. Lab., Acoust. Div., Code 7142, 4555 Overlook Ave. SW, Washington, DC 20375, USA, jason.summers@nrl.navy.mil)

Rough surface analogs to ocean bottom interfaces with two contrasting power-law roughness spectra were fabricated from slabs of PVC. A tank experiment with a nearly monostatic geometry and transmitted signals in the band 100-300 kHz was performed, with the source and receiver positioned to produce acoustic interactions on multiple locations on the surfaces. Models of scattering strength and

the received time series, using deterministic and stochastic representations of the surface, are used to verify the predicted dependence of the scattering, with emphasis on the sub-critical angle (< 50 degrees grazing) region, where the predicted difference in scattering strength due to the contrast in roughness between the two fabricated surfaces is on the order of 10 dB. The numerical models employed were perturbation theory, a second-order small-slope calculation using the power-law roughness parameters, and a fourth-order small-slope calculation using the actual grid of heights as an input. The experimental effort also focused on the near-critical angle region where the predictions of the numerical models differed markedly. [Work supported by ONR and NURC.]

6:40

4aUWe13. Shallow-water tank experiments and model comparisons over range-dependent elastic bottoms. Jon M. Collis (Boston University, Department of Aerospace and Mechanical Engineering, 110 Cummington Street, Boston, MA 02215, USA, jcollis@bu.edu), Michael D. Collins (U.S. Naval Res. Lab., Acoust. Div., Code 7142, 4555 Overlook Ave. SW, Washington, DC 20375, USA, michael.collins@nrl.navy.mil), Harry J. Simpson (U.S. Naval Res. Lab., Acoust. Div., Code 7142, 4555 Overlook Ave. SW, Washington, DC 20375, USA, harry.simpson@nrl.navy.mil), Raymond J. Soukup (U.S. Naval Res. Lab., Acoust. Div., Code 7142, 4555 Overlook Ave. SW, Washington, DC 20375, USA, soukup@abyss.nrl.navy.mil), William L. Siegmann (Rensselaer Polytechnic Institute, 110 8th Street, Troy, NY 12180, USA, siegmw@rpi.edu)

A series of tank experiments has been conducted in order to obtain high quality data for acoustic propagation in shallow-water environments with elastic bottoms. Such problems can now be solved accurately with the parabolic equation method, which is being used for comparisons with measured transmission loss. Results from the initial experiment with a flat or sloped slab of PVC demonstrated both benchmark quality agreement between computed solutions and data, and the necessity of accounting for elasticity in the bottom [J. M. Collis, *et al.*, JASA **122**]. This paper will present results of a second experiment, conducted in the same manner as the first, but modified to allow for variable bottom slopes. Time series were collected at 100-300 kHz on horizontal arrays for two source positions. Parabolic equation solutions for treating variable slopes, using coordinate transformation methods of mapping and axis rotations, will be benchmarked against the new data. [Work supported by the Office of Naval Research.]

7:00

4aUWe14. The Broadband In-Water Structural Acoustics of Unexploded Ordinance. Harry J. Simpson (U.S. Naval Res. Lab., Acoust. Div., Code 7142, 4555 Overlook Ave. SW, Washington, DC 20375, USA, harry.simpson@nrl.navy.mil), Brian H. Houston (Naval Research Laboratory, 4555 Overlook Ave, Washington, DC 20375, USA, houston@code7136.nrl.navy.mil), Michael L. Saniga (U.S. Naval Res. Lab., Acoust. Div., Code 7142, 4555 Overlook Ave. SW, Washington, DC 20375, USA, saniga@code7136.nrl.navy.mil), Joseph A. Bucaro (U.S. Naval Res. Lab., Acoust. Div., Code 7142, 4555 Overlook Ave. SW, Washington, DC 20375, USA, joseph.bucaro@nrl.navy.mil)

The Laboratory for Structural Acoustics (LSA) at the Naval Research Laboratory consists of a 1 million gallon, deionized water, indoor cylindrical tank (17m diameter by 15m deep). The key features include: 1) vibration and temperature isolation, 2) feedback controlled heating and adiabatic materials (temperature variability $<0.01°C$), and 3) reverberation reducing anechoic materials. This laboratory has computer controlled robotic scanners and manipulators used for precision freefield measurements including nearfield acoustic holography and compact range scattering. The precision robotics, environmental control, and painstaking measures to insure homogeneity and stability result in a high fidelity, versatile, and unique underwater acoustic measurement laboratory. The LSA also contains an indoor rectangular tank (10m by 8m) laboratory, with a 3m deep sand bottom and 4m of water column. In a similar fashion to the freefield laboratory, this laboratory is used to study target scattering in a marine bottom environment. We discuss such databases focused on the challenging problem of unexploded ordinance (UXO) in water where we use the structural acoustic response measured in a series of laboratory experiments to detect and identify several common UXOs. The 360 degree broadband (1-140 kHz) compact range monostatic and bistatic measurements taken in both laboratories will be discussed.

7:20

4aUWe15. Benchmarking of computational scattering models using underwater acoustic data from a corrugated wax slab. David C. Calvo (U.S. Naval Res. Lab., Acoust. Div., Code 7142, 4555 Overlook Ave. SW, Washington, DC 20375, USA, david.calvo@nrl.navy.mil), Gaetano Canepa (NATO Undersea Research Centre, Viale San Bartolomeo 400, 19126 La Spezia, Italy, canepa@nurc.nato.int), Raymond J. Soukup (U.S. Naval Res. Lab., Acoust. Div., Code 7142, 4555 Overlook Ave. SW, Washington, DC 20375, USA, soukup@abyss.nrl.navy.mil), Edward L. Kunz (U.S. Naval Res. Lab., Acoust. Div., Code 7142, 4555 Overlook Ave. SW, Washington, DC 20375, USA, kunz@abyss.nrl.navy.mil), Jean-Pierre Sessarego (Laboratory for Mechanics and Acoustics CNRS, 31 chemin Joseph Aiguier, 13009 Marseille, France, sessarego@lma.cnrs-mrs.fr), Kevin Rudd (U.S. Naval Res. Lab., Acoust. Div., Code 7142, 4555 Overlook Ave. SW, Washington, DC 20375, USA, kevin.rudd@nrl.navy.mil)

Measured time series for underwater acoustic scattering from a 30 cm x 30 cm x 5 cm wax slab with a two-dimensional corrugated (rippled) surface are compared with simulation results. The experimental geometry and directionality of the sensors allowed for ensonification of the rippled surface and the appearance of shadowing effects at low grazing angles. The acoustic source transmitted impulses at 200-800 kHz (wavelengths between 0.75-0.19 cm). The height and spacing of the ripples were 0.3 cm and 3 cm, respectively, and the slab had negligible shear speed and a measured attenuation. We simulate the experiment with the following methods listed in increasing levels of physical accuracy and computational cost: Kirchhoff Approximation (KA), Second-order Small-Slope approximation (SSA2), the Wide-angle On-Surface Radiation Condition method (WOSRC), a Pseudo-differential Impedance Operator method (PIO), a 2-domain Integral Equation method (IE-2DOM), and an Elastodynamic Finite Integration Technique (EFIT). The range of techniques allowed us to examine effects such as reflections off the interior bottom or ends of the slab and the effectiveness of the asymptotic (KA/SSA2) and pseudo-differential (WOSRC/PIO) methods for cases that include shadowing. (Work sponsored by ONR and NURC.)

Session 4pAAa

Architectural Acoustics: Archeological Acoustics I

David Lubman, Cochair
DL Acoustics, 14301 Middletown Lane, Westminster, CA 92683, USA

Jens Holger Rindel, Cochair
Odeon A/S, Scion DTU, Diplomvej Buildling 381, Lyngby, DK-2800, Denmark

Invited Papers

1:20

4pAAa1. Sound resonance in prehistoric times: A study of Paleolithic painted caves and rocks. Iegor Reznikoff (Université de Paris X, Département de Philosophie, 92001 Nanterre, France, dominiqueleconte@yahoo.fr)

Caves have natural properties of resonance: some parts sound very well, the sound lasts for some seconds or gives several echoes, some other parts have a dull resonance or no resonance at all. It is extremely interesting to compare in a given cave the map of the most resonant locations with the map of the locations of the paintings: are there correlations between resonance and paintings? We have studied many Paleolithic caves in France in which the answer was remarkably positive; stated shortly: the more resonant the location, the more paintings or signs are situated in this location. Here are presented some studies and results in the caves of Isturitz and Oxocelhaya in Pays Basque and in some other caves. Some considerations are given about the resonance - pictures relationship in open spaces with prehistoric painted rocks. Bibliography I. Reznikoff: Prehistoric Paintings, Sound and Rocks in Studien zur Musikarchäologie III: 2nd International Symposium on Music Archaeology, Sept. 2000, ed. E. Hickmann, Berlin, Rahden, 2002, 39-56. The Evidence of the Use of Sound Resonance from Palaeolithic to Medieval Times, Archaeoacoustics, C. Scarre & G. Lawson ed., University of Cambridge, Cambridge, 2006, 77-84. On Primitive Elements of Musical Meaning, www.musicandmeaning.net, JMM 3 (Invited papers), 2005.

1:40

4pAAa2. Architectural and acoustic restoration of the 'Benevento' Roman Theatre. Luigi Maffei (Built Environment Control Laboratory Ri.A.S., Second University of Naples, Abazia di S. Lorenzo, 81031 Aversa, Italy, luigi.maffei@unina2.it), Gino Iannace (Built Environment Control Laboratory Ri.A.S., Second University of Naples, Abazia di S. Lorenzo, 81031 Aversa, Italy, gino.iannace@unina2.it), Leda De Gregorio (Built Environment Control Laboratory Ri.A.S., Second University of Naples, Abazia di S. Lorenzo, 81031 Aversa, Italy, ledadegreg@libero.it), Umberto Palmieri (Built Environment Control Laboratory Ri.A.S., Second University of Naples, Abazia di S. Lorenzo, 81031 Aversa, Italy, uzy@libero.it)

Acoustics as well as the extraordinary architecture are substantial part of the heritage of ancient Greek and Roman theatres. These archaeological areas are more often used for classical and modern performing activities but to emphasise the original acoustics, restoration of the original shape, reconfiguration of the space and introduction of new technologies and materials may be needed. These activities must happen taking into account the ″International Charter for The Conservation and Restoration of Monuments and Sites″ as main tools defining conservation, use and maintenance guidelines in matter of discipline for ancient performing places. This paper presents some proposals for the stage reconstruction of the Benevento Roman Theatre and examine the associated effects on the theatre acoustics. Design proposals, minded to preserve the place authenticity, improving the acoustics and keeping intact the surrounding atmosphere for spectators, are the result of archaeological data, contemporary performances requirements, state of the art in matter of stage setting design. Acoustic field prediction is based on numerical models and auralization aiming to reproduce the real listening conditions.

Contributed Paper

2:00

4pAAa3. Acoustic characterization of the ancient theatre at Syracuse. Marco Gullo (DREAM, Univ. of Palermo, Viale delle Scienze, Edificio 9, 90128 Palermo, Italy, mgullo@dream.unipa.it), Armando La Pica (DREAM, Univ. of Palermo, Viale delle Scienze, Edificio 9, 90128 Palermo, Italy, lapica@unipa.it), Giuseppe Rodono' (DREAM, Univ. of Palermo, Viale delle Scienze, Edificio 9, 90128 Palermo, Italy, rodon@unipa.it), Vincenzo Vinci (DREAM, Univ. of Palermo, Viale delle Scienze, Edificio 9, 90128 Palermo, Italy, vincenzo_vinci@hotmail.it)

The ancient theatre at Syracuse, the largest open air theatre in Sicily, experienced many structural changes along its history. Today its very renowned drama festival attracts visitors from all the world that fill the entire cavea: customized seats accomodation and a prominent stage play an important role in the theatre acoustics. Because no data were available in literature on its acoustical perfomance a measurement session was carried out by our team in the framework of a wide research project on ancient theatres acoustics in the modern use. From data recorded ″room criteria″ parameters have been evaluated together with spectral analysis in order to gain a deeper information on the acoustic field. Main results are listed and commented and a comparison among data collected on field during the team experience in the past years is reported.

Invited Paper

2:20

4pAAa4. On the use of ancient theatres for modern performances: a scale model approach. Andrea Farnetani (Engineering Dept. - Univ. of Ferrara, Via Saragat, 1, 44100 Ferrara, Italy, andrea.farnetani@unife.it), Nicola Prodi (Engineering Dept. - Univ. of Ferrara, Via Saragat, 1, 44100 Ferrara, Italy, nicola.prodi@unife.it), Roberto Pompoli (Engineering Dept. - Univ. of Ferrara, Via Saragat, 1, 44100 Ferrara, Italy, roberto.pompoli@unife.it)

Ancient theatres are widely used today for modern performances including drama, music and ballets. Despite the state of conservation of the stage, the scenery is seldom designed with little care about its acoustical efficiency. Moreover, depending on the specific venue, a sound system can be employed in the performance. To clarify the acoustical impact of all these elements in ancient theatres, different stage settings and a sound sytem were investigated by means of scale model measurements. The scale model is a 1:20 scale reproduction of the ancient theatre of Siracusa (Italy). It is conceived as modular structure so that different configurations of the cavea and of the stage can be reproduced. To investigate the stage-set effects different groups of reflecting panels were arranged on the platform and an orchestra shell was tested too. Then, to simulate the sound system, two directional high frequency sources were assembled and optimized. The interplay of stage, sound system and theatre architecture was outlined by a comprehensive set of acoustical measurements.

Contributed Paper

2:40

4pAAa5. ″Acoustics vases in ancient theatres: disposition, analysis from the ancient tetracordal musical system″. Arturo Barba Sevillano (Grup d'Acustica Arquitectònica, Ambiental i Industrial, E.T.S.I.I, Univ. Politécnica de Valencia, Camino de Vera, s/n, 46022 Valencia, Spain, arbarse@doctor.upv.es), Radu Lacatis (Grup d'Acustica Arquitectònica, Ambiental i Industrial, E.T.S.I.I, Univ. Politécnica de Valencia, Camino de Vera, s/n, 46022 Valencia, Spain, rala1@doctor.upv.es), Alicia Giménez (Grup d'Acustica Arquitectònica, Ambiental i Industrial, E.T.S.I.I, Univ. Politécnica de Valencia, Camino de Vera, s/n, 46022 Valencia, Spain, agimenez@fis.upv.es), José Romero (Grup d'Acustica Arquitectònica, Ambiental i Industrial, E.T.S.I.I, Univ. Politécnica de Valencia, Camino de Vera, s/n, 46022 Valencia, Spain, romerof@fis.upv.es)

The acoustics of the ancient Greek and Roman theatres has always been rated as excellent by experts, without discussion. Beyond the purely architectural aspects, in this kind of outdoor theatres some mechanisms were used in order to improve the acoustics. In this paper we have studied the texts about ″theatre's vases″ of the famous book ″On Architecture″ by Vitruvius. Different interpretations and illustrations of these vases, that several translators carried out in the sixteenth to the eighteenth centuries, have been researched. From the wide bibliography consulted in this regard we have developed a plane with the disposition of the bronze vases in the theatres. In this plane we have specified the frequency of each one of them, and explained their disposition from the tetracordal musical system acquired from the Greek culture. Finally, an analysis of the disposition of the vases has been made. We have studied and looked for the musical intervals and harmonic relations among adjacent vases.

Invited Papers

3:00

4pAAa6. Musical granite pillars in ancient Hindu temples. Paul Calamia (Rensselaer Polytechnic Institute, Greene Bldg., 110 8th St., Troy, NY 12180, USA, calamp@rpi.edu), Jonas Braasch (Rensselaer Polytechnic Institute, Greene Bldg., 110 8th St., Troy, NY 12180, USA, braasj@rpi.edu)

In some ancient Hindu temples built in India between the 7th century and the 16th century can be found a fascinating architectural element: intricately designed musical pillars of solid granite. These pillars, clusters of which were often carved from a single piece of stone, were tuned by means of their length, width, and tension (induced by a load from above) and were played to accompany devotional readings and dance performances. Various tunings and sound characteristics were employed based on the intended purpose. In this paper, examples of extant pillars will be presented and discussed within the context of their acoustical and architectural significance.

3:20

4pAAa7. Convolution-scattering model for staircase echoes at the temple of Kukulkan. David Lubman (DL Acoustics, 14301 Middletown Lane, Westminster, CA 92683, USA, dlubman@dlacoustics.com)

Chirped echoes from staircases at the temple of Kukulkan at Chichen Itza have stimulated much interest since first reported at scientific meetings by the author in 1998. Among them are Declercq et al (J. Acoust. Soc. Am. 116, (6) 2004). They correctly observed that the echo depends strongly on the ″type″ of incident sound, but offered no explanation. Those authors overlooked an earlier explanation given at the First Pan-American/Iberian Meeting on Acoustics at Cancun, Mexico (Lubman, J. Acoust. Soc. Am. 112, (5) (2002). It included a mathematical model of the chirped echo effect and a full simulation of the chirped echo, including auralization. This model explicitly shows echo dependence on the time-frequency structure of the impinging sound. With it, ethnomusicologists and others can conveniently simulate the staircase echo for any recorded sound stimulus, including handclaps, voices, and ethnic sound instruments. The clap-echo system is modeled as a time-invariant linear system. The echo time series is found by convolving the stimulus (e.g., handclap) with the staircase impulse response. This earlier model is far more computationally efficient than the Declercq model, and achieves greater accuracy by avoiding the false and needless assumptions of plane wave propagation and infinite corrugated periodic surfaces.

3:40-5:00 Posters

Lecture sessions will recess for presentation of poster papers on various topics in acoustics. See poster sessions for topics and abstracts.

Invited Paper

5:00

4pAAa8. On the Acoustics of the Underground Galleries of Ancient Chavín de Huántar, Peru. Jonathan S. Abel (Stanford Univ., Center for Computer Research in Music and Acoustics (CCRMA), Dept. of Music, Stanford, CA 94305-8180, USA, abel@ccrma.stanford.edu), John W. Rick (Stanford University, Archaeology Center, P.O. Box 20446, Stanford, CA 94309, USA, johnrick@stanford.edu), Patty P. Huang (Stanford Univ., Center for Computer Research in Music and Acoustics (CCRMA), Dept. of Music, Stanford, CA 94305-8180, USA, pph@ccrma.stanford.edu), Miriam A. Kolar (Stanford Univ., Center for Computer Research in Music and Acoustics (CCRMA), Dept. of Music, Stanford, CA 94305-8180, USA, kolar@ccrma.stanford.edu), Julius O. Smith (Stanford Univ., Center for Computer Research in Music and Acoustics (CCRMA), Dept. of Music, Stanford, CA 94305-8180, USA, jos@ccrma.stanford.edu), John M. Chowning (Stanford Univ., Center for Computer Research in Music and Acoustics (CCRMA), Dept. of Music, Stanford, CA 94305-8180, USA, jc@ccrma.stanford.edu)

Chavín de Huántar is a monumental World Heritage archaeological site in the Peruvian highlands predating Inca society by over 2000 years. The importance of site acoustics is suggested by distinctive architectural features, notably an extensive network of underground galleries used in part for ritual purposes. The labyrinthine galleries are arranged in a series of small rectangular alcoves off narrow corridors. Here we focus on measuring and modeling the acoustics at Chavín to understand the implications of auditory experiences within the galleries as related to the site's role in developing religious authority. Acoustic measurements and models of a site can be used to archive site acoustics, estimate the acoustics of inaccessible or alternative site architectures, and reconstruct original site acoustics; they may also be used to corroborate aspects of rituals suggested by other archaeological data. Preliminary acoustic measurements at Chavín show a short reverberation time, dense and energetic early reflections, and a large lateral energy fraction. The short reverberation time would enable rhythmically articulated group performance using Strombus shell trumpets found onsite. The early reflections would provide strong acoustic reinforcement and consistent resonances for participants in gallery alcoves. The wide soundfield would envelop participants, contributing to the ritual experience.

Contributed Paper

5:20

4pAAa9. Assessment of Acoustical Characteristics for Historical Baths (Hammams). Asuman Aydin (Middle East Technical University, Dept of Architecture, METU (ODTU), Inonu Blvd, 06531 Ankara, Turkey, aydinasuman@yahoo.com), Ayse Tavukcuoglu (Middle East Technical University, Dept of Architecture, METU (ODTU), Inonu Blvd, 06531 Ankara, Turkey, aysetavukcuoglu@yahoo.com), Mehmet Caliskan (Middle East Technical University, Dept of Architecture, METU (ODTU), Inonu Blvd, 06531 Ankara, Turkey, caliskan@metu.edu.tr)

Comprehensive studies are necessary to better understand the original acoustical characteristics of historical baths (hammams) in order to discover the historical technologies establishing acoustical properties in these structures and keep their proper functioning for long periods of time. The study was conducted on five historical Turkish hammams, belonging to the Ottoman period. Their acoustical performances were examined in terms of basic acoustical parameters, such as, reverberation time, early decay time, clarity, lateral fraction, sound transmission index. The 3D computer modelling and acoustics simulation were done for each structure by ″ODEON combined 8.5″. Their audio performance was evaluated by taking into consideration of the volume, materials use and environmental conditions. The analyses were done for the case of the unoccupied condition while one of the structures, Sengul Hammam in Ankara, was analysed both for non- and fully-occupied conditions. The joint interpretation of the results was done in order to define the acoustical features of the hammam structures. The potentials for improving the acoustical performance of interiors were also discussed. The use of 3D computer modeling and acoustical simulation, adapted for the case of historical hammam structures, provided a good opportunity for the assessment of their acoustical performance on quantitative basis.

Invited Papers

5:40

4pAAa10. History and acoustics of the Asian free-reed mouth organs. James Cottingham (Coe College, 1220 First Avenue NE, Cedar Rapids, IA 52402, USA, jcotting@coe.edu)

Mouth-blown instruments employing a free reed coupled to a pipe resonator have long been known and used throughout East and Southeast Asia. Details of the origin and development of these instruments are not known, but are closely connected with the history and prehistory of a multitude of ethnic groups. Free reed instruments have been employed in a variety of ways, from simple signaling devices to use in the court music of Japan and China. The pipe resonators vary from the buffalo horn to bamboo pipes of nearly cylindrical cross section. The instruments exemplify a pipe-resonator coupling significantly different from that of the standard wind instruments of European origin. In some cases the reed is at or near one end of an open or closed pipe resonator, but in other examples the reed is mounted in the side of the resonator away from the ends. A summary of recent experimental investigations of these instruments will be presented, along with musical examples.

6:00

4pAAa11. The mridangam: A study of the history and acoustics of an ancient South Indian drum. Rohan Krishnamurthy (Kalamazoo College, 544 Sunrise Circle, Kalamazoo, MI 49009, USA, rohan@rohanrhythm.com), Ian Hempe (Coe College, 1220 First Avenue NE, Cedar Rapids, IA 52402, USA, ikhempe@coe.edu), James Cottingham (Coe College, 1220 First Avenue NE, Cedar Rapids, IA 52402, USA, jcotting@coe.edu)

The acoustical properties of the South Indian drum, the mridangam, were studied. The barrel-shaped mridangam has been described in ancient Hindu scriptures and depicted in cave paintings and temple sculptures. With a claimed antiquity dating back to the Vedic period, it is the principal percussion instrument in South Indian classical music and dance and possesses unique tonal properties. The mridangam is comprised of three primary parts: The tonal head (valanthalai), the bass head (thoppi), and the central shell (kattai), to which the two heads are traditionally fastened by leather rope. Measurements of modes and mode frequencies were made on traditional drums, as well as on drums where the heads were remounted using a new and user-friendly design. Measurements of drumhead vibration and sound spectra were also made when the drumhead was excited by a skilled player using standard strokes. The frequencies of the first few modes of the tonal head were found, as expected, to be tuned approximately harmonic. Practical performance variables, including effects of altering mounting tension and coupling between the drumheads, were also studied. Results from the study will be followed by a practical demonstration of the instrument.

6:20

4pAAa12. Auditory capacities of human fossils: A new approach to the origin of speech. Ignacio Martínez ((1) Universidad de Alcala de Henares; (2) Centro UCM-ISCIII de Evolución y Comportamiento Humanos, Centro UCM-ISCIII de Evolución y Comportamiento Humanos, C/ Sinesio Delgado, N° 4, Pabellón 14, 28029 Madrid, Spain, imartinezm@isciii.es), Rolf Michael Quam ((1) American Museum of Natural History; (2) Centro UCM-ISCIII de Evolución y Comportamiento Humanos, Division of Anthropology, American Museum of Natural History, Central Park West @ 79th St., New York, NY 10024, USA, rquam@amnh.org), Manuel Rosa (Universidad de Alcalá de Henares, Edificio de Ciencias, Campus Universitario, 28871 Alcalá de Henares, Spain, manuel.rosa@uah.es), Pilar Jarabo (Universidad de Alcalá de Henares, Edificio de Ciencias, Campus Universitario, 28871 Alcalá de Henares, Spain, mpilar.jarabo@uah.es), Carlos Lorenzo ((1) Universitat Rovira i Virgili (2) Centro UCM-ISCIII de Evolución y Comportamiento Humanos, Universitat Rovira i Virgili, Facultat de Lletres Institut de Paleoecologia Humana, Area de Prehistoria, i Evolució Social, Imperial Tarraco, 1, 43005 Tarragona, Spain, clorenzo@prehistoria.urv.es), Juan Luis Arsuaga ((1) Universidad Complutense de Madrid; (2) Centro UCM-ISCIII de Evolución y Comportamiento Humanos, Centro UCM-ISCIII de Evolución y Comportamiento Humanos, C/ Sinesio delgado, N° 4, Pabellón 14, 28029 Madrid, Spain, jlarsuag@isciii.es)

The origin and evolution of human language has mainly dealt with the reconstruction of the upper respiratory tract of human fossils. After decades of controversy no clear results have arisen from these studies. We propose a new approach to this issue based on the possibility to reconstruct the sound power transmission, through the external and middle ear, in fossil specimens. The results thus obtained in the more than 500 ky old fossils from the Sima de los Huesos site (Sierra de Atapuerca, Spain) show that this hominins had the same auditory capacities as modern human, suggesting an older origin for speech than any previous study.

6:40

4pAAa13. The marvellous sound world in the 'Phonurgia Nova' of Athanasius Kircher. Lamberto Tronchin (DIENCA - CIARM, University of Bologna, viale Risorgimento, 2, I-40136 Bologna, Italy, tronchin@ciarm.ing.unibo.it), Ilaria Durvilli (DIENCA - CIARM, University of Bologna, viale Risorgimento, 2, I-40136 Bologna, Italy, ilaria.durvilli@mail.ing.unibo.it), Valerio Tarabusi (DIENCA - CIARM, University of Bologna, viale Risorgimento, 2, I-40136 Bologna, Italy, ciarm02@hotmail.com), Galia Mastromatteo (DIENCA - CIARM, University of Bologna, viale Risorgimento, 2, I-40136 Bologna, Italy, gam@ciarm.ing.unibo.it)

Athanasius Kircher, Jesuit, was born in Geisa, Thüringen, in 1608. He spent a large amount of his life in Rome, where he died in 1680. He was active in many different topics, ranging from geology to philosophy. He was the author of many books at his time, among all the Musurgia Universalis, written in 1650, and the Phonurgia Nova, of 1673. Whilst the Musurgia Universalis gathered a wide attention also in recent years, the Phonurgia Nova, which means ″ a new method of sound production″, was only recently rediscovered. In this paper the original Latin version of the Phonurgia Nova, which comprises two different books, i.e. the ″Phonosophia nova″ and the ″Phonosophia anacamptica″, is analyzed. The first book deals with the influence of music in the human being, whereas the second book analyses the sound propagation in enclosure. This book reveals some interesting acoustic apparatus for sound production and propagation, as the ″tuba stentorophonica″ (the loud trumpet), the ″statua citofonica″ (the talking statue). Some of these phonic apparatus are described, analyzed and commented.

Session 4pAAb

Architectural Acoustics: Archeological Acoustics II (Poster Session)

David Lubman, Cochair
DL Acoustics

Jens Holger Rindel, Cochair
Odeon A/S

All posters will be on display from 3:40 p.m. to 5:20 p.m. To allow contributors an opportunity to see other posters, contributors of odd-numbered papers will be at their posters from 3:40 p.m. to 4:30 p.m. and contributors of even-numbered papers will be at their posters from 4:30 p.m. to 5:20 p.m.

Contributed Papers

4pAAb1. Acoustics of Unique Baroque Theatre in Český Krumlov. Jana Dolejsi (Studio D - Akustika s.r.o., Zizkova 12, 371 22 Ceske Budejovice, Czech Republic, jana.dolejsi@akustikad.com), Pavel Slavko (Státní hrad a zámek, 381 01 Cesky Krumlov, Czech Republic, castle@ckrumlov.cz), Ladislav Pouzar (Chvalšinská 231, 381 01 Cesky Krumlov, Czech Republic, ladislav@pouzar.cz), Monika Rychtarikova (Lab. ATF, Katholieke Universiteit Leuven, Celestijnenlaan 200D, B-3001 Leuven, Belgium, Monika.Rychtarikova@bwk.kuleuven.be)

The castle theater in the Český Krumlov is a unique historical site in Europe which represents a valuable example of a theater with Baroque scenes from the late 18th century. It was preserved with exceptional completeness and authenticity since it has never burned, and during the last two centuries it was not modernized. The baroque period must be understood as a universal style with many methods of expression which act in harmony, and the individual elements must complement each other and be interconnected to produce an effective unit. It was a challenge to experimentally prove these relationships and connections in as wide context as possible (i.e. relations between the architecture, contemporary scene lighting, perspectives and proportions, roomacoustic properties, contemporary musical interpretations and vocal techniques, placing of the orchestra and other. According to musicians, actors and audience is this theatre known as a hall with excellent acoustic condition. However, no room acoustic measurements were performed in the theatre in the last century. This article report on results from the acoustical measurements and simulation in the main hall of the theatre which help us to understand which acoustical values people find pleasant in the room of this character.

4pAAb2. Acoustical reconstruction of San Petronio Basilica in Bologna during the Baroque period: the effect of festive decorations. Francesco Martellotta (DAU - Politecnico di Bari, via Orabona 4, 70125 Bari, Italy, f.martellotta@poliba.it), Ettore Cirillo (DAU - Politecnico di Bari, via Orabona 4, 70125 Bari, Italy, e.cirillo@poliba.it), Sabrina Della Crociata (DAU - Politecnico di Bari, via Orabona 4, 70125 Bari, Italy, sadel1984@libero.it), Emanuele Gasparini (via Centurare 33, 37062 Dossobuono, Italy, emanuele.gasparini@libero.it), Daniela Preziuso (DAMS - Alma Mater Studiorum Univ. di Bologna, via Barberia, 4, 40123 Bologna, Italy, aleinad2002@libero.it)

The Basilica of San Petronio in Bologna (Italy) is a large Gothic church characterized by three naves divided by cluster piers made of brick and flanked by square chapels. It is 130 m long, 60 m wide and 44 m high, developing a volume of 170000 m^3. The widespread use of smooth plaster and the substantial lack of decoration give rise to a reverberation time (in unoccupied conditions) which varies from about 13 s at 125 Hz to 5 s at 4 kHz, with an average of 10.7 s at mid frequencies. In occupied conditions the expected mid-frequency reverberation time should lower to about 7 s. Nonetheless, these acoustic conditions appear scarcely compatible with the characteristics of the Baroque music which was composed for the ″Cappella musicale″ during the 17th century. However, historical research pointed out how, in that period, rich draping and curtains were often used during the major religious and civil celebrations. The analysis of the acoustic consequences of such temporary installations was performed by means of acoustic simulation based on historical records calibrated on the current configuration of the church. The paper presents the results of such reconstruction.

4pAAb3. Assessment of strong reflections in ancient theatres: Spatial information from parallel measurement data. Giuseppe Rodonò (DREAM, Univ. of Palermo, Viale delle Scienze, Edificio 9, 90128 Palermo, Italy, rodon@unipa.it), Marco Gullo (DREAM, Univ. of Palermo, Viale delle Scienze, Edificio 9, 90128 Palermo, Italy, mgullo@dream.unipa.it), Armando La Pica (DREAM, Univ. of Palermo, Viale delle Scienze, Edificio 9, 90128 Palermo, Italy, lapica@unipa.it), Vincenzo Vinci (DREAM, Univ. of Palermo, Viale delle Scienze, Edificio 9, 90128 Palermo, Italy, vincenzo_vinci@hotmail.it)

The sound field in ancient open-air theatres shows a finite time-response in a transient. The structure of the time-response depends on geometrical characteristics of the theatre and source-receiver position: upon geometry dimension of the stage area its possible to observe nearly strong reflections and quantify the associated delay time. Sampling the theatre space with a single microphone does not allow any directional information on the sound field but the parallel use of more microphones and software post-processing could add spatial information. Dataset consists of four syncronized impulse response measured along a radial direction in the theatre plan for differents source positions. A directional receiver system based on a post-processing method has been implemented and applied to measurement data. The obtained experimental results are reported and discussed.

4pAAb4. Ultrasonic quantitative strength assessment of artificially aged and archaeological wood samples. Ari Salmi (Univ. of Helsinki / Dept. of Physical Sciences, POB 64 (Gustaf Hällströmin katu 2), 00014 Helsinki, Finland, edward.haeggstrom@helsinki.fi), Kari Steffen (P.O.B 56 University of Helsinki, 00014 Helsinki, Finland, kari.steffen@helsinki.fi), Joona Eskelinen (Univ. of Helsinki / Dept. of Physical Sciences, POB 64 (Gustaf Hällströmin katu 2), 00014 Helsinki, Finland, joona.eskelinen@helsinki.fi), Edward Hæggström (Electronics Research Unit, University of Helsinki, P.O.Box 64 (Gustaf Hällströmin katu 2), FIN-00014 Helsinki, Finland, edward.haeggstrom@helsinki.fi)

A large fraction of discovered archaeological artefacts are wooden. Since materials grow brittle and their stiffness decreases over time, it is vital for archaeologists to have methods that assess the strength of the object prior to

moving it. We present preliminary shear and elastic modulus data measured using 100 kHz longitudinal and shear ultrasonic tone burst through-transmission. Artificially aged wooden samples and archaeological samples of known age were used to validate the aging procedure by comparison of the shear and elastic modulus. We also measured the modulae of water-logged samples obtained from the ship wreck Vrouw Maria sunken in the Finnish archipelago in 1771, and compared to samples artificially aged to similar age. Scanning electron microscopy (SEM) was used to compare the structure of artificially and naturally aged samples. The results presented may be used to create an artefact model for strength assessment, and to give guidelines of strength vs. age for archaeologists to support their logistics decisions.

4pAAb5. The Parpalló Cave: A singular archaeological acoustic site. Noé Jiménez González (Universidad Politécnica de Valencia, C/ La trampa N° 2, 02520 Chinchilla de Montearagón, Spain, nojigon@epsg.upv.es), Rubén Picó (EPSG - Univ. Politécnica de Valencia, c/ Nazaret-Oliva s/n, 46780 Grau de Gandia, Spain, rpico@fis.upv.es), Javier Redondo (IGIC - Universitat Politècnica de València, Cra. Nazaret-Oliva S/N, E-46730 Gandia, Spain, fredondo@fis.upv.es)

The Parpalló Cave is located in the slopes of Montdúber, in Valencia (Spain). It is one of the most important Palaeolithic sites, not only in Spain, but in the world. It was a privileged location for its inhabitants from the Upper Palaeolithic onwards. It has one of the most spectacular collections of Palaeolithic art mobilier found to date. The Parpalló cave features a considerably large opening which, undoubtedly, influences its acoustic properties. Indeed, the sound pressure field inside the cave is not excessively reverberant and intelligibility is significantly better than in similar enclosures. In this work a study of the acoustic properties of the Parpalló cave is performed by using numerical simulation.

THURSDAY AFTERNOON, 3 JULY 2008 P2-B, LEVEL 2, 3:40 TO 5:20 P.M.

Session 4pAAc

Architectural Acoustics and Psychological and Physiological Acoustics: Speech Segregation in Rooms II (Poster Session)

Barbara Shinn-Cunningham, Cochair
Boston University Hearing Research Center

Mathieu Lavandier, Cochair
Cardiff University

All posters will be on display from 3:40 p.m. to 5:20 p.m. To allow contributors an opportunity to see other posters, contributors of odd-numbered papers will be at their posters from 3:40 p.m. to 4:30 p.m. and contributors of even-numbered papers will be at their posters from 4:30 p.m. to 5:20 p.m.

Contributed Papers

4pAAc1. Effects of spatial factors of speech, noise, and reverberation sounds on listening difficulty. Hayato Sato (Environmental Acoustics Laboratory, Graduate School of Engineering, Kobe University, Rokkodai 1-1, Nada, 657-8501 Kobe, Japan, hayato@kobe-u.ac.jp), Tomoyasu Takaoka (Environmental Acoustics Laboratory, Graduate School of Engineering, Kobe University, Rokkodai 1-1, Nada, 657-8501 Kobe, Japan, Tomoyasu.Takaoka@mb2.seikyou.ne.jp), Masayuki Morimoto (Environmental Acoustics Laboratory, Graduate School of Engineering, Kobe University, Rokkodai 1-1, Nada, 657-8501 Kobe, Japan, mrmt@kobe-u.ac.jp)

It is well known that the amount of auditory masking in binaural listening is affected by spatial factors of signal and masking sounds such as the degree of interaural cross-correlation and the arriving direction. The amount of auditory masking for speech signal are usually measured using speech intelligibility tests. However, in the sound fields that appears in everyday life, speech intelligibility are usually close to 100%. Therefore, it was unclear how much the effects of spatial factors on speech communication in everyday life are. Listening tests were performed to clarify the effects of spatial factors on listening difficulty ratings [M. Morimoto *et al*., J. Acoust. Soc. Am. **116**, 1607-1613 (2004)] focussing on the degree of interaural cross-correlations of speech, noise, and reverberation sounds, and on the arriving direction of speech signal. The two spatial factors were controlled by several loudspeakers which are horizontally installed in an anechoic room. The results of listening tests showed that the effects of the two spatial factors on listening difficulty ratings decreased with improving listening conditions, and the effects can be ignored in the sound fields that often appears in everyday life.

4pAAc2. Binaural enhancement of speech intelligibility metrics. Florent Deux (Chalmers University of Technology, Division of Applied Acoustics, Chalmers Room Acoustic Group, SE-41296 Göteborg, Sweden, florentdeux@gmail.com), Mendel Kleiner (Chalmers Rm. Acoust. Group, Dept. of Appl. Acoust., Chalmers Univ. of Technology, 41296 Gothenburg, Sweden, mendel.kleiner@chalmers.se)

Efficient methods of quantifying speech intelligibility are needed for designing and understanding functional architectural spaces. All current measures of speech intelligibility are based on monaural impulse response, which excludes consideration of important binaural aspects of human hearing, including dereverberation and decoloration. Acquisition of binaural data has increasingly become common practice, using dummy heads or in-ear microphones, making the development of binaural intelligibility measures especially timely. The need for such a measure is illustrated by calculations of speech transmission index (STI) with a single energy-based impulse obtained through combination of binaural data channels. Each method of

combination produces significantly different STI values that illustrate the impact of orientation and location on intelligibility calculations. The relationship between such estimation variation and subjective experience must be studied to determine the research direction for a much needed, uniquely binaural speech intelligibility measure. The aim of this research is then to provide a guide to be used in comparing values obtained by the various methods. The project will then involve measurements of psychoacoustic metrics for speech intelligibility by objective methods as well as determination of speech intelligibility by subjective methods using tests with binaural recording and playback listening.

THURSDAY AFTERNOON, 3 JULY 2008 P2-B, LEVEL 2, 3:40 TO 5:20 P.M.

Session 4pAAd

Architectural Acoustics: Architectural Acoustics Potpourri III (Poster Session)

Ingo Witew, Cochair
Institute of Technical Acoustics, Templergraben 55, Aachen, 52056, Germany

Byron Harrison, Cochair
Talaske, 1033 South Boulevard, Oak Park IL 60302, USA

All posters will be on display from 3:40 p.m. to 5:20 p.m. To allow contributors an opportunity to see other posters, contributors of odd-numbered papers will be at their posters from 3:40 p.m. to 4:30 p.m. and contributors of even-numbered papers will be at their posters from 4:30 p.m. to 5:20 p.m.

Contributed Papers

4pAAd1. Analysis of the impact of sound diffusion in the reverberation time of an architectural space - A proposal for the characterization of diffusive surfaces using scale models. Elisa Garay-Vargas (Program of Graduate Studies in Design, CyAD - Universidad Autónoma Metropolitana, Av. San Pablo 180, Edificio D 101, Col. Reynosa Tamaulipas, Delegacion Azcapotzalco, 02200 Mexico, D.F., Mexico, elisagaray@gmail.com) , Fausto E. Rodriguez-Manzo (Departamento de Procesos y Tecnicas, CyAD, Universidad Autonoma Metropolitana-Azcapotzalco, Av. San Pablo 180, Edificio H-PB, Col. Reynosa Tamaulipas, Delegacion Azcapotzalco, 02200 Mexico, D.F., Mexico, rfme@correo.azc.uam.mx)

The acoustic quality of architectural spaces has been related directly with the reverberation phenomenon, in order to understand more about sound in architecture, this proposal tries to conclude how diffusion acts on the reverberation time. The fact that architects deal with absorption coefficients and change the reverberation time by playing and designing with materials, opens a door to the possibility of new ways of architectural design, knowing how simple or complex and even natural diffusion surfaces will act in space. Several examples of the use of diffusion and reverberation in architectural spaces can be found in buildings like the Jewish Museum from Daniel Libeskind or the Therme Vals from Peter Zumthor, the use of big surfaces of concrete in the first and uneven surfaces in the second, transform each of these places in one with very interesting sound qualities. To create spaces like these we can take diffusion as a design argument but, How will certain diffusive surfaces influence on the reverberation time of an architectural space? To answer this question it is necessary to experiment with scale models measuring the reverberation time, and not the diffusion itself.

4pAAd2. Re-evaluating Noise Criterion in Digital Audio Recording Environments. Linda Gedemer (5930 Penfield Ave., Woodland Hills, CA 91367, USA, gedeml@rpi.edu)

The absence of audible noise in recording studios is highly desirable. For this reason, the acoustic design of recording facilities usually involves an accurate assessment of the audibility of background noise. However, noise criterion that sets levels for inaudible noise do not take in account the sensitivity of today's digital recording equipment and post production processing. Noise-level criterion and measurement techniques exist in order to created an atmosphere where noise is rated at a level of audibility with respect to the type of space being measured. In this paper these criterion will be analyzed in terms of critical recording spaces. The criterion will be considered in terms of current building practices and digital audio recording equipment used. A set of questions were sent to working sound engineers in order to received first hand opinions regarding noise issues in recording studios. It is not the intention of this report to suggest a new noise criterion but rather to better understand existing problems which could then help in the creation of a more relevant noise criterion to be developed in the future.

4pAAd3. Possible correlation between acoustic and thermal performances of building structures. Giovanni Semprini (University, DIENCA Dept. Facoltà di Ingegneria, Viale Risorgimento 2, 40136 Bologna, Italy, giovanni.semprini@mail.ing.unibo.it), Alessandro Cocchi (University, DIENCA Dept. Facoltà di Ingegneria, Viale Risorgimento 2, 40136 Bologna, Italy, alessandro.cocchi@mail.ing .unibo.it), Cosimo Marinosci (DIENCA - Univ. of Bologna, Viale Risorgimento 2, 40136 Bologna, Italy, cosimo.marinosci@mail.ing.unibo.it)

Most European standards required high performance values for sound and thermal insulation in building structures, according to Directive EEC 89/106. Sound transmission and heat transfer in structures have different physical and analytical approach and specific parameters of performance (i.e. sound transmission loss or thermal transmittance) are not directly correlated each others; many kind of structures have also different behaviour depending on mechanical properties of materials, numbers of layers of materials, etc. The aim of this work is to analyse possible correlation between sound transmission performances and thermal properties values in order to evaluated common trends related to physical properties of the various building components, like for example density or surface mass.

4pAAd4. On the use of a corrugated ceiling for noise reduction in rooms. Nico F. Declercq (Georgia Tech Lorraine - G.W. Woodruff School of ME, UMI Georgia Tech - CNRS 2958, 2 rue Marconi, 57070 Metz, France, nico.declercq@me.gatech.edu), Katelijn Vanderhaeghe (Georgia Tech Lorraine - G.W. Woodruff School of ME, UMI Georgia Tech - CNRS

2958, 2 rue Marconi, 57070 Metz, France, declercq@ieee.org),Katrien Dewijngaert (Georgia Tech Lorraine - G.W. Woodruff School of ME, UMI Georgia Tech - CNRS 2958, 2 rue Marconi, 57070 Metz, France, declercq@ieee.org), Patricia Verleysen (Ghent University, Mechanics of Materials and Structures, Sint-Pietersnieuwstraat 41, 9000 Ghent, Belgium, Patricia.Verleysen@ugent.be)

In certain halls the acoustics is dominated by distinct frequencies having disturbingly high intensities caused by yelling children, such as in an indoor swimming pool, or by industrial production processes. The use of damping materials to cover the ceiling, floor and side walls is not always permitted because of esthetic reasons or because of safety grounds or even humidity. The current study shows that in those cases the use of a corrugated surface is possible and is actually more effective in filtering out very distinct frequencies. An example is presented for frequencies at 3 to 4 kHz and numerical results are obtained in support of the use of a corrugated structure rather than classic damping materials such as baffles.

4pAAd5. Musicians' Adjustment of Performance to Room Acoustics, Part III: Understanding the Variations in Musical Expressions. Kosuke Kato (Center for Advanced Science and Innovation, Osaka University, Yamadaoka 2-1, Suita-shi, 565-0871 Osaka, Japan, kato@casi.osaka-u.ac.jp), Kanako Ueno (Institute of Industrial Science, University of Tokyo, Komaba 4-6-1, Meguro-ku, 153-8505 Tokyo, Japan, ueno@iis.u-tokyo.ac.jp), Keiji Kawai (Graduate School of Science and Technology, Kumamoto University, Kurokami 2-39-1, Kumamoto-shi, 860-8555 Kumamoto, Japan, kawai@arch.kumamoto-u.ac.jp)

This paper attempts to investigate the acoustic variations in the musical sound signals produced by professional performers under different room acoustic conditions. The sound signals produced by four professional instrumentalists and an operatic baritone singer under simulated concert hall sound fields were recorded by placing a unidirectional microphone close to either the instruments or the mouth of the opera singer. In order to quantify the extent of the variations in the resulting sound signals due to the adjustment of the musical expressions, an acoustic analysis was conducted. The results indicated that the ″note-on ratio,″ defined as the ratio of tone duration and inter-onset interval, of several staccato tones was decreased in reverberant halls. The higher harmonics of tones of an oboist and a flutist were suppressed in reverberant sound fields, while the vibrato extent of a violinist was considerably varied as was reported in our previous study (Part II). Based on the results of the interviews with the performers during the recordings, it was inferred that the variations in the musical sound signals were produced by the performers to adjust to the room acoustic conditions.

4pAAd6. In situ measurement of acoustic parameters with smart devices. Karl Van Nieuwenhuyse (Vrije Universiteit Brussel, Acoustics and Vibration Research Group, Dept. of Mechanical Engineering, Pleinlaan 2, BE-1050 Brussels, Belgium, karl.van.nieuwenhuyse@skynet.be), Patrick Guillaume (Vrije Universiteit Brussel, Acoustics and Vibration Research Group, Dept. of Mechanical Engineering, Pleinlaan 2, BE-1050 Brussels, Belgium, Patrick.Guillaume@vub.ac.be), Steve Van Landuit (Vrije Universiteit Brussel, Acoustics and Vibration Research Group, Dept. of Mechanical Engineering, Pleinlaan 2, BE-1050 Brussels, Belgium, svanlandui@vub.ac.be), Cedric Vuye (Hogeschool Antwerpen, Dept. of Industrial Sciences, Paardenmarkt 92, BE-2000 Antwerpen, Belgium, c.vuye@ha.be), Gert De Sitter (Vrije Universiteit Brussel, Acoustics and Vibration Research Group, Dept. of Mechanical Engineering, Pleinlaan 2, BE-1050 Brussels, Belgium, gert.de.sitter@vub.ac.be)

Instruments for in situ analysis of the acoustic parameters of a room are, due to their high prime cost, not widely accessible. In an effort to change this, new software was developed to enable these measurements by use of highly portable consumer electronics such as PDA's and Smart phones. The newly developed software calculates the reverberation time using the impulse method and aims at delivering accurate results using the built-in microphone or an external one. This paper will discuss the accuracy of the new software in comparison with professional equipment through several case studies, even as the different techniques used to overcome the inherent problems forthcoming the equipment used, i.e. microphone quality and automatic gain control.

4pAAd7. Efficiency of two-dimensional interpolation algorithms for high-quality dynamic binaural synthesis. Karim Helwani (Department of Audio Communication, Technical University of Berlin, Sekr. EN-08, Einsteinufer 17c, 10587 Berlin, Germany, karim.helwani@gmx.de), Alexander Lindau (Department of Audio Communication, Technical University of Berlin, Sekr. EN-08, Einsteinufer 17c, 10587 Berlin, Germany, alexander.lindau@tu-berlin.de), Stefan Weinzierl (Department of Audio Communication, Technical University of Berlin, Sekr. EN-08, Einsteinufer 17c, 10587 Berlin, Germany, stefan.weinzierl@tu-berlin.de)

Binaural synthesis of acoustical environments is based on binaural room impulse responses (BRIRs) measured with an angular resolution of typically between 1° and 15°. Considering the size of the resulting BRIR database used for auralization and the long measurement duration for its acquisition, it is reasonable to use interpolation from a lower resolution BRIR grid. Based on a mathematical formulation of the interpolation problem for BRIRs, a set of different solutions for two-dimensional spaces is described and compared with regard to efficiency and real time performance. In order to evaluate the degradation introduced by interpolation, different methods have been implemented and applied to a HRTF and a BRIR database measured in two degrees of freedom with 1°/1° horizontal/vertical resolution. These are bilinear interpolation (i.e. nearest neighbour, inverse distance weighting), spherical spline interpolation, wavelet interpolation, and interpolation based on principal component analysis (PCA). A listening test following an ABX procedure has been performed to evaluate the efficiency of the different interpolation methods according to the detection rates of interpolated versus measured BRIR databases in a dynamically auralized acoustical environment.

4pAAd8. Perception of teachers and pupils to the acoustics of classrooms. Carmen L. Loro (Federal University of Parana, Centro Politécnico - Setor de Tecnologia, Bairro Jardim das Américas, 81531-990 Curitiba, Brazil, loro@arnet.com.br), Paulo Henrique Trombetta T. Zannin (Federal University of Parana, Centro Politécnico - Setor de Tecnologia, Bairro Jardim das Américas, 81531-990 Curitiba, Brazil, paulo.zannin@pesquisador.cnpq.br)

The present survey has evaluated the acoustic characteristics of classrooms built as modular classrooms. The study has focused on the background noise, reverberation time, noise insulation and interviews with teachers and pupils. The acoustic comfort of classrooms in a Brazilian public school has been evaluated through interviews with 62 teachers and 464 pupils. Acoustic measurements have revealed the poor acoustic quality of the classrooms. The walls between the classrooms and the corridor have permanent ventilation openings on glassy bricks. The measured weighted apparent sound reduction index (ISO 140-4; ISO 717-1) for the wall, with a door and glassy brick, was R'w = 17 dB. The low value of the weighted apparent sound reduction index R'w= 17 dB contributes significantly to the noise transmission from one room to the other, contributing to the elevated levels of background noise inside the classrooms. Interviews with teachers and pupils have shown that the main noise sources noted in the classrooms originate inside the school: voices of students and of the teacher of the neighboring classroom.

4pAAd9. Comparing the sound absorption of different objects. Robert Hickling (Sonometrics Inc., 8306 Huntington Road, Huntington Woods, MI 48070-1643, USA, sonometrics@comcast.net), John Kopko (Kolano and Saha Engineers Inc., 3559 Sashabaw Road, Waterford, MI 48329, USA, jkopko@kandse.com), Pranab Saha (Kolano and Saha Engineers Inc., 3559 Sashabaw Road, Waterford, MI 48329, USA, prsaha@kandse.com)

Current methods of measuring sound absorption involve a piece of material. Small pieces are tested in impedance tubes. Larger pieces are tested in a reverberation room, using the reverberation-time decay method, as in ISO Standard 354. However these procedures do not determine the absorption of a complete object. It is proposed to determine the absorption of

an object by measuring the negative sound power of the object in a reverberation room using sound intensity. It has been shown that sound power using sound intensity can be measured accurately in reverberation rooms (R. Hickling, Proceedings NOISE-CON 97, pages 483-488). Negative sound power on its own, however, cannot provide a satisfactory comparison indicator between objects because it depends on the room. It is necessary, therefore, to develop a normalization procedure to make the negative sound-power measurement independent of the room. A procedure is described which was tested for the same object (a car seat) in two different reverberation rooms. The results are encouraging. It is planned to conduct further tests using a variety of objects in different rooms to check the validity of the normalization procedure.

THURSDAY AFTERNOON, 3 JULY 2008 P2-B, LEVEL 2, 3:40 TO 5:20 P.M.

Session 4pAAe

Architectural Acoustics and Noise: Acoustics and Privacy in Healthcare Facilities II: Emerging Research Around the World II (Poster Session)

William Cavanaugh, Cochair
Cavanaugh Tocci Associates, Inc.

Kerstin Persson Waye, Cochair
Dept. of Environ. Medicine, The Sahlgrenska Acad. of Gothenburg Univ.

All posters will be on display from 3:40 p.m. to 5:20 p.m. To allow contributors an opportunity to see other posters, contributors of odd-numbered papers will be at their posters from 3:40 p.m. to 4:30 p.m. and contributors of even-numbered papers will be at their posters from 4:30 p.m. to 5:20 p.m.

Contributed Paper

4pAAe1. The noise control in laboratories and health areas: A keyword in order to pratice biosafety. Marta Ribeiro Valle Macedo (Fundaçào Oswalso Cruz, Avenida Brasil 4365 - Manguinhos, 21040-360 Rio de Janeiro, Brazil, mribeiro@fiocruz.br)

The noise control in laboratories and health areas: a keyword in order to pratice biosafety Marta Ribeiro Valle Macedo Coordenação de Saúde do trabalhador, Fundação Oswaldo Cruz, Av. Brasil 4365, Manguinhos-Rio de Janeiro, Brasil, CEP.21040-360 The environmental noise control is an increasing preoccupation at the international level in order to observing the effects on the human health. At the outdoor environment or in habitations, in work places and health areas, these effects are verified, as mentioned by World Health Organization (1995; 1999) and in rich bibliography about this subject. In areas with biological and chemical risk, where the development of activities need of great concentration, noise is a stressor agent and causes direct and indirect effects on the human health as well as affecting the intelligibility of the speech, the performance of activities and causing work accidents. However, the exposition to the main sound sources found in laboratories and hospitals located at the Fundação Oswaldo Cruz (Fiocruz), a Brazilian health institution, could have been avoided if some noise control measures had been employed. This paper presents the main situations observed at the evaluation devoloped during 2007, in 744 environments of work and shows how environmental noise comes interfering at the workers performance in Fiocruz.

Session 4pAAf

Architectural Acoustics: Case Studies and Design Approaches II (Poster Session)

Ingo Witew, Cochair
Institute of Technical Acoustics, Templergraben 55, Aachen, 52056, Germany

Byron Harrison, Cochair
Talaske, 1033 South Boulevard, Oak Park IL 60302, USA

All posters will be on display from 3:40 p.m. to 5:20 p.m. To allow contributors an opportunity to see other posters, contributors of odd-numbered papers will be at their posters from 3:40 p.m. to 4:30 p.m. and contributors of even-numbered papers will be at their posters from 4:30 p.m. to 5:20 p.m.

Contributed Papers

4pAAf1. Predicting the acoustics of historic Istanbul Tunnel: Simulation, calculation methods and geometrical details. Filiz Bal Kocyigit (Karabuk University, 232. Str. No: 5/5 Ilkbahar Mah., Cankaya, 06550 Ankara, Turkey, filizbkocyigit@yahoo.com), Sertan Senturk (20th Street 17/6 Bahçelievler, 06490 Ankara, Turkey, sertansenturk@yahoo.com)

The Istanbul Tunnel, which was designed and constructed by Eugene Henry Gavand at 1875 is the 3rd. Metro and 2nd underground railway system in the world after Washington Metro (1868). In this paper, the acoustics of the Istanbul Tunnel are investigated. This is a special case which sets up a challenge to these prediction methods. The shape of the tunnel and therefore focusing the sound, reverberant wall, and therefore fluctuation effect demands high accuracy in predicting the early reflections. The energy dissipates quickly in this type of enclosures and there is little masking effect of the reverberation. Another aspect that has been shown to give very different results in this case study is the geometrical detailing of the models. When the Istanbul Tunnel is compared with modern metro systems; nowadays railway systems are controlled by modern electronic and mechanical system, but in the 19th century these electronic systems were not available. A solution could be found with the shape of the building. The aim of this paper is to clarify some of the problems that can arise in this type of constructions, and give guidelines for how they can be overcome / avoided. Another objective is to emphasize that room acoustic computer simulations although very useful, need careful consideration about the underlying calculation methods.

4pAAf2. The Royal Church of San Lorenzo in Turin: Guarino Guarini and the Baroque architectural acoustics. Marco Caniato (University of Trieste, Piazzale Europa, 34100 Trieste, Italy, caniatomarco @vodafone.it), Federica Bettarello (Engineering Dept. - Univ. of Ferrara, Via Saragat, 1, 44100 Ferrara, Italy, federica.bettarello@unife.it), Marco Masoero (Politecnico di Torino, Corso Duca degli Abruzzi 24, 10123 Torino, Italy, marco.masoero@polito.it)

In 1666 the architect Guarino Guarini received from Carlo Emanuele II, Duke of Savoy, the appointment to build in Turin a new church dedicated to S. Lorenzo. The architect conceived a design in Baroque style with a very particular ribbed dome and this peculiarity is a very hard to find feature throughout Europe. Acoustics measurements were performed in S. Lorenzo in order to investigate how this unique architecture affects the response parameters used in architectural acoustics. Results are discussed in the paper, comparing to the methodology suggested by Cirillo and Martellotta in order to characterize the acoustics of churches.

4pAAf3. Bernardo Antonio Vittone: acoustics and architecture in the XVIII century. Marco Caniato (University of Trieste, Piazzale Europa, 34100 Trieste, Italy, caniatomarco@vodafone.it), Vilma Fasoli (University of Trieste, Piazzale Europa, 34100 Trieste, Italy, fasoli@tin.it)

Contemporary critics have identified Savoy architect Bernardo Vittone as a major contributor to the establishment of the concept and experience of architecture as the ″art of construction″ in the 18th century. Vittone grew and worked under the guidance of mathematician Guarino Guarini, whose mastery of theoretical and scientific aspects he was never credited to have matched. Vittone's approach to architecture was mainly practical, his plans chiefly derived from the rules of mechanics and descriptive geometry. Experience was his main source of inspiration. Designs, plans, domes and vaults are but ways to achieve balance and harmony and so are precision and control of the relation between geometry and acoustics, architecture and music. In his book ″Alternative instructions on the civil Architecture″ morover he included in the second appendix the ″Armonic instructions″, within a dissertation on the nature of sound, its propagation in open spaces, in closed ones and its relation with music. In this paper a commented overview is given matching his description of acoustics with present-day knowledge.

4pAAf4. The engineering method of sound field control for amplifications in sports arena. Jian Peng (Guangzhou Radio, 231 Huanshi Zhong Road, 510000 Guangzhou, China, zp24@drexel.edu), Zhao Peng (Drexel Univ., 3175 JFK Blvd, APT 707, Philadelphia, PA 19104, USA, zp24@drexel.edu)

This paper discusses the engineering method of sound field control for amplifications in sports arena, which includes the selection, assembly and adjustment of the loudspeaker system. It also includes the site characteristics of the sports arena, as well as the relations between the loudspeaker and the site. Through the measurements of the rated sensitivity and maximum noise power, the loudspeaker system can be determined as distributed or central system, linear or plane array. With the adjustments on parameters such as the directivity $D(\Theta)$and the directivity factor Q, the loudspeaker system will be able to effectively control the sound field during amplification process and to achieve better sound quality in sports arena. Besides determining the effective engineering method for sound field control in the amplification process, this paper also considers the acoustical characteristics of sound sources and coupling effect in the sound field.

4pAAf5. Correlation between architectural and acoustical parameters in Catholic churches of the colonial era in Ayacucho, Peru. Carlos R. Jimenez (Pontificia Universidad Catolica Del Peru, Av. Universitaria 1801, San Miguel, 32 Lima, Peru, cjimene@pucp.edu.pe)

The paper reports the analysis of the results of an acoustic survey carried out on several Catholic Churches in the city of Ayacucho, a southern city in the Peruvian Andes, built during the colonial era through centuries XVI to XVIII. The study is performed taking into account both room-average values and individual position values of many acoustical parameters measured according to ISO 3382. Effects among architectural characteristics of each church as lenght, height, room volume, interior surfaces area, total absorbing area, mean absorption coefficient, and some objective acoustical parameters as reverberation time, early decay time, clarity, definition and center time, are investigated.

4pAAf6. Simulation of the reverberation time of an existing architectural space using a 1:10 scale model. Luz Del Carmen Gonzalez-Rodriguez (Program of Graduate Studies in Design, CyAD - Universidad Autonoma Metropolitana, Av. San Pablo 180, Edificio D 101, Col. Reynosa Tamaulipas, Delegacion Azcapotzalco, 02200 Mexico, D.F., Mexico, loozie@gmail.com), Fausto E. Rodriguez-Manzo (Departamento de Procesos y Tecnicas, CyAD, Universidad Autonoma Metropolitana-Azcapotzalco, Av. San Pablo 180, Edificio H-PB, Col. Reynosa Tamaulipas, Delegacion Azcapotzalco, 02200 Mexico, D.F., Mexico, rfme@correo.azc.uam.mx)

Recently the science of acoustics has been reconsidered and valued more than just a tool concerning physics, telecommunications, and music. It is now an important topic of research for the acoustic comfort of places where people work and live, and it is also considered as an essential issue for the physical and mental health of human beings. Sound has to be integrated as a design concept in architecture, but architects need tools for understanding more the way to reach not only good acoustics but also good architectural design. It has been proven that physical scale models are very useful for the prediction of the acoustical behaviour of rooms, therefore this process is analyzed and studied at the Acoustic Design and Analysis Laboratory of the UAM-Azcapotzalco in Mexico City, in order to promote further investigations that provide useful data for the design of architectural spaces as well as the design of sound control devices. This paper shows the work of a master degree thesis where the main objective is to present the measurements of reverberation time taken in an existing room compared with those taken in the physical scale model of the same room.

4pAAf7. Architectural Acoustics Design using Diffusing Surfaces. James Heddle (James Heddle Pty Ltd, Unit 2315 / 180 Grey Street, South Bank, 4101 Brisbane, Australia, acousticdesign@gmail.com)

This paper reviews the design challenges and development of acoustic treatments for three acoustical design projects in Australia. The projects that will be outlined were a surround sound widescreen lecture theatre, a contemporary council chambers and the rectification of a problematic brass band practice room. The treatments included sound diffusing surfaces of the geometric type with or without embedded amplitude reflection gratings. Where the gratings were used in multiples the designs also addressed periodicity issues using modulation of the grating patterns with the best known merit factors. The design approach and the development of the acoustical surface features and treatments to solve the design issues, including problems experienced in the building phase, will be discussed.

4pAAf8. Evaluation of existing sound system designs in mosques and alternative modern solutions. Wasim Orfali (Nordmannzeile 12, 12157 Berlin, Germany, orfaliwasim@hotmail.com), Wolfgang Ahnert (Ahnert Feistel Media Group, Arkonastr. 45-49, 13189 Berlin, Germany, wahnert@ada-acousticdesign.de)

Sound intelligibly and audibility was from the old days and will remain a central issue in any sound system design especially in mosques. In other worship spaces sound system may not be needed during specific worshiping modes like congregational prayers. In mosques all worshiping modes require professionally designed sound system to maintain the needed intelligibility and audibility levels in such spaces. Here the current used sound systems in mosques will be discussed and pro and cons will be highlighted. Also, the effect of these systems on mosques applicable sound parameter will be introduced. In the same time, modern sound system design solution for different mosques architectural form and size will be suggested. Case study examples will be used to show the advantages of the new suggested sound system configurations.

4pAAf9. Room acoustics enhancement system in a Multifunctional Cultural Centre. Géza Balogh, Jr. (Interton Electroacoustics, Major u. 63, H-1119 Budapest, Hungary, balogh@interton.hu), Géza Balogh, Dr. (Interton Electroacoustics, Major u. 63, H-1119 Budapest, Hungary, drbalogh@interton.hu)

In the lecture, we present our system called DCR (Digital Control of Reverberation), which is capable of changing the reverberation of a room by means of electroacoustical devices. Using the DCR system, we are able to change the enclosure, i.e. we create an electroacoustical enclosure on the walls and on the ceiling. The parameters of the electroacoustical enclosure can be changed in several steps. The system was installed in Hungary for the first time in the city of Debrecen, in the Kölcsey Cultural Centre. The principle of the DCR and the problems and their solutions will be presented via this specific installation. We study the effect of the distance between the microphones and the loudspeakers, and the factors that influence this effect. We also analyse the room acoustics parameters in respect to the frequency, in the different status of the auditorium. Our room acoustics enhancement DCR system is based on the non-inline principle, thus the room acoustics of the large auditorium (1100 seats) of the Kölcsey Centre remained absolutely natural. We use several numbers of independent digital channels in the system, and each channel consists of one microphone, one or two loudspeakers, a power amplifier and a DSP.

4pAAf10. Translating acoustics into architecture. Ewart A. Wetherill (Ewart A. Wetherill, AIA, 28 Cove Road, Alameda, CA 94502-7416, USA, redwetherill@sbcglobal.net)

Ever since Wallace Clement Sabine's first presentation to the American Institute of Architects in 1898, a substantial gap has often existed between available information on building acoustics and its successful application to the design of buildings. Experience over at least the past 40 years suggests that one of the reasons for this has been the difficulty of adapting construction methods, that were selected to meet other criteria, to satisfy specific acoustical conditions. In a complex project it is important that requirements for individual spaces be identified and resolved early in the design process so that they can be integrated successfully into the overall building design. This paper discusses a procedure that has been found very convenient for establishing acoustical requirements during the schematic design and transferring recommendations efficiently for inclusion in the construction documents. The information is compiled in a book-style format for ease of distribution and for fast reference at any time in design and construction.

Session 4pAAg

Architectural Acoustics: Prediction Methods in Building Acoustics III (Poster Session)

Berndt Zeitler, Cochair
NRC - Institute for Research in Construction

Catherine Guigou-Carter, Cochair
CSTB

All posters will be on display from 3:40 p.m. to 5:20 p.m. To allow contributors an opportunity to see other posters, contributors of odd-numbered papers will be at their posters from 3:40 p.m. to 4:30 p.m. and contributors of even-numbered papers will be at their posters from 4:30 p.m. to 5:20 p.m.

Contributed Papers

4pAAg1. Determination of unknown parameters in impervious layers by inverse method. Eva Escuder Silla (Escola Politècnica Superior de Gandia, Universitat Politècnica de València, Crtra Natzaret-Oliva s/n, 46730 Gandia, Spain, evescude@fis.upv.es), Jesús Alba Fernandez (Escola Politècnica Superior de Gandia, Universitat Politècnica de València, Crtra Natzaret-Oliva s/n, 46730 Gandia, Spain, jesalba@fis.upv.es), Jaime Ramis Soriano (DFISTS. Univ. de Alicante, Carretera de Sant Vicent del Raspeig s/n, 03690 San Vicente del Raspeig, Spain, jramis@ua.es), Romina Del Rey Tormos (Escola Politècnica Superior de Gandia, Universitat Politècnica de València, Crtra Natzaret-Oliva s/n, 46730 Gandia, Spain, roderey@doctor.upv.es)

In this work, a novel procedure is shown for the determination of unknown parameters in impervious layers used in multilayer structures by inverse method and using scale models. Experimental pressure and velocity data are obtained by Nearfield Acoustic Holography (NAH) for the calculation of the transmission loss of the different multilayer structures mounted on the window of a wooden box designed for that end. These data are used as input data in the inverse method. The forecast model of acoustic insulation in multilayered structures used in this work was Trochidis&Kalaroutis model based on Spatial Fourier Transform (SFT). By applying Trochidis&Kalaroutis model and adjusting by numerical methods the variables that define the impervious layers of the system, the values of the unknown magnitudes of the layers are calculated. For validation purposes the results are compared to those obtained with Ookura&Saito model.

4pAAg2. New Roadway noise modeling to predict noise propagation in front of urban façade. Hany Hossam Eldien (Suez Canal Univ., 25500 Suez, Egypt, hany.hossam@gmail.com), Philippe Woloszyn (UMR ESO, Université de Haute Bretagne - Rennes II, Place du Recteur Henri Le Moal, CS 24307, 35043 Rennes Cedex, France, philippe.woloszyn@univ-rennes2.fr)

Roadway noise is the most important example of a linear noise source, since it comprises about 80 percent of the environmental noise exposure for humans worldwide. Due to the complexity of the variables, a line source acoustic model is realized by a computer model . In this paper we propose a new approach system based upon Schröder's quadratic residue diffuser modeling for modeling a linear traffic source. 1/10th scale model has been used to simulate the traffic noise propagation in front of the building façade and for a free field. The line source directivity is made quasi-uniform in the aperture angle of interest. The line source directivity measurements were made using a 1/4″ microphone Larson Davis type 2530. The sequence of the quadratic residue diffusor is calculated following the Schröder's modulo formula and with 1.60m length, 0.14m height, and 0.11m width. The line source has also been weighted by a full-size equivalent normalised traffic noise spectrum according to the French standard NF EN 1793-3.

4pAAg3. Influence of the conservation state of the facade elements as a variable of prediction of acoustic insulation to airborne sound. Leonardo Meza (Pontificia Universidad Católica de Chile, Av. Vicuña Mackena 4860, Macul, 7820436 Santiago, Chile, lmezam@uc.cl)

The different prediction methods of acoustic insulation are based on the acoustic properties of the constituent materials of the buildings, however, they don't usually consider the conservation state as a variable within the prediction, ignoring the natural process of degradation that the material and the construction elements suffer which sometimes are increased by the deterioration due to the use of itself. At this paper, the behavior of some construction elements is analyzed by means of acoustic insulation measurements in-situ, such as windows and its woodwork, which presents in many cases a diminish in the acoustic performance due to the damage and deterioration. Finally, the incorporation of this variable is proposed in future prediction models of acoustic insulation.

4pAAg4. Variable Source-Directivity Using Dodecahedron-Loudspeakers. Gottfried K. Behler (RWTH Aachen University, Templergraben 55, D-52056 Aachen, Germany, gkb@akustik.rwth-aachen.de), Martin Pollow (RWTH Aachen University, Templergraben 55, D-52056 Aachen, Germany, martin.pollow@akustik.rwth-aachen.de)

For room-acoustical measurements dodecahedron loudspeakers are commonplace to achieve a uniform directivity. Therefore all transducers are fed with the same signal. If the signals for the twelve transducers are individually adjustable, the variation of amplitude and phase offers the possibility to achieve a predefined directivity. The goal is to calculate the twelve frequency dependent amplitude- and phase-coefficients for any given directivity with the least possible error. A simple approach like superposition unfortunately does not reveal a correct result, since all transducer interact with each other. The decomposition of spherical functions into spherical harmonics, however, leads to an analytic solution for the prediction of the sound radiation. The acoustical components - like sound pressure and sound velocity - are split up into weighted, orthogonal base functions which can be combined in a way that the mutual coupling between different membrane vibrations is respected. Under these conditions complex filter transfer functions, individually optimized for each one of the twelve transducers can be

computed with respect to the target directivity function. Different approaches for the optimization procedure are discussed. Besides the more theoretical approach measurements with a real multichannel system are shown.

4pAAg5. In situ evaluation of the vibration reduction index Kij. Arianna Astolfi (Politecnico di Torino, Department of Energetics, Corso Duca degli Abruzzi, 24, 10129 Turin, Italy, arianna.astolfi@polito.it), Alessandro Schiavi (Istituto Nazionale di Ricerca Metrologica, str. delle Cacce, 91, 10135 Turin, Italy, a.schiavi@inrim.it), Cristiana Taricco (Via Tapparelli 31, 12038 Savigliano (CN), Italy, c.taricco@fastwebnet.it), Simone Geroso (Politecnico di Torino, Department of Energetics, Corso Duca degli Abruzzi, 24, 10129 Turin, Italy, geroso@alice.it), Fabrizio Bronuzzi (Politecnico di Torino, Department of Energetics, Corso Duca degli Abruzzi, 24, 10129 Turin, Italy, fabrizio.bronuzzi@polito.it), Andrea Savio (Via Madonnina, 12, 10090 Gassino Torinese (TO), Italy, andrea.savio_84@alice.it)

As stated in EN 12354-1 and 2 Standards the vibration reduction index Kij is a quantity related to the vibrational power transmission over a junction between structural elements, normalized in order to make it invariant. This quantity allows to quantify the flanking transmission both in air-borne and impact sound insulation between rooms. It is important to underline that the measurement method reported in the EN 10848-1 Standard is only referred to the laboratory measurement, anyway in the Annex E of the EN 12354-1 Standard is indicated that the same methodology is probably useble also in in situ condition. In this work several measurements of the vibration reduction index in situ are reported in order to verify if the methodology is also suitable in uncontrolled conditions as in the field. The measured results are compared with the previsional model results according to the EN 12354-1. In particular the case studies are the T-junctions and the cross-junctions between the ceilings and the vertical walls in some typical rooms in dwellings. From the first experimental results some peculiar building features, influencing the measurement and the calculation data, have been evidenced, expecially with reference to the south European building typologies in brick and concrete.

4pAAg6. High sound pressure models for microperforated panels backed by an air cavity. Rostand Tayong (Lab. de Recherche en Mécanique et Acoustique, I.S.A.T - Univ. de Bourgogne, 49, rue Mademoiselle Bourgeois, 58000 Nevers, France, rostand.tayong@u-bourgogne.fr), Thomas Dupont (Lab. de Recherche en Mécanique et Acoustique, I.S.A.T - Univ. de Bourgogne, 49, rue Mademoiselle Bourgeois, 58000 Nevers, France, thomas.dupont@u-bourgogne.fr), Marie-Annick Galland (Centre Acoustique du LMFA, Ecole Centrale de Lyon, 36 avenue Guy de Collongue, 69134 Ecully cedex, France, marie-annick.galland@ec-lyon.fr), Philippe Leclaire (Lab. de Recherche en Mécanique et Acoustique, I.S.A.T - Univ. de Bourgogne, 49, rue Mademoiselle Bourgeois, 58000 Nevers, France, philippe.leclaire@gmail.com)

When submitted to relatively high sound pressure amplitudes, Micro Perforated Panels (MPP) are influenced by certain effects, which are non negligible (vibration of the panel, end radiation and also proximity of the perforations). A model of the total impedance of the MPP is derived from the sum of the contributions of each effect in the case of relatively high sound pressure. The effect of end radiation is supposed to be independent of the propagation inside the apertures. The model is applicable for low Mach numbers. In order to validate the models, various steel MPP specimens were built with different aperture diameters, interstices (distance between two near apertures) and thickness sizes. The experimental method consists in measuring the acoustical pressure before the specimen and the velocity at the aperture entrance. The experimental setup is based on the use of an impedance circular tube. A loudspeaker capable of delivering high sound pressure is used as a source. The excitation is a white noise in a frequency range between 500 Hz and 5000 Hz and the detection is performed with microphones. The comparison between measurements and simulations for the impedance and absorption coefficient is done and discussed.

THURSDAY AFTERNOON, 3 JULY 2008 P2-B, LEVEL 2, 3:40 TO 5:20 P.M.

Session 4pAAh

Architectural Acoustics: Measuring Methods and Uncertainty in Building Acoustics II (Poster Session)

Brandon Tinianow, Cochair

Werner Scholl, Cochair
Physikalisch-Technische Bundesanstalt

All posters will be on display from 3:40 p.m. to 5:20 p.m. To allow contributors an opportunity to see other posters, contributors of odd-numbered papers will be at their posters from 3:40 p.m. to 4:30 p.m. and contributors of even-numbered papers will be at their posters from 4:30 p.m. to 5:20 p.m.

Contributed Papers

4pAAh1. The examination of the influence of standing waves on reverberation time measurements in small reverberant rooms. Marko Horvat (Faculty of EE and Computing, Unska 3, Department of Electroacoustics, HR-10000 Zagreb, Croatia, marko.horvat@fer.hr), Kristian Jambrosic (Faculty of EE and Computing, Unska 3, Department of Electroacoustics, HR-10000 Zagreb, Croatia, kristian.jambrosic@fer.hr), Hrvoje Domitrovic (Faculty of EE and Computing, Unska 3, Department of Electroacoustics, HR-10000 Zagreb, Croatia, hrvoje.domitrovic@fer.hr)

The measurements of reverberation time are performed in a small and rather reverberant shoe-box type room in order to determine the spatial distribution of reverberation time with respect to the formation of standing waves in the room itself. The measurements are made in a two-axes raster with equidistant distribution of measurement points. The goal is to investigate the conclusions made in an earlier work by Graber et al. that the distribution of reverberation time values along the fore mentioned raster reaches maximum values at the points of minimum sound pressure level andvice versa. The room in which the measurements are made is deliberately chosen to be relatively small in order to examine the lowest modes of standing waves that form in the room.

4pAAh2. Effect of the estimation of the wall/floor junction type on the acoustic isolation. Jesús Alba Fernandez (Escola Politècnica Superior de

Gandia, Universitat Politècnica de València, Crtra Natzaret-Oliva s/n, 46730 Gandia, Spain, jesalba@fis.upv.es), Jaime Ramis Soriano (DFISTS. Univ. de Alicante, Carretera de Sant Vicent del Raspeig s/n, 03690 San Vicente del Raspeig, Spain, jramis@ua.es), Eva Escuder Silla (Escola Politècnica Superior de Gandia, Universitat Politècnica de València, Crtra Natzaret-Oliva s/n, 46730 Gandia, Spain, evescude@fis.upv.es), Romina Del Rey Tormos (Escola Politècnica Superior de Gandia, Universitat Politècnica de València, Crtra Natzaret-Oliva s/n, 46730 Gandia, Spain, roderey@doctor.upv.es)

Deviations between the laboratory measurement and the final in situ measurement, are common in the acoustic isolation. A fundamental difference between both cases is the effect of the lateral flanks. This effect produce that the global acoustic insulation changes substantially. With the standard UNE-EN-12354-1, it can be estimated the effect of the flank, obtaining the vibration reduction indexes and evaluating the insulation of every way. It is also possible to carried out a measurement procedure with the Standard ISO 10848, in it the index is measured and then the index is calculated. This paper shows the differences of results of airborne sound insulation and impact insulation with in situ measurements of the vibration reduction index and the different estimations that the Standard allow. Different unions are studied, and the influence of these in the global result of the insulation is evaluated.

4pAAh3. Study in the measurement of noise air insulation in laboratory of the effect in the diffuse field. Romina Del Rey Tormos (Escola Politècnica Superior de Gandia, Universitat Politècnica de València, Crtra Natzaret-Oliva s/n, 46730 Gandia, Spain, roderey@doctor.upv.es), Jesús Alba Fernandez (Escola Politècnica Superior de Gandia, Universitat Politècnica de València, Crtra Natzaret-Oliva s/n, 46730 Gandia, Spain, jesalba@fis.upv.es), Jaime Ramis Soriano (DFISTS. Univ. de Alicante, Carretera de Sant Vicent del Raspeig s/n, 03690 San Vicente del Raspeig, Spain, jramis@ua.es), Eva Escuder Silla (Escola Politècnica Superior de Gandia, Universitat Politècnica de València, Crtra Natzaret-Oliva s/n, 46730 Gandia, Spain, evescude@fis.upv.es)

We can obtain, in a transmission chamber, the air transmitted noise insulation. In the standard 140-1 the characteristics of these chambers are described. One of these characteristics tries to ensure diffuse field inside these chambers. Nevertheless, we cannot assure an incident angle between 0° and 90° on the test wall, there is a limit angle lower than 90°. In this paper, we study the valuation of the committed mistake by limit angle in transmission chambers. Expressions used for calculating the insulation in transmission chambers are obtained from transmission description in diffuse field, in which case the angle is 90°. In this work, for different materials commonly used in transmission chambers tests, the influence of the indetermination of a mistake and the global mistake evolution with limit angle is studied.

4pAAh4. Student project of building an impedance tube. Mia Suhanek (Faculty of EE and Computing, Unska 3, Department of Electroacoustics, HR-10000 Zagreb, Croatia, mia.suhanek@fer.hr), Kristian Jambrosic (Faculty of EE and Computing, Unska 3, Department of Electroacoustics, HR-10000 Zagreb, Croatia, kristian.jambrosic@fer.hr), Hrvoje Domitrovic (Faculty of EE and Computing, Unska 3, Department of Electroacoustics, HR-10000 Zagreb, Croatia, hrvoje.domitrovic@fer.hr)

This paper describes a student project of building an impedance tube for measuring the absorption coefficient using the transfer-function method, in accordance with the standard ISO 10534-2. This method is well-established and has many advantages compared to the older method using standing wave ratio (ISO 10354-1) in terms of measurement speed and accuracy. For the tube, only inexpensive materials and transducers were used. The tube was designed for the frequency range between 90 and 2000 Hz. In order to achieve this range with one tube, three microphone positions have been used. The resulting absorption coefficient has been calculated using the one- and two-microphone method. Different broadband excitation signals have been used in order to compare their robustness, such as MLS, frequency sweep and white noise. Various problems with the design and construction are addressed and the optimal configuration is discussed.

4pAAh5. Uncertainty of airborne sound insulation index measurement in laboratory conditions. Tadeusz Wszolek (University of Science and Technology, Department of Mechanics and Vibroacoustics, Al.Mickiewicza 30, 30-059 Krakow, Poland, twszolek@agh.edu.pl)

In buildings, airborne sound insulation is used to define the acoustic quality of walls between rooms. However the evaluation of sound insulation is sometimes difficult or even ambiguous, both in field and laboratory measurements, in spite of the fact that there are some unified measurement procedures specified in the ISO 140 standards. There are problems with the reproducibility and repeatability of the measured results. Some difficulties may be caused by non-diffuse acoustic fields, non uniform reverberation time or large spread of the reverberation time measurements especially in low frequency band. Some minor problems are also posed by flanking transmission and the S/N ratio. In the present work partial uncertainty analysis has been carried out for all the above mentioned factors and their influence has been evaluated on the combined uncertainty in 1/3 octave bands and the Rw index, using the uncertainty propagation law

4pAAh6. Blind estimation method of reverberation time based on concept of modulation transfer function. Masashi Unoki (JAIST, 1-1 Asahidai, 923-1292 Nomi, Japan, unoki@jaist.ac.jp), Sota Hiramatsu (JAIST, 1-1 Asahidai, 923-1292 Nomi, Japan, s0610073@jaist.ac.jp)

This paper proposes a method for blindly estimating the reverberation time based on the concept of the modulation transfer function (MTF). This method estimates the reverberation time from the reverberant signal without measuring room acoustics. In the MTF-based speech dereverberation method, proposed by the authors, a process for estimating a parameter related to the reverberation time was incorporated. In this paper, we investigate whether the estimation process, previously presented by authors, works as a blind estimation method and point out a problem with their method. We then propose a new method for blindly estimating the reverberation time to resolve the problem. In the proposed method, the reverberation time is correctly estimated by inverse-MTF filtering in the modulation frequency domain. We evaluated the proposed method with their method using both artificial MTF-based signals and speech signals to show how well the proposed method correctly estimates the reverberation time in artificial reverberant environments. Results suggested that the proposed method correctly estimates reverberation times from the observed reverberant signals. [Work supported by a Grant-in-Aid for Science Research from the Japanese Ministry of Education (No. 18680017).]

4pAAh7. Realization of a measurement system for physical and acoustic measurements on brick walls. Luca Barbaresi (DIENCA - Univ. of Bologna, Viale Risorgimento 2, 40136 Bologna, Italy, luca.barbaresi@mail.ing.unibo.it), Massimo Garai (DIENCA - Univ. of Bologna, Viale Risorgimento 2, 40136 Bologna, Italy, massimo.garai@mail.ing.unibo.it), Paolo Guidorzi (DIENCA - Univ. of Bologna, Viale Risorgimento 2, 40136 Bologna, Italy, paolo.guidorzi@mail.ing.unibo.it), Giovanni Semprini (University, DIENCA Dept. Facoltà di Ingegneria, Viale Risorgimento 2, 40136 Bologna, Italy, giovanni.semprini@mail.ing.unibo.it)

Aim of this study is the development of a system for the measurement of frequency values of some physical variables such as the damping factor, the thickness of a structural element, the structural reverberation time and the longitudinal wave speed propagation in light brick walls. Such variables are required by the UNI EN 12354-1 normative for the analytical estimation of the sound reduction index R of monolithic elements in the laboratory. The results of the calculation, as a function of frequency, will be shown and compared with the measured values of the sound reduction index R.

4pAAh8. Swept Sine against MLS in room acoustics with music signals as background noise. Joel P. Paulo (ISEL, R. Conselheiro Emídio Navarro,1, 1959-007 Lisbon, Portugal, jpaulo@deetc.isel.ipl.pt), J. Luis Bento Coelho (CAPS, Instituto Superior Técnico, TU Lisbon, Av. Rovisco Pais, P-1049-001 Lisbon, Portugal, bcoelho@ist.utl.pt)

The Swept Sine and the MLS techniques are very popular in room acoustic measurement set-ups. Advantages and disadvantages of both methods have been well investigated and can be found in the literature. However, information regarding the performance of these techniques in the presence of high background music levels is scarce. Since the estimation of the room impulse response is based on the correlation between signals, the likelihood between the test signal and the music contents has an important role on the results accuracy. This paper explores these issues by taking into account the semantic information of the music signals when used as disturbance. The method used for the assessment of the gain between the two techniques consists on splitting each frame in segments and applying a weighting function depending on a likelihood function. The features used for the likelihood function are the rms value of each segment, spectral energy envelope relation, bandwidth and harmonic structure. Several examples are presented for comparison of the performance of the Swept Sine and the MLS techniques. Advantages and disadvantages of each technique are discussed for music signals as noise.

4pAAh9. Effects of filtering of room impulse responses on room acoustics parameters by using different filter structures. Csaba Huszty (Budapest University of Technology and Economics, BME Dept. of Telecommunications, Magyar tudósok körútja 2, H-1117 Budapest, Hungary, huszty@hit.bme.hu), Norbert Bukuli (Budapest University of Technology and Economics, BME Dept. of Telecommunications, Magyar tudósok körútja 2, H-1117 Budapest, Hungary, bukuli.norbert@gmail.com), Ákos Torma (Budapest University of Technology and Economics, BME Dept. of Telecommunications, Magyar tudósok körútja 2, H-1117 Budapest, Hungary, tormakos@gmail.com), Fülöp Augusztinovicz (Budapest University of Technology and Economics, BME Dept. of Telecommunications, Magyar tudósok körútja 2, H-1117 Budapest, Hungary, fulop@hit.bme.hu)

Room acoustic evaluation is usually based on post-processing of measured room impulse responses (RIRs), and this often requires some kind of filtering, for instance to derive fractional octave band parameters of a room. In this paper it is shown that the considerable variance of room acoustic parameters of almost any hall is partly caused by the filtering method and the filter properties used in the course of post-processing. The paper proposes new qualification methods and parameters for determining the quality of FIR filter banks, taking their use for acoustic evaluation into account. It suggests practical considerations for the design as well, and shows the analysis and comparison of effects of various filter properties -- such as filter types and topology structures -- on some room acoustics parameters. By using the suggested methods, it is possible to derive more accurate and reliable results in room acoustic evaluation.

4pAAh10. Reverberation time measuring methods. Kristian Jambrosic (Faculty of EE and Computing, Unska 3, Department of Electroacoustics, HR-10000 Zagreb, Croatia, kristian.jambrosic@fer.hr), Marko Horvat (Faculty of EE and Computing, Unska 3, Department of Electroacoustics, HR-10000 Zagreb, Croatia, marko.horvat@fer.hr), Hrvoje Domitrovic (Faculty of EE and Computing, Unska 3, Department of Electroacoustics, HR-10000 Zagreb, Croatia, hrvoje.domitrovic@fer.hr)

In this paper different well-established methods of reverberation time measurement are compared. Furthermore, the results obtained using these methods are compared to the results provided by some additional methods which could serve as an in situ tool if, for any reason, the reverberation time measurements cannot be carried out using the standardized methods. The methods compared in this paper include the standardized methods (EN ISO 3382:2000), namely the impulse response measured with pink noise, exponential sweep, MLS, but also pistol shots of different calibers, balloon bursts, gated external pink noise, and the B&K filtered burst method. In order to make the comparison, the measurements were performed in four acoustically very different spaces - a rather small and well-damped listening room, a much bigger damped listening room, a rather reverberant atrium, and a large and very reverberant shoebox-shaped room. The results were evaluated according to signal-to-noise ratio criterion as well. Special attention has been given to the influence of room modes on measurement results.

THURSDAY AFTERNOON, 3 JULY 2008 P2-B, LEVEL 2, 3:40 TO 6:40 P.M.

Session 4pAAi

Architectural Acoustics and the National Council of Acoustical Consultants: Student Design Competition

Byron W. Harrison, Cochair
The Talaske Group Inc., 1033 South Boulevard, Oak Park, IL 60302, USA

Anders Christian Gade, Cochair
Dept. of Acoustic Technology, Technical University of Denmark, Building 352, DK 2800 Lyngby, Denmark

The Technical Committee on Architectural Acoustics of the Acoustical Society of America, the National Council of Acoustical Consultants, and the Robert Bradford Newman Student Award Fund are sponsoring the 2008 Student Design Competition that will be professionally judged at this meeting. The purpose of this design competition is to encourage students enrolled in architecture, engineering, physics, and other university curriculums that involve building design and/or acoustics to express their knowledge of architectural acoustics in the design of a new theater performance space as part of a university building project.

This competition is open to undergraduate and graduate students from all nations. Submissions will be poster presentations that demonstrate room acoustics, noise control, and acoustic isolation techniques in building planning and room design. The submitted designs will be displayed in this session and they will be judged by a panel of professional architects and acoustical consultants. An award of USD$1250.00 will be made to the entry judged "First Honors." Four awards of USD$700.00 will be made to each of four entries judged "Commendation."

Session 4pABb

Animal Bioacoustics, Psychological and Physiological Acoustics, and ECUA: Auditory Brainstem Response and Behavior Correlation III (Poster Session)

Elizabeth Brittan-Powell, Cochair
University of Maryland

Alexander Supin, Cochair
Institute of Ecology and Evolution

All posters will be on display from 3:40 p.m. to 5:20 p.m. To allow contributors an opportunity to see other posters, contributors of odd-numbered papers will be at their posters from 3:40 p.m. to 4:30 p.m. and contributors of even-numbered papers will be at their posters from 4:30 p.m. to 5:20 p.m.

Contributed Papers

4pABb1. Intense sonar pings induce temporary threshold shift in a bottlenose dolphin (Tursiops truncatus). T Aran Mooney (University of Hawaii, Hawaii Institute of Marine Biology, P.O. Box 1106, Kailua, HI 96734, USA, mooneyt@hawaii.edu), Paul E. Nachtigall (University of Hawaii, Hawaii Institute of Marine Biology, P.O. Box 1106, Kailua, HI 96734, USA, nachtiga@hawaii.edu), Stephanie Vlachos (University of Hawaii, Hawaii Institute of Marine Biology, P.O. Box 1106, Kailua, HI 96734, USA, vlachos@hawaii.edu)

For over a decade it has been suggested that high intensity anthropogenic sounds, such as sonar, could induce a temporary threshold shift (TTS) in odontocetes. Although TTS has been examined in marine mammals, the temporary physiological effects of sonar sounds have yet to be established. This study explored the effects of high-intensity (up to 203 dB re: 1 μPa), mid-frequency sweeps (2-4 kHz) on the hearing of a bottlenose dolphin (Tursiops truncatus). The goal was to determine if these sounds could induce TTS and what sound exposure levels (SEL; dB re: 1 $\mu Pa^2 s$) were necessary for TTS to be induced. Fatiguing sounds were presented to mimic that of mid-frequency sonar. Hearing thresholds were measured before and after exposures using auditory evoked potentials to determine amount of shift and rate of recovery. Temporary threshold shifts of 5-6 dB were measured using SELs of 214 dB, in situations when 15 sonar pings were presented in series. Recovery to normal hearing was rapid, typically within 5 to 10 min. Exposure levels required to induce TTS were high, supporting the notion that relatively short sounds must be of relatively high intensity to induce threshold shifts.

4pABb2. The auditory time resolution in bottlenose dolphins: Behavioral experiments versus auditory evoked potential methods. Gennadi L. Zaslavski (University Authority for Applied Research, RAMOT, Tel-Aviv University, str. Gordon 51 app 7, 42442 Netanya, Israel, gennadi.zaslavski@gmail.com)

Non-invasive auditory evoked potentials (AEP) methods are now widely used to study dolphins' hearing because some auditory characteristics can be obtained much faster compare to behavioral methods. The bottlenose dolphin auditory time resolution assessed using evoked potentials responses to a double click, amplitude modulated tone and periodic click is generally believed to be around 300 microseconds. This assessment is claimed to be in full agreement with behavioral measurements. The intention of this paper is to reevaluate behavioral results which are believed to support AEP methods in light of numerous behavioral results indicative of the bottlenose dolphin time resolution as high as 20-30 microseconds. We found that as long as there are differences in waveforms, bottlenose dolphins are able to discriminate between very short (as short as a bottlenose dolphin sonar click) signals with identical energy spectra as well as between brief noise signals with random energy spectra. Auditory evoked responses do not reveal any differences between such signals whereas the differences are readily indicated by behavioral responses of the dolphins. The auditory temporal analysis of brief signals in bottlenose dolphins seems to be inaccessible by AEP methods, at least in their present form.

Session 4pABc

Animal Bioacoustics and ECUA: Odontocete Acoustics II (Poster Session)

David Mellinger, Cochair
Oregon State Univ. and NOAA

Michel Andre, Cochair
Laboratori d'Aplicacions Bioacústiques (Universitat Politècnica de Catalunya)

All posters will be on display from 3:40 p.m. to 5:20 p.m. To allow contributors an opportunity to see other posters, contributors of odd-numbered papers will be at their posters from 3:40 p.m. to 4:30 p.m. and contributors of even-numbered papers will be at their posters from 4:30 p.m. to 5:20 p.m.

Contributed Papers

4pABc1. Decalcifying Protocol of Odontocete Ear Samples with RDO®. Maria Morell (Laboratori d'Aplicacions Bioacústiques (Universitat Politècnica de Catalunya), avda. Rambla Exposició s/n, 08800 Vilanova i la Geltrú, Spain, maria.morell@lab.upc.edu), Eduard Degollada (Laboratori d'Aplicacions Bioacústiques (Universitat Politècnica de Catalunya), avda. Rambla Exposició s/n, 08800 Vilanova i la Geltrú, Spain, edmaktub @edmaktub.com), Josep Maria Alonso (Laboratori d'Aplicacions Bioacústiques (Universitat Politècnica de Catalunya), avda. Rambla Exposició s/n, 08800 Vilanova i la Geltrú, Spain, jmalonso@iim.csic.es), Thierry Jauniaux (Université de Liège, Place du 20-Aout, 9, B-4000 Liège, Belgium, T.Jauniaux@ulg.ac.be), Mardik Leopold (Imares, P.O. Box 167, 1790 AD Den Burg, Texel, Netherlands, Mardik.Leopold@wur.nl), Kees Camphuysen (Royal NIOZ (Netherlands Inst. for Sea Research), 1790 AB Den Burg, Texel, Netherlands, camphuys@nioz.nl), Michel Andre (Laboratori d'Aplicacions Bioacústiques, Universitat Politècnica de Catalunya, avda. Rambla Exposició s/n, 08800 Vilanova i la Geltrú, Spain, michel.andre@upc.edu)

The study of the organ of Corti is essential to assess the impact of underwater noise on cetaceans. While classical histology techniques (including EDTA decalcification) have been previously considered, the process is time consuming and artifacts, probably directly deriving from the protocol, often appear and difficult the analysis. However, no matter the choice of the analysis technique, one of the challenging step after extraction and fixation of the samples is to decalcify the bone envelope to access the cochlea without damaging the soft tissues. Here, we propose to use a fast commercial decalcifier (RDO®). 103 ears from 12 different odontocetes species stranded in the Mediterranean, Spanish North Atlantic and North Sea have been used to precisely determine the decalcification time. Specifically, the species processed were: Phocoena phocoena (n=45), Stenella coeruleoalba (n=12), Stenella frontalis (n=12), Tursiops truncatus (n=13), Delphinus delphis (n=4), Kogia simus (n=3), Kogia breviceps (n=2), Globicephala macrorhynchus (n=3), Globicephala melas (n=2), Steno bredanensis (n=4), Lagenodelphis hosei (n=2) and Ziphius cavirostris (n=1). Depending on the species, the decalcification time ranged from several hours to a few days, allowing a subsequently faster observation of the cochlear structures through routine microscope techniques.

4pABc2. Mesoplodon densirostris transmission beam pattern estimated from passive acoustic bottom mounted hydrophones and a DTag recording. Jessica Ward (NAVSEA, Newport Undersea Warfare Center, Newport, RI RI 02841, USA, wardja@npt.nuwc.navy.mil), David Moretti (NAVSEA, Newport Undersea Warfare Center, Newport, RI RI 02841, USA, MorettiDJ@npt.nuwc.navy.mil), Ronald P. Morrissey (Naval Undersea Warfare Center Division Newport, 1176 Howell Street, Bldg 1351, 2nd Floor, Newport, RI 02841, USA, morrisseyrp@npt.nuwc .navy.mil), Nancy A. Dimarzio (Naval Undersea Warfare Center Division Newport, 1176 Howell Street, Bldg 1351, 2nd Floor, Newport, RI 02841, USA, dimarziona@npt.nuwc.navy.mil), Peter Tyack (Woods Hole Oceanographic Institution, Applied Ocean Physics & Engineering Dept., Woods Hole, MA 02543, USA, ptyack@whoi.edu), Mark Johnson (Woods Hole Oceanographic Institution, Applied Ocean Physics & Engineering Dept., Woods Hole, MA 02543, USA, majohnson@whoi.edu)

The transmission beam pattern of a female Mesoplodon densirostris tagged on October 23, 2006 in the Tongue of the Ocean, Bahamas is estimated using data from a Woods Hole Oceanographic Institution DTag and simultaneous recordings from broadband, bottom mounted hydrophones at the Atlantic Undersea Test and Evaluation Center, Andros Island, Bahamas. The bottom mounted hydrophones are used to localize the tagged animal and measure the received level of each click. Pitch, roll and heading from the DTag are used to determine the horizontal and vertical aspect angles relative to the hydrophone. An estimate of the M. densirostris horizontal and vertical transmission beam pattern based on four dives will be presented.

Session 4pABd

Animal Bioacoustics: General Topics in Animal Bioacoustics I

Richard R. Fay, Cochair
Loyola University Chicago, Parmly Hearing Institute, 6525 N. Sheridan Rd., Chicago, IL 60626, USA

Michel Andre, Cochair
Laboratori d'Aplicacions Bioacústiques, Universitat Politècnica de Catalunya, avda. Rambla Exposició s/n, Vilanova i la Geltrú, 08800, Spain

Contributed Papers

5:20

4pABd1. Vocalizations of the Spotted Hyena (Crocuta crocuta): Eliciting Acoustic Variation in Groans. Frédéric E. Theunissen (UC Berkeley, Dept. of Psychology, 3210 Tolmant Hall, Berkeley, CA 94720-1650, USA, theunissen@berkeley.edu), Steve Glickman (UC Berkeley, Dept. of Psychology, 3210 Tolmant Hall, Berkeley, CA 94720-1650, USA, glickman@berkeley.edu), Suzanne Page (UC Berkeley, Dept. of Psychology, 3210 Tolmant Hall, Berkeley, CA 94720-1650, USA, mweldele @berkeley.edu)

Spotted hyenas (Crocuta crocuta) are highly social animals possessing a complex vocal repertoire. Vocal signals of different types correlate with distinct social circumstances. Groans constitute a very large category in the spotted hyena repertoire which is not well understood. Sounds labeled as groans vary in their acoustical quality from more growling sounds to more tonal vocalizations. Groans are also elicited in many different social interactions. To begin to decipher the meaning of these vocal signals, we examined how the variation in the acoustic properties of groans was correlated with experimentally controlled eliciting conditions. Groans were elicited in adult hyenas presented with three objects: unfamiliar spotted hyena cubs, meaty bones, and the empty transport cage used to contain bones or cubs on other trials. Cubs elicited more groans from more adults than other objects but all objects elicited vocal responses. More importantly, discriminant analysis revealed differences in the acoustic characteristics of groans elicited by cubs and those elicited by other objects. Cubs elicited more prolonged and more tonal groans with higher fundamental frequency. Our study shows that groans can be classified into different groups and that these different sounds were produced in different behavioral contexts.

5:40

4pABd2. The relationship between complex vocal signaling and immunocompetence in the brown-headed cowbird (Molothrus ater). Samantha Levinson (UC Santa Barbara, 6689 El Colegio Rd. Apt. 46, Goleta, CA 93117, USA, slevinson@umail.ucsb.edu), Loren Merrill (UC Santa Barbara, 6689 El Colegio Rd. Apt. 46, Goleta, CA 93117, USA, lmerrill@lifesci.ucsb.edu)

Male brown-headed cowbirds (Molothrus ater) use song in mate attraction and in male-male competition to signal their quality to potential mates and competitors. Singing is an energetically expensive activity for birds, so repertoire size, singing rate, and complexity of songs should be honest indicators of a male's overall quality. Resistance to parasites is a major component of male quality, and some aspects of immunity are inherited by his offspring. Females obtain indirect benefits from mating with healthy males by having healthy offspring, so song may signal immune condition to females. Male cowbirds usually sing between four and six different song types when displaying to females. These songs differ in the amount of frequency modulation required during singing, which indicates that the difficulty of production of these songs by the syrinx also varies. In this study, we investigate the correlation between immune function and singing behavior, specifically the size of a bird's repertoire and the complexity of his songs. Understanding the relationship between repertoire size, song complexity, and immune function is important to understanding the role of vocal signaling in mate attraction in songbirds.

6:00

4pABd3. The statistics of plant echoes as perceived by echolocating bats. Yossi Yovel (Eberhard-Karls-Universität Tübingen, Zool. Institut, Abt. Tierphysiologie, Auf der Morgenstelle 28, 72076 Tübingen, Germany, yossiyovel@hotmail.com), Matthias O. Franz (University of Applied Sciences, Konstanz, Germany, HTWG Konstanz, Brauneggerstr. 55, D-78462 Konstanz, Germany, mfranz@htwg-konstanz.de), Peter Stilz (Eberhard-Karls-Universität Tübingen, Zool. Institut, Abt. Tierphysiologie, Auf der Morgenstelle 28, 72076 Tübingen, Germany, peter.stilz@uni-tuebingen.de), Hans-Ulrich Schnitzler (Eberhard-Karls-Universität Tübingen, Zool. Institut, Abt. Tierphysiologie, Auf der Morgenstelle 28, 72076 Tübingen, Germany, hans-ulrich.schnitzler@uni-tuebingen.de)

To explore the statistics of complex natural plant echoes, we emitted bat-like downsweeps (200-0 kHz) and recorded the echoes of various tree species. A Hilbert transform was used to calculate the envelope of the echoes impulse responses. This corresponds to a one-dimensional representation of the spatial reflector arrangement of the plant. We then calculated the envelope's power spectrum to asses the amount of periodic structures. In control experiments we compared power spectra of a single leaf, a branch and a few branches, and tested the effect of systematically decreasing the leaf density of a plant. On a bi-logarithmic plot, the averaged power spectra of all trees have a sigmoid shape with three approximately linear domains that represent different scales of structure, but differ between species. We hypothesize that the first domain is influenced by the gross skeleton of branches, while the others are associated with smaller scale structures. The control experiments showed a similar dependence between leaf density and power spectrum. Modeling plants as simple three-dimensional textures with stationary statistics was sufficient to predict the characteristics of the spectra. Our findings suggest an interpretable relation between the power spectrum of the echo's envelope and the spatial statistics of the plant.

6:20

4pABd4. Modelling of the echo generation process in bat echolocation. Timos Papadopoulos (University of Southampton, SPCG-ISVR, SO17 1BJ Southampton, UK, tp@isvr.soton.ac.uk), Robert Allen (University of Southampton, SPCG-ISVR, SO17 1BJ Southampton, UK, R.Allen@soton .ac.uk)

Very few studies exist that attempt to model the detailed shape of the echoes generated by real targets in bat echolocation. The modelling becomes even more complicated when one attempts to take into account the specific acoustic characteristics of the bat as a source and receiver. Hence, the exact physical acoustics basis that underpins the target detection and classification capabilities demonstrated by bats remains a largely open research question. We use previously published work on real target echo measurement (Simmons and Chen, JASA 1989) as a starting point but modify their ex-

perimental method in a way that allows the incorporation of the bat's source and receiver characteristics in the modelling. Furthermore, we compare our measurements with analytically predicted results and show good agreement. We discuss how our experimental method can be used for the prediction of the binaural signals that constitute the actual input to the bat's auditory system during echolocation.

6:40

4pABd5. The simulation of bat-oriented auditory processing using the experimental data of echolocating signals. Su Yeon Kim (University of Southampton, SPCG-ISVR, SO17 1BJ Southampton, UK, syk@isvr.soton.ac.uk), Robert Allen (University of Southampton, SPCG-ISVR, SO17 1BJ Southampton, UK, R.Allen@soton.ac.uk), Daniel Rowan (University of Southampton, SPCG-ISVR, SO17 1BJ Southampton, UK, dr@isvr.soton.ac.uk)

There are various approaches to understanding the echolocation phenomenon of bats. A part of the echolocating process is assessed here by determining what acoustic signal a bat's ears receive during echolocation. It is simplified in an experimental rig to measure the reflections from objects in different horizontal angles which represents a sound localisation task in bats. It has been assumed in this study that the remarkable echolocating ability of bats, which is not shown in the most other mammalian species, is achieved by their different physical shape of head and ears, and specialised auditory processing of echolocating signals. In human studies in terms of sound localisation, physical characteristics are usually modelled as a head-related transfer function (or HRTF) and gammatone filter banks are widely used to simulate auditory processing in the cochlear. A modified filterbank is used here to represent the auditory processing in bats and combined with the experimental data of object reflections. Bat HRTFs will be used subsequently to determine the acoustic reflections at both ears.

7:00

4pABd6. Steady streaming near model cod otoliths. Charlotte Kotas (Georgia Institute of Technology, Mechanical Engineering, 771 Ferst Drive, Atlanta, GA 30332-0405, USA, charlotte.kotas@gatech.edu), Peter H. Rogers (Georgia Institute of Technology, Mechanical Engineering, 771 Ferst Drive, Atlanta, GA 30332-0405, USA, peter.rogers@me.gatech.edu), Minami Yoda (Georgia Institute of Technology, Mechanical Engineering, 771 Ferst Drive, Atlanta, GA 30332-0405, USA, minami.yoda@me.gatech.edu)

Typical fish distinguish sounds at about 10-1000 Hz with particle motions as small as 0.1 nm and angular separation near 10° using their ears, which contain dense, bony otoliths weakly suspended in endolymph and tissue. The otoliths oscillate relative to incident sound, inducing flows in the surrounding fluid which are in turn sensed by the hair cells on the overlying macular membrane which project into the groovelike sulcus on the otolith. These fluid flows are then sampled by the hair cells and ''heard'' by the fish. The irregular geometry of the otolith shapes the flow patterns. The hair cells, which are organized into different ciliary orientation groups on the macula, preferentially sample the flow patterns along their axes. The steady component of the fluid motion near enlarged models of an actual cod otolith oscillated at 2--20 Hz along different directions was studied in the vicinity of the hair cells using phase-locked particle-image velocimetry (PIV) and pathline visualizations. The possible relationship between the flow patterns and hearing capabilities is discussed. Although the oscillation amplitudes studied are much larger than those for underwater sound, evidence suggests that the flow patterns are amplitude independent. [Supported by ONR.]

7:20

4pABd7. Sound source segregation by goldfish: Two simultaneous tones. Richard R. Fay (Loyola University Chicago, Parmly Hearing Institute, 6525 N. Sheridan Rd., Chicago, IL 60626, USA, rfay@luc.edu)

In 1964, van Bergeijk asked, ″...given that a fish can discriminate between sounds A and B when they are presented separately, can he still discriminate either one when both are presented simultaneously? Or do the two sounds blend to form a new entity (such as a chord).″ This question was a very early query about sound source segregation by fishes. We have investigated the role that frequency separation plays in this phenomenon using classical respiratory conditioning with a stimulus generalization paradigm. Groups of animals were first conditioned to 2-tone mixtures comprised of 150 Hz (A) and another frequency (B) ranging from 300 Hz to 750 Hz. Generalization tests were then carried out using single tones between 50 and 900 Hz. Group mean generalization gradients showed that the two tones were segregated at the widest A-B spacings, and tended to be segregated as the A-B spacing was reduced. The limited resolution of the test procedure did not allow an answer at the narrowest spacings. Source segregation, even of abstract tones, may be a fundamental feature of the sense of hearing of all organisms, and occurs in the absence of auditory cortex and complex cognitive abilities.

7:40

4pABd8. Passive Acoustic Detection and Monitoring of Schools of Herring. Thomas R. Hahn (University of Miami, RSMAS, 4600 Rickenbacker Causeway, Miami, FL 33149, USA, t.hahn@miami.edu), Gary L. Thomas (University of Miami, RSMAS, 4600 Rickenbacker Causeway, Miami, FL 33149, USA, gthomas@rsmas.miami.edu)

Passive acoustic detection and monitoring of various marine fishes has recently received much attention in the literature. It has been recognized that passive acoustic techniques have the potential to complement traditional active acoustic surveys and to significantly increase their overall efficiency, if the acoustic signatures of the considered species are well understood. In this paper, the potential of passive acoustic techniques is explored for the specific case of Pacific herring (Clupea palassii). It is demonstrated that schools of herring can acoustically be detected by observing the sound of coordinated bubble release, triggered, e.g., by predator activity. This sound not only has identifiable features that can be exploited for determining the presence or absence by simple means, but could also carry abundance and size information. Work supported by ONR and the NMFS via the PWSSC.

Session 4pAOa

Acoustical Oceanography, Underwater Acoustics, and ECUA: Rapid Environmental Assessment

John C. Osler, Cochair
Defence R&D Canada - Atlantic, P.O. Box 1012, Dartmouth, NS B2Y3Z7, Canada

Yann Stephan, Cochair
SHOM, 13 rue du Chatellier, CS 92803, Brest cedex 2, 29228, France

Invited Paper

2:00

4pAOa1. Overview of U.S. Navy Operational Oceanographic Models in Support of Acoustic Applications. Richard Allard (Naval Research Laboratory, NRL Code 7322, Stennis Space Center, MS 39571, USA, allard@nrlssc.navy.mil), Charlie Barron (Naval Research Laboratory, NRL Coded 7323, Stennis Space Center, MS 39529, USA, barron@nrlssc.navy.mil), Frank Bub (Naval Oceanographic Office, Balch Blvd, Stennis Space Center, MS 39529, USA, frank.bub@navy.mil), Emanuel F. Coelho (University of Southern Mississippi, Balch Blvd, Stennis Space Center, MS 39529, USA, coelho@nrlssc.navy.mil), James Cummings (Naval Research Laboratory, NRL Code 7322, Stennis Space Center, MS 39571, USA, cummings@nrlmry.navy.mil), J. Pacquin Fabre (Naval Research Laboratory, NRL Code 7322, Stennis Space Center, MS 39571, USA, josie.fabre@nrlssc.navy.mil), Robert Helber (Naval Research Laboratory, NRL Code 7322, Stennis Space Center, MS 39571, USA, helber@nrlssc.navy.mil), Clark Rowley (Naval Research Laboratory, NRL Code 7322, Stennis Space Center, MS 39571, USA, rowley@nrlssc.navy.mil)

The Naval Oceanographic Office operational global 1/8° Navy Coastal Ocean Model assimilates satellite and in-situ data to produce daily 72-hr forecasts. Output includes 3D fields of temperature, salinity, u- and v-components of ocean currents at standard depth levels, and these support derived fields including sound speed and sonic layer depth. The global model provides initial/boundary conditions for nested regional models, primarily relocatable NCOM. The relocatable NCOM modeling system can be set up quickly for areas of interest, includes river and tidal forcing, and is forced with a high-resolution atmospheric mesoscale model. Local and remote observations are incorporated into the models through the Navy Coupled Ocean Data Assimilation system, which assimilates sea surface temperature data from satellite, ships and buoys, profile data from floats and gliders, xbt's, CTD's, fixed and drifting buoys as well as altimeter-derived sea surface heights and ice concentration. In this presentation we will discuss how the operational ocean models feed into acoustic prediction models and tactical decision aids, the role glider observations will play in the modeling strategy, the use of ensembles to provide improved prediction error estimates and guide new observations, and future plans.

Contributed Paper

2:20

4pAOa2. High-frequency multibeam echosounder classification for rapid environmental assessment. Kerstin Siemes (Acoustic Remote Sensing Group, Delft Institute of Earth Observation and Space Systems, Delft University of Technology, Kluyverweg 1, 2629 HS Delft, Netherlands, k.siemes@tudelft.nl), Mirjam Snellen (Acoustic Remote Sensing Group, Delft Institute of Earth Observation and Space Systems, Delft University of Technology, Kluyverweg 1, 2629 HS Delft, Netherlands, m.snellen @tudelft.nl), Dick G. Simons (Delft University of Technology, P.O. Box Postbus 5048, 2600 GA Delft, Netherlands, d.g.simons@tudelft .nl), Jean-Pierre Hermand (Université libre de Bruxelles (U.L.B.) - Environmental hydroacoustics lab, av. Franklin D. Roosevelt 50, CP 194/5, 1050 Bruxelles, Belgium, jhermand@ulb.ac.be), Matthias Meyer (Royal Netherlands Naval College (NLDA) - REA group, PO Box 10000, 1780 Den Helder, Netherlands, mmeyer@ulb.ac.be), Jean-Claude Le Gac (NATO Undersea Research Center, Viale San Bartolomeo 400, 19126 La Spezia, Italy, legac@nurc.nato.int)

For shallow-water naval operations, obtaining rapidly an accurate picture of the environmental circumstances often is of high importance. Hereto a multi-sensor approach is required. In this context, the MREA/BP'07 experiment has been carried out south of Elba (Mediterranean Sea), where several techniques of environmental characterization covering the fields of underwater acoustics, physical oceanography and geophysics have been combined [Le Gac&Hermand, 2007]. The required information typically concerns water-column properties, sea surface roughness, and sediment geo-acoustic properties. Estimating these geo-acoustic parameters from inversion of acoustic data received on drifting sparse arrays has proved to be a promising approach. Part of MREA/BP'07 was therefore dedicated to this type of measurement. For validating the resulting geo-acoustic estimates sediment samples were collected. Additionally, measurements were carried out using a multibeam-echosounder. This system provides depth information, but also allows for seafloor classification. The classification approach taken is model-based employing the backscatter data. It discriminates between sediments in the most optimal way by applying the Bayes decision rule for multiple hypotheses, implicitly accounting for backscatter-strength ping-to-ping variability. Here, results of seafloor classification using the multibeam data and a preliminary comparison with the sediment sample analysis and the geo-acoustic parameter estimates as obtained from the drifting arrays are presented.

2:40

4pAOa3. Integrated scheme of rapid environmental assessment for shallow water acoustics. Jean-Claude Le Gac (NATO Undersea Research Center, Viale San Bartolomeo 400, 19126 La Spezia, Italy, legac@nurc.nato.int), Jean-Pierre Hermand (Université libre de Bruxelles (U.L.B.) - Environmental hydroacoustics lab, av. Franklin D. Roosevelt 50, CP 194/5, 1050 Bruxelles, Belgium, jhermand@ulb.ac.be), Frans Absil (Royal Netherlands Naval College (NLDA) - REA group, PO Box 10000, 1780 Den Helder, Netherlands, fgj.absil@nlda.nl)

Predicting sound propagation in shallow or very shallow water environments requires that the frequency-dependent acoustic properties be assessed for all components of the waveguide, i.e., the water column, sea bottom and sea surface interface. During the Maritime Rapid Environmental Assessment MREA/BP'07 sea trial in April-May 2007, south of Elba Island in the Mediterranean Sea, an integrated MREA scheme has been implemented to provide a full 4D (3D+T) environmental picture that is directly exploitable by acoustic propagation models. Based on a joint multi-disciplinary effort, several standard and advanced techniques of environmental characterization covering the fields of underwater acoustics, physical oceanography and geophysics have been combined within a coherent scheme of data acquisition, processing and assimilation. The paper presents the whole architecture of the implemented scheme. Based on a preliminary analysis of MREA/BP'07 data, advantages and drawbacks of the approach will be discussed. Ways ahead for further improvement and perspectives are finally drawn.

3:00

4pAOa4. The application of rapid environmental assessment to sonar performance. Paul C. Hines (Defence R&D Canada - Atlantic, P.O. Box 1012, Dartmouth, NS B2Y3Z7, Canada, Paul.Hines@drdc-rddc.gc.ca), Sean Pecknold (Defence R&D Canada - Atlantic, P.O. Box 1012, Dartmouth, NS B2Y3Z7, Canada, sean.pecknold@drdc-rddc.gc.ca), John C. Osler (Defence R&D Canada - Atlantic, P.O. Box 1012, Dartmouth, NS B2Y3Z7, Canada, john.osler@drdc-rddc.gc.ca)

Naval sonar operations and planning in littoral environments requires information from historical databases, in situ sampling of environmental parameters, and models capable of estimating sonar performance and the uncertainty in the estimate. Defence R&D Canada's approach to enable rapid environmental assessment (REA) for sonar incorporates three components: (1) a GIS-enabled database to manage historical environmental data, (2) measurement tools that operate while underway to provide in situ sampling of water column and seabed properties, and (3) a sensitivity model that examines the relative importance of different environmental parameters in order to quantify the impact of incomplete or degraded environmental information, and to specify the appropriate spatial and temporal scales for sampling. In this presentation, the integration of these aspects of REA will be demonstrated using transmission loss data collected in shallow water. Predictions made using REA data provide a substantially better fit to the measurements than those using historical databases.

3:20

4pAOa5. Systemic approach to performance prediction and the exploitation of environmental information in naval systems. Patrick Grenard (DGA/DET/CTSN, BP28, 83800 Toulon Armées, France, Patrick.Grenard@dga.defense.gouv.fr)

Interoperability of systems and implementation of network enabled capabilities are at the heart of defense transformation. By providing extensive capabilities for data gathering, processing and presentations, they achieve a greater tactical advantage through superior knowledge of and use of the operational environment. Within the framework of the deployment of the new French Navy information system SIC21, a system of systems is being developed in order to support the implementation of the NATO concept of Recognized Environmental Picture (REP). The metasystem established allows for the assimilation of Rapid Environmental Assessment (REA) data, and for a local or remote production of the REP. In order to support decision making and to guide actions local exploitation of the REP is carried out through embedded tactical decision aids. They rely on advanced performance prediction tools including propagation modelling capabilities called in simulation scenarios. The aims of the implemented models are to predict performances at the appropriate level of granularity, to provide a confidence level on the proposed tactical picture, to define the appropriate level of marine environmental knowledge that should be acquired, to optimise sensor settings, and finally to provide inversion tools for the REA, ensuring consistency with forward modelling used in performance prediction.

Session 4pAOb

Acoustical Oceanography, Signal Processing in Acoustics, and ECUA: Passive Acoustic Tomography I (Poster Session)

Karim Sabra, Cochair
Georgia Institute of Technology, School of Mechanical Engineering

Sergio Jesus, Cochair
ISR

All posters will be on display from 3:40 p.m. to 5:20 p.m. To allow contributors an opportunity to see other posters, contributors of odd-numbered papers will be at their posters from 3:40 p.m. to 4:30 p.m. and contributors of even-numbered papers will be at their posters from 4:30 p.m. to 5:20 p.m.

Contributed Paper

4pAOb1. Low-frequency acoustic signature of hurricane Ernesto. James Traer (Marine Physical Laboratory, Scripps Institute of Oceanography, 8602 La Jolla Shores Drive, La Jolla, CA 92093-0238, USA, jtraer@ucsd.edu), Peter Gerstoft (Marine Physical Laboratory, Scripps Institute of Oceanography, 8602 La Jolla Shores Drive, La Jolla, CA 92093-0238, USA, gerstoft@ucsd.edu), Laura Brooks (Marine Physical Laboratory, Scripps Institute of Oceanography, 8602 La Jolla Shores Drive, La Jolla, CA 92093-0238, USA, lbrook02@gmail.com), William Hodgkiss (MPL, Scripps Institution of Oceanography, University of California, San Diego, La Jolla, CA 92093-0238, USA, wsh@mpl.ucsd.edu), David Knobles (Applied Research Laboratories, UT at Austin, P. O. Box 8029, Austin, TX 78713, USA, knobles@arlut.utexas.edu)

The ambient noise level variations produced by Hurricane Ernesto were observed by the SWAMI32, SWAMI52 and SHARK arrays as the storm passed over the SW06 shallow water site. Microseism signals were detected in the water column near 0.1 Hz and were tracked with a beamformer over a period of several days observing variations that were very closely linked to measured surface waves. 5-75 Hz beamforming showed a sound-field dominated by local surface-noise punctuated by brief surges of noise from distant sources. Beamforming and time-domain cross-correlations showed that changes in acoustic environment on the time-scale of hours occurred at all three arrays with good correlation in time and directionality suggesting the storm induced noise-field is homogeneous over many kilometers.

Session 4pAOc

Acoustical Oceanography and ECUA: General Topics in Acoustical Oceanography I (Poster Session)

Andone Lavery, Cochair
Woods Hole Oceanographic Institution

Yann Stephan, Cochair
SHOM

All posters will be on display from 3:40 p.m. to 5:20 p.m. To allow contributors an opportunity to see other posters, contributors of odd-numbered papers will be at their posters from 3:40 p.m. to 4:30 p.m. and contributors of even-numbered papers will be at their posters from 4:30 p.m. to 5:20 p.m.

Contributed Papers

4pAOc1. The sea and ocean 3D acoustic waveguide: rays dynamics and chaos phenomena. Alexander V. Glushkov (Odessa University, P.O.Box 24a, 65009 Odessa-9, Ukraine, glushkov@paco.net), Andrey A. Svinarenko (Odessa University, P.O.Box 24a, 65009 Odessa-9, Ukraine, glushkov@paco.net), Olga Y. Khetselius (Odessa University, P.O.Box 24a, 65009 Odessa-9, Ukraine, glushkov@paco.net), Nikoly S. Serbov (Odessa University, P.O.Box 24a, 65009 Odessa-9, Ukraine, glushkov@paco.net)

It has been carried out modeling of the sea and ocean 3D acoustic waveguide. On the basis of Hamiltonian equations of rays it is studied a dynamics of rays. It has been shown that for acoustic waveguide in a shallow sea with non-level bottom under the rays propagation in a waveguide dependence of the of temporal frequency upon the output angle represents a fractal measure in accordance with Abdullaev-Zaslavsky result. For the ocean 3D acoustic waveguide on the basis of solving the eiconal equations in the Hamiltonian form it has been studied the fractal dynamics, including the chaotic one. There are presented the data of numerical solution of equations for the typical acoustic channel in the North-Atlantic region. The conditions for the Arnold diffusion effect realization are discussed.

4pAOc2. Fuzzy Clustering of Oceanographic Sound Speed Profiles for Acoustic Characterization. John Dubberley (Naval Research Laboratory, Bldg. 1005 Rm D-23, Stennis Space Center, MS 39529, USA, john.dubberley@nrlssc.navy.mil), Robert Zingerelli (Naval Research Laboratory, Bldg. 1005 Rm D-23, Stennis Space Center, MS 39529, USA, robert.zingerelli@nrlssc.navy.mil)

Historic oceanographic sound speed profiles have traditionally been grouped by area and time period, usually one degree square area and monthly time. After grading the profiles, mean profiles and standard deviations are calculated from the accepted profiles and in the acoustics community they are then used to predict the expected acoustic response of the region. Here the historic profiles in NOAA's World Ocean Database 2005 (WOD2005) will be divided into the same area and time periods, but in subsets with a sufficient number of profiles, fuzzy clustering will be employed on acoustically relevant oceanographic parameters (mixed layer depth, surface temperature, sound speed gradient, etc) to divide the population into multiple clusters. A parabolic equation acoustic transmission model is then applied on the WOD2005 statistical profiles and on the fuzzy cluster populations. Conclusions will be drawn about the suitability of this clustering to capture the variability of acoustic response at a given time and place.

4pAOc3. On the consideration of motion effects in underwater geoacoustic inversion. Nicolas Josso (GIPSA-lab, dep. DIS, 961, rue de la Houille Blanche, 38402 St Martin d'Hères, France, nicolas.josso@gispa-lab.inpg.fr), Cornel Ioana (GIPSA-lab, dep. DIS, 961, rue de la Houille Blanche, 38402 St Martin d'Hères, France, cornel.ioana@gipsa-lab.inpg.fr), Cédric Gervaise (E3I2 - EA3876, 2 rue François Verny, 29806 Brest Cedex, France, cedric.gervaise@ensieta.fr), Jérôme I. Mars (GIPSA-lab, dep. DIS, 961, rue de la Houille Blanche, 38402 St Martin d'Hères, France, jerome.mars @gipsa-lab.inpg.fr)

The estimation of an impulse response (IR) of a propagation channel is necessary for a large number of underwater acoustic applications: underwater communication, sonar detection and localization, marine mammal monitoring, etc. Basically, it informs us about the distortions of a transmitted signal in one underwater channel. This operation is usually subject to additional distortions due to the motion of the transmitter-channel-receiver configuration. This paper points on the effects of the motion while estimating the IR for shallow water environments in the very low frequencies bandwidth with matching filtering between the transmitted and the received signals. We propose a methodology to compare between the IR estimation in motionless and motion contexts, respectively. Using this methodology an objective criterion for motion effect analysis is proposed in order to measure the distortions due to the motion phenomena. The proposed methodology is applied to real data sets issued from PASSTIME campaign (SHOM, Bay of Biscaie, 2005) proving also its interest for motion effect analysis.

Session 4pAOd

Acoustical Oceanography and ECUA: Acoustic Characterization of Sea Floor Habitats I (Poster Session)

Christian De Moustier, Cochair
UNH, Center for Coastal and Ocean Mapping

Dick Simons, Cochair
Delft University of Technology

Xavier Lurton, Cochair
Institut Français de Recherche pour l'Exploitation de la Mer

All posters will be on display from 3:40 p.m. to 5:20 p.m. To allow contributors an opportunity to see other posters, contributors of odd-numbered papers will be at their posters from 3:40 p.m. to 4:30 p.m. and contributors of even-numbered papers will be at their posters from 4:30 p.m. to 5:20 p.m.

Contributed Paper

4pAOd1. Hierarchical spline technique application for real time 3D displaying of seafloor using multibeam sonar data. Jerzy Demkowicz (Gdansk University of Technology, ul. Narutowicza 11/12, 80-952 Gdansk, Poland, demjot@eti.pg.gda.pl)

Multibeam sonar records have a high resolution raster character. Unfortunately, interpolating and approximating and eventually displaying scattered 3D raster data of high volume leads to some difficulties related to a computer processing power. Usually the problem solution leads to multiresolution wavelet approach. The paper presents some advantages of using hierarchical splines as applied to real data from multibeam EM 3002 sonar acquired during acoustic survey on Southern Baltic. The proposed approach is two folded: firstly, all acquired multibeam sonar raw data are interpolated with high density uniform spline interpolation. The knots and control points of interpolated network are saved for defined resolution level. In the next stage, preprocessed high resolution data are combined with low resolution data sets after knot decimation process. Such approach allow real time 3D displaying of multibeam sonar data for different zoom levels

Session 4pAOg

Acoustical Oceanography and ECUA: Acoustic Characterization of Sea Floor Habitats II

Christian De Moustier, Cochair
UNH, Center for Coastal and Ocean Mapping, Chase Ocean Engineering Lab, 24 Colovos Road, Durham, NH 03824, USA

Dick G. Simons, Cochair
Delft University of Technology, P.O. Box Postbus 5048, Delft, 2600 GA, Netherlands

Xavier Lurton, Cochair
Institut Français de Recherche pour l'Exploitation de la Mer, NSE/AS, BP 70, Plouzané, 29280, France

Invited Paper

5:20

4pAOg1. High frequency scattering measurements for mussel bed characterisation. M. Snellen (Delft Institute of Earth Observation and Space Systems, Delft University of Technology, Kluyverweg 1, 2629 HS Delft, Netherlands, M.Snellen@tudelft.nl), Dick G. Simons (Delft University of Technology, P.O. Box Postbus 5048, 2600 GA Delft, Netherlands, d.g.simons@tudelft.nl), Rolf Riethmueller (Institute for Coastal Research, GKSS Research Centre Geesthacht, Max-Planck-Str. 1, D-21502 Geesthacht, Germany, rolf.riethmueller@gkss.de)

Several approaches exist towards seafloor classification using high-frequency backscattering measurements. The classification approach taken in this paper is a model-based classification employing backscatter data measured by a multibeam-echosounder (MBES) system. The method discriminates between sediments in the most optimal way by applying the Bayes decision rule for multiple hypotheses, implicitly accounting for the backscatter strength ping-to-ping variability. The method's applicability for seafloor classification has been demonstrated by using 300 kHz MBES data collected in the Cleaver-Bank area (North Sea). The area is well-known from a geological point of view due to extensive sampling campaigns and is characterized by a wide variety of seafloor types. Here we apply the classification method to MBES data acquired in the Oosterschelde estuary (the Netherlands) which is known to contain mussel culture spots. Also recordings using a video camera towed close to the seafloor and core measurements have been taken. From the video recordings estimates of mussel coverage as a function of position were derived. Analysis of the MBES results shows that they clearly reveal the presence of the mussel beds, indicating the usefulness of acoustic classification for habitat mapping. A comparison between MBES analysis results, video recordings and sample analysis will be presented.

Contributed Papers

5:40

4pAOg2. Vertical echosounder versus side-scan sonar mapping of Posidonia Oceanica fields. Noela Sanchez-Carnero (Universidade da Coruña, Campus de Zapateira s/n, E-15071 A Coruña, Spain, noesanchez@udc.es), Víctor Espinosa (IGIC - Universitat Politècnica de València, Cra. Nazaret-Oliva S/N, E-46730 Gandia, Spain, vespinos@fis.upv.es), Miguel Rodilla (IGIC - Universitat Politècnica de València, Cra. Nazaret-Oliva S/N, E-46730 Gandia, Spain, mrodilla@hma.upv.es), Ester Soliveres (IGIC - Universitat Politècnica de València, Cra. Nazaret-Oliva S/N, E-46730 Gandia, Spain, essogon@epsg.upv.es), Juan Freire (Universidade da Coruña, Campus de Zapateira s/n, E-15071 A Coruña, Spain, jfreire@udc.es)

Posidonia fields in the ″Cabo de Gata″ marine natural park, located in the south-east mediterranean spanish coast, have been mapped by means of two different acoustical tools: a vertical single-beam scientific echosounder and a side-scan sonar. The measured transects have been dived and recorded with a video camera in order to validate the predictions from the extracted acoustical data. We compare both the results obtained from the application of commercial software for bottom classification, and the processing with alternative algorithms in the case of the vertical echosounder, with those derived from the analysis of the side-scan sonar data.

6:00

4pAOg3. Comparison of multi-beam and single-beam seabed backscatter and sampling resolution near normal incidence. Rudy Kloser (GPO Box 1538, 7001 Hobart, Australia, rudy.kloser@csiro.au)

The seabed backscatter difference near normal incidence (<30°) is compared between two multibeams (EM300 and EM1002) and two on-axis calibrated single beam EK60 (38 and 120 kHz) echo sounders and found to differ by 7 to 10 dB. A seabed backscatter model supported the calibration of the single beam backscatter near normal incidence. Potential errors due to incorrectly applied equivalent area compensation were found to contribute to this difference but not significantly. Estimating the equivalent area of sampling from multibeam and single beam echosounders highlights the complexities of sampling resolutions as a function of incidence angle and pulse length. These variable sample sizes influence the measured backscatter due to the patchy nature of seabed substrate and fauna. The current backscattering processing method for a national upper slope mapping program relies on producing metrics at the highest spatial resolution. Calibration errors on these metrics for seabed classification for a national mapping program are discussed.

6:20

4pAOg4. Using the MBES for classification of riverbed sediments. Alireza Amiri-Simkooei (Acoustic Remote Sensing Group, Delft Institute of Earth Observation and Space Systems, Delft University of Technology, Kluyverweg 1, 2629 HS Delft, Netherlands, a.amirisimkooei@tudelft.nl), Mirjam Snellen (Acoustic Remote Sensing Group, Delft Institute of Earth Observation and Space Systems, Delft University of Technology, Kluyverweg 1, 2629 HS Delft, Netherlands, m.snellen@tudelft.nl), Dick G. Simons (Delft University of Technology, P.O. Box Postbus 5048, 2600 GA Delft, Netherlands, d.g.simons@tudelft.nl)

For keeping the Dutch rivers suitable for commercial activities measures are required. For example, the bottom of the river Waal, connecting Rotterdam with German industrial areas, is subsiding. Since the subsidence varies along the river, dangerous shoals occur. Sediment suppletions are planned to counteract the subsidence. Appropriate suppletion material is expected to keep the bottom more stable. To monitor the suppletion effectiveness, multibeam-echosounder (MBES) measurements are planned, allowing for simultaneous estimation of bathymetry and sediment composition. For the latter, we apply a method employing the MBES backscatter data. It estimates the number of sediment types present in the survey area and discriminates between them by applying the Bayes decision rule for multiple hypotheses, implicitly accounting for the backscatter strength ping-to-ping variability. The method's applicability was demonstrated in a well-surveyed test area (North Sea). In 2007, MBES measurements were acquired at the Waal, accompanied with extensive sediment grabbing. Contrary to the test area, water depths are very shallow and significant bottom slopes exist, requiring corrections. The lower water depths correspond to smaller beam-footprints, resulting in a higher ping-to-ping variability. Consequently the discriminating power between sediments will decrease. The performance of the classification method for this river environment is assessed.

6:40

4pAOg5. Analysis of Backscatter and Seafloor Acoustical Properties for Geosciences and Biodiversity Mapping Studies in Cook Strait, New Zealand. Xavier Lurton (Institut Français de Recherche pour l'Exploitation de la Mer, NSE/AS, BP 70, 29280 Plouzané, France, lurton@ifremer.fr), Geoffroy Lamarche (National Institute of Water and Atmospheric Research (NIWA), Private bag 14-901, 6021 Wellington, New Zealand, g.lamarche@niwa.co.nz), Anne-Laure Verdier (National Institute of Water and Atmospheric Research (NIWA), Private bag 14-901, 6021 Wellington, New Zealand, a.verdier@niwa.co.nz), Jean-Marie Augustin (Institut Français de Recherche pour l'Exploitation de la Mer, NSE/AS, BP 70, 29280 Plouzané, France, augustin@ifremer.fr), Ian Wright (National Institute of Water and Atmospheric Research (NIWA), Private bag 14-901, 6021 Wellington, New Zealand, i.wright@niwa.co.nz), Ashley Rowden (National Institute of Water and Atmospheric Research (NIWA), Private bag 14-901, 6021 Wellington, New Zealand, a.rowden@niwa.co.nz), Alan Orpin (National Institute of Water and Atmospheric Research (NIWA), Private bag 14-901, 6021 Wellington, New Zealand, a.orpin@niwa.co.nz), Miles Dunkin (National Institute of Water and Atmospheric Research (NIWA), Private bag 14-901, 6021 Wellington, New Zealand, m.dunkin@niwa.co.nz)

A quantitative analysis was conducted over sonar backscatter data collected on the Cook Strait region, central New Zealand, featuring multibeam (~ 30 kHz) bathymetry and backscatter data, groundtruthed by an extensive geological database (photographs, seabed samples, high-resolution seismics). A first processing step removes the effects of the sounder, seafloor topography, and water column. A second step includes sonar image mosaicing, signal calibration and compensation, speckle noise filtering, image segmentation and textural analysis. Backscatter angular dependence is then extracted from the raw data accounting for the co-registered multibeam bathymetry; it is linked to the various facies of this geologically very active region, forming a catalogue usable for future investigation. Some local features are analysed in details, referring to the geological local context. Also the backscatter data from the Haungaroa volcano were used for a proof-of-concept biodiversity mapping exercise. Ecological theory was utilised to predict biodiversity from the seabed substrate heterogeneity, derived from the segmentation of the backscatter data properly pre-processed. The backscatter analysis resulted in the identification of local features with geological, sedimentological, topographic, and possibly biological significance, otherwise not recognised with conventional surveying. This emphasises the potential of backscatter data in submarine seismic hazard studies and large-scale biodiversity mapping.

7:00

4pAOg6. Seabed biotope mapping using multi-beam backscatter based on reference sites. Rudy Kloser (GPO Box 1538, 7001 Hobart, Australia, rudy.kloser@csiro.au)

A multibeam sonar (MBS) was used to discriminate ecological relevant seabed characteristics based on 62 reference sites spanning depths 50 m to 400 m sampled with georeferenced video, sediment grab and rock dredge. The simple ecologically derived terrain characteristics of soft, hard, smooth and rough were found to have the most predictive power for discrimination of the biota using data from video and physical sampling. The acoustic data were corrected for range and incidence angle effects and analysed based on phenomenological characteristics and inversion of a seabed scattering model. Near normal incidence ($<16°$) the seabed backscatter showed poor correlation to seabed characteristics (cross validation error 32%) and was sensitive to the estimation of the correct seabed incidence angle. Using the trend in backscatter near normal incidence ($<30°$) greatly improved (cross validation error 4%) the classification but also increased the spatial scale of classification. The length of biotope scales were derived from the video transects with 50% of patches less than 18 m. Referencing the seabed backscatter to a consistent incidence angle (40°) gave the highest spatial resolution derived metric and minimised range, incident angle and beam compensation errors. Using this simple metric, high probabilities of prediction of fauna functional groups were recorded.

7:20

4pAOg7. Statistics of seafloor backscatter measured with multibeam sonar systems. John D. Penrose (Curtin University of Technology, Centre for Marine Sci & Tech, GPO Box U1987, 6845 Perth, WA, Australia, j.penrose@cmst.curtin.edu.au), Alexander Gavrilov (Curtin University of Technology, Centre for Marine Sci & Tech, GPO Box U1987, 6845 Perth, WA, Australia, a.gavrilov@cmst.curtin.edu.au), Iain M. Parnum (Curtin University of Technology, Centre for Marine Sci & Tech, GPO Box U1987, 6845 Perth, WA, Australia, i.parnum@cmst.curtin.edu.au)

A number of theoretical models for seafloor backscatter statistics developed for the recent years show a good agreement with experimental measurements made with sonar systems. However, methods of data collection used in multibeam systems are commonly not taken into consideration when analysing backscatter statistics. Using data collected with a Reson Seabat 8125 system and based on theoretical considerations, it is shown that the seafloor backscatter strength derived from the peak intensity measured as a single value for each beam leads to considerable backscatter overestimation at oblique angles of incidence when the beam footprint is much larger than the insonification area. This occurs because variations of the peak intensity are extreme value distributed, which can be well approximated by the Gumbel distribution. The location parameter of the Gumbel distribution depends on the ratio of the footprint and insonification areas, which results in distorted angular dependence of backscatter strength estimates. On the other hand, the average backscatter strength derived from the integral intensity, i.e. backscatter energy, is a consistent estimate of the actual seafloor backscatter strength. The Gamma distribution is demonstrated to be a good approximation for statistics of the integral intensity, even when the scattering regime is expected to be non-Rayleigh.

Session 4pAOh

Acoustical Oceanography, Signal Processing in Acoustics, and ECUA: Passive Acoustic Tomography II

Karim G. Sabra, Cochair
Georgia Institute of Technology, School of Mechanical Engineering, 771 Ferst Drive, NW, Atlanta, GA 30332-0405, USA

Sergio Jesus, Cochair
ISR, Universidade do Algarve, Faro, PT-8005-139, Portugal

Invited Papers

5:40

4pAOh1. Analysis of passive seabed imaging techniques. Thomas M. Siderius (HLS Research Inc., 3366 N. Torrey Pines Ct, Suite 310, La Jolla, CA 92037, USA, siderius@hlsresearch.com)

Recently, a passive technique has been developed to image seabed layering. The method exploits naturally occurring acoustic noise generated on the sea-surface, primarily from breaking waves. The processing exploits the noise coherence through cross-correlations between sensors to recover travel times to significant seabed reflectors. To make this a practical tool, beamforming is used with a vertical array of hydrophones and this greatly reduces the required averaging times. Several data sets using moored arrays have shown stable returns from the seabed. Imaging seabed layering over extended areas requires the array to move which has been accomplished by allowing the array to drift. This, however, introduces a number of complications. If the array moves too rapidly, there is potential for the ensonified seabed (in the beam) to change within the averaging time. Another potential problem could be caused by vertical motion of the array (e.g. by surface coupling). In this case, Doppler shifts may cause degradation in the cross-correlation peaks. In some cases, these degrading factors may be reduced through signal processing. In this presentation potential mechanisms that degrade passive seabed imaging will be described with possible mitigating signal processing. Numerical modeling and measured data sets will be analyzed.

6:00

4pAOh2. Passive tomography of the oceanic environment using ambient noise cross-correlations. Karim G. Sabra (Georgia Institute of Technology, School of Mechanical Engineering, 771 Ferst Drive, NW, Atlanta, GA 30332-0405, USA, karim.sabra@me.gatech.edu)

The random nature of noise and scattered fields tends to suggest limited utility. Indeed, acoustic fields from random sources or scatterers are often considered to be incoherent, but there is some coherence between two sensors that receive signals from the same individual source or scatterer. An estimate of the Green's function (or impulse response) between two points can be obtained from the cross-correlation of ambient noise recorded at these two points. Recent theoretical and experimental studies in ultrasonics, civil engineering, underwater acoustics and seismology have investigated this technique in various environments and frequency ranges. These results provide a means for passive tomography of the ocean environment using only the ambient noise field, without the use of active sources. The coherent wavefronts emerge from a correlation process that accumulates contributions over time from noise sources whose propagation paths pass through both receivers. We will examine the background physics of extracting these coherent structures and present experimental results confirming these theoretical arguments. Further we will present experimental results such as using noise for time synchronization and localization of unconnected acoustic receivers, and for constructing passive tomographic images of the environment.

6:20

4pAOh3. Passive Geoacoustic Inversion using broadband ship noise in Bay of Biscay shallow water environment. Cédric Gervaise (E3I2 - EA3876, 2 rue François Verny, 29806 Brest Cedex, France, cedric.gervaise@ensieta.fr)

Our communication proposes a new geoacoustic inversion method for shallow water environments (100 to 300 m). The method relies on the inversion of broadband noise produced by ships of opportunity. The interference patterns generated by the ship movement and the propagation properties of the waveguide are exploited to extract the relative dispersion curves on a chosen bandwidth. These curves are then inverted to estimate geoacoustic properties. This inversion scheme was previously tested (with success) against real data from a very shallow water (10 to 30 m) trial performed off the Southern coast of Barcelona, Spain [1]. To deal with shallow waters, our inversion scheme is improved and tests against real data from PASSTIME trial performed in Bay of Biscay during October 2005. Inversion's results are compared with ground truth and the results showed to be accurate and robust. The proposed technique, which is suitable to a small number of hydrophones and quite easy to implement, offers interesting perspectives for passive geoacoustic inversion. [1] S. Vallez, C. Gervaise, Y. Stephan, M. Andre, Inversion géoacoustique d'un canal très petits petits fonds à partir des navires en mouvement - traitement incohérent, accepté pour publication Revue Traitement du Signal

6:40

4pAOh4. The passive mode tomography of the ocean using data from short vertical arrays bent by the ocean currents. Andrey Shurup (Department of Acoustics, Physics Faculty, Moscow State University, Leninskie Gory, 119991 Moscow, Russian Federation, burov@phys.msu.ru), Sergey Sergeev (Department of Acoustics, Physics Faculty, Moscow State University, Leninskie Gory, 119991 Moscow, Russian Federation, sergeev@su29.ru), Valentin Burov (Department of Acoustics, Physics Faculty, Moscow State University, Leninskie Gory, 119991 Moscow, Russian Federation, burov@phys.msu.ru)

The possible realization of passive ocean tomography based on the widely discussed relation between the Green's function and ambient noise cross-correlation is discussed. The problem is considered in the mode representation of acoustic field in adiabatic approximation. The estimated time of signal accumulation required to determine the Green's function with sufficient accuracy reveals the possibility of implementing the schemes of the mode tomography of the ocean based on the measuring the ambient noise field of the ocean. It is shown that the use of the vertical arrays with vector receivers allows a decrease in the accumulation time to one or several hours, depending on the conditions of experiment. The mode structure of acoustic field is determined from the cross-correlation matrix of the noise field received by the hydrophones of short vertical arrays bent by the ocean currents and covering only the part of the sound channel. The proposed algorithm differs from the commonly used mode-filtering procedure and allows a compensation of antenna declination from the vertical profile and takes into account of the finite length of antenna aperture, that is ordinary explored in ocean experiments.

7:00

4pAOh5. Emergence of the deterministic Green's function from thermal noise in inhomogeneous solids and fluid-solid structures. Oleg A. Godin (NOAA/ESRL, 325 Broadway, Mail Code R/PSD99, Boulder, CO 80305-3328, USA, Oleg.Godin@noaa.gov)

S. M. Rytov [*A Theory of Electrical Fluctuations and Thermal Radiation* (USSR Academy of Sciences, Moscow, 1953)] was apparently the first to establish theoretically a simple relation between deterministic Green's function and cross-correlation of fluctuations of wave fields generated by random sources. He used reciprocity considerations to analyze fluctuations of electromagnetic fields. An acoustic counterpart of the Rytov's approach was applied in [O. A. Godin, Emergence of the acoustic Green's function from thermal noise, J. Acoust. Soc. Am. **121**, EL96-EL102 (2007)] to derive exact and asymptotic relations between acoustic Green's functions and cross-correlation of thermal noise in inhomogeneous moving or motionless fluids. In this paper, these results are extended to solid and fluid-solid media and compared to experimental and theoretical results previously reported in the literature. It is shown that, with the averaging time being sufficiently large, the two-point correlation function of thermal noise contains as much information about the environment as can be obtained acoustically by placing transceivers at the two points. A possibility of retrieving parameters of a fluid motion, such as a flow in a pipe or an oceanic current, from cross-correlations of diffuse noise fields is addressed.

7:20

4pAOh6. Comparing time domain Green's functions with simulated noise and ambient noise data cross-correlation for a horizontal array. Stephanie Fried (MPL, Scripps Institution of Oceanography, University of California, San Diego, La Jolla, CA 92093-0238, USA, sefried@ucsd.edu), Karim G. Sabra (Georgia Institute of Technology, School of Mechanical Engineering, 771 Ferst Drive, NW, Atlanta, GA 30332-0405, USA, karim.sabra@me.gatech.edu), Philippe Roux (LGIT - CNRS - Université Joseph Fourier, Maison des Géosciences, 1381 rue de la Piscine, BP 53, 38041 Grenoble, France, philippe.roux @obs.ujf-grenoble.fr), William A. Kuperman (MPL, Scripps Institution of Oceanography, University of California, San Diego, La Jolla, CA 92093-0238, USA, wkuperman@ucsd.edu)

Previous work has shown that an approximation of the Green's function can be extracted from ambient noise data through cross-correlating the received signals along an array. The resulting Green's function approximation gives accurate time-of-arrivals for the multipaths between hydrophones but can only approximate the magnitude of the arrivals in the time domain Green's function. Nevertheless, some useful information can be obtained from the relative amplitudes of the correlated returns assembled. Further, a Monte Carlo noise model simulation for a similar environment for which noise data was collected reproduces the same cross-correlation arrival structure for the processed ambient noise data and the theoretical time domain Green's function arrival structure. [Research supported by ONR].

7:40

4pAOh7. Acoustic modeshape inversion using deep water ambient noise measurements. Kathleen E. Wage (George Mason University, 4400, University Drive, Fairfax, VA 22030, USA, kwage@gmu.edu), Khalid Almuhanna (George Mason University, 4400, University Drive, Fairfax, VA 22030, USA, kalmuha1@gmu.edu)

Assuming that ambient noise can be represented by a sum of uncorrelated acoustic modes, the eigenvectors of the noise covariance matrix for a vertical line array should correspond to the sampled modeshapes. In previous work several authors have investigated using an eigendecomposition of the noise covariance to estimate the mode functions in shallow water, e.g., Wolf et al. [Proc. of the 1993 IEEE Oceans Conf.,vol. I, pp. 99-104], Hursky et al. [J. Acoust. Soc. Am., 109(4), pp. 1355-1366], and Nielsen and Westwood [J. Acoust. Soc. Am., 111(2), pp. 748-756]. While the same approach should work for deep water scenarios, only few deep water experiments have deployed arrays with sufficient aperture to resolve the modes, e.g., the work D'Spain et al. [Pure appl. geophys., Vol. 158, pp. 475-512]. This paper explores the problem of inverting for the acoustic modes of a deep water waveguide using ambient noise measurements. In particular the paper focuses on important signal processing issues, including data snapshot requirements, and the effects of array tilt. Data from a deep water propagation experiment will be used to quantify how well the empirical modes match the true modes derived from measured environmental data. [Work supported by an ONR Young Investigator Award.]

Session 4pBBa

Biomedical Ultrasound/Bioresponse to Vibration: Ultrasonic Characterization of Bone I

Keith A. Wear, Cochair
U.S. Food and Drug Administration, Center for Devices and Radiological Health, 10903 New Hampshire Ave, Bldg 62, Rm 3108, Silver Spring, MD 20993, USA

Kay Raum, Cochair
Martin Luther University of Halle-Wittenberg, Dept. of Orthopedics, Q-BAM Group, Magdeburger Str. 22, Halle, 06097, Germany

Invited Papers

2:00

4pBBa1. Present state and future trends in ultrasonic characterization of bone. Pascal Laugier (Université Paris 6, Laboratoire d'Imagerie Paramétrique, 15, rue de l'Ecole de Médecine, 75006 Paris, France, laugier@lip.bhdc.jussieu.fr)

Although it has been over 20 years since the first recorded use of a quantitative ultrasound (QUS) technology to predict bone fragility, the field has not yet reached its maturity. QUS have the potential to predict fracture risk in a number of clinical circumstances and has the advantages of being non-ionizing, inexpensive, portable, highly acceptable to patients and repeatable. However, the wide dissemination of QUS in clinical practice is still limited and suffering form the absence of clinical consensus on how to integrate QUS technologies in bone densitometry armamentarium. There are a number of critical issues that need to be addressed in order to develop the role of QUS within rheumatology. These include issues of technologies adapted to measure the central skeleton, data acquisition and signal processing procedures to reveal bone properties beyond bone mineral quantity and elucidation of the complex interaction between ultrasound and bone structure. In this presentation, we review recent developments to assess bone mechanical properties. We conclude with suggestions of future lines and trends in technology challenges and research areas such as new acquisition modes, advanced signal processing techniques, and models.

2:20

4pBBa2. Ultrasonic guided waves in bone. Petro Moilanen (University of Jyväskylä, Department of Physics, PO. Box 35, 40014 Jyväskylä, Finland, pemoilan@cc.jyu.fi)

Recent progress in quantitative ultrasound (QUS) has shown increasing interest towards measuring long bones by ultrasonic guided waves. This technology is widely used in the field of non-destructive testing and evaluation of different waveguide structures. Cortical bone provides such an elastic waveguide and its ability to sustain loading and resist fractures is known to relate to its mechanical properties at different length scales. As guided waves could yield diverse characterization of bone's mechanical properties at the macroscopic level, the method of guided waves has a strong potential over the standardized bone densitometry as a tool for bone assessment. Despite this, development of guided wave methods is challenging, e.g., due to interferences and multiparametric inversion problem. This paper discusses the promises and challenges related to bones characterization by ultrasonic guided waves.

Contributed Papers

2:40

4pBBa3. Dual frequency ultrasound measurement of bone - a technique for elimination of soft tissue effects on pulse-echo measurements. Ossi Riekkinen (University of Kuopio, POB 1627, 70211 Kuopio, Finland, Ossi.Riekkinen@uku.fi), Mikko Hakulinen (University of Kuopio, POB 1627, 70211 Kuopio, Finland, Mikko.Hakulinen@uku.fi), Juha Töyräs (Kuopio University Hospital, POB 1777, 70211 Kuopio, Finland, Juha.Toyras@kuh.fi), Jukka Jurvelin (University of Kuopio, POB 1627, 70211 Kuopio, Finland, Jukka .Jurvelin@uku.fi)

Quantitative ultrasound (US) measurements have been suggested for screening of osteoporosis. However, soft tissues overlying bones affect reliability of the measurements. In this in vitro study, a novel dual frequency ultrasound (DFUS) technique is introduced for elimination of the errors induced by soft tissues on bone pulse-echo US measurements. In DFUS, US reflection from soft tissue-bone interface is measured with two different US frequencies. By knowing the frequency specific US attenuation and speed in adipose and lean tissues, the effect of soft tissue can be determined. DFUS, conducted at frequencies of 2.25 MHz and 5.0 MHz, was validated using human trabecular bone samples ($n = 25$) covered with heterogeneous soft tissues. DFUS, reduced ($p < 0.01$) the mean error induced by soft tissues from 58.6% to -4.9% and from 127.4% to 23.8% in broadband ultrasound backscattering and integrated reflection coefficients (at 5.0 MHz), respectively. Our results suggest that DFUS is a technique capable to minimize the errors induced by the soft tissue overlying the bone. As no reflection information within soft tissue (adipose-lean tissue interface) is needed in pulse-echo measurements DFUS may enhance the accuracy of ultrasound measurements. Thereby, DFUS shows a significant clinical potential.

3:00

4pBBa4. Improved standardization methods for clinical measurements of BUA and SOS. Keith A. Wear (U.S. Food and Drug Administration, Center for Devices and Radiological Health, 10903 New Hampshire Ave, Bldg 62, Rm 3108, Silver Spring, MD 20993, USA, keith.wear@fda.hhs .gov)

BACKGROUND: Although calcaneal broadband ultrasound attenuation (BUA) and speed of sound (SOS) are good predictors of osteoporotic fracture risk, BUA and SOS measurements exhibit substantial inter-system

variability. PURPOSE: 1) Compare phase insensitive (PI) detection, which suppresses phase cancellation, and conventional phase sensitive (PS) detection for measurement of BUA. 2) Test a new compensation formula for reducing variability in SOS measurements. METHODS: Data from 73 women were acquired using a GE Lunar Achilles Insight bone sonometer. Radio frequency data were processed off-line using both PI and PS algorithms. RESULTS: BUA measurements (mean ± sd) were 81.4 ± 21.4 dB/MHz (PS) and 67.2 ± 9.7 dB/MHz (PI). Compensation of SOS measurements reduced 1) average transit-time-marker-related SOS variability by 75% in 73 women and 2) bandwidth-related SOS variability by 80% in a bone-mimicking phantom. CONCLUSION: These new methods will enable a substantial improvement in consistency in bone sonometry. The mention of commercial products, their sources, or their use in connection with material reported herein is not to be construed as either an actual or implied endorsement of such products by the Department of Health and Human Services.

3:20

4pBBa5. Characterization of Ultrasound Propagation Through Ex-vivo Human Temporal Bone. Azzdine Y. Ammi (University of Cincinnati, Biomedical Engineering, MSB, 231 Albert Sabin Way, Cincinnati, OH 45267-0586, USA, azzdine.ammia@uc.edu), Douglas T. Mast (University of Cincinnati, Biomedical Engineering, MSB, 231 Albert Sabin Way, Cincinnati, OH 45267-0586, USA, masttd@email.uc.edu), I-Hua Huang (1415 2nd Aveue, Unit 1804, Seattle, WA 98101, USA, helloihua@gmail.com), Todd A. Abruzzo (University of Cincinnati, Dept.s of Radiol., Neurosurg. & Biomed. Engineer., Cincinnati, OH 45267, USA, Todd.Abruzzo@Healthall.com),Constantin C. Coussios(University of Oxford, Medical Engineering Unit, 43 Banbury Road, OX2 6PE Oxford, UK, constantin.coussios@eng.ox.ac.uk), George J. Shaw (University of Cincinnati, Biomedical Engineering, MSB, 231 Albert Sabin Way, Cincinnati, OH 45267-0586, USA, SHAWGE@UCMAIL.UC.EDU), Christy K. Holland (University of Cincinnati, Biomedical Engineering, MSB, 231 Albert Sabin Way, Cincinnati, OH 45267-0586, USA, Christy.Holland@uc.edu)

Knowledge of cranial and intracranial ultrasonic properties is essential for optimal results in brain vasculature imaging and therapy. The aims of this study were to perform measurements of the intracranial acoustic pressure field, to identify ultrasound parameters that maximize penetration and minimize beam aberration, and to estimate the speed of sound and the attenuation per unit length in the temporal bone (TB). In vitro experiments were conducted on five human skulls. In a water-filled tank, two unfocused (0.12 and 1.03 MHz) and one focused (2.00 MHz) transducers were consecutively placed near the TB of each skull. The acoustic pressure field was measured in a volume estimated to encompass the middle cerebral artery (MCA). For each measurement, the intracranial distance from the position of maximum acoustic pressure to the estimated MCA origin was quantified. The pressure reductions at these locations relative to the free field were also estimated. The intracranial -3 dB depth of field and beam width were investigated as a function frequency. The speed of sound in TB at 1.03 MHz was 1752.1 to 3285.3 m/s. This work provides quantitative information on the cranial and intracranial ultrasound properties, which are needed for optimal insonation of the brain vasculature.

3:40-5:20 Posters

Lecture sessions will recess for presentation of poster papers on various topics in acoustics. See poster sessions for topics and abstracts.

Contributed Papers

5:20

4pBBa6. Estimation of femoral bone density from trabecular direct wave and cortical guided wave ultrasound velocities measured at the proximal femur in vivo. Reinhard Barkmann (Medizinische Physik, Diagnostische Radiologie, Universitätsklinikum Schleswig-Holstein, Arnold-Heller-Str.9, 24105 Kiel, Germany, barkmann@rad.uni-kiel.de), Stefanie Dencks (Medizinische Physik, Diagnostische Radiologie, Universitätsklinikum Schleswig-Holstein, Arnold-Heller-Str.9, 24105 Kiel, Germany, dencks@rad.uni-kiel.de), Alexander Bremer (Medizinische Physik, Diagnostische Radiologie, Universitätsklinikum Schleswig-Holstein, Arnold-Heller-Str.9, 24105 Kiel, Germany, Alexander.Bremer@gmx.net), Pascal Laugier (Université Paris 6, Laboratoire d'Imagerie Paramétrique, 15, rue de l'Ecole de Médecine, 75006 Paris, France, laugier@lip.bhdc.jussieu.fr), Frederic Padilla (Université Paris 6, Laboratoire d'Imagerie Paramétrique, 15, rue de l'Ecole de Médecine, 75006 Paris, France, Frederic.Padilla@lip.bhdc.jussieu.fr), Kim Brixen (Odense University Hospital, Department of Endocrinology, 5000 Odense, Denmark, Kim.Brixen@ouh.regionsyddanmark.dk), Jesper Ryg (Odense University Hospital, Department of Endocrinology, 5000 Odense, Denmark, Jesper.Ryg@ouh.regionsyddanmark.dk), Claus C. Glüer (Medizinische Physik, Diagnostische Radiologie, Universitätsklinikum Schleswig-Holstein, Arnold-Heller-Str.9, 24105 Kiel, Germany, glueer@rad.uni-kiel.de)

Bone mineral density (BMD) of the proximal femur is a predictor of hip fracture risk. We developed a Quantitative Ultrasound (QUS) scanner for measurements at this site with similar performance (FemUS). In this study we tested if ultrasound velocities of direct waves through trabecular bone and of guided waves through cortical bone could be used to estimate BMD. In two centres, Kiel and Odense, we measured time-of-flight (TOF) of waves through the trabecular greater trochanter and cortical intertrochanter as well as a wave through soft tissue only. TOF was adjusted for leg width using ultrasound echoes reflected from the skin of the leg to yield speed-of-sound (SOS) of different wave components. Data were cross-calibrated and pooled (62 women). Bivariate correlations and a multivariate model were calculated for the estimation of femur BMD. BMD correlated both with trabecular and cortical SOS but not soft tissue SOS. Coefficient of determination, percentage residual error (RMSE) and level of significance (p) were $R^2=0.51$, RMSE=12.6%, $p<0.0001$ for trabecular and $R^2=0.53$, RMSE=12.3%, $p<0.0001$ for cortical measurements. The combination of trabecular, cortical and soft tissue SOS improved the correlation to $R^2=0.69$, RMSE=10.4%, $p<0.0001$. Multiwave ultrasound methods allow estimation of femoral BMD with a low residual error.

5:40

4pBBa7. Estimation of in vivo cancellous bone elasticity. Takahiko Otani (Doshisha University, 1-3, Tatara Miyakodani, 610-0321 Kyotanabe, Japan, totani@oyoe.jp), Isao Mano (Oyo Electric Co., Ltd., 63-1, Nakamichiomote Hirakawa, 610-0101 Joyo, Japan, imano@oyoe.jp), Toshiyuki Tsujimoto (Horiba, Ltd., 2, Miyanohigashi-cho, Kisshoin, Minami-ku, 601-8510 Kyoto, Japan, toshiyuki.tsujimoto@horiba.com)

Effect of decreasing bone density (a symptom of osteoporosis) is greater for cancellous bone than for dense cortical bone, because cancellous bone is metabolically more active. Therefore, bone density or bone mineral density at cancellous bone is generally used to estimate the onset of osteoporosis. Elasticity or elastic constant is one of fundamental mechanical parameters and directly related to the mechanical strength of bone. Accordingly, elasticity is a preferable parameter to assess the fracture risk. A novel ultrasonic bone densitometer LD-100 has been developed to obtain mass density and elasticity of cancellous bone with a spatial resolution comparable to that of the peripheral quantitative computed tomography system. Bone mass density and bone elasticity are evaluated using ultrasonic parameters based on fast and slow waves in cancellous bone using a modeling of ultrasonic wave propagation path. Elasticity is deduced from measured bone mass density and propagation speed of fast wave. Thus, elasticity of cancellous bone is approximately expressed by a cubic equation of bone mass density.

6:00

4pBBa8. Fracture and bone defect assessment using quantitative ultrasound wave propagation. Mikey Szczupak (Stony Brook University, SUNY, Department of Biomedical Engineering, 350 Psychology-A Building, Stony Brook, NY 11794, USA, mszczupak90@yahoo.com), Yi Xia (Stony Brook University, SUNY, Department of Biomedical Engineering, 350 Psychology-A Building, Stony Brook, NY 11794, USA, xia.yi76@gmail.com), Jiqi Cheng (Stony Brook University, SUNY, Department of Biomedical Engineering, 350 Psychology-A Building, Stony Brook, NY 11794, USA, chengjiqi@yahoo.com), Yi-Xian Qin (Stony Brook University, SUNY, Department of Biomedical Engineering, 350 Psychology-A Building, Stony Brook, NY 11794, USA, yi-xian.qin@sunysb.edu)

Nondestructive evaluation of early fracture and monitoring its healing, particularly in non-typical fracture, is critical yet challenge. Quantitative ultrasound test along the long bone is largely dependant on bone density, gap size, the level of maturity of the callus, and mineralized status. We propose that the ultrasonic velocity (UV) is dependent on fracture gap size and the degree of porosity. The objective of the study was to develop an analytical and a multiple ultrasound sensing system for non-invasive fracture assessment. An analytical model was generated as a function between UV and the gap size in long bone. The ultrasound measurements were performed in the intact pig femur with controlled fracture sizes, e.g., 1mm, 3mm and 5mm. A serial ultrasound transducers were aligned 3 cm above bone with an angle approximately equal to the critical angle. The results indicated that the UV decreased with increase of fracture size in a linear manner ($r=0.96$), in which UV decreased 6.7%, 16.3% and 26.8% for 1, 3 and 5 mm gaps, respectively. The simulation result significantly matched the experiment measurement ($r=0.98$). The results demonstrated that quantitative ultrasound has potential to the diagnosis of fracture, monitoring fracture healing, and other bone disorders.

6:20

4pBBa9. Monitoring of trabecular bone induced microdamage using a nonlinear wave-coupling technique. Guillaume Renaud (LUSSI, 10 Bd Tonellé, 37032 Tours, France, guillaume.renaud28@etu.univ-tours.fr), Samuel Callé (LUSSI, 10 Bd Tonellé, 37032 Tours, France, calle_s@med.univ-tours.fr), Jean-Pierre Remenieras (LUSSI, 10 Bd Tonellé, 37032 Tours, France, remenier@med.univ-tours.fr), David Mitton (Laboratoire de biomécanique, 151, Boulevard de l'hopital, 75013 Paris, France, david.mitton@paris.ensam.fr), Julie Blanchi (Laboratoire de biomécanique, 151, Boulevard de l'hopital, 75013 Paris, France, julieblanchi@gmail.com), Marielle Defontaine (LUSSI, 10 Bd Tonellé, 37032 Tours, France, defontai@med.univ-tours.fr)

Bone tissue contains microcracks which may affect its mechanical properties as well as the whole trabecular structure. The relationship between crack density and bone strength is nevertheless poorly understood. Efficient nonlinear (NL) ultrasound methods have been widely developed for nondestructive testing and geophysical applications to detect microdamage. Moreover it has been reported that elastic nonlinearities increase with induced damage. We propose to monitor trabecular bone microdamage using a NL wave coupling technique. Ultrasonic short bursts times of flight (TOF) are modulated as result of NL interaction with a low-frequency (LF) wave in the medium. TOF modulation (TOFM), or propagation velocity variations, are directly related to NL elasticity variations. This technique allows measuring the instantaneous TOFM as a function of the LF pressure. It is thus possible to analyze separately elasticity variations in tension and in compression, and to distinguish the tension to compression phase from the compression to tension phase (hysteresis). In several trabecular bone samples, different TOFM amplitudes in tension and in compression are observed, probably due to microdamage. For increasing damage levels progressively induced by quasi-static compression testing, linear and nonlinear ultrasound parameters are compared to biomechanical parameters.

6:40

4pBBa10. Local measurements of the diffusion constant in multiple scattering media: Application to human trabecular bone imaging. Alexandre Aubry (Laboratoire Ondes et Acoustique, ESPCI, Université Paris 7, CNRS, 10 rue Vauquelin, 75005 Paris, France, alexandre.aubry@espci.fr),Arnaud Derode(Laboratoire Ondes et Acoustique, ESPCI, Université Paris 7, CNRS, 10 rue Vauquelin, 75005 Paris, France, arnaud.derode@ujf-grenoble.fr), Frederic Padilla (Université Paris 6, Laboratoire d'Imagerie Paramétrique, 15, rue de l'Ecole de Médecine, 75006 Paris, France, Frederic.Padilla@lip.bhdc.jussieu.fr)

Multiple scattering of ultrasound can occur in trabecular bones. A typical signature of multiple scattering is the coherent backscattering effect, and the average trajectory of a wave undergoing multiple scattering can be characterized by the diffusion constant D. In this work, we present local measurements of the diffusion constant for ultrasonic waves in human trabecular bone, based on near-field observation of the backscattered intensity. The experimental set up consists in an array of programmable transducers placed in front of a slice of bone that we want to image. By achieving Gaussian beamforming both at emission and reception, an array of virtual sources and receivers located in the near-field is constructed. The time evolution of the incoherent component of the intensity backscattered on this virtual array is shown to represent directly the growth of the diffusive halo as $(Dt)^{1/2}$. A matrix treatment is proposed to separate the incoherent intensity from the coherent backscattering peak. Once the incoherent contribution is isolated, local measurements of the diffusion constant D are achieved around 3 MHz and then a D-map of the bone is built. These measurements are shown to be strongly correlated with the bone mineral density.

7:00

4pBBa11. Relationship Between Mechanical Properties and Acoustic Parameters Obtained from Fast and Slow Waves for Cancellous Bone. Masaki Harada (Doshisha University, 1-3, Tatara Miyakodani, 610-0321 Kyotanabe, Japan, dth0315@mail4.doshisha.ac.jp), Kazuto Tanaka (Doshisha University, 1-3, Tatara Miyakodani, 610-0321 Kyotanabe, Japan, ktanaka@mail.doshisha.ac.jp), Tsutao Katayama (Doshisha University, 1-3, Tatara Miyakodani, 610-0321 Kyotanabe, Japan, tkatayam@mail.doshisha.ac.jp), Katsunori Mizuno (Doshisha University, 1-3, Tatara Miyakodani, 610-0321 Kyotanabe, Japan, dtg0151@mail4.doshisha.ac.jp), Hiroki Soumiya (Doshisha University, 1-3, Tatara Miyakodani, 610-0321 Kyotanabe, Japan, mmatsuka@mail.doshisha.ac.jp), Mami Matsukawa (Doshisha University, 1-3, Tatara Miyakodani, 610-0321 Kyotanabe, Japan, mmatsuka@mail.doshisha.ac.jp)

The bone-density measuring equipment using the characteristics of the ultrasound has been applied for the diagnosis of osteoporosis. The propagated ultrasonic wave in the cancellous bone changes dramatically due to its complicated structure, and is separated into fast wave and slow wave. The parameters obtained from two-waves are closely related to the structure properties and the elastic properties of bone, which is considered to provide important information related to bone strength. However, the relationship between the strength obtained by the mechanical tests and the fast and slow wave properties is not clearly investigated. In this study, compression tests of the cancellous bovine bone were conducted to determine the compressive strength in addition to the ultrasonic measurements. Our results showed that amplitude ratio of fast and slow wave significantly correlated ($r2=0.88$) with the compressive strength, which reasonably indicates that the bone strength increases in proportional to the density of the cancellous bone.

7:20

4pBBa12. Two-dimensional simulation of circumferential wave propagation in cortical bone at the femoral neck: sensitivity to bone geometry. Julien Grondin (Université Paris 6, Laboratoire d'Imagerie Paramétrique, 15, rue de l'Ecole de Médecine, 75006 Paris, France, Julien.Grondin@lip.bhdc.jussieu.fr), Quentin Grimal (Université Paris 6, Laboratoire d'Imagerie Paramétrique, 15, rue de l'Ecole de Médecine, 75006 Paris, France, quentin.grimal@lip.bhdc.jussieu.fr), Pascal Laugier (Université Paris 6, Laboratoire d'Imagerie Paramétrique, 15, rue de l'Ecole de Médecine, 75006 Paris, France, laugier@lip.bhdc.jussieu.fr)

Assessment of bone status using ultrasound techniques has proved to be efficient to quantify the risk of osteoporotic fracture. A prototype scanner is currently developed (European FEMUS project) to assess bone quality at the hip. Circumferential waves in femoral neck cortical bone are expected to propagate in the prototype configuration. In this work, the relationships

between time of flight (TOF) of circumferential waves and femoral neck cross-section geometrical parameters were investigated. Two-dimensional finite-difference time-domain simulations of through transmission propagation of a plane wave at 0.5 MHz central frequency were performed on eight femoral neck cross-section models reconstructed from X-ray computed tomography data of one human femur. An ellipse with major radius (a) and minor radius (b) was fitted on the external circumference of each cross-section. The TOF was highly correlated to the ellipticity a/b (R = -0.9607, p<10-3) and to the area delineated by the endosteal surface (R = -0.9717, p<10-4). These results indicate that the TOF is sensitive to the shape of the femoral neck cross-section. This is interesting insofar as previous studies highlighted the importance of the relationships between geometrical parameters and bone strength. In future works, these 2-D results will be challenged in 3-D configurations.

7:40

4pBBa13. Array transducer applied to low-frequency guided wave ultrasonography: An in vivo study on human radius and tibia. Vantte Kilappa (University of Jyväskylä, Department of Physics, PO. Box 35, 40014 Jyväskylä, Finland, warma@iki.fi), Petro Moilanen (University of Jyväskylä, Department of Physics, PO. Box 35, 40014 Jyväskylä, Finland, pemoilan@cc.jyu.fi), Tianhui Chen (University of Jyväskylä, Department of Health Sciences, PO. Box 35, 40014 Jyväskylä, Finland, cth006@hotmail.com), Hongqiang Ma (University of Jyväskylä, Department of Health Sciences, PO. Box 35, 40014 Jyväskylä, Finland, mhqsir0827@hotmail.com), Jussi Timonen (University of Jyväskylä, Department of Physics, PO. Box 35, 40014 Jyväskylä, Finland, Jussi.Timonen @phys.jyu.fi), Sulin Cheng (University of Jyväskylä, Department of Health Sciences, PO. Box 35, 40014 Jyväskylä, Finland, Sulin.Cheng@sport.jyu.fi)

Velocity (V_{FAS}) of a first arriving signal for $f < 0.5$ MHz is expected to have an enhanced sensitivity to endosteal osteoporotic changes as compared to using higher frequencies. In this study a group of males and females (aged 10-87 years) was measured by using a new array probe ($f_c = 0.4$ MHz) on the radius and tibia. In addition, peripheral quantitative computed tomography was used to assess the bone mineral density (BMD) and cortical thickness (CTh) at the same bone locations. Initial results (n=57) showed that the repeatability error of the V_{FAS} data (CV_{rms}) was 0.5%. When V_{FAS} data for the radius was plotted by age it characterized well, yet better than BMD or CTh, the typical growth and loss curve of bone. V_{FAS} for the radius was strongly correlated with total BMD ($r = 0.84$, $p < 0.001$), cortical BMD ($r = 0.77$, $p < 0.001$), subcortical BMD ($r = 0.66$, $p < 0.001$) and CTh ($r = 0.59$, $p < 0.001$). Corresponding results for the tibia were similar but clearly weaker than those for the radius. In conclusion, the low-frequency V_{FAS} had good accuracy and it predicted well both the geometry and material properties throughout the cortex.

THURSDAY AFTERNOON, 3 JULY 2008 P3-B, LEVEL 3, 3:40 TO 5:20 P.M.

Session 4pBBb

Biomedical Ultrasound/Bioresponse to Vibration: Ultrasonic Characterization of Bone II (Poster Session)

Keith Wear, Cochair
U.S. Food and Drug Administration, Center for Devices and Radiological Health

Frederic Padilla, Cochair
Université Paris 6

All posters will be on display from 3:40 p.m. to 5:20 p.m. To allow contributors an opportunity to see other posters, contributors of odd-numbered papers will be at their posters from 3:40 p.m. to 4:30 p.m. and contributors of even-numbered papers will be at their posters from 4:30 p.m. to 5:20 p.m.

Contributed Papers

4pBBb1. Cross-sectional ultrasonic tomography of the medullary cavity of child bones - Limits of resolution. Philippe Lasaygues (Laboratory for Mechanics and Acoustics CNRS, 31 chemin Joseph Aiguier, 13009 Marseille, France, lasaygues@lma.cnrs-mrs.fr), Régine Guillermin (Laboratory for Mechanics and Acoustics CNRS, 31 chemin Joseph Aiguier, 13009 Marseille, France, guillermin@lma.cnrs-mrs.fr), Eric Debieu (Laboratory for Mechanics and Acoustics CNRS, 31 chemin Joseph Aiguier, 13009 Marseille, France, debieu@lma.cnrs-mrs.fr), Jean-Pierre Lefebvre (Laboratory for Mechanics and Acoustics CNRS, 31 chemin Joseph Aiguier, 13009 Marseille, France, lefebvre@lma.cnrs-mrs.fr), Philippe Petit (Pediatric radiology department, 'Timone' Children's Hospital, 13006 Marseille, France, philippe.petit@mail.ap-hm.fr)

In children with bone diseases, ultrasonography has proved to be a highly effective tool for assessing congenital disorders. However, with standard devices, this method of examination is limited and not suitable for diagnostic large purposes as tumors or sub-periostal infectious. Authors dealt with the imaging of more adult bones than children, and the main aim has usually been to assess the thickness of the diaphysis and/or to estimate the wave velocity crossing the structure. Our group has been focusing on the cross-sectional radial imaging process, using ultrasonic computed tomography, of child bones. Although this method is known to provide a potentially valuable means of imaging objects with similar acoustical impedance, problems arise when it is proposed to obtain quantitative tomograms of more highly contrasted media. Finding solutions involves either using non-linear schemes. In this paper, we recall the advantages and limitations of ultrasonic computed tomography methods when dealing with highly contrasted scatterers. The results obtained are promising and suggest that the geometrical and acoustical characteristics of children's bones can be efficiently determined using this ultrasonic computed tomography method.

4pBBb2. Model study on assessment of bone by ultrasonic guided waves through a varying layer of soft tissue. Alexey Tatarinov (Artann Laboratories, 1753 Linvale-Harbourton, Lambertville, NJ 08350, USA, tatarinov@artannlabs.com), Armen Sarvazyan (Artann Laboratories, 1753 Linvale-Harbourton, Lambertville, NJ 08350, USA, armen@artannlabs.com)

Propagation parameters of ultrasonic guided waves in long bones are sensitive to changes of the cortical thickness, which is one of bone parameters affected by osteoporosis. Meanwhile, the guided waves in bone can be masked by the longitudinal waves in the overlying soft tissues, especially in obese patients. The goal of this study was to explore a possibility to minimize the effect of soft tissue on quantitative assessment of propagation parameters of axial guided waves in long bones. Phantoms and animal bone fragments modeling the axial gradients of the cortical thickness in the human proximal tibia were used. The specimens were covered by a layer of soft tissue of varied thickness. Ultrasonic signals were acquired in the pulse mode at 0.1 MHz by the surface transmission. The specimens were scanned lengthwise and the acquired signals were plotted versus the scanned distance. Analysis of the obtained waveform profiles along the tested specimens allowed quantitative evaluation of the variations of the cortical thickness despite the presence of a 5-6 mm soft tissue layer. The ratio of the acoustic wavelength to the soft tissue layer thickness defines the level of the soft tissue effect.

4pBBb3. Using Singular Value Decomposition to analyse a low frequency contribution on human cortical bone with a 1MHz axial transmission probe. Magali Sasso (Echosens, R&D department, 153 avenue d'Italie, 75013 Paris, France, magali.sasso@echosens.com), Maryline Talmant (Université Paris 6, Laboratoire d'Imagerie Paramétrique, 15, rue de l'Ecole de Médecine, 75006 Paris, France, talmant@lip.bhdc.jussieu.fr), Guillaume Haiat (CNRS, Laboratoire de Recherches Orthopédiques, 10, Avenue de Verdun, 75010 Paris, France, haiat@univ-paris12.fr), Pascal Laugier (Université Paris 6, Laboratoire d'Imagerie Paramétrique, 15, rue de l'Ecole de Médecine, 75006 Paris, France, laugier@lip.bhdc.jussieu.fr), Salah Naili (Université Paris 12, B2OA, 61, Avenue du Général de Gaulle, 94010 Créteil, France, naili@univ-paris12.fr)

The configuration of axial transmission technique dedicated to cortical bone characterization generates multiple contributions, associated with different propagation modes. The first arriving signal velocity is classically evaluated using time-of-flight measurements while the analysis of later arrivals requires the development of specific signal processing tools. We focus here on an Energetic Low Frequency (ELF) later contribution acquired by a 1-MHz multi-element bi-directional probe devised in the LIP. Using a procedure adapted from the Singular Value Decomposition (SVD), the ELF contribution was separated from the rest of the signal. The ability of the method to provide an accurate phase velocity estimate of a dispersive wave was established in a controlled-case study on the propagation of Lamb waves on plates using FDTD (Finite-Difference Time-Domain) simulations. The method applied on signals acquired previously in vitro on human radii using the bidirectional device show that the ELF is consistent with the A0 Lamb mode and that its velocity is related to cortical bone thickness ($R2 = 0.6$, $p < 10\text{-}5$). Identification of A0 type wave agree with results reported in the literature obtained with a mono-element device which operates in the 100-300 kHz frequency band.

4pBBb4. Variability of velocities provided by axial transmission due to irregular geometry of cortical bones. Thiên-Ly Pham (Université Paris 6, Laboratoire d'Imagerie Paramétrique, 15, rue de l'Ecole de Médecine, 75006 Paris, France, pham@lip.bhdc.jussieu.fr), Maryline Talmant (Université Paris 6, Laboratoire d'Imagerie Paramétrique, 15, rue de l'Ecole de Médecine, 75006 Paris, France, talmant@lip.bhdc.jussieu.fr), Pascal Laugier (Université Paris 6, Laboratoire d'Imagerie Paramétrique, 15, rue de l'Ecole de Médecine, 75006 Paris, France, laugier@lip.bhdc.jussieu.fr)

Early predictions of the velocities of axially transmitted waves on cortical bones were based on waveguides such as plate and tube of regular geometry and uniform thickness. We investigate the role of the actual irregular geometry by means of numerical simulations comparing monodirectional and bidirectional multielement modalities. Propagation was simulated using a finite difference method in a set of human radii previously examined by a bidirectional device. Individual geometry of the samples was reconstructed from X Ray tomography (pixel=100mm). The material constituting the bone models was considered to be a transverse isotropic medium with chosen fixed elastic properties taken from literature. In addition simulations were performed on plate of either constant or variable thickness. Preliminary results perfomed on 9 samples show that bidirectional technique reduces the variability of the velocities of axially transmitted waves compared to monodirectional array when irregular geometries are involved. Whereas bidirectional velocity is significantly correlated to the velocity obtained in plates whose thickness is equal to the mean thickness of the specimen ($r^2 = 0.77$, $p = 0.0018$, RMSE=29m/s), no significant correlation is found for monodirectional velocity. The effect is mainly attributed to the irregular external surface of real samples.

4pBBb5. A finite element model of the lamellar osteonal structure based on ultrahigh frequency acoustic impedance data. Kay Raum (Martin Luther University of Halle-Wittenberg, Dept. of Orthopedics, Q-BAM Group, Magdeburger Str. 22, 06097 Halle, Germany, kay.raum@medizin.uni-halle.de), Quentin Grimal (Université Paris 6, Laboratoire d'Imagerie Paramétrique, 15, rue de l'Ecole de Médecine, 75006 Paris, France, quentin.grimal@lip.bhdc.jussieu.fr), Alf Gerisch (Martin Luther University of Halle-Wittenberg, Institut für Mathematik, 06099 Halle, Germany, alf.gerisch@medizin.uni-halle.de)

Materials: A finite element (FE) model was developed, in which the osteon is considered to consist of a central Haversian canal filled with an incompressible fluid and surrounding sets of lamellar units. Each lamellar unit was further subdivided in five sublayers, whereas the orientation of the symmetry axis between adjacent sublayers was shifted clockwise. A sublayer consists of one to ten layers of parallel oriented mineralized collagen fibrils (thickness: 0.2 μm, constant transverse isotropic stiffness tensor). Results: A variation of the sublayer thicknesses results in either isotropic or anisotropic tissue compound properties. By changing the individual layer thicknesses various degrees of anisotropy could be produced. A good agreement with the lamellar pattern obtained in 1.2-GHz SAM images as well as with the anisotropic elastic coefficients measured at the tissue level (50-MHz ultrasound) was obtained by choosing an asymmetric lamellar unit. Conclusions: With the proposed combination of experimentally derived microelastic and microstructural data by 1.2 GHz SAM and a micromechanical FE the homogenized elastic stiffness tensor of lamellar bone tissue was derived. The tissue anisotropy was explained by the asymmetric twisted plywood structure.

4pBBb6. Distribution and anisotropy of fast wave speed in the cancellous bone of bovine femur. Katsunori Mizuno (Doshisha University, 1-3, Tatara Miyakodani, 610-0321 Kyotanabe, Japan, dtg0151@mail4.doshisha.ac.jp), Hiroki Soumiya (Doshisha University, 1-3, Tatara Miyakodani, 610-0321 Kyotanabe, Japan, mmatsuka@mail.doshisha.ac.jp), Mami Matsukawa (Doshisha University, 1-3, Tatara Miyakodani, 610-0321 Kyotanabe, Japan, mmatsuka@mail.doshisha.ac.jp), Takahiko Otani (Doshisha University, 1-3, Tatara Miyakodani, 610-0321 Kyotanabe, Japan, totani@oyoe.jp), Masahiko Takada (Omihachiman Community Medical Center, 1379 Tsuchida-cho, 523*0082 Omihachiman, Japan, takada@design.kyushu-u.ac.jp), Isao Mano (Oyo Electric Co., Ltd., 63-1, Nakamichiomote Hirakawa, 610-0101 Joyo, Japan, imano@oyoe.jp), Toshiyuki Tsujimoto (Horiba, Ltd., 2, Miyanohigashi-cho, Kisshoin, Minami-ku, 601-8510 Kyoto, Japan, toshiyuki.tsujimoto@horiba.com)

The ultrasonic longitudinal wave in the cancellous bone is separated into two waves, fast and slow waves [1]. In this study, the relationship between the fast wave speed and the cancellous bone structure is experimentally investigated. A conventional ultrasonic pulse measurement was performed using a PVDF focus transmitter (Custom made, Toray) and a self-made PVDF receiver. Cylindrical specimens of cancellous bone were taken from the head of bovine femur in the distal part, along the three orthogonal directions. The distribution of fast wave speed was obtained by changing the measurement position along the cylindrical axis. The anisotropy of speed was also investigated by rotating the specimens. The structural parameters

of each specimen were also measured by X-ray micro CT (MCT-12505MF, Hitachi), which gave us the trabecular length and alignment from MIL (mean intercept length) parameters through TRI/3D-Bon software (Ratoc). We found that the fast wave showed large distribution and strong anisotropy depending on the measurement positions and wave propagation directions in the specimens. The fast wave showed the maximum speed in case of wave propagation along the load direction. Reference [1] A. Hosokawa and T. Otani, J. Acoust. Soc. Am., 101, 558 (1997).

4pBBb7. Ultrasonic wave properties in the bone axis direction of bovine cortical bone. Kazufumi Yamamoto (Orthopaedic Surgery, Hamamatsu University School of Medicine, 1-20-1 Handayama Higasi-ku, 431-3192 Hamamatsu, Japan, kazyama2323@hotmail.com), Yuichiro Yaoi (Doshisha University, 1-3, Tatara Miyakodani, 610-0321 Kyotanabe, Japan, yuichiro_y0306@hotmail.co.jp), Yu Yamato (Orthopaedic Surgery, Hamamatsu University School of Medicine, 1-20-1 Handayama Higasi-ku, 431-3192 Hamamatsu, Japan, kazyama2323@hotmail.com), Takahiro Yanagitani (Graduate school of engineering, Tohoku University, 28 Kawauchi Aoba-ku, 980-8579 Sendai, Japan, mmatsuka@mail.doshisha.ac.jp), Takaaki Koizumi (Doshisha University, 1-3, Tatara Miyakodani, 610-0321 Kyotanabe, Japan, mmatsuka@mail.doshisha.ac.jp), Mami Matsukawa (Doshisha University, 1-3, Tatara Miyakodani, 610-0321 Kyotanabe, Japan, mmatsuka@mail.doshisha.ac.jp), Kaoru Yamazaki (Orthopaedic Surgery, Hamamatsu University School of Medicine, 1-20-1 Handayama Higasi-ku, 431-3192 Hamamatsu, Japan, kazyama2323@hotmail.com), Akira Nagano (Orthopaedic Surgery, Hamamatsu University School of Medicine, 1-20-1 Handayama Higasi-ku, 431-3192 Hamamatsu, Japan, kazyama2323@hotmail.com)

Quantitative ultrasound (QUS) is a good method to measure elastic properties of bone (one indicator of bone quality) in vivo. Bovine cortical bone has two typical microstructures, plexiform and Haversian. In the nanoscopic level, bone consists of calcium phosphate, which forms incomplete hydroxyapatite (HAp) crystal. The preferred orientation of c-axis of HAp crystallites induces anisotropy and inhomogeneity of elastic properties in bone. In this study, relationship between speed of sound (SOS) and HAp crystallites orientation in the axial direction were investigated in two foreign age bovine cortical bones. The dependence of attenuation on the anatomical position was also investigated. Two ring shaped cortical bone samples were made from 36 and 24-month-old bovine femur. SOS was measured by a conventional ultrasonic pulse system, using self-made PVDF transducers. The integrated intensity of (0002) peak obtained using X-ray diffraction was estimated to evaluate the amount of preferred orientation. Regardless of age, a significant correlation between SOS and preferred orientation of HAp crystallite was observed in the parts of the plexiform structure, and gradient of the relation showed a similar tendency. Attenuation seemed to strongly depend on bone microstructure because of its porosity.

4pBBb8. Anisotropy of ultrasonic longitudinal wave in the cortical bone of bovine femur. Yuichiro Yaoi (Doshisha University, 1-3, Tatara Miyakodani, 610-0321 Kyotanabe, Japan, yuichiro_y0306@hotmail.co.jp), Kazufumi Yamamoto (Orthopaedic Surgery, Hamamatsu University School of Medicine, 1-20-1 Handayama Higasi-ku, 431-3192 Hamamatsu, Japan, kazyama2323@hotmail.com), Takaaki Koizumi (Doshisha University, 1-3, Tatara Miyakodani, 610-0321 Kyotanabe, Japan, mmatsuka@mail.doshisha.ac.jp), Mami Matsukawa (Doshisha University, 1-3, Tatara Miyakodani, 610-0321 Kyotanabe, Japan, mmatsuka@mail.doshisha.ac.jp), Kaoru Yamazaki (Orthopaedic Surgery, Hamamatsu University School of Medicine, 1-20-1 Handayama Higasi-ku, 431-3192 Hamamatsu, Japan, kazyama2323@hotmail.com), Akira Nagano (Orthopaedic Surgery, Hamamatsu University School of Medicine, 1-20-1 Handayama Higasi-ku, 431-3192 Hamamatsu, Japan, kazyama2323@hotmail.com)

Quantitative ultrasound (QUS) is a good method to measure elastic properties of bone. It is known that the mammalian cortical bone shows strong anisotropy and inhomogeneity. We have investigated the distribution of ultrasonic longitudinal wave properties in bovine femur, considering the structure in the nanoscopic level [Yamato et al. Calcified Tissue International, Accepted]. In this study, the anisotropy in the axial-tangential plane of bovine cortical bone is experimentally investigated using an ultrasonic pulse technique. The ultrasonic pulse measurement was performed using a PVDF focus transmitter (Custom made, Toray) and a self-made flat PVDF receiver. Three ring-shaped cortical bone samples were made from a 32-month-old bovine femur. Four cylindrical specimens were taken from one ring-shaped cortical bone sample along the radial direction. The anisotropy of speed was investigated by rotating the specimens. We found that directivities of ultrasonic longitudinal wave in these specimens were similar. In addition, the direction of the fastest wave speed was a little different from the bone axis. The results indicate the complicated anisotropy of the cortical bone.

4pBBb9. Ultrasonic velocity dispersion in bovine cortical bone. Guillaume Haiat (CNRS, Laboratoire de Recherches Orthopédiques, 10, Avenue de Verdun, 75010 Paris, France, haiat@univ-paris12.fr), Magali Sasso (Echosens, R&D department, 153 avenue d'Italie, 75013 Paris, France, magali.sasso@echosens.com), Salah Naili (Université Paris 12, B2OA, 61, Avenue du Général de Gaulle, 94010 Créteil, France, naili@univ-paris12.fr), Kazufumi Yamamoto (Orthopaedic Surgery, Hamamatsu University School of Medicine, 1-20-1 Handayama Higasi-ku, 431-3192 Hamamatsu, Japan, kazyama2323@hotmail.com), Mami Matsukawa (Doshisha University, 1-3, Tatara Miyakodani, 610-0321 Kyotanabe, Japan, mmatsuka@mail.doshisha.ac.jp)

The evaluation of cortical bone quality has become possible in clinical practice, but the interaction between a broadband ultrasonic pulse and this complex multiscale medium remains poorly understood. Specifically, the frequency dependence of phase velocity has been sparsely investigated. This study aims at evaluating the determinants of the frequency dependence of phase velocity in bovine femoral cortical bone samples using an in vitro ultrasonic transmission device. Phase velocity is shown to vary quasi linearly in a 1 MHz restricted bandwidth around 4 MHz, which enables dispersion evaluation. Axial dispersion is significantly higher than radial and tangential dispersions. Significant differences in dispersion are obtained according to the anatomical location. The microstructure of each sample is determined using an optical microscope, which allows assessing the dependence of dispersion on the type of bone microstructure. Mostly positive, but also negative values of dispersion are measured. Negative dispersion is obtained mostly in samples constituted of mixed microstructure, which may be explained by phase cancellation effects due to the presence of different microstructures within the same sample. Dispersion is shown to be related to broadband ultrasonic attenuation values, especially in the radial direction. This dependence is compared with results derived from the local Kramers-Krönig relationships.

4pBBb10. Diffuse ultrasonic backscatter from cortical bone. Joseph A. Turner (University of Nebraska, Dept. of Engineering Mechanics, W317.4 NH, Lincoln, NE 68588, USA, jaturner@unl.edu), Goutam Ghoshal (University of Nebraska, Dept. of Engineering Mechanics, W317.4 NH, Lincoln, NE 68588, USA, goutamghoshal@rediffmail.com)

Diffuse ultrasonic backscatter techniques have been used primarily for characterization of microstructure in structural materials such as polycrystalline metals. Such measurements exploit the spatial variance of the signals from a modified pulse-echo technique. In this presentation, experiments are discussed using this technique on samples of porcine cortical bone at center frequencies of 15, 20, and 25 MHz. The time domain results obtained are analyzed with respect to a single-scattering model that includes statistical information about the microstructure. In addition, the model includes a rigorous description of the transducer beam pattern as it interacts with the liquid-sample. These results provide information regarding the ability of single-scattering models to capture the ultrasound propagation in such materials.

4pBBb11. Effects of bone marrow on the ultrasonic propagation in the cancellous bone - Comparative study on experiment and simulation. Takashi Saeki (Doshisha University, 1-3, Tatara Miyakodani, 610-0321 Kyotanabe, Japan, dth0915@mail4.doshisha.ac.jp), Masahiro Emura (Doshisha University, 1-3, Tatara Miyakodani, 610-0321 Kyotanabe, Japan, dth0915@mail4.doshisha.ac.jp), Katsunori Mizuno (Doshisha University, 1-3, Tatara Miyakodani, 610-0321 Kyotanabe, Japan, dtg0151@mail4.doshisha.ac.jp), Mami Matsukawa (Doshisha University, 1-3, Tatara Miyakodani, 610-0321 Kyotanabe, Japan, mmatsuka@mail.doshisha.ac.jp), Yoshiki Nagatani (Nara Medical University, 840 Shijo-cho, 634-8522 Kashihara, Japan, naramed-u@nagatani.ne.jp)

Longitudinal ultrasonic wave in cancellous bone separates into fast and slow waves depending on the bone structure. This phenomenon seems useful for the diagnosis of osteoporosis. In this study, we have investigated the influences of soft tissue (bone marrow) in the cancellous bone on the propagation of waves, in order to investigate the mechanism of this phenomenon. First, we have experimentally investigated the temperature dependence of longitudinal wave velocity and attenuation in bovine bone marrow, using a conventional ultrasonic pulse method. We used the ultrasonic wave at 1MHz. Then, we simulated the wave propagation in cancellous bone. For simulation, we used the 3 dimensional elastic FDTD (Finite Difference Time Domain) method. Here, we used the X-ray CT pictures of actual cancellous bone obtained from the head of left bovine femur as the bone model. By changing the velocity and the attenuation values in the soft tissue among trabeculae from those of marrow to the water, we have found the changes in the waveforms of both fast and slow waves. This indicates the changes in both wave properties, due to the properties of soft tissue.

4pBBb12. Measurement of the tortuosity and the viscous characteristic length of human cancellous bone via transmitted waves. Naima Sebaa (Laboratoire d'Acoustique de l'Université du Maine, Avenue Olivier Messiaen, 72085 Le Mans, France, naima.sebaa@univ-lemans.fr), Laurens Boeckx (Lab. ATF, Katholieke Universiteit Leuven, Celestijnenlaan 200D, B-3001 Leuven, Belgium, laurens.boeckx@fys.kuleuven.be), Zine Fellah (CNRS-Laboratoire de Mécanique et d'Acoustique, 31 Chemin Joseph Aiguier, 13402 Marseille, France, fellah@lma.cnrs-mrs.fr), Mouna Naas (Laboratoire d'Acoustique de l'Université du Maine, Avenue Olivier Messiaen, 72085 Le Mans, France, mouna.naas.etu@univ-lemans.fr), Tom L. Goossens (Technische Universiteit Eindhoven, Den Dolech 2, 5600 MB Eindhoven, Netherlands, tomgoos@gmail.com), Steven Boonen (Afdeling Geriatrie, UZ Herestraat, 3000 Leuven, Belgium, Steven.Boonen@med.kuleuven.be), Georges Van Der Perre (Afd. Biomechanica en Grafisch Ontwerpen, Celestijnenlaan 300, 3000 Leuven, Belgium, Georges.VanderPerre@mech.kuleuven.be), Philippe Leclaire (Lab. de Recherche en Mécanique et Acoustique, I.S.A.T - Univ. de Bourgogne, 49, rue Mademoiselle Bourgeois, 58000 Nevers, France, philippe.leclaire@gmail.com), Claude Depollier (Laboratoire d'Acoustique de l'Université du Maine, Avenue Olivier Messiaen, 72085 Le Mans, France, claude.depollier@univ-lemans.fr), Walter Lauriks (Lab. ATF, Katholieke Universiteit Leuven, Celestijnenlaan 200D, B-3001 Leuven, Belgium, Walter.Lauriks@fys.kuleuven.be)

For a few years several authors have proposed the model of Biot to describe the ultrasonic wave propagation in cancellous bone. One drawback of this model is the number of parameters which it needs. Two significant parameters to describe the geometry of the trabeculae are tortuosity and viscous characteristics length. In this communication, we propose two methods to measure these parameters. The first method consists in estimating these two parameters by inversion from the transmission coefficient. In the second method, we get the tortuosity from direct measurement using the focused transducers. The scan of a layer of cancellous bone shows a good correlation between direct measurements and the results of the inversion.

4pBBb13. Simulation of ultrasound wave propagation through trabecular bone samples with and without bone marrow. Liesbet Goossens (Afdeling Biomechanica en Grafisch Ontwerpen, Departement Werktuigkunde, Katholieke Universiteit Leuven, Afd. Biomechanica en Grafisch Ontwerpen, Celestijnenlaan 300, 3000 Leuven, Belgium, liesbet.goossens@mech.kuleuven.be), Jef Vanderoost (K.U.Leuven, Celestijnenlaan 300c, bus 2419, 3001 Heverlee, Belgium, jef.vanderoost@mech.kuleuven.be), Siegfried Jaecques (Department of Dentistry, Oral Pathology and Maxillo-Facial Surgery, BIOMAT Research Cluster, Katholieke Universiteit Leuven, Kapucijnenvoer 7 - bus 7001, 3000 Leuven, Belgium, siegfried.jaecques@med.kuleuven.be), Steven Boonen (Afdeling Geriatrie, UZ Herestraat, 3000 Leuven, Belgium, Steven.Boonen@med.kuleuven.be), Jan D'Hooge (Division of Cardiovascular Imaging and Dynamics, Katholieke Universiteit Leuven, UZ Herestraat 49 - bus 7003, 3000 Leuven, Belgium, jan.dhooge@uz.kuleuven.be), Walter Lauriks (Lab. ATF, Katholieke Universiteit Leuven, Celestijnenlaan 200D, B-3001 Leuven, Belgium, Walter.Lauriks@fys.kuleuven.be), Georges Van Der Perre (Afd. Biomechanica en Grafisch Ontwerpen, Celestijnenlaan 300, 3000 Leuven, Belgium, Georges.VanderPerre@mech.kuleuven.be)

For the clinical assessment of osteoporosis, ultrasound has been proposed as an alternative or supplement to the Dual-Energy X-ray Absorptiometry technique. However the interaction of ultrasound waves with (trabecular) bone remains relatively poorly understood. The aim of the present study was to improve the understanding of this interaction by simulating ultrasound wave propagation in fifteen trabecular bone samples from the human lumbar spine, using μCT based Finite Elements Modelling. The model included only the solid bone, without the bone marrow. Two structural parameters were calculated: the bone volume fraction (BV/TV) and the structural (apparent) elastic modulus (E_s), and the ultrasound parameter Speed Of Sound (SOS). At 1 MHz, correlations between SOS and the parameters BV/TV and E_s were rather weak but the results can be explained from the specific features of the trabecular structure and the intrinsic material elastic modulus E_i. The correlation found between the simulated SOS values and those calculated from the simple bar equation was poor when the three directions are considered separately. However at lower frequencies (50-300 kHz), this correlation significantly improved. Currently we investigate the correlations between SOS and the structural parameters when the bone marrow is included in the FE model.

4pBBb14. Modeling the ultrasonic scattering in trabecular bone. Andrzej Nowicki (Institute of Fundamental Technological Research, Swietokrzyska 21, 00-049 Warsaw, Poland, anowicki@ippt.gov.pl), Jerzy Litniewski (Institute of Fundamental Technological Research, Swietokrzyska 21, 00-049 Warsaw, Poland, jlitn@ippt.gov.pl)

Computer simulations conducted to investigate the properties of the ultrasound pulse-echo signal, as it is received on the transducer surface after scattering in trabecular bone was developed. It can be used to yield an ideal environment in which, the effects of various parameters (scatterer mechanical and geometrical properties, scatterers' concentration), the shape of incident wave and experimental conditions influencing the scattering of ultrasonic waves in trabecular bone structure can be examined individually. The Wear's scattering model of a cancellous bone was applied with modifications that allow for changes of mechanical and geometrical properties of individual trabeculae as well as their spatial density variation. The model also enables considering the groups of scatterers with varying mean values, e.g. thick and thin trabeculae of cancellous bone. Also, the real interrogating pulses are considered, thus the pulse shape, the emitted field structure and the frequency transfer function of the transmitting-receiving transducer are applied in simulations. The results proved that the computer simulation is a useful tool for gaining a better understanding of the scattering of ultrasonic waves in biological tissue and has a particular relevance in studying scattering in cancellous bone which may be approximated as a collection of cylindrical trabeculae.

4pBBb15. Dual frequency ultrasound technique enables determination of soft tissue composition and improves reliability of *in vivo* ultrasound bone densitometry. Janne P. Karjalainen (University of Kuopio, POB 1627, 70211 Kuopio, Finland, janne.karjalainen@uku.fi), Juha Töyräs (Kuopio University Hospital, POB 1777, 70211 Kuopio, Finland, Juha.Toyras@kuh.fi), Toni Rikkonen (University of Kuopio, POB 1627, 70211 Kuopio, Finland, toni.rikkonen@uku.fi), Jukka Jurvelin (University of Kuopio, POB 1627, 70211 Kuopio, Finland, Jukka.Jurvelin@uku.fi), Ossi Riekkinen (University of Kuopio, POB 1627, 70211 Kuopio, Finland, Ossi.Riekkinen@uku.fi)

Soft tissues diminish reliability of the bone ultrasound backscatter measurements. In this study, the ability of a single broadband transducer dual frequency ultrasound (DFUS) technique to monitor the changes in soft tissue was investigated in a body builder during a 21 week training and dieting period, inducing a weight loss of 16.5 kg (18%). Then, DFUS was applied to correct the errors induced by soft tissues on the measurements of integrated reflection coefficient (IRC) in human distal femur. In DFUS, US reflection from soft tissue-bone interface is determined with two different US frequencies and, by knowing the frequency specific US attenuation and speed in adipose and lean tissues, their content can be determined. The dual energy X-ray absorptiometry (DXA) indicated that significant changes in quantity and composition of soft tissue, but not in bone density, took place during the diet. As compared with DXA, the single transducer DFUS could determine local soft tissue composition ($r^2 = 0.88$, $n=8$, $p < 0.01$). The change in uncorrected IRC associated significantly with the change in body composition ($r^2 = 0.56$, $n=8$, $p < 0.05$). The IRC values, corrected by DFUS, showed only minor variation (SD = $\pm$ 1.26 dB) during the diet.

4pBBb16. Simulation and modeling of a new quantitative ultrasound imaging device using cylindrical crossed beam forming arrays. Sylvain Haupert (Université Paris 6, Laboratoire d'Imagerie Paramétrique, 15, rue de l'Ecole de Médecine, 75006 Paris, France, sylvain.haupert@lip.bhdc.jussieu.fr), Djelloul Reguieg (Université Paris 6, Laboratoire d'Imagerie Paramétrique, 15, rue de l'Ecole de Médecine, 75006 Paris, France, reguieg@gmail.com), Frederic Padilla (Université Paris 6, Laboratoire d'Imagerie Paramétrique, 15, rue de l'Ecole de Médecine, 75006 Paris, France, Frederic.Padilla@lip.bhdc.jussieu.fr), Marielle Defontaine (LUSSI, 10 Bd Tonellé, 37032 Tours, France, defontai@med.univ-tours.fr), Pascal Laugier (Université Paris 6, Laboratoire d'Imagerie Paramétrique, 15, rue de l'Ecole de Médecine, 75006 Paris, France, laugier@lip.bhdc.jussieu.fr)

Real-time quantitative ultrasound imaging (QUI) produces images of bone properties with the advantages of being non-ionizing, portable and repeatable. A real-time QUI technique has been proposed, based on two 2-D arrays (24x24 transducer elements) to produce a confocal spherical focusing in transmit and receive modes. However, the electronics to manage beam scanning and focusing is complex and remains expensive. To overcome these disadvantages, a new device has been developed, based on two 1-D transducer arrays (72x1 transducer elements) and confocal cylindrical crossed-beam forming. The intersection of two orthogonal cylindrical focus lines replaces the spherical focused beams. Initial results obtained with this approach showed a distortion and a shift of the spectrum in the low frequency range compared to the reference confocal spherical focusing technique. The aim of the study was to explain the observed differences between spherical and cylindrical focusing techniques using numerical simulations of elementary impulse responses calculated in the confocal and reception planes. The orthogonal configuration of the transmit and receive focusing line results in orthogonal curvatures of the transmitted wavefront and receiving aperture, with summation by the receiving aperture of an out-of-phase wavefront. We show that this effect is the major source for the frequency response artifacts.

4pBBb17. Longitudinal assessment of human bone quality using scanning confocal quantitative ultrasound. Yi-Xian Qin (Stony Brook University, SUNY, Department of Biomedical Engineering, 350 Psychology-A Building, Stony Brook, NY 11794, USA, yi-xian.qin@sunysb.edu), Yi Xia (Stony Brook University, SUNY, Department of Biomedical Engineering, 350 Psychology-A Building, Stony Brook, NY 11794, USA, xia.yi76@gmail.com), Wei Lin (Stony Brook University, SUNY, Department of Biomedical Engineering, 350 Psychology-A Building, Stony Brook, NY 11794, USA, wei.lin@sunysb.edu), Jiqi Cheng (Stony Brook University, SUNY, Department of Biomedical Engineering, 350 Psychology-A Building, Stony Brook, NY 11794, USA, chengjiqi@yahoo.com), Jesse Muir (Stony Brook University, SUNY, Department of Biomedical Engineering, 350 Psychology-A Building, Stony Brook, NY 11794, USA, jmuir@ic.sunysb.edu), Clint Rubin (Stony Brook University, SUNY, Department of Biomedical Engineering, 350 Psychology-A Building, Stony Brook, NY 11794, USA, crubin@sunysb.edu)

Microgravity and aging induced bone loss is a critical skeleton complication occurred particularly in the weight-supporting skeleton, which leads to osteoporosis and fracture. Advents in quantitative ultrasound (QUS) provide a unique method for evaluating both bone strength and density. Using an imaging-base confocal scanning ultrasound diagnostic system (SCAD), the goals of this work were to non-invasively characterize bone quality at proximal femur, and longitudinally monitor effectives of calcaneus bone loss in a 90-day bedrest. QUS scanning was performed at proximal femur (cadaver) and calcaneus (bedrest subjects) regions with QUS images of 80x80 mm^2 for hip and 40x40 mm^2 for calcaneus. QUS was processed to calculate the ultrasound attenuation (ATT; dB), wave ultrasound velocity (UV), and the broadband ultrasound attenuation (BUA; dB/MHz). Human cadaver proximal femurs have been measured with the SCAD, micro-CT, DXA, and mechanical strength test. Human calcaneus of bedrest subjects were measured using SCAD and DXA in day 0 (baseline), day 60 and day 90. Results demonstrated that QUS measurement has the capability to predict bone BMD, microstructure and mechanical properties in human bone, and indicated significant sensitivity to the progressive change of bone quality, particularly in the trabecular bone region with remodeling activities.

Session 4pBBc

Biomedical Ultrasound/Bioresponse to Vibration: Theoretical and Computational Models of Ultrasonic Propagation in Bones II (Poster Session)

James Miller, Cochair
Washington University

Pascal Laugier, Cochair
Université Paris 6

All posters will be on display from 3:40 p.m. to 5:20 p.m. To allow contributors an opportunity to see other posters, contributors of odd-numbered papers will be at their posters from 3:40 p.m. to 4:30 p.m. and contributors of even-numbered papers will be at their posters from 4:30 p.m. to 5:20 p.m.

Contributed Papers

4pBBc1. Investigation of effect of trabecular microstructure on ultrasound propagation through cancellous bone using finite-difference time-domain simulations. Atsushi Hosokawa (Akashi National College of Technology, 679-3 Nishioka, Uozumi, 674-8501 Akashi, Japan, hosokawa@akashi.ac.jp)

Using finite-difference time-domain (FDTD) numerical simulations, it was investigated how the trabecular microstructure could affect the propagation of ultrasound waves through cancellous bone. Three-dimensional (3D) numerical models of cancellous bone were reconstructed from 3D micro-computed tomography images of bovine femoral bone with oriented trabecular structure. In these models, the trabecular elements were eroded to increase porosity using an image processing technique. Three erosion procedures were given to realize different changes in the trabecular microstructure with increasing porosity. FDTD simulations of the ultrasound pulse waves propagating through the cancellous bone models were performed in two cases of the propagations parallel and perpendicular to the main trabecular orientation, and the porosity dependences of the propagation properties, attenuation and propagation speed, were derived for various trabecular changes. It was demonstrated from the simulated results that the propagation properties in both directions parallel and perpendicular to the trabecular orientation could be affected by the trabecular microstructure. In addition, the effects of the major (or plate-like) and minor (or rod-like) trabecular elements on the ultrasound propagation were respectively investigated for both the parallel and perpendicular propagations.

4pBBc2. Excess ultrasonic attenuation due to inhomogeneities in porous media. Mouna Naas (Laboratoire d'Acoustique de l'Université du Maine, Avenue Olivier Messiaen, 72085 Le Mans, France, mouna.naas.etu@univ-lemans.fr), Naima Sebaa (Laboratoire d'Acoustique de l'Université du Maine, Avenue Olivier Messiaen, 72085 Le Mans, France, naima.sebaa@univ-lemans.fr), Zine Fellah (CNRS-Laboratoire de Mécanique et d'Acoustique, 31 Chemin Joseph Aiguier, 13402 Marseille, France, fellah@lma.cnrs-mrs.fr), Mohamed Fellah (Laboratoire de Physique Théorique, Institut de Physique, USTHB, BP, 16111 Alger, Algeria, fellah1@yahoo.com), Walter Lauriks (Lab. ATF, Katholieke Universiteit Leuven, Celestijnenlaan 200D, B-3001 Leuven, Belgium, Walter.Lauriks@fys.kuleuven.be), Claude Depollier (Laboratoire d'Acoustique de l'Université du Maine, Avenue Olivier Messiaen, 72085 Le Mans, France, claude.depollier@univ-lemans.fr)

While Biot's theory seems well adapted to model the acoustical waves propagation in cancellous bone, some of its predictions do not agree with the experimental results. The excess of attenuation of the fast wave is one of these discrepancies. In this paper we propose a modified Biot's model which takes into account the fluctuations of the physical parameters and their correlations. As a result of this model, we show that this excess of attenuation is due to several processes: i) classical Biot's attenuation, ii) scattering leading to the extension of the wave path, iii) mode conversion. Some comparison between experimental results and numerical simulations are proposed.

4pBBc3. Relationship between QUS parameters and a cellular model-based estimation of bone strength. Guillaume Haiat (CNRS, Laboratoire de Recherches Orthopédiques, 10, Avenue de Verdun, 75010 Paris, France, haiat@univ-paris12.fr), Frederic Padilla (Université Paris 6, Laboratoire d'Imagerie Paramétrique, 15, rue de l'Ecole de Médecine, 75006 Paris, France, Frederic.Padilla@lip.bhdc.jussieu.fr), Pascal Laugier (Université Paris 6, Laboratoire d'Imagerie Paramétrique, 15, rue de l'Ecole de Médecine, 75006 Paris, France, laugier@lip.bhdc.jussieu.fr)

The final goal of quantitative ultrasound (QUS) techniques is to assess bone strength. However, the translation of QUS results into bone strength remains elusive because the physical principles of ultrasonic propagation in bone are not fully understood yet. Here, the sensitivity of Broadband Ultrasonic Attenuation and Speed of Sound to variations of bone strength is derived. Therefore, a cellular model is combined to a multiple regression analysis resulting from the analysis of finite-difference time domain (FDTD) simulations coupled with imaging techniques. The variation of QUS variables induced by a variation of strength of 10%, realized either by a change in material properties or a change in bone volume fraction (BV/TV) is investigated. Except when BV/TV is high, the variations of BUA in response to a variation in strength realized by a pure change of BV/TV is higher than the technique imprecision and thus can be detected. When the variation of strength is realized by changes of elastic properties, the response in QUS properties is dominated by the variation in C11 over C44. The interpretation of these data, however, is not straightforward due to sparse description of elastic properties at the tissue level, which is a limitation of the cellular model.

4pBBc4. Bulk waves velocities are dependent on frequency in cortical bone. Cécile Baron (Université Paris 6, Laboratoire d'Imagerie Paramétrique, 15, rue de l'Ecole de Médecine, 75006 Paris, France, norabelic@yahoo.fr), Quentin Grimal (Université Paris 6, Laboratoire d'Imagerie Paramétrique, 15, rue de l'Ecole de Médecine, 75006 Paris, France, quentin.grimal@lip.bhdc.jussieu.fr), Maryline Talmant (Université

Paris 6, Laboratoire d'Imagerie Paramétrique, 15, rue de l'Ecole de Médecine, 75006 Paris, France, talmant@lip.bhdc.jussieu.fr), Pascal Laugier (Université Paris 6, Laboratoire d'Imagerie Paramétrique, 15, rue de l'Ecole de Médecine, 75006 Paris, France, laugier@lip.bhdc.jussieu.fr)

Any model of ultrasound propagation in cortical bone requires the knowledge of the effective elastic properties of bone at, let's say, the mm scale. It is well known that the porous network of cortical bone interacts with ultrasonic waves and plays a major role in the mechanical behaviour. The purpose of the present work is to emphasize that, in cortical bone, there is some variation of the effective bulk wave velocities, and consequently of the elastic properties, with frequency in the MHz range due to the effect of the porous network. A Finite Difference Time Domain (FDTD) code is used to simulate the ultrasonic propagation of compression and shear waves, transverse to, and along the bone axis, in cortical bone volumes reconstructed from micro-computed tomography (microCT). The resolution of the microCT data allowed to model the 3D networks of resorption cavities and Haversian pores. It is found that, for porosities typically above 5-6 %, the effective phase velocity is dependent on the frequency. Preliminary results indicate that the influence of the frequency is more important in the range 1-5 MHz.

Session 4pBBd

Biomedical Ultrasound/Bioresponse to Vibration and Physical Acoustics: Light and Sound for Medical Imaging and Therapy II (Poster Session)

Ronald Roy, Cochair
Boston University

Emmanuel Bossy, Cochair
Laboratoire Photons et Matière, ESPCI/CNRS

All posters will be on display from 3:40 p.m. to 5:20 p.m. To allow contributors an opportunity to see other posters, contributors of odd-numbered papers will be at their posters from 3:40 p.m. to 4:30 p.m. and contributors of even-numbered papers will be at their posters from 4:30 p.m. to 5:20 p.m.

Contributed Papers

4pBBd1. Selective ultrasonic focusing towards an optical contrast agent by use of photoacoustic-guided time-reversal. Arik R. Funke (Laboratoire Photons et Matière, ESPCI/CNRS, 10 rue Vauquelin, 75231 Paris Cedex 05, France, arik.funke@espci.fr), Emmanuel Bossy (Laboratoire Photons et Matière, ESPCI/CNRS, 10 rue Vauquelin, 75231 Paris Cedex 05, France, emmanuel.bossy@espci.fr), Jean-François Aubry (Laboratoire Ondes et Acoustique, ESPCI, Université Paris 7, CNRS, 10 rue Vauquelin, 75005 Paris, France, jean-francois.aubry@espci.fr), Mathias Fink (Laboratoire Ondes et Acoustique, ESPCI, Université Paris 7, CNRS, 10 rue Vauquelin, 75005 Paris, France, mathias.fink@espci.fr), Albert-Claude Boccara (Laboratoire Photons et Matière, ESPCI/CNRS, 10 rue Vauquelin, 75231 Paris Cedex 05, France, boccara@optique.espci.fr)

We recently demonstrated experimentally that optically absorbing regions embedded at centimetric depths in an optically diffusive medium can be used, through the photoacoustic effect, as ultrasound sources for time-reversal techniques [Bossy *et al.*, APL **89**(18), 2006]. If the optically absorbing region is spatially localized, the emission of the time-reversed photoacoustic waves provides a method to automatically focus ultrasound towards the absorbing region. In biological tissue, this approach has the potential to automatically guide high-intensity focused ultrasound (HIFU) beams towards a targeted region labelled with an optically absorbing contrast agent. However, such an approach is conceivable only if the HIFU beam is guided towards the sole targeted region, and not towards other potentially strong endogenous optical absorbers (such as blood vessels). In this work, we present a method to selectively focus time-reversed photoacoustic waves towards an exogenous wavelength-dependent optical contrast agent. Experiments were performed *in vitro* on tissue-mimicking phantoms, with nanoparticles as contrast agents. A tunable nanosecond pulsed laser was used with different optical wavelengths to generate photoacoustic waves. A multichannel time-reversal ultrasound system was used to emit ultrasound signals derived from time-reversed photoacoustic signals obtained with different optical wavelengths.

4pBBd2. Point spread function of the limited-view array transducers in optoacoustic tomography: numerical and experimental studies. Ivan Pelivanov (International Laser Center of Moscow State University, Vorob'yovy Gory, 1, 119992 Moscow, Russian Federation, pelivanov@ilc.edu.ru), Tatiana Khokhlova (International Laser Center of Moscow State University, Vorob'yovy Gory, 1, 119992 Moscow, Russian Federation, t_khokhlova@ilc.edu.ru), Varvara Simonova (International Laser Center of Moscow State University, Vorob'yovy Gory, 1, 119992 Moscow, Russian Federation, simvar@mail.ru), Alexei Podolsky (International Laser Center of Moscow State University, Vorob'yovy Gory, 1, 119992 Moscow, Russian Federation, uzh@yandex.ru), Alexander Karabutov (Moscow State University, MSU, 1, building 2, GSP-2, Leninskiye Gory, 119992 Moscow, Russian Federation, akarabutov@gmail.com)

Optoacoustic (OA) tomography utilizes pulsed laser radiation for thermoelastic excitation of wideband ultrasonic pulses. The distribution of laser-induced heat release can be reconstructed if the ultrasonic pulses are detected by an array of transducers. The resolution provided by an array depends on various aspects of its design - the number of elements, element size, spacing and arrangement - and is determined by the point spread function (PSF) of the array. In present work PSFs of arrays with different characteristics are calculated using the Rayleigh integral for simulating the direct problem, and backprojection algorithm for solving the inverse problem of OA tomography. Universal dependencies of the resolution provided by an array on the dimensions and arrangement of its elements are found. Numerical studies are validated by experimental measurements of PSFs of different arrays.

4pBBd3. A combined platform for b-mode and real-time optoacoustic imaging based on raw data acquisition. Marc Fournelle (Fraunhofer IBMT, Ensheimer Strasse 48, 66386 Sankt Ingbert, Germany, marc.fournelle@ibmt.fhg.de), Kirsten Maass (Fraunhofer IBMT, Ensheimerstrasse 48, 66386 Sankt Ingbert, Germany, kirsten.maass@ibmt.fhg.de), Heinrich Fonfara (Fraunhofer IBMT, Ensheimerstrasse 48, 66386 Sankt Ingbert, Germany, heinrich.fonfara@ibmt.fhg.de), Hans-Joachim Welsch (Fraunhofer IBMT, Ensheimerstrasse 48, 66386 Sankt Ingbert, Germany, hansjoachim.welsch@ibmt.fhg.de), Holger J. Hewener (Fraunhofer IBMT, Ensheimer Strasse 48, 66386 Sankt Ingbert, Germany, holger.hewener@ibmt.fraunhofer.de), Christian Günther (Fraunhofer IBMT, Ensheimerstrasse 48, 66386 Sankt Ingbert, Germany, christian.guenther@ibmt.fhg.de), Robert M. Lemor (Fraunhofer IBMT, Ensheimer Strasse 48, 66386 Sankt Ingbert, Germany, robert.lemor@ibmt.fhg.de)

Optoacoustic imaging is a new promising medical imaging modality combining the benefits of optical and acoustical methods. Optoacoustics allow to make the high intrinsic optical contrast in biological tissue accessible to acoustical detection. In addition, the possibility of using nanoscaled contrast agents makes of optoacoustics an ideal candidate for molecular imaging. While optoacoustics are an emerging imaging modality with poor clinical experience, ultrasound is widely used for diagnosis. Accordingly, optoacoustic images are much harder to interpret than b-mode images. For this reason, we developed a hardware platform which allows combined b-mode and optoacoustic imaging using a 2-in-1 transducer with arrays of different frequency for the two modalities. The system supports simultaneous data acquisition of 128 channels with a sample rate of 80 MSamples allowing the usage of transducers with frequencies up to 20 MHz. The unprocessed data is transferred to a PC where the images are reconstructed with algorithms adapted to both modalities. A software for hardware control, data processing and visualization in real-time was developed. B-mode and optoacoustic images of tissue phantoms were generated and different types of nanoparticles were used as optoacoustic contrast agent. Further, first invivo measurements underlying the high potentials of the combined system were obtained.

4pBBd4. A maximum likelihood method for obtaining integrated attenuation from ultrasound transmission mode measurements. Rene G. Willemink (University of Twente, Signals and Systems Group (SaS), Faculty of Electrical Engineering, Mathematics and Computer Sciences (EWI), P.O. Box 217, 7500AE Enschede, Netherlands, G.H.Willemink@utwente.nl), Srirang Manohar (University of Twente, Biophysical Engineering Group (BPE), Faculty of Science and Engineering (TNW), P.O. Box 217, 7500 AE Enschede, Netherlands, s.manohar@tnw.utwente.nl), Kees H. Slump (Univ. of Twente, P.O. Box 217, 7500 AE Enschede, Netherlands, c.h.slump@utwente.nl), Ferdi Van Der Heijden (Univ. of Twente, P.O. Box 217, 7500 AE Enschede, Netherlands, f.vanderheijden@utwente.nl), Ton G. Van Leeuwen (Univ. of Twente, P.O. Box 217, 7500 AE Enschede, Netherlands, a.g.j.m.vanleeuwen@tnw.utwente.nl)

In photoacoustic imaging applications an image is reconstructed of the optical absorption distribution the imaged object. The photoacoustic measurements however are also dependent on acoustic properties of the imaged object. By estimating the acoustic properties from photoacoustic measurements, we can improve the performance of the optical absorption reconstruction and allow for the imaging of separate acoustic modalities. We derive and evaluate a maximum likelihood estimator for the measurements of integrated acoustic attenuation. This estimator is applicable to media like soft tissue. In this kind of media, the attenuation due to dissipative effects obeys a frequency power law. By measuring the propagation of ultrasound signals through such a medium, the parameters that describe the attenuation can be estimated. In this paper a new method is introduced for estimating the attenuation of ultrasound media by means of transmission mode measurements. The method is based on analyzing the noise characteristics of the received signals and the formulation of a maximum likelihood estimator. The new estimator is compared to existing methods and was found to be a better estimator in terms of the RMS error than previous methods.

THURSDAY AFTERNOON, 3 JULY 2008 ROOM 353, 2:00 TO 7:40 P.M.

Session 4pEAa

Engineering Acoustics: Transducers I

Robert M. Koch, Chair
NUWC, 1176 Howell Street, Code 8232, Bldg. 1302, Newport, RI 02841-1708, USA

Contributed Papers

2:00

4pEAa1. Analytical modeling of piezoelectric ceramic transducers based on coupled vibration analysis. Boris Aronov (UMassD, 22 Seabeds Way, apt. 12, Needham, MA 02494, USA, baronov@comcast.net)

The energy method for analyzing piezoelelctric ceramic transducers [B. S. Aronov, JASA, 117(1), 210-220.] is applied to the treatment of transducers with mechanical systems that can be cobsidered as two-dimensional. Analysis is made following the general outline of the theory of coupled vibration in two degree-of-freedom systems and its extention to calculating the resonance frequencies of elastic bodies, as suggested by Gibbe and Blechshmidt [Ann. Physik, Ser. 5, 18, No. 5, 417-485 (1933)]. The approach to the problem is illustrated with examples of piezoelectric rectangular plates, stripes and thin-walled cylinders at various orientations relative to crystallographic coordinate system. For all of the examples the resonance frquencies and effective coupling coefficients are presented as functions of the dimensional aspect ratios. Equivalent electromechanical circuits are introduced that permit calculation of the transducers performance under different loading conditions. Practical recommendations for improving the electromechanical properties of the transducers by use of appropriate aspect ratios are discussed.

2:20

4pEAa2. Resonance frequencies of the multilayered piezotransducers. Francisco J. Arnold (CESET - Unicamp, R. Paschoal Marmo, 1888 - JD. Nova Italia, 13484332 Limeira, Brazil, arnold@ceset.unicamp.br)

Piezoelectric transducers used in high power ultrasonic applications are composed of piezoelectric ceramics, metallic blocks and a central bolt that pre-stresses the assembly. The impedance characterization of these transducers has been done by using numerical methods but, in many cases, one-dimensional simplified models are enough to a good physical interpretation of the problem. In this work was used the Mason's equivalent electric circuit for one-dimensional modeling of composed transducers. It was derived Thevénin's equivalent circuit to simplify the problem and evaluate the ef-

fects of the central bolt on the resonances. Some transducers were mounted and the transmission line circuit was used to measure the resonance frequencies. The results show a good fitting between the experimental and simulated by electric circuit. By using the presented model it was identify other longitudinal vibration modes further that considered in previous models and, so that, it was increased the possibility of investigate the behavior of the transducers using the frequency spectrum.

2:40

4pEAa3. Integrated transducers for marine animal tags using thick film PZT. Rasmus Lou-Møller (Ferroperm Piezoceramics A/S, Hejreskovvej 18A, 3490 Kvistgaard, Denmark, rm@ferroperm.net), Erling Ringgaard (Ferroperm Piezoceramics A/S, Hejreskovvej 18A, 3490 Kvistgaard, Denmark, er@ferroperm.net), Tomasz Zawada (Ferroperm Piezoceramics A/S, Hejreskovvej 18A, 3490 Kvistgaard, Denmark, tz@ferroperm-piezo.com), Sigmar Gudbjoernsson (Star-Oddi, Vatnagardar 14, 104 Raykjavik, Iceland, sigmar@star-oddi.com), Haraldur Hilmarsson (Star-Oddi, Vatnagardar 14, 104 Raykjavik, Iceland, sigmar @star-oddi.com)

The technology of printing PZT ceramic layers onto curved substrates using pad printing is demonstrated by the application of a transmitter/receiver system printed on alumina cylinders. The cylinder is used as housing for a Data Storage Tag (DST) for marine animals. DST's are used for monitoring behaviour and lifecycle of animals, providing valuable knowledge for marine biologists and researchers. Electrodes and PZT ceramic is printed directly onto the alumina housing using the pad printing technique, which eliminates the need for complex assembly procedures and other post processing steps. Since the PZT is situated on the external surface of the housing, direct contact between the acoustic elements and the marine animal is ensured and the elements do not take up valuable space inside the tag. The manufacturing of the active elements and the technology of pad printing PZT thick film is presented. The piezoelectric properties of the film and the acoustic properties have been tested under laboratory conditions. According to the obtained results one can conclude that the transmitter/receiver system was able to assure sufficient sensitivity in the required distance keeping the power consumption on an extremely low level. Second generation devices will be ready for commercialisation in the near future.

3:00

4pEAa4. High-Output and High-Fidelity Microsized Driver System. Keehoon Kim (Physical Optics Corporation, 20600 Gramercy Pl #103, Torrance, CA 90501, USA, kkim@poc.com), Tao Xu (Physical Optics Corporation, 20600 Gramercy Pl #103, Torrance, CA 90501, USA, txu@poc.com),Reginald Daniels(Air Force Research Laboratory, 2610 Seventh St. Bldg 441, Wright Patterson AFB, OH 45433, USA, Reginald .Daniels@WPAFB.AF.MIL)

Active noise reduction (ANR) for aircrew hearing protection in harsh noise environments such as military and civilian flight operations requires a high-performance, microsized driver that provides not only high acoustic power, at least 130 dB SPL, but also high fidelity sound quality, especially in low-frequency ranges below 100 Hz. A new microsized smart material actuator (MSMA) is being developed by using high-density and direct-conversion piezoelectric exciters combined with a unique acoustic structure, unlike conventional moving coil/magnet-type drivers. The dimensions of the MSMA are 6 mm in diameter by 7 mm long, small enough for ear-canal application as an earplug driver, maximizing ANR effectiveness. The MSMA system consists of a microscale earplug driver, a protective package made of medical-grade stainless steel, and a compact actuation amplifier easily connected to or embedded in an external ANR controller. Performance tests show the system produces over 130 dB SPL in a 1 cc trapped cylindrical volume with very flat frequency responses even below 100 Hz. The total harmonic distortion of the MSMA is lower than 4% over all audible frequency ranges, without phase delay or discontinuities.

3:20

4pEAa5. MEMS-based magnetic and electrostatic acoustic microspeakers. Michael Pedersen (Novusonic Corporation, P.O. Box 183, Ashton, MD 20861, USA, info@novusonic.com)

Acoustic microspeakers remains a challenging application area for MEMS technology. This is mostly due to the inherently low transduction factors normally achievable in MEMS technology. While established electromagnetic transduction principles may be adapted for MEMS technology, there are also other transduction methods, such as electrostatic, with high performance potential. In this paper, the design, fabrication, and testing of two different types of MEMS microspeakers is presented. Firstly, an electromagnetic microspeaker is shown consisting of a MEMS diaphragm with integrated moving and an external rare earth permanent magnet and yoke structure. Secondly, a novel MEMS electrostatic microspeaker based on rolling contact is presented. In this device, high transduction forces are achieved by the strong electrical field over a solid insulator, and the forces are translated to a MEMS diaphragm by an integrated cantilever structure. Measurements on the electromagnetic microspeakers show a sensitivity of 83 dB SPL/mW at 1 kHz in a B&K 4153 acoustic coupler. The resonance frequency of the 6mm diameter diaphragm was 3.2 kHz. Numerical simulations suggest that simple changes to the moving coil geometry and material may increase the sensitivity to 108 dB SPL/mW.

3:40-5:20 Posters

Lecture sessions will recess for presentation of poster papers on various topics in acoustics. See poster sessions for topics and abstracts.

Contributed Papers

5:20

4pEAa6. Sound pressure estimation at an electroacoustic transducer's voicing face by way of all-electrical sensing. Florian Sandoz (Ecole Polytechnique Fédérale de Lausanne, EPFL STI LEMA, Station 11, CH 1015 Lausanne, Switzerland, florian.sandoz@epfl.ch), Hervé Lissek (Ecole Polytechnique Fédérale de Lausanne, EPFL STI LEMA, Station 11, CH 1015 Lausanne, Switzerland, herve.lissek@epfl.ch)

When it comes to designing active control disposals, sound pressure sensing is usually required. In the framework of active control of acoustic impedance, this work aims at conceiving a digital estimator that processes voltage and current measurement to compute an estimation of the pressure in the vicinity of the diaphragm of an electro-dynamic speaker. After dealing with modeling concerns of the actuator, the bilinear transform is used to obtain equations of two IIR filters. An adaptive identification using the LMS algorithm and a SVD-based identification are tested to compute filters coefficient, both leading to poor experimental results. Accordingly, the actual transfer functions of the speaker are measured and optimal IIR filters are designed using the simulated annealing algorithm. It is then shown that good results can be achieved experimentally when the speaker is loaded electrically by a short circuit or an open circuit. Finally, performances of the process are discussed regarding other operating conditions.

5:40

4pEAa7. Virtual Prototyping of Electrodynamic Loudspeakers by Utilizing a Finite Element Method. Reinhard Lerch (Univ. Erlangen-Nuremberg, Dept. of Sensor Technology, Paul-Gordan-Str. 3/5, 91052 Erlangen, Germany, reinhard.lerch@lse.eei.uni-erlangen.de), Manfred Kaltenbacher (Univ. Erlangen-Nuremberg, Dept. of Sensor Technology, Paul-Gordan-Str. 3/5, 91052 Erlangen, Germany, manfred.kaltenbacher @lse.eei.uni-erlangen.de), Martin Meiler (Simetris GmbH, Am Weichselgarten 7, 91058 Erlangen, Germany, martin.meiler@simetris.de)

To speed up the development of electrodynamic loudspeakers, computer tools have to be applied. With appropriate computer simulations, the costly and lengthy fabrication of prototypes, as required within conventional experimental design, can be reduced tremendously. Present computer modeling tools are mainly based on equivalent circuit representations. The main drawback of these models, however, stems from the fact that the circuit element parameters have to be measured on a prototype, first. Therefore, the need for appropriate numerical simulation tools based on finite element method (FEM) arises, since as input parameters they suffice with geometrical and material data. However, present finite element tools suffer from their incompleteness in respect to full field couplings and nonlinear features. In this paper, a new finite element scheme is introduced and its utilization within the computer-aided design of electrodynamic loudspeakers is demonstrated. This scheme allows the precise and efficient calculation of the electromagnetic, mechanical and acoustic fields, including their couplings. Furthermore, nonlinear effects in the mechanical behavior of the spider as well as magnetic nonlinearities due to the nonhomogeneity of the magnetic field are taken into account.

6:00

4pEAa8. Tactile Touch Plate with Variable Boundary Conditions. Ros Kiri Ing (Laboratoire Ondes et Acoustique, ESPCI, Université Paris 7, CNRS, 10 rue Vauquelin, 75005 Paris, France, ros-kiri.ing@espci .fr), Didier Cassereau (Laboratoire Ondes et Acoustique, 10, rue Vauquelin, 75231 Paris, France, didier.cassereau@espci.fr), Mathias Fink (Laboratoire Ondes et Acoustique, ESPCI, Université Paris 7, CNRS, 10 rue Vauquelin, 75005 Paris, France, mathias.fink@espci.fr), Jean-Pierre Nikolovski (Laboratoire Ondes et Acoustique, ESPCI, Université Paris 7, CNRS, 10 rue Vauquelin, 75005 Paris, France, jean-pierre.nikolovski@cea .fr)

The touch screen device is becoming more and more widespread because it is a very user friendly human/machine interface. In acoustic domains, several approaches are used to realize such a device. Triangulation or Rayleigh waves absorption are such classical methods. However, these approaches are limited because they need a large number of sensors and are only applicable to plates of constant thickness and homogeneous materials. To remedy these limitations, a new approach is proposed using only two sensors. In this approach, one sensor is used to excite the plate, either continuously or impulsively. The second sensor is used to detect the acoustic waves generated in the plate. When an object comes into contact with the plate, some acoustic wave characteristics change. These changes affect different frequencies and depend on the position of the contact point. Comparing these changes with pre-recorded values, it is possible to achieve a tactile touch plate that only responds to specific touch locations. Several experiments with different types of plates were conducted and the results will be presented.

6:20

4pEAa9. Personal sound system design for mobile phone, monitor, and television set: cylindrical shape approach. Ji-Ho Chang (Center for Noise and Vibration Control, Korea Advanced Institute of Science and Technology, Dep. of Mechanical Engineering, Guseong-dong, Yuseong-gu, 305-701 Daejon, Republic of Korea, chang.jiho@gmail.com), Jin-Young Park (Center for Noise and Vibration Control, Korea Advanced Institute of Science and Technology, Dep. of Mechanical Engineering, Guseong-dong, Yuseong-gu, 305-701 Daejon, Republic of Korea, jypark1979 @kaist.ac.kr), Yang-Hann Kim (Center for Noise and Vibration Control, Korea Advanced Institute of Science and Technology, 4114, Department of Mechanical Engineering, Guseong-dong, Yuseong-gu, 305-701 Daejon, Republic of Korea, yanghannkim@kaist.ac.kr)

Personal sound system that focuses sound on the user and reduces in the other zone has great interest in these days because it has significant needs to be applied in personal devices such as mobile phone, monitor, and television set. We have shown the feasibility of the personal sound system using a line array of loudspeaker units [C.-H. Lee et. al., J. Acoust. Soc. Am., 122, 3053 (2007)] based on acoustic contrast control [J.-W. Choi, Y.-H. Kim, J. Acoust. Soc. Am. 111, 1695(2002)], with the successful result of about 20dB difference between the front and the side region for 800-5kHz range. Continuing this research, we try to apply acoustic contrast control in cylindrical shape instead of two-dimensional planar shape that was used before in order to reduce the level of side lobes more. That is, acoustically bright zone and dark zone are determined as cylindrical shape surrounding the array of loudspeakers. Computer simulation and experimental result will be addressed and evaluated by comparing to the previous result. (This work was supported by the Korea Science and Engineering Foundation(KOSEF) through the National Research Lab. Program funded by the Ministry of Science and Technology(M10500000112-05J0000-11210).)

6:40

4pEAa10. Efficient Directivity Pattern Control for Spherical Loudspeaker Arrays. Franz Zotter (Institute of Electronic Music and Acoustics, Inffeldgasse 10 / 3, 8010 Graz, Austria, zotter@iem.at), Hannes Pomberger (Institute of Electronic Music and Acoustics, Inffeldgasse 10 / 3, 8010 Graz, Austria, pom@sbox.tugraz.at), Andrew Schmeder (Center for New Music and Audio Technologies, 1750 Arch Street, Berkeley, CA 94720, USA, andy@cnmat.berkeley.edu)

With an appropriate control system, directivity pattern synthesis can be accomplished with spherical loudspeaker arrays, e.g. in the shape of Platonic solids or spheres. The application of such devices for the reproduction of natural or artificial directivity patterns poses a relatively young field of research in computer music and acoustic measurements. Using directivity measurements with microphones, the directivity patterns of the individual speakers on the array can be determined. Usually, the directivity of the whole array may be regarded as a linear combination of these patterns. In order to gain control, the measurement data of the linear system need to be inverted. Given L loudspeakers and M microphones, this inversion yields the desired control system, an expensive LxM multiple-input-multiple-output (MIMO) filter. We introduce discrete spherical harmonics transform and decoder matrices to reduce the number of channels required for this control system, thus reducing the computational effort. However, this step often leads to a sparse MIMO-system, in which many off-diagonal transfer functions vanish. If applicable, the computation of the non-zero transfer functions only can be done at even much lower cost. A case study for an icosahedral loudspeaker array is given, showing the properties of the sparse MIMO-system.

7:00

4pEAa11. Effects of enclosure design on the directivity synthesis by spherical loudspeaker arrays. Alexander Mattioli Pasqual (Universidade Estadual de Campinas, Rua Mendeleiev, 200, Cidade Universitária ″Zeferino Vaz″, 13083-970 Campinas, Brazil, pasqual@fem.unicamp.br), José Roberto Arruda (Universidade Estadual de Campinas, Rua Mendeleiev, 200, Cidade Universitária ″Zeferino Vaz″, 13083-970 Campinas, Brazil, arruda@fem.unicamp.br), Philippe Herzog (Laboratoire de Mécanique et d'Acoustique - CNRS, 31 chemin Joseph Aiguier, 13402 Marseille, France, herzog@lma.cnrs-mrs.fr)

Spherical loudspeaker arrays have been used to generate non-uniform directivity patterns. It is known that the poor radiation efficiency of spherical sources and the loudspeaker electroacoustic behavior impose constraints on the directivity synthesis at low frequencies, which are aggravated as the source volume is made smaller. In this work, the effects of the enclosure design on the loudspeaker signal powers are analyzed. Two different approaches have been reported in literature, although quantitative comparisons

have not been provided. In the first approach, the drivers share the same enclosure volume and in the second, they have their own independent sealed cavities. Here, an analytical model that takes into account the interior and exterior acoustic coupling is used in order to evaluate the voltages that must feed the array drivers. It is shown that the signal powers can be reduced at low frequencies by letting the drivers share the same enclosure volume. However, this leads to controllability problems, since some natural frequencies of the enclosure are in the operation range of the spherical array. If controllability at natural frequencies is neglected, a simple lumped parameter model of the enclosure presents good agreement with the continuous model, indicating that heavy calculations may be unnecessary.

7:20

4pEAa12. Relative calibration and characterization of 1/4″ condenser microphones under different environmental conditions. Cécile Guianvarc'H (Institut National de Métrologie (LNE-INM/Cnam), 61 rue du Landy, 93210 La Plaine Saint Denis, France, cecile.guianvarch@cnam.fr) , Paolo Alberto Giuliano Albo (Istituto Nazionale di Ricerca Metrologica (INRiM), Strada delle Cacce, 91, 10135 Torino, Italy, albo@inrim .it), Roberto Gavioso (Istituto Nazionale di Ricerca Metrologica (INRiM), Strada delle Cacce, 91, 10135 Torino, Italy, r.gavioso@inrim.it), Giuliana Benedetto (Istituto Nazionale di Ricerca Metrologica (INRiM), Strada delle Cacce, 91, 10135 Torino, Italy, gbenedet@inrim.it), Laurent Pitre (Institut National de Métrologie (LNE-INM/Cnam), 61 rue du Landy, 93210 La Plaine Saint Denis, France, pitre@cnam.fr), Arnaud Guillou (Institut National de Métrologie (LNE-INM/Cnam), 61 rue du Landy, 93210 La Plaine Saint Denis, France, guillou.arnaud@gmail.com),Michel Bruneau (Laboratoire d'Acoustique de l'Université du Maine, Avenue Olivier Messiaen, 72085 Le Mans, France, michel.bruneau@univ-lemans.fr), Anne-Marie Bruneau (Laboratoire d'Acoustique de l'Université du Maine (LAUM, UMR CNRS 6613), Avenue Olivier Messiaen, 72085 Le Mans, France, anne-marie.bruneau@univ-lemans.fr)

Measurement condenser microphones are commonly used in air at ambient temperature and pressure. However, several applications require to use such microphones in environments which are significantly different. In particular, for the determination of the Boltzmann constant by an acoustic method, measurements take place in a cavity filled with pure argon or helium over a wide pressure range at the temperature of the triple point of water. For this application, it is important to determine the microphone frequency response and acoustic input impedance with a low uncertainty in these gas conditions. A few previous works have examined the influence of static pressure, temperature and gas composition on microphone sensitivity. In one case, these results were supported by a theoretical investigation using a lumped-element model. The aim of the present work is to compare theoretical results from different lumped-element models with experimental relative calibration results obtained using an electrostatic actuator technique. Measurements are performed on 1/4″ condenser microphones maintained in argon and helium environments, at 273.16 K, in the pressure range between 50 kPa and 700 kPa. The results are used to test the existing theoretical models and to compare the microphone properties with the manufacturer's data.

THURSDAY AFTERNOON, 3 JULY 2008 ROOM 342B, 2:20 TO 3:40 P.M.

Session 4pEAb

Engineering Acoustics, Underwater Acoustics, Acoustical Oceanography, and ECUA: Acoustics in Marine Archeology

Kenneth Walsh, Cochair
K & M Engineering LTD, 51 Bayberry Lane, Middletown, Rhode Island 02842, USA

Tuncay Akal, Cochair
SUASIS: Underwater Systems Technology Development, Tubitak-Marmara Research Center, Tech. D. Free Zone, Block A - L4, Gebze, Kocaeli, 41470, Turkey

Invited Papers

2:20

4pEAb1. Green's theorem as the foundation of interferometry. Adriana Citlali Ramírez (WesternGeco, 10001 Richmond Ave, Houston, TX 77042, USA, aperez50@slb.com), Arthur B. Weglein (University of Houston, Physics Department, 617 S&R Bldg1, Houston, TX 77204-5005, USA, aweglein@uh.edu)

A prerequisite for applying full wavefield theory to marine exploration is the completeness and proper sampling of recorded data, which can be satisfied with data extrapolation/interpolation techniques. Green's theorem can be applied to acoustic measurements of the Earth's subsurface to obtain exact equations that incorporate boundary conditions for the retrieval of the Earth's Green's function in positions where it was not measured. Recently, a number of papers on seismic interferometry have shown methods to reconstruct the Green's function between a pair of receivers by using data cross correlations. Current interferometry methods require dual measurements (pressure field and its normal derivative) which are not always available. The lack of dual measurements has encouraged the arrival of algorithms using high frequency and one-way wave approximations to the normal field derivative. The approximations are compromises to the exact theory and, hence, produce artifacts. We present a unifying framework for a broad class of interferometry techniques using Green's theorem. This framework and foundation allows errors and artifacts to be anticipated and fully explained as a consequence of approximations made within Green's theorem. We also develop a set of more effective interferometry methods, where fewer (or none) approximations are made and the result is improved.

2:40

4pEAb2. Surveillance and Protection of Underwater Archaeological Sites: Sea-Guard. Tuncay Akal (SUASIS: Underwater Systems Technology Development, Tubitak-Marmara Research Center, Tech. D. Free Zone, Block A - L4, Gebze, 41470 Kocaeli, Turkey, tuakal@yahoo.com), Piero Guerrini (NURC Nato Undersea Research Centre, Viale San Bartolomeo 400, 19026 La Spezia, Italy, guerrini@nurc.nato.int), William A. Kuperman (MPL, Scripps Institution of Oceanography, University of California, San Diego, La Jolla, CA 92093-0238, USA, wkuperman@ucsd.edu), Kerem Koprulu (SUASIS: Underwater Systems Technology Development, Tubitak-Marmara Research Center, Tech. D. Free Zone, Block A - L4, Gebze, 41470 Kocaeli, Turkey, keremkpr@yahoo.com), Philippe Roux (LGIT - CNRS - Université Joseph Fourier, Maison des Géosciences, 1381 rue de la Piscine, BP 53, 38041 Grenoble, France, philippe.roux@obs.ujf-grenoble.fr), Karim G. Sabra (Georgia Institute of Technology, School of Mechanical Engineering, 771 Ferst Drive, NW, Atlanta, GA 30332-0405, USA, karim.sabra@me.gatech.edu)

Recent advances in underwater detection and survey techniques have increased the possibility of finding the wrecks of vessels and their cargoes. Since prehistoric times, many populations have used vessels for transportation and trade and built harbors and it is now estimated that there are about a million antique wrecks that lie underwater, still to be discovered. Many of these wrecks and ancient harbours lie within shallow depths and can be discovered and accessed easily by humans using available hardware such as side-scan sonars, multi-beam echo sounders, ROVs, GPS navigation, diving gear. Even though the majority of known archaeological sites on land are well protected by guards and high tech equipment, there is no technology for surveillance and protection of underwater archeology sites. This paper presents a new system specifically adapted for the surveillance and protection of underwater archaeological sites (SEA-GUARD). Options available to the acoustic sensor suite of this system are pressure hydrophones and/or vector sensors. The system is based on an underwater acoustic monitoring of the noise field near an archaeological site sending preprocessed signals as an alarm to the authorities on shore via GSM/GPRS or Satellite network.

Contributed Paper

3:00

4pEAb3. Acoustic methods in extremely shallow water for reconstruction of ancient environments. Fantina Madricardo (CNR-Istituto di Scienze Marine, Riva Sette Martiri - Castello 1364/a, 30122 Venice, Italy, fantina.madricardo@ismar.cnr.it), Sandra Donnici (CNR-Istituto di Scienze Marine, Riva Sette Martiri - Castello 1364/a, 30122 Venice, Italy, sandra.donnici@ismar.cnr.it), Alberto Lezziero (PHAROS sas, Via della Libertà 12, 30175 Venice, Italy, alezziero@gmail.com), Federica De Carli (CNR-Istituto di Acustica 'O,M .Corbino', Via del Fosso del Cavaliere, 100, 00133 Rome, Italy, federica .decarli@gmail.com)

A large area of the Venice Lagoon was surveyed through a modified traditional echosounder. For the first time, acoustic methods together with geological analysis were used systematically to investigate natural and anthropogenic morphologies buried in the lagoonal sediments. The shallowness (with depths often < 1m) of the Venice Lagoon represents a challenge for underwater acoustic methods. The results we present in this paper show that such methods are very useful for detailed geomorphological and archaeological reconstruction and can be extended to other similar environments. In this context, a general methodology of multidisciplinary data collection was developed. As a synthesis of our acoustic and geoarchaeological investigation, maps of the ancient lagoonal environment were produced.

Invited Paper

3:20

4pEAb4. Precision positioning for deep-water archaeology. Brian Bingham (Franklin W. Olin College of Engineering, 1000 Olin Way, MH 368, Needham, MA 02492, USA, bbing@olin.edu)

Underwater archaeology makes use a variety of tools for deep-water exploration, but the defining characteristic of archaeology, what distinguishes the endeavor as scientific in purpose, is the quantifiable techniques employed for precision navigation. Precise positioning enables the collocation of archaeological results into a common reference frame, creating a persistent data products with the spatial context to enable interpretation. With this common context, data products such as site-maps, micro-bathymetric maps and photomosaics afford the capability to perform measurements with known accuracy and resolution, a key differentiator of the science of archaeology. Acoustic ranging is the meter stick of marine archeology. Archaeology has leveraged standard navigation techniques: long baseline (LBL) positioning, ultra-short baseline (USBL) tracking, Doppler velocity log (DVL) dead-reckoning, etc. However, the extreme precision required for archaeology has driven the development of new precise ranging instruments. This paper presents the capabilities and limitations of today's precision ranging instruments which use discrete sequence spread spectrum (DSSS) signal processing to provide the requisite performance. In addition to a technical discussion, the paper presents the results of recent field work in the Aegean, the Mediterranean and the East Coast of the Unites States.

Session 4pEAc

Engineering Acoustics: Ultrasonic Acoustic MEMS II (Poster Session)

F. Levent Degertekin, Cochair
Georgia Institute of Technology

Dominique Certon, Cochair
Lab. LUSSI Inserm U930 CNRS FRE 2448 Univ. François Rabelais

All posters will be on display from 3:40 p.m. to 5:20 p.m. To allow contributors an opportunity to see other posters, contributors of odd-numbered papers will be at their posters from 3:40 p.m. to 4:30 p.m. and contributors of even-numbered papers will be at their posters from 4:30 p.m. to 5:20 p.m.

Contributed Papers

4pEAc1. A surface acoustic wave impedance loaded sensor for wireless humidity measurement. Rung-De Wang (Institute of Applied Mechanics, National Taiwan University, No. 1, Sec. 4, Roosevelt Road, 106 Taipei, Taiwan, r94543020@ntu.edu.tw), Yung-Yu Chen (Department of Mechanical Engineering, Tatung University, No. 40, Sec. 3, Chungshan N. Rd., 104 Taipei, Taiwan, yychen@ttu.edu.tw), Tsung-Tsong Wu (Institute of Applied Mechanics, National Taiwan University, No. 1, Sec. 4, Roosevelt Road, 106 Taipei, Taiwan, wutt@ndt.iam.ntu.edu.tw)

The control of humidity is required in various areas such as the smart living space, industry, agriculture, and medicine. To reduce cost and increase lifetime, a wireless humidity sensor without an additional power supply should be developed to fulfill their needs. Recently, there are more and more efforts on surface acoustic wave (SAW) based radio frequency identification (RFID) system. The RFID system primarily consists of a reader and transponders, composed of SAW tags and antennas. Due to the capabilities of passive operation and wireless connection, SAW tags are also suitable for remote sensing. Therefore, in this study, a wireless humidity sensor is accomplished by integrating a 433MHz 128°YX-LiNbO3 SAW tag with a resistive humidity sensor. The SAW tag is designed as an impedance loaded sensor. Moreover, because nanostructure sensing materials possess high surface-to-volume ratio, large penetration depth, and fast charge diffusion rate, CSA-doped polyaniline nanofibers are synthesized by the interfacial polymerization method and further deposited on the resistive humidity sensor as sensitive film to enhance the sensitivity. Finally, the humidity sensor was constructed and measured. Results indicate that our proposed sensor exhibits not only good linearity but also high sensitivity. Furthermore, it is indeed capable of passive remote sensing.

4pEAc2. Periodically poled transduction structures built on thinned single crystal Lithium Niobate layers bonded onto Silicon. Emilie Courjon (CNRS FEMTO-ST, 32 Avenue de l'Observatoire, 25044 Besançon, France, emilie.courjon@femto-st.fr), Gwenn Ulliac (CNRS FEMTO-ST, 32 Avenue de l'Observatoire, 25044 Besançon, France, gwenn.ulliac@femto-st.fr), Jérôme Hauden (Photline Technologies, 16 rue Jouchoux, 25000 Besançon, France, jerome.hauden@photline.com), Sylvain Ballandras (CNRS FEMTO-ST, 32 Avenue de l'Observatoire, 25044 Besançon, France, sylvain.ballandras@femto-st.fr)

The demand for highly coupled high quality acoustic wave devices has generated a strong innovative activity, yielding the investigation of new excitation principles and wave guide structures. In a recent work, we have investigated the interest of periodically poled transducers (PPTs) on single crystal $LiNbO_3$ Z-cut plates. The PPT simply consists of a periodically poled ferroelectrics layer metallized on its two faces for acoutoelectric excitation. In this work, we have fabricated PPTs on single crystal $LiNbO_3$ Z-cut thinned layers reported on Silicon to develop a new kind of wave guide. Their fabrication is based on a home-made wafer bonding technique based on a metal-metal adhesion, the lithium niobate being lapped and polished in order to obtain a layer exhibiting a few tenth micrometer thick. The corresponding devices have successfully fabricated and tested in the frequency range 100-300 MHz. Comparison between experimental measurements and theoretical analysis (using a combination of finite and boundary element analysis) show that the modes are well controlled and that different kind of wave polarization may be excited.

4pEAc3. Acoustical properties characterization of a composite made of SU-8 and nanoparticules for BioMEMS application. Julien Carlier (IEMN - DOAE, Université de Valenciennes, Le Mont - Houy, 59313 Valenciennes, France, julien.carlier@univ-valenciennes.fr), Pierre Campistron (IEMN - DOAE, Université de Valenciennes, Le Mont - Houy, 59313 Valenciennes, France, pierre.campistron@univ-valenciennes.fr), Dorothée Callens (IEMN - DOAE, Université de Valenciennes, Le Mont - Houy, 59313 Valenciennes, France, dorothee.callens@univ-valenciennes.fr), Caroline Soyer (IEMN - DOAE, Université de Valenciennes, Le Mont - Houy, 59313 Valenciennes, France, caroline.soyer@univ-valenciennes.fr), Bertrand Nongaillard (IEMN - DOAE, Université de Valenciennes, Le Mont - Houy, 59313 Valenciennes, France, Bertrand.Nongaillard@univ-valenciennes.fr), Shengxiang Wang (IEMN - DOAE, Université de Valenciennes, Le Mont - Houy, 59313 Valenciennes, France, shx_wang@126.com), Xingzhong Zhao (Department of Physics, Wuhan University, 430072 Wuhan, China, xzzhao@whu.edu.cn)

The photoresist SU-8 (often used in microtechnology) has been acoustically characterized at the frequency of 1 GHz thanks to ZnO transducers. This material will be used to achieve acoustical matching between silicon and water at this frequency and a gain of about 5 dB has been obtained using the combination of this material with a silicon oxyde layer. The acoustical characterization of a composite material made of this photoresist SU-8 doped with nanoparticules (TiO_2 for example) is also presented. The aim is to achieve matching layers with specific mechanical impedance around 5 MRay and depending on the nanoparticules concentration. The targeted application concerns the integration of high frequency ultrasonic transducer in Lab-on-Chip for biological cell characterization, especially adhesion properties or biological cells mechanical behaviour. The mechanical impedance and the attenuation of this composite material are characterized around 1 GHz thanks to a standing wave ratio method measuring S11 parameter and extracting the targeted parameters thanks to signal processing.

4pEAc4. High Overtone Bulk Acoustic Resonators Based on Thinned Single-crystal Piezoelectric Layers: Filters and Frequency Sources Applications. Dorian Gachon (CNRS FEMTO-ST, 32 Avenue de l'Observatoire, 25044 Besançon, France, dorian.gachon@femto-st.fr), Jeremy Masson (CNRS FEMTO-ST, 32 Avenue de l'Observatoire, 25044 Besançon, France, jeremy.masson@femto-st.fr), Emilie Courjon (CNRS FEMTO-ST, 32 Avenue de l'Observatoire, 25044 Besançon, France, emilie.courjon@femto-st.fr), Sylvain Ballandras (CNRS FEMTO-ST, 32 Avenue de l'Observatoire, 25044 Besançon, France, sylvain.ballandras@femto-st.fr)

The thin film bulk acoustic wave resonators exploiting the thickness-extensional vibration mode of piezoelectric thin films is a key technology as alternative solutions to standard SAW resonators. Lakin have emphasized the capability of High Overtone Bulk Acoustic Resonators to present high quality factors at frequencies in the GHz range. HBAR spring from the conjugation of the strong coupling coefficient of deposited piezoelectric thin films and of the high intrinsic quality of used substrates. The piezoelectric film and the two electrodes on its both sides are used as transducer whereas the acoustic energy is mainly trapped in the substrate. The resonant frequency corresponds to a half wavelength in the entire thickness of the device and, in opposition to FBAR, we can utilized both odd and even harmonics. The fundamental, generally in the vicinity of 10 MHz, has no specific interest but Q.f products around 1.1×10^{14} have already been obtained for high overtones using aluminum nitride thin films deposited onto sapphire. In view of improving the Q factor of thin films, it is desirable to use a single-crystal piezoelectric material such as lithium niobate. We show and compare the fabrication in both approaches. Different measurement results are exposed for both approaches for the fabrication of oscillator and filters are shown and discussed.

4pEAc5. Micromachined probe performance assessment. Mathieu Legros (Vermon SA, 180 rue Général Renault, 37000 Tours, France, m.legros@vermon.com), Cyril Meynier (Vermon SA, 180 rue Général Renault, 37000 Tours, France, c.meynier@vermon.com), Guillaume Ferin (Vermon SA, 180 rue Général Renault, 37000 Tours, France, g.ferin@vermon.com), Rémi Dufait (Vermon SA, 180 rue Général Renault, 37000 Tours, France, r.duvait@vermon.com)

In recent years, Capacitive Micromachined Ultrasound Transducer (CMUT) technology was widely investigated and functional prototypes have been released by several R&D teams. CMUT technology offers outstanding characteristics in acoustic, interconnect packaging capabilities or in integration features that are exciting criteria for new medical applications. We propose a full acoustic characterization report of a CMUT probe. A linear array was fully packaged with electronic preamplifier boards integrated. A complete acoustic characterization of the probe is then performed and presented. In a second phase, a linear probe with piezocomposite technology is realized. The conception is done in regard to the geometric characteristics and to the acoustic response of the micromachined probe. Then an electro-acoustical benchmark CMUT / piezocomposite is realized in the closest conditions. Using a commercial ultrasound imaging platform, an image assessment is performed. The images are first analysed in a quantitative way with a tissue mimicking phantom, using a computerized tool who considered imaging parameters such as contrast, resolution or signal to noise ratio. In a second way, a clinical perspective is discussed with in vivo images.

4pEAc6. CMUT membrane model based on theory of stratified plates. Nicolas Senegond (Lab. LUSSI Inserm U930 CNRS FRE 2448 Univ. François Rabelais, 10, Boulevard Tonnellé, 37032 Tours, France, nicolas.senegond@univ-tours.fr), Franck Teston (Lab. LUSSI Inserm U930 CNRS FRE 2448 Univ. François Rabelais, 10, Boulevard Tonnellé, 37032 Tours, France, franck.teston@univ-tours.fr), Cyril Meynier (Vermon SA, 180 rue Général Renault, 37000 Tours, France, c.meynier@vermon.com), Dominique Certon (Lab. LUSSI Inserm U930 CNRS FRE 2448 Univ. François Rabelais, 10, Boulevard Tonnellé, 37032 Tours, France, dominique.certon@univ-tours.fr)

To optimize and characterize capacitive micromachined transducers, static and dynamic mechanical behavior of the membrane have to be considered and modeled. Most of cMUT models are based on the classical plate equation. The flexural rigidity is homogenized for multi-layer structure taking into account properties of each material. Homogenization relations are available provided the flexural plate equation can be separated from the in-plane deformation equation, so-called the membrane-like behavior equation. Practically, for membrane partially covered with electrode, at the metallized/non-metallized discontinuity, these equations cannot be solved separately and homogenization procedure is no more available. Moreover, initial membrane deflection introduces supplementary coupling between in-plane and flexural displacements requiring modification of homogenization relations. A complete analytical formulation of the plate equation is developed in this paper. A finite difference meshing has been used to numerically solve the new set of plate equations. First, a cMUT with simple geometry is modeled for validation and comparison with Finite Element simulation (COMSOL Multiphysics software). Then, the validity domain of the ″simple″ flexural plate equation is discussed. Finally, an example of membrane optimization is given, where a multi-layer structure is proposed to reduce influence of static pre-stresses in the membrane on collapse voltage and resonance frequency.

4pEAc7. Pure-shear mode BAW resonators consisting of (11-20)textured ZnO films. Takahiko Yanagitani (Faculty of Engineering Tohoku University, 6-6-05 Aramaki Aoba Aoba-ku, 610-0321 Kyotanabe, Japan, yanagi@ecei.tohoku.ac.jp), Kiuchi Masato (National Institute of Advanced Industrial Science and Technology, 1-8-31 Midorigaoka, Osaka, 563-8577 Ikeda, Japan, yanagitani@usl.doshisha.ac.jp), Mami Matsukawa (Doshisha University, 1-3, Tatara Miyakodani, 610-0321 Kyotanabe, Japan, mmatsuka@mail.doshisha.ac.jp), Yoshiaki Watanabe (Faculty of Engineering, Doshisha Univ., 1-3 Miyakodani Tatara, 610-0321 Kyotanabe, Japan, kwatanab@mail.doshisha.ac.jp)

Thickness pure-shear mode film bulk acoustic wave resonators (FBARs) made of (11-20) textured ZnO films have been fabricated. We have also fabricated FBAR structure consisting of two layers of the (11-20) textured ZnO film with opposite polarization directions. This FBAR structure operated in second overtone pure-shear mode, and allowed shear-mode FBARs at higher frequency. The effective electromechanical coupling coefficients k_{eff}^2 of pure-shear mode FBAR and second overtone pure-shear mode FBAR in this study were found to be 3.3% and 0.8%, respectively. The temperature coefficient of frequency (TCF) of thickness extensional mode FBAR, pure-shear mode FBAR, and second overtone pure-shear mode FBAR were measured in the temperature range of 10-60 °C. TCF values of -63.1 ppm/°C, -34.7 ppm/°C, and -35.6 ppm/°C were found for the thickness extensional mode FBAR, the pure-shear mode FBAR, and the second overtone pure-shear mode FBAR, respectively. These results demonstrated that pure-shear mode ZnO FBARs have more stable temperature characteristics than the conventional thickness extensional mode ZnO FBARs.

4pEAc8. Influence of the shape of the membrane of computed cMUT using FEA/BEM analysis. Stanislas Clatot (CNRS FEMTO-ST, 32 Avenue de l'Observatoire, 25044 Besançon, France, stanislas.clatot@femto-st.fr), Emeline Sadoulet (CNRS FEMTO-ST, 32 Avenue de l'Observatoire, 25044 Besançon, France, emeline.sadoulet-reboul@univ-fcomte.fr), Olivia Arbey (CNRS FEMTO-ST, 32 Avenue de l'Observatoire, 25044 Besançon, France, olivia.arbey@femto-st.fr), William Daniau (CNRS FEMTO-ST, 32 Avenue de l'Observatoire, 25044 Besançon, France, william.daniau@femto-st.fr), Julien Garcia (CNRS FEMTO-ST, 32 Avenue de l'Observatoire, 25044 Besançon, France, julien.garcia@femto-st.fr), Joseph Lardies (FEMTO-ST Applied Mechanics, 24 chemin de l'épitaphe, 25000 Besançon, France, joseph.lardies@univ-fcomte.fr), Sylvain Ballandras (CNRS FEMTO-ST, 32 Avenue de l'Observatoire, 25044 Besançon, France, sylvain.ballandras@femto-st.fr), Marc Berthillier (University of Franche-Comté, Institute FEMTO - LMARC, 24 rue de l'Epitaphe, 25000 Besançon, France, marc.berthillier@univ-fcomte.fr)

The possibility to excite and detect acoustic waves in fluids using capacitive micro-machined ultrasonic transducers (cMUT) built on silicon using clean room techniques offers attractive opportunities for manufacturing high quality low cost imaging probes. CMUTs developed for acoustic imaging exploit the first flexural mode of thin and stiff membranes, leading to

bandwidth larger than 100%. These transducers can be accurately designed using mixed finite element analysis/boundary element methods (FEA/BEM). Periodic FEA particularly allows for the simulation of devices exhibiting complicated shape interfaces and involving materials of different nature. BEM also are particularly well-suited to provide an accurate description of any stacked medium assuming flat interfaces for the radiation area and the layer interface for 2 and 3D structures as well. In this work, we have analysed the influence of the shape of the MUT membrane on the spectral response of the transducer. 3D Computations have been conducted considering radiation coniditions in the substrate on the backside (silicon) and in viscous water on the front side. we have particularly focused the computation on solutions allowing for reducing parasitic modes in the actual operation of the transducer. The efficiency of the different configuration are compared in termes of emitted pressure contributions.

THURSDAY AFTERNOON, 3 JULY 2008 P3-C, LEVEL 3, 3:40 TO 5:20 P.M.

Session 4pEAd

Engineering Acoustics and Signal Processing in Acoustics: Transducers and Signal Processing for the Oil and Gas Industry II (Poster Session)

Fernando Garcìa-Osuna, Cochair
Schlumberger

Benoit Froelich, Cochair
Etudes et Productions Schlumberger

All posters will be on display from 3:40 p.m. to 5:20 p.m. To allow contributors an opportunity to see other posters, contributors of odd-numbered papers will be at their posters from 3:40 p.m. to 4:30 p.m. and contributors of even-numbered papers will be at their posters from 4:30 p.m. to 5:20 p.m.

Contributed Papers

4pEAd1. Multimode evaluation of cement behind steel pipe. Benoit Froelich (Etudes et Productions Schlumberger, 1, rue Becquerel, BP 202, 92142 Clamart, France, bfroelich@clamart.oilfield.slb.com)

Oil wells are usually cased with a steel pipe, and cement is injected in the annulus between pipe and rock in order to provide hydraulic isolation of the reservoir. The traditional ultrasonic technique to evaluate cement behind steel pipe has been to excite the pipe thickness mode, and to extract the acoustic impedance of the material from the pulse-echo response. However, this technique suffers from some limitations, such as a limited depth of investigation or a poor discrimination between mud and light cement. To alleviate such limitations, the thickness mode can be combined with the pipe flexural mode. Although dispersive, the flexural mode has the unique property of a quasi constant group velocity in a specific frequency domain which is high enough to provide azimuthal resolution. Such property provides the means for an accurate measurement of the time of arrival and the amplitude of the different echoes generated by a particular geometry. In particular, the echo traveling within the annulus and reflected by the rock can be easily detected from within the pipe, and provide novel information on the annulus fill.

4pEAd2. Data fusion technique applied to steam wastage estimation and fault detection in an industrial process heating application. Sivaram Nishal Ramadas (Institute of Sound and Vibration Research, University of Southampton, University Road, Highfield, S017 1BJ Southampton, UK, nishal@ieee.org)

Data fusion, the process of combining information obtained together from many heterogeneous sensors to form a single composite picture of the environment, is used widely in many applications. Modern steam heating systems consist of mechanical devices known as 'traps', which are robust and reliable but inevitably over time can wear and fail, with the possibility of leaking steam. To diagnose such faulty steam traps and the level of leakage under operating conditions in a closed system is difficult. This paper presents the preliminary work carried out to integrate together data recorded from commercial sensors (such as piezoelectric acoustic emission devices, pressure transmitters, and thermocouples) to estimate steam wastage and fault detection in a steam system. Experimental data were acquired from a purpose built steam wastage test rig (built similar to the method outlined in the British Standard for determination of steam loss from traps), capable of simulating varying condensate loads by injecting preheated water into a steam test line. The captured composite data is then used to develop a signal processing algorithm to diagnose effective trap operation and quantify the rate of steam loss in the system and the results are discussed.

Session 4pEAe

Engineering Acoustics: Transducers II (Poster Session)

Robert M. Koch, Chair
NOWC

All posters will be on display from 3:40 p.m. to 5:20 p.m. To allow contributors an opportunity to see other posters, contributors of odd-numbered papers will be at their posters from 3:40 p.m. to 4:30 p.m. and contributors of even-numbered papers will be at their posters from 4:30 p.m. to 5:20 p.m.

Contributed Papers

4pEAe1. Condenser microphone as parametric electroacoustic system and its time-domain modelling via equivalent electrical circuit in SPICE software. Michal Vlk (Czech Technical University, Faculty of Electrical Engineering, Department of Radioengineering, Technická 2, 166 27 Praha 6 - Dejvice, Czech Republic, vlkm3@fel.cvut.cz)

Condenser microphone usually works with constant polarisation voltage. Where special attentions are prescribed for spectrum of self noise there may be useful to use high frequency voltage (pump) applied to transducer instead of DC charge. When frequency of pump is orders of higher than frequency of acoustic signals, large parametric gain occurs in the transducer. Method for describing such a system via equivalent electric network with approach of electronic filter design blocks was developped and special analogies were used for convergency improvement. Method was applied to time-domain simulation of pressure transducer with current-mode diode discriminator in SPICE computer analysis software. Simulations of transient behavior after switching system on was demonstrated.

4pEAe2. Modelling of radiofrequency MEMS bulk acoustic wave resonators with Legendre polynomial method. Antoine A. Raherison (IEMN - DOAE, Université de Valenciennes, Le Mont - Houy, 59313 Valenciennes, France, raherson_antoine@yahoo.fr), Faniry Emilson F. Ratolojanahary (LAPAUF, Universite de Fianarantsoa, 301 Fianarantsoa, Madagascar, faniry@univ-fianar.mg), Jean-Etienne J. Lefebvre (IEMN - DOAE, Université de Valenciennes, Le Mont - Houy, 59313 Valenciennes, France, jean-etienne.lefebvre@univ-valenciennes.fr), Lahoucine L. Elmaimouni (Faculte polydisciplinaire d'Ouarzazate, Universite Ibn Zohr, BP 638, Ouarzazate, Morocco, la_elmaimouni@yahoo.fr), Tadeusz T. Gryba (IEMN - DOAE, Université de Valenciennes, Le Mont - Houy, 59313 Valenciennes, France, tadeusz.gryba@univ-valenciennes.fr)

Radio-Frequency electro-acoustic resonators and filters are key components for wireless communication devices. The next generation of mobile systems requires for these components a strict size reduction, higher operating frequency and better power resistance. So, MEMS BAW (Bulk Acoustic Wave) devices have emerged as an efficient alternative to established Surface Acoustic Wave filtering solutions. Knowledge of the electromechanical coupling coefficient and the Q-factor are of primary importance for the MEMS BAW device design. In our model, the Legendre polynomial method which describes the structure and incorporates automatically the boundary conditions in constitutive and propagation equations is used to calculate these parameters. It is the first time this method is applied to study standing rather than propagative waves. The advantage of this approach are, in a unique formulation, to take into account the presence of sources, existence of electrodes' losses and dissimilarity of the constituent materials of the resonator. To validate this approach, it is applied to a Al/ZnO/Al resonator. Through harmonic and modal analysis, the influence of electrodes properties on MEMS BAW resonator performances are illustrated; the results are compared with those published earlier. This method is an efficient tool for designing MEMS BAW filter.

4pEAe3. Design of dispersive layered SAW filters with CMOS low noise amplifier. Tadeusz T. Gryba (IEMN - DOAE, Université de Valenciennes, Le Mont - Houy, 59313 Valenciennes, France, tadeusz.gryba@univ-valenciennes.fr), Julien Carlier (IEMN - DOAE, Université de Valenciennes, Le Mont - Houy, 59313 Valenciennes, France, julien.carlier@univ-valenciennes.fr), Etienne Ntagwirumugara (IEMN - DOAE, Université de Valenciennes, Le Mont - Houy, 59313 Valenciennes, France, entagwir@yahoo.fr), Victor Y. Zhang (IEMN-CNRS, Av. Poincare, Cite Scientifique, B.P. 60069, 59652 Villeneuve d'Ascq Cedex, France, victor.zhang@iemn.univ-lille1.fr), Jean-Etienne J. Lefebvre (IEMN - DOAE, Université de Valenciennes, Le Mont - Houy, 59313 Valenciennes, France, jean-etienne.lefebvre@univ-valenciennes.fr)

Up to now, RF front-end surface acoustic wave (SAW) filters for mobile communication are mainly fabricated on $LiNbO_3$ and $LiTaO_3$ substrates. A monolithic integration of these filters on Si substrates is highly desirable, but Si is non piezoelectric. One alternative is the deposition of a piezoelectric film on the semiconductor substrate. CMOS technology is very attractive for integrating the radio frequency modules in a single chip. This paper presents the analysis and realisation of a SAW passband filter on silicon substrate based on a piezoelectric ZnO thin film working near 1 GHz , integrated with a CMOS low-noise amplifier. We propose a modified coupling of modes (COM) approach for a layered ZnO/Si surface acoustic wave filter. The COM parameters in this formulation are the Rayleigh wave velocity, the electromechanical coupling coefficient, the complex reflection coefficient, the transduction coefficient and the inter-digital capacitance C. This is a dispersive SAW layered filter some parameters of which become frequency dependent due to the phase velocity dispersion. We present the theoretical and experimental results of the filter integrated with a CMOS low noise amplifier.

4pEAe4. A stepped plate transducer as ultrasonic range sensor. Yub Je (Postech, San 31, Hyoja-Dong, Namgu, 790-784 Pohang, Republic of Korea, effortjy@postech.ac.kr), Jong-Kyu Park (Postech, San 31, Hyoja-Dong, Namgu, 790-784 Pohang, Republic of Korea, chong@postech.ac.kr) , Dong Hoon Yi (Postech, San 31, Hyoja-Dong, Namgu, 790-784 Pohang, Republic of Korea, effortjy@hotmail.com), Haksue Lee (Postech, San 31, Hyoja-Dong, Namgu, 790-784 Pohang, Republic of Korea, jolary@postech.ac.kr), Wonkyu Moon (Postech, San 31, Hyoja-Dong, Namgu, 790-784 Pohang, Republic of Korea, wkmoon@postech.ac.kr)

A new type of highly directional ultrasonic transducer is designed and tested as an ultrasonic range sensor by using the parametric acoustic arrays. To get intensive primary waves, a modified stepped plate transducer is proposed. Gallego-juarez et al.(1978) first proposed stepped plate transducer for high power radiation at one frequency. The steps with the height of half-

wavelength of sound in air compensate discrete phase difference on the vibrating plate. However, two collimated beams are required for the parametric acoustic array. The position and height of the steps are modified to compensate the flexural vibration for two frequencies in this transducer. The transducer diameter is 50mm. The optimal primary frequencies are designed as 80kHz and 120kHz to generate difference frequency of 40kHz efficiently. The proposed transducer has the HPBW of 5° that is much higher directivity than general ultrasonic range sensor(Generally 20° on same size). The maximum SPL is 130dB at primary frequencies and 95dB at difference frequency on 75Vpk input. These experimental results show that the proposed transducer can successfully improve the spatial resolution of ultrasonic sensor. [Research is partly supported by MIC/IITA Intelligent Robot Sensor and partly supported by DAPA and ADD UD070054AD]

4pEAe5. A study on the adaptive design of loudspeaker driver parameters for a given enclosure. Seokjin Lee (Applied Acoustics Lab., INMC, 132-302, Seoul National University, San 56-1, Sillim-dong, Kwanak-gu, 151-742 Seoul, Republic of Korea, sjlee@acoustics.snu.ac.kr), Junguk Noh (Applied Acoustics Lab., INMC, 132-302, Seoul National University, San 56-1, Sillim-dong, Kwanak-gu, 151-742 Seoul, Republic of Korea, junoh37@acoustics.snu.ac.kr), Koeng-Mo Sung (Applied Acoustics Lab., INMC, 132-302, Seoul National University, San 56-1, Sillim-dong, Kwanak-gu, 151-742 Seoul, Republic of Korea, kmsung@snu.ac.kr)

In the conventional methods of electro-dynamic loudspeaker design, driver units are selected first and then the enclosures are designed for the best compensation of frequency responses of the given drivers. However, in the industry of nowadays, these conventional methods are not appropriate; the enclosure design is determined first, and after that, a proper driver unit is selected by trial and error. In this paper, an adaptive design method of loudspeaker driver parameters for a given enclosure is studied. We estimated loudspeaker parameters such as diaphragm size, acoustic compliance, acoustic resistance, etc., to obtain an optimal alignment or desired response curve for a given enclosure. In the proposed method, the target frequency response curve in low-frequency range is determined first. Second, the optimal size of driver is calculated. The other driver parameters, such as driver suspension, Q of driver, etc., are designed lastly. Easier and faster design can be achieved by the proposed design method of electro-dynamic loudspeakers.

4pEAe6. Consideration on design of the sensitivity in piezoelectric vibratory tactile sensor. Subaru Kudo (School of Science and Engineering, Ishinomaki Senshu University, 1 Shinmito, Minamisakai, 986-8580 Ishinomaki-city, Miyagi, Japan, kudou@isenshu-u.ac.jp)

The piezoelectric vibratory tactile sensors have been used for measuring the softness and hardness of an object. They make use of changes in the resonance frequency when their vibrating sections are brought into contact with an object. In this study, the sensitivity of the frequency change on the tactile sensors is experimentally considered. The longitudinal-bar-type and the fixed-free-bar type resonators are used as the tactile sensors. Then, the experimental characteristics of the manufactured tactile sensors are shown by measuring the softness and hardness of the test pieces. The differences of the characteristics of the sensitivity are discussed from the viewpoint of the resonance frequency, vibration mode and the dimensions of the resonator. It is clarified that the sensitivity on the tactile sensor is inversely proportional to the mass of the resonator. Moreover, the effects of the resonance frequency change on the tactile sensor by the load force and the additional mass, in case of contacting with an object, are analyzed using the finite element method. The obtained results will be useful for designing the piezoelectric vibratory tactile sensor.

4pEAe7. Improvement of low frequency signal radiation performance for piezoelectric loudspeakers. Juro Ohga (2-24-3, Tamanawa, 247-0071 Kamakura, Japan, johga@nifty.com)

Piezoelectric loudspeaker is characterized by their very simple constructions, but their radiation performance at low frequency region is poor because their diaphragms are too stiff for large amplitude vibration. This paper proposes two innovative methods for improvement of low frequency radiation performance of piezoelectric direct-radiator loudspeakers. One is a flat-shape loudspeaker unit with a tuck-shaped flexible diaphragm by a sheet of piezoelectric film. The other is a paper cone loudspeaker unit with a large radiator driven by revolution of piezoelectric ultrasonic motors. A loudspeaker system with satisfactorily wide frequency range for music is constructed by combination of these two sorts of loudspeaker units.

4pEAe8. Geometrical optimization of vented boxes. Guillaume Pellerin (CNAM Paris, 5, rue du Vert Bois, 75003 Paris, France, guillaume.pellerin@cnam.fr)

Today, low frequency reproduction with loudspeakers in vented box is limited by two factors: the volume of the box, and non-linear airflow through the vent. We propose a novel approach that takes into account aerodynamical parameters, leading to original profiles and an improved functioning of the vented box. For example, under certain alignment conditions, there exits a second cut-off frequency below the first one, localized on the lower impedance hump. Using this lower cut-off frequency and an adapted vent profile makes it possible to radiate frequencies under 40 Hz with box volumes smaller than 1 liter and small drivers. A prototype will be demonstrated.

Session 4pEAf

Engineering Acoustics: Sound Fields II (Poster Session)

Raymond Kirby, Chair
Brunel University

All posters will be on display from 3:40 p.m. to 5:20 p.m. To allow contributors an opportunity to see other posters, contributors of odd-numbered papers will be at their posters from 3:40 p.m. to 4:30 p.m. and contributors of even-numbered papers will be at their posters from 4:30 p.m. to 5:20 p.m.

Contributed Papers

4pEAf1. Application of Advanced Features in Computational Acoustics. Reinhard Lerch (Univ. Erlangen-Nuremberg, Dept. of Sensor Technology, Paul-Gordan-Str. 3/5, 91052 Erlangen, Germany, reinhard.lerch @lse.eei.uni-erlangen.de), Manfred Kaltenbacher (Univ. Erlangen-Nuremberg, Dept. of Sensor Technology, Paul-Gordan-Str. 3/5, 91052 Erlangen, Germany, manfred.kaltenbacher@lse.eei.uni-erlangen.de), Martin Meiler (Simetris GmbH, Am Weichselgarten 7, 91058 Erlangen, Germany, martin.meiler@simetris.de)

Modern numerical simulation tools allow the analysis of the generation and propagation of sound. However, a variety of computational features enhancing their applicability are missing in these codes. Therefore, it is sometimes cumbersome to come to practically useful results when applying such codes to real life problems. Here, some of these lacking features will be addressed and, furthermore, their implementation in a new finite element code is reported. These features are: Frequency dependent damping propagation medium, nonmatching grids for computing sound in neighbouring domains with quite different propaga-tion velocities and perfectly matched layers (for handling of open domain problems without reflections at boundaries of the computational domain). A finite element environment including pre- and post-processing has been established to support the development of electroacoustic devices. The following real life examples will be reported: electrodynamic loudspeakers, noise emission from power transformers, ultrasound devices for medical imaging such as conventional piezoceramic arrays as well as CMUTs (capacitive micromachined ultrasound transducers). It will be also shown that the code is able to handle nonlinear effects in transducing mechanisms and acoustic wave propagation, as occurring in HIFU (high intensive focused ultrasound) applications.

4pEAf2. Theoretical Study of Near 3D Sound Field Reproduction Based on Wave Field Synthesis. Toshiyuki Kimura (National Institute of Information and Communications Technology, 4-2-1, Nukui-Kitamachi, Koganei, 184-8795 Tokyo, Japan, t-kimura@nict.go.jp), Yoko Yamakata (National Institute of Information and Communications Technology, 4-2-1, Nukui-Kitamachi, Koganei, 184-8795 Tokyo, Japan, yamakata@nict.go.jp), Michiaki Katsumoto (National Institute of Information and Communications Technology, 4-2-1, Nukui-Kitamachi, Koganei, 184-8795 Tokyo, Japan, katumoto@nict.go.jp)

It is very important to develop near 3D sound field reproduction techniques in order to realize the ultra-realistic communication such as 3D TV and 3D tele-conference. In this report, the principle of the near 3D sound field reproduction technique using wave field synthesis is defined from Kirchhoff-Helmholtz integral equation and two methods (dipole control method and directional point control method) are proposed. The performance of two proposed methods is studied by computer simulation and it is shown that the dipole control method has good performance and that the directional point control method has good performance if the directivity of loudspeakers is unidirectional or shotgun.

4pEAf3. Performance Evaluation of 3D Sound Field Reproduction System with a Few Loudspeakers and Wave Field Synthesis. Munenori Naoe (National Institute of Information and Communications Technology, 4-2-1, Nukui-Kitamachi, Koganei, 184-8795 Tokyo, Japan, nm.s512.ex@nict.go.jp), Toshiyuki Kimura (National Institute of Information and Communications Technology, 4-2-1, Nukui-Kitamachi, Koganei, 184-8795 Tokyo, Japan, t-kimura@nict.go.jp), Yoko Yamakata (National Institute of Information and Communications Technology, 4-2-1, Nukui-Kitamachi, Koganei, 184-8795 Tokyo, Japan, yamakata @nict.go.jp), Michiaki Katsumoto (National Institute of Information and Communications Technology, 4-2-1, Nukui-Kitamachi, Koganei, 184-8795 Tokyo, Japan, katumoto@nict.go.jp)

A conventional 3D sound field reproduction system using wave field synthesis places a lot of loudspeakers around the listener. However, since such a system is very expensive and loudspeakers come into the listener's field of vision, it is very difficult to construct an audio-visual system with it. We developed and evaluated a 3D sound field reproduction system using eight loudspeakers placed at the vertex of cube and wave field synthesis. We compared the sound localization of a loudspeaker array with that of seventeen loudspeakers placed around the listener and found that their localization capabilities were equivalent except the normal direction of cube's planes.

4pEAf4. Synthesis of wave front in the sound field recording/reproduction system based on the boundary surface control principle. Seigo Enomoto (Advanced Telecommunication Research Institute International, 2-2-2 Hikaridai, 'Keihanna Science City', 6190288 Kyoto, Japan, seigo.enomoto@atr.jp), Yusuke Ikeda (Advanced Telecommunication Research Institute International, 2-2-2 Hikaridai, 'Keihanna Science City', 6190288 Kyoto, Japan, yusuke.ikeda@atr.jp), Shiro Ise (Urban and Envronemental Engineering, Graduate School of Engeneering, Kyoto University, C1-386, Kyodai-Katsura, Nisikyo-ku, Kyoto-si, 6158540 Kyoto, Japan, ise@archi.kyoto-u.ac.jp), Satoshi Nakamura (Advanced Telecommunication Research Institute International, 2-2-2 Hikaridai, 'Keihanna Science City', 6190288 Kyoto, Japan, satoshi.nakamura@atr.jp)

Based on the boundary surface control (BSC) principle, a new recording/reproduction system is developed to realize high fidelity three-dimensional sound field reproduction. Theoretically, by using this new system, physically faithful reproduction could be achieved in any acoustic environments. Sound recording/reproduction systems based on the BSC principle require many loudspeakers and many microphones. In this new system, the microphone array system to record 3D sound field consists of 70 microphones, and the loudspeaker system to reproduce the recorded 3D sound field consists of 62 full-range units and 8 sub-woofer units. To evaluate the ability of this system, the wave front which is measured in the sound-

proofed room is compared with the reconstructed wave front within this system. The experiment shows that the reconstructed secondary wave front is very similar to the primary wave front in lower frequency.

4pEAf5. Three-Dimensional FDTD Method for Analysing of the acoustic characteristics of Compact Acoustic Reproduction Systems. Yuichiro Koga (Kansai University, Kobe-Nishiku-Gakuenhigasimati5-1-512, 651-2102 Kobe, Japan, koga0814@joho.densi.kansai-u.ac.jp)

We propose a method for analysing of the acoustic characteristics of compact acoustic reproduction systems with Three-Dimensional FDTD method. We reproduce actual structure of compact acoustic reproduction systems and take the frequency characteristic of sound pressure level at a point with Three-Dimensional FDTD method. To compare the frequency characteristic of sound pressure level of actual measurement of compact acoustic reproduction systems to measurement of the proposed method, we show availability of the proposed method for analysing of the acoustic characteristics of compact acoustic reproduction systems. The proposed method could explain actual phenomena on compact acoustic reproduction systems well.

4pEAf6. Sound localization in multiple regions: theory and applications. Yang-Hann Kim (Center for Noise and Vibration Control, Korea Advanced Institute of Science and Technology, 4114, Department of Mechanical Engineering, Guseong-dong, Yuseong-gu, 305-701 Daejon, Republic of Korea, yanghannkim@kaist.ac.kr), Ji-Ho Chang (Center for Noise and Vibration Control, Korea Advanced Institute of Science and Technology, Dep. of Mechanical Engineering, Guseong-dong, Yuseong-gu, 305-701 Daejon, Republic of Korea, chang.jiho@gmail.com), Jin-Young Park (Center for Noise and Vibration Control, Korea Advanced Institute of Science and Technology, Dep. of Mechanical Engineering, Guseong-dong, Yuseong-gu, 305-701 Daejon, Republic of Korea, jypark1979@kaist.ac.kr)

It is often required to have several listening zones, which allows us to have different sounds that we select. For example, in a room, someone wants to listen sound from TV set, and other wants to listen music. In a car, a driver might wants to hear the information coming from his/her navigator system, and the passenger at the back side wants have a quiet zone so that he/she can sleep. To accomplish this kind of acoustic zones, we need to generate multiple sound zones by using multiple speakers. The performance has to be evaluated in accordance with how well one can listen the sound that is expected to have. We proposed to maximize the acoustic contrast between the zones that are defined. The basic concept associated with this approach was proposed by Choi and Kim [J. Acoust. Soc. Am., Vol.111(4), 1695-1700, Apr. 2002.], but this paper extend this fundamental idea to multiple zone cases. Theoretical formulation which shows what we have proposed is well addressed and several practical cases, including car audio system will be demonstrated. [This work was supported by the Korea Science and Engineering Foundation (KOSEF) through the National Research Lab. Program funded by the Ministry of Science and Technology (M10500000112-05J0000-11210)]

4pEAf7. Sound focused personal audio system design: Performance improvement in acoustic contrast control by spatial weighting for obtaining spatially averaged acoustic potential energy. Jin-Young Park (Center for Noise and Vibration Control, Korea Advanced Institute of Science and Technology, Dep. of Mechanical Engineering, Guseong-dong, Yuseong-gu, 305-701 Daejon, Republic of Korea, jypark1979@kaist.ac.kr), Ji-Ho Chang (Center for Noise and Vibration Control, Korea Advanced Institute of Science and Technology, Dep. of Mechanical Engineering, Guseong-dong, Yuseong-gu, 305-701 Daejon, Republic of Korea, chang.jiho@gmail.com), Chan-Hui Lee (Center for Noise and Vibration Control, Korea Advanced Institute of Science and Technology, Dep. of Mechanical Engineering, Guseong-dong, Yuseong-gu, 305-701 Daejon, Republic of Korea, Chance99@kaist.ac.kr), Yang-Hann Kim (Center for Noise and Vibration Control, Korea Advanced Institute of Science and Technology, 4114, Department of Mechanical Engineering, Guseong-dong, Yuseong-gu, 305-701 Daejon, Republic of Korea, yanghannkim@kaist.ac.kr)

In acoustic contrast control [J.-W. Choi and Y.-H. Kim, J. Acoust. Soc. Am. 111. 1695 (2002)], spatially averaged acoustic potential energy is used as a representative spatial parameter because acoustic contrast control aims to maximize spatially averaged acoustic potential energy ratio between acoustically bright and dark zone. Therefore, spatial averaging process should be concerned carefully because control performance is sensitive to how to determine bright and dark zone. We have already got successful result in feasibility study for personal audio system with over 20dB difference between bright (frontal) and dark (side) zone [C.-H. Lee et al., J. Acoust. Soc. Am. 111, 3053 (2007)], without any spatial weighting in spatial averaging of acoustic potential energy. Recently, we're trying to improve the control performance by giving spatial weighting in spatial averaging process because how to give spatial weighting has to do with the improvement of control performance to satisfy the original purpose of personal audio system more closely. In this paper, it will be covered the investigation for how to give spatial weighting in averaging process and shown experimental evaluations for a sound focused personal audio system. [Supported by the Korea Science and Engineering Foundation (KOSEF) through the National Research Lab. Program funded by the Ministry of Science and Technology (M10500000112-05J0000-11210)]

4pEAf8. 3D sound field rendering under non-idealized loudspeaker arrangements. Alois Sontacchi (Institute of Electronic Music and Acoustics, Inffeldgasse 10 / 3, 8010 Graz, Austria, sontacchi@iem.at), Franz Zotter (Institute of Electronic Music and Acoustics, Inffeldgasse 10 / 3, 8010 Graz, Austria, zotter@iem.at), Robert Höldrich (Institute of Electronic Music and Acoustics, Inffeldgasse 10 / 3, 8010 Graz, Austria, hoeldrich@iem.at)

The approach to realise periphonic sound field reproduction based on spherical harmonics (multi-pole theory) has already been well-known as Ambisonics and Higher Order Ambisonics, respectively. By the aid of an N-dimensional orthogonal set of vectors any arbitrary source free sound field can be described. Reproduction is realized by projection of the encoded sound field on a regular loudspeaker distribution over a spherical surface. The used set of vectors exhibits a defined hierarchic with interesting symmetries. In the original scheme sound sources represented by plane waves (sources in far distance) can be encoded independent of the decoding process on the regular loudspeaker layout. Usually, in practice - in contrast to theory, 3D loudspeaker layouts are requested for the upper hemisphere. This restriction is caused by the physical configuration. First of all that demand bounds the reproduction of sound sources to the upper area. Furthermore caused by these facts idealized regular layouts considering the 3 dimensions are impossible. Within this contribution we will show how the symmetries of the spherical harmonics can be used to obtain optimized decoding rules and to overcome insufficient irregular loudspeaker arrangements.

4pEAf9. Measurements of head-related transfer function in sagittal and frontal coordinates. Takashi Nakado (Nagoya University, Furo-cho, Chikusa-ku, 4648603 Nagoya, Japan, nakado@sp.m.is.nagoya-u.ac.jp), Takanori Nishino (Nagoya University, Furo-cho, Chikusa-ku, 4648603 Nagoya, Japan, nishino@media.nagoya-u.ac.jp), Kazuya Takeda (Nagoya University, Furo-cho, Chikusa-ku, 4648603 Nagoya, Japan, kazuya.takeda@nagoya-u.jp)

3D sounds can be generated by using a head-related transfer function (HRTF), which is defined as the acoustic transfer function between a sound source and the entrance to the ear canal. Since HRTF depends on a subject and the sound source direction, many HRTF measurements were conducted. In most case, HRTFs were measured in horizontal coordinates. However, HRTF measurements in other coordinates are also useful. In previous researches, HRTFs measured in sagittal coordinates were used to investigate the relation between spectral cues and vertical angle perception. Although HRTF measurement in frontal coordinates is rarely conducted, there is an advantage to measure HRTFs densely in the front and rear where sound localizations are very sensitive. Therefore, we measured HRTFs for about

2,300 directions in sagittal and frontal coordinates and constructed a database. The measurements were conducted in a soundproof chamber with two head-and-torso simulators (B&K 4128 and KEMAR). The HRTF database can be downloaded at http://www.sp.m.is.nagoya-u.ac.jp/HRTF/ .

4pEAf10. A New Sound Field Reproduction Method Based on the Spatial Covariance. Yoshinori Takahashi (NHK Science & Technical Research Laboratories, 1-10-11 Kinuta, Setagaya-ku, 157-8510 Tokyo, Japan, yoshinori@ieee.org), Akio Ando (NHK Science & Technical Research Laboratories, 1-10-11 Kinuta, Setagaya-ku, 157-8510 Tokyo, Japan, ando.a-io@nhk.or.jp)

This work investigates a sound field reproduction method based on the sound field statistics. The covariance among recorded multi-channel signals might represent the relative relationship and the mutual magnitude characteristics between each point in the sound field that time invariant. The author Y. Takahashi et al. proposed a reproduction method minimizing the difference in the spatial covariance between the original and reproduced sound fields [19th ICA, RBA15-012]. We call the method ″SOund field Reproduction method based on the sPAtial Covariance (SORPAC)″. However it has not been clarified that the theoretical background and the characteristics in listening. The SORPAC doesn't require the information of sound source locations and transfer functions. In this work, we described the reproduction theory of SORPAC in frequency domain. And we showed the relationship between SORPAC and the general wave surface control. Then we confirmed that the SORPAC is able to reproduce the sound source direction without the wave surface control. As a application of SORPAC, we demonstrated a multi-channel contents down-mixing experiment and evaluated the result from the binaural-listening point of view.

4pEAf11. Optimal array pattern synthesis with desired magnitude response. Alexander Mattioli Pasqual (Universidade Estadual de Campinas, Rua Mendeleiev, 200, Cidade Universitária ″Zeferino Vaz″, 13083-970 Campinas, Brazil, pasqual@fem.unicamp.br), José Roberto Arruda (Universidade Estadual de Campinas, Rua Mendeleiev, 200, Cidade Universitária ″Zeferino Vaz″, 13083-970 Campinas, Brazil, arruda@fem.unicamp.br), Philippe Herzog (Laboratoire de Mécanique et d'Acoustique - CNRS, 31 chemin Joseph Aiguier, 13402 Marseille, France, herzog@lma.cnrs-mrs.fr)

Letting Euclidean norm be the performance parameter, the task of finding the best approximation of a complex function in a finite dimension subspace leads to a convex optimization problem that can be easily solved by the least-squares method. However, this procedure leads to a sub-optimal solution in applications that have no phase requirements on the approximated function. In this case, semidefinite programming has been used to obtain optimal magnitude responses. In this work, this non-convex optimization problem is dealt with by using an iterative method based on the least-squares, which is illustrated on directivity synthesis by spherical loudspeaker arrays. Usually, instead of synthesize directly the desired pattern, the strategy adopted is to reproduce its truncated spherical harmonic representation. The truncation order is determined by the number of drivers of the spherical array. It is shown that truncation error and signal powers can be significantly reduced if phase error is neglected, providing potential means to improve directivity synthesis for applications requiring only magnitude response.

THURSDAY AFTERNOON, 3 JULY 2008 ROOM 202/203, 2:20 TO 6:20 P.M.

Session 4pED

Education in Acoustics: Acoustics Education Software

Ralph T. Muehleisen, Cochair
Illinois Institute of Technology, Civil, Architectural and Environmental Engineering, 3201 S. Dearborn St., Room 228, Chicago, IL 60616, USA

Catherine Potel, Cochair
Laboratoire d'Acoustique de l'Université du Maine, Avenue Olivier Messiaen, Le Mans, 72085, France

Invited Papers

2:20

4pED1. Education software for numerical acoustics. Olivier Dazel (Laboratoire d'Acoustique de l'Université du Maine, Avenue Olivier Messiaen, 72085 Le Mans, France, olivier.dazel@univ-lemans.fr)

Numerical computations tools and scientific computing programs are more and more used by acousticians. This induces that higher education institutions have to include numerical techniques in their programs. Several general aspects should be considered while designing such courses; they are the initial level of the students, their ability with mathematics and/or physics and the aim of the formation. Particular aspects on the choice of a type of software and the methodology need also to be studied. This talk will detail these aspects around the numerical courses at Université du Maine in Le Mans (France) whose formations ranges are from sound and vibration technicians to PhD students. Some typical examples and numerical tools will be presented to illustrate the purpose.

2:40

4pED2. Computer tools for architectural acoustics education. Jian Kang (School of Architecture, University of Sheffield, Western Bank, S10 2TN Sheffield, UK, j.kang@sheffield.ac.uk)

Calculating/simulating acoustic performance of architectural spaces and building elements plays an important role in architectural education. Unfortunately, architectural students often hesitate to use theoretical formulae/models commonly applied by acousticians. This study aims to develop simple calculation/simulation tools to help architectural students to understand basic acoustic principles.

Focusing on the effectiveness of various key parameters, as well as on scientific visualisation way of presenting teaching materials, five tools have been developed: (1) sound distribution behind an environmental noise barrier, with parameters including barrier height, source-barrier distance, and source height; (2) sound distribution in a rectangular street canyon, with parameters including street length, width, building height, boundary absorption coefficient, air absorption, and the height of receiver plane; (3) reverberation time calculation in a rectangular space, with parameters including room dimensions and boundary absorption coefficients, where a database of absorption coefficients is also included; (4) absorption of perforated panel absorbers, especially micro-perforated panel absorbers, with parameters including hole size, hole spacing, panel thickness, and depth of airspace; (5) digital audio animation for urban soundscape design, considering idealised cross-streets and squares in a 2D environment, where the sound file with multiple sources can be played back, with reverberation effects. [Work supported by the Theodore John Schultz Grant]

3:00

4pED3. Live computer-based demonstrations in musical acoustics education. Donald M. Campbell (Edinburgh University, 4201 JCMB, Kings Buildings, Mayfield Road, EH9 3JZ Edinburgh, UK, d.m.campbell@ed.ac.uk), David Skulina (Edinburgh University, 4201 JCMB, Kings Buildings, Mayfield Road, EH9 3JZ Edinburgh, UK, dskulina@ph.ed.ac.uk)

Live demonstrations play a vital pedagogical role in any science education programme. For a subject as interdisciplinary as musical acoustics, embracing as it does mathematics, physics, engineering, psychology, cognitive science, neurophysiology, musicology and music technology, demonstrations of psychoacoustical phenomena and performances on musical instruments provide invaluable methods for involving and intriguing a general audience. The recent dramatic increase in the memory and speed of laptop computers has opened new possibilities for live computer-based demonstrations. This talk explores some of these possibilities, including demonstrations of the analysis and display of musical instrument sounds using real-time spectrographic programs and the explanation of important musical instrument characteristics using physical modelling synthesis.

3:20

4pED4. A computer model to study the properties of guided waves. Michael J. Lowe (Imperial College London, Department of Mechanical Engineering, SW7 2AZ London, UK, m.lowe@imperial.ac.uk)

The author's research group has a specialist interest in developing guided wave techniques for the Non Destructive Testing (NDT) of structures. Guided waves travel along the structure and so can be used to inspect large lengths or areas very much faster then the traditional point-by-point ultrasonic methods. The development of these inspection methods requires careful study and understanding of the properties of the guided waves. To address this need, the author's team has created a general purpose modelling tool. This can model waves in waveguides consiting of an arbitrary number of layers which can be flat or cylindrical, elastic or damped, isotropic or anisotropic solids, or perfect or viscous fluids, and can be immersed in a fluid or embedded in a solid. The primary output of the program is the dispersion curves, that is the frequency-velocity relationships of any modes which could travel in the structure. The program also predicts the attenuation of the modes, caused by leakage into surrounding materials or by material damping, and the mode shapes The presentation will explain the basis of the modelling tool and illustrate the way in which it can be used to understand the guided waves.

3:40-5:20 Posters

Lecture sessions will recess for presentation of poster papers on various topics in acoustics. See poster sessions for topics and abstracts.

Invited Paper

5:20

4pED5. DELTAEC is also an acoustics teaching tool. Steven Garrett (Penn State, Applied Research Laboratory, PO Box 30, State College, PA 16804, USA, sxg185@psu.edu)

A major revision of the Los Alamos thermoacoustics code, renamed DELTAEC, was released in 2007. It takes advantage of a user-friendly, menu-driven Windows environment and has indigenous plotting capabilities. DELTAEC is a differential equation solver that analyzes one-dimensional acoustical networks defined by a series of ″segments″ representing ducts, compliances, speakers, etc. This talk will relate experiences using this software to teach a first-year graduate core course on acoustics in fluids. Examples include illustration of effective length and quality factor of Helmholtz resonators, as well as the more challenging standing wave solutions within a resonator of variable cross-section. The plotting feature allows immediate illustration of the pressure and velocity fields as well as power flow within the resonator. DELTAEC will also adjust gas mixture concentration to match a specified frequency. Segments representing electrodynamic loudspeakers, radiation loading, and flow resistance in porous media will be used to demonstrate the coupled-oscillatory behavior of a bass-reflex enclosure's complex electrical impedance *vs.* frequency. Calculation of the modes of a catenoidal horn of finite length will be presented. The ″thermo-physical property″ feature provides fluid and solid properties at the students' choice of pressure, temperature and frequency, making it useful as a ″handbook″ for other assignments.

5:40

4pED6. CNAQ: a MATLAB acquisition tool for computing transfer functions over audio cards. Guillaume Pellerin (CNAM Paris, 5, rue du Vert Bois, 75003 Paris, France, guillaume.pellerin@cnam.fr)

Since transfer function measurements require very precise buffer management, it is not easy to find any free and/or educational software which processes them with consumer audio cards, cheaper than professional ones but useful. Some people often use musical sequencers to generate and acquire signals but data can't be easily analyzed in other specific engineering codes because the lengths of the samples can't be easily fixed for example. Therefore, we decided to develop a specific software for general audio acoustic measurements with these main constraints: choose a programming language compatible with existing educational and professional tools, promote multi-platform interpreted languages, be able to use consumer audio cards, publish the source code under the terms of a free software license. CNAQ provides a graphical interface under MATLAB to process sweep sine measurements for any kind of acoustical or electronic application in the audio range. The current features of the software and some development ideas, such as implementing convolution based Farina's method, will be also presented.

6:00

4pED7. Noise Metric - Environmental Noise Analysis Software. Milan Stojiljković (Faculty of Technical Sciences, Department of Environmental Engineering, Trg Dositeja Obradovića 6, 21000 Novi Sad, Yugoslavia, noisemetric@gmail.com),Vlado Delic(Faculty of Technical Sciences, Department of Tellecomunications, Laboratory for Acoustics and Speech Technologies, Trg Dositeja Obradovića 6, 21000 Novi Sad, Yugoslavia, vdelic @uns.ns.ac.yu)

Noise Metric software suite addresses the need for a modern low-cost acquisition, post-processing and analysis system that accommodates professional grade instruments used in typical environmental noise assessments. Software is designed to comply with national and international legislation and to provide a comprehensive overview of environmental acoustics theory in an interactive help file. Educational use is emphasized by providing measurement wizards and example case histories, with included demonstration measurement files for student self study. Acknowledging tight student financial budgets, the system is not limited to use with professional grade equipment. It can be configured for less expensive and less precise operation by providing integration with standard PC sound boards and low-cost microphones. Current beta version focuses on community noise and traffic noise assessment, with future modules planned for occupational noise and basic acoustic calculations. Off line analysis module is supplemented by a real time module for recording and logging the measurements and a browser for viewing the analysis results, noise rating level calculation and report generation. Every attempt is being made to automate as many analysis tasks as possible and thus minimize the human induced errors in the assessment process. Preliminary product testing was successfully completed by comparison with proprietary software products.

THURSDAY AFTERNOON, 3 JULY 2008 AMPHI MAILLOT, 1:40 TO 7:00 P.M.

Session 4pMUa

Musical Acoustics: Control of Natural and Synthetic Musical Sounds I

Marcelo M. Wanderley, Cochair
Centre for Interdisciplinary Research in Music Media & Technology (CIRMMT) - Schulich School of Music - McGill Univ., 555 Sherbrooke Street West, Montreal, QC H3A1E3, Canada

Jean Kergomard, Cochair
Laboratoire de Mécanique et d'Acoustique CNRS UPR-7051, 31, Chemin Joseph Aiguier, Marseille Cedex 20, 13402, France

Invited Papers

1:40

4pMUa1. Systems control theory for sound synthesis: an overview. Brigitte D'Andréa-Novel (Ecole des Mines de Paris, 60 Bd. Saint-Michel, 75006 Paris, France, brigitte.dandrea-novel@ensmp.fr), Denis Matignon (Univ. Toulouse; ISAE. Dept. MIA, 10 av. Edouard Belin, 31055 Toulouse, France, denis.matignon@isae.fr)

The aim of this talk is to present some classical techniques and methods from control theory to deal with the problem of sound synthesis based on physical models. A first part will be devoted to the case of finite-dimensional state space, illustrated by: 1. Kelly-Lochbaum structure for 1D wave equations; 2. Realization theory for passive impedance of rational type. The second part considers the infinite-dimensional case. More precisely the authors will present: 1. The operator associated to PDEs in acoustics, its diagonalization leading to ″Riemann invariants″ useful to study stability properties; 2. A Lyapunov method to elaborate boundary control to ensure stabilization of an equilibrium regime and some kind of robustness; 3. Diffusive realizations of fractional time derivatives, useful when modeling visco-thermal losses in acoustical ducts. These tools are well adapted to the class of ″wind instruments″.

2:00

4pMUa2. Extracting Reed Control Parameters Using Acoustic Measurements and Inverse Filtering. Tamara R. Smyth (Simon Fraser University, 2728 West 5th Ave, Vancouver, BC V6K 1T4, Canada, tamaras@cs.sfu.ca), Jonathan Abel (Stanford University, 752 College Ave, Menlo Park, CA 94025, USA, jonathan.abel@comcast.net)

The control of virtual musical instruments often relies on either a specially-developed controller on which the performer has usually not gained sufficient virtuosity to play musically, or an existing multipurpose general controller with control parameters not always easily, or intuitively, mapped to the synthesis parameters of the virtual instrument being performed. A response to this problem is to obtain control information from a musical performance where the performer uses an instrument with which s/he is sufficiently familiar. In this work, we incorporate a previously developed measurement technique to transform a measured clarinet signal into a sequence of pulses corresponding to the reed displacement as a function of time. The measurement technique, shown to obtain accurate reflection functions from various tube structures, is used to obtain a filter modeling the bore and bell of the wind instrument used in the performance. The ″reed pulse″ waveform is then isolated by inverse filtering the measured clarinet signal. The characteristics of this residual waveform, which evolve with the performer's control of the instrument, may be extracted and remapped to the synthesis parameters of a physical model.

Contributed Papers

2:20

4pMUa3. Modeling and automatic control of a slide flute. Brigitte D'Andréa-Novel (Ecole des Mines de Paris, 60 Bd. Saint-Michel, 75006 Paris, France, brigitte.dandrea-novel@ensmp.fr), Benoit Fabre (Institut Jean Le Rond d'Alembert / LAM (UPMC / CNRS / Ministère Culture), 11, rue de Lourmel, 75015 Paris, France, fabreb@ccr.jussieu.fr), Jean-Michel Coron (Lab. Jacques-Louis Lions, UPMC and Institut Universitaire de France, 4 place Jussieu, 75005 Paris, France, Jean-Michel.coron@math.u-psud.fr)

In this paper, we consider the problem of modeling and control of a slide flute: a kind of recorder without finger holes but which is ended by a piston mechanism to modify the length of the resonator. A previous study has been done, but with a very simple boundary condition for the mouth, corresponding to an ideal situation assuming that the acoustic pressure is zero at the entrance of the resonator. In this work, we have taken into account a more realistic model, describing the coupling effects between the jet and the pipe. The jet is obtained by blowing through a flue channel and formed by flow separation at the flue exit, and finally directed towards a sharp edge, called the labium. The resulting structure will be described by two linear PDEs coupled with nonlinear ODEs describing the boundary conditions: for the mouth, taking into account the jet dynamics, and for the piston. A modal analysis is performed using the linearized boundary conditions which can also be used to compute the suitable blowing pressure and the suitable pipe length to obtain a desired fundamental frequency or equivalently a desired pitch. This will constitute the basis of our control algorithm.

2:40

4pMUa4. Physical parameters of the violin bridge changed by active control. Henri Boutin (Institut Jean le Rond d'Alembert, Lab. d'Acoustique Musicale, 11, rue de Lourmel, 75015 Paris, France, boutin@lam.jussieu.fr), Charles Besnainou (Institut Jean le Rond d'Alembert, Laboratoire d'Acoustique Musicale, 11, rue de Lourmel, 75015 Paris, France, chbesnai@ccr.jussieu.fr)

The physical parameters of a violin bridge have a significant influence on the tonal colouration of its sound. The resonance peaks of the bridge shape the response of the violin body. Reinicke and Cremer developed a simple bridge model that shows a typical broad frequency peak around 2.5kHz, because it incorporates the coupling to the violin body and the soundpost. By using the same model, Jim Woodhouse revealed the effect of some parameters of the bridge (mass, stiffness and foot spacing) on the instrument frequency response. Here the parameters of the violin resonance peaks are changed in real time, by applying an active control method. Such a technique, very useful in noise reduction, enabled to change separately the position and the shape of each peak of the bridge input admittance. On the bridge, 2 actuators and an accelerometer are placed at strategic positions in order to change the peak frequency and the damping factor values. The system behaviour is controlled by a Digital Signal Processor. Some sound results achieved with a real violin back up the theoretical equations.

Invited Paper

3:00-3:20 Break

3:20

4pMUa5. Between the frog and the tip - bowing gestures and bow-string interaction in violin playing. Anders Askenfelt (Dept. of Speech, Music and Hearing, Royal Institute of Technology (KTH), Lindstedtsvägen 24, SE-100 44 Stockholm, Sweden, andersa@speech.kth.se)

The motion of the bow gives a natural visualization of a string performance. Watching the player's bowing may augment the communicative power of the music, but all relevant bow control parameters are not easy to capture by a spectator. The string player controls volume of sound and tone quality continuously by coordination of three basic bowing parameters (bow velocity, bow-bridge distance, and bow force), which set the main conditions for the bow-string interaction. At a more detailed level of description, the tilting of the bow, which among other things controls the effective width of the bow hair, enters into the model. On a longer time scale, pre-planned coordination schemes ('bowing gestures'), including the basic bowing parameters and the angles between the path of the bow and the strings, builds the performance. Systems for recording bowing parameters will be reviewed and results from old and current studies on bowing gestures presented. The player's choice and coordination of bowing parameters are constrained both in attacks and 'steady-state' according to bow-string interaction models. Recent verifications of these control spaces will be examined. Strategies for starting notes and examples of how players do in practice will be presented and compared with listeners' preferences.

3:40-5:00 Posters

Lecture sessions will recess for presentation of poster papers on various topics in acoustics. See poster sessions for topics and abstracts.

Invited Papers

5:00

4pMUa6. The guitar as an extension of the voice - Phonetic gestures underlying guitar timbre perception and description. Caroline Traube (Laboratoire informatique, acoustique et musique, Faculté de musique, Université de Montréal, C.P. 6128, succursale Centre-Ville, Montréal, QC H3C 3J7, Canada, caroline.traube@umontreal.ca), Maryse Lavoie (Laboratoire informatique, acoustique et musique, Faculté de musique, Université de Montréal, C.P. 6128, succursale Centre-Ville, Montréal, QC H3C 3J7, Canada, maryse.lavoie@umontreal.ca)

The guitar is an instrument that gives the player great control over timbre. Different plucking techniques involve varying the finger position along the string and the inclination between the finger and the string. Guitarists perceive subtle variations of these parameters and have developed a rich vocabulary to describe the tones they produce on their instrument. Vocal imitations - onomatopoeias - is another way to intuitively describe instrumental tones. The data that we collected showed that guitar tones can be consistently associated with different types of vowels depending on instrumental gesture parameters, suggesting that guitar tones can evoke ″phonetic gestures″ as defined in the motor theory of speech perception. In addition, these phonetic gestures seem to be at the origin of a large subset of commonly used verbal descriptors: open, oval, round, thin, closed, nasal, hollow, etc. These analogies can be explained by the comb-filter shaped spectral envelope of plucked-string instruments which emphasizes energy in the region of vocal formants. We conclude that, when technical difficulties have been surmounted, performers can use their musical instrument as an extension of their voice, the musical instruments allowing a virtuosic control of sound parameters similar to those involved in the paralinguistic elements of speech.

5:20

4pMUa7. Production and perception of goal-points and coarticulations in music. Rolf Inge Godøy (University of Oslo, Department of Musicology, P.B. 1017 Blindern, N-0315 Oslo, Norway, r.i.godoy@imv.uio.no), Alexander Refsum Jensenius (University of Oslo, Department of Musicology, P.B. 1017 Blindern, N-0315 Oslo, Norway, a.r.jensenius@imv.uio.no), Kristian Nymoen (University of Oslo, Department of Musicology, P.B. 1017 Blindern, N-0315 Oslo, Norway, krisny@hf.uio.no)

From our studies of sound-related movement (http://musicalgestures.uio.no), we have reason to believe that both sound-producing and sound-accompanying movements are centered around what we call goal-points, meaning certain salient events in the music such as downbeats, or various accent types, or melodic peaks. In music performance, these goal-points are reflected in the positions and shapes of the performers' effectors (fingers, hands, arms, torso, etc.) at certain moments in time, similar to what is known as keyframes in animation. The movement trajectories between these goal-points, similar to what is known as interframes in animation, may often demonstrate the phenomenon of coarticulation, i.e. that the various smaller movement are subsumed under more superordinate and goal-directed movement trajectories. In this paper, we shall present a summary of recent human movement research in support of this scheme of goal-points and coarticulations, as well as demonstrate this scheme with data from our ongoing motion capture studies of pianists' performance and other researchers' motion capture data.

5:40

4pMUa8. Perception, verbal description and gestural control of piano timbre. Caroline Traube (Laboratoire informatique, acoustique et musique, Faculté de musique, Université de Montréal, C.P. 6128, succursale Centre-Ville, Montréal, QC H3C 3J7, Canada, caroline.traube@umontreal.ca), Michel Bernays (Laboratoire informatique, acoustique et musique, Faculté de musique, Université de Montréal, C.P. 6128, succursale Centre-Ville, Montréal, QC H3C 3J7, Canada, michel.bernays@gmail.com), Madeleine Bellemare (Laboratoire informatique, acoustique et musique, Faculté de musique, Université de Montréal, C.P. 6128, succursale Centre-Ville, Montréal, QC H3C 3J7, Canada, madeleine.bellemare@umontreal.ca)

Musical expressivity in virtuosic pianistic performance relies heavily on timbre and performers call upon a vast vocabulary to describe the nature of their sound; examples of adjectives include velvety, metallic, bright, round and dark. The present study aims to determine whether this vocabulary, its perceptual meaning and the gesture applied to obtain the sounds it describes, stand as consensual among pianists. The relations between timbre, articulation, register and dynamics are also examined. Nearly 100 verbal descriptors were collected as well as the description of the associated gestures. Some timbres are specific to certain dynamic levels and others are the result of a combination of at least two sonic elements into one resulting sound object, where articulation, - the relation between one note to the next - plays a crucial role. A subset of these adjectives has been selected for further study. A professional pianist performed, on a computer-controlled recording acoustic piano, three short project-designed pieces with several timbres, as designated by adjectives. The excerpts were also captured with microphones to serve as stimuli for a timbre recognition task, both in free form and by selection, to which a group of 17 pianists performed with great accuracy.

Contributed Paper

6:00

4pMUa9. Study of brass performer gestures. René E. Causse (IRCAM, 1 Place Igor Stravinsky, 75004 Paris, France, causse@ircam.fr), Vincent Freour (IRCAM -CNRS (UMR 9912 STMS), 1, Place Igor Stravinsky, 75004 Paris, France, Vincent.Freour@ircam.fr)

Brass instrument playing requires the musican to control his respiratory gesture and the elastic properties of his lips. This raises the question of musician gesture optimisation and strategy in order to complete a musical exercise. It also makes gesture characterization very hard to conduct in a non-invasive way. On the other hand, it is possible to measure some control parameters (linked to the respiratory and lip-adjustment gesture) like lip force applied on the mouthpiece and mouth air pressure. Theses parameters measurements and also the specific mouthpiece receiver developed to measure lip force with a minimum interference to the player are presented. Respiratory flows during live playing are also evaluated thanks to the calibration of respiratory belts used on the thoracial and abdominal regions of musicians. Details of the method for carrying out this type of measurement and preliminary results are reported. During this measurement sound recording and analysis are also conducted thanks to a set of audio descriptors. Links between control parameters measurements and sound characterisation are examined. Parallel development of a automated artificial mouth, used for experimental validations, is also outlined. [Work, within the CONSONNES project, is lead with the support of the French Research National Agency ANR].

Invited Papers

6:20

4pMUa10. Refining mapping strategies to improve the sound quality of physically controlled synthesis. Vincent Verfaille (Centre for Interdisciplinary Research in Music Media & Technology (CIRMMT) - Schulich School of Music - McGill Univ., 555 Sherbrooke Street West, Montreal, QC H3A1E3, Canada, vincent@music.mcgill.ca), Arnaud Rebillout (4 le Cabut, 33390 Cars, France, arnaud.rebillout@gmail.com), Philippe Guillemain (Laboratoire de Mécanique et d'Acoustique CNRS UPR-7051, 31, Chemin Joseph Aiguier, 13402 Marseille Cedex 20, France, guillemain@lma.cnrs-mrs.fr), Marcelo M. Wanderley (Centre for Interdisciplinary Research in Music Media & Technology (CIRMMT) - Schulich School of Music - McGill Univ., 555 Sherbrooke Street West, Montreal, QC H3A1E3, Canada, marcelo.wanderley@mcgill.ca)

A new technique, called 'physically controlled synthesis', is being developed to improve the controllability and sound quality of digital sound synthesis. It can be seen as a mapping strategy that combines a synthesis model based on a physical model (controllability) with a signal model based on additive synthesis (sound quality), and a database of pre-analyzed natural instrumental sounds. A key point is the computation of perceptually relevant timbre descriptors that interface the two synthesizers to provide additive synthesis data by navigating the database and selecting neighbour additive frames to morph. To limit the latency introduced, we developed specific algorithms to extract sound features from the physical model; the database size was increased offline by using a higher control sampling rate. In addition to previous works by the authors, devoted to the permanent regime and using a 2D indexation of the additive database, transients handling is achieved through a 3D search in a frame-by-frame basis that ignores the natural time unfolding, hence allowing to choose the best frame with the proper pitch in addition to the two other sound descriptors.

6:40

4pMUa11. Inverse problem: Recovering the full-state of a simplified model of a trumpet-like instrument from the radiated pressure. Thomas Hélie (IRCAM, 1, place Igor Stravinsky, 75004 Paris, France, thomas.helie@ircam.fr), Brigitte D'Andréa-Novel (Ecole des Mines de Paris, 60 Bd. Saint-Michel, 75006 Paris, France, brigitte.dandrea-novel@ensmp.fr)

We consider a simplified model of a trumpet-like instrument composed of a valve (including the mechanics of the lips), a jet (coupled with the valve dynamics), and an acoustic pipe excited by the jet and radiating in the air. A special care is devoted to the energy balance of the whole system and its dissipative property. This leads us to introduce a model of a non-stationary jet. In a second step, the problem of the observation of the full-state (that is, the position and the velocity of the lips, the flow and the pressure in the jet and in the acoustic pipe) from the radiated pressure is analyzed. This problem can be recasted as a problem of control engineering, using a so-called neutral system (differential system including the delayed state and its time derivative). We show how the energy balance can help to solve this problem and define a naturally well-posed observator. As a last step, this work is recasted in the context of a more general inverse problem: What control input (pressure in the mouth, parameter of the lips, etc) must be used to feed the model in order to recover a target sound?

Session 4pMUb

Musical Acoustics: Bowed and Keyboard Stringed Instruments II (Poster Session)

Seiji Adachi, Cochair
Fraunhofer Institute for Building Physics

Simon Félix, Cochair
Laboratoire d'Acoustique de l'Université du Maine

All posters will be on display from 3:40 p.m. to 5:20 p.m. To allow contributors an opportunity to see other posters, contributors of odd-numbered papers will be at their posters from 3:40 p.m. to 4:30 p.m. and contributors of even-numbered papers will be at their posters from 4:30 p.m. to 5:20 p.m.

Contributed Papers

4pMUb1. Experimental modal analysis of bows. Enrico Ravina (University of Genoa - Centre of Research on Choral and Instrumental Music (MUSICOS), Via Opera Pia 15 A, 16145 Genova, Italy, enrico.ravina@unige.it), Paolo Silvestri (Univ. of Genoa - DIMEC, Via Opera Pia 15 A, 16145 Genova, Italy, p.silvestri@unige.it), Antonino Airenti (Bow Maker, Via Marussig 13, 16100 Genova, Italy, inf @baroquebows.net)

The vibration performances of bow instruments are usually studied developing numerical and experimental modal analyses of the body of the instrument or of their parts (tailpiece, bridge, fingerboard, neck). The dynamic contribution of the bow is less considered, but the mutual actions generated between bow and strings are conditioned by the mechanical features of the bow. The paper analyzes the dynamic behaviour of different kind of bows (clip-in frog and screw-driven frog) and different geometries (baroque, modern,...) through experimetal modal analyses. Bows are instrumented with micro-accelerometers and excited by a micro-hammer. Frequency Response Functions up to 2500 Hz allow a good characterization of the bow and show significant differences about the modal shapes. The study is integrated with the experimental strain analysis, based on micro strain gauges glued on the body; the very small dimensions of the transducers (2.5 mm) allow, from one side, a not intrusive analysis but, from another side, require specific contrivances of mounting. Details on the integrated experimentations are focussed and discussed.

4pMUb2. Spherical mapping of violins. Enrico Ravina (University of Genoa - Centre of Research on Choral and Instrumental Music (MUSICOS), Via Opera Pia 15 A, 16145 Genova, Italy, enrico.ravina@unige.it), Paolo Silvestri (Univ. of Genoa - DIMEC, Via Opera Pia 15 A, 16145 Genova, Italy, p.silvestri@unige.it), Pio Montanari (Master Violinmaker, Via delle Compere 2, 16100 Genova, Italy, montanaripio@libero.it), Guido De Vecchi (Musician, Via S. Maria di Castello 37, 16100 Genova, Italy, ensemble@ilfalcone.com)

An original experimental approach oriented to the evaluation of the acoustic performances of violins is described. Starting from 14th Century the violins family have passed through significant changing, strongly influencing their sound. The ″instrumental music″ requires different parts for different voices: the violin family changes its mechanical structure following this requirement. The structural elements are modified in order to adequate the sound to the aesthetic taste of the historical period. Mechanical modifications involve geometry, relative positions and structural characteristics of fixed and mobile parts. The consequence is a significant alteration of vibration and acoustic responses. The paper describes a systematic approach oriented to evaluate the acoustic performances of differently mounted violins (baroque, classical, modern) by means a spherical mapping of the generated sound. A workbench based on a semicircular structure carrying an array of 10 microphones interfaced to a portable acquisition unit, has been designed and realized. The violin, played by the musician in anechoic chamber or in representation room, is located at the centre of this semicircle: changing the relative angular position between the violin and the array acoustic spherical maps describing the actual sound emission are generated. A systematic comparison among differently mounted violins is shown and discussed.

4pMUb3. On the generation of axial modes in the nonlinear vibration of strings. Alexandre Watzky (Laboratoire de Mécanique Physique, Université Paris 12 - Fac. des Sciences & Technologie, 61 av. du Gal. de Gaulle, 94010 Créteil, France, watzky@univ-paris12.fr)

Vibrating strings are known to be nonlinear. Transverse vibrations induce axial motion as well as a modulation of the string's tension. An overview of the nonlinear models of the vibrating string has been presented at the 150th Meeting of the ASA. It has been shown that if temporal considerations are prevalent from an acoustical point of view, the involved coupling mechanisms are mainly ruled by the spatial shape of the modes. The purpose of this communication is to investigate the specific case of transverse-axial interactions and to examine the possible generation of axial modes through transverse vibrations. It also gives the opportunity to discuss the common hypotheses. Despite the complex modal couplings that can occur, this results enable to avoid or favor axial modes in the design of the string itself or of the boundary conditions i.e. the bridge.

4pMUb4. The application of thin plate theory to the time evolution of musical instruments. Christopher Gorman (Rollins College, Department of Physics, Winter Park, FL 32789, USA, cgorman@rollins.edu), David Parker (Rollins College, Department of Physics, Winter Park, FL 32789, USA, dparker@rollins.edu), Connor Ballance (Rollins College, Department of Physics, Winter Park, FL 32789, USA, ballance@vanadium.rollins.edu), Donald Griffin (Rollins College, Department of Physics, Winter Park, FL 32789, USA, griffin@vanadium.rollins.edu), Thomas Moore (Rollins College, Department of Physics, Winter Park, FL 32789, USA, tmoore@rollins.edu)

The steady state dynamics of many musical instruments can be modeled using thin-plate theory. It has been shown that the normal-mode frequencies of systems as diverse as the orchestral crotale and piano soundboard can be accurately calculated within this approximation, and it is therefore reasonable to ask if thin-plate theory can be applied to model the time evolution of these instruments. To answer this question we have modeled a struck flat plate using finite differences and compared the decay of the eigenmodes to experimental results. We find that the time evolution of the motion of a struck thin plate is not well described under the thin-plate approximation even when the modal frequencies are predicted accurately. We propose that

mode coupling between longitudinal and transverse modes requires that a full three dimensional model be used to predict the time evolution even when the plate is thin.

4pMUb5. Considering the effect of hammer shank flexibility using a multibody dynamic simulation model of a piano action mechanism with string contact. Chandrika P. Vyasarayani (University of Waterloo, Department of Systems Design Engineering, Waterloo, ON N2L 3G1, Canada, cpvyasar@engmail.uwaterloo.ca), Stephen Birkett (University of Waterloo, Department of Systems Design Engineering, Waterloo, ON N2L 3G1, Canada, sbirkett@real.uwaterloo.ca), John McPhee (University of Waterloo, Department of Systems Design Engineering, Waterloo, ON N2L 3G1, Canada, mcphee@real.uwaterloo.ca)

A piano action mechanism converts a pianist's mechanical input into acceleration of the piano hammer, which impacts the string for tone generation. We present a multibody dynamic model of the mechanism, considering the differences when hammer shank flexibility is included as compared to a rigid shank. The model is developed using the graph theoretic approach and includes the hammer-string interaction. A Rayleigh beam model including complete second order deformation field is used for simulating hammer shank flexibility. The governing partial differential equation is discretized using Ritz approach considering Taylor monomials as assumed modes. A convergence study confirms that two bending modes and one axial mode are sufficient to represent the hammer shank deformation. The vibrating string is modeled using a standard modal analysis procedure. The many contacts between components of the mechanism include significant sliding during contact; for these contacts a modified Hunt-Crossley law is used to represent the normal force, and interface friction is handled using a Cull and Tucker friction model. The results of parametric studies show the effect of hammer head friction on the dynamics of the mechanism during string impact, as well as the influence of hammer shank flexibility on the frequency response of the string.

4pMUb6. A complex model for piano action. José Lozada (Laboratoire de Mécanique des Solides, Ecole Polytechnique, 91128 Palaiseau Cedex, France, jose.lozada@cea.fr), Xavier Boutillon (Laboratoire de Mécanique des Solides, Ecole Polytechnique, 91128 Palaiseau Cedex, France, boutillon@lms.polytechnique.fr), Moustapha Hafez (Laboratoire des Interfaces Sensorielles, CEA-LIST, 18 route du Panorama, BP 6, 92265 Fontenay-aux-Roses Cedex, France, moustapha.hafez@cea.fr)

Available mechanical models of piano action are extremely simplified in view of the complexity of an actual mechanism. Several arguments will be presented which indicate that more dynamical complexities than those offered by the current models are considered as intrinsic properties of good piano actions. A more complete model of a grand piano action during the attack of a note will be presented which includes the six degrees of freedom of the action, all considered as rigid bodies: the key, the damper, the whippen, the repetition lever, the jack, and the hammer. In this model, coupling features are represented by lumped elements: Coulomb friction, linear and nonlinear springs. Methods for characterizing each element of the model will be presented. The final result will be given in terms of dynamical equations, coupling equations, and geometrical constrains.

4pMUb7. Feature exaggeration in scale performance on the piano. Shinya Morita (Graduate School of Science and technology, Ryukoku University, 1-5, Yokotani, Oe-cho, Seta, 520-2194 Otsu, Shiga, Japan, t040550@mail.ryukoku.ac.jp), Norio Emura (Faculty of Engineering, Doshisha University, 1-3, Tataramiyakodani, 610-0321 Kyo-tanabe, Kyoto, Japan, etf1702@mail4.doshisha.ac.jp), Masanobu Miura (Graduate School of Science and technology, Ryukoku University, 1-5, Yokotani, Oe-cho, Seta, 520-2194 Otsu, Shiga, Japan, miura@rins.ryukoku.ac.jp), Seiko Akinaga (Department of Education, Shukugawa Gakuin College, 6-58, Kosikiiwa-cho, 662-8555 Nishinomiya, Hyogo, Japan, akinaga@shukugawa-c.ac.jp), Masuzo Yanagida (Faculty of Engineering, Doshisha University, 1-3, Tataramiyakodani, 610-0321 Kyo-tanabe, Kyoto, Japan, myanagid@mail.doshisha.ac.jp)

This paper proposes a set of parameters for describing features of scale-playing on the piano. The parameter set consists of 15 parameters, among which 12 are three sets of four parameters pi1 through pi4 where i ={1, 2, 3} distinguishes three basic features; onset time, velocity, and duration. Each of these basic features is modeled as the sum of a global curve and the deviation from it, where the spline interpolation is employed using locally averaged points, or representative points, as the points to be passed. The local average is calculated for each sequence of notes played without finger crossing. The suffix j in pij distinguishes the standard deviations (j=0), the rms deviation from the spline curve (j=1), the range of the curve (j=2), the rms difference between successive notes (j=3), and the rms of the spline curve from the metronomic line (j=4). All parameters are made controllable with slider bars from 0% to 200% for synthesizing suppressed performance or exaggerated performance, where 100% represents the original performance. Proposed parameter set is expected to be useful in self-training of piano, as it can indicate the features and undesirable habits of the player by setting values above 100% in exaggerated form.

Session 4pMUc

Musical Acoustics: Plucked Stringed Instruments II (Poster Session)

François Gautier, Cochair
Laboratoire d'Acoustique de I'Université du Maine

Chris Waltham, Cochair
University of British Columbia

All posters will be on display from 3:40 p.m. to 5:20 p.m. To allow contributors an opportunity to see other posters, contributors of odd-numbered papers will be at their posters from 3:40 p.m. to 4:30 p.m. and contributors of even-numbered papers will be at their posters from 4:30 p.m. to 5:20 p.m.

Contributed Papers

4pMUc1. The physics of the American five-string banjo. Laurie Stephey (Rollins College, Department of Physics, Winter Park, FL 32789, USA, lstephey@rollins.edu), Thomas Moore (Rollins College, Department of Physics, Winter Park, FL 32789, USA, tmoore@rollins.edu)

We report on a systematic study of the American five-string banjo, which was undertaken in an effort to understand the dynamics of this complex instrument. The deflection shapes of the membranic head were studied and catalogued using time-averaged electronic speckle pattern interferometry. The impedance presented to the strings was measured using laser Doppler vibrometry coupled with an integrated force sensor and harmonic driver. Additionally, time resolved spectral analysis of the plucked strings was used to quantify the characteristic decay of the coupled string/membrane system, while time-resolved interferometric studies of the membrane have led to a better understanding of the motion after a string is plucked. All of these investigations help to reveal the importance of the various parameters that affect the sound of this unusual instrument.

4pMUc2. The interaction between the strings and soundboard of a harp. Chris Waltham (University of British Columbia, Department of Physics & Astronomy, Vancouver, BC V6T 1Z1, Canada, cew@phas.ubc.ca)

The harp is an instrument with a set of plucked strings that excite the sound board directly, without the medium of a bridge. The strings are positioned at an acute angle to the plane of the sound board. The quality of the sound produced depends on the motion of the string, which is non-planar, and its interaction with the resonances of the sound board. The interaction is intrinsically non-linear as the soundboard responds to changes in both the angle and the tension of the string. To avoid the difficulties of string-string interactions on a real harp, a small test ″instrument″ has been constructed with a single string and a variable-angle sound board. The string and sound board motions have been measured simultaneously. Preliminary results will be presented.

4pMUc3. Categorization of guitars from bridge admittance measurements. François Gautier (Laboratoire d'Acoustique de l'Université du Maine, Avenue Olivier Messiaen, 72085 Le Mans, France, francois.gautier@univ-lemans.fr), Jean-Loic Le Carrou (Laboratoire d'Acoustique de l'Université du Maine, Avenue Olivier Messiaen, 72085 Le Mans, France, jean-loic.le_carrou@univ-lemans.fr),Maarten Hol(LAUM, CNRS, Université du Maine, Lab. d'Acoustique Université du Maine, UMR CNRS 6613, 72085 Le Mans Cedex 9, France, M.Hol@student .tue.nl), Vincent Doutaut (Institut Technologique Européen des Métiers de la Musique, 71 Av. O. Messiaen, 72000 Le Mans, France, Vincent.Doutaut @itemm.fr)

The acoustical characteristics of the guitar depend on the instrument makers' choices concerning the geometry, the material and the assembly techniques. The aim of this paper is to define criteria permitting the discrimination of guitars according to their acoustic characteristics. These criteria can be used, for example, by instrument makers to test the repeatability of their making process. Evaluation of the guitars' quality from this categorization is beyond the scope of this paper. A low-cost portable system allowing bridge admittance measurements has been designed and used on 4 groups of classical guitars, each being composed of about 10 similar instruments. A statistical study shows that the tested instruments can clearly be differentiated according to (1) the modal parameters associated to the first 2 vibroacoustic modes (air mode A0 and first soundboard mode T1), and to (2) a 'merit indicator', close to the one defined by C. Barlow (Proc.I.O.A., vol 19, Pt 5, 1997, 69-78). This 'merit indicator' is computed from the mean value of the bridge admittance and an estimation of the critical frequency of the soundboard.

4pMUc4. Modal analysis and transient string response of solid body electric bass guitars with effects of the instrumentalist. Dave Woolworth (Oxford Acoustics, Inc., 356 CR 102, Oxford, MS 38655, USA, dave@oxfordacoustics.com), Henry A. Scarton (Rensselaer Polytechnic Institute, Department of Mechanical Engineering, Troy, NY 12180, USA, scarton@rpi.edu)

This paper documents modal analysis of seven solid body electric basses. The basses are modeled in one dimension of motion normal to the face of the instrument in both free-free state and with boundary conditions imposed by a musician. The results are compared and analyzed in terms of bending and torsion. Analysis is done regarding open string harmonic content of the electromagnetic output over time versus the resonant frequencies of the instruments. Results of finite element analysis modeling of a simplified bass guitar structure will be presented, and significance of damping effects on harmonic output will be considered in terms of the listener.

Session 4pMUd

Musical Acoustics: Wind Instruments II (Poster Session)

Seiji Adachi, Cochair
Fraunhofer Institute for Building Physics

Simon Félix, Cochair
Laboratoire d'Acoustique de l'Université du Maine

All posters will be on display from 3:40 p.m. to 5:20 p.m. To allow contributors an opportunity to see other posters, contributors of odd-numbered papers will be at their posters from 3:40 p.m. to 4:30 p.m. and contributors of even-numbered papers will be at their posters from 4:30 p.m. to 5:20 p.m.

Contributed Papers

4pMUd1. Controllable pitch-bending effects in the accordion playing. R. Llanos-Vazquez (Dpto. Física Aplicada 1. Escuela Técnica Superior de Ingeniería, Alameda de Urquijo s/n, 48013 Bilbao, Spain, rucurdu@orange.es), M. J. Elejalde-García (Dpto. Física Aplicada 1. Escuela Técnica Superior de Ingeniería, Alameda de Urquijo s/n, 48013 Bilbao, Spain, mariajesus.elejalde@ehu.es), E. Macho-Stadler (Dpto. Física Aplicada 1. Escuela Técnica Superior de Ingeniería, Alameda de Urquijo s/n, 48013 Bilbao, Spain, erica.macho@ehu.es)

The accordion employs reeds in which the tongue is mounted outside the reed frame in such a way that sounding is normally possible only on one direction of airflow. Under normal operating conditions the reeds behave as blown-closed. Pitch bending technique allows players to make a controllable glide, non tempered glissando, from one pitch to another. Pitch-bending frequency shift, defined as the percentage of the ratio of the frequency change and the original frequency has been measured in a series of experiments. Some of the results involving the dependence of the function on pitch, direction of the bellows movement, cassoto possibilities and harmonic number are reported here. If the player qualifies, he/she can make controllable pitch-bending effects where the glissando may fall an exact semitone.

4pMUd2. Study the mouthpiece of the txistu. A. Agos-Esparza (Dpto. Física Aplicada 1. Escuela Técnica Superior de Ingeniería, Alameda de Urquijo s/n, 48013 Bilbao, Spain, bckagesa@ikasle.ehu.es), M. J. Elejalde-García (Dpto. Física Aplicada 1. Escuela Técnica Superior de Ingeniería, Alameda de Urquijo s/n, 48013 Bilbao, Spain, mariajesus.elejalde@ehu.es), E. Macho-Stadler (Dpto. Física Aplicada 1. Escuela Técnica Superior de Ingeniería, Alameda de Urquijo s/n, 48013 Bilbao, Spain, erica.macho@ehu.es)

The txistu is a three finger holed recorder from the Basque Country. The evolution of the txistu involves different kinds of wood, bore length, finger hole positioning and it being made of two or three pieces. The txistu also has a unique mouthpiece, made up by a small metallic piece of the pipe and also a metal reed which was introduced centuries ago. The distance between the pipe and the reed can be adjusted to fit the user's preferences. By using a blowing machine and data acquisition software, experiments study the influence of the shape and inclination of the reed on the values of the harmonic content and the sonority of the final note.

4pMUd3. Automated fingering services for woodwinds: development of a "virtual clarinet". Yakov Kulik (University of New South Wales, Music Acoustics, School of Physics, NSW 2052 Sydney, Australia, ykulik@phys.unsw.edu.au),Andrew Botros(University of New South Wales, Music Acoustics, School of Physics, NSW 2052 Sydney, Australia, ABotros@phys.unsw.edu.au), John Smith (University of New South Wales, Music Acoustics, School of Physics, NSW 2052 Sydney, Australia, john.smith@unsw.edu.au)

The Virtual Flute is a popular web service that recommends alternative fingerings for difficult passages, timbre variations, intonations or multiphonics. Its database was generated by a machine-learned expert system analysing waveguide models for all 39,744 fingerings. The relatively simple geometry of the flute and its tone holes allowed a simple yet accurate model. The development of similar systems for other woodwinds faces greater modelling and computational challenges. For example, the clarinet has a more complex geometry, with tone holes whose radius and length vary by factors of 4.2 and 2.8. Further, it has several million different fingerings. To achieve the required accuracy, individual measurements of each hole separately and of mouthpiece and bell, as well as several dozen fingering examples, were used to determine parameters of a still simple waveguide model. The model uses conical and cylindrical segments with parallel and shunt impedances at junctions, representing tone holes. This approach of incrementally enhancing our waveguide model allows computational advantages: an efficient, woodwind-generic software framework is built that can adapt to the instrument of interest. We report interim results with such a system, with further potential applications in the design of woodwind instruments and other acoustic duct systems.

4pMUd4. Source-resonator modeling: a rough paradox. Laurent P. Millot (IDEAT (University Paris 1), ENS Louis-Lumière, 7 allée du Promontoire, 93161 Noisy-le-grand, France, l.millot@ens-louis-lumiere.fr)

Using the example of a short pipe loaded by a free reed located upwards, we will underline the fact that a reflection function based modeling will not give the same results (and synthesized sounds) as an unsteady incompressible and lossless Bernoulli description while this model is commonly assumed to be a low-frequency limit case of the first one, and that the second description is the only valid one. This paradox will be explained and it will be underlined why the so-called electro-acoustical analogies do not constitute a low-frequency limit case of reflection function or input impedance descriptions, based on a waves paradigm. Extension to striking reeds and/or longer pipes, as found in saxophone, clarinet or sheng for instance, will be discussed and a strange coupling between a priori incompatible models, commonly used in Musical Acoustics notably, will be described.

4pMUd5. Sound quality of the 16'' french bagpipe: wood influence. Mathieu Paquier (LISyC EA 3883, 6 avenue Victor Le Gorgeu, CS 93837, 29238 Brest Cedex 3, France, mathieu.paquier@univ-brest.fr), Raphaël Jeannin (LISyC EA 3883, 6 avenue Victor Le Gorgeu, CS 93837, 29238 Brest Cedex 3, France, jeanninraphael@yahoo.fr)

The most played among the bagpipes from the centre of France is the 16-inch musette, called in this way because of the length of the melodic pipe (oboe). Though these instruments are less known than the biniou from Brittany or the Great Highland Bagpipe, the number of players and makers is, nowadays, in increase because of their easy play and quasi-chromatic scale. Whereas the Breton and Scottish bagpipes are always made of very hard woods, some 16'' musettes are fabricated with softer woods. This difference is certainly related to the flexibility of the 16'' oboe double-reed. At first, we recorded some short musical sequences played on 16'' musettes made of 5 different woods (African Ebony, Santos Rosewood, Boxwood, African Blackwood and Service Tree), then some listeners (specialist and naïve) were asked to give their feedback about the quality of the recorded sounds. In a second set of experiments, we recorded some single notes played with these various bagpipes and analyzed the acoustic features of the recorded signals. At last, the perceptual results were compared with the physical parameters obtained in the second experiment.

THURSDAY AFTERNOON, 3 JULY 2008 P2-D, LEVEL 2, 3:40 TO 5:20 P.M.

Session 4pMUe

Musical Acoustics: Control of Natural and Synthetic Musical Sounds II (Poster Session)

Marcelo Wanderley, Cochair
Centre for Interdisciplinary Research in Music Media & Technology (CIRMMT) - Schulich School of Music - McGill Univ.

Jean Kergomard, Cochair
Laboratoire de Mécanique et d'Acoustique CNRS UPR-7051

All posters will be on display from 3:40 p.m. to 5:20 p.m. To allow contributors an opportunity to see other posters, contributors of odd-numbered papers will be at their posters from 3:40 p.m. to 4:30 p.m. and contributors of even-numbered papers will be at their posters from 4:30 p.m. to 5:20 p.m.

Contributed Papers

4pMUe1. Exploration of timbre variations in music performance. Mathieu Barthet (CNRS-Laboratoire de Mécanique et d'Acoustique, 31 Chemin Joseph Aiguier, 13402 Marseille, France, barthet@lma.cnrs-mrs.fr), Philippe Guillemain (Laboratoire de Mécanique et d'Acoustique CNRS UPR-7051, 31, Chemin Joseph Aiguier, 13402 Marseille Cedex 20, France, guillemain@lma.cnrs-mrs.fr), Richard Kronland-Martinet (CNRS-LMA, 31, chemin Joseph Aiguier, 13402 Marseille, France, kronland@lma.cnrs-mrs.fr), Solvi Ystad (CNRS-LMA, 31, chemin Joseph Aiguier, 13402 Marseille, France, ystad@lma.cnrs-mrs.fr)

Timbre has seen during the twentieth century a growing attention from both musicians and scientists, the former to expand a traditional music system until now governed by the structures of pitches, the latter to better understand how timbre is produced and how it is processed by the perceptive and cognitive systems. In the music performance context, many studies deal with the role of timing and dynamics, but much fewer are dedicated to the one of timbre. The works presented here aim at showing the importance of timbre variations from two points of view: the production of sounds and their perception. The relations between the control parameters (mouth pressure and reed aperture) of a simplified physics-based clarinet synthesis model and the generated timbres have been investigated. Experiments have further been done to measure the within-individual consistency of timbre variations of a clarinet player repeating several instances of a musical excerpt from a Bach piece while keeping the same musical intention. Brightness variations characterized by the time-varying Spectral Centroid showed a strong consistency across the repetitions. The influence of such brightness variations on the perceived musical quality of a performance was then assessed thanks to an analysis-transformation-synthesis paradigm.

4pMUe2. Active Sound Design of a Bassoon. Frederic Konkel(TU Berlin, Institute of Fluid Mechanics and Engineering Acoustics, Einsteinufer 25, Sekr. TA 7, D-10587 Berlin, Germany, f.konkel@advacoustics.de), Andre Jakob (TU Berlin, Institute of Fluid Mechanics and Engineering Acoustics, Einsteinufer 25, Sekr. TA 7, D-10587 Berlin, Germany, kontakt@advacoustics.de), Frank Heintze (Staatskapelle Berlin, Staatsoper Unter den Linden, Unter den Linden 7, D-10117 Berlin, Germany, f.heintze@advacoustics.de), Michael Möser (TU Berlin, Institute of Fluid Mechanics and Engineering Acoustics, Einsteinufer 25, Sekr. TA 7, D-10587 Berlin, Germany, moes0338@mailbox.tu-berlin.de)

Possibilities of influencing the sound characteristics of a woodwind by means of active noise control were investigated. The woodwind used in this investigation was a bassoon. The first step of the investigation consisted of a set of measurements of the sound spectra of different tones and volumes by means of measurement microphones inside and outside the instrument. Additionally measurements of the radiation characeristics of the instrument were performed by means of the acoustic camera. An experimental setup was designed with the instrument driven mechanically by compressed air. The aim of the work was to change the sound characteristics of the bassoon by changing individual harmonics of the tones by means of a loudspeaker attached to the bassoon. The loudspeaker was attached to the bassoon via a tube. Suitable positions for the connection of the tube to the instrument were examined as well as suitable possibilites for the generation of the reference signal neccessary for the feedforward control scheme. The experimental setup will be presented here as well as results of the measurements with and without active sound design with an analog controller.

4pMUe3. The influence of control parameters and physical parameters on reed instruments playing. Jean Kergomard (Laboratoire de Mécanique et d'Acoustique CNRS UPR-7051, 31, Chemin Joseph Aiguier, 13402 Marseille Cedex 20, France, kergomard@lma.cnrs-mrs.fr), Philippe Guillemain (Laboratoire de Mécanique et d'Acoustique CNRS UPR-7051, 31, Chemin Joseph Aiguier, 13402 Marseille Cedex 20, France, guillemain@lma.cnrs-mrs.fr), Fabrice Silva (CNRS-Laboratoire de Mécanique et d'Acoustique, 31 Chemin Joseph Aiguier, 13402 Marseille, France, silva@lma.cnrs-mrs.fr), Christophe Vergez (CNRS-Laboratoire de Mécanique et d'Acoustique, 31 Chemin Joseph Aiguier, 13402 Marseille, France, vergez@lma.cnrs-mrs.fr)

An attempt to summarize the influence of both control and physical parameters on production and radiation of sound of reed instruments is given. Some parameters, such as the shape of the resonator, are fixed by the instrument maker, or chosen by the instrumentalist itself: the the reed, and the fixation of the reed on the mouthpiece. These parameters, named physical parameters, are fixed when playing. The second kind of parameters can be totally or partially controlled when playing: the fingering is an obvious one, then the way the reed is pinched by the lip, with an effect on both the reed opening and the reed dynamics, finally the mouth pressure and the shape of the vocal tract. The influence of these parameters is discussed with respect to several attributes of the sound: the various thresholds (normal sound at pianissimo level, extinction at fortissimo level), the control of different regimes, the shape of transients, the playing frequency, the spectrum. The state of present knowledge is given, with emphasis of further research that should be done, and a comparison with the cases of sound controllers and artificial mouth is discussed.

4pMUe4. A setup for measurement of bowing parameters in bowed-string instrument performance. Erwin Schoonderwaldt (Dept. of Speech, Music and Hearing, Royal Institute of Technology (KTH), Lindstedtsvägen 24, SE-100 44 Stockholm, Sweden, schoondw@kth.se), Matthias Demoucron (IRCAM, 1 Place Igor Stravinsky, 75004 Paris, France, demoucron@ircam.fr), Nicolas Rasamimanana (IRCAM, 1 Place Igor Stravinsky, 75004 Paris, France, rasamimanana@ircam.fr)

An accurate measurement of instrumentalists' actions in playing situations is the basis for several research topics such as musical performance analysis, control of sound synthesis algorithms or effective validation of theoretical results in musical acoustics. We present a setup for a complete and accurate measurement of bowing parameters in bowed-string instrument performance, with minimum interference for the player. The method is based on the combined use of motion capture and sensors attached to the bow. An optical motion capture system was used to track the position and orientation (6 DOF) of the bow and the instrument. In addition, sensors were attached to the frog of the bow for measuring bow acceleration in different axes and bow force exerted on the strings. Both sensors can be easily attached to any bow. We will describe how the data from the different systems are combined for an accurate calculation of bowing parameters, such as bow-bridge distance, bow velocity, bow acceleration, bow angles and bow pressure. Finally, we will present examples of measurements and briefly discuss some potential applications.

THURSDAY AFTERNOON, 3 JULY 2008 P2-D, LEVEL 2, 3:40 TO 5:20 P.M.

Session 4pMUf

Musical Acoustics: Virtual Musical Instruments II (Poster Session)

Julius Smith, Cochair
Stanford Univ.

Antoine Chaigne, Cochair
ENSTA

All posters will be on display from 3:40 p.m. to 5:20 p.m. To allow contributors an opportunity to see other posters, contributors of odd-numbered papers will be at their posters from 3:40 p.m. to 4:30 p.m. and contributors of even-numbered papers will be at their posters from 4:30 p.m. to 5:20 p.m.

Contributed Papers

4pMUf1. Simulation of Acoustic Pressure and Flow Velocity in Human Glottis. Petr Sidlof (Academy of Sciences of the Czech Republic, Narodni 3, 11720 Prague, Czech Republic, sidlof@it.cas.cz), Antoine Chaigne (ENSTA, Chemin de la Hunière, 91761 Palaiseau, France, antoine.chaigne@ensta.fr), Olivier Doare (ENSTA, Chemin de la Hunière, 91761 Palaiseau, France, olivier.doare@ensta.fr), Olivier Cadot (ENSTA, Chemin de la Hunière, 91761 Palaiseau, France, olivier.cadot@ensta.fr)

The pressure and velocity fields in coronal plane along the vibrating vocal folds were studied using a finite element mathematical model. The shapes of the vocal folds were specified according to data measured on excised human larynges in phonation position. The mathematical model of the flow is based on 2D incompressible Navier-Stokes equations adapted to deal with the time-variable shape of the domain, caused by vocal fold vibration. The numerical simulations allow to observe closely various flow features related to phonation - flow separation in the glottis, Coanda effect or vortex shedding. The numerical results were verified experimentally by Particle Image velocimetry (PIV) on a physical vocal fold model. In addition to acoustic, subglottal pressure and impact intensity measurements, flow velocity fields were recorded in the domain immediately above glottis. Analysis of the PIV images gives good insight into the dynamics of the supraglottal flow. Among other applications, the results should be used in the future for singing voice simulations based on physical models.

4pMUf2. A synthesis and analysis framework for wind instrument sounds based on the digital pulse forming principle. Michael Oehler (Institute for applied Musicology and Psychology, Saarstrasse 1A, 50677 Koeln, Germany, michael.oehler@iamp.info), Christoph Reuter (University of Cologne - Musicological Institute, Beethovenstrasse 4, 50674 Koeln, Germany, info@chr-reuter.de)

A digital real-time-capable analysis- and synthesis-system for wind instrument sounds, based on the pulse forming theory, has been developed. The rediscovered model for the sound generating process of wind instruments rests upon the idea, that wind instrument sounds can basically be put down to its excitation impulses, which independently of the fundamental always behave according to the same principles. First realised in the analogue wind instrument synthesizer Realton Variophon (1975), the sound synthesis method has currently been transferred onto a digital platform [supported by the German Research Foundation]. Instrument specific algorithms control the pulse width and shape according to the applied pitch and dynamic values. That way subtle sound nuances that can be produced on acoustic wind instruments as well as real timbre modulation may be synthesized by just modifying a single parameter (i.e. breath pressure). In order to validate the performance of the developed framework, several perception experiments were conducted subsequently.

4pMUf3. Perceptual effects of radiation control with a multi-louspeaker device. Nicolas Misdariis (IRCAM - UMR CNRS 9912, Equipe Perception et Design Sonores, 1, place Igor Stravinsky, 75004 Paris, France, misdarii@ircam.fr), Alexandre Lang (Université de Technologie de Compiègne, E.A. Costech - Groupe de Suppléance Perceptive, BP 60319, 60206 Compiègne Cedex, France, lang.alexandre@gmail.com), Brian F. Katz (LIMSI-CNRS, B.P. 133, 91403 Orsay, France, brian.katz@limsi.fr), Patrick Susini (IRCAM - UMR CNRS 9912, Equipe Perception et Design Sonores, 1, place Igor Stravinsky, 75004 Paris, France, susini@ircam.fr)

This study investigates the perceptual issue of acoustical radiation control with the following hypothesis: radiation control can reduce the perceptual gap between a sound coming from an acoustical source (e.g., an instrument) and a sound coming from an electro-acoustical device (e.g., the recording of an instrument played by a loudspeaker). The work is technically supported by a generic multi-loudspeaker device that allows sound reproduction with controlled directivity patterns in a given number of spatial dimensions. The conducted experiment involves two distinct sound corpus: speaking/singing voice (recorded and spatially measured) and a struck plate (synthesized and spatially computed with modeled directivity). Incremental levels of radiation pattern control, in terms of precision of the reproduction, are also considered by combining several diffusion systems and different directivity patterns. Participants are asked to evaluate the stimuli on three semantic differential scales: source width (largeur), distance (distance) and realism (réalisme). The results show a global significant effect of radiation on sound perception: the acoustical/electro-acoustical gap is significantly reduced through radiation control, especially when considering the scales of width and distance. Theoretical principles, technical elements, experimental set-up and overall results will be presented, detailed and discussed during the presentation.

4pMUf4. Measuring and Modeling Violin Sound Radiation for Sound Equalization. Alfonso Perez Carrillo (Pompeu Fabra University, Ocata 1,3°, 08003 Barcelona, Spain, aperez@iua.upf.edu), Jordi Bonada (Pompeu Fabra University, Ocata 1,3°, 08003 Barcelona, Spain, jbonada@iua.upf.edu), Esteban Maestre (Pompeu Fabra University, Ocata 1,3°, 08003 Barcelona, Spain, emaestre@iua.upf.edu), Enric Guaus (Pompeu Fabra University, Ocata 1,3°, 08003 Barcelona, Spain, eguaus@iua.upf.edu), Merlijn Blaauw (Pompeu Fabra University, Ocata 1,3°, 08003 Barcelona, Spain, mblaauw@iua.upf.edu)

During a performance a violin is put into vibration and this vibration is radiated to the air. Depending on the distance and direction of the listener, he perceives a slightly different sound. Sound radiation at each point in the space is determined by the impulse response or transfer function between vibration of the violin and sound pressure at that point. There is variety of methodologies to obtain acoustic impulse responses of violins. They differ mainly in the way of exciting the violin, the point of excitation, the position where the acoustic response is measured and how excitation and response signals are deconvolved. In this work we measure violin vibration with a bridge pickup and we 1) propose a method to calculate the transfer function between signals from the bridge pickup and a microphone, 2) use a 3D motion tracker to get the position of the microphone respect to the violin so that we can calculate the response for different directions and distances and 3) we model sound radiation as a ″reference″ impulse response and a parametric filter whose response depends on distance and orientation with respect to the ″reference″ position.

4pMUf5. Virtual electric guitars and associated audio effects in Faust and C++. Julius O. Smith (Stanford Univ., Center for Computer Research in Music and Acoustics (CCRMA), Dept. of Music, Stanford, CA 94305-8180, USA, jos@ccrma.stanford.edu)

Advances in computing technology, both in hardware and software, are enabling new levels of performance in real-time for virtual musical instruments based on acoustic principles. This paper is concerned with software implementation technology for such instruments, written in high-level languages that compile down to efficient low-level implementations on a wide variety of platforms. Specific results will be presented for the case of virtual electric guitars and associated digital audio effects expressed in the Faust and C++ languages, and compiled to become plugins for VST, Pure Data, and other real-time performance environments. This work builds upon a previous paper at the Linux Audio Conference (LAC-2008), and laboratory module written for the RealSimple project at CCRMA (http://ccrma.stanford.edu/realsimple/).

4pMUf6. Fine tuning of guitar sounds with changed top plate, back plate and rim geometry using a whole body 3D Finite-Difference model. Rolf Bader (University of Hamburg, Institute of Musicology, Neue Rabenstr. 13, 20354 Hamburg, Germany, R_Bader@t-online.de)

The change of radiated sounds from guitars is investigated in terms of the fine tuning of these sounds applying slight changes to the guitar body, instrument builders would do with their guitars. As changes of these geometries of real guitars can only be perceived when the instrument is put together, the question is mostly open how different the whole instrument would have sounded with slight changes. So here the virtual guitar can be of great use. In the model, the top plate thickness, fan bracing, rim thickness and back plate geometry were changed in a linear way. Then these results could be associated directly to a change in only one geometry parameter. It is not assumed, that the sounds fit one existing guitar perfectly. Rather th overall influence of these changes on the sounds is investigated to show an overall behaviour. As the eigenfrequencies of the guitar body are that many, that a more or less closed resonance curve is achieved (without so-called 'dead spots'), the changes in the sounds are measured in the following terms: changes in the initial transient of the sounds, its brightness using the spectral centroid, its density using a spectral entropy measurement and amplitude fluctuations of the different sound partials.

4pMUf7. Nonlinear vibrations of impacted rectangular plates. Comparison between numerical simulation and experiments. Cédric Camier (ENSTA, Chemin de la Hunière, 91761 Palaiseau cedex, France, cedric.camier@ensta.fr), Kevin Arcas (ENSTA, Chemin de la Hunière, 91761 Palaiseau, France, arcas@ensta.fr), Stefan Bilbao (University of Edinburgh, Room 7306B, JCMB, King's Bldgs., Mayfield Rd., EH9 3JZ Edinburgh, UK, sbilbao@staffmail.ed.ac.uk)

Large amplitude vibrations of free-edge rectangular plates, subjected to an impulse excitation is addressed. In particular, this work is devoted to the analysis and simulation of a nonlinear von Kármán plate equations and by associate experimental investigations. Time domain simulations are achieved using implicit finite differences (FD) schemes recently developed by Bilbao. These energy-conserving methods guarantee the stability of the algorithm. To compare with simulations results, an experimental setup which allows reproducible impulse excitation and measurements by laser vibrometry has been developed. The time history of the force applied to a rectangular steel plate is recorded and this signal is used as excitation term in the simulations. We perform a parametric study, with both experimental and

numerical approaches, by increasing gradually the amplitude of forcing. Non-linear phenomena, such as pitch glide and chaotic behaviour are observed and discussed.

4pMUf8. Active control of a vibrating string. Edgar Berdahl (Stanford Univ., Center for Computer Research in Music and Acoustics (CCRMA), Dept. of Music, Stanford, CA 94305-8180, USA, eberdahl@ccrma.stanford.edu), Guenter Niemeyer (Stanford Univ., Mech. Eng., Bldg. 530, Stanford, CA 94305, USA, gunter.niemeyer@stanford.edu), Julius O. Smith (Stanford Univ., Center for Computer Research in Music and Acoustics (CCRMA), Dept. of Music, Stanford, CA 94305-8180, USA, jos@ccrma.stanford.edu)

We discuss the specifics of applying active feedback control to a vibrating string. Using sensors, actuators, and digital controller hardware, we make the acoustics of the string programmable, yet the string retains its tangible qualities. As a consequence, fretting, bowing, and plucking controlled and uncontrolled strings have similar physical consequences. Consider that any controller emulating a network of springs, masses, and dashpots attached to the string is a passive controller. To allow the string's acoustics to be programmable over a wide range, we should be able to implement passive controllers. This means that there must be at least one linear and collocated sensor/actuator pair. We explain how to construct such a pair in the laboratory. Finally, we explain one controller particular to one-dimensional systems such as vibrating strings. Whenever the sensor detects a pulse arriving, the actuator emits a new pulse. The output spectrum consists of a harmonic series proportional to the sampling of the product of the pulse's Fourier transform and the transfer function from the actuator to the sound recording device. Sound examples are presented. Finally, we discuss an open source environment we have created for adjusting controller parameters in real time from standard computer music software.

4pMUf9. Interfacing Digital Waveguide with CORDIS ANIMA networks. Alexandros Kontogeorgakopoulos (ACROE-ICA (Institut National Polytechnique de Grenoble), 46 av. Félix Viallet, 30031 Grenoble, France, alexandros.kontogeorgakopoulos@imag.fr), Claude Cadoz (ACROE-ICA (Institut National Polytechnique de Grenoble), 46 av. Félix Viallet, 30031 Grenoble, France, claude.cadoz@imag.fr)

The aim of this article is mainly to offer a link between the Digital Waveguide and the CORDIS-ANIMA physical modeling formalism. The first one is highly a modular lumped physical modeling and simulation system based on the mass-interaction paradigm while the second one offers accurate and efficient discrete time distributed models synthesized typically by delay lines and scattering junctions, in combination with digital filters. Both of them are widely developed and used in the domain of computer music field by scientists and artists. Although Digital Waveguide models have already been combined with Wave Digital Filters, they have never been exploited and integrated with CORDIS ANIMA networks. Wave Digital Filters are lumped models which are based on a scattering theoretic formulation which simplifies interfacing to Digital Waveguide models in contrast with the CORDIS ANIMA models. This research investigates the similarities of those formalisms, as well as focuses on the advantages of each modeling technique and proposes a real time computable interface between them. Moreover it results as well in a common convenient structural representation of their computational algorithms using signal processing block diagrams. These hybrid models were designed directly by their block diagrams, simulated and run in differ time using the Simulink software package of the matlab technical computing language.

THURSDAY AFTERNOON, 3 JULY 2008 ROOM 250A, 2:00 TO 3:40 P.M.

Session 4pNSa

Noise and EURONOISE: Vibration Perception I

Patricia Davies, Cochair
Ray W. Herrick Lab., School of Mechanical Engineering, Purdue Univ., 140 S. Martin Jischke Drive, West Lafayette, IN 47907-2031, USA

Michael J. Griffin, Cochair
Institute of Sound and Vibration Research, University of Southampton, Human Factors Research Unit, Southampton, SO17 1BJ, UK

Invited Papers

2:00

4pNSa1. Recent research activities for the assessment of vibration in living environment with respect to human perception in Japan. Yasunao Matsumoto (Saitama University, 255 Shimo-Ohkubo, Sakura, 338-8570 Saitama, Japan, ymatsu@mail.saitama-u.ac.jp), Sunao Kunimatsu (National Institute of Advanced Industrial Science and Technology, Tsukuba Central 7, 1-1-1 Higashi, 305-8567 Tsukuba, Japan, s.kunimatsu@aist.go.jp), Takashige Ishikawa (Japan Women's University, 2-8-1 Mejirodai, Bunkyou, 112-8681 Tokyo, Japan, ishikawa@fc.jwu.ac.jp), Yoshihiro Hirao (Kobayashi Institute of Physical Research, 3-20-41 Higashi-Motomachi, 185-0022 Tokyo, Japan, hirao@kobayasi-riken.or.jp)

The number of complaints against vibration has been increasing gradually in recent years in Japan. This fact may imply problems of the Vibration Regulation Law that was implemented almost 30 years ago so as to regulate vibrations caused by factories and construction works and to mitigate vibration problems caused by road traffic. A group of experts has been investigating an assessment method that may be able to assess recent vibration problems reasonably since 2004. This paper presents a part of group activity that aims at improving the understanding of human vibration perception and applying it in vibration assessment in living environment. Results obtained from experiments involving human subjects to determine perception thresholds of whole-body vibration are summarised.

2:20

4pNSa2. Development of a social survey questionnaire of reactions to vibration in residential buildings. Henrietta Howarth (Institute of Sound and Vibration Research, University of Southampton, Human Factors Research Unit, SO17 1BJ Southampton, UK, h.howarth@soton.ac.uk), Michael J. Griffin (Institute of Sound and Vibration Research, University of Southampton, Human Factors Research Unit, SO17 1BJ Southampton, UK, M.J.Griffin@soton.ac.uk)

A social survey questionnaire has been developed to determine human responses to vibration in residential environments. The overall aim was to produce a robust methodology for obtaining responses that could be combined with vibration measurements so as to investigate dose-response relationships for vibration in residential buildings. The vibration considered included that from sources outside the control of residents (e.g., road, rail, industrial, construction). This paper describes the development of the questionnaire and explains its structure and content. A review of social surveys and field and laboratory studies of vibration and noise is included. Methods of analysing responses obtained to the questionnaire are summarised.

2:40

4pNSa3. Cross-modality matching of loudness and whole-body vibration strength. Stephan Töpken (Oldenburg University, Institute of Physics - Acoustics, Carl-von-Ossietzky Str. 9-11, 26111 Oldenburg, Germany, stephan.toepken@uni-oldenburg.de), Michael Bellmann (ITAP GmbH, Marie-Curie Str. 8, 26129 Oldenburg, Germany, Bellmann@itap.de), Reinhard Weber (Oldenburg University, Institute of Physics - Acoustics, Carl-von-Ossietzky Str. 9-11, 26111 Oldenburg, Germany, Reinhard.Weber@uni-oldenburg.de)

In every day live humans are often exposed to noise and vibration simultaneously. Regarding comfort issues inside a car, it is of interest to know, whether the simultaneous perceptions of noise and vibration interfere. Laboratory tests have been carried out with temporally overlapping, partially overlapping and non overlapping presentations of acoustic and whole-body vibration stimuli. Sitting on a rigid chair on a vibration test bench, participants are asked to judge the strength of the excited whole-body vibrations in comparison to the loudness of noise presented via closed headphones. An adaptive method is employed to determine the subjective point of equality (PSE) between both sensory channels. The acoustic stimulus is a 1/2-octave band-pass noise centred at 100 Hz with a fixed noise level, the vibration stimulus is a narrowband noise, also 1/2-octave broad with a centre frequency of 31,5 Hz. The signals have an equal duration of one second. The signal parameters are chosen with respect to specific situations in a car. The PSE's of the loudness and the vibration strength as a function of the temporal order of the acoustic and vibration stimuli exhibit no dependency on the degree of temporal overlap of the stimulus presentation.

3:00

4pNSa4. Thresholds for the perception of fore-and-aft, lateral and vertical vibration by seated persons. Miyuki Morioka (Institute of Sound and Vibration Research, University of Southampton, Human Factors Research Unit, SO17 1BJ Southampton, UK, M.Morioka@soton.ac.uk), Michael J. Griffin (Institute of Sound and Vibration Research, University of Southampton, Human Factors Research Unit, SO17 1BJ Southampton, UK, M.J.Griffin@soton.ac.uk)

Vibration experienced in transport and in buildings can yield discomfort or annoyance if the vibration exceeds the threshold for vibration perception. Knowledge of thresholds makes it possible to determine which frequencies and directions of low magnitude vibration give rise to perception. The effect vibration frequency (2 to 315 Hz) on absolute thresholds for the perception of whole-body vibration has been determined experimentally with 12 seated persons for each of the three axes of excitation (fore-and-aft, lateral and vertical). The frequency-dependence of the thresholds differed between the three axes. At frequencies, greater than 10 Hz, sensitivity was greatest for vertical vibration. At frequencies less than 3.15 Hz, sensitivity was greatest to fore-and-aft vibration. In all three axes, the acceleration threshold contours at frequencies greater than 80 Hz were U-shaped, suggesting the same psychophysical channel mediated high frequency thresholds for fore-and-aft, lateral and vertical vibration. It is shown that the frequency-dependence of absolute thresholds for the perception of whole-body vibration are not consistent with the frequency weightings used in current standards.

Contributed Paper

3:20

4pNSa5. Is there a perceptive signature of vehicles vibrations? Maël Amari (PSA Peugeot Citroën, Centre Technique de Vélizy, Route de Gisy, 78943 Vélizy-Villacoublay, France, mael.amari@mpsa.com), Etienne Parizet (Laboratoire Vibrations Acoustique, Insa Lyon, 25 bis, av. J. Capelle, 69621 Villeurbanne Cedex, France, etienne.parizet @insa-lyon.fr), Vincent Roussarie (PSA Peugeot Citroën, Centre Technique de Vélizy, Route de Gisy, 78943 Vélizy-Villacoublay, France, vincent .roussarie@mpsa.com)

The vibro-acoustic comfort of vehicles running at low speed has been studied for several years by car manufacturers. Even if car passengers are exposed to a complex environment involving sight, hearing and touch, it is generally agreed that vibrations transmitted through the seat is a very significant parameter in such situations. Previous laboratory experimentations revealed that vehicles were strongly discriminated even when subjects were submitted to seat vibrations only. The ranking of vehicles was also identical for different tested roads. All these observations raised the question of the existence of an identifiable signature of vehicles, independent of the road type. A perceptive experiment designed to evaluate the influence of such phenomenon was conducted. Subjects were submitted to a free sorting test. The categorisation task consisted in grouping vibrations stimuli recorded in 9 cars running on 3 differents roads according to their similarity. The RMS level of stimuli was normalised so that its effect was not predominant during the experiment. Results showed that stimuli groups corresponded to the 3 tested roads, and were correlated to time envelopes of vibrations. Vehicles were not significantly discriminated.

Session 4pNSb

Noise, Architectural Acoustics, and EURONOISE: Noise, Vibration and Acoustics for Medical and Research Facilities and Their Occupants I

James West, Cochair
Johns Hopkins University, Department of Electrical Engineering, 3400 North Charles Street, Baltimore, MD 21218, USA

Jack B. Evans, Cochair
JEAcoustics, 1705 West Koenig Lane, Austin, TX 78756, USA

Marc Asselineau, Cochair
Peutz & Associés, 10 rue des Messageries, Paris, F75010, France

Erica Ryherd, Cochair
Woodruff School of Mechanical Engineering, Georgia Institute of Technology, Atlanta, GA 30332-0405, USA

Invited Papers

2:00

4pNSb1. Toward a comprehensive hospital noise reduction research program. Ilene Busch-Vishniac (McMaster University, 1280 Main Street West, Hamilton, ON L9G 4X6, Canada, provost@mcmaster.ca), James West (Johns Hopkins University, Department of Electrical Engineering, 3400 North Charles Street, Baltimore, MD 21218, USA, jimwest@jhu.edu)

Over the last few years there has been a growing interest in the control of hospital noise. This is prompted by a number of drivers: the recognition that hospital noise is a top complaint of patients, staff, and visitors; the move to a digital hospital and the impediment of speech recognition in very noisy environments; the implications of HIPAA and speech privacy on hospitals; and concerns about safety when communication is compromised by noise. Although there are now a number of studies of various issues associated with hospital noise, each views only a small piece of the very complicated problem. This presentation outlines a comprehensive noise research program designed to link acoustical measures with noise interventions and with staff and patient outcomes. Only through such an approach will it be possible to answer important questions such as which noise interventions are most effective and what hospital design strategies are most effective in terms of noise mitigation.

2:20

4pNSb2. Describing the sound environment of the neurological intensive care unit and personnel response. Erica Ryherd (Woodruff School of Mechanical Engineering, Georgia Institute of Technology, Atlanta, GA 30332-0405, USA, erica.ryherd@me.gatech.edu), Kerstin Persson Waye (Dept. of Environ. Medicine, The Sahlgrenska Acad. of Gothenburg Univ., Box 414, 405 30 Gothenburg, Sweden, kerstin.persson-waye@amm.gu.se)

The hospital soundscape is populated with a number of noise sources that may be detrimental to the occupational environment, including medical equipment, alarms, portable carts, activities, paging/communication, and ventilation systems. This paper describes a study in which sound measurements were made over five days and occupant evaluations were conducted in a neurological intensive care unit (ICU). Forty-seven nursing staff members completed questionnaires regarding general reactions to the ICU environment as well as perceived psychological and physiological reactions to the noise. Acoustical characteristics such as level distributions, restorative periods, and spectral content were explored in addition to overall equivalent, minimum, maximum, and peak sound pressure levels. Results showed the mean length of restorative periods (LAeq below 50 dB for more than 5 min) was 9 and 13 minutes for day and night, respectively. Sound measurements near the patients showed LAeq values of 53 - 58 dB, and dosimeters worn by the personnel revealed higher noise levels. Questionnaire results indicated that 91% of those surveyed felt that the noise negatively affected them in their daily work environment. They perceived the noise as contributing to stress symptoms such as irritation, fatigue, tension headaches, and difficulties concentrating. [Work supported by ASA and Swedish FAS].

2:40

4pNSb3. Indoor environment and acoustic conditions in two Finnish hospital wards. Annu Haapakangas (Finnish Institute of Occupational Health, Lemminkäisenkatu 14-18 B, 20520 Turku, Finland, annu.haapakangas@ttl.fi), Riikka Helenius (Finnish Institute of Occupational Health, Lemminkäisenkatu 14-18 B, 20520 Turku, Finland, riikka.helenius@ttl.fi), Valtteri O. Hongisto (Finnish Institute of Occupational Health, Lemminkäisenkatu 14-18 B, 20520 Turku, Finland, valtteri.hongisto@ttl.fi)

The aim of this study was to determine the acoustic conditions of two typical Finnish wards. The methods included long-term noise measurements, building acoustical measurements and questionnaires for patients (N=33) and nurses (N=27). The average sound pressure levels were within 49 and 58 dBA in the corridors, office and patient rooms. Personal noise exposure levels among nurses were within 56 and 70 dBA. The noise was mainly caused by people. Ventilation noise level was 28 dBA. Building acoustic measurements

showed reasonable agreement with national directions. Indoor environment was not a problem for most patients. Some disturbance from thermal conditions, dry air and noise was experienced. From daytime noise sources, other patients' snore and groans caused annoyance in some patients. Night-time sleep was disturbed most by anxiety, pain, noise, thermal conditions and an uncomfortable bed. Patients were, on average, quite satisfied with the overall room conditions. Nurses were more bothered by environmental factors than patients, giving highest annoyance ratings to thermal conditions, air quality and noise. Noises were experienced to cause some distraction when concentrating to work tasks. Sounds of phones ringing were experienced as particularly detrimental. Lack of privacy was the most obvious problem in both staff and patient evaluations.

3:00

4pNSb4. Eliminating environmental stressors in hospitals: managing noise through different interventions. Michael Phiri (The University of Sheffield, School of Architecture, Arts Tower, Western Bank, S10 2TN Sheffield, UK, m.phiri@sheffield.ac.uk)

There is growing body of knowledge of over 1,000 scientific studies which provide evidence that patients experience positive health outcomes in an environment that incorporates natural light, elements of nature, soothing colours, meaningful and varying stimuli, peaceful sounds, pleasant views and a sense of beauty. This paper reviews the research, its practical applications in order to enhance acoustics comfort and quality of care in healthcare settings. Healthcare planners can carry out small-scale, medium- and large-scale evidence-based design interventions. Small-scale interventions which minimise cost maximise impact on acoustic comfort can be implemented relatively quickly and easily e.g. provision of rubbish bins with a damping system to close lids slowly, dimming lights on the wards etc. Control measures include strategies to reduce noise levels in healthcare facilities with or without physical environmental alterations including specification of appropriate absorbent materials (e.g. acoustic ceiling tiles). Medium-scale interventions e.g. inpatient or nursing unit design involve consideration of the shape, geometry and other characteristics of a room in order to deal with background noise, speech intelligibility and other elements which promote acoustic comfort. Large-scale interventions involve large capital works notably entire hospital complexes, assemblies of departments/specialties but have evidence extrapolated from the small- and medium-scale interventions.

3:20

4pNSb5. Improved perception of sound environments through room acoustic interventions. Marc R. Janssen (Saint-Gobain Ecophon AB, Box 500, 26061 Hyllinge, Sweden, marc.janssen@ecophon.se)

Noise in hospitals is apparently among the top complaints of patients, visitors, and staff. An increasing amount of evidence shows the negative effects of sound within health care environments, affecting the quality of care in the end. Very few hospitals have actually been able to characterize hospital noise and to find effective noise control approaches. This paper will show international results of room acoustic interventions on the patients and staff perception of the sound environment. Next to that the suggestions will be presented on the use of relevant acoustical parameters to support the performance and well-being of staff and patients. One specific example will deal with a case study at the Thorax ICU at the Karolinska University Hospital in Stockholm. The purpose of the study has been to clarify how room acoustics in a patient ward affect the staff's perception of the noise situation in that ward. Another purpose has been to develop a better understanding of how a set of requirements for room acoustics should be formulated in order to obtain a supportive health care environment. It is possible to conclude that, by adding more absorption to the room, the noise situation has been positively influenced and perceived.

3:40-5:20 Posters

Lecture sessions will recess for presentation of poster papers on various topics in acoustics. See poster sessions for topics and abstracts.

Contributed Paper

5:20

4pNSb6. Aural Connectivity: Enhancing sound environments in critical care settings for effective nurse auditory monitoring. Selen Okcu (Georgia Institute of Technology, College of Architecture, Atlanta, GA 30332-0155, USA, okcuse@yahoo.com), Craig Zimring (Georgia Institute of Technology, College of Architecture, Atlanta, GA 30332-0155, USA, craig.zimring@coa.gatech.edu), Erica Ryherd (Woodruff School of Mechanical Engineering, Georgia Institute of Technology, Atlanta, GA 30332-0405, USA, erica.ryherd@me.gatech.edu)

In intensive care unit (ICU) settings, the sound environment is critically important to nurses accomplishing their tasks. In earlier studies by the authors, it was found that non-amplified environmental sounds such as patient bodily sounds, patient threatening/unusual sounds, and help calls from patients and other caregivers are critically important auditory cues that nurses must listen for and respond to immediately. These sounds do not exist in isolation but matter as a pattern of aural connectivity that can support a nurse's critical monitoring abilities as she moves through her workplace. Aural connectivity is a network measure that reflects the overall pattern of where users can hear and respond to different key sounds within a setting. This paper describes the sound environments of two ICU hospital settings with similar patient acuity levels but differing layout designs. Preliminary results regarding the patterns of aural connectivity and the role that layout design might play in those patterns are discussed and potential implications for layout design are proposed.

5:40

4pNSb7. Vibration Effects on Laboratory Mice during Building Construction. Richard A. Carman (Wilson, Ihrig & Associates, 5776 Broadway, Oakland, CA 94618, USA, rcarman@wiai.com), Deborah A. Jue (Wilson, Ihrig & Associates, 5776 Broadway, Oakland, CA 94618, USA, djue@wiai.com), Gary M. Glickman (Wilson, Ihrig & Associates, 65 Broadway, Suite 401, New York, NY 10006, USA, gglickman@wiai.com)

Laboratory animals, in particular mice, are an integral part of medical and scientific research. Genetic research involving mice can be substantially affected by disruptions to the animals' environment. A new research facility is being built in close proximity to an existing one and the work will involve both demolition and new construction. Prior to construction, a study was conducted at the research facility to establish acceptable vibration levels in the vivaria areas. The study involved an experiment using an electrodynamic shaker to determine the effect of whole-body vibration on pregnant mice. The results of that study have been published. During construction, continuous vibration monitoring was conducted and the program and instrumentation used for monitoring are described. Results are presented, which include the researchers' data on the observed effects on the mice as well as the measured vibration levels during the construction.

6:00

4pNSb8. ″Vibration Kills″ and other lessons from the trenches. Hal Amick (Colin Gordon & Associates, P. O. Box 39, San Bruno, CA 94066, USA, hal.amick@colingordon.com), Michael L. Gendreau (Colin Gordon & Associates, P. O. Box 39, San Bruno, CA 94066, USA, michael.gendreau@colingordon.com)

In many areas of acoustics and vibration design, criteria are based upon parameters such as comfort, privacy, intelligibility, productivity, or machine precision. One can approach these criteria with a somewhat dispassionate attitude. However, when working with the biological research communities, one is periodically reminded by the researchers and medical practitioners that much of their work ultimately deals with life-and-death issues, either for patients for whom a drug or medical device is intended, or for organisms used in test protocols. The authors will share a collection of case studies in which these issues are illustrated. These include: Death of cells due to excessive vibration during electrophysiology. Vibration-induced nausea experienced by a surgeon using a surgical microscope for spine surgery. A life-saving medical technology resulting from a serendipitous discovery in a low-vibration lab environment. These case studies highlight the need for care in the specification, design, and construction of biological and biomedical research and healthcare facilities.

6:20

4pNSb9. Don't forget the quench pipe when installing an MRI. Carel Ostendorf (Cauberg-Huygen R.I. BV, Postbus 480, 6200 AL Maastricht, Netherlands, c.ostendorf@chri.nl)

An MRI is a useful medical device but it makes a lot of noise. A sound level of 90 dB(A) or more in the MRI room is not unusual. Placing an MRI in an existing hospital means that extra care has to be taken to prevent the noise from the MRI causing nuisance in adjacent rooms. In this paper the situation is discussed in which complaints appeared after the installation of the MRI. First sound measurements were done to see if the sound level in the office above the MRI fulfils the noise ratings. This way it would be clearer if the acoustic measures were doing their job. Whatever the outcome, the hospital wanted to put an end to the complaints. So, more sound measurements were done to establish the cause of the nuisance and to point out what extra measures have to be taken to solve the problem. It turned out that the quench pipe played an important role in this situation.

6:40

4pNSb10. Generic noise criterion curves for sensitive equipment. Michael L. Gendreau (Colin Gordon & Associates, P. O. Box 39, San Bruno, CA 94066, USA, michael.gendreau@colingordon.com)

Electron beam-based instruments are sensitive to the environment in which they operate. Adverse environments may limit their achievable resolution. Many equipment manufacturers provide specifications for the acceptable level of various environmental conditions, such as vibration, EMI, and acoustic noise. However, the quality of the specifications vary significantly, from well-defined to conjectural. Additionally, during the design of a facility, the specific instruments that will be used may not yet be known. Thus, it is useful to have ″generic″ criteria, intended to represent entire classes of instruments, to use in the design of facilities. Generic vibration criteria exist to aid in the design of laboratories, though there have been no such instrument-based generic criteria available for acoustic noise. The generic noise criteria that are currently used in lab design (NC, NR, dBA, etc.) were established to address the effect of noise on human beings. Using noise specifications for a significant number of instruments with varying resolving powers, correlation of resolution with environmental noise is demonstrated. Based on the data reviewed, generic noise criterion curves have been developed and presented for use in the design of facilities that contain noise-sensitive equipment. These are applicable when other well-defined and specific criteria are not available.

Session 4pNSc

Noise and EURONOISE: Potential to Reduce Tire/Road Noise I

J. Stuart Bolton, Cochair
Ray W. Herrick Labs., School of Mech. Eng., Purdue University, 140 S. Martin Jischke Drive, West Lafayette, IN 47907-2031, USA

Ernst-Ulrich Saemann, Cochair
Continental AG, Jaedekamp 30, Hannover, 30419, Germany

Invited Papers

2:00

4pNSc1. The influence of tyre design on tyre/road noise - some fundamental thoughts. Wolfgang Kropp (Chalmers University of Technology, Division of Applied Acoustics, SE-41296 Gothenburg, Sweden, wolfgang.kropp@chalmers.se), Patrick Sabiniarz (Chalmers University of Technology, Division of Applied Acoustics, SE-41296 Gothenburg, Sweden, patrick.sabiniarz@chalmers.se)

Tyre/road noise generation mechanisms are divided into two categories, tyre vibrations (due to time varying contact forces) and airflow related processes (e.g. air-pumping) in the contact between tyre and road. The paper only focuses on tyre vibrations. An existing model for the simulation of tyre/road interaction is used to investigate the influence of tyre design on the vibrational energy stored in the tyre structure during rolling. It can be shown that ,although design is changed substantially, very little changes can be observed with respect to input power through the contact into the tyre structure. Changes in driving point mobilities of tyres are not directly related to changes in noise generation. Geometry changes leading to different contact geometry and in this way to different modal composition of the vibrational field as well as design changes leading to changes in wave speed are of higher importance. These changes have a strong influence on the radiation efficiency of tyres.

2:20

4pNSc2. Development of low noise tyres in EC project SILENCE. Ernst-Ulrich Saemann (Continental AG, Jaedekamp 30, 30419 Hannover, Germany, Ernst-Ulrich.Saemann@conti.de)

A lot of efforts were made in the last two decades to lower the tire/road noise. The tire industry has optimized the tread pattern as the main influence parameter so that nowadays the radiated sound pressure of a modern tire in the far field is very close to that of a blank tire with the same construction. Because the tread pattern is needed to achieve the required safety level further noise reduction has to be addressed mainly by tire construction. For many years tire manufacturers have been searching for a construction, which fulfils the targets of the automotive industry and generates less noise. The research was done not only in house but also with public projects. In the EC Project SILENCE a subproject has provided design solutions and hardware solutions for noise reduction, with respect to vehicle/tyre/road integration, under typical urban and suburban traffic conditions. This improvement is based on an increased understanding of noise generation and radiation mechanisms gained by the further development of experimental and simulation techniques. A series of low noise tyres (prototypes) has been developed and tested on a selection of appropriate low noise road surfaces.

2:40

4pNSc3. The ranking of rolling noise from passenger car tyres - a comparison between measurements and modelling results. Truls Berge (SINTEF ICT Dept. of Acoustics, O.S. Bragstads pl., NO-7465 Trondheim, Norway, truls.berge@sintef.no)

Tyres are type approved with regard to rolling noise on an ISO-test track, according to the EU-directive 2001/43/EC. The test track is basically a rather smooth road surface with maximum chipping size of 8 mm. However, most surfaces normally used on roads, especially in the northern European countries, are rougher surfaces, typically Stone Mastic Asphalt (SMA) with 11 to 16 mm stones. A project has been initiated to compare the noise levels of a selection of highly used after market summer tyres (in Norway). Noise measurements of 12 tyres have been performed on a selection of new and old SMA-road surfaces. The 3D texture of the same road surfaces has been measured with laser profile equipment. In addition, the point mobility and other design features of the tyres have been measured to be used as input data to the SPERoN tyre/road noise model. Then, comparison will be made between measurements and modelling results. Preliminary results from the noise measurements show a difference of 2.5-3 dB(A) on SMA-surfaces, between the tyres. The project is a co-operative between SINTEF (Norway), MüllerBBM (Germany), and Chalmers University (Sweden).

3:00

4pNSc4. Sound Radiation Modes of a Tire on a Reflecting Surface. J. Stuart Bolton (Ray W. Herrick Labs., School of Mech. Eng., Purdue University, 140 S. Martin Jischke Drive, West Lafayette, IN 47907-2031, USA, bolton@purdue.edu), Kiho Yum (Hyundai Motor Company, Chassis & Powertrain Engineering Team 3, Hyundai-Kia Motors Corporate R&D Division, Hwasung-Si, Gyeonggi-Do, 772-1, 445-706 Jangduk-Dong, Republic of Korea, kihoyum@hyundai-motor.com)

Wave number decomposition of a tire's radial vibration can be used to reveal the wave propagation characteristics of tires. In this paper, the relationship between the structural wave propagation characteristics of a tire excited at one point and its sound radiation is considered. The sound radiation resulting from structural vibration of a tire in contact with the ground was investigated by using boundary element analysis. In particular, the orthogonal radiation modes of a tire in the presence of a reflecting surface, along with their radiation efficiency characteristics, were calculated by applying an eigenvector analysis to the tire's radiation resistance matrix. The latter analysis made use of acoustic transfer vectors and a recovery surface appropriate for a pass-by noise test. The radiation mode results reveal that it is the vibration in the region close to the contact patch that primarily controls sound radiation. In particular, to reduce pass-by noise levels, it is necessary to mismatch the tire's structural ring mode and the radiation modes with high radiation efficiencies. It has also been found that the radiation from a tire is controlled by a relatively small number of radiation modes (although the number of contributing modes increases with frequency).

3:20

4pNSc5. Analysis of truck tire rolling noise and structural vibrations. Samuel Blanc (Goodyear, Technical Center, L - 7750 Colmar-Berg, Luxembourg, samuel_blanc@goodyear.com), Jan Leyssens (Goodyear, Technical Center, L - 7750 Colmar-Berg, Luxembourg, jan.leyssens@goodyear.com)

Legislators are increasingly demanding towards the vehicle and tire industry for further reduction of tire/road noise emissions. With the need to develop quieter tires, noise has become one of the driving performance criteria in the design process, together with safety, wear and rolling resistance. Next generation truck tires will have to meet more severe legal requirements. In this context, noise has to be improved both at constant speed for the tire regulation and under acceleration for the vehicle legislation. Field test results of different tire tread designs under accelerated and constant speed conditions are given in this presentation. Noise mechanisms and effects of rolling conditions are discussed based on pass-by and near-field microphones. In addition, the dynamic vibration of a truck tire casing is analysed using both detailed FEA modelling and experimental results.

3:40-5:20 Posters

Lecture sessions will recess for presentation of poster papers in various topics in acoustics. See poster sessions for topics and abstracts.

Invited Paper

5:20

4pNSc6. Simulation of tire tread block dynamics with respect to complex contact phenomena. Gunnar Gäbel (Institute of Dynamics and Vibration Research, Leibniz University Hannover, Appelstr. 11, 30167 Hannover, Germany, gaebel@ids.uni-hannover.de), Patrick Moldenhauer (Institute of Dynamics and Vibration Research, Leibniz University Hannover, Appelstr. 11, 30167 Hannover, Germany, moldenhauer@ids.uni-hannover.de), Matthias Kröger (Institute of Dynamics and Vibration Research, Leibniz University Hannover, Appelstr. 11, 30167 Hannover, Germany, kroeger@ids.uni-hannover.de)

Vibrations of the tire structure are caused by the interaction between the rolling tire and the road surface. The tread block is the only tire component which is directly in contact with the cleft road surface texture and therefore of special interest. The contact due to the rough surface leads to complex contact phenomena e.g. friction characteristics depending on normal contact pressure and relative velocity, non-linear contact stiffness and wear effects changing the tread block geometry and in hence the local contact forces. These contact phenomena strongly influence the dynamical behaviour of the tread block and the whole tire. A modular model based on a modal reduction method will be presented to investigate the tread block dynamics under consideration of the local friction characteristic, the non-linear contact stiffness and wear which are also analyzed experimentally on a concrete road surface to identify the model parameters.

Contributed Papers

5:40

4pNSc7. Transmissibility of a deformed rotating tyre. Ruud Van Doorn (Eindhoven University of Technology, Dept. of Mechanical Engineering, Dynamics & Control, P.O. Box 513, 5600MB Eindhoven, Netherlands, r.r.j.j.v.doorn@student.tue.nl), Ines Lopez (Eindhoven University of Technology, Dept. of Mechanical Engineering, Dynamics & Control, P.O. Box 513, 5600MB Eindhoven, Netherlands, i.lopez@tue.nl), René Van Der Steen (Eindhoven University of Technology, Dept. of Mechanical Engineering, Dynamics & Control, P.O. Box 513, 5600MB Eindhoven, Netherlands, r.v.d.steen@tue.nl), N.b. Roozen (Eindhoven University of Technology, Dept. of Mechanical Engineering, Dynamics & Control, P.O. Box 513, 5600MB Eindhoven, Netherlands, n.b.roozen@tue.nl), Henk Nijmeijer(Eindhoven University of Technology, Dept. of Mechanical Engineering, Dynamics & Control, P.O. Box 513, 5600MB Eindhoven, Netherlands, h.nijmeijer@tue.nl)

The major source of environmental noise exposure is road traffic noise. Of all noise sources, tyre rolling noise is dominant for speeds above 30 km/h for passenger cars. Tyre rolling noise can be subdivided into interior and exterior noise. For the interior noise to which the passengers are exposed to, the tyre transmissibility is essential since it relates the contact forces with the axle forces. These axle forces are responsible for the structure borne interior noise. Here, a Finite Element tyre model, including a fully coupled air column, is used to examine the transmissibility in the frequency domain 0-300 Hz. It is shown that three aspects are essential in mod-

eling the axle forces resulting from tyre-road interaction: 1) the tyre deformation since it leads to a set of non-axisymmetric eigenmodes, 2) the relatively low-damped non-axisymmetric acoustic resonance, and 3) rotation. A methodology using substructuring techniques is presented to include rotational effects both in the case of an undeformed and deformed tyre. These effects of rotation on the transmissibility differ in the deformed and undeformed case: frequency loci veering occurs in the deformed case, while in the undeformed case rotation results in a pure split of the eigenfrequencies.

6:00

4pNSc8. Simulation and analysis of tire road noise, finite element results and validation. Maik Brinkmeier (Institut für Baumechanik und Numerische Mechanik, Appelstraße 9A, 30167 Hannover, Germany, brinkmeier@ibnm.uni-hannover.de), Udo Nackenhorst (Institut für Baumechanik und Numerische Mechanik, Appelstraße 9A, 30167 Hannover, Germany, nackenhorst@ibnm.uni-hannover.de), Jan Biermann (Institut für Modellierung und Berechnung, Denickestraße 17, 21073 Hamburg, Germany, biermann@tu-harburg.de), Otto Von Estorff (Institut für Modellierung und Berechnung, Denickestraße 17, 21073 Hamburg, Germany, estorff@tu-harburg.de)

This presentation shows the methods and results of the German research project ″Silent Traffic″. The main topics are the simulation of tire road noise as well as the validation of the methods and finite element models. The target is to understand the mechanisms of sound generation and to get suggestions to reduce the traffic noise resulting from the virtual system. The investigations are based on a physical modeling of the tire road system rather then on the processing of statistical data. The simulation procedure can be decomposed into four steps: The computation of non-linear stationary rolling, the eigenvalue analysis in the deformed state, the analysis of road surface textures, and the calculation of the noise radiation including a modal superposition approach with an excitation by deterministic functions. Thereby, the numerical model enables for a detailed analysis of certain effects of the sound generation and radiation that contribute to the overall tire road noise. The simulation results are compared to measurements, both for structural dynamics and acoustics, to show the quality of the model und to indicate possible improvements for further development.

6:20

4pNSc9. A contact solver suitable for tyre/road noise analysis. Arjan Schutte (University of Twente, Dept. Mechanical Engineering, P.O. Box 217, 7500 AE Enschede, Netherlands, j.h.schutte@utwente.nl), Ysbrand H. Wijnant (University of Twente, Dept. Mechanical Engineering, P.O. Box 217, 7500 AE Enschede, Netherlands, Y.H.Wijnant@ctw.utwente.nl), André De Boer (University of Twente, Dept. Mechanical Engineering, P.O. Box 217, 7500 AE Enschede, Netherlands, a.deboer@utwente.nl)

Road traffic noise is a major environmental problem in modern society. The interaction between tyre and road surface, the major noise source, is non-linear and is best described in the time domain. The currently used contact models for acoustic analyses have problems with either accuracy or calculation speed. At the Structural Dynamics and Acoustics group of the University of Twente an alternative contact algorithm has been developed. The characteristic feature of this algorithm is that, while solving the set of equations, the contact condition, i.e. the condition stating that there is no overlap between the bodies, is satisfied exactly. Hence, there is no need for contact elements or contact parameters. The possibility to optimize and speed up the algorithm, using multigrid is the major advantage of the new approach. In this paper the contact algorithm is applied to a two-dimensional finite element model. Coulomb friction is taken into account. Some test simulations illustrate the ease of the algorithm. The model will be extended and nonlinear material behaviour will be added. Multigrid and multilevel will be used to speed up the calculation. The goal is to compute the vibrations and radiated noise pattern of a profiled tyre rolling on a road.

Invited Paper

6:40

4pNSc10. The effect of porous road surfaces on radiation and propagation of tyre noise. Bert Peeters (M+P - consulting engineers, PO Box 2094, 5260 CB Vught, Netherlands, BertPeeters@mp.nl), Ard Kuijpers (M+P - consulting engineers, PO Box 2094, 5260 CB Vught, Netherlands, ArdKuijpers@mp.nl)

It is well-known that porous road surfaces are very effective for the abatement of tyre/road noise. However, the physical principles behind the noise-reducing properties of these surfaces are not well understood and often even misinterpreted. Lack of understanding becomes a problem when developing a prediction model for tyre/road noise to be able to optimize the road surface for noise abatement. In the framework of the EU SILENCE project and the Dutch IPG program a model has been developed to predict the influence of road surface porosity on the radiation and propagation of tyre/road noise. First step in the model development was to gain physical insight from stationary and vehicle measurements with passenger car and truck tyres on both dense and porous surfaces. Next step was to qualitatively and quantitatively describe the observed physical phenomena in a mathematical model according to the KISS principle: avoid unnecessary complexity, both in input parameters and in the mathematical model. The end result is a mathematical model that describes the noise reduction potential for a standard tyre on various (porous) road surfaces, using a sound absorption spectrum as input. This model is available for a broad audience in the recently launched SPERoN acoustic optimization tool.

Session 4pNSd

Noise and EURONOISE: Cultural Variations in Sound/Noise Assessment I (Poster Session)

Catherine Guastavino, Cochair
Centre for Interdisciplinary Research in Music Media & Technology (CIRMMT) - School of Information Studies - McGill Univ.

Danièle Dubois, Cochair
CNRS

All posters will be on display from 3:40 p.m. to 5:20 p.m. To allow contributors an opportunity to see other posters, contributors of odd-numbered papers will be at their posters from 3:40 p.m. to 4:30 p.m. and contributors of even-numbered papers will be at their posters from 4:30 p.m. to 5:20 p.m.

Contributed Papers

4pNSd1. Noise exposition in the daily life. José Romero(Grup d'Acustica Arquitectònica, Ambiental i Industrial, E.T.S.I.I, Univ. Politécnica de Valencia, Camino de Vera, s/n, 46022 Valencia, Spain, romerof@fis.upv.es), Alicia Giménez (Grup d'Acustica Arquitectònica, Ambiental i Industrial, E.T.S.I.I, Univ. Politécnica de Valencia, Camino de Vera, s/n, 46022 Valencia, Spain, agimenez@fis.upv.es), Salvador Cerdá (Grup d'Acustica Arquitectònica, Ambiental i Industrial, E.T.S.I.I, Univ. Politécnica de Valencia, Camino de Vera, s/n, 46022 Valencia, Spain, salcerjo@mat.upv.es), Joaquin Navasquillo (Facultad de Ciencias, Univ. de Valencia, Blasco Ibañez, 15, 46010 Valencia, Spain, joaquin.navasquillo@uv.es), Radu Lacatis (Grup d'Acustica Arquitectònica, Ambiental i Industrial, E.T.S.I.I, Univ. Politécnica de Valencia, Camino de Vera, s/n, 46022 Valencia, Spain, rala1@doctor.upv.es), Arturo Barba Sevillano (Grup d'Acustica Arquitectònica, Ambiental i Industrial, E.T.S.I.I, Univ. Politécnica de Valencia, Camino de Vera, s/n, 46022 Valencia, Spain, arbarse@doctor.upv.es)

Nowadays, the man lives exposed in a world of sounds (pleasant - disagreeable, nonannoying - annoying) throughout the time, during the 24 hours a day. The man is exposed to the noise in his daily life, since he awakes, moves, works, entertains itself, rests, and to sleep. We have made a survey of levels of exhibition to the noise, having distinguished they are leisure, work or rest, in a amog young population of 20-35 years without hearing problems, and of both sexes. The results show us and agree with other authors, that the exhibition levels are highest in the activities chosen, like for example the leisure. In addition, the levels of exhibition, to the noise are related with the diverses activities of the population.

4pNSd2. Noise(s) and sound(s): comparing various conceptualizations of acoustic phenomena across languages. Danièle S. Dubois (CNRS, LCPE/LAM 11 rue de Lourmel, 75015 Paris, France, ddubois@ccr.jussieu.fr), Catherine Guastavino (Centre for Interdisciplinary Research in Music Media & Technology (CIRMMT) - School of Information Studies - McGill Univ., 3459 McTavish, Montreal, QC H3A1Y1, Canada, Catherine.Guastavino@mcgill.ca)

Musical listening focuses on perceptual attributes of the sound itself (e.g. pitch, loudness), whereas everyday listening focuses on events to gather relevant information about what happens in our environment (e.g. car approaching), that is, not about the sound itself but rather about noise as produced by sources and actions, and the effect of sound/noise on listeners. Previous linguistic analyses of discourses identified different conceptualizations of everyday/environmental noises and of musical sounds, as well as different conceptualizations for acousticians and non-acousticians. A more extensive psycholinguistic investigation was conducted to evaluate how different languages (not only consensual vocabularies) differently structure the semantic space of acoustic phenomenon. An open questionnaire was administered to expert listeners (acousticians) and naïve listeners from 5 different languages (French, Italian, Spanish, German and English) to collect linguistic resources available in each language and used in discourse to describe acoustic phenomena in their native languages. Presented in this paper are the first results of the comparative psycholinguistic analysis, in terms of linguistic devices and correlated conceptualizations, focusing on - the distinction between noise(s) and sound(s) across languages - the difference between scientific discourses and common sense discourses within and across languages.

Session 4pNSf

Noise and EURONOISE: Car Acoustics III (Poster Session)

Luc Mongeau, Cochair
McGill University

Virginie Maillard, Cochair
RENAULT

All posters will be on display from 3:40 p.m. to 5:20 p.m. To allow contributors an opportunity to see other posters, contributors of odd-numbered papers will be at their posters from 3:40 p.m. to 4:30 p.m. and contributors of even-numbered papers will be at their posters from 4:30 p.m. to 5:20 p.m.

Contributed Papers

4pNSf1. New vehicule noise emission values to update the French 'Guide du bruit'. Sonia Doisy (Laboratoire des Ponts et Chaussées, 11, rue Jean Mentelin, BP 9, 67035 Strasbourg, France, sonia.doisy@equipement.gouv.fr), Joel Lelong (INRETS, 25 av. F. Mitterrand, case 24, 69675 Bron, France, lelong@inrets.fr), Jean-François Hamet (INRETS, 25 av. F. Mitterrand, case 24, 69675 Bron, France, hamet@inrets.fr)

French traffic noise prediction models are based on vehicle noise emission values defined by the ″Guide du Bruit des Transports Terrestres″, issued in 1980. A research programme was established in order to update these values and take into account developments in car and road technology. The methodology followed to output emission values has been developed by successive steps, as the processing performed on the collected data went along. After several attempts the shape adopted for the emission formulas considers the vehicle pass-by LAmax as the sum of two subsource contributions: the power unit contribution which varies with acceleration and the road gradient, and the tyre/road contribution which varies with speed and the road surface type. New emission values are now completely defined, and ready to be used in noise prediction models.

4pNSf2. Acoustical Parameters of Automotive Interiors using Hybrid Fleeces basing on natural fibres. Christian R. Koenig (University of Bremen, Badgasteiner Str. 1, FZB - Room 2140, 28359 Bremen, Germany, chkoenig@uni-bremen.de), Dieter H. Müller (University of Bremen, Badgasteiner Str. 1, FZB - Room 2140, 28359 Bremen, Germany, ml@biba.uni-bremen.de), K.-D. Thoben (University of Bremen, Badgasteiner Str. 1, FZB - Room 2140, 28359 Bremen, Germany, tho@biba.uni-bremen.de)

Hybrid fleeces are often used to produce composites and layered structures for car interiors. The fleeces consist of reinforcement fibres and polymeric fibres as matrix material. The utilization of natural fibres as a reinforcement for composite may be regarded as an emerging research area in polymer science. An important range of application can be found in the automotive industry. Despite of ecological gains like less environmental impact of the later product within the formation, usage and disposal period further technical and economical advantages result from this strategy. In addition to a reduction of the component's cost and net weight or an improvement of driving safety due to the crash behaviour of the composite material, natural fibre reinforced polymers offer increased recycling capabilities over conventional polymers used in that area. The presentation concentrates on the possibilities by using different materials, different ratios of thermoplastic and natural fibre material and different process parameters. Layers are especially investigated to demonstrate how the fleeces and the techniques to bond the fleeces can influence the acoustical behaviour and mechanical properties. Based on the results of the measurements optimised, multi-layered sandwiches were developed and will be presented.

4pNSf3. Statistical energy analysis limits for acoustic radiation car: an alternative approach. Gérard Borello (InterAC, 10 impasse Borde-Basse, ZA. La Violette, 31240 L'Union, France, gerard.borello@interac.fr), Alex Borello (InterAC, 10 impasse Borde-Basse, ZA. La Violette, 31240 L'Union, France, info@interac.fr), Julien Primus (InterAC, 10 impasse Borde-Basse, ZA. La Violette, 31240 L'Union, France, info@interac.fr), Laurent Gagliardini (PSA Peugeot Citroën, Route de Gisy, 78943 Vélizy-Villacoublay Cedex, France, laurent.gagliardini@mpsa.com)

Due to a new pass-by noise regulation, Vehicle exterior noise will have to be reduced in the coming years. This may be achieved by optimizing underbody and underhood absorption and screening apertures. There is then a need for numerical techniques able to predict sound reduction related to acoustic absorption and transmission loss changes. Through a work supported by ADEME and headed by PSA, energy-based predictive techniques such as Analytical Statistical Energy Analysis (ASEA) and discretized Energy Flow Analysis (DEFA) were tested against the actual physical problem to be solved through a series of benchmarks. Both theories are compared across several simple acoustic problems. It is concluded that both methods do not fit to the initial acoustic optimization requirement due to their intrinsic assumptions that restrict their applicative range. More fitted numerical techniques are now investigated: among new candidates, the Virtual SEA (VSEA) technique that allows the creation of a numerical model of coupled acoustic cavities from the finite element global modes without the serious limitations of ASEA and a matrix approach based on Craigh-Bampton substructuration of the cavities.

4pNSf4. A multiple regression model for predicting rattle noise subjective rating from in-car microphones measurements. Benoît Gauduin (Genesis S.A., Bâtiment Gérard Mégie, Domaine du Petit Arbois - BP 69, 13545 Aix-en-Provence Cedex 4, France, benoit.gauduin@genesis.fr), Christophe Noel (Genesis S.A., Bâtiment Gérard Mégie, Domaine du Petit Arbois - BP 69, 13545 Aix-en-Provence Cedex 4, France, christophe.noel@free.fr), Jean-Louis Meillier (Renault, Centre Technique d'Aubevoye, Parc de Gaillon, 27940 Aubevoye, France, jean-louis.meillier@renault.com), Patrick Boussard (Genesis S.A., Bâtiment Gérard Mégie, Domaine du Petit Arbois - BP 69, 13545 Aix-en-Provence Cedex 4, France, patrick.boussard@genesis.fr)

In some situations when the road is deformed, the shock absorbers of vehicles may produce a specific sound, called rattle noise. It may be perceived by the driver and wrongly considered as a malfunction of the vehicle.

This sound is part of the global acoustic comfort of the vehicle and hence is studied by RENAULT. The approach presented here aims at predicting the rattle noise subjective rating given by a RENAULT expert on a scale from 0 to 10, by developing a model based on in-car binaural microphones measurements in the ears if the driver. First, a set of 11 metrics has been build, related to temporal aspects, spectral components and time-frequency information of the rattle noise recorded. The corpus is made of 19 different configurations of shock absorbers of a given car. The method used to select the most relevant metrics for the multiple regression model is presented. This selection is based on a statistical robustness estimation of the model. Hence, it appears that only 6 metrics are sufficient to build the model. Finally, the performance of the model is evaluated on 5 new configurations of shock absorbers.

4pNSf5. Structure borne noise inside a coach. Joanes Berasategi (Mondragon University, Loramendi 4, Apdo 23, 20500 Arrasate, Spain, joanes.berasategui@alumni.eps.mondragon.edu), Unai Galfarsoro (Mondragon University, Loramendi 4, Apdo 23, 20500 Arrasate, Spain, ugalfarsoro@eps.mondragon.edu), María Jesús Elejabarrieta (Mondragon University, Loramendi 4, Apdo 23, 20500 Arrasate, Spain, mjelejabarrieta@eps.mondragon.edu), Igor Insausti (Mondragon University, Loramendi 4, Apdo 23, 20500 Arrasate, Spain, ugalfarsoro@eps.mondragon.edu)

Nowadays the use of coaches as ground collective transport is generalizing in society and besides, its use is encouraged by all public institutions. Users of this type of vehicles request that they are comfortable, even more in long trips. Therefore, decreasing noise and vibrations inside the coach is a essential requirement to obtain a good quality of the vehicle and the satisfaction of the traveller. To increase the vibroacoustic comfort it is necessary to know qualitatively and quantitatively the noise and vibration sources, as well as their transmission paths. Thus, in this work a procedure has been defined and applied to measure and analyse the vibration and acoustic behaviour of a coach in different operating modes: idling, three constant speeds, acceleration and deceleration. 32 acceleration and sound pressure signals have been acquired, corresponding to different interior and exterior points of the coach. The analysis of the acceleration autospectra has allowed to determine the contribution of elements like floor, glasses and lateral panels to the sound pressure perceived by the traveller in the passenger compartment in the different studied operating modes.

4pNSf6. Experimental approach for reducing uncertainties associated with road vehicle noise according to ISO 362. Louis-Ferdinand Pardo (UTAC, Autodrome de Linas-Montlhéry, BP 20212, 91311 Montlhéry, France, louis-ferdinand.pardo@utac.com), Thierry Ageron (UTAC, Autodrome de Linas-Montlhéry, BP 20212, 91311 Montlhéry, France, ageron@utac.com), Serge Ficheux (UTAC, Autodrome de Linas-Montlhéry, BP 20212, 91311 Montlhéry, France, ficheux@utac.com), Celine Berthou (UTAC, Autodrome de Linas-Montlhéry, BP 20212, 91311 Montlhéry, France, berthou@utac.com)

This paper proposes an approach for reduction uncertainties related to sound pressure levels measured in accordance with procedures given in ISO 362 for noise emitted by road vehicles under acceleration This approach is based on an experimental assessing of several disturbing factors that lead to variation in the resulting level observed day to day and site to site for the same vehicle. The assessment of corrections to build the model is based on an independent analysis on each influent factor (test track, noise measuring device and temperature) taking into account of vehicle noise behaviour depending on power unit and tyres.

Session 4pNSg

Noise, Architectural Acoustics, and EURONOISE: Noise, Vibration and Acoustics for Medical and Research Facilities and Their Occupants II (Poster Session)

James West, Cochair
Johns Hopkins University

Jack Evans, Cochair
JEAcoustics

Marc Asselineau, Cochair
Peutz & Associés

Erica Ryherd, Cochair
Georgia Institute of Technology

All posters will be on display from 3:40 p.m. to 5:20 p.m. To allow contributors an opportunity to see other posters, contributors of odd-numbered papers will be at their posters from 3:40 p.m. to 4:30 p.m. and contributors of even-numbered papers will be at their posters from 4:30 p.m. to 5:20 p.m.

Contributed Papers

4pNSg1. Noise control of laboratories: case studies. Marc Asselineau (Peutz & Associés, 10 rue des Messageries, F75010 Paris, France, m.asselineau@peutz.fr)

Laboratories for research and production usually feature work areas complete with exhaust equipment as well as specific equipment (e.g. heaters, shakers, etc.). More to the point, such research and production areas are often linked to open plan offices where workers process their results, as well as partitioned offices where supervising engineers or researchers work. Suchfitting out is supposed to help circulate information around the team and save valuable space. Unfortunately, it easily can be noisy and rather uncomfortable, especially when coming from older fully partitioned laboratories and offices. This paper aims to illustrate a few acoustical highlights of laboratories through a few cases studies, looking at such parameters as spatial sound level decay, background noise level and reverberation time, but also at such additional factors as general background and psychological aspects, and looking at tentative standards. It turns out that both the acoustical quality of the room and the space planning must be developed according to the users' needs.

4pNSg2. Noise reduction in an operating room: A case study. James West (Johns Hopkins University, Department of Electrical Engineering, 3400 North Charles Street, Baltimore, MD 21218, USA, jimwest@jhu.edu), Ilene Busch-Vishniac (McMaster University, 1280 Main Street West, Hamilton, ON L9G 4X6, Canada, provost@mcmaster.ca), Joseph King (Shamoon College of Engineering, Math. Department, Bialik/Basel Sts., 84100 Beer Sheva, Israel, joseph.a.king@usa.dupont.com), Natalia Levit (DuPont, 5401 Jefferson Davis Highway, Richmond, VA 23234, USA, natalia.v.levit@usa.dupont.com)

In our previous study reported in INTER-NOISE 2006 we found that operating rooms are among the most problematic areas in the healthcare industry. The maximum peak levels measured during various surgical procedures are extremely high - 100-120 dB, which can potentially lead to the hearing damage and interfere with the speech communication during surgery. Neurosurgery and orthopedic operating rooms are found to be among the noisiest overall. However, introduction of the acoustical materials to the operating room is very difficult due to the strict infectious control requirements. We report here a case study on using sound absorptive panels protected by DuPont Tyvek®, a unique flash spun plexifilamentary film-fibril sheet, combining excellent barrier properties with distinctive porous structure to make it acoustically transparent in the voice frequency range.

4pNSg3. Case Study of MRI Installation in Existing Hospitals. James Perry (Cerami & Associates, 404 Fifth Avenue, New York, NY 10018, USA, jperry@ceramiassociates.com)

Medical facilities frequently seek to add function and capacity to their imaging facilities. The addition of new MRI units into existing hospital spaces is quite common, however many manufacturers impose and stringent low-frequency vibration limits which must be met before a unit can be delivered and installed. Vibration sources such as mechanical systems and external transit can degrade the achievable imaging resolution at levels undetectable by unaided humans. A case study is presented for one such project which required significant vibration controls to existing ventilation, water, and electrical systems to ensure acceptable vibration levels at an unlikely equipment installation.

4pNSg4. Nanotechnology research facility- A vibration and noise control design case study. Jack B. Evans (JEAcoustics, 1705 West Koenig Lane, Austin, TX 78756, USA, Evans@JEAcoustics.com), Chad N. Himmel (JEAcoustics, 1705 West Koenig Lane, Austin, TX 78756, USA, Himmel@JEAcoustics.com), Daniel J. Kupersztoch (JEAcoustics, 1705 West Koenig Lane, Austin, TX 78756, USA, Kupersztoch@JEAcoustics.com)

Vibration and noise control would be critical to the success of a proposed nanotechnology and molecular research facility. Roadway traffic, a nearby power generation plant and buildings in the vicinity were potential sources of ground borne vibration disturbances. Mechanical equipment, occupant installed support apparata and occupant activities were potential sources of internally generated vibration disturbances. On-site ground borne vibration was measured for comparison with generic floor vibration criteria for sensitive installations. Results were analyzed relative to criteria for

potential disturbance of sensitive equipment, perception by occupants, audible radiated structure borne noise in acoustically sensitive spaces and resolution-degrading motion for scanning and for transmission electron microscopes and other nanotechnology clean room equipment. Design guidelines and structural vibration control concepts were recommended to the structural engineers, including de-tuning, damping and isolation methods. Recommendations were provided for mechanical noise control and vibration isolation. Architectural noise control, sound isolation and room acoustics guidelines were provided for research, office and meeting spaces. This case study will discuss the desired vibration and noise control objectives and the design solutions that were implemented. Building photographs will be presented. Post-construction measurement results will be graphically compared with pre-construction conditions to demonstrate apparent degree of success in mitigating vibration.

THURSDAY AFTERNOON, 3 JULY 2008 P2-A, LEVEL 2, 3:40 TO 5:20 P.M.

Session 4pNSh

Noise, ASA Committee on Standards, and EURONOISE: Measurement of Occupational Noise Exposure II (Poster Session)

William Murphy, Cochair
National Institute for Occupational Safety and Health

Beat Hohmann, Cochair
Suva, Physics Section

All posters will be on display from 3:40 p.m. to 5:20 p.m. To allow contributors an opportunity to see other posters, contributors of odd-numbered papers will be at their posters from 3:40 p.m. to 4:30 p.m. and contributors of even-numbered papers will be at their posters from 4:30 p.m. to 5:20 p.m.

Contributed Papers

4pNSh1. New findings on noise exposure in the construction trades. Reimer Paulsen (BGIA - Institut für Arbeitsschutz, Alte Heerstr. 111, 53757 Sankt Augustin, Germany, reimer.paulsen@dguv.de)

The degree to which employees on construction sites are exposed to noise often depends on a variety of individual activities. The calculation of the average noise exposure for different construction trades in this sector calls for an enhanced level of work analysis and measurement. Recommended here are personal measurements with simultaneous recording of the various activities and machines employed. With the subsequent assignment of average sound pressure levels and activities, it is then possible to draw conclusions about part exposures and mean exposure. At euronoise 2006 in Tampere, findings for a series of construction trades were presented. In the meantime, this series of measurements has been extended to include further trades. Furthermore subsequent measurements have been performed for individual trades, this was considered necessary because certain machines and working methods have changed in these fields in the last 20 years. The findings show that technical progress does not necessarily result in a reduction in noise exposure.

4pNSh2. Who can guaranty compliance with the Exposure Limit Value of 87 dB(A)? Fabien Krajcarz (Gamba Acoustique, 2 rue de la Découverte, BP 163, 31676 Labege Cedex, France, fabien.krajcarz@acoustique-gamba.fr)

The level of daily exposure (Lex8h) of workers has to be measured in accordance with French standard NFS 31084. The attenuation of personal noise protection has to be determined according to standard NF EN ISO 4869-2. In addition to the difficulties of applying these methods, one has to be aware that the actual effectiveness of the protection can deviate considerably from its theoretical effectiveness and, ultimately, it is the effective duration of wearing the protection that really determines the protection of workers. We have provided modest evidence, more than a survey in the strictest sense of the term, of the conditions in which the protectors are worn (or not) at a large French industrial company. The results have shown that the wearing of hearing protectors is far from being routine, even when the noise levels are high. Thus, the question then arises as to the guarantee which the entity or person responsible for measuring bears for compliance with the Exposure Limit Value of 87 dB (A), when wearing the protection.

4pNSh3. Measurement Method for Noise Exposure of Jobs of the Construction Sector. Samuel Quintana (Universidad de Castilla-La Mancha, Campus Universitario, 16071 Cuenca, Spain, Samuel.Quintana @uclm.es), Marcos D. Fernandez (Universidad de Castilla-La Mancha, Campus Universitario, 16071 Cuenca, Spain, Marcos.Fernandez @uclm.es), Noelia Chavarria (Universidad de Castilla-La Mancha, Campus Universitario, 16071 Cuenca, Spain, noe_chava@hotmail.com), Jose A. Ballesteros (Universidad de Castilla-La Mancha, Campus Universitario, 16071 Cuenca, Spain, Josea.Ballesteros@uclm.es), Isabel Gonzalez (Universidad de Castilla-La Mancha, Campus Universitario, 16071 Cuenca, Spain, Isabel.Gonzalez@uclm.es)

Noise is one of the physical contaminants with a high presence in the construction sector. Nowadays, several negative effects produced by the exposure to noise are known, mainly regarding hearing. Although there is evidence of the existence of many other effects, some of them are not characterized precisely yet. Due to the importance that these effects have on the worker's health and well-being, it is necessary to develop some mechanisms to study and suggest preventive solutions on these questions. In this work, it has been studied the most appropriate measurement method for taking, as precisely as possible, the noise levels that the workers of the construction sector are exposed to. Several measures have been taken and analyzed to determine the best indexes and parameters to characterize the noise in the construction. For which, the current European regulations regarding the noise exposure (Directive 2003/10 of the EU) have always been taken into account.

4pNSh4. Impulsive occupational exposure for workers in drop-forge foundries. Edward L. Zechmann (National Institute for Occupational Safety and Health, 4676 Columbia Parkway, Mailstop C-27, Cincinnati, OH 45226-1998, USA, cri6@cdc.gov), Scott Brueck (National Institute for Occupational Safety and Health, 4676 Columbia Parkway, Mailstop C-27, Cincinnati, OH 45226-1998, USA, zcd6@cdc.gov), William J. Murphy (National Institute for Occupational Safety and Health, 4676 Columbia Parkway, Mailstop C-27, Cincinnati, OH 45226-1998, USA, wjm4 @cdc.gov)

Occupational noise exposure limits for impulsive sounds in the United States are established by the Occupational Safety and Health Administration and recommended by the National Institute for Occupational Safety and Health to permit no impulsive exposure in excess of 140 dB peak SPL. Peak pressure levels in excess of this limit can be found in industrial sectors such as construction, law enforcement and manufacturing. Taylor et al. [J. Acoust. Soc. Am 76:807-819, 1984] reported equivalent A-weighted levels, L_{Aeq}, of 108 dB for forge operators sampled in seven drop-forge foundries in the United Kingdom. In a recent study of noise exposure at two drop-forge manufacturing plants in the U.S., peak impulse levels were measured in a range of 117 to 154 dB peak SPL and 8-hour equivalent A-weighted levels, L_{Aeq8}, for forge operators between 95 and 116 dB and for press operators between 95 and 105 dB. Kurtosis, A, B C and D-durations were assessed for the impulsive and continuous noise samples. This paper will present the results of measurement and analysis of noise exposures typical for a drop-forge facility.

THURSDAY AFTERNOON, 3 JULY 2008 P2-A, LEVEL 2, 3:40 TO 5:20 P.M.

Session 4pNSi

Noise, Structural Acoustics and Vibration, Signal Processing in Acoustics, and EURONOISE: Airframe Noise Measurement, Prediction, and Control II (Poster Session)

Joe Posey, Cochair
NASA

Denis Gely, Cochair
ONERA

All posters will be on display from 3:40 p.m. to 5:20 p.m. To allow contributors an opportunity to see other posters, contributors of odd-numbered papers will be at their posters from 3:40 p.m. to 4:30 p.m. and contributors of even-numbered papers will be at their posters from 4:30 p.m. to 5:20 p.m.

Contributed Papers

4pNSi1. Overview of revolutionary aircraft for quiet communities workshop. Joe W. Posey (NASA, Langley Research Center, MS 461, Hampton, VA 23681, USA, joe.w.posey@nasa.gov)

At some time in the future, technical advances, environmental imperatives, societal expectations for mobility, and economic drivers will dictate that radically different aircraft will be built and flown. Therefore, aircraft designs will change even if low noise were not one of the environmental imperatives, and acousticians must be aware of the possible directions for aircraft design and the resulting opportunities and challenges for noise control. To address this need, the National Aeronautics and Space Administration sponsored a workshop entitled Revolutionary Aircraft for Quiet Communities in Hampton, VA, 24-26 July 2007. Twenty-six talks covered aircraft design, interior noise challenges, airframe noise, propulsion, and aircraft noise prediction. Revolutionary aircraft will employ dramatically improved materials, propulsion systems, and flow control technology to improve efficiency and enhance mobility. Five hours of discussion surfaced many concerns and recommendations, including the increasing need for acousticians to be involved on highly integrated teams throughout the vehicle design process. Also, other discipline experts participating in aircraft design need some education in acoustics to increase their sensitivity to noise control issues. The National Institute of Aerospace hosted the event, and the Council of European Aerospace Societies and the American Institute of Aeronautics and Astronautics were co-sponsors.

4pNSi2. Adaptive closed-loop control of cavity flows. Louis Cattafesta (University of Florida, 231 MAE-A, P.O. Box 116250, Gainesville, FL 32611, USA, cattafes@ufl.edu), Srinivasan Arunajatesan (Combustion Research and Flow Technology, Inc., 6210 Keller's Church Road, Pipersville, PA 18947, USA, ajs@craft-tech.com), Qi Song (University of Florida, 231 MAE-A, P.O. Box 116250, Gainesville, FL 32611, USA, song@ufl.edu), Cesar Moreno (University of Florida, 231 MAE-A, P.O. Box 116250, Gainesville, FL 32611, USA, cesargm@ufl.edu), Miguel Palaviccini (University of Florida, 231 MAE-A, P.O. Box 116250, Gainesville, FL 32611, USA, mrp1124@ufl.edu)

Results from a combined experimental and computational study are presented on the development of an adaptive feedback controller for the suppression of cavity pressure loads. The experiments are performed in a variable-sized cavity in a high-speed wind tunnel, while the computations are performed using the CRAFT CFD flow solver. The adaptive control system incorporates recursive algorithms for system identification with disturbance rejection algorithms for feedback control. Results are presented using unsteady surface pressure sensors on the cavity walls and an array of zero-net mass-flux (ZNMF) actuators at the leading edge. The experimental data are used to compare with and validate the computations. These novel simulations form a virtual experiment testbed that is used to assess, for example, actuator type, placement, and requirements and also candidate identification and control algorithms.

Session 4pNSj

Noise and EURONOISE: Soundscape in the Heritage of Urban and Natural Areas II (Poster Session)

Bennett Brooks, Cochair
Brooks Acoustics Corp.

Giovanni Brambilla, Cochair
CNR Institute of Acoustics

All posters will be on display from 3:40 p.m. to 5:20 p.m. To allow contributors an opportunity to see other posters, contributors of odd-numbered papers will be at their posters from 3:40 p.m. to 4:30 p.m. and contributors of even-numbered papers will be at their posters from 4:30 p.m. to 5:20 p.m.

Contributed Papers

4pNSj1. Noise masking as a soundscaping measuring procedure. Mohammed Boubezari (CAPS, Instituto Superior Técnico, TU Lisbon, Av. Rovisco Pais, P-1049-001 Lisbon, Portugal, boubezari@gmail.com), J. Luis Bento Coelho (CAPS, Instituto Superior Técnico, TU Lisbon, Av. Rovisco Pais, P-1049-001 Lisbon, Portugal, bcoelho@ist.utl.pt)

Loudness is the perceived intensity of a sound that could solve the problem of measuring a sound that is already filtered by the listening procedure. However, technically it is impossible to separate physically the sources of a noise into its components as well as human perception does. Loudness cannot be operative if a sound is merged with other noises. The principle of the proposed solution consists on gradually mixing a white noise during listening until the selected sound that one wants to measure is totally masked. The level of the masking white noise is controlled independently from the listener and measured with dB(A). The listener controls the limit of audibility of the selected sound, which is masked by the white noise. This paper describes the patent deposited around this method and shows the results obtained so far, and how this technique can be helpful in a visual translation of the sound space composition.

4pNSj2. Adaptive Characterization of Near and Far field Elements in the Soundscape. David R. Barclay (Marine Physical Lab, Scripps Institution of Oceanography, UCSD, 9500 Gilman Dr. M/C 0238, La Jolla, CA 92093-0238, USA, dbarclay@mpl.ucsd.edu)

Characterization of a soundscape through objective parameters relies on our understanding of psychoacoustics and ability to model the complex signal processing of the mind. Certain physical parameters such as loudness and timbre are easily retrieved from data while other descriptive parameters are more difficult to measure objectively. Several signal processing algorithms are presented here in the context of describing a soundscape in terms of keynote sounds (background noise) and sound signals (foreground sounds). Simulations and stereo field data recorded in San Diego are analyzed. Adaptive matched field processing is used in conjunction with conventional spectral analysis for the detection and categorization of near field events. These sounds are then removed to provide a more accurate description of keynote sounds. Spatial distribution of the soundscape is measured using conventional beamforming algorithms.

4pNSj3. Internet and mobile technologies for a public role in noise surveying. Charlie Mydlarz (The University of Salford, C.S.E., Salford University, The Crescent, M5 4WT Manchester, UK, c.mydlarz@salford.ac.uk),Ian Drumm(The University of Salford, C.S.E., Salford University, The Crescent, M5 4WT Manchester, UK, i.drumm@salford.ac.uk), Trevor J. Cox (University of Salford, Acoustics Research Centre, Newton Building, M5 4WT Salford, UK, t.j.cox@salford.ac.uk)

The traditional method of noise surveying is to use trained professionals to go to a specific site to measure and assess noise levels using dedicated and expensive equipment. This project aims to enfranchise the public by providing them with the opportunity to play an active role in noise measurement and assessment, as well as how their soundscapes are shaped. With the implementation of mobile phone, PDA and PC applications, alongside web based collation techniques; we aim to empower the public in the gathering of context specific data on soundscapes. The methodology will provide a case study for the wider research community in developing public participation-based research activities of this kind. This will provide a better understanding of the public's relationship with their soundscape and how this relationship varies with location and demographic data. Inferences will be compared from the analysis of data sets generated with other soundscape research with a view towards validating the techniques and gaining new insights into the field.

4pNSj4. From Descriptive to Predictive Soundscape Representation. Mohammed Boubezari (CAPS, Instituto Superior Técnico, TU Lisbon, Av. Rovisco Pais, P-1049-001 Lisbon, Portugal, boubezari@gmail.com), J. Luis Bento Coelho (CAPS, Instituto Superior Técnico, TU Lisbon, Av. Rovisco Pais, P-1049-001 Lisbon, Portugal, bcoelho@ist.utl.pt)

Regarding the knowledge on psychoacoustics (Zwickers), on phenomenology of perception (Gibson. J. J.) and the results obtained at CAPS-IST (Boubezari-Bento Coelho), a descriptive and qualitative sound map was drawn and a predictive procedure was developed. The method shows that the introduction of human perception during the process of analysis and signal processing makes it possible to target measurements on one or more noise sources selected separately from their background noise. Contrary to conventional measurements, which yield overall values of LAeq, without distinguishing the sources, the method presented here allows a space description of a sound space by making each sound stand out from its context. The method allows the measurement of the range of a noisy source in a given place, the testing of the range or the masking of an urban device (fountain) or contribute to the decision and the design of a specific architectural project, for example. This paper describes the method (and its limits) and the results obtained and shows how a predictive qualitative sound map with low cost is now feasible.

Session 4pNSk

Noise and EURONOISE: Potential to Reduce Tire/Road Noise II (Poster Session)

J. Stuart Bolton, Cochair
Ray W. Herrick Labs., School of Mech. Eng., Purdue University

Ernst-Ulrich Saemann, Cochair
Continental AG

All posters will be on display from 3:40 p.m. to 5:20 p.m. To allow contributors an opportunity to see other posters, contributors of odd-numbered papers will be at their posters from 3:40 p.m. to 4:30 p.m. and contributors of even-numbered papers will be at their posters from 4:30 p.m. to 5:20 p.m.

Contributed Papers

4pNSk1. Frequency loci veering in deformed rotating tyres. Ruud Van Doorn (Eindhoven University of Technology, Dept. of Mechanical Engineering, Dynamics & Control, P.O. Box 513, 5600MB Eindhoven, Netherlands, r.r.j.j.v.doorn@student.tue.nl), Ines Lopez (Eindhoven University of Technology, Dept. of Mechanical Engineering, Dynamics & Control, P.O. Box 513, 5600MB Eindhoven, Netherlands, i.lopez@tue.nl), René Van Der Steen (Eindhoven University of Technology, Dept. of Mechanical Engineering, Dynamics & Control, P.O. Box 513, 5600MB Eindhoven, Netherlands, r.v.d.steen@tue.nl), N.b. Roozen (Eindhoven University of Technology, Dept. of Mechanical Engineering, Dynamics & Control, P.O. Box 513, 5600MB Eindhoven, Netherlands, n.b.roozen@tue.nl), Henk Nijmeijer (Eindhoven University of Technology, Dept. of Mechanical Engineering, Dynamics & Control, P.O. Box 513, 5600MB Eindhoven, Netherlands, h.nijmeijer@tue.nl)

In previous work [1] a methodology to model tyre vibrations has been developed, which exploits a modal base determined in a standard FE package and includes rotational effects by a coordinate transformation. In the present paper, the effect of rotation on the eigenfrequencies of a deformed tyre is examined. It is well-known that rotation splits the eigenfrequencies of an undeformed tyre symmetrically around the eigenfrequencies of the non-rotating tyre, where the slope of the eigenfrequency-lines is determined by the circumferential wave number and tyre radius only. However, the eigenfrequency-lines of a deformed tyre demonstrate a fascinating mutual repulsion behaviour if the velocity is increased. This phenomenon is known as frequency loci veering and is induced by the a-periodicity resulting from the tyre deformation. Besides the effect of veering on the eigenfrequencies, the corresponding eigenmodes interact in the transition zones and finally interchange. The effects of veering are extremely intensified by the high modal density of the tyre structure, which results in a decreasing eigenfrequency distribution when the rotational velocity increases. [1] I. Lopez et al, JSV 307, 481-494, (2007)

4pNSk2. A model to evaluate the importance of tangential contact forces for tyre/road noise generation. Patrick Sabiniarz (Chalmers University of Technology, Division of Applied Acoustics, SE-41296 Gothenburg, Sweden, patrick.sabiniarz@chalmers.se), Wolfgang Kropp (Chalmers University of Technology, Division of Applied Acoustics, SE-41296 Gothenburg, Sweden, wolfgang.kropp@chalmers.se)

The interaction between tyre and road is a complex non-linear process including radial and tangential contact forces between tyre and road surface. During recent years models have been developed which allow for predicting radial forces as function of surface and tyre properties. These models can be used to quantify the influence of radial forces on the noise generation. Whereas in many cases time varying radial forces are the main reason for the generation of tyre noise, in some cases other mechanisms seem to be dominant. This paper aims on understanding the influence of tangential contact on tyre/road noise generation. For this reason the model developed by the Chalmers Tyre Road Noise Group has been extended to also include tangential interaction. The model is based on the same concept as that used by McIntyre and Woodhouse for modelling string/bow contact of musical instruments. It computes the time varying normal and tangential contact forces for a tyre rolling over a rough surface at constant speed. A small selection of simulation results are presented aiming at showing the effect of different parameters, such as friction coefficient and normal load, on the occurrence of instability phenomena such as stick/slip vibrations.

Session 4pNSl

Noise and EURONOISE: Noise from Wind Power Projects II (Poster Session)

Eddie Duncan, Cochair
Resource Systems Group (RSG)

Kerstin Persson Waye, Cochair
Dept. of Environ. Medicine, The Sahlgrenska Acad. of Gothenburg Univ.

All posters will be on display from 3:40 p.m. to 5:20 p.m. To allow contributors an opportunity to see other posters, contributors of odd-numbered papers will be at their posters from 3:40 p.m. to 4:30 p.m. and contributors of even-numbered papers will be at their posters from 4:30 p.m. to 5:20 p.m.

Contributed Papers

4pNSl1. A rational approach for regulating windturbine noise. Martin Van Den Berg (Ministry VROM, Po. Box 30945, IPC 635, 2500GX Den Haag, Netherlands, martin.vandenberg@minvrom.nl)

Windturbines have evolved from the cosy, wooden Dutch windmill type to large industrial generators of sustainable energy. Their noise production luckily did not evolve in step, but in some cases they can be a perhaps unsustainable nuisance for population living nearby. Presently the local and national authorities are trying to get a hold on the problem, often still using methods from the wooden machine age. The paper describes a modern approach for dealing with windturbine noise, using harmonized methods and recently acquired insights in the reaction of people to this particular noise. Tentative dose-effect relations in terms of Lden and Lnight enable comparisons with noise from transport.

4pNSl2. Wind farm aural and visual impact in the Netherlands. Frits Van Den Berg (University of Groningen - Science & Society Group, Nijenborgh 4, 9747AG Groningen, Netherlands, fvdberg@ggd.amsterdam.nl), Eja Pedersen (Occupational and Environmental Medicine, Göteborg University, PO Box 100, SE-405 30 Göteborg, Sweden, eja.pedersen@set.hh.se), Roel Bakker (Northern Centre for Healthcare Research, University Medical Centre Groningen, PO Box 30001, 9700 RB Groningen, Netherlands, R.H.Bakker@med.umcg.nl), Jelte Bouma (Northern Centre for Healthcare Research, University Medical Centre Groningen, PO Box 30001, 9700 RB Groningen, Netherlands, j.bouma@med.umcg.nl)

The WINDFARM perception project, carried out in 2006 in the Netherlands, aimed to explore the impact of wind farms on people living close to wind farms. The study sample was selected in three types of area (countryside, countryside with major road, built up area) by means of a Geographic Information System (GIS). Each selected address was within 2.5 km of a wind turbine of at least 500 kW electric power and a similar turbine within 500 m of the first. Aural impact was calculated according to three different sound propagation models: the international ISO-9613 standard, the model legally required in the Netherlands, and a simplified model as in the New Zealand Standard NZS-6808. Visual impact was quantified in two ways: the vertical angle determined by the height of the apparently tallest turbine, and the solid angle determined by all turbines where each turbine was replaced by a vertical rectangle just enclosing the turbine. Immission sound levels from the wind farms at 1948 receiver locations varied from 21 to 54 dB(A), relative size from 0.01% to 30% of the total field of view. Results show that all impact measures are highly correlated with distance to the nearest wind turbine.

4pNSl3. Dispersal of measured sound power levels for wind turbines. René Gamba (Gamba Acoustique, 2 rue de la découverte, BP 163, 31676 Labege Cedex, France, rene.gamba@acoustique-gamba.fr), Sébastien Garrigues (Gamba Acoustique, 2 rue de la découverte, BP 163, 31676 Labege Cedex, France, sebastien.garrigues@acoustique-gamba.fr)

The standard IEC 61400-11 provides guidance in the measurement, analysis and reporting of acoustic emissions (sound power levels) from wind turbine generator systems. The application of this standard aims to provide accurate results that can be replicated by others. We did several measurement operations according to this standard on various wind farms fitted with many turbine manufacturers on different ground types. Important differences have been noticed with equal working conditions between the most and the less noisy wind turbine on a single farm. We will present these results compared to the manufacturers' guaranteed values and initiate explanations (like the difficulties to link the wind speed at 10m above ground with the wind speed received at hub height; or the influence of wind incidence on blades).

Session 4pNSm

Noise and EURONOISE: Vibration Perception II (Poster Session)

Patricia Davies, Cochair
Ray W. Herrick Lab., School of Mechanical Engineering, Purdue Univ.

Michael Griffin, Cochair
Institute of Sound and Vibration Research, University of Southampton

All posters will be on display from 3:40 p.m. to 5:20 p.m. To allow contributors an opportunity to see other posters, contributors of odd-numbered papers will be at their posters from 3:40 p.m. to 4:30 p.m. and contributors of even-numbered papers will be at their posters from 4:30 p.m. to 5:20 p.m.

Contributed Papers

4pNSm1. Hand-arm equal sensation curves for steering wheel translational and axial vibration. Mickael Sauvage (PSA Peugeot Citroën, Centre Technique de Vélizy, Route de Gisy, 78943 Vélizy-Villacoublay, France, mickael.sauvage@mpsa.com), Elise Gressant (PSA Peugeot Citroën, Centre Technique de Vélizy, Route de Gisy, 78943 Vélizy-Villacoublay, France, elise.gressant@u-cergy.fr), Olivier Lescop (PSA Peugeot Citroën, Centre Technique de Vélizy, Route de Gisy, 78943 Vélizy-Villacoublay, France, olivier.lescop@mpsa.com), Vincent Roussarie (PSA Peugeot Citroën, Centre Technique de Vélizy, Route de Gisy, 78943 Vélizy-Villacoublay, France, vincent.roussarie@mpsa.com)

The aim of the study was to determine the hand-arm equal sensation curves for steering wheel translational and axial vibration. A sensory panel of 10 trained judges performed a two-step procedure. The test stimuli used were sinusoidal vibrations in the range from 4 to 60 Hz, with amplitude of 0.2 m/s^2 rms. The first step was to determine perceived sensations for each frequency. Four families of vibration were defined (pumping movement, shaking sensation, trembling sensation and prickling sensation). The second step was a three-down-one-up test based on these families to determine the equal sensation level. Results showed that perceived intensity depends on vibration family, frequency and excitation direction (translational or axial).

4pNSm2. A new instrument for the measurement of occupational vibration. Laurent Faiget (01dB-Metravib, 200 Chemin des Ormeaux, F-69578 Limonest, France, laurent.faiget@01db-metravib.com), Fernand Dupont(01dB-Metravib, 6 Avenue Louis Blériot, F-31570 Ste Foy D'Aigrefeuille, France, fernand.dupont@01db-metravib.com), Christine Aujard (01dB-Metravib, 200 Chemin des Ormeaux, F-69578 Limonest, France, christine.aujard@01db-metravib.com)

Directive 2002/44/CE relative to the risks arising from vibration has been transcribed into national laws of most Member States. This directive deals with the determination of limits and action values for the daily exposure to vibration. Two physiological domains are addressed: the ″hand-arm″ and the ″whole-body″ domains, the acceptable statutory values of which are specified in the text. The experimental protocol, as well as indicators relevant for assessment, is defined in Standards ISO 5349-2 and ISO 2631-1. The equivalent frequency-weighted acceleration shall be measured on the 3 axes x, y and z, the bandwidth of which is defined for each domain. 01dB-Metravib introduces a new portable instrument that perfectly meets the requirements of this statutory application. A blind metrological instrument connected to a triaxial accelerometer is installed on site. The instrument is remotely controlled by the operator using a wireless remote control of the Pocket PC type. This remote control is used to manage measurement configurations (″whole-body″, hand-arm″), to start acquisitions (immediate, delayed mode) and to collect measured data for post-processing and archiving purposes. We will present metrological and operational advancements of this new instrument and describe a real case study dealing with the assessment of daily exposure to vibration.

Session 4pNSn

Noise, Computational Acoustics, and EURONOISE: Source Identification in Radiation and Scattering II (Poster Session)

J. Stuart Bolton, Cochair
Ray W. Herrick Labs., School of Mech. Eng., Purdue University

Peter Juhl, Cochair
Institute of Sensors, Signals and Electrotechnics, University of Southern Denmark

All posters will be on display from 3:40 p.m. to 5:20 p.m. To allow contributors an opportunity to see other posters, contributors of odd-numbered papers will be at their posters from 3:40 p.m. to 4:30 p.m. and contributors of even-numbered papers will be at their posters from 4:30 p.m. to 5:20 p.m.

Contributed Papers

4pNSn1. Adaptation of the propagator for numerical acoustic holography of a wheel type object. Thibault Le Bourdon (Institut Jean Le Rond d'Alembert, UMR CNRS 7190, UPMC, 2 Place de la Gare de Ceinture, 78210 Saint-Cyr l'Ecole, France, lbourdon@ccr.jussieu.fr), Vincent Martin (Institut Jean Le Rond d'Alembert, UMR CNRS 7190, UPMC, 2 Place de la Gare de Ceinture, 78210 Saint-Cyr l'Ecole, France, vmartin@ccr.jussieu.fr)

Holography procedure of a vibrating object can be geometrically interpreted resulting in a guarantee of its identified vibratory velocity, the quality of which depends on the pressure measurement at an array of microphones and on the propagation model. In case of a wheel with the panel body, a plane array parallel to the visible side is the only one possible. The velocity is then accessible on the side concerned and needs a propagation model with adequate acoustic conditions over the whole plane with the visible side (source plane). Having in mind such a configuration, a theoretical work in the 3D space has shown the surrounding influence on the reconstructed velocity on the visible side. It has appeared that vibrations other than the ones of the front side and the rear acoustic load can be described with an admittance on the source plane. We present here an exhaustive search for the adequate admittance concerned leading to a correct propagator and a correct velocity identified. The success achieved in the procedure may rely on the single velocity and single model liable to radiate a given pressure on a sufficiently large antenna.

4pNSn2. Exact solutions to the acoustic source reconstruction problem. Cédric Maury (Université de Technologie de Compiègne, Centre de Recherche Royallieu, BP20529, 60205 Compiègne, France, cedric.maury@utc.fr), Teresa Bravo (Université de Technologie de Compiègne, Centre de Recherche Royallieu, BP20529, 60205 Compiègne, France, teresa.bravo-maria@utc.fr)

In this study analytical solutions are derived for the singular radiation and velocity patterns of a baffled elastic beam, thus leading to closed-form expressions for the singular value expansion of a number of integral operators which map a boundary velocity onto the acoustic pressure distribution radiated in far-field or intermediate regions. Exact solutions to this problem involve prolate spheroidal wave functions which correspond to a set of independent distributions with finite spatial support and with maximal energy concentration in a given bandwidth in the wavenumber domain. A stable solution to the inverse source reconstruction problem is obtained by decomposing the unknown boundary velocity into a number of efficiently radiating singular velocity patterns which corresponds to the number of degrees of freedom of the radiated field. It is found that the degree of ill-posedness of the inverse problem is significantly reduced when considering a hemicircular observation arc with respect to a linear array of sensors, by a factor scaling on the small angular aperture subtended by the observation line. Estimates are derived of the spatial resolution limits that can be achieved in the source reconstruction problem from the dimension of the efficiently radiating subspace.

Session 4pNSo

Noise, ASA Committee on Standards, and EURONOISE: Prominent Discrete Tones II (Poster Session)

Robert Hellweg, Cochair
Wellesley, MA

Lothar Schmidt, Cochair
Currenta GmbH & Co. OHG

All posters will be on display from 3:40 p.m. to 5:20 p.m. To allow contributors an opportunity to see other posters, contributors of odd-numbered papers will be at their posters from 3:40 p.m. to 4:30 p.m. and contributors of even-numbered papers will be at their posters from 4:30 p.m. to 5:20 p.m.

Contributed Papers

4pNSo1. Tonalness perception of harmonic complex tones. Sebastian Fingerhuth (Institute of Technical Acoustics, RWTH Aachen University, Neustrasse 50, 52066 Aachen, Germany, sfi@akustik.rwth-aachen.de), Etienne Parizet (Laboratoire Vibrations Acoustique, Insa Lyon, 25 bis, av. J. Capelle, 69621 Villeurbanne Cedex, France, etienne.parizet@insa-lyon.fr)

Many everyday sounds have a more or less tonal characteristic. This normally means they have some peaks in the spectrum and generate one or more of the pitch sensations. In this work we present the results of a listening test which deals with the perception of tonalness of harmonic complex sounds. It consisted in presenting sounds via headphones to the 30 listeners who had to evaluate the tonalness using magnitude estimation with a reference sound. The sounds presented to the listeners varied in some parameters which modified the perception of tonalness. The parameters are: i) tone to noise level (3dB steps), ii) number of harmonics (1, 2, 4, 8 and 8 with f0 and f1 removed) and iii) spectral shape of the harmonics (constant, -5dB/oct and 5dB/oct). The loudness of the stimuli were equalized. Tonalness increases for higher tone to noise ratio. A change in the spectral shape is most important for a high number of harmonics. More harmonics also increase tonalness mostly for constant and increasing spectral shape. The results of the test were also compared with the tonalness calculation algorithm from Aures' and the german DIN45681 model. Both gave a correlation coefficient $>$ 0.95.

4pNSo2. Methods for automating prominent tone evaluation and for considering variations with time or other reference quantities. Wade R. Bray (HEAD acoustics, Inc., 6964 Kensington Road, Brighton, MI 48116, USA, wbray@headacoustics.com)

Information Technology acoustic protocols include identifying prominent tones according to likely subjective importance. Most existing methods for calculating tone-to-noise ratio (TNR) require a suspect tone to be selected by the analyst, who must also mark the width; both are potential sources of uncertainty and variability. One purpose of this paper is to present an automatic tone-detection and width-assessment methodology for more robust, less operator-intensive TNR calculation in accordance with ECMA-74. The paper will also present a process giving a complete spectral representation of the prominence ratio (a specific prominence ratio) by iterating the calculation at each frequency bin of the Fourier transform of the time-signal. The ECMA-74 tone-detection procedure for TNR is also applicable to the specific prominence ratio and is automatable, yielding tones-only prominence results without user intervention for any or all tones qualifying as prominent. The conventional average prominent tone evaluation over an operating interval can cause mis-assessment or no assessment of subjectively prominent tones which change frequency and/or level with time. We will therefore also discuss applying the described procedures as functions of time or other reference quantities, and suggest considering the subjective significance of time-domain effects such as modulation occurring from certain multiple prominent tone situations.

Session 4pNSp

Noise and EURONOISE: Tire-Road Noise from the Road Perspective II (Poster Session)

Paul Donavan, Cochair
Illingworth & Rodkin, Inc.

Fabienne Anfosso-Ledee, Cochair
Laboratoire Central des Ponts et Chaussées

All posters will be on display from 3:40 p.m. to 5:20 p.m. To allow contributors an opportunity to see other posters, contributors of odd-numbered papers will be at their posters from 3:40 p.m. to 4:30 p.m. and contributors of even-numbered papers will be at their posters from 4:30 p.m. to 5:20 p.m.

Contributed Papers

4pNSp1. Dense road surfaces with small aggregate size - tyre/road noise reduction after repaving. Nils-Åke Nilsson (Acoustic Control AB, Tumstocksvägen 1, SE-187 66 Taeby, Sweden, na.nilsson@acoustic.se), Nils Ulmgren (NCC Roads Sweden AB, R&D Center, Bryggervägen 13, SE194 36 Upplands Väsby, Sweden, nils.ulmgren@ncc.se)

Open, porous road surfaces normally suffers from pore clogging particularly in inner city situations with low vehicle speed. After a relatively short time pore clogging could almost eliminate the noise reduction effect. A dense low noise road surface with smaller aggregate stone size could here offer substantial noise reduction due to reduced surface roughness, despite its low sound absorption factor. In this paper is presented data on the ″repaving insertion loss″ in dB(A) when exchanging a worn older SMA16 by a newly paved dense SMA8. Comparative results will also be shown for various types of newly paved SMA16 in comparison to the a newly paved SMA8. The technique for noise reduction mentioned above could be believed to have an ″improved long term endurance″ as compared to the same degree of noise reduction achieved by open graded technique particularly in city centres. For the Scandiavian countries where studded tyres are allowed, further reduction of stone size could be possible at acceptable wear rate if studded tyres are taxed or prohibited e.g. in environmental zones. This could lead to a further increased reduction of tyre/road noise in such zones. Grant from European Commission to Project Quiet City Transport (QCITY) is acknowledged.

4pNSp2. Measurement of pavement absorption using ISO 13472-2. Andrew F. Seybert (University of Kentucky, Dept. of Mech. Engineering, 151 RGAN Bldg., Lexington, KY 40506, USA, seybert@engr.uky.edu), Jun Han (University of Kentucky, Dept. of Mech. Engineering, 151 RGAN Bldg., Lexington, KY 40506, USA, jhan@engr.uky.edu)

This paper discusses some recent experience with ISO draft standard 13472-2 for the measurement of the absorption of pavements. The draft standard is meant to be used for the measurement of the sound absorption coefficient of ″reflective″ pavements, e.g., pavements of test tracks used for passby noise measurements of vehicles, tires, etc. An impedance tube has been constructed based on the requirements of the draft standard, and the device has been used in the laboratory (with pavement samples) and in situ to measure pavement absorption. The papers discusses these results and other important features of the draft standard including microphone calibration, parasitic tube absorption, and the construction features of the impedance tube and source.

4pNSp3. A first step toward a close proximity noise map. Moises Bueno (Laboratory of Acoustics Applied to Civil Engineering (LA2IC), Universidad de Castilla-La Mancha, Department of Applied Physics, 13071 Ciudad Real, Spain, moises.bueno@uclm.es), Urbano Viñuela (Laboratory of Acoustics Applied to Civil Engineering (LA2IC), Universidad de Castilla-La Mancha, Department of Applied Physics, 13071 Ciudad Real, Spain, urbano.vinuela@uclm.es), Fernando Terán (Laboratory of Acoustics Applied to Civil Engineering (LA2IC), Universidad de Castilla-La Mancha, Department of Applied Physics, 13071 Ciudad Real, Spain, fernando.teran @uclm.es), S. E. Paje (Laboratory of Acoustics Applied to Civil Engineering (LA2IC), Universidad de Castilla-La Mancha, Department of Applied Physics, 13071 Ciudad Real, Spain, santiago.exposito@uclm.es), Jeane Luong (Mecanique d'ingenierie des systemes, Université Pierre et Marie Curie, 75252 Paris, France, jeanne.luong@etu.upmc.fr)

In recent years, environmental noise has become a serious issue for civil infrastructure and environmental administration due to public concern over the subject of noise pollution. The most significant deterioration of environmental acoustics conditions comes from road traffic transportation. The predominant noise source is the combination of the tire/pavement interaction and the propulsion systems of the vehicles. Generally, tire/pavement interaction is the principal source of noise for speeds above 40 km/h in the case of most modern cars. In this research, geo-referenced close proximity rolling noise is used for acoustical characterization of asphalt concrete surfaces in an urban environment. A close proximity noise map of streets with low speed limits is presented for a reference speed of 50 km/h. Different pavements and pavement conditions, common in urban streets, are analyzed: dense and semidense asphalt concrete, with Spanish denomination D-8 and S-12, respectively, and on the other hand, dense pavement at the end of its service life (D-8*). Noise levels from dense surfaces (D-8) increase significantly over time, principally due to the appearance of surface defects such as cracks and ruts.

4pNSp4. Road pavement classification based on noise emission characteristics. Joel P. Paulo (ISEL, R. Conselheiro Emídio Navarro,1, 1959-007 Lisbon, Portugal, jpaulo@deetc.isel.ipl.pt), J. Luis Bento Coelho (CAPS, Instituto Superior Técnico, TU Lisbon, Av. Rovisco Pais, P-1049-001 Lisbon, Portugal, bcoelho@ist.utl.pt)

The measurement procedure to evaluate the influence of road surface characteristics on vehicle and traffic noise is designated by Close-Proximity (CPX) method, as described in the ISO 11819-2 draft. This procedure consists on acquiring the vehicle rolling noise signal near the tires and close to the surface by means of at least two microphones, in a special arrangement for the determination of the Close-Proximity Sound Index (CPXI). Road

traffic noise is estimated by taking into account the absorption characteristics of road surface on the propagation of sound and the speed and type of vehicles. However, the particular characteristics of the different pavement types, which may influence the sound radiation, are not considered. The main goal of this research is to identify and classify different types of road pavements, for different stress conditions, using the CPX method. Such information can be used as a guideline for calibrating noise mapping models in order to achieve more realistic and accurate results. The classification of the different road surfaces consists on a supervised learning technique based on the Support Vector Machine, SVM, algorithms. Results based on error analysis are presented and discussed.

4pNSp5. A single wheel trailer for tire/road noise measurements enabling both the CPX- and pass-by methods. Martin Höjer (Acoustic Control AB, Tumstocksvägen 1, SE-187 66 Taeby, Sweden, martin.hojer@acoustic.se), Nils-Åke Nilsson (Acoustic Control AB, Tumstocksvägen 1, SE-187 66 Taeby, Sweden, na.nilsson@acoustic.se)

A single wheel trailer for tyre/road noise measurements has been developed. It has a towing beam, up to 8 m long, which ensures low background noise from support wheels and towing vehicle. Shielding hood is not necessary. The single wheel trailer can thus be used both for CPX-measurements with on-board carried microphones and pass-by measurements using stationary road-side microphones. The advantage of measuring in the free field with a minimum influence from the suspension attachments etc. is that the emission frequency spectra will be almost undisturbed. It can thus be more easily compared to the sound levels at road-side residents. Due to the long towing beam, tyre prototypes $>$10 dB quieter can be studied without disturbing background noise. The trailer has been specially designed to ensure stable vehicle dynamics, even though the normally loaded measurement tyre is rolling up to 8 meters behind the support trailer. Another interesting feature is the telescopic design of the towing beam, which enable compaction of the trailer so that the measurement wheel is landed on the trailer support part, enabling convenient transportation to the measurement site.

4pNSp6. A noise classification system for low-noise road surfacings - experiences and status. Bent Andersen (Danish Road Institute/Road Directorate, Guldalderen 12, 2640 Hedehusene, Denmark, bea@vd.dk), Jørgen Kragh (Danish Road Institute/Road Directorate, Guldalderen 12, 2640 Hedehusene, Denmark, kragh@vd.dk), Sigurd N. Thomsen (Danish Road Institute/Road Directorate, Guldalderen 12, 2640 Hedehusene, Denmark, snt @vd.dk)

As a result of an increasing pressure from the population as well as from road administrations a noise classification system for road surfacings was put into operation in the autumn 2006. The so-called SRS-system (a Danish abbreviation for noise reducing wearing courses) is provisional and non-committal for a couple of years until sufficient experience has been collected. It is a comprehensive system including: ˙Guidelines on the use of low-noise asphalt surfacings for noise abatement. ˙Method for declaration and documentation of noise reduction based on the CPX (close proximity)-method. ˙Paradigm for use in preparation of tendering documents and contracts. The measurement method is based upon the ISO draft standard describing the CPX-method, but includes further specification. Reference values for dense asphalt concrete are defined, and 2 dB wide noise reduction classes A, B, and C are defined at 50 and 80 km/h. The method also specifies an inter-calibration procedure (including definition of reference road sections) to be applied for different CPX measurement devices. Each year a specific calibration constant is issued for each device. The paper will also discuss the recent developments in the selection of future reference tyres for CPX measurements. Finally, a status of the classified surfacings will be presented.

THURSDAY AFTERNOON, 3 JULY 2008 P2-A, LEVEL 2, 3:40 TO 5:20 P.M.

Session 4pNSq

Noise and EURONOISE: Fan Noise and Low-Mach Number Rotating Blade Noise II (Poster Session)

Scott Morris, Cochair
Notre Dame

Michel Roger, Cochair
Ecole Centrale de Lyon

All posters will be on display from 3:40 p.m. to 5:20 p.m. To allow contributors an opportunity to see other posters, contributors of odd-numbered papers will be at their posters from 3:40 p.m. to 4:30 p.m. and contributors of even-numbered papers will be at their posters from 4:30 p.m. to 5:20 p.m.

Contributed Papers

4pNSq1. Prediction of blade trailing-edge noise of an axial flow fan. Alain Guedel (CETIAT, BP 2042, 69603 Villeurbanne Cedex, France, alain.guedel@cetiat.fr), Arthur Finez (Ecole Centrale de Lyon, 36 Avenue Guy de Collongue, Centre Acoustique, 69134 Ecully, France, arthur.finez@gmail.com), Gérald Perrin (CETIAT, BP 2042, 69603 Villeurbanne Cedex, France, gerald.perrin@cetiat.fr), Michel Roger (Ecole Centrale de Lyon, 36 Avenue Guy de Collongue, Centre Acoustique, 69134 Ecully, France, michel.roger@ec-lyon.fr)

Broadband noise is a major part of the noise radiated by low-speed fans such as industrial and domestic fans. One of the main mechanisms of broadband noise is blade trailing-edge noise, which is due to the convection of the turbulent flow of the boundary layer past the blade trailing edge. The objective of this work is to predict trailing-edge noise of an axial flow-fan with an analytical model adapted from Amiet's formulation. The input data of the model are the spectra and correlation length scales of the wall pressure fluctuations on the blade suction side close to the trailing edge. These data are measured with small pressure transducers flush mounted on the blade suction side. A first study was performed on a 800-mm axial fan without shroud. The comparison between the predicted and measured far-field sound pressure spectra proved quite good, which validated the model in this impeller configuration. The next stage in progress is to insert a shroud on the

same impeller and validate the noise prediction in this case for different fan operating points. The importance of additional broadband noise sources, such as blade tip noise, could also be assessed on this fan configuration.

4pNSq2. Fan Blade Trailing-Edge Noise Prediction Using RANS Simulations. Yannick Rozenberg (ONERA, BP 72 - 29 avenue de la Division Leclerc, 92322 Chatillon Cedex, France, yannick.rozenberg@onera.fr), Michel Roger (Ecole Centrale de Lyon, 36 Avenue Guy de Collongue, Centre Acoustique, 69134 Ecully, France, michel.roger@ec-lyon.fr), Stéphane Moreau (Valeo Thermal Systems, rue Louis Normand, 8, 78321 La Verrière, France, stephane.moreau@valeo .com)

An analytical model based on Paterson & Amiet's work dealing with the trailing-edge noise of a blade has been previously validated thanks to a dedicated experiment on a low speed axial fan. Wall-pressure spectra near the trailing-edge of the blade and at different radii are needed for an accurate prediction. Only experiments and LES simulations are able to provide them. In an industrial context, both methods can not be applied since they are too expensive and time-consuming. To overcome this difficulty, RANS simulations are combined with semi-empirical wall-pressure spectra to obtain the needed input data. The effect of the mean-pressure gradient is taken into account. The model is applied first to the noise radiated by an airfoil placed in the open-jet of an anechoic wind tunnel, then to an automotive cooling fan and finally to an aircraft engine fan. RANS simulations are post-processed to run the analytical model with appropriate input data. The noise predictions are then compared with experimental results.

4pNSq3. Experimental investigation of wind turbine noise. Maud Leroux (Laboratoire d'Etudes Aérodynamiques (LEA), Université de Poitiers - ENSMA - CNRS, Bâtiment K, 40 Avenue du Recteur Pineau, 86022 Poitiers, France, maud.leroux@lea.univ-poitiers.fr), Yves Gervais (Laboratoire d'Etudes Aérodynamiques (LEA), Université de Poitiers - ENSMA - CNRS, Bâtiment K, 40 Avenue du Recteur Pineau, 86022 Poitiers, France, yves.gervais@lea.univ-poitiers.fr), Jacques Borée (Laboratoire d'Etudes Aérodynamiques (LEA), Université de Poitiers - ENSMA - CNRS, Bâtiment K, 40 Avenue du Recteur Pineau, 86022 Poitiers, France, jacques.boree@lea.ensma.fr), Arnaud Ménoret (Signal Developpement, 12 Boulevard Chasseigne, 86000 Poitiers, France, a.menoret @signal-developpement.com)

Broadband noise is nowadays the major contribution to the total spectrum of noise generated by wind turbines. The mechanisms that generate airfoil self-noise have been studied through years and many authors agree that dominant noise comes from inflow turbulence, and interaction between turbulent boundary layer and trailing edge of the airfoil. This study presents results from combined experimental techniques in order to better identify and predict noise issuing from a NACA 0012. Noise from trailing edge is most investigated in a 2D configuration in an anechoic wind tunnel, using microphone array (far field measurements), wall pressure fluctuations, hot wire. The data base turns out to be useful in order to improve extensions of Amiet and Brooks models. Some aspects of noise mechanisms and their characteristics are better identified and refined when wind tunnel results are compared to measurements of noise on full scale wind turbines. Measurements in situ achieved with a microphone array of 30 meters wide are used to provide complementary informations on 3D rotating source in terms of localisation and specific directivity.

4pNSq4. Measurement of wall pressure fluctuations for noise prediction in axial flow fans. Jérémy Hurault (Lab. d'Energétique et de Mécanique des Fluides Interne, Arts et Métiers ParisTech, 151 Boulevard de l'Hôpital, 75013 Paris, France, jeremy.hurault@paris.ensam.fr), Smaine Kouidri (LIMSI-CNRS, BP 133, 91403 Orsay Cedex, France, smaine.kouidri@limsi.fr), Farid Bakir (Lab. d'Energétique et de Mécanique des Fluides Interne, Arts et Métiers ParisTech, 151 Boulevard de l'Hôpital, 75013 Paris, France, farid.bakir@paris.ensam.fr), Robert Rey (Lab. d'Energétique et de Mécanique des Fluides Interne, Arts et Métiers ParisTech, 151 Boulevard de l'Hôpital, 75013 Paris, France, robert .rey@paris.ensam.fr)

The unsteady pressure field on fan blades is an important investigation topic. Both numerical simulation and experimental techniques are used in order to achieve this purpose. However neither has given yet entire satisfaction. The CFD tools using the resolution of the averaged Navier Stokes equations do not really give the unsteady aerodynamic characteristics of the flow needed for an accurate noise prediction. In addition, tools using large eddy simulation are still expensive for industrial users in the case of a complex geometry such as turbomachinery. When a lifting surfaces goes through turbulence, pressure fluctuations occur on their surfaces that can radiate noise. To calculate these fluctuations and thus the noise requires a theoretical model of the unsteady aerodynamics. The validation and development of these models require data and understanding from experiments. Unsteady surface pressure measurements were carried out on one fan blade with an array of pressure transducers with high sensitivity. The fan studied is a low pressure and low Mach number axial flow fan. Investigations of unsteady surface pressure are carried out in different configuration, spanwise, chordwise, pressure side and suction side. Data are gathered through a slip ring by an analyser. The unsteady wall pressure spectra is used as an input for trailing edge noise analytical prediction model.

Session 4pNSr

Noise and EURONOISE: Cultural Variations in Sound/Noise Assessment II

Catherine Guastavino, Cochair
Centre for Interdisciplinary Research in Music Media & Technology (CIRMMT) - School of Information Studies - McGill Univ., 3459 McTavish, Montreal, QC H3A1Y1, Canada

Danièle S. Dubois, Cochair
CNRS, LCPE/LAM 11 rue de Lourmel, Paris, 75015, France

Invited Papers

5:20

4pNSr1. Acoustical Variety of Soundscapes - Comparison of Soundscapes. Klaus Genuit (HEAD acoustics GmbH, Ebertstrasse 30a, 52134 Herzogenrath, Germany, klaus.genuit@head-acoustics.de), André Fiebig (HEAD acoustics GmbH, Ebertstrasse 30a, 52134 Herzogenrath, Germany, andre.fiebig@head-acoustics.de)

Noise of urban places varies not only with regard to its physical parameters, but also it is perceived and assessed differently because of cultural, sociological, historical and economic influences. The physical description of a soundscape does not cover the complexity of human perception in a specific environmental setting. Therefore, the task of soundscape researchers has to consider more aspects than the measurement and interpretation of the acoustical differences caused by location-specific noise sources. Moreover, semantic and cognitive aspects relating to culture, tradition and economy must be extensively analyzed. Cultural and sociological conditions influence the people's evaluations of their surroundings. A deeper understanding is necessary to adequately analyze soundscapes, especially where specific noise phenomena - e.g. temporal and spectral effects - are of more importance to the listeners' well-being than an averaged SPL value. The presented paper compares and analyses environmental sounds of different cities scattered all over the world by means of conventional and advanced acoustical analyses. The results could provide reliable data for further investigations covering sociological and cultural issues.

5:40

4pNSr2. Naïve and expert listeners use different strategies to categorize everyday sounds. Guillaume Lemaitre (IRCAM - UMR CNRS 9912, Equipe Perception et Design Sonores, 1, place Igor Stravinsky, 75004 Paris, France, lemaitre@ircam.fr), Olivier Houix (IRCAM - UMR CNRS 9912, Equipe Perception et Design Sonores, 1, place Igor Stravinsky, 75004 Paris, France, olivier.houix@ircam.fr), Nicolas Misdariis (IRCAM - UMR CNRS 9912, Equipe Perception et Design Sonores, 1, place Igor Stravinsky, 75004 Paris, France, misdarii@ircam.fr), Patrick Susini (IRCAM - UMR CNRS 9912, Equipe Perception et Design Sonores, 1, place Igor Stravinsky, 75004 Paris, France, susini@ircam.fr)

We report an experiment investigating the influence of the expertise of listeners on the strategy used to categorize sounds. A set of sixty kitchen sounds was selected, based on their causal uncertainty (ranging from very well identified to ambiguous). Thirty listeners were selected on the basis of their expertise in sound and music: fifteen ″experts″ and fifteen ″naïves″. First, they had to group together the sounds. Second, they had to describe the properties shared by the sounds in each category. Finally, they were provided with a description of different strategies of classification previously identified (acoustical, causal or semantic similarity), and required to indicate, for each category, which one they had used. The results show a strong influence of the expertise of the participants: while naive listeners made categories mainly on the basis of the events that they identified as having caused the sounds, experts made mainly categories of sounds on the basis of the perceived acoustical properties (timbre, time patterns, etc.). This result is coherent with the available literature demonstrating the coexistence of different strategies of listening, and links these strategies to the skills of the listeners. [This work is founded by the FP6 NEST Pathfinder European project CLOSED]

Contributed Paper

6:00

4pNSr3. Cultural variations and constants in emotional reactions to sounds. Daniel Vastfjall (Chalmers University of Technology, Division of Applied Acoustics - Chalmers Room Acoustics Group, Sven Hultins gata 8a, 41296 Gothenburg, Sweden, daniel.vastfjall@psy.gu.se)

In this talk I will argue that emotional reactions to sounds can be both constant and vary between different cultures. A model of sound perception that was developed by Chalmers room acoustics group, the Emotional Reaction Model (ERM) will be reviewed. The ERM predicts that emotional reactions to auditory events can be both elicited by 1) certain form features (eg. a steep rise time, a loud sound, a rough sound) and 2) content features (eg. the qualitative experience of the sound source; the loud, rough sound is a tiger roaring). The influence of form features are expected to be rather constant across people and cultures, while content features are expected to vary more between people. Empirical evidence supporting these predicitions will be reviewed and the implications for our understanding sound perception will be discussed.

Invited Papers

6:20

4pNSr4. When exposed to sounds, would perceived loudness not be affected by social context? Pieter Jan Stallen (Leiden University, PX Box 9555, 2300 RB Leiden, Netherlands, stallen@fsw.leidenuniv.nl)

After decades of predominantly correlation studies of non-auditory factors and environmental noise annoyance, Maris, Stallen, Vermunt and Steensma (2007a,2007b) have demonstrated experimentally that a negative and positive relationship between producer and receiver of environmental sounds can cause the receiver to be more and less annoyed by the sound, respectively. This finding raises the question whether the context of environmental sound, and social context in particular, could already be determining responses to environmental sounds at earlier stages of auditory processing. This paper will present answers regarding perceived loudness, which is generally considered to be a more immediate (and less evaluative) response to sound exposure than the feeling of annoyance. From a statistics point of view, there is room for early influences as isophones which are based upon equal loudness judgments seem to hide no less, if not more, variation than the mean annoyance score at various sound pressure levels (cf. Berglund and Preis, 1997). It will be argued that seemingly conflicting empirical findings could be reconciled by postulating different attentional mechanisms as they vary with task characteristics and demands. Ideas will be presented by which the presumed theoretical model could be tested experimentally.

6:40

4pNSr5. Comparison of Japanese and English language descriptions of piano performances captured using popular multichannel microphone arrays. William L. Martens (McGill University, Schulich School of Music, 555 Sherbrooke Street West, Montreal, QC H3A 1E3, Canada, wlm@music.mcgill.ca), Sungyoung Kim (Yamaha, 203 Matsunokijima, 438-0192 Iwata, Japan, sungyoung_kim@gmx.yamaha.com), Atsushi Marui (Tokyo University of the Arts, 1-25-1 Senju, Adachi, 120-0034 Tokyo, Japan, marui@ms.geidai.ac.jp)

In a cross-cultural comparison of musical sound evaluations, the way in which bipolar adjective pairs are used by native speakers of Japanese and English language was studied via a subjective rating task. These ratings were collected in response to eight solo piano performances that had been captured using four popular multichannel microphone arrays, reproduced via a standard 5-channel loudspeaker array, re-recorded binaurally, and finally presented via headphones. This allowed nearly identical stimuli to be presented to all listeners, without any modulation of the loudspeaker signals via listener head movements. Average ratings were compared to acoustical measures made on the 32 binaural stimuli, and to salient perceptual dimensions that previously had been derived from pairwise dissimilarity ratings between the stimuli. Results showed close agreement in how the selected terms were used by native speakers of Japanese and English language in the context of this study.

THURSDAY AFTERNOON, 3 JULY 2008 P3-A, LEVEL 3, 3:40 TO 5:20 P.M.

Session 4pPAa

Physical Acoustics: Ultrasonics: Material Characterization II (Poster Session)

Jim A. Tencate, Cochair
Los Alamos National Laboratory

Koen Van Den Abeele, Cochair
K. U. Leuven, Campus Kortrijk

All posters will be on display from 3:40 p.m. to 5:20 p.m. To allow contributors an opportunity to see other posters, contributors of odd-numbered papers will be at their posters from 3:40 p.m. to 4:30 p.m. and contributors of even-numbered papers will be at their posters from 4:30 p.m. to 5:20 p.m.

Contributed Papers

4pPAa1. Structure and ultrasonic properties of vanadium tellurite glasses containing cupper oxide. Nadia Abd El-Aal (National Institute of Standards, 136 Tersa St, El-Haram, 12211 Giza, Egypt, n_nadia_99@yahoo.com), Hisham Afifi (National Institute of Standards, 136 Tersa St, El-Haram, 12211 Giza, Egypt, hmafifi@hotmail.com)

The elastic properties of vanadium tellurite (65TeO2-(35-x) V2O5-xCuO) glasses with different compositions of cupper (x= 7.5 to 17.5 mol% in steps of 2.5 mol %) have been studied at room temperature (300K). The ultrasonic velocity measurements have been made using a transducer having resonating frequency of 4 MHz (both longitudinal and shear). The density, molar volume, and ultrasonic velocities show an interesting observations, which are used to explore the structural changes in the network. Elastic moduli, Poisson ratio, crosslink density, microhardnes, and Debye temperature of the glasses have been determined using the experimental data. The composition dependence of the elastic properties explores useful information about the physical properties of the vanadium tellurite glasses doped with cupper. Quantitative analysis has been carried out in order to obtain more informations about the structure of the glass under the study, based on bond compression model, and ring deformation model, i.e., the cation-anion bond of each oxide. The observed results through ultrasonic non-destructive evaluation investigate the structural changes and mechanical properties of the glass.

4pPAa2. Elastic characterization of ceramic balls using resonant ultrasound spectroscopy of spheroidal modes. François Deneuville (Institut d'Electronique de Microélectronique et de Nanotechnologie, Département Opto-Acousto-Electronique (UMR CNRS 8520), Université de Valenciennes et du Hainaut-Cambrésis, Le Mont-Houy, 59313 Valenciennes cedex 9, France, francois.deneuville@gmail.com), Marc Duquennoy (Institut d'Electronique de Microélectronique et de Nanotechnologie, Département Opto-Acousto-Electronique (UMR CNRS 8520), Université de Valenciennes et du Hainaut-Cambrésis, Le Mont-Houy, 59313 Valenciennes cedex 9, France, Marc.Duquennoy@univ-valenciennes.fr), Mohammadi Ouaftouh (Institut d'Electronique de Microélectronique et de Nanotechnologie, Département Opto-Acousto-Electronique (UMR CNRS 8520), Université de Valenciennes et du Hainaut-Cambrésis, Le Mont-Houy, 59313 Valenciennes cedex 9, France, mohammadi.ouaftouh@univ-valenciennes.fr), Frédéric Jenot (Institut d'Electronique de Microélectronique et de Nanotechnologie, Département Opto-Acousto-Electronique (UMR CNRS 8520), Université de Valenciennes et du Hainaut-Cambrésis, Le Mont-Houy, 59313 Valenciennes cedex 9, France, frederic.jenot@univ-valenciennes.fr), Mohamed Ourak (Institut d'Electronique de Microélectronique et de Nanotechnologie, Département Opto-Acousto-Electronique (UMR CNRS 8520), Université de Valenciennes et du Hainaut-Cambrésis, Le Mont-Houy, 59313 Valenciennes cedex 9, France, Mohamed.Ourak@univ-valenciennes.fr),Sébastien Desvaux(SKF Group, Z.I. n°2 Batterie 900 Rouvignies, 59309 Valenciennes, France, sebastien.desvaux@snfa.com)

The use of ceramic balls, in particular silicon nitride balls, allows a substantial improvement of bearing performances. For critical aerospace and space applications, there is a need for developing new nondestructive techniques for the characterization of these balls. We propose in this work to study the possibilities offered by a specific technique of resonant ultrasound spectroscopy of spheroidal modes. As shown by the theoretical study on elastic sphere vibrations, these modes allow to characterize the whole volume of balls or only the close-to-surface layers, according to the considered frequency range. To acquire the resonance spectra of these modes, a specific measurement system composed of a piezoelectric ultrasonic probe and an optical interferometer was developed. A self-implemented numerical processing of measured spectra allows to detect the resonance frequencies and to deduce from them the propagation velocity of the spheroidal waves in each inspected subsurface layers. Then, we propose a method based on these results that permit to estimate the elastic coefficients of the balls according to various inspection depths. This method has the advantage of providing very high precision evaluations of the elastic coefficients over a wide frequency range.

Session 4pPAb

Physical Acoustics and Computational Acoustics: Combustion Noise and Thermo-Acoustics II (Poster Session)

Tim Lieuwen, Cochair
Georgia Institute of Technology

Maria Heckl, Cochair
Keele University

Rafael Piscoya, Cochair
Technische Fachhochschule Berlin, Univ. of Applied Sciences

All posters will be on display from 3:40 p.m. to 5:20 p.m. To allow contributors an opportunity to see other posters, contributors of odd-numbered papers will be at their posters from 3:40 p.m. to 4:30 p.m. and contributors of even-numbered papers will be at their posters from 4:30 p.m. to 5:20 p.m.

Contributed Papers

4pPAb1. Inversion of the bulk viscosity in nonequilibrium media with heat release and new acoustical properties of such media. Nonna Molevich (P.N. Lebedev Physical Institute Samara branch, Pervomaiskaya Str 21-36, 443100 Samara, Russian Federation, molevich@fian.smr.ru)

New acoustical properties, which are caused by the inversion of the bulk (second) viscosity in nonequilibrium media, are investigated. Negative bulk viscosity can take place due to the positive feedback between the sound perturbation and the nonequilibrium heat release. During previous years, the conditions for the negative bulk viscosity existence were found in a large number of nonequilibrium media such as a vibrationally excited gas with stationary nonequilibrium, nonisothermal plasma, chemical active mixtures with irreversible reactions, media with nonequilibrium phases, upper atmosphere layers, and earth magma with bubbles. The following phenomena are discussed for gaseous media with negative viscosity: (1) New dispersion characteristics (in particular, the low-frequency sound speed can exceed the high-frequency one); (2) Acoustically instability of nonequilibrium media, nonlinear mechanisms of the wave growth stabilization and stationary self-sustaining structures; (3) Linear and non-linear sound beam refraction including the self-focusing (due to two self-action mechanisms in acoustically active media: the gas cooling by sound and the excitation of acoustical streaming in direction opposite to sound propagation) and the anomalous reflection (with reflection coefficient $R>1$) on a boundary between equilibrium and nonequilibrium media; (4) The vortex and thermal wave amplification due to intensive parametric interactions in acoustically active media.

4pPAb2. Stationary structures in acoustically active nonequilibrium media with one relaxation process. Rinat Galimov (Samara State Aerospace University, Magnitnaya st. 15, 443017 Samara, Russian Federation, renrk@mail.ru), Nonna Molevich (P.N. Lebedev Physical Institute Samara branch, Pervomaiskaya Str 21-36, 443100 Samara, Russian Federation, molevich@fian.smr.ru)

Chemical active mixtures with irreversible reactions, vibrationally excited gases, and nonisothermal plasmas are examples of acoustically active nonequilibrium media. In such media it is possible the existence of stationary nonlinear structures that are different from the step-wise shock wave structures. In the first part of the present paper it is investigated the solutions of a general acoustical equation, describing in the second order perturbation theory a nonlinear evolution of wide spectrum acoustical disturbances in nonequilibrium media with one relaxation process. Its low- and high- frequency limits correspond to Kuramoto-Sivashinsky equation and the Burgers equation with a source, respectively. Stationary structures of general equation, the conditions of their establishment and all their parameters are found analytically and numerically. In acoustically active media it is predicted the existence of the stationary solitary pulse. Then, we consider 1-D relaxing gas dynamics system of equations with simple Landau-Teller model of relaxation. The possible stationary profiles are shown in nonequilibrium degree- stationary wave speed bifurcation diagram. The boundaries of this diagram are obtained in analytical forms. The field of weak shock wave instability is shown in this bifurcation diagram. Unstable shock wave disintegrates into the sequence of solitary pulses described by the general acoustical equation.

4pPAb3. Thermoacoustic waves near the liquid-vapor critical point. Pierre Carles (Université Pierre et Marie Curie, 4 Place Jussieu, 75005 Paris, France, carles@ccr.jussieu.fr)

The thermal relaxation in a fixed-volume cell filled with a near-critical fluid is governed by the rapid expansion of thermal boundary layers, which drive a series of thermo-acoustic waves in the bulk fluid. The long-term cumulative effect of these waves is to increase the pressure in the cell, which in turn leads to a global temperature increase (a process named the Piston Effect). Recently and for the first time, the thermo- acoustic waves produced by the Piston Effect have been measured experimentally using interferometric methods [Y. Miura et al., to appear in Phys. Rev. E (2006)]. In the present work, we use asymptotic methods in order to derive a complete theoretical model of the Piston-Effect-driven acoustic waves, applicable to real fluid equations of state and to arbitrary reduced temperatures. The predictions of this model are compared to the above-mentioned experimental data, and an excellent agreement is observed without any fitting parameter. This result confirms the high precision of the data in question, and shows that asymptotic models such as ours can be a powerful tool for analyzing the results of such experiments.

4pPAb4. Prediction of noise emissions from industrial flares. Carl-Christian Hantschk (Müller-BBM GmbH, Robert-Koch-Str. 11, 82152 Planegg, Germany, Carl-Christian.Hantschk@MuellerBBM.de), Edwin Schorer (Müller-BBM GmbH, Robert-Koch-Str. 11, 82152 Planegg, Germany, Edwin.Schorer@MuellerBBM.de)

In many industries where combustible waste gases are obtained, flares are used to burn these gases in a controlled manner. Among other environmental aspects, the noise emissions associated with flaring are becoming increasingly important in many countries as population density goes up and residential and industrial areas move closer together. Installing noise control equipment on flares is almost impossible while they are in service, since flares are typically a safety related plant component that can only be turned off after the connected plant has been shut down. Accordingly, in order to plan appropriate noise control measures in time and to avoid unnecessary costs, predicting the noise emissions of flares as early in the design process as possible is crucial. This requires knowledge of the relevant individual noise sources associated to the flare system and the ability to calculate their respective contribution - in the operating condition in question - to the overall noise emission, based on the data available in the planning stage. The present paper summarizes these sources and outlines some of the individual effects and parameters having an influence on the acoustical characteristics of flares.

4pPAb5. Modelling of acoustic losses with the wave equation for the analysis of combustion instabilities. Elke Wanke (Lehrstuhl für Thermodynamik, Technische Universität München, Boltzmannstrasse 15, 85747 Garching, Germany, wanke@td.mw.tum.de), Fabian Weyermann (Lehrstuhl für Thermodynamik, Technische Universität München, Boltzmannstrasse 15, 85747 Garching, Germany, weyermann@td.mw.tum.de), Christoph Hirsch (Lehrstuhl für Thermodynamik, Technische Universität München, Boltzmannstrasse 15, 85747 Garching, Germany, hirsch@td.mw.tum.de), Thomas Sattelmayer (Lehrstuhl für Thermodynamik, Technische Universität München, Boltzmannstrasse 15, 85747 Garching, Germany, sattelmayer@td.mw.tum.de)

A numerical design tool for the assessment of the stability of combustion chambers has been developed, which is able to compute geometrically complex systems with thermoacoustic feedback in the time domain. It is shown that internal acoustic losses can be considered although the method is based on the solution of the wave equation. The presented method overcomes a serious limitation of the original approach and allows to make quantitative predictions. The model is based on the Bernoulli equation and derives the required information from the spatial distribution of the loss of total pressure. For the purpose of a comprehensive validation of the model, simulations were carried out in the frequency domain before the model was implemented. As the internal acoustic losses in combustors stem almost completely from the flow separation at the exit of the burners the losses are independent from temperature. For this reason the influence of the flame was neglected in the study to only focus on the modelling of acoustic losses. The numerical results are validated with single burner test rig experiments.

Session 4pPAc

Physical Acoustics: Quantum Acoustics II (Poster Session)

Michel DeBilly, Cochair
Institut Jean le Rond d'Alembert

Walter Lauriks, Chair
Katholieke Universiteit Leuven

All posters will be on display from 3:40 p.m. to 5:20 p.m. To allow contributors an opportunity to see other posters, contributors of odd-numbered papers will be at their posters from 3:40 p.m. to 4:30 p.m. and contributors of even-numbered papers will be at their posters from 4:30 p.m. to 5:20 p.m.

Contributed Papers

4pPAc1. Acoustic studies of the martensite phase transition in Ti-Ni alloys. Andrew A. Abramovich (St. Petersburg State Technological University of Plant Polymers, Chernykh str., 4, Vasenko str., 5/15, apt.32, 195197 St. Petersburg, Russian Federation, andrew@ns2740.spb.edu), Elena V. Charnaya (Department of Physics, St. Petersburg State University, Petrodvorets, Ulianovskaya, 1, 198504 St. Petersburg, Russian Federation, charnaya@paloma.spbu.ru), Sergei P. Belyaev (Department of Mathematics and Mechanics, St. Petersburg State University, Petrodvorets, Ulianovskaya, 1, 198504 St. Petersburg, Russian Federation, belyaev@paloma.spbu.ru), Aleksander E. Volkov (Department of Mathematics and Mechanics, St. Petersburg State University, Petrodvorets, Ulianovskaya, 1, 198504 St. Petersburg, Russian Federation, volkov@paloma.spbu.ru)

Acoustic studies of elastic properties and attenuation of ultrasonic waves (longitudinal and transverse) at the martensite phase transition were carried out in the Ti-Ni based polycrystalline alloys. Measurements were carried out using a pulse ultrasonic technique within a temperature range of 190 to 440 K upon continuous warming and cooling the samples after various hardening and annealing treatment. Anomalies of ultrasound velocity and attenuation were observed through the martensite phase transition which depended on wave polarization and thermal history of the samples, peaks of attenuation were seen only for transverse waves. A pronounced thermal hysteresis of acoustic features was also observed upon warming and cooling. The obtained results were treated on the basis of the phenomenological Landau theory for the B2-B19' ferroelastic phase transition.

4pPAc2. Observation of induced shear acoustic phonons by Brillouin scattering. Taisuke Yoshida (Faculty of Engineering Doshisha University, 1-3 Tatara Miyakodani, 610-0321 Kyotanabe, Japan, dth0186@mail4.doshisha.ac.jp), Sigeo Murata (Faculty of Engineering Doshisha University, 1-3 Tatara Miyakodani, 610-0321 Kyotanabe, Japan, dth0186@mail4.doshisha.ac.jp), Takahiko Yanagitani (Faculty of Engineering Tohoku University, 6-6-05 Aramaki Aoba Aoba-ku, 610-0321 Kyotanabe, Japan, yanagi@ecei.tohoku.ac.jp), Mami Matsukawa (Doshisha University, 1-3, Tatara Miyakodani, 610-0321 Kyotanabe, Japan, mmatsuka@mail.doshisha.ac.jp)

The Brillouin scattering measurement is an efficient nondestructive and noncontact method which enables the simultaneous measurement of longitudinal and shear wave velocities at hypersonic frequencies. However, the measurement accuracy of shear wave velocities is low because of the weak Brillouin scattering from the thermal phonons. In this study, therefore, we have tried to overcome this problem by making use of the induced coherent shear phonons. We have adopted the Reflection Induced θA (RIθA) scattering geometry for Brillouin scattering measurement. To induce shear acoustic phonons, we used an uniaxially aligned ZnO film transducer developed in our laboratory, which can be fabricated on any solid materials without the epitaxy technique. As a result, we obtained the intense Stokes peak in case of silica glass sample which is larger than that obtained from the thermal phonons. It means that observation of induced shear acoustic phonons was achieved. Because the RIθA geometry enables the simultaneous measurement of longitudinal and shear phonons in plane, this technique opens the new feature for the nondestructive elasticity measurement.

4pPAc3. Study of acoustical phonon modes in superlattices with SiGe QDs. Anatoliy Yaremko (Lashkaryov Institute of Semiconductor Physics, NAS of Ukraine, Prospekt Nauky 45, 03028 Kyiv, Ukraine, yaremko@isp.kiev.ua), Volodymyr Yukhymchuk (Lashkaryov Institute of Semiconductor Physics, NAS of Ukraine, Prospekt Nauky 45, 03028 Kyiv, Ukraine, yukhym@isp.kiev.ua), Volodymyr Dzhagan (Lashkaryov Institute of Semiconductor Physics, NAS of Ukraine, Prospekt Nauky 45, 03028 Kyiv, Ukraine, dzhagan@isp.kiev.ua), Mykhailo Valakh (Lashkaryov Institute of Semiconductor Physics, NAS of Ukraine, Prospekt Nauky 45, 03028 Kyiv, Ukraine, valakh@isp.kiev.ua)

Multilayers with SiGe nanoislands (QD's) grown in a broad temperature range are studied using Raman spectroscopy, HRXRD and compared with similar multilayers without islands. As the growth temperature increases, Si content in the islands increases, partially relieving strain. These structural transformations manifest themselves in both the intensity and frequency of the low-frequency Raman peaks. Due to composition- and strain-induced changes in the island band structure, excitation conditions come out of resonance, reducing Raman peak intensity. We have shown that at the interpretation of the Raman scattering by folded acoustic phonons for structures with nanoislands the real morphology of the island layer should be considered. The observed series of the low-frequency Raman peaks, for the multilayered structures with the number of QD layers below ten, is due to the acoustic phonon modes within the islands. The enhancement of the scattering intensity due to resonance of the excitation light with the electronic transitions within the islands plays a significant role. Theoretical analysis was fulfilled in the framework of microscopic approach with using Green function method and taking into account the real structure of QD's and their interaction with surrounding matrix.

4pPAc4. Evolution of ultrasound transmission during the sol-gel transition. Bożena Gadomska (University of Warsaw, Department of Chemistry, Laboratory of Physicochemistry of Dielectrics and Magnetics, ul. Żwirki i Wigury 101, 01-905 Warsaw, Poland, bogad@chem.uw.edu.pl), Wojciech Gadomski (University of Warsaw, Department of Chemistry, Laboratory of Physicochemistry of Dielectrics and Magnetics, ul. Żwirki i Wigury 101, 01-905 Warsaw, Poland, gado@chem.uw.edu.pl)

The velocity of the ultrasound wave has been detected during the gelation process of the aqueous gelatin solution. We observe monotonic decrease of the ultrasound transmission in train of the gel network formation. In order to find the dependance of the ultrasound velocity on the number of the intermolecular bonds, responsible for gel formation, we have performed the simultaneous measurements of the optical activity evolution. The experiments have been performed in the gelatin gel and in the silica gel. We have described the process in terms of the percolation theory by power law, according to Landau theory of the second order phase transitions, and by fitting the theoretical results to the experimental curves we have found the appropriate critical exponents. We have also shown how the ultrasound velocity depends on the concentration of the gelling substance and on the temperature, in which the process of the sol-gel transition has been performed.

4pPAc5. Acoustic wave propagation in cubic piezoelectric semiconductor plates. Bernard Collet (Université Pierre et Marie Curie - Institut Jean le Rond d'Alembert-UMR-CNRS 7190, T65-Case 162, 4 place Jussieu, 75252 Paris Cedex 05, France, bc@ccr.jussieu.fr)

Piezoelectric materials can be either dielectric or semiconductors. An acoustic wave propagating in a piezoelectric crystal is usually accompanied by an electric field. When the crystal is also a semiconductor, the electric field produces currents and space charges, resulting in dispersion and acoustic loss. The interaction between a travelling acoustic wave and mobile charges in piezoelectric semiconductors is currently called the acoustoelectric effect. It was shown experimentally and proved theoretically that an acoustic wave travelling in a piezoelectric semiconductor can be amplified by the application of an initial dc electric field. Piezoelectric semiconductors devices often have structural design of plates or rods. Here we study the thin piezoelectric semiconductor plates. Two-dimensional equations for coupled extensional, flexural and thickness-shear motions are obtained systematically from the three-dimensional equations by retaining lower order terms in power series expansions in the plate thickness coordinate. The two-dimensional equations are specialized to crystals of cubic (43m) symmetry. Propagation of extensional, flexural and thickness-shear waves and their amplification by a dc electric field are analyzed.

4pPAc6. Ultrasonic annealing of radiation defects in silicon. Artem Podolian (T Shevchenko Kiev National University, Dept of Physics, 03680 Kiev, Ukraine, gogi@univ.kiev.ua), Oleg Korotchenkov (T Shevchenko Kiev National University, Dept of Physics, 03680 Kiev, Ukraine, olegk@univ.kiev.ua)

Cold annealing of radiation defects in silicon is reported and the likely origin of the effect is suggested. The data on photocurrent transients and photoluminescence spectra are contrasted in γ-irradiated float zone and Czochralski silicon. The ultrasonic load is shown to slow down the current decay, indicative of the decreased defect densities. The microscopic model includes the likely pathways for E-center annealing in zone and C-O-V_2 complex redistribution in Czochralski materials. The carbon involvement into the annealing effect is further evidenced by taking the photoluminescence spectral evolution with applied ultrasonic loads. The usage of the presented technique in improving the performance of radiatively damaged silicon detectors is furthermore discussed.

THURSDAY AFTERNOON, 3 JULY 2008 P3-A, LEVEL 3, 3:40 TO 5:20 P.M.

Session 4pPAd

Physical Acoustics: General Topics in Nonlinear Acoustics II (Poster Session)

Thomas Matula, Cochair
University of Washington

Murray Korman, Cochair
U.S. Naval Academy

All posters will be on display from 3:40 p.m. to 5:20 p.m. To allow contributors an opportunity to see other posters, contributors of odd-numbered papers will be at their posters from 3:40 p.m. to 4:30 p.m. and contributors of even-numbered papers will be at their posters from 4:30 p.m. to 5:20 p.m.

Contributed Papers

4pPAd1. Parametric audible sounds by phase-cancellation excitation of primary waves. Tomoo Kamakura (Dept. of Electronic Eng., Univ. of Electro-Communications, 1-5-1, Chofugaoka, 182-8585 Chofu-shi, Japan, kamakura@ee.uec.ac.jp), Shinichi Sakai (Dept. of Electronic Eng., Univ. of Electro-Communications, 1-5-1, Chofugaoka, 182-8585 Chofu-shi, Japan, sakashin@ew3.ee.uec.ac.jp), Hideyuki Nomura (Dept. of Electronic Eng., Univ. of Electro-Communications, 1-5-1, Chofugaoka, 182-8585 Chofu-shi, Japan, nomu@ee.uec.ac.jp), Masahiko Akiyama (Dept. of Electronic Eng., Univ. of Electro-Communications, 1-5-1, Chofugaoka, 182-8585 Chofu-shi, Japan, akiyama@ew3.ee.uec.ac.jp)

An ultrasound source with a simple configuration is considered as a theoretical model. The source with a circular aperture consists of two coaxially arranged planar emitters: i.e., one is an inner disc emitter and the other is an outer ring emitter. The active areas of these emitters are the same. The outer diameter of the source is 20 cm. Both the emitters are driven individually at the same frequencies of 40 and 42 kHz but different phase angles. Especially, we focus on two extreme cases of the usual in-phase driving and out-of-phase driving. Numerical computation using the KZK equation demonstrates that when the driving signals are in phase the difference frequency beam of a 2-kHz wave has a candle-flame-like directivity. The beam has a

similar directivity when the signals are out-of-phase by 180 degrees, although the peak of the sound pressure level decreases by few decibels. Interestingly, the second harmonic pressure level of the difference frequency reduces by ten decibels and more. Needless to say, the pressure amplitudes of the primary waves are suppressed considerably near the beam axis. Experimental verification is done using an airborne ultrasound source with a 19.2-cm circular aperture.

4pPAd2. The Generation of Acoustic Waves and Cavitation Processes in Regime of Phase Synchronization During Multichannel Discharges in Electrolyte. Vyacheslav S. Teslenko (Lavrentyev Institute of Hydrodynamics SB RAS, Lavrentyev ave., 15, 630090 Novosibirsk, Russian Federation, vteslenko@academ.org), Alexey P. Drozhzhin (Lavrentyev Institute of Hydrodynamics SB RAS, Lavrentyev ave., 15, 630090 Novosibirsk, Russian Federation, ruslan@hydro.nsc.ru), Ruslan N. Medvedev (Lavrentyev Institute of Hydrodynamics SB RAS, Lavrentyev ave., 15, 630090 Novosibirsk, Russian Federation, drozh@hydro.nsc.ru)

In the paper the problems of acoustic waves generation of required frequency, amplitude and profile by the phase synchronization of multichannel discharges are considered. The phase synchronization of discharges is supplied by the implementation in the discharge circuit of additional inductance which acts as a dynamic feedback and ensures the selfsynchronization of N generated bubbles and acoustic wave's radiation [1]. The devices of such types may be used to form acoustic fields with required frequency and shape. References: 1. V. S. Teslenko, R. N. Medvedev, and A. P. Drozhzhin, Self-Synchronization of Electrohydrodynamic Autooscillations during Multichannel Discharges in Electrolyte // ISSN 1063-7850, Technical Physics Letters, 2007, Vol. 33, No. 10, pp. 833-836. http://www.swsl.newmail.ru/publ/TEPL833.pdf

4pPAd3. Acoustic properties of TaCl - TaBr mixed crystals. Farkhad Akhmedzhanov (Navoi State Mine Institute, 27a Yuzhnaya Street, 210100 Navoi, Uzbekistan, farkhad2@yahoo.com)

Attenuation coefficient and phase velocity of transversal and longitudinal acoustic waves in TaCl - TaBr mixed crystals have been investigated by Bragg light diffraction on the acoustic waves. The measurements were carried out at the frequencies from 200 to 1200 MHz at home temperature. Moreover, the phase velocity was determined by using Raman-Nath diffraction and optical heterodyning at 10 MHz. The investigations shown, that the change of acoustic properties in the investigated mixed crystals is nonadditive. Nonlinear interaction constants have been calculated taking into consideration various factors, which can influence on the propagation of acoustic waves in mixed crystals. The results were compared with similar investigations in NaCl - NaBr mixed crystals.

4pPAd4. Adjusting the phase of the signals transmitted from dual frequency probe for reducing second harmonic during propagation. Pasovic Mirza (Université de Lyon, 43 boulevard du 11 Novembre 1918, 69622 Villeurbanne, France, mirza.pasovic@creatis.insa-lyon.fr), Christian Cachard (Université de Lyon, 43 boulevard du 11 Novembre 1918, 69622 Villeurbanne, France, christian.cachard@creatis.insa-lyon.fr), Guillaume Matte (Biomedical Engineering, Erasmus MC, P.O. Box 2040, 3000 CA Rotterdam, Netherlands, g.matte@erasmusmc.nl), René Van Der Steen (Eindhoven University of Technology, Dept. of Mechanical Engineering, Dynamics & Control, P.O. Box 513, 5600MB Eindhoven, Netherlands, r.v.d.steen@tue.nl), Nico De Jong (Erasmus MC, Dr Molewaterplein 50 room Ee2302, 3015GE Rotterdam, Netherlands, n.dejong@erasmusmc.nl), Olivier Basset (Université de Lyon, 43 boulevard du 11 Novembre 1918, 69622 Villeurbanne, France, olivier.basset@creatis.insa-lyon.fr)

During propagation of the ultrasound wave, nonlinearities of the medium, causes rise of higher harmonics that are seen in amplitude spectrum. In ultrasound contrast harmonic imaging this is unwanted effect, since it is expected to image only higher harmonics produced by contrast agents. In previous studies Christopher, Krishnan and Shen proposed transmitting either an inverted signal (collected by hydrophone), transmitting 2nd harmonic with broadband transducer or transmitting third harmonic to reduce the second harmonic at measurement point. Our study uses a dual frequency probe which transmits one wave at frequency f0 and one wave at double frequency 2f0 named second harmonic reduction signal (SHRS) for reducing the second harmonic in the propagating signal. The hardest task is the appropriate adjustment of the phase of the SHRS to reduce second harmonic during propagation in the focal area. We outline how to set phase and established that the phase of the SHRS in not affected by the nonlinear parameter B/A and excitation pressure P0 but rather by the excitation frequency and the ultrasound system geometry (transducer size and distance to focal area). A reduction of 25dB has been obtained in simulation (Po=100kPa, fo=2.25 MHz). Experiments in water tank, have shown the reduction of 2nd harmonic by 30dB.

4pPAd5. Energy pumping in acoustics. Romain Bellet (Laboratoire de Mécanique et d'Acoustique - CNRS, 31 chemin Joseph Aiguier, 13402 Marseille, France, bellet@lma.cnrs-mrs.fr), Bruno Cochelin (Laboratoire de Mécanique et d'Acoustique - CNRS, 31 chemin Joseph Aiguier, 13402 Marseille, France, bruno.cochelin@ec-marseille.fr), Pierre-Olivier Mattei (Laboratoire de Mécanique et d'Acoustique - CNRS, 31 chemin Joseph Aiguier, 13402 Marseille, France, mattei@lma.cnrs-mrs.fr), Philippe Herzog (Laboratoire de Mécanique et d'Acoustique - CNRS, 31 chemin Joseph Aiguier, 13402 Marseille, France, herzog@lma.cnrs-mrs.fr)

Energy pumping corresponds to a particular vibratory regime of a nonlinear system coupled to a linear primary structure. Its non-linear behaviour allows to reduce vibrations of the primary structure, and is thus a new passive vibration control technique. This phenomenon has mainly been studied in mechanical engineering, so we transposed its principle to noise control in an acoustic medium. The presentation will focus on results about acoustic energy pumping that we observed both experimentally and numerically, in the time and frequency domains. These results highlight two main points: physically, energy pumping corresponds to an irreversible transfer of energy from the primary system to the non-linear absorber, and practically, its effects are a noise level limitation in the acoustic medium in permanent regime and a much faster sound extinction in transient regime.

4pPAd6. Shock wave propagation in heterogeneous medium, from ultrasound to sonic boom. Lili Ganjehi (Institut Jean Le Rond d'Alembert, Université Pierre et Marie Curie, Boites 161 et 162, 4 place Jussieu, 75252 Paris Cedex 05, France, ganjehi@lmm.jussieu.fr), François Coulouvrat (Institut Jean Le Rond d'Alembert, Université Pierre et Marie Curie, Boites 161 et 162, 4 place Jussieu, 75252 Paris Cedex 05, France, coulouvr@ccr.jussieu.fr), Jean-Louis Thomas (Centre National de la Recherche Scientifique, Institut des NanoSciences de Paris, Université Pierre et Marie Curie, 4 place Jussieu, 75252 Paris Cedex 05, France, thomasjl@ccr.jussieu.fr), Régis Marchiano (Institut Jean Le Rond d'Alembert, Université Pierre et Marie Curie, Boites 161 et 162, 4 place Jussieu, 75252 Paris Cedex 05, France, marchi@lmm.jussieu.fr)

Strong variability of sonic boom due to the atmospheric turbulence is known since the first test flight recordings in the 1960's. To simulate this, a laboratory scale experiment is conducted with ultrasonic shock waves in water at 1 MHz. The experiment is designed for an optimal 1:100,000 scaling with sonic boom. It includes single or multiple heterogeneities of varying sizes but comparable to the acoustical wavelength. Its deterministic aspect allows detailed comparisons with the results of a numerical model based on a nonlinear wide angle parabolic approximation. The experiments show the following features of the shock wave propagation : wavefront folding, local amplification (acoustical lens effect), increase of the rise time, strong variability of the time waveforms. All these features are in qualitative agreement with sonic boom observations. They are observed for a single heterogeneity provided this one is sufficiently large, but are amplified in case of multiple heterogeneities. Comparisons with results of numerical simulations show good agreement in various configurations. Improvements provided by the wide angle approach with respect to the standard parabolic approximation will also be discussed. Preliminary simulations for N wave propagation in a randomly heterogeneous medium will finally be presented.

4pPAd7. A route to chaotic state on an electrodynamic loudspeaker. Antonio Petosic (Faculty of Electrical Engineering and Computing, Unska 3, 10000 Zagreb, Croatia, antonio.petosic@fer.hr), Ivan Djurek (Faculty of Electrical Engineering and Computing, Unska 3, 10000 Zagreb, Croatia, ivan.djurek@fer.hr), Djurek Danijel (AVAC, Kesten brijeg 15, 10000 Zagreb, Croatia, danijel.djurek@zg-net.hr)

The low frequency electrodynamic loudspeaker (EDL) unit has been measured and analyzed in terms of chaotic behavior. It was found that an electrodynamic loudspeaker can function as a chaotic system. Loudspeaker impedance and vibration amplitude as function of driving frequency were measured at various driving currents, and well-know cut-off effect from nonlinear dynamical systems has been noticed. In the frequency region near cut-off and at higher driving currents the period doubling and later chaotic state occur. The experimentally obtained chaotic state was confirmed theoretically solving nonlinear equation of motion with strong nonlinear effective stiffness spatial dependency. It was found that statically measured suspension effective stiffness does not enables chaotic state when included in differential equation, and it has been concluded that membrane viscoelastic properties enhance the restoring force far enough to obtain chaos. The nonlinear equation describing anharmonic periodically driven oscillator has been solved numerically and the theoretical results were compared to experimental results.

4pPAd8. Analysis of the effects of the oscillations of a rigid sphere inside a cylindrical cavity containing a standing acoustic wave. Edgar A. Torres (Universidad Nacional Autonoma de Mexico, Centro de Ciencias Aplicadas y Desarrollo Tecnologico, CCADET-UNAM, Circuito Exterior s/n, Cd. Universitaria, A. P. 70-186, 02510 Mexico, D.F., Mexico, edgar.augusto.torres.gallegos@gmail.com), Arturo Santillan (Universidad Nacional Autonoma de Mexico, Centro de Ciencias Aplicadas y Desarrollo Tecnologico, CCADET-UNAM, Circuito Exterior s/n, Cd. Universitaria, A. P. 70-186, 02510 Mexico, D.F., Mexico, arturo.orozco@ccadet.unam.mx)

Under certain driving conditions of a single-axis acoustic levitation device, a suspended sample leaves its stability state and starts to oscillate vertically around the initial equilibrium position. A published theory on such instabilities [J. Rudnick and M. Barmatz, ″Oscillational instabilities in single-mode acoustic levitators,″ J. Acoust. Soc. Am., 87(1), 81-92, 1990] predicts the occurrence of time delays between the response of the cavity of the device and the motion of the sample inside it. In this paper, a theoretical and experimental investigation on similar time delay effects will be described. A solid sphere was moved in a controlled way inside a closed cylindrical cavity by means of a rod connecting the object to the outside of the system. A standing wave was generated inside the cavity by using a speaker. In this way, oscillations of the sphere were produced and the response of the sound field to such movement was studied. The effect of the frequency of the oscillations of the sphere on the time delay between the sound pressure and the movement of that object will be reported. In addition, the relations between the obtained results and the published theory on oscillational instabilities will be discussed.

4pPAd9. Manipulation of the behavior of SiC particles and oil bubbles using ultrasonic standing wave field. Seung Hyun Cho (Korea Research Institute of Standards and Science, Doryong dong 1, Yuseong gu, 305-340 Daejon, Republic of Korea, seungcho@kriss.re.kr), Dae-Cheol Seo (Korea Research Institute of Standards and Science, Doryong dong 1, Yuseong gu, 305-340 Daejon, Republic of Korea, dcseo@kriss.re.kr), Bong Young Ahn (Korea Research Institute of Standards and Science, Doryong dong 1, Yuseong gu, 305-340 Daejon, Republic of Korea, ahnby@kriss.re.kr)

Using ultrasound, particles submerged or flowing in fluid can be manipulated since ultrasound has an effect on the behavior of particles. Specifically, in standing wave field, particles generally move to pressure nodes or pressure antinodes due to acoustic radiation force. In this work, the behavior of SiC particles and oil bubbles in flowing water by standing wave field was investigated. Standing wave field in frequencies between 2 and 2.5 MHz was formed in a few mm narrow flow channel using a water coupled ultrasonic transducer and a steel reflector. We observed the effect of the standing wave parameters such as frequency, flow channel width, or sound intensity on the behavior of the particles. Various interesting results were obtained through some experiments. We separated SiC particles and oil bubbles. It was shown that the operating frequency of standing wave can control the particle moving location. Sound intensity increase also leads to the entrapment of moving particles. The resulted observations reveal the possibility of various applications of the ultrasonic standing wave to the manipulation of particles.

Session 4pPAe

Physical Acoustics: Ultrasonics: NDT and Layered Systems II (Poster Session)

Vincent Pagneux, Cochair
Laboratoire d'Acoustique de l'Université du Maine

Claire Prada, Cochair
Université Paris 7

All posters will be on display from 3:40 p.m. to 5:20 p.m. To allow contributors an opportunity to see other posters, contributors of odd-numbered papers will be at their posters from 3:40 p.m. to 4:30 p.m. and contributors of even-numbered papers will be at their posters from 4:30 p.m. to 5:20 p.m.

Contributed Papers

4pPAe1. Dual frequency ultrasound- A pulse-echo technique for analysis of layered material. Ossi Riekkinen (University of Kuopio, POB 1627, 70211 Kuopio, Finland, Ossi.Riekkinen@uku.fi), Mikko Hakulinen (University of Kuopio, POB 1627, 70211 Kuopio, Finland, Mikko.Hakulinen@uku.fi), Juha Töyräs (Kuopio University Hospital, POB 1777, 70211 Kuopio, Finland, Juha.Toyras@kuh.fi), Jukka Jurvelin (University of Kuopio, POB 1627, 70211 Kuopio, Finland, Jukka .Jurvelin@uku.fi)

Ultrasound (US) thickness gauges typically analyse layered materials by utilizing ultrasound reflections between different layers and prior knowledge for the material order within the layered structure. In this study, a dual frequency ultrasound (DFUS) technique is applied to eliminate the effect of overlying layered structure on the measurements of the object of interest without prior knowledge of the order of materials within the multilayered structure. DFUS technique utilizes prior knowledge on US attenuation coefficient and speed at two frequencies in multilayered materials, consisting of two different material types. Then, US reflection from the front (first) and the back (last) surfaces of the multilayered structure is measured using two different US frequencies. No reflections from the internal interfaces are needed. The technique was validated using several elastomer samples and their combinations, measured at 2.25 MHz and 5.0 MHz. DFUS reduced the mean error, induced by the overlying elastomers, in reflection from the object of interest from 103.6 - 289.4% to -15.9 - 5.6% and from 37.5 - 77.5% to -12.0 - 4.9% with 5.0 MHz and 2.25 MHz, respectively. Based on these results, DFUS is a straightforward technique to analyse the multilayered structure without the need for echoes from internal interfaces.

4pPAe2. Ultrasonic pulse propagation in a bonded three-layered structure. Jose Luis San Emeterio (Instituto de Acustica CSIC, Serrano 144, 28006 Madrid, Spain, jluis@ia.cetef.csic.es), Antonio Ramos (Instituto de Acustica CSIC, Serrano 144, 28006 Madrid, Spain, aramos@ia.cetef.csic.es), Emilia Pardo (Instituto de Acustica CSIC, Serrano 144, 28006 Madrid, Spain, empargo@ia.cetef.csic.es), Julio C. Leite (COPPE, Universidad Federal Rio de Janeiro, 68501 Rio de Janeiro, Brazil, juliobastosleite@jahoo.com.br), Jose Miguel Alvarez (INTA, Carretera Ajalvir, Km 4, 28850 Madrid, Spain, miguelalj@inta.es), Carlos Perez Trigo (INTA, Carretera Ajalvir, Km 4, 28850 Madrid, Spain, pereztrc @inta.es)

Bonded layers are used in the assembly of many critical functional parts of industrial equipment. In this work, ultrasonic pulse propagation in a steel-rubber-rubber bonded composite structure is investigated by means of computer simulation and pulse echo experimental evaluation. Ultrasonic pulse propagation is modelled using a 2D time domain finite-difference software. For the experimental measurements, two test samples were fabricated by bonding a thin layer of steel and two thin layers of rubber, including debonded areas at marked regions of each interface. Several ultrasonic traces were acquired by contact pulse-echo testing, using a 5 MHz wideband transducer, from the external steel surface. The large acoustic impedance mismatch existing between steel and rubber layers makes that only a very small part of the ultrasonic energy is transmitted through the first (steel-rubber) interface. The high attenuation in rubber materials and the possible overlapping of multiple echoes are additional characteristics of the complex ultrasonic pulse propagation in this flat structure. Some differences in time and frequency domains, between the received signals from normal bonded areas and completely debonded areas are discussed, looking for defect detection at the first (steel-rubber) and second (rubber-rubber) interfaces.

4pPAe3. Inverse Problem to Determine an Epoxy Film Parameters in a Tri-Layer Metal/Adhesive/Metal Structure. Naima Ismaili Alaoui (Laboratoire d'Electronique Signaux-Systemes et Informatique LESSI, Université Sidi Mohammed Ben Abdellah, Faculté des Sciences Dhar el Mehraz, 30000 Fes, Morocco, nanialaoui@hotmail.com), Mounsif Ech-Cherif El-Kettani (LOMC FRE-3102 CNRS, Groupe Ondes Acoustiques, University of Le Havre, Place Robert Schuman, BP 4006, 76610 Le Havre, France, elkettani@univ-lehavre.fr), Driss Chenouni (Laboratoire d'Electronique Signaux-Systemes et Informatique LESSI, Université Sidi Mohammed Ben Abdellah, Faculté des Sciences Dhar el Mehraz, 30000 Fes, Morocco, d_chenouni@yahoo.fr), Zakia Lakhlii (Laboratoire d'Electronique Signaux-Systemes et Informatique LESSI, Université Sidi Mohammed Ben Abdellah, Faculté des Sciences Dhar el Mehraz, 30000 Fes, Morocco, zlakhliai@hotmail.fr), Jean-Louis Izbicki (LOMC FRE-3102 CNRS, Groupe Ondes Acoustiques, University of Le Havre, Place Robert Schuman, BP 4006, 76610 Le Havre, France, jean-louis.izbicki @univ-lehavre.fr), Bruno Morvan (LOMC FRE-3102 CNRS, Groupe Ondes Acoustiques, University of Le Havre, Place Robert Schuman, BP 4006, 76610 Le Havre, France, bruno.morvan@univ-lehavre.fr)

The aim of this work is to give the elastic parameters and the thickness of a slim epoxy film of a tri-layer metal/adhesive/metal structure, by inverse problem on the experimental data, knowing the characteristic equation of the structure. This equation is firstly solved and the sensitivity of some modes to the parameters of interest is studied. The couple of solutions wavenumber-frequency obtained from the direct problem are reintroduced in the characteristic equation, looking for the longitudinal and shear waves velocities, and the epoxy thickness that minimise this equation. A criterion that takes into account the averaged and the variance values of each parameter is deduced and allows these parameters determination in $\pm 3\%$ of the used values. To test the reliability of the method, the wavenumber solution is randomly perturbed in $\pm 5\%$ range, as the experimental wavenumber is expected to be weakly different from the theoretical one. The velocities and the thickness obtained still in the $\pm 3\%$ range around the used values. This

method is then applied on experimental data obtained from a Duraluminum/epoxy/Duraluminum structure. The longitudinal and shear velocities and the thickness of the epoxy film obtained are in ±3% around the given values.

4pPAe4. The analysis of diffraction effects of acoustic waves on the crack's top. Yulia V. Zhitlukhina (Institute of Metal Physics, 18, Sofia Kovalevskaya St., GSP-170, 620041 Ekaterinburg, Russian Federation, julika_sun@mail.ru), Dmitry V. Perov (Institute of Metal Physics, 18, Sofia Kovalevskaya St., GSP-170, 620041 Ekaterinburg, Russian Federation, peroff@imp.uran.ru), Anatoly B. Rinkevich (Institute of Metal Physics, 18, Sofia Kovalevskaya St., GSP-170, 620041 Ekaterinburg, Russian Federation, rin@imp.uran.ru)

Diffraction effects and features of acoustic wave propagation in elastic media with microcrack were investigated in detail for pulse probing signals. The crack's plane was oriented across the direction of longitudinal ultrasonic wave incidence so that the detection of such a crack with so ″inconvenient″ spatial location is difficult enough by using traditional acoustic techniques. By using laser interferometer, the set of instantaneous pictures of acoustic field on the specimen's surface, corresponding to different time moments was obtained what allowed investigating and visualizing of acoustic field propagation and diffraction's effects on the crack's top in dynamics. Using various methods of numerical modeling of diffraction processes of acoustic wave on the crack's edge and top for pulse signals the origin of V-like structures on the snapshots of acoustic fields was explained and analyzed.

4pPAe5. Structural Health Monitoring using cross-correlation of an ambient noise field. Najib Abou Leyla (UVHC, IEMN-DOAE, Le Mont Houy, 59313 Valenciennes, France, najib.abouleyla@univ-valenciennes.fr), Emmanuel Moulin (UVHC, IEMN-DOAE, Le Mont-Houy, 59313 Valenciennes, France, emmanuel.moulin@univ-valenciennes.fr), Jamal Assaad (UVHC, IEMN-DOAE, Le Mont-Houy, 59313 Valenciennes, France, jamal.assaad@univ-valenciennes.fr), Sébastien Grondel (UVHC, IEMN-DOAE, Le Mont-Houy, 59313 Valenciennes, France, sebastien.grondel@univ-valenciennes.fr), Pascal Poussot (UVHC, IEMN-DOAE, Le Mont Houy, 59313 Valenciennes, France, pascal.poussot@univ-valenciennes.fr)

Theoretical and experimental studies in underwater acoustic, seismology and more recently ultrasonic have demonstrated that an estimate of the Time Domain Green Function (TDGF) between two receivers could be obtained from the cross-correlation of a diffuse acoustic noise field of these two receivers. The aim of the work is to exploit this technique in order to characterize Structural Health Monitoring (SHM) of aeronautic structures without the use of active sources. In this case, the aero-acoustic and/or mechanical sources (engine) generate an ambient noise field with some imperfections for the application. Indeed, source concentrations, source directivity and non-random components in time can appear which leads to an erroneous estimate of the TDGF. A key point to the study is thus to understand the influence of such imperfections. Therefore, experimental measurements have been performed using different types of acoustic noise sources (localized or diffuse). Cross-correlation results obtained in each case are then compared and theoretically interpreted. Finally, the potential of this technique in terms of damage detection is verified.

4pPAe6. Prediction of ultrasonic noise and attenuation for the simulation of non destructive testing. Frédéric Jenson (CEA-LIST, Centre de Saclay, 9119 Gif-sur-Yvette, France, frederic.jenson@cea.fr), Vincent Dorval (CEA-LIST, Centre de Saclay, 9119 Gif-sur-Yvette, France, vincent.dorval@cea.fr), Gilles Corneloup (LCND - Université de la Méditerranée, IUT Aix Provence, Avenue Gaston Berger, 13625 Aix en Provence Cedex, France, gilles.corneloup@univmed.fr)

Ultrasonic non destructive testing of some polycrystalline materials can be significantly affected by their microstructure. In such materials a fraction of the acoustic energy is redirected in all directions, which leads to both attenuation and structural noise and causes significant loss in detection performances. Consequently, being able to predict these phenomena would help in designing better testing procedures. During previous works at CEA-LIST, noise and attenuation models have been developped and implemented into the simulation software for non destructive testing CIVA. The noise model describes the microstructure of the material as a set of point-like scatterers and the attenuation model uses a filtering approach. They both require reference ultrasonic measurements to reproduce the behaviour of a given material. The connection of this approach to a scattering model relating noise and attenuation to microstructural characteristics is studied in this work. The selected model is based on the Born approximation and allows one to relate physical quantities such as the scattering cross section and the attenuation coefficient to second order statistical properties of the microstructure and to elastic properties of a single crystallite. This model accounts for important effects such as anisotropic scattering and mode conversions, but neglects multiple scattering events. Simulation results obtained with this approach are compared to experimental results.

4pPAe7. Ultrasonic control of the adhesion quality of two aluminium sheets. Naima Taifi (Fac. des sciences; Univ. Chouaib Doukkali, B.P: 20, 24000 El Jadida, Morocco, taifinaima@yahoo.fr), Bouazza Faiz (Ibn Zohr University, FS Agadir, 80000 Agadir, Morocco, faizbou@hotmail.com), Ali Moudden (Ibn Zohr University, FS Agadir, 80000 Agadir, Morocco, ali_moudden@yahoo.fr), Gerard Maze (LAUE, Université du Havre, Place Robert Schuman, F-76610 Le Havre, France, gerard.maze@univ-lehavre.fr), Dominique Decultot (LOMC FRE 3102 CNRS Groupes Ondes Acoustiques, Université du Havre (IUT), Place Robert Schuman, 76610 Le Havre, France, dominique.decultot@univ-lehavre.fr), Driss Izbaim (Ibn Zohr University, FS Agadir, 80000 Agadir, Morocco, driss_izbaim@yahoo.fr)

In this work, we present two ultrasonic methods allowing to control the quality of adhesion of two aluminium sheets with the same thickness. These methods are based on the analysis of the ultrasonic signals retrodiffused by the Al/glue/Al structure. The first method consists in controlling the behaviour of the mode of the sheets which is splitted. Two parameters controlling the transfers were allowed to characterize any type of adhesion: good, bad and intermediate. The second method is based on control of the width of the mode of the adhesive. The representation of this width by Argan diagram allows to control the quality of adhesion from the measurement of the diagram diameter.

Session 4pPAf

Physical Acoustics: Ultrasonics: Industrial NDT II (Poster Session)

Bertrand Nongaillard, Cochair
IEMN-DOAE

Christophe Aristegui, Cochair
Université Bordeaux

All posters will be on display from 3:40 p.m. to 5:20 p.m. To allow contributors an opportunity to see other posters, contributors of odd-numbered papers will be at their posters from 3:40 p.m. to 4:30 p.m. and contributors of even-numbered papers will be at their posters from 4:30 p.m. to 5:20 p.m.

Contributed Papers

4pPAf1. Simultaneous Sum-Frequency and Vibro-Acoustography Imaging for Nondestructive Evaluation (NDE) and Testing (NDT) Applications. Farid Mitri (Dep. of Physiology and Biomed. Eng., Mayo Clinic College of Medicine, 200 First Street SW, Rochester, MN 55905, USA, mitri.farid@mayo.edu), Glauber T. Silva (Instituto Nacional de Matematica Pura e Aplicada, 22460 Rio de Janeiro, Brazil, mitri@ieee.org), James Greenleaf (Dep. of Physiology and Biomed. Eng., Mayo Clinic College of Medicine, 200 First Street SW, Rochester, MN 55905, USA, jfg@mayo.edu), Mostafa Fatemi (Dep. of Physiology and Biomed. Eng., Mayo Clinic College of Medicine, 200 First Street SW, Rochester, MN 55905, USA, fatemi@mayo.edu)

High-resolution ultrasound imaging systems for inspection of defects and flaws in materials are of great demand in many industries. Among these systems, Vibro-acoustography (VA) has shown excellent capabilities as a non-contact method for non-destructive high-resolution imaging applications. This method consists of mixing two confocal ultrasound beams, slightly shifted in frequency, to produce an acoustic emission field at the difference frequency of the primary incident ultrasound beams. In addition to the difference frequency signal, there exists another signal at the sum frequency, formed in the intersection region of the two primary beams. The goal of this study is to investigate the formation of high-resolution images using the sum frequency of ultrasound waves in VA while concurrently forming the conventional difference-frequency VA image, thereby increasing the amount of information acquired during a single scan. A theoretical model describing the sum frequency wave propagation, including beam forming and image formation in the confocal configuration is developed and verified experimentally. Moreover, sample experiments are performed on a flawed fiber-reinforced ceramic composite plate. Images at both the difference and sum frequencies are compared and discussed. Results show that the sum frequency image produces a high-resolution C-scan of the plate by which the flaws and structural details of the plate can be detected.

4pPAf2. Ultrasonic polar c-scan system for range of material sizes and its capabilities for non-destructive testing. Kyle Barbour (Georgia Tech Lorraine - G.W. Woodruff School of ME, UMI Georgia Tech - CNRS 2958, 2 rue Marconi, 57070 Metz, France, nfdaaa@gmail.com), John M. Vander Weide (Georgia Tech Lorraine - G.W. Woodruff School of ME, UMI Georgia Tech - CNRS 2958, 2 rue Marconi, 57070 Metz, France, nico.declercq@me.gatech.edu), Sarah W. Herbison (Georgia Tech Lorraine - G.W. Woodruff School of ME, UMI Georgia Tech - CNRS 2958, 2 rue Marconi, 57070 Metz, France, sherbison@gatech.edu), Nico F. Declercq(Georgia Tech Lorraine - G.W. Woodruff School of ME, UMI Georgia Tech - CNRS 2958, 2 rue Marconi, 57070 Metz, France, nico .declercq@me.gatech.edu)

The principle of multi-directional incident ultrasound has already shown to be a promising technique for the nondestructive evaluation of composites and other materials. The advantage is the correspondence between stiffness, damage and the registered double through transmission patterns. C-scans are widely used as a tool for the detection of defects in materials. A new ultrasonic scanner has been developed, called the Polar C-Scan, which enables efficient polar scan measurements in combination with C-scan capabilities. The scanner opens many possibilities for nondestructive testing by means of polar scans, C-scans, single transmission, double through transmission and even reflection. Furthermore the system produces almost no noise, which enables highly sensitive measurements in the time domain and the frequency domain. The presented work shows a thorough investigation of all the capabilities of the system and presents results for fiber reinforced composites after different fatigue cycles.

4pPAf3. Ultrasonic and acoustic method for viscoelastic complex media characterization. Georges Nassar (IEMN - DOAE, Université de Valenciennes, Le Mont - Houy, 59313 Valenciennes, France, gnassar@univ-valenciennes.fr), Fabrice Lefebvre (IEMN - DOAE, Université de Valenciennes, Le Mont - Houy, 59313 Valenciennes, France, Fabrice.Lefebvre@univ-valenciennes.fr), Alain Skaf (IEMN - DOAE, Université de Valenciennes, Le Mont - Houy, 59313 Valenciennes, France, alain.skaf@univ-valenciennes.fr), Bertrand Nongaillard (IEMN - DOAE, Université de Valenciennes, Le Mont - Houy, 59313 Valenciennes, France, Bertrand.Nongaillard@univ-valenciennes.fr)

In this paper, the potentialities of a low frequency ultrasonic/acoustic technique devoted to the study and characterization of the viscoelastic complex media is investigated. This work shows the limit of the use of ultrasound in a viscoelastic media with a complex matrix. In this context the cheese was indicated as a model of propagation medium, such a product having a very complex matrix in term of texture, openings, crystallization, moisture,... . Theoretical basis of sound attenuation in cheese is recalled, especially the effects of the matrix viscoelasticity and the scattering of ultrasonic energy by holes and cracks. Depending on the degree of openness, ultrasonic velocity or attenuation is chosen to represent the evolution of the cheese. For very high degree of openness, ultrasounds are no longer usable and a tap-test acoustic technique is employed and allows a quality indicator to be constructed. Experimental validations were done with optical images of cut cheeses and rheological measurements. The results indicate that a high degree of sensitivity can be reached with ultrasonic / acoustic non destructive technique.

Session 4pPAg

Physical Acoustics: Nonlinear Acoustics of Consolidated Materials and Non Destructive Testing II (Poster Session)

James Tencate, Cochair
EES-11 (Geophysics) - Los Alamos National Laboratory

Koen Van Den Abeele, Cochair
K.U.Leuven Campus Kortrijk

All posters will be on display from 3:40 p.m. to 5:20 p.m. To allow contributors an opportunity to see other posters, contributors of odd-numbered papers will be at their posters from 3:40 p.m. to 4:30 p.m. and contributors of even-numbered papers will be at their posters from 4:30 p.m. to 5:20 p.m.

Contributed Papers

4pPAg1. Theoretical investigations into the use of linear and nonlinear inhomogeneous waves for non-destructive testing. John M. Vander Weide (Georgia Tech Lorraine - G.W. Woodruff School of ME, UMI Georgia Tech - CNRS 2958, 2 rue Marconi, 57070 Metz, France, nico.declercq@me.gatech.edu), Nico F. Declercq (Georgia Tech Lorraine - G.W. Woodruff School of ME, UMI Georgia Tech - CNRS 2958, 2 rue Marconi, 57070 Metz, France, nico.declercq@me.gatech.edu)

Following the shift to incorporate more materials by design into modern engineering is the theoretical need to model an increasingly more complicated material structure and predict a design life for complex engineered materials. The presence of defects, interface cracks and delaminations adds to the inherent nonlinearity of a structure by degrading material stiffness and other physical properties contributing to fracture. The presence of local defects either at interfaces between two different materials or grain boundaries within the bulk material provide a natural location for the formation and subsequent propagation of cracks. This work provides initial theoretical investigations into the use of ultrasonic inhomogeneous waves to nondestructively probe such interface defects. Characterized theoretically by a complex valued wave number, the inhomogeneous wave is the more general plane wave solution of the wave equation. The complex valued wave number allows for the material effects of damping along the propagation direction and wave inhomogeneity or amplitude decay along the wavefront. To study the interaction with cracks, a singular integral equation formulation like that of Krenk and Schmidt is extended to farfield simulations with ultrasonic inhomogeneous waves.

4pPAg2. Acoustic emission of structures basis on the A3B5 compounds. Vitaly V. Veleschuk (Institute of Semiconductors Physics, NASU, Prospect Nauki 45, 03028 Kyiv, Ukraine, vvvit@ukr.net), Oleg V. Lyashenko (Institute of Semiconductors Physics, NASU, Prospect Nauki 45, 03028 Kyiv, Ukraine, lyashenk@mail.univ.kiev.ua), Olexander I. Vlasenko (Institute of Semiconductors Physics, NASU, Prospect Nauki 45, 03028 Kyiv, Ukraine, vvvit@pochta.ru)

Failure of internal mechanical pressure at origin and movement of dislocations in processes of fast degradation and defect formation in LED and semiconductor lasers lead to occurrence of acoustic emission (AE) - to the phenomenon of radiation of pulse spontaneous acoustic wave's noise character. This failure of internal mechanical pressure in local volumes with occurrence AE is possible only at action of external fields (influences) of the certain physical nature, in our case - non-uniform fields of the thermomechanical pressure created by a constant direct current. In work were investigated n+-n-p- structures basis on the GaP:N, GaP0,85As0,15:N, Zn-O, InGaN/GaN and p+-p-n- structures basis on the Ga0,7Al0,3As and Ga0,65Al0,35As. During step-by-step increase of a current 10-25 multiple change of AE occurrence threshold and a destruction threshold of structures was revealed at natural ageing structures after 6˙108 s. For some samples of structures at low temperatures (77) AE occurrence threshold came nearer or even corresponded to a destruction threshold. The given effect explains gradual saturation of dislocations by atoms of impurity with formation of Cottrell cloud, that considerably lowers their mobility and increases activation energy and accordingly a AE occurrence threshold

4pPAg3. Polar scans as a nonlinear acoustics tool. John M. Vander Weide (Georgia Tech Lorraine - G.W. Woodruff School of ME, UMI Georgia Tech - CNRS 2958, 2 rue Marconi, 57070 Metz, France, nico.declercq@me.gatech.edu), Nico F. Declercq (Georgia Tech Lorraine - G.W. Woodruff School of ME, UMI Georgia Tech - CNRS 2958, 2 rue Marconi, 57070 Metz, France, nico.declercq@me.gatech.edu)

Nonlinear acoustic wave response provides a powerful means of assessing material properties. One very interesting area of application is testing for material damage. While an undamaged material may have a very linear acoustic response, damage such as crack formation creates strong nonlinearity with acoustic excitation amplitude. Many nonlinear acoustics techniques for nondestructive testing analyze the harmonic content in the wave scattered from a crack. A planar c-scan can be used in conjunction with the nonlinear acoustics techniques to provide defect detection and imaging. Polar scans are a complementary technique for damage assessment which has not yet found application in nonlinear acoustics. In the polar scan, the sound field in the hemisphere around a material point is measured and plotted to display a unique signature of local material properties. This work provides initial investigations into the use of the polar scan technique in nonlinear acoustics by detection of the second harmonic.

4pPAg4. Detection of the nonlinearity evolution in concrete samples subject to quasi-static loadings. Paola Antonaci (Politecnico di Torino, Corso Duca degli Abruzzi 24, 10129 Torino, Italy, paola.antonaci@polito.it), Pietro Bocca (Politecnico di Torino, Structural Engineering Department, 10129 Torino, Italy, pietro.bocca@polito.it), Caterina Bruno (Politecnico di Torino, Structural Engineering Department, 10129 Torino, Italy, caterina.bruno@polito.it), Antonio S. Gliozzi (Politecnico di Torino, Corso Duca degli Abruzzi 24, 10129 Torino, Italy, antonio.gliozzi@polito.it), Davide Masera (Politecnico di Torino, Structural Engineering Department, 10129 Torino, Italy, davide.masera@polito.it), Marco Scalerandi (Politecnico di Torino, Corso Duca degli Abruzzi 24, 10129 Torino, Italy, marco.scalerandi@infm.polito.it)

The signature of nonlinearity in the elastic response of a specimen to an impingent ultrasonic wave is usually determined through Fourier analysis, which provides low amplitude signals, often below noise level. We suggest here an alternative, based on the amplitude dependence of the response of the system. Our procedure is conceptually simple and easy to implement. In addition, it keeps simultaneously into account the nonlinear signature effects on phases, amplitudes and frequencies of the response. The procedure is described and used to analyse the variation of the nonlinearity in a concrete bar subject to quasi-static loadings of increasing amplitude. The sensitivity of the approach allows to distinguish the compaction phase (up to a load of 30% of the rupture loading) from a microdamage progression (up to a load of 60%) and the pre-rupture phases.

4pPAg5. Nondestructive tests of cylindrical steel samples using the ultrasonic projection method and the ultrasound transmission tomography method. Krzysztof J. Opielinski (Wroclaw University of Technology/Institute of Telecommunications, Teleinformatics and Acoustics, Wybrzeze Wyspianskiego 27, 50-370 Wroclaw, Poland, krzysztof.opielinski@pwr.wroc.pl), Tadeusz Gudra (Wroclaw University of Technology/Institute of Telecommunications, Teleinformatics and Acoustics, Wybrzeze Wyspianskiego 27, 50-370 Wroclaw, Poland, Tadeusz.Gudra @pwr.wroc.pl)

The paper presents some methods of NDT of cylindrical steel samples by means of ultrasonic projection (UP) method and ultrasound transmission tomography (UTT) method. Some ways of scanning were proposed, using different measurement geometries and rendering possible the characterization and visualization of the inner structure of steel samples by projection and tomographic images of measured acoustic parameters. The measurements proposed in the paper allow us to obtain at the same time the distributions of mean values of a number of acoustic parameters characterizing the structure of samples: the mean amplitude of the ultrasonic wave after running through the sample, the mean runtime on the transmitter-receiver path, and the mean decrease of the ultrasonic wave frequency after running through the sample. These parameters measured in the tomographic scanning setup from many directions around the samples allow us to reconstruct the distributions of the local values of acoustic parameters such as respectively: the ultrasonic wave attenuation coefficient, the group velocity of the ultrasonic wave, the derivative of attenuation coefficient along the frequency. The reconstructed distributions of the local values of acoustic parameters render possible the imaging of the samples' internal structure cross-sections, each of the parameters characterizing different features of the structure.

4pPAg6. Use of point-source/point-receiver elastic waves in NDT-application. Alexandr I. Korobov (Dept. of Acoustics, Physics Faculty, M.V. Lomonosov Moscow State University, Leninskie gory 1, 119991 Moscow, Russian Federation, akor@acs465a-1.phys.msu.ru), Natalya I. Odina (Dept. of Acoustics, Physics Faculty, M.V. Lomonosov Moscow State University, Leninskie gory 1, 119991 Moscow, Russian Federation, niodina@mail.ru), Anna V. Abramova (Dept. of Acoustics, Physics Faculty, M.V. Lomonosov Moscow State University, Leninskie gory 1, 119991 Moscow, Russian Federation, akor@acs465a.phys.msu.ru)

The ultrasonic automated experimental setup and technique for research of anisotropy of elastic properties of micro- and nanocrystalline metals and residual stresses are developed. Setup works in range of frequencies of 0.2-5 MHz. Accuracy of measurement of propagation time of elastic wave is equal to 0.2 ns, amplitude - 1%. Setup allows to make diagnostics of metals using volume, Raleigh and Lamb waves and to carry out scanning on linear and angular coordinates. Use of point source and receiver of acoustic waves and the high time resolution allows to carry out research of anisotropy and residual pressure with high spatial resolution. The x-y-coordinate device operated by personal computer, allows to carry out two-dimensional scanning of the sample by elastic waves with step of 10 micron. Experimental results of diagnostics of anisotropy of elastic properties in a number of microcrystalline constructional materials with residual stresses (alloys of aluminum and steel), and also a steel plate in the field of welded seam are presented. Significant anisotropy of elastic properties caused by these defects is revealed in investigated samples. The work is supported by RFBR.

4pPAg7. Acoustic attenuation in silicon and silicon oxide. Anatolij P. Onanko (Taras Shevchenko Kyiv National University, physics faculty, prosp. Glushkova, 2/1, 03028 Kyiv, Ukraine, onanko@univ.kiev.ua), Oleg V. Lyashenko (Institute of Semiconductors Physics, NASU, Prospect Nauki 45, 03028 Kyiv, Ukraine, lyashenk@mail.univ.kiev.ua), Inna O. Lyashenko (Taras Shevchenko Kyiv National University, physics faculty, prosp. Glushkova, 2/1, 03028 Kyiv, Ukraine, lyashik@ukr.net), Yurij A. Onanko (Taras Shevchenko Kyiv National University, physics faculty, prosp. Glushkova, 2/1, 03028 Kyiv, Ukraine, onanko@univ.kiev.ua)

In the present work the non-destructive acoustic attenuation (AA) method of the technological control the structure defects of semiconductor plates after various dozes of the x-ray irradiation is developed. For measurement of temperature dependences of AA the method of resonant fluctuations of a plate on frequency 1.5 kHz was used at elastic deformation in vacuum. Measurements of temperature dependences AA in silicon plate a 460–470 micron thick after drawing a 600 nm layer of silicon oxide. Disk of a p-type silicon, doped B, orientation (100) with specific electroresistance 7,5 ohm·cm. The small maximums of AA were observed at temperature 346 K and 380 K. The main maximum of AA was observed at temperature 510 K. The affinity received by us of value of energy of activation 0,8 eV of AA at 510 K to energy of migration interstitial atoms 0,85 eV of silicon allows to assume the relaxation mechanism caused by reorientation interstitial atoms of silicon in dumbbell configurations.

4pPAg8. Nondestructive Evaluation of heterogeneous materials using acoustic emission and ultrasound. Adil Faiz (ENSIM - LAUM, Université du Maine, rue Aristote, 72085 Le Mans, France, adil.faiz@univ-lemans.fr), Rachid El Guerjouma (ENSIM - LAUM, Université du Maine, rue Aristote, 72085 Le Mans, France, Rachid.El_Guerjouma@univ-lemans.fr), Mouras Bentahar (Université du Maine LAUM, Lab. d'Acoustique Université du Maine, UMR CNRS 6613, 72085 Le Mans Cedex 9, France, mourad.bentahar@univ-lemans.)

Heterogeneous materials as Composites and concrete are advantageous as structural components in many applications. However, damage detection in such materials is difficult due to their heterogeneity and anisotropy. Furthermore, conventional non destructive technique as X-radiographic is mostly not very sensitive to early damage and very time consuming and expensive. The purpose of this contribution is to study the capabilities of several methods, non destructive and very sensitive for damage characterisation, as Acoustic Emission (AE) and ultrasonic for the structural health monitoring of heterogeneous materials as polymer based composite materials and concrete. These materials are instrumented by piezoelectric sensors in order to detect acoustic emission and to measure the ultrasonic velocity. The mechanisms of the damage events and their space-time localizations are identified from AE. Simultaneously, the longitudinal ultrasonic velocity is measured in situ by transmission through the composites thickness. The AE is very well correlated with the loss of stiffness determined from ultrasonic velocity measurements showing the potentiality of this combined approach for in situ structural health monitoring.

4pPAg9. In-situ measured Q- factor dependence from load in short and long time periods. Nora A. Vilchinska (LAA-Latvian Acoustics Association, 3 Kurzemes pr, LV-1064 Riga, Latvia, vilcinska@hotmail.com)

Dynamic loaded large object is under research. Long time periods (8 years) measurements are made by variety loads: from quasi static till strong motion. Short time measurements start from quasi static and load goes step-by-step till strong motion- maximum loaded- and return in the same way to quasi static. This experiment longs 60 minutes. An assessment of material quality factor (Q-factor) in places of measurements was made taking into account the absorbed and emitted energy. The Q-factor for energy is calculated from RMS response spectra curves. The Q-factor and its changes in long time and short time experiments in some MPs are compared. The smaller is the Q-factor, the higher is the concentration of interior invisible cracks. Structural alterations, opening of fractures and their closure under load, and transitional processes are reflected in the spectra of emitted acoustic signals and in the nonlinearity of response Q-factor.

Session 4pPAh

Physical Acoustics: Acoustic Probes of Planetary Environments II (Poster Session)

Andi Petculescu, Cochair
University of Louisiana

Martin Towner, Cochair
PSSRI

All posters will be on display from 3:40 p.m. to 5:20 p.m. To allow contributors an opportunity to see other posters, contributors of odd-numbered papers will be at their posters from 3:40 p.m. to 4:30 p.m. and contributors of even-numbered papers will be at their posters from 4:30 p.m. to 5:20 p.m.

Contributed Papers

4pPAh1. An ultrasonic anemometer for Mars. Colin Wilson(University of Oxford, Department of Atmospheric, Oceanic and Planetary Physics, OX1 3PU Oxford, UK, wilson@atmos.ox.ac.uk), David Hutchins (University of Warwick, School of Engineering, CV4 7AL Coventry, UK, D.A.Hutchins@warwick.ac.uk), Lee A. Davis (University of Warwick, School of Engineering, CV4 7AL Coventry, UK, lee.davis@warwick.ac.uk), Martin C. Towner (PSSRI, The Open University, Walton Hall, MK7 6AA Milton Keynes, UK, m.c.towner@open.ac.uk)

Ultrasonic anemometers are often used for studies of 3-D atmospheric turbulence on Earth, due to their robust calibration and fast operation (>10 Hz). The same qualities make ultrasonic anemometry attractive for use on Mars, where similar atmospheric turbulence is found. The low density of Martian atmosphere - a hundredth that of the Earth's - is problematic, because of the large acoustic impedance mismatch between the atmosphere and piezoelectric transducers. One solution to this problem is to use piezoelectric transducers with a hornlike resonator bonded to their front surface. Another solution is to use a capacitive membrane transducer instead. We report on performance of various ultrasonic transducers in carbon dioxide Martian pressures, and present an instrument design capable of meeting the stringent mass, power, and environmental requirements of the European ExoMars lander.

4pPAh2. Acoustic tomography of the internal wave-ssociated fluctuations in the lower atmosphere. Igor Chunchuzov (Obukhov Institute of Atmospheric Physics, 3 Pyzhevskii Per., 119017 Moscow, Russian Federation, igor.chunchuzov@gmail.com), Sergey Kulichkov (Obukhov Institute of Atmospheric Physics, 3 Pyzhevskii Per., 119017 Moscow, Russian Federation, snk@ifaran.ru),Vitaly Perepelkin(Obukhov Institute of Atmospheric Physics, 3 Pyzhevskii Per., 119017 Moscow, Russian Federation, vitaliper54@gmail.com), Astrid Ziemann (Leipzig Institute for Meteorology, Stephanstr. 3, 04103 Leipzig, Germany, ziemann@uni-leipzig.de), Klaus Arnold (Leipzig Institute for Meteorology, Stephanstr. 3, 04103 Leipzig, Germany, Arnold@uni-leipzig.de), Anke Kniffka (Leipzig Institute for Meteorology, Stephanstr. 3, 04103 Leipzig, Germany, kniffka@rz.uni-leipzig.de)

The two different schemes of acoustic tomography of the atmospheric boundary layer (ABL) were used in the field experiments conducted near Melpitz (Germany) and Zvenigorod (Russia). The mesoscale effective sound speed fluctuations (periods 1min-1h) averaged over different acoustic ray paths were retrieved from the fluctuations of sound travel time between sources and receivers. It was found that a major contribution to the retrieved fluctuations comes from the wind speed fluctuations. By using a coherence analysis of the retrieved and measured wind speed fluctuations in the spatially distanced points the wave like fluctuations with periods of 16-20min, 8-10min, 4-5min, 1-2min have been filtered, and their horizontal translation velocities and scales have been estimated. Similar periods were also found in the variations of the vertical turbulent fluxes of momentum and heat near ground. The mechanism of origination of these periods in the observed fluctuations is proposed. The effect of the wind shear variations induced by internal waves on the turbulence intensity was observed. This effect showed a substantial role played by internal waves in the origin of an intermittency of turbulence in the stably stratified ABL. This work was supported by RFBR, grants 06-05-64229, 05-05-64973, 07-05-91555.

Session 4pPAi

Physical Acoustics, Acoustical Oceanography, and Biomedical Ultrasound/Bioresponse to Vibration: Acoustically Activated Bubble Dynamics and Applications II (Poster Session)

Erich Everbach, Cochair
Swarthmore College

Joachim Holzfuss, Cochair
Institute of Applied Physics, TU Darmstadt

All posters will be on display from 3:40 p.m. to 5:20 p.m. To allow contributors an opportunity to see other posters, contributors of odd-numbered papers will be at their posters from 3:40 p.m. to 4:30 p.m. and contributors of even-numbered papers will be at their posters from 4:30 p.m. to 5:20 p.m.

Contributed Papers

4pPAi1. Sound propagation in viscoelastic pipe with liquid-bubble mixture. Semyon Levitsky (Shamoon College of Engineering, Math. Department, Bialik/Basel Sts., 84100 Beer Sheva, Israel, levits@sce.ac.il), Rudolf Bergman (Shamoon College of Engineering, Math. Department, Bialik/Basel Sts., 84100 Beer Sheva, Israel, rudolf@sce.ac.il), Jehuda Haddad (Shamoon College of Engineering, Math. Department, Bialik/Basel Sts., 84100 Beer Sheva, Israel, jehuda@sce.ac.il)

Propagation of acoustic waves in thin-walled polymeric tube with viscous liquid is investigated. Dynamics of the tube - liquid interaction is studied within conjugated quasi-one-dimensional formulation; the tube material is supposed to follow linear viscoelastic model with appropriate choice of the compliance function. It is assumed that the liquid contains fine air bubbles; the concentration of free gas is supposed to be small. Compressibility of liquid in the wave in the presence of bubbles can be almost entirely attributed to compressibility of the gas phase; it is accounted for within dispersion equation for bubbly liquid. Both heat and viscous losses are included in the phase interaction description at the liquid-gas interface. The resulting dispersion equation for the waveguide with liquid-gas mixture is studied in the long-wave range, where sound length is larger from the waveguide diameter. Results of simulations illustrate strong influence of the pipe mechanical properties and parameters of the gas phase on sound dispersion and attenuation.

4pPAi2. Acoustic measurement of bubble size and position in an ink jet printhead. Arjan Van Der Bos (Physics of Fluids, University of Twente, P.O. Box 217, 7500 AE Enschede, Netherlands, j.a.vanderbos@tnw.utwente.nl), Roger Jeurissen (Physics of Fluids, University of Twente, P.O. Box 217, 7500 AE Enschede, Netherlands, r.j.m.jeurissen@tnw.utwente.nl), Jos De Jong (Oce Technology, P.O. Box 101, 5900 MA Venlo, Netherlands, jos.dejong@oce.com), Detlef Lohse (Physics of Fluids, University of Twente, P.O. Box 217, 7500 AE Enschede, Netherlands, d.lohse@utwente.nl), Michel Versluis (Physics of Fluids, University of Twente, P.O. Box 217, 7500 AE Enschede, Netherlands, m.versluis@utwente.nl), Hans Reinten (Oce Technology, P.O. Box 101, 5900 MA Venlo, Netherlands, hans.reinten@oce.com), Marc Van Den Berg (Oce Technology, P.O. Box 101, 5900 MA Venlo, Netherlands, marc.van.den.berg@oce.com), Herman Wijshoff (Oce Technology, P.O. Box 101, 5900 MA Venlo, Netherlands, herman.wijshoff@oce.com), Richard Stevens (Physics of Fluids, University of Twente, P.O. Box 217, 7500 AE Enschede, Netherlands, r.j.a.m.stevens@student.utwente.nl)

An acoustic measurement method of the volume and position of a bubble in an ink jet print head, is presented. The system is driven by a piëzo actuator. The actuator is also used as a sensor by measuring the current through the piëzo. The method used to determine the volume and position of the bubble is based on a linear model of the investigated system. This model predicts the current for a given position and volume of the bubble. The inverse problem is to infer the position and volume of the bubble from the measured current through the piëzo actuator. The solution of the inverse problem is demonstrated. Thus, an acoustical measurement method of these properties is obtained. The results from the acoustical measurement method correspond closely with results from optical measurements. This indicates validity of the presented method.

4pPAi3. Single bubble oscillations in viscoelastic media. Anatoliy Strybulevych (Dept. of Physics and Astronomy, Univ. of Manitoba, Winnipeg, MB R3T 2N2, Canada, anatoliy@physics.umanitoba.ca), Valentin Leroy (Univ. of Manitoba, Dept. of Physics and Astronomy, Univ. of Manitoba, Winnipeg, MB R3T 2N2, Canada, valeroy77@yahoo.fr), Martin G. Scanlon (Univ. of Manitoba, Dept. of Food Science, 250 Ellis Bldg., Winnipeg, MB R3T 2N2, Canada, scanlon@cc.umanitoba.ca), John H. Page (Dept. of Physics and Astronomy, Univ. of Manitoba, Winnipeg, MB R3T 2N2, Canada, jhpage@cc.umanitoba.ca)

We report a new ultrasonic technique for determining the viscoelasticity of soft materials based on the oscillations of single bubbles injected into the material of interest. It is known that bubbles in a liquid act as strong acoustic scatterers that exhibit a low frequency resonance known as the Minnaert resonance. In the case of viscoelastic media, the complex frequency-dependent shear modulus causes the Minnaert frequency to be shifted to a higher value and leads to additional ultrasonic absorption. Therefore, both storage and loss shear moduli can be determined from the resonance frequency and the damping rate of the acoustic oscillations of a single bubble that has been injected into the sample. Experiments were performed on optically transparent commercial hair gel, agar gel, and PDMS rubber, allowing independent measurements of the bubble sizes to be made by an optical imaging technique. The acoustical properties of the samples were measured by sweeping the frequency of a continuous sinusoidal signal from 4 to 50 kHz. Because the Minnaert frequency is inversely proportional to the radius of the bubble, experiments on bubbles of different sizes enabled the frequency dependence of the complex shear moduli of the materials to be determined.

4pPAi4. Experimental examination on the interactive force between two bubbles under ultrasound irradiation: Influence of the distance between two bubbles on bubble behavior. Takaaki Fujikawa (Faculty of Engineering, Doshisha Univ., 1-3 Miyakodani Tatara, 610-0321 Kyotanabe, Japan, dth0106@mail4.doshisha.ac.jp), Kenji Yoshida (Faculty of Engineering, Doshisha Univ., 1-3 Miyakodani Tatara, 610-0321 Kyotanabe, Japan, etf1103@mail4.doshisha.ac.jp), Yoshiaki Watanabe (Faculty of Engineering, Doshisha Univ., 1-3 Miyakodani Tatara, 610-0321 Kyotanabe, Japan, kwatanab@mail.doshisha.ac.jp)

The interactive force called the secondary Bjerknes force works among multiple bubbles under ultrasound irradiation, which results in the complicated behaviors of bubbles. In this study, we have experimentally examined the direction of the interactive force depending on the distance between two bubbles. When two bubbles vibrate individually, the direction of the interactive force depends on the phase difference between vibrations of these bubbles. In addition to this theory, considering the influence of the radiated acoustic wave from a bubble vibration on the other bubble vibration, Ida has pointed that this influence induces a change in the direction of the interactive force [M. Ida et al., Phys. Rev. E 67, 056617 (2003)]. In order to examine this theoretical prediction, the behaviors of both a free bubble and a bubble adhered to the polymer were observed under ultrasound irradiation, using a high-speed video camera. From the results, we found the reversal of the direction of the interactive force due to the variation in the distance between two bubbles. These innovative experimental results give an interesting point of view to understand the dynamics of multiple bubbles.

4pPAi5. Destruction of the gas-filled capsule using effects of the collapsing bubble near the capsule. Jun Miyabe (Faculty of Engineering, Doshisha Univ., 1-3 Miyakodani Tatara, 610-0321 Kyotanabe, Japan, dth0144@mail4.doshisha.ac.jp), Kenji Yoshida (Faculty of Engineering, Doshisha Univ., 1-3 Miyakodani Tatara, 610-0321 Kyotanabe, Japan, etf1103@mail4.doshisha.ac.jp), Daisuke Koyama (Tokyo Institute of Technology, 4259 Nagatsuda, 226-8503 Yokohama, Japan, dkoyama@sonic.pi.titech.ac.j), Yoshiaki Watanabe (Faculty of Engineering, Doshisha Univ., 1-3 Miyakodani Tatara, 610-0321 Kyotanabe, Japan, kwatanab@mail.doshisha.ac.jp)

A new technique to destroy the gas-filled capsule is proposed, making use of the collapsing bubble near the capsule in the ultrasound field. At the moment of collapses under the ultrasound irradiation, the bubble causes flow and acoustic wave radiation. These phenomena are expected to assist the destruction of the capsule. We observed the effect of the bubble on this destruction, using a high-speed video camera which enables the real-time imaging. In this experiment, we use gas-filled capsule made of polyvinyl chloride. When no bubble was near the capsule at sound pressure of 60kPa, the capsule showed no vibration. However, in the presence of neighboring bubble, the capsule showed the destruction behavior of the deformation and the emission of internal gas. At higher sound pressure such as over 100kPa, the capsule showed above destruction behavior even if the bubble was not located near the capsule. In the presence of the bubble, however, the capsule was destructed in a shorter time. These experimental results give significant knowledge to a technique manipulating the gas-filled capsule destruction in the drug delivery system.

4pPAi6. Acoustic transmission through one plane of bubbles. Valentin Leroy (Univ. of Manitoba, Dept. of Physics and Astronomy, Univ. of Manitoba, Winnipeg, MB R3T 2N2, Canada, valeroy77@yahoo.fr), Anatoliy Strybulevych (Dept. of Physics and Astronomy, Univ. of Manitoba, Winnipeg, MB R3T 2N2, Canada, anatoliy@physics.umanitoba.ca), Martin G. Scanlon (Univ. of Manitoba, Dept. of Food Science, 250 Ellis Bldg., Winnipeg, MB R3T 2N2, Canada, scanlon@cc.umanitoba.ca), John H. Page (Dept. of Physics and Astronomy, Univ. of Manitoba, Winnipeg, MB R3T 2N2, Canada, jhpage@cc.umanitoba.ca)

We measured the transmission of ultrasonic waves through one layer of bubbles, for frequencies ranging from 30 to 250 kHz. The layer was a true 2D structure obtained by injecting very monodisperse bubbles (with radius $r=100$ μm) into a yield-stress polymer gel. Even for layer with a low concentration of bubbles (areal fraction, $n\pi r^2$, of 10-20%, where n is the number of bubbles per unit area), the transmission was found to be significantly reduced by the presence of bubbles (-20 to -50 dB) and showed a sharp minimum at a particular frequency. Interestingly, this frequency did not correspond to the individual Minnaert resonance of the bubbles, but depended on the concentration, which we interpret as an indication of strong coupling between the bubbles. We propose a simple model, based on a self-consistent relation, which takes into account the coupling between the bubbles and gives good agreement with the measured transmission.

4pPAi7. Nonlinear ultrasonic waves in water-air mixtures. Christian Vanhille (Universidad Rey Juan Carlos, Tulipán, s/n., 28933 Móstoles, Madrid, Spain, christian.vanhille@urjc.es), Cleofé Campos-Pozuelo (Instituto de Acústica, CSIC, Serrano, 144, 28006 Madrid, Spain, ccampos@ia.cetef.csic.es)

In this paper we present some features of nonlinear ultrasonic waves in water-air mixtures. This analysis is based on the coupling of the linear wave equation to the bubble equation in a volume formulation. The system is solved via the development of a numerical model (SMOW-BL code). The main restrictions of the model are: the nonlinear behaviour comes exclusively from the bubble vibration, all the bubbles have the same size, air inside the bubbles is adiabatic. Continuous waves at low ultrasonic frequency and wide band pulses propagation in an open domain are analysed. Results obtained by considering several bubbly layers in water are given. The existence of soliton in a water-air mixture is demonstrated. Some results corresponding to standing waves are also presented. A model which allows us to consider the self-generation of air bubbles in water, i.e., cavitation, is proposed.

Session 4pPAj

Physical Acoustics: Ultrafast Acoustics II (Poster Session)

David Hurley, Cochair
Materials Characterization Department, Idaho National Laboratory

Clément Rossignol, Cochair
LMP, UMR CNRS 5469, Université Bordeaux I

All posters will be on display from 3:40 p.m. to 5:20 p.m. To allow contributors an opportunity to see other posters, contributors of odd-numbered papers will be at their posters from 3:40 p.m. to 4:30 p.m. and contributors of even-numbered papers will be at their posters from 4:30 p.m. to 5:20 p.m.

Contributed Papers

4pPAj1. Complete characterization in thin film using picosecond ultrasonics and nanostructured transducer. Pierre-Adrien Mante (IEMN-CNRS, Cité Scientifique - Avenue Poincaré, BP 60069, 59652 Villeneuve d'Ascq Cedex, France, pierre-adrien.mante @isen.fr), Jean-François Robillard (IEMN-CNRS, Cité Scientifique - Avenue Poincaré, BP 60069, 59652 Villeneuve d'Ascq Cedex, France, jean-francois.robillard@isen.fr), Arnaud Devos (IEMN-CNRS, Cité Scientifique - Avenue Poincaré, BP 60069, 59652 Villeneuve d'Ascq Cedex, France, arnaud.devos@isen.fr), Isabelle Roch-Jeune (IEMN-CNRS, Cité Scientifique - Avenue Poincaré, BP 60069, 59652 Villeneuve d'Ascq Cedex, France, isabelle.roch-jeune@iemn.univ-lille1.fr)

Picosecond ultrasonics is an efficient method to excite and detect vibrations within a thin film. A strong optical pulse warms a material surface, which leads to the creation of an acoustic wave propagating at the sound velocity. The waves propagation modifies the optical properties of the material that can be detected by a second time-shifted optical pulse. With an usual metallic transducer, only longitudinal waves can be generated. The use of this technique on a nanostructured transducer adds in-plane propagating waves. In the case of an isotropic medium, we have access to all acoustic properties. In order to confirm this statement, we realized and studied 2D lattices of metallic nanostructures. We used e-beam lithography to obtain defect free lattices of aluminum nanocubes. Both cubes width and lattice parameters were chosen to optimize the properties measurements [1]. This nanostructuration allows us to get information about longitudinal and in-plane waves, in the gigahertz frequency range. The experiments where carried out with an aluminum lattice on a 600nm-thick silica film. This method, demonstrated on a well-known material, is suitable for any thin film. [1] J.-F. Robillard, A. Devos and I. Roch-Jeune ″Time-resolved vibrations of two-dimensional hypersonic phononic crystals″, Phys. Rev. B. 76, 092301 (2007)

4pPAj2. Generation of acoustical phonons by femtosecond laser pulses in GaAs in the presence of external electric field. Philippe Babilotte (LPEC/UMR 6087/CNRS/Université du Maine, Avenue Olivier Messiaen, 72085 Le Mans Cedex 09, France, philippe.babilotte.etu @univ-lemans.fr), Pascal Ruello (LPEC/UMR 6087/CNRS/Université du Maine, Avenue Olivier Messiaen, 72085 Le Mans Cedex 09, France, pascal.ruello@univ-lemans.fr), Denis Mounier (LPEC/UMR 6087/CNRS/Université du Maine, Avenue Olivier Messiaen, 72085 Le Mans Cedex 09, France, denis.mounier@univ-lemans.fr), Daniel Pugliese (LPEC/UMR 6087/CNRS/Université du Maine, Avenue Olivier Messiaen, 72085 Le Mans Cedex 09, France, Daniel.Pugliese@univ-lemans.fr), Mathieu Edely (LPEC/UMR 6087/CNRS/Université du Maine, Avenue Olivier Messiaen, 72085 Le Mans Cedex 09, France, mathieu.edely@univ-lemans .fr), Alain Bulou (LPEC/UMR 6087/CNRS/Université du Maine, Avenue Olivier Messiaen, 72085 Le Mans Cedex 09, France, alain.bulou @univ-lemans.fr), Jean-Marc Breteau (LPEC/UMR 6087/CNRS/Université du Maine, Avenue Olivier Messiaen, 72085 Le Mans Cedex 09, France, jean-marc.breteau@univ-lemans.fr), Vitali Gusev (LPEC/UMR 6087/CNRS/Université du Maine, Avenue Olivier Messiaen, 72085 Le Mans Cedex 09, France, vitali.goussev@univ-lemans.fr)

Experimental results on the generation and the detection by fs laser pulses of the acoustical phonons at frequencies from tens to hundreds GHz in GaAs in the presence of external electric field are presented. The influence of the magnitude and the direction of the applied electric field on the parameters of ps ultrasound is investigated. Results obtained in GaAs and low-temperature GaAs are compared. The experimental opportunities to discriminate the acoustical phonons produced by laser-induced inverse piezoelectrical effect and the acoustical phonons due to the thermoelastic mechanism and to the mechanism of electron-phonon deformation potential are discussed. This study was supported by ANR project BLAN06-3-136284.

4pPAj3. Temperature Dependence of Elastic Constant Measurements on Thin Films by Picosecond Ultrasonics. Patrick Emery (IEMN-CNRS, Cité Scientifique - Avenue Poincaré, BP 60069, 59652 Villeneuve d'Ascq Cedex, France, patrick.emery@isen.fr), Arnaud Devos (IEMN-CNRS, Cité Scientifique - Avenue Poincaré, BP 60069, 59652 Villeneuve d'Ascq Cedex, France, arnaud.devos@isen.fr)

The temperature dependence of mechanical parameters is well-known for bulk materials. New methods have to be developed to access such characteristics on thin films. These measurements are needed for understanding the temperature behavior of acoustic components in microelectronics, as for Bulk Acoustic Wave (BAW) resonators used in wireless communication. A BAW resonator uses the thickness mode resonance of a piezoelectric layer (Aluminium Nitride). In the radio-frequency range, a BAW resonator is a complex stack of various materials in thin film. The temperature dependences measurements offer a way to regulate the performances' drift induced by the warming of the device and to design temperature-independent components. Here, we present a method based on a variable temperature picosecond ultrasonics setup. The procedure is first validated on silica, then applied on various BAW technology materials (AlN, Mo, SiN, W).

4pPAj4. Photothermal and photoacoustic imaging by ultrafast optical sampling. Stefan Dilhaire (LMP, UMR CNRS 5469, Université Bordeaux I, 351, cours de la Libération, 33405 Talence, France, stefan.dilhaire @u-bordeaux1.fr), Jean-Michel Rampnoux (LMP, UMR CNRS 5469,

Université Bordeaux I, 351, cours de la Libération, 33405 Talence, France, jm.rampnoux@cpmoh.u-bordeaux1.fr), Gilles Pernot (LMP, UMR CNRS 5469, Université Bordeaux I, 351, cours de la Libération, 33405 Talence, France, g.pernot@cpmoh.u-bordeaux1.fr), Gaetan Calbris (LMP, UMR CNRS 5469, Université Bordeaux I, 351, cours de la Libération, 33405 Talence, France, g.calbris@cpmoh.u-bordeaux1.fr), Stephane Grauby (LMP, UMR CNRS 5469, Université Bordeaux I, 351, cours de la Libération, 33405 Talence, France, s.grauby@cpmoh.u-bordeaux1.fr), Clément Rossignol (LMP, UMR CNRS 5469, Université Bordeaux I, 351, cours de la Libération, 33405 Talence, France, c.rossignol@lmp.u-bordeaux1.fr), Sebastien Ermeneux (Alphanov, 351 cours de la Libération, 33405 Talence, France, sebastien.ermeneux@alphanov.com), Eric Mottay (Amplitudes Systèmes, 6, allée du doyen Georges Brus, 33600 Pessac, France, emottay@amplitude-systemes.com)

We describe a new ultrafast imaging technique based on the use of two new generation Ytterbium lasers emitting at 1030 nm at 50 MHz repletion rate. Ultrafast acquisition is achieved by slightly shifting the repetition rate of the ″pump″ and the ″probe″ beams. In that conditions a single shot response is acquired in 1ms that allows sweeping the surface of the device or the material and obtain movies of the reflectivity field of the surface. This technique allows filming the reflectance changes of a material at very high speed typically 1 Tera frame per second during 20ns. We will show applications of this technique in acoustic imaging of surface waves and non destructive evaluation of microelectronic materials.

4pPAj5. The role of coherent phonons in the vibronic laser. Wojciech Gadomski (University of Warsaw, Department of Chemistry, Laboratory of Physicochemistry of Dielectrics and Magnetics, ul. Żwirki i Wigury 101, 01-905 Warsaw, Poland, gado@chem.uw.edu.pl), Bożena Gadomska (University of Warsaw, Department of Chemistry, Laboratory of Physicochemistry of Dielectrics and Magnetics, ul. Żwirki i Wigury 101, 01-905 Warsaw, Poland, bogad@chem.uw.edu.pl)

Herewith we present the quantum theory of the vibronic laser, which is based on the crucial role played by the host crystal phonons in the laser dynamics. In the solid state transition-metal ion laser the operation takes place between the vibronically broadened electronic levels of the gain center, thus the laser action is accompanied by the creation or annihilation of the host lattice phonons. The nonequilibrium coherent phonons, produced in the process of the nonradiative energy transition from the photoexcited impurity ion, pump the energy level, from whivh the laser action takes place. One can say that the laser photons are produced at the cost of lattice phonons. This is the reason why the coherent phonons strongly influence the character of the laser action and govern the complicated laser dynamics. In the laser equations, derived by us, the number of coherent phonons is treated as one of dynamical variables coupled with the number of photons. In solution we observe the effect of energy pulling between photons and phonons. Phonons follow all forms of the photon dynamics including self-pulsations and chaotic dynamics.

4pPAj6. Picosecond ultrasonics signal in biological materials: Comparison between predictions and experiments. Mathieu Ducousso (LMP, UMR CNRS 5469, Université Bordeaux I, 351, cours de la Libération, 33405 Talence, France, m.ducousso@lmp.u-bordeaux1.fr), Clément Rossignol (LMP, UMR CNRS 5469, Université Bordeaux I, 351, cours de la Libération, 33405 Talence, France, c.rossignol@lmp.u-bordeaux1.fr), Bertrand Audoin (LMP, UMR CNRS 5469, Université Bordeaux I, 351, cours de la Libération, 33405 Talence, France, b.audoin@lmp.u-bordeaux1.fr), Fabien Guillemot (INSERM U577, Université Victor Segalen Bordeaux 2, 146, rue Léo-Saignat, Case 45, 33076 Talence, France, fabien.guillemot@bordeaux.inserm.fr), Marie-Christine Durrieu (INSERM U577, Université Victor Segalen Bordeaux 2, 146, rue Léo-Saignat, Case 45, 33076 Talence, France, durrieumc@bordeaux.inserm.fr)

Picosecond ultrasonics is a non-destructive method for measuring mechanical properties such as velocity or stiffness coefficients for nanometric materials [1]. This technique uses femtosecond laser pulses for generating and detecting acoustics waves from GHz to THz. Its resolution is about nanometers in depth and a few micrometers laterally. For transparent materials it allows generating the so-called Brillouin oscillations, which frequencies are determined by the material sound velocity and the light beam wavelength. In this paper this technique is applied to biological cells. Measurements suggest promising perspectives for the imaging inside a single living cell; frequency content is from 5 to 20 GHz. A theoretical model based on Fourier heat and acoustic wave equations has been developed. These equations include heat diffusion and acoustic propagation respectively. It permits numerical simulations in time domain. First experimental results on animal and vegetal cells are presented and confronted with these calculated waveforms. [1] C. Thomsen, H. T. Grahn, H. J. Maris, J. Tauc, Phys. Rev. B 34, 4129, 1986

Session 4pPAk

Physical Acoustics: Thermoacoustics II (Poster Session)

Steven Garrett, Cochair
Penn State University

Philippe Blanc-Benon, Cochair
Ecole Centrale de Lyon

All posters will be on display from 3:40 p.m. to 5:20 p.m. To allow contributors an opportunity to see other posters, contributors of odd-numbered papers will be at their posters from 3:40 p.m. to 4:30 p.m. and contributors of even-numbered papers will be at their posters from 4:30 p.m. to 5:20 p.m.

Contributed Papers

4pPAk1. Experimental evaluation of the wavenumber in stacked screen regenerators. Yuki Ueda (Tokyo University of Agriculture and Technology, Nakacho 2-24-16, 187-8588 Koganei, Tokyo, Japan, uedayuki@cc.tuat.ac.jp)

The experimental method to evaluate the wavenumber of the acoustic wave propagating in pores media is proposed. The method was applied to four types of stacks composed of square channels and seven types of regenerators consisting of stacked mesh screens. The experimental results of the stacks agreed well with the theoretical results. The experimentally obtained wavenumber in the stacked screen regenerators were found to be similar to that in circular channels. However, it was found that they depend on the types of regenerators. Based on the dependence on the regenerator types of the evaluated wavenumber, the effective radius in the stacked screen regenerators was addressed.

4pPAk2. A thermoacoustic device for sound reproduction. Fotios Kontomichos (Audio and Acoustic Technology Group, Wire Communications Laboratory, Electrical Engineering & Computer Technology Department, University of Patras, 26500 Patras, Greece, fotkon@wcl.ee.upatras.gr), Alexandros Koutsioubas (University of Patras Dept. of Physics, Rio, 26500 Patras, Greece, alexandk@physics.upatras.gr), John Mourjopoulos (Audio and Acoustic Technology Group, Wire Communications Laboratory, Electrical Engineering & Computer Technology Department, University of Patras, 26500 Patras, Greece, mourjop@wcl.ee.upatras.gr), Nikolaos Spiliopoulos (University of Patras Dept. of Physics, Rio, 26500 Patras, Greece, nspiliop@physics.upatras.gr), Alexandros Vradis (University of Patras Dept. of Physics, Rio, 26500 Patras, Greece, vradis@physics.upatras.gr)

Many current research efforts focus on alternative electroacoustic transduction devices having no moving parts, in order to achieve sufficient audio performance from compact solid state devices. Thermoacoustic loudspeakers are transducers based on the conversion of A/C current signals to thermal energy, causing a local fluctuation of air pressure which generates acoustic waves. A thermoacoustic actuator does not involve any movement of solid components in order to generate an acoustic wave and it is based on a mechanism of a ″virtual″ piston produced by vibrating air molecules via alternating heat transfer to the medium. This work examines such novel and alternative audio transduction technologies based on a novel hybrid thermoacoustic transducer prototype which was developed at the University of Patras through the cooperation between Audio and Acoustic Technology Group and Solid State Physics Laboratory. This hybrid solid state device without moving parts is based on the thermoacoustic method of sound reproduction and preliminary measurements of its performance are presented. The theoretical principles of these systems are also simulated, resulting into comparisons with the measured performance of the prototype.

4pPAk3. Numerical modelling of acoustic streaming in resonators. Abdennour Boufermel (Laboratoire d'Acoustique de l'Université du Maine, Avenue Olivier Messiaen, 72085 Le Mans, France, boufermel@hotmail.fr), Nicolas Joly (Laboratoire d'Acoustique de l'Université du Maine, Avenue Olivier Messiaen, 72085 Le Mans, France, nicolas.joly@univ-lemans.fr), Pierrick Lotton (Laboratoire d'Acoustique de l'Université du Maine, Avenue Olivier Messiaen, 72085 Le Mans, France, Pierrick.Lotton@univ-lemans.fr)

The acoustic wave propagation in thermoviscous fluid can generate slow phenomena, such as streaming and thermoacoustic effects, by nonlinear processes localised mainly in the viscous and thermal boundary layers. The model presented consists in computing numerically by the finite element method, (i) first, the harmonic solution for linear acoustics in thermoviscous fluid including the boundary layers, and (ii) second, the unsteady solution for the acoustic streaming and heat transfer. The model formulation is based on the mass and momentum conservation equations for the streaming, and the energy conservation equation for heat transfer. The streaming is presented as a standard form of an incompressible flow for velocity vector for mass transport, where the nonlinear effects of acoustics are considered as excitation forces for the streaming and sources for heat transfer. As the performance of thermoacoustic devices is limited by the convective heat transfer of the streaming, this study is suited for the optimisation of these systems. Another application is the development of microfluidic devices.

4pPAk4. Experimental validations of a new thermoacoustic simulation software CRISTA. Adrien Bétrancourt (LIMSI-CNRS, BP 133, F-91403 Orsay, France, adrien.betrancourt@limsi.fr), Thierry Le Pollès (Hekyom SARL, 2 rue Jean Rostand, 91400 Orsay, France, thlepolles@hekyom.com), Gérard Defresne (LIMSI-CNRS, BP 133, F-91403 Orsay, France, defresne@limsi.fr), Diana Baltean-Carlès (LIMSI-CNRS, BP 133, F-91403 Orsay, France, baltean@limsi.fr), Patxi Duthil (Institut de Physique Nucléaire d'Orsay, 15 rue Georges Clémenceau, 91400 Orsay, France, duthil@ipno.in2p3.fr), Jean-Pierre Thermeau (Institut de Physique Nucléaire d'Orsay, 15 rue Georges Clémenceau, 91400 Orsay, France, thermeau@ipno.in2p3.fr), Maurice-Xavier François (LIMSI-CNRS, BP 133, F-91403 Orsay, France, mxf@limsi.fr)

A new simulation software CRISTA has been developed at LIMSI-CNRS. It is based on the Rott's equations approximation. It computes all thermal and acoustic parameters of a given thermoacoustic device whose geometry is previously designed with another program TADESIGN. To realize

the simulation, the user needs only to define a drive ratio at some point of the system and the heat exchanger temperatures. Note that for a prime mover the hot heat exchanger temperature is a simulation result. Every converged solution guarantees the physical principles. Moreover, CRISTA allows computing the quality factor of the resonator. The experimental validations have been successfully performed on different devices coupled to the same prime mover: a simple RLC load, an acoustic amplifier, a pulse tube refrigerator and a lumped boost pulse tube refrigerator.

4pPAk5. Numerical simulation of a thermoacoustic wave amplification. Omar Hireche (LIMSI-CNRS, BP 133, F-91403 Orsay, France, hireche@limsi.fr), Catherine Weisman (LIMSI-CNRS, BP 133, F-91403 Orsay, France, weisman@limsi.fr), Diana Baltean-Carlès (LIMSI-CNRS, BP 133, F-91403 Orsay, France, baltean@limsi.fr), Luc Bauwens (University of Calgary, Departement of Mechanical and Manufacturing Engineering, 2500 University Drive NW, Calgary, AB AB T2N 1N4, Canada, bauwens@ucalgary.ca), Maurice-Xavier François (LIMSI-CNRS, BP 133, F-91403 Orsay, France, mxf@limsi.fr), Patrick Le Quere (LIMSI-CNRS, BP 133, F-91403 Orsay, France, plq@limsi.fr)

We performed a numerical study of the thermal and physical phenomena occurring in thermoacoustic wave generators. The goal of the simulation is to predict the amplification due to thermoacoustics of a wave initially of small amplitude. Therefore, we focus on the stack and the two heat exchangers, which we call the active cell, which is acoustically compact. The resonator area is split into two parts: the active cell, in which heat transfer takes place, and a resonator, in which the flow is acoustic. The flow in the two-dimensional active cell can be approximated as a low Mach number viscous, conductive flow, subjected to spatially uniform pressure fluctuations. This model is formally derived using asymptotic expansions in terms of Mach number. The focus here is heat transfer between two successive stack plates. The two-dimensional time-dependent problem resulting from this model is solved numerically. Outside the active cell, flow in the resonator is described by a reversible acoustic one-dimensional model. The coupling between the two zones is obtained by matching the velocity at the interface. The acoustics in the resonance tube can be solved using the d'Alembert solution, relating velocities at the interface to velocity values at an earlier time.

4pPAk6. Green chillies: a practical thermoacoustic refrigerator in day-to-day use since February 2007. Philip Spoor (CFIC-Qdrive, 302 Tenth St., Troy, NY 12180, USA, pspoor@cficinc.com)

CFIC, Inc. recently designed and built a thermoacoustic food refrigerator for the U.S. Army's Combat Feeding program (based at the Natick Soldier Center in Natick, MA). The Army wants a more combat-hardy alternative to standard vapor-compression devices, which have many leak-prone braze joints. However, the thermoacoustic ″Army Fridge″ has generated increasing commercial and public interest as the search for environmentally benign alternatives to conventional refrigeration has intensified. The Army fridge uses helium as its working fluid, and it has no pumps or cirulating fluids, only heat pipes and fans for heat exchange with the air. Unlike all other thermoacoustic prototypes known to us, this device is expressly designed like a product, with all the thermoacoustic hardware and controls confined to a relatively small enclosure on top of a large (17 cubic foot) cabinet, and operation accomplished by a single power switch and a thermostat. In early 2007 the Army fridge went into long-term testing at CFIC, Inc. as our auxiliary refrigerator. By March 2007 it will have surpassed 1 year (8760 hours) of continuous running. We will present details of construction, performance history, and recommendations for higher efficiency and lower cost.

4pPAk7. Effect of an obstacle on Rayleigh acoustic streaming cells. Solenn Moreau (Laboratoire d'Etudes Aérodynamiques (LEA), Université de Poitiers, ENSMA, CNRS, Bat K, 40 avenue du recteur Pineau, 86022 Poitiers, France, solene.moreau@lea.univ-poitiers.fr), Helene Baillet (Laboratoire d'Etudes Aérodynamiques (LEA), Université de Poitiers, ENSMA, CNRS, Bat K, 40 avenue du recteur Pineau, 86022 Poitiers, France, helene.baillet@lea.univ-poitiers.fr),Jean-Christophe Valière (Laboratoire d'Etudes Aérodynamiques (LEA), Université de Poitiers, ENSMA, CNRS, Bat K, 40 avenue du recteur Pineau, 86022 Poitiers, France, jean-christophe.valiere@lea.univ-poitiers.fr)

Acoustic streaming has harmful consequences on thermoacoustic machines behaviour because of the associated heat transfers. A preliminary study was carried out in order to study the effect of an obstacle on the Rayleigh cells to help in understanding the role of such phenomena in thermoacoustic machines. An obstacle was introduced in a half-wavelength cylindrical wave guide to study its effects on acoustic streaming. The obstacle was placed at various positions along the wave guide axis and experiments were carried out at various acoustic levels. The axial streaming velocity was measured using Laser Doppler Velocimetry (LDV). It was observed that adding an obstacle in the streaming pattern modifies the latter and that new streaming vortices appear in the vicinity of the obstacle. When the obstacle position approaches a maximum of the Rayleigh streaming velocity the number and the amplitude of acoustic streaming vortices at the ends of the obstacle increase. Similar tendencies were observed when the acoustic velocity amplitude was increased. Because streaming in the vicinity of the obstacle end is complex and has a high amplitude, heat effects can be expected to be important and complex at the ends of the thermaoacoustic stack where heat exchangers are located.

4pPAk8. Experimental study of the thermoacoustic effect using infrared thermography. Vincent Feuillet (Laboratoire d'Acoustique de l'Université du Maine, Avenue Olivier Messiaen, 72085 Le Mans, France, vincent.feuillet@univ-lemans.fr), Guillaume Penelet (Laboratoire d'Acoustique de l'Université du Maine, Avenue Olivier Messiaen, 72085 Le Mans, France, guillaume.penelet@univ-lemans.fr), Pierrick Lotton (Laboratoire d'Acoustique de l'Université du Maine, Avenue Olivier Messiaen, 72085 Le Mans, France, Pierrick.Lotton@univ-lemans.fr), Lionel Camberlein (Laboratoire d'Acoustique de l'Université du Maine, Avenue Olivier Messiaen, 72085 Le Mans, France, lionel.camberlein@univ-lemans.fr)

The thermal metrology used to study experimentally the thermoacoustic effect is almost always based on thermoelectric junctions. This kind of measurement is intrusive and provides a few information in space. This paper presents an experimental set-up where temperature measurement on the thermoacoustic stack is acquired by infrared thermography. This measurement provides more information in space and time to study complex physical phenomena, such as heat transfer through both ends of the stack, non linear edge effects, or optimal spacing between stack and heat exchangers. The experimental set-up consists of a half-wavelength resonator with a square cross section closed by a rigid wall at one end and coupled to an electrodynamic loudspeaker at the other end. The thermoacoustic core is either a single plate or a stack of parallel plates made of Kapton. Temperature measurements are carried out along the stack by the use of an infrared camera. The acoustic pressure is measured by a microphone flush-mounted on the wall at the exit of the resonator. First results show the essential role played by the edge effects and the heat generated by viscous losses.

4pPAk9. LDV measurements of acoustic streaming in a traveling wave, closed-loop resonator. Cyril Desjouy (Laboratoire d'Acoustique de l'Université du Maine, Avenue Olivier Messiaen, 72085 Le Mans, France, cyril.desjouy@univ-lemans.fr), Pierrick Lotton (Laboratoire d'Acoustique de l'Université du Maine, Avenue Olivier Messiaen, 72085 Le Mans, France, Pierrick.Lotton@univ-lemans.fr), Guillaume Penelet (Laboratoire d'Acoustique de l'Université du Maine, Avenue Olivier Messiaen, 72085 Le Mans, France, guillaume.penelet@univ-lemans.fr), James Blondeau (Laboratoire d'Acoustique de l'Université du Maine, Avenue Olivier Messiaen, 72085 Le Mans, France, james.blondeau@univ-lemans.fr)

The first part of this work deals with the study of an annular acoustic resonator, where the acoustic field is controlled by two loud-speakers in order to generate a purely traveling wave. The results of a complete electroacoustic modeling of this device, where the acoustic field is accurately defined, are compared to the experimental results. The second part deals with the characterization of various non-linear effects occurring in such a device. The generation of acoustic streaming is especially investigated in our study.

Laser Doppler Velocimetry measurements are performed in order to characterize both first order (acoustic) and second order (acoustic streaming) velocity fields. Works are now in progress in order to improve accuracy of streaming measurement and to compare the experimental data to the available theories. This study should contribute to enhance the designing of thermoacoustic devices and should be also useful for its potential applications in microfluidics, especially for the development of micro-pumps and micro-mixers.

4pPAk10. Weakly non-linear thermoacoustics for general porous media. Peter In 'T Panhuis (Eindhoven University of Technology, P.O. Box 513, 5600 MB Eindhoven, Netherlands, p.h.m.w.panhuis @tue.nl), Sjoerd Rienstra (Eindhoven University of Technology, P.O. Box 513, 5600 MB Eindhoven, Netherlands, s.w.rienstra@tue.nl), Han Slot (Eindhoven University of Technology, P.O. Box 513, 5600 MB Eindhoven, Netherlands, j.j.m.slot@tue.nl), Jos Zeegers (Eindhoven University of Technology, Den Dolech 2, 5612 AZ Eindhoven, Netherlands, j.c.h .zeegers@tue.nl)

A weakly nonlinear theory for thermoacoustics, including acoustic streaming, a temperature-dependent viscosity and slowly varying pores with arbitrarily shaped cross-sections, has been constructed by systematically applying dimensional analysis and small-parameter asymptotics. In this way a set of equations for the acoustic and streaming variables can be derived. For some simple cases explicit solutions can be found, such as the short-stack approximation, but for the more advanced applications we have to resort to a numerical solution. The theory has been implemented both for standing-wave and traveling-wave applications. For the case of a standing-wave system we have compared our computations with experimental data and found a remarkable agreement.

4pPAk11. Viscous and thermal effects in acoustic radiation problems. Husnain Inayat Hussian (INSA de Lyon - LVA, Bâtiment St. Exupéry, 25 bis avenue Jean Capelle, F-69621 Villeurbanne Cedex, France, husnain .inayat-hussain@insa-lyon.fr), Jean-Louis Guyader (INSA de Lyon - LVA, Bâtiment St. Exupéry, 25 bis avenue Jean Capelle, F-69621 Villeurbanne Cedex, France, jean-louis.guyader@insa-lyon.fr)

The thermal and viscous effects are generally neglected in acoustic radiation problems. In the present work we observe if these effects have any significance on acoustic radiation characteristics. Several researches have been materialised in this respect, notably, Bruneau, Beltman et al. These models study factors like inertial and viscous terms for example and then keep some while neglect others based on their significance. Our approach is quite general and we take all the factors into consideration. Our model not only deals with the thermal and viscous effects but compressibility and all other terms are taken into consideration. A system of differential equations issuing from conservation principles is linearized. Next harmonic dependence is assumed and a linear system is obtained. This linear system generates different waves among which only those are kept, which follow the sommerfeld condition. These waves produce an equal number of linear systems, and consequently; pressure, temperature, and the normal and tangential acoustic veocities are determined, using the boundary conditions of no slip, isothermal wall and matching normal acoustic velocity. Our aim is to apply these findings to a viscothermal fluid within a double wall to see if acoustic transmission is improved.

4pPAk12. Physical mechanism and theoretical model of thermoacoustic heat exchangers. Ercang Luo (Technical Institute of Physics and Chemistry, CAS, Beiyitiao Rd., Zhongguancun St., P.O.Box 2711, 100080 Beijing, China, Ecluo@cl.cryo.ac.cn), Bo Gao (Graduate University of Chinese Academy of Sciences, Zhongguancun St., 100049 Beijing, China, gaobozaihit@163.com)

Unlike a regenerator, there are both oscillating heat exchange flux (first order) and non-zero time-averaged heat exchange flux (second order) in the hot and cold end heat exchangers of thermoacoustic systems. The non-zero time-averaged heat flux just reflects the net heat exchange between the working substance and external heat sinks, which is more important and interesting for design. In this paper, the physical mechanism of oscillating flow heat exchanger is first analyzed. Based on understanding of the heat transfer mechanism, the theoretical model of heat transfer is then developed; in this part, the key of the problem is to obtain transversal distribution of the second order time-averaged temperature, T20(y). Eventually, an analytical expression of Nusselt number for the thermoacoustic heat exchangers is obtained under the assumption of laminar flow.

Session 4pPPa

Psychological and Physiological Acoustics: Role of Temporal Fine Structure in Speech and Non-Speech Perception for Normal and Hearing-Impaired People I

Christian Lorenzi, Cochair
Univ Paris Descartes, CNRS, Ecole Normale Superieure, DEC, 29 rue d'Ulm, Paris, 75005, France

Brian Moore, Cochair
University of Cambridge, Department of Experimental Psychology, Downing Street, Cambridge, CB2 3EB, UK

Invited Papers

2:00

4pPPa1. Role of temporal fine structure cues in speech intelligibility. Christian Lorenzi (Univ Paris Descartes, CNRS, Ecole Normale Superieure, DEC, 29 rue d'Ulm, 75005 Paris, France, lorenzi@ens.fr)

A number of studies have investigated the role of two temporal features of the narrowband speech signals at the output of auditory filters in speech identification: temporal envelope (E) and temporal fine structure (TFS) cues. To assess the contribution of each feature to speech identification, speech stimuli were split into an array of contiguous analysis bands and processed using several techniques to remove, as far as possible, either E or TFS cues within each band. Overall, the outcome of these studies indicated that, after moderate to subtantial training, high levels of speech identification measured in quiet could be obtained for normal-hearing listeners on the basis of E cues or TFS cues alone. The results obtained with TFS cues only may appear surprising, because it is generally considered that, at least for non-tonal languages, E cues carry most of the phonetic information required for speech identification in quiet whereas TFS cues play mainly a role in conveying the pitch cues required for the segregation of speech and background sounds. Further work assessing the extent to which TFS cues alone can convey useful linguistic information in addition to these pitch cues will be reviewed.

2:20

4pPPa2. Role of temporal fine structure in speech perception. Fan-Gang Zeng (University of California Irvine, 364 Med Surge II, Irvine, CA 92697, USA, fzeng@uci.edu)

Recent studies have shown that lack of access to the temporal fine structure cue is a major reason for the difficulty in speech perception in noise by hearing-impaired listeners. To further understand the role of temporal fine structure, we need to define the temporal fine structure and to delineate its relationship to the temporal envelope in both acoustical and perceptual domains. This talk will first examine the relationship between temporal envelope and temporal fine structure in signal processing terms and then relate it to speech production and perception. Acoustically, the temporal fine structure primarily contributes to changes in fundamental frequency, harmonics, and formant transition. Perceptually, while the temporal fine structure can contribute to speech intelligibility via the formant transition cue, it contributes to speech perception in noise by enhancing auditory objection formation rather than increasing speech intelligibility directly.

2:40

4pPPa3. Temporal fine structure coding for pitch and speech perception. Andrew J. Oxenham (University of Minnesota, Department of Psychology, 75 E. River Road, Elliott Hall N218, Minneapolis, MN 55455, USA, oxenham@umn.edu)

Temporal fine structure can be defined mathematically with relative ease. Understanding its perceptual importance, or even how it is coded in the peripheral auditory system, is another matter. This talk will review recent work from our lab that addresses some of these issues. The focus will be on the use and representation of temporal fine structure in complex pitch perception with spectrally resolved and unresolved components, and on the importance of temporal fine structure when using F0 information in speech to segregate target speech for competing talkers and other complex interfering sounds. [Supported by National Institutes of Health grant R01 DC 05216.]

3:00

4pPPa4. The contribution of temporal fine structure information to the intelligibility of speech in noise. Kathryn Hopkins (University of Cambridge, Department of Experimental Psychology, Downing Street, CB2 3EB Cambridge, UK, kh311@cam.ac.uk), Brian Moore (University of Cambridge, Department of Experimental Psychology, Downing Street, CB2 3EB Cambridge, UK, bcjm@cam.ac.uk)

Temporal fine structure (TFS) information in speech may be particularly useful when listening to a target in a background that contains temporal 'dips'. A change in TFS may allow identification of signal portions where the target-to-background ratio is high. This hypothesis was tested. Speech reception thresholds were measured with steady and an 8-Hz amplitude-modulated noise background for signals processed to contain variable amounts of TFS information. Signals were filtered into channels and channel signals for channel numbers above a 'cut off channel' (CO) were tone-vocoded to remove TFS information, while channel signals with channel numbers of CO and below were left unprocessed. Signals from all channels were combined. Five values of CO were tested for each noise type, with

ten normal-hearing subjects. Subjects benefited more from TFS information when listening in the modulated masker than the steady masker. For steady noise, addition of TFS information above 548 Hz did not improve performance, whereas for modulated noise, addition of TFS at high frequencies did improve performance. The greater benefit from TFS information when listening in modulated noise is consistent with the idea that TFS information is important for listening in the dips of a fluctuating masker.

3:20

4pPPa5. Discrimination of stochastic patterns of frequency modulation relevant to speech perception. Stanley Sheft (Parmly Hearing Inst., Loyola Univ. Chicago, 6525 N. Sheridan Road, Chicago, IL 60626, USA, ssheft@luc.edu), Christian Lorenzi (Univ Paris Descartes, CNRS, Ecole Normale Superieure, DEC, 29 rue d'Ulm, 75005 Paris, France, lorenzi@ens.fr)

Recent work has suggested involvement of temporal fine structure (TFS) information in speech perception, especially in adverse listening conditions. However, little is known regarding discrimination of pattern of TFS modulation, an ability that would underlie robust contribution to speech processing. The present study evaluated the ability to discriminate among stochastic patterns of frequency modulation (FM). Contrasting modulators were different samples of lowpass noise that shared a common bandwidth and resulted in the same maximum frequency excursion. Performance levels declined in an orderly manner with modulator bandwidth, similar to results obtained when lowpass noise is used to modulate amplitude (i.e., AM) rather than fine structure. Modeling, however, indicated that the similarity was not simply a result of FM-to-AM conversion at the output of auditory filters. In additional conditions, discrimination of stochastic FM was measured in the presence of wideband noise which in some cases was sinusoidally amplitude modulated at either 4 or 20 Hz. With both unmodulated and modulated maskers, little effect on performance was noted, even with a signal carrier level as low as 15-20 dB above detection threshold. Absence of a substantial masking effect indicates availability of TFS cues for speech perception in noise. [Work supported by NIH.]

3:40-5:20 Posters

Lecture sessions will recess for presentation of poster papers on various topics in acoustics. See poster sessions for topics and abstracts.

Invited Paper

5:20

4pPPa6. The role of temporal fine structure in speech source segregation. Joshua G. Bernstein (Walter Reed Army Medical Center, Army Audiology and Speech Center, 6900 Georgia Ave. NW, Washington, DC 20307-5001, USA, joshua.bernstein@amedd.army.mil), Kenneth W. Grant (Walter Reed Army Medical Center, Army Audiology and Speech Center, 6900 Georgia Ave. NW, Washington, DC 20307-5001, USA, grant@tidalwave.net)

Normal-hearing (NH) listeners show better speech recognition when a stationary noise masker is replaced by an opposite-gender competing talker at the same signal-to-noise ratio (SNR). Hearing-impaired (HI) listeners often do not show this interfering-talker benefit (ITB). This may be due to a reduced ability to use temporal fine structure (TFS). Consistent with this idea, NH listeners also show little ITB when TFS is removed. We hypothesized that TFS underlies the ITB by providing source-segregation cues. To test this hypothesis, non-auditory segregation cues were introduced in the form of a video of the talker's face. Speech intelligibility was estimated in NH listeners as a function of SNR for sentences spoken by a female talker and masked by speech-spectrum shaped stationary noise or a single male talker. Target and masker were summed before processing by a 15-channel noise vocoder to remove TFS, and presented with or without accompanying video. Without video, listeners received little ITB, consistent with previous results. Auditory-visual conditions yielded as much as 9 dB of ITB, supporting the hypothesis that a diminished ability to perceptually segregate sources contributes to the lack of ITB in the absence of TFS. Similar results were obtained for unprocessed speech in HI listeners.

Contributed Paper

5:40

4pPPa7. Relative importance of E and TFS speech cues in low and high-frequency channels. Marine Ardoint (Univ Paris Descartes, CNRS, Ecole Normale Superieure, DEC, 29 rue d'Ulm, 75005 Paris, France, marine.ardoint@ens.fr), Christian Lorenzi (Univ Paris Descartes, CNRS, Ecole Normale Superieure, DEC, 29 rue d'Ulm, 75005 Paris, France, lorenzi@ens.fr)

Previous studies have shown that perfect speech identification in quiet could be obtained for broadband speech processed using the Hilbert transform to preserve either temporal envelope (E) or temporal fine structure (TFS) cues only in narrow frequency bands. However, little is known regarding the respective contribution of each cue to speech intelligibility in low and high frequency bands. The goal of the present study was to assess the contribution of E and TFS cues of the low- and high-frequency channels to consonant identification. Vowel-consonant-vowel stimuli were split into an array of 16 analysis bands spanning the range 80-8,020 Hz and processed using the Hilbert transform to keep either E or TFS cues only within each band. Identification scores were measured for low-pass and high-pass filtering of the processed stimuli for a group of normal-hearing listeners. Results will be discussed in light of phase-locking properties to E and TFS. In most mammals, phase-locking of auditory-nerve fibers begins to decline above 1 kHz and disappears above 4-5 kHz. TFS-coded speech intelligibility should therefore drop when stimuli are high-pass filtered above 1 kHz and be at chance level for high-pass filtering above 5 kHz. No such drop should be expected for E-coded speech.

6:00

4pPPa8. The importance of temporal fine structure coding for speech perception in listeners with sensorineural hearing impairment as compared to normal hearing listeners. Emily Buss (University of North Carolina, School of Medicine, 1115 Bioinformatics. Bldg., CB7070, 130 Mason Farm Rd., Chapel Hill, NC 27599, USA, ebuss@med.unc.edu), Joseph W. Hall (University of North Carolina, School of Medicine, 1115 Bioinformatics. Bldg., CB7070, 130 Mason Farm Rd., Chapel Hill, NC 27599, USA, jwh@med.unc.edu), John H. Grose (University of North Carolina, School of Medicine, 1115 Bioinformatics. Bldg., CB7070, 130 Mason Farm Rd., Chapel Hill, NC 27599, USA, jhg@med.unc.edu)

Physiological data suggest that the neural representation of temporal fine structure could benefit speech recognition in normal hearing listeners. Conversely, it has been hypothesized that deficits in the encoding of fine structure could play a role in the poor speech perception of patients with sensorineural hearing loss, particularly for speech presented at moderate to high levels and speech presented in background noise. Experiments on the psychoacoustical abilities of adults with hearing loss have shown a correlation between performance on tasks thought to rely on fine structure cues (e.g., low rate FM detection) and ability to understand speech or lowpass filtered speech, lending support to this hypothesis. This talk will review these data, as well as the mechanisms proposed to account for this result, and will consider the relation of these findings to experiments with normal-hearing listeners.

6:20

4pPPa9. Fine-structure processing, frequency selectivity and speech perception in hearing-impaired listeners. Olaf Strelcyk (Centre for applied hearing research, Technical University of Denmark, DTU, Bygn. 352, 2800 Lyngby, Denmark, os@oersted.dtu.dk), Torsten Dau (Centre for applied hearing research, Technical University of Denmark, DTU, Bygn. 352, 2800 Lyngby, Denmark, tda@oersted.dtu.dk)

Hearing-impaired people often experience great difficulty with speech communication when background noise is present, even if reduced audibility has been compensated for. Other impairment factors must be involved. In order to minimize confounding effects, the subjects participating in this study consisted of groups with homogeneous, symmetric audiograms. The perceptual listening experiments assessed the intelligibility of full-spectrum as well as low-pass filtered speech in the presence of stationary and fluctuating interferers, the individual's frequency selectivity and the integrity of temporal fine-structure processing. The latter was addressed in a binaural and a monaural experiment. In the binaural experiment, the lateralization threshold was measured for low-frequency tones with ongoing interaural phase delays. In the monaural experiment, detection thresholds for low-rate frequency modulation were obtained. In addition, these binaural and monaural thresholds were measured in a stationary background noise in order to assess the persistence of the fine-structure processing to interfering noise. Apart from elevated speech reception thresholds, the hearing impaired listeners showed poorer performance than the normally hearing in terms of frequency selectivity and fine-structure processing, despite normal audiometric thresholds at the test frequencies. However, the binaural fine-structure processing was not found to be particularly vulnerable to interfering noise in these listeners.

Session 4pPPb

Psychological and Physiological Acoustics: Role of Temporal Fine Structure in Speech and Non-Speech Perception for Normal and Hearing-Impaired People II (Poster Session)

Christian Lorenzi, Cochair
Univ Paris Descartes, CNRS, Ecole Normale Superieure

Brian Moore, Cochair
University of Cambridge

All posters will be on display from 3:40 p.m. to 5:20 p.m. To allow contributors an opportunity to see other posters, contributors of odd-numbered papers will be at their posters from 3:40 p.m. to 4:30 p.m. and contributors of even-numbered papers will be at their posters from 4:30 p.m. to 5:20 p.m.

Contributed Papers

4pPPb1. Facilitation of intensity discrimination of short stimuli in noise occurs not far from a stimuli detection threshold. Liudmila Rimskaya-Korsakova (N. N. Andreyev Acoustics Institute, Shvernika 4, 117036 Moscow, Russian Federation, lkrk@akin.ru)

Adaptation is a main property of sensory receptors. In a basis of adaptation are properties of peripheral receptors and central neuron. There is a question: what is the auditory adaptation mechanism to short high frequency stimuli? How the auditory system can trace stimulus amplitude changes? The probable answer is: stimuli are mixed with noise of different origin. Noise adapts hearing and improves discrimination of stimulus. Simulation researches of peripheral encoding were shown the amplitude structure of short stimulus acting in isolation or in noise could be preserved when intensity are not far from thresholds of fibers. For each stimulus level there is the certain noise level, when amplitude structure can be detected without losses. In this work the validity of these statements was checked up in auditory experiments. The thresholds of intensity discrimination (ID) for short stimulus presented in silence and in conditions of simultaneous and forward masking have been estimated. In a range of average stimulus intensity and for each stimulus level there is the certain noise level when ID is better in noise but not in silence. The ID facilitation is registered near to the stimulus detection thresholds and after adaptation of hearing by noise. Results of auditory researches correspond to the simulation results.

4pPPb2. Intelligibility of temporal fine structure speech signals with restricted FM excursion. Gaëtan Gilbert (Equipe audition LPP UMR CNRS 8158, 29, rue d'Ulm, 75005 Paris, France, gaetan.gilbert@ens.fr), Agnes Leger (Equipe audition LPP UMR CNRS 8158, 29, rue d'Ulm, 75005 Paris, France, legeragnes@gmail.com), Christian Lorenzi (Univ Paris Descartes, CNRS, Ecole Normale Superieure, DEC, 29 rue d'Ulm, 75005 Paris, France, lorenzi@ens.fr)

The Hilbert transform is the most common demodulation technique to derive temporal fine structure (TFS) signals. However, for speech stimuli, the Hilbert transform generally leads to results that have no clear physical meaning, generating undesired artefacts; for instance, instantaneous frequency may vary well beyond the analysis filters bandwidth. This study examined the intelligibility in quiet of TFS-coded Vowel-Consonants-Vowel signals generated with a demodulation technique minimizing these artefacts. Speech items were passed through a 16 FIR filters (750th order) filterbank. A Greenwood mapping was used to set filters bandwidth between 80-8020 Hz (approximately 2 ERBs wide). A frequency-modulation function was extracted at the output of each filter, hard limited within the analysis bandwidth and lowpass filtered. Spectral cues were removed by equating the rms across bands. Identification scores ranged between chance level (6.25%) with no improvement across sessions for the least experienced listeners and 50% correct for the most experienced listeners. Further experiments will investigate these between-listeners differences.

4pPPb3. Hard times for the pitch of complex sounds in reverberant environments. Mark Sayles (Centre for the Neural Basis of Hearing, The Physiological Laboratory, Downing Street, CB2 3EG Cambridge, UK, ms417@cam.ac.uk), Ian M. Winter (Centre for the Neural Basis of Hearing, The Physiological Laboratory, Downing Street, CB2 3EG Cambridge, UK, imw1001@cam.ac.uk)

Reverberation is present in most everyday listening environments, with sound reaching our ears directly from the source(s), and indirectly after reflecting from nearby surfaces. Reverberation smears spectral transitions through time and disrupts temporal envelope modulation in harmonic complex sounds such as voiced portions of speech. Envelope modulation can provide a cue to the pitch of complex sounds and is relied upon by hearing impaired listeners. We have examined the effects of reverberation on the temporal representation of the dynamic pitch of frequency-modulated harmonic complex sounds in the responses of single units from the ventral cochlear nucleus. Without reverberation most units provide a strong representation of the modulated pitch in their short-term interspike interval distributions. Relatively mild reverberation degrades the representation based on envelope modulation, whilst more severe reverberation removes it. The representation of pitch based on fine structure is more robust to the effects of reverberation; however, this representation is smeared in time by indirect sound energy. The effects of reverberation are critically dependent on the neuron's best-frequency, source-to-receiver distance, fundamental frequency and frequency modulation rate. We observe comparable results in human listeners using the same sounds.

4pPPb4. Effect of speech rate on speech-on-speech masking. Jing Chen (Dept. of Machine Intelligence, Speech and Hearing Research Center, 2 Science Building, Peking Univ., 5 Yeheyuan Road, Haidian District, 100871 Beijing, China, chenj@cis.pku.edu.cn), Xihong H. Wu (Dept. of Machine Intelligence, Speech and Hearing Research Center, 2 Science Building, Peking Univ., 5 Yeheyuan Road, Haidian District, 100871 Beijing, China, wxh@cis.pku.edu.cn), Xuefei F. Zou (Dept. of Machine Intelligence, Speech and Hearing Research Center, 2 Science Building, Peking Univ., 5 Yeheyuan Road, Haidian District, 100871 Beijing, China, zouxf@cis.pku.edu.cn), Zhiping P. Zhang (Dept. of Machine Intelligence, Speech and Hearing Research Center, 2 Science Building, Peking Univ., 5

Yeheyuan Road, Haidian District, 100871 Beijing, China, zhangzp@cis.pku.edu.cn), Lijuan J. Xu (Dept. of Psychology, Peking Univ., 5 Yeheyuan Road, Haidian District, 100871 Beijing, China, lijuan179021@yahoo.com.cn), Mengyuan Y. Wang (Dept. of Psychology, Peking Univ., 5 Yeheyuan Road, Haidian District, 100871 Beijing, China, motoluto@163.com), Liang Li (Dept. of Psychology, Peking Univ., 5 Yeheyuan Road, Haidian District, 100871 Beijing, China, liangli@pku.edu.cn), Huisheng S. Chi (Dept. of Machine Intelligence, Speech and Hearing Research Center, 2 Science Building, Peking Univ., 5 Yeheyuan Road, Haidian District, 100871 Beijing, China, chi@pku.edu.cn)

Target speech can be better recognized under speech-on-speech masking conditions if certain differences between target and masker (e.g. in loudness, pitch, location) can be used as cues for streaming. This study examined whether the speech rate can be used by listeners as a cue for unmasking target speech. The rate difference between target and masking speech was manipulated by changing the rate of masking speech using the Synchronized Overlap-Add Fixed Synthesis (SOLAFS) algorithm, and consequently, the ratio of target speech to masking speech (the speech rate ratio, SRR) was quantified. Both target and masker speech were Chinese nonsense sentences and they were co-presented with the signal-to-masker ratio of -7 dB. The results show that speech recognition was significantly increased with the SRR increase from 1 to 1.5 or the SRR decreased from 1 to 0.5. Moreover, the unmasking effect of precedence-induced perceived spatial separation on target-speech recognition was increased monotonically with the increase of the SRR from 0.5 to 1.5. These results suggest that the speech rate is one of the factors influencing both energetic masking and informational masking of Chinese speech. [Supported by the NSFC 60435010; 60535030; 60605016; 30670704]

4pPPb5. Charactering the individual ear by the ″Auditory Profile″. Wouter A. Dreschler (AMC, Clinical and Experimental Audiology, 1105 Amsterdam, Netherlands, w.a.dreschler@amc.uva.nl), Thamar E. Esch Van (AMC - Dept. of Clinical and Experimental Audiology, Meibergdreef 9, 1105AZ Amsterdam, Netherlands, t.e.vanesch@amc.nl), Birgitta Larsby (Linkoepings Universitet, Hus Origo Campus Valla, 581 83 Linkoeping, Sweden, birgitta.larsby@inr.liu.se), Mathias Hallgren (Linkoepings Universitet, Hus Origo Campus Valla, 581 83 Linkoeping, Sweden, mathias.hallgren@inr.liu.se), Mark E. Lutman (University of Southampton, University Road, Highfield / ISVR, SO17 iBJ Southampton, UK, mel@isvr.soton.ac.uk), Johannes Lyzenga (Vrije Universiteit Medical Center, Boelelaan 1117, 1081 HV Amsterdam, Netherlands, j.lyzenga@vumc.nl), M Vormann (Hoerzentrum Oldenburg, Hoerzentrum Oldenburg, 26129 Oldenburg, Germany, matthias.vormann@web.de), Birger Kollmeier (Universität Oldenburg, Medizinische Physik, Carl-von-Ossietzky Str. 9-11, 26111 Oldenburg, Germany, birger.kollmeier@uni-oldenburg.de)

This paper describes a new approach to auditory diagnostics, which is one of the central themes of the EU-project HEARCOM. For this purpose we defined a so-called ″Auditory Profile″ that can be assessed for each individual listener using a standardized battery of audiological tests that - in addition to the pure-tone audiogram - focus on loudness perception, frequency resolution, temporal acuity, speech perception, binaural functioning, listening effort, subjective hearing abilities, and cognition. For the sake of testing time only summary tests are included from each of these areas, but the broad approach of characterizing auditory communication problems by means of standardized test is expected to have an added value above traditional testing in understanding the reasons for poor speech reception. The Auditory profile may also be relevant in the field of auditory rehabilitation and for design of acoustical environments. The results of an international 5-center study (in 4 countries and in 4 languages) will be presented and the relevance of a broad but well-standardized approach will be discussed.

4pPPb6. Evidence of neural processing of the interaural correlation between long-duration noises in humans. Wenjie J. Wang (Dept. of Psychology, Peking Univ., 5 Yeheyuan Road, Haidian District, 100871 Beijing, China, wenjie@pku.edu.cn), Lingzhi Z. Kong (Dept. of Psychology, Peking Univ., 5 Yeheyuan Road, Haidian District, 100871 Beijing, China, konglingzhi@gmail.com), Jingyu Y. Li (Dept. of Machine Intelligence, Speech and Hearing Research Center, 2 Science Building, Peking Univ., 5 Yeheyuan Road, Haidian District, 100871 Beijing, China, lijy@cis.pku.edu.cn), Qiang Huang (Dept. of Machine Intelligence, Speech and Hearing Research Center, 2 Science Building, Peking Univ., 5 Yeheyuan Road, Haidian District, 100871 Beijing, China, QIANG.HUANG@SPREADTRUM.COM), Xihong H. Wu (Dept. of Machine Intelligence, Speech and Hearing Research Center, 2 Science Building, Peking Univ., 5 Yeheyuan Road, Haidian District, 100871 Beijing, China, wxh@cis.pku.edu.cn), Liang Li (Dept. of Psychology, Peking Univ., 5 Yeheyuan Road, Haidian District, 100871 Beijing, China, liangli@pku.edu.cn)

When the delay between two correlated sounds is sufficiently short, attributes of the lagging sound are perceptually captured by the leading sound, causing a fused image as coming from the leading-sound location. To investigate neural processing of the interaural correlation between long-duration sounds in humans, we recorded scalp event-related potentials (ERPs) to a transient silent gap that was inserted in long-duration broadband noises presented via headphones. The noises at the two ears were either correlated or uncorrelated. When the noises were correlated but not uncorrelated, participants mainly perceived only one gap image whose inside-head position was modulated by the interaural time difference (ITD). Compared to ERPs when the noises were uncorrelated, the amplitude of the N1/P2 component to the gap was smaller and amplitudes in the latency range of 100 to 200 ms were more imbalanced between the two hemispheres when the noises were correlated. When the ITD for the correlated noises was increased to 16 ms, which was beyond the ITD range for fusion, two gap images were perceived, and the amplitude of the N1/P2 component to the gap became larger and the sustained potentials during 300-500 ms after the gap onset became more negative. [Supported by NSFC].

Session 4pPPc

Psychological and Physiological Acoustics: General Topics in Psychological and Physiological Acoustics VI (Poster Session)

Elizabeth Strickland, Cochair
Purdue University

Armin Kohlrausch, Cochair
Philips Research Europe

Alain De Cheveigne, Cochair
CNRS, Universite Paris 5, Ecole Normale Superieure

All posters will be on display from 3:40 p.m. to 5:20 p.m. To allow contributors an opportunity to see other posters, contributors of odd-numbered papers will be at their posters from 3:40 p.m. to 4:30 p.m. and contributors of even-numbered papers will be at their posters from 4:30 p.m. to 5:20 p.m.

Contributed Papers

4pPPc1. A computational model of binaural speech intelligibility level difference. Kalle J. Palomäki (Adaptive Informatics Research Centre, Helsinki University of Technology, P.O. Box 5400, 02015 Espoo, Finland, kalle.palomaki@tkk.fi), Guy J. Brown (University of Sheffield, Dept. of Computer Science, Regent Court, 211 Portobello Street, S1 4DP Sheffield, UK, g.brown@dcs.shef.ac.uk)

This study addresses two questions relating to the binaural intelligibility level difference (BILD). First, we ask whether the BILD is underlain by an equalization-cancellation (EC) mechanism, in which a disparity between the interaural time difference of the target and masker is exploited within each frequency channel, rather than across channels. Second, we consider the effects of three sources of internal noise on the EC mechanism: jitter in neural delays, noise in the equalization process and nonlinearities in the auditory pathway. These issues are investigated using a computational model consisting of peripheral auditory model, binaural processor, auditory scene processor and automatic speech recognition system. The binaural model is based on EC processing, with performance limited by internal noise. The auditory scene processor groups speech harmonics by common F0 and identifies 'glimpses' in which the signal-to-noise ratio is favorable for speech. The performance of human listeners and the computational model are compared on the same speech intelligibility test (Edmonds & Culling, 2005, JASA 117 (5), 3069-3078). The BILD of human listeners can be replicated by adjusting parameters that determine the internal noise in the EC model; however, the speech reception threshold of the model is lower than that of human listeners.

4pPPc2. Bernoulli coding on the auditory nerve and its implications for central auditory processing. Robert A. Houde (Center for Communications Research, 125 Tech Park Drive, Rochester, NY 14623, USA, rahoude@gmail.com), James M. Hillenbrand (Western Michigan University, Dept of Speech Path & Aud., 1903 W. Michigan Ave., Kalamazoo, MI 49008, USA, james.hillenbrand@wmich.edu)

The auditory periphery is well represented as a bank of band pass filter/inner hair cell (IHC) channels, with each IHC providing half wave rectification, amplitude compression, and conversion to firing probability on the auditory nerve (AN) fibers innervating that IHC. Frequency resolution varies dramatically with sound intensity, ranging from sharp tuning near threshold to very broad at high intensities. Cochlear filtering provides a satisfactory representation of broadband characteristics such as timbre but not the fine frequency resolution required for perceptual frequency discrimination. High resolution frequency analysis must, therefore, be provided by post-AN processes. We present a model of AN coding in which fine frequency analysis is carried out at central auditory stages. By this model the stochastic process on each AN fiber resulting from the IHC's firing probability is modeled by a Bernoulli process. As a result, the IHC output signal is transferred to the cochlear nucleus (CN) without further filtering, where it can be recovered by a simple summation over those AN fibers from the region of that IHC. We present a neurally plausible process for narrow band analysis at the CN using the regular pulses of chopper cells.

4pPPc3. The first effect of pitch shift as a function of component spacing. Adam Mielczarek (Acoustics Division, Wroclaw University of Technology, Wybrzeze Wyspianskiego 27A, 50-370 Wroclaw, Poland, adam.mielczarek@pwr.wroc.pl)

The paper presents the results of an experiment regarding the influence of component spacing on the first effect of pitch shift. During the adjustment procedure, the listeners matched the pitch of the three-component complex to the same sensation produced by pure tone. The stimuli were composed of the 3rd, 4th and 5th harmonics of 100, 200 or 400 Hz shifted up in the frequency domain by 30 Hz. The level of each component was 50 dB SPL. The subject was presented with a 5-s sample of the test complex, and after a 500 ms break he had to define the pitch of the three-component complex using the matching tone. The results of the experiment suggest that the pitch shift phenomenon is based on the relative frequency rather than on the absolute frequency or the dominant component number.

4pPPc4. Neuronal representation of pitch ambiguity. Mark Sayles (Centre for the Neural Basis of Hearing, The Physiological Laboratory, Downing Street, CB2 3EG Cambridge, UK, ms417@cam.ac.uk), Ian M. Winter (Centre for the Neural Basis of Hearing, The Physiological Laboratory, Downing Street, CB2 3EG Cambridge, UK, imw1001@cam.ac.uk)

Iterated rippled noise (IRN) is produced by delaying a broadband noise by time d, multiplying by gain g, adding the delayed noise to the original, and repeating this process for n iterations. When $g=+1$ IRN has a well-defined pitch at $1/d$ Hz. If $g=-1$ the pitch can be ambiguous. A gain of -1 is equivalent to applying a frequency-independent phase shift ϕ of π rads to the delayed noise ($g=+1 \equiv \phi=0$). We recorded spike-trains from single units in the ventral cochlear nucleus in response to IRN with varying ϕ. Units with high best frequencies represented waveform envelope modula-

tion (independent of ϕ), however, units in the phase-locking range of best frequencies represented stimulus fine structure (which varies with ϕ). Fine structure responders show a gradual transition from a well-defined peak in the interspike interval distribution at d when $\phi=0$ to two equal-amplitude peaks flanking d when $\phi=\pi$, and a gradual shift back to a well-defined peak at d as ϕ approaches 2π. Within the dominance region for pitch interspike interval distributions account for psychophysical pitch matches of $1.07/d$ and $0.94/d$ Hz for $\phi=\pi/2$ and $3/2\pi$ respectively, as well as the ambiguous pitches of $0.88/d$, $1.14/d$, and $1/2d$ Hz heard when $\phi=\pi$ rads.

4pPPc5. The effect of regional dialect on the psychometric reliability and validity of two sets of Mandarin speech audiometry materials. Shawn L. Nissen (Brigham Young University, 138 TLRB, 1190 North 900 East, Provo, UT 84602, USA, shawn_nissen@byu.edu), Richard W. Harris (Brigham Young University, 138 TLRB, 1190 North 900 East, Provo, UT 84602, USA, richard_harris@byu.edu), Jamie Garlick (Brigham Young University, 138 TLRB, 1190 North 900 East, Provo, UT 84602, USA, jamie.garlick@gmail.com), Nathan Richardson (Brigham Young University, 138 TLRB, 1190 North 900 East, Provo, UT 84602, USA, nathan000000@yahoo.com)

Previous research has shown conflicting evidence on the effect of testing an individual's hearing acuity with speech perception materials created in a mutually intelligible, yet non-regional dialect. Thus, the aim of this study is to examine the validity and reliability of using previously developed psychometrically equivalent speech audiometry materials in Mainland Mandarin and Taiwan Mandarin to evaluate the speech perception abilities (word recognition and speech reception threshold) of regional and non-regional listeners of the presented dialects. In addition, this study will investigate whether a native speaker of one Mandarin dialect is able to accurately administer and score the results from listeners of a different regional dialect. Some aspects of the listeners' performance on materials from a non-regional Mandarin dialect were found to be significantly different statistically. However, it is unclear if such differences are large enough to make a difference in the clinical testing of speech perception. In terms of scoring accuracy, a high percentage of agreement was found between the two interpreters from different dialectal backgrounds. [Work supported by research funding from Brigham Young University School of Education]

4pPPc6. Estimating the effective frequency of cochlear implant electrodes using contralateral residual acoustic hearing. Tim Green (UCL, Wolfson House, 4, Stephenson Way, NW1 2HE London, UK, tim.green@ucl.ac.uk), Andrew Faulkner (UCL, Wolfson House, 4, Stephenson Way, NW1 2HE London, UK, andyf@phon.ucl.ac.uk), Stuart Rosen (UCL, Wolfson House, 4, Stephenson Way, NW1 2HE London, UK, stuart@phon.ucl.ac.uk)

For some cochlear implant (CI) users a contralateral hearing aid provides significantly improved speech perception. Important factors in the bimodal transmission of speech spectral information are likely to include the extent to which the frequency selectivity of residual hearing allows additional place-coded channels, and mismatches between frequency-to-place maps across modalities. When acoustic place coding extends above around 500 Hz an overlap of frequency coverage between acoustic and electric hearing may result in interaural conflicts. However, addressing this issue requires accurate knowledge of CI frequency-to-place maps. Effective characteristic frequencies of CI electrodes have previously been estimated using comparisons of the pitch produced by electrical stimulation with that produced by contralateral acoustic sinusoids In the present work, the acoustic stimuli used for pitch comparisons are either sinusoids or 1/3 octave bands of noise. The latter minimize temporal pitch cues and may reduce differences in perceived quality between electrical and acoustical auditory sensations. Electrical stimuli are high-rate (900 pps or greater) single-electrode pulse trains. Comparisons are performed at different levels spaced over the dynamic range and both paired-comparison and adjustment tasks are used. Results will be discussed in relation to speech processing approaches for optimally combining an implant and contralateral hearing aid.

4pPPc7. Performance on auditory temporal-processing tasks for speech and non-speech stimuli by young and elderly listeners. Diane Kewley-Port (Indiana University, Speech and Hearing Sciences, 200 S. Jordan, Bloomington, IN 47405, USA, kewley@indiana.edu), Larry Humes (Indiana University, Speech and Hearing Sciences, 200 S. Jordan, Bloomington, IN 47405, USA, humes@indiana.edu), Daniel Fogerty (Indiana University, Speech and Hearing Sciences, 200 S. Jordan, Bloomington, IN 47405, USA, dfogerty@indiana.edu), Dana Kinney (Indiana University, Speech and Hearing Sciences, 200 S. Jordan, Bloomington, IN 47405, USA, danakin@indiana.edu)

Results from three auditory tasks are presented from a larger series of temporal-processing tasks completed in three sensory modalities by young and older adults. The first task measured temporal gap detection in noise bands. The second and third tasks used digitally processed vowels in four words (pit, pet, pot, put) as the stimuli. The second task required listeners to identify the order of either two- or four-vowel sequences presented monaurally or dichotically. The third task measured the identification of these four vowels when presented either before or after a noise or vowel-like masker (forward- or backward-masking tasks). Altogether, performance was obtained for 14 auditory temporal-processing measures. Young ($N=20$) and older ($N=50$) adults participated. Preliminary analyses (based on data from 50 of the 70 subjects) indicate that young listeners performed significantly better and with less variability than elderly listeners on all tasks. For most tasks, there was considerable overlap between the data from young and elderly listeners, indicating a modest negative impact of aging. At the individual level, correlational analyses among the older adults indicated that pure-tone thresholds were not predictive of temporal-processing performance and that performance on many of the temporal-processing tasks was moderately correlated. [Supported by NIA R01 AG022334.]

4pPPc8. MEG measures of the auditory steady-state response: Sinusoidal and non-sinusoidal stimuli. Garreth Prendergast (The University of York, Heslington, YO10 5DD York, UK, garreth.prendergast@ynic.york.ac.uk), Sam R. Johnson (The University of York, Heslington, YO10 5DD York, UK, sam@ynic.york.ac.uk), Gary G. Green (The University of York, Heslington, YO10 5DD York, UK, gary.green@ynic.york.ac.uk)

Human sensitivity to amplitude modulation has long been of interest to researchers, both in behavioural and neurological measures. Processing of amplitude modulation is implicated in the process of speech perception and sinusoidal amplitude modulation is used extensively to probe the mechanisms involved in encoding this information. The temporal envelope of speech is more accurately described as bursts of modulation rather than continuous modulation and the current work exposes participants to a continuum of modulation waveforms; from sinusoidal to pulsatile. Waveforms were amplitude modulated at 4 Hz and imposed upon a 500 Hz pure-tone carrier. The waveforms were generated using raised-cosine pulses with different half-durations. Half-durations of 8, 16, 24, 32, 64 and 125 ms were used (125 ms producing sinusoidal amplitude modulation at 4 Hz). Stimuli were 240 seconds in duration and responses were collected on a 248 channel whole-head MEG scanner. The frequency domain steady-state response was analysed from each condition in 14 participants, and results confirmed that the response to sinusoidal amplitude modulation was significantly lower than to modulations more representative of those found in speech signals. This suggests that non-sinusoidal stimuli may be more effective when investigating these auditory mechanisms.

4pPPc9. Laboratory synthesis of industrial noise environments with predetermined statistical properties. Wei Qiu (State University of New York, 101 Broad Street, Plattsburgh, NY 12901, USA, wei.qiu@plattsburgh.edu), Bob Davis (State University of New York, 101 Broad Street, Plattsburgh, NY 12901, USA, davisri@plattsburgh.edu), Roger P. Hamernik (State University of New York, 101 Broad Street, Plattsburgh, NY 12901, USA, roger.hamernik@plattsburgh.edu)

High-level nonGaussion noise is commonly found in a variety of industrial environments. Recent experiments have shown that for a given energy level, the statistical properties of a noise can have a strong effect on the extent of hearing loss produced in exposed individuals. In order to study, in an

animal model, the effects on hearing of such noise environments, the statistical properties of the noise as embodied in the kurtosis metric must be under experimental control. For a fixed value of kurtosis and energy level the following four variables will have a strong effect on hearing loss: (1) peak histogram; (2) interval histogram; (3) duration of noise transients; and (4) level of any background Gaussian noise. Simulations have shown that the relations among kurtosis and these variables are nonlinear. However, under certain restricted conditions, these relations may be linear. Accordingly, two strategies for designing controlled industrial noise exposures are presented: (1) the interval-priority model and (2) the duration-priority model. Computer simulations and measurements of actual acoustic environments showed that these two models could be effectively used to simulate a wide variety of realistic industrial noises.

4pPPc10. Intervention for restricted dynamic range and reduced sound tolerance. Charles Formby (University of Alabama, 700 University Boulevard East Suite 315, Tuscaloosa, AL 35487, USA, cformby@as.ua.edu), Monica Hawley (University of Maryland, 16 S. Eutaw St, Suite 500, Baltimore, MD 21201, USA, moncia@hawleyonline.net), Laguinn Sherlock (University of Maryland, 16 S. Eutaw St, Suite 500, Baltimore, MD 21201, USA, gsherlock@smail.umaryland.edu), Susan Gold (University of Maryland, 16 S. Eutaw St, Suite 500, Baltimore, MD 21201, USA, sgold@smail.umaryland.edu), Allyson Segar (University of Maryland, 0100 Lefrak Hall, College Park, MD 20742, USA, asegar@hesp.umd.edu), Christine Gmitter (University of Maryland, 0100 Lefrak Hall, College Park, MD 20742, USA, cgmitter@hesp.umd.edu), Justine Cannavo (University of Maryland, 0100 Lefrak Hall, College Park, MD 20742, USA, jcannavo@hesp.umd.edu)

Hyperacusis is an abnormal condition of sound intolerance that may cause some persons to reject amplified sound from their hearing aids. A significant secondary benefit reported for many patients receiving Tinnitus Retraining Therapy (TRT) is increased Loudness Discomfort Levels (LDLs). TRT involves both counseling and sound therapy (i.e., daily exposure to soft sound from bilateral noise generators (NGs)). We implemented a randomized, double-blind, placebo-controlled clinical trial to assess the efficacy of TRT as an intervention to improve sound tolerance in hearing-aid eligible persons with hyperacusis and/or restricted dynamic ranges. Subjects were assigned to one of four treatment groups: 1) full treatment, both counseling and NGs, 2) counseling and placebo NGs, 3) NGs without counseling, and 4) placebo NGs without counseling. They were evaluated at least monthly, typically for five months or more, on a variety of audiometric tests, including LDLs, the Contour Test for Loudness, and word recognition measured at comfortable and loud levels. Over 80% of the subjects assigned to full treatment achieved significant benefit (defined as shifts of greater than 10 dB in LDLs or the Contour Test uncomfortable level); whereas, most subjects assigned to a partial treatment group did not benefit from their treatment. [Supported by NIH].

4pPPc11. Relationship between a visual stimulus with a feeling of depth and its equivalent sound pressure level (ESPL). Hiroshi Hasegawa (Utsunomiya Univ., 7-1-2 Yoto, Tochigi-ken, 321-8585 Utsunomiya-shi, Japan, hasegawa@is.utsunomiya-u.ac.jp), Hirotaka Ono (Utsunomiya Univ., 7-1-2 Yoto, Tochigi-ken, 321-8585 Utsunomiya-shi, Japan, hasegawa@is.utsunomiya-u.ac.jp), Takumi Ito (Utsunomiya Univ., 7-1-2 Yoto, Tochigi-ken, 321-8585 Utsunomiya-shi, Japan, hasegawa@is.utsunomiya-u.ac.jp), Ichiro Yuyama (Utsunomiya Univ., 7-1-2 Yoto, Tochigi-ken, 321-8585 Utsunomiya-shi, Japan, yuyama@is.utsunomiya-u.ac.jp), Masao Kasuga (Utsunomiya Univ., 7-1-2 Yoto, Tochigi-ken, 321-8585 Utsunomiya-shi, Japan, kasuga@is.utsunomiya-u.ac.jp), Miyoshi Ayama (Utsunomiya Univ., 7-1-2 Yoto, Tochigi-ken, 321-8585 Utsunomiya-shi, Japan, nakatsue@is.utsunomiya-u.ac.jp)

This study investigated the equivalent perception between a visual stimulus and its associated sound. Experiments of an auditory-visual stimulus presentation using an audio-video clip of a man beating a drum on a road were performed. The visual stimulus had a feeling of depth with a perspective view of the road. The visual stimulus was projected onto a screen that had the viewing angles of 43.8 deg.(W) * 25.4 deg.(H). Four kinds of distance between the subject and the visual stimulus from 5 to 40 m, seven kinds of the delay time between auditory and visual stimulus from -8 F to 8 F (1 F = 1/30 s), where "+" indicates that the visual event preceded the sound, and nine levels of the sound stimulus from -12 dB to 12 dB of the standard sound pressure level (SPL) were combined and presented. We evaluated the sound pressure level matching with each presentation pattern (equivalent sound pressure level; ESPL). As a result, we obtained that the ESPL tended to decrease when the delay time increased (the sound was delayed). This result shows a possibility that the visual stimulus was a little shifted to the direction of the sound.

4pPPc12. Temporal dynamics of stimulus specific processing in the human auditory cortex as revealed by electroencephalography. Paul M. Briley (MRC Institute of Hearing Research, University Park, NG7 2RD Nottingham, UK, paul@ihr.mrc.ac.uk), Katrin Krumbholz (MRC Institute of Hearing Research, University Park, NG7 2RD Nottingham, UK, katrin@ihr.mrc.ac.uk)

When the same sound is presented repeatedly, the electrical brain response recorded over the scalp decreases in amplitude, an effect known as adaptation. Adaptation is dependent on both the similarity of the sounds and the time between them. It has been particularly well studied for a deflection of the electrical response known as the N100, which peaks about 100 ms after sound onset and receives major contributions from auditory cortical sources. Adaptation may reflect decreased sensitivity to repetitive stimuli, but could also indicate more efficient processing of familiar events. Research on adaptation has often employed an alternating tone paradigm (A-B-A-B), examining the effects of changing inter-stimulus interval (ISI) or the frequency separation between A and B tones. Decreasing the frequency separation leads to an increase in N100 adaptation, and it has been suggested that the frequency specificity of this adaptation sharpens with decreasing ISI. In contrast, some studies have used A-B pairs with long inter-pair gaps and have found an enhancement of the N100 response to the B tone at short ISIs. In order to gain a better understanding of the processes contributing to adaptation and enhancement, this study investigates the temporal dynamics and the frequency selectivity of these effects.

4pPPc13. An Investigation of Width and Depth Perception toward a Sound Image Constructed of Multiple Variant Sound Waves Emitted from a Loudspeaker Array. Yoko Yamakata (National Institute of Information and Communications Technology, 4-2-1, Nukui-Kitamachi, Koganei, 184-8795 Tokyo, Japan, yamakata@nict.go.jp), Toshiyuki Kimura (National Institute of Information and Communications Technology, 4-2-1, Nukui-Kitamachi, Koganei, 184-8795 Tokyo, Japan, t-kimura@nict.go.jp), Munenori Naoe (National Institute of Information and Communications Technology, 4-2-1, Nukui-Kitamachi, Koganei, 184-8795 Tokyo, Japan, nm.s512.ex@nict.go.jp), Michiaki Katsumoto (National Institute of Information and Communications Technology, 4-2-1, Nukui-Kitamachi, Koganei, 184-8795 Tokyo, Japan, katumoto@nict.go.jp)

Many musical instruments, including violins and guitars, vibrate their resonant bodies differently over their surface when they make a sound. This paper aims to reveal the influences of such vibration variation of a soundboard surface on the width and depth perception of the sound image when listeners were in a near-field 50 cm or 1 m away from the soundboard. In this paper, a loudspeaker array mimicked the surface vibration as each loudspeaker makes a corresponding sound independently and cooperatively. Three types of sounds, synthesized single-tone, multi-tone, and instrumental, were used as sources. To know what factors affect the perception of the sound image, various test sound sets were prepared by varying an original sound set in amplitude or delay for each frequency for each loudspeaker. Eight subjects were asked to identify which sound image in a pair of test sounds was wider or farther than the other according to Scheffe's pair comparison method. The results shows that a test sound set with a delay varia-

tion, which mimics sounds emitted by bending vibrations propagating on a soundboard, obviously influences the perception of sound image width and that the amplitude variation does not have much influence.

4pPPc14. MEG Recordings of Amplitude-modulated Noise and Tonal Stimuli in Healthy Adult Listeners. Yang Zhang (University of Minnesota, Dept. of Speech-Language-Hearing Sci. & Center for Neurobehavioral Development, Minneapolis, MN 55455, USA, zhang470@umn.edu), Yingjiu Nie (University of Minnesota, Dept. of Speech-Language-Hearing Sci. & Center for Neurobehavioral Development, Minneapolis, MN 55455, USA, niex0008@umn.edu), Toshiaki Imada (University of Washington, Dept. of Speech & Hearing Sciences, and Institute for Learning & Brain Sciences, Box 357988, Seattle, WA 98195, USA, imada@u.washington.edu), Keita Tanaka (Tokyo Denki University, Research Center for Advanced Technologies, 270-1382 Inzai, Japan, ktanaka@rcat.dendai.ac.jp), Masaki Kawakatsu (Tokyo Denki University, School of Information Environment, 270-1382 Inzai, Japan, kawakatu@asrl.dendai.ac.jp)

Amplitude modulation (AM) provides very important auditory information for the perception of complex sounds by normal listeners as well as cochlear implant users. The present study used a 122-channel whole-head magnetoencephalography (MEG) system to record auditory responses to amplitude-modulated pure tones and broadband noises in six healthy male adult subjects. The stimuli were presented in blocks of twenty with a brief silence in between, and the AM rates for both types of stimuli were at 20, 40, and 80 Hz. At least 80 artifact-free trials were collected for each stimulus. As expected, the MEG data showed a significant bilateral effect of AM rate in the N1m component. There was also strong evidence that the neural representations of both the unmodulated pure tone and noise stimuli in the auditory regions of both hemispheres could be significantly affected by the global context of block design stimulus presentation.

4pPPc15. Critical-band compression method of speech enhancement for elderly people: Investigation of syllable and word intelligibility. Keiichi Yasu (Dept. of Electrical and Electronics Engineering, Sophia University, 7-1 Kiyoi-cho, Chiyoda-ku, 102-8554 Tokyo, Japan, k-yasu@sophia.ac.jp), Hideki Ishida (Dept. of Electrical and Electronics Engineering, Sophia University, 7-1 Kiyoi-cho, Chiyoda-ku, 102-8554 Tokyo, Japan, ishida-h@sophia.ac.jp), Ryosuke Takahashi (Dept. of Electrical and Electronics Engineering, Sophia University, 7-1 Kiyoi-cho, Chiyoda-ku, 102-8554 Tokyo, Japan, ryo.t.sust@gmail.com), Takayuki Arai (Dept. of Electrical and Electronics Engineering, Sophia University, 7-1 Kiyoi-cho, Chiyoda-ku, 102-8554 Tokyo, Japan, arai@sophia.ac.jp), Kei Kobayashi (Dept. of Electrical and Electronics Engineering, Sophia University, 7-1 Kiyoi-cho, Chiyoda-ku, 102-8554 Tokyo, Japan, kei-koba@ba2.so-net.ne.jp), Mitsuko Shindo (Sophia Univ. Research Center for Communication Disorders, 7-1 Kiyoi-cho, Chiyoda-ku, 102-8554 Tokyo, Japan, shindo-m@sophia.ac.jp)

Auditory filters for the hearing impaired tend to be wider than those of normal hearing people. Thus, the frequency selectivity decreases because of increased masking effects [Glasberg and Moore, J. Acoust. Soc. Am., 79(4), 1020-1033, 1986]. We have developed a method, called ″critical-band compression,″ in which the critical band is compressed along the frequency axis [Yasu et al., Handbook of the International Hearing Aid Research Conference (IHCON), 55, Lake Tahoe, 2004]. We investigated whether our method improves syllable and word intelligibility. Thirty one elderly people participated in experiments. First, we measured the auditory filter bandwidth using a notched noise method [Patterson, J. Acoust. Soc. Am., 59(3), 640-654, 1976]. Second, we conducted syllable and word intelligibility tests. The compression rates of critical-band compression were set to 0% for the original, and 25%, 50%, and 75%. The results were that the percentages of correct responses were almost the same at 0%, 25% and 50% compression rates for syllable and word intelligibility. A significant correlation was not obtained between the compression rate of processing and the auditory filter bandwidth. [Work supported by JSPS.KAKENHI (16203041) and Sophia University Open Research Center from MEXT.]

4pPPc16. Speaker size discrimination for acoustically scaled versions of whispered words. Yoshie Aoki (Faculty of Systems Engineering, Wakayama University, 930 Sakaedani, 640-8510 Wakayama, Japan, s085065@sys.wakayama-u.ac.jp), Toshio Irino (Faculty of Systems Engineering, Wakayama University, 930 Sakaedani, 640-8510 Wakayama, Japan, irino@sys.wakayama-u.ac.jp), Hideki Kawahara (Faculty of Systems Engineering, Wakayama University, 930 Sakaedani, 640-8510 Wakayama, Japan, kawahara@sys.wakayama-u.ac.jp), Roy D. Patterson (Centre for the Neural Basis of Hearing, Department of Physiology, Development and Neuroscience, University of Cambridge, Downing Site, CB23EG Cambridge, UK, rdp1@cam.ac.uk)

Humans can extract the message from the voices of men, women, and children without being confused by the size information, and they can extract the size information without being confused by the message. This suggests that the auditory system can extract and separate information about vocal tract shape from information about vocal tract length. Smith et al. [J. Acoust. Soc. Am. 117(1), 305-318 (2005)], Ives et al. [J. Acoust. Soc. Am. 118(6), 3816-3822 (2005)], and Aoki et al. [ARO, 31st Midwinter meeting (2008)] performed discrimination experiments with acoustically scaled vowels, syllables, and naturally spoken words, respectively, and demonstrated that the ability to discriminate speaker size extends beyond the normal range of speaker sizes. Smith and Patterson [BSA Cardiff (2005)] demonstrated that performance on the size-discrimination task is only marginally reduced when the vowels are unvoiced. We extended these size-discrimination experiments to whispered versions of naturally spoken, four-mora Japanese words. The just-noticeable-difference for the whispered words was about 6 %, which is roughly the same as that for voiced words. The results show that voicing is not required for effective extraction of the size information. Research supported by JSPS Grant-in-Aid [B18300060] and the UK-MRC [G0500221].

4pPPc17. Effects of modality-dependent cuing and eye movements on sound localization. Beáta Tomoriová (Laboratory of Perception and Cognition, Technical University of Košice, Letná 9, 042 00 Košice, Slovakia, beata.tomoriova@gmail.com), Rudolf Andoga (Laboratory of Perception and Cognition, Technical University of Košice, Letná 9, 042 00 Košice, Slovakia, rudolf.andoga@tuke.sk), Norbert Kopčo (Laboratory of Perception and Cognition, Technical University of Košice, Letná 9, 042 00 Košice, Slovakia, kopco@tuke.sk)

A previous study of visual and auditory hemispheric cuing in horizontal sound localization found modality-dependent effects of cuing resulting in biases in responses [Kopco, Tomoriova, Andoga, J. Acoust. Soc. Am. 121, 3094, 2007]. The previous study also suggested that some of the effects might be due to eye movements as eye fixation was not controlled. The goal of the current study was to isolate the attentional effects from the eye movement effects. An experiment identical to the previous one was performed, with the exception that the subjects were fixating the center of the audiovisual display. Localization performance was measured for transient auditory stimuli originating in the frontal horizontal plane. In most runs, a cue preceded the stimulus and indicated (correctly or incorrectly) the hemisphere (left vs. right) from which the subsequent target arrived. The cues differed by modality and the cue-to-target onset asynchrony. The listeners were instructed to focus their attention to the cued side. Compared to the previous study, a reduction in some effects was observed. However, modality-dependent biases in performance persisted, confirming that auditory spatial attentional control is modality dependent and operating on time scale of seconds. [Supported by the Slovak Science Grant Agency.]

4pPPc18. Synchrony-asynchrony discrimination of audio-visual signals in auditory streaming. Maori Kobayashi (R.I.E.C., Tohoku University, 2-1, Katahira, Aoba-ku, 980-8577 Sendai, Japan, maori@ais.riec.tohoku.ac.jp), Shuichi Sakamoto (R.I.E.C., Tohoku University, 2-1, Katahira, Aoba-ku, 980-8577 Sendai, Japan, saka@ais.riec.tohoku.ac.jp), Yôiti Suzuki (R.I.E.C., Tohoku University, 2-1, Katahira, Aoba-ku, 980-8577 Sendai, Japan, yoh@ais.riec.tohoku.ac.jp)

Temporal synchrony is a critical condition for integrating information presented in different sensory modalities. In this study, the effect of tonal organization on synchrony-asynchrony discrimination was examined. The auditory sequences were four repetitions of a triplet pattern comprising a low-frequency tone (L) and a high-frequency tone (H). The frequency difference (ΔF) between L and H was either approximately 1/12, 1/6, 1/3, 1/2, or 1 octave, centered at 1 kHz. Each tone was of 33.2 ms duration including rising and falling raised-cosine ramps of 5 ms. The stimulus onset asynchrony (SOA) of adjacent tones was randomized between 33.2 and 332 ms. The tone sequences were presented diotically via headphones at 65 dB SPL. The visual stimulus was a luminance-modulated Gaussian blob presented on a CRT monitor. The visual stimulus duration was 8.3 ms. Synchrony-asynchrony discrimination thresholds of visual-auditory stimulus onsets were measured using the 2IFC paradigm with a 2-up 1-down method under six ΔF conditions. The results demonstrated that synchrony-asynchrony discrimination improved for audio-visual pulse trains at ΔF between L and H greater than 1/3 octave, suggesting that audio-visual synchrony perception is influenced by the build-up of auditory streaming.

4pPPc19. Voice quality of emphatics in comparison with non-emphatics in Morrocan Arabic. Karim Shoul (Lab. LPP UMR 7018 CNRS, 19, rue des bernardins, 75005 Paris, France, shoulkarim@hotmail .com)

Based on acoustic and physiological data, this study examines the voice quality of emphacized (also called pharyngealized) vowels in Moroccan Arabic. The aim is to determine whether, as argued by some authors (Heath 1987, Fre woldu 1986), these vowels are creaky or glottalized. For this purpose, the /a/ vowel is considred in syllables after initial and intervocalic /t, d, s/ and their emphatic counterparts for an acoustic study as well as a physiological one (Fourcin's EGG 1974). The cues axamined inculde F0 values, duration and amplitude of the acoustic and glottalic signals, as well as the open quotien (0q) (as seen by Henrich 2001). Results of the acoustic analysis show no significant differences between emphacized and non-emphacized vowels as far as F0 values, duration and amplitude of the acoustic signal are concerned. The same absence of difference is observed from the EGG experiment, which indicate that 0q represents half of the whole glottal phase. These findings sugget that emphacized vowels, just like the corresponding non-emphacized counterparts, are characterized by a modal voice quality. They imply that 'secondary' pharyngealization does not require a narrowing of the supra-glottic cavity which would affect the mode of vocal-fold vibrations.

4pPPc20. Influence of multi-channel dynamic range compression on intelligibility: effect of envelope modulation bandwidth. Michael A. Stone (University of Cambridge, Department of Experimental Psychology, Downing Street, CB2 3EB Cambridge, UK, mas19@cam.ac.uk), Christian Füllgrabe (University of Cambridge, Department of Experimental Psychology, Downing Street, CB2 3EB Cambridge, UK, cf277@cam.ac.uk), Brian Moore (University of Cambridge, Department of Experimental Psychology, Downing Street, CB2 3EB Cambridge, UK, bcjm@cam.ac.uk)

Stone and Moore [J. Acoust. Soc. Am. (in press)] showed that, as the speed and number of channels in a multi-channel compressor increased, intelligibility of noise-vocoded signals in a competing speech task decreased. The noise vocoder is often used to simulate the information conveyed by cochlear implants. However, the vocoder of Stone and Moore preserved only low-rate ($<$45 Hz) envelope modulations whereas some implantees show sensitivity to envelope modulation rates up to about 300 Hz. Furthermore, intrinsic fluctuations in the noise carriers affect the reception of low-rate modulations of the signal (Whitmal et al. [J. Acoust. Soc. Am. 122: 2376-2388, (2007)]). Here, a tone vocoder with N=8 or N=16 channels was used. Vocoding was preceded by N/8, N/4, or N/2 channels of compression, each using one of three speeds, affecting modulation rates up to about 2, 6, or 18 Hz, respectively. The lowpass filters extracting the channel envelopes had corner frequencies of 45 or 180 Hz. Intelligibility was measured using IEEE sentences with a competing speaker. The deleterious effect of compression with increasing channel number and speed was greater for the lower corner frequency. Compression of rates below 6 Hz affected intelligibility, independent of the presence of higher modulation rates.

4pPPc21. Characterizing lexical interferences in informational masking during speech-in-speech comprehension. Michel Hoen (Laboratoire d'Etude des Mécanismes Cognitifs (EMC). EA 3082 CNRS, Université Lumière Lyon 2, 5, Avenue Pierre Mendès-France, 69676 Bron Cedex, France, Michel.Hoen@univ-lyon2.fr), Claire Grataloup (Laboratoire Dynamique du Langage (DDL), UMR 5596 CNRS, Université de Lyon et Lyon 2, Institut des Sciences de l'Homme - 14 avenue Berthelot, 69363 Lyon Cedex 07, France, Claire.Grataloup@pse.unige.ch), François Pellegrino (Laboratoire Dynamique du Langage (DDL), UMR 5596 CNRS, Université de Lyon et Lyon 2, Institut des Sciences de l'Homme - 14 avenue Berthelot, 69363 Lyon Cedex 07, France, Francois.Pellegrino@univ-lyon2.fr), Lionel Collet (Univ. Lyon 1 - Lab. Neurosciences, Service Pr Collet, Pavillon U, Hôpital Edouard Herriot, F-69003 Lyon, France, iakhoun@olfac.univ-lyon1.fr), Fanny Meunier (Laboratoire Dynamique du Langage (DDL), UMR 5596 CNRS, Université de Lyon et Lyon 2, Institut des Sciences de l'Homme - 14 avenue Berthelot, 69363 Lyon Cedex 07, France, fanny.meunier@univ-lyon2.fr)

Results from our former research on the characterization of informational masking effects occurring during speech-in-speech comprehension showed that phonological and lexical information create specific informational masking effects, depending on the number of speakers involved (Hoen et al., 2007). The goal of the present study was to better characterize purely lexical factors potentially participating into informational masking phenomena. We evaluated speech-in-speech comprehension performances of 40 normal hearing participants listening to isolated lexical items presented together with different speech babble sounds. Lexicality of target items was controlled by using words of variable lexical frequency, high- vs. low-frequency items, as well as pseudowords. The interaction between lexicality of target items and lexicality of words in background noise was controlled by creating babble sounds made of high- or low-frequency words. Results show that, as in silence, lexicality of target items plays a determinant role, high-frequency words being always more intelligible (70%) than low-frequency words (50%), or pseudowords (37%). Conversely, the frequency of lexical items present in the babble had an effect only on the comprehension of pseudowords, the latter being more intelligible in a background of low-frequency items. Together, these results give new precisions on the detailed informational masking effects occurring during speech-in-speech comprehension.

4pPPc22. Perceived plausibility of a multi-modal musical performance with introduced auditory-visual spatial and temporal mismatch. Daniel Valente (Rensselaer Polytechnic Institute, Greene Bldg., 110 8th St., Troy, NY 12180, USA, danvprod@gmail.com), Jonas Braasch (Rensselaer Polytechnic Institute, Greene Bldg., 110 8th St., Troy, NY 12180, USA, braasj @rpi.edu)

One of the biggest problems for multi-modal virtual musical performance is that of auditory-visual mismatch. Often such performances place musicians in a dry, studio-like environment and rely on acoustic room modeling techniques to place the musician's sound in an environment more conducive to musical performance. The problem, for example occurs when the musician sounds as if he/she is in a large performance space but from a visual standpoint appears to be located in a very small studio environment. This experiment aimed to reveal the impact of such mismatches on the perceived plausibility of a multi-modal musical performance. Listeners were confronted with three contrasting musical excerpts presented in a virtual environment with varying degrees of auditory visual mismatch. In the first phase, listeners were able to adjust the acoustic modeling algorithm using the salient parameters of direct to reverberant ratio and reverberation time. As the visual space volume that the performance was presented in increased, the listeners repeatedly increased reverberation time and decreased direct to reverberant ratio. During the second phase, where varying levels of spatial

and temporal mismatch were purposefully introduced, the level of repeatability and accuracy of the listening group decreased despite subjective responses indicating accurate perceived performance realism.

4pPPc23. Haircell non-functionality and dead regions in the cochlea: an exploring study. Bastiaan Warnaar (AMC - Dept. of Clinical and Experimental Audiology, Meibergdreef 9, 1105AZ Amsterdam, Netherlands, b.warnaar@amc.nl), Wouter A. Dreschler (AMC, Clinical and Experimental Audiology, 1105 Amsterdam, Netherlands, w.a.dreschler@amc.uva.nl)

Dead regions (DRs) refer originally to regions in the cochlea without evoked electrical potentials due to non-functional inner hair cells and/or fibers of the auditory nerve. The focus of this study is to characterize hair cell non-functionality in the cochlea by means of psychophysical tests. A battery of tests was administered to a group of 13 subjects with a steep sloping tone threshold (>50 dB/octave) between 1 and 2 kHz and severe loss (>60 dB HL) at high frequencies. Psychophysical Tuning Curves (PTC) and Threshold Equalizing Noise (TEN) are the classical tests to diagnose dead regions. Both use as criteria the phenomenon of off-frequency listening. Based on the results of complementary tests like Notched Noise measurements (NN) and Otoacoustic Emissions (OAE), it is argued that off-frequency listening is not necessarily connected to loss of inner hair cells and/or nerve fibers. Furthermore, combination tones produced by well functioning outer hair cells at places of severe hearing loss (>60 dB HL) are found. This may be explained by the presence of a dead region, which is verified with PTC and/or TEN measurements in 3 out of 4 of the cases.

4pPPc24. Audio-visual quality model for internet protocol television services. Marieneige Garcia (Deutsche Telekom Laboratories, Berlin Institute of Technology, Ernst-Reuter-Platz 7, 10587 Berlin, Germany, marie-neige.garcia@telekom.de), Alexander Raake (Deutsche Telekom Laboratories, Berlin Institute of Technology, Ernst-Reuter-Platz 7, 10587 Berlin, Germany, alexander.raake@telekom.de)

This paper presents a model for predicting the perceived audio-visual quality of IPTV services. Our model follows a modular approach and audio-visual quality is deduced from the perceived audio quality, the perceived video quality, the interaction between the audio quality and the video quality and the quality of the interaction between audio and video (lip-synchronization). In its current form, the model covers H.264 video codec, Standard Definition and High Definition video resolutions, MP2 audio codec and wav audio format. Addressed degradations, which generate different visual and auditory perceptual dimensions, are compression artifacts, packet losses, reduced bandwidth and delay between audio and video. Results demonstrate a mutual influence of the perceived audio and video qualities and the predominance of the video quality on the overall audio-visual quality. We analyze the interaction between visual perceptual dimensions, like blockiness, blurriness, slicing and freezing, and auditory perceptual dimensions, like frequency content (brightness), interruptedness, and freezing. We also study the influence of the type of the degradation on the interaction between perceived audio and video qualities. At last, we examine the influence of the audio-visual content (music video, news, etc.) on the perceived audio-visual quality. An outlook highlights future model extensions.

4pPPc25. Neural coding of envelope and fine structure in noise degraded speech. Jayaganesh Swaminathan (Purdue University, 500 Oval Drive, West Lafayette, IN 47907, USA, jswamy@purdue.edu), Michael Heinz (Purdue University, 500 Oval Drive, West Lafayette, IN 47907, USA, mheinz@purdue.edu)

Numerous perceptual studies have revealed that envelope is sufficient for speech perception in quiet, but that temporal fine structure (TFS) is required for speech perception in noise. However, the neural correlates of these perceptual observations remain unknown. The primary focus of the present work was to develop and evaluate neural cross correlation coefficient (CCC) metrics to quantify envelope and TFS coding in auditory-nerve responses to noise degraded speech. Shuffled auto- and cross-correlogram analyses were used to compute separate CCCs to quantify stimulus-related envelope and fine structure based on neural spike train data from a computational auditory-nerve model. The neural CCCs have a wide dynamic range as revealed by near-zero values for uncorrelated conditions and near-one values for correlated conditions based on broadband noise responses. Spectrally matched noise was systematically added to a speech sentence at different signal-to-noise ratios (SNRs). Initial analyses reveal that CCC_ENV > CCC_TFS for positive SNRs, whereas CCC_TFS > CCC_ENV for negative SNRs. Predicted effects of hearing loss on envelope and TFS coding will also be discussed. These neural metrics can be used to evaluate temporal coding of speech with implications for cochlear-implant and hearing-aid strategies. Supported by NIH-NIDCD.

4pPPc26. The effect of masker type and word-position on word recall and sentence understanding. Payam Ezzatian (University of Toronto Mississauga, 3359 Mississauga rd N., Mississauga, ON L5L 1C6, Canada, payam.ezzatian@utoronto.ca), Liang Li (University of Toronto Mississauga, 3359 Mississauga rd N., Mississauga, ON L5L 1C6, Canada, liang.li@utoronto.ca), Kathy Pichora-Fuller (University of Toronto Mississauga, 3359 Mississauga rd N., Mississauga, ON L5L 1C6, Canada, k.pichora.fuller@utoronto.ca), Bruce Schneider (University of Toronto Mississauga, 3359 Mississauga rd N., Mississauga, ON L5L 1C6, Canada, bruce.schneider@utoronto.ca)

Speech understanding is influenced by not only the presence, but also the specific nature of maskers. Noise maskers primarily result in energetic masking, whereas speech maskers create additional interference due to linguistic and acoustic similarities to the target. The present study examined the influence of different types of maskers and target word position on the immediate recall of words in sentences by normal-hearing younger adults. In Experiment 1, nonsense sentences with 3 keywords (e.g., A ″house″ should ″dash″ to the ″bowl″.) were presented against a background of speech-spectrum noise or two-talker nonsense speech. With the speech masker, accuracy increased with word position. With the speech-spectrum noise masker, performance was highest for the first word and did not vary linearly with word position. In Experiment 2, when the speech-masker was noise-vocoded to preserve envelope information while disrupting fine structure cues and minimizing semantic content, performance was similar to that found with the speech-spectrum masker. The results suggest that the ability to track a target sentence in conditions of informational masking improves as the target utterance unfolds over time.

4pPPc27. Training-induced auditory plasticity measured using auditory steady-state responses. Karolina Kluk (The University of Manchester, Human Communication and Deafness Research Group, Ellen Wilkinson Building, Oxford Road, M13 9PL Manchester, UK, karolina.kluk@manchester.ac.uk), Christine M. Tan (University of Essex, Department of Psychology, Wivenhoe Park, CO4 3SQ Colchester, UK, ctan@essex.ac.uk), Michael S. John (Rotman Research Institute, Baycrest Centre for Geriatric Care, 3560 Bathurst Street, Toronto, AB M6A 2E1, Canada, sjohn@rotman-baycrest.on.ca), Terence W. Picton (Rotman Research Institute, Baycrest Centre for Geriatric Care, 3560 Bathurst Street, Toronto, AB M6A 2E1, Canada, tpicton@rotman-baycrest.on.ca)

Re-mapping of the primary auditory cortex may be induced by extensive training. For example, training of monkeys to perform frequency discrimination (FD) at one carrier frequency expands the representation of that frequency region in the auditory cortex. This study was intended to demonstrate training-induced auditory plasticity using auditory steady-state responses (ASSRs) in humans. Right-handed, non-musicians underwent FD training in their left ear only at 1 kHz. ASSRs were recorded to 1- and 2-kHz amplitude modulated tones (100 % AM depth at rates of 41, 83 and 45, 87 Hz, across two conditions). ASSRs recorded at the start of the experiment were compared with the ASSRs recorded after three two-hour sessions of FD training scheduled 24 hours apart. The results revealed significant increase in the amplitude of ASSRs recorded to 41- and 45-Hz AM tones (at 1 kHz only) presented to the trained left ear. There was no significant change in the amplitude of ASSRs recorded to the 2-kHz tones or to any stimuli presented to the un-trained right ear. As expected FD training

had no effect on 83- and 87-Hz ASSRs (which are generated mainly in the brainstem). These results support the idea of training-induced reorganization of the auditory cortex.

4pPPc28. Hearing-screening tests based on filtered sounds and on speech-in-noise intelligibility tests. Bozena Kostek (Gdansk University of Technology, Multimedia Systems Department, 11/12 Gabriela Narutowicza Street, 80-952 Gdansk, Poland, bozenka@sound.eti.pg.gda.pl), Andrzej Czyzewski (Gdansk University of Technology, Multimedia Systems Department, 11/12 Gabriela Narutowicza Street, 80-952 Gdansk, Poland, andcz@sound.eti.pg.gda.pl), Lukasz Kosikowski (Gdansk University of Technology, Multimedia Systems Department, 11/12 Gabriela Narutowicza Street, 80-952 Gdansk, Poland, kosiq@sound.eti.pg.gda.pl), Krzysztof Kochanek (The Institute of Physiology and Pathology of Hearing, Pstrowskiego 1, 01-943 Warsaw, Poland, k.kochanek@ifps.org.pl), Henryk Skarzynski (The Institute of Physiology and Pathology of Hearing, Pstrowskiego 1, 01-943 Warsaw, Poland, h.skarzynski@ifps.org.pl)

A hearing-screening system dedicated to small-children in pre-schools and primary schools is described in the paper. It uses as a hardware a palmtop computer supplemented with a small sound calibrating device. The described application provides tests that employ automatic questionnaire analysis, audiometric test procedures, and assessment of speech intelligibility in noise. In the speech-in-noise intelligibility tests, pictures are used for young children, and the screening tests are supervised by adults. Apart from the standardized audiometric tests, the screening tests employ environmental sounds filtered in audiometric frequency bands and calibrated as to their levels. When all the testing is completed, the system automatically analyzes the results for each child examined. The decision is made automatically by the expert system taking into account the number of incorrect answers. Children whose hearing impairment is confirmed are referred to treatment in rehabilitation centers. The project presented is a part of the large-scale ″I can hear...″ screening tests program carried out in Poland for the last few years. This may help to increase awareness and inspire action against noise at a very early age. The methods employed for filtering and calibration environmental sounds and results achieved are presented in the paper.

4pPPc29. The effect of masker type and word-position on word recall and sentence understanding. Payam Ezzatian (University of Toronto Mississauga, 3359 Mississauga rd N., Mississauga, ON L5L 1C6, Canada, payam.ezzatian@utoronto.ca), Liang Li (University of Toronto Mississauga, 3359 Mississauga rd N., Mississauga, ON L5L 1C6, Canada, liang.li@utoronto.ca), Kathy Pichora-Fuller (University of Toronto Mississauga, 3359 Mississauga rd N., Mississauga, ON L5L 1C6, Canada, k.pichora.fuller@utoronto.ca), Bruce Schneider (University of Toronto Mississauga, 3359 Mississauga rd N., Mississauga, ON L5L 1C6, Canada, bruce.schneider@utoronto.ca)

Speech understanding is influenced by not only the presence, but also the specific nature of maskers. Noise maskers primarily result in energetic masking, whereas speech maskers create additional interference due to linguistic and acoustic similarities to target speech. The present study examined the influence of different types of maskers and target word position on the immediate recall of words in sentences by normal-hearing younger adults. In Experiment 1, nonsense sentences with 3 keywords (e.g., A ″house″ should ″dash″ to the ″bowl″.) were presented against a background of speech-spectrum noise or two-talker nonsense speech. With the speech masker, accuracy increased with word position in a linear fashion. With the speech-spectrum noise masker, performance was highest for the first word but the same for the second keyword and third keyword. In Experiment 2, when the speech-masker was noise-vocoded to preserve envelope information while disrupting fine structure cues and minimizing semantic content, performance was similar to that found with the speech-spectrum noise masker. The results suggest that the ability to track a target sentence in conditions of informational masking improves as the target utterance unfolds over time.

4pPPc30. Empirical comparisons of pitch patterns in music, speech, and birdsong. Adam T. Tierney (UC San Diego Dept. of Cognitive Science, Neurosciences Institute, 9500 Gilman Drive, La Jolla, CA 92093-0515, USA, AdamTierney@gmail.com), Frank A. Russo (Ryerson University Department of Psychology, 350 Victoria Street, Toronto, ON M5B 2K3, Canada, russo@ryerson.ca), Aniruddh D. Patel (Neurosciences Institute, 10640 John Jay Hopkins Drive, La Jolla, CA 92121, USA, apatel@nsi.edu)

In music, large intervals (″pitch skips″) are often followed by reversals, and phrases often have an arch-like shape and final durational lengthening. These regularities could reflect motor constraints on pitch production or could reflect the melodic characteristics of speech. To distinguish between these possibilities we compared pitch patterns in instrumental musical themes, sentences, and birdsongs. Patterns due to production-related constraints should be common to all three domains, whereas patterns due to statistical learning from speech should be present in speech but not birdsong. Sequences were taken from English and French instrumental classical music, sentences from 4 languages, and songs of 56 songbird families. For sentences and birdsongs each syllable/note was assigned one pitch. For each sequence, we quantified patterns of post-skip reversals, the direction of the initial and final interval, the relative duration of the final syllable/note, and the pitch contour shape. Post-skip reversals predominated in all domains, likely reflecting a shared constraint: skips frequently take melodies toward the edges of the pitch range, forcing a subsequent reversal (as suggested by Von Hippel & Huron, 2000). Arch-like contours and final lengthening were found in music and speech but not birdsong, possibly reflecting an influence of speech patterns on musical structure.

4pPPc31. Form and content in emotional reactions to sounds. Daniel Vastfjall (Chalmers University of Technology, Division of Applied Acoustics - Chalmers Room Acoustics Group, Sven Hultins gata 8a, 41296 Gothenburg, Sweden, daniel.vastfjall@psy.gu.se), Erkin Asutay (Chalmers University of Technology, Division of Applied Acoustics, Sven Hultinsgata 8a, 41296 Gothenburg, Sweden, erkin@student.chalmers.se), Anders Genell (Chalmers University of Technology, Division of Applied Acoustics, Sven Hultinsgata 8a, 41296 Gothenburg, Sweden, Anders.Genell@ta.chalmers.se), Ana Tajadura (Chalmers University of Technology, Division of Applied Acoustics, Sven Hultinsgata 8a, 41296 Gothenburg, Sweden, ana.tajadura@chalmers.se)

People react emotionally to auditory stimuli. Despite this fact relatively little is known how sounds can create emotional reactions in listeners. We have developed a framework, the Emotion Reaction Model (ERM), that predict that both form features (i.e classical psychophysical attributes such as loudness, sharpness etc) and content feratures (i.e. psychological associations to the sound producing source). Using ERM we tested the relative contribution of form vs. content in producing emotional reactions to sounds. In a first experiment, participants rated their emotional reactions to sounds from qualitatively different categories (animals, humans, machine noise) and to same sounds with time or frequency scrambling applied (thus rendering them difficult to identify, but with retained psychoacoustical properties). Experiments 2 used the same sounds but with a priming procedure and experiment 3 assessed emotional reactions using physiological measures. Overall, content, rather than form, appeared to have the biggest impact on emotional reactions. This research may complement traditional psychoacoustical theories that focus solely on form features.

4pPPc32. Learning to read; attaching your ear to your tongue. Eugene Galanter (Children's Progress, Inc./ Columbia University, 460 Riverside Drive, New York, NY 10027, USA, eg53@columbia.edu)

Really early learning predicts later success in school, life, and society (1), (2). Speech fluency, measured by accuracy, rate, and prosody (3), predicts reading comprehension (4) and reading proficiency (5). Speech fluency may be improved by one-on-one teacher interactions. When properly administered they give teachers useful information, but are time-consuming and subject to teacher's expectations. The results are commonly norm-referenced; a ″wait to fail″ model where teachers find deficits later in ″high-stakes tests″ (6). These failures led us to develop ″voice mirroring (VM).″ (7) V-M lets children self-correct their speech by hearing it mirrored after amplification. The child hears discrepancies between their own speech and

their teacher's to self-correct. Children supported by V-M demonstrate better reading skills as estimated by their teachers; (single-blind). Well-spoken children read well

4pPPc33. Temporal response of a simplified bidimensional numerical model of the cochlea. Christine Lepine (Université Paul Sabatier, PHASE, 118, route de Narbonne, 31062 Toulouse cedex 9, France, salmets@aol.com), Vincent Gibiat (Université Paul Sabatier, PHASE, 118, route de Narbonne, 31062 Toulouse cedex 9, France, gibiat@cict.fr)

Within the framework of a study related to bone conduction, numerical simulations have been performed in the time domain, with the aim of comparing the cochlear partition displacement in the case of different places of stimulation. An oversimplified 2D model of the cochlea is used. It is first excited with pulses centered on various audible-range frequencies with a localisation of the source which is analogous to the position of the oval window. Secondly, new sets of calculations introduce different localisations and/or spatial extensions of the sources. An analogy with seismology being adequate to simulate the solid-fluid (cochlear partition-perilymph) coupling, a finite difference numerical simulation based upon the Virieux scheme for elastic waves propagation has been used. The movement of the simplified basilar membrane is observable when excited via air or bone conduction. Results of the propagation of a single pulse within the model will be presented and discussed through information available in literature.

4pPPc34. Modelling of the cochlea response as a versatile tool for acoustic signal processing. Marinus M. Boone (University of Technology Delft, Lorentzweg 1, 2628 CJ Delft, Netherlands, m.m.boone @tudelft.nl), Diemer De Vries (University of Technology Delft, Lorentzweg 1, 2628 CJ Delft, Netherlands, d.devries@tudelft.nl), Tjeerd C. Andringa (University of Groningen, Dept. Artificial Intelligence, P.O. Box 407, 9700 AK Groningen, Netherlands, t.andringa@ai.rug.nl), Anton Schlesinger (University of Technology Delft, Lorentzweg 1, 2628 CJ Delft, Netherlands, A.Schlesinger@tudelft.nl), Jasper Van Dorp Schuitman (University of Technology Delft, Lorentzweg 1, 2628 CJ Delft, Netherlands, J.vanDorpSchuitman@tudelft.nl), Bea Valkenier (University of Groningen, Dept. Artificial Intelligence, P.O. Box 407, 9700 AK Groningen, Netherlands, bea@ai.rug.nl), Hedde Van De Vooren (University of Groningen, Dept. Artificial Intelligence, P.O. Box 407, 9700 AK Groningen, Netherlands, h.van.de.vooren@ai.rug.nl)

The inner ear or cochlea processes the acoustic signals that enter the oval window into a specific time-frequency pattern. Many acoustic signal processing methods are based on this behaviour. A fundamental method is to calculate this time-frequency response by solving the differential equation of the movement of the basilar membrane, followed by a visualisation of the excitation patterns in a time-frequency plot. For that purpose Continuity Preserving Signal Processing (CPSP) is a promising method. In the presentation an overview will be given of a project that is carried out by TUD (University of Technology Delft) together with RUG (University of Groningen) being sponsored by STW (Dutch Technology Foundation). The project divides into four sub-projects which are closely related: Automatic Keyword Spotting, Machine Analysis and Diagnostics, Speech Intelligibility Enhancement for Hearing Aids and Quality Assessment of Room Acoustics. Results that have been obtained in the project will be summarised. Detailed results of the sub-projects will be presented in separate presentations.

4pPPc35. Improving speech intelligibility based on a conjunction of multiple perceptual models. Anton Schlesinger (University of Technology Delft, Lorentzweg 1, 2628 CJ Delft, Netherlands, A.Schlesinger @tudelft.nl), Marinus M. Boone (University of Technology Delft, Lorentzweg 1, 2628 CJ Delft, Netherlands, m.m.boone@tudelft.nl)

The enhancement of speech intelligibility is crucial to the success of hearing aids and other speech transmission systems. Such systems often have to operate in real-world situations, in which noise, reverberation and competing talkers impair the signal-to-noise ratio and therewith the degree of intelligibility. Psychoacoustic and neuropsychological models progressively explain the working principle of the auditory path. In order to technologically achieve the mammalian hearing-performance, Computational Auditory Scene Analysis (CASA), a vivid field of research in acoustics, converts these models into technical approaches. Asking for neuropsychological evidence that underlies the extraction of sound-objects in reverberation and noise, two models are essential. These are echo-suppression, which is subject to the precedence effect, and modulation perception, performed by a neural mapping of time-information of the auditory input into a periodotopical organization. The models have been applied and successfully tested in enhancing the signal-to-noise ratio, respectively. In this work, we conjunct both models and obtain a temporal and lateral inhibition system, which successfully suspends interferences. An evaluation of the proposed approach verifies the consistency with psychoacoustical experiments of the precedence effect and modulation perception; the resulting speech intelligibility benefits considerably in acoustically adverse situations.

4pPPc36. Tinnitus: one problem that can be solved. G. Mario Mattia (Bruel Acoustics S.r.l. - EuroAcustici, Viale Cesare Pavese 304, 00144 Roma, Italy, m.mattia@euroacustici.org)

The author axplains the origin of idiopathic or subjective tinnitus. After more than ten years of research (at a personal centre and at Rome University ″La Sapienza″ Faculty of Medicine ...) we have solved more than 80% of tinnitus problems for a thousand people. We have found that the perceived sound can be a source of stress and can be recorded in the brain as ″dangerous″. We illustrate that a psychological and neurological rehabilitation implemented in a multifactors approach can give health and offer a new normal quality of life. With biofeedback EEG, EMG and GSR we are implementing our therapy. The biofeedback helps people understand the effects of stress on tinnitus and how to manage this stress to optimize performance and improve health. Previous studies have shown an enhancement of human performance and faster rehabilitation when physiological measures (respiration rate, heart rate, skin conductance, temperature, and surface electromyography) were fed back in sessions of Autogenic Training.

4pPPc37. Subjective evaluation of accelerating car interior noise using brain magnetic field. Kenji Takami (Univ. of Hyogo, 2167 Shosha, 671-2201 Himeji, Japan, hyogo.takami@aist.go.jp), Shunsuke Ishimitsu (Hiroshima City University / National Institute of Advanced Industrial Science and Technology, 3-4-1 Ozuka-Higashi, Asa-Minami-Ku, 731-3194 Hiroshima, Japan, ishimitu@hiroshima-cu.ac.jp), Seiji Nakagawa (National Institute of Advanced Industrial Science and Technology (AIST), 1-8-31 Midorigaoka, 563-8577 Ikeda, Osaka, Japan, s-nakagawa@aist.go.jp), Toshihiko Asami (Univ. of Hyogo, 2167 Shosha, 671-2201 Himeji, Japan, asami@eng.u-hyogo.ac.jp)

Recently, the production concept of car engine sound has been changing to the sound design from the cure against noise. Although most work has concentrated on comfortable engine sound, the psychoacoustic effects of time-varying rate of frequency in accelerating engine sound have not been sufficiently studied. Thus we investigated the effects of time-frequency-changing rate in car interior noise on auditory impression using psychological and neurophysiological methods. Harmonic complex tones which simulated accelerating car noise were used as stimuli. Frequencies of the stimuli were time-varying by 15, 25, 35, 50, and 70 Hz/s, like accelerating-engine sounds. First, subjective evaluations were examined using a SD method. Second, neuronal activities of the auditory cortex evoked by these stimuli were measured by magnetoencephalography(MEG). The results indicated that time-varying rate of frequency has significant effects on subjective impression and neuronal activities of the auditory cortex.

4pPPc38. Subjective experiment on auditory localization for traffic alarm sounds. Sakae Yokoyama (Chiba Institute of Technology, 2-17-1, Tsudanuma, Narashino, 275-0016 Chiba, Japan, sakae@iis.u-tokyo .ac.jp), Hideki Tachibana (Chiba Institute of Technology, 2-17-1, Tsudanuma, Narashino, 275-0016 Chiba, Japan, tachibana@acoust.cs.it-chiba.ac.jp)

When riding a motorbike with a helmet or driving a car, it is often experienced that the judgment of directions of alarm sounds like a horn and sirens of engine truck and ambulance car becomes difficult. This kind of auditory localization is seriously related to traffic safety. In this study, therefore, the effects of covering the driver' s head with a helmet and sound transmission into a car on the auditory localization for traffic alarm sounds

were examined by laboratory tests. To simulate a 3-dimensional sound field, the 6-channel recording/reproduction technique was applied and the incident direction of the test sounds was varied in twelve horizontal directions.

4pPPc39. Development of pure-tone auditory threshold in school children. Reinhard Müller (University of Giessen, Aulweg 123, 35392 Giessen, Germany, reinhard.mueller@audio.med.uni-giessen.de)

The overwhelming majority of publications concerning hearing in children is related to diseases, but normal development of hearing attracts little attention. Normal hearing, as defined by ISO 7029, refers to persons at the age of 18. While aging effects of hearing may be estimated by the use of formulas, children are not included. A field-study at a primary school in Germany showed a notably lower hearing sensitivity for children than for young adults. First graders did not hear well, but auditory performance improved with rising age. For validating this result, the first graders of the field study were again tested 3 years later. The second tests showed the expected improvement of their hearing threshold. So the hearing sense starts not with the full capability but underlies a certain development. Maybe training effects are the key to understanding this topic, as in other human skills.

4pPPc40. Problems in sound quality evaluation in Brazil: general or cultural ones? Stephan Paul (Lab. of Vibrations and Acoustics, Fed. Univ. of Santa Catarina, CTC, EMC, Campus Trindade, 88040 Florianópolis, Brazil, stephan.paul.acoustic@gmail.com)

Within modern sound engineering the individual perception of sound events has to be considered. Within sound and vibration related research all over the world several instruments were already developed, but this instruments are subject to several restrictions, especially their language. When sound evaluations are to be made in Brazil adequate evaluation instruments are necessary. This article is intended to discuss some of the problems encountered by the author and its co-workers when developing assessment procedures and especially instruments for evaluation of sound quality with Brazilian subjects. Especially the work undertaken to study descriptors for sound and vibration and the problems resulting in this work will be discussed. We consider the present congress, with participants from all over the world, to be a suitable platform to discuss some of the problems and results obtained.

THURSDAY AFTERNOON, 3 JULY 2008 P2-C, LEVEL 2, 3:40 TO 5:20 P.M.

Session 4pPPd

Psychological and Physiological Acoustics: Auditory Perception of Sound Source Properties II (Poster Session)

John Neuhoff, Cochair
The College of Wooster

Anna Preis, Cochair
Institute of Acoustics, Adam Mickiewicz University

All posters will be on display from 3:40 p.m. to 5:20 p.m. To allow contributors an opportunity to see other posters, contributors of odd-numbered papers will be at their posters from 3:40 p.m. to 4:30 p.m. and contributors of even-numbered papers will be at their posters from 4:30 p.m. to 5:20 p.m.

Contributed Papers

4pPPd1. Auditory-guided reaching movements in the peripersonal frontal space. Florian Dramas (IRIT, Univ. Toulouse 3 - INPT - Univ. Toulouse 1 - CNRS Equipe Diamant, Univ. Paul Sabatier, 31062 Toulouse, France, florian.dramas@irit.fr), Brian F. Katz (LIMSI-CNRS, B.P. 133, 91403 Orsay, France, brian.katz@limsi.fr), Christophe Jouffrais (IRIT, Univ. Toulouse 3 - INPT - Univ. Toulouse 1 - CNRS Equipe Diamant, Univ. Paul Sabatier, 31062 Toulouse, France, jouffrais@irit.fr)

Previous studies on auditory localization processes have shown that humans can localize sound sources accurately, including distance in certain situations. Few studies have examined auditory localization by binaural mechanisms in the peripersonal space. Numerous studies have examined auditory localization through verbal report or various pointing movements. This study examines the precision of hand ″reaching″ movement towards an auditory object. An experimental platform (semicircle, radius 1m) was constructed with 35 small loudspeakers placed under an acoustically transparent grid. Blindfolded subjects were seated within the platform at table height. Test protocol consisted of a brief audio stimulus presented via a single loudspeaker followed by the subject placing their index finger (preferred hand) at the location of the sound object. Optical finger tracking was used during the course of the experiment. Two test variables were investigated: different audio stimuli, Gaussian noise bursts varying the number and the duration of each burst; room acoustic conditions, with and without acoustical damping for reflection suppression. Preliminary results show precision of localization does not grow indefinitely with the number of burst repetitions but reaches a limit. Azimuth precision remains accurate, even with short burst conditions, contrary to the distance perception which increases with the stimuli duration.

4pPPd2. In-situ observation of the perceptive process linked to dashboard tapping sounds. Francois Montignies (Renault Technocentre, FR TCR LAB 252, 1 avenue du Golf, 78288 Guyancourt Cedex, France, francois.montignies@insa-lyon.fr), Valery Nosulenko (Institute of Psychology, Russian Academy of Science, 129366 Moscow, Russian Federation, valery.nosulenko@gmail.com), Etienne Parizet (Laboratoire Vibrations Acoustique, Insa Lyon, 25 bis, av. J. Capelle, 69621 Villeurbanne Cedex, France, etienne.parizet@insa-lyon.fr)

It is well-known that in show-rooms some people might tap on the dashboard of vehicles. The aim of this study was to determine the importance of this phenomenon and to identify which properties of the vehicle are perceived through the sound thus produced. An ethomethodological observation

was conducted to collect data about the action/perception process of a subject exploring a static vehicle. The work was based on the methodology developed by Nosulenko and Saymolenko to evaluate perceived quality using free verbalisations in a comparison task. 52 naive subjects were placed in ecologically valid conditions. Their task consisted in freely exploring two vehicles and selecting their preferred one. From a qualitative analysis of audiovisual recordings, a data base was built. It linked verbalisations, operations and perceived objects, and allowed the quantification of indicators related to activity and perception. The analysis of operations validated that the tapping operation was not anecdotal. Moreover, dashboard was one of the main perceived objects linked to to the auditive dimension. Finally, a significative effect of the tapping operation on the evaluation of dashboard material quality was observed, suggesting an implicite influence of sound on this perceived property.

4pPPd3. Hemispheric Differences in the Recognition of Environmental Sounds. Julio Gonzalez (Universitat Jaume I, Dept. Psicologia Basica, Clinica y Psicobiologia, Campus Riu Sec. Facultad CC. Humanas y Sociales, 12071 Castellon de la Plana, Spain, gonzalez@psb.uji.es), Conor T. McLennan (Cleveland State University, Dpt. Psychology, 2121 Euclid Ave. CB 175, Cleveland, OH 44115, USA, c.mclennan@csuohio.edu)

In the visual domain, Marsolek and colleagues have provided support for their claim that two dissociable and parallel neural subsystems underlie abstract and specific object recognition [Marsolek, 1999; Marsolek & Burgund, 2003]. According to their dissociable subsystems theory, an abstract-category subsystem operates more effectively in the left hemisphere (LH) and is less sensitive to the specific surface characteristics of the stimuli, whereas a specific-exemplar subsystem operates more effectively in the right hemisphere (RH) and is more sensitive to specific stimulus characteristics. In the present study, we tested this hypothesis in the auditory domain by conducting 2 long-term repetition-priming experiments on the recognition of environmental sounds. Participants attempted to identify target sounds from an initial 750 ms sound stem. Target stems were primed by either an identical or a different exemplar sound (e.g., the same or different tokens of a bagpipe). Target stems were presented monaurally in both experiments; however, in Exp. 2 white noise was simultaneously administered to the opposite ear. Our results are consistent with Marsolek's framework. In particular, in both experiments an exemplar specificity effect was obtained when the sounds were presented to the left ear (RH), but not when the sounds were presented to the right ear (LH).

4pPPd4. Perception of speech properties from extremely brief segments. Sue Harding (Sheffield University, Computer Science Department, Regent Court, 211 Portobello St., S1 4DP Sheffield, UK, s.harding@dcs.shef.ac.uk), Martin Cooke (Sheffield University, Computer Science Department, Regent Court, 211 Portobello St., S1 4DP Sheffield, UK, m.cooke@dcs.shef.ac.uk)

A glance at a visual scene enables observers to become rapidly aware of its most important characteristics. Here, we describe experiments using very brief segments of natural speech which demonstrate that a surprising amount of information can be determined from only a few milliseconds of the auditory signal. Segments with durations ranging from 2.5 to 80 ms were extracted from six vowels and six fricatives spoken by males and females. Listeners identified the phoneme and/or gender, or whether a vowel or consonant had been presented. While listeners' performance dropped close to chance for the 2.5 ms stimuli for most tasks, for the vowel/fricative distinction listeners obtained scores above 70% even for such short segments. Listeners performed well above chance for the 10 ms stimuli for three out of four tasks. Combining results within tasks showed that listeners also distinguished voiced from unvoiced phonemes in less than 10 ms. Threshold values from logistic fits indicate the order in which information becomes available: vowel/fricative distinction (3.0 ms), voicing distinction (6.7 ms), phoneme identification (11.9 ms) and gender identification (15.3 ms). By exploiting the ″gist″ of an auditory scene, listeners may be able to deploy prior knowledge rapidly to constrain further interpretation.

4pPPd5. Comparison of headphones and equalization for virtual auditory source localization. David Schonstein (Arkamys, 5 rue Frédéric Bastiat, 75008 Paris, France, dschonstein@arkamys.com), Laurent Ferré (LIMSI-CNRS, B.P. 133, 91403 Orsay, France, laurent.ferre @limsi.fr), Brian F. Katz (LIMSI-CNRS, B.P. 133, 91403 Orsay, France, brian.katz@limsi.fr)

This study investigates the variation in localization performance between different headphone styles. Eight different headphones (including various in-ear, circumaural open and closed, and bone conduction headphones) were tested. In addition, the effect of headphone equalization (aiming to produce an approximately flat frequency response) was investigated. Localization was examined for 24 locations distributed on a sphere surrounding the listener. A single subject participated in the study using a single chosen non-individual HRTF set. Each location was repeated 6 times, resulting in a total of 144 localization reports. Overall, results were relatively consistent for 3 out of the 8 headphones tested. For these headphones, there was no significant difference in lateral angle error, associated with ITD and ILD cues. Polar angle errors, associated with the cone of confusion, however did vary significantly for these headphones. The headphone equalization had varying effects on localization accuracy depending on the headphone. Globally, headphone equalization showed no significant effect on localization accuracy. The results serve as a preliminary investigation, highlighting consistent results for only a select group of headphones tested for effective sound rendering in virtual auditory space. In addition, the results suggest that headphone equalization has a minimal influence on localization accuracy under these conditions.

4pPPd6. Perception of Sound Source Distance and Loudness in a Coherent Field of a Reverberant Field. Yoshifumi Hara (Kogakuin University, 1-24-2, Nishi-Shinjuku, Shinjuku-ku, 185-0012 Tokyo, Japan, kuro5hiron@ymail.plala.or.jp), Yoshinori Takahashi (Kogakuin University, 1-24-2, Nishi-Shinjuku, Shinjuku-ku, 185-0012 Tokyo, Japan, yoshinori@ieee.org), Hiroaki Nomura (Kure National College of Technology, 2-2-11, Aga-Minami Kure City, 737-8506 Hiroshima, Japan, hnomura@kure-nct.ac.jp), Mikio Tohyama (Waseda University, 1-3-10, Bldg. 29-7, Nishi-Waseda, Shinjuku-ku, 169-0051 Tokyo, Japan, m_tohyama@waseda.jp), Kazunori Miyoshi (Kogakuin University, 1-24-2, Nishi-Shinjuku, Shinjuku-ku, 185-0012 Tokyo, Japan, miyoshi@cc .kogakuin.ac.jp)

Perception of reverberant sound field changes with a sound source distance (SSD). This article describes SSD perception in a coherent region close to the sound source in the reverberation field. We performed listening tests for SSD perception and loudness of speech and carried out transfer functions analysis using a reverberant room. We confirm that both SSD perception and loudness are correlated to the standard deviation of the magnitude frequency response of the transfer function in the coherent region. That is SSD erception and loudness increase as SSD becomes long in the coherent region. However loudness decreases in an incoherent region. Consequently, we surmise SSD perception in the coherent region might be due to increase in loudness.

4pPPd7. The influence of pinna position on head-related transfer function. Przemyslaw Plaskota (Wroclaw University of Technology, Wybrzeze Wyspianskiego 27, 50-370 Wroclaw, Poland, przemyslaw.plaskota@pwr.wroc.pl), Andrzej B. Dobrucki (Wroclaw University of Technology, Wybrzeze Wyspianskiego 27, 50-370 Wroclaw, Poland, andrzej.dobrucki@pwr.wroc.pl)

The changes of spectrum of sound at listener ear are one of the major cues for sound source localization. Head Related Transfer-Function (HRTF) describes the influence of torso, head and pinna on sound spectrum. It is possible to recognize HRTF using computational method, e.g. Boundary Elements Method (BEM). The numerical model used for calculation of HRTF is constructed by transfer geometrical shape of head and pinna into numerical domain. Important question during geometry reconstruction process is

the accuracy of shape mapping. The pinna has significant influence on HRFT. In the paper, the influence of accuracy of pinna geometry transformation and pinna position on HRTF is presented. Particularly, the pinna flare angle, pinna rotation angle and position of ear entrance were taking into considerations. Measurements have been done on numerical model with the invariable pinna and head shapes, using BEM method.

4pPPd8. Environmental Enrichment Increases Response Strength And Paired-Pulse Depression Of Auditory Cortex Neurons. Cherie R. Percaccio (Univ. of Texas, 800 W. Campbell Rd, Richardson, TX 75080, USA, cheriep@u.washington.edu), Autumn L. Pruette (Univ. of Texas, 800 W. Campbell Rd, Richardson, TX 75080, USA, autumn.pruette@utsouthwestern.edu), Shilpa T. Mistry (Univ. of Texas, 800 W. Campbell Rd, Richardson, TX 75080, USA, shilpa.mistry@utsouthwestern.edu), Yeting H. Chen (Univ. of Texas, 800 W. Campbell Rd, Richardson, TX 75080, USA, superhelen@gmail.com), Daniel L. Rathbun (Univ. of Texas, 800 W. Campbell Rd, Richardson, TX 75080, USA, dlrathbun@ucdavis.edu), Michael P. Kilgard (Univ. of Texas, 800 W. Campbell Rd, Richardson, TX 75080, USA, kilgard@utdallas.edu)

A wide variety of sensory gating impairments have been associated with autism. Abnormal brain development may alter patterns of interaction between the child and the environment and hinder the acquisition of critical language skills. After several months of therapy, autistic symptoms may subside as children advance to higher cognitive stages. This study modeled the physiological changes associated with therapy-related gains in children by investigating enrichment-induced plasticity in rat auditory cortex. Evoked potential response strength and paired-pulse depression were enhanced by exposure to an enriched environment and degraded by exposure to a standard environment. While neither exercise nor social stimulation, specifically, resulted in any plasticity, rats that heard the enriched environment from a distance also exhibited enhanced responses. The degree of enrichment-induced plasticity was not reduced by a substantial and persistent cholinergic deficit. The finding that enrichment increases response strength and paired-pulse depression in the auditory cortex of rats is consistent with earlier clinical observations, suggesting that proper sensory development is necessary for higher cognitive processes. In the future we will investigate if clinical gains during and after therapy are associated with increased event-related potential discrimination and hemispheric localization of speech stimuli in children with autism.

4pPPd9. Directional loudness measurements for a multichannel system. Densil Cabrera (University of Sydney, Faculty of Architecture, Design and Planning, NSW 2006 Sydney, Australia, densil@usyd.edu.au), Luis Miranda (University of Sydney, Faculty of Architecture, Design and Planning, NSW 2006 Sydney, Australia, lmir9852@mail.usyd.edu.au), Ian Dash (Australian Broadcasting Corporation, Technology Research & Standards, Level 11, Ultimo Building, 2001 Sydney, Australia, Dash.Ian@abc.net.au)

Loudness matching listening tests were conducted to quantify the difference in loudness level from a constant signal played from various horizontal directions. The multichannel system used for this tests was a 5-channel system, set up according to the ITU Recommendation BS.116-1 Methods for the subjective assessment of small impairments in audio systems including multichannel sound systems and the test signals were octave bands of noise with centre frequencies from 63 Hz to 8000 Hz. These tests were conducted as part of ongoing research for the ITU Recommendation BS.1770 Algorithms to measure audio programme loudness and true-peak level. The aim of this experiment is to contribute to the design of a loudness meter by providing channel weightings, and results indicate that listeners are more sensitive to the surround channels than the other channels in the mid and high frequency range.

4pPPd10. Investigating the potential of human echolocation in virtual sonic trigonometry. Flaithri E. Neff (University College Cork, Western Road, IRL Cork, Ireland, fn2@cs.ucc.ie), Ian Pitt (University College Cork, Western Road, IRL Cork, Ireland, i.pitt@cs.ucc.ie)

Describing a mathematical problem often involves visual diagrams. For blind students this accentuates the challenges they face. Projects such as LAMBDA have used linear speech and Braille to convey algebraic equations. However, spatial features, for example in trigonometry, are difficult to map to a linear-based system. Traditional tactile methods (e.g. German film) convey simple shapes but need Braille support and speech-tactile interfaces (e.g. NOMAD) require unconventional equipment. Cognitive issues regarding tactile interpretation of 3D shapes also persist. Blind students interact regularly with speech technology and audio games. This exposure means that the auditory system is potentially becoming accustomed to sonic interpretation of computer-based information. Some of our research has looked at expanding the sonic environment to include spatial information aimed at trigonometry. The next stage is to provide interactive user control. Our system is based on a user interface model in order to consider the cognitive issues involved. We use Microsoft's XNA/XACT environment to create our auditory scene. In this paper we discuss how to implement sonic-based user interaction while further simplifying our auditory scene. In order to achieve this, we examine the potential of human echolocation to orient within the virtual walls and corners of a triangle.

4pPPd11. Toward synthesis tools using 'evocation' as control parameters. Adrien Merer (CNRS-LMA, 31, chemin Joseph Aiguier, 13402 Marseille, France, merer@lma.cnrs-mrs.fr), Mitsuko Aramaki (CNRS - INCM and Université de Provence, 31, chemin Joseph Aiguier, 13402 Marseille, France, aramaki@lma.cnrs-mrs.fr), Richard Kronland-Martinet (CNRS-LMA, 31, chemin Joseph Aiguier, 13402 Marseille, France, kronland@lma.cnrs-mrs.fr), Solvi Ystad (CNRS-LMA, 31, chemin Joseph Aiguier, 13402 Marseille, France, ystad@lma.cnrs-mrs.fr)

This study addresses the design of synthesis tool controlled by high-level parameters, such as mental evocations induced by sounds. As a first approach, we considered sounds evoking motions and we addressed 3 main questions: What are the different categories of motion? What are the common acoustic features of sounds within a category? How to synthesize sounds that evokes specific motions? We gathered samples used by electro-acoustic music composers as a framework for their compositions and synthesized sounds. Then we effectuated a two-steps listening test. The first part aims at determining these different motion categories. It consisted in a free categorization task in which listeners build their own groups of sounds as function of evoked motions. The second part aims at determining a set of sounds characteristic of each of these categories. It consisted in a constrained categorization task with predefined categories represented by prototypical sounds (deduced from free categorization task). We used a feature selection method to highlight most relevant signal descriptors for each category. Finally, designing a synthesis tool implies the calibration of these descriptors (a specific range of values for each category) and their control (leading to address the inverse problem). These aspects are currently being investigated.

4pPPd12. Human recognition by active and passive acoustic signatures. Alexander Ekimov (University of Mississippi, NCPA, 1 Coliseum Drive, University, MS 38677, USA, aekimov@olemiss.edu), James M. Sabatier (University of Mississippi, NCPA, 1 Coliseum Drive, University, MS 38677, USA, sabatier@olemiss.edu)

Recognition of different sensed objects is a problem that often appears in practice. One of the solutions is based on analysis of the signatures of the specific objects. This method was applied for the acoustic detection of walking humans. Human footsteps excite envelopes of broadband acoustic signals in the air due to periodic friction forces between the foot and the ground/floor. The repetition frequency of these envelopes is equal to the footstep rate and usually lies below 3 Hz. High frequencies in these envelopes allow detection and localization of a walker using a narrowband ultrasonic receiver with a high directivity pattern. Consequently, periodic low frequency human motion results in passive ultrasonic detection using this

method. This motion has also unique Doppler signatures and is measured using ultrasonic sonar. Common analyses of passive and Doppler signatures allow the extraction of the specific cadence in human motion and recognition of a human while rejecting other moving or stationary objects. [Work supported by Department of the Army, Army Research Office contract W911NF-04-1-0190].

4pPPd13. Strategic listener movement in a model of auditory distance perception. Yan-Chen Lu (Sheffield University, Computer Science Department, Regent Court, 211 Portobello St., S1 4DP Sheffield, UK, y.c.lu@dcs.shef.ac.uk), Martin Cooke (Sheffield University, Computer Science Department, Regent Court, 211 Portobello St., S1 4DP Sheffield, UK, m.cooke@dcs.shef.ac.uk)

A mobile listener has the potential to exploit dynamic auditory cues to judge sound source distance. One such cue is motion parallax, which employs a sequence of azimuth estimates from interaural time differences to triangulate sound source location. However, distortions due to reverberation and competing sources complicate matters, so it is of interest to know what active strategies listeners might adopt to arrive at robust location estimates. One hypothesis is that not all listener motion trajectories are equally-beneficial for distance estimation. Trajectories designed via certain optimisation criteria might lead to faster and more robust estimates in a wider range of environments. Eight listener motion strategies were tested, from naive approaches such as random walks and head-rotation only to more sophisticated techniques based on sequential Monte Carlo methods. In the latter case, strategies included movement towards the expected source location, or in the most informative direction, or movement reducing overall uncertainty. Evaluation in a simulated acoustic environment with single sources under both anechoic and reverberant conditions demonstrated that moving towards the most likely source location led to the most accurate estimation of distance and subsequent tracking of a moving source. Significant problems remain in estimating distance in multi-source conditions.

THURSDAY AFTERNOON, 3 JULY 2008 P2-B, LEVEL 2, 3:40 TO 5:20 P.M.

Session 4pSAa

Structural Acoustics and Vibration, Computational Acoustics, and EURONOISE: Efficient Boundary Element Methods II (Poster Session)

Ramani Duraiswami, Cochair
University of Maryland Institute for Advanced Computer Studies

Haike Brick, Cochair
TFH Berlin - University of Applied Sciences

All posters will be on display from 3:40 p.m. to 5:20 p.m. To allow contributors an opportunity to see other posters, contributors of odd-numbered papers will be at their posters from 3:40 p.m. to 4:30 p.m. and contributors of even-numbered papers will be at their posters from 4:30 p.m. to 5:20 p.m.

Contributed Papers

4pSAa1. Application of the fast multipole method for solving very large acoustic radiation problems. Raphael Hallez (LMS International, Researchpark Z1, Interleuvenlaan 68, 3001 Leuven, Belgium, raphael.hallez@lmsintl.com), Koen De Langhe (LMS International, Researchpark Z1, Interleuvenlaan 68, 3001 Leuven, Belgium, koen.delanghe@lmsintl.com), Michel Tournour (LMS International, Researchpark Z1, Interleuvenlaan 68, 3001 Leuven, Belgium, michel.tournour@lmsintl.com), Toufic Abboud (IMACS, Ecole Polytechnique, 91128 Palaiseau Cedex, France, abboud@imacs.polytechnique.fr)

Boundary element method is well known and extensively used to solve acoustic radiation problems. It is especially appropriated for exterior radiation since the fluid domain does not need to be meshed, as opposed to the finite element method. However, the mathematical formulation leads to a dense matrix system of equations. Therefore, the size of the model increases drastically as the frequency of analysis increases and huge computer resources are required to solve complex models in the mid-frequency range. The fast multipole method can be used to extend the boundary element model and solve such problems. For a model with N nodes, this technique brings the number of operations down to O(N*LogN) instead of O(N**3) for conventional boundary elements. This new methodology has been applied here to study the acoustic radiation of a complete car in the mid-frequency range. The accuracy of the results as well as the computation time demonstrate the great potential of this new method to solve very large acoustic radiation problems.

4pSAa2. FE-Model Reduction for FE-BE Coupling with Large Fluid-Structure Interfaces. Michael Junge (Institute of Applied and Experimental Mechanics, University of Stuttgart, Pfaffenwaldring 9, 70550 Stuttgart, Germany, junge@iam.uni-stuttgart.de), Jens Becker (Institute of Applied and Experimental Mechanics, University of Stuttgart, Pfaffenwaldring 9, 70550 Stuttgart, Germany, becker@iam.uni-stuttgart.de), Dominik Brunner (Institute of Applied and Experimental Mechanics, University of Stuttgart, Pfaffenwaldring 9, 70550 Stuttgart, Germany, brunner@iam.uni-stuttgart.de), Lothar Gaul (Institute of Applied and Experimental Mechanics, University of Stuttgart, Pfaffenwaldring 9, 70550 Stuttgart, Germany, gaul@iam.uni-stuttgart.de)

For the finite element method model, reduction techniques exist to represent the dynamic behavior of component substructures. Depending on the type of reduction method, the reduction basis contains constraint or attachment modes, which are computed for all structural degrees of freedom on an interface. The interface can either be defined by adjacent substructures or by coupling interfaces to other physical domains, as it is the case for FE-BE coupled systems. A large interface thus leads to an increased size of the reduced order model and limits standard model reduction techniques to applications with small interfaces. In this work, interface reduction methods are investigated. Here, the size of the reduced order model is decreased by reducing the number of retained interface modes, while marginally increasing the reduction error. A direct reduction method based on strain--energy considerations is presented. Additionally, an iterative reduction scheme is pro-

posed which only adds a basis vector to the reduction basis, if the spanned subspace is sufficiently enlarged. The applicability of the proposed methods is shown for an example structure.

4pSAa3. Modeling of the acoustic eigenproblem with sound absorption using boundary element method. Antoine Lavie (Univ. d'Artois, Faculté des Sciences Appliquées - Lab. LAMTI, Technoparc Futura, 62400 Bethune, France, antoine.lavie@univ-artois.fr), Alexandre Leblanc (ISAE, 10, av Edouard Belin, 31055 Toulouse, France, alexandre.leblanc@isae.fr), Abdelkader Haddi (Univ. d'Artois, Faculté des Sciences Appliquées - Lab. LAMTI, Technoparc Futura, 62400 Bethune, France, abdelkader.haddi@univ-artois.fr)

This paper deals with determination of resonant frequencies for absorbant 3D acoustic cavities. The behaviour of the sound absorbing boundary can be described with a Robin condition as proposed by Rajakumar et al. [Int. J. Numer. Methods Eng., 36, 3957-3072 (1993)]. This approach is inaccurate, especially for low frequencies because the absorption coefficient is assumed to be constant. We observed the acoustic admittance for foam and fibrous type materials varies linearly for low frequencies. The introduction of a new absorption coefficient allows to take into account this behavior in order to improve the accuracy in the determination of the first modes (typically less than 500 Hz in car interior). This formulation has been implemented in a boundary element program we have developed. The results are compared with those given by the finite element program ANSYS. Computations are carried out for rectangular parallelepiped and Sedan car interior.

THURSDAY AFTERNOON, 3 JULY 2008 P2-B, LEVEL 2, 3:40 TO 5:20 P.M.

Session 4pSAb

Structural Acoustics and Vibration and EURONOISE: Distributed Active Noise and Vibration Control II (Poster Session)

Kenneth Cunefare, Cochair
Georgia Institute of Technology

Manuel Collet, Cochair
FEMTO-ST UMR CNRS

All posters will be on display from 3:40 p.m. to 5:20 p.m. To allow contributors an opportunity to see other posters, contributors of odd-numbered papers will be at their posters from 3:40 p.m. to 4:30 p.m. and contributors of even-numbered papers will be at their posters from 4:30 p.m. to 5:20 p.m.

Contributed Papers

4pSAb1. Active noise control in turbofan aircrafts: theory and experiments. Ernesto Monaco (Dept. of Aerospace Engineering - University of Naples, Via Claudio, 21, 80125 Naples, Italy, ermonaco@unina.it), Leonardo Lecce (Dept. of Aerospace Engineering - University of Naples, Via Claudio, 21, 80125 Naples, Italy, leonardo@unina.it), Ciro Natale (Dipartimento di Ingegneria dell'Informazione - Seconda Università degli Studi di Napoli, Via Roma 29, I-81031 Aversa (CE), Italy, ciro.natale@unina2.it), Salvatore Pirozzi (Dipartimento di Ingegneria dell'Informazione - Seconda Università degli Studi di Napoli, Via Roma 29, I-81031 Aversa (CE), Italy, salvatore.pirozzi@unina2.it), Chris May (Laboratory of Process Automation (LPA) - Saarland University, Gebäude A5 1, D-66123 Saarbrücken, Germany, c.may@zip.uni-sb.de)

This paper presents the activities developed by the authors within the research project M.E.S.E.M.A. funded by the European Commission. A noise and vibration control system using magnetostrictive actuators has been designed and experimentally tested on a large scale (fuselage mock-up) test article, for controlling noise and vibrations between 150 - 500 Hz. The environmental noise and vibration excitation was representative of a small/medium turbofan aircraft. Firstly a numerical model of the test article has been developed in MSC/NASTRAN coupling the structural part with the interior acoustic volume. Furthermore the experimental characterisation of the test-article has been carried on. The model, updated by the mean of the experimental results, was employed to derive the required control actuators performances in order to achieve the best control predicted using a well consolidated ″feed-forward″ approach. Genetic Algorithms have been employed in order to optimise the positioning of the actuators. Dedicated magnetostrictive actuators have been designed together with light power amplifiers meeting the specifications; on each actuator an optoelecronic sensor, based on Bragg grating, has been integrated to optimize the actuator performance. A two-level ANVC system has been designed and tested on a full scale fuselage mock-up. The paper present an overview of the activities developed as well as of the achieved results.

4pSAb2. Active vibration control for the identification-based model of a circular plate. Lucyna Leniowska (University of Rzeszow, Rejtana 16, PL35-310 Rzeszow, Poland, lleniow@univ.rzeszow.pl), Pawel Kos (University of Rzeszow, Rejtana 16, PL35-310 Rzeszow, Poland, pkos@univ.rzeszow.pl)

An active vibration control system is proposed for suppressing the small amplitude vibration of circular plate. An experimental set-up consists of a hard-walled cylinder with a thin metallic plate at one end. Primary excitation is provided by a low frequency loudspeaker installed centrally at the bottom of the cylinder. The vibrations of the plate are measured by the application of strain sensors and accelerometers. Intelligent materials such as 2-layer piezo disk elements are used as the actuators. For the considered system the OE (Output Error) method of discrete-time model identification for real-time active vibration control have been applied. The mathematical model obtained by this method identification is then employed for the linear pole placement controller design. Numerical simulations describing the attenuation effects are presented and discussed.

4pSAb3. Adaptive predictive feedback control of circular plate vibrations. Lucyna Leniowska (University of Rzeszow, Rejtana 16, PL35-310 Rzeszow, Poland, lleniow@univ.rzeszow.pl), Pawel Kos (University of Rzeszow, Rejtana 16, PL35-310 Rzeszow, Poland, pkos@univ.rzeszow.pl)

Adaptive predictive controller, consists of an on-line identification technique coupled with a control scheme, is used in this paper for a plate vibration suppression. It is assumed, that the system to be regulated is unknown and the control schemes presented have the ability to identify and suppress the plate vibrations with only an initial estimate of the system order. The choice of structure is motivated by its representative nature. This configuration has also been well studied by the authors both analytically and experimentally, using several kind of controllers (PID, PI2D, fuzzy, LQR). There are two fundamental steps involved in the closed-loop system. The first step is to identify a mathematical model. The second step is to use the identified model to design a controller. One drawback of this approach is that, the control signal is fed to the actuator after updates of the control law expression, which always leads to some delay. In order to align better the updating process, the authors introduce the prediction of plant output with established error convergence. The one-step ahead system output prediction is calculated from the recursive formulas of the interpolation functions chosen. Simulations are included and discussed.

4pSAb4. Vibration control of flexible 3D robot arm with join and distributed actuators. Ryszard Leniowski (Rzeszow University of Technology, W.Pola 2, PL 35-902 Rzeszow, Poland, lery@prz-rzeszow.pl)

An active vibration control system is proposed for suppressing amplitude vibration of flexible 3D robot arm. This system integrates control algorithms, intelligent materials and software technologies. The mathematical model of physical system is based upon the geometry and properties of an experimental set-up consisting of a Flex3D robot with a flexible joints and flexible arm. The tip of the arm is loaded by eccentric mass. The vibrations of the plate are measured by the application of a grid of strain sensors and pair of coupled gyroscope-accelerometer. Two kinds of actuators are used. The first is a grid of PZT elements which form a local segments of compensators. Second is a standard BLDC motor located in the join. For the considered system the linear and non-linear (Neural Network of Runge-Kutta type models) of discrete-time model identification for real-time active vibration control have been applied. The mathematical model obtained by this method identification is then employed for the two class of controllers: linear pole placement controller for local segments compensators and non-linear reduced model reference for servo-controller. Virtual simulations are included and discussed.

THURSDAY AFTERNOON, 3 JULY 2008 P2-B, LEVEL 2, 3:40 TO 5:20 P.M.

Session 4pSAc

Structural Acoustics and Vibration, Computational Acoustics, and EURONOISE: Fluid-Structure Interaction III (Poster Session)

Noureddine Atalla, Cochair
Univ. de Sherbrooke

Vicente Cutanda Henriquez, Cochair
Institute of Sensors, Signals and Electrotechnics, University of Southern Denmark

Stefan Schneider, Cochair
Laboratoire de Mécanique et d'Acoustique, UPR 7051 CNRS

All posters will be on display from 3:40 p.m. to 5:20 p.m. To allow contributors an opportunity to see other posters, contributors of odd-numbered papers will be at their posters from 3:40 p.m. to 4:30 p.m. and contributors of even-numbered papers will be at their posters from 4:30 p.m. to 5:20 p.m.

Contributed Papers

4pSAc1. Modified amplitude and strouhal number scaling for correction of turbulent wall pressure fluctuations. Thomas Galib (NUWC, Howell St, Newport, RI 02841, USA, galibta@npt.nuwc.navy.mil)

Pressure fluctuations were measured in an external turbulent boundary layer over a buoyantly propelled axisymmetric body of revolution. Data were measured for three cases, resulting in axial length Reynolds numbers of 6.88x10 , 4.27x10 , and 3.21x10 at the measurement locations. The fresh water measurements were made in a fully developed turbulent boundary layer, following natural transition, with a near zero (very mildly adverse) pressure gradient. The salt water measurements were made in a favorable pressure gradient following a flow trip to force transition. The momentum thickness Reynolds number was greater than 4400 for all measurements, and the data were scaled with outer variables. The turbulence data were corrected using Corcos correction factors and then further scaled in both amplitude and frequency by the square root of (transducer radius/displacement thickness), in an attempt to resolve spatial resolution effects. This resulted in excellent agreement among the spectra to a modified Strouhal number of 1, which was the range of validity for the data. A second data set (constant freestream velocity and increasing displacement thickness with downstream measurement location), scaled somewhat better with the ratio of transducer radius to displacement thickness.

4pSAc2. The stability of nonequilibrium supersonic boundary layer. Igor Zavershinsky (Samara State Aerospace University, 34 Moskow Str., 443086 Samara, Russian Federation, zav@smr.ru)

The present work looks at the influence of molecular vibrational energy nonequilibrium on the instability of boundary layer. The boundary layer loses its stability at supercritical Reinolds numbers. At small Mach numbers

$M < 2$ can be unstable only Tollmien-Schlichting waves, which phase velocity in relation of mean flow is subsonic. The recent studies were shown that in the acoustically active gas the critical Reynolds number for subsonic disturbances is decreased in comparison with equilibrium media [1,2]. At large Mach numbers $M > 2$ in addition to Tollmien-Schlichting waves we must take into account both falling and reflecting acoustic waves (Mach waves). As a result the interaction between vortical structure and acoustic waves leads to shift of critical Reinolds number in comparison to subsonic case. Here the dependence of critical Reynolds number on thin flat plane from degree of nonequilibrium for spatial supersonic disturbances is founded. It was shown that acoustical activity of media has a large destabilizing influence. The increment of this instability is raised with growth of the degree of non-equilibrium. 1. Bertolotti F.P. J. Fluid Mech., 1998, V. 372. P. 93. 2. Knestyapin V.N., Kogan E.Ya., Zavershinsky I.P. High Temperatures. 2007. V.45. N2. P.1.

4pSAc3. Coupled wavenumbers of structural acoustic waveguides: A unified asymptotic approach. Abhijit Sarkar (Indian Institute of Science, FRITA Lab, Dept. of Mechanical Engg., Indian Institute of Science, 560012 Bangalore, India, asarkar@mecheng.iisc.ernet.in), Venkata R. Sonti (Indian Institute of Science, FRITA Lab, Dept. of Mechanical Engg., Indian Institute of Science, 560012 Bangalore, India, sonti@mecheng.iisc.ernet.in)

In the literature, the coupled wavenumbers in flexible-walled acoustic waveguides have been found mainly using numerical methods for a fixed set of parameters. These solutions, although useful, do not continuously track the coupled wavenumbers as the fluid-loading parameter is varied from small to large values. Such a continuous tracking is possible by applying the asymptotic methods to the coupled dispersion relation. Analytical formulae for the coupled wavenumbers can also be found. In this work, we present a consistent, unified and physically insightful view of structural acoustic coupling in the context of a planar structural-acoustic waveguide (with two different BCs), the axisymmetric and beam modes of a fluid-filled circular cylindrical shell and finally a fluid-filled elliptic cylindrical shell. In all the five cases, we use a single fluid-structure-coupling asymptotic parameter (ϵ). The regular perturbation method is used to solve the coupled dispersion relation for small and large values of ϵ. The circular and the elliptic cylinders necessitate the use of additional asymptotic parameters. A general trend in all systems is that a given wavenumber branch transits from a rigid-walled solution to a pressure-release solution with increasing ϵ. Also, the wavenumber curves veer where the earlier uncoupled wavenumbers intersected.

4pSAc4. Boundary element model to study sound transmission provided by a single panel in the presence of an elastic interlayer. Andreia Pereira (University of Coimbra, Department of Civil Engeneering - Pólo II da Universidade - Rua Luís Reis Santos, 3030-788 Coimbra, Portugal, apereira@dec.uc.pt), António Tadeu (University of Coimbra, Department of Civil Engeneering - Pólo II da Universidade - Rua Luís Reis Santos, 3030-788 Coimbra, Portugal, tadeu@dec.uc.pt)

In this paper the Boundary Element Method is applied to develop a numerical model which may be used to study the airborne and impact sound insulation provided by a single panel of infinite extent bounded by two fluid media, with an elastic interlayer (joint) inserted into the partition. The elastic interlayer is placed in the panel, perpendicular to the its surfaces and fully occupying the panel thickness. When the interlayer assumes the properties of a resilient material, it is able to reduce the wave propagation through the elastic medium of the partition. The model is excited by a harmonic line load that acts either in the fluid medium or in the elastic medium in the direction perpendicular to the panel's surface. The model is developed following a direct frequency domain formulation which assumes full coupling between the fluid media and the elastic media. Analytical Green's functions for an elastic single layer bounded by fluid media are used to avoid having to discretize the horizontal surfaces of the partition. Numerical simulations are displayed in order to illustrate the applicability of the proposed model to the analysis of airborne and impact sound insulation when an elastic interlayer is inserted into a single partition.

4pSAc5. Numerical analysis of airborne and impact sound insulation between non-contiguous acoustic spaces using the Boundary Element Method. Andreia Pereira (University of Coimbra, Department of Civil Engeneering - Pólo II da Universidade - Rua Luís Reis Santos, 3030-788 Coimbra, Portugal, apereira@dec.uc.pt), António Tadeu (University of Coimbra, Department of Civil Engeneering - Pólo II da Universidade - Rua Luís Reis Santos, 3030-788 Coimbra, Portugal, tadeu@dec.uc.pt), Paulo Santos (University of Coimbra, Department of Civil Engeneering - Pólo II da Universidade - Rua Luís Reis Santos, 3030-788 Coimbra, Portugal, pfsantos@dec.uc.pt)

In this paper a Boundary Element Method (BEM) is used to predict the acoustic behaviour provided by four two-dimensional acoustic closed spaces separated by slabs and walls, surrounded by an elastic infinite medium. The walls and slabs are modelled as single partitions. The model is excited by cylindrical loads in the form of an airborne sound source placed in the acoustic space or an impact sound source acting on the slab, perpendicular to its surface. The formulation is developed following a direct BEM approach which assumes full coupling between the fluid medium and the elastic medium. The model requires the discretization of all interfaces and allows the analysis in the low and medium frequency range. A numerical analysis is performed to study airborne and impact sound insulation between acoustic non-contiguous spaces, where the sound pressure level which is established in the receiving room is due to flanking transmission. The influence of the structure's stiffness on the sound insulation is discussed for varying thicknesses of slabs and walls. The acoustic behaviour of the structure is described by sound insulation curves and average vibration velocity level curves of the walls and slabs and the results are discussed.

4pSAc6. Influence of temperature on sound transmission through viscoelastic sandwich plates. Samir Assaf (ESTACA, 34 rue Victor Hugo, 92300 Levallois Perret, France, sassaf@estaca.fr), Mohamed Guerich (ESILV, 92916 Paris la Défense, France, mohamed.guerich @devinci.fr)

A numerical study to investigate the effects of temperature on the diffuse sound transmission loss (TL) of sandwich plates is presented. The numerical prediction tool used is based on a finite element formulation for the sandwich plate coupled to a boundary element method for the acoustic medium. The plate formulation is derived from Kirchhoff's theory for the elastic faces and Mindlin's theory for the core. The frequency-temperature dependence of the viscoelastic material properties are taken into account using an experimentally derived viscoelastic constitutive law. The results presented deal with a laminated glass subjected to a diffuse sound field. It is found that the dip of the TL curve at the coincidence frequency of the plate is totally removed for temperatures where this frequency is in the transition region of the used viscoelastic material. Indeed, the relative low value of the storage modulus and the high value of the loss factor in this region induce high transverse shear deformations of the viscoelastic interlayer and thus high energy losses.

4pSAc7. A transmission loss definition based on the root mean squared intensity. Ysbrand H. Wijnant (University of Twente, Dept. Mechanical Engineering, P.O. Box 217, 7500 AE Enschede, Netherlands, Y.H.Wijnant @ctw.utwente.nl)

Numerical simulation enables the calculation of the sound power transmitted through any structure for any arbitrary source but it can not be used to determine transmission loss, which is based on the transmitted power divided by the incident power. One can calculate the active power (= incident minus reflected power), but one generally can not determine the incident and reflected power themselves. In fact, apart from 1 dimensional analysis, transmission loss is only defined for diffuse sound fields and it only quantifies the acoustical performance of the structure for this field and not for the actual, in-situ, source. While the incident power can not be determined, the active and root mean squared power can. The latter quantity is introduced and is a measure for the total energy flow per period, i.e. the net energy flow and the energy flowing back and forth. A transmission loss definition based on the ratio between the active power and the root mean squared power is

shown to closely resemble the transmission loss in the 1 dimensional case. Results for a 2 dimensional case show that the ratio is a quantity which does characterize the transmission of the structure as it is excited by the source.

4pSAc8. Fast solutions in FSI-Problems using CMS-Methods. Johannes Guggenberger (Mueller-BBM, Robert-Koch-Str. 11, 82152 Planegg, Germany, johannes.guggenberger@muellerbbm.de)

Parameter studies in FSI-problems may often become quite time consuming. In most cases the fluid parameters are well defined and only the influence of the parameters of the solid is subject to investigate. Therefore it would be desirable to investigate the fluid and solid part separately and finally combine them using CMS-Methods. This approach would also provide a good physical insight into the individual and combined behaviour of the components fluid and solid. Generally for each interface DOF one constraint mode must be added to the modal base. Since in most problems in FSI the fluid-structure interface involves many DOF the general CMS approach becomes inefficient. To reduce the number of constraint modes it is proposed to use the mode shapes of each component as a load function on the other domain. The static solution provides the modal based constraint modes. Their number corresponds to the number of total component modes which is in most cases much less then in the classic approach. The application is shown in optimization, updating, and monte-carlo-simulation problems.

THURSDAY AFTERNOON, 3 JULY 2008 ROOM 250B, 2:00 TO 3:40 P.M.

Session 4pSCa

Speech Communication: Articulatory Modeling and Control of Speech and Singing Organs

Maureen Stone, Cochair
Vocal Tract Visualization Lab, Depts of Biomedical Sciences and Orthodontics, University of Maryland Dental School, 650 W. Baltimore St., Baltimore, MD 21201, USA

Phil Hoole, Cochair
Institut für Phonetik und Sprachverarbeitung, Schellingstr. 3, München, 80799, Germany

Invited Papers

2:00

4pSCa1. Issues in the acoustic modeling of the vocal tract - a progress report on APEX. Björn Lindblom (Stockholm University, Universitetsvägen 10C, SE10691 Stockholm, Sweden, lindblom@ling.su.se), Johan Sundberg (KTH, Department of Speech, Music and Hearing, Lindstedtsvägen 24, SE-100 44 Stockholm, Sweden, jsu@csc.kth.se)

Faced with an acoustic record of the human voice an investigator is often led to wonder: How was this sample produced? Direct articulatory measurements lacking, the researcher may nonetheless find information of value by resorting to numerical models that relate cavity shapes to acoustic parameters. The classical 'three-parameter models' exemplify this type of tool. The APEX model is another example, developed to help answering questions about the acoustic consequences of articulatory movements. Based on X-ray measurements from a single speaker, APEX converts input specifications for articulatory parameters such as jaw, lips, larynx, tongue tip and tongue body into formant frequencies. The introduction of independent control of the jaw and the tongue and the fact that possible tongue shapes are specified relative to a neutral reference tongue have made significant insights into various topics possible (e.g., coordination jaw/tongue in singing, compensatory articulations). Recently we have been able to increase the physiological realism of APEX representations using MRI and X-ray data. We have also investigated physical models to improve the treatment of certain 3-D front cavity configurations such as raised tongue blade and spread lips. The goal of our paper is to present an overview of the most recent version of APEX.

2:20

4pSCa2. Articulatory comparison of spoken and sung vowels based on MRI. Pierre Badin (Département Parole & Cognition, GIPSA-lab, 46, avenue Félix Viallet, 38031 Grenoble Cedex, France, pierre.badin@gipsa-lab.inpg.fr), Nathalie Henrich (Département Parole & Cognition, GIPSA-lab, 46, avenue Félix Viallet, 38031 Grenoble Cedex, France, Nathalie.Henrich@gipsa-lab.inpg.fr), Laurent Lamalle (Plateforme régionale IRM 3Tesla, IFR n° 1, RMN Biomédicale : de la cellule à l'homme, CHU de Grenoble, BP 217, 38043 Grenoble Cedex 9, France, Laurent.Lamalle@ujf-grenoble.fr)

Understanding the differences of articulatory strategies between spoken and sung vowels is of interest to both speech and singing research. We have thus used MRI to record midsagittal images from three subjects producing sustained vowels with various characteristics. The subjects were a professional lyric soprano, a semi-professional soprano, and a semi professional bass. They were instructed to produce combinations of (1) the ten French or the five Italian oral vowels, (2) speaking, amateur singing, or professional singing modes, (3) chest or falsetto registers, (4) pitch levels varying from B2 (120 Hz) to F5 (700 Hz). Any combination that the subject would not feel comfortable with was excluded from the corpus. The midsagittal contours of the vocal organs (jaw, lips, tongue, velum, pharyngeal wall, hyoid bone, etc.) were manually traced on each image, and a number of articulatory measurements (jaw or hyoid bone height, lip aperture, tongue position, etc.) were automatically derived. Our contribution analyses the influence of the various production conditions on these articulatory characteristics, such as the jaw aperture increase related to pitch increase, or the lower position of the larynx for singing in comparison to speech. Some acoustics considerations will be discussed as well.

2:40

4pSCa3. Resonance characteristics of the hypopharyngeal cavities. Kiyoshi Honda (Phonetics & Phonology Laboratories, UMR-7018-CNRS & University of Paris III, 19, rue des Bernardins, 75005 Paris, France, honda@atr.jp), Tatsuya Kitamura (Konan University, Okamoto 8-9-1, Higashinada, 658-8501 Kobe, Japan, t-kitamu@konan-u.ac.jp), Hironori Takemoto (ATR Cognitive Information Science Laboratories, 2-2-2 Hikaridai, Seika-cho Soraku-gun, 619-0288 Kyoto, Japan, takemoto@atr.jp), Parham Mokhtari (ATR Cognitive Information Science Laboratories, 2-2-2 Hikaridai, Seika-cho Soraku-gun, 619-0288 Kyoto, Japan, parham@atr.jp), Seiji Adachi (Fraunhofer Institute for Building Physics, Nobelstrasse 12, 70569 Stuttgart, Germany, seiji.adachi@ibp.fraunhofer.de)

The hypopharyngeal cavities are the narrow, complex parts of the lower vocal tract that include the supraglottal laryngeal cavity and bilateral cavities of the piriform fossa. These small regions exhibit rather strong acoustic influence on vowel spectra in the higher frequencies and contribute to determining voice quality and speaker characteristics. The laryngeal cavity functions nearly as a Helmholtz resonator to generate an extra formant in the vicinity of 3 kHz, and the piriform fossa forms a pair of side-branches of the vocal tract to cause spectral zeros in the vicinity of 4-5 kHz. Vocal-tract models without employing these acoustic effects can hardly simulate natural-sounding voices of a particular speaker. Therefore, realistic acoustic models of vowel production must include the three functional components: glottal source sounds, hypopharyngeal-cavity coupling, and resonance of the vocal-tract proper. This presentation demonstrates the results from acoustic experiments on solid vocal-tract models and computer simulations of the cavities' effects based on our MRI-based visualization of the vocal tract. A possible control for singing voice qualities will be discussed based on the three-component model.

3:00

4pSCa4. Observation of voice registers. Ken-Ichi Sakakibara (Health Sciences University of Hokkaido, 2jo-5chome, Kita-ku, 002-8072 Sapporo, Japan, quesokis@gmail.com), Hiroshi Imagawa (Department of Otolaryngology, University of Tokyo, 7-3-1, Hongo, Bunkyo-ku, 113-8655 Tokyo, Japan, imagawa@m.u-tokyo.ac.jp), Miwako Kimura (Department of Otolaryngology, University of Tokyo, 7-3-1, Hongo, Bunkyo-ku, 113-8655 Tokyo, Japan, mkimu-tky@umin.ac.jp), Isao Tokuda (Japan Advanced Institute of Science and Technology, 1-1 Asahidai, Nomi-shi, 923-1292 Ishikawa, Japan, isao@jaist.ac.jp), Takaharu Nito (Department of Otolaryngology, University of Tokyo, 7-3-1, Hongo, Bunkyo-ku, 113-8655 Tokyo, Japan, taka.nito@nifty.com), Niro Tayama (International Medical Center of Japan, 1-21-1, Toyama, Shinjuku-ku, 162-8655 Tokyo, Japan, ntayama@imcj.hosp.go.jp)

In singing, voice register is one of the most salient aspects of voice quality, and it has therefore generated a lot of debates, acoustically, physiologically, and pedagogically. In singing, the voice registers can be physiologically classified into four categories: vocal fry, modal, falsetto, and whistle. In this study, vocal fold vibratory patterns appeared in each register were observed using high-speed images and simulated using the two-mass model. In vocal fry, three different vibratory patterns (aperiodic, subharmonic, and periodic with small open quotient) were observed. In addition, the simulation showed that transitions between the three different vibratory patterns are easy. In whistle, closure of the posterior part of glottis and rapid vibration of the anterior part were observed.

3:20

4pSCa5. Voice production modes and vocal tract shape in South-Siberian throat-singing. Sven Grawunder (Max Planck Institute for Evolutionary Anthropology, Deutscher Platz 6, 04103 Leipzig, Germany, grawunder@eva.mpg.de)

South-Siberian throat-singing features reinforced harmonics as carrier of sung melodies and enforced phonation modes. Available articulatory studies of throat-singers suggest that throat-singing makes use of three voice production mechanisms which result in two basic voice modes (mid tensed vs. low rough). Thus all three mechanisms share an excessive constriction of the larynx entrance i.e. approximation of the aryepiglottic folds and the epiglottis. The current study comprises acoustic data from 69 male singers. 25 singer were recorded by use of a field setting for acoustic, electroglottographic and subglottal resonance signal acquisition. Perturbation measures show dominance of individual variability over areal (cultural) factors, but strong influence of articulatory reinforcement strategies. The data also provide evidence for a model of reinforcement of harmonics by means of (1) voice source variation (closing phase, excitation strength), i.e. increased subglottal pressure, while air flow remains constant or lowered for the tensed mode; and double cycle modes involving mass bodies of upper laryngeal structures for the low mode; (2) formant merging due to multiple vocal tract constrictions including a coupling of source to the adjacent epilaryngeal tube of 1/6 vocal-tract length and bandwidth tuning as a result of adjustment of lip radiation.

Session 4pSCb

Speech Communication: General Topics in Speech Communication III (Poster Session)

Christine Shadle, Cochair
Haskins Laboratories

Sharon Coffey-Corina, Cochair
Center for Mind and Brain UC Davis

Bart De Boer, Cochair
Amsterdam, Netherlands

All posters will be on display from 3:40 p.m. to 5:20 p.m. To allow contributors an opportunity to see other posters, contributors of odd-numbered papers will be at their posters from 3:40 p.m. to 4:30 p.m. and contributors of even-numbered papers will be at their posters from 4:30 p.m. to 5:20 p.m.

Contributed Papers

4pSCb1. Feature extraction for vowel recognition using mellin transform. Mahdi Jamaati (Technical University of Shahrood, 12345 Shahrood, Iran, mahdi.jamaati@gmail.com), Milad Lankarany (Technical University of Shahrood, 12345 Shahrood, Iran, milad.lankarany@gmail .com), Hossein Marvi (Technical University of Shahrood, 12345 Shahrood, Iran, h_marvi@shahroodut.ac.ir)

This paper proposed a new feature extraction algorithm for vowel recognition using Mellin transform and MFCC. The scale transform is a particular restriction of the Mellin transform. The key property of the scale transform is the scale invariance. This algorithm consists of 3 main stages which are as follow. First stage contains, Extraction spectral envelope from vowels, by using cepstrum method. In the second stage, Mellin transform is used for mapping same vowels with different pitch and different vocal tract to the same waveforms. In third stage, we used a new MFCC algorithm in order to extract main parameters from the output of second stage. The new MFCC algorithm contains third and fourth order cumulant of log-mel-amplitudes. This new MFCC coefficients are robust in presence of additive white noise. Moreover, The LPC method has been used instead of MFCC method in third stage, Experimental result indicates that the new MFCC algorithm produced better result than LPC and original MFCC.

4pSCb2. Empirical articulatory-acoustic relations for vowels. Richard S. McGowan (CReSS LLC, 1 Seaborn Place, Lexington, MA 02420, USA, rsmcgowan@earthlink.net), Michael A. Berger (Dept. of Linguistics, Univ. of Rochester, 503 Lattimore Hall, Rochester, NY 14627-0096, USA, m.a .berger@sms.ed.ac.uk)

Vowels tokens were extracted from four talkers in the Wisconsin X-ray Microbeam Speech Production Database. The neighboring phonemes of these vowels were restricted to be non-nasal and non-liquid. The first three formant frequencies were measured using LPC analysis with manual corrections at a rate corresponding to the pellet trajectory sampling rate, thus yielding large amounts of simultaneous formant frequency and pellet position data points (between 11,000 and 20,000 for each talker.) Principal components analysis was performed for both the formant frequencies and the pellet position data, to produce three orthogonal acoustic components and four orthogonal articulatory components. A local linear regression technique, known as loess [Cleveland, W. S. and Devlin, S. J. (1988), J. Amer. Stat. Assoc., 83, 596 - 610], was applied to orthogonal components to map between the acoustic and articulatory domains. This technique permits regression slopes to vary within the domain of the independent variables. The results will be discussed in terms of optimization of loess parameters (e.g. size of local neighborhoods), goodness of fit of the mappings, and the degree to which slopes in the mappings vary. Manually corrected formant frequencies will be compared with fully automatic Line Spectral Frequencies. [Supported by NIDCD-001247 to CReSS LLC]

4pSCb3. Cross-language study of age perception by elderly listeners. Kyoko Nagao (Center for Pediatric Auditory and Speech Sciences, Nemours Biomedical Reserach, A.I. du Pont Hospital for Children, 1600 Rockland Road, Wilmington, DE 19803, USA, nagao@asel.udel.edu), Amanda K. Riley (Indiana University, Department of Speech and Hearing Sciences, 200 S Jordan Avenue, Bloomington, IN 47405, USA, mandieriley@gmail .com)

Recent studies show that perception of speaker's age is influenced by a listener's familiarity with the speaker's language. However, these results were based on young adult listeners. The current study examines whether language familiarity influences the perception of speaker's age in elderly listeners. The vowel stimuli was prepared from the sustained vowel /i/ collected from 30 native speakers of American English and 30 native speaker of Japanese. The sentence stimuli was taken from the reading of the North Wind and the Sun by these 60 speakers (in their native language). Fifteen elderly native speakers of English (mean age 73.5 years, range from 67 to 84 years) listened to both stimuli types and estimated the age of speakers. Correlation between perceived age and chronological age was moderate for the sentence stimuli, but weak for the vowel stimuli. Correlation between perceived age and chronological age was stronger when the listeners judged sentence stimuli in their native language than when they judged sentence stimuli in the foreign language ($r=0.74$ versus $r=0.63$). The vowel stimuli did not show the effect of speaker language. The results suggest that linguistic information has a critical role in age perception, regardless of listener's age.

4pSCb4. Acoustic tubes with maximal and minimal resonance frequencies. Bart De Boer (Spuistraat 210, 1012VT Amsterdam, Netherlands, b.g.deboer@uva.nl)

This paper presents a theoretical derivation of acoustic tract shapes that minimize and maximize resonance frequencies. The derivation is based on a symmetry of Webster's horn equation and on Ehrenfest's adiabatic invariance hypothesis. It is shown that for minimizing formant frequencies, abrupt transitions are necessary, while for maximizing resonance frequencies, gradual transitions are needed. It is argued that this has implications for modeling human, animal and prehistoric vocal tracts. Such models should

represent the anatomic (in)ability to produce abrupt and gradual transitions correctly, otherwise they would have biases towards different sets of formant frequencies than real vocal tracts.

4pSCb5. Rhythmic characteristics of prose and verse in varieties of Portuguese. Zinny Bond (Ohio University, 18 Maplewood Drive, Athens, OH 45701, USA, bond@ohio.edu), Verna Stockmal (Ohio University, 384 Gordy Hall, Athens, OH 45701, USA, grannymeem@hotmail.com), Emilia A. Marks (Ohio University, Department of Modern Languages, Athens, OH 45701, USA, markse@ohio.edu), Audra Woods (Ohio University, Speech and hearing sciences, Athens, OH 45701, USA, aw365402@ohio.edu)

Whether varieties of Portuguese differ in their rhythmic classification is not entirely clear. European Portuguese is generally considered to employ stress-based rhythm whereas the rhythmic classification of Brazilian Portuguese is disputed. Acoustically-based measures of rhythm have usually employed spoken prose passages for language samples. Possibly, the apparent rhythmic characteristics of language varieties may be clarified by employing different types of language materials. We selected spoken prose and traditional verse for investigation. Five native speakers of European Portuguese and five native speakers of Brazilian Portuguese recorded a sonnet consisting of 154 syllables and a short prose passage consisting of 270 syllables. From these recordings, acoustically based rhythm metrics, as suggested by Ramus, et al. [Cognition 73, 1999, 265-292] and Ling, et al. [Language and Speech 43, 2000, 377-401] were calculated. Measures of consonantal duration variability increased from spoken prose to spoken verse, suggesting that the talkers employed slower, more clearly articulated speech in reading the poem than in reading the prose passage. However, the two tasks did not clearly distinguish between the two varieties of Portuguese.

4pSCb6. Experimental study of turbulent flow sound production in presence of a simplified vocal tract constriction. Olivier Estienne (Département Parole & Cognition, GIPSA-lab, 46, avenue Félix Viallet, 38031 Grenoble Cedex, France, olivier.estienne @gipsa-lab.inpg.fr), Annemie Van Hirtum (Département Parole & Cognition, GIPSA-lab, 46, avenue Félix Viallet, 38031 Grenoble Cedex, France, annemie.vanhirtum@gipsa-lab.inpg.fr), Xavier Pelorson (Département Parole & Cognition, GIPSA-lab, 46, avenue Félix Viallet, 38031 Grenoble Cedex, France, pelorson@icp.inpg.fr), Helène Bailliet (Laboratoire d'Etudes Aerodynamiques - CNRS, Bat K, 40 avenue du recteur Pineau, 86022 Poitiers, France, helene.bailliet@lea.univ-poitiers.fr)

Sound production due to turbulence is widely shown to be an important phenomenon involved in a.o. fricatives, singing, whispering and speech pathologies. In spite of it relevance, only a few recent models are dealing with turbulence consequences during voiced sound production. The current study presents preliminary results of an experimental characterisation of the aeroacoustical effects of a turbulent flow in case of a constricted channel flow, by means of measuring the velocity fluctuations and the acoustic field downstream of the constriction. Aiming a future application in speech production, the influence of typical vocal tract shape parameters on the velocity distribution and sound field is explored: the tube shape and length as well as the degree, geometry and position of the constriction. The influence of the Reynolds number of the upstream flow is also observed. Results are discussed with respect to the upper airways and human sound production and will be exploited with respect to simplified models for velocity fluctuations and sound production.

4pSCb7. Influences of perceived racial identity on human talker identification. Tyler K. Perrachione (Massachusetts Institute of Technology, 77 Massachusetts Avenue, Cambridge, MA 02139, USA, tkp@mit.edu), Joan Y. Chiao (Northwestern University, 2029 Sheridan Road, Evanston, IL 60208, USA, jchiao@northwestern.edu), Patrick C. Wong (Northwestern University, 2240 Campus Drive, Evanston, IL 60208, USA, pwong@northwestern.edu)

Talker identification, the process by which human listeners recognize individuals by their voice, is one of the most poorly understood abilities of the human auditory system. Current psychological models of talker identification rely on strict analogies to face perception and the visual system, despite differences in the objects of perception in these two modalities. Here we investigate the existence of an own-race bias in voice perception - a phenomenon which has been pivotal in the study of face perception. Our results demonstrate an own-race bias in talker identification: listeners of different ethnic backgrounds show an advantage for identifying individual voices of the same race as themselves. However, unlike in vision, the own-race bias in talker identification manifests based specifically on the perceived, but not actual, race of a talker. The influence of perceived race suggests physical (voice structural) cues do not give rise to this effect. Instead, the own-race bias in talker identification is a result of listeners' asymmetric exposure to talkers' socially-acquired manners of expression (i.e. the dynamic features of voice and speech). Such manners of expression may be stereotypically associated with a particular ethnic group, although not actually exhibited by all members of that group. [Work supported by NIH]

4pSCb8. Signal densities and criterion variance in speech and nonspeech perception. Luis E. Lopez-Bascuas (Universidad Complutense Madrid, Facultad Psicologia, Campus Somosaguas, 28223 Madrid, Spain, lelopezb@psi.ucm.es)

The actual shape of signal densities has become an important issue when studying speech perception within the framework of Signal Detection Theory (SDT). Using an SDT model that allowed unequal criterion variances, López-Bascuas [Proc. Eurosp. 3, 2281-2283 (1995)] found that speech signals did not accommodate to the standard Gaussian assumption. However, Schouten and van Hessen [J. Acoust. Soc. Am. 104, 2980-2990 (1998)] measured response distributions directly and, assuming an interval scale, concluded that the Gaussian assumption held for both continua. Nevertheless, Pastore and Macmillan [J. Acoust. Soc. Am. 111, 2432 (2002)] applied ROC analysis to Schouten and van Hessen's data and their curves supported the Gaussian assumption for the nonspeech signals only. Later, López-Bascuas et al. [J. Acoust. Soc. Am. 115, 2465 (2004)] showed that non-linear z-transformed ROCs are not sufficient evidence for postulating non-gaussian signal densities. In this paper we try to figure out whether unequal criterion variances could underlie non-linear z-transformed ROCs by fitting a restricted Thurstonian SDT-like model to a nonspeech continuum composed by white noise and a square wave. The results indicate that unequal criterion variances is the possible cause of the deviant ROCs for nonspeech.

4pSCb9. Perception of reduced speech: Approximated stops. Natasha Warner (University of Arizona, MPI NIjmegen, Box 210028, Dept. of Linguistics, Tucson, AZ 85721-0028, USA, nwarner@u.arizona.edu), Tucker V. Benjamin (University of Alberta, Dept. of Linguistics, 4-32 Assiniboia Hall, Edmonton, AB T6G 2E7, Canada, bvtucker@ualberta.ca), Amy Fountain (University of Arizona, MPI NIjmegen, Box 210028, Dept. of Linguistics, Tucson, AZ 85721-0028, USA, avf@u.arizona.edu)

Natural, spontaneous speech often shows extreme reductions of many speech segments, to the point of apparent deletion. Where the flap allophone of /t/ and /d/ is expected in American English, one frequently sees an approximant-like or even vocalic pattern, rather than a clear flap. Still, such tokens are usually perceived as containing a /t/ or /d/ (e.g. 'needle' even with a very reduced /d/ is usually not perceived as 'kneel'). The current work identifies acoustic characteristics of reduced 'flaps' and presents phonetic identification data for continua that manipulate these characteristics. Presence vs. absence of a dip in intensity, duration of that dip, and degree of that dip in decibels are manipulated. Degree of intensity dip has the strongest effect, with a minimal dip in intensity more likely to be perceived as 'kneel' and a strong dip in intensity more likely to be perceived as 'needle.' The results indicate that all three of these characteristics do affect listeners' percept of a consonant, but not sufficiently to completely account for the percept. Listeners are sensitive to the acoustic characteristics of consonant reduction, but they are also very skilled at evaluating variability along the acoustic dimensions that realize reduction.

4pSCb10. Amplitude modulation shape and speech intelligibility. Garreth Prendergast (The University of York, Heslington, YO10 5DD York, UK, garreth.prendergast@ynic.york.ac.uk), Sam R. Johnson (The University of York, Heslington, YO10 5DD York, UK, sam@ynic.york.ac.uk), Gary G. Green (The University of York, Heslington, YO10 5DD York, UK, gary.green@ynic.york.ac.uk)

Research has demonstrated that low frequency amplitude modulations in speech signals are crucially important to maintaining intelligibility. The current work demonstrates a flexible way of characterising the pulsatile bursts of energy found in the temporal envelopes of sub-band filtered speech. Speech was passed through a 128-filter Gammatone filterbank and the temporal envelope of each filter extracted using the Hilbert transform. Thirty-five raised cosine pulses were fitted to model the envelope of each filter and each pulse was defined by its amplitude, half-duration and centre position. The distribution of these pulses demonstrates that the most commonly found pulse half-duration in speech is around 10 ms and few pulses have half-durations longer than 25 ms. Highly intelligible vocoded speech is generated using the extracted pulses and these measures suggest that the auditory system may signal the position in time of the amplitude modulations rather than representing low-frequency information. This method creates a flexible framework within which to further probe the mechanisms involved and allows the ability to focus on cross-channel information in the time domain.

4pSCb11. Training English vowels for French speakers with varying English experience. Paul Iverson (University College London, Department of Phonetics and Linguistics, 4, Stephenson Way, NW1 2HE London, UK, p.iverson@ucl.ac.uk), Melanie Preece-Pinet (University College London, Department of Phonetics and Linguistics, 4, Stephenson Way, NW1 2HE London, UK, m.pinet@ucl.ac.uk)

It is clear that high-variability phonetic training can improve speech perception for adult second-language learners, but it is uncertain what levels of processing are responsible for this change and whether this interacts with the previous experience of the learners. The present study investigated these issues by giving auditory training to French speakers with varying degrees of English experience. Listeners completed 8 sessions of high-variability identification training with clusters of minimal-pair words (e.g., sleet, slit, slight, slate) and a different speaker in each session. The pre/post tests evaluated changes in vowel perception using open-set identification in quiet and noise, a 3-interval category discrimination task, and a task in which individuals mapped their best exemplars for English vowels in a space that included formant movement and duration. The preliminary results suggest that French speakers improved substantially in their identification performance (about 20 percentage points), without having large changes in their ability to discriminate these categories. The results support a view that training improves the process of applying phonetic category knowledge, without changing the underlying categories themselves.

4pSCb12. Computerized assessment and training of the perception of American English (AE) speech sounds by adult learners of English. James Miller (Communication Disorders Technology, Inc., Indiana Univeristy Research Park, 501 N. Morton Street Sta 215, Bloomington, IN 47404, USA, jamdmill@indiana.edu), Roy Sillings (Communication Disorders Technology, Inc., Indiana Univeristy Research Park, 501 N. Morton Street Sta 215, Bloomington, IN 47404, USA, rsillings@comdistec.com), Charles S. Watson (Communication Disorders Technology, Inc., Indiana Univeristy Research Park, 501 N. Morton Street Sta 215, Bloomington, IN 47404, USA, watson@indiana.edu), Isabelle Darcy (Indiana University, Dept. of Second Language Studies, Memorial Hall 315, 1021 E. Third Street, Bloomington, IN 47405, USA, idarcy@indiana.edu), Kathleen Bardovi-Harlig (Indiana University, Dept. of Second Language Studies, Memorial Hall 315, 1021 E. Third Street, Bloomington, IN 47405, USA, bardovi@indiana.edu)

Fourteen volunteer students, with first languages other than English and enrolled in English pronunciation classes, used a specialized software program, the ″Speech Perception Assessment and Training System (SPATS).″ The software was made available in a language laboratory for seven weeks. Students used the program between 3 and 19 hours, the mean being 13 hours. The goal of SPATS is to train the perception of English words as they are produced in naturally spoken, fluent sentences. The average student correctly identified 1723 words in 313 different sentences as spoken by 10 different talkers and also attempted to identify a total of 7530 presentations of syllable onsets, nuclei, or codas as spoken by 8 different talkers in several phonetic contexts. These syllable constituents were presented in quiet, the sentences in moderate amounts of 12-talker babble. All showed significant progress in perception of AE speech sounds, a few approaching the levels of native speakers. By extrapolation, with 20 to 30 hours of program use nearly all might approach the perceptual performance of native speakers. Those that returned post-training questionnaires viewed the program favorably and recommended its use in regular classes. Speech samples were collected. Accent ratings and spectrographic analyses will be presented.

4pSCb13. Integrated magnetic resonance imaging methods for speech science and technology. Shinobu Masaki (ATR Cognitive Information Science Laboratories, 2-2-2 Hikaridai, Seika-cho Soraku-gun, 619-0288 Kyoto, Japan, masaki@atr.jp), Yukiko Nota (National Institute of Information and Communications Technology/ATR Cognitive Information Science Laboratories, 2-2-2 Hikaridai, Seika-cho, 619-0288 Kyoto, Japan, ynota@atr.jp), Sayoko Takano (ATR Cognitive Information Science Laboratories, 2-2-2 Hikaridai, Seika-cho Soraku-gun, 619-0288 Kyoto, Japan, tsayoko@atr.jp), Hironori Takemoto (ATR Cognitive Information Science Laboratories, 2-2-2 Hikaridai, Seika-cho Soraku-gun, 619-0288 Kyoto, Japan, takemoto@atr.jp), Tatsuya Kitamura (Konan University, Okamoto 8-9-1, Higashinada, 658-8501 Kobe, Japan, t-kitamu@konan-u.ac.jp), Kiyoshi Honda (Phonetics & Phonology Laboratories, UMR-7018-CNRS & University of Paris III, 19, rue des Bernardins, 75005 Paris, France, honda@atr.jp)

This presentation introduces our integration of magnetic resonance imaging (MRI) techniques at ATR Brain Activity Imaging Center (Kyoto, Japan) toward research into speech science and technology. The first breakthrough in our application of MRI to speech research was the motion imaging of the speech organs in articulation using a cardiac cine-MRI method. It enables us to acquire information in the time-space domain to reconstruct successive image frames using utterance repetitions synchronized with MRI scans. This cine-technique was further improved for high-quality imaging and expanded into three-dimensional (3D) visualization of articulatory movements. Using this technique, we could successfully obtain temporal changes of vocal-tract area function during a Japanese five-vowel sequence. This effort also contributed to developing other techniques to overcome the limitations of MRI, such as the post-hoc inclusion of teeth images in 3D volumes or the phonation-synchronized scan for crystal-sharp static imaging. Further, a custom high-sensitivity coil was developed to visualize the fine structures of the lip muscles and laryngeal airway. The potentials of new MRI approaches such as ultra-high-resolution imaging with a higher-field scanner or real-time motion imaging during a single utterance will be discussed toward future contributions to speech science and technology.

4pSCb14. Acoustic characteristics of solid vocal tracts modeled from ATR MRI database of Japanese vowel production. Tatsuya Kitamura (Konan University, Okamoto 8-9-1, Higashinada, 658-8501 Kobe, Japan, t-kitamu@konan-u.ac.jp), Hironori Takemoto (ATR Cognitive Information Science Laboratories, 2-2-2 Hikaridai, Seika-cho Soraku-gun, 619-0288 Kyoto, Japan, takemoto@atr.jp), Kiyoshi Honda (Phonetics & Phonology Laboratories, UMR-7018-CNRS & University of Paris III, 19, rue des Bernardins, 75005 Paris, France, honda@atr.jp)

″ATR MRI database of Japanese vowel production″ provides volumetric magnetic resonance images and speech data of the five Japanese vowels produced by a male native Japanese speaker. In this study, the database was used to evaluate acoustic characteristics of vocal tracts for five Japanese vowels; we measured frequency responses of realistic vocal tract solid models formed by a stereo-lithographic technique. The model's glottis was sealed with a plastic plane with a 1.2-mm hole. A time-stretched pulse signal generated from a horn driver unit was introduced into the solid model at the lip end. The response signals of the models were recorded at the model's glottis from the hole by a probe microphone. This method permits accurate measurement of acoustic characteristics of the vocal tract including the laryngeal cavity, which generates the laryngeal cavity resonance during closed-glottis periods of phonation [H. Takemoto et al., JASA, 120, 2228-

2238 (2006), T. Kitamura et al., JASA, 120, 2239-2249 (2006)]. The results provide a benchmark for evaluating numerical analysis methods, such as transmission line models, finite element methods, and finite difference-time domain-methods, which have been used to study vocal tract acoustics. [Work supported by SCOPE (071705001) of Ministry of Internal Affairs and Communications, Japan.]

4pSCb15. Linguistic versus non-linguistic processing of speech prosody in dichotic listening. Ritsu Kanamura (Graduate School of Comprehensive Scientific Research, Prefectural Univ. of Hiroshima at Mihara, 1-1 Gakuen-machi, 723-0053 Mihara, Japan, bulle.de.savon.von.von@gmail.com), Satoshi Imaizumi (The Prefectural Univ. of Hiroshima, 1-1 Gakuen-machi, 723-0053 Mihara, Japan, imaizumi@pu-hiroshima.ac.jp)

Linguistic and non-linguistic information processing of speech prosody are studied using two dichotic listening tasks, a Word task and a F0 task. During the Word task, subjects were required to identify either right- or left-ear stimulus from two-syllable homophonic words presented with different pitch accents. During the F0 task, subjects were required to identify either right- or left-ear stimulus from F0 partials extracted from the words used in the Word task. The correct percent of responses was high and RT was short for high familiarity words presented to the right ear rather than the others under the Word task, while no such differences were found under the F0 task. RT of the Word task was shorter than the F0 task. These results suggest that the processing of linguistic speech prosody under dichotic listening conditions is based on the interactive auditory and linguistic neural resources with right- ear or left-hemispheric dominance, and are faster than auditory F0 pattern identification. The tasks developed can be used to detect central auditory processing disorders.

4pSCb16. Broader range of training voices improves performance of HMM model of phonemic identification. J Parchment (University of Arizona, Dept. of Linguistics, Douglass Building, Room 200E, Tucson, AZ 85721, USA, jparch@u.arizona.edu)

A model proposed by Lin (2005) learns phonetic categories from waveform input. Recorded speech from a set of male talkers is divided into training and test sets. The training set is separated into phonemes, subjected to cepstral analysis, and used as the input to a Hidden Markov Model, which clusters the phonemes into phonemic categories. After this unsupervised learning process, the model is then able to accurately identify speech segments in the test set, showing that relevant acoustic information is captured by the model. The current study explores the outcome when a model of this type is trained on a range of talkers differing in sex and vocal tract configuration. Preliminary results suggest that this approach can improve performance when testing is generalized to a wider range of new talkers. However, too wide a range of training voices reduces accurate categorization, while too narrow a range reduces generalizability. Continuing efforts seek to quantify the optimum range of training voices and to identify the variables that can predict the degree of improvement in performance on test voices. This work has implications for automatic speech recognition models as well as for issues of speaker normalization.

4pSCb17. A Method of Co-registering Multiple Magnetic Resonance Imaged Vocal Tract Volumes for Fricatives. Michael I. Proctor (Haskins Laboratories, 300 George St, New Haven, CT 06511, USA, proctor@haskins.yale.edu), Christine Shadle (Haskins Laboratories, 300 George St, New Haven, CT 06511, USA, shadle@haskins.yale.edu), Khalil Iskarous (Haskins Laboratories, 300 George St, New Haven, CT 06511, USA, iskarous@haskins.yale.edu)

In a study of fricative production, Magnetic Resonance Imaging was used to acquire three-dimensional tract geometries of fricatives produced in four different vowel contexts. Short scan sequences were used to image multiple productions of each fricative in a single session. Although minimizing the number of tokens, this resulted in a coarser spatial resolution in some parts of the tract, which required a different approach to assembling vocal tract volumes. Sagittal, axial and oblique-coronal imaging orientations were chosen to best resolve the tract in the mid-sagittal plane, the pharynx, and around the fricative constriction. Each fricative token was acquired using a 37 second imaging sequence. Dental impressions were imaged separately. Three corresponding point clouds were created by sampling air-tissue boundaries in each image stack, and aligned using anatomical landmarks on the face and spinal column, creating a single, multiply-sampled volume. Area functions were estimated using the most suitable data source at each region of the tract. Vocal tract models were constructed for eight fricatives produced in four vowel contexts by four speakers of American English. The advantages of this method of tract modeling, and its automatic application to potentially variable MRI data sources will be discussed. [Funded by NIH-NIDCD-RO1-DC006705]

4pSCb18. Acoustical analysis of Canadian and Parisian French word-final vowel productions in varying phonetic contexts. Franzo Law (CUNY Graduate Center, 365 5th Avenue, Program in Speech-Language-Hearing Sciences, New York, NY 10016, USA, flaw@gc.cuny.edu), Winifred Strange (CUNY Graduate Center, 365 5th Avenue, Program in Speech-Language-Hearing Sciences, New York, NY 10016, USA, strangepin@aol.com)

Dialects can differ greatly in their phonetics and phonology, and can diverge to a great degree in vowel production. This study explores the acoustic nature of Canadian French (CF) vowels in word-final position, relative to those of Standard Parisian French (PF). CF and PF male participants were recorded producing minimal sets of words, differing in the final vowels /i y e ″epsilon″ a ″o-bar″ o u/, embedded in carrier phrases. Real-word minimal sets were constructed using words with final vowels preceded by labial, coronal, and back stops and fricatives. (Monosyllabic CV words were used whenever possible; VCV and CCV words were used when no CV word was available.) Nonsense disyllabic minimal sets were also recorded with vowels preceded by labial, coronal, and back stops in the following context: /gisCV/. Of particular interest was the stability of the /e - ″epsilon″/ distinction in word-final position for Parisian French, which was maintained in preliminary results. Across-syllable boundary coarticulatory effects are also discussed. This is the first part of a larger study investigating second-language lexical and morphosyntactic CF vowel perception by English learners of French. [Work supported by NIH F31DC008075]

4pSCb19. An MRI Study of the Effect of Vowel Context on English Fricatives. Christine Shadle (Haskins Laboratories, 300 George St, New Haven, CT 06511, USA, shadle@haskins.yale.edu), Michael I. Proctor (Haskins Laboratories, 300 George St, New Haven, CT 06511, USA, proctor@haskins.yale.edu), Khalil Iskarous (Haskins Laboratories, 300 George St, New Haven, CT 06511, USA, iskarous@haskins.yale.edu)

To gain a better understanding of the long-observed effects of vocalic context, the articulation of fricatives was investigated using Magnetic Resonance Imaging. Five speakers of American English were imaged while producing eight fricatives in the contexts [i-a-u-schwa]. Sagittal, axial and oblique-coronal volumes were acquired for each vowel-fricative combination. Acoustic recordings were made during scans and separately in an anechoic chamber. Vocal tract models were generated by aligning and superimposing all three stack orientations. The models reveal that a variety of articulatory strategies are employed in the production of English fricatives, and that vocalic context is significant. For some subjects, tongue shape differs little with vowel context; other subjects show highly varied tongue shape differences but little difference in lip rounding. Two subjects show significant variation with vowel context for every fricative, including [θ]; two show very little difference, even for [f]. The sublingual cavity in [sh] is extensive for two subjects, but only slightly bigger than in [s] for two other subjects. Tongue grooving in and behind the constriction also varies, and is especially evident in the oblique scans. Overall, more variation and effect of vowel context was observed than expected from the literature. [Funded by NIH-NIDCD-RO1-DC006705]

4pSCb20. F0 contour estimation based on time-varying complex speech analysis. Keiichi Funaki (Univ. of the Ryukyus, Senbaru 1, Nishihara, 903-0213 Okinawa, Japan, funaki@cc.u-ryukyu.ac.jp)

Robust F0 (Fundamental frequency) estimation plays an important role in speech processing such as speech coding and tonal speech recognition. We have already proposed robust F0 estimation algorithm based on time-varying complex AR (TV-CAR) speech analysis for analytic signal, in

which the weighted autocorrelation function is calculated using the complex residual and then the F0 is searched as the peak sample for each frame [IEICE Trans. on Fundamentals, Vol.E91-A.No.3] [IEICE Trans. on Fundamentals, Vol.E90-A, No.8]. Although the algorithm can estimate more robust F0 estimation for IRS filtered speech corrupted by additive noise, the algorithm cannot perform better for non-IRS filtered speech or slightly contaminated IRS-filtered speech. In addition, the frame-based F0 estimation cannot extract the F0 trajectories in the time-domain. In order to cope with the drawbacks, this paper proposes quite simple F0 contour estimation algorithm based on the TV-CAR speech analysis, in which the F0 contour is estimated by peak-picking for the estimated time-varying spectrum that is the same manner as formant frequency estimation. The experimental results demonstrate that the proposed method leads to more accurate continuous F0 estimation than the conventional one for high-pitched speech due to the nature of analytic signal for non-IRS filtered high-pitched female speech.

4pSCb21. Extraction of vocal tract area function from three-dimensional magnetic resonance images using digital waveguide mesh. Kenji Inoue (Osaka Institute of Technology, 4-18-15, Tanabe, Higashisumiyosi-ku, 546-0031 Osaka, Japan, chikuwa.bushi@gmail.com), Hironori Takemoto (ATR Cognitive Information Science Laboratories, 2-2-2 Hikaridai, Seika-cho Soraku-gun, 619-0288 Kyoto, Japan, takemoto@atr.jp), Tatsuya Kitamura (Konan University, Okamoto 8-9-1, Higashinada, 658-8501 Kobe, Japan, t-kitamu@konan-u.ac.jp), Shinobu Masaki (ATR Cognitive Information Science Laboratories, 2-2-2 Hikaridai, Seika-cho Soraku-gun, 619-0288 Kyoto, Japan, masaki@atr.jp), Hirotake Nakashima (Osaka Institute of Technology, 1-79-1, Kitayama, Hirakata, 573-0196 Osaka-fu, Japan, nakas@is.oit.ac.jp)

A method is proposed in this paper to extract the vocal tract area function from the three-dimensional magnetic resonance images. The proposed method uses the digital waveguide mesh, an implementation of the finite-difference time-domain (FDTD) method, to simulate wave propagation in the vocal tract from the glottis to the lips. The dimensions of the vocal tract areas are then calculated along the traveling wavefront that emerges from the simulation. Formant analysis has been conducted for Japanese vowels to show the validity of the proposed method. The calculated formant frequencies of the area functions obtained by the proposed method and other existing methods have been compared to those measured from the acoustic utterance of the imaged person.

4pSCb22. Increasing speech alignment through crossmodal speaker familiarity. Rachel M. Miller (University of California, Riverside, Department of Psychology, 900 University Ave., Riverside, CA 92521, USA, rmill002@ucr.edu), Kauyumari Sanchez (University of California, Riverside, Department of Psychology, 900 University Ave., Riverside, CA 92521, USA, ksanc004@student.ucr.edu), Lawrence D. Rosenblum (University of California, Riverside, Department of Psychology, 900 University Ave., Riverside, CA 92521, USA, rosenblu@citrus.ucr.edu)

In speech alignment phenomena, individuals inadvertently imitate aspects of another talker's utterances. Recent research has shown that when asked to shadow words, subjects not only align to the speech they hear, they also align to the speech they see when shadowing words by lipreading [Miller, et al., J. Acoust. Soc. Am., 120, 5, Pt. 2 (2006)]. This research also showed that some of the dimensions to which subjects align are the same whether based on shadowing of auditory or visual speech stimuli. This might mean that subjects can align to a speaker's idiolectic dimensions available in both modalities. To examine this possibility, an experiment was conducted to see if alignment increased with exposure to the same or a different speaker, across two blocks of presentations that were: a) both auditory; b) both visual; or c) one auditory and one visual. If subjects align to amodal, idiolectic speaker style, then alignment should be comparable across presentation types in the same speaker condition. Results revealed that alignment increased when the speaker was the same over the course of the two blocks regardless of presentation type. These results suggest that alignment can be based on amodal, idiolectic dimensions which are available across modalities.

4pSCb23. Perception of Japanese consonants by native speakers of American English. Takeshi Nozawa (Ritsumeikan University, College of Economics, 1-1-1 Nojihigashi, Kusatsu, 525-8577 Shiga, Japan, t-nozawa@ec.ritsumei.ac.jp)

Four native speakers of Japanese produced Japanese multi-syllable words and non-words, which include stops, fricatives, affricates, nasals and the liquid. Twelve native speakers of American English, who had never learned Japanese, heard their utterances and spelled out what they heard in English alphabet. What was of interest was whether native speakers of American English would perceive Japanese consonants in a way they are transcribed in English alphabet. The results revealed that Japanese stops were equated with generally the phonetically closest English stops, but voiceless stops were more likely to be equated with voiced stops of the same place of articulation than the other way around. Among voiced stops, /b/ and /d/ respectively were equated with /v/ and /l/. The word-initial /ts/, though words like ″tsunami″ have become part of English, was predominantly equated with /s/ rather than /ts/. The Japanese liquid, which is usually transcribed as /r/, was predominantly equated with /l/ rather than /r/. This agrees with results of previous research that demonstrate that English /r/ is more dissimilar from Japanese /r/ than English /l/ (See Aoyama et al. 2004).

4pSCb24. Synchronous speech and speech rate. Miran Kim (Suny, Dept. Linguistics, S201, SBS building, Stony Brook, NY 11794-4376, USA, mrkim@ic.sunysb.edu), Hosung Nam (Haskins Laboratories, 300 George St., Suite 900, New Haven, CT 06511, USA, nam@haskins.yale.edu)

Synchronously read speech has shown to reduce a high degree of speaker variability of reading exhibited by speakers in laboratory recording; e.g., pause placement and duration, and speech rate. However, quantitative analysis of speech rate has rarely been found in studies on synchronous speech. This study examines Mandarin Chinese (2 dialects from Taiwan and Shanghai), which is a syllable-time language and thus expected to exhibit a relatively stable speech rate, in both read-alone and read-together speech. Consistency and variability of speech rate are compared in both reading types across repetitions within a subject, across subjects, and across dialects. The results show that speech rate is more stable in read-together than in read-alone speech, and that speech rate in synchronous reading falls on a constant value of speech rate rather than on the average between the speakers' rates in pair. This global pattern is consistent across dialects, and stylized local variation of speech rate over prosodic units (Intonational phrase) is also observed unique to each dialect. We discuss how timing in synchronous speech cannot be accounted for only by dynamic entrainment of speakers with different speech rates and how there should also be rhythmic information shared by speakers of a language.

4pSCb25. Effects of auditory, visual, and audio-visual training on nonnative perception of English fricatives. Yue Wang (Simon Fraser Univ., RCB 9224, 8888 Univ. Dr., Burnaby, BC V5A 1S6, Canada, yuew@sfu.ca), Dawn Behne (Norwegian University of Science and Technology, Psychology Dept, NO 7491 Trondheim, Norway, dawn.behne@svt.ntnu.no), Angela Cooper (Simon Fraser Univ., RCB 9224, 8888 Univ. Dr., Burnaby, BC V5A 1S6, Canada, akcooper@sfu.ca), Haisheng Jiang (Simon Fraser Univ., RCB 9224, 8888 Univ. Dr., Burnaby, BC V5A 1S6, Canada, hdjiang@sfu.ca), Nina Leung (Simon Fraser Univ., RCB 9224, 8888 Univ. Dr., Burnaby, BC V5A 1S6, Canada, nhleung@alumni.sfu.ca), Jung-Yueh Tu (Simon Fraser Univ., RCB 9224, 8888 Univ. Dr., Burnaby, BC V5A 1S6, Canada, jta31@sfu.ca)

This study examines the effects of auditory (A), visual (V), and audio-visual (AV) training on nonnative speech perception. Mandarin Chinese natives were trained to perceive English voiceless fricatives (in monosyllabic words and nonwords) of three visually distinct places of articulation: interdentals nonexistent in Mandarin, labiodentals and alveolars common in both languages. Participants were randomly assigned to a control group or one of three 2-week (six sessions, 40 minutes/session) training groups with a dif-

ferent input modality: A, V, or AV. In pre- and post-tests, the fricatives are presented in four ways for an identification task: A-only, V-only, AV congruent (AVc), and AV incongruent (AVi). Additionally, three generalization posttests are administered testing voiced fricatives, new real words, and a new speaker. Results show that post-training, the trainees reveal: (1) improvements corresponding to training type (e.g., the V-training group improves most for the V-only stimuli), (2) greater improvements for the familiar (but less visually distinct) alveolars than for the new interdentals, (3) decreased AV-fusion for the AVi stimuli, and (4) consistent patterns in the generalization tests. Results are discussed in terms of the effects of speech input modality, experience, and L1 on L2 AV speech learning. [Research supported by SSHRC]

4pSCb26. Comparison of the brain regions for consonant processing in Japanese and English subjects. Yoshikazu Oya (Faculty of Systems Engineering, Wakayama University, 930 Sakaedani, 640-8510 Wakayama, Japan, s085067@sys.wakayama-u.ac.jp), Toshio Irino (Faculty of Systems Engineering, Wakayama University, 930 Sakaedani, 640-8510 Wakayama, Japan, irino@sys.wakayama-u.ac.jp), Alexis G. Hervais-Adelman (Centre for the Neural Basis of Hearing, Department of Physiology, Development and Neuroscience, University of Cambridge, Downing Site, CB23EG Cambridge, UK, alexis.hervais-adelman@mrc-cbu.cam.ac.uk), David T. Ives (Centre for the Neural Basis of Hearing, Department of Physiology, Development and Neuroscience, University of Cambridge, Downing Site, CB23EG Cambridge, UK, dti20@cam.ac.uk), Hideki Kawahara (Faculty of Systems Engineering, Wakayama University, 930 Sakaedani, 640-8510 Wakayama, Japan, kawahara@sys.wakayama-u.ac.jp), Roy D. Patterson (Centre for the Neural Basis of Hearing, Department of Physiology, Development and Neuroscience, University of Cambridge, Downing Site, CB23EG Cambridge, UK, rdp1@cam.ac.uk)

A recent fMRI study on speech-sound processing by Uppenkamp et al. [Neuroimage, 31(3), 1284-1296 (2006)] revealed that regions of the left and right, superior temporal gyri (STG) and anterior, superior temporal sulci (STS) respond preferentially to speech-like stimuli. Hervais-Adelman et al. [BSA London (2007)] extended this research to investigate the processing of consonant-vowel (CV) and vowel-consonant (VC) syllables and determine the locus of consonant-processing in the brain of English speakers. This paper reports an experiment with the same stimuli but with Japanese subjects for whom VC syllables are a novelty. In both the English and Japanese subjects, there was enhanced activity in left STS for vowels over non-speech sounds, as in Uppenkamp et al. (2006). A significant difference was observed between the responses to CV and VC syllables in left STS and planum temporale (PT). There was almost no CV-VC difference in the English subjects. The activity regions for VC syllables were larger than for CV syllables in Japanese subjects, probably because the Japanese subjects would have heard the VCs as two syllable speech sounds. Research supported by JSPS Grant-in-Aid [B18300060] and the UK-MRC [G0500221, G9900369].

4pSCb27. Influence of music education on second language acquisition. Barbara Pastuszek-Lipinska (Adam Mickiewicz University, al .Niepodleglosci 4, 61-874 Poznan, Poland, energin@wp.pl)

To explore the extent to which music education influences second-language acquisition, two groups of native Polish speakers, musicians and non-musicians, were asked to reproduce sentences in six languages: English, French, Italian, Spanish, Japanese, and Belgian Dutch. The speech stimuli were developed with a text-to-speech application and differed phonemically, phonostylistically, and in length. The paper includes results of a general auditory analysis of subjects' productions as well as the results of a web-based listening test with a panel of native speakers of the involved languages. All collected data were also analyzed with statistical tools. The results revealed that music education exerted a measurable impact on speech perception and production. Musicians outperformed non-musicians in the study. From the results, it appears that the influence of musical expertise extends beyond music processing to speech processing, and the strength of this influence is connected not only to auditory training. Therefore, the superior performance of the musicians in the task may be interpreted as evidence that music education is an enabling factor in the successful acquisition of a second language. It also indicates that the impact of musical training is not a myth, but has a scientific basis.

4pSCb28. The relation between articulatory and aerodynamic properties of single /t/, /S/ and their combination in /tS/ and /St/. Susanne Fuchs (ZAS, Schuetzenstr. 18, 10117 Berlin, Germany, fuchs@zas.gwz-berlin.de), Laura L. Koenig (Haskins Labs. and Long Island Univ., Brooklyn, New York, NY 11201-8423, USA, koenig@haskins .yale.edu)

Intraoral pressure changes during speech production are a result of different factors, such as articulatory movements (place and manner of articulation), subglottal pressure, and laryngeal-oral coordination. This study attempts to provide a better understanding of the relation between aerodynamics and articulation in single voiceless consonants and their combinations. We gathered electropalatographic data simultaneously with intraoral pressure data for 9 native speakers of German. During voiceless aspirated stop production intraoral pressure equalizes with subglottal pressure since an oral closure is formed and the glottis is open. During voiceless fricative production intraoral pressure is lower than in stop production since the air can escape through the oral constriction. In /t, S, St/ the intraoral pressure changes are highly correlated with the articulatory behaviour. However, the affricate /tS/ shows an unusual relationship with aerodynamics and articulation. Although an oral closure is formed, pressure rises at a later point and reaches its peak during the fricative. We interpret these findings with respect to a special laryngeal - oral coordination in affricates as reported in Hoole et al. (2003) who found a relatively late glottal opening during the stop portion of the affricate.

4pSCb29. Experimental study of the fluid-structure-acoustic interaction in a human voice model. Stefan Kniesburges (University Erlangen-Nuremberg, Institute of Fluid Mechanics, Cauerst. 4, 91058 Erlangen, Germany, stefan.kniesburges@lstm.uni-erlangen.de), Stefan Becker (University Erlangen-Nuremberg, Institute of Fluid Mechanics, Cauerst. 4, 91058 Erlangen, Germany, stefan.becker@lstm.uni-erlangen .de), Stefan Mueller (University Erlangen-Nuremberg, Institute of Fluid Mechanics, Cauerst. 4, 91058 Erlangen, Germany, stefan.mueller@lstm .uni-erlangen.de), Antonio Delgado (University Erlangen-Nuremberg, Institute of Fluid Mechanics, Cauerst. 4, 91058 Erlangen, Germany, adelgado@lstm.uni-erlangen.de), Gerhard Link (Univ. Erlangen-Nuremberg, Dept. of Sensor Technology, Paul-Gordan-Str. 3/5, 91052 Erlangen, Germany, gerhard.link@lse.eei.uni-erlangen.de), Manfred Kaltenbacher (Univ. Erlangen-Nuremberg, Dept. of Sensor Technology, Paul-Gordan-Str. 3/5, 91052 Erlangen, Germany, manfred.kaltenbacher @lse.eei.uni-erlangen.de), Michael Doellinger (University Hospital Erlangen, Department of Phoniatrics and Pediatric Audiology, Medical School, Bohlenplatz 21, 91054 Erlangen, Germany, michael.doellinger@uk-erlangen.de)

A fluid-structure-coupled in-vitro model was developed for the investigation of the physical processes of the human phonation. The setup enables to simulate self-sustained vocal fold oscillation and to analyse the resulting supraglottal flow field. Measurement techniques like high-speed flow visualization, Particle Image Velocimetry (PIV) of the time-dependent flow field, unsteady pressure measurement, vibration measurement by a Laser-Scanning-Vibrometer were applied. The acoustic field was simultaneously recorded. Analysis was performed regarding correlations between the acoustic field, the flow velocity and the displacement of the vocal folds. The results support the existence of the Coanda-effect during phonation as assumed in previous work. The flow attaches to one vocal fold just past the glottis and forms a spacious vortex behind the vocal folds. This behaviour is not linked to one vocal fold and changes stochastically from cycle to cycle. The analysis indicates, that the acoustic sound is primarily produced by the pressure fluctuation caused by the pulsating flow rate due to the opening and closing process of the vocal folds. We assume, that the structural sound and the turbulence-induced sound do have minor acoustical implication.

4pSCb30. FEM simulation of tongue deformation for /i/ with a four-cube model applied to tagged cine-MRI data. Sayoko Takano (ATR Cognitive Information Science Laboratories, 2-2-2 Hikaridai, Seika-cho Soraku-gun, 619-0288 Kyoto, Japan, tsayoko@atr.jp), Hiroki Matsuzaki (Hokkai-Gakuen University, 1-1, Minami-26, Nishi-11, Chuou-ku, 064-0926 Sapporo, Japan, matsu@eli.hokkai-s-u.ac.jp), Kunitoshi Motoki (Hokkai-Gakuen University, 1-1, Minami-26, Nishi-11, Chuou-ku, 064-0926 Sapporo, Japan, motoki@eli.hokkai-s-u.ac.jp)

Roles of extrinsic and intrinsic tongue muscles in the production of vowel /i/ were examined using a finite element method (FEM) applied to the tagged cine-MRI data. It has been thought that tongue tissue deformation for /i/ is mainly due to the combined actions of the genioglossus muscle bundles advancing the tongue root to elevate the dorsum with a mid-line grooving. A recent study with the tagging-MRI revealed earlier, faster and greater tissue deformation at anterior top of the tongue than posterior part during /ei/ production. This result implies the contribution of the intrinsic tongue muscle (transverse anterior) with an independent hydrostat mechanism from that of the genioglossus muscle bundles. In this study, a simple four-cube model is built to examine the co-contraction effect of the genioglossus and transverse muscles using using the FEM. The simulation result with the anterior transverse muscle (Ta) showed good agreement with the pattern of the tongue deformation obtained from the tagged-MRI data, suggesting that transverse anterior also plays an important role for the realization of the tongue shape for the production of vowel /i/.

4pSCb31. Classification of normal and pathological vocal fold vibrations using Phonvibrograms. Jörg Lohscheller (University Hospital Erlangen, Department of Phoniatrics and Pediatric Audiology, Medical School, Bohlenplatz 21, 91054 Erlangen, Germany, joerg.lohscheller@uk-erlangen.de), Daniel Voigt (Dept. Phoniatrics and Pediatric Audiology, Bohlenplatz 21, 91054 Erlangen, Germany, daniel.voigt@uk-erlangen.de), Michael Doellinger (University Hospital Erlangen, Department of Phoniatrics and Pediatric Audiology, Medical School, Bohlenplatz 21, 91054 Erlangen, Germany, michael.doellinger@uk-erlangen.de)

Clinical examination of voice disorders demands an endoscopical observation of vocal fold vibrations. High-speed endoscopy is the state-of-the-art technology for investigation of vocal fold vibrations. A novel visualization strategy is proposed which transforms the segmented contours of vocal fold edges into a set of two dimensional images, denoted Phonovibrograms (PVG). Within PVGs the individual type of vocal fold vibration becomes uniquely characterized by specific geometric patterns which can be seen as fingerprints of vocal fold vibration. The PVGs give an intuitive access on the type and degree of the laryngeal asymmetry which is essential to quantify the effects of functional and organic voice disorders. To determine the vibration characteristics within the computed PVG pattern recognition algorithms are applied. Thus, for each vocal fold the vibration type can be quantified and classified. The results of the PVG classification will be presented in 80 subjects (normal and pathological voices). It will be shown, that a classification of the vibration type can be performed very precisely even in disturbed vocal fold vibrations. The obtained PVG images can be documented and stored on a hard-disc using a lossless image data-format. The quantitative description of PVG patterns has the potential to realize a novel classification of vocal fold vibrations.

4pSCb32. Glottal-opening and airflow pattern during production of voiceless fricatives: a new non-invasive instrumentation. Kiyoshi Honda (Phonetics & Phonology Laboratories, UMR-7018-CNRS & University of Paris III, 19, rue des Bernardins, 75005 Paris, France, honda@atr.jp), Shinji Maeda (CNRS & ENST, 46, rue Barrault, 75634 Paris, France, maeda@tsi.enst.fr)

In the production of voiceless fricatives, the airflow passing through the vocal tract is controlled by reciprocal open-close patterns of the glottal and oral constriction. In order to observe such coordinated patterns, the authors have developed a combined method using a non-invasive (external-lighting and sensing) photoglottographic (ePGG) technique and a pressure-difference airflow mask. The former technique has the advantage of no restriction of phonetic environments (improvement from the standard PGG) and can be further combined with instrumentation of intraoral air pressure and/or of articulatory movements. Our PGG-airflow data are examined to address a question: It has been known that the glottis opens always wider for word-initial fricatives than for word-medial ones despite no obvious difference in acoustic and physiological requirements. It will be discussed whether the degrees of glottal opening during a fricative co-vary with other aerodynamic and articulatory controls in CVCV utterances with V = nonclose vowels.

4pSCb33. Mucosal wave analysis of a human vocal fold in the hemilarynx experiment. Michael Doellinger (University Hospital Erlangen, Department of Phoniatrics and Pediatric Audiology, Medical School, Bohlenplatz 21, 91054 Erlangen, Germany, michael.doellinger@uk-erlangen.de), David A. Berry (The Laryngeal Dynamics Laboratory, Division of Head & Neck Surgery, David Geffen School of Medicine at UCLA, 31-24 Rehab Center, 1000 Veteran Ave., Los Angeles, 90095-1794, USA, daberry@ucla.edu), Jörg Lohscheller (University Hospital Erlangen, Department of Phoniatrics and Pediatric Audiology, Medical School, Bohlenplatz 21, 91054 Erlangen, Germany, joerg.lohscheller@uk-erlangen.de)

The mucosal wave propagation was investigated in laboratory experiments across a variety of phonatory conditions. The focus was on the medial and superior surface dynamics of the vocal fold, which quantify mucosal wave propagation, but have been relatively little studied. High-speed, digital imaging of the entire surface of the vocal fold was performed using an excised human hemilarynx setup. Surface dynamics were characterized and differentiated across a variety of phonatory conditions. During sustained, flow-induced oscillation, the local maxima of vocal fold mucosal displacements, velocities and acceleration and their particular phase delays in the glottal cycle were investigated. Statistical analysis was performed, examining the influence of applied stimulations. Increasing the airflow yielded higher values for lateral displacements as well as higher velocity/acceleration values. Elongating the vocal fold resulted in decreased lateral displacements. The mucosal wave propagation apparently increased for higher flow, elongated folds, and higher adduction forces. While an understanding of the correlation between vocal fold dynamics and phonatory physiology/pathology is still in its infancy, the data presented here help to establish such connections. The data are also useful for the development and evaluation of physical and numerical models of vocal fold vibration.

4pSCb34. Categorical and non-categorical perception of speech: Behavioural and neural evidence. Jack C. Rogers (MRC Cognition and Brain Sciences Unit, 15 Chaucer Road, CB2 7EF Cambridge, UK, jack.rogers@mrc-cbu.cam.ac.uk), Matthew H. Davis (MRC CBU, 15 Chaucer Rd., CB2 7EF Cambridge, UK, matt.davis@mrc-cbu.cam.ac.uk)

What effects do within- and between-category variations have on the perception of speech? Using audio-morphing and the ″Straight″ channel vocoder (Kawahara, 2004), we produced 320 high-quality phonetic continua varying in place, manner and voicing including word/word (blade/glade), word/pseudo (blouse/glouse), pseudo/word (bown/gown) and pseudo/pseudo (blem/glem) pairs. A 2AFC task confirmed the category boundary shift for word/pseudo and pseudo/word pairs (Ganong, 1980), equivalent for onset (bench/gench) and offset (flad/flag) pairs. This suggests that lexical influences on categorical perception are not produced on-line but rather occur post-perceptually, consistent with top-down effects. Sensitivity to within- and between-category phonological variation was investigated using sparse fMRI in a paired auditory repetition priming paradigm. Minimal pairs (48 across the 4 stimulus groups) were presented to participants who listened in the context of a semantic monitoring task. Between-category pairs with a phonological change produced a greater neural response compared to within-category same pairs with the same magnitude of acoustic difference. This response to phonologically different pairs provides a neural correlate of categorical perception in left middle temporal, inferior frontal and pre-central regions. These responses in inferior frontal regions may contribute towards top-down influences on categorical perception of speech (cf Ganong Effect).

4pSCb35. Distinguishing Place of Consonant Articulation using the Aurora System. Yana Yunusova (University of Toronto, 160-500 University Ave, Toronto, ON M5G 1V7, Canada, yana.yunusova@utoronto.ca), Jeff Stanley (Northern Digital Inc, 103 Randall Drive, Waterloo, ON N2V 1C5, Canada, jstanley@ndigital.com), Jordan R. Green (University of Nebraska, 318O Barkley Center, Lincoln, NE 68583-0738, USA, jgreen4@unl.edu)

The goal of this project is to determine the effect of bite-block and speaking rate manipulation on lingual targets for consonants using a recently developed Aurora, a 3-D electromagnetic movement tracking system (NDI). Bite-block and speaking rate manipulations are common intervention techniques with speakers with dysarthria and apraxia of speech. Therefore, understanding their effect on consonant target regions is essential for predicting the outcomes of articulatory training in these clinical populations. In this project, articulatory positions of two sensors on the tongue tip and dorsum will be recorded independent of the head. Stops /t, k/ and fricatives /s, sh/ will be embedded in aCa syllables. A bite block condition will be used to eliminate jaw contribution to tongue movements. The location and size of articulatory regions associated with each consonant will be compared in bite block and no-block conditions. Additionally, the rate effect on the location and size of the consonant articulatory regions will be examined. Potential clinical implication of the finding on articulatory intervention will be considered.

4pSCb36. Discrimination of Mandarin tone 1 vs. tone 4 in disyllables by adult speakers of English. Shari Berkowitz (CUNY Graduate Center, Speech Acoustics and Perception Lab, 365 Fifth Avenue, New York, NY 10016, USA, shariellen@nyc.rr.com)

Previous research on cross-language perception of lexical tone has mainly used monosyllabic stimuli; however disyllables may be more difficult for non-natives to discriminate due to coarticulation and context effects (Berkowitz & Strange, 2007). Preliminary work suggests that there is an effect of context on discrimination of tone 1 vs. 4, despite the fact that this is usually considered an easy contrast when tested with monosyllabic stimuli. Disyllabic Mandarin nonsense words served as stimuli in a categorial same/different task. Pairings of tone 1 and tone 4 in initial and final position were tested in the context of all four tones. American English listeners with no background in tone languages completed the experiment without feedback. Data was scored with A' and was analyzed for effect of tone, initial vs. final position in the disyllable, and height and contour of the fundamental frequency. The results of this paradigm will be used to design a study of tone perception in preschool groups who speak Mandarin as their L1, English as their L1, and internationally adopted children who were previously exposed to Mandarin.

4pSCb37. Articulatory features influencing regressive place assimilation across word-boundaries in German. Marion Jaeger (Institut für Phonetik und Sprachverarbeitung, Schellingstr. 3, 80799 München, Germany, jaeger@phonetik.uni-muenchen.de), Phil Hoole (Institut für Phonetik und Sprachverarbeitung, Schellingstr. 3, 80799 München, Germany, hoole@phonetik.uni-muenchen.de)

Within current phonological theories the greater tendency of C1 nasals vs. C1 plosives to undergo regressive place assimilation is often treated as the consequence of acoustic-perceptual properties of nasality (e.g. Steriade, 2001). Little is known about the articulatory patterns underlying this asymmetry. Our current EMA study aims to test and compare the effects of manner of articulation of C1 (alveolar nasal vs. alveolar plosive), place of articulation of C2 (labial vs. dorsal plosive), vowel context (palatal /i/ vs. non-palatal vowel /a/), and word frequency upon the intra- and intergestural timing and movement magnitude of various articulators in C1C2 sequences across word-boundaries in German subjects. Our analyses of non-palatal vowel contexts in three speakers showed a greater likelihood of reduction of the tongue tip both in words with a nasal C1 and in high frequency words. For those word pairs in which tongue tip displacement was measurable, tongue tip - tongue back overlap was significantly greater in word pairs with a nasal C1 and in word pairs with high frequency words. On the other hand, tongue tip - lower lip overlap was only significantly greater in word pairs with high frequency words.

4pSCb38. Time-frequency detection of stridence in fricatives and affricates. Slobodan Jovicic (School of Electrical Engineering, University of Belgrade, Bulevar kralja Aleksandra 73, 11000 Belgrade, Serby, jovicic@etf.bg.ac.yu), Silvana Punisic (Institute for Experimental Phonetics and Speech Pathology, Gospodar Jovanova 35, 11000 Belgrade, Serby, iefpgmir@eunet.yu), Zoran Saric (Institute for Experimental Phonetics and Speech Pathology, Gospodar Jovanova 35, 11000 Belgrade, Serby, sariczoran@yahoo.com)

As wheezes in abnormal breath sounds observed in patients with obstructive pulmonary diseases, the stridence in voice is manifested as excessively sharp, conspicuous, usually habitual hiss that is especially distinct with whispering. This paper reviews the articulator and acoustics features of stridence in unvoiced fricatives and affricates, and presents an algorithm for detection of stridence. Detection of stridence was based on: time-frequency representation by FFT power spectra, time-frequency representation by AR-Burg power spectra, and power trajectory of signals in characteristic frequency bands. Many features are extracted from this analysis, as: the local power spectra maximum to average surrounding power ratio, the correlation coefficient between spectral and power maxima in signal, the spectral power slope in selected frequency band, spectral entropy in selected frequency band, and phoneme duration. The extracted set of features is input to the nonlinear classificator that decides about stridence in voice and the level of pathology. The algorithm was tested with speech database of normal and pathology voices. The speakers were both sex and the different ages. The results of automatic stridence detection showed high level of coincidence with the judgment of speech therapists.

4pSCb39. Adaptive microphone array free of the desired speaker cancellation combined with postfilter. Slobodan Jovicic (School of Electrical Engineering, University of Belgrade, Bulevar kralja Aleksandra 73, 11000 Belgrade, Serby, jovicic@etf.bg.ac.yu), Zoran Saric (Institute for Experimental Phonetics and Speech Pathology, Gospodar Jovanova 35, 11000 Belgrade, Serby, sariczoran@yahoo.com)

The optimal microphone array includes two processing blocks - minimum variance distortionless response (MVDR) beamformer and the single-channel Wiener filter, which acts as post-filter. The main drawback of MVDR beamformer is the cancellation of the desired speech signal and its degradation in multi-path wave propagation environment. To make the adaptive algorithm robust against room reverberation and to prevent desired signal cancellation, an estimation of the unknown desired speaker's transfer function was proposed. The estimation is based on the imperfect signal and the interference covariance matrices estimated from available microphone signals during speaker activity and pause of speech respectively. As MVDR beamformer suppresses coherent interference, post-filter has to reduce diffuse acoustic noise. The post-filter proposed in this paper is developed under assumption that complex coherence function is unknown but time invariant. The additional improvement of the post-processing algorithm on low frequencies is obtained by combining a priori noise power attenuation factor for diffuse noise field with estimated one. The proposed algorithm is tested on simulated room with reverberation, and compared with some known post-processing algorithms with rather good results.

4pSCb40. The role of source and filter cues in emotion recognition in speech. Disa Sauter (Birkbeck College London, Henry Wellcome Building, Malet Street, WC1E 7HX London, UK, d.sauter@bbk.ac.uk), Frank Eisner (University College London, Institute of Cognitive Neuroscience, 17 Queen Square, WC1N 3AR London, UK, f.eisner@ucl.ac.uk), Stuart Rosen (Department of Phonetics and Linguistics, University College London, Gower Street, WC1E 6BT London, UK, s.rosen@ucl.ac.uk), Sophie K. Scott (University College London, Institute of Cognitive Neuroscience, 17 Queen Square, WC1N 3AR London, UK, sophie.scott@ucl.ac.uk)

In the context of the source-filter theory of speech, it is well established that intelligibility is heavily reliant on information carried by the filter, that is, spectral cues (e.g., Faulkner et al., 2001; Shannon et al., 1995). However,

the extraction of other types of information in the speech signal, such as emotion and identity, is less well understood. In this study we investigated the extent to which emotion recognition in speech depends on filter-dependent cues, using a forced-choice emotion identification task at ten levels of noise-vocoding ranging between one and 32 channels. In addition, participants performed a speech intelligibility task with the same stimuli. Our results indicate that compared to speech intelligibility, emotion recognition relies less on spectral information and more on cues typically signaled by source variations, such as voice pitch, voice quality, and intensity. We suggest that, while the reliance on spectral dynamics is likely a unique aspect of human speech, greater phylogenetic continuity across species may be found in the communication of affect in vocalizations.

4pSCb41. Model of the configurations of intonation movements in Danish - suggesting an 'intoneme'. Sophia Frovin (SLK, English Department, University of Aarhus, Jens Chr. Skous Vej 5, 8000 Aarhus C, Denmark, sophiafrovin@yahoo.com)

This study examines the inventory of intonation movements in Danish. The aim is to identify the micro intonation and to produce a model of the movement patterns in Danish, which would predict the intonation of synthetic speech in order to establish a close-to-natural intonation. The theoretical background is a modified version of the ″close copy theory″ ('t Hart et al.), in which movements are tendency lines in the intonation pattern. A new movement starts when the tendency line shifts direction. The acoustic analysis comprises measurements of time, semitones and slope (semitones/second = slope) and a description of the (parts of) phones in intonation movements of actual speech. The analysis suggests that the slope of the movement is one of the most important features of intonation, and that speakers are aiming to produce one of a set of 5 standard slopes, depending mainly on the phonetic segment, suggesting an underlying unit - an ″intoneme″- displaying the same relationship as that of phoneme and phone.

4pSCb42. Influences of manner and voicing on articulatory coordination in German and French initial consonant clusters. Barbara Kuehnert (Laboratoire de Phonétique et Phonologie - UMR 7018 CNRS - Paris 3, 19, rue des Bernadins, 75005 Paris, France, barbara.kuhnert@univ-paris3.fr), Phil Hoole (Institut für Phonetik und Sprachverarbeitung, Schellingstr. 3, 80799 München, Germany, hoole@phonetik.uni-muenchen.de), Christine Mooshammer (Haskins lab and MIT Research lab of electronics, 300 George street suite 900, New Haven, CT 06511, USA, tine@haskins.yale.edu), Lasse Bombien (Institut für Phonetik und Sprachverarbeitung, Schellingstr. 3, 80799 München, Germany, lasse@phonetik.uni-muenchen.de)

This study aims for improved understanding of whether and how coordination patterns of supraglottal gestures in complex syllable onsets are driven by competing demands of motor economy for the speaker and high recoverability for the listener. Specifically, EMA data for four German and three French speakers was acquired for C1C2 clusters where manner of articulation was varied for C2 (/l/ vs. /n/) and voicing for C1 (/p/ vs. /b/, /k/ vs. /g/). Results (1): A robust effect of less overlap of the constriction gesture for C1 and C2 when C2 is nasal. Clusters with nasal C2 may require less overlap in order to avoid compromising the acoustic characteristics of the C1 burst by early velar lowering. Interestingly, such clusters appear to be less stable diachronically and may be less favoured for the formation of complex onsets because of reduced scope for efficient parallel transmission of segmental information. Results (2): For German, a consistent effect of less overlap for voiceless compared to voiced C1. Discussion here will centre on whether possible cross-language differences between German and French can be related to differences in timing of voice onset and resulting differences in the acoustic properties of the C1-C2 transitions.

4pSCb43. Characterisation of the velocity distribution on rigid in-vitro upper airway replicas. Annemie Van Hirtum (Département Parole & Cognition, GIPSA-lab, 46, avenue Félix Viallet, 38031 Grenoble Cedex, France, annemie.vanhirtum@gipsa-lab.inpg.fr), Xavier Grandchamp (Département Parole & Cognition, GIPSA-lab, 46, avenue Félix Viallet, 38031 Grenoble Cedex, France, xavier.grandchamp@gipsa-lab.inpg.fr),David Marx(Laboratoire d'Etudes Aerodynamiques - CNRS, Bat K, 40 avenue du recteur Pineau, 86022 Poitiers, France, david.marx@lea.univ-poitiers.fr), Xavier Pelorson (Département Parole & Cognition, GIPSA-lab, 46, avenue Félix Viallet, 38031 Grenoble Cedex, France, pelorson@icp.inpg.fr), Helène Bailliet (Laboratoire d'Etudes Aerodynamiques - CNRS, Bat K, 40 avenue du recteur Pineau, 86022 Poitiers, France, helene.bailliet@lea.univ-poitiers.fr)

Qualitative and quantitative characterisation of the velocity distribution is an important aspect in order to study respiration related flow phenomena in the upper airways as well as for human speech production. Classical phonation models exploit one-dimensional flow descriptions in order to estimate the pressure forces exerted on the vocal folds tissues. In this case, the velocity distribution is expressed as an analytical relationship depending on volume velocity airflow, geometry and pressure distribution. Therefore simplified flow models can be validated by measuring the relevant quantities. However, more detailed and quantitative velocity predictions, aiming e.g. to improve phonation modelling or to study turbulent sound production, require increased precision for both the qualitative and quantitative characterisation of the velocity distribution. The current paper presents preliminary in-vitro measurements of the velocity distribution obtained by Particle Image Velocimetry combined with hot film anemometry. Several simplified rigid geometries are assessed in order to represent different portions of the upper airway. Besides qualitative results a first quantitative comparison between simulated and measured velocities is provided and discussed.

4pSCb44. Experimental analysis of the relationship between the glottal flow and glottal area waveforms. Raphael Schwarz (University of South Carolina, 1621 Greene St, Williams Brice Building, 6th Fl, Columbia, SC 29208, USA, rschwarz@gwm.sc.edu), Dimitar D. Deliyski (University of South Carolina, 1621 Greene St, Williams Brice Building, 6th Fl, Columbia, SC 29208, USA, deliyski@gwm.sc.edu)

A very important but little studied aspect of human voice production is the relationship between the vocal fold vibration and the transglottal airflow. To analyze this relationship, in this study we combined high-speed videoendoscopy of the glottis for determining the glottal area waveform (GAW) with inverse filtering of the acoustic signal for estimating the glottal flow waveform (GFW). The high-speed camera system, recording at 20,000 pps, and the audio recording hardware were triggered by the same quartz oscillator to achieve synchronization with an unprecedented accuracy within 25 μs. We developed an image processing algorithm for automatic extraction of the GAW from the high-speed images. The high-speed video samples and the corresponding acoustic signals were obtained from 12 normophonic individuals (6 male, 6 female) for different voicing conditions: register (pulse, modal, falsetto); adductory adjustment (loose, normal, pressed); longitudinal tension within modal register (low, comfortable, high pitch); non-stationary phonation (variation in pitch and loudness). To compare the resulting GAWs and GFWs, the waveforms were parameterized concerning their temporal and spectral features. It is shown, that the revealed relationships between the vocal fold vibrations and the transglottal flow are comprehensible by accounting the different phonation conditions. [Work supported by NIH.]

4pSCb45. Pitch production by bilingual Mandarin-Min speakers and monolingual Mandarin speakers in speaking Taiwan Mandarin and Min. E-Chin Wu (Graduate Institute of Linguistics, National Taiwan Univ, Grad. Inst. of Linguistics, National Taiwan Univ., 1, Roosevelt Rd. Sec. 4, 106 Taipei, Taiwan, r95142002@ntu.edu.tw), Janice Fon (Grad. Inst. of Linguistics, National Taiwan Univ., 1, Roosevelt Rd. Sec. 4, 106 Taipei, Taiwan, jfon@ntu.edu.tw)

In this study, Mandarin produced by bilingual Mandarin-Min speakers and monolingual Mandarin speakers were compared to see whether the presence of Min would pose influence on the pitch range utilized by bilingual Mandarin-Min speakers in speaking Mandarin. The results showed that bilingual Mandarin-Min speakers and monolingual Mandarin speakers did indeed differ in their pitch values when speaking Mandarin. Intriguingly, however, the difference did not go in the same direction for males and females.

It is proposed here that the difference found in the male group was due to influence of Min, while the difference found in the female groups was due to social factors. The results of this study indicate that both language experiences and social constraints are important factors that influence a person's use of pitch.

4pSCb46. Probing the independence of formant control. Ewen Macdonald (Queen's University, 62 Arch St, Dept. of Psychology, Humphrey Hall, Kingston, ON K7L 3N6, Canada, ewen.macdonald@queensu.ca), Bryan P. Burt (Queen's University, 62 Arch St, Dept. of Psychology, Humphrey Hall, Kingston, ON K7L 3N6, Canada, bryan.burt@queensu.ca), Kevin G. Munhall (Queen's University, 62 Arch St, Dept. of Psychology, Humphrey Hall, Kingston, ON K7L 3N6, Canada, kevin.munhall@queensu.ca)

Previous experiments in speech motor learning have demonstrated that acoustic feedback is used to control formant frequencies (Houde and Jordan 1998; Purcell and Munhall 2006; Villacorta, Perkell, and Guenther 2007). In these studies, the formants of a vowel were shifted using a real-time signal processing system. When subjects spoke a vowel, they heard themselves saying a different vowel. The talkers spontaneously compensated for this auditory feedback perturbation by producing formants in the opposite direction in frequency to the perturbation. The purpose of the present study was to investigate if compensating for a perturbation in either the first or second formant also leads to a change in production of the other formant. A between-subjects experiment was conducted where half the participants had a perturbation applied only to the first formant and the other half had a perturbation applied only to the second formant. As in previous experiments, both groups compensated for the perturbed formant. In compensating for the perturbed formant, the production of the other, unperturbed, formant was also affected. However, the change in frequency was quite small. The results will be discussed in terms of the independent variables of speech motor planning

4pSCb47. Pitch Tracking using the Generalized Harmonicity Indicator. Darren Haddad (Air Force Research Lab, 525 Brooks Road, Rome, NY 13441, USA, darren.haddad@rl.af.mil), Andrew Noga (525 Brooks Road, Rome, NY 13441, USA, Andrew.Noga@rl.af.mil), Tappan Sarkar (323 Link Hall, Syarcuse University, Syracuse, NY 13244-1240, USA, tksarkar@syr.edu)

For many audio applications, a process is required to obtain an accurate estimate of the fundamental and harmonics of periodic sections of the audio signal. The Generalized Harmonicity Indicator (GHI) is to determine, assess and track the fundamental and harmonic frequencies of consecutive time segments of a speech signal using the Matrix Pencil (MP) technique[i]. Various methods of fundamental and harmonic frequency tracking have been proposed and developed, but most have been based on other low resolution techniques such as FFT and cepstral analyses. This is opposed to using a super-resolution frequency estimation technique as provided by the MP. The prior art in the area of super-resolution speech fundamental determination consists of the ″super resolution pitch determinator″ (SRPD)[ii] and the ″enhanced SRPD″ (eSRPD) methods. Because these prior methods do not explicitly process a spectral representation or decomposition of the input audio signal, they are not considered to be in the same class as the MP GHI, although they provide a baseline for comparing different estimation techniques. [i] Haddad, D.M., Sarkar, T.K., Noga, A.J.; ″Speech Compression Using the Matrix Pencil Technique″; IEEE 12th DSP Workshop; Sept. 2006; Page(s):218-221. [ii] Y. Medan, E., Yair, D., Chazan, ″Super Resolution Pitch Determination of Speech Signals,″ IEEE Trans. On Signal Processing, ASSP-39(1):40-48, 1991.

4pSCb48. Intraglottal pressures in a static physical model of the converging glottis: entrance loss coefficients, exit coefficients, Bernoulli effects, and viscous effects. Lewis P. Fulcher (Bowling Green State University, Department of Physics and Astronomy, Bowling Green, OH 43403, USA, fulcher@bgsu.edu), Ronald C. Scherer (Bowling Green State University, Department of Physics and Astronomy, Bowling Green, OH 43403, USA, ronalds@bgnet.bgsu.edu)

Pressure distributions were obtained with a static physical model (M5) at diameters d = 0.005, 0.01, 0.02, 0.04, 0.08, 0.16, and 0.32 cm for converging angles of 5, 10, 20, and 40 degrees. At each diameter and angle, transglottal pressures typically ranged from 3 to 15 cm H_2O. For each angle, diameter, and transglottal pressure, the measured pressure at the glottal entrance was used to calculate an entrance loss coefficient, and the measured pressure near the glottal exit was used to determine an exit coefficient. Previous work with the uniform glottis, where the only important physical effect was viscosity, found linear fits to the intraglottal pressures to be excellent approximations. Since the widening channel of the converging glottis produces Bernoulli effects as well as viscous effects, a parabolic form for intraglottal pressures is explored. Such an analytic form for the intraglottal pressures when accompanied by tables of entrance loss and exit coefficients would be a useful tool for researchers needing expressions easily included in numerical models of phonation. The validity of the new analytic treatment will be assessed by comparing the calculated pressures with the observed M5 pressures. [Work supported by NIH R01DC03577.]

4pSCb49. Mitigation of Nonlinear Distortion in Speech Signals Using Histogram Matching. Brett Smolenski (RADC, 2433 Forest Lane, Schwenksville, PA 19473, USA, bsmolens@gmail.com)

Nonlinear distortion is a common artifact in audio communication equipment. In addition, it is well know that the normalized amplitude distribution of speech signals converges to approximately a gamma distribution after a few seconds. Hence, the transfer function of any memoryless nonlinearity distorting the speech signal can easily be estimated, provided one has buffered enough data. This research shows how both parametric and nonparametric histogram matching algorithms can be employed to remove the effects of these types of distortions. Further, the improvement these algorithms have on speaker identification performance is also studied. This approach represents a radical departure from the traditional approach taken in speech enhancement. The traditional approach has been to first acquire a model or representation of the distortion, noise, or interference that is corrupting the signal, and then attempt to remove this from the signal, usually introducing other forms of distortion in the process. With this approach a model of clean undistorted speech is used that the distorted speech is then matched to.

4pSCb50. Fricative synthesis investigations using the transmission line matrix method. Athanasios Katsamanis (National Technical University of Athens, School of Electrical and Computer Engineering, Zografou campus, 15773 Athens, Greece, nkatsam@cs.ntua.gr), Petros Maragos (National Technical University of Athens, School of Electrical and Computer Engineering, Zografou campus, 15773 Athens, Greece, maragos@cs.ntua.gr)

We investigate the potential of properly applying the Transmission Line Matrix method to simulate the 3D acoustic field in the vocal tract especially for the synthesis of fricatives. For fricatives, we are mainly interested in the higher end of the spectrum where the planar wave propagation assumption that is accepted in the one-dimensional simulation cannot provide accurate results. This is the main reason why we explore 3D acoustic field simulation. Proper incorporation of noise sources is considered to account for frication. Their placement and acoustic properties are investigated. Motivated by measurements of the airflow during fricative production, we also explore the influence of mean flow to acoustics in the tract. Sound propagation in moving medium is considered for this purpose. The applied vocal tract geometry is determined from 3D MRI images. We present computational considerations for the analyzed framework in parallel to potential benefits compared to the one-dimensional vocal tract simulation.

4pSCb51. Acquisition of the production of 'new' and 'similar' vowels: the case of /u/ and /y/ in French by Japanese-speaking learners. Takeki Kamiyama (Laboratoire de phonétique et phonologie (UMR 7018), 19, rue des Bernardins, 75005 Paris, France, takekik@phiz.c.u-tokyo.ac.jp)

French /y/ (F2/F3 close around 2000 Hz for males) does not have an equivalent phoneme in Japanese and English, whereas /u/ (F1/F2 close $<$ 1000 Hz) has a phonemic counterpart (high back) in both Japanese and English, but its phonetic realization is different from French /u/, with a higher F2. Flege (1987) found out that it was easier for American English

speakers to acquire a native-like production of French /y/ (″new″ phone) than that of /u/ (″similar″ phone). Our recording of two groups of adult Japanese-speaking learners of French (JLF) shows a similar tendency. We measured the formants of isolated vowels embedded in a carrier sentence read 3 times by JLFs. In the first group, consisting of 3 elementary learners who volunteered for the task, 2 learners pronounced /y/ with close F2/F3, but none of them produced a low F2 (< 1000 Hz) for /u/. In the second group, consisting of 50 JLFs in 4 different classes and levels (elementary to upper intermediate), only 4 of them, who had all lived in a French-speaking country except one, produced /u/ with a low F2 (< 1000 Hz), whereas a dozen of them pronounced /y/ with close F2/F3.

4pSCb52. On the influence of vocal fold collision on phonation. Juergen Neubauer (School of Medicine, University of California, 31-24 Rehab Center, 1000 Veteran Ave., Los Angeles, CA 90095-1794, USA, jneubauer@mednet.ucla.edu), Zhaoyan Zhang (School of Medicine, University of California, 31-24 Rehab Center, 1000 Veteran Ave., Los Angeles, CA 90095-1794, USA, zyzhang@ucla.edu)

For laryngoscopic observations show that the closed time of the glottis is significantly long, especially for low-frequency vocal fold vibrations in the vocal fry and chest register. Vocal fold contact appears to be a major part of the phonatory cycle and may play an important role for self-sustained vocal fold oscillations. Using a 2D, finite element, self-oscillating model of the coupled vocal fold-glottal flow system, we studied the influence of the mechanical impact on phonation onset mechanisms and vocal fold vibratory behavior. The air flow was assumed to be laminar and the compressible Navier-Stokes equations were solved for the flow domain. For fixed values of the Young's modulus of the vocal fold we found that vocal fold contact significantly increased the vibration frequency as compared to the case of no contact. The changed total pressure forces on the vocal fold in medial-lateral (lift force) and inferior-superior (drag force) directions resulted in different phonation threshold pressure values and vocal fold vibration patterns. The increase in phonation frequency due to contact will be discussed based on the theory of impact oscillators.

4pSCb53. ERPs to words correlate with behavioral measures in children with Autism Spectrum Disorder. Sharon Coffey-Corina (Center for Mind and Brain UC Davis, 267 Cousteau Pl, Davis, CA 95618, USA, sccorina@ucdavis.edu), Denise Padden (I-LABS, University of Washington, Box 357920, Seattle, WA 98195, USA, dpadden@u.washington.edu), Patricia K. Kuhl (University of Washington, Dept. of Speech & Hearing Sciences, and Institute for Learning & Brain Sciences, Box 357988, Seattle, WA 98195, USA, pkkuhl@u.washington.edu)

Children with Autism Spectrum Disorder (ASD) participated in a research study that involved both electrophysiological and behavioral measures. Event related brain potentials (ERPs) were recorded during auditory presentation of known and unknown words. Behavioral measures of language/cognitive function and severity of autism symptoms were also collected at the time of ERP testing and again one year later. In general, higher functioning children with ASD exhibited more localized brain effects for differences between known and unknown words. Lower functioning children with ASD had more diffuse patterns of response to the different word classes and also exhibited a stronger right hemisphere lateralization. That is, they showed differences between known and unknown words at many electrode sites and larger differences in the right hemisphere. In addition, significant correlations were obtained between specific brain wave measurements for both known and unknown words and the various behavioral measures. Patterns of ERPs effectively predicted later behavioral scores.

4pSCb54. Magnetoencephalography as a tool to study speech perception in awake infants. Toshiaki Imada (University of Washington, Dept. of Speech & Hearing Sciences, and Institute for Learning & Brain Sciences, Box 357988, Seattle, WA 98195, USA, imada@u.washington.edu), Alexis N. Bosseler (University of Washington, Dept. of Speech & Hearing Sciences, and Institute for Learning & Brain Sciences, Box 357988, Seattle, WA 98195, USA, bosseler@u.washington.edu), Samu Taulu (Elekta-Neuromag Oy, 22 Elimäenkatu, 00510 Helsinki, Finland, samu@squid.neuromag.fi),Elina Pihko(BioMag Laboratory, Helsinki University Central Hospital, 00029 Helsinki, Finland, pihko@biomag.hus.fi), Jyrki Mäkelä (BioMag Laboratory, Helsinki University Central Hospital, 00029 Helsinki, Finland, jyrki.makela@hus.fi), Antti Ahonen (Elekta-Neuromag Oy, 22 Elimäenkatu, 00510 Helsinki, Finland, antti.ahonen@elekta.com), Patricia K. Kuhl (University of Washington, Dept. of Speech & Hearing Sciences, and Institute for Learning & Brain Sciences, Box 357988, Seattle, WA 98195, USA, pkkuhl@u.washington.edu)

Magnetoencephalography (MEG) provides a safe, noninvasive method for studying the developing brain by offering reliable localization of the brain regions activated during speech processing. However technical challenges make recording awake infants difficult. The small size of the infant head in the adult-sized helmet results in a low signal-to-noise ratio. Head and limb movement, which is typical of young infants, produces signal artifact that is difficult to overcome during signal processing. This study used MEG to study phonetic processing in awake, non-sedated typically developing infants from 5 to 16 months. The recordings were made using the Elekta Neuromag® 306-channel instrument at BioMag Laboratory, Helsinki University Central Hospital, Finland. Infants listened to speech syllables produced by a loudspeaker inside the magnetically shielded room. Newly developed signal processing methods and behavioral entertainment greatly improved the quality of the data, producing 29 successful infant recordings out of 35 attempts. We describe the methods, as well as removal of movement-modulated artifacts, efficient interference suppression, and movement compensation during data analysis. Whole-head MEG recordings in awake babies a few months old are now feasible.

4pSCb55. Adapting second language phonemic perception training to common instructional situations: A progress report. Thomas R. Sawallis (Univ. of Alabama, English Dept., Box 870244, Tuscaloosa, AL 35487, USA, tsawalli@bama.ua.edu), Michael W. Townley (Univ. of Alabama, English Dept., Box 870244, Tuscaloosa, AL 35487, USA, townl003@bama.ua.edu)

Although current L2 pedagogy de-emphasizes phoneme-level pronunciation training, laboratory experiments demonstrate benefits from training non-natives in perception of difficult target-language phonemic contrasts. Specifically, evidence shows that: learners' perceptual performance improves (Jamieson & Morosan, 1986; Flege, 1995), improvements generalize to new talkers and words (Lively, Logan, & Pisoni, 1993), perceptual training triggers production improvements (i.e., without production training, Bradlow et al., 1997), and both perceptual (Lively et al., 1994) and production improvements (Bradlow et al., 1999) are maintained over several months. We are adapting perceptual training methods from such studies for use in common instructional situations, starting with Japanese students learning the English /l-r/ contrast. This paper addresses three practical concerns. First, studies show that the perceptual training needs tokens with multiple kinds of variation. We discuss phonological variation in corpus design, sociolinguistic variation in talker recruitment, and inducement of within-talker variations. Second the training must be usable both independently and in classrooms. We discuss the design of sessions short enough for inclusion as part of daily classroom activities. Third, the training must be computer-controlled. We discuss necessary functions, available programs, and our choice. Finally, we briefly demonstrate the training, and give a sketch of interim results.

4pSCb56. ″Polyaural″ array processing for robust automatic speech recognition in noisy and reverberant environments. Richard M. Stern (Carnegie Mellon University, Department of Electrical and Computer Engineering and Language Technologies Institute, 5000 Forbes Avenue, Pittsburgh, PA 15213, USA, rms@cs.cmu.edu), Evandro B. Gouvea (Carnegie Mellon University, Department of Electrical and Computer Engineering and Language Technologies Institute, 5000 Forbes

Avenue, Pittsburgh, PA 15213, USA, egouvea@cs.cmu.edu),Kshitiz Kumar (Carnegie Mellon University, Department of Electrical and Computer Engineering and Language Technologies Institute, 5000 Forbes Avenue, Pittsburgh, PA 15213, USA, kshitizk@cs.cmu.edu)

It is well known that human binaural processing is very useful for separating incoming sound sources as well as for improving the intelligibility of speech in reverberant environments. In this paper we present a new method of signal processing for robust speech recognition using multiple microphones. The method, loosely based on the human binaural hearing system, consists of passing the speech signals detected by multiple microphones through bandpass filtering and nonlinear halfwave rectification operations, and then cross-correlating the outputs from each channel within each frequency band. These operations provide rejection of off-axis interfering signals. These operations are repeated (in a non-physiological fashion) for the negative of the signal, and an estimate of the desired signal is obtained by combining the positive and negative outputs. We demonstrate that the use of this approach provides substantially better recognition accuracy than delay-and-sum beamforming using the same sensors for target signals in the presence of additive broadband and speech maskers, and it provides substantial improvements in specific reverberant environments as well. [Supported by NSF and DARPA]

4pSCb57. Coupled 2D-Fluid-Structure-Acoustic Simulation of the Human Voice. Gerhard Link (Univ. Erlangen-Nuremberg, Dept. of Sensor Technology, Paul-Gordan-Str. 3/5, 91052 Erlangen, Germany, gerhard.link @lse.eei.uni-erlangen.de), Manfred Kaltenbacher (Univ. Erlangen-Nuremberg, Dept. of Sensor Technology, Paul-Gordan-Str. 3/5, 91052 Erlangen, Germany, manfred.kaltenbacher@lse.eei.uni-erlangen.de), Michael Doellinger (University Hospital Erlangen, Department of Phoniatrics and Pediatric Audiology, Medical School, Bohlenplatz 21, 91054 Erlangen, Germany, michael.doellinger@uk-erlangen.de), Reinhard Lerch (Univ. Erlangen-Nuremberg, Dept. of Sensor Technology, Paul-Gordan-Str. 3/5, 91052 Erlangen, Germany, reinhard.lerch@lse.eei.uni-erlangen.de)

The human voice is a key factor in social life. If the phonation process is disturbed due to a disease as e.g. hoarseness, communication and social life are strongly affected. Therefore, it is necessary to enhance therapies in order to minimize affliction caused by a disease. There exist different approaches to improve therapies. Experimental field studies of different physical parameters, like acoustic pressure or vocal fold displacements are one possibility. Another promising approach to advance insight into laryngeal dynamics is given by numerical simulations. Due to the growing computing power the complexity of numerical phonation models is steadily increasing and full fluid-structure-acoustic interacting models are now feasible. Therefore, we have developed a two-dimensional numerical model for the human phonation process, which includes the complete fluid-structure-acoustic interaction. As discretization method the finite-element method was applied for all possible three physical fields. The fluid-structure and the structure-acoustic interactions are based on general continuum mechanical principles; the fluid-acoustic interaction is based on Lighthill's acoustic analogy. Therewith, the analysis of all sound mechanisms, which consist of the eddy-induced, the volume-induced, and the mechanical-induced sound can be performed. First simulation results will be presented and discussed.

THURSDAY AFTERNOON, 3 JULY 2008 P3-C, LEVEL 3, 3:40 TO 5:20 P.M.

Session 4pSPa

Signal Processing in Acoustics, Acoustical Oceanography, and ECUA: Model-Based Signal Processing III (Poster Session)

Sean Lehman, Cochair
Pleasanton, CA

Christian Pichot, Cochair

All posters will be on display from 3:40 p.m. to 5:20 p.m. To allow contributors an opportunity to see other posters, contributors of odd-numbered papers will be at their posters from 3:40 p.m. to 4:30 p.m. and contributors of even-numbered papers will be at their posters from 4:30 p.m. to 5:20 p.m.

Contributed Papers

4pSPa1. Detection and classification using the Estimated Ocean Detector. Richard Lee Culver (ARL Penn State, PO Box 30, State College, PA 16804, USA, rlc5@psu.edu), Colin W. Jemmott (ARL Penn State, PO Box 30, State College, PA 16804, USA, cwj112@psu.edu), Brett E. Bissinger (ARL Penn State, PO Box 30, State College, PA 16804, USA, beb194@psu.edu), Nirmal K. Bose (ARL Penn State, PO Box 30, State College, PA 16804, USA, bkn@engr.psu.edu)

We have developed the Estimated Ocean Detector, a likelihood ratio receiver with an estimator-correlator structure, and applied it to detection and classification of underwater acoustic signals. The receiver requires that the noise probability density function (pdf) to belong to the exponential class but need not be Gaussian. A composite hypothesis is employed in order to incorporate knowledge (or predictions) of the signal parameter statistics. Previously, receiver performance was demonstrated for Gaussian noise and sinusoidal signals with known frequency and phase and whose amplitude pdfs were predicted using knowledge of the ocean environment and an acoustic propagation program. In order for the receiver to be useful operationally, it must be able to accommodate unknown signal phase and incorporate numerical estimates of noise and signal parameter pdfs. Progress toward satisfying these requirements is reported in this talk. Work supported by the Office of Naval Research Undersea Signal Processing.

4pSPa2. Fractal analysis of signals of the seismic acoustic emission. Alexander V. Glushkov (Odessa University, P.O.Box 24a, 65009 Odessa-9, Ukraine, glushkov@paco.net), Andrey A. Svinarenko (Odessa University, P.O.Box 24a, 65009 Odessa-9, Ukraine, glushkov@paco.net), Yaroslav I. Lepikh (Odessa University, P.O.Box 24a, 65009 Odessa-9, Ukraine, glushkov@paco.net)

Paper is devoted to analysis fractal properties of signals of the seismic acoustic emission in periods between earthquakes. Earlier it has been carried out an analysis of natural data on distribution of the earthquake hypercenters (Mukhamedov, 1992; Salimi et al, 1993). To reveal the fractal properties for signals of the seismic acoustic emission the joint wavelet analysis is carried out by using the non-decimated wavelet transform (Glushkov et al, 2004, 2005). We present the fractal processing data for envelopes of signal of the seismic acoustic emission in different ranges of frequencies. The dependences of the Herst indicator and fractal dimension curve on the lengths of considered intervals are presented. It takes a place crossover upon a behaviour with the Herst indicator H=0,4-0,6. It is given the physical interpretation of the seismic acoustic emission. References: Mukhamedov V.A., Izv. Russian Acad.Sci. 3, 39 (1992). Salimi M., Robertson M., Sammis S., Phys .Rev.Lett. 70, 2186 (1993). Glushkov A.V. etal, Nonlinear Processes in Geophys. 11, 285 (2004). Glushkov A.V. et al, Atmospheric Res. (Elseiver). 77, 100 (2005).

4pSPa3. A torpedo detection and 3-D tracking system. Nico Roosnek (Roosnek Research & Development, Vlaskamp 82, 2592 AC The Hague, Netherlands, nico@roosnek.nl)

Ship torpedo defence systems are ideally based on 3D information of incoming torpedoes. Therefore a Torpedo Detection and Location (TDL) sonar system has been designed based on a transmitting transducer, two receiving arrays and optimal signal processing with 3D-tracking capabilities with optimal estimation. The transmitted signal is a chirp. The signal processing with intrinsic beamforming is based on the phase of the signal and on optimal estimation (Kalman filtering). For testing the capabilities of such a design a test system on detection and tracking of a torpedo-like object in the atmosphere has been developed. Some figures about its capability, which can be extrapolated to underwater situations, will be given.

4pSPa4. Chirplet Transform Analysis for Ultrasonic Inspection of Composite Materials. Abdessalem Benammar (Image and signal processing laboratory. Welding and NDT Centre, Route de Dely-Ibrahim, BP 64, Chéraga, 16035 Alger, Algeria, Abs_benammar@yahoo.fr), Redouane Drai (Image and signal processing laboratory. Welding and NDT Centre, Route de Dely-Ibrahim, BP 64, Chéraga, 16035 Alger, Algeria, drai_r@yahoo.fr), Ahmed Kechida (Image and signal processing laboratory. Welding and NDT Centre, Route de Dely-Ibrahim, BP 64, Chéraga, 16035 Alger, Algeria, Abs_benammar@yahoo.fr), Abderrezak Guessoum (Image and signal processing laboratory. Welding and NDT Centre, Route de Dely-Ibrahim, BP 64, Chéraga, 16035 Alger, Algeria, Abs _benammar@yahoo.fr)

In this work, a successive parameter estimation algorithm based on the chirplet transform is presented. The chirplet transform is used not only as a means for time frequency representation, but also to estimate the echo parameters, including the amplitude, time-of-arrival, center frequency, bandwidth, phase, and chirp rate. We initially apply this method to simulated signals with additional structural noise. These signals contain several echo defects, closer between them. This stage permits to see the robustness of the developed algorithm. Thereafter, we validate all simulated results by experimental results obtained on composite material with and without delamination defects.

4pSPa5. Source localisation on a single hydrophone. Grégoire Le Touzé (GIPSA-lab, dep. DIS, 961, rue de la Houille Blanche, 38402 St Martin d'Hères, France, gregoire.letouze@lis.inpg.fr), Barbara Nicolas (GIPSA-lab, dep. DIS, 961, rue de la Houille Blanche, 38402 St Martin d'Hères, France, barbara.nicolas@gipsa-lab.inpg.fr), Jérôme I. Mars (GIPSA-lab, dep. DIS, 961, rue de la Houille Blanche, 38402 St Martin d'Hères, France, jerome.mars@gipsa-lab.inpg.fr)

The aim of the study is to localise an undewater Ultra Low Frequency (ULF) source in a shallow water environement. The acoustic signal is recorded on a single hydrophone and the source, which has to be short in time, is unknown. To perform the localisation, we have developed modal filters based on time-frequency techniques. Different localisation techniques are proposed: - Conventional Matched Mode Processing: results are good for range estimation but contain error on source depth estimation. We show that those errors are due to the ULF band. - Source depth estimation technique based on mode amplitude estimation: this estimation is precise but presents ambiguities. - Range estimation technique using mode phase estimation: we recently developed this method which also estimates mode signs. The source range is precisely estimated and mode sign estimation avoids ambiguity on source depth estimation combined with the previous method. These methods are validated on real data comming from the North Sea.

4pSPa6. Analyze effects of the flow on the vocalic reduction and the coarticulation in sequences CV of pharyngal Arabic. L Falek (Université des sciences et de la technologie Houari Boumédiène (USTHB), Laboratoire de communication parlée et de traitement du signa, Faculté d'Electronique et d'Informatique, BP 32, El Alia, Alger, Algeria, lilalcpts@yahoo.fr), O. Bouferroum (Université des sciences et de la technologie Houari Boumédiène (USTHB), Laboratoire de communication parlèe et de traitement du signa, Faculté d'Electronique et d'Informatique, BP 32, El Alia, Alger, Algeria), A. Djeradi (Université des sciences et de la technologie Houari Boumédiène (USTHB), Laboratoire de communication parlèe et de traitement du signa, Faculté d'Electronique et d'Informatique, BP 32, El Alia, Alger, Algeria)

The degree of coarticulation and the vocalic reduction (RV) are indices related to good engine control (Gay 1978). Fowler (1998) explains why locus equation (LE) is used to characterize, at the same time, the place of articulation and the degree of coarticulation between consonants and vowels: a strong slope (m=1) indicates a maximum coarticulation between consonants and vowels (i.e. minimal resistance of the coarticulation), while a weak slope (m=0) indicates absence of coarticulation between consonants and vowels (maximum resistance of the coarticulation). The bond between the degree of coarticulation and the RV can be explained according to the linear relation between F2onset and F2milieu: the modifications of values of F2milieu will affect those of F2onset and consequently those of the slopes. In this study, the analysis of the vocalic reduction and slopes of the equations of locus, carried out on CV (extracts starting from sentences) in standard Arabic pronounced by speakers having different mother tongues (near to Arabic standard and very far away from standard Arabic), and at speed of variable elocution, revealed a vocalic reduction and a variation of the slope of the locus equation, specific to each speaker, who seems to be related to his mother tongue. El Tamimi (2006) carried out a similar study with normal flow, in dialectical Arabic and in French, with normal flow, an influence of the mother tongue showed on the vocalic reduction and the slope of the equation of locus.

Session 4pSPb

Signal Processing in Acoustics: Advances in Acoustic Sensors and Networks for Defense Applications II (Poster Session)

Brian Ferguson, Cochair
Defence Science and Technology Organisation

Pierre Naz, Cochair
ISL

All posters will be on display from 3:40 p.m. to 5:20 p.m. To allow contributors an opportunity to see other posters, contributors of odd-numbered papers will be at their posters from 3:40 p.m. to 4:30 p.m. and contributors of even-numbered papers will be at their posters from 4:30 p.m. to 5:20 p.m.

Contributed Papers

4pSPb1. Aircrafts localisation and tracking with arrays of microphones. Gaetano Caronna (Università La Sapienza - Dept. Fisica Tecnica, Via Eudossiana 18, 00184 Roma, Italy, gaetano.caronna@uniroma1.it), Pierluigi Testa (Università La Sapienza - Dept. Fisica Tecnica, Via Eudossiana 18, 00184 Roma, Italy, pierluigi.testa@uniroma1.it)

University of Roma ″La Sapienza″ will participate in a project, financed by the Italian Ministry of Research, aiming to detect and to track aircrafts near the airport using the acoustic emissions of the aircraft and the technique of acoustic beam-forming. Although the principle is well known and some applications are reported in literature and explored also by our group in a previous European FP6 project (″Safe Airport″), the final performance and the engineering value are not assessed. In this reseach effort the problem is again raised aiming to create a more realistic model including wind and temperature gradient that, in particular conditions, can drastically impair the validity of the results, estimating the related errors. A simulation software was written considering the steering drive on the microphones outputs, being the mechanical rotation of the array prohibited, due to the aerodynamic noises induced. At least two arrays, opportunely located, are requested in order to perform a triangulation and detect the source of the acoustic wave emitted by the aircraft. The precision in the localisation of the acoustic source was estimated in a simulation where real aircraft acoustic emissions and environmental noise were used as imput.

4pSPb2. Acoustic Source Localization via Distributed Sensor Networks using Tera-scale Optical-Core Devices. Neena Imam (Oak Ridge National Laboratory, 1 Bethel Valley Road, Oak Ridge, TN 37831-6015, USA, imamn@ornl.gov), Jacob Barhen (Oak Ridge National Laboratory, 1 Bethel Valley Road, Oak Ridge, TN 37831-6015, USA, barhenj@ornl.gov)

For real-time acoustic source localization applications, one of the primary challenges is the considerable growth in computational complexity associated with the emergence of ever larger, active or passive, distributed sensor networks. The complexity of the calculations needed to achieve accurate source localization increases dramatically with the size of sensor arrays, resulting in substantial growth of computational requirements that cannot be met with standard hardware. One option to meet this challenge builds upon the emergence of digital optical-core devices. The objective of this work was to explore the implementation of key building block algorithms used in underwater source localization on optical-core digital processing platform recently introduced by Lenslet Inc. We investigate key concepts of threat-detection algorithms such as Time Difference Of Arrival (TDOA) estimation via sensor data correlation in both time and frequency domains with the purpose of implementation on the optical-core processor. We illustrate our results with the aid of numerical simulation and actual optical hardware runs. The major accomplishments of this research, in terms of computational speedup and numerical accuracy achieved via the deployment of optical processing technology, should be of substantial interest to the acoustic signal processing community.

4pSPb3. Performance of high-resolution sensor array processing algorithms in the localization of acoustic sources. Joseph Lardies (FEMTO-ST Applied Mechanics, 24 chemin de l'épitaphe, 25000 Besançon, France, joseph.lardies@univ-fcomte.fr), Hua Ma (University of Franche-Comté, Institute FEMTO - LMARC, 24 rue de l'Epitaphe, 25000 Besançon, France, rosyhorse@hotmail.fr), Marc Berthillier (University of Franche-Comté, Institute FEMTO - LMARC, 24 rue de l'Epitaphe, 25000 Besançon, France, marc.berthillier@univ-fcomte.fr), Emmanuel Foltete (FEMTO-ST Applied Mechanics, 24 chemin de l'épitaphe, 25000 Besançon, France, emmanuel.foltete@univ-fcomte.fr)

The localization of noise sources from a specified direction may often be accomplished with an array of sensors. One commonly used processor consists of delay and add networks: a conventional beamformer, however its spectrum suffers from the Rayleigh resolution and its performance is highly degraded, specially in lower frequency range. In the communication, the performance of some typical high-resolution sensor array processing algorithms: Minimum Variance, MUSIC, Mini-Norm algorithms are investigated for wideband source location. Their performances are compared with a new source localization algorithm which is based on a sparse representation of sensor measurements with an overcomplete basis composed of samples from the array manifold. The key of the method is the use of the SVD for data reduction and the formulation of a joint multiple-sample sparse representation problem in the signal subspace domain. Increased resolution and improved robustness to noise is obtained with this algorithm applied to various numerical examples.

Session 4pSPc

Signal Processing in Acoustics: Filter Design, Detection, and Estimation II (Poster Session)

Michael Roan, Cochair
Virginia Tech

Jorge Quijano, Cochair
NEAR Lab-Portland State University

All posters will be on display from 3:40 p.m. to 5:20 p.m. To allow contributors an opportunity to see other posters, contributors of odd-numbered papers will be at their posters from 3:40 p.m. to 4:30 p.m. and contributors of even-numbered papers will be at their posters from 4:30 p.m. to 5:20 p.m.

Contributed Papers

4pSPc1. Averaged Lagrange Method for interpolation filter. Jonathan Andrea (LIEN - BP 239, Université Henri Poincaré, 54506 Vandoeuvre, France, jonathan.andrea@lien.uhp-nancy.fr), Frederic Coutard (LIEN - BP 239, Université Henri Poincaré, 54506 Vandoeuvre, France, frederic.coutard@lien.uhp-nancy.fr), Patrick Schweitzer (LIEN - BP 239, Université Henri Poincaré, 54506 Vandoeuvre, France, patrick.schweitzer@lien.uhp-nancy.fr), Etienne Tisserand (LIEN - BP 239, Université Henri Poincaré, 54506 Vandoeuvre, France, etienne.tisserand @lien.uhp-nancy.fr)

This paper presents a new method for Lagrange interpolation for reducing distortions without introducing any complexity. The aim is to improve the linearity of the phase and the gain responses of the interpolation filter by an averaging method. A first FIR interpolation filter of the second order computes the values between three successive samples of the input signal. At the same time, a second filter, identical to the first, computes the values between (xk–2 , xk–1 , xk). Finally, the common values between (xk–2 , xk–1) provided by the two filters are averaged two by two. This double interpolation can be simply done with a single third order filter and with a Farrow structure filter. Compared to the usual Lagrange's third order interpolation filter, the behaviour of the filter we propose is more regular especially in the high frequencies of the Nyquist band. More, the filter coefficients are easier to calculate. The designed filter is tested on a FPGA of Altera. The results shows that the method significantly reduces distortions and improves quality of the frequency response.

4pSPc2. Application of digital filters for measurement of nonlinear distortions in loudspeakers using Wolf's method. Rafal Siczek (Wroclaw University of Technology, Wybrzeze Wyspianskiego 27, 50-370 Wroclaw, Poland, rafal.siczek@pwr.wroc.pl)

The design of digital filters used for measurement of nonlinear distortions in loudspeakers by the Wolf's method is presented in the paper. The Wolf's method has been developed in 1953 and originally the analog filters was applied. This method requires particularly steep slopes of both band-reject filters (at the transmitting part of the measurement system) and band-pass filters (at the receiving part). The digital filters allows for achievement of such steep slopes with a relatively small cost in comparison with analog ones. The very high attenuation in the barrage bands can be achieved. In the very narrow transition band any irregularities do not appear. The design procedures using MATLAB package have been described. Then, the digital filter allow for achievement of a high accuracy of measurement.

4pSPc3. Objective quality measurement of the excitation of impact sounds in a source/filter model. Mathieu Lagrange (Centre for Interdisciplinary Research in Music Media & Technology (CIRMMT) - Schulich School of Music - McGill Univ., 555 Sherbrooke Street West, Montreal, QC H3A1E3, Canada, mathieu.lagrange@mcgill.ca), Bruno L. Giordano (Centre for Interdisciplinary Research in Music Media & Technology (CIRMMT) - Schulich School of Music - McGill Univ., 555 Sherbrooke Street West, Montreal, QC H3A1E3, Canada, bruno.giordano@music.mcgill.ca), Philippe Depalle (Centre for Interdisciplinary Research in Music Media & Technology (CIRMMT) - Schulich School of Music - McGill Univ., 555 Sherbrooke Street West, Montreal, QC H3A1E3, Canada, depalle@music.mcgill.ca), Stephen McAdams (Centre for Interdisciplinary Research in Music Media & Technology (CIRMMT) - Schulich School of Music - McGill Univ., 555 Sherbrooke Street West, Montreal, QC H3A1E3, Canada, smc@music.mcgill.ca)

For the modeling of percussive (non-sustained) sounds, the excitation signal can be estimated from an original sound in several ways, usually by a time-domain deconvolution process. The source signal obtained by such a process cannot be compared with the original excitation because it is usually unknown. Hence in most of the approaches available in the literature, the validation of the deconvolution process is quantifed in terms of spectral flatness, i.e. a source signal is considered as a good estimation of the excitation when most of the resonant content has been removed. However, the excitation signal is usually a percussive burst, the time domain properties of which are known to be very important, at least perceptually speaking. To evaluate the time domain properties of the estimated excitation, we propose in this paper to compare the estimated excitation to the recording of the acceleration of the hammer hitting a plate. In the recordings considered, the evolution of the acceleration of the hammer has a specifc pattern with several peaks due to the bouncing of the hammer on the suspended plate. This specifc pattern allows us to propose a metric that can be useful for objectively measuring the quality of the estimation process.

4pSPc4. Detecting Scenes in Lifelog Videos based on Probabilistic Models of Audio data. Kiichiro Yamano (Hosei University, 3-7-2 Kajino-cho, 184-8584 Koganei, Japan, n04k1035@cis.k.hosei.ac.jp), Katunobu Itou (Hosei University, 3-7-2 Kajino-cho, 184-8584 Koganei, Japan, itou @hosei.ac.jp)

Lifelog videos are recorded every activity in everyday lives. To utilize them efficiently, it is required to be indexed automatically. To index continuous shots of the lifelog, significant scenes are detected automatically. For detection, many researches employ image features such as color and edge, however, the accuracy is insufficient. In this study, we propose

probabilistic models for scene detection from lifelog video. In this method, mel-frequency filter bank output of audio tracks of the lifelog videos is modeled statistically with hand-labeled training data. We tested the proposed method to use train station scene. We collected 11 hour sound data for such scenes. To analyze them, we defined seven categories, such as stopping trains, passing trains, starting trains, waiting, and so on. Our method achieved to 100% for waiting scene and 18.4% in average.

4pSPc5. Estimation of reflection location by the correlation coefficient function. Hideo Shibayama (Shibaura Institute of Technology, 3-7-5, Toyosu, Koto-ku, 135-8548 Tokyo, Japan, sibayama@sic.shibaura-it.ac.jp), Takeshi Araya (Hitachi Information & Communication Engineering, Ltd, 393 Totsukamati Totsuka-ku, 244-8502 Yokohama Kanagawa, Japan, takeshi.araya.tx@hitachi.com), Yoshiaki Makabe (Hitachi Information & Communication Engineering, Ltd, 393 Totsukamati Totsuka-ku, 244-8502 Yokohama Kanagawa, Japan, yoshiaki.makabe.hd@hitachi.com), Eiji Okarura (Hitachi Information & Communication Engineering, Ltd, 393 Totsukamati Totsuka-ku, 244-8502 Yokohama Kanagawa, Japan, eiji.okamura.mh@hitachi.com)

Gas is supplied to households through gas pipes that branch out from a main pipe. It is essential to carry out maintenance of these branch pipes to ensure the safe supply of gas. However, there are many cases in which the state of buried gas pipes and the connection condition of a large number of pipes are unknown because no detailed information is included in piping drawings or only plan views are available. If the piping arrangement can be estimated on the basis of response waves originating from an acoustic wave travelling in a gas pipe emitted by a loudspeaker, which is placed at one end of the pipe, this method will be important for the maintenance of branch pipes. To realize this, we report a method of estimating the length of gas pipes using correlation coefficient between a driving signal and measured waves. And, we show the experimental results with high accuracy.

4pSPc6. An experiment for signal identification of the MIMO communication by sonic waves. Daisuke Hayashi (Shibaura Institute of Technology, 3-7-5, Toyosu, Koto-ku, 135-8548 Tokyo, Japan, m107077@sic.shibaura-it.ac.jp), Yasukazu Maeda (Shibaura Institute of Technology, 3-7-5, Toyosu, Koto-ku, 135-8548 Tokyo, Japan, m107092@sic.shibaura-it.ac.jp),Toru Itakura(Shibaura Institute of Technology, 3-7-5, Toyosu, Koto-ku, 135-8548 Tokyo, Japan, m106009@sic.shibaura-it.ac.jp), Hideo Shibayama (Shibaura Institute of Technology, 3-7-5, Toyosu, Koto-ku, 135-8548 Tokyo, Japan, sibayama@sic.shibaura-it.ac.jp)

Recently, the communication method by MIMO works in a field of the wireless communication. We do research on application to the MIMO system in an acoustic field by sonic wave. As the transmission method, we use the space division multiplexing (SDM) that is the method for the purpose of the improvement of the transmission rate that accepted the number of the transmission elements by sending plural signals at the same time. It is important to identify each signal from several different signals that are transmitted at the same frequency band. And, we study method for detecting each signal. This paper describes influence of the signal detection for the different conditions of the multi-path propagation.

4pSPc7. Transverse vectorization of fast Fourier transforms on multicore architectures. Travis Humble (Oak Ridge National Laboratory, 1 Bethel Valley Road, Oak Ridge, TN 37831-6015, USA, humblets@ornl.gov), Jacob Barhen (Oak Ridge National Laboratory, 1 Bethel Valley Road, Oak Ridge, TN 37831-6015, USA, barhenj@ornl.gov), Michael Traweek (Office of Naval Research, 875 North Randolph Street, Arlington, VA 22203, USA, Mike.Traweek@navy.mil)

Single-instruction, multiple-data (SIMD) multicore computing architectures, such as the IBM Cell Broadband Engine Architecture, offer new opportunities for quickly and efficiently calculating the 1D-FFT of acoustic signals, as time-sampled data arrays can be naturally partitioned across the multiple cores on which vectorized implementations of the FFT operate. Building on this parallel pipeline model, we consider the case that M data arrays of length N reside within each core. Whereas the cost of sequentially executing these M FFT's conventionally scales as $\alpha MN\log_2 N$, we demonstrate a transverse vectorization solution whose cost scales as $\alpha\beta N\log_2 N$, where α and β are constant scaling factors. Our approach makes use of the SIMD instruction set and large vector register file inherent to each core of the IBM Cell in order to calculate the FFT of M data arrays simultaneously. By efficiently using all the available vector registers in performing the FFT, this transverse SIMD vectorization solution further reduces the computational complexity of the conventional parallel pipeline model.

Session 4pUWa

Underwater Acoustics and ECUA: Image and Signal Processing

Ivars Kirsteins, Cochair
NUWC, 1176 Howell St, Newport, RI 02841, USA

Ioannis Koukos, Cochair
Hellenic Naval Academy, Telecommunications Lab, Terma Hatzikyriakou Street, Piraeus, 18539, Greece

Contributed Papers

2:00

4pUWa1. Physics-based signal processing methodologies for separating target echoes into their constituent elastic and geometric components. Ivars Kirsteins (NUWC, 1176 Howell St, Newport, RI 02841, USA, kirsteinsip@npt.nuwc.navy.mil), Alessandra Tesei (NATO Undersea Research Centre, Viale San Bartolomeo 400, 19126 La Spezia, Italy, tesei @nurc.nato.int)

Echoes from even simple canonical symmetric shapes such as solid elastic spheres are highly complex, consisting of a superposition of specular, elastic, and geometric diffractive components closely spaced in time and frequency. Although measurement of the individual elastic and geometric components is important for analysis of scattering physics and object identification, in practice individual components are often hard to measure because of mutual interference between components. When an object interacts with a boundary, such as the sea floor, additional interfering echoes make the object signature even more complicated to interpret. Motivated by this problem, a frequency-domain technique is developed for separating an echo into its constituent elastic and geometric components, and for isolating specular reflections from a possibly interacting boundary. It is based on modelling the echo components in the frequency domain as amplitude-modulated piecewise-linear chirps, utilizing physically-inspired group delay models and constraints, and then using a modified Costas' residual signal analysis (RSA) algorithm in combination with chirp transform analysis to decompose the echo. The RSA scheme is demonstrated on actual echoes collected in the NURC EVA-06 sea trial from spherical and cylindrical target shapes and is shown to work well with the separated components verified against modelling predictions.

2:20

4pUWa2. Two Dimensional Wavelet Coefficient Statistics for Sea Bottom Classification. Ioannis Koukos (Hellenic Naval Academy, Telecommunications Lab, Terma Hatzikyriakou Street, 18539 Piraeus, Greece, jalex_14u@hotmail.com), Theodoros Mavroidis (Hellenic Naval Academy, Telecommunications Lab, Terma Hatzikyriakou Street, 18539 Piraeus, Greece, tmavroid@tellas.gr), Georgios Vardoulias (Hellenic Naval Academy, Telecommunications Lab, Terma Hatzikyriakou Street, 18539 Piraeus, Greece, ggvard@gmail.com)

In this paper we examine the classification of different seafloors based on the analysis of images obtained by side-scan sonar. For this purpose, we apply various two dimensional multilevel wavelet decomposition schemes on images obtained from three different seafloor types, i.e., sand ripples, rocks and sands, and then we examine the statistics of the corresponding wavelet coefficients. The observed Probability Density Functions (pdf) are modeled using various theoretical distributions such as the Alpha Stable, Sum of Gaussians, Log-normal. The parameters of the fit are subsequently used to classify the side scan sonar images according to well known cluster analysis techniques. The use of the energy of the wavelet coefficients as a tool for side scan sonar image classification is also evaluated. A new unsupervised classification scheme based on the pdf fitting parameters is proposed.

2:40

4pUWa3. Computer Vision Techniques Applied for Reconstruction of Seafloor 3D Images from Side Scan and Synthetic Aperture Sonars Data. Krzysztof Bikonis (Gdansk University of Technology, Department of Geoinformatics, Narutowicza 11/12, 80-952 Gdansk, Poland, binio@eti.pg.gda.pl), Andrzej Stepnowski (Gdansk University of Technology, Department of Geoinformatics, Narutowicza 11/12, 80-952 Gdansk, Poland, astep@pg.gda.pl), Marek Moszynski (Gdansk University of Technology, Department of Geoinformatics, Narutowicza 11/12, 80-952 Gdansk, Poland, marmo@eti.pg.gda.pl)

The Side Scan Sonar and Synthetic Aperture Sonar are well known echo signal processing technologies that produce 2D images of the seafloor. Both systems combines a number of acoustic pings to form a high resolution image of seafloor. It was shown in numerous papers that 2D images acquired by such systems can be transformed into 3D models of seafloor surface by algorithmic approach using intensity information, contained in a grayscaled images. The paper presents the concept of processing the Side Scan Sonar and Synthetic Aperture Sonar records for detailed reconstruction of 3D seafloor using Shape from Shading techniques. Shape from Shading is one of the basic techniques used in computer vision for the objects reconstruction. The algorithms proposed in the paper use the assumed Lambert model of backscattering strength dependence on incident angle and utilize additionally the information from shadow areas for solving obtained set of equations. The idea was verified by simulation study. The obtained results of 3D shape reconstruction are presented and the performance of the algorithms is discussed.

3:00

4pUWa4. Underwater vehicle attitude estimation using Hough transformation. Hisashi Shiba (Radio Application Division, NEC Corporation, 1-10, Nisshin-cho, Fuchu, 183-8501 Tokyo, Japan, h-shiba@aj.jp.nec .com)

In these decades various imaging sonar systems have been developed. They are very effective for underwater investigations such as geologies, fisheries, resource surveys and securities. To extend these system abilities we studied new imaging sonar applications and found they are also useful in underwater vehicle navigations. In this presentation I propose a new method of estimating vehicle attitude parameters relative to the ocean surface or the seafloor by the onboard imaging sonar. The ocean surface or the seafloor is often obtained as a plane in sonar images. However, the images are sometimes too noisy to identify the plane locations because of ambient noise and reverberations by texture patterns on the planes. The new method describes these planes with plane equation parameters connected to attitude parameters, and searches the most appropriate parameter sets using a voting procedure which is a three dimensional expansion of the Hough transformation widely applied in line detections on noisy two dimensional images. The method provides the plane location and attitude parameters simultaneously without other sensors. After the algorithm explanation multi-beam imaging sonar simulations are shown and accuracies are evaluated.

3:20

4pUWa5. Adaptive coding/modulation for shallow-water UWA communications. Sanjay Mani (Arizona State University, Dept. of Electrical Engineering, Tempe, AZ 85287-5706, USA, sanjay.mani@asu.edu), Tolga M. Duman (Arizona State University, Dept. of Electrical Engineering, Tempe, AZ 85287-5706, USA, duman@asu.edu), Paul Hursky (HLS Research, Inc., 3366 N. Torrey Pines Ct., Ste. 310, La Jolla, CA 92037, USA, paul.hursky@hlsresearch.com)

We consider adaptive modulation and coding techniques for Phase Shift Keying (PSK) transmission schemes over underwater acoustic (UWA) channels. Adaptive modulation and coding can be an effective means of obtaining higher data rates while retaining acceptable error levels by exploiting knowledge of the channel state. This is particularly significant in the UWA scenario, where attained spectral efficiencies are critical since usable bandwidth is a severe limitation. We examine the use of channel capacity and post-equalization signal to noise ratio (SNR) as adaptation metrics. We illustrate the ideas both through simulations and using the results of a recent experiment (AUVfest 2007). In the experiment, in order to evaluate effectiveness of adaptive coding/modulation for UWA communications, we have transmitted a bank of signals with varying spectral efficiencies (obtained by changing the number of transmit elements, modulation scheme, and code rate) back to back. Using the received signals, we illustrate the relevance of the channel condition metrics under consideration, that is, we evaluate the proposed metrics for various scenarios, and provide indications of the transmission rates that could have been achieved reliably.

THURSDAY AFTERNOON, 3 JULY 2008 AMPHI BORDEAUX, 3:00 TO 5:40 P.M.

Session 4pUWb

Underwater Acoustics and ECUA: High Frequency Variability II

Marcia Isakson, Cochair
Applied Research Laboratories, University of Texas, PO Box 8029, Austin, TX 78713-8029, USA

Thomas Folégot, Cochair
NATO Undersea Research Center, Viale San Bartolomeo 400, La Spezia, 19126, Italy

Invited Papers

3:00

4pUWb1. Examples of high frequency variability in underwater acoustic systems. Peter Stein (Scientific Solutions, Inc., 99 Perimeter Rd., Nashua, NH 03063, USA, pstein@scisol.com)

Invited paper for the structured (special) session UW09 High Frequency Variability In this paper we will look at examples of high frequency variability encountered by the author during the design and implementation of underwater acoustic systems over the last 20 years. These systems include those for radiated noise measurements, short baseline tracking, tomographic correction of numerical ocean models, marine mammal detection, and diver detection. The examples will highlight the different physical sources of variability and their effects on system performance. Methods used for mitigating the effects both in the physical design of the sensor system and in the signal processing will also be discussed.

3:20

4pUWb2. Gaussian beam tracing for high-frequency acoustics. Michael B. Porter (HLS Research, Inc., 3366 N. Torrey Pines Ct., Ste. 310, La Jolla, CA 92037, USA, michael.porter@hlsresearch.com), Martin Siderius (HLS Research, Inc., 3366 N. Torrey Pines Ct., Ste. 310, La Jolla, CA 92037, USA, martin.siderius@hlsresearch.com), Paul Hursky (HLS Research, Inc., 3366 N. Torrey Pines Ct., Ste. 310, La Jolla, CA 92037, USA, paul.hursky@hlsresearch.com)

Gaussian beam tracing is an approach that constructs full-wave beams around the skeleton of conventional ray theory. This Gaussian beam approach leads to a very simple algorithm and provides remarkable accuracy and speed. For high-frequency, broadband applications, Gaussian beams are often the only practical approach, as the standard full-wave modeling alternatives are often thousands of times slower. Gaussian beams are derived using high-frequency asymptotics, and therefore fit naturally to certain current areas of interest in HF acoustics, such as acoustic communications. However, what often surprises people who are not familiar with the technique is that it works quite well at lower frequencies, depending on the water depth. That fact, is really a consequence of 20 years of continued advances in the Gaussian beam method. We will review those developments in the context of HF variability, considering effects of boundary, volume, and source/receiver dynamics.

3:40-5:00 Posters
Lecture sessions will recess for presentation of poster papers in various topics in acoustics. See poster sessions for topics and abstracts.

Invited Papers

5:00

4pUWb3. Field-calibration: exploiting high-frequency mobile platform transmissions for source localization at lower frequency with arrays. Paul Hursky (HLS Research, Inc., 3366 N. Torrey Pines Ct., Ste. 310, La Jolla, CA 92037, USA, paul.hursky@hlsresearch.com), Michael B. Porter (HLS Research, Inc., 3366 N. Torrey Pines Ct., Ste. 310, La Jolla, CA 92037, USA, michael.porter@hlsresearch.com)

Multipath arrivals in an ocean waveguide with a reflective enough bottom can be used as a fingerprint for source range and depth and this has been demonstrated by many researchers using matched field processing. However, MFP relies upon acoustic propagation models to produce the Green's functions to be used as steering vectors for this processing. We have proposed to instead directly measure these Green's functions using wideband acoustic comms signals from mobile platforms such as AUVs that are increasingly part of naval applications. Thus we measure the multipath arrival pattern at 8-16 kHz from the many locations AUVs are visiting, and then apply such measurements for locating other sources at low frequency. A key factor in this process is being able to capture the essential features of the impulse response function at high frequency, where fluctuations are much more severe than at low frequency. We have previously presented experimental results of applying this technique using a single hydrophone receiver. Here we will report on a continuation of that work, using vertical arrays and data from the RADAR '07 experiment.

5:20

4pUWb4. The effects of sediment variability on reflection coefficient measurements. Marcia Isakson (Applied Research Laboratories, University of Texas, PO Box 8029, Austin, TX 78713-8029, USA, misakson@arlut.utexas.edu), Nicholas P. Chotiros (Applied Research Laboratories, University of Texas, PO Box 8029, Austin, TX 78713-8029, USA, chotiros@arlut.utexas.edu)

The statistical distribution of specularly scattered acoustic energy, commonly known as the reflection coefficient, is an important parameter when developing models for shallow water propagation and acoustic communications. The distribution of measured reflection coefficient data from 5 to 50 kHz and 10 to 70 degrees grazing angles was taken from a sea bottom recently perturbed by hurricane off the coast of Florida at the Sediment Acoustic Experiment 2004 (SAX04). The width and shape of the distributions are attributed to varying sediments in the experimental area and interface roughness. These distributions are analyzed to determine the scattering from different types of sediments including sand and mud. The effects of both roughness scattering and sediment variability on the mean value and distribution of the measured reflection coefficient will be explored. [Work sponsored by ONR Ocean Acoustics.]

THURSDAY AFTERNOON, 3 JULY 2008 P3-C, LEVEL 3, 3:40 TO 5:20 P.M.

Session 4pUWc

Underwater Acoustics and ECUA: Tank Experiments II (Poster Session)

Raymond Soukup, Cochair
U.S. Naval Res. Lab.

Jean-Pierre Sessarego, Cochair
Laboratory for Mechanics and Acoustics CNRS

All posters will be on display from 3:40 p.m. to 5:20 p.m. To allow contributors an opportunity to see other posters, contributors of odd-numbered papers will be at their posters from 3:40 p.m. to 4:30 p.m. and contributors of even-numbered papers will be at their posters from 4:30 p.m. to 5:20 p.m.

Contributed Papers

4pUWc1. Acoustical and optical measurements on a mixture of air microbubbles in water. Vincent Duro (LOMC FRE 3102 CNRS Groupes Ondes Acoustiques, Université du Havre (IUT), Place Robert Schuman, 76610 Le Havre, France, vincent.duro421@univ-lehavre.fr), Dominique Rajoana (LOMC FRE 3102 CNRS Groupes Ondes Acoustiques, Université du Havre (IUT), Place Robert Schuman, 76610 Le Havre, France, raphael.rajaona@univ-lehavre.fr), Dominique Decultot (LOMC FRE 3102 CNRS Groupes Ondes Acoustiques, Université du Havre (IUT), Place Robert Schuman, 76610 Le Havre, France, dominique.decultot@univ-lehavre.fr), Gerard Maze (LAUE, Université du Havre, Place Robert Schuman, F-76610 Le Havre, France, gerard.maze@univ-lehavre.fr)

An important challenge for current naval research is the modernization of battleships. Their target detection system must be increasingly efficient and they must be increasingly undetectable. Due to turbulent flows and bubbles, ship wakes are a detectable acoustic signature and ship bow waves disturb sonar detection. In this work, we study sound propagation through bubble clouds in water. We have developed an experimental set-up which permits us to acquire, in synchronization, acoustical signals and optical images. The phenomenon of bubble monopole resonance in very low frequency, related to bubble size, provokes effects of strong sound damping and sound speed dispersion. These experimental results, related to theoretical results, permit to estimated sizes and concentrations of bubbles. The ac-

quired bubble images permit to know the real bubble sizes and concentrations, in order to correlate with the experimental acoustical results. Air bubbles are generated with a high pressure water jet introduced into the host liquid medium. A hydrodynamic study is done to characterize the bubble jet. We present in this work, theoretical results establishing a complex effective wave number characterizing the sound propagation in an effective medium. All results are discussed and compared with results of others papers on this subject.

4pUWc2. Acoustic methods in extremely shallow water: validity of the far field approximation. Fantina Madricardo (CNR-Istituto di Scienze Marine, Riva Sette Martiri - Castello 1364/a, 30122 Venice, Italy, fantina.madricardo@ismar.cnr.it), Silvano Buogo (CNR-Istituto di Acustica 'O,M.Corbino', Via del Fosso del Cavaliere, 100, 00133 Rome, Italy, silvano.buogo@idac.rm.cnr.it), Paola Calicchia (CNR-Istituto di Acustica 'O,M.Corbino', Via del Fosso del Cavaliere, 100, 00133 Rome, Italy, paola.calicchia@idac.rm.cnr.it), Emiliano Boccardi (CNR-Istituto di Scienze Marine, Riva Sette Martiri - Castello 1364/a, 30122 Venice, Italy, E.Boccardi@lse.ac.uk)

In this paper we present some experimental results concerning the possibility of using traditional echosounder in extremely shallow water environments. In the framework of the Echos Project, a collaboration between ISMAR and IA, a wide area of the Venice Lagoon has been explored with a traditional echosounder. Since the explored area was extremely shallow (up to 50 cm), it became necessary to check experimentally whether the far field approximation was still valid in such conditions. In this work the acoustic field of the echosounder ELAC LAZ72 used for the sub bottom investigation is experimentally characterized and the validity of the far field approximation is verified.

4pUWc3. Acoustic measurements of bubbles in the wake of ship model in tank. Alexander Sutin (Stevens Institute of Technology, Castle Point on Hudson, Hoboken, NJ 07030, USA, asutin@stevens.edu), Alexander Benilov (Stevens Institute of Technology, Castle Point on Hudson, Hoboken, NJ 07030, USA, Alexander.Benilov@stevens.edu), Heui-Seol Roh (Stevens Institute of Technology, Castle Point on Hudson, Hoboken, NJ 07030, USA, Heui-Seol.Roh@stevens.edu), Young In Nah (Agency of Defense Development, P.O.Box, ChinHae, 645-600 Kyung Nam, Republic of Korea, yinah@add.re.kr)

The interest to bubble generation by moving ships is connected with large area of bubble wake reaching several kilometers that can be used for ship detection. We developed acoustic system for the measurements of bubble density and conducted measurements in 100 m long towing tank. The developed system measured attenuation of ultrasound in wide frequency band from 50 to 800 kHz between two acoustic sensors placed on the distance 20cm. The attenuation of sound produced by bubbles was observed during several minutes after model of ship passed the point of measurement. The attenuation was recalculated to the bubble size distribution for bubbles from 4 to 65 microns using theory of resonance bubble attenuation. The measured bubble size distribution can be interpolated by power dependence $n(R) \sim R^{(-3.5)}$ that is typical for bubbles at sea subsurface layer. The dependencies of bubble concentration of model ship speed and type of propeller were investigated. The generation of bubbles was observed when the model speed exceeds definite threshold that can be connected with the cavitation threshold. The theory describing dynamics of wake turbulence based on the shear-free turbulent wake was developed. The measured bubble concentration was in good agreement with the developed theory.

THURSDAY AFTERNOON, 3 JULY 2008 P3-C, LEVEL 3, 3:40 TO 5:20 P.M.

Session 4pUWd

Underwater Acoustics and ECUA: Determination of Acoustic Properties of Materials for Sonar Applications II (Poster Session)

Kenneth Foote, Cochair
Woods Hole Oceanographic Institution

Stephen Robinson, Cochair
National Physical Laboratory

All posters will be on display from 3:40 p.m. to 5:20 p.m. To allow contributors an opportunity to see other posters, contributors of odd-numbered papers will be at their posters from 3:40 p.m. to 4:30 p.m. and contributors of even-numbered papers will be at their posters from 4:30 p.m. to 5:20 p.m.

Contributed Paper

4pUWd1. Experimental study on resistance and noise reduction of low functional surfaces hydrophobic coatings. Lin Zhang (Harbin Engineering University, 31st Building Wenmiao Street, 150001 Harbin, China, zhanglin8624@yahoo.com.cn), Ting Jiang (Harbin Engineering University, 31st Building Wenmiao Street, 150001 Harbin, China, jianfly@163.com)

The object moves in viscous fluid will accepting two kinds of resistance, one kind is the friction drag that the fluid applied to the object directly, another kind is the pressure drag that because of separating the fluid and taking from, and this drag force can create the flow noise. On theoretical aspect, this article analyses the relation between physical properties of the material and flow resistance and flow noise. The conclusion is that the surface material has the effect of reducing the flow resistance and noise because of its experimental on reducing the mutual action between fluid and solid surface under given conditions. On experimental aspect, use the gravitational low noise water tunnel test condition and adopt torpedo model, many times have the test on the drag and noise reduction of the torpedo model under diversity flow rate, have coating and not coating situation. Indicate by analysis that the low surface energy dewatering coatings used in experiment have the certain drag and noise reduction effect under the high flow rate, and with the flow rate power-up, the effect of the drag and noise reduction becomes better and better.

Session 4pUWe

Underwater Acoustics and ECUA: General Topics in Underwater Acoustics (Poster Session)

David L. Bradley, Cochair
Pennsylvania State University

Kevin LePage, Cochair
Naval Research Laboratory

All posters will be on display from 3:40 p.m. to 5:20 p.m. To allow contributors an opportunity to see other posters, contributors of odd-numbered papers will be at their posters from 3:40 p.m. to 4:30 p.m. and contributors of even-numbered papers will be at their posters from 4:30 p.m. to 5:20 p.m.

Contributed Papers

4pUWe1. A solution to the problem of simultaneous classification and localization of underwater objects from their acoustic field. Andrey I. Mashoshin (Central Scientific and Research Inst. 'Elektropribor', 30, Malaya Posadskaya Street, 197046 St. Petersburg, Russian Federation, amashoshin@eprib.ru)

This paper presents one of the solutions to the problem of simultaneous classification and localization of underwater objects from its acoustical field. It was shown that both problems (classification and localization) have some common features that allow to consider them as one mutual problem which can be solved by maximum likelihood method. The solution takes into account: - the fundamental physical representations of the transmission, propagation, reception of signals, and the measurement of their parameters against the noise background; - the target parameters vector describing features of its noise radiation and motion; - the parameters vector characterizing the observation conditions; - the errors vector of the signal parameter measurements. The theoretical solution is illustrated by solving a relatively simple but practically important problem of classification and ranging of an underwater object from passive underwater acoustic observation data.

4pUWe2. On acoustic tomography method physical advantages in long range ocean inhomogeneities control. Andrew Semenov (Acad. N.N. Andreev's Acoustics Institute, Russ. Acad. of Sci., 4 Shvernik Street, 117036 Moscow, Russian Federation, asemen@akin.ru)

An acoustic tomography method based on observation of signals transecting an inhomogeneity is discussed. While for various inhomogeneities (ships, underwater objects, sea mammals etc.) short range monitoring of back scattered sonar reflections could be used, their monitoring at longer ranges is still a problem. This is due to the fast decay of sonar signals with distance, especially in unfavorably absorbing shallow water regions where there is functional distance dependence of optimum frequency. New perspectives on ocean climate change measurement (ATOC) require monitoring of extra long (500 - 1000 km) tomography traces, where ocean vortices and icebergs could hamper the progress. The physical limits (optimum frequencies and efficiencies) for two tomographic methods for deep and, most unfavorable in the author's view, shallow ocean regions are compared. For several types of inhomogeneities tomorgaphic measurement optimization estimates are discussed. For ranges up to 500 km the acoustic tomography method has substantial advantages with respect to conventional sonar monitoring even for unfavorable shallow water regions at least up to 300 km distance and in all deep water regions. Tomographic measurements are also indispensable in long-range ocean vortices monitoring.

4pUWe3. A hydrophone calibration centre for the Mediterranean area. Giovanni Bosco Cannelli (CNR-Istituto di Acustica 'O,M.Corbino', Via del Fosso del Cavaliere, 100, 00133 Rome, Italy, giovannibosco.cannelli@idac.rm.cnr.it), Silvano Buogo (CNR-Istituto di Acustica 'O,M.Corbino', Via del Fosso del Cavaliere, 100, 00133 Rome, Italy, silvano.buogo@idac.rm.cnr.it), Paola Calicchia (CNR-Istituto di Acustica 'O,M.Corbino', Via del Fosso del Cavaliere, 100, 00133 Rome, Italy, paola.calicchia@idac.rm.cnr.it)

The Underwater Acoustics Laboratory of the Institute of Acoustics ″O. M. Corbino″ in Rome, Italy, has recently achieved accreditation for hydrophone calibration. It can offer hydrophone calibration services operating under a management system compliant with UNI EN ISO/IEC standard and traceability of measurements to NPL primary standards. Precise, traceable measurements are needed today in all applications of underwater acoustics, where a faithful response of measuring devices is essential for a correct evaluation of the system performance and for a rigorous assessment of the environmental impact of man-made activities at sea. To attain these requirements the Laboratory has a water tank 6 m long, 4 m wide and 5,5 m deep, equipped with a motorized two-trolley positioning system capable of handling loads of up to 100 kg. A variety of test and measurement equipment is available, controlled by a computer acoustic calibration system, and standalone instruments for signal generation, acquisition and analysis. Besides, two windows are provided on one of the tank walls for combined acoustical and optical measurements, which can be performed using the available Laser Doppler Vibrometer (up to 100 kHz) and the 16-mm film rotating prism high-speed camera (up to 10 000 frames per second).

4pUWe4. Characteristics of sound pressure field focused by an acoustic aplanat lens. Toshiaki Nakamura (National Defense Academy, 1-10-20 Hashirimizu, 239-8686 Yokosuka, Japan, toshiaki@nda.ac.jp), Yuji Sato (Tsukuba Univ., Tsukuba Science City, 305-8573 Ibaraki, Japan, yuji@aclab.esys.tsukuba.ac.jp), Ayano Miyazaki (National Defense Academy, 1-10-20 Hashirimizu, 239-8686 Yokosuka, Japan, g44044@nda.ac.jp), Kazuyoshi Mori (National Defense Academy, 1-10-20 Hashirimizu, 239-8686 Yokosuka, Japan, kmori@nda.ac.jp)

In this paper, we describe the characteristics of an acoustic aplanat lens which can eliminate both spherical and coma aberrations. A singlet aplanat lens was designed using a ray theory in paraxial area. Sound pressure fields of the bi-concave aplanat lens and a spherical lens with 160 mm in diameter for the frequency of 500 kHz were evaluated by a three-dimensional finite difference time domain (3-D FDTD) method. The aplanetic lens showed better convergence characteristics than spherical lens. Two bi-concave lenses of aplanat and spherical lenses were made by acrylic resin and water tank experiment was conducted to compare the on-axis characteristics and

beam patterns at the focus of them. As a result, the aplanat lens could focus higher sound pressure than the spherical one within the incident angle of 10 degrees.

4pUWe5. Echo analysis of objects on the seafloor. Xiukun Li (College of Underwater Acoustic Engineering, Harbin Engineering University, 150001 Harbin, China, xiukun_li@yahoo.com.cn), Huiguang Chi (College of Underwater Acoustic Engineering, Harbin Engineering University, 150001 Harbin, China, xiukun_li@yahoo.com.cn)

Echoes from elastic objects on the seafloor comprise two kinds of acoustic components as well as bottom reverberation. One is elastic scattering echoes, and the other is geometric echoes. These echoes are called highlights, which can be used for identification of objects. Because time delay among highlights from small objects is very short, neither the wavelets resolved highlights structure nor suppressed bottom reverberation according to research. In order to obtain highlights structure and decay reverberation, the Hilbert Huang Transform (HHT), which is a new idea for analyzing nonlinear and nonstationary is applied in the paper. The HHT can describe the data from the instantaneous frequency and energy rather than the global frequency and energy defined by the Fourier spectral analysis, and the adjustable window Fourier spectral analysis defined by the wavelet. The results from both extensive simulations and real data show that the HHT has the highest resolution in time and frequency domain, and may prove to be a vital method for identification of objects on the sea floor.

4pUWe6. Tidal Effect of Reciprocal Sound Propagations at the Experiment in Hashirimizu Port. Hanako Ogasawara (National Defense Academy, 1-10-20 Hashirimizu, 239-8686 Yokosuka, Japan, ogasawar@nda.ac.jp), Toshiaki Nakamura (National Defense Academy, 1-10-20 Hashirimizu, 239-8686 Yokosuka, Japan, toshiaki@nda.ac.jp), Kazuyoshi Mori (National Defense Academy, 1-10-20 Hashirimizu, 239-8686 Yokosuka, Japan, kmori@nda.ac.jp), Koichi Mizutani (Tsukuba Univ., Tsukuba Science City, 305-8573 Ibaraki, Japan, mizutani@esys.tsukuba.ac.jp)

Acoustical monitoring method could monitor wide area such as ocean because it can spatially measure the measurement object with a few sensors. It is important to monitor ocean structure changes for understanding global climate changes and for controlling aquatic resources. We investigated sound propagation characteristics using sound propagated data measured at Hashirimizu port of Yokosuka, Japan in August 2006 and 2007. The experimental area was very shallow water with the average depth of 5 m and travel distance of 110 m. M-sequence signal alternately propagated every 30 seconds from each bank side. Water depth change caused by tide affected received signal amplitude traveled with the frequency of 12 kHz and 80 kHz. It was also confirmed from simulated sound pressure by FDTD method through the change of assumed water depth. Furthermore, water temperature fluctuation could be confirmed from the travel time changes.

4pUWe7. Reduced Scale Experiment of Frequency Dependence of Single Spherical Biconcave Acoustic Lens for Ambient Noise Imaging. Kazuyoshi Mori (National Defense Academy, 1-10-20 Hashirimizu, 239-8686 Yokosuka, Japan, kmori@nda.ac.jp), Hanako Ogasawara (National Defense Academy, 1-10-20 Hashirimizu, 239-8686 Yokosuka, Japan, ogasawar@nda.ac.jp), Toshiaki Nakamura (National Defense Academy, 1-10-20 Hashirimizu, 239-8686 Yokosuka, Japan, toshiaki@nda.ac.jp)

By the numerical analysis results using the Finite Difference Time Domain method in our previous studies, it was supposed that the spherical biconcave lens with an aperture diameter of 2.0 m has sufficient directional resolution (for example, the beam width is 1 deg at 60 kHz) for realizing the Ambient Noise Imaging (ANI) system. In this study, to confirm the directional resolution of the lens in a wide frequency band of 20-100 kHz, we performed a reduced scale experiment of one-fifth space in a water tank. The lens, made of acrylic resin, has an aperture diameter of 400 mm and a radius of curvature of 500 mm. A burst pulse of 25 cycles at 100, 200, 300, and 500 kHz, in which the frequency increases 5 times, was radiated from the sound source to the lens. The results show that the -3 dB area, whose pressure is 3 dB lower than the maximum at the image point, does not overlap each other at 300 and 500 kHz. It is supposed that the lens of 2.0 m aperture has the fine resolution over 60 kHz in the original scale.

4pUWe8. Suppression of side lobe level on the cone characteristics of the directivity pattern of an antenna as an important factor in its directivity index and effective aperture. Zvonimir M.S. Milosic (MORH, Trg kralja Petra Kresimira IV, HR-10000 Zagreb, Croatia, zvonimir.milosic@morh.hr)

This paper will present a universal procedure for precise de-embedding of the directivity index and effective aperture dependence of the suppressed side lobes on measured cone directivity patterns of sonar antennas. The procedure is derived on an idealized model of cone characteristics and directivity patterns of antennas. It is universally applicable to any contemporary sonar or hydroacoustic communication system with a cone directivity pattern. In accordance with the given expressions of directivity index and effective aperture of circle baffled pistons, this paper will present substitute analytical functions for hypothetical circle antennas with suppressed minor lobes. The presented graphs of functional behavior in a two-dimensional system, and in a three-dimensional coordinate system, are an excellent base for standardization, unification and quality evaluation of sonar or radar systems and also medical scanners. Key words: directivity index of sonar antenna, idealized model of cone directivity pattern, level of suppressed side lobes, effective aperture

Session 4pUWf

Underwater Acoustics and ECUA: Sound Propagation in 3-Dimensional Environments I (Poster Session)

David Calvo, Cochair
U.S. Naval Res. Lab.

Michael Taroudakis, Cochair
University of Crete & FORTH/IACM

All posters will be on display from 3:40 p.m. to 5:20 p.m. To allow contributors an opportunity to see other posters, contributors of odd-numbered papers will be at their posters from 3:40 p.m. to 4:30 p.m. and contributors of even-numbered papers will be at their posters from 4:30 p.m. to 5:20 p.m.

Contributed Paper

4pUWf1. On a new approach to numerical modeling of a low-frequency underwater sound in 2 and 3-dimensional oceanic waveguides. Oleg E. Gulin (Il'ichev Pacific Oceanological Institute of Far-East Branch of Russian Academy of Sciences, 43, Baltiyskaya st., 690068 Vladivostok, Russian Federation, gulinoe@rambler.ru)

A new method to compute underwater sound fields in irregular planar waveguides is proposed. It realizes the full two-way propagation approach and exploits an idea of a problem solution dependence on a certain variable parameter that is the position of a boundary of the irregular region. With respect to this parameter for waveguide modes, an initial value problem can be formulated in the horizontal plane that is completely equivalent to the boundary value problem for the original wave equation (Helmholtz equation). This fact allows simulation of sound fields in waveguides based on ordinary differential equations with traditional approximations and for arbitrary source distance from the irregular region and the degree of irregularities. Examples of a simulation for a 2-D irregular waveguide model with an upslope rigid or absorbing penetrable bottom are presented for low frequencies and shallow sea conditions. They illustrate the strong difference between our solution and approximate solutions that arise due to both mode coupling and considerable backscattering within the considered irregular waveguide models

Session 4pUWg

Underwater Acoustics and ECUA: Nonlinear Acoustic Methods in Searching for Buried Objects

Benjamin R. Dzikowicz, Cochair
Naval Surface Warfare Center, Panama City Division, Code HS-11, 100 Vernon Ave., Panama City, FL 32407, USA

Eugeniusz Kozaczka, Cochair
Univ., Narutowicza 11/12, Gdansk, 80-952, Poland

Invited Papers

5:20

4pUWg1. Parametric sonars in searching of buried objects. Eugeniusz Kozaczka (Univ., Narutowicza 11/12, 80-952 Gdansk, Poland, kozaczka@pg.gda.pl)

The subject of this paper is the description of usage of the parametric sonar for searching of the objects that are on the surface of the seabed or very close to it. Searching of underwater objects, especially these ones buried in the seabed has a very practical meaning. Presently more often mass destruction weapon is placed in the very difficult way to find it. Moreover searching of the objects of the archaeological character at sea requires usage of devices those have possibility of penetration of sediment which covers the searched object. In this case the most useful of acoustic means are parametric sonars that due to their specific features are good tools for underwater searching. The principle of detection of buried objects is similar to detection in the case of usage of the classical sonars. The dispersion of the sound field enables to track the object and sometimes enables to define the shape of the searched object. The measurement equipment can be connected to the Global Positioning System (GPS) and complementary equipment that is necessary in such kind of investigations. There will be presented experimental results that were obtained during the trials in the Gdansk Bay. Also will be shown the typical images for chosen objects.

5:40

4pUWg2. Observation of sub-bottom sediments in the Southern Baltic by means of nonlinear acoustic method. Grazyna Grelowska (Polish Naval Academy, Smidowicza 69, 81-103 Gdynia, Poland, ggrel@wp.pl), Eugeniusz Kozaczka (Univ., Narutowicza 11/12, 80-952 Gdansk, Poland, kozaczka@pg.gda.pl), Ignacy Gloza (Polish Naval Academy, Smidowicza 69, 81-103 Gdynia, Poland, i.gloza@amw.gdynia.pl)

The aim of the paper is to present results of preliminary experimental investigation using parametric echosounder in natural conditions for profiling the subbottom sediments in the Gulf of Gdansk. The ability to predict seabed properties: seafloor roughness, subbottom structure and discrete scatterers laying on the seafloor or buried into sediments, from remotely sensed data is important especially in regions that need permanent monitoring. Precise determination of seabed structure or localisation of buried objects in the sand requires the use of a low frequency signal to penetrate the sediment and a narrow beam to provide high-resolution data. Both requirements can be achieved with a parametric (nonlinear) technique. The special experimental setup has been arranged allowing penetration of bottom sediments as well as precise positioning and following a given route. Measurements were conducted exactly along given routes, for that geological profiles have bean taken by means of another method. It allow as to compare detailed date obtained by means of parametric echosounding to ones given at geological map. In all investigations the primary frequency of the array was of 100 kHz, whereas the secondary frequency changed in range 5 kHz - 15 kHz.

6:00

4pUWg3. Transmission of low frequency sounds from ships into water environment. Ignacy Gloza (Polish Naval Academy, Smidowicza 69, 81-103 Gdynia, Poland, i.gloza@amw.gdynia.pl)

The main goal is presentation the broad experimental research associated with the transmission of acoustic energy generated by moving objects into the water. I present the methodology of evoluation of the transmission of low frequency vibration from the mechanisms of ship into the water environment. For that purpose the research of vibration distribution over ship's hull were conducted along with the hydroacoustic field. The underwater sound measurements were performed both for sailing condition and during anchorage. The hull is source of complex surface shape inducing waves of different frequencies depending on the working parameters of ship's machinery. As a result of mechanical incitement of the hull's surface a complex distribution of vibration is created depending on vibration spectra of the primary sources as for the main propulsion units, generators or other mechanisms. This research allowed to determine the transmission coefficient for the mechanical vibration energy going through the ship's hull and the evaluation of influence on the hydroacoustic field of a ship. The values signaling the changes of the technical condition of machinery and propulsion system.

6:20

4pUWg4. Detection of a resonant target buried in sediment using iterative time reversal: mid-frequency pond experiments. Benjamin R. Dzikowicz (Naval Surface Warfare Center, Panama City Division, Code HS-11, 100 Vernon Ave., Panama City, FL 32407, USA, benjamin.dzikowicz@navy.mil), Zachary J. Waters (Boston University, Dept. of Aerosp. and Mech. Eng., 110 Cummington St., Boston, MA 02215, USA, zjwaters@bu.edu), R. Glynn Holt (Boston University, Dept. of Aerosp. and Mech. Eng., 110 Cummington St., Boston, MA 02215, USA, rgholt@bu.edu), Ronald A. Roy (Boston University, Dept. of Aerosp. and Mech. Eng., 110 Cummington St., Boston, MA 02215, USA, ronroy@bu.edu)

Iterative time reversal techniques developed at smaller scales, [Waters et al., J. Acoust. Soc. Am. 122, 3023 (2007)], are applied to the detection of a 15 cm diameter stainless steel shell buried in sandy sediment at the acoustic test pond at the Naval Surface Warfare Center - Panama City Division. A mid-frequency, directional projector is located 1.5 m above the sediment and directed normally to it. A hydrophone is located midway between the sediment and the projector. This system gives a response between 20 kHz and 200 kHz. A calibration filter is designed using the direct path response between the projector and hydrophone. This filter is applied at each time reversal iteration to prevent the time reversal technique from converging to the transducer resonance. Application of iterative time reversal allows the detection of the target at greater depths than otherwise possible due to the resonance scattering of the target. Additional experiments explore the application of filters, and the effect of different window sizes. Also, comparisons with similar laboratory experiments and comments on real world applications are discussed. [Work supported by the Office of Naval Research.]

6:40

4pUWg5. Sonar detection of targets buried under seafloor ripple at shallow grazing angles. Joseph Lopes (Naval Surface Warfare Center - Panama City Division, 110 Vernon Ave, Panama City, FL 32407, USA, joseph.l.lopes@navy.mil), Raymond Lim (Naval Surface Warfare Center - Panama City Division, 110 Vernon Ave, Panama City, FL 32407, USA, raymond.lim@navy.mil), Carrie Dowdy (Naval Surface Warfare Center - Panama City Division, 110 Vernon Ave, Panama City, FL 32407, USA, carrie.dowdy@navy.mil), Kevin L. Williams (Applied Physics Laboratory, University of Washington, 1013 NE 40th St, Seattle, WA 98105, USA, williams@apl.washington.edu), Eric Thorsos (Applied Physics Laboratory, University of Washington, 1013 NE 40th St, Seattle, WA 98105, USA, eit@apl.washington.edu)

This paper summarizes results from modeling and measurement efforts investigating shallow grazing angle reverberation levels from a rippled bottom and subcritical detection of targets buried under such interfaces. The focus of this work is associated with frequencies less than 10 kHz where evanescent transmission is important. Measurements were performed in a 13.7-m deep, 110-m long, 80-m wide test-pool with a 1.5-m layer of sand on the bottom. Rippled contours were artificially formed with the aid of a sand scraper. A parametric sonar that generated difference frequency signals in the 1 to 20 kHz frequency range was placed onto a rail system permitting acquired data to be processed and displayed similar to that of a side scan sonar. The buried target was a solid aluminum cylinder. The seabed roughness was measured to assess ripple fidelity and to estimate the small-scale roughness spectrum which was used in scattering models to calculate the backscattered signal levels from the target and bottom. Acoustic backscatter data obtained for various ripples parameters (wavelengths, heights, orientation, etc.) were compared to model predictions based on perturbation theory. [Work supported by the Office of Naval Research and the Strategic Environmental Research and Development Program, USA].

7:00

4pUWg6. Changing of scattering properties of underwater objects covered by elastic shell. Grazyna Grelowska (Polish Naval Academy, Smidowicza 69, 81-103 Gdynia, Poland, ggrel@wp.pl), Ignacy Gloza (Polish Naval Academy, Smidowicza 69, 81-103 Gdynia, Poland, i.gloza@amw.gdynia.pl)

In certain situations it is of a great importance to decrease reflection properties of underwater objects positioned into water, deployed on a seabed or buried into sediments. This effect could be achieved by means of covering shell changing acoustic parameters of considered object. The aim of the paper is to present the idea of performing the covering material for underwater objects as well as results of experimental investigation of its scattering characteristics. Acoustic scattering measurements were performed in laboratory condition on solid air-filled objects of sphere or ellipsoidal shape with or without covering shell. The objects were insonified by acoustic source at frequency in range of 60 kHz - 150 kHz.

Contributed Paper

7:20

4pUWg7. Experimental study of parametric transmission: Simultaneous generation of two beams. Maud Amate (GESMA, BP42, 29240 Brest Armées, France, maud.amate@dga.defense.gouv.fr), Pierre Cervenka (Institut Jean le Rond D'Alembert, UMR 7190, 2 Place de la Gare de Ceinture, 78210 Saint Cyr L'Ecole, France, cvk@ccr.jussieu.fr), Jacques Marchal (Institut Jean le Rond D'Alembert, UMR 7190, 2 Place de la Gare de Ceinture, 78210 Saint Cyr L'Ecole, France, jmarchal@ccr.jussieu.fr)

In order to respond to the buried mines threat, an approach of GESMA (Groupe d'Etudes Sous-Marines de l'Atlantique) is to take advantage of the parametric transmission in sonar imagery. This technique allows producing narrow beamwidths at low frequencies. Such a parametric transmitter has been designed and calibrated in collaboration with an academic laboratory of Paris VI, and the targeted benchmark is fulfilled: 2° @ 20 kHz, with sufficient source level. The design of the complete sonar system is based on a sequential multibeam transmission associated with a synthetic aperture technique at receive. However, the shortfall of the sweeping technique lies in the timing limitation. One solution to increase the coverage rate is the simultaneous generation of several parametric beams in different directions. Experimentations have been conducted in a tank with different signals: CW, LFM, Ricker. This presentation addresses the results of these experimentations in the context of buried mines detection and classification.

THURSDAY AFTERNOON, 3 JULY 2008 ROOM 362/363, 5:20 TO 7:40 P.M.

Session 4pUWh

Underwater Acoustics, Computational Acoustics, and ECUA: Numerical Methods in Underwater Scattering

Andrew F. Seybert, Cochair
University of Kentucky, Dept. of Mech. Engineering, 151 RGAN Bldg., Lexington, KY 40506, USA

Martin Ochmann, Cochair
Technische Fachhochschule Berlin, Univ. of Applied Sciences, Luxemburger Str. 10, Berlin, 13353, Germany

Bodo Nolte, Cochair
Forschungsanstalt der Bundeswehr für Wasserschall und Geophysik, Klausdorfer Weg 2-24, Kiel, 24148, Germany

Invited Papers

5:20

4pUWh1. BIE and coupled BIE-FEM methods for scattering from underwater objects. Ilkka Karasalo (FOI, Gullfossgatan 6, SE 16490 Stockholm, Sweden, ilkka.karasalo@foi.se)

Two techniques are described for computation of acoustic scattering by a smooth elastic object in a fluid space or a fluid layer of a layered fluid-solid medium. Both techniques use a frequency-domain boundary integral equation (BIE) method for the exterior layered medium, with the Green's function computed numerically by adaptive high-order transform integration and exact finite elements. The surface of the object is parameterized by a smooth map of the unit sphere, and the BIE is discretized by B-splines, point collocation and numerical integration in polar-like coordinates centered at the collocation point. Two approaches for handling the interior dynamics of the object are described. In the first, applicable to objects structured into homogeneous layers separated by closed smooth interfaces, the interior dynamics is formulated as a system of BIEs with displacements and tractions at the interfaces as unknowns. In the second, the interior is discretized by a general-purpose finite element (FEM) method, and an impedance matrix connecting tractions and displacements on the exterior surface is computed by eliminating interior degrees of freedom by Gaussian elimination. Computational results on test cases of the 2006 target strength benchmark workshop at NURC are presented.

5:40

4pUWh2. Calculation of the acoustic target strength of elastic objects based on BEM-BEM-coupling. Ralf Burgschweiger (Technische Fachhochschule Berlin, Univ. of Applied Sciences, Luxemburger Str. 10, 13353 Berlin, Germany, burgi@tfh-berlin.de), Martin Ochmann (Technische Fachhochschule Berlin, Univ. of Applied Sciences, Luxemburger Str. 10, 13353 Berlin, Germany, ochmann@tfh-berlin.de), Bodo Nolte (Forschungsanstalt der Bundeswehr für Wasserschall und Geophysik, Klausdorfer Weg 2-24, 24148 Kiel, Germany, bodonolte@bwb.org)

Based on a BEM-BEM-coupling method, the scattered pressure from elastic objects placed in water and partially buried in the sediment is calculated. For this reason, a special variant of the boundary element method (BEM) is implemented. It contains a pre- and a postprocessor with 3D visualization, in order to define the geometry of the scattering objects in the interface layer between fluid and sediment and the parameters needed for characterizing the fluid and the elastic material. The solver is able to perform numerical calculations in a multiple parallel manner. For the solution of the underlying system of linear equations, we use different kinds of approximate and direct solution techniques. Simple acoustical exterior problems, for example, the sound scattering by elastic solid cylinders and spheres placed in a fluid are treated by the BEM-BEM-coupling method. The results will be compared with analytical solutions or solutions obtained from other numerical methods.

Contributed Papers

6:00

4pUWh3. Modeling of scattering from targets in an oceanic waveguide using Kirchhoff/diffraction method. Keunhwa Lee (Seoul National University, San 56-1, Silim, Kwanak, 11111 Seoul, Republic of Korea, nasalkh2@snu.ac.kr), Woojae Seong (Seoul National University, Room. 306, Bd. 34, San 56-1, Sillim-dong, Kwanak-gu, College of Engineering, Dept. of Naval Architecture and Ocean Engineering, 151-744 Seoul, Republic of Korea, wseong@snu.ac.kr), Yongtaek Joo (Daewoo shipbuilding & marine engeineering CO.,LTD., Aju-dong, Geoje city, 11111 Geoje, Republic of Korea, yhsaga@dsme.co.kr)

The target scattering model in an oceanic waveguide is presented. The target scattered pressure field is formulated using the generalized Green's function method [F. Ingenito, J. Acoust. Soc. Am. 82, 2051-2059 (1987)]. The concept of Kirchhoff/diffraction method is introduced in order to simplify the Fredholm integral equation. In numerical analysis, complex target is divided into numerous polygon facets, whose analytic solution for scattered field is derived based on the waveguide solution by the ray or normal mode theory. This solution is used in constructing the target scattered field for complex target. Comparison between ray and normal mode based target scattering model is shown. Finally discussion for conditions of the source/receiver and target which improves the numerical efficiency is given.

6:20

4pUWh4. Modeling ocean reverberation under short pulse conditions. Henry Weinberg (Alion Science Incorporated, 23 Colonial Drive, Waterford, CT 06385, USA, chic@ct.metrocast.net)

The Comprehensive Acoustic System Simulation (CASS) is a standard model for predicting ocean reverberation. However, the current version, CASS V4.1, is known to have theoretical and numerical difficulties when investigating short pulse lengths. This is due to two model requirements: (1) the time increment for sampling reverberation should not exceed the pulse length; and (2) the range increment for sampling the environment should not exceed half the sound speed-pulse length product. Unless these requirements are met, certain phenomena, such as time splitting, may not be accurately modeled. In addition, the predicted results may have an unrealistic step function appearance. On the other hand, very small time and range increments often lead to excessive computational requirements. A simple modification to CASS V4.1 appears to have relaxed the current increment requirements substantially. The range increment must still be small enough to sample environmental features, but not to the extent dictated by small pulse lengths. Although the modification is based on a well known mathematical method for accelerating convergence, its success in modeling reverberation was unexpected.

6:40

4pUWh5. Comparison of two monostatic reverberation models based on ray theory. Youngmin Chu (Seoul National University, Room. 306, Bd. 34, San 56-1, Sillim-dong, Kwanak-gu, College of Engineering, Dept. of Naval Architecture and Ocean Engineering, 151-744 Seoul, Republic of Korea, sks655@snu.ac.kr), Woojae Seong (Seoul National University, Room. 306, Bd. 34, San 56-1, Sillim-dong, Kwanak-gu, College of Engineering, Dept. of Naval Architecture and Ocean Engineering, 151-744 Seoul, Republic of Korea, wseong@snu.ac.kr), Won Tchon Oh (Agency for Defense Development, 645-016 Jinhae, Republic of Korea, wontchon@chollian.net)

Two monostatic reverberation models applicable for range dependent environment are presented. Considering the roughness of both the sea surface and bottom, we calculate the reverberation signal, based on the ray propagation model and scattering model using the composite-roughness theory and/or other empirical formulae. First model computes the reverberation time signal using two-way eigenray searching between source/receiver position along the discrete scattering area (dA). The other model uses one-way eigenray searching along the discrete ray angle ($d\theta$) which generates a non-uniform scattering area providing less accurate solution at a reduced computational burden. The time series calculated from both models are shown and compared with the solutions presented in the Reverberation Modeling Workshop (Nov. 2006, Austin, TX).

7:00

4pUWh6. A novel modelling approach for sound propagation analysis in a multiple scatterer environment. Bert Van Genechten (K.U.Leuven - Dept. of Mechanical Engineering, Celestijnenlaan 300B - bus 2420, 3001 Heverlee, Belgium, Bert.VanGenechten@mech.kuleuven.be), Bart Bergen (K.U.Leuven - Dept. of Mechanical Engineering, Celestijnenlaan 300B - bus 2420, 3001 Heverlee, Belgium, Bart.Bergen@mech.kuleuven.be), Bert Pluymers (K.U.Leuven - Dept. of Mechanical Engineering, Celestijnenlaan 300B - bus 2420, 3001 Heverlee, Belgium, Bert.Pluymers@mech.kuleuven.be), Dirk Vandepitte (K.U.Leuven - Dept. of Mechanical Engineering, Celestijnenlaan 300B - bus 2420, 3001 Heverlee, Belgium, Dirk.Vandepitte@mech.kuleuven.be), Wim Desmet (K.U.Leuven - Dept. of Mechanical Engineering, Celestijnenlaan 300B - bus 2420, 3001 Heverlee, Belgium, Wim.Desmet@mech.kuleuven.be)

In the past decades element-based numerical modelling techniques have become a commonly used and invaluable tool for the analysis of acoustic radiation and scattering problems. However, the pollution errors associated with the element discretisation inherent to these methods increase with the increasing size of the problem domain. As a result, the applicability of these methods for radiation and scattering problems in which the source and receiver positions are located far from each other is often prohibited. The Wave Based Method (WBM) is an alternative deterministic prediction method for the analysis of steady-state acoustic problems. It is based on an indirect Trefftz approach in that wave functions, which are exact solutions of the underlying differential equation, are used to describe the dynamic response. The enhanced computational efficiency of the WBM as compared to the element based methods has been shown already for the analysis of both finite and (semi-)infinite acoustic problems. This paper introduces a novel WBM-based methodology to model the acoustic source-receiver transfer path functions in a multiple scatterer environment. A sound propagation validation case illustrates the potential of the proposed approach.

7:20

4pUWh7. The basis choice and the reconstruction of combined refractive-kinetic inhomogeneities in the problems of ocean acoustic tomography. Andrey Shurup (Department of Acoustics, Physics Faculty, Moscow State University, Leninskie Gory, 119991 Moscow, Russian Federation, burov@phys.msu.ru), Sergey Sergeev (Department of Acoustics, Physics Faculty, Moscow State University, Leninskie Gory, 119991 Moscow, Russian Federation, sergeev@su29.ru), Valentin Burov (Department of Acoustics, Physics Faculty, Moscow State University, Leninskie Gory, 119991 Moscow, Russian Federation, burov@phys.msu.ru)

The characteristics of the acoustical signal in ocean are determined by both the refractive inhomogeneities (the perturbation of sound velocity) and the presence of ocean currents. The methods of acoustical tomography can be applied to the simultaneous reconstruction of both refractive and kinetic inhomogeneities. In this paper the problem of the combined refractive-kinetic inhomogeneites reconstruction by the tomography methods is considered. For the realization of proposed scheme so called band basis consisted of a number of intersected stripes is applied. The advantage of the band basis in tomographic applications is conditioned by the simplicity of solving the direct problem and the possibility of describing all types of inhomogeneities in a unified manner. The comparison of the band basis with the commonly used basis composed of nonoverlapping squares is considered. The results of the reconstruction of model kinetic and combined refractive-kinetic inhomogeneities in band basis are presented. The possibility of complete tomography reconstruction of two-dimensional flows based on the scattering data only is illustrated.

Session 5aAAa

Architectural Acoustics: New Frontiers in Room Acoustical Modeling I

Murray Hodgson, Cochair
The University of British Columbia, Department of Electrical and Computer Engineering, 2332 Main Mall, Vancouver, BC V6T 1Z4, Canada

Vincent Valeau, Cochair
Laboratoire d'Etudes Aérodynamiques (LEA), Université de Poitiers - ENSMA - CNRS, Bâtiment K, 40 Avenue du Recteur Pineau, Poitiers, F-86022, France

Contributed Papers

8:00

5aAAa1. Multiresolution geometrical-acoustics modeling. Benjamin Markham (Rensselaer Polytechnic Institute, Greene Bldg., 110 8th St., Troy, NY 12180, USA, markhb@rpi.edu), Paul Calamia (Rensselaer Polytechnic Institute, Greene Bldg., 110 8th St., Troy, NY 12180, USA, calamp@rpi.edu)

Geometrical-acoustics (GA) modeling techniques assume that surfaces are large relative to the wavelengths of interest. For a given scenario, practitioners typically create a single 3D model with large, flat surfaces that satisfy the assumption over a broad range of frequencies. Such geometric approximations lead to errors in the spatial distribution of the simulated sound field because geometric details that influence reflection and scattering behavior are omitted. To compensate for the approximations, modelers typically estimate scattering coefficients for the surfaces to account stochastically for the actual, wavelength-dependent variations in reflection directionality. A more deterministic approach could consider a series of models with increasing geometric detail, each to be analyzed at a corresponding frequency band for which the requirement of large surface dimensions is satisfied. Thus, to improve broadband spatial accuracy for GA simulations, we propose a multiresolution modeling approach. Using scale model measurements of a corrugated wall, comparisons of our method with non-GA techniques, and some simple listening tests, we will demonstrate that multiresolution geometry provides more spatially accurate results than single-resolution approximations when using GA techniques, and that this improved accuracy is aurally significant.

8:20

5aAAa2. On the analysis of the time spreading of sound diffusers. Javier Redondo (IGIC - Universitat Politècnica de València, Cra. Nazaret-Oliva S/N, E-46730 Gandia, Spain, fredondo@fis.upv.es), Rubén Picó (EPSG - Univ. Politécnica de Valencia, c/ Nazaret-Oliva s/n, 46780 Grau de Gandia, Spain, rpico@fis.upv.es), Mark R. Avis (University of Salford, Acoustics Research Centre, Newton Building, M5 4WT Salford, UK, m.r.avis@salford.ac.uk)

Since the invention of sound diffusers three decades ago a substantial effort has been made to predict the acoustic behaviour of these structures. BEM methods are well established for this purpose after a systematic comparison between simulations and experimental data. Volumetric methods such as finite element methods (FEM) or the finite difference time domain method (FDTD) are not often used, due to their large computational cost. However, near to far field transformations (NFFT) can overcome that problem. Recently some of the authors have shown that the FDTD method is a useful technique to analyse the time domain signature of sound diffusers. In this paper a careful analysis of the performance of diffusers in the time domain ("time spreading") are reported, opening a new field of research.

Invited Papers

8:40

5aAAa3. Diffraction modeling in acoustic radiance transfer method. Samuel Siltanen (Helsinki University of Technology, P.O. Box 5400, 02015 TKK, Finland, Samuel.Siltanen@tml.hut.fi), Tapio Lokki (Helsinki University of Technology, P.O. Box 5400, 02015 TKK, Finland, Tapio.Lokki@tkk.fi)

The room acoustic radiance transfer method is a solution to recently presented room acoustic rendering equation which formulates the mathematical basis for all the ray-based (geometrical) room acoustic modeling algorithms. The basic acoustic transfer method gives as accurate results as the state-of-the-art commercial room acoustic modeling software. However, the basic method still lacks, e.g., diffraction modeling and modeling of complex reflections from surfaces. In this paper we discuss different diffraction modeling methods in the light of the acoustic radiance transfer method. The problems as well as benefits of each diffraction modeling method are summarized to understand which one of them can be implemented together with acoustic radiance transfer. Finally, some implementation examples are given.

9:00

5aAAa4. Can also diffracted sound be handled as flow of particles? Some new results of a beam tracing approach based on the uncertainty principle. Uwe M. Stephenson (Hafen City University Hamburg, Nelkenweg 10, 23843 Bad Oldesloe, Germany, post@umstephenson.de)

In computational room acoustics as well as noise immission prognosis efficient ray or beam tracing methods are well approved - but the problem of the neglected diffraction is still unsolved in general. The author's successful approach of 1986 based on Heisenbergs uncertainty principle was extended to the more efficient beam tracing technique and presented at the ICA 2007. The algorithm has now been generalized to recursive higher order diffraction. Now, not only single edge, but also multiple edge diffraction could be simulated

(slit and "wide obstacle" with two edges). The results have again been compared with Svensson's exact wave-theoretical secondary edge source model. With some restrictions, they seem to indicate, that indeed even diffraction of sound - like light - may be handled as flow of particles. To avoid the feared explosion of computation time with higher order diffraction, a beam reunification may now be achieved by Quantized Pyramidal Beam Tracing.

Contributed Paper

9:20

5aAAa5. General impedance boundary conditions in pseudospectral time-domain methods for room acoustics. Carlos Spa (Universitat Pompeu Fabra - Fundació Barcelona Media, Ocata, 1, 08003 Barcelona, Spain, carlos.spa@upf.edu), Toni Mateos (Universitat Pompeu Fabra - Fundació Barcelona Media, Ocata, 1, 08003 Barcelona, Spain, toni.mateos@barcelonamedia.org), Adan Garriga (Universitat Pompeu Fabra - Fundació Barcelona Media, Ocata, 1, 08003 Barcelona, Spain, adan .garriga@barcelonamedia.org)

Finite-differences in the time domain (FDTD) are among the most accurate numerical techniques to simulate wave phenomena. The main drawback of FDTD numerical schemes is their computational cost in large scale simulations. The recently developed Fourier pseudospectral time-domain (PSTD) techniques, by approximating the spatial derivatives more efficiently, have improved significantly the accuracy and time costs of the simulations of electromagnetic fields. As a step towards applying PSTD techniques to room acoustic problems, we present here a framework to properly deal with material modeling in terms of generic impedance boundary conditions, beyond the common perfectly matched layer absorbing boundaries. We apply our results to a few representative cases (simple but reverberant rooms) and analyse its performance in terms of accuracy and computational resources. In particular we analyse whether the mild constraints that PSTD imposes on space-time discretization lead to good enough results in room acoustic simulations.

9:40-11:00 Posters

Lecture sessions will recess for presentation of poster papers on various topics in acoustics. See poster sessions for topics and abstracts.

Invited Papers

11:00

5aAAa6. Ray-tracing prediction of sound-pressure and sound-intensity fields in empty and fitted rooms. Murray Hodgson (The University of British Columbia, Department of Electrical and Computer Engineering, 2332 Main Mall, Vancouver, BC V6T 1Z4, Canada, mhodgson@interchange.ubc.ca), Owen Cousins (The University of British Columbia, Department of Electrical and Computer Engineering, 2332 Main Mall, Vancouver, BC V6T 1Z4, Canada, owencousins@hotmail.com), Gary Chan (The University of British Columbia, Department of Electrical and Computer Engineering, 2332 Main Mall, Vancouver, BC V6T 1Z4, Canada, gakachan@interchg.ubc.ca), Vincent Valeau (Laboratoire d'Etudes Aérodynamiques (LEA), Université de Poitiers - ENSMA - CNRS, Bâtiment K, 40 Avenue du Recteur Pineau, F-86022 Poitiers, France, vincent.valeau@lea.univ-poitiers.fr)

A Monte-Carlo ray-tracing model has been adapted to the prediction of sound-pressure and sound-intensity fields in rooms with surfaces of arbitrary surface impedance, and containing parallelepiped obstacles. Phase changes due to propagation distance and wall reflection were accounted for. Diffraction around obstacle edges was modeled by the Unified Theory of Diffraction. The model was also extended to include the out-of-phase secondary sound source of a single-channel, global active-noise-control (ANC) system. The new model was validated in comparison with predictions by reference models (e.g. FEM) and with the results of experiments in an anechoic chamber and in real rooms. It was used to predict the effectiveness of ANC. This paper discusses the development of the new models, the results of the validation tests and ANC predictions.

11:20

5aAAa7. The intensity in a reverberant field as an acoustic energy-density gradient. Vincent Valeau (Laboratoire d'Etudes Aérodynamiques (LEA), Université de Poitiers - ENSMA - CNRS, Bâtiment K, 40 Avenue du Recteur Pineau, F-86022 Poitiers, France, vincent.valeau@lea.univ-poitiers.fr), Matthieu Boirlaud (ESIP, Av. du Recteur Pineau, 86022 Poitiers Cedex, France, matthieu.boirlaud@etu.univ-poitiers.fr), Judicaël Picaut (Lab. Central des Ponts et Chaussées, Division Entretien, Sécurité et Acoustique des Routes, Route de Bouaye - BP 4129, 44341 Bouguenais Cedex, France, Judicael.Picaut@lcpc.fr), Murray Hodgson (The University of British Columbia, Department of Electrical and Computer Engineering, 2332 Main Mall, Vancouver, BC V6T 1Z4, Canada, mhodgson@interchange.ubc.ca)

The classical assumption for diffuse reverberant sound fields is that the acoustic energy flow at any location in a room -- i.e., the acoustic intensity -- is null. For rooms with disproportionate dimensions and/or uneven absorption distributions, this assumption no longer holds. Over the past few years, a room-acoustic diffusion model has been developed that can be seen as an extension of the statistical theory to nondiffuse sound fields. This work investigates the basic gradient-equation underlying this diffusion theory: it states that the energy-flow vector is proportional to both the gradient of the acoustic energy density, and to the room diffusion constant. The gradient equation for the acoustic intensity is confirmed numerically by comparison with calculations of the intensity vector using a particle-tracing model and a ray-tracing model. Examples are presented for a room with a diffuse sound field, and for elongated rooms where the sound field is strongly non-diffuse, in the case of both diffuse and specular reflections.

11:40

5aAAa8. Prediction and tailoring of steady-state broadband sound fields in enclosures using absorption scaling and energy-intensity boundary elements. Donald B. Bliss (Duke University, Mechanical Engineering and Materials Science, 148B Hudson Hall, Durham, NC 27708, USA, dbb@duke.edu), Krista A. Michalis (Duke University, Mechanical Engineering and Materials Science, 148B Hudson Hall, Durham, NC 27708, USA, kam49@duke.edu), Linda P. Franzoni (Duke University, Mechanical Engineering and Materials Science, 148B Hudson Hall, Durham, NC 27708, USA, franzoni@duke.edu)

Enclosures with diffuse reflection boundaries are modeled with an energy-intensity boundary element method using uncorrelated broadband directional sources. An absorption-based perturbation analysis shows the spatial variation of the acoustic field obeys certain scaling laws. A series expansion in terms of average absorption gives separate boundary integral problems at each order. The lowest-order solution has a uniform level proportional to the reciprocal of the average absorption. The next-order solution is independent of average absorption and primarily responsible for spatial variation of the acoustic field. This solution depends on the spatial distribution of absorption and input power sources, but not their overall level. For the primary spatial variation, the effects of the relative distributions of absorption and input power are linear and uncoupled. These distributions can be expressed in terms of constituent spatial modes corresponding to the ways absorption and input power can be distributed. Solved numerically once for each mode, the acoustic field can be expressed in terms of the modal amplitudes in closed form. These amplitudes can be adjusted to tailor the spatial variation. Examples include how to distribute absorption to minimize sound levels in one location, or how to achieve a uniform interior field. (Sponsor: NSF)

Contributed Papers

12:00

5aAAa9. Analysis of room transfer function and reverberant signal statistics. Eleftheria Georganti (Acoustic Technology Department, Technical University of Denmark, Ørsted Plads, B352, DK-2800 Lyngby, Denmark, ege@oersted.dtu.dk), John Mourjopoulos (Audio and Acoustic Technology Group, Wire Communications Laboratory, Electrical Engineering & Computer Technology Department, University of Patras, 26500 Patras, Greece, mourjop@wcl.ee.upatras.gr), Finn Jacobsen (Acoustic Technology Department, Technical University of Denmark, Ørsted Plads, B352, DK-2800 Lyngby, Denmark, fja@oersted.dtu.dk)

For some time now, statistical analysis has been a valuable tool in analyzing room transfer functions (RTFs). This work examines existing statistical time-frequency models and techniques for RTF analysis (e.g., Schroeder's stochastic model and the standard deviation over frequency bands for the RTF magnitude and phase). RTF fractional octave smoothing, as with 1/3 octave analysis, may lead to RTF simplifications that can be useful for several audio applications, like room compensation, room modeling, auralisation purposes. The aim of this work is to identify the relationship of optimal response smoothing (e.g., as in complex smoothing) with respect to the original RTF statistics. More specifically, the RTF statistics, derived after the complex smoothing calculation, are compared to the original statistics across space inside typical rooms, by varying the source, the receiver position and the corresponding ratio of the direct and reverberant signal. In addition, this work examines the statistical quantities for speech and audio signals prior to their reproduction within rooms and when recorded in rooms. Histograms and other statistical distributions are used to compare RTF minima of typical "anechoic" and "reverberant" audio speech signals, in order to model the alterations due to room acoustics. The above results are obtained from both in-situ room response measurements and controlled acoustical response simulations.

12:20

5aAAa10. On the implementation of room acoustics modeling software using Digital Waveguide Mesh. José J. Lopez (Tech. Univ. of Valencia, Camino de Vera S/N, 46021 Valencia, Spain, jjlopez@dcom.upv.es), José Escolano (University of Jaén, Alfonso X, 28, E-23700 Linares, Spain, escolano@ujaen.es), Basilio Pueo (University of Alicante, Signals, Systems and Telecommunications, Cta San Vicente del Raspeig s/n, E-03690 Alicante, Spain, basilio@ua.es)

The Digital Waveguide Mesh (DWM) method for room acoustic simulation has been introduced in the last years to solve sound propagation problems numerically. However, the huge computer power needed in the modeling of large rooms and the complexity to incorporate realistic boundary conditions has delayed their general use, being restricted to the validation of theoretical concepts using simple and small rooms. This paper presents a complete DWM implementation where all the stages needed to analyze a room are discussed. The software starts the analysis from the architectural model of the room importing its geometry directly from a CAD file. After that, it generates the rectangular mesh of individual cells that conforms the volume to be simulated. Next, the time domain recursion is carried out using parallel computer techniques. Also the software includes a serious treatment of boundary conditions using different material with frequency dependence characteristics. Finally, the software can export the results. Additionally, some room simulation examples are presented and analyzed in detail. The work carried out demonstrate how it is possible, with the current power of the personal computer, to start to simulate real rooms with high amount of geometric details and frequency dependent boundary.

12:40-2:00 Lunch Break

2:00

5aAAa11. Defining perceptual requirements of dynamic (real-time) acoustic modeling and auralization. Linda Gedemer (5930 Penfield Ave., Woodland Hills, CA 91367, USA, gedeml@rpi.edu)

Acoustic modeling is evolving from static sources and receivers to dynamic sources and receivers as computational speeds allow for faster renderings. Current research has focused on creating highly accurate dynamic models and auralizations but still struggle with the trade-off between accuracy and available processing speed. The question remains as to how accurate do these models need to be if the receiver (listener) is moving dynamically through the acoustic model. The focus of this paper is to address the accuracy required of dynamic models and/or auralizations from a perceptual standpoint. From this, the necessity for creating models that are perhaps more accurate than required will be considered.

2:20

5aAAa12. The scanning and voxellisation of complex 3D objects for incorporation within finite difference time domain based acoustic prediction. Ian Drumm (The University of Salford, C.S.E., Salford University, The Crescent, M5 4WT Manchester, UK, i.drumm@salford.ac.uk)

This paper presents techniques developed to incorporate complex 3D objects within the author's own finite difference time domain based acoustic prediction software application. Using a combination of 3D laser scanning, ray based voxellisation and a least pth norm based filter design approach to emulate the absorption profiles of non-rigid boundaries; complex objects can be incorporated into a variety of FDTD based acoustic prediction scenarios. The paper will evaluate the success of the approach and explore its application. Of particular interest is the emulation of furniture, people, acoustic modifiers and other complex non planer structures within room acoustics predictions.

Invited Paper

2:40

5aAAa13. Localization and mesoscopics in structures and rooms II. Richard Weaver (Dept. of Physics, University of Illinois, Urbana, IL 61801, USA, r-weaver@uiuc.edu)

A new theory is developed which makes quantitative predictions for energy transport that are consistent with localization. The theory promises ultimately to apply to a wide variety of systems. It is based on an assumption of S-matrices that are incoherent - as conventional diffuse field theories would have it - but then corrected to assure exact energy conservation. It is shown that the resulting system responses (they are concatenations of S matrices) have coherence, are consistent with localization, and predict Greens function retrieval. Localization emerges naturally from competition between rates of transport and rate of eigen-mode resolution. Examples are presented corresponding to coupled rooms and to diffusion in a multiply scattering medium. Future generalizations are discussed and the mathematical challenges are outlined. This is the second talk in a pair begun in a different session. Work supported by NSF CMS 05-28096.

FRIDAY MORNING, 4 JULY 2008 ROOM 243, 8:00 A.M. TO 3:20 P.M.

Session 5aAAb

Architectural Acoustics and Noise: Airborne and Impact Sound Insulation I

Berndt Zeitler, Cochair
NRC - Institute for Research in Construction, 1200 Montreal Road, Building M-27, Ottawa, ON K1A 0R6, Canada

Patrizio Fausti, Cochair
Engineering Dept. - Univ. of Ferrara, Via Saragat, 1, Ferrara, 44100, Italy

Contributed Paper

8:00

5aAAb1. Maximizing field performance of thin, light-weight partition and floor assemblies. Ronald Eligator (Acoustic Dimensions, 145 Huguenot Street, New Rochelle, NY 10801, USA, religator@acousticdimensions.com)

Laboratory test reports are an important source of information regarding anticipated performance of a sound barrier construction. However, differences in construction conditions between the laboratory and a real building can greatly affect, usually negatively, the performance of a sound barrier assembly in the field. This reality, combined with the typical client's focus on reducing construction costs, requires that for a sound barrier construction to be successful, the effect of abutting constructions must be well understood. This paper reports on our firm's experience in translating lab-tested lightweight sound barrier assemblies to the field, relating design conditions to field results in terms of physical construction and noise reduction results.

Invited Paper

8:20

5aAAb2. Monitoring field and laboratory performance for airborne and impact sound insulation for 110,000 homes per annum. Sean Smith (BPC, Napier University, 42 Colinton Road, EH10 5BT Edinburgh, UK, se.smith@napier.ac.uk), Dave Baker (Robust Details Ltd, Davy Avenue, Knowlhill, MK5 8NB Milton Keynes, UK, dbaker@robustdetails.com), David Panter (Robust Details Ltd, Davy Avenue, Knowlhill, MK5 8NB Milton Keynes, UK, dpanter@robustdetails.com)

This paper provides an overview of a unique monitoring system used in England and Wales for tracking the sound insulation performance for 110 000 new build homes per annum. The regulatory approach, known as Robust Details was established within the building regulations and passed by parliament in 2004 after an 18 month initial research project. Annually over 5000 construction sites now use this system approach for separating walls and floors for attached houses and apartments. Acoustic site inspections and sound insulation field testing reports provide systematic feedback to the design and performance review. Since the RD systems inception on-site sound insulation compliance rates have risen from 40% to 97%. This paper will discuss the role of laboratory benchmark testing for products and also the role of acoustic ″field″ inspectors in tracking the airborne and impact performance. In addition the role of intervention and statistical analysis in upgrading or withdrawing specific wall and floor constructions will be presented.

Contributed Paper

8:40

5aAAb3. Changed sound properties due to minor construction changes in a lightweight building. Fredrik Ljunggren (Luleå Univ. of Technology, Div. of Sound and Vibration, S-97187 Luleå, Sweden, fredrik.ljunggren@ltu.se)

This paper relates to building acoustic measurement inside a two-story office house. The construction, which is known as lightweight, is prefabricated in volumes at a factory and is then transported to the building yard for assembling. It is build up of a wooden frame with particle boards and plaster boards attached. The building consists of a number of nominally, or almost nominally, identical rooms with assumed identical sound properties. In the projection stage, the construction was slightly modified in some of the rooms in order to see in what way the sound properties would be affected. In total eight impact sound pressure level measurements and eight sound reduction index measurements were performed and analysed for the different setups.

Invited Papers

9:00

5aAAb4. The drying process influence on the brick walls sound reduction index: laboratory evaluations and theoretical analysis. Chiara Scrosati (Construction Technologies Institute of Italian National Research Council, Viale Lombardia, 49, 20098 San Giuliano Milanese (MI), Italy, labacustica@itc.cnr.it), Fabio Scamoni (Construction Technologies Institute of Italian National Research Council, Viale Lombardia, 49, 20098 San Giuliano Milanese (MI), Italy, Fabio.Scamoni@itc.cnr.it), Fabrizio Valentini (Construction Technologies Institute of Italian National Research Council, Viale Lombardia, 49, 20098 San Giuliano Milanese (MI), Italy, Fabrizio.Valentini@itc.cnr.it)

This paper presents experimental results showing the sound reduction index of different types of brick walls; the analysis was in particular carried out on double walls, single walls, and single walls with external lining. Its main purpose is to find the minimum drying time of the structure necessary to obtain the sound reduction indexes of brick walls as close as possible to laboratory real values. Moreover, it aims at making results of different laboratories as comparable as possible in terms of repeatability and reproducibility. All the fundamental quantities, such as the sound reduction index (R), the weighted sound reduction index (R_{w}), the spectrum adaptation terms C and C_{tr}, and temperature (T) and relative moisture, have been analyzed. A qualitative analysis of the curves slope of the sound reduction index versus frequency has been conducted for each drying time for each type of evaluated wall. The measurements were carried out in the acoustic laboratory of ITC-CNR (the Construction Technologies Institute of the Italian National Research Council) in Milan, according to the procedures of ISO 140 part 3.

9:20

5aAAb5. Acoustical proprieties of light brick walls and its effects on flanking transmission. Giovanni Semprini (University, DIENCA Dept. Facoltà di Ingegneria, Viale Risorgimento 2, 40136 Bologna, Italy, giovanni.semprini@mail.ing.unibo.it), Luca Barbaresi (DIENCA - Univ. of Bologna, Viale Risorgimento 2, 40136 Bologna, Italy, luca.barbaresi@mail.ing.unibo.it)

Light brick walls 8-10 cm thick are typical structures frequently used in Italian building constructions as a internal partitions between dwellings and as internal layer of double façade walls. Due to low surface mass and rigid connection to other horizontal and vertical structures, light brick walls are often responsible of high flanking transmission. The simplest acoustic modeling of this structure for the evaluation of sound transmission in buildings, is the approach proposed by the EN 12354 standards, where the brick wall can be considered as a homogeneous structure and main acoustic parameters required are the sound reduction index and the vibration reduction index Kij. The aim of this paper is to analyse results of physical and acoustical properties (sound reduction index, structural reverberation time, radiation efficiency) of a typical 8 cm thick brick wall measured in laboratory testing facility, used as a partition in different test configuration: single layer wall, double brick layer wall with internal thermal layer and as a component of lateral wall, where the Kij index flanking transmission were also evaluated. Experimental results are then compared with theoretical values in order to analyse difference with homogeneous structures.

9:40-11:00 Posters

Lecture sessions will recess for presentation of poster papers on various topics in acoustics. See poster sessions for topics and abstracts.

Contributed Paper

11:00

5aAAb6. Lightweight system Technostar specified in the CCTV tower Beijing. Andrew Koster (Saint-Gobain Insulation, Parallelweg 20, 4878AH Etten-Leur, Netherlands, andrew.koster@saint-gobain.com)

The role and possibilities of lightweight mineral wool is known for quite some years, acting as the optimum spring in a mass spring mass system one can reach high acoustic values. Compared to the massive constructions (e.g., concrete) the use of a mass spring mass construction has also other advantages (e.g., logistic, dimension of foundation and labour costs). Saint-Gobain Isover developed a wall system called Technostar, originally defined for cinema walls. In this construction an optimal mass spring mass construction is created. The theory of mass spring mass systems will shortly come up. All elements of the system are described. The acoustical performance of the Technostar construction is calculated with acoustic software (Stiff) and compared with laboratory measurements; the influence of different parameters on the measured acoustical performance will be shown. The practical use of the Technostar wall will be shown on the basis of the project CCTV tower in Beijing. For this project the acoustic requirements, the translation in terms of the wall construction with the specific details will be shown. The system will be build in March 2008.

Invited Paper

11:20

5aAAb7. Influence of static-load on airflow resistivity determination. Alessandro Schiavi (Istituto Nazionale di Ricerca Metrologica, str. delle Cacce, 91, 10135 Turin, Italy, a.schiavi@inrim.it), Claudio Guglielmone (Istituto Nazionale di Ricerca Metrologica, str. delle Cacce, 91, 10135 Turin, Italy, c.guglielmone@inrim.it), Piercarlo Miglietta (FIAT Group Automobiles S.p.A., Corso G. Agnelli, 220, 10135 Turin, Italy, piercarlo.miglietta@fiat.com), Franco Alasia (Istituto Nazionale di Ricerca Metrologica, str. delle Cacce, 91, 10135 Turin, Italy, f.alasia@inrim.it)

Dynamic stiffness of resilient materials used as underlayer in floating floors give useful knowledge on the acoustical behaviour of a floor in impact sound insulation. In previous works the influence of the static load and the compressive behaviour of the resilient layers on dynamic stiffness evaluation has been shown. A new measurement technique of the airflow resistance (according to ISO 9053) in terms of static load applied on the resilient materials with open cells is proposed. Usually the airflow resistance of porous materials used as underlayers is evaluated on unloaded samples of material. In dynamic stiffness measurements the material is subject to a static load of 2 kPa. Because the dynamic stiffness value depends on airflow resistivity r [Pa×s/m^2] (in particular when 10 kPas/m^2< r <100 kPas/m^2) through the material, it is important to evaluate the airflow resistivity behaviour in the same condition of the dynamic stiffness measurement, i.e., under a static load of 2 kPa. A new apparatus to evaluate the airflow resistivity in terms of different static loads has been designed and realized at I.N.RI.M. of Turin. The first experimental results show evidence of the dependence of the airflow resistivity of the resilient materials on the applied load.

Contributed Papers

11:40

5aAAb8. Compression of felt-type thermal insulation layer for underfloor heating system and floor impact sound. Tongjun Cho (SKEC, Jung-Gu, Soonhwa-Dong 66, SK Soonhwa B/D, R&D Center, 100130 Seoul, Republic of Korea, tjc@skec.co.kr), Hyun-Min Kim (SKEC, Jung-Gu, Soonhwa-Dong 66, SK Soonhwa B/D, R&D Center, 100130 Seoul, Republic of Korea, thek80@skec.co.kr)

In Korea, almost every house uses underfloor heating, which has advantages of thermal comfort and energy efficiency. However, when it is constructed for high-rise apartment houses, it yields a problem in floor impact sound insulation. It accounts for the fact that a foam-type thermal insulator sandwiched between structural slab and heating floor functions as a spring and easily transmits impacts on the floor to the slab. In that case, the system's transmissibility is determined by dynamic stiffness of the thermal insulation layer and the lower the dynamic stiffness is, the more the floor impact is isolated. For that reason, apartments construction companies are attempting to lower the dynamic stiffness of the thermal insulation layer for impact sound reduction. As part of the attempt, felt-type materials with relatively low dynamic stiffness such as glass wool or polyester felt are considered as a substitution for the foam-type thermal insulator. However, there is a possibility that compression of the felt-type materials would increase the dynamic stiffness and the impact sound insulation effect at early stage might be weakened in the long term. This paper investigates the correlation between gradual compression of the felt-type thermal insulation layer and the impact sound variation.

12:00

5aAAb9. Acoustic and vibration characteristics of floated floors concrete structures. Seungyup Y. Yoo (Hanyang University, 133-791 Seoul, Republic of Korea, syrus81@hanyang.ac.kr), Jin Yong Jeon (Hanyang University, Department of Architectural Engineering, 133-791 Seoul, Republic of Korea, jyjeon@hanyang.ac.kr)

The floating floor with multilayers of resilient materials was investigated for the isolation of floor impact sound. The floor structures were evaluated in the reduction of the heavy-weight impact sound, which is mainly affected by the boundary conditions of the tested floors. The values of single-number ratings for floor impact sounds decrease dramatically for floated floors. Insertion loss is determined by the vibration characteristics of a bare slab, such as transmissibility. The logarithmic decrement (ξ) of the vibration responses was 4 times higher than that of the bare slab. Above 125 Hz, the vibration between the slab structure and floating floor is isolated effectively. It was revealed that the resonant frequency of the slab structure and the damping factor of the floating floor are important aspects for impact sound isolation.

Invited Paper

12:20

5aAAb10. Interactions between floor and ceiling panels in presence of a fibrous material in the cavity. Thomas Scelo (Marshall Day Acoustics LTD, P. O. Box 5811, Wellesley St., 1000 Auckland, New Zealand, thomas.scelo@marshallday.co.nz)

The mechanisms governing the acoustic transmission through building elements such as floor/ceiling assemblies are complex. The vibroacoustic interactions between the finite size structure and the enclosed volume are, in particular, rendered more complex at low frequencies when the finite dimensions of the building are taken into consideration. A model developed to predict the low frequencies vibroacoustics response of mutliplates systems offers the opportunity to explore, among other geometrical and material parameters, the effects of a fibrous material in the ceiling plenum on the acoustics behaviour of the whole structure. This paper presents the theoretical approach employed to predict the interactions between the floor, the ceiling panel and the enclosed volume. It also explores the effects of varying the material characteristics and overall thickness on these interactions.

12:40-1:40 Lunch Break

Invited Paper

1:40

5aAAb11. Methods to control low frequency impact noise in wood-frame construction. Berndt Zeitler (NRC - Institute for Research in Construction, 1200 Montreal Road, Building M-27, Ottawa, ON K1A 0R6, Canada, berndt.zeitler@nrc-cnrc.gc.ca), Trevor Nightingale (NRC - Institute for Research in Construction, 1200 Montreal Road, Building M-27, Ottawa, ON K1A 0R6, Canada, Trevor.Nightingale@nrc-cnrc.gc.ca), Frances King (NRC - Institute for Research in Construction, 1200 Montreal Road, Building M-27, Ottawa, ON K1A 0R6, Canada, Frances.King@nrc-cnrc.gc.ca)

The control of low frequency impact noise is of great importance in Japan and Korea. For impact noise rating, both countries use standardised heavy and soft impactors that inject high levels of low frequency power into a wood-frame floor due to the high force applied and "good" impedance match between the source and the floor. This paper reports on a parametric study designed to confirm the important parameters for controlling low frequency impact noise and how these parameters are affected by changes to construction details. The paper shows that increasing the drive point impedance floor surface while minimising the structural coupling between the gypsum board ceiling and the structural framing (joists) are important elements. Additionally, a well-designed floor topping can be very effective when applied to a suitable floor. The paper presents data to show the relative importance of direct and flanking transmission paths. Furthermore, it is shown that repeated impacts by the Bang Machine physically change the floor assembly and as a consequence resulting impact sound pressure levels in the receive room also change. The paper concludes with a general discussion and recommendations.

Contributed Papers

2:00

5aAAb12. Field airborne and impact sound insulation of wood truss floor systems. Chad N. Himmel (JEAcoustics, 1705 West Koenig Lane, Austin, TX 78756, USA, Himmel@JEAcoustics.com), Daniel J. Kupersztoch (JEAcoustics, 1705 West Koenig Lane, Austin, TX 78756, USA, Kupersztoch@JEAcoustics.com)

A series of field measurements on wood truss floors of various types was recently completed at four residential apartment complexes. About 40 floors with different floor finishes, gypsum concrete underlayment, noise control underlayment systems, truss span lengths, ceiling types, and resilient metal channel types were constructed and measured. Trusses were all similar engineered prefabricated parallel chord wood trusses. Room volumes and room absorptive characteristics are varied and nonstandard. Measurements are normalized according to ASTM E 1007 and proposed normalized impact sound rating (NISR) procedures to provide a reasonably consistent set for analysis. Low frequency measurements were conducted to 12.5 Hz one-third octave band. For both transmission loss and impact sound, many of the results compare well with predictions using simple regression analysis developed by others using variables such as the mass of the layers, truss depth and spacing, insulation thickness and density, and resilient metal channel spacing. The measurements and results will be presented in the paper.

2:20

5aAAb13. Impact sound insulating performance of access floors. Francesco Asdrubali (Università degli studi di Perugia, Via G. Duranti 67, 06125 Perugia, Italy, fasdruba@unipg.it), Francesco D'Alessandro (Università degli studi di Perugia, Via G. Duranti 67, 06125 Perugia, Italy, dalessandro.unipg@ciriaf.it)

Access floor are raised floor systems consisting of modular panels supported by posts at a certain height to create a gap below the floor surface. Electrical wires and pipes can be placed inside the gap in order to avoid exposed installations and to simplify operations involving the inspection, repair, changing, or adding of system elements. This paper presents the results of the measurement campaign carried out on seven different access floor configurations, obtained by changing different floor elements: panels, surface finishes, damping materials under the posts base. Impact sound insulating properties of access floors combined with false ceilings were also tested and are reported in the paper. The tests were executed in two overlapping reverberating rooms available at the Acoustics Laboratory of the University of Perugia using the procedures given by ISO 140-6 Standard. The results are expressed in terms of normalized sound impact pressure level Ln and of the corresponding single number index Ln,W.

Invited Papers

2:40

5aAAb14. Measurement of room-to-room airborne sound insulation with an access floor in a dwelling unit of condominium. Takashi Koga (Kajima Technical Research Institute, 2-19-1 Tobitakyu, Chofu, 182-0036 Tokyo, Japan, tkoga@kajima.com)

It is preferred covering a wooden access floor on the concrete floor for condominium apartments in Japan. The access floor usually installed after every partition in each dwelling unit. If access floor and ceiling were done before partition, one can obtain accuracy of construction and reduce waste material. Therefore, one can provide building more green. But, there is concern that may deteriorate sound insulation because of flanking path through under the access floor. On the other hand, there is also another dominant flanking path irrespectively to these construction methods: via doors leading into hallway. A number of field measurements of sound insulation were done with opening/closing doors to evaluate the flanking transmission via the doors. These results show that the doors affect especially in high frequency, but not significant in low-mid frequency. Next, the sound transmission performances of access floors and ceilings measured at laboratory are compared with direct sound transmission through wall itself. As a conclusion, field measurement results show that this construction method difference less affect to airborne sound insulation performance.

3:00

5aAAb15. The acoustical effect of reveal blocks, from measuring method to prediction. Frigyes Reis (Budapest University of Technology and Economics, Lab. of Building Acoustics, Mûegyetem rakpart 3., 1111 Budapest, Hungary, reis@mail.bme.hu), Balázs Tóth (Wienerberger Co., Bártfay str. 34, 1119 Budapest, Hungary, balazs.toth@wienerberger.hu)

The analysis of the efforts to create high quality building from the point of view of energy-efficiency, and the resulting variety of new products, building constructions and systems leads to the conclusion: there are characteristic deficiencies in the field of measuring and prediction methods related to sound insulation, and there is a need to stop the gap. The example on which the problem is shown is

the acoustical effects of reveal blocks, used around window openings, to reduce heat propagation and increase energy efficiency. The reveal blocks include more sound propagation paths, the sound insulation of which can not be determined using the existing measuring standards. The paper describes new measuring concept and method to characterise the sound insulation characteristics of reveal blocks in their built-in form. The methods are fitted to the standardised measuring methods of sound insulation. Proposal is presented for the modification in the prediction procedure of sound insulation of façade constructions, utilising the results of the new measuring method.

FRIDAY MORNING, 4 JULY 2008 P2-B, LEVEL 2, 9:40 TO 11:20 A.M.

Session 5aAAc

Architectural Acoustics and Noise: Airborne and Impact Sound Insulation II (Poster Session)

Berndt Zeitler, Cochair
NRC - Institute for Research in Construction

Patrizio Fausti, Cochair
Engineering Dept. - Univ. of Ferrara

All posters will be on display from 9:40 a.m. to 11:20 a.m. To allow contributors an opportunity to see other posters, contributors of odd-numbered papers will be at their posters from 9:40 a.m. to 10:30 a.m. and contributors of even-numbered papers will be at their posters from 10:30 a.m. to 11:20 a.m.

Contributed Papers

5aAAc1. Enhancement of impact sound insulation for "Gründerzeit-Häuser" build around 1900 during refurbishment using concrete-wood composite floors or suspended ceilings. Thomas Bednar (University of Technology, Karlsplatz 13/206, A-1040 Vienna, Austria, thomas.bednar@tuwien.ac.at)

During refurbishment of Viennese buidlings that have been erected around 1900 an important aspect is to enhance the impact sound insulation of the old wooden floors. Usually the floors are wood beam floors and the uppermost floor is a massive wooden floor called Dippelbaumdecke. Two important measures are taken to increase the impact sound insulation to achieve the minimum requirement of LnTw<=48≤dB. The paper describes the design of an optimal suspended ceiling to avoid additional measures and as an alternative the impact of an additional thin concrete floor on top of the Dippelbaum-floor to achive minimum floor heights. As the thin concrete floor has a much larger area than the rooms below the measured results showed a big influence of concrete floor area on the impact sound level.

5aAAc2. Sound insulation properties of building elements, considering the frequency range below 100 Hz. Herbert Muellner (TGM Federal Institute of Technology, Wexstrasse 19-23, 1200 Vienna, Austria, herbert.muellner@tgm.ac.at), Anna Frey (University of Applied Sciences, FH Campus Vienna, Daumegasse 3, 1100 Vienna, Austria, anna.frey@chello.at), Catrin Humer (TGM Federal Institute of Technology, Wexstrasse 19-23, 1200 Vienna, Austria, catrin.humer@tgm.ac.at)

The constantly increasing standard of comfort in general and the rising number of apartment buildings in lightweight mode of construction directed the focus of research to the sound insulation properties of timber frame and massive wood element buildings. The complaints of the residents of terraced houses and multiple dwellings in lightweight buildings mainly concern noise events characterised by dominant low frequency. This problem regards airborne sound insulation as well as impact sound insulation. Based on empirical data the comparison of the sound insulation properties of the building elements investigated shows the specific problem of each category of construction mode in the frequency range below 100 Hz. The typical sound insulation characteristics regarding the low frequency range are discussed in the light of the current applied sound insulation requirements as well as in relation to the problem to comply with the resident's apperception of sound insulation quality.

5aAAc3. Effect of the frequency spectrum trend on the determination of the weighted normalized impact sound pressure level for floor structures. Federica Bettarello (Engineering Dept. - Univ. of Ferrara, Via Saragat, 1, 44100 Ferrara, Italy, federica.bettarello@unife.it), Patrizio Fausti (Engineering Dept. - Univ. of Ferrara, Via Saragat, 1, 44100 Ferrara, Italy, patrizio.fausti@unife.it)

The most common floor constructions in Italian buildings are composed of two parts: the structural one, made of concrete beams and perforated bricks, and the floating floor. The results of the in situ measurements of the impact sound pressure level, realized on the structural part of the floors, show a frequency spectrum trend that increases with the frequency. The spectrum is also characterized by many peaks and dips at the high frequency range that strongly influence the determination of the weighted normalized impact sound pressure level, also for structures with similar mass and geometry. The frequency trend of the beam and brick structures is completely different from the characteristic spectrum of homogeneous concrete slabs or lightweight structures. Considerations on how those differences can influence the obtainable results in terms of the reduction of impact sound pressure level referred to the same floating floor typology, the spectrum adaptation terms and the other acoustic quantities described in the standards are reported.

5aAAc4. Influence of flanking transmission in typical Italian constructions. Simone Secchi (Univ. of Florence, Via San Niccolò 89/a, 50125 Florence, Italy, simone.secchi@taed.unifi.it), Gianfranco Cellai (Univ. of Florence, Via San Niccolò 89/a, 50125 Florence, Italy, gianfranco.cellai@unifi.it), Elisa Nannipieri (Univ. of Florence, Via San Niccolò 89/a, 50125 Florence, Italy, elisa.nannipieri@taed.unifi.it)

Actually acoustic performance of building components are analysed with reference to standardised conditions, in laboratories with suppressed flanking transmission. Laboratory results often show values of the performances quite different from those measured in real buildings, as a consequence of flanking transmission and of different conditions of realisation in

situ. Moreover, in spite of all efforts aimed to standardise laboratory test conditions, often we find different certified performances of same building components obtained in different laboratory. In some cases, these differences may be very relevant. Besides, the Italian decree on acoustic requirement of buildings prescribes limiting values to be measured in situ. For these reasons, many producers of building materials and components more frequently presents in their depliants both laboratory values and in situ values of acoustic performances of their products. The paper shows the preliminary results of an research aimed to verify acoustic performances of partition walls and floors in a laboratory which respect conditions of ISO 140-1, but with the presence of relevant flanking transmission, similar to real buildings. The relevance of the flanking transmission has also been modified by means of a lining applied to the ceiling of the receiving room of the laboratory.

5aAAc5. Survey on the insulation performance of acoustic louvres. Lieven De Geetere (Belgian Building Research Institute, Lombardstraat 42, B-1000 Brussel, Belgium, lieven.de.geetere@bbri.be), Bart Ingelaere (BBRI, rue du Lombard, 42, B-1000 Brussel, Belgium, bart .ingelaere@bbri.be)

Machinery such as compressors, boilers and generators require adequate ventilation and extract. To avoid excessive noise breakout, acoustic louvres are frequently used. These are usually made of tilted hollow metallic blades filled with absorptive materials and perforated at the inside face. This study investigates the important characteristics of common shaped acoustic louvres with regard to sound insulation. First, a market survey on 109 existing acoustic louvres of 24 producers worldwide is made. Second, laboratory measurements of sound insulation on 38 prototypes of 1 m^2 acoustic louvres are compared. The influence of several parameters are studied such as louvre depth, blade angle, blade shape, blade thickness, blade spacing, kind of absorptive material, perforation degree, and edge filling.

5aAAc6. Sound insulation characteristics of shipboard windows. Sangryul R. Kim (Acoustics Team, Korea Institute of Machinery and Materials, 171 Jang-dong, Yuseong-gu, 305-343 Daejeon, Republic of Korea, srkim@kimm.re.kr), Hyun-Sil Kim (Acoustics Team, Korea Institute of Machinery and Materials, 171 Jang-dong, Yuseong-gu, 305-343 Daejeon, Republic of Korea, hskim@kimm.re.kr),Hyun-Ju Kang(Acoustics Team, Korea Institute of Machinery and Materials, 171 Jang-dong, Yuseong-gu, 305-343 Daejeon, Republic of Korea, kanghj@kimm.re.kr)

Although small-size windows are used in a ship, shipboard windows are a multilayered structure with glasses and air-gaps for high sound insulation. This paper discusses how to improve the sound insulation performance of shipboard windows. First, the sound transmission loss (STL) obtained from various experiments with shipboard windows are introduced and studied. The results show the layer arrangement as well as the material property of each layer makes an effect on the window's STL. It is also found that the higher the sound insulation performance of the window is, the more important the effect of the window frame is. Next, theoretical investigations are carried out and discussed in comparison with the experimental results. The comparison provides possible clues to increase the STL of the window.

5aAAc7. Acoustic analysis of the framework and walls stage in the construction of a housing block. Maria Jesus Ballesteros (Universidad de Castilla-La Mancha, Campus Universitario, 16071 Cuenca, Spain, MJesus.Ballesteros1@alu.uclm.es), Samuel Quintana (Universidad de Castilla-La Mancha, Campus Universitario, 16071 Cuenca, Spain, Samuel.Quintana@uclm.es), Marcos D. Fernandez (Universidad de Castilla-La Mancha, Campus Universitario, 16071 Cuenca, Spain, Marcos.Fernandez@uclm.es), Jose A. Ballesteros (Universidad de Castilla-La Mancha, Campus Universitario, 16071 Cuenca, Spain, Josea.Ballesteros@uclm.es), Laura Rodriguez (Universidad de Castilla-La Mancha, Campus Universitario, 16071 Cuenca, Spain, Laura.Rodriguez @uclm.es)

The noise in the construction process is one of the main environmental and industrial noise sources. There are no specific regulations in several European countries for assessing such kind of noise, neither reference indexes for its evaluation. Therefore, the limits adopted are those for environmental and industrial noise, although they do not take into account the intrinsic characteristics of this noise. A measurement procedure has been stated for assessing the noise in building sites in which, the most appropriate indexes for this noise have been analyzed and used to derive the acoustic characteristics of the framework and walls stage. This stage is considered as one of the most annoying in the construction process of a housing block.

Session 5aAAd

Architectural Acoustics: Coupled Volume Acoustics I (Poster Session)

Jason Summers, Cochair
U.S. Naval Res. Lab.

Alexis Billon, Cochair
Universite de Liege

All posters will be on display from 9:40 a.m. to 11:20 a.m. To allow contributors an opportunity to see other posters, contributors of odd-numbered papers will be at their posters from 9:40 a.m. to 10:30 a.m. and contributors of even-numbered papers will be at their posters from 10:30 a.m. to 11:20 a.m.

Contributed Paper

5aAAd1. Investigations on real-size coupled rooms based on Bayesian estimation method. Zuhre Su (Russ Berger Design Group, 4006 Belt Line Road Suite 160, Addison, TX 75001, USA, tayasu7@yahoo.com), Dave Woolworth (Oxford Acoustics, Inc., 356 CR 102, Oxford, MS 38655, USA, dave@oxfordacoustics.com), Ning Xiang (Rensselaer Polytechnic Institute, Greene Building, School of Architecture, 110 8th Street, Troy, NY 12180, USA, xiangn@rpi.edu)

As a case study, this work aims to experiment coupled-volume systems with scientifically grounded quantifiers using Bayesian analysis, a reliable analysis method in evaluating effects of different parameters on sound energy decays of coupled rooms [Xiang & Goggans, J. Acoust. Soc. Am. **110**, 1415 - 1424 (2001)]. This research uses the well-defined indicators developed by Xiang and Goggans to assess sound energy decays in a real-size hall. Derived from the model-based Bayesian inference, level differences (ΔL), diverse decay times, and decay time ratios are the quantitative descriptors of sound energy decays in acoustically coupled spaces. The room impulse responses of Howorth Theater in Oxford, Mississippi coupled to the adjacent lobby are experimentally measured in the case study. The two rooms are connected with two separate apertures and have distinct natural reverberation times that allow experimenting different setups for probable acoustical coupling at certain locations. In this paper, frequency, and location dependence of double-slope characteristics of sound energy decays are discussed.

Session 5aAAe

Architectural Acoustics: New Frontiers in Room Acoustical Modeling II (Poster Session)

Murray Hodgson, Cochair
University of British Columbia

Vincent Valeau, Cochair
Laboratoire d'Etudes Aérodynamiques (LEA)

All posters will be on display from 9:40 a.m. to 11:20 a.m. To allow contributors an opportunity to see other posters, contributors of odd-numbered papers will be at their posters from 9:40 a.m. to 10:30 a.m. and contributors of even-numbered papers will be at their posters from 10:30 a.m. to 11:20 a.m.

Contributed Papers

5aAAe1. Predıctıng the acoustıcs of hıstorıc Istanbul Tunnel: Sımulatıon, calculatıon methods and geometrıcal detaıls. Filiz Bal Kocyigit (Karabuk University, 232. Str. No: 5/5 Ilkbahar Mah., Cankaya, 06550 Ankara, Turkey, filizbkocyigit@yahoo.com)

Istanbul Tunnel was designed and constructed by Eugene Henry Gavand in 1875 is the third Metro and second underground railway system in the world after Washington Metro (1868). In this paper, the acoustics of Istanbul Tunnel is investigated. This is a special case which sets up a challenge to these prediction methods. The shape of the tunnel and therefore focusing the sound, reverberant wall, and therefore fluctuation effect demands high accuracy in predicting the early reflections. The energy dissipates quickly in this type of enclosures and there is little masking effect of the reverberation. Another aspect that has been shown to give very different results in this case study is the geometrical detailing of the models. When Istanbul Tunnel compared with modern metrosystems; nowadays railway systems are controlled by modern electronic and mechanical system, but in the 19th century this electronic systems could not used. Solutions could be with the shape of the building. The aim of this paper is to clarify some of the problems that can arise in this type of constructions, and give guidelines for how they can be overcome/avoided. Another objective is to emphasize that room acoustic computer simulations, although very useful, need careful consideration about the underlying calculation methods.

5aAAe2. Size-adaptive spherical receptor acceleration method for acoustical ray tracing. Stéphane Lesoinne (University of Liège - INTELSIG, Institut Montéfiore, Sart-Tilman, Batiment 28, 4000 Liège, Belgium, s.lesoinne@ulg.ac.be), Jean-Jacques Embrechts (University of Liège - INTELSIG, Institut Montéfiore, Sart-Tilman, Batiment 28, 4000 Liège, Belgium, jjembrechts@ulg.ac.be)

Randomized ray tracing in room acoustics can be used to compute echograms, but the results computed at the receptor are affected by statistical errors [1]. To decrease these statistical errors, the usual solution is to increase the number of rays, but this also increases the computation time. Another solution is to increase the receptor size, but this lowers the spatial resolution of the computed sound field, which is particularly important for the early part of the echogram. In order to decrease the computation time and keep a sufficient resolution, the method proposed in this paper is based on a progressive modification of the receptor size (spherical type) as long as the ray's travel grows. At the same time, the number of rays into the room can be decreased as the sound ray lengths increase while keeping the statistical errors more or less constant. The consequence is that the sound field spatial resolution evolves from "precise" at the beginning of the echogram to "rough" at its end. The first applications of this new method show a significant gain of CPU time. [Broad spectrum diffusion model for room acoustics ray-tracing algorithms, J. J. Embrechts, Jnl. Acoust. Soc. Am. **107**(4) 2068-2081 (2000)].

5aAAe3. Variation of mean free path length over time and its effect on room impulse response. Miomir Mijic (Faculty of Electrical Engineering, Bulevar Kralja Aleksandra 73, 11000 Belgrade, Serby, emijic@etf.bg.ac.yu), Dragana Sumarac Pavlovic (Faculty of Electrical Engineering, Bulevar Kralja Aleksandra 73, 11000 Belgrade, Serby, dsumarac@etf.bg.ac.yu)

In their previous paper (Forum acusticum 2005, Proceedings, 2399-2404) the authors presented the local effect found in a large sports hall, described as significantly shorter reverberation time in the first 400-500 ms than that in the rest of the hall's long impulse response. To analyse this phenomenon, a new measure - mean free path length (MFPL) variation in time over the impulse response - was introduced. It is identified as the function of time obtained as an ensemble average in some fixed interval traced along the impulse response duration. The ray tracing simulation was used to calculate ray paths approaching the receiver in time. Analyzing MFPL variations over time is a new insight into the structure of room impulse response, and this paper presents its main characteristics, its dependence on geometrical properties of rooms, and also its relation to statistically defined mean free path length (4 V/S). The paper also presents a correlation between MFPL variation over time and the sound decay curve. The MFPL variation over time reveals the causes of the local effect introduced in the previous paper, but it is generally useful in explaining the sound decay monotony deviations.

5aAAe4. Towards a realistic ray tracing for room acoustics. Jaume Durany (Universitat Pompeu Fabra - Fundació Barcelona Media, Ocata, 1, 08003 Barcelona, Spain, jaume.durany@upf.edu), Adan Garriga (Universitat Pompeu Fabra - Fundació Barcelona Media, Ocata, 1, 08003 Barcelona, Spain, adan.garriga@barcelonamedia.org), Toni Mateos (Universitat Pompeu Fabra - Fundació Barcelona Media, Ocata, 1, 08003 Barcelona, Spain, toni.mateos@barcelonamedia.org)

We present a recently developed ray tracing engine for room acoustics computations whose improved physics provide more realistic results than present state of the art methods. Ray tracing has been widely applied within the graphics community to obtain realistic shadings, but the computational cost reduction has oriented efforts towards fast computations of apparently realistic images rather than physically correct results. In the case of audio ray tracers, a similar tendency has led to relatively fast shading algorithms that often miss its physical basis, preventing the resulting impulse responses from converging to physically correct solutions. Our engine improves this situation by focusing on two main issues. First, it ensures the mathematical convergence of the algorithms by maintaining the coherence between the

computation of the direction of the reflected rays and the computation of the contribution of the sources to a given point in the environment. Second, the engine works directly in the frequency domain. This allows for the implementation of frequency-dependent phenomena, from surface impedance and reflections to frequency-dependent source directivity patterns. We present a comparative study of the proposed ray tracing engine with the state of the art, emphasizing properties like realism, coherence and convergence.

5aAAe5. A geometric acoustics simulation proposal for curved geometry. Arthur Van Der Harten (Rensselaer Polytechnic Institute, Greene Bldg., 110 8th St., Troy, NY 12180, USA, Arthur.vanderharten@gmail.com), Paul Calamia (Rensselaer Polytechnic Institute, Greene Bldg., 110 8th St., Troy, NY 12180, USA, calamp@rpi.edu)

Current methods for acoustical simulations based on geometrical acoustics are designed to ascertain the properties of rooms using models comprising large flat polygons. Typically these same methods are used on models of spaces with curved surfaces in which the curves are approximated using planar facets. In such cases, errors are introduced in the simulation when the infinitely varying normal of a curve is replaced with a finite number of piecewise constant normals, one for each facet. NURBS - nonuniform rational B-splines - offer an alternative geometric representation that allows curves to be represented with precision. Using Rhinoceros, a commonly used NURBS-based CAD program, as a platform for an acoustic simulation tool for models of both NURBS and polygon geometry, we can begin to discover whether it is possible to conceptualize a geometrical acoustics method that is more accurate for curved surfaces. This talk will cover the implementation and early testing of an acoustic-simulation plug-in for Rhinoceros.

FRIDAY MORNING, 4 JULY 2008 P2-B, LEVEL 2, 9:40 TO 11:20 A.M.

Session 5aAAf

Architectural Acoustics and Musical Acoustics: New Measurement Parameters in Performing Arts Spaces I (Poster Session)

Lily Wang, Cochair
University of Nebraska - Lincoln

Brian Katz, Cochair
LIMSI-CNRS

All posters will be on display from 9:40 a.m. to 11:20 a.m. To allow contributors an opportunity to see other posters, contributors of odd-numbered papers will be at their posters from 9:40 a.m. to 10:30 a.m. and contributors of even-numbered papers will be at their posters from 10:30 a.m. to 11:20 a.m.

Contributed Papers

5aAAf1. Converging evidence in evaluating acoustical intimacy. Bobby E. Gibbs (Rensselaer Polytechnic Institute, Greene Bldg., 110 8th St., Troy, NY 12180, USA, gibbsb@rpi.edu), Jonas Braasch (Rensselaer Polytechnic Institute, Greene Bldg., 110 8th St., Troy, NY 12180, USA, braasj@rpi.edu), Ted Krueger (Rensselaer Polytechnic Institute, Greene Bldg., 110 8th St., Troy, NY 12180, USA, krueger@rpi.edu)

Previously, we presented a novel interactive pilot experiment in which participants modified parameters in a virtual acoustical environment so that they corresponded to three intimacy settings: low, medium, and high. Additionally, participants were asked to rank the -- yet unknown -- parameters (volume, direct-to-reverberant energy ratio, frequency attenuation, and room size) in terms of the importance in making their judgments. Based on a larger body of data, the direct-to-reverberant energy ratio emerges as the strongest acoustical correlate of intimacy. A repeated-measures test revealed that the "preservation" of this parameter (the degree to which a participant changed the value from an optimum setting) varies the least across intimacy levels and across levels of previous training. Additionally, this parameter is consistently ranked as being the most important in the ranking portion of the test. We also found that salience of some of the other parameters varied significantly across intimacy levels, possibly suggesting a weighting system is warranted. These results are compared with binaural measurements of the virtual system. In particular, we will address disparities from the pilot experiment and recent data that resulted from differences in measuring the direct-to-reverberant energy ratio. [Work supported by RPI HAAS Fellowship and ASA Minority Fellowship.]

5aAAf2. Effects of multiple directional sources on quantitative and qualitative analyses of concert hall acoustics. Youngmin Kwon (Acoustic Dimensions, 15505 Wright Brothers Drive, Addison, TX 75001, USA, ykwon@acousticdimensions.com), Gary W. Siebein (Univ. of Florida, 231 Arch, PO Box 115702, Gainesville, FL 32611, USA, gsiebein@siebeinacoustic.com), Martin A. Gold (Univ. of Florida, 231 Arch, P.O. Box 115702, Gainesville, FL 32611, USA, mgold@ufl.edu)

The "orchestral impulse reponse" measurement technique using multiple directional sources and its effects on quantitative analysis of concert hall acoustics were discussed earlier [Kwon and Siebein, J. Acoust. Soc. Am. **120**, 3263(A) (2006)]. An array with 16 directional loudspeakers approximating overall sound radiation patterns of each instrumental group of an orchestra was incorporated for room acoustical measurements and analyses. As a continuous study, this paper discusses qualitative assessments of concert hall acoustics over room subjective parameters including reverberance, clarity, warmth, spaciousness, envelopment, etc. The music signals binaurally recorded in a performance hall with the same source array were evaluated by means of subjective listening tests in comparison to those recorded with the single omni-directional source (dodec). The results showed that some perceived differences are present between the array with multiple directional sources and the one with a single omni-directional source. In the main orchestra seating, in particular, reverberance and clarity are perceived more but warmth is perceived less when compared to the recordings through the single omni-source. The results will be further discussed in conjunction with their quantitative measures resulted from the above measurement technique.

5aAAf3. Room acoustics measurements with an approximately spherical source of 120 drivers. Roger Schwenke (Meyer Sound Laboratories, 2832 San Pablo Ave, Berkeley, CA 94702, USA, rogers@meyersound.com), Franz Zotter (Institute of Electronic Music and Acoustics, Inffeldgasse 10/3, 8010 Graz, Austria, zotter@iem.at), David Wessel (Center for New Music and Audio Technologies, 1750 Arch Street, Berkeley, CA 94720, USA, wessel@cnmat.berkeley.edu.), Andrew Schmeder (Center for New Music and Audio Technologies, 1750 Arch Street, Berkeley, CA 94720, USA, andy@cnmat.berkeley.edu)

An approximately spherical source of 120 individually controlled drivers is used to perform impulse response measurements in a room with a 1.4 s reverberation time and a distinct echo. The signal to the drivers is processed to produce both omni-directional and unidirectional patterns. The omni-directional pattern is compared with measurements made with a traditional 12 sided source. The unidirectional patterns are measured both pointed towards and away from the listener position. Intelligibility metrics for the different directionalities and orientations are measured. The unidirectional pattern is aimed in different directions to minimally and maximally excite the distinct echo in the room, and locate it's origin.

5aAAf4. Measurement-based fuzzy interpolation of room impulse responses. Csaba Huszty (Budapest University of Technology and Economics, BME Dept. of Telecommunications, Magyar tudósok körútja 2, H-1117 Budapest, Hungary, huszty@hit.bme.hu), Bottyán Németh (Budapest University of Technology and Economics, BME Dept. of Telecommunications, Magyar tudósok körútja 2, H-1117 Budapest, Hungary, bottyan@tmit.bme.hu), Péter Baranyi (Budapest University of Technology and Economics, BME Dept. of Telecommunications, Magyar tudósok körútja 2, H-1117 Budapest, Hungary, baranyi@tmit.bme.hu), Fülöp Augusztinovicz (Budapest University of Technology and Economics, BME Dept. of Telecommunications, Magyar tudósok körútja 2, H-1117 Budapest, Hungary, fulop@hit.bme.hu)

Application of room impulse responses (RIRs) to acoustic evaluation and auralization often requires many measurements to get enough information about the hall, or to provide enough flexibility for virtual sound source placements in convolution reverberation. In this paper we propose a measurement-based fuzzy modeling method to approximate the RIR function at an arbitrary location between available measured points, without a priori information on the hall geometry or wall reflection parameters. For the fuzzy model identification we define an accuracy indicator of the spatial density of the source positions and predict the required number of them in a selected hall. This indicator quantifies the relationship of the early reflections, determined for various measured positions. This paper also proposes a method that treats nonuniform spatial sampling of the measurement positions, and its implementation for 2D cases is shown. Nonuniform spatial sampling can be useful when RIRs at some source positions -- e.g. positions of musicians on a stage of a concert hall -- are known or have to be measured precisely, but RIRs at locations in between require an approximation only. The proposed fuzzy model of RIRs actually transforms the measured information into a uniform and tensor product form, enabling the analyst to use further matrix and tensor algebra based numerical methods.

FRIDAY MORNING, 4 JULY 2008 AMPHI BLEU, 8:00 A.M. TO 5:40 P.M.

Session 5aABa

Animal Bioacoustics: General Topics in Animal Bioacoustics II

Richard R. Fay, Cochair
Loyola University Chicago, Parmly Hearing Institute, 6525 N. Sheridan Rd., Chicago, IL 60626, USA

Michel Andre, Cochair
Laboratori d'Aplicacions Bioacústiques (Universitat Politècnica de Catalunya), avda. Rambla Exposició s/n, Vilanova i la Geltrú, 08800, Spain

Contributed Papers

8:00

5aABa1. Acoustic production mechanisms in pinnipeds. Marija Spasikova (Centre for Social Learning and Cognitive Evolution, University of St. Andrews, School of Psychology, KY16 9JP St. Andrews, Fife, UK, marija.spasikova@gmail.com), William T. Fitch (Centre for Social Learning and Cognitive Evolution, University of St. Andrews, School of Psychology, KY16 9JP St. Andrews, Fife, UK, wtsf@st-andrews.ac.uk), Colleen Reichmuth (UCSC Institute of Marine Sciences, Long Marine Lab - University of California, 100 Shaffer Road, Santa Cruz, CA 95060, USA, coll@ucsc.edu), Ronald J. Schusterman (UCSC Institute of Marine Sciences, Long Marine Lab - University of California, 100 Shaffer Road, Santa Cruz, CA 95060, USA, rjschust@ucsc.edu)

The ability to develop articulate speech relies on capabilities that became available to our ancestors through changes in both peripheral mechanisms (vocal acoustics and anatomy) and neural mechanisms (vocal control and imitation). Few distantly related species (cetaceans, birds and pinnipeds) have shown the ability of vocal imitation, but of the three, only the pinnipeds use the same vocal tract as us humans. For this reason we choose to study two closely related pinniped species: the harbour seal (*Phoca Vitulina*), a good vocal imitator (capable of complex vocal learning), and the Californian sea lion (*Zalophus californicus*), a close relative with very limited vocal imitation capabilities (no evidence of complex vocal learning) to look at the acoustical production mechanisms of the species as well as the neural mechanisms underlying the same. Using previously acquired data gathered in California at the Long Marine Lab, we performed video and acoustic analysis to show correlation between jaw opening and formants frequencies in the harbour seal (*Phoca Vitulina*), in speech like vocalisations. We are examining the involvement of tongue movement during these vocalisations, hypothesising that it will account for the remaining residuals in the correlation between the formants excursions and the jaw movements.

8:20

5aABa2. Habitat occupation time-series of St. Lawrence belugas from passive acoustic monitoring. Nathalie Roy (Fisheries and Oceans Canada & ISMER-UQAR, 850 route de la Mer, P.O. Box 1000, Mont-Joli, QC G5H-3Z4, Canada, royn@dfo-mpo.gc.ca), Yvan Simard (Fisheries and Oceans Canada & ISMER-UQAR, 850 route de la Mer, P.O. Box 1000, Mont-Joli, QC G5H-3Z4, Canada, simardy@dfo-mpo.gc.ca), Catherine

Bédard(Marine Science Institute, University of Québec, 310 Allée des Ursulines, P.O. Box 3300, Rimouski, QC G5L-3A1, Canada, catherine.becard01@uqar.qc.ca), Elisabeth Leblanc (Marine Science Institute, University of Québec, 310 Allée des Ursulines, P.O. Box 3300, Rimouski, QC G5L-3A1, Canada, elisabeth.leblanc@uqar.qc.ca)

Passive acoustic monitoring (PAM) was used to generate a six-week continuous time-series of occupation of a segment of the St. Lawrence Estuary by belugas. The PAM data were acquired from a cabled hydrophone deployed at mid-depth into the 300-m deep Laurentian channel off Cap-de-Bon-Desir during summer 2003. Beluga vocalisation activity time-series was obtained from the [0.5-5.0 kHz] bandpassed PAM data that were processed to filter out noise from the heavy shipping on the nearby St. Lawrence Seaway and from occasional whale watching boats, and low-frequency traces of clicks, via adaptive spectral subtraction and image processing methods applied to the spectrogram. The remaining traces on the binary image of the spectrogram were summed up to generate a vocalisation index, which was essentially due to belugas in this region. The vocalisation index time-series was then analysed for presence of circadian rhythms and correlations with the semi-diurnal tidal cycle, currents from an acoustic Doppler current profiler and wind. Results are interpreted from the knowledge of the biological and physical oceanographic processes occurring in the monitored area.

8:40

5aABa3. Comparison of automatic classification methods for beluga whales vocalizations. Elisabeth Leblanc (Marine Science Institute, University of Québec, 310 Allée des Ursulines, P.O. Box 3300, Rimouski, QC G5L-3A1, Canada, elisabeth.leblanc@uqar.qc.ca), Mohammed Bahoura (Eng. Dept., Université du Québec, 300 Allée des Ursulines, P.O. Box 3300, Rimouski, QC G5L-3A1, Canada, mohammed_bahoura@uqar.qc.ca), Yvan Simard (Fisheries and Oceans Canada & ISMER-UQAR, 850 route de la Mer, P.O. Box 1000, Mont-Joli, QC G5H-3Z4, Canada, simardy@dfo-mpo.gc.ca)

The beluga whale is a loquacious marine mammal with a complex vocal repertory. It produces a wide variety of whistles and pulsed tones as well as high-frequency echolocation clicks. Automatic detection of the long-distance propagating communication calls are desirable for implementing passive acoustic monitoring (PAM) systems in their environment, for habitat utilisation studies and real-time early warning devices in anthropogenic impact mitigation systems. Signal processing methods were developed to classify beluga vocalizations from a PAM data set recorded in Cap-de-Bon-Désir in the Saguenay-St. Lawrence Marine Park in summer 2003 using a 6-hydrophones array with a 10-100 kHz sampling rate. The performance of an MFCC-based HMM system and a polynomial model applied to extracted time-frequency contours of vocalizations will be evaluated. The feasibility of real-time implementation will then be analysed for both methods.

9:00

5aABa4. One plus one equals one: The beluga whale (Delphinapterus leucas) produces two pulses to form its echolocation click. Marc O. Lammers (Hawaii Institute of Marine Biology, P. O. Box 1106, Kailua, HI 96734, USA, lammers@hawaii.edu), Manuel Castellote (L'Oceanografic, C/. Junta de Murs i Valls, s/n, 46013 Valencia, Spain, mcastellote @oceanografic.org)

Empirical results have shown that two sound generators exist in the nasal system of delphinids. It had been previously assumed that these function independently, with one primarily involved in pulse production and the other in the generation of tonal signals. Here we report that in the beluga whale both generators appear to be simultaneously involved in the production of the echolocation click measured in front of the animal. A study was conducted that examined the propagation of the echolocation click of a captive 12 year-old female beluga whale at 15°, 30°, 45°, 60°, 75°, and 90° off the center axis of both sides of the outgoing beam. The results reveal that at angles greater than 30° two distinct pulses are measured that cannot be attributed to multipath reflections from the surface or any structure in the tank. The two pulses are maximally separated in time at 90° off-axis and gradually converge with each 15° measurement closer to the beam center. At 30° the two pulses begin to form a single, albeit distorted pulse. The phenomenon is symmetrical on both sides of the animal. These findings shed new light on how beluga whales and perhaps other odontocetes form their echolocation pulse.

9:20

5aABa5. The nanomechanics of mechanosensory neurones in vivo. James F. Windmill (University of Bristol, D34 School of Biological Sciences, Woodland Road, BS8 1UG Bristol, UK, james.windmill@bristol.ac.uk), Victoria G. Pook (University of Bristol, School of Biological Sciences, Woodland Road, BS8 1UG Bristol, UK, vicky.pook@bristol.ac.uk), Daniel Robert (University of Bristol, D34 School of Biological Sciences, Woodland Road, BS8 1UG Bristol, UK, d.robert@bris.ac.uk)

The ability to detect and process sound is a sense particularly important in many animals, including insects, playing a key role in predator, prey and mate detection. Acute hearing, both in the sense of extreme sensitivity to sound and sharp frequency selectivity, relies on the active participation of auditory mechanoreceptors. In insects, active auditory mechanics was first demonstrated in mosquitoes, whereby auditory sensitivity is enhanced by the action and reaction of mechanosensory neurones to sound-induced vibrations. The mosquito's auditory neurones can generate motions that mechanically drive the antenna and tune it to biologically relevant sounds. The mechanosensory neurones are capable of detecting exquisitely small mechanical displacements, down to 100 picometres. In the mosquito's Johnston's organ (300 μm in diameter) there is a high density of these neurones (16 000 units). The mechanical response of the mechanoreceptors was measured in vivo using an atomic force microscope, in response to stimulation of the external antenna. The work establishes the link between the previously measured non-linearities of the mosquito's antennal vibrations and the nanoscale mechanics of the mechanosensory neurones.

9:40-11:00 Posters

Lecture sessions will recess for the presentation of poster papers on various topics in acoustics. See poster sessions for topics and abstracts

Contributed Paper

11:00

5aABa6. Computer aided design of audio signal classifier systems. Sebastian V. Huebner (Pestalozzistrasse 5, 14482 Potsdam, Germany, sebastian@sejona.de)

The problem of programming classifier systems for deterministic events in bioacoustic signals is seen as a knowledge engineering problem. Advantages and disadvantages of traditional approaches are discussed. A knowledge engineering approach for interactive visual classifier system design is described and advantages of the approach are highlighted. The basic architecture of a general purpose knowledge engineering framework for the acoustics domain is outlined. Emphasis is placed on both expert knowledge and on the role of data mining within the classifier system design process. Several examples illustrate how the approach can be used to create classifier systems for bioacoustic patterns in the time-frequency domain. Examples include multiscale spectrographic visualization, techniques to create and interactively modify subsymbolic and symbolic classifier systems for time-frequency patterns as well as the usage of three-dimensional visualizations to display hierarchical dependencies within complex classifier systems.

Invited Paper

11:20

5aABa7. Sounds from a neonate harbour porpoise and their potential use in acoustic monitoring. Magnus Wahlberg (Fjord&Bælt / University of Southern Denmark, Margrethes Plads 1, 5300 Kerteminde, Denmark, magnus@fjord-baelt.dk)

Harbour porpoises (Phocoena phocoena) emit ultrasonic (130 kHz) clicks with a stereotyped source parameters for echolocation and communication. Recently it was observed that the first days of living, a neonate harbour porpoise emitted contact calls of much a much lower frequency emphasis, around a few kHz. The echolocation clicks produced by the calf significantly differed in duration and band width during the first four months postpartum. The acoustic signals from harbour porpoise calves are ideal for automated detection and therefore as a tool in population studies of this species. Both hydrophone array systems towed from boats, and automated click detectors (such as T-PODs) may incorporate routines for automated detection of young calves. These findings may have a large potential for facilitating biologists in gathering important biological data from this otherwise very difficult-to-study species of marine mammals.

Contributed Papers

11:40

5aABa8. Two-dimensional sonar beam characteristics of single harbour porpoise (Phocoena phocoena) echolocation clicks measured with a 16 hydrophone array. Jens C. Koblitz (Eberhard-Karls-Universität Tübingen, Zool. Institut, Abt. Tierphysiologie, Auf der Morgenstelle 28, 72076 Tübingen, Germany, Jens.Koblitz@uni-tuebingen.de), Magnus Wahlberg (Fjord&Bælt/University of Southern Denmark, Margrethes Plads 1, 5300 Kerteminde, Denmark, magnus@fjord-baelt.dk), Peter T. Madsen (University of Aarhus, Biological Sciences, Zoophysiology, C. F. Møllers Allé, Building 1131, DK-8000 Aarhus, Denmark, peter.madsen@biology.au.dk), Peter Stilz (Eberhard-Karls-Universität Tübingen, Zool. Institut, Abt. Tierphysiologie, Auf der Morgenstelle 28, 72076 Tübingen, Germany, peter.stilz@uni-tuebingen.de), Hans-Ulrich Schnitzler (Eberhard-Karls-Universität Tübingen, Zool. Institut, Abt. Tierphysiologie, Auf der Morgenstelle 28, 72076 Tübingen, Germany, hans-ulrich.schnitzler@uni-tuebingen.de)

For the first time, the beam structure of single harbour porpoise echolocation clicks was simultaneously measured in both the vertical and horizontal plane. Echolocation clicks of a stationed animal and free-swimming animals catching fish were recorded with a "plus-shaped" array consisting of 16 hydrophones. The -3 dB beam width in the horizontal and vertical planes is in most cases similar to what has been previously measured by Au et al. (1999). However, individual clicks are sometimes broader or narrower than what has been previously reported. This may be caused by either voluntary control of the animal's beam width, or it may be a secondary effect of variations in intensity and air content within the sound production system.

12:00

5aABa9. Dolphin modulation rate transfer functions resulting from exposure to frequency modulated signals. Dorian S. Houser (Biomimetica, 7951 Shantung Dr., Santee, CA 92071, USA, dhouser@spawar.navy.mil), James J. Finneran (US Navy Marine Mammal Program, Space and Naval Warfare Systems Center, 53560 Hull St., Code 71510, San Diego, CA 92152, USA, james.finneran@navy.mil)

Frequency modulated (FM) signals are useful in audiometric studies where the test environment contributes to multipath interference and produces spatial variations in the sound pressure field. Rhythmic FM stimuli are useful in evoked potential audiometry because of the auditory steady state response (ASSR) that is created within the auditory system. Although some research on dolphin ASSRs resulting from rhythmic FM signals has been performed, relationships between modulation depth, modulation rate, and ASSR amplitude have not been fully explored. To address this, two dolphins were exposed to rhythmic FM signals (120 dB SPL and center frequency=40 kHz) and the resulting ASSR recorded. The modulation depth (peak-to-peak) and modulation rate were varied from 0.1-10% and 200-2500 Hz, respectively. A total of 512 epochs were recorded for each stimulus presentation and the averaged waveform was analyzed in the frequency domain. The amplitude peak corresponding to the modulation rate was used to create the modulation rate transfer function (MRTF). Both dolphins showed a MRTF peak at a 1 kHz modulation rate, while one dolphin showed a second peak at 500 Hz. The use of rhythmic FM signals in ASSR studies may be a useful for testing in less than ideal acoustic environments.

12:20-1:40 Lunch Break

Contributed Papers

1:40

5aABa10. Correcting gray whale (Eschrichtius robustus) call rates in San Ignacio Lagoon, using sound exposure level measurements of ambient noise. Melania Guerra (Marine Physical Laboratory, Scripps Institution of Oceanography, 9500 Gilman Dr, MC 0238, La Jolla, CA 92093-0238, USA, meguerra@ucsd.edu), Aaron Thode (Marine Physical Laboratory, Scripps Institution of Oceanography, 9500 Gilman Dr, MC 0238, La Jolla, CA 92093-0238, USA, athode@ucsd.edu), Jorge Urban (Laboratorio de Mamiferos Marinos, Universidad Autonoma de Baja California Sur, La Paz, Apartado Postal 19-B, 23080 La Paz, Mexico, jurban@uabcs.mx), Sergio Gonzalez (Laboratorio de Mamiferos Marinos, Universidad Autonoma de Baja California Sur, La Paz, Apartado Postal 19-B, 23080 La Paz, Mexico, sergiog@uabcs.mx)

Autonomous acoustic recordings of gray whales (Eschrichtius robustus) were made in San Ignacio Lagoon, in February 2005-2008, while animals were present to breed and raise calves. Counts were made of the gray whales' most common vocalization, type S1. A sequence of semi-automated procedures was implemented to assist with call detection. Hourly call rates were computed for all seasons and adjusted for expected changes in detection range, caused by variations in the ambient background noise level. In this environment, the underwater acoustic background combines biological, oceanographic and man-made sources and can present changes of 10 dB above the average base level of 96dB re 1uPa 2-s between 350 and 750 Hz over semidiurnal scales. The relative changes in call rates in 2006 and 2008 are compared with visual survey counts conducted over the same period. The definition of SNR in the present study develops from energy flux densities or sound exposure levels (SEL). SEL were calculated experimentally through even sampling in time and individual sampling for each call. By assuming that the background masks a proportion of the detected calls, corrections were applied to determine the vocal activity within a fixed detection range.

2:00

5aABa11. The acoustic field on the melon of echolocating Atlantic bottlenose dolphin (Tursiops truncatus). Whitlow W. Au (Univ. of Hawaii, P.O. Box 1106, Kailua, HI 96734, USA, wau@hawaii.edu), Dorian S. Houser (Biomimetica, 7951 Shantung Dr., Santee, CA 92071, USA, dhouser@spawar.navy.mil), James J. Finneran (US Navy Marine Mammal Program, Space and Naval Warfare Systems Center, 53560 Hull St., Code 71510, San Diego, CA 92152, USA, james.finneran@navy.mil), Lois Dankiewicz (SAIC, 4065 Hancock Street, MS: Q1-A, San Diego, CA 92110, USA, lois.dankiewicz@saic.com), Wu-Jung Lee (MIT-WHOI Joint Program, 266 Woods Hole Road, Woods Hole, MA 02543, USA, wjlee@whoi.edu), Patrick W. Moore (US Space & Naval Warfare Systems Center, 49620 Beluga Road, San Diego, CA 92151, USA, pmoore@spawar.navy.mil)

An array of five broadband suction cup hydrophones were placed on the melon of two bottlenose dolphins to determine where on the melon the echolocation beam emerges and to examine how signals in the acoustic near-field relate to signals in the far-field at 1 m. Four different array geometries were used: a linear one with hydrophones arranged along the midline of the melon between 2.8 and 3.7 cm apart, and two around the front of the melon at 1.4 and 4.2 cm above the melon-rostrum crease and one across the melon in certain locations not measured by other configurations. The beam axis was found to be close to the mid-line of the melon, approximately 5.4 cm above the melon-rostrum crease for both animals. The signal path coincided with the low-density, low-velocity core of the melon supporting the melon hypothesis postulated many years ago by Kenneth Norris. Slight asymmetry in the signal was found with higher amplitudes on the starboard side of the melon. Although the signal waveform measured on the melon appeared distorted, when they were mathematically summed in the far-field while preserving the relative time of arrival, the resultant waveform matched that measured by the hydrophone located at 1 m.

2:20

5aABa12. Detection of beaked whales using near surface towed hydrophones: prospects for survey and mitigation. Douglas Gillespie (Sea Mammal Research Unit, Gatty Marine Laboratory, University of St. Andrews, KY16 8LB St. Andrews, UK, dg50@st-andrews.ac.uk), Jonathan Gordon (Sea Mammal Research Unit, Gatty Marine Laboratory, University of St. Andrews, KY16 8LB St. Andrews, UK, jg20@st-andrews.ac.uk), Marjolaine Caillat (Sea Mammal Research Unit, Gatty Marine Laboratory, University of St. Andrews, KY16 8LB St Andrews, UK, marjolaine.caillat@club-internet.fr), Diane Claridge (Bahamas Marine Mammal Research Organisation, P.O. Box AB-20714, Abaco, 0 Marsh Harbour, Bahamas, bmms@oii.net), David Moretti (NAVSEA, Newport Undersea Warfare Center, Newport, RI RI 02841, USA, MorettiDJ@npt.nuwc.navy.mil), Ian Boyd (Sea Mammal Research Unit, Gatty Marine Laboratory, University of St Andrews, KY16 8LB St Andrews, UK, ilb@st-andrews.ac.uk)

Beaked whales are extremely difficult to sight at sea and this hampers attempts to study them, and makes real time mitigation difficult. Passive acoustic monitoring could improve detection efficiency. Blainville's beaked whales, (Mesoplodon densirostris) are known to produce most of their vocalizations at depth. They are routinely detected on bottom mounted hydrophones arrays but the extent to which they can be detected using near-surface hydrophones is not known. Continuous recordings were made at a sampling rate of 192 kHz from towed hydrophone arrays during line transect surveys in the Bahamas in conjunction with teams monitoring bottom-mounted hydrophones at the AUTEC Tongue of the Ocean navy range. A beaked whale click detector and classifier was developed within Rainbow Click and PAMGUARD and this was both run in real time and used to analyze recordings to pick out beaked whale click trains. Detected click trains correlated well with detection of beaked whales on bottom-mounted hydrophones. Three species of beaked whale were encountered visually and detected acoustically: Mesoplodon densirostris, Ziphius cavirostris and Mesoplodon europaeus. Target motion analysis of bearings to sequences of clicks suggests a maximum detection range of approximately three kilometers and preliminary results indicate that clicks can be identified to species.

2:40

5aABa13. Acoustic localization of two distinct blue whale (Balaenoptera musculus) subspecies in the South-West Indian Ocean. Flore Samaran (CEBC-CNRS, Centre d'Etude Biologique de Chizé, 79360 Villiers en Bois, France, samaran@cebc.cnrs.fr), Olivier Adam (Université Paris Est, 61, avenue de Gaulle, 94000 Creteil, France, adam@univ-paris12.fr), Jean-François Motsch (Université Paris Est, 61, avenue de Gaulle, 94000 Creteil, France, motsch@univ-paris12.fr), Yves Cansi (Commissariat à l'Energie Atomique, Centre DAM - Ile de France, Bruyères-le-Châtel, 91297 Arpajon Cedex, France, yves.cansi@cea.fr), Gérard Ruzié (Commissariat à l'Energie Atomique, Centre DAM - Ile de France, Bruyères-le-Châtel, 91297 Arpajon Cedex, France, gerard.ruzie@cea.fr), Christophe Guinet (CEBC-CNRS, Centre d'Etude Biologique de Chizé, 79360 Villiers en Bois, France, guinet@cebc.cnrs.fr)

Analysis of one year of acoustic signal recordings from the five permanent autonomous hydrophones of the International Monitoring System in the South-West Indian Ocean reveals low frequency with high intensity calls produced by two blue whale subspecies. The "Antarctic" or "true" blue whale (B. m. intermedia) calls and the "Madagascar-type" Pygmy blue whale calls (B. m. brevicauda) were automatically detected through the matched filtering method. The potential movements were investigated by using the time difference of arrival (TDOA) of calls to assess the bearing of the sound source. The fully range dependent parabolic equation code (RAM - range-dependent acoustic model) and the PMCC code (progressive multichannel correlation) are applied to estimate the range between our system and the vocalising animals. Our results show that (1) the variation of call number revealed two distinct patterns of seasonal whale occurrences and (2) the distances from the hydrophones to the blue whales reached up to 50 km. Tracking whales is possible when whales are concentrated of the hydrophone array.

3:00

5aABa14. Biosonar performance of a false killer whale (Pseudorca crassidens) improved with practice. Robert Gisiner (Marine Mammal Commission, 4340 East-West Highway, Room 700, Bethesda, CA 20814, USA, bgisiner@mmc.gov)

Cylinder wall thickness discrimination tasks have been used to assess the limits of dolphin biosonar. An attempt to replicate the benchmark data from a bottlenose dolphin (Tursiops truncatus) resulted in a surprising order of magnitude better performance by a false killer whale. The improvement came over multiple testing episodes, which suggests that initial limits to discrimination were overcome by learning; either through better understanding of the reinforcement contingencies, attention to novel sources of information within the returning echoes, or both. These results offer important insights into methodological considerations for testing animal psychophysical performance, especially for sensory performances like echolocation in which the subject exercises active control over the sensory input. The ability to improve sensory performance with practice also offers insights into the way the echo information is processed into an internal representation of external physical reality by the central nervous system, a process that is very likely open to improvement through experience, or learning, throughout the individual's life.

3:20

5aABa15. An analysis of Humpback whale songs for individual classification. Suleman Mazhar (URA Laboratory, Institute of Industrial Science, The University of Tokyo, 4-6-1, Komaba, Meguro, 153-8505 Tokyo, Japan, suleman@iis.u-tokyo.ac.jp), Tamaki Ura (URA Laboratory, Institute of Industrial Science, The University of Tokyo, 4-6-1, Komaba, Meguro, 153-8505 Tokyo, Japan, ura@iis.u-tokyo.ac.jp), Rajendar Bahl (Indian Institute of Technology, Delhi, Hauz Khas, 110016 New Delhi, India, rbahl@care.iitd.ernet.in)

Acoustics based tracking systems are in use for studying cetacean behaviour. Such noninvasive techniques can also prove efficient for population assessment of vocally active species. One problem in this regard is to distinguish already counted reappearing cetaceans, even if reappearance occurs after a brief interval. In this connection we propose development of in-

dividual identification system for humpback whales (*Megaptera novaeangliae*) based on unique acoustic features underlying a song. Earlier we analyzed recognition performance of cepstrum based voice signature in seven humpback whales. The results were based on training and test data sampled from the same song. In this work, we test our hypothesis using data from different songs (i.e., recording timings of training and test data sets do not overlap) for two different individuals. Recognition rates for two individuals are above 80% and 95%, respectively. However an eight years old song gives degraded recognition rate of around 58%. The results give an insight into the effects of temporal song evolution on accuracy of our system. Our observations are followed by harmonic analysis of song units in two individuals. Cepstral coefficients and support vector machine (SVM) were used for classification and signal band-crossing rate was used for segmenting song units.

3:40

5aABa16. Phonemic segment characterization of Norwegian killer whale call types. Ari D. Shapiro (Woods Hole Oceanographic Institution, Applied Ocean Physics & Engineering Dept., Woods Hole, MA 02543, USA, ashapiro@whoi.edu), Stephanie Seneff (Massachusetts Institute of Technology, Computer Science and Aritifical Intelligence Laboratory, Spoken Language Systems Group, Cambridge, MA 02139, USA, seneff@csail.mit.edu), Peter Tyack (Woods Hole Oceanographic Institution, Applied Ocean Physics & Engineering Dept., Woods Hole, MA 02543, USA, ptyack@whoi.edu)

An important issue in animal vocal communication concerns the fundamental unit used to build signals into a repertoire and the syntactic rules associated with that assembly. Killer whale vocal production has traditionally been categorized by human observers into a set of discrete call types. These call types often contain internal spectral shifts, silent gaps and synchronously produced low and high frequency components. Such features motivated the analysis here which tested whether call types could be represented by a set of flexibly arranged and smaller phonemic segments. We evaluated whether segmented characterizations of stereotyped Norwegian killer whale calls yielded automated classification results of contour traces that paralleled a classification scheme using whole call type designations. Representations of calls in their entirety or as sets of either distinct or shared syllables did achieve similar performance. Calls composed of shared segments may provide a more parsimonious approach to parsing the vocal stream since there were fewer segments than call types, nearly 75% of all call types contained at least one shared syllable, and some syntactic patterns were evident. Such a system could flexibly generate new call types and contain the killer whale vocal repertoire within a subset of the possible combinations of segments.

4:00

5aABa17. AFM and BSEM: Novel approaches to the Basilar Membrane. Darlene R. Ketten (NIH/NIDCD and WHOI, Section on Auditory Mechanics, Bldg 10-5D49, Bethesda, MD 20892, USA, dketten@whoi.edu), Emilios K. Dimitriadis (NIH/NIDCD and WHOI, Section on Auditory Mechanics, Bldg 10-5D49, Bethesda, MD 20892, USA, dimitria@helix.nih.gov), Richard S. Chadwick (NIH/NIDCD and WHOI, Section on Auditory Mechanics, Bldg 10-5D49, Bethesda, MD 20892, USA, chadwick@helix.nih.gov), David Mountain (Boston University, Biomedical Engineering Dept., 44 Cummington St., Boston, MA 02215, USA, dcm @bu.edu)

For over a half century, researchers have probed cochlear biophysics with increasingly sophisticated technologies. Recently, we brought two new approaches, atomic force microscopy (AFM) and backscatter electron microscopy (BSEM), to bear on the question of how basilar membrane structural variations affect mechanical responses. Hemi-cochleae and basilar membrane segments were obtained from rat, guinea pig, and gerbil ears by temporal bone microdissection. Hemi-cochleae in PBS or formalin were imaged in a hydrated, uncoated state (VP wet mode) in Petri dishes mounted on boutons using an Hitachi S3400 N-1 SEM. Membrane segments were excised, trimmed of laminae and ligament remnants, and mounted on polylysine/albumin-coated glass for AFM imaging and force measurements. Both BSEM and AFM data indicate two distinct regions consistent with softer ground substance separating relatively stiff, ordered fiber bundles oriented radially in pectinate regions. Fibers and bundles ranged 0.3 to 1 μm in diameter with elasticity values, based on a Hertzian contact model, in the hundreds of kPa range, consistent with mixed elastin and collagen. Greatest variations occurred in matrix spacing, suggesting differences are attributable largely to packing density. Middle turn ground substance spacing averaged 1.5 μm, consistent with previously reported values (Naidu and Mountain, 2007; Fung, 1993).

4:20

5aABa18. Depth, orientation, and acoustics of sperm whales (Physeter macrocephalus) under natural and depredation foraging conditions in the Gulf of Alaska. Delphine Mathias (Marine Physical Laboratory, Scripps Institution of Oceanography, 9500 Gilman Dr, MC 0238, La Jolla, CA 92093-0238, USA, delphine.mathias@gmail.com), Aaron Thode (Marine Physical Laboratory, Scripps Institution of Oceanography, 9500 Gilman Dr, MC 0238, La Jolla, CA 92093-0238, USA, athode@ucsd.edu), Jan Straley (University of Alaska SE, 1332 Seward Ave, Sitka, AK 99835, USA, jan.straley@uas.alaska.edu), Kendall Folkert (PO Box 6497, Sitka, AK 99835, USA, kendallcobra@yahoo.com), John Calambokidis (Cascadia Research Collective, 218 1/2 W. 4th Ave., Olympia, WA 98501, USA, calambokidis@cascadiaresearch.org), Greg Schorr (Cascadia Research Collective, 218 1/2 W. 4th Ave., Olympia, WA 98501, USA, GSchorr@cascadiaresearch.org), William C. Burgess (Greeneridge Sciences Inc, 6060 Graham Hill Rd, suite f, Felton, CA 95018, USA, burgess@greeneridge.com), Chris Lunsford (National Marine Fisheries Service Auke Bay Laboratory, 11305 Glacier Hwy, Juneau, AK 99801-8626, USA, chris.lunsford@noaa.gov)

In July 2007 bioacoustic tags were attached to adult sperm whales in the Gulf of Alaska under both natural foraging conditions, and situations wherein the animals were depredating sablefish from commercial longlining vessels. A small Rigid-Hull Inflatable was used to approach and attach a suction-cup acoustic recording tag on 13 occasions and stayed on animals for a total of 168 hours, yielding 80 h of depth, orientation, and acoustic data. These results, combined with passive acoustic tracking and underwater video-camera data, indicate that sperm whales depredate at depths shallower than 50 m, compared to natural foraging depths of 300-400 m in the area. During depredation the animals demonstrate changes in pitch and roll that are greater when compared with normal foraging behavior. Observations on the acoustic behavior of the animals are noted as well. The fact that these normally deep-diving animals depredate so close to the surface has interesting implications for both depredation-reduction strategies and biosonar research. [Work conducted under the SEASWAP program, supported by the North Pacific Research Board and the National Geographic Society.]

4:40

5aABa19. Fin whale (Balaenoptera physalus) movements along the Spanish mediterranean coast. Manuel Castellote (L'Oceanografic, C/. Junta de Murs i Valls, s/n, 46013 Valencia, Spain, mcastellote @oceanografic.org), José-Antonio Esteban (Research Department, Parques Reunidos Valencia S. A. L'Oceanogràfic, Ciudad de las Artes y las Ciencias, 46013 Valencia, Spain, investigacion@oceanografic.org), Christopher W. Clark (Cornell University Laboratory of Ornithology, Bioacoustics Research Program, 159 Sapsucker Woods Road, Ithaca, NY 14850, USA, cwc2 @cornell.edu)

The Ligurian-Corsican-Provençal Basin is a fin whale summer feeding ground, but little is known about the seasonal movement patterns of this population. We acoustically monitored two regions off Spain (eastern and southern) during summer-fall-winter 2006 using seafloor autonomous recording units. Long patterned sequences of 20 Hz pulses and back-beats from Mediterranean fin whales were identified in both study regions using acoustic features as indicators of population identity. Eastern area: fin whale sounds were detected at very high rates (122 pulses/hour) and between 40-80% of time/day. The detection pattern can be explained by whales moving gradually through the acoustic recorder's detection area, suggesting that the area is probably used as a passage between summer and winter grounds. Southern area: detections from the same population were less abundant (21 pulses/hour) and between 10-35 % of time/day. The detection pattern shows a highly variable distribution with no clear trend, suggesting that Mediter-

ranean fin whales continuously remained in and moved out of the detection area of the recorder from November to January. These results show that this southern area is potentially used as a winter ground. This work documents a new dispersion path towards the Alboran sea, a new potential winter ground.

5:00

5aABa20. Accurate estimation of the duration of tonal signals emitted by marine mammals. Nicolas Sentenac (Thales Underwater Systems, 525, route des dolines, BP 157, 06903 Sophia Antipolis, France, nicolas .sentenac@fr.thalesgroup.com)

Passive acoustic marine mammals detection and classification is of great importance nowadays. The goal of this article is to present a tool that can be used to accurately measure the duration of tonal emissions from marine mammals, helping to classify them. Marine mammals emissions can be split into two different kinds and one of them is tonal emission. It can be defined by its narrow band frequency pattern. Narrow band signals can be detected in the time/frequency space thanks to the use of the spectrogram and thanks to a quadratic contrast criterion. The expression of this criterion for signal-only and noise-only is straightforward. This article will introduce the expression of a lower bound of the expectation of the criterion when signal and noise are mixed. As this lower bound is a function of signal to noise ratio, it can be used to threshold the criterion with the desired signal to noise ratio value. When the criterion is computed along time on a sliding window, narrow band signals with a higher snr than the thresholding one are detected as soon as they appear and until they vanish, giving an accurate estimation of the duration of such signals.

Invited Paper

5:20

5aABa21. Ultrasonic production and reception in frogs: Lessons from Asia. Peter Narins (UCLA, Dept. of Physiological Science, 621 Charles E. Young Drive S., Los Angeles, CA 90095-1606, USA, pnarins@ucla.edu)

Among the vertebrates, only microchiropteran bats, cetaceans and some rodents are known to produce and detect ultrasonic (US) frequencies for the purpose of communication and/or echolocation, suggesting that this capacity may be restricted to mammals. We have recently provided the first evidence of ultrasonic communication in an amphibian - the concave-eared torrent frog, Amolops tormotus (Ranidae) from Huangshan Hot Springs, China. Males of A. tormotus produce diverse birdlike melodic calls with pronounced frequency modulations that often contain spectral energy in the US range. Acoustic playback experiments conducted in the animal's natural habitat confirmed that the audible as well as the US components of an A. tormotus call could effectively evoke males' vocal responses. Electrophysiological recordings from the auditory midbrain confirmed the US hearing capacity of these frogs and that of a sympatric species facing similar environmental constraints. This extraordinary upward extension into the ultrasonic range of both the harmonic content of the advertisement calls and the frog's hearing sensitivity is likely to have coevolved in response to the intense, predominately low-frequency ambient noise from local streams. Supported by NIH grant DC-00222.

FRIDAY MORNING, 4 JULY 2008 P3-C, LEVEL 3, 9:40 TO 11:20 A.M.

Session 5aABb

Animal Bioacoustics: General Topics in Animal Bioacoustics III (Poster Session)

Richard Fay, Cochair
Loyola University Chicago

Michel Andre, Cochair
Laboratori d'Aplicacions Bioacústiques (Universitat Politècnica de Catalunya)

All posters will be on display from 9:40 a.m. to 11:20 a.m. To allow contributors an opportunity to see other posters, contributors of odd-numbered papers will be at their posters from 9:40 a.m. to 10:30 a.m. and contributors of even-numbered papers will be at their posters from 10:30 a.m. to 11:20 a.m.

Contributed Papers

5aABb1. A brownian energy depot model of the basilar membrane oscillation. Chul Koo Kim (Yonsei University, Department of Physics, Shinchon-dong, 120-749 Seoul, Republic of Korea, ckkim@yonsei.ac.kr)

Response of a living basilar membrane (BM) is significantly different from that of the cadaver and is known to be essentially active. The best candidate for a generator of the active force in mammals is the outer hair cells. By employing the outer hair cells as the energy depot, we newly propose an interactive energy depot model for the basilar membrane. In this model, the nonlinear responses and the spontaneous basilar membrane oscillation are obtained. In the regime of small vibration, this model is reduced to the well-known Hopf bifurcation model. Our model suggests two-fold roles of the outer hair cells in hearing: an amplification for a weak stimulation and a protection for a strong stimulation.

5aABb2. Slow chaotic changes in the excitability of the auditory units. Nikolay G. Bibikov (N.N. Andreyev Acustical Institute, Shvernik st. 4, 117036 Moscow, Russian Federation, bibikov@akin.ru), Alexandre B. Dymov (N.N. Andreyev Acustical Institute, Shvernik st. 4, 117036 Moscow, Russian Federation, dymov@mail.ru)

We explored the statistical properties of the spontaneous and evoked firing activity in the brainstem auditory units of the grass frog (Rana t temporaria). We estimated the properties of spontaneous firing using the following functions: interspike interval distribution, hazard function, autocorrelation functions for original and shifted sequence of interspike intervals, function of interdependence of neighboring intervals. The dependences of Fano and Allans factors upon the values of counting time (window size) were also obtained. We observed a considerable deviation of the spontane-

ous activity from the renewal process for the majority of units located both in the dorsal medullar nucleus (homolog of cochlear nucleus in the mammals) and in torus semicircularis (homolog of inferior colliculus). The negative correlation between the neighboring short interspike intervals was typical for some (mainly toral) units. However, generally week but quite reliable positive correlation between neighboring intervals was typical for the great majority of neurons. The values of Fano and Allan factors were close to 1 at window size less than 100-500 ms and increased in proportion to some power for larger window sizes. The exponents of these power dependences were different for different units.

5aABb3. Synchrony and neuromechanical sensitivity in the mosquito hearing organ. Joseph C. Jackson (University of Bristol, D34 School of Biological Sciences, Woodland Road, BS8 1UG Bristol, UK, j.c.jackson@bris.ac.uk), Daniel Robert (University of Bristol, D34 School of Biological Sciences, Woodland Road, BS8 1UG Bristol, UK, d.robert@bris.ac.uk)

Sound detection is a fundamental tool for many biological organisms to sense their environment. Sensing the particle velocity component of sound waves has led to the evolution of exquisitely sensitive auditory organs: small oscillators that are driven resonantly by the sound field. The sound detection threshold is often indistinguishable from Brownian motion. To achieve such low thresholds, the mammalian cochlea incorporates active mechanisms, adding energy to the sound oscillations, and so enhancing sensitivity and selectivity. Mosquito antennae are also endowed with active auditory mechanics. Males use these highly sensitive external antennae to detect the flight sound of females. Sound-induced oscillation of the antenna stimulates thousands of mechanosensory neurones. The antenna exhibits dynamic responses remarkably similar to vertebrate auditory systems: self-oscillation and amplitude-dependent bandwidth both occur. They also exhibit hitherto unseen nonlinear responses including mid-level amplification and hysteresis. The mechanisms for these effects are thought to derive from ciliary motility in the mechanosensory neurones. We show that synchronization in the motile neurones generates large stable coherent forces that provide the antenna with its nonlinear response characteristics. Synchronization ensures a coherent neuronal output, improving signal fidelity. Finally, coherent force modifies the dissipation of antennal energy, changing the bandwidth and enhancing sensitivity.

5aABb4. Changes in structure of Redwing's (Turdus iliacus) local dialect in time. Ludmila Osipova (St. Petersburg State University, Universitetskaya emb., 7/9, 199034 St. Petersburg, Russian Federation, osipoval@yandex.ru)

The question of the period of existance of a local dialect is yet to be answered. Were there a changes in time-and-frequency parameters of dialects with time? If there were, what parameters had changed? On the basis of original data for 2005 - 2007 period, and archives of Department of Vertebrate Zoology of Saint-Petersburg State University, the history of local dialect of Redwing (Turdus iliacus) from Saint-Petersburg's outskirt (Peterhof) was investigated.The archive contains recordings of local dialects of Peterhof for 1960-1991 period. Until now, the longest period of local dialect observation for this species did not exceed 10 years (Bjerke, 1981). In observed period of 48 years several changes were found. Number of elements in phrase, it's duration, frequency modulation of all elements, their configuration, duration and frequency range. The major changes occurred to the first element of song. It is gradual reduction with time is obvious.

5aABb5. Microacoustics: maintaining an ecologically relevant scale in insect bioacoustics. Erica L. Morley (University of Bristol, D34 School of Biological Sciences, Woodland Road, BS8 1UG Bristol, UK, Erica.Morley@bristol.ac.uk), Thorin Jonsson (University of Bristol, School of Biological Sciences, Woodland Road, BS8 1UG Bristol, UK, t.jonsson@bristol.ac.uk), Daniel Robert (University of Bristol, D34 School of Biological Sciences, Woodland Road, BS8 1UG Bristol, UK, d.robert@bris.ac.uk)

A major challenge when studying an organism is to maintain its environment and context as reliably as possible. When looking at sensory systems it is crucial not to assume the animal's perception the same as ours and instead measure and mimic more accurately the natural stimuli driving the sensors. In insect bioacoustics the usual practice in playback and recording techniques overlooks differences in scale and context in which the organism's sensory system evolved. Here we present an approach to emit and record low-amplitude near-field sound, while maintaining an ecologically relevant scale, in *Drosophila melanogaster*. To mimic the effect of male courtship song on the female sound receiver (antennae) a mechanical microwing was constructed simulating, in power and geometry, particle velocity signals emitted by singing males, with its efficacy tested by behavioural assay. Development of a miniature particle velocity microphone was also initiated for recording signals in the fly's immediate vicinity (<2 mm) to elucidate the magnitude, temporal and radiation characteristics of the produced sound-field.

5aABb6. The effect of courtship song components in Drosophila melanogaster. Yu-Po Chen (University of Bristol, D34 School of Biological Sciences, Woodland Road, BS8 1UG Bristol, UK, Yu-po.Chen@bristol.ac.uk), Joseph C. Jackson (University of Bristol, D34 School of Biological Sciences, Woodland Road, BS8 1UG Bristol, UK, j.c.jackson@bris.ac.uk), James F. Windmill (University of Bristol, D34 School of Biological Sciences, Woodland Road, BS8 1UG Bristol, UK, james.windmill@bristol.ac.uk), Daniel Robert (University of Bristol, D34 School of Biological Sciences, Woodland Road, BS8 1UG Bristol, UK, d.robert@bris.ac.uk)

Courtship between male and female Drosophila melanogaster involves a complex emission of sounds produced by the male. This song comprises two aspects: a low-frequency sine song followed by a series of intense pulses. These songs increase the chances of the female accepting the male. However, the reason for the complexity of the song, and the effect on the female of the song's components, is poorly understood. Using measurements of the male courtship song for a canonical stimulus, we investigate the importance of the sine song on both the mechanical and electrophysiological responses of the female antenna: the nonlinear auditory sensor. While stimulating the antenna with modified courtship songs, antennal motion was measured using laser Doppler vibrometry, and compound potentials were simultaneously measured from the auditory neurones. Results show that, even at the periphery, there exists a significant change in the way the antenna responds to the pulses as a function of the sine song intensity, most emphatically through the neurophysiological signals. Results indicate that the sine song is an advantageous trait used to increase the female perception of the pulses in both time and amplitude sensitivity, and therefore improve the male's chance of successfully courting a female.

5aABb7. The Locust's tympanal mechanics. James F. Windmill (University of Bristol, D34 School of Biological Sciences, Woodland Road, BS8 1UG Bristol, UK, james.windmill@bristol.ac.uk), Samuel D. Bockenhauer (Stanford University, 208 Rosse Ln, #305, Stanford, 94305, USA, sbockenhauer@gmail.com), Thomas R. McDonagh (University of Bristol, School of Biological Sciences, Woodland Road, BS8 1UG Bristol, UK, tm3377@bristol.ac.uk), Daniel Robert (University of Bristol, D34 School of Biological Sciences, Woodland Road, BS8 1UG Bristol, UK, d.robert@bris.ac.uk)

In the ear of the desert locust frequency analysis arises from the mechanical properties of the tympanal membrane. Incident sound is spatially decomposed into discrete frequency components through a tympanal travelling wave that funnels mechanical energy to specific tympanal locations, where distinct groups of mechanoreceptor neurones project. Initial analysis of the travelling waves employs conventional, steady state FFT, allowing a detailed analysis of the spatial composition of different frequencies onto the membrane. To further understand the exact mechanics of the tympanal travelling wave, its motion was also measured in the time domain to characterise its response to single impulse and single frequency stimuli, with a resolution of 390 ns. This allows the measurement of instantaneous wave velocity and the direct observation of wave compression across the tympanum. The locust tympanal membrane locust exploits tonotopic frequency analysis, in a similar sense to that of the travelling waves of von Békésy on the mammalian basilar membrane. However, von Békésy's wave is born from interactions between the anisotropic basilar membrane and surrounding incom-

pressible fluids, whereas the locust's wave rides on an anisotropic membrane suspended in air. The locust's tympanum thus combines the functions of both sound reception and frequency analysis.

5aABb8. Automated acoustic identification of beetle larvae in imported goods using time domain analysis. James Schofield (University of York, Department of Electronics, Heslington, YO10 5DD York, UK, js517@york.ac.uk), David Chesmore (University of York, Department of Electronics, Heslington, YO10 5DD York, UK, edc1@ohm.york.ac.uk)

The detection of insect pests in imported goods is of considerable economic importance and the automation of this process is becoming more viable both technologically and financially. As a result, the Department for Environment, Food and Rural Affairs in the UK has funded a research project to develop instrumentation facilitating real-time acoustic detection of the feeding activity of insect larvae inside imported goods, such as timber. The instrumentation will also be capable of species-level identification. Previous work at York has shown that detection of beetle larvae in wood is possible using low cost piezoelectric sensors. The project described here extends this work by investigating a number of signal analysis methods for robust detection of biting events, including fractal dimension analysis. Identification is currently being carried out using time domain signal coding and artificial neural networks. This paper will concentrate on the results of various algorithms for the estimation of fractal dimension and their relative suitability for bite detection. The effects of varying sampling rates, threshold levels and signal-to-noise ratio on the detection rate will be demonstrated.

5aABb9. Sound insulation of artificial and natural sound signals in reeds habitats. Igor Ianovschi (Universitetskaja nab. 7/9, Dep. Vertebrate Zoology, 199034 St. Petersburg, Russian Federation, igorul@mail.ru), Ludmila Osipova (St. Petersburg State University, Universitetskaya emb., 7/9, 199034 St. Petersburg, Russian Federation, osipoval @yandex.ru)

From the point of view of acoustical communication, dense fields of reeds are strong acoustical filtre which distorts original sound signal. In this research the rate of sound signals sound insulation in massives of reeds was estimated. As a models were used artificially synthesized, modulated by frequency signals of three frequency lines: 1-2 kHz, 2-4 kHz, and 4-8 kHz with duration of 0.1 and 0.25 msec. For comparison were also used elements of bird songs. The least damping was noted in signals with descending frequency modulation in 8 - 4 kHz range in the upper level of reeds (6 db on 10 m). The most damping were noted in signals with descending frequency modulation in 2 - 1 kHz in the middle level of juncaceous massive(18 db to 10 m). The signals with frequency modulation of 4-2 kHz were extending better in the upper level of reeds (7-8 db), whereas in the lower and upper levels were noted dependence of damping rate on duration of sound impulse - the signals with duration of 0.25 mec were damping less than signals with duration of 0.1 msec . The elements of bird songs during their emission in the middle level of juncaceous massive were damping by 15-20 db on 10 m.

5aABb10. Echolocation and flight strategies of Japanese house bats (Pipistrellus abramus) to attack a prey in the field revealed by a microphone array. Emyo Fujioka (Faculty of Engineering, Doshisha Univ., 1-3 Miyakodani Tatara, 610-0321 Kyotanabe, Japan, dth0902@mail4.doshisha.ac.jp), Shigeki Mantani (Faculty of Engineering, Doshisha Univ., 1-3 Miyakodani Tatara, 610-0321 Kyotanabe, Japan, bte2058@mail4.doshisha.ac.jp), Michihiro Fukuda (Faculty of Engineering, Doshisha Univ., 1-3 Miyakodani Tatara, 610-0321 Kyotanabe, Japan, dtg0108@mail4.doshisha.ac.jp), Shizuko Hiryu (Faculty of Engineering, Doshisha Univ., 1-3 Miyakodani Tatara, 610-0321 Kyotanabe, Japan, shiryu@mail.doshisha.ac.jp), Hiroshi Riquimaroux (Faculty of Engineering, Doshisha Univ., 1-3 Miyakodani Tatara, 610-0321 Kyotanabe, Japan, hrikimar@mail.doshisha.ac.jp), Yoshiaki Watanabe (Faculty of Engineering, Doshisha Univ., 1-3 Miyakodani Tatara, 610-0321 Kyotanabe, Japan, kwatanab@mail.doshisha.ac.jp)

Bats are supposed to have effective strategies for achieving a good balance between echolocation and flight behaviors while capturing small moving insects in the field. To reveal their strategies for catching insects, we successfully reconstructed 3-D flight trajectories for the bat to forage in the field by a four-microphone array system, and conducted both acoustical and behavioral analyses for capturing behavior. Data show that the flying bats changed their flight direction flexibly, and sometime repeated capturing insects every two to three seconds. During the search phase, the bat moved 0.5-0.8 m during an interval between successive pulses (IPI) and then decreased that the moving distance during an IPI up to 0.1 m just before capturing a prey. Interestingly, we found that the bat tended to descend toward a prey from above when the approach phase started. This suggests that foraging bats may effectively utilize gravity for an easy acceleration toward the prey to concentrate on the complex echolocation for capturing moving insects. [Supported by a grant to RCAST at Doshisha Univ. from MEXT of Japan: Special Research Grants for Development of Characteristic Education from the Promotion and Mutual Aid Corporation for Private Schools Japan, Innovative Cluster Creation Project.]

5aABb11. Optimization of the characteristics of receiving echoes by free-flying echolocating bats, revealed by onboard pulse-echo recordings. Shizuko Hiryu (Faculty of Engineering, Doshisha Univ., 1-3 Miyakodani Tatara, 610-0321 Kyotanabe, Japan, shiryu@mail.doshisha.ac.jp), Yu Shiori (Faculty of Engineering, Doshisha Univ., 1-3 Miyakodani Tatara, 610-0321 Kyotanabe, Japan, dtg0165@mail4.doshisha.ac.jp), Tatsuro Hosokawa (Faculty of Engineering, Doshisha Univ., 1-3 Miyakodani Tatara, 610-0321 Kyotanabe, Japan, dtg0119@mail4.doshisha.ac.jp), Hiroshi Riquimaroux (Faculty of Engineering, Doshisha Univ., 1-3 Miyakodani Tatara, 610-0321 Kyotanabe, Japan, hrikimar@mail.doshisha.ac.jp), Yoshiaki Watanabe (Faculty of Engineering, Doshisha Univ., 1-3 Miyakodani Tatara, 610-0321 Kyotanabe, Japan, kwatanab@mail.doshisha.ac.jp)

To understand complex sensory-motor behavior underlying echolocation by bats, we need to precisely measure acoustic characteristics of echoes that the bats actually listen to during flight. However, it has been technically-difficult to develop a small and light enough microphone set at the position of the bat's ear, and information about the echoes is so far virtually lacked. Here, we have successfully monitored these returning echoes by means of an onboard telemetry microphone mounted on the bats, and we confirmed that the free-flying horseshoe bats compensated for Doppler-shifts by adjusting their call frequency, thus maintaining the echo frequency at constant. Furthermore, we found that the bats also adjusted pulse amplitude with the distance to maintain the echo intensity within the narrow range. Receiving echoes with stable amplitude could help the bats to sustain consistent analysis of successive echoes, and combined frequency and amplitude compensation may be for optimization of successive echoes for target range estimation to control approach and landing. [Supported by a grant to RCAST at Doshisha Univ. from MEXT of Japan: Special Research Grants for the Development of Characteristic Education from the Promotion and Mutual Aid Corporation for Private Schools of Japan and the Innovative Cluster Creation Project.]

5aABb12. Some problems of analyzing bio-sonar echolocation signals generated by echolocating animals living in the water and in the air. Tadeusz Gudra (Wroclaw University of Technology/Institute of Telecommunications, Teleinformatics and Acoustics, Wybrzeze Wyspianskiego 27, 50-370 Wroclaw, Poland, Tadeusz.Gudra@pwr.wroc.pl), Krzysztof Herman (Wroclaw University of Technology/Institute of Telecommunications, Teleinformatics and Acoustics, Wybrzeze Wyspianskiego 27, 50-370 Wroclaw, Poland, krzysztof.herman@pwr.wroc.pl)

In this paper some similarities and differences of bio-sonar echolocation signals generated in the water and in the air are presented. The echolocation cues of marine mammals and bats are usually frequency and amplitude signals modulated simultaneously. The main problems of the analysis of such type of signals are envelope detecting and time-frequency decomposition. In this paper some digital signal processing (DSP) algorithms that may be used to analyze this type of signals are presented. The basic linear spectrogram (STFS), the nonlinear Winger-Vill'e spectrogram and some time-scale representations of signals using wavelets methods of estimation of the fre-

quency modulation function have been compared. An analysis of possibilities for acoustic identification of particular species of bats by means of echolocation is also presented.

5aABb13. Blue whale calls characterization using chirplet transform. Mohammed Bahoura (Eng. Dept., Université du Québec, 300 Allée des Ursulines, P.O. Box 3300, Rimouski, QC G5L-3A1, Canada, mohammed_bahoura@uqar.qc.ca), Yvan Simard (Fisheries and Oceans Canada & ISMER-UQAR, 850 route de la Mer, P.O. Box 1000, Mont-Joli, QC G5H-3Z4, Canada, simardy@dfo-mpo.gc.ca)

The blue whale, Balaenoptera musculus, frequently produce distinctive low-frequency (<100 Hz) signature calls that propagate over large distances in deep oceans. Their efficient detection and identification under variable noise conditions in long-term recordings is a basic requirement of passive acoustic monitoring systems used for studying distributional ecology and habitat selection of these large-scale migrant animals. In North Atlantic, blue whale signature calls are the A and B infrasounds (15-20 Hz), which often occur together in AB phrases, and the audible D-call (35-120 Hz), also known as arch sound. Given the distinction of these calls by their frequency band and rate of change in frequency, the chirplet transform appears well adapted to characterize such calls. We test here this new approach from subset of vocalizations of blue whale sounds recorded in St. Lawrence Estuary. The recordings are band-pass filtered and segmented to isolate individual calls. Then, a feature vector based on the chirplet transform is extracted from each call. Finally, vector quantization (VQ) is used to classify the calls into A, B, and D vocalizations. The performance of the method is compared for various VQ code book sizes. Small code book sizes using only 3 features produced classification rates exceeding 92%.

5aABb14. Burst pulses produced by free-ranging bottlenose dolphins in Tampa Bay, Florida and Mississippi Sound, Mississippi. Natalija Lace (University of Southern Mississippi, 118 College Drive, Box 5025, Hattiesburg, MS 39406, USA, kodzaks@yahoo.com), Stan A. Kuczaj (University of Southern Mississippi, 118 College Drive, Box 5025, Hattiesburg, MS 39406, USA, s.kuczaj@usm.edu), Marc O. Lammers (Hawaii Institute of Marine Biology, P.O. Box 1106, Kailua, HI 96734, USA, lammers@hawaii.edu)

Investigations of the bottlenose dolphin's acoustic repertoire have mainly focused on whistles and echolocation clicks. However, despite their widespread occurrence, burst pulses have not received much attention. The primary function of burst pulses remains unknown and a comparative analysis can be used to advance our knowledge of the function of burst pulses. We recorded the acoustic repertoires of free-ranging bottlenose dolphins in the Tampa Bay and Mississippi Sound areas using broadband recording equipment. The two habitats differ in their environmental features, including water temperature, ambient noise levels and water turbidity. Our preliminary data show that several acoustic parameters such as peak frequency and center frequency of burst pulses differ among habitats. We also report other acoustic parameters, such as the number of clicks, inter-click interval, 3-dB and rms bandwidth. In our ongoing study, we will examine relationships between environmental features of the habitats and the acoustic characteristics of burst pulses.

5aABb15. First report of burst-pulse vocalizations from white-beaked dolphins (*Lagenorhynchus albirostris*). Peter Simard (University of South Florida, College of Marine Science, 140 7th Ave. S., St. Petersburg, FL 33701, USA, psimard@marine.usf.edu), David Mann (University of South Florida, College of Marine Science, 140 7th Ave. S., St. Petersburg, FL 33701, USA, dmann@marine.usf.edu), Shannon Gowans (Eckerd College, Galbraith Marine Science Laboratory, 4200 54th Ave South, St. Petersburg, FL 33711, USA, gowanss@eckerd.edu)

Dolphin vocalizations are generally categorized as tonal whistles or pulsed clicks. Pulsed signals in dolphins are usually associated with echolocation, however an increasing number of species are found to produce burst pulse signals which may be used for communication. Groups of white-beaked dolphins (*Lagenorhynchus albirostris*) were recorded from a 4.2 m rigid inflatable boat near Halifax, Canada with a hydrophone towed 25 m behind the boat at a depth of approximately 5m, and an M-Audio 24/96 digital recorder (16 bit, 96 kHz). During one 23-minute encounter, 11 burst pulse segments were recorded. Mean burst pulse duration was 0.83s (SD 0.51, range 0.22s - 1.74s). Seven segments with high signal to noise ratios were manually selected for analysis in Matlab. Mean pulse rate was 765 Hz (SD 182.2, range 552 Hz - 941 Hz). These durations and pulse rates are similar to those reported for other dolphin species. These vocalizations were made immediately before the group began actively swimming away from the boat at high speed, suggesting that these vocalizations are used in agonistic encounters as suggested for other species of dolphins. This is the first time burst-pulse vocalizations have been reported in this species.

5aABb16. Real-time acoustic monitoring of the deep-ocean environment. Michel Andre (Laboratori d'Aplicacions Bioacústiques (Universitat Politècnica de Catalunya), avda. Rambla Exposició s/n, 08800 Vilanova i la Geltrú, Spain, michel.andre@upc.edu), Mike Van Der Schaar (Laboratori d'Aplicacions Bioacústiques (Universitat Politècnica de Catalunya), avda. Rambla Exposició s/n, 08800 Vilanova i la Geltrú, Spain, mike.vanderschaar@upc.edu), A. Mas (Laboratori d'Aplicacions Bioacústiques (Universitat Politècnica de Catalunya), avda. Rambla Exposició s/n, 08800 Vilanova i la Geltrú, Spain, alex.mas@lab.upc.edu), A. Roma (Laboratori d'Aplicacions Bioacústiques (Universitat Politècnica de Catalunya), avda. Rambla Exposició s/n, 08800 Vilanova i la Geltrú, Spain, agnes.roma@lab.upc.edu), J.v. Castell (Laboratori d'Aplicacions Bioacústiques (Universitat Politècnica de Catalunya), avda. Rambla Exposició s/n, 08800 Vilanova i la Geltrú, Spain, joan.v.castell@lab.upc.edu), Maria Morell (Laboratori d'Aplicacions Bioacústiques (Universitat Politècnica de Catalunya), avda. Rambla Exposició s/n, 08800 Vilanova i la Geltrú, Spain, maria.morell@lab.upc.edu), M. Solè (Laboratori d'Aplicacions Bioacústiques (Universitat Politècnica de Catalunya), avda. Rambla Exposició s/n, 08800 Vilanova i la Geltrú, Spain, marta.sole@lab.upc.edu), J.f. Rolin (IFREMER, Centre de Brest, BP 70, 29280 Plouzane, France, jean.francois.rolin@ifremer.fr), Roland Person (IFREMER, Centre de Brest, BP 70, 29280 Plouzane, France, roland.person@ifremer.fr)

ESONET is a European Network of Excellence (NoE) associating 50 partners (research centres, universities, industrials and SMEs) from 14 countries: France, Germany, Italy, UK, Spain, Portugal, Greece, Belgium, Ireland, the Netherlands, Norway, Sweden, Bulgaria, and Turkey. More than 300 scientists and engineers will participate to its activities. The aim of the ESONET NoE is the lasting integration of European research on deep-sea multidisciplinary observatories. ESONET is particularly sensitive on the effects of noise on marine organisms. Because our knowledge is still quite limited, ESONET is developing a Demonstration Mission, called LIDO, *Listening to the Deep-Ocean Environment*, a research program that will help establishing a scientific base to allow (1) the real-time automatic identification and classification of nonbiological and biological sounds, (2) the monitoring of marine organisms and population dynamics, (3) the assessment and control of the long term effects of anthropogenic sources on marine organisms, (4) the education of the public, end-users and the administration, and (5) the approval of ethical guidelines and procedures. This latter point constitutes a major criterion to award the ESONET LABEL to the observatories. This paper presents the data management architecture and the RT analysis processes that will be carried out at the observatories.

5aABb17. The acoustic role of supralaryngeal air sacs. Bart De Boer (Spuistraat 210, 1012VT Amsterdam, Netherlands, b.g.deboer@uva.nl)

This paper investigates the acoustic effect of supralaryngeal air sacs on the range of sounds that a given vocal tract can generate. Humans do not have supralaryngeal air sacs, whereas apes (chimpanzees, orangutans and gorillas) do. It has also been found that the anatomy of the hyoid bone of Neanderthals (the Kebara hyoid) is consistent with the absence of air sacs, while that of Australopithecines (the Dikika baby) is consistent with their presence. As an important difference between humans and all other primates is that humans speak, it has been suggested that the loss of air sacs has something to do with the evolution of speech. Here an articulatory model is used to compare the acoustic properties of a humanlike vocal tract with and without a chimpanzeelike air sac. The articulatory model is based on the Mermelstein model, and the air sac is a simplified model of a side branch with the approximate size of a chimpanzee air sac. It is found that the air sac reduces the range of articulations, and decreases the average formant

frequency. This would provide an explanation for the presence of air sacs in apes (size exaggeration) and their disappearance in humans (increased articulatory range).

5aABb18. Quantitative assessment of bone properties during defect healing in an animal defect model after augmentation with different bone graft materials using scanning acoustic microscopy. Mathias Schulz (ZHBO Universitätsklinikum Halle, Dept. of Traumatology and Reconstructive Surgery, Ernst-Grube-Str. 40, 06120 Halle, Germany, mathias.schulz@medizin.uni-halle.de), Kay Raum (Martin Luther University of Halle-Wittenberg, Dept. of Orthopedics, Q-BAM Group, Magdeburger Str. 22, 06097 Halle, Germany, kay.raum@medizin.uni-halle.de), Joerg Brandt (Martin Luther University of Halle-Wittenberg, Dept. of Orthopedics, Q-BAM Group, Magdeburger Str. 22, 06097 Halle, Germany, joerg.brandt@medizin.uni-halle.de), Kay Brehme (ZHBO Universitätsklinikum Halle, Dept. of Traumatology and Reconstructive Surgery, Ernst-Grube-Str. 40, 06120 Halle, Germany, kay.brehme@medizin.uni-halle.de)

The aim of this study was to evaluate the dynamic process of bone healing and bone remodeling in an animal defect model. A nanocrystalline hydroxyapatite in an aqueous suspension paste and mixed with either autogenous or allogenic bone was implanted. The investigation was performed using quantitative acoustic microscopy at a frequency of 50 MHz. 4-mm diameter defects were prepared on each femur at distal metaphysis in 60 white New Zealand rabbits. The animals were sacrificed after 2, 4, 6, 8, or 12 weeks. The influences on the acoustic impedance values only in the newly formed bone were analyzed by two-factor analysis of variance and post-hoc multiple comparison tests. Moreover, the kinetics of bone stiffening was evaluated by fitting the impedance data to an exponential growth model. In all treatment groups the impedance increased with healing time. Significant differences between the treatment groups were observed 4, 6, and 8 weeks after treatment ($p<0.05$). The experimental results agreed with the exponential growth model with coefficients of correlation (R2) between 0.6 and 0.8. Nanocrystalline hydroxyapatite paste in combination with autogenous bone was found to be superior to the other evaluated treatment strategies.

5aABb19. An opportunistic passive acoustics study of the spatial and temporal distribution and vocal behavior of Blainville's beaked whale ("Mesoplodon densirostris") in the presence of mid-frequency active sonar. David Moretti (NAVSEA, Newport Undersea Warfare Center, Newport, RI RI 02841, USA, MorettiDJ@npt.nuwc.navy.mil), Ronald P. Morrissey (Naval Undersea Warfare Center Division Newport, 1176 Howell Street, Bldg 1351, 2nd Floor, Newport, RI 02841, USA, morrisseyrp@npt.nuwc.navy.mil), Nancy A. Dimarzio (Naval Undersea Warfare Center Division Newport, 1176 Howell Street, Bldg 1351, 2nd Floor, Newport, RI 02841, USA, dimarziona@npt.nuwc.navy.mil), Jessica Ward (NAVSEA, Newport Undersea Warfare Center, Newport, RI RI 02841, USA, wardja@npt.nuwc.navy.mil),Susan Jarvis(Naval Undersea Warfare Center Division Newport, 1176 Howell Street, Bldg 1351, 2nd Floor, Newport, RI 02841, USA, Sjarvis@wpi.edu), Elena McCarthy (Naval Undersea Warfare Center Division Newport, 1176 Howell Street, Bldg 1351, 2nd Floor, Newport, RI 02841, USA, mccarthy@nurc.nato.int), Annamaria Izzi (Naval Undersea Warfare Center Division Newport, 1176 Howell Street, Bldg 1351, 2nd Floor, Newport, RI 02841, USA, izzia.ctrmccarthy@nurc.nato.int)

The effect of mid-frequency active sonar, has increasingly become an issue with navies worldwide. The U.S. navy ranges have been used to develop passive acoustic algorithms and tools to detect, classify, and localize marine mammal vocalizations which have been applied to an opportunistic passive acoustic study of Blainville's beaked whales. Based on Woods Hole Oceanographic Digital Tags (Dtags), these animals are known to produce echo-location clicks only during deep foraging dives. Using passive acoustics detection of vocalizations, foraging groups of animals were isolated and the duration of vocalizations was used as a measure of foraging behavior. The animals' vocal behavior and spatial and temporal distribution were characterized during periods with no active sonar on range. These results are compared to those derived from opportunistic data obtained during multiship active mid-frequency sonar operations.

5aABb20. Testing the acoustic tolerance of harbour porpoise hearing for impulsive sounds. Klaus Lucke (FTZ Westkueste/University of Kiel, Hafentoern 1, 25761 Buesum, Germany, lucke@ftz-west.uni-kiel.de), Paul A. Lepper (Loughborough University, Electronic & Electrical Engineering, LE11 3TU Leicestershire, UK, p.a.lepper@lboro.ac.uk), Marie-Anne Blanchet (Fjord&Bælt / University of Southern Denmark, Margrethes Plads 1, 5300 Kerteminde, Denmark, marie@fjord-baelt.dk), Ursula Siebert (FTZ Westkueste / University of Kiel, Hafentoern 1, 25761 Buesum, Germany, ursula.siebert@ftz-west.uni-kiel.de)

The planned construction of offshore wind turbines in the North and Baltic Seas involves the emission of high numbers of intense impulsive sounds when the foundations of the turbines are being driven into the ground by pile driving. Based on information from other odontocete cetaceans it can be assumed that the source levels which will on average exceed 225 dB re 1 μPa pose a risk at least for temporary threshold shift (TTS) on harbour porpoises which inhabit these waters. In order to base the definition of noise exposure criteria on information on the tolerance of the hearing of this species a TTS study was conducted on one of the harbour porpoises held at the Fjord and Baelt in Kerteminde, Denmark. The hearing data were collected by using the AEP method. An airgun was chosen as sound source for the fatiguing sound stimulus to simulate the impulsive sounds at sufficiently high levels. This study comprises the testing of the animals normal hearing sensitivity and subsequent repetitions of these tests after an exposure to single impulsive sounds from the airgun at increasing levels. The baseline hearing data, thresholds for behavioural reactions and the resulting TTS levels will be presented.

Session 5aAO

Acoustical Oceanography and ECUA: General Topics in Acoustical Oceanography II

Andone Lavery, Cochair
Woods Hole Oceanographic Institution, Applied Ocean Physics & Engineering Department, 98 Water Street, MS #11, Woods Hole, MA 02543, USA

James H. Miller, Cochair
University of Rhode Island, Department of Ocean Engineering, Narragansett Bay Campus, Narragansett, RI 02882, USA

Contributed Papers

11:00

5aAO1. Analysis of Munk waveguide normal modes based on the Rayleigh-Schrödinger perturbation and adiabatic invariant theories. Luiz Guimarães (Dept. Física Nuclear, Instituto de Física, Universidade Federal do Rio de Janeiro, Cx Postal 68528, 21945-970 Rio de Janeiro, Brazil, LULA@IF.UFRJ.BR)

This work concerns to obtain accurate explicit formulas related to discrete spectrum of the Munk deepwater acoustic wave guide problem. To this end, based on the Rayleigh-Schrödinger perturbation theory, we developed analytic results related to the discrete values of the radial wave numbers as well as to the eigen pressure felds. We compare these previous results with JWKB ones. In addition, based on invariant adiabatic theory to wave equation [1,2], we tried to improve the accuracy of the JWKB calculation applying Olver's uniform asymptotic expansion (UAE) theory for the solution of the second-order differential equation with two turning points [3-5]. Comparing these three above particular frameworks, we conclude that UAE theory is accurate and it well describes the Munk wave guide normal modes. [1] L. M. Brekhovskikh and Yu. P. Lysanov, Fundamentals of Ocean Acoustics, Spinger, NY, 2001. [2] B. G. Katsnelson and V. G. Petnikov, Shallow Water Acoustics. Spinger, UK, 2002. [3] F. W. J. Olver, Asymptotics and special functions, Academic Press, London, 1974. [4] L. G. Guimarães and H. M. Nussenzveig, J. Mod. Optic., **41**, 625 (1994). [5] P. C. G. de Moraes and L. G. Guimarães, JQSRT, **74** 757 (2002).

11:20

5aAO2. High-resolution population density imaging of random scatterers through cross-spectral coherence in matched filter variance. Mark Andrews (Northeastern University, 302 Stearns Center, Rm 311, 360 Huntington Ave, Boston, MA 02115, USA, Andrews.mar@neu.edu), Zheng Gong (Northeastern University, 302 Stearns Center, Rm 311, 360 Huntington Ave, Boston, MA 02115, USA, zgong@ece.neu.edu), Daniel Cocuzzo (Northeastern University, 302 Stearns Center, Rm 311, 360 Huntington Ave, Boston, MA 02115, USA, dcocuzzo@ece.neu.edu), Purnima Ratilal (Northeastern University, 302 Stearns Center, Rm 311, 360 Huntington Ave, Boston, MA 02115, USA, purnima@ece.neu.edu)

The matched filter enables imaging with high spatial resolution and high signal-to-noise ratio by coherent correlation with the expected field from what is assumed to be a discrete scatterer. In many imaging systems, however, returns from large numbers of scatterers are received together and the coherent or expected field vanishes. This is the case when imaging schools of fish, other groups of marine life, or other diffuse scatterers in sonar or ultrasound applications. Here we show that despite the absence of an expected field, cross spectral coherence in the matched filter variance retains a pulse compression property that enables high-resolution imaging of scatterer population density. Both analytic and numerical models are developed for active imaging systems. We show the conditions for when the coherent intensity can be neglected. The model is implemented for several scenarios where single scattering dominates and also for cases where multiple scattering is important. It can applied to imaging in both free space and waveguide environments.

11:40

5aAO3. Using angular dependence of multibeam echo features in seabed classification. Zbigniew Lubniewski (Gdansk University of Technology, Department of Geoinformatics, Narutowicza 11/12, 80-952 Gdansk, Poland, lubniew@eti.pg.gda.pl), Andrzej Chybicki (Gdansk University of Technology, Department of Geoinformatics, Narutowicza 11/12, 80-952 Gdansk, Poland, andrzej.chybicki@eti.pg.gda.pl)

The approach to seabed classification based on processing multibeam sonar echoes is presented. The multibeam sonars, besides their well verified and widely used applications like high resolution bathymetry measurements or underwater object imaging, are also the promising tool in seafloor identification and classification, having several advantages over conventional single beam echosounders. The proposed seabed classification method assumes calculation of a set of parameters of an echo envelope, similarly as in single beam classification. These parameters include echo energy, echo length, statistical moments of echo energy and the set of echo shape descriptors. They are extracted for each consecutive beam allowing the estimation of their dependence on seafloor incident angle. The characteristic features of this dependence are described quantitatively and constitute the input information for an automatic supervised seabed classifier. The results of the simple classification procedure applied for multibeam data records acquired from several bottom types in Gdańsk Bay region are presented and discussed.

12:00

5aAO4. Applications of compression techniques for reducing the size of multibeam sonar records. Andrzej Chybicki (Gdansk University of Technology, Department of Geoinformatics, Narutowicza 11/12, 80-952 Gdansk, Poland, andrzej.chybicki@eti.pg.gda.pl), Marek Moszynski (Gdansk University of Technology, Department of Geoinformatics, Narutowicza 11/12, 80-952 Gdansk, Poland, marmo@eti.pg.gda.pl)

High efficiency of multibeam sonar system (MBS) hardware due to operational requirements (i.e., high frequency, high ping rate, and high resolution of collected data) results in very large volumes of datasets stored on local hard drives of operator's station. In this context, the process of archiving of such warehouse of data collected in previous surveys becomes crucial problem. The paper investigates various lossy and lossless compression methods that can be applied to multibeam sonar data to reduce the size of acquired files without loosing relevant information. The specific character of MBS data allows applying various signal, image, and video compression methods to achieve better results than when using standard ones. Various techniques of reordering the data were analysed to achieve best possible compression ratio.

Session 5aBBa

Biomedical Ultrasound/Bioresponse to Vibration and Engineering Acoustics: Transducers for Medical Imaging and Therapy I

Jeffrey A. Ketterling, Cochair
Frederic L. Lizzi Center for Biomedical Engineering, Riverside Research Institute, 156 William St., New York, NY 10038, USA

Marc Lethiecq, Cochair
LUSSI, 10 Bd Tonellé, Tours, 37032, France

Invited Papers

8:00

5aBBa1. Designing advanced piezoelectric ceramics for novel ultrasonic applications. Erling Ringgaard (Ferroperm Piezoceramics A/S, Hejreskovvej 18A, 3490 Kvistgaard, Denmark, er@ferroperm.net), Wanda W. Wolny (Ferroperm Piezoceramics A/S, Hejreskovvej 18A, 3490 Kvistgaard, Denmark, ww@ferroperm.net), Torsten Bove (Ferroperm Piezoceramics A/S, Hejreskovvej 18A, 3490 Kvistgaard, Denmark, tb@ferroperm.net)

As new applications of medical ultrasound continue to emerge and the development of electronics continues, there is an increased interest in specialised piezoelectric ceramics with optimised properties. With the present level of knowledge about piezoceramics it is possible to design materials combining selected characteristics - although of course the laws of physics prevent changing certain properties independently. The main parameters in the design process are composition modification and controlled porosity. One of the new types of materials developed is especially intended for high-intensity focused ultrasound (HIFU) applications, where the ability to continuously generate high acoustic power should be combined with specifications for electrical impedance matching. Since the first requirement calls for very low dielectric and mechanical losses (hard doping), whereas for typical applications the second one calls for a high permittivity (soft material), a new combination was needed. The new PZT-based materials Ferroperm Pz52 and Pz54 fulfil these requirements and are already being extensively used for HIFU applications. Another example of new materials is the commercial family of porous PZT. The introduction of porosity affects all properties, and by optimising composition and porosity level it is possible to design materials that can replace lead metaniobate-based ceramics for a number of applications.

8:20

5aBBa2. Dual-mode ultrasound array (DMUA) systems for noninvasive surgery. John Ballard (University of Minnesota, 200 Union St SE, Rm 4-174 EECS Bldg, Minneapolis, MN 55455, USA, ball250@umn.edu), Yayun Wan (University of Minnesota, 200 Union St SE, Rm 4-174 EECS Bldg, Minneapolis, MN 55455, USA, wanx0028@umn.edu), Emad S. Ebbini (University of Minnesota, 200 Union St SE, Rm 4-174 EECS Bldg, Minneapolis, MN 55455, USA, emad@umn.edu)

Advances in microelectronics and piezocomposite transducer technology have made it possible to design, fabricate, and test therapeutic arrays with imaging capabilities suitable for image-guided noninvasive surgery. Prototype DMUAs have been recently tested and were shown to be capable of generating therapeutic HIFU beams suitable for tissue ablation while intermittently imaging the target volume before, during, and after lesion formation. An additional advantage of imaging with DMUAs is the potential for identifying critical regions in the treatment field for targeting or avoidance by the HIFU beam. We have developed an image-based refocusing algorithm that allows for maximizing the power deposition at the location of HIFU focus while minimizing the power deposition at critical targets to be avoided. Grayscale images obtained using the DMUA are used to define the coordinate of the target and the grid points in the treatment region. A major application of this capability is the targeting of liver tumors by large-aperture arrays in the presence of the rib cage. In this paper, we present experimental validation of this algorithm in vitro. Quantitative analysis of the improvements in the quality of the HIFU beam at the target will be presented and discussed.

8:40

5aBBa3. High power sources for ultrasound thermal therapy and shock wave lithotripsy. Neil Owen (INSERM, U556, 151 Cours Albert Thomas, 69003 Lyon, France, Neil.Owen@lyon.inserm.fr), Dominique Cathignol (INSERM, U556, 151 Cours Albert Thomas, 69003 Lyon, France, cathignol@lyon.inserm.fr), David Melodelima (INSERM, U556, 151 Cours Albert Thomas, 69003 Lyon, France, melodelima@lyon.inserm.fr), Alain Birer (INSERM, U556, 151 Cours Albert Thomas, 69003 Lyon, France, birer@lyon.inserm.fr), Jean Yves Chapelon (INSERM, U556, 151 Cours Albert Thomas, 69003 Lyon, France, chapelon@lyon.inserm.fr), Cyril Lafon (INSERM, U556, 151 Cours Albert Thomas, 69003 Lyon, France, lafon@lyon.inserm.fr)

We present a summary of Inserm's experience with high power sources, which are necessary for ultrasound thermal therapy and lithotripsy. Moreover, generating high intensity pseudo-continuous waveforms or high pressure pulses imposes different constraints on the transducer materials, specifically heat and mechanical stress. For thermal therapy, miniature piezoceramic transducers were used for interstitial, intratumoral, and endoluminal applicators. These probes operated at surface intensities up to 50 W/cm^2 and generated elementary lesions in vivo within tens of seconds. Piezocomposite transducers were developed for large-aperture, highly-focused beams used in extracorporeal or intraoperative treatments. Focal intensities were 1000 W/cm^2 or higher and up to 256 elements were utilized. Miniaturized piezocomposite transducers are currently being developed for dual-mode imaging and therapy. For lithotripsy, piezoelec-

tric shock wave generators were developed as alternatives to electrohydraulic or electromagnetic generators. Using piezocomposite materials and a novel prestraining method increased transducer surface pressure compared to a multielement piezoceramic design, and therefore halved the aperture diameter. In in vitro tests, plaster kidney stone models were comminuted with ~200 shock waves, a number comparable to values published for electrohydraulic generators, the current "gold" standard. This work contributes to the advancement of transducer performance in therapeutic ultrasound. [Supported by Inserm Post-doctoral Fellowship.]

9:00

5aBBa4. An eight-element annular array for image-guided high intensity focused ultrasound therapy. Peter Kaczkowski (Center for Industrial and Medical Ultrasound, Applied Physics Lab., University of Washington, 1013 NE 40th St., Seattle, WA 98105, USA, peter@apl.washington.edu), Bryan Cunitz (Center for Industrial and Medical Ultrasound, Applied Physics Lab., University of Washington, 1013 NE 40th St., Seattle, WA 98105, USA, bwc@apl.washington.edu), George Keilman (Sonic Concepts, 11807 North Creek Parkway South - Suite 111, Bothell, WA 98011, USA, gkeilman@sonicconcepts.com)

The investigation of high intensity focused ultrasound (HIFU) as a tool for noninvasive thermally ablative therapy has required deeper understanding of the relative roles of nonlinear mechanisms involved in heat deposition. Attempts at quantifying the dose response to particular exposure conditions in vitro are complicated by the interplay of several mechanisms. These include microbubble cavitation, nonlinear acoustic propagation and attenuation, dependence of tissue parameters on temperature and temperature history, and formation and evolution of vapor bubbles due to boiling. One immediately evident consequence of such effects is distortion of coagulative lesion shape and size, colloquially evolving from "cigars" to "tadpoles". Developing a quantitative understanding of the relative roles of relevant nonlinear mechanisms is not straightforward, yet is desirable for design of algorithms for therapy planning and real time monitoring using ultrasound. A historical perspective of research toward this end will be presented along with a recommendation for suitable terminology for the various physical acoustic regimes encountered in HIFU therapy. [Work supported by Army MRMC, NIH DK43881, NSBRI SMS00402, and RFBR.]

9:20

5aBBa5. Transducers for reduced aberration in HIFU by nonlinear harmonic focusing. Gregory Clement (Harvard Medical School, Focused Ultrasound Lab - BWH Radiology, 221 Longwood Ave RM 521, Boston, MA 02115, USA, gclement@hms.harvard.edu), Jason White (Harvard Medical School, Focused Ultrasound Lab - BWH Radiology, 221 Longwood Ave RM 521, Boston, MA 02115, USA, white@bwh.harvard.edu)

We have been investigating a low-frequency transducer design that promotes the *divergence* of the low frequency beam while promoting the *focusing* of nonlinear-induced higher harmonic frequencies. In this manner, a low frequency - and thus less absorbed and less distorted - beam is passed through the near field, peaking before the buildup of higher-frequency components. The high frequency components are then focused by means of the wavefront design. Using this approach, we expect reduced distortion of the ultrasound focus, while allowing a beam that uses mechanical or thermal effects for ablation, as opposed to cavitation. In our preliminary study we have been working to establish feasibility of the approach. Two source transducers (0.272 MHz and 0.272 MHz) with identical geometries were used to propagate through *ex vivo* human skull, representing strong nearfield aberration. Transmitted fields were scanned after transsskull propagation with a pvdf needle hydrophone. Reconstructions were performed at the fundamental frequencies for both scans, and for the 0.272 MHz transducer, an additional reconstruction was performed at its second harmonic (by design 0.544 MHz). The harmonic signal was observed to be significantly less distorted than the same frequency directly propagated from the transducer. A numeric study for optimizing the method will also be presented.

9:40-11:00 Posters

Lecture sessions will recess for presentation of poster papers on various topics in acoustics. See poster sessions for topics and abstracts.

Contributed Papers

11:00

5aBBa6. Combined two frequency array for optoacoustics and acoustics. Kirsten Maass (Fraunhofer IBMT, Ensheimerstrasse 48, 66386 Sankt Ingbert, Germany, kirsten.maass@ibmt.fhg.de), Christian Degel (Fraunhofer IBMT, Ensheimer Strasse 48, 66386 Sankt Ingbert, Germany, christian.degel@ibmt.fraunhofer.de), Marc Fournelle (Fraunhofer IBMT, Ensheimer Strasse 48, 66386 Sankt Ingbert, Germany, marc.fournelle@ibmt.fhg.de), Heinrich Fonfara (Fraunhofer IBMT, Ensheimerstrasse 48, 66386 Sankt Ingbert, Germany, heinrich.fonfara@ibmt.fhg.de), Robert M. Lemor (Fraunhofer IBMT, Ensheimer Strasse 48, 66386 Sankt Ingbert, Germany, robert.lemor@ibmt.fhg.de)

A combined transducer for optoacoustics and b-mode ultrasound has to be built according to the specific requirements of both modalities. In order to combine the two tasks in one transducer, we have designed a probe consisting of a PZT array and a PVDF array in a sandwich assembly. The 20 MHz PZT array is a linear array with 128 elements bearing a 150 μm pitch. It operates as a high resolution transmit and receive array for the visualization of geometrical structures in biological tissue. A thin piezoelectric polymer film (PVDF) that is structured as receiving array is superposed to the PZT array. The PVDF array allows to detect the small optoacoustic pressure transients resulting of laser irradiation of small biological structures. Its acoustic impedance of approximately 4-4,5 MRayl allows to use it in a double function as optoacoustic receiving array and matching layer for the PZT array. The combined array is driven by a custom made multichannel read-out system supporting sampling frequencies of 80 MHz and combined imaging with b-mode and optoacoustics. This combined probe integrates the benefits of a high resolution PZT array and gives access to the specificity of optoacoustic signal generation.

11:20

5aBBa7. Dual-frequency driving transducer for ultrasonic echography. Iwaki Akiyama (Shonan Institute of Technology, 1-1-25 Tsujido-nishikaigan, 251-8511 Fujisawa, Japan, akiyama@iwaki.org), Natsuki Yoshizumi (Shonan Institute of Technology, 1-1-25 Tsujido-nishikaigan, 251-8511 Fujisawa, Japan, yoshizumi@pari.go.jp), Shigemi Saito (Tokai University, 3-20-1 Orito, Shimizu-ku, 424-8610 Shizuoka, Japan, ssaito@scc.u-tokai.ac.jp), Daisuke Koyama (Tokyo Institute of Technology, 4259 Nagatsuda, 226-8503 Yokohama, Japan, dkoyama@sonic

.pi.titech.ac.j),Kentarou Nakamura(Tokyo Institute of Technology, 4259 Nagatsuda, 226-8503 Yokohama, Japan, knakamur@sonic.pi.titech.ac.jp)

We propose a novel ultrasonic imaging technique by transmitting ultrasonic pulse of dual-frequency and receiving multifrequency echoes from the biological tissues. When the ultrasonic pulse of two frequencies is transmitted from a transducer, the secondary waves are generated during the nonlinear propagation through the biological media. A choice of f_0 and $4f_0$ as the dual-frequency results in the generation of $2f_0$, $3f_0$, and $5f_0$ components as the secondary waves. Multifrequency echoes are capable of improving the image quality by reducing the speckle noise. We have developed the following annular type transducer. The PZT disk of 7 mm in diameter is coaxially arranged in the PZT ring of 9 mm in inner diameter and 17 mm in outer diameter. The ring and circular transducers transmit the pulses of 2 and 8 MHz, respectively. It was confirmed that this transducer formed the ultrasonic beams of 4, 6, and 10 MHz as well as the beams of 2 and 8 MHz in degassed water. Then the experiments of imaging the agar-gel phantom and pork meat were carried out by mechanical scanning. As a result, we also confirmed the improvement of image quality by reducing the speckle noise.

11:40

5aBBa8. Progress towards transducers and arrays for real-time high frequency biomedical ultrasound imaging. Sandy Cochran (Institute for Medical Science and Technology, University of Dundee, Wilson House, 1 Wurzburg Loan, DD2 1FD Dundee, UK, s.cochran@dundee.ac.uk), Jeff Bamber (Institute of Cancer Research, 15 Cotswold Road, Belmont, Sutton, SM2 5NG Surrey, UK, jeff.bamber@icr.ac.uk), Anne L. Bernassau (Institute for Medical Science and Technology, University of Dundee, Wilson House, 1 Wurzburg Loan, DD2 1FD Dundee, UK, a.l.bernassau@dundee.ac.uk), Nigel Bush (Piezo Composite Transducers Ltd, Aberdeen Science Park, Balgownie Drive, Bridge of Don, AB22 8GU Aberdeen, UK, nigel.bush@icr.ac.uk), Tim W. Button (Functional Materials Group, IRC in Materials Processing, The University of Birmingham, Edgbaston, B15 2TT Birmingham, UK, t.w.button@bham.ac.uk), Christine E. Demore (Institute for Medical Science and Technology, University of Dundee, Wilson House, 1 Wurzburg Loan, DD2 1FD Dundee, UK, c.demore@dundee.ac.uk), Luis Garcia-Gancedo (Tritech International Ltd, Peregrine Road, Westhill Business Park, Westhill, AB32 6LJ Aberdeen, UK, l.garciagancedo@bham.ac.uk), David Hutson (Institute for Medical Science and Technology, University of Dundee, Wilson House, 1 Wurzburg Loan, DD2 1FD Dundee, UK, d.hutson@dundee.ac.uk), Duncan P. Maclennan (University of Strathclyde, DTC in Medical Devices, Bioengineering Department, Wolfson Building, 106 Rottenrow, G4 0NW Glasgow, UK, duncan.p.maclennan@strath.ac.uk), Paul M. Maher (Tritech International Ltd, Peregrine Road, Westhill Business Park, Westhill, AB32 6LJ Aberdeen, UK, paulmichaelmaher@hotmail.com), Carl Meggs (Tritech International Ltd, Peregrine Road, Westhill Business Park, Westhill, AB32 6LJ Aberdeen, UK, c.meggs@bham.ac.uk), Rhiannon A. Webster (Tritech International Ltd, Peregrine Road, Westhill Business Park, Westhill, AB32 6LJ Aberdeen, UK, raw160@bham.ac.uk)

As research into transducers and arrays for real-time high frequency biomedical ultrasound imaging continues, it is becoming increasingly clear that major applications exist for systems with significantly higher spatial resolution than those already available for human clinical imaging. A key area of research remains the design and fabrication of the transducer or array. It is now accepted that piezocomposite is the material of choice and composite design and conventional dice-and-fill fabrication techniques have been optimised to allow 40 MHz operation, corresponding to wavelengths around 40 um. This expands the range of applications of piezocomposites but is still limited in terms of resolution of fine structures, for example at cellular level and to explore harmonic imaging. In this paper, we report continuing progress in work on new design techniques and fabrication processes with the potential for fabricating arrays that operate up to 100 MHz. The net-shape micromoulding fabrication technique for the ceramic within our composites is outlined, new single element transducer designs and array fabrication based on advanced surface finishing and photolithographic processes are described, and results are presented illustrating key performance data such as the point spread function, insertion loss and imaging of post mortem human tissue.

12:00

5aBBa9. Micromachined linear array with 100 MHz center frequency. Eike C. Weiss (Fraunhofer IBMT, Ensheimer Strasse 48, 66386 Sankt Ingbert, Germany, eike.weiss@ibmt.fraunhofer.de), Anette Jakob (Fraunhofer IBMT, Ensheimerstrasse 48, 66386 Sankt Ingbert, Germany, anette.jakob@ibmt.fraunhofer.de), Steffen H. Tretbar (Fraunhofer IBMT, Ensheimerstrasse 48, 66386 Sankt Ingbert, Germany, steffen.tretbar@ibmt.fraunhofer.de), Werner Haberer (Fraunhofer IBMT, Ensheimerstrasse 48, 66386 Sankt Ingbert, Germany, werner.haberer@ibmt.fraunhofer.de), Thorsten Knoll (Fraunhofer IBMT, Ensheimerstrasse 48, 66386 Sankt Ingbert, Germany, thorsten.knoll@ibmt.fraunhofer.de), Frank Bauerfeld (Fraunhofer IBMT, Ensheimerstrasse 48, 66386 Sankt Ingbert, Germany, frank.bauerfeld@ibmt.fraunhofer.de), Joerg Herrmann (Fraunhofer IBMT, Ensheimerstrasse 48, 66386 Sankt Ingbert, Germany, joerg.herrmann@ibmt.fraunhofer.de), Robert M. Lemor (Fraunhofer IBMT, Ensheimer Strasse 48, 66386 Sankt Ingbert, Germany, robert.lemor@ibmt.fhg.de)

High-frequency ultrasound systems based on single element transducers in the frequency range of 50-120 MHz and mechanical scanning of the transducer. Linear arrays with electrical scanning can be used to increase the speed of scanning and reduce the size of the transducers. We present a linear array combined with multiplexer and single channel electronics. Working at 100 MHz, lateral resolution better than 100 μm is possible with an aperture of 1 mm^2. The 100 MHz array is based on silicon micro machining with a ZnO membrane as active material. The most important steps are the deposition of a 26 μm-thick ZnO thin film by magnetron sputtering and the anisotropic etching of the backside of the silicon wafer to fabricate the ZnO membrane. The individual elements of the transducer are defined by patterning a gold electrode with the desired array structure via photolithography and subsequently wet etching. Results from 32 element arrays with an 8 element 500 by 500 μm aperture agree well with numerical simulations and the shifting of the aperture works as well. Due to the cost-effectiveness of the process, a large number of applications have come now into reach for high-frequency ultrasound imaging.

12:20

5aBBa10. Lead magnesium niobate-lead titanate single crystal thick films on silicon substrate for high-frequency micromachined ultrasonic transducers. Jue Peng (Department of Applied Physics and Materials Research Centre, The Hong Kong Polytechnic University, Hunghom, Kowloon Hong Kong, China, aperica@inet.polyu.edu.hk), Chen Chao (Department of Applied Physics and Materials Research Centre, The Hong Kong Polytechnic University, Hunghom, Kowloon Hong Kong, China, rikeynes@inet.polyu.edu.hk), Jiyan Dai (Department of Applied Physics and Materials Research Centre, The Hong Kong Polytechnic University, Hunghom, Kowloon Hong Kong, China, apdaijy@inet.polyu.edu.hk), Helen L. W. Chan (Department of Applied Physics and Materials Research Centre, The Hong Kong Polytechnic University, Hunghom, Kowloon Hong Kong, China, apahlcha@inet.polyu.edu.hk), Haosu Luo (The Shanghai Institute of Ceramics, Chinese Academy of Sciences, 201800 Shanghai, China, hsluo@mail.sic.ac.cn)

Some new clinical applications requiring ultrasonic frequencies higher than 30 MHz are emerging, such as ophthalmological and dermatological imaging and intravascular imaging with probes mounted on catheter tips. High frequency ultrasonic transducer (HFUT) has thus been a growing research area in recent years. Most of the HFUTs reported are using piezoelectric PZT ceramic thin plates, ZnO films or PVDF films as the transducer materials. The PMN-PT ($(1-x)Pb(Mg_{1/3}Nb_{2/3})O_{3-x}PbTiO_3$) single crystal, although possessing the highest piezoelectric coefficients, has seldom been used for this purpose because it is difficult to lap down the brittle single crystals to thin plates and handle them in conventional way of transducer fabrication. In this work, a novel high-frequency ultrasonic transducer structure is realized by using PMN-PT-on-silicon technology and silicon micromachining. A hybrid processing method involving wafer bonding, mechanical lapping and wet chemical thinning is successfully developed. PMN-PT thick films with thickness ranging from several to tens of microns have been demonstrated and they have properties comparable to those of PMN-PT bulk samples. A prototype high frequency ultrasonic transducer is being fabricated and characterized. Acknowledgement Financial support from the Innovation and Technology Fund (K-ZP21) is acknowledged.

Session 5aBBb

Biomedical Ultrasound/Bioresponse to Vibration: Ultrasonic Characterization of Bone III

Keith A. Wear, Cochair
U.S. Food and Drug Administration, Center for Devices and Radiological Health, 10903 New Hampshire Ave, Bldg 62, Rm 3108, Silver Spring, MD 20993, USA

Emmanuel Bossy, Cochair
Laboratoire Photons et Matière, ESPCI/CNRS, 10 rue Vauquelin, Paris Cedex 05, 75231, France

Invited Paper

8:20

5aBBb1. Microelastic imaging of mineralized tissues - Principles and applications in musculoskeletal research. Kay Raum (Martin Luther University of Halle-Wittenberg, Dept. of Orthopedics, Q-BAM Group, Magdeburger Str. 22, 06097 Halle, Germany, kay.raum@medizin.uni-halle.de)

High frequency ultrasound has become one of the most powerful tools for microelastic characterization of hard biological materials. A major advantage is the possibility to map not only the microstructure, but also the heterogeneous anisotropic elasticity of mineralized tissues. Quantitative concepts for deriving anisotropic elastic parameters with frequencies from 50 MHz to the GHz range will be presented. Due to the scalability ultrasound can be applied for large animal studies, e.g., to predict the mechanical stability in sheep tibiae after callus distraction, as well as for small animal models, e.g., to study the effects of genetic differences in inbred strain mice. Moreover, SAM data are suitable for numerical deformation or sound propagation analyses on "real- life" models. Such models are crucial for the development and validation of new non-invasive diagnostic tools dedicated to the prediction of an individual fracture risk. For example, it has been shown that the velocity of the first arriving signal - measured with the axial transmission technique at the radius - can be predicted by a nonlinear combination of fracture determining parameters, i.e., porosity, cortical thickness and tissue elasticity, assessed by 50-MHz SAM. These findings may lead to the establishment of pathology specific treatment and regeneration monitoring strategies.

Contributed Papers

8:40

5aBBb2. Assessment of cortical bone density and anisotropy in human femur using ultrasound and x-ray. Dorian Cretin (Furuno Electric Co., Ltd, 9-52 Ashihara-cho, 662-8580 Nishinomiya, Japan, dorian.cretin@furuno.co.jp), Ryouichi Suetoshi (Furuno Electric Co., Ltd, 9-52 Ashihara-cho, 662-8580 Nishinomiya, Japan, ryohichi.suetoshi@furuno.co.jp), Atsushi Uodome (Furuno Electric Co., Ltd, 9-52 Ashihara-cho, 662-8580 Nishinomiya, Japan, atsushi.uodome@furuno.co.jp), Shinji Ogawa (Furuno Electric Co., Ltd, 9-52 Ashihara-cho, 662-8580 Nishinomiya, Japan, shinji.ogawa@furuno.co.jp), Sakaya Miyabe (Graduate School of Engineering, Osaka Univ., Division of Materials and Manufacturing Science, 2-1 Yamadaoka, Suita, 565-0871 Osaka, Japan, miyabe@mat.eng.osaka-u.ac.jp), Takayoshi Nakano (Graduate School of Engineering, Osaka Univ., Division of Materials and Manufacturing Science, 2-1 Yamadaoka, Suita, 565-0871 Osaka, Japan, nakano@mat.eng.osaka-u.ac.jp)

The purpose of this research is to investigate the contribution of the intrinsic properties of human bone to the ultrasound velocities in the axial, radial, and tangential directions. Samples of cortical bone were cut from 19 human medial femurs and polished to a rectangular parallelepiped shape. The orientation of apatite crystallites was assessed by microbeam x-ray diffraction, the density with a densitometer using the Archimedes' principle. Bone mineral density (BMD) was also measured with peripheral quantitative computed tomography (pQCT) and dual-x-ray absorptiometry (DXA). The speed of sound (SOS) for each three directions was measured with 3 MHz ultrasonic broadband transducers. Radial and tangential SOS demonstrated a strong correlation with density ($R=0.83, p<0.0001$ and $R=0.85, p<0.0001$, respectively). In the axial direction, the correlation between density and SOS was moderate ($R=0.59$). However, a significant correlation was found by using density and apatite orientation of c-axis in a multiple regression analysis ($R=0.85, p<0.001$). Axial SOS can be explained by contributions of both density and crystal orientation.

9:00

5aBBb3. Experimental determination of Young modulus and Poisson ratio in cortical bone tissue using high resolution scanning acoustic microscopy and nanoindentation. Fabienne Rupin (Université Paris 6, Laboratoire d'Imagerie Paramétrique, 15, rue de l'Ecole de Médecine, 75006 Paris, France, fabienne.rupin@lip.bhdc.jussieu.fr), Amena Saied (Université Paris 6, Laboratoire d'Imagerie Paramétrique, 15, rue de l'Ecole de Médecine, 75006 Paris, France, saied@lip.bhdc.jussieu.fr), Davy Dalmas (CNRS/Saint-Gobain, SVI Saint-Gobain Recherche, 93303 Aubervilliers Cedex, France, Davy.Dalmas@saint-gobain.com), Françoise Peyrin (Creatis, UMR CNRS 5515, INSERM U630, 69621 Villeurbanne Cedex, France, peyrin@esrf.fr), Sylvain Haupert (Université Paris 6, Laboratoire d'Imagerie Paramétrique, 15, rue de l'Ecole de Médecine, 75006 Paris, France, sylvain.haupert@lip.bhdc.jussieu.fr), Etienne Barthel (CNRS/Saint-Gobain, SVI Saint-Gobain Recherche, 93303 Aubervilliers Cedex, France, Etienne.Barthel@saint-gobain.com), Georges Boivin (Unité INSERM U831, Faculté de Médecine R. Laennec, 69372 Lyon Cedex 08, France, Georges.boivin@sante.univ-lyon1.fr), Pascal Laugier (Université Paris 6, Laboratoire d'Imagerie Paramétrique, 15, rue de l'Ecole de Médecine, 75006 Paris, France, laugier@lip.bhdc.jussieu.fr)

Nanoindentation allows measurements of local mechanical properties of bone tissue. Scanning acoustic microscopy (SAM) provides images related to bone density and elasticity. In both techniques, the estimation of Young modulus (E) relies on the accuracy of Poisson's ratio value (σ). In cortical bone, σ varies between 0.15 and 0.45 but, is classically set to 0.3, resulting in an approximate value of E. This study describes a new method combining SAM and nanoindentation techniques to locally evaluate σ in human femo-

ral cortex. A 200 MHz SAM-based acoustic impedance (8 μm lateral resolution) was combined with synchrotron microtomography (to provide local bone mineral density) to map the distribution of near surface elastic modulus. Whereas, nanoindentation modulus was calculated on several osseous regions. Assuming the equalization rule, the intersection of both modulus curves versus σ permits to accurately derive σ. The method was tested on aluminium, PMMA and polycarbonate samples of known σ and provided experimental σ values with a precision better than 3%. In bone, σ was 0.42 ± 0.01 corresponding to $E = 20 \pm 1$ GPa. Our preliminary results indicate that combination of high-resolution SAM and nanoindentation may be relevant to accurately determine both Poisson ratio and Young modulus of bone tissue.

9:20

5aBBb4. Vibration spectroscopy and guided wave propagation data as indicators of structural and mechanical degradation of human bones. Erick Ogam (Laboratoire de Mécanique et d'Acoustique CNRS UPR-7051, 31, Chemin Joseph Aiguier, 13402 Marseille Cedex 20, France, ogam@lma.cnrs-mrs.fr), Armand Wirgin (CNRS-Laboratoire de Mécanique et d'Acoustique, 31 Chemin Joseph Aiguier, 13402 Marseille, France, wirgin@lma.cnrs-mrs.fr), Zine Fellah (CNRS-Laboratoire de Mécanique et d'Acoustique, 31 Chemin Joseph Aiguier, 13402 Marseille, France, fellah@lma.cnrs-mrs.fr), Catherine Masson (INRETS - Laboratoire de Biomécanique Appliquée- UMRT 24, Faculté de Medecine, Bd. Pierre Dramard, 13916 Marseille, France, catherine.masson@inrets.fr), Philippe Guillemain(Laboratoire de Mécanique et d'Acoustique CNRS UPR-7051, 31, Chemin Joseph Aiguier, 13402 Marseille Cedex 20, France, guillemain@lma.cnrs-mrs.fr), François Gabrielli (INRETS - Laboratoire de Biomécanique Appliquée- UMRT 24, Faculté de Medecine, Bd. Pierre Dramard, 13916 Marseille, France, francois.gabrielli@inrets.fr), Jean-Philippe Groby (DRE/L2S - UMR8506 CNRS/Supelec/Univ. Paris Sud 11, Département de Recherche en Electromagnétisme/Laboratoire des signaux et systèmes, 3 rue Joliot-Curie, 91192 Gif-sur-Yvette cedex, France, groby@lss.supelec.fr), Robert Gilbert (University of Delaware, Department of Mathematics, 317 Ewing Hall, Newark, DE 19716, USA, gilbert @math.udel.edu)

Vibration spectroscopy and guided wave modes analysis of long bones are investigated as tools to assess bone quality or integrity. Two different methods of vibroacoustic experiments are undertaken to determine the health of dry human tibia bones. The first method involves vibratory modes of the bone, excited and measured by piezoelectric transducers and sensors respectively. The measured frequency response is validated using finite element simulation (FES), also used in the inverse problem for retrieval of the bone material properties. The principle of in-plane (IP) and out-of-plane (OP) mode splitting to determine the degree of the damage, that we developed in an earlier study, is applied to classify the bones according to their degree of damage. The second method involves the analysis of the guided wave phase velocities recovered using the reassigned Gabor spectrogram from signals measured along the diaphysis of the tibias. The frequency difference between the peaks of the split modes are then correlated to the phase velocities of the retrieved Lamb modes.

FRIDAY MORNING, 4 JULY 2008 P3-B, LEVEL 3, 9:40 TO 11:20 A.M.

Session 5aBBc

Biomedical Ultrasound/Bioresponse to Vibration and Engineering Acoustics: Transducers for Medical Imaging and Therapy II (Poster Session)

Jeffrey Ketterling, Cochair
Frederic L. Lizzi Center for Biomedical Engineering

Marc Lethiecq, Cochair
LUSSI

All posters will be on display from 9:40 a.m. to 11:20 a.m. To allow contributors an opportunity to see other posters, contributors of odd-numbered papers will be at their posters from 9:40 a.m. to 10:30 a.m. and contributors of even-numbered papers will be at their posters from 10:30 a.m. to 11:20 a.m.

Contributed Papers

5aBBc1. High performance ultrasound arrays assessment through in vitro imaging performance. Mathieu Legros (Vermon SA, 180 rue Général Renault, 37000 Tours, France, m.legros@vermon.com), Guillaume Ferin (Vermon SA, 180 rue Général Renault, 37000 Tours, France, g.ferin@vermon.com), Leong Ratsimandresey (Vermon SA, 180 rue Général Renault, 37000 Tours, France, l.ratsi@vermon.com), Rémi Dufait (Vermon SA, 180 rue Général Renault, 37000 Tours, France, r.duvait @vermon.com)

Probes are well-known to be a capital element for ultrasound image quality. During design, many parameters can be tuned on the acoustic stack to optimise the electrical, electroacoustical and acoustical performance measurements. But the effects on image quality of these performances are not so well identified. To overcome such a limitation, we developed a quantitative method for image quality assessment. A set of algorithms was developed to assess in vitro images. The goal of this investigation is to link the electroacoustical, acoustical performances and transducer parameters to the imaging performance. Ultrasound test objects were used to quantify the ultrasound images. The acquisition was carried out on a commercial scanner and imaging parameters were set constant in order to benchmark the probes in the same environment. From B-mode images, key parameters such as axial and lateral resolutions, contrast, statistic or metric parameters, and signal to noise ratio are established. Data from transducers, exhibiting different trade-offs on their performances (bandwidth, bandwidth shape, center frequency, elementary directivity) were characterized. Using the algorithms developed, all identified image properties were analysed with regard to these performances. The impact of each electroacoustical parameter on image quality have been identified and discussed.

5aBBc2. Modeling of different transducer configurations with combined pseudospectral and finite-difference time-domain methods. Erwan Filoux (LUSSI, 10 Bd Tonellé, 37032 Tours, France, erwan.filoux@etu.univ-tours.fr), Franck Levassort (LUSSI, 10 Bd Tonellé, 37032 Tours, France, franck.levassort@univ-tours.fr), Samuel Callé (LUSSI, 10 Bd Tonellé, 37032 Tours, France, calle_s@med.univ-tours.fr), Marc Lethiecq (LUSSI, 10 Bd Tonellé, 37032 Tours, France, lethiecq@univ-tours.fr)

The numerical simulation of acoustic waves propagating in inhomogeneous media is often achieved using pseudospectral (PS) algorithms, which require few nodes per wavelength to converge, while complex piezoelectric structures are simulated with finite-difference (FD) or finite-element (FE) methods. A combination of the PS and FD algorithms, retaining their advantages, is presented in order to simulate the behavior of various piezoelectric transducers used in ultrasonic imaging with one single model. The theory is exposed and the algorithm is applied to simulate PZT resonators flooded into water. Perfectly matched layers are developed to absorb the mechanical waves at the borders of the computational domain, and space-shifted grids are used to reduce Gibbs phenomenon. The electrical impedance and various physical parameters (displacements, electric potentials) are calculated. Different high frequency transducer configurations have been modeled. In the case of a simple two-dimensionnal plate, described in Cartesian coordinates, the results are satisfactorily compared to those obtained with a commercial FE software. Then, simulations of an axisymmetrical single-element transducer are favorably compared to FE simulations and experimental measurements. The hybrid algorithm is also used to calculate the large radiation pattern of an annular array with little time-processing, which illustrates the efficiency of the method.

FRIDAY MORNING, 4 JULY 2008 P3-B, LEVEL 3, 9:40 TO 11:20 A.M.

Session 5aBBd

Biomedical Ultrasound/Bioresponse to Vibration: General Topics in Biomedical Ultrasound/Bioresponse to Vibration I (Poster Session)

Michael Bailey, Cochair
Center for Industrial and Medical Ultrasound, Applied Physics Lab.

Oleg Sapozhnikov, Cochair
Center for Industrial and Medical Ultrasound, Applied Physics Lab.

All posters will be on display from 9:40 a.m. to 11:20 a.m. To allow contributors an opportunity to see other posters, contributors of odd-numbered papers will be at their posters from 9:40 a.m. to 10:30 a.m. and contributors of even-numbered papers will be at their posters from 10:30 a.m. to 11:20 a.m.

Contributed Papers

5aBBd1. 1 kHz sound stimulates nitric oxide and prostaglandin E2 production by rat mesenchymal stem cells. Dorothée Bossis (Université Paris 6, Laboratoire d'Imagerie Paramétrique, 15, rue de l'Ecole de Médecine, 75006 Paris, France, dorothee.bossis@lip.bhdc.jussieu.fr), Frederic Padilla (Université Paris 6, Laboratoire d'Imagerie Paramétrique, 15, rue de l'Ecole de Médecine, 75006 Paris, France, Frederic.Padilla@lip.bhdc.jussieu.fr), Bertrand David (Faculté de Médecine Paris 7- Denis Diderot, Laboratoire Biomécanique et Biomatériaux Ostéo-Articulaires - B2OA, 10 avenue de Verdun, 75010 Paris, France, bertrand.david@paris7.jussieu.fr), Hervé Petite (Faculté de Médecine Paris 7- Denis Diderot, Laboratoire Biomécanique et Biomatériaux Ostéo-Articulaires - B2OA, 10 avenue de Verdun, 75010 Paris, France, hpetite@infobiogen.fr), Pascal Laugier (Université Paris 6, Laboratoire d'Imagerie Paramétrique, 15, rue de l'Ecole de Médecine, 75006 Paris, France, laugier@lip.bhdc.jussieu.fr)

Pulsed ultrasound has become a common therapy for delayed unions and non unions. Currently available clinical devices use modulated (1 kHz) 1.5 MHz ultrasound stimulation that produces a 1 kHz radiation force vibration. It was hypothesized that this radiation force is responsible for the stimulatory effect on bone formation. Therefore, we have investigated the effect of 1 kHz stimulation in rat mesenchymal stem cells (MSCs) by measuring the production of on nitric oxide (NO) and prostaglandin E2 (PGE2). Continuous wave 1 kHz low power sound was applied to cultured rat MSCs for 20 min. NO concentration was determined by amperometry and PGE2 was assayed by ELISA in the supernatant. The stimulation produced a significant increase in both NO and PGE2 concentration compared to controls. We conclude that rat MSCs respond to the mechanical stress produced by 1 kHz continuous wave as evidenced by the increase in NO and PGE2 production. This study provides evidence for the action of 1 kHz stimulation on bone cells.

5aBBd2. Accurate ultrasonic measurement of two-dimensional displacement of heart wall motion for estimation of myocardial regional strain rate. Yasunori Honjo (Department of Electronic Engineering, Graduate School of Engineering, Tohoku University, 6-6-05 Aramaki-aza-Aoba, Aoba-ku, 980-8579 Sendai, Japan, honjo@us.ecei.tohoku.ac.jp), Hideyuki Hasegawa (Department of Electronic Engineering, Graduate School of Engineering, Tohoku University, 6-6-05 Aramaki-aza-Aoba, Aoba-ku, 980-8579 Sendai, Japan, hasegawa@us.ecei.tohoku.ac.jp), Hiroshi Kanai (Department of Electronic Engineering, Graduate School of Engineering, Tohoku University, 6-6-05 Aramaki-aza-Aoba, Aoba-ku, 980-8579 Sendai, Japan, hasegawa@us.ecei.tohoku.ac.jp)

Methods for imaging of strain rate in the heart wall are useful for quantitative evaluation of regional heart function. We developed a method which can accurately measure the heart wall motion along an ultrasonic beam based on phase changes in rf echoes. However, there are some components in the wall motion which are not along each ultrasonic beam. Therefore, the measurement of motion in the direction perpendicular (lateral) to the beam has been required in addition to that in the axial direction, but some unsolved problems remain in estimation of lateral motion of the wall. In this study, two-dimensional displacement was estimated by 2D cross-correlation between rf echoes. Important parameters, the sizes of a region-of-interest and search region, which determine tracking accuracy, were adaptively op-

timized by referring to instantaneous wall velocities, in the respective cardiac phases. The correlation coefficient between the lateral displacement estimated by the 2D tracking with optimized parameters in longitudinal-axis view and axial displacement in apical view (corresponding to lateral displacement in longitudinal-axis view) separately and accurately estimated by the 1D phase-based method was 0.93. These results show possibility of this method for accurate measurement of two-dimensional heart motion to assess the regional myocardial strain rate.

5aBBd3. Flow-mediated change in viscoelasticity of radial arterial wall measured by 22-MHz ultrasound. Kazuki Ikeshita (Department of Electronic Engineering, Graduate School of Engineering, Tohoku University, 6-6-05 Aramaki-aza-Aoba, Aoba-ku, 980-8579 Sendai, Japan, ikeshita@us.ecei.tohoku.ac.jp), Hideyuki Hasegawa (Department of Electronic Engineering, Graduate School of Engineering, Tohoku University, 6-6-05 Aramaki-aza-Aoba, Aoba-ku, 980-8579 Sendai, Japan, hasegawa@us.ecei.tohoku.ac.jp), Hiroshi Kanai (Department of Electronic Engineering, Graduate School of Engineering, Tohoku University, 6-6-05 Aramaki-aza-Aoba, Aoba-ku, 980-8579 Sendai, Japan, hasegawa@us.ecei.tohoku.ac.jp)

The endothelial dysfunction is considered to be an initial step of atherosclerosis. Moreover, it was reported that the smooth muscle, which constructs the media of the artery, changes its characteristics due to early-stage atherosclerosis. Therefore, it is essential to develop a method for assessing the regional endothelial function and mechanical property of the arterial wall. There is an ultrasound-based conventional technique to measure the change in inner diameter of the brachial artery caused by flow-mediated dilation (FMD) after release of avascularization. In this study, the transient change in the mechanical property of the arterial wall was further revealed by measuring the stress-strain relationship during each heartbeat. For this measurement, the minute change in thickness (strain) of the radial artery was measured using the ultrasonic phased tracking method, together with the waveform of blood pressure (stress) which was continuously measured at the radial artery. From in vivo experiments, it has been founded the slope of the stress-strain hysteresis loop decreases due to FMD and the area increase depends on the ratio of elastic modulus and loss modulus (depends on viscosity). These results show a potential of the proposed method for thorough analysis of the transient change in viscoelasticity due to FMD.

5aBBd4. Experimental investigation of the scattering of sound by solid spheres in a liquid. Jason Bach (Georgia Tech Lorraine - G.W. Woodruff School of ME, UMI Georgia Tech - CNRS 2958, 2 rue Marconi, 57070 Metz, France, jsbach82@yahoo.com), Nico F. Declercq (Georgia Tech Lorraine - G.W. Woodruff School of ME, UMI Georgia Tech - CNRS 2958, 2 rue Marconi, 57070 Metz, France, nico.declercq@me.gatech.edu), David Ku (Georgia Tech Lorraine - G.W. Woodruff School of ME, UMI Georgia Tech - CNRS 2958, 2 rue Marconi, 57070 Metz, France, david.ku@me.gatech.edu)

The framework of this investigation is the characterization of spheres in a liquid by means of ultrasound. Experiments are performed to study the effectiveness of the use of bounded ultrasonic pulses in single transmission and in double through transmission to characterize size and shape of spheres. Special attention is paid to the influence of the beam width and frequency in comparison with the size of the sphere. The research is performed by means of a new generation polar c-scan apparatus. In a first step the interaction of sound with a single sphere is studied. In a second step two spheres are studied where one sphere crosses the sound path through the other sphere. Limitations for detection and characterization of spheres depending on their relative position and on the characteristics of the applied ultrasonic pulse are described in detail. The research is performed in the framework of the use of ultrasound for biomedical applications.

FRIDAY MORNING, 4 JULY 2008 P3-B, LEVEL, 9:40 TO 11:20 A.M.

Session 5aBBe

Biomedical Ultrasound/Bioresponse to Vibration: Biomedical Applications of Acoustic Radiation Force I (Poster Session)

Mostafa Fatemi, Cochair
Dep. of Physiology and Biomed. Eng., Mayo Clinic College of Medicine

Mathias Fink, Cochair
Laboratoire Ondes et Acoustique

All posters will be on display from 9:40 a.m. to 11:20 a.m. To allow contributors an opportunity to see other posters, contributors of odd-numbered papers will be at their posters from 9:40 a.m. to 10:30 a.m. and contributors of even-numbered papers will be at their posters from 10:30 a.m. to 11:20 a.m.

Contributed Papers

5aBBe1. Comparative study of vibro-acoustography and B-mode ultrasound in prostate imaging. Azra Alizad (Dept. of Physiology and Biomed. Eng., Mayo Clinic College of Medicine, 200 First Street SW, Rochester, MN 55905, USA, aza@mayo.edu), Farid Mitri (Dept. of Physiology and Biomed. Eng., Mayo Clinic College of Medicine, 200 First Street SW, Rochester, MN 55905, USA, mitri.farid@mayo.edu), Brian Davis (Dep. of Radiation Oncology, Mayo Clinic College of Medicine, 200 1st St. SW, Rochester, MN 55905, USA, davis.brian@mayo.edu), James Greenleaf (Dept. of Physiology and Biomed. Eng., Mayo Clinic College of Medicine, 200 First Street SW, Rochester, MN 55905, USA, jfg@mayo.edu), Mostafa Fatemi (Dept. of Physiology and Biomed. Eng., Mayo Clinic College of Medicine, 200 First Street SW, Rochester, MN 55905, USA, fatemi@mayo.edu)

Vibro-acoustography (VA) is an imaging modality that uses the radiation force of ultrasound to vibrate tissue at a low frequency and records the resulting acoustic field to produce an image that is represents object characteristics at both ultrasound as well as low (audio) frequencies. Currently, B-mode ultrasound is used for prostate imaging. This imaging method has some limitations, including the speckle noise, which limit its ability in detection of lesions and calcifications. The purpose of this study is to explore the potentials of VA for prostate imaging. VA, B-mode ultrasound, and radiography were performed on 12 excised human prostate samples and the

resulting images were compared. VA system parameters were, center frequency 3 MHz, $\Delta f = 50$ kHz, image area 5×5 cm, pixel size 0.2×0.2 mm. Images evaluated in terms of visibility of anatomical and pathological structures and contrast. Results showed that prostate anatomical structures, mass lesions, and calcifications were visible in the VA images taken at different depths, and VA image quality was superior to B-mode. VA images exhibited significant contrast between the central and peripheral zones with enhanced borders. It is concluded that, with further development, VA may become suitable modality for in prostate imaging.

5aBBe2. Acoustic radiation forces in monitoring of milk composition. Diana Priev (Hebrew University, HaGomeh 16/4, 98537 Maale Adumim, Israel, diana.priev@mail.huji.ac.il), Victor Ponomarev (NDT Instruments Ltd, HaGomeh 16/4, 98537 Maale Adumim, Israel, viktora @aaanet.ru), Aba Priev (Hebrew University, Hadassah Medical School, Ein Kerem, 91120 Jerusalem, Israel, abbap@ekmd.huji.ac.il)

High sensitivity of ultrasonic velocity and attenuation to composition and state of milk and other liquid food products is now well established. Unfortunately, existing devices include measurements of the acoustic properties of milk at different temperatures and therefore require waiting for temperature equilibration of the milk when the sample is heated or cooled and cannot be used for real-time monitoring. In this paper ultrasonic particles analyzer of NDT Instruments, AcoMilk-02, used for continuous monitoring of fat globules and somatic cells of raw milk in computerized milking station of cowsheds has been described. This device is based on high intensity standing wave for preliminary separation and concentration of the fat globules and somatic cells by the acoustic radiation forces and low intensity standing wave to measure their content. Testing of analyzer was carried out on 5 cows during one-month period. It was found that milk production level, stage of lactation, and outside temperature have significant influence on the milk composition. Continuous monitoring of milk fat and somatic cells count that typically have high day-to-day variation, provide a much-needed tool for dairy management and for veterinary diagnostic purposes.

5aBBe3. Ultrasound-enhanced latex immunoassay of pathogens in water. Danny Bavli (Hebrew University, Hadassah Medical School, Ein Kerem, 91120 Jerusalem, Israel, danny.bavli@mail.huji.ac.il), Yechezkel Barenholz (Hebrew University, Hadassah Medical School, Ein Kerem, 91120 Jerusalem, Israel, yb@cc.huji.ac.il), Noam Emanuel (Hebrew University, Hadassah Medical School, Ein Kerem, 91120 Jerusalem, Israel, noam.emanuel@mail.huji.ac.il), Victor Ponomarev (NDT Instruments Ltd, HaGomeh 16/4, 98537 Maale Adumim, Israel, viktora@aaanet.ru),Aba Priev (Hebrew University, Hadassah Medical School, Ein Kerem, 91120 Jerusalem, Israel, abbap@ekmd.huji.ac.il)

Real-time knowledge of contaminants in water is an essential component of any potable water security system. Latex immunoassay is the basic technique in rapid identification of pathogens. We used acoustic radiation to accelerate the latex immunoassay and to bring about separation between free and bound antigen (rotavirus SA-11) in less than one minute. The ultrasonic cylindrical standing-wave device of NDT Instruments, UltraAssay 101, creates areas of maximum and minimum potential energy (nodes). Acoustic radiation forces acting on the pathogens drive them directly to the central node. In this manner, antibody-antigen complexes accumulate in the nodes in 40-60 sec. The nonbound antibodies are washed out of the separation area by the buffer flow. The forces responsible for separation of particles in the UltraAssay 101 depend on the frequency of the standing-wave resonator and on the density, compressibility and size of the immune complexes. Additionally, UltraAssay 101 is able to directly monitor water salinity, turbidity and specific gravity.

5aBBe4. Wave propagation modes and arterial stiffness. Miguel Bernal (Dept. of Physiology and Biomed. Eng., Mayo Clinic College of Medicine, 200 First Street SW, Rochester, MN 55905, USA, bernalrestrepo.miguel@mayo.edu), James Greenleaf (Dept. of Physiology and Biomed. Eng., Mayo Clinic College of Medicine, 200 First Street SW, Rochester, MN 55905, USA, jfg@mayo.edu)

Arterial elasticity is an independent predictor of cardiovascular disease and mortality. Measurment of waves in thin shells can be used to estimate the circumferential and the longitudinal elastic moduli. Latex tubes and excised pig arteries were used as isotropic and anisotropic models. Waves were generated using focused ultrasound (1 ms, 3 MHz) in different locations of the wall. The modes of propagation of the waves were detected with a laser vibrometer or an ultrasound pulse echo tool while the excitation was moved known distances. Bending waves were predominant when exciting in the center of the wall, while a combination of torsion and bending waves resulted from exciting off center. Wave speeds of 15 m/s and 5 m/s respectively, were measured for the bending waves. Using the Moens-Korteweg equation, values of 1.1 and 0.350 MPa were found for the longitudinal elastic modulus in the tube and artery respectively. Generation of different modes in the tubes and arteries is possible using focused ultrasound. Elastic components of the tubes and vessels in the longitudinal and the circumferential direction can be estimated from the speed of propagation and the frequency of the bending and the torsional waves.

Session 5aBBf

Biomedical Ultrasound/Bioresponse to Vibration: Biomedical Applications of Acoustic Radiation Force II

Mostafa Fatemi, Cochair
Dep. of Physiology and Biomed. Eng., Mayo Clinic College of Medicine, 200 First Street SW, Rochester, MN 55905, USA

Mathias Fink, Cochair
Laboratoire Ondes et Acoustique, ESPCI, Université Paris 7, CNRS, 10 rue Vauquelin, Paris, 75005, France

Invited Paper

11:00

5aBBf1. Biomedical applications of radiation force generated in standing ultrasonic waves. Lev Ostrovsky (Zel Technol./Univ. of Colorado, 325 Broadway, R/PSD99, Boulder, CO 80305, USA, Lev.A.Ostrovsky@noaa.gov), Armen Sarvazyan (Artann Laboratories, 1753 Linvale-Harbourton, Lambertville, NJ 08350, USA, armen@artannlabs.com)

This talk presents an overview of physical basis for the action of acoustic radiation force on particles in standing waves in relation to biomedical applications. The effect itself is known since the 19th century (Kundt, 1974) and its biomedical significance was demonstrated in 1971 by Dyson et al. However, despite a long history, extensive studies of particle behavior in standing ultrasonic waves have started only during the last decade due to numerous emerging biomedical applications. The range of currently explored applications is broad: targeted drug and gene delivery, increasing sensitivity of biosensors and immunochemical tests, manipulating cells in suspensions, microstirring, and others. The presentation will focus on theoretical analysis and applications of radiation force acting on particles and bubbles in the standing ultrasonic fields. Dynamics of particle motion induced by ultrasonic radiation force as a function of frequency, intensity, and other variables will be considered. The principal difference in interaction of ultrasonic standing wave field with solid particles and with bubbles due to resonant properties and high compressibility of the latter will be quantitatively analyzed. Several specific biomedical applications of the analyzed phenomena will be discussed.

Contributed Papers

11:20

5aBBf2. Radiation force on spheres in acoustic beams and related aspects of scattering. Philip L. Marston (Washington State University, Physics and Astronomy Department, Pullman, WA 99164-2814, USA, marston@wsu.edu), David B. Thiessen (Washington State University, Physics and Astronomy Department, Pullman, WA 99164-2814, USA, thiessen@wsu.edu)

The close connection between the acoustic radiation force on objects in fluids and the angular distribution of the farfield scattering is especially useful in cases where dissipative effects are weak in the surrounding fluid. This connection also applies to objects illuminated by acoustic beams and has been used to extend the analysis of scattering by spheres in Bessel beams [P. L. Marston, J. Acoust. Soc. Am. **121**, 753-757 (2007); **122**, 247-252 (2007)] to the evaluation of the radiation force on spheres [P. L. Marston, J. Acoust. Soc. Am. **120**, 3518-3524 (2006); **122**, 3162-3165 (2007)]. The quantitative predictions (which include situations of negative radiation force) have been verified by nearfield analysis of the radiation force using the finite element method. We have also examined the radiation force on a sphere for a special case of co-propagating Bessel beams having unequal beam parameters. The scattering of a higher order Bessel beam by a sphere placed on the axis has also been analyzed. The backscattering in that case vanishes in agreement with prior predictions [B. T. Hefner and P. L. Marston, J. Acoust. Soc. Am. **106**, 3313-3316 (1999)] for a general class of helicoidal acoustic beams. [Supported by NASA and ONR.]

11:40

5aBBf3. Modeling the modulated acoustic radiation force distribution in a viscoelastic medium driven by a spherically focused ultrasound transducer. Faik Can Meral (University of Illinois, 842 West Taylor St. MC 251, Chicago, IL 60607, USA, fmeral2@uic.edu), Thomas J. Royston (University of Illinois at Chicago, 842 W. Taylor St. ERF 1072, Chicago, IL 60607, USA, troyston@uic.edu),Richard L. Magin (University of Illinois, 842 West Taylor St. MC 251, Chicago, IL 60607, USA, rmagin@uic.edu)

Acoustic radiation force created by focused ultrasound transducers is gaining great interest in medical diagnosis. This study aims to clarify the acoustic power delivery by means of a modulated focused transducer and to predict the performance of such systems. A spherical-cap shaped transducer, made of piezoelectric material, is used to create ultrasonic waves at a focal point. Different modulation methods, given in the literature and reviewed here, are available for creating a concentrated alternating force due to the acoustic radiation pressure. The relationship between the voltage input to the piezoelectric transducer and its resulting mechanical deformation is examined using a finite element model (FEM) for high frequency harmonic excitation (3 - 10 MHz). The oscillating surface of the transducer drives the contacting media, which exerts an acoustic load on the transducer that is also considered in the FE analysis. Also, the motion of resulting acoustic waves in a lossy medium is studied for a more accurate estimation of the induced force distribution and energy dissipation within the medium. Ultimately, the intention of this work is to relate the electrical power input to the transducer to the resulting dynamic force generated in the coupling medium. [Research supported by NIH Grant # EB004885.]

12:00

5aBBf4. Biomedical applications of acoustic radiation force based on somatosensory reception. Leonid R. Gavrilov (N.N. Andreyev Acoustics Institute, 4, Shvernik Street, 117036 Moscow, Russian Federation, gavrilov@akin.ru), Jeffrey W. Hand (Imperial College London, Hammersmith Campus, Ducane Road, W12 0NN London, UK,

j.hand@imperial.ac.uk),Efim M. Tsirulnikov(I.M. Sechenov Institute of Evolutionary Physiology and Biochemistry, 44 Torez ave., 194223 St. Petersburg, Russian Federation, tsiruln@iephb.ru)

We have previously shown that short pulses of focused ultrasound may be used to stimulate locally receptor neural structures and thereby induce sensations that humans can perceive through the skin (for example tactile, warmth and cold, tickling, pain, etc.). Furthermore, ultrasound modulated by sound signals (tone, speech, music, etc.) can induce sound sensations corresponding to the nature of the modulation in persons with normal hearing. The mechanism underlying these effects that have been used in clinical diagnostic practice is related to the radiation force. We also showed recently that the phenomenon of the radiation force could be used in perspective robotic systems, sensors, and automated control systems, based on the use of tactile sensations in the human-machine interface, as well as in devices that may allow blind and visually impaired persons to perceive textual information presented on a tactile display. The research was supported by INTAS (05-1000008-7841) and RFBR (06-02-16079).

Invited Paper

12:20

5aBBf5. Ultrasound stimulated vibrometry for measuring tissue properties. James Greenleaf (Dept. of Physiology and Biomed. Eng., Mayo Clinic College of Medicine, 200 First Street SW, Rochester, MN 55905, USA, jfg@mayo.edu), Shigao Chen (Dept. of Physiology and Biomed. Eng., Mayo Clinic College of Medicine, 200 First Street SW, Rochester, MN 55905, USA, chen.shigao@mayo.edu), Xiaoming Zhang (Dept. of Physiology and Biomed. Eng., Mayo Clinic College of Medicine, 200 First Street SW, Rochester, MN 55905, USA, Zhang.xiaoming@mayo.edu)

Harmonic or pulsed radiation pressure and subsequent measurement of the tissue response can be used to accurately quantitatively measure fundamental material properties of tissue. The measurement of shear wave dispersion can be used to estimate elastic shear moduli of tissue using an appropriate model. Fundamental model free properties such as complex modulus can also be measured. Ultrasound radiation pressure is used to induce free propagating shear waves. The measurable properties of the shear waves such as speed are sensitive to only the local material properties of the tissue under certain circumstances. A model relating the shear wave speed as a function of frequency is related to the elastic and viscous moduli within small regions of tissue according to, for instance, the Voigt model. Shear and elastic moduli in tissue are measured with high accuracy and precision given appropriate models of wave propagation within the geometry of the tissue. Complex modulus in liver of live pig and other tissues have been made. Careful use of shear wave propagation and subsequent measurements can provide fundamental quantitative measurements of tissue mechanical properties if models are accurate. An application of this method is the noninvasive measurement of liver stiffness as a surrogate for fibrosis.

12:40-2:00 Lunch Break

Invited Papers

2:00

5aBBf6. Supersonic shear imaging: a multiwave imaging example. Mathias Fink (Laboratoire Ondes et Acoustique, ESPCI, Université Paris 7, CNRS, 10 rue Vauquelin, 75005 Paris, France, mathias.fink@espci.fr), Mickael Tanter (Laboratoire Ondes et Acoustique, ESPCI, Université Paris 7, CNRS, 10 rue Vauquelin, 75005 Paris, France, michael.tanter@espci.fr), Jeremy Bercoff (Supersonic Imagine, 13857 Aix en Provence, France, jeremy.bercoff@supersonicimagine.fr)

A new imaging method that relies on the simultaneous use of both a low frequency shear wave and a high frequency ultrasound is described. The shear waves have typically centimetric wavelengths and they propagated at low velocity in tissues. They are progressively distorted by the viscoelastic inhomogeneities of encountered tissues. When coupled to an ultrafast ultrasound scanner (5000 images per second), it allows for the follow up of the propagation of these waves with a millimetric resolution over a large zone of interest. From the spatiotemporal evolution of the shear displacement fields, inversion algorithms are used to recover the shear modulus and viscosity map with submillimetric resolution. These techniques are no more diffraction limited because, the near field of the transient waves is directly observed. In this multivave technique, the shear wave gives the contrast while the ultrasonic wave gives the spatial resolution. Shear waves are generated leveraging the innovative use of the ultrasonic radiation force generated by an ultrasound probe. A supersonic shear source is remotely created in tissues. Such a moving source creates two plane shear waves propagating in a Mach cone. In vivo images obtained in breast, liver, muscles will be presented that show the great interest of this quantitative imaging technique.

2:20

5aBBf7. Image quality assessment: Vibro-acoustography versus B-mode. Mostafa Fatemi (Dept. of Physiology and Biomed. Eng., Mayo Clinic College of Medicine, 200 First Street SW, Rochester, MN 55905, USA, fatemi@mayo.edu)

Vibro-acoustography (VA) is based on conversion of ultrasound energy from high frequency to a low frequency. This conversion, which results from the nonlinear nature of wave equation, gives VA some key advantages over linear ultrasound imaging such as B-mode. Two key features of VA are analyzed: lack of speckle noise, and angle-independency, which is the ability of imaging specular reflectors regardless of their orientation. Both the speckle noise and angle dependency are major artifacts in B-mode. Lack of speckle noise results from the fact that VA images are constructed from the low frequency acoustic signal. Using an acoustical model, it is shown that the random scatterers within soft tissue do not promote speckle noise in VA as they do in B-mode; thus VA generally produces high contrast images. Angle-independency results from the broad beam pattern of the low-frequency acoustic field. A model is constructed describing the amplitude of the acoustic signal versus object orientation angle. It is shown that the signal amplitude is relatively insensitive to object orientation; thus VA may be suitable for imaging specular objects such as implants. It is concluded that VA may be advantageous in applications where speckle noise and angle dependency are of concern.

2:40

5aBBf8. In vivo feasibility of local harmonic motion imaging and its use for thermal surgery control. Kullervo Hynynen (University of Toronto, Sunnybrook Health Sciences Centre, Suite S6 65b, 2075 Bayview Ave, Toronto, ON M4N 3M5, Canada, khynynen@sri.utoronto.ca), Laura Curiel (University of Toronto, Sunnybrook Health Sciences Centre, Suite S6 65b, 2075 Bayview Ave, Toronto, ON M4N 3M5, Canada, lcuriel@sri.utoronto.ca), Rajiv Chopra (University of Toronto, Sunnybrook Health Sciences Centre, Suite S6 65b, 2075 Bayview Ave, Toronto, ON M4N 3M5, Canada, chopra@sri.utoronto.ca)

A local harmonic motion can be generated within the tissues by the periodic induction of radiation force using a focused ultrasound (FUS) transducer. Tissue motion can then be tracked by collecting rf signals during the excitation using a separate transducer. Finally, displacement estimates can be obtained by cross-correlating the collected rf signals. The characteristics of the induced LHM depend on the local elastic properties of the tissues making it an attractive tool for imaging and therapy control applications. LHM measurements have been obtained in vivo on rabbit muscle and it was observed that the amplitude of the motion was significantly reduced after coagulation. LHM was successfully used to spatially detect the presence of the coagulation lesions within the tissues as a drop in LHM amplitude. It was also possible to detect the location of an implanted VX2 tumor when a spatial scan was performed as the LHM amplitude was lower inside the tumor because of an increased stiffness. Measurements of LHM during tissue heating using FUS reflected the changes in stiffness and revealed the apparition of coagulation showing the potential of these measurements as an alternative control for the FUS exposure. [Work supported by NIH Grant R33 CA102884 and the Canadian Research Chair Program.]

3:00

5aBBf9. Impulsive acoustic radiation force: imaging approaches and clinical applications. Kathryn Nightingale (Biomedical Engineering, Duke Univ., 136 Hudson Hall, Durham, NC 27708, USA, kathy.nightingale@duke.edu), Mark Palmeri (Duke University, P.O. Box 90281, Durham, NC 27708, USA, mlp6@duke.edu), Liang Zhai (Duke University, P.O. Box 90281, Durham, NC 27708, USA, liang.zhai@duke.edu), Kristin Frinkley (Biomedical Engineering, Duke Univ., 136 Hudson Hall, Durham, NC 27708, USA, kdf2@duke.edu), Michael Wang (Duke University, P.O. Box 90281, Durham, NC 27708, USA, michael.h.wang@duke.edu), Jeremy Dahl (Duke University, P.O. Box 90281, Durham, NC 27708, USA, jjd@duke.edu), Brian Fahey (Duke University, P.O. Box 90281, Durham, NC 27708, USA, bjf8@duke.edu), Stephen Hsu (Duke University, P.O. Box 90281, Durham, NC 27708, USA, sjh6@duke.edu), David Bradway (Duke University, P.O. Box 90281, Durham, NC 27708, USA, david.bradway@duke.edu), Gregg Trahey (Duke University, P.O. Box 90281, Durham, NC 27708, USA, gregg.trahey@duke.edu)

Focused acoustic radiation force can be used to locally mechanically excite tissue, and the tissue response can be monitored with conventional ultrasonic displacement estimation methods. Many groups are currently exploring the potential for radiation force based methods to derive information about tissue stiffness associated with different pathologies. These techniques can be implemented on a modified diagnostic ultrasound scanner, using the same transducer for both generating the radiation force excitation and monitoring the tissue response. Multiple locations within an imaging field of view can be interrogated sequentially, by electronically controlling the push and track apertures and beam locations. A variety of data processing and imaging approaches are under investigation. Images are generated of the tissue displacement magnitude within the region of excitation at a given time after radiation force application. These images portray relative differences in tissue stiffness, and provide interesting structural information that is well correlated with, and often exhibits improved contrast over, matched B-mode images. Methods for quantifying tissue stiffness through monitoring shear wave propagation, as originally proposed by Sarvazyan, are also under investigation. Results from ongoing clinical studies using these methods in a variety of organs (e.g., liver, prostate, breast, and heart) will be presented.

3:20

5aBBf10. Experimental validation of the amplitude-modulated harmonic motion imaging for tissues stiffness estimation. Caroline Maleke (Columbia University Dept. of Biomedical Engineering, 622 W 168th SSt, PH-7, Room 200 Center, New York, NY 10032, USA, cm2243@columbia.edu), Jianwen Luo (Columbia University Dept. of Biomedical Engineering, 622 W 168th St, PH-7, Room 200 Center, New York, NY 10032, USA, jl2767@columbia.edu), Viktor Gamarnik (Columbia University Dept of Biomedical Engineering, 622 W 168th st, PH-7, room 200 center, New York, NY 10032, USA, vg2125@columbia.edu), Elisa Konofagou (Dept. of Biomedical Engineering, Columbia Univ., 351 Engineering Terrace MC 8904, 1210 Amsterdam Ave., New York, NY 10027, USA, ek2191@columbia.edu)

It has been previously shown that amplitude-modulated harmonic motion imaging (AM-HMI) has the capability of induce and image tissue displacement during the application of an oscillatory radiation force. Here, we aim at validating theoretical HMI findings with experimental results on similar phantoms. A finite-element-method (FEM) was first used to model a dynamic response of phantoms with inclusions at different stiffnesses and sizes. The FEM and experimental results were compared and used to describe the behavior of the locally displaced tissue. The radiation force was generated by a 4.68 MHz FUS transducer modulated at 50 Hz with acoustic pressure levels varied between 1.2 and 4 MPa. A 7.5 MHz pulse-echo transducer was placed through the center of the FUS transducer and used to image the displaced tissue. A 1D-cross-correlation method on successive RF signals was used to estimate the axial-displacement. The FEM and experimental results displayed good agreement in displacement patterns, i.e., the highest localized displacement occurred at the focus and was symmetrically distributed. In addition, mechanical testing was performed to estimate the phantom-gels moduli. A linear relationship between HMI displacements and tissue Young's moduli was established within the range of 13-to-50kPa. Further studies will involve the implementation of 1D linear-array transducer for full-view imaging.

3:40

5aBBf11. An integrated system to deliver impulsive radiation force and to image induced transient strain for monitoring focused ultrasound surgery. Gearoid Berry (Institute of Cancer Research, 15 Cotswold Road, Belmont, Sutton, SM2 5NG Surrey, UK, gearoid.berry@icr.ac.uk), Jeff Bamber (Institute of Cancer Research, 15 Cotswold Road, Belmont, Sutton, SM2 5NG Surrey, UK, jeff.bamber@icr.ac.uk), Yixin Ma (Institute of Cancer Research, 15 Cotswold Road, SM2 5NG Sutton, UK, yixin.ma@icr.ac.uk), Ian Rivens (Institute of Cancer Research, 15 Cotswold Road, SM2 5NG Sutton, UK, ian.rivens@icr.ac.uk), Gail Ter Haar (Institute of Cancer Research, 15 Cotswold Road, Belmont, Sutton, SM2 5NG Surrey, UK, gail.terhaar@icr.ac.uk)

Thermal coagulation of tissue causes an approximate three-fold increase in stiffness, which can be easily detected by various elasticity imaging methods. Advantages have been reported, for application to breast cancer diagnosis, of an elasticity imaging method that applies a highly localised transient stress deep within the tissue using a low frequency focused ultrasound radiation force impulse, and uses relatively high frequency echo imaging to measure the transient strain generated in the tissue placed between the transducers. In this paper we describe a new system that implements this concept using a focused ultrasound surgical transducer to apply the transient ($<$10 ms) load, synchronized by a customised field programmable gate array to a Zonare C5-2 probe to image the strain. Both transducers are on the same side of the tissue and locked together for scanning to create transient strain elastograms. Performance measurements, obtained using gelatine phantoms and ex vivo thermally ablated liver tissue, indicate an elastogram spatial resolution of 2 mm, and acceptable contrast for detecting regions of thermally coagulated tissue. An advantage of this configuration is that it may be easily integrated into focused ultrasound therapy.

4:00-4:20 Break

4:20

5aBBf12. Ultrasonic imaging of displacements inside objects induced by continuously applied fluctuating acoustic radiation forces. Hideyuki Hasegawa (Department of Electronic Engineering, Graduate School of Engineering, Tohoku University, 6-6-05 Aramaki-aza-Aoba, Aoba-ku, 980-8579 Sendai, Japan, hasegawa@us.ecei.tohoku.ac.jp), Yoshitaka Odagiri (Department of Electronic Engineering, Graduate School of Engineering, Tohoku University, 6-6-05 Aramaki-aza-Aoba, Aoba-ku, 980-8579 Sendai, Japan, hasegawa@us.ecei.tohoku.ac.jp), Hiroshi Kanai (Department of Electronic Engineering, Graduate School of Engineering, Tohoku University, 6-6-05 Aramaki-aza-Aoba, Aoba-ku, 980-8579 Sendai, Japan, hasegawa@us.ecei.tohoku.ac.jp)

Recently, many studies are conducted to measure the response of soft tissue to applied ultrasonic acoustic radiation force. However, the change in position of a target is dominantly induced by a radiation force applied from only one direction, particularly when the target is much harder than surrounding medium. In this case, elasticity of the target cannot be evaluated because the change in position does not relate to target's elasticity. In this study, 1-MHz continuous-wave ultrasound whose envelope fluctuated at 5 Hz was used to apply the radiation force fluctuating at 5 Hz. By applying two radiation forces from two opposite horizontal directions, the object would be effectively deformed (compressed) in the horizontal direction and vertically expanded due to its incompressibility. Resultant vertical displacements were measured by ultrasonic pulses at 22 MHz in center frequency which can be easily separated from 1-MHz ultrasound by filtering. In in vitro experiments using chicken muscle and porcine liver, displacements at 5 Hz were clearly imaged. Amplitudes of displacements in liver are similar to those in muscle, whereas applied radiation force was one-fifth. Furthermore, shear wave propagating in liver was clearly visualized because liver was much softer than muscle, i.e., the wavelength was much shorter.

4:40

5aBBf13. Viscoelastic properties of myocardium tissue with surface and shear wave methods. Xiaoming Zhang (Dep. of Physiology and Biomed. Eng., Mayo Clinic College of Medicine, 200 First Street SW, Rochester, MN 55905, USA, Zhang.xiaoming@mayo.edu), Shigao Chen (Dep. of Physiology and Biomed. Eng., Mayo Clinic College of Medicine, 200 First Street SW, Rochester, MN 55905, USA, chen.shigao@mayo.edu), Matthew Urban (Dep. of Physiology and Biomed. Eng., Mayo Clinic College of Medicine, 200 First Street SW, Rochester, MN 55905, USA, urban.matthew@mayo.edu), Randall Kinnick (Dep. of Physiology and Biomed. Eng., Mayo Clinic College of Medicine, 200 First Street SW, Rochester, MN 55905, USA, kinnick.randall@mayo.edu), James Greenleaf (Dep. of Physiology and Biomed. Eng., Mayo Clinic College of Medicine, 200 First Street SW, Rochester, MN 55905, USA, jfg@mayo.edu)

Considerable interest in the elastic properties of soft tissue has increased in medicine due to their clinical relevance for monitoring various diseases as well as a biomarker for cancer. A recent emerging field is the use of acoustic radiation force for imaging and estimating the elastic properties of tissue. Newly developed imaging modalities include shear wave elasticity imaging, supersonic shear wave imaging, acoustic radiation force impulse imaging, and vibro-acoustography. In these new methods, the shear wave is used to estimate the elasticity of tissue. We have developed a novel surface wave method for noninvasively estimating the elasticity of tissue [X. Zhang et al., J. Acoust. Soc. Am., **122**, 2522-2525 (2007)]. In this method, a localized ultrasound radiation force is remotely and noninvasively applied inside the tissue. The surface wave speed is used to estimate the elasticity of tissue. This method has been further developed and applied to estimate the viscoelasticity of animal myocardium tissue. In this abstract, we report our recent results of in vitro studies on animal myocardium tissue. Both the surface wave and shear wave are measured and analyzed. Noninvasive characterization of viscoelastic properties of myocardium tissue may be a very important tool for assessing heart function.

Invited Papers

5:00

5aBBf14. Use of radiation force for enhancing efficacy of molecular targeted ultrasound contrast agents - in vitro and in vivo. John A. Hossack (University of Virginia, Biomedical Engineering, MR5, 415 Lane Rd, Charlottesville, VA VA 22908-0759, USA, jh7fj@virginia.edu)

Intravenously injected modified ultrasound microbubbles possessing molecule specific targeting ligands hold significant promise as a method for "molecular imaging." Unfortunately, although microbubbles can achieve specific adhesion in regions of vascular pathology, the method breaks down in high blood flow regions where the bond formation process is more problematic. I present results indicating that acoustic radiation does increase the specific targeted adhesion of microbubbles by pushing the bubbles towards the periphery of a vessel. During in vitro studies, radiation force enhanced microbubble adhesion up to 60-fold. Microbubble adhesion is observed to increase approximately with the square of acoustic pressure between 25 and 122 kPa, but decreases at higher pressures as the bubbles rupture. Our in vivo studies involved using intravital microscopy to assess the adherence of P-selectin targeted microbubbles in the mouse cremaster microcirculation and femoral vessels. Acoustic radiation force enhanced microbubble retention four-fold in cremaster venules and in the femoral vein. A 20-fold enhancement was observed in the femoral artery. I discuss the potential for derivatives of the technique to provide molecular targeted therapeutic contribution.

5:20

5aBBf15. Assessment of tissue viscoelasticity using acoustically interrogated laser-induced microbubble. Stanislav Y. Emelianov (Applied Research Laboratories, The University of Texas, P.O. Box 8029, Austin, TX 78713-8029, USA, emelian@mail.utexas.edu), Salavat R. Aglyamov (Applied Research Laboratories, The University of Texas, P.O. Box 8029, Austin, TX 78713-8029, USA, aglyamov@mail.utexas.edu), Andrei B. Karpiouk (Applied Research Laboratories, The University of Texas, P.O. Box 8029, Austin, TX 78713-8029, USA, Andrei.Karpiouk@engr.utexas.edu), Yurii A. Ilinskii (Applied Research Laboratories, The University of Texas, P.O. Box 8029, Austin, TX 78713-8029, USA, yura@arlut.utexas.edu), Evgenia A. Zabolostkaya (Applied Research Laboratories, The University of Texas, P.O. Box 8029, Austin, TX 78713-8029, USA, zhenia@arlut.utexas.edu)

Lasers are used in many biomedical and clinical applications, ranging from diagnosis to therapy. In eye microsurgery, for example, a pulsed laser beam produces a localized surgical effect through the formation of a cavitation microbubble as a result of tissue photodisruption occurring in the focal zone. However, to insure successful presurgical planning, surgical procedure, and postoperative stages of pathology treatment, the mechanical properties of the tissue must be analyzed before selective laser intervention. Since microbubbles are already produced during laser surgery, we have developed an integrated approach utilizing these laser-induced microbubbles as reporters of tissue viscoelasticity. Specifically, we have derived a general model of gas bubble dynamics in viscoelastic media to describe both translation and oscillations of the microbubble exposed to the acoustic radiation force. Furthermore, an ultrasound method based on temporal measurement of passive acoustic emission from cavity during laser-tissue interaction and simultaneous active pulse-echo ultrasound probing of the cavitation bubble was developed to detect and characterize the laser-induced microbubbles. The results of our theoretical, numerical, and experimental studies demonstrate that measurements of gas bubble behavior exposed to acoustic radiation force can be used to assess the mechanical properties of the surrounding tissue.

Contributed Papers

5:40

5aBBf16. Acoustic radiation force manipulation of PC12 cells In vitro. Robert Muratore (Frederic L. Lizzi Center for Biomedical Engineering, Riverside Research Institute, 156 William St. Fl 9, New York, NY 10038-2609, USA, muratore@rrinyc.org), Erin Szulman (Frederic L. Lizzi Center for Biomedical Engineering, Riverside Research Institute, 156 William St. Fl 9, New York, NY 10038-2609, USA, erin.szul@gmail.com), Nina Xu (Dept. of Biomedical Engineering, Columbia Univ., 351 Engineering Terrace MC 8904, 1210 Amsterdam Ave., New York, NY 10027, USA, xu.nina@gmail.com), Melissa J. Simon (Dept. of Biomedical Engineering, Columbia Univ., 351 Engineering Terrace MC 8904, 1210 Amsterdam Ave., New York, NY 10027, USA, mjs2150@columbia.edu), Barclay Morrison (Dept. of Biomedical Engineering, Columbia Univ., 351 Engineering Terrace MC 8904, 1210 Amsterdam Ave., New York, NY 10027, USA, bm2119@columbia.edu)

To understand and prevent brain injuries from head trauma, researchers study mechanically stressed neuronal tissue. To anticipate future application of controllable ultrasonic in-vivo stress, we investigated the effects of acoustic radiation force on in-vitro PC12 cells. Undifferentiated PC12 cells were serum-cultured in DMEM/F12 on poly-L-lysine-coated polystyrene. Some cultures were DAPI stained. The culture plates were placed on an inverted phase-contrast microscope. An f/1.1 ultrasound transducer with a water-filled coupling cone was focused on the culture at a 45-degree angle-of-incidence, and excited with 30-ms 4.7-MHz pulses. Acoustic power was 8 W, and peak pressure was estimated at 300 kPa. Digital images were recorded before, during, and after insonification. Incident-light and fluorescence images revealed three populations: cells that were stationary (apparently outside the effective force field region), cells that elongated about 2 μm under radiation force and returned to approximately their original shapes when the force was removed (apparently adhered to the substrate), and cells that moved about 50 μm with each pulse and did not return (apparently free-floating). We conclude that cell morphology can be influenced reversibly with acoustic radiation force. (Support was provided by the Riverside Research Institute Fund for Biomedical Engineering Research and the Gatsby Initiatives in Brain Circuitry.)

6:00

5aBBf17. Enhancement of bead-based immunoassays by the use of acoustic radiation force. Martin Wiklund (Royal Institute of Technology, Biomedical and X-Ray Physics, KTH - AlbaNova, Roslagstullsbacken 21, SE-106 91 Stockholm, Sweden, martin@biox.kth.se)

Radiation forces generated by ultrasonic standing waves have long been used for increasing the speed and sensitivity of bead-based immunoagglutination tests. More recently, detection methods based on confocal laser-scanning fluorometry and single-step homogeneous bead-based immunoassays show promise for fast, easy and sensitive bioanalytics. If such methods are combined with ultrasonic enhancement, very high sensitivity can be obtained. Here, we analyze and compare the characteristics, performance and limitations of ultrasonic enhancement used in agglutination-based and fluorescence-based immunoassays. Both radiation force aspects, as well as reaction kinetics aspects, are discussed. Finally, we report on novel results where ultrasonic enhancement is performed in microtiter plates, using a fluorescence-based assay. Here, the ultrasound enriches the sample a factor 10^6-10^7, and a detection limit of 60 femtomolar is obtained for a thyroid stimulating hormone (TSH) assay. Our results are compared with the results from a high-performance commercial instrument (Luminex xMAP technology).

Session 5aED

Education in Acoustics: General Topics in Education in Acoustics

William M. Hartmann, Chair
Michigan State University, Dept. of Physics and Astronomy, East Lansing, MI 48824, USA

Contributed Papers

8:00

5aED1. Education for professional career in acoustics. Marion Burgess (Acoustics and Vibration Unit, University of NSW @ Aust Defence Force Academy, 2600 Canberra, Australia, m.burgess@adfa.edu.au), Matthew Stead (Bassett Acoustics, Level 6, 100 Pirie St, 5000 Adelaide, Australia, m.stead@bassett.com.au)

There is a demand around the world for staff for acoustical consulting companies as evidenced by the "positions available" listings. Companies would ideally like to hire staff with a good engineering, physics or building background plus an understanding of acoustics. Programs of study at University may deal with the principles of acoustics and vibration but there is usually a need for supplementary education and training for new staff in practical applications of those principles. While larger companies may provide this "in house" smaller companies do not have such resources and seek to supplement the basic knowledge with short courses or other educational opportunities. Most of these are available at specific times which may limit their applicability. In this paper we will discuss an approach to address this educational need with a fully flexible distance learning program. The program is loosely based on the UK Institute of Acoustics Diploma program. The modules comprising the program have been developed with the assistance of the senior consultants and from the acoustic consulting industry body. The early experiences with implementing the program will be discussed.

8:20

5aED2. The need to integrate speech acoustics course work across the speech-language pathology curriculum. Kathleen Siren (Loyola College in Maryland, 4501 North Charles Street, Department of Speech-Language Pathology/Audiology, Baltimore, MD 21210, USA, ksiren@loyola.edu)

The profession of speech-language pathology faces two critical challenges: (1) the lack of sufficient evidence-based practice due to limited clinical research in the field and (2) the dramatic decline in recent years in the number of students pursuing PhDs. Although speech acoustics courses are a part of most undergraduate programs in speech-language pathology, these courses are often disassociated from students' additional undergraduate and graduate course work and clinical training. These isolated speech science courses may inadequately prepare speech-language pathology students for future research-based course work and clinical practice. This paper reports results of a survey of 140 former undergraduate students who took a speech acoustics course between 1994 and 2003. The survey asks students about additional speech acoustics course work, related research experience, and use of speech science information in clinical practice. The majority of students surveyed report that speech acoustics information is largely isolated in one undergraduate course. This paper concludes that programs must consider better harmonizing speech science course work with other undergraduate and graduate course work and clinical training to meet the current research related challenges to the profession.

8:40

5aED3. Interdisciplinary teamwork, "Soundscaping": A pedagogical challenge. Jan Tro (Norwegian University of Science and Technology, O.S. Bragstad plass 2B, NO-7491 Trondheim, Norway, tro@iet.ntnu.no)

For seven years the Norwegian University of Science and Technology, NTNU, has offered the Master course Interdisciplinary Teamwork ("Eksperter i Team", EiT). EiT is organized into "villages" (consisting of up to thirty students). The Acoustics Group, NTNU, is in charge of a village named "Soundscaping" mainly dealing with sound design in public areas. The students in each village are divided into teams of five. The team members may represent very different fields of study like history, philosophy, literature, religion, music, electronics, architecture, physics, medicine, chemistry, computer science and more. The paper will discuss aspects of interdisciplinary teamwork training in acoustics and gives visual and sound examples of very different and interesting results and sound products ranging from pure sound art installations and interactive educational programs to talking waste basket and new developed sound absorbers.

9:00

5aED4. Noise induced hearing loss amongst classical music students - An audiometry study of students of the Royal Academy of Music. Georgia Zepidou (London South Bank University, FESBE, Borough Road, SE1 0AA London, UK, zepidoug@lsbu.ac.uk), Stephen Dance (London South Bank University, FESBE, Borough Road, SE1 0AA London, UK, dances@lsbu.ac.uk), Salvador Morant (London South Bank University, FESBE, Borough Road, SE1 0AA London, UK, salpelmo@hotmail.com)

Under the new UK guidance for Control of Noise at Work, entertainment noise now has to be considered for all employees. Health surveillance has been undertaken as part of the induction for all 1st year students studying at the Royal Academy of Music in London, as of September 2007. Seminars were arranged and details of the audiometric tests given prior to the health surveillance, so that only valid data was collected. A total of 350 students were asked to fill out questionnaires on their particular habits. Analysis of the audiograms showed double the incidence of health surveillance warning levels of hearing loss amongst men compared to women, although both had significantly better hearing than general population for their age. When early signs of noise induced hearing loss were considered, a loss of more than 20 dB at any high frequency, was indicated for more than half of the brass musicians.

9:20

5aED5. Problem based Masters Programme in Acoustics - ten years of experience. Sofus Birkedal Nielsen (Aalborg University, Fredrik Bajers Vej 7 B, 9220 Aalborg Ø, Denmark, sbn@es.aau.dk)

The Section of Acoustics at Aalborg University in Denmark has more that ten years of experience in offering a masters programme in Acoustics. The programme provides students with classical and modern aspects of physical acoustics, psychoacoustics and electro acoustics. Also signal processing which today is a major tool in understanding and utilizing of the newest sound technology is a compulsory part of the study. The language is English and the programme is open for all students with the appropriate background. So far half of the students have been non-Danish citizens coming from four continents. The pedagogical concept is problem based learning, with all students organized in groups of 4 - 6 students (having their own group rooms). Each semester has its own theme with relevant courses and suggested projects from the supervisors, industry or the students themselves. The project work is a considerable part of the workload at a semester, one could say that the courses give the theoretical background for the projects which are "learning by doing" with access to the best facilities, rooms and equipment.

Session 5aMUa

Musical Acoustics: Control of Natural and Synthetic Musical Sounds III

Marcelo M. Wanderley, Cochair
Centre for Interdisciplinary Research in Music Media & Technology (CIRMMT) - Schulich School of Music - McGill Univ., 555 Sherbrooke Street West, Montreal, QC H3A1E3, Canada

Jean Kergomard, Cochair
Laboratoire de Mécanique et d'Acoustique CNRS UPR-7051, 31, Chemin Joseph Aiguier, Marseille Cedex 20, 13402, France

Invited Papers

8:00

5aMUa1. Indirect acquisition of flutist gestures: a case study of harmonic note fingerings. Vincent Verfaille (Centre for Interdisciplinary Research in Music Media & Technology (CIRMMT) - Schulich School of Music - McGill Univ., 555 Sherbrooke Street West, Montreal, QC H3A1E3, Canada, vincent@music.mcgill.ca), Marcelo M. Wanderley (Centre for Interdisciplinary Research in Music Media & Technology (CIRMMT) - Schulich School of Music - McGill Univ., 555 Sherbrooke Street West, Montreal, QC H3A1E3, Canada, marcelo.wanderley@mcgill.ca), Philippe Depalle (Centre for Interdisciplinary Research in Music Media & Technology (CIRMMT) - Schulich School of Music - McGill Univ., 555 Sherbrooke Street West, Montreal, QC H3A1E3, Canada, depalle@music.mcgill.ca)

The indirect acquisition of musicians' gestures consists in retrieving information about gestures from the sound. Inspired by previous studies investigating clarinetists' gestures, we focus on the flute, which features numerous playing modes and a rich palette of sounds. Our goal is to provide musicians with guidelines for using indirect acquisition. For a variety of playing modes, we collected information about gestures, body parts involved, and effects on the acoustical signal. We then designed signal processing algorithms for recognizing which gesture is involved in a given sound; later we will quantize related movement by combining direct acquisition, indirect acquisition and motion capture. Focusing on harmonic note fingerings, a first experiment investigated octave-related harmonic note fingerings with 1 nonexpert performer (ff dynamics and normal articulation). A target F_0-guided PCA on the amplitude of the first six harmonics of $F_0/4$ from 1 semi-tone frequency bands retrieved the correct fingering with two principle components in all trials. A second experiment investigated octave and non-octave related harmonic note fingerings with four expert performers. A target F_0-guided PCA on the sum of energies around iF_0/k ($k=2,...,6$; $i=1,...,12$) provided wider clusters, making more difficult to retrieve the correct fingering in some specific cases that we will discuss.

8:20

5aMUa2. Control parameters of a generalized vibrato model with modulations of harmonics and residual. Vincent Verfaille (Centre for Interdisciplinary Research in Music Media & Technology (CIRMMT) - Schulich School of Music - McGill Univ., 555 Sherbrooke Street West, Montreal, QC H3A1E3, Canada, vincent@music.mcgill.ca), Catherine Guastavino (Centre for Interdisciplinary Research in Music Media & Technology (CIRMMT) - School of Information Studies - McGill Univ., 3459 McTavish, Montreal, QC H3A1Y1, Canada, Catherine.Guastavino@mcgill.ca), Philippe Depalle (Centre for Interdisciplinary Research in Music Media & Technology (CIRMMT) - Schulich School of Music - McGill Univ., 555 Sherbrooke Street West, Montreal, QC H3A1E3, Canada, depalle@music.mcgill.ca)

Our previous research focused on vibrato modeling of the harmonics of musical sounds. We demonstrated the need to account for fundamental frequency modulation, global amplitude modulation, but also spectral envelope modulation linked to brightness modulations. This may result from nonlinearities between the excitation signal and the resonating body, and/or from variable spectral sampling of the impedance function as F_0 varies. For instance on flute, vibrato results from air pressure modulations. We also observed in sounds with vibrato of wind instruments that the residual also exhibits amplitude modulation, somehow due to air pressure modulations that are responsible vibrato. In a pilot listening test on shakuhashi sounds (for which the residual is obviously modulated), we asked participants to discriminate between the original modulated harmonics plus the amplitude modulated residual, and the original modulated harmonics plus a non-modulated residual, in a AB comparison task (same/different test). Preliminary results show that participants can hear the difference, suggesting that the amplitude modulation on the residual is audible. Subsequently, we developed a generalized vibrato model incorporating modulations on harmonics and residual. This model is presented here with an emphasis on its control parameters.

8:40

5aMUa3. Why practice scales? Details of fingering transitions in flute playing. André Almeida (University of New South Wales, Music Acoustics, School of Physics, NSW 2052 Sydney, Australia, aalmeida@phys.unsw.edu.au), Renee Chow (University of New South Wales, Music Acoustics, School of Physics, NSW 2052 Sydney, Australia, z3130148@student.unsw.edu.au), John Smith (University of New South Wales, Music Acoustics, School of Physics, NSW 2052 Sydney, Australia, john.smith@unsw.edu.au)

Mastering a wind instrument requires not only expert blowing and embouchure, but also many hours of practice of exercises that improve the fingering speed, regularity and coordination. Many note transitions involve the motion of several fingers, often in opposite directions. The order of finger movement can sometimes affect the transitions between notes and produce short, spurious notes between the original and destination notes. We adapted a transverse flute for real time measurement (with a resolution of 3 ms) of all key positions using reflected light sensors. Beginner and advanced players were asked to perform a phrase including multifinger transitions. The detailed motion, average speed and intervals between finger motion were analysed. The comparison among players is not surprising: an experienced player was found to have more regular time intervals between fingers moving in a same direction (within 10 ms) than an amateur (within 25 ms). Contrary fingering motions are slightly less regular (15 ms for an experienced player against 50 ms for an amateur), but still unperceptible to the ear in the case of the experienced musician. A range of details will be reported, for instance the influence of scale exercises.

9:00

5aMUa4. Gesture synthesis: basic control of a flute physical model. Nicolas Montgermont (Institut Jean Le Rond d'Alembert/LAM (UPMC/CNRS/Ministère Culture), 11, rue de Lourmel, 75015 Paris, France, montgermont@lam.jussieu.fr), Benoit Fabre (Institut Jean Le Rond d'Alembert/LAM (UPMC/CNRS/Ministère Culture), 11, rue de Lourmel, 75015 Paris, France, fabreb@ccr.jussieu.fr), Patricio De La Cuadra (Centro de Investigación en Tecnologias de Audio (CITA), Universidad Católica de Chile, Alameda 340, Oficina 13, Casilla 114-D Santiago, Chile, pcuadra@uc.cl)

In the flute family, the oscillation is due to the instability of a jet at the output of a channel coupled with an acoustic resonator. Recent physical models allows to simulate the behavior of the complete instrument, but we still lack a convincing way to drive them. The simulation of the isolated instrument must be completed with a modelization of the control exerted by the flutist. Depending of the instrument of the flute family, the number and type of control parameters are differents. For example, in a recorder the player blows inside a fixed channel built by the instrument maker and in the case of the transverse flute, the channel is shaped by the player's lips during the playing. This paper presents a simple model of flute player, based on measurements carried on instrumentalists playing on a recorder or a transverse flute. The model is generating the basic features of the instrument control in order to produce given pitches and dynamics. The coupling with a flute physical model allows to study its validity.

FRIDAY MORNING, 4 JULY 2008 P2-D, LEVEL 2, 9:40 TO 11:20 A.M.

Session 5aMUb

Musical Acoustics: General (Mode Conversion, Radiation and Perception of Musical Sound) (Poster Session)

All posters will be on display from 9:40 a.m. to 11:20 a.m. To allow contributors an opportunity to see other posters, contributors of odd-numbered papers will be at their posters from 9:40 a.m. to 10:30 a.m. and contributors of even-numbered papers will be at their posters from 10:30 a.m. to 11:20 a.m.

5aMUb1. Subjective evaluations of the performance proficiency for fluctuating musical sounds using fluctuation strength or roughness. Nozomiko Yasui (Graduate School of Science and Technology, Ryukoku University, 1-5, Yokotani, Oe-cho, Seta, 520-2194 Otsu, Shiga, Japan, n-yasui@mail.ryukoku.ac.jp), Masafumi Kinou (Graduate School of Science and Technology, Ryukoku University, 1-5, Yokotani, Oe-cho, Seta, 520-2194 Otsu, Shiga, Japan, kino@rins.ryukoku.ac.jp), Masanobu Miura (Graduate School of Science and Technology, Ryukoku University, 1-5, Yokotani, Oe-cho, Seta, 520-2194 Otsu, Shiga, Japan, miura@rins.ryukoku.ac.jp)

The "Fluctuation Strength (FS)" and the "Roughness" were suggested as evaluation indices of hearing sensation concerning fluctuated sounds of low or high frequencies. Past studies have been investigated FS and roughness of modulated pure tones and broadband noise. However, few studies have been reported concerning FS and roughness of attenuating sounds produced by musical instruments and performance proficiency for them. Therefore, the tremolo played on the mandolin and the closed roll played on the snare-drum are employed here as fluctuating musical sounds of low or high frequencies. Introduced here is the FS and roughness as indices for the evaluation of the performance proficiency for tremolo and roll. Specifically, experts of mandolin or snare-drum are asked to play tremolo of various plucking rate (number of plucking per second) and closed roll of various stroking rate (number of stroking per second). An evaluation experiment using the 2AFC method is conducted to evaluate performance proficiency for tremolo and roll. Aesthetic performances of tremolo and roll are described as "smooth, or not fluctuated" by trained players. The amount of physical FS for tremolo and physical roughness for roll are calculated by an original procedure to investigate relations between physical indices and evaluation results.

5aMUb2. Musical perception within a highly reverberant room. Nelia Valverde (Universidad de Castilla-La Mancha, Campus Universitario, 16071 Cuenca, Spain, Nelia.Valverde@uclm.es), Marcos D. Fernandez (Universidad de Castilla-La Mancha, Campus Universitario, 16071 Cuenca, Spain, Marcos.Fernandez@uclm.es), Javier Ariza (Universidad de Castilla-La Mancha, Campus Universitario, 16071 Cuenca, Spain, Javier.Ariza@uclm.es), Jose A. Ballesteros (Universidad de Castilla-La Mancha, Campus Universitario, 16071 Cuenca, Spain, Josea.Ballesteros@uclm.es), Juan P. Ruiz (Universidad de Castilla-La

Mancha, Campus Universitario, 16071 Cuenca, Spain, Juanpedro.Ruiz @uclm.es)

The listening of a musical composition generates a unique and different perception in every listener, but, at the same time, the specific acoustic conditions of the room chosen for its performance have a decisive influence in that perception, which can fit in, almost completely, with the acoustic qualification of the room. The aim of this work is to find out how the high reverberance of a room can have a strong influence on the perception of a musical composition. For that aim, the St. Peter's church (in Cuenca, Spain) with a circular plan, a reduced volume and a high reverberance time has been chosen for the performance. A musical composition for voice and electroacoustics has been created specifically for this church. This has been recorded within the church using a HATS in the listener position and a set of music experts have been asked a survey about their impressions on perception after listening the recording using headphones. The results of the psychoacoustic analysis reveal that the high reverberance of this church leads to an extremely low intelligibility and an unclear sound of the recording. This, together with an unbereable background noise, gives a general acoustic perception not very attractive.

5aMUb3. Foundations of sound therapy. Iegor Reznikoff (Université de Paris X, Département de Philosophie, 92001 Nanterre, France, dominiqueleconte@yahoo.fr)

In the practice of music therapy, the use of the sounds of a live naturally singing voice appears to be the most effective; in some cases, results are obtained whereas there are no results using musical sounds, and generally results are obtained in a much shorter time. Sounds and singing in just intonation are particularly efficient. This practice introduces to a deep understanding of sound therapy. Sketched here are the vocal sound/body relationship and the vocal sound / consciousness relationship, which are relevant in this therapy. Finally clinical examples are given (coma states, loss of speech, old persons, states close to death, mind handicapped persons, depression, etc.). Bibliography I. Reznikoff: On Primitive Elements of Musical Meaning, www.musicandmeaning.net, Journal of Music and Meaning 3 (Invited papers), 2005.

5aMUb4. Broadband directive sources modeling for acoustic discrete-time domain methods. José Escolano (University of Jaén, Alfonso X, 28, E-23700 Linares, Spain, escolano@ujaen.es),José J. Lopez (Tech. Univ. of Valencia, Camino de Vera S/N, 46021 Valencia, Spain, jjlopez@dcom.upv.es)

The use of sources with complex directivities in discrete-time domain methods, such as the finite-difference time-domain method or the digital waveguide mesh, is a recently open topic. However, so far, the provided solutions work for discrete frequencies or frequency-independent sources. Both solutions are useful for very particular cases and in most cases, far from real sources. This paper provides an extension in the use of a monopole source combination for broadband directive sources in discrete-time domain simulations. This method results very effective for frequency-independent and dependent sources, even in cases where the directivity diagrams have considerable lobules. Finally, this method will be tested through several examples.

5aMUb5. Auditory resolution in virtual environments: Effects of spatialization algorithm, off-center listener positioning and speaker configuration. Georgios Marentakis (Centre for Interdisciplinary Research in Music Media & Technology (CIRMMT) - Schulich School of Music - McGill Univ., 555 Sherbrooke Street West, Montreal, QC H3A1E3, Canada, gmarentakis@music.mcgill.ca), Nils Peters (Centre for Interdisciplinary Research in Music Media & Technology (CIRMMT) - Schulich School of Music - McGill Univ., 555 Sherbrooke Street West, Montreal, QC H3A1E3, Canada, nils.peters@mcgill.ca), Stephen McAdams (Centre for Interdisciplinary Research in Music Media & Technology (CIRMMT) - Schulich School of Music - McGill Univ., 555 Sherbrooke Street West, Montreal, QC H3A1E3, Canada, smc@music.mcgill.ca)

We present the results of an empirical study on the effects of room and off-center listener positioning on sound localization in two virtual environments, VBAP and Ambisonics. Localization accuracy has been assessed by estimating Minimum Audible Angles and Minimum Audible Movement Angles for the two spatialization algorithms and for three directions of sound incidence, in the studio and a concert hall for listeners in off-center listener positions, with two loudspeaker setups. A model of localization accuracy as a function of the experimental variables is presented, that can be used to quantify the effects of the room and off-center listening positions on sound localization and auditory movement detection.

Session 5aMUc

Musical Acoustics: Plucked and Struck Idiophones I (Poster Session)

Thomas D. Rossing, Cochair
Stanford University

Charles Besainou, Cochair
Institut Jean le Rond d'Alembert

All posters will be on display from 9:40 a.m. to 11:20 a.m. To allow contributors an opportunity to see other posters, contributors of odd-numbered papers will be at their posters from 9:40 a.m. to 10:30 a.m. and contributors of even-numbered papers will be at their posters from 10:30 a.m. to 11:20 a.m.

Contributed Papers

5aMUc1. Analysis of drum player's motion. Hiroshi Kawakami(Nihon University, 2-42-1 Asahigaoka, Nerima, 176-8525 Tokyo, Japan, hkawakami@eva.hi-ho.ne.jp), Yuki Mito (Nihon University, 2-42-1 Asahigaoka, Nerima, 176-8525 Tokyo, Japan, mitotic@hotmail.com), Reiji Watanuma (Nihon University, 2-42-1 Asahigaoka, Nerima, 176-8525 Tokyo, Japan, VFE16733@nifty.ne.jp), Mieko Marumo (Nihon University, 2-42-1 Asahigaoka, Nerima, 176-8525 Tokyo, Japan, marumo@rg8.so-net.ne.jp)

In this experiment, the motion of a drum player's arm was measured by the optical motion capture system in various performance types. From these actual movement data, we analyzed about the acceleration and sound energy flux of the stick before and after excitation. Moreover, the snap of a wrist which is very important at the time of a high drum performance and the relation of acceleration, and the relation of sound energy flux were also analyzed. From those results, it was suggested that the snap of the wrist was important at the time of a high drum performance, and it was concerned with sound power. Especially, the performance which player hit the drum speedy and repeatedly was concerned with the acceleration of stick before and after excitation.

5aMUc2. Dampening vibration modes of the snare drum batter head. Barry Larkin (Iowa State University, Department of Music, Music Hall, Ames, IA 50011, USA, blarkin@iastate.edu), Andrew Morrison (Illinois Wesleyan University, Department of Physics, 1312 N. Park St., Bloomington, IL 61701, USA, amorriso@iwu.edu)

Percussionists have always had to contend with an undesirable ringing sound while performing on the snare drum. It is usually referred to as the "edge ring." A common method to eliminate this sound comes from placing some type of dampening material on the edge of the drum head. Manufacturers of drums have provided many ways of dealing with this problem including internal dampening devices, customized drums heads or material designed to be placed on the drum head. Using electronic television holography, it was revealed the source of this "ring" to be the third mode of vibration that produces a pitch approximately one octave and a half step above the fundamental [Larkin and Morrison, JASA, **122**, #5, p 3056]. In this update to the previous work, we will show the effect of dampening devices on the third and other modes.

5aMUc3. Finite element modelling of steelpan acoustics. Derek A. Gay (The University of The West Indies, Department Civil Engineering, St Augustine, Trinidad and Tobago, derek.gay@sta.uwi.edu)

In this paper the finite element method is used to model acoustic vibrations of steelpan shells. The steelpan surface is characterized as a three-dimensional compound shell, comprising notes (surfaces with reverse curvature) on a concave ellipsoidal surface attached to a cylindrical shell (the skirt). In this model note and inter-note surfaces are defined by geometric parameters which can be varied to define complex surface geometries. The geometric mesh model is used develop tenor, cello and bass steelpans instruments and a 3D finite element shell vibration algorithm is used to demonstrate their vibration characteristics. Modes shapes and frequencies of the composite shell structures are computed for typical configurations of note and skirt geometry. The model demonstrates that there exist many composite natural modes of a playing surface involving the interaction between two or more notes. In addition, it is found that the frequency range of mode shapes associated primarily within skirt vibration overlaps with the musical range of the notes underscoring the potential for "skirt-note" coupling. The degree of frequency overlap was found to be largely dependent on skirt length and configuration.

Session 5aMUd

Musical Acoustics and Signal Processing in Acoustics: Signal Representations and Models of Musical Sounds I (Poster Session)

James Beauchamp, Cochair
University of Illinois

Bertrand David, Cochair
Télécom Paristech (ENST) / TSI - CNRS LTCI

All posters will be on display from 9:40 a.m. to 11:20 a.m. To allow contributors an opportunity to see other posters, contributors of odd-numbered papers will be at their posters from 9:40 a.m. to 10:30 a.m. and contributors of even-numbered papers will be at their posters from 10:30 a.m. to 11:20 a.m.

Contributed Papers

5aMUd1. The perceptual and cognitive nonlinearities underlying musical preference across multiple exposures. Elizabeth H. Margulis (University of Arkansas, Department of Music - MUSC 109, Fayetteville, AR 72701, USA, ehm@uark.edu), Anil K. Roy (Northwestern University, 2240 Campus Drive, Evanston, IL 60208, USA, a-roy@u.northwestern.edu), Patrick C. Wong (Northwestern University, 2240 Campus Drive, Evanston, IL 60208, USA, pwong@northwestern.edu)

Repetition is a fundamental part of engagement with the auditory world. Repeated exposures influence what gets perceived as important and what features are singled out for attention. That repetition can also influence the mysterious phenomenon of aesthetic enjoyment is a longstanding observation to which much intellectual attention has been paid. A special case of repetition and perceptual learning is music, a domain in which people choose to be exposed to the identical stimulus again and again. This apparent preference for repeated exposures connects fundamentally to notions of human identity, affect, cognitive processing, and neural function. We report on a set of experiments that uses behavioral measures to assess perceptual changes across multiple exposures (five over one week) of a 20-minute piece for orchestra. Across the five exposures, we found an inverted U-shape preference response, which possibly is decomposable to the complex interaction of multiple nonlinear components, represented by performance on tasks relating to memory, attention, affect, syntax, and error detection We argue that musical preference has remained a puzzle because the behavior depends on an underlying complex system with numerous nonlinear cognitive components revealed by our results. [Work supported by NIH, NSF, and Northwestern University.]

5aMUd2. Single sensor singer/music separation using a source/filter model of the singer voice. Jean-Louis Durrieu (Télécom Paristech (ENST) / TSI - CNRS LTCI, 46, rue Barrault, 75634 Paris Cedex 13, France, durrieu@enst.fr), Bertrand David (Télécom Paristech (ENST) / TSI - CNRS LTCI, 46, rue Barrault, 75634 Paris Cedex 13, France, bertrand.david@enst.fr), Gaël Richard (Télécom Paristech (ENST) / TSI - CNRS LTCI, 46, rue Barrault, 75634 Paris Cedex 13, France, gael.richard @enst.fr)

Separating the singer voice from polyphonic music signals has many useful applications, such as demixing/remixing, desoloing or audio indexing. In the works of Benaroya on single sensor blind source separation, the signals are modeled by Gaussian mixtures (GMM) such that each state is characterized by a spectral shape. The separation itself is then done by adaptive Wiener filtering. However, to better fit general signals, the number of states for the vocal model should be equal to the number of notes multiplied by the number of vowels (or canonical vocal tract shapes) that the singer uses. Therefore, in order to separate a singer voice from background music, we suggest a source/filter model for the singer signal, keeping the same models as used by Benaroya for the background music signal. Assuming the presence of only one singer, we separate the desired part from the rest by first estimating the sung melody thanks to the source part of our model and then re-evaluating the parameters of our model. This research is partly supported by the European Commission under contract FP6-027026-K-SPACE and by the French AII (Quaero project).

5aMUd3. What/when causal expectation modelling applied to percussive audio. Amaury Hazan (Pomeu Fabra University, Ocata 1, 08003 Barcelona, Spain, ahazan@iua.upf.edu), Paul Brossier (Pomeu Fabra University, Ocata 1, 08003 Barcelona, Spain, piem@piem .org), Ricard Marxer (Pomeu Fabra University, Ocata 1, 08003 Barcelona, Spain, rmarxer@iua.upf.edu), Hendrik Purwins (Pomeu Fabra University, Ocata 1, 08003 Barcelona, Spain, hpurwins@iua.upf.edu)

A causal system for representing a musical stream and generating further expected events is presented. Starting from an auditory front-end which extracts low-level (e.g., spectral shape, mel frequency cepstral coefficients) and midlevel features such as onsets and beats, an unsupervised categorisation process builds and maintains a set of symbols aimed at representing musical stream events using both timbre and time descriptions. The time events are represented using inter-onset intervals relative to the beats. These symbols are then processed by an expectation module based on predictive partial match, a multiscale technique derived from N-grams. The system capacity to generate an expectation that matches its transcription is evaluated using drum recordings from the ENST-drums database. We show that the MFCC-based representation leads to a more compact set of symbols and a better match between transcription and expectation. Also, we suggest that the system is sensitive to exposure and illustrate some properties of the expectation entropy while attending percussive audio patterns.

5aMUd4. Dynamical hierarchical self-organization of harmonic and motivic musical categories. Ricard Marxer (Pomeu Fabra University, Ocata 1, 08003 Barcelona, Spain, rmarxer@iua.upf.edu), Piotr Holonowicz (Pomeu Fabra University, Ocata 1, 08003 Barcelona, Spain, pholonow@iua.upf.edu), Amaury Hazan (Pomeu Fabra University, Ocata 1, 08003 Barcelona, Spain, ahazan@iua.upf.edu), Hendrik Purwins (Pomeu Fabra University, Ocata 1, 08003 Barcelona, Spain, hpurwins@iua.upf.edu)

We introduce a generic model of emergence of musical categories during the listening process. The model is based on a preprocessing and a categorization module. Preprocessing results in a perceptually plausible representation of music events extracted from symbolic input. The categorization

module lets a taxonomy of musical entities emerge according to a cognitively plausible online learning paradigm. We show the advantages of using a conceptual clustering method in the musical domain. The system extracts multilevel hierarchies and can be tuned to clustering at various resolutions. The potential of the model is exemplified by exposing it to two different datasets resulting in music harmonic and motivic categorization consistent with music theory.

5aMUd5. A comparison of molecular approaches for generating sparse and structured multiresolution representations of audio and music signals. Bob Sturm (University of California, Box 117, Department of Electrical and Computer Engineering, Santa Barbara, CA 93106, USA, boblsturm@ece.ucsb.edu), John J. Shynk (University of California, Box 117, Department of Electrical and Computer Engineering, Santa Barbara, CA 93106, USA, shynk@ece.ucsb.edu), Aaron McLeran (University of California, Media Arts and Technology Program, Santa Barbara, CA 93106, USA, amcleran@gmail.com), Curtis Roads (University of California, Media Arts and Technology Program, Santa Barbara, CA 93106, USA, clang@mat.ucsb.edu), Laurent Daudet (UPMC Univ Paris 06, LAM / IJLRA, 11 rue de Lourmel, 75015 Paris, France, daudet@lam.jussieu.fr)

The authors investigate the characteristics and performance of joint (single-step) and sequential (two-step) approaches to creating sparse and structured multiresolution representations of audio and music signals derived using sparse overcomplete methods. A joint approach, such as molecular matching pursuit, attempts to find structures in a signal as part of the decomposition process, while a sequential approach, such as agglomerative clustering, attempts to find structures in the completed decomposition of a signal. Each of these approaches have different benefits and drawbacks. For a joint approach, it is computationally convenient that the decomposition and structuring are done simultaneously, but usually only simple structural relations are possible. For a sequential approach, one is working in a parameter space of much smaller dimension than the original signal, but the computation is higher since the decomposition and the structure building are two separate processes. Results from these approaches using real audio and music signals will be compared and contrasted, and will contribute to our goal of creating an enhanced interface between the content of audio and music signals, e.g., onsets, notes, voices, and their multiresolution sparse atomic decompositions.

5aMUd6. Initialization, distances and local minima in audio applications of the non-negative matrix factorization. Nancy Bertin (Télécom Paristech (ENST) / TSI - CNRS LTCI, 46, rue Barrault, 75634 Paris Cedex 13, France, nbertin@enst.fr), Roland Badeau (Télécom Paristech (ENST) / TSI - CNRS LTCI, 46, rue Barrault, 75634 Paris Cedex 13, France, roland.badeau@enst.fr)

The use of the non-negative matrix factorization (NMF) as a decomposition technique has dramatically grown in various signal processing applications over the last years. Its computation, based on the iterative minimization of a cost function, relies on several choices, among which the distance involved in the cost function itself but also the initialization of the algorithm. These choices are all the more crucial as the usual algorithms, iterative, only ensure convergence to a local minimum. In this work, we compare three typical distances in the NMF problem (namely Euclidian, Kullback-Leibler divergence and Itakura-Saito distance) and their combination with different initializations, in an audio context: decomposition of the time-frequency representation for the transcription of polyphonic music. Both the existence of global and local minima, and the efficiency of transcription are examined. Moreover, NMF update rules can be formulated in a unified framework for the three aforementioned cost functions. This formulation allows figuring out new NMF algorithms which could address the local minima question.

5aMUd7. Automatic morphological description of sounds. Geoffroy G. Peeters (Ircam, 1, pl. Igor Stravinsky, 75004 Paris, France, peeters@ircam.fr), Emmanuel Deruty (Ircam, 1, pl. Igor Stravinsky, 75004 Paris, France, emmanuel.deruty@gmail.com)

Morphological description has been proposed by Pierre Schaeffer. It consists in describing sounds by identifying the temporal evolution of their acoustical properties to a set of profiles. This kind of description is especially useful for indexing sounds with unknown cause such as SoundFX. The present work deals with the automatic estimation of this morphological description from audio signal analysis. In this work, three morphological descriptions are considered: - dynamic profiles (ascending, descending, ascending/descending, stable, impulsive), - melodic profiles (asc., desc. fixed, up/down, down/up) - repetition profiles. For each case we present the most appropriate audio features (loudness, pitch, pitch salience, temporal increase/decrease, lag-matrix-periodicity, ...) and mapping algorithm (slope computed from spline approximations of temporal profiles, ...) used to automatically estimate the profiles. We demonstrate the use of these descriptions for automatic indexing (using decision trees) and search-by-similarity of SoundFX.

5aMUd8. Sound feature extraction to distinguish between a grand and an upright piano. Grigorios Plitsis (Greece, grigoriosplitsis@merseymail.com)

The sound of a grand piano differs from that of an upright piano. In order to find what characterizes the produced sound, an instrument recognition system capable of producing a model of the sound features should be created. Feature extraction can be performed with the use of the Mel frequency cepstral coefficients (MFCCs). This method is useful as it approximates the mechanism of human hearing. Statistical modeling can be further applied using the Gaussian mixture model (GMM) so as to train the system. In order to decide whether the under test instrument is a grand or an upright piano the log-likelihood should be calculated. This study could assist in the identification of the parameters defining the sound of a grand and an upright piano.

5aMUd9. Instrument sound description and modelisation in the context of computer aided orchestration. Damien Tardieu (Ircam, 1, pl. Igor Stravinsky, 75004 Paris, France, Damien.Tardieu@ircam.fr), Grégoire Carpentier (Ircam, 1, pl. Igor Stravinsky, 75004 Paris, France, Gregoire.Carpentier@ircam.fr), Geoffroy G. Peeters (Ircam, 1, pl. Igor Stravinsky, 75004 Paris, France, peeters@ircam.fr)

We present a work related to the description of instrumental sound in the context of computer aided orchestration. We define the orchestration problem as the search of instrument sound combinations that sound close to a given target. In the presented approach, instrument sounds are described by a set of acoustic features that are extracted from large sound sample databases. The features are then modeled by a probabilistic distribution. Finally the models are combined to approximate the description of a combination of instrument sounds. We discuss the requirement induced by the orchestration problem on the choice of the acoustic features and detail the chosen set of features. In a second part we describe the method used to learn the probabilistic model of different instruments and playing techniques and show that it allows to learn the models from few samples and to deduce the models of some playing techniques, pitches or dynamics that are not available in the training set. Finally we evaluate the proposed method on classification tasks and describe its integration in a computer assisted orchestration program.

Session 5aMUe

Musical Acoustics and Signal Processing in Acoustics: Signal Representations and Models of Musical Sounds II

James W. Beauchamp, Cochair
University of Illinois, 1002 Eliot Drive, Urbana, IL 61801, USA

Bertrand David, Cochair
Télécom Paristech (ENST) / TSI - CNRS LTCI, 46, rue Barrault, Paris Cedex 13, 75634, France

Contributed Paper

11:00

5aMUe1. Early use of the Scott-Koenig phonautograph for documenting performance. George Brock-Nannestad (Patent Tactics, Resedavej 40, DK-2820 Gentofte, Denmark, pattac@image.dk), Jean-Marc Fontaine (Université UPMC - Ministère de la Culture - CNRS - IJRA - LAM, 11, rue de Lourmel, F-75015 Paris, France, jmfontai@ccr.jussieu.fr)

Acoustics in the 1850s combined listening, observation and notation. This was "real-time", catching any phenomenon as it appeared. If it was repeatable, one could prepare for it. Continuous data rather than observation data enabled a very different analysis from observation and notebooks. Édouard-Léon Scott's invention of the phonautograph enabled this. A surface moved below a stylus that was vibrated by sound in air. Originally a blackened glass plate, the scientific instrument maker Rudolph Koenig contributed by devising a very long axis representing time, because now blackened paper was wrapped around a cylinder on a threaded shaft. A two-dimensional representation of the individual vibrations was obtained. Scott both deposited a sealed letter with the Paris Academy of Sciences in January, 1857 and filed a patent application in April, 1857. Later he deposited a further sealed letter and in 1859 he filed an application for patent of addition. Following the thoughts expressed and documented in his manuscripts here analyzed in context and comparing with Koenig's production it is feasible to see how they were dependent on each other, although they had different purposes in mind. The paper concentrates on Scott's interests in performance, and a number of original tracings are discussed.

Invited Papers

11:20

5aMUe2. Sparse representations of audio: from source separation to wavefield compressed sensing? Remi Gribonval (INRIA, IRISA, Campus de Beaulieu, 35042 Rennes Cedex, France, remi.gribonval@irisa.fr)

Sparse signal representations, which are at the heart of today's coding standards (JPEG, MPEG, MP3), are known to have had a substantial impact in signal compression. Their principle is to represent high-dimensional data by a combination of a few elementary building blocks, called atoms, chosen from a large collection called a dictionary. Over the last five years, theoretical advances in sparse representations have highlighted their potential to impact all fundamental areas of signal processing. We will discuss some current and emerging applications of sparse models in musical sound processing including: signal acquisition (Compressed Sensing - sampling wave fields at a dramatically reduced rate) and signal manipulation (e.g., source separation and enhancement for digital remastering). We will conclude by discussing the new algorithmic and modeling challenges raised by these approaches.

11:40

5aMUe3. Towards a hierarchically sparse model for audio signals. Laurent Daudet (UPMC Univ Paris 06, LAM / IJLRA, 11 rue de Lourmel, 75015 Paris, France, daudet@lam.jussieu.fr)

In this paper we discuss a major issue that arises when building sparse atomic models for music signals: in which space (/ dictionary) should we represent the signals? Having extremely redundant dictionaries is very informative for the locally most important atoms, but is irrelevant for the detail atoms that represent residual signals. Also, what are the advantages of dictionaries composed of learned atoms (which brings the issue of representativeness) compared to generic dictionaries? We here advocate for non-fixed dictionaries, with a multi-layered hierarchical decomposition: the first layer roughly describes the signal, in an extremely redundant, signal-tailored, structured dictionary. This layer is also very sparse, most of the information being carried by the atoms' parameters, similarly to parametric representations. Subsequent layers give more and more details, increasing the data amount while reducing overcompleteness and structural model constraints. These techniques have obvious applications for audio coding, but are also useful for scalable music data mining. This research is supported by the French ANR (DESAM project).

12:00

5aMUe4. Bayesian inference in hierarchical non-negative matrix factorisation models of musical sounds. Ali Taylan Cemgil (University of Cambridge, Trumpington Street, CB2 1PZ Cambridge, UK, atc27@cam.ac.uk), Tuomas Virtanen (Tampere University of Technology, Inst. of Signal Processing, FI-33101 Tampere, Finland, tuomas.virtanen@tut.fi)

There has been a surge of interest to efficient audio and music modeling using tools from statistical machine learning. One such technique, that has been particularly successful, is non-negative matrix factorisation (NMF). However, a detailed theoretical understanding of this success is missing, as well as links to other modeling strategies such as sinusoidal or harmonic models. To fill this gap,

we describe NMF in a statistical framework, as a hierarchical generative model consisting of an observation and a prior component. We show that particular choices lead to standard NMF algorithms as special cases, where parameter estimation is carried out via maximum likelihood. Starting from this view, we develop extensions that facilitate more realistic acoustic modeling (such as spectral smoothness or harmonicity of natural sounds) and alternative inference techniques via Gibbs sampling and variational Bayes, which allow us to do principled comparisons between alternative models via Bayesian model selection. Our novel construction, where we make use of Markov chains of Gamma random variables, retains conjugacy and enables us to develop models that fit better to real data while retaining attractive features of standard NMF such as fast convergence and easy implementation. We illustrate our approach on polyphonic pitch estimation.

12:20

5aMUe5. On sinusoidal modeling of nonstationary signals. Axel Roebel (IRCAM, 1, pl. Igor-Stravinsky, 75004 Paris, France, roebel@ircam.fr)

In this presentation we are going to give an overview over a number of techniques that have been developed in our group to improve the modeling of musical (nonstationary) signals using sinusoidal models. One of the basic problems with sinusoidal models is the fact that the underlying theory is derived assuming stationary sinusoids, while in the real world all sinusoidal components are non stationary. The two topics that will be covered main are, first a technique that allows to distinguish between nonstationary sinusoidal components, noise and transients, and second a new technique for parameter estimation of nonstationary sinusoids using frequency domain demodulation.

12:40-1:40 Lunch Break

Invited Papers

1:40

5aMUe6. Advances in the tracking of partials for the sinusoidal modeling of musical sounds. Sylvain Marchand (LaBRI - CNRS, University of Bordeaux 1, 351 cours de la Liberation, F-33405 Talence, France, sylvain.marchand@labri.fr)

Whereas sinusoidal modeling is widely used for sounds, polynomial models are still used for the model parameters, which can hardly handle modulations (vibrato and tremolo) present in musical sounds. Moreover, the partial tracking algorithms are often designed under stationarity assumptions. Advances in partial tracking may come out of the modeling of the partials themselves. We consider their parameters (frequencies and amplitudes) as predictable and slow time varying: First, the future of any partial can be determined from its past evolutions; second, no audible frequency should appear in the spectral content of these evolutions, otherwise it would question the perceptive consistency of the model. We then choose to handle nonstationary sinusoidal modeling by a deterministic approach based on linear prediction of the partial evolutions and partial discrimination based on the spectral properties of these evolutions. The underlying model for each partial is now a sum of sinusoids, thus leading to a two-level sinusoidal modeling, well suited for musical sounds, where modulations are important. The enhanced partial tracking algorithm also handles the case of crossing partials, without the need for any probabilistic approach. Better modeling the deterministic part of polyphonic sounds leads to enhanced source separation and time scaling algorithms.

2:00

5aMUe7. Adaptive subspace methods for high resolution analysis of music signals. Roland Badeau (Télécom Paristech (ENST) /TSI - CNRS LTCI, 46, rue Barrault, 75634 Paris Cedex 13, France, roland.badeau@enst.fr), Bertrand David (Télécom Paristech (ENST)/TSI - CNRS LTCI, 46, rue Barrault, 75634 Paris Cedex 13, France, bertrand.david@enst.fr)

In the field of music signals analysis, the tonal part of a broad variety of sounds is often represented as a sum of slowly varying sinusoids. The Fourier transform remains a prominent tool for estimating the parameters of this model, due to its robustness and to the existence of fast algorithms. Its main drawback relies in its spectral resolution, bounded by the length of the analysis window. Subspace-based high resolution (HR) methods are conversely not constrained by this limit, since they rely on the particular geometrical structure of the signal model. Nevertheless, they have been seldom used in audio signal processing, mainly due to their high computational cost. Based on recent advances in the field of subspace tracking, enhanced adaptive algorithms for HR analysis have thus been developed, leading to a high resolution time-frequency representation of the signal, called HR-ogram. The application of these algorithms to music signals, made difficult by the high dynamics and the presence of colored noise, has required the tuning of well-adapted preprocessing techniques. The whole tool is now mature, and allows a high quality separation of the tonal part of various musical sounds. This research is supported by the French ANR under contract ANR-06-JCJC-0027-01 (DESAM).

2:20

5aMUe8. Towards an adaptive subspace-based representation of musical spectral content. Bertrand David (Télécom Paristech (ENST)/TSI - CNRS LTCI, 46, rue Barrault, 75634 Paris Cedex 13, France, bertrand.david@enst.fr), Roland Badeau (Télécom Paristech (ENST)/TSI - CNRS LTCI, 46, rue Barrault, 75634 Paris Cedex 13, France, roland.badeau@enst.fr)

This study presents an algorithm based on an adaptive framework model for musical sound signals assumed to be composed of slowly varying frequency components surrounded by additive noise. These components appear as contours in a time-frequency representation, as for instance, a spectrogram. To extract these contours, an often used solution is to estimate the parameters (amplitude, frequency, and phase) of each component at each frame and then to link them from one to the next with the help of a distance measure or an HMM. Conversely, our method attempts to *update* the estimated values from one time instant to the next. It relies on principal subspace tracking (with respect to time) together with gradient descent to individually update each of the component parameters. Finally, each extracted contour, which represents the frequency and amplitude variation of a single component, is available for subsequent

processing. Applications are demonstrated in the fields of harmonic plus noise decomposition and analysis/transformation/synthesis. This research is supported by the french Institut Telecom, TAMTAM project.

2:40

5aMUe9. Damped sinusoids and subspace based approach for lossy audio coding. Olivier Derrien (Université de Toulon, Av Georges Pompidou, BP 56, 83162 La Valette du Var, France, olivier.derrien@univ-tln.fr), Gaël Richard (Télécom Paristech (ENST) /TSI - CNRS LTCI, 46, rue Barrault, 75634 Paris Cedex 13, France, gael.richard@enst.fr), Roland Badeau (Télécom Paristech (ENST)/TSI - CNRS LTCI, 46, rue Barrault, 75634 Paris Cedex 13, France, roland.badeau@enst.fr)

The new subspace-based techniques recently introduced appear to be well adapted for the parameters estimation of a damped sinusoids + noise signal model. These high-resolution (HR) methods have a better frequency resolution than the Fourier analysis, but they are rarely used in audio coding. Although HR methods would be suitable for parametric coding at low bitrates, we show that they are also efficient for high-bitrate coding where state-of the art codecs are usually transform-based. Our coding scheme first includes a 8-band PQMF filter-bank decomposition. Then, each subband signal is segmented in onsets and a maximum-order HR analysis is performed on each segment with the ESPRIT algorithm. For each component of the model, frequency, damping, amplitude and phase are quantized. The residual signal is not coded. This codec is compared to a MDCT framework, where transform and quantization are the same as in a MPEG-AAC but without inclusion of perceptual modelling and entropy coding. Preliminary objective and subjective tests show the potential of this approach which requires, on mostly tonal signals, significantly less bits than the traditionnal MDCT method for a given quality.

3:00

5aMUe10. Auditory model based analysis of polyphonic music. Anssi Klapuri (Tampere University of Technology, Korkeakoulunkatu 1, 33720 Tampere, Finland, anssi.klapuri@tut.fi)

This study is about the use of an auditory model to extract multiple pitches from polyphonic music signals. One goal was to identify the conditions where pitch analysis using an auditory model is advantageous over more conventional time or frequency domain approaches. It is shown that these conditions include especially the processing of band-limited signals or signals where important parts of the audible spectrum are corrupted by band-limited interference. An efficient implementation strategy is described which reduces the computational complexity of the auditory model roughly by factor 10. Further prospects of bandwise processing and redundant signal representations in general are discussed.

3:20

5aMUe11. On perceptual distortion measures and parametric modeling. Mads G. Christensen (Aalborg University, Niels Jernes Vej 12 A, DK-9220 Aalborg, Denmark, mgc@es.aau.dk)

Over the past two decades, there has been much interest in incorporating human sound perception in signal processing algorithms, often in the form of perceptual distortion measure or an approximation thereof. An example of this is MDCT-based audio coding where a good quality can be achieved at very low bit-rates by taking masking effects into account. More recently, the same principles have been applied to parametric modeling and coding of audio signals. We discuss the inherent tradeoffs in choosing a perceptual distortion measure and a parametric model and the pros and cons of various ways of implementing such perceptual distortion measures is discussed. An important question that we seek to answer is whether perception should be taken into account in the estimation of model parameters or this should be done in a separate step.

Contributed Paper

3:40

5aMUe12. Efficient coding of a xylophone sound using spikogram nonredundent coding. Rolf Bader (University of Hamburg, Institute of Musicology, Neue Rabenstr. 13, 20354 Hamburg, Germany, R_Bader@t-online.de)

Sensory systems try to use the incoming data most efficiently. Studies of Lewicki et al. lately showed, that a representation of a spike train just representing the sound and not having any redundancy is how the auditory system of the cat represents incoming sounds. To compare this theory with musical instruments, a xylophone sound was analyzed in terms of a spikogram. Here, gammatones of a 64 channel filterbank with different attack and decay values are superposed in a way to reconstruct the original sound. Only those gammatones were used which are needed to result in the sound used as input and so no redundancy is present in the analysis of the sound. It was found, that the most reasonable fit of the gammatone shape with the empirical data indeed made the representation most efficient and so the xylophone sound is most easily represented by the auditory system. Although more analysis are needed here, musical instruments could show up to be built in a way to fit a most efficient coding by listeners and so fulfill a middle-of-the-road rule of not too much and not too few information so that listeners are interested in but not overtaxed by the sounds.

4:00-4:20 Break

4:20

5aMUe13. A frequency shifting model of pitch. Paris Smaragdis (Adobe Systems Inc., 275 Grove St., Newton, MA 02466, USA, paris@media.mit.edu)

We present a model useful for tracking of melodies of sounds that can have arbitrary harmonic structure (including inharmonic instruments and noise sources). This model is based on a spectral shift assumption which is capable of tracking melodic movements of an instrument regardless of the irregularity of its spectrum. This technique can be used to simultaneously estimate the spectral character of the instrument to be analyzed in addition to its melody. It is capable of dealing with multiple instances of the same instrument, thereby recognizing chords as well as notes, and can also extract multiple melodies in audio signals composed out of many instruments.

4:40

5aMUe14. Modeling vocal sounds in polyphonic musical audio signals. Masataka Goto (National Institute of Advanced Industrial Science and Technology (AIST), IT, 1-1-1 Umezono, Tsukuba, 305-8568 Ibaraki, Japan, m.goto@aist.go.jp), Hiromasa Fujihara (National Institute of Advanced Industrial Science and Technology (AIST), IT, 1-1-1 Umezono, Tsukuba, 305-8568 Ibaraki, Japan, h.fujihara@aist.go.jp)

This paper describes our research aimed at modeling vocal sounds (singing voices) in available music recordings and its applications to singer identification, singer similarity, and lyrics synchronization. Our predominant-F0 estimation method, PreFEst, can obtain the melody line by modeling the input sound mixture as a weighted mixture of harmonic-structure tone models (probability density functions) of all possible F0s and estimating their weights and the tone models by MAP estimation. Since the PreFEst was designed for general melodies, we extended it to specialize in vocal melodies by using vocal timbre models --- vocal and nonvocal GMMs. Those GMMs are trained beforehand and used to evaluate the vocal probability. The GMMs are also used to identify vocal regions, but its strategy should depend on applications. For singer identification and singer-similarity calculation, since the purpose is to model singer's identity by training each singer's vocal GMM, certainly reliable vocal regions should be identified even if most true regions were missed. On the other hand, for lyrics synchronization, since the purpose is to align each phoneme to the estimated vocal melody, vocal regions should be identified without missing any true regions. We achieved this by biasing log likelihoods provided by vocal and non-vocal GMMs.

5:00

5aMUe15. Music and speech signal processing using harmonic-temporal clustering. Jonathan Le Roux (University of Tokyo, Sagayama/Ono Laboratory, 7-3-1 Hongo, Bunkyo-ku, 113-8656 Tokyo, Japan, leroux@hil.t.u-tokyo.ac.jp), Hirokazu Kameoka (NTT Communication Science Laboratories, NTT Corporation, 3-1 Morinosato wakamiya, 243-0198 Atsugi, Kanagawa, Japan, kameoka@eye.brl.ntt.co.jp), Nobutaka Ono (University of Tokyo, Sagayama/Ono Laboratory, 7-3-1 Hongo, Bunkyo-ku, 113-8656 Tokyo, Japan, onono@hil.t.u-tokyo.ac.jp), Alain De Cheveigne (CNRS, Universite Paris 5, Ecole Normale Superieure, 29 rue d'Ulm, 75230 Paris, France, alain.de.cheveigne@ens.fr), Shigeki Sagayama (University of Tokyo, Sagayama/Ono Laboratory, 7-3-1 Hongo, Bunkyo-ku, 113-8656 Tokyo, Japan, sagayama@hil.t.u-tokyo.ac.jp)

We present here the principle of the recently introduced harmonic-temporal clustering (HTC) framework and its applications in both music and speech signal processing. HTC relies on a precise parametric description of the harmonic parts of the power spectrum through constrained Gaussian mixture models. The model parameters of all the elements of the acoustical scene are estimated jointly by an unsupervised 2D time-frequency clustering of the observed power density. HTC is effective for multi-pitch analysis of music signals and F0 estimation of single and multiple speaker speech signals in various noisy environments. It also enables to perform extra processing of monaural music and speech signals, such as isolation or cancellation of a particular part, noise reduction and source separation.

5:20

5aMUe16. Timbre transposition based on time-varying spectral analysis of continuous monophonic audio and precomputed spectral libraries. James W. Beauchamp (University of Illinois, 1002 Eliot Drive, Urbana, IL 61801, USA, jwbeauch@uiuc.edu), Mert Bay (University of Illinois, 212 W. Healey, Apt. 303, Champaign, IL 61820, USA, mertbay@uiuc.com)

A sinusoidal model for solo musical sounds consisting of time-varying harmonic amplitudes and frequencies allows for convenient temporal and spectral modifications. With a harmonic model, analysis frames can be grouped by fundamental frequency (F0) and then clustered in terms of their harmonic spectra. The resulting cluster centroid spectra are used as spectral libraries. When continuous audio monophonic passages are analyzed in the form of harmonic components, F0 vs. time data are used to guide the extraction of parameters from the sound in order to find appropriate library spectra for resynthesis. Two methods for finding appropriate spectra are: (1) best rms match with the incoming spectra and (2) best spectral centroid match. These give similar results, but centroid matching yields smoother spectra over time. Timbre transposition is performed by using a library that belongs to another instrument. We have found that when the target instrument has a unique timbral quality based on its spectrum, the synthesis sounds mostly like that instrument. However, if the target instrument's spectral characteristic is not sufficiently differentiated from the source, the source timbral quality may dominate, probably due to its temporal behavior being transmitted. Results will be demonstrated by audio examples.

5:40

5aMUe17. Comparison of the sound of a grand and an upright piano using wavelets. Grigorios Plitsis (Greece, grigoriosplitsis@merseymail.com)

Wavelet analysis is useful for extracting patterns and thus analyzing signals. Although the Fourier analysis can reveal different features of a signal, it is less appropriate for describing transient phenomena and sudden sound changes. As a result, Fourier-based music reconstruction cannot exactly imitate the physical sound, as it is not possible to know at the same time a specific frequency as well as the time of occurrence of this frequency. Wavelet analysis is capable of highlighting different attributes of a signal. Different types of wavelets are thus used in the present study in order to compare the sound produced by a grand piano with that produced by an upright piano.

6:00

5aMUe18. Modeling of piano sounds using FEM simulation of soundboard vibration. Luis I. Ortiz-Berenguer (Universidad Politecnica de Madrid, Ctra.Valencia km7, 28031 Madrid, Spain, lortiz@diac.upm.es), Francisco J. Casajus-Quiros (Universidad Politecnica de Madrid, Ctra.Valencia km7, 28031 Madrid, Spain, javier@gaps.ssr.upm.es),David Ibanez-Cuenca (Universidad Politecnica de Madrid, Ctra.Valencia km7, 28031 Madrid, Spain, dibanez@alumnos.euitt.upm.es)

Pattern-matching methods for polyphonic transcription of piano sounds require a set of patterns that can be obtained by modeling the piano-sound spectra. The modeling should take into account not only the string stiffness but also the effect of the soundboard impedance on the string vibration. Studies on that effect corresponding to a wide range of impedance values have previously been carried out by the authors. However, actual impedance values for real pianos must be used in the model. Although the impedance value of a few grand-pianos have been measured by the authors, these results are not significative enough to create a model. Thus, a FEM simulation of soundboard vibration is proposed to obtain nearly-actual impedance values. The simulation considers several cases of vibrating plates from the simplest rectangular one and increasing the similarity to real piano soundboards. The quality of the simulation is verified comparing the obtained results with either recognized theoretical results for the simplest cases or measured values for the more complex ones. The complexity of the simulated soundboard is limited to the case that produces only slight variations in the modeled spectrum. [This work has been supported by Spanish National Project TEC2006-13067-C03-01/TCM.]

FRIDAY MORNING, 4 JULY 2008 ROOM 202/203, 11:00 A.M. TO 12:00 NOON

Session 5aMUf

Musical Acoustics: Plucked and Struck Idiophones II

Thomas D. Rossing, Cochair
Stanford University, CCRMA, Department of Music, Stanford, CA 94305, 26464 Taaffe Rd, Los Altos Hills, CA 94022, USA

Charles Besnainou, Cochair
Institut Jean le Rond d'Alembert, Laboratoire d'Acoustique Musicale, 11, rue de Lourmel, Paris, 75015, France

11:00

5aMUf1. Characterizing the sound of an African thumb piano (kalimba). David M.f. Chapman (Scientific Consultant, 8 Lakeview Avenue, Dartmouth, NS B3A 3S7, Canada, dave.chapman@ns.sympatico.ca)

The kalimba is an African percussion instrument whose notes are generated by vibrating metal tines of various lengths attached to sound board or sound box. Unlike a vibrating string or organ pipe, the overtone structure is anharmonic, that is, the overtone frequencies (which determine sound quality) are not simple integer multiples of the fundamental frequency (which determines pitch). The ratio of the first overtone to the fundamental is in the range 5.3-5.9, depending on the tine geometry. The vibrating tines are modeled as a clamped-supported-free beam and the observed overtone structure is shown to be in accordance with this model. Audio examples will be provided.

11:20

5aMUf2. The jew's harp, experimental study and modeling. Charles Besnainou (Institut Jean le Rond d'Alembert, Laboratoire d'Acoustique Musicale, 11, rue de Lourmel, 75015 Paris, France, chbesnai@ccr.jussieu.fr), Joel Frelat (Institut Jean le Rond d'Alembert, Lab. d'Acoustique Musicale, 11, rue de Lourmel, 75015 Paris, France, frelat@lmm.jussieu.fr),Adrien Mamou-Mani(Institut Jean le Rond d'Alembert, Lab. d'Acoustique Musicale, 11, rue de Lourmel, 75015 Paris, France, mamou-mani@lmm.jussieu.fr)

Under its archaic aspects jew's harp is a musical instrument highly subtle. Indeed, a metal blade (or wooden) attached to a rigid frame put into vibration by the musician, and coupled to the buccal resonator allow nice tune. The skilt of the jew's harp focuses on the conformations of this cavity whose function is to select the right components of the vibration to be amplify. In our study, we have modelled a playing technique which involves blowing during the blade vibrates. In the lake of breath, the spectre of sound produced by the blade is odd, i.e., it includes at first approximation odd components (n+1) multiple the fundamental. Whereas when the musician adds breath the spectrum turns into a spectrum containing all components of basic integer multiples (n). This work takes place in the context of studies of vibrating systems under prestress and loaded. In that case the load, and the prestress are generated by the musician breath by bending the blade On the other hand, experimental studies are compare with the model results.

11:40

5aMUf3. Sound of the HANG. Thomas D. Rossing (Stanford University, CCRMA, Department of Music, Stanford, CA 94305, 26464 Taaffe Rd, Los Altos Hills, CA 94022, USA, rossing@ccrma.stanford.edu), David

Wessel(Center for New Music and Audio Technologies, 1750 Arch Street, Berkeley, CA 94720, USA, wessel@cnmat.berkeley.edu.)

Previous studies of the HANG [T. D. Rossing, U. Hansen, F. Rohner, and S. Schärer, 142nd ASA meeting, December 2001; T. D. Rossing, A. Morrison, U. Hansen, F. Rohner, and S. Schärer, Proceedings of ISMA07, Barcelona, 2007] have discussed the modes of vibration and the sound radiation field of the HANG when note areas are excited by sinusoidal force. Since the HANG is a hand-played steel instrument, a wide variety of playing techniques are used by various performers. We report on the sound of the HANG when played in various ways. Recordings of the HANG were made with a hemispheric microphone array. The instrument was excited by taking multiple samples of each of a number of striking techniques with the hand. These include single strokes from the soft part of the finger, as well as, the finger nail itself. Various grace note techniques like flams were also investigated. Damping was controlled by the time the finger remained in contact with the instrument, as well as, by using the palm. Force hammer measurements were also included. We report on these measurements and incorporate them in to an excited-resonance model of the instrument. Demonstrations of the real and modeled instrument will be provided.

Session 5aNSa

Noise and EURONOISE: Soundscape & Community Noise I

Bennett Brooks, Cochair
Brooks Acoust. Corp., 27 Hartford Turnpike, Vernon, CT 06066, USA

Brigitte Schulte-Fortkamp, Cochair
TU Berlin, Institute of Fluid Mechanics and Engineering Acoustics, Einsteinufer 25, Sekr. TA 7, Berlin, D-10587, Germany

Invited Papers

8:00

5aNSa1. Soundscapes: from noise annoyance to the music of urban life. Catherine Guastavino (Centre for Interdisciplinary Research in Music Media & Technology (CIRMMT) - School of Information Studies - McGill Univ., 3459 McTavish, Montreal, QC H3A1Y1, Canada, Catherine.Guastavino@mcgill.ca), Danièle S. Dubois (CNRS, LCPE/LAM 11 rue de Lourmel, 75015 Paris, France, ddubois@ccr.jussieu.fr)

Through an overview of empirical research over the past ten years, we present an interpretation of the evolution of the concept of soundscape. From a strictly acoustic definition in terms of physical descriptors, it evolved into a more complex notion integrating the effects of noise on citizens. Soundscape research therefore requires the contribution of human sciences (psychology of perception, cognitive psychology, sociology, anthropology of senses). There is converging evidence that people judgments of noise is related to the meaning given to the activities producing the noise. Consequently, physical descriptions in acoustics have to face the diversity of human reactions to noise correlated with the diversity of activities, the diversity of source producing noises within a diversity of physical environments (natural, architectural). This paper focuses on major emerging issues in soundscapes research, namely - the integration of such a diversity of pieces of knowledge within a general knowledge - the translation of these diverse conceptualizations into physical descriptions - the elaboration of convincing physical measurements for decision makers. We will draw consequences for further developments in the cooperative and pluridisciplinary research and for producing guidelines for new orientations in community policies.

8:20

5aNSa2. The soundscape of church bells - sound community or culture clash. Brenda H. Kiser (DL Acoustics, 14301 Middletown Lane, Westminster, CA 92683, USA, brendakiser@ix.netcom.com), David Lubman (DL Acoustics, 14301 Middletown Lane, Westminster, CA 92683, USA, dlubman@dlacoustics.com)

Church bells have long communicated important information to the surrounding community, creating a sound neighborhood. The community relied on the sound neighborhood to learn of events such as weddings, births and deaths, impending danger, church services, and the curfew. The bells thus provided communal identity. This paper reviews the sound neighborhood created by the bells of the church of St. Mary-le-Bow in the City of London, popularly known as "Bow Bells." The ringing of these bells has for centuries defined London's Cockneys and has featured in London's folklore and history since the 14th century. The current status of the soundscape is presented. Sound examples are given. This paper also discusses the future of the soundscape of church bells in light of current societal changes.

8:40

5aNSa3. How is hearing heard in second year architectural design education? Juergen Bauer (Waterford Institute of Technology, Cork Road, IRE - 00000 Waterford, Ireland, jbauer@wit.ie)

Architects are often accused of "not being interested in acoustics because it is invisible". Surely, architectural design, particularly at preliminary stage, has always been driven visually: architects usually develop a project by vision, not by hearing. On the other hand, designing architects have to deal creatively with more or less invisible parameters: sociocultural demands, climatic aspects as wind or temperature, or even daylight which can be considered to be visible but certainly is everything but constant. If an architect's design

ability is about observation and awareness, and to give an example, if light is considered to be much more than just being bright or dark, how then could we implement early awareness that sound is much more than noise or silence, and that sound planning is much more than just using anti-noise-panels? We asked second year architecture students at Waterford Institute of Technology to (re-)think the architecture of schools and to question the sound qualities and their own sound recollection of such an environment. The paper will outline the teaching approach and present some student's responses to the given aims and brief. Finally, the lessons learnt by teaching staff will be summarized.

9:00

5aNSa4. Using the soundscape approach to develop a public space in Berlin - perception and evaluation. Brigitte Schulte-Fortkamp (TU Berlin, Institute of Fluid Mechanics and Engineering Acoustics, Einsteinufer 25, Sekr. TA 7, D-10587 Berlin, Germany, brigitte.schulte-fortkamp@tu-berlin.de), Rudi Volz (Advacoustics, Leibnizstr.21, Dr. Rudi Volz, 10625 Berlin, Germany, volz@advacoustics.de), Andre Jakob (TU Berlin, Institute of Fluid Mechanics and Engineering Acoustics, Einsteinufer 25, Sekr. TA 7, D-10587 Berlin, Germany, kontakt@advacoustics.de)

In Berlin the Soundscape Project "Nauener Platz" is carried out to rebuild a difficult public space into a space which is dominated by social freedom. A designed space related procedure is developed following the soundscape approach, which will provide acoustical indicators and parameters describing urban and other outdoor living areas with respect to physical conditions and their relevance for life. The measurement of outdoor sound quality will take into consideration not only the sound pressure but also the characteristics of the sounds which lead to specific human reactions, both positive and negative: calmness, inspiration, annoyance, discontentment, anxiety, etc. and the pathogenic effects. Qualitative evaluations through soundwalks and open interviews have been conducted introducing the new experts. Framework and procedure will be discussed. The Soundscape Project is a module of the Project "Nauener Platz - Remodelling for Young and Old"in the framework of the research program "Experimental Housing and Urban Development (ExWoSt)" of the "Federal Ministry of Transport, Building, and Urban Affairs (BMVBS)" by the "Federal Office for Building and Regional Planning (BBR)". It is related to the fields of research (ExWoSt) concerned with ″Innovation of Urban Neighbourhoods for Families and the Elderly″. The project executing organization is the Regional Office Berlin-Mitte.

9:20

5aNSa5. Using the soundscape approach to develop a public space in Berlin - measurement and calculation. Rudi Volz (Advacoustics, Leibnizstr.21, Dr. Rudi Volz, 10625 Berlin, Germany, volz@advacoustics.de), Andre Jakob (TU Berlin, Institute of Fluid Mechanics and Engineering Acoustics, Einsteinufer 25, Sekr. TA 7, D-10587 Berlin, Germany, kontakt@advacoustics.de), Brigitte Schulte-Fortkamp (TU Berlin, Institute of Fluid Mechanics and Engineering Acoustics, Einsteinufer 25, Sekr. TA 7, D-10587 Berlin, Germany, brigitte.schulte-fortkamp@tu-berlin.de)

In this contribution the Soundscape Project "Nauener Platz" in Berlin is subject to different measurement- and calculation methods to develop acoustical indicators and parameters into a database describing urban and other outdoor living areas with respect to physical conditions and their relevance for life. The "Nauener Platz" is carried out to rebuilt a difficult open space into a space which is dominated by social freedom. To obtain the physical quantities sound pressure levels in 1/3-octave bands were measured and artificial head recordings were taken to describe the current state. Combined with calculations using noise prediction software it was possible to verify the sound propagation data outside according to the measurements and allow predictions about planned arrangements. First estimations of these measurements and calculations will be presented. The Soundscape Project is a module of the Project "Nauener Platz - remodelling for young and old". This project is in the framework of the research program "Experimental Housing and Urban Development (ExWoSt)" of the "Federal Ministry of Transport, Building, and Urban Affairs (BMVBS)" by the "Federal Office for Building and Regional Planning (BBR)". It is related to the fields of research (ExWoSt) concerned with "Innovation of Urban Neighbourhoods for Families and the Elderly". The project executing organization is the Regional Office Berlin-Mitte.

9:40-11:00 Posters

Lecture sessions will recess for presentation of poster papers on various topics in acoustics. See poster sessions for topics and abstracts.

Invited Papers

11:00

5aNSa6. Applicability of advanced measurement techniques to soundscape studies. André Fiebig (HEAD acoustics GmbH, Ebertstrasse 30a, 52134 Herzogenrath, Germany, andre.fiebig@head-acoustics.de), Klaus Genuit (HEAD acoustics GmbH, Ebertstrasse 30a, 52134 Herzogenrath, Germany, klaus.genuit@head-acoustics.de)

A wide range of measurement systems and analysis techniques were applied in previous soundscape studies to document and describe the physical conditions of the scrutinized area. Monaural and binaural recording systems positioned at different measurement points are frequently used, and the collected recordings are played back with headphones or sophisticated loudspeaker arrangements in specific surroundings for further analyses. In the paper, an overview of measurement and playback technologies applied in soundscape studies will be given and the immanent problems related to certain recording and playback systems will be discussed, e.g., measurement accuracy and expense, costs, etc. Furthermore, soundscape researchers have started to establish more and more a pool of specific analyses, which allows - at least partially - the detection of relevant (acoustical) patterns and features as well as a first classification of soundscapes. This allows even the detection of positively experienced environments. However, varying measurement technologies and procedures used in different soundscape studies lead to the problem that the studies and the obtained analysis results are often difficult to compare. The present paper takes up this problem and deals with developing a common basis of measurement techniques and procedures.

11:20

5aNSa7. Analysis and evaluation of traffic sounds. Jens Guettes (TU Berlin, Institute of Fluid Mechanics and Engineering Acoustics, Modersohnstr.64, 10245 Berlin, Germany, jensguettes@gmx.de)

This work focuses on a residential area in Friedrichshain, a district close to the centre of Berlin. A soundscape analysis was made in this area, where the neighbours spent most of their free time, especially their leisure time. Basically, our measurements pointed out that immissions into the flats are mainly due to the low-frequency range under 200 Hz, in particular in the case of closed windows. In addition, this low-frequency range initiates standing waves and vibrations within the flats, causing annoying secondary sounds. Furthermore, effects arose, caused by an impulsive signal structure and a discontinuity in the time structure of the source signals, depending on the street pavement and on the traffic situation. With regard to that point, different physical and perceptive measurement and analysis methods were compared and interviews within the neighbourhood were conducted. Moreover, we tried to correlate the results of the survey with those of our measurements in order to see advantages and disadvantages of the applied methods. The scope of A-weighted measurements was then critically considered. Different ways will be discussed about how the complex evaluation of traffic sounds in the future could be based more on neighbours' perception and needs.

11:40

5aNSa8. Soundscape design methods to acheive net zero environmantal noise impacts. Gary W. Siebein (Univ. of Florida, 231 Arch, P.O. Box 115702, Gainesville, FL 32611, USA, gsiebein@siebeinacoustic.com), Robert M. Lilkendey (Siebein Associates, Inc., 625 NW 60th Street, Suite C, Gainesville, FL 32607, USA, rlilkendey@siebeinacoustic.com), Hyun Paek (Siebein Associates, Inc., 625 NW 60th Street, Suite C, Gainesville, FL 32607, USA, hpaek@siebeinacoustic.com)

Soundscape design methods were developed to approach net zero environmental noise impacts for significant building projects in complex settings. Auralization methods for various design alternatives were presented for stake holder review in a large auditorium and in a full size demonstration in the actual environment. Innovative acoustical design and analysis methods were developed to economically reduce source noise levels to the vicinity of the ambient sound level. Methods to determine the nature of the ambient sound level as it varies with time of day, time of year, and other natural and community factors included a series of long term average A-weighted sound levels as well as more detailed octave band measurements and calibrated aural recordings of specific acoustic events. Sound walks were conducted at various times of day to understand the dynamics of the acoustical environment and to identify issues. Focus group discussions among stakeholders and team members developed the long term plans for the community and appropriate architectural and acoustical design criteria for the project.

12:00

5aNSa9. The influence of subjective response on the choice of measurement for aircraft arrival noise at Nantucket Airport. Nancy Timmerman (Nancy S. Timmerman, P.E., 25 Upton Street, Boston, MA 02118-1609, USA, nstpe@hotmail.com)

The Nantucket Airport in Massachusetts serves primarily turboprop commuter aircraft, and private or charter jets, with most of its operations in the summer. A seasonal homeowner was severely affected by arrival flight noise and requested noise measurements and noise control recommendations for this architect-designed residence. Time was spent with the homeowner to understand steps already taken, and problems still causing trouble. Standard measurement procedures for aircraft operations in the United States call for the use of A-weighted, slow response for the assessment of noise impact. Since the noise sources at this airport have strong tonal components (from the propellers), and noise control recommendations were sought, one-second 1/3-octave band levels were used to both document the observed problem, and to estimate the field transmission loss of the windows and doors. Measurements were made during a Friday afternoon, when arriving aircraft were mostly 1.5 to 2 min apart. A-weighted maximum and single event levels (SELs) were also measured for each overflight, for comparison with published aircraft data. A "short circuit" was found due to an exposed vent pipe, which resulted in no transmission loss in the 100 Hz band. Appropriate recommendations were made.

Contributed Paper

12:20

5aNSa10. Are perceived soundscapes within urban parks restorative? Sarah R. Payne (The University of Manchester, SED, MARC, Oxford Road, M13 9PL Manchester, UK, sarah.payne@postgrad.manchester.ac.uk)

The perceived quality of urban park soundscapes is starting to be explored, and attention restoration research has shown which environments are generally restorative. Yet the effect of perceived soundscapes on individuals' restorative experiences is hardly known. Natural environments, in general, provide restoration for people, including recovery from attentional fatigue and enabling reflection. Therefore the visually "natural" environment of urban parks provides a useful setting to explore the role of varying soundscapes in restoration. Four hundred park users within Sheffield, UK, were surveyed as they left two urban parks. Data were collected on aspects of their park visit, along with measures of their current perceived restoration. Participants' perceived soundscapes were described by the amount of time they heard certain sound types in the park, and the volume at which they heard them. Sound levels [LAeq, dB(A)] within the parks were also monitored on a number of days to provide contextual information. Results of the study will be discussed along with the importance of soundscape quality and individuals' restorative experiences in helping to provide a productive and positive quality of urban life.

12:40-2:00 Lunch Break

2:00

5aNSa11. Perceptive relevance of soundscape descriptors: a morpho-typological approach. Jean-Dominique Polack (Institut Jean le Rond d'Alembert, Laboratoire d'Acoustique Musicale, 11, rue de Lourmel, 75015 Paris, France, polack@ccr.jussieu.fr), Jacuqes Beaumont (INRETS - Laboratoire Transports et Environnement, 25, avenue François Mitterrand, 69675 Bron Cedex, France, jacques.beaumont@inrets.fr), Christine Arras (Acouphen, 33 route de Jonage - BP 30, 69 891 Pusignan Cedex, France, christine.arras@acouphen.fr), Mikael Zekri (Institut Jean le Rond d'Alembert, Laboratoire d'Acoustique Musicale, 11, rue de Lourmel, 75015 Paris, France, mikael.zekri@gmail.com), Benjamin Robin (INRETS - Laboratoire Transports et Environnement, 25, avenue François Mitterrand, 69675 Bron Cedex, France, benjamin.robin@inrets.fr)

For assessing the validity of a morpho-typological classification of urban sounds with respect to sound assessment, factor analysis was applied to a database compiled in the city of Lyon and lead to a four-classes classification based on the number of lanes and whether a street is one-way or not. Free categorisation was then carried out on sound excerpts recorded in different sites corresponding to different classes. The main results are: a corpus of 42 h of five-channel recordings of a choice of sites from the classification at different times of the day; the validation of the relevance of the morpho-typological classification for perception; and a confirmation of the semantic oppositions between sources and background noise, as well as holistic and event sequences. Further, annoyance is controlled by the absence or the presence of human or nature sound sources, pleading for research toward automatic identification of sources. Last, categorisation confirms earlier investigations based on variance analysis: in narrow and large streets, traffic increase differently governs the increase of both noise level and annoyance.

2:20

5aNSa12. Environmental management of a large construction site in a densely populated urban area: an innovative approach to noise and vibration mitigation. Marco Masoero (Politecnico di Torino, Corso Duca degli Abruzzi 24, 10123 Torino, Italy, marco.masoero@polito.it), Carlo Alessandro Bertetti (Studio Progetto Ambiente s.r.l., Corso Rosselli 44, 10128 Torino, Italy, ac.bertetti@progambiente.it)

An innovative approach to noise and vibration mitigation has been applied to the construction of a new underground railway. The aim is to overcome the difficulties in respecting noise level limits in densely populated areas, as specified by current legislation, even with state-of-the-art technology (e.g., low-emission machinery, noise barriers, etc.). The proposed approach aims at integrating the construction activity in the urban soundscape, placing maximum emphasis on construction organisation measures (e.g., construction activity scheduling and execution, training and information of contractor's personnel, etc.) and on communication and involvement of the exposed population. In this respect, two key figures have been identified: the first is an environmental engineer permanently assisting the construction manager in all the environmental impact issues; the second consists of a sample of population for which the subjective reaction to noise is monitored and fed back to the construction manager. Results are presented and discussed for one of the main construction sites in central Turin.

2:40

5aNSa13. The application of the soundscape approach in the evaluation of the urban public spaces. Monika Rychtarikova (Lab. ATF, Katholieke Universiteit Leuven, Celestijnenlaan 200D, B-3001 Leuven, Belgium, Monika.Rychtarikova@bwk.kuleuven.be), Gerrit Vermeir (Lab. ATF, Katholieke Universiteit Leuven, Celestijnenlaan 200D, B-3001 Leuven, Belgium, Gerrit.Vermeir@bwk.kuleuven.be), Markieta Domecka (Centre for Sociological Research, K.U. Leuven, Parkstraat 45, 3001 Leuven, Belgium, markieta.domecka@soc.kuleuven.be)

An important issues in the development of European cities is the design and renovation of the urban public areas. Typically, broad variety of approaches (sociological, ecological, environmental, physical, etc.) is needed. Earlier studies show the necessity of the transversal multidisciplinary approach in this issue. In order to study the acoustical dimension, the concept of soundscape needs to be proposed and elaborated. Soundscape approach differs from the classical statistical noise analysis in the evaluation of a context-related noise and in the extrapolation of environmental sounds in its complexity. Nowadays, even by using recently developed sophisticated acoustical and psycho-acoustical measurable and quantifiable parameters, it still remains difficult to grasp the complete meaning of a soundscape in words only or by numbers only. Our hypothesis is that the description of the city soundscape might be successfully done by combination of acoustical numbers and words. This article will propose a method for acoustical characterization of urban areas in the framework of the Belgian federal project: SD/TA/05A Design and renovation of urban public spaces towards sustainable cities (DRUPSSuC).

3:00

5aNSa14. Subjective evaluation of community noise in Canada's National Capital Region and its relation to waking levels of salivary biomarkers. David S. Michaud (Health Canada, 775 Brookfield Road, Ottawa, ON, Ottawa, ON K1A1C1, Canada, dmichaud@hc-sc.gc.ca), Stephen E. Keith (Health Canada, 775 Brookfield Road, Ottawa, ON, Ottawa, ON K1A1C1, Canada, skeith@hc-sc.gc.ca), Jason Tsang (Health Canada, 775 Brookfield Road, Ottawa, ON, Ottawa, ON K1A1C1, Canada, jtsang@hc-sc.gc.ca), Anne Konkle (Health Canada, 50 Columbine Driveway, Tunney's Pasture, Ottawa, ON K1AOK9, Canada, akonkle@hc-sc.gc.ca)

Some research has suggested an association between long-term exposure to traffic noise and relative risk of cardiovascular disease (Babisch et al., 2005; Willich et al., 2006). It has been assumed that noise may act as a nonspecific stressor. Acute exposure to noise can evoke physiological and behavioural changes reminiscent of a stress response in rodents (Michaud et al., 2003), but it is equivocal that this occurs in humans chronically exposed to traffic noise. This pilot project examined annoyance to community noise and salivary biomarkers known to be influenced by stressor exposure. A face-to-face interview subjectively assessed community noise for 60 residents (30 males, 30 females; mean age 41.3, SD = 14.98). Traffic sound levels will be determined and respondents categorized into high ($>$65 dBA, Leq24) and low ($<$50 dBA) noise areas. Participants also provided saliva samples upon awakening, 30-min after awakening, and prior to bedtime. Concentrations of salivary biomarkers of alpha-amylase and cortisol were spectrophotometrically determined using commercial enzyme-linked immunosorbant assays. Two-way (high-noise versus low-noise) mixed-model analyses of variance will examine differences in questionnaire and salivary responses. Sex differences will be evaluated with independent t-tests, and polynomial regression analyses will relate salivary biomarker levels to high- or low-noise areas.

3:20

5aNSa15. Processing of long-term acoustic measurements. Laurent Faiget (01dB-Metravib, 200 Chemin des Ormeaux, F-69578 Limonest, France, laurent.faiget@01db-metravib.com), Benoit Plassat (01dB-Metravib, 200 Chemin des Ormeaux, F-69578 Limonest, France, benoit.plassat@01db-metravib.com), Stéphane Bloquet (01dB-Metravib, 200 Chemin des Ormeaux, F-69578 Limonest, France, stephane.bloquet@01db-metravib.com), Christine Aujard (01dB-Metravib, 200 Chemin des Ormeaux, F-69578 Limonest, France, christine.aujard@01db-metravib.com)

Many standards and European directives relative to noise are used to assess an acoustic situation, based on long-term indicators such as Lday, Lnight or Levening. These indicators are defined mainly as the mean yearly equivalent acoustic level on a particular part of the day. Acoustic measurements are performed on reference periods representative of the typical acoustic situation. An Oper@ monitoring system performed measurements for two years on several points. An acoustic database of the one-second integration time measurement was created. Different kinds of calculations were performed on these data, the variant being the measurement time considered. This study evaluates the convergence of the classic equivalent level with these long-term indicators.

3:40

5aNSa16. The association between residential quality of life and aircraft noise annoyance around Frankfurt Airport. Dirk Schreckenberg (ZEUS GmbH, Sennbrink 46, 58093 Hagen, Germany, schreckenberg@zeusgmbh.de)

A large field study on aircraft noise annoyance with 2312 residents from 66 areas within a radius of 40 km around Frankfurt Airport was performed between the announcement and implementation of the airport extension (4th runway). For the address of each participant aircraft noise levels were calculated. This presentation concentrates on results with regard to the relationship between perceived - not noise-related - environmental situation and social quality of life in the residential area (i.e. infrastructure, economic development, neighbours, attractiveness of the area) and aircraft noise annoyance. Furthermore the impact of actual perceived residential situation and the expected future situation after airport extension on noise annoyance before the change in aircraft noise exposure occurs is compared. Results of the analyses will be presented and discussed.

4:00-4:20 Break

4:20

5aNSa17. Ergonomics of intern environments: privacy and reactions to noise pollution. G. Mario Mattia (Bruel Acoustics S.r.l. - EuroAcustici, Viale Cesare Pavese 304, 00144 Roma, Italy, m.mattia@euroacustici.org) , Per V. Bruel (Bruel Acoustics S.r.l. - EuroAcustici, Viale Cesare Pavese 304, 00144 Roma, Italy, bruel@mclink.it)

The acoustical ergonomic is an important target for any room acoustics, intelligibility and community noise. The authors explain the experience on metrological and neuropsychological approach to the human reaction to noise. Environmental sound quality, room acoustics and interference of perceived sound (interference with the privacy) can start subjective effects and strong reaction by humans. The author explains experience and research of human reactions on noise interference, privacy, stress, ... annoying sounds (also with very low levels), rooms with stationary waves, long reverberation time, low acoustical building insulation, are the first cause of complain from the community. We suggest noise limits, international standards, neuropsychological interpretation of the acoustical annoyance.

4:40

5aNSa18. Noise annoyance indicators for various industrial noise sources: Results and comparisons. Marion Alayrac (EDF R&D, 1 avenue général de Gaulle, 92141 Clamart Cedex, France, marion.alayrac@edf.fr), Stéphanie Viollon (EDF R&D, 1 avenue général de Gaulle, 92141 Clamart Cedex, France, stephanie.viollon @edf.fr), Catherine Marquis-Favre (Université de Lyon, Ecole Nationale des Travaux Publics de l'Etat, CNRS, URA 1652, Département Génie Civil et Bâtiment, 3, rue Maurice Audin, 69120 Vaulx-en-velin, France, Catherine .MARQUIS@entpe.fr)

Characterizing the environmental impact of an industrial plant goes through a better understanding of the noise annoyance caused by industrial noise sources, which are numerous and various. A first step was to construct a perceptive typology of various industrial noise sources from a categorization test and based on perceived similarities. Now, laboratory tests are carried out, for each perceptive category separately, through the same experimental procedure, by testing the influence of the sound pressure level and of the noise spectral characteristics (low frequency noise, tonal noiseœ) on noise annoyance. The effect of spectral modifications due to the noise propagation on noise annoyance is also assessed. Subjects have also to judge the annoyance induced by an ambient noise exposure, built with a background noise and an industrial noise for which the emergence level is controlled. Different types of background noises are studied. Through a statistical analysis, indicators are developed for each perceptive category, based on classical indicators such as sound pressure level or loudness (for instance), or on indicators improved to suit spectral characteristics noticed. In this paper, the results of those listening tests are detailed and compared.

5:00

5aNSa19. Soundscape characterization in selected areas of Central London. Gianluca Memoli (Imperial College London, Department of Chemical Engineering, Exhibition road, SW7 2AZ London, UK, g.memoli@imperial.ac.uk), Alan Bloomfield (Greater London Authority (GLA), City Hall, The Queen's Walk, SE1 2AA London, UK, Alan.Bloomfield@london.gov.uk), Max Dixon (Greater London Authority (GLA), City Hall, The Queen's Walk, SE1 2AA London, UK, max.dixon @london.gov.uk)

The Mayor of London's Ambient Noise Strategy 'Sounder City' is the first UK public policy document to promote, not just noise reduction, but positive soundscape management. For its prescriptions to be put into full effect, psychoacoustic methods are needed to characterize existing areas where action may be needed to counteract existing noise pollution. To this aim, the soundscape characterization of two different areas in Central London will be presented in this work, where the two selected parks have in common the presence of a heavily trafficked road nearby. The acoustical experience of passers-by will be mapped using an indicator related to the time history of sound energy, related in previous studies to people's perceptions. Comparison with the same description performed by classical psychoacoustic parameters and perspectives for innovative, positive soundscape based actions will be discussed.

5:20

5aNSa20. Social survey on the road traffic noise effect on the quality of life in Moroccan cities. Weam Kharbaoui (Ecole Supérieure de Technologie de Salé, Laboratoire Energétique Matériaux et Environnement, Avenue du Prince Héritier, BP 227, 10000 Salé, Morocco, alex_weam @yahoo.es), Mohammed Garoum (Ecole Supérieure de Technologie de Salé, Laboratoire Energétique Matériaux et Environnement, Avenue du Prince Héritier, BP 227, 10000 Salé, Morocco, garoum1 @yahoo.fr), Abdelaziz Bahoussa (Ecole Supérieure de Technologie de Salé, Laboratoire Energétique Matériaux et Environnement, Avenue du Prince Héritier, BP 227, Salé, Morocco, abahoussa@yahoo.fr), Mohammed Rhachi (Ecole Supérieure de Technologie de Salé, Laboratoire Energétique Matériaux et Environnement, Avenue du Prince Héritier, BP 227, 10000 Salé, Morocco, mrhachi@hotmail.com)

Because of the fast growth of the urbanisation, the noise road traffic causes annoyance, and a wide range of negative effects on the health in many Moroccan urban areas. This problem becomes so serious that it is necessary to develop an adequate global noise policies, regulations, and laws. Unfortunately there is a lack of sufficiently technical, scientific, and social data allowing a precise evaluation of this pollution. The objective of this work is to complete our preliminary social survey and make a further step in the evaluation of the Moroccan urban community response to road traffic noise. The questionnaire used contains 55 closed and open questions and was performed using the ISO-15666 recommendations. The sample was composed of 1200 adults chosen randomly in Rabat, Salé and Tetouen cities. The targeted population consisted on persons of both sexes of 18 and more years old. According to the road traffic condition in Moroccan cities, results were analysed and compared with those obtained in several European cities.

5:40

5aNSa21. Advanced acoustical material tuned for low frequency noise reduction: a case study. Kathleen Kondylas (NEVA Associates Noise Control, 15 Beck Street, Newburyport, MA 01950, USA, kondylas@earthlink.net), Natalia Levit (DuPont, 5401 Jefferson Davis Highway, Richmond, VA 23234, USA, natalia.v.levit@usa.dupont .com), Joseph A. King (DuPont, 5401 Jefferson Davis Highway, Richmond, VA 23234, USA, joseph.a.king@usa.dupont.com), Chris R. Fuller (Virginia Tech, 131 Durham Hall, Blacksburg, VA 24061, USA, christopher.r.fuller@nasa.gov)

Low frequency noise is a significant annoyance at very low amplitudes, particularly when outdoor community noise from mechanical equipment penetrates commercial and residential building structures. Mid and high frequencies are selectively attenuated by the exterior walls. However, mitigation of the low frequency noise has been very challenging due to the longer wavelength and higher energy. This work presents case studies of an ad-

vanced acoustical material in typical metal panels to mitigate community noise from outdoor mechanical equipment. These advanced materials were developed with a unique combination of patented acoustical and vibration absorbing technology, based of distributed absorbers, layered with standard acoustic materials. The materials provide enhanced low frequency noise (below 300 Hz) over state of the art 10 cm metal panels filled with the fiberglass absorber. The case studies demonstrate superior acoustic performance in low frequency without substantial increase in weight.

6:00

5aNSa22. A study on the adaptation of soundscape to covered spaces: Part 2. Asli Ozcevik (Yildiz Technical University Faculty of Architecture, Chair of Building Physics, Besiktas, 34349 Istanbul, Turkey, aozcevik@hotmail.com), Zerhan Yuksel Can (Yildiz Technical University Faculty of Architecture, Chair of Building Physics, Besiktas, 34349 Istanbul, Turkey, karabi@yildiz.edu.tr)

This study is the second part of a research on the Adaptation of soundscape to covered spaces. A modern and a historical shopping center were compared and evaluated by means of subjective and objective evaluations. The consistency of the objective (time histories) and subjective (listening tests) findings showed that covered commercial areas may have a specific sound environment. The formation of streets is generally the basic spatial design concept that connects open and closed shopping areas. Therefore one of the studies that authors proposed at the previous paper was the comparison of open and closed shopping areas. In this study the soundscapes of a modern and a traditional street having shopping as a basic function will be determined by soundwalks and listening tests, and the findings will be compared with those of the previous studies.

FRIDAY MORNING, 4 JULY 2008 ROOM 251, 8:00 TO 10:00 A.M.

Session 5aNSb

Noise, Architectural Acoustics, and EURONOISE: Noise, Vibration and Acoustics for Medical and Research Facilities and Their Occupants III

James West, Cochair
Johns Hopkins University, Department of Electrical Engineering, 3400 North Charles Street, Baltimore, MD 21218, USA

Jack B. Evans, Cochair
JEAcoustics, 1705 West Koenig Lane, Austin, TX 78756, USA

Marc Asselineau, Cochair
Peutz & Associés, 10 rue des Messageries, Paris, F75010, France

Erica Ryherd, Cochair
Woodruff School of Mechanical Engineering, Georgia Institute of Technology, Atlanta, GA 30332-0405, USA

Invited Papers

8:00

5aNSb1. Realistic floor vibration criteria for MRI operation: A compilation of case studies. Basel Jurdy (Sparling, 720 Olive Way Suite 1400, Seattle, WA 98101-1853, USA, bjurdy@sparling.com), Michael Yantis (Sparling, 720 Olive Way Suite 1400, Seattle, WA 98101-1853, USA, myantis@sparling.com)

Vibration criteria published by various magnetic resonance imaging (MRI) manufacturers have been found to be too conservative with respect to allowable floor vibration resulting from MRI operation. The floor vibration produced by the MRI operation is greater than the published criteria. Previous experience by the authors has shown that there is an allowable threshold for MRI operation induced vibration, above which the MRI will not operate properly. This paper reports results of a survey of structural floor systems for 1.5T and 3.0T MRIs that are working satisfactorily. The most common floor systems have been analyzed structurally using finite element analysis to determine the forced response to a standardized input. Measurement results for some of the floors during MRI operation is also included.

8:20

5aNSb2. Vibration case study - design challenges for meeting medical imaging manufacturer specifications. Chris Papadimos (Papadimos Group, 818 Fifth Avenue, Suite 207, San Rafael, CA 94901, USA, chris@papadimosgroup.com)

Manufacturer vibration specifications for medical imaging equipment impose formidable challenges particularly when locating such equipment on elevated floors, which is increasingly desirable for work flow and proximity to operating rooms and other support spaces in healthcare facilities. Urban sites can further complicate matters as such sites tend to often be near busy roads that are sources of vibration. Other internal sources of vibration that must be taken into consideration include occupant activities and operating building mechanical systems. All these conflicting interests need to be properly balanced and clearly evaluated; developing solutions requires a diligent and experienced design team. Some of the challenges that had to be overcome in order to develop vibration designs to accom-

modate medical imaging equipment such as CT Scanners and MRI's on elevated floors of a new healthcare facility are presented in this paper. Extensive site testing to evaluate design constraints and pre-existing conditions, avoidance of incompatible adjacencies and proper considerations in terms of space layouts, development of specialized floor designs and a clear understanding of imaging equipment manufacturer specifications are the key elements addressed in this paper.

Contributed Paper

8:40

5aNSb3. Noise in an Emergency treatment ward. Sergio Beristain (Mexican Institute of Acoustics, P.O. Box 12-1022, Narvarte, 03001 Mexico, D.F., Mexico, sberista@hotmail.com)

It is beign assessed the noise inside a typical social service Hospital in Mexico City, several sources and relevant areas have been identified and evaluated. This paper presents a detailed description of the Adults Urgency Room, where all the emergency cases are received and attended arround the clock. In this section of the hospital, forty to sixty patients are attended at the same time in a large open plan room, separated only by curtains, with only a few private rooms for doctors in order to attend incoming patients, trying to solve each case immediatelly, allow him/her entrance into the main room for full emergency treatment, or find a bed inside the hospital for a longer treatment. Noise sourcees are all over the place, and noise variablity is large.

Invited Papers

9:00

5aNSb4. Study case of a centre for biomedical analyses: the importance of an acoustic analysis of the current situation and definition of the targets to be achieved. Fabien Krajcarz (Gamba Acoustique, 2 rue de la Découverte, BP 163, 31676 Labege Cedex, France, fabien.krajcarz@acoustique-gamba.fr)

The French regulations concerning the limits on noise levels in medical establishments include the acoustic performances of existing buildings used to accommodate defined medical activities and in which the regulations are normally observed. Nevertheless, there are cases which are either outside the list of the buildings covered, or merit special treatment. One example is described here: a centre for biomedical analyses in a large regional teaching hospital covering a technical area of several hundreds square meters. This concentration of human activities and technical equipment without any acoustic attenuation measures was the spark for a considerable labour movement. In this article we describe the challenges of these situations, the pitfalls to be avoided and any post-project and design stage measures to be implemented.

9:20

5aNSb5. Use of a versatile acoustic room for audiology applications. Chantal Laroche (University of Ottawa, 451 Smyth Road, room 3062, Guindon Hall, Ottawa, ON K1H 8M5, Canada, claroche@uottawa.ca), Christian Giguère (University of Ottawa, 451 Smyth Road, room 3062, Guindon Hall, Ottawa, ON K1H 8M5, Canada, cgiguere@uottawa.ca), Véronique Vaillancourt (University of Ottawa, 451 Smyth Road, room 3062, Guindon Hall, Ottawa, ON K1H 8M5, Canada, vaillancourt@mail.health.uottawa.ca)

For several decades, hearing tests have been carried out in audiometric test rooms which must meet acoustical requirements set forth in standards on ambient noise levels (i.e., ANSI S3.1-1999 (R2003)). It is however generally accepted that acoustical environments in which individuals with hearing loss function daily seldom correspond to environments found in audiometric rooms. Constraints regarding the sound attenuation by room walls (i.e., costs) can thus be minimized with a more rigorous control over certain acoustical characteristics within the sound room (i.e., reverberation time), thereby allowing to recreate more realistic environments of daily living. During the planning stage of the Research Unit on Noise and Communication at the University of Ottawa, the researchers opted for a versatile acoustic room with reversible panels that not only offers adequate sound attenuation by walls but also some control over reverberation time, thereby allowing to recreate more typical acoustic environments. The characteristics of this versatile acoustic room, as well as examples describing applications of use (effect of repetition on speech recognition, attenuation by headphones used with portable audio systems, effect of hearing protection on speech recognition within military noise environments) will be presented.

Contributed Paper

9:40

5aNSb6. NMR sensitivity to floor vibration. Yuval Ben-Dov (IDE, 68 Mazzeo Drive, Randolph, MA 02368, USA, yuval.ben-dov@ideworld.com), Peter Heiland (IDE, 68 Mazzeo Drive, Randolph, MA 02368, USA, peter.heiland@ideworld.com), Srinivasan Rajan (Novartis Institutes for BioMedical Research, 250 Massachusetts Avenue, Building #600 Room # 6C-172, Cambridge, MA 02139, USA, srinivasan.rajan@novartis.com)

NMR is widely used in the determination of molecular structures in solution. Floor vibrations interfere with the NMR measurements and are coupled with the signal of interest. To minimize the effect of floor vibrations, NMR spectrometers are typically installed on a solid floor with minimal structurally induced vibrations. However, in some cases this is not possible, and the tool is exposed to structural vibrations. We study the NMR sensitivity to floor vibrations. A Bruker 500 MHz installed on IDE active isolation platform is used. By exciting the platform in a controlled manner we can measure the noise as observed in the NMR spectrum due to the platform vibrations. The sensitivity highly depends on the excitation frequency, and is not well reflected in a typical requirements specification. Revised requirements are presented for the floor vibration both for a tool installed as is, and for a tool on top of our isolation platform.

Session 5aNSc

Noise and EURONOISE: Acoustic Performance of Energy Efficient Building Products I

Anthony Hoover, Cochair
McKay Conant Hoover, Inc., 5655 Lindero Canyon Road, Suite 325, Westlake Village, CA 91362, USA

Jacques Roland, Cochair
Centre Scientifique et Technique du Bâtiment, 24 rue Joseph Fourier, Saint Martin d'Hères, 38400, France

Invited Papers

8:00

5aNSc1. Buildings thermal and acoustics insulation: friends or enemies. Jacques Roland (Centre Scientifique et Technique du Bâtiment, 24 rue Joseph Fourier, 38400 Saint Martin d'Hères, France, jacques.roland@cstb.fr)

The increasing concern on climate changes and greenhouse gas accumulation has urged most of countries to enforce new thermal regulation to improve the energy efficiency of existing and new buildings. This improvement shall not at least induce a reduction of the acoustic comfort, and possibly increase it by a careful choice of products and a relevant design. The new products and technologies involve the building envelop insulation, the thermal bridges suppression, the improvement of air conditioning efficiency, and the renewable energy sources attached to the building. The author will review these new products and technologies and show what are the expected benefit or threat for the acoustic performance of buildings. This will include triple glazing, bulk insulating materials, natural fibrous materials, vacuum insulation panels, phase change materials, thermal bridge isolators, integrated photovoltaic cells, light weight construction, passive house concept, heat pumps, and air conditioning with heat exchangers.

8:20

5aNSc2. Acoustic behavior of triple glazings. Marc Rehfeld (Saint Gobain Glass, CRDC, B.P. 40103, 60777 Thourotte Cedex, France, marc.rehfeld@saint-gobain.com), David Fournier (Saint Gobain Glass, CRDC, B.P. 40103, 60777 Thourotte Cedex, France, david.fournier@saint-gobain.com)

Making of triple glazings is the only way to still improve thermal performances of Insulating Glass Units. Possible ways with double glazings are already in use: increase the space between glasses, use low emissivity coatings and special gas with lower thermal conductivity as argon or krypton. Specific acoustic weak point of double glazings is the resonance between the two panes which works as a mass spring mass system, and coupling of eigenmodes of panes through the air (gas) cavity. These phenomena are of course still more important with triple glazings, as there are two resonances. The paper will give all comparative data concerning thermal and acoustic performances, and describe a way to achieve the same single number values of sound transmission loss with triple glazing that with double glazing by adding absorption in the gas cavities.

Contributed Paper

8:40

5aNSc3. Acoustic design criteria for naturally ventilated buildings. Chris D. Field (Arup Acoustics, 901 Market Street, Suite 260, San Francisco, CA 94103, USA, chris.field@arup.com)

This paper proposes satisfactory indoor noise level criteria for office buildings which are compatible with achieving minimum natural ventilation standards set out in green building rating systems for sustainable building design. Indoor air quality standards related to the use of natural ventilation in buildings conflict with the control of ingress of external noise through ventilation openings to meet internationally recognized background noise limits for building use. These standards generally assume, however, that buildings are sealed and air conditioned to meet the stated recommended indoor noise levels. It is not feasible, however, that these noise standards can be expected or are appropriate to be achieved in naturally ventilated buildings. Therefore, to account for the thermal comfort benefit of natural ventilation and the ability to locally control natural ventilation and noise levels by closing of windows, an allowable exceedance of the recommended indoor noise levels is explored. The allowable deviation from existing background noise level guidelines is determined, which is considered to be an acceptable compromise for increased thermal comfort.

Invited Paper

9:00

5aNSc4. R+D for the integration of high acoustic-thermal performances in spanish building products. Marta Fuente (Labein-Tecnalia, C/Geldo - Parque Tecnológico de Bizkaia, Edificio 700, 48160 Derio, Spain, mfuente@labein.es)

Many EU countries are introducing new national regulations aimed at complying with the European Directive "Energy Performance of Buildings" (EPBD). Subsequently, in Spain a new normative has been recently approved (CTE-HE), compiling new requirements for energy saving in buildings. In this framework, energy efficiency considerations will have an increasing impact on the design of buildings and the choice of materials and products. In the same way, the acoustical quality of dwellings in Spain is going to be guaranteed with the compliance of the new Spanish Building Regulation (CTE-HR). Searching a higher level of comfort in dwellings the CTE is in-

creasing its requirements and is considering the building as a product itself. These new developments involve efforts and resources for the upgrading of the constructive materials and systems, demanding investments for R&D activities. Therefore manufacturers of the constructive sector in Spain are launching many innovative research strategies for the development of better products, addressing key factors for the energy efficiency of buildings.

Contributed Paper

9:20

5aNSc5. Sound insulation of traditional roof constructions considering energy efficiency requirements. Beáta Mesterházy (Budapest University of Technology and Economics, Lab. of Building Acoustics, Mûegyetem rakpart 3., 1111 Budapest, Hungary, bmester@mail.bme.hu), Frigyes Reis (Budapest University of Technology and Economics, Lab. of Building Acoustics, Mûegyetem rakpart 3., 1111 Budapest, Hungary, reis@mail.bme.hu), Gábor Szlávik (URSA Salgótarján zRt., Budapesti út 31, 3104 Salgótarján, Hungary, gabor.szlavik@uralita.com)

The efforts for energy efficiency result changes in building constructions, also in case of roof constructions. The most important constructional conclusion is the growth of the thickness of the heat insulating layer. Beside heat insulation, inner ventilation between the layers is the other important parameter, which has a great effect on sound insulation behaviour. In regular product information sheets, either in internet or in printed forms, the effect of these later parameter is not present and this way the laboratory data do not show the reality. For the purpose of modeling the reality, a new installation method has been developed, which considers the effects of ventilation usually used in our climate conditions. This new installation method has been realised and used in laboratory experiments. The results based on the new installation method approach the reality better and reflect the acoustical importance of the certain constructional components.

9:40-10:40 Posters

Lecture sessions will recess for presentation of poster papers on various topics in acoustics. See poster sessions for topics and abstracts.

Invited Paper

10:40

5aNSc6. Acoustic performance of membrane based multilayered systems with improved thermal inertia characteristics. Catherine Guigou-Carter (CSTB, 24, rue Joseph Fourier, 38400 Saint Martin D'Hères, France, catherine.guigou@cstb.fr), Hebert Sallee (CSTB, 24, rue Joseph Fourier, 38400 Saint Martin D'Hères, France, hebert.sallee@cstb.fr), Xavier Normand (IFTH, Avenue Guy de Collongue, 69134 Ecully Cedex, France, xnormand@ifth.org)

In this paper the development of double membrane based systems, including phase change materials (denoted-PCM) is discussed. The cavity between the two membranes is filled with a new type of absorbing material: a 3D, nonwoven, complex structure made of two or three fibrous mats that allows the inclusion of small granulated particles while being fabricated. Granulated phase change materials are therefore included in this 3D, nonwoven structure in order to increase thermal properties by the heat storage/restoring principle. The PCMs introduced in this nonwoven structure act to store part of the heat when it is in excess, and then, to restore it when the temperature inside the room is too low. The intermediate temperature chosen to correspond to a desired comfort temperature (for example around 20 °C) corresponds to the phase transition temperature of the PCM. Lightweight membranes are then fixed on each side of this complex 3D, nonwoven structure, including the PCMs. The acoustic performance of such systems is investigated in terms of the sound transmission loss, both experimentally and analytically. The thermal performance is also briefly presented.

Contributed Paper

11:00

5aNSc7. Sound transmission loss of vacuum insulation panels. Waldemar Maysenhölder (Fraunhofer Institute for Building Physics, Dept. of Acoustics, Nobelstraße 12, 70569 Stuttgart, Germany, maysenhoelder @ibp.fraunhofer.de)

The sound transmission loss of a variety of vacuum insulation panels (VIP) has been measured in the laboratory. Core materials of the VIP include silica, polyurethane, micro fleece, and glass fibers. Mass law behavior and minima due to bending-wave coincidence and thickness resonance have been observed. Destroying the vacuum may reduce the sound insulation drastically. Since in practical applications the VIP need protection, the predominant interest lies in the transmission loss of multilayered assemblies, e.g., VIP sandwiched between aluminum plates. Calculations performed by the software LAYERS show that with additional "decoupling" layers (air, rubber) the coincidence dip can be avoided or shifted to higher frequencies, where it is less critical. Preliminary experimental realizations indicate the important role of a proper gluing of the layers. According to further LAYERS calculations, attachment of VIP to massive walls and protection by a plaster layer does not change the transmission loss of the wall appreciably, except for the VIP with the soft polyurethane core material.

Invited Papers

11:20

5aNSc8. Vibration reduction of thermal break balcony connections. Martin Schneider (University of Applied Sciences, Schellingstr. 24, 70174 Stuttgart, Germany, martin.schneider@hft-stuttgart.de), Heinz-Martin Fischer (University of Applied Sciences, Schellingstr. 24, 70174 Stuttgart, Germany, heinz-martin.fischer@hft-stuttgart.de)

In energy efficient buildings concrete balconies have to be thermally insulated from the concrete floor to reduce heat loss and to increase surface temperature. This thermal break is obtained by polystyrene in combination with high-strength concrete thrust-force bearings and an arrangement of stainless steel straight and bent bars to act as tension and shear reinforcement. The acoustic performance of such thermal break units was investigated under laboratory conditions. Therefore the vibration level difference at different junctions

between balcony and the thermal isolated concrete floor as well as the normalized impact sound pressure level of the floor when the balcony is excited with the standard tapping machine are measured. The influence of the number of tension and shear steel bars and the type of thermal insulating material was studied on typical sized balconies connected to small test floors. The vibration isolation at low frequencies was determined using modal testing.

11:40

5aNSc9. Using high light reflectance acoustical ceilings to increase the energy efficiency of buildings. Marsha S. Bischel (Armstrong Building Products, 2500 Columbia Ave, Lancaster, PA 17603, USA, msbischel@armstrong.com), William E. Beakes (Armstrong Building Products, Retired, 4057 Woodcrest Lane, Columbia, 17512, USA, beakeswe@embarqmail.com)

Acoustical ceilings with white, highly light-reflecting surfaces can be used as an effective, passive means to significantly improve the energy efficiency of a space. When a ceiling with high light reflectance is coupled with an indirect lighting system, illumination can be increased by 20%, or the energy directly associated with lighting can be reduced by 20%. In addition, lower lighting loads can reduce cooling costs by 7%. A highly light reflective ceiling can also be used to reflect daylight into a space, increasing the amount of light in interior areas away from the windows by as much as 20%; alternatively, the surface area of windows may be reduced by 14% while maintaining the same illumination levels. In all cases, the increased reflectance of light allows the number of fixtures to be decreased, further increasing the savings related to both energy and maintenance. The percentage of energy savings associated with lighting is proportional to the percentage increase in the light reflectance value; therefore, even small increases in light reflectance provide increases in energy efficiency. When the acoustical performance of two products is comparable, light reflectance could be a critical differentiator in determining total building performance and occupant comfort.

12:00

5aNSc10. High sound and thermal insulation constructions with dB-deck. Bart Ingelaere (BBRI, rue du Lombard, 42, B-1000 Brussel, Belgium, bart.ingelaere@bbri.be), Gerrit Vermeir (Lab. ATF, Katholieke Universiteit Leuven, Celestijnenlaan 200D, B-3001 Leuven, Belgium, Gerrit.Vermeir@bwk.kuleuven.be), Debby Wuyts (BBRI, rue du Lombard, 42, B-1000 Brussel, Belgium, debby.wuyts@bbri.be)

The new Belgian requirements demand $DnT,w \geqslant 58$ dB and $L'nT,w \leqslant 50$ dB between apartments for enhanced acoustic comfort. At the same time the Energy Performance Regulations impose strict requirements for the thermal insulation between apartments. Higher demands on sound insulation can be realized in practice by using higher surface weights for walls and floors and by applying failure free floating floors. However requiring higher weights for floors is in contradiction with the technique of concrete hollow floor elements. A thermal and acoustical solution was found in the development of dB-deck, a prefab double floor element with intermediate supporting elastic pads, cutting structural vibration paths between superposed apartments. In combination with double walls without anchors (allowing for a high sound reduction index and no structural transmission in the horizontal sense), this construction technique allowed for $DnT,w > 63$ dB and $L'nT,w < 47$ dB without a floating floor in experimental setups This solution was developed by a team of the BBRI, KULeuven, and CDM for an important producer of hollow floor elements. This technique has now been used for real constructions. The paper presents technical details, the results of the acoustical measurements and the acoustical advantages and difficulties met in the construction of this apartment block.

12:20

5aNSc11. The effect of additional thermal lining on the acoustic performance of a wall. Jacek Nurzynski (Building Research Institute, Filtrowa Str. 1, 00-611 Warsaw, Poland, j.nurzynski@itb.pl)

External thermal insulation systems (ETICS) are commonly used in Poland mainly for thermorenovation of multifamily residential buildings constructed in seventies using industrialized methods. Additional layer improves thermal performance of a wall but also causes decrease of sound insulation in certain frequency range. Usually the acoustic effect of thermorenovation is unnoticed by inhabitants, but in the case of noisy locations it is sometimes perceived as an appearance of a new tonal outside noise source. The paper presents results of investigation on the influence of additional lining on the acoustic performance of massive wall based on laboratory tests. Resonance frequency, its location and influence on single number quantities is discussed. The problem of sound reduction index improvement prediction acc. to EN 12354-1, separate acoustical characteristics of lining and testing acc. to ISO 140-16 is also considered.

12:40

5aNSc12. Development of thermoacoustic floating floors for use between parking and dwellings. Catherine Guigou-Carter (CSTB, 24, rue Joseph Fourier, 38400 Saint Martin D'Hères, France, catherine.guigou@cstb.fr), Jean-Baptiste Chene (CSTB, 84, Avenue Jean-Jaurès, 77447 Marne-la-Vallée Cedex 2, France, jean-baptiste.chene@cstb.fr)

The French thermal regulation (RT2005) is favoring thermal floating floor between spaces such as parking or stores, and dwelling units. However, these solutions do not fulfill the French acoustic regulation with regards to airborne noise. This paper discusses the development of solutions allowing fulfilling both the thermal and the acoustic regulation. To achieve this goal, a mixed approach combining measurements and numerical predictions is used. Furthermore, the laboratory characterization of such floating systems usually involves a concrete base floor 140 mm in thickness (following the NF EN 140-8 standard) and a floating concrete layer 40 mm in thickness. However, in situ the concrete base floor as well as the floating concrete layer can be thicker. Therefore, some laboratory measurements are performed on a thermal floating floor system combining a 200 mm thick concrete base floor, a thermal insulation layer (polystyrene or polyurethane based foam for example) and a 60 mm thick floating concrete layer. The prediction method shows that this type of thermal floating systems is not acceptable with respect to the acoustic regulation. The behaviour of such multilayered systems is investigated using a wave approach based prediction tool in order to develop solutions allowing fulfilling the acoustic regulation.

Session 5aNSd

Noise, ASA Committee on Standards, Architectural Acoustics, and EURONOISE: Classroom Acoustics I (Poster Session)

Louis Sutherland, Cochair
Consultant in Acoustics

Luigi Maffei, Cochair
Built Environment Control Laboratory Ri.A.S., Second University of Naples

All posters will be on display from 9:40 a.m. to 11:20 a.m. To allow contributors an opportunity to see other posters, contributors of odd-numbered papers will be at their posters from 9:40 a.m. to 10:30 a.m. and contributors of even-numbered papers will be at their posters from 10:30 a.m. to 11:20 a.m.

Contributed Papers

5aNSd1. Comparisons of predicted and measured values of speech, noise, reverberation and early reflections in optimized classrooms. Sooch San Souci (AiA - Audition, Intelligibility, Acoustics, 35 bis rue de Fay, 77140 St Pierre Les Nemours, France, s.sansouci@wanadoo.fr), Line Guerra (AiA - Audition, Intelligibility, Acoustics, 47 rue Le Corbusier, 92100 Boulogne, France, line.guerra@aiacoustique.com), Richard Campbell (Bang-Campbell Associates, 26-G Chilmark Drive, East Falmouth, MA 02536, USA, rhcamp@rcn.com)

12 newly renovated classrooms have been studied to determine the accuracy of prediction software used to guide architects, acousticians and interior designers. Several variations in renovation techniques based on traditional precepts were compared. After the renovations were complete, measurements and recordings were made of speech, noise, and reverberation when the rooms were both occupied and nonoccupied by students. A systematic map of the results was compiled, which when presented on a seat by seat basis, defined values of merit for the presumed optimizations and were compared to the predicted values. The two principle indices chosen as targets were increases in total speech level and decreases in total noise level (including late reverberation). When referred to these targets, several novel strategies proved to offer higher value/cost ratios while a few traditional strategies proved to be deficient and in some cases detrimental to at least one of the principle indices. Emerging from this study is what appears to be evidence for two points: (1) that some common acoustic criteria are inadequate for classrooms and (2) there are several strategies that might offer significant advantages over some of the traditional guidelines for acoustic treatments for learning spaces.

5aNSd2. The use of U50 to calculate the optimal absorption in a classroom. Lau Nijs (Delft University of Technology, Berlageweg 1, 2628 BG Delft, Netherlands, L.Nijs@tudelft.nl), Monika Rychtarikova (Lab. ATF, Katholieke Universiteit Leuven, Celestijnenlaan 200D, B-3001 Leuven, Belgium, Monika.Rychtarikova@bwk.kuleuven.be), Gerrit Vermeir (Lab. ATF, Katholieke Universiteit Leuven, Celestijnenlaan 200D, B-3001 Leuven, Belgium, Gerrit.Vermeir@bwk.kuleuven.be)

Common measures for the speech intelligibility predict increasing values with increasing absorption in empty classrooms. Measurements confirm this relation, so it seems as if an anechoic room is the best place to teach. However, there are two problems: the sound pressure level at the back row is too low when compared to the levels on the front row or when compared to the noise level caused by pupils plus ventilation systems. A simple method is proposed based on U50, which gives the relation between the sound energy from direct sound (from a teacher or a pupil) plus early reflections on one side and late reflections plus noise on the other. Barron's formula for the sound level decrease in a concert hall is included to predict the sound level drop through the classroom. Model results indicate that the absorption coefficient should be in the order of 20 to 30% if the signal to noise ratio is in the range between +5 to -5 dB. These values seem low, but measurements in existing classrooms show low signal to noise levels as well.

5aNSd3. The Nordic voice ergonomic group: legislation and vocal health. Valdis Inigbjörg Jonsdottir (Tad er Malid, Furuvellir 13, 601 Akureyri, Iceland, valdisj@ismennt.is)

Research has revealed a number of factors which have a negative impact on voice function (e.g., activity noise, background sound, poor acoustics, long duration of voice usage, speaking distance). In these circumstances vocal loading increases, potentially giving rise to voice disorders. Currently, practical measures within society for the improvement of speakers' working conditions and the prevention of voice loading are not satisfactory. Voice experts from the five Nordic countries met in Reykjavik in May 2006 to inaugurate the Nordic Voice Ergonomic Group, with the aim of investigating the current situation within voice ergonomics, with a particular focus on sound-related problems. The group found that occupational safety and health legislation relating to speech communication in educational working environment differs between Nordic countries. Moreover, this legislation does not specifically deal with speech communication or the risk of voice disorders. This presentation will report on the details of the current legislation and the Group's suggestions for legislative change which might prevent disturbance in speech communication and decrease the risk of vocal disorder as an occupational hazard.

Session 5aNSe

Noise and EURONOISE: Examples of Noise Control I (Poster Session)

Brigitte Schulte-Fortkamp, Cochair
TU Berlin, Institute of Fluid Mechanics and Engineering Acoustics

Pierre Etienne Gautier, Cochair
SNCF DIR

All posters will be on display from 9:40 a.m. to 11:20 a.m. To allow contributors an opportunity to see other posters, contributors of odd-numbered papers will be at their posters from 9:40 a.m. to 10:30 a.m. and contributors of even-numbered papers will be at their posters from 10:30 a.m. to 11:20 a.m.

Contributed Papers

5aNSe1. Jet noise prediction using RANS CFD input. Magdi Omais (Airbus/ONERA, 64 avenue de Paris, 92320 Châtillon, France, magdi.omais@onera.fr), Stephane Redonnet (ONERA (French aerospace Center), CFD & Aeroacoustics Department, BP 72, 29 avenue de la division Leclerc, 92322 Chatillon Cedex, France, stephane.redonnet @onera.fr), Bastien Caruelle (Airbus S.A.S, Department of Acoustic & Environment, 316 route de Bayonne, 31000 Toulouse, France, bastien.caruelle@airbus.com), Eric Manoha (ONERA (French aerospace Center), CFD & Aeroacoustics Department, BP 72, 29 avenue de la division Leclerc, 92322 Chatillon Cedex, France, eric.manoha@onera.fr)

In the present work, a volume source model based on the SNGR approach, first proposed by Bailly, has been implemented and developed for jet noise prediction purposes. This method presenting the advantage of providing unsteady three-dimensional turbulent data from a RANS computation, it shall be compatible with industrial development processes. First, the theoretical aspects of the original SNGR model were revisited. More particularly, analytical developments showed that considerable modifications were needed to take local flow effects into account while generating unsteady turbulent data. Moreover, the way to include anisotropy effects in the model, as originally proposed by Billson, was improved by using a nonlinear extension of Boussinesq approximation to recover the local Reynolds stress tensor. In a second step, the potentialities of the stochastic tool for jet noise simulations have been evaluated against existing numerical and experimental databases. In addition to that concern, its sensitivity to a slight modification of the RANS input data was studied. As a last step, the possibility of accounting for high frequency dynamics in reasonable CPU times has been deeply investigated. The main results obtained from this study show that the stochastic approach should be a promising method for future applications to industrial nozzle configurations.

5aNSe2. The primary noise sources associated with turbulent Coanda wall jets. Caroline Lubert (James Madison University, Department of Mathematics & Statistics, MSC 1911, Harrisonburg, VA 22807, USA, lubertcp@jmu.edu)

A wide variety of aeronautical and aerospace applications utilize the Coanda effect. However, due to the enhanced turbulence levels observed with devices using this effect, turbulent mixing noise is a primary noise source. For supersonic jets close to Coanda surfaces, shock-associated noise (both broadband and screech tones) is also a significant source of sound. A theory has been developed to predict the turbulent mixing noise emitted by unit-volume of jet-type shear-layer turbulence close to a rigid plane, and extended to a plane two-dimensional wall-jet. However, most flows of practical interest are three-dimensional and, in the case of the Coanda jets, exhibit significant curvature. This paper extends the previous models for turbulent mixing noise to predict the aeroacoustic characteristics of a three-dimensional turbulent flow over a Coanda surface. Details of experimental observations of the shock-cell structure associated with supersonic Coanda wall jets, and a method of modeling the corresponding shock-associated noise, is also discussed.

5aNSe3. Efficiency of shielding effect on installed double stream nozzles. Sébastien Aeberli (SNECMA - groupe SAFRAN, Villaroche - Rond-point R. Ravaud, 77550 Moissy-Cramayel, France, sebastien.aeberli @snecma.fr)

In spite of acoustic improvements on jet noise brought by innovative technologies such as chevrons, a way to ensure important acoustic gains is to optimize the power plant integration on aircrafts in order to benefit of the shielding effect due to wing, empennage and fuselage surfaces. In this presentation, these effects are illustrated thanks to a jet noise test campaign at 1/10th scale in an anechoic chamber as part of a European project. This campaign gives a better understanding of shielding effect by a wing and also of the acoustic impact of pylon azimutal direction on two representative BPR 9 nozzles (Baseline - smooth - and Low Noise - with chevrons). The efficiency of shielding effect on jet noise sources in these configurations is assessed.

5aNSe4. Automatic segmentation of traffic noise. Fernando José Mato-Méndez (Universidad de Vigo, E.T.S.I.Telecomunicación C./ Maxwell S/N, 36200 Vigo (Pontevedra), Spain, fmato@tsc.uvigo.es)

The state of the art in audio source separation reflects a growing interest towards developing tools oriented to speech and music applications. However, its application to the study of noise, and more specifically to the study of traffic noise, is scarce. The source separation in this work environment is a key process for subsequent classification and analysis, and has motivated the present research carried out. This paper is intended to present, therefore, the different strategies followed in the implementation of an automatic segmentator for traffic noise, focusing the research on two main aspects: The removal of components of noise unrelated with the sources of study and, by other side, the detection and separation of audio sources acquired. For this purpose, measures of traffic noise are made and results are analyzed for the running system, achieving a high level of performance in real work conditions.

5aNSe5. Real time evaluation of soft microphones on a local active noise control system. Stelios M. Potirakis (Intracom Defense Electronics, 21km Peania-Markopoulo Street, GR-19400 Koropi - Attica, Greece, spoti@intracomdefense.com), Maria Rangoussi (T.E.I. Piraeus/Department of Electronics, 250, Thivon str., GR-12244 Athens-Aigaleo, Greece,

mariar@teipir.gr),Stylianos Savvaidis(T.E.I. Piraeus/Department of Electronics, 250, Thivon str., GR-12244 Athens-Aigaleo, Greece, ssavaid@teipir.gr), Nikos Zafeiropoulos (T.E.I. Piraeus / Department of Electronics, 250, Thivon str., GR-12244 Athens-Aigaleo, Greece, nikoszafeiropoulos@yahoo.gr)

Systems for the active control of acoustic noise (ANC) rely on measurements of the noise signal in order to produce the required "quiet zone." Soft microphones (SM) are a virtual microphone alternative already proposed by the authors, employing estimates rather than measurements of the noise signal obtained from room impulse responses based on measurements. Therefore, a single microphone can be used to estimate the noise signal at multiple points. This has already been successfully applied on single microphone noise mapping. In the present work, the SM method is evaluated on a real time local ANC system. The proposed scheme is a filtered-s least mean square (FXLMS) based control structure, incorporating SM. Following the proposed system design-simulation with Matlab-Simulink, a three-dimensional enclosure (office-simulating) and a real electroacoustic ANC system based on a TI® TMS320C6713 DSP, developed for this purpose, were built in the laboratory to carry out the experiments. Different options of estimating the SM signals and exploiting them into the control structure are experimentally evaluated as to their ability to enlarge the silence zone and their noise reduction performance around the listener ear zone (using a head and torso simulator) and compared to the standard FX-LMS solution.

5aNSe6. Application examples of beamforming method. Andrea Cerniglia (Euroacoustic srl, via Gandhi, 13, 10013 Avigliana, Italy, a.cerniglia@euroacoustic.com)

Acoustical beamfoming technique is a powerful method for noise source investigation, suitable for many different applications. Thanks to this technology is possible to identify where the noise is coming from, in a very clear and understandable form, both in static or dynamic situations. In addition on standard features, some advanced functions can helps to make correlation between subjective and objective parameters, for better understanding of acoustical phenomena. The paper describes some real applications of a very innovative beamforming system, based on a spherical antenna. The described measurements coming from several fields as automotive, enviromental noise, occupational noise, architectural acoustic, noise barriers investigation.

FRIDAY MORNING, 4 JULY 2008 P2-A, LEVEL 2, 9:40 TO 11:20 A.M.

Session 5aNSf

Noise and EURONOISE: Soundscape & Community Noise II (Poster Session)

Bennett Brooks, Cochair

Brigitte Schulte-Fortkamp, Cochair
TU Berlin, Institute of Fluid Mechanics and Engineering Acoustics

All posters will be on display from 9:40 a.m. to 11:20 a.m. To allow contributors an opportunity to see other posters, contributors of odd-numbered papers will be at their posters from 9:40 a.m. to 10:30 a.m. and contributors of even-numbered papers will be at their posters from 10:30 a.m. to 11:20 a.m.

Contributed Papers

5aNSf1. The influence of meteorological conditions on noise propagation outdoors and sustainable planning of roads and motorways. Barbara Joanna Lebiedowska (Warsaw University of Technology, ul. Lukasiewicza 17, 09-400 Plock, Poland, barbara_lebiedowska@yahoo.fr)

Adequate road planning that allows for the separation of built-up areas and travel routes is one of the basic prevention strategies of hazards resulting from road usage. If possible, the roads should never be routed across cities and residential districts. However, if for some reason a busy road must be located near a built-up area, long-term meteorological conditions, characteristic of the area, must be examined prior to the execution of any work. Road planning on the basis of the analysis of the "rose of conditions favourable" to noise propagation will help minimise the road's negative acoustic influence on the adjacent buildings and facilities. The acoustic profile of two selected sites (in Poland and in France) is examined in the paper. Conditions favourable to propagation differ significantly in both cases depending on the position of the source-to-receiver direction in relation to the directions of the world

5aNSf2. Community response to military shooting noise immissions. Mark Brink (ETH Zürich, Center for Organizational and Occupational Sciences, LEO B 9.1, 8092 Zürich, Switzerland, brink@ethz.ch), Jean Marc Wunderli (EMPA - Materials Science and Technology, Ueberlandstr. 129, CH-8600 Duebendorf, Switzerland, jean-marc.wunderli@empa.ch), Hans Boegli (Federal Office for the Environment, BAFU, 3003 Bern, Switzerland, hans.boegli@bafu.admin.ch)

The assessment of the impact of any kind of noise exposure on the population is a fundamental step in the process of noise abatement. Data about the exposure-response relationship for annoyance due to noise emissions from military shooting grounds are rather scarce at the time. In order to establish new legal exposure limit values for shooting noise from heavy and light weapons, we conducted an extensive telephone interview survey in several - mostly rural - municipalities affected by military shooting noise in Switzerland. The exposure assessment for each respondent was calculated based on the source models of a range of weapons and ammunitions of the Swiss army. Preliminary results suggest that although the responses of the population to noise from military weapons are rather dispersed, data should be sufficiently consistent to establish an exposure-response relationship which can help in defining a binding exposure limit value.

5aNSf3. Investigation of traffic noise from additional tolling lanes at Portage toll plaza. Silas Bensing (Columbia College Chicago, 370 Millport Drive, Valparaiso, IN 46385, USA, silas.bensing@loop.colum.edu)

Electronic toll collecting systems quickly and efficiently move traffic through toll facilities by automatically collecting tolls from individual vehicle transponders. An ongoing study investigates the addition of three electronic toll lanes to the existing twelve lanes at the Portage toll plaza on the Indiana Toll Road (Portage, Indiana, USA), scheduled to be completed by December 2008. The study aims to predict noise levels of the plaza after the addition of the lanes, the hypothesis being that the additional lanes will have little or no effect on the toll plaza noise levels. Noise measurements are be-

ing made at locations in the vicinity of the existing plaza with consideration for a nearby residential area. An outdoor noise propagation software (SoundPlan) is used to create a comprehensive traffic noise model for the area under investigation. Test data from the existing site will be compared to the model and used to predict future noise levels.

5aNSf4. Assessment of military shooting noise. Hans Boegli (Federal Office for the Environment, BAFU, 3003 Bern, Switzerland, hans.boegli @bafu.admin.ch), Jean Marc Wunderli (EMPA - Materials Science and Technology, Ueberlandstr. 129, CH-8600 Duebendorf, Switzerland, jean-marc.wunderli@empa.ch), Mark Brink (ETH Zürich, Center for Organizational and Occupational Sciences, LEO B 9.1, 8092 Zürich, Switzerland, brink@ethz.ch)

The assessment of the impact of noise exposure on the population is a fundamental step in noise abatement. It includes the establishing of an exposure-response relationship and the setting of an impact threshold that specifies the protection level for the population and triggers eventually mitigating measures to reduce noise exposure. In Switzerland, the impact thresholds should be set so that, in the light of current scientific knowledge and experience, noise exposure below these thresholds will not seriously disturb the well-being of the population. For most current noise sources such as roads, railways and airports there already exist impact thresholds as part of the noise abatement legislation. Yet, no impact thresholds for military shooting grounds have been specified so far. Therefore a study was carried out in order to assess the impact of military noise exposure. The research included the calculation of noise exposure of eight military shooting grounds ranging from small infantry shooting ranges to expanded artillery and tank training facilities and a survey at over 1000 residents in the neighbourhood of these installations. Preliminary results suggest that although the responses of the population to military noise are rather dispersed, data should be sufficiently consistent to establish an exposure-response relationship.

5aNSf5. Design and evaluation of novel barriers. George Bamnios (Electronics Dept. ATEI of Thessaloniki, P.O. Box 141, Sindos, 57400 Thessaloniki, Greece, bamnios@el.teithe.gr), Ioannis Rekanos (Physics Devision, Dept. of Mathematics, Physics and Computational Sciences, School of Engineering, Aristotle Univ. of Thessaloniki Campus, 54124 Thessaloniki, Greece, rekanos@auth.gr), Konstantinos Zacharias (Physics Devision, Dept. of Mathematics, Physics and Computational Sciences, School of Engineering, Aristotle Univ. of Thessaloniki Campus, 54124 Thessaloniki, Greece, zachark@gen.auth.gr), Athanasios Trochidis (Physics Devision, Dept. of Mathematics, Physics and Computational Sciences, School of Engineering, Aristotle Univ. of Thessaloniki Campus, 54124 Thessaloniki, Greece, trohidis@gen.auth.gr)

This work presents the results of a project for the design of novel noise barriers with improved performance. The aim of the project was twofold. First, to optimize the performance of barriers by appropriately modifying both the shape and the acoustical conditions at the edge to suppress the sound pressure. Second, to quantify the acoustic performance of the novel barriers both mathematically and experimentally in a standardized, well controlled process. The insertion loss of different types of barriers with modified edge shapes and acoustical conditions were investigated systematically in comparison with conventional ones using a method based on BEM. The comparison highlighted the influence of shape and edge configuration on barrier efficiency and allowed the design of novel barriers with optimal performance. The novel barriers were tested and their efficiency was quantified experimentally using the Maximum Length Sequence (MLS) technique, which offers the advantage of in-situ measurements in the presence of extraneous noise. The experimental results are shown to be in good agreement with the experiments. Based on the aforementioned procedure, a unified framework was established, witch allows the design of potentially improved noise barriers.

5aNSf6. Nuisance control of leisure activities. Robert Barti(LEM Laboratory, Pol. Ind. Cova Solera, Av. Can Sucarrats, 110 nau 11, 08191 Rubi, Spain, robert@lem-sl.com)

In Spain there are more than 345 000 leisure activities with more than 1.2 M jobs. This economical sector produces the 2.2% of the PIB overall Spanish economic production. Tourism is a big source of money for many Spanish cities. Leisure activities is the most common economic activity related with this sector. Typical Spanish good weather let's people to remain for a long time up to early morning in the streets. Human activity produces always noise. Acoustic noise control measurements uses dB(A) scale for evaluation. Low noise levels dB(A) has no correlation with acoustic perception of people because people can "follow" the rhythm of the music. Increase the TL of structures let's to reduce the noise from activities, but increasing the power amplifier the problem remains still in the same point. The solution checked is to use an acoustic limiter as a warranty of no contamination to neighbours from the activity. Some results about this technique are discussed in this paper. In order to solve a complain between neighbours an leisure activity, a political solution is more effective than technical solution is. The main objective is to set the correct balance between perception of sounds and acoustic comfort at home.

5aNSf7. Perspectives for a strategical mapping of soundscapes. Gianluca Memoli (Imperial College London, Department of Chemical Engineering, Exhibition road, SW7 2AZ London, UK, g.memoli@imperial .ac.uk), Gaetano Licitra (ARPAT - Dept. Firenze, Via Porpora, 22, 50144 Firenze, Italy, g.licitra@arpat.toscana.it), Mauro Cerchiai (ARPAT - Dept. Pisa, Via V. Veneto, 27, 56127 Pisa, Italy, m.cerchiai@arpat.toscana.it)

The transposition of the European Noise Directive by Member States gives a new way to action plans of urban areas, underlying (article 6 and Annex III) that dose-effect relations should be used to assess the effect of noise on populations. Particular interest, in this sense, has the relationship between annoyance and perceived soundscape: it is now almost accepted that a higher annoyance is not always proportional to higher noise levels. This paper will demonstrate that a way to move from mapping noise exposure to a map of annoyance passes through the characterization of the soundscapes present on the territory. A numerical indicator ("slope"), derived from the time history of the measured sound/noise, will in fact be used to characterize the evolution along the day of the soundscapes present in the city of Pisa (I). In particular, "slope" (correlated to annoyance in previous studies) will be used to prepare a map of the annoyance in selected areas of Pisa: predicted annoyance will be to be compared with the one extrapolated by noise levels. Differences, similarities and their effects on action plans will be discussed.

5aNSf8. Analysis and evaluation of noise reaction in open public spaces in Mexico City. Miriam German (Universidad Nacional Autonoma de Mexico-Facultad de Arquitectura, Circuito Interior S/N, Ciudad Universitaria, Delegacion Coyoacan, 02410 Mexico D.F., Mexico, lydmgg@yahoo .com.mx)

Mexico City, with a population estimated in 19 millions, is part of one of the largest metropolitan areas in the world. Unfortunately, scientific work on urban noise in Mexico City is scarce. A study on people reaction to urban noise carried out in open public spaces of two different zones of Mexico City will be presented. A previous survey in those zones showed that the noise levels exceeded the values recommended by international organizations to protect public health and welfare. The general objective of the study to be presented was to identify the sound sources perceived by the pedestrians, and to evaluate their response to urban noise pollution in the two mentioned areas. The results show that for most of the people (a) urban noise is not considered a relevant aspect to improve the quality in the city, although urban noise has a negative effect on the decision of using open public spaces; (b) the people with knowledge of the negative effects of noise pollution are more annoyed; (c) vehicular traffic is the most annoying noise source, contributing significantly the public transportation; (d) one of the principal strategies to confront urban noise is to get used to it.

Session 5aNSg

Jérôme Defrance, Chair
CSTB

Noise and EURONOISE: Propagation and Urban Noise I (Poster Session)

All posters will be on display from 9:40 a.m. to 11:20 a.m. To allow contributors an opportunity to see other posters, contributors of odd-numbered papers will be at their posters from 9:40 a.m. to 10:30 a.m. and contributors of even-numbered papers will be at their posters from 10:30 a.m. to 11:20 a.m.

Contributed Papers

5aNSg1. Perception of noise in suburban and urban areas. Elaine C. Paz (Federal University of Parana, Centro Politécnico - Setor de Tecnologia, Bairro Jardim das Américas, 81531-990 Curitiba, Brazil, epaz@bol.com.br), Paulo Henrique Trombetta T. Zannin (Federal University of Parana, Centro Politécnico - Setor de Tecnologia, Bairro Jardim das Américas, 81531-990 Curitiba, Brazil, paulo.zannin@pesquisador.cnpq.br)

This work analyses, using a comparative approach, the environmental noise perception in the daily lives of inhabitants of a residential area, with that of a mixed (residential and commercial) area (downtown), in a large Latin America city. The goal was to confront an ideal urban environment with one acoustically polluted, as function of noise descriptors. Concomitant with the evaluation of noise perception (subjective analysis), noise levels were measured (objective analysis) in both areas. The single average equivalent noise level (Leq) found for downtown was 73 dB(A), and 53 dB(A) for the residential area. A random sample of the populations of both areas was taken, through a questionnaire. Questionnaire data was treated statistically through a factorial multivariate analysis. This analysis has generated three statistical indicators: time perception, atypical noise perception, and sources and disturbances. Over 50% of both populations sampled have the perception that high frequency noise levels are gradually increasing, with higher contribution from traffic noise. The dominant organic effects reported were irritability and loss of concentration ability, these last being precursors of hearing loss.

5aNSg2. Traffic noise in shielded urban areas: comparison of experimental data with model results. Ando Randrianoelina (TNO Science and Industry, Stieljesweg 1, 2628CK Delft, Netherlands, ando.randrianoelina@tno.nl), Erik Salomons (TNO Science and Industry, Stieljesweg 1, 2628CK Delft, Netherlands, erik.salomons@tno.nl)

Noise maps of cities are commonly produced with rather simple engineering models for sound propagation. These models may be inaccurate in complex urban situations, in particular in situations with street canyons. Street canyons are urban areas that are partly or completely enclosed by buildings, for example a street between two buildings or a backyard surrounded by buildings. In this paper we study sound propagation from a city bus in a street canyon to a receiver in a nearby street canyon. Multiple reflections of sound waves in both the source canyon and the receiver canyon play an important role in the sound propagation. Experimental data are compared with three types of model results: (i) results of a numerical boundary element model, (ii) results of a 1:30 scale model experiment in a semi-anechoic room, and (iii) results of the Dutch standard engineering model, which is similar to the international standard ISO 9613-2. The data are in reasonable agreement with model results (i) and (ii), while the engineering model yields sound levels that are about 10 dB too low.

5aNSg3. Reflection of sound from a forest: comparison of experimental data to scattering theory. Erik Salomons (TNO Science and Industry, Stieljesweg 1, 2628CK Delft, Netherlands, erik.salomons@tno.nl),Jean Marc Wunderli (EMPA - Materials Science and Technology, Ueberlandstr. 129, CH-8600 Duebendorf, Switzerland, jean-marc.wunderli@empa.ch)

Reflection of sound by a forest has been investigated by means of measurements near Thun in Switzerland. Sound pulses were generated at 50 and 150 m from the forest, and reflected sound was recorded at distances of 100, 200, and 300 m from the forest. By comparison with numerical calculations of reflection of sound from a hard wall, using a parabolic-equation model for sound propagation in an atmosphere with wind and temperature as recorded during the measurements, the attenuation of sound waves upon reflection at the forest was determined. It was found that the reflection attenuation decreases from about 20 dB at low frequency to about 10 dB at high frequency. The experimental results for the reflection attenuation are compared with results of a theoretical model for scattering of spherical sound waves by a single row of cylinders. The model employs an effective spacing between the cylinders, to account for trees that are not at the edge of the forest, i.e., inside the forest. The model results are in good agreement with the experimental results. The comparison indicates that the effective spacing decreases with decreasing frequency, as low-frequency waves penetrate deeper into a forest than high-frequency waves do.

5aNSg4. Reflection of sound from a forest: Effective tree spacing for a scattering model with a single line of cylinders. Jean Marc Wunderli (EMPA - Materials Science and Technology, Ueberlandstr. 129, CH-8600 Duebendorf, Switzerland, jean-marc.wunderli@empa.ch), Erik Salomons (TNO Science and Industry, Stieljesweg 1, 2628CK Delft, Netherlands, erik.salomons@tno.nl)

A scattering model for the reflection of sound at forest rims is presented by the authors in another contribution to this conference. The forest is thereby modeled by a single row of cylinders with the effective spacing as single free parameter. In the present article an engineering scheme for this effective tree spacing is presented. The scheme is based on results of numerical calculations with the Euler model for sound propagation in a model forest consisting of cylinders. The numerical results show that forests are widely transparent for incoming as well as reflected sound waves. Multiple reflections can be neglected. Reflections from trees deep inside the forest experience additional propagation attenuation and are therefore weakened relative to contributions from trees in the first row. Apart from geometrical spreading foliage attenuation is the most prominent effect. The penetration depth of the forest reflection is proportional to the wavelength. The frequency dependent penetration depth is derived by means of a statistical analysis for numerous situations. Assuming the effective tree spacing to be inversely proportional to the penetration depth, the engineering scheme for the effective tree spacing is derived. Comparisons of the frequency response with measurements show good agreement.

Session 5aNSh

Noise, Structural Acoustics and Vibration, Physical Acoustics and EURONOISE: Sound and Vibration from Explosions in Air I (Poster Session)

Roger Waxler, Cochair
University of Mississippi

Keith Attenborough, Cochair
Open University

All posters will be on display from 9:40 a.m. to 11:20 a.m. To allow contributors an opportunity to see other posters, contributors of odd-numbered papers will be at their posters from 9:40 a.m. to 10:30 a.m. and contributors of even-numbered papers will be at their posters from 10:30 a.m. to 11:20 a.m.

Contributed Papers

5aNSh1. Environmental noise reduction means of weapons. Rauno Pääkkönen (Finnish Institute of Occupational Health, P.O. Box 486, 33101 Tampere, Finland, rauno.paakkonen@ttl.fi)

Noise from hand-held weapons is generated by their muzzle blast, the noise of the bullet in flight and on impact. The muzzle blast of almost all powder guns exceeds 140 dB near the ear of the shooter, which is considered to be able to generate a risk of hearing defects. The muzzle brake decreases recoil, but at the same time it forces the sound sideways and backwards. One novel aspect of noise attenuation is the use of active noise cancelling system at shooting ranges and in hearing protectors. The noise data has been collected on different shooting ranges in Finland. Both front and reflection types of suppressors were used. Silencers that attenuate noise to the sides and back have a significant effect, where as the noise to the front is not significantly attenuated because of the bullet noise. It is also possible to reach an attenuation of a few decibels of the maximum level of the muzzle blast with ANC headsets. The noise created by shotguns is the most significant source of environmental noise at many shooting ranges. It would be especially important to attain new ideas and innovations in the noise prevention of shotgun ranges.

5aNSh2. The development of a bespoke gunfire noise model for a military training area and the vibration impacts through the air on ancient structures. Graham Parry (ACCON UK Limited, Unit B, Fronds Park, Frouds Lane, Aldermaston, RG7 4LH Reading, UK, graham.parry@accon-uk.com)

This paper describes the development of a bespoke weapons system noise model known as the gunfire noise analysis tool (GNAT). The requirements for such a model came out of an expansion of military training within a National Park and the need to demonstrate that noise impacts could be modeled with reasonable accuracy out to distances of 10 kms and without the need for specialist acousticians or meteorologists to run the model. Additionally, the requirement was to ensure that noise modeling could be carried out within a matter of minutes thus allowing military training decisions to be made while protecting sensitive receptor locations from very high noise levels. The model utilised best practice and acoustic theory available at the time within the specific requirements of noise modeling outlined above. The model was validated against a number of noise measurements exercises carried out using controlled military noise events and for a live military exercise.

5aNSh3. Transducers for acoustical impulse measurements. Per Rasmussen (G.R.A.S. Sound & Vibration A/S, Skovlytoften 33, 2840 Holte, Denmark, pr@gras.dk)

The measurement of impulsive noise signals as for example from gunshots or airbag deployments requires special considerations when selecting transducer. The high frequency content in short impulses requires high bandwidth to correctly capture high rise times and small dimensions of the transducer to avoid diffraction. For high level impulses with very rapid rise time, the wide frequency range requires the use of preamplifiers with high slew rate capabilities and the capacitance and length of cables must be considered carefully. Slew rate limitations and bandwidth limitations can drastically change the peak value of an impulse. It is thus necessary to consider the whole measurement chain from transducer to AD-converter to ensure the correct measurement of the impulse.

5aNSh4. Large weapon source emission data protocols and results. Michael James (Blue Ridge Research and Consulting, 13 1/2 W. Walnut St., Asheville, NC 28801, USA, michael.james@blueridgeresearch.com), Micah Downing (Blue Ridge Research and Consulting, 13 1/2 W. Walnut St., Asheville, NC 28801, USA, micah.downing@blueridgeresearch.com), Pater Larry (U.S. Army Engineer Research and Development Center, 2902 Farber Drive, Champaign, IL 61821, USA, Larry.L.Pater@erdc.usace.army.mil)

The U.S. Army needs detailed information about the blast pressure field created by large weapons to avoid negative impacts on testing and training mission capabilities due to noise. The noise software tools BNOISE2™ and RMTK Noise Tool, which the Department of Defense (DoD) uses to predict and assess impacts of large weapon noise, require accurate acoustic source emission models. A free-field representation of the sound source acoustical emission, containing no waveform signal perturbations due to the ground, other reflecting surfaces, ballistic waves, or propagation anomalies, is required. The measurement protocols have been developed to collect the free-field source emission data. These protocols are described along with acoustical data and emission source results for the 120 mm M-1 tank gun, the 105 mm Stryker gun, and various weights of C-4 explosives. In addition, the measured acoustic data are compared with an idealized Friedlander curve. The overall results demonstrate that the protocols do provide sufficient free-field blast waveforms.

Session 5aNSi

Noise and EURONOISE: Acoustic Performance of Energy Efficient Building Products II (Poster Session)

Anthony Hoover, Cochair
McKay Conant Brooks, Inc.

Jacques Roland, Cochair
Centre Scientifique et Technique du Bâtiment

All posters will be on display from 9:40 a.m. to 11:20 a.m. To allow contributors an opportunity to see other posters, contributors of odd-numbered papers will be at their posters from 9:40 a.m. to 10:30 a.m. and contributors of even-numbered papers will be at their posters from 10:30 a.m. to 11:20 a.m.

Contributed Paper

5aNSi1. Roof-top urban wind turbines in London. Stephen Dance (London South Bank University, FESBE, Borough Road, SE1 0AA London, UK, dances@lsbu.ac.uk), Linda Liviani (RBA Acoustics, 104 The Foundry Annexe, 65 Glasshill Street, SE1 0QR London, UK, lindalive2@hotmail.com)

With the Mayor of London's office decision to allow planning permission only if 10% of the building's energy consumption is from renewable sources, wind turbines are starting to be erected on rooftops of residential blocks. A Proven 6 kW, 6m horizontal axis turbine was positioned on an 11 story 1960s concrete construction block of flats in the summer of 2007. Noise and vibration measurements were taken on the roof-top and in the nearest flat. In addition, energy performance was monitored, wind speed and direction recorded and weather noted. Results confirm that central London is a 24 h city and, given the right conditions, the turbine generators meaningful amounts of electricity.

Session 5aNSj

Noise and EURONOISE: Examples of Noise Control II

Karl Hirsch, Cochair
Cervus Consult, Kolpingstrasse 13, Wuerselen, D-52146, Germany

Pierre Etienne Gautier, Cochair
SNCF DIR, 45, rue de Londres, Paris, 75379, France

Contributed Papers

11:00

5aNSj1. Monitoring of noise reduction from traffic speed control. J. Jabben (RIVM, A. van Leeuwenhoeklaan 9, 3720 BA Bilthoven, Netherlands, jan.jabben@rivm.nl), C. Potma (RIVM, A. van Leeuwenhoeklaan 9, 3720 BA Bilthoven, Netherlands, charlos.potma@rivm.nl)

In November 2005, at the Hague, Amsterdam, Rotterdam and Utrecht, a 80 km/u speed limit was introduced on sections of motorways in the Netherlands. The aim was to evaluate the effects on noise, air quality and the circulation of the traffic. RIVM investigated the effects of noise emission by direct measurement at the sections with speed limit. This paper gives the results from continuous monitoring of noise levels that was started at July 2005 and continued up to November 2006. In the presentation the average measured effects on the equivalent noise emissions at the different sites will be given. Also the effects of traffic speed reduction on dwellings in the neighborhood of the motorways were evaluated using noise maps. Furthermore, apart from the average equivalent noise levels, the statistical noise indicators L5, L10, L70, and L95 were continuously monitored. It was found that speed reduction induces more reduction on maximum noise levels than on the average (equivalent) noise levels, probably due to a more steady and even distribution of traffic speeds.

11:20

5aNSj2. Automatic classification of traffic noise. Manuel A. Sobreira-Seoane (University of Vigo, E.T.S.I de Telecomunicación, Rúa Maxwell s/n, 36310 Vigo, Spain, msobre@gts.tsc.uvigo.es), Alfonso Rodríguez Molares (University of Vigo, E.T.S.I de Telecomunicación, Rúa Maxwell s/n, 36310 Vigo, Spain, amolares@gts.tsc.uvigo.es), José Luis Alba Castro (University of Vigo, E.T.S.I de Telecomunicación, Rúa Maxwell s/n, 36310 Vigo, Spain, jalba@gts.tsc.uvigo.es)

When modeling a city or a secondary road to calculate a noise map, the information about the number of heavy/light vehicles and the average speed it is not always available. In this paper, a first approach to get an automatic classification of vehicles is presented. The system is based on the classifi-

cation of the audio signal that a noise source produces. Some basic classifiers have been tested (k-nearest neighbours, FLD (Fischer linear discriminator) and principal components. As first approach, the aim of the job was to determine if the different classes (trucks, cars, and motorbikes) could be separable using different time and frequency characteristics: zero crossing ratios, spectral centroids, spectral rolloff, subband energies and mel frequency cepstral coefficients. The results shows that for some of the characteristics tested, the signals are separable, so a continuous traffic noise signal could be processed to get the information of the number of heavy trucks, cars, and motorbikes that passed by during the recording time. Information of a stereo recording could be used to get information of the direction of the vehicle. At this moment, combining three characteristics and FLD, errors bellow 9% can be reported.

11:40

5aNSj3. Remarks on a blast sound propagation model for noise management purposes at military training areas. Karl Hirsch (Cervus Consult, Kolpingstrasse 13, D-52146 Wuerselen, Germany, hirsch@cervus.de)

Germany will introduce a daily shooting noise management at its military training areas. Roughly speaking, this management adopts the basic ideas of ISO 17201-5 but uses in addition a rating scheme that allows 18 exceedance days per year (5%). For management purposes, the underlying sound prediction scheme must support two decision (1) Whether or not, the noise load of the daily planned occupancy is within certain noise limits. (2) Whether or not, the daily changing occupancy is close to a low noise minimum for the requested training options. The propagation model must consider particular weather conditions and the terrain shielding to enable the operator to optimise the occupancy with respect to these important conditions on a daily basis. The prediction must be fast enough to run several alternatives within minutes. Therefore, the prediction could not base on a sophisticated physical propagation model but must be done along a reasonable technical scheme. This paper discusses a ray tracing approach that is expected to substitute the currently in-use formula based on fitted empirical parameters. This model will at least provide one parameter to describe the sound refraction (radius of curvature) and a rule on how to estimate up wind propagation.

12:00

5aNSj4. Simulation of highway traffic noise with utilization of equivalent sound level of pass-by vehicle. Pichai Pamanikabud (King Mongkut U. of Technology-Thonburi, Dept. of Civil Engineering, Faculty of Engineering, Pracha-u-tid Road, Thungkru, 10140 Bangkok, Thailand, pichai.pam@kmutt.ac.th), Marupong Tansatcha (Dept. of Public Works and Town & Country Planning, Ministry of Interior, Rama 9 Rd., Huai-Khwang, 10320 Bangkok, Thailand, t_marupong@yahoo.com)

This paper presents study and building of a highway traffic noise simulation model by utilizing equivalent sound level over 20 s of passing-by vehicular noise in the analysis of nine types of vehicular basic noise. The basic noise of each vehicle type is applied into the formulation of the main highway traffic noise simulation model. The coefficient of propagation and ground effect for this model is also estimated and applied to the highway traffic noise model. This highway traffic noise model is then tested for its goodness-of-fit to field observations. The testing result shows that this model provides an effective prediction for highway noise in Thailand.

12:20

5aNSj5. Identification of noise sources in centrifugal blower with acoustic camera. Jurij Prezelj (University of Ljubljana, Faculty of Mechanical Engineering, Aškerčeva 6, 1000 Ljubljana, Slovenia, jurij.prezelj@fs.uni-lj.si), Mirko Čudina (University of Ljubljana, Faculty of Mechanical Engineering, Aškerčeva 6, 1000 Ljubljana, Slovenia, mirko.cudina@fs.uni-lj.si)

A centrifugal blower represents the main noise source in a vacuum cleaner. Noise emitted by the centrifugal blower working as a suction unit has aerodynamic, mechanical, and electromagnetic noise origins. Noise emitted by a suction unit consists of airborne and structure-borne noise. The contribution of the individual noise source to the total noise level depends on the geometry of the suction unit, rotational speed and on the operating conditions. Operating conditions of a suction unit depend on the amount of dust particles in the dust bag and are constantly changing during operation until a zero flow rate is reached. In order to reduce noise of suction unit at broad range of operating conditions, an identification of noise sources needs to be performed. Identification of most important noise sources on the centrifugal blower was performed with an acoustic camera at the design and off-design operation conditions. From the analyses we can conclude that the rotational noise usually prevails at the design point of operation, and that the nonrotational noise prevails at off-design operation. The main source of noise within a suction unit can be attributed to the aerodynamically generated noise, at the design as well as at off-design operation.

12:40-2:00 Lunch Break

Contributed Papers

2:00

5aNSj6. Buzz-saw noise : propagation of shock waves in aero-engine inlet ducts. Rasika Fernando (Institut Jean Le Rond d'Alembert, Université Pierre et Marie Curie, Boites 161 et 162, 4 place Jussieu, 75252 Paris Cedex 05, France, fernando@lmm.jussieu.fr), Régis Marchiano (Institut Jean Le Rond d'Alembert, Université Pierre et Marie Curie, Boites 161 et 162, 4 place Jussieu, 75252 Paris Cedex 05, France, marchi@lmm.jussieu.fr), François Coulouvrat (Institut Jean Le Rond d'Alembert, Université Pierre et Marie Curie, Boites 161 et 162, 4 place Jussieu, 75252 Paris Cedex 05, France, coulouvr@ccr.jussieu.fr), Yann Druon (Airbus S.A.S, Department of Acoustic & Environment, 316 route de Bayonne, 31000 Toulouse, France, yann.druon@airbus.com)

When high bypass ratio aircraft engines run at takeoff operating conditions, blade relative flow velocities can exceed sonic speed, thus generating forward propagating shock waves that spiral inside the intake before being radiated. "Buzz-saw" or "multiple pure tone" noise then occurs, and measured acoustic spectra close to the fan display tones at the blade passing frequency and its harmonics, along with those of the engine shaft rotation frequency. This work first attempts to reformulate McAlpine and Fisher's frequency domain model for the propagation of a sawtooth waveform spiralling inside a hard-walled and lined cylindrical duct with uniform flow. The nondissipative Burgers equation is solved, and modal attenuation and dispersion are added using a split-step computational method. In practice, shocks do not only occur at blade tips, but on a significant portion of the blade span. The plane wave hypothesis being no longer valid, a new three-dimensional model is presented for a no-flow case. This model is based on the computation of the axial variations of the mode amplitudes under the influence of the nonlinear modal interactions. The formalism of this new model, along with the preliminary results are also presented.

2:20

5aNSj7. Numerical simulation of aerodynamical noise generated by a cylindrical cavity. Daniel-Ciprian Mincu (ONERA (French aerospace Center), CFD & Aeroacoustics Department, BP 72, 29 avenue de la division Leclerc, 92322 Chatillon Cedex, France, dmincu@onera.fr), Stephane Redonnet (ONERA (French aerospace Center), CFD & Aeroacoustics Department, BP 72, 29 avenue de la division Leclerc, 92322 Chatillon Cedex, France, stephane.redonnet@onera.fr), Ivan Mary (ONERA (French aerospace Center), CFD & Aeroacoustics Department, BP 72, 29 avenue de la

division Leclerc, 92322 Chatillon Cedex, France, ivan.mary @onera.fr), Lionel Larcheveque (Universite de Provence, 29, avenue Robert Schuman, 13621 Aix-en-Provence, France, lionel.larcheveque @polytech.univ-mrs.fr), Eric Manoha (ONERA (French aerospace Center), CFD & Aeroacoustics Department, BP 72, 29 avenue de la division Leclerc, 92322 Chatillon Cedex, France, eric.manoha@onera.fr)

Cylindrical cavities are mounted at some positions on fuselage and wings of commercial transport aircraft for various service functions. Such cavities were identified as potential airframe noise sources generating high intensity whistles at frequencies situated in the audible range of 0.5-0.8 kHz. The present paper focuses on the numerical simulation of the far field noise generated by the unsteady flow passing over a cylindrical cavity with an aspect ratio (diameter/height) equal to unity, using a numerical methodology combining a LES and a Kirchhoff integration method. The LES computation was done using ONERA's cell-center/finite-volume/CFD code named FLU3M. A laminar boundary layer profile was applied upstream the computational domain, without forcing any turbulence. The LES results were coupled with a 3D Kirchhoff method in the frequency domain. The computed far field noise was compared to dedicated experimental data, showing very good agreement, especially regarding the emission frequency. The final paper will present in detail the involved numerical methods, the computational procedure, and several comparisons to experimental data. This study was completed in the framework of the AEROCAV (AEROacoustique d'une CAVité cylindrique) project funded by the FRAE (Fondation Recherche Aéronautique et Espace).

2:40

5aNSj8. Efficient method for harmonics estimation of car engine sounds: application to high quality real-time synthesis. Stephane Molla (Genesis S.A., Bâtiment Gérard Mégie, Domaine du Petit Arbois - BP 69, 13545 Aix-en-Provence Cedex 4, France, stephane.molla @genesis.fr), Florent Jaillet (Genesis S.A., Bâtiment Gérard Mégie, Domaine du Petit Arbois - BP 69, 13545 Aix-en-Provence Cedex 4, France, florent.jaillet@gmail.com), Benoît Gauduin (Genesis S.A., Bâtiment Gérard Mégie, Domaine du Petit Arbois - BP 69, 13545 Aix-en-Provence Cedex 4, France, benoit.gauduin@genesis.fr)

Additive synthesis is the most popular method for the resynthesis of sounds containing slowly evolving harmonics or partials, such as car engine noise and more generally rotating machines sounds. The most important step lies in the estimation of the amplitude and frequency of each sinusoidal component. It appears that insufficiently precise estimation often leads to unsatisfactory results in terms of sound fidelity. A method providing the time and frequency evolution of the amplitude of the harmonics of a recorded sound is presented. This technique is based on a joint time and frequency chaining of amplitude's extrema of amplitudes coming from a short-time Fourier transform, using forward and backward estimation. The proposed method is compared to a rough estimation, and to an estimation based on measured tachometric data, all carried out over the same car engine sound. This estimation method is implemented into the LEA software, which thus allows fast and precise computations of the parameters. Moreover, it also helps in estimating the frequency content of the "background" noise, which depends on the speed, allowing the extraction of the partials from the original sound in an easy and efficient way. Once these characteristics are found, a high quality real-time synthesis is possible.

3:00

5aNSj9. A simple acoustic model to characterize the internal sound field in centrifugal pumps originated by blade-tongue interaction. Jorge Parrondo (Universidad de Oviedo, Dep. de Energía, Campus de Viesques s/n, 33203 Gijón, Spain, parrondo@uniovi.es), Javier Perez (Universidad de Oviedo, Dep. de Energía, Campus de Viesques s/n, 33203 Gijón, Spain, javier.perez_castillo@siemens.com), Raul Barrio (Universidad de Oviedo, Dep. de Energía, Campus de Viesques s/n, 33203 Gijón, Spain, barrioraul @uniovi.es)

Conventional centrifugal pumps with volute casing generate fluid-dynamic noise particularly at the so-called blade-passing frequency, due to the interaction of the flow exiting the pump impeller with the volute tongue. The amplitude of the sound generated is very dependent on the pump operating point. Following previous studies by the authors, a methodology has been applied to quantify the generation of tonal noise for a given centrifugal pump, previously tested in laboratory. The procedure is based on a simple acoustic model for the pump, in which one or several ideal point sources are located at some arbitrary position in the volute. These ideal sources are assumed to radiate plane sound waves along the volute, which was considered to be composed by a succession of slices, each of them equivalent to a linear three-port acoustic system with sound transmission and reflexion coefficients according to the corresponding port areas. A series of tests was conducted to check the assumptions of the acoustic model, by applying external acoustic loads onto the pump outlet duct and measuring the noise reflected. The resulting reflection coefficient was in good agreement with the predictions of the acoustic model.

3:20

5aNSj10. Performance evaluation method for high noise environment intercom headsets. Stelios M. Potirakis (Intracom Defense Electronics, 21km Peania-Markopoulo Street, GR-19400 Koropi - Attica, Greece, spoti@intracomdefense.com), Yiannis Moisiadis (Intracom Defense Electronics, 21km Peania-Markopoulo Street, GR-19400 Koropi - Attica, Greece, gmoy@intracomdefense.com), Antonis Varagis (Intracom Defense Electronics, 21km Peania-Markopoulo Street, GR-19400 Koropi - Attica, Greece, avar@intracomdefense.com)

Intercoms' use in high noise environments (HNE) is typical since direct speech communication of individuals is difficult or even impossible. The headset selection for such an application is crucial since it serves both for noise attenuation and voice reproduction. It has been recently acknowledged in telecommunications (ITU-T/P.380) that headset electroacoustic measurements should be performed on head and torso simulator (HATS). However, in military applications where headsets are mainly used in HNE there is not a standard performance evaluation method but only for the earphone elements (MIL-PRF-25670B), thus excluding the acoustics of the earcup cavity, absorbing materials and face fitting quality. It is well known that the reproduced speech level should be of about 10 dB above noise level to achieve good intelligibility, so both sensitivity and noise reduction capability should be measured on a HATS to evaluate such a headset. In this work, a systematic methodology for measurement and performance evaluation of HNE headsets is proposed based on HATS. Critical aspects that may affect the test procedure, such as HATS response and the right headset placement are examined. Finally, a series of measurements prove the value of the proposed method. Large differences are revealed even for headsets following the same standard.

Session 5aPAa

Physical Acoustics: Infrasound I

Henry E. Bass, Cochair
The University of Mississippi - NCPA, 1 Coliseum Drive, University, MS 38677, USA

Alexis Le Pichon, Cochair
CEA-DASE, Arpajon Cedex, Bruyères-le-Châtel, 91297, France

Invited Paper

8:00

5aPAa1. Monitoring hurricanes using infrasound. Carrick L. Talmadge (The University of Mississippi - NCPA, 1 Coliseum Drive, University, MS 38677, USA, clt@olemiss.edu), Claus Hetzer (National Center for Physical Acoustics, University of Mississippi, University, MS 38677, USA, claus@olemiss.edu), Henry E. Bass (The University of Mississippi - NCPA, 1 Coliseum Drive, University, MS 38677, USA, pabass@olemiss.edu)

In spite of recent technological advances, forecasting the intensity of a hurricane remains a challenging problem. Knowledge of the location and the strength of the storm at the moment where it makes landfall is critical for civil defense planning and public safety. Part of the reason for this is that storms that are well away from land can only be monitored intermittently (e.g., three times per day). Infrasound signals are produced by the interaction of the hurricane with the sea-state and hold promise for characterizing sudden changes in hurricane strength on a time scale not possible with current sensing technologies. The University of Mississippi is leading a US national collaboration to monitor hurricanes using infrasound in the Gulf of Mexico and in the Western Atlantic Ocean. The results of measurements by from our group will be summarized, and the technical challenges associated with these measurements will be discussed.

Contributed Papers

8:20

5aPAa2. Infrasonic precursor of tropical cyclone. Konstantin A. Naugolnykh (University of Colorado/Zeltech, 325 Broadway, Boulder, CO 80305, USA, konstantin.naugolnykh@noaa.gov), Samuil A. Rybak (N. Andreev Acoustics Institute, 4 Schwernik St., 117420 Moscow, Russian Federation, am_rybak@hotmail.com)

Intense infrasonic emission was observed prior to the birth of a tropical cyclone (Netreba, 1991). It is connected apparently with instability of atmospheric layers in cyclone area. There are different mechanisms of this effect. Stratified compressional flow is unstable (Rybak, 2002), providing amplification of its potential component. Cooling of air in upward convection flow makes water vapor supersaturated. This is a nonequilibrium state of fluid where effect of instability can be developed. The equation of infrasonic propagation in such a medium is developed. (Naugolnykh, Rybak, 2006). Solutions of instability equation indicates the effect of radiation instability which produces infrasonic wave generation and its nonlinear evolution. Corresponding analyses of this equation make it possible to clarify the principally important aspects of cyclone infrasonic precursors. [Work supported by ESP.NR.NRCLG982524.]

8:40

5aPAa3. Origin of the sound prduced by volcanic eruptions. Sylvie Vergniolle (Institut de Physique du Globe, 4 Place Jussieu, 75252 Paris, France, vergniolle@ipgp.jussieu.fr)

Volcanic eruptions present different regimes, which can be understood and classified in the framework of a two-phase flow, either an annular flow such as in hawaiian fire fountains or a slug flow in strombolian explosions. The gas, exsolved at depth, carries physical information about the dynamics of strombolian activity, which in turn may lead to a better understanding of volcanic systems. The sound produced by volcanic eruptions is mostly infrasonic, although the landing of magma fragments on the ground is in the audible range. The first cause for sound generation is related to the gas overpressure when the sound waves are produced by a slug breaking at the surface. Gas overpressure induces oscillations of the gas volume and pushes passively the liquid film above the slug, and has been modeled accordingly. Sometimes the overpressure is small and the bubble vibration prior to breaking does not exist. In that case, the sound is produced by the gas escaping through a small hole on the bubble nose and is modeled as an Helmholtz resonator. The second class of sound source is related to the expulsion of a gas-ejecta mixture at a large velocity. Examples of volcanic sound waves will be presented.

9:00

5aPAa4. Implications from the analysis of meteoric infrasound. Laeslo G. Evers (Royal Netherlands Meteorological Institute (KNMI), PO Box 201, 3730 AE De Bilt, Netherlands, evers@knmi.nl), Hein Haak (Royal Netherlands Meteorological Institute (KNMI), PO Box 201, 3730 AE De Bilt, Netherlands, haak@knmi.nl), Alexis Le Pichon (CEA-DASE, Arpajon Cedex, 91297 Bruyères-le-Châtel, France, alexis.le-pichon@cea.fr), Karl Antier (CEA-DASE, Arpajon Cedex, 91297 Bruyères-le-Châtel, France, karl.antier@cea.fr)

Monitoring of infrasound has been widely applied in the past to detect nuclear tests. The Limited (Partial) Test Ban Treaty of 1963 confined nuclear test explosions to the underground marking the end of the global interest in infrasound. During the negotiation of the Comprehensive Nuclear-Test-Ban Treaty, in 1995-1996, it became gradually clear that infrasound monitoring should be become one of the four techniques for the treaty's verification system. The global interest in infrasound has increased significantly since the signature of the CTBT. Meteors are one of the few natural sources mimicking a nuclear. Therefore, it is an ideal object to test detection capability, phase identifiers, localization procedures and propagation models of infrasound and their processing techniques. In this presentation, we will show the results of studies on meteoric-generated infrasound and their implications for infrasound as verification technique. In addition, results of the 2007 .09.15 meteor in Peru will be discussed which is one of the few meteoroids in recent times leaving an impact crater.

Invited Paper

9:20

5aPAa5. Infrasound monitoring and global atmospheric dynamics. Elisabeth Blanc (Commissariat à l'Energie Atomique, DASE/SLDG/LSEG, Centre DAM-Ile de France, 91297 Arpajon Cedex, France, elisabeth.blanc@cea.fr), Alexis Le Pichon (CEA-DASE, Arpajon Cedex, 91297 Bruyères-le-Châtel, France, alexis.le-pichon@cea.fr), Lars Ceranna (Federal Institute of Geosciences and Natural Ressources, Section B3.11 Seismology, Stilleweg 2, 30655 Hannover, Germany, ceranna@sdac.hannover.bgr.de)

The development of the Infrasound International Monitoring System, used for the verification of the Comprehensive Test Ban Treaty, offers a powerful way to measure, atmospheric waves permanently and at a global scale. Infrasonic waves propagate in the channel formed by the temperature and wind gradients of the atmosphere. Long term observations provide information about the evolution of the propagation conditions and then of atmospheric parameters. The monitoring of continuous sources, as ocean swell, gives the characteristics of the stratospheric wave duct submitted to stratospheric warming effects. Large scale gravity waves, which are also observed by the network, produce a forcing of the stratosphere at low and middle latitudes and long-lived changes in the stratospheric circulation towards high latitudes, leading to fluctuations in the strength of the polar vortex. These fluctuations move down to the lower stratosphere with possible effects on the tropospheric temperature. Gravity wave monitoring in Antarctica reveals a gravity wave system correlated with the wind and the temperature gradients in the stratosphere. Gravity waves associated with magnetic storms are generally not observed. However, wave systems coming from North could reveal other processes related with the global dynamics of the stratosphere.

9:40-10:40 Posters

Lecture sessions will recess for presentation of poster papers on various topics in acoustics. See poster sessions for topics and abstracts.

Contributed Paper

10:40

5aPAa6. Locating infrasound events in wind with dense distributed arrays. Wheeler Howard (Mil-tec Research and Technology, 9 Industrial Park Dr, Oxford, MS 38655, USA, whoward@mil-tec.com), Kevin Dillion (Mil-tec Research and Technology, 9 Industrial Park Dr, Oxford, MS 38655, USA, kdillion@mil-tec.com), F. Douglas Shields (University of Mississippi/ NCPA, 1 Coliseum Dr, University, MS 38677, USA, dshields @olemiss.edu)

Applications for infrasound suffer due to the presence of wind noise in the sensor data. Several techniques have been and are being used to mitigate the influence of wind noise in locating infrasonic signals of interest. One of these methods is the averaging of data from multiple sensors in a distributed array. A distributed array was employed to study infrasonic signals from airborne sources. Wind noise during testing masked the location of the infrasonic signals in the time domain. Postprocessing techniques using statistical measures for dense arrays were employed to recover the onset of the infrasonic events. Data from these tests and an explanation of the postprocessing techniques will be discussed.

Invited Papers

11:00

5aPAa7. Detection and localization capability of the European infrasound network. Lars Ceranna (Federal Institute of Geosciences and Natural Ressources, Section B3.11 Seismology, Stilleweg 2, 30655 Hannover, Germany, ceranna@sdac.hannover .bgr.de), Alexis Le Pichon (CEA-DASE, Arpajon Cedex, 91297 Bruyères-le-Châtel, France, alexis.le-pichon@cea.fr), Julien Vergoz (CEA-DASE, Arpajon Cedex, 91297 Bruyères-le-Châtel, France, julien.vergoz@cea.fr), Laslo Evers (KNMI, PO Box 201, 3730 De Bilt, Netherlands, laslo.evers@knmi.nl)

The infrasound network of the International Monitoring Network (IMS) for the compliance with the Comprehensive Nuclear-Test-Ban Treaty (CTBT) is currently not fully established. However, it has demonstrated its capability for detecting and locating infrasonic sources like meteorites, as well as volcanic eruptions on a global scale. Such ground-truth events are rare; therefore regions providing a dense network of infrasound stations have to be considered to test and to calibrate detection and location procedures. In central Europe, several years of continuous infrasound waveform data are available for nine stations in Sweden, the Netherlands, France, and Germany, whereas only one of them is part of the IMS. This exquisite setting with an average interstation distance below 500 km allows the analysis of natural and artificial infrasonic activity in Europe. The results of the association of multiple arrays demonstrate the need of continuous infrasound monitoring on a regional scale to advance the development of automatic location procedures. Beside the seasonal variation of the network's detection capability, which is dominated by the prevailing stratospheric winds, dominant source regions showing repeating events will be discussed in detail considering the next recording stations.

11:20

5aPAa8. Continuous infrasound monitoring for atmospheric studies. Alexis Le Pichon (CEA-DASE, Arpajon Cedex, 91297 Bruyères-le-Châtel, France, alexis.le-pichon@cea.fr), Nicolas Brachet (CTBTO PTS/IDC Vienna International Centre, P.O. Box 1200, A-1400 Vienna, Austria, Nicolas.Brachet@ctbto.org), Lars Ceranna (Federal Institute of Geosciences and Natural Ressources, Section B3.11 Seismology, Stilleweg 2, 30655 Hannover, Germany, ceranna@sdac.hannover.bgr.de)

Infrasound data processing on a routine-basis provides a powerful tool to quantify relationships between infrasonic observables and atmospheric specification problems. In particular, studies of continuous sources of infrasonic waves provide further evidence that long-range propagation primarily depends on the seasonal variability of the prevailing zonal winds. It confirms that most of the detected infrasound energy propagates in the stratospheric waveguide. The observed detection capability of the IMS network is compared to the

predicted one using near-real time atmospheric updates. Moreover, on regional scales, signals from volcanic activities open up new fields for investigations into inverse problems for atmospheric remote sensing in a range of altitude where routine ground based or satellite measurements are rare. With the increasing number of IMS and experimental arrays deployed around the globe, a valuable contribution can be anticipated in the understanding of the dynamics of the upper atmosphere. In return, such studies will help to optimize the siting of infrasound arrays with respect to both the number and configuration in order to monitor infrasonic sources of interest.

11:40

5aPAa9. Inversion of infrasound signals for atmospheric remote sensing. Douglas Drob (Naval Research Laboratory, Space Science Division, 4555 Overlook Avenue, Washington, DC 20375, USA, douglas.drob@nrl.navy.mil), Milton Garces (Infrasound Laboratory, University of Hawaii, 73-4460 Queen Kaahumanu Highway #119, Kailua-Kona, HI 96740, USA, milton@isla.hawaii.edu), Robert Meier (Naval Research Laboratory, Space Science Division, 4555 Overlook Avenue, Washington, DC 20375, USA, robert.meier@nrl.navy.mil), Michael Picone (Naval Research Laboratory, Space Science Division, 4555 Overlook Avenue, Washington, DC 20375, USA, j.picone@nrl.navy.mil)

This paper investigates the utilization of observed long-range infrasound signals to improve our knowledge of upper atmospheric winds and temperatures. A series of numerical experiments designed to provide a mathematical framework for implementation of this idea is presented. The statistical performance of a realistic infrasonic upper atmospheric remote sensing network over a range of different environmental and propagation modeling assumptions, source types, and geophysical variables (season, local-time, latitude, etc) is quantified. For a series of fictitious events, infrasonic observables are calculated with 3D Cartesian ray tracer and a series of atmospheric profiles spanning the range of geophysical parameters. These synthetic measurements are then inverted to estimate the original atmospheric background fields.

Contributed Papers

12:00

5aPAa10. The influence of shallow atmospheric structure on tropospheric ducted infrasound from the Buncefield oil depot explosion. David N. Green (AWE Blacknest, Brimpton, RG7 4RS Reading, UK, dgreen@blacknest.gov.uk), Matthew Hort (Met Office, FitzRoy Road, EX1 3PB Exeter, UK, matthew.hort@metoffice.gov.uk), David Bowers (AWE Blacknest, Brimpton, RG7 4RS Reading, UK, bowers@blacknest.gov.uk)

The vapour cloud explosion which destroyed the Buncefield oil depot, UK, on 11th December 2005, has proven to be a benchmark ground truth event for infrasonic studies. The regional infrasonic returns, those that propagated in the stratosphere and thermosphere, have been analysed in detail elsewhere. Here, we present the results of a study into infrasound ducted in the troposphere, recorded within 250 km of the source as air-to-ground coupled waves by a dense seismometer network. These tropospheric arrivals exhibit large waveform differences across the UK, both in amplitude and waveform shape. We numerically model these infrasound arrivals using a wave number integration method, incorporating a velocity profile derived from the UK Met Office numerical weather prediction model. Although some of the waveform variability is due to ground conditions at the recording site, we show that consistent changes in waveform shape across a 200 km swath of stations are correlated with a change in the wind vector in the lowermost 2 km of the atmosphere. Also, small amplitude, high-frequency precursors to the dominant acoustic signal, which might be misinterpreted as evidence of a small initial explosion, are shown to be consistent with the dispersion expected from a thin, shallow wind jet.

12:20

5aPAa11. Regional and telesonic propagation of volcano-acoustic signals. Milton Garces (Infrasound Laboratory, University of Hawaii, 73-4460 Queen Kaahumanu Highway #119, Kailua-Kona, HI 96740, USA, milton@isla.hawaii.edu), David Fee (Infrasound Laboratory, University of Hawaii, 73-4460 Queen Kaahumanu Highway #119, Kailua-Kona, HI 96740, USA, dfee@isla.hawaii.edu)

Volcanic explosions are reliable sources for studying infrasonic propagation. Large amplitude acoustic explosions with known locations and onset times provide useful constraints for the signal changes induced by atmospheric variability. As part of the Acoustic Surveillance of Hazardous Eruptions (ASHE) project, two four-element infrasound arrays with collocated seismometers have been deployed 37 and 251 km from Tungurahua Volcano, Ecuador since February 2006. During this period Tungurahua has been in near-constant eruption, with energetic tremor signals and a multitude of energetic explosions. A combination of array processing and energy threshold detectors have been used to identify over 12 000 explosions at the nearby array (RIOE, 37 km), with the peak pressure of the largest explosion around 24 Pa. Many of the larger explosions are recorded at the more distant LITE (251 km) array as well. To further supplement the dataset, select data from infrasonic sensors at distances of 3-5 km from the crater will be used. State-of-the-art wave propagation and atmospheric models will be used to assess the influence of long-range propagation on the volcanic signals. By selecting a data subset with high signal to noise ratios, it should be possible to infer statistically significant atmospheric propagation effects.

12:40-1:40 Lunch Break

Contributed Papers

1:40

5aPAa12. Gravity and rumble of distant sources. Philippe Delorme (ONERA/DSNA, 29, avenue de la Division Leclerc, 92322 Chatillon, France, Philippe.delorme@onera.fr), Geraldine Menexiadis (ONERA/DSNA, 29, avenue de la Division Leclerc, 92322 Chatillon, France, geraldine.menexiadis@onera.fr)

The subject of this paper is the comprehension of this physical phenomenon: Let an atmospheric source emiting an impulsive signal (such as thunder, explosion...). The received signal at short distance is itself impulsive but at long distance one can hear a rumble which can last up to one minute. If one models the propagation of the sound by the traditional equation of the waves, as the Green function is a distribution whose support is the sphere of radius CT (C: speed of sound, T: the travel time), the received signal (calculated by convolution) should last only the duration of emission. If one uses ray tracings to take into account the heterogeneity of the medium, one obtains the same conclusion (only the time of arrival is modified) in contradiction with the experimental results such as those obtained for example during the First World War to detect the position of the enemy batteries. A similar phenomenon can be observed in the study of the propagation of a sonic boom (although less obvious because the support of the

two-dimensional Green function is not a circle). We thus propose a critic of the physical models, and our conclusion lays on the need for taking into account gravity.

2:00

5aPAa13. Study of Infrasound Propagation from the Shuttle Atlantis using a large Seismic Network. Michael A. Hedlin (University of San Diego California, Scripps Institute of Oceanography, 9500 Gilman Drive, La Jolla, CA 92093, USA, hedlin@ucsd.edu), Catherine D. Degroot-Hedlin (University of San Diego California, Scripps Institute of Oceanography, 9500 Gilman Drive, La Jolla, CA 92093, USA, chedlin@ucsd.edu), Kris Walker (University of San Diego California, Scripps Institute of Oceanography, 9500 Gilman Drive, La Jolla, CA 92093, USA, walker@ucsd.edu), Douglas Drob (Naval Research Laboratory, Space Science Division, 4555 Overlook Avenue, Washington, DC 20375, USA, douglas.drob@nrl.navy.mil), Mark A. Zumberge (University of San Diego California, Scripps Institute of Oceanography, 9500 Gilman Drive, La Jolla, CA 92093, USA, mzumberge@ucsd.edu)

Inclement weather in Florida forced the shuttle Atlantis to land at Edwards Air Force base in southern California on June 22, 2007, passing near three infrasound stations and several hundred seismic stations in northern Mexico, southern California, and Nevada. The high signal-to-noise ratio, broad receiver coverage, and Atlantis' positional information allowed us to test our ability to model infrasound propagation through the atmosphere to regional distances. We predicted shadow zones and arrival times using rays launched at right angles to the conical shock front surrounding the shuttle, and traced through a standard atmospheric model, as well as a global G2S model. Comparison of predictions vs observations shows agreement over much of the study area for both atmospheric specifications. To the east of the shuttle trajectory, there were no detections beyond the primary acoustic carpet. Infrasound energy was detected hundreds of kilometers to the west and northwest of the shuttle trajectory, consistent with the predictions of ducting due to the westward summer-time stratospheric jet. Both atmospheric models predict regions of ensonification alternating with shadow zones to the northwest. However, infrasound energy was detected tens of kilometers beyond predicted zones of ensonification, possibly due to uncertainties in stratospheric wind speeds.

2:20

5aPAa14. Nonlinear propagation modeling of infrasound. David Norris (BBN Technologies, 1300 N. 17th St., Ste. 400, Arlington, VA 22209, USA, dnorris@bbn.com), Kevin Bongiovanni (BBN Technologies, 4 John Clarke Rd, Middletown, RI 02842, USA, kbongiov @bbn.com), James Masi (BBN Technologies, 4 John Clarke Rd, Middletown, RI 02842, USA, jmasi@bbn.com)

The significance of nonlinear propagation effects on infrasound is studied using the Nonlinear Progressive Wave Equation (NPE) [B. E. McDonald and W. A. Kupperman, J. Acoust. Soc. Am., **81**, 1406--1417 (1987)]. The NPE model accounts for nonlinear effects associated with a weak shock front, including shock-driven energy loss and self refraction. Numerical implementation is accomplished using a pseudospectral approach, which provides excellent computational efficiency while still maintaining acceptably small numerical errors. The nonlinear effects are isolated by generating NPE predictions with the nonlinear terms turned on and off. With the nonlinear terms off, the NPE reduces to a standard linear PE formulation. Waveform predictions through a realistic atmosphere are compared to ground truth observations to evaluate the NPE model performance and assess the influence of the nonlinear effects along the propagation path.

2:40

5aPAa15. Misty picture: A unique experiment for the interpretation of the infrasound propagation from large explosive sources. Olaf Gainville (Commissariat à l'Energie Atomique, DASE/SLDG/LSEG, Centre DAM-Ile de France, 91297 Arpajon Cedex, France, olaf.gainville@ec-lyon.fr), Philippe Blanc-Benon (Ecole Centrale de Lyon, LMFA, UMR CNRS 5509, Ecully, 69134 Lyon, France, Philippe.Blanc-Benon@ec-lyon.fr), Elisabeth Blanc (Commissariat à l'Energie Atomique, DASE/SLDG/LSEG, Centre DAM-Ile de France, 91297 Arpajon Cedex, France, elisabeth.blanc@cea.fr), Roger Roche (Commissariat à l'Energie Atomique, DASE/SLDG/LSEG, Centre DAM-Ile de France, 91297 Arpajon Cedex, France, roger.roche @cea.fr), Christophe Millet (Commissariat à l'Energie Atomique, DASE/SLDG/LSEG, Centre DAM-Ile de France, 91297 Arpajon Cedex, France, christophe.millet@cea.fr), Francoise Le Piver (Commissariat à l'Energie Atomique, DASE/SLDG/LSEG, Centre DAM-Ile de France, 91297 Arpajon Cedex, France, francoise.lepiver@cea.fr), Bruno Despres (Commissariat à l'Energie Atomique, DSSI, Centre DAM-Ile de France, 91297 Arpajon Cedex, France, bruno.despres@cea.fr), Pierre-Franck Piserchia (Commissariat à l'Energie Atomique, DASE/SLDG/LSEG, Centre DAM-Ile de France, 91297 Arpajon Cedex, France, pierre-franck .piserchia@cea.fr)

In the framework of the Comprehensive Nuclear-Test-Ban Treaty, the International Monitoring System develops a 60 micro-barometric stations network. These stations, which records infrasound, detect various powerful natural and artificial sources like long range explosions, oceanic swell, and volcano eruptions. For data analysis, the CEA, in collaboration with the LMFA, develops specific methods based on measurements, data processing and numerical simulation. The Misty Picture experiment is a high explosive event (4685 Tons of ANFO) realized in 1987 in New Mexico (US). Infrasounds were recorded by 22 sensors until a distance of 1000 km in a quiet background noise condition. Multireflected tropospheric, stratospheric and thermospheric phases are detected. Signals recorded near the source (1 km away) and observed in the geometrical shadow zone (between 150 km and 250 km from the point source) are of particular interest. This reference experiment very well documented is used to improve our understanding of the atmospheric propagation of infrasound as well as to evaluate our models. Using various methods such as ray tracing, parabolic equation and finite differences, we investigate effects of the wind, atmospheric absorption, nonlinearity, refraction, (2D and 3D) and scattering by small atmospheric scales on observed phase kinds, their travel time and their waveform.

Invited Paper

3:00

5aPAa16. A low power and low noise infrasound sensor for temporary measurements. Damien Ponceau (CEA/DASE, BP12, Service TMG, 91680 Bruyères le Chatel, France, damien.ponceau@cea.fr)

Temporary infrasound measurements require low power consumption, reliable, and compact equipments. As a consequence, these equipments are not always as accurate as equipments operating on long term stations. Measurements quality can be affected. DASE has developed a portable infrasound sensor from MB2005 microbarometer. This new microbarometer consists in improved mechanics from MB2005 and in a movement transducer providing a voltage directly proportional to pressure derivate all over infrasound bandwidth and even more: sensor response phase is purely independent from environment (temperature, condensationœ) all over the same bandwidth. Moreover, thanks to its very simple design this sensor needs very low power and is lighter, smaller and cheaper than previous generation sensors. It reaches Infrasound Low Noise Model (IS LNM) down to 0.02 Hz and is very portable as it weights less than 3 kg with less than 1 L. A batch of prototypes has been manufactured and evaluated in lab thanks to an infrasound generator used for routine calibration of microbarometers installed by DASE on some International Monitoring System stations (IMS). Sensors field evaluation is running. First results are promising.

Session 5aPAb

Physical Acoustics: Time Reversal Acoustics for Nonlinear Imaging I

Alexander Sutin, Cochair
Stevens Institute of Technology, Castle Point on Hudson, Hoboken, NJ 07030, USA

Serge Dos Santos, Cochair
ENI Val de Loire, Université François Rabelais de Tours, LUSSI CNRS, rue de la Chocolaterie, Blois, 41034, France

Invited Papers

8:00

5aPAb1. Time reversal of acoustic waves in the nonlinear regime: basic physics and application to ultrasound contrast imaging. Mickael Tanter (Laboratoire Ondes et Acoustique, ESPCI, Université Paris 7, CNRS, 10 rue Vauquelin, 75005 Paris, France, michael.tanter@espci.fr), Olivier Couture (Laboratoire Ondes et Acoustique, ESPCI, Université Paris 7, CNRS, 10 rue Vauquelin, 75005 Paris, France, olivier.couture@espci.fr), Mathias Fink (Laboratoire Ondes et Acoustique, ESPCI, Université Paris 7, CNRS, 10 rue Vauquelin, 75005 Paris, France, mathias.fink@espci.fr)

Time reversal invariance of acoustic waves propagation remains valid even in the nonlinear regime in nondissipative media. This very interesting property that was extensively used in linear acoustics can also find potential applications in the nonlinear regime. Harmonic imaging coupled to the use of contrast agents is a topic of wide interest in ultrasonic medical imaging. Images are built at twice the excitation frequency that corresponds to the resonance frequency of the bubbles embedded in the medium. Consequently, the contrast becomes important between areas of low and high concentration of bubbles. However, at a high mechanical index, the harmonic components of backscattered echoes depends on the intrinsic nonlinear properties of tissues as well as the bubble's resonance. The focused beam is generating harmonics during its nonlinear propagation. It results in a degradation of the harmonic image contrast. Time reversal is an elegant way to find the emission codes allowing us to cancel the harmonic components due to nonlinear propagation of the ultrasonic beam. In the absence of bubbles, if the backscattered echoes are time-reversed and reemitted by the array, the harmonic components of the resulting wavefront are transferred back to the fundamental frequency during propagation. Experiments conducted with 1D-linear arrays illustrate these cancellation techniques.

8:20

5aPAb2. Localized nonlinearity time reversal imaging with chaotic cavities. Olivier Bou Matar (IEMN, UMR CNRS 8520, avenue Poincaré, BP 60069, 59652 Villeneuve d'Ascq, France, olivier.boumatar@iemn.univ-lille1.fr), Yifeng Li (IEMN - LEMAC UMR CNRS 8520, Ecole Centrale de Lille, BP 48, Cite scientifique, 59651 Villeneuve D'Ascq, France, Yifeng.li@iemn.univ-lille1.fr), Vladimir L. Preobrazhensky (IEMN, UMR CNRS 8520, avenue Poincaré, BP 60069, 59652 Villeneuve d'Ascq, France, vladimir.preobrajenski@iemn.univ-lille1.fr), Philippe Pernod (IEMN, UMR CNRS 8520, avenue Poincaré, BP 60069, 59652 Villeneuve d'Ascq, France, philippe.pernod@iemn.univ-lille1.fr)

Recent results have shown that nonlinear elastic wave spectroscopy (NEWS) and time reversal (TR) techniques can be combined to localize defects. NEWS techniques can be used either as a post-treatment of TR used as a tool for generating strong localized stress (TR-NEWS), or as a pretreatment, of TR used as a tool for defect identification (NEWS-TR). The TR process can be implemented with a programmable multielements ultrasonic system. But recently, it has been demonstrated that a single PZT ceramic glued on the sample can also be used as a TR mirror. In this case the quality of the retrofocusing process, and so the microdamage localization, depends on the sample geometry. In this study, numerical and laboratory studies, performed in order to determine and enhance the possibility to localize microdamage based on a combination of a time reversal technique using an emitter with a chaotic shape and nonlinear elastic wave response, will be presented. The benefit of using such emitters is clearly found in breaking the symmetry of the problem, leading to an unambiguous retrofocusing. Moreover, chirp-coded excitation, instead of short pulses, is studied in order to transmit more energy on the defect without increasing the peak intensity of the excitation.

8:40

5aPAb3. Landmine detection using nonlinear vibrations excited by time reversal techniques. Brad Libbey (U.S. Army RDECOM CERDEC NVESDS, 10221 Burbeck Rd, Fort Belvoir, VA 22060, USA, brad.libbey@us.army.mil), Alexander Sutin (Stevens Institute of Technology, Castle Point on Hudson, Hoboken, NJ 07030, USA, asutin@stevens.edu), Armen Sarvazyan (Artann Laboratories, 1753 Linvale-Harbourton, Lambertville, NJ 08350, USA, armen@artannlabs.com)

Time reversal focuses seismic waves and excites nonlinear surface vibrations that are large in the presence of a landmine. These soil vibrations provide an accurate localization cue when contrasted with measurements made without a mine. Traditionally nonlinear effects were investigated by measuring the interaction of harmonic waves and nonlinear resonance frequency shifts. These methods provide high signal to noise ratios, but required tuning of excitation frequencies resulting in test times unsuitable for field applications. Time reversal is capable of providing broad band excitation at amplitudes large enough to drive the nonlinear mechanisms at measurable levels while reducing the overall measurement time. Spatial and temporal focusing data will be presented for three different time reversal systems compromising speakers and vibrators for seismic excitation and a Doppler laser vibrometer and geophones for signal

recording. The high amplitude signals generated by these systems adequately drive the nonlinear responses. Special processing techniques, phase inversion and varied amplitude, have been developed to extract the nonlinear responses from the broadband response by cancelling the linear part. The remaining nonlinear response shows greater mine/no mine contrast than the linear data. Practical implementations of the developed methods will be discussed.

9:00

5aPAb4. Separation of multiple scatterers in NEWS-TR experiments. Sigfried Vanaverbeke (K.U.Leuven Campus Kortrijk, E. Sabbelaan 53, 8500 Kortrijk, Belgium, Sigfried.Vanaverbeke@kuleuven-kortrijk.be), Lieven De Lathauwer (K.U.Leuven Campus Kortrijk, E. Sabbelaan 53, 8500 Kortrijk, Belgium, Lieven.DeLathauwer@kuleuven-kortrijk.be), Herbert De Gersem (K.U.Leuven Campus Kortrijk, E. Sabbelaan 53, 8500 Kortrijk, Belgium, Herbert.DeGersem@kuleuven-kortrijk.be), Koen Van Den Abeele (K.U .Leuven Campus Kortrijk, E. Sabbelaan 53, 8500 Kortrijk, Belgium, koen.vandenabeele@kuleuven-kortrijk.be)

Nonlinear elastic wave spectroscopy combined with acoustic time reversal (NEWS-TR) is a promising new methodology for detecting microdamage at an early stage. When dealing with structures which could potentially contain many pointlike nonlinear scatterers, there is a need to develop techniques for separately imaging the defects using a distributed sensor network which acts as a time-reversal mirror. In this contribution, we present numerical simulations of a newly developed version of the DORT method for nonlinear imaging and also discuss the possibility of applying PARAFAC (parallel factor analysis) and ICA (independent component analysis) methods to solve the problem of separating multiple nonlinear scatterers in the time-frequency domain.

9:20

5aPAb5. Wide band time reversal acoustic nonlinear diagnostics. Tj Ulrich (EES-11 (Geophysics) - Los Alamos National Laboratory, MS D443, Los Alamos, NM 87545, USA, tju@lanl.gov), Alexandr Sutin (Stevens Institute of Technology, Castle Point on Hudson, Davidson Laboratory, Hoboken, NJ 07030, USA, asutin@stevens-tech.edu), Jim A. Tencate (EES-11 (Geophysics) - Los Alamos National Laboratory, MS D443, Los Alamos, NM 87545, USA, tencate@lanl.gov)

Time reversal acoustics (TRA) techniques provide a means to focus energy at a localized time and space, or at an unknown location (i.e., source or scatterer not known a priori) without the need to calculate time delays, as is necessary for phased arrays. The experiments demonstrate that time reversal focusing provides localized surface vibration with amplitude sufficient to induce measurable nonlinear effects and does so over a wide frequency band. Because the amplitude is spatially focused, time reversal enables local probing of this nonlinearity that can be used for nonlinear imaging. The nonlinear effects for wide band frequency signals were measured by phase-inversion method combining two signals of opposite sign in order to cancel the linear response and preserve quadratic nonlinearities. The method works effectively for nonlinear NDE of thin plates where laser Doppler Vibrometer can be used for measurements of the surface vibration and TRA focusing of acoustic waves. Presented results include crack and delamination diagnostic is epoxy graphite composites, diffusion bonded metallic disks and impact surface damage in glass. Scanning electron microscopy and optical images are also shown to demonstrate the types of damage features detected using this method.

9:40-11:00 Posters

Lecture sessions will recess for presentation of poster papers on various topics in acoustics. See poster sessions for topics and abstracts.

Contributed Papers

11:00

5aPAb6. Time reversal use in detection of buried cracks. Pierre-Yves Le Bas (EES-11 (Geophysics) - Los Alamos National Laboratory, MS D443, Los Alamos, NM 87545, USA, pylb@lanl.gov), Brian E. Anderson (EES-11 (Geophysics) - Los Alamos National Laboratory, MS D443, Los Alamos, NM 87545, USA, bea@lanl.gov), Michele Griffa (EES-11 (Geophysics) - Los Alamos National Laboratory, MS D443, Los Alamos, NM 87545, USA, mgriffa@lanl.gov), Tj Ulrich (EES-11 (Geophysics) - Los Alamos National Laboratory, MS D443, Los Alamos, NM 87545, USA, tju@lanl.gov), Paul A. Johnson (EES-11 (Geophysics) - Los Alamos National Laboratory, MS D443, Los Alamos, NM 87545, USA, paj@lanl.gov)

Time reversal has the potential to become a powerful tool in nondestructive evaluation. Coupled with nonlinear properties of cracks in a technique known as time reverse nonlinear elastic wave spectroscopy (TRNEWS), it provides the means to detect defects in complex structures. This experimental study explores the capabilities of TR to focus energy inside a 3D medium in order to activate nonlinear features or defects. Special attention is given to buried cracks. The current challenge is introducing sufficient energy in order to excite the buried feature and produce nonlinear scattering. We will provide an overview of the problem.

11:20

5aPAb7. Computational time reversal acoustics imaging of embedded defects in solid media. Michele Griffa (EES-11 (Geophysics) - Los Alamos National Laboratory, MS D443, Los Alamos, NM 87545, USA, mgriffa@lanl.gov), Brian E. Anderson (EES-11 (Geophysics) - Los Alamos National Laboratory, MS D443, Los Alamos, NM 87545, USA, bea@lanl.gov), Tj Ulrich (EES-11 (Geophysics) - Los Alamos National Laboratory, MS D443, Los Alamos, NM 87545, USA, tju@lanl.gov), Pierre-Yves Le Bas (EES-11 (Geophysics) - Los Alamos National Laboratory, MS D443, Los Alamos, NM 87545, USA, pylb@lanl.gov), Paul A. Johnson (EES-11 (Geophysics) - Los Alamos National Laboratory, MS D443, Los Alamos, NM 87545, USA, paj@lanl.gov), Lianjie Huang (EES-11 (Geophysics) - Los Alamos National Laboratory, MS D443, Los Alamos, NM 87545, USA, ljh@lanl.gov)

Time reversal acoustics (TRA) techniques can exploit the nonlinear processes emerging from the interaction between the incident waves and nonlinear scatterers in solid media in order to localize and characterize the scatterers themselves. When nonlinear scatterers are embedded, their localization can be obtained through a mixed experimental/numerical TRA procedure: the forward propagation is performed experimentally, while the time reversal (TR) backward propagation is simulated using computational codes and a reference model of the solid. The synergetic use of dedicated processing of the forward propagation signals collected at the time reversal mirror (TRM), for example with nonlinear elastic wave spectroscopy (NEWS) techniques, and the calculation of the backpropagated wave fields at each point within the specimen leads to imaging of the nonlinear scatterers. We show examples of nonlinear scatterer (macroscopic cracks, distributed microcracks) imaging by such a procedure, exploiting high per-

formance (parallel) computational codes. We address issues in the imaging method related to the discrepancy between the reference model of the specimen and the real specimen itself. Finally, we address the implementation of the technique for non-destructive Evaluation (NDE) real-world applications using multi-threaded computational codes to be run on common multicore desktop computers.

Invited Paper

11:40

5aPAb8. Improving signal analysis for nonlinear time reversed acoustics: simulation results. Marco Scalerandi (Politecnico di Torino, Corso Duca degli Abruzzi 24, 10129 Torino, Italy, marco.scalerandi@infm.polito.it), Antonio S. Gliozzi (Politecnico di Torino, Corso Duca degli Abruzzi 24, 10129 Torino, Italy, antonio.gliozzi@polito.it)

Nonlinear time reversed acoustics have attracted attention as a tool to localize and identify nonlinear defects in solids [1-4]. The procedure is based on extracting the features due to the nonlinear scatterers from the signals received at the transducer array and back-propagate only the resulting portion of the signals. The usual approach is to filter the received signals to keep only contributions due to higher order harmonics or sidebands. As a result, the signals are very small in amplitude and can be not detectable if transducers are located far from the scatterers. It is evident the need for novel signal processing tools to increase the signal-to-noise ratio of the nonlinear contributions. We have recently proposed a scaling subtraction method [5], which is applied here to nonlinear time reversal virtual experiments, showing the improvements in the signal-to-noise ratio, with resulting better imaging of the nonlinear scatterer. Results will be presented for two approaches to nonlinear time reversal. [1] A. S. Gliozzi et al., J. Acoust. Soc. Am. 120, 2506-2517 (2006). [2] T. J. Ulrich et al., J. Acoust. Soc. Am. 119, 1514-18 (2006). [3] T. J. Ulrich et al., Phys. Rev. Lett. 98, 10430 (2007). [4] T. Goursolle et al., J. Acoust. Soc. Am. 122, 3220 (2007). [5] M. Scalerandi et al., submitted to Appl. Phys. Lett. (2008).

Contributed Papers

12:00

5aPAb9. 3D numerical study for defect detection with nonlinear elastic wave spectroscopy and time reversal techniques. Thomas Goursolle (ENI Val de Loire, Université François Rabelais de Tours, LUSSI CNRS, rue de la Chocolaterie, 41034 Blois, France, thomas.goursolle@univ-tours.fr), Samuel Callé (LUSSI, 10 Bd Tonellé, 37032 Tours, France, calle_s@med.univ-tours.fr), Serge Dos Santos (ENI Val de Loire, Université François Rabelais de Tours, LUSSI CNRS, rue de la Chocolaterie, 41034 Blois, France, serge.dossantos@univ-tours.fr), Olivier Bou Matar (IEMN, UMR CNRS 8520, avenue Poincaré, BP 60069, 59652 Villeneuve d'Ascq, France, olivier.boumatar@iemn.univ-lille1.fr)

Nonlinear elastic wave spectroscopy (NEWS) techniques have been developed to study the anomalously high level of "nonclassical" nonlinearity of cracked materials. Within AERONEWS project (http://www.kuleuven-kortrijk.be/aeronews), more recent innovative nondestructive NEWS techniques have been proposed to detect microinhomogeneities like cracks. It has been notably shown that NEWS and time reversal (TR) techniques can be combined to precisely localize cracks with a high sensitivity. NEWS techniques can be used either as a post-treatment of TR used as a tool for strong localized stress generation (TR-NEWS), or as a pre-treatment of TR used as a tool for defect (nonlinear source) identification (NEWS-TR). A 3D multiscale pseudo-spectral time domain (PSTD) code has been developed to simulate nonlinear acoustic propagation in heterogeneous nonlinear hysteretic solids. The hysteretic nonlinearity is introduced owing to a PM space model, based on a multiscale approach, extended in 3D owning to Kelvin notations. Using this algorithm, the influence of various parameters such as the defect position or the filtering method is particularly described for NEWS-TR and TR-NEWS methods. Finally, the sensitivity and feasibility of both methods are discussed.

12:20

5aPAb10. Varied amplitude method in time reversal acoustic land mine. Laurent Fillinger (Artann Laboratories/ Stevens Institute of Technology, 711 Hudson St, Hoboken, NJ 07030, USA, laurent.fillinger@artannlabs.com), Alexander Sutin (Stevens Institute of Technology, Castle Point on Hudson, Hoboken, NJ 07030, USA, asutin@stevens.edu), Brad Libbey (U.S. Army RDECOM CERDEC NVESDS, 10221 Burbeck Rd, Fort Belvoir, VA 22060, USA, brad.libbey@us.army.mil), Armen Sarvazyan (Artann Laboratories, 1753 Linvale-Harbourton, Lambertville, NJ 08350, USA, armen@artannlabs.com)

Acoustic methods of land mine detection are being developed for non-metal mines where conventional electromagnetic methods fail. One such method, based on time reversal acoustic principles, is the hhase-inversion method; which detects quadratic and even ordered harmonic nonlinearities in the surface vibration above a mine. While this has shown higher sensitivity than linear methods it cannot detect all nonlinear components. These components can be detected by the Varied Amplitude method that is based on wide band excitation of surface vibration using the principles of time reversal acoustics. The nonlinear effects are measured for surface vibrations with different amplitudes and the normalized received signals can then be subtracted to reveal all the nonlinear components. We conducted a set of experiments using a box with six loudspeaker and an array of spatially distributed geophones to measure the linear and nonlinear components for various types of mines in different soils. Information about nonlinear components' spatial distribution allows one to observe greater mine/no mine contrast than with linear and other nonlinear techniques. [Work was supported by the U.S. Army RDECOM CERDEC Night Vision and Electronic Sensors Directorate.]

Session 5aPAc

Physical Acoustics: Vibrations in Plates I

Daniel Royer, Cochair
Laboratoire Ondes et Acoustique, ESPCI, Université Paris 7, CNRS, 10 rue Vauquelin, Paris, 75005, France

Olivier Poncelet, Cochair
LMP, UMR CNRS 5469, Université Bordeaux I, 351, cours de la Libération, Talence, 33405, France

Contributed Papers

8:00

5aPAc1. Discussion on the validity domain of SEA. Alain Le Bot (CNRS, LTDS Ecole centrale de Lyon 36, av. Guy de Collongue, 69134 Ecully, France, alain.le-bot@ec-lyon.fr), Vincent Cotoni (ESI Group, 12555 High Bluff Dr., suite 250, San Diego, CA 92130, USA, vincent.cotoni @esi-group-na.com)

This paper is concerned with the validity domain of SEA which is defined in terms of four criteria. The mode count N and the modal overlap M must be high, the normalized attenuation factor m and the coupling strength gamma must be small. The application of the dimensional analysis on the governing equations of plates gives the space of dimensionless parameters in which the validity domain of SEA must be delimited. This domain is discussed on the basis of the geometric properties of the surfaces delimiting it. The diagrams of validity of SEA are introduced and proposed as a tool for a practical use of SEA.

8:20

5aPAc2. Lamb waves filtering by waveguides with linear varying section. Zahia Hamitouche (LOMC FRE-3102 CNRS, Groupe Ondes Acoustiques, University of Le Havre, Place Robert Schuman, BP 4006, 76610 Le Havre, France, zahia.hamitouche@univ-lehavre.fr), Mounsif Ech-Cherif El-Kettani (LOMC FRE-3102 CNRS, Groupe Ondes Acoustiques, University of Le Havre, Place Robert Schuman, BP 4006, 76610 Le Havre, France, elkettani@univ-lehavre.fr), Hakim Djelouah (Faculty of Physics, University of Science and Technology Houari Boumedienne, BP 32 El Allia, Bab-Ezzouar, 16000 Algiers, Algeria, djelouah_hakim @yahoo.fr), Jean-Louis Izbicki (LOMC FRE-3102 CNRS, Groupe Ondes Acoustiques, University of Le Havre, Place Robert Schuman, BP 4006, 76610 Le Havre, France, jean-louis.izbicki@univ-lehavre.fr)

This experimental and numerical work deals with the study of Lamb modes propagating in a plate with a linear variation of thickness. The varying section area exhibits a filtering phenomenon for Lamb modes having a frequency-thickness cutoff. If the incident Lamb wave, excited at a given frequency and propagating downslope, reaches its thickness cutoff in the varying section area, it is reflected and propagates upslope. Otherwise, it is transmitted outside the varying section domain with modes conversion. The S2 incident mode is a particular case: when it reaches its cutoff, it is converted into the S1 mode with negative groupe velocity and a downslope propagation; then the S1 Lamb wave is reflected at its cutoff. The experimental and numerical studies are in good agreements.

8:40

5aPAc3. Experimental study of lamb mode conversions at the junction of two joined plates. Taoufiq Belhoussine Drissi (LOMC FRE-3102 CNRS, Groupe Ondes Acoustiques, University of Le Havre, Place Robert Schuman, BP 4006, 76610 Le Havre, France, taoufiq_belhoussine_drissi@yahoo.fr), Bruno Morvan (LOMC FRE-3102 CNRS, Groupe Ondes Acoustiques, University of Le Havre, Place Robert Schuman, BP 4006, 76610 Le Havre, France, bruno.morvan@univ-lehavre.fr), Pascal Pareige (LOMC FRE-3102 CNRS, Groupe Ondes Acoustiques, University of Le Havre, Place Robert Schuman, BP 4006, 76610 Le Havre, France, pascal.pareige@univ-lehavre.fr)

In this study we are interested in a welded junction of two plates. Plates have the same thickness and are joined along their edges. Some previous theoretical studies have shown that guided Lamb waves are suitable for the characterisation of the interface between two plates [C. Scandrett and N. Vasudevan & M.V Predoi and M. Rousseau]. In a first time a junction perpendicular to the plates is experimentally investigated. Aluminum, copper and steel plates are used. Incident S0 Lamb wave is excited by a contact piezocomposite transducer and the surface displacements of the plate are detected by use of a laser vibrometer on both side of the junction. Converted waves are observed. From the measured normal surface displacements, reflection and transmission energy coefficients of the incident S0 wave through the junction are calculated. These coefficients are in a good agreement with the theoretically predicted ones. In a second time, the studied junction is not perpendicular to the plate. Experimental results are presented and compare to numerical ones obtained with the Comsol® Finite Element code.

9:00

5aPAc4. Second order dispersive effect on zero-group velocity Lamb modes. Daniel Royer (Laboratoire Ondes et Acoustique, ESPCI, Université Paris 7, CNRS, 10 rue Vauquelin, 75005 Paris, France, daniel.royer@espci.fr), Dominique Clorennec (Laboratoire Ondes et Acoustique, ESPCI, Université Paris 7, CNRS, 10 rue Vauquelin, 75005 Paris, France, dominique.clorennec@espci.fr), Claire Prada (Laboratoire Ondes et Acoustique, ESPCI, Université Paris 7, CNRS, 10 rue Vauquelin, 75005 Paris, France, claire.prada-julia@espci.fr)

After a local and transient loading of a plate, the acoustic energy decay in the source area can be explained by three mechanisms: the energy transport phenomenon at the Lamb wave group velocity, the material damping and the second-order dispersive effect. Generally, the first mechanism dominates the other two. However, some dispersion curves of Lamb modes present a minimum frequency for a nonzero wave number. Since at these points the group velocity vanishes, no energy transport occurs, and the slower other two phenomena can be observed. Using laser-based ultrasonic techniques, we show that the mechanical response of various thin metallic plates to a laser pulse impact is dominated by the resonance of the zero group velocity S_1-Lamb mode. In the first microseconds, we observed a $t^{-1/2}$ decay of the local vibration amplitude, which cannot be explained by the material damping. We demonstrated that this effect is ascribed to the second-order term in the dispersion relation. After this power law decay, the

mechanical displacement undergoes an exponential decay corresponding to the wave damping. Then, we show that the local attenuation of the plate material can be measured without any mechanical contact.

9:20

5aPAc5. Guided waves in plates with linear variation of thickness. Mihai Valentin M. Predoi (University Politechnica of Bucharest, Department of Mechanics, 060032 Bucharest, Romania, predoi @cat.mec.pub.ro), Mounsif Ech Cherif El Kettani (LOMC FRE-3102 CNRS, Groupe Ondes Acoustiques, University of Le Havre, Place Robert Schuman, BP 4006, 76610 Le Havre, France, mounsif.elkettani @univ-lehavre.fr), Zahia Hamitouche (LOMC FRE-3102 CNRS, Groupe Ondes Acoustiques, University of Le Havre, Place Robert Schuman, BP 4006, 76610 Le Havre, France, zahia.hamitouche@univ-lehavre.fr) , Cristian Catalin Petre (University Politechnica of Bucharest, Department of Mechanics, 060032 Bucharest, Romania, cristian.petre@promteh.ro)

Guided waves represent promising nondestructive evaluation (NDE) techniques. Their advantage of long distance propagation is however hampered by complex wave scattering at each discontinuity along the investigated structure. These scattered waves can be used to locate and size possible defects. Theoretical investigation is a prerequisite step in the development of a NDE technique. Planar metallic structures with localized thickness variation imposed by design represent possible new industrial structures that could be tested using guided waves. The waves scattered at the region of variable thickness must be theoretically predicted and experimentally measured before any defect could be detected. Very few authors have investigated waveguides with continuous variation of thickness. Our previous numerical and experimental studies have proven the complexity of the scattering phenomenon in such cases. Among other remarks is the curved shape of the wave front. The present work investigates properties of the waves in the linear thickness variation region of the waveguide. A plain strain model, developed in polar coordinates is theoretically developed and numerically tested using specialized finite elements based algorithms. Specific properties such as stress and displacements fields are determined by numerical simulation at several frequencies and dihedral angles.

9:40-10:40 Posters

Lecture sessions will recess for presentation of poster papers on various topics in acoustics. See poster sessions for topics and abstracts.

Contributed Papers

10:40

5aPAc6. Refracting characteristics of backward propagating Lamb modes. Massimo Germano (Sapienza Università di Roma, Via A. Scarpa, 14, 00161 Rome, Italy, massimo.germano@uniroma1.it), Adriano Alippi (Sapienza Università di Roma, Via A. Scarpa, 14, 00161 Rome, Italy, adriano.alippi@uniroma1.it), Andrea Bettucci (Sapienza Università di Roma, Via A. Scarpa, 14, 00161 Rome, Italy, andrea.bettucci@uniroma1 .it), Annunziata D'Orazio (Sapienza Università di Roma, Via A. Scarpa, 14, 00161 Rome, Italy, annunziata.dorazio@uniroma1.it)

Lamb waves are acoustic modes propagating along thin plates or shells and result from the coupling of longitudinal waves and shear vertical waves (polarized along the thickness direction), taking place at the surface boundaries for satisfying the boundary conditions of the waveguide. Their nature being a composition of two differently polarized components, it permits that, for some combination of frequency and wavenumber, a Lamb mode is propagating which has its group velocity contradirected with respect to the phase velocity. These are the so-called "backward" Lamb modes, and one of them takes place at the starting region (low wave number) of the S_1 mode dispersion curve in aluminum. Peculiar features of a wave packet of a symmetric Lamb mode S_1, backward propagating in an aluminum waveguide, are observed and anomalous behavior in refraction, diffraction and interference of this peculiar mode is experimentally put in evidence. Particularly, contradirected refraction is put in evidence, as it takes place at the boundary where a forward propagating mode is coupled to a backward propagating one, and change from forward to backward mode is obtained in case of a wedge shaped laminar plate, which goes through a zero point of the group velocity.

11:00

5aPAc7. Conversion of a Scholte - Stoneley wave at the extremity of a fluid loaded plate: comparison between finite element method, radiation mode theory and experiments. Ebrahim Lamkanfi (Ghent University, Sint-Pietersnieuwstraat 41, 9000 Ghent, Belgium, Ebrahim.Lamkanfi @ugent.be), Nico F. Declercq (Georgia Tech Lorraine - G.W. Woodruff School of ME, UMI Georgia Tech - CNRS 2958, 2 rue Marconi, 57070 Metz, France, nico.declercq@me.gatech.edu), Wim Van Paepegem (Ghent University, Sint-Pietersnieuwstraat 41, 9000 Ghent, Belgium, wim.vanpaepegem@ugent.be), Joris Degrieck (Ghent University, Sint-Pietersnieuwstraat 41, 9000 Ghent, Belgium, joris.degrieck@ugent.be)

The radiation theory has proved to produce results in agreement with experiments when the conversion is investigated of a Scholte - Stoneley wave at the extremity of a fluid loaded plate. The drawback of the radiation mode theory is that it is not universally applicable and is also very cumbersome. The advantage is that it is an exact method. There is a trend in acoustics to develop finite element models to describe the interaction of sound waves with materials. This investigation compares a newly developed finite element model to simulate the considered effect. Results are compared with the exact results obtained by the radiation mode theory [J. Acoust. Soc. Am. **101**(3), 1347-1357, 1997] and experimental observations [J. Acoust. Soc. Am. **95**(1), 13-20, 1994]. The study shows correspondence between the finite element analysis and earlier obtained experimental and theoretical results as a function of a relationship between mesh properties and the evanescence (rather than the wave length) of the considered Stoneley waves.

Session 5aPAd

Physical Acoustics: Time Reversal Acoustics for Nonlinear Imaging II (Poster Session)

Alexander Sutin, Cochair
Stevens Institute of Technology

Serge Dos Santos, Cochair
ENI Val de Loire, Université François Rabelais de Tours, LUSSI CNRS

All posters will be on display from 9:40 a.m. to 11:20 a.m. To allow contributors an opportunity to see other posters, contributors of odd-numbered papers will be at their posters from 9:40 a.m. to 10:30 a.m. and contributors of even-numbered papers will be at their posters from 10:30 a.m. to 11:20 a.m.

Contributed Papers

5aPAd1. Nonlinear phase conjugate ultrasonic waves in moving media. Vladimir L. Preobrazhensky (IEMN, UMR CNRS 8520, avenue Poincaré, BP 60069, 59652 Villeneuve d'Ascq, France, vladimir.preobrajenski@iemn.univ-lille1.fr), Philippe Pernod (IEMN, UMR CNRS 8520, avenue Poincaré, BP 60069, 59652 Villeneuve d'Ascq, France, philippe.pernod@iemn.univ-lille1.fr), Yuri Pyl'Nov (Moscow Institute of Radio Engineering, Electronics & Automation, Vernadsky prosp., 78, 119454 Moscow, Russian Federation, pylnov@yandex.ru), Nikolay Smagin (Moscow Institute of Radio Engineering, Electronics & Automation, Vernadsky prosp., 78, 119454 Moscow, Russian Federation, pylnov@yandex.ru)

The basic principle of acoustic wave phase conjugation provides compensation of phase incursions during back propagation of the phase conjugate waves (PCW) towards the source of the primary emission. This feature of PCW results from time reversal invariance of acoustic field in a stationary medium. In moving media or in the presence of flows the time reversal invariance is broken resulting in essential modification of PCW properties. The incident wave spatial distribution is not reproduced completely by the phase conjugate wave and the phase incursions are not compensated any more. In the present paper the general theory of PCW propagation in moving nonlinear media is developed. The theory is applied for description of PCW acoustic rays and calculation of noncompensated phase shift of PCW on the source of the primary probing wave. The treatment of the phase shift of the PCW is developed as a new method of diagnostics and imaging of flow velocity distributions in liquid. The method is approved experimentally on examples of laminar and vortex flows and immersed fluid jet in water. Improvement of quality of the images of flows using nonlinear modes of propagation and interaction of phase conjugate waves is demonstrated.

5aPAd2. Evaluation of local nonlinearity using time reversal acoustic focusing. Serge Dos Santos (ENI Val de Loire, Université François Rabelais de Tours, LUSSI CNRS, rue de la Chocolaterie, 41034 Blois, France, serge.dossantos@univ-tours.fr), Alexander Sutin (Stevens Institute of Technology, Castle Point on Hudson, Hoboken, NJ 07030, USA, asutin@stevens.edu), Armen Sarvazyan (Artann Laboratories, 1753 Linvale-Harbourton, Lambertville, NJ 08350, USA, armen@artannlabs.com), Thomas Goursolle (ENI Val de Loire, Université François Rabelais de Tours, LUSSI CNRS, rue de la Chocolaterie, 41034 Blois, France, thomas.goursolle@univ-tours.fr)

Time reversal acoustic focusing can be used for local assessment of nonlinear properties of media [Sarvazyan A., Sutin A. , JASA, **115** (5): 2595 (2004)]. Time Reversal focusing provides high acoustic pressure leading to a nonlinear response localized in space and time. Interaction area of two overlapping focused beams acts as a virtual localized source generating ultrasonic waves with combination frequencies. Measurements of the intensity of this signal allow estimation of the nonlinear parameter in the focal region. The first experiment was conducted in water with spatially varying acoustical nonlinearity produced by a microbubble column or contrast agent Optison. We used two synchronized TRA aluminium reverberators to focus ultrasonic waves with frequencies 660 kHz and 776 kHz. Various parameters such as amplitude and frequency of the primary field, the position and number of emitters, choice of initial excitation (tone burst, binary, shirp-coded) were optimized for the nonlinear signature extraction. The second experiment was conducted in steel samples where surface vibration were measured by laser vibrometer. Excitation frequencies were between 490 kHz and 860 kHz . These experiments show again that amplitude dependence of nonlinear generated components was slightly less than the product of primary component that is predicted by classical nonlinear theory.

Session 5aPAe

Albert Migliori, Cochair
Los Alamos National Laboratory

Claude Boutin, Cochair
École Nationale des Travaux Publics de État

Physical Acoustics: Ultrasonics: Transducers and Instruments I (Poster Session)

All posters will be on display from 9:40 a.m. to 11:20 a.m. To allow contributors an opportunity to see other posters, contributors of odd-numbered papers will be at their posters from 9:40 a.m. to 10:30 a.m. and contributors of even-numbered papers will be at their posters from 10:30 a.m. to 11:20 a.m.

Contributed Papers

5aPAe1. An ultrasonic technique using shear waves interactions to characterize new hybrid gels. Philippe Banet (ECIME Université de Cergy-Pontoise, rue d'Eragny, 95031 Neuville-sur-Oise, France, philippe.banet@u-cergy.fr), Pascal Griesmar (ECIME Université de Cergy-Pontoise, rue d'Eragny, 95031 Neuville-sur-Oise, France, pascal.griesmar@u-cergy.fr), Frederic Vidal (LPPI - Université de Cergy-Pontoise, rue d'Eragny, 95031 Neuville-sur-Oise, France, frederic.vidal@u-cergy.fr), Jean-Yves Le Huerou (ECIME Université de Cergy-Pontoise, rue d'Eragny, 95031 Neuville-sur-Oise, France, jean-yves.lehuerou@u-cergy.fr), Claude Chevrot (LPPI - Université de Cergy-Pontoise, rue d'Eragny, 95031 Neuville-sur-Oise, France, claude.chevrot@u-cergy.fr), Dominique Teyssie (LPPI - Université de Cergy-Pontoise, rue d'Eragny, 95031 Neuville-sur-Oise, France, dominique.teyssie@u-cergy.fr), Stéphane Serfaty (ECIME Université de Cergy-Pontoise, rue d'Eragny, 95031 Neuville-sur-Oise, France, stephane.serfaty@u-cergy.fr)

Thickness shear mode transducer techniques using AT-cut quartz crystal can be used to measure viscoelastic parameters of soft materials (gels, colloidal suspensions œ) during their formation. Today the control of hybrid materials synthesis and evolution has a great interest, particularly for biomedical applications such as drug delivery. With those materials, a challenge is to obtain new structures constituted by interpenetrating organic- inorganic polymers networks (IPN) to get novel therapeutic behaviours. In this paper, the monitoring of ultrasonic shear waves propagation in the material at 6 MHz is presented for different thermosensible hybrid (poly-N-isopropylacrylamide (PNIPAM) - silica). We show that at a mesoscopic scale it is possible to analyze mechanical interactions between different networks related to chemical bounds. The network evolution observed with our technique is in good agreement with the Fourier transform infrared analysis of NIPAM polymerization. As shown in previous work for silica gels, a precursor characteristic time of gelation process (in liquid phase) can be determined to describe the polymerization kinetic. By its nondestructive character and its simplicity of measurement, this technique allows an online optimization of new hybrid materials.

5aPAe2. Effects of materials conductivity on the viscosity measurement using a QCM. Stéphane Serfaty (ECIME Université de Cergy-Pontoise, rue d'Eragny, 95031 Neuville-sur-Oise, France, stephane.serfaty@u-cergy.fr), Emmanuel Caplain (ECIME Université de Cergy-Pontoise, rue d'Eragny, 95031 Neuville-sur-Oise, France, emmanuel.caplain@u-cergy.fr), Pascal Griesmar (ECIME Université de Cergy-Pontoise, rue d'Eragny, 95031 Neuville-sur-Oise, France, pascal.griesmar@u-cergy.fr), Jean-Yves Le Huerou (ECIME Université de Cergy-Pontoise, rue d'Eragny, 95031 Neuville-sur-Oise, France, jean-yves.lehuerou@u-cergy.fr), Marcel Gindre (ECIME Université de Cergy-Pontoise, rue d'Eragny, 95031 Neuville-sur-Oise, France, marcel.gindre@u-cergy.fr)

Quartz crystal microbalance (QCM) is commonly used to characterize the viscosity of soft materials. For biomedical applications the modified BVD model of QCM is unsuitable due to the conductivity of the biomaterial. In order to take into account the electrical effects, a new model including a static lossy capacitor is proposed. A theoretical study of the shear wave propagation in the quartz shows that these effects modify the static and the motional branches of the BVD circuit. The conductivity effects of the material at the surface of the QCM can be modeled by same parallel elements added in both branches. In the motional branch the electromechanical coupling factor is applied to these elements. To validate the new lumped element model measurements for KCl mixtures are achieved. The results show that an accurate extraction of viscosity ($<5\%$) can be obtained for a middle of conductivity less than 0.3 S/m. In addition for water-/glycerol mixtures the resonant frequency shift and damping follow an accurate linear shape ($<5\%$) according to the square root of the liquid viscosity and density product. These results increase (up to 200 times) the validity domain of viscosity compared to the classical modified BVD model.

5aPAe3. Viscosimetry using a new electromagnetic-acoustic microbalance. Emmanuel Caplain (ECIME Université de Cergy-Pontoise, rue d'Eragny, 95031 Neuville-sur-Oise, France, emmanuel.caplain@u-cergy.fr), Stéphane Serfaty (ECIME Université de Cergy-Pontoise, rue d'Eragny, 95031 Neuville-sur-Oise, France, stephane.serfaty@u-cergy.fr), Pascal Griesmar (ECIME Université de Cergy-Pontoise, rue d'Eragny, 95031 Neuville-sur-Oise, France, pascal.griesmar@u-cergy.fr), Jean-Yves Le Huerou (ECIME Université de Cergy-Pontoise, rue d'Eragny, 95031 Neuville-sur-Oise, France, jean-yves.lehuerou@u-cergy.fr), Nicolas Wilkie-Chancellier (ECIME Université de Cergy-Pontoise, rue d'Eragny, 95031 Neuville-sur-Oise, France, Nicolas.Wilkie-Chancellier@u-cergy.fr)

The nanostructure evolution of gels, biomaterials or porous media can be characterized by its mechanical properties. Few nondestructive techniques are developed to investigate the viscosity evolution. This paper present a new electromagnetic-acoustic technique using a wireless thickness shear mode transducer. A suitable model of the measurement is also presented to characterize the viscosity of the nanostructure in contact with the transducer. This transducer is a double copper-clad PVDF substrate resonator, designed to operate over a wide radiofrequency range without lumped tuning capacitors. This architecture constitutes an alternative solution to design a high-Q ultrasonic microbalance. To characterize the material at the surface of the transducer, the evolution of the induced complex impedance is measured. From this evolution, the mechanical energy storage and dissipa-

tion in the material can be extracted. In order to validate the lumped element model used, a series of glycerol/water mixtures is studied. We show that the resonant frequency shift and damping follow an accurate linear shape (<5%) according to the square root of the liquid viscosity and density product. This result is in good agreement with the classical prediction of Martin and Kanazawa obtained with a quartz crystal microbalance.

5aPAe4. Functionally graded plates studied by laser ultrasonic technique. Yongdong Pan (Institute of Acoustics, Tongji University, 1239 Siping Road, 200092 Shanghai, China, ypan@mail.tongji.edu.cn), Qian Wang (Institute of Acoustics, Tongji University, 1239 Siping Road, 200092 Shanghai, China, wang_qian_@126.com), Zheng Zhong (School of Aerospace Engineering and Applied Mechanics, Tongji University, 1239 Siping Road, 200092 Shanghai, China, zhongk@mail.tongji.edu.cn), Clément Rossignol (LMP, UMR CNRS 5469, Université Bordeaux I, 351, cours de la Libération, 33405 Talence, France, c.rossignol@lmp.u-bordeaux1.fr), Bertrand Audoin (LMP, UMR CNRS 5469, Université Bordeaux I, 351, cours de la Libération, 33405 Talence, France, b.audoin@lmp.u-bordeaux1.fr)

In a functionally graded plate, the composition and structure change continuously along the thickness direction, resulting in corresponding changes of the acoustic impedance of the material. The study of the wave propagation in such a plate is important for both the nondestructive evaluation of properties of functionally gradient materials and engineering. In this work, the experimental system of laser ultrasonic measurement is introduced, and a theoretical model is proposed to predict the transient displacement field generated by laser in a functionally graded plate (FGP). After the laser line source is assumed as an idea transient force, and the FGP is considered as an inhomogeneous plate along its thickness direction, the transient displacement field is numerically solved by the Peano expansion method. Laser ultrasonic measurement was carried on several FGPs, and the direct arrivals of longitudinal and shear waves were observed in the experimental displacement field. The agreement between experimental and calculated theoretical waveforms provides a promise for both experimental and theoretical methods.

5aPAe5. Genetic manipulation engineers the elasticity of arabidopsis thaliana. Ari Salmi (Univ. of Helsinki / Dept. of Physical Sciences, POB 64 (Gustaf Hällströmin katu 2), 00014 Helsinki, Finland, edward.haeggstrom@helsinki.fi), Kimmo Mustonen (University of Helsinki, Gustaf Hällströmin Katu 2, 00015 Helsinki, Finland, kimmo.mustonen@helsinki.fi), Juha Immanen (Dept. of Biological and Environmental Sciences, P.O.B 65, 00014 Helsinki, Finland, juha.immanen@helsinki.fi), Yrjö Helariutta (Dept. of Biological and Environmental Sciences, P.O.B 65, 00014 Helsinki, Finland, yrjo.helariutta@helsinki.fi), Edward Hæggström (Electronics Research Unit, University of Helsinki, P.O.Box 64 (Gustaf Hällströmin katu 2), FIN-00014 Helsinki, Finland, edward.haeggstrom@helsinki.fi)

Arabidopsis thaliana is a model species widely used in plant science studies. It grows fast and exhibits wood formation in its stem and root resembling softwood produced by angiosperm trees. The Arabidopsis model allows rapid testing of methods for wood composition modification possibly adaptable for tree breeding. We estimated ultrasonically the modulus of elasticity in Arabidopsis stems and roots in both radial and in-plane direction for two commonly used ecotypes (Columbia and Landsberg erecta). Plants were grown in greenhouse conditions and six inflorescence stems per ecotype were measured in vivo applying 4 MHz out-of-plane and 2 MHz in-plane ultrasonic tone bursts. The effects of AtCAD1 gene expression silencing in Col ecotype were tested using the same method. We recorded a (10%, $p=0.1$) decrease in the elastic modulus of the lignin-decreased Atcad 1 samples (10-20% decrease in lignin content), and a significant (29%, $p=0.02$) difference between the sound velocities in the two ecotypes. In-plane elasticity results are also presented. The results are the first ultrasonically measured modulus values for this commonly used plant model species, creating a quantitative mechanical measure for the effects of wood composition modification.

5aPAe6. Nondestructive evaluation of heterogeneous materials using acoustic emission and ultrasound. Adil Faiz (ENSIM - LAUM, Université du Maine, rue Aristote, 72085 Le Mans, France, adil.faiz@univ-lemans.fr), Rachid El Guerjouma (ENSIM - LAUM, Université du Maine, rue Aristote, 72085 Le Mans, France, Rachid.El_Guerjouma@univ-lemans.fr), Mouras Bentahar (Université du Maine LAUM, Lab. d'Acoustique Université du Maine, UMR CNRS 6613, 72085 Le Mans Cedex 9, France, mourad.bentahar@univ-lemans.)

Heterogeneous materials as composites and concrete are advantageous as structural components in many applications. However, damage detection in such materials is difficult due to their heterogeneity and anisotropy. Furthermore, conventional non destructive technique as x-radiographic is mostly not very sensitive to early damage and very time consuming and expensive. The purpose of this contribution is to study the capabilities of several methods, nondestructive and very sensitive for damage characterisation, as acoustic emission (AE) and ultrasonic for the structural health monitoring of heterogeneous materials as polymer based composite materials and concrete. These materials are instrumented by piezoelectric sensors in order to detect acoustic emission and to measure the ultrasonic velocity. The mechanisms of the damage events and their space-time localizations are identified from AE. Simultaneously, the longitudinal ultrasonic velocity is measured in situ by transmission through the composite thickness. The AE is very well correlated with the loss of stiffness determined from ultrasonic velocity measurements showing the potentiality of this combined approach for in situ structural monitoring.

5aPAe7. Development of a system using ultrasonic waves for assessing the quality of frying oil and salad oil during frying. Driss Izbaim (Ibn Zohr University, FS Agadir, 80000 Agadir, Morocco, driss_izbaim@yahoo.fr), Bouazza Faiz (Ibn Zohr University, FS Agadir, 80000 Agadir, Morocco, faizbou@hotmail.com), Adil Hamine (Ibn Zohr University, FS Agadir, 80000 Agadir, Morocco, adil.hamine@Gmail.com), Naima Taifi (Fac. des sciences; Univ. Chouaib Doukkali, B.P: 20, 24000 El Jadida, Morocco, taifinaima@yahoo.fr), Ali Moudden (Ibn Zohr University, FS Agadir, 80000 Agadir, Morocco, ali_moudden@yahoo.fr)

The design and construction of a real-time system is described with reference to applications in quality control of frying oil. This system, developed using the LabVIEW™ software, controls the ultrasonic velocity by receiving the signals backscattered by a recipient full of oil. Measurements on samples of frying oil and salad oil are described and the results of velocity measurements on a group of samples of varying frying time taken in 160 °C are reported. The new system is built around three main elements: acquiring the oil signals, automating the signals control, and several calculations to determine in real-time the phase velocity of the oil. The results obtained show the feasibility of assessing the quality of oils using ultrasonic waves through monitoring the frying process. This system can be used also to control other industry products such as the canned fish oil, milk, and the cement.

5aPAe8. Influence of polymeric nanocomposite film on acoustic waves in piezoelectrics. Iren E. Kuznetsova (Institute of Radio Engineering and Electronics of RAS, Saratov Branch, Zelyonaya str., 38, 410019 Saratov, Russian Federation, kuziren@yandex.ru), Boris D. Zaitsev (Institute of Radio Engineering and Electronics of RAS, Saratov Branch, Zelyonaya str., 38, 410019 Saratov, Russian Federation, zai-boris@yandex.ru), Anastasia S. Kuznetsova (Institute of Radio Engineering and Electronics of RAS, Saratov Branch, Zelyonaya str., 38, 410019 Saratov, Russian Federation, tigrnasya@yandex.ru)

At present the attention of researchers is attracted by investigation of multilayer acoustical waveguides with using of well known as well as novel materials. Also in present time there exist a lot of papers devoted to novel nanocomposite polymeric materials. But the influence of such materials on parameters of acoustic waves in piezoelectrics did not study. In this connec-

tion the paper is devoted to theoretical investigation of acoustic waves in structure "piezoelectric - polymeric nanocomposite film." The analysis was carried out by the example of polymeric nanocomposite film with various contents of Fe and CdS nanoparticles and lithium niobate plate or substrate. As a result of conducted calculation the velocity and attenuation per wavelength have been found for acoustic waves propagating in aforementioned structure. The conducted analysis has showed that for certain value of nanocomposite film thickness d the attenuation of investigated waves has the resonant behavior. The obtained results allow choose such values of d for which the acoustic wave does not practically attenuate in the presence of the film. This opens, for example, the prospects of development of undisturbed substrates of nanocomposite materials for thin piezoelectric plates. This work is supported by RFBR 06-08-01011, RNP.2.1.1.8014 (Russia), contract 2007-3-1.3-07-15-036 (Russia).

FRIDAY MORNING, 4 JULY 2008 P3-A, LEVEL 3, 9:40 TO 11:20 A.M.

Session 5aPAf

Physical Acoustics: Infrasound II (Poster Session)

Henry Bass, Cochair
The University of Mississippi - NCPA

Alexis Le Pichon, Cochair
CEA-DASE

All posters will be on display from 9:40 a.m. to 11:20 a.m. To allow contributors an opportunity to see other posters, contributors of odd-numbered papers will be at their posters from 9:40 a.m. to 10:30 a.m. and contributors of even-numbered papers will be at their posters from 10:30 a.m. to 11:20 a.m.

Contributed Papers

5aPAf1. Close listening of a permanently degassing volcano: Yasur (Vanuatu). Christelle Zielinski (Institut de Physique du Globe, 4 Place Jussieu, 75252 Paris, France, zielinski@ipgp.jussieu.fr), Sylvie Vergniolle (Institut de Physique du Globe, 4 Place Jussieu, 75252 Paris, France, vergniolle@ipgp.jussieu.fr), Michel Lardy (IRD Center, BPA5, Cedex, 98848 Noumea, New Caledonia, lardy@noumea.ird.nc), Alexis Le Pichon (CEA-DASE, Arpajon Cedex, 91297 Bruyères-le-Châtel, France, alexis.le-pichon@cea.fr), Michel Frogneux (IPGS, 5, rue René Descartes, 67084 Strasbourg Cedex, France, michel.frogneux@eost.u-strasbg.fr)

Acoustic measurement is a very powerful technique to monitor gas volume and pressure at a safe distance of a volcano. Since eruptions are driven by a gas phase, acoustic recordings of eruptions can provide insights into the degassing processes. The permanent activity of Yasur volcano (Vanuatu) has been acoustically monitored continously to detect and understand the sudden increases in the volcanic degassing. In the absence of appropriate modeling of the sound source, we have used a dimensionless analysis of our infrasonic records close to the source to relate acoustic power and the velocity of the gas - ejecta mixture. Our one-year dataset at the source shows several sudden increases in gas flux over one week as well as more progressive evolution, over several months. Explosions are also detected using a method based on wavelet decomposition. This shows that most of the changes in gas flux are related to strong changes in the number of explosions. Understanding the origin of these variations has strong implications for hazards assessments.

5aPAf2. Low frequency airplane noise measurement. Xiao Di (National Center for Physical Acoustics, University of Mississippi, University, MS 38677, USA, xiaodi@olemiss.edu), Claus Hetzer (National Center for Physical Acoustics, University of Mississippi, University, MS 38677, USA, claus@olemiss.edu), Ronald A. Wagstaff (National Center for Physical Acoustics, University of Mississippi, University, MS 38677, USA, rwagstaf@olemiss.edu), Ali M. Mir (National Center for Physical Acoustics, University of Mississippi, University, MS 38677, USA, mali1 @olemiss.edu)

Low frequency airplane noise during takeoff and landing periods is a serious environment hazard. Also, the low frequencies originating from the airplanes could potentially be an easy target for detection. Since there is very little attenuation at the low frequencies, the low frequency sound can propagate to relatively long distances. Several field experiments were conducted to identify the low frequency signal and noise content from many different airplanes. What is different in our experiment from most other noise experiments is that we will identify the very low frequency content of the airplane noise spectrum, from 200 Hz down to the infrasound range, 0.02 Hz. During the experiments, two infrasound microphone systems were used: Chaparral 50, which has a bandwidth from 0.02 to 50 Hz, and Chaparral 2.5, which has a bandwidth from 0.1 to 200 Hz. In addition to the infrasound systems, a recording system with B&K microphones was also used. The data were collected before, during, and after landing and takeoff periods. The low frequency signal and noise content during each of those periods will be analyzed and reported on.

5aPAf3. Experimental study on the effects of N-wave sonic-boom signatures on window vibration. Yusuke Naka (Japan Aerospace Exploration Agency, 6-13-1 Osawa, Mitaka, 181-0015 Tokyo, Japan, ynaka@chofu.jaxa.jp), Yoshikazu Makino (Japan Aerospace Exploration Agency, 6-13-1 Osawa, Mitaka, 181-0015 Tokyo, Japan, makino@chofu.jaxa.jp), Takeshi Ito (Japan Aerospace Exploration Agency, 6-13-1 Osawa, Mitaka, 181-0015 Tokyo, Japan, ito@chofu.jaxa.jp)

For fulfillment of overland supersonic flight, it is important to understand the effects of sonic booms on buildings, since these effects, including vibration of walls and rattling noise from windows, are believed to be the main causes of annoyance in indoor spaces. In this study, the vibration of windows impacted by sonic booms is investigated through in-laboratory experiments by using a device developed at Japan Aerospace Exploration Agency (JAXA). Rattle is captured as high-frequency components of the acceleration of the windows. The effects of sonic booms having *N*-shape signatures with various values of peak overpressure, rise time, and duration are investigated. Results show general tendency of increase of rattle with increasing peak overpressure and decreasing rise time, as expected. However,

the results also indicate a possibility that these parameters, as well as duration, affect the time-frequency structure of the acceleration (and hence rattle) of windows in a somewhat complicated manner.

5aPAf4. Correlating electromagnetical and infrasonic signals from thunderstorms. Jelle Assink (Royal Netherlands Meteorological Institute (KNMI), PO Box 201, 3730 AE De Bilt, Netherlands, jelle.assink@gmail.com), Laeslo G. Evers (Royal Netherlands Meteorological Institute (KNMI), PO Box 201, 3730 AE De Bilt, Netherlands, evers@knmi.nl), Iwan Holleman (Royal Netherlands Meteorological Institute (KNMI), PO Box 201, 3730 AE De Bilt, Netherlands, holleman@knmi.nl)

During thunderstorm activity, electromagnetical and infrasonic signals are emitted due to the process of lightning and thunder. It is shown that correlating infrasound detections with results from a electromagnetical lightning detection network is successful up to distances of 50 km from the infrasound array. Infrasound recordings clearly show blast wave characteristics, relatable to CG discharges, with a dominant frequency between 1-5 Hz. Amplitude measurements can partly be explained by the beam pattern of a line source. The ability to measure thunderstorm activity with infrasound arrays has both positive and negative implications for infrasound verification purposes.

5aPAf5. Coherency of infrasound studied with a large aperture infrasound array in the Netherlands. Johan Mentink (Royal Netherlands Meteorological Institute (KNMI), PO Box 201, 3730 AE De Bilt, Netherlands, mentink@knmi.nl), Laeslo G. Evers (Royal Netherlands Meteorological Institute (KNMI), PO Box 201, 3730 AE De Bilt, Netherlands, evers@knmi.nl)

A large aperture infrasound array (LAIA) is being constructed in the Netherlands as geophysical part of an astronomical low frequency array, i.e., the LOFAR project. This array extends the detection capabilities of infrasound up to the mHz range, including acoustic-gravity and gravity waves as well. Owing to its large aperture (80 km) and number of interstation distances, this 30 element microbarometer array is ideally suited to study the coherency of infrasound as function of frequency under various atmospheric conditions. Based on conventional and modern correlation techniques, the ultimate aim is to experimentally determine and quantify infrasound propagation characteristics. As a result, we gain understanding in the physical mechanisms responsible for decoherence, which in turn will be used to develop infrasound as a passive atmospheric probe. Knowledge on the coherency length as function of the state of the atmosphere also has direct implications for the design of optimal infrasound arrays. This study will outline the characteristics of LAIA and present the first results of the coherency studies.

5aPAf6. Modeling real porous tube infrasonic arrays. Timothy Marston (The Graduate Program in Acoustics, The Pennsylvania State University, PO Box 30, State College, PA 16804, USA, tmm357@psu.edu), Thomas Gabrielson (The Graduate Program in Acoustics, The Pennsylvania State University, PO Box 30, State College, PA 16804, USA, tbg3@psu.edu)

Measured values of acoustic resistance in porous hoses have been implemented into a previously developed porous tube model for infrasonic arrays [J. Acoust. Soc. Am. **122**, 2960 (2007)]. Garden soaker hoses are commonly used in porous infrasonic arrays, and a simple method for the measurement the acoustic resistance of a segment of soaker hose will be presented. This experimentally determined resistance value can be implemented into the porous tube model for an improved array response prediction. It is anticipated that this analysis will give rise to improved phase and magnitude predictions for this type of array. Applications include design optimization of porous tube arrays, and infrasonic propagation through porous ducts. [Research funded by the Applied Research Laboratory Educational and Foundational Fund.]

5aPAf7. Finite difference time domain synthesis of infrasound propagation through an absorbing atmosphere. Catherine D. Degroot-Hedlin (University of San Diego California, Scripps Institute of Oceanography, 9500 Gilman Drive, La Jolla, CA 92093, USA, chedlin@ucsd.edu)

Equations applicable to finite difference time domain (FDTD) computation of infrasound propagation through an absorbing atmosphere are derived and examined in this paper. It is shown that over altitudes up to 160 km, and at frequencies relevant to global infrasound propagation, i.e., 0.02-5 Hz, the acoustic absorption in dB/m varies approximately as the square of the propagation frequency plus a small constant term. A second-order differential equation is presented for an atmosphere modeled as a compressible Newtonian fluid with low shear viscosity, acted on by a small external damping force. It is shown that the solution to this equation represents pressure fluctuations with the observed form for infrasound propagation, i.e., sound is attenuated as $(\beta+\gamma f^2)$. Increased dispersion is predicted at altitudes over 100 km. The equation is separated into two partial differential equations that are first order in time for FDTD implementation. A numerical analysis of errors inherent to this FDTD method shows that the attenuation term imposes additional stability constraints on the FDTD algorithm. Comparison of FDTD results for models with and without attenuation shows that the predicted transmission losses for the attenuating media agree with those computed from the synthesized waveforms.

Session 5aPAg

Physical Acoustics: Ultrasonics Under Extreme Conditions I (Poster Session)

Albert Migliori, Cochair
LANL

Frédéric Decremps, Cochair
IMPMC, Université Paris VI

All posters will be on display from 9:40 a.m. to 11:20 a.m. To allow contributors an opportunity to see other posters, contributors of odd-numbered papers will be at their posters from 9:40 a.m. to 10:30 a.m. and contributors of even-numbered papers will be at their posters from 10:30 a.m. to 11:20 a.m.

Contributed Papers

5aPAg1. Guided modes modeling in multilayered composites plates. Morched Ben Amor (Faculté des Sciences de Sfax, Laboratoire de Physique des Matériaux, BP 802, 3018 Sfax, Tunisia, morched_benamor@yahoo.fr)

Due to the periodicity of the composite structure the Floquet wave approach seems well suited for medium characterization. The pass and stop band domains for [0/45/90/-45] cross ply composites have been plotted. Dispersive guided wave propagation through a lossy composite laminates immersed in water have been investigated. Our interest is focused on a guided mode in the frequency range from 1.6 MHz to 5 MHz. This mode has been pointed out by both reflection coefficient and energy vector analysis in term of incident angle. In this paper it is investigated how by fine-tuning the frequency and the incident angle, internal displacement and stress field vary in the multilayer. When the frequecy is increased the mode changes from a plate mode to a surface mode. The description includes real Floquet wave numbers as well as complex wave numbers.

5aPAg2. Influence of the calorimetric system setup on the output acoustic power measurement results. Antonio Petosic (Faculty of Electrical Engineering and Computing, Unska 3, 10000 Zagreb, Croatia, antonio.petosic@fer.hr), Bojan Ivančević (Faculty of Electrical Engineering and Computing, Unska 3, 10000 Zagreb, Croatia, bojan.ivancevic@fer.hr),Dragoljub Svilar(Brodarski Institut, Avenija Većeslava Holjevca bb, 10000 Zagreb, Croatia, dsvilar@hrbi.hr)

The problem of measuring an output acoustic power using calorimetric method has been considered in different regimes of transmitter working. The transmitter has been driven at different excitation electrical power levels and the influence of sonotrode tip position in the different calorimetric systems on the measurement results is considered. Two calorimetric systems with different volumes of loading liquid (water) and different geometries (having influence on thermodynamical losses) have been used in the experiments. The exponential experimental temperature-time curves have been fitted with theoretical and time constants, losses, output acoustic power and electroacoustic efficiency factor have been found assuming that all ultrasound energy is absorbed in the system. The pressure field in the box is complicated and radiation impedance (radiated power) depends on the position in the complex ultrasound field where the point source is located. In the nonlinear regime of working strong cavitation activity occur with oscillating bubles in the front of vibrating tips and the radiated power is decreased because the tip is only partially radiating due to radiation impedance variations. The electroacustic efficiency factor has been compared with equivalent circuit approach where parameters of transmitter have been found for unloaded and loaded transmitter.

Session 5aPAh

Physical Acoustics: Ducts and Waveguides I (Poster Session)

Marc Deschamps, Cochair
LMP

Olivier Dazel, Cochair
Laboratoire d'Acoustique de I'Université du Maine

All posters will be on display from 9:40 a.m. to 11:20 a.m. To allow contributors an opportunity to see other posters, contributors of odd-numbered papers will be at their posters from 9:40 a.m. to 10:30 a.m. and contributors of even-numbered papers will be at their posters from 10:30 a.m. to 11:20 a.m.

Contributed Papers

5aPAh1. The design and modeling of a lateral acoustic particle manipulator exhibiting quarter-wave operation. Peter Glynne-Jones (University of Southampton, School of Engineering Sciences, University Road, SO17 1BJ Southampton, UK, p.glynne-jones@soton.ac.uk), Martyn Hill (University of Southampton, School of Engineering Sciences, University Road, SO17 1BJ Southampton, UK, m.hill@soton.ac.uk), Nicholas R. Harris (University of Southampton, Electronics and Computer Science, SO17 1BJ Southampton, UK, nrh@ecs.soton.ac.uk), Rosemary J. Townsend (University of Southampton, School of Engineering Sciences, University Road, SO17 1BJ Southampton, UK, R.J.Townsend@soton.ac.uk), Surendra K. Ravula (Sandia National Laboratories, Eubank Blvd, Albuquerque, NM 87123, USA, skravul@sandia.gov)

Prior work [Petersson et al., 2004] has demonstrated the operation of a half-wave acoustic particle manipulator, whose forces act in the plane of a silicon substrate. In a half-wave device particles are directed to the centre of a channel. Devices acting in plane have manufacturing advantages, and lend themselves to many microfluidic applications. We demonstrate, for the first time, such a device with a quarter-wave mode that is able to manipulate particles to the side of a channel in addition to a near half wave mode. The design utilises resonant "islands" to create the necessary pressure release boundary condition. The device is conventionally milled in brass, permitting cheaper and quicker fabrication than in silicon. Finite element modelling is presented to elucidate the operation of both half and quarter-wave devices. In contrast to essentially one-dimensional planar devices, the two-dimensional distribution of the velocity and pressure fields result in particles being constrained to a line within the channel.

5aPAh2. A semianalytical finite element method for elastic guided waves propagating in helical structures. Fabien Treyssède (Nantes Atlantique University - LCPC, Division for Metrology and Instrumentation, Route de Pornic - BP 4129, 44341 Bouguenais, France, fabien.treyssede@lcpc.fr), Ahmed Frikha (Nantes Atlantique University - LCPC, Division for Metrology and Instrumentation, Route de Pornic - BP 4129, 44341 Bouguenais, France, ahmed.frikha@lcpc.fr)

Steel multiwire cables are widely used in civil engineering as load-carrying members. The basic element of these cables is usually a simple straight strand made of a straight core and one layer of helical wires. Several difficulties arise in the understanding of guided ultrasonic waves in such structures, partly due to the helical geometry and the interwire coupling effects. In the context of nondestructive evaluation, this paper aims at theoretically investigating the propagation of elastic waves in helical waveguides. A numerical method is chosen based on a semianalytical finite element technique that relies on a specific nonorthogonal curvilinear coordinate system. This system is shown to be translationally invariant along the helix centerline so that a spatial Fourier transform can be explicitly performed along the axis and the problem is reduced to two dimensions. A single helical wire is first considered. The convergence and accuracy of the proposed method are assessed by comparing finite element results with reference solutions. The method is then extended to study a seven wire cable with simplified contact conditions. Dispersion curves are presented for wave numbers as well as energy velocities. Significant differences with the infinite straight cylinder are observed.

5aPAh3. Numerical simulation of acoustic wave propagation via a liquid with gas bubbles. Nikolai Kudryashov (Department of Applied Mathematics, Moscow Engineering and Physics Institute (State University), 31, Kashirskoe Shosse, 115409 Moscow, Russian Federation, kudryashov@mephi.ru), Nikolai Teterev (Department of Applied Mathematics, Moscow Engineering and Physics Institute (State University), 31, Kashirskoe Shosse, 115409 Moscow, Russian Federation, us_tet@mail.ru)

Wave propagation through a liquid with gas bubbles is numerically investigated, in 1D and 2D cases. The mathematical model is constructed in one-velocity, two-temperature approximation. The liquid is described by the empiric Tait equation. The bubble oscillations are described by Rayleigh-Plesset-type equation. The heat exchange between bubbles and the liquid is taking into account. Comparison of analytical solutions to results of numerical simulation has shown, that the developed model adequately describes dynamics of the wave propagation in a gas-liquid mixture. In the 2D case different regimes of wave propagation through a liquid containing gas bubbles are found. The leading wave with damped wave train is formed in a gas-liquid mixture out of bell-shaped impulse. The pressure splash can appear behind, on and before initial solitary wave in a liquid with a bubble channel and exist for a long time. The heat exchange effect on wave propagation is investigated. It is shown that properties of the wave propagation and it structure depend on the gas volume content, wavelength and on the bubble area width.

5aPAh4. Transmission gaps and Fano resonances in a simple acoustic waveguide: Analytical model. El Houssaine El Boudouti (Faculté des Sciences, Département de Physique, Université Mohamed I, 60000 Oujda, Morocco, elboudouti@yahoo.fr), Tarik Mrabti (Faculté des Sciences, Département de Physique, Université Mohamed I, 60000 Oujda, Morocco, t.mrabti@yahoo.fr), Hosni Al-Wahsh (Faculty of Engineering, Benha University, 11241 Cairo, Egypt, alwahsh2003@yahoo.com), Bahram Djafari-Rouhani (IEMN, UMR CNRS 8520, avenue Poincaré, BP 60069, 59652 Villeneuve d'Ascq, France, Bahram.Djafari-Rouhani@univ-lille1

.fr),Abdellatif Akjouj(IEMN, UMR CNRS 8520, avenue Poincaré, BP 60069, 59652 Villeneuve d'Ascq, France, abdellatif.akjouj@univ-lille1 .fr), Leonard Dobrzynski (IEMN, UMR CNRS 8520, avenue Poincaré, BP 60069, 59652 Villeneuve d'Ascq, France, leonard.dobrzynski@univ-lille1 .fr)

A simple acoustic device consisting of two dangling side resonators grafted at two sites on a slender tube is designed to obtain possibly transmission stop bands where the propagation of longitudinal acoustic waves is forbidden. Contrary to all known systems of this kind, a spectral transmission gap of nonzero width occurs here even with this simple structure. This is obtained by combining appropriately the zeros of transmission of the side resonators. Sharp resonant states inside the gaps can be achieved without introducing any defects in the structure. This results from an internal resonance of the structure when such a resonance is situated in the vicinity of a zero of transmission or placed between two zeros of transmission, the so-called Fano resonances. A general analytical expression for the transmission coefficient is given for these systems within the framework of the Green's function method. The amplitude and the phase time of the transmission are discussed as a function of frequency and it is shown that the width of the stop bands is very sensitive to the number of the side resonators. These results should have important consequences for the suppression of low-frequency noise and for designing filters.

5aPAh5. Complex edge resonance in elastic waveguides. Vincent Pagneux (Laboratoire d'Acoustique de l'Université du Maine, UMR CNRS 6613, AV. O. Messiaen, 72085 Le Mans, France, vincent.pagneux@univ-lemans.fr)

The resonance for different configurations of elastic waveguides with a free edge is studied from the point of view of complex resonance. We determine numerically the variations of the real part and of the imaginary part of the complex resonance frequency as a function of the Poisson ratio. For three different configurations, semi-infinite 2D plates, elastic cylinder and circular hole through a plate, the results show similar behaviours which are: a real resonance frequency for a zero Poisson ratio and a real resonance frequency that corresponds to a Lamé mode at one positive value of the Poisson ratio. In all the configurations, these free edges have complex resonances which have very high quality factors. The two Poisson ratio where the complex resonance frequency has a zero imaginary part (infinite quality factors) corresponds to trapped modes for which there is a decoupling between the propagating waves and the evanescent waves. The first decoupling at zero Poisson ratio is due to the special structure of the elasticity equations there and the second decoupling is due to the decoupling between the propagating Lamé mode and the higher order evanescent modes.

5aPAh6. Measurements on quarterwavelength tubes and Helmholtz resonators. Alberto Soto-Nicolas (Nokia Co, Sinivaival 5, 33720 Tampere, Finland, alberto.soto-nicolas@nokia.com)

The aim of this work is to determine what are factors limiting the prediction of the resonance frequency in unflanged quarter wavelength tubes and cylindrical Helmholtz resonators. When Helmholtz resonators are cylindrical, the frequency resonance may be predicted by solving a frequency 4th order polynomial equation. This formula may be used in quarter wavelength tubes too by just eliminating the value of the internal end correction. Some measurements were carried out showing that the accuracy in the prediction of the frequency resonance is limited by three factors: The uncertainty of values of end corrections, the visco-thermal effects not considered by the formula and the error in the estimation of the sound speed.

FRIDAY MORNING, 4 JULY 2008 P3-A, LEVEL 3, 9:40 TO 11:20 A.M.

Session 5aPAi

Physical Acoustics: General Topics in Physical Acoustics I (Poster Session)

Walter Lauriks, Cochair
Katholicke Univsiteit Leuven

Andi Petsculescu, Cochair
University of Louisiana

All posters will be on display from 9:40 a.m. to 11:20 a.m. To allow contributors an opportunity to see other posters, contributors of odd-numbered papers will be at their posters from 9:40 a.m. to 10:30 a.m. and contributors of even-numbered papers will be at their posters from 10:30 a.m. to 11:20 a.m.

Contributed Papers

5aPAi1. Focused borehole radiator. Dmitry Kas'Yanov(Radiophysical Research Inst., 25 Bolshaya Pecherskaya, 603950 Nizhny Novgorod, Russian Federation, vo-kak@yandex.ru)

A promising type of borehole acoustic radiators intended for both stimulating borehole geotechnological processes and investigating the borehole environment is considered. The basic difference of the radiators under consideration from the existing ones is the possibility of focusing the acoustic field into a preset region of borehole environment. Elastic fields produced by focusing borehole radiators in rock are studied. Limiting abilities of focusing borehole systems are investigated. Optimal type of focusing borehole radiator is shown for well stimulation. It is demonstrated that borehole radiators with a variable focal distance can be designed, which provides a real opportunity to control the distribution of elastic fields in the borehole environment. This property may be very important in developing the acoustic technologies for stimulating productive reservoirs of geotechnological boreholes.

5aPAi2. Experimental study of the convergence of two-point cross-correlation toward the Green's Function. Pierre Gouedard (LGIT

- CNRS - Université Joseph Fourier, Maison des Géosciences, 1381 rue de la Piscine, BP 53, 38041 Grenoble, France, pierre.gouedard @ujf-grenoble.fr), Philippe Roux (LGIT - CNRS - Université Joseph Fourier, Maison des Géosciences, 1381 rue de la Piscine, BP 53, 38041 Grenoble, France, philippe.roux@obs.ujf-grenoble.fr), Michel Campillo (LGIT - CNRS - Université Joseph Fourier, Maison des Géosciences, 1381 rue de la Piscine, BP 53, 38041 Grenoble, France, Michel.Campillo@obs.ujf-grenoble.fr), Arie Verdel (Shell International Exploration and Production B.V., Kessler Park 1, 2288 Rijswijk, Netherlands, arie.verdel@shell.com), Xander Campman (Shell International Exploration and Production B.V., Kessler Park 1, 2288 Rijswijk, Netherlands, xander.campman@shell.com)

Cross-correlation of seismic noise recorded at two points yields the Green's Function (GF) between the two points when seismic noise is spatially and temporally diffuse. Seismic events yield the same result (1) when direct waves are cross-correlated from sources that are azimuthally distributed or (2) when coda waves are cross-correlated whatever the source distribution. In this work, the question of convergence toward the GF is investigated with real data. From a high-resolution survey with dense arrays of geophones and sources, we select different sets of sources and time windows to compute the cross-correlation between two receivers. We compare correlations derivative with the actual GF, and show the influence of source locations and scattering on the GF reconstruction. For direct waves, sources located in the endfire lobes of the receiver pair have an essential contribution. With sources located outside the endfire lobes, the GF can nevertheless be retrieved using coda waves.

5aPAi3. Spectral properties of the surface SH waves in a vertically periodic half-space. Stanislav V. Golkin (LMP, UMR CNRS 5469, Université Bordeaux I, 351, cours de la Libération, 33405 Talence, France, s.golkin@lmp.u-bordeaux1.fr), Olivier Poncelet (LMP, UMR CNRS 5469, Université Bordeaux I, 351, cours de la Libération, 33405 Talence, France, o.poncelet@lmp.u-bordeaux1.fr), Alexander Shuvalov (LMP, UMR CNRS 5469, Université Bordeaux I, 351, cours de la Libération, 33405 Talence, France, a.shuvalov@lmp.u-bordeaux1.fr)

We consider shear horizontal (SH) waves propagating under a free surface of semi-infinite medium with vertically periodical continuous or discrete variation of material properties. This case is marked by certain special features. It is known that the dispersion spectrum embracing 'physical' and "non-physical" (in the sense of radiation condition) surface SH waves precisely coincides with another spectrum, which describes the SH waves in a single period with traction-free edges and which is relatively straightforward to calculate [1]. Of a particular interest for possible applications is that the distribution of those spectral bands, where the surface SH waves are "physical" and hence do exist, depends essentially on the profile of variation of material properties across the unit cell. In the present paper, we analyze the link between the periodic-inhomogeneity profile and the existence of surface SH waves in the frequency-wave number domain, and we show how this feature manifests itself in the time-space response. [1] A. L. Shuvalov, O. Poncelet, and A. N. Podlipenets, "On the guided and surface shear horizontal waves in monoclinic transversely periodic layers and halfspaces with arbitrary variation of material properties across the unit cell," Stud. Geophys. Geod. **50** 381-398 (2006)

5aPAi4. SH surface wave in multicracked solids. Olivier Poncelet (LMP, UMR CNRS 5469, Université Bordeaux I, 351, cours de la Libération, 33405 Talence, France, o.poncelet@lmp.u-bordeaux1.fr), Stanislav V. Golkin (LMP, UMR CNRS 5469, Université Bordeaux I, 351, cours de la Libération, 33405 Talence, France, s.golkin @lmp.u-bordeaux1.fr), Christophe Aristegui (LMP, UMR CNRS 5469, Université Bordeaux I, 351, cours de la Libération, 33405 Talence, France, c.aristegui@lmp.u-bordeaux1.fr), Mihai Caleap (LMP, UMR CNRS 5469, Université Bordeaux I, 351, cours de la Libération, 33405 Talence, France, m.caleap@lmp.u-bordeaux1.fr),Alexander Shuvalov(LMP, UMR CNRS 5469, Université Bordeaux I, 351, cours de la Libération, 33405 Talence, France, a.shuvalov@lmp.u-bordeaux1.fr)

We focus on the dispersion spectra of surface coherent waves in damaged semi-infinite elastic solids. The damage region is located within the surface layer containing depth-depending concentration of parallel closed cracks. The dispersion equation is similar to that for the Love waves in a coated substrate, except that the layer's effective elastic properties, being deduced from multiple scattering theory, are frequency-dependent and complex. For healthy elastic solids, the grazing SH wave is nondispersive. The dispersion under study is induced by the presence of cracks. The effect of both the magnitude of crack-concentration and its profile into the depth is investigated. The reliability of the semianalytical predictions is also discussed through a comparison with the numerical results obtained by using a finite-difference code.

5aPAi5. The acoustical research of shear viscoelastic properties of nanoparticles suspensions. Bair Damdinov (Buryat State University, Smolina Str., 24A, 670000 Ulan-Ude, Russian Federation, dababa@rambler.ru), Tuyana Dembelova (Buryat State University, Smolina Str., 24A, 670000 Ulan-Ude, Russian Federation, lmf@ofpsrv .bsc.buryatia.ru), Badmaev Badma (Buryat State University, Smolina Str., 24A, 670000 Ulan-Ude, Russian Federation, lmf@ofpsrv.bsc.buryatia.ru)

The acoustical research of some physical properties of nanoparticles suspensions has been carried out in this work. Mechanical properties of the SiO_2 and YAG particles suspensions have been investigated. Resonance method is used for measurement of viscoelastic properties (shear modulus and shear viscosity) of the suspensions. It was shown that the viscosity and elasticity depend on size and concentration of particles. Colloid suspension of nanoparticles of silica dioxide (SiO_2) and yttrium alumina garnet doped by neodymium (Nd:YAG) are synthesized. The shear viscoelastic properties of the colloid suspensions have been measured by acoustical method. The researching of colloid suspension of SiO_2 nanoparticles of different concentration by the acoustical resonance method is shown that viscosity and shear modulus decrease with nanoparticle concentration increasing. The nonlinear behavior of viscosity and elasticity in depending on shear influence amplitude has been shown. Investigation of viscosity of suspensions of Nd:YAG nanoparticles in ethanol in depending on concentration has been carried out. The decreasing of shear modulus of the suspensions with concentration decrease has been shown. The work was supported by RFBR 05-02-16584a and 07-02-90103-Mong-a.

5aPAi6. Modelization of acoustic waves radiation from sources of complex geometry aperture. Rafik Serhane (Université des Sciences et de la Technologie Houari Boumediene; Faculté de Physique, BP 32, El-Alia, DZ-16111 Alger, Algeria, rafik_serhane@hotmail.com), Tarek Boutkedjirt (Université des Sciences et de la Technologie Houari Boumediene; Faculté de Physique, BP 32, El-Alia, DZ-16111 Alger, Algeria, tarek_boutkedjirt@hotmail.com)

The Rayleigh integral giving the impulse response for the acoustic velocity potential cannot always be determined analytically for all types of transducer apertures. The shape of the transducer surface and the spatial distribution of the excitation on its surface can complicate the calculation. This makes using numeric methods indispensable. One of these methods consists in discritizing the aperture surface in polygonal shape elements. Our work makes use of both methods of Jensen and Faure [IEEE UFFC 39-2(1992) 262, Acta Acustica 2(1994)257]. In the former, the transducer surface is subdivided in triangles. The latter one uses additional virtual triangles one side of which is that of the physical element and its summit is the field point projection on the plane containing the considered physical element. Additionally, a rotation of the virtual triangle around the field point projection is performed. In this work, the orientations of those virtual triangles are considered according to Jensen method and their contributions to the impulse response are calculated according to the two situations described by Faure. The combination of the two methods is, then, generalized to the case of non-planar complex surfaces such as concave phased arrays.

Session 5aPAj

Physical Acoustics: Scattering and Diffraction I (Poster Session)

Michael L. Oelze, Cochair
University of Illinois at Urbana-Champaign

Jean-Marc Conoir, Cochair
Université Paris 6

All posters will be on display from 9:40 a.m. to 11:20 a.m. To allow contributors an opportunity to see other posters, contributors of odd-numbered papers will be at their posters from 9:40 a.m. to 10:30 a.m. and contributors of even-numbered papers will be at their posters from 10:30 a.m. to 11:20 a.m.

Contributed Papers

5aPAj1. Time-domain acoustic pressure fields from axisymmetric impulse sources by Rayleigh's Integral. Stephen I. Warshaw (40 West 15th St. Loft 1C, New York, NY 10011, USA, siw1939@yahoo.com)

This paper shows how Rayleigh's Integral is used to efficiently and rapidly calculate time-domain pressure waveforms and wavefronts radiated from a planar baffle due to axisymmetric normal impulse accelerations that converge toward or expand away from a fixed center of symmetry. These accelerations are prescribed with simple functional forms and histories. The Rayleigh Integrals are evaluated by Gaussian integrations that seem peculiarly suited to the integrands. The acoustic fields are presented as "snapshots" of pressure contours of the evolving wavefront structures emerging from the baffle surface, and as functions of time at selected key points. As a bonus, significant insights are provided by graphs of slant range versus time that clearly identify key signal paths from the source points to the field points. The presented methods avoid the complexities inherent in more standard transform and harmonic source treatments. They also provide insights into actual acoustic fields generated by impulsive sources, as, e.g., above the ground surface over a deeply buried explosion. [J. R. Banister and W. V. Hereford, J. Geophys. Res. **96**(D3), 5185-5193 (1991)] Simpler examples were reported earlier. [S. I. Warshaw, JASA **77**, S60 (1985); JASA **79**, S90 (1986); JASA **80**, S106 (1986), and 12 ICA Toronto, L3-6 (1986)]

5aPAj2. Unified and stable scattering matrix formalism for acoustic waves in piezoelectric stacks. Victor Y. Zhang (IEMN-CNRS, Av. Poincare, Cite Scientifique, B.P. 60069, 59652 Villeneuve d'Ascq Cedex, France, victor.zhang@iemn.univ-lille1.fr), Vincent Laude (Institut FEMTO-ST/CNRS, 32 avenue de l'Observatoire, 25044 Besançon cedex, France, vincent.laude@femto-st.fr)

This paper presents a unified and full scattering matrix (s-matrix) formalism. A stable recursive algorithm is derived for computation of the total s-matrix of a multilayered stack in terms of the interface s-matrix, both referring to the eigen-modes amplitudes. The derivation is direct and succinct, the derived expressions of the s-matrix are terse and concise, and the recursion is efficient and convenient for implementation. By combining the s-matrix formalism and the surface impedance matrix of the external media, various terminations of the stack can be easily handled. Numerical examples are given to show its numerical superiority over other currently used matrix formalisms: including unconditional stability throughout large and small thicknesses and pole-free feature.

5aPAj3. Temperature-dependent diffusing acoustic wave spectroscopy with resonant scatterers. Valentin Leroy (Laboratoire Ondes et Acoustique, ESPCI, Université Paris 7, CNRS, 10 rue Vauquelin, 75005 Paris, France, valeroy77@yahoo.fr),Arnaud Derode(Laboratoire Ondes et Acoustique, ESPCI, Université Paris 7, CNRS, 10 rue Vauquelin, 75005 Paris, France, arnaud.derode@ujf-grenoble.fr)

The influence of a slight temperature change on the correlation of multiply scattered acoustic waves is studied, and experimental results are discussed. The technique presented here, similar to diffuse acoustic wave spectroscopy, is based on the sensitivity of a multiple scattering medium to a slight change. Ultrasonic waves around 3 MHz are transmitted through a sample made of steel rods in water and recorded by an array of transducers at different temperatures. The cross-correlations between highly-scattered signals are computed. The main effect of the temperature change is a simple dilation of the times of arrival, due to a change of the sound velocity in water. But the scatterers also play a role in the progressive decorrelation of waveforms. An analysis resolved in both time and frequency shows that at some particular frequencies, the resonant behavior of the scatterers are responsible for a significantly larger decorrelation. Interestingly, the experimental results allow one to detect the presence of a small resonance that was not detected earlier on the same scatterers with classical measurement of the scattering mean freepath. A simple model is proposed to interpret the experimental results.

5aPAj4. Ultrasonic wave propagation in heterogeneous solid media. Mathieu Rossat (LCND - Université de la Méditerranée, IUT Aix Provence, Avenue Gaston Berger, 13625 Aix en Provence Cedex, France, mathieu.rossat@univmed.fr), Jean-François Chaix (LCND - Université de la Méditerranée, IUT Aix Provence, Avenue Gaston Berger, 13625 Aix en Provence Cedex, France, jean-francois.chaix@univmed.fr), Vincent Garnier (LCND - Université de la Méditerranée, IUT Aix Provence, Avenue Gaston Berger, 13625 Aix en Provence Cedex, France, vincent.garnier @univmed.fr)

To check up concrete structures "in situ" engineers often employ ultrasonic waves. The implementation of tests and analysis of results even inversion of the problem need good knowledge about propagation phenomena. These phenomena require understanding interaction between ultrasonic waves and scatters, such as granular, porosity, and cracks. This defect can come from fabrication or mechanical damage. The size and the shape of obstacle have an influence on the spatial scattering of ultrasonic waves. We propose to show you the possible using multiple scattering in homogeneous models of propagation and the last work on a sphere in a hard media. Our objective is to bring obstacle geometries closer to the reality. Consequently, we study spheroidal scatters with various aspect ratios.

5aPAj5. Comparisons between multiple scattering methods and time-domain numerical simulations for elastic waves. Mathieu Chekroun (EDF R&D - LCPC, LCPC centre de Nantes BP4129, 44341 Bouguenais, France, mathieu.chekroun@lcpc.fr), Loic Le Marrec (Institute of Mathematical Research of Rennes IRMAR, Campus de Beaulieu, 35042 Rennes, France, loic.lemarrec@univ-rennes1.fr), Bruno Lombard (Laboratoire de Mécanique et d'Acoustique LMA, 31 chemin Joseph Aiguier, 13402 Marseille, France, lombard@lma.cnrs-mrs.fr), Odile Abraham (LCPC, Centre de Nantes BP4129, 44341 Bouguenais, France, odile.abraham@lcpc.fr), Joel Piraux (Laboratoire de Mécanique et d'Acoustique LMA, 31 chemin Joseph Aiguier, 13402 Marseille, France, piraux@lma.cnrs-mrs.fr)

Propagation of elastic waves in heterogeneous medium composed of scatterers embedded in a homogeneous matrix is considered. Both matrix and scatterers are isotropic elastic media. The multiple scattering regime is assumed, and the focus is put on the coherent field obtained by averaging several equivalent realizations of disorder. Classical methods, such as Independent Scattering Approximation, Foldy or Waterman-Truell's model, provide expressions of the complex effective wave number of the coherent field, leading to an effective phase velocity and effective damping factor. Two-dimensional time-domain numerical simulations are performed for studying the validity of these analytical or semianalytical methods. To reduce spurious effects, such as numerical diffraction, to a negligible level, a high-order numerical scheme and an immersed interface method are used together. Comparisons between theoretical and numerical values of the effective phase velocity and damping factor are proposed and analyzed in terms of the frequency, the scatterer density, and the propagation length.

5aPAj6. Coherent elastic wave propagation through nonuniform spatial distributions of cracks. Christophe Aristegui (LMP, UMR CNRS 5469, Université Bordeaux I, 351, cours de la Libération, 33405 Talence, France, c.aristegui@lmp.u-bordeaux1.fr), Mihai Caleap (LMP, UMR CNRS 5469, Université Bordeaux I, 351, cours de la Libération, 33405 Talence, France, m.caleap@lmp.u-bordeaux1.fr), Olivier Poncelet (LMP, UMR CNRS 5469, Université Bordeaux I, 351, cours de la Libération, 33405 Talence, France, o.poncelet@lmp.u-bordeaux1.fr), Stanislav V. Golkin (LMP, UMR CNRS 5469, Université Bordeaux I, 351, cours de la Libération, 33405 Talence, France, s.golkin@lmp.u-bordeaux1 .fr), Alexander Shuvalov (LMP, UMR CNRS 5469, Université Bordeaux I, 351, cours de la Libération, 33405 Talence, France, a.shuvalov@lmp.u-bordeaux1.fr)

Models for multiple scattering of elastic waves usually concern uniform distributions of scatterers. The aim of this work is to predict the propagation of SH coherent waves through nonuniform distribution of parallel closed cracks. The spatial variation of the distribution properties is taken into account via replacing heterogeneous media by stacks of effective homogeneous layers. Propagation in each layer is then governed by the effective acoustic impedance and the effective wave number, derived in the framework of Waterman and Truell approach. On this basis, the reflection and transmission coefficients of the nonuniform distributions are calculated by using the transfer matrix method. We focus especially on distributions of crack size and concentration. Impact of the distribution profiles is also investigated. The semianalytical predictions are compared with numerical results obtained by using a finite-difference code.

5aPAj7. New approach to the problem on long-wave sound scattering by a Rankine vortex. Ivan Belyaev (Central Aerohydrodynamics Institute (TsAGI), Acoustic Division, 17 Radio str., 105005 Moscow, Russian Federation, belyaev_iv@bk.ru), Victor Kopiev (Central Aerohydrodynamics Institute (TsAGI), Acoustic Division, 17 Radio str., 105005 Moscow, Russian Federation, vkopiev@mx.iki.rssi.ru)

The well-known problem of sound scattering by a Rankine vortex at small Mach number M is considered. Despite the long history of the problem (Pitaevskii 1958, O'Shea 1975 etc.), solutions obtained by different authors still are not free from essential objections. The main difficulty is that the slow decay of the mean velocity field at infinity hinders a correct formulation of the problem. Most authors use a plane wave as the incident field in the leading approximation in M (Sakov 1993, Ford and Smith 1999, Howe 1999), however to obtain a physically reasonable solution the second approximation in the incident field is to be chosen beforehand. It is shown that instead of the plane wave condition, the condition of a point source far from the vortex should be posed. In the new formulation the correct solution of the problem of nonresonant sound scattering by the Rankine vortex is determined from the matching procedure in M. This solution is compared with the previous results, and areas where these results hold are revealed. Existing solutions for resonant scattering (Kopiev and Leontiev1987, Sozou 1990) are analyzed too and a result unifying the previous ones is found.

5aPAj8. Scattering of seismic waves by a fracture zone containing randomly distributed frictional cracks. Mihai Caleap (LMP, UMR CNRS 5469, Université Bordeaux I, 351, cours de la Libération, 33405 Talence, France, m.caleap@lmp.u-bordeaux1.fr), Christophe Aristegui (LMP, UMR CNRS 5469, Université Bordeaux I, 351, cours de la Libération, 33405 Talence, France, c.aristegui@lmp.u-bordeaux1.fr)

An investigation is conducted how the geometrical properties of a crack distribution in a fault fracture zone and the frictional characteristics of the crack surface are reflected in the attenuation and dispersion of incident seismic waves. All cracks are assumed to be either aligned or randomly oriented. The crack width is assumed to obey a power law distribution, according to seismological knowledge. The crack surface is assumed to be stress-free, or to undergo viscous friction. To deal with cracks under high confining pressure, the latter case will be more realistic than the stress-free crack, due to the existence of fluid in the earth's crust and the viscoelastic response of contacting solid material to seismic waves under high confining pressure. When the crack distribution is statistically homogeneous, the calculated dispersion and attenuation exhibit that the variance of crack size affects in different way the coherent wave. The analysis on the effect of the friction shows that the crack scattering decreases as the viscosity increases, which is expected since for high viscosity, the crack faces remain almost welded to each other. The results obtained in this work will be applicable to the state close to the occurrence time in large earthquakes.

5aPAj9. Identification and characterisation of the scholte A and circumferential S0 waves from the time-frequency analysis of an acoustic experimental signal backscattered by a tube. Rachid Latif (ESSI - ENSA, BP 1136, Ibn Zohr University, 80000 Agadir, Morocco, latif@ensa-agadir.ac.ma), Elhoucien Aassif (Ibn Zohr University, FS Agadir, 80000 Agadir, Morocco, aassif@hotmail.com), Mustapha Laaboubi (Ibn Zohr University, FS Agadir, 80000 Agadir, Morocco, laaboubi@gmail.com), Ali Moudden (Ibn Zohr University, FS Agadir, 80000 Agadir, Morocco, ali_moudden@yahoo.fr), Gerard Maze (LAUE, Université du Havre, Place Robert Schuman, F-76610 Le Havre, France, gerard.maze@univ-lehavre.fr)

The problem of the acoustic diffusion by a tube is a theoretical problem which had known since few years a considerable interest. A good comprehension of the acoustic diffusion makes it possible the study of the opposite problem. Many theoretical and practical works were made by a tube in the acoustic diffusion field. These works showed in particular that the resonance phenomenons are directly related to the physical and geometrical properties of the target. The interest of the study presented in this paper is the identification of the circumferential wave. Several frequential analysis techniques were applied to characterize the target. These analysis techniques currently used present the major disadvantage to not be able to highlight the temporal structure of the field diffused by the target. Reciprocally the acoustic temporal analysis of the target ca not always separate the successive arrivals of the various type waves in the signal and to have information on their frequential contents. The joint time-frequency representations provide this need. In this paper, the time-frequency of Wigner-Ville is applied to analyse the acoustic experimental signal backscattered by a steel tube with radii radio b/a=0.97 (a: external radius, b: internal radius) immersed in water. Through the Wigner-Ville image we have identified the scholte A and the circumferential S0 waves.

Session 5aPAk

Physical Acoustics: Vibrations in Plates II (Poster Session)

Daniel Royer, Cochair
Université Paris 7

Oliver Poncelet, Cochair
Université Bordeaux

All posters will be on display from 9:40 a.m. to 11:20 a.m. To allow contributors an opportunity to see other posters, contributors of odd-numbered papers will be at their posters from 9:40 a.m. to 10:30 a.m. and contributors of even-numbered papers will be at their posters from 10:30 a.m. to 11:20 a.m.

Contributed Papers

5aPAk1. Study and development of a low-frequency acoustic sensor dedicated to the vibratory analysis and the mechanical characterization of the plates. Georges Nassar (IEMN - DOAE, Université de Valenciennes, Le Mont - Houy, 59313 Valenciennes, France, gnassar@univ-valenciennes.fr), Bassam Merheb (IEMN - DOAE, Université de Valenciennes, Le Mont - Houy, 59313 Valenciennes, France, bassam.merheb@univ-valenciennes.fr), Alain Skaf (IEMN - DOAE, Université de Valenciennes, Le Mont - Houy, 59313 Valenciennes, France, alain.skaf@univ-valenciennes.fr), Fabrice Lefebvre (IEMN - DOAE, Université de Valenciennes, Le Mont - Houy, 59313 Valenciennes, France, Fabrice.Lefebvre@univ-valenciennes.fr), Bertrand Nongaillard (IEMN - DOAE, Université de Valenciennes, Le Mont - Houy, 59313 Valenciennes, France, Bertrand.Nongaillard@univ-valenciennes.fr)

A low-frequency acoustic method was implemented for the purpose of nondestructive control and evaluation of metal plates coating. In this method, a mechanical pulse (acoustic impact) is used to generate acoustic vibrations on a frequency band between 100 Hz to 20 kHz, and a compact acoustic sensor, constructed with by composite materials with an embedded ferroelectric disk, is used to receive the acoustic vibrations. The technique consists in setting in resonance the integrality of a reduced size mechanical structure. The modal frequencies of plates are calculated by two methods: analytically and by finite element method. Then, a numerical modeling of the acoustic behaviour of the sensor is presented. Finally, experimental trials are described and results showing the sensitivity of the method to evaluate coating of metal plates are analyzed.

5aPAk2. Construction of symmetrical and asymmetrical notches from elementary steps in isotropic plates. Farouk Benmeddour (UVHC, IEMN-DOAE, Le Mont-Houy, 59313 Valenciennes, France, farouk_benmeddour@yahoo.fr), Sébastien Grondel (UVHC, IEMN-DOAE, Le Mont-Houy, 59313 Valenciennes, France, sebastien.grondel@univ-valenciennes.fr), Jamal Assaad (UVHC, IEMN-DOAE, Le Mont-Houy, 59313 Valenciennes, France, jamal.assaad@univ-valenciennes.fr), Emmanuel Moulin (UVHC, IEMN-DOAE, Le Mont-Houy, 59313 Valenciennes, France, emmanuel.moulin@univ-valenciennes.fr), Lucie Dupont (UVHC, IEMN-DOAE, Le Mont Houy, 59313 Valenciennes, France, lucie.dupont@univ-valenciennes.fr)

The interactions of the fundamental Lamb modes with discontinuities in an isotropic structure will be presented and analyzed in a simple and a fast way. The key point is to decompose the symmetrical or asymmetrical notch into two elementary steps. The fundamental antisymmetrical and symmetrical Lamb modes contributions are separated by means of the simple arithmetic operations of addition and subtraction. The power reflection and transmission coefficients are then computed with the well-known average power flow equation described in a previous work [NDT&E international, Vol. **41**, p.1-9 (2008)]. Using these coefficients, the symmetrical notch can be constructed from one elementary symmetrical step while the asymmetrical notch is constructed from the superposition of asymmetrical down- and up-steps. Mode conversions phenomena are observed and analyzed for the asymmetrical steps and notches case. Finally, an experimental device is realized to test aluminum plates with different notch depths. Good agreement is found between experimental and numerical results.

5aPAk3. Lamb and Stoneley wave interactions with a fluid droplet. Loic Martinez (ECIME Université de Cergy-Pontoise, rue d'Eragny, 95031 Neuville-sur-Oise, France, loic.martinez@u-cergy.fr), Nicolas Wilkie-Chancellier (ECIME Université de Cergy-Pontoise, rue d'Eragny, 95031 Neuville-sur-Oise, France, Nicolas.Wilkie-Chancellier@u-cergy.fr), Christ Glorieux (Lab. ATF, Katholieke Universiteit Leuven, Celestijnenlaan 200D, B-3001 Leuven, Belgium, christ.glorieux@fys.kuleuven.be)

In order to analyse wetting aspects from an acoustical point of view, the present work investigates the interaction of a liquid droplet with Lamb and Stoneley waves propagating on a plane plate. A horizontal plane plate is in contact with a liquid on its lower interface, air in contact with its upper interface, the droplet lying on the top interface. Lamb waves are generated by a pulse trough a contact transducer placed at one edge of the plate. This generates in a wide range the high wave numbers of the Lamb modes A0, A1, S0 and the fluid born Sholte Stoneley wave (A-wave). For low wave numbers, the transducer is placed at normal incidence, under both the plate and the droplet. Signals obtained by emission/reception with the same transducer (2 MHz) clearly exhibits a coupling effect between acoustic modes inside the droplet and Lamb modes. Laser Doppler scans around the droplet show reflection/refraction/diffraction patterns of the incident line wavefront through the droplet. These experiments carried out with various wetting conditions point out a good correlation between the parameters of the acoustical resonances and the wetting properties, enabling an acoustic estimation of the wetting in a wide frequency range.

Session 5aPAl

Physical Acoustics: Ultrasonics: Transducers and Instruments II

Albert Migliori, Cochair
Los Alamos National Laboratory, Los Alamos, NM, 87545, USA

Claude Boutin, Cochair
École nationale des travaux publics de l'État, Rue Maurice Audin, F- 69518 Vaulx-en-Velin Cedex, FRANCE

Contributed Papers

11:20

5aPAl1. Analysis of wavefronts for the piston source acoustic fields. Dmitry V. Perov (Institute of Metal Physics, 18, Sofia Kovalevskaya St., GSP-170, 620041 Ekaterinburg, Russian Federation, peroff@imp.uran.ru), Anatoly B. Rinkevich (Institute of Metal Physics, 18, Sofia Kovalevskaya St., GSP-170, 620041 Ekaterinburg, Russian Federation, rin@imp.uran.ru)

The development of modern acoustic methods is based to a great extent on a thorough investigation of the structure of acoustic fields and on the refinement of methods of their analysis and calculation. The study of the local features of acoustic field and its space-time structure is an urgent problem of physical acoustics. This work is dedicated to analytical investigation of space-time structure of wavefronts corresponding to the acoustic fields which are radiated by the piston source into elastic media. It is assumed that the spatial distributions. Various spatial distributions of acoustic field over the surface of the transducer are taken into consideration.

11:40

5aPAl2. Miniature, high efficiency transducers for ultrasonic flow meter applications. Shrinivas G. Joshi (Marquette University, EECE Department, College of Engineering, P. O. Box 1881, Milwaukee, WI 53201-1881, USA, shri.joshi@mu.edu), Boris D. Zaitsev (Institute of Radio Engineering and Electronics of RAS, Saratov Branch, Zelyonaya str., 38, 410019 Saratov, Russian Federation, zai-boris@yandex.ru), Iren E. Kuznetsova (Institute of Radio Engineering and Electronics of RAS, Saratov Branch, Zelyonaya str., 38, 410019 Saratov, Russian Federation, kuziren@yandex.ru)

This paper is concerned with the development of novel, miniature, high efficiency transducers for use in ultrasonic flow meters. Theoretical and experimental work done in our laboratory has shown that a flat, planar transducer that has minimal protrusion into the flow pipe can be realized based on conversion of plate acoustic waves (PAWs) to bulk acoustic waves (BAWs) and vice versa. The transducer is essentially a thin plate of a suitable piezoelectric material on which intedigital transducers (IDTs) are fabricated to generate and detect plate acoustic waves. With proper design very efficient conversion of energy from plate waves in the piezoelectric material to bulk waves in the fluid (and vice versa) can be achieved. For example, using lithium niobate as the piezoelectric material and water as the fluid, total conversion loss (PAW to BAW and back from BAW to PAW) of less than 2.5 dB has been obtained. An important advantage of plate waves is that since wave energy is present on both plate surfaces, the IDT can be on the surface opposite from that which is in contact with the fluid. Details of the theoretical analysis used, experimental results obtained, and potential applications will be presented.

12:00

5aPAl3. Free-field calibration of microphones: theoretical and experimental determination of the acoustic center. Dominique Rodrigues (Laboratoire Nationale de métrologie et d'Essais (LNE), 29 avenue Roger Hennequin, 78197 Trappes Cedex, France, dominique.rodrigues@lne.fr),Jean-Noel Durocher(Laboratoire Nationale de métrologie et d'Essais (LNE), 29 avenue Roger Hennequin, 78197 Trappes Cedex, France, jean-noel.durocher@lne.fr), Michel Bruneau (Laboratoire d'Acoustique de l'Université du Maine, Avenue Olivier Messiaen, 72085 Le Mans, France, michel.bruneau@univ-lemans.fr), Anne-Marie Bruneau (Laboratoire d'Acoustique de l'Université du Maine (LAUM, UMR CNRS 6613), Avenue Olivier Messiaen, 72085 Le Mans, France, anne-marie.bruneau@univ-lemans.fr)

The concept of acoustic center is closely linked to the free-field calibration of microphones and have a great influence on the final results for the free-field sensitivity of the calibrated microphones. The international standard IEC 1094-3 defines the acoustic center of a reciprocal transducer as the point from which spherical waves seem to be diverging when the transducer is acting as a source. In the literature, the principal procedure used to measure the acoustic center of a reciprocal transducer is based on the measurement of the modulus of electrical transfer impedance at various distances of three pairs of microphones coupled by a free field. This paper presents a new procedure to determine the acoustic center of a reciprocal transducer assuming a source without any acoustic center and measuring the modulus of the electrical transfer impedance at various distances between this source and the transducer to be tested. Finally, the position of the acoustic center is deduced from the inverse distance law. Experimental values are presented and compared with theoretical values obtained using a theoretical model of the laboratory standard microphones (mounted on a semi-infinite rod) derived from those available in the literature.

12:20

5aPAl4. Study of acoustoelasticity behavior of concrete material under uniaxial compression. Jean-François Chaix (LCND - Université de la Méditerranée, IUT Aix Provence, Avenue Gaston Berger, 13625 Aix en Provence Cedex, France, jean-francois.chaix@univmed.fr), Ivan Lillamand (LCND - Université de la Méditerranée, IUT Aix Provence, Avenue Gaston Berger, 13625 Aix en Provence Cedex, France, ivan.lillamand@univmed.fr), Marie-Aude Ploix (LCND - Université de la Méditerranée, IUT Aix Provence, Avenue Gaston Berger, 13625 Aix en Provence Cedex, France, marie-aude.ploix@univmed.fr), Vincent Garnier (LCND - Université de la Méditerranée, IUT Aix Provence, Avenue Gaston Berger, 13625 Aix en Provence Cedex, France, vincent.garnier@univmed.fr), Gilles Corneloup (LCND - Université de la Méditerranée, IUT Aix Provence, Avenue Gaston Berger, 13625 Aix en Provence Cedex, France, gilles.corneloup@univmed.fr)

The general subject concerns the non destructive testing of prestressed structures in civil engineering. In this topic we are interested in the feasibility of stress evaluation in concrete by ultrasonic methods. To do that, we use the acoustoelasticity theory which exploits the nonlinear behaviour of media to establish the link between stress and ultrasonic velocity. This theory has been validated in homogeneous media and used in steel (to evaluated stresses in steel bolt for example). Concrete is a heterogeneous medium where the ultrasonic velocity measurement is more difficult than in steel. The scattered waves induce uncertainty in the measured values but the nonlinear behaviour of concrete is more important than the one of steel. We

show an application in high performance concrete submitted to uniaxial compression. We measure velocities of longitudinal and transversal transmitted ultrasonic waves in the direction and perpendicularly to the stress at different level of the stress test. The sensibility of the different velocities is observed and the potential to evaluate stress in concrete is shown. Prospects particularly concern extension of tested formulations and in situ measurements. This study is supported by ANR-ACTENA, a French research program.

12:40-2:00 Lunch Break

Contributed Papers

2:00

5aPAl5. Analysis of the backscattered waves in an heterogeneous material: Application on concretes. Vincent Garnier (LCND - Université de la Méditerranée, IUT Aix Provence, Avenue Gaston Berger, 13625 Aix en Provence Cedex, France, vincent.garnier@univmed.fr), Stéphane Morières (LCND - Université de la Méditerranée, IUT Aix Provence, Avenue Gaston Berger, 13625 Aix en Provence Cedex, France, stephane.moriere@gadz.org), Jean-François Chaix (LCND - Université de la Méditerranée, IUT Aix Provence, Avenue Gaston Berger, 13625 Aix en Provence Cedex, France, jean-francois.chaix@univmed.fr), Gilles Corneloup (LCND - Université de la Méditerranée, IUT Aix Provence, Avenue Gaston Berger, 13625 Aix en Provence Cedex, France, gilles.corneloup @univmed.fr)

In heterogeneous materials, ultrasonic waves can be scattered forward or backward. The set of the backscattered contribution generates a wave that is attenuated over time. We make the measurement of this attenuation with the envelope of the backscattered signal. This information evolves with the nature, shape, and size of the scatterers so with the material state. First, we propose the simulation of the signal in which we introduce the attenuation dependence on the frequency. Second, we develop this application on concretes in which many scatterers contribute to the signal's generation. We apply the technique with differents tools to generate and exploit the backscattered waves. The attenuation evolutions with the material's nature, porosity, damage and saturation rate of the concrete are analysed.

2:20

5aPAl6. Airborne phased array for airborne applications based on cellular polymer. Christian Degel (Fraunhofer IBMT, Ensheimer Strasse 48, 66386 Sankt Ingbert, Germany, christian.degel@ibmt.fraunhofer.de) , Franz Josef Becker (Fraunhofer IBMT, Ensheimer Strasse 48, 66386 Sankt Ingbert, Germany, franz.becker@ibmt.fraunhofer.de), Martin Heinz (Fraunhofer IBMT, Industriestrasse 5, 66280 Sulzbach, Germany, martin.heinz@ibmt.fraunhofer.de), Heinrich Fonfara (Fraunhofer IBMT, Ensheimerstrasse 48, 66386 Sankt Ingbert, Germany, heinrich.fonfara@ibmt.fhg.de), Robert M. Lemor (Fraunhofer IBMT, Ensheimer Strasse 48, 66386 Sankt Ingbert, Germany, robert.lemor@ibmt.fhg .de)

Object recognition, advanced distance measurements and other inspection scenarios have an increasing demand in versatile airborne ultrasonic phased arrays for acoustic scanning without moving parts. Based on cellular polymer film with high piezoelectric effect we have realized an array structure with a pitch of 0.5 mm and element length of 10 mm. The working frequency of the material was measured to 250 kHz. From pointspread simulation with the small ratio of pitch/wavelength of 0.35 we could expect good beam steering and focusing characteristics. A first test array was realized and characterized. There was good agreement between measurement results and simulations. Additionally a low frequency electronic beamformer system was developed for generating the first B-image of an airborne phased array. Measurements showed that cellular polymer is a well suitable material for airborne applications. It can easily be structured to the desired shape. It allows especially the realization of phased arrays for applications like surface or profile measurement, access control, attendance check, robot guidance etc. New airborne array types like linear, phased, curved, or circular arrays are now possible. Also single element transducers with varying apertures (rectangular, oval), shaped apertures [focusing (line- or point-focusing), defocusing] or combinations of both are possible.

2:40

5aPAl7. Nonlinear focal shift in focused ultrasonic transducers and its dependence on the Fresnel number. Yuri Makov (Moscow State University, Dept. of Acoustics, 46730 Moscow, Russian Federation, yuri_makov@mail.ru), Victor Sánchez-Morcillo (IGIC - Universitat Politècnica de València, Cra. Nazaret-Oliva S/N, E-46730 Gandia, Spain, victorsm@fis.upv.es), Francisco Camarena (IGIC - Universitat Politècnica de València, Cra. Nazaret-Oliva S/N, E-46730 Gandia, Spain, fracafe@fis.upv.es), Víctor Espinosa (IGIC - Universitat Politècnica de València, Cra. Nazaret-Oliva S/N, E-46730 Gandia, Spain, vespinos@fis .upv.es)

In this work we present a systematic study of the on-axis location of the maximum pressure and intensity points in the field radiated by a focused transducer. We report the motion of these characteristic points as the transducer voltage is increased. Different initial distributions, ranging from uniform to Gaussian cases, are considered. The numerical analysis is based on the solutions of the KZK equation with different initial conditions. Experimental results have been obtained for three different Fresnel number focused transducers in linear and nonlinear regime in order to analyze the focal shift effect. An analytical expression of the initial (linear) shift of the maximum pressure position is given. This expression, and the results of the numerical simulations, shows a good agreement with the experimental data. As a main conclusion, we demonstrate that the axial range of the nonlinear shift of pressure is larger for strong initial focal shifts, occurring for small Fresnel number transducers. Theoretical and numerical predictions of the focal shift effect in Gaussian beams are also presented. In this work we have established the relation between the focal shift (both in linear and nonlinear regime) with the Fresnel number of the transducer.

3:00

5aPAl8. Linking static and dynamic NDT through fractional derivatives. Ari Salmi (Univ. of Helsinki / Dept. of Physical Sciences, POB 64 (Gustaf Hällströmin katu 2), 00014 Helsinki, Finland, edward.haeggstrom@helsinki.fi), Tuomas Hintikka (Electronics Research Unit, University of Helsinki, P.O. Box 64 (Gustaf Hällströmin katu 2), FIN-00014 Helsinki, Finland, tuomas.hintikka@yahoo.com), Pekka Saranpaa (Finnish Forest Research Institute METLA, Vantaa Research Unit, Vantaa, FI-01301 Helsinki, Finland, pekka.saranpaa@metla.fi), Timo Karppinen (Electronics Research Unit, University of Helsinki, P.O. Box 64 (Gustaf Hällströmin katu 2), FIN-00014 Helsinki, Finland, timo.karppinen@helsinki.fi), Edward Hæggström (Electronics Research Unit, University of Helsinki, P.O. Box 64 (Gustaf Hällströmin katu 2), FIN-00014 Helsinki, Finland, edward.haeggstrom@helsinki.fi), Ritva Serimaa (Univ. of Helsinki / Dept. of Physical Sciences, POB 64 (Gustaf Hällströmin katu 2), 00014 Helsinki, Finland, ritva.serimaa@helsinki.fi)

Static testing of mechanical properties of materials is widely used and well documented. Several extensively employed NDT techniques relying on induced mechanic wave motion (dynamic strain) exist. Comparing results obtained with dynamic NDT techniques to each other and to certified static tests is problematic especially for polymer materials whose absolute mechanical moduli depend on loading frequency. We present a study performed on 102 block-shaped dry samples of Norwegian spruce wood (Picea Abies [L.] Karst., a complex natural polymer) using ultrasound propagated in the longitudinal wood direction with frequencies ranging from 50 kHz to 8 MHz. The samples were also tested using a standardized three-point bending test providing longitudinal elasticity estimates at near-zero frequency (static MOE). We validate experimentally the Pritz[1] five-parameter fractional derivative model and we link together the static test and the ultrasonic NDT

technique. Our results allow predicting the static MOE from the dynamic MOE obtained with ultrasonic test equipment, and permit comparison of data obtained with ultrasonic methods applying different frequencies. [1] T. Pritz, Five-parameter fractional derivative model for polymeric damping materials, Journal of Sound and Vibration, **265**(5), 935-952 (2003)

3:20

5aPAl9. Influence of low temperature cycles on the integrity of pretreated 2024 T3 aluminium joints by an ultrasonic method. Martine Rousseau (Institut Jean Le Rond d'Alembert Université Paris 6 CNRS UMR 7190, 4, Place Jussieu, Case 162, 75252 Paris cedex 05, France, mrousse@ccr.jussieu.fr), Valentina Vlasie Belloncle (Institut Jean Le Rond d'Alembert Université Paris 6 CNRS UMR 7190, 4, Place Jussieu, Case 162, 75252 Paris cedex 05, France, vlasie_valentina@yahoo.fr)

Many authors have considered the problem of adhesive bond durability over a long period of time or under special environmental conditions, and all have conclued that surface preparation is of paramount importance. Here, 2024 T3 aluminium alloy bonded joints, whose metallic plates underwent phosphoric acid pretreatment prior to bonding, are investigated before and after exposure to -40 °C for 67 h. This procedure of ageing is repeated several times and the samples are examined by ultrasonic Lamb waves after each cycle. In particular, the position of the cutoff-frequencies of ultrasonic guided waves which propagate into the bonded aluminum/epoxy/aluminium structure allows us to calculate the stiffnesses of the metal/adhesive interfaces with a rheological model. Thus, after exposure, a progressive decrease in the value of the stiffnesses is observed even for pretreated surfaces. Two complementary mechanical explanations are proposed. First, the cold exposure of the sample and the difference between thermal dilatation coefficients of aluminum and epoxy produce a damage of the interfacial zone. Second, the cooling introduces microcracks in the epoxy then caracterized by a smaller Young modulus.

FRIDAY MORNING, 4 JULY 2008 ROOM 241, 8:00 TO 11:40 A.M.

Session 5aPPa

Psychological and Physiological Acoustics: Cross-Spectral Auditory Integration: Physiological, Psychophysical, and Clinical Evidence I

Blas Espinoza-Varas, Cochair
CommunicationSciences & Disorders, OU Health Sciences Ctr., 825 NE 14th St., Oklahoma City, OK 73126-0901, USA

Alain De Cheveigne, Cochair
CNRS, Universite Paris 5, Ecole Normale Superieure, 29 rue d'Ulm, Paris, 75230, France

Contributed Paper

8:00

5aPPa1. Sensitivity of high-frequency inferior colliculus neurons to sinusoidal amplitude-modulation of low-frequency tones. Laurel H. Carney (University of Rochester, Depts. of Biomedical Engineering and Neurobiology & Anatomy, 601 Elmwood Ave., Box 603, Rochester, NY 14642, USA, Laurel.Carney@Rochester.edu)

Responses of neurons in the inferior colliculus of awake rabbit were studied using sinusoidally amplitude-modulated (SAM) tones with a wide range of carrier and modulation frequencies. Neurometric thresholds for detection of modulation were estimated by applying both average rate and temporal metrics to neural responses. For neurons tuned to high frequencies, neurometric thresholds for SAM detection were substantially lower for mid- to high-level carriers at frequencies in the tail of the tuning curves than for carriers near the characteristic frequency (CF). Sensitivity to SAM for low carrier frequencies was often superior to sensitivity for near-CF carriers at low sound levels. These results suggest that psychophysical SAM detection thresholds at sound levels above approximately 60 dB SPL may be supported by "tail" responses of neurons tuned octaves above the carrier frequency. Improvement of psychophysical SAM detection thresholds with sound level is thus consistent with the contribution of a large population of responsive and sensitive "off-CF" neurons as level is increased. The fact that many auditory neurons, in both the peripheral and central nervous system, respond across several octaves at mid-to-high SPLs must be taken into account when considering "across-channel" interactions in tasks that involve both simple and complex sounds.

Invited Paper

8:20

5aPPa2. Role of peripheral nonlinearities in across-frequency processing of envelope fluctuations in normal hearing and hearing impaired listeners. Jesko Verhey (Universität Oldenburg, Medizinische Physik, Carl-von-Ossietzky Str. 9-11, 26111 Oldenburg, Germany, jesko.verhey@uni-oldenburg.de), Jesko Rennies (Universität Oldenburg, Medizinische Physik, Carl-von-Ossietzky Str. 9-11, 26111 Oldenburg, Germany, jan.rennies@uni-oldenburg.de), Stephan M. Ernst (Universität Oldenburg, Medizinische Physik, Carl-von-Ossietzky Str. 9-11, 26111 Oldenburg, Germany, stephan.ernst@uni-oldenburg.de)

A psychoacoustical phenomenon related to the ability of the auditory system to compare information across frequency is comodulation masking release (CMR). CMR describes the effect that signal detectability of a sinusoidal signal embedded in a masker at the signal frequency can be improved by simultaneously presenting additional maskers in off-frequency regions if the additional maskers and the on-frequency masker (OFM) component have the same temporal envelope. Recently it was proposed that peripheral nonlinear processes such as suppression may account for large proportions of the CMR in conditions with a large spectral distance between the masker components. The aim of the present study was to test this hypothesis by measuring suppression and CMR within the same subjects for various frequency-level combinations of the off-frequency masker component. Average data for normal hearing listeners

show a large overlap between the existence regions for suppression and CMR. The hearing impaired subjects with a sensorineural hearing loss show a negligible suppression and CMR. The data support the hypothesis that peripheral nonlinearities play an important role in CMR experiments with large spectral distances and large level differences between the masker components.

Contributed Paper

8:40

5aPPa3. Frequency modulated harmonics induces informational masking of Chinese speech. Xihong H. Wu (Dept. of Machine Intelligence, Speech and Hearing Research Center, 2 Science Building, Peking Univ., 5 Yeheyuan Road, Haidian District, 100871 Beijing, China, wxh@cis.pku.edu.cn), Jing Chen (Dept. of Machine Intelligence, Speech and Hearing Research Center, 2 Science Building, Peking Univ., 5 Yeheyuan Road, Haidian District, 100871 Beijing, China, chenj@cis.pku.edu.cn), Xuefei F. Zou (Dept. of Machine Intelligence, Speech and Hearing Research Center, 2 Science Building, Peking Univ., 5 Yeheyuan Road, Haidian District, 100871 Beijing, China, zouxf@cis.pku.edu.cn), Jingyu Y. Li (Dept. of Machine Intelligence, Speech and Hearing Research Center, 2 Science Building, Peking Univ., 5 Yeheyuan Road, Haidian District, 100871 Beijing, China, lijy@cis.pku.edu.cn), Lijuan J. Xu (Dept. of Psychology, Peking Univ., 5 Yeheyuan Road, Haidian District, 100871 Beijing, China, lijuan179021@yahoo.com.cn), Liang Li (Dept. of Psychology, Peking Univ., 5 Yeheyuan Road, Haidian District, 100871 Beijing, China, liangli@pku.edu.cn), Huisheng S. Chi (Dept. of Machine Intelligence, Speech and Hearing Research Center, 2 Science Building, Peking Univ., 5 Yeheyuan Road, Haidian District, 100871 Beijing, China, chi@pku.edu.cn)

Informational masking (IM) occurs when target speech is co-presented with competing speech. It is important to know what acoustic characteristics of a speech masker are essential to induce IM. This study investigated whether frequency modulation (FM) of speech is associated with IM. Nonsense Chinese Mandarin sentences were spoken by a young female as target stimuli and maskers were tone harmonics whose fundamental frequency (F0) was modulated sinusoidally and number of harmonic streams was varied. The magnitude of IM was evaluated by measuring the precedence-induced releasing effect of perceived spatial separation on target speech. The results show that the releasing effect reached the highest level when F0 became 252 Hz, which was the mean pitch of target speech. In addition, the releasing effect was significantly higher when the masker contained two harmonic streams than when one stream. These results suggest that because frequency-modulated harmonics can be used to inducing IM of speech, the FM component of speech is an important acoustic factor underlying IM. [Supported by the NSFC 60435010; 60535030; 60605016; 30670704.]

Invited Papers

9:00

5aPPa4. Cross-spectral synergy and consonant identification. Thomas Ulrich Christiansen (Technical University of Denmark, Center for Applied Hearing Research, Ørsteds Plads, Building 352, 2800 Lyngby, Denmark, tuc@oersted.dtu.dk), Steven Greenberg (Technical University of Denmark, Center for Applied Hearing Research, Ørsteds Plads, Building 352, 2800 Lyngby, Denmark, steveng@silicon-speech.com)

The auditory processing of consonants was investigated using an information-theoretic approach. Listeners identified eleven different Danish consonants spoken in a Consonant + Vowel + [l] environment. Each syllable was processed so that only a portion of the original audio spectrum was present. Three-quarter-octave bands of speech, with center frequencies of 750, 1500 and 3000 Hz, were presented individually and in combination with each other. Confusion matrices were computed, and from these the amount of information transmitted for each of three phonetic-features - voicing, manner and place of articulation - was computed for each condition. From such analyses one can determine whether information associated with any given phonetic feature combines linearly across the acoustic spectrum or not. Our results indicate that information associated with voicing and manner-of-articulation combines in quasi-linear fashion across the frequency spectrum. In contrast, place-of-articulation cues are integrated synergistically - information associated with two or three channels combined is far greater than predicted from the amount of information associated with individual spectral bands. Because consonants are essential for understanding speech, and place-of articulation information is crucial for decoding consonants, spoken language perception is likely to reflect highly non-linear processes.

9:20

5aPPa5. Across-frequency integration of speech information in listeners with sensorineural hearing loss. Joseph W. Hall (University of North Carolina, School of Medicine, 1115 Bioinformatics. Bldg., CB7070, 130 Mason Farm Rd., Chapel Hill, NC 27599, USA, jwh@med.unc.edu), Emily Buss (University of North Carolina, School of Medicine, 1115 Bioinformatics. Bldg., CB7070, 130 Mason Farm Rd., Chapel Hill, NC 27599, USA, ebuss@med.unc.edu), John H. Grose (University of North Carolina, School of Medicine, 1115 Bioinformatics. Bldg., CB7070, 130 Mason Farm Rd., Chapel Hill, NC 27599, USA, jhg@med.unc.edu)

At very poor signal-to-noise ratios, good speech perception may depend critically upon the ability of the listener to combine relatively brief glimpses of the signal that are separated both in terms of frequency and time. This presentation will review past research that has addressed the ability of normal-hearing and hearing-impaired listeners to integrate speech information in this way. The presentation will also consider recent studies from our laboratory that have investigated spectral/temporal integration of speech signals in listeners with mild-to-moderate sensorineural hearing losses. One of these studies focused upon the integration of speech information that was asynchronous across frequency and the other focused upon the integration of synchronous information arising from two relatively narrow bands that were widely separated in frequency. The results from these studies indicated that although the hearing- impaired listeners exhibited some characteristics suggestive of poor processing of speech, there was little indication of essential deficits in the ability to integrate synchronous or asynchronous across-frequency speech information.

9:40-11:00 Posters

Lecture sessions will recess for presentation of poster papers on various topics in acoustics. See poster sessions for topics and abstracts.

Invited Papers

11:00

5aPPa6. Cross-spectral integration of speech patterns by normal and impaired listeners. Eric W. Healy (University of South Carolina, Speech Psychoacoustics Laboratory, Department of Communication Sciences and Disorders, William Brice Bldg., 1621 Greene St., Columbia, SC 29208, USA, ewh@sc.edu)

According to the current session description, "Recent evidence suggests that speech recognition depends importantly on the ability to integrate information across the frequency spectrum, which is not accounted for by the sensitivity (information content) of the respective spectral regions." Indeed, temporal speech patterns that yield near zero intelligibility when presented individually can provide intelligibility in excess of 80% when presented in pairs. These and other recent data involving the integration of speech patterns across the spectrum by the normal auditory system will be described. In addition, "speech-recognition data supporting the existence of a cross-spectral integration deficit in hearing-impaired patients" will be discussed and contrasted against similar experiments involving non-speech stimuli.

11:20

5aPPa7. Integration of acoustic cues for consonant identification by cochlear implant users. Mario Svirsky (New York University, Dept. of Otolaryngology, NYUSOM, 550 First Ave., NBV-5E5, New York, NY 10016, USA, mario.svirsky@nyumc.org), Elad Sagi (New York University, Dept. of Otolaryngology, NYUSOM, 550 First Ave., NBV-5E5, New York, NY 10016, USA, elad.sagi@med.nyu.edu)

Users of cochlear implants (CIs) obtain substantial benefit from their devices, but their speech perception is (on average) less than perfect and there are significant individual differences among patients. In particular, their consonant identification levels are lower than those of normal hearing listeners, or even most users of hearing aids. We have developed a simple quantitative model (multidimensional Phoneme Identification or MPI model) to predict consonant confusion matrices for individual cochlear implant users based on their discrimination of three consonantal acoustic cues: place of stimulation in the cochlea, silent gap duration, and percentage of energy above 800 Hz. Despite using only three degrees of freedom (i.e., JND for each cue) the model can explain most of the consonant pairs that are confused (or not confused) by individual CI users. However, when a listener's measured JNDs are used as inputs to the model, the predictions that result tend to have a higher percentage of correct responses than shown by the listener. One possible explanation is that CI users' speech perception may be limited not only by their basic psychophysical capabilities but also by their imperfect integration of different acoustic cues. [Work supported by NIDCD (R01-DC03937).]

FRIDAY MORNING, 4 JULY 2008 ROOM 242A, 8:00 A.M. TO 12:20 P.M.

Session 5aPPb

Psychological and Physiological Acoustics: Otoacoustic Emissions, from Cochlear Modeling to Experimental Techniques, and Back I

Christopher A. Shera, Cochair
Eaton-Peabody Laboratory, 243 Charles St, Boston, MA 02114, USA

Arturo Moleti, Cochair
University of Roma Tor Vergata - Physics Department, Via della Ricerca Scientifica, 1, Roma, 00133, Italy

Invited Papers

8:00

5aPPb1. Testing coherent reflection in chinchilla. Christopher A. Shera (Eaton-Peabody Laboratory, 243 Charles St, Boston, MA 02114, USA, shera@epl.meei.harvard.edu), Arnold Tubis (Institute for Nonlinear Science, University of California, San Diego, La Jolla, CA 92093, USA, tubisa@aol.com), Carrick L. Talmadge (The University of Mississippi - NCPA, 1 Coliseum Drive, University, MS 38677, USA, clt@olemiss.edu)

Coherent-reflection theory explains the generation of stimulus-frequency and transient-evoked otoacoustic emissions by showing how they emerge from the coherent "backscattering" of forward-traveling waves by mechanical irregularities in the cochlear partition. Recent published measurements of stimulus-frequency otoacoustic emissions (SFOAEs) and estimates of near-threshold basilar-membrane (BM) responses derived from Wiener-kernel analysis of auditory-nerve responses allow for comprehensive tests of the theory in chinchilla. Model predictions are based on: (1) an approximate analytic expression for the SFOAE signal in terms of the BM traveling

5a FRI. AM

wave and its complex wave number; (2) an inversion procedure that derives the wave number from BM traveling waves; and (3) estimates of BM traveling waves obtained from the Wiener-kernel data and local scaling assumptions. At frequencies above 4 kHz, predicted median SFOAE phase-gradient delays are in excellent agreement with the SFOAE measurements. At frequencies below 4 kHz, chinchilla SFOAEs show strong evidence of interference between short- and long-latency components. Approximate unmixing of these components, and association of the long-latency component with the predicted SFOAE, yields close agreement throughout the cochlea.

8:20

5aPPb2. Two-tone suppression of stimulus frequency otoacoustic emissions in human ears with sensorineural hearing loss. Douglas H. Keefe (Boys Town National Research Hospital, 555 North 30th Street, Omaha, NE 68131, USA, keefe@boystown.org), John C. Ellison (Boys Town National Research Hospital, 555 North 30th Street, Omaha, NE 68131, USA, ellisonj@boystown.org), Denis F. Fitzpatrick (Boys Town National Research Hospital, 555 North 30th Street, Omaha, NE 68131, USA, fitzpatrickd@boystown.org)

Two-tone suppression (2TS) of stimulus frequency otoacoustic emissions (SFOAEs) recorded in normal-functioning human ears is a noninvasive measure of cochlear nonlinearity. This study investigates 2TS SFOAE response properties in 63 subjects with sensorineural hearing loss and normal middle-ear function. SFOAEs were measured using tones at frequencies (f_p) from 0.5 to 8 kHz and levels from 40-60 dB SPL. For interpreting SFOAEs, hearing status was classified at each frequency according to degree of hearing loss, with losses ranging from within normal limits to 95 dB HL. SFOAE suppression was measured as a function of suppressor frequency (f_s) and level (L_s), with results analyzed in terms of a SFOAE suppression tuning curve. A tip-to-tail difference (TTD) was defined between the L_s needed to produce a criterion decrement in SFOAE level at f_s one octave below f_p and the L_s needed to produce a criterion decrement near f_p. The TTD estimates cochlear-amplifier gain in normal-functioning ears, but its properties in impaired ears based on SFOAEs have not been examined. Results will be analyzed as a function of the hearing status to assess the relative impact of outer-hair cell dysfunction in the SFOAE source region at tonotopic place. [Work supported by NIH.]

8:40

5aPPb3. Species differences in low-level otoacoustic emissions may be explained by "hot regions" in the cochlea. Jon Siegel (Northwestern Univ, 2240 Campus Drive, Evanston, IL 60208, USA, j-siegel@northwestern.edu)

Otoacoustic emissions evoked by low-level transients (TEOAE) and single tones (SFOAE) appear to excite the same emission mechanism, a concept originally formulated by Kemp and others and confirmed quantitatively by Kalluri and Shera (JASA **121**, 2097–2110 (2007)). We have studied emissions evoked by single tones (SFOAE) measured using the suppression method. In humans, 50-70 dB SPL tones most readily suppress SFOAE evoked by lower-level tones when the suppressor is near the frequency of the evoking tone, suggesting that most of the emission originates near the peak of mechanical activity induced by the evoking tone. However, in chinchillas, Mongolian gerbils and mice, emission components originating basal to the peak appear to be relatively larger than in humans. The range of frequencies evoking the largest SFOAE correspond to those where spontaneous emissions are detected, from roughly 0.5 - 6 kHz in humans, 4-12 kHz in chinchillas, 15-30 kHz in mice and still higher in bats. Stimulus tones below this "hot" frequency range appear to generate the largest SFOAE components basal to the peak. The existence of "hot regions" in the cochlea may explain the apparent species differences in emission behavior between humans and small mammals. (Supported by NIH grant DC-00419 and Northwestern University.)

9:00

5aPPb4. 5 mHz oscillations in OAE intensity following sound exposure. David Kemp (UCL Ear Institute, UCL Centre for Auditory Research, 332 Gray's Inn Road, WC1X8EE London, UK, d.kemp@UCL.ac.uk), Oliver J. Brill (UCL Ear Institute, UCL Centre for Auditory Research, 332 Gray's Inn Road, WC1X8EE London, UK, Oliver@otodynamics.com)

Otoacoustic emission (OAE) intensity is highly stable in healthy ears but can be temporarily reduced following noise exposure. This reduction in OAE intensity is well correlated with temporary noise induced hearing threshold elevation and is presumed to be due to metabolic fatigue in the outer hair cells. These cells are responsible for the generation of OAEs and are essential for the maintenance of normal hearing threshold. The severity and recovery of post exposure OAE reduction in an individual is therefore of interest for hearing protection purposes. This paper concerns the regulation of outer hair cell status and the effect of overstimulation on that regulation. We measured OAE level fluctuations following mild over stimulation (e.g., 100 dBSPL for 2 ms) in order to observe the dynamics of OAE regulation. We propose this parallels outer hair cell physiological regulation. Under-damped oscillations in OAE level occur typically at a frequency of 5 milliHertz after sound exposure. We find oscillations are excited by both the onset and offset of overstimulation and a linear model explains our observations. The oscillation is clearly not itself a fatigue process but fatigue is revealed by the need for a small depression of the baseline of the OAE oscillations.

9:20

5aPPb5. Several properties of distortion product otoacoustic emissions can be modeled by simple input/output functions. Paul Fahey (University of Scranton, Dept. of Physics/Electrical Engineering, Scranton, PA 18510, USA, faheyp1@scranton.edu), Glen K. Martin (Jerry Pettis Memorial Veterans Medical Center, Research Service (151), 11201 Benton Street, Loma Linda, 92357, USA, glen.martin2@va.gov)

Distortion product otoacoustic emissions (DPOAEs) often exhibit regular patterns in both amplitude and phase as functions of both the levels and frequencies of the generating primary tones. Many of these patterns can be approximated when modeled by simple input/output functions. In particular, nulling patterns in rabbit DPOAEs and their modifications upon noise damage or fatiguing tonal exposures can be modeled at the level of input/output functions. Also, input/output functions can be used to propose the possible physics that underlies some complicated DPOAE patterns in level/frequency space that occur in the presence of a third tone. Both data and models will be reviewed.

9:40-11:00 Posters

Lecture sessions will recess for presentation of poster papers on various topics in acoustics. See poster sessions for topics and abstracts.

Invited Papers

11:00

5aPPb6. Using the frequency dispersive properties of otoacoustic emissions to facilitate separation of different components. Glenis R. Long (Graduate Center of the City University of New York, Speech-Language-Hearing Program, 365 Fifth Ave, New York, NY 10016, USA, glong@gc.cuny.edu), Carrick L. Talmadge (The University of Mississippi - NCPA, 1 Coliseum Drive, University, MS 38677, USA, clt@olemiss.edu)

Otoacoustic emissions (OAE) are frequency dispersive (different frequencies have different latencies), because of the properties of the basilar membrane. These frequency-dependent latency differences, are used to separate the transient otoacoustic emissions (TEOAE) from the stimulus, but have not been used with stimulus frequency (SFOAE) and distortion product (DPOAE) otoacoustic emissions. If continuously-sweeping tones are used to generate DPOAE and SFOAE, the frequency dispersive properties of these OAE cannot only be used to separate the evoking stimuli from the OAE, but also to separate OAE coming from different cochlear regions. Modifications of the LSF procedure to extract OAE (Long &Talmadge, 1997: JASA, 102:2831-2848; Talmadge et al. 1999: JASA,105:275-292) permit not only the extraction of the different OAE components, but also provide an estimate of the latency of the OAE, which does not depend on group delay. DPOAE and SFOAE extracted using sweeping tones in normal and impaired adults and infants provide information about the nature of cochlea function in these populations

11:20

5aPPb7. Does overexposure modify the fine structure of distortion product otoacoustic emissions? Karen Reuter (Acoustics, Aalborg University, Fredrik Bajers Vej 7 B5, 9220 Aalborg Ø, Denmark, kr@es.aau.dk), Dorte Hammershøi (Acoustics, Aalborg University, Fredrik Bajers Vej 7 B5, 9220 Aalborg Ø, Denmark, dh@es.aau.dk)

It is investigated, whether the pattern of distortion product otoacoustic emission (DPOAE) fine structure (quasiperiodic variations across frequency) is altered by an acoustical overexposure. DPOAE fine structures are determined in 16 normal-hearing humans using a high frequency-resolution and primary levels of L1/L2=65/45 dB. DPOAEs are measured both before and after the subjects are monaurally exposed to a 1 kHz tone lasting for 3 min at an equivalent threshold sound pressure level of 105.5 dB. After the exposure the DPOAE levels are shifted to lower values and recover to the initial levels within 20 min. The DPOAE fine structure pattern is analyzed by an automatic classification algorithm, which determines ripple center frequency, ripple spacing, ripple height, and ripple prevalence. For some individuals, an alteration of some of the parameters could be observed after the exposure, i.e., either a more pronounced or a less pronounced fine structure could be observed after the exposure. Across subjects, no shift of the fine structure pattern in frequency could be observed, also none of the calculated parameters changed consistently after the exposure. The results do not support the idea that the DPOAE fine structure might contain more information about the state of hearing than the DPOAE level.

11:40

5aPPb8. Changes in distortion product otoacoustic emission (DPOAE) fine structure due to contralateral acoustic stimulation. Manfred Mauermann (Universität Oldenburg, Medizinische Physik, Carl-von-Ossietzky Str. 9-11, 26111 Oldenburg, Germany, manfred.mauermann@uni-oldenburg.de), Birger Kollmeier (Universität Oldenburg, Medizinische Physik, Carl-von-Ossietzky Str. 9-11, 26111 Oldenburg, Germany, birger.kollmeier@uni-oldenburg.de)

Contralateral acoustic stimulation (CAS) can cause changes in the amplitude of the $2f_1$-f_2 DPOAE in humans - most probably mediated by the medial olivocochlear reflex. DPOAE amplitude changes due to CAS show large interindividual variability and large changes from suppression to enhancement for small changes of the primary levels. The underlying mechanisms of these effects are still not fully understood. We hypothesize that the two interacting DPOAE sources might be differently affected by the CAS. If so, CAS will cause specific changes in DPOAE fine structure. Therefore, DPOAE fine structures were measured using frequency-modulated primaries (f_2: 1500-3000 Hz, f_2/f_1: 1.2; L_2: 60 dB SPL; L_1: 58, 63, 68 dB SPL) without and with a broadband CAS (50 dB SPL). The fine structure changes and shifts according to CAS were analyzed in detail - including latency windowing to separate the contributions from the two interacting DPOAE sources. The results indicate, e.g., that there is no "true" enhancement in terms of enhanced cochlear activity during broadband CAS. Rather there are slight frequency shifts in DPOAE fine structure due to changes in the relative contribution of the two DPOAE sources. This shift can lead to observations of "pseudo" enhancement of up to 20 dB for isolated frequencies.

Contributed Paper

12:00

5aPPb9. Otoacoustic emission latency and cochlear mechanics. Arturo Moleti (University of Roma Tor Vergata - Physics Department, Via della Ricerca Scientifica, 1, 00133 Roma, Italy, moleti@roma2.infn.it), Renata Sisto (ISPESL - Occupational Hygiene Department, Via di Fontana Candida, 1, 00040 Monte Porzio Catone (RM), Italy, renata.sisto@ispesl.it)

Otoacoustic emission (OAE) latency data provide important information about several aspects of cochlear mechanics. Time-frequency analysis techniques, euther based on the wavelet transform or on Matching Pursuit algorithms, permit to get accurate estimates of the latency of transient evoked OAEs (TEOAEs). Wavelet estimates of the TEOAE latency of 14 young subjects, recorded at different stimulus levels from 60 to 90 dB pSPL, are used here to test several predictions of transmission line cochlear models. The experimental relation between latency, frequency, and stimulus level, is used to get estimates of cochlear tuning at different stimulus levels, which can be compared with behavioral and other OAE-based estimates.

These estimates can be used to get information about the functional form of the cochlear amplifier nonlinearity. The comparison between the TEOAE latency and the auditory brainstem response (ABR) latency may help discriminating between different models for the OAE backward propagation. Wavelet latency and phase-gradient delay may be estimated on the same TEOAE waveforms. The comparison between these two characteristic times permits, in principle, to identify the place-fixed or wave-fixed nature of the TEOAE generation mechanisms.

FRIDAY MORNING, 4 JULY 2008 P2-C, LEVEL 2, 9:40 TO 11:20 A.M.

Session 5aPPc

Psychological and Physiological Acoustics: Otoacoustic Emissions, from Cochlear Modeling to Experimental Techniques, and Back II (Poster Session)

Christopher Shera, Cochair
Eaton-Peabody Laboratory

Arturo Moleti, Cochair
University of Roma Tor Vergata - Physics Department

All posters will be on display from 9:40 a.m. to 11:20 a.m. To allow contributors an opportunity to see other posters, contributors of odd-numbered papers will be at their posters from 9:40 a.m. to 10:30 a.m. and contributors of even-numbered papers will be at their posters from 10:30 a.m. to 11:20 a.m.

Contributed Papers

5aPPc1. Hemispheric Laterality and Peripheral Auditory Asymmetry studied by Transiently Evoked Otoacoustic Emissions. Annie M. Moulin (Neurosciences Sensorielles Comportement Cognition UMR5020 CNRS, Université de Lyon, 50, avenue Tony Garnier, 69366 Lyon Cedex 07, France, amoulin@olfac.univ-lyon1.fr), Jean-Bertrand Nottet (Hôpital du service de santé des Armées Desgenettes, Boulevard Pinel, 69000 Lyon, France, jean-bertrand.nottet@wanadoo.fr)

A peripheral left-right assymetry has been shown at the cochlear level: Transiently evoked otoacoustic emissions (TEOAEs) amplitudes are greater in the right ear than in the left ear of right-handed subjects, whereas no difference is obtained in left-handed subjects (Khalfa et al., 1998). This study sought to investigate a possible link between peripheral auditory assymetry and hemispheric laterality assessed by a dichotic listening task. Peripheral auditory laterality was investigated by comparing TEOAEs from both ears of each subject in 289 normally hearing subjects, with 94 left-handed subjects (52 women), and 194 right-handed subjects (129 women). Results show significantly greater OAE amplitude in right ear than in left ears for both right-handers (12.93 dB, SD=4.46 versus 11.89, SD=4.6) and left-handers (11.62 SD=3.8 versus 10.44, SD=3.8, whereas average hearing loss across frequencies did not show any significant difference. However, in the left-handers, only the subgroups of subjects presenting a right-ear advantage at the dichotic tasks, presented a significantly greater TEOAE amplitude in the right ear versus the left ear. Those results suggest a definite link between peripheral auditory assymetry and hemispheric laterality.

5aPPc2. Temporal suppression and augmentation of click-evoked otoacoustic emissions. Sarah Verhulst (Centre for applied hearing research, Technical University of Denmark, DTU, Bygn. 352, 2800 Lyngby, Denmark, sv@oersted.dtu.dk), James M. Harte (Centre for applied hearing research, Technical University of Denmark, DTU, Bygn. 352, 2800 Lyngby, Denmark, jha@oersted.dtu.dk), Torsten Dau (Centre for applied hearing research, Technical University of Denmark, DTU, Bygn. 352, 2800 Lyngby, Denmark, tda@oersted.dtu.dk)

This study investigates and models temporal suppression of click-evoked otoacoustic emissions (CEOAEs). This suppression-effect is created when a suppressor-click is presented close in time to a test-click. The analysis was carried out for short time-frames of short- and long-latency CEOAEs. The latter is defined as a CEOAE with duration greater than 20 ms, typically observed for test subjects with spontaneous otoacoustic emissions (SOAEs). Previous studies have tended to exclude these test subjects but they are incorporated here. The results from six exemplary subjects demonstrate that temporal suppression is present in all CEOAEs for inter-click intervals (ICIs) less than 8 ms. The long-latency CEOAEs showed augmentation (i.e., negative suppression) for ICIs of 6-7 ms which was not reported for the short-latency CEOAE at these ICIs. A phenomenological approach is adopted here to explain both temporal suppression and augmentation of CEOAEs. Recently, a feedback automatic gain control (AGC) system has been used to model CEOAE suppression. However, this system cannot account for augmentation and therefore another, dynamic nonlinear model was developed. Suppression and augmentation were modeled phenomenologically using compression or expansion of the system output. This was obtained by shifting the operating-point on the input/output-characteristic in relation to the ICI.

5aPPc3. A psychophysical test of the Kummer primary-level rule for measuring distortion-product otoacoustic emission input/output functions. Enrique A. Lopez-Poveda (University of Salamanca, Instituto de Neurociencias de Castilla y León, Avda. Alfonso X 'El Sabio' s/n, 37007 Salamanca, Spain, ealopezpoveda@usal.es), Peter T. Johannesen (University of Salamanca, Instituto de Neurociencias de Castilla y León, Avda. Alfonso X 'El Sabio' s/n, 37007 Salamanca, Spain, peter@usal.es)

The standard procedure for measuring distortion-product otoacoustic emission (DPOAEs) input/output (I/O) curves involves using primaries whose levels conform to the rule of Kummer [Kummer et al., J. Acoust. Soc. Am. **103**, 3431-44 (1998)]. The assumption is that the DP originates at the F2 cochlear site and primaries that conform to this rule produce equal excitation at that site, which maximizes the DP amplitude. These ideas were tested psychophysically by measuring temporal masking curves (TMCs) for masker frequencies equal to the primary frequencies. A TMC-based level rule was obtained by plotting the levels of the F1 masker against those for the F2 one for corresponding masker-probe intervals. DPOAE I/O curves were then measured using the Kummer rule, the TMC-based rule, and pri-

mary levels optimized individually to maximize DP amplitude. DPOAEs for the TMC-based and the Kummer rule had statistically similar amplitudes, but they were both lower than those measured with individually-optimized levels. This undermines the assumption that maximum DP responses occur for primaries that produce equal excitation at the F2 cochlear site. Individually-optimized levels showed that L1 should be higher than prescribed by the Kummer rule. [Work supported by IMSERSO-131/06, PROFIT-CIT-390000-2005-4, and MEC-BFU-2006-07536, and The Oticon Foundation.]

5aPPc4. Cochlear nonlinearity in normal-hearing subjects as inferred psychophysically and from distortion-product otoacoustic emissions. Peter T. Johannesen (University of Salamanca, Instituto de Neurociencias de Castilla y León, Avda. Alfonso X 'El Sabio' s/n, 37007 Salamanca, Spain, peter@usal.es), Enrique A. Lopez-Poveda (University of Salamanca, Instituto de Neurociencias de Castilla y León, Avda. Alfonso X 'El Sabio' s/n, 37007 Salamanca, Spain, ealopezpoveda@usal.es)

The aim was to investigate the correlation between estimates of compression ratio, compression threshold, and cochlear gain for normal-hearing subjects inferred from temporal masking curves (TMC) and distortion-product otoacoustic emission (DPOAEs) input-output (I/O) curves. Special care was given to reduce the influence of DPOAE fine structure on the I/O curves. Data were collected for 10 subjects and for cochlear places with characteristic frequencies (CFs) of 0.5, 1, 2, and 4 kHz. Except at 4 kHz, little correlation was found between ratio estimates obtained with the two methods. One reason is that the DPOAE I/O curves show plateaus or dips which result in unexpectedly high compression estimates. Moderately high correlation was found between the compression-threshold estimates obtained with the two methods, although DPOAE-based values were systematically lower than those based on the TMCs. Both methods confirmed that compression ratio and threshold are approximately constant across the CF range considered. Cochlear gain could be estimated from TMCs only and it was found to increase slightly with increasing CF. It is discussed that DPOAE I/O curves may be inappropriate to infer precise individual nonlinear cochlear characteristics in normal-hearing listeners, particularly at low CFs [Work supported by IMSERSO 131/06, PROFIT CIT-390000-2005-4, MEC BFU-2006-07536, and The Oticon Foundation.]

5aPPc5. Recovery of distortion product otoacoustic emissions (DPOAE) with high time-resolution from a moderate monaural-exposure to 2-kHz in human subjects. Miguel Angel Aranda De Toro (Acoustics, Aalborg University, Fredrik Bajers Vej 7 B5, 9220 Aalborg Ø, Denmark, maat@es.aau.dk), Rodrigo Ordoñez (Acoustics, Aalborg University, Fredrik Bajers Vej 7 B5, 9220 Aalborg Ø, Denmark, rop@es.aau.dk), Karen Reuter (Acoustics, Aalborg University, Fredrik Bajers Vej 7 B5, 9220 Aalborg Ø, Denmark, kr@es.aau.dk), Dorte Hammershøi (Acoustics, Aalborg University, Fredrik Bajers Vej 7 B5, 9220 Aalborg Ø, Denmark, dh@es.aau.dk)

The amplitude of distortion product otoacoustic emissions (DPOAE) decreases temporarily after exposure to a sound of moderate level. These changes show similarities to the changes observed in absolute hearing thresholds after similar sound exposures. This paper presents the experimental protocol to study how DPOAEs in human subjects are affected after a monaural exposure of ten minutes to a pure tone of 2 kHz. The experimental protocol allows to measure fine structures of the DPOAE with high time-resolution in a limited frequency range. Thus, the results give a detailed description of the DPOAE recovery process and can be used to develop a mathematical model of the recovery. This is the first approximation to study the recovery of more complex exposures. [Work supported by the Danish Research Council for Technology and Production.]

5aPPc6. Analysis of time-frequency fine structure of transiently evoked otoacoustic emissions to study the effects of exposure to GSM radiofrequency fields. Alessia Paglialonga (Institute of Biomedical Engineering CNR - Polytechnic Univ. Milan, Piazza Leonardo da Vinci, 32, I-20133 Milan, Italy, alessia.paglialonga@polimi.it), Gabriella Tognola (Institute of Biomedical Engineering CNR - Polytechnic Univ. Milan, Piazza Leonardo da Vinci, 32, I-20133 Milan, Italy, gabriella.tognola@polimi.it), Marta Parazzini (Institute of Biomedical Engineering CNR - Polytechnic Univ. Milan, Piazza Leonardo da Vinci, 32, I-20133 Milan, Italy, marta.parazzini@polimi.it), Federica Sibella (Institute of Biomedical Engineering CNR - Polytechnic Univ. Milan, Piazza Leonardo da Vinci, 32, I-20133 Milan, Italy, federica.sibella@polimi.it), Steven L. Bell (University of Southampton, University Road, Highfield/ISVR, SO17 iBJ Southampton, UK, alessia.paglialonga@polimi.it), Mark E. Lutman (University of Southampton, University Road, Highfield / ISVR, SO17 iBJ Southampton, UK, mel@isvr.soton.ac.uk), Gyorgy Thuroczy (National Research Institute for Radiobiology and Radiohygiene NIRR, Department of Non-Ionizing Radiation, Anna u. 5, 1775 Budapest, Hungary, alessia.paglialonga@polimi.it), Paolo Ravazzani (Institute of Biomedical Engineering CNR - Polytechnic Univ. Milan, Piazza Leonardo da Vinci, 32, I-20133 Milan, Italy, paolo.ravazzani@polimi.it)

Mobile phones have become very commonly used throughout the world within a short period of time. To date there is only limited knowledge about interaction between electromagnetic fields (EMFs) emitted by mobile phones and the auditory function. Moreover, there is widespread concern that there may be potential for harm. The aim of this study, performed in the framework of the European Commission Project GUARD "Potential adverse effects of GSM cellular phones on hearing" (5FP, QLK4-CT-2001-00150, 2002-2004), was to assess potential subtle changes in cochlear function of normal hearing subjects by measuring the time-frequency fine structure of TEOAEs after exposure to low-intensity EMFs emitted by GSM mobile phones. TEOAEs were recorded in 27 healthy young adults before and after 10 min of real or sham exposure in a double-blind design. TEOAE data were analyzed both globally (broadband analysis) and using the wavelet transform (analysis of time-frequency fine structure). The broadband analysis revealed no significant effect on TEOAEs related to exposure, confirming results of previous studies; in addition, no significant change was detected in the analysis of the elementary wavelet components, suggesting that a 10-min exposure to EMFs emitted by GSM mobile phones has no immediate after-effect on TEOAE time-frequency fine structure.

5aPPc7. Simulating electrically evoked emissions in the cochlea. Julien Meaud (University of Michigan, 2250 G G Brown Bldg, 2350 Hayward St., Ann Arbor, MI 48109, USA, jmeaud@umich.edu), Karl Grosh (University of Michigan, 2250 G G Brown Bldg, 2350 Hayward St., Ann Arbor, MI 48109, USA, grosh@umich.edu)

Electrical stimulation of the cochlea is a means for investigating the electromechanics of the organ. In this study, we use a mechanical-electrical-acoustic cochlear model to make predictions of the effect of intracochlear bipolar electrical stimulation on the basilar membrane velocity and stapes velocity. Bipolar stimulation provides for a localized means of stimulating the outer hair cells (OHC) and is a well-established technique for evoking otoacoustic emissions. We show that both fast, fluid-borne, and slow, fluid-structure waves are possible. Whether the fast or slow waves dominate the overall response depends on the level of activity in the cochlea, the frequency and location of excitation, and the boundary conditions at the stapes and round window. We show that forward propagating traveling waves may dominate the basilar membrane response even with intracochlear stimulation apical to the measurement site. These results bear direct impact on the interpretation of noninvasive measurements using otoacoustic emissions.

5aPPc8. Otoacoustic emissions in sheep (Ovis aries): Sex differences and prenatal androgen effects. Dennis McFadden (University of Texas, Psychology Dept, SEA 4.110, Austin, TX 78712-0187, USA, mcfadden@psy.utexas.edu), Edward Pasanen (University of Texas, Psychology Dept, SEA 4.110, Austin, TX 78712-0187, USA, pasanen

@psy.utexas.edu),Michelle D. Valero(University of Texas, Department of Biology, San Antonio, TX 78249, USA, bonfire_2002@hotmail.com), Eila K. Roberts (University of Michigan, Department of Psychology and Reproductive Sciences Program, Ann Arbor, MI 48109, USA, ekrobert@umich.edu), Theresa M. Lee (University of Michigan, Department of Psychology and Reproductive Sciences Program, Ann Arbor, MI 48109, USA, terrilee@umich.edu)

Otoacoustic emissions (OAEs) were measured in Suffolk sheep (*Ovis aries*), the first ruminant species tested for OAEs to our knowledge. Some sheep had been administered testosterone or estradiol during prenatal development, some had been gonadectomized after birth, and some had been allowed to develop normally. The click-evoked otoacoustic emissions (CEOAEs) exhibited by the female control group (N=11) were stronger than those in the male control group (N=15), which is the same direction of effect reported for other mammals, including humans. The females administered testosterone prenatally (N=13) had substantially weaker (masculinized) CEOAEs than control females. Both outcomes suggest that prenatal exposure to androgens weakens the cochlear amplifiers. The CEOAEs of males administered testosterone prenatally (N=5) were not different from those of control males, which is contrary to expectation, but in accord with data from similarly treated rhesus monkeys. Seven males (of 24) and seven females (of 34) had no measurable DPOAEs at any frequency or level of primary tones tested, even though all did have normal-appearing CEOAEs. No spontaneous otoacoustic emissions (SOAEs) were found in any ears, a common finding in non-human species. [Supported by NIDCD (DM) and NICHD (TML).]

5aPPc9. Potential adverse effects of UMTS electromagnetic fields generated by mobile phones on the human inner ear: A European project (EMFNEAR). Annie M. Moulin (Neurosciences Sensorielles Comportement Cognition UMR5020 CNRS, Université de Lyon, 50, avenue Tony Garnier, 69366 Lyon Cedex 07, France, amoulin@olfac.univ-lyon1.fr), Marta Parazzini (Institute of Biomedical Engineering CNR - Polytechnic Univ. Milan, Piazza Leonardo da Vinci, 32, I-20133 Milan, Italy, marta.parazzini@polimi.it),Mark E. Lutman(University of Southampton, University Road, Highfield/ISVR, SO17 iBJ Southampton, UK, mel@isvr.soton.ac.uk), Gyorgy Thuroczy (National Research Institute for Radiobiology and Radiohygiene NIRR, Department of Non-Ionizing Radiation, Anna u. 5, 1775 Budapest, Hungary, alessia.paglialonga@polimi.it), Mariola Sliwinska-Kowalska (Nofer Institute of Occupational Medicine, PL-90-950 Lodz, Poland, marsliw@imp.lodz.pl), Georgy Tavarkiladze (National Research Centre for Audiology and Hearing Rehabilitation, 117513 Moscow, Russian Federation, gtavartkiladze@audiology.ru), Ingrida Uloziene (Kaunas University of Medicine, LT44307 Kaunas, Lithuania, uloziene@kmu.lt), Virgilius Uloza (Kaunas University of Medicine, LT44307 Kaunas, Lithuania, uloza@kmu.lt), Shrikanta Mishra (University of Southampton, University Road, Highfield / ISVR, SO17 iBJ Southampton, UK, sm2@isvr.soton.ac.uk), Lionel Collet (Univ. Lyon 1 - Lab. Neurosciences, Service Pr Collet, Pavillon U, Hôpital Edouard Herriot, F-69003 Lyon, France, iakhoun@olfac.univ-lyon1.fr), Paolo Ravazzani (Institute of Biomedical Engineering CNR - Polytechnic Univ. Milan, Piazza Leonardo da Vinci, 32, I-20133 Milan, Italy, paolo.ravazzani@polimi.it)

To answer concerns as to the potential effects of electromagnetic fields (EMF) generated by third generation mobile phones on the inner ear, the European Commission funded project ″EMFNEAR″ assessed potential changes in auditory function induced by UMTS field both in humans and in laboratory animals. The purpose of this paper is to present the final outcomes of the project in humans. Normally hearing subjects (18-30 years old) were exposed to 20 min UMTS or sham exposure in a double-blind controlled study. Two different EMF field strengths were used: SAR of 0.069 W/kg using a commercially available phone and SAR of 1.75 W/kg using a patch antenna. Audiological assessment, involving pure tone audiometry, distortion product otoacoustic emissions, effects of contralateral acoustic stimulation on Transiently evoked otoacoustic emissions and late cognitive potentials (P300), were performed before and immediately after real or sham exposures. Results showed no effects of acute UMTS electromagnetic fields exposure on the inner auditory system of humans.

Session 5aPPd

Psychological and Physiological Acoustics: General Topics in Psychological and Physiological Acoustics VII (Poster Session)

Elizabeth Strickland, Cochair
Purdue University

Armin Kohlrausch, Cochair
Philips Research Europe

Alain De Cheveigne, Cochair
CNRS, Universite Paris 5, Ecole Normale Superieure

All posters will be on display from 9:40 a.m. to 11:20 a.m. To allow contributors an opportunity to see other posters, contributors of odd-numbered papers will be at their posters from 9:40 a.m. to 10:30 a.m. and contributors of even-numbered papers will be at their posters from 10:30 a.m. to 11:20 a.m.

Contributed Papers

5aPPd1. Phase interactions between auditory filter and complex stimuli: psychophysical evidence for level dependence in cochlear phase response. Yi Shen (Indiana Univ., 200 S. Jordan Ave., Dept. of Speech and Hearing Sciences, Bloomington, IN 47405-7000, USA, shen2@indiana.edu), Jennifer Lentz (Indiana Univ., 200 S. Jordan Ave., Dept. of Speech and Hearing Sciences, Bloomington, IN 47405-7000, USA, jjlentz@indiana.edu)

Harmonic complexes with the same power spectrum and different phase spectra lead to significant differences in their efficiency in masking pure-tone signals. This process is presumably due to phase interactions between the masker and the cochlea, leading to internally represented waveforms with different amounts of modulation. The present study applied this idea to estimate the phase characteristic of the auditory system at different stimulus levels. Two masking experiments were conducted for estimating whether auditory-filter phase curvatures are level dependent at 2 and 4 kHz. Curvatures were measured at fixed masker levels ranging between 50 and 90 dB SPL in one experiment and at fixed signal levels (25 - 50 dB SPL) in a second experiment. Results from both experiments suggest a level dependence in the auditory-filter phase curvature at both frequencies, which shifts from a negative value towards zero with increasing excitation level. A plausible explanation for this observed level dependence was proposed with the use of a nonlinear cochlear model. This modeling approach indicated that the behaviorally measurable phase curvature is affected by level dependent alterations in the magnitude and phase response of the basilar membrane.

5aPPd2. Is auditory intensity discrimination a comparison of entropy changes? Iftikhar Nizami (1312 Grayson Place, Decatur, GA 30030, USA, nizamii2@aol.com)

In JASA (**97**, 1995), Wong & Norwich presented a Weber-fraction equation derived from McConville, Norwich, & Abel (Int J Biomed Comput **27**, 1991). The latter modeled two-alternative forced-choice discrimination between stimuli of identical spectra and identical durations "t" but differing intensities I and $I+\Delta I$. Discrimination depended on $\Delta H(I,t)$, the change in the information-theoretic entropy over t and ΔI. $\Delta H(I,t)$, assumed constant over intensities, emerged as one of five unknowns in a Weber-fraction equation, $(\Delta I)/I=f(t_0,t_W,n,\beta,\Delta H(I,t))$. McConville et al. *presumed* values for n and t_W. Using $(\Delta I)/I\approx\Delta H(I,t)/(I\Delta t[\partial^2 H/\partial I\partial t])$ and setting $\Delta t=t$, $f(t_0,t_W,n,\beta,\Delta H(I,t))$ was *approximated* as $g(n,(\beta/t),\Delta H(I,t))=\Delta H(I,t)/(It[\partial^2 H/\partial I\partial t])$, which was then curvefitted to one listener's Weber fractions. The obtained $\Delta H(I,t)$ alone was substituted back into $f(t_0,t_W,n,\beta,\Delta H(I,t))$, which was then substantiated by curvefitting to the data to reveal the remaining unknowns, t_0 and β. McConville et al. *had* to curvefit, because they model only a *single*, unspecified forced-choice trial, making ΔI *any* intensity change; and *none* of the unknowns could legitimately be presumed. The curvefitting was flawed: the assumption $\Delta H(I,t)=$constant affirms Fechner's postulate; and $\partial^2 H/\partial I\partial t<0$, giving a *negative* Weber fraction. McConville et al. fail to explain auditory intensity discrimination as a comparison of entropy changes, casting doubt on Wong & Norwich (1995).

5aPPd3. Does Norwich's Entropy Theory of Perception avoid the use of mechanisms, as required of an information-theoretic model of auditory primary-afferent firing? Iftikhar Nizami (1312 Grayson Place, Decatur, GA 30030, USA, nizamii2@aol.com)

Norwich et al.'s Entropy Theory (1975-present) stipulates that (1) the auditory receptor is uncertain about the stimulus' intensity, (2) uncertainty, given by the "entropy" H, relates to primary afferent neuronal firing-rate F as $F=\text{constant}\times H$. H was calculated according to Garner & Hake (Psychological Review **58**, 1951; after Shannon, Bell System Technical Journal **27**, 1948) using Information Theory. H is available *any time* events, their outcomes, and the appropriate probabilities of occurrence are known, precisely because Information Theory ignores *mechanisms*, such as sensory transduction. Hence, any "information-theoretic" hearing model must avoid physiological mechanisms, and Norwich et al. claim to comply. But do they? The Entropy Theory was scrutinized for avoidance of physiological mechanisms. Norwich et al. stipulated throughout that (1) "We can envisage a steady sensory stimulus as a stationary stochastic sequence of microscopic sensory events" (Norwich & Wong, Annales de la Fondation Louis de Broglie **22**, 1997), (2) those events (representing different intensities) are repeatedly *sampled* by the receptor. Sampling *is* a mechanism, not separable from transduction, the event's (presumed) "outcome". Also, Norwich et al.'s attempts to separate events from outcomes produces inconsistent identification of "events." The Entropy Theory is not an information-theoretic model of primary-afferent firing.

5aPPd4. Slopes of psychometric functions for forward-masked tones with and without a suppressor. Ifat Yasin (UCL Ear Institute, 332 Gray's Inn Road, WC1X 8EE London, UK, i.yasin@ucl.ac.uk), Christopher J. Plack (Psychology Department, Lancaster University, LA1 4YF Lancaster, UK, c.plack@lancaster.ac.uk)

The compressive nonlinearity defined by the basilar membrane (BM) input-output (I/O) function is evident in the slopes of psychometric

functions for forward-masked tones. A suppressor tone may reduce compression by linearizing the compressive portion of the BM I/O function, or reduce cochlear gain without affecting the value of maximum compression. The present study compared slopes of psychometric functions obtained for a fixed low-level signal in the presence of a variable masker with or without a suppressor gated with the masker. Thresholds and psychometric functions were obtained for four normal-hearing listeners using a 2I-AFC task. The sinusoidal signal was a low-level 4-kHz tone (0-ms steady state, 2-ms $\cos^2$ ramps) masked by a sinusoidal masker (100-ms steady state, 2-ms $\cos^2$ ramps). The maskers were either on frequency (4 kHz) or off frequency (2.2 kHz) and were presented at masker-signal intervals of 20-100 ms. Initial analyses suggest that as masker levels increase, the slopes of psychometric functions become increasingly shallow (on-frequency masker) or remain relatively steep (off-frequency masker). The effect of a suppressor on the slopes of the psychometric functions appears to be minimal. Results will be discussed in the context of a cochlear model of peripheral nonlinearity.

5aPPd5. An effect of top-down processing on intensity discrimination in the sensory-trace mode. Ervin R. Hafter (University of California, Department of Psychology, 3210 Tolman Hall, Berkeley, CA, CA 94720-1650, USA, hafter@berkeley.edu), Anne-Marie Bonnel (University of California, Department of Psychology, 3210 Tolman Hall, Berkeley, CA, CA 94720-1650, USA, AMBonnel@berkeley.edu), Swapan Gandhi (University of California, Department of Psychology, 3210 Tolman Hall, Berkeley, CA, CA 94720-1650, USA, swapangandhi@berkeley.edu)

A traditional measure of intensity discrimination presents a standard stimulus followed by a test. In one perceptual strategy, the subject compares the test to a coded version of the standard in long-term "context-coded memory" while, in another, the comparison is to a copy of the standard held in short-term "trace memory" [Durlach and Braida, J. Acoust. Soc. Amer, **46**, 372-383 (1969)]. Subjects can be induced to use trace memory by roving the level of the standard randomly from trial to trial. It is well known that roving lowers overall performance, but by parsing individual standards we find that the loss is not uniform. Rather, an inverse correlation with the roved levels shows a severe departure from Weber's Law, with slopes of about -6 dB over 20 dB of roving. This can be modeled in terms of an additive noise that, unlike the multiplicative noise implied by Weber's Law, is constant across levels. We believe this represents top-down processes involved in the use of stimuli held in rehearsal memory.

5aPPd6. Contribution of very low modulation frequencies to speech intelligibility in a competing speech task. Christian Füllgrabe (University of Cambridge, Department of Experimental Psychology, Downing Street, CB2 3EB Cambridge, UK, cf277@cam.ac.uk), Michael A. Stone (University of Cambridge, Department of Experimental Psychology, Downing Street, CB2 3EB Cambridge, UK, mas19@cam.ac.uk), Brian Moore (University of Cambridge, Department of Experimental Psychology, Downing Street, CB2 3EB Cambridge, UK, bcjm@cam.ac.uk)

Vocoder studies have demonstrated that low-rate temporal-envelope cues (below $\sim$ 50 Hz) in a few frequency bands are sufficient for good speech identification in quiet. From the effects of low pass and high pass filtering of the temporal envelopes extracted from band pass filtered sentences, Drullman et al. [J. Acoust. Soc. Am. **95**, 2670-2680 (1994); J. Acoust. Soc. Am. **95**, 1053-1064 (1994)] argued that modulation frequencies between 4 and 16 Hz are the most important for speech identification in a steady background noise. However, Stone and Moore (JASA, in press) found that modulation frequencies below 2 Hz were also beneficial when the speech signal was processed through an 8-channel (but not a 12-channel) noise vocoder. The present study investigated speech identification for nine normal-hearing listeners using IEEE sentences presented with a competing talker; the mixed signal was processed using a 6-, 9-, or 15-channel noise vocoder. Low-rate temporal-envelope cues were manipulated using a compressor for each channel. Compression speed varied from slow to fast, so as to progressively degrade modulation frequencies below 4 Hz. Independent of the spectral resolution of the vocoder, mean intelligibility decreased as the compression speed increased; even modulation frequencies below 1.3 Hz contributed significantly to speech intelligibility.

5aPPd7. Comodulation masking release and its representation in human auditory cortex. Stephan M. Ernst (Universität Oldenburg, Medizinische Physik, Carl-von-Ossietzky Str. 9-11, 26111 Oldenburg, Germany, stephan.ernst@uni-oldenburg.de), Jesko Verhey (Universität Oldenburg, Medizinische Physik, Carl-von-Ossietzky Str. 9-11, 26111 Oldenburg, Germany, jesko.verhey@uni-oldenburg.de), Stefan Uppenkamp (Universität Oldenburg, Medizinische Physik, Carl-von-Ossietzky Str. 9-11, 26111 Oldenburg, Germany, stefan.uppenkamp@uni-oldenburg.de)

The aim of the present study was to find a correlate of the psychoacoustical effect of comodulation masking release (CMR) in human auditory cortex using functional magnetic resonance imaging (fMRI). The target stimulus was a sinusoidal signal embedded in a band limited white noise which was either unmodulated or multiplied with an irregular square-wave modulator with mean modulation frequency of 40 Hz (comodulated condition). For all listeners participating in the fMRI study, the average psychoacoustic threshold difference between the unmodulated and the comodulated condition (i.e., the CMR) was 20 dB. Similar to the results from a previous fMRI study on pure-tone masking (Ernst, Verhey, Uppenkamp, ARO abstracts 30 (2007), p. 302(A)), a spatial dissociation of changes of overall level and signal-to-noise ratio in auditory cortex was found. The comparison of the fMRI activation maps for a signal presented in modulated and in unmodulated noise reveals that those regions in the antero-lateral part of Heschl's gyrus previously shown to represent the audibility of a target (rather than overall level) exhibit a stronger activation for the modulated than for the unmodulated conditions. This result is interpreted as a physiological correlate of the psychoacoustical CMR effect at the level of the auditory cortex.

5aPPd8. Behavioral evidence for off-frequency compression at 4 kHz. Dhany Arifianto (University of Zagreb, Psychology Department, Lancaster University, LA1 4YF Lancaster, UK, arifianto@ieee.org), Christopher J. Plack (Psychology Department, Lancaster University, LA1 4YF Lancaster, UK, c.plack@lancaster.ac.uk)

Most behavioral techniques for estimating the basilar-membrane response rely on the assumption that the response to an off-frequency masker is linear at the signal place. To test this assumption, we modified the additivity of forward masking technique. The signal was a 4-kHz, 10-ms pure tone, presented at 10 dB sensation level. The maskers were 500-Hz-wide bands of noise centered on 1.5, 2, or 4 kHz. Masker 1 had a duration of 200 ms and was followed immediately by masker 2 with a duration of 20 ms. The masker 2-signal silent interval ranged from 10 to 60 ms. For each interval, the masker level required to mask the signal was determined, for each masker presented individually, and for the two maskers combined. In the combined case, the levels of the two maskers were set to be roughly equally effective, and adaptively varied together. Combining two equally effective maskers should produce a 3-dB reduction in masker level at threshold if the system is linear. A reduction greater than this indicates compression. Although compression was greatest for the 4-kHz maskers, compression was also observed at 1.5 and 2 kHz, suggesting that the assumption of a linear off-frequency response may not valid.

5aPPd9. Multiple looks in spectrotemporal integration. Evelyn Hoglund (The Ohio State University, 110 Pressey Hall, 1070 Carmack Road, Columbus, OH 43210, USA, hoglund.1@osu.edu), Lawrence Feth (The Ohio State University, 110 Pressey Hall, 1070 Carmack Road, Columbus, OH 43210, USA, feth.1@osu.edu)

The multiple looks hypothesis was originally developed as an explanation for temporal integration and resolution. Our preliminary work supports its extension to spectral integration as well spectrotemporal integration. The current study was designed to measure detection of tonal signals that vary in both spectral and temporal dimensions. Preliminary work began by measuring thresholds in quiet. Elementary signals consisted of 10 ms tone bursts centered on one of eight frequencies spaced 1 ERB apart. Complexes were constructed by adding two to eight individual tone bursts along the temporal or spectral dimension, or both. The signals varied along both dimensions in several ways to focus on the relative salience of each dimension for

detection. In quiet, the spectrotemporal integration conditions showed threshold improvement to be limited by spectral integration. Surprisingly, even trial-by-trial randomization of frequencies did not negatively influence detection. For this study, the same tone complexes from the preliminary work were used to measure thresholds in a wide band energetic masker. As expected, threshold improvement was most dependent on increasing the number of tones, with less effect from other variables. Subtle differences between quiet and masked integration performance will be discussed. Research supported by a grant from NIH/NIDCD R01-DC006879.

5aPPd10. Estimating the basilar-membrane input/output-function in normal-hearing and hearing-impaired listeners using forward masking. Morten L. Jepsen (Centre for Applied Hearing Research, Technical University of Denmark, DTU, Bygn. 352, 2800 Lyngby, Denmark, mlj@oersted.dtu.dk), Torsten Dau (Centre for Applied Hearing Research, Technical University of Denmark, DTU, Bygn. 352, 2800 Lyngby, Denmark, tda@oersted.dtu.dk)

To partly characterize the function of cochlear processing in humans, the basilar membrane (BM) input-output (I/O) function can be estimated. In recent studies, forward masking has been used to estimate BM compression. If an on-frequency masker is processed compressively, while an off-frequency masker is transformed more linearly, the ratio between the slopes of growth of masking (GOM) functions provides an estimate of BM compression at the signal frequency. In this study, this paradigm is extended to also estimate the knee-point of the I/O-function between linear processing at low levels and compressive processing at medium levels. If a signal can be masked by a low-level on-frequency masker such that signal and masker fall in the linear region of the I/O-function, then a steeper GOM function is expected. The knee-point can then be estimated in the input level region where the GOM changes significantly. Data were collected from eight normal-hearing (NH) and five hearing-impaired (HI) listeners with mild to moderate sensorineural hearing loss. Both groups showed large inter-subject but low intra-subject variability. When the knee-point could be estimated for the HI listeners it was shifted towards higher input levels and compression was similar to that of NH listeners.

5aPPd11. Unpredictable interruption can enhance the auditory continuity illusion. Maori Kobayashi (R.I.E.C., Tohoku University, 2-1, Katahira, Aoba-ku, 980-8577 Sendai, Japan, maori@ais.riec.tohoku.ac.jp), Makio Kashino (NTT Communication Science Laboratories, NTT Corporation, 3-1, Morinosato Wakamiya, 243-0198 Atsugi, Japan, kashino@avg.brl.ntt.co.jp)

It was examined whether the predictability of interruption timing affects the limit of perceiving the continuity illusion. The stimulus consisted of a 500-Hz sinusoidal inducee and a 200-ms, 500-Hz, 1/3-octave noise band inducer, which were alternated repeatedly, with a fixed interval (400 ms) between adjacent inducers (regular condition) or with random intervals (irregular condition). The continuity limit (CL) was measured in terms of the maximum level of the inducee for the illusory continuity to be perceived while maintaining the inducer level at 60 dB SPL. In Experiment 1, the listeners' task was to judge whether the inducee appeared continuous or discontinuous. In Experiment 2, the task was to discriminate illusory and physical continuity in a two-interval forced choice paradigm. In both experiments, the mean CLs in the irregular condition were significantly higher than those in the regular condition. In Experiment 3, when an identical irregular interval pattern was used repeatedly in successive trials, the mean CL gradually declined, and reached the level of the regular condition in approximately 80 trials. These results suggest that unpredictability, not mere irregularity, in interruption timing promotes the continuity illusion, implying the involvement of the short-term plasticity of the auditory system.

5aPPd12. A filterbank model of human nonlinear auditory frequency selectivity. Almudena Eustaquio-Martín (University of Salamanca, Instituto de Neurociencias de Castilla y León, Avda. Alfonso X 'El Sabio' s/n, 37007 Salamanca, Spain, aeustaquio@usal.es), Enrique A. Lopez-Poveda(University of Salamanca, Instituto de Neurociencias de Castilla y León, Avda. Alfonso X 'El Sabio' s/n, 37007 Salamanca, Spain, ealopezpoveda@usal.es)

Filterbank models of human nonlinear auditory frequency selectivity are useful in a variety of applications. Existing filterbanks are almost certainly flawed because they do not account for the recent observation that compression extends to a wider range of stimulus frequencies in apical than in basal cochlear sites [Lopez-Poveda et al. (2003), J. Acoust. Soc. Am. 113, 951-960]. Here, we present a filterbank based on the forward-masking data from which this observation was made. A forward-masking model was constructed by cascading a linear "outer/middle-ear" filter, followed by a dual-resonance nonlinear (DRNL) filter, followed by a linear temporal window. The temporal window was assumed to be identical across listeners and cochlear places. Only the parameters of the DRNL filter were adjusted to simulate the absolute threshold and the masking data of three listeners for probe frequencies of 0.5, 1, 2, 4, and 8 kHz. A bank of DRNL filters was then constructed by linear or quadratic regression of the optimum parameters. It is discussed that this filterbank is the best possible approximation of human level-dependent auditory frequency selectivity to date. Additionally, the results support the linearity of the temporal window. [Work supported by IMSERSO 131/06, PROFIT CIT-390000-2005-4, MEC BFU-2006-07536.]

5aPPd13. Object's width and distance distinguished by the blind using auditory sense while they are walking. Takahiro Miura (Graduate School of Information Science and Technology, University of Tokyo, 7-3-1 Hongo, Bunkyo-ku, 113-8654 Tokyo, Japan, miura@human.rcast.u-tokyo.ac.jp), Kazutaka Ueda (Research Center for Advanced Science and Technology, University of Tokyo, 4-6-1 Komaba, Meguro-ku, 153-8904 Tokyo, Japan, ueda@human.rcast.u-tokyo.ac.jp), Teruo Muraoka (Research Center for Advanced Science and Technology, University of Tokyo, 4-6-1 Komaba, Meguro-ku, 153-8904 Tokyo, Japan, muraoka@human.rcast.u-tokyo.ac.jp), Shuichi Ino (Research Center for Advanced Science and Technology, University of Tokyo, 4-6-1 Komaba, Meguro-ku, 153-8904 Tokyo, Japan, ino@human.rcast.u-tokyo.ac.jp), Tohru Ifukube (Research Center for Advanced Science and Technology, University of Tokyo, 4-6-1 Komaba, Meguro-ku, 153-8904 Tokyo, Japan, ifukube@human.rcast.u-tokyo.ac.jp)

Mobility aid has recently become important for the blind because of increasing their outgoing opportunity. It is necessary for the blind to acquire "obstacle sense" by which they can recognize surrounding objects auditorily. In particular, it is indispensable to investigate the characteristics of the obstacle sense while they are walking. However, training method for the mobility has not been systematically proposed yet because factors regarding the obstacle sense while walking remain unknown. Final goal of this study is to propose a systematic training method for their mobility using the obstacle sense. In this study, the authors particularly focused on a relation of interaural differences between both ears to the ability of the obstacle sense while walking toward the obstacles. In the experiments, the blind subjects were asked to answer when they find the obstacle made of wooden plate with various widths in both conditions of head moving and head fixing. Auditory discrimination ability of the obstacles was measured as a function of the obstacle's width and the distance from the blind subject. From the experimental results, it was found that blind people generally can recognize the obstacles better in the head moving case than the head fixing case.

5aPPd14. Amplitude modulation depth discrimination in hearing-impaired and normal-hearing listeners. Stephan D. Ewert (Carl von Ossietzky Universität Oldenburg, Ammerländer Heerstraße 114-118, 26111 Oldenburg, Germany, stephan.ewert@uni-oldenburg.de), Jutta Volmer (Universität Oldenburg, Medizinische Physik, Carl-von-Ossietzky Str. 9-11, 26111 Oldenburg, Germany, jutta.volmer@uni-oldenburg.de), Torsten Dau (Centre for applied hearing research, Technical University of Denmark, DTU, Bygn. 352, 2800 Lyngby, Denmark, tda@oersted.dtu.dk), Jesko Verhey (Universität Oldenburg, Medizinische Physik, Carl-von-Ossietzky Str. 9-11, 26111 Oldenburg, Germany, jesko.verhey@uni-oldenburg.de)

The processing of amplitude modulations (AM) of sounds is assumed to be crucial for decoding and understanding of speech in humans. Since hearing-impaired (HI) listeners often suffer from severely hampered speech intelligibility, particularly in reverberant or noisy environments, they might also show degraded performance in AM processing tasks. However, several

studies indicated a similar or even better performance in AM detection tasks for sensorineural HI listeners than for normal hearing (NH) listeners when reduced audibility was compensated. In addition to AM detection, this study investigates the differential processing of amplitude modulation depth in HI and NH listeners. AM-depth discrimination of a 4-, 8-, and 30-Hz sinusoidal AM, imposed on a 1- or 4-kHz pure-tone carrier, was measured. The AM of the standard ranged from being well detectable to near threshold. AM-depth discrimination thresholds strongly varied among HI listeners and were elevated in comparison to NH for high standard depths. A model of AM processing is suggested incorporating an individually adjusted simulation of the auditory periphery. To account for the data of HI listeners, however, the key element appeared to be an increased internal noise in the AM-depth domain. Consequences for speech perception are discussed.

5aPPd15. Exploring the psychophysical temporal effect in masking using a model of the auditory periphery. Skyler Jennings (Purdue University, 500 Oval Drive, West Lafayette, IN 47907, USA, sgjennin@purdue.edu), Michael Heinz (Purdue University, 500 Oval Drive, West Lafayette, IN 47907, USA, mheinz@purdue.edu), Elizabeth Strickland (Purdue University, 500 Oval Drive, West Lafayette, IN 47907, USA, estrick@purdue.edu)

Under some conditions, normal hearing individuals can detect a short duration signal in a simultaneous masker at a lower signal-to-masker ratio when there is preceding stimulation (either a precursor or an extension of the masker). This effect has been referred to as overshoot or the temporal effect. It has been hypothesized the neural adaptation may account for some but not all of the temporal effect. Recent psychophysical data suggest that cochlear gain may decrease over the course of the masker and improve detection. This could be mediated by the medial olivocochlear reflex (MOCR). In the present study, a model of peripheral auditory processing [Zilany and Bruce, J. Acoust. Soc. Am. **120**, 1446-1466 (2006)] using a d'-type metric was used to assess the relative contributions of these processes. Although the model includes neural adaptation, initial results indicate that it does not predict a temporal effect. The potential role of the MOCR will be simulated by decreasing the gain of the cochlear amplifier, to see if this will produce a temporal effect in the model predictions. [Work supported by NIH.]

5aPPd16. Intelligibility of whispered speech interleaved with speech or noise maskers. Nandini Iyer (AFRL, 2610 Seventh Street, WPAFB, OH 45433, USA, nandini.iyer@wpafb.af.mil), Douglas S. Brungart (AFRL, 2610 Seventh Street, WPAFB, OH 45433, USA, douglas.brungart @wpafb.af.mil), Brian D. Simpson (AFRL, 2610 Seventh Street, WPAFB, OH 45433, USA, Brian.Simpson@wpafb.af.mil)

When an interrupted speech signal is alternated with a noise masker, performance is generally improved relative to the condition where the speech and noise are presented continuously. However, when two interrupted speech signals are alternated, performance declines relative to the continuous presentation condition. One possible explanation for this result is that listeners in the alternated speech and noise condition use the contrast between the periodic temporal structure of voiced speech and the random temporal structure of noise to segregate the time intervals associated with the speech target and noise masker. In the current experiment, a whispered speech signal was either presented continuously in the presence of a noise masker or alternated with a noise masker at an 8-Hz rate. The results show near perfect performance in the alternated whisper and noise condition, suggesting that harmonic structure due to voicing is not necessary to segregate a speech signal from an interleaved random-noise masker. Indeed, when whispered speech was interleaved with voiced speech, performance decreased relative to the continuous condition when the target talker was voiced but not when it was whispered, suggesting that listeners are better at selectively attending to unvoiced intervals and ignoring voiced intervals than the converse.

5aPPd17. Temporal integration functions of amplitude modulation depth discrimination: can multiple-looks model explain this? Jungmee Lee (Univ. of Arizona, 1131 E. 2nd Street, Tucson, AZ 85721, USA, jmlee6@email.arizona.edu), Derek Edwards (Univ. of Arizona, 1131 E. 2nd Street, Tucson, AZ 85721, USA, derek09@email.arizona.edu), Jennifer Andrews (Univ. of Arizona, 1131 E. 2nd Street, Tucson, AZ 85721, USA, andrewsj@email.arizona.edu), Heather Murray (Univ. of Arizona, 1131 E. 2nd Street, Tucson, AZ 85721, USA, hmurray@email.arizona.edu)

Lee and Bacon (1994) applied a multiple looks model (Viemeister and Wakefield, 1990) as a mechanism of AM depth discrimination when the carrier and the modulator were presented at the same time (gated condition). The model provided a reasonable prediction, but the performance (d') was underpredicted when the number of modulation cycles changed from two to four. They speculated that onset information loss due to gating with two modulation cycles lead to a greater improvement with four modulation cycles. Following this, one would expect that AM depth discrimination can be better predicted by the multiple-looks model for the condition where there is no loss of modulation information at onset. This study compared psychometric functions of AM depth discrimination with different modulation cycles for the gated and onset-only conditions (carrier was presented for 250 ms prior to the modulation to preserve onset information). The slop of the psychometric functions with two modulation cycles was shallower than those with greater modulation cycles for the gated condition, while the slop of the psychometric functions was similar for all modulation cycles for the onset-only condition. The data will be discussed with multiple looks model. [This work was supported by NIDCD Grant No. R03 DC06605-02.]

Session 5aPPe

Psychological and Physiological Acoustics and Computational Acoustics: Computational Auralization I (Poster Session)

Durand Begault, Cochair
NASA Ames Research Center

Lauri Savioja, Cochair
Helsinki University of Technology

All posters will be on display from 9:40 a.m. to 11:20 a.m. To allow contributors an opportunity to see other posters, contributors of odd-numbered papers will be at their posters from 9:40 a.m. to 10:30 a.m. and contributors of even-numbered papers will be at their posters from 10:30 a.m. to 11:20 a.m.

Contributed Papers

5aPPe1. Effect of sound spatialisation on multitasking in remote meetings. Stuart N. Wrigley (University of Sheffield, Regent Court, Dept. of Computer Science, 211 Portobello Road, s1 4dp Sheffield, UK, s.wrigley@dcs.shef.ac.uk), Simon Tucker (University of Sheffield, Dept. of Information Studies, Regent Court, 211 Portobello Street, S1 4DP Sheffield, UK, s.tucker@dcs.shef.ac.uk), Guy J. Brown (University of Sheffield, Dept. of Computer Science, Regent Court, 211 Portobello Street, S1 4DP Sheffield, UK, g.brown@dcs.shef.ac.uk), Steve Whittaker (University of Sheffield, Dept. of Information Studies, Regent Court, 211 Portobello Street, S1 4DP Sheffield, UK, s.whittaker@shef.ac.uk)

Participants in a teleconference often multitask during meetings, e.g., they work on a text-based "foreground" task whilst listening in the 'background' for a topic of interest to appear. Audio material should therefore be presented in a manner that has the smallest possible impact on the foreground task without affecting topic detection. Here, we ask whether spatialised audio presentation of a meeting is less disruptive than the single-channel mixture of talkers that is normally used in teleconference audio. Head-related impulse responses are used to synthesise a stereo signal in which each meeting participant is placed at a spatially distinct location. A number of talker location configurations are used, and we examine how these impact upon a text-based foreground task: finding all letter "e" occurrences in a block of text as quickly as possible. We also examine the effect of listening task (e.g., "listen for keyword x" versus "listen for keyword x spoken by talker on left") and record listener preferences for audio presentation style. Our results suggest that single-channel and spatialised audio are equally disruptive when listeners are unaware of the audio presentation style. We also report studies in which presentation type and target direction-/gender are cued.

5aPPe2. The use of virtual acoustics in the evaluation and development of binaural hearing aid algorithms. Monika Rychtarikova (Lab. ATF, Katholieke Universiteit Leuven, Celestijnenlaan 200D, B-3001 Leuven, Belgium, Monika.Rychtarikova@bwk.kuleuven.be), Tim Van Den Bogaert (ExpORL, Dept. Neurosciences, K.U. Leuven, Herestraat 49 bus 721, O. & N2, B-3000 Leuven, Belgium, tim.vandenbogaert@med.kuleuven.be), Gerrit Vermeir (Lab. ATF, Katholieke Universiteit Leuven, Celestijnenlaan 200D, B-3001 Leuven, Belgium, Gerrit.Vermeir@bwk.kuleuven.be), Koen Eneman (ExpORL, Dept. Neurosciences, K.U. Leuven, Herestraat 49 bus 721, O. & N2, B-3000 Leuven, Belgium, koen.eneman@med.kuleuven.be), Walter Lauriks (Lab. ATF, Katholieke Universiteit Leuven, Celestijnenlaan 200D, B-3001 Leuven, Belgium, Walter.Lauriks@fys.kuleuven.be),Marc Moonen(ESAT/SISTA, K.U. Leuven, Kasteelpark Arenberg 10, B-3001 Leuven, Belgium, marc.moonen@esat.kuleuven.be), Jan Wouters (ExpORL, Dept. Neurosciences, K.U. Leuven, Herestraat 49 bus 721, O. & N2, B-3000 Leuven, Belgium, jan.wouters@med.kuleuven.be)

The development of noise reduction algorithms for hearing aids (HA) is not longer only related to the improvement of signal to noise ratio, but also to the quality of hearing, e.g., binaural aspects of hearing. This is very important for the recognition of the localization of sound sources but also for an improved speech intelligibility in noisy situations due to spatial release from masking effects. New design and signal processing algorithms for binaural HA's need to be tested and validated in different acoustical scenarios. As it is too laborious and time consuming to perform sufficient numbers of perceptual evaluations in different rooms with different acoustical parameters, advanced acoustic modeling of different virtual acoustical environments might be needed. Virtual acoustics in our research relates to the convolution of the measured or simulated binaural signals (head related transfer functions - HRTF's) with the impulse response generated from a computer model of a room (using ODEON® software) to simulate binaural sounds. This study investigates the usage of virtual acoustics in the framework of developing algorithms for binaural hearing aids. It evaluates and quantifies the fidelity of binaural signals generated by commercially available virtual acoustics software with respect to the localization of sound and speech intelligibility in different acoustical scenarios.

5aPPe3. Auralization of urban soundscaping designs using the Arup SoundLab. Seb Jouan (Arup Acoustics, Bergius House, 11-12 Claremont Terrace, G3 7XR Glasgow, UK, seb.jouan@arup.com)

Noise is unwanted sound (from an urban planning point of view). The standard practice to control noise, while valuable, is a negative process (i.e., reducing unwanted "noise"). In response, there is a drive by several authorities to take a more positive approach to improve and manage soundscapes in cities and civic spaces. Urban soundscape design consists of planning, shaping and managing the sound to fit each area of the masterplan in terms of civic, cultural, and social character. Arup uses its SoundLab, a 3D sound facility (ambisonic), to design and auralise (the sound equivalent to visualisation) soundscapes with planners, architects or artists and demonstrate to Local Planning Authorities or clients the results of the design. An example of urban soundscaping design is Dark Neville Street, Leeds for Leeds City Council where architectural, lighting design, acoustical soundscaping design were integrated together with an artistic sonic piece by Hans-Peter Kuhn which was auralised in the Arup SoundLab. An example of "indoor" sonic art and soundscape design installation is "Harmonic Bridge" by

Bill Fontana and Arup Acoustics in the Turbine Hall of the Tate Modern (June-August 2006) where the sonic art piece was composed in the SoundLab.

5aPPe4. Salience of spatial attributes on quality evaluation of multichannel audio processing devices. Inyong Choi (Seoul National University, ENG 420-025, Gwanak PO Box 34, 151-600 Seoul, Republic of Korea, inyongchoi@gmail.com), Jung-Hun Seo (Seoul National University, ENG 420-025, Gwanak PO Box 34, 151-600 Seoul, Republic of Korea, pollini@acoustics.snu.ac.kr), Koeng-Mo Sung (Applied Acoustics Lab., INMC, 132-302, Seoul National University, San 56-1, Sillim-dong, Kwanak-gu, 151-742 Seoul, Republic of Korea, kmsung@snu.ac.kr)

Objective quality assessment methods for audio signal processing devices, e.g. ITU-R BS.1387-1, measure perceived quality by using various types of test excerpts and incorporating a number of psychoacoustic metrics for evaluating various attributes of quality degradations. As many multichannel audio processing devices are being developed, recent quality assessment methods include not only timbral features but also spatial features, such as analysis on interaural disparities. In this paper, the importance of the newly proposed spatial - interaural - features are studied for different types of multichannel test signals. The spatial features have bigger salience on directly recorded sound sources than artificially manipulated multichannel contents.

5aPPe5. Assessment of simulation quality of three different auralization procedures. Stephan Paul (Lab. of Vibrations and Acoustics, Fed. Univ. of Santa Catarina, CTC, EMC, Campus Trindade, 88040 Florianópolis, Brazil, stephan.paul.acoustic@gmail.com)

When acoustical problems occur in architectural spaces acousticians are often requested to help. The help is often complicated by very different knowledge in acoustics and problems in communication between architect, musicians and acousticians. Auralization of sound sources is considered to be a powerful tool to solve the problem, making acoustic information accessible for hearing. The present research assessed the quality of the output of different simulation procedures by subjective assessment of similarity with a reference sound, considering different perceptual dimensions (localization, reverberation, and timbre). The reference sound was obtained by binaural recording in the room that was auralized using ray-tracing, mirror sources or a hybrid pyramid tracing method. Two different types of sound sources, human speech and a guitar, were auralized. The results show that the subjective quality of the simulation procedure depends on the type of sound source and the perceptive dimension that was assessed. In general the mirror source method performed best for localization of speech, whereas ray-tracing was the preferred method for the guitar sound. Overall mirror sources also outperform the other methods when good localization is required. Independent from the source the hybrid method was considered the best for the reverberation dimension.

5aPPe6. Effects of hardware on optimal filter segmentations for the segmented convolution. Frank Wefers (Institute of Technical Acoustics, RWTH Aachen University, Neustrasse 50, 52066 Aachen, Germany, Frank.Wefers@akustik.rwth-aachen.de)

The segmented convolution is a commonly used method for the auralisation in interactive virtual acoustic environments. Typically the auralisation of a virtual scene is done by convolution of the scenes' sound sources signals with impulse responses, that describe the sound transmission paths. The segmented convolution algorithm allows an efficient computation of the convolution in real-time, by segmentation of the impulse response into several parts. In order to allow the realistic simulation of complex acoustical scenes, the convolutions' computational effort must be minimised. It is a fact that the segmentation of the impulse response is a key parameter to the algorithm and has great effects on its computational load, stability and even realisability in real-time. Considerations on optimal filter segmentations mainly founded on a theoretical point, like the runtime complexity of operations or the number of required floating point operations. However, practical systems behave differently: Calculations on real hardware suffer cache losses and memory bandwidth. In this contribution, the influence of real hardware on optimal filter segmentations is examined. An optimisation algorithm is presented, that allows to gain optimal filter segmentations for a dedicated target system. The consequences of efficiency losses to the structure of optimal filter segmentations are discussed.

Session 5aPPf

Psychological and Physiological Acoustics and Speech Communication: Acoustic Features and Speech Perception I (Poster Session)

Jont Allen, Cochair
University of Illinois

Sarah Hawkins, Cochair
University of Cambridge

All posters will be on display from 9:40 a.m. to 11:20 a.m. To allow contributors an opportunity to see other posters, contributors of odd-numbered papers will be at their posters from 9:40 a.m. to 10:30 a.m. and contributors of even-numbered papers will be at their posters from 10:30 a.m. to 11:20 a.m.

Contributed Papers

5aPPf1. English speech intelligibility test among persons of Arabic native language. Mohammed Abd-Elbasseer (National Institute of Standard (NIS) - Acoustics Department, Teras Street/Al Ahram Street/Giza, 202 Cairo, Egypt, mbacir@yahoo.com), Sanaa Barakat (National Institute of Standard (NIS) - Acoustics Department, Teras Street/Al Ahram Street / Giza, 202 Cairo, Egypt, s43223@yahoo.com)

English language as a non-native language is the most common language over the world, it is the language of conferences, business and the airports. While the Arabic language is the native language of Egypt, the English language is considered as the second language. This research will conduct to investigate the effect of speech level, rate and repetition on the intelligibility of English language among some highly educated Egyptian persons. 34 males and females subjects are participated in this test. 40 sentences of BKB sentences were used with three scored words per sentence. First, they are subjected to the speech rate of about 220, 190, 160, and 100 words per minute at the speech level of about 60 dBA, which is considered as the normal level. Second,they are subjected to the speech level of 60, 70, and 80 dBA at speech rate of 190 words per minute, which is considered as the normal rate. It was found that the intelligibility score increased with decreasing the rate and increasing the level respectively. It was found that scores of the worst scored sentence for the first 15 subjects did not change, whatever we repeat the tested sentence at normal rate and level.

5aPPf2. Spectral masking release with HiRes120 sound processing in cochlear implant users. Julie Bestel (Advanced Bionics, 76 rue de Battenheim, 68170 Rixheim, France, julieb@abionics.fr), Olivier Sterkers (Hôpital Beaujon, service ORL, 100 bd du Général Leclerc, 92118 Clichy, France, olivier.sterkers@bjn.ap-hop-paris.fr), Bruno Frachet (Hôpital Avicenne, Service ORL et de chirurgie cervico-faciale, 125 rue de Stalingrad, 93009 Bobigny, France, bruno.frachet@club-internet.fr), Bernard Meyer (Hôpital Saint-Antoine, Service ORL, 184 rue du Faubourg St Antoine, 75012 Paris, France, bernard.meyer@sat.ap-hop-paris.fr), Eric Truy (Hôpital Edouard Herriot, Service ORL, Place d'Arsonval, 69003 Lyon, France, eric.truy@chu-lyon.fr), Patrick Boyle (Advanced Bionics, 76 rue de Battenheim, 68170 Rixheim, France, patrickb@abionics.fr), Christian Lorenzi (Univ Paris Descartes, CNRS, Ecole Normale Superieure, DEC, 29 rue d'Ulm, 75005 Paris, France, lorenzi@ens.fr)

Current sound processors in cochlear implants show poor frequency resolution compared to normal auditory processes. They smooth spectral gaps within background maskers, thereby preventing implant users from experiencing release from masking (i.e., improved speech identification in maskers showing spectral gaps compared to maskers with continuous spectra). The Advanced Bionics' HiRes120 coding scheme aims to increase the transmission of fine-grain spectral information using a strategy based upon current steering. If HiRes120 improves the precision of spectral coding compared to the standard HiRes strategy, listeners should show improved release from masking for the slowest spectral modulations in a noise masker. This hypothesis is tested in newly implanted adults who alternately use HiRes and HiRes120 sound processing for a period of 10 months. Every two or three months, consonant identification is measured in each implantee in the presence of a stationary speech-shaped noise (SSN) masker at a fixed signal-to-noise ratio yielding 30-40% correct identification with unmodulated noise. The SSN masker is either unmodulated or spectrally modulated to produce periodic, three ERB-wide "spectral gaps" in the noise masker. Masking release scores defined as the change in consonant identification performance in modulated versus unmodulated noise will be presented and discussed.

5aPPf3. Comparison of speech vs speech-analogue temporal encoding in human: An auditory brainstem response and categorical perception assessment. Idrick Akhoun (Univ. Lyon 1 - Lab. Neurosciences, Service Pr Collet, Pavillon U, Hôpital Edouard Herriot, F-69003 Lyon, France, iakhoun@olfac.univ-lyon1.fr), Céline Richard (Univ. Lyon 1 - Lab. Neurosciences, Service Pr Collet, Pavillon U, Hôpital Edouard Herriot, F-69003 Lyon, France, iakhoun@olfac.univ-lyon1.fr), Annie Moulin (Univ. Lyon 1 - Lab. Neurosciences, Service Pr Collet, Pavillon U, Hôpital Edouard Herriot, F-69003 Lyon, France, iakhoun@olfac.univ-lyon1.fr), Evelyne Veuillet (Univ. Lyon 1 - Lab. Neurosciences, Service Pr Collet, Pavillon U, Hôpital Edouard Herriot, F-69003 Lyon, France, iakhoun@olfac.univ-lyon1.fr), Stéphane Gallégo (Univ. Lyon 1 - Lab. Neurosciences, Service Pr Collet, Pavillon U, Hôpital Edouard Herriot, F-69003 Lyon, France, iakhoun@olfac.univ-lyon1.fr), Christian Berger-Vachon (Univ. Lyon 1 - Lab. Neurosciences, Service Pr Collet, Pavillon U, Hôpital Edouard Herriot, F-69003 Lyon, France, iakhoun@olfac.univ-lyon1.fr), Lionel Collet (Univ. Lyon 1 - Lab. Neurosciences, Service Pr Collet, Pavillon U, Hôpital Edouard Herriot, F-69003 Lyon, France, iakhoun@olfac.univ-lyon1.fr), Hung Thai-Van (Univ. Lyon 1 - Lab. Neurosciences, Service Pr Collet, Pavillon U, Hôpital Edouard Herriot, F-69003 Lyon, France, iakhoun@olfac.univ-lyon1.fr)

Temporal speech cues, such as periodicity and voice onset time (VOT), are particularly salient information for speech intelligibility. In addition, speech elicited auditory brainstem response (Speech ABR) to consonant vowels (CV) has been shown to mimic the temporal periodicity of the acoustic signal very accurately. Consequently, Speech ABR has been described as a potential objective tool to explore the temporal integration of speech excerpts in human brainstem. We aimed at putting in evidence the specialization of temporal encoding of speech vs nonspeech signals through clinical and behavioral measurements. A sum of five sinusoids, at the five

formant frequencies, modulated by the corresponding CV temporal envelope, was taken as speech-analogue. Accordingly, Speech and Analogue ABRs components were compared, although a priori due to be similar. Furthermore, categorical perception assessment was processed to both analogue and full-speech continuums. If confirmed, these preliminary results (seven normal hearing adults for physiological ABRs and behavioral categorical perception) would bring further evidence of an early specialization of temporal processing of speech, in line with previous research [Kraus and Nicol, Trends in Neuroscience 28(4), 176--81 (2005)]. [Work supported by CNRS, Cochlear & Univ.Lyon 1.]

5aPPf4. Modulation of the voice-cuing effect on releasing speech from informational masking. Lijuan J. Xu (Dept. of Psychology, Peking Univ., 5 Yeheyuan Road, Haidian District, 100871 Beijing, China, lijuan179021@yahoo.com.cn), Jingyu Y. Li (Dept. of Machine Intelligence, Speech and Hearing Research Center, 2 Science Building, Peking Univ., 5 Yeheyuan Road, Haidian District, 100871 Beijing, China, lijy@cis.pku.edu.cn), Ying Huang (Dept. of Psychology, Peking Univ., 5 Yeheyuan Road, Haidian District, 100871 Beijing, China, innhuang@gmail.com), Xihong H. Wu (Dept. of Machine Intelligence, Speech and Hearing Research Center, 2 Science Building, Peking Univ., 5 Yeheyuan Road, Haidian District, 100871 Beijing, China, wxh@cis.pku.edu.cn), Liang Li (Dept. of Psychology, Peking Univ., 5 Yeheyuan Road, Haidian District, 100871 Beijing, China, liangli@pku.edu.cn)

In cocktail-party environments, familiarity or knowledge of target talker's voice is useful for reducing speech-on-speech masking (Yang et al., Speech Communication, **49**, 892-904, 2007). In addition, the onset asynchrony between target speech and masking speech is an effective cue for unmasking target speech. The present study examined whether the voice-cuing effect can be modulated by either the degree of familiarity/knowledge of target talker's voice or the speech onset asynchrony. When target speech started one second after masking speech, prepresenting a priming sentence voiced by the target talker significantly improved the recognition of the target speech which was copresented with masking speech. However, reinforcing the familiarity/knowledge of the target-talker's voice did not further improve the recognition. When target speech and masking speech started at the same time, a single presentation of voice-priming speech did not change participants' speech recognition against masking speech unless the familiarity-/knowledge of target-talker's voice was reinforced by either a learning procedure or repeated presentation of the target-talker's voice before testing. These results suggest that the voice-cuing effect on releasing speech from informational masking is graded, depending on both the degree of familiarity/knowledge of the target-talker's voice and the modulation by other cues such as speech-onset asynchrony.

5aPPf5. Consequences of regional accent differences for speech perception studies. Richard Wright (University of Washington, 1417 NE 42nd Street, Seattle, WA 98105, USA, rawright@u.washington.edu), Pamela Souza (University of Washington, 1417 NE 42nd Street, Seattle, WA 98105, USA, psouza@u.washington.edu), Stephanie Bor (University of Washington, 1417 NE 42nd Street, Seattle, WA 98105, USA, stebor@u.washington.edu), Star Reed (University of Washington, 1417 NE 42nd Street, Seattle, WA 98105, USA, starreed@u.washington.edu)

Sociophonetic research has demonstrated effects of regional accent on vowels. However, little attention is paid to regional accent in hearing and speech perception studies that use standard vowel stimuli. This poster illustrates the importance of these factors to perception. A library of synthetic vowels from nine different regions of the U.S. (e.g., southern California, upper Midwest) was generated according to published formant values. The vowels were categorized into three groups (near, medium, far) according to Euclidean distance in an F1 by F2 space relative to Pacific Northwest (PNW) vowels. Based on several experimental factors, two vowel pairs representing the high back and low front vowels were chosen as stimuli. The near, medium and far exemplars and PNW exemplars were presented to native PNW listeners in a forced-choice identification task. Dependent variables were identification accuracy and reaction time. Task difficulty was manipulated using background noise level. Results indicate that recognition scores were poorer, and reaction time was longer, for vowels that were spectrally distant from the listener's regional accent. These data suggest that researchers should take into account regional accent in selecting vowel stimuli or generating synthetic vowels for general-use speech perception tests. Supported by NIDCD (DC00033, RO1 DC006014).

5aPPf6. Factors affecting recognition of vocoded speech: Effect of envelope cutoff frequency and carrier type. Pamela Souza (University of Washington, 1417 NE 42nd Street, Seattle, WA 98105, USA, psouza@u.washington.edu), Stuart Rosen (UCL, Wolfson House, 4, Stephenson Way, NW1 2HE London, UK, stuart@phon.ucl.ac.uk)

Multiband vocoded signals are used to study temporal cues as well as to simulate information available to cochlear implant wearers, but different implementations of these signals may affect results. This series of experiments varied envelope cutoff frequency (30 or 300 Hz), carrier type (tone or noise) and number of frequency bands (2-5) for vocoded speech presented to normal-hearing subjects. Dependent measures were consonant recognition (vowel-consonant-vowel syllables), vowel recognition (/b/-vowel-/d/ words), and sentence recognition. Results indicated better performance with a high envelope cutoff for tone-vocoded signals, and no effect of envelope cutoff for noise-vocoded signals. When only low-frequency envelope cues were available, performance was better for noise-vocoded than for tone-vocoded signals. When higher-frequency envelope cues were available, performance was better for tone-vocoded than for noise-vocoded signals. To understand the source of the observed differences, a follow-up study tested the relative contributions of comodulation across bands (as in the 30- and 300-Hz tone-vocoded conditions) and spectral sidebands (as in the 300-Hz tone-vocoded conditions). Those data indicated that comodulation across bands did not contribute to performance. The presence of sidebands which provided more spectral detail improved performance over a sparser spectrum. [Supported by the Bloedel Hearing Research Center and NIH RO1 DC006014.]

5aPPf7. When and how disyllables are contracted into monosyllables in Taiwan Mandarin? Chierh Cheng (University College London, Department of Phonetics and Linguistics, Gower Street, WC1E 6BT London, UK, chiacheng.fl86@nctu.edu.tw), Yi Xu (University College London, Wolfson House, 4 Stephenson Way, NW1 2HE London, UK, yi.xu@ucl.ac.uk)

In Taiwan Mandarin, a disyllabic word or phrase is often contracted into a monosyllabic unit in conversational speech, just as "do not" is often contracted into "don't" in English. The goal of this research is to a) test the hypothesis that contraction is directly related to time pressure, and so it can be elicited in the laboratory from nonsense disyllabic units, and b) search for the underlying mechanisms of contraction. We devised four groups of nonsense disyllabic combinations according to the level of obstruction in the intervocalic consonant: (1) zero obstruction - CV+V; CV+VN; CV+VV, (2) nasal consonant - CVN+V; CV+NV, (3) non-nasal consonant - CV+CV, where C is a stop, fricative or affricate, and 4) nasal + non-nasal consonant-CVN+CV. These disyllabic units were embedded in carriers that would impose different degrees of time pressure on them. Four speakers of Taiwan Mandarin read aloud these sentences at three articulatory modes: clear, natural and fast. Preliminary examinations showed that contraction occurred more frequently as speech rate increased and as intervocalic obstruction decreased. Detailed acoustic analyses are being conducted to search for evidence of the underlying mechanism of such contraction, and the results will be reported.

5aPPf8. Estimation model for the speech-quality dimension "Noisiness." Lu Huo (Institute for Circuit and System Theory, Christian-Albrechts-University of Kiel, Kaiserstrasse 2, 24143 Kiel, Germany, lhu@tf.uni-kiel.de), Marcel Wältermann (Deutsche Telekom Laboratories, Berlin Institute of Technology, Ernst-Reuter-Platz 7, 10587 Berlin, Germany, marcel.waeltermann@telekom.de), Ulrich Heute (Institute for Circuit and System Theory, Christian-Albrechts-University of Kiel, Kaiserstrasse 2, 24143 Kiel, Germany, uh@tf.uni-kiel.de), Sebastian

Möller(Deutsche Telekom Laboratories, Berlin Institute of Technology, Ernst-Reuter-Platz 7, 10587 Berlin, Germany, sebastian.moeller@telekom.de)

State-of-the-art assessment method of speech-transmission quality (e.g., PESQ or TOSQA) predict the mean-opinion score (MOS) quite accurately, but cannot provide diagnostic information, which is, however, highly desirable for system developers. In our research project, we aim at the development of an attribute-based speech-quality measure, which provides estimates of different attributes of speech samples and then maps them to one integral-quality estimate. Three dominant, mutually orthogonal perceptual dimensions were firstly identified by auditory experiments and multidimensional analysis (MDA) for narrow-band speech transmission: "directness/ frequency content," "continuity," and "noisiness." The present paper focuses on the further decomposition and measurement of the global dimension "Noisiness." Therefore, an auditory test including samples degraded by different kinds of noises has been conducted. The subsequent MDA indicates that at least two sub-dimensions (SD), "Speech Contamination" and (perceived) "Additive-Noise Level," are further describing the global dimension "Noisiness." The first SD characterizes the degree the noise distorts the speech signal as such, whereas the second SD reflects the degree the additive circuit or background noise itself annoys the listener. The instrumental estimation methods for both SDs and the mapping to the integral-quality ratings are presented in this paper.

5aPPf9. Across-ear grouping of speech bands in quiet and in the presence of interference. Erol Ozmeral (Boston University Hearing Research Center, 677 Beacon Street, Boston, MA 02215, USA, ozmeral@bu.edu), Virginia Best (Univ. of Sydney, Dept. of Physiology, NSW 2006 Sydney, Australia, ginbest@physiol.usyd.edu.au), Jaime McCoin (Boston University Hearing Research Center, 677 Beacon Street, Boston, MA 02215, USA, jmsushigirl@gmail.com), Barbara Shinn-Cunningham (Boston University Hearing Research Center, 677 Beacon Street, Boston, MA 02215, USA, shinn@cns.bu.edu)

Speech was filtered into 16 frequency bands. Three bands were randomly selected on each trial as the LOW (two low-frequency bands) and HIGH (one high-frequency band) target components. LOW and HIGH were either presented to the same (SAME) or opposite (SPLIT) ears. Four randomly selected, nonoverlapping frequency bands from a different utterance were time reversed, and summed. When present, this masker was either played to the same ear as LOW and HIGH (SAME-MASK), same ear as LOW with HIGH opposite (SPLIT-MASKLOW), or same ear as HIGH with LOW opposite (SPLIT-MASKHIGH). Intelligibility was best in the SAME and SPLIT conditions and much better than with either LOW or HIGH presented alone. Thus, in quiet, listeners can perceptually integrate information across target components with little spectro-temporal correlation, even when spatial cues promote segregation of these components. Performance in the SAME-MASK condition was generally better than either SPLIT-MASKLOW or SPLIT-MASKHIGH conditions (although worse than in SAME and SPLIT conditions). Furthermore, performance in the two SPLIT-MASK conditions was comparable to performance with LOW or HIGH alone. Thus, when spatial cues oppose grouping of the target and there is a competing off-frequency interference, listeners have difficulty integrating information across target components.

5aPPf10. The role of consonant duration and amplitude processing on speech intelligibility in noise. Jeffrey J. Digiovanni (Ohio University, W218 Grover Center, Athens, OH 45701, USA, digiovan@ohio.edu), Ashley K. Stover (Ohio University, W218 Grover Center, Athens, OH 45701, USA, as357803@ohio.edu)

The effects of hearing loss on speech intelligibility have led researchers to search for methods to ameliorate these effects. Clear speech has been studied extensively to determine the specific acoustic and phonetic differences between speech spoken in a conversational versus a clear-speech mode. Two characteristics of clear speech, increased consonant duration and selective-consonant amplification were investigated. These components were applied individually to Hearing-in-Noise Test sentences and consonant-vowel (CV) pairs. Stimuli were presented in sound field to hearing-impaired and normal-hearing individuals in the presence of speech-shaped noise. Percent correct was measured for HINT sentences and confusion matrices were developed for the CV pair intelligibility tests. An information transmission analysis was performed. During HINT sentence presentations, subjects benefited most from lengthening the duration of the consonant, maximally in the 30 ms condition, beyond which significant degradation in intelligibility was observed. Consonant specific amplification of 10 dB resulted in improved intelligibility for sentences. These data suggest that the two processing components are viable to improve speech intelligibility and they, however, also suggest that there is a limit to the processing whereby benefits are no longer observed.

5aPPf11. The role of combined consonant duration and amplitude processing on speech intelligibility in noise. Jeffrey J. Digiovanni (Ohio University, W218 Grover Center, Athens, OH 45701, USA, digiovan@ohio.edu), Jessica A. Wolfanger (Ohio University, W218 Grover Center, Athens, OH 45701, USA, jw241702@ohio.edu)

Reduced speech intelligibility in noise, especially consonant perception, is a well documented phenomenon. Research in clear speech has revealed many acoustic and phonetic differences between speech spoken in a conversational versus clear-speech mode. In the present study two components were tested in combination, namely increases in consonant duration (and respective decreases in adjacent vowel duration) and selective-consonant amplification. Conditions in which intelligibility improvements were observed for the individual processing of duration and amplitude modifications were chosen and tested in combination. The components were applied to Hearing-in-Noise Test sentences and consonant-vowel (CV) pairs. Stimuli were presented in sound field to normal-hearing individuals in the presence of speech-shaped noise. Percent correct was measured for HINT sentences and confusion matrices were developed for the CV pair intelligibility tests. An information transmission analysis was performed. Results will be discussed with regard to the greater body of research in clear speech.

5aPPf12. Effect of amplification on the intelligibility of speech in hearing impaired children with and without dead regions in the cochlea. Alicja N. Malicka (The University of Manchester, School of Psychological Sciences, Ellen Wilkinson Building, M13 9PL Manchester, UK, alicja.malicka@manchester.ac.uk), Kevin J. Munro (The University of Manchester, School of Psychological Sciences, Ellen Wilkinson Building, M13 9PL Manchester, UK, kevin.j.munro@manchester.ac.uk), Thomas Baer (University of Cambridge, Department of Experimental Psychology, Downing Street, CB2 3EB Cambridge, UK, tb107@cus.cam.ac.uk)

Adults with high-frequency (HF) sensorineural hearing impairment with and without dead regions (DRs) in the cochlea differ in benefit from amplification of speech presented in quiet [Vickers et al., J. Acoust. Soc. Am. **110**, 1164-1175 (2001)]. Subjects with HF DRs showed no improvement in speech intelligibility when spectral components of the speech above about 1.7 times the edge frequency of the DR were amplified according to a hearing-aid prescription formula while performance of those without DRs showed improvement with addition of amplified frequency components up to 7.5 kHz. In the present study we tested a group of six children (8-12 years old) who were experienced hearing-aid users with moderate-to-severe sensorineural hearing impairment. The presence of DRs was diagnosed using the TEN(HL) test and "fast" psychophysical tuning curves. Four children showed evidence for DRs (two unilateral and two bilateral). The vowel-consonant-vowel stimuli (65-dB SPL) were subjected to the frequency-gain characteristic prescribed by the DSL prescription formula then low-pass filtered with various cutoff frequencies and presented via headphones. The results showed that in ears with or without DRs the performance improved with increasing cutoff frequency up to 7.5 kHz.

5aPPf13. Acoustic correlates of fricative perception. Shira Katseff (University of California, Department of Linguistics, 1203 Dwinelle Hall, Berkeley, CA 94720, USA, skatseff@berkeley.edu)

A number of spectral attributes have been proposed as correlates of fricative place of articulation. However, these attributes have difficulty distinguishing fricatives in noncanonical speech, e.g., from children. Because child speech is intelligible, it is possible that some of these characteristics

are not used in speech perception. This study collected a corpus of /s/ and /S/-containing words from children between 3 and 5. Adults categorized fricatives extracted from this corpus. A series of regressions are used to compare the ability of spectral attributes to predict (1) human categorization of /s/ and /S/ productions, and (2) the intended fricative production. The analysis reveals that mistakes in perception are driven by overuse of a single spectral attribute, spectral slope. This result suggests caution in equating methods of computational separation with methods of human perception, and provides a simple method for investigating relationships between the two.

FRIDAY MORNING, 4 JULY 2008 P2-C, LEVEL 2, 9:40 TO 11:20 A.M.

Session 5aPPg

Psychological and Physiological Acoustics: Cross-spectral Auditory Integration: Physiological, Psychophysical, and Clinical Evidence II (Poster Session)

Blas Espinoza-Varas, Cochair
CommunicationSciences & Disorders, OU Health Sciences Ctr.

Alain De Cheveigne, Cochair
CNRS, Universite Paris 5, Ecole Normale Superieure

All posters will be on display from 9:40 a.m. to 11:20 a.m. To allow contributors an opportunity to see other posters, contributors of odd-numbered papers will be at their posters from 9:40 a.m. to 10:30 a.m. and contributors of even-numbered papers will be at their posters from 10:30 a.m. to 11:20 a.m.

Contributed Papers

5aPPg1. Stimulus effects on spectral shape discrimination. Mini N. Shrivastav (University of Florida, 336 Dauer Hall, Dept. of Communication Sciences and Disorders, Gainesville, FL 32611, USA, mnarendr@csd.ufl.edu), David A. Eddins (University of Rochester, Department of Otolaryngology, Rochester, NY 14618, USA, David_Eddins @URMC.Rochester.edu)

For a single stimulus such as shaped broadband noise, spectral-shape discrimination can vary based on the nature of the spectral feature that is being detected. For example, Shrivastav et al. (2006) found a significant difference in thresholds for broadband noise with a narrow localized spectral peak and those with a broad overall spectral change. They also found a moderate association between discrimination thresholds and speech-identification scores in older hearing-impaired listeners, but only for the stimuli with a narrow spectral peak. It is not clear whether these stimulus-dependent effects were associated with the bandwidth of the spectral peak, the slope of the peak, or a combination of these features. In the present study, spectral shape discrimination thresholds and speech recognition scores will be measured for ten young normal-hearing and ten older hearing-impaired listeners. The broadband noise will vary systematically in the bandwidth and the slope of a single spectral peak. The results will determine if and how spectral-shape perception changes with the nature of the stimulus paradigm used to measure it. Further, the results will also indicate if the association between spectral shape perception and speech identification is observed for all stimuli or only to a subset.

5aPPg2. Resolution, spectral weighting, and integration of information across tonotopically remote cochlear regions: hearing-sensitivity, sensation level, and training effects. Blas Espinoza -Varas (CommunicationSciences & Disorders, OU Health Sciences Ctr., 825 NE 14th St., Oklahoma City, OK 73126-0901, USA, blas-espinoza-varas@ouhsc.edu)

This paper examines how listeners resolve, weight, and integrate redundant sensory information from tonotopically remote cochlear regions, one in the mid (m) the other in the high (h) frequencies. Subjects listened to two-component complexes and attempted to resolve and integrate simultaneous differences in frequency (DFm) at ≈1000 Hz and in duration (DTh) at ≈3500 Hz. Discrimination performance was studied as a function of hearing sensitivity, sensation level (SL) and training. Normal hearing listeners tend to resolve both DFm and DTh and integrate the information if the component SLs are equal, but resolve only the louder component difference if the SLs are very unequal; i.e., spectral weighting is biased and integration is limited or nil. Much the same pattern obtains when the low SL in H results from high-frequency impaired sensitivity (IS). Once established, equating the component SLs (e.g., by high-frequency amplification) is often ineffective to rectify the weighting bias; doing so requires extensive discrimination training with the low SL component. With IS, an anomalous trend obtains when the SL is much lower for (m) than for (h): the resolution of DFm is equal to or better than that of DTh, and integration is quite efficient, possibly reflecting tonotopic map reorganization.

5aPPg3. Pitch discrimination of simultaneous and nonsimultaneous complexes across spectral regions. Elizabeth Borchert (University of Minnesota, Department of Psychology, 75 E. River Road, Elliott Hall N218, Minneapolis, MN 55455, USA, olsen064@umn.edu), Andrew J. Oxenham (University of Minnesota, Department of Psychology, 75 E. River Road, Elliott Hall N218, Minneapolis, MN 55455, USA, oxenham@umn.edu), Christophe Micheyl (University of Minnesota, Department of Psychology, 75 E. River Road, Elliott Hall N218, Minneapolis, MN 55455, USA, cmicheyl@umn.edu)

Detecting differences in fundamental frequency (F0) across different spectral regions may be important in the perceptual organization of both simultaneous and sequential sounds, but it is unknown whether the same mechanisms are involved in these two cases. Here we directly compare the detection of pitch differences between pairs of complex tones presented either simultaneously or sequentially. 28 normal-hearing listeners heard two pairs of complex tones in each trial and indicated the pair in which the pitches of the two tones differed. The complex tones in each pair were band-pass filtered to have nonoverlapping spectra, but at least some resolved harmonics in all cases. Performance was generally better in the simultaneous than in the sequential condition. In a follow-up condition, it was found that introducing an onset asynchrony between the two spectral regions in the si-

multaneous condition resulted in impaired performance, approaching that found in the sequential case, despite the duration of the simultaneous portion remaining the same. The results suggest that perceived fusion, rather than an explicit F0 extraction and comparison may underlie the detection of F0 differences between simultaneous groups of harmonics in distinct spectral regions. [Work supported by NIH grant R01 DC 05216.]

5aPPg4. Across-frequency processes involved in auditory detection of coloration. Jörg M. Buchholz (CAHR, Department of Electrical Engineering, DTU, Ørsteds Plads, Bygning 352, 2800 Kgs. Lyngby, Denmark, jb@oersted.dtu.dk), Paris Kerketsos (CAHR, Department of Electrical Engineering, DTU, Ørsteds Plads, Bygning 352, 2800 Kgs. Lyngby, Denmark, paris_kerketsos@hotmail.com)

When an early wall reflection is added to a direct sound, a spectral modulation is introduced to the signal's power spectrum. This spectral modulation typically produces an auditory sensation of coloration or pitch. Throughout this study, auditory spectral-integration effects involved in coloration detection are investigated. Coloration detection thresholds were therefore measured as a function of reflection delay and stimulus bandwidth. In order to investigate the involved auditory mechanisms, an auditory model was employed that was conceptually similar to the peripheral weighting model [Yost, JASA, 1982, 416-425]. When a "classical" gammatone filterbank was applied within this spectrum-based model, the model largely underestimated human performance at high signal frequencies. However, this limitation could be resolved by employing an auditory filterbank with narrower filters. This novel filterbank was designed to approximate auditory filter-shapes measured by Oxenham and Shera [JARO, 2003, 541-554], derived from forward masking data. The results of the present study demonstrate that a "purely" spectrum-based model approach can successfully describe auditory coloration detection even at high signal frequencies.

5aPPg5. Phoneme recognition as a function of the number of auditory filter outputs. Frederic Apoux (University of South Carolina, Speech Psychoacoustics Laboratory, Department of Communication Sciences and Disorders, William Brice Bldg., 1621 Greene St., Columbia, SC 29208, USA, apoux@sc.edu), Eric W. Healy (University of South Carolina, Speech Psychoacoustics Laboratory, Department of Communication Sciences and Disorders, William Brice Bldg., 1621 Greene St., Columbia, SC 29208, USA, ewh@sc.edu)

It has been proposed that listeners take advantage of brief "coups d'oeil" when processing speech in noise. These glimpses can be characterized both in time and frequency. The obligatory role of the auditory filters in determining the nature of any further processing suggests that the frequency extent of a glimpse should be equivalent to that of an auditory filter. Accordingly, it is hypothesized that the spectral characteristics of glimpses primarily relate to the available number of auditory channels. The present study investigated the number of auditory filter outputs needed to identify phonemes in quiet. Stimuli were first restricted to 80-8000 Hz and then split into 30 contiguous auditory filter width bands. Normal-hearing listeners were presented with N bands whose spectral location was selected randomly from trial to trial. No signal was presented in the other bands. Consistent with previous studies, performance gradually increased with the number of bands. An asymptote was reached with 24 and 16 bands for vowels and consonants, respectively. While high levels of speech understanding are typically observed with as few as 4 channels of spectral information, our results indicate that accurate phoneme recognition requires combination of a much larger number of auditory filter outputs.

FRIDAY MORNING, 4 JULY 2008 ROOM 252B, 8:00 A.M. TO 12:40 P.M.

Session 5aSAa

Structural Acoustics and Vibration, ASA Committee on Standards, and EURONOISE: Ground Vehicle Noise and Vibration I

Donald B. Bliss, Cochair
Duke University, Mechanical Engineering and Materials Science, 148B Hudson Hall, Durham, NC 27708, USA

Paul De Vos, Cochair
DHV BV, Postbus 1132, Amersfoort, NL 3800 BC, Netherlands

Invited Papers

8:00

5aSAa1. Contribution of the tyre to further lowering tyre/road noise. Ernst-Ulrich Saemann (Continental AG, Jaedekamp 30, 30419 Hannover, Germany, Ernst-Ulrich.Saemann@conti.de)

The tyre is the only part of a vehicle that must be originally and primarily designed to transmit forces to outside the vehicle. At the same time the amount of energy a tyre consumes per kilometre in operation and for production has to be minimized. On dry, wet, and snow-covered roads, the safety of traffic can only be ensured by a sufficient capability for acceleration and braking deceleration, cornering stability, tracking on acceleration and braking, steering precision and direction stability. The high requirements on safety, economy, and durability limit the possible reduction in the emission of tyre/road noise. Nevertheless, nowadays patterned tires can be constructed which are not more than 1-3 dB(A) louder than smooth tires. As a further reduction of tire excitation by tread pattern optimization cannot be expected and a soft tread compound cannot be used due to the customer's requirements, the only possibility to build tyres with less sound radiation is to lower the noise already from the blank tyre. Considerably more tyre/road noise reduction can be gained if the excitation by road is addressed, too.

8:20

5aSAa2. Prediction and audio synthesis of vehicle pass-by noise. Estelle Bongini (SNCF DIR, 45, rue de Londres, 75379 Paris, France, estelle.bongini@sncf.fr), Stephane Molla (Genesis S.A., Bâtiment Gérard Mégie, Domaine du Petit Arbois - BP 69, 13545 Aix-en-Provence Cedex 4, France, stephane.molla@genesis.fr), Cédric Herviou (SNCF DIR, 45, rue de Londres, 75379 Paris, France, cedric.herviou@gmail.com), Dominique Habault (LMA CNRS, 31 chemin Joseph Aiguier, 13402 Marseille, France, habault@lma.cnrs-mrs.fr), Franck Poisson (SNCF DIR, 45, rue de Londres, 75379 Paris, France, franck.poisson@sncf.fr)

The European project SILENCE is dedicated to the reduction of railway and roadway noise in urban areas. Within this context, SNCF and LMA (Laboratoire de mécanique et d'acoustique, Marseille) collaborate into the subproject B to develop a pass-by sound simulation software. This global modelling tool will support parametric studies on the reduction of the noise of a train or a car pass-by, by providing standard indicators (time signature, equivalent sound pressure level) and sound samples. These sound samples are computed in B-Format, which allows, after a short postprocessing, to provide various listening formats (mono-aural, binaural, œ). The software is now operational and the sources characterisation has been carried out on an AGC bi-mode BOMBARDIER train and a passenger car. Equivalent sources have been defined in various operating conditions. Simulated pass-by indicators (signature, Leqtp(A)) in various configurations have been compared to measured one and show very good agreement. A perceptive validation has been carried out with listening tests, by indirectly comparing recorded samples corpus and corresponding simulated samples corpus. It shows that the arrangement made by the listeners of the simulated corpus and the arrangement of the recorded corpus are closely the same and are based on the same perceptive criterion.

Contributed Papers

8:40

5aSAa3. Dependence of the contact area on the velocity of a rolling tire. Hong Hai Nguyen (ENPC, UR Navier, 6 et 8 Avenue Blaise Pascal, Cité Descartes, Champs sur Marne, 77455 Marne la Vallée, France, nguyen.hong-hai@lami.enpc.fr), Julien Cesbron (Université d'Evry - Val d'Essonne, Laboratoire de Mécanique d'Evry, EA3332, 40, rue du Pelvoux, 91 020 Evry Cedex, France, cesbron.julien@neuf.fr), Fabienne Anfosso-Ledee (Laboratoire Central des Ponts et Chaussées, BP 4129, 44341 Bouguenais Cedex, France, fabienne.anfosso@lcpc.fr), Hai Ping Yin (ENPC, UR Navier, 6 et 8 Avenue Blaise Pascal, Cité Descartes, Champs sur Marne, 77455 Marne la Vallée, France, yin@lami.enpc.fr), Silvano Erlicher (Université Paris-Est, 6 et 8 avenue Blaise Pascal, Cité Descartes - Champs sur Marne, 77455 Marne la Vallée Cedex 2, France, erlicher@lami.enpc.fr), Denis Duhamel (ENPC, UR Navier, 6 et 8 Avenue Blaise Pascal, Cité Descartes, Champs sur Marne, 77455 Marne la Vallée, France, duhamel@lami.enpc.fr)

It is known that the eigenfrequencies of a rolling tire depend on the velocity of rotation. We distinguish two causes for the stiffness increase: the frequency dependence of the complex modulus of the materials and the geometrical stiffness. The real part of the Young's modulus is monotonic according to the frequency. It contributes for an important part to the stiffening. The geometrical stiffness also increases with the rotational velocity. A consequence of these effects is the modification of the size of the contact area for different velocities of a rolling tire. Here we first present experimental results estimating the size of the contact area for a tire in statics and for different rolling velocities. Differences of 20% can be observed. Then the viscoelastic behaviours of the tire materials are presented and experimental results showing the frequency dependence of the complex modulus of the tire constitutive materials are given. Then finite element computations are presented with a real distribution of materials in the tire section and the size of the contact area is estimated and compared to experimental measurements. These results could improve the modelling of tire road interaction for tire noise predictions.

9:00

5aSAa4. Deploying successfully Laser Doppler Vibrometry techniques within the automotive NVH process. Mehdi Batel (Polytec, 32 rue Delizy, 93694 Pantin Cedex, France, l.korn@polytec.fr)

Laser Doppler Vibrometry is becoming today an established technique and the gold-standard for noncontact measurements in the automotive industry. These methodologies are widely used to characterize the mechanical behaviour of structures in vibration or strain, with always zero mass loading. They provide high precision results with very low operating costs as well as optimized setup times. The applications of laser vibrometry in the automotive industry are extremely various, and are helping today automotive professionals to improve dramatically the NVH performance of components and full vehicles. This paper explains how these methodologies are fitting today in the everyday challenge of automotive NVH Test & CAE engineers: providing best in class noise and vibration quality with mass reductions constraints. A new laser scanning technique including the use of a 3D robot is also presented, providing an innovative way to characterize the dynamics of body structures with very high precision and rapidity. The paper will present a measurement performed on a full vehicle (43 robot positions done in 1h30 hour), with 1094 points of vibration data at 1 Hz resolution.

9:20

5aSAa5. Application of digital speckle interferometry for vibration analysis of a statically loaded vehicle tyre. Dan Borza (National Institute of Applied Sciences of Rouen, INSA Rouen, LMR, Ave l'Universite, BP8 76800 Rouen, France, dan.borza@insa-rouen.fr), Ioana Nistea (Institut National des Sciences Appliquées de Rouen, BP8 avenue de l'Université, 76801 Saint-Etienne du Rouvray, France, ioana.nistea@insa-rouen.fr)

Vehicle noise has, as one of its main sources, tyres and their interaction with the road. Experimental analysis of tyre vibroacoustic behaviour may provide useful information on the contributions of various regions of the tyre to the resultant noise. Digital speckle interferometry represents a reliable and efficient choice for vibration analysis, providing full field and real time information on surface displacement. The optical configuration used for this study is a standard out-of-plane sensitive setup, based on a continuous wave YAG laser. A 4 bucket phase stepping algorithm is applied, with the use of a piezo actuator, in order to eliminate the random phase difference between the object and the reference wave. The measurement results are images of the tested tyre, covered with interference fringes, representing contour maps of out of plane vibration amplitudes. This paper presents measurements for the case of a tyre subjected to a point excitation at the limit of the contact surface with the road, under statical load of 4 kN. The principal resonant modes and frequencies are presented, then difficulties related to sensibility vector variation over the test surface and coupled mode resonances are discussed.

9:40-11:00 Posters

Lecture sessions will recess for presentation of poster papers on various topics in acoustics. See poster sessions for topics and abstracts.

Contributed Papers

11:00

5aSAa6. An energy-based updated modal approach for the efficient analysis of large trimmed models. Gregory Lielens (Free Field Technologies, Rue Emile Francqui 1 - batiment B - AXIS PARC LLN, 1435 Mont-Saint-Guibert, Belgium, gregory.lielens@fft.be), Benoit Van Den Nieuwenhof (Free Field Technologies, Rue Emile Francqui 1 - batiment B - AXIS PARC LLN, 1435 Mont-Saint-Guibert, Belgium, benoit.vandennieuwenhof@fft.be), Fabien Acher (Free Field Technologies, Rue Emile Francqui 1 - batiment B - AXIS PARC LLN, 1435 Mont-Saint-Guibert, Belgium, fabien.acher@fft.be), Jean-Pierre Coyette (Free Field Technologies, Rue Emile Francqui 1 - batiment B - AXIS PARC LLN, 1435 Mont-Saint-Guibert, Belgium, jean-pierre.coyette@fft.be)

Large trimmed models, widely encountered in the automotive industry, generally involve a body-in-white structure coupled to an acoustic cavity and covered by a set of trim components. Due to the large number of degrees of freedom of such models, the direct analysis in physical coordinates, though theoretically correct, is not feasible on current computers. The paper presents an alternative and efficient solution strategy in modal coordinates that relies on an update of the modal parameters of the car body and the acoustic cavity, based on the energetic behaviour of the trim components. The description of the trim component in terms of an energetic database simplifies the data exchange between the automotive manufactor and the trim provider. Furthermore, it enables a fast frequency analysis of various loadcases/trim scenarios and makes optimisation possible. The updated modal approach implemented in Actran/Trim is applied on a simplified car model on which various trim components are applied. The application shows how the stiffening, added mass and damping effects of each trim component can be derived from the energetic database and can guide an optimisation process.

11:20

5aSAa7. Critical assessment of operational path analysis: mathematical problems of transmissibility estimation. Peter Gajdatsy (LMS International, Interleuvenlaan 68, 3001 Leuven, Belgium, peter.gajdatsy@lmsintl.com), Karl Janssens (LMS International, Interleuvenlaan 68, 3001 Leuven, Belgium, Karl.Janssens@lmsintl.com), Ludo Gielen (LMS International, Interleuvenlaan 68, 3001 Leuven, Belgium, ludo.gielen@lms.be), Peter Mas (LMS International, Interleuvenlaan 68, 3001 Leuven, Belgium, peter.mas@lms.be), Herman Van Der Auweraer (LMS International, Interleuvenlaan 68, 3001 Leuven, Belgium, Herman .VanderAuweraer@lmsintl.com)

Classical transfer path analysis (TPA) is a widely used and reliable method for tackling noise and vibration problems. But due to its complexity and time-consuming measurement procedure there is an ongoing research for simpler and faster methods. One such method, most often referred to as operational path analysis (OPA), was presented two years ago and has quickly gained popularity in the NVH field for its speed and ease of use. To estimate path contributions transmissibilities are calculated from the measured operational reference and target accelerations and sound pressures. This new method is now critically examined and compared to a reliable classical TPA measurement. The results of this examination reveal three significant weaknesses. This paper focuses on the problems related to the estimation of transmissibilities which mostly arise from the limited amount of orders present in the signal and the coherence between inputs. It is shown that despite the advantages of the method, it is not applicable in many situations and has to be used with care for it can easily give misleading results.

11:40

5aSAa8. IC engine velocity fields, spherical harmonics and evanescent waves. Igor Machetta (Centro Ricerche FIAT, Strada Torino, 50, 10043 Orbassano (TO), Italy, igor.machetta@fptpowertrain.crf.it), Eugenius Nijman (Centro Ricerche FIAT, Strada Torino, 50, 10043 Orbassano (TO), Italy, eugenius.nijman@fptpowertrain.crf.it)

Spherical nearfield acoustical holography (SNAH) has been used to reconstruct the volume acceleration distribution close to the surface of an IC engine from the measured sound pressure distribution on a sphere enclosing the engine. Such reconstruction frequently requires the calculated target spheres to intercept the strongly nonspherical powertrain structure violating, at first sight, the conventional rules of SNAH. In this paper the SNAH results are compared with the results of two alternative, i.e., an inverse and a power based, source reconstruction methods. Notwithstanding the alleged violation of the rules it is shown that surprisingly good results may be obtained provided the spherical spectrum components associated with evanescent waves are omitted from the back propagation calculation.

12:00

5aSAa9. Influence of bolted items on modal analysis performed on a car body. Miguel Colomo (Universidad Politécnica de Madrid, Avda. Constitución n° 62 1°D, 28931 Móstoles, Spain, miguelcolomo @gmail.com), Andrzej Pietrzyk (Volvo Car Corporation, NVH CAE Noise & Vibration Center Dept 91620, PV2C2, 405 31 Gothenburg, Sweden, apietrzy@volvocars.com), Wolfgang Kropp (Chalmers University of Technology, Division of Applied Acoustics, SE-41296 Gothenburg, Sweden, wolfgang.kropp@chalmers.se)

When performing Modal Analysis testing on a BIG (body-in-gray), some bolted items are included to better take into account their influence on body stiffness. However, their contribution to the stiffness is not relevant in the frequency range accessible for modal analysis (usually up to 70 Hz on a BIG). On the other hand, these bolted items increase the dispersion between results obtained for nominally identical test objects. The question which arises is whether the items should be included in the BIG definition to perform modal analysis and, in this case, which is their influence on the results? MIMO (multi-input-multi-output) measurements were carried out over three, nominally identical, Volvo S80 BIGs. Several configurations were measured for each BIG, starting from the complete body the bolted items were progressively removed. A version of LMS PolyMAX method was programmed by Matlab to analyze the measured data. Conclusions about bolted items influence are drawn based on the study of stabilization diagrams and modal parameters. The poles selection by the stabilization diagrams is one of PolyMAX method keys. The method understanding obtained from programming allows studying the ins and outs of poles selection. Polynomial order plays an important role in physical poles identification, especially for closely spaced modes. Results are shown to highlight its relevance.

12:20

5aSAa10. Analysis of structure borne transmission in a railway vehicle using Energy Flow Method. Pascal Bouvet (Vibratec, 28 Chemin du Petit Bois, BP 36, 69131 Ecully Cedex, France, pascal.bouvet@vibratec.fr)

The Energy Flow Method (EFM) is a computationally efficient method, by which the results of a Finite Element Analysis (FEA) may be postprocessed to form energy flow models. It can be used to study structure borne transmission in structures, based on modal descriptions of the structure and the internal cavity. The EFM allows to form a Energy Influence Coefficient model (EIC) or an inverse SEA model. A first issue consists in partitioning the FE model into SEA subsystems, with respect to the SEA assumptions (particularly the weak coupling assumptions). An automatic technique based

on cluster analysis, can be used to determine an appropriate SEA substructuring, before calculating the Coupling Loss Factors (CLF) between mechanical subsystem. A second issue is to calculate the CLF between structural and acoustic subsystems. This paper presents an industrial application of these techniques, for the analysis of structure borne transmission inside a tramway vehicle. The EFM technique is used to calculate the vibroacoustic transfer of the car body of the tramway, and comparison with measurements on a vehicle are presented.

FRIDAY MORNING, 4 JULY 2008 ROOM 253, 8:00 A.M. TO 4:00 P.M.

Session 5aSAb

Structural Acoustics and Vibration and EURONOISE: Active Noise Control: New Strategies and Innovative Concepts I

Alain Berry, Cochair
Univ. de Sherbrooke, Mechanical Engineering Depart., 2500 Boulevard de l'Université, Sherbrooke, QC J1K 2R1, Canada

Marie-Annick Galland, Cochair
Centre Acoustique du LMFA, Ecole Centrale de Lyon, 36 avenue Guy de Collongue, Ecully cedex, 69134, France

Invited Papers

8:00

5aSAb1. Active structural-acoustic control of laminated cylindrical panels using vertically/obliquely reinforced 1-3 piezoelectric composite. Manas C. Ray (Indian Institute of Technology, Mechanical Engineering Department, 721302 Kharagpur, India, mcray@mech.iitkgp.ernet.in)

The performance of active constrained layer damping (ACLD) treatment for active structural-acoustic control of vibrating thin laminated cylindrical panels has been investigated. The constraining layer of the ACLD treatment has been considered to be made of vertically/obliquely reinforced 1-3 piezoelectric composite material. A finite element model has been developed for the laminated panels integrated with the patches of ACLD treatment to describe the coupled structural-acoustic behavior of the panels enclosing an acoustic cavity. Both velocity and pressure rate feedback controls have been implemented to activate the patches. Symmetric and antisymmetric cross-ply and antisymmetric angle-ply panels have been considered for evaluating the numerical results. Emphasis has also been placed on investigating the effect of the piezoelectric fiber orientation in the constraining layer and the shallowness angle of the cylindrical panels on the performance of the patches.

8:20

5aSAb2. Decentralized control of sound radiation from an aircraft-style panel using iterative loop recovery. Noah H. Schiller (NASA Langley Research Center, 2 North Dryden Street, Hampton, VA 23681, USA, noah.h.schiller@nasa.gov), Randolph H. Cabell (NASA Langley Research Center, 2 North Dryden Street, Hampton, VA 23681, USA, randolph.h.cabell@nasa.gov), Chris R. Fuller (Virginia Tech, 131 Durham Hall, Blacksburg, VA 24061, USA, christopher.r.fuller@nasa.gov)

A decentralized LQG-based control strategy is designed to reduce low-frequency sound transmission through periodically stiffened panels. While modern control strategies have been used to reduce sound radiation from relatively simple structural acoustic systems, significant implementation issues have to be addressed before these control strategies can be extended to large systems such as the fuselage of an aircraft. For instance, centralized approaches typically require a high level of connectivity and are computationally intensive, while decentralized strategies face stability problems caused by the unmodeled interaction between neighboring control units. Since accurate uncertainty bounds are not known a priori, it is difficult to ensure the decentralized control system will be robust without making the controller overly conservative. Therefore, an iterative approach is suggested, which utilizes frequency-shaped loop recovery. The approach accounts for modeling error introduced by neighboring control loops, requires no communication between subsystems, and is relatively simple. The control strategy is validated using real-time control experiments performed on a built-up aluminum test structure representative of the fuselage of an aircraft. Experiments demonstrate that the iterative approach is capable of achieving 12 dB peak reductions and a 3.6 dB integrated reduction in radiated sound power from the stiffened panel.

8:40

5aSAb3. Experimental tests on smart panels for the reduction of sound radiation. Paolo Gardonio (ISVR, University of Southampton, Highfield, SO17 1BJ Southampton, UK, pg@isvr.soton.ac.uk), Cristobal Gonzalez Diaz (ISVR, University of Southampton, Highfield, SO17 1BJ Southampton, UK, cgd@isvr.soton.ac.uk), Neven Alujevic (ISVR, University of Southampton, Highfield, SO17 1BJ Southampton, UK, na2@isvr.soton.ac.uk), Yohko Aoki (ISVR, University of Southampton, Highfield, SO17 1BJ Southampton, UK, ya@isvr.soton.ac.uk)

This paper presents a comparative experimental study carried out on four types of smart panels for the reduction of sound radiation. The four panels are equipped with decentralized velocity feedback control units that are designed to generate active damping. In this way the frequency averaged response and sound radiation produced by stochastic disturbances can be effectively reduced at low audio

frequencies. The first smart panel is composed of a 4×4 array of square piezoelectric patch actuators with accelerometer sensors at their centres. The second smart panel is composed of sixteen triangularly shaped piezoelectric patch actuators with base edges evenly distributed along the perimeter of the panel and accelerometer sensors located on the top vertices of the actuators. The third panel is composed of five electrodynamic inertial actuators with accelerometer sensors located under their footprints. The fourth panel is equipped with a light honeycomb trim panel mounted on four stiff mounts. A set of nine reactive electrodynamic actuators is located in the shallow cavity between the two panels. Accelerometer sensors are mounted at the two footprints of each actuator. The sensor-actuator pairs mounted in the four panels are used to implement analogue local feedback loops.

9:00

5aSAb4. Extremal harmonic active control of power. Philippe Micheau (Univ. de Sherbrooke, Mechanical Engineering Depart., 2500 Boulevard de l'Université, Sherbrooke, QC J1K 2R1, Canada, Philippe.Micheau@USherbrooke.ca), Jean-Philippe Gauthier (Univ. de Sherbrooke, Mechanical Engineering Depart., 2500 Boulevard de l'Université, Sherbrooke, QC J1K 2R1, Canada, Jean-Philippe.Gauthier@cta-brp-udes.com)

The extremal harmonic active control of power consists to define an energetic criterion at the main harmonic and to extremalize it on-line by commanding a secondary source of power. The term extremal means that the optimal criterion value is reached with an on-line optimization algorithm. Without loss of originality, the context of rotating machines oscillation in synchronization with rotor position is used to illustrate this approach. A second commanded torque source, attached to the shaft, is used to control speed oscillation due to torque disturbance. Such configuration can be found in hybrid automotive for example. The energetic criterion can be the kinetic energy (for conventional active speed oscillation cancelling), the reactive power (to add a virtual flywheel on the shaft) or the active power (for energy harvesting to charge a battery). The optimization algorithm is the method of steepest descent implemented with implicit or explicit gradient computation. But, in the case of reactive power, the implicit controller is not practically achievable. The experimental results with a test bed show that the explicit controllers converge at the extremum of each criterion. To conclude, the presented explicit extremal controller is a good candidate to be used for energetic criterion control.

9:20

5aSAb5. Control of harmonic distortion in a motor driven subsonic acoustic source. Marty Johnson (Virginia Tech, Mechanical Engineering, 143 Durham 0238, Blacksburg, VA 24061, USA, martyj@vt.edu), Alessandro Toso (Virginia Tech, Mechanical Engineering, 143 Durham 0238, Blacksburg, VA 24061, USA, aletoso@vt.edu), Vincent Blandea (ISVR, University of Southampton, University Road, Highfield, S017 1BJ Southampton, UK, vblandea@gmail.com)

This paper presents a comparison of active control strategies used to reduce the harmonic distortion of a motor driven subsonic source. The source consists of a DC motor that drives a pair of speaker diaphragms through a belt drive system which in turn drives a pair of passive radiators through an acoustic enclosure. The motor drive system is inherently nonlinear with significant losses in force at polarity changes. A number of control strategies were tested both theoretically and experimentally in order to determine the best strategy for linearizing the output from the speaker. The methodologies tested were: (i) an FXLMS based adaptive time domain controller using a linear plant model, (ii) an FXLMS based adaptive frequency domain harmonic controller using a linear plant model, (iii) an FXLMS based adaptive frequency domain harmonic controller using a nonlinear plant model and (iv) a simplex based adaptive frequency domain harmonic controller. The time domain system is shown to suffer from slow adaption rates for the higher harmonics, the model based FXLMS harmonic controllers were shown to suffer from the nonstationarity of the nonlinear plant and the simplex method was shown to provide good results while being robust to slow variations in the plant.

9:40-11:00 Posters

Lecture sessions will recess for presentation of poster papers on various topics in acoustics. See poster sessions for topics and abstracts.

Invited Papers

11:00

5aSAb6. Variable area jet nozzle for noise reduction using shape memory alloy actuators. James Mabe (Boeing Phantom Works, M/C 42-51, PO BOX 3707, Seattle, WA 98124-2207, USA, james.h.mabe@boeing.com)

A significant reduction in noise and improved fuel consumption can be achieved by varying the area of a commercial jet engine's fan nozzle. A larger diameter at takeoff and approach can reduce jet velocity reducing noise. Adjusting the diameter in cruise, to account for varying Mach number, altitude, etc, can optimize fan loading and reduce fuel consumption. Boeing recently tested a scaled variable area jet nozzle capable of a 20% area change. Shape memory alloy actuators were used to position 12 interlocking panels at the nozzle exit. A closed loop control system was used to maintain a range of constant diameters with varying flow conditions and to vary the diameter under constant flow conditions. Acoustic data by side line microphones and flow field measurements at several cross-sections using PIV was collected at each condition. In this paper the variable area nozzle's design is described. The effect of the nozzle's diameter on its acoustic performance is presented for a range of Mach numbers and mass flow rates. Flow field data is shown including the effects of the joints between the interlocking panels.

11:20

5aSAb7. Concept of active reverberation box. Hisaharu Suzuki (Kyushu University, 4-9-1, Shiobaru, Minamiku, 815-8540 Fukuoka, Japan, hisaha@souldsp.jp), Akira Omoto (Kyushu University, 4-9-1, Shiobaru, Minamiku, 815-8540 Fukuoka, Japan, omoto@design.kyushu-u.ac.jp)

A quite small reverberation box with active controller system is proposed. If we try to measure the characteristics of acoustic materials, such as glass wool, in a small sized enclosure, there are few dominant modes which cause the condition that the incident wave to target material is biased toward the specific direction. As a result, the measured result shows the irregular distribution which depends on measuring point or evaluating method such as the reverberation time reading. The proposed system which utilized the active control enables us to create a plane wave with arbitrary direction in the enclosure. Therefore it has possibilities of solving the problems caused by insufficient incident condition. Also, in this study, the two evaluating strategies that the traditional reverberation time method and the steady state analysis method are concerned.

11:40

5aSAb8. Active control of engine noise transmitted into cavities: simulation, experimental validation and sound quality assessment. Leopoldo P. De Oliveira (KU Leuven, Celestijnenlaan 300B, Departement Werktuigkunde - PMA, 3001 Leuven, Belgium, leopoldo.deoliveira@mech.kuleuven.be), Paul Sas (KU Leuven, Celestijnenlaan 300B, Departement Werktuigkunde - PMA, 3001 Leuven, Belgium, Paul.Sas@mech.kuleuven.be), Wim Desmet (K.U.Leuven - Dept. of Mechanical Engineering, Celestijnenlaan 300B - bus 2420, 3001 Heverlee, Belgium, Wim.Desmet@mech.kuleuven.be), Karl Janssens (LMS International, Interleuvenlaan 68, 3001 Leuven, Belgium, Karl.Janssens@lmsintl.com), Peter Gajdatsy (LMS International, Interleuvenlaan 68, 3001 Leuven, Belgium, peter.gajdatsy@lmsintl.com), Herman Van Der Auweraer (LMS International, Interleuvenlaan 68, 3001 Leuven, Belgium, Herman.VanderAuweraer@lmsintl.com)

Active control has been proposed as a possible solution to cope with low frequency noise reduction in vehicles. Active noise control systems tend to be designed with a target on the sound pressure level reduction. However, the perceived control efficiency for the occupants can be more accurately assessed if psychoacoustic metrics are taken into account. The aim of this paper is to evaluate, numerically and experimentally, the effect of a collocated velocity feedback controller on the sound quality of engine noise in a vehicle mockup. The simulation scheme is described and experimentally validated. The engine excitation is provided by a sound quality equivalent engine simulator, running on a real-time platform that delivers harmonic excitation in function of the driving condition. The controller performance is evaluated in terms of sound quality metrics such as specific loudness and roughness. As a result of the control action, loudness is significantly reduced and roughness slightly spread, with an overall improvement on the perceived engine sound.

12:00

5aSAb9. Reproduction of loud low-frequency soundfields with Boundary Surface Control. Emmanuel Friot (Laboratory for Mechanics and Acoustics CNRS, 31 chemin Joseph Aiguier, 13009 Marseille, France, friot@lma.cnrs-mrs.fr), Régine Guillermin (Laboratory for Mechanics and Acoustics CNRS, 31 chemin Joseph Aiguier, 13009 Marseille, France, guillermin@lma.cnrs-mrs.fr), Cédric Pinhède (CNRS - LMA, 31 Chemin Joseph Aiguier, 13009 Marseille, France, pinhede@lma.cnrs-mrs.fr)

Many research works have focused on multichannel soundfield reproduction during the past decade, and complete systems are now commercially available for 3D sound control e.g., with Wave Field Synthesis. However, the usual underlying approximation of free-field propagation is not valid when reproducing high level low frequency noise, such as a sonic boom, inside a closet; a specific sound control strategy is required in this case. In this context the paper presents an experiment of low-frequency soundfield reproduction with open-loop control of the acoustic pressure at a set of 30 microphones enclosing a listening area. It is shown that this so-called Boundary Surface Control strategy allows an accurate reproduction of 3D soundfields inside the LMA sonic boom closet, equipped with 16 wall-embedded noise sources, at frequencies from 3 to 200 Hz.

12:20

5aSAb10. Experimental assessment of the performance of a "smart foam" absorber. Pierre M. Leroy (Laboratoire de Mécanique et d'Acoustique - CNRS, 31 chemin Joseph Aiguier, 13402 Marseille, France, leroy@lma.cnrs-mrs.fr), Philippe Herzog (Laboratoire de Mécanique et d'Acoustique - CNRS, 31 chemin Joseph Aiguier, 13402 Marseille, France, herzog@lma.cnrs-mrs.fr), Alain Berry (Univ. de Sherbrooke, Mechanical Engineering Depart., 2500 Boulevard de l'Université, Sherbrooke, QC J1K 2R1, Canada, alain.berry@usherbrooke.ca), Noureddine Atalla (Univ. de Sherbrooke, Mechanical Engineering Depart., 2500 Boulevard de l'Université, Sherbrooke, QC J1K 2R1, Canada, Nouredinne.Atalla@Usherbrooke.ca)

The signal processing implementation of a hybrid passive/active absorber (smart foam) made up from the combination of a passive absorbent (poroelastic melamine foam) typically efficient at the high frequencies, and a bonded, curved PVDF film, to enhance low frequency performance is considered. Three methods for obtaining the control signal are experimentally compared in the case of a plane wave excitation. A prototype of such smart foam has been built and tested in a waveguide (rectangular impedance tube) at frequencies between 100 Hz and 1000 Hz. The performances in term of the ratio of reflected to incident sound pressure are presented and discussed, comparing the three methods. The first method uses estimations of the transfer functions between the sources and two microphones in the tube to calculate off-line an optimal filter in the frequency domain. It is then compared with numerical simulations, based on a 3D FE model of the smart foam. The two other methods are based on a real-time adaptive control using a FXLMS algorithm, a unidirectional microphone as error sensor, and the primary source signal as reference signal. The control filter is obtained after the initial convergence, using either pure tone disturbance (secnd method) or broad band disturbance (third method).

12:40-2:00 Lunch Break

2:00

5aSAb11. Active vibration reduction applied to the compressor of an air-conditioning unit for trams. Joachim Bös (Fraunhofer Institute for Structural Durability and System Reliability LBF, Bartningstr. 47, 64289 Darmstadt, Germany, joachim.boes@lbf.fraunhofer.de), Enrico Janssen (Fraunhofer Institute for Structural Durability and System Reliability LBF, Bartningstr. 47, 64289 Darmstadt, Germany, enrico.janssen@lbf.fraunhofer.de), Michael Kauba (Fraunhofer Institute for Structural Durability and System Reliability LBF, Bartningstr. 47, 64289 Darmstadt, Germany, michael.kauba@lbf.fraunhofer.de), Dirk Mayer (Fraunhofer Institute for Structural Durability and System Reliability LBF, Bartningstr. 47, 64289 Darmstadt, Germany, dirk.mayer@lbf.fraunhofer.de)

Within the framework of the European Integrated Project InMAR (intelligent materials for active noise reduction) active vibration control and active structural acoustic control approaches are applied to an HVAC (heating, ventilation, and air conditioning) unit used to air-condition the driver's cab of a tram. Measurements previously performed by the manufacturer of the unit indicated that annoying tonal noise in the 50 Hz and 100 Hz 1/3 octave bands inside the driver's cab is mainly caused by the vibration of the compressor mounted in the HVAC unit on the roof of the tram. Therefore, two different concepts for the design of active compressor mounts were developed that are used to reduce the vibration excitation of the HVAC unit's housing. The first one is an active tuned vibration absorber whose natural frequency can be adapted by means of piezoelectric patch actuators and which behaves as a vibration compensator at higher frequencies. The second one is an active mount based on four piezoelectric stack actuators and an elastomer part that deflects the effective direction of the piezo stack displacement by 90 degrees while amplifying the displacement by a factor of approximately 30. These two concepts are compared with each other.

2:20

5aSAb12. Training by research - program of, and experiences in, the Smart Structures Research Training Network project. Fülöp Augusztinovicz (Budapest University of Technology and Economics, BME Dept. of Telecommunications, Magyar tudósok körútja 2, H-1117 Budapest, Hungary, fulop@hit.bme.hu)

Smart Structures is a Marie Curie Research Training network (RTN) named "A Computer Aided Engineering Approach to Smart Structures Design". The overall objective of the RTN is to develop an educational and research framework for developing macroscale noise control applications based on intelligent material systems. The scientific and technological objective of the network is to advance the state-of-the-art in smart materials research to the level of system integration and industrial applicability, with a specific focus on solutions for noise and vibration reduction and for vibration-based damage detection. The paper gives a short overview of the project partners' activity and summarizes the experiences of the researchers and their tutors after the first 18 months of the network.

2:40

5aSAb13. Intelligent interfaces for sound insulation: Numerical and experimental optimisation. Cedric Batifol (Centre Acoustique du LMFA, Ecole Centrale de Lyon, 36 avenue Guy de Collongue, 69134 Ecully cedex, France, cedric.batifol@ec-lyon.fr), Marie-Annick Galland (Centre Acoustique du LMFA, Ecole Centrale de Lyon, 36 avenue Guy de Collongue, 69134 Ecully cedex, France, marie-annick.galland@ec-lyon.fr), Mohamed Ichchou (Centre Acoustique du LMFA, Ecole Centrale de Lyon, 36 avenue Guy de Collongue, 69134 Ecully cedex, France, mohamed.ichchou@ec-lyon.fr)

Sound insulation is actually achieved thanks to passive multilayers. These ones are classically made of elastic, acoustic and poroelastic media. Good results are obtained in medium and high frequencies, but low frequencies disturbances still remain a problem. Indeed, local and global resonant behaviours of the panel, such as plate bending mode or the double-leaf phenomenon, occur and lower the performances. An active concept has already been proposed and validated. Piezoelectric components are added to the interface and act a secondary source aiming at minimising the sound transmitted. In this contribution, a double-plate system is studied. A reduced finite element model of an elementary cell is presented. This one relies on modal projection and classical component mode synthesis (CMS) procedures. This model is first updated and validated thanks to measurements performed on a dedicated test bench. The use of active control allows a 15 dB enhancement of sound insulation at low resonant frequencies. Numerical experiments are designed. Response surfaces are obtained thanks to kriging procedures. Finally, the configuration of the optimal interface is discussed in a physical point of view.

3:00

5aSAb14. Practical implementation of low-latency DSP for feedback control of sound in research contexts. Edgar Berdahl (Stanford Univ., Center for Computer Research in Music and Acoustics (CCRMA), Dept. of Music, Stanford, CA 94305-8180, USA, eberdahl@ccrma.stanford.edu), Nelson Lee (Stanford Univ., Center for Computer Research in Music and Acoustics (CCRMA), Dept. of Music, Stanford, CA 94305-8180, USA, nalee@stanford.edu), Guenter Niemeyer (Stanford Univ., Mech. Eng., Bldg. 530, Stanford, CA 94305, USA, gunter.niemeyer@stanford.edu), Julius O. Smith (Stanford Univ., Center for Computer Research in Music and Acoustics (CCRMA), Dept. of Music, Stanford, CA 94305-8180, USA, jos@ccrma.stanford.edu)

Feedback control of sound requires low-latency signal processing. In addition, because the human range of hearing extends roughly from 20 Hz to 20 kHz, controller hardware must process signals with relatively large bandwidths in comparison with common control applications. Over the past decade, the appropriate embedded hardware has become a niche product, so its cost has actually increased. The open source community has developed an excellent alternative: a general-purpose computer runs Linux with the real-time application interface (RTAI). Open source drivers (see www.comedi.org) enable software to communicate efficiently with data acquisition cards. For the first time, we describe in detail from start to finish how to configure such a system. In particular, we explain how to run control code from user space while still disabling interrupts. We further explain how to reserve a processor for running only feedback control code. This configuration achieves less than one sample of total system delay at sampling rates as high as 50 kHz. Other processors remain free to run standard Linux programs, allowing researchers to control sound with calls to many generic software libraries. We present detailed measurements of system jitter for various configurations and provide an example open-source toolbox demonstrating all these aspects at http://ccrma.stanford.edu/~eberdahl/Projects/TFCMI.

3:20

5aSAb15. From the electrical shunting of a loudspeaker to active impedance control. Hervé Lissek (Ecole Polytechnique Fédérale de Lausanne, EPFL STI LEMA, Station 11, CH 1015 Lausanne, Switzerland, herve.lissek@epfl.ch), Florian Sandoz (Ecole Polytechnique Fédérale de Lausanne, EPFL STI LEMA, Station 11, CH 1015 Lausanne, Switzerland, florian.sandoz@epfl.ch)

Variable acoustic properties can be obtained on an electroacoustic transducer's voicing face by very basic control strategies, among which are the shunting of the loudspeaker (shortcut, variable electric load, or negative resistance disposals). It is proven that better performances with enhanced controllability can be obtained by way of hybrid feedback control, consisting in a double feedback loop, one on acoustic pressure at the diaphragm and the other on its velocity, leading to a global acoustic impedance control. The present work describes the theory of the hybrid feedback control, by way of block diagrams aiming at visualizing the control principle, starting from the shunted loudspeaker. Simulations of performances obtained on Matlab/Simulink are presented, and compared to experimental results obtained on analog prototypes mounted at the end of a dedicated impedance tube. A last, a discussion on stability issues follows, leading to concluding remarks on the disposal behavior and possible means of enhancements.

3:40

5aSAb16. Active-passive multilayered panels for reduction of both acoustic reflection and transmission. Azzedine Sitel (Centre Acoustique du LMFA, Ecole Centrale de Lyon, 36 avenue Guy de Collongue, 69134 Ecully cedex, France, azzedine.sitel@ec-lyon.fr), Ying Hu (Centre Acoustique du LMFA, Ecole Centrale de Lyon, 36 avenue Guy de Collongue, 69134 Ecully cedex, France, ying.hu@ec-lyon.fr), Marie-Annick Galland (Centre Acoustique du LMFA, Ecole Centrale de Lyon, 36 avenue Guy de Collongue, 69134 Ecully cedex, France, marie-annick.galland@ec-lyon.fr)

The design of panels reducing both acoustic reflection and transmission for a wide frequency range is a problem of considerable practical interest for building or transport industries. Classically, these panels are made up of elastic plates bonded to poroelastic layers. Such structures are efficient in the middle and high frequency range but exhibit a lack of performance at low frequency. Hybrid passive/active cells previously developed at the LMFA have proved their efficiency for global noise reduction. They combine passive means (elastic plates, poroelastic material) and active control through a piezoelectric actuator to ensure high panel performance throughout the whole frequency range. In this paper, two systems are described. The first one is a multilayered panel combining two cells: the first cell on the emission side ensures high absorption, the second cell located at the rear face aims at reducing transmission. The second structure consists of a double-plate system using a microperforated plate on the emission side and an active plate on the transmission side. The performance of the two systems are examined through analytical or numerical simulations developed for plane waves and diffuse field conditions, and through experiments carried out for plane waves under normal incidence.

FRIDAY MORNING, 4 JULY 2008 P2-B, LEVEL 2, 9:40 TO 11:20 A.M.

Session 5aSAc

Structural Acoustics and Vibration and EURONOISE: Active Noise Control: New Strategies and Innovative Concepts II (Poster Session)

Alain Berry, Cochair
Univ. de Sherbrooke

Marie-Annick Galland, Cochair
Centre Acoustique du LMFA

All posters will be on display from 9:40 a.m. to 11:20 a.m. To allow contributors an opportunity to see other posters, contributors of odd-numbered papers will be at their posters from 9:40 a.m. to 10:30 a.m. and contributors of even-numbered papers will be at their posters from 10:30 a.m. to 11:20 a.m.

Contributed Papers

5aSAc1. New multichannel modified filtered-x algorithms for active noise control using the dichotomous coordinate descent method. Felix Albu (Politehnica University of Bucharest, Bd. Iuliu Maniu, no. 1-3, 061102 Bucharest, Romania, felix_albu@ieee.org), Constantin Paleologu (Politehnica University of Bucharest, Bd. Iuliu Maniu, no. 1-3, 061102 Bucharest, Romania, pale@comm.pub.ro)

In this paper, several multichannel modified filtered-x algorithms for active noise control or acoustic equalization systems using the dichotomous coordinate descent method (DCD) are introduced. This multiplierless and divisionless method is used for avoiding the matrix inversion that appears in adaptive algorithms such us fast transversal filters (FTF), recursive least square (RLS) based algorithms, affine projection (AP) or its fast versions. The study is focused on the important computational savings given by the use of DCD method, the effect on the convergence properties and stability of the investigated algorithms. A comparison of their convergence performance in case of using non-ideal noisy acoustic plants is also given. It is proved by simulations that the use of the dichotomous coordinate descent method can be an interesting option for reducing the computational cost of practical multichannel algorithms for ANC or acoustic equalization algorithms.

5aSAc2. Use of peak filter for online secondary path modeling in a feedforward active ship-noise cancellation system. Xueshan Bao (Department of Electronics and Telecommunications, Norwegian University of Science and Technology, Sem Sælands vei 5, 7491 Trondheim, Norway, xbao@iet.ntnu.no)

The injected auxiliary noise used in online secondary path modeling method often disturbs the convergence of control filter and increases the residual sound field energy of the active noise cancellation (ANC) system. To mitigate this problem, an improved online secondary path modeling method is proposed, in which the transfer function of secondary path is reconstructed by a peak filter. The frequency response of new transfer function remains unchanged at the frequency band of the noise to be cancelled; while the other bands are attenuated deeply. With this system the simulation experiment of active ship-radiated noise cancellation is accomplished. The result shows that new system's noise cancellation capability is improved and residual sound field energy (including channel response to injected auxiliary noise) is smaller than conventional system without peak filter because of the simplified transfer function of secondary path and reduced energy disturbance between control filter and modeling filter.

5aSAc3. Adaptive active noise control incorporating with a transfer function method for reducing acoustic feedback in a duct. Yun-Hui Liu (Southern Taiwan University, 1 Nan-Tai St, Yung-Kang City, 710 Tainan Hsien, Taiwan, yhliu@mail.stut.edu.tw)

In most practical applications of active noise control, the acoustic feedback is a major problem that often interferes with the operation of the control system and even renders it unstable. We propose a frequency-domain method based on transfer function to reduce the influence of acoustic feedback based on plane wave transmission theory of sound in a duct. The origi-

nal signal of primary noise is obtained from the measured signals of reference microphone and error microphone which are transformed to frequency domain by FFT and operated by the proposed method. In this study, Filtered-X LMS algorithm is applied to carry out the active noise controller incorporating with this transfer function method. Experimental results of active noise control show that the system has achieved 18.5 dB maximal attenuation in the frequency band 200-600 Hz. On the contrary, it is only attenuate 3-4 dB if acoustic feedback is present. Therefore, it was to verify that the proposed method of acoustic feedback cancellation incorporating with the Filtered-X LMS algorithm can effectively reduce the influence of acoustic feedback and obtains a better performance of active noise control in a duct.

5aSAc4. Secondary source distribution effect on active noise control robustness. Mahdi Azarpeyvand (Institute of Sound and Vibration Research, University of Southampton, University Road, SO17 1BJ Southampton, UK, ma@isvr.soton.ac.uk)

Arrangement of secondary sources and microphones play an important role in effectiveness and robustness of any active noise control (ANC) system. This paper concerns effective distribution of secondary sources for a typical ANC system so that provides a robust and acceptable level of noise reduction for different types of primary source, namely monopole, dipole and multipole, radiating at 100 Hz and 250 Hz. Two sets of secondary sources are considered here: planar distribution, and dome-type distribution. Results have shown that utilization of planar distribution model leads to more effective and stable noise reduction for most of the cases, while using a dome-type set of secondary sources is not able to effectively reduce noise from dipole and multipole primary sources. In addition, it was found that implementation of dome-type arrangement is more difficult than the planar distribution and is also very likely to become unstable for some particular source arrangements (i.e., or mathematically ill-conditioned).

5aSAc5. Improvement of acoustic transmission loss by active modal mass control. Vincent Lhuillier (Laboratoire Vibrations Acoustique - INSA Lyon, 25 bis avenue Jean Capelle, Bâtiment Saint-Exupéry, F-69621 Villeurbanne cedex, France, vincent.lhuillier@insa-lyon.fr), Charles Pezerat (Laboratoire Vibrations Acoustique - INSA Lyon, 25 bis avenue Jean Capelle, Bâtiment Saint-Exupéry, F-69621 Villeurbanne cedex, France, charles.pezerat@insa-lyon.fr), Simon Chesne (LaMCoS - INSA-Lyon - CNRS UMR5259, 18-20, rue des Sciences, Bâtiment Jean d'Alembert, F-69621 Villeurbanne, France, simon.chesne@insa-lyon.fr), Luc Gaudiller (LaMCoS - INSA-Lyon - CNRS UMR5259, 18-20, rue des Sciences, Bâtiment Jean d'Alembert, F-69621 Villeurbanne, France, luc .gaudiller@insa-lyon.fr)

This paper deals with an alternative modal control approach to reduce the sound transmission through a structure excited by an acoustic wave. Active control enables to conserve the characteristics of lightness while improving acoustic performances. For light and small structures having small modal overlap, the ″modal mass damping control″ is proposed. The aim of this control is to modify the modal distribution of high radiation efficiency modes with modal virtual mass and modal virtual damping. The interest of this approach is that at low frequencies, the active virtual mass effects shift down eigen frequencies to less audible frequency range while reducing vibration amplitudes in a broad frequency range. The modal virtual mass control appears to be a good complement to a standard damping control which is exclusively efficient at resonances. In order to detail the concept of the proposed method, an application is presented on a double panel equipped with piezoelectric patches. The structure is excited by a distributive acoustic plane wave. Acoustic transmission loss factors of the simulated controlled and the non-controlled smart structure are shown and optimization is discussed.

5aSAc6. A two-dimensional ANC system - from simulation to application. Christian Kleinhenrich (Univ. of Wuppertal, Rainer-Gruenter-Str. 21, 42119 Wuppertal, Germany, c.kleinhenrich @uni-wuppertal.de), Detlef Krahé (Univ. of Wuppertal, Rainer-Gruenter-Str. 21, 42119 Wuppertal, Germany, krahe@uni-wuppertal.de), Arndt Niepenberg (WaveScape Technologies GmbH, Lise-Meitner-Str. 1-9, 42119 Wuppertal, Germany, niepenberg@wavescape-technologies.com)

An existing two-dimensional active noise control (ANC) system attenuates a given noise (primary field) inside a certain area and frequency range by an additionally generated sound (secondary field). The two-dimensional ANC system consists of several modules containing a pair of microphones and a line array of loudspeakers each. The configuration of the modules depends on the acoustical environment and the desired shape of the protection area. Planning this is supported by a tool based on simulating the superposition of both sound fields. This spatial, close to reality simulation for predicting the achievable noise attenuation and determining important system parameters is implemented in MATLAB. With this planning tool it is possible to place all required acoustic sources and sinks into a virtual room and analyze the properties of the resulting sound field concerning real application scenarios. This paper draws a comparison between the results given by simulation and the subsequently realized ANC system within the scope of a typical application.

5aSAc7. Active noise control in light jet aircraft. Oliver Pabst (Helmut-Schmidt-Universität - Universität der Bundeswehr Hamburg, Holstenhofweg 85, 22043 Hamburg, Germany, opabst@hsu-hh.de), Thomas Kletschkowski (Helmut-Schmidt-Universität - Universität der Bundeswehr Hamburg, Holstenhofweg 85, 22043 Hamburg, Germany, thomas .kletschkowski@hsuhh.de), Delf Sachau (Helmut-Schmidt-Universität - Universität der Bundeswehr Hamburg, Holstenhofweg 85, 22043 Hamburg, Germany, sachau@hsuhh.de)

Active systems for noise reduction are especially of interest when considering applications in which low-frequency noise is a main source of disturbance and only limited amounts of installation space and payload are available. This makes the adaptation and implementation of such systems plausible in vehicles such as automobiles and aircraft where passive reduction methods are restricted. In order to achieve effective active control in these environments, aspects such as the control method and actuator- and sensor-type as well as positioning must be considered. The noise characteristics are often known beforehand or are easily accessible by measurement. Using this data, an upper bound for possible noise reduction may be determined, e.g., by means of linear prediction methods. A current research project is aimed at developing an audiosystem for the cabin area of a light jet aircraft which, at the same time, should also function as an effective noise reduction system in order to enhance the cabin comfort as well as the audio quality. Using data from a measurement flight in a typical light jet aircraft, limitations of active control are determined. Furthermore, the testbed, an acoustic mockup, is presented, currently beholding a multichannel ANC- Audio system for tonal and broadband noise.

Session 5aSAd

Structural Acoustics and Vibration, ASA Committee on Standards, and EURONOISE: Ground Vehicle Noise and Vibration II (Poster Session)

Donald Bliss, Cochair
Duke University

Paul De Vos, Cochair
DHV BV

All posters will be on display from 9:40 a.m. to 11:20 a.m. To allow contributors an opportunity to see other posters, contributors of odd-numbered papers will be at their posters from 9:40 a.m. to 10:30 a.m. and contributors of even-numbered papers will be at their posters from 10:30 a.m. to 11:20 a.m.

Contributed Papers

5aSAd1. An hybrid method for sound transmission inside trains. Philippe A. Jean (CSTB, 24 rue Joseph Fourier, 38400 Saint-Martin-d'Hères, France, philippe.jean@cstb.fr), Michel Villot (CSTB, 24 rue Joseph Fourier, 38400 Saint-Martin-d'Hères, France, michel.villot@cstb.fr)

Hybrid methods mixing ray-tracing and energy approaches have been implemented and validated in the case of sound transmission inside a train. Generally, validation is proposed against measurements where it may be difficult to assess precisely the importance of the various assumptions and simplifications. In this paper, the proposed hybrid approach is compared to more precise numerical computations based on BEM and analytic models. This allows studying the importance of assumptions made on the computations of incident power and transmitted power. The case of a train in a tunnel has also been analysed where the sound field in the tunnel is computed by means of 2.5D BEM.

5aSAd2. Critical assessment of operational path analysis: effect of coupling between path inputs. Peter Gajdatsy (LMS International, Interleuvenlaan 68, 3001 Leuven, Belgium, peter.gajdatsy@lmsintl.com), Karl Janssens (LMS International, Interleuvenlaan 68, 3001 Leuven, Belgium, Karl.Janssens@lmsintl.com), Ludo Gielen (LMS International, Interleuvenlaan 68, 3001 Leuven, Belgium, ludo.gielen@lms.be), Peter Mas (LMS International, Interleuvenlaan 68, 3001 Leuven, Belgium, peter.mas@lms.be), Herman Van Der Auweraer (LMS International, Interleuvenlaan 68, 3001 Leuven, Belgium, Herman.VanderAuweraer@lmsintl.com)

Classical transfer path analysis (TPA) is a widely used and reliable method for tackling noise and vibration problems. But due to its complexity and time-consuming procedure the industry is constantly seeking for simpler and faster methods. One such method, often referred to as operational path analysis (OPA), was presented in 2006 and has quickly gained popularity in the NVH field. The method works with measured operational input and output accelerations and sound pressures and the transmissibilities calculated from these. The claim for its accuracy is based on being able to reproduce the original output signal by summing the calculated partial contributions but it has not yet been compared to other TPA methods. This new method is now critically examined and compared to a reliable classical TPA measurement. The results of this examination reveal three significant weaknesses. This paper deals with the effect of the cross-coupling between the input signals. Due to modal behavior a single force will cause vibrations at all inputs. Thus, there is not a simple one-to-one relationship between loads and inputs. This coupling then can easily lead to false identification of significant paths in case of the OPA method.

Session 5aSCa

Speech Communication: Speaker Identification by Machine

Jaime Hernández-Cordero, Cochair
US Department of Defense, PO BOX 183, Odenton, MD 21113, USA

Louis-Jean Boë, Cochair
GIPSA-lab, Université Stendhal, 1180, avenue Centrale, 38031 Grenoble CEDEX 9, France

Contributed Papers

8:00

5aSCa1. Adaptive threshold estimation for speaker verification systems. Eduardo Castilllo-Guerra (University of New Brunswick, P.O. Box 4400, 15 Dineen Dr., D36 Head Hall, Fredericton, NB E3B 5A3, Canada, ecastill@unb.ca), Roberto Díaz-Amador (Central University of Las Villas, Carr. a Camajuaní km 5.5, 50100 Santa Clara, Cuba, ramador@uclv.edu.cu), Cárdenas-Barreras L. Julian (Central University of Las Villas, Carr. a Camajuaní km 5.5, 50100 Santa Clara, Cuba, jcardenas @uclv.edu.cu)

This paper describes an adaptive threshold estimation mechanism for speaker authentication systems. The mechanism estimates speaker-dependent thresholds based on successful verifications considering the minimization of a relation-based cost function. Speaker authentication systems commonly use a threshold to decide whether a claimed identity matches a voice-print previously enrolled. Speaker independent threshold is a common option but it does not consider specific speaker characteristics that are relevant to achieve better system performance. Speaker dependent threshold on the contrary, uses speaker-specific data to estimate individual thresholds but the system performance can also suffer from suboptimal threshold conditioned by limited number of true scores. The algorithm reported in this paper starts with the speaker dependent threshold and use an adaptive algorithm to perform online re-estimation of the initial threshold based on speaker-dependent data. The threshold is re-estimated in each successful authentication transaction according to a custom-made confidence score. The reported technique keep the voice print up-to-date while is less sensitive to score outliers than traditional speaker dependent threshold. The algorithm provided a performance enhancement of up to 36.2% when compared to traditional speaker independent or dependent threshold using an ad-hoc database involving cell and land-line utterances from male and female speakers.

8:20

5aSCa2. Estimation of target-to-interferer ratio using the Auditory Image Model. Michael Carlin (Air Force Research Laboratory, 525 Brooks Road, Rome, NY 13441, USA, Michael.Carlin@rl.af.mil)

Performance in speech processing applications such as speaker recognition becomes severely degraded when the short-time audio being analyzed contains more than one speaker. However, it has been shown that if the audio is only minimally-corrupted by the interfering speech, i.e., the target-to-interferer ratio (TIR) is sufficiently large, then accurate recognition results can still be achieved. During phonation, estimation of TIR is especially critical since uncorrupted vowel sounds contain important speaker-discriminating information. This research investigates a method to estimate the relative intensity of interfering speech using the Auditory Image Model (AIM) of Patterson et al. (J. Acoust. Soc. Am., **98**, 1890-1894 (1995)). The proposed TIR estimator attempts to exploit both the apparent high resolution in the simulated Neural Activity Pattern and variation in cross-channel Strobe Point correlation when observing overlapping vowel sounds. Experiments were conducted for five canonical male vowels which were perceptually-scaled using the STRAIGHT algorithm (Chapter in Speech Separation by Humans and Machines, P. Divenyi, ed., Kluwer Academic Publishers, 2005) and superimposed at varying levels of TIR. Results suggest that the proposed approach is a promising step towards both detecting the presence and relative intensity of an interfering speaker.

8:40

5aSCa3. Extraction of likelihood-ratio forensic evidence from the formant trajectories of diphthongs. Geoffrey Stewart Morrison (Australian National University, School of Language Studies, Building 110, ACT 0200 Canberra, Australia, geoff.morrison@anu .edu.au), Phil Rose (Australian National University, School of Language Studies, Building 110, ACT 0200 Canberra, Australia, philip.rose@anu.edu.au), Yuko Kinoshita (University of Canberra, School of Languages and International Studies, ACT 2601 Canberra, Australia, yuko.kinoshita@canberra.edu.au)

The likelihood-ratio approach to forensic speaker recognition seeks to determine the likelihood that one would observe the evidence, the acoustic difference between suspect and offender speech samples, under the hypothesis that they were produced by the same speaker versus under the hypothesis that they were produced by different speakers. Before the results of a scientific forensic technique can be presented in court, it is necessary to demonstrate its efficacy. This presentation tests the efficacy of extracting information from the formant trajectories of diphthongs. Differences in physiology and learned motor patterns could potentially lead to different speakers producing quite different formant trajectories which could in turn lead to strong forensic evidence. The data tested were /aI/, /aʊ/, /eI/, /″open o″I/, /oʊ/, /i″schwa″/, and /ɛ″schwa″/ tokens produced in several phonetic contexts by 27 male speakers of Australian English. Cubic polynomials were fitted to each vowel token, and the coefficient values were used in a multivariate-kernel-density procedure which calculated likelihood ratios. Cross-validated same-speaker and different-speaker comparisons were made, resulting in a series of same-speaker and different-speaker likelihood ratios for each vowel phoneme. Results indicated that substantial strength of evidence with respect to speaker identity can be extracted from diphthong formant trajectories.

9:00

5aSCa4. Identifying speaker-dependent acoustic parameters in Spanish vowels. Victoria Marrero (Universidad Nacional Educación a Distancia, Desp. 707A. C/ Senda del Rey, 7, 28040 Madrid, Spain, vmarrero@flog.uned.es), Elena Battaner (URJC, C/Tulipan s/n, 28345 Móstoles (Madrid), Spain, elena.battaner@urjc.es), Juana Gil (Universidad Nacional Educación a Distancia, Desp. 707A. C/ Senda del Rey, 7, 28040 Madrid, Spain, mgil@flog.uned.es), Joaquim Llisterri (UAB, Filologia. Edifici B. Campus Bellaterra, 08193 Barcelona, Spain, Joaquim .Llisterri@uab.cat), María Machuca (UAB, Filologia. Edifici B. Campus Bellaterra, 08193 Barcelona, Spain, MariaJesus.Machuca@uab .es), Montserrat Marquina (UAB, Filologia. Edifici B. Campus Bellaterra, 08193 Barcelona, Spain, Montserrat.Marquina@campus.uab.es), Carme De La Mota (UAB, Filologia. Edifici B. Campus Bellaterra, 08193 Barcelona, Spain, Carme.delaMota@uab.cat), Antonio Rios (UAB, Filologia. Edifici B. Campus Bellaterra, 08193 Barcelona, Spain, Antonio.Rios@uab.cat)

In the frame of VILE Projects (Inter-and-Intra-Speaker-Variation-in-Spanish for automatic speaker identification), we try to identify what

vowel's acoustic parameters depend more on the individual characteristics of the speaker and less of the linguistic variables. Variations on standard deviation (SD), when grouping together parameters by speaker or by phoneme, are analysed. 30 speakers (from AHUMADA database) read the same text in three sessions. Mean value (Hz) of four formants (F1-F2-F3-F4) and fundamental frequency (F0) are analysed in Spanish vowels (except /u/), surrounded by unvoiced stops or /s/ (1850 samples). Hypothesis: Individual parameters will show less SD when grouping by speaker/session; vowel quality parameters, when grouping by phoneme. F1 and F2 are timbre-dependent parameters. F3 and F4 are speaker-dependent parameters. F0 has characteristics of both. The most variable parameter is F2. The opposite is F4. -No significant differences grouping by session or by speakers in none of the parameters. -F0 has the highest variability between vowel qualities, even if stressed and unstressed vowels are separated. -When clustering data by speaker/sessión (all vowels together), by comparison with clustering by vowel (all speakers together), SD is *50% higher in F1-F2 *75% lesser in F4 *66% lesser in F0 *F3 shows no significant differences

9:20

5aSCa5. The question of disguised voice. Patrick Perrot (Telecom Paris Tech, 46 rue Barrault, 75013 Paris, France, perrot@tsi.enst.fr), Gerard Chollet (Telecom Paris Tech, 46 rue Barrault, 75013 Paris, France, chollet @enst.fr)

State of the art automatic speaker recognition systems show very good results in the discrimination between different speakers under controlled recording conditions. In a forensic context, the conditions are uncontrolled and voice can be disguised. In cases of terrorism claim, extortion or kidnapping, it is of great interest for offenders to conceal their identity. Voice disguise is an important constraint to speaker discrimination. Some disguises produce a great variation of parameters and change the perception of an identity. The main risk is to confound a disguised voice and a normal voice and accuse an innocent individual. This paper proposes on one hand to present the impact of voice disguise on automatic speaker recognition and, on the other hand a statistical study in order to detect and identify four disguises among the most common. The first step consists in extracting features and the second step to classify them. MFCC (Mel Frequency Cepstral Coefficient) are considered as features and different classification algorithms have been tested. The studied disguises are based on a deliberated and non electronic way. The proposed analysis of disguised voice classification provides interesting results in detection by the use of SVM (Support Vector Machine) and in identification by the use of GMM (Gaussian mixture models).

9:40

5aSCa6. Speaker identification on the SCOTUS corpus. Jiahong Yuan (University of Pennsylvania, 609 Williams Hall, Philadelphia, PA 19104, USA, jiahong@ling.upenn.edu), Mark Liberman (University of Pennsylvania, 609 Williams Hall, Philadelphia, PA 19104, USA, myl@cis .upenn.edu)

This paper reports the results of our experiments on speaker identification in the SCOTUS corpus, which includes oral arguments from the Supreme Court of the United States. Our main findings are as follows: 1) a combination of Gaussian mixture models and monophone HMM models attains near-100% text-independent identification accuracy on utterances that are longer than one second; (2) the sampling rate of 11025 Hz achieves the best performance (higher sampling rates are harmful); and a sampling rate as low as 2000 Hz still achieves more than 90% accuracy; (3) a distance score based on likelihood numbers was used to measure the variability of phones among speakers; we found that the most variable phone is the phone UH (as in good), and the velar nasal NG is more variable than the other two nasal sounds M and N; 4.) our models achieved "perfect" forced alignment on very long speech segments (one hour). These findings and their significance are discussed.

10:00

5aSCa7. Dependency of recognition rate on number of words for text-independent speaker recognition using vector quantization. Hidenori Shimizu (Div. of Electronic Eng. and Computer Sci., Kanazawa Univ., Kakuma-machi, 920-1192 Kanazawa-shi, Japan, shimizu@oak .ec.t.kanazawa-u.ac.jp), Tetsuo Funada (Div. of Electronic Eng. and Computer Sci., Kanazawa Univ., Kakuma-machi, 920-1192 Kanazawa-shi, Japan, funada@t.kanazawa-u.ac.jp)

In this research, we discuss speaker recognition using the Kohonen feature map. The map is constructed for each speaker, and it is trained by using log-power and fourteenth-order mel-frequency cepstral coefficients (MFCC) and their temporal difference. The quantization distortion is computed between the input speech and a specific vector on the feature map of each speaker. We conduct speaker recognition experiment based on VQ distortion. Utterances of prefectural name in Japan are used as speech data. We examine particularly the dependency of recognition rate on number of words used for recognition. According to our experiments of speaker identification, this system correctly recognizes 98.9% by using a single word for 40 male speakers, while it attains 100% by using more than three words. Moreover, we confirmed superiority of using VQ over HMM under the same experimental conditions.

Session 5aSCb

Speech Communication: Cross-Language Speech Perception and Production

Yue Wang, Cochair
Simon Fraser Univ., RCB 9224, 8888 Univ. Dr., Burnaby, BC V5A 1S6, Canada

Dawn Behne, Cochair
Norwegian University of Science and Technology, Psychology Dept, Trondheim, NO 7491, Norway

Invited Papers

8:40

5aSCb1. Sound structure and function of English as a global language. Ann Bradlow (Northwestern University, Department of Linguistics, 2016 Sheridan Road, Evanston, IL 60208, USA, abradlow@northwestern.edu)

Many English conversations across the globe today involve non-native speakers. To understand the sound structure of English in a global context, we asked native and non-native listeners to rate the similarity of various languages (n=17) to English. In general, the native and non-native listeners' distance-from-English ratings were positively correlated; but, the non-natives tended to rank languages as more distant from English than the natives. Native and non-native listeners then rated the accents of native and non-native speakers. Again, the native and non-native listener ratings were positively correlated, but the non-native listeners generally rated both native and non-native speakers as more foreign-accented than did the native listeners. Together, these data suggest that both native and non-native English generally sound less "marked" to native listeners than to non-native listeners. As a means of understanding how English functions as a global language, we examined communicative efficiency in task-oriented dialogues between various combinations of natives and non-natives. All pairs successfully completed the task; yet, when one or more non-native talkers were involved, the task took about twice as long to complete as when both were native talkers. Together, these studies help characterize the structure and function of English as a twenty-first century lingua franca.

9:00

5aSCb2. Maintainance vs. "loss" of the perceptual bias favoring natural reference vowels. Ocke-Schwen Bohn (Aarhus University, English Department, J.-C.-Skous Vej 5, DK-8000 Århus C, Denmark, engosb@hum.au.dk), Linda Polka (McGill University, School of Communication Sciences and Disorders, Beatty Hall, 1266 Pine Avenue West, Montreal, QC H3G 1A8, Canada, linda.polka@mcgill.ca)

Previous infant vowel discrimination studies (Polka & Bohn, 2003) have shown that babies are perceptually biased to favor vowels with more extreme articulations such that a change from a more peripheral vowel ("natural reference vowel" - NRV) to a vowel located more centrally in the vowel space is less discriminable than a change presented in the reverse direction. Recent studies of adult vowel perception suggest that the universal bias favoring NRVs is maintained in the absence of specific language experience and but "lost" if native or non-native language experience causes a reset of the perceptual default favoring NRVs. This presentation reports on vowel discrimination experiments which examined whether absence or presence of specific vowel experience is related to maintenance or loss of this perceptual bias in Danish infants (age 6-12 months). For two Danish vowel contrasts, asymmetries were observed for younger infants, but not for infants older than 10 months. For an English vowel contrast that does not exist in Danish, the asymmetry was maintained in infants up to 12 months and in adult Danish listeners. Results confirm the assumption that the perceptual bias favoring NRVs is maintained throughout the lifespan unless specific vowel experience causes on override. [Work supported by the Danish Research Council for the Humanities.]

9:20

5aSCb3. Cross-language auditory-visual speech perception development. Denis Burnham (MARCS Auditory Laboratories, University of Western Sydney, Locked Bag 1797, Penrith South, NSW, 1797 Sydney, Australia, d.burnham@uws.edu.au), Kaoru Sekiyama (Kumamoto University, Division of Cognitive Psychology, Faculty of Letters, 861-0000 Kumamoto, Japan, sekiyama@kumamoto-u.ac.jp), Dogu Erdener (MARCS Auditory Laboratories, University of Western Sydney, Locked Bag 1797, Penrith South, NSW, 1797 Sydney, Australia, d.erdener@uws.edu.au)

Speech perception is auditory-visual (AV), but there is more visual information use by English than Japanese language perceivers (Sekiyama & Tohkura, 1993). This raises two questions: (1) when and (2) why do such differences emerge? In Experiment 1 with English- and Japanese-language children (6, 8, 11 years) and adults, AV speech perception (AVSP) was equivalent in English and Japanese 6-year-olds, significantly increased between 6 and 8 years in English- but not Japanese-language children, and remained stable over all ages for the Japanese. The origin of the Japanese-English adult difference in English language children's dramatic rise in AVSP between 6 and 8 years was investigated in Experiment 2. English-language children (5 to 8 years) and adults were tested for AVSP,

reading, articulation, and language-specific speech perception (focus on native and away from non-native speech sounds, a known correlate of reading, Burnham, 2003). Regressions showed that language specific speech perception reliably predicted AVSP. It appears children use extra information (AVSP) in the face of challenging linguistic hurdles (learning to read), but only when the language is phonetically complex and the phoneme-to-grapheme conversion rules of the script are not transparent (English, but not Japanese).

Contributed Paper

9:40

5aSCb4. Dependence of corresponding phonetic categories in native bilingual speakers and in monolingual overhearers of English and French. Carol A. Fowler (Haskins Laboratories, 300 George St, Suite 900, New Haven, CT 06511, USA, carol.fowler@haskins.yale.edu)

Our research addresses two main questions. First, among phonetic categories that correspond, but are not identical, in the two languages of native bilingual speakers, are there cross-language influences on speech production? Specifically, are the voiceless voice-onset times (VOTs) of bilingual speakers of English and French in Montreal longer in their French speech and shorter in their English speech than the VOTs of monolingual speakers of the two languages in Montreal? Our findings suggest a positive answer. Second, does mere overhearing of a language that one does not speak have an impact on production of phonetic categories? To answer this, we examined the voiceless VOTs of monolingual speakers of French and English in Montreal (who hear substantial unaccented English and French, respectively) with those, respectively, of monolingual speakers of French in Paris and of English in Connecticut. Our answer here was no. I discuss the implications of these findings for an understanding of the phonetic knowledge systems of monolingual and natively bilingual speakers.

Invited Paper

10:00

5aSCb5. Plurality and plasticity of neural representation for speech sounds. Yang Zhang (University of Minnesota, Dept. of Speech-Language-Hearing Sci. & Center for Neurobehavioral Development, Minneapolis, MN 55455, USA, zhang470@umn.edu)

High-density event-related potential (ERP) and magnetoencephalography (MEG) data are presented here to illustrate the plurality and plasticity of speech representation in the spatio-temporal dynamics of neural responses. First, there is evidence for both continuous and discrete processing of speech sounds depending on the acoustic parameters and experimental conditions. Speech discrimination and neural sensitivity measures suggest that the perceptual organization of within-category variations is based on both phonetic knowledge and acoustic analysis. Second, attention plays an important role in determining the neural response patterns. Focused attention significantly changes the hemispheric laterality and strength of neural activation for speech processing. Selectively attending to the different aspects (phonetic vs social-indexical information) of the same speech stimuli shows different regional recruitment, hemispheric involvement and temporal characteristics. Third, the nature of language input and experience can significantly affect learning outcome. Enriched exposure alters the neural representations for speech sounds and plasticity of the system. Theoretical and practical implications for language learning and treatment are discussed.

Session 5aSCc

Speech Communication: General Topics in Speech Communication IV (Poster Session)

Linda Polka, Cochair
McGill University

Christine Mooshammer, Cochair
Haskins Lab and MIT Research Lab of Electronics

Suzanne Boyce, Cochair
Department of Communication Sciences and Disorders, University of Cincinnati

All posters will be on display from 10:20 a.m. to 12:00 a.m. To allow contributors an opportunity to see other posters, contributors of odd-numbered papers will be at their posters from 10:20 a.m. to 11:10 a.m. and contributors of even-numbered papers will be at their posters from 11:10 a.m. to 12:00 p.m.

Contributed Papers

5aSCc1. Call early in the evening on a spring day. Maxine Eskenazi (Language Technologies Institute Carnegie Mellon University, 4619 Newell Simon Hall, 5000 Forbes Ave, Pittsburgh, PA 15213, USA, max@cs.cmu.edu), Antoine Raux (Language Technologies Institute Carnegie Mellon University, 4619 Newell Simon Hall, 5000 Forbes Ave, Pittsburgh, PA 15213, USA, antoine@cs.cmu.edu)

The CMU Let's Go Spoken Dialogue System has been used daily for about three years to answer calls to the Pittsburgh Port Authority for bus information in the evening and on weekends. This has resulted in a database of over 50 000 spoken dialogues as of January 2008, one of the largest publicly available sets of this type of data. While retraining the system with part of this data, it became apparent that there are times of the day, of the week and of the year when the average number of successful calls is significantly higher. We will present evidence, using these three measures of time (hour, day of week, month of year) and criteria such as signal-to-noise ratio, estimated success rate, number of turns per dialogue, number of non-understandings per dialogue, and barge-in rate to detect the regular, predictable appearance of high and low success rates and to suggest methods for palliating this effect in order to increase overall dialogue success rates.

5aSCc2. Duration modeling for English letters embedded in Chinese speech. Wen-Hsing Lai (National Kaohsiung First University of Science and Technology, No. 2, Jhuoyue Rd., Nanzih District, 811 Kaohsiung, Taiwan, lwh@ccms.nkfust.edu.tw)

A review of existing multilingual TTS (text-to-speech) systems shows that the secondary language inserted into the primary language sounds more like isolated individual words in an alien language environment and not congruous with the primary language's prosody. Since the letter-by-letter spelling of English words or acronyms appears in Chinese speech quite often, a duration modeling approach for English letters embedded in Chinese speech is proposed to make the English congruous with the primary language's tempo. It takes several major factors as additive factors and estimates all model parameters by an EM (expectation-maximization) algorithm. Experimental results showed that the standard deviation of the duration from the test set was greatly reduced from 59.82 to 9.37 ms by the duration modeling while eliminating effects from factors. The root mean squared error between the original and estimated durations was 9.35 ms for the open tests. Experimental results have confirmed its effectiveness on isolating several main factors that seriously affects the duration. Moreover, the estimated value of the factors agreed well to our prior linguistic knowledge. Besides, the hidden state labels produced by the EM algorithm were linguistically meaningful.

5aSCc3. Modeling perception of breathy voice quality in vowels using data obtained in an adaptive matching task. Rahul Shrivastav (University of Florida, Dauer Hall, P.O. Box 117420, Dept. of Communication Sciences and Disorders, Gainesville, FL 32611, USA, rahul@csd.ufl.edu), Arturo Camacho (University of Florida, Dauer Hall, P.O. Box 117420, Dept. of Communication Sciences and Disorders, Gainesville, FL 32611, USA, arturocl@yahoo.com), Sona A. Patel (University of Florida, Dauer Hall, P.O. Box 117420, Dept. of Communication Sciences and Disorders, Gainesville, FL 32611, USA, sona09@ufl.edu), David A. Eddins (University of Rochester, Department of Otolaryngology, Rochester, NY 14618, USA, David_Eddins@URMC.Rochester.edu)

A computational model of breathy voice quality has been developed based on perceptual judgments of synthetic /a/ vowels [Shrivastav, Camacho, and Patel, JASA **120**(5), 3248]. This model is based on the ratio of the loudness of aspiration noise ("noise loudness;" NL) to the loudness of the periodic components of the vowel when masked by the aspiration noise ("partial loudness;" PL) [Shrivastav and Sapienza, JASA, **114**(1), 2218-2224 (2005)]. Results showed that the model accounted for a large amount of variance in perceptual ratings of training data (R-square=0.92) but not for testing data (R-square=0.59). It was hypothesized that this reduction was partly related to the use of a magnitude estimation task to obtain perceptual judgments, since magnitude estimates are biased by the range of the quantity measured and are prone to inconsistencies in how subjects assign numbers to items [Poulton, 1989; Guilford, 1954]. To minimize such biases, a matching task may be used to obtain ratio level estimates of breathiness [Patel, Shrivastav and Eddins, JASA, **119**(5), 3340 (2006)]. The present study describes a model to predict breathy voice quality derived from perceptual judgments obtained using a matching task.

5aSCc4. The effect of training in noise on foreign language consonant acquisition. M. Luisa Garcia Lecumberri (University of the Basque Country, Paseo de la Universidad 5, Facultad de Filologia, 01006 Vitoria, Spain, garcia.lecumberri@ehu.es), Martin Cooke (Sheffield University, Computer Science Department, Regent Court, 211 Portobello St., S1 4DP Sheffield, UK, m.cooke@dcs.shef.ac.uk)

Formal exposure to second language sounds normally takes place in clean, laboratory conditions, but at issue is the transfer of such learning to everyday situations. Categories learned in non-natural settings may be fragile, raising the question as to whether learning in noise leads to greater category robustness. The current study compared two groups of Spanish learners of English who were trained in either quiet or noise backgrounds on a 24 consonant discrimination task. Learners' performance was measured in pre- and post-tests and monitored over the course of nine weeks' training. Both groups showed continual improvement during training with similar overall gains of 6-7 percentage points, suggesting that training in adverse conditions is as effective as in quiet. Tests involving consonant identification in quiet and noise revealed no significant differences in pre-post improvement between the two groups. However, voiceless obstruents benefited more from training in noise while voiced obstruents experienced more improvement when trained in a quiet background regardless of the testing condition (quiet vs noise). The noise-trained disadvantage is consistent with masking of voicing in noise, while the quiet-trained deficit for voiceless obstruents may derive from overgeneralisation during the acquisition of new contrasts.

5aSCc5. Analyze effects of the flow on the vocalic reduction and the coarticulation in sequences CV of pharyngal Arabic. Leila Falek (USTHB, Faculté d'électronique et d'Informatique, 16111 Algiers, Algeria, lilalcpts@yahoo.fr), Othmane Bouferroum (USTHB, Faculté d'électronique et d'Informatique, 16111 Algiers, Algeria, lilalcpts@yahoo.fr), Amar Djeradi (USTHB, Faculté d'électronique et d'Informatique, 16111 Algiers, Algeria, lilalcpts@yahoo.fr)

The degree of coarticulation and the vocalic reduction (RV) are indices related to a good engine control (Gay, 1978). Fowler (1998) explains why locus equation (LE) is used to characterize, at the same time, the place of articulation and the degree of coarticulation between consonants and vowels: a strong slope (m=1) indicates a maximum coarticulation between consonants and vowels (i.e., minimal resistance of the coarticulation), while a weak slope (m=0) indicates absence of coarticulation between consonants and vowels (maximum resistance of the coarticulation). The bond between the degree of coarticulation and the RV can be explained according to the linear relation between F2onset and F2milieu: the modifications of values of F2milieu will affect those of F2onset and consequently those of the slopes of. In this study, the analysis of the vocalic reduction and slopes of the equations of locus, carried out on CV (extracts starting from sentences) in standard Arabic pronounced by speakers having different mother tongues (near to Arabic standard and very far away from standard Arabic), and at speed of variable elocution, revealed a vocalic reduction and a variation of the slope of the locus equation, specific to each speaker, who seems to be related to his mother tongue. El Tamimi (2006) carried out a similar study with normal flow, in dialectical Arabic and in French, with normal flow, an influence of the mother tongue showed on the vocalic reduction and the slope of the equation of locus.

5aSCc6. A comparison between two cases of voicing neutralization: Final devoicing and voicing assimilation in obstruent clusters. Rebeka Campos-Astorkiza (Ohio State University, Dept. Spanish & Portuguese, 298 Hagerty Hall, 1775 College Rd, Columbus, OH 43210, USA, campos-astorkiza.1@osu.edu)

This study compares two processes that result in voicing neutralization, namely final obstruent devoicing and regressive voicing assimilation in obstruent clusters in Lithuanian. The goal is to find out whether both neutralizing environments present similar acoustic patterns. Acoustic data was collected from native speakers of Lithuanian in order to analyze /k/ and /g/ in word final position (final devoicing) and in the word medial clusters /gs/, /ks/, /kz/ and /gz/ (voicing assimilation). Three main acoustic cues to obstruent voicing were measured: obstruent closure duration, voicing during closure and duration of preceding vowel. The statistical results show that, although both final devoicing and voicing assimilation result in incomplete voicing neutralization, they use the acoustic cues differently. In the case of voicing assimilation, there are statistically significant differences in closure duration, voicing during closure and preceding vowel duration between the stops in /ks, gz/ and their assimilated counterparts in /gs, kz/. As for final devoicing, underlyingly voiceless obstruents and devoiced obstruents show differences in their closure duration and voicing during closure but not in their preceding vowel duration. These results suggest that final devoicing and voicing assimilation have different acoustic realizations in Lithuanian, supporting their analysis as two different processes.

5aSCc7. Effectiveness of prosodic features in the perception of mandarin utterance-final particles. Bin Li (Department of Chinese, Translation & Linguistics, City University of Hong Kong, 83 Tat Chee Ave. Kowloon Tong, 220 Hong Kong, China, binli2@cityu.edu.hk), Jinping Zhu (TsingHua University, 104 Main Acadamic building, 100084 Beijing, China, yx@abcd.edu.cn)

Utterance-final particles (UFPs) in Mandarin are regarded as discourse markers, whose "elusive" meanings and functions have been investigated in different perspectives such as pragmatics and semantics. Our study focuses on two most frequently used UFPs: NE and A, both of which can occur in identical utterances. The difference lies in that NE implies a shared common ground between the speaker and the hearer, whereas such commonness lacks for A. A preliminary acoustic analysis found that prosodic features of an utterance were more salient when a UFP was not used. The current study aims at the effectiveness of these prosodic features in perceiving these particles. Native speakers of Mandarin are asked to listen to sentences, which may originally contain a UFP that is removed. Their tasks are to decide whether a UFP, and which one, is needed in a given sentence. It is hypothesized that without textual cues, speakers will reply on prosodic features in their judgment; therefore, they will perform better in sentences where UFPs are not used originally and where prosodic cues are more salient.

5aSCc8. The effect of learning on listening to ultra-Fast speech. Takuya Nishimoto (Graduate School of Information Science and Technology, The University of Tokyo, 7-3-1 Hongo, Bunkyo-ku, 113-8656 Tokyo, Japan, nishi@hil.t.u-tokyo.ac.jp), Yukika Kariya (Department of Communication, Tokyo Woman's Christian University, 2-6-1 Zenpukuzi, Suginami-ku, 167-8585 Tokyo, Japan, g04c043@cis.twcu.ac.jp), Takayuki Watanabe (Department of Communication, Tokyo Woman's Christian University, 2-6-1 Zenpukuzi, Suginami-ku, 167-8585 Tokyo, Japan, nabe@cis.twcu.ac.jp)

We investigated the intelligibility of ultrafast speech which may be used for screen reader for persons with visual disability. The subjects were 35 women who are university students and are not visually/hearing impaired. They were divided into four groups and they listened to 150 words with the speed of approximately 20 morae/s. The vocabulary contained the tasks of high and low familiarity words, and the orders of tasks were different by the groups. Four morae Japanese words from the FW03 database were used as the vocabulary of the recall test. As a result, significant learning effect was observed in cases where the subject listened the high familiarity words in succession. This indicates that the learning effect to the ultrafast speech is promoted when the mental lexical access is easy. We also investigated the mental workloads of the listening task using the NASA-TLX method. As the results, significantly high workload scores were observed at the listening of low familiarity words. The results also suggested that the mental workload decreases when the subject was aware that the mental lexical access was difficult.

5aSCc9. Speech segmentation in monolingual and bilingual infant learners of Canadian English and Canadian French. Linda Polka (McGill University, School of Communication Sciences and Disorders, Beatty Hall, 1266 Pine Avenue West, Montreal, QC H3G 1A8, Canada, linda.polka@mcgill.ca), Jennifer Proulx (McGill University, School of Communication Sciences and Disorders, Beatty Hall, 1266 Pine Avenue West, Montreal, QC H3G 1A8, Canada, Jennifer.proulx@mail.mcgill.ca), Megha Sundara (UCLA Department of Linguistics, 3125 Campbell Hall, Los Angeles, CA 90095-1543, USA, megha.sundara@humnet.ucla.edu)

Speech segmentation skills emerging in infancy are influenced by the infant's native language. English infants favor a stress-based strategy (Jusczyk et al., 1999) whereas French infants favor a syllable-based strategy (Nazzi et al., 2006). Cross-linguistic findings from our lab, based on between group comparisons, show that monolingual 8-month-olds learning either Canadian English or Canadian French segment bisyllabic words in their native lan-

guage but not in a rhythmically-different non-native language. Canadian French infants fail to segment Canadian English; Canadian English infants fail to segment Canadian French. Bilingual infants (exposed to both languages) were tested in each language on separate days. Although they appear to segment in both languages, attrition has high in the second test session. To assess cross-language segmentation more directly we tested monolingual and bilingual 8-month-olds using a task designed to assess segmentation in both languages in the same infant within a single test session. Findings confirm that monolingual 8-month-olds fail to segment bisyllabic words in a rhythmically-different non-native language. Preliminary data show that bilingual 8-month-olds segment only in the language that is favored in their language input. Thus, in early stages of speech processing all infants appear to develop speech segmentation strategies that are optimal for one language.

5aSCc10. Clear speech intelligibility and accentedness ratings for native and non-native talkers and listeners. Rajka Smiljanic (Northwestern University, Department of Linguistics, 2016 Sheridan Road, Evanston, IL 60208, USA, rajka@northwestern.edu), Ann Bradlow (Northwestern University, Department of Linguistics, 2016 Sheridan Road, Evanston, IL 60208, USA, abradlow@northwestern.edu)

This study investigated how native language background (L1) interacts with speaking style in determining levels of speech intelligibility. In four experiments, we explored whether native and non-native hyper-articulation clear speech strategies provide similar intelligibility benefits for native and high proficiency non-native listeners. The sentence-in-noise perception results revealed that native speech was preferred over non-native speech by both listener groups even when non-native talkers and listeners shared the same L1. Clear speech was shown to be beneficial for both the native and fluent non-native listeners. However, non-native clear speech enhanced intelligibility less than native clear speech, supporting the hypothesis that clear speech production strategies involve enhancement of language-specific phonological contrasts. In order to assess the relationship between objective intelligibility measures and subjective accentedness ratings, we obtained accentedness ratings of native and non-native conversational and clear speech by native and non-native listeners. The results showed that objective intelligibility and subjective accentedness were independent. Overall, these results provide strong evidence that clear speech involves language-specific modifications. Nevertheless, native and high proficiency non-native clear speech modifications are generally helpful for both native and high proficiency non-native listeners even when the objective intelligibility and subjective accentedness levels diverged for various listener and talker groups.

5aSCc11. Vietnamese monophthong vowel production by native speakers and American adult learners. Matthew Winn (University of Maryland College Park, Department of Hearing & Speech Sciences, 0100 Lefrak Hall, College Park, MD 20742, USA, mwinn@hesp.umd.edu), Allison Blodgett (University of Maryland College Park, Center for Advanced Study of Language, 7005 52nd Ave, College Park, MD 20742, USA, ablodgett@casl.umd.edu), Jessica Bauman (University of Maryland College Park, Center for Advanced Study of Language, 7005 52nd Ave, College Park, MD 20742, USA, jbauman@hesp.umd.edu), Anita Bowles (University of Maryland College Park, Center for Advanced Study of Language, 7005 52nd Ave, College Park, MD 20742, USA, abowles@casl.umd.edu), Lykara Charters (University of Maryland College Park, Center for Advanced Study of Language, 7005 52nd Ave, College Park, MD 20742, USA, lykarac@mac.com), Anton Rytting (University of Maryland College Park, Center for Advanced Study of Language, 7005 52nd Ave, College Park, MD 20742, USA, crytting@casl.umd.edu), Jessica Shamoo (University of Maryland College Park, Center for Advanced Study of Language, 7005 52nd Ave, College Park, MD 20742, USA, jshamoo@casl.umd.edu)

This study provides new native speaker data regarding the vowel space and duration contrasts of Vietnamese monophthongs. These data add to existing empirical accounts and raise questions about descriptions aimed at adult language learners. In addition, specific acoustic measures target difficulties that English-speaking adults encounter when producing Vietnamese vowels. These measures include the rounding distinction for back vowels, height distinction for central vowels, and duration distinction between short and long vowels. Results show that adult learners exhibit greater variability and overall less accurate production than native speakers for the high-back unrounded vowel u', with slightly better performance for the mid-back unrounded vowel o', perhaps because it is similar to English / Λ /. Additionally, these learners demonstrate varying levels of success with regard to the production of central vowel height but generally fail to distinguish the two vowel duration categories exhibited by native speakers.

5aSCc12. The role of segmental and intonational cues in dialect discrimination. Chad Vicenik (UCLA Department of Linguistics, 3125 Campbell Hall, Los Angeles, CA 90095-1543, USA, cvicenik@humnet.ucla.edu), Megha Sundara (UCLA Department of Linguistics, 3125 Campbell Hall, Los Angeles, CA 90095-1543, USA, megha.sundara@humnet.ucla.edu)

Research indicates that adult listeners are able to use intonation to discriminate between two languages when one of the languages is familiar (Ramus and Mehler, 1999; Pijper, 1983). In this paper, we test adults to determine whether they use segmental or intonational cues to distinguish their native dialect from a foreign one. In three experiments, American English listeners were asked to categorize American and Australian English sentences when (a) segmental and supra-segmental cues are available, (b) sentences are re-synthesized with flat intonation, leaving only segmental cues, (c) segmental information is stripped away, leaving only intonation. Results will be discussed in the context of infant research demonstrating that five month olds are able to distinguish different dialects of the same language (Nazzi, Jusczyk, and Johnson 2000).

5aSCc13. Effects of syllable structure on reaction times in a delayed naming task. Christine Mooshammer (Haskins Lab and MIT Research Lab of Electronics, 300 George Street Suite 900, New Haven, CT 06511, USA, tine@haskins.yale.edu), Louis Goldstein (Haskins Laboratories, 300 George St., Suite 900, New Haven, CT 06511, USA, goldstein@haskins.yale.edu), Mark Tiede (Haskins Lab and MIT Research Lab of Electronics, 300 George Street Suite 900, New Haven, CT 06511, USA, tiede@haskins.yale.edu), Hosung Nam (Haskins Laboratories, 300 George St., Suite 900, New Haven, CT 06511, USA, nam@haskins.yale.edu), Man Gao (Haskins Laboratories, 300 George St., Suite 900, New Haven, CT 06511, USA, gao@haskins.yale.edu)

Syllable complexity has been found to affect the time the speaker needs for planning and initiating utterance production. Shorter latencies for complex onsets (CCV) as compared to simple onsets (CV) have been explained by effects of segment-specific biomechanical constraints at the level of motor execution, and by neighborhood density at the planning level. Within the framework of Articulatory Phonology, shorter planning latencies for CV syllables (compared to VC) have been attributed to quicker stabilization for tighter gestural coupling hypothesized for in-phase coupling of the onset consonant and release with the vowel. We attempted to test both onset complexity (C vs CC) and coda complexity (open vs. closed syllables) within a single experiment, so that we could evaluate the relative magnitudes of these effects and uncover potential interactions. To do so, American English monosyllabic words varying in syllable structure were presented using a delayed naming paradigm. The results replicated both effects, showing additive effects of roughly comparable magnitudes. Whether these effects are due to planning or motor execution will be tested by further simple naming and picture naming experiments.

5aSCc14. Breathy and whispery voicing in White Hmong. Sean Fulop (California State Univ. Fresno, 5245 N. Backer Ave., Linguistics PB92, Fresno, CA 93705, USA, sfulop@csufresno.edu), Chris Golston (California State Univ. Fresno, 5245 N. Backer Ave., Linguistics PB92, Fresno, CA 93705, USA, chrisg@csufresno.edu)

Two phonatory strategies are acknowledged to involve a superposition of periodic vocal cord vibration with excessive airflow generating turbulent noise. Breathy voice has the vocal folds vibrating along their entire length, but incomplete closure allows a constant airflow. Whispery voice has the vocal folds vibrating modally along an anterior segment, while the arytenoids maintain a posterior hole which allows a constant airflow. In linguistic phonetics, these are standardly regarded as variant strategies of a

single "breathy voice'' specification, and have never been noted to coexist in one language in an important way. They do in White Hmong. One of the seven "tones'' of White Hmong is breathy. Syllables bearing this tone display breathy voicing (of the first type) on the vowel. White Hmong also has a stop [d^h], which sounds like whispery voicing during the release phase. In this study, the breathy tone is shown to have a higher H1 amplitude relative to H2 (compared to modal voice), while the whispery voiced stop is even more extreme in this measure. Whispery voiced stops are also shown to display less harmonicity than the breathy tone, which in turn has less harmonicity than modal voicing in a similar syllable.

5aSCc15. Developing a bilingual communication aid for a Japanese ALS patient using voice conversion technique. Akemi Iida (School of Media Science, Tokyo University of Technology, 1404-1, Katakura-cho, Hachiouji, 192-0982 Tokyo, Japan, ake@media.teu.ac.jp), Shimpei Kajima (Dept. of Electrical and Electronics Engineering, Sophia University, 7-1 Kiyoi-cho, Chiyoda-ku, 102-8554 Tokyo, Japan, s.kajima@gmail.com), Keiichi Yasu (Dept. of Electrical and Electronics Engineering, Sophia University, 7-1 Kiyoi-cho, Chiyoda-ku, 102-8554 Tokyo, Japan, k-yasu@sophia.ac.jp), John M. Kominek (Language Technologies Institute, Carnegie Mellon University, 5000 Forbes Ave. West, Pittsburgh, PA 15213, USA, jkominek@cs.cmu.edu), Yasuhiro Aikawa (1-36-2, Shinjuku, Shinjuku-ku, Shinjuku dai-nana-biru 7F, 160-0022 Tokyo, Japan, aikawa@loopedpicture.com), Takayuki Arai (Dept. of Electrical and Electronics Engineering, Sophia University, 7-1 Kiyoi-cho, Chiyoda-ku, 102-8554 Tokyo, Japan, arai@sophia.ac.jp)

A bilingual communication aid for a Japanese amyotrophic lateral sclerosis (ALS) patient has been developed. From our previous research, a corpus-based speech synthesis method was ideal for synthesizing speech with voice quality identifiable as the patient's own. However, a recording of a large amount of speech, which is a burden for the patient, is required for such system. In this study, a voice conversion technique was applied so that a smaller amount of recording is needed for synthesis. An English speech synthesis system with the patient's voice was developed using Festival, a corpus-based speech synthesizer with voice conversion technique. Two methods for Japanese speech synthesis were attempted using HTS toolkit. The first used an acoustic model built from all 503 recordings of the patient. The second used an acoustic model built from 503 wavefiles of which voice was converted to the patient's from a native speaker's. The latter method requires fewer recordings of the patient's. The result of the perceptual experiment showed that the voice synthesized with the latter was perceived to have a closer voice quality to the patient's natural speech. Last, GUI on windows was developed for the patient to synthesize speech by typing in the text.

5aSCc16. Individual differences in perception of emotions from nonsense speech. Sona A. Patel (University of Florida, Dauer Hall, P.O. Box 117420, Dept. of Communication Sciences and Disorders, Gainesville, FL 32611, USA, sona09@ufl.edu), Rahul Shrivastav (University of Florida, Dauer Hall, P.O. Box 117420, Dept. of Communication Sciences and Disorders, Gainesville, FL 32611, USA, rahul@csd.ufl.edu)

Identification of the acoustic cues used to perceive emotions in speech is important for a number of applications including rehabilitation, natural speech modeling, and speech synthesis. In a recent experiment, Patel, Shrivastav, Harnsberger, and Shrivastav (2007) found that a four-dimensional solution accounted for 90% of the variance in similarity judgments for 19 emotional categories in nonsense speech. This solution was determined for averaged judgments across twelve listeners. The present study investigated individual differences in the perception of emotions for speech devoid of semantic information but rich in suprasegmental cues. Six male and six female listeners participated in a same-different discrimination test of a set of nonsense sentences produced in nineteen emotional contexts by two actors. Nonsense sentences were used in order to avoid any biases caused by semantics. The perceptual distance between each stimulus pair was computed in terms of d' values for each listener. These distances were submitted to a multidimensional scaling analysis using the INDSCAL algorithm. The INDSCAL analysis reports the best fitting solution for all listeners as a group, along with the weights assigned to each dimension by individual listeners. The results of this analysis will be presented.

5aSCc17. Phonological representation of negation in Sakizaya. Wen-Chi Shen (Grad. Inst. of Linguistics, National Taiwan Univ., 1, Roosevelt Rd. Sec. 4, 106 Taipei, Taiwan, r94142007@ntu.edu.tw), Wen-Yu Chiang (Graduate Institute of Linguistics, Grad. Inst. of Linguistics, National Taiwan Univ., 1, Roosevelt Rd. Sec. 4, 106 Taipei, Taiwan, countryroad0509@hotmail.com)

This paper aims at investigating phonological representation of negation in Sakizaya, an endangered Formosan language in Taiwan. Defying Yaeger-Dror's "Cognitive prominence principles" (2003), Chiang (2006) examines negators in Saisiyat, a SVO language as English, and finds the sentential subjects are more prominent acoustically rather than negators. Thus, I will adopt Chiang's modal (2006) and analyze phonological representation of six negators in Sakizaya to see where the pitch accent falls. Besides, if falling on the negators, I will see whether it is because of either cognitive prominence properties or its sentence-initial position? Six informants (three male and three female), from 50-74 years old, participated in the experiment, recorded by DAT, analyzed by Praat and digitized at a 22050-Hz sampling rate. Affirmative and negative sentences are asked in Mandarin while the informants are instructed to translate them into Sakizaya. Besides, they are asked to produce iterative -ay sentences since the negator ca'ay is the most frequently used negator with higher prominent syllable -ay. The results show negators are more prominent in Sakizaya compared to sentential subjects. I conclude it is word order that influences the prominence of pitch contour since Saisiyat is an SVO language and Sakizaya a VSO one.

5aSCc18. The effect of vowel duration on formant frequencies - data from Hakka Chinese. Wai-Sum Lee (Phonetics Lab, Dept. of Chinese, Translation and Linguistics, City University of Hong Kong, 83 Tat Chee Avenue, Kowloon Hong Kong, Hong Kong, w.s.lee@cityu.edu.hk), Eric Zee (Phonetics Lab, Dept. of Chinese, Translation and Linguistics, City University of Hong Kong, 83 Tat Chee Avenue, Kowloon Hong Kong, Hong Kong, eric.zee@cityu.edu.hk)

In the target undershoot model, vowel duration is considered as the main determinant of vowel reduction, resulting in undershoot in formant frequencies relative to the "bull's-eye formant pattern" (Lindblom, 1963). The model predicts more schwa-like formant frequencies as vowel duration is shortened. In Hakka Chinese, vowel phonemes /i e a o u/ may be realized as long [i: e: a: o: u:] in the CV: syllables and short [i e a o u] in the CVS syllables (S=a stop consonant). Results of a formant frequency analysis of the long and short vowel sets in Hakka Chinese from ten male and ten female speakers show that (i) in all the short vowels there is a displacement of vowel formant frequencies away from the target frequencies associated with the long vowels; and (ii) relative to the target frequencies, F1F2 do not become more schwa-like for all the short vowels, with [u] being the only vowel that undergoes centralization in the F1F2 plane and with [i e o a] displaying a significant rise in F1, [i e] an insignificant decrease in F2, and [o] an insignificant increase in F2. It appears that the Hakka data do not support the target undershoot model.

5aSCc19. An experimental and modeling study of anticipatory coarticulation in VCV sequences. Liang Ma (Labaratoire Parole et Language, 29, Avenue Robert Schuman, 13621 Aix-en-Provence, France, liang.ma@lpl.univ-aix.fr), Pascal Perrier (ICP/GIPSA-lab, INPG, 46 Avenue Félix Viallet, 38031 Grenoble Cedex 01, France, Pascal.Perrier@gipsa-lab.inpg.fr), Jianwu Dang (Japan Advanced Institute of Science and Technology, 1-1 Asahidai, Nomi, 923-1292 Ishikawa, Japan, jdang@jaist.ac.jp)

Anticipatory coarticulation within V1CV2 sequences is studied for EMMA data in French and in Mandarin Chinese. The corpus was designed consistently for both languages. V1 and V2 were /i, a, u/ and C was either /t/ or /k/. The influences of V2 on tongue position of V1 and of C were analyzed for three French and two Chinese speakers. For French speakers vowel V2 influences the whole sequence V1CV2, while its influence is strictly limited to the syllable CV2 for Mandarin speakers. These suggested

that speech planning strategies in French and in Chinese are different and that differences could arise from differences in the status of the syllable in the analyzed languages. A speech production model has been then used for testing quantitatively these conclusions. It involves a forward model and optimization techniques to infer optimal motor commands from the phonemic targets in the perceptual space. Different hypotheses about planning and execution of movement were tested on this model. The comparison of simulations and data supports the hypothesis that the syllable could be a basic unit for planning for Mandarin speakers, while it suggests that larger sequences such as VCV should be considered in the planning of French sequences.

5aSCc20. Psychoacoustic measures of blind audio source separation performance. Mingu Lee (Applied Acoustics Lab., INMC, 132-302, Seoul National University, San 56-1, Sillim-dong, Kwanak-gu, 151-742 Seoul, Republic of Korea, klugh34@acoustics.snu.ac.kr), Inseok Heo (Applied Acoustics Lab., INMC, 132-302, Seoul National University, San 56-1, Sillim-dong, Kwanak-gu, 151-742 Seoul, Republic of Korea, hisherz@acoustics.snu.ac.kr), Nakjin Choi (Applied Acoustics Lab., INMC, 132-302, Seoul National University, San 56-1, Sillim-dong, Kwanak-gu, 151-742 Seoul, Republic of Korea, nakjin@acoustics.snu.ac.kr), Koeng-Mo Sung (Applied Acoustics Lab., INMC, 132-302, Seoul National University, San 56-1, Sillim-dong, Kwanak-gu, 151-742 Seoul, Republic of Korea, kmsung@snu.ac.kr)

In this paper, an improved method for evaluating the performance of blind audio source separation (BASS) is discussed. In previous studies, such as described in E. Vincent et al., IEEE Transactions on Speech and Audio Processing, 2006, several computation methods for measuring quality of BASS algorithms e.g., defined by source-to-distortion ratio (SDR), source-to-interferences ratio (SIR), sources-to-noise ratio (SNR) and sources-to-artifacts ratio (SAR) are introduced. However, those methods do not take human auditory system into consideration. An improved method is developed by applying preprocessing and using weighted-inner product in frequency domain instead of simple inner-product in time domain. The proposed method incorporates well-known psychoacoustic characteristics e.g., masking effect and equal loudness contours. In comparison with the conventional quality measures, the proposed method shows better correlation with the results of carefully designed listening tests.

5aSCc21. The acoustic manifestation of consonant gradation in Northern Sami. Fredrik Karlsson (Umeå University, Department of Language Studies, SE90187 Umeå, Sweden, fredrik.karlsson@ling.umu.se), Kirk P. Sullivan (Umeå University, Department of Language Studies, SE90187 Umeå, Sweden, kirk.sullivan@ling.umu.se), Mikael Svonni (Umeå University, Department of Language Studies, SE90187 Umeå, Sweden, mikael.svonni@samiska.umu.se), Jan Van Doorn (Umeå University, Department of Clinical Sciences, SE90187 Umeå, Sweden, jan.vandoorn@logopedi.umu.se), Ola Wennstedt (Institute for Language and Folklore, Onomastics and Folklore Research in Umeå, Länsmansvägen 5, SE90420 Umeå, Sweden, ola.wennstedt@sofi.se)

Consonant gradation is a feature of Sami and is realised in Northern Sami in changes from nominative singular to genitive plural form, e.g., "heavdni" (spider) and "heavnni-t" (spiders). The data examined in this paper was collected in 2007 and represents the first acoustic analysis of consonant gradation in Northern Sami. The data was collected in Övre Soppero in Northern Sweden using an elicitation technique that was designed to collect phonetically controlled material for analysis. The nouns were elicited in singular or plural form using picture prompts and the participants were asked to give the word in the carrier sentences "Lea okta __ govas" ("There is a ___ in the picture") and "Leat guokte __ govas" ("There are two ___ in the picture"). The recordings were labeled in Wavesurfer at a phonetic level and the segments relating to consonant gradation extracted for acoustic analysis. In the paper we present our initial findings.

5aSCc22. The use of fundamental frequency information by cochlear implant patients with residual low-frequency hearing. Stephanie Herf (Arizona State University, Dept. of Speech and Hearing Science, Box 87-0102, Tempe, AZ 85287-0102, USA, spitzer@asu.edu), Julie Liss (Arizona State University, Dept. of Speech and Hearing Science, Box 87-0102, Tempe, AZ 85287-0102, USA, julie.liss@asu.edu), Anthony Spahr (Arizona State University, Lattie F. Coor Hall, Room 3462, Tempe, AZ 85287, USA, Tony.Spahr@Asu.Edu), Michael Dorman (Arizona State University, Dept. of Speech and Hearing Science, Box 87-0102, Tempe, AZ 85287-0102, USA, michael.dorman@asu.edu)

Recent studies have demonstrated significant benefits of complementing the electric hearing provided by a cochlear implant (CI) with residual low-frequency acoustic hearing. It has been suggested that the benefit of low-frequency hearing ($<$250 Hz) is due to improved representation of fundamental frequency (F0). It was hypothesized that removing F0 information would negatively impact speech perception in bimodal CI patients (EAS) more so when they are using both modes of perception. It was further hypothesized that these patients' more effective use of F0 information would result in higher intelligibility scores and less unpredicted lexical boundary errors (LBEs) in a speech transcription task. Six EAS patients transcribed normal and F0-flattened phrases. Results indicate EAS patients demonstrated a significant benefit from the residual low-frequency acoustic hearing and perform better in this mode. Five of the six EAS patients were able to transcribe the normal phrases with greater accuracy than the flat F0 phrases in both conditions. These patients correctly parsed lexical boundaries and transcribed phonemic targets with greater accuracy in the bimodal condition. These results demonstrate the importance of pitch and low frequency spectral information in the perception of speech.

5aSCc23. Digital acquisition of ultrasound imaging of the tongue. Aude Noiray (Haskins Laboratories, 300 George St., New Haven, CT 06511, USA, aude.noiray@haskins.yale.edu), Khalil Iskarous (Haskins Laboratories, 300 George St., New Haven, CT 06511, USA, iskarous@haskins.yale.edu), D.h. H. Whalen (Haskins Laboratories, 300 George St., New Haven, CT 06511, USA, whalen@haskins.yale.edu)

One of the goals of speech production research is to understand the functioning of the tongue in the production of overlapping lingual segments. This is especially important since all vocalic and most consonantal contrasts involve a tongue gesture. An obstacle to progress in this area has been the difficulty of observing tongue motion in enough spatial and temporal detail to develop theory on its linguistic functioning. Ultrasound has become increasingly popular in tongue imaging, since it allows the researcher to observe most of the tongue dynamically, while being clinically safe. However, a limitation of this technique is the slow 30 Hz rate of analog acquisition. We have developed a new method for digital acquisition of ultrasound data at over 100 Hz, with simultaneous synchronized acquisition of audio and Optotrak data. Acquisition of the ultrasound digital video data is externally triggered using a novel pulse sequence that is simultaneously captured by the audio and Optotrak acquisition device. We will illustrate the detail of the dynamics of the tongue in an experiment on the coproduction of rhotic and vocalic segments (seven American English subjects), where digital ultrasound was captured at 127 Hz (Funded by NIH DC-02717).

5aSCc24. Vocal tract normalization in articulatory space using thin-plate spline method. Jianguo Wei (LTCI/CNRS, TSI/ENST, DB407, 37/39, rue Dareau, 75014 Paris, France, wei@enst.fr), Jianwu Dang (Japan Advanced Institute of Science and Technology, 1-1 Asahidai, Nomi, 923-1292 Ishikawa, Japan, jdang@jaist.ac.jp)

Inter-subject normalization is a key issue of group analysis of articulatory data to obtain a general description of kinematic properties of human speech production. Multisubject articulatory study however is scarce due to the difficulty of normalization in articulatory domain. In order to reduce intersubject variations among articulatory space, a simple normalization procedure was proposed using a Thin-plate spline method. The purpose of this normalization processing is to reduce the morphological differences of vocal tracts such as shape and size among different subjects. Nonlinear factors of the reduction are considered in this normalization procedure. The electromagnetic Articulographic (EMMA) data were used in our experiments,

which were obtained from the NTT EMMA database for three subjects data included. A physiological articulatory model has been used to serve as the template. The landmarks were defined consistently in vocal tract space over the template and all subjects. The evaluations showed that the variances over subjects have been reduced 2.1 mm for consonants and 2.3 mm for vowels averaged over all tongue pellets.

5aSCc25. A comparison of coarticulation in conversational and clear speech. Jean E. Andruski (Wayne State University, 207 Rackham Bldg, 60 Farnsworth Ave., Department of Communication Sciences and Disorders, Detroit, MI 48202, USA, ag0611@wayne.edu)

Coarticulation may either hinder speech perception by increasing variability and altering the distinctive features of speech sounds, or enhance speech perception by providing additional cues to nearby sounds and spreading these cues out over time. This study examines the clear and conversational speech of 16 English speakers (8 females and 8 males) to compare the amount of coarticulation in clear and conversational speech when distinctive features are changed, as opposed to when nondistinctive features are changed. Devoicing of voiced fricatives and voicing of /t/ are investigated as examples of distinctive feature changes. Vowel nasalization and lip rounding in /s/ and /z/ are examined as examples of nondistinctive feature changes. Percentage of voicing during frication noise is used as a measure of fricative devoicing; voice onset time and percentage of voicing during the closure are used as measures of voicing in /t/; amplitude of the nasal formant and nasal formant onset time are used as measures of vowel nasalization; and center of gravity of the final 50% of the frication noise is used as a measure of lip rounding in /s/ and /z/. Results are compared across clear and conversational speech and across speaker gender. Individual speaker differences are also examined.

5aSCc26. The development of measurable speech rhythm during second language acquisition. Francisco Gutiérrez Díez (Universidad de Murcia, Departmento de Filología Inglesa, C/ Santo Cristo 1, 30009 Murcia, Spain, fgdiez@ono.com), Volker Dellwo (UCL, Wolfson House, 4, Stephenson Way, NW1 2HE London, UK, v.dellwo@ucl.ac.uk), Núria Gavaldà (Universitat de Barcelona, Departament de Filologia Anglesa i Alemanya, Granvia de les Corts Catalanes 585, 08007 Barcelona, Spain, nuria.gavalfe@gmail.com), Stuart Rosen (UCL, Wolfson House, 4, Stephenson Way, NW1 2HE London, UK, stuart@phon.ucl.ac.uk)

It has been demonstrated repeatedly that durational characteristics of consonantal (C) and vocalic (V) intervals are robust acoustic correlates of rhythm class (stress-timed, syllable-timed, mora-timed). Here, we investigate how objective rhythm measures develop during the acquisition of a second language. In a longitudinal study, nine native speakers of Spanish were recorded reading a text in English before and after a year of English language training at university level. A control group of nine native English speakers read the same text. Automatic forced alignment of speech segment boundaries using hidden Markov models allowed the calculation of C and V interval durations. Standard rhythm metrics (%V, deltaC, deltaV, PVI) were calculated for all recordings. First results show that durational C interval characteristics between native English and Spanish English (pre- and post-training) do not differ. However, V interval characteristics (deltaV, nPVI, %V) are lowest for English natives, higher for the Spanish post training group and highest for the Spanish pretraining group. The results suggest that (a) deficits of speech rhythm competence in a second language are mostly revealed on a vocalic level and (b) an increase in competence in a second language is reflected well by measurable speech rhythm.

5aSCc27. Transforming modal voice into irregular voice by amplitude scaling of individual glottal cycles. Tamás Bőhm (Dept. of Telecommunications and Media Informatics, Budapest Univ. of Technology and Economics, Magyar Tudósok krt. 2, H-1117 Budapest, Hungary, bohm@tmit.bme.hu), Nicolas Audibert (GIPSA-lab, Speech & Cognition Dept (ICP), INPG/UJF/Stendhal/CNRS UMR 5216, Université Stendhal, 1180 av. Centrale, 38040 Grenoble Cedex 9, France, Nicolas.Audibert@gipsa-lab.inpg.fr), Stefanie Shattuck-Hufnagel (Massachusetts Institute of Technology, Research Laboratory of Electronics, Speech Communication Group, 77 Massachusetts Ave., Cambridge, MA 02139, USA, stef@speech.mit.edu), Géza Németh (Dept. of Telecommunications and Media Informatics, Budapest Univ of Technology and Economics, Magyar Tudósok krt. 2, H-1117 Budapest, Hungary, nemeth@tmit.bme.hu), Véronique Aubergé (GIPSA-lab, Speech & Cognition Dept. (ICP), INPG/UJF/Stendhal/CNRS UMR 5216, Université Stendhal, 1180 av. Centrale, 38040 Grenoble Cedex 9, France, Veronique.Auberge@icp.inpg.fr)

Irregular phonation can serve as a cue to segmental contrasts and prosodic structure as well as to the affective state and identity of the speaker. Thus algorithms for transforming between voice qualities, such as regular and irregular phonation, may contribute to building more natural sounding, expressive and personalized speech synthesizers. We describe a semiautomatic transformation method that introduces irregular pitch periods into a modal speech signal by amplitude scaling of the individual cycles. First the periods are separated by windowing, then multiplied by scaling factors, and finally overlapped and added. Thus, amplitude irregularities are introduced via boosting or attenuating selected cycles. The abrupt, substantial changes in cycle lengths that are characteristic of naturally-occurring irregular phonation can be achieved by removing (scaling to zero) one or more consecutive periods. A freely available graphical tool has been developed for copying stylized pulse patterns (glottal pulse spacings and amplitudes) from an irregular recording to a regular one, allowing the scaling factors to be refined and the waveform regenerated interactively. We present the effects of the transformation on harmonic structure, and perceptual test results showing that transformed signals are similar to natural irregular recordings in both roughness and naturalness.

5aSCc28. Speech transcription for Embodied Conversational Agent animation. Leila Zouari (Telecom Paris Tech, 46 rue Barrault, 75013 Paris, France, zouari@enst.fr), Gerard Chollet (Telecom Paris Tech, 46 rue Barrault, 75013 Paris, France, chollet@enst.fr)

This article investigates speech transcription within a framework of Embodied Conversational Agent (ECA) animation by voice. The idea is to detect some pronounced expressions/keywords in order to animate automatically the face and the body of an avatar. Extensibility, speed and precision are the main constraints of this interactive application. So after defining the set of the relevant words (to the application), a fast large vocabulary speech recognition system was developped and the keyword detection was evaluated. In order to fasten the recognition system without decreasing its efficiency, the acoustic models have been shortened by an original process. It consists in decreasing the number of shared central states of context dependant models which are considered stationary. The shared states situated in the border of the models remain inchanged. Then all the models are retrained. The system is evaluated on an hour of the ESTER database (a French broadcast news database). The experiments show that reducing the number central states of triphones is advantageous. Indeed, the length of models is reduced by 20% with no loss of accuracy.

5aSCc29. A cross-dialect acoustic description of vowels: Peruvian versus European Spanish. Katerina Chladkova (Palacky University Olomouc, Dept. of English and American Studies, Krizkovskeho 10, 771 80 Olomouc, Czech Republic, katerina.chladkova@seznam.cz), Paola Escudero (University of Amsterdam, Institute of Phonetic Sciences, Spuistraat 210, 1012 VT Amsterdam, Netherlands, P.R.EscuderoNeyra@uva.nl), Paul Boersma (University of Amsterdam, Institute of Phonetic Sciences, Spuistraat 210, 1012 VT Amsterdam, Netherlands, P.P.G.Boersma@uva.nl)

This paper aims to provide acoustic description and comparison of vowel properties of two major dialects of Spanish: Peruvian and European. The method of data collection and acoustic analyses reported in Escudero et al. (submitted) for Portuguese is replicated in order to allow for future comparisons across languages. Each of the five Spanish monophthongs /i, e, a, o, u/ was produced in stressed position in the first syllable of a CVCV (consonant-vowel-consonant-vowel) frame. The CVCV words were read both in isolation and in a carrier sentence. Vowel tokens were examined between voiceless stops /p, t, k/ and fricatives /f, s/, which supplied five

variable consonantal contexts. We analyzed the vowels' first and second formants (F1 and F2) as well as their fundamental frequency and duration. Unsurprisingly, a main effect of vowel identity and gender on formant values was found. Most importantly, unlike Morrison and Escudero (2007), we found for Spanish an interaction between dialect and vowel identity, implying that the F1 and F2 values of some vowels are significantly different between dialects.

5aSCc30. Contextual influences: Perception of sentences in noise is facilitated similarly in young and older listeners by meaningful semantic context; neural correlates explored via functional magnetic resonance imaging (fMRI). Heather Macdonald (Queen's University, Dept Psychology, 62 Arch Street, Kingston, ON K7L 3N6, Canada, hpmacdonald@gmail.com), Matthew H. Davis (MRC CBU, 15 Chaucer Rd., CB2 7EF Cambridge, UK, matt.davis@mrc-cbu.cam.ac.uk), Kathy Pichora-Fuller (University of Toronto Mississauga, 3359 Mississauga rd N., Mississauga, ON L5L 1C6, Canada, k.pichora.fuller@utoronto.ca), Ingrid S. Johnsrude (Queen's University, Dept Psychology, 62 Arch Street, Kingston, ON K7L 3N6, Canada, ingrid.johnsrude@queensu.ca)

Meaningful semantic context has been demonstrated to improve comprehension of spoken sentences by young and old adults, especially in difficult listening conditions. Evidence for this benefit is based largely on data collected using SPIN sentences, highly structured sentences with a predictable or unpredictable final word. We asked young (14 participants, aged 18-25) and older adults (20 participants, aged 60-75) to report entire sentences which were less structured in nature and contained either a meaningful or anomalous global semantic context. Sentences were mixed with signal-correlated noise, at 9 signal-to-noise ratios (-6 to +2 dB), and also presented without noise. Comprehension by both groups benefited from meaningful context, without a clear overall difference in the amount of benefit obtained. We used fMRI to look at neural activity associated with deriving benefit from meaningful context. Whole-brain EPI data were acquired from young (16 participants, aged 19-26) adults using a sparse imaging design. Word-report data obtained in the scanner were used as intelligibility measures in data analysis. In addition to activity associated with meaningful context, we observe a large left inferior-frontal region in which BOLD signal correlated more strongly with the intelligibility of anomalous compared to coherent prose, presumably reflecting challenged semantic integration processes.

5aSCc31. Landmark-based analysis of sleep-deprived speech. Suzanne Boyce (Department of Communication Sciences and Disorders, University of Cincinnati, Mail location 0394, Cincinnati, OH 45267, USA, boycese@email.uc.edu), Joel Macauslan (S.T.A.R. Corporation, 54 Middlesex Tnpk, Bedford, 01730, USA, joelM@starspeech.com), Ann Bradlow (Northwestern University, Department of Linguistics, 2016 Sheridan Road, Evanston, IL 60208, USA, abradlow@northwestern.edu), Rajka Smiljanic (Northwestern University, Department of Linguistics, 2016 Sheridan Road, Evanston, IL 60208, USA, rajka@northwestern.edu)

The speech of sleep-deprived persons has been variously described as more "slurred" or "tired-sounding" than speech by the same speakers in a rested condition. Although sleep deprivation is a major focus of research for public safety and health reasons, there has been notably little research on the connection between sleep deprivation and speech. Using an automatic system for detecting "landmarks", i.e., important perceptual and articulatory events in the acoustic signal, we compared sleep-deprived and rested speech recorded during two well-controlled studies of sleep deprivation. Our results show that sleep-deprived speech is significantly different from rested speech for both the number and pattern of landmarks detected. These results are similar in detail to differences previously found between clear and conversational styles of speech. The relevance of these findings for speech as a marker of sleep-deprivation will be discussed, along with potential applications in public safety and health. [Research supported by NIH.]

5aSCc32. Vowel duration as a cue for coda voicing and the perception of second-language vowel quantity. Vaclav Jonas Podlipsky (Dept. of English and American Studies, Palacky Univ., Krizkovskeho 10, 77180 Olomouc, Czech Republic, vaclavjonaspodlipsky@centrum.cz)

When acquiring the phonology of a second language (L2), a learner may have to dissociate a perceptual cue from what it marked in the first language (L1) and attach it to another linguistic entity. This study examined the acquisition of Czech vowel quantity by native speakers of American English. In Czech, vowel duration is reserved for cuing short/long vowel (V/V:) contrasts, while in English it is an important cue for coda obstruent voicing. It is not certain whether in Czech, as in many other languages, voiced codas lengthen the preceding vowels; if they do, a vowel should be more likely to be perceived as short before a voiced obstruent and as long before a voiceless one. A perceptual V/V: categorization experiment showed that for Czech listeners ($n=54$) the V/V: boundary came slightly (3.3 ms) but consistently ($p<0.001$) later before a voiced coda. If English learners transfer L1 perceptual strategies to their L2 Czech, the V/V: boundary shift should be even larger. However, this study found no significant effect of coda voicing on the perception of vowel quantity for the non-native listeners. It is concluded that the learners redefined the value of vowel duration as a perceptual cue.

5aSCc33. Talker-specific and accent-general perceptual adaptation to Korean-accented English. Sabrina K. Sidaras (Dept. of Psychology, Emory University, 532 Kilgo Cir, Atlanta, GA 30322, USA, ssidara@emory.edu), Jessica E. Alexander (Dept. of Psychology, Emory University, 532 Kilgo Cir, Atlanta, GA 30322, USA, jessica.alexander@emory.edu), Lynne C. Nygaard (Dept. of Psychology, Emory University, 532 Kilgo Cir, Atlanta, GA 30322, USA, lnygaar@emory.edu)

The present study investigated the relative contribution of talker-specific and accent-general learning to the perceptual adaptation of accented speech. Adult native English-speaking listeners were asked to transcribe Korean-accented English words in a brief, high variability perceptual learning paradigm. During training, listeners transcribed individual words produced by six Korean-accented speakers and were given feedback on their transcription performance. Controls were either trained with native English speakers or were given no training. At test, listeners were presented with Korean-accented speech produced by both familiar and unfamiliar talkers. The results suggest that listeners learned accent-general properties of non-native speech. Listeners showed better transcription performance for both familiar and unfamiliar accented talkers relative to English and no training controls. However, talker-specific properties such as individual talker familiarity and baseline intelligibility also influenced transcription performance at test. These findings suggest that although listeners are sensitive to multiple sources of variation in speech, they appear to engage in accent-general perceptual adaptation to non-native speech.

5aSCc34. Effect of musical experience on Mandarin tone and vowel discrimination and imitation. Terry L. Gottfried (Lawrence University, P. O. Box 599, Dept. of Psychology, Appleton, WI 54912-0599, USA, gottfrit@lawrence.edu), Yangqing Xu (Lawrence University, P. O. Box 599, Dept. of Psychology, Appleton, WI 54912-0599, USA, xuy@lawrence.edu)

Recent studies have demonstrated a relation between musical experience and accuracy in speaking and perceiving unfamiliar speech contrasts. For example, Gottfried [in Bohn and Munro, Eds., John Benjamins, 221-237 (2007)) found that native speakers of American English with musical training perform better than non-musicians when discriminating and imitating the four lexical tones of Mandarin Chinese. In this study, four native speakers of Mandarin (Chengdu region) produced target words in a fixed carrier sentence. Their productions of high unrounded /i/ and high rounded /u/ were significantly affected by the initial consonant, especially /u/ (which is often transcribed as two different vowels in pinyin, u and ü, according to the initial consonant). Vowels that followed consonants with more anterior articulation (pinyin j, q, x) had lower F1 and higher F2 than vowels that followed more posterior consonants (pinyin zh, ch, sh). The F0 of the word immediately preceding the target words (kan4) was significantly affected by

the tone of the target word. Current research tests whether musicians and nonmusicians differ in their ability to discriminate and imitate these phonemic contrasts according to native speakers' phonemic categories, which allow contextual variation in acoustic information.

5aSCc35. Expanding the set of acoustic features of the post-vocalic voicing contrast in English. Blake Rodgers (University of Wisconsin, 1168 Van Hise, 1220 Linden Drive, Madison, WI 53706, USA, brodgers@wisc.edu), Thomas Purnell (University of Wisconsin, 1168 Van Hise, 1220 Linden Drive, Madison, WI 53706, USA, tcpurnell@wisc.edu), Joseph Salmons (University of Wisconsin, 1168 Van Hise, 1220 Linden Drive, Madison, WI 53706, USA, jsalmons@wisc.edu)

The literature on post-vocalic voicing contrasts indicates that no single acoustic characteristic or perceptual cue captures the phonological distinction [e.g., Nittrouer 2004]. Previous perceptual studies examined such acoustic characteristics as vowel duration, percent and duration of closure voicing, formant, and F0 transitions. Detailed acoustic examination reveals additional variation. It is hypothesized that these understudied acoustic characteristics also play a role in the family of voicing cues. In the present study, two laryngeal characteristics are measured and modeled: glottalization (here, an abrupt drop in rate of vocal fold vibration by tensed vocal folds) and a sharp amplitude drop (due to abrupt spreading of vocal folds). Examination of American English data reveals that speakers tend to have at least one of these two characteristics in their final voiceless obstruents, but generally not both. Results suggest a process of laryngeal enhancement of final voiceless obstruents in addition to the traditional cues of vowel duration, formant transitions, etc. Implications for the categorization of laryngeal features and trading relations within the family of final voicing cues are discussed.

5aSCc36. Providing simultaneous visual feedback may ameliorate speech disruptions caused by exposure to delayed auditory feedback. Jeffery Jones (Wilfrid Laurier University, 75 University Ave. West, Waterloo, ON N2L 3C5, Canada, jjones@wlu.ca), Danielle Striemer (Wilfrid Laurier University, 75 University Ave. West, Waterloo, ON N2L 3C5, Canada, dstriemer@gmail.com)

Speakers exposed to delayed auditory feedback (DAF) are often dysfluent. We investigated the possibility that providing visual feedback in addition to DAF would reduce speech disruption. Participants repeated sentences while they heard their auditory feedback delayed with and without simultaneous visual feedback. Replicating previous work, DAF led to increased sentence durations and an increased number of speech disruptions. Results showed that visual feedback did not reduce DAF effects on duration, however, a nonsignificant trend was observed that indicated fewer speech disruptions occurred when visual feedback was provided. This trend was significant in speakers who were overall less affected by DAF. These results suggest the possibility that speakers can strategically use alternative sources of feedback.

5aSCc37. Acoustic characteristics of Swedish dorsal fricatives. Ryan Shosted (University of Illinois, 4080 FLB, 707 S Mathews Ave; MC-160, Urbana, IL 61801, USA, rshosted@uiuc.edu)

The identity of ["hooktop heng"], the "voiceless dorso-palatal/velar fricative" or "simultaneous" ["esh"] and [x], is controversial (IPA 2009: 140, 203). The present study attempts to acoustically differentiate ["esh"], [x], and (non-labialized) ["hooktop heng"]. A female speaker of Stockholm Swedish produced VCV nonsense words with balanced V and alternating C. Windowed spectra were obtained and averaged at various locations in the fricatives. ["esh"] can be reliably differentiated from [x] and ["hooktop heng"] based on center of gravity measures in the middle of the fricative. However, center of gravity differences between [x] and ["hooktop heng"] are not revealing, confirming Lindblad's x-ray tracings (1980: 89). The most robust acoustic difference between the two dorsal fricatives is the presence of erratic, high-amplitude disturbances during [x]. These may be attributed to sudden explosions of saliva and ephemeral contact with the uvula, more likely for slightly-retracted [x] than for ["hooktop heng"]. It seems unlikely that ["hooktop heng"] is produced with a second simultaneous constriction that is of acoustic relevance. International Phonetic Association. 1999. *Handbook of the International Phonetic Association*. Cambridge: Cambridge University Press. Lindblad, P. 1980. Svenskans sje- och tje-ljud i ett Allmänfonetisk perspektiv. *Travaux de l'Institut de linguistique de Lund 16*. Lund: LiberLäromedel/Gleerup.

5aSCc38. Audiovisual speech perception in children with autism spectrum disorders and typical development. Julia Irwin (Haskins Laboratories, 300 George Street, New Haven, CT 06511, USA, julia.irwin@haskins.yale.edu)

For typically developing perceivers, visual speech information influences what listeners hear. When the place of articulation of visual and auditory speech tokens are incongruent, perceivers often report hearing a visually influenced response (the "McGurk effect", McGurk and MacDonald, 1976). Children with autism spectrum disorders (ASD) appear to be less susceptible to the McGurk effect than their typically developing peers (e.g., Mongillo, Irwin, Whalen, Klaiman, Carter and Schultz, in press). Given the gaze aversion characteristic of children with ASD, eye-tracking methodology was employed to extend our previous research on the McGurk effect to examine: (1) sensitivity to mismatched auditory and visual speech (McGurk), (2) visual gain in the presence of auditory noise, and (3) detection of auditory and visual asynchrony. Children with ASD and their chronological age-matched and verbal mental age-matched typically developing controls (ranging in age from 7-12 years) were assessed. Implications for the development of audiovisual speech processing in typically developing and children with ASD will be discussed. [Work supported by NIH.]

5aSCc39. Attentional modulation of the perception of illusory vowels and sound onsets: A functional magnetic resonance imaging (fMRI) study. Antje Heinrich (University of Cambridge, Department of Linguistics, Sidgwick Avenue, CB3 9DA Cambridge, UK, ah540@cam.ac.uk), Matthew H. Davis (MRC CBU, 15 Chaucer Rd., CB2 7EF Cambridge, UK, matt.davis@mrc-cbu.cam.ac.uk), Robert P. Carlyon (MRC CBU, 15 Chaucer Rd., CB2 7EF Cambridge, UK, bob.carlyon@mrc-cbu.cam.ac.uk), Ingrid S. Johnsrude (Queen's University, Dept Psychology, 62 Arch Street, Kingston, ON K7L 3N6, Canada, ingrid.johnsrude@queensu.ca)

In a previous study, we exploited the Gestalt principle of closure to create illusory vowel sounds and examined the neural correlates of their perception using fMRI. When two formants of a synthetic vowel are presented in an alternating pattern, filling the gaps in each formant with bursts of noise causes the formants to be heard as continuous and more vowel-like. When this ″Illusion″ condition was modified by increasing the formant-to-noise ratio (FNR), the formants were heard as interrupted ("Illusion Break" condition) and less vowel-like. BOLD signal in the Middle Temporal Gyrus (MTG) was greater for Illusion than for Illusion-Break stimuli, reflecting the difference in speechlikeness. Primary auditory areas (PAC) exhibited the opposite pattern, probably because Illusion-Break stimuli contain more perceived sound onsets than the Illusion stimuli. In the current study we examine whether the neural activation to illusory vowels and sound onsets is modulated by attention. Participants were scanned while listening to Illusion, Illusion Break, and two types of intact vowels and simultaneously directing their attention either to the vowel stimuli or to auditory or visual distractors. Preliminary analyses suggest that activation to intact and illusory vowels in MTG, and to sound onset in PAC, is modulated by attention.

5aSCc40. Effect of head covers on directivity pattern of human head. Dejan Todoroviæ (Dirigent Acoustics, Takovska 45A, 11000 Beograd, Serby, dgtdejan@yahoo.com)

In this paper are presented the experimental results of changes in directivity patterns of artificial head with three different types of head covers. The mathematical model of human head approximated by radially vibrating spherical cap set in a sphere is discussed. For the purpose of this research, the physical model of a human speaker head is constructed, and the far-field detailed directivity patterns of the model with and without head covers is measured. Hair as porous absorber, cap and straw hat, as sound barriers, are discussed, and their influence on sound wave propagation is considered. Measured detailed directivity pattern changes affected by head covers in far

field are calculated in step of ten degrees for spherical coordinates (polar angle and azimuth) and presented in form of two- and three-dimensional polar plots.

5aSCc41. English and Polish glides compared. Anna Balas (Adam Mickiewicz University, al. Niepodleglosci 4, 61-874 Poznan, Poland, abalas@ifa.amu.edu.pl)

This paper compares acoustic features of (1) Polish and English glides before vowels, and (2) Polish glides in vowel-plus-glide sequences with English diphthong offglides. Contrary to traditional articulatory descriptions, the results presented, based on acoustic measurements and vector length calculations, do not reveal that Polish glides in vowel-plus-glide sequences are characterized by more extreme formant values than English diphthong offglides. The difference between English diphthongs and Polish vowel-plus-glide sequences is attributed to timing properties, which are shown to be relatively easily acquired by Polish learners of English, probably because of a universal tendency for the first element to be longer than the second one. Preliminary results, however, point to acoustic differences between Polish glides before and after vowels, the former being more consonantal than the latter.

5aSCc42. Correlations among three audiovisual (AV) speech tasks. Julia Irwin (Haskins Laboratories, 300 George Street, New Haven, CT 06511, USA, julia.irwin@haskins.yale.edu), Lawrence Brancazio (Southern Connecticut State University and Haskins Laboratories, 300 George Street, New Haven, CT 06511, USA, brancaziol@southernct.edu)

Visual speech information influences what listeners hear. When the place of articulation of visual and auditory speech tokens are incongruent, perceivers often report hearing a visually influenced response (the "McGurk effect", McGurk and MacDonald, 1976). However, individual differences in this visual influence are poorly understood. Extending work by Grant & Seitz (1998) and Conrey and Pisoni (2006), we examined correlations between susceptibility to the "McGurk effect" and performance on three related audiovisual tasks. (1) AV speech in noise: we assessed visual gain by comparing word identification in audio-only and AV conditions. (2) AV asynchrony detection: Participants made asynchrony judgments of speech and nonspeech stimuli with asynchronies ranging from +250 ms visual to +250 ms auditory lead. The speech stimuli were CV syllables and the nonspeech stimuli consisted of lissajous circles paired with sine waves. In one set of nonspeech stimuli, the lissajous was modeled on the lip aperture of the CV and the sine wave, amplitude and frequency were derived from the CV. For the other set, the lissajous and sine wave were derived from clapping hands. (3) Speechreading: Participants identified isolated words presented visually. Factors associated with a strong McGurk effect will be discussed. [Work supported by NIH.]

5aSCc43. Factors influencing French schwa deletion and duration: A corpus-based study. Audrey Bürki (Laboratoire de Psycholinguistique, Université de Genève, 40, Bvd Pont d'Arve, 1201 Geneva, Switzerland, audrey.buerki@pse.unige.ch), Mirjam Ernestus (Radboud University Nijmegen & Max Planck Institute for Psycholinguistics, P.O. Box 310, 6500 Nijmegen, Netherlands, Mirjam.Ernestus@mpi.nl), Cécile Fougeron (Laboratoire de Phonétique et Phonologie, UMR 7018, CNRS-Paris 3/Sorbonne Nouvelle, 19 rue des Bernardins, 75005 Paris, France, cecile.fougeron@univ-paris3.fr), Cédric Gendrot (Laboratoire de Phonétique et Phonologie, UMR 7018, CNRS-Paris 3/Sorbonne Nouvelle, 19 rue des Bernardins, 75005 Paris, France, cedric.gendrot@univ-paris3.fr), Ulrich H. Frauenfelder (Laboratoire de Psycholinguistique, Université de Genève, 40, Bvd Pont d'Arve, 1201 Geneva, Switzerland, ulrich.frauenfelder@pse.unige.ch)

Numerous factors have been advanced to account for the alternance of schwa with zero in French, such as lexical frequency, sonority, syllable structure, phonotactic constraints, etc. ... In the present study we use a recently developed statistical modeling technique, mixed effects models with crossed random effects, to capture the relative contributions of multiple linguistic factors on both, schwa deletion and schwa's physical duration when present. This study is based on the analysis of 4300 occurrences, extracted from the production of more than 300 speakers in a broadcast corpus. The implications of these findings for the debate on the nature of the processes involved in schwa deletion as well as for the nature of lexical representations will be discussed.

5aSCc44. Perceptual clarity of speech modulates activity in left temporal-lobe regions: fMRI correlates of top-down influences. Conor Wild (Queen's University, Centre for Neuroscience Studies, 62 Arch Street, Kingston, ON K7L3N6, Canada, 9cw13@queensu.ca), Matthew H. Davis (MRC CBU, 15 Chaucer Rd., CB2 7EF Cambridge, UK, matt.davis@mrc-cbu.cam.ac.uk), Alexis G. Hervais-Adelman (Centre for the Neural Basis of Hearing, Department of Physiology, Development and Neuroscience, University of Cambridge, Downing Site, CB23EG Cambridge, UK, alexis.hervais-adelman@mrc-cbu.cam.ac.uk), Ingrid S. Johnsrude (Queen's University, Dept Psychology, 62 Arch Street, Kingston, ON K7L 3N6, Canada, ingrid.johnsrude@queensu.ca)

Behavioral evidence supports the idea that perception is guided by mechanisms that compute an input's most probable interpretation. For example, four-band noise-vocoded speech, which is largely unintelligible to naive listeners, becomes perceptually clear when listeners possess prior knowledge of the signal content - a phenomenon we call "pop-out". Feedback connections within and among auditory cortical regions may allow cognitively "higher" levels of processing to predict and thus "explain" the bottom-up signal. In the present study, we use fMRI to investigate the network underlying pop-out. We use written primes (matching or nonmatching text strings) to manipulate a subject's perception of single noise-vocoded words, thereby creating acoustically matched conditions that elicit the perceptions of intelligible or unintelligible speech. Whole brain fMRI data were gathered from 21 subjects using a sparse-imaging procedure. Preliminary analysis reveals regions of statistically significant signal change along the left superior and middle temporal gyri and superior temporal sulcus for matching trials that induce perceptual popout. Functional connectivity analysis will allow us to investigate coupling among these auditory regions, and how connectivity is modulated depending on the perceptual coherence of a noise-vocoded utterance.

5aSCc45. Some acoustic cues in the detection of the Nepalese aspiration. Rajesh Khatiwada (LPP UMR CNRS- 7018 Université Sorbonne Nouvelle, 19 rue des bernardins, 75005 Paris, France, rajesh.khatiwada@free.fr)

In terms of laryngeal setting, most languages have only two types of stops. In the Nepalese sound inventory there are four types of stops: voiceless unaspirated, voiced unaspirated, voiceless aspirated, and voiced aspirated (or breathy voiced). The main objective of this paper is to present the prominent and consistent acoustic cues that differentiate the aspirated segments from their unaspirated counterparts of the Nepalese coronals - the dental-alveolar (t,th,d,dh), retroflex (T,Th,D,Dh) and affricates (ts,tsh,dz,dzh). VOT (Voice Onset Time) (Lisker and Abramson 1964) is the familiar model used to characterize three of these phonation types - voiced, voiceless, and aspiration stops. Some authors have pointed out that this method is not able to distinguish the plain voiced and voiced aspirated stops. An alternative segmentation model proposed by Mikuteit and Reetz (2007) is adopted here. Beside the analysis of the closure duration of segments, measuring the beginning of the burst or its release, we use other acoustic cues to characterize Nepalese aspiration such as F0 lowering, the structure of the lower harmonics and spectral tilt (Hanson 1997, Stevens 1998). This experimental work is based on the corpus based on four native speakers of Nepali.

5aSCc46. Prosodic realization of focus on verbal phrases in two Chinese dialects. Yiya Chen (LUCL, Phonetics Laboratory, Cleveringaplaats 1, P. O. Box 9515, 2300 RA Leiden, Netherlands, yiya.chen@let.leidenuniv.nl)

A well-established observation in West-Germanic languages is that when a verbal phrase (e.g., likes movies) is uttered as new information (i.e., focused), speakers often accent (via F0 changes) the noun only (e.g., Ladd 1980 and 1996). Listeners, in turn, find that a single accent on noun sounds as appropriate as when both verb and object are accented (e.g., Gussenhoven

1987, Birch and Clifton 1995, Welby 2003). This study will report results of an experiment which was designed to examine the prosodic realization of focus on verbal phrases in two tonal dialects - Beijing Mandarin and Shanghai Chinese. Both dialects use F0 changes to indicate word meanings, but they differ in tone sandhi patterns. That is, they differ in how words group into phrasal tonal domains and how lexical tones undergo changes within the domain. Two types of focus were elicited: One provides new information to Wh-questions and the other corrections of wrong information in the preceding discourse. The goal of the study is to contribute to the development of a cross-linguistic theory of the prosodic realization of focus. [Work supported by the VENI research grant from the Netherlands Organization for Scientific Research.]

5aSCc47. On nasal onset time (NOT) duration of French nasal vowels in function of the preceding consonant types. Julie Montagu (Laboratoire de Phonétique et Phonologie UMR 7018-CNRS/Université Paris 3, 5, rue des Bernardins, 75005 Paris, France, julie_montagu@yahoo.com)

Aerodynamic requirement, a high intra-oral air pressure (Pio), for the production of stop and fricative consonants delays the nasalization (velum opening) of the subsequent nasal vowel. We call this time delay between the onset of the nasal vowel and that of its nasalization as nasal onset time (NOT). The NOT was expected to be longer after voiceless consonants (higher Pio) than after voiced counterparts. The measurement of NOT on simultaneous recordings of speech and nasal signals for 24 Parisian speakers have unexpectedly shown that a greater NOT after voiced stops (38 ms in average corresponding to 17% of total nasal vowel duration) and voiced fricatives (7%) than after voiceless ones, respectively, 14.5% for stops and 4.1% for fricatives. This order is observed regardless of changes in speech rate: NOT is 11.1% with the voiced and 9.3% with the voiceless stops in slow, 17% and 14.5% in normal, and 22.4% and 18.6% in rapid rate. These results suggest that not only the Pio, but also some other factors are involved in the determination of NOT. We shall discuss possible such factors in perception and in production.

5aSCc48. Sustained and transient brain activations in bilingual control. Yapeng Wang (State Key Laboratory for Cognitive Neuroscience and Learning, Beijing Normal University, 100875 Beijing, China, Institute for Learning and Brain Sciences, University of Washington, Seattle, WA 98115, USA, yapengw@u.washington.edu), Patricia K. Kuhl (University of Washington, Dept. of Speech & Hearing Sciences, and Institute for Learning & Brain Sciences, Box 357988, Seattle, WA 98195, USA, pkkuhl@u.washington.edu), He Li (State Key Laboratory for Cognitive Neuroscience and Learning, Beijing Normal University, 100875 Beijing, China, Institute for Learning and Brain Sciences, University of Washington, Seattle, WA 98115, USA, her2003@163.com),Qi Dong(State Key Laboratory for Cognitive Neuroscience and Learning, Beijing Normal University, 100875 Beijing, China, Institute for Learning and Brain Sciences, University of Washington, Seattle, WA 98115, USA, dongqi@bnu.edu.cn)

Behavioral and neuroimaging evidence shows that bilinguals experience interference and competition during bilingual processing. The neural basis of bilingual language control is not well understood. Using mixed blocked and event-related design, the present study explored the sustained and transient activations during bilingual control. 15 Chinese-English bilingual speakers were scanned when they performed language switching tasks. The results showed that, compared to single language condition, the mixed language condition (sustained control) induced the activation in the bilateral prefrontal (BA6/BA8/BA10), middle frontal (BA45/46) and parietal lobes (BA7/ BA40/BA49); In contrast, relative to the no switch condition, language switching (transient control) activated the left superior, inferior parietal lobe (BA2/ BA40) and middle frontal (BA11/46). These results suggested that sustained and transient language control induced differential lateral activation patterns.

5aSCc49. Automatic acoustic analysis of substitute speech characteristica by speech recognition technique. Maria Schuster (Dpt. Phoniatrics and Pedaudiology, Bohlenplatz 21, 91054 Erlangen, Germany, maria.schuster@uk-erlangen.de), Andreas Maier (Dpt. Phoniatrics and Pedaudiology, Bohlenplatz 21, 91054 Erlangen, Germany, maier@informatik.uni-erlangen.de), Tino Haderlein (Dpt. Phoniatrics and Pedaudiology, Bohlenplatz 21, 91054 Erlangen, Germany, tino.haderlein@informatik.uni-erlangen.de), Ulrich Eysholdt (Dpt. Phoniatrics and Pedaudiology, Bohlenplatz 21, 91054 Erlangen, Germany, ulrich.eysholdt@uk-erlangen.de), Elmar Noeth (Dpt. for Pattern Recognition, Martensstr. 5, 91052 Erlangen, Germany, noeth@informatik.uni-erlangen.de)

Tracheo-esophageal (TE) substitute speech is often used after total laryngectomy as it resembles normal speech more than other substitute speech methods. However, TE speech still shows restrictions and is perceived as hoarse, rough, with strain, and usually monotone, e.g., due to augmented irregularity of the voice signal. Commonly used diagnostic tools to describe the acoustic properties of TE speech are mostly not applicable. Before, automatic speech recognition has been shown to serve as a appropriate acoustic tool for the quantification of TE speech intelligility. We now applied an automatic speech recognition system with prosody module on speech data of 41 laryngectomees. The prosody module extracted 150 parameters. Factor analysis revealed five principal components. They show high correlation to perceptively described TE speech characteristica. Automatic prosody analysis by speech recognition technique allows to detect and quantify characteristics of highly disordered speech.

Session 5aUWa

Underwater Acoustics, Signal Processing in Acoustics, and ECUA: Broadband Underwater Communications I

Heechun Song, Cochair
MPL, Scripps Institution of Oceanography, University of California, San Diego, La Jolla, CA 92093-0238, USA

Sergio Jesus, Cochair
ISR, Universidade do Algarve, Faro, PT-8005-139, Portugal

Invited Papers

8:00

5aUWa1. Multiinput multioutput OFDM for shallow-water UWA communications. Yunus Emre (Arizona State University, Dept. of Electrical Engineering, Tempe, AZ 85287-5706, USA, yunus.emre@asu.edu), Vinod Kandasamy (Arizona State University, Dept. of Electrical Engineering, Tempe, AZ 85287-5706, USA, vinod.kandasamy@asu.edu), Tolga M. Duman (Arizona State University, Dept. of Electrical Engineering, Tempe, AZ 85287-5706, USA, duman@asu.edu), Paul Hursky (HLS Research, Inc., 3366 N. Torrey Pines Ct., Ste. 310, La Jolla, CA 92037, USA, paul.hursky@hlsresearch.com), Subhadeep Roy (Qualcomm Flarion Technologies, Bridgewater, NJ 08807, USA, subhadee@qualcomm.com)

We investigate performance of turbo coded multiple-input multiple-output (MIMO)-OFDM systems with layered space time (LST) architectures for underwater acoustic (UWA) channels by using simulations and results from the AUVfest experiment performed in June 2007. MIMO systems have been shown to be promising in the sense that they increase the reliable transmission rates significantly without consuming additional bandwidth and power. Robustness of OFDM systems with cyclic prefix or zero padding to ISI channels are also well known; so the combination of MIMO techniques and OFDM can be regarded as a promising technology for shallow water UWA communications which is characterized by severe bandwidth limitations and long intersymbol interference (ISI) spans. The paper reviews necessary components of a MIMO-OFDM communication system, including, time and frequency synchronization, channel estimation, and tracking of the varying channel parameters. Modifications necessary to make the system suitable for UWA channels are summarized. Results of the AUVFest 2007 experiment are very promising; for instance, 2×2 MIMO-OFDM can reach up to 60 Kbps transmission for a bandwidth of 16 KHz with simple receiver structures for a range of 2000 m. In addition to the coherent system, differential and unitary space-time coded MIMO-OFDM scenarios are also considered.

8:20

5aUWa2. High rate acoustic communications based on orthogonal frequency division multiplexing. Milica Stojanovic (Massachusetts Institute of Technology E38-376, 292 Main St., Cambridge, MA 02139, USA, millitsa@mit.edu)

Orthogonal frequency division multiplexing (OFDM) offers simplicity of FFT-based implementation with frequency-domain channel equalization, and has emerged as a standard in many terrestrial systems. Its application to underwater systems, however, is challenged by the motion-induced Doppler distortion, which creates nonuniform frequency offset in a wideband acoustic signal. To counteract this problem, recent research has focused on synchronization methods, demonstrating the feasibility of wideband OFDM in initial sea trials. We consider the design of a complete OFDM receiver based on three key techniques: adaptive carrier tracking, spatial diversity combining, and sparse channel estimation. In particular, we focus on time-domain channel estimation, which provides a natural platform for channel sparsing. Sparsing of the impulse response, or discarding of its insignificant coefficients, is shown to offer performance gains on acoustic channels, since they are often naturally sparse. Decision-directed operation, which is made possible by adaptive carrier tracking, yields a low overhead, and further improves the performance of channel estimation beyond that of nonadaptive pilot-based schemes. The technique proposed is applied to experimental data recorded in a shallow water channel over 1 km. Results show excellent performance of coded OFDM signals, transmitted in the 19-31 kHz band with a varying number of subcarriers.

8:40

5aUWa3. Experimental assessment of time-reversed OFDM underwater communications. Joao Gomes (ISR - Instituto Superior Tecnico, Av. Rovisco Pais, Torre Norte 7.22, 1049-001 Lisboa, Portugal, jpg@isr.ist.utl.pt), Antonio Silva (ISR, Universidade do Algarve, PT-8005-139 Faro, Portugal, asilva@ualg.pt), Sergio Jesus (ISR, Universidade do Algarve, PT-8005-139 Faro, Portugal, sjesus@ualg.pt)

OFDM communication has recently been demonstrated in underwater channels at rates exceeding 7 kbps. This is a popular modulation in wireless communications due to its flexibility for spectrum management and the simplicity of transmitters/receivers. Despite widespread interest, experimental data on the performance of underwater OFDM are scarce. This work aims to contribute to a better understanding of this technique by examining results from the UAB'07 experiment, conducted in Norway in September 2007. Data were transmitted in a fjord using several formats with bandwidths of 3 and 7.5 kHz, and recorded at a range of 800 m in a 16-hydrophone array. Significant multipath was observed over at least 40 ms, which would call for a rather large OFDM prefix/guard interval and hence drastically reduce the data rate. Passive time reversal is used here as a computationally inexpensive scheme to shorten the channel length

to less than 10 ms, so that moderate guard intervals can be used with a conventional OFDM receiver. The same preamble/postamble signals used for synchronization and Doppler precompensation are reused as probes for passive time reversal, so the latter entails no loss in efficiency. The performance of time-reversed OFDM is compared with plain QPSK modulation using either time reversal or multichannel equalization at the receiver.

9:00

5aUWa4. Linear and circular adaptive beamforming arrays for high bandwidth acoustic communications. Jeffrey Neasham (Newcastle University, School of Electrical, Electronic and Computer Engineering, Merz Court, NE1 7RU Newcastle upon Tyne, UK, j.a.neasham@ncl.ac.uk), David Howarth (Tritech International, Morecambe Road, Ulverston, LA12 9BN Cumbria, UK, davidhowarth@tritechulverston.co.uk), Bayan Sharif (Newcastle University, School of Electrical, Electronic and Computer Engineering, Merz Court, NE1 7RU Newcastle upon Tyne, UK, bayan.sharif@ncl.ac.uk), Oliver Hinton (Newcastle University, School of Electrical, Electronic and Computer Engineering, Merz Court, NE1 7RU Newcastle upon Tyne, UK, oliver.hinton@ncl.ac.uk)

This paper will discuss the development of a new generation of high bandwidth (up to 32 kbits/s) underwater communication products for ranges up to 4 km. Multipath propagation is the dominant factor in system performance in both shallow water, horizontal channels and deep water, vertical channels. The properties of such channels will be analysed and the design of both linear and circular receiver arrays will be discussed to maximise reliability. We will then describe how these arrays are combined with the latest "software" receiver principles to create a powerful and flexible system, incorporating adaptive signal processing with minimal hardware complexity. Finally the performance of this system will be illustrated with results from experimental trials.

9:20

5aUWa5. Channel estimation for underwater acoustic communications: sparse channels, soft input data, and Bayesian techniques. James Preisig (Woods Hole Oceanographic Institution, Bigelow 404, MS#9, Woods Hole, MA 02543, USA, jpreisig@whoi.edu), Ballard Blair (Woods Hole Oceanographic Institution, Bigelow 404, MS#9, Woods Hole, MA 02543, USA, bjblair@mit.edu), Weichang Li (Woods Hole Oceanographic Institution, Bigelow 404, MS#9, Woods Hole, MA 02543, USA, wli@whoi.edu)

The problem of estimating the time-varying impulse response of the communications channel is central to creating reliable and high-rate communications links. Past work has shown that by jointly accounting for channel dynamics and sparse channel characteristics, the accuracy of the channel impulse response estimate is improved with a corresponding improvement in communications systems performance. Following a survey of the basic techniques that have been developed, these basic techniques are extended in two ways. The first allows for a more complete accounting for the channel characteristics via apriori distributions on the probabilities of the complex channel tap values and optimized basis functions for sparse channel structure. The second allows for the use of soft input data in the channel estimation process thus making the techniques feasible for iterative channel estimation and data estimation algorithms. The extensions are developed and their performance compared using data from recent shallow water acoustic communications experiments.

Contributed Paper

9:40

5aUWa6. Investigation of modal processing for low frequency acoustic communications in shallow water. Andrey Morozov (Woods Hole Oceanographic Institution, Bigelow 404, MS#9, Woods Hole, MA 02543, USA, amorozov@whoi.edu), James Preisig (Woods Hole Oceanographic Institution, Bigelow 404, MS#9, Woods Hole, MA 02543, USA, jpreisig@whoi.edu), Joseph Papp (Woods Hole Oceanographic Institution, Bigelow 404, MS#9, Woods Hole, MA 02543, USA, jpapp@whoi.edu)

Acoustic receptions at a vertical line array collected during the SW06 experiment were processed to show the feasibility of broadband mode decomposition as a preprocessing method to shorten time-spread and concentrate received signal energy in a small number of independent channels. The vertical array spanned the water column from 12 m depth to the bottom. PSK m-sequence modulated signals with different carrier frequencies were transmitted from a distance of 19.2 km. Signals were processed for both the case of ordinary internal waves activity and the case with abnormally strong internal wave solitons. The measured sound velocity and known bottom properties were accounted for. Mode filtering was based on a broadband pseudo-inverse processing of the received VLA signals. The broadband mode filtering decomposed the received signal into a number of independent signals with a reduced time-spread. The constellation of signals from the output of mode filters showed that a simple demodulator can achieve a high quality reception. Even during strong internal waves activity the acoustic energy was concentrated in a small number of the first acoustical modes. The receiver estimated the mode-time intensity distribution and used the strongest modes for demodulation. High quality reception is demonstrated with the data.

10:00-11:00 Posters

Lecture sessions will recess for the presentation of poster papers on various topics on acoustics. See poster sessions for topics and abstracts.

11:00

5aUWa7. Basin-scale time reversal communications. Heechun Song (MPL, Scripps Institution of Oceanography, University of California, San Diego, La Jolla, CA 92093-0238, USA, hcsong@ucsd.edu), William A. Kuperman (MPL, Scripps Institution of Oceanography, University of California, San Diego, La Jolla, CA 92093-0238, USA, wkuperman@ucsd.edu), William Hodgkiss (MPL, Scripps Institution of Oceanography, University of California, San Diego, La Jolla, CA 92093-0238, USA, wsh@mpl.ucsd.edu)

During November 1994, broadband acoustic signals were transmitted from a 75-Hz source to a 20-element, 700-m vertical array at approximately 3250 km range in the eastern North Pacific Ocean as part of the Acoustic Engineering Test (AET) of the Acoustic Thermometry of Ocean Climate (ATOC) program [Worcester et al., J. Acoust. Soc. Am. **105**, 3185-3201 (1999)]. The AET tomography signal can be treated as a binary-phase shift-keying (BPSK) communication signal with an information rate of 37.5 bits/s. With the multipath arrivals spanning 5-8 s, this data represents an extreme case of intersymbol interference (ISI). The AET array data are processed using time reversal combined with frequent channel updates to accommodate channel variations over the 20-min long reception, followed by a single channel decision-feedback equalizer (DFE). The almost error-free performance using all 20 array elements demonstrates the feasibility of time reversal communications. Further, comparable performance of single receive element communications integrating over multiple transmissions indicates that the ocean provided temporal diversity as well as the spatial diversity provided by the array.

11:20

5aUWa8. Coherent time reversal communications in a shallow multipath environment. Slawomir Jastrzebski (University of Technology and Life Sciences, ul. Kordeckiego 20, 85-225 Bydgoszcz, Poland, sj@utp.edu.pl)

Underwater acoustic channel is one of the less reliable communication channels due to its reverberant properties produced by the surface and the bottom of the sea and Doppler spreading caused by the transmitter and the receiver movements. Strong intersymbol interference (ISI) caused by time-varying multipath environments and relatively fast channel variations are two of the major challenges for practical implementation of coherent underwater acoustic communications. In this paper a phase conjugation is considered as a method for mitigating intersymbol interference in coherent communication and this technique reducing the complexity of underwater receivers. Phase conjugation uses time reversal to remove intersymbol interferences. This method performs the time reversal operation in the computer at the receiver instead of time reversed propagation through the sea. This paper presents numerical simulations results of coherent communications using this technique. Phase conjugation processing in acoustic communications was demonstrated with the transmission of BPSK and QPSK modulation schemes. Different messages were sent simultaneously to different depths at different ranges in 100 m deep shallow water. Simulation results suggest that the phase conjugation technique may be used as a potential application to undersea communications, especially in an environment with significant multipath.

11:40

5aUWa9. Very broadband high frequency underwater acoustic communications. Lee Freitag (Woods Hole Oceanographic Inst., 266 Woods Hole Road, MS 18, Woods Hole, MA 02543, USA, lfreitag@whoi.edu), Sandipa Singh (Woods Hole Oceanographic Inst., 266 Woods Hole Road, MS 18, Woods Hole, MA 02543, USA, ssingh@whoi.edu), Keenan Ball (Woods Hole Oceanographic Inst., 266 Woods Hole Road, MS 18, Woods Hole, MA 02543, USA, kball@whoi.edu)

Many new applications for underwater observatories and sensor systems do not require long ranges, but do require very power-efficient, high-throughput communications. Recent work in phase-coherent underwater acoustic communications has shown that signal bandwidths of 10-40 khz at carrier frequencies from 80 to 120 khz may be used to achieve throughputs of up to 80 kbps at ranges of 100-500 m in shallow water. The work has included channel impulse response measurements over time and with respect to range, and application of the adaptive decision feedback equalizer using signals at multiple bandwidths. The broadband, high-frequency propagation environment is characterized, and its impact on the reliability of very wide band signals (relative to the signal carrier) is presented.

12:00

5aUWa10. Experiments of wideband color image transmission. Hiroshi Ochi (JAMSTEC, 2-15, Natsushima-cho, 237-0061 Yokosuka, Japan, ochi@jamstec.go.jp), Yoshitaka Watanabe (JAMSTEC, 2-15, Natsushima-cho, 237-0061 Yokosuka, Japan, yoshitakaw@jamstec.go.jp), Takuya Shimura (JAMSTEC, 2-15, Natsushima-cho, 237-0061 Yokosuka, Japan, shimurat@jamstec.go.jp), Takehito Hattori (Nippon Marine Enterprises, Ltd., 14-1, Ogawa-cho, 238-0004 Yokosuka, Japan, hattorit@nme.co.jp)

In JAMSTEC, we have been studying about a high-speed underwater acoustic communication for color image transmission from underwater vehicle of deep water. The objective of our research is to transmit a JPEG compressed color image within once a second. Experiments were carried out at the depth of 1000 m area. The distance of transmission was 250 - 600 m. Four omni-directional hydrophones were used for receiving. QPSK and 8PSK were used as its modulation method. The four-channel decision feedback equalizer with phase compensator was applied for the demodulation algorithm. Because of this experiment was carried out at deep sea environment, the communication channel characteristics was relatively simple. In these experiment, when the SNR was higher than 12 dB, error free communication was carried out in case of QPSK. And also when the SNR was higher than 20 dB, error free communication was carried out in case of 8PSK

12:20

5aUWa11. Robust time-division channel-access approach for an ad hoc underwater network. Kae Yeet Foo (University of Birmingham, Department of Electronic, Electrical and Computer Engineering, Edgbaston, B15 2TT Birmingham, UK, kyf740@bham.ac.uk), Philip Atkins (University of Birmingham, Department of Electronic, Electrical and Computer Engineering, Edgbaston, B15 2TT Birmingham, UK, p.r.atkins@bham.ac.uk), Steve A. Pointer (Qinetiq, Winfrith Technology Centre, DT2 8XJ Dorchester, UK, sapointer@qinetiq.com), Carl P. Tiltman (Dstl, Winfrith Technology Centre, DT2 8WX Dorchester, UK, cptiltman@dstl.gov.uk)

An ad hoc underwater network is formed by a cluster of stationary nodes that can act as a source, destination, or a relay, in which data packets usually travel across multiple hops. Using a time-division scheme where the propagation delay between the nodes is used as a packet queuing buffer optimizes throughput. This requires accurate knowledge of the relative ranges of all the nodes, a high level of accuracy in time-synchronization, and restricts changes in the position of the nodes especially in the absence of a central server or master node within the network. A method that offers greater robustness is by using a time-slotted approach, where each node is offered a time-slot sufficient for one transmission to reach its maximum effective range. A passive acknowledgment scheme is implemented where a node listens for acknowledgment when the transmitted packet is being relayed. Nodes monitor other time-slots for the opportunity to contend for idle slots in order to enhance throughput. Results obtained from simulations demonstrate that this method is robust in supporting changes in the relative distances between the nodes, and can typically operate with a time synchronization error of up to 1 s.

Session 5aUWb

Underwater Acoustics and ECUA: Environmental Impact on Propagation

Bashar Mohammad, Cochair
Heriot Watt University, School of Engineering and Physical Sciences, Riccarton, Edinburgh, EH14 4AS, UK

Jinshan Xu, Cochair
MIT Mechanical Engieerning Department, 77 Massachusett Ave., Cambridge, MA 02139, USA

Contributed Papers

8:00

5aUWb1. Spatial and temporal variations in acoustic propagation in Dabob Bay during PLUSNet'07 Exercise. Jinshan Xu (MIT Mechanical Engieerning Department, 77 Massachusett Ave., Cambridge, MA 02139, USA, jinshan@mit.edu), Pierre Lermusiaux (MIT Mechanical Engieerning Department, 77 Massachusett Ave., Cambridge, MA 02139, USA, pierrel@MIT.EDU), Patrick Haley (MIT Mechanical Engieerning Department, 77 Massachusett Ave., Cambridge, MA 02139, USA, phaley@MIT.EDU), Wayne Leslie (MIT Mechanical Engieerning Department, 77 Massachusett Ave., Cambridge, MA 02139, USA, wgleslie@MIT.EDU), Oleg Logutov (MIT Mechanical Engieerning Department, 77 Massachusett Ave., Cambridge, MA 02139, USA, logutov @mit.edu)

We present spatial and temporal variability of the acoustic field in Dabob Bay during the PLUSNet'07 (Persistent Littoral Undersea Surveillance Network) Exercise. The study uses a 4D (3D in space plus 1D in time) data-assimilative numerical ocean model to provide inputs to an acoustic propagation model. The Havard-Ocean-Prediction-System with in-situ CTD measurement assimilation provided output forecasts with a 300-m and 1-to-5-m resolution in the horizontal and vertical direction, for a 3-h interval within a 15-day period. This environmental data as the input to acoustic modeling allowed prediction and study of the (semi-)diurnal temporal variations of the acoustic field, as well as the varying spatial structures of the field. Using the one-way coupled-normal-mode code, along- and across-sections in the Dabob Bay acoustic field structures at 100, 400, and 900 Hz were forecasts and studied for various source depths. Interesting propagation effects such as the acoustic transmission-loss fluctuations with respect to the source depth and frequency as a result of the regional ocean variability, wind forcing, and tidal effects are discussed. The novelty of this work lies in the accuracy of the acoustic transmission-loss prediction in the littoral region by physically coupling the real-time ocean prediction system to acoustic modeling. This work also offers a potential extension to a 4D acoustic modeling.

8:20

5aUWb2. On shallow water ocean acoustic tomography system based on parametric arrays physical properties evaluation. Andrew Semenov (Acad. N.N. Andreev's Acoustics Institute, Russ. Acad. of Sci., 4 Shvernik Street, 117036 Moscow, Russian Federation, asemen@akin.ru)

Unsophisticated acoustic tomography system properties using envelope of radiated acoustic signal for ocean long-range inhomogeneities control, presumably, in most unfavorable, in the author view, shallow water regions, are evaluated. Unique solution to be used there is a narrow directional parametric radiation array. When pump wave signal decay range to array Frauengopher zone dimension ratio exceeds pump wave frequency to radiated signal frequency ratio, parametric radiation array operation model turns to "horn" model instead of "traveling wave" model conventionally used for consumed power prediction. For utmost distance achievement both ends of tomography system should be designed as narrow directional parametric arrays working on optimal frequency basic propagation (first) mode. For instance, signal optimum frequency 40 Hz. is shown to be necessary for model inhomogeneity (100 m long cylinder) control on 500-km radiation array distance in water layer of depth 200 m with unfavorable attenuation properties. Major lobe solid angle should be chosen not wider than 0,03 radians. Array frequency ratio is advised to be of an order of 10, while array length - 100 half wavelength for pump sound field frequency. Then estimate of power consumption looks like 180-200 kWt of pump signal acoustic power.

8:40

5aUWb3. The analysis of underwater environmental factors in relation to the harbor protection in Tzoin-Kaohsiung areas. Jin-Yuan Liu (Department of Marine Environmental Informatics/National Taiwan Ocean University, 2 Pei-Ning Road, 202 Keelung, Taiwan, jimliu@faculty.nsysu.edu.tw), Chen-Fen Huang (Department of Marine Environmental Informatics/National Taiwan Ocean University, 2 Pei-Ning Road, 202 Keelung, Taiwan, chenfen@mail.ntou.edu.tw)

Harbor is an important shipping traffic area. The intrusion or threatening by outsiders in the harbor area will certainly cause great panic of the society, and therefore, the protection of harbor and its nearby water is utterly important. The Tzoin harbor is primarily serviced for navy, and is under planning for further expansion. Therefore, a complete control of the Tzoin-Kaohsiung marine environment, both geographical and acoustical, is necessary for military applications. The purpose of this study is to conduct a complete survey of the environment in the designated area, covering the first seaway of the Kaohsiung harbor and off coast water of the Si-Tze bay area. The survey of the marine environment includes seafloor topography, morphology, subbottom profile, waves, currents, and wind fields. In acoustic aspect, the survey emphasizes the harbor ambient noise measurement. The data obtained shall be thoroughly examined and analyzed. The results provide a foundation for future underwater experimental studies, including target localization, geoacoustic inversion, and active sonar reverberation.

9:00

5aUWb4. The effects of a shallow-water acoustic channel on Right whale vocalisations. Bashar Mohammad (Heriot Watt University, School of Engineering and Physical Sciences, Riccarton, EH14 4AS Edinburgh, UK, mb41@hw.ac.uk), Ron McHugh (Heriot Watt University, School of Engineering and Physical Sciences, Riccarton, EH14 4AS Edinburgh, UK, r.mchugh@hw.ac.uk), Judith Bell (Heriot Watt University, School of Engineering and Physical Sciences, Riccarton, EH14 4AS Edinburgh, UK, j.bell @hw.ac.uk)

For mitigation and monitoring of Right whales, identifying their presence from their vocalisations is a key research issue. Their vocalisations are characterized as frequency modulated up-sweeps with duration of ~1s and a frequency range from 50Hz to 200Hz. Acoustic methods to classify these received calls are assessed by the variation in the received data set. As well as the natural variation in vocalisation within the species, the received acoustic signals are also influenced by the effect of the acoustic channel. The shallow water of Cape Cod Bay is one of the favoured habitats for the Northern Right whale. Such waters act as an acoustic waveguide where multiple reflections off boundaries cause calls to become dispersive in nature. In this paper we discuss the effects of channel environmental parameters such as water depth and sediment type on first the FM deviation and second on

the time difference of arrival between the first and second modes, which in turn influences acoustic range estimation. Such channel effects were studied using the normal mode acoustic propagation model (PROSIM). An analysis of real acoustic data recorded in Cape Cod Bay (2001 obtained from IFAW) will be also presented in terms of dispersion results.

9:20

5aUWb5. Development of an ocean surveillance system. V. Ananthakrishnan (Department of Electronics, Cochin University of Science & Technology, Thrikkakara, 682 022 Ernakulam, India, ananthanmattathil@gmail.com), C Prabha (Department of Electronics, Cochin University of Science & Technology, Thrikkakara, 682 022 Ernakulam, India, prabhasuma@cusat.ac.in), Supriya M. Hariharan (Department of Electronics, Cochin University of Science & Technology, Thrikkakara, 682 022 Ernakulam, India, supriya@cusat.ac.in), Saseendran Pillai (Department of Electronics, Cochin University of Science & Technology, Thrikkakara, 682 022 Ernakulam, India, prspillai@cusat.ac.in)

Now-a-days, underwater sensor networks are gaining considerable importance, for Ocean Surveillance applications. A minimally configurable three-node sensor network is found to be capable of performing localization as well as tracking of underwater targets. Each node comprises of a surface buoy having processing modules, controller hardware and support electronics for estimating the direction of arrival. The development of the node system comprising of controller and processing modules is presented in this paper. The controller hardware, consisting of a gear assembly, magnetic compass and a precision digital signal controller, helps in sampling the ocean by way of steering the hydrophone arrays and capturing the target emanations, while the processing module performs the computation of the direction of arrivals. The target emissions picked up by the hydrophone arrays are analyzed and processed for computing the direction of signal arrival with reference to the geomagnetic meridian. The direction of maximum signal arrivals computed by the three nodes, lead to the estimation of the target position. Localization of the target is carried out by effectively utilizing the information furnished by Global Positioning System incorporated in the node hardware, which has an efficient power management mechanism, as well.

FRIDAY MORNING, 4 JULY 2008 ROOM 342A, 8:00 A.M. TO 12:40 P.M.

Session 5aUWc

Underwater Acoustics and ECUA: High Frequency Scattering I

Anthony P. Lyons, Cochair
Applied Research Laboratory, The Pennsylvania State University, P.O. Box 30, State College, 16804, USA

Philippe Blondel, Cochair
University of Bath, Department of Physics, Claverton Down, Bath, BA2 7AY, UK

Nicholas Pace, Cochair
Department of Physics, University of Bath, Bath BA2 7AY, UK

Contributed Paper

8:00

5aUWc1. Classification of angular backscattered responses obtained at sea with a forward looking sonar system. Pierre Cervenka (Institut Jean le Rond D'Alembert, UMR 7190, 2 Place de la Gare de Ceinture, 78210 Saint Cyr L'Ecole, France, cvk@ccr.jussieu.fr), Jacques Marchal (Institut Jean le Rond D'Alembert, UMR 7190, 2 Place de la Gare de Ceinture, 78210 Saint Cyr L'Ecole, France, jmarchal@ccr.jussieu.fr)

The prototype of a multibeam front-scan sonar has been developed within the frame of a MAST contract (n° MAS3-CT97-0090 DG12-ESCY, acronym COSMOS). A large amount of data has been collected at sea. With the forward looking geometry of acquisition, the foot-prints of successive pings overlap largely, so that most parts of the surveyed areas are seen under a large range of incidence angles. It gives the capability to derive the local angular response of the bottom, which is indeed an important information for characterizing the nature of the seafloor. This presentation addresses the successive steps that were undergone to classify the backscattered responses: Data are conditioned to perform principal component analyzis; an original clustering identification process is also described; resulting maps are finally presented.

Invited Papers

8:20

5aUWc2. A comparison between modeled and measured high frequency bottom backscattering. Dick G. Simons (Delft University of Technology, P.O. Box Postbus 5048, 2600 GA Delft, Netherlands, d.g.simons@tudelft.nl), M. Snellen (Delft Institute of Earth Observation and Space Systems, Delft University of Technology, Kluyverweg 1, 2629 HS Delft, Netherlands, M.Snellen@tudelft.nl)

Compared to taking many sediment grabs, classification techniques based on acoustic remote sensing allow for significant cost reductions, providing the required information at much denser spatial scale. An attractive approach hereto is to use the multibeam-echosounder (MBES) which measures sediment backscatter strengths as a function of angle. By maximizing the match between this backscatter strength and model results, sediment properties can be derived. The backscatter model used here accounts for both surface roughness and volume scattering. MBES measurements (300 kHz) were taken in the Cleaver-Bank area (North Sea), characterized by a wide variety of sediment types for which a large number of grabs is collected. For the majority of the sediment types occurring, well-defined single-sediment-type areas can be discerned. Based on MBES measurements in these areas and corresponding geotechnical

sediment parameters provided by grab grain size analysis, calibration curves are derived, representing the mismatch between modeled and measured backscatter strengths. These curves are found to be similar for all sediment types considered. By applying these correction curves to the MBES measurements, they show good agreement with the model for all observed sediment types. It is shown that after this correction the model can be used for sediment classification purposes.

8:40

5aUWc3. Acoustic scattering by deformed elongated objects: bent or rough finite cylinders, bent edges, and other stuff. Timothy K. Stanton (Woods Hole Oceanographic Institution, Applied Ocean Physics & Engineering Department, 98 Water Street, MS #11, Woods Hole, MA 02543, USA, tstanton@whoi.edu), Dezhang Chu (NOAA/NMFS/NWFSC/FRAMD, Montlake Blvd., E. Seattle, WA 98112, USA, dchu@whoi.edu), Guy Norton (Naval Research Laboratory, Code 7181, Stennis Space Center, MS 39529, USA, guy.norton@nrlssc.navy.mil)

Predicting acoustic scattering by deformed elongated objects remains a challenge as there are no exact analytical solutions. Numerical solutions are also challenged through various computational issues. In this research, we have developed and applied an approximate analytical approach for predicting scattering by various deformed elongated objects, including bent or rough finite cylinders and deformed edges. The formulation is based on a line integral in which the scattering or diffraction per unit length of the exact solution to an infinitely long, straight undeformed object is integrated along the length of the finite-length deformed object, accounting for variations along the length of phase and certain local properties of the object. Predictions concerning various types of deformed finite cylinders are first discussed (including Stanton, J. Acoust. Soc. Am. **86**, 691-705 (1989) and subsequent papers), followed by recent predictions concerning deformed finite edges (Stanton et al., J. Acoust. Soc. Am. **122**, 3167-3176 (2007)). These latter predictions using the approximate line integral compare favorably with predictions based on the T-matrix numerical method, which is formally exact. Also discussed are: dependences upon length, orientation, bend, and roughness; comparisons with experimental data concerning machined objects and marine life; and range of validity of the approach.

9:00

5aUWc4. High frequency scattering from discrete inclusions in marine sediments. Anatoliy N. Ivakin (Applied Physics Laboratory, University of Washington, 1013 NE 40th Street, Seattle, WA 98105, USA, ivakin@apl.washington.edu)

A model of high frequency scattering from sediments with discrete inclusions (such as shells and shell fragments) having an arbitrary size-depth distribution is developed. The model assumes also knowledge of a depth-dependent individual scattering function of inclusions. It is more general than in previous models and includes discrete scatterers located both below and on the water-sediment interface (partially buried). Some simple results are obtained for the case of high enough frequencies using approaches of geometry acoustics. Frequency-angular dependencies of the bottom backscattering strength are calculated for sediments with different size-depth distributions of inclusions. Inputs for the size distribution of inclusions (shell fragments) are obtained from granulometric analysis of coarse fractions of the sediment samples taken at the SAX99/SAX04 site (near Ft Walton Beach, Florida). It is shown that taking into account partially buried shells is important and can significantly enhance estimates of the bottom scattering strength especially at grazing angles below critical (about 30 degrees for sand). [Work supported by ONR, Ocean Acoustics].

Contributed Paper

9:20

5aUWc5. A review of the scattering properties of suspended sandy sediments for the application of acoustics to sediment transport studies. Peter D. Thorne (Proudman Oceanographic Laboratory, Joseph Proudman Building, 6, Brownlow Street, L3 5DA Liverpool, UK, pdt@pol.ac.uk), Ramazan Meral (Kahramanmaras Sutcu Imam University, Faculty of Agriculture, Department of Agricultural, Structures and Irrigation, 46060 Kahramanmaras, Turkey, rmeral@ksu.edu.tr)

Multi-frequency acoustics backscattering has been used for over a decade, to quantitatively measure, in the marine environment, near-bed profiles of suspended sediment particle size and concentration. Central to obtaining the sediment parameters from the backscattered signal, is a description of the scattering properties of irregularly shaped particles randomly distributed in space. Formulations are therefore required for both the attenuation and backscattering properties of suspensions of sedimentary particles with size and acoustic frequency. There is no rigorous analytical solution or single formulation for these scattering properties and different researchers have used somewhat different expressions. However, all these expressions are based on a variation of sphere scattering, modified to fit available scattering data. Here we bring together four decades of published data on the acoustic scattering properties of suspensions of sandy sediments. These data are reformulated in terms of the usual acoustic scattering nomenclature, that is the form function and the normalised total scattering cross-section and simple heuristic generic expressions, based on a sphere scattering model, are formulated to describe the sediment scattering properties. The expressions are not limited to sand particles, but should have broad applicability to irregularly shaped particle scattering.

Invited Paper

9:40

5aUWc6. On the angular dependence of sound scattering from natural sand in turbulent suspensions. Alex E. Hay (Dalhousie University, Department of Oceanography, Halifax, NS B3H 4J1, Canada, alex.hay@dal.ca), Stephanie A. Moore (Dalhousie University, Department of Oceanography, Halifax, NS B3H 4J1, Canada, Stephanie.Moore@phys.ocean.dal.ca), Wesley Paul (Dalhousie University, Department of Oceanography, Halifax, NS B3H 4J1, Canada, Wes.Paul@Dal.Ca)

We report on measurements of the variation with scattering angle of the differential scattering cross section of particles embedded in turbulence. The experimental apparatus consists of a turbulent round water jet carrying the particles, and a pair of broadband MHz-frequency transducers operating as transmitter and receiver and arranged in a bistatic geometry centred on the jet axis. The purpose of the jet is to confine the scatterers within a restricted range interval and thereby eliminate the need to correct the signal for attenuation due to scattering along the transmit and receive paths. Measurements were made at scattering angles between 90 and 170 degrees, for

both natural sand grains and spherical glass beads in narrow size distributions with median diameters ranging from 200 to 500 μm. Particle size distributions were determined using different methodologies to obtain both volumetric and projected area estimates of equivalent spherical size. The results are compared to the theory for scattering by a solid sphere. Implications regarding the choice of equivalent sphere size for sound scattering by natural sand grains in suspension are discussed.

10:00-11:00 Posters

Lecture sessions will recess for presentation of poster papers on various topics in acoustics. See poster sessions for topics and abstracts.

Contributed Papers

11:00

5aUWc7. Measurements of the scattering characteristics of sediment suspensions having broad particle size distributions. Benjamin D. Moate (Proudman Oceanographic Laboratory, Joseph Proudman Building, 6, Brownlow Street, L3 5DA Liverpool, UK, bdm@pol.ac.uk), Peter D. Thorne (Proudman Oceanographic Laboratory, Joseph Proudman Building, 6, Brownlow Street, L3 5DA Liverpool, UK, pdt@pol.ac.uk)

Profiles of suspended sediment concentration and mean size can be measured in underwater environments using Acoustic Backscatter Systems (ABS). Inversion of ABS measurements into sediment size and concentration requires knowledge of the backscattering form function, f, and the total normalised scattering cross section, χ. Previous studies have measured these parameters for sediments sieved over narrow size ranges only. Narrow size ranges are unrealistic compared to the broad Particle Size Distributions (PSD) that typically occur in nature however, and it is known that f and χ are significantly altered by changes from narrow to broad PSDs. Theoretically, these changes can be accounted for in ABS inversions by taking values of f and χ obtained from narrow size ranges, and integrating them over the suspended PSD, though this theory has not been validated for real suspended sediments. Here, we compare the results of this integration with measured values of f and χ for suspensions of (irregularly shaped) sandy sediments having broad PSDs. The results show that as the standard deviation of the size distribution increases, acoustic scattering is increased in the Rayleigh regime whilst being reduced in the geometric regime. These changes significantly affect acoustic estimates of suspended sediment concentration and size.

11:20

5aUWc8. Acoustic scattering from double-diffusive microstructure. Andone Lavery (Woods Hole Oceanographic Institution, Applied Ocean Physics & Engineering Department, 98 Water Street, MS #11, Woods Hole, MA 02543, USA, alavery@whoi.edu), Tetjana Ross (Dalhousie University, Department of Oceanography, 1355 Oxford Street, Halifax, NS B3H 4JI, Canada, tetjana.ross@dal.ca)

Laboratory measurements of high-frequency broadband acoustic backscattering (200-600 kHz) from the diffusive regime of double-diffusive microstructure have been performed. This type of microstructure, which was characterized using direct microstructure and optical shadowgraph techniques, is identified by sharp density and sound speed interfaces separating well-mixed layers. Acoustic backscattering measurements were performed for a range of physical parameters controlling the double-diffusive microstructure. The echoes have been analyzed in both the frequency domain, providing information on the spectral response of the scattering, and in the time domain, using pulse compression techniques. High levels of variability were observed, associated with interface oscillations and turbulent plumes, with many echoes showing significant spectral structure. Acoustic estimates of interface thickness, obtained for the echoes with exactly two peaks in the compressed pulse output, were in good agreement with estimates based on direct microstructure and optical shadowgraph measurements. Predictions based on a one-dimensional weak-scattering model that includes the actual density and sound speed profiles agree reasonably with the measured scattering. A remote-sensing tool for mapping oceanic microstructure, such as high-frequency broadband acoustic scattering, could lead to a better understanding of the extent and evolution of double-diffusive layering, and to the importance of double diffusion to oceanic mixing.

Invited Papers

11:40

5aUWc9. Clustered scatterers: the effect on the mean acoustic field. Thomas C. Weber (University of New Hampshire, Ctr. for Coastal and Ocean Mapping, 24 Colovos Road, Durham, NH 03824, USA, weber@ccom.unh.edu)

Clustering, or spatially dependent correlation in the fluctuating number density of discrete scatterers of sound, is commonly found to occur in nature. In the ocean, clustering can occur as a result of scatterer entrainment in fluid flows, as in the case of particles and bubbles, or, in the case of fish, as a result of the behaviour of the scatterer. In either case, the presence of clustering can dramatically alter the effect of the scatterers on acoustic fields from that which would be predicted from the same scatterer population but without clustering. The effect of scatterers on the mean acoustic field is often treated using an effective medium wave number. In this paper, a modification to the effective medium number that accounts for clustering is presented and examined for the case of propagation through bubble clouds. Attenuation predictions over a broad range of frequencies (10-350 kHz) using observations of bubble clustering under oceanic breaking waves will be discussed.

12:00

5aUWc10. A very shallow water ray propagation model. Lucie Pautet (7A/01 Attemsgasse, 1220 Vienna, Austria, luciepautet@yahoo.com), Alessandra Tesei (NATO Undersea Research Centre, Viale San Bartolomeo 400, 19126 La Spezia, Italy, tesei@nurc.nato.int)

For applications such as minehunting, communications, high frequency time-reversal, there has been a need for reliable and fast propagation models able to correctly treat scattering at the rough waveguide boundaries. Data and scattering models have shown that as signal frequency or surface roughness increases, the scattering pattern from the ocean bottom and ocean surface evolves from specular to quasi omni-directional. Ray propagation models are fast but, a priori, they would treat surface bounces as perfectly specular which would not account for the angular spread observed on multipath structures. The idea followed by the authors over the past few years has

been to introduce in the Bellhop ray tracing model a reflection kernel including deterministic properties of the sea surface and bottom. Simulations using this kernel display a significant effect of the multipath structure similar to the angular spread observed in in-situ data. Simulation results are compared with a recent experimental study at 10-20 KHz (BARRIER'04 at NURC) on the influence of wind strength on surface bounce spreading and subsequent TR-focus spread.

12:20

5aUWc11. Broadband acoustic scattering from nonlinear internal solitary waves. Andone Lavery (Woods Hole Oceanographic Institution, Applied Ocean Physics & Engineering Department, 98 Water Street, MS #11, Woods Hole, MA 02543, USA, alavery@whoi.edu)

High-frequency broadband (150-600 kHz) acoustic scattering techniques have been used to obtain high-resolution images of nonlinear internal solitary waves (ISWs) propagating shoreward over the New Jersey continental shelf. In contrast to traditional single-frequency measurements, broadband acoustic scattering allows the frequency spectrum of the scattering to be determined, which, in combination with scattering models and direct ground-truthing measurements, allows regions in which the scattering is dominated by biology versus microstructure to be distinguished. Multiple ISWs were tracked and imaged acoustically at different stages of their generation, propagation, and dissipation. Simultaneous microstructure and zooplankton net sampling measurements were performed. Multiple scattering layers and distinct scattering patches were often associated to the ISWs, often exhibiting distinct frequency responses. Clear day/night differences in the scattering from the ISWs were observed due to the daily vertical migration of zooplankton. Though high turbulence levels are associated with ISWs, the strongest scattering returns were not always associated to the highest turbulence levels. Instead, the strongest scattering, at some frequencies, was sometimes associated to large temperature gradients. In regions in which the scattering was dominated by either microstructure or zooplankton, acoustic inversions have been performed for the dissipation rate of turbulent kinetic energy and zooplankton size and abundance.

FRIDAY MORNING, 4 JULY 2008 ROOM 342B, 8:00 TO 11:40 A.M.

Session 5aUWd

Underwater Acoustics and ECUA: Low-Frequency and High-Frequency Synthetic Aperture Sonar

Peter T. Gough, Cochair
University of Canterbury, Private Bag 4800, Christchurch, 8022, New Zealand

Roy E. Hansen, Cochair
Norwegian Defence Research Establishment, P O Box 25, Kjeller, NO-2027, Norway

Invited Paper

8:00

5aUWd1. Ten key papers in synthetic aperture sonar. Peter T. Gough (University of Canterbury, Private Bag 4800, 8022 Christchurch, New Zealand, peter.gough@canterbury.ac.nz), Michael Hayes (University of Canterbury, Private Bag 4800, 8022 Christchurch, New Zealand, michael.hayes@canterbury.ac.nz)

There are now hundreds of patents and papers on synthetic aperture sonar; some of them of key importance whereas many others are of peripheral or minor interest. Here we take what we consider to be the top ten publications in synthetic aperture sonar and explain why we believe they are important and how they have made a significant contribution to the developing discipline or have made some leap of imagination in the area. This paper is more than a catalogue of the top ten citations since not all the real advances in the field have been published in academic peer-review journals.

Contributed Papers

8:20

5aUWd2. Multifrequency interferometry on synthetic aperture sonar images. Torstein Olsmo Sæbø (Norwegian Defence Research Establishment, P O Box 25, NO-2027 Kjeller, Norway, torstein-olsmo.sabo@ffi.no), Roy E. Hansen (Norwegian Defence Research Establishment, P O Box 25, NO-2027 Kjeller, Norway, roy-edgar.hansen@ffi.no), Hayden J. Callow (Norwegian Defence Research Establishment, P O Box 25, NO-2027 Kjeller, Norway, hayden-john.callow@ffi.no)

Interferometric processing on synthetic aperture sonar (SAS) images can provide accurate bathymetric maps with very high spatial resolution. Often, bathymetric precision is limited by two-pi phase ambiguities in the interferogram. Several phase-unwrapping algorithms exist, but they all depend on some type of continuity throughout the interferogram. The locations of the phase ambiguities are dependent on the carrier frequency of the transmitted signal. Dividing the frequency band into multiple subbands provides multiple interferograms, each with a unique carrier frequency and thus differing ambiguity positions. In this paper, we investigate how to take advantage of subband interferograms to reduce phase ambiguities at the expense of accuracy. This is performed by using the phase differences between the individual subband interferograms. We also present a method were we use the differences in subband interferograms to eliminate the phase ambiguities in both the original interferogram, and in the subband interferograms themselves. Both methods are tested on simulated data and field data collected by the HUGIN autonomous underwater vehicle carrying the Kongsberg HISAS 1030.

8:40

5aUWd3. Circular synthetic aperture sonar results from autonomous underwater vehicle trials. Roy E. Hansen (Norwegian Defence Research Establishment, P O Box 25, NO-2027 Kjeller, Norway, roy-edgar.hansen @ffi.no), Torstein Olsmo Sæbø (Norwegian Defence Research Establishment, P O Box 25, NO-2027 Kjeller, Norway, torstein-olsmo.sabo @ffi.no), Hayden J. Callow (Norwegian Defence Research Establishment, P O Box 25, NO-2027 Kjeller, Norway, hayden-john.callow@ffi.no)

The principle of synthetic aperture sonar (SAS) is to combine successive pings coherently from different observation angles in order to increase the azimuth resolution. By collecting data along a circular track, a circular SAS (CSAS) image, or tomographic image, can be made. The image reconstruction can be done either incoherently, fully coherently, or partially coherently where each subaperture of coherent processing consists of a section of the circle. In target classification, CSAS has several benefits: the object is observed from all aspect angles giving a better perception; the resolution in the image increases. In this paper, we calculate required accuracy in navigation, bathymetry and sound velocity for successful circular SAS. Finally, we show circular SAS images of small targets from real data collected by the HUGIN autonomous underwater vehicle carrying the Kongsberg HISAS 1030. We test different beamforming strategies, and show the effect of coherent and incoherent tomographic imaging.

9:00

5aUWd4. Autofocus of synthetic aperture sonar data using the phase adjustment by contrast enhancement algorithm. Hayden J. Callow (Norwegian Defence Research Establishment, P O Box 25, NO-2027 Kjeller, Norway, hayden-john.callow@ffi.no), Torstein Olsmo Sæbø (Norwegian Defence Research Establishment, P O Box 25, NO-2027 Kjeller, Norway, torstein-olsmo.sabo@ffi.no), Roy E. Hansen (Norwegian Defence Research Establishment, P O Box 25, NO-2027 Kjeller, Norway, roy-edgar.hansen@ffi.no)

Imagery from synthetic aperture systems often suffers from imperfect image formation due uncertainties in the collection geometry or environmental parameters. Autofocus techniques aim to estimate and subsequently eliminate the effect of these uncertainties---automatically adjusting focus parameters to obtain a "better" image. Typically, autofocus algorithms will optimise for reduced Doppler phase gradients or improved image contrast. The phase adjustment by contrast enhancement (PACE) algorithm belongs to the second class and was first proposed for use in synthetic aperture radar (SAR) autofocus. The algorithm is somewhat unusual for a contrast optimisation in that it avoids lengthy computation through directly solving the equations for optimum contrast. This advance allows for rapid autofocus without the need for complicated iterative optimisers. We compare results from using the PACE algorithm on local region of strip-map synthetic aperture sonar (SAS) data collected with the HUGIN AUV and compare against a benchmark phase gradient autofocus (PGA) algorithm. We also demonstrate the effect of using the algorithm in circular SAS imagery, something not currently possible with standard PGA-based autofocus.

9:20

5aUWd5. Planar synthetic aperture processing (P-SAS) to real acoustic data of underwater imaging. Adel Jammali (Faculté des Sciences de Monastir μEi Lab Tunisia, Avenue de l'environnement, 5019 Monastir, Tunisia, adel.jam@voila.fr), Afif Belkacem (Faculté des Sciences de Monastir μEi Lab Tunisia, Avenue de l'environnement, 5019 Monastir, Tunisia, afif_bel@yahoo.fr), Kamel Besbes (Faculté des Sciences de Monastir μEi Lab Tunisia, Avenue de l'environnement, 5019 Monastir, Tunisia, Kamel.Besbes@fsm.rnu.tn), Manell E. Zakharia (French Naval Acadamey, BP 600, 29240 Brest-Armees, France, manell.zakharia@ecole-navale.fr)

Planar synthetic aperture technique has been validated on both simulated and tank data. It showed a significant improvement of 3D representation of bottom and subbottom. In this paper we present its application to real data acquired during sea experiments on a dump site. Data were acquired during the SITAR (Seafloor Imaging and Toxicity: Assessment of Risks caused by buried waste) project. The transmitter was a parametric array (TOPAS). Two central frequency were explored, 10 kHz and 20 kHz. The transmitter was fixed on a ROV which position was monitored. As P-SAS algorithm was designed for data obtained on a regular planar grid important modification were required to handle real sea data and "realistic" navigation conditions (irregular grid): a "re-arrangement" algorithm was designed for preprocessing actual data and correct for trajectory disturbances (in 2D). This algorithm is the re-projection of data to a new (virtual) regularly grid. The algorithm was validated on tank experimental data prior to application to sea data. Both conventional and SAS data will be presented. A strata representation technique was used for analyzing the seafloor, the subbottom and the localization of buried objects on a dump site in the Baltic sea.

9:40-11:00 Posters

Lecture sessions will recess for presentation of poster papers on various topics in acoustics. See poster sessions for topics and abstracts.

Contributed Paper

11:00

5aUWd6. Towards an understanding of how a synthetic aperture sonar images buried targets. Peter T. Gough (University of Canterbury, Private Bag 4800, 8022 Christchurch, New Zealand, peter.gough@canterbury .ac.nz), Michael Hayes (University of Canterbury, Private Bag 4800, 8022 Christchurch, New Zealand, michael.hayes@canterbury.ac.nz)

One of the useful features of synthetic aperture sonar (SAS) is that in the reconstructed image, the cross-track resolution is inversely proportional to the bandwidth and the along-track resolution is proportional to the transducer's along-track extent and that these are more or less independent of the center frequency. An unexpected aspect of SAS imaging so far is that objects buried in sand/sediment are sometimes visible even at geometries where the incident angle far exceeds the critical angle for the bulk materials. It is surmised that the roughness of the sea/sea-floor interface is the significant contributing factor. So as an adjunct to the main Kiwi SAS programme, a seafloor "document" camera colocated with a three-transducer active sonic probe has been designed and deployed in controlled circumstances. The intention is to estimate the critical parameters that best describes the roughness of the sea floor and perhaps how these parameters relate to the way the SAS images shallow buried targets. In regions of reasonable visibility, the camera is used to provide ground-truth. The paper details the construction of the camera and sonic probe as well describes some preliminary results using smooth and raked sand.

Invited Paper

11:20

5aUWd7. Imaging buried objects using synthetic aperture processing. Steven Schock (Florida Atlantic University, Dept of Ocean Engineering, 777 Glades Rd, Boca Raton, FL 33431, USA, schock@oe.fau.edu)

FM sonar generates images of buried objects using synthetic aperture processing. A spherical projector illuminates objects buried in the seabed out to the range associated with the critical angle. Scattering off buried targets is measured with one meter long line hydrophone arrays embedded in sonar vehicle wings. The histories of the projector and hydrophones positions, used for compensating acoustic data during synthetic aperture processing, are calculated based on navigation data provided by an inertial measurement unit and Doppler velocity log. Three orthogonal image projections of the seabed containing 5, 7.5, 10, and 15 cm diameter cylinders, buried up to 30 cm in seabeds consisting of sand and sandy mud in three meters of water, show the burial depth and orientation of the cylinders. The temporal resolution of the imagery is approximately 6 cm. The azimuthal resolution varies between 5 and 20 cm and is a function of target range and relative bearing with respect to the sonar vehicle. This imaging technique can be applied to marine archeological investigations in water depths of two meters and greater.

FRIDAY MORNING, 4 JULY 2008 ROOM 362/363, 8:00 TO 9:40 A.M.

Session 5aUWe

Underwater Acoustics and ECUA: Monitoring Systems and Ambient Noise

Mark K. Prior, Cochair
CTBTO, Vienna International Centre, P.O. Box 1200, Vienna, 1400, Austria

David Deveau, Cochair
Naval Undersea Warfare Center - AUTEC, PSC 1012 Box 701, FPO, AA, FL 34058, USA

Contributed Papers

8:00

5aUWe1. An optimization approach to the automatic identification of signals originating from underwater explosions. Mark K. Prior (CTBTO, Vienna International Centre, PO Box 1200, 1400 Vienna, Austria, Mark.Prior@CTBTO.ORG)

Data recorded by the International Monitoring System (IMS) of the Comprehensive Test-Ban Treaty Organization are used to illustrate the different types of signal that are routinely received on IMS hydrophone stations. It is shown that automated methods for characterizing the source of these signals sometimes fail to identify signals arising from underwater explosions. A new approach to the automatic identification of such signals is presented. The approach uses Receiver Operating Characteristic (ROC) curves to investigate the trade-off between false-alarm rate and probability of detection. It applies a threshold to a parameter developed as a measure of the likelihood of a signal being associated with an explosion. A numerical Measure of Performance (MoP) is derived from the ROC curves and the definition of the likelihood parameter is tuned so as to maximize this MoP. Optimization of the parameter definition is achieved using an approach based on genetic algorithms.

8:20

5aUWe2. Seafloor Geodetic Networks for monitoring tectonic plate motion and deformation. Stavroula Peroutsea (School of Rural and Surveying Engineering, National Technical University of Athens, Ch. Mantika 1, 11362 Athens, Greece, ROK2POK5G@INTERNET.GR), Efstratios Doukakis (School of Rural and Surveying Engineering, National Technical University of Athens, Ch. Mantika 1, 11362 Athens, Greece, EDOUK @CENTRAL.NTUA.GR)

This paper argues that seafloor geodetic networks, monitoring tectonic plate motion and deformation, supplementing terrestrial geodetic networks, can provide important information for the understanding of crustal processes, globally. The proposed monitoring system consists of three main components: real-time kinematic-differential GPS ship positioning, precise acoustic ranging between ship and seafloor transponders - which establish the network nodes- and near-bottom direct acoustic measurements of the network baselines. The coordinates of the transponders in a goedetic reference system can be determined from these observations and a sound-speed structure model. The motion and deformation of the tectonic plate can be traced as a change of coordinates and/or the internal geometry of the network. Stochastic and mathematic models, algorithms and data analysis are crucial for achieving the necessary accuracy in such a demanding process regarding seafloor position estimation.

8:40

5aUWe3. Confined deep water acoustic noise study within the Bahamian TOTO. David Deveau (Naval Undersea Warfare Center - AUTEC, PSC 1012 Box 701, FPO, AA, FL 34058, USA, david.deveau@autec .navy.mil)

The three-sided deep coral reef that borders Andros Island, Bahamas is populated with deep water acoustic sensors that presents a unique opportunity to study the impact of wind and wave in a physical environment with limited man-made noise sources over a wide acoustic band (50-40 kHz). This area is known as the "Tongue of the Ocean" (TOTO) for its unique satellite viewed shape. The region's deep acoustic channel (~1550 m) is surrounded by steep walls and only one outlet suggesting a highly reverberant cavity where weather produced ambient noise signatures may persist over greater periods producing levels greater than typically observed in the open ocean. In this study, daily acoustic spectra are gathered on two sensors spaced 20 km apart with accompanied wind and weather information. The spectra will be correlated to advancing and receding weather fronts in an effort to relate the surface changes to the deep water ambient noise levels. This study also serves as a precursor to a shallow water acoustic noise intensity study where similar weather comparisons will be made and compared to the deep water counterpart.

9:00

5aUWe4. Historical ambient noise levels in a topographically isolated basin. D. Benjamin Reeder (Naval Postgraduate School, Department of Oceanography, 833 Dyer Road, Rm 328, Monterey, CA 93943-5738, USA, dbreeder@nps.edu), Susan M. Mach (Naval Undersea Warfare Center Detachment AUTEC, P.O. Box 24619, West Palm Beach, FL 33416, USA, Susan.Mach@autec.navy.mil), Edmond S. Sheffield (Naval Undersea Warfare Center Detachment AUTEC, P.O. Box 24619, West Palm Beach, FL 33416, USA, Edmond.Sheffield@autec.navy.mil)

During the late 1970s and early 1980s, careful measurements of ambient noise were made in the Tongue of the Ocean (TOTO) in the Bahamas. The measurements were made using a vertical array of five omni-directional hydrophones moored in 2200 m water depth with an average hydrophone depth of 122 m. Data were collected within a 20 Hz - 20 kHz band at ten specific 1/3 octave band frequencies, and then reported in spectrum level as a function of surface wind speed. Records contaminated by anthropogenic sources (e.g., local vessel traffic), biological sources (e.g., marine mammal vocalizations) and other sources (e.g., rain) were eliminated to allow analysis of background ocean ambient noise only. TOTO is a deep basin, topographically isolated from the Atlantic Ocean, and therefore largely acoustically decoupled from the Atlantic Ocean deep sound channel. The basin's geographical isolation and the controlled data collection methodology employed over a four-year period make this three-decade-old data set a potential proxy for preindustrial era ocean noise levels. The environmental setting, data collection methodology, analysis methodology and results are presented and discussed within the context of historical ocean ambient noise levels.

9:20

5aUWe5. Analysis of wind generated shallow water ambient noise. Ari Poikonen (Finnish Naval Research Institute (FNRI), P.O. Box 116, FIN-02631 Espoo, Finland, ari.poikonen@mil.fi), Seppo Madekivi (Finnish Naval Research Institute (FNRI), P.O. Box 116, FIN-02631 Espoo, Finland, seppo.madekivi@mil.fi)

Underwater ambient noise measurements were carried out in very shallow water (10-20 m) in the archipelago of the Gulf of Finland during the full year. Weather conditions varied from calm sea to near gale winds. The lowest spectral levels were obtained under the ice cover during the coldest winter months. No seasonal effect was observed in the measured spectra. The role of water depth was modeled with several bottom sediments in order to identify possible channel effects at lower frequencies of the noise spectra. The ambient noise spectra are typically bandlimited. A bandpass filter model was thus fitted to the noise spectra. The filter model provides several useful parameters to characterize the effect of wind speed on the noise spectra. The cutoff frequency of the high-pass part of the spectra decreases from ca 400 Hz down to below 200 Hz as wind increases from light breeze to near gale force. The corresponding spectral slopes get steeper with increasing winds saturating to the value of 12 dB/oct already in fresh breeze. The other parameters used in the analysis are high frequency (low-pass) spectral slope, the frequency of maximum spectral level, noise bandwidth and total power in the band.

FRIDAY MORNING, 4 JULY 2008 P3-C, LEVEL 3, 9:40 TO 11:20 A.M.

Session 5aUWf

Underwater Acoustics, Signal Processing in Acoustics, and ECUA: Broadband Underwater Communications II (Poster Session)

Heechun Song, Cochair
MPL

Sergio Jesus, Cochair
ISR

All posters will be on display from 9:40 a.m. to 11:20 a.m. To allow contributors an opportunity to see other posters, contributors of odd-numbered papers will be at their posters from 9:40 a.m. to 10:30 a.m. and contributors of even-numbered papers will be at their posters from 10:30 a.m. to 11:20 a.m.

Contributed Papers

5aUWf1. Basic at-sea experiment for long horizontal time-reversal communication in deep ocean. Takuya Shimura (JAMSTEC, 2-15, Natsushima-cho, 237-0061 Yokosuka, Japan, shimurat@jamstec.go.jp), Yoshitaka Watanabe (JAMSTEC, 2-15, Natsushima-cho, 237-0061 Yokosuka, Japan, yoshitakaw@jamstec.go.jp), Hiroshi Ochi (JAMSTEC, 2-15, Natsushima-cho, 237-0061 Yokosuka, Japan, ochi@jamstec.go.jp), Takehito Hattori (Nippon Marine Enterprises, Ltd., 14-1, Ogawa-cho, 238-0004 Yokosuka, Japan, hattorit@nme.co.jp)

In our research program, a long cruising autonomous underwater vehicle (AUV) has been developed and a project on a second AUV is planned, for wide-areal observation in the deep ocean. In such AUV operation, it is preferred to ensure acoustic communication with AUV even at low data-transmission rate. Time-reversal techniques have a possibility to achieve such long horizontal communication. We have proposed a method of combining time reversal and an adaptive equalizer to realize communication even with a sparse time-reversal array (TRA) and communication with a moving target. To verify the performance of such time-reversal communication, at-sea experiments were executed at the various distances. In the experiment of 10 km at a water depth of 1000 m, bidirectional time-reversal communication between the focus point and TRA was achieved successfully and the effects of the TRA depth and its channel number are investigated. In the experiments of 20, 30, 40 km at the slight sloping area, the performance on the distances are discussed. In the experiment of 100 km at a water depth of 4000 m, the convergence by passive time reversal was verified.

5aUWf2. High data rate coherent underwater acoustic communications during KauaiEx and MakaiEx. Aijun Song (University of Delaware, College of Marine and Earth Studies, S. College Street, Newark, DE 19716, USA, ajsong@udel.edu), Mohsen Badiey (University of Delaware, College of Marine and Earth Studies, S. College Street, Newark, DE 19716, USA, badiey@udel.edu), Heechun Song (MPL, Scripps Institution of Oceanography, University of California, San Diego, La Jolla, CA 92093-0238, USA, hcsong@ucsd.edu), William Hodgkiss (MPL, Scripps Institution of Oceanography, University of California, San Diego, La Jolla, CA 92093-0238, USA, wsh@mpl.ucsd.edu)

During two acoustic communications experiments conducted around Kauai Island, Hawaii (KauaiEx, 2003 and MakaiEx, 2005), various coherent communications data with concurrent environmental measurements were collected under different experimental settings. The collected communications data are processed by a newly proposed receiver, which consists of time-reversal multichannel combining followed by a single channel DFE. Continuous channel updates along with Doppler tracking are used prior to time reversal combining to combat fast channel variations. The receiver can successfully demodulate different types of coherent communications signals, including phase shift keying (PSK) and quadrature amplitude modulation (QAM) signals, at different symbols rates for different source/receiver settings, such as fixed source/receiver, drifting source/receiver, and towed source. Selected high data rate communication results will be presented to show the effectiveness of the receiver. The receiver performance in relation to the environmental variability also will be shown.

5aUWf3. Optimal placement of array elements for time-reversal mirror. Jae Hoon Joo (LIG Nex1 Co., Ltd, 102-18 Mabuk-dong Giheung-gu, 446-912 Yongin, Republic of Korea, jhjub@lignex1.com), Jea Soo Kim (Dept. of Ocean Engineering, Korea Maritime Univ., 1 Dongsam-dong Youngdo-ku, 606-791 Busan, Republic of Korea, jskim@hhu.ac.kr)

In the application of time-reversal mirror (TRM) to the underwater acoustic communication, the optimal placement of the transmit/receive array can enhance the signal-to-noise ratio at the foci when a number of array elements is limited. In this presentation, the optimal location of individual elements is determined by maximizing contrast between the focal location and the area of interest using genetic algorithm. As a result of optimization, the contrast as well as the intensity at foci is increased when compared to the conventional TRM. The optimal number of array elements is also investigated based on the objective function of genetic algorithm in connection with finding optimal placement of array. Numerical examples for TRM and contrast-maximization are presented and discussed.

5aUWf4. Experimental analysis of statistical characteristics of a very shallow underwater acoustic channel. Sea-Moon Kim (MOERI/KORDI, 171 Jang-dong, Yuseong-gu, 305-343 Daejeon, Republic of Korea, smkim@moeri.re.kr), Sung-Hoon Byun (MOERI/KORDI, 171 Jang-dong, Yuseong-gu, 305-343 Daejeon, Republic of Korea, byunsh@moeri.re.kr), Yong-Kon Lim (MOERI/KORDI, 171 Jang-dong, Yuseong-gu, 305-343 Daejeon, Republic of Korea, yklim@moeri.re.kr)

Underwater acoustic channel is characterized as a time-varying and multipath environment. Not only each propagation path changes randomly but also the scattered waves from the surface and bottom deteriorate signal transmission resulting in fading channels and poor communication performance. In order to design communication algorithms and determine modem parameters the characteristics of random ocean channel must be analyzed in advance. In this paper we investigate the statistical channel properties with experimental data gathered in a very shallow water near the southern coast of South Korea using band-limited signals with center frequencies of 20-40 kHz. The impulse responses at several distances up to 4km are estimated and their statistical characteristics in the complex domain are analyzed. We found that the statistical properties are highly dependent on the channel impulse response and the carrier frequency.

5aUWf5. Characterization of long-range time-varying underwater acoustic communication channels. Morten Smedsrud (FFI, Karljohansvern, P.O. Box 115, 3192 Horten, Norway, morten.smedsrud@ffi.no), Trond Jenserud (FFI, Karljohansvern, P.O.Box 115, 3192 Horten, Norway, trond .jenserud@ffi.no)

We present communication channel characterizations performed on in-situ measurements from the Baltic and North Sea. The communication channels were probed using pseudorandom binary sequences (PRBS), obtaining time-variant channel impulse responses through wideband matched filtering. Characteristics central to communications were obtained. Included are: scattering functions, coherence-times and coherence bandwidths. The validity of the quasi wide sense stationary uncorrelated scattering (quasi-WSSUS) assumption was also investigated for the measured channels. Measurements were acquired in the joint European project "UUV Covert Acoustic Communications." The project aims to design an acoustic communication system between an unmanned underwater vehicle (UUV) and a support mother ship. The first sea trials of the project focused on the acquisition of noise and long-range, low-frequency communication channel data for the explicit purpose of building an acoustic channel simulator.

5aUWf6. A novel architecture for multihops routing ad hoc underwater acoustic sensor networking. Roee Diamant (Technion - Israel Institute of Technology, RAFAEL, POB 2250, 31021 Haifa, Israel, diamantr@rafael.co.il), Azriel Sinai (Technion - Israel Institute of Technology, RAFAEL, POB 2250, 31021 Haifa, Israel, azrielsi@rafael.co.il)

Underwater acoustic communication networks are an innovative issue, which faces difficult medium problems, such as long propagation time and dynamic network topology. In addition, due to high error probabilities typical for this channel it is preferred to use anti collision network mechanism. Because of the long propagation time, methods such as CTS/RTS, requiring transmissions of pre-messages, achieve relatively low network efficiency. Moreover, TDMA methods do not utilize the network resources allowing reuse in the code domain (using CDMA) and in the spatial domain in case of nonhomogenic network topology which includes obstructions in the acoustic line of sight. In this paper we introduce a network concept based on the CDMA method confronting the acoustic underwater network challenges, such as the "near-far" problem, fast time varying topology, multihops routing and message distribution protection. Using this concept, a sea trial including broadcast, multicast and unicast transmissions of SMS and navigation control messages was carried out in various scenarios including multihops near the shores of Israel. We present results from this sea trial demonstrating the efficacy of the proposed networking scheme.

5aUWf7. Capacity estimations for underwater acoustic communication systems with source power constraints. Haibin Wang (National Laboratory of Acoustics, Institute of Acoustics, Chinese Academy of Sciences, NO .21, Northwest 4th Ring Road, 100080 Beijing, China, whb@mail.ioa.ac.cn), Di Meng (National Laboratory of Acoustics, Institute of Acoustics, Chinese Academy of Sciences, NO.21, Northwest 4th Ring Road, 100080 Beijing, China, whb@mail.ioa.ac.cn), Hua Yang (National Laboratory of Acoustics, Institute of Acoustics, Chinese Academy of Sciences, NO.21, Northwest 4th Ring Road, 100080 Beijing, China, yh@mail.ioa.ac.cn)

Channel capacity is an important parameter of underwater acoustic communication (UWAC) systems. For a certain channel and source power, water-filling algorithm of information-theory can be used to estimate the capacity. However, in practice, there are many constraints of the source transmission power. One of the most important constraints is that many communication nodes may exist in a local area, which means that the source power of each node should be confined in order to keep all nodes working normally. Considering this constraint and applying acoustic propagation modeling, this paper estimates the capacities of an UWAC system in some typical propagation conditions. The results are very useful for analyzing the maximum data rate of a practical acoustic channel and providing the optimal parameters of an UWAC system.

5aUWf8. Synchronisation of underwater communication receivers by means of broadband sweep-spread pulses. Konstantin G. Kebkal (EvoLogics GmbH/Technical University Berlin, Ackerstrasse 76 (ACK1), 13355 Berlin, Germany, kebkal@bionik.tu-berlin.de), Rudolf Bannasch (EvoLogics GmbH/Technical University Berlin, Ackerstrasse 76 (ACK1), 13355 Berlin, Germany, bannasch@evologics.de), Alexey G. Kebkal (EvoLogics GmbH/Technical University Berlin, Ackerstrasse 76 (ACK1), 13355 Berlin, Germany, kebkal@gmail.com)

Using sweep spread pulses a variety of multipath components of a receive signal can be often resolved in time-frequency domain. In result of synchronisation of the receiver with the most powerful component, other multipaths can be effectively suppressed by means of a matched filter. Owing to exact synchronisation, the difference frequency will be equal to zero and outputs of matched filters will be good for estimation of (information) parameters. However, the synchronous component (as well as others) can occasionally turn out to be composite and to contain energy of several non-resolved multipaths. In this case, the synchronisation time of the receiver will be not exact and the difference frequency of demodulated signal will differ from zero. This effect will cause a systematic error in estimation of the information parameter. This paper represents the results of mathematic modeling of the systematic error (for receivers, utilising the sweep-spread carrier technology), as well as, experiments on synchronisation of the receiver by means of wideband sweep spread pulses.

5aUWf9. Measurement of angular power profile at an array receiver in a shallow underwater acoustic channel. Sung-Hoon Byun (MOERI/KORDI, 171 Jang-dong, Yuseong-gu, 305-343 Daejeon, Republic of Korea, byunsh@moeri.re.kr), Sea-Moon Kim (MOERI/KORDI, 171 Jang-dong, Yuseong-gu, 305-343 Daejeon, Republic of Korea, smkim@moeri.re.kr), Yong-Kon Lim (MOERI/KORDI, 171 Jang-dong, Yuseong-gu, 305-343 Daejeon, Republic of Korea, yklim@moeri.re.kr), Woojae Seong (Seoul National University, Room. 306, Bd. 34, San 56-1, Sillim-dong, Kwanak-gu, College of Engineering, Dept. of Naval Architecture and Ocean Engineering, 151-744 Seoul, Republic of Korea, wseong@snu.ac.kr)

In the design of broadband underwater acoustic communication system, proper analysis of underwater acoustic channel characteristics is required to determine communication system parameters. Especially for high channel capacity transmissions such as multiinput multioutput (MIMO) systems, the spatial correlation characteristics among multiple sensors determine communication performance and they are affected by the angular power distribution of the incoming acoustic waves. In this study, we suggest a model-based array signal processing technique for measuring the angular power profile and apply it to experimental data gathered from very shallow water of 20 to 30 m water depth near the southern coast of South Korea. At first we show the variation of the angular power profile over different transmitter/receiver ranges and then its impact on the spatial correlation characteristics between two different array elements. Finally we discuss the expected spatial diversity effects from the viewpoint of underwater acoustic channel modeling.

FRIDAY MORNING, 4 JULY 2008 P3-C, LEVEL 3, 9:40 TO 11:20 A.M.

Session 5aUWg

Underwater Acoustics and ECUA: High Frequency Scattering II (Poster Session)

Anthony Lyons, Cochair
Applied Research Laboratory

Philippe Blondel, Cochair
University of Bath

Nicholas Pace, Cochair
SACLANT Undersea Research Centre

All posters will be on display from 9:40 a.m. to 11:20 a.m. To allow contributors an opportunity to see other posters, contributors of odd-numbered papers will be at their posters from 9:40 a.m. to 10:30 a.m. and contributors of even-numbered papers will be at their posters from 10:30 a.m. to 11:20 a.m.

Contributed Papers

5aUWg1. Modeling high-frequency reverberation and propagation loss in support of a submarine target strength trial. Boris Vasiliev (DRDC Atlantic, 9 Grove St., Dartmouth, NS B2Y 3Z7, Canada, boris.vasiliev@drdc-rddc.gc.ca), Art Collier (DRDC Atlantic, 9 Grove St., Dartmouth, NS B2Y 3Z7, Canada, art.collier@drdc-rddc.gc.ca)

The presentation reviews the environmental modeling conducted in support of a submarine acoustic target strength trial. The measurements at 20-40 kHz were collected at a shallow site in North West Atlantic. The site bottom was gravel; surface winds were 2-6 m/s. For ranges less than 1.8 km, the CW reverberation at 24, 28, and 39 kHz agreed with CASS-GRAB predictions; beyond 1.8 km, the model output underestimated the measurements. The predictions were computed for APL-UW surface and bottom models appropriate for trial conditions: negligible surface reflection loss and scattering strength, low bottom reflection loss and high bottom scattering strength. The LFM reverberation at 21, 28, and 36 kHz for 2 kHz bandwidth signals matched the CW reverberation after compensation for the pulse range resolution and frequency differences in the beam responses and volume attenuation. Agreement among CASS-GRAB prediction and data verified the assumed sonar and environmental parameters used in propagation loss modeling and increased confidence in the target strength estimates. The latter were consistent with previously reported values.

5aUWg2. Performances of a multistatic model of sound scattering by rough surfaces. Virginie Jaud (E3I2 - EA3876, 2 rue François Verny,29806 Brest Cedex, France, virginie.jaud@ensieta.fr), Cédric Gervaise (E3I2 - EA3876, 2 rue François Verny, 29806 Brest Cedex, France, cedric.gervaise@ensieta.fr), Ali Khenchaf (E3I2 - EA3876, 2 rue François Verny, 29806 Brest Cedex, France, ali.khenchaf@ensieta.fr)

The ocean floor is far from being a smooth and perfectly rigid surface. That is why its sound scattering properties are a useful input to the analysis of this medium as for acoustic data inversion. Thus, multi-static scattering coefficients have been investigated in a frequency range of order of 10 kHz to 300 kHz. The Kirchhoff Approximation and the Small Perturbation Method could be cited respectively in the case of dimensions of a rough surface larger and smaller than the wavelength. Nevertheless, for those frequencies, hence for those wavelengths, a rough surface should be considered at different scales compared to the wavelength. As a part of the incident wave is transmitted to the seabed medium, it is also important to know the effect of the scattering coming from the volume. Jackson's scattering model takes these considerations into account. The aim of the study is first to show an improvement of the surface scattering method using the Small Slope Approximation and keeping the initial method of Jackson's model to describe the scattering from the volume. Comparisons with well-known models are presented to show the performances of this new approach and comparisons between different multistatic geometries are analyzed to show the most useful configuration of the model.

5aUWg3. Complex interfaces of granular media: multiscale characterization and effective medium modeling. Yves Le Gonidec (Géosciences Rennes, Bât. 15, Campus de Beaulieu, 35042 Rennes, France, yves.legonidec@univ-rennes1.fr)

Seafloor is a complex geological interface : the acoustic reflectivity strongly depends on the sonar frequency which can be from few to hundreds kHz. In order to understand the physical processes involved, we have developed a multiscale acoustic method based on the wavelet transform properties: we introduce this theoretical approach first applied on homogeneous discontinuities. Then, we have developed acoustic experiments where the discontinuties are complex interfaces: we present the experimental setup and describe the results measured on granular media made of monodisperse glass beads. For this seafloor modeling, where all parameters are known, we put in evidence five frequency ranges corresponding to particular acoustic regimes: we give physical interpretations based on the analysis of effective medium modeling. From low to high frequencies, a strong transition is observed between propagation and scattering phenomena. Going further in this study, we illustrate the results on a bimodal glass bead distribution where high frequency scattering can be isolated using an original experimental approach.

FRIDAY MORNING, 4 JULY 2008 ROOM 341, 11:00 A.M. TO 12:40 P.M.

Session 5aUWh

Underwater Acoustics and ECUA: Sensor Coalition

Henrik Schmidt, Cochair
MIT, 77 Mass Ave, 5-204, Cambridge, MA 02139, USA

Stéphane Jespers, Cochair
Délégation Générale de l'Armement, 7-9 rue des Mathurins, Bagneux, 92220, France

Contributed Paper

11:00

5aUWh1. A review of approaches towards effective underwater sensor networks. Michel Leonard (NURC, Viale San Bartolomeo 400, 19121 La Spezia, Italy, leonard@nurc.nato.int), Diego Merani (NURC, Viale San Bartolomeo 400, 19121 La Spezia, Italy, merani@nurc.nato.int), Alessandro Berni (NURC, Viale San Bartolomeo 400, 19121 La Spezia, Italy, merani @nurc.nato.int)

The still largely unexplored vastness of the ocean, covering about two-third of the surface of earth, has fascinated humans for as long as we have records for. Its currents, chemical composition, and ecosystems are all highly variable at different locations and times. New paradigms for the monitoring of the undersea environment, based on autonomous underwater sensor nodes organized in ad-hoc coalitions, offer a promising approach towards the development of scalable networks for underwater sensing, monitoring, reconnaissance and surveillance. This promise has however to be balanced against important challenges, which need to properly addressed in order to devise a credible system concept. Some challenges worth mentioning are the difficulty in ensuring a low error-rate end-to-end path between source and destination for the duration of the communications session, the negative impact of communications performance characteristics at applications level, and energy constraints for battery-operated nodes. The requirement is therefore to design new protocols to provide network flexibility and reliability through self-organization and reconfiguration, as well as new energy-efficient routing schemes, including geographic and data-centric routing, to maximize the operational lifespan of autonomous power-constrained nodes. In this paper we will present the state of the art and approaches being investigated at NURC.

Invited Papers

11:20

5aUWh2. Nested Autonomy - Adaptive and collaborative sensing with hybrid sensing networks. Arjuna Balasuriya (MIT, 77 Mass Ave, 5-204, Cambridge, MA 02139, USA, arjunab@mit.edu), Henrik Schmidt (MIT, 77 Mass Ave, 5-204, Cambridge, MA 02139, USA, henrik@mit.edu), Michael B. Benjamin (MIT, 77 Mass Ave, 5-204, Cambridge, MA 02139, USA, mikerb@csail.mit .edu)

Control of undersea sensing networks is restricted by the limited acoustic communication capacity and the need for surfacing "datamules" for communicating with the operators. Adaptive sampling of episodic events must therefore be performed fully autonomously. Similarly, collaboration between nodes is limited by the communication horizon. These constraints favor the use of a nested operational paradigm, with clusters of highly autonomous nodes capable of detecting, classifying, and localizing episodic events, if possible collaborating with neighboring nodes without operator intervention. Such a Nested Autonomy operational paradigm is being developed for capturing episodic oceanographic events by AUVs and gliders in the NSF ORION ocean observatory. Based on the portable, open-source MOOS-IvP autonomous control framework, the same paradigm is being applied for distributed acoustic surveillance networks in the ONR PLUSNet program. In either case the nested autonomy enables the autononomous exploitation of the environmental and tactical situation, and collaborative tracking of targets or oceanographic events. The operator control is limited to very simple deploy and prosecute commands. The performance of the nested autonomy paradigm is demonstrated by examples using a high-fidelity simulation environment, and by results from recent field experiments. [Work supported by ONR.]

11:40

5aUWh3. Performance modeling and tradeoffs studies for hybrid sensing networks. Stéphane Jespers (Délégation Générale de l'Armement, 7-9 rue des Mathurins, 92220 Bagneux, France, stephane.jespers@dga.defense.gouv.fr)

The transformation of naval forces in support of expeditionary operations requires substantial endurance enhancement of their existing undersea reconnaissance and surveillance functions. Concepts of operations for distributed sensor fields - to be deployed in littoral waters - are now being proposed, encouraged by the favourable outlook for network technologies. The renewed attention for multistatic sonar is one example of this trend. Predicting the performance of distributed sensor fields for ASW applications, with sensors involving the use of acoustics and non-acoustics is complex. Though it is a great chance for optimizing the use of assets, the impact of sensor platforms' mobility (AUVs or gliders) adds yet another level of space-time complexity. Prior to any large scale test or development, system and operational studies must be able to determine optimal architectures and node placement as function of mission requirements. A major constraint is that of the limitations imposed on autonomous and covert data exchange in the maritime and underwater domains. This speeks for the design of hybrid sensor network architectures, as they appear to be well suited in dealing with substantial sensor data and command control data (e.g., backseat-driver paradigm) communication requirements.

Contributed Paper

12:00

5aUWh4. Acoustics for underwater neutrino telescopes. Miguel Ardid (IGIC - Universitat Politècnica de València, Cra. Nazaret-Oliva S/N, E-46730 Gandia, Spain, mardid@fis.upv.es), Manuel Bou-Cabo (IGIC - Universitat Politècnica de València, Cra. Nazaret-Oliva S/N, E-46730 Gandia, Spain, maboca3@doctor.upv.es), Juan Antonio Martínez-Mora (IGIC - Universitat Politècnica de València, Cra. Nazaret-Oliva S/N, E-46730 Gandia, Spain, jmmora@fis.upv.es), Francisco Camarena (IGIC - Universitat Politècnica de València, Cra. Nazaret-Oliva S/N, E-46730 Gandia, Spain, fracafe@fis.upv.es), Víctor Espinosa (IGIC - Universitat Politècnica de València, Cra. Nazaret-Oliva S/N, E-46730 Gandia, Spain, vespinos@fis .upv.es)

In this communication we present the research activities in underwater acoustic sensors and arrays used in underwater neutrino telescopes. These activities are developed in two areas. First, in optical based underwater neutrino telescopes, an acoustic positioning system is used in order to monitor the position and orientation of the optical modules in deep sea. In the second field, there is the idea to build underwater telescopes composed of arrays of acoustic sensors in order to detect the weak thermoacoustic pulse which will be produced when a very high energy neutrino interacts in the water. For both, a challenging and very specific acoustic system is needed. After the description of these systems and a brief review of the status of the field, our work in the area in the frames of ANTARES and KM3NeT neutrino collaborations is shown.

Invited Paper

12:20

5aUWh5. The applicability of a small autonomous vehicle towed array system to ocean acoustic measurements and signal processing. William M. Carey (College of Enginering, Boston University, 110 Cummington St, Boston, MA 02215, USA, wcarey @bu.edu), Jason D. Holmes (BBN Technologies, 10 Moulton St., Cambridge, MA 02318, USA, jholmes@bbn.com), Edmund J. Sullivan (EJS Consultants, 46 Lawton Brook Lane, Portmouth, RI 02871, USA, PADDYPRIEST@aol.com), James F. Lynch (Woods Hole Oceanographic Institution, 98 Water Street, Bigelow 203A, MS-11, Woods Hole, MA 02543, USA, jlynch@whoi.edu)

An array was developed to demonstrate, and quantify the performance characteristics of an autonomous-vehicle towed-array system. This technology provides for a cost effective tool for the measurement of coherent signal propagation, depth dependent and directional noise fields and to establish quantitative limits on array performance. The tangential drag on a 40-m length array composed of a reinforced tube with an outer diameter of 2.8 cm is extrapolated to be between 20-28 N for diameter Reynold's number of approximately 4 104. The hydrophone- preamplifier groups have a sensitivity of –174±1.5 dB re 1μPa/V between 100 Hz to 10 kHz. with an adjustable spacing between 0.5 and 1.5 m. The system tow stability enabled the use of the synthetic Hankel transform to estimate the modal

horizontal wave number spectrum and the identification of interface wave speeds at frequencies up to 1000 Hz. The formation of synthetic apertures combined with model based extended Kalman filter techniques was found to demonstrate both narrow band and broadband tracking. Finally the system is shown to provide a unique measurement capability for directional noise measurement in shallow water environments.

FRIDAY MORNING, 4 JULY 2008 ROOM 342B, 11:40 A.M. TO 1:00 P.M.

Session 5aUWi

Underwater Acoustics and ECUA: Synthetic Aperture Sonar and Radar Convergences

James Candy, Cochair
P.O. Box 808, L-156, Univ. of California, Lawrence Livermore Natl. Lab., Livermore, CA 94551, USA

Hugh Griffiths, Cochair
Defense college of, management and Technology, Academy of United Kingdom, Cranfield University, Swindon, UK

René Garello, Cochair
ENST-Bretagne, Dpt ITI, CS 83818, Brest Cedex 03, 29238, France

Contributed Paper

11:40

5aUWi1. Several imaging algorithms for synthetic aperture sonar and forward looking gap-filler in real-time and post-processing on IXSEA's "Shadows" sonar. Frédéric Jean (IXSEA, 46, quai François Mitterrand, 13600 La Ciotat, France, frj@ixsea.com)

SHADOWS is a new sonar system developed by IXSEA SAS. It is a towed composed of a synthetic aperture side-scan sonar and a forward-looking sonar. The system produces SAS images with a constant resolution 15 cm from 30 m to 300 m on each side. It also fills the nadir gap from 0 to 30 m with images having 40×15 cm resolution. The images are provided in real-time and are georeferenced. The synthetic aperture sonar algorithm uses INS data combined with the Displaced Phase Center Algorithm (DPC). Differences between INS and DPC navigations can be used to compute a topography profile of the ground. The post processing and real-time modes differ on the weight given between INS and DPC, and on the approximations to be done. The real-time beam-forming algorithm used is the time-domain fast factorized back projection which can be pushed to an exact back projection in the post processing mode. The forward-looking sonar uses a patented "sectorized emission" architecture. The images are side-scanlike. The real-time algorithm can be customized to make some incoherent integration on several pings increasing the contrast but slightly decreasing the resolution. A post processing algorithm can also provide an animation on a specific contact on the floor.

Invited Paper

12:00

5aUWi2. Passive synthetic aperture as an experimental tool. Edmund J. Sullivan (EJS Consultants, 46 Lawton Brook Lane, Portmouth, RI 02871, USA, PADDYPRIEST@aol.com), William M. Carey (College of Enginering, Boston University, 110 Cummington St, Boston, MA 02215, USA, wcarey@bu.edu), Jason D. Holmes (BBN Technologies, 10 Moulton St., Cambridge, MA 02318, USA, jholmes@bbn.com), James F. Lynch (Woods Hole Oceanographic Institution, 98 Water Street, Bigelow 203A, MS-11, Woods Hole, MA 02543, USA, jlynch@whoi.edu)

The use of autonomous undersea vehicle towed arrays offer an inexpensive way to carry out oceanographic measurements. Due to the small size and limited power of such vehicles, the physical aperture of the array is necessarily limited and the tow speed is low. However, there is an advantage in that short arrays at low speeds can have no flow noise. In addition the use of passive synthetic aperture (PSA) to provide spatial resolution and gain can play a major role. Here, we describe the use of two forms of passive synthetic array processing used in a shallow-water experiment. A six-element towed array, with 0.75 m spacing, was used to estimate the horizontal wave numbers of a propagation channel. A narrow-band form of PSA will be described which was used to generate coherent spatial gain by generating an aperture hundreds of wavelengths and provided accurate estimates of the horizontal modal wave numbers at frequencies les than 600 Hz. A broadband form of PSA was used to provide bearing estimation of a ferry passing through the area. The ferry's broadband propulsion noise, which was in the 900 Hz region, was used as the source. An overall increase in gain is demonstrated.

12:20

5aUWi3. Radar and sonar interferometry. René Garello (ENST-Bretagne, Dpt ITI, CS 83818, 29238 Brest Cedex 03, France, rene.garello@telecom-bretagne.eu), Christophe Sintes (ENST-Bretagne, Dpt ITI, CS 83818, 29238 Brest Cedex 03, France, christophe.sintes @enst-bretagne.fr), Didier Gueriot (Telecom Bretagne, Dept iTi - Technopole Brest-Iroise, CS 83818, 29238 Brest, France, didier.gueriot @telecom-bretagne.eu), Jean-Marie Nicolas (Ecole Nationale Supérieure des Télécommunication de Paris, Telecom ParisTech, Département TSI, 46 rue Barrault, 75634 Paris Cedex 13, France, nicolas@enst.fr)

This paper is an attempt to compare two interferometric processings. The first one is applied to traditional space-borne radar (SAR) and the second on recent interferometric sonar data. Few comparisons between those tech-niques have already been made, despite the fact that they share many similar principles, only a. Thus, the key idea of this article is to present both techniques with assets, drawbacks and specific "tricks" used in dataprocessing. The first part introduces briefly both sensors and compares signal and processing techniques used for both of them. The second part deals with interferometry, and more precisely with underwater and satellite interferometry. Then a noise-pollution analysis is performed on both techniques followed by bias removal methods for getting interferometric information. The conclusion summarizes the similarities between sonar and radar processing, pointing at the techniques that can applied to both.

12:40

5aUWi4. Interferometric synthetic aperture processing: a comparison of sonar and radar. Michael Hayes (University of Canterbury, Private Bag 4800, 8022 Christchurch, New Zealand, michael.hayes @canterbury.ac.nz), Peter T. Gough (University of Canterbury, Private Bag 4800, 8022 Christchurch, New Zealand, peter.gough@canterbury.ac.nz)

Interferometric aperture synthesis is an inverse problem that attempts to form an elevation map of the earth (in the case of radar) or a bathymetric map of the seafloor (in the case of sonar). In both cases, a pair of (nominally) vertically displaced transducers is configured as an interferometer. After aperture synthesis is performed to produce a pair of images, the height of each resolvable scatterer can be estimated using time delay estimation between the image pairs and knowledge of the system geometry. While interferometric synthetic aperture sonar (InSAS) seems like an obvious extension of the methods of interferometric synthetic aperture radar (InSAR), the height estimation algorithms are surprisingly different. In this paper we start with the principle of generalised correlation for optimal time delay estimation. This filters the signals to maximise their coherence since the accuracy of the time delay estimates, and thus the height estimates, strongly depends upon the signal coherence. We then consider the fundamental differences between InSAR and InSAS; namely the relative signal bandwidth, aperture sampling rate, and geometry and show how application of generalised correlation time delay estimation leads to the differences in how InSAS and InSAR signals are processed.

FRIDAY AFTERNOON, 4 JULY 2008 ROOM 242B, 3:20 TO 6:20 P.M.

Session 5pAAa

Architectural Acoustics and Musical Acoustics: New Measurement Parameters in Performing Arts Spaces II

Lily M. Wang, Cochair
University of Nebraska - Lincoln, 1110 S. 67th St., Omaha, NE 68182-0681, USA

Brian F. Katz, Cochair
LIMSI-CNRS, B.P. 133, Orsay, 91403, France

Invited Paper

3:20

5pAAa1. Determining acoustical parameters using cochlear modeling and auditory masking. Jasper Van Dorp Schuitman (University of Technology Delft, Lorentzweg 1, 2628 CJ Delft, Netherlands, J.vanDorpSchuitman@tudelft.nl), Diemer De Vries (University of Technology Delft, Lorentzweg 1, 2628 CJ Delft, Netherlands, d.devries@tudelft.nl)

The acoustical qualities of a concert hall or any other room are generally expressed using acoustical parameters determined from impulse responses. From microphone array measurements it turned out that these parameters can fluctuate severely over small distances, whereas the perceptual cues for which these parameters are supposed to be a measure remain constant. This means that a local parameter value has a very low predictive value for acoustic quality. In this research, cochlear modeling techniques and simulations of auditory masking effects have been applied to model human hearing. These techniques together model various stages in the auditory path, like the movement of the basilar membrane inside the cochlea and mechanisms inside the brains. It turns out that determining acoustical parameters using this representation leads to results which show much less spatial fluctuations, and are closer to human perception.

3:40

5pAAa2. Sound strength and reverberation time in small concert halls. Marc Aretz (RWTH Aachen University, Institute for Technical Acoustics, Neustraße 50, 52066 Aachen, Germany, Marc.Aretz@akustik.rwth-aachen.de), Raf Orlowski (Arup Acoustics, St. Giles Hall Pound Hill, CB3 0AE Cambridge, UK, Raf.Orlowski@arup.com)

Many small concert halls are being built in music departments in schools and universities and these have to cater for a wide variety of musicalensembles ranging from orchestras to solo performers. Such diverse musical forces require different acoustic conditions in terms of reverberation and loudness and so variable acoustics are frequently provided. However, introducing absorption decreases reverberation and loudness and so a careful balance needs to be struck between controlling loudness and maintaining reverberation. In the course of this study a series of measurements was carried out in six small concert halls in Cambridge, UK, which accommodate a range of sizes of musical ensembles from quartets to orchestras, in order to determine the range of reverberation times and sound strengths, including changes due to variable absorption. The measured strength levels were compared to values derived from traditional and revised theory on strength calculations in order to assess the accuracy of the theories for small chamber music halls. The measured values of strength levels were observed to be mostly lower than the predicted ones. In order to account for this difference (particularly in spaces with added absorption) a combination of Barron's revised theory and the Vorländer correction factor is proposed.

4:00

5pAAa3. Proposition of new acoustical parameters to analyze the 3D spatial composition of sound in music spaces. Alban A. Bassuet (Arup Acoustics, 155 Avenue of the Americas, New York, NY 10013, USA, alban.bassuet@arup.com)

From acoustic measurements conducted in more than 100 renowned historical music spaces, for the Constellation Project, this paper proposes new acoustical parameters created to better describe the 3D spatial composition of sound in music spaces. Using B-format recordings, the author is proposing a visualization algorithm to plot the acoustic intensity at specific time frames and ranges. The acoustic energy is decomposed into relevant space segments and energy ratio parameters LH (lateral frontal high versus lateral frontal low), and FR (lateral rear high versus lateral rear low) are deduced and proposed for analyzing the distribution of sound and the envelopment characteristics of the room. Examples of intensity plots and of the proposed 3D acoustical parameters are given for various room types ranging from small to large concert halls, small to large opera houses, famous organ churches and Roman basilicas.

4:20-4:40 Break

Invited Paper

4:40

5pAAa4. Early reflection surfaces in Concert Halls - a new quantitative criterion. Yann Jurkiewicz (Kahle Acoustics, 188 avenue Molière, 1050 Brussels, Belgium, yjurkiewicz@kahle.be), Eckhard Kahle (Kahle Acoustics, 188 avenue Molière, 1050 Brussels, Belgium, kahle@kahle.be)

A new acoustic parameter has been defined for the acoustic brief of the Philharmonie de Paris Concert Hall. With a seating capacity of 2400 and the audience enveloping the performers on all sides, the new hall will be at the upper limit of the ideal range for symphonic music, and an efficient acoustic design was called for. In order to relate architectural design to acoustic efficiency, and based on quantitative study of existing halls, an early efficiency parameter was developed. For the Paris Philharmonie the brief requested a total area of 1400 m^2 of surfaces being able to create early reflections, with 500 m^2 being less than 15 m from the stage. The studies leading to the definition and the justificantion of the parameter will be presented. Another, more accurate definition expresses the early efficiency parameter in terms of the solid angle for a source on stage, allowing generalization of the new criterion for all hall sizes.

Contributed Paper

5:00

5pAAa5. Diffuseness and intensity analysis of spatial impulse responses. Tapio Lokki (Helsinki University of Technology, P.O. Box 5400, 02015 TKK, Finland, Tapio.Lokki@tkk.fi)

Spatial impulse responses, meaning responses measured with a microphone grid, were measured in seven concert halls. The microphone array consisted of 12 omni-microphones, enabling a construction of three intensity pairs (in x, y, and z directions) with 1 cm spacing and three intensity pairs with 10 cm spacing. In each hall impulse responses were measured with at least three loudspeaker and four microphone positions. They were analyzed with directional audio coding methodology, which enables analysis of diffuseness and instantaneous intensity as a function of time and frequency. In other words, with this analysis it is possible to analyze the directions of early reflections and to estimate diffuseness of sound field in a measurement position. Preliminary results indicate that diffuseness is quite similar in different positions in one hall, but it varies more between halls. The directions of early reflections are hard to visualize, however some example videos are shown to get an idea about the possibilities of such an analysis technique.

Invited Paper

5:20

5pAAa6. Experiments with the orchestral impulse response. Gary W. Siebein (Univ. of Florida, 231 Arch, PO Box 115702, Gainesville, FL 32611, USA, gsiebein@siebeinacoustic.com), Robert M. Lilkendey (Siebein Associates, Inc., 625 NW 60th Street, Suite C, Gainesville, FL 32607, USA, rlilkendey@siebeinacoustic.com), Hyun Paek (Siebein Associates, Inc., 625 NW 60th Street, Suite C, Gainesville, FL 32607, USA, hpaek@siebeinacoustic.com), Chris Jones (Siebein Associates, Inc., 625 NW 60th Street, Suite C, Gainesville, FL 32607, USA, cjones@siebeinacoustic.com), Joshua Fisher (Siebein Associates, Inc., 625 NW 60th Street, Suite C, Gainesville, FL 32607, USA, jfisher@siebeinacoustic.com), Youngmin Kwon (Univ. of Florida, 231 Arch, PO Box 115702, Gainesville, FL 32611, USA, ymkwon@hotmail.com)

Experiments were conducted in a large multipurpose performance hall to examine the differences in listening quality and physical acoustical measurements that resulted from using a single dodecahedral loudspeaker as the sound source and an array of multiple

directional loudspeakers spread across the stage to simulate the various sections of an orchestra. Significant differences in listening qualities were recorded by listeners at three locations in the hall. The impulse responses recorded using the two systems varied dramatically in structure and in some of the typical acoustic metrics measured. However, there were also similarities among many measurements using the two systems. The research indicates the need for new measurement parameters to express the significant architectural features of the room and the physical acoustical difference that caused the perceived qualities of the sound field to vary. Preliminary analysis of the existing and proposed parameters will be presented.

Contributed Papers

5:40

5pAAa7. Relevance of acoustic parameters for musician communication. Anne Guthrie (1926 5th Ave, Troy, NY 12180, USA, guthra2@rpi.edu), Jonas Braasch (Rensselaer Polytechnic Institute, Greene Bldg., 110 8th St., Troy, NY 12180, USA)

In situations of indeterminate musical performance (particularly in telepresence, where acoustic degradation is a frequent concern), autonomous musical communication, both practical and artistic, forms the crux of the musical material. The relevance of stage acoustic and psychoacoustic parameters to contemporary performance situations must be re-examined with regards to the heightened importance of communication. Parameters developed by A. C. Gade, J. Meyer, and D. Brungart are starting points for this examination. Experiments are conducted with four instrumentalists playing excerpts from a composition by Christian Wolff (open notation allows for measurable variations depending on communication quality), communicating telematically between two virtual environments. Parameters determined by questionnaire to have the strongest effect on quality and efficiency of communication are varied at intervals and evaluated by the performers. Five parameters are tested: Self-to-Others Ratio, Commonality of Aural Space, Masking of Individual Voices, Visual-Audio Synchrony, and Position/Directivity. The performances are recorded and analyzed for variations in musical content, such as dynamics, rhythm, register, and density. The three sets of data (objective parameters, performer evaluation, and musical analysis) are compared to determine the effects of the selected parameters on musical communication.

6:00

5pAAa8. A qualitative and quantitative analysis of impulse responses from balloon bursts. Dominique J. Cheenne (Columbia College Chicago, Department of Audio Arts & Acoustics, 33 East Congress, Suite 601, Chicago, IL 60605, USA, dcheenne@colum.edu), Mauricio Ardila (Columbia College Chicago, Department of Audio Arts & Acoustics, 33 East Congress, Suite 601, Chicago, IL 60605, USA, mardila@colum.edu), Connie G. Lee (Columbia College Chicago, Department of Audio Arts & Acoustics, 33 East Congress, Suite 601, Chicago, IL 60605, USA, miss.connie.lee@gmail.com), Ben Bridgewater (Columbia College Chicago, Department of Audio Arts & Acoustics, 33 East Congress, Suite 601, Chicago, IL 60605, USA, captain.cranium@gmail.com)

Anechoic recordings of balloon bursts were systematically acquired for various conditions of balloon diameters, puncture location, and inflation pressure. The recordings were analyzed to derive the average frequency spectrum over the effective duration of the acoustic impulse. Although the data show the well-known limitations for the impulse responses (in terms of repeatability and directional behavior) when viewed at high resolution, the results are quite consistent when averaged over one-third octave bands and reveal that the diameter factor (the ratio between the diameter of the inflated balloon to that of its stated maximum), rather than the overall diameter of the balloon, is a good indicator of the sound pressure level, especially above 200 Hz. The study proposes some simple empirical formulas to predict the quantitative sound pressure level and the qualitative spectral response (using the spectral centroid and skewness) from balloon bursts, based on the inflation factor as a variable. The study also offers suggestions to maximize the value of the balloon-burst methodology in building acoustics measurements by describing an effective way to measure reverberation time while simultaneously acquiring useful directional information associated with the reflected sound.

Session 5pAAb

Architectural Acoustics: Coupled Volume Acoustics II

Jason E. Summers, Cochair
U.S. Naval Res. Lab., Acoust. Div., Code 7142, 4555 Overlook Ave. SW, Washington, DC 20375, USA

Alexis Billon, Cochair
Universite de Liege, INTELSIG group - Département E.E.I., B28 Sart-Tilman, Liege, 4000, Belgium

Invited Papers

3:40

5pAAb1. Soundfields in coupled rooms: A theoretical and phenomenological synopsis. Jason E. Summers (U.S. Naval Res. Lab., Acoust. Div., Code 7142, 4555 Overlook Ave. SW, Washington, DC 20375, USA, jason.summers@nrl.navy.mil)

In systems of acoustically coupled rooms, energy in the reverberant field is exchanged between constituent rooms via transondentboundaries. Energy in the direct field can be distributed between rooms by the same mechanism. These exchanges of energy have been able to explain the phenomenon of multiple-slope decay curves. Likewise, they result in spatial and spectral variations in steady-state SPL and decay-curve shape. The basic form of the decay curve is governed by the gross locations of the source(s) and receiver: which room(s) they occupy, in addition to properties of the rooms themselves: volume, surface area, and absorption. Historically, these basic dependencies have been well explained by statistical-acoustics (SA) models. More subtle variations in decay-curve shape result from the fine-scale locations of source(s) and receivers relative to one another and boundary regions through which energy is exchanged (e.g., apertures). By accounting for radiation from boundaries, and propagation delays within and between rooms, more sophisticated SA models can reproduce these effects. Even so, these models fail when SA assumptions are violated or energy transfer becomes so great (e.g., large aperture areas) that room boundaries are ambiguous. In these cases, newer computational models yield accurate predictions and physical insight. [Work supported by ONR.]

4:00

5pAAb2. On the use of diffusion equations to model the acoustics of coupled rooms. Alexis Billon (Universite de Liege, INTELSIG group - Département E.E.I., B28 Sart-Tilman, 4000 Liege, Belgium, abillon@ulg.ac.be), Vincent Valeau (Laboratoire d'Etudes Aérodynamiques (LEA), Université de Poitiers - ENSMA - CNRS, Bâtiment K, 40 Avenue du Recteur Pineau, F-86022 Poitiers, France, vincent.valeau@lea.univ-poitiers.fr), Judicaël Picaut (Lab. Central des Ponts et Chaussées, Division Entretien, Sécurité et Acoustique des Routes, Route de Bouaye - BP 4129, 44341 Bouguenais Cedex, France, Judicael.Picaut@lcpc.fr), Cédric Foy (CEBTP-SOLEN, 12 Avenue Gay Lussac, ZAC La Clef Saint Pierre, 78990 Elancourt, France, c.foy@cebtp.fr), Anas Sakout (LEPTIAB Université de La Rochelle, Avenue Michel Crépeau, 17042 La Rochelle Cedex 01, France, asakout@univ-lr.fr)

The acoustics of coupled rooms are characterized by energy exchanges through apertures and/or partition walls. The use of systems of diffusion equations allows to predict the temporal and spatial energy distributions in these configurations quite accurately. In this presentation, the diffusion formalism for room acoustics-prediction is summarized. The systems of equations to be solved in the case of coupling through an aperture and through a partition wall are presented. For two rooms coupled through an aperture (two classrooms connected through an open door), the results obtained with the diffusion model are compared to experimental data, in terms of sound pressure levels and sound decays. On the other hand, for the case of two classrooms connected through a partition wall, the diffusion model is compared to experimental data in terms of sound pressure level difference only. Finally, an engineering application is presented in the configuration involving a workroom including multiple sound sources (e.g., machines) connected to offices through open and closed doors.

4:20

5pAAb3. Modeling and analysis of acoustically coupled spaces using a diffusion equation model. Yun Jing (Rensselaer Polytechnic Institute, Greene Building, School of Architecture, 110 8th Street, Troy, NY 12180, USA, jingy@rpi.edu), Ning Xiang (Rensselaer Polytechnic Institute, Greene Building, School of Architecture, 110 8th Street, Troy, NY 12180, USA, xiangn@rpi.edu)

Acoustically coupled spaces have been studied and applied to concert halls due to a number of interesting phenomena inside the spaces, including nonexponential energy decays, which are believed to benefit both desired clarity and reverberance. A diffusion equation model has been recently applied to acoustically coupled spaces to predict both steady-state and time-dependent sound field [A. Billon, et. al., J. Acoust. Soc. Am., **120**, 2006, pp. 2043-2054], good agreements between simulations and experimental measurements have been found. In this paper, the diffusion equation along with a recently proposed modified boundary condition [Y. Jing and N. Xiang, J. Acoust. Soc. Am., **123**, 145-153 (2008)] is used, to reveal intriguing characteristics of coupled spaces, including the sound pressure level distribution along the aperture, energy flow in both rooms, and location dependence of the acoustic source on energy decay characteristics. Experimental results are employed to verify the model, and show the capability of the diffusion equation model for guiding the design of coupled spaces.

4:40

5pAAb4. Low frequency evaluation of steady-state pressure distribution and reverberation time in two-room coupled system. Miroslaw Meissner (Institute of Fundamental Technological Research PAS, Swietokrzyska 21, 00-049 Warsaw, Poland, mmeissn@ippt.gov.pl)

A modal expansion method supported by a numerical implementation has been used for studying acoustic properties of coupled room system composed of two connected rectangular enclosures. In a theoretical model a low frequency limit was considered, where modes are lightly damped, thus they were approximated by eigenmodes of a hard-walled room. Eigenfunctions and eigenfrequencies were computed numerically via an application of the forced oscillator method. Calculation results have shown a great influence of absorbing material location and sound source position on the distribution of acoustic pressure and sound decay inside enclosures. As was shown it is the result of a modal localization caused by a generation of modes with eigenfrequencies very close to frequencies of modes in rectangular prisms having the same dimensions as enclosures. When one of enclosures was much more absorbent than the other one, calculation data have demonstrated an interaction of modes during a sound decay that produces reverberant curves with a rapid initial decay and a shallow late decay slope. As was found a "sagging" appearance of decay curves occurs when a late sound decay is dominated by a decay of eigenmodes localized in an enclosure with a weak sound damping.

Contributed Paper

5:00

5pAAb5. The application of acoustically coupled spaces in concert hall design. Christopher Jaffe (167 East Rocks Road, Norwalk, CT 06851, USA, ADK117@GMAIL.COM)

At mid-twentieth century, a hall having a reverberation decay curve with a late arriving extended second slope was considered an acoustical failure. It was assumed that that the level of the extended reverberation in the hall would interfere with the ongoing running music of the ensemble and reduce orchestral clarity, definition and transparency. To my knowledge, only two practitioners pioneered the utilization of physical acoustic coupling in concert shell and concert hall design during those early years. One was Russell Johnson, when he was with Bolt Beranek and Newman and later with his own firm Artec. The other was me with both my firms Stagecraft Corporation and Jaffe Acoustics. This paper discusses how the need to improve the concert hall environment of American multi-use theatres led to the application of coupling techniques in these halls and how both Mr. Johnson and I later applied physical acoustic coupling in single room concert spaces.

Invited Paper

5:20

5pAAb6. Multivariable analysis of energy decay in coupled volume rooms: How can we objectively describe what we perceive in coupled volume performance spaces? Todd L. Brooks (Artec Consultants Inc, 114 W 26th ST FL 12, New York, NY 10001, USA, tlb@artecconsultants.com), Ted Pyper (Artec Consultants Inc, 114 W 26th ST FL 12, New York, NY 10001, USA, tap@artecconsultants.com), Kelly A. Aston (Artec Consultants Inc, 114 W 26th ST FL 12, New York, NY 10001, USA, ka@artecconsultants.com), Damian J. Doria (Artec Consultants Inc, 114 W 26th ST FL 12, New York, NY 10001, USA, dd@artecconsultants.com)

The behavior of coupled volumes in room acoustics is commonly characterized by multiple slopes observed in sound energy decay curves, as measured (or modeled) using an omnidirectional receiver. This characterization is often limiting and can not adequately explain the change in character of sound energy decay with time that we perceive as listeners in music performance spaces that employ coupled volumes. By investigating energy decay as a function of several independent variables, including time, frequency, and direction of energy arrival, we seek to forge new objective measures that relate to what a listener actually hears in a coupled volume concert hall. We will discuss relevant geometry and materials of several coupled volume performance spaces designed by Artec Consultants Inc, describe subjective phenomena we have observed in these halls, and present results of our ongoing investigation of new objective metrics geared to better characterize coupled volume music performance spaces.

Contributed Paper

5:40

5pAAb7. Theoretical considerations in the prediction of decay times for the Philharmonie de Paris. Thomas Scelo (Marshall Day Acoustics LTD, P O Box 5811, Wellesley St., 1000 Auckland, New Zealand, thomas.scelo@marshallday.co.nz), Harold Marshall (Marshall Day Acoustics LTD, P O Box 5811, Wellesley St., 1000 Auckland, New Zealand, harold.marshall@marshallday.co.nz), Joanne O. Valentine (Marshall Day Acoustics LTD, P O Box 5811, Wellesley St., 1000 Auckland, New Zealand, joanne.valentine@marshallday.co.nz)

The brief for the Philharmonie de Paris includes the requirement that the hall should combine great clarity with high reverberation. The proposed solution, which won the design competition, consists of two nested chambers: an inner space producing acoustical intimacy and an outer space with its own architectural and acoustical presence. The interaction between these two spaces gives the possibility for the full range of acoustical adaptability required in the acoustical brief. This paper reports on some theoretical modelling work for the hall where the geometry considered is first described in the context of coupled space modelling. The predicted range of the variability achieved in the design by closure of the coupling openings is then presented. Finally, the paper discusses the appropriateness of these models when predicting the decay times in such a complex geometry.

Invited Paper

6:00

5pAAb8. Adjustable acoustics --- Coupled volumes in Artec concert halls: an extravagance or necessity? Tateo Nakajima (Artec Consultants Inc, 114 W 26th ST FL 12, New York, NY 10001, USA, tn@artecconsultants.com), Damian J. Doria (Artec Consultants Inc, 114 W 26th ST FL 12, New York, NY 10001, USA, dd@artecconsultants.com), Edward Arenius (Artec Consultants Inc, 114 W 26th ST FL 12, New York, NY 10001, USA, ea@artecconsultants.com), Andrew Morgan (Artec Consultants Inc, 114 W 26th ST FL 12, New York, NY 10001, USA, ajm@artecconsultants.com)

Led by its founder, Russell Johnson, Artec has developed an unequalled body of experience in the practical application of coupled volumes in the design and construction of concert halls. This paper will present a survey of selected past and future Artec projects from the point of view of the artists and venue managers that perform and work in these halls on a daily basis. Are adjustable acoustics an extravagance or a necessity? What practical problems have been encountered and are they inherent in the concept of adjustability or can they be avoided? How have the musicians reacted? And what is the future of adjustable acoustics?

FRIDAY AFTERNOON, 4 JULY 2008 ROOM 343, 1:40 TO 4:20 P.M.

Session 5pAO

Acoustical Oceanography and ECUA: Acoustical Tomography and Long Range Propagation

Timothy Duda, Cochair
Woods Hole Oceanographic Institution, 98 Water Street, Bigelow 107, MS-12, Woods Hole, MA 02543, USA

Yann Stephan, Cochair
SHOM, 13 rue du Chatellier, CS 92803, Brest cedex 2, 29228, France

Contributed Papers

1:40

5pAO1. Ocean acoustic tomography using a double-beamforming algorithm. Ion Iturbe (GIPSA-lab, dep. DIS, 961, rue de la Houille Blanche, 38402 St Martin d'Hères, France, ion.iturbe@gipsa-lab.inpg .fr), Philippe Roux (LGIT - CNRS - Université Joseph Fourier, Maison des Géosciences, 1381 rue de la Piscine, BP 53, 38041 Grenoble, France, philippe.roux@obs.ujf-grenoble.fr), Barbara Nicolas (GIPSA-lab, dep. DIS, 961, rue de la Houille Blanche, 38402 St Martin d'Hères, France, barbara.nicolas@gipsa-lab.inpg.fr), Jérôme I. Mars (GIPSA-lab, dep. DIS, 961, rue de la Houille Blanche, 38402 St Martin d'Hères, France, jerome .mars@gipsa-lab.inpg.fr)

Since Munk and Wunsch proposed the basis for ocean acoustic tomography, many experiments have been performed to estimate sound speed fluctuations in the ocean, using ray identification and measurement of their travel times. However, technical limitations appeared such as the precision of the arrival time measurements or the number of ray arrivals that can be extracted from the signal. Recently, technical improvements allowed more complete experiments using two vertical arrays of sensors (source array and hydrophone array). In this configuration, the signals between each source and receiver are recorded which greatly improve the available information to identify the acoustic rays. One way to increase the number of rays in the tomography algorithm is to perform double-beamforming on the source and receive arrays. With double-beamforming, ray arrivals are separated by emission angle, reception angle and arrival time. Thus, we solve more ray arrivals than with a single beamforming or with a point-to-point approach. In order to avoid previous limitations and to explore acoustical limitations, we study two simple cases through the double-beamforming algorithm: with simulated data and with ultrasonic small-scale experimental data.

2:00

5pAO2. A simulation study of shallow water tomography for coastal monitoring. Olivier Carrière (Université libre de Bruxelles (U.L.B.) - Environmental hydroacoustics lab, av. Franklin D. Roosevelt 50, CP 194/5, 1050 Bruxelles, Belgium, ocarrier@ulb.ac.be), Jean-Pierre Hermand(Université libre de Bruxelles (U.L.B.) - Environmental hydroacoustics lab, av. Franklin D. Roosevelt 50, CP 194/5, 1050 Bruxelles, Belgium, jhermand@ulb.ac.be), Yann Stephan (SHOM, 13 rue du Chatellier, CS 92803, 29228 Brest cedex 2, France, yann.stephan@shom.fr)

Developing operational oceanographic models for coastal environment is an exciting challenge for the next decades. The typical sparsity of assimilated *in-situ* observations often creates biases in the model predictions reducing the overall accuracy of the forecasting. In such a highly dynamic environment, acoustic tomography can be a good candidate to provide synoptic measurements over wide areas while a range-dependent inversion scheme allows to achieve a reasonable spatial resolution. In this work, we present simulation results of a Kalman-based assimilation of ocean-acoustic data for a basic model of the Ushant front west off Britanny. In a first part, a single vertical slice tomography experiment is simulated for a static front model to study in which way the modal propagation of a multifrequency acoustic signal is affected by the characteristics of the front (position, intensity). In a second part, the problem of assimilating full-field acoustic data into a dynamic model and tracking of the range-dependent sound-speed field is addressed.

2:20

5pAO3. Sound-speed estimation from RAFOS transmissions. Emmanuel Skarsoulis (FORTH / IACM, N. Plastira 100, Vasilika Voutes, GR-70013 Heraklion, Greece, eskars@iacm.forth.gr), George Piperakis (FORTH / IACM, N. Plastira 100, Vasilika Voutes, GR-70013 Heraklion, Greece, piperak@iacm.forth.gr)

Acoustic navigation of Lagrangian (moving) floats is carried out by measuring travel times from a number of fixed stations/moorings. A minimum of two fixed stations are needed for location estimation in the horizontal, whereas an additional fixed station is commonly used to remove left-right ambiguity. The signals (RAFOS) and sampling schemes used in ocean acoustic navigation are characterized by limited time resolution (order of 200 msec), much smaller than the resolution used in travel-time tomography (order of 1-10 msec). The possibility of combining navigation signals (travel

times) from three fixed stations to multiple moving floats for simultaneous sound-speed estimation and float localization is examined here. The redundant travel-time information in this case offers a significant advantage and makes the accurate estimation of the speed of sound feasible. It is shown that the estimation error for the sound speed decreases with the number of floats, and thus the estimation accuracy improves as the set of floats grows larger. This procedure also leads to improved location estimates for the individual floats. A number of numerical experiments are used to demonstrate the performance of the method. [Work supported by EU/FP6 Damocles project.]

2:40

5pAO4. Using Seagliders for acoustic receiving and communication. Bruce M. Howe (Applied Physics Lab., Univ. of Washington, 1013 Northeast 40th St., Seattle, WA 98105, USA, howe@apl.washington.edu), Michael L. Boyd (Applied Physics Lab., Univ. of Washington, 1013 Northeast 40th St., Seattle, WA 98105, USA, mike@apl.washington.edu)

Underwater gliders are beginning to be used as tools in ocean acoustics and acoustical oceanography. Results from several experiments conducted in summer 2006 with Seagliders equipped with acoustic modems and receivers are described. Off Kauai, a glider received signals from the Acoustic Thermometry of Ocean Climate/North Pacific Acoustic Laboratory 75 Hz source; subsequent coherent processing showed close to theoretical gain for 12 min records while moving away from the source at ranges >100 km with velocity 20 cm/s (measured by travel time, Doppler, and dead reckoning). In the Monterey Bay MB06 experiment, two-way communications between other subsea platforms and shore via the acoustic modem-equipped glider was demonstrated (albeit with latency). The results support the future use of gliders as precision navigated platforms, communication and time distribution nodes, and thermometry/tomography mobile receivers. Work supported by the Office of Naval Research.

3:00

5pAO5. A decade of acoustic thermometry in the North Pacific Ocean: Using long-range acoustic travel times to test gyre-scale temperature variability derived from other observations and ocean models. Peter Worcester (MPL, Scripps Institution of Oceanography, University of California, San Diego, La Jolla, CA 92093-0238, USA, pworcester@ucsd.edu), Brian D. Dushaw (Applied Physics Lab., Univ. of Washington, 1013 Northeast 40th St., Seattle, WA 98105, USA, dushaw@apl.washington.edu), Rex K. Andrew (Applied Physics Lab., Univ. of Washington, 1013 Northeast 40th St., Seattle, WA 98105, USA, randrew@apl.washington.edu), Bruce M. Howe (Applied Physics Lab., Univ. of Washington, 1013 Northeast 40th St., Seattle, WA 98105, USA, howe@apl.washington.edu), James A. Mercer (Applied Physics Lab., Univ. of Washington, 1013 Northeast 40th St., Seattle, WA 98105, USA, mercer@apl.washington.edu), Robert C. Spindel (Applied Physics Lab., Univ. of Washington, 1013 Northeast 40th St., Seattle, WA 98105, USA, spindel@apl.washington.edu), Bruce Cornuelle (MPL, Scripps Institution of Oceanography, University of California, San Diego, La Jolla, CA 92093-0238, USA, bdc@ucsd.edu), Matthew Dzieciuch (MPL, Scripps Institution of Oceanography, University of California, San Diego, La Jolla, CA 92093-0238, USA, mad@ucsd.edu), Theodore G. Birdsall (Univ. of Michigan, Electrical Engineering and Computer Science Dept., 1301 Beal Ave., Ann Arbor, MI 48109-2122, USA, birdsall@umich.edu), Kurt Metzger (Univ. of Michigan, Electrical Engineering and Computer Science Dept., 1301 Beal Ave., Ann Arbor, MI 48109-2122, USA, metzger@umich.edu), Dimitris Menemenlis (Jet Propulsion Laboratory, California Institute of Technology, 4800 Oak Grove Dr., Pasadena, CA 91109, USA, menemenlis@jpl.nasa.gov)

Large-scale, range- and depth-averaged temperatures in the North Pacific Ocean were measured by long-range acoustic transmissions over the decade 1996-2006. Acoustic sources off central California and north of Kauai transmitted to receivers throughout the North Pacific. Even though acoustic travel times are spatially integrating, suppressing mesoscale variability and providing a precise measure of large-scale temperature, the travel times sometimes vary significantly on time scales of only a few weeks. The interannual variability is large, with no consistent warming or cooling trends. Comparison of the measured travel times with travel times derived from (i) the World Ocean Atlas 2005 (WOA05), (ii) an upper ocean temperature estimate derived from satellite altimetry and in situ profiles, (iii) an analysis provided by the Estimating the Circulation and Climate of the Ocean (ECCO) project, and (iv) simulation results from a high-resolution configuration of the Parallel Ocean Program (POP) show similarities, but also reveal substantial differences. The differences suggest that the data can provide significant additional constraints for numerical ocean simulations. The acoustic data show that WOA05 is a much better estimate of the time-mean hydrography than either the ECCO or POP estimates and provide significantly better time resolution for large-scale ocean variability than can be derived from satellite altimetry and in situ profiles.

3:20

5pAO6. Coherence of tracked arrivals in SPICEX. Matthew Dzieciuch (MPL, Scripps Institution of Oceanography, University of California, San Diego, La Jolla, CA 92093-0238, USA, mad@ucsd.edu), Bruce Cornuelle (MPL, Scripps Institution of Oceanography, University of California, San Diego, La Jolla, CA 92093-0238, USA, bdc@ucsd.edu), Peter Worcester (MPL, Scripps Institution of Oceanography, University of California, San Diego, La Jolla, CA 92093-0238, USA, pworcester@ucsd.edu)

In the fall of 2004, 250 Hz broadband signals were received at 500 km and 1000 km ranges on a near full water-column vertical array in the North Pacific ocean. Individual ray arrivals of very high SNR could easily be identified and tracked using a turning-point filter (time-delay beamforming accounting for channel structure), thus providing accurate vertical coherence estimates. The observations can be compared to standard Monte Carlo estimates of coherence made using accurate parabolic-equation acoustic propagation in an ensemble of ocean states consistent with the standard Garrett-Munk ocean internal-wave spectrum. Acoustic coherence can also be expressed as a depth- dependent structure function. This is naturally estimated by the full-wave travel-time sensitivity kernel (TSK) which provides a linearized transformation from the internal wave spectrum to the structure function. Environmental measurements were conducted almost concurrently with the acoustic trials, constraining the acceptable ocean variability. Allowances must be made for scattering by sound-speed variability along isopycnals (spiciness) in the upper mixed layer. The most important conclusion to date is that the vertical coherence is depth-dependent but this statement must be qualified by the ability of the beamformer to separate arrivals.

3:40

5pAO7. Travel-time sensitivity kernels in long-range propagation. Emmanuel Skarsoulis (FORTH/IACM, N. Plastira 100, Vasilika Voutes, GR-70013 Heraklion, Greece, eskars@iacm.forth.gr), Bruce Cornuelle (MPL, Scripps Institution of Oceanography, University of California, San Diego, La Jolla, CA 92093-0238, USA, bdc@ucsd.edu), Matthew Dzieciuch (MPL, Scripps Institution of Oceanography, University of California, San Diego, La Jolla, CA 92093-0238, USA, mad@ucsd.edu)

The effect of increasing range on the sensitivity of finite-frequency travel-time observables to sound-speed perturbations is studied using the notion of wave-theoretic sensitivity kernels based on the first Born approximation of the Green's function and the notion of peak arrivals. Travel-time sensitivity kernels are examined in a range-independent background ocean environment. While at medium ranges the kernels exhibit zero-sensitivity cores on the eigenrays, these cores shrink and disappear at long ranges due to refraction and the kernels converge in the vertical towards the corresponding eigenrays; this behavior is not observed in free space. On the other hand the kernels expand in the horizontal cross-range direction and attain their maximum extent at the midpoint between source and receiver, similar to the behavior of the Fresnel volume in free space. Thus, stratification affects the shape of the sensitivity kernel in the vertical preventing expansion with increasing range but not in the horizontal such that the sensitivity kernel takes the form of a folded rug expanding the eigenray in the horizontal cross-range direction. [Work supported by ONR.]

4:00

5pAO8. High-frequency broadband acoustic current tomography in shallow water. Jing Luo (University of Delaware, College of Marine and Earth Studies, S. College Street, Newark, DE 19716, USA, luojing@udel.edu), Entin A. Karjadi (College of Marine and Earth Studies, University of Delaware, Newark, DE 19716, USA, karjadi@udel.edu), Mohsen Badiey (University of Delaware, College of Marine and Earth Studies, S. College Street, Newark, DE 19716, USA, badiey@udel.edu)

To study current tomography in very shallow water regions a simultaneous oceanographic and broadband (1-25 kHz) acoustic experiment was conducted in the Delaware Bay. The mean water depth was 15 m and the source-receiver range was 760 m. In this paper, we discuss the feasibility of using reciprocal acoustic transmission for current tomography applications. A beamforming technique is used to resolve the arrival time of direct and surface-bounced rays since in shallow water the received acoustic signals are more complicated due to multiple interactions with bottom and sea surface. Using the experimental data, the accuracy of travel time measurements for variable environmental conditions is examined for different center frequencies and bandwidths. The current velocity prediction results are compared with ADCP measurements to determine the feasibility of current tomography in shallow water.

FRIDAY AFTERNOON, 4 JULY 2008 ROOM 353, 2:00 TO 5:20 P.M.

Session 5pBB

Biomedical Ultrasound/Bioresponse to Vibration: General Topics in Biomedical Ultrasound/Bioresponse to Vibration II

Michael R. Bailey, Cochair
Center for Industrial and Medical Ultrasound, Applied Physics Lab., University of Washington, 1013 NE 40th St., Seattle, WA 98105, USA

Oleg A. Sapozhnikov, Cochair
Center for Industrial and Medical Ultrasound, Applied Physics Lab., University of Washington, 1013 NE 40th St., Seattle, WA 98105, USA

Contributed Papers

2:00

5pBB1. Dual confocal ultrasound system for shear wave elastography. Michael D. Gray (Georgia Institute of Technology, Mechanical Engineering, 771 Ferst Drive, Atlanta, GA 30332-0405, USA, michael.gray@me.gatech.edu), James S. Martin (Georgia Institute of Technology, Mechanical Engineering, 771 Ferst Drive, Atlanta, GA 30332-0405, USA, james.martin@me.gatech.edu), Peter H. Rogers (Georgia Institute of Technology, Mechanical Engineering, 771 Ferst Drive, Atlanta, GA 30332-0405, USA, peter.rogers@me.gatech.edu)

A dual confocal transducer system for ultrasound-based elastography is presented. The system is intended to noninvasively measure the complex shear speed in cetacean head tissues, including brain, jaw fat, and melon. The system instrumentation features a pair of dual-element confocal ultrasound transducers, one of which is used to remotely generate low frequency (100-1000 Hz) shear waves in soft tissues via radiation force, and the other is used to measure the resulting shear wave displacements using Doppler techniques. One transducer is configured as an open ring into which the other transducer can be placed and translated. The relative positions of the transducers are mechanically manipulated in order to measure short-path propagation and estimate shear wave speed and loss. Work supported by ONR.

2:20

5pBB2. Simulated response of the human lung to low-frequency underwater sound using a finite-element-based thoracic model. Mark S. Wochner (Applied Research Laboratories, The University of Texas, P.O. Box 8029, Austin, TX 78713-8029, USA, mwochner@mail.utexas.edu), Yurii A. Ilinskii (Applied Research Laboratories, The University of Texas, P.O. Box 8029, Austin, TX 78713-8029, USA, yura@arlut.utexas.edu), Mark F. Hamilton (Applied Research Laboratories, The University of Texas, P.O. Box 8029, Austin, TX 78713-8029, USA, hamilton@mail.utexas.edu), Evgenia A. Zabolotskaya (Applied Research Laboratories, The University of Texas, P.O. Box 8029, Austin, TX 78713-8029, USA, zhenia@arlut.utexas.edu)

In a previous paper, inhomogeneity within the lungs and its influence on the lung's response to low-frequency underwater sound using a finite-element-based model was discussed [Wochner, *et al*., J. Acoust. Soc. Am. **122**, 2957 (2007)]. Here we report an extension of the previous work that adds surrounding organs to the finite element model. It is hypothesized that the significant damage that can occur at relatively low amplitudes when the lung is in resonance is due primarily to the shear stresses that can occur in the lung through its interactions with surrounding organs. In particular, the heart, diaphragm, and ribs, all of which have considerably different material properties compared to lung, may have a sizable effect on the lung's response to low-frequency underwater sound. This paper will discuss the resonance frequency, motion, and stress and strain fields produced using this new finite-element-based thoracic model. [Work supported by ONR and ARL:UT IR&D.]

2:40

5pBB3. Dual apodization technique for improved contrast. Jesse Yen (University of Southern California, 1042 Downey Way, Los Angeles, CA 90089, USA, jesseyen@usc.edu), Chi Seo (University of Southern California, 1042 Downey Way, Los Angeles, CA 90089, USA, chiseo@usc.edu)

We propose a method to use dual apertures or dual apodization functions to reduce side lobes and clutter for ultrasound imaging. Using a common transmit aperture but different receive apodizations or apertures, we create two point spread functions with very similar main lobes and different side-lobe and clutter signals. Main lobe signals can be distinguished from clutter signals using normalized cross-correlation of the raw radio-frequency data. The normalized cross-correlation coefficient is used as a pixel-by-pixel weighting to pass main-lobe signals and suppress side lobe and clutter

signals. Main lobe signals will have a high cross-correlation coefficient near 1 and clutter signals will have coefficients between 0 and -1. Point target simulations show a narrowing of the main beam compared to conventional beamforming at beamwidths -20 dB and lower. Using a 5 MHz 128-element linear array, improvements of contrast-to-noise ratio (CNR) of an anechoic cyst compared to delay and sum beamforming exceed 130% in both simulations and experiments. We also evaluated this method for robustness in the presence of phase aberration. Aberrators ranging from 25-45 ns rms with correlation lengths of 3-5 mm were used. Here, improvements in CNR also exceed 100% in many cases.

3:00

5pBB4. Nonlinear ultrasonic imagery of high contrast objects. Régine Guillermin (Laboratory for Mechanics and Acoustics CNRS, 31 chemin Joseph Aiguier, 13009 Marseille, France, guillermin@lma.cnrs-mrs.fr), Philippe Lasaygues (Laboratory for Mechanics and Acoustics CNRS, 31 chemin Joseph Aiguier, 13009 Marseille, France, lasaygues@lma.cnrs-mrs.fr)

This study is concerned whith the ultrasonic imagery of elastic materials like cylinders or tubes by diffraction tomography technic. The aim of this work is then to solve a nonlinear inverse scattering problem. Various methods can be employed, generally involving a minimization of the differences between modeling data and measurements. The Distorted Born Iterative (DBI) method belongs to the class of algebraic reconstruction algorithms and have therefore been investigated in literature. Very promising results have been obtained both on synthetic and experimental data especially for electromagnetic inverse diffraction problems, but as far as the authors know few ultrasonic experimental results are available. This method was developed to increase the domain of application of the Born approximation to high contrast targets. Iterations are performed numerically solving a forward and an inverse problems at every iteration. This yields quantitative information about the scatterer, such as the speed of sound. Inversions of both numerical and experimental data are presented.

3:20

5pBB5. Inverse scattering in modern ultrasound imaging. Francesco Simonetti (Imperial College London, Department of Mechanical Engineering, South Kensington Campus, SW7 2AZ London, UK, f.simonetti@imperial.ac.uk)

Progress in solid state electronics and sensor manufacturing has led to the rapid development of ultrasound arrays over the last decade resulting in prototypes with thousands of transreceivers. Ultrasound scanners that use this technology are widely used in medical imaging and are based on beamforming techniques. In a similar fashion to an optical lens, the array forms an aperture which can focus and steer an ultrasound beam in space as it is done by microscopes and telescopes. The beamforming process can be seen as an inverse scattering problem whereby the scattering measurements are used to reconstruct the structure of the object being probed. To achieve this, a model that describes the interaction of the probing wave with the object is required. Beamforming assumes that scattering events occurring at different locations within the object are independent of each other, thus neglecting multiple scattering. Here, it is argue that accounting for more accurate wave-matter interaction models in the inverse scattering problem leads to greater image quality than that obtained with conventional beamforming. Experimental images with unprecedented resolution beyond the classical diffraction limit are presented along with tomographic reconstructions of a complex 3D breast phantom that show striking similarities with x-ray CT.

3:40

5pBB6. Deconvolution of freehand 3D ultrasound data using improved reconstruction techniques in consideration of ultrasound point spread functions. Holger J. Hewener (Fraunhofer IBMT, Ensheimer Strasse 48, 66386 Sankt Ingbert, Germany, holger.hewener@ibmt.fraunhofer.de), Robert M. Lemor (Fraunhofer IBMT, Ensheimer Strasse 48, 66386 Sankt Ingbert, Germany, robert.lemor@ibmt.fhg.de)

Medical ultrasound data suffers from blur caused by the volume expansion of the pressure field of the mechanical wave. This blur is dependent on the used excitation pulse and focusing of the ultrasonic wave and can therefore be examined. In order to improve the overall system resolution for 3D ultrasound reconstructions we have to know this signal degeneration to compensate it using deconvolution techniques or multicode compounding during the volume reconstruction step. Looking at the ultrasound transfer function we can focus on the simulation and measurement of the "point spread function" especially in the lateral and elevational direction. To understand its effects on a 3D reconstruction we compute a simulation of freehand-ultrasound slices based on synthetic phantom structures and given US parameters. Computing a 3D reconstruction of these simulated slices we are able to optimize the reconstruction algorithm itself to archive better resolution in the volume data sets considering ultrasound parameters like beamforming and the excitation pulses.

4:00-4:20 Break

4:20

5pBB7. Noninvasive monitoring of mesenchymal stem cells by 1.2 GHz acoustic microscopy. Moritz Von Buttlar (Institute of Experimental Physics II, University of Leipzig, Linnéstr. 5, 04103 Leipzig, Germany, vbuttlar@physik.uni-leipzig.de), Evgeny Twerdowski (Institute of Experimental Physics II, University of Leipzig, Linnéstr. 5, 04103 Leipzig, Germany, twerdowski@physik.uni-leipzig.de), Reinhold Wannemacher (Institute of Experimental Physics II, University of Leipzig, Linnéstr. 5, 04103 Leipzig, Germany, wannemacher@physik.uni-leipzig.de), Wolfgang Grill (Institute of Experimental Physics II, University of Leipzig, Linnéstr. 5, 04103 Leipzig, Germany, grill@physik.uni-leipzig.de)

Cell-based therapies can benefit from noninvasive and marker-free monitoring techniques for living cells. For this purpose a phase-sensitive scanning acoustic microscope operating at a frequency of 1.2 GHz was combined with a commercial confocal laser scanning microscope. The system is equipped with a live-support system for the long-term observation of living cells. Confocal acoustic imaging with phase and magnitude contrast and confocal laser scanning microscopy can be performed simultaneously. Both techniques are used in reflection from opposing sides of the object. Time-lapsed acoustic microscope images of ovine mesenchymal stem cells are presented. For this purpose, a pseudo-3D representation is generated by encoding the unwrapped phase in the height and the magnitude in the brightness. In the case of highly reflective substrates and sufficiently low reflection from the interface between the cells and the surrounding fluid the echo from the top of the cells can be neglected and the phase contrast image can be transformed to a time-of-flight image. In the same approximation the magnitude image provides information about the gradual extinction of the echo signal due to absorption in the cells. The two images can be combined to generate a new form of contrast representing the product of the absorption coefficient and the velocity of sound inside the observed cells.

4:40

5pBB8. Transverse vibration of prestressed beams: An experimental technique for the determination of dynamic viscoelastic material properties of tissue mimicking materials. Yigit Yazicioglu (Middle East Technical University, Orta Dogu Teknik Universitesi, Makine Muhendisligi Bolumu B-313, 06531 Ankara, Turkey, yigit@metu.edu.tr), Bryn A. Martin (University of Illinois at Chicago, 2923 W. 71st Street, Woodridge, IL 60517, USA, flux@ebryn.com), Karen Navarro-Castillo (University of Illinois at Chicago, 842 W. Taylor St. ERF 1072, Chicago, IL 60607, USA, knc_001@yahoo.com.mx), Umit Kutluay (Tubitak-Sage, Samsun Yolu 25.Km, Tilkicak Tepe Mevkii P.K.16, 06261 Ankara, Turkey, ukutluay@sage.tubitak.gov.tr), Thomas J. Royston (University of Illinois at Chicago, 842 W. Taylor St. ERF 1072, Chicago, IL 60607, USA, troyston@uic.edu)

An experimental dynamic material property identification technique is presented that is based on the theoretical formulations of a vibrating prestressed beam. The technique determines the viscoelastic material properties of tissue mimicking materials that govern their dynamic behavior. Results are presented for silicone-based materials (Sylgard 184, Dow Corning, Midland, MI) that are formed in the lab using a range of mixing ratios and cast in the form of a thick string held between fixed supports under tensile pre-

stress. The specimens are excited through the transverse harmonic displacement of the boundary. Transverse vibration at an arbitrary location is measured and compared with theory to identify material viscoelastic moduli valid up to at least several hundred Hertz. The presented technique can aid in providing accurate viscoelastic parameter values for phantoms that are used in the development of a range of medical diagnostic techniques that attempt to identify pathology or tissue differentiation via changes in mechanical stiffness and viscosity.

5:00

5pBB9. Air-borne and tissue-borne sensitivity of skin-radiation acoustic sensors. Matias Zanartu (School of Electrical and Computer Engineering, Purdue University, 206 South Martin Jischke Drive, West Lafayette, IN 47907, USA, mzanartu@purdue.edu), Julio C. Ho (Weldon School of Biomedical Engineering, Purdue University, 206 South Martin Jischke Drive, West Lafayette, IN 47907, USA, hoj@purdue.edu), Steve Kraman (Department of Internal Medicine, University of Kentucky, 740 South Limestone Street, Lexington, KY 40536, USA, sskram01@email.uky.edu), Hans Pasterkamp (Department of Pediatrics and Child Health, University of Manitoba, CS516-840 Sherbrook St, Winnipeg, MB R3A 1S1, Canada, pasterkamp@umanitoba.ca), Jessica E. Huber (Department of Speech, Language, and Hearing Sciences, Purdue University, 500 Oval Drive, West Lafayette, IN 47907, USA, jhuber@purdue.edu), George R. Wodicka (Weldon School of Biomedical Engineering, Purdue University, 206 South Martin Jischke Drive, West Lafayette, IN 47907, USA, wodicka@purdue.edu)

Measurements of body sounds on the skin surface have been widely used in the medical field and continue to be a topic of current research, ranging from the diagnosis of the respiratory and cardiovascular diseases to the monitoring of voice dosimetry. These measurements are normally acquired by means of light-weight accelerometers and/or air-coupled microphones attached to the skin. Such recordings can be corrupted by air-borne sounds that are generated by the subject or by other sources of background noise. In this project, the sensitivity of various commonly used bioacoustic sensors to airborne sounds was evaluated and compared with their sensitivity to tissue-borne body sounds. To delineate the sensitivity to each pathway, the sensors were first tested in-vitro, and then on human subjects. The results indicated that in many cases the air-borne sensitivity is sufficiently high to significantly corrupt body sound signals. The effectiveness of different air-borne insulation devices was also evaluated. Spectral analysis showed that simple acoustic insulators (e.g., passive hearing protectors) provide significant attenuation within the range of frequencies of interest for most applications, particularly when using air-coupled microphones.

FRIDAY AFTERNOON, 4 JULY 2008 ROOM 252A, 2:00 TO 6:20 P.M.

Session 5pNSa

Noise, ASA Committee on Standards, Architectural Acoustics, and EURONOISE: Classroom Acoustics II

Louis C. Sutherland, Cochair
Consultant in Acoustics, 27803 Longhill Dr., Rancho Palos Verdes, CA 90275-3908, USA

Luigi Maffei, Cochair
Built Environment Control Laboratory Ri.A.S., Second University of Naples, Abazia di S. Lorenzo, Aversa, 81031, Italy

David Lubman, Cochair
DL Acoustics, 14301 Middletown Lane, Westminster, CA 92683, USA

Invited Paper

2:00

5pNSa1. Are classrooms in historical buildings compatible with good acoustics standards? Luigi Maffei (Built Environment Control Laboratory Ri.A.S., Second University of Naples, Abazia di S. Lorenzo, 81031 Aversa, Italy, luigi.maffei@unina2.it), Gino Iannace (Built Environment Control Laboratory Ri.A.S., Second University of Naples, Abazia di S. Lorenzo, 81031 Aversa, Italy, gino.iannace@unina2.it), Massimiliano Masullo (Built Environment Control Laboratory Ri.A.S., Second University of Naples, Abazia di S. Lorenzo, 81031 Aversa, Italy, ing.masullo@libero.it)

Many surveys and researches have underlined that the acoustic characteristics of classrooms are strictly connected to performances of students and to the stress of the teachers during lessons. In standard classrooms sound quality can be easily reached without sound amplification but introducing appropriate sound absorbing/scattering materials at the ceiling and/or at the vertical walls. Nevertheless in historical buildings with vaults or trusses, high walls and many architectural restrictions imposed by district superintendent, it could be very difficult to achieve good acoustics standards with widespread solutions. In this paper the acoustic performances of different classrooms in an historical Monastery actually center of the Faculty of Architecture of the Second University of Naples are analysed. After these analysis, compatible architectural and acoustic solutions to improve the sound quality were developed and tested in laboratory measurements and then applied in some classrooms to verify the benefits.

Contributed Paper

5pNSa2. Results of acoustical treatments in existing classrooms. Arianna Astolfi (Politecnico di Torino, Department of Energetics, Corso Duca degli Abruzzi, 24, 10129 Turin, Italy, arianna.astolfi@polito.it), Alessia Griginis (Onleco srl, Via Pigafetta, 3, 10129 Turin, Italy, griginis@onleco.com)

In 2001, 2002, and 2005, the Department of Energetics of the Politecnico di Torino has carried out in-field objective and subjective surveys with the aim of evaluating the acoustical quality in secondary-school classrooms of the Province of Turin (Italy). From the results the following main problems emerged: high reverberation times, high background noise levels caused mainly by low sound insulation between classrooms and corridors and between adjacent classrooms, low façade sound insulation, excessive teachers' vocal efforts. In this work results of acoustical treatments in some of these existing classrooms are reported. Measurements are made before and after the restorations. The case studies are chosen with reference to different building typologies and urban contexts, and consisted of improvements in sound absorption, sound insulation of internal partitions, doors and façades, and acoustic bridges elimination. They are divided in "light" and "heavy" types. The first, less expensive, with the aim to obtain good acoustical conditions, the latter, more expansive, focused to obtain optimal conditions. In fact, mainly in restoration of public schools, a good level of acoustical quality with contained costs is requested. The treatments are carried out with the aim to constitute a repertory of solutions to apply primarily in school restoration.

Invited Papers

2:40

5pNSa3. Speech perception in classroom noise and reverberation by children with typical and impaired hearing - Preliminary results. Frank Iglehart (Clarke School for the Deaf, 47 Round Hill Road, Northampton, MA 01060, USA, figlehart@clarkeschool.org)

A child's ability to perceive speech in the classroom influences academic progress. In this study, students with a various degrees of hearing loss perceive spoken words in sentences in a classroom. The room contains multiple noise levels and reverberation times (RTs). Classroom reverberation is measured using standardized procedures (with slight modifications to ASTM C423-02a: X2). RTs are controlled by quantities of acoustic panels in the room. Using the BKB-SIN Test, the speech-to-noise ratio at which the students perceive 50% words correctly (i.e., SNR-50) are measured in three reverberant conditions. Data collected to date indicate that students with severe-to-profound hearing loss (n=15; ages 8-16 years) demonstrated average SNR-50s of +12 dB (SD=4), +13 dB (SD=4), and +17 dB (SD=4) for conditions of 0.3, 0.6 and 0.9 s RT, respectively. Students with typical hearing (n=14; ages 8-16 years) had SNR-50s that averaged -4 dB (SD=2), -3 dB (SD=2) and -2 dB (SD=2), respectively. Performance/intensity curves are also calculated in order to estimate minimal optimal listening conditions for each RT. This is an ongoing study. The session presentation will include emerging data on children with other degrees of hearing loss.

3:00

5pNSa4. Vocal symptoms in preschool teachers and the working environment. Valdis Inigbjörg Jonsdottir (Tad er Malid, Furuvellir 13, 601 Akureyri, Iceland, valdisj@ismennt.is)

Research has shown that teachers experience a high risk of developing voice problems. Noise levels in classrooms with young children are higher than in classrooms with older students, indicating preschool teachers' voices may be at greater risk. Questionnaires were sent to 88 preschool teachers in five preschools in Akureyri, and the parents of the 424 children in daycare. The study was aimed to obtain information about (1) teachers: experienced vocal symptoms, occurrence of vocal symptoms, opinions on working environment; air quality, noise, heat, acoustics. (2) parents: children's hearing problems. The study also aimed to ascertain noise levels and reverberation time in pre-school classrooms, and to compare teachers' reported ages, teaching experience, vocal symptoms and frequency with findings in other studies. Sound and reverberation-time measurements were taken by the Icelandic Department of Occupational Health and Safety. Reported vocal symptoms were more common among preschool teachers than other teachers, even though their youth and lack of teaching experience was marked. They appeared to be workrelated. 40% of the children had a history of hearing problems. Noise levels measured were very high. Correlation was found between voice fatigue and high temperature, bad indoor air, and poor acoustics.

3:20

5pNSa5. Acoustical requirements of classrooms and new concepts of teaching. Kurt Eggenschwiler (Empa, Laboratory of Acoustics, Ueberlandstrasse 129, CH-8600 Duebendorf, Switzerland, kurt.eggenschwiler@empa.ch), Markus Cslovejcsek (School of Teacher Education at the University of Applied Sciences FHNW, Kuettigerstrasse 42, CH-5000 Aarau, Switzerland, markus.cslovjecsek@fhnw.ch)

In recent years acoustic requirements for classrooms were published in various guidelines. Of course it is important that the present knowledge will be implemented, but how should this be done? And what is the correspondence of acoustic requirements and new concepts of learning? These questions are the basis of a cooperation of the Laboratory of Acoustics at Empa, Dübendorf and the School of Teacher Education, Aarau in Switzerland. The cooperation itself is one possibility to transfer knowledge. In addition it was planned but not yet realized to develop concepts of knowledge transfer by student work (diploma thesis). Classroom acoustics were discussed in seminars and there were completed some diploma theses. One project dealt with the acoustic problems of a new teaching concept. Part of the concept is that teaching of four groups of pupils takes place in three classrooms and in the corridor. The doors of the classrooms remain open and at the same time pupils work individually, in groups, and a small group is instructed by a teacher. There were found suggestions for improving the acoustics, but for different reason the realization was not possible.

3:40

5pNSa6. An Ambiophonics system for the study of intelligibility in the virtual classrooms. Nicola Prodi (Engineering Dept. - Univ. of Ferrara, Via Saragat, 1, 44100 Ferrara, Italy, nicola.prodi@unife.it), Andrea Farnetani (Engineering Dept. - Univ. of Ferrara, Via Saragat, 1, 44100 Ferrara, Italy, andrea.farnetani@unife.it), Patrizio Fausti (Engineering Dept. - Univ. of Ferrara, Via Saragat, 1, 44100 Ferrara, Italy, patrizio.fausti@unife.it), Roberto Pompoli (Engineering Dept. - Univ. of Ferrara, Via Saragat, 1, 44100 Ferrara, Italy, roberto.pompoli@unife.it)

In recent years the investigations on the intelligibility has profited by the increasing efficiency of the simulation and rendering technologies of virtual acoustics. In particular the latest systems are well suited to reproduce sound fields whose tridimensional characteristics are quite close to the real ones both objectively and subjectively. In this framework the Ambiophonics system, consisting of the merging of a double stereo-dipole and of an first order Ambisonics system, has gained particular attention. In the configuration used in this work the system employs twelve loudspeakers and is fed either with measured binaural and B-format data or by simulated ones. Based on this apparatus listening tests have been prepared in the Italian language to investigate the acoustics of classrooms and to focus on the effect of the directional characteristics of noise (i.e., fan-coils or tapping from the upper floor) on the intelligibility of words. The whole apparatus is driven by a Labview application which has also the aim of collecting the responses by the testers.

4:00-4:20 Break

4:20

5pNSa7. Noise - A stress factor? Acoustic ergonomics at schools. Gerhart Tiesler (University of Bremen/ISF, Grazer Str. 4, D-28359 Bremen, Germany, tiesler@uni-bremen.de), Markus Oberdoerster (Saint-Gobain Ecophon GmbH, Taschenmacherstr. 8, D-23556 Luebeck, Germany, markus.oberdoerster@ecophon.de)

Description of teaching reality is the main topic of this interdisciplinary examination about "acoustic ergonomics of schools." In the first step we analyse how different teaching methods affect basic noiselevel and working noise level. Which effect has an altered room acoustics on the sound levels in the context of each teaching method. The data records available as timeseries allows for the first time analysing single phases of lessons, which are characterized by certain pedagogical characteristics or individual instruction phases. Is it correct to speak of "noise stress" or is this stress an emotional reaction to the kind of? Based on recordings of teachers heartrate we analyse in the third step the effects of noise level on the workload of the teachers as a stress reaction. A distinction is made on the subject of different teaching methods, and on the basis the different room acoustic conditions. In one primary school we had four classes with a RT$>$0.5 s and four further classes with a RT$<$0.5s. At a second primary school we analysed the effect of the room acoustic refurbishment. Finally we investigate factors of fatigue. Which effect has CO_2 in the classroom on all people, and the working noise level?

4:40

5pNSa8. Acoustical evaluation of nonclassroom university learning spaces. Murray Hodgson (The University of British Columbia, Department of Electrical and Computer Engineering, 2332 Main Mall, Vancouver, BC V6T 1Z4, Canada, mhodgson@interchange.ubc.ca), Jorge Garcia Moreno (The University of British Columbia, Department of Electrical and Computer Engineering, 2332 Main Mall, Vancouver, BC V6T 1Z4, Canada, 123calabaza@gmail.com)

This paper reports the results of an acoustical evaluation of non-classroom learning spaces at UBC. In twelve buildings, 25 indoor spaces -- a restaurant, a cafeteria, libraries, dedicated study spaces, building atria, etc. -- used for learning activities by at least 50 people were studied. The evaluation involved physical and acoustical (reverberation time, sound propagation, Speech Intelligibility Index) measurements, and occupant activity and satisfaction questionnaires. Questionnaires were administered three times (morning, lunchtime, and afternoon) on one day. The questionnaires asked about satisfaction with, and the effects of, the acoustical and nonacoustical environments. The acoustical measurement results were compared with established acceptability criteria. Questionnaires were analyzed for differences between times of day, test space, etc. The questionnaire responses and acoustical-measurement results were correlated. Using both as possible predictors, multivariable-regression models for predicting and explaining occupant satisfaction with, and the effects of, the acoustical environment were developed.

5:00

5pNSa9. The effect of amplification on children's performance in the classroom. Bridget M. Shield (London South Bank University, Borough Road, SE1 0AA London, UK, shieldbm@lsbu.ac.uk), Julie E. Dockrell (Institute of Education, 25 Woburn Square, WC1H 0AA London, UK, j.dockrell@ioe.ac.uk)

The use of amplification systems in the classroom has the potential to reduce the impact of poor classroom acoustics for typically developing pupils and those with special educational needs (SENs). The immediate benefits of amplified acoustic signals on the performance of 253 primary school children, including 24 children with special needs, were examined. All participants were familiar with the use of the amplification systems. Children's performance was assessed on two verbal measures (spelling and oral comprehension) and one non-verbal measure, using a balanced repeated measures design. It was predicted that the effects of amplification would be evident for spelling and oral language comprehension, but that there would be no discernable effect on speed of processing. Children with SEN were expected to have an added advantage with amplification. The predictions were partially supported. Both gain score analysis and ANOVAs of performance scores with amplification, controlling for performance without amplification, revealed an effect on spelling only for the typically developing children, while children with SENs benefited in both the spelling and the oral comprehension tasks. When installed appropriately, amplification improves children's ability to decode single words; SEN children also benefit in terms of their ability to process oral input.

5:20

5pNSa10. Soundfield amplification is a poor substitute for good classroom acoustics. David Lubman (DL Acoustics, 14301 Middletown Lane, Westminster, CA 92683, USA, dlubman@dlacoustics.com), Louis C. Sutherland (Consultant in Acoustics, 27803 Longhill Dr., Rancho Palos Verdes, CA 90275-3908, USA, lou-sutherland@juno.com)

Soundfield (amplification) systems are widely and often aggressively marketed for small classrooms. In June 2006, the Acoustical Society of America (ASA) issued a public position statement on the use of sound amplification in typical small classrooms http://asa.aip.org/amplification.pdf. This paper attempts to explain why the ASA found that soundfield systems are poor substitutes for good acoustics. Good acoustics for learning requires unoccupied classroom noise levels of 35 dBA or less and midfrequency reverberation times of 0.6 s or less. At the same time, it is recognized that centralized amplifiers and sound distribution systems can provide valuable educational benefits in small classrooms with good acoustics. Such systems are useful for multimedia presentations and voice reinforcement. The authors urge that this message be brought to the attention of educators and educational facility decision makers.

Contributed Papers

5:40

5pNSa11. Subjective evaluation of acoustical quality of lecture rooms with respect to the quality of the sound reinforcement system and the level of background noise. Sanja Grubesa (Faculty of EE and Computing, Unska 3, Department of Electroacoustics, HR-10000 Zagreb, Croatia, sanja.grubesa@fer.hr), Marko Horvat (Faculty of EE and Computing, Unska 3, Department of Electroacoustics, HR-10000 Zagreb, Croatia, marko.horvat@fer.hr), Hrvoje Domitrovic (Faculty of EE and Computing, Unska 3, Department of Electroacoustics, HR-10000 Zagreb, Croatia, hrvoje.domitrovic@fer.hr)

As a part of a general questionnaire on the quality of lecturing on the Faculty of EE and Computing in Zagreb, Croatia, the students have to grade the acoustical quality of lecture rooms in an indirect way by giving answers to several questions included in that questionnaire. As the sound reinforcement system in two largest lecture halls is in rather bad condition, it is to be replaced in the near future with a new one of significantly better quality. The goal of this paper is to examine whether this change is reflected in the grades of acoustical quality given by the students. In the second part of the paper, the students' grades on acoustical quality of two smaller lecture rooms of identical size and acoustic treatment are compared. The comparison is made with respect to the position of these rooms relative to the nearby street as the source of traffic noise. The overall level and spectral content of noise are measured in those lecture rooms. The correlation is then examined between the results of these measurements and the grades given by the students.

6:00

5pNSa12. Education vs cost - Difficulties in implementing acoustical design standards in classrooms. Patricia M. Scanlon (Cerami & Associates, 404 Fifth Avenue, New York, NY 10018, USA, pscanlon@ceramiassociates.com), James Perry (Cerami & Associates, 404 Fifth Avenue, New York, NY 10018, USA, jperry@ceramiassociates.com), Victoria J. Cerami (Cerami & Associates, 404 Fifth Avenue, New York, NY 10018, USA, vcerami@ceramiassociates.com)

Good acoustical design standards for classrooms are established - quiet background noise levels due to mechancial systems and exterior sources, use of absorptive finishes to control reverberation, walls, doors and floors able to control airborne and impact noise transmission. So why do so many schools fail to follow these guidelines? Are private schools even less likely to adhere to these standards? What are the construction and equipment options? We will discuss various educational standards, as well as the reticence of school planners to comply. We will discuss what schools often build, versus what one might say they should build, together with cost comparison. We will review case studies where guidelines were, and were not, followed - examples that reflect the acoustician's mission to educate educators on the value of acoustical design considerations in classrooms.

Session 5pNSb

Noise, Structural Acoustics and Vibration, Physical Acoustics, and EURONOISE: Sound and Vibration from Explosions in Air II

Roger Waxler, Cochair
University of Mississippi, NCPA, 1 Coliseum Drive, University, MS 38677, USA

Keith Attenborough, Cochair
Open University, Department of Design, Development, Materials and Environment, Walton Hall, Milton Keynes, MK7 6AA, UK

Invited Papers

2:00

5pNSb1. High-altitude infrasound calibration experiments. Henry E. Bass (The University of Mississippi - NCPA, 1 Coliseum Drive, University, MS 38677, USA, pabass@olemiss.edu), Eugene T. Herrin (Southern Methodist University, P. O. Box 750395, Dallas, TX 75275, USA, herrin@passion.isem.smu.edu), Paul Golden (Southern Methodist University, P. O. Box 750395, Dallas, TX 75275, USA, pgolden@mail.smu.edu), Robert Woodward (Incorporated Research Institutions for Seismology, 1200 New York Avenue, NW, Suite 800, Washington, DC 20005, USA, woodward@iris.edu), Douglas Drob (Naval Research Laboratory, Space Science Division, 4555 Overlook Avenue, Washington, DC 20375, USA, douglas.drob@nrl.navy.mil), Michael A. Hedlin (University of San Diego California, Scripps Institute of Oceanography, 9500 Gilman Drive, La Jolla, CA 92093, USA, hedlin@ucsd.edu), Catherine De Groot-Hedlin (University of San Diego California, Scripps Institute of Oceanography, 9500 Gilman Drive, La Jolla, CA 92093, USA, cdghedlin@gmail.com), Kris Walker (University of San Diego California, Scripps Institute of Oceanography, 9500 Gilman Drive, La Jolla, CA 92093, USA, walker@ucsd.edu), Milton Garces (Infrasound Laboratory, University of Hawaii, 73-4460 Queen Kaahumanu Highway #119, Kailua-Kona, HI 96740, USA, milton@isla.hawaii.edu), Curt Szuberla (University of Alaska, 903 Koyukuk Drive, Fairbanks, AK 99775, USA, cas@gi.alaska.edu), Rod Whitaker (Los Alamos National Laboratory, EES-2 MS J577, Los Alamos, NM 87545, USA, rww@lanl.gov)

At the 152nd Meeting of the Acoustical Society of America, Andre and Bass reported an infrasound experiment conducted at White Sands Missile Range during the 2005-2006 time frame. The experiment consisted of exploding a 22.4 kg charge at altitudes from 31.3 km to 49.6 km then recording the waveforms at 30 infrasound arrays (not all at the same time) at distances up to 1200 km from the source. The analysis is not yet complete but some preliminary observations have been reported in the most recent issue of Acoustics Today. This talk will summarize the findings published in Acoustics Today and offer suggestions to others who might want to access and analyze the data.

2:20

5pNSb2. Infrasonic and seismic signals from explosions in Northwestern Europe. Laeslo G. Evers (Royal Netherlands Meteorological Institute (KNMI), PO Box 201, 3730 AE De Bilt, Netherlands, evers@knmi.nl), Hein Haak (Royal Netherlands Meteorological Institute (KNMI), PO Box 201, 3730 AE De Bilt, Netherlands, haak@knmi.nl)

Large explosions often generate both seismic and infrasound signals that can be detected over large ranges, i.e., hundreds of kilometers. Ground truth of such explosions is available from direct observations and/or seismic signals and can be used to get insight in the propagation of infrasound. Long range infrasound propagation is controlled by the state of the atmosphere. Tropospheric, stratospheric, and thermospheric ducts might exist and have implications on the signal characteristics and their detectability. In this study, we will show results of studies on explosions in Northwestern Europe using both seismic and infrasound data. These observations are used to derive source characteristics like: location, origin time and yield. Furthermore, the propagation characteristics of infrasound will be addressed.

2:40

5pNSb3. Infrasound propagation in the zone of silence. Paul Golden (Southern Methodist University, P. O. Box 750395, Dallas, TX 75275, USA, pgolden@mail.smu.edu), Petru Negraru (Southern Methodist University, P. O. Box 750395, Dallas, TX 75275, USA, pnegraru@smu.edu), Eugene T. Herrin (Southern Methodist University, P. O. Box 750395, Dallas, TX 75275, USA, herrin@passion.isem.smu.edu)

Two controlled source experiments were conducted in Nevada in 2006 and 2007 to study infrasound signal propagation at distances less than 300 km from the source. In 2006 three temporary infrasound arrays were deployed at distances of 76, 108, and 157 from the source. In 2007 the site at 157 km was reoccupied, and data was also recorded at 288 km from the source. Interesting results were derived from the travel time analysis. In 2006 the site at 76 km recorded both tropospheric and stratospheric arrivals, while at 108 and 157 km only stratospheric arrivals were recorded. In 2007 the site at 157 km recorded both tropospheric and stratospheric arrivals, while at 288 km both stratospheric and thermospheric arrivals were recorded. Atmospheric modeling with the InfraMAP software failed to predict returning rays or pressure levels similar to the observed data. Because of the large amplitude variations we attempt to estimate the yields of the explosions using the predominant frequency content of the signals. The physical basis for such a method is found in an increased acoustic transit time of the explosion blast radius with increased yield. Preliminary results suggest this is possible.

3:00

5pNSb4. Validating upper-wind models using infrasound from active volcanoes. Alexis Le Pichon (CEA-DASE, Arpajon Cedex, 91297 Bruyères-le-Châtel, France, alexis.le-pichon@cea.fr), Karl Antier (CEA-DASE, Arpajon Cedex, 91297 Bruyères-le-Châtel, France, karl.antier@cea.fr), Sylvie Vergniolle (Institut de Physique du Globe, 4 Place Jussieu, 75252 Paris, France, vergniolle@ipgp.jussieu.fr), Michel Lardy (IRD Center, BPA5, Cedex, 98848 Noumea, New Caledonia, lardy@noumea.ird.nc), Douglas Drob (Naval Research Laboratory, Space Science Division, 4555 Overlook Avenue, Washington, DC 20375, USA, douglas.drob@nrl.navy.mil)

Known and quasipermanent infrasonic sources are needed to evaluate and improve upper-wind models. Infrasounds generated by active volcanoes offer a unique opportunity for atmospheric studies. The Yasur volcano in the Vanuatu archipelago is an outstanding source of infrasonic waves due to its regular activity. This volcano is permanently monitored by the IS22 infrasound station located in New Caledonia and by one microbarometer installed close to its crater. A five-year monitoring period of Yasur at short and large propagation range provides new insights on quantitative relationships between infrasonic observables and atmospheric specifications. This experimental setting is proposed to validate consistently the Naval Research Laboratory Ground to Space (NRL-G2S) semi-empirical atmospheric model up to the stratosphere. The propagation modeling results accurately explain seasonal changes as well as small short-timescale variations of the infrasonic observables. This study demonstrates that the use of appropriate propagation tools along with the NRL-G2S specifications provides accurate enough results for most of the long-range observations for the purpose of operational infrasound monitoring.

3:20

5pNSb5. Semianalytical modeling of plate flexural waves generated by laser-initiated air shock waves. Vasil B. Georgiev (Loughborough University, Department of Aeronautical and Automotive Engineering, Ashby Road, LE11 3TU Loughborough, UK, V.Georgiev@lboro.ac.uk), Victor V. Krylov (Loughborough University, Department of Aeronautical and Automotive Engineering, Ashby Road, LE11 3TU Loughborough, UK, V.V.Krylov@lboro.ac.uk), Qin Qin (University of Hull, Department of Engineering, Cottingham Road, HU6 7RX Hull, UK, q.qin@hull.ac.uk), Keith Attenborough (Open University, Department of Design, Development, Materials and Environment, Walton Hall, MK7 6AA Milton Keynes, UK, Keith.Attenborough@ioa.org.uk)

The paper describes the results of the semianalytical modeling of the interaction of laser-initiated air shock waves with an infinite elastic plate. The impact of the incident shock wave on the plate has been approximated by an equivalent cylindrically diverging surface force resulting from the combined surface pressure of the incident and reflected shock waves. This force has been then represented in the wave number-frequency domain by means of Hankel and Fourier transforms which have been carried out numerically - and the problem has been solved using the Green's function method applied to an infinite plate. The resulting frequency spectra and time histories of the generated flexural wave pulses have been calculated for different values of laser pulse energy and for different heights of the laser beam focusing above the plate surface. The obtained theoretical results have been compared with the results of the reduced-scale model experiments on shock wave interaction with the ground in which large plastic and wooden plates have been used to represent the ground surface. The comparison shows that the obtained semi-analytical results are in good agreement with the experimental ones.

3:40

5pNSb6. Ground effects on sound and vibration from explosions. Christian Madshus (NGI, P.O. Box 3930 Ullevaal Stadion, Sognsveien 72, 0806 Oslo, Norway, cm@ngi.no), Finn Løvholt (NGI, P.O. Box 3930 Ullevaal Stadion, Sognsveien 72, 0806 Oslo, Norway, flo@ngi.no), Ra Cleave (NGI, P.O. Box 3930 Ullevaal Stadion, Sognsveien 72, 0806 Oslo, Norway, rc@ngi.no), Karin Rothschild (NGI, P.O. Box 3930 Ullevaal Stadion, Sognsveien 72, 0806 Oslo, Norway, kmr@ngi.no), Zenon Cetina-Medina (NGI, P.O. Box 3930 Ullevaal Stadion, Sognsveien 72, 0806 Oslo, Norway, zmc@ngi.no)

Low frequency sound from military activity and explosions do propagate over large distances. The sound pressure may induce substantial vibration in the ground and particularly in buildings. Such vibrations turn out to be a major cause of complaints among neighbouring communities around training fields and blast sites. We will present investigations on long range propagation of low frequency sound and sound-induced vibration, based on a substantial amount of data collected during a series of full scale tests performed in Norway over the last 14 years. All data are assembled in the NORTRIAL database, which is now publicly available. Meteorology and ground interaction largely influence the sound propagation and vibration response. At low frequency meteorological- and ground effects may intricately interact and lead to large, apparently random variability in sound pressure at large distances. Statistically based investigations on the sound propagation and its variability will be presented. Particular focus will be on the ground interaction effects, and a new and more extensive system for ground classification, based on cartographic data, empirical and numerical modeling will be introduced. Findings on building response to outdoor low frequency sound and transfer mechanisms from outdoor pressure to indoor sound and vibration will be presented.

4:00-4:20 Break

4:20

5pNSb7. Deducing ground structure using seismic pulses originating from an outdoor explosive source. Shahram Taherzadeh (The Open University, Faculty of Mathematics, Computing and Technology, Walton Hall, MK7 6AA Milton Keynes, UK, s.taherzadeh@open.ac.uk), Keith Attenborough (Open University, Department of Design, Development, Materials and Environment, Walton Hall, MK7 6AA Milton Keynes, UK, Keith.Attenborough@ioa.org.uk)

Near-surface layering of ground soil can influence propagation of acoustic and seismic pulses originating from above-surface sources. Simultaneous recording of acoustic air pressure and seismic radial and vertical particle velocities resulting from a small, above ground explosion is used to obtain information about soil structure near the surface. Assuming nonlinear effects to be small at the ranges

of interest here, a numerical model called Fast Field Program for Layered Air Ground Systems (FFLAGS), developed originally for continuous sound sources above a porous elastic ground is used to model a porous elastic layered ground system. Suitable optimisation methods were used to predict a set of best fit parameters for the near-surface ground structure. It is shown that the model can explain multiple seismic arrivals and give a reasonable prediction of wave speeds and layer depths while the pressure pulse can predict permeability of the surface soil.

4:40

5pNSb8. Predictions for the influence of the nocturnal jet on the long range propagation of impulsive signals. Roger Waxler (University of Mississippi, NCPA, 1 Coliseum Drive, University, MS 38677, USA, rwax@olemiss.edu), Kenneth E Gilbert (National Center for Physical Acoustics, University of Mississippi, University, MS 38677, USA, kgilbert@olemiss.edu), Carrick L. Talmadge (The University of Mississippi - NCPA, 1 Coliseum Drive, University, MS 38677, USA, clt@olemiss.edu), Xiao Di (National Center for Physical Acoustics, University of Mississippi, University, MS 38677, USA, xiaodi@olemiss.edu)

On clear nights, inland over flat ground, one generally finds a temperature inversion in the first hundred meters or so of the atmosphere. Near the ground, winds tend to be light, increasing with altitude. Above the temperature inversion one finds a stiff geostrophic wind known as the nocturnal jet. Theoretical predictions, based on ray theory and expansions in vertical modes, for the effect of the nocturnal jet on the long range propagation of impulsive signals are presented. For sufficiently short ranges, less than 3 km or so, the nocturnal jet has no effect. At these ranges only the temperature inversion and the light winds in the inversion play a role. At longer ranges the nocturnal jet significantly alters the arrival structure of the propagated signal. It is predicted that, due to coincident arrivals from the inversion and from the nocturnal jet, there is a segment of ranges about 1 km long, beginning at about 4 km, in which the amplitude of the first arrival becomes anomalously large and then splits into two distinct arrivals.

5:00

5pNSb9. The physics of pulse propagation in the nocturnal atmospheric boundary layer: measurement and theory. Carrick L. Talmadge (The University of Mississippi - NCPA, 1 Coliseum Drive, University, MS 38677, USA, clt@olemiss.edu), Roger Waxler (University of Mississippi, NCPA, 1 Coliseum Drive, University, MS 38677, USA, rwax@olemiss.edu), Kenneth E Gilbert (National Center for Physical Acoustics, University of Mississippi, University, MS 38677, USA, kgilbert@olemiss.edu), Jin So (National Center for Physical Acoustics, University of Mississippi, University, MS 38677, USA, jso@olemiss.edu), Rommel Stribling (National Center for Physical Acoustics, University of Mississippi, University, MS 38677, USA, eercs@olemiss.edu), Xiao Di (National Center for Physical Acoustics, University of Mississippi, University, MS 38677, USA, xiaodi@olemiss.edu)

A series of experiments designed to probe the effect of the nocturnal atmosphere on low-frequency (10- 500 Hz) sound propagation will be discussed, and their ramifications explored. These experiments involve detecting arrivals from a propane cannon on a vertical array of microphones 1-3 km from the source, which were collected simultaneously with meteorological experiments designed to measure the vertical temperature and horizontal wind velocity profiles. Chief among the results of these experiments is the observation of a nocturnal model structure that has a significant surface wave component at frequencies below 150 Hz. At higher frequencies and longer propagation distances ($>$1.5 km), the surface wave is not observed due to attenuation from its interaction with the ground. At higher frequencies, the model structure displays a characteristic "quiet height" first described in Waxler et al. (2006). The potential application of these results for remote sensing the atmospheric boundary layer are discussed, and contrasted with other methods of measurement of the atmospheric profile.

Contributed Paper

5:20

5pNSb10. Nonlinear parabolic equation model for finite-amplitude sound propagation in an inhomogeneous medium over a nonflat, finite-impedance ground surface. Thomas Leissing (CSTB, 24 rue Joseph Fourier, 38400 Saint-Martin-d'Hères, France, thomas.leissing@cstb.fr), Philippe A. Jean (CSTB, 24 rue Joseph Fourier, 38400 Saint-Martin-d'Hères, France, philippe.jean@cstb.fr), Jérôme Defrance (CSTB, 24 rue Joseph Fourier, 38400 Saint-Martin-d'Hères, France, jerome.defrance@cstb.fr), Christian Soize (Université de Marne la Vallée, 5, Boulevard Descartes, 77454 Marne la Vallée, France, soize@univ-mlv.fr)

A nonlinear parabolic equation (NPE) model for weakly nonlinear sound propagation in an inhomogeneous medium is described. The model being formulated in the time domain, complex impedances cannot be used to simulate ground surfaces. A second NPE model is thus derived to include the medium in the computational system. Based on a nonlinear extension of the Zwikker-Kosten model for rigidly-framed porous media, it allows to include Forchheimer's nonlinearities. Both models are then adapted to terrain-following coordinates, and used together with an interface condition, allow to simulate finite-amplitude sound propagation over a nonflat, finite-impedance ground surface. Numerical examples show that the NPE model is in good agreement with the solutions of the frequency domain boundary element method. Applications of this model to the simulation of sound propagation from explosions in air are then discussed.

Invited Papers

5:40

5pNSb11. Mean vs event sound-level prediction: obtaining consistency between atmospheric data inputs, propagation models, and the predictand. David K. Wilson (U.S. Army Engineer Research and Development Center, 72 Lyme Rd., Hanover, NH 03755-1290, USA, D.Keith.Wilson@usace.army.mil), Chris L. Pettit (U.S. Naval Academy, Aerospace Engineering Dept., 590 Holloway Rd., MS 11-B, Annapolis, MD 21402, USA, petitcl@usna.edu), Vladimir E. Ostashev (NOAA/Earth System Research Laboratory, 325 Broadway, Boulder, CO 80305, USA, vladimir.ostashev@noaa.gov), Matthew S. Lewis (U.S. Army Engineer Research and Development Center, 72 Lyme Rd., Hanover, NH 03755-1290, USA, Matthew.S.Lewis@usace.army.mil)

The following, deceptively challenging, questions are addressed: What are the most suitable atmospheric data resources and propagation models for predicting event (explosion and other short duration) sound-exposure levels? Do these differ from those most suitable for predicting mean sound levels? Atmospheric data typically consist either of single, "snapshot" samples of the vertical profiles, as from a weather balloon, or average vertical profiles, as from climatology or a numerical weather model. Recent statistical studies, based on high-resolution atmospheric simulation, demonstrate the superiority of mean profiles for prediction of *both mean and event* sound levels, even when single-sample profiles are synchronized to and collected along the path of the propagation event. Running propagation models "blind" to the nature of the atmospheric inputs is shown to be hazardous: predictions from mean profiles lack turbulent scattering, thus underestimating sound levels near the ground, whereas predictions from single-sample profiles implicitly assume the turbulence has infinite horizontal extent, thus overestimating sound levels. Some desirable consistency results from numerically solving parabolic equations (PEs) for statistical *moments* of the sound pressure, rather than conventional deterministic PEs. The moment PEs directly predict mean sound levels or the expected value and variability of event sound-exposure levels.

6:00

5pNSb12. Beam-forming and dispersion measurements at the edge of a pine forest. Michael J. White (US Army Engineer Research and Development Center, 2902 Newmark Drive, Champaign, IL 61826, USA, Michael.J.White@usace.army.mil), Michelle E. Swearingen (Norwegian Defense Research Establishment/US Army, Postboks 25, 2027 Kjeller, Norway, michelle.swearingen@ffi.no)

Beam-forming analyses were performed on four-microphone linear arrays placed just within the interior of a pine forest to separate signal arrivals by direction from an impulsive sound source in an open field. The arrays were deployed in three configurations: transverse, longitudinal, and vertical. The arrays spacings were organized in a pattern that provides six baselines with four microphones. Longitudinal and transverse configurations show arrivals scattered from trunks, and the vertical configurations indicate some refraction and scattering by the canopy. Signal dispersion curves developed using the four-microphone arrays had greater variation in trace velocity at higher frequencies in each configuration.

FRIDAY AFTERNOON, 4 JULY 2008 ROOM 251, 4:20 TO 6:20 P.M.

Session 5pNSc

Noise and EURONOISE: Propagation and Urban Noise II

Jérôme Defrance, Chair
CSTB, 24 rue Joseph Fourier, Saint-Martin-d'Hères, 38400, France

Contributed Papers

4:20

5pNSc1. Road traffic noise from viaducts in mountainous areas. Jérôme Defrance (CSTB, 24 rue Joseph Fourier, 38400 Saint-Martin-d'Hères, France, jerome.defrance@cstb.fr), Matthieu Beyret (CSTB, 24 rue Joseph Fourier, 38400 Saint-Martin-d'Hères, France, matthieu.beyret @cstb.fr), Marine Baulac (CSTB, 24 rue Joseph Fourier, 38400 Saint-Martin-d'Hères, France, marine.baulac@cstb.fr), Philippe A. Jean (CSTB, 24 rue Joseph Fourier, 38400 Saint-Martin-d'Hères, France, philippe.jean @cstb.fr)

Mountainous zones in Europe, such as the Alps, represent huge areas where many viaducts are built, most of them for motorways. The way the sound grazes the asphalt surface from the low and high traffic equivalent sources up to the road edges, and how it then diffracts towards dwellings is a complex mechanism. The standard approaches are suited to plain situations but fail in predicting finely sound propagation behaviour for such geometries. In this paper, one gives the main trends of received noise levels from viaducts as a function of both their geometry and the receiver location. A 2D Boundary Element Method is used for predictions since meteorological effects can be neglected for the short propagation (a few hundreds meters). This assumption makes sense since the viaduct considered in this work is sufficiently high (20 m) and the ground effect is weakly affected by refraction. Different configurations are then simulated in order to address and discuss several geometrical effects, such as: platform elevation, low height barriers addition, complex shape barriers and presence of a central gap in the platform.

4:40

5pNSc2. Characteristics of road traffic noise level statistics for shielded areas. Jens Forssén (Division of Applied Acoustics, Chalmers University of Technology, 41296 Göteborg, Sweden, jens.forssen@chalmers .se), Maarten Hornikx (Applied Acoustics, Chalmers University of Technology, Sven Hultins Gata 8a, SE-41296 Gothenburg, Sweden, maarten .hornikx@chalmers.se)

For noise immission, it is of interest to study other noise level statistics besides the long-term equivalent levels and maximum levels. By further analysis of the time variations of the noise level, an improved description of the negative effects of the noise may be achieved, for instance concerning perceived annoyance. Here, noise level histograms, i.e., probability density

functions of sound pressure levels, from controlled recordings have been investigated. This has been made for a situation of special interest, which is a courtyard shielded from a dominating road traffic noise source. It has been reported previously that many shielded urban areas show levels that are considerably higher than the equivalent level, described as an upward tail of the histogram, which is not a usual characteristic of directly exposed areas. From the analysis made here, it is shown that the upward tail, i.e., the higher levels, of the shielded area is caused by locally occurring, unshielded road traffic events. It is concluded that the upward tail as a common characteristic of shielded urban areas may well be due to locally occurring noise events, for instance due to local road traffic.

5:00

5pNSc3. Use of the transmission line matrix method for the sound propagation modeling in urban area. Gwenaël Guillaume (Lab. Central des Ponts et Chaussées, Division Entretien, Sécurité et Acoustique des Routes, Route de Bouaye - BP 4129, 44341 Bouguenais Cedex, France, Gwenael.Guillaume@lcpc.fr), Judicaël Picaut (Lab. Central des Ponts et Chaussées, Division Entretien, Sécurité et Acoustique des Routes, Route de Bouaye - BP 4129, 44341 Bouguenais Cedex, France, Judicael.Picaut@lcpc.fr), Guillaume Dutilleux (Lab. Régional des Ponts et Chaussées, 11, rue Jean Mentelin, BP 9, 67035 Strasbourg Cedex 2, France, Guillaume.Dutilleux@equipement.gouv.fr)

This paper deals with the sound propagation modeling in urban area. This problematic requires to take into account many phenomena that can have a substantial impact as well in semienclosed spaces as on long-range outdoor sound propagation, such as reflections and absorption on the frontages and on the ground, atmospheric attenuation, sound velocity variations related with wind and temperature vertical gradients, atmospheric turbulences. The numerical method used is the TLM (transmission line modeling), which has been originated in electromagnetism and adapted for acoustics applications. It consists in a physical rendering of the waves propagation based on the Huygens' principle. It is established on a spatiotemporal discretization of the domain using an iterative temporal process for sound pressure propagation, instead of the resolution of mathematical equations. The TLM model has then been developed in two and three dimensions allowing to combine all the phenomena affecting the sound propagation in urban area. Numerical simulations are given for canyon streets.

5:20

5pNSc4. Predictions of sound pressure levels in streets using a diffusion model: numerical validations and experimental comparisons. Alexis Billon (Universite de Liege, INTELSIG group - Département E.E.I., B28 Sart-Tilman, 4000 Liege, Belgium, abillon@ulg.ac.be), Judicaël Picaut (Lab. Central des Ponts et Chaussées, Division Entretien, Sécurité et Acoustique des Routes, Route de Bouaye - BP 4129, 44341 Bouguenais Cedex, France, Judicael.Picaut@lcpc.fr)

Predictions of sound propagation in urban areas have attracted a considerable over the years. If the sound energy is assimilated to particles with a constant energy, their movement can be described by a transport equation. In canyon streets, this transport equation can be reduced to a diffusion equation whose expression is more simple. In this presentation, sound absorption at the boundaries (buildings facades and ground), as well as atmospheric sound attenuation are introduced. The problem is then solved numerically using a finite elements method for the configuration of a canyon street. A systematic validation of the obtained model is carried out in terms of sound pressure level by comparison to numerical simulations taken from the literature. Comparisons with experimental data are then conducted. Finally, applications in more complex configurations are presented.

5:40

5pNSc5. A cellular automaton for urban traffic noise. Erik Salomons (TNO Science and Industry, Stieljesweg 1, 2628CK Delft, Netherlands, erik.salomons@tno.nl)

Propagation of traffic noise in a city is a complex phenomenon, due to multiple reflection, diffraction, and scattering at irregular facades of buildings. These effects may be calculated with computer models based on numerical integration of the basic acoustic equations, but in practice these models can be applied only to small urban regions due to limited computer power. Here we propose a new approach for simulating urban traffic noise: a cellular automaton (CA) based on simple update rules for the configuration of cars in a city, and simple rules for propagation of sound to receivers. An example is presented for a square model city of 25 km^2, consisting of 10^6 square cells. The CA employs a time integration step of 0.3 s, and includes noise contributions from all cars in the city. The fluctuating sound level is computed for a period of 24 h, both for a receiver along a street and for a receiver that is screened by buildings. While the sound level at the first receiver shows sharp peaks corresponding to passages of cars, the sound level fluctuations at the screened receiver are much smaller as most of the sound energy comes from distant cars in this case.

6:00

5pNSc6. Numerical prediction of the effect of traffic lights on the vehicle noise at urban street intersections. Jorge Parrondo (Universidad de Oviedo, Dep. de Energía, Campus de Viesques s/n, 33203 Gijón, Spain, parrondo@uniovi.es), Ruben Zurita (Universidad de Oviedo, Dep. de Energía, Campus de Viesques s/n, 33203 Gijón, Spain, ZURITA@lsi.uniovi.es), Jose A. Corrales (Universidad de Oviedo, Dep. de Energía, Campus de Viesques s/n, 33203 Gijón, Spain, JA@lsi.uniovi.es), Joaquin Fernandez (Univ. de Extremadura, Escuela de Ing. Industriales, 06071 Badajoz, Spain, ffrancos@unex.es)

Intersections of urban streets are particularly noisy locations due to the addition of the noise from vehicles at different streets, a long period of noise emission from queuing vehicles with traffic lights in red and the noise from accelerating vehicles. Besides, the traffic lights impose a modulation in the passage of the vehicles, so that the subsequent noise variability along time contributes to increase the annoyance degree. This paper presents a code especially developed to simulate both the spatial and temporal distribution of the sound pressure levels induced by the vehicle traffic in street intersections. The algorithm combines a traffic model with vehicles in dynamic motion through the domain with a model for sound propagation, based on the method of virtual images in which the determination of the location of the successive image sources was reduced to a reference horizontal plane. Sound emission from each vehicle was established according to the Harmonoise guidelines. After verifying the code predictions by comparison with measurements at several street intersections, the method was applied systematically to investigate the effect of varying the regulation parameters of the traffic lights on the Leq and L10 distributions for some particular cases.

Session 5pPAa

Physical Acoustics: Ducts and Waveguides II

Marc Deschamps, Cochair
LMP, Lab. de Mécanique et Physique (LMP), 351, Place de la Libération, Talence, 33405, France

Olivier Dazel, Cochair
Laboratoire d'Acoustique de l'Université du Maine, Avenue Olivier Messiaen, Le Mans, 72085, France

Contributed Papers

2:00

5pPAa1. A higher order parabolic equation for predicting in-duct propagation in high frequencies. Patrice Malbéqui (ONERA, 29 avenue de la Division Leclerc, 92322 Châtilllon, France, patrice.malbequi@onera.fr)

Complementary methods are required to predict the in-duct propagation in a large frequency range including the linear absorption and the flow effects. Numerical methods solving the Euler's equations are pertinent for rotational flow but limited to the low frequencies. The Boundary Element Method is applicable in a large frequency range assuming a homogeneous flow. The ray-model is valid in high frequencies but scattering effects are difficult to implement. This paper presents the capabilities of a Higher-Order Parabolic Equation (HOPE) to handle duct propagation in the high frequency range. In contrast with the so-called standard PE and the wide-angle PE, the HOPE improves the accuracy of the solution due to its wider propagation aperture angle, especially close to the cutoff frequency. Several duct propagation configurations including flow and liner are considered. Using a marching algorithm, the HOPE computes in a very short CPU time the sound propagation and represents an attractive alternative to the ray-model in the high frequency range. [Work supported by Airbus-France.]

2:20

5pPAa2. An integrated multimodal acoustic particle manipulator and optical evanescent field waveguide. Peter Glynne-Jones (University of Southampton, School of Engineering Sciences, University Road, SO17 1BJ Southampton, UK, p.glynne-jones@soton.ac.uk), Martyn Hill (University of Southampton, School of Engineering Sciences, University Road, SO17 1BJ Southampton, UK, m.hill@soton.ac.uk), Rosemary J. Townsend (University of Southampton, School of Engineering Sciences, University Road, SO17 1BJ Southampton, UK, R.J.Townsend@soton.ac.uk), Nicholas R. Harris (University of Southampton, Electronics and Computer Science, SO17 1BJ Southampton, UK, nrh@ecs.soton.ac.uk), James S. Wilkinson (University of Southampton, Optoelectronics Research Centre, SO17 1BJ Southampton, UK, jsw@ecs.soton.ac.uk), Fan Zhang (University of Southampton, Optoelectronics Research Centre, SO17 1BJ Southampton, UK, faz@orc.soton.ac.uk), Tracy Melvin (University of Southampton, Optoelectronics Research Centre, SO17 1BJ Southampton, UK, tm@ecs.soton.ac.uk)

A new acoustic/optical/microfluidic system is presented for the manipulation of bead-tagged DNA molecules. Acoustic radiation forces are used to manipulate microspheres into and away from the evanescent field of a laser coupled waveguide that is integrated into the reflector of the acoustic chamber. With suitable fluorophores the presence of the target DNA can be detected with a fluorescence microscope enabling large populations of beads to be examined simultaneously. The integrated waveguide and multimodal acoustic chamber are presented here, with results showing that the microspheres can be successfully detected as they are brought into the evanescent field using a quarter-wave acoustic configuration. It is also shown that by measuring the time of flight of a microsphere between the half- and quarter-wave nodal planes the bead size can be determined, providing a means of multiplexing the detection (detecting a range of different target DNA sequences).

2:40

5pPAa3. Trapped wave in plan waveguides including gaussian varying section domain. Patrick Marical (LOMC FRE-3102 CNRS, Groupe Ondes Acoustiques, University of Le Havre, Place Robert Schuman, BP 4006, 76610 Le Havre, France, patrick.marical368@univ-lehavre.fr), Mounsif Ech-Cherif El-Kettani (LOMC FRE-3102 CNRS, Groupe Ondes Acoustiques, University of Le Havre, Place Robert Schuman, BP 4006, 76610 Le Havre, France, elkettani@univ-lehavre.fr), Zahia Hamitouche (LOMC FRE-3102 CNRS, Groupe Ondes Acoustiques, University of Le Havre, Place Robert Schuman, BP 4006, 76610 Le Havre, France, zahia.hamitouche@univ-lehavre.fr), Mihai Valentin M. Predoi (University Politechnica of Bucharest, Department of Mechanics, 060032 Bucharest, Romania, predoi@cat.mec.pub.ro)

In previous works on plan waveguides including an area of varying section of Gaussian shape, we have observed experimentally and numerically the existence of a trapped wave in the Gaussian varying section domain in the case of the A1 incident Lamb mode. The purpose of this work is to highlight the existence of this trapped wave, depending on the equation of the Gaussian profile of the varying section domain. This study is carried out numerically using FEM, as our numerical model has been previously validated. The results obtained show that the phenomenon of trapped wave is strongly linked to the Lamb wave conversion phenomenon: when the incident Lamb wave gives rise to a trapped wave, it is systematically converted into other Lamb waves transmitted outside the area of varying section. Otherwise, it is totally transmitted without any conversion and in this case, any trapped wave exists. The conversion phenomenon is quantified and we show that it is important and depend on the breaking symmetry of the incident Lamb mode by the varying section area.

3:00

5pPAa4. Intermodal coupling in a dissipative fluid filling a rough-walled waveguide. Tony Valier-Brasier (Laboratoire d'Acoustique de l'Université du Maine, Avenue Olivier Messiaen, 72085 Le Mans, France, tony.valier-brasier.etu@univ-lemans.fr), Catherine Potel (Laboratoire d'Acoustique de l'Université du Maine, Avenue Olivier Messiaen, 72085 Le Mans, France, catherine.potel@univ-lemans.fr), Michel Bruneau (Laboratoire d'Acoustique de l'Université du Maine, Avenue Olivier Messiaen, 72085 Le Mans, France, michel.bruneau@univ-lemans.fr), Claude Depollier (Laboratoire d'Acoustique de l'Université du Maine, Avenue Olivier Messiaen, 72085 Le Mans, France, claude.depollier@univ-lemans.fr)

The present study follows recent works dealing with the analytical model of an acoustic field in fluid-filled waveguides with rough walls. In these works, the acoustic field is obtained from the coupling between Neumann eigenmodes of the regularly shaped waveguide which bounds outwardly the rough walls of the waveguide considered, using integral formulation with suitable Green function. The effect of the roughness is expressed

in such a way that two intermodal coupling mechanisms are highlighted: a bulk coupling and a surface coupling, the first one depending on the depth of the roughness and the second one depending in addition on the local slope. Moreover, a phonon relation is involved when the rough profile is periodic. The aim of the present study is to account for the thermo-viscous boundary layer effects through eigenmodes which satisfy appropriate mixed boundary conditions, leading to a better understanding of the physical mechanisms when resonances and phonon relationship are involved.

3:20

5pPAa5. Evaluation of the lined duct performances based on a 3D two port scattering matrix. Mohamed Taktak (Université de Technologie de Compiègne, Centre de Recherche Royallieu, BP20529, 60205 Compiègne, France, mohamed.taktak@utc.fr), Jean Michel Ville (Université de Technologie de Compiègne, Centre de Recherche Royallieu, BP20529, 60205 Compiègne, France, jean-michel.ville@utc.fr), Mohamed Haddar (Unité de Modélisation, Mécanique et de Production (U2MP), Ecole Nationale d'Ingénieurs de Sfax, BP 3038, 3038 Sfax, Tunisia, mohamed.haddar@enis.rnu.tn), Félix Foucart (Université de Technologie de Compiègne, Centre de Recherche Royallieu, BP20529, 60205 Compiègne, France, felix.foucart@utc.fr)

The scattering matrix constitutes a good tool to characterize a lined duct. In fact, this matrix relates the incoming modal pressures to the out coming ones and contains detailed information and per mode about the transmission, reflection, and conversion properties of the duct. It depends only on the geometric and acoustic properties of the duct. The two port acoustic dissipation and attenuation interest the designers of lined duct like aircraft engine manufacturers to evaluate the duct performances. These values can be deduced from the two port scattering matrix and from the vector of incoming modal pressures. In this work, a study about the two port acoustic dissipation and attenuation computed from the scattering matrix and for different cases of incoming modal pressures are presented. Scattering matrices used in this study are measured by an experimental procedure developed at the University of Technology of Compiègne based upon the experimental setup realized during the European Project DUCAT. The experimental acoustic power dissipation and attenuation are computed for different cases of modal structure on the both side of the duct. Then, these results were confronted with ones given by a theorical study of the problem based on the finite element method.

3:40-4:00 Break

4:00

5pPAa6. Elaboration of a sacttering matrix measurement procedure using the p-v probe. Yamen Kchaou (Université de Technologie de Compiègne, Centre de Recherche Royallieu, BP20529, 60205 Compiègne, France, yamen.kchaou@yahoo.fr), Mohamed Taktak (Université de Technologie de Compiègne, Centre de Recherche Royallieu, BP20529, 60205 Compiègne, France, mohamed.taktak@utc.fr), Jean Michel Ville (Université de Technologie de Compiègne, Centre de Recherche Royallieu, BP20529, 60205 Compiègne, France, jean-michel.ville@utc.fr), Mohamed Haddar (Unité de Modélisation, Mécanique et de Production (U2MP), Ecole Nationale d'Ingénieurs de Sfax, BP 3038, 3038 Sfax, Tunisia, mohamed.haddar@enis.rnu.tn), Félix Foucart (Université de Technologie de Compiègne, Centre de Recherche Royallieu, BP20529, 60205 Compiègne, France, felix.foucart@utc.fr)

The scattering matrix which relates traveling waves amplitudes as state variables has been shown to be more attractive than transfer or mobility matrices since it reflects the fundamental duct nature: it gives a more complete description of the transmission, reflection, and conversion properties of the duct. In the University of Technology of Compiègne, an experimental procedure was developed to measure this matrix: a p-p probe mounted on a setup designed during DUCAT project is used to measure pressures at two cross sections on the both side of the test lined duct, then by using a modal decomposition and separation techniques, the scattering matrix is deduced. In this paper, a method to measure the multimodal scattering matrix based on the use of a p-v probe getting simultaneously the acoustic pressure and velocity at one section on the both side of the test duct is developed. A comparison of some acoustics values (scattering matrix coefficients, acoustic powersœ) of a hard wall duct straight duct obtained by each technique with the theory is presented to evaluate its advantages and limitations.

4:20

5pPAa7. Axisymmetrical and nonaxisymmetrical guided waves propagating in a solid elastic cylinder embedded in a solid medium. Slah Yaacoubi (LCPC, Lab. Central des Ponts et chaussées (LCPC), Route de Bouaye-BP 4129, 44341 Bouguenais, France, slah.yaacoubi@lcpc.fr), Laurent Laguerre (LCPC, Lab. Central des Ponts et chaussées (LCPC), Route de Bouaye-BP 4129, 44341 Bouguenais, France, laurent.laguerre@lcpc.fr), Eric Ducasse (LMP, Lab. de Mécanique et Physique (LMP), 351, Place de la Libération, 33405 Talence, France, e.ducasse@lmp.u-bordeaux1.fr), Marc Deschamps (LMP, Lab. de Mécanique et Physique (LMP), 351, Place de la Libération, 33405 Talence, France, m.deschamps@lmp.u-bordeaux1.fr)

For NDT of rods and pipes, fundamental characteristics of guided waves are to be known, especially dispersion relations between frequency and wave number. A necessary step before detecting defects is to be able to calculate the propagated elastodynamical field in healthy waveguides. Thus, the goal of this work is the calculation of this field propagating in a cylindrical stratified waveguide. The incident field is generated at the end of the cylinder by a force or velocity source which is off-axis and Gaussian distributed. First, Vector Hankel transform and Fourier series are combined to decompose this field with respect to the angular position. Second, each component is decomposed into an infinite sum of rays, i.e., elementary generalized conical waves. These waves undergo multiple reflections with the guiding surface of the waveguide. Third, we use Generalized Debye Series (GDS) for calculating the global reflection coefficients resulting from these multiple reflections. Finally, the total field is synthesized by the summation of the incident and reflected rays. Many outputs of this code can be exploited like velocity field, stress field, energy field in 2D or 3D spatiotemporal or frequential simulations. Diagrams obtained by this code are compared with results from DISPERSE software.

4:40

5pPAa8. Coupling transfer matrix method to finite element method for the analysis of hollow body networks with passive or reactive elements. Fabien Chevillotte (Groupe d'Acoustique de l'Université de Sherbrooke, 2500, Boul. de l'Université, Département de génie mécanique, Sherbrooke, QC J1K-2R1, Canada, fabien.chevillotte@usherbrooke.ca), Raymond Panneton (Groupe d'Acoustique de l'Université de Sherbrooke, 2500, Boul. de l'Université, Département de génie mécanique, Sherbrooke, QC J1K-2R1, Canada, raymond.panneton@usherbrooke.ca), Hakim Bougrab (Groupe d'Acoustique de l'Université de Sherbrooke, 2500, Boul. de l'Université, Département de génie mécanique, Sherbrooke, QC J1K-2R1, Canada, Hakim.Bougrab@USherbrooke.ca), Christophe Chaut (Henkel Technologies, Acoustics Center, 58203 Cosne sur Loire, France, Christophe.Chaut@fr.Henkel.com), Jean-Luc Wojtowicki (Henkel Technologies, Acoustics Center, 58203 Cosne sur Loire, France, Jean-Luc .Wojtowicki@fr.Henkel.com)

This work shows how to couple transfer matrix method to finite element method with a view to analyze the acoustic response of hollow body structures with a minimum of memory requirements and computational time. An hollow body structure is made up from a series of elongated rigid-walled fluid partitions (i.e., waveguides). These fluid partitions are separated by any passive (e.g., multilayered sound barrier) or reactive elements (e.g., expansion chamber). In the proposed hybrid model, the elongated fluid partitions are modeled using 1D fluid finite elements, and the passive or reactive elements using transfer matrices. From the weak integral formulation of the acoustic problem, it is shown how the coupling with the transfer matrix is taken into account through a mixed boundary condition. After discretization of the acoustic pressure and application of the variational principle, the finite element matrix system is obtained, where only the nodal pressures in the fluid partitions remain. The transfer matrix has been converted into a kind of admittance matrix, where no additional degrees of freedom are necessary to account for the passive or reactive elements. The method is used to predict the acoustic response of a real hollow body structure. Good correlations are obtained with experimentations.

Session 5pPAb

Physical Acoustics: Ultrasonics Under Extreme Conditions II

Albert Migliori, Cochair
NHMFL, Los Alamos Natl. Lab. Los Alamos, NM 87545, USA

Frédéric Decremps, Cochair
IMPMC, Université Paris VI, 140, rue de Lourmel, Paris, 75015, France

Invited Papers

3:20

5pPAb1. Gigahertz ultrasonic interferometry at high pressure and temperature: Geophysical implications. Anastasia P. Kantor (Bayerisches Geoinstitut, University Bayreuth, 95440 Bayreuth, Germany, Anastasia.Kantor@Uni-Bayreuth.de), Steven D. Jacobsen (Department of Earth and Planetary Sciences, Northwestern University, Evansto, IL 60208-2150, USA, steven@earth.northwestern.edu), Innokenty Y. Kantor (Bayerisches Geoinstitut, University Bayreuth, 95440 Bayreuth, Germany, Innokenty.Kantor@uni-bayreuth.de), Leonid S. Dubrovinsky (Bayerisches Geoinstitut, University Bayreuth, 95440 Bayreuth, Germany, Leonid.Dubrovinsky@uni-bayreuth.de), Hans Josef Reichmann (Geoforschungszentrum Potsdam, Telegrafenberg, Division 4, 14473 Potsdam, Germany, hanni@gfz-potsdam.de)

High-frequency acoustic interferometry is widely used to penetrate a medium and measure the reflection signature, which can reveal details about the inner structure of the medium. It is a very helpful and one of the most accurate techniques for determination elastic properties of different materials being capable to measure sound wave velocities in very small samples under high pressures. The ultrasonic interferometry system operating at 0.6-2.1 gigahertz (GHz) frequencies was developed in the Bavarian Geoinstitute of the University of Bayreuth for in situ high pressure and temperature experiments. High pressures are reached by using diamond anvil cell, and a Pt-resistive heater allows reaching high temperatures. The experimental setup is equipped with a laser system, which allows measuring a shift of ruby fluorescence line at every given temperature.

3:40

5pPAb2. Estimation of thermophysical properties of fluids under high pressure from speed of sound measurements. Jean Luc Daridon (Université de Pau et des Pays de l'Adour, Laboratoire des Fluides Complexes, UMR 5150, BP 1155, 64000 Pau, France, jean-luc.daridon@univ-pau.fr)

The thermophysical properties of pure substances in fluid state as functions of temperature and pressure are of great interest not only for industrial applications (for example in the oil and gas industry), but also for fundamental aspects in view of developing models for an accurate representation of dense fluids. Now these measurements are difficult to perform under pressure, particularly for non single-phase systems, at atmospheric pressure. An interesting alternative consists in using the ultrasonic velocity which can be determined experimentally with a high degree of accuracy including at high pressures and high temperatures, and which presents the advantage of giving access to various derived properties. This potential, which is specific to ultrasonic velocity in fluids, has been the starting point for the investigation of a large number of pure liquids and gases as well as of several types of mixtures by ultrasonic measurements. In this work we will review the procedures used to evaluate thermophysical properties as a function of pressure from speed of sound measurements. The validity of the different approaches will be checked by comparison to several thermophysical properties measured in an extended pressure range. The accuracy reached for each property by the different procedures will be bring out.

Contributed Papers

4:00

5pPAb3. New results on the sound velocity measurements under extreme conditions using time-resolved picosecond acoustic technique. Frédéric Decremps (IMPMC, Université Paris VI, 140, rue de Lourmel, 75015 Paris, France, frederic.decremps@impmc.jussieu.fr), Laurent Belliard (INSP - UMR 7588 CNRS & Université Pierre et Marie Curie, 140 Rue de Lourmel, 75015 Paris, France, lbelliar@ccr.jussieu.fr), Bernard Perrin (INSP - UMR 7588 CNRS & Université Pierre et Marie Curie, 140 Rue de Lourmel, 75015 Paris, France, bernard.perrin@insp.jussieu.fr), Michel Gauthier (IMPMC, Université Paris VI, 140, rue de Lourmel, 75015 Paris, France, michel.gauthier@impmc.jussieu.fr)

In this presentation, recent works on the pressure and temperature dependence of the sound velocity will be discussed. We have used a newly developed method combining the time-resolved picosecond optical technique and a diamond anvil cell [1]. This setup makes possible accurate measurements of the attenuation and velocity of longitudinal waves in the Ghz range, and opens the elastic investigations of all materials (opaque, transparent, single- or polycrystal, liquids) up to several Mbar and thousands of K. The experimental method will be first described, with a discussion of the factors limiting the possibilities and the technique accuracy. [1] F. Decremps, L. Belliard, B. Perrin, and M. Gauthier, Phys. Rev. Lett, to be pubished in January 2008.

4:20-4:40 Break

4:40

5pPAb4. Elastic moduli at high temperatures with two different ultrasonic methods. Ludivine Bourgeois (Commissariat à l'Energie Atomique (CEA), Centre de Valduc, 21120 Is sur Tille, France, ludivine.bourgeois@cea.fr)

"The elastic moduli and specially the shear modulus G is one of the parameters needed to implement the constitutive relations. These mechanical

properties can be measured for a solid or a liquid with different ultrasonic methods. This paper deals with the determination of G(T) with two different methods: a contact delay-line ultrasonic device which has been developed to measure the shear and compression waves velocities up to 1000 K on cylindrical specimens and a contactless (laser) ultrasonic device which can measure surface acoustic waves velocities in metals up to the melting point. Results on metals such as Al without phase transition and for Co through the phase transition will be presented."

5:00

5pPAb5. Measurements under high pressure of ultrasonic velocity in glycerol. Hassina Khelladi (Faculty of Physics, University of Science and Technology Houari Boumedienne, BP 32 El Allia, Bab-Ezzouar, 16000 Algiers, Algeria, hassinakhelladi@yahoo.fr), Frédéric Plantier (Université de Pau et des Pays de l'Adour, Laboratoire des Fluides Complexes, UMR 5150, BP 1155, 64000 Pau, France, frederic.plantier@univ-pau.fr), Jean Luc Daridon (Université de Pau et des Pays de l'Adour, Laboratoire des Fluides Complexes, UMR 5150, BP 1155, 64000 Pau, France, jean-luc.daridon@univ-pau.fr), Hakim Djelouah (Faculty of Physics, University of Science and Technology Houari Boumedienne, BP 32 El Allia, Bab-Ezzouar, 16000 Algiers, Algeria, djelouah_hakim@yahoo.fr)

Glycerol has been the subject of significant scientist interest. Indeed, glycerol is a polyalcohol and the presence of three hydroxyl groups per molecule makes glycerol a complex system to explore. The purpose of this investigation is to measure under high pressure the ultrasonic wave velocity in glycerol, from which a number of important thermodynamic properties could be derived and determined as a function of pressure and temperature. Pressure and temperature ranges exploited in this experimental investigation of various glycerol properties, are extended respectively from 0.1 MPa to 100 MPa and from 10 °C to 100 °C. A high pressure measurement cell equipped with temperature and pressure monitoring and control instrumentation was used. A time of flight method was exploited to measure, under high pressure, the ultrasonic wave velocity at different temperatures. The resulting experimental data of ultrasonic wave velocity in glycerol combined with measurements at atmospheric pressure, of density, specific heat and thermal expansion coefficient were used to derive density at elevated pressures. As isentropic compressibility is linked to ultrasonic wave velocity and density by means of the Newton-Laplace equation, this intrinsic physical property is easily deduced. These results led to the behavior of each physical property as a function of temperature and pressure.

5:20

5pPAb6. Laser optoacoustic study of near-critical states and phase transitions in metals. Alexander Y. Ivochkin (Moscow State University International Laser Centre, Leninskie gory, 1, 119992 Moscow, Russian Federation, ivochkin@yandex.ru), Alexander G. Kaptilniy (Joint Institute for High Temperatures, Russian Academy of Science, Izhorskaya str., 13/19, 125412 Moscow, Russian Federation, drc@pochta.ru), Alexander Karabutov (Moscow State University, MSU, 1, building 2, GSP-2, Leninskiye Gory, 119992 Moscow, Russian Federation, akarabutov@gmail.com)

Pulsed laser optoacoustic technique is used for generation and study of near-critical states and phase transitions in metals. Metal surface is confined by a layer of transparent dielectric. In this case the efficiency of pressure generation is much greater than in case of the free surface so it is possible to achieve states of metals with relatively high thermodynamic parameters: P $\sim 10^4$ atm and T ~ 10^4 K with a table-top laser system. The experimental setup for simultaneous measurements of pressure, temperature, and reflectivity of metal surface with nanosecond temporal resolution was assembled. Q-switched Nd:YAG laser with pulse duration ~ ~10 ns and pulse energy ~1 J was used. Pressure was measured using $LiNbO_3$ piezotransducer. Temperature was obtained with optical pyrometer. Lead and mercury were chosen as test metals. Pressure pulses up to 1 kbar in lead and up to 7 kbar in mercury (with T ~2400 K - super-critical area of the phase diagram for Hg) were obtained. The curve of laser heating process in P-T coordinates was plotted. The measurements of optical properties showed considerable decrease of surface reflectivity both for lead and mercury at high laser fluences due to increase of temperature and density decrease.

5:40

5pPAb7. Effect of intense neutron dose radiation on piezoceramics. Franck P. Augereau (IES/Université Montpellier II, Université Montpellier II, Place Eugène Bataillon, 34095 Montpellier, France, Franck.Augereau@ies.univ-montp2.fr), Jean-Yves Ferrandis (Radio Application Division, NEC Corporation, Université Montpellier II, Place Eugène Bataillon, 34095 Montpellier, France, ferrandi@lain.univ-montp2.fr), Jean-François Villard (CEA Saclay, 91191 Gif sur Yvette Cedex, France, jean-francois.villard@cea.fr), Damien Fourmentel (CEA Saclay, 91191 Gif sur Yvette Cedex, France, damien.fourmentel@cea.fr), Mark Dierckx (SCK-CEN, Boeretang 200, B-2400 Mol, Belgium, mdierckx@sckcen.be), Jan Wagemans (SCK-CEN, Boeretang 200, B-2400 Mol, Belgium, jwageman@SCKCEN.BE)

Four grades of commercial PZT materials have been exposed to nuclear radiation during five months in an irradiation channel of the BR1 research reactor at SCK·CEN (Belgium). This experimental study was performed in the framework of the Joint Instrumentation Laboratory with the CEA French Commission of Atomic Energy to validate these materials for future applications in severe conditions such as online measurements in irradiation experiments performed in research reactors. For this purpose, thin piezoelectric discs were irradiated while a remote network analyser continuously monitored the frequency response of their electrical impedance. The total neutron dose has reached a level of 1.5.1017 neutrons/cm^2. Positive and negative shifts of the peak resonance frequency have been recorded but in any case with a variation lower than 1%. On the other hand, the amplitude of the electrical impedance at resonance frequency has largely decreased with even a reduction by factor two or three for some piezoelectric cells. Transitory effects have also been detected for these two parameters as function of the reactor activity. Additional thermal and gamma radiation effect have been investigated. Similarly, some piezoelectric cells glued on glass delay line have been tested with satisfactory results to these stresses.

6:00

5pPAb8. Ultrasonic exploration at extreme shallow underground in submerged soil. Kunihiko Seo (Toin University of Yokohama, 1614 Kurogane-cho, Aoba-ku, 225-8502 Yokohama, Japan, seo.ylk@gmail.com), Takashi Shirakawa (Toin University of Yokohama, 1614 Kurogane-cho, Aoba-ku, 225-8502 Yokohama, Japan, t_shira7@yahoo.co.jp), Tsuneyoshi Sugimoto (Toin University of Yokohama, 1614 Kurogane-cho, Aoba-ku, 225-8502 Yokohama, Japan, tsugimot@cc.toin.ac.jp)

Now a lot of land mines remain buried in the world, so that the clearance of them is required. As a tool of removing land mines, equipments using electromagnetic radiation are often employed. However, there is a problem that the land mines in the flooded soil such as in Southeast Asia cannot be detected in the rainy season. Therefore, the new way using sound waves will be profitable to detect the land mines in the flooded soil. In this research, the acoustic exploration at very shallow area in submerged sand is examined at a water tank in the lab. First we measure the propagation property of ultrasound of 120 kHz in the shallow submerged sand, and examine underground imaging. As a result, the acoustic velocity is measured at about 1500 m/s and the attenuation is measured at about -19 dB/m. And next, shallow underground exploring by using acoustic shielding boards is carried out. As a result, underground images in the water tank simulating the submerged soil are obtained. Then acoustic shielding boards can block wave which propagates specific route. This will make another exploration method possible.

Session 5pPAc

Physical Acoustics: General Topics in Physical Acoustics II

Walter Lauriks, Cochair
Lab. ATF, Katholieke Universiteit Leuven, Celestijnenlaan 200D, Leuven, B-3001, Belgium

Andi Petsculescu, Cochair
University of Louisiana, Department of Physics, P.O. Box 44210, Lafayette, LA 70504, USA

Contributed Papers

4:00

5pPAc1. An automated 3 dimensional scanning system for validation of acoustical simulation results. Simo-Pekka Simonaho (University of Kuopio, P.O.Box 1627, 70211 Kuopio, Finland, simo-pekka.simonaho@uku.fi)

To validate acoustical simulation results, a great number of measurement points are needed especially in 3 dimensional cases. These measurements can be extremely laborious when done manually. Also, the spatial information of the measurement points has to be accurate. In this work, an automated 3-D scanning system with high spatial resolution for validation of acoustical simulation results is introduced. The system consists of a multi channel data acquisition hardware, a microphone array and a 3-D scanning system. The movement of the microphone array is controlled by the data acquisition hardware. The performance of the automated 3-D scanning system is demonstrated and the experimentally measured pressure fields are compared to simulation results.

4:20

5pPAc2. Signal processing of impedance spectrum for speed of sound and pressure measurement in plane or radial resonators. Eric Rosenkrantz (Radio Application Division, NEC Corporation, Université Montpellier II, Place Eugène Bataillon, 34095 Montpellier, France, eric.rosenkrantz@ies.univ-montp2.fr), Jean-Yves Ferrandis (Radio Application Division, NEC Corporation, Université Montpellier II, Place Eugène Bataillon, 34095 Montpellier, France, ferrandi@lain.univ-montp2.fr), Gerard Leveque (Institut d'Electronique du Sud UMR-CNRS 5214, Université Montpellier II, Place Eugène Bataillon, 34095 Montpellier, France, Gerard.leveque@ies.univ-montp2.fr)

The impedance of gas contained between two plane walls is a periodic function of the frequency. The frequency interval between two resonances of the gas is equal to c/2D. Furthermore, the amplitude of the resonances is proportional to the pressure. We describe a signal processing to easily deduce the speed of sound and the pressure of the gas from the impedance spectrum. We show that the modulus of the Fourier transform of the modulus of impedance, called "Tempograph," contains all information about the gas. In some industrial cases the container is a cylinder or a sphere which can be used as a radial resonator exited by a radial wave [1, 2]. The frequency response of such resonator at high frequencies is quasi-periodic and thus the same signal processing can be used. [1] M. F. Narbey, et al., "Determination of the composition of a gas mixture in a nuclear fuel rod by an acoustic method." INSIGHT, **42**(9), 603-605 (2000). [2] A. Olson, "Helium bottle pressure measurement by portable ultrasonic technique." 1989, Rapport de Boeing n°AD-A208 994, http://stinet.dtic.mil/str/index.html.

4:40

5pPAc3. Absorption and velocity of acoustical waves in binary solutions of poly (ethylene glycol) and water. Rajendra Kumar Singh (Department of Physics, Banaras Hindu University, 221005 Varanasi, India, rksingh_17@rediffmail.com), Manish Pratap Singh (Banaras Hindu University, 221005 Varanasi, India, mps_bhu@yahoo.co.in),Rishi Pal Singh (Banaras Hindu University, 221005 Varanasi, India, rishisingh80@rediffmail.com)

A resonator technique has been devoleped to measure ultrasonic velocity and absorption for aqueous solutions of PEG of different molecular weights. The velocity has been measured at different frequencies and the concentrations (by weight) ranged from 1% to 10% of poly (ethylene glycol) in water. Adiabatic compressibility has been obtained at different temperatures, using experimental value of velocity and density. Viscocity has also been measured in wide temperature range . Ultrasonic absorption has been measured in the frequency range 400 KHz-50 MHz, using resonator technique and pulse technique in temperature range 400-650 °C. Observations showed that the ultrasonic absorption decreases with increasing temperature at a given concentration and also increases with concentration at a given temperature. The velocity increases with increasing temperature and concentration. Shear viscosity has been found to decrease with temperature but increases with concentration. Velocity studies show that as the polymer concentration increases a more rigid molecular structure is formed by bonding between the large polymer molecules.

5:00

5pPAc4. Acoustic field in a spherical resonator: effect of modal coupling due to small perturbations. Cécile Guianvarc'H (Institut National de Métrologie (LNE-INM/Cnam), 61 rue du Landy, 93210 La Plaine Saint Denis, France, cecile.guianvarch@cnam.fr), Laurent Pitre (Institut National de Métrologie (LNE-INM/Cnam), 61 rue du Landy, 93210 La Plaine Saint Denis, France, pitre@cnam.fr), Arnaud Guillou (Institut National de Métrologie (LNE-INM/Cnam), 61 rue du Landy, 93210 La Plaine Saint Denis, France, guillou.arnaud@gmail.com), Michel Bruneau (Laboratoire d'Acoustique de l'Université du Maine, Avenue Olivier Messiaen, 72085 Le Mans, France, michel.bruneau@univ-lemans.fr), Anne-Marie Bruneau (Laboratoire d'Acoustique de l'Université du Maine (LAUM, UMR CNRS 6613), Avenue Olivier Messiaen, 72085 Le Mans, France, anne-marie.bruneau@univ-lemans.fr)

The international community recently recommended a re-definition of the kelvin referring to the value of the Boltzmann constant k, which must thus be known with a relative uncertainty of 10^{-6}. The measurement of the acoustic resonance properties of a gas filled spherical or quasi-spherical resonator is an appropriate method to do this with these requirements. Actually, a detailed modeling of the acoustic field in the resonator is required for the determination of k. Several phenomena must be taken into account including heat conduction, shear and bulk viscosity of the gas, the real shape of the resonator, the acoustic input impedance of small acoustic elements flush-mounted on the wall (tubes, transducers)... . Significant theoretical studies have already been done in which these perturbations are accounted for separately, the coupling between them being neglected. The scope here is thus to provide a unified model for the acoustic field in the cavity including all these perturbations and the resulting modal coupling, and applying it on a simple practical configuration: a spherical resonator filled with argon, acoustic transducers being flush-mounted on the wall.

5:20

5pPAc5. Towards a theory for arbitrarily shaped sound field reproduction systems. Sascha Spors (Deutsche Telekom Laboratories, Ernst-Reuter-Platz 7, 10587 Berlin, Germany, sascha.spors@telekom.de), Jens Ahrens (Deutsche Telekom Laboratories, Ernst-Reuter-Platz 7, 10587 Berlin, Germany, jens.ahrens@telekom.de)

The simple source approach predicts that a distribution of appropriately driven loudspeakers (secondary sources) enclosing a given listening area is suitable for the physical recreation of any desired exterior virtual sound field within that listening area. A specific class of sound reproduction approaches (e.g., higher-order Ambisonics) is based upon the explicit solution of the simple source formulation with respect to the secondary source driving function. To the knowledge of the authors, such an explicit solution is currently only available for specific geometries of the sound reproduction system. This contribution presents a theoretical framework for the derivation of the explicit solution for the driving function of arbitrarily shaped secondary source arrangements. It is based upon the expansion of the reproduced wave field into a series of orthogonal basis functions. These basis functions emerge from the respective underlying geometry. It is shown that most of the sound reproduction systems that are based upon the simple source formulation can be seen as specialization of the presented approach to a particular geometry and basis function.

5:40

5pPAc6. Numerical computation of reflected and transmitted waves at a fluid/solid interface. Laure Bossy (AREVA - CEZUS Research Center, Avenue Paul Girod, 73403 Ugine Cedex, France, laure.bossy@espci.fr), Marie-Françoise Cugnet (AREVA - CEZUS Research Center, Avenue Paul Girod, 73403 Ugine Cedex, France, mariefrancoise.cugnet@areva.com), Emmanuel Bossy (Laboratoire Photons et Matière, ESPCI/CNRS, 10 rue Vauquelin, 75231 Paris Cedex 05, France, emmanuel.bossy@espci.fr), Didier Cassereau (Laboratoire Ondes et Acoustique, 10, rue Vauquelin, 75231 Paris, France, didier.cassereau @espci.fr)

In this paper, we propose a numerical computation of the different waves generated when a spherical incident pulse is reflected and transmitted by a fluid/solid interface. In addition to the standard reflected and transmitted waves that propagate inside the volume, various surface waves can also be found in both propagation media. In the fluid, we can observe the longitudinal and transverse head waves, and the so-called leaky Rayleigh wave that generalizes the Rayleigh wave in a semi-infinite free solid medium to the case of an immersed interface. Similar effects can also be observed on the transmitted displacement field inside the solid material. We compare different numerical approaches, including semianalytic methods (high-frequency approximation coupled to ray modeling approach) and implicit methods (finite elements and/or finite differences scheme), each method having its own advantages and inconvenients, and domains of validity. These different methods are used to evaluate the field reflected by the interface ; the transmitted displacement field is also analyzed from the same point of view. The plane and curved geometries will be analyzed and the influence of the curvature of the interface will be pointed out.

6:00

5pPAc7. V(z) oscillations in acoustic microscope at upward defocusing. Anton V. Kozlov (MSU, Leninskie Gory, Bld. 1-2, 119991 GSP-1 Moscow, Russian Federation, av_kozlov@inbox.ru), Vladimir G. Mozhaev (MSU, Leninskie Gory, Bld. 1-2, 119991 GSP-1 Moscow, Russian Federation, vgmozhaev@mail.ru)

Acoustic microscopy is widely used for imaging and study of elastic properties of transparent and opaque materials. As a rule, multiple periodic oscillations in the output signal V of a reflection acoustic microscope can be observed in the case of negative defocusing of the wide-angle acoustic lens, i.e., when its focus is a distance z below the solid sample surface. The main well-known mechanism for $V(z)$ oscillations is the interference of radiation reflected perpendicularly from the sample surface and re-radiation of leaky Rayleigh waves generated on the sample by the lens. This effect explains high contrast imaging in reflection scanning acoustic microscopy, and it is a popular method to study properties of solids by measuring Rayleigh wave speeds. As it is shown in this work, bulk acoustic waves in the sample can also give rise to $V(z)$ oscillations. A new mechanism of such oscillations is predicted in the case of positive defocusing (focusing above the sample surface) in acoustic microscopy of anisotropic plates exhibiting negative acoustic refraction. The ray model of this effect shows a possibility to find a relationship between extrema of $V(z)$ curve and separate points on the acoustic slowness surface of the sample.

FRIDAY AFTERNOON, 4 JULY 2008 ROOM 351, 5:00 TO 6:20 P.M.

Session 5pPAd

Physical Acoustics: Scattering and Diffraction II

Michael L. Oelze, Cochair
University of Illinois at Urbana-Champaign, Beckman Institute, 405 N Mathews, Urbana, IL 61801, USA

Jean-Marc Conoir, Cochair
Institut Jean Le Rond d'Alembert-UMR CNRS 7190, Université Paris 6, tour 55-65, 4 place Jussieu, Paris, 75005, France

Contributed Papers

5:00

5pPAd1. The physics of wedge diffraction: A model in terms of elementary diffracted waves. Mitsuhiro Ueda (Predio Meguro Science Laboratory, 4-20-13 Meguro, Meguro-ku, 153-0063 Tokyo, Japan, ueda-mt @nifty.com)

A model for wedge diffraction is constructed using the virtual discontinuity principle of diffraction [1]. In the model diffracted waves are described by the sum of two elementary diffracted waves that are calculated by integrating the potential along the half line issued from the vertex of wedge. The wedge of aperture angle π/n (n=1,2,3,...) is nondiffractive since its potential can be expressed by the sum of direct waves from the point source and its mirror images. The nondiffractive wedges are useless in the conventional analysis of diffraction since there are no diffracted waves in the potential. But in this model diffracted waves of these wedges are cancelled out in the summing process. Thus the elementary diffracted waves are existed even in these wedges and far field solution for them is obtained for the nondiffractive wedge. Due to its simple structure it can be extended to the arbitrary wedge without any modification and the far field solution of diffracted waves is derived by summing the extended elementary diffracted waves in the model and it coincides with the rigorous one literally. Thus the model is verified firmly by this simple calculation. 1. M. Ueda, JASA, 95, p.2354 (1994).

5:20

5pPAd2. A global search tool for the equivalent source method and its applications to the scattering problem. Yves J.r. Gounot (UFRJ/COPPE, Universidade Federal do Rio de Janeiro, 21941-972 Rio de Janeiro, Brazil, ygounot@mecanica.ufrj.br), Ricardo E. Musafir (UFRJ/COPPE, Universidade Federal do Rio de Janeiro, 21941-972 Rio de Janeiro, Brazil, rem @serv.com.ufrj.br)

Low computational-cost solutions to the acoustic scattering problem can be obtained with the equivalent source method (ESM), provided the sources are adequately positioned. Because this last point represents often a complicated task - mainly responsible for the not much widespread use of the method - a technique that hurdles this difficulty, called ESGA, has been previously proposed (Gounot and Musafir, Internoise 2004). Based on a combination of genetic algorithm with ESM, the ESGA is a global search tool that provides, given a set of monopoles, their 'optimal' positioning and complex amplitudes. The technique efficiency is here shown through a number of three-dimensional scattering problems. The algorithm is also used in order to identify, for each of the different cases considered, typical geometrical arrangements of monopoles which provide good solutions.

5:40

5pPAd3. Convergence of correlations in multiply scattering media. Eric Larose (LGIT - CNRS - Université Joseph Fourier, Maison des Géosciences, 1381 rue de la Piscine, BP 53, 38041 Grenoble, France, Eric.Larose@obs.ujf-grenoble.fr), Arnaud Derode (Laboratoire Ondes et Acoustique, ESPCI, Université Paris 7, CNRS, 10 rue Vauquelin, 75005 Paris, France, arnaud.derode@ujf-grenoble.fr), Philippe Roux (LGIT - CNRS - Université Joseph Fourier, Maison des Géosciences, 1381 rue de la Piscine, BP 53, 38041 Grenoble, France, philippe.roux@obs.ujf-grenoble.fr), Michel Campillo (LGIT - CNRS - Université Joseph Fourier, Maison des Géosciences, 1381 rue de la Piscine, BP 53, 38041 Grenoble, France, Michel.Campillo@obs.ujf-grenoble.fr)

Correlations of ambient seismic or acoustic noise are now widely used to reconstruct the impulse response between two passive receivers as if a source was placed at on of them. Applications include terrestrial and solar seismology, underwater acoustics and structural health monitoring. Nevertheless, for a given set of data, correlations do not only yield automatically the Green function between the sensors, but also contains residual fluctuations that might ″blur″ the images. [Gizon et al, Astrophys. J. 614 (2004); Weaver and Lobkis, J. Acoust. Soc. Am. **117** (2005); Sabra et al., J. Acoust. Soc. Am. 118 (2005)]. We propose a model to describe the "signal-to-fluctuations" ratio in the correlations in the case of nonstationary wavefields, and more particularly in the case of scattering media. The work includes theoretical derivations and numerical simulations. The role of multiple scattering in the rate of convergence of the correlations toward the Green function is quantitatively evaluated [Larose et al, (submitted 2008)].

6:00

5pPAd4. Reflection and transmission coefficients of a fluid slablike region containing a depth-varying random distribution of cylinders. Jean-Marc Conoir (Institut Jean Le Rond d'Alembert-UMR CNRS 7190, Université Paris 6, tour 55-65, 4 place Jussieu, 75005 Paris, France, conoir@lmm.jussieu.fr), Sébastien Robert (LOA, UMR CNRS 7587, ESPCI, 10 rue Vauquelin, 75231 Paris, France, Sebastien.Robert@espci.fr), Abdelhak El Mouhtadi (LOMC- FRE CNRS 3102- Groupe Ondes Acoustiques, Université du Havre, place R. Schuman, 76610 Le Havre, France, abdelhak.ilel@gmail.com), Francine Luppé (LOMC- FRE CNRS 3102- Groupe Ondes Acoustiques, Université du Havre, place R. Schuman, 76610 Le Havre, France, francine.luppe @univ-lehavre.fr)

This work deals with multiple scattering by a random distribution of parallel elastic cylinders immersed in a fluid slablike region. The concentration of scatterers inside the slab is supposed to vary slowly with depth, and the WKB method is used to calculate the reflection and transmission coefficients of the slab. In order to do so, the continuity conditions on the boundaries between the slab and the surrounding fluid are needed. They follow from the application of Twersky's theory to the case of a slab with a given constant concentration of scatterers, which shows that both pressure and normal displacement are continuous, provided an effective mass density of the slab is correctly defined. The results of the WKB are successfully compared to those obtained from the discretization of the slab into layers of constant concentrations of cylinders and the use of Twersky's theory.

FRIDAY AFTERNOON, 4 JULY 2008 ROOM 241, 2:00 TO 6:20 P.M.

Session 5pPPa

Psychological and Physiological Acoustics and Speech Communication: Acoustic Features and Speech Perception II

Jont B. Allen, Cochair
University of IL, 405 N. Mathews, Room 2061 Beckman Inst. (MC 251), Urbana, IL 61801, USA

Sarah Hawkins, Cochair
University of Cambridge, Department of Linguistics, Sidgwick Avenue, Cambridge, CB3 9DA, UK

Invited Papers

2:00

5pPPa1. Reception of phonetic features in fluctuating background noise maskers. Christian Lorenzi (Univ Paris Descartes, CNRS, Ecole Normale Superieure, DEC, 29 rue d'Ulm, 75005 Paris, France, lorenzi@ens.fr)

We will review recent studies investigating the reception of phonetic features (voicing, manner and place of articulation) in nonstationary background maskers. In each study, consonant identification was assessed in steady and amplitude-modulated speech-shaped noise at signal-to-noise ratios yielding about 50% correct in steady noise. The rate and depth of amplitude modulation applied to the noise masker were either fixed or systematically varied. Confusion matrices were compiled across listeners and the amount of release from masking (percent information received in nonsteady minus steady noise) was calculated for each phonetic feature and experimental condition. Speech and noise mixtures were (i) left intact (unfiltered), (ii) lowpass filtered (<1.5 kHz), or iii) processed in order to

degrade spectral (place of excitation in the cochlea) and/or temporal fine structure cues. Overall, the results indicate that release from masking typically reported in normal-hearing listeners (i.e., the substantial improvement in speech reception in fluctuating noise compared to steady noise) is not identical across phonetic features. This suggests that the ability to "glimpse" into background noise valleys involves multiple auditory processes constrained by both peripheral and central factors.

2:20

5pPPa2. Identification of intervocalic consonants in stationary and nonstationary noise. Martin Cooke (Sheffield University, Computer Science Department, Regent Court, 211 Portobello St., S1 4DP Sheffield, UK, m.cooke@dcs.shef.ac.uk), Odette Scharenborg (Centre for Language and Speech Technology, Radboud University Nijmegen, Erasmusplein 1, 6525 HT Nijmegen, Netherlands, O.Scharenborg@let.ru.nl)

The factors which underlie the perception of consonants in noise remain poorly understood. In this study, native listeners identified 24 English consonants spoken by eight talkers presented in nine intervocalic contexts with varying stress position. Listeners were tested in 5 noise conditions: tokens were masked by stationary speech-shaped noise, a competing talker, three and eight speaker babble and speech-modulated noise, all of which have the long-term spectrum of speech. The rank ordering of consonant identification scores in stationary noise was highly-correlated ($r=0.9$, $p<0.0001$) with a similar condition reported by Phatak and Allen [JASA **121**: 2312-2326, 2007], but less so in the four nonstationary noise backgrounds ($r=0.74$, $p<0.001$). In particular, /y/, /r/, /l/, /f/, /ch/, /sh/, /m/ and most of the plosives showed a wide variation in ranking. These findings suggest that, in addition to the long-term spectrum of the masker, consonant identification is noise is affected by other factors such as temporal fluctuations in the masker, misallocation of foreground-/background components and attention.

2:40

5pPPa3. The interaction of glimpsing, pitch and vocal tract length in the recognition of concurrent syllables. Martin D. Vestergaard (Centre for the Neural Basis of Hearing, Department of Physiology, Development and Neuroscience, University of Cambridge, Downing Site, CB23EG Cambridge, UK, mdv23@cam.ac.uk), Nicolas R. Fyson (Centre for the Neural Basis of Hearing, Department of Physiology, Development and Neuroscience, University of Cambridge, Downing Site, CB23EG Cambridge, UK, nickfyson@gmail.com), Roy D. Patterson (Centre for the Neural Basis of Hearing, Department of Physiology, Development and Neuroscience, University of Cambridge, Downing Site, CB23EG Cambridge, UK, rdp1@cam.ac.uk)

In multispeaker environments, human listeners use the temporal misalignment of competing speech signals to improve recognition-an effect referred to as "glimpsing." When the temporal envelopes of concurrent syllables pairs are carefully matched to preclude glimpsing, listeners were observed to use vocal tract length (VTL) and glottal pulse rate (GPR) cues to improve recognition. This paper reports an investigation of the interaction between glimpsing and these vocal cues. Syllables were synthesized with a vocoder to simulate speakers with widely different combinations of GPR and VTL. Recognition of one syllable in the presence of a concurrent syllable was measured as the vocal cues and the temporal alignment of the syllables were varied. The effect of glimpsing was most pronounced when the vocal cue differences between the target and distracter syllables were small. Furthermore, there was a strong effect of consonant type (stops, fricatives, or sonorants) and an asymmetry between consonant-vowel (CV) and vowel-consonant (VC) syllables. The lowest recognition rate was observed, not at perfect temporal alignment but rather at a distracter lag of -50 ms for CVs and 100 ms for VCs. The results are analyzed with confusion matrices. Research supported by the UK MRC [G0500221, G9900369].

3:00

5pPPa4. Phoneme confusions as a function of noise, spectral resolution and L2 experience. Robert Shannon (House Ear Institute, 2100 W. Third St., Los Angeles, CA 90057, USA, shannon@hei.org), Monica Padilla (House Ear Institute, 2100 W. Third St., Los Angeles, CA 90057, USA, mpadilla@hei.org)

Consonant and vowel confusion matrices were measured from normal hearing listeners with varying degrees of experience in English. There were five listeners each in the following categories: native English speakers, and Spanish speakers who were immersed in English at the ages of 0-5 years, 5-10 years, 10-18 years, and over 18 years. 12 vowels (hVd) or 18 consonants (vCv) were presented and responses were collected in a confusion matrix. Spectral resolution was varied by using a noise-band vocoder with 2, 4, 6, 8, and 16 channels, as well as unprocessed speech. All stimuli were presented in speech shaped noise at SNR levels of -5 dB to +15 dB in 5 dB steps as well as in quiet. Noise and spectral resolution had a similar effect on voicing, manner and place of articulation, and also had similar effects as a function of L2 experience. For native speakers of Spanish the duration of L2 experience had the largest effect on voicing cues, less effect on manner cues, and almost no effect on place cues.

3:20

5pPPa5. The perceptual flow of phonetic feature processing. Steven Greenberg (Technical University of Denmark, Center for Applied Hearing Research, Ørsteds Plads, Building 352, 2800 Lyngby, Denmark, steveng@silicon-speech.com), Thomas Ulrich Christiansen (Technical University of Denmark, Center for Applied Hearing Research, Ørsteds Plads, Building 352, 2800 Lyngby, Denmark, tuc@oersted.dtu.dk)

How does the brain process spoken language? It is our thesis that word intelligibility and consonant identification are insufficient by themselves to model how the speech signal is decoded - a finer-grained approach is required. In this study, listeners identified 11 different Danish consonants spoken in a Consonant + Vowel + [l] environment. Each syllable was processed so that only a portion of the original audio spectrum was present. Three-quarter-octave bands of speech, centered at 750, 1500, and 3000 Hz, were presented individually and in combination with each other. The conditional, posterior probabilities associated with phonetic-feature decoding were computed from confusion matrices in order to deduce the temporal flow of phonetic processing. Decoding the feature, Manner-of-Articulation, depends on accurate decoding of the feature Voicing (but not vice-versa), and decoding Place-of-Articulation requires

precise decoding of Manner (but not the converse). From these data, we conclude that Voicing is processed prior to Manner-of-Articulation, and that Manner is decoded prior to Place-of-Articulation. Voicing and Manner cues are often correctly decoded in conditions where Place is not. This asymmetric pattern of feature decoding may provide extra-segmental information of utility for speech processing, particularly in adverse listening conditions.

3:40

5pPPa6. Understanding the complex modulation spectrum for consonants and consonant features. Kenneth W. Grant (Walter Reed Army Medical Center, Army Audiology and Speech Center, 6900 Georgia Ave. NW, Washington, DC 20307-5001, USA, grant@tidalwave.net), Sandeep A. Phatak (Walter Reed Army Medical Center, Army Audiology and Speech Center, 6900 Georgia Ave. NW, Washington, DC 20307-5001, USA, s.a.phatak@gmail.com), Elena Grassi (Walter Reed Army Medical Center, Army Audiology and Speech Center, 6900 Georgia Ave. NW, Washington, DC 20307-5001, USA, elena.grassi@gmail.com)

Speech intelligibility is highly dependent on the magnitude and phase characteristics of the low-frequency modulation spectrum. However, unlike more traditional representations of speech, such as the spectrogram, associating details of the modulation spectrum to specific phonemes and subphonemic units of speech has not been readily forthcoming. In the present study we used local time reversals of the speech waveform between 20-160 ms to selectively distort portions of the complex modulation spectrum. Normal-hearing subjects were tested on a consonant recognition task and a detailed analysis of the perceptual confusions was performed. Consistent with earlier results using sentence-length materials, average consonant intelligibility declined as the length of the time reversal segment increased. Further analyses were conducted to determine the effect of time-reversal segment duration on the amount of information transmitted for individual consonants (including specific consonant productions) and acoustic features for voicing, manner of articulation, and place of articulation. An acoustic analysis using a biologically motivated auditory processing model was also performed to determine the effect of time reversals on cochlear and cortical representations of speech. The relations between changes to the complex modulation spectrum and the percent information transmission of selected speech segments and features are discussed.

4:00-4:20 Break

4:20

5pPPa7. Can CV intelligibility predict speech intelligibility? Sarah Hawkins (University of Cambridge, Department of Linguistics, Sidgwick Avenue, CB3 9DA Cambridge, UK, sh110@cam.ac.uk)

This paper begins by reviewing the speech perception literature to predict cues that would and would not be expected to survive energetic masking of various types. The focus is especially (but not exclusively) on spectrotemporal cues to stops in the vicinity of the segment boundary in CV syllables. The second part of the paper discusses influences that can restrict the generality of research findings from isolated CV syllables. This includes ways in which CV syllables change in different phonetic contexts and styles of speech, contributions of the visual modality, and other uses of top-down information, such as phonotactic, lexical, semantic and syntactic probability. The paper concludes by asking whether-and how-simple measures such as CV intelligibility can be used to reflect intelligibility of speech in real-life communicative situations.

4:40

5pPPa8. The role of the cochlear processing in human speech recognition. Jont B. Allen (University of IL, 405 N. Mathews, Room 2061 Beckman Inst. (MC 251), Urbana, IL 61801, USA, jontallen@ieee.org), Marion Regnier (208 S. 3rd St. Apt 5A, Brooklyn, NY 11211, USA, marion.regnier@gmail.com), Sandeep Phatak (Walter Reed Hospital, Silver Springs, MD 20901, USA, s.a.phatak@gmail.com), Feipeng Li (University of IL, 405 N. Mathews, Room 2061 Beckman Inst. (MC 251), Urbana, IL 61801, USA, fli2@uiuc.edu)

Little is know about how the auditory system decodes speech. We may think of speech communication re Shannon's source-channel model, thus viewed, the most complex part of the speech communication channel is the auditory system (the receiver). In my speech-perception research, I have attempted to limit the assumptions, and have thus fallen back on Shannon's basic source-channel model. The basic tool is the confusion matrix (CM) for isolated natural consonant and vowels (CV), as a function of the speech to noise ratio (SNR), with several types of masking noise. We have used large numbers of talkers and listeners (i.e., 20). In a second experiment we selectively remove islands of speech in time-frequency, and then correlate the resulting modified speech against subject scores. Our most important conclusions are: (1) The across-frequency onset transient portion of the signal is typically the most important. (2) The spectral regions of these transient are used to code different consonants. (3) While the frequency regions for a given consonant are correlated to the following vowel, this may not be important for perception. (4) Compact spectral-temporal amplitude modulations components (e.g., a 10 Hz modulation) do not seem to play a significant role, at least above 1-2 kHz.

Contributed Papers

5:00

5pPPa9. Spectral and temporal modulations essential to spoken word, gender and timbre identification. Frédéric E. Theunissen (UC Berkeley, Dept. of Psychology, 3210 Tolmant Hall, Berkeley, CA 94720-1650, USA, theunissen@berkeley.edu), Taffeta Elliott (UC Berkeley, Dept. of Psychology, 3210 Tolmant Hall, Berkeley, CA 94720-1650, USA, taffeta@berkeley.edu)

Human speech and musical sounds contain complex spectral and temporal modulations. Speech intelligibility, perception of melody, and identification of source characteristics (e.g., speaker gender or musical timbre) depend on spectrotemporal modulations but can be surprisingly robust to drastic spectral and temporal degradations. We systematically explored which restricted spectral and temporal modulations are essential to the perception of complex sounds. Degraded sentences and musical sounds were obtained by a novel modulation filtering procedure performed on the sound spectrogram. Temporal modulation filtering smeared the amplitude envelope by removing changes above particular Hz. Spectral modulation filtering smeared the spectral energy across frequency bands by removing changes above particular cyc/kHz. We further complemented this low-pass filtering with more specific notch-filtering. Speech intelligibility, gender recognition

and musical instrument identification were assessed in psychophysical experiments. We determined that spectral modulations below ~3.75 cyc/kHz, and temporal modulations between 1 and 7 Hz are essential for speech comprehension. Gender identification however required the presence of higher spectral modulations. Similarly the timbre and pitch of instruments was affected differentially by notch filters in these two regions of the modulation spectrum. Our research could be used to guide the design of optimal signal processing in hearing aids and cochlear implants.

5:20

5pPPa10. A model with compression for estimating speech intelligibility in quiet and in noise. Koenraad S. Rhebergen (AMC - Dept. of Clinical and Experimental Audiology, AMC, Clinical and Experimental Audiology, 1105 Amsterdam, Netherlands, k.s.rhebergen @amc.uva.nl), Johannes Lyzenga (Vrije Universiteit Medical Center, Boelelaan 1117, 1081 HV Amsterdam, Netherlands, j.lyzenga@vumc.nl)

For speech reception thresholds (SRTs), measured in normally-hearing listeners using various types of stationary noise, the Speech Intelligibility Index (SII, ANSI S3.5-1997) model predicts a fairly constant speech proportion (of about 0.3) necessary for sentence intelligibility. For SRTs in quiet, the estimated speech proportions are often lower, and show a larger inter-subject variability, than found for speech in noise near normal speech levels. This might be related to the fact that cochlear compression is larger at normal speech levels than near the threshold for speech in quiet. The SII model does not take this into account. The present model attempts to alleviate this problem by including cochlear compression. It is based on a loudness model for normally-hearing and hearing-impaired listeners [ANSI S3 .4-2007]. It estimates internal excitation levels of the speech, accounts for the compressed effective dynamic range of the internal speech signal, and calculates the proportion of speech above threshold using similar spectral weighting as used in the standard SII. The present model and the standard SII were used to predict SRTs in quiet and noise for both normally-hearing and hearing-impaired listeners. The present model predicted speech intelligibility with less variability than the standard SII.

5:40

5pPPa11. Listeners' sensitivity to talker differences in voice-onset-time: Segments versus features. Rachel M. Theodore (Northeastern University, Dept. of Psych. - 125 NI, 360 Huntington Ave., Boston, MA 02115-5000, USA, r.theodore@neu.edu), Joanne L. Miller(Northeastern University, Dept. of Psych. - 125 NI, 360 Huntington Ave., Boston, MA 02115-5000, USA, j.miller@neu.edu)

Recent findings indicate that listeners are sensitive to talker differences in phonetic properties of speech, including voice-onset-time (VOT) in word-initial voiceless stop consonants. Here we extend earlier findings from our laboratory [J. S. Allen and J. L. Miller, J. Acoust. Soc. Am. **115**, 3171-3813 (2004)] by examining the level of representation underlying this sensitivity. In familiarization phases, listeners heard two talkers produce pain. Critically, word-initial VOTs were manipulated such that one talker produced short VOTs and the other talker produced long VOTs. In test phases, listeners were presented with a short-VOT and long-VOT variant of either pain or cane; in both cases, listeners were asked to select which of the two VOT variants was most representative of a given talker. Results to date indicate that which variant of pain is selected at test is in line with listeners' exposure during training (replicating earlier findings), and that this effect holds even when listeners are tested on cane, which begins with a different voiceless stop than heard during training. These results suggest that listeners are sensitive to talker differences in VOT at the level of a phonetic feature, rather than at the level of a particular phonetic segment.

6:00

5pPPa12. Amplitude modulation of noise cues voicing distinction in fricatives. Jonathan Pincas (University of Surrey, GU2 7XH Guildford, UK, jon@pincas.co.uk), Philip J. Jackson (University of Surrey, Centre for Vision, Speech and Signal Processing, GU2 7XH Guildford, UK, p.jackson @surrey.ac.uk)

The aperiodic noise source in fricatives is characteristically amplitude modulated by voicing. Previous psychoacoustic studies have established that observed levels of AM in voiced fricatives are detectable, and its inclusion in synthesis has improved speech quality. Phonological voicing in fricatives can be cued by a number of factors: the voicing fundamental, duration of any devoicing, duration of frication, and formant transitions. However, the possible contribution of AM has not been investigated. In a cue trading experiment, subjects distinguished between the nonsense words "ahser" and "ahzer." The voicing boundary was measured along a formant-transition duration continuum, as a function of AM depth, voicing amplitude and masking of the voicing component by low-frequency noise. The presence of AM increased voiced responses by approximately 30%. The ability of AM to cue voicing was strongest at greater modulation depths and when voicing was unavailable as a cue, as might occur in telecommunication systems or noisy environments. Further work would examine other fricatives and phonetic contexts, as well as interaction with other cues.

Session 5pPPb

Psychological and Physiological Acoustics and Computational Acoustics: Computational Auralization II

Durand R. Begault, Cochair
NASA Ames Research Center, Mail Stop 262-2, NASA ARC, Moffett Field, CA 94035, USA

Lauri Savioja, Cochair
Helsinki University of Technology, Department of Media Technology, PO Box 5400, TKK, 02015, Finland

Contributed Papers

2:00

5pPPb1. Externalization in binaural synthesis: effects of recording environment and measurement procedure. Florian Völk (AG Technische Akustik, MMK, TU München, Arcisstr. 21, 80333 München, Germany, florian.voelk@mytum.de), Fabian Heinemann (AG Technische Akustik, MMK, TU München, Arcisstr. 21, 80333 München, Germany, hef@mmk.ei.tum.de), Hugo Fastl (AG Technische Akustik, MMK, TU München, Arcisstr. 21, 80333 München, Germany, fastl@mmk.ei.tum.de)

Databases of head related impulse responses (HRIRs) for binaural synthesis can be measured either in anechoic or reflective environments. If high synthesis quality is needed, miniature microphone measurements are performed in the ear canals of each individual user (individual measurement). Sometimes impulse responses measured in the ear canals of one individual are used for synthesis for other persons (nonindividual measurement). In most other cases artificial head measurements are used. This paper considers the dependence of the perceived distance of auditory images (externalization) on the measurement procedure (individual, nonindividual, artificial head) and on the recording environment (anechoic, reflective). For each measurement the same system and the same setup, especially the same geometric parameters, are used. Differences in the corresponding impulse response databases are determined and related to the subjective relative externalization differences in the front, in the back, and to both sides. For each direction a seven point rating scale was used. Statistical analysis suggests that the measurement parameters applied influence the externalization of auditory images.

2:20

5pPPb2. Smart sound environments: merging intentional soundscapes, nonspeech audio cues and ambient intelligence. Ralf Jung (Universität des Saarlandes, LS Wahlster, FB Informatik, Bldg. E 1 1, Room 1.18, 66123 Saarbrücken, Germany, rjung@cs.uni-sb.de)

We introduce an intelligent audio notification system for multiuser environments that provides users with information about events (e.g., important emails) in a more discreet and non-distracting way. The peripheral awareness of individual-related events is done by using nonspeech audio cues which can be seamlessly integrated into artificial background soundscapes. These ambient soundscapes are self-composed with respect to well-known perceptual constraints such as auditive Gestalt laws as well as music psychological findings. To follow a hierarchical approach for the notification sounds we use notification instruments, ambient noises and traditional alert signals that are grouped by their level of intrusiveness. Since the notification system also follows a human-centered approach it takes parameters like user preferences, his/her current position in the environment and the type of event into consideration to decide which notification is the appropriate at this time. In the paper, we will describe the architecture of the personalized ambient audio notification service, compositional constraints as well as some findings of a user study in which we tested successfully the efficiency of our system with 25 subjects.

2:40

5pPPb3. A virtual auditory environment for investigating the auditory signal processing of realistic sounds. Sylvain Favrot (CAHR, Department of Electrical Engineering, DTU, Ørsteds Plads, Bygning 352, 2800 Kgs. Lyngby, Denmark, sf@oersted.dtu.dk), Jörg M. Buchholz (CAHR, Department of Electrical Engineering, DTU, Ørsteds Plads, Bygning 352, 2800 Kgs. Lyngby, Denmark, jb@oersted.dtu.dk)

In the present study, a novel multichannel loudspeaker-based virtual auditory environment (VAE) is introduced. The VAE aims at providing a versatile research environment for investigating the auditory signal processing in real environments, i.e., considering multiple sound sources and room reverberation. The environment is based on the ODEON room acoustic simulation software to render the acoustical scene. ODEON outputs are processed using a combination of different order Ambisonic techniques to calculate multichannel room impulse responses (mRIR). Auralization is then obtained by the convolution of the mRIR with an acoustic signal. The derivation of the mRIRs takes into account that (i) auditory localization is most sensitive to the location of the direct sound and (ii) that auditory localization performance is rather poor for early reflections and even worse for late reverberation. Throughout the VAE development, special care was taken in order to achieve a realistic auditory percept and to avoid "artifacts" such as unnatural coloration. The performance of the VAE has been evaluated and optimized on a 29 loudspeaker setup using both objective and subjective measurement techniques.

3:00

5pPPb4. Real-time auralization system based on beam-tracing and mixed-order Ambisonics. Markus Noisternig (LIMSI-CNRS, B.P. 133, 91403 Orsay, France, markus.noisternig@limsi.fr), Lauri Savioja (Helsinki University of Technology, Department of Media Technology, PO Box 5400, 02015 TKK, Finland, Lauri.Savioja@tkk.fi), Brian F. Katz (LIMSI-CNRS, B.P. 133, 91403 Orsay, France, brian.katz@limsi.fr)

Auralization, the final step in computational room acoustic simulations, aims to make audible the acoustics of complex virtual architectural spaces in a realistic and accurate manner. This paper presents a novel real-time auralization system comprising a geometry engine, a beam-tracer, and an audio renderer. The computation of early reflection paths is based on an efficient beam-tracing algorithm capable of real-time detection of specular reflection paths in a static geometry with one or several moving listener(s). For simpler rooms, the real-time performance is maintained even with dynamic geometries and sources. Results of the beam-tracer, sent to the audio renderer, consist of visible reflection paths and their accumulated material attenuation. From this geometrical and acoustical data, listener position-related 3D room impulse responses are generated applying a higher-order virtual Ambisonics approach. Final rendering of the binaural room impulse response (BRIR) is made taking into account the listener's head-orientation. As higher order reflections are more diffuse in nature, they may be encoded using lower Ambisonic orders, thereby reducing computational load. The environment combines high quality audio with visual rendering realized using the open source platforms Pure Data and VirChor respectively. This auralization framework provides direct audio-visual feedback in real-time for VR environments.

Invited Papers

3:20

5pPPb5. Real-time auralization of modifiable rooms. Dirk Schröder (Institute of Technical Acoustics, RWTH Aachen University, Neustr. 50, 52066 Aachen, Germany, dsc@akustik.rwth-aachen.de), Ingo Assenmacher (Virtual Reality Group, RWTH Aachen University, Seffenter Weg 23, 52074 Aachen, Germany, assenmacher@rz.rwth-aachen.de)

Immersive virtual environments are a powerful tool for acousticians and architects to design buildings if the virtual reality system provides an interactive imaging of virtual sound sources with respect to the rooms' physical aspects. Current implementations using hybrid room acoustic simulation methods (e.g., combining image sources and ray tracing) enable the user to walk freely in such virtual architectural spaces, whereby the position/orientation of sound sources are interactively manipulable to detect possible acoustic defects, e.g., flutter echoes. In the case of coupled rooms, sound transmission effects must be included into the real-time simulation in order to identify deficient airborne sound insulation, whereby current implementations only support a change of state (open/closed) of fixed room-connecting elements, e.g., doors and windows. However, in scenarios like an architectural planning stage, it is convenient to manipulate the room geometry more freely, e.g., via the interactive positioning of stage reflector panels, but common spatial data structures, e.g., BSP- or Octrees do not efficiently support these operations. For this purpose, the concept of Spatial Hashing, which originates from computer graphics for collision detection of deformable objects, is applied to the simulation process. This adaptation also features an efficient identification and update process of image sources.

3:40

5pPPb6. Comparison of auralisation results betwee measurements and simulations of line arrays with high resolution modeling data. Wolfgang Ahnert (Ahnert Feistel Media Group, Arkonastr. 45-49, 13189 Berlin, Germany, wahnert@ada-acousticdesign.de), Stefan Feistel (Ahnert Feistel Media Group, Arkonastr. 45-49, 13189 Berlin, Germany, sfeistel@afmg.eu), Ralph Bauer-Diefenbach (Ahnert Feistel Media Group, Arkonastr. 45-49, 13189 Berlin, Germany, rbauer@ada-acousticdesign.de)

In a concert hall a direct comparison of several line arrays for a new sound system has been made. At different locations the binaural impulse response has been measured and used for auralisation. In a computer model of the hall the measured line array was implemented. The single array sources have been modeled in different modes like far-field cluster, simple module array or as a high-resolution loudspeaker array. By means of the new developed SpeakerLab Module these source simulators have been created and afterwards used to calculate binaural impulse responses at the corresponding seats equal to the measurements. After that an auralisation routine has been used. The results are compared for the different degrees of source resolution and with the measurements. Beside acoustic measures the subjective sound quality of the different auralisation results is reported.

4:00-4:20 Break

Contributed Paper

4:20

5pPPb7. Investigation on the restitution system influence over perceived Higher Order Ambisonics sound field: a subjective evaluation involving from first to fourth order systems. Stephanie Bertet (IRCAM, 1 Place Igor Stravinsky, 75004 Paris, France, Stephanie.Bertet@ircam.fr), Jérôme Daniel (France Telecom R&D, 2 avenue Pierre Marzin, 22300 Lannion, France, jerome.daniel@orange-ftgroup.com), Etienne Parizet (Laboratoire Vibrations Acoustique, Insa Lyon, 25 bis, av. J. Capelle, 69621 Villeurbanne Cedex, France, etienne.parizet@insa-lyon.fr), Olivier Warusfel (IRCAM, 1 Place Igor Stravinsky, 75004 Paris, France, Olivier.Warusfel@ircam.fr)

Among the spatial audio reproduction techniques over loudspeakers, the Higher Order Ambisonics (HOA) approach is based on a sound field spherical harmonics decomposition. By truncating the decomposition to the Mth order, it remains a finite number of components that form the spatial HOA format. The more components are used to encode the sound field, the finer the spatial resolution is. Similarly, the size of the area where the sound field is accurately recreated is proportional to the order. For an Mth encoding order, $N=2M+2$ equally distributed loudspeakers are recommended for a homogeneous reproduction in the horizontal plane. Adding loudspeakers does not change the spatial resolution. However, what is the influence of the restitution system on the perceived sound field? An experiment was designed in order to compare four systems (from first to fourth order) and a reference one, using similarity ratings obtained from pairwise comparisons. Two sound scenes were used, simulating an audio conference and a scene in a kitchen at home. 25 listeners participated to the experiment. The results were analysed using the Indscal method. The perceptual space appeared to be a two dimensional one, highlighting the influence of the order and the number of loudspeakers on the reproduced scenes.

Invited Papers

4:40

5pPPb8. Recording of anechoic symphony music. Tapio Lokki (Helsinki University of Technology, P.O. Box 5400, 02015 TKK, Finland, Tapio.Lokki@tkk.fi), Jukka Pätynen (Helsinki University of Technology, P.O. Box 5400, 02015 TKK, Finland, jpatynen@tml.hut.fi), Ville Pulkki (Helsinki University of Technology, P.O. Box 5400, 02015 TKK, Finland, Ville.Pulkki@tkk.fi)

When designing the acoustics of a concert hall, it would be beneficial to be able to use real recording of a symphony orchestra in auralization. The technical constraints for such recordings are high. First, the instruments have to be recorded separately, as in simultaneous recording the cross talk between microphones could not be avoided. Second, the recording room should be anechoic. Third, the instruments have different sound radiation patterns, thus they should be recorded with multiple microphones around them. Therefore, we end up recording each instrument individually in an anechoic chamber with multiple microphones. The remaining problem is to achieve a common timing as an ensemble between the individually recorded instruments. This was solved by first recording a video of a conductor conducting a pianist playing the whole score. The players in an anechoic chamber then followed the conductor in a monitor while

listening the pianist on headphones. Four short passages, from two to four minutes, from different music styles were recorded. The recordings were made with 20 low-self-noise microphones, mounted on the shape of a dodecahedron. Finally, we discuss the musical and technical quality of recorded sound, and the response by the musicians, who were professional orchestra players.

5:00

5pPPb9. Uni-Verse Acoustic Simulation System: interactive real-time room acoustic simulation is dynamic 3D environments. Peter Lundén (Interactive Institute, Box 1197, SE-164 26 Kista, Sweden, plu@tii.se)

Uni-Verse Acoustic Simulation System (UVAS) is a newly developed interactive room acoustic simulation system that can handle dynamically changing 3D geometric models in real-time. The system can share such models with other application, such as visual renderers or 3D modeling tools, over a network using the Verse protocol. UVAS is implemented using the beam-tracing method. It is build as two separate but highly integrated parts. The first part is handling the geometry, it's responsibility is to find audible sound sources and relevant reflection paths in the simulated environment. The second part is handling the audio rendering, producing the audible result of the simulation based on information given by the first part. This paper will focusing on the first part

5:20

5pPPb10. Case study of measurements and computer modeling auralization results for medium-sized multipurpose halls. Hari V. Savitala (Charles M Salter Associates, Inc., 130 Sutter St, Suite 500, San Francisco, CA 94104, USA, hari.savitala@cmsalter.com), Jason Duty (Charles M Salter Associates, Inc., 130 Sutter St, Suite 500, San Francisco, CA 94104, USA, jason.duty@cmsalter.com), Christopher Peltier (Charles M Salter Associates, Inc., 130 Sutter St, Suite 500, San Francisco, CA 94104, USA, christopher.peltier@cmsalter.com)

This case study focuses on auralizations and their accuracy in modeling medium-sized multipurpose halls (400-600 seats). Within each hall, impulse response measurements were taken with drapes deployed and retracted. The same configurations were modeled in the room acoustics program ODEON. Acoustical parameters, such as T20, T30, C50, C80, were used to check the agreement of the model to the measurements. A systematic approach was then used to adjust model parameters to match the real-world measurements. The modified and unmodified auralizations were then used to determine if any differences could be perceived in an informal listening evaluation. The auralizations and listening evaluation results are presented to better understand how to accurately auralize medium-sized multipurpose halls.

Contributed Papers

5:40

5pPPb11. Real-time 3D audio for digital cinema. Pau Arumi (Universitat Pompeu Fabra - Fundació Barcelona Media, Ocata, 1, 08003 Barcelona, Spain, parumi@iua.upf.edu), David Garcia (Fundacio Barcelona Media, Carrer Ocata n° 1, 08003 Barcelona, Spain, dgarcia@iua.upf.edu), Toni Mateos (Universitat Pompeu Fabra - Fundació Barcelona Media, Ocata, 1, 08003 Barcelona, Spain, toni.mateos@barcelonamedia.org), Adan Garriga (Universitat Pompeu Fabra - Fundació Barcelona Media, Ocata, 1, 08003 Barcelona, Spain, adan.garriga@barcelonamedia.org), Jaume Durany (Universitat Pompeu Fabra - Fundació Barcelona Media, Ocata, 1, 08003 Barcelona, Spain, jaume.durany@upf.edu)

We present a real-time 3D audio system with a number of nice features: it is suited for plausible reference with the visual environment, it is real-time capable, it can process multiple moving sound sources and listeners in a normal CPU. In our approach, a database of pressure and velocities impulse-responses (IRs) is computed offline for each (architectural) environment using physically based ray-tracing techniques. During playback, the real-time system retrieves IRs corresponding to the sources and target positions, performs a low-latency partitioned convolution and smoothes IR transitions with cross-fades. Finally, the system is flexible enough to decode to any surround exhibition setup. The software has been developed within the CLAM open-source audio framework. We present a real scenario where these techniques were successfully applied: an augmented-reality film with 3D audio within the context of the IP-RACINE project for digital cinema. The shooting was done with a high-end prototype camera with zoom and position tracking which enabled the real-time motion of a subjective listener within the scene. Our technology enabled the film director to both pre-hear surround audio of an augmented-reality scene shooting and fine-tune audio rendering in post-production.

6:00

5pPPb12. Near-field binaural synthesis, experimental progress report. Dylan Menzies-Gow (De Montfort University, Queens Building, LE1 9BH Leicester, UK, dylan@dmu.ac.uk)

A methodology was previously presented for displaying high quality binaural images of near-field complex sources, using wave reconstruction. Multipole representations of objects are transformed to Fourier-Bessel and plane wave expansions at the listener, before conversion to binaural signals. One advantage of this approach is that does not require special HRTF information other than the planewave HRTFs, and can fully render the complex field of a near object. As a first step towards a full working system, a real-time implementation is described here for displaying a monopole source using a six degrees-of-freedom infrared head tracking device.

Session 5pSC

Speech Communication: Multimodal Speech Technology

Gerasimos Potamianos, Cochair
IBM T. J. Watson Research Center, RTE 134, Yorktown Heights, NY 10598, USA

Gerard Bailly, Cochair
GIPSA-lab. Dept Speech & Cognition, INPG, 46, av. Félix Viallet, Grenoble, 38031, France

Contributed Paper

2:00

5pSC1. An ultrasound-based silent speech interface. Thomas Hueber (ESPCI - Telecom Paris, 10 rue Vauquelin, 75005 Paris, France, hueber@ieee.org), Gerard Chollet (Telecom Paris Tech, 46 rue Barrault, 75013 Paris, France, chollet@enst.fr), Bruce Denby (Université Paris VI, ESPCI - Laboratoire d'Electronique, 10 rue Vauquelin, 75005 Paris, France, denby@ieee.org), Gerard Dreyfus (Université Paris VI, ESPCI - Laboratoire d'Electronique, 10 rue Vauquelin, 75005 Paris, France, gerard.dreyfus@espci.fr), Maureen Stone (Vocal Tract Visualization Lab, Depts of Biomedical Sciences and Orthodontics, University of Maryland Dental School, 650 W. Baltimore St., Baltimore, MD 21201, USA, mstone @umaryland.edu)

The paper proposes the use of ultrasound scans of tongue movement and video sequences of the lips to synthesize speech. A speech synthesizer driven only by video acquisitions may be qualified as a "silent speech interface," which could be used by laryngectomyzed patient as an alternative to tracheo-esophageal speech, for voice communication where silence must be maintained, or in very noisy environments. Our system is based on the building of a one-hour audiovisual corpus of phonetic units, which associates visual features extracted from video with acoustic observations. The ultrasound and optical images are interpreted as a linear combination of standard configurations obtained by principal components analysis (PCA) from a phonetically balanced subset of typical frames. HMM-based stochastic models trained on these visual features sequences are subsequently used to predict phonetic targets from video-only data. Finally, a Viterbi unit selection algorithm is used to find the optimal sequence of acoustic units given both this phonetic prediction and the sequence of visual features. The system is able to perform phonetic transcription from video-only speech data with over 55% correct recognition, on continuous speech, using neither phonotactic nor linguistic constraints.

Invited Papers

2:20

5pSC2. Multimodal control of talking heads. Gerard Bailly (GIPSA-lab. Dept Speech & Cognition, INPG, 46, av. Félix Viallet, 38031 Grenoble, France, gerard.bailly@gipsa-lab.inpg.fr), Oxana Govokhina (GIPSA-lab. Dept Speech & Cognition, INPG, 46, av. Félix Viallet, 38031 Grenoble, France, oxana.govokhina@gipsa-lab.inpg.fr), Gaspard Breton (Orange R&D, 4 rue du Clos Courtel, 35512 Cesson-Sévigné, France, gaspard.breton@orange-ftgroup.com)

Multimodal speech synthesis has been devoted for years to the rendering of linguistic or paralinguistic content - i.e., parametrized but discrete information - by continuous audible and visible consequences of speech articulation, eventually complemented by facial expressions, gaze and other body gestures including head, hand, and arm movements. Articulatory synthesizers (producing sounds from gestures) intrinsically compute coherent audiovisual signals but do not presently compete with data-driven techniques: most talking heads are nowadays controlled by models built using human audiovisual data. These control models should replicate the laws governing the coherence of observed multimodal signals and the correct phasing relations between salient events of the multimodal stream. We will report on two comparative evaluations of various lip-sync models (dealing with post-synchronization between speech sounds and articulatory movements) and present a trainable control model that learns automatically phasing relations between acoustic and gestural events. This model can be further extended to capture the fine temporal structure of multimodal scores and a first application to the synchronization between speech and head, face and hand movements during cued speech production will be presented.

2:40

5pSC3. Statistical conversion of speech parameter trajectory for mapping between features of different modalities. Tomoki Toda (Nara Institute of Science and Technology, 8916-5 Takayama-cho, Ikoma, 630-0192 Nara, Japan, tomoki@is.naist.jp)

A state-of-the-art speech parameter conversion technique and its application to a mapping between features of different modalities are reviewed. Many statistical approaches to the parameter conversion have been studied particularly for voice conversion in speech synthesis research. A typical method conducts the parameter conversion frame by frame based on the minimum mean square error using a Gaussian mixture model of the joint probability density of input and output parameters [Y. Stylianou et al., IEEE Trans. SAP, **6**(2), 131-142 (1998)]. Although this method is reasonably effective, the deterioration of the conversion accuracy is caused by essential problems of the frame-based conversion process. Recently a conversion method based on the maximum likelihood estimation of a parameter trajectory has been proposed [T. Toda et al., IEEE Trans. ASLP, **15**(8), 2222-2235 (2007)]. This method realizes the appropriate converted parameter sequence by (1) using not only static but also dynamic feature statistics and (2) considering a global variance feature

of the converted parameters. It has been reported that this method is effective in several applications such as a spectral determination from articulatory movements, an acoustic-to-articulatory inversion mapping, and a conversion of body-transmitted speech into air-transmitted speech.

Contributed Paper

3:00

5pSC4. A comparison of visual features for audiovisual automatic speech recognition. Nasir Ahmad (Loughborough Univ, LE11 3TU Leicestershire, UK, n.ahmad@lboro.ac.uk), Sekharjit Datta (Loughborough Univ, LE11 3TU Leicestershire, UK, s.datta@lboro.ac.uk), David Mulvaney (Loughborough Univ, LE11 3TU Leicestershire, UK, d.j.mulvaney@lboro.ac.uk), Omar Farooq (Loughborough Univ, LE11 3TU Leicestershire, UK, o.farooq@lboro.ac.uk)

The use of visual information from speaker's mouth region have shown to improve the performance of automatic speech recognition (ASR) systems. This is particularly important in presence of noise which even in moderate form severely degrades the speech recognition performance of systems using only audio information. Various sets of features extracted from speaker's mouth region have been used to improve upon the performance of an ASR system in such challenging conditions and have met many successes. To the best of authors knowledge, the effect of using these techniques on recognition performance on the basis of phonemes have not been investigated yet. This paper presents a comparison of phoneme recognition performance using visual features extracted from mouth region-of-interest using discrete cosine transform (DCT) and discrete wavelet transform (DWT). New DCT and DWT features have also been extracted and compared with the previously used one. These features were used along with audio features based on Mel frequency cepstral coefficients (MFCC). This work will help in selecting suitable features for different application and identify the limitations of these methods in recognition of individual phonemes.

3:20-3:40 Break

Invited Paper

3:40

5pSC5. Spatial rendering of audiovisual synthetic speech use for immersive environments. Markus Noisternig (LIMSI-CNRS, B.P. 133, 91403 Orsay, France, markus.noisternig@limsi.fr), Brian F. Katz (LIMSI-CNRS, B.P. 133, 91403 Orsay, France, brian.katz@limsi.fr), Christophe D'Alessandro (LIMSI-CNRS, B.P. 133, 91403 Orsay, France, cda@limsi.fr)

Synthetic speech is usually delivered as a mono audio signal. In this project, audiovisual speech synthesis is attributed to a virtual agent moving in a virtual three-dimensional scene. More realistic acoustic rendering is achieved by taking into account the position of the agent in the scene, the acoustics of the room depicted in the scene, and the orientation of the virtual character's head relative. 3D phoneme dependant radiation patterns have been measured for two speakers and a singer. These data are integrated into a Text-To-Speech system using a phoneme to directivity pattern transcription module which also includes a phoneme to viseme model for the agent. In addition to the effects related to agent's head orientation for the direct sound, a room acoustics model allows for realistic rendering of the room effect as well as the apparent distance as depicted in the virtual scene. Real-time synthesis is implemented in a 3D audio rendering system.

4:00

5pSC6. Audiovisual automatic speech recognition: Progress and challenges. Gerasimos Potamianos (IBM T. J. Watson Research Center, RTE 134, Yorktown Heights, NY 10598, USA, gpotam@us.ibm.com)

The paper overviews recent progress and challenges in a number of audiovisual speech processing technologies with main emphasis on the problem of automatic speech recognition. It is well known that visual channel information can improve automatic speech processing for human-computer interaction. To automatically process and incorporate such information into automatic systems, a number of steps are required that are surprisingly similar accross speech technologies. Crucial above all is the issue of feature representation of visual speech and its robust extraction. In addition, appropriate integration of the audio and visual representations is required, in order to ensure improved performance of the bimodal systems over audio-only baselines. These topics are discussed in detail in the talk, with main emphasis on their application to the speech recognition problem in the challenging environments of automobiles and smart rooms.

Contributed Paper

4:20

5pSC7. Analysis and synthesis of nonverbal facial motion. Jonas Beskow (KTH Speech, Music and Hearing, Lindstedtsvägen 24, 10044 Stockholm, Sweden, beskow@kth.se), Björn Granström (KTH Speech, Music and Hearing, Lindstedtsvägen 24, 10044 Stockholm, Sweden, bjorn@speech.kth.se)

Until recently, most efforts in audio-visual speech synthesis have been concerned with verbal content. However, in human-human communication it is obvious that nonverbal signals plays an important role, such as when expressing emotions and attitudes. Interaction is also often regulated using facial cues, for example gaze, head and eyebrow movements. Some of these cues have a direct coupling to the speech signal, while other occur during both while speaking and listening. When applying interactive talking agents in man-machine systems, nonverbal signals may be very important in easing the flow of communication. In a series of experiments we have been exploring the function of nonverbal facial motion. These studies include an experiment on the interaction between expressive speech and prominence, as well as an attempt to synthesize emotions and attitudes in a talking head, using 3D motion capture data. Further we will report on a real-time experiment with human-human avatar-mediated conversation, where the subjects' turn-taking behavior is affected by facial motion in the avatars.

Session 5pUWa

Underwater Acoustics and ECUA: Sound Propagation in 3D Environments II

David C. Calvo, Cochair
U.S. Naval Res. Lab., Acoust. Div., Code 7142, 4555 Overlook Ave. SW, Washington, DC 20375, USA

Michael Taroudakis, Cochair
University of Crete & FORTH/IACM, Vassilika Vouton, P.O. Box 1385, Heraklion, 711 10, Greece

Invited Paper

1:40

5pUWa1. Stability of wavefronts at sound propagation in highly structured three-dimensional environments. Oleg A. Godin (NOAA/ESRL, 325 Broadway, Mail Code R/PSD99, Boulder, CO 80305-3328, USA, Oleg.Godin@noaa.gov)

Extensive numerical modeling of long-range propagation of sound and seismic waves as well as observations of underwater acoustic fields with line arrays reveal that wavefronts are often much more stable and predictable than the rays comprising these wavefronts. This paper considers multiple scattering of sound by environmental inhomogeneities with spatial scales small compared to the propagation range but large compared to the wavelength. These inhomogeneities include 3D variations in sound speed and current velocity that are small compared to the average sound speed, can be either random or deterministic, and are superimposed on an arbitrary slowly-varying background. A theoretical explanation of wavefront stability in highly-structured environments is achieved by demonstrating that end points of rays launched from a point source and having a given eikonal (phase) are scattered primarily along the wavefront corresponding to the same eikonal in the unperturbed environment. The ratio of displacements of the ray end points along and across the unperturbed wavefront is proportional to the number of uncorrelated scattering events. The results apply to conventional rays and to horizontal rays describing propagation of adiabatic normal modes in almost-layered media. The origin of relative stability of wavefronts compared to rays is traced back to Fermat's principle.

Contributed Paper

2:00

5pUWa2. Range and cross-range propagation effects in a liquid wedge overlaying an elastic bottom. Piotr Borejko (Vienna University of Technology, Karlsplatz 13/E206/3, A-1040 Vienna, Austria, pb@allmech.tuwien.ac.at)

The penetrable-wedge model, a constant density isospeed layer of fluid with a pressure-release horizontal surface and a sloping elastic bottom, provides an extensive insight into the role of the ocean bottom in acoustic propagation from an underwater source. In particular, it is a realistic model of a rock-bottom ocean near a shoreline that accounts for horizontal refraction and allows for a ground wave. This paper discusses some new results for small and large range propagation for two penetrable-wedge models: one where the shear wave speed in the bottom is lower than the sound speed in the fluid and the other where the shear wave speed is higher. The operational representation of the ray-integral solution for the acoustic field from a point source in a penetrable wedge of fluid is further developed to the stage at which one can compute the exact, other than the omission of diffraction at the wedge apex, pressure response curve, as recorded at a receiver, due to an arbitrary time variation of the pressure at the source in a 3° wedge. The three-dimensional propagation effects are examined for range transmission when the receivers are located up-slope and down-slope of the source, and for cross-range transmission when the receivers are located cross-slope of the source.

Invited Papers

2:20

5pUWa3. Depth-dependent resonant target strength analysis of a dense Atlantic Herring school from wide-area OAWRS and localized 3D morphology sensing. Daniel Cocuzzo (Northeastern University, 302 Stearns Center, Rm 311, 360 Huntington Ave, Boston, MA 02115, USA, dcocuzzo@ece.neu.edu), Zheng Gong (Northeastern University, 302 Stearns Center, Rm 311, 360 Huntington Ave, Boston, MA 02115, USA, zgong@ece.neu.edu), Mark Andrews (Northeastern University, 302 Stearns Center, Rm 311, 360 Huntington Ave, Boston, MA 02115, USA, Andrews.mar@neu.edu), Ioannis Bertsatos (Massachusetts Institute of Technology, Room 5-435, 77 Massachusetts Avenue, Cambridge, MA 02139, USA, ibertsat@mit.edu), Tianrun Chen (Massachusetts Institute of Technology, Room 5-212, 77 Massachusetts Avenue, Cambridge, MA 02139, USA, trchen@mit.edu), Hector Pena (Institute of Marine Research, PO Box 1870, 5817 Bergen, Norway, hector.pena@imr.no), Thomas C. Weber (University of New Hampshire, Ctr. for Coastal and Ocean Mapping, 24 Colovos Road, Durham, NH 03824, USA, weber@ccom.unh.edu), Nicholas Makris (Massachusetts Institute of Technology, Room 5-212, 77 Massachusetts Avenue, Cambridge, MA 02139, USA, makris@mit.edu), Purnima Ratilal (Northeastern University, 302 Stearns Center, Rm 311, 360 Huntington Ave, Boston, MA 02115, USA, purnima@ece.neu.edu)

The depth-dependent target strength of Atlantic Herring is estimated at several distinct bandwidths close to their resonance frequency for a localized, highly dense school observed during the NOPP-sponsored Gulf of Maine Experiment on September 22, 2006. An ocean acoustics waveguide remote sensing (OAWRS) system was deployed near George's Bank to investigate the migration and spawning behavior of fish over wide areas. In conjunction with OAWRS, a Simrad EK60 conventional fish-finding echosounder (CFFS)

and a Reson Seabat 7125 multibeam sonar system were deployed to provide local depth extent and 3D volume morphology of the dense herring school. The calibration of low-frequency target strength derived from OAWRS data using localized CFFS density and multibeam 3D volume estimates as inputs is discussed. The correlation between the mean depth of the vertically migrating herring school and its resonance frequency is investigated. The results are compared with a theoretical model for 3D resonance scattering from fish swimbladder modeled as a spheroidal bubble. This analysis may allow inference of fish depth and species classification based on the scattered frequency response of targets imaged by OAWRS. Implications for classifying general localized targets, biological or man-made, are discussed further.

2:40

5pUWa4. Multiple forward scattering through an ocean waveguide with 3D random inhomogeneities. Nicholas Makris (Massachusetts Institute of Technology, Room 5-212, 77 Massachusetts Avenue, Cambridge, MA 02139, USA, makris@mit.edu), Purnima Ratilal (Northeastern University, 302 Stearns Center, Rm 311, 360 Huntington Ave, Boston, MA 02115, USA, purnima@ece.neu.edu), Tianrun Chen (Massachusetts Institute of Technology, Room 5-212, 77 Massachusetts Avenue, Cambridge, MA 02139, USA, trchen@mit.edu)

Analytic expressions have been derived for the mean and spatial covariance of the acoustic field multiply forward scattered though a stratified ocean waveguide containing 3D random surface or volume inhomogeneities [Ratilal and Makris, J. Acoust. Soc. Am. **118**, 3532-3559 (2005)]. These expressions are further used to derive the temporal coherence of an acoustic signal propagated through 3D random inhomogeneities. Field moments are given in terms of moments of the scatter function density of the 3D random inhomogeneities, which enables straightforward application to a broad range of 3D scatterers. Here we give examples of the attenuation, dispersion and loss of temporal coherence expected after multiple forward scattering through (1) random internal waves in both continental shelf and deep ocean environments, (2) fish schools, and (3) random wind-generated bubbles in continental shelf and surf-zone area. We show that 3D scattering effects become important when the Fresnel width exceeds the cross-range coherence scale of the inhomogeneities, and can lead to substantial power loss.

Contributed Papers

3:00

5pUWa5. Application of the matrix Rytov method to the calculation of the coherence function of a sound field in an oceanic waveguide. Alex G. Voronovich (NOAA/Earth System Research Laboratory, 325 Broadway, Boulder, CO 80305, USA, alexander.voronovich@noaa.gov), Vladimir E. Ostashev (NOAA/Earth System Research Laboratory, 325 Broadway, Boulder, CO 80305, USA, vladimir.ostashev@noaa.gov)

Closed equations for the coherence function of a monochromatic sound field propagating in a statistically inhomogeneous 3D oceanic waveguide have high dimensions and are difficult to solve even with the use of modern computers. Significant reduction of the dimension of the problem was achieved by assuming that sound speed fluctuations are statistically isotropic in a horizontal plane. However, even in this case calculation of the coherence function for a megameter range takes about a day. In this paper, we develop an approximate solution of the closed equations for the coherence function which is similar to a matrix version of the Rytov method. An explicit expression for the coherence function is obtained which contains exponent of an ″interaction″ matrix. This matrix is determined in terms of the acoustic and internal wave modes and spatial spectrum of the sound speed fluctuations. It is shown that the matrix Rytov method provides an accurate solution for the coherence function which coincides with the solution of the closed equations within a few percent. Calculation of the coherence function now takes only about an hour. This allows us to study in detail the dependence of the coherence function on parameters of the problem.

3:20

5pUWa6. Measurements of 3D propagation in the shelf environment. Kevin D. Heaney (Oasis Inc., 11006 Clara Barton Dr., Fairfax Station, VA 22039, USA, oceansound04@yahoo.com)

In the Fall of 2007 measurements were made to calibrate the acoustic environment on the shallow water shelf off the coast of Florida. The continental shelf is quite flat (less than 1 degree slope) for a region approximately 10 km wide. Transmissions to a cross-shelf 900 m horizontal line array were made from a source transiting along the shelf. The signal transmissions include broadband LFM (20-420 Hz) and a comb of narrow band frequencies spanning the same range. Narrowband beamforming results show the clearly identified source. The arrival angle for the source is as expected until a distance of approximately 30-40 km when there is an apparent bearing shift in-shore of up to 25 degrees. This behavior is expected in propagation on a shelf (of greater slope) but its behavior is surprising. The phenomenon was observed for several runs at various source and water depths. In order to explain the phenomenon, a hybrid adiabatic normal mode-Parabolic Equation method will be applied to the environment. This model computes the vertical modes and phase speeds at each location and then uses the PE to propagate each mode individually using it's spatially varying phase speed and attenuation. Comparisons of theory and data will be made.

3:40

5pUWa7. Observations of out of plane arrivals for long range low frequency transmission in shallow water. Harry Deferrari (Univ. of Miami, 4600 Rickenbacker Causeway, Miami, FL 33149, USA, hdeferrari@rsmas.miami.edu)

Two recent experiments have used long horizontal arrays to receive broadband low frequency signals propagated over long ranges in shallow water. Both used m-sequence signals that resolve pulse arrivals in time with each arrival associated with a single acoustic mode of propagation. At moderate propagation ranges, out to 20 km, wave fronts for all modes are observed to be parallel, implying an orderly two-dimensional propagation. At a much longer range, 80 km, a number of separable arrivals are observed but not necessarily with a one-to-one correspondence with modes. The paths appear to be stable and coherent in time implying that they are true Fermat paths, but their wavefront arrival angles differ suggesting the same mode is arriving from several directions, that is, by curved (out of plane paths). The paths could result from wedge effects from gentle slopes perpendicular to the propagation path or possibly from chaotic interaction with random facets of the bottom. In any case, the ultimate limitation for horizontal spatial coherence and array resolution may be the multipath interference of bundles of out of plane arrivals.

4:00-4:20 Break

Invited Papers

4:20

5pUWa8. Hydroacoustic blockage prediction and measurement at Diego Garcia using the Adiabatic Mode Parabolic Equation Model. Zachary Upton (BBN Technologies, 1300 N. 17th Street, Suite 400, Arlington, VA 22209, USA, zupton@bbn.com), Michael D. Collins (U.S. Naval Res. Lab., Acoust. Div., Code 7142, 4555 Overlook Ave. SW, Washington, DC 20375, USA, michael.collins@nrl.navy.mil), Jay Pulli (BBN Technologies, 1300 N. 17th Street, Suite 400, Arlington, VA 22209, USA, jpulli@bbn.com)

Underwater explosion monitoring with sparse sensors at long ranges relies on the efficient propagation of acoustic energy in the sound fixing and ranging (SOFAR) channel. When sound traveling in this channel encounters an island or seamount, it will either diffract, scatter, or be converted into seismic energy. Signals observed on the opposite side of these obstructions have been affected by some combination of these processes, and models of global detection and localization depend on knowing these effects. We present a study using the Adiabatic Mode Parabolic Equation (AMPE) model to predict these processes in three dimensions at the Chagos Archipelago. Predictions at 5, 10, and 20 Hz are compared with measurements of approximately 300 T-wave signals from six years of earthquakes on either side of the Chagos Archipelago. These have been recorded at the hydrophone arrays around Diego Garcia. The result of this 360-degree analysis, and the agreement with observed data, demonstrate the utility of the model in understanding the physical effects of these obstructions.

4:40

5pUWa9. Investigation of 3D benchmark problems in underwater acoustics: a uniform approach. Frederic Sturm (Laboratoire de Mécanique des Fluides et d'Acoustique (UMR CNRS 5509), Ecole Centrale de Lyon, Centre acoustique, 36, avenue Guy de Collongue, 69134 Ecully Cedex, France, frederic.sturm@ec-lyon.fr)

In underwater acoustics, most of the three-dimensional effects on sound wave propagation are usually described by modelers considering one of the following shallow-water benchmark problems: a wedge-shaped waveguide, a canyon, a seamount, and a sinusoidal (corrugated) bottom. These test cases have been thoroughly analyzed individually considering both harmonic point sources (emitting at very low frequencies, for some obvious problems of CPU time and memory limitation) and broadband source pulses (with also very-low central frequencies). In the present work, we report numerical results corresponding to the propagation of broadband pulses in the four above-mentioned test cases. The numerical simulations are performed using a fully 3D parabolic equation based model coupled with a Fourier synthesis technique to handle the time dependence of the source signal. The objective is to propose a uniform representation of the numerical results so as to facilitate the comparison of the 3D effects present in each of the four benchmarks. Snapshots of the propagating pulses at very close successive times are compared with 2D results. In addition, movies of the propagating pulses are shown for each test case and compared to each other. Movies strongly facilitate the observation and thus the understanding of the 3D effects experienced by all the propagating waves.

Contributed Paper

5:00

5pUWa10. Using parallel programming and a three-dimensional visualization cave to map the acoustic energy distribution from a seismic array in the ocean. Natalia Sidorovskaia (Department of Physics, University of Louisiana, UL BOX 44210, Lafayette, LA 70504-4210, USA, nas@louisiana.edu), Arslan Tashmukhambetov (Department of Physics, University of New Orleans, New Orleans, LA 70148, USA, atashmuk@uno.edu), George E. Ioup (Department of Physics, University of New Orleans, New Orleans, LA 70148, USA, geioup@uno.edu), Juliette W. Ioup (Department of Physics, University of New Orleans, New Orleans, LA 70148, USA, jioup@uno.edu)

Modeling and visualization of the dynamic acoustic field during a seismic exploration survey represent a computational challenge due to broadband, directional nature of the acoustic signal radiated by a seismic array. Standard acoustic propagation models (RAM and SWAMP) are upgraded for parallel processing and tested in the LONI (the Louisiana Optical Network Initiative) environment, using the Louisiana fiber optics grid computing network to model the three-dimensional time-varying acoustic field in the ocean during a seismic exploration survey. The generated volume of data is transferred and visualized in the advanced immersive visualization environment, supported by Louisiana Immersive Technology Enterprise (LITE) facilities. The proposed technology is one of the first steps in developing real-time monitoring of the acoustic energy distribution in a large oceanic volume. This can be beneficial for environmental impact assessment and regulation and for seismic survey design. [Research supported in part by the Joint Industry Project through OGP and by ITI of University of Louisiana at Lafayette.]

Invited Paper

5:20

5pUWa11. Effects of solitons on acoustic energy flow in three dimensions. Kevin B. Smith (Naval Postgraduate School/Naval Undersea Warfare Center, Code PH/Sk, Department of Physics, Monterey, CA 93943, USA, kbsmith@nps.edu), John A. Colosi (Naval Postgraduate School, Code OC/Cj, Department of Oceanography, Monterey, CA 93943, USA, jacolosi@nps.edu)

The impact of a train of nonlinear solitons on the propagation of acoustic energy in shallow water is examined. The soliton perturbations are based on an analytic formulation that produces a train of five soliton waves. Each wave front is parallel and has infinite extent in the horizontal direction. The acoustic field is modeled using a three-dimensional (3D) split-step Fourier parabolic equation (SSF/PE) approach defined in Cartesian coordinates. The standard PE approximation is employed in both depth and cross-range directions. Both pressure and particle velocity fields are computed in a self-consistent manner, allowing a full description of the 3D acoustic intensity field which describes the flow of energy in the presence of the solitons. Individual, low-order modes are extracted from the propagating field so that the impact on specific modes may be examined. The analysis is performed at various frequencies and

for various source-receiver geometries relative to the soliton train. Emphasis is placed on the focusing and defocusing of acoustic energy between the various soliton waves. The impact of such soliton perturbations on signal variability and bearing resolution at the receiver will be quantified. [Work supported by ONR 321OA.]

Contributed Papers

5:40

5pUWa12. High-frequency underwater acoustic propagation in a port using the three-dimensional method of images. Pierre-Philippe J. Beaujean (Florida Atlantic University, SeaTech Campus, 101 North Beach Road, Dania Beach, FL 33004, USA, pbeaujea@seatech.fau.edu), Matthew D. Staska (International Transducer Corporation, 869 Ward Drive, Santa Barbara, CA 93111, USA, MStaska@channeltech.com)

A computer-efficient model for underwater acoustic propagation in a shallow, three-dimensional rectangular duct closed at one end has been developed using the method of images. The duct simulates a turning basin located in a port, surrounded with concrete walls and filled with sea water. The channel bottom is composed of silt. The modeled impulse response is compared with the impulse response measured between 15 kHz and 33 kHz. Despite small sensor-position inaccuracies and an approximated duct geometry, the impulse response can be modeled with a relative echo magnitude error of 1.62 dB at worst, and a relative echo location error varying between 0% and 4% when averaged across multiple measurements and sensor locations. This is a sufficient level of accuracy for the simulation of an acoustic communication system operating in the same frequency band and in shallow waters, as time fluctuations in echo magnitude commonly reach 10 dB in this type of environment.

6:00

5pUWa13. Acoustic mode beam effects of nonlinear internal gravity waves in shallow water. Timothy Duda (Woods Hole Oceanographic Institution, 98 Water Street, Bigelow 107, MS-12, Woods Hole, MA 02543, USA, tduda@whoi.edu), Ying-Tsong Lin (Woods Hole Oceanographic Institution, 98 Water Street, Bigelow 107, MS-12, Woods Hole, MA 02543, USA, ytlin@whoi.edu), James F. Lynch (Woods Hole Oceanographic Institution, 98 Water Street, Bigelow 203A, MS-11, Woods Hole, MA 02543, USA, jlynch@whoi.edu)

Ducting of sound between short-wavelength nonlinear internal gravity waves in coastal environments has been demonstrated by substantial evidence. The ducting takes a unique form for each of the acoustic normal modes. Some consequences of this are examined here using three-dimensional parabolic equation modeling and theory. For a pair of waves having a broadband 200-Hz source placed between (i.e., in the duct), strong interference patterns within the duct are developed for each mode after a few kilometers. Some of the energy escapes at high angle with respect to the duct direction. Termination of the internal wave duct, an observed feature, results in beams of energy unique to each mode to radiate outward. Specific cases having water depths of order 80 m and propagation distances of 20 to 30 km are examined. Situations where one or more modes are completely absent at selected positions are compared with similar events observed in the field.

FRIDAY AFTERNOON, 4 JULY 2008 ROOM 342A, 1:40 TO 6:20 P.M.

Session 5pUWb

Underwater Acoustics and ECUA: Scattering From Objects Near Boundaries

Eric Thorsos, Cochair
Applied Physics Laboratory, University of Washington, 1013 NE 40th St, Seattle, WA 98105, USA

Mario Zampolli, Cochair
NATO Undersea Research Centre, Viale San Bartolomeo 400, La Spezia, 19126, Italy

Invited Papers

1:40

5pUWb1. Measurement and modeling of targets deployed on and within sand sediments. Kevin L. Williams (Applied Physics Laboratory, University of Washington, 1013 NE 40th St, Seattle, WA 98105, USA, williams@apl.washington.edu), Eric Thorsos (Applied Physics Laboratory, University of Washington, 1013 NE 40th St, Seattle, WA 98105, USA, eit@apl.washington.edu), Steven Kargl (Applied Physics Laboratory, University of Washington, 1013 NE 40th Street, Seattle, WA 98105, USA, kargl@troutmask.apl.washington.edu), Joseph Lopes (Naval Surface Warfare Center - Panama City Division, 110 Vernon Ave, Panama City, FL 32407, USA, joseph.l.lopes@navy.mil), Raymond Lim (Naval Surface Warfare Center - Panama City Division, 110 Vernon Ave, Panama City, FL 32407, USA, raymond.lim@navy.mil), Carrie Dowdy (Naval Surface Warfare Center - Panama City Division, 110 Vernon Ave, Panama City, FL 32407, USA, carrie.dowdy@navy.mil)

Acoustic signatures of elastic targets located near sediment interfaces include effects due to energy interacting with the sediment. Therefore, modeling target response also requires models of scattering from, penetration into and propagation within ocean sediments. We first describe at-sea and test pond measurements carried out on "proud" (target resting on the sediment) and buried targets at frequencies in the range of 2 to 50 kHz. The results from some of these measurements are then compared to models incorporating various levels of sophistication relative to both the target and the sediment physics. The modeling hierarchy includes the following: (1) simple sonar equation estimates that treat the target physics via a frequency dependent target strength and use formally averaged results for sediment scattering, (2) realization level modeling that allows calculation of sediment and target scattering for individual pings with

sufficient fidelity to carry out synthetic aperture processing (for a proud target only its geometrical scattering is considered while the elastic response can be included for a buried target), (3) T-matrix and finite element modeling in which the target elastic response is included but sediment scattering is treated using formal averages and/or flat surface approximations. [Work supported by the Office of Naval Research and the Strategic Environmental Research and Development Program, USA.]

2:00

5pUWb2. Synthetic aperture sonar imaging of simple finite targets near a sediment-water interface. Steven Kargl (Applied Physics Laboratory, University of Washington, 1013 NE 40th Street, Seattle, WA 98105, USA, kargl@troutmask.apl.washington.edu), Kevin L. Williams (Applied Physics Laboratory, University of Washington, 1013 NE 40th St, Seattle, WA 98105, USA, williams@apl.washington.edu), Eric Thorsos (Applied Physics Laboratory, University of Washington, 1013 NE 40th St, Seattle, WA 98105, USA, eit@apl.washington.edu), Darrell R. Jackson (Applied Physics Laboratory, University of Washington, 1013 NE 40th Street, Seattle, WA 98105, USA, drj@apl.washington.edu), Dajun Tang (Applied Physics Laboratory, University of Washington, 1013 NE 40th St, Seattle, WA 98105, USA, djtang@apl.washington.edu)

Synthetic aperture sonar (SAS) is used often to detect targets that are either proud or buried below a sandy sediment interface where the nominal grazing angle of incidence from the SAS to the point above a buried target is below the critical grazing angle. A numerical model for scattering from simple targets in a shallow water environment will be described, and can be used to generate pings suitable for SAS processing. For buried targets, the model includes reverberation from the rough seafloor, penetration through the interface, target scattering, and propagation back to the SAS. The reverberation and penetration components are derived from first order perturbation theory where small-scale roughness and superimposed ripple can be accommodated. For proud targets, the simulations include the scattering from the target where interaction with the seafloor is included through simple acoustic ray models. The interaction of the target with an incident field is based on a free field scattering model. Simulations will be compared to both benchmark problems and measurements over a frequency range of 10-30 kHz. These comparisons further support sediment ripple structure as the dominant mechanism for subcritical penetration in this frequency range. [Work supported by the US Office of Naval Research.]

2:20

5pUWb3. Experiments and numerical modeling of low to midfrequency scattering from elastic objects near the sea floor. Mario Zampolli (NATO Undersea Research Centre, Viale San Bartolomeo 400, 19126 La Spezia, Italy, zampolli@nurc.nato.int), Alessandra Tesei (NATO Undersea Research Centre, Viale San Bartolomeo 400, 19126 La Spezia, Italy, tesei@nurc.nato.int), Finn B. Jensen (NATO Undersea Research Centre, Viale San Bartolomeo 400, 19126 La Spezia, Italy, jensen@nurc.nato.int), Gaetano Canepa (NATO Undersea Research Centre, Viale San Bartolomeo 400, 19126 La Spezia, Italy, canepa@nurc.nato.int)

The scattering of low to mid-frequency sound (1-10's of kHz) from submerged elastic structures of size O(1m) is a topic of interest to the underwater acoustics community. In the first part of the presentation, a brief description of the relevant components of the EVA experiment is given. The purpose of the sea trial was the acquisition of high-fidelity echoes from submerged spherical and cylindrical targets, made of composite materials with internal layered structure. The second part of the presentation is focused on the finite-element modeling technique developed at NURC for investigating the scattering from axially symmetric submerged elastic objects. Particular attention is dedicated to the computation of the far field at a distance from the target via the Helmholtz-Kirchhoff integral, using the near field sampled on the target surface, together with Green's functions capable of describing a two-layered water-sediment fluid medium. Those geometries, for which the overall axial symmetry is broken by the presence of the water-sediment boundary, can be treated approximately by taking into account the boundary-reflected incident field, as well as the first order interaction between the target-scattered echo and the sea floor. The numerical technique is validated by comparison with data collected during the EVA trial.

2:40

5pUWb4. Modeling bottom penetration for buried target detection. Raymond Lim (Naval Surface Warfare Center - Panama City Division, 110 Vernon Ave, Panama City, FL 32407, USA, raymond.lim@navy.mil), Gary S. Sammelmann (Naval Surface Warfare Center - Panama City Division, 110 Vernon Ave, Panama City, FL 32407, USA, gary.sammelmann@navy.mil)

Sonar detection of targets buried in underwater sediments has been found to be complicated by surface roughness. In particular, current-induced ripples can diffract energy down into sandy sediments to enhance buried target detection at shallow sonar grazing angles. To validate these effects, models encompassing the dominant propagation mechanisms as well as faithfully representing the target in the environment have been used. This paper describes our efforts to adapt transition matrix and perturbation theory models to provide realistic predictions of buried target response for spherical and cylindrical shapes. Combining these models of scattering and penetration required adopting some approximations to reduce computation time while retaining accuracy. Steps taken to verify and exercise the resulting models reveal some sensitivities that accentuate the need for accurate environmental and setup ground truth for validation of detection mechanisms. [Work supported by the Office of Naval Research and the Strategic Environmental Research and Development Program, USA.]

3:00

5pUWb5. Scattering by a partially exposed nearly rigid cylinder: Experiments and analysis. Kyungmin Baik (Washington State University, Physics and Astronomy Department, Pullman, WA 99164-2814, USA, nupho27@dreamwiz.com), Philip L. Marston (Washington State University, Physics and Astronomy Department, Pullman, WA 99164-2814, USA, marston@wsu.edu)

The backscattering from a partially exposed circular cylinder was measured for broad side illumination under conditions where the contributions associated with the elastic response of the cylinder were expected to be weak. Grazing illumination was used. Since the objective was to investigate the transition in the number of reflected rays with increasing exposure, it was convenient to partially submerge the cylinder through the free surface of a tank of water. The magnitude of the scattering was measured for ka between 9.6 and 16 where k is the acoustic wave number and a is the radius of the cylinder. The scattering varied smoothly as a function of the cylinder's

exposure in agreement with analytical results based on a Kirchhoff approximation [K. Baik and P. L. Marston, IEEE J. Oceanic Eng. (accepted)]. The analysis is easily modified for the case a cylinder breaking through a flat hard interface. For the different types of rays, path length calculations (as a function of the exposure) that are part of that analysis are also relevant to identifying echoes in SAS images of partially exposed cylinders and spheres. [Research supported by ONR.]

3:20

5pUWb6. Elastic and interfacial contributions to SAS images of tilted metal cylinders: Laboratory experiments. Jon La Follett (Washington State University, Physics and Astronomy Department, Pullman, WA 99164-2814, USA, LAFOLLEJ@mail.wsu.edu), Kyungmin Baik (Washington State University, Physics and Astronomy Department, Pullman, WA 99164-2814, USA, nupho27@dreamwiz.com), Philip L. Marston (Washington State University, Physics and Astronomy Department, Pullman, WA 99164-2814, USA, marston@wsu.edu)

Laboratory experiments were carried out to explore interfacial and elastic contributions to synthetic aperture sonar (SAS) images of a solid aluminum circular cylinder having flat ends. Some of the elastic responses for free field backscattering as a function of tilt angle could be interpreted using prior ray-based theory of generalized Rayleigh wave contributions [K. Gipson and P.L. Marston, J. Acoust. Soc. Am. 106, 1673-1680 (1999); 107, 112-117 (2000)]. Simplified acoustic holography was also used to interpret aspects of the free field bistatic response. To study the effects of proximity to a flat reflecting surface, the cylinder was hung through the free surface of a water tank and monostatic SAS images were acquired by scanning the transducer location along a horizontal line. This arrangement partially simulates SAS images of cylinders on the ocean bottom at grazing incidence. There were bright contributions to the SAS images of tilted cylinders associated with direct elastic rays as well as with indirect elastic rays due to acoustic reflections from the free surface of the water tank. [Research supported by ONR.]

3:40

5pUWb7. Elastic scattering by partially-solid-filled spherical shell on the seabed: Model-data comparison and physical understanding. Alessandra Tesei (NATO Undersea Research Centre, Viale San Bartolomeo 400, 19126 La Spezia, Italy, tesei@nurc.nato.int), Mario Zampolli (NATO Undersea Research Centre, Viale San Bartolomeo 400, 19126 La Spezia, Italy, zampolli@nurc.nato.int), Gaetano Canepa (NATO Undersea Research Centre, Viale San Bartolomeo 400, 19126 La Spezia, Italy, canepa@nurc.nato.int)

Low- to mid-frequency elastic scattering measurements were conducted in the range from 5 to 40 ka on a spherical composite shell deployed proud on a sandy seabed. The object consists of a thin-walled shell made of layers of a random-fiber material, and then filled partially with an isotropic solidified epoxy resin and partially with sea water. A scaled version of the object was measured in a water tank under free field conditions. The target responses obtained with and without interaction with the seafloor boundary were compared to simulations achieved by the NURC modeling tool Axiscat. The temporal echoes of the objects were analyzed in terms of elastic waves supported by the structure, on the basis of a ray model. The strongest elastic components come from the interior solid filler. The experimental data of the sphere on the seabed were acquired in October 2006 during the EVA'06 trial off the Island of Elba. The free field data were collected in the NURC water tank.

4:00-4:20 Break

4:20

5pUWb8. Robust recognition and characterization of man-made objects in shallow water using time-frequency analysis. Shaun D. Anderson (Georgia Institute of Technology, Woodruff School of Mechanical Engineering, Graduate Box 1000, Atlanta, GA 30332, USA, sanderson49@gatech.edu), Karim G. Sabra (Georgia Institute of Technology, School of Mechanical Engineering, 771 Ferst Drive, NW, Atlanta, GA 30332-0405, USA, karim.sabra@me.gatech.edu), Manell E. Zakharia (French Naval Acadamey, BP 600, 29240 Brest-Armees, France, manell.zakharia@ecole-navale.fr), Mario Zampolli (NATO Undersea Research Centre, Viale San Bartolomeo 400, 19126 La Spezia, Italy, zampolli@nurc.nato.int), Henrik Schmidt (MIT, 77 Mass Ave, 5-204, Cambridge, MA 02139, USA, henrik@mit.edu), William A. Kuperman (MPL, Scripps Institution of Oceanography, University of California, San Diego, La Jolla, CA 92093-0238, USA, wkuperman@ucsd.edu)

For underwater sonar, time-frequency analysis, in particular Wigner-Ville analysis, has been shown to be a relevant tool for discriminating a man made target (shell) from a natural one of the same shape (solid) and even to estimate some target characteristics (shell thickness, shear velocity...). This processing tool takes advantage of the evolutional, time dependent aspect of the echo spectrum. The estimated time-frequency patterns can be used for detection and wideband classification of sonar echoes in order to reduce false alarms. In particular, the so-called "coincidence pattern" appearing for specific frequency range is a robust time-frequency signature of man-made shells. A time-frequency analysis will be presented to understand echo formation mechanisms using a standard spherical shell model target model. The influence of the medium parameters as well as the source-receiver configuration will be investigated in free space and then extended to the case of a shallow water waveguide. The proposed approach will be tested using target scattering data collected during Experiments for Validation of Acoustic modeling techniques (EVA) sea test on the north shore of Isola D'Elba, Italy. Application to mine-hunting sonar systems will be discussed.

4:40

5pUWb9. Bi-static scattering from buried, elastic objects in shallow water waveguides. Henrik Schmidt (MIT, 77 Mass Ave, 5-204, Cambridge, MA 02139, USA, henrik@mit.edu), Deep Ghosh (MIT, 77 Mass Ave, 5-204, Cambridge, MA 02139, USA, dghosh @mit.edu)

The emerging autonomous network technology is enabling new operational paradigms for the concurrent detection, classification and localization of seabed objects by collaborating AUVs. Thus, such networks can exploit the bi-static enhancement of targets which are stealthy to conventional mono-static sonars, and the resonance properties of manmade targets. Under the GOATS and SWAMSI programs MIT in collaboration with NURC have addressed the fundamental issues associated with the development of such a new sonar concept. Through a series of joint experiements, various aspects of the interaction of elastic targets, completely or partially buried in the seabed have been investicated, including the evanescent coupling of low-frequency sound (1-10 kHz) into the seabed, the coupling with structural waves in the targets, and the 3D scattering back into the water column. The analysis is performed using a spectral virtual source scattering model with an embedded spectral Green's function generator which incorporates all multiple scattering effects between the target and the seabed. The target response is represented uniquely by an impedance matrix which may be computed separately using analytical or numerical methods, depending on the target geometry. The scattering model has been combined with the OASES code to provide a comprehensive simulation environment including all the shallow water waveguide physics.[Work Supported by ONR].

Contributed Paper

5:00

5pUWb10. Full field modeling of multiaspect scattering from buried objects. Ilkka Karasalo (FOI, Gullfossgatan 6, SE 16490 Stockholm, Sweden, ilkka.karasalo@foi.se)

Results are presented from a computational study of imaging of objects buried in the seabed under shallow water, using a rail-mounted active sonar and synthetic aperture processing. The medium is modeled as range independent, composed of a shallow water layer above a seabed of a muddy sediment containing the objects, and deeper subbottom layers. The objects have simple shape and structure, with diameters in the range 15-195 cm. From selected positions along the rail, the sonar insonifies the objects by LFM pulses from a directive transmitter, and records the backscattered echoes with a horizontal uniform line array (ULA), or optionally a pair of vertically separated ULAs. The signals from all sonar positions are integrated coherently by synthetic aperture processing for enhanced azimuthal resolution in the images of the objects. The parameters of the models of the medium, the objects and the experimental geometry are chosen to approximate those of a sea trial conducted in the Stockholm archipelago in 2004. The model-predicted scattered field is computed using the XFEM-S code, based on a frequency-domain boundary integral equation (BIE) formulation of scattering from a smooth object in a layered fluid-solid medium. Comparisons of model predictions with experimental results are presented.

Invited Papers

5:20

5pUWb11. Broadband scattering from spherical shells in a waveguide: modeling and classification. John A. Fawcett (DRDC Atlantic, PO Box 1012, Dartmouth, NS B2Y 3Z7, Canada, john.fawcett@drdc-rddc.gc.ca)

In this presentation, the exact expression for scattering from a sphere in a Pekeris waveguide (e.g., Sammelmann and Hackman, J. Acoust. Soc. Am., 82, 1987) is discussed. The importance of the sphere/interface rescattering terms is considered. A computationally faster multipath expansion approach is derived and its accuracy compared with the exact approach. For sufficiently high frequencies and in the case where the rescattering terms can be ignored, the multipath approach yields accurate predictions. The broadband scattering from an elastic-shelled sphere in a Pekeris waveguide is considered as a function of the frequency (or time for a pulse) and the sphere's range and depth in the waveguide. The classification problem is also discussed. The echos (time series or spectra) from a large set of spheres with varying parameters are generated and grouped into six classes corresponding to the various shell thicknesses and materials. Simple classifiers based upon temporal or spectral representations are considered for the spheres in free space and in a waveguide

5:40

5pUWb12. Backscattering from an elastic target near a water-sediment interface at oblique incidence: First results of tank experiments. Jean-Pierre Sessarego (Laboratory for Mechanics and Acoustics CNRS, 31 chemin Joseph Aiguier, 13009 Marseille, France, sessarego@lma.cnrs-mrs.fr), Anatoliy N. Ivakin (Applied Physics Laboratory, University of Washington, 1013 NE 40th Street, Seattle, WA 98105, USA, ivakin@apl.washington.edu), Régine Guillermin (Laboratory for Mechanics and Acoustics CNRS, 31 chemin Joseph Aiguier, 13009 Marseille, France, guillermin@lma.cnrs-mrs.fr)

Sound scattering from a target situated near a water-sediment interface was studied in laboratory conditions in order to control separately all the parameters involved in the scattering process. Targets of different sizes were ensonified with wide band transducers covering the frequency range 200 kHz to 1 MHz. First, the target scattering strength was measured in the free space conditions, and the scattering strength of the water-sediment interface was measured at oblique incidence. These characteristics were used to provide a rough estimate for the signal-to-noise ratio for the second set of experiments where the target was situated near the interface to study effects of target-boundary interactions. The intensity of the total scattered field was measured as a function of the beamwidth, transducer/object and object/interface distances, frequency, grazing angle, target size and the interface roughness parameters. The interface considered here is a flattened sand surface which was studied earlier [Ivakin and Sessarego, High frequency scattering from flattened sand sediments: effects of granular structure, J. Acoust. Soc. Am., **122**, (5) 2007]. The targets were spherical glass beads of different size. Side scan sonar images are presented and possibilities of their qualitative interpretation are discussed.

Contributed Paper

6:00

5pUWb13. Estimates of scattering strength for buried cylindrical targets ensonified by evanescent waves. David C. Calvo (U.S. Naval Res. Lab., Acoust. Div., Code 7142, 4555 Overlook Ave. SW, Washington, DC 20375, USA, david.calvo@nrl.navy.mil), Mario Zampolli (NATO Undersea Research Centre, Viale San Bartolomeo 400, 19126 La Spezia, Italy, zampolli@nurc.nato.int), Alessandra Tesei (NATO Undersea Research Centre, Viale San Bartolomeo 400, 19126 La Spezia, Italy, tesei@nurc.nato.int)

It is known that low-frequency subcritical sound waves can significantly scatter from targets buried in a seabed due to the significant penetration depth of the incident evanescent wave. Past computational work on scattering by buried spherical shells has been done, for example, using a T-matrix Method [R. Lim et al., J. Acoust. Soc. Am. **93**, 1762-1783 (1993)], a Virtual Source Method [I. Lucifredi and H. Schmidt., J. Acoust. Soc. Am. **120**, 3566-3583 (2006)], or finite-element methods [Zampolli et al., J. Acoust. Soc. Am., in press]. In addition to high-fidelity results which are expected from the preceding numerical methods, it desirable to have approximate analytical/asymptotic predictions of multistatic scattering strength for a variety of homogeneous or layered buried targets. Focusing on buried cylinders of infinite or finite-length, we first compute scattering using an approximate method that makes use of separation of variables and neglects multiple scattering between the interface and the target. Results are compared with those generated using the Axiscat/NURC/COMSOL finite-element method. Asymptotic estimates are then presented for scattering strength for objects completely buried in the seafloor for a flat interface (Work sponsored by ONR and NURC.)

FRIDAY AFTERNOON, 4 JULY 2008 ROOM 341, 2:00 TO 6:00 P.M.

Session 5pUWc

Underwater Acoustics and ECUA: Automatic Target Recognition, Sensors and Algorithms

Gerald Dobeck, Cochair
Naval Surface Warfare Ctr., Coastal Systems Station, Dahlgren Div., Panama City, FL 32407-7001, USA

Marc Pinto, Cochair
NATO Undersea Research Centre, Viale San Bartolomeo 400, La Spezia, 19126, Italy

Yvan Petillot, Cochair
School of Engineering and Physical Sciences, Heriot-Watt University, Edinburgh, EH14 4AS, UK

Invited Paper

2:00

5pUWc1. A track-before-detect algorithm for active sonar based on a hidden Markov model. Nigel H. Parsons (Thales Underwater Systems Ltd., Dolphin House, Ashurst Drive, Bird Hall Lane, Cheadle Heath, SK3 0XB Stockport, UK, nigel.parsons@uk.thalesgroup.com)

An active sonar track-before-detect algorithm is described. It is based on a hidden Markov model which uses a Viterbi algorithm to estimate the log-likelihood ratio of the presence or absence of a target in tracks within a state space representing a set of ranges, bearings, range rates and bearing rates, assuming a set of transition probabilities of changes in range rate and bearing rate. A detection is declared if the log-likelihood ratio exceeds a certain threshold and subsequently an HMM tracker, operating on a much smaller state space, is then employed. The performance of this algorithm on simulated data is evaluated. It is shown that, for moving and manoeuvring targets, the detection performance is significantly better than that of a conventional algorithm.

Contributed Paper

2:20

5pUWc2. Forward looking techniques for environment modeling, obstacle detection and characterization. Isabelle Quidu (ENSIETA - E3I2 Lab., 2 rue François Verny, 29806 Brest Cedex 9, France, isabelle.quidu@ensieta.fr), Yann Dupas (Groupe d'Etudes Sous-Marines de l'Atlantique (GESMA), BP 42, 29240 Brest Armées, France, yann.dupas@dga.defense.gouv.fr)

Military underwater robots are designed to perform complex underwater missions in both known and unknown environments. To achieve these tasks, an Autonomous Underwater Vehicle (AUV) must be supplied with appropriate sensors to deal with unpredictable events that can put it in danger, and with a high degree of decisional autonomy. In this paper, we have studied the architecture of forward looking sensors to allow the creation of a 3D model of the environment presenting the seabed and the obstacles that are on the path of the AUV. Our approach is based on experimental trials using different and complementary ways (sonars with several configurations) to gather an information as complete as possible. This information will be processed by the vehicle during a survey mission. Practically, we create a reference model of a static environment using a multibeam system which produces bathymetric images at different grazing angles. In the same environment we then use a Forward Looking Sonar intended for the recognition of detected echoes in comparison with the reference model. If an echo cannot be related to a known object on the reference map, it is considered as an obstacle, and the map is updated.

Invited Paper

2:40

5pUWc3. Automated change detection with area matching. John Dubberley (Naval Research Laboratory, Bldg. 1005 Rm D-23, Stennis Space Center, MS 39529, USA, john.dubberley@nrlssc.navy.mil), Marlin Gendron (Naval Research Laboratory, Bldg. 1005 Rm D-23, Stennis Space Center, MS 39529, USA, marlin.gendron@nrlssc.navy.mil), Maura Lohrenz (Naval Research Laboratory, Bldg. 1005 Rm D-23, Stennis Space Center, MS 39529, USA, maura.lohrenz@nrlssc.navy.mil)

When resurveying a geographic area of the seafloor during sidescan change detection operations, an automated method to match bottom objects imaged previously with objects imaged in the resurvey can increase efficiency and accuracy. The geographic position of a new object relative to a historical object is a good indicator of a match. However, due to position error within either survey, there may be more than one spatially-close object in the new imagery. To complicate matters further, the reflected energy from the new object may be significantly different given a different incidence angle in the resurvey or the partial burial of the object. In addition, the resurveyed object image may be below the threshold set for automatic recognition and falsely eliminated. This presentation will address these problems and suggest possible methods for matching "constellations" of bottom objects by Dijkstra's minimum cost - maximum flow algorithm, control point matching, and the data-association procedure.

Contributed Paper

3:00

5pUWc4. An acoustic barrier based on amplitude variations of the ray paths and double beamforming. Barbara Nicolas (GIPSA-lab, dep. DIS, 961, rue de la Houille Blanche, 38402 St Martin d'Hères, France, barbara.nicolas@gipsa-lab.inpg.fr), Philippe Roux (LGIT - CNRS - Université Joseph Fourier, Maison des Géosciences, 1381 rue de la Piscine, BP 53, 38041 Grenoble, France, philippe.roux@obs.ujf-grenoble.fr), Ion Iturbe (GIPSA-lab, dep. DIS, 961, rue de la Houille Blanche, 38402 St Martin d'Hères, France, ion.iturbe@gipsa-lab.inpg.fr), Jérôme I. Mars (GIPSA-lab, dep. DIS, 961, rue de la Houille Blanche, 38402 St Martin d'Hères, France, jerome.mars@gipsa-lab.inpg.fr)

The objective of this work is to build an acoustic barrier to detect and localize a target between two vertical arrays of sensors. To perform this detection/localisation, we record the signal between each source (of the source array) and each reveiver (of the receiver array). Using these data, we extract the different ray paths between sources and receivers thanks to a new signal processing method: double beamforming. Then, we show that ray paths and their arrival times are not affected by a target in the medium but that ray amplitudes change. As a result, it is possible to use amplitude variation of the rays to find the target localisation. To validate these methods we perform ultrasonic experiments in a tank. These experiments are often used in underwater acoustics as they emulate shallow water waveguides: indeed, by multiplying the frequency by a factor x, distances are divided by the same factor. As acoustic and elastic propagation properties are not affected by this scaling down, it is possible to achieve "oceanic experiments" in a simple tank. Results of double beamforming and target detection are shown.

Invited Papers

3:20

5pUWc5. Advanced ATR techniques based on High-Resolution SAS Sensors. Enrique Coiras (NATO Undersea Research Centre, Viale San Bartolomeo 400, 19126 La Spezia, Italy, coiras@nurc.nato.int), Johannes Groen (NATO Undersea Research Centre, Viale San Bartolomeo 400, 19126 La Spezia, Italy, groen@nurc.nato.int), Benjamin Evans (NATO Undersea Research Centre, Viale San Bartolomeo 400, 19126 La Spezia, Italy, evans@nurc.nato.int), Marc Pinto (NATO Undersea Research Centre, Viale San Bartolomeo 400, 19126 La Spezia, Italy, pinto@nurc.nato.int)

Automatic Target Recognition (ATR) is a key element of expeditionary Mine Countermeasures (MCM) and port protection operations. Most existing approaches to ATR are currently based on high resolution sonar sensors, which provide enough information to obtain satisfactory detection and classification performance for the large World War 2 mine types (e.g., 2 m long cylinder). False alarm rates, however, are still unacceptably high for modern mines, which constrains the way operations are undertaken and often requires either confirmation or re-evaluation by a human operator. The introduction of new AUV-mounted Synthetic Aperture Sonars (SAS) increases the resolution, quality and range of acquired sonar images, which broadens the set of machine vision and computer image analysis techniques that can be used for underwater ATR operations. In this paper we study the impact that the increased quality and resolution have on performance gains and false alarm reduction. A number of classification algorithms are selected to represent the pool of existing approaches to target detection and classification, and their performances are estimated using both simulated and real image data in order to quantify the benefits associated to the new SAS technology. Evolution and near-future plans are discussed, introducing emerging bio-sonar sensors, anomaly detectors and autonomous AUV systems.

3:40

5pUWc6. Rapid distinction of dumpsite objects using Multiple-Aspect Scattering - Results from scaled tank experiments. Philippe Blondel (University of Bath, Department of Physics, Claverton Down, BA2 7AY Bath, UK, pyspb@bath.ac.uk)

Toxic dumpsites on the seafloor are causing increasing environmental concern, but traditional sonar imaging strains to distinguish objects in unconsolidated sediments, in particular in cluttered terrains. Scaled tank experiments were conducted with four different cylinders (fluid-filled and solid aluminium, air-filled and solid stainless steel, respectively) and two seabed types (silt and gravel), using the facilities at the University of Bath. The setup was a 10:1 scaled version of the EC-SITAR sea trials site in the Stockholm Archipelago (Sweden). The main aim of these experiments was to design efficient surveying strategies, later used at sea. Our studies showed large variations depending on the aspect of these targets and their bistatic imaging configuration. These variations can be directly related to the shapes of the targets (e.g., dimensions, presence of ribs), their content (hollow or solid) and the material of the shells (e.g.,

stainless steel or aluminium). They are quantified using the combined L4 norm of the time-domain signals at each aspect. Using appropriate ranges of multistatic configurations and imaging each target at three distinct aspects (45° apart), it is possible to successfully distinguish between similar targets with distinct contents and/or material, even in cluttered terrains.

4:00-4:20 Break

Contributed Papers

4:20

5pUWc7. Target detection of man made objects in side scan sonar images - segmentation based false alarm reduction -. Max Neumann (Freie Universität Berlin, Takustr. 9, 14195 Berlin, Germany, papperlapapp@gmail.com), Christian Knauer (Freie Universität Berlin, Takustr. 9, 14195 Berlin, Germany, christian.knauer@inf.fu-berlin.de), Bodo Nolte (Forschungsanstalt der Bundeswehr für Wasserschall und Geophysik, Klausdorfer Weg 2-24, 24148 Kiel, Germany, bodonolte@bwb.org), Dieter Brecht (Forschungsanstalt der Bundeswehr für Wasserschall und Geophysik, Klausdorfer Weg 2-24, 24148 Kiel, Germany, dieterbrecht@bwb.org), Wolfgang Jans (Forschungsanstalt der Bundeswehr für Wasserschall und Geophysik, Klausdorfer Weg 2-24, 24148 Kiel, Germany, wolfgangjans@bwb.org), Alfons Ebert (FGAN-FOM, Gutleuthausstraße 1, 76275 Ettlingen, Germany, a.ebert@fom.fgan.de)

This paper presents a fast and robust algorithm for significantly reducing the number of false detections caused by screening algorithms for side scan sonar (SSS) images. The presented algorithm consists of two processing steps. First, an iterative segmentation process is carried out for seperating the image into shadow and background. This segmentation is based on an energy function which combines the local neighborhood segment information and the amplitude of a pixel. By minimizing this function, a clear shadow, the most significant target characteristic, will be extracted. Second, based on the region of interest (ROI) and the shadow contour, a robust classification approach is applied, utilizing the area of the shadow, the first two statistical moments of the pixel amplitude and the existence of parallel lines (Hough transformation). This algorithm was tested using a data set with approx. 2400 ROIs containing about 200 targets and 270 targetlike stones or sandrippel. This data set was gathered during five different measurement campaigns in the Baltic Sea and the Mediterranean Sea using three different SSS systems Benthos C3D, Klein2000 and Marine Sonics). These data were collected by FWG and WTD71 as well as by Atlas Electronik with the SeaOtter MK1 AUV.

4:40

5pUWc8. Sonar target-phase measurement and effects of transducer-matching. Philip Atkins (University of Birmingham, Department of Electronic, Electrical and Computer Engineering, Edgbaston, B15 2TT Birmingham, UK, p.r.atkins@bham.ac.uk), Alan Islas (University of Birmingham, Department of Electronic, Electrical and Computer Engineering, Edgbaston, B15 2TT Birmingham, UK, AXI743@bham.ac.uk), Kenneth G. Foote (Woods Hole Oceanographic Institution, Woods Hole, MA 02543, USA, kfoote@whoi.edu)

Active sonar systems normally detect and classify a target based on the amplitude of the received echo or the induced Doppler shift. However, additional classification information may be available from the phase shift introduced by some targets as a result of the boundary conditions. For example, reverberation from the sea surface and scattering from fish swimbladders introduce an additional phase shift that may not be present in returns from an acoustically stiffer seabed or synthetic target. Algorithms based on the use of subband correlators are presented for measuring the phase shifts introduced by the boundary conditions on stationary and moving targets when insonified by broadband transmissions. These techniques are used to remove the phase shifts introduced by the unknown target. However, the unknown phase characteristics of the transducer, matching circuit, and electronic circuitry of a sonar system imply that target-phase measurements are very difficult to make in any practical system. The effects of adding a Butterworth-derived matching circuit to a Reson TC2130 transducer are presented for the case of sinusoidal frequency-modulated excitation of solid elastic and thin elastic-shelled hollow spheres. It is concluded that target-phase measurements can enhance the classification performance of a suitably calibrated sonar system.

Invited Papers

5:00

5pUWc9. Evaluation of portable high-frequency sonars for diver identification. Anna Crawford (Defence R&D Canada Atlantic, P.O. Box 1012, 9 Grove St, Dartmouth, NS B2Y 3Z7, Canada, anna.crawford@drdc-rddc.gc.ca), Vance Crowe (Defence R&D Canada Atlantic, P.O. Box 1012, 9 Grove St, Dartmouth, NS B2Y 3Z7, Canada, vance.crowe@drdc-rddc.gc.ca), Thomas Pastore (NATO Undersea Research Centre, Viale San Bartolomeo 400, 19126 La Spezia, Italy, Pastore@nurc.nato.int), Ronald Kessel (NATO Undersea Research Centre, Viale San Bartolomeo 400, 19126 La Spezia, Italy, Kessel@nurc.nato.int)

Obtaining a positive identification is a critical step in most tiered harbour protection strategies for countering underwater intruders. It is generally recognised that sonar is one of the best tools for underwater imaging, however operating in a harbour environment presents challenges. As part of an on-going harbour protection research project, small easily portable high-frequency sonar systems are being investigated as a means to equip small response craft with intruder identification capability. Several systems are being considered, with the most comprehensive testing by DRDC to date being done on small Canadian-made sonars. Tests were conducted in local harbour waters in Halifax, Canada, and in La Spezia, Italy, through participation in the NATO Undersea Research Centre Response Against Diver Intrusions (RADI) joint trial, conducted in November 2007. A variety of small sonars and manned and unmanned response craft were used during the RADI trial. Evaluation of the performance of these devices for the task of diver identification in realistic conditions will be discussed.

5:20

5pUWc10. Features for propagation-invariant classification of underwater targets. Patrick Loughlin (University of Pittsburgh, 348 Benedum Engineering Hall, Dept. of Electrical & Computer Engineering, Pittsburgh, PA 15261, USA, loughlin@engr.pitt.edu), Greg Okopal (University of Pittsburgh, 348 Benedum Engineering Hall, Dept. of Electrical & Computer Engineering, Pittsburgh, PA 15261, USA, gno1@pitt.edu)

As sound propagates in shallow water, it is subject to frequency-dependent spreading and attenuation (dispersion and damping). In active sonar, these propagation-induced changes can be detrimental to automatic classification because the observed backscatter depends on the propagation environment and how far the wave has traveled. One way to address this problem is to develop propagation-invariant

features of the wave that can be used in automatic classification. In this talk, we present temporal, spectral, and cepstral moment-like features of a wave that are invariant per mode to dispersion and damping. Classification results on numerical simulations of the backscatter from different steel shells propagating in a Pekeris waveguide with damping and random variations will be presented. [Supported by ONR grants N00014-06-1-0009 and N00014-07-10355]

Contributed Paper

5:40

5pUWc11. MCM sensor requirements: performance measures. Samantha Dugelay (Dstl, Building A32, Winfrith Technology Centre, DT2 8WX Dorchester, UK, sdugelay@dstl.gov.uk)

This paper presents a comparison of two measures of performance suitable to characterise operational performance of mine hunting sonars in various environmental conditions. The first measure is a direct adaptation of information theory and bounds the capability of a sonar to distinguish between objects, i.e., a classification capability. The bounds take into account the amount of distinguishable pixels between objects and the statistical information content of each pixel. Successfully applied in Radar, this approach has also demonstrated the performance of synthetic aperture sonar at NURC using a Rayleigh distribution for statistical pixel distribution. The measure is now being further developed to include high resolution distributions such as K-law which readily appear in high resolution images. The second measure, Johnson's criteria aims to provide guidance on resolution required for operator detection, classification and identification. This measure originally derived from experiments on night vision images is now being modified to simultaneously incorporate target highlight and shadow information in varying environmental conditions. Finally, the predictions of these measures will in the future be compared to each other and to current system performances.

FRIDAY AFTERNOON, 4 JULY 2008 ROOM 342B, 2:20 TO 3:40 P.M.

Session 5pUWd

Underwater Acoustics and ECUA: Acoustic Data Fusion

Eric Maillard, Cochair
Reson Inc, Golet, CA, USA

Benoit Zerr, Cochair
DGA/GESMA, BP42, Brest Armées, 29240, France

Contributed Papers

2:20

5pUWd1. Multisegmentation of sonar images using belief function theory. Mounir Dhibi (ENSIETA E3I2, 2 rue François Verny, 29806 Brest Cedex 9, France, mounir.dhibi@ensieta.fr), Romain Courtis (I2ETA Romain Courtis, GESMA/SDP/GDM, BP 42, 29240 Brest Armées, France, Romain.Courtis@dga.defense.gouv.fr), Arnaud Martin (ENSIETA E3I2, 2 rue François Verny, 29806 Brest Cedex 9, France, arnaud.martin@ensieta.fr), Isabelle Quidu (ENSIETA - E3I2 Lab., 2 rue François Verny, 29806 Brest Cedex 9, France, isabelle.quidu@ensieta.fr)

Today side scan sonar is one of the most efficient sensors for Rapid Environment Assessment missions. Unfortunately, features extracted from a given area are strongly dependent on the relative position of the sensor (e.g., due to the shadow or the gain variation). That could conduct to a bad segmentation of the seabed. However, due to the fact that operational systems give very often multiple views of the same area we use the redundancy. In this work, we propose to fuse multiview segmentations in order to outperform the seabed classification. First we present a way to characterize the seabed using as a start point, a texture analysis in order to extract parameters on images. Then, a classification method allows allocating a class according to the type of sediment for the different standpoints. The proposed classifier fusion is based on the belief function theory. We present results from a set of experiments conducted to evaluate the proposed approach with real sonar images and we discuss them.

2:40

5pUWd2. Elimination of corner-turning in FFT-based sonar array beamforming. Jacob Barhen (Oak Ridge National Laboratory, 1 Bethel Valley Road, Oak Ridge, TN 37831-6015, USA, barhenj@ornl.gov), Travis Humble (Oak Ridge National Laboratory, 1 Bethel Valley Road, Oak Ridge, TN 37831-6015, USA, humblets@ornl.gov), Michael Traweek (Office of Naval Research, 875 North Randolph Street, Arlington, VA 22203, USA, Mike.Traweek@navy.mil)

The expected availability, in the near future, of an ultralow power version of the revolutionary IBM CELL multicore processor opens unprecedented opportunities for implementing sophisticated signal processing algorithms faster and within a much lower energy budget. The concept of "corner turning" has been, for many decades, at the heart of array beamforming via Fourier transforms. As widely reported in the open literature (both for sonars and radars), the computational sequence involving corner turning operations, i.e., the sequence: temporal Fourier transforms --> data cube corner turning --> spatial Fourier transforms, constitutes one of the primary obstacles to achieving high-performance and lower power dissipation (by reducing the number of times memory is accessed). Even with the emergence of novel multicore processors, leading providers (e.g., Mercury Computers) still include explicit corner turning stages in their computational flow architectures for multidimensional array processing. The primary innovation reported in this paper addresses the development of a computational scheme that avoids altogether the corner turning stage. We discuss its implementation on currently available CELL technology (65 nm SOI) and demonstrate close to an order of magnitude speed-up compared to the scheme with corner turning implemented on the same processor.

3:00

5pUWd3. Multiple-sensor fusion approach to seabed classification. Benoit Zerr (DGA/GESMA, BP42, 29240 Brest Armées, France, benoit.zerr@dga.defense.gouv.fr), David Kerneis (ENST Bretagne Dept. ITI, Technopôle Brest-Iroise - CS 83818, 29238 Brest Cedex 3, France, david.kerneis@enst-bretagne.fr), Basel Solaiman (ENST Bretagne Dept. ITI, Technopôle Brest-Iroise - CS 83818, 29238 Brest Cedex 3, France, basel.solaiman@enst-bretagne.fr)

Seabed classification is key issue for civilian and military underwater applications, from offshore exploitation to mine counter measure. Most of the existing automated classification techniques relies on the analysis of the data provided by a single sensor, supposed to unambiguously separate the different classes of seabed. In this paper we present a different approach which considers that, even if a sensor cannot tell the differences between two classes, classification will improve by considering that the seabed belongs to one of these two classes, and, further, that the analysis of the data from another sensor can resolve the ambiguity. For each sensor, the classification is achieved in a conventional way by feature extraction and supervised classification. The fusion of the results implements the theory of evidence through Dempster-Shafer method. After a description of the method, the paper discusses the experimental results from the fusion of information delivered by three sensors: an imaging sidescan sonar, a vertical echo sounder and an interferometric bathymetric sonar. The major part of the experimental data has been acquired by towed or hull mounted sensors. As these sensors are a subset of the payloads operated simultaneously by the new DGA-SHOM DAURADE AUV, preliminary seabed classification results in covert REA missions will also be presented and discussed.

3:20

5pUWd4. Acoustic data fusion devoted to underwater vegetation mapping. Claire Noel (Semantic TS, 39 Ch Buge, 83110 Sanary, France, noel@semantic-ts.fr), Christophe Viala (Semantic TS, 39 Ch Buge, 83110 Sanary, France, viala@semantic-ts.fr), Michel Coquet (Semantic TS, 39 Ch Buge, 83110 Sanary, France, coquet@semantic-ts.fr), Benoit Zerr (DGA/GESMA, BP42, 29240 Brest Armées, France, benoit.zerr @dga.defense.gouv.fr), Thierry Perrot (CEVA, Presqu'île de Pen Lan BP3, 22710 Pleubian, France, thierry.perrot@ceva.fr)

This paper presents research tasks conducted by SEMANTIC TS, in collaboration with GESMA, aimed to develop a mapping method for underwater vegetation lying on seabed. First stage is to develop a method for detecting and characterizing vegetation on the seabed using the acoustic response from a conventional single beam echo sounder. This new method is then operated simultaneously with multibeam sonar producing micro-relief information and side scan sonar providing gray scale levels associated with bottom reflectivity. Then fusion of these three data is processed. We show efficiency of these multisensor data fusion concept to get very precise seabed vegetation mapping in a way reducing truth control (video and diving investigations). Sensors and method accuracy allow obtaining, like in biomedical field, real 3D scan pictures of seabed vegetation. This study is first applied to posidonia and cymodocea, which play a key role in Mediterranean's echosystem. Then, extension of the method is investigated to address laminaria which may significantly affect the performance of acoustic and optical sensors used for sea-mines detection and this paper presents results of data fusion mapping on an Atlantic sea area covered by luminaria, studied and well known by the CEVA.

FRIDAY AFTERNOON, 4 JULY 2008 ROOM 342B, 4:00 TO 6:20 P.M.

Session 5pUWe

Underwater Acoustics and ECUA: Noise Suppression, Robust Direction of Arrival, and Target Strength Estimation

Georges Bienvenu, Cochair
Thales Naval Division, Thales Underwater Systems, France

Ronald A. Wagstaff, Cochair
National Center for Physical Acoustics, University of Mississippi, University, MS 38677, USA

Contributed Papers

4:00

5pUWe1. "Venus's-noisetrap" high-gain adaptive processor. Ronald A. Wagstaff (National Center for Physical Acoustics, University of Mississippi, University, MS 38677, USA, rwagstaf@olemiss.edu), Heath E. Rice (National Center for Physical Acoustics, University of Mississippi, University, MS 38677, USA, herice@olemiss.edu)

The Venus's-noisetrap is a high gain adaptive signal processor inspired by Venus's-flytrap, an insect eating plant. The Venus's-noisetrap utilizes single sensor or beamformed spectral data. It "traps" the data samples by modifying the governing equations in a manner that each spectral sample is adaptively "trapped" before averaging. The trapping process is a fluctuation-based temporal coherence determination of whether the time history in each spatial or spectral bin is signal or noise. Signals are set "free", while the noise remains trapped, blocking it from participating in the averaging process. For ocean acoustic data, the processor automatically identifies signals from submerged sources. In addition, the Venus's-noisetrap achieves large signal-to-noise ratio (SNR), high spectral and spatial resolution, and auto-identification of signals. The techniques that cause this processor to mimic the Venus's-flytrap will be discussed, and the method of continuously adapting the governing equations to the unpredictable signal and noise environment will be illustrated. Results will be presented to show the processor's large SNRs and corresponding enhancements in spectral and spatial resolution.

4:20

5pUWe2. Suppression of oceanic reverberation by subspace methods. Xuan Li (Institute of Acoustics, Chinese Academy of Sciences, 100080 Beijing, China, happyxuanli@hotmail.com), Xiaochuan Ma (Institute of Acoustics, Chinese Academy of Sciences, 100080 Beijing, China, maxc@mail.ioa.ac.cn), Chaohuan Hou (Institute of Acoustics, Chinese Academy of Sciences, 100080 Beijing, China, hch@mail.ioa.ac.cn)

Acoustic signal processing in shallow water environments is a challenging problem because of the presence of reverberation. Based on some models of reverberation, data from sensors array is pretreated to suppress reverberation. Considering reverberation as a sum of echoes of transmitted

signal, the principal component inverse (PCI) algorithm deletes the largest singulars of data matrix, which is constructed from array data. However, estimating a threshold which is needed in PCI is difficult in practice. In this paper, two new subspace methods, Deleting Big Eigenvalues and Subspace Projection are proposed. The two novel methods, substituting automatic signal-number estimation for threshold estimation, are operated via eigendecomposition. According to a simulation which takes broadband linear modulated frequency signal as transmitted signal, these two methods show a similar performance but smaller computing quantity compared with PCI.

4:40

5pUWe3. Coherent effects of flow- and pressure-hull of a generic submarine on target scattering in an active sonar performance model. Pieter Schippers (TNO-D&V-Underwater Technology, Oude Waalsdorperweg 63, Post Box 96864, 2509 JG The Hague, Netherlands, pieter.schippers @tno.nl)

Since the late eighties the sonar performance model ALMOST for active and passive sonar is under development at TNO. For active detection performance, first a point target was used, with a single target strength value dependent on parameters like aspect angle, based on measurements or other sources. However by now there is a demand for TS of ships and wakes with realistic dimensions and characteristics. A generic sub was modeled with additional software routines, as a pixel file. A newly developed time domain model for hull reflection was implemented, also using scattering pixels, assuming multiple scattering with damping in the metal hull layer. This extension of the pixel modelling is evaluated versus literature data. Some modeling results of target strength computations are shown, for a generic submarine with pressure hull, with aspect angle, frequency and bandwidth as parameters.

5:00

5pUWe4. Robust capon beamformer for port/starboard discrimination of twin-line array. Zaixiao Gong (National Laboratory of Acoustics, Institute of Acoustics, Chinese Academy of Sciences, NO.21, Bei-Si-huan-Xi Road, 100080 Beijing, China, gzx@mail.ioa.ac.cn)

Compared with the single-line array, the twin-line array have the potential to solve the port/starboard discrimination problem. Conventional method of geometric phase shifting has been used to distinguish the port/starboard of the target. But it can only be used to solve the problem when the frequency bandwidth is limited. The method based on optimum beamforming for hydrophone triplets can hardly be applied with the twin-line arrays. Aimed at the twin-line arrays port/starboard discrimination problem, a method based on the robust capon beamformer is proposed in this paper, which has advantages of concise algorithm and robustness against the aberration of the array shape. And the method works better with wider frequency bandwidth. Simulation and on sea experiment data are analyzed to verify the method.

5:20

5pUWe5. A numerical method for array sensor noise field calculation in detection performance optimization. Chao Sun (Institute of Acoustic Engineering, Northwestern Polytechnical University, 710072 Xi'an, China, csun@nwpu.edu.cn), Bo Yang (Institute of Acoustic Engineering, Northwestern Polytechnical University, 710072 Xi'an, China, yangbo@mail.nwpu.edu.cn), Yixin Yang (Institute of Acoustic Engineering, Northwestern Polytechnical University, 710072 Xi'an, China, yxyang @nwpu.edu.cn)

Different from the generally adopted criteria of minimizing the sidelobe level and maximizing the array gain in the weighting design of a sonar array, an approach was proposed recently to optimize the shading weights with the aim of maximizing the deflection coefficient in the square-law detector, which in essence suppresses the self-noise by including the noise information at array sensors in the optimization procedure. When several noise sources are present and/or an analytical expression of the noise transfer function is not available, the sensor noise needs to be measured in forming the sensor noise response cross correlation matrix required in the optimization which is very demanding when an array with large number of sensors is considered. To avoid the tedious work of noise measurement, a numerical method is developed in this paper. In this method, the main self-noise sources are assigned with different positions and strengths and the noise field at the array sensors is calculated via either the finite element method or the boundary element method. Tank experiment validated the effectiveness of this method. By using this method, the detection performance of a sensor array can be predicted before it is physically built and tested in under practical conditions.

5:40

5pUWe6. Improving spatial resolution of interferometric bathymetry in multibeam echosounders. Gerard Llort-Pujol (ENST-Bretagne, Dpt ITI, CS 83818, 29238 Brest Cedex 03, France, gerard.llort @enst-bretagne.fr), Christophe Sintes (ENST-Bretagne, Dpt ITI, CS 83818, 29238 Brest Cedex 03, France, christophe.sintes @enst-bretagne.fr), Xavier Lurton (Institut Français de Recherche pour l'Exploitation de la Mer, NSE/AS, BP 70, 29280 Plouzané, France, lurton @ifremer.fr)

Most multibeam echosounders used in seafloor mapping use the interferometry method for bathymetry measurement, based on the zero-crossing of the phase difference between two sub-arrays. In this approach, only one sounding is computed per formed beam, and the spatial resolution is linked to the beam footprint extent. Using the whole content of the phase difference signal vs time makes it possible ideally to get a bathymetry data sampled at the very resolution of the digitised signal. A trade-off is however to be found between this resolution improvement and the increase in the measurement noise. The performances of interferometric bathymetry are presented, together with the constraints of the resolution-accuracy trade-off, and a presentation of a high-resolution algorithm for interferometric bathymetry applicable to multibeam systems. This is illustrated by results obtained on a wreck, showing the remarkable improvement achievable in resolution over a real target. The potentialities for this method are promising, since it allows to process, in the same beam, targets on the seafloor and inside the water column; simplifications in multibeam sounders array structure and processing are also to consider.

6:00

5pUWe7. Adaptive removal of a known interference and its scattered energy. Yung P. Lee (SAIC, 4001 N. Fairfax Dr, Suite 175, mail stop 1-11-1, Arlington, VA 22203, USA, yung.p.lee@saic.com), William Lee (Duke University, Department of Electrical and Computer Engineering, Durham, NC 27708, USA, wwl3@duke.edu)

In underwater passive processing, the nearby fast moving loud surface ships produce nonstationary interference field and limit most sonar performance. After 9/11, AIS (automatic identify system) is required for ships larger than 60's, providing ground truth of positions, speeds, and other ancillary information for the nearby surface ships. This study investigates adaptive removal of a known loud signal using the ground truth information and acoustic propagation modeling. In addition, scattered energy away from the loud signal is identified through a delay correlation processing and is also removed. In a segment of MAPEX2k experiment conducted by SACLANT Centre off the west coast of Italy on November 28, 2000, the research vessel ALLIANCE towed an array at 2 m/s passing by a moored controlled source. The controlled source transmitted a loud 1-s 150-500 Hz LFM sequence every 15 s. In this setting, the fixed controlled source generated a nonstationary interference field received on the towed array. With the knowledge of the array tow track and source position the performance of removing the known interference and its scattered energy in a real shallow water environment is examined.

Session 5pUWf

Underwater Acoustics and ECUA: Sound Generation and Attenuation

Theodore G. Jones, Cochair
U.S. Naval Research Laboratory, Code 6795, 4555 Overlook Ave. SW, Washington, DC 20375, USA

Andrzej Zak, Cochair
Polish Naval Academy, Smidowicza 69, Gdynia, 81-103, Poland

Contributed Papers

4:40

5pUWf1. Neural classification of ships hydroacoustic signatures. Andrzej Zak (Polish Naval Academy, Smidowicza 69, 81-103 Gdynia, Poland, a.zak@amw.gdynia.pl)

The paper presents method of classification of hydroacoustic signatures generated by moving ship. Classification is a procedure in which individual items are placed into groups based on quantitative information on one or more characteristics inherent in the items. In this paper the hydroacoustics signals classification is understood as the process of automatically recognition what kind of object is generating acoustics signals on the basis of individual information included in generated sounds. Hydroacoustics signal classification is a difficult task and it is still an active research area. Automatic signal classification works based on the premise that sounds emitted by object to the environment are unique for that object. However this task has been challenged by the highly variant of input signals. The paper includes discussion about unique of sound generated by moving ships. To solve problem of hydroacoustic signatures classification the Kohonen networks which belongs to group of self organizing networks where chosen. Hydroacoustic signals were acquired on the Polish Navy Range during the complex ship measurement. At the end the results of classification of underwater noises made by ship were presented.

5:00

5pUWf2. Underwater acoustic generation with narrow and broadband lasers. Theodore G. Jones (U.S. Naval Research Laboratory, Code 6795, 4555 Overlook Ave. SW, Washington, DC 20375, USA, ted.jones@nrl.navy.mil), Melissa K. Hornstein (U.S. Naval Research Laboratory, Code 6795, 4555 Overlook Ave. SW, Washington, DC 20375, USA, melissa.hornstein@nrl.navy.mil), Antonio C. Ting (U.S. Naval Research Laboratory, Code 6795, 4555 Overlook Ave. SW, Washington, DC 20375, USA, antonio.ting@nrl.navy.mil), Zachary W. Wilkes (Research Support Instruments, Inc., 4325 Forbes Blvd, Ste B, Lanham, MD 20706, USA, zachary.wilkes@nrl.navy.mil), Dennis A. Lindwall (U.S. Naval Research Laboratory-Stennis, Marine Geosciences Division, Code 7432, Stennis Space Center, Stennis, MS 39529, USA, lindwall@nrlssc.navy.mil)

Underwater laser acoustic sources, generated by intense pulsed lasers on above-water and underwater platforms, are under investigation. In a novel configuration, a tailored intense broadband laser pulse can be designed to propagate many meters underwater and compress at a predetermined remote location. Controlled compression of these optical pulses is governed by a combination of optical group velocity dispersion (GVD) and nonlinear Kerr self-focusing, resulting in photoionization, localized heating, and shock generation. Recent and ongoing experiments include near-field acoustic source characterization using lens-focused pulses of a broadband 400 nm Ti: sapphire laser, as well as 1064 nm and 532 nm narrowband YAG laser pulses. Also, the nonlinear optical Kerr index of water at 400 nm was precisely measured. Acoustic source characterization includes measurements of photoacoustic energy conversion efficiency, acoustic power spectrum, and directivity. Experimental results will be presented, and laser sources and techniques for underwater acoustic generation will be compared. [This work is supported by the U.S. Office of Naval Research.]

5:20

5pUWf3. Recent progress on the theoretical modeling of underwater acoustics induced by sonic booms. Johnson C. Wang (The Aerospace Corporation, System Planning and Engineering, El Segundo, CA 90245-4691, USA, Johnson.C.Wang@aero.org), Charles P. Griffice (The Aerospace Corporation, System Planning and Engineering, El Segundo, CA 90245-4691, USA, Charles.P.Griffice@aero.org), Adam M. Fincham (University of Southern, Aerospace & Mechanical Engineering, 854 W Downey way, Los Angeles, CA 90089-1191, USA, afincham@usc.edu), John R. Edwards (U. S. Air Force, Air Force Space Command, 483 N. Aviation Blvd., El Segundo, CA 90245-2808, USA, John.Edwards@LOSANGELES.AF.MIL), Adel A. Hashad (U. S. Air Force, Air Force Space Command, 483 N. Aviation Blvd., El Segundo, CA 90245-2808, USA, Adel.Hashad@LOSANGELES.AF.MIL)

This paper, review and status in nature, consists of three parts: (1) The salient nature and results of the published papers from an ocean sonic boom (OSB) project will be reviewed including theoretical and experimental studies of the wavy surface effect on the underwater acoustics, a three-dimensional theory of underwater acoustics and the underwater acoustics induced by a sonic boom traveling at hyper-velocity speeds. (2) New unpublished results will be reported including studies of sonic boom underwater overpressures affected by ocean finite depth and ocean stratification (variable sound speed). These studies are possible due to the derivation of a semi-similar transformation for the underwater acoustics governing equations and the application of high performance computers. (3) The preliminary results of the work-in-progress will also be discussed including three-dimensional extensions of former professor H. K. Cheng's two-dimensional wavy surface theory and laboratory verification.

5:40

5pUWf4. Influence of a resonance changer on the sound radiation of a submarine. Sascha Merz (University of New South Wales, School of Mechanical and Manufacturing Engineering, 2052 Kensington, Australia, sascha.merz@gmx.net), Roger Kinns (University of New South Wales, School of Mechanical and Manufacturing Engineering, 2052 Kensington, Australia, roger.kinns@aol.com), Nicole J. Kessissoglou (University of New South Wales, 2052 Sydney, Australia, n.kessissoglou@unsw.edu.au)

In order to reduce the excitation of the submarine hull through the shaft, a vibration attenuation system, called a resonance changer, can be implemented in the propeller/propulsion system. The effectiveness of such a system in reducing the low frequency sound radiation characteristics of a submarine is investigated. Only sound radiation due to fluctuating propeller forces, which are generated by the operation of the propeller in a nonuniform wake, is considered. These fluctuating forces are transmitted to the submarine hull through the fluid, as well as through the propeller shaft. Both

types of excitation cause hull vibration and sound radiation. The accordion modes of the pressure hull, are particularly efficient sound radiators. Parameters for the resonance changer system have been optimised previously by considering only excitation of the hull through the shaft. It is shown that the effectiveness of the resonance changer at different frequencies is modified significantly in a typical full-scale implementation, due to the sound radiation from the propeller. The effect on performance is increased further when the vibration of the propeller itself is taken into account. Therefore overall optimisation of any resonance changer system requires a comprehensive model. Some of the principal effects are explored in this paper.

6:00

5pUWf5. The research on measuring the coefficient of sound absorption in turbid seawater. Qi Li (Harbin Engineering University, College of Underwater Acoustic Engineering, 150001 Harbin, China, chizhafengyun1979@126.com), Yongwei Liu (Harbin Engineering University, College of Underwater Acoustic Engineering, 150001 Harbin, China, chizhafengyun1979@126.com)

When naval mine-hunting sonars and side-scan surveying sonars operating at 20~60 kHz are working in shallow coastal waters, the viscothermal absorption of sound by suspended mud in the water may greatly decrease their detection properties. This kind of water is also characterized as turbid seawater. However, the research on measuring the coefficient of sound absorption in turbid seawater has little been done. The main difference between turbid seawater and clear seawater is that there are mud particles suspending in turbid seawater. It is also the main reason why sound absorption in turbid seawater is greater than that in clear seawater. In the paper, the coefficient of sound absorption at 20~60 kHz in turbid seawater has been measured by the reverberation technique. Results demonstrate that if the concentration of the mud is bellow 0.11 kg/m^3, the mud in turbid seawater doesn't cause additional absorption. When the concentration of the mud is between 0.14 and 0.49 kg/m^3, the coefficient of sound absorption in turbid seawater is as twice at least as that in clear seawater.